JOURNAL OF AGRICULTURAL AND FOOD CHEMISTRY

Editorial

pubs.acs.org/JAFC

Future Has Tradition in *JAFC*, but Tradition, Too, Has a Future!

The landscape of scientific publishing is continually changing. A vast number of new journals are sprouting out of the ground. Many of these new journals are miniaturized in scope or limited by a narrow readership. In comparison, the *Journal of Agricultural and Food Chemistry* (*JAFC*) is firmly rooted in a long tradition of publication excellence in the broader chemistry and (bio)technology of agricultural and biobased materials all the way up to food products including bioactivity, nutritional, and health aspects. Since its foundation in 1953 with Walter J. Murphy as the first Editor-in-Chief, *JAFC* has become the most influential journal in agricultural and food chemistry. Over 5500 world-leading scientists serve as peer reviewers each year. In 2013, the journal had over 82000 citations, over 2 million article requests, and published more than 1500 papers, the most ever.

As new Editor-in-Chief, there is no better purpose for my first Editorial than to acknowledge the contributions of Jim Seiber to *JAFC*. Jim successfully navigated *JAFC* for 15 years; under his tenure the journal developed greatly with an increase of yearly manuscript submissions by more than 300%, yearly published article content by more than 45%, total number of citations to *JAFC* by nearly 375%, and a rise of the impact factor to 3.107. Backed with the excellent support of the ACS, Jim decreased the time it took accepted papers to reach our global readership.

Acting in wise foresight, Jim and *JAFC*'s passionate Associate Editors widened the scope of the journal and reacted flexibly to the ever-changing multidisciplinary arena of agricultural and food chemistry by timely introduction of new categories such as metabolomics, new formats such as Letters, and new author recognition tools such as the *JAFC* Research Article of the Year Award. Not only has the number of Associate Editors grown from 5 to 12, but also the global presence of *JAFC* has increased significantly. As cutting-edge research in *JAFC* continues to become more global, the composition of the team of Associate Editors is more international than ever before, and I expect this trend to continue: Hanne Christine Bertram (Denmark), Zhen-Yu Chen (China), John W. Finley (USA), Chi-Tang Ho (USA), Yoshinori Mine (Canada), Russell Molyneux (USA), Peter Schieberle (Germany), Taka Shibamoto (USA), Veronika Somoza (Austria), Francisco Tomás-Barberán (Spain), Elisabeth Waters (Australia), Liangli (Lucy) Yu (USA). Jim and the Associate Editors could always build on the contributions of the engaged members of the Editorial Advisory Board supporting *JAFC* in agenda setting and manuscript decision making. In an extraordinary show of service to the journal, Fereidoon Shahidi, Gow-Chin Yen, and Michael Clifford have provided more than 30 manuscript reviews over the past 3 years. Backed by all of these active supporters and continually refreshed with new science and innovative features, it is not surprising that *JAFC* retained leadership as the most cited journal in the three ISI categories "Agriculture", "Applied Chemistry", and "Food Science and Technology". Jim deserves our hearty thanks for these achievements!

So, as a welcome to 2015, first let me share an Editor's overarching goal for the coming year - that the Associate Editors and I will work hard to ensure that *JAFC* remains the premier journal in which to publish authors' most impactful and innovative science. Although submissions are increasing from all around the globe, the submitted manuscripts will be handled by an Associate Editor having the appropriate expertise, no matter where the authors are from or where the Editor is geographically located. Thus, while we have an increasingly international team of excellent Associate Editors, the defining aspect of the manuscripts we publish should be their outstanding science, not the country of origin. *JAFC* will further expand its tradition to develop strong, largely ramified roots. These will help our fundamental knowledge to continuously flourish, while concurrently germinating internationally to reach best-in-class scientists developing and applying new molecular tools and technologies to solve global challenges in agricultural and food research. *JAFC* is more than ever on the spot. Here's to an exciting 2015!

Thomas F. Hofmann, Editor

AUTHOR INFORMATION

Notes

Views expressed in this editorial are those of the author and not necessarily the views of the ACS.

Published: January 14, 2015

ACS Publications © 2015 American Chemical Society

DOI: 10.1021/jf506125u
J. Agric. Food Chem. 2015, 63, 1−1

JOURNAL OF AGRICULTURAL AND FOOD CHEMISTRY

Editorial

pubs.acs.org/JAFC

Reviewer List 2014

The Editor and Associate Editors gratefully acknowledge the following scientists for reviewing manuscripts during 2014. Many of these individuals reviewed several manuscripts. We thank all of the reviewers for their contributions of time and talent. Note: this list reflects reviews received between November 11, 2013, and November 30, 2014.

Kjersti Aaby
Lotfi Aarab
John A. B. Aasen
Margit D. Aaslyng
Javier Abadía
Antonio Abad-Somovilla
Faridah Abas
Mohamed Saad Abbady
Ouissam Abbas
A. M. Abd El-Aty
El-Sayed M. Abdel Aal
Anas Abdel Rahman
Emilia Abdulmalek
Keiko Abe
Saman Abeysekara
K. R. W. Abeywickrama
Maher Abou Hachem
Ehab A. Abourashed
Sameh Fekry AbouZid
Veronika Abram
Christelle Absalon
Marijana M. Ačanski
Cesare Accinelli
Maurizio Aceto
Durga Acharya
Bradley Ackermann
Rita Acquistucci
Shuji Adachi
Douglas O. Adams
Adeleke A. Adeniyi
Bibhutosh Adhikary
Steffen Adler
Marielle Adrian
A. G. Gopalakrishna
Giovanni Agati
Evgenios Agatokleous
Agnes Ageorges
Eduardo Agosin
Gennaro Agrimi
Julio C. Aguilar-Cordero
Yolanda Aguilera
Vivek Ahluwalia
Dong U. Ahn
Guomin Ai
Yongfeng Ai
Mitsugu Akagawa
Miki Akamatsu
Humayoun Akhtar
Tsunehiro Aki
Nagao Akihiko
Jaap Akkerdaas
Casimir C. Akoh
Ozlem Akpinar
Abdurrahman Aktumsek
Samsul Alam
Cesarettin Alasalvar
Saphwan Al-Assaf
Triantafyllos A. Albanis
Katherine T. Alben
Poreda Aleksander
Katerina Aleksieva
F. Alen
Herve Alexandre
W. Russ Algar
Jafar Al-Hakkak
Ahmed M. Al-Jabr
Jeremy Allen
Ana Allende
Günter Allmaier
Agostinho Almiro Almeida
Leonor Almeida
Luis Almela
Diego López Alonso
Gonzalo L. Alonso
Jose L. Alonso
Rosa Maria Alonso-Salces
Prof. Rotimi Aluko
Rotimi E. Aluko
Renato Amadò
Yoshiaki Amakura
Edna Regina Amante
Joana Soares Amaral
Ryszard Amarowicz
Jennifer M. Ames
Dragan Amić
Antonella Amicucci
Jose Manuel Amigo
Lourdes Amigo
Tejraj M. Aminabhavi
Mahmoud Aminlari
Kamalakannan Anbarasu
Gaby Andersen
Øyvind M. Andersen
James V. Anderson
Mirjana Andjelkovic
Anna Andolfi
Jose M Andrade
José Paulo Andrade
Juan E. Andrade
Paula B. Andrade
Silvana Andreescu
Anders Andren
Sonia Andrés
Donato Andueza
Isabel Andujar
Skelte G. Anema
Monica Anese
Laura Anfossi
Cristina Angeloni
Alberto Angioni
Caroli Anna
María Cristina Añón
Enriqueta Antico
Maria N. Antipina
M. Carmen Antolín
Andrea Antonelli
Zofia Antoszkiewicz
Takayoshi Aoki
Reşat Apak
Ramon Aparicio
Constantin Apetrei
Zeno Apostolides
Michael Appell
Eugenio Aprea
Farrukh Aqil
Juan Alberto Arancibia
Mirta Ines Aranguren
Panagiotis Arapitsas
Maria Eduarda Machado Araujo
André Araújo
Michel Mozeika Araújo
Vicent Arbona
Lourdes Arce
Douglas D. Archbold
Anna Ardevol
Ardiansyah Ardiansyah
Dimitris S. Argyropoulos
Renée Silvia Arias
Sakae Arimoto-Kobayashi
Ana C. M. Arisi
Kaoru Ariyama
V. Arjunan
Marco Arlorio
Kevin Armbrust
John Thor Arnason
Tim Arndt
Juergen Arnhold
Anna Arnoldi
Susan D. Arntfield
Luis Arola
Naveen Arora
Daniel Arrieta-Baez
Javier Arrizon
Francisco Teodoro Arroyo
Francisco Noé Arroyo López
Derya Arslan
Idris Arslan
Alejandro Arteaga
William E. Artz
Joseph Arul
Tomiko Asakura
Stefan Asam
Tadao Asami
Maxwell Darko Asante
Maria Asensio Ramos
Muhammad Asgher
Hitoshi Ashida
Vincent M. Asiago
Ramon Asis
Ruhan Askin Uzel
Iciar Astiasaran
Linda S. Aston
Thierry Astruc
Vessela Atansova-Penichon
Anne-Marie Aucour
Joong-Hyuck Auh
Anna-Marja Aura
Pinarosa Avato
Khalijah Awang
Joseph Awika
Mehmet Ay
J. Fernando Ayala-Zavala
Rahim Aydin
Belen Ayestarán Iturbe
June E. Ayling
Maria Jose Ayora-Cañada
Arash Azarfar
Ricardo Antunes Azevedo
Elena Azzini
K. Suresh Babu
Sabulal Baby
Benoit Bach
Thomas Bach
Michael Backes
Charles Wilson Bacon
Tomasz Baczek
Melissa A. Badding
Vladimir Badmaev
Kwang-Hyun Baek
Seung Joon Baek
Hyung Hee Baek
Scott Baerson
Jeroen J. Baert
Maria E. Baez
Bojlul Bahar
Theeshan Bahorun
Naisheng Bai
Roberto Baigorri
Istvan Bak
Alan T. Bakalinsky
Mikhail Yurievich Balakshin
Rafael Balart
Manimalha Balasubramani
Susanne Baldermann
Rafik Balti
Takeshi Bamba
Charles William Bamforth
Benjamin Bandowe
Brian Bandy
Punam Bandyopadhyay
Kaushik Banerjee
Vassya S. Bankova
Grigor B. Bantchev
Jie Bao
Jinsong Bao
Ning Bao
William E. Barbeau
Reyes Barbera
Luiz Claudio Almeida Barbosa
Biancamaria Baroli
María Verónica Baroni

Published: January 14, 2015

ACS Publications © 2015 American Chemical Society

DOI: 10.1021/jf506178r
J. Agric. Food Chem. 2015, 63, 2−18

Leila M. Barraj
Célia Barril
Sheryl Barringer
Russell A. Barrow
Veronique J. Barthet
Elena Bartkiene
John P. Bartley
Begoña Bartolome
Veronika Bartova
Eduardo Bárzana
K. Husnu Can Baser
Deborah Helena Markowicz Bastos
Soumalee Basu
Arpita Basu
Samita Basu
Max Batenburg
Ian Batey
Graeme D. Batten
Maurizio Battino
Stefan Bauer
Sabine Baumgartner
Ana-Belen Bautista-Ortin
Luigi Bavaresco
Kaleab Baye
Taner Baysal
Isabel López Bazzocchi
Daniel W. Bearden
Jonathan Beauchamp
Adilson Beatriz
Aurelie Bechoff
John J. Beck
Emilene Becker
J. Ole Becker
Gudrun Beckh
Diane M. Beckles
Sabina Maria Bednarska
Mohammad Behbahani
Ross C. Beier
Donald Clarence Beitz
Horacio Ramon Beldomenico
Leonard N. Bell
Luke Bell
Nacer Bellaloui
Denis Bellenot
José María Belles
Luis A. Bello-Perez
Josefina Belloque
Isabel Belo
Rachid Bel-Rhlid
Peter S. Belton
James Noble BeMiller
Aladar F. Bencsath
Justin Garfield Bendall
Alessandra Bendini
Carlos Bengoechea
Vanesa Benítez
Soottawat Benjakul
Ofir Benjamin
Noureddine Benkeblia
Catherine Bennetau-Pelissero
Rodney M. Bennett
Abby D. Benninghoff
Mekki F. Bensaci
Shimshon Ben-Yehoshua
Bjorn J. A. Berendsen
Alexander Berestetskiy
Thorsten Berg
Enrico Bergamaschi
Ralf Günter Berger
Gary Bergstrom
Mark A. Berhow
Maria Dolores Bermejo
Pilar Bermejo-Barrera
José Bernal
Mark A. Bernards
Matthew W. Bernart
Houda Berrada
Lucia Bertacchini
Davide Bertelli
Franz Berthiller
Michele Correa Bertoldi
Claire Berton
Paula Berton
Hanne C. Bertram
Pascale Besse
Joseph M. Betz
Till Beuerle
Dejan Bezbradica
Vijai Bhadauria
Ritu Bhalla
Rakesh Bhardwaj
Mahalingeshwara Bhat
Rajeev Bhat
Prashant Kumar Bhattacharya
Haq Bhatti
Kamlesh Kumar Bhutani
Kaishun Bi
Dobroslawa Bialonska
Armandodoriano Bianco
Martin Biendl
Ross Bierer
Sebastiaan Karel An Bijttebier
Katarina Bíliková
Andrew Billin
Gerald F. Bills
Keren A. Bindon
Lucia Birosova
Marc Birringer
Bruce R. Bistrian
Ashim Kumar Biswas
H.C. Bittenbender
Barbara A. Blackwell
Diane A. Blake
Barry Blakely
Pilar Blanco
Andreas Blank
Ralf Harald Blank
Georgios Blekas
Eric Block
Louis Bluhm
Frank D. Blum
Linda Blythe
Maria Amélia Diamantino Boaventura
Otilia Bobis
Vivian Caetano Bochi
Ulrike Böcker
Volker Boehm
Rafal Bogel-Lukasik
Paolo Bogoni
Eduardo Boido
Bradley Warren Bolling
Ivana Bonaccorsi
Giovana Bonat Celli
Isabel Bondia-Pons
Pascal Bonnarme
Jean-Louis Bonnemain
Estelle Bonnin
Francesco Bonomi
Monica Bononi
Josep Serra Bonvehí
Graham Bonwick
Lee Boon-Beng
Miguel Angel Bootello García
Melike Bor
Matteo Bordiga
Alessandra Bordoni
Albert Bordons
Wlodzimierz Borejsza-Wysocki
Søren Borg
Grethe Iren A. Borge
Daniel L. G. Borges
Laurent F. Bornaghi
Katalin Böröczky
Giorgio Borreani
Giovanna Boschin
Sankhadip Bose
Geertrui Bosmans
Paul Kenneth Boss
Goreti Botelho
Christo Botha
Alessandro Botton
Ricard Bou
Mohamed Bouaziz
Stephen M. Boue
Dominique L. Bouglé
Annaïg Bouguennec
Mohamed Bouhache
Renaud Boulanger
Nathalie Bourgougnon
I. Bousova
Rachel Boutrou
Michael Bowman
Mara Elga Medeiros Braga
Neura Bragagnolo
Gianfranco Brambilla
Peter Michael Bramley
Ferdinando Branca
Adriano Brandelli
Andrea Brandolini
Vincenzo Brandolini
David L. Brandon
Kirsten Brandt
Marcus Brandt
Eleonora Braschi
Annett Braune
Laura Bravo
Andreas Breidbach
Harald Breivik
Andrew P. Breksa
Harald Brelid
Beatriz Margarita Brena
Manuel Brenes
Barbara Brezna
Ana Briones Perez
Michel Britten
Steven Britz
Karlis Briviba
C. Leigh Broadhurst
Stefania Brocca
Jens Brockmeyer
Andre Brodkorb
Inge Broer
Elvino Brosio
Chantal Brossard
Nicolas Brosse
Eleanor M. Brown
Paul D. Brown
James H. Bruce
Roque Bru-Martínez
Eva María Brun
Philip D. Brune
Pascal Brunerie
Markus Brunnbauer
Rolfe J. Bryant
Wayne Bryden
Marcin Bryła
Franz Bucar
Grazyna Budryn
Mark Buecking
Carmen Bueno
Andrea Buettner
C. Bugaud
Astrid Buica
Metin Bulbul
Mirko Bunzel
Katia Buonasera
Giovanna G. Buonocore
Hester Burger
Kent Burkey
Maksim A. Burkin
Betty Burri
Britt M. Burton-Freeman
Ulrich Busch
Lowell P. Bush
Rodney J. Bushway
Mark Busman
Pablo Busti
Jesus H. Busto
Guadalupe Bustos
Vito Macayan Butardo
Ronald G. Buttery
Peter Butz
Christian Butzke
Jean-Claude Bwanganga Tawaba
Michal Bystrzejewski
Ana Isabel Cabañero
Pierluigi Caboni
Maria Fiorenza Caboni
Gustavo Cabrera
Estrella Cadahía
Solange Cadore
Yves Cadot
Keith R. Cadwallader
Thomas Michael Cahill
Kezhou Cai
Shumei Cai
Yizhong Cai
Stefano Caldarelli
Angela I. Calderón
Ana María Calderón De La Barca
Augusta Caligiani
Ángel Calín Sánchez
Damien L. Callahan
Antonis C. Calokerinos
Marta M. Calvo
José Sousa Câmara
Alejandra B. Camargo
Maria Manuela Camino Feltes
Mary Ellen Camire
M. Cammarata
Jerry Campbell
Natalia Campillo
Nafiz Oncu Can
Joan-Miquel Canals
Beatriz Cancho
Alan A.G. Candlish
Ramon Canela-Garayoa
Joaquin Canizares
Francis Canon
Maria H. G. Canteri
Celia Maria Cantin
Charles Lowell Cantrell
Aocheng Cao
Jay Cao
Min-Jie Cao
Rihui Cao
Shifeng Cao
Yuhua Cao
Flavio Capettini
Jack C. Cappozzo
Ivana Caputo
Leonardo Caputo
Katya Carbone
Ángel A. Carbonell-Barrachina

DOI: 10.1021/jf506178r
J. Agric. Food Chem. 2015, 63, 2−18

Marie-Annette Carbonneau
Marcella L. Card
Anaberta Cardador-Martinez
Vladimiro Cardenia
Daniel Rodrigues Cardoso
Susana Maria Cardoso
Mercedes Careche
Anna L. Carew
Amanda N. Carey
Reinhold Carle
Celia R. Carlini
Manuel Carmona
Didac Carmona
Francisco M. Carrau
Mary C. Carson
Elena Cartea
Donatella Caruso
John A. Carver
Julio Casado
Susana Casal
Monica Casale
Isidre Casals
Agostino Casapullo
Osvaldo Cascone
E. Casero
Araceli Castañeda-Ovando
Jose Maria Castellano
Massimo Castellari
Maria Antonietta Castiglione Morelli
Patrice Castignolles
Laurence Castle
Inar Alves Castro
Lucia Castro-Vazquez
Pablo Federico Cavagnaro
Roberta Cavalli
Ivana Cavoski
José Antonio Cayuela Sánchez
Tommy Licht Cederberg
Mehmet Fatih Cengiz
Ana M. Cenzano
Alberto Cepeda
Christoph Cerny
Zoran Cerovic
Fátima Cerqueira
Miguel A. Cerqueira
Lorenzo Cerretani
Carlos L. Cespedes
Carlos Leonardo Cespedes-Acuna
Juan Manuel Cevallos-Cevallos
Yong Jun Cha
Brigitte Chabbert
Ming Chai
Kelly D. Chamberlin
Odile Chambin
Verawat Champreda
Jerry Chun Chung Chan
Anuj Chandel
Prtap Chandran
Rufus Chaney
Chen-Tien Chang
Shang-Tzen Chang
Yuhua Chang
Yuan-Shiun Chang
Yung-Ho Chang
Tsu-Chung Chang
Tsong-Min Chang
Shu-Wei Chang
Sam K.C. Chang
Pahn-Shick Chang
Ke Liang Bruce Chang
Hong Chang
Hee-Ra Chang
Fang-Rong Chang
Hebron C. Chang
Saksit Chanthai
Louis Kuoping Chao
Pei-Min Chao
Yun-Peng Chao
Maria José Chapela
Denis Charlebois
Stefan Chassaing
Parnali K. Chatterjee
Subrata Chattopadhyay
Chi Fai Chau
Abdul Shakoor Chaudhry
Qasim Chaudhry
Rajinder Singh Chauhan
Anurag Chaurasia
Clemencia Chaves-Lopez
C. T. Che
Kranthi Chebrolu
Luis Chel-Guerrero
Prasanth Chelikani
Duraisamy Chellappa
Farid Chemat
H.-C. Chen
Quansheng Chen
Wei-Jen Chen
Wei Chen
Tianfeng Chen
Tao Chen
Shouwen Chen
Shiguo Chen
X. Q. Chen
Shao-Nong Chen
Ruei-Ming Chen
Qing-Xi Chen
Qihe Chen
Po Ting Chen
Pei Chen
Lingyun Chen
Lingxin Chen
Xiao-chun Chen
Ligang Chen
Yen-Chou Chen
Liang-Yu Chen
Lih-Geeng Chen
Yi-Chen Chen
Liang Chen
Zhongxiu Chen
Zhongxiao Chen
Zhi-Gang Chen
Zhen-Yu Chen
Zhao Chen
Yu-Kuo Chen
Yue-Hwa Chen
Yanyi Chen
Yi-Chen Chen
Xiaohui Chen
Xiaoyan Chen
Yeming Chen
Yanping Chen
Yang Chen
Xiaoyan Chen
Xiaoxin (Luke) Chen
Xiaowen Chen
Xiao-Qing Chen
Xiaoqiang Chen
YiWen Chen
Cong-gui Chen
Hongda Chen
Bing Huei Chen
Haifeng Chen
Xin Chen
Guonan Chen
Gu Chen
Feng Chen
Hong-Jhang Chen
C.-Y. Oliver Chen
Haimin Chen
Chun-Jung Chen
Chung-Yi Chen
Chu-Chin Chen
Ching-Shih Chen
Ching-Hsein Chen
Charles Huang Chen
Bo Chen
Bingcan Chen
Li Chen
Diejun Chen
Jiluan Chen
Lei Chen
Lanzhen Chen
Kunsong Chen
Kuan-Chou Chen
Kai Chen
Junhui Chen
Jonathan Chen
Guoying Chen
Jin-Chung Chen
Hongping Chen
Jih-Jung Chen
Hsi-Jen Chen
Hongzhang Chen
Jiping Chen
Hsien-Jung Chen
Jie Chen
Huadong Chen
Hu-biao Chen
Hui Chen
Ih-Sheng Chen
Jian-ye Chen
Hsiao-Ling Chen
Luisa W. Cheng
Zhiliang Cheng
Zhihong Cheng
Yu Cheng
Yongqiang Cheng
Pi Cheng
Ning-hui Cheng
Kun Cheng
Kuan-Chen Cheng
Juei-Tang Cheng
H. N. Cheng
Baohui Baco Cheng
Chun-Wen Cheng
Lai Hoong Cheng
Gita Cherian
Lesley Ann Chesson
Irene Chetschik
Hon-Yeung Cheung
Peter C. K. Cheung
Francois Chevalier
Eng-Hui Chew
Veronique Cheynier
Y.-J. Chi
Meng-Tsan Chiang
Wen-Dee Chiang
Chung-Jen Chiang
Emma Chiavaro
Kazuhiro Chiba
Lee I. Chiba
Ravindra Nath Chibbar
Yoshito Chikaraishi
Koo B. Chin
Young-Won Chin
Robin Y.-Y. Chiou
Chureeporn Chitchumroon-chokchai
Wan-Chun Chiu
Myeong-Cheoul Cho
Chung Y. Cho
Suwimol Chockchaisawasdee
DuBok Choi
Jae Sue Choi
Sang-Won Choi
Wahn Soo Choi
Woo-Jung Choi
Young Hae Choi
Jean-François Chollet
Meng Nan Chong
Jaebum Choo
Nikolaos Chorianopoulos
Jyh-Ching Chou
Shen-Chieh Chou
Tzung-Han Chou
Moncef Chouaibi
Partha Pratim Choudhury
Ashim Chowdhury Chowdhury
Lars Porskjær Christensen
Soren Brogger Christensen
Kathrine Bisgaard Christensen
Philip Christenson
Miltiaidis V. Christopoulos
Ching-Liang Chu
Ivan K. Chu
Yung-Lin Chu
Pin Ju Chueh
Sung Hyun Chung
Namhyun Chung
Yun-Chin Chung
Stephen Wai Cheung Chung
Donghwa Chung
Ching-Hu Chung
Hau Yin Chung
Charng-Cherng Chyau
Raúl Esteban Cian
M. Ciani
Maria Antonietta Ciardiello
Margit Cichna-Markl
Alicia Graciela Cid
Lukasz M. Ciesla
Victor Cifuentes
Blaz Cigic
Antonio Cilla
Francesco Cimino
Alessio Cimmino
Bruno Cinel
Ewa Ciska
Fausto H. Cisneros
Debra Arwood Clare
Andrew C. Clark
David Alan Clark
Robert Daniel Clark
Morten R. Clausen
Keith Clay
Gary Clayton
Alain Clement
Alfonso Clemente
Michael N. Clifford
Paola Coccetti
L. Cocolin
Mehmet Coelhan
Seth Cohen
Manuel A. Coimbra
Mary Florence Cole
Steven Mark Colegate
M. D. Coleman
Mark G. Collett
Sonia Collin

DOI: 10.1021/jf506178r
J. Agric. Food Chem. 2015, 63, 2−18

Luiz Alberto Colnago
Ian J. Colquhoun
Stefania Colombini
Mario Colucci
Emilie Combet
Giuseppe Comi
Michael A. Conlon
John M. Conner
Sean Connor
Roberto Consonni
Lanfranco Conte
Pellegrino Conte
Paolo Conti
Sandro Conticelli
María del Mar Contreras
Daniel Cook
Jo Marie Cook
Daniel Cooley
Jamie A. Cooper
Valerie Copie
Jana Copikova
Zulema Coppes
Juan-José R. Coque
Rodrigo Coqui da Silva
Beatriz Rosana Cordenunsi
Roger Corder
Chiara Cordero
Daniel Cordova
Harold Corke
Claus Cornett
Danilo Corradini
Benedito Correa
Roberta Targino Pinto Correia
Manuela Correia
Nieves Corzo
Fernanda Cosme
Joana Costa
Greg L. Cote
Paul Counce
Dirk Courtheyn
Daniel Cozzolino
Rosaria Cozzolino
Benedikt Cramer
Rebecca Creamer
Glen L. Creasy
Darren J. Creek
Mauro Andrea Cremonini
Carlo Crescenzi
P. Cressey
Claudia Crestini
Colin Crews
Kevin D. Croft
Thomas Croguennec
Timothy R. Croley
Paul Cronje
Quentin Cronk
Gerard Cros
Jean-Claude Crouzet
Stephen J. Crozier
Alan Crozier
Adriano Cruz
Rui Cruz
Hugo Cruz-Hipolito
Carmen Cuadrado
Rosa Paula Odejar Cuevas
Jian Dong Cui
Paolo Curir
Elena Curti
Chris Curtin
Theresa Curtis
Andreas Czepa
Jaroslaw Czubinski
Agata Czyżowska
Neil C. Da Costa
Maria Fátima das Graças Fernandes Da Silva
Roberta Claro da Silva
Maria Daglia
Zhiyuan Dai
Ziyu Dai
Susie Y. Dai
Bojie Dai
Grazyna Dajbrowska
Bruce E. Dale
Brian Dalrymple
Trine Kastrup Dalsgaard
Norelle Daly
Julie Dalziel
Robert G. Dambergs
Stefano D'Amico
Ji Dan
Martin Danaher
Olivier Dangles
Dganit Danino
Dennis Dannehl
Dirk Dannenberger
Alessandro D'Annibale
Hussein Gehad Daood
Philippe Darriet
Kishore Das
Undurti N. Das
Manashi Das Purkayastha
Swagata Dasgupta
Sukalyan Dash
Keyvan Dastmalchi
Maurizio D'Auria
Alberto Davalos
Michel Daveau
Tomas Davidek
Noel W. Davies
Peter L. Davies
Kevin Davies
Mark Franklin Davis
Corinna Dawid
Martin Day
Franck E. Dayan
Godwin Basil D'Cunha
Ignacio de Alfonso
Begoña De Ancos
Dalene De Beer
Johan De Boever
Luc De Cooman
Victor De Freitas
Annalisa De Girolamo
Denis De Keukeleire
Norbert De Kimpe
José Pedro De La Cruz
Natalia de las Heras
Ana Cristina Silva De Lima
Sidney G. De Limaa
Vincenzo De Luca
Elvira González De Mejía
Bruno De Meulenaer
Fabiana F. De Moura
Lívia de Lacerda de Oliveira Pineli
Sonia de Pascual-Teresa
Alexandre De Paula Rogerio
Rafael De Prado
Eva De Rijke
Maria C. De Rosa
Sarah De Saeger
Diana De Santis
Stefaan De Smet
André J. de Villiers
Ric C. H. De Vos
Pierre de Wit
Lisa L. Dean
Laurent Debrauwer
Eric A. Decker
Geneviève Défago
Alexandre Dehaut
Monica Deiana
Mark A. Dekeyser
Matthijs Dekker
Maria del Alamo-Sanza
M. Del Bubba
Daniele Del Buono
Jose Carlos Del Rio
Daniele Del Rio
Manuel del Valle
Philippe Delahaut
Bryan Delaney
Cristina Delgado-Andrade
Francisco Delgado-Vargas
Mario Dell'Agli
Nicolò Dellarosa
Pierluigi Delmonte
Stephen Richard Delwiche
Tigst Demeke
Fatih Demirci
Ozlem Demirkiran
Ze-yuan Deng
Anping Deng
Bowen Deng
Qian Deng
Wei Deng
Xiaojuan Deng
Yu Deng
Zeyuan Deng
Ana Denicola
Yann Desfougères
Tom Desmet
Renu Deswal
Edenio Detmann
C. Devakumar
Sridevi Devaraj
Audrey Devatine
Jonathan W. Devries
Tristan Dew
Molly Dewey
Ralph Dewey
Karaj Singh Dhillon
Sushil Dhital
Claudie Dhuique-Mayer
Christophe d'Hulst
Rong Di
Chiara Di Lorenzo
Aldo Di Luccia
Carla Di Mattia
Maria Paz Diago
Jinling Diao
Daniel Anthony Dias
Isabel Díaz
M. J. Díaz
Rocio I. Diaz de la Garza
Marta E. Diaz-Garcia
Eric Dickinson
Leslie C. Dickson
John Didzbalis
Sandra C. Dieguez
Ana Maria Díez-Pascual
Madhu P. Dikshit
Steven R. Dimler
Shangwu Ding
Yousong Ding
Shuangyang Ding
Qiang (John) Ding
Ming-Wu Ding
Kan Ding
Huanzhong Ding
Wang-Hsien Ding
Harun-Diraman
Gianfranco Diretto
Nomusa Rhoda Dlamini
Yang Do Choi
Ronaldo F. do Nascimento
Gary Dobson
Mahmut Doğan
Piero Dolara
Gregory G. Dolnikowski
Jose Luis Domingo
Pedro Domingues
Valentina Fernandes Domingues
Xiangchao Dong
Zizheng Dong
Dario Donno
Francesco Donsì
Sonia Dopico-García
Olena Doran
Gregory Doran
Peter Dörmann
Giniani Carla Dors
Antonio dos S. Silva
Michael Dowd
Patrick F. Dowd
Floyd Dowell
Gerard Downey
Melanie L. Downs
Pascale Dozolme
Silvina R. Drago
William Mason Draper
Vlasta Drevenkar
Darcy R. Driedger
Michel Dron
Stephan Drusch
Ming Du
Yuguang Du
Qizhen Du
Hongwu Du
Wei Du
Maret Du Toit
Wessel Johannes Du Toit
Hongwei Duan
Jin-Ao Duan
Jingjing Duan
Jinyou Duan
Xuewu Duan
Juan Duarte
Maria Fatima Duarte
Montserrat Duenas
Laurent Dufosse
Tammy R. Dugas
Stephen O. Duke
Andreas Dunkel
Julie Dunne
David Edwin Dunstan
Rosa Duran-Patron
Marcello Duranti
Prem Dureja
Ksenija Durgo
Pradip Kumar Dutta
Jens Duus
Jolon M. Dyer
Gary A. Dykes
Krzysztof Dziedzic
Jerzy Dziuba
Stephen D. Ebbs
Susan E. Ebeler
Klaus Eder
John Alexander Edgar
Indika Edirisinghe
RuAngelie Edrada-Ebel
Florence Edwards-Levy

DOI: 10.1021/jf506178r
J. Agric. Food Chem. 2015, 63, 2−18

Kah Yaw Ee
Sergei Eermin
Thelma Egan
Einar Skarstad Egeland
Stefan Ehling
Jerry Eichler
Wolfgang Eisenreich
Brian David Eitzer
Ali M. El Halawany
Abdelfatteh El Omri
Thomas Elder
Pedro Elez-Martinez
Lutz Elflein
Seham S. El-Hawary
Ryan J. Elias
Fred Joseph Eller
Sabine Ellinger
Christopher T. Elliott
Gamal ElMasry
Stephen John Elmore
Ali Elshafei
K. Elumalai
Naushad Mohammad Emmambux
Karl-Heinz Engel
Ulrich H. Engelhardt
Wim J. M. Engels
Søren Balling Engelsen
Tomas Erban
Mustafa Erbas
Helmut Erbersdobler
John W. Erdman
John Erdman, Jr.
Xabier Erdocia
Sergei A. Eremin
Seda Ersus Bilek
Abdulselam Ertaş
Per Ertbjerg
M. Teresa Escribano-Bailon
Ana Escudero
Rosa Escudero
Omid Esmaeilipour
Michael Graham Espey
Juan C. Espín
Judith Dolores Espinoza-Perez
Patricia Esquivel
Nour-Eddine Es-Safi
Melanie Esselen
Mario Estévez
Jose Maria Estrela
E. Etxeberria
D. Evan Evans
Christian C. Evans
David W. Everett
J. M. Evers
Antonio Evidente
Trevor Austin Faber
Greta Faccio
George C. Fahey
Jed W. Fahey
Mark L. Failla
Robert John Falconer
Maria L. Faleiro
James F. Faller
Biagio Fallico
Marie-Helene Famelart
Zhen-Chuan Fan
Peihong Fan
Titan S. Fan
Wenlai Fan
Chiara Fanali
Anne-Laure Fanciullino
Zhenglai Fang
Binghu Fang
Jian-Min Fang
Jim Fang
Liqiong Fang
Yapeng Fang
Yong Fang
Martín Fanzone
Franco Faoro
Mohamed A. Farag
Adriana Farah
Mir Ali Farajzadeh
A. Fardet
Ana Paula Farinha
Harold M. Farrell
Majekodunmi Oladeji Fatope
Cameron Faustman
John F. Federici
Marini Federico
Bruno Fedrizzi
Urs Feller
Antoni Femenia
Jiwen Feng
Tao Feng
Jie Feng
Jianguo Feng
Fengqin Feng
Yu-Qi Feng
Katia Valevski Sales Fernandes
M. A. Fernandez
Victoria Fernandez
Brígida Fernández De Simón
Maria Angeles Fernandez-Arche
Jesus Dionisio Fernández-Bayo
Juan Fernández-Bolaños
Roberto Fernandez-Lafuente
Miguel A. Fernandez-Muino
María-Soledad Fernández-Pachón
Juan Fernandez-Tajes
Juan Pablo Fernández-Trujillo
Alessandra Ferrandino
Isabel M. P. L. V. O. Ferreira
Vicente Ferreira
Isabel C. F. R. Ferreira
Edilene Cristina Ferreira
Dulcineia Ferreira
Daneel Ferreira
Leonardo Cesar Ferreira
Evelina G. Ferrer
Federico Ferreres
Cristina Ferrero
James A. Ferretti
Daniel Festring
Badr El-Sabah A. Fetoh
Joerg Fettke
Oliver Fiehn
P. G. Fields
Inês Figueira
Ana Cristina Silva Figueiredo
Michael Filigenzi
John W. Finley
John Weldon Finley
Christine Finnie
Michaela Fiol
Antonio Fiorentino
Joan G. Fischer
Thilo C. Fischer
Markus Fischer
Lutz Fischer
Marc J. C. Fischer
Ian Denis Fisk
Richard J. Fitzgerald
Mario Flaig
Riccardo Flamini
Peter Fleischmann
Leonard Flendrig
Mary T. Fletcher
Dimitrios John Fletouris
Erico Marlon Moraes Flores
Monica Flores
Giorgia Foca
Alexandrina Ligia Focsan
Terence Lee Fodey
Edward Allen Foegeding
Petra Foerst
Vincenzo Fogliano
Ariel R. Fontana
Angelo Fontana
Debora Fontanini
Kevin A. Ford
Fabio Forlani
Monica Forni
Isabel M. I. Fortea
Luca Forti
Torgils Fossen
Mario C. Foti
Vasileios Fotopoulos
Imogen Foubert
Glen P. Fox
Daniela Fracassetti
Cesar G. Fraga
I. Leigh Francis
Marta Francisco
Dayan Franck
Célia Maria Landi Franco
Octávio Luiz Franco
Laura Franitza
Damian Conrad Frank
Jan Frank
Oliver Frank
Stephanie Frank
Alessandra Fratianni
Felix Frauendorfer
Katrin Frauenstein
Rupert Fray
Giuseppe Fregapane
Carmen Sofia Rocha Freire
Ana C. Freitas
Alfred D. French
Eric Frerot
Xavier C. Frette
Russell David Frew
Carl Frey
Juana Frias
Kristina Fricke
Mendel Friedman
Helge Fritsch
Jona Ines Fritz
Guglielmina Froldi
Andrej Frolov
María José Frutos
Frederick Fry
Yu-Jie Fu
Shu-Ling Fu
Yu-Jie Fu
Peng Fu
Peter P. Fu
Sigfredo Fuentes
E. Patrick Fuerst
Ko Fujimori
Yoshinori Fujimura
Ken-ichi Fujita
Shuji Fujita
Harukazu Fukami
Eiichiro Fukusaki
Masao Fukushima
Claudia Maria Furlan
Samuel Furse
Takeshi Furuta
Gabriele Gadermaier
Priyadarshini Gadgil
Stefan Gafner
Nico Galaffu
Samy M. Galal
Carlos Galan-Vidal
Roberta Galarini
Gianni Galaverna
Teresa Galeano-Díaz
Silvia Galindez-Najera
Catarina Galinha
Sophie Gallier
Vito Gallo
Christophe Claude Galopin
Roger Galve
Julio Galvez
Lena Galvez Ranilla
Angelita Gambuti
Tamer Gamel
Jay J. Gan
Girish Ganjyal
Vaishnavi Ganti
Michael G. Gänzle
Feng Gao
Xue-Jun Gao
Wen-Yuan Gao
Kun Gao
Jin-Ming Gao
Hao Gao
Silvio Garattini
Hugo Garcia
José Maria Garcia
Maria Alejandra Garcia
Guadalupe Garcia Llatas
María Carmen García Parrilla
Francisco García-Cánovas
María Teresa García-Conesa
Diego Luis Garcia-Gonzalez
José María García-Mina
Juan F. Garcia-Reyes
A. Garcia-Ruiz
P. Garcia-Segovia
Cristina Garcia-Viguera
Rocio Garcia-Villalba
Jorge L. Gardea-Torresdey
Teresa Garde-Cerdán
Dale R. Gardner
Cristiano Garino
Antonio Garrido-Fernández
María Carmen Garrigós
Arthur Garrison
Gil Garrote
David F. Garvin
Klaus Gase
Mattia Gasperotti
Klaus Gassenmeier
Francesco Gilberto Gatti
Giuseppe Gattuso
Joel Gautron
Rafael Gavara
Terrence Gavin
Marija Gavrovic-Jankulovic

DOI: 10.1021/jf506178r
J. Agric. Food Chem. 2015, 63, 2−18

Urszula Gawlik-Dziki
Zuzana Gazova
Gabriella Gazzani
Alain Geffard
Wentzel Ca Gelderblom
Eva Gelenser
Pierre Gelinas
Goran Gellerstedt
Nahit Gencer
ZengChao Geng
Anli Geng
Annamaria Genga
Claude Genot
Alessandro Genovese
Maria I. Genovese
Susan Genualdi
Zhang Genyi
Milen Ivanov Georgiev
Clarissa Gerhauser
Katrin Gerlach
Jared Quinton Gerlach
Juliet A. Gerrard
Arjen Gerssen
Zev Gerstl
Andreas J. Gescher
Jan M. C. Geuns
Ashraf Ghanem
Kamal Ghanemi
Mosad Ahmed Ghareeb
Greg Gharst
Mahdi Ghasemi-Varnamkhasti
Masomeh Ghassem
Mohammadreza Ghomi
Amit K. Ghosh
Banibrata Ghosh
Koushik Ghosh
Mahua Ghosh
Cecilia Giacomini
Thomas J. Gianfagna
Carmen Gianfrani
Alberto Gianinetti
Valentina Gianotti
Monika Gibis
Donna Gibson
Michael J. Gidley
Thomas Giersch
Maria Isabel Gil
Nicolas Gil
Robert G. Gilbert
Alexis Romain Gilbert
Bienvenida Gilbert-López
Brendon Gill
Chris I. R. Gill
Sarjeet S. Gill
Juan Antonio Gimenez Bastida
Rosa M. Giner
Edgardo Giordani
Guillermo Giovambattista
Alfonso Giovane
Manuela Giovannetti
Adriana Castello Costa Girardi
Gözde Girgin
Julio Giron-Calle
M. Monica Giusti
Raymond Philip Glahn
Hansruedi Glatt
Robert Glew
Marcus A. Glomb
Julie M. Goddard
Rolf Gerhard Godelmann
Michał Marek Godlewski
Mary An Godshall
Danica Erin Goggin
Yolanda Gogorcena
Vural Gökmen
Carlos Alberto Gomez Aldapa
Ana Maria Gómez-Caravaca
Agustina Gomez-Hens
Leobardo Manuel Gómez-Oliván
Encarna Gomez-Plaza
Andrea Gómez-Zavaglia
Sónia Gonçalves
Florence Gondret
Yi Gong
Yuansheng Gong
Karine Gontier
Roxana Elizabeth Gonzalez
Antonio Gonzalez
Maria Jose Gonzalez
Carmen Gonzalez-Barreiro
María Reyes González-Centeno
Antonio Gonzalez-Sarrias
Cynthia L. Goodman
Madhuban Gopal
T. Gopinandhan
Belén Gordillo
Ahmet Ceyhan Gören
Shela Gorinstein
Stanislava Gorjanovic
Irina Goryacheva
Fabio Gosetti
Alexander Gosslau
Tetsuhisa Goto
Lalitha R. Gowda
Luis Goya
Aymeric Goyer
Franco Gozzo
John H. Grabber
Jose Graca
Fernando Granado-Lorencio
Daniel Granato
Antonio Granell
Sebastian Granica
Michael Granvogl
Benoit Graulet
Heinrich Grausgruber
David A. Gray
Marion L. Greaser
Ralf Greiner
Paola Grenni
Jonathan Gressel
Gordon W. Gribble
D. Grierson
Gerhard Gries
Casey C. Grimm
Konrad Grob
Maria Victoria Eiras Grossmann
Clara Grosso
Christian W. Gruber
Nicolas Gruyer
Stanislaw Gryglewicz
Hai-Ying Gu
Liwei Gu
Zhengrong Gu
Hongxia Guan
Yongguang Guan
Aytaç Güder
Muralikrishna Gudipati
Miguel Gueimonde
Matthias Guentert
Helmut Guenther
Laurence Guérin
Leonor Guerra-Guimarães
Raúl F Guerrero
Nicoletta Guerrieri
Riccardo Guidetti
Lucia Guidi
Luís F. Guido
Jose M. Guillamon
Dominique Guillaume
Marti Guillaume
María D. Guillén
Claude Guillou
José Manuel Guisán
Hardeep Singh Gujral
Ashu Gulati
Atilla Gulec
Piotr Gulewicz
Maria Gullo
Ziya Gunata
Shouwu Guo
Zhiyong Guo
Shuntang Guo
Qing-Long Guo
Lei Guo
Jiangfeng Guo
Hongyan Guo
Dongwei Guo
Zheng Guo
Ramesh C. Gupta
Vinod K. Gupta
Ozan Gurbuz
Anilda Guri
Maristella Gussoni
Brian Guthrie
Janet A. Gutierrez-Uribe
Francois Guyon
Nicolas Guyot
Sylvain Guyot
Z. Guzel-Seydim
Ivette Guzman
Valeria Guzsvany
Zoltan Gyori
Jae-Ho Ha
Ilka Haase
Norbert Haase
Paul Timo Haase
S. Habimana
Mary Hadley
Guido R. M. M. Haenen
Ann E. Hagerman
Per M. Hägglund
Young Tae Hahm
Martin Hajduch
Jayanta Haldar
Mintu Halder
Heather Hallen-Adams
A. Halmemies-Beauchet-Filleau
Dietmar Haltrich
Sandra Halwacks
Jun-Sang Ham
Michael R. Hamblin
Matthias Hamburger
John F. Hammerstone
Earl G. Hammond
Daniela Hampel
Lamia Hamrouni
Rui-Min Han
Zhenlin Han
Xianghui Han
Quan-Bin Han
Qian Han
Kyoung Sik Han
Heyou Han
Yi-Fan Han
Dong-Wook Han
Bo Han
Lujia Han
Akihiro Handa
Rachel L. Hanlin
Abdelali Hannoufa
Christophe Hano
F. Hanschen
Chad Hansen
Laura Hansen
Xiao-Jiang Hao
Zhigang Hao
Hiroshi Hara
Kazutomo Haraguchi
James F. Harbertson
Wanda Hardman
Kevin Hardouin
George G. Harrigan
Peter de Boves Harrington
James M. Harrington
Howard Harrison
Rogers Emughedi Harry-O'kuru
Sandra Hartmann
Rob Haselberg
Jovin Hasjim
G. Haskaraca
Sahar Hassani
Neuza Mariko Aymoto Hassimotto
Tadashi Hatanaka
Tsutomu Hatano
Ronald D. Hatfield
Fani Hatjina
Ryota Hattori
Efimia Hatzidimitriou
Gary Hausman
Shigeru Hayakawa
Yoji Hayasaka
Kenshi Hayashi
Saeed A. Hayek
Heiko Hayen
Andrew Hayhurst
Diana Haynes
Lynn Haynes
El Akrem Hayouni
David B. Haytowitz
Douglas G. Hayward
Jan Hazebroek
Hong-Ju He
Xiangjiu He
Rong-rong He
Qinghua He
Limin He
Lili He
Kan He
Hongwu He
Hongmei He
Xu-Sheng He
Hong-Ping He
David Heber
Karoly Heberger
Elvira María Hebert
Vincent Robert Hebert
Rikke Hedegaard
Adrian D. Hegeman
Daniela Heimler
Marina Heinonen
Patrick Heist
Michael Hellwig
Richard Helm
Fernando Henao
Gregg Henderson
Suzanne Hendrich
Constance Hendrickson
Hanne Vang Hendriksen
Matt Hengel

DOI: 10.1021/jf506178r
J. Agric. Food Chem. 2015, 63, 2−18

Thomas Henle
Geneive Elizabeth Henry
Markus J. Herderich
Francisco José Heredia
Rod A. Herman
Armin Hermann
Isidro Hermosín-Gutiérrez
Manuel Hernandez-Cordoba
Blanca Hernández-Ledesma
Purificacion Hernandez-Orte
Humberto Hernández-Sánchez
Tomas Herraiz
Maria Lidia Herrera
Braulio Edgar Herrera-Cabrera
Miguel Herrero
Miguel Herrero
C. Herrero Latorre
John L. Hess
Mona Hafez Hetta
Kasper Arthur Hettinga
Francisco J. Hidalgo
Christopher P. Higgins
Art Hill
Camilla Hill
Donald Hilton
Max Hincke
Simon Hird
Kendal D Hirschi
Salim Hiziroglu
Frantisek Hnilicka
Hsiao-Yung Ho
Su-Chen Ho
Yuan-Soon Ho
S. Hobdey
Rodrigo Barcellos Hoff
Angela Hoffman
Karin Hoffman-Sommergruber
Thomas Hofmann
Valérie Hofstetter
Petra Hogger
Peter Hojrup
M. Holasova
Michal Holcapek
Askild Lorentz Holck
Aline Holder
Paul Holford
Robert Hollingworth
Hannah Holscher
Carl Holt
Kevin M. Holtman
Bruno Holzapfel
Thomas Holzhauser
Stefan Holzmayr
Ellen M. Hondrogiannis
Jungil Hong
Yan Hong
Young Shick Hong
Francisco Hontoria
Antony M. Hooper
Helene Hopfer
Naoko Hori-Tamura
Peter Horlacher
Damaso Hornero-Mendez
Carl Friedrich Horst Longin
Eva Horvathova
Carl Hoseney
Karim Hosni
Farah Hosseinian
Junchang Hou
Qingxi Hou
Harry Hou
Wen-Chi Hou
Tzyh-Chyuan Hour
Norma Houston
Siew Eng How
Luke R. Howard
Kate Howell
David Hoyland
Geza Hrazdina
Silvana Hrelia
Zuzana Hruska
You-Cheng Hseu
Chia-wen Carmen Hsieh
Jung-Feng Hsieh
Wen-Chuan Hsieh
Yih-Shou Hsieh
Yun-Hwa Peggy Hsieh
Yue-Ie Hsing
Chun-Hua Hsu
Yuan-Man Hsu
Jue-Liang Hsu
Chin-Lin Hsu
Shi-lan Hsu
Miao-Lin Hu
Jiahuai Hu
Zhoujian Hu
Shengshui Hu
Meizhong Hu
Lihong Hu
Jun Hu
Jiye Hu
Baolan Hu
Hongbo Hu
Bin Hu
Wanfeng Hu
Bing Hu
Chien-An Hu
Fenglin Hu
Yufei Hua
Huiming Hua
Shauku Huang
Kexuan Huang
Nan Huang
Qiliang Huang
Qingrong Huang
Ron Huang
Tzou-Chi Huang
Wei-Dong Huang
Wei-Fong Huang
Wen-Lii Huang
Kehe Huang
Yang Huang
Guan-Jhong Huang
Wuyang Huang
Fang Huang
B. K. Huang
Ching-Tsan Huang
Huazhang Huang
Yi-Chia Huang
Jianying Huang
Feng-Hong Huang
Hsiu-Chen Huang
Huiling Huang
Dejian Huang
Martin Allen Hubbe
Machteld Huber
Miriam Hubinger
Christian W. Huck
Isis Hueza
Glenna J. Hughes
Guohua Hui
Jowita Humin
Hans-Ulrich Humpf
Xu Hun
Wei-Lun Hung
Melvin C. Hunt
Christopher G. Hunt
Thom Huppertz
William Jeffrey Hurst
Andrew Hursthouse
Søren Husted
Kevin Huvaere
Tsong-Long Hwang
Geum-Sook Hwang
Hong-Sik Hwang
Kwontack Hwang
Stefania Iametti
Marco Iammarino
Gabrela A. Ibanez
Elena Ibañez
David Ibarra
Mwafaq Ibdah
Young Bassey Ibiang
Hisham R. Ibrahim
Christèle Icard-Vernière
Filiz İçier
Nagatoshi Ide
Taisen Iguchi
Takashi Iimure
Shinya Ikeda
Tsukasa Ikeda
Shinichi Ikushiro
Julius Kwagh-har Ikya
Nebojsa M. Ilic
Shinsuke Imai
Katsumi Imaizumi
Jona Ines Fritz
Marzia Innocenti
Hiroyasu Inoue
Koichi Inoue
David Inouye
Takako Inui
Carla Eliete Iochims dos Santos
Richard Ipsen
Gabriela Irazoqui
Marcello Iriti
José Hipólito Isaza Martínez
Mamoru Isemura
Norio Ishida
Atsushi Ishihara
Takeshi Ishii
Tsutomu Ishikawa
Kanji Ishimaru
Ciro Isidoro
Murray Bruce Isman
Shirou Itagaki
Hideyuki Ito
Hiroaki Itoh
Ken Itoh
Saotomo Itoh
Violeta Ivanova-Petropulos
Takashi Iwafune
Nick Jackowetz
Scott Harding Jackson
Lauren S. Jackson
Daniel A. Jacobo-Velázquez
Rosangela Assis Jacques
Walter Jäger
Margaretha Ingeborg Jägerstad
Rakesh Jaiswal
Lidija Jakobek
Greta Jakobsdottir
Michael A. Jakupec
Mahbubul Alam Foizul Jalal
Delano James
Kuo-Ching Jan
Srinivas Janaswamy
Jay-lin Jane
Eric Jang
Jae-Hyuk Jang
Jerzy Jankun
Amol V. Janorkar
B. Janoszka
Koen J. A. Jansens
Geert Janssens
Klaus-Dieter Jany
Rie Bak Jäpelt
Aneta Jastrzębska
G. K. Jayaprakasha
Chamila Jayasinghe
Lee-Ann Jaykus
Jae-Young Je
Philippe Jeandet
Peter M. Jeffers
David William Jeffery
Elizabeth H. Jeffery
Henryk H. Jelen
G. Ronald Jenkins
Hanne Bak Jensen
Henrik Max Jensen
Ida Johanne Jensen
Soren Krogh Jensen
Tae Cheon Jeong
Woo-Sik Jeong
Rajesh Jha
Yewei Ji
Baoping Ji
Junfeng Ji
Li Jia
Dong Jiang
Longfa Jiang
Zhiliang Jiang
Zhi-Hong Jiang
Yueming Jiang
Weiying Jiang
Tianjia Jiang
Shu Jiang
Shann-Tzong Jiang
Dingxin Jiang
Deshou Jiang
Bo Jiang
Aimin Jiang
Ren-Wang Jiang
Guangling Jiao
Elisa Jimenez
Ana Jimenez-Araujo
Jose C. Jimenez-Lopez
Rodrigo Jiménez-Saiz
Maria Luisa Jimeno
Zhao Jin
Zhuang Jin
Peng Jin
Fen Jin
Chang-Hai Jin
Maojun Jin
Hao Jing
Linhong Jing
Vladimir Jiranek
Leopold Frieda Jirovetz
Franz Jirsa
Maik A. Jochmann
Heran Johnson
Richard M. Johnson
Elizabeth J. Johnson
John J. Johnston
Jouni Jokela
K. Jomova
Michaela Jonas
Joanna Jones
Russell L. Jones
Shuna Jones
Owen Jones
Graham P. Jones
Andrew Maxwell Phineas Jones
Huw Dylan Jones
Sisse Jongberg
Ramakanth S. Jonnala

DOI: 10.1021/jf506178r
J. Agric. Food Chem. 2015, 63, 2−18

Ilona Jonuskiene
Juana Dolores Jorda
Maria Jose Jordan
António M. Jordão
Elizabeth Joubert
Daniel Joulain
Xingrong Ju
B. Juan
ChiChang Juan
M. Emilia Juan
Rong-Huay Juang
B. O. Juliano
Riitta Julkunen-Tiitto
Mira Jun
Sang Hoon Jung
Sung-Keun Jung
Kyung-Hwan Jung
J. Marcos Jurado
Jerzy Juskiewicz
Lesław Juszczak
John A. Juvik
Piotr Kachlicki
Pawel Kafarski
Ebru Kafkas
Shinzo Kagabu
Isabelle Ann Kagan
Norihiko Kageyama
Kenji Kai
Mitali Kakran
Panagiotis Kalaitzis
Sathya Kalambur
Jana P. Kalinova
Diganta Kalita
Heikki Kallio
Wilhelmina Kalt
Alaa Kamel
Senem Kamiloglu
Werner Kaminsky
Suchitra Kamle
Alexander A. Kamnev
M. Kanai
Kazuki Kanazawa
Satoshi Kaneco
Hirotaka Kaneda
Shu Kaneko
Hideo Kaneko
Young-Hee Kang
Ji Kang
KuiDong Kang
Joseph Kanner
Yossi Kanner
Yung-Hsi Kao
Muammer Kaplan
Constantina Panayioti Kapnissi-Christodoulou
C. Tissa Kappagoda
Özlem Karadeniz
S. Karagoz
Haralabos Karantonis
Thomas Karbowiak
Lutvija Karić
Keikhosro Karimi
Reijo Karjalainen
John Karlik
Peter Karuso
Sashi G. Kasimsetty
Christina Kast
Hiroyuki Kataoka
Shigeru Katayama
Atsushi Kato
Tomoyuki Katsube-Tanaka
Stanley E. Katz
Maninder Kaur
Diksha Kaushik
Nat N. V. Kav
Nickolas G. Kavallieratos
Jun Kawabata
Michiko Kawakami
Akira Kawamura
Joanna Kawa-Rygielska
Masami Kawase
Colin D. Kay
Shin-ichi Kayano
Shaoyong Ke
Matthias Keck
Michael J. Keenan
Panagiotis Kefalas
Joshua Kellogg
Roger Kelly
Mitch Kelly
Alan L. Kelly
Mary Kelly
Mark Kelm
Ivan R. Kennedy
James A. Kennedy
Philip G. Kerr
William L. Kerr
Fiona Kerslake
Serhat Keser
Emre Keskin
Agnes Keszler
Michael Keusgen
Žarko S. Kevrešan
Frederick Khachik
Abdul Latif Khan
Avik Khan
Ratchaneewan Khiaosa-Ard
Boris N. Khlebtsov
Saeid Khodadoust
Ali Khoddami
Ali Khoshab
Ashot Khrimian
Johanes Kiefl
Hiroe Kikuzaki
Jane Kilcoyne
Matthew J. Killeen
Paul Andrew Kilmartin
Rachel Kilmister
Pekka Kilpeläinen
Sung Hoon Kim
Young-Suk Kim
Youngmok Kim
Yong-Tae Kim
Tack-Joong Kim
Se-Jae Kim
Sang Moo Kim
Kyong-Su Kim
Junheon Kim
Jun Tae Kim
Jeong-Han Kim
Beom Seok Kim
Jaeyoung Kim
Jae Kwang Kim
Hyunsook Kim
Hyun-Soo Kim
Hyun-Jin Kim
Hyun Jung Kim
Yeong Shik Kim
Doman Kim
Chong-Tai Kim
Cheorl-Ho Kim
Jang-Eok Kim
Bruce Kimball
Athanasios C. Kimbaris
Yoshinobu Kimura
Jerry W. King
A. Douglas Kinghorn
Ramachandra K. Kini
Vassilis Kiosseoglou
Ara Kirakosyan
Lara Kirsch
Takao Kishimoto
Nand Kishore
Anna K. Kiss
Alecia M. Kiszonas
Kazumi Kitta
David Kitts
David D. Kitts
Barbara P. Klein
Dieter Klemm
Jennifer Kloepper
Sappasith Klomklao
T. J. Klopfenstein
Grzegorz Kłosowski
James Levi Klotz
Alicja Kluczyk
Anthony Knight
Dietmar Knopp
Knud Erik Bach Knudsen
Chun-Han Ko
Jiunn Liang Ko
Sanghoon Ko
Yuan-Tih Ko
Kenji Kobata
Tolgahan Kocadağlı
Matthias Koch
Jan P. Kochansky
Gabor Kocsy
Heike Koehler
Peter Koehler
Eunmi Koh
P. Köhler
Peter Köhler
Noriko Kohyama
Marja E. Koivunen
Milan Kojic
Shosuke Kojo
Michalis Komaitis
Michael Komárek
Masaaki Komatsu
Tamas Komives
Ewald Komor
Nevzat Konar
Izabela Konczak
Fumio Kondo
Chuihua Kong
Ling-Yi Kong
Xiangzhen Kong
Baohua Kong
Chang-Suk Kong
Paul Kong Thoo Lin
Yasuko Kawamura Konishi
Katharina Konitzer
Vassilis Kontogiorgos
Michael George Kontominas
Rachel E. Kopec
Randall A. Kopper
Thomas Koppmann
Olivera Koprivnjak
Dean Adam Kopsell
Takuya Koseki
Iztok Joze Kosir
William C. Koskinen
Georgina Kosturkova
Yorgos Stelios Kotseridis
Yiannis Kourkoutas
Georgios Koutsidis
Martin F. Kovacs
Mariusz Kowalczyk
P. Kowalski
Moritz Krahl
Barbara Krajewska
Catherine M. Kramer
Gerhard E. Krammer
Bernhard Kräutler
Dietmar Krautwurst
Ivan Kreft
Johanna Kreissl
Robert Kremer
Michael Kreuzer
Ulrich Krings
Suresh Babu Krishna Moorthy
Hari B. Krishnan
Lothar Wilfried Kroh
Dana A. Krueger
Johanita Kruger
Vladimir Krylov
Alexander J. Krynitsky
Jolanta Krzyczkowska
Kuo-Lung Ku
Yau Hoong Kuan
Yu-Hsiang Kuan
Roman Kubec
Kikue Kubota
Annette Kuehn
Jan Kuhlmann
Shirley Kuhnen
Nikolai Kuhnert
Tea Kulisic-Bilusic
Ulrich Kulozik
B. Dinesh Kumar
Rajesh Kumar
S. Naresh Kumar
Sanjeet Kumar
Dipak Kumar Sahoo
Gabriela Kuncova
Alina Kunicka
Gotthard Kunze
Chia-Feng Kuo
Jen Min Kuo
Ping-Chung Kuo
Shiu-Ming Kuo
Tsun-Yung Kuo
Yao-Haur Kuo
Takashi Kuribayashi
Keisuke Kurita
László Kursinszky
Sudarshan Tanaji Kurwadkar
Thomas Kurz
Markus Küsters
Barbara Kusznierewicz
U. Baris Kutman
Frantisek Kvasnicka
M. Kverka
Veronika Kwiatkowski
Sung Won Kwon
Oran Kwon
Petri Kylli
James J. La Clair
John Marcus Labavitch
Helene Laboure
Marie-Aleth Lacaille-Dubois
Dirk W. Lachenmeier
Jaromir Lachman
Markus Lacorn
Florence Lacoste
Monique Lacroix
Gregory S. Ladics
Michael R Ladisch
Helle N. Lærke
M. Jesús Lagarda
Camel Lagnika
Mickaël Laguerre
Marc Lahaye
Li-Chuan Lai
Ching-Shu Lai
William A. Laing
Franco Maria Lajolo
Jean Paul Lalles
René Lametsch
Santosh Lamichhane
Rosa M. Lamuela-Raventós
Maria C. Lanari

DOI: 10.1021/jf506178r
J. Agric. Food Chem. 2015, 63, 2−18

Rosalba Lanciotti
Sophie Landaud
Rikard Landberg
Roman Lang
Swen Langer
Daniel Langos
Peter Harald Langsjoen
Ravishanker Lankallapaly
Wenjian Lao
Moisés Laparra
Moshe Lapidot
Isabel Lara
João Laranjinha
María Angélica Larraín
Mar Larrosa
Kim Lambertsen Larsen
Mette Larsen
Camille Larue
Ola Lasekan
Barbara Lata
Vincenzo Lattanzio
Gladys O. Latunde-Dada
Ching Shuan Lau
V. Felipe Laurie
John H. Lauterbach
Bryan Lavarack
Vera Lavelli
Tao Le
Thien Trung Le
Jean-Luc Le Quere
Vijittra Leardkamolkarn
Blaise Wayne LeBlanc
Ming-Fen Lee
Jungmin Lee
Junsoo Lee
Ki Won Lee
Kwang Ho Lee
Kwang Youl Lee
Kwang-Geun Lee
Kyung-Min Lee
Maw-Rong Lee
Wen-Sen Lee
Mi Kyeong Lee
Robert J. Lee
S. K. Lee
Sang Kook Lee
Sanghyun Lee
Stephen T. Lee
Sung-Eun Lee
Tzu-Tai Lee
Joonhee Lee
Meng-Shiou Lee
Hong Jin Lee
Chang Yong Lee
Chihoon Lee
Ching-Kuo Lee
Chong-Kil Lee
Choong Hwan Lee
Cindy M. Lee
Dongho Lee
Jung-Kul Lee
GullLee Lee
Chan Lee
Hui-Young Lee
Hyoung S. Lee
Jae-Won Lee
Jinwok Lee
Jong hun Lee
Jung-Bum Lee
Jung Hoon Lee
Dong-Sun Lee
Naruemon Leelayuwat
Wolf Dieter Lehmann
Steven J. Lehotay
Hongtao Lei
Xingen Lei
Yang Lei
Yu Lei
Erich Leitner
Gerald Lelong
Ann T. Lemley
Federico Lemmetti
Valfredo Lemos
Leondios Leondiadis
Hrvoje Lepedus
Bob Lerch
Patrice Lerouge
Sittiwat Lertsiri
Uri Lesmes
Gene E. Lester
Thomas Leustek
Grazyna Lewandowicz
Paul Lewer
Anna Lewinska
Jakob Ley
Peiwu Li
Laura Li
Li Li
Liya Li
Minhui Li
Nianguang Li
Jianfa Li
Pengcheng Li
Ping Li
Ping Li
Pingliang Li
Qian Li
Qing Xiao Li
Rong Li
Na Li
Deqiang Li
Robert W. Li
Betty W. Li
Bin Li
Binchun Li
Bo Li
Can-Peng Li
Chunjie Li
Jihong Li
Defa Li
Jian-Xin Li
Fangbai Li
Fu Li
Gang Li
Genxi Li
Gongke Li
Guoliang Li
Guolin Li
Hua-Bin Li
Chunyang Li
Yanling Li
Zhong Li
Zheng-Ming Li
Zheng Li
Zhanlin Li
Yunqi Li
Yun Cheng Li
Yue Li
Youran Li
Qun-Yi Li
Yanshen Li
Yan Vivian Li
Xiaoxi Li
Xiangyang Li
Sheng-Hong Li
Sen Li
Yihan Li
Shenghe Li
Xiang Li
Shiming Li
Shuping Li
Shuyi Li
Si-Quan Li
Tsung-Lin Li
Wei Li
Weijia Li
Wen-Lin Li
Xian Li
Tianhu Li
Shaoping Li
H. C. Liang
Yu-Chih Liang
Jin Liang
Haojun Liang
Jianfen Liang
James C. Liao
Xun Liao
Xiaojun Liao
Vivian Hsiu-Chuan Liao
Pao-Chi Liao
Hui-Fen Liao
Dan-Kui Liao
Chia-Ding Liao
Kuang-Wen Liao
Erica Liberto
Birgit Lichtenberg-Kraag
Fernando Cebola Lidon
Gérard Liger-Belair
Angelo Liguori
Chong-Kuei Lii
Mary Ann Lila
Seung-Taik Lim
Wallace Lim
Marta R. M. Lima
Andreas Limbeck
Li-Yun Lin
Yongcheng Lin
Yong Lin
Chih-Cheng Lin
Yaw-Huei Lin
Yun-Lian Lin
Wun-Yuan Lin
Shih-Bin Lin
Mengshi Lin
Meei-Yn Lin
Li Lin
Jin-Yuarn Lin
Jianming Na Lin
Hai-Shu Lin
Daohui Lin
Da-Gin Lin
Chih-Li Lin
Chi-Chen Lin
Cheng-Wen Lin
Chun-Mao Lin
J. Lindberg
Torbjorn Linden
Christian Lindinger
Chang-Chun Ling
Celeste M. Lino
Jozef P. H. Linssen
John E. Linz
Carolyn E. Lister
Kathrin Ingrid Liszt
John H. Litchfield
Grzegorz Litwinienko
Xiaoya Liu
Xiaoli Liu
Xiaofei Liu
Xiaodan Liu
Xiangfei Liu
Wei Liu
Xingang Liu
Shiu-Mei Liu
Yanlin Liu
Shing-Hwa Liu
Shangzhong Liu
Songqin Liu
Xinghai Liu
Rutao Liu
Yanhong Liu
Songbai Liu
Yiming Liu
Yonghong Liu
Yu Liu
Yun Liu
Yung-Chuan Liu
Zheng Liu
Zhenghui liu
Zhiqian Liu
Zhiqiang Liu
Yahong Liu
Chun-Ting Liu
Aiping Liu
Bao-Sheng Liu
Wei Liu
Chan-Min Liu
Quan Liu
Donghong Liu
Dongting Liu
Fang Liu
Gang Liu
Guang-Ming Liu
Guodong Liu
Je-Ruei Liu
Jiaren Liu
Jingbo Liu
Jingfu Liu
Jun Liu
Kwang-Hyeon Liu
Lei Liu
Long Liu
Ming Liu
Ming-Qi Liu
Mingzhu Liu
Peng Liu
Pengfei Liu
Dasen Liu
Bensheng Liu
Jian zhu Liu
Alessandro Liverani
Gérard Hubert Lizard
Juan M. Llobet
Chih-Yu Lo
Yi-Chen Lo
Angela Roberta Lo Piero
Roberto Lo Scalzo
Alexandre Rodrigues Lobo
Monica Locatelli
Anne Loccisano
Amy Logan
Jack J. Lohne
Monica Rosa Loizzo
Mette Marie Løkke
Ante Loncaric
Julian Londoño-Londoño
Danfeng Long
Vincenzo Longo
Lucia Maria Xavier Lopes
Christelle Lopez
Francisco Lopez
Sergio Lopez
Luisa López
María Dolores López
María Liza López
Agustin Lopez Munguia
José M. López Vilariño
Camilo López-Alarcón
Gracia López-Carballo
Rosina Lopez-Fandino
E. Lopez-Huertas
Miguel Angel Lopez-Manchado
A. A. López Mañanes
Jose Eugenio Lopez-Periago
Mario Lorenz

DOI: 10.1021/jf506178r
J. Agric. Food Chem. 2015, 63, 2−18

Peter Christian Lorenzen
Chrystel Loret
Natalia Loscos
Jack N. Losso
Blas Lotina-Hennsen
Lili Lou
Qiaojun Lou
S. N. Lou
Vasiliki Louli
Simon M. Loveday
Douglas W. Lowman
Bożena Lozowicka
Ting-Jang Lu
Shin Lu
Yingjian Lu
Yan-Hua Lu
Yanbin Lu
Xiuling Lu
Xiaonan Lu
Min Lu
Baiyi Lu
Jian Lu
Hongfei Lu
Fachuang Lu
Chi-Hua Lu
Chao Lu
Weiying Lu
Juan J. Lucena
Rafael Lucena
Luigi Lucini
Richard D. Ludescher
Deivis Lujan-Rhenals
Marcin Łukaszewicz
Ed Lulai
Aderval Luna
Xiao-Dong Luo
Zisheng Luo
Yi Luo
Yangchao Luo
Wenhong Luo
Shaojun Luo
Xiaolan Luo
Sara J. Lupton
María Dolores Luque De Castro
Sue Lurie
Douglas Luster
Jens Lütjohann
Jiagen Lv
Junli Lv
Yi Lv
John W. Lyga
Graham Henry Lyons
Xi Ma
Zhonghua H. Ma
Yongqiang Ma
Qing-Hu Ma
Xiaoyuan Ma
Zhongjun Ma
Jun Ma
Haile Ma
Gang Ma
Dongying Ma
Baiping Ma
Yingjun Ma
Mingming Ma
Allan Patrick Gose Macabeo
Wade Mace
Maria Ligia Rodrigues Macedo
Olga Lima Tavares Machado
Ángela Machuca
Shaun MacMahon
Tilak R. Madaan
Lucia Maddau
Ronald L. Madl
Yolanda Madrid
Osamu Maeda
Britt Maestroni
Isabel Mafra
Filippo Maggi
Prokopios Magiatis
Kanjana Mahattanatawee
Behnoush Maherani
Andrea Mahn
Pitchaon Maisuthisakul
Michael S. Majewski
Tarun Kumar Maji
Yoshio Makino
Antonios M. Makris
Donald Makus
Mario Malagoli
Mery Malandrino
Julia Maldonado-Valderrama
Soheila J. Maleki
Veronika Mall
Alexandre Maller
Paul Kamba Malumba
Joao Malva
Jan Malyszko
Stefano Mammi
Mark J. Mamula
Richard A. Mancini
Khakhathi Mandiwana
Jordi Manes
Panagiotis Manesiotis
George Manganaris
Amruta Manke
Catarina Mansilha
Catarina Mansilha
Sébastien Manteau
Casimiro Mantell
Fani Mantzouridou
Paloma Manzanares
Frank Chiahung Mao
Takashi Maoka
Sameer A. S. Mapari
Matteo Marangon
Axel Marchal
Stéphanie Marchand
R. Marchant
Andrea Marchetti
Maria L. Marco
Pauline Marcq
Tim Marczylo
Castro María
Panagiota Markaki
Doris Marko
Nelson Marmiroli
José Carlos Marques
Catarina Marques
Raymond T. Marsili
Stefan Martens
J. M. Martina
Antonio Martin-Esteban
E. Nora Martinez
Enrique Martínez Force
Maria Rosa Martinez-Larranaga
Jose M. Martinez-Rivas
Silvana Martini
Joana T. Martins
Maria João Martins
Erwin Märtlbauer
Melanie Marty
Sue Masayuki
Rodolfo Horacio Mascheroni
Pellegrino Masiello
Jorge C. Masini
Francesca Masino
Riccardo Massantini
Tetsuya Masuda
Toshiya Masuda
Tsutomu Masujima
Kristen E. Matak
Narumol Matan
Raquel Mateos
Nuno Mateus
Michael L. Mathai
James M. Mathews
Fumio Matsuda
Kazuhiko Matsuda
Hiroshi Matsufuji
Kenji Matsui
Toshiro Matsui
Kentaro Matsumiya
Kinzo Matsumoto
Kiyoshi Matsumoto
Monica Mattarozzi
James Mattheis
Susan Matthew
Paul Matthews
Pirjo Helena Mattila
D. Scott Mattinson
Fulvio Mattivi
J. Matuz
Jeng-Leun Mau
Ronald Maul
Gianluigi Mauriello
Thomas P. Mawhinney
Carl A. Maxwell
Paul Stanley May
Jiri Mazac
Miguel Angel Mazorra-Manzano
Maria Fiorella Mazzeo
Kristi McCallum
Pearse McCarron
Shaunna McCauley
David Julian McClements
James McClung
Gregeory McCollum
Laura L. McConnell
Susan Patricia McCormick
Armando G. McDonald
Gordon J. McDougall
Murray James McEwan
Andrew McEwen
Tony Kevin Mcghie
Tony K. McGhie
Robert J. McGorrin
Mitch McGrath
Marla McIntosh
Ian R. McKinnon
Donald McMahon
Ken Mcmillin
Mary Ellen P. Mcnally
Jacqui M. McRae
Sharifudin Md. Shaarani
Giuseppe Meca
Rosaria Medda
Jand Venes Rolim Medeiros
R. M. Medeiros
Roger Meder
Manuel Medina
Miguel Ángel Medina
Roxana Beatriz Medina
Kumudini M. Meepagala
Emira Mehinagic
Mohamed Mehiri
Payam Mehrshahi
Alka Mehta
Sebastian Meier
Urs Meier
Wolfram Meier-Augenstein
Steven Wayne Meinhardt
Ghozlene Mekhloufi
Antonio J. Meléndez-Martínez
Carla Mello
Matthias F. Melzig
Maria Carmen Mena
Pedro Mena
Fabio Mencarelli
Ana Mendes
Rogerio O. Mendes
Lilia Mendez Lagunas
Jose Antonio Mendiola
Leonora Mendoza
Sandra Olimpia Mendoza
Jiangfei Meng
Ourania Menkisoglou
Simonetta Menotta
Elena B. Menshchikova
James Menzies
Adriana Zerlotti Mercadante
Giovana Domeneghini Mercali
Jeffrey A. Mertens
Marta Mesías
Frédéric Mestdagh
Ákos Mesterházy
Montse Mestres
Manfred Metzler
Barbara U. Metzler-Zebeli
Stamatios F. Mexis
Wolfgang Meyerhof
Samia Mezouari
Bruno Mezzetti
Ming Miao
Alain Michel
Sylvie Michel
Alex Michels
Johanna Michl
Ján A. Miernyk
Jorn Dalgaard Mikkelsen
Rene Mikkelsen
Susan R. Mikkelsen
Alexandr Mikyska
Paul E. Milbury
Magdalena Milczarek
Luigi Milella
Jocelyn G. Millar
Glenn Miller
J. David Miller
Kenneth B. Miller
Rebecca Miller
Rick Miller
George Milliken
Tanja Mimmo
Byungrok Min
Byung Sun Min
Yoshinori Mine
Ramón Mira de Orduña
Beatriz Miralles
M. Miriani
Sidney S. Mirvish
Devesh K. Misra
Alyson Elayne Mitchell
Richard Mithen
Kamila Mitrowska
Hisashi Miyagawa
Makoto Miyahara
Yusaku Miyamae
Sayuri Miyamoto
Masahiro Miyashita
Hitoshi Miyazaki
Norio Miyazawa

DOI: 10.1021/jf506178r
J. Agric. Food Chem. 2015, 63, 2−18

Norio Miyoshi
Takayuki Mizuno
Huanbiao Mo
Alejandra Moenne
Emmanuel Mogusu
Ali I. Mohamed
Jemima Beryl Mohankumar
A. Molina
Norhaizan Mohd Esa
Isabel Molina
Joachim Molkentin
Peter Molnar
Philip Molyneux
Linda Monaci
Yulia B. Monakhova
Pravakar Mondal
Luigi Mondello
Mei-chin Mong
Vincent M. Monnier
Manami Monobe
Sabine Montaut
Cinzia Montemurro
Paola Montoro
Angel Montoya
Javier Marcelo Montserrat
Sergio Montserrat-de la Paz
Hyo-Bang Moon
Jae-Hak Moon
Joon-Kwan Moon
Jeffrey C. Moore
Amram Mor
Leticia Mora
Maria Veronica Mora
Mohammad Moradi
Adela Mora-Gutierrez
Simone Morais
Francisco J. Morales
Juan C. Morales
Antonio Morata
Antonio Moreda-Piñeiro
Ricardo F.A. Moreira
Michael J. Morello
Diego A. Moreno
María Jesús Moreno
F. Javier Moreno
Maria Victoria Moreno Arribas
Antonio Moreno Herrera
Marcelo Antonio Morgano
Ágnes M. Móricz
Kenji Morimoto
Masanori Morimoto
Kyoji Morita
Tatsuya Morita
Takanori Moriyama
Andrea Moro
Matthew Morra
Mohamed A. Morsy
A. Mortazavian
Grith Mortensen
Claudio Moser
Sergio Moser
Magdi Mossoba
Amira Abdel Motaal
Maria José Motilva
Donald S. Mottram
Hongyan Mou
Hani Moubasher
Maria Alejandra Moya-Leon
Encarnación Moyano
Patrick Moyna
Xindong Mu
Irene Mueller-Harvey
Laura Mugnai
Michael Muhitch
Eric S. Muise
Fungai N. D. Mukome
Maurizio Mulas
Nadia Mulinacci
Bill Mullen
William Mullen
Christopher A. Mullin
John Peter Munafo
Gerald Münch
Sakthivel Muniyan
Edvani Curti Muniz
Francisco J. Muñoz
Rocio Gil Muñoz
Rosario Muñoz
Akira Murakami
Koji Muramoto
Masatsune Murata
Michael Murkovic
Cormac D. Murphy
Ghulam Murtaza
Mohd Rais Mustafa
Nor Afizah Mustapha
Franco Mutinelli
Kyung Myung
Koji Nagao
Masaya Nagao
Lakshmi S. Nair
Muraleedharan Gopalan Nair
Bai Naisheng
Yoshiaki Nakagawa
Kazuhiko Nakamura
Kozo Nakamura
Soichiro Nakamura
Yoshimasa Nakamura
Yoshio Nakatani
Sitthipong Nalinanon
Myung Hee Nam
Jacek Namiesnik
Vijay Nandula
Alessandra Napolitano
Serenella Nardi
Mirella Nardini
J. Roberto Oliveira Nascimento
Robert J. Nash
Atef M. K. Nassar
Françoise Nau
Giovanna Navarra
Duroy A. Navarre
Juan Carlos Navarro
Miguel Navarro-Alarcon
Inmaculada Navarro-González
Daniele Naviglio
Eiji Nawata
Monica Azucena Nazareno
Vidushi Neergheen
Giuseppina Negri
Tatsuo Nehira
Lembit Nei
Jonathan Wesley Neidigh
Andrew Peter Neilson
Jim A. Nelson
Agnes Sz. Nemeth
Bee Keat Neoh
Cristina Nerin
Eirik Nestaas
Catherine C. Neto
Michael Netzela
Susanne Neugart
Ralf Neumann
Klaus Gerald Neumuller
Valdir Augusto Neves
Maria Teresa Neves-Petersen
Lee A. Newman
Tzi Bun Ng
Sai-Ming Ngai
Thanh Dong Nguyen
Hui Ni
Xinzhi Ni
Yongnian Ni
Taco Nicolai
Maria Cristina Nicoli
Luca Nicolotti
Shaoping Nie
Xiaohua Nie
Michel W.F. Nielen
Kristian Fog Nielsen
David C. Nieman
Ludwig Niessen
Pedro M. Nieto
Helene H. Nieuwoudt
Etsuo Niki
Maria Nikolantonaki
Dilara Nilufer-Erdil
Kiyofumi Ninomiya
Jun Nishihira
Naomichi Nishimura
Hisashi Nishiwaki
N. Nitin
Bing Niu
Junfeng Niu
Yuge Niu
Patrick Njobeh
Emmanuel Njumbe Ediage
Joaquim de Araújo Nóbrega
Koji Noge
Sang Noh
Hitoshi Nohta
Kiyoshi Nokihara
Kei Nomiyama
Cassana Seimi Nomura
Keiichi Nomura
Yoshihiro Nomura
Eliane Ferreira Noronha
Natalja P. Nørskov
Violeta Nour
Johannes Novak
Enrico Novelli
Vittorino Novello
Esther Novo-Uzal
Nikoletta G. Ntalli
Roberto Nucci
Karin Nuernberg
Fernando Milheiro Nunes
Itaciara Nunes
Alberto Nunez
Estrella Nuñez-Delicado
George J. E. Nychas
Laura Nystroem
D. Obenland
A. Oberholster
Hassan K. Obied
Jose Maria Obon
Nora M. O'Brien
Masaru Ochiai
F. Ocloo
Tatsuya Oda
Isabel Odriozola-Serrano
A. C. Oehlschlager
Indrawati Oey
Masahiro Ogawa
Yasumitsu Ogra
Nives Ogrinc
Myung Sook Oh
Seikwan Oh
Suk-Heung Oh
Deok-Kun Oh
Hideo Ohkawa
Yusei Ohshima
Yoshito Ohtani
Akira Oikawa
Yong Sik Ok
Keiki Okazaki
A. Olad
Agustin Olano
Wieslaw Oleszek
Cornelius Olieman
Jose Oliva
Carla Marques Oliveira
Joana Oliveira
Jose T. A. Oliveira
Àngels Olivella
Alberto de Jesus Oliveros Bastidas
Teresa Oliviero
Velimatti Ollilainen
Nuria Del Olmo
Rafal Olszanecki
Tomasz Krzysztof Olszewski
John O'Mahony
Sesselja Omarsdottir
Gemma Oms-Oliu
Baran Onal-Ulusoy
H. V. Masey O'Neill
Tooru Ooizumi
Carl E. Orazio
Greg Organ
José de Jesús Ornelas-Paz
Valerie Orsat
George González Ortega
Natividad Ortega
Abel Ortiz
Cristian Ortiz
M. J. Oruna
Kazufumi Osako
Tatsuya Oshima
Ali Osman
Coralia Osorio Roa
Henrik Ostdal
Maurice O'Sullivan
Maria D. Osuna
Jan Oszmienski
Yuzuru Otsuka
Don E. Otter
Daniel E. Otzen
Shiyi Ou
Dasharath P. Oulkar
Simon Ovenden
Janel Elizabeth Owens
Fatih Oz
Özgül Özdestan
Peggy Ozias-Akins
Sibel A. Ozkan
Yoshihisa Ozoe
Ismet Ozturk
Nadine Pabian
Fernando Pablos
Deborah Pacetti
Maurizio Paci
Daniela Pacifico
Severina Pacifico
Man-Hui Pai
Alicia Paini
Paulina Pajączkowska
Natalia Palacios-Rojas
Marimuthu Palanisamy

DOI: 10.1021/jf506178r
J. Agric. Food Chem. 2015, 63, 2−18

Gopinadhan Paliyath
Mercè Pallàs
Jose Manuel Palma
Miguel Palma
Luisa Palmieri
Andreu Palou
Min-Hsiung Pan
Xiao Pan
Cheol-Ho Pan
Tzu-Ming Pan
Yibin Pan
Tai-Long Pan
Guoqing Pan
Chorng-Liang Pan
Canping Pan
Daodong Pan
Jiaomai Pan
Daniel G. Panaccione
Min Pang
Xiao-Yan Pang
Xue-qun Pang
Kip E. Panter
Jitendra Panwar
Lucia Panzella
Ioannis N. Papadoyannis
Emmanouil H. Papaioannou
Adele Papetti
Efstathia Paramera
Adamantini Paraskevopoulou
Gabriel Pardo
Octavio Paredes-Lopez
Lucia Pareja
Teodor Parella
Bram Pareyt
Seung K. Park
Yong Kun Park
Yeonhwa Park
Seung-Chun Park
Sang Un Park
Kyoung-Chan Park
Kyechung Park
Jongtae Park
Jae B. Park
Il-Kwon Park
Tae Jung Park
Eunyoung Park
Doo Hyun Park
Cheon-Seok Park
Bosoon Park
Kwan-Hwa Park
Jane K. Parker
Michelangelo Pascale
Sophie Pascal-Lorber
Jonas A. R. Paschoal
Inmaculada Pascual
Sonia Pascual-Teresa
P. Paseiro-Losada
Antonella Pasqualone
Edgar Pastene
Chiara Pastore
Glaucia M. Pastore
Petra Patakova
G. Pataro
Bhimanagouda S. Patil
Ioannis S. Patrikios
Harold E. Pattee
Ralf Pätzold
Moushumi Paul
Anneleen Pauly
Hrvoje Pavlović
Elke Pawelzik
M. Soledade C. Pedras
Maria Angeles Pedreno
Franco Pedreschi
Renjun Pei
Richard Peigler
Rafael Peinado
Jaroslav Pejchal
Federica Pellati
Nicoletta Pellegrini
Carlos Peña
Dungeng Peng
Robert Y. Peng
Hailong Peng
Chi-Chung Peng
Kou-Cheng Peng
Chiung-Huei Peng
Juan Peragón
Ana Luisa Pereira
Fabíola Verbi Pereira
José Alberto Pereira
Ricardo Nuno Pereira
António Manuel Peres
Montse Perez
María Dolores Pérez
María del Carmen Pérez-Camino
Laura Pérez-Fons
Antonio Pérez-Gálvez
Marina Perez-Gordo
Jara Pérez-Jiménez
Trinidad Perez-Palacios
Cristina Perez-Ternero
Míriam Pérez-Trujillo
María Jesús Periago
Nebojsa Perisic
Penelope Perkins-Veazie
Javier Sanchez Perona
Clarisse Perrin
Daniel Perrone
Irena Perucka
Miklos Pesti
Clemens K. Peterbauer
Mikael Agerlin Petersen
Devin G. Peterson
Jeremy Petit
Carmen L. O. Petkowicz
Giacomo Petretto
Rita Petrucci
Hans Pettersson
Alessandro Pezzella
James A. Pfister
Hanh Phan-Thi
Kim-Yen Phan-Thien
Tom D. Phillips
Melissa M. Phillips
Brigitte Picard
Gianluca Picariello
Anna Lisa Piccinelli
Clara Piccirillo
Matthew J. Picklo
Yolanda Pico
Adeline Picot
Anne Marita Pihlanto
Fernando Pina
Samantha Pinho
Jorge Antonio Pino
Manuela E. Pintado
Edgar Pinto
Glaucia Maria Ferreira Pinto
Carlo Pirola
Monika Pischetsrieder
Gina Cecilia Pistol
Emanuela Pitzalis
Roberto Pizzala
Javier Plasencia
Merichel Plaza
Patricia Plaza-Bolaños
Przemysław Mieszko Płonka
Anne Plotto
Maria de Fatima Poças
Ewa Pociecha
Lynda Podhorniak
Juergen Poerschmann
Pawel Pohl
Luigi Poisson
Julio Polaina
Tomaz Polak
Krzysztof Polewski
M. G. Polissiou
Palmiro Poltronieri
Anandh Babu Pon Velayutham
Céline Poncet-Legrand
David G. Popovich
John R. Porter
María P. Portillo
Nebojsa I. Potkonjak
Patrick Poucheret
Nina Aagaard Poulsen
Martin S. Pour Nikfardjam
Elena Poverenov
Andrew Clifford Povey
Malcom J. W. Povey
Jonathan J. Powell
Joseph Robert Powers
Maria Angeles Pozo-Bayon
Abani Pradhan
Marta Prado
Md. Habibur Rahman Pramanik
K. Nagendra Prasad
Christophe Praz
Paul David Prenzler
Nigel D. Priestley
Ronald L. Prior
D. Procházková
Darwin J. Prockop
Andrew Proctor
Marin Prodanov Prodanov
Charalampos Proestos
Ludger Beerhues
Jaime Prohens
Peter Proksch
Nicholas William Proschogo
Dov Prusky
Yunqiao Pu
Allen E. Puchalski
Eduardo Puértolas
Eero Puolanne
L. L. A. Purcena
Roger W. Purchas
W. Ronald Purdum
Lesley Putman
Alina Pyka
Synan Abu Qamar
Hongyan Qi
Zeming Qi
Wei Qi
Phoebe X. Qi
Lian-Wen Qi
Lichun Qian
Michael C. Qian
Tianxiu Qian
Xuhong Qian
Bo Qin
Ruijun Qin
Yuchang Qin
Zhaohai Qin
Jian-Wen Qiu
Jing Qiu
Ning Qiu
Xi Qiu
Xiangyun Qiu
Carmen Quero
Jesus Alberto Quezada-Gallo
Yun Qui
Stephane Quideau
Alain Quinsac
Cristina Quintelas
Jose Maria Quiroga
Juliana Neves Rodrigues Ract
Elena Rada
Nadia Raffaelli
María Dolores Raffo
Arthur Jonas Ragauskas
Neera Raghav
Sivakumar Raghavan
Pullakhandam Raghu
Mohammed M. Rahman
Merl Raisbeck
Smita Raithore
C. Rajashekar
Moganty R. Rajeswari
Sveto Rakic
Jean-Philippe Ral
Ranjith Ramanathan
Diky Ramdani
Lina M. Ramirez-Lopez
Guillermo Ramis Ramos
Daniel Ramon
Fernando Ramos
Sonia Ramos
Gideon Ramtahal
Gurinder Jit Randhawa
Natarajan Ranganathan
Archna Rani
Scott A. Rankin
A. G. Appu Rao
Jiajia Rao
Qinchun Rao
Srinivasa P. S. Rao
Vietla Satyanarayana Rao
Zhiming Rao
Paolo Rapisarda
Rie Romme Rasmussen
Peter Have Rasmussen
Javier Raso
Shiva Kumar Rastogi
Luca Rastrelli
Bakhtiyor Rasulev
Marion Raters
Wajira S Ratnayake
Gabriela Ratz
Doris Rauhut
Catherine Ravel
Lidia M. Ravelo-Pérez
Harshadrai M. Rawel
Ashish Rawson
Ramesh M. Ray
Marilyn Rayner
Saleh Rayyan
Maria José Ferreira Rebelo
Isidra Recio
Manuel Suarez Recio
rita redaelli
Araceli Redondo
Jess D. Reed
R. Neil Reese
Carlos Regalado
Klaas Reglitz
Jorge Regueiro
Sophie Marie Réhault-Godbert
Aune Rehema
Manuel Joaquín Reigosa

DOI: 10.1021/jf506178r
J. Agric. Food Chem. 2015, 63, 2−18

Peter J. Reilly
Gary Reineccius
Vernon N. Reinhold
Mariza Gomes Reis
Wojciech Rejmer
Perla Relkin
Maurizio Remelli
Di-Feng Ren
Guixing Ren
Jiaoyan Ren
Denis Renard
Manuel Rendueles
Scott Renneckar
Derek Renshaw
T. Requena
Teresa Requena
Martin Resano
Patrizia Restani
Eugenio Revilla
Wim Paul Reybroeck
Nicholas P. Reynolds
Claudia M. Rezende
Leila Rezig
Neil Rhodes
John J. Riascos
Alain Riaublanc
António Ribeiro
Caue Ribeiro
Jorge Manuel Ricardo-Da-Silva
Florence Richard-Forget
Mark P. Richards
Elke Richling
Pascal Richomme
C. W. Rico
Cyren M. Rico
Lars Ridder
William P. Ridley
Franklin Riet-Correa
Ivonne Magdalena Catharina Maria Rietjens
Maria Pia Rigobello
Agnes M. Rimando
Gerald Rimbach
Frank Rinaldi
Jose Luis Rios
Sara J. Risch
Patrizia Riso
Patricia Risso
Renata Ristic
Alberto Ritieni
Syed Ibrahim Rizvi
George P. Rizzi
Angela Maria Rizzo
Roberto Rizzo
Harry Robberecht
Sue A. Roberts
Thomas Hugh Roberts
Simon P. Robinson
Gilles Robitaille
John F. Robyt
María Roca
João Batista Rocha
Victor Rodov
P. Rodrigues
S. Rodrigues
Edson Rodrigues-Filho
Rosalia Rodriguez
Jason D. Rodriguez
Arantxa Rodriguez
Victor M. Rodriguez
Francisco Rodríguez
Isaac Rodríguez
Juan Miguel Rodriguez Patino
Luis Miguel Rodríguez-Alcalá
Delia B. Rodriguez-Amaya
Encarnación Rodríguez-Gonzalo
Ana Rodriguez-Mateos
Maria Luz Rodriguez-Mendez
María Janeth Rodríguez-Roque
Rogelio Rodríguez-Sotres
Deborah E. Rogers
ChangHyun Roh
Gu Seob Roh
Barbara Rohm
Sascha Rohn
Manuel Roig
Luca Rolle
Iván P. Román Falcó
Gianfranco Romanazzi
Ine Rombouts
Concepcion Romero
Hernán Mauricio Romero
Maria-Paz Romero
Roberto Romero-Gonzalez
Corinne Rondeau
Carlo Rosati
Devin Jerrold Rose
Cristina M. Rosell
Moshe Rosenberg
Charles Rosenkrans
José María Ros-García
Ahmad Rosma
Andrew S. Ross
Carolyn Felicity Ross
Mark M. Ross
Maddalena Rossi
Mauro Rossi
John T. Rossiter
Andreas Rossmann
Valerie Rota
Christophe Rothan
Jean-Max Rouanet
Antoine Rouilly
Russell Rouseff
Ioannis G. Roussis
Sevastianos Roussos
Kenneth H. Roux
Giovanni N. Roviello
Nicolas Rozes
Zhenhua Ruan
Diego Rubiales
Antonio Rubies
Fernando Rubio
María del Carmen Rubio
Soledad Rubio
Patrizia Rubiolo
David R. Rudell
Alisa Rudnitskaya
José A. Rufián-Henares
Zebao Rui
Héctor A. Ruiz
Juan Manuel Ruiz
Maria Victoria Ruiz
Maria Luisa Ruiz del Castillo
Yolanda Ruiz-García
Antonio Ruiz-Medina
Wilson Rumbeiha
Prithy Rupa
Gordana Rusak
Gian Luigi Russo
Maria Russo
Mariateresa Russo
Nino Russo
Turid Rustad
Shane M. Rutherfurd
Elizabeth P. Ryan
Dave Ryan
Michael E. Rybak
Michael Rychlik
Mojmir Rychtera
Shi Yong Ryu
Nazamid Saari
Shyam S. Sablani
Cristina M. Sabliov
Ozlem Sacan
Gianattilio Sacchi
Joseph R. Sachleben
Gavin L. Sacks
Hiroki Saeki
Leonard Martin Sagis
Gianni Sagratini
Elena Saguer
Vinod Saharan
Buket Sahin
Stefan Sahlstrom
Ai Egusa Saiga
Kaori Sakamoto
Miho Sakamoto
Tatsuji Sakamoto
Shohei Sakuda
Angelo Sala
Joaquín J. Salas
Muhammad Saleem
Mahmoud Saleh
András Salgó
Ligia Salgueiro
M. Rosario Salinas
Christian Salles
Bolesław Przybysław Salmanowicz
Serafina Salvati
Roberto Samperi
Ana Sanches-Silva
Lourdes Sánchez
Ana Sánchez
Ana Cristina Sánchez Gimeno
M. Teresa Sánchez-Ballesta
Laura Sánchez-Hernández
Cortes Sanchez-Mata
Maria Cortes Sanchez-Mata
Eva Sanchez-Palomo
Maria Teresa Sancho
Wolfgang Sand
Melanie Sanders
Amandeep K. Sandhu
Pilar Sandin-España
Pat Sandra
Harold H. Sandstead
Shengmin Sang
Anderson de Souza Sant'Ana
Léa Silvia Sant'Ana
Celso Santanna
Véronique Santé-Lhoutellier
Antonello Santini
Sónia A. O. Santos
Sara Ribeiro Santos
Ana Cristina Santos
Valentín Santos
Celestino Santos-Buelga
Lucas Santos-Juanes
Carlos Sanz
Maria Luz Sanz
Gautam Sarath
P. S. Saravana
Abdelwareth A. O. Sarhan
Simo Sarkanen
Ujjal Sarkar
Rakrudee Sarnthima Sartini
Jutamaad Satayavivad
Shridhar Krishna Sathe
Ramalingam Sathishkumar
Kenji Sato
Kiyotaka Sato
Mayumi Sato
Pawel Satora
Tulasi Satyanarayana
Cédric Saucier
James A. Saunders
Fulgencio Saura-Calixto
Brett J. Savary
Elif Savas
Jean-Michel Savoie
Francesco Savorani
Akiyoshi Sawabe
Masayoshi Sawamura
Yoriko Sawano
Sedat Sayar
Andrea Scaloni
Christine H. Scaman
Alessio Scarafoni
Andrea Scartazza
Sebastian Schaffer
K. M. Schaich
Alexander G. Schauss
Hugo Scheer
Frank Schenck
Michela Schiavon
Andreas Schieber
Peter Schieberle
Elisabetta Schievano
Stefan Schillberg
Jurgen Schiller
Wes Schilling
Romana Schirhagl
Jean-Paul Schirlé-Keller
Erwin D. Schleicher
Hedwig Schlichtherle-Cerny
Philipp Schmidberger
Hans-Peter Schmidt
Christophe Schmitt
Rainer Schmitt
Marilyn Schneider
Rudolf J. Schneider
Ewald Schnug
Sebastian Schoenauer
Carola Schoenknecht
Margit Schollenberger
Henk A. Schols
Katharina Scholz-Ahrens
Monika Schreiner
Peter Schröder
Christian Schuh
Hartwig Schulz
Claude Schummer
Wilfried G. Schwab
Wolfgang Schwack
Heidi Schwartz
Steven J. Schwartz
Christiane Schwarz
Karin Schwarz
Monica Scognamiglio
Geoffrey Robert Scollary
Corey E. Scott
Paul Scott
Ian Melville Scott
M. Paul Scott
Alan Seawright
Natividad Sebastià

DOI: 10.1021/jf506178r
J. Agric. Food Chem. 2015, 63, 2−18

Marek Šebela
Ronnald R. Sederoff
Navindra P. Seeram
Philippe Seguin
Juan Segura
Antonio Segura-Carretero
Verena Seidl-Seiboth
David Seigler
Jasreen K. Sekhon
Serkan Selli
Gordon W. Selling
María V. Selma
Maria Germanovna Semenova
Deepak Kumar Semwal
Marcelo M. Sena
Thomas Senn
Enrique Sentandreu
Jolanta Sereikaite
Lucrezia Sergio
Sergio O. Serna-Saldivar
Maria Serrano
Jéssica Serrano-Díaz
Maurizio Servili
Mitsutoshi Setou
Feride Severcan
Stefano Sforza
Cristina Sgherri
Barbara Sgorbini
Amita Shah
Utkarsh Shah
Nahid Shahabadi
Muhammad Adnan Shahid
Fereidoon Shahidi
Guomin Shan
Bing Shao
Suqin Shao
Xusheng Shao
Xueguang Shao
Xi Shao
Maged Sharaf
Arun Sharma
Ashok K. Sharma
Nick Shaw
Kinnari Shelat
Krista Shellie
Weilin L. Shelver
Ya-Ching Shen
Guoqing Shen
Hao Shen
Jianzhong Shen
Lirong Shen
Rui-Ling Shen
Wen-Biao Shen
Chwan-Li Shen
Carolina Shene
Long Sheng
Jiali Shentu
Gordon Seymour Shephard
Robert Sheridan
Alexander F. Shestakov
Kalidas Shetty
Joen Rong Sheu
M. L. Sheu
Fuu Sheu
Peter R. Shewry
Haiming Shi
Junling Shi
Linqi Shi
Shu Yun Shi
YeuChing Shi
Chyuan-Yuan Shiau
Sy-Yu Shiau
Takayuki Shibamoto
Mark Shigenaga
Jae Han Shim
Hidehisa Shimizu
Kuniyoshi Shimizu
Bun-ichi Shimizu
Makoto Shimoyamada
Eui-Cheol Shin
Gye Hwa Shin
Kazutoshi Shindo
Kazuo Shiomi
Prachand Shrestha
Tatsiana G. Shutava
Youbin Si
Alfonso Siani
Rosa Anna Siciliano
Leonard M. Sidisky
Karl J. Siebert
Caroline Siefarth
David Siegel
Barbara Siegmund
Carmen Sieiro
Hartwig Sievers
Giovanni Signore
Ewa Sikorska
Slavica Siler-Marinkovic
Carlos Peres Silva
Dilson Silva
Marcia Messias da Silva
Alessandra Silvani
Armando Jorge Domingues Silvestre
Jesus Simal-Gandara
Vida Šimat
Mario J. Simirgiotis
Charlotte Simmler
Monique S. J. Simmonds
Amber L. Simmons
Ryan R. Simon
Breda Simonovska
Jean-Pierre Simorre
Andre J. Simpson
Sebnem Simsek
Jozef Simuth
Andrew J. Sinclair
Gurmit Singh
Sridevi Annapurna Singh
Samunder Singh
Rakesh Kumar Singh
Harminder Pal Singh
Birbal P. Singh
Balram Singh
Anand Singh
Ajay Pratap Singh
Abhay Narayan Singh
Neera Singh
Maxim Sinkevich
Aki Sinkkonen
Srinivas Sistla
Mahmoud Z. Sitohy
Raseetha Siva
Pandian Sivakumar
John D. Sivey
K Skalicka-Wozniak
Helen Skaltsa
Mojca Škerget
Jørgen Skibsted
Leif H. Skibsted
George Skouroumounis
Louise Slade
Joanne L. Slavin
Margaret Slavin
Rune Slimestad
Jens J. Sloth
David R. Smart
Joseph L. Smilanick
Alison M. Smith
Brenda J. Smith
Christopher Smith
Christopher John Smith
Darrin Lee Smith
David J. Smith
Jason A. Smith
J. Scott Smith
Paul A. Smith
Philip C. Smith
Rachelle Smith
Irina P. Smoliakova
Heather Eunice Smyth
Nicholas Harrer Snow
Jae-Young So
Sandra Sobocanec
Anatoly Petrovich Sobolev
Anatoly P. Sobolev
Rafel Socias i Company
Sirirath Sodngam
D. S. Sogi
Marina Sokovi
Daniel K. Y. Solaiman
Cristina Soler Rivas
Michele Solfrizzo
Emad Ali Soliman
Robert Soliva-Fortuny
Alexei E. Solovchenko
Leellen Solter
Ferenc Somogyvári
Mark M. Somoza
Veronika Somoza
Joo-Hiuk Son
Bao-An Song
Baoan Song
Yuanda Song
Yang Song
Xiaojin Song
Xiao Yan Song
Benito Soto-Blanco
Mustafa Soylak
Martien C. Spanjer
Karl Speer
Giorgia Spigno
Jennifer Spinler
Kurt Spokas
Apostolos Spyros
Fábio M. Squina
Keerthi Srinivas
Rajendra Prasad Srivastava
George Srzednicki
Franz St. John
Richard Herman Stadler
Marc Stadler
Dan Staerk
Wilhelm Stahl
Henrik Stalbrand
Apryll M. Stalcup
Angelique Stalmach
Larry H. Stanker
Ruth E. Stark
Timo D. Stark
Christian Starkenmann
Erika Staudacher
Eleftheria Stavridou
Marina Stefova
Bryan L. Stegelmeier
Hans H. Stein
Martin Steinhaus
Petra Steinhaus
Siegrid Steinkellner
Havard Steinshamn
Katherine Stenerson
Marcus Stensmyr
Irina Stepanov
Cheryl Stephenson
Tracy Sterling
Rudolf Stetina
Martin Steup
Roberto Stevanato
Tatjana Stevanovic
Jan F. Stevens
Philip C. Stevenson
Maria L. Stewart
Derek Stewart
Susanne Stingl
Robert D. Stipanovic
Maciej Stobiecki
Anna Stochmal
Klaus Stolze
Michael Stout
Robert E. Stratford
Cecil Stushnoff
Nan-Wei Su
Zhengquan Su
Zheng-Yuan Su
Kuan-Pin Su
Belen Suarez-Valles
Bikram Subedi
Venkataraman Subramanian
R. Subramanian
Koji Sugawara
Yasushi Sugimoto
Manickam Sugumaran
Shaida Fariza Sulaiman
Joanna Suliburska
Michael Sulyok
Surendranath P. Suman
Baoshan Sun
Hongnan Sun
Jian Sun
Jianghao Sun
Qingjie Sun
Run-Cang Sun
Runcang Sun
Shangde Sun
Shang-De Sun
Shao-Long Sun
Weiqing Sun
Yuanxia Sun
Zewei Sun
Ulrik Sundekilde
Ulrik Kræmer Sundekilde
Jih-Min Sung
S. M. Sunil
Lakshmi Sunkara
Stefano Superchi
Vipa Surojanametakul
Somyote Sutthivaiyakit
Ei-Ichiro Suzuki
Shunji Suzuki
Jisnuson Svasti
Stuart Swanston
Ken Sweat
Michael Sweedman
Mark Sykes
Tore Syversen
Y. T. Szeto
Arkadiusz Paweł Szterk
Aleksandra Barbara Szydłowska-Czerniak
Monika Szymańska-Chargot
J. Szymońska
Amani Taamalli
Sartaj Tabassum
Louisa Tabatabai
Maria Tabernero
Zeynep Tacer-Caba
José L. Tadeo
Hessy L. Taft
Davide Tagliazucchi
Reza Tahergorabi
Heidar-Ali Tajmir-Riahi
Umeo Takahama

DOI: 10.1021/jf506178r
J. Agric. Food Chem. 2015, 63, 2−18

Koretaro Takahashi
Makoto Takahashi
Nobuyuki Takahashi
Yoko Takahashi
Tsujita Takahiro
Tomoyuki Takaku
Gary R. Takeoka
Miklós Takó
Kiyoshi Takoi
Stephen T. Talcott
Pasquale Tamborra
Tarja Tamminen
Hirotoshi Tamura
Fa-Jui Tan
Li-Feng Tan
Hiroyuki Tanaka
Keijitsu Tanaka
Makoto Tanaka
Mitsuru Tanaka
Naoki Tanaka
Takashi Tanaka
Takuji Tanaka
Vishnu K. Tandon
Chih-Hsin Tang
Chuan-He Tang
Hao Tang
Mingliang Tang
Shengan Tang
Wenping Tang
Gregory J. Tanner
Masaru Tanokura
Anna L. Tan-Wilson
Liang Tao
Sijia Tao
Yi-Ming Tao
Petros Taoukis
Javier Tardaguila
Eden Tareke
Lee Tarpley
Marko Tapio Tarvainen
Fernando Tateo
Bernhard Tauscher
Aldo Tava
Marcos Taveira
Andy Taylor
John R. N. Taylor
Mark A. Taylor
Saad Tayyab
Vera Tchakalova
Piero Andrea Temussi
Noelia Tena
Maija Tenkanen
Gian Carlo Tenore
Alexandra Ter Halle
Norihiko Terahara
Junji Terao
Waldemar Ternes
Frederic J. Tessier
Richard F. Tester
Theresia Thalhammer
Li Thao
Nishanth Tharayil
Dil Thavarajah
Laetitia Theron
Martin Gustavo Theumer
Usha Thiyam-Hollander
Nikolaos S. Thomaidis
Karin Thomas
Olivier Paul Thomas
Henry J. Thompson
Tom S. Thompson
Jasmine Thorkildsen
Ulf Thrane
Linwei Tian
Yaoqi Tian
Louis X. Tiefenauer
Axel Tiessen
Rohan V. Tikekar
Michael M. Tilley
Yuwen Ting
Sheryl A. Tittlemier
Kyoko Toda
Masako Toda
Aldo Todaro
Setsuko Todoriki
Peter M. A. Toivonen
M. Tomas
Francisco Tomas-Barberan
Patrick L. Tomco
Qing-Xiao Tong
Zhaohui Tong
Pietro Tonutti
Ondulla Tyvette Toomer
Fatih Tornuk
Alba Torrents
Patricia Torres
R. Torres
Josep Lluis Torres
Bohn Torsten
Paola Tosi
Ildikó V. Tóth
Juscelino Tovar
Ioan Cristian Trelea
Réjean Tremblay
Réda Triqui
Antonio Dario Troise
Jurij Trontelj
Patrick Trouillas
Pilar Truchado
Van-Den Truong
Pijen Tsai
Shau-Wei Tsai
Tsung-Yu Tsai
Tung-Hu Tsai
Ying-Chieh Tsai
Rong Tsao
Karl W. K. Tsim
Maria Z Tsimidou
Emmanouil Dimitrios Tsochatzis
Koichiro Tsuchiya
Tsuyoshi Tsuduki
Chein-Hsiun Tu
Maobing Tu
Yunfei Tu
Zheng-Chao Tu
Kayimbi M. Tubajika
Franco Tubaro
Carlo I. G. Tuberoso
Ludmila Tuckova
Jose Tudela Serrano
Artemio Zabala Tulio
Sara Tulipani
Rosa Tundis
Yen-Chen Tung
Michael H. Tunick
Sherri B. Turnipseed
Christian Turra
Amit K. Tyagi
Oxana Tyapkova
Bor-Show Tzang
Fabiola Ubillus
Janice Y. Uchida
Minori Uchimiya
Peter Uden
Chibuike C. Udenigwe
Mariko Uehara
Daisuke Ueno
Toshio Ueno
Maurizio Ugliano
Hiroyuki Ukeda
Detlef Ulrich
Shahid Umar
Takayuki Umemoto
Noriharu Ken Umetsu
Patrick R. Unwin
Brad L. Upham
Tadasu Urashima
Jaime Uribarri
Paulina Urrutia
Ewald Usleber
Yoshinosuke Usuki
U. Uthumporn
Uchechukwu Anastasia Utoh Nedosa
Tamer Uyar
Fabrice Vaillant
M. Vairamani
Athanasios Valavanidis
Jesus Valcarcel
M. Valdivia-López
Patrícia Valentão
Kateřina Valentová
Stefania Valenzano
Francesca Valerio
Daniel Valero
Edelmira Valero
Manuel Valero
Luca Valgimigli
Fernando Vallejo
M. D. Vallejo
Steven Valles
Anna Vallverdu-Queralt
Victoriano Valpuesta
Juan Valverde
Antonio Valverde
Marie-Rose Van Calsteren
Nicole M. van Dam
Koen van de Wetering
Lambertus A. M. van den Broek
Erik van der Linden
A. F. B. van der Poel
Cees Van Dijk
John P. M. van Duynhoven
Mark E. Van Dyke
Leo J. L. D. van Griensven
François Van Hove
John Van Klink
Filip Van Opstaele
Els Van Pamel
Christof Van Poucke
Steven C. Van Sluyter
Gordon van't Slot
Ewoud J. J. van Velzen
Jairam Vanamala
Jelena Vancetovic
Rob Vandebriel
Luciana Vandenberghe
Aila Vanhatalo
M. Pilar Vaquero
Patroklos Vareltzis
Elisabeth Varga
Prasad S. Variyar
Isabel Vasconcelos
Alina Mihaela Vasilescu
Todor Vasiljevic
Daniel Giddings Vassão
Martha Vaughan
Steven F. Vaughn
Sílvio Vaz Jr.
Manuel Vazquez
Robert Veberic
Eva Veiseth-Kent
Nigel Veitch
Anne Vejux
Joaquin Velasco
Leonardo Velasco
Pablo Velasco
Edwin J. A. Veldhuizen
Carmen Venegas
Dharuman Venkataraman
Tyamagondlv V. Venkatesh
Petras Rimantas Venskutonis
Vittoria Ventrella
Jorge Ventura Ferreira Cardoso
Vito Verardo
Germano Veras
John R. Vercellotti
Roland Verhe
Mahendra Kumar Verma
Mario A. Vermeer
Aude Vernhet
Veronique Verrez-Bagnis
Joran Verspreet
Kevin J. Verstrepen
Vaclav Vetvicka
Fabio Vianello
Ariel Roberto Vicente
Stefania Vichi
Melita Vidaković
Jean Claude Vidal
Rajko Vidrih
Margarida C. Vieira
Marco Vighi
Louise Vigsnæs
Martin Vila-Aiub
Ricardo Villalobos
Mar Villamiel
Débora Villaño
Francisco J. Villarreal
Juan José Villaverde
Pierre Villeneuve
Pilar Viñas
Joe A. Vinson
Francesco Violi
Francesco Visioli
Ramin Vismeh
Meththika Vithanage
Marlize Zaretha Viviers
Rudi F. Vogel
Johann Vollmann
Dietrich Von Baer
Christoph Von-Holst
Kenneth A. Voss
Paul Voziyan
Urska Vrhovsek
Frank Vriesekoop
Zisis G. Vryzas
James Wachira
Koji Wada
Wim Waetjen
Yuhya Wakasa
Masataka Wakayama
Toshiyuki Wakimoto
Czesla Walawson
Richard Brian Walker
Mandy Walker
D. Eric Walters
Rosemary L Walzem
Wayne G. Wamer
Jie Wan
Qian-Hong Wan
Xiaochun Wan
Janitha P. D. Wanasundara
Aiqin Wang
Bin Wang
Bor-Sen Wang
Bao-Lei Wang
Chau-Jong Wang

DOI: 10.1021/jf506178r
J. Agric. Food Chem. 2015, 63, 2−18

Chi-Chiu Wang
Chin-Kun Wang
ChongZhi Wang
Dongfeng Wang
Dongjie Wang
Daoquan Wang
Daowen Wang
Dayong Wang
Feng Wang
Guang Wang
Haiyan Wang
Haizhen Wang
Hui-Min David Wang
Jian Wang
Jia-Sheng Wang
Jianhua Wang
Jian ping Wang
Lisheng Wang
Jing Wang
Juan Fei Wang
Jun Wang
Junfeng Wang
Liangsheng Wang
Lifeng Wang
Lin (Lynn) Wang
Lisa Wang
Mei Wang
Min Wang
Mingfu Wang
Ming-Hua Wang
Peng Wang
Qiaomei Wang
Qin Wang
Qingmin Wang
Qiquan Wang
Selina C. Wang
ShaoYun Wang
Sheng-Yang Wang
Shih-Wei Wang
Shu Wang
Shu-Guang Wang
Shujun Wang
Shuo Wang
Steven S.-S. Wang
Tao Wang
Thomas T. Y. Wang
Tiejun Wang
Wen-Xiong Wang
Weiqun Wang
Xiangyu Wang
Xiaojun Wang
Xiao Wang
Xiaoyong Wang
Xingguo Wang
Xinquan Wang
Ya-Jane Wang
Yi Wang
Ying-Jan Wang
Youping Wang
Yu Wang
Yuan-Kai Wang
Yuhong Wang
Yuh-Tai Wang
Zhouping Wang
Zhongfu Wang
Zhezhi Wang
Zhenyu Wang
Zhanzhong Wang
S. M. Wani
Supason Pattanaargson Wanichwe-charungruang
Akira Wanikawa
Umesh Wankhade
Daniel W. Warner
Benedikt Warth
Kenji Washio
Agnieszka Waskiewicz
Tatsuo Watanabe
Eiki Watanabe
Fumio Watanabe
Naoharu Watanabe
Andrew L. Waterhouse
Daniel L. E. Waters
Wim Wätjen
C. B. Watkins
Tzong-Der Way
Amanda Weaver
Connie M. Weaver
Mark A. Weaver
Stefan Weckx
David E. Wedge
Deepthi Weerasinghe
Monthana Weerawatthanakorn
Cunxu Wei
Fang Wei
Guor-Jien Wei
Zhaojun Wei
K. Weingartner
Randy Alan Weintraub
Kevin D. Welch
Aalim M. Weljie
Saskia Welter
Stéphane Welti
Bernhard Welz
Bei Wen
Jie Wen
Zhiyou Wen
Chia-Jui Weng
Meng-Shih Weng
Barend Wentzel
Leslie Ann Weston
Edwin Westreicher Kristen
Wolfgang Wetscherek
David Wetzel
Natasha Whenham
Monica Whent
Thomas B. Whitaker
Jason C. White
Andrew K. Whittaker
Macdonald Wick
Margaret E. Wickham-St. Germain
Wieslaw Wiczkowski
Wilbur Warren Widmer
Elisabeth Wiesen
Melanie Wiesner
Lars Wiking
Peter James Wilde
Eric Wilkes
Frank Will
David John Williams
Kristina M. Williams
Roderick P. W. Williams
Gary Williamson
Kyle R. Willian
Christina Wilson
Karl A. Wilson
Ted E. F. Wilson
Zdenìk Wimmer
Michael Wink
Carl K. Winter
Peter Winterhalter
Ana Louise Winters
René Wintjens
Agata Witczak
Renger Witkamp
Regina-Michaela Wittich
Ken Witwer
Ursula Woelwer-Rieck
Aneta Wojdylo
E. J. Wolfrum
Mesay Mulugeta Wolle
Jeffrey D. Wolt
Charles S. Wong
Dominic W. S. Wong
Jack Ho Wong
Jon W. Wong
Ka Hing Wong
Po Keung Wong
Prinya Wongsa
Kwan Kit Woo
Delilah F. Wood
James E. Woodrow
Jan Byron Wooten
Randy Worobo
Amanda J. Wright
Katarzyna Wrobel
Ronald E. Wrolstad
Aibo Wu
Ben-Hong Wu
Chang-Jer Wu
Changlong Wu
Changqing Wu
Chi-Hao Wu
ChunFu Wu
Di Wu
Gang Wu
Hou Wu
Hui Wu
Jianping Wu
Jing Wu
Jiu-Lin Wu
Kangbing Wu
Kuen-Yuh Wu
Liming Wu
Mei-Li Wu
Minchen Wu
Ming-Chang Wu
Ming-Jiuan Wu
Qi Wu
Qing-Li Wu
Ren'an Wu
She-Ching Wu
ShiBiao Wu
Shih-Hsiung Wu
Shimin Wu
Tao Wu
Wei Wu
Xianli Wu
Xiaomeng Wu
Xiaorong Wu
Xiaoqin Wu
Xi-Yang Wu
Yan Wu
Yang-Chang Wu
Ying Wu
Yongjiang Wu
Yongning Wu
Zhen Wu
Ziyun Wu
Matthias Wuest
Daniel A. Wunderlin
Slawomir Wybraniec
Rimo Xi
Min Xia
Shuqin Xia
Feng Xiao
Hang Xiao
Hui Xiao
Jianbo Xiao
Kai Xiao
Rui Xiao
Zhuping Xiao
De-Yu Xie
Fuliang Xie
Fu-Wei Xie
Guoxiang Xie
Jingwu Xie
M. Y. Xie
Ruliang Xie
Yan Xie
Zhuohong Xie
Xiaoping Xing
Hua Xiong
Youling L. Xiong
Baojun Xu
Bin Xu
Changmou Xu
Chengdong Xu
Chunlin Xu
Feng Xu
Guobao Xu
Guowang Xu
Han Xu
Hanhong Xu
Hong Xu
Hongxia Xu
Hui Xu
Jian-guo Xu
Jimmy Xu
Juan Xu
Ming Xu
Ping Xu
Xiangqun Xu
Xiaoyong Xu
Xiaoyun Xu
Xinglian Xu
Xueming Xu
Xurong Xu
Yan Xu
Yingda Xu
Zhimin Xu
Richeng Xuan
Jing Xue
Ming Xue
Yemin Xue
Ioannis Nickolaos Xynias
Montarop Yamabhai
Haruki Yamada
Tatsuhiko Yamada
Fumio Yamaguchi
Yoshimasa Yamaguchi
Norio Yamamoto
Tatsuyuki Yamamoto
Rumi Yamaoki
Satoshi Yamauchi
Yadollah Yamini
Chunyan Yan
Congqi Yan
Cuie Yan
Hongyuan Yan
Ya-Xian Yan
Yeong-Yu Yan
Yue-Ming Yan
Bao Yang
Chao-Hsun Yang
Cheng Yang
Ching-Ping Yang
Deng-Jye Yang
Guang-Fu Yang
Hong Yang
Hongshun Yang
Hsueh-Hui Yang
Hui-Ting Yang
Jun Yang
Kaiguang Yang
Ling Yang
Litao Yang
Nianjun Yang
Nicole Yang
Qing Yang
Raymond Yang
Rong-Ling Yang
Ruijin Yang
Runqiang Yang
T. Yang
Tiankui Yang
Tsung-Shi Yang
Wen-Jen Yang

DOI: 10.1021/jf506178r
J. Agric. Food Chem. 2015, 63, 2−18

Wensheng Yang
Wenzhu Yang
Woong-Mo Yang
Xiaogen Yang
Xiao-Quan Yang
Xinghao Yang
Xinling Yang
Yaling Yang
Yan Yang
Yanjun Yang
Yi-Ling Yang
Yiqi Yang
Yuechao Yang
Z. Y. Yang
Ziyin Yang
Zhenfeng Yang
Linxing Yao
Zhong-Ping Yao
C. K. Yap
Midori Yasuda
Varoujan A. Yaylayan
Christian C. Yde
Aiqian Ye
Jiannong Ye
Ran Ye
Xingqian Ye
Yonghao Ye
Maria Yebra
An-I Yeh
Chi-Tai Yeh
Ting-Feng Yeh
Ahmet Yemenicioglu
Gow-Chin Yen
Jui-Hung Yen
Mao-Hsiung Yen
Chahan Yeretzian
Caixia Yin
Jie Yin
Mei-Chin Yin
Xiang-sheng Yin
Xuebin Yin
Yulong Yin
You-Min Ying
Robert A. Yokley
Kazushige Yokota
Tomoya Yokoyama
Wallace Yokoyama
Alejandra Yommi
Koichi Yoneyama
Jirawat Yongsawatdigul
Hye Hyun Yoo
In Sun Yoon
J. S. Yoon
Soon-Do Yoon
Yeongkeng Yoon
Hiroo Yoshida
Kumi Yoshida
Midori Yoshida
Mitsuru Yoshida
Munehiro Yoshida
Tadashi Yoshihashi
Masaaki Yoshikawa
Tomoya Yoshinari
Jin-Mao You
Youngjae You
Xiong Youling
Carolyn Young
Jette Feveile Young
Niall Young
Aimin Yu
Bi Yu
Bin Yu
Chi Chung Yu
Deyue Yu
Feng-Yih Yu
Guanping Yu
Hailong Yu
Jianmei Yu
Junhong Yu
Liangli Yu
Long Yu
Zhiqiang Yu
Yunlong Yu
Yung-Luen Yu
Youwei Yu
Xiaobin Yu
Shuqin Yu
Rongmin Yu
Peiqiang Yu
Huaibo Yuan
Huizhu Yuan
Jian-Ping Yuan
John Yuan
Tao Yuan
Tong-Qi Yuan
Yang Yuan
Ying-Jin Yuan
Toshifumi Yui
Onder Yumrutas
A. W. Yunus
María del Mar Yust
Dimitrios Zabaras
Pilar Zafrilla
Amaya Zalacain
Aleksandra Zambrowicz
Rosario Zamora
Fernando Zamora
Maurizio Zandomeneghi
Daniel Basilio Zandonadi
Ru Zang
Emanuele Zannini
Everton Fernando Zanoelo
Vincenzo Zara
Martin Zarnkow
Robert Zarnowski
Olfa Zarrouk
Zenon Zdunczyk
Luis Zea
Qendrim Zebeli
Reinhard Zeleny
Wei-Cai Zeng
Xin-An Zeng
Edgar Zenteno
Giuseppe Zeppa
Long-ying Zha
Xue-Qiang Zha
Zha-Jun Zhan
Aijun Zhang
Aiping Zhang
Boce Zhang
Bolin Zhang
Dabing Zhang
Genyi Zhang
Guo-Lin Zhang
Guowen Zhang
Haixia Zhang
Heping Zhang
Hongyan Zhang
Hongyin Zhang
Hui Zhang
Jian-An Zhang
Jingyan Zhang
Jin-lan Zhang
Jun Zhang
Junzeng Zhang
Kai Zhang
Mingwei Zhang
Quanbin Zhang
Shiwei Zhang
Suxia Zhang
Wei Zhang
Xiaoming Zhang
Xiaoyu Zhang
Xingxu Zhang
Xinzhong Zhang
Xiuli Zhang
Xue-Hong Zhang
Xuewu Zhang
Xunli Zhang
Yan Zhang
Yanjun Zhang
Ying Zhang
Yu Zhang
Yuan-Xing Zhang
Yue Zhang
Yuzhu Zhang
Zhaohui Zhang
Bao Yu Zhao
Chunchang Zhao
Chunchao Zhao
Ercheng Zhao
Feng-Qi Zhao
Guanghua Zhao
Guohua Zhao
Haifeng Zhao
Hongwei Zhao
Jian Zhao
Mouming Zhao
Nan Zhao
Qin-Shi Zhao
Wei Zhao
Wei-Guang Zhao
Wei-jun Zhao
Xinrui Zhao
Yan Zhao
Yang Zhao
Yang Zhao
Zongbao Kent Zhao
Guodong Zheng
Jinkai Zheng
Yonghua Zheng
Yu-Guo Zheng
Zuoxing Zheng
Fan Zhijin
Xu Zhixiang
Cheng Zhong
Dafang Zhong
Fang Zhong
Lin-xin Zhong
Ailing Zhou
Bin Zhou
Dongmei Zhou
Guangxiong Zhou
Jingwen Zhou
Jinjin Zhou
Kequan Zhou
Ming Zhou
Peng Zhou
Qixin Zhong
Qiang Zhou
Qingxiang Zhou
Ximin Zhou
Xuelin Zhou
Yan Zhou
Yipin Zhou
Yu-Ting Zhou
Zhiqin Zhou
Beiwei Zhu
Biao Zhu
Guonian Zhu
Hongjun Zhu
JunYong Zhu
Shusheng Zhu
Xudong Zhu
Xuntao Zhu
Yan Zhu
Yang Zhu
Yingdong Zhu
You-quan Zhu
Zaifang Zhu
Zhichen Zhu
Zhiguang Zhu
Hong Zhuang
Shiwen Zhuang
Shulin Zhuang
Christian Zidorn
Acácio Antonio Ferreira Zielinski
Ana Lucia Zimbardi
Benno Zimmermann
Ouliana Ziouzenkova
Hubert Zipper
Bogdan Zisu
Bruce Zoecklein
Min-Hua Zong
Holger Zorn
Long Zou
Xiaoyong Zou
Shi Zu Hao
Jesus Zueco
Magdalena Zuk
Julio Alberto Zygadlo

DOI: 10.1021/jf506178r
J. Agric. Food Chem. 2015, 63, 2−18

JOURNAL OF AGRICULTURAL AND FOOD CHEMISTRY

Review

pubs.acs.org/JAFC

Effect of Production Phase on Bottle-Fermented Sparkling Wine Quality

Belinda Kemp,*[,†] Hervé Alexandre,[§] Bertrand Robillard,[#] and Richard Marchal[⊥]

[†]Cool Climate Oenology and Viticulture Institute (CCOVI), Brock University, 500 Glenridge Avenue, St. Catharines, Ontario, Canada L2R 5N3

[§]Institut Universitaire de la Vigne et du Vin Jules Guyot, Université de Bourgogne, Rue Claude Ladrey, 21078 Dijon, France

[#]Institut Oenologique de Champagne (IOC), ZI de Mardeuil, Route de Cumières, B.P. 25, 51201 Épernay Cédex Champagne, France

[⊥]Laboratoire d'Oenologie et de Chimie appliquée, Unité de Recherche sur la Vigne et les Vins de Champagne (URVVC), EA 4707, Moulin de la Housse, B.P. 1039, 51687 Reims Cédex 02, France

ABSTRACT: This review analyzes bottle-fermented sparkling wine research at each stage of production by evaluating existing knowledge to identify areas that require future investigation. With the growing importance of enological investigation being focused on the needs of the wine production industry, this review examines current research at each stage of bottle-fermented sparkling wine production. Production phases analyzed in this review include pressing, juice adjustments, malolactic fermentation (MLF), stabilization, clarification, *tirage*, lees aging, disgorging, and *dosage*. The aim of this review is to identify enological factors that affect bottle-fermented sparkling wine quality, predominantly aroma, flavor, and foaming quality. Future research topics identified include regional specific varieties, plant-based products from vines, grapes, and yeast that can be used in sparkling wine production, gushing at disgorging, and methods to increase the rate of yeast autolysis. An internationally accepted sensory analysis method specifically designed for sparkling wine is required.

KEYWORDS: *sparkling wine, wine production, aroma, flavor, foaming*

INTRODUCTION

Bottle-fermented wine production is increasing on a global scale, and there is a growing focus on alternative grape varieties in emerging sparkling wine regions that can produce quality sparkling wine. The more famous sparkling wines include Champagne and crémants from France, cava from Spain, prosecco from Italy, sekt from Germany, Cap Classique from South Africa, and sparkling icewine from Ontario (made with grapes picked by hand and pressed in their natural frozen state at approximately −10°C). Semi-sparkling wines such as Frizzante are found in Italy and white Vinho Verde in Portugal. Bottle-fermented sparkling wine quality, defined as flavor, aroma, and foaming height and stability, can be affected both positively and negatively at every stage of production. Factors that affect the quality of sparkling wine include grape variety, yeast strain, oxygen management, malolactic fermentation (MLF), fining, filtration, *tirage* recipe, length of lees aging, *dosage* recipe, and lees aging post-disgorging. The current literature has been critically analyzed to identify previous research regarding bottle-fermented/méthode champenoise/traditional method sparkling wine at every stage of production (Figure 1). Additionally, the authors aim to identify areas of future research that will benefit winemakers, contribute to increased wine quality, and advance scientific knowledge.

VITICULTURAL EFFECTS ON SPARKLING WINE QUALITY

This section of the review is a summary of viticultural effects of grape variety, clone, grape maturity, leaf removal (specifically fruit exposure), and yield and their impact on sparkling wine flavor, aroma, and foaming of sparkling wine.

The selection of grape variety for sparkling wine takes into consideration climate, foaming properties of the juice, the base wine composition (sugar, acidity, and pH levels), aging ability, and the wine style required. Cava wine is predominantly produced from white varieties, Macabeo/Viura, Xarel.lo, Parellada, and Verdejo with a small proportion of Chardonnay and Malvasia Riojana/Subirat Parent. Red varieties in cava wine production include Monastrell, Pinot noir, Garnacha, and Trepat.[1,2] The traditional Champagne grapes are Chardonnay, Pinot noir, and Pinot meunier, but a revival in interest of varieties such as Petit meslier, Arbane, Pinot blanc, and Pinot gris in Champagne is taking place.[3] An increase in the use of alternative grape varieties for sparkling wine is underway. Research has recently focused on varieties such as Albariño, Verdejo, Godello, Garnacha, and Prieto Picudo in Spain,[4] Baga and Ferñao-Pires in Portugal,[5] Italian Riesling/Welschriesling, Manzoni Bianco, and Moscato Embrapa in Brazil[6,7] Mieli in China,[8] and Emir and Dimrit in Turkey.[9,10] This increase in monovarietal sparkling wines is resulting in cultivar-specific, regionally focused research at various stages of the sparkling wine process.

Chardonnay clones in California, used for sparkling wine, were compared to Champagne clones in a 4 year study.[11]

Received: September 4, 2014
Revised: November 22, 2014
Accepted: December 14, 2014
Published: December 15, 2014

ACS Publications © 2014 American Chemical Society

DOI: 10.1021/jf504268u
J. Agric. Food Chem. 2015, 63, 19−38

Figure 1. Simplified flowchart of bottle-fermented wine production stages.

American clones had higher acidity at harvest, which was attributed to climatic differences of the two regions. The significant difference between reproductive factors was greatest between the American clones.[11] Pinot noir clone performance in California was found to be significantly different in a 3 year study, with some clones suffering from excessive vegetative growth and others from high yields.[12] Making a viable comparison of the performance of clones for sparkling wines in different countries is extremely difficult because studies rarely have more than a few clones in common.[11] Vine spacing, row orientation, training system, canopy management, and soil and climate differences in each country or region or even from one vineyard to another are all factors that influence clone and rootstock performance.[11,12]

A study in Portugal investigated the impact of soil type and grape maturity on sparkling wine aroma quality. More herbaceous notes were apparent in sparkling wines made from grapes picked one week before commercial harvest. Unfortunately, sugar levels, acidity, and pH values of the grapes were not presented in the study.[13] Esteruelas et al.[14] recently reported that sparkling wines produced from early harvested Macabeo/Viura, Xarel.lo, Parellada, and Chardonnay vines had higher foaming properties compared to those harvested later. However, the first grape harvest was determined by acidity levels and the second harvest by sugar levels, so alcohol differences also contributed to differences in foaming properties.

Viticultural Effects on Phenolic Compounds. Several studies have investigated the effect of viticultural practices on phenolic compounds in sparkling wines due to their importance on rosé, red, and white sparkling wine color and their impact on foaming and flavor.[15,16] Preflowering leaf removal resulted in higher levels of hydroxycinnamates in Chardonnay base wines and increased anthocyanin levels in Pinot noir base wines in Tasmania, Australia.[15] Hydroxycinnamates are the major class of phenolic compounds in Champagne and cava wines. They affect the texture and mouthfeel of sparkling wines, thereby affecting quality.[1,14,16−19] With regard to yield effects, Parellada sparkling wines from high-yielding vineyards in Spain had higher levels of phenolic compounds and fusel alcohols compared to low-yielding ones.[17] Sensory panelists preferred wines from the low-yielding vineyard, although this may have been due to the spontaneous malolactic fermentation that took place in the high-yielding wines, making direct comparison to low-yielding wines difficult.

Phenolic compounds in grape skins and seeds can be a result of environmental factors, vintage, training system, clonal selection, light, temperature, canopy management, and water availability.[5,14−16] Tastes and textures elicited by the presence of phenolic compounds in still white table wines are more prominent at lower alcohol levels and at moderate pH levels, indicating that the presence of phenolics is more important in the context of lighter bodied wines.[20] This could have implications for the quality of sparkling wines with low alcohol levels.

Nineteen phenolic compounds were identified in both Chardonnay and Pinot noir monovarietal Champagne wines from 2000 and 2001 vintages, although the quantity of each varied between the grape varieties.[16] In agreement with a previous study, the variation between phenolic concentrations in the wines was due to variety and vintage, but press pressure (which affects phenolic extraction) was not considered.[14,15]

Although common in many regions, mechanical harvesting is banned in Champagne. This is due to detrimental anthocyanin extraction from red grapes destined for white sparkling wine. Limited space between the grapevine rows in the Champagne region prohibits mechanical access, so this is unlikely to change in the future. Excessive anthocyanin extraction from mechanical harvesting can result in juice requiring charcoal or polyvinylpolyprrolidone (PVPP) treatment and can cause a loss of aromas and foamability in the final wine.[4] Additionally, an increase of pathogensis-related (PR) proteins from mechanically harvested white grapes compared to hand-picked fruit has been reported.[21−23] Results were attributed to their exraction from skins as opposed to physiological wounding response by the berry. PR proteins are largely responsible for protein haze, have low isoelectric points (p*I*) and molecular weights (MW), and are resistant to low pH as well as enzymatic and non-enzymatic proteolysis.[23] Phenolic compounds negatively affect foaming properties and have been implicated in "gushing" during disgorging (see Gushing).[1,24]

Recently, a comprehensive review regarding viticulture for sparkling wine production was published that highlights viticultural research including grape varieties, clones, rootstocks, soil impact on flavor, precipitation in cool/cold climates, and training systems as part of climate change adaptations.[25]

PRESSING

Traditional Champagne wine production uses gentle whole bunch pressing due to the use of red grapes for white wine production to prevent excessive anthocyanin extraction. A study in 1980 compared musts pressed by screw press, cylindrical Willmes press, and Willmes press with pressing aids and reported pressing effects on aroma constituents.[26] It is known that high pressures at pressing increase proteins and polyphenol

DOI: 10.1021/jf504268u
J. Agric. Food Chem. 2015, 63, 19−38

oxidase (PPO) and that oxidation of phenolic compounds is the main source of browning in wines due to PPO activity.[27] An increase in browning of cava wine (measured at 420 nm) due to the oxidation of phenolics has been previously reported.[18] A comparison of three presses, two traditional basket presses (with and without an outflow central star, respectively), and a pneumatic press, revealed that oxidation level of musts obtained from traditional Champagne presses were high as early as the press exit.[27] Crushed and destemmed juice from Spanish Albariño, Verdejo, Godello, Garnacha, and Prieto Picudo grapes was found to have high levels of phenolic compounds, which were later removed from base wines with PVPP.[4]

A study of a central membrane press compared to a side membrane press on red grapes for still table wine found that the central membrane press produced a higher juice yield as well as lower phenolic levels in juice fractions.[28] Few studies have compared flavor, aroma, and foaming properties of sparkling wines processed using different presses, yet this technology has vastly improved in the past decade. Additionally, comparisons of press performances have been discussed but not with specific regard to sparkling wine quality.[29] The addition of pressing aids, such as rice hulls, to the press with the grapes has been found to increase free run juice from 5 to 15%.[29,30] However, their addition may influence aroma development in sparkling wine, and their use may be dependent on the type of press being used as well as the press cycle program.[29]

Recent grape processing innovations have been developed that include automatic grape box unloading in Champagne in addition to the separation of press fractions partitioned into distinct juice trays using gravity flow with automatic SO_2 addition.[31] Further technological methods to preserve potential grape aromas and quality of the wine have been developed and are currently used in Champagne wine production. These include vibrating hoppers that deliver grapes directly to the press and inert gas (nitrogen) to protect grapes from oxidation in press.[31]

PRESS FRACTIONS

The main objective of grape pressing, as previously mentioned, is to use minimal rotation to avoid oxidation and minimal mechanical pressure on the grapes to minimize total insoluble solids that negatively affect wine quality. Studies have found a decrease in protein concentration and an increase in browning of the juice in the crumbling cycle of a Willmes press.[32−35] This oxidation could affect the foaming ability of the final wine if these fractions are included in the *cuvee* (first press fraction) or *taille* (subsequent press fractions referred to as first *taille* and second *taille* in Champagne). Further studies identified *Vitis vinifera* proteins including a class of IV chitinase, thaumatin-like proteins, putative thaumatin-like protein, and several uncategorized proteins in Pinot noir press fractions of *Botrytis*-contaminated grapes.[34−37] These proteins decreased in the return/retroussé cycle, which could have a negative impact on foaming. Most proteins have a p*I* ranging from 2.5 to 4.5 and MWs of 12−65 kDa.[36−38] Some grape-derived proteins may not survive two fermentations. However, grape pathogenesis (PR)-related proteins, found in high concentrations in grapes, are thought to be the main contributors to protein haze in still white table wines.[38−40] Although if numerous proteins were isolated and characterized according to their MW, p*I*, hydrophobicity, glycans, amino acid composition, and origin, there would still be little information concerning foaming properties of specific proteins or those responsible for foaming height and stability.[38−42] Turbidity levels decreased during the pressing but increased at the return/retroussé stage.[35] In the same study, post-pressing and after 24 h of flocculation, the early fractions had settled and decreased dramatically, from 300 to 20 nephelometric turbidity units (NTU), whereas the return/retroussé fractions were only marginally reduced. Foamability decreased during pressing, probably due to protein reduction or proteins binding to phenolic compounds.[35] Acidity decreased during sparkling grape pressing and pH increased. Additionally, phenolic extraction increased during the length of the pressing with increased pressure of each press cycle.[35] Press-fractioning impact on base wine and sparkling wine chemical composition will depend on grape variety, type of press, the pressure exerted during each cycle, and the length of each cycle.

CHAPTALIZATION, ACIDIFICATION, AND DEACIDIFICATION

Chaptalization. Chaptalization (sugar addition to increase final alcohol level) using cane or beet sugar is common in some cool-climate sparkling wine production regions, that is, Champagne and England. It is often suggested that 17 g/L additional sugar is required for white wines to reach 1% volume increase in alcohol content.[44] However, for low-temperature fermentations such as sparkling base wines, 16 g/L sugar likely contributes 1% volume of alcohol to the wine.[39] Guidelines regarding the level of chaptalization and its timing are controlled by regulatory bodies in each wine region. Sugar addition is not permitted in cava production, but rectified grape must (RGM) is allowed, but only in difficult years when climate conditions have affected grape ripeness.[14,44] Brazilian legislation allows the addition of sugar to grape must during the initial fermentation to increase ethanol content by up to 3 °GL [Gay-Lussac (GL) is the volumetric percentage of alcohol in a beverage].[42] However, in California, legislation permits sugar addition only for the second fermentation.[42] One study found that juice chaptalization had a significant influence on the perceived sweetness, body, and balance between acidity and flavor in still table wines.[45] The study investigated fruit ripeness and juice chaptalization on the sensory properties and typicality of Sauvignon blanc wines in Marlbourough, New Zealand. Since Goresline and Champlin,[46] there have been few studies regarding the effect of sugar type (i.e., cane, beet, dextrose) added prefermentation on sparkling wine quality. Chemical analysis of sparkling wines pre- and post-sugar addition, at first and/or secondary fermentation, investigating its effect on aroma, flavor, and wine quality has not been completed. However, it is likely that any required sugar addition prior to first fermentation will not affect aroma but increase alcohol and enhance the balance of acidity and sweetness.

Acidification. Acidification of juice is carried out by the addition of tartaric acid or, in some countries, cation exchange and is legal in some warm wine regions (i.e., California, Australia). Tartaric acid addition decreases the potassium ions and increases equivalently the concentration of hydrogen ions.[47] The pH reduction from acid addition is not directly related to the amount of acid added due to variations in the buffering capacity of different wines.[44] However, it is possible to make calculations for additions based on the level of pH reduction required.[44] Tartaric acid has also been found to positively affect foaming.[43,47−49] Lowering the pH without lowering titratable acidity requires the addition of calcium

DOI: 10.1021/jf504268u
J. Agric. Food Chem. 2015, 63, 19−38

sulfate ($CaSO_4$).[47] However, this is more suited to juice, and wines, to be aged prior to bottling and is not authorized by OIV regulations (except in Jerez, Spain, for historical reasons). The effect of acidification with tartaric acid on long-term sparkling wine quality and flavor remains unclear due to a lack of studies. However, any long-term effect on sparkling wine is likely to be minimal due to high tartaric acid being beneficial for sparkling wine foaming and stability.

Deacidification. Uncommon in cool and cold climates except in exceptionally poor growing seasons, the removal of tartaric acid or excess L-malic acid before or after fermentation may be necessary to balance wine acidity and stability.[4] Blending wines with high-acid wines or musts is not always possible, and amelioration (water addition) is detrimental.[50] Double-salt precipitation treatment (Acidex or DICALCIC) uses a 1% calcium tartrate and malic acid salt mixture as a seeding agent and is used to treat a small quantity of the wine, which is blended back into the untreated sample.[50] Boulton[51] advocated that treatment of juice is preferable to treatment of wine and stated that a juice with a pH of >3.8 and a titratable acidity of >10 g/L requires addition of tartaric acid after the double-salt method. This encourages potassium bitartrate crystal (KHTa) precipitation during and after fermentation, to lower the extent of exchange and pH.[46] Further details of deacidification can be found in a review by Volshenck et al.[50]

Malolactic Fermentation (MLF). MLF carried out post-first fermentation or simultaneously with alcoholic fermentation [cofermentation of yeast with lactic acid bacteria (LAB)] is common among winemakers in Champagne but results in a change in acid that may contribute to a reduction in aging.[52] Nonetheless, in difficult years in some wine regions when juice has high acidity, or for stylistic reasons, wineries might consider MLF. MLF not only reduces the acidity but improves the biological stability of the wine and modifies sparkling wine texture.[53] *Oenococcus oeni* is the main LAB that conducts MLF by the decarboxylation of L-malic to L-lactic acid.[54] *Lactobacillus* and *Pediococcus* LAB can conduct MLF but can be associated with wine spoilage and off-flavors.[54] Malic acid has been found to positively affect foaming height but negatively affect foam stability,[1,24,55,56] whereas lactic acid has been found to be beneficial for foaming stability but negatively affects foaming height.[24,56] Furthermore, malic acid and citric acid have both been found to inhibit calcium tartrate precipitation in model wine.[57] Several extensive reviews regarding MLF chemistry have been published but are not the subject of this review.[58,59] They detail bacterial strain performance, inoculation timing, and factors that affect MLF, those being ethanol, sulfur dioxide (SO_2), medium-chain fatty acid MLF inhibition, pH, temperature, nutritional requirements, and phenolic compounds as well as effects on wine aroma and lysozyme.

To prevent MLF, hen egg lysozyme (peptidoglycan *N*-acetylmuramylhydrolase, EC 3.2.1.17) can be used to reduce SO_2 levels in must or wine and prevents MLF due to the sensitivity of *O. oeni* to it. It is not permitted for use in all wine regions (i.e., Canada), and its high cost can be prohibitory.[60,61] Two genetically modified yeasts for MLF have been released onto the market but have limited availability in only a few countries due to public perception and lack of acceptance.[62,63]

Anecdotally, manufacturers of LAB are investigating the use of region-specific strains for MLF by identifying strains in vineyards/wineries, isolating suitable candidates and testing them on wines prior to their manufacture. MLF technological innovations include a study that used a two-stage nanofiltration technique (demalication) and compared its efficiency to inoculated MLF in six grape varieties, including Chardonnay.[64] Further research is required, though, because volatile aroma compounds, flavor analysis, and sensory analysis were not carried out in the study. Provided that aroma and flavor are not negatively affected, and beneficial compounds such as proteins for foaming are not removed in this process, it could have application in sparkling wine production.

An immobilized lactic acid bacterium continues to be investigated for MLF due to its ability to perform MLF in a low-pH environment.[65,66] Materials used to suspend lactic acid bacteria have included grape skins, corn cobs, and delignified cellulosic material (DCM) from sawdust, but they are not yet available commercially.[65,66] Sequential alcoholic and MLF using immobilized cells have been found to increase the speed of wine production, but fermentations were influenced by the pH of the medium, with higher pH levels being less successful.[67] This method may be more suitable for large-scale wineries, but further research is required regarding the flavor and aroma profile of the finished sparkling wines. The selection criterion for LAB has been highlighted and includes stress resistance, technological performance, and safety.[68] With recent progress being made on the stress adaptations, survival rate of *O. oeni*, and proteome map of *O. oeni*, future research is focused on decreasing the time and improving the success rate of MLF in high-acid wines to improve production efficiency.[69]

Recently, *Schizosaccharomyces pombe* yeast with malic dehydrogenase activity that metabolizes malic acid with the production of ethanol has been trialled.[47,63,70] Traditionally described as wine spoilage yeast, *S. pombe* has malic dehydrogenous activity, produces pyruvic acid, breaks down ethyl carbamate precursors, and has a cell wall structure that ensures the autolytic release of mannoproteins and polysaccharides during lees aging, yet only a limited number of commercial strains are available.[63,70] Its main drawback is the strong acetic acid production from unselected strains currently used in wine research.[70] However, it has potential use in sparkling wine production including the partial reduction of malic acid in wine. Instead of using it for a complete MLF, it could be used to start MLF, which could be followed by inoculation with *O. oeni* when acidity is reduced. Additionally, sequential inoculation with selected *Saccharomyces cerevisiae* strains at fermentation and the selection of low acetic acid forming strains for sparkling wine are further options. Further information regarding MLF and LAB can be found in published reviews.[50,59,71] The effect of these various deacidification methods on long-term sparkling wine flavor, aroma, and quality remain unclear due to a lack of comparative published research.[47]

ALCOHOLIC FERMENTATION OF SPARKLING BASE WINES

Alcoholic fermentation wine kinetics has been extensively investigated.[62,71] The key metabolic process during winemaking is alcoholic fermentation, the conversion of sugars into ethanol and carbon dioxide by yeast: $C_6H_{12}O_6 \rightarrow 2CH_3CH_2OH + 2CO_2$.[72] Base wine flavor composition, aroma, and foaming potential are influenced by many factors that include grape variety, clone, rootstock, yield, the health of the grapes (i.e., disease severity), sugar levels, acid levels, nutrient levels, choice of yeast, and press fractions. The alcohol level of sparkling wine has been found to have a negative effect on foam. Chardonnay and Parellada wines made from less ripe grapes in Spain had

DOI: 10.1021/jf504268u
J. Agric. Food Chem. 2015, 63, 19−38

higher foamability, due to lower sugar levels at harvest, compared to the grapes picked later.[14] Fermentability of botrytized base wine is reduced because of compositional effects including grape metabolites and protein composition of the *Botrytis*-affected berries.[73] *Botrytis* has been implicated in the destabilization of sparkling wine foam in several studies as well as organoleptic properties, thereby affecting final wine flavor and quality.[73−76] *Botrytis*-affected grapes also require higher SO_2 additions during pressing, which itself is known to negatively affect foaming.[1,49,56,77] The addition of a mixture of potassium caseinate, bentonite, and microcrystalline cellulose mixture to Parellada and Macabeo/Viura juice prefermentation produced wines with lower polyphenol content (less browning capacity), high foam stability time, less foamability, and foam collar persistence than the ones treated with bentonite.[78] It was reported that volatile aroma profiles of the wines treated with the caseinate mixture were different in comparison to the bentonite-treated wines, even though the study did not report any effect on sparkling wine quality.

Enzymatic preparations are used in winemaking to increase color extraction and filterability and improve aroma release due to β-glycosidase activity.[76] Pectolytic enzymes (added to juice during or after pressing) can increase juice yield and are used to settle solids in juice by breaking down pectins to smaller compounds. Grape protopectin and pectin levels are affected by climatic conditions and affect extraction of phenolic compunds. Insoluble protopectin is high in unripe grapes and is converted to pectin by hydrolyzation during ripening. Pectins are linear polymers of galacturonic acid, often possessing multiple esterified methyl groups, and complexed to various degrees with rhamnogalacturonan and chains consisting of arabinans and arabinoglactan.[29] However, pectolytic enzyme addition to Macabeo/Viura, Xarel.lo, and Parellada juice had a negative impact on foaming, possibly due to the settling and removal of solids that included polysaccharides and/or proteins.[79]

Few comparative published studies exist regarding the effect of oak barrels, steel tanks, and cement eggs and their impact on the final sparkling wine flavor and aroma, undoubtedly due to the number of vessels required and the length of time needed from base wine to finished wine for comprehensive chemical and sensory wine analysis. House style (reductive/oxidative) will dictate percent of oak used during production, which ranges from 10 to 100% depending on style. However, a study of the phenolic profiles of Chardonnay and Picapoll varieties of still wines fermented in stainless steel and American oak barrels has been published.[80] Unsurprisingly, total phenolics were found to be higher in wines fermented in oak, which may have detrimental effects on the finished wine foam qualities.[55,79] Several aromatic volatile compounds were reported in the oak-fermented wines [coniferaldehyde, sinapinaldehyde, syingaldehyde, 4-ethylguaiacol, 4-vinylphenol, eugenol, β-methyl-γ-octalactone, furan compound, and a coumarin (scropoletin)] but not in the stainless steel wines, but their impact on sparkling wine aroma and flavor by sensory analysis was not examined.

The effects of six commercial yeast strains were investigated using Macabeo/Viura, Xarel.lo, and Parellada base wines.[81] Yeasts produced wines with different aroma concentrations of esters, glycerol, phenylethanol, terpenes, isoamyl acetate, medium-chain fatty acids, and alcohols. The study illustrates chemical compositional changes attributed to yeast strain. The dynamics of *S. cerevisiae* in controlled and spontaneous fermentations, of two base wines from wineries in Franciacorta, Italy, were investigated.[82] The highest level of biodiversity of yeast isolates was found in the spontaneous fermentation, but the study did not investigate the sensory impact on the final wines. Although it is known that *pied de cuvée* is carried out in some sparkling wine regions (grapes are picked earlier and used to inoculate the first fermentation), there remains a lack of published studies concerning this inoculation method on yeast profile and its effect on sparkling wine foaming, flavor, or aging ability. The potential benefits of non-*Saccharomyces* yeasts (i.e., *Torulaspora delbrueckii*, *Pichia kluyveri*, *Lachancea thermotolerans*, *Candida/Metschnikowia pulcherrima*) on still table wine are well-known.[83] Nevertheless, their effect on bottle-fermented sparkling wines (if used for first fermentation) remains unclear, particularly in regard to their effect on glycerol (important for mouthfeel) that affects wine viscosity, foaming, and volatile aroma compounds.

Low nitrogen concentration in must and excessive ammonium addition have both been found to affect fermentation length, volatile acidity, and glycerol content and wine aroma profile.[84] A study in Australia with Chardonnay investigated nutrient concentration effects on fermentation kinetics and composition.[85] The project surveyed Chardonnay juice composition from cool and warm climates destined for still and sparkling wines, so there was a wide range of pH and acidity levels. They found that low potassium concentrations at low pH negatively affected fermentation performance of some yeasts, thereby affecting the wine quality due to acetic acid production. However, the study did not include the effect of yeast strain or type of nutrient addition on aroma compounds. Grape variety has an influence on nitrogen concentrations, which influences the fermentation kinetics and aromatic profile of the wines.[86] For instance, cava wines manufactured from Monastrell grapes had lower concentrations of fatty acids and ethyl esters as well as different nitrogen concentrations compared to wines produced from Trepat and Macabeo/Xarel.lo/Parellada blend.[86]

Alternatives to SO_2 addition to wine to prevent oxidation and microbial instability are a major focus of current enology research, and studies have used ascorbic acid, glutathione, yeast lees, and yeast autolysate.[87] The yeast derivative glutathione (GSH) (a tripeptide composed of glutamic acid, cysteine, and glycine) was found to be the one additive that performed most like SO_2 in a base wine in Prosecco DOCG when added to Pinot noir and Chardonnay must and base wine.[88] The study found that addition to must had greater oxidation protection than base wines, but addition to base wines resulted in retained free SO_2 levels. Phenolic levels were found to be lower in the sparkling wine that had GSH addition to must. The authors suggest further studies to assess the influence of GSH on MLF and to elucidate the effect of GSH on the levels of free SO_2. These preliminary results indicate that GSH has a promising role in future sparkling wine production, particularly due to the possible reduction of SO_2 use. However, studies into its effect on sparkling wine flavor, aroma, and lees aging are also needed. Additionally, the consequences of oxygenation of must and base wines on the synthesis and preservation of varietal aromas in the finished sparkling wine remain unclear, despite a comprehensive review of wine aroma aging in still wines by Ugliano.[89]

With regard to sparkling base wine aroma, different yeasts produce wines with different base wine aromas, particularly ethyl esters of fatty acids, depending upon yeast strain, fermentation temperature, oxygen management, and sugar

DOI: 10.1021/jf504268u
J. Agric. Food Chem. 2015, 63, 19−38

contents.[90] They are predominantly produced during alcoholic fermentation from reactions between alcohols and acetyl-CoA catalyzed by alcohol acetyltransferase.[13] The most important ethyl esters found in Chardonnay base wines were ethyl butanoate, ethyl hexanoate, ethyl octanoate, ethyl decanoate, ethyl lactate, and diethyl succinate.[90] Higher molecular weight alcohols found in Brazilian Chardonnay base wines included the aliphatic alcohols propanol, hexanol, dodecanol, 2,3-butanediol, and 2-phenylethanol.[90]

Grape variety has an effect on the aroma of base and sparkling wines. As an example, Ferñao-Pires grapes produced sparkling wines with higher aroma potential than Baga grapes in Portugal.[13] Although there are differences in the aroma compounds between base and sparkling wines, the main volatile compounds that differed between Brazilian Chardonnay base wines and the finished sparkling wines were C_{13}-norisprenoids (TDN, vitisparine, and β-damascenone), esters (laurate, 2-hydroxybutanoate, decanoate, 2-hydroxypropanoate, pentanoate ethyl esters), alcohols (4-butoxybutanol, 1-propanol, methaniol), aldehydes (3-phenyl-2-propenal, nonanal, undecanal), acids (acetic, 2-ethylhexanoic, butanoic), ketones (acetoin, diacetyl), and phenols (4-vinylguaiacol, 4-ethylphenol).[91] With regard to the color of wines after the first fermentation, Girbau et al.[92] suggested that base wine color intensity of white wines produced from black grapes should be similar to that of wines made from white grapes, between 140 and 160 absorbance units (AU).

STABILIZATION, CLARIFICATION, FINING, AND FILTRATION

Blending of base wines has not been an area of scientific research because the blends are specific to the winery style, so in-house trials are usually conducted. Post-blended wines are stabilized to test for tartrate and protein stability, and several studies have investigated methods to assist in wine stability prior to fining (if required) and filtering.

Stabilization and Clarification. In grape juice and wine, tartaric acid (H2T) and its salt, potassium hydrogen tartrate (KHT), are naturally present.[93] Tartrate instability leads to crystal formation in wine bottles, and the most common method to avoid crystals is cold stabilization (chilling wines to −4° for 10 days to 3 weeks using jacketed blankets or seeding crystals).[95] Other methods include electrodialysis, ion exchange, yeast mannoproteins, metartaric acid, and carboxymethylcellulose (CMC).[93,95] Stabilization and clarification along with the first 6 months on lees reduced polyphenol concentrations in sparkling wines, but the reduction was reversed by 9 months of lees aging, probably because some phenolic compounds were released back into the wine.[96] Cross-flow microfiltration is becoming more widely used for clarification and microbiological stabilization in wine production, although its effect on sparkling wine quality is unclear, particularly the effect on foaming ability and stability.[97,98] Clarification of Champagne base wines using wheat, alfalfa, and lupine proteins reported improved clarification compared to bentonite treatment. Pea protein is now commercially available and is currently being used by some English winemakers and so could be considered.[98]

CMC was authorized in 2008 by the International Organisation of Vine and Wine (OIV) at a concentration limit of 100 mg/L tartrate stabilization. It is made of polymers of β-D-glucose units on which the primary or secondary alcohol groups are esterified by sodium acetate groups (−CH_2−COONa).[99] However, it is not yet available or permitted in all wine regions.[93,100] The use of CMC can decrease winery energy costs due to a reduction in cooling while also preventing the loss of acidity. Yet CMC has been found to remove phenolics and proteins if CMC is added in high quantities, which may affect foaming. The stabilizing effect of CMC on tartrate salt precipitation results from its capacity to reduce the transfer of bitartrate molecules from the wine supersaturated with salt to the growing crystals and to decrease the speed with which crystals grow.[94,99] The effect of CMCs with different degrees of substitution and molecular weights on tartaric stability, tartaric acid, mineral content, phenolic compounds, and chromatic and sensory charactersistics of white still wines was recently investigated.[101] All CMCs significantly reduced conductivity, and a higher addition of CMCs resulted in higher tartaric stability. In wines with high tartaric instability associated with tartaric acid and potassium concentrations, CMC is beneficial. However, a deeper understanding is necessary with regard to their structure. This will allow winemakers to choose the appropriate CMC for a given tartaric acid instability issue.[101]

Flotation is a solid−liquid separation process used when the density of the particles is lower than the liquid containing them and is commonly used in wastewater treatment.[99] It has grown in popularity for wine production in recent years for must clarification due to the subsequent reduction/elimination of fining. Flocculating agents are used to bind particles including mineral adjuvants and proteins isolated from plants.[99] It has been suggested that natural plant-based vegetable compounds can replace animal products, for example, gelatin, and could reduce phenolic content and browning in white juices destined for base wines prior to fermentation.[98,99,102] Chitine derivatives are new biopolymers recently described as good flotation adjuvants.[103]

Fining. Grape variety, vintage, grape maturity, pH, and processing techniques affect must and wine proteins.[99] Trials on still wines to remove proteins using carrageenan, wheat proteins, lupine proteins, pea proteins, pectin, laccase, aspartic acid protease, and zirconium have taken place.[99,104−108] Aspartic acid protease BcAP8, from the fungal pathogen *Botrytis cinerea*, has recently been found to remove heat-precipitated proteins from Semillon still wines but not adequately in Sauvignon blanc still wines.[109] Nonetheless, Marchal et al.[110] showed that *Botrytis* protease negatively affects wine foaming by removing proteins, although a direct causal relationship between *Botrytis* proteases and wine protein content has not yet been found.[109] It is unlikely that sparkling winemakers would use *Botrytis*-associated enzymes due to possible effects on foamability and flavor.

The foamability of still base wines (Pinot noir and Chardonnay) decreases when the dose of bentonite increases. Generally speaking, base wine for the production of sparkling wine should have no proteoic haze risk, so bentonite fining is not required. Overfining with bentonite causes large bubbles and poor bubble stability and will affect wine aroma.[99] Bentonite treatment has a deleterious effect on wine foaming properties as the foamability of wines obtained from musts treated with bentonite at the concentration of 50 g/hL decreased by 40−60% and, correlatively, the protein content of the same wines diminished by 20−60%.[77] Bentonite, although commonly used by winemakers in the production of sparkling wines, should be avoided for sparkling base wines. This is because of its concentration of heavy metals potentially released over time and its negative effect on foaming, and it

DOI: 10.1021/jf504268u
J. Agric. Food Chem. 2015, 63, 19−38

should not be used for fining if bentonite is to be used as a riddling agent. The most commonly used protein stability test is the one referred to by Pocock and Rankine.[105,106] Wine is subjected to 80 °C for 6 h, cooled, and then visually checked for haze with a strong beam of light.[105,106] Unfortunately, there is currently no recommended protein level in base wines at bottling, probably due to the many variables involved including grape variety and production techniques. Unlike bentonite treatment, fining with gelatin−tannins or gelatin−silica gel significantly increases the foaming properties of the fined wines when compared to the nontreated wines.[111] The current interest in natural, plant-based winemaking products means further studies in this area are likely in the future.

Many sparkling base wines produced with Pinot noir and Pinot meunier grapes are pink in color. This is especially true for the wines produced with (1) grape berries having a high maturity level (less common in cool regions where the potential alcohol is between 8 and 10.5% v/v) or (2) the grape juice obtained in the second part of the pressing cycle. In the Champagne area, Pinot noir and Pinot meunier grape berries represent approximately two-thirds of all grapes, and many winemakers use vegetable charcoal for base wine color removal. Treatments with charcoal always diminish the Pinot noir base wine foamability.[77,114,115] It has been shown that 40 g/hL charcoal, used to remove color from Pinot noir base wines, was required for sufficient color removal.[114] The amount of charcoal needed to treat base wines will depend on the type of charcoal used, the wine chemical composition, and timing of addition. Charcoal contains a large quantity of air, and oxidation can occur from charcoal use due to the reduced protection that can occur when the protective phenolic compounds have been removed.[101] Wine oxidation can be reduced and prevented if the charcoal is rapidly and meticulously removed.[101] As with all fining agents, winery trials using different types of charcoal to determine the final type and quantity of charcoal addition are recommended.

A logarithmic relationship was found between the pink color and wine protein content. Foamability decreased by 54% with charcoal addition, and protein content decreased by 20%, suggesting that proteins in Pinot noir base wines are not solely responsible for foam quality. Nicolini et al.[115] found that a smaller amount of active carbon (20 mg/L) added during fermentation to still white wines produced from Chardonnay and Pinot gris did not negatively affect wine color or aroma. Differences in the grape color, charcoal product, analysis method, grape variety, vintage, and ripeness parameters (pH, TA, sugar level, phenolic composition) could all contribute to the difference in results. Some considerations that should be given to base wine charcoal additions include the timing of addition (must or base wine), the grape variety, and whether during alcoholic fermentation or to the blend before bottling. Additionally, it was not established whether the color from some red grapes would diminish during bottle fermentation and/or lees aging because phenolics are absorbed by yeast cells, with tannins being absorbed before anthocyanins.[112] This could mean charcoal addition to base wine is unnecessary for some varieties, especially as carbon used to remove color has been shown to be detrimental to wine foaming ability.[114]

Studies into the impact of specific grape (endogenous and exogenous) phenolics on foaming, phenolic characterization of different grape varieties, and their foaming ability, along with products capable of removing anthocyanins without removing beneficial proteins, could be areas of future study.[114] Occasionally carbon can also be used to reduce base wine off-flavors (mushroomy/moldy/earthy odors), but the carbon used for color removal and that used for off-flavor treatments have different characteristics. Not all forms of charcoal can absorb aroma compounds and polyphenols.

New fining agents include yeast protein extracts for clarification and stabilization including phenolic removal but are not yet available for trials on sparkling base wines.[116] PVPP is a high molecular weight fining agent made of cross-linked polypyrrolidone and attracts phenolic compounds by adsorption.[99] It is used to decrease bitterness in wine and oxidative browning in white wines. Potassium caseinate, either alone or in combination with other fining agents (gelatin or bentonite), was studied using Parellada juice for cava wine production. Juice filtration was found to be the most effective form of clarification, but potassium caseinate had less influence on aroma compounds and removed more phenolic compounds than other fining agents.[113] More recently, chitine derivatives have been described as interacting with some polyphenols and transition metals such as iron and copper so they could act as a preservative in regard to the wine oxidation process.[117,118]

Filtration. After cold stabilization and fining (if required), the turbidity of the wine is generally too high for bottling or secondary in-bottle fermentation so it is necessary to filter it (except for some rare wines vinified/produced and/or matured in barrels). Filtration is important for the brilliance of white wines, but results show that it modifies the turbidity of the sparkling wine. Additionally, foam formation depends on the type of filtration the wine has been subjected to.[48] Different foaming behavior has been reported in sparkling wine after different types of filtration.[119] Two base wines were laboratory filtered (0.2, 0.45, 0.65, and 3 μm and unfiltered), and it was found that foaming substantially decreased with filtering, no doubt due to removal of compounds required for foaming. The 0.2 μm filtered wine had very poor foam, and 0.45−3 μm range results were less clear, but the 0.45 μm filtered wine had the least foam collapse and best collar stability. It has been demonstrated that the smaller the filter pore size, the lower the foaming properties.[48] These differences are due to a different rate of film rupture. Foam expansion (E) is defined as the ratio of foam volume on liquid volume under standard conditions. During foam formation, the films are still thick and are drained mainly by gravity. Assuming that the nucleation is constant, the difference of slopes (during foam formation) depends on filtration.[48] These different coalescence rates occur because during foam formation, bubbles trap substances such as proteins to stabilize their interfaces.[120,121] If these components are lacking, the films are not stable and the surface tension is high, so coalescence takes place more easily.[48,122]

A comparison of diatomaceous earth (DE) filtration to cross-flow filtration in the food and drink industry found that DE filtering requires a low skill level and low maintenance and is cost-effective, but it is a risk to workers due to dust exposure from fine diatomaceous earth.[123] Apart from storage space for the DE filter and earth, consideration must be made for the spent cake disposal. Cross-flow filtration has a cost implication. It has been suggested that wine flavor and aroma can be lost in wines filtered by a cross-flow system.[123] However, a recent study in California using red and white still wines found minimal sensory differences between cross-filtered and unfiltered white wines.[124] Yet the red unfiltered wine changed after 2 months of post-filtration. A study of three membranes for cross-flow membrane filtration found that 0.1 μm was the

DOI: 10.1021/jf504268u
J. Agric. Food Chem. 2015, 63, 19−38

optimum cut-off point for white Riesling wines.[125] Filtering base wines to such a low level will most likely negatively affect foaming due to removal of foam-active compounds such as proteins. A review of cross-flow microfiltration in enology includes wine composition, membrane fouling, and membrane characteristics.[126] However, the effect of cross-flow filtration on sparkling wine foam, flavor, and volatile aromas remains unclear. Lenticular filtration is a relatively recent innovation rapidly replacing DE filtration in Champagne. It has no moving parts and fewer health hazards for workers than DE due to lack of dust inhalation risk and fewer disposal issues. These filters have large internal surfaces capable of retaining considerable volumes of turbid liquid (up to 3 L/m^2).[127] A comparative study using the same sparkling base wine filtered using different filtration methods would increase our knowledge and understanding of how the filtration systems affect sparkling wine volatile aroma compounds, foaming, and flavor.

BOTTLING AND *TIRAGE* (BOTTLING FOR BOTTLE FERMENTATION)

After fermentation, the sugar level at bottling affects the bottle pressure, especially with the more permeable crown caps available to producers.[128] An amount of 22−24 g/L sugar is used in the *tirage*, although in commercial wineries it may be 22−23 g/L to avoid excess pressure that can be high if the CO_2 loss is low from a crown cap. Depending on the crown cap permeability, the loss or transfer of CO_2 from inside the bottle to the outside can be from 0.12 to 0.68 mL/day. This CO_2 permeability is correlated with the O_2 intake.[129,130] Crown caps have been designed with seals with a range of permeability related to the desired O_2 intake depending on the quality objectives requested by the winemakers; that is, if the *cuvée* is to have long lees aging, the winemaker will choose a "closed to oxygen" crown cap to avoid oxidation during aging of the wine in the cellar. With the current crown caps on the market, the scale of O_2 intake ranges from 500 ppb to >3000 ppb (accumulated oxygen over 2 years).

All sparkling wines, but particularly rosé wines, are photosensitive and suffer from degradation over time on shelves, resulting in color, flavor, and aroma changes. Several studies have investigated the role of bottle color in wine quality.[131−133] Low-density polyethylene films (LDPE) have been found to protect wines for 60.4% longer than bottles without photoprotection, increasing the wine's shelf life from 6 to 12 months.[131] During storage Chardonnay still wine has been shown to be affected by temperature and light. The order of protection reported is Flint < Arctic Blue < French Green and Antique Green with low-wavelength visible, ultraviolet light being primarily responsible for the color changes.[132] Bottle weight was found to have only a minor impact on rosé sparkling wine color development.[133] These results have implications for producers of bottle-fermented sparkling wine when choosing colored bottles for wines, especially rosé sparkling wines, when color, flavor, and aroma retention is required for quality wine.

Tirage. *Tirage* ingredients are a closely guarded secret in many wineries, but the *tirage* recipe from two studies were *S. cerevisae* var. *bayanus* yeast (0.30 g/L) with sucrose (23 g/L) and bentonite (0.10 g/L) as a riddling aid.[96,134] This level of bentonite addition (at 0.10 g/L) is not reflective of all commercial wineries because if a winery uses bentonite as a riddling aid, it is more likely to be between 0.01 and 0.04 g/L.[34,35] Nutrient additions such as diammonium phosphate (DAP) and/or thiamin can be made along with tannin to prevent reductive notes and provide structure to sparkling wine while increasing antioxidant ability of the wine.[135] Other studies have not included *tirage* or *dosage* ingredients in their experimental design, making comparisons of chemical analysis results difficult.[136,137] The CIVC has demonstrated that the initial oxygen level at the *tirage* stage is not a limiting factor for yeast growth and fermentation kinetics. However, the initial CO_2 level in the mixing tank can be problematic for the normal development of the cells during *prise de mousse* (secondary fermentation in bottle).[139,140] A study of the influence of the method of starter culture preparation and level of inoculation with viable yeast assessed the kinetics of yeast growth and sugar utilization in *tirage* found that starter cultures prepared aerobically (in juice or wine) started fermentations that finished at similar times.[141] At similar levels of inoculation, the anaerobically prepared culture resulted in fermentations being completed 8−10 h earlier, due to the short period of exponential growth and earlier onset of linear growth, where 65−90% of the total sugar is utilized. Consideration must be given to alcohol level prior to sugar addition to ensure the required bottle pressure at the end of secondary fermentation is reached.[135] Researchers used a stable carbon isotope method to detect sugar additions in sparkling wines from Chile, Australia, Brazil, the United States, and Europe (France, Germany, Portugal, and Spain).[43] They identified sugar beet as being used for secondary fermentation in European and Chilean wines as opposed to sugar cane in Brazilian and Argentinian sparkling wines. There is unikely to be any effect on wine flavor or volatile aroma compounds from these two forms of sugar (see Chaptalization).

Winemakers generally use active dried yeast for bottle fermentation, and many suitable strains are available on the market. The direct yeast preparation for *tirage* avoids the risk of contamination compared to a multiplication procedure from one initial batch of yeast. Yeast flocculation ability is an important consideration to facilitate sediment removal at disgorging. This explains why some companies have developed "agglomerated yeast" to avoid riddling agents and to facilitate the riddling step.[142,143] However, the use of this particular yeast is decreasing due to some negative organoleptic effects on sparkling wine generated by some agglomerated yeast strains.[144]

Some researchers blend bottles of sparkling wines to allow for bottle variation prior to volatile aroma analysis, whereas others use two to three separate bottles for replication without opening and blending them.[137,145,146] Standardizing representative bottle numbers (i.e., three to five) to reduce bottle variation factors in addition to reporting *tirage* and *dosage* ingredients would improve direct comparisons of wines, research results, their treatments, and other factors associated with quality sparkling wines.

RIDDLING AIDS/ADJUVANTS

Bentonite. Bentonite not only is used as a fining agent for still wines (see Fining) but is also the most frequently used riddling agent for bottle fermentation. This clay efficiently removes proteins from wine due to the cation exchange capacity of the bentonite (a negatively charged adsorbent that at wine pH binds the positively charged grape proteins).[108] Calcium bentonite produces more compact lees than sodium bentonite and so is the preferred riddling agent for wineries that choose to use it in their Champagne sparkling wines.[99] A

DOI: 10.1021/jf504268u
J. Agric. Food Chem. 2015, 63, 19−38

study carried out by Jeandet et al.[146] investigated suspended particles (*voltigeurs*) thought to be bentonite in Champagne wines post-riddling. The particles were larger than bentonite, not protein related, but due to the concentration of aluminum and silicon concentration were found to be of a similar atomic composition to bentonite used in the *tirage liqueur*; however, it remains unclear why these particles did not settle during *remuage*. The use of bentonite as a riddling aid was investigated in cava monovarietal sparkling wines.[147] It decreased foaming height and stability in Chardonnay, Macabeo/Viura, and Xarel.lo. This was because bentonite removed favorable foaming proteins in the wine, although no significant differences were reported in Parellada and Pinot noir wines. The protein fraction, F2 and F3, which comprised proteins with molecular weights of 60 kDa (F2) and between 20−30 kDa (F3), were most affected by bentonite treatment, eliminating >80% of total soluble proteins.[147] These results are in agreement with another study that reported an almost complete removal of low molecular weight proteins from Chardonnay wines, illustrating that bentonite effects are different depending upon grape variety and the blend of grape varieties of the bottled sparkling wine.[148,149] A study found that just 3 g/hL of sodium bentonite added to cava sparkling wine (blend of Macabeo/Viura, Parellada, and Xarel.lo) did not greatly affect the volatile aroma compounds.[144] Nevertheless, sensory analysis showed that panelists preferred the wines produced without bentonite, in agreement with Martinez-Rodriguez and Polo.[150] It was found that even an addition of 3 g/hL bentonite reduced the foaming capacity of cava sparkling wines, which affected the visual and sensorial properties of the wine although the grape varieties in the wines were not mentioned.[150] This suggests bentonite affected mouthfeel, flavor, and aroma, possibly due to the change in nitrogen content, ethyl octanoate, and ethyl decanoate concentrations and other smaller volatile aroma compounds.

Bentonite and Alginate. Some other riddling agents can contain a percentage of potassium alginate. This polysaccharide has the ability to form gel in acidic conditions or very stable gels with calcium cation.[150] This enables a rapid formation of film-type sediments allowing quicker riddling. This particular riddling agent is often dedicated to mechanical riddling, and a pure bentonite riddling agent is used for manual riddling.

Immobilized Yeast. Methods for encapsulated yeast in alginate matrix dedicated to the bottle fermentation were patented in the mid-1970s.[151−154] Valade[155] conducted a study into riddling methods and compared (1) classical yeast and hand riddling, (2) classical yeast and mechanical riddling, (3) mechanical riddling and agglomerated yeast, (4) technique using included yeasts, and (5) the "Millispark" cartridge (developed by Micropore in 1993). The author found no difference in the wines, and no negative effect was observed on the sparkling wine flavor quality. More recently, a study compared the use of biocapsules (co-immobilization of filamentous fungi *Pencillium chrysogenum* and *S. cerevisiae* yeast), calcium alginate beads (immobilized *S. cerevisiae* yeast trapped in calcium alginate beads), and free yeast cells with bentonite.[156] Calcium alginate beads completed riddling in 15 s, biocapsules in 2 min, but free yeast with bentonite took several days. Yeast cells with bentonite produced wines with reduced foaming in agreement with other studies.[146] Calcium alginate wines had slightly higher foamability values than those made with biocapsules. This was attributed to the matrix support of the biocapsules formed by fungus hyphae that may have absorbed proteins required for foaming. Several studies have investigated the use of different support casings for immobilized yeasts in the beer and bioethanol industries, and these include clay and poly(potassium acrylate), but their effectiveness and impact on sparkling wine have not been investigated.[157,158]

SECONDARY FERMENTATION

Yeast chosen for secondary fermentation can sometimes be the same as the first fermentation (depending on wine style and the preference of the winemaker). Invariably, yeast is chosen for its ability to ferment wines high in acid, with low pH and possessing a high ethanol tolerance. *S. cerevisiae* strains able to carry out secondary fermentation in bottle were isolated from spontaneously fermenting Macabeo/Viura, Xarel.lo, and Parellada musts in El Penedes, Spain.[159] The use of non-*Saccharomyces* yeast is becoming more common in winemaking, but less so for secondary fermentation in bottle. There is a lack of published research regarding their use in sparkling winemaking, possibly due to an expected increase in glycerol, which could affect viscosity (that can affect foaming), mouthfeel, and wine flavor.[160] The effect of conventional versus non-conventional selected wild yeast for secondary fermentation was investigated with isolated yeasts from Sicilian Malvasia delle Lipari wine.[161] The yeasts produced sparkling wine with different aroma profiles easily distinguished in a triangle test. Further studies using wild yeast are likely to be a focus of future research, particularly with alternative varieties.

The kinetics of a second fermentation has been monitored using Attenuated Total Reflectance−Fourier Transform Infrared (ATR-FTIR) microspectroscopy to observe the degradation of lipids, proteins, and polysaccharides in Chardonnay base wine.[162] These authors suggested the technique could be used to select yeast strains according to their autolytic capacity, but wineries are unlikely to have this technology. The transcriptome profiling of secondary fermentation included the expression of genes involved in respiratory metabolism, oxidative stress response, autophagy, and peroxisomal function consistent with ethanol being the main environmental factor influencing transcriptional responses to winemaking conditions.[163] The majority of genes down-regulated during secondary fermentation are related to cell growth, linked to the biosynthesis of nucleic acids and proteins, and gene expression.[163] The study found that low pH or CO_2 pressure was not a relevant constraint for the adaptation of wine yeast cells as expected. However, phenolic compounds suppress yeast metabolism during the secondary fermentation in the bottle, which can cause gushing problems for sparkling red, rosé, and white wines.[164] The lower the temperature of a solution, that is, after secondary fermentation, the higher the gas solubility. After secondary fermentation, a standard 75 cL Champagne bottle has close to 9 g of dissolved CO_2 molecules.[72]

AGING ON YEAST LEES

The lees present in still wine during aging are composed of tartaric acid salts, organic residues, and cells of various species of yeasts and bacteria. In contrast, sparkling wine lees are mainly composed of cells from a single species of yeast, along with the technological co-adjuvants, which help to flocculate and eliminate the yeast lees at the end of aging. The aging of sparkling wine in the bottle on yeast lees is generally longer than still wine aging, and yeast autolysis occurs under pressure

DOI: 10.1021/jf504268u
J. Agric. Food Chem. 2015, 63, 19−38

commonly at 6 standard atmospheres (atm). Yeast autolysis is considered a lytic event. It is an irreversible process catalyzed by yeast intracellular enzymes. Autolysis generally takes place at the end of the stationary phase of growth and is usually associated with cell death. The scientific basis of yeast autolysis has been the subject of numerous reviews and is not the subject of this paper.[165−168]

Natural autolysis takes time. This is especially true in wines, in which the autolytic conditions from pH 3 to 4, aging temperature of 15°C, and presence of ethanol (12% v/v) are not the ideal conditions of 45°C at pH 5.[168] In sparkling wines, yeast autolysis does not begin until 2−4 months after the completion of secondary fermentation.[165,169] Yeast autolysis can be promoted by using a mixture of "killer" and sensitive yeast for the secondary fermentation. In these conditions, the sensitive yeast cells rapidly die in the presence of the killer strains.[169]

Hydrolytic enzymes play a major role in autolysis. Proteases are the most extensively studied of all the enzymes involved in autolysis. In sparkling wines, proteolytic activity decreases during active bottle fermentation and in the following months, but after 9 months of fermentation and aging, it gradually increases.[170] Leroy et al.[171] reported that proteolytic activity during Champagne aging may also depend on the yeast strain used.

The yeast cell wall is degraded during autolysis, but few studies have investigated the enzymes involved in this process during wine production. In still wines aged on lees, it has been shown that glucanases are involved in yeast cell wall degradation.[172,173] Cell wall degradation during autolysis results in the release of both amino acids and macromolecules, suggesting that both proteolytic and polysaccharides are involved in the degradation of enzymes.[176] However, in sparkling wine conditions, these activities have not been studied. A recent study investigated the evolution of polysaccharides and their molecular weights during sparkling winemaking.[96] The highest amount of mannoproteins and polysaccahrides with high concentrations of arabinose and galactose with a shift to low molecular weights was reported after 6 months of lees aging, which could positively effect foaming.

Recently, it was reported that the addition of enzyme preparation rich in β-glucanase increases aging characteristic of sparkling wine and would also enhance the antioxidant properties of sparkling wine.[174,175] Indeed, addition of exogenous β-glucanases promotes release of yeast components in sparkling wine during aging.[176] The optimal temperature for proteolysis in the Champenoise method has been reported to be between 10 and 12°C.[114] Another factor that influences yeast autolysis is the yeast strain. One study suggested that yeast strains with a high autolytic capacity would produce better quality sparkling wine than yeasts with a low autolytic capacity.[178] They also suggested that autolytic capacity and foaming analysis should be used for selecting yeasts for sparkling wine production. The importance of the autolytic capacity of yeast strains for sparkling wine quality was confirmed by Nunez et al.[179] A mutant strain with accelerated autolysis was used to conduct the secondary fermentation. The resulting wine had better foaming properties than that produced with the control strain. The aging period was also reduced from 9 to 6 months with this mutant, potentially decreasing production costs.

The use of high-pressure homogenization (HPH) to accelerate yeast autolysis in sparkling wines in Franciacorta, Italy, was investigated. Results showed that HPH-treated yeast strains (except L951) significantly modified the ester profile with lower medium- and long-chain fatty acid concentrations compared to wines without HPH treatment.[138] HPH reduced aging time for most yeast strains without enzyme addition. Its role in reducing medium- and long-chain fatty acids could be utilized in the future to reduce high levels of medium-chain fatty acids to prevent stuck MLF.[59] Although the volatile aroma profile of sparkling wine is dependent upon the kinetics of volatile retention and release by yeast lees during aging, further research is needed to study the effects of HPH on sensory attributes of sparkling wine and foaming ability.[76]

YEAST AUTOLYSIS COMPOUNDS AND THEIR IMPACT ON SPARKLING WINE QUALITY

The autolysis of yeast during aging results in the release of various compounds that modify the physical and organoleptic properties of sparkling wine.

Changes in the Nitrogen Compounds Present at Different Stages in the Traditional Method. Nitrogen release is thought to reflect the autolytic activity of the yeast-proteolytic activity in particular. Yeast autolysis does not begin until 3−4 months after the end of the secondary fermentation. The total amino acid concentration increases before the increase in free amino acid concentration. Thus, peptides are released into the medium and then broken down into amino acids. The change in the various nitrogen fractions during bottle-fermented sparkling wine aging has been studied.[180] Between 3 and 9 months after addition of the *tirage* solution, no change in free amino acid concentration had been observed, regardless of the grape variety used. Free amino acid concentration increased after 9 months, indicating the start of autolysis, and these results have been confirmed.[179] Peptide content fluctuates, peaking after 12−15 months of aging on the lees and decreasing thereafter. This behavior may reflect an initial release of peptides that are subsequently broken down. The amount of peptides released by yeast autolysis during sparkling wine aging is variable and depends on grape variety and aging time.[181] The nature of the peptides released also changes with aging; the length of the peptides released decreased with increased aging time.[182,183]

The amino acid composition of the peptides present in sparkling wines has been investigated.[180−184] The peptides mostly originate from the breakdown of yeast proteins rather than grape juice proteins. An increase in protein and polypeptide levels during the first 3 months, followed by a decrease attributed to protease activity, has been reported.[182] Protein and peptide contents then increased again after 6 months. Amino acid enrichment of the medium may improve the aromatic potential of sparkling wine, as amino acids are the precursors of aroma compounds. Aroma compounds may be generated by the deamination or decarboxylation of amino acid.[165] The levels of one lactone compound, 3-hydroxy-4, 5-dimethyl-2(5*H*)-furanone, also known as sotolon (green nut, curry odor), gradually increase during the aging of sparkling wine. Pham et al.[185] showed that sotolon is generated from threonine, which is transformed into α-ketobutyric acid that reacts with acetaldehyde. Vitispirane, a norisoprene-derived compound imparting eucalyptus aromas, is synthesized from methionine and has been detected in aged cava wine.[186]

DOI: 10.1021/jf504268u
J. Agric. Food Chem. 2015, 63, 19−38

The characteristics of foam are an extremely important property of sparkling wine that is usually measured for foam height, foam area, and foam collar.[179] Moreno-Arribas et al.[187] suggested that the hydrophobicity of peptides might account for the foaming properties of sparkling wine. A few years later it was found that foam characteristics were positively correlated with the concentrations of most free amino acids and proteins, confirming the results of Malvy et al.[183,188] However, no relationship was found between foam characteristics and the concentration of wine peptides.

Polymers. Glucanases and proteases release polysaccharides from the yeast cell wall during autolysis in sparkling wines. These macromolecules contain mainly glucose (74%) and mannose (26%). Polysaccharide concentrations in wines vary. An increase in polysaccharide content from 366 mg/L in base wine to 602 mg/L after 9 months of aging has been reported.[189] The effect of colloids (macromolecules) on foam quality has also been investigated.[190] Neutral polysaccharides are important for foam quality due to their highly significant, positive effect on foam stability.[187] A recent study investigated the impact of polysaccharides from Spanish varieties (Verdejo, Macabeo/Viura, Malvasía, Albarín, Godello, Prieto Picudo, Tempranillo, and Garnacha) on foaming properties.[184] Polysaccharides (mannoproteins, polysaccharides rich in arabinose and galactose, homogalacturons, glucans, and rhamnogalacturons type II) did not correlate with foamability [maximum height reached by foam after CO_2 injection (HM) or foam stability height during CO_2 injection (HS)].[184] The model to explain HS in the study was only predicted by polysaccharides rich in arabinose and galactose. However, there were positive correlations between all of the wine polysaccharides and foam stability time [defined as the time that elapsed before bubble collapse and the appearance of liquid after the interruption by CO^2 (TS)], except for rhamnogalacturonans type II. The optimum aging time for obtaining a high-quality, stable foam appears to be 18 months. Foam quality decreases after 18 months, which coincides with an increase in the level of monomeric compounds, such as fructose, that probably arise from the hydrolysis of grape components by yeast enzymes released during autolysis.[55]

Lipids are important components of sparkling wines because they are a major source of flavor compounds and affect foam stability.[191] Changes in the lipid content of sparkling wine have been the focus of several studies. Lipid content increases during the secondary fermentation, and qualitative changes occur during aging in the bottle in contact with the lees.[192,193] The concentration of polar lipids decreases, whereas the concentration of neutral lipids increases (monoglycerides, diglycerides, triglycerides). Conflicting results have been published concerning the influence of lipids on foam. Octanoic and decanoic fatty acids have been found to reduce foam stability, but it was also reported that the addition of a lipid mixture did not affect the foam.[77,194] It has been noted that linolenic and palmitoleic acid levels were the best indicators of foam stability, and the effect of fatty acids on the foaming properties of wine was investigated.[49,195] The C8, C10, and C12 acids had a negative effect on foam quality, whereas ethyl esters of hexanoic, octanoic, and decanoic acids had a positive effect.

RNase is active during autolysis in Champagne, but data on the extent of nucleic acid degradation should be interpreted with caution because organic acids, phenolic compounds, peptides, and other compounds in wine can interfere with the measurement of nucleotides.[171] Monophosphate nucleotides (5′-UMP, 5′-GMP, and 5′-IMP) have unequivocally been identified in Champagne wine aged on lees.[196,197] Nucleotide monophosphate concentration ranged from 50 to 500 μg/L. Recently it was demonstrated that aging on lees leads to an increase in uridine concentration, whereas purines appear as fermentative catabolites, which are derived from nucleosides or ATP degradation.[198] The nucleotides, especially monophosphate nucleotides, are used as flavorings in the food industry, but further studies are required to evaluate their impact on wine flavor.[199]

Volatile Compounds Released during Autolysis. Heavy acyl chain esters have been identified in model and sparkling wines.[177] Terpenic alcohols and higher alcohols are also released during autolysis. Geraniol and α-terpineol, citronellol, and farnesol have all been identified. These compounds are perceived by tasters at low concentrations, from 100 to 300 μg/L. Molnar et al.[177] suggested that farnesol could greatly contribute to the aromatic quality of sparkling wine, and Loyaux et al.[200] suggested that nerolidol makes a similar contribution to Champagne wines. Approximately 10 aldehydes have been identified in sparkling wines.[168] Methyl-3-butanal is the most abundant, accounting for 40% of all aldehydes present, and may be formed through a mechanism involving isoamyl alcohol oxidation. Most of the aldehydes identified are present at levels close to, or greater than, the detection threshold of the human nose for aqueous solutions, but their odor active values in ethanolic solution with CO_2 (sparkling wine) is unknown.

Volatile aroma compounds released during autolysis were characterized in 221 cava wines (classified into four groups according to their aging time), and diethyl succinate was identified as a possible age marker throughout the aging period.[201] Acetates appeared to decrease during aging, whereas diethyl succinate, vitispirane, and 1,1,6-trimethyl-1,2-dihydronaphthalene (TDN) levels increased over time. Hexanol and 2-phenylethanol were also released during autolysis. Compounds such as vitispirane, TDN, and diethyl succinate may be good age markers and can discriminate between young and aged sparkling wines. Similar results have been obtained, and the researchers reported that some high molecular weight acetates and ethyl and isoamyl esters are typical aroma compounds in young cava wines, whereas vitispirane, diethyl succinate, TDN, hexenol, and ethyl acetate are typical aroma compounds in cava wines aged over a prolonged period.[202] The release of these aromas by yeast enzymes acting on glycoside precursors has been identified as a possible mechanism for their formation, with C13-norisoprenoids and vitispirane being derived from glycoside-bound carotenoids and megastigma, respectively.[202]

The concentration of esters has been found to decrease with aging in the presence of lees, especially 5-hydroxymethyl-2-furfural (5-HMF), synthesized from the dehydration of sugar (mainly fructose) and formed from the intermediate stage of the Maillard reaction.[203−205] This stage begins with the Amadori/Heyns products leading to sugar fragmentation products, that is, 5-HMF, in aged bottled-fermented sparkling wines.[204−206] 5-HMF has been described as contributing caramel, butter, musty, sharp, animal, and soap aromas to wines.[204,208,209] However, its odor activity threshold in sparkling wine and contribution to aged sparkling wine aroma, flavor, and quality remain to be determined. Fedrizzi et al.[210] found that different lengths of time on lees did not affect sulfur compounds in Chardonnay or Chardonnay/Pinot noir sparkling wines, but ethyl pyroglutamate was found to be

DOI: 10.1021/jf504268u
J. Agric. Food Chem. 2015, 63, 19−38

much higher in lees aged wines than still table wines aged on lees, which correlated with aging. Still table wines can age on lees in stainless steel tanks or oak barrels, depending on wine style and variety, but bottled-fermented sparkling wines age on lees that are in the bottle from secondary fermentation.

Benzenemethanethiol, 2-furanmethanethiol, and ethyl 3-mercaptopropionate were found in concentrations higher than their perception thresholds in aged wines, suggesting an important role in the aroma of aged Champagne wines.[211] In the study 3-mercaptohexan-1-ol (3MH) in aged Champagne wines was 4−10 times its perception threshold, which can contribute to the fruity aroma of Champagne wine. Differences in the phenolic concentration of various sparkling wine grape varieties have been reported.[211] However, lees aging did not significantly affect phenolic composition; rather, viticultural effects, vintage variation, and grape variety are responsible for phenolic differences in wines.

RIDDLING/*REMUAGE*

Prior to riddling, "Le Coup de Poigné" or "Poignettage" was used in Champagne but is less common today.[207] The process involves taking the bottle and shaking it to stir up yeast lees and then placing it on its side so that lees are dispersed over 80 cm^2.[207] This practice may break apart tartaric crystals if cold stabilization was not carried out on the base wine and could possibly assist with loosening yeast "streaks" to consolidate lees sediment.

Lees aging in bottle can be from 9 months to several years, depending on the regulations of the wine region and the wine style, and is followed by *remuage* (riddling) to move sediment to the neck of the bottle.[176] The gradual and controlled turning of the slanted and inverted bottles brings the yeast and adjuvants (bentonite or bentonite/alginate) together.[146] Riddling time has been reduced to 3−4 days with free yeasts and to 2 days with agglomerated yeasts, using automated riddling machines with 504 bottles in each cage.[146] The method of riddling does not affect O_2 intake. A recent promising innovation in sparkling wine technology has been developed.[212] Researchers attached to yeast cells magnetic iron oxide maghemite (γ-Fe_2O_3) that did not penetrate the yeast cell wall. These magnetized yeasts increased secondary fermentation time, and simplified and accelerated yeast removal from the bottle.[212] The iron oxide nanoparticles are considered nontoxic and are approved by the U.S. Food and Drug Administration (FDA) for in vivo medical applications and did not exceed the permissible iron limit in European wine regulations.[212] However, the effect on sparkling wine quality as well as yeast multiplication, foaming, oxidative potential, and long-term lees aging is currently unclear. This new magnetized yeast removal method could have a significant impact on production costs by removing the need for riddling, gyropalette equipment, and freezing bottleneck in glycol, decreasing riddling time and production costs (especially equipment and energy costs) of bottle-fermented wine production.

DISGORGING/*DÉGORGEMENT*

Disgorging is the removal of the yeast sediment and adjuvants from the bottle. It is currently performed by inserting the neck of the bottle into a glycol or calcium chloride solution, which freezes (−25°C) the yeast sediment in the *bidule* (a small plastic cap that fits inside the crown cap to catch yeast sediment).[76] Bottles are then picked up and quickly placed neck up; the crown cap is removed, and pressure ejects the *bidule* along with the iced sediment.[76] Marks and Morris investigated the use of ascorbic acid and SO_2 additions at disgorging on *V. vinifera* Chardonnay and Riesling sparkling wines and four sparkling wines made from hybrid cultivars (Cayuga white, Vidal, Chancellor, and Chardonnel) in Arkansas (USA). The aim was to assess the efficiency of ascorbic acid, SO_2, and a combination of the two on the oxidation of sparkling wine post-disgorging after 11 months of lees aging. SO_2 levels declined in all cultivars after the storage period, but there was no added benefit of including ascorbic acid in the *dosage*. Higher acetaldehyde levels were reported in wines after storage with SO_2 only added. Wines made from Cayuga white and Chancellor grape varieties had reduced browning and reduced color intensity when ascorbic acid was added compared to Chardonnay, Riesling, Vidal, and Chardonnel. The results indicated that ascorbic acid could be used in sparkling wine production to prevent oxidation, but only for certain cultivars.[213] Some studies suggest that closure is mainly responsible for the SO_2 decline and post-bottling oxidation.[214−216,218−220] In addition to the closure effect, the presence of the yeast (*sur lattes* bottles) in the traditional method can explain the rapid decrease of SO_2 over time. Some CO_2 is also lost at disgorging, but rapid closing with traditional cork, technical cork, or other closures prevents excessive CO_2 loss. After corking the bottle, dissolved and gaseous CO_2 quickly recovers equilibrium.[72]

"Gushing". Gushing during disgorging has been attributed to a number of factors, specifically tannin from red grape varieties, bottle shaking, ambient temperature during disgorging, insufficient bottle cleaning, cork dust, ultraviolet (UV) lighting in the disgorging area (especially natural sunlight from open doors or through windows on bottles waiting to be disgorged), incomplete riddling, lack of tartaric stabilization, and protein instability.[217,221,222] However, there is a lack of published studies fully investigating the causes in sparkling wine.[221,222] The effect of gushing causes financial loss due to reduction of wine and a decrease of bottling-line speed and efficiency, but its impact on foam, volatile compounds, and flavor in the finished product has not been researched (gushing can generate various levels of O_2 intake before corking.[220] Recent studies focused on beer gushing found that some proteins (hydrophobins and LTP) can be responsible even at very low levels (ppb scale) for beer gushing.[223−225] These particular compounds, the hydrophobic biopolymers of medium MW, are excreted from some fungi (*Fusarium* and other barley contaminants) and remain stable during beer production process. No evidence exists of work being conducted into the link between hydrophobic biopolymers and gushing in sparkling wine. It is likely that some grape contaminants could exhibit the same behavior as that previously described in beer. This would provide further information about "unexplainable gushing" in sparkling wines that lack tartaric crystals, turbidity, MLF in bottle, or riddling issues as suggested by Liger Belair et al.[226,227] The beer foaming gene, *CFG1*, has been isolated from *Saccharomyces pastorianus*, and similar fermentation foaming genes in *S. cerevisiae* are *Awa1p* and *Fpg1p*. These are cell wall mannoproteins, although their contribution, if any, to gushing and effervescence in sparkling wine remains unknown.[228,229]

"Jetting". Oxygen is a major contributor to wine quality; therefore, managing oxygen ingress is of utmost importance during bottle-fermented sparkling wine production.[230] Jetting has been developed to reduce flavor and aroma bottle variability

DOI: 10.1021/jf504268u
J. Agric. Food Chem. 2015, 63, 19−38

from the oxygen in the neck of the bottle at disgorging.[231] The beer industry has used this technology for several decades to avoid air intake (beer is very sensitive to oxidation). Immediately after disgorging when the headspace is 25 mL, there is potentially >7 mg of O_2 per bottle.[232] When the wine is removed, there is potentially >10 mg of O_2 per bottle. Jetting is the insertion of 100 μL of wine into the bottleneck to induce foaming and is being used in some Champagne wine production at bottling.[231] The foam acts as a piston, reducing oxygen ingress in the neck space because the cork is then inserted when the foam is high. Results of a blind test sensory analysis in Champagne found that 31 of 41 panelists preferred the jetted samples, describing them as *fresh* and *fruity*.[230,231]

Liqueur d'Expedition/Dosage. Prior to corking, the *liqueur d'expedition* (*dosage* solution) is inserted into each bottle, and it can give each wine its own unique flavor, for example, ice wine *dosage* in Ontario. The recipe for the *dosage* varies among wineries but can consist of sugar (cane or beet), the oldest sparkling wine in the cellar, oaked/unoaked still Chardonnay wine, wines aged in stainless steel, oak, or/and concrete vessels, with SO_2, citric acid, and very occasionally brandy (now illegal in Champagne), tannins, and/or copper sulfate.[19,76] To date there are no published studies regarding sugar types/sources in *dosage* on sparkling wine quality. *Zero-dosage* is becoming more popular and contains no added sugar. This type of "no-*dosage*" is reserved for special *premium* wines in Champagne. However, it has also recently been used in a scientific study of alternative varieties for sparkling wine. In the study *liqueur d'expedition* was not added to any of the research wines. Each bottle was filled with the same wine to produce Brut Nature wines for the laboratory and sensory analysis.[4] A recent study that used a range of wine styles in the *dosage* solutions found no difference in ethyl ester concentrations in brut sparkling wines (8 g/L residual sugar) by 15 weeks post-disgorging.[232] Interestingly, the *zero-dosage* wines (same wine inserted without sugar) showed an increase in ethyl isovalerate (fruity/minty), which the sugar added wines lacked. The wines with the same wine inserted but with sugar addition (8 g/L) showed slight increased in ethyl butyrate (artificial fruit/candy/strawberry) and ethyl isobutyrate (apple/tropical fruit/citrus). However, the effect on volatile wine compounds when aging under cork post-disgorging or the effect on sensory properties of the wines was not studied. Higher sugar additions may have more of an impact on volatile aroma compounds in sparkling wine than the 8 g/L residual sugar in the trial wines. The contribution of fusel alcohol pathways (anabolic and catabolic) that arise primarily from hexoses in wine fermentation has recently been studied.[233] The rate of sugar hydrolysis has been found to differ between grape varieties. It has been suggested that the natural hydolysis of a 10 g/L sucrose addition to a still wine (pH 3−3.4) devoid of invertase acitivity will take 2.5−5.5 months.[234] The length of time between disgorging and release of sparkling wine for sale is a decision by the wine producer, but the flavor of sparkling wine during the post-disgorging time is known to differ from 1 to 3 months and continuously in bottle thereafter. However, further flavor analysis of sparkling wine aging post-disgorging will clarify the aroma and flavor chemistry occurring in the bottle. It has been demonstrated that disgorging leads to a significant increase in the concentrations of thiols, specifically 2-furanmethanethiol (toasty aroma), benzenemethanethiol (smoky aroma), and ethyl 3-mercaptopropinate (foxy aroma), in two Champagne wines across a range of vintages.[235] Oxygen ingress at disgorging can negatively affect sparkling wine quality, and comprehensive reviews about oxidation mechanisms in wines have already been published.[219,236,237]

SENSORY ANALYSIS OF SPARKLING WINES

There is no internationally accepted or recognized sensory analysis method that has been specifically designed for sparkling wine and no published criteria to evaluate effervescence and foam of sparkling wines.[238] Hedonic scales following panelist training to obtain consensus-based descriptors have been used by visual assessment of foam formation and effervescence as well as questionnaires during tastings, but the method utilized depends on the aims and objectives of the research.[136,238−240] Although serving temperature, bottle opening method, pouring method, room temperature, and lighting are controlled, studies lack attention to glass type, sample order effect on foam and flavor, and the time between opening bottles and then pouring and imbibing.[90,240,242] Sparkling wine descriptors have been generated in studies and used in sparkling wine sensory analysis that includes olfactory intensity, equilibrium, fruity, full body, vegetal, acidity, persistence, floral, varietal, bitterness, freshness, and astringency.[96,243] Foam attributes have included initial foam, foam collar, bubble size, effervescence, and foam and require panelists to be trained in the use of these descriptors.[96,244] A fixed-choice profiling (FCP) method was used whereby each descriptor definition was built from the consesus of the panelists.[245] Initially 64 descriptors were generated, but this was reduced to 19. Wines were poured 5 min before panelists entered the room, so foaming height and stability were not included in the sensory analysis, which are essential to sparkling wine quality. A modified-descriptive analysis method for sparkling wine sensory analysis using calibrated glasses (cm/mm) to measure foam height would help with standardizing a sparkling wine sensory method. Criteria suggestions for consideration include (1) a specific time between opening pouring and tasting the wines or (2) immediate assessment of each wine by panelists as soon as their sample is poured, (3) set room and bottle temperature, (4) storage guidelines before tasting, (5) standardized bubble and foam classifications including persistence, stability, and collar, (6) agreed visual, aroma, and palate descriptors for sparkling wine styles, and (7) number of times to taste the same wine while minimizing bottle variation by allowing panelists to taste at least three bottles for replication purposes.

The odor activity value (OAV) of an aroma compound is an indication of the importance of a specific compound to the aroma of a wine, calculated as the ratio between the concentration of an individual compound and the perception thereshold described in the literature.[7] Until perception thresholds of volatile aroma compounds are determined in a range of sparkling wines (monovarietal and blends) for each compound, it is difficult to state with any certainty their contribution to sparkling wine aroma profile. For instance, the two 3MH enantiomers, *R* and *S*, have different aromas: *R* is fruitier with a grapefruit aroma, and *S* produces aromas reminiscent of passion fruit, which are likely to contribute differently to sparkling wine aroma profiles.[211] However, although OAVs can provide important information, they do not take into account the interactions between volatile compounds and other wine compounds that can enhance or suppress aromas.[241] It is also likely that CO_2 affects odor detection when compared to the same aroma compound in an aqueous or ethanolic solution.

DOI: 10.1021/jf504268u
J. Agric. Food Chem. 2015, 63, 19−38

This review of sparkling wine production has discussed current knowledge and highlighted areas for future research that include grape varieties, *tirage* and *dosage* effects on sparkling aroma and flavor chemical composition, the need for a specific sensory analysis method for sparkling wine, markers associated with sparkling wine quality (especially fermentation byproducts from secondary fermentation), and reducing the time and efficiency of MLF.[62] Future studies are likely to include chemical and sensory analysis related to post-disgorging aging effects on wine flavor and aroma, research related to red and rosé sparkling wines, length of lees aging for *zero-dosage* wines, low-SO_2 wines, SO_2 alternatives for sparkling wines, the effect of using different yeasts for first and secondary fermentations, acceleration of yeast autolysis, reduction of time for MLF, and enzymes involved in yeast autolysis. The mechanism for induction of yeast autolysis remains elusive as are the kinetics of glucanase activity linked to wine quality by its ability to release mannoproteins and the effect on the release of nucleotides, nucleosides, and lipids. If the chemical profile of Chardonnay including acids, genes, and proteins can be identified, then similar varieties with similar traits, and therefore aging characteristics, could be sought in sparkling wine regions. Research regarding phenolic compounds in sparkling wine is likely to focus on different grape varieties to provide information for phenolic management techniques to wine-makers, especially for color stability of rosé and red sparkling wines. Research is likely to focus on "alternative" or "resurrected" varieties for sparkling wines and is likely to include the impact of non-*Saccharomyces* yeast on sparkling wine aroma, flavor, and foaming. Studies that investigate natural plant-based products from vines/grapes/yeast for use in the production process are already underway and likely to continue. The authors are aware of an international sensory analysis method currently being developed with a team of international sensory scientists, specifically for sparkling wine assessment. Although not covered in this review, organic and biodynamic effects on sparkling wine quality, plus the economical, financial, and ecological sustainablility of sparkling wine production practises, are likely to be a focus of future research.

AUTHOR INFORMATION

Corresponding Author

*(B.K.) E-mail: bkemp@brocku.ca. Phone: (905) 688-5550. Fax: (905) 328-2792.

Funding

We express our gratitude to the Cool Climate Oenology and Viticulture Institute (CCOVI), Brock University, Ontario, Canada; Universty of Dijon, France; Institut Oenologique de Champagne (IOC); University of Reims, France; Région Champagne-Ardenne; and the Association Recherche Oenologie Champagne et Université for financial support for more than 25 years.

Notes

The authors declare no competing financial interest.

REFERENCES

(1) Girbau-Solà, M.; Lopez-Tamames, E.; Bujan, J.; Buxaderas, S. Foam aptitude of Trepat and Monastrell red varieties in cava elaboration. 1. Base wine characteristics. *J. Agric. Food Chem.* **2002**, *50* (20), 5596−5599.

(2) Gramona, J. Autolysis and its impact on the sensory qualities of sparkling wines made from the traditional method. In *Proceedings of the 1st International Sparkling Wine Symposium*, Denbies Estate, Surrey, UK; Goode, J., Ed.; Flavour Press: UK, 2012; pp 62.

(3) Audeguin, L. Grape production in France; from blockbuster varieties to indigenous cultivars. Presented at the *Ontario Fruit and Vegetable Convention*, Niagara Falls, Ontario, Canada, Feb 19−20, 2014.

(4) Martínez-Lapuente, L.; Guadalupe, Z.; Ayestaran, B.; Ortega-Heras, M.; Perez-Magarino, S. Sparkling wine produced from alternative varieties: sensory attributes and evolution of phenolics during winemaking and aging. *Am. J. Enol. Vitic.* **2013**, *64* (1), 39−49.

(5) Coelho, E.; Reis, A.; Domingues, R. M.; Rocha, S. M.; Coimbra, M. A. Synergistic effect of high and low molecular weight molecules in the foamability and foam stability of sparkling wines. *J. Agric. Food Chem.* **2011**, *59* (3), 3168−3179.

(6) Stefenon, C. A.; Bonesi, C.; De, M.; Marzarotto, V.; Barbabe, D.; Spinelli, F. R.; Webber, V.; Vanderlinde, R. Phenolic composition and antioxidant activity in sparkling wines: modulation by the aging on lees. *Food Chem.* **2014**, *145*, 292−299.

(7) Caliari, V.; Burin, V. M.; Rosier, J. P.; Bordignon Luiz, M. T. Aromatic profile of Brazilian sparkling wine grapes produced from classical and innovative grape varieties. *Food Res. Int.* **2014**, *62*, 965−973.

(8) Song, J. Q.; Li, H.; Liang, Y. Y.; Tao, Y. Y.; Mi, C. Q.; Qian, M. C.; Wang, H. Characterisation of volatile components of red and sparkling wines from a new white cultivar 'Meili' (*Vitis vinifera* L.). *Vitis* **2013**, *52* (1), 41−48.

(9) Bozdogan, A.; Canbas, A. Influence of yeast strain, immobilisation and ageing time on the changes of free amino acids and amino acids in peptides in bottle-fermented sparkling wines obtained from *Vitis vinifera* cv. Emir. *Int. J. Food Sci. Technol.* **2011**, *46*, 1113−1121.

(10) Bozdogan, A.; Canbas, A. The effect on yeast strain, immobilisation, and aging time on the amount of free amino acids and amino acids in peptides of sparkling wines obtained from cv. Dimrit grapes. *S. Afr. J. Enol. Vitic.* **2012**, *33* (2), 257−163.

(11) Anderson, M. M.; Smith, R. J.; Williams, M. A.; Wolpert, J. A. Viticultural evaluation of French and California Chardonnay clones grown for production of sparkling wine. *Am. J. Enol. Vitic.* **2008**, *59* (1), 73−77.

(12) Mercado-Martín, G. I.; Wolpert, J. A.; Smith, R. J. Viticultural evaluation of eleven clones and two field selections of Pinot noir grown for production of sparkling wine in Los Carneros, California. *Am. J. Enol. Vitic.* **2006**, *57*, 371−376.

(13) Coelho, E.; Coimbra, M. A.; Nogueria, J. M. F.; Rocha, S. M. Quantification approach for assessment of sparkling wine volatiles from different soils, ripening stages, and varieties by stir bar sorptive extraction with liquid desorption. *Anal. Chim. Acta* **2009**, *635*, 714−221.

(14) Esteruelas, M.; González-Royo, E.; Kontoudakis, N.; Orte, A.; Cantos; Miquel Canals, J.; Zamora, F. Influence of grape maturity on the foaming properties of base wines and sparkling wines (cava). *J. Sci. Food Agric.* **2014**, DOI: 10.1002/jsfa.6922.

(15) Kerslake, F. L.; Jones, J. E.; Close. D. C.; Dambergs, R. G. Bunch exposure effects on the quality of Pinot noir and Chardonnay fruit and base wines for cool climate sparkling wine production. Presented at the Ciência e Técnica Vitivinícola, Proceedings 18th International Symposium GiESCO, Porto, Portugal, July 7-11, 2013; Vol. 28, pp 471−477.

(16) Chamkha, M.; Cathala, B.; Cheynier, V.; Douillard, R. Phenolic composition of Champagnes from Chardonnay and Pinot noir vintages. *J. Agric. Food Chem.* **2003**, *51*, 3179−3184.

(17) Pozo-Bayón, M. A.; Polo, M. C.; Martin-Alvarez, P. J.; Pueyo, E. Effect of vineyard yield on the composition of sparkling wines produced from the grape cultivar Parellada. *Food Chem.* **2004**, *86*, 413−419.

(18) Ibern-Gomez, M.; Anrdés-Lacueva, C.; Lamuela-Raventos, R.; Buxaderas, S.; Singleton, V.; de la Torre-Boronet, M. Browning of cava (sparkling wine) during aging in contact with lees due to the phenolic composition. *Am. J. Enol. Vitic.* **2000**, *51* (1), 29−36.

DOI: 10.1021/jf504268u
J. Agric. Food Chem. 2015, 63, 19−38

(19) Bosch-Fusté, J.; Sartini, E.; Flores-Rubio, C.; Caixach, J.; Lopez-Tamames, E.; Buxaderas, S. Viability of total phenol index value as quality marker of sparkling wines, "cavas". *Food Chem.* **2009**, *114*, 782−790.
(20) Gawel, R.; Van Sluyter, S. C.; Smith, P. A.; Waters, E. J. The effect of pH and alcohol on perception of phenolic character in white wine. *Am. J. Enol. Vitic.* **2003**, *64* (4), 425−429.
(21) Pocock, K. F.; Hayasaka, Y.; Peng, Z.; Williams, P. J.; Waters, E. J. The effect of harvesting and long-distance transport on the concentration of haze-forming proteins in grape juice. *Aust. J. Grape Wine Res.* **1998**, *4*, 23−29.
(22) Pocock, K. F.; Waters, E. J. The effect of mechanical harvesting and transport of grapes and juice oxidation. *Aust. J. Grape Wine Res.* **1998**, *4*, 136−139.
(23) Waters, E. J.; Alexander, G.; Muhlack, R.; Pocock, K. F.; Colby, C.; O'Neill, B. K.; Høj, P. B.; Jones, P. Preventing protein haze in bottled white wine. *Aust. J. Grape Wine Res.* **2005**, *11* (2), 215−225.
(24) Andres-Lacueva, C.; Lopez-Tamames, E.; Lamuela-Raventos, R.; Buxaderas, S.; Torre-Boronat, M. Characteristics of sparkling base wines affecting foam behaviour. *J. Agric. Food Chem.* **1996**, *44* (4), 989−995.
(25) Jones, J.; Kerslake, F. L.; Close, D. C.; Dambergs, R. G. Viticulture for sparkling wine production: a review. *Am. J. Enol. Vitic.* **2014**, DOI: 10.5344/ajev.2014.13099.
(26) Kinzer, G.; Schreier, P. Influence of different pressing systems on the composition of volatile constituents in unfermented grape musts and wines. *Am. J. Enol. Vitic.* **1980**, *1*, 7−13.
(27) Cheynier, V.; Masson, G.; Rigaud, J.; Moutounet, M. Estimation of must oxidation during pressing in Champagne. *Am. J. Enol. Vitic.* **1993**, *44*, 393−399.
(28) Gibson, R.; Baggio, P. Central membrane press technology − a comparative study. *Aust. N. Z. Grape Grower Winemaker* **2003**, *475*, 101−104.
(29) Jackson, R. S. Fermentation. In *Wine Science: In Principles and Applications*, 4th ed.; Academic Press/Elsevier: Hoboken, NJ, USA, 2014; Vol. 1, pp 328− 441.
(30) Rao, M. A.; Cooley, H. J. Role of cultivar and press aid in pressing characteristics and juice yields of crushed grapes. *J. Food Process. Eng.* **1992**, *15*, 65−79.
(31) Cossanteli, G. New developments in sparkling wine presses. In *Proceedings of 1st International Sparkling Wine Symposium*, Denbies Estate, Surrey, UK; Goode, J., Ed.; Flavour Press: UK, 2009; pp 63−66.
(32) Luguera, C.; Moreno-Arribas, V.; Pueyo, E.; Bartolome, B.; Polo, M. C. Fractionation and partial characterisation of protein fractions present at different stages of the production of sparkling wines. *Food Chem.* **1998**, *63* (4), 465−471.
(33) Marchal, R.; Menissier, R.; Oluwa, S.; Becart, B.; Jeandet, P.; Kemp, B.; Foss, C.; Robillard, B. Impact on Pinot noir grape juice and wine composition. Presented at the Macrowine Conference, Bordeaux, France, June 18−21, 2012.
(34) Marchal, R.; Salmon; Parmentier, M.; Jegou, S.; Rivero Granados, F. J.; Vrigneau, C.; Robillard, B. Impact of press fractioning on Pinot Meunier grape juice composition. Presented at the III International Conference of Wine Active Compounds, Dijon, Bourgogne, France, 2014.
(35) Marchal, R.; Kemp, B.; Ménissier, R., Oluwa, S.; Pannetier, B.; Whitehead, D.; Whitehead, C. Foss, C. Press fraction composition of sparkling must and base wine. Presented at the International Cool Climate Symposium (ICCS), Hobart, Tasmania, 2012.
(36) Brissonnet, F.; Maujean, A. Characterisation of foaming proteins in a Champagne base wine. *Am. J. Enol. Vitic.* **1993**, *44*, 297−301.
(37) Marchal, R.; Warchol, M.; Cilindre, C.; Jeandet, P. Evidence for protein degradation by *Botrytis cinerea* and relationships with alteration of synthetic wine foaming properties. *J. Agric. Food Chem.* **2006**, *54*, 5157−5165.
(38) Ferreira, R.; Picarra-Pereira, M.; Monteiro, S.; Loureiro, V.; Teixeira, A. The wine proteins. *Trends Food Sci. Technol.* **2002**, *12* (7), 230−239.
(39) Pérez-Cerrada, M.; Casp, A.; Maquieira, A. Chromatographic determination of the anion content in Spanish rectified concentrated musts. *Am. J. Enol. Vitic.* **1993**, *44* (3), 292−296.
(40) Le Bourse, D.; Conreux, S.; Villaume, S.; Lameriras, J.-M.; Jeandet, P. Quantification of chitinase and thaumatin-like proteins in grape juices. *Anal. Bioanal. Chem.* **2011**, *401*, 1541−1549.
(41) Kwon, S. Profiling of soluble proteins in wine by nano-high-performance liquid chromatography/tandem mass spectrometry. *J. Agric. Food Chem.* **2004**, *52* (24), 7258−7263.
(42) Rizzon, L. A.; Meneguzzo, J.; Abarzua, C. E. In *Elaboraciüão de Vinho Espumante na Propriedade Vitıcola*; Embrapa-Centro Nacional de Pesquisa de Uva e Vinho: Bento Goncüalvez, Brazil, 2000; p 24.
(43) Martinelli, L. A.; Moreira, M. Z.; Ometto, J. P. H. B.; Alcarde, A. R.; Rizzon, L. A.; Stange, E.; Ehleringer, J. R. Stable carbon isotopic composition of the wine and CO_2 bubbles of sparkling wines: detecting C_4 sugar additions. *J. Agric. Food Chem.* **2003**, *51*, 2625−2631.
(44) Rankine, B. In *Making Good Wine*, 3rd ed.; Pan MacMillian Australia: Sydney, Australia, 2004; pp 117.
(45) Pineau, B.; Trought, M. C.T.; Stronge, K.; Beresford, M. K.; Wohlers, M. W.; Jaeger, S. R. Influence of fruit ripeness and juice chaptalisation on the sensory properties and degree of typicality expressed by Sauvignon blanc wines from Marlborough, New Zealand. *Aust. J. Grape Wine Res.* **2011**, *17*, 358−367.
(46) Goresline, H. E.; Champlin, F. M. Sugars in Champagne production. *J. Ind. Eng. Chem.* **1938**, 112−113.
(47) Boulton, R. Understanding and adjusting acidity measures in cool climate juices and wines. Presented at the Seventh Cool Climate Symposium (ICCS), Seattle, WA, USA, June 20−22, 2010.
(48) Robillard, B.; Delpuech, E.; Viaux, L.; Malvy, J.; Vignes-Adler, M.; Duteurtre, B. Improvements for sparkling base wine foam measurements and effect of wine filtration on foam behaviour. *Am. J. Enol. Vitic.* **1993**, *44* (4), 387−393.
(49) Pueyo, E.; Martin-Alvarez, P.; Polo, M. C. Relationship between foam characteristics and chemical composition in wines and cavas (sparkling wine). *Am. J. Enol. Vitic.* **1995**, *46*, 518−524.
(50) Volschenk, H.; van Huuren, H. J. J.; Viljoen-Bloom, M. Malic acid in wine: origin, function and metabolism during vinification. *S. Afr. J. Enol.* **2006**, *27* (2), 123−136.
(51) Boulton, R. Managing acidity and pH in wine. Presented at the Winemaking for Challenging Environments Symposium, 65th ASEV National Conference, Austin, TX, USA, June 27, 2014.
(52) Auge, D.; Valade, M.; Moncomble, D. Acidity of Champagne wines: use of malolactic fermentation? *Vigneron Champenois Epernay* **2000**, *121* (2), 44−56.
(53) Lasik, M. The application of malolactic fermentation process to create good quality grape wine produced in cool-climate countries: a review. *Eur. Food Res. Technol.* **2013**, *237*, 843−850.
(54) Bartowsky, E. J.; Borneman, A. R. Genomic variations of *Oenococcus oeni* strains on the potential to impact on malolactic fermentation and aroma compounds in wine. *Appl. Microbiol. Technol.* **2011**, *92* (3), 441−447.
(55) Andreas-Lacueva, C.; Lamuela-Raventos, R. M.; Buxaderas, S.; del Carmen de la Torre-Boronat, M. Influence of variety and aging on foaming properties of cava (sparkling wine). 2. *J. Agric. Food Chem.* **1997**, *45*, 2520−2525.
(56) López-Barajas, M.; López-Tamames, E.; Buxaderas, S.; De La Torre-Boronat, M. Effect of vinification and variety on foam capacity of wine. *Am. J. Enol. Vitic.* **1998**, *49* (4), 397−402.
(57) McKinnon, A. J.; Scollary, G. R.; Solomon, D. H.; Williams, P. J. The influence of wine components on the spontaneous precipitation of calcium L-(+)-tartrate in a model wine solution. *Am. J. Enol. Vitic.* **1995**, *46*, 509−517.
(58) Bauer, R.; Dicks, L. M. T. Control of malolactic fermentation in wine. A review. *S. Afri. J. Enol. Vitic.* **2004**, *25* (2), 74−88.
(59) Lerm, E.; Engelbrecht, L.; du Toit, M. Malolactic fermentation: the ABC's of MLF. *S. Afr. J. Enol. Vitic.* **2010**, *31* (2), 186−212.

DOI: 10.1021/jf504268u
J. Agric. Food Chem. 2015, 63, 19−38

(60) Gerbaux, V.; Villa, A.; Monamy, C.; Bertrand, A. Use of lysozyme to inhibit malolactic fermentation and to stabilise wine after malolactic fermentation. *Am. J. Enol. Vitic.* **1997**, *48*, 49−53.
(61) Marchal, R.; Chaboche, D.; Douillard, R.; Jeandet, P. Influence of lysozyme treatments on Champagne base wine foaming properties. *J. Agric. Food Chem.* **2002**, *50* (6), 1420−1428.
(62) Sablayrolles, J. M. Control of alcoholic fermentation in winemaking: current situation and prospect. *Food Res. Int.* **2009**, *42*, 418−424.
(63) Suarez-Lepe, J. A.; Palomero, F.; Benito, S.; Calderon, F.; Morata, A. Review: Oenological versatility of *Schizosaccharomyces* spp. *Eur. Food Res. Technol.* **2012**, *235*, 375−383.
(64) Ducruet, J.; Fast-Merlier, K.; Noilet, P. New application for nanofiltration: reduction of malic acid in grape must. *Am. J. Enol. Vitic.* **2010**, *61* (2), 278−283.
(65) Agouridis, N.; Bekatorou, A.; Nigam, P.; Kanellaki, M. Malolactic fermentation in wine with *Lactobacillis casei* cells immobilised on de-lignified cellulosic material. *J. Agric. Food Chem.* **2005**, *53*, 2546−2551.
(66) Genisheva, Z.; Mussatto, S. I.; Oliveira, J. M.; Texeira, J. A. Malolactic fermentation of wines with immobilised lactic acid bacteria − influence of concentration, type of support material and storage conditions. *Food Chem.* **2013**, *138*, 1510−1512.
(67) Genisheva, Z.; Mota, A.; Mussatto, S. I.; Oliveira, J. M.; Texeira, J. A. Integrated continuous winemaking process involving sequential alcoholic and malolactic fermentations with immobilised cells. *Process Biochem.* **2014**, *49*, 1−9.
(68) Torriani, S.; Felis, C. E.; Fracchetti, F. Selection criteria and tools for malolactic fermentation starter development: an update. *Ann. Microbiol.* **2011**, *61*, 33−39.
(69) De la Luz Mohedano, M.; Russon, M.; de los Rios, V.; Capozzi, V.; Fernandez de Palencia, P.; Spano, G.; Lopez, P. A partial proteome reference map of the wine lactic acid bacterium *Oenococcus oeni* ATCC BAA-1163. *Open Biol.* **2014**, *4* (130154), 1−10.
(70) Benito, S.; Palomero, F.; Morata, A.; Calderon, F.; Suarez-Lepe, J. New applications for *Schizosaccharomyces pombe* in the alcoholic fermentation of red wines. *Int. J. Food Sci. Technol.* **2012**, *47*, 2101−2108.
(71) Moreno-Arribas, M. V.; Polo, M. C. Winemaking biochemistry and microbiology: current knowledge and future trends. *Crit. Rev. Food Sci. Nutr.* **2005**, *45*, 265−286.
(72) Liger-Belair, G.; Polidoric, G.; Zéninaria, V. Unraveling the evolving nature of gaseous and dissolved carbon dioxide in Champagne wines: a state-of-the-art review, from the bottle to the tasting glass. *Anal. Chim. Acta* **2012**, *732*, 1−15.
(73) Hong, Y. S.; Cilindre, C.; Liger-Belair, G.; Jeandet, P.; Hertkorm, N.; Schmitt-Kopplin, P. Metabolic influence of *Botrytis cinerea* infection in Champagne base wine. *J. Agric. Food Chem.* **2011**, *59*, 7237−7245.
(74) Marchal, R.; Warchol, M.; Cilindre, C.; Jeandet, P. Evidence for protein degradation by *Botrytis cinerea* and relationships with alteration of synthetic wine foaming properties. *J. Agric. Food Chem.* **2006**, *54*, 5157−5165.
(75) Cilindre, C.; Castro, A.; Clement, C.; Jeandot, P.; Marchal, R. Influence of *Botrytis cinerea* infection on Champagne wine proteins (characterised by two-dimensional electrophoresis/immunodetection) and wine foaming properties. *Food Chem.* **2007**, *103*, 139−149.
(76) Torresi, A.; Frangipane, M. T.; Anelli, G. Biotechnologies in sparkling wine production. Interesting approaches for quality improvement: a review. *Food Chem.* **2011**, *129*, 1232−1241.
(77) Maujean, A.; Poinsaut, P.; Dantan, H.; Brissonnet, F.; Cossiez, E. Etude de la tenue et de la qualité de mousse des vins effervescents. II: Mise au point d'une technique de mesure de la moussabilité, de la tenue et de la stabilité de mousse des vins effervescents. (Study of the performance and quality of the foam in sparkling wines. II: Perfecting of a measuring technique for foamability, performance and stability of the foam in sparkling wines). *Bull. O.I.V.* **1990**, *63*, 405−427.
(78) Puig-Deu, M.; López-Tamames; Buxaderas, S.; Torre-Boronat, M. C. Quality of base and sparkling wines as influenced by the type of fining agent added pre-fermentation. *Food Chem.* **1999**, *66*, 35−42.
(79) Lao, C.; Santamaria, A.; López-Tamames, E.; Bujan, J.; Buxaderas, S.; De la Torre-Boronat, M. Effect of grape pectic enzyme treatment on foaming properties of white musts and wines. *Food Chem.* **1999**, *65* (2), 169−173.
(80) Ibern-Gomez, M.; Andrés-Lacueva, C.; Lamuela-Raventos, R.; Lao-Luque, C.; Buxaderas, S.; de la Torre-Boronet, M. C. Differences in phenolic profile between oak wood and stainless steel fermentation in white wines. *Am. J. Enol. Vitic.* **2001**, *52* (2), 159−164.
(81) Torrens, J.; Urpi, P.; Riu-Aumatell, M.; Vichi, S.; Lopez-Tamames, E.; Buxaderas, S. Different commercial yeast strains affecting the volatile and sensory profile of cava base wine. *Int. J. Food Microbiol.* **2008**, *124*, 48−57.
(82) Vigentini, I.; Fabrizio, V.; Faccincani, M.; Picozzi, C.; Comasio, A.; Foshiona, R. Dynamics of *Saccharomyces cerevisiae* populations in controlled and spontaneous fermentations for Franciacorta D.O.C.G. base wines. *Ann. Microbiol.* **2014**, *64*, 639−651.
(83) Jolly, N. P.; Varela, C.; Pretorius, I. S. Not your ordinary yeast: non-*Saccharomyces* yeasts in wine production uncovered. *FEMS Yeast Res.* **2014**, *14*, 215−237.
(84) Martínez-Moreno, R.; Quiros, M.; Morales, P.; Gonzalez, R. New insights into the advantages of ammonium as a winemaking nutrient. *Int. J. Food Microbiol.* **2014**, *177*, 128−135.
(85) Schmidt, S.; Dillon, S.; Kolouchava, R. H.; Chambers, P. Impacts of variations in elemental nutrient concentration of Chardonnay musts on *Saccharomyces cerevisiae* fermentation kinetics and wine composition. *Appl. Microbiol. Cell Physiol.* **2011**, *91*, 365−375.
(86) Pozo-Bayón, M. A.; Martin-Ālvarez, P. J.; Moreno-Arribas, M. V.; Andujar, I.; Pueyo, E. Impact of using Trepat and Monastrell red grapes on the volatile and nitrogen composition during the manufacture of rosé cava sparkling wines. *Food Sci. Technol.* **2010**, *43*, 1526−1532.
(87) Comuzzo, P.; Battistutta, F.; Vendrame, M.; Silvina Páez, M.; Luisi, G.; Zironi, R. Antioxidant properties of different products and additives in white wine. *Food Chem.* **2014**, *168*, 107−114.
(88) Webber, V.; Valduga Dutra, S.; Rodrigues Spinelli, F.; Rossi Marcon, A.; Joao Carnieli, G.; Vanerlinde, R. Effect of glutathione addition in sparkling wine. *Food Chem.* **2014**, *159*, 391−398.
(89) Ugliano, M. Oxygen contribution to wine aroma evolution during bottle aging. *J. Agric. Food Chem.* **2013**, *61*, 6125−6136.
(90) Welke, J. E.; Zanus, M.; Lazarotto, M.; Schmitt, K. G.; Zini, C. A. Volatile characterisation by multivariate optimization of headspace-solid phase microextraction and sensorial evaluation of Chardonnay base wines. *J. Braz. Chem. Soc.* **2012**, *23* (4), 678−687.
(91) Welke, J. E.; Zanus, M.; Lazarotto, M.; Pulgati, F. H.; Zini, C. A. Main differences between volatiles of sparkling and base wines accessed through comprehensive two dimensional gas chromatography with time-of-flight mass spectrometric detection and chemometric tools. *Food Chem.* **2014**, *164*, 427−437.
(92) Girbau-Solà, M.; Lopez-Tamames, E.; Bujan, J.; Buxaderas, S. Foam aptitude of Trepat and Monastrell red varieties in cava elaboration. 2. Second fermentation and aging. *J. Agric. Food Chem.* **2002**, *50* (20), 5600−5604.
(93) Greeff, A. E.; Robillard, B.; du Toit, W. J. Short and long-term efficiency of carboxymethylcellulose (CMC) to prevent crystal formation in South African wine. *Food Addit. Contam. Part A* **2012**, *29* (9), 1374−1385.
(94) Low, L.; O'Niell, B.; Ford, C.; Godden, J.; Gishen, M.; Colby, C. Economic evaluation of alternative technologies for tartrate stabilisation of wines. *Int. J. Food Sci. Technol.* **2008**, *43*, 1202−1216.
(95) Gonçlaves, F.; Fernandes, C.; Camerira dos Santos, P.; de Pinho, M. N. Wine tartaric stabilisation by electrodialysis and its assessment by the saturation temperature. *J. Food Eng.* **2003**, *59*, 229−235.
(96) Martinez-Lapuente, L.; Guadalupe, Z.; Ayestaran, B.; Ortega-Heras, M.; Perez-Magarino, S. Changes in polysaccharide composition

DOI: 10.1021/jf504268u
J. Agric. Food Chem. 2015, 63, 19−38

during sparkling winemaking and aging. *J. Agric. Food Chem.* **2013**, *61* (50), 12362−12373.
(97) Salazar, F. N.; de Bruijn, J. P. F.; Seminario, L.; Guell, C.; Lopez, F. Improvement of wine crossflow microfiltration by a new hybrid process. *J. Food Eng.* **2007**, *79* (4), 1329−1336.
(98) Marchal, R.; Lallement, A.; Jeandet, P.; Establet, G. Clarification of Muscat musts using wheat proteins and the flotation technique. *J. Agric. Food Chem.* **2003**, *51*, 2040−2048.
(99) Marchal, R.; Jeandet, P. Use of enological additives for colloid and tartrate salt stabilisation in white wines and for improvement of sparkling wine foaming properties. Chapter 5. In *Wine Chemistry and Biochemistry*; Moreno, M. V., Polo, M. C., Eds.; Springer: New York, 2009; Vol. 1, pp 127−158.
(100) Claus, H.; Tenzer, S.; Sobe, M.; Schlander, H.; Konig, H.; Frohlich, J. Effect of carboxymethylcellulose on tartrate salt, protein and other colour stability of red wine. *Aust. J. Grape Wine Res.* **2014**, *20*, 186−193.
(101) Guise, R.; Filipe-Ribeiro, L.; Nascimento, D.; Bessa, O.; Nunes, F. M.; Cosme, F. Comparison between different types of carboxymethylcellulose and other oenological additives used for white wine tartaric stabilisation. *Food Chem.* **2014**, *156*, 250−257.
(102) Kemp, B. Sparkling wine research trials in the UK. *Aspects Appl. Biol.* **2011**, *111*, 29−30.
(103) Delavigne, N.; Sonn, P.; Barbera, N.; Soave, M.; Robillard, B. Les dérivés de chitine comme nouvelle génération d'adjuvant de flottation. *Rev. Oenol.* **2014**, *151*, 1−4.
(104) Cabello-Pasini, A.; Victoria-Cota, N.; Macias-Carranza, V.; Hernandez Garibay, E.; Muñiz-Salazar, R. Clarification of wines using polysaccharides extracted from seaweeds. *Am. J. Enol. Vitic.* **2005**, *56*, 52−59.
(105) Pocock, K. F.; Rankine, B. C. Heat test for detecting protein instability in wine. *Aust. Wine, Brew. Spirit Rev.* **1973**, *91* (5), 42−43.
(106) Salazar, F.; Zamora, F.; Canals, J. M.; López, F. Protein stabilisation in sparkling base wine using zirconia and bentonite: influence on the foam parameters and protein fractions. *J. Int. Sci. Vigne Vin* **2010** June (Special issue Macrowine), 51−58.
(107) Minussi, R. C.; Rosi, M.; Bologna, L.; Rotillo, D.; Pastore, G. M.; Duran, N. Phenols removal in musts: strategy for wine stabilisation by laccase. *J. Mol. Catal. B: Enzym.* **2007**, *45*, 102−107.
(108) Marangon, M.; Lucchetta, M.; Duan, D.; Stockdale, V. J.; Hart, A.; Rogers, P. J.; Waters, E. J. Protein removal from a Chardonnay juice by addition of carrageenan and pectin. *Aust. J. Grape Wine Res.* **2012**, *18*, 194−202.
(109) Van Slyter, S. C.; Warnock, N. I.; Schmidt, S.; Anderson, P.; Van Kan, J. A. L.; Bacic, A.; Waters, E. Aspartic acid protease from *Botrytis cinerea* removes haze-forming proteins during white wine-making. *J. Agric. Food Chem.* **2013**, *61*, 9705−9711.
(110) Marchal, R.; Berthier, L.; Legendre, L.; Marchal-Delahunt, P.; Jeandet, P.; Maujean, A. Effects of *Botrytis cinerea* infection on the must protein electrophoretic characteristics. *J. Agric. Food Chem.* **1998**, *46*, 4945−4949.
(111) Marchal, R.; Marchal-Delahaut, L.; Michels, F.; Parmentier, M.; Lallement, A.; Jeandet, P. Wheat gluten used as clarifying agent of musts and white wines. *Am. J. Enol. Vitic.* **2002**, *53*, 308−314.
(112) Mauzauric, J. P.; Salmon, J. M. Interactions between yeast lees and yeast polyphenols during simulation of wine aging. I. Analysis of remnant polyphenolic compounds in the resulting wines. *J. Agric. Food Chem.* **2005**, *53*, 5647−5653.
(113) Puig-deu, M.; López-Tammes, E.; Buxadreas, S.; Torre-Boronat, M. C. Influence of must racking and fining procedures on the composition of white wine. *Vitis* **1996**, *35* (3), 141−145.
(114) Parmentier, M.; Salmon, T.; Kemp, B.; Foss, C.; Deroy, A.; Marchal, R. Charcoal treatment on Pinot noir sparkling base wine: effect on colour, protein content and foaming properties. Presented at the Vino Analytica Scientia Symposium, Reims, Champagne, France, July 3−5, 2013.
(115) Nicolini, G.; Tonidandel, L.; Moser, S.; Roman, T.; Larcher, R. The use of carbon during fermentation: the effects on fungicide residues, aroma composition and the colour of white wines. Presented at the OIV 36th World Congress of Vine and Wine, Bucharest, Romania, June 2−8, 2013.
(116) Fernandes, J.; Neto, R.; Centeno, F.; Teixeira, F.; Gomes, A. C. Protein yeast extract: alternative to white wine clarification and stabilisation. Presented at the III International Conference of Wine Active Compounds, Dijon, Bourgogne, France, 2014.
(117) Eder, R. Neues unbekanntes Weinbehandlungsmittel. *Der Winzer* **2011**, Sept, 10−13.
(118) Bornet, A.; Delavigne, N.; Robillard, B. Chitin-glucan and chitosan: two new bio-tools for mineral contaminants reduction in wine. Presented at the OIV 36th World Congress of Vine and Wine, Bucharest, Romania, June 2−8, 2013.
(119) Viaux, L.; Morard, C.; Robillard, B.; Duteurtre, B. The impact of foam base wine filtration on Champagne foam behaviour. *Am. J. Enol. Vitic.* **1994**, *45* (4), 407−409.
(120) Douillard, R.; Lefebvre, J.; Tran, V. Applicability of Gibb's law to protein adsorption isotherms. Presented at the 7th International Conference on Surface and Colloid Science, Compiègne, France, July 8−13, 1991.
(121) Graham, D. E.; Philips, M. C. Proteins at liquid interfaces: I. Kinetics of adsorption and surface denaturation. II. Adsorption isotherm. III. Molecular structure of adsorbed films. *J. Colloid Interface Sci.* **1979**, *70*, 403−439.
(122) Jordan, A. D.; Napper, D. H. Some aspects of the physical chemistry of bubbles and foam phenomena in sparkling wines. Presented at the 6th Australian Wine Indunstry Technological Conference, Adelaide, Australia, 1988; pp 237−246.
(123) Mirliss, M. A. Comparison of DE and cross-flow filtration: just the facts, ma'am. Water conditioning and purification; www.wcponline.com/pdf/0702mirliss.pdf, 2002 (accessed Aug 9, 2014).
(124) Buffon, P.; Heymann, H.; Block, D. E. Sensory and chemical effects of cross-flow filtration on white and red wines. *Am. J. Enol. Vitic.* **2014**, *65*, 305−314.
(125) Peri, C.; Riva, M.; Decio, P. Cross-flow membrane filtration of wines: comparison of the performance of ultrafiltration, microfiltration and intermediate cut-off membranes. *Am. J. Enol. Vitic.* **1988**, *39* (2), 162−168.
(126) El Rayess, Y.; Albasi, C.; Bacchin, P.; Taillandier, P.; Raynal, J.; Mietton-Peuchot, M.; Devatine, A. Cross-flow microfiltration applied to oenology: a review. *J. Membr. Sci.* **2011**, *382*, 1−19.
(127) Ribéreau-Gayon, P.; Glories, G.; Maujean, A.; Dubourdieu, D. Chemical nature, origins and consequences of the main organoleptic defects. In *Handbook of Enology. The Chemistry of Wine Stabilisation and Treatment*, 2nd ed.; Wiley: Chichester, UK, 2006; Vol. 2, 340 pp.
(128) Liger-Belair, G. The physics and chemistry behind the bubbling properties of Champagne and sparkling wines: a state-of-the-art review. *J. Agric. Food Chem.* **2005**, *53*, 2788−2802.
(129) Valade, M.; Bunner, D.; Tribaut-Sohier, I.; Tusseau, D.; Moncomble, D. Le gaz carbonique et l'oxygène lors de l'élaboration du champagne. *Rev. Fr. Oenol.* **2011**, *246* (April/May), 1−10.
(130) Bunner, D.; Tribaut-Sohier, I.; Valade, M.; Rouchaussé, J.-M.; Tusseau, D.; Moncomble, D. *Le Vigneron Champenois* **2008**, *4*, 40−63.
(131) Cristofoli, K.; Brandalise, R. N.; Zeni, M. Photo stabilised LDPE films with UV absorber and HALS as protection against the light for rosé sparkling wine. *J. Food Process. Technol.* **2012**, *3* (7), 1−7.
(132) Dias, D. A.; Smith, T. A.; Ghiggino, K. P.; Scollary, G. R. The role of light, temperature and wine bottle colour on pigment enhancement in white wine. *Food Chem.* **2012**, *135*, 2934−2941.
(133) Dias, D. A.; Clark, A. C.; Smith, T. A.; Ghiggino, K. P.; Scollary, G. R. Wine bottle colour and oxidative spoilage: whole bottle light exposure experiments under controlled and uncontrolled temperature conditions. *Food Chem.* **2013**, *138*, 2451−2459.
(134) Pérez-Magaiño, S.; Ortega-Heras, M.; Martinez-Lapuente, L.; Guadalupe, Z.; Ayestaran, B. Multivariate analysis for the differentiation of sparkling wines elaborated from autochthonous Spanish grape varieties: volatile compounds, amino acids and biogenic amines. *Eur. Food Res. Technol.* **2013**, *236*, 827−841.
(135) Valade, M.; Laurent, M. The *tirage*-mixture to carry out fermentation of sparkling wine. Part 1. Calculation of *tirage*

DOI: 10.1021/jf504268u
J. Agric. Food Chem. 2015, 63, 19−38

ingredients. Part 2: The production of the mixture and control of second fermentation. *Vigneron Champenois, Epernay, France* **2001**, *22* (3), 40−57.
(136) Torrens, J.; Riu-Aumatell, M.; Vichi, S.; Lopez-Tamames, E.; Buxaderas, S. Assessment of volatile and sensory profiles between base and sparkling wines. *J. Agric. Food Chem.* **2010**, *58*, 2455−2461.
(137) Gallardo-Chacon, J.; Vichi, S.; Lopez-Tamames, E.; Buxaderas, S. Analysis of sparkling wine lees surface volatiles by optimized headspace solid-phase micro-extraction. *J. Agric. Food Chem.* **2009**, *57*, 3279−3285.
(138) Patrignani, F.; Ndagijimana, M.; Vernocchi, P.; Gianotti, A.; Riponi, C.; Gardini, F.; Lanciotti, R. High-pressure homogenization to modify yeast performance for sparkling wine production according to the traditional method. *Am. J. Enol. Vitic.* **2013**, *64* (2), 258−267.
(139) Valade, M.; Tribaut-Sohier, I.; Bunner, D.; Pierlot, C.; Moncomble, D.; Tusseau, D. Les apports d'oxygène en vinification et leurs impacts sur les vins. Le cas particulier du Champagne. *Rev. Fr. Oenol.* **2008**, *221*, 1−6.
(140) Valade, M.; Tribaut-Sohier, I.; Bunner, D.; Pierlot, C.; Moncomble, D.; Tusseau, D. Les apports d'oxygène en vinification et leurs impacts sur les vins. Le cas particulier du Champagne. *Rev. Fr. Oenol.* **2008**, *222*, 17−28.
(141) Monk, P.; Storer, J. The kinetics of yeast growth and sugar stabilisation in *tirage*: the influence of different methods of starter culture preparation and inoculation levels. *Am. J. Enol. Vitic.* **1986**, *37* (1), 72−76.
(142) Caillet, M. M. Les nouvelles techniques de tirage. Levures agglomérantes. *Le Vigneron Champenois* **1991**, *1*, 27−39.
(143) Duteurtre, B. *Le Champagne − de la Tradition à la Science*; Tec & Doc. Lavoisier: Paris, France, 2011; pp133−134.
(144) Pozo-Bayón, M. A.; Pueyo, E.; Martin-Alvarez, P. J.; Martinez-Rodríguez, A.; Carmen-Polo, M. Influence of yeast strain, bentonite addition, and aging time on volatile compounds of sparkling wines. *Am. J. Enol. Vitic.* **2003**, *54* (4), 273−278.
(145) Pozo-Bayón, M. A.; Monagas, M.; Carmen-Polo, M.; Gomez-Cordoves. Occurrence of pyranoanthocyanains in sparkling wines manufactured from red grape varieties. *J. Agric. Food Chem.* **2004**, *52*, 1300−1306.
(146) Jeandet, P.; Lenfant, J. C.; Caillet, M.; Liger-Belair, G.; Vasserot, Y.; Marchal, R. Contribution to the study of the *remuage* procedure in Champagne wine production: identification of *voltigeurs* particles in suspension in the wine. *Am. J. Enol. Vitic.* **2000**, *1* (4), 418−419.
(147) Vanrell, G.; Canals, R.; Esteruelas, M.; Fort, F.; Canals, J. M.; Zamora, F. Influence of the use of bentonite as a riddling agent on foam quality and protein fraction of sparkling wines (cava). *Food Chem.* **2007**, *104*, 148−155.
(148) Lambri, M.; Dordoni, R.; Giribaldi, M.; Violetta, M. R.; Giuffrida, M. G. Heat-unstable protein removal by different bentonite labels in white wines. *LWT−Food Sci. Technol.* **2012**, *46*, 460−467.
(149) Pozo-Bayón, M. A.; Hernandez, M. T.; Martin-Alvarez, P. J.; Carmen-Polo, M. Study of low molecular weight phenolic compounds during the aging of sparkling wines manufactured with red and white grape varieties. *J. Agric. Food Chem.* **2003**, *51*, 2089−2095.
(150) Martinez-Rodríguez, A. J.; Polo, M. C. Effect of the addition of bentonite to the tirage solution on the nitrogen composition and sensory quality of sparkling wines. *Food Chem.* **2003**, *81*, 383−388.
(151) Fundueanu, G.; Nastruzzi, C.; Carpov, A.; Desbrières, J.; Rinaudo, M. Physico-chemical characterization of Ca-alginate micro-particles produced with different methods. *Biomaterials* **1999**, *20* (15), 1427−1435.
(152) Lallement, A. Les levures incluses pour la prise de mousse. *Rev. Œnol.* **1991**, *58*, 29−31.
(153) Divies, C. Procédé enzymatique utilisant des micro-organismes inclus. Patent 75245 09, 1975.
(154) Robillard, B. Impacts of disgorging on quality, oxidation and heterogeneity. *Vigneron Champenois, Epernay* **2003**, *124*, 11, 58−60, 62, 64−67.
(155) Valade, M. Technical and economical approaches of different procedures of bottle fermentation. *Rev. Oenol.* **1995**, *21* (75), 19−23.
(156) Puig-Pujol, A.; Bertran, E.; Garcia-Martinez, T.; Capdevila, F.; Minguez, S.; Mauricio, J. C. Application of new organic yeast method for sparkling wine production. *Am. J. Enol. Vitic.* **2013**, *64* (3), 386−394.
(157) Poreda, A.; Tuszynski, T.; Zaniewicz, M.; Sroka, P.; Jakubowski, M. Support materials for yeast immobilisation affect the concentration of metal ions in the fermentation medium. *J. Inst. Brew.* **2013**, *119*, 164−171.
(158) Owsawemwenze, L. A.; Adogbo, G. M. Ethanol synthesis using yeast anchored on calcium alginate and clay support. *Int. J. Sci. Eng. Res.* **2013**, *4* (4), 479−484.
(159) Nadal, D.; Carro, D.; Fernández-Larrea, J.; Piña, B. Analysis and dynamics of chromosomal complements of wild sparkling wine yeast strains. *Appl. Environ. Microbiol.* **1999**, *65* (4), 1688−1695.
(160) Fleet, G. Wine yeasts for the future. *FEMS Yeast Res.* **2008**, *8* (7), 979−985.
(161) Lombardo, A.; Guarrera, N. Conventional versus non-conventional selected wild yeasts effect on Champenois method sparkling wine aroma. *Riv. Vitiol. Enol., Conegliano* **2012**, *65* (1), 37−52.
(162) Cavagna, M.; Dell Anna, R.; Monti, F.; Rossi, F.; Torriani, S. Use of ATR-FTIR Micro spectroscopy to monitor autolysis of *Saccharomyces cerevisiae* cells in base wine. *J. Agric. Food Chem.* **2010**, *58*, 39−45.
(163) Penacho, V.; Valero, E.; Gonazalez, R. Transcription profiling of sparkling wine second fermentation. *Int. J. Food Microbiol.* **2012**, *153*, 176−182.
(164) Hialgo, P.; Pueyo, E.; Pozo-Bayon, M. A.; Martinez-Rodriguez, A. J.; Martin-Alvarez, P.; Polo, M. C. Sensory and analytical study of rosé sparkling wines manufactured by second fermentation in the bottle. *J. Agric. Food Chem.* **2004**, *52*, 6640−6645.
(165) Charpentier, C.; Feuillat, F. Yeast autolysis. In *Wine Microbiology and Biotechnology*; Fleet, G. H., Ed.; Harwood Academic Publishers: Chur, Switzerland, 1993; pp 243−264.
(166) Fornairon-Bonnefond, C.; Camarasa, C.; Moutounet, M.; Salmon, J. M. Etat des connaissances scientifiques actuelles sur le phénomène d'autolyse des levures et l'élevage des vins sur lies. *J. Int. Sci. Vigne Vin* **2001**, *35*, 57−78.
(167) Babayan, T. L.; Bezrukov, M. G. Autolysis in yeast. *Acta Biotechnol.* **1985**, 129−136.
(168) Alexandre, H.; Guilloux-Benatier, M. Yeast autolysis in sparkling wine. *Aust. J. Grape Wine Res.* **2006**, *12*, 119−127.
(169) Todd, B.; Fleet, G. H.; Henschke, P. A. Promotion of autolysis through the interaction of killer and sensitive yeasts: potential application in sparkling wine production. *Am. J. Enol. Vitic.* **2000**, *51*, 65−72.
(170) Feuillat, M.; Charpentier, C. Autolysis of yeasts in Champagne. *Am. J. Enol. Vitic.* **1982**, *33*, 6−13.
(171) Leroy, M. J.; Charpentier, M.; Duteurtre, B.; Feuillat, M.; Charpentier, C. Yeast autolysis during Champagne aging. *Am. J. Enol. Vitic.* **1990**, *41*, 21−28.
(172) Arnold, W. N. The structure of the yeast cell wall. Solubilisation of a marker enzyme, α-fructofuranosidase, by the autolytic system. *J. Biol. Chem.* **1972**, *4*, 1161−1169.
(173) Hien, N. H.; Fleet, G. H. Separation and characterisation of six (1 leads to 3)-β-glucanases from *Saccharomyces cerevisiae*. *J. Bacteriol.* **1983**, *156* (3), 1204−1213.
(174) Rodriguez-Nogales, J. M.; Fernández-Fernández, E.; Gómez, M.; Vila-Crespo, J. Antioxidant properties of sparkling wines produced with β-glucanase and commercial yeast preparations. *J. Food Sci.* **2012**, *77*, C1005−C1010.
(175) Rodriguez-Nogales, J. M.; Fernández-Fernández, E.; Vila-Crespo, J. Effect of the addition of β-glucanase and commercial yeast preparations on the chemical and sensorial characteristics of traditional sparkling wine. *Eur. Food Res. Technol.* **2012**, *235*, 729−744.
(176) Torresi, S.; Frangipane, M. T.; Garzillo, A. M.V.; Massantini, R.; Contini, M. Effects of a β-glucanase enzymatic preparation on yeast

DOI: 10.1021/jf504268u
J. Agric. Food Chem. 2015, 63, 19−38

lysis during aging of traditional sparkling wines. *Food Res. Int.* **2014**, *55*, 83−92.
(177) Molnar, I.; Oura, E.; Suomalainen, H. Study of the volatile substances produced during the autolysis of Champagne yeasts. *Acta Aliment.* **1981**, *10*, 27−36.
(178) Martinez-Rodriguez, A. J.; Carrascosa, A. V.; Barcenilla, J. M.; Pozo-Bayon, M. A.; Polo, M. C. Autolytic capacity and foam analysis as additional criteria for the selection of yeast strains for sparkling wine production. *Food Microbiol.* **2001**, *18*, 183−191.
(179) Nunez, Y. P.; Carrascosa, A. V.; Gonzalez, R.; Polo, M. C.; Martinez-Rodriguez, A. J. Effect of accelerated autolysis of yeast on the composition and foaming properties of sparkling wines elaborated by a Champenoise method. *J. Agric. Food Chem.* **2005**, *53*, 7232−7237.
(180) Moreno-Arribas, V.; Pueyo, E.; Polo, M. C. Peptides in musts and wines. Changes during the manufacture of cavas (sparkling wines). *J. Agric. Food Chem.* **1996**, *44*, 3783−3788.
(181) Moreno-Arribas, V.; Pueyo, E.; Polo, M. C.; Martin-Alvarez, P. J. Changes in the amino acid composition of the different nitrogenous fractions during the aging of wine with yeasts. *J. Agric. Food Chem.* **1998**, *46*, 4042−4051.
(182) Martinez-Rodriguez, A. J.; Polo, M. C. Characterisation of the nitrogen compounds released during yeast autolysis in a model wine system. *J. Agric. Food Chem.* **2000**, *48*, 1081−1085.
(183) Moreno-Arribas, M. V.; Bartolomé, B.; Pueyo, E.; Polo, M. C. Isolation and characterisation of individual peptides from wine. *J. Agric. Food Chem.* **1998**, *46*, 3422−3425.
(184) Martínez-Lapuente, L.; Guadalupe, Z.; Ayestarána, B.; Pérez-Magariño, S. Role of major wine constituents in the foam properties of white and rosé sparkling wines. *Food Chem.* **2014**, DOI: 10.1016/j.foodchem.2014.10.080.
(185) Pham, T. T.; Guichard, E.; Schlich, P.; Charpentier, C. Optimal conditions for the formation of sotolon from α-cetobutyric acid in the French "Vin Jaune". *J. Agric. Food Chem.* **1995**, *43*, 2616−2619.
(186) Francioli, S.; Torrens, J.; Riu-Aumatell, M.; Lopez-Tamanez, E.; Buxaderas, S. Volatile compounds by SPME-GC as age markers of sparkling wines. *Am. J. Enol. Vitic.* **2003**, *54*, 158−162.
(187) Moreno-Arribas, V.; Pueyo, E.; Nieto, F. J.; Martin-Alvarez, P. J.; Polo, M. C. Influence of the polysaccharides and the nitrogen compounds on foaming properties of sparkling wines. *Food Chem.* **2000**, *70*, 309−317.
(188) Malvy, J.; Robillard, B.; Duteurtre, B. Influence des protéines sur le comportement de la mousse des vins de Champagne. *Sci. Aliment.* **1994**, *14*, 87−98.
(189) Charpentier, C. Yeast autolysis and yeast macromolecules? Their contribution to wine flavour and stability. *Am. J. Enol. Vitic.* **2000**, *51*, 271−275.
(190) Brissonnet, F.; Maujean, A. Identification of some foam active compounds in Champagne base wines. *Am. J. Enol. Vitic.* **1991**, *42*, 97−102.
(191) Forss, D. A. Role of lipids in flavours. *J. Agric. Food Chem.* **1969**, *17*, 681−685.
(192) Troton, D.; Charpentier, M.; Robillard, B.; Calvayrac, R.; Duteurtre, B. Evolution of the lipid contents of Champagne wine during the second fermentation of *Saccharomyces cerevisiae*. *Am. J. Enol. Vitic.* **1989**, *40*, 175−182.
(193) Piton, F.; Charpentier, M.; Troton, D. Cell wall and lipid changes in *Saccharomyces cerevisiae* during ageing of Champagne wine. *Am. J. Enol. Vitic.* **1998**, *39*, 221−226.
(194) Dussaud, A.; Robillard, B.; Carles, B.; Duteurtre, B. Exogenous lipids and ethanol influences on the foam behaviour of sparkling base wines. *J. Food Sci.* **1994**, *59*, 148−151.
(195) Gallart, M.; Lopez-Tamames, E.; Suberbiola, G.; Buxaderas, S. Influence of fatty acids on wine foaming. *J. Agric. Food Chem.* **2002**, *50*, 7042−7045.
(196) Aussenac, J.; Chassagne, D.; Claparol, C.; Charpentier, M.; Duteurtre, B.; Feuillat, M.; Charpentier, C. Purification method for the isolation of monophosphate nucleotides from Champagne wine and their identification by mass spectrometry. *J. Chromatogr., A* **2001**, *907*, 155−164.
(197) Charpentier, C.; Aussenac, J.; Charpentier, M.; Prome, J. C.; Duteurtre, B.; Feuillat, M. Release of nucleotides and nucleosides during yeast autolysis: kinetics and potential impact on flavor. *J. Agric. Food Chem.* **2005**, *53*, 3000−3007.
(198) Tudela, R.; Riu-Aumatell, M.; Castellari, M.; Buxaderas, S.; Lopez-Tamames, E. Changes in RNA catabolites of sparkling wines during the biological aging. *J. Agric. Food Chem.* **2013**, *61*, 6028−6035.
(199) Abbas, C. A. Production of antioxidants, aromas, colours, flavours, and vitamins by yeasts. In *Yeasts in Food and Beverages*; Querol, A., Fleet, G. H., Eds.; Springer: Berlin, Germany, 2006; pp 285−334.
(200) Loyaux, D.; Roger, S.; Adda, J. The evolution of champagne volatiles during aging. *J. Sci. Food Agric.* **1981**, *32*, 1254−1258.
(201) Francoli, S.; Torrens, J.; Riu-Aumatell, M.; Lopez-Tamames, E.; Buxaderas, S. Volatile compounds by SPME-GC as age markers of sparkling wines. *Am. J. Enol. Vitic.* **2003**, *5* (3), 158−162.
(202) Riu-Aumatell, M.; Bosch-Fusté, J.; Lopez-Tamames, E.; Buxaderas, S. Development of volatile compounds of cava (Spanish sparkling wine) during long ageing time in contact with lees. *Food Chem.* **2006**, *95*, 237−242.
(203) Bautista, R.; Fernandez, E.; Falque, E. Effect of the contact with fermentation lees or commercial lees on the volatile composition of white wines. *Eur. Food Res. Technol.* **2007**, *244*, 405−413.
(204) Serra-Cayuela, A.; Castellari, M.; Bosch-Fuste, J.; Riu-Aumatell, M.; Buxaderas, S.; Lopez-Tamames, E. Identification of 5-hydroxymethyl-2-furfural (5-HMF) in cava sparkling wines by LC-DAD-MS/MS and NMR spectrometry. *Food Chem.* **2013**, *141*, 3373−3380.
(205) Van Boekel, M. A. J. S. Formation of flavour compounds in the Maillard Reaction. *Biotechnol. Adv.* **2006**, *24*, 230−233.
(206) Villamiel, M.; Del Castillo, M. D.; Corzo, N. Browning reactions. In *Food Biochemistry and Food Processing*; Yui, Y. H., Nipe, W.-K., Nollet, L. M. L., Paliyath, G., Simpson, B. K., Eds.; Wiley-Blackwell: Oxford, UK, 2006.
(207) Gramona, J. Autolysis and its importance on the sensory qualities of sparkling wines made with the traditional method. Presented at the 2nd International Sparkling Wine Symposium, Denbies Estate, Surrey, UK; Goode, J., Ed.; Flavour Press: UK, 2011; pp 59−64.
(208) Mendes, B.; Gonclaves, J.; Camara, J. Effectiveness of high through-put miniaturised sorbent- and solid phase micro-extraction techniques combined with gas chromatography-mass spectrometry analysis for a rapid screening of volatile and semi-volatile composition of wines − a comparative study. *Talanta* **2012**, *88*, 79−94.
(209) Paravisini, L.; Gourrat-Pernin, K.; Gouttefangeas, C.; Moretton, C.; Nigay, H.; Dacremont, C.; Guichard, E. Identification of compounds responsible for the odorant properties of aromatic caramel. *Flavour Fragance J.* **2012**, *27*, 424−432.
(210) Fedrizzi, B.; Magno, F.; Finato, F.; Versini, G. Variation of fermentative sulfur compounds in Italian "Millesieme" classic sparkling wines during aging and storage on lees. *J. Agric. Food Chem.* **2010**, *58*, 9716−9722.
(211) Tominaga, T.; Nicolass, Y.; Frerot, E.; Dubourdieu, D. Stereoisometric distribution of 3-mecaptoheaxan-1-ol and 3-mercatohexyl acetate in dry and sweet white wines made from *Vitis vinifera* (var. Sauvignon blanc and Semillon). *J. Agric. Food Chem.* **2006**, *4*, 7251−7255.
(212) Berovic, M.; Berlot, M.; Kralj, S.; Makovec, D. A new method for the rapid separation of magnetised yeast in sparkling wine. *Biochem. Eng. J.* **2014**, *88*, 77−84.
(213) Marks, A. C.; Morris, J. R. Ascorbic acid effects on the post-disgorgement oxidative stability of sparkling wine. *Am. J. Enol. Vitic.* **1993**, *44* (2), 227−231.
(214) Kwiatkowski, M. J.; Skouroumounis, K. A.; Waters, E. The impact of closures, including screw cap with three different HS volumes, on the composition, colour and sensory properties of a Cabernet Sauvignon wine during two years' storage. *Aust. J. Grape Wine Res.* **2007**, *13*, 81−94.
(215) Lopes, P.; Silva, M. A.; Pons, A.; Tominaga, T.; Lavigne, V.; Saucier, C.; Darriet, P.; Teissedre, P. L.; Dubourdieu, D. Impact of

DOI: 10.1021/jf504268u
J. Agric. Food Chem. 2015, 63, 19−38

oxygen dissolved at bottling and transmitted through closures on the composition and sensory properties of a Sauvignon blanc wine during bottle storage. *J. Agric. Food Chem.* **2009**, *57*, 10261−10270.
(216) Casey, J. Controversies about corks. *Aust. N. Z. Grapegrower Winemaker* **1993**, *375*, 68−74.
(217) Salgues, M. The UK sparkling wine project: strategy and recommendations. Presented at the 1st International Sparkling Wine Symposium, Denbies Estate, Surrey, UK; Goode, J., Ed.; Flavour Press: UK, 2009; pp 24−30.
(218) Casey, J. Is cork a good seal for wine? *Aust. N. Z. Grapegrower Winemaker* **1994**, *372*, 37−41.
(219) Casey, J. The 'random oxidation' myth. *Aust. N. Z. Grapegrower Winemaker* **2009**, *548*, 77−81.
(220) Brevot, M.; Labbé, J.; Viaux, L.; Bournérias, P.-Y.; Marcoult, A.; Robillard, B. Mastering oxygen at bottle stage − a proposal for sparkling wine. Presented at the 13th Australian Wine Industry Technical Conference, Adelaide, Australia, June 2007.
(221) Robillard, B.; Liger Belair, G. Les gaz dans la bouteille. Part 1/2. *Rev. Œnol.* **2007**, *122*, 39−42.
(222) Liger Belair, G.; Robillard, B. Les gaz dans la bouteille. Part 2/2. *Rev. Œnol.* **2008**, *126*, 33−35.
(223) Sarlin, T.; Nakari-Setala, T.; Linder, M.; Penttila, M.; Haikara, A. Fungal hydrophobins as predictors of the gushing activity of malt. *J. Inst. Brew.* **2005**, *111* (2), 105−111.
(224) Sarlin, T. Detection and characterisation of Fusarium hydrophobins inducing gushing in beer. Ph.D. thesis, University School of Chemical Technology, Espoo, Finland, 2012; 82 pp.
(225) Shokribousjein, Z.; Deckers, S. M.; Gebuers, K.; Lorgouilloux, Y.; Baggerman, G.; Verachtert, H.; declour, J. A.; Etienne, P.; Rock, J. M.; Michiels, C.; Derdelinckx, G. Review: Hydrophobins, beer foaming and gushing. *Cerevisia* **2011**, *35*, 85−101.
(226) Liger-Belair, G.; Barbier, J.-E.; Polidori, G.; Chaudruc, D.; Robillard, B. Le gerbage des vins effervescents. Part 1/2. L'origine du phénomène et quelques solutions pratiques pour y remédier. *Rev. Œnol.* **2013**, *39* (147), 47−52.
(227) Liger-Belair, G.; Barbier, J. E.; Robillard, B. Le gerbage des vins effervescents. Part 2/2. Vers la construction d'un modèle théorique. *Rev. Œnol.* **2013**, *39* (148), 46−48.
(228) Basco, L.; Veiga-Crespo, P.; Sánchez-Pérez, A.; Villa, T. G. FPG1, a gene involved in foam formation in *Saccharomyces cerevisiae*. *Yeast* **2011**, *28*, 437−451.
(229) Basco, L.; Veiga-Crespo, P.; Sánchez-Pérez, A.; Villa, T. G. Cloning and characterisation of the beer foaming gene *CFG1* from *Saccharyomces pastorianus*. *J. Agric Food Chem.* **2012**, *60*, 10796−10807.
(230) Robillard, B. The use of jetting technology for a better quality management at bottle (disgorging) stage. Presented at the 1st International Sparkling Wine Symposium, Denbies Estate, Surrey, UK; Goode, J., Ed.; Flavour Press: UK, 2009; pp 85−90.
(231) Robillard, B.; Bournerias, P. Y. The use of "jetting" technology for better quality management at bottle stage. Presented at the International Cool Climate Symposium (ICCS), Hobart, Tasmania, Australia, Jan 31−Feb 4, 2012.
(232) Hogan, C.; Kemp, B.; Xu, S.; Inglis, D.; McFadden-Smith, W. The effect of wine-based *dosage* solutions on the volatile aroma composition and flavour of Ontario sparkling wine. Presented at the 65th ASEV National Conference, Austin, TX, USA, 2014; 126 pp.
(233) Nisbet, M. A.; Tobias, J.; Brenna, J. T.; Sacks, G.; Mansfield, A. K. Quantifying the contribution of grape hexoses to wine volatiles by high-precision [$U_{13}C$]-glucose tracer studies. *J. Agric. Food Chem.* **2014**, *62* (28), 6820−6827.
(234) Wilker, K. Hydrolysis of sucrose in eastern U.S. table wines. *Am. J. Enol. Vitic.* **1992**, *43* (4), 81−383.
(235) Tominaga, T.; Guimbertau, G.; Dubourdieu, D. Role of certain volatile thiols in the bouquet of aged Champagne wines. *J. Agric. Food Chem.* **2003**, *51*, 1016−1020.
(236) Du Toit, W.; Marais, J.; Pretorius, I.; du Toit, M. Oxygen in must and wine: a review. *S. Afr. J. Enol. Vitic.* **2006**, *27* (1), 76−94.
(237) Oliveira, C. C.; Silva Ferreira, A. C.; De Freitas, V.; Silva, A. M. S. Oxidation mechanisms occurring in wine. *Food Res. Int.* **2011**, *44*, 1115−1126.
(238) Buxaderas, S.; López-Tamames, E. Managing the quality of sparkling wine. *Managing Wine Quality, Vol. 2: Viticulture and Wine Quality*; Reynolds, A., Ed.; Woodhead Food Series: Canada, 2010; pp 553−588.
(239) Hardy, G. Production methods in Champagne. Presented at the 1989 New York Sparkling Wine Symposium; Henick-Kling, T., Baroody, E., Woodbury, R., Eds.; New York State Agricultural Experimental Station, Geneva, NY, 1991; pp 23−27.
(240) Harrar, V.; Smith, B.; Deroy, O.; Spence, C. Grape expectations: how the proportion of white grapes in Champagne affects ratings of experts and social drinkers in a blind tasting. *Flavour* **2013**, *2* (25), 1−10.
(241) Francis, I.; Newton, J. Determining wine aroma from compositional data. *Aust. J. Grape Wine Res.* **2005**, *11*, 114−126.
(242) Obiols, J. M.; de la Presa-Owens, C.; Buxadreas, S.; Bori, J. L.; de la Torre-Boronet, M. C. Protocol d'avaluació de la formació d'efervescéncia I escuma en vins escumoses. *ACE Rev. Enol.* **1998**, *15*, 3−8.
(243) González-San José, M. L.; Oretga-Heras, M.; Pérez-Marariño, S. Micro-oxygenation treatment and sensory properties of young red wines. *Food Sci. Technol. Int.* **2008**, *14*, 123−130.
(244) Gallart, M.; Tomás, X.; Suberiola, G.; López-Tamames, E.; Buxaderas, S. Relationship between foam parameters obtained by the gas-sparging method and sensory evaluation of sparkling wines. *J. Sci. Food Agric.* **2004**, *84*, 127−133.
(245) Vannier, A.; Brun, O. X.; Feinberg, M. H. Application of sensory analysis to champagne wine characterisation and discrimination. *Food Qual. Pref.* **1999**, *10*, 101−107.

DOI: 10.1021/jf504268u
J. Agric. Food Chem. 2015, 63, 19−38

JOURNAL OF AGRICULTURAL AND FOOD CHEMISTRY

Letter

pubs.acs.org/JAFC

Colorimetric Assay for Heterogeneous-Catalyzed Lipase Activity: Enzyme-Regulated Gold Nanoparticle Aggregation

ABSTRACT: Lipase is a neglected enzyme in the field of gold nanoparticle-based enzyme assays. This paper reports a novel colorimetric probe to rapidly visualize lipase activities by using Tween 20 functioned GNPs (Tween 20-GNPs) as a reporter. The present strategy hence could overcome the limitations caused by the heterogeneous interface in lipase assay. Catalytic hydrolytic cleavage of the ester bond in Tween 20-GNPs by lipase will trigger the rapid aggregation of GNPs at a high salt solution. The color change from red to purple could be used to sense the activity of lipase. The detection limit (3σ) is as low as 2.8×10^{-2} mg/mL. A preliminary enzyme activity screening was carried out for seven commercially purchased lipase samples. It also has been successfully applied to detecting lipase in fermentation broth of *Bacillus subtilis* without any pretreatment.

KEYWORDS: *assays, enzymes, gold nanoparticles, tween 20*

INTRODUCTION

Lipases constitute the most important groups of biocatalysts for biotechnological applications, such as the synthesis of pharmaceuticals, agrochemicals, flavouring compounds, biopolymers, and biodiesel.[1−6] Developing technically simple yet effective assays for real-time lipase activity is of critical importance both for the industrial lipases optimization and for the drug discovery and medical diagnosis of diseases. In traditional lipase engineering, fluorogenic or chromogenic substrates and indicator assays have been used as the main screening tool.[7−9]

Gold nanoparticles (GNPs) have been used for a variety of enzyme assays.[10−17] In particular, GNP-based colorimetric assays have become excellent candidates for in vitro measurements[18] because of simple and rapid measurement, cheap instrumentation, robustness, and potential for high-throughput assay.

In the field of GNP-based enzyme assays, the lipase activity assay is still virgin ground.[19,20] Unlike the bond-cleaving enzymes, such as protease or endonuclease which work in homogeneous aqueous phase, the lipases are one such class of enzymes that catalyze hydrolysis of hydrophobic substrates at the lipid−water interface. The assay for lipase is complicated by difficulties associated with emulsifying the lipid substrates, which often produce signal interference and/or compound−lipid interactions.[21]

Tween 20 (polysorbates 20) is an amphipathic, nonionic surfactant composed of fatty acid esters of polyoxyethylene sorbitan monolaurate, the stability, biocompatibility, and relative nontoxicity of which allow it to be used as emulsifier in a number of scientific and pharmacological applications.[22,23] Although Tween 20 was previously investigated, such as in stabilizing gold nanoparticles,[24−28] and in synthesis nanomaterial,[29,30] as well as in turbidimetric assay of lipolytic enzymes,[31] no work has reported their multifunctional roles in the fabrication of GNP-based probe for lipase activity.

Herein, we developed a GNP-based colorimetric assay, which allows real-time measurement of lipase activity/kinetics. The presented strategy exploits the multifunctional properties of Tween 20 as an amphiphilic stabilizing agent as well as substrate for lipase and hence could overcome the limitations caused by the lipid−water interface in lipase assay. By using Tween 20-modified gold nanoparticles (Tween 20-GNPs) as substrate, the system can easily perform in homogeneous phase like the bond-cleaving enzymes did. It exhibits the possibility of overcoming the limitations of traditional lipase assay caused by lipid−water interface. To our knowledge, this is the first use of Tween 20-GNPs as colorimetric indicators to evaluate lipase activity. We believe that the research of screening lipase activity would not only broaden the spectrum of GNP-based enzyme assays but also stimulate the development of GNP-based assays for new targets.

Colorimetric lipase activity assay was performed under the following procedures. The lipases with different activities were added to the above Tween 20-GNP solution consisting of PBS (20 μL, 0.5 M, pH 6.5) and NaCl (50 μL, 2 M). Immediately, the mixture solutions were incubated at 50 °C for 5 min, and the UV−vis spectra were recorded.

For real sample detections, we conducted a preliminary screening using the developed strategy to test the activity of seven commercial purchased lipase samples (BCL, CRL, PPL, RNL, ANL, TLL, and PCL). We also evaluated whether Tween 20-GNPs would respond to lipase in living bacterial cells using inactivated and activated fermentation broth of *Bacillus subtilis*.

RESULTS AND DISCUSSION

Scheme 1 describes the sensing mechanism employed in this study. The GNPs were modified by Tween 20. We used Tween 20 here to act not only as the substrate for lipase but also as the stabilizer for GNPs. Tween 20-GNPs are stable at high salt concentrations (e.g., 0.1 M NaCl) because of the electrostatic and steric stabilization provided by tethered negatively charged Tween 20 polymers. The hydrolytic cleavage of the ester bond in Tween 20 catalyzed by lipase will trigger the rapid aggregation of GNPs at the same salt solution. The color change from red to purple associated with this event can therefore be used to sense the activity of the lipase.

The UV−vis spectroscopy was monitored to reveal the functional roles of Tween 20 in the assay. As shown in Figure 1, GNPs in aqueous solution were monodispersed (Eppendorf

Received: November 5, 2014
Revised: December 14, 2014
Accepted: December 17, 2014
Published: December 17, 2014

ACS Publications © 2014 American Chemical Society

DOI: 10.1021/jf505339q
J. Agric. Food Chem. 2015, 63, 39−42

Scheme 1. Schematic Illustration of the Mechanism of Sensing the Activtiy of Lipase Based on Tween 20-GNPs

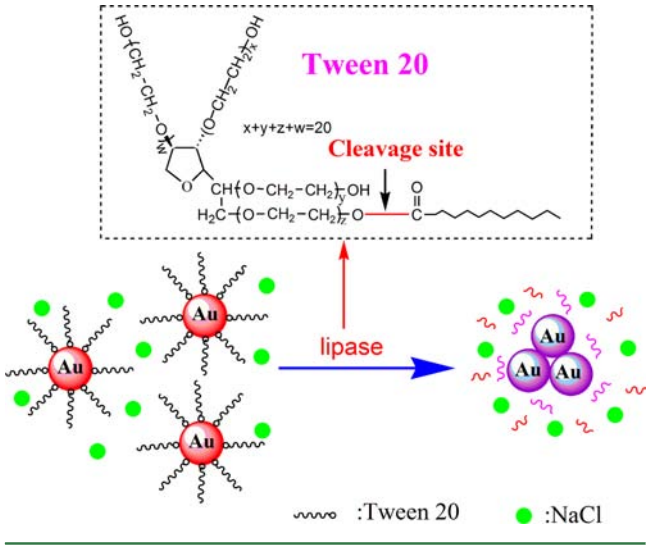

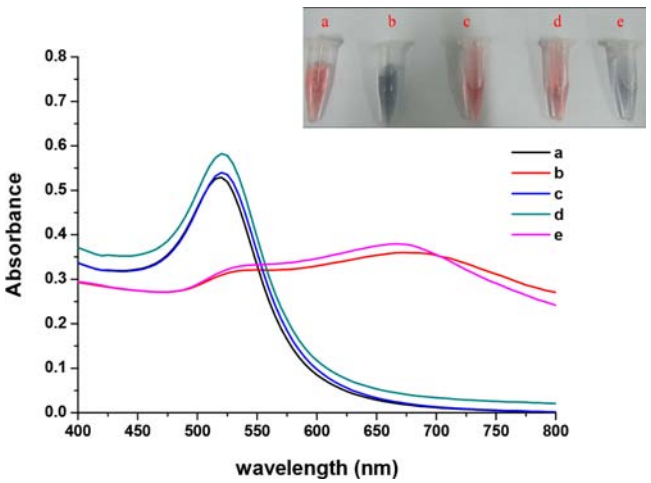

Figure 1. UV−vis spectra of solutions of (a) GNPs in aqueous solution, (b) GNPs, in 0.1 M NaCl, (c) Tween 20-GNPs, 0.1 M NaCl, (d) Tween 20-GNPs, 0.1 M NaCl, and 2 mg inactivated lipase, and (e) Tween 20-GNPs, 0.1 M NaCl, and 2 mg lipase. The phosphate in solution is at pH 6.5, and the incubation time is 5 min. (Inset) Corresponding visual color of these solutions.

tube a, curve a), and they aggregated in 0.1 M NaCl (Eppendorf tube b, curve b). However, for Tween 20-GNP solution, the position of the SPR maxima exhibited almost no change, indicating that the steric repulsion of Tween 20 can resist high salt strength (Eppendorf tube c, curve c). This result is consistent with previous reports that Tween 20 can be adsorbed onto the surface of GNPs to shield the citrate ions and prevent the aggregation of GNPs.[32−35] The addition of lipase can result in the aggregation of Tween 20-GNPs due to the catalysis of hydrolytic Tween 20 on the surface of GNPs (Eppendorf tube e, curve e). In the case of inactivated lipase, which was deactivated in high temperature (100 °C), there is no color change and no peak red shift (Eppendorf tube, curve d), demonstrating that the lipase catalysis cleavage of the ester bond in Tween 20 causes the GNP aggregation. The aggregation of the Tween 20-GNPs was also confirmed by TEM (Supporting Information, Figure S1).

Effects of salt concentration, Tween 20 concentration, GNP size, pH, and reaction temperature were investigated. The ratio value (E_{650}/E_{520}) of the extinction is used to quantify the aggregation process or color change. The optimal detection conditions for salt concentration, Tween 20 concentration, GNP size, pH, and reaction temperature were 0.1 M NaCl, 82.28 μM, 13 nm, 6.5, and 50 °C, respectively, for sensitive and rapid detection (Supporting Information, Figures S2 and S3). This result is also confirmed by zeta-potential experiments. The zeta potentials of Tween 20-GNP solution without NaCl were found to be −9.86 ± 0.50 and −3.52 ± 0.65 mV with 0.1 M NaCl, indicating that the electrostatic repulsion between Tween 20-GNPs was screened by NaCl.

Kinetic studies of the color change in the presence of various amounts of lipase were carried out (Supporting Information, Figure S4). It was found that the rate of color change was directly related to the amount of lipase used in the assay; faster color changes were observed when more lipase was used. The red shift was found to gradually increase on the lipase concentration (Figure 2A) and the rate of color change was directly related to the amount of lipase used in the assay. According to the calibration curve (Figure 2B), the response to the increasing amounts of lipase was linear in the range of from 0.15 to 1.80 mg/mL (R^2 = 0.9934). The detection limit (3σ) of this assay is as low as 2.8 × 10^{-2} mg/mL. One important feature of this assay is that the color change is sensitive and rapid. A comparison was made between our system and

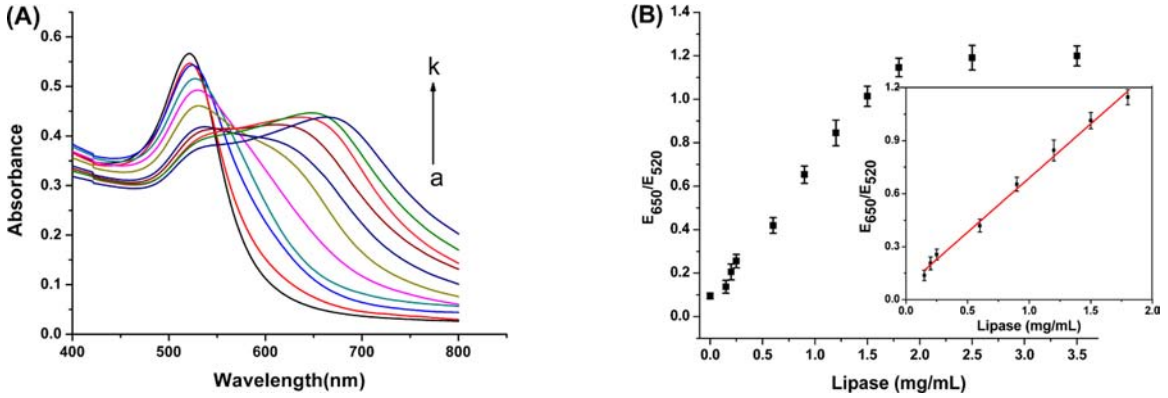

Figure 2. (A) UV−vis spectra of Tween 20-GNPs in the presence of different concentrations of lipase: (a) 0 mg/mL; (b) 0.15 mg/mL; (c) 0.2 mg/mL; (d) 0.25 mg/mL; (e) 0.6 mg/mL; (f) 0.9 mg/mL; (g) 1.2 mg/mL; (h) 1.5 mg/mL; (i) 1.8 mg/mL; (j) 2.5 mg/mL; (k) 3.5 mg/mL. (B) Calibration curve of E_{650}/E_{520} versus the concentration of lipase. (Inset) Expanded linear region.

DOI: 10.1021/jf505339q
J. Agric. Food Chem. 2015, 63, 39−42

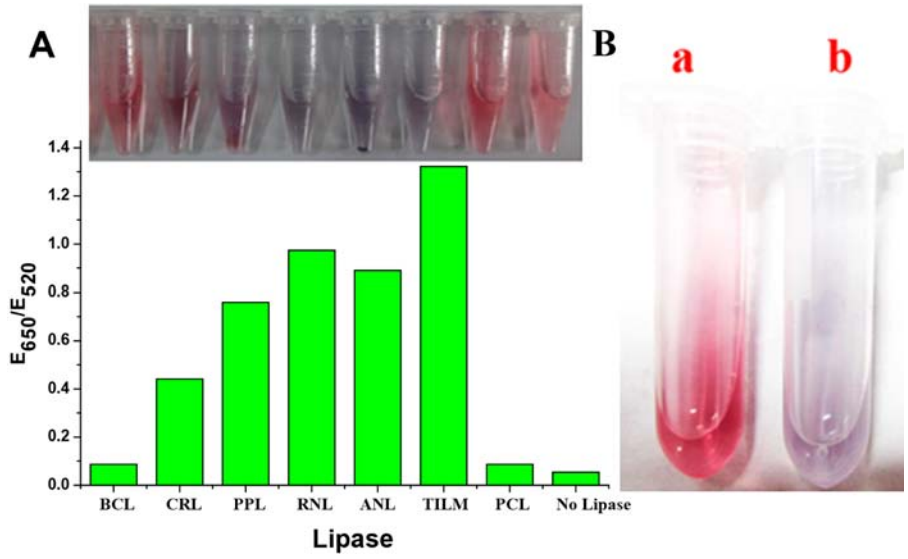

Figure 3. (A) Plot of E_{650}/E_{520} intensity of Tween 20-GNPs upon the addition of a fixed concentration (1 mg/mL) of commercial lipase samples, respectively, and within a interval of 10 min. (Inset) Corresponding visual color. (B) Visual color of Tween 20-AuNP solutions upon adding (a) inactivated and (b) activated fermentation broth of *Bacillus subtilis* after 10 min of incubation.

turbidimetric assay for lipase activity using Tween 20 as substrate.[31] The results showed that at the same lipase concentration our system is 1000 times more sensitive than the turbidimetric assay. The time to reach maximum color change was just 5 min in our system, whereas the turbidimetric assays required around 30 min (Supporting Information, Figure S5).

A preliminary screening was carried out using this system to test the activities of seven commercial purchased lipase samples (BCL, CRL, PPL, RNL, ANL, TLL, and PCL). The color and the E_{650}/E_{520} value of Tween 20-GNP solution in the presence of a fixed concentration (1 mg/mL) of lipase samples were monitored, respectively, within a fixed time interval. As shown in Figure 3A, Tween 20-GNPs incubated with TLL, ANL, and RNL led to significant color changes, whereas with PCL and BCL no color changes were observed. Moreover, the different color changes (violet blue in TLL, ANL, and RNL and reddish purple in CRL and PPL) were attributed to the different lipase activities. With UV−vis spectroscopy quantitative detection, we conclude that the lipase activity decreases in the following order: TLL > RNL > ANL > PPL > CRL > BCL > PCL. This order is consistent with the results detected with a pH-stat method (Supporting Information, Table S1), demonstrating the possibility that the colorimetric assay protocol can be used as an alternative to conventional methods for a sensitive assay of lipase activity.

The assay was also applied to fermentation broth of *B. subtilis*. The supernatant of the crude sample without any pretreatment was incubated with Tween 20-GNPs. A pronounced color change from red to blue was observed (Figure 3B-b), but inactivated sample solution, which was deactivated by boiling, did not lead to any color change (Figure 3B-a). This shows that the Tween 20-GNPs system provides a particularly useful probing approach for real samples that usually have significant background activities, which might cause false-positive signals during the measurements. The new Tween 20-GNP colorimetric assay has potential in the routine quantification of lipase in biochemistry industrial and medical applications.

In conclusion, we have developed a new colorimetric assay for screening lipase activity; it does not require specific instrumentation or complicated experimental steps. Furthermore, as opposed to a fluorogenic or chromogenic derivative of the substrate, it is desirable to carry out the assay without emulsification.

Wei Zhang[†]
Yan Tang[†]
Jia Liu[†]
Ling Jiang[‡]
Wei Huang[#]
Feng-Wei Huo*[,#,§]
Danbi Tian*[,†]

[†]College of Science, [‡]College of Food Science and Light Industry, and [#]Key Laboratory for Flexible Electronics and Institute of Advanced Materials (IAM), National Synergistic Innovation Center for Advanced Materials (SICAM), Nanjing Tech University, Nanjing 211816, China

[§]School of Materials Science and Engineering, Nan yang Technological University, 50 Nan yang Avenue, 639798 Singapore

■ ASSOCIATED CONTENT

Supporting Information

Materials and methods, Figures S1−S5, and Table S1. This material is available free of charge via the Internet at http://pubs.acs.org.

■ AUTHOR INFORMATION

Corresponding Authors

*(D.T.) E-mail: danbi@njtech.edu.cn. Phone/fax: +86 25 86210899.

*(F.-W.H.) E-mail: fwhuo@ntu.edu.sg. Phone: (+65) 6316-8921. Fax: (+65) 6790-9081.

Funding

This work was supported by the Natural Science Foundation of Jiangsu Province, China (No. BK2012822), the National

DOI: 10.1021/jf505339q
J. Agric. Food Chem. 2015, 63, 39−42

Science Foundation for Distinguished Young Scholars of China (No. 21225626), the National High Technology Research, Development Program of China (No. 2012AA021700), and the National Natural Science Foundation of China for Young Scholars (No. 21106064).

Notes

The authors declare no competing financial interest.

■ ACKNOWLEDGMENTS

We appreciate Jiangsu province college students' practice and innovation training platform.

■ REFERENCES

(1) Yang, G.; Wu, J.; Xu, G.; Yang, L. Comparative study of properties of immobilized lipase onto glutaraldehyde-activated amino-silica gel via different methods. *Colloid Surf. B* **2010**, *78*, 351−356.

(2) Shah, S.; Gupta, M. N. Lipase catalyzed preparation of biodiesel from jatropha oil in a solvent free system. *Process Biochem.* **2007**, *42*, 409−414.

(3) Gupta, R.; Gupta, N.; Rathi, P. Bacterial lipases: an overview of production, purification and biochemical properties. *Appl. Microbiol. Biotechnol.* **2004**, *64*, 763−781.

(4) Bajaj, A.; Lohan, P.; Jha, P. N.; Mehrotra, R. Biodiesel production through lipase catalyzed transesterification: an overview. *J. Mol. Catal. B−Enzym.* **2010**, *62*, 9−14.

(5) Lu, X.; Luo, Z.; Yu, S.; Fu, X. Lipase-catalyzed synthesis of starch palmitate in mixed ionic liquids. *J. Agric. Food Chem.* **2012**, *60*, 9273−9279.

(6) Chen, B.; Liu, H.; Guo, Z.; Huang, J.; Wang, M.; Xu, X.; Zheng, L. Lipase-catalyzed esterification of ferulic acid with oleyl alcohol in ionic liquid/isooctane binary systems. *J. Agric. Food Chem.* **2011**, *59*, 1256−1263.

(7) Zupan, A.; Trobec, S.; Gaberc-Porekar, V.; Menart, V. High expression of green fluorescent protein in *Pichia pastoris* leads to formation of fluorescent particles. *J. Biotechnol.* **2004**, *109*, 115−112.

(8) Jette, J. F.; Ziomek, E. Determination of lipase activity by a rhodamine-triglyceride-agarose assay. *Anal. Biochem.* **1994**, *219*, 256−260.

(9) Surribas, A.; Resina, D.; Ferrer, P.; Valero, F. Rivoflavin may interfere with on-line monitoring of secreted green fluorescence protein fusion proteins in *Pichia pastoris*. *Microb. Cell Fact.* **2007**, *6*, 15.

(10) Tiwari, N.; Rathore, A.; Prabhune, A.; Kulkarni, S. Gold nanoparticles for colorimetric detection of hydrolysis of antibiotics by penicillin G acylase. *Adv. Biosci. Biotechnol.* **2010**, *1*, 322−329.

(11) Wang, M.; Gu, X.; Zhang, G.; Zhang, D.; Zhu, D. Continuous colorimetric assay for acetylcholinesterase and inhibitor screening with gold nanoparticles. *Langmuir* **2009**, *25*, 2504−2507.

(12) Oishi, J.; Asami, Y.; Mori, T.; Kang, J.-H.; Niidome, T.; Katayama, Y. Colorimetric enzymatic activity assay based on noncrosslinking aggregation of gold nanoparticles induced by adsorption of substrate peptides. *Biomacromolecules* **2008**, *9*, 2301−2308.

(13) Wang, Z.; Lévy, R.; Fernig, D. G.; Brust, M. Kinase-catalyzed modification of gold nanoparticles: a new approach to colorimetric kinase activity screening. *J. Am. Chem. Soc.* **2006**, *128*, 2214−2215.

(14) Baron, R.; Zayats, M.; Willner, I. Dopamine-, L-DOPA-, adrenaline-, and noradrenaline-induced growth of Au nanoparticles: assays for the detection of neurotransmitters and of tyrosinase activity. *Anal. Chem.* **2005**, *77*, 1566−1571.

(15) Xu, X.; Han, M. S.; Mirkin, C. A. A gold-nanoparticle-based real-time colorimetric screening method for endonuclease activity and inhibition. *Angew. Chem., Int. Ed.* **2007**, *119*, 3538−3540.

(16) Zhang, L.; Zhao, J.; Jiang, J.; Yu, R. Enzyme-regulated unmodified gold nanoparticle aggregation: a label free colorimetric assay for rapid and sensitive detection of adenosine deaminase activity and inhibition. *Chem. Commun.* **2012**, *48*, 10996−10998.

(17) Zeng, Z.; Mizukami, S.; Kikuchi, K. Simple and real-time colorimetric assay for glycosidases activity using functionalized gold nanoparticles and its application for inhibitor screening. *Anal. Chem.* **2012**, *84*, 9089−9095.

(18) Xie, X.; Xu, W.; Liu, X. Improving colorimetric assays through protein enzyme-assisted gold nanoparticle amplification. *Acc. Chem. Res.* **2012**, *45*, 1511−1520.

(19) Hutter, E.; Maysinger, D. Gold-nanoparticle-based biosensors for detection of enzyme activity. *Trends Pharmacol. Sci.* **2013**, *34*, 497−507.

(20) Saha, K.; Agasti, S. S.; Kim, C.; Li, X.; Rotello, V. M. Gold nanoparticles in chemical and biological sensing. *Chem. Rev.* **2012**, *112*, 2739−2779.

(21) Tam, J.; Henault, M.; Li, L.; Wang, Z.; Partridge, A. W.; Melnyk, R. A. An activity-based probe for high-throughput measurements of triacylglycerol lipases. *Anal. Biochem.* **2011**, *414*, 254−260.

(22) Duy, J.; Connell, L.; Eck, W.; Collins, S.; Smith, R. Preparation of surfactant-stabilized gold nanoparticle−peptide nucleic acid conjugates. *J. Nanopart. Res.* **2010**, *12*, 2363−2369.

(23) Aslan, K.; Pérez-Luna, V. H. Surface modification of colloidal gold by chemisorption of alkanethiols in the presence of a nonionic surfactant. *Langmuir* **2002**, *18*, 6059−6065.

(24) Zhang, Z.; Zhang, J.; Qu, C.; Pan, D.; Chen, Z.; Chen, L. Label free colorimetric sensing of thiocyanate based on inducing aggregation of Tween 20-stabilized gold nanoparticles. *Analyst* **2012**, *137*, 2682−2686.

(25) Xu, S.; Yuan, H.; Xu, A.; Wang, J.; Wu, L. Rapid synthesis of stable and functional conjugates of DNA/gold nanoparticles mediated by Tween 80. *Langmuir* **2011**, *27*, 13629−13634.

(26) Wu, Z.-H.; Tseng, W.-L. Combined cloud point extraction and Tween 20-stabilized gold nanoparticles for colorimetric assay of silver nanoparticles in environmental water. *Anal. Methods* **2011**, *3*, 2915−2920.

(27) Liu, C.-Y.; Tseng, W.-L. Colorimetric assay for cyanide and cyanogenic glycoside using polysorbate 40-stabilized gold nanoparticles. *Chem. Commun.* **2011**, *47*, 2550−2552.

(28) Zhao, Y.; Wang, Z.; Zhang, W.; Jiang, X. Adsorbed Tween 80 is unique in its ability to improve the stability of gold nanoparticles in solutions of biomolecules. *Nanoscale* **2010**, *2*, 2114−2119.

(29) Hormozi-Nezhad, M. R.; Karami, P.; Robatjazi, H. A simple shape-controlled synthesis of gold nanoparticles using nonionic surfactants. *RSC Adv.* **2013**, *3*, 7726−7732.

(30) Zuaznabar-Gardona, J. C.; Cao, R.; Suarez, M. Vertical self-assembly of modified multiwalled carbon nanotubes on gold surfaces induced by chitosan and Tween. *Chem. Commun.* **2012**, *48*, 1910−1912.

(31) Tigerstrom, R. G. v.; Stelmaschuk, S. The use of Tween 20 in a sensitive turbidimetric assay of lipolytic enzymes. *Can. J. Microbiol.* **1989**, *35*, 511−514.

(32) Ye, Y.; Liu, H.; Yang, L.; Liu, J. Sensitive and selective SERS probe for trivalent chromium detection using citrate attached gold nanoparticles. *Nanoscale* **2012**, *4*, 6442−6448.

(33) Lin, C.-Y.; Yu, C.-J.; Lin, Y.-H.; Tseng, W.-L. Colorimetric sensing of silver(I) and mercury(II) ions based on an assembly of Tween 20-stabilized gold nanoparticles. *Anal. Chem.* **2010**, *82*, 6830−6837.

(34) Li, M.-D.; Tseng, W.-L.; Cheng, T.-L. Ultrasensitive detection of indoleamines by combination of nanoparticle-based extraction with capillary electrophoresis/laser-induced native fluorescence. *J. Chromatogr., A* **2009**, *1216*, 6451−6458.

(35) Kerwin, B. A. Polysorbates 20 and 80 used in the formulation of protein biotherapeutics: structure and degradation pathways. *J. Pharm. Sci.* **2008**, *97*, 2924−2935.

DOI: 10.1021/jf505339q
J. Agric. Food Chem. 2015, 63, 39−42

JOURNAL OF AGRICULTURAL AND FOOD CHEMISTRY

Article

pubs.acs.org/JAFC

Effect of 5-*n*-Alkylresorcinol Extracts from Durum Wheat Whole Grain on the Growth of Fusarium Head Blight (FHB) Causal Agents

Roberto Ciccoritti, Marina Pasquini, Daniela Sgrulletta, and Francesca Nocente*

Consiglio per la Ricerca e la sperimentazione in Agricoltura, Unità di Ricerca per la Valorizzazione Qualitativa dei Cereali (CRA-QCE), Via Cassia 176, 00191 Roma, Italy

ABSTRACT: In an approach toward the identification of ecofriendly compounds for fusarium head blight biocontrol, the in vitro antifungal activity of 5-*n*-alkylresorcinol (AR) extracts, obtained from durum wheat intact kernels, was tested. In comparison with ethyl acetate and acetone extracts containing AR, total inhibition of *Fusarium graminearum* spore germination was observed with cyclohexane extract, which also exhibited a significant fungistatic activity against *F. graminearum*, *Fusarium culmorum*, *Fusarium avenaceum*, and *Fusarium poae*. Additionally, the study of the influence of such variables as predrying of seeds and durum wheat genotype on AR cyclohexane extract properties allowed the association of its highest antifungal activity with the AR homologue composition and, in particular, with the presence of a higher C21:0/C23:0 ratio. The interesting finding of this study suggests a potential application of the AR homologues in crop protection systems and could be an important step toward the development of commercial formulations suitable to the prevention of fungal diseases.

KEYWORDS: *5-n-alkylresorcinols, antifungal activity, AR extraction, AR homologue composition, durum wheat*

INTRODUCTION

Fungal diseases are by far the most serious threat to global crop production and cause heavy losses that can result in enormous socioeconomic hardship. Presently, it has been estimated that each year fungal infections destroy at least 125 million tons of the top five food crops (rice, wheat, maize, potatoes, and soybeans), which provide the majority of calories consumed by people. Among fungal diseases, fusarium head blight (FHB) is considered the most serious disease of common and durum wheat and other small-grain cereals worldwide, resulting in significant quality, safety, and yield reductions. The disease is caused by various filamentous fungi including *Microdochium nivale* and many *Fusarium* species; in Europe *Fusarium graminearum*, *Fusarium culmorum*, *Fusarium avenaceum*, and *Fusarium poae* are predominant.[1,2] Moreover, under favorable environmental conditions, the scabby grain is often contaminated by tricothecene mycotoxins (e.g., deoxynivalenol, T-2, HT-2, and zearalenone), making it unsuitable for human foods or animal feeds.

The control of FHB has relied on the use of resistant varieties and chemical fungicides. As resistant cultivars are very rare, the chemical fungicides have an important role in an integrated FHB control program,[3] but they represent a serious threat leading to disturbed biodiversity, outbreaks of secondary pests, development of resistance in the pathogens, and contamination of the food chain in the ecosystem.[4] In consideration of the environmental and economical implications associated with the use of chemical fungicides, there has been an increased interest in discovering biologically active natural compounds and extracts from higher plants as new classes of pesticides. Plant secondary metabolites, once not considered important compounds, are now thought to mediate chemical defense mechanisms by providing chemical barriers against animal and microbial predators and have enormous potential to inspire and influence modern agrochemical research.[5−8] Among the secondary plant constituents, alkylresorcinols (ARs) and their derivatives are considered to serve as phytoanticipins and allelochemicals, although direct evidence is still lacking.[9] ARs belong to an extensive family of bioactive compounds, referred to as nonisoprenoid phenolic lipids, which occur primarily in plants, fungi, and bacteria.[10] Structurally the 5-*n*-alkylresorcinols of cereals are characterized by two hydroxyl groups, at positions C1 and C3 of the aromatic ring, and a lipophilic alkyl chain at the C5 position. The amphiphilic nature of their structure could be responsible for their ability to interact with biological membranes, nucleic acids, or enzymes[11] and related to their antimicrobial, antiparasitic, antitumor, and antifungal activities.[10−14] In cereal grains, 99% of resorcinolic lipids occur only in an intermediate layer of caryopsis, including the hyaline layer, inner pericarp, and testa and are not detected in other parts of the grain, including endosperm and germ.[15] The localization of ARs at the surface of plant tissues could enhance their protective effect as a chemical barrier to infection; in fact, they are constitutively present in plants, but their biosynthesis may be triggered during seedling stage by fungal infection.[16] Antifungal activity of 5-*n*-alkylresorcinols extracted from rye has been reported against *Aspergillus niger*, *Aspergillus versicolor*, *Penicillium chrysogenum*, *Penicillium roqueforte*, *Rhizoctonia solani*, *Rhizoctonia cerealis*, and *F. culmorum*.[17−19] The resistance of barley seeds to the pathogenic fungi *A. niger* and *P. crysogenum* was attributed to resorcinolic lipids present in the seed epicuticular wax.[20] Alkylresorcinols isolated from etiolated rice seedling showed antifungal activity against spore germination of *Pyricularia oryzae*.[21] The occurrence of 5-*n*-(heptadec-12-enyl) and 5-*n*-pentadecylresorcinols in the peel was considered to be responsible for the resistance of mango fruits to fungal infections

Received: July 11, 2014
Accepted: December 11, 2014
Published: December 11, 2014

ACS Publications © 2014 American Chemical Society

DOI: 10.1021/jf5054518
J. Agric. Food Chem. 2015, 63, 43−50

by *Alternaria alternata*.[22,23] The capability of these natural compounds to inhibit fungal growth could be exploited to control plant diseases, avoiding the presence of fungicidal residues.

This work has been carried out with the aim to evaluate the antifungal activity of durum wheat whole grain extracts containing 5-*n*-alkylresorcinols against four species of *Fusarium* (*F. graminearum* Schwabe, *F. culmorum* (W.G. Smith) Sacc, *F. avenaceum* (Fr.) Sacc., and *F. poae* (Peck) Wollenw.) using in vitro assays. To the best of our knowledge this is the first study that examines the inhibitory effect of different alkylresorcinol extracts on the in vitro vegetative growth of four important *Fusarium* fungi. In addition, the possibility of using these extracts in seed treatment to control *Fusarium* diseases has been evaluated. The effects of variability factors such as the wheat genotype used and the seed-drying process on AR content, relative homologue composition, and antifungal activity of the durum wheat extracts are also discussed.

MATERIALS AND METHODS

Chemicals. All organic solvents used for AR extraction and pyridine were purchased from Carlo Erba (Italy). Methyl behenate (C22:0, methyl docosanoate) and 4-hexylresorcinol (4-hexyl-1,3-dihydroxybenzene) were purchased from Sigma-Aldrich (Milan, Italy). Trimethylchlorosilane (TMCS), which was used to prepare the trimethylsilyl ether derivates of AR extracts, was purchased from Restek (Milan, Italy). Standards 5-*n*-pentadecylresorcinol (C15:0), 5-*n*-heptadecylresorcinol (C17:0), 5-*n*-nonadecylresorcinol (C19:0), 5-*n*-heneicosylresorcinol (C21:0), 5-*n*-tricosylresorcinol (C23:0), and 5-*n*-pentacosylresorcinol (C25:0) were purchased from ReseaLife Chem. Science (Burgdorf, Switzerland).

Plant and Fungal Materials. For AR extraction, experimental plant material consisted of seeds of two commercial durum wheat cultivars, Tirex, grown during the crop years 2012 and 2013, and Simeto, grown during 2013. In addition, cv. Iride was used for the seed treatment with wheat extract for FHB protection. Kernels were kept at 4 °C until extraction and analysis.

Four isolates of *F. graminearum* (Fg_QCE2, Fg_QCE3, Fg_QCE5, Fg_QCE11) and of *F. culmorum* (Fc_QCE1, Fc_QCE2, Fc_QCE3, Fc_QCE7) and one isolate of *F. avenaceum* (Fav_QCE8) and of *F. poae* (Fp_QCE3), collected throughout Italy from infected durum wheat seeds from 2009 to 2011, were maintained and used in this study. Each isolate was cultured on potato dextrose agar (PDA) (Formedium, Hunstanton, UK) supplemented with neomycin and streptomycin sulfate (0.3 g L^{-1}) and incubated at 22 °C with a 12 h photoperiod for 7−14 days. The mycelium was then transferred onto fresh PDA plates and placed under near-ultraviolet for 10 days under 12/12 h alternate cycles of light and darkness to favor sporulation. All *Fusarium* isolates were identified on the basis of conidial morphology[24,25] and PCR analysis using species-specific primers for *F. graminearum*,[26] *F. culmorum*,[27] *F. avenaceum*,[27] and *F. poae*.[28]

For the bioassays, conidia or mycelial disks from 7-day-old cultures were used. Conidial concentration was adjusted with the aid of a hemocytometer to a concentration of 1×10^5 conidia/mL.

Extraction of Alkylresorcinols. Three organic solvents (acetone, ethyl acetate, and cyclohexane) were used to extract ARs from intact kernel at a ratio 1:4 (w/v) by continuous mechanical shaking for 24 h at 28 °C temperature. The extraction was repeated one more time with fresh solvent, and the products of the two consecutive extractions were combined. The extracts were filtered through Whatman no. 42 paper and used for gas chromatography−mass spectrometry (GC-MS) analysis and antifungal assays.

A successive test was carried out to increase AR extraction yield. Briefly, kernels of cultivars Tirex and Simeto (from 2013 harvest) were weighed and placed in a hot air oven at 50, 105, and 130 °C for 90 min and at 105 °C for 180 and 300 min. The decrease in moisture amount was evaluated as weight difference before and after heat treatment. Seeds were immediately used for AR extraction with cyclohexane or acetone as described above.

Chemical Analysis by GC−MS. Total AR content and relative homologue composition in wheat extracts were determined by GC-MS analysis, according to Landberg et al.[29] using 200 μg of methyl behenate as internal standard (IS). AR extracts (10 mL) were dried under nitrogen and silylated with a mixture (400 μL) of pyridine and TMCS (9:1 v/v). The mixture was then shaken and heated at 70 °C for 60 min. GC-MS analysis was performed with the gas chromatograph GC Clarus 600 series coupled to a mass spectrometer Clarus 580D (PerkinElmer, Milan, Italy) equipped with a split/splitless injector, an RTX-5MS column (0.25 mm × 30 m, 0.25 μm film thickness, Restek, Milan, Italy), and a quadrupole mass spectrometer (Clarus 580D, PerkinElmer) operating in electronic impact (EI) ionization mode (70 eV). Helium was used as the carrier gas (1 mL min^{-1}). The column temperature was programmed from 250 to 320 °C (hold for 2 min) at a 3.5 °C min^{-1} heating rate and then to 330 °C at a 1.1 °C min^{-1} heating rate. Ion source and detector temperatures were 250 and 350 °C, respectively. The injector temperature was 325 °C. Total ion current (TIC) mode was used to record the positive ion mass spectra of the samples in the range between m/z 40 and 620. AR homologue content was quantified according to the method of Ross et al.,[30] using a fragment ion m/z 268, which is characteristic for 5-*n*-alkylresorcinol homologues.

Antifungal Activity of AR Extracts. Extracts obtained from cv. Tirex (from 2012 harvest) by using acetone, cyclohexane, and ethyl acetate were evaporated to dryness at 60 °C in a rotary evaporator (Buchi R-114, Switzerland) and redissolved in the respective solvent to obtain 1100 μg/mL ARs. PDA plates (60 mm) were prepared, according to the method of Yin et al.,[31] by spreading 500 μL of acetone, ethyl acetate, or cyclohexane extracts from wheat whole grain, respectively, after solidification of medium (10 mL for plate). Media plates spread with 500 μL of solvents served as controls.

The antifungal activity was evaluated by considering the inhibiting effect of the AR extracts both on spore germination and on mycelial growth.

In the first experiment, 4 μL of a conidial suspension (1×10^5 mL^{-1}) of Fg_QCE2 isolate was used to inoculate the central surface of the plates and incubated in the dark at 22 °C. Three replications were prepared for each treatment, and each treatment was replicated twice. The spore germination was evaluated on the basis of the fungal ability to form a colony at 4 days after inoculation, compared with the control. The colony diameter was measured by electronic digital calliper (0−150 mm), and all values were recorded in two directions at right angles to each other; then the colony average diameter was calculated. Data are expressed as percentage growth inhibition in reference to the growth of untreated control.

Control experiments were carried out under similar conditions by using the standard 4-hexylresorcinol (positive control). A concentrated acetone stock solution of 4-hexylresorcinol was made and progressively diluted to obtain a 1 mg/mL solution. From this solution 10, 50, and 100 μL were brought to a volume of 500 μL with acetone and spread on PDA plates (60 mm).

The three extracts were also bioassayed to test their effect on conidial germination of *F. graminearum* using the method of Belding et al.[32] About 100 μL of the three extracts was applied respectively onto glass coverslips and then air-dried to form a film. Acetone, ethyl acetate, cyclohexane, and sterile distilled water were used as negative control. All of the coverslips were inoculated with 2 μL of 1×10^5 spores mL^{-1} of Fg_QCE2 isolate and placed in the lid of an inverted Petri dish filled with 0.95 M NaCl−2% agar, to maintain the relative humidity (RH) at 97.5% at 22 °C, and the coverslips were positioned about 3 mm below the agar surface. Two coverslips per treatment were used. Petri dishes were then incubated for 18 h in the dark at 22 °C. The number of germinated spores was examined by light microscope.

The second assay was carried out to evaluate the fungistatic activity of cyclohexane extract on the mycelial growth of four isolates of *F. graminearum* and *F. culmorum*, respectively, one isolate of *F. avenaceum*, and one isolate of *F. poae*. One 4 mm diameter plug of each isolate growing on PDA was placed in the center of 60 mm PDA plates, prepared as previously described. The plates were incubated at 22 °C in

DOI: 10.1021/jf5054518
J. Agric. Food Chem. 2015, 63, 43−50

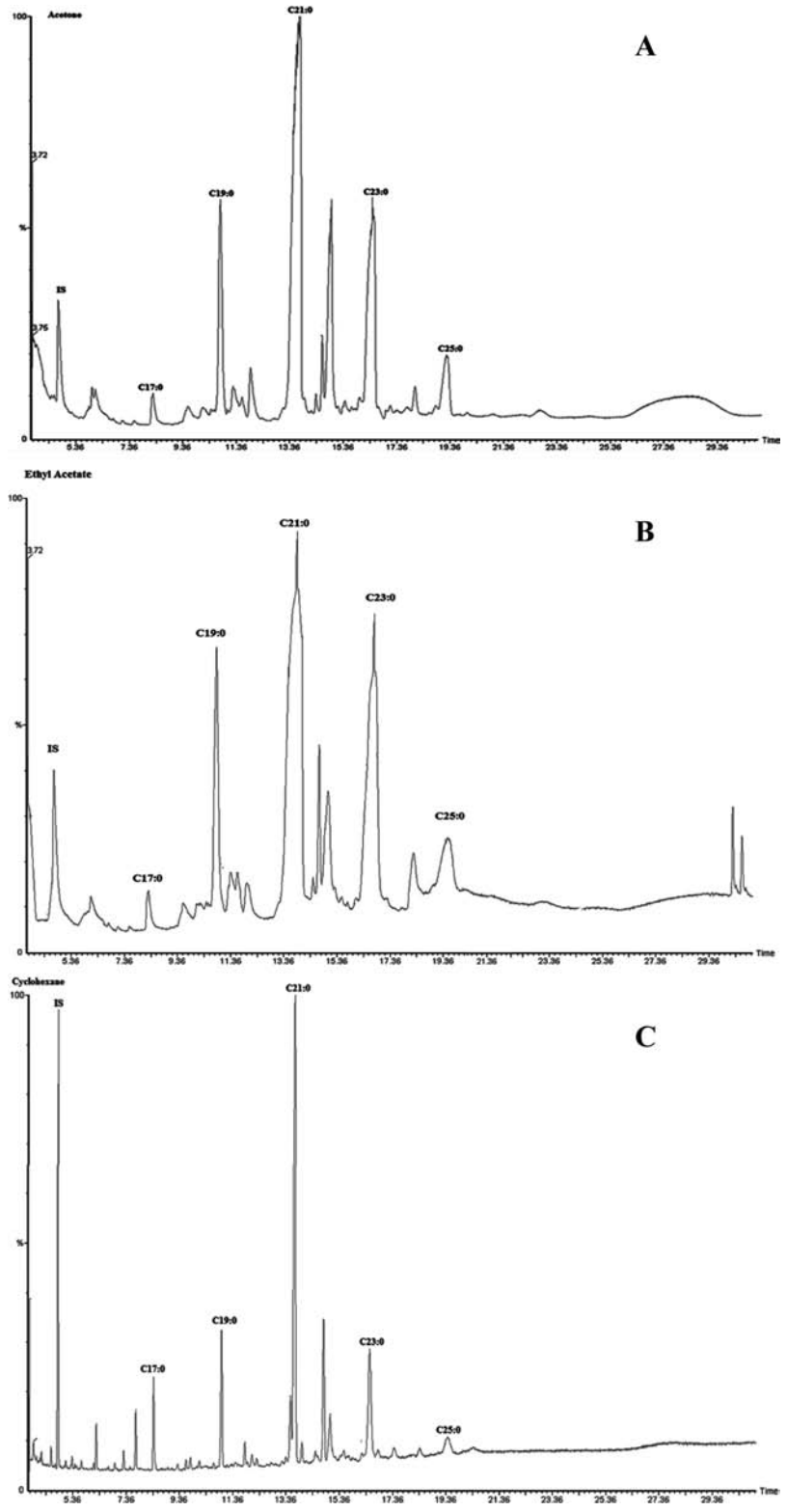

Figure 1. Total ion current (TIC) chromatograms of alkylresorcinols in acetone (A), ethyl acetate (B), and cyclohexane (C) extract from whole durum wheat kernel. Peak identification: IS, internal standard; 1, 5-heptadecylresorcinol C17:0; 2, 5-nonadecylresorcinol, C19:0; 3, 5-heneicosylresorcinol, C21:0; 4, 5-*n*-tricosylresorcinol, C23:0; 5, 5-pentacosylresorcinol, C25:0.

the dark, and at 4 and 6 days after inoculation the colony diameters were measured and the percentage growth inhibition was calculated. Three replications were prepared for each treatment, and each experiment was replicated twice.

Antifungal Activity Assay of Mixtures of Standard Homologue Chains of ARs. Two mixtures of AR homologue chains were obtained by dissolving different quantities of standard homologues in acetone to have 1100 μg/mL total AR. The objective was to reproduce similar qualitative and quantitative compositions in AR homologue in comparison with the natural extracts isolated from durum wheat whole grain by using cyclohexane and acetone solvents.

DOI: 10.1021/jf5054518
J. Agric. Food Chem. 2015, 63, 43−50

Table 1. Total AR Content and Relative Homologue Composition of Cyclohexane, Acetone, and Ethyl Acetate Extracts from Durum Wheat Grain (Mean Value and Standard Deviation)[a]

	homologue composition (%)						
solvent	C15:0	C17:0	C19:0	C21:0	C23:0	C25:0	total AR (μg/g DM)
cyclohexane	nd	0.51 ± 0.10	12.36 ± 0.63	59.91 ± 2.20	21.02 ± 1.21	6.20 ± 0.75	109.44 ± 8.89
acetone	tr	0.69 ± 0.08	18.02 ± 0.78	37.94 ± 2.91	32.80 ± 1.12	10.55 ± 1.85	273.27 ± 30.43
ethyl acetate	tr	1.15 ± 0.09	22.34 ± 0.52	34.98 ± 2.65	30.73 ± 1.44	10.80 ± 1.00	371.30 ± 30.00
LSD		0.86	2.33	4.52	3.06	2.90	10.53

[a]nd, not detected; tr, trace; LSD, least significant difference ($p < 0.05$).

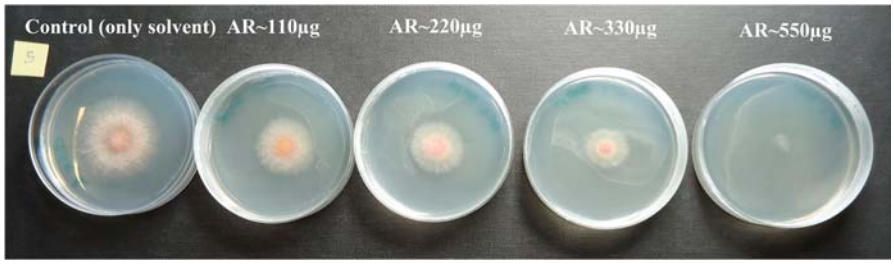

Figure 2. Growth of *F. graminearum* on PDA plates, containing different quantities (from 100 to 500 μL) of cyclohexane AR extracts.

The effect on fungal growth was evaluated by spreading 500 μL of both AR solutions on PDA plates. The center of air-dried plates was inoculated with 4 μL of a conidial suspension (1×10^5 mL^{-1}) of Fg_QCE2 isolate, and after 4 days, the inhibition percentage of mycelial growth was calculated as previously described.

A further experiment was performed to assess the effect of the addition of synthetic C21:0 homologue on the antifungal activity of acetone and ethyl acetate natural extracts. The solutions were prepared by adding 250 and 500 μg of C21:0 homologue standard to 1 mL of acetone or ethyl acetate natural extract, containing about 1100 μg of total AR. The antifungal activity assay against Fg_QCE2 isolate was performed as described above.

Seed Treatment with Cyclohexane AR Extract. One hundred seeds of the durum wheat cv. Iride, susceptible to FHB, were surface-sterilized by washing with 2% sodium hypochlorite for 10 min, followed by three water rinses (5 min each), and dried under a laminar flow hood. Ten milliliters of the cyclohexane extract (3 mg/mL of AR) obtained from the cv. Tirex were previously dried and redissolved in 10 mL of acetone. The extract was added to the seeds with stirring at room temperature until acetone was evaporated. Seeds treated with 10 mL of acetone or 10 mL of distilled sterile water were used as control. Seed infection with Fg_QCE2 isolate was performed using 10 mL of a macroconidia suspension at the concentration of 2×10^4 spores mL^{-1}. After 15 min of incubation, the conidial suspension was removed, and the seeds were plated on a paper disk kept in 90 mm Petri plates containing agar 0.5% (w/v) (10 seeds for plates). Seeds were incubated in a growth chamber at 22 °C, for 6 days under 12/12 h alternate cycles of light and darkness. The experiment was repeated twice. Recording of the infected seeds was done 4 and 6 days after infection using a stereomicroscope.

Statistical Analysis. The analysis of variance (ANOVA) performed with the MSTATC program (Michigan State University, East Lansing, MI, USA) was used to evaluate the significance of the antifungal activity of the AR extracts.

RESULTS

GC-MS Characterization of AR Extracts. ARs extracted from cv. Tirex (grown during 2012) with ethyl acetate, acetone, and cyclohexane were analyzed by GC-MS. The TIC chromatograms of the three extracts are shown in Figure 1. The mass spectra of alkylresorcinols show Mclafferty base fragment at m/z 268, and the identity of the ARs was confirmed by molecular ion at m/z 478 (C15:0), 492 (C17:0), 534 (C19:0), 548 (C21:0), 576 (C23:0), and 604 (C25:0). The three solvents exhibited different abilities to extract ARs, and the highest amount of ARs was found in ethyl acetate. The hierarchy of the AR content in the three extracts was ethyl acetate ≫ acetone ≫ cyclohexane. Moreover, the GC-MS analysis showed that the cyclohexane extract was characterized by lower contents of ballast substances or other unidentified compounds (Figure 1). Ethyl acetate and acetone extracts furnished comparable results for homologue chain composition, whereas the cyclohexane extract contained a significantly higher proportion of C21:0 homologue, representing 59.9 ± 2.2% of AR homologues, and significantly lower percentages of the other homologues, if compared with acetone and ethyl acetate extracts (Table 1).

Antifungal Activity of AR Extracts. The in vitro assay results showed that all of the AR extracts were able to inhibit the growth of *F. graminearum*, although presenting different levels of activity (cyclohexane, 100 ± 0%; acetone, 27 ± 3%; ethyl acetate, 17 ± 2%). As a matter of fact, a total inhibition of spore germination was observed only with cyclohexane extract in the dose between 300 and 500 μL, containing about 330−550 μg of ARs (Figure 2). In this study the 4-*n*-hexylresorcinol was used as positive control to verify the assay conditions; as expected, a total inhibition of spore germination was observed at amounts <10 μg. In addition, the efficacy of the three extracts to inhibit the spore germination of *F. graminearum* was estimated by using the method of Belding et al.[32] Germination of 90 ± 4% of conidia was observed in the presence of ethyl acetate extract and 70 ± 5% in the presence of acetone extract, whereas the presence of cyclohexane extract completely inhibited spore germination.

The relationship between homologue composition of AR extracts and their antifungal activity was also tested by using two homologue standard solutions, containing the same qualitative and quantitative compositions identified in crude durum wheat cyclohexane and acetone extracts. The results showed a different inhibition activity of the two solutions against Fg_QCE2 isolate. In particular, the solution reproducing cyclohexane homologue composition, containing a higher percentage of C21:0 chain, showed a greater antifungal efficacy (growth inhibition of 37 ±

DOI: 10.1021/jf5054518
J. Agric. Food Chem. 2015, 63, 43−50

1%) in comparison to the solution reproducing the acetone extract (growth inhibition of 19 ± 1%).

The role of C21:0 homologue on the AR antifungal activity was evaluated by adding synthetic C21:0 to the acetone and ethyl acetate natural extracts. At 4 days after inoculation, the addition of C21:0 standard in the acetone extract determined a complete inhibition of Fg_QCE2 isolate spore germination, already at the lowest concentration (250 μg). No significant variation of antifungal activity of ethyl acetate extract enriched with synthetic C21:0, at both concentrations, was observed (23 ± 1% of growth inhibition) with respect to natural extract (22 ± 0%).

The fungistatic activity of cyclohexane extract on mycelial growth of *F. graminearum*, *F. culmorum*, *F. avenaceum*, and *F. poae* was also tested and statistically evaluated. The analysis of variance (ANOVA) performed on the colony diameter, measured 4 and 6 days after inoculation, showed statistically significant differences in the effect of the extract against the pathogens compared with the controls (Figure 3). In particular, the mean values of growth inhibition percentage were 47 ± 4% for *F. graminearum*, 41 ± 5% for *F. culmorum*, 55 ± 6% for *F. avenaceum*, and 40 ± 3% for *F. poae*.

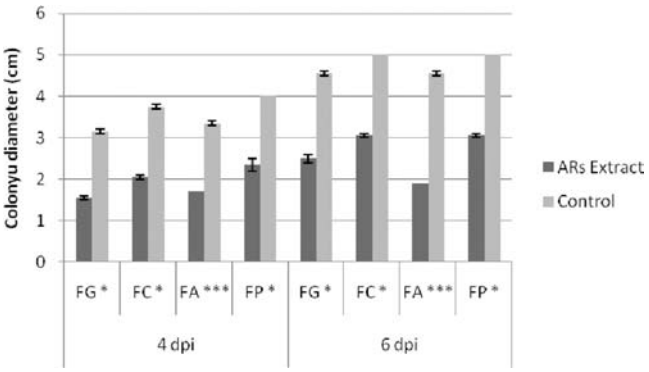

Figure 3. Effects of cyclohexane AR extract (~500 μg of AR) on mycelial growth of *Fusarium* spp. (FG, *F. graminearum*; FC, *F. culmorum*; FA, *F. avenaceum*; FP, *F. poae*): colony diameter (cm) 4 and 6 days after inoculation (mean values of triplicate experiments are given). (***) P = 0.001; (**) P = 0.01; (*) P = 0.05.

The antifungal activity of the extract against the four isolates of *F. graminearum* and the four isolates of *F. culmorum* is shown in Table 2. The AR extract exhibited antifungal activity against all of the tested *Fusarium* isolates, although some significant differences among the isolates were observed. The *F. graminearum* isolates showed the major variability of growth inhibition that ranged from 51 ± 1% for Fg_QCE2 to 32 ± 5% for Fg_QCE11 isolate. With regard to *F. culmorum* isolates, the highest antifungal activity was observed against Fc_QCE1 (growth inhibition = 45 ± 2%).

Protective Role of AR Cyclohexane Extract on Durum Wheat Seeds. The efficacy of the cyclohexane extract to protect seeds was evaluated. Seeds of the durum wheat cv. Iride were preliminarily treated with this extract and successively infected with a conidial suspension of Fg_QCE2 isolate. At 4 and 6 days after inoculation, respectively 77 ± 4 and 55 ± 5% of the treated seeds were not infected compared with untreated seeds, all completely infected after 4 days (Figure 4). The effect of this treatment on seed germination was evaluated by a static-type germinability assay. Four days after treatment, a reduction of 13 ± 4% of germinability was observed compared to the control seeds (2 ± 1%), treated with the solvent. Furthermore, in the treated seeds a slowdown in germination, with a day of delay compared to the control seeds, was observed.

Table 2. Antifungal Activity of AR Cyclohexane Extract versus Different Isolates of *F. graminearum* and *F. culmorum*[a]

	colony diameter (cm)		
	ARs	control	growth inhibition (%)
Fg_QCE2	1.55 ± 0.05	3.15 ± 0.05	50.79 ± 1.20
Fg_QCE3	1.80 ± 0.05	2.90 ± 0.05	37.93 ± 3.74
Fg_QCE5	1.60 ± 0.05	2.55 ± 0.05	36.00 ± 2.83
Fg_QCE11	1.70 ± 0.05	2.50 ± 0.05	32.00 ± 4.57
LSD			5.20
Fc_QCE1	2.05 ± 0.05	3.75 ± 0.05	45.33 ± 2.00
Fc_QCE2	2.25 ± 0.05	3.50 ± 0.05	35.71 ± 0.73
Fc_QCE3	2.40 ± 0.10	3.50 ± 0.10	31.43 ± 5.33
Fc_QCE7	2.15 ± 0.05	3.55 ± 0.05	39.44 ± 3.20
LSD			4.21

[a]LSD, least significant difference (p < 0.05).

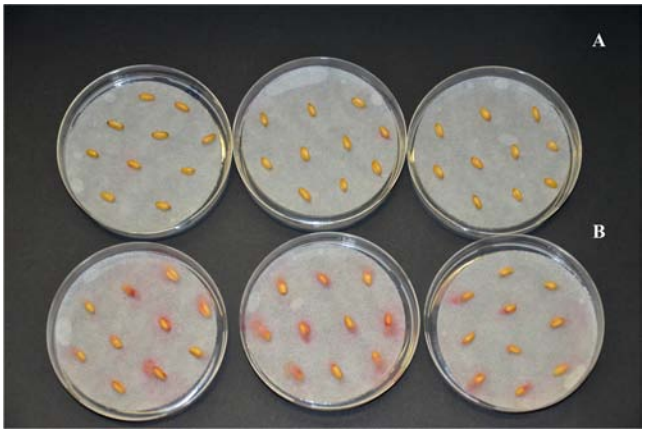

Figure 4. Effect of seed treatment with cyclohexane AR extract (A) and with solvent (B) on *F. graminearum* infection at 4 days after inoculation.

Effect of Seed-Drying Treatment and Durum Wheat Genotype on Antifungal Activity of AR Extracts. To increase the accessibility of cyclohexane solvent to the AR compounds, seed matrices (moisture content about 11.5%) of two durum wheat cultivars (Tirex and Simeto) were treated with high temperatures to reduce the moisture amount under 8% and facilitate AR extraction.[33] Measurements of AR content in acetone and cyclohexane extracts from predried seeds showed that an increased temperature (from 50 to 130 °C, moisture content about 9.4 and 5.2%, respectively) always resulted in increased AR content, and 105 °C for 90 min appeared to be the optimum conditions for an efficient AR extraction (Figure 5); in fact, in these conditions a proper seed moisture reduction (moisture content about 6.7%) was obtained, without undesirable variations in raw material. Changes in homologue profiles in the extracts obtained from predried and not dried seeds were also observed. In particular, the GC-MS data showed that the AR homologue profile presented a consistent decrease of C19:0 and C21:0 homologues and a significant increase of C23:0 chain in predried seeds; in addition, increased amounts of saturated ARs were evidenced in predried extracts (data not reported).

DOI: 10.1021/jf5054518
J. Agric. Food Chem. 2015, 63, 43−50

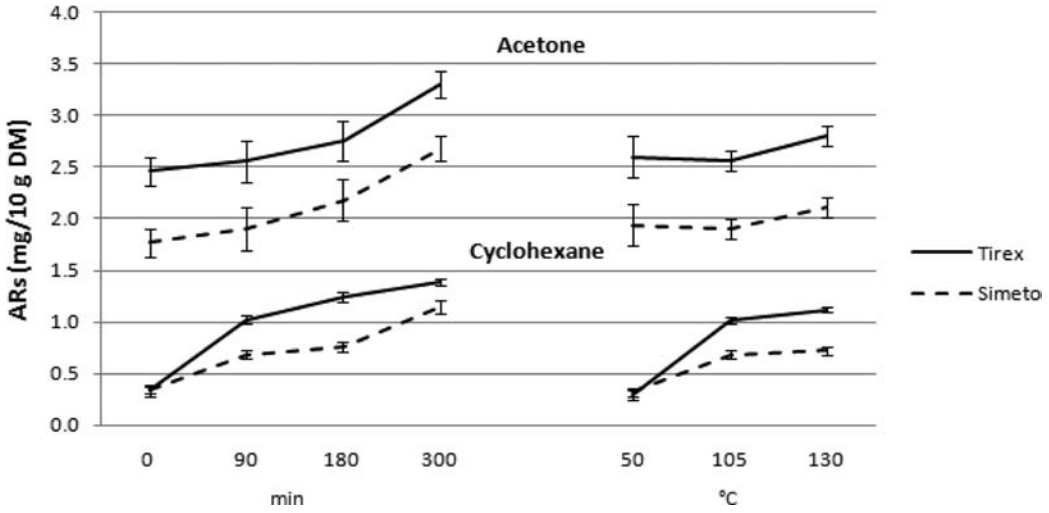

Figure 5. Effect of drying time and temperature on AR extractability with acetone and cyclohexane solvent from two durum wheat cultivars (Tirex and Simeto). (Mean values of triplicate experiments are given.)

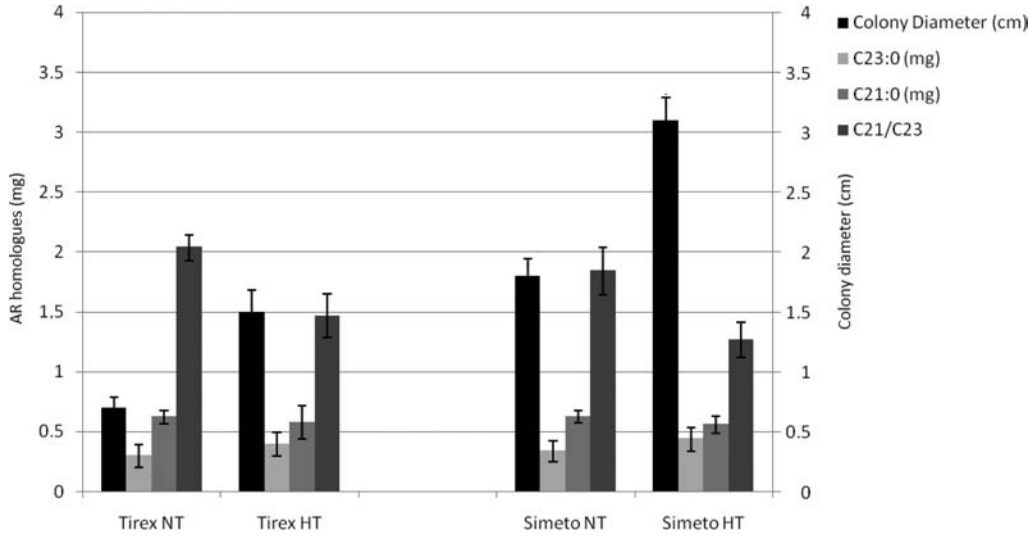

Figure 6. Effect of seed-drying treatment on the amount of C21:0 and C23:0 homologue of the AR cyclohexane extracts, obtained from the cultivars Tirex and Simeto, and on their antifungal activity against *F. graminearum* (colony diameter). NT, not dried seed; HT, dried seed.

The effect of predrying process on the antifungal activity of AR cyclohexane extract against *F. graminearum* is shown in Figure 6. At 4 days after inoculation, the AR extract obtained from predried seeds showed a lower antifungal activity with respect to the extract obtained from untreated kernels; the significant decrease in antifungal activity in dried samples always matched a decrease of the C21:0 and an increase of C23:0 homologue. In addition, as represented in Figure 6, significant differences in fungal growth inhibition activity between the extracts obtained from the two durum wheat cultivars were observed (82 ± 2% Tirex and 53 ± 7% Simeto).

DISCUSSION

The beneficial antifungal and antibacterial activities have led to the general assumption that alkylresorcinols play a defensive role during plant growth. Our results demonstrate the antifungal activity of durum wheat grain extracts, suggesting AR homologue composition as target of this activity. It is difficult to extract alkylresorcinols free of contaminants from cereal grain;[34] among the suggested organic solvents, in the present investigation ethyl acetate, acetone, and cyclohexane were chosen as extractants of 5-*n*-alkylresorcinols. According to previous papers,[35,36] intact kernels were preferred for the extraction. The results of GC-MS showed that the durum wheat grain extracts were always a mixture of contaminating coextracted compounds, soluble in the solvents used for the experiments. The data also indicated significant differences in AR content among ethyl acetate, acetone, and cyclohexane likely due to the different polarities of these solvents.[37] Zarnowski and Suzuki,[34] examining the efficiency of various solvents for the best total alkylresorcinols yield, also stated higher extraction ability of acetone and ethyl acetate with respect to cyclohexane, although this last extract was characterized by low ballast substances. Nevertheless, the interesting finding of this study was that only the relative amount of the C21:0 homologue increased using cyclohexane. This might be due to the middle chain length of lipophilic tail of C21:0 that could favor its solubility in the hydrocarbon solvent; on the other hand, the biological matrix and the individual cellular environment in which C21:0 and other ARs were embedded could affect their release depending on the protocol of

DOI: 10.1021/jf5054518
J. Agric. Food Chem. 2015, 63, 43−50

extraction. Moreover, the data confirmed cyclohexane as the most efficient solvent for minimizing coextraction of interfering compounds, which may have reduced the inhibitory effects of 5-*n*-alkylresorcinols on fungal growth. In fact, the antifungal activity was found to differ among the extracts, and the order of activity was cyclohexane ≫ acetone ≫ ethyl acetate. The high fungistatic activity of the cyclohexane extract was evidenced against *F. graminearum*, *F. culmorum*, *F. poae*, and *F. avenaceum*, this last species appearing to be the most sensitive one to AR activity. Moreover, the results of tests with different *F. culmorum* and *F. graminearum* isolates confirmed the antifungal properties of ARs despite the capacity of some *Fusarium* species to metabolize these molecules as previously described by Zarnowski et al.,[18,38] who suggested for *F. culmorum* a possible mechanism of tolerance to ARs. Therefore, studies on AR biosynthesis and biodegradation into fungal metabolism will be also needed in future projects concerned with the improvement of their applicability for fungal biocontrol.

The study on the influence of the predrying of seeds and the durum wheat genotype used on AR properties has further allowed the highest antifungal activity of the cyclohexane extract to be associated with the presence of a higher C21:0/C23:0 ratio. In fact, the predrying treatment significantly enhanced the recovery of total and saturated ARs, in agreement with the data of Agil et al.[39] In addition, significant modifications of the homologue composition in the AR cyclohexane extract with significant variations in C21:0 and C23:0 chains were evidenced. These changes in homologue composition appeared critical for the described antifungal activity, and the experiment with the standard homologues of AR supported this hypothesis. As part of the review process of this research, the results of the new tests showed that the addition of synthetic C21:0 increased the antifungal activity of the acetone extract, whereas no variation in the ethyl acetate extract activity was evidenced. In this last case likely the undesired interactions between ARs and coextracted compounds could also affect the activity of added C21:0 homologue. Accordingly, the data suggested that the higher antifungal activity of the cyclohexane extract might be due to the reduced presence of contaminants and the different AR composition, characterized by a higher amount of C21:0 homologue chain. These results were in agreement with Stasiuk and Kozubek,[40] who observed a higher ability to solubilize the erythrocyte membranes of homologue C21:0 extracted from rye compared to the other homologues. Moreover, previous studies on fatty acids proved the importance of the chain length in relation to antimicrobial activity.[41,42] On the basis of the trends of this study, AR antifungal activity seemed to be also influenced by factors such as genetic and environmental variables;[43−45] the choice of the durum wheat cultivar used for AR extraction and/or crop environment appeared to be important for optimizing and improving both the content of alkylresorcinols and their biological properties. However, our data did not exclude that other compounds present in the extracts might also play a role in the antifungal activity.

The role of ARs in plant defense is recognized, and their potential application in crop protection systems could appear as an alternative to chemical pesticides, in particular in "conscious agriculture". Our results indicated that seed treatment with cyclohexane extract could reduce the infection incidence of about 50%, suggesting the AR extract as potential control agent of *Fusarium* fungi. However, other agroecological aspects must be considered. In fact, the application of these compounds could affect chemical-mediated communication in the rhizosphere, both between plants and between plants and the soil microbial consortium,[46] that is a crucial contributor to soil quality, favoring long-term sustainability and resistance to perturbation.[47] Thus, the behavior of these molecules in crop field conditions will request future experiments to evaluate their stability and activity and their effects on soil communities.

In conclusion, the identification of the most effective AR homologue composition in inhibiting *Fusarium* growth suggested a potential application of the AR homologues in crop protection systems and could be an important step toward the development of commercial formulations suitable to prevent fungal diseases. Moreover, these findings supported the idea to include ARs in innovative cereal breeding programs to obtain new genotypes with increased resistance to fungal diseases and enhanced bioactive compounds.[44]

AUTHOR INFORMATION

Corresponding Author

*(F.N.) E-mail: francesca.nocente@entecra.it. Phone: +39 06 3295705. Fax: +39 06 36306022.

Notes

The authors declare no competing financial interest.

ABBREVIATIONS USED

ANOVA, analysis of variance; AR, alkylresorcinol; C15:0, 5-*n*-pentadecylresorcinol; C17:0, 5-*n*-heptadecylresorcinol; C19:0, 5-*n*-nonadecylresorcinol; C21:0, 5-*n*-heneicosylresorcinol; C22:0, methyl behenate; C23:0, 5-*n*-tricosylresorcinol; C25:0, 5-*n*-pentacosylresorcinol; cv., cultivar; cvs, cultivars; DM, dry matter; IS, internal standard; *m*/*z*, mass/charge; nd, not detected; PDA, potato dextrose agar; 4-hexylresorcinol, 4-hexyl-1,3-dihydroxybenzene; RH, relative humidity; TIC, total ion current; TMCS, trimethylchlorosilane; tr, trace

REFERENCES

(1) Parry, D. W.; Jenkinson, P.; McLeod, L. Fusarium earblight (scab) in small grain cereals: a review. *Plant Pathol.* **1995**, *44*, 207−238.

(2) Bottalico, A.; Perrone, G. Toxigenic *Fusarium* species and mycotoxins associated with head blight in small-grain cereals in Europe. *Eur. J. Plant Pathol.* **2002**, *108*, 611−624.

(3) Müllenborn, C.; Steiner, U.; Ludwig, M.; Oerke, E. C. Effect of fungicides on the complex of *Fusarium* species and saprophytic fungi colonizing wheat kernels. *Eur. J. Plant Pathol.* **2008**, *120*, 157−166.

(4) Lyon, G. P.; Reglinski, T.; Newton, A. C. Novel disease control compounds: the potential to immunize plants against infection. *Plant Pathol.* **1995**, *44*, 407−427.

(5) Jing, L.; Lei, Z.; Li, L.; Xie, R.; Xi, W.; Guan, Y.; Zhou, Z. Antifungal activity of citrus essential oils. *J. Agric. Food Chem.* **2014**, *62*, 3011−3033.

(6) Suchowilska, E.; Wiwart, M.; Grabowska, G. Antifungal activity of methanol extracts from spikes of *Triticum spelta* and *Triticum aestivum* genotypes differing in their response to *Fusarium culmorum* inoculation. *Biologia* **2008**, *63*, 471−476.

(7) Arif, T.; Bhosalea, J. D.; Kumara, N.; Mandala, T. K.; Bendreb, R. S.; Lavekara, G. S.; Dabura, R. Natural products − antifungal agents derived from plants. *J. Asian Nat. Prod. Res.* **2009**, *11*, 621−638.

(8) Boutigny, A. L.; Pénichon, A. V.; Benet, M.; Barreau, C.; Forget, F. R. Natural phenolic acids from wheat bran inhibit *Fusarium culmorum* trichothecene biosynthesis *in vitro* by repressing *Tri* gene expression. *Eur. J. Plant Pathol.* **2010**, *127*, 275−286.

(9) Baerson, S. R.; Schroder, J.; Cook, D.; Rimando, A. M.; Pan, Z.; Dayan, F. E.; Noonan, B. P.; Duke, S. O. Alkylresorcinol biosynthesis in plants: new insights from an ancient enzyme family. *Plant Signal Behav.* **2010**, *5*, 1−4.

DOI: 10.1021/jf5054518
J. Agric. Food Chem. 2015, 63, 43−50

(10) Kozubek, A.; Tyman, J. H. P. Resorcinolic lipids, the natural non-isoprenoid phenolic amphiphiles and their biological activity. *Chem. Rev.* **1999**, *99*, 1−25.
(11) Stasiuk, M.; Kozubek, A. Biological activity of phenolic lipids. *Cell. Mol. Life Sci.* **2010**, *67*, 841−860.
(12) Ross, A. B.; Shepherd, M. J.; Schupphaus, M.; Sinclair, V.; Alfaro, B.; Kamal-Eldin, A.; Aman, P. Alkylresorcinols in cereals and cereal products. *J. Agric. Food Chem.* **2003**, *51*, 4111−4118.
(13) Linko, A. M.; Juntunen, K. S.; Mykkanen, H. M.; Aldercreutz, H. Whole-grain rye bread consumption by women correlates with plasma alkylresorcinols and increases their concentration compared with low-fiber wheat bread. *J. Nutr.* **2005**, *135*, 580−583.
(14) Zhu, Y.; Conklin, D. R.; Chen, H.; Wang, L.; Sang, S. 5-Alk(en)ylresorcinols as the major active components in wheat bran inhibit human colon cancer cell growth. *Bioorg. Med. Chem.* **2011**, *19*, 3973−3982.
(15) Landberg, R.; Kamal-Eldin, A.; Salmenkallio-Marttila, M.; Rouau, X.; Åman, P. Localization of alkylresorcinols in wheat, rye and barley kernels. *J. Cereal Sci.* **2008**, *48*, 401−406.
(16) Suzuki, Y.; Yamaguchi, I. Antimicrobial agents (phytoanticipins) in *Gramineae* crops produced specifically during seedling stage. *J. Pestic. Sci.* **1998**, *23*, 316−321.
(17) Reiss, J. Influence of alkylresorcinols from rye and related compounds on the growth of food-borne molds. *Cereal Chem.* **1989**, *66*, 491−493.
(18) Zarnowski, R.; Kozubek, A.; Pietr, S. J. Effect of rye 5-*n*-alkylresorcinols on in vitro growth of phytopathogenic *Fusarium* and *Rhizoctonia* fungi. *Bull. Pol. Acad. Sci.: Biol. Sci.* **1999**, *47*, 231−235.
(19) Dey, E. S.; Ahmadi-Afzadi, M.; Nybom, H.; Tahir, I. Alkylresorcinols isolated from rye bran by supercritical fluid of carbon dioxide and suspended in a food-grade emulsion show activity against *Penicillium expansum* on apples. *Arch. Phytopathol. Plant Prot.* **2013**, *46*, 105−119.
(20) Garcìa, S.; Garcìa, C.; Heinzen, H.; Moyna, P. Chemical basis of the resistance of barley seeds to pathogenic fungi. *Phytochemistry* **1997**, *44*, 415−418.
(21) Suzuki, Y.; Esumi, Y.; Hyakutake, H.; Kono, Y.; Sakurai, A. Isolation of 5-(8′*Z*-heptadecenyl)-resorcinol from etiolated rice seedlings as an antifungal agent. *Phytochemistry* **1996**, *41*, 1485−1489.
(22) Cojocaru, M.; Droby, S.; Glotter, E.; Goldman, A.; Gottlieb, H. E.; Jacoby, B.; Prusky, D. 5-(12-Heptadecenyl)-resorcinol, the major component of the antifungal activity in the peel of mango fruit. *Phytochemistry* **1986**, *25*, 1093−1095.
(23) Kienzle, S.; Carle, R.; Sruamsiri, P.; Tosta, C.; Neidhart, S. Occurrence of alk(en)ylresorcinols in the fruits of two mango (*Mangifera indica* L.) cultivars during on-tree maturation and postharvest storage. *J. Agric. Food Chem.* **2014**, *62*, 28−40.
(24) Leslie, J. F.; Summerell, B. A. *The Fusarium Laboratory Manual*; Blackwell Publishing: Ames, IA, USA, 2006.
(25) Balmas, V.; Vitale, S.; Marcello, A.; Corazza, L. La fusariosi della spiga. *Inf. Agrario* **2000**, *35*, 27−29.
(26) Nicholson, P.; Simpson, D. R.; Weston, G. E.; Rezanoor, H. N.; Lees, A. K.; Parry, D. W.; Joyce, D. Detection and quantification of *Fusarium culmorum* and *Fusarium graminearum* in cereals using PCR assay. *Physiol. Mol. Plant Pathol.* **1998**, *53*, 17−37.
(27) Schilling, A. G.; Moller, E. M.; Geiger, H. H. Polymerase chain reaction-based assays for species-specific detection of *Fusarium culmorum*, *F. graminearum*, and *F. avenaceum*. *Phytopathology* **1996**, *86*, 515−522.
(28) Parry, W.; Nicholson, P. Development of a PCR assay to detect *Fusarium poae* in wheat. *Plant Pathol.* **1996**, *45*, 383−391.
(29) Landberg, R.; Andersson, A. A. M.; Aman, P.; Kamal-Eldin, A. Comparison of GC and colorimetry for the determination of alkylresorcinol homologues in cereal grains and products. *Food Chem.* **2009**, *113*, 1363−1369.
(30) Ross, A.; Aman, P.; Andersson, R.; Kamal-Eldin, A. Chromatographic analysis of alkylresorcinols and their metabolites. *J. Chromatogr., A* **2004**, *1054*, 157−164.
(31) Yin, Y.; Bi, Y.; Chen, S.; Li, Y.; Wang, Y.; Ge, Y.; Ding, B.; Li, Y.; Zhang, Z. Chemical composition and antifungal activity of cuticular wax isolated from Asian pear fruit (cv. Pingguoli). *Sci. Hortic. (Amsterdam, Neth.)* **2011**, *129*, 577−582.
(32) Belding, R. D.; Sutton, T. B.; Blankenship, S. M.; Young, E. Relationship between apple fruit epicuticular wax and growth of *Peltaster fructicola* and *Leptodontidium elatius*, two fungi that cause sooty blotch disease. *Plant Dis.* **2000**, *84*, 767−772.
(33) Shahidi, F.; Wanasundara, P. K. J. P. D. Extraction and analysis of lipids. In *Food Lipids. Chemistry, Nutrition, and Biotechnology*, 2nd ed.; Akoh, C. C., Min, D. B., Eds.; Dekker: New York, 2008; pp 151−156.
(34) Zarnowski, R.; Suzuki, Y. Expedient Soxhlet extraction of resorcinolic lipids from wheat grains. *J. Food Compos. Anal.* **2004**, *17*, 649−663.
(35) Ross, A. B.; Kamal-Eldin, A.; Jung, C.; Shepherd, M. J.; Aman, P. Gas chromatographic analysis of alkylresorcinols in rye (*Secale cereale* L.) grains. *J. Sci. Food Agric.* **2001**, *81*, 1405−1411.
(36) Landberg, R.; Dey, E. S.; Francisco, J. D. C.; Aman, P.; Kamal-Eldin, A. Comparison of supercritical carbon dioxide and ethyl acetate extraction of alkylresorcinols from wheat and rye. *J. Food Compos. Anal.* **2007**, *20*, 534−538.
(37) Francisco, J. D. C.; Danielsson, B.; Kozubek, A.; Dey, E. S. Application of supercritical carbon dioxide for the extraction of alkylresorcinols from rye bran. *J. Supercrit. Fluids* **2005**, *35*, 220−226.
(38) Zarnowski, R.; Lewicka, T.; Pietr, S. J. Production and secretion of 5-*n*-alkyl-resorcinols by *Fusarium culmorum*. *Z. Naturforsch.* **2000**, *55*, 846−848.
(39) Agil, R.; Oomah, D. B.; Mazza, G.; Hosseinian, F. S. Optimization of alkylresorcinols extraction from triticale bran using response surface methodology. *Food Bioprocess. Technol.* **2012**, *5*, 2655−2664.
(40) Stasiuk, M.; Kozubek, A. Membrane perturbing properties of natural phenolic and resorcinolic lipids. *FEBS Lett.* **2008**, *582*, 3607−3613.
(41) Malina, A.; Shai, Y. Conjugation of fatty acids with different lengths modulates the antibacterial and antifungal activity of a cationic biologically inactive peptide. *Biochem. J.* **2005**, *390*, 695−702.
(42) Williams, A. A.; Sugandhi, E. W.; Macri, R. V.; Falkinham, J. O., III; Gandour, R. D. Antimicrobial activity of long-chain, water-soluble, dendritic tricarboxylato amphiphiles. *J. Antimicrob. Chemother.* **2007**, *59*, 451−458.
(43) Bellato, S.; Ciccoritti, R.; Del Frate, V.; Sgrulletta, D.; Carbone, K. Influence of genotype and environment on the content of 5-*n*-alkylresorcinol on the antiradical activity of whole grain durum wheat grain. *J. .Cereal Sci.* **2013**, *57*, 162−169.
(44) Ciccoritti, R.; Bellato, S.; Carbone, K.; Sgrulletta, D. Content and relative composition of some phytochemicals in diploid, tetraploid and hexaploid *Triticum* species with potential nutraceutical propertis. *J. Cereal Sci.* **2013**, *57*, 200−206.
(45) Zarnowski, R.; Suzuki, Y.; Yamaguchi, I.; Pietr, S. J. Alkylresorcinols in barley (*Hordeum vulgare* L. distichon) grains. *Z. Naturforsch.* **2002**, *57C*, 57−62.
(46) Magnucka, E. G.; Oksińska, M. P.; Lewicka, T. Resorcinolic lipids in winter wheat grains and roots. *EJPAU [Online]* **2014**, *17*, 12, http://www.ejpau.media.pl/volume17/issue3/art-12.html (accessed Sept 3, 2014).
(47) Lynch, J. M.; Benedetti, A.; Insam, H.; Nuti, M. P.; Smalla, K.; Torsvik, V.; Nannipieri, P. Microbial diversity in soil: ecological theories, the contribution of molecular techniques and the impact of transgenic plants and transgenic microorganims. *Biol. Fertil. Soils* **2004**, *40*, 363−385.

DOI: 10.1021/jf5054518
J. Agric. Food Chem. 2015, 63, 43−50

JOURNAL OF AGRICULTURAL AND FOOD CHEMISTRY

Article

pubs.acs.org/JAFC

Effect of *Plum pox virus* on Chemical Composition and Fruit Quality of Plum

Valentina Usenik,*[,†] Damijana Kastelec,[‡] Franci Stampar,[†] and Mojca Virscek Marn[§]

[†]Biotechnical Faculty, Department of Agronomy, Chair for Fruit, Wine and Vegetable Growing, University of Ljubljana, Jamnikarjeva 101, SI-1000 Ljubljana, Slovenia

[‡]Biotechnical Faculty, Department of Agronomy, Chair for Genetics, Biotechnology, Statistics and Plant Breeding, University of Ljubljana, Jamnikarjeva 101, SI-1000 Ljubljana, Slovenia

[§]Plant Protection Department, Agricultural Institute of Slovenia, Hacquetova 17, SI-1000 Ljubljana, Slovenia

ABSTRACT: The quality of fruit from PPV (*Plum pox virus*)-infected plum (*Prunus domestica* L.) trees was investigated during the last 3 weeks of ripening using healthy tree (T3), tree with short-term infection (T2), and tree with long-term infection (T1). The pomological variables (presence of necrosis on fruit, color of fruit, color of flesh, firmness, soluble solids content, and fruit weight) and composition of nutritive compounds (sugars and organic acids) and bioactive compounds (phenolics: anthocyanins, flavonols, and hydroxycinnamic acids) were evaluated. The results indicated that the PPV infection modified the ripening process (the most in T1) and the composition of nutritive and bioactive compounds in the healthy-looking part of the fruit. Long-term infected tree (T1) yielded fruit with the poorest pomological traits and with the most modified composition of nutritive and phenolic compounds. The short-term PPV infected tree also produced fruit with significantly altered phytochemicals composition, although the pomological traits had not changed significantly.

KEYWORDS: *Plum pox virus, Prunus domestica, pomological characteristics, phytochemicals, nutritive compounds, phenolics, composition data analysis*

INTRODUCTION

Sharka (plum pox), caused by the *Plum pox virus* (PPV), is the most serious viral disease threatening the stone fruit industry, particularly because it causes severe losses in susceptible cultivars and is spread efficiently by aphids.[1] Over an approximately 80-year period since the description of the sharka disease, PPV has been thoroughly studied at various stages of the infection cycle.[2] On unripe fruit, shallow depressions of darker color appear. During ripening, these develop into deep rings and irregular lines, which cause deformation of the fruit. The epidermal tissue and underlying cells become necrotic, and the flesh turns brownish-red. The necrotic tissue often extends down to the seed. These fruits are tasteless and fibrous.[3] The diseased fruits contain more organic acids but less sugar and, especially, less sucrose. The fruits of infected susceptible varieties are also smaller in size.[4]

The influence of viruses on trees depends on the pathogen and its strain, as well as the fruit species, cultivar, rootstock, nutrition supply, time and mode of infection, vector species, and age of the tree when infected.[5] Trees newly infected with PPV show minor symptoms, usually only on one part of the tree, but with passing years infection of the tree increases.[6] The 'Požegača' cultivar is known to be very susceptible to PPV. This cultivar is widely distributed in Europe and has many synonyms, like 'Vânăt Românesc', 'Vinete Românești', or 'Bistrițene' in Romania; 'Kiustendilska' in Bulgaria; 'Vengerka' in Moldova; 'Quetsche' in France; 'Hauszwetsche' in Germany; 'Madjarica' in Croatia; 'Domača češplja' in Slovenia; etc.[7] Severe premature fruit drop (80−100%) has been reported for this cultivar. The dropping of the fruit begins 30−40 days before ripening.[4]

A number of physiological, biochemical, and structural changes occur during the ripening of plum,[8] resulting in modifications to pomological traits as well as to phytochemicals, which are dependent on the species,[9,10] cultivar,[9,11−13] ripening stage,[11−15] part of the fruit,[13,16] and rootstock.[17,18] Phytochemicals, particularly phenolics, are also good indicators of changed plant metabolism, owing to stress caused by infection; however, there has been no report about the effect of the PPV infection on phytochemicals in plum fruit.

In this study the effect of the PPV-Rec strain on external and internal quality of 'Brkinska češpa' was studied during the last 3 weeks of ripening. The quality of fruit from a tree that has been infected with PPV for at least 5 years and from a recently infected tree was compared to that of fruit from a healthy tree grown at the same location. To our knowledge this is the first report about the effect of PPV infection on composition of sugars, organic acids, and phenolics (anthocyanins, flavonols, and hydroxycinnamic acids) in plum fruit during the last stages of ripening. The results will improve the knowledge regarding the impact of PPV infection on the ripening process, the pomological traits, and especially the composition of phytochemicals in the healthy-looking part of the susceptible *Prunus domestica* plum fruit.

MATERIALS AND METHODS

Sample Collection. Fruit of 'Brkinska češpa', the local biotype of 'Domača češplja' (*Prunus domestica* L.), were collected from August 20

Received: July 17, 2014
Accepted: December 12, 2014
Published: December 15, 2014

ACS Publications © 2014 American Chemical Society

DOI: 10.1021/jf505330t
J. Agric. Food Chem. 2015, 63, 51−60

Table 1. Identification of Phenolic Compounds in Plum Fruit in Negative and Positive Ionization with HPLC-MS, MS^2, and MS^3

phenolic group	M^+ or $[M-H]^-$ (m/z)[a]	MS^2 (m/z)	MS^3 (m/z)	tentative identification	expressed in
anthocyanins	449	287		cyanidin-3-*O*-glucoside	cyanidin-3-*O*-galactoside
	595	449	287	cyanidin-3-*O*-rutinoside	cyanidin-3-*O*-galactoside
	463	301		peonidin-3-*O*-glucoside	peonidin-3-*O*-glucoside
	609	463	301	peonidin-3-*O*-rutinoside	peonidin-3-*O*-glucoside
hydroxycinnamic acids	353	191, 179		3-*O*-caffeoylquinic acid (neochlorogenic acid)	3-*O*-caffeoylquinic acid
	337	173		4-*O*-*p*-coumaroylquinic acid	*p*-coumaric acid
	353	191, 179		5-*O*-caffeoylquinic acid (chlorogenic acid)	chlorogenic acid
	353	173, 179		4-*O*-caffeoylquinic acid (cryptochlorogenic acid)	chlorogenic acid
flavonols	609	301		quercetin-3-*O*-rutinoside (rutin)	quercetin-3-*O*-rutinoside
	463	301		quercetin-3-*O*-galactoside	quercetin-3-*O*-galactoside
	463	301		quercetin-3-*O*-glucoside	quercetin-3-*O*-glucoside
	593	285		kaempferol-3-*O*-rutinoside	kaempferol-3-*O*-glucoside
	623	315		isorhamnetin-3-*O*-rutinoside	isorhamnetin-3-*O*-glucoside

[a]M^+ (m/z) anthocyanins were obtained in the positive ion mode; other phenolics were obtained in the negative ion mode.

to September 19 in 2013 from a plum orchard in the southwestern part of Slovenia (45°32′ latitude, 14°15′ longitude; 600 m altitude), with 1500 mm of average annual precipitation. Three trees growing on their own roots in close vicinity were selected based on the abundance of symptoms.

All the trees were over 30 years old and propagated through root suckers. The rate of infection on leaves and fruits was estimated visually on each sampling time. One tree showed severe symptoms of PPV infection on almost all fruit and severe premature dropping of fruit, and it was infected by PPV for at least 5 years (T1) (long-term infection), since the owner discovered symptoms on the leaves in spring 2009. The sharka symptoms on the recently infected tree were less severe. Mild symptoms were observed on few fruits. The first symptoms of PPV infections on leaves of this tree were observed by the owner in 2012 (T2) (short-term infection). On the third tree symptoms of PPV infection were absent (T3) (control).

The visual observations of PPV symptoms were confirmed by laboratory analyses. The presence/absence of PPV and other viruses that might cause similar symptoms or aggrevate the symptoms of PPV was checked on March 12, 2014, in buds collected throughout the canopy using double-antibody sandwich enzyme-linked immunosorbent assay (DAS-ELISA). Antibodies (Bioreba AG, Reinach, Switzerland) for detection of *Plum pox virus* (PPV), *Prune dwarf virus* (PDV), *Prunus necrotic ringspot* virus (PNRSV), *Apple chlorotic virus* (ACLSV), and *Apple mosaic virus* (ApMV) were used. Total RNA isolated from the two PPV positive samples was used in reverse transcriptase polymerase chain reaction (RT-PCR) using PPV3MODIF/P3M and PPV3MODIF/P3D primer pairs.[19,20] Obtained amplicons were directly sequenced. Strain designations of all sequences were determined based on the 99% nucleotide identity to sequences in the National Center for Biotechnology Information (NCBI) database using the blastn tool.

Fruits were picked at 8−13-day intervals through the last 3 weeks of ripening—August 20 (*d0*; in figures, 0), August 29 (*d9*; in figures, 9), September 11 (*d22*; in figures, 22), and September 19 (*d30*; in figures, 30, only T3)—and immediately transferred to the laboratory for further analytical determinations. For each sampling date and each tree, 30 fruits were selected randomly. The sample of 30 fruits was randomly divided into five repetitions (subsamples). The percentage of premature dropping of fruit was estimated for each tree and each sampling date.

Pomological Variables. Pomological variables (color of fruit, color of flesh, firmness, fruit weight, and soluble solids content (SSC)) were measured, and the presence of necrosis on plum fruit was assessed visually on each fruit using the following scale: 0 = without symptoms, 1 = symptoms covering <10% of the fruit skin, 2 = symptoms covering 10−30% of the skin, 3 = symptoms covering >30% of the skin. Using a Konica Minolta Portable Color Reader CR-10 (Konica Minolta, Inc., Osaka, Japan; measuring diameter 8 mm), hue (h^*) was measured in fruit with an uninjured blush on two sides of each fruit and the values were averaged (h_{peel}) and in flesh (h_{flesh}). With a penetrometer (Chatillon penetrometer model DFG 50, John Chatillion & Sons, New York, U.S.A.; insertion depth 5 mm), equipped with a round jagged stainless steel probe (diameter 6 mm), firmness was measured on two sides of each fruit immediately after the measurement of h_{peel}, and the values were averaged. SSC was measured in fruit juice with a digital refractometer (WM-7, Atago Co. Ltd., Tokyo, Japan).

Fruit weight was measured only on September 11 and September 19. The water content of the edible part was calculated as a difference from the fresh and dry weight of each subsample.

Samples (peel + flesh) for further determination of sugars, organic acids, and phenolic compounds were taken on four sides of each fruit with a round stainless steel probe (diameter 6 mm). In fruit with necrosis, the healthy-looking part of the fruit was taken for analyses. Fruit tissue of each subsample (4 parts of 6 fruits) was frozen and kept at −20 °C until the extraction. The extraction was made for each subsample at once: from one part of the fruit tissue for determination of sugars and organic acids and from the other part for determination of phenolic compounds. Determination of sugars, organic acids, and phenolic compounds was therefore made on the same plant material.

Sugars and Organic Acids. One g of plum tissue was homogenized in 5 mL of twice-distilled water and left for 30 min at room temperature with frequent stirring. The extracts were centrifuged at 12 800*g* for 7 min at 10 °C (Eppendorf Centrifuge 5810R, Hamburg Germany). The supernatants were filtered through a 0.20 μm cellulose ester filter (Macherey-Nagel; Düren, Germany) and transferred into a vial, and 20 μL of the sample was used for the analysis.

The analysis of sugars was carried out using a Surveyor high-performance liquid chromatography (HPLC) system with a refractive index (RI) detector (Thermo Finnigan). Separation of sugars was carried out using Rezex-RCM-monosaccharide column (300 × 7.8 mm; Phenomenex, Torrance, CA) operated at 65 °C. The mobile phase was double distilled water. The flow rate was 0.6 mL/min. The run time was 30 min.

Organic acids were analyzed with the same HPLC system, equipped with a UV detector set at 210 nm using a Rezex ROA column from Phenomenex HPLC (Thermo Scientific, Finnigan Spectra system, Waltham, MA, U.S.A.) operated at 65 °C. The elution solvent was 4 mM sulfuric acid at a flow rate of 0.6 mL min^{-1}. The duration of the analysis was 30 min.

The concentration of an individual metabolite was calculated according to a calibration curve of corresponding standard solution. The concentrations of sugars and organic acids were expressed as grams per kilogram of fresh weight (g kg^{-1} of FW). From the data of individual sugars and individual organic acids, sum of sugars (SUG) and sum of acids (ACID) and their ratio SUG/ACID were calculated.

DOI: 10.1021/jf505330t
J. Agric. Food Chem. 2015, 63, 51−60

Table 2. Average Score of Premature Dropping of Fruit (Fruit Drop), Median of Necrosis (Nec), and Averages with Standard Errors of h_{peel}, Firmness, h_{flesh}, Soluble Solids Content (SSC), Water Content of Edible Part (%), and Fruit Weight (g) for Three Levels of PPV Infection (T1, Long-Term Infection; T2, Short-Term Infection; T3, Control) during the Last Stages of Fruit Ripening (Day); $n = 30$[a]

				h_{peel}		firmness		h_{flesh}		SSC		water content		fruit weight	
	day	fruit drop	nec	$\bar{x}$	SE	$\bar{x}$	SE	$\bar{x}$	SE	$\bar{x}$	SE	$\bar{x}$	SE	$\bar{x}$	SE
T1	0	20	2	277.4 cd	8.8	1.0 b	0.4	91.4 b	7.5	18.8 cd	1.3	81.2	1.3		
	9	45	3	270.5 cd	6.5	0.9 bcd	0.3	87.0 c	9.2	19.0 cd	0.8	81.0	0.8		
	22	60	2	268.7 d	9.0	0.5 e	0.1	85.2 cd	5.0	19.4 bc	0.2	80.6	0.2	10.8	2.2
T2	0	2	0	310.3 a	24.7	1.6 a	0.4	96.4 a	6.4	18.4 de	0.5	81.7	0.5		
	9	10	0	278.2 c	9.5	0.9 cd	0.3	82.8 de	5.5	18.2 de	0.3	81.8	0.2		
	22	30	0	270.9 cd	12.8	0.6 e	0.2	78.0 f	6.3	20.4 a	0.8	79.6	0.8	11.1	1.8
T3	0	2	0	303.5 a	20.1	1.6 a	0.5	94.5 ab	3.3	18.6 cd	0.2	81.4	0.2		
	9	5	0	295.0 b	11.6	1.0 bc	0.2	80.0 ef	5.7	17.6 e	0.4	82.4	0.4		
	22	5	0	306.9 a	28.5	0.8 d	0.2	76.8 f	6.5	18.1 de	0.4	81.9	0.4	15.9	2.0
	30	8	0	272.3 cd	4.0	0.9 cd	0.2	70.0 g	3.5	19.9 ab	0.4	80.1	0.4	16.5	1.5

[a]a–f = No statistically significant differences between averages denoted with the same letter.

Phenolics. Plum tissue was ground to a fine paste in a mortar chilled with liquid nitrogen. One gram was extracted with 2.4 mL of methanol containing 3% (v/v) formic acid and 1% (w/v) 2.6-di-*tert*-butyl-4-methylphenol (BHT) in a cooled ultrasonic bath for 1 h. BHT was added to the samples to prevent oxidation during the extraction and formic acid was added for anthocyanin stabilization. After extraction, samples were centrifuged at 12 800*g* for 5 min at 4 °C and filtered through Chromafil A0-20/25 polyamide filters (Macherey-Nagel; Düren, Germany).

The analysis was performed immediately after extraction on a Surveyor HPLC system with a photodiode array (PDA) detector (Thermo Scientific, San Jose, CA, U.S.A.). The column was a Gemini C_{18} (150 × 4.6 mm; 3 μm; Phenomenex, Torrance, CA, U.S.A.) protected with a Phenomenex security guard column and operated at 25 °C. The elution solvents were aqueous 0.1% formic acid in double-distilled water (A) and 0.1% formic acid in acetonitrile (B). Samples were eluted using a linear gradient from 5 to 20% B in the first 15 min, followed by a linear gradient from 20 to 30% B for 5 min, then an isocratic mixture for 5 min, followed by a linear gradient from 30 to 90% B for 5 min, and then an isocratic mixture for 15 min before returning to the initial conditions[21] with some modifications, with an injection amount of 20 μL and a flow rate of 0.6 mL min^{-1}. Detected and quantified were hydroxycinnamic acids at 280 nm, flavonol derivatives at 350 nm, and anthocyanins at 530 nm.

Phenolic compounds were identified using a mass spectrometer (Thermo Scientific, LCQ Deca XP MAX) with an electrospray ionization (ESI) operating in positive (anthocyanins) and negative (all the other phenolics) ionization mode. Analyses were carried out using full-scan, data-dependent MS^n scanning from m/z 100 to 1000. The MS data are presented in Table 1. The capillary temperature was 250 °C, the sheath gas and auxiliary gas were 60 and 15 units, respectively, and the source voltage was 3 kV for negative and 4 kV for positive ionization.

The identification of compounds was confirmed by comparing retention times and their spectra as well as by adding the standard solution to the sample and by fragmentation. The concentrations of phenolics were calculated from peak areas of samples and corresponding standards. For compounds lacking standards, quantification was carried out using similar compounds as standards (Table 1). Concentrations were expressed in milligrams per kilogram fresh weight (mg kg^{-1} of FW). For the general presentation of the results, the sum of four hydroxycinnamic acids (HCA), the sum of five flavonols (FLAVO), and the sum of four anthocyanins (ANTH) were calculated.

Chemicals. The following standards were used for the quantification of sugars, organic acids, and phenolic compounds: sucrose, fructose, glucose, sorbitol, citric acid, malic acid, fumaric acid, *p*-coumaric acid, quercetin-3-*O*-galactoside, quercetin-3-*O*-glucoside, kaempferol-3-*O*-glucoside, cyanidin-3-*O*-galactoside, and peonidin-3-*O*-glucoside from Fluka Chemie GmBH (Buchs, Switzerland); shikimic acid, neochlorogenic (3-caffeoylquinic) acid, chlorogenic (5-caffeoylquinic) acid, and rutin (quercetin-3-*O*-rutinoside) from Sigma–Aldrich Chemical (St. Louis, MO, U.S.A.), and isorhamnetin-3-*O*-glucoside from Extrasynthese (Genay Cedex, France). Methanol for the extraction of phenolics was acquired from Sigma–Aldrich Chemical. The chemicals for the mobile phases were HPLC–MS grade acetonitrile and formic acid from Fluka Chemical GmBH. Water for the mobile phase was twice distilled and purified with the Milli-Q system (Millipore, Bedford, MA, U.S.A.).

Statistical Analysis. The data were analyzed as a two-factor experiment design, with the first factor expressing the level of PPV infection with three levels: T1, T2, and T3; the second factor expresses the time during ripening and also has three levels (*d0*, *d9*, and *d22*). In the case of pomological variables, there were 30 replications, and one plum represents an experimental unit. In the case of sugars, organic acids, and phenolic compounds, there were 5 replications; samples of flesh + peel were prepared from 6 plums. The impact of two fixed factors on pomological and chemical variables was examined on the basis of statistical analysis, performing linear models with one categorical explanatory variable (PPV infection) and one numeric explanatory variable (time). In most cases the interaction between PPV infection and time was statistically significant, indicating differing time trends for variables at different levels of PPV infection. The influence of PPV infection during the last stage of ripening on sugars, organic acids, and phenolic composition (relative values) was examined on the basis of compositional data analysis.[22] Three out of the four components in the four-part subcompositions of sugars, acids, and groups of phenolic components were first transformed using isometric log-ratio transformation (*ilr*) based on sequential binary partition. Multivariate and further univariate analysis of variance (MANOVA and ANOVA) was performed on *ilr* coordinates. Statistical analysis was done with the R program.[23] For compositional data analysis, the "compositions" package was used.[24,25]

RESULTS/DISCUSSION

DAS-ELISA testing showed the absence of all tested viruses with the exception of PPV. The presence of PPV was confirmed in both trees showing sharka symptoms (T1 and T2). The symptomless tree (T3) proved to be PPV-free. Owing to the absence of other viruses that can affect stone fruit, all the differences found can be ascribed to the effect of PPV. The 1226 nucleotide long sequences from both PPV-positive trees obtained with the primers PPV3MODIFIED[19] and P3M[20] were found to be identical and to belong to the PPV-Rec strain. Strain identification is important, because PPV isolates are diverse and have been assigned to 9 strains,[26] which differ in

DOI: 10.1021/jf505330t
J. Agric. Food Chem. 2015, 63, 51–60

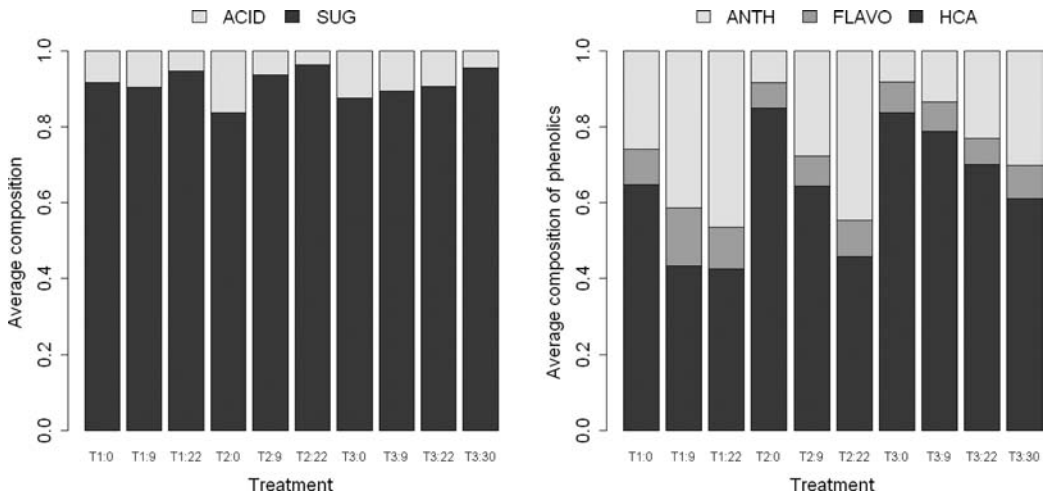

Figure 1. Effect of PPV infection (T1, long-term infection; T2, short-term infection; T3, control) on the average composition of nutritive compounds (left) and phenolics (right) of plum 'Brkinska češpa' during the last stages of fruit ripening (day) (0; 9; 22; 30, only T3).

Table 3. Average Contents with Standard Errors (g/kg of FW) of Individual Sugars and Sum of Sugars (SUG) for Three Levels of PPV Infection (T1, Long-Term Infection; T2, Short-Term Infection; T3, Control) during the Last Stages of Fruit Ripening (Day); $n = 5$[a]

		sucrose		glucose		fructose		sorbitol		SUG	
	day	$\bar{x}$	SE	$\bar{x}$	SE	$\bar{x}$	SE	$\bar{x}$	SE	$\bar{x}$	SE
T1	0	30.5 d	4.9	34.4 bA	2.6	17.6 a	1.5	19.0 a	3.2	101.4 bB	7.7
	9	44.6 bc	4.5	28.8 bB	0.9	15.7 ab	1.6	15.0 b	3.1	104.1 bAB	6.6
	22	49.7 ab	5.1	31.3 bB	1.4	13.0 cd	1.8	10.6 c	1.1	104.7 bA	7.4
T2	0	31.5 d	4.4	40.3 aA	8.3	11.5 d	2.4	19.4 a	2.1	102.6 aB	15.0
	9	43.7 c	2.2	37.6 aB	2.2	13.7 bcd	1.2	14.4 b	2.1	109.4 aAB	2.4
	22	54.8 a	3.5	36.1 aB	4.1	17.7 a	1.9	9.8 c	2.9	118.3 aA	9.2
T3	0	33.5 d	5.1	43.2 aA	4.7	11.6 d	2.2	21.2 a	2.0	109.5 aB	10.4
	9	41.3 c	2.9	39.2 aB	2.8	12.2 cd	1.1	19.3 a	2.5	112.0 aAB	8.6
	22	43.8 c	2.0	34.0 aB	3.0	14.5 bc	0.8	19.0 a	2.0	111.2 aA	4.0
	30	45.5	2.7	38.4	1.0	17.3	0.5	18.8	0.9	119.9	2.3

[a]a–d = No statistically significant differences between averages denoted with the same letter. For the variables with statistically significant infection/time interaction, only small letters are used for indication of differences between treatments. If the interaction was not statistically significant, small letters indicate differences between rates of infection and capital letters indicate the differences between different time points.

their pathogenicity, host range, aphid transmissibility, and geographic distribution. The results show that premature fruit drop is higher in infected trees and that it increases with the duration of infection (Table 2).

Pomological Variables. Our results show the effect of PPV infection on the pomological characteristics during the final phases of ripening (Table 2). The analysis of variance for all pomological characteristics show that the interaction between infection and ripening stage (time) was statistically significant. This means that the level of PPV infection does influence the process of ripening.

The medians of the necrosis score evaluated for 30 plums of each tree/time combination differed from 0 only for T1 (Table 2). At the first sampling date, no necrosis was found on T2 and T3 fruit, but all fruit from T1 showed necrotic symptoms: score 1, 12 plums; score 2, 12 plums; and score 3, 6 plums. At the second sampling (*d9*), 12 plums from T1 got a score of 2 and 18 plums a score of 3. Two fruit from T2 got a score of 1, all others 0. At the last sampling (*d22*), 10 plums from T1 got a score of 1, 14 plums a score of 2, and 5 plums a score of 3; 5 plums from T2 got a score of 1, 1 a score of 2, and 1 a score of 3. This shows that the severity of symptoms increases with the duration of infection. These results also confirmed our estimation of infection rate done in the field. It is known that the infection of trees and the symptom expression increases with years;[6] thus, the relative differences in the rate of infection among trees of the same cultivar and rootstock on the same location can be estimated based on the abundance of symptoms on the leaves and on the fruit.

Significantly the lowest average values of h_{peel} were observed in T1 at first measurement (*d0*) (Table 2). The color of T1 at *d0* was magenta–blue and did not change significantly over the next 22 days. Ripening of T2 fruit resulted in changed color of fruit peel from magenta (*d0*) to magenta–blue (*d22*). The color of T3 changed to magenta–blue at *d30*. When plums become more highly colored, the h_{peel} decreases.[15] These results show the faster process of fruit ripening in fruit from infected trees (T1 and T2) and confirm the observations of Atanassov (cited in ref 4) that plums from PPV infected trees ripen from 10–15 days or more ahead of fruit from healthy trees.

Color intensity of flesh (h_{flesh}) significantly decreased during ripening (the color changed from green to yellow), more evidently in T2 and T3 than in T1 fruit. The fruit of T1 on *d22* had significantly higher values of h_{flesh} than T2 and T3, showing a more greenish flesh. The h_{flesh} of T3 decreased the most from

DOI: 10.1021/jf505330t
J. Agric. Food Chem. 2015, 63, 51–60

Table 4. Average Contents with Standard Errors (g/kg of FW) of Individual Organic Acids, Sum of Organic Acids (ACID), and SUG/ACID Ratio with 95% Confidence Intervals (CIs) for Three Levels of PPV Infection (T1, Long-Term Infection; T2, Short-Term Infection; T3, Control) during the Last Stages of Fruit Ripening (Day); $n = 5$[a]

		citric acid		malic acid		shikimic acid		fumaric acid		ACID		SUG/ACID ratio	
	day	$\bar{x}$	SE	$\bar{x}$	SE	$\bar{x}$	SE	$\bar{x}$	SE	$\bar{x}$	SE	$\bar{x}$	95% CI
T1	0	0.16 bA	0.03	9.1 de	0.9	0.02 d	0.01	0.014 bcd	0.001	9.3 de	0.9	10.9	9.2. 12.9
	9	0.21 bB	0.04	11.0 cd	2.9	0.02 d	0.01	0.016 bc	0.003	11.2 cd	3.0	9.8	8.1, 11.3
	22	0.08 bC	0.02	5.8 fg	1.9	0.01 e	0.00	0.008 f	0.002	5.9 fg	2.0	19.1	15.5, 21.7
T2	0	0.29 abA	0.05	19.6 a	3.0	0.05 a	0.01	0.023 a	0.002	20.0 a	3.0	5.2	4.3, 6.1
	9	0.11 abB	0.02	7.3 ef	1.6	0.02 d	0.00	0.011 def	0.001	7.4 ef	1.7	15.3	12.7, 17.8
	22	0.09 abC	0.01	4.4 g	0.5	0.01 e	0.00	0.011 ef	0.002	4.5 g	0.5	26.4	22.2, 31.1
T3	0	0.32 aA	0.11	15.0 b	1.0	0.04 a	0.00	0.017 b	0.002	15.4 b	1.1	7.2	6.0, 8.4
	9	0.16 aB	0.04	12.9 bc	0.9	0.04 b	0.00	0.013 cde	0.001	13.1 bc	0.9	8.6	7.2, 10.1
	22	0.14 aC	0.02	11.2 cd	1.2	0.03 c	0.00	0.017 b	0.003	11.4 cd	1.2	9.9	8.3, 11.6
	30	0.14	0.03	5.4	1.1	0.01	0.00	0.011	0.001	5.6	1.1	22.1	18.4, 25.8

[a]a–d = No statistically significant differences between averages denoted with the same letter. For the variables with statistically significant infection/time interaction, only small letters are used for indication of differences between treatments. If the interaction was not statistically significant, small letters indicate differences between rates of infection and capital letters indicate the differences between different time points.

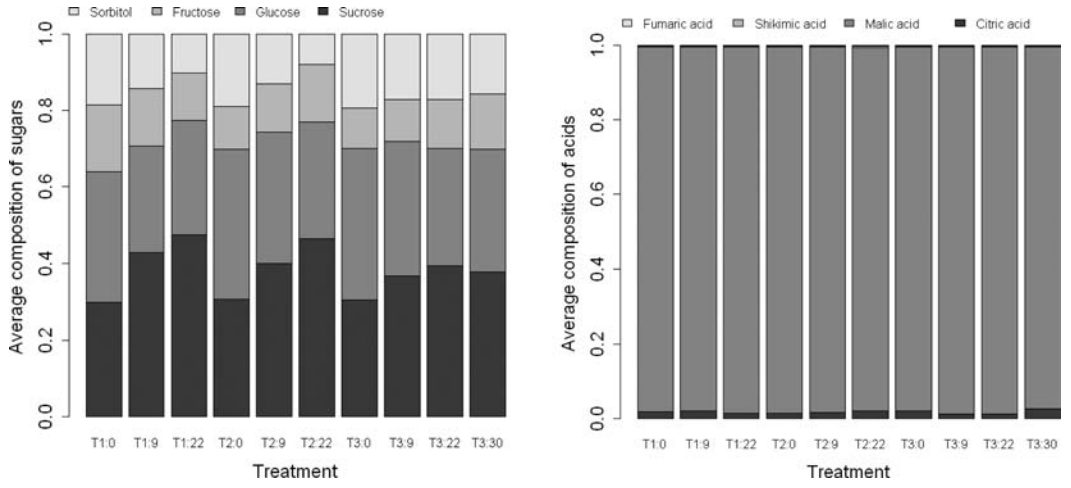

Figure 2. Effect of PPV infection (T1, long-term infection; T2, short-term infection; T3, control) on the average composition of sugars (left) and organic acids (right) of plum 'Brkinska češpa' during the last stages of fruit ripening (day) (0; 9; 22; 30, only T3).

d22 to *d30*. Assessment of ripeness using flesh color is consistent with the results of other pomological characteristics.

Our results show variation in reduction of firmness among fruit with various levels of infection. At the first measurement (*d0*), fruit from the PPV-free (T3) and from the tree infected for only a short time (T2) showed equal levels of firmness. Fruits from the long-term infected tree (T1) were statistically softer. After 9 days, differences in firmness among the fruit almost disappeared, but after 22 days the firmness of T1 and T2 fruit decreased to almost the same level, while T3 fruit remained firmer. The results for firmness also show that a high level of PPV infection causes earlier ripening of fruit, since during the final ripening phases a change in firmness is the only useful indicator of plum maturity.[15]

Ripening did not change soluble solids content (SSC) in T1 but increased it significantly in T2 between *d9* and *d22* and in T3 between *d22* and *d30*. Given that ripening increases SSC,[11] it can be assumed that PPV infection caused earlier ripening of T1 and T2 fruit. SSC is an essential quality variable in stone fruit,[27,28] which has been proposed as the most reliable maturation parameter for plums.[29,30] The average SSC of 10 selections of 'Brkinska češpa' varied from 16.2 to 19.8.[31]

Infection had no impact on the water content of the edible part of the plum fruit (Table 2). The level of PPV infection did influence average fruit weight, which was measured only on *d22* and *d30*. The fruit of T1 and T2 on *d22* had a similar fruit weight (10.8 and 11.1 g), which was much lower compared to T3 (15.9 g). By the last sampling day (*d30*), the average fruit weight of T3 had increased to 16.5 g. The ripening process increases fruit weight.[11] The average fruit weight of 10 selections of 'Brkinska češpa' varied from 17.4 to 21.4 g.[31]

Nutritive Compounds. Our results show the effect of PPV infection on the composition of nutritive compounds in the plum fruit of 'Brkinska češpa' during the final ripening phases. Two groups of nutritive compounds were identified: sugars and organic acids. In general, the relative content of sugars increased and the relative content of acids decreased during ripening (Figure 1 and Tables 3 and 4). T1 fruit had significantly less SUG than T2 and T3 fruit (Table 3).

The average content of individual sugars is shown in Table 3, and their average composition is shown in Figure 2. Glucose, fructose, sorbitol, and sucrose were detected.[13] Relative content of sucrose during the final phases of ripening generally increased (30.0% to 47.5%), but it decreased in the case of

DOI: 10.1021/jf505330t
J. Agric. Food Chem. 2015, 63, 51–60

Table 5. Average Contents with Standard Errors (mg/kg of FW) of Individual Hydroxycinnamic Acids and Sum of Hydroxycinnamic Acids (HCA) for Three Levels of PPV Infection (T1, Long-Term Infection; T2, Short-Term Infection; T3, Control) during the Last Stages of Fruit Ripening (Day); $n = 5$[a]

		neochlorogenic acid		*p*-coumaroylquinic acid		chlorogenic acid		cryptochlorogenic acid		HCA	
	day	$\bar{x}$	SE	$\bar{x}$	SE	$\bar{x}$	SE	$\bar{x}$	SE	$\bar{x}$	SE
T1	0	222.6 de	32.6	13.8 aA	1.5	43.5 bB	5.3	9.9 a A	2.3	289.7 de	34.6
	9	166.9 e	66.5	14.3 aA	3.5	59.3 bB	21.6	8.1 aB	3.6	248.5 e	91.6
	22	220.4 de	46.7	14.5 aA	0.9	67.6 bA	7.8	8.3 aB	0.9	310.8 de	52.9
T2	0	383.5 a	44.9	14.3 bA	1.6	78.0 aB	23.8	9.4 aA	2.4	485.1 a	61.8
	9	270.1 cd	24.1	11.3 bA	1.4	67.6 aB	14.4	6.0 aB	0.3	354.9 cd	37.6
	22	241.7 d	22.2	11.5 bA	2.0	83.4 aA	13.1	5.6 aB	0.5	342.1 cd	24.9
T3	0	320.8 bc	55.5	12.1 bA	2.1	53.0 aB	15.0	11.5 aA	5.2	397.4 bc	75.1
	9	331.3 ab	30.8	10.6 bA	1.0	66.8 aB	12.2	8.2 aB	0.6	416.8 abc	32.2
	22	335.4 ab	34.5	11.0 bA	0.8	83.5 aA	7.9	6.5 aB	1.1	436.4 ab	40.0
	30	321.6	24.9	8.6	0.8	64.1	8.8	6.3	0.8	400.6	32.8

[a]a–d = No statistically significant differences between averages denoted with the same letter. For the variables with statistically significant infection/time interaction, only small letters are used for indication of differences between treatments. If the interaction was not statistically significant, small letters indicate differences between rates of infection and capital letters indicate the differences between different time points.

glucose (39.5% to 27.8%), fructose (17.4% to 10.5%), and sorbitol (19.4% to 8.0%).

The interaction between infection and time was significant for sucrose; the increase of sucrose during ripening was the slowest for T3. The average glucose content significantly linearly decreased during ripening, with the same rate for all levels of infection. At first measurement (*d0*), there was a significant difference in average glucose between T1 and the other two infection rates; T3 had on average 10.4 g/kg more and T2 had on average 7.3 g/kg more glucose than T1. The average content of fructose increased during ripening in T2 and T3 and decreased in T1. Only in T1 and T2 did ripening significantly decrease sorbitol.

In general, the results for sugars show similarities between T2 and T3, but in the case of sucrose at *d22* there are similarities between T1 and T2. Fruit of T1 had less total sugars, glucose, and sorbitol than T2 and T3. Fruit of T1 and T2 had at *d22* more sucrose than T3 (Table 3).

To examine relative changes in the composition of sugars, the analysis was also done on the *ilr* (isometric log-ratio transformation) transformed four-component sugar composition (Figure 2). The MANOVA for the *ilr* coordinates shows that the infection/time interaction was statistically significant. This means that sugar composition changes during ripening are not the same for all levels of PPV infection. The three *ilr* coordinates were calculated: ilr_1 represents the balance between glucose and sucrose $ilr_1 = c_1 \times \ln(\text{glucose}/\text{sucrose})$; ilr_2 represents the balance between fructose and the group of sucrose and glucose) $ilr_2 = c_2 \times \ln(\text{fructose}/g(\text{sucrose} \times \text{glucose}))$; and ilr_3 represents the balance between sorbitol and the other three components $ilr_3 = c_3 \times \ln(\text{sorbitol}/g(\text{sucrose} \times \text{glucose} \times \text{fructose}))$. The constants c_1, c_2, and c_3 are determined on the basis of sequential binary partition and play a normalization role. The function $g(\,)$ represents the geometric mean of the composition components. The univariate ANOVA for ilr_1 showed a significant influence of infection and time; the highest occurred in T3 and the lowest in T1, and it decreased with time, owing to increased sucrose content relative to glucose. The infection/time interaction was statistically significant for ilr_2. The ilr_2, which for T1 at *d0* was significantly higher than T2 and T3 during ripening, decreased significantly in T1, but in T2 and T3 it increased slightly. The ilr_3 differed among levels of infection (the highest was in T3) and decreased over time—the most in T1 and T2, owing to a reduction in sorbitol concentration relative to the other sugars. The ilr_1 and ilr_2 coordinates show more similarities between T2 and T3, but the ilr_3 coordinate shows similarity between T1 and T2.

The average content of individual organic acids and the sum of acids (ACID) are shown in Table 4, and their average composition is shown in Figure 2. In general, the relative concentration of acids during ripening decreased:[11,13] from 98.4% to 97.5% malic acid, from 2.0% to 1.2% citric acid, from 0.3% to 0.2% shikimic acid, and from 0.2% to 0.1% fumaric acid.

The infection/time interaction was significant for ACID (Table 4). Fruit of T2 and T3 had significantly higher average ACID (20.0 and 15.4 g/kg, respectively) than T1 (9.3 g/kg) at first measurement (*d0*). Ripening decreased organic acids in plum, the most in T1 and T2. Fruit of T3 had significantly higher average ACID than T1 and T2 at *d22*. There is evident decrease of ACID in T3 between *d22* and *d30*.

The ANOVA for each acid separately (Table 4) showed that the citric acid content of T3 was significantly higher compared to T1. During ripening the content significantly decreased, the most in T2. The ANOVAs for average levels of malic acid, shikimic acid, and fumaric acid show that the infection/time interaction was statistically significant. The content of malic acid and shikimic acid of T2 and T3 was significantly higher than that of T1. The negative time trend (from *d0* to *d22*) was significant for all acids. There was an evident decrease in the main organic acid, malic acid, and ACID in T3 between *d22* and *d30*.

In general, the results for organic acids show that PPV infection causes earlier ripening of fruit. More similarities were between T1 and T2.

Four-component organic acid composition (Figure 2) was transformed into three *ilr* coordinates: $ilr_1 = c_1 \times \ln(\text{malic}/\text{citric})$, $ilr_2 = c_2 \times \ln(\text{fumaric}/\text{shikimic})$, and $ilr_3 = c_3 \times \ln(g(\text{citric} \times \text{malic})/g(\text{shikimic} \times \text{fumaric}))$. MANOVA showed that the infection/time interaction was statistically significant for all *ilr* coordinates. The ilr_1 was, at first measurement, lowest in T3 and highest in T2, but at *d22* it was highest in T3, owing to the higher relative concentration of malic acid against citric acid, and it was lowest in T2. There were significant differences among the levels of infection in ilr_2;

DOI: 10.1021/jf505330t
J. Agric. Food Chem. 2015, 63, 51–60

Table 6. Average Contents with Standard Errors (mg/kg of FW) of Individual Anthocyanins and Sum of Anthocyanins (ANTH) for Three Levels of PPV Infection (T1, Long-Term Infection; T2, Short-Term Infection; T3, Control) during the Last Stages of Fruit Ripening (Day); $n = 5$[a]

		cyanidin-3-glucoside		cyanidin-3-rutinoside		peonidin-3-rutinoside		peonidin-3-rutinoside		ANTH	
	day	$\bar{x}$	SE	$\bar{x}$	SE	$\bar{x}$	SE	$\bar{x}$	SE	$\bar{x}$	SE
T1	0	26.8 c	6.1	52.3 cd	18.0	8.6 aC	2.4	29.9 d	6.0	117.6 cd	27.6
	9	65.7 b	14.5	111.6 b	31.3	16.6 aB	2.7	34.0 bc	8.5	227.9 b	50.9
	22	113.8 a	20.9	167.9 a	39.9	19.6 aA	6.4	37.5 ab	6.9	338.8 a	57.8
T2	0	4.5 d	2.6	19.4 e	4.1	4.4 aC	0.9	19.3 d	3.0	47.5 e	6.4
	9	26.4 c	10.7	69.9 c	16.2	14.4 aB	2.3	45.3 c	15.0	156.0 c	39.7
	22	99.6 a	33.1	151.1 a	32.8	19.6 aA	4.3	69.6 a	13.1	339.9 a	76.6
T3	0	4.3 d	1.7	14.0 e	5.5	4.0 bC	1.1	16.8 d	2.6	39.0 e	10.2
	9	6.4 d	1.9	26.3 de	2.9	8.7 bB	4.2	31.4 c	15.1	72.8 de	19.9
	22	14.6 cd	4.2	63.3 c	8.6	11.8 bA	4.9	53.8 c	4.8	143.4 c	13.5
	30	29.5	11.1	98.0	28.6	17.1	4.4	56.7	8.4	201.3	49.1

[a]a–e = No statistically significant differences between averages denoted with the same letter. For the variables with statistically significant infection/time interaction, only small letters are used for indication of differences between treatments. If the interaction was not statistically significant, small letters indicate differences between rates of infection and capital letters indicate the differences between different time points.

Table 7. Average Contents with Standard Errors (mg/kg of FW) of Individual Flavonols and Sum of Flavonols (FLAVO) for Three Levels of PPV Infection (T1, Long-Term Infection; T2, Short-Term Infection; T3, Control) during the Last Stages of Fruit Ripening (Day); $n = 5$[a]

		rutin		quercetin-3-galactoside		quercetin-3-glucoside		kaempferol-3-rutinoside		isorhamnetin-3-rutinoside		FLAVO	
	day	$\bar{x}$	SE	$\bar{x}$	SE	$\bar{x}$	SE	$\bar{x}$	SE	$\bar{x}$	SE	$\bar{x}$	SE
T1	0	33.6 aB	7.0	1.7 aB	0.3	2.2 c	0.8	1.6 aB	0.6	2.9 aB	0.8	42.0 aB	8.9
	9	66.5 aA	24.5	2.6 aAB	0.9	8.8 a	2.2	2.5 aAB	0.8	5.6 aA	1.8	86.0 aA	29.2
	22	59.9 aA	11.5	2.6 aA	0.4	10.9 a	3.6	2.3 aA	0.7	5.3 aA	1.5	81.1 aA	15.7
T2	0	34.4 abB	19.2	2.0 abB	1.0	1.8 c	1.3	1.7 aB	1.2	3.4 aB	2.0	43.3 bB	24.5
	9	36.7 abA	11.7	1.6 abAB	0.4	2.4 c	0.7	1.7 aAB	0.5	3.5 aA	1.0	45.9 bA	14.2
	22	56.7 abA	18.6	2.7 abA	0.9	6.4 b	2.3	3.1 aA	1.4	5.0 aA	1.2	73.9 bA	23.8
T3	0	31.0 bB	5.4	1.7 bB	0.4	1.6 c	0.5	1.7 aB	0.4	3.2 aB	0.6	39.2 bB	7.1
	9	35.9 bA	16.6	1.7 bAB	0.6	1.8 c	1.0	1.6 aAB	0.9	3.6 aA	1.6	44.5 bA	20.6
	22	36.0 bA	10.5	1.7 bA	0.4	1.8 c	0.6	1.6 aA	0.6	3.8 aA	0.8	44.9 bA	12.9
	30	43.1	8.8	4.2	1.5	3.7	1.3	2.3	0.6	4.9	1.1	58.2	12.7

[a]a–d = No statistically significant differences between averages denoted with the same letter. For the variables with statistically significant infection/time interaction, only small letters are used for indication of differences between treatments. If the interaction was not statistically significant, small letters indicate differences between rates of infection and capital letters indicate the differences between different time points.

it was higher in T1 and T2, thus explaining the higher relative concentration of fumaric acid against shikimic acid. Ripening decreased the ilr_3 of T2 and T3 due to decreased relative concentrations of malic acid and citric acid.

The coordinates ilr_1 and ilr_2 show more similarities between T1 and T2, but ilr_3 shows similarity between T2 and T3. Additionally, the ratio SUG/ACID (Table 4) shows that the level of PPV infection influences the process of ripening. To consider the assumptions of ANOVA, the log-ratio was analyzed. The average SUG/ACID ratio of T1 increased significantly between *d9* and *d22* to 19.1 (95% CI is 15.5–21.7); the average SUG/ACID ratio of T2 increased linearly from *d0* to *d22*, and the average SUG/ACID ratio of T3 increased slowly between *d0* and *d22* and then jumped to 22.1 (95% CI is 18.4–25.8) by d30, owing to the increase in SUG and the decrease in ACID between *d22* and *d30*.

Phenolics. Three main groups of phenolics were detected in the edible part of 'Brkinska češpa' fruit: anthocyanins, flavonols, and the most abundant, hydroxycinnamic acids. The average composition according to these groups (sum of anthocyanins (ANTH), sum of flavonols (FLAVO)m and sum of hydroxycinnamic acids (HCA)) is shown in Figure 1 (right). Average concentrations, along with standard errors for individual phenolics inside groups, are shown in Tables 5–7, and the average composition within the phenolic group is shown in Figure 3.

Two *ilr* coordinates were calculated: $ilr_1 = c_1 \times \ln(\text{FLAVO}/\text{HCA})$ and $ilr_2 = c_2 \times \ln(\text{ANTH}/g(\text{HCA} \times \text{FLAVO}))$. The MANOVA for the *ilr* coordinates showed that the infection/time interaction was statistically significant. The phenolic composition of T3 was significantly different from that of T1 and T2. Ripening significantly increased the ilr_1 of T1 and T2, owing to the decreased relative content of HCA and increased FLAVO. This resulted in significantly higher ilr_1 in T1 and T2 than in T3 at *d22*. The ilr_2 was significantly increased during ripening, owing to increased ANTH and decreased HCA, evidently more in T1 and T2 than in T3 (Figure 1).

The four hydroxycinnamic acid derivatives were identified in 'Brkinska češpa' fruit: the main neochlorogenic acid,[13,31] *p*-coumaroylquinic acid, chlorogenic acid, and cryptochlorogenic acid, in accordance with the results of Slimestad et al.[10]

The ANOVA for each hydroxycinnamic acid separately shows that infection/time interaction was statistically significant for the average HCA and neochlorogenic acid prevailed: T2

DOI: 10.1021/jf505330t
J. Agric. Food Chem. 2015, 63, 51–60

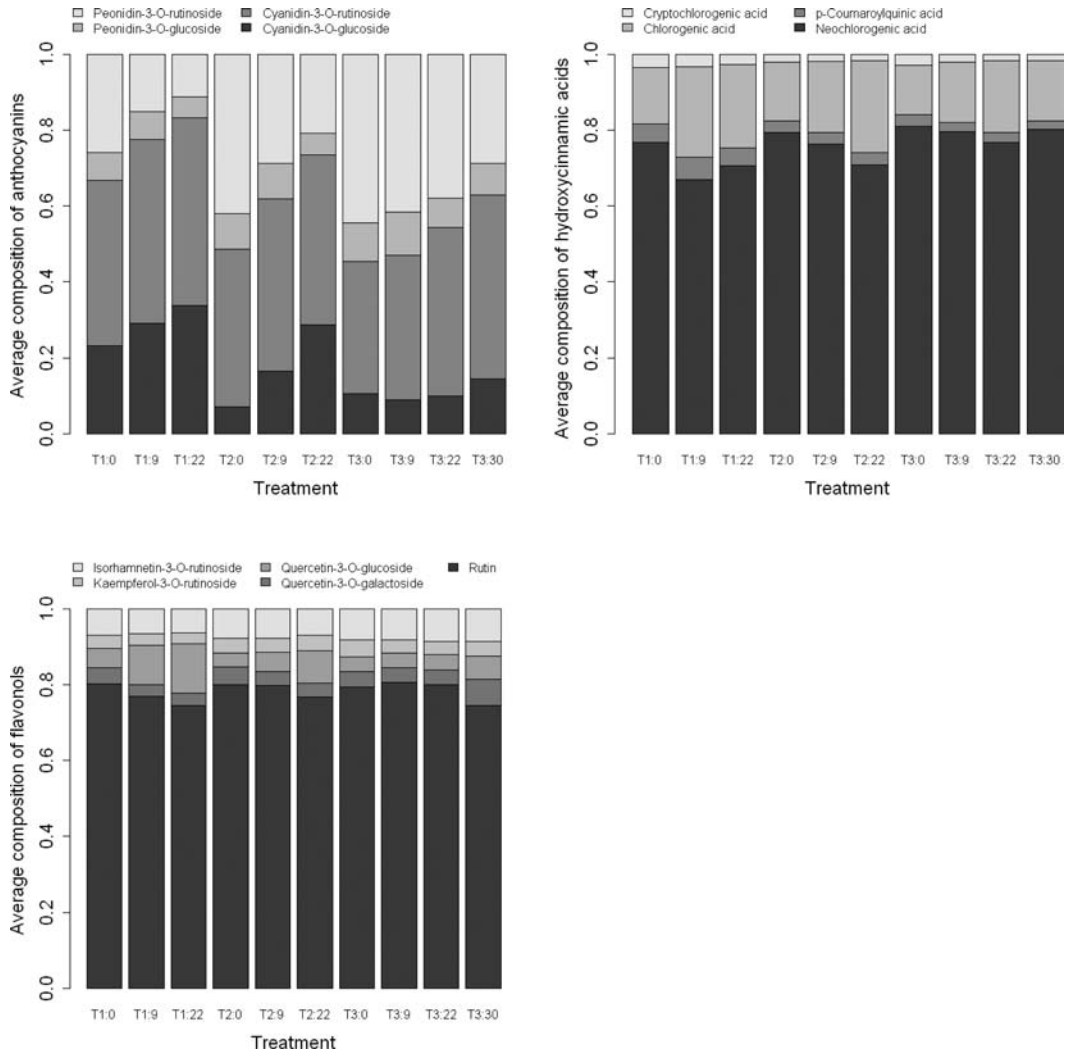

Figure 3. Effect of PPV infection (T1, long-term infection; T2, short-term infection; T3, control) on the average composition of hydroxycinnamic acids (top left), flavonols (top right), and anthocyanins (bottom right) of plum 'Brkinska češpa' during the last stages of fruit ripening (day) (0; 9; 22; 30, only T3).

and T3 had significantly more HCA than T1 (T2 more than T3) at *d0*. Ripening significantly decreases HCA and neochlorogenic acid only in T2. At the last sampling (*d22*), T3 had a significantly higher content of neochlorogenic acid and HCA than T2 and especially T1 (Table 5).

The PPV infection significantly influenced the average content of *p*-coumaroylquinic acid. Fruit of T1 had a significantly higher average content of *p*-coumaroylquinic acid than T2 and T3. There was no time trend.

Infection and time significantly influenced average content of chlorogenic acid. Fruit of T2 and T3 had significantly more chlorogenic acid than T1. Analysis shows a positive time trend.

There were no significant differences among the levels of infection in content of cryptochlorogenic acid. The content significantly decreased during ripening (the most in T3).

In the case of HCA (Figure 3), three *ilr* coordinates were calculated: $ilr_1 = c_1 \times \ln(p\text{-coumaroylquinic/neochlorogenic})$, $ilr_2 = c_2 \times \ln(\text{cryptochlorogenic/chlorogenic})$, and $ilr_3 = c_3 \times \ln(g(\text{neochlorogenic} \times p\text{-coumaroylquinic})/g(\text{chlorogenic} \times \text{cryptochlorogenic}))$. The MANOVA for *ilr* coordinates showed that the infection/time interaction was statistically significant. The coordinate ilr_1 was significantly influenced by infection—the greatest in T1 and the lowest in T3, owing to the higher relative content of neochlorogenic acid. Ripening had no significant influence on ilr_1.[13] The coordinate ilr_2 was significantly influenced by infection (the greatest in T1 and the lowest in T2) and time (ripening decreased the ilr_2). Our results show a negative time trend for the ilr_3 coordinate, with no significant effect from infection. The coordinates ilr_1 and ilr_3 show similarities between T2 and T3, but ilr_2 shows similarity between T1 and T3 on *d0* and *d9* and similarity between T2 and T3 on *d22*.

Four anthocyanins, cyanidin-3-*O*-glucoside, cyanidin-3-*O*-rutinoside, peonidin-3-*O*-glucoside, and peonidin-3-*O*-rutinoside, were identified in 'Brkinska češpa' fruit, which is in accordance with previous reports.[13,32] The relative concentration ranges were 34.8−49.4% for cyanidin-3-*O*-rutinoside, 11.1−44.4% for peonidin-3-*O*-rutinoside, 7.0−33.8% for cyanidin-3-*O*-glucoside, and 5.6−11.5% for peonidin-3-*O*-glucoside (Figure 3). Cyanidin-3-*O*-rutinoside was ascertained as the main anthocyanin in *Prunus domestica* plum.[10,12,13]

Ripening significantly increased ANTH,[11−13] in T1 and T2 more than in T3. At the beginning of the measurements, the highest content of ANTH was measured in T1. A higher content of ANTH in infected fruit shows a stress-protective role of anthocyanins in plant tissue given that they are acting as

DOI: 10.1021/jf505330t
J. Agric. Food Chem. 2015, 63, 51−60

general antioxidants in various stress situations. The measurement of h_{peel} shows similar results; T1 fruit was colored more than T2 and T3 at *d0*.

The ANOVA for each anthocyanin separately shows that infection/time interaction was statistically significant for the average cyanidin-3-*O*-glucoside and cyanidin-3-*O*-rutinoside. The highest content of both compounds was measured in T1 and T2. Ripening from *d0* to *d22* increased the content of both compounds significantly only in T1 and T2. In T3 the content of both cyanidins increased between *d22* and *d30*. The content of peonidin-3-*O*-glucoside, which increased with time, was significantly higher in T1 and T2 than in T3. The infection/time interaction was statistically significant for peonidin-3-*O*-rutinoside; the content increased with time, the most in T2 and T3.

In the case of ANTH (Figure 3), three *ilr* coordinates were calculated: $ilr_1 = c_1 \times \ln$(cyanidin-3-*O*-rutinoside/cyanidin-3-*O*-glucoside), $ilr_2 = c_2 \times \ln$(peonidin-3-*O*-rutinoside/peonidin-3-*O*-glucoside), and $ilr_3 = c_3 \times \ln(g$(cyanidin-3-*O*-glucoside × cyanidin-3-*O*-rutinoside)/g(peonidin-3-*O*-glucoside × peonidin-3-*O*-rutinoside)). The infection/time interaction was statistically significant for the ilr_1; the log-ratio of T1 and T2 during ripening decreased because of a relative increase in cyanidin-3-*O*-glucoside, but that of T3 increased slightly, owing to a relative increase in cyanidin-3-*O*-rutinoside. The ilr_2 was significantly affected by infection; the least effect was in T1 and the greatest was in T3, owing to the higher relative content of peonidin-3-*O*-rutinoside. The infection/time interaction was statistically significant for the coordinate ilr_3; ripening increased the log-ratio and resulted in a higher relative content of cyanidins in T1 and T2 but not in T3. The ilr_1, ilr_2, and ilr_3 coordinates show significant differences in the composition of anthocyanins between T1 and T3. T2 shows more similarities with T1.

The following five flavonols were identified in 'Brkinska češpa' fruit: rutin, quercetin-3-*O*-galactoside, quercetin-3-*O*-glucoside, kaempferol-3-*O*-rutinoside, and isorhamnetin-3-*O*-rutinoside. Rutin was the main flavonol compound (Figure 3).[13,32] Quercetin-3-*O*-galactoside and quercetin-3-*O*-glucoside have been previously identified in plums of *Prunus domestica*[32] and *Prunus salicina*.[33] Two novel compounds in plum fruit were identified: kaempferol-3-*O*-rutinoside and isorhamnetin-3-*O*-rutinoside (Table 1).

Infection and time significantly influenced average FLAVO (Table 7). T1 had a significantly higher content of FLAVO than T2 and T3. The increase in FLAVO during ripening was highest in T1 and lowest in T3. The levels of PPV infection, which represent various levels of stress, do influence the content of FLAVO. A higher content of FLAVO in infected fruit shows the stress-protective role of flavonols.

The ANOVA for each individual flavonol shows that infection and time significantly influenced the average content of rutin and quercetin-3-*O*-galactoside. T1 had a significantly higher content of rutin and quercetin-3-*O*-galactoside than T3. The time trend for both compounds was positive.

The infection/time interaction was statistically significant for quercetin-3-*O*-glucoside. The content was significantly the highest in T1. Ripening increased quercetin-3-*O*-glucoside—the most in T1 and the least in T3.

Infection had no significant effect on kaempferol-3-*O*-rutinoside and isorhamnetin-3-*O*-rutinoside. A positive time trend was significant for both compounds. The content of kaempferol-3-*O*-rutinoside increased the most in T2 and the least in T3. The content of isorhamnetin-3-*O*-rutinoside increased the most in T1 and the least in T3.

In the case of FLAVO (Figure 3), four *ilr* coordinates were calculated: $ilr_1 = c_1 \times \ln$(quercetin-3-*O*-galactoside/rutin), $ilr_2 = c_2 \times \ln$(kaempferol-3-*O*-rutinoside/quercetin-3-*O*-glucoside), $ilr_3 = c_3 \times \ln(g$(quercetin-3-*O*-glucoside × kaempferol-3-*O*-rutinoside)/isorhamnetin-3-*O*-rutinoside), and $ilr_4 = c_4 \times \ln(g$(quercetin-3-*O*-glucoside × kaempferol-3-*O*-rutinoside × isorhamnetin-3-*O*-rutinoside)/g(rutin × quercetin-3-*O*-galactoside)). There was no statistically significant effect of infection on the coordinate ilr_1, which from *d0* to *d22* decreased due to decreased relative content of rutin (Figure 3). The infection/time interaction was statistically significant for the ilr_2, ilr_3, and ilr_4 coordinates. The ilr_2 coordinate decreased during ripening in T1 and T2 owing to a higher increase in quercetin-3-*O*-glucoside. In T1 and T2, the ilr_3 and ilr_4 coordinates decreased significantly during ripening due to increased relative content of quercetin-3-*O*-glucoside and decreased relative content of rutin. Evident changes in the ilr_3 and ilr_4 of T3 occurred only between *d22* and *d30*, when the relative content of rutin decreased but quercetin-3-*O*-galactoside and quercetin-3-*O*-glucoside increased. These results confirm the other data; T3 fruit was ripe by *d30*, but the infection forced the process of ripening—T1 and T2 fruit ripened earlier.

Our results show that the level of PPV infection did modify the ripening process, especially fruit coloration, fruit softening, and fruit weight. The ripening process was the most forced in the long-term infected tree (T1) but resulted in inferior pomological traits. The fruits from the short-term infected tree (T2) were softer, smaller, and riper than fruit from the healthy tree (T3), but the percentage of fruit showing serious symptoms on fruit peel and in the flesh was lower than for T1.

PPV infection significantly modified the composition of nutritive and phenolic compounds, the most in fruit from the long-term PPV-infected tree (T1). The long-term infected tree (T1) yielded fruit with less glucose, malic acid, shikimic acid, sum of organic acids, neochlorogenic acid, and sum of hydroxycinnamic acids, but with more anthocyanins and flavonols than both T2 and T3. The healthy tree yielded fruit with more neochlorogenic acid and sum of hydroxycinnamic acids and less cyanidin-3-*O*-glucoside, cyanidin-3-*O*-rutinoside, peonidin-3-*O*-glucoside, and sum of anthocyanins than the short-term infected tree (T2).

Additionally, the short-term PPV infected tree produces fruit with a significantly changed phytochemicals composition. The visual appearance of such fruit has not changed significantly, but the composition of phytochemicals has, and this does determine the taste of plum, the quality of products processed from fruit, and, ultimately, human health.

AUTHOR INFORMATION

Corresponding Author

*Tel.: +386 1 320 31 43. Fax: +386 1 423 10 88. E-mail: valentina.usenik@bf.uni-lj.si.

Funding

This work is part of program Horticulture no. P4-0013-0481 funded by the Slovenian Research Agency. The work was financially supported also by the FP7 Project CropSustain, grant agreement FP7-REGPOT-CT2012-316205.

Notes

The authors declare no competing financial interest.

DOI: 10.1021/jf505330t
J. Agric. Food Chem. 2015, 63, 51−60

REFERENCES

(1) Garcìa, J. A.; Glasa, M.; Cambra, M.; Candresse, T. *Plum pox virus* and sharka: A model potyvirus and a major disease. *Mol. Plant Pathol.* **2014**, *15*, 226−241.

(2) Subr, Z.; Glasa, M. Unfolding the secrets of plum pox virus: from epidemiology to genomics. *Acta Virol.* **2013**, *57*, 217−228.

(3) Németh, M. Plum pox (Sharka). In *Virus, mycoplasma and rickettsia like diseases of fruit trees*; Akadémiai Kiadó: Budapest, Hungary, 1986; pp 463−478.

(4) Kamenova, I.; Milusheva, S. Sharka disease in Bulgaria: Past, present and future. *Biotechnol. Biotechnol. Equip.* **2005**, *19*, 22−40.

(5) Németh, M. Economic consequences of fruit tree viruses, mycoplasma- and rickettsia-like organisms. In *Virus, mycoplasma and rickettsia like diseases of fruit trees*; Akadémiai Kiadó: Budapest, Hungary, 1986; pp 43−50.

(6) Trifonov, D. Susceptibility of plum varieties to Plum pox disease. *Acta Hort.* **1975**, *44*, 163−164.

(7) Drkenda, P.; Kurtović, M. Pomological characteristics of autochthonous plum genotypes (*Prunus domestica*) from Bosnia and Herzegovina. *Acta Hort.* **2012**, *968*, 81−83.

(8) Nunes, C.; Rato, A. E.; Barros, A. S.; Saraiva, J. A.; Coimbra, M. A. Search for suitable maturation parameters to define the harvest maturity of plums (*Prunus domestica* L.): A case study of candied plums. *Food Chem.* **2009**, *112*, 570−574.

(9) Diaz-Mula, H. M.; Zapata, P. J.; Guillén, F.; Castillo, S.; Martinez-Romero, D.; Valero, D.; Serrano, M. Changes in physicochemical and nutritive parameters and bioactive compounds during development and on tree ripening of eight plum cultivars: A comparative study. *J. Sci. Food Agric.* **2008**, *88*, 2499−2507.

(10) Slimestad, R.; Vangdal, E.; Brede, C. Analysis of phenolic compounds in six Norwegian plum cultivars (*Prunus domestica* L.). *J. Agric. Food Chem.* **2009**, *57*, 11370−11375.

(11) Usenik, V.; Kastelec, D.; Veberič, R.; Štampar, F. Quality changes during ripening of plums (*Prunus domestica* L.). *Food Chem.* **2008**, *111*, 830−836.

(12) Usenik, V.; Štampar, F.; Veberič, R. Anthocyanins and fruit colour in plums (*Prunus domestica* L.) during ripening. *Food Chem.* **2009**, *114*, 529−534.

(13) Usenik, V.; Štampar, F.; Kastelec, D. Phytochemicals in fruits of two *Prunus domestica* L. plum cultivars during ripening. *J. Sci. Food Agric.* **2013**, *93*, 681−692.

(14) Tomás-Barberán, F. A.; Gil, M. I.; Cremin, P.; Waterhouse, A. L.; Hess-Pierce, B.; Kader, A. A. HPLC-DAD-ESIMS analysis of phenolic compounds in nectarines, peaches and plums. *J. Agric. Food Chem.* **2001**, *49*, 4748−4760.

(15) Usenik, V.; Štampar, F.; Kastelec, D. Indicators of plum maturity: When do plums become tasty? *Sci. Hortic. (Amsterdam, Neth.)* **2014**, *167*, 127−134.

(16) Khallouki, F.; Haubner, R.; Erben, G.; Ulrich, C. M.; Owen, R. W. Phytochemical composition and antioxidant capacity of various botanical parts of the fruits of *Prunus* × *domestica* L. from the Lorraine region of Europe. *Food Chem.* **2012**, *133*, 697−706.

(17) Rato, A. E.; Agulheiro, A. C.; Barroso, J. M.; Riquelme, F. Soil and rootstock influence on fruit quality of plums (*Prunus domestica* L.). *Sci. Hortic. (Amsterdam, Neth.)* **2008**, *118*, 218−222.

(18) Milošević, T.; Milošević, N. The physical and chemical attributes of plum influenced by rootstock. *Acta Aliment. Acad. Sci. Hung.* **2012**, *41*, 293−303.

(19) Viršček Marn, M.; Mavrič Pleško, I.; Zindović, J.; Miladinović, Z. Diversity of *Plum pox virus* isolates in Montenegro. *J. Plant Pathol.* **2012**, *94*, 201−204.

(20) Candresse, T.; Cambra, M.; Dallot, S.; Lanneau, M.; Asensio, M.; Gorris, M. T.; Revers, F.; Macquaire, G.; Olmos, A.; Boscia, D.; Quiot, J. B.; Dunez, J. Comparison of monoclonal antibodies and PCR assays for the typing of isolates belonging to the D and M serotypes of *Plum Pox Potyvirus*. *Phytopathology* **1998**, *88*, 198−204.

(21) Wang, S. Y.; Zheng, W.; Galletta, G. J. Cultural system affects fruit quality and antioxidant capacity in strawberries. *J. Agric. Food Chem.* **2002**, *50*, 6534−6542.

(22) Egozcue, J. J.; Pawlowsky-Glahn, V. Groups of parts and their balances in compositional data analysis. *Math Geol.* **2005**, *37*, 795−828.

(23) R Development Core Team. R, a language and environment for statistical computing. R Foundation for Statistical Computing: Vienna, Austria, 2013; http://www.R-project.org/.

(24) Van den Boogart, K. G.; Tolosana-Delgado, R. Compositional data analysis with the R. In *Compositional data analysis: From theory and practise*; Buccianti, A., Mateu-Figueras, G., Pawlowsky-Glahn, V., Eds.; Special Publication of the Geological Society of London; The Geological Society: London, **2006**; pp 119−127.

(25) Van den Boogart, K. G.; Tolosana-Delgado, R. "Compositions": A unified R package to analyze compositional data. *Comput. Geosci.* **2008**, *34*, 320−333.

(26) James, D.; Varga, A.; Sanderson, D. Genetic diversity of *Plum pox virus*: Strains, disease and related challenges for control. *Can. J. Plant Pathol.* **2013**, *35*, 431−441.

(27) Di Miceli, C.; Infante, R.; Inglese, P. Instrumental and sensory evaluation of eating quality of peaches and nectarines. *Eur. J. Hort. Sci.* **2010**, *75*, 97−102.

(28) Infante, R.; Contador, L.; Rubio, P.; Mesa, K.; Meneses, C. Non-destructive monitoring of flesh softening in the black-skinned Japanese plums 'Angeleno' and 'Autumn beaut' on-tree and postharvest. *Postharvest Biol. Technol.* **2011**, *61*, 35−40.

(29) Prasanna, V.; Prabha, T. N.; Tharanathan, R. N. Fruit ripening phenomena—An overview. *Crit. Rev. Food Sci. Nutr.* **2007**, *47*, 1−19.

(30) Casquero, P. A.; Guerra, M. Harvest parameters to optimize storage life of European plum 'Qullins Gage'. *Int. J. Food Sci.* **2009**, *44*, 2049−2054.

(31) Usenik, V.; Štampar, F.; Fajt, N. Pomological and phenological characteristics of some autochthonous Slovenian plum cultivars. *Acta Hortic.* **2007**, *734*, 53−59.

(32) Treutter, D.; Wang, D. W.; Farag, M. A.; Baires, G. D. A.; Ruhmann, S.; Neumuller, M. Diversity of phenolic profiles in the fruit skin of *Prunus domestica* plums and related species. *J. Agric. Food Chem.* **2012**, *60*, 12011−12019.

(33) Venter, A.; Joubert, E.; de Beer, D. Characterisation of phenolic compounds in South African plum fruits (*Prunus salicina* Lindl.) using HPLC coupled with diode-array, fluorescence, mass spectrometry and on-line antioxidant detection. *Molecules* **2013**, *18*, 5072−5090.

DOI: 10.1021/jf505330t
J. Agric. Food Chem. 2015, 63, 51−60

JOURNAL OF AGRICULTURAL AND FOOD CHEMISTRY

Article

pubs.acs.org/JAFC

Identification and Structural Elucidation of Ergotryptamine, a New Ergot Alkaloid Produced by Genetically Modified *Aspergillus nidulans* and Natural Isolates of *Epichloë* Species

Katy L. Ryan,[†] Novruz G. Akhmedov,[‡] and Daniel G. Panaccione*[,†]

[†]Division of Plant and Soil Sciences, West Virginia University, 1090 Agricultural Sciences, Morgantown, West Virginia 26505-6108, United States

[‡]Department of Chemistry, West Virginia University, 217 Clark Hall, Morgantown, West Virginia 26505-6045, United States

Supporting Information

ABSTRACT: Ergot alkaloid pathway reconstruction in *Aspergillus nidulans* is an approach used to better understand the biosynthesis of these mycotoxins. An engineered strain named *A. nidulans* WFC (expressing ergot alkaloid synthesis genes *dmaW*, *easF*, and *easC*) produced the established intermediate *N*-methyl-4-dimethylallyltryptophan, as well as an uncharacterized ergot alkaloid. We investigated the chemical structure of the new metabolite and its role in the ergot alkaloid pathway. Mass spectrometry, labeling, and NMR studies showed that the unknown ergot alkaloid, designated here as ergotryptamine, differed from *N*-methyl-4-dimethylallyltryptophan by the loss of the carboxyl group, addition of a hydroxyl group, and shift in position of a carbon−carbon double bond. Feeding studies with *Aspergillus* mutants did not show ergotryptamine turnover, suggesting it is a pathway byproduct as opposed to an authentic intermediate. Several *Epichloë* species also produced this metabolite, and further investigations revealed the equivalency of ergotryptamine with an *Epichloë*-derived ergot alkaloid provisionally described as 6,7-secolysergine.

KEYWORDS: *ergot alkaloids, mycotoxins, ergotryptamine, 6,7-secolysergine, Aspergillus, Epichloë, NMR*

INTRODUCTION

Ergot alkaloids are a class of indole-derived mycotoxins with agricultural and pharmaceutical significance. Several fungi in the family Clavicipitaceae (order Hypocreales) and a few fungi in the distantly related family Trichocomaceae (order Eurotiales) produce these secondary metabolites.[1,2] The *Epichloë* spp. (Clavicipitaceae) are endophytes of turf and forage grasses (Poaceae, subfamily Poöideae) and synthesize a variety of compounds toxic to vertebrates and invertebrates.[3] Ergot alkaloids in these grass symbionts cause toxicoses in grazing animals and are responsible for significant economic loss to livestock industries.[4,5] The phylogenetically divergent fungus *Aspergillus fumigatus* (Trichocomaceae) is a common saprotroph and opportunistic human pathogen that causes spoilage of feed in agricultural settings.[1,6,7] Compared to the *Epichloë* spp., *A. fumigatus* produces a different subset of ergot alkaloids but can serve as a prominent model organism for studying ergot alkaloid biosynthesis.[8−12]

There is considerable diversity in the later steps of the ergot alkaloid pathway due to genetic variation within ergot alkaloid gene clusters of different fungi; however, there is strong evidence that the early steps of the pathway leading to the formation of intermediate chanoclavine I, **7**, are conserved (Figure 1).[1,2,13] It was recently discovered that four genes, *dmaW*, *easF*, *easC*, and *easE*, amplified from the *A. fumigatus* genome are sufficient to direct synthesis of **7** when transgenically expressed in *Aspergillus nidulans*, a model fungus that does not contain ergot alkaloid-synthesizing genes or produce ergot alkaloids.[11] DmaW performs the determinant step of ergot alkaloid synthesis by prenylating tryptophan, **2**, to produce dimethylallyltryptophan, **3**.[9,10,14] The *easF* gene encodes a methyltransferase responsible for converting **3** into *N*-methyl-4-dimethylallyltryptophan, **4**.[12] The exact reactions catalyzed by EasE and EasC have not yet been determined, but genetic analyses demonstrate that these two genes are required to convert **4** to **7**.[8,11,15] Bioinformatics suggest that EasC is a catalase, whereas EasE is an oxidoreductase.[8,11,15] A scheme of conversion from **4** to **7** has been proposed by Kozikowski et al.[16] (Figure 1).

Previously Ryan et al.[11] investigated the roles of EasC and EasE, as well as the intermediates they produced, by reconstructing the early steps of ergot alkaloid synthesis in *A. nidulans*. A mutant strain named *A. nidulans* WFC (containing the genes *dmaW*, *easF*, and *easC* from *A. fumigatus*) accumulated ergot alkaloid pathway intermediate **4** as well as an uncharacterized ergot alkaloid of *m*/*z* 259 (referred to here as alkaloid X) not seen in control strains or the nearly isogenic transformant *A. nidulans* WFE (expressing *dmaW*, *easF*, and *easE*), which synthesized **4** but no unusual metabolites. On the basis of the genetic background of the modified *A. nidulans* strain that produces this compound and the compound's chromatographic and fluorescence properties, alkaloid X was proposed to be a derivative of **4**. In this study, we investigated the chemical structure of this new ergot alkaloid, its role as a

Received: September 22, 2014
Revised: December 8, 2014
Accepted: December 10, 2014
Published: December 10, 2014

ACS Publications © 2014 American Chemical Society

DOI: 10.1021/jf505718x
J. Agric. Food Chem. 2015, 63, 61−67

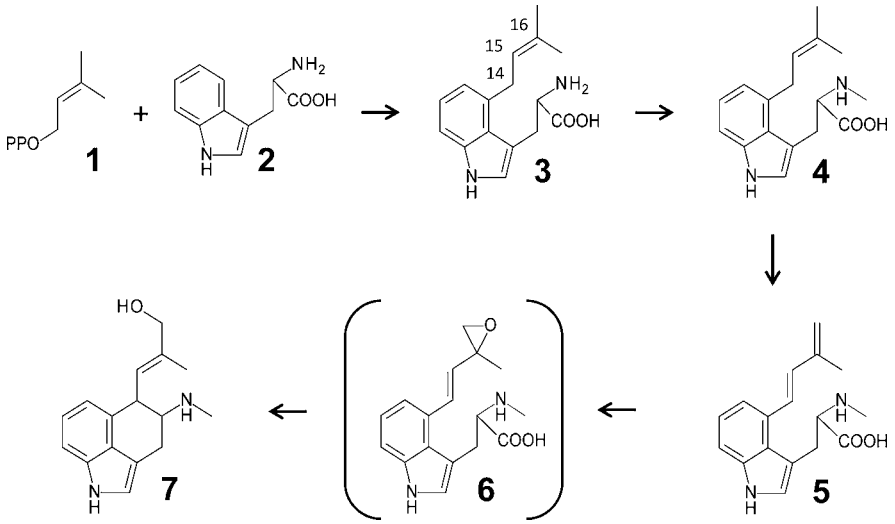

Figure 1. Early steps of ergot alkaloid synthesis (modified from Kozikowski et al.):[16] **1**, dimethlyallylpyrophosphate; **2**, L-tryptophan; **3**, dimethylallyltryptophan; **4**, *N*-methyl-4-dimethylallyltryptophan; **5**, dienyl tryptophan intermediate; **6**, hypothetical epoxide-containing intermediate; **7**, chanoclavine I.

pathway intermediate or byproduct, and whether natural ergot alkaloid producers accumulated this metabolite.

MATERIALS AND METHODS

Large-Scale Extraction and Isolation of Ergot Alkaloids. *Aspergillus nidulans* strain WFC was previously generated by Ryan et al.[11] Cultures were grown on modified ST medium (20 g/L sucrose, 20 g/L tryptone, 1 g/L $MgSO_4$, 2 mL/L trace element solution,[17] 50 mg/L nicotinic acid, 1 g/L tryptophan, 20 mL/L corn steep liquor, and 15 g/L agar) for 7 d at 37 °C. Ergot alkaloids were extracted by incubating fungal mats in 10% aqueous ammonium carbonate (25 mL of solvent per 100 × 15 mm Petri dish) for 2 h, followed by centrifugation at 5000 rpm for 10 min to pellet spores and mycelium. The extract was purified over an Isolute C18 SPE column (500 mg/3 mL) (Biotage, Charlotte, NC) as described previously.[19] Alkaloid X was eluted in 3 mL of 98% methanol/2% (v/v) glacial acetic acid for NMR spectroscopy or in 99.95% methanol/0.05% (v/v) glacial acetic acid for *Aspergillus* feeding studies. For NMR analyses, alkaloid X was purified in batches by analytical high-performance liquid chromatography (HPLC), reapplied to an Isolute C18 column, and, after elution, dried under vacuum. For *Aspergillus* feeding studies, eluate was concentrated to a final volume of 10 μL.

Feeding Studies with Labeled Tryptophan and *A. nidulans* WFC. Ten milligrams of L-tryptophan-d_5 (indole-d_5) or L-tryptophan-*1*-^{13}C (both from Sigma–Aldrich, St. Louis, MO) was dissolved in 1 mL of water, filter-sterilized through a 0.22-μm filter, and added to 99 mL of SYE agar (20 g/L sucrose, 20 g/L yeast extract, 1 g/L $MgSO_4$, 50 mg/L nicotinic acid, and 2 mL/L trace element solution) after autoclaving but prior to solidification of the medium. This medium was inoculated with *A. nidulans* WFC and incubated for 1 week at 37 °C. No deleterious effects of growing *A. nidulans* on these labeled derivatives of tryptophan were noted. Ergot alkaloids were extracted by repeatedly washing the fungal culture surface with 2 mL of methanol. The suspended cultures were incubated in methanol for 30 min, clarified by centrifugation, concentrated in a vacuum centrifuge to 50 μL, and analyzed by electrospray ionization liquid chromatography/mass spectrometry (ESI LC/MS).

Feeding Study with Alkaloid X and *Aspergillus* Mutants. *A. nidulans* strain WFE was described in Ryan et al.,[11] and *A. fumigatus easC* and *easE* knockout mutants were previously generated by Goetz et al.[8] A total of 1 × 10^6 spores was inoculated in 200 μL of liquid sucrose malt medium (15 g/L malt extract broth and 20 g/L sucrose) supplemented with 50 μmol alkaloid X and incubated for 5 days at 37 °C. Ergot alkaloids were extracted by addition of 200 μL of methanol, vortexed briefly, and incubated for 30 min at room temperature, followed by centrifugation for clarification. Samples were then analyzed by HPLC.

Yield of Alkaloid X. *A. nidulans* strain WFC was grown on ST agar for 10 days at 37 °C. One square centimeter (surface area) of fungal culture was vortexed in 400 μL of methanol and incubated for 30 min. The number of spores per microliter of suspension, which is a measure of fungal growth, was counted on a hemacytometer (Hausser Scientific, Horsham, PA). Samples were centrifuged to remove fungal matter, followed by HPLC analysis. Metabolite yield was calculated by comparison of peak areas to an ergonovine (Sigma, St. Louis, MO) standard curve and normalized to the concentration of conidia per microliter.

Extraction of Ergot Alkaloids from *Epichloë* sp.-Infected Grasses. An *lpsA* knockout strain of *Epichloë festucae* var. *lolii* × *Epichloë typhina* isolate Lp1 (henceforth called *E.* sp. Lp1), was previously generated and inoculated into perennial ryegrass (*Lolium perenne*).[18,19] Other *Epichloë* spp.-infected grasses were provided by Christopher Schardl (University of Kentucky). The *Epichloë* species studied included several species recently realigned from the genus *Neotyphodium* that have previously been known by their *Neotyphodium* sp. names.[20] Ergot alkaloids were extracted from fungal-infected grass pseudostems as previously described.[21]

High-Performance Liquid Chromatography. Samples were loaded onto a 150 mm × 4.6 mm i.d., 5-μm ODS3 Prodigy C18 column (Phenomenex, Torrance, CA) and subjected to a gradient of mobile phases A (5% acetonitrile/95% 50 mM ammonium acetate, v/v) and B (75% acetonitrile/25% 50 mM ammonium acetate) as previously described.[21] Ergot alkaloids were detected by their fluorescence at two detector settings: 272 nm excitation and 372 nm emission or 310 nm excitation and 410 nm emission. For purification of alkaloid X, *A. nidulans* WFC extracts purified by Isolute column chromatography were applied to the analytical HPLC column and runoff was collected for 30 s after alkaloid X was visualized by the detectors. Multiple batches (>10) were processed, and runoff was concentrated together for a final yield of 200 μg.

Electrospray Ionization Liquid Chromatography/Mass Spectrometry. For most analyses (other than comparison of alkaloid X from *A. nidulans* WFC to compounds extracted from *Epichloë* sp.-infected grasses), 10 μL of concentrated fungal extract was injected into a Finnigan LCQ DecaXP plus mass spectrometer equipped with a Surveyor HPLC system. Analytes were separated on a 150 mm × 2 mm i.d., 4 μm polar-RP C18 column (Phenomenex) maintained at 30 °C, by combining mobile phases A (5% acetonitrile/0.1% formic acid/94.9% water) and B (75% acetonitrile/0.1% formic acid/24.9% water) as described by Ryan et al.[11] The flow rate was 200 μL/min. Analytes

DOI: 10.1021/jf505718x
J. Agric. Food Chem. 2015, 63, 61−67

were ionized by electrospray ionization in positive mode and were detected by scanning for ions between m/z 200 and 400. MS^2 scans for compounds exhibiting m/z 259.0 also were conducted. For isotope incorporation, m/z intensities were recorded at peak retention time (alkaloid X retention time = 22 min; **4** retention time = 33 min) for the following peaks: m/z 259.0 $[\text{alkaloid X} + \text{H}]^+$; m/z 260.0 $[\text{alkaloid X} + 1 + \text{H}]^+$; m/z 263.0 $[\text{alkaloid X} + 4 + \text{H}]^+$; m/z 287.0 $[\mathbf{4} + \text{H}]^+$; m/z 288.0 $[\mathbf{4} + 1 + \text{H}]^+$; and m/z 291.0 $[\mathbf{4} + 4 + \text{H}]^+$. Eight intensity readings for each metabolite were recorded around peak intensity. Student's t test was performed with JMP (SAS, Cary, NC) to compare sample means of m/z intensity ratios for alkaloid X and **4** between samples grown on labeled **2** supplemented medium and unsupplemented medium.

Analyses of alkaloid X from *A. nidulans* WFC in comparison to compounds extracted from *Epichloë* sp.-infected grasses were conducted with different instrumentation and methods. Concentrated sample (20 μL) was analyzed on a ThermoScientific Q Exactive mass spectrometer (ThermoScientific, Waltham, MA). Analytes were separated on a 50 × 2.1 mm i.d., 1.9-μm particle size, end-capped, Hypersil Gold column (Thermo Scientific) maintained at 30 °C, by combining mobile phases A (5% acetonitrile/0.1% formic acid/94.9% water) and B (75% acetonitrile/0.1% formic acid/24.9% water) over a 10 min linear gradient of 0−100% B. The flow rate was 300 μL/min. Analytes were ionized by electrospray ionization in positive mode and were detected by scanning for ions between m/z 200 and 400. Alkaloid X had an accurate mass of 258.17337 Da, which deviated by only 0.62 ppm from the theoretical mass of $C_{16}H_{22}N_2O$.

NMR Measurements. One- and two-dimensional (1D and 2D) NMR spectra were recorded on a Varian Inova 600 MHz spectrometer at 25 °C operating at 599.67 and 150.79 MHz for proton and carbon, respectively, and equipped with a triple-resonance z-axis pulsed field gradient 5-mm probe. Sample concentration was 0.2 mg/0.7 mL (0.001 M). The free induction decays (FIDs) of the 1D and 2D NMR spectra were processed by use of the commercially available NMR software package ACD/SpecManager, Product Version 12 (Advanced Chemistry Development, Inc., Toronto, Ontario, Canada). ^{1}H NMR chemical shifts are reported relative to the tetramethylsilane (TMS) internal standard peak at 0 ppm. ^{13}C NMR chemical shifts are reported in deuterated dimethyl sulfoxide (DMSO-d_6) relative to the central peak of the septet set to 39.5 ppm. Typical parameters for acquiring ^{1}H NMR spectra were as follows: spectral width 7807.16 Hz, acquisition time 4.0 s, pulse width 3.16 μs (45°), relaxation time 2 s, and number of transients 128. The parameters for the gradient-selected 1D total correlation spectroscopy (TOCSY) were applied by use of the TOCSY1D program with spectral width 7807.16 Hz, acquisition time 4.0 s, pulse width 9.5 μs (90°), relaxation time 1 s, mixing time 80 ms, and number of transients 128. The FIDs were processed with a line broadening (lb) function of 1 Hz. The gradient-selected gCOSY spectra were acquired over both $F2$ and $F1$ with spectral width 7807.16 Hz, pulse width 9.0 μs (90°), relaxation delay 1 s, and 512 time increments of 64 transients each in magnitude mode. The FIDs were zero-filled to give a 4K × 4K data matrix, and a sine-bell function was applied in both dimensions ($F1$ and $F2$) prior to Fourier transformations giving a digital resolution of 3.81 Hz. Adiabatic versions of gradient-selected heteronuclear single quantum coherence (gHSQCAD) and heteronuclear multiple-bond correlation (gHMBCAD) spectra were acquired in phase-sensitive mode with spectral widths of 7807.16 kHz for ^{1}H ($F2$ dimension) and 37 700 Hz for ^{13}C ($F1$ dimension) by using a 2048 × 512 data matrix size and 128 transients for each $t1$ value. The carbon decoupler 90° pulse width was 10.4 μs, and one-bond coupling *j1xh* was set to 145 Hz. For evolution of long-range correlation, the multiple-bond CH coupling constant *jnxh* was set to 8 Hz and relaxation delay was set to 1.5 s. The FIDs of proton-detected gHSQCAD were processed with a Gaussian weighting function in both dimensions, whereas the FIDs of proton-detected gHMBCAD were processed with a sine-bell weighting function in $F2$ and with a Gaussian weighting function in $F1$ (carbon dimension).

NMR parameters (chemical shifts and coupling constants) for alkaloid X were determined by iterative analysis by use of the gNMR program. As starting data, the iterative process used ^{1}H NMR chemical shifts and coupling constants estimated from the experimental spectra.

RESULTS AND DISCUSSION

Insights on the Structure of Alkaloid X. *Aspergillus nidulans* WFC cultures grown on ST medium with or without d_5-labeled tryptophan, **2**, were analyzed by ESI LC/MS for the incorporation of deuterated **2** into alkaloid X as well as into the known ergot alkaloid intermediate *N*-methyl-4-dimethylallyltryptophan, **4**. During the first step of ergot alkaloid synthesis, DmaW replaces a deuterium on indole carbon 5 with a prenyl group, resulting in accumulation of ions with m/z values consistent with $[\text{M} + 4 + \text{H}]^+$ rather than $[\text{M} + 5 + \text{H}]^+$ in cultures supplemented with d_5-labeled **2**. Fungal cultures grown on medium supplemented with d_5-labeled **2** contained a significantly higher ratio of intensity values of m/z 291.0 $[\mathbf{4} + 4 + \text{H}]^+$ to m/z 287.0 $[\mathbf{4} + \text{H}]^+$ compared to control cultures grown on medium lacking d_5-labeled **2** (Figure 2). Similarly,

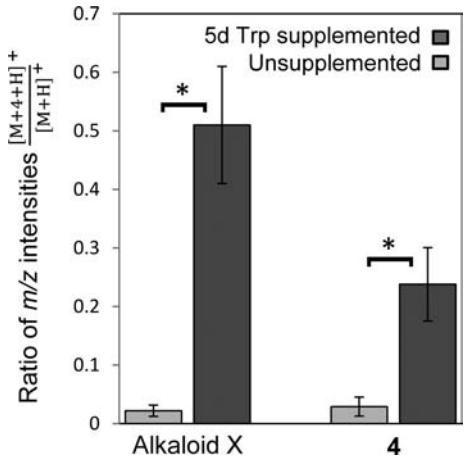

Figure 2. Derivation of alkaloid X, **8**, from L-tryptophan, **2**. Incorporation of four **2**-derived deuterium atoms into alkaloid X and *N*-methyl-4-dimethylallyltryptophan, **4**, was measured by recording intensity values for compounds with m/z 259.0 and 263.0 (for alkaloid X) and m/z 287.0 and 291.0 (for **4**). Error bars represent the standard error. Statistical significance in Student's t test is represented by * ($P < 0.05$).

extracts from fungi grown on medium supplemented with d_5-labeled **2** had a significantly higher ratio of intensity values of m/z 263.0 $[\text{alkaloid X} + 4 + \text{H}]^+$ to m/z 259.0 $[\text{alkaloid X} + \text{H}]^+$, compared to controls (Figure 2). In conjunction with genetic data that demonstrated accumulation of alkaloid X is dependent on expression of three ergot alkaloid biosynthesis genes,[11] the incorporation of deuterated **2** into alkaloid X confirms the new alkaloid is a derivative of **2**, and the accretion of m/z values consistent with $[\text{M} + 4 + \text{H}]^+$ rather than $[\text{M} + 5 + \text{H}]^+$, similar to what was observed with **4**, supports its membership in the ergot alkaloid family.

Based on high-resolution ESI LC/MS analyses, alkaloid X has a molecular formula of $C_{16}H_{22}N_2O$. When considered in relation to **4**, the molecular formula of alkaloid X is consistent with loss of the carboxyl group and addition of an oxygen. The absence of the carboxyl group in alkaloid X was tested by culturing *A. nidulans* WFC on medium supplemented with L-tryptophan-*1*-^{13}C. The presence of **4** in these cultures provided a positive control for incorporation of L-tryptophan-*1*-^{13}C. ESI LC/MS analyses of extracts from these cultures showed a

DOI: 10.1021/jf505718x
J. Agric. Food Chem. 2015, 63, 61−67

significantly greater ratio of intensity values of m/z 288.0 $[\mathbf{4} + 1 + H]^+$ to m/z 287.0 $[\mathbf{4} + H]^+$ compared to extracts from nonsupplemented control cultures (Figure 3), consistent with

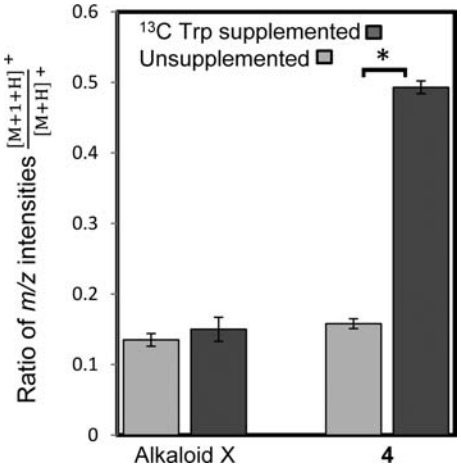

Figure 3. Lack of a carboxyl group derived from L-tryptophan, **2**, in alkaloid X, **8**. The presence of the carboxyl group was investigated by recording intensity values for compounds of m/z 259.0 and 260.0 (for alkaloid X) and compounds of m/z 287.0 and 288.0 (for **4**). Error bars represent standard error. Statistical significance in Student's t test is represented by * ($P < 0.05$).

presence of the **2**-derived carboxyl group in **4**. However, there was no difference in the ratio of intensity values of m/z 260.0 [alkaloid X + 1 + H]$^+$ to m/z 259.0 [alkaloid X + H]$^+$ in cultures grown on supplemented medium compared to controls (Figure 3). The lack of increased ^{13}C isotope incorporation into alkaloid X demonstrated the absence of the carboxyl group derived from **2** in the compound.

When genetic data on the origin of alkaloid X[11] are considered along with mass spectrometric, labeling, and fluorescence data, certain aspects of the structure of the compound can be proposed. The compound appears to be a derivative of **4**, containing a double bond conjugated to the indole ring, and lacking the carboxyl group. The compound also has an additional oxygen, which we hypothesized was located on the dimethylallyl-derived carbon 16 (customarily called carbon 8 in ergot alkaloids) as seen in **8** (Figure 4). Oxidation of **4** at this position would result in the double bond shifting

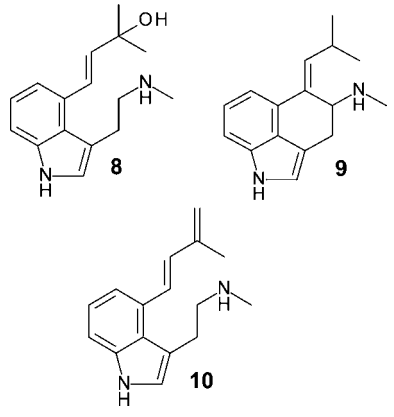

Figure 4. Chemical structures of alkaloid X or ergotryptamine, **8**; the previously proposed[19] 6,7-secolysergine, **9**; and the dehydrated derivative, **10**, of ergotryptamine.

from the 15,16 position to the 14,15 position (conjugated to the indole ring), accounting for the fluorescent properties of the molecule.

Structural Elucidation of Alkaloid X by NMR Techniques. Both 1D and 2D NMR techniques, including ^{1}H 1D TOCSY, gradient-selected ^{1}H−^{1}H gCOSY, and adiabatic versions of proton-detected gHSQCAD and gHMBCAD experiments, were used to investigate the chemical structure of alkaloid X, more specifically to identify the positions of the hydroxyl group and carbon double bond. In order to support the structural integrity of the new metabolite, ^{1}H and ^{13}C NMR spectra of **2** acquired in DMSO-d_6 were accomplished with the aid of 2D NMR techniques including gCOSY, gHSQCAD, and gHMBCAD. The lack of downfield proton H5 (δ 7.57) of the indole moiety of **2** confirms H5 substitution by the prenyl group (Figure 5). The ^{13}C NMR spectrum of alkaloid X was not acquired due to insufficient quantities (concentration 0.001 M). *A. nidulans* WFC cultures produced a low concentration of alkaloid X, with an average yield of 58 fg/spore.

The ^{1}H NMR spectrum (Figure 5) of alkaloid X in DMSO-d_6 exhibited four distinct aromatic protons downfield of the indole moiety at δ 7.10 (doublet, J = 2.4 Hz), δ 7.20 (doublet of doublets, J = 7.5, 0.8 Hz), δ 6.99 (doublet of doublets, J = 7.9, 7.5 Hz), and δ 7.01 (doublet of doublets, J = 7.9, 0.8 Hz) assigned as H2, H6, H7, and H8, respectively. Proton−proton connectivity (H6−H7−H8) through three bonds deduced from gCOSY spectrum was supported by 1D TOCSY experimental subspectra. Similarly, the contour plot of the gCOSY spectrum revealed cross peaks between the doublets, integrating for one proton each at δ 6.20 and δ 7.17 with a coupling constant of $^3J_{trans}$= 15.8 Hz, which were assigned to H14 and H15, respectively. Two upfield singlets integrating for six and three protons at δ 1.31 and 2.33, respectively were assigned to H13, H17, and H18. In the ^{1}H NMR spectrum, two aliphatic methylene (CH_2) protons appeared at δ 2.77 (triplet, J = 7.5 Hz) and δ 2.98 (triplet, J = 7.5 Hz). The chemical shift assignments of these methylene protons (10-CH_2 and 11-CH_2) were based on the observed two- and three-bond gHMBCAD correlations. The methylene protons at δ 2.98 showed long-range correlations to the carbon resonances C2, C3, and C4 of the indole moiety at δ 123.75, 113.80, and 124.24, respectively, and this peak at δ 2.98 was immediately assigned to the 10-CH_2. Due to unresolved coupling between 16-CH_3 and H15, the doublet lines at δ 7.17 were broadened and it was assigned to H15. Similarly, the doublet of doublets at δ 7.01 is broadened due to unresolved small couplings ($^5J_{HH}$) and was assigned to H8. Unambiguous assignments of H6 and H8 can be also accomplished by use of double pulsed field gradient spin echo nuclear Overhauser effect (DPFGSE NOE) spectra. Since the concentration of alkaloid X was very low (0.001 M, or 0.2 mg/0.7 mL), this experiment was not performed. NH (position 12) and OH protons are exchangeable with water in solution and consequently did not appear in the ^{1}H NMR spectrum. However, the NH (position 1) proton of the indole ring showed a broad singlet at δ 10.80. The assigned NMR parameters [^{1}H and ^{13}C chemical shifts (δ, in parts per million, ppm) and coupling constants (J, in hertz, Hz)] are listed in Table 1.

Utilization of gradient-selected 1D TOCSY experiment permitted a sequential assignment of the spin systems for different structural segments [(C_{10}−C_{11}), (C_6−C_7−C_8), and

DOI: 10.1021/jf505718x
J. Agric. Food Chem. 2015, 63, 61−67

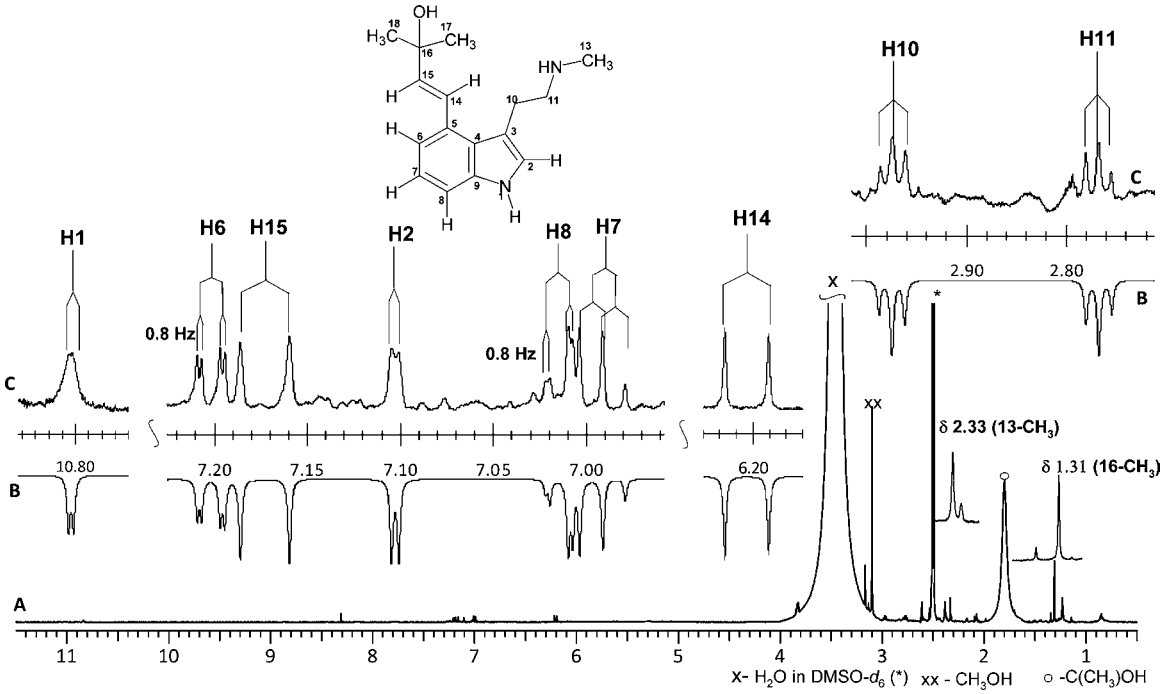

Figure 5. (A) ^{1}H NMR spectrum of alkaloid X in DMSO-d_6. The inset spectra are back-to-back representations of the expanded portions of (B) calculated and (C) experimental spectra.

Table 1. ^{1}H and ^{13}C NMR Data (Chemical Shifts and Coupling Constants) of Alkaloid X in DMSO-d_6

proton	δ_H, ppm	carbon	δ_X, ppm[a]	$^nJ_{HH}$ (n = 3, 4)	J_{Hz}
H1	10.83	C2	123.75	^3J, H1−H2	2.4
H2	7.1	C3	113.8	^3J, H6−H7	7.5
H6	7.2	C4	124.23	^3J, H7−H8	7.9
H7	6.99	C5	133.25	^4J, H6−H8	0.8
H8	7.01	C6	110.69	^3J, H10−H11	7.5
10-CH_2	2.98	C7	122.93	$^3J_{trans}$, H14−H15	15.8
11-CH_2	2.77	C8	115.87		
N−CH_3	2.33	C9	136.74		
H14	6.2	C10	27.1		
H15	7.17	C11	53.84		
H17/H18	1.31	C13	35.74		
OH	n.o.[b]	C14	129.05		
NH	n.o.	C15	140.25		
		C16	69.62		
		C17/C18	30.38		

[a] ^{13}C NMR chemical shifts are extracted from the 2D NMR spectra. [b] n.o., not observed.

(C_{14}−C_{15})] of alkaloid X by means of bond connectivities. Use of the 1D TOCSY technique removed all undesired proton frequencies and gave a clean, selective excitation ^{1}H NMR subspectrum. All selective excitation subspectra showed only those hydrogens that are in the same ^{1}H coupling network.

Once all proton connectivities were established, an iterative procedure was used to extract precise values of coupling constants for resonances of each proton (Figure 5). The determined values of couplings derived from the experimental ^{1}H NMR spectrum were used as starting couplings for an iteration of multiplicity patterns for each proton peak, generating accurate values of coupling constants. A good match between calculated and experimental splitting patterns of these protons confirmed their chemical shift assignments are correct.

A gradient version of proton-detected gHSQCAD spectrum was recorded to identify proton-bearing carbons (2-CH, 6-CH, 7-CH, 8-CH, 10-CH_2, 11-CH_2, 13-CH_3, 14-CH, 15-CH, 17-CH_3, and 18-CH_3) on the basis of one-bond correlations. The assignment of five quaternary carbons (C3, C4, C5, C9, and C16) was extracted on the basis of two ($^2J_{H-C}$) or three ($^3J_{H-C}$) gHMBCAD correlations. The contour plot of the gHMBCAD spectrum revealed a two-bond correlation between 16-CH_3 at δ 1.31 and carbon peak at δ 69.62, which is a typical chemical shift for tertiary carbon atom connected to OH group.

Complementary to the MS data, the analysis of 1D and 2D NMR spectra confirm that alkaloid X is compound **8** (Figure 4). This unique ergot alkaloid produced by *A. nidulans* WFC, (3*E*)-2-methyl-4-{3-[2-(methylamino)ethyl]-1*H*-indol-4-yl}-but-3-en-2-ol, was given the trivial name ergotryptamine due to its origin in the ergot alkaloid pathway and its structural similarity to tryptamine.

Role of Ergotryptamine (Alkaloid X) in the Ergot Alkaloid Pathway. Ergotryptamine, **8**, is a new member of the ergot alkaloid family. Genetic data[11] indicate that **8** is derived from **4**. Structural data reveal that **8** is a bicyclic ergot alkaloid lacking the carboxyl group found in precursor **4**. The biochemical scheme proposed for synthesis of chanoclavine I, **7** (Figure 1), suggests that decarboxylation coincides with closure of the third ergoline ring.[16] Here we show that decarboxylation can occur without ring closure, revealing that under some conditions these events may occur via independent reactions. Through comparison of ergot alkaloid profiles of *A. nidulans* WFE and *A. nidulans* WFC (which differ only in the presence of EasC versus EasE and the accumulation of **8** exclusively in *A. nidulans* WFC), we propose that decarboxylation of **4** or its oxidized derivative requires EasC. Enzymatic studies need to be performed to test the hypothesis that EasC can act as a decarboxylase.

DOI: 10.1021/jf505718x
J. Agric. Food Chem. 2015, 63, 61−67

The role of **8** as a pathway intermediate or byproduct was tested by feeding the metabolite to *Aspergillus* mutants, followed by HPLC analyses for the detection of downstream pathway products. *A. nidulans* WFE transformants and *A. fumigatus easC* knockout (ko) and *A. fumigatus easE* ko strains, all of which contain downstream pathway enzymes, failed to turn over **8**. These data indicate that **8** accumulates as a pathway byproduct (or spur product) that is incapable of being enzymatically converted to **7** or other pathway products.

Accumulation of Ergotryptamine in *Epichloë* Species and Equivalency with Provisional 6,7-Secolysergine. HPLC analyses revealed that ergotryptamine, **8**, displayed the same retention time (41 min) and fluorescence properties as a molecule previously observed in *E.* sp. Lp1 and provisionally named 6,7-secolysergine, **9**.[19] (Figures 4 and 6). This molecule

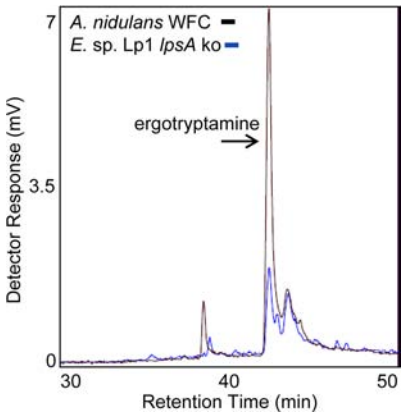

Figure 6. Accumulation of ergotryptamine, **8**, in *E. sp.* Lp1 *lpsA* ko. Ergot alkaloids produced by *A. nidulans* WFC (black) and *E.* sp. Lp1 *lpsA* ko-infected perennial ryegrass (blue) were analyzed by HPLC with fluorescence detected via 310 nm excitation and 410 nm emission.

accumulated twice as abundantly in *E.* sp. Lp1 *lpsA* ko as compared to wild-type *E.* sp. Lp1,[19] so extracts of that mutant were studied to test the identity of **8** with provisional **9**. Extracts from *E.* sp. Lp1 *lpsA* ko-infected grasses were analyzed by ESI LC/MS to further investigate potential accumulation of **8**. The Q Exactive high-resolution ESI LC/MS revealed coeluting peaks from *A. nidulans* WFC and *E.* sp. Lp1 *lpsA* ko-infected grasses with near-identical m/z values of 259.18065 and 259.18066 (Figure 7). Ionization of **8** from *A. nidulans* WFC and the coeluting molecule from *E.* sp. Lp1 *lpsA* ko led to an abundance of ionized fragment of m/z 241.17, corresponding to $[\mathbf{8} - H_2O + H]^+$ (Figure 7) and also to the apparent molecular ion previously observed for **9**.[19] This fragment was also visualized during analyses of **8** on the Finnigan LCQ LC/MS used previously and was found to be the dominant ion formed from selective fragmentation of **8**. Extracts from *E.* sp. Lp1 *lpsA* ko-infected grasses displayed similar ratios of m/z 259 parent ion to m/z 241 fragment ion (3.5:1) when compared to **8** from *A. nidulans* WFC (3.7:1). These results demonstrate the accumulation of **8** as a natural product in the fungal endophyte *E.* sp. Lp1 and provide support for the identity of **8** with the provisionally identified **9**. We propose that the apparent molecular ion detected by Panaccione et al.[19] was the dehydrated fragment of ergotryptamine, **10** (Figure 4), and that a provisional structure was proposed for the m/z 241 compound without considering bicyclic ergot alkaloids.

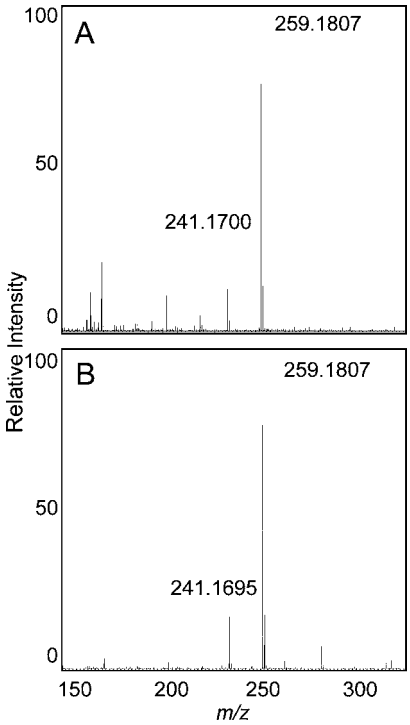

Figure 7. High-resolution ESI LC/MS spectra of ergotryptamine, **8**, in (A) *A. nidulans* WFC and (B) *Epichloë* sp. Lp1 *lpsA* ko-infected perennial ryegrass.

Several other *Epichloë* species contained a metabolite that coeluted with **8** when analyzed by fluorescence HPLC (Table 2). Fungal extracts from two asexual hybrid species, *Epichloë coenophiala* in tall fescue (*Lolium arundinaceum*) and *Epichloë funkii* in sleepy grass (*Achnatherum robustum*), contained an analyte characteristic of **8**. The sexual nonhybrid *Epichloë elymi* produced **8** in its host Canadian wild rye (*Elymus canadensis*). Although the genes necessary for synthesis of **8** are common to all ergot alkaloid producers, the accumulation of this metabolite appears to be species-specific, as we did not detect **8** in multiple extracts of *Epichloë gansuensis* in drunken horse grass (*Epichloë inebrians*) or *Epichloë festucae* var. *lolii* in perennial ryegrass (*Lolium perenne*).

Table 2. Concentrations of Ergotryptamine, 8, in Plants Containing Various *Epichloë* Species

host plant	*Epichloë* species and isolate	no. of samples	**8** (μg/g; mean ± SE)[a]
Lolium arundinaceum	*E. coenophiala* 4163	3	0.16 ± 0.04
Lolium arundinaceum	*E. coenophiala* e19	23	0.27 ± 0.08
Achnatherum robustum	*E. funkii*	5	0.32 ± 0.03
Elymus canadensis	*E. elymi*	2	1.76 ± 0.22
Lolium perenne	*E.* sp. Lp1	3	0.90 ± 0.20
Achnatherum inebrians	*E. gansuensis*	9	nd[b]
Lolium perenne	*E. festucae* var. *lolii*	8	nd

[a]All assays were conducted in the same way with same instrumentation, though tissues were of different ages and harvested at different times of year. [b]nd, not detected.

Agricultural Perspective. Ergot alkaloids cause toxicoses in livestock by interacting with multiple neurotransmitter receptors. The biological activities of ergotryptamine, **8**, are unknown, yet they remain of interest due to the accumulation

DOI: 10.1021/jf505718x
J. Agric. Food Chem. 2015, 63, 61−67

of this metabolite in prominent grass endophytes in the genus *Epichloë*. Feeding preference studies utilizing various mutant *E.* sp. Lp1-infected grasses have shown that rabbits prefer to feed on non-ergot-alkaloid-producing *E.* sp. Lp1 *dmaW* ko infected grasses rather than *E.* sp. Lp1 *lpsA* ko-infected grasses, which contained significant quantities of **7** and **8**.[22] The relative contributions of **8** relative to **7** in this feeding deterrence is unknown. Further research into the biological effects of this metabolite are needed to assess its bioactivity.

■ ASSOCIATED CONTENT

Supporting Information

One table, listing exact masses of ergotryptamine and dehydrated fragment, and five figures, showing NMR parameters of tryptophan in DMSO-d_6, gCOSY spectrum of alkaloid X, experimental 1D TOCSY subspectra of alkaloid X, gHSQCAD and gHMBCAD specta of alkaloid X, and ergotryptamine fragment from MS^2. This material is available free of charge via the Internet at http://pubs.acs.org.

■ AUTHOR INFORMATION

Corresponding Author

* Telephone 304-293-8819; e-mail danpan@wvu.edu.

Funding

This study was supported by Grant 2012-67013-19384 from USDA NIFA.

Notes

The authors declare no competing financial interest.

■ ACKNOWLEDGMENTS

This work was published with permission of the West Virginia Agriculture and Forestry Experiment Station as scientific article 3224. We thank Simona Florea, Li Chen, Padma Nagabhyru, and Christopher Schardl (University of Kentucky) for generously providing samples of endophyte-infected grasses. We also thank Brian Tapper and Geoff Lane (AgResearch, New Zealand) for confirmatory analyses and helpful comments on the manuscript. We gratefully acknowledge the use of the WVU Shared Research Facilities and the assistance of Huiyuan Li.

■ REFERENCES

(1) Panaccione, D. G. Ergot Alkaloids. In *The Mycota, Industrial Applications*; 2nd ed.; Hofrichter, M., Ed.; Springer-Verlag: Berlin, 2010; Vol. *X*, pp 195−214.

(2) Schardl, C. L.; Young, C. A.; Hesse, U.; Amyotte, S. G.; Andreeva, K.; Calie, P. J.; Fleetwood, D. J.; Haws, D. C.; Moore, N.; Oeser, B.; Panaccione, D. G.; Schweri, K. K.; Voisey, C. R.; Farman, M. L.; Jaromczyk, J. W.; Roe, B. A.; O'Sullivan, D. M.; Scott, B.; Tudzynski, P.; An, Z.; Arnaoudova, E. G.; Bullock, C. T.; Charlton, N. D.; Chen, L.; Cox, M.; Dinkins, R. D.; Florea, S.; Glenn, A. E.; Gordon, A.; Güldener, U.; Harris, D. R.; Hollin, W.; Jaromczyk, J.; Johnson, R. D.; Khan, A. K.; Leistner, E.; Leuchtmann, A.; Li, C.; Liu, J. G.; Liu, J.; Liu, M.; Mace, W.; Machado, C.; Nagabhyru, P.; Pan, J.; Schmid, J.; Sugawara, K.; Steiner, U.; Takach, J. E.; Tanaka, E.; Webb, J. S.; Wilson, E. V.; Wiseman, J. L.; Yoshida, R.; Zeng, Z. Plant-symbiotic fungi as chemical engineers: Multi-genome analysis of the Clavicipitaceae reveals dynamics of alkaloid loci. *PLoS Genet.* **2013**, *9*, No. e1003323.

(3) Schardl, C. L.; Florea, S.; Pan, J.; Nagabhyru, P.; Bec, S.; Calie, P. J. The epichloae: Alkaloid diversity and roles in symbiosis with grasses. *Curr. Opin. Plant Biol.* **2013**, *16*, 480−488.

(4) Strickland, J. R.; Brown, K. R.; Aiken, G. E.; Klotz, J. L.; Flythe, M. D. Ergot alkaloids: Toxicokinetics and vascular effects. In *International Symposium on Fungal Endophytes of Grasses*; Young, C. A., Aiken, G. E., McCulley, R. L., Strickland, J. R., Schardl, C. L., Eds.; Noble Foundation: Ardmore, OK, 2012; pp 14−19.

(5) Thompson, R. W.; Fribourg, H. A.; Waller, J. C.; Sanders, W. I.; Reynolds, J. H.; Phillips, J. M.; Schmidt, S. P.; Crawford, R. J.; Allen, V. G.; Faulkner, D. B. Combined analysis of tall fescue steer grazing studies in the eastern United States. *J. Anim. Sci.* **1993**, *71*, 1940−1946.

(6) Latgé, J. P. *Aspergillus fumigatus* and aspergillosis. *Clin. Microbial. Rev.* **1999**, *12*, 310−350.

(7) Scudamore, K. A.; Livesey, C. T. Occurrence and significance of mycotoxins in forage crops and silage: A review. *J. Sci. Food Agric.* **1997**, *77*, 1−17.

(8) Goetz, K. E.; Coyle, C. M.; Cheng, J. Z.; O'Connor, S. E.; Panaccione, D. G. Ergot cluster-encoded catalase is required for synthesis of chanoclavine-I in *Aspergillus fumigatus*. *Curr. Genet.* **2011**, *57*, 201−211.

(9) Unsöld, I. A.; Li, S.-M. Overproduction, purification and characterization of FgaPT2, a dimethylallyltryptophan synthase from *Aspergillus fumigatus*. *Microbiology* **2005**, *151*, 1499−1505.

(10) Coyle, C. M.; Panaccione, D. G. An ergot alkaloid biosynthesis gene and clustered hypothetical genes from *Aspergillus fumigatus*. *Appl. Environ. Microbiol.* **2005**, *71*, 3112−3118.

(11) Ryan, K. L.; Moore, C.; Panaccione, D. G. Partial reconstruction of the ergot alkaloid pathway by heterologous gene expression in *Aspergillus nidulans*. *Toxins* **2013**, *5*, 445−455.

(12) Rigbers, O.; Li, S.-M. Ergot alkaloid biosynthesis in *Aspergillus fumigatus*: Overproduction and biochemical characterization of a 4-dimethylallyltryptophan N-methyltransferase. *J. Biol. Chem.* **2008**, *283*, 26859−26868.

(13) Lorenz, N.; Haarmann, T.; Pažoutová, S.; Jung, M.; Tudzynski, P. The ergot alkaloid gene cluster: Functional analyses and evolutionary aspects. *Phytochemistry* **2009**, *70*, 1822−1832.

(14) Wang, J.; Machado, C.; Panaccione, D. G.; Tsai, H.-F.; Schardl, C. L. The determinant step in ergot alkaloid biosynthesis by an endophyte of perennial ryegrass. *Fungal Genet. Biol.* **2004**, *41*, 189−198.

(15) Lorenz, N.; Olšovská, J.; Šulc, M.; Tudzynski, P. Alkaloid cluster gene *ccsA* of the ergot fungus *Claviceps purpurea* encodes chanoclavine I synthase, a flavin adenine dinucleotide-containing oxidoreductase mediating the transformation of *N*-methyl-dimethylallyltryptophan to chanoclavine. *Appl. Environ. Microbiol.* **2010**, *76*, 1822−1830.

(16) Kozikowski, A. P.; Chen, C.; Wu, J.-P.; Shibuya, M.; Kim, C.-G.; Floss, H. G. Probing ergot alkaloid biosynthesis: Intermediates in the formation of ring C. *J. Am. Chem. Soc.* **1993**, *115*, 2482−2488.

(17) Hunter, S. H.; Provasoli, L.; Schatz, A.; Haskins, C. P. Some approaches to the study of the role of metals in the metabolism of microorganisms. *Am. Philos. Soc. Proc.* **1950**, *94*, 152−170.

(18) Panaccione, D. G.; Johnson, R. D.; Wang, J.; Young, C. A.; Damrongkool, P.; Scott, B.; Schardl, C. L. Elimination of ergovaline from a grass-*Neotyphodium* endophyte symbiosis by genetic modification of the endophyte. *Proc. Natl. Acad. Sci. U.S.A.* **2001**, *98*, 12820−12825.

(19) Panaccione, D. G.; Tapper, B. A.; Lane, G. A.; Davies, E.; Fraser, K. Biochemical outcome of blocking the ergot alkaloid pathway of a grass endophyte. *J. Agric. Food Chem.* **2003**, *51*, 6429−6437.

(20) Leuchtmann, A.; Bacon, C. W.; Schardl, C. L.; White, J. F.; Tadych, M. Nomenclatural realignment of *Neotyphodium* species with genus *Epichloë*. *Mycologia* **2014**, *106*, 202−215.

(21) Panaccione, D. G.; Ryan, K. L.; Schardl, C. L.; Florea, S. Analysis and modification of ergot alkaloid profiles in fungi. *Methods Enzymol.* **2012**, *515*, 267−290.

(22) Panaccione, D. G.; Cipoletti, J. R.; Sedlock, A. B.; Blemings, K. P.; Schardl, C. L.; Machado, C.; Seidel, G. E. Effects of ergot alkaloids of food preference and satiety in rabbits, as assessed with gene knockout endophytes in perennial ryegrass (*Lolium perenne*). *J. Agric. Food Chem.* **2006**, *54*, 4582−4587.

DOI: 10.1021/jf505718x
J. Agric. Food Chem. 2015, 63, 61−67

JOURNAL OF AGRICULTURAL AND FOOD CHEMISTRY

Article

pubs.acs.org/JAFC

Nematicidal Activities of 4-Quinolone Alkaloids Isolated from the Aerial Part of *Triumfetta grandidens* against *Meloidogyne incognita*

Ja Yeong Jang,[†,‡] Quang Le Dang,[§] Yong Ho Choi,[∥] Gyung Ja Choi,[∥] Kyoung Soo Jang,[∥] Byeongjin Cha,[‡] Ngoc Hoang Luu,[⊥] and Jin-Cheol Kim*[,†]

[†]Division of Applied Bioscience and Biotechnology, Institute of Environmentally Friendly Agriculture, College of Agriculture and Life Sciences, Chonnam National University, 77 Yongbong-Ro, Buk-Gu, Gwangju 500-757, Republic of Korea

[‡]Department of Plant Medicine, Chungbuk National University, 52 Naesudong-Ro, Heungdeok-Gu, Cheongju, Chungbuk 361-763, Republic of Korea

[§]Department of Phytochemistry, Vietnam Institute of Industrial Chemistry, 2 Pham Ngu Lao, Hoan Kiem District, Hanoi 10999, Vietnam

[∥]Eco-friendly New Materials Research Group, Korea Research Institute of Chemical Technology, Yuseong-Gu, Post Office Box 107, Daejeon 305-600, Republic of Korea

[⊥]Vietnam Chemicals Agency, Ministry of Industry and Trade, 91 Dinh Tien Hoang Street, Hanoi 10000, Vietnam

Supporting Information

ABSTRACT: The methanol extract of the aerial part of *Triumfetta grandidens* (Tiliaceae) was highly active against *Meloidogyne incognita*, with second-stage juveniles (J2s) mortality of 100% at 500 μg/mL at 48 h post-exposure. Two 4-quinolone alkaloids, waltherione E (**1**), a new alkaloid, and waltherione A (**2**), were isolated and identified as nematicidal compounds through bioassay-guided fractionation and instrumental analysis. The nematicidal activities of the isolated compounds against *M. incognita* were evaluated on the basis of mortality and effect on egg hatching. Compounds **1** and **2** exhibited high mortalities against J2s of *M. incognita*, with EC_{50} values of 0.09 and 0.27 μg/mL at 48 h, respectively. Compounds **1** and **2** also exhibited a considerable inhibitory effect on egg hatching, which inhibited 91.9 and 87.4% of egg hatching, respectively, after 7 days of exposure at a concentration of 1.25 μg/mL. The biological activities of the two 4-quinolone alkaloids were comparable to those of abamectin. In addition, pot experiments using the crude extract of the aerial part of *T. grandidens* showed that it completely suppressed the formation of gall on roots of plants at a concentration of 1000 μg/mL. These results suggest that *T. grandidens* and its bioactive 4-quinolone alkaloids can be used as a potent botanical nematicide in organic agriculture.

KEYWORDS: *Meloidogyne incognita, nematicidal activity, Triumfetta grandidens, 4-quinolone alkaloids*

INTRODUCTION

Nematode infestation is one of the major stresses affecting crop production worldwide. Plant parasitic nematodes, the most devastating pest groups responsible for insidious disease symptoms in different crops, are causing significant economic losses. Estimated annual yield losses in the world's major crops because of plant parasitic nematodes is about 12.3%.[1] Root knot nematodes (RKNs; *Meloidogyne* spp.), plant parasitic nematodes, have caused an estimated annual loss to world crop yields of U.S. $118 billion.[2] *Meloidogyne incognita* (Kofoid and White) Chitwood is regarded as one of the most important species in RKNs.[3] They cause plants to wither through inducing the formation of giant cells in roots of infected plants and taking nutrients from host plant roots. In addition, they cause physiological plant disorders by aiding infection of pathogenic microorganisms.

It is difficult to control RKNs because they spend their lives in the soil or plant roots. The nematode cuticle and other surface organizations make it difficult for many organic molecules to pass through.[4] Even though many synthetic nematicides, such as methyl bromide, aldicarb, and oxamyl, can be used to control RKNs, most of them are considerably toxic or volatile. Methyl bromide, the most widely used fumigant, faces prohibition of use in 2015 because of its ozone depletion and human health concern in most countries.[5,6] The demand for environmentally acceptable nematicides that can be applied in organic farm is increasing.[7] Thus, a search for alternatives, such as botanical nematicides, has recently received much attention, even though their toxic effects should be carefully evaluated before commercialization.

Plants are capable of resisting the invasion of plant parasitic nematodes by producing active substances because they live in the soil as stationary organisms.[8] These compounds can be directly used as botanical nematicides or served as templates for chemically synthesized derivatives to enhance their activity and reduce their environmental impact.[4] Plant-derived nematicidal metabolites were chemically classified into aldehydes, ketones, alkaloids, glycosides, glucosinolates, isothiocyanates, limonoids, quassinoids, saponins, phenolics, flavonoids, quinones, piperamides, polyacetylenes, polythienyls, and terpenes.[8] Research on developing phytochemical-based nematicides was attempted

Received: September 23, 2014
Revised: December 5, 2014
Accepted: December 12, 2014
Published: December 12, 2014

 © 2014 American Chemical Society

for control of nematodes. Recently, bionematicides derived from plants, such as Sincocin and NemaKILL, were developed using plant extracts and essential oils, respectively.[9] Sincocin, an environmentally friendly pesticide, is able to control citrus nematode, reniform nematode, and cyst nematode. However, it has weak activities against *M. incognita*.[9] NemaKILL, an organic nematicide for the control of soil nematodes of crops, is highly active to RKN and root lesion nematode.

In the search for botanical nematicides from Vietnamese plants, a methanol (MeOH) extract of the aerial part of *Triumfetta grandidens* Hance (Tiliaceae) showed strong activity against *M. incognita*. *Triumfetta* species, widespread across tropical regions, is reported to produce biologically active metabolites, such as triterpenoids, ceramides, alkaloids, triterpenes, polyols, steroids, lupeol, tormentic and oleanolic acids, heptadecanoic acid, β-carotene, and glycosides.[10−17] However, whether they have nematicidal compounds was not clear. Therefore, the purpose of this study was to isolate and identify nematicidal compounds from *T. grandidens* and evaluate their *in vitro* and *in vivo* activities against *M. incognita*.

MATERIALS AND METHODS

Chemicals. Abamectin was purchased from Supelco (Bellefonate, PA). Tween 20 was obtained from Sigma-Aldrich (St. Louis, MO). Sunchungtan 150EC (active ingredients: 30% fosthiazate and 70% surfactant) was purchased from Dongbu Farm Hannong (Daejeon, Korea). All organic solvents used in the study, such as MeOH, ethyl acetate (EtOAc), *n*-butanol (BuOH), chloroform ($CHCl_3$), and acetone, were of analytical grade. They are commercially available from E. Merck (Darmstadt, Germany) or Daejung Chemicals (Siheung, Korea).

Plant Materials. The aerial part of *T. grandidens* was collected by the Department of Phytochemistry, Vietnam Institute of Industrial Chemistry, and dried. Plant species was identified, and voucher specimens were deposited in the laboratory.

Extraction and Isolation of Nematicidal Metabolites. The dried material of *T. grandidens* (100 g) was chopped and then extracted twice with 70% MeOH (2 × 3 L) for 24 h at room temperature. The extracts were filtered through a Whatman No. 2 filter paper and concentrated using a rotary evaporator under vacuum to yield crude extracts (11.26 g). The MeOH extract was dissolved in 500 mL of distilled water and then successively partitioned twice with EtOAc and BuOH. The three layers were assayed for nematicidal activity against second-stage juveniles (J2s) of *M. incognita*. Of the three layers, the EtOAc layer showed the strongest nematicidal activity against *M. incognita*. Therefore, the EtOAc layer was used for further isolation of active compounds.

The EtOAc fraction (3.19 g) was subjected to chromatography on a silica gel column (3.5 × 60 cm, Kieselgel 60, 200 g, 70−230 mesh, E. Merck) with elution with $CHCl_3$/MeOH (95:5, v/v), yielding 11 fractions, F1−F11. The fractions were monitored using thin-layer chromatography (TLC) with the developing solvent $CHCl_3$/MeOH (9:1, v/v). The TLC plate used was a Kieselgel 60GF 254 with 0.25 mm layer thickness (E. Merck). The nematicidal activity of the fractions were also performed using the second-stage juvenile (J2s) of *M. incognita*. The active spot was detected by ultraviolet (UV) light (254 nm) at a R_f value of 0.4. Five fractions (F4−F8) containing the active spot were combined. The combined F4−F8 fractions (454.5 mg) were subjected to Sephadex LH 20 column chromatography. The column used was a 62 × 2.8 cm inner diameter, glass column, which was packed with 70 g of Sephadex LH20 resin (70−100 μm, Sigma-Aldrich, Vienna, Austria) and eluted with methylene chloride/*n*-hexane/MeOH (5:5:1, v/v/v). It yielded four fractions named F4-1−F4-4. The four fractions were combined (49.3 mg) and injected into Shimadzu LC-6AD prep-high-performance liquid chromatography (HPLC) equipped with a SPD-M10AVP photodiode array detector (Shimadzu, Tokyo, Japan). The column for prep-HPLC was a C_{18} reversed-phase column (Atlantis T3, 5 μm, OBD 19 × 250 mm, Waters, Co., Ireland). The solvent system was isocratic of MeOH/0.05% trifluoroacetic acid in water (55:45, v/v) at a flow rate of 3.5 mL/min. Peaks were collected for nematicidal activity bioassays. Eventually, two pure compounds **1** (8.5 mg) and **2** (9.0 mg) were isolated as nematicidal metabolites.

Structure Determination of Nematicidal Metabolites. Chemical structures of the isolated compounds were determined by one- and two-dimensional nuclear magnetic resonance (NMR) spectroscopy and electrospray ionization mass spectrometry (ESI−MS) analyses. ^{1}H and ^{13}C NMR spectra were measured in $CDCl_3$ (Cambridge Isotope Laboratories, Inc., Woburn, MA) with a Bruker AMX-500 spectrometer (Bruker Analytiche Messtechnik Gmbh, Rheinstetten, Germany) at 500 MHz for ^{1}H NMR spectra and 125 MHz for ^{13}C NMR spectra. Chemical shifts were calculated using tetramethylsilane (TMS) as the internal standard. ^{1}H and ^{13}C NMR assignments were supported by ^{1}H−^{1}H correlation spectroscopy (COSY), heteronuclear multiple-quantum coherence (HMQC), nuclear Overhauser effect spectrometry (NOESY), and heteronuclear multiple-bond correlation (HMBC) experiments. ESI−MS analyses were performed on a MSD1100 single-quadruple mass spectrometer equipped with ESI (Hewlett−Packard Co., Palo Alto, CA). The high-resolution molecular mass values of the two compounds were determined by a Synapt G2 HDMS quadrupole time-of-flight (QTOF) mass spectrometer equipped with an electrospray ion source (Waters, Milford, MA).

Nematode Juveniles. *M. incognita* was reared on tomatoes (*Lycopersicum esculentum* Mill. cv. Seokwang) for 2 months in a greenhouse at 25 ± 3 °C. Eggs were collected from infected tomato roots and extracted with 1% NaOCl solutions. The nematode eggs were obtained by passing through a 45 μm sieve. Eggs were collected on a 25 μm sieve. Surface-sterilized eggs were allowed to hatch in modified Bearmann funnels[18] at 28 °C within 5 days to obtain J2s.

Mortality Bioassay. Stock solutions of test materials obtained from aerial parts of *T. grandidens* were prepared using MeOH or acetone as the solvent. The final concentration of organic solvents did not exceed 1% of the volume. In all cases, working solutions were prepared 2 times higher than the test concentration. Nematicidal activities of the MeOH extract and solvent layers were tested at a concentration range of 7.8−500 μg/mL. Purified compounds were tested at a concentration range of 0.02−10 μg/mL. Distilled water containing MeOH or acetone alone was used as a negative control. Abamectin, a natural nematicide, was used as a positive control. Freshly hatched J2s were used within 24 h for the bioassay using 96-well tissue culture plates (Becton Dickinson, Franklin Lakes, NJ). Aliquots of 25 μL of J2s suspensions (about 50) were placed in each well. Working solutions were then added at a ratio of 1:1 (v/v). Plates were smoothly shaken and exposed to 100% of humidity in a plastic box to avoid evaporation of each well. Plates were incubated in the dark at 28 °C. Juveniles were observed under a light microscope after 24, 48, and 72 h after treatment. Nematodes were judged as dead if their bodies were straight with no movement even if physically stimulated with a fine needle. The experiment using pure compound was conducted twice with five replicates, and the other experiments using solvent layers and the fractions obtained during isolation were performed once with three replicates. The value was presented as a percentage of corrected mortality (±standard deviation). Mortality values were corrected according to Abbott's formula.[19]

$$\text{mortality (\%)} = [(\text{mortality percentage in treatment} - \text{mortality percentage in control}) / (100 - \text{mortality percentage in control})] \times 100$$

Hatching Bioassay. Egg suspension was obtained using a sieve combination of 45 and 25 μm mesh sizes. Eggs on the 25 μm sieve were collected in a beaker using distilled water. Approximately 150 eggs in 25 μL of egg suspension were transferred to each well of a 96 well plate, followed by the addition of the working solutions of purified compounds at a ratio of 1:1. Plates were gently mixed and covered with a film to prevent evaporation. The plates were incubated in the

dx.doi.org/10.1021/jf504572h | J. Agric. Food Chem. 2015, 63, 68−74

dark at 28 °C. Nematode egg hatch inhibition rate was assessed with the aid of a light microscope at 3, 7, and 14 days after treatment. Experiments were conducted twice with five replicates. Hatch inhibition (HI) was calculated using the following formula:[20]

$$\mathrm{HI}\ (\%) = [(C - T)/C] \times 100$$

where C and T represented the percentages of egg hatch in the control and treatment, respectively.

Egg hatch was calculated as follows:

$$\text{percentage of egg hatch} = 100 \times \text{juveniles}/[\text{eggs} + \text{juveniles}]$$

***In Vivo* Experiment.** Pot experiments were performed in a greenhouse at 25 °C. A total of 400 g of air-dried and steam-sterilized soil (sand/nursery soil, 1:1, v/v) was added in 9 cm plastic pots. Tomato seedlings grown on clay−loam soil in a greenhouse for 2 weeks were transplanted into the pot. Eggs of *M. incognita* were obtained from the 2 month old tomato roots. About 5000 eggs were applied to the roots of tomato seedlings using a micropipette. The MeOH extract obtained from the aerial part of *T. grandidens* was dissolved in MeOH and then diluted with 0.025% (v/v) Tween 20. Sunchungtan 150EC (active ingredients: 30% fosthiazate and 70% surfactant) was diluted 2000-fold (150 μg/mL fosthiazate) with distilled water and served as a positive control. Negative controls were treated with 0.025% (v/v) Tween 20 containing 5% MeOH. Each sample was treated at a rate of 20 mL/pot by root drench application after inoculating eggs of *M. incognita*. Experiments were performed twice with five replicates. Pots were treated after 2 weeks with 50 mL of a 0.1% solution of 20−20−20 (N−P−K) fertilizer. Experiments were terminated 6 weeks after inoculation. Galling index (GI) was assessed, and a 0−5 galling scale was used, where 0 represents no galls on roots, 1 refers to 1−2 galls per root, 2 indicates 3−10 galls per root, 3 indicates 11−30 galls per root, 4 indicates 31−100 galls per root, and 5 indicates more than 100 galls per root.[21] On the other hand, phytotoxicity, such as deformation, discoloration, and reduced growth of the plant treated, was observed.

Statistical Analysis. One-way analysis of variation (ANOVA) with Turkey's honest significant difference (HSD) test was used for multiple comparisons ($p = 0.05$). The median effective concentration (EC_{50}) values were calculated using Microsoft Excel (version 2010 software). Regression analyses were conducted using a linear regression model implemented in Excel. Statistical analyses were performed using SAS software (version 12.0, SAS Institute, Cary, NC). Statistical difference was considered when a p value was less than 0.05.

RESULTS AND DISCUSSION

Isolation and Identification of Compounds from *T. grandidens*. The MeOH extract of the aerial part of *T. grandidens* exhibited strong nematicidal activity against J2s of *M. incognita*, with 100% mortality at a concentration of 500 μg/mL after 48 h of exposure (Figure 1). To our knowledge, the biological activity of *T. grandidens* has not yet been reported. In this study, we report nematicidal activity of the MeOH extract from the aerial part of *T. grandidens* against *M. incognita*.

To isolate active nematicidal compounds, the MeOH extract was sequentially fractionated with EtOAc and BuOH. Two organic layers and one aqueous layer were tested for their nematicidal activity against *M. incognita* together with MeOH extract. Their activities against J2s of *M. incognita* are summarized in Figure 1. The MeOH extract and the EtOAc and BuOH layers showed dose-dependent activity against J2s. However, the water layer was virtually inactive. The EtOAc layer showed the strongest activity against J2s of *M. incognita*. The EC_{50} values for the EtOAc layer, MeOH extract, and BuOH layer were 8.35, 56.62, and 120.18 μg/mL, respectively.

Bioassay-guided column chromatography with instrumental analyses led to the isolation of two nematicidal compounds

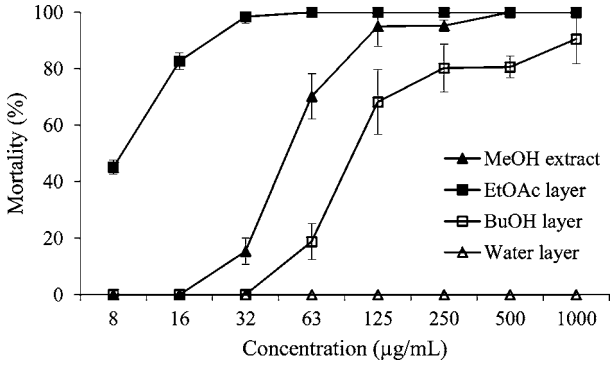

Figure 1. Nematicidal activities of the MeOH extract of the aerial part of *T. grandidens* and its three solvent extracts against the J2s of *M. incognita*. The mortalities were measured 48 h after treatment. Each value represented the mean ± standard deviation from three replicates.

(waltherione A and a new analogue named wlatherione E) from the EtOAc layer of the aerial part of *T. grandidens*.

Compound **1** was obtained as a white amorphous powder. $[\alpha]_D^{25}$ −29.0 (*c* 0.003, $CHCl_3$). ESI−MS *m/z*: 422.06 $[M - H]^-$. ^1H and ^{13}C NMR data are summarized in Table 1, which are similar to those of waltherione A and its analogues.[22−24] Compound **2** was obtained as a white amorphous powder. $[\alpha]_D^{25}$ −25.1 (*c* 0.004, $CHCl_3$). ESI−MS *m/z*: 394.26 $[M + H]^+$. ^1H and ^{13}C NMR spectra are listed in Table 1. These data were in agreement with those of waltherione A reported previously.[22,23]

^{13}C and ^1H NMR, COSY, HSQC, and HMBC spectra and the specific rotation value of compound **2**, waltherione A, were consistent with its reported literature values.[19] High-resolution ESI−QTOF mass spectrometry gave the molecular formula $C_{23}H_{23}NO_5$ ($[M + H]^+$, calcd., *m/z* 394.1654; found, *m/z* 394.1652). ^1H and ^{13}C NMR data of isolated compounds **1** and **2** are summarized in Table 1.

Compound **1**, waltherione E, was obtained as an off-white solid. High-resolution ESI−QTOF mass spectrometry gave the molecular formula $C_{24}H_{25}NO_6$ ($[M + H]^+$, calcd., *m/z* 424.1760; found, *m/z* 424.1756). ^{13}C NMR, distortionless enhancement by polarization transfer (DEPT), and HMQC spectra indicated the presence of 14 aromatic carbons between δ 111.43 and 153.06, carbonyl carbon at δ 171.06, two oxygenated methine carbons at δ 75.62 and 80.11, an oxygenated quaternary carbon at δ 78.06, two methylene carbons at δ 22.22 and 34.06, and three methoxy groups at δ 55.42, 55.86, and 60.46. The ^1H NMR spectrum of compound **1** revealed the presence of five aromatic hydrogens between 5.89 and 7.66 ppm. The ^1H NMR spectrum also revealed four methyl singlets [three at δ 3.95, 3.78, and 3.54 (3C−OMe, 2′C−OMe, and 5′C−OMe) and one at δ 2.46 (2C−Me)], two diastereotopic methylene groups at δ 2.03/2.43 and 2.01/2.33, and two methine hydrogens at δ 4.69 and 6.61. The ^1H NMR spectrum allowed for the assignment of one hydroxyl group at δ 5.12. There was no signal as a result of an amino group, probably because of rapid proton exchange rates. The ^1H and ^{13}C NMR data of compounds **1** and **2** were very similar to each other. However, compound **1** had an additional methoxy group attached to C-5′ (Table 1). ^1H NMR spectra of compound **1** indicated the presence of a trisubstituted benzene spin system, H-3′, H-4′, and H-6′, showing a doublet of a doublet, doublet, and doublet, respectively. In comparison, compound **2** showed a disubstituted benzene spin system. The homonuclear $^1H-^1H$

dx.doi.org/10.1021/jf504572h | J. Agric. Food Chem. 2015, 63, 68−74

Table 1. ^{1}H and ^{13}C NMR Data for Waltherione E and Waltherione A in $CDCl_3$ (J in Hz)

	waltherione E		waltherione A	
position	δ_C	δ_H (mult; J, Hz)	δ_C	δ_H (mult; J, Hz)
2	140.96, C		141.16. C	
3	144.09, C		143.41, C	
4	171.06, C		171.97, C	
4a	118.50, C		118.83, C	
5	141.33, C		141.54, C	
6	132.35, C		132.24, C	
7	133.17, CH	7.66, d (7.5)	133.06, CH	7.64, d (8.5)
8	117.63, CH	7.38, d (7.0)	117.52, CH	7.52, d (8.0)
8a	138.52, C		138.09, C	
9	77.95, C		78.06, C	
10	80.05, CH	4.69, d (7.5)	80.11, CH	4.70, d (7.5)
11	22.22, CH_2	a (2.03, m), b (2.43, m)	22.22, CH_2	a (2.08, m), b (2.41, m)
12	34.05, CH_2	a (2.01, m), b (2.33, m)	34.06, CH_2	a (2.01, m), b (2.35, m)
13	75.61, CH	6.61, br s	75.62, CH	6.67, d (6.0)
1′	135.53, C		134.21, C	
2′	150.48, C		156.19, C	
3′	111.43, CH	6.70, dd (9.0, 2.5)	110.89, CH	6.96, d (8.0)
4′	111.43, CH	6.88, d (8.5)	128.71, CH	7.21, dd (7.5,7.5)
5′	153.06, C		120.67, CH	6.73, dd (7.5, 7.5)
6′	119.37, CH	5.89, d (2.0)	131.64, CH	6.33, d (7.5)
2C−CH_3	14.67, CH_3	2.46, s	14.68, CH_3	2.46, s
3C−OMe	60.46 CH_3	3.78, s	60.29, CH_3	3.77, s
2′C−OMe	55.86, CH_3	3.95, s	55.51, CH_3	4.00, s
5′C−OMe	55.42, CH_3	3.54, s		

COSY spectrum of compound **1** did not show a vicinal coupling between C-5′ and C-6′ (at δ 6.70/6.88 ppm), which was observed in compound **2** (Figure 2). Furthermore, HMBC correlation of C-5′ was not observed. The relevant COSY and HMBC correlations in compounds **1** and **2** are shown in Figure 3. Thus, compound **1** was identified as 5-methoxywaltherione A and named waltherione E (Figure 2). It is reported for the first time in this study.

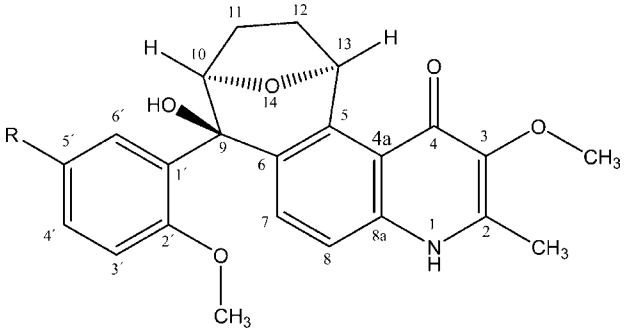

Figure 2. Chemical structures of nematicidal metabolites isolated from the aerial part of *T. grandidens*.

Waltherione A, a 4-quinolone alkaloid compound previously isolated from *Waltheria douradinha*, *Melochia chamaedrys*, and *Melochia odorata*,[23−26] has only been isolated from the Hermannieae tribe of the Sterculiaceae family. To our knowledge, the isolation of 4-quinolone alkaloids, such as waltherione A and E from *T. grandidens* of Tiliaceae, is reported for the first time in this study.

J2s Mortality and Hatch Inhibition of Compounds 1 and 2. The time course effects of the purified nematicidal metabolites on J2s are summarized in Table 2. The two compounds isolated from the aerial part of *T. grandidens* exhibited very strong nematicidal activity at 48 h post-exposure, with EC_{50} values of 0.09 μg/mL for waltherione E and 0.27 μg/mL for waltherione A, which were comparable to the abamectin positive control (EC_{50} = 0.13 μg/mL; Table 2). Nematicidal activities were increased when the exposure time increased to

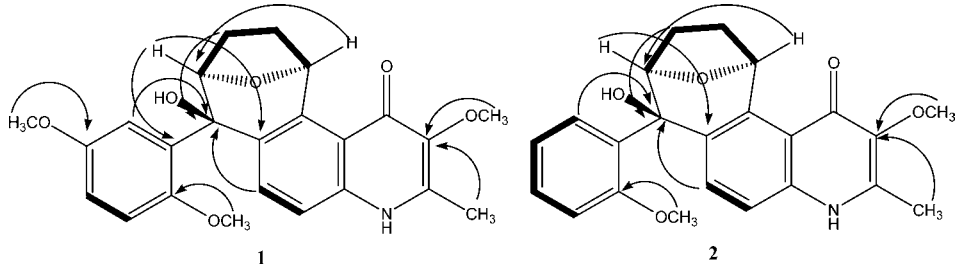

Figure 3. Significant correlation in COSY (solid lines) and HMBC (arrows) spectra of compounds **1** and **2**.

dx.doi.org/10.1021/jf504572h | J. Agric. Food Chem. 2015, 63, 68−74

Table 2. EC_{50} and R^2 Values of Purified Nematicidal Metabolites of *T. grandidnes* and Abamectin against *M. incognita* at 24, 48, and 72 h after Treatment

	EC_{50} (μg/mL)		EC_{50} (μg/mL)		EC_{50} (μg/mL)	
	24 h	R^2	48 h	R^2	72 h	R^2
waltherione E	0.15	0.96	0.09	0.94	0.08	0.96
waltherione A	0.26	0.94	0.27	0.96	0.18	0.95
abamectin	0.96	0.91	0.13	0.95	0.11	0.96

72 h, with EC_{50} values of 0.08 μg/mL for waltherione E and 0.18 μg/mL for waltherione A. The EC_{50} value for abamectin was 0.11 μg/mL at 72 h. These results revealed that waltherione E isolated from *T. grandidens* had a stronger activity than abamectin against J2s of *M. incognita*.

The two 4-quinolone alkaloids isolated from the aerial part of *T. grandidens* have stronger activities compared to other plant-derived compounds based on data reported in the literature. Caboni et al.[5] reported that phthalaldehyde, the most active aldehyde among selected aromatic aldehydes, showed a LC_{50} value of 11 ± 6 μg/mL against J2s of *M. incognita*, followed by salicylaldehyde and cinnamic aldehyde, with LC_{50} values of 11 ± 1 and 12 ± 5 μg/mL, respectively. Le Dang et al.[27] reported that squamosin G among various annonaceous acetogennins from *Annona squamosa* seeds showed nematicidal activity against *M. incognita*, with a LC_{50} value of 0.287 μg/mL after 72 h of exposure.

The two purified compounds in this study also displayed a significant inhibitory effect on egg hatching, with an inhibitory effect of over 90% at a concentration of 1.25 μg/mL on day 7 compared to the negative control (Figure 4), which was similar

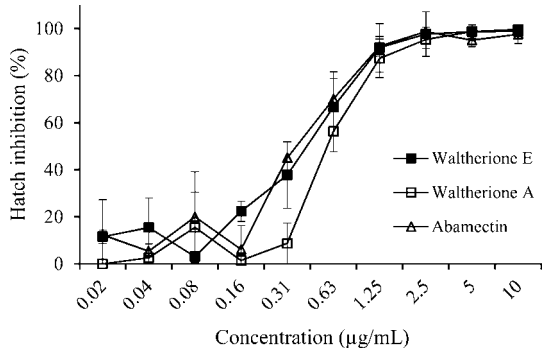

Figure 4. Inhibitory effects of waltherione E and waltherione A on egg hatching of *M. incognita* 7 days after treatment. Each value represented the mean ± standard deviation of two runs with five replicates each.

to that of abamectin. In this study, we clearly demonstrated *in vitro* that the two 4-quinolone alkaloids produced by *T. grandidens* possessed strong killing activities against J2s and an inhibitory effect on egg hatching of *M. incognita*.

Waltherione A was reported to possess antifungal activity against *Candida albicans*, *Cryptococcus neoformans*, and *Saccharomyces cerevisiae* and acetylcholinesterase inhibitory activity.[26,28] In addition, waltherione A and its analogue waltherione C displayed *in vitro* anti-human immunodeficiency virus (HIV) activity.[24] The killing effect on J2s and inhibitory effect on egg hatching of waltherione A and E from *T. grandidens* are reported for the first time in this study. The nematicidal activity of quinolone alkaloids has not been previously reported. Only thiazolidinones based on fluoroquinolone is known to have activities against *Ditylenchus myceliophagus* and *Caenorhabditis elegans*, with LD_{50} values of 210 and 240 μg/mL, respectively.[29]

The mode of action of 4-quinolone alkaloids on nematicidal activity is likely to involve acetylcholinesterase inhibition. Nematode locomotion depends upon an array of various neurons and interneurons employing the neurotransmitters acetylcholine and γ-aminobutyric acid. The effects of acetylcholine can be reduced by numerous acetylcholinesterase inhibitors, such as carbamate and organophosphate nematicides.[30−32] Even though the degree of acetylcholinesterase inhibition and nematicidal activity of the carbamate and organophosphate pesticides does not always correlate,[33,34] there is a general agreement that their toxic action upon nematodes is caused by their ability to inhibit acetylcholinesterase.[31,35,36] However, other mechanisms of the two 4-quinolone alkaloids involved in their nematicidal activity against *M. incognita* should also be considered.[33,34]

***In Vivo* Experiments.** Disease control efficacy of the MeOH extract of the aerial part of *T. grandidens* was evaluated *in vivo* using the GI index and compared to Sunchungtan, a commercial nematicide with fosthiazate as the active ingredient. The crude extract of *T. grandidens* at concentrations of 500, 1000, and 2000 μg/mL effectively reduced the formation of gall on roots of tomato plants (Figure 5). At concentrations of 1000 and 2000 μg/mL, the MeOH extract completely suppressed gall formation, which was comparable to the efficacy of Sunchungtan. In contrast, control plants had heavily galled roots (Figure 5). No phytotoxic effect of the crude extract to

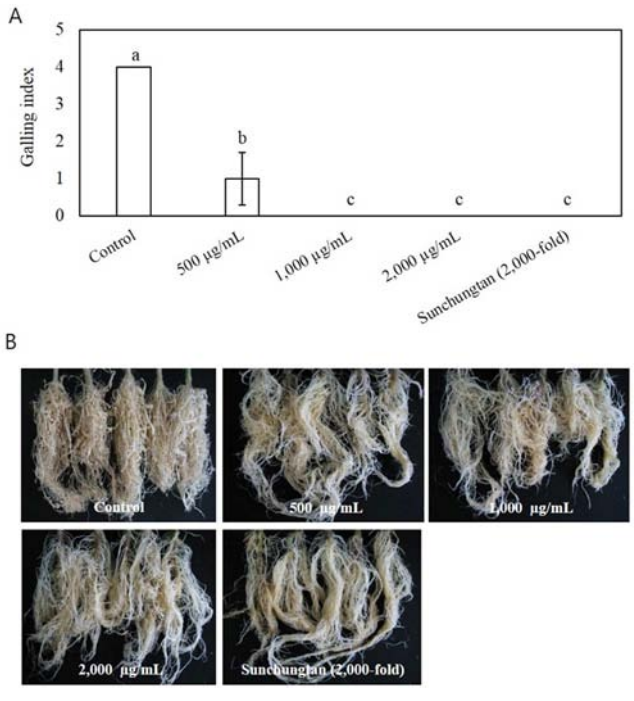

Figure 5. Effect of the MeOH extract from the aerial part of *T. graindidens* at concentrations of 500−2000 μg/mL on (A) gall formation on tomato plant roots by *M. incgonita* and (B) treated plants 6 weeks after inoculation. Sunchungtan (active ingredient 30% fosthiazate), a commercial nematicide, was diluted 2000-fold (150 μg/mL fosthiazate) as a positive control. Values were the mean ± standard deviation of combined results from two experiments with five replicates. Relationships among means were analyzed with one-way ANOVA and Turkey's HSD test (p = 0.05). Means with the same letter were not significantly different.

dx.doi.org/10.1021/jf504572h | J. Agric. Food Chem. 2015, 63, 68−74

the plants was observed. These results indicate that the crude extract of *T. grandidens* has potential as a botanical nematicide.

For the first time, our research has provided potent nematicidal activities of the crude extract of the aerial part of *T. grandidens* and its compounds waltherione E and waltherione A against *M. incognita*. The crude extract of *T. grandidens* effectively suppressed gall formation on tomato plant roots. Thus, our results suggest that the solvent extract of the aerial part of *T. grandidens* and their 4-quinolone alkaloids could be used as botanical nematicides for the control of RKNs.

■ ASSOCIATED CONTENT

Supporting Information

Typical HPLC chromatogram and UV spectra of waltherione E (**1**) and waltherione A (**2**) (Figure S1), high-resolution ESI−QTOF mass spectrum of waltherione E (**1**) (Figure S2), NMR spectra of waltherione E (**1**) (Figure S3), and contents of waltherione E (**1**) and waltherione A (**2**) in the MeOH and EtOAc extracts of *T. grandidens* (Table S1). This material is available free of charge via the Internet at http://pubs.acs.org.

■ AUTHOR INFORMATION

Corresponding Author

*Telephone: +82-62-530-2132. Fax: +82-62-530-2139. E-mail: kjinc@chonnam.ac.kr.

Funding

This study was performed with support from the Cooperative Research Program for Agricultural Science and Technology Development (Project PJ01020702), Rural Development Administration, Republic of Korea.

Notes

The authors declare no competing financial interest.

■ ACKNOWLEDGMENTS

The authors thank Dr. Young Hye Kim [Korea Basic Science Institute (KBSI)] for high-resolution ESI−QTOF mass spectrometry analysis.

■ REFERENCES

(1) Sasser, J. N.; Freckman, D. W. A world perspective on nematology: The role of the society. In *Vistas on Nematology*; Veech, J. A., Dickson, D. W., Eds.; Society of Nematologists: Hyattsville, MD, 1987; pp 7−14.

(2) McCarter, J. P. Molecular approaches toward resistance to plant-parasitic nematdoes. In *Cell Biology of Plant Nematode Parasitism*; Berg, R. H., Taylor, C. G., Eds.; Springer: St. Louis, MO, 2009; Plant Cell Monographs, Vol. *15*, pp 239−267.

(3) Hu, Y.; Zhang, W.; Zhang, P.; Ruan, W.; Zhu, X. Nematicidal activity of chaetoglobosin a produced by *Chaetomium globosum* NK102 against *Meloidogyne incognita*. *J. Agric. Food Chem.* **2013**, *61*, 41−46.

(4) Chitwood, D. J. Phytochemical based strategies for nematode control. *Annu. Rev. Phytopathol.* **2002**, *40*, 221−249.

(5) United Nations Environmental Programme (UNEP). Synthesis report of the methyl bromide interim scientific assessment and methyl bromide interim technology and economic assessment. In *Montreal Protocol Assessment Supplement*; UNEP: Nairobi, Kenya, 1992; p 33.

(6) Nyczepir, A. P.; Thomas, S. H. Current and future management strategies in intensive crop protection systems. In *Root Knot Nematodes*; Perry, R. N., Moens, M., Starr, J. L., Eds.; Cab International: Oxfordshire, U.K., 2009; pp 412−443.

(7) Oka, Y.; Ben-Daniel, B.; Cohen, Y. Nematicidal activity of the leaf powder and extracts of *Myrtus communis* against the root-knot nematode *Meloidogyne javanica*. *Plant Pathol.* **2012**, *61*, 1012−1020.

(8) Ntalli, N. G.; Caboni, P. Botanical namaticides: A review. *J. Agric. Food Chem.* **2012**, *60*, 9929−9940.

(9) Chitwood, D. J. Nematicides. In *Encyclopedia of Agrochemicals*; Plimmer, J. R., Ed.; John Wiley and Sons: New York, 2003; Vol. 3, pp 104−115.

(10) Mbosso, E. J. T.; Wintjens, R.; Lenta, B. N.; Ngouela, S.; Rohmer, M.; Tsamo, E. Chemical constituents from *Glyphaea brevis* and *Monodora myristica*: Chemotaxonomic significance. *Chem. Biol.* **2013**, *10*, 224−232.

(11) Nair, A. G. R.; Seetharaman, T. R.; Voirin, B.; Favre-Bonvin, J. True structure of triumboidin, a flavone glycoside from *Triumfetta rhomboidea*. *Phytochemistry* **1986**, *25*, 768−769.

(12) Sandjo, L. P.; Hannewald, P.; Yemloul, M.; Kirsh, G.; Ngadjui, B. T. Triumfettamide and triumfettoside Ic, two ceramides and other secondary metabolites from the stems of wild *Triumfetta cordifolia* A. Rich. (Tiliaceae). *Helv. Chim. Acta* **2008**, *91*, 1326−1335.

(13) Sandjo, L. P.; Simo, I. K.; Kuete, V.; Hannewald, P.; Yemloul, M.; Rincheval, V.; Ngadjui, B. T.; Kirsch, G.; Couty, F.; Schneider, S. Triumfettosterol Id and triumfettosaponin, a new (fatty acyl)-substituted steroid and a triterpenoid 'dimer' bis(β-D-glucopyranosyl) ester from the leaves of wild *Triumfetta cordifolia* A. Rich. (Tiliaceae). *Helv. Chim. Acta* **2009**, *92*, 1748−1759.

(14) Sandjo, L. P.; Tchoukoua, A.; Ntede, H. N.; Yemloul, M.; Perspicace, E.; Keumedjio, F.; Couty, F.; Kirsch, G.; Ngadjui, B. T. New nortriterpenoid and ceramides from stems and leaves of cultivated *Triumfetta cordifolia* A Rich (Tiliaceae). *J. Am. Oil Chem. Soc.* **2010**, *87*, 1167−1177.

(15) Sandjo, L. P.; Rincheval, V.; Ngadjui, B. T.; Kirsch, G. Cytotoxic effect of some pentacyclic triterpenes and hemisynthetic derivatives of stigmasterol. *Chem. Nat. Compd.* **2011**, *47*, 731−734.

(16) Tchoukoua, A.; Sandjo, L. P.; Keumedjil, F.; Ngadjui, B. T.; Kirsch, G. Triumfettamide B, a new ceramide from the twigs of *Triumfetta rhomboidea*. *Chem. Nat. Compd.* **2013**, *49*, 811−814.

(17) Williams, R. B. Searching for anticancer natural products from the rainforest plant of Suriname and Madagascar. Ph.D. Dissertation, Department of Chemistry, Virginia Polytechnic Instituite and State University, Blacksburg, VA, 2005; p 177.

(18) Viglierchio, D. R.; Schmitt, R. V. On the methodology of nematode extraction from field samples: Baermann funnel modifications. *J. Nematol.* **1983**, *15*, 438−444.

(19) Abbott, W. S. A method of computing the effectiveness of and insecticide. *J. Econ. Entomol.* **1925**, *18*, 265−267.

(20) Nguyen, D. M. C.; Seo, D. J.; Kim, K. Y.; Park, R. D.; Kim, D. H.; Han, Y. S.; Kim, T. H.; Jung, W. J. Nematicidal activity of 3,4-dihydroxybenzoic acid purified from *Terminalia nigrovenulosa* bark against *Meloidogyne incognita*. *Microb. Pathog.* **2013**, *59*, 52−59.

(21) Taylor, A. L.; Sasser, J. N. *Biology, Identification and Control of Root-Knot Nematodes (Meloidogyne Species)*; Department of Plant Pathology, North Carolina State University: Raleigh, NC, 1978; Vol. 2, p 111.

(22) Gressler, V.; Stuker, C. Z.; Dias, G. C. D.; Dalcol, I. I.; Burrow, R. A.; Schmidt, J.; Wessjohann, L.; Morel, A. F. Quinolone alkaloids from *Waltheria douradinha*. *Phytochemistry* **2008**, *69*, 994−999.

(23) Hoelzel, S. C.; Vieira, E. R.; Giacomelli, S. R.; Dalcol, I. I.; Zanatta, N.; Morel, A. F. An unusual quinolinone alkaloid from *Waltheria douradinha*. *Phytochemistry* **2005**, *66*, 1163−1167.

(24) Jadulco, R. C.; Pond, C. D.; Van Wagoner, R. M.; Koch, M.; Gideon, O. G.; Matainaho, T. K.; Piskaut, P.; Barrows, L. R. 4-Quinolone alkaloids from *Melochia odorata*. *J. Nat. Prod.* **2014**, *77*, 183−187.

(25) Dias, G. C. D.; Gressler, V.; Hoenzel, S. C. S. M.; Silva, U. F.; Dalcol, I. I.; Morel, A. F. Constituents of the root of *Melochia chamaedrys*. *Phytochemistry* **2007**, *68*, 668−672.

(26) Emile, A.; Waikedre, J.; Herrenknecht, C.; Fourneau, C.; Gantier, J.-C.; Hnawia, E.; Cabalion, P.; Hocquemiller, R.; Fournet, A. Bioassay-guided isolation of antifungal alkaloids from *Melochia odorata*. *Phytother. Res.* **2007**, *21*, 398−400.

(27) Le Dang, Q.; Kim, W. K.; Nguyen, C. M.; Choi, Y. H.; Choi, G. J.; Jang, K. S.; Park, M. S.; Lim, C. H.; Luu, N. H.; Kim, J.-C.

Nematicidal and antifungal activities of annonaceous acetogenins from *Annona squamosa* against various plant pathogens. *J. Agric. Food Chem.* **2011**, *59*, 11160−11167.
(28) Lima, M. M. C.; Lopez, J. A.; David, J. M.; Silva, E. P.; Giulietti, A. M.; Queiroz, L. P.; David, J. P. Acetylcholinesterase activity of alkaloids from the leaves of *Waltheria brachypetala*. *Planta Med.* **2009**, *75*, 335−337.
(29) Srinivas, V.; Nagaraj, A.; Reddy, C. H. Synthesis and biological evaluation of novel methylene-bisthiazolidinone derivatives as potential nematicidal agents. *J. Heterocycl. Chem.* **2008**, *45*, 999−1003.
(30) Debell, J. T. A long look at neuromuscular junctions in nematodes. *Q. Rev. Biol.* **1965**, *40*, 233−251.
(31) Johnson, C. D.; Stretton, A. O. W. Neural control of locomotion in *Acaris*: Antomy, electrophysiology, and biochemistry. In *Nematodes as Biological Models*; Zuckerman, B. M., Ed.; Academic Press: New York, 1980; Vol. *1*, pp 159−195.
(32) Russell, R. L.; Burns, R. H. Nematode responses to anti-AChE anthelminthics: Genetic analysis in *C. elegans*. In *Molecular Paradigms for Eradicating Helminthic Parasites*; MachInnis, A., Ed.; Alan R. Liss: New York, 1987; pp 407−420.
(33) Opperman, C. H.; Chang, S. Plant-parasitic nematode acetylcholinesterase inhibition by carbamate and organophosphate nematicides. *J. Nematol.* **1990**, *22*, 481−488.
(34) Nordmeyer, D.; Dickson, D. W. Biological activity and acetylcholinesterase inhibition by nonfumigant nematicides and their degradation products on *Meloidogyne incognita*. *Rev. Nematol.* **1990**, *13*, 229−232.
(35) Del Castillo, J.; De Mello, W. C.; Morales, T. Inhibitory action of γ-aminobutyric acid (GABA) on *Ascaris* muscle. *Experientia* **1964**, *20*, 141−143.
(36) Johnson, C. D.; Stretton, A. O. W. GABA-immunoreactivity in inhibitory motor neurons of the nematode *Ascaris*. *J. Neurosci.* **1987**, *7*, 223−235.

JOURNAL OF AGRICULTURAL AND FOOD CHEMISTRY

Article

pubs.acs.org/JAFC

Potential Toxicity of Phthalic Acid Esters Plasticizer: Interaction of Dimethyl Phthalate with Trypsin in Vitro

Yaping Wang, Guowen Zhang,* and Langhong Wang

State Key Laboratory of Food Science and Technology, Nanchang University, Nanchang 330047, China

ABSTRACT: Dimethyl phthalate (DMP) is widely used as a plasticizer in industrial processes and has been reported to possess potential toxicity to the human body. In this study, the interaction between DMP and trypsin in vitro was investigated. The results of fluorescence, UV−vis, circular dichroism, and Fourier transform infrared spectra along with cyclic voltammetric measurements indicated that the remarkable fluorescence quenching and conformational changes of trypsin resulted from the formation of a DMP−trypsin complex, which was driven mainly by hydrophobic interactions. The molecular docking and trypsin activity assay showed that DMP primarily interacted with the catalytic triad of trypsin and led to the inhibition of trypsin activity. The dimensions of the individual trypsin molecules were found to become larger after binding with DMP by atomic force microscopy imaging. This study offers a comprehensive picture of DMP−trypsin interaction, which is expected to provide insights into the toxicological effect of DMP.

KEYWORDS: *dimethyl phthalate, trypsin, interaction, spectroscopy, molecular docking, atomic force microscopy*

INTRODUCTION

Phthalic acid esters (PAEs), also known as dialkyl or alkyl aryl esters of 1,2-benzenedi-carboxylic acid, are a class of refractory organic compounds frequently added to plastics to enhance the flexibility of the materials. PAEs also serve as solvents and emulsifiers used in pharmaceuticals, pesticides, health and beauty products, and children's toys.[1,2] Because of their wide applications and growing demand, PAEs have become one of the highest yielding chemicals in the world. Their worldwide production amounts to approximately 6 million tonnes per year.[3] Because of the existence of noncovalent bonds between the phthalate plasticizers and their parent materials, PAEs can be significantly leached into the environment and lead to environmental contamination, which may cause common exposures in the general population.[4] As a kind of environmental endocrine disrupting chemical, PAEs show estrogen effects and a variety of biological toxicity. Investigations have shown that PAEs can reduce fertility and pregnancy rates in humans and animal models and can increase miscarriages and other gestational complications.[5] Epidemiologic studies have also found that early phthalate exposure can induce neurodevelopmental damage.[6] Moreover, they are suspected to cause liver, kidney, and thyroid gland tissue damage.[7] Some PAEs, such as dimethyl phthalate, diethyl phthalate, dibutyl phthalate, benzylbutyl phthalate, and di(2-ethylhexyl) phthalate, have been classified as priority environmental pollutants by the U.S. Environmental Protection Agency, European Union, and the China National Environmental Monitoring Center.[8] In recent years, excess of some PAEs has been detected sometimes in liquor and beverage in China, and their safety has attracted much attention, thus most PAEs have been listed as kinds of illegal food additives by the Ministry of Health, China.

Dimethyl phthalate (DMP, structure shown in Figure 1A) is one of the most frequently used PAEs. The impact of this chemical on the environment and its toxicity to living organisms is of great concern. DMP and its intermediates are suspected to be responsible for functional disturbances in the nervous systems and liver in animals.[9] Known for endocrine-disrupting and estrogenic activity, it may also promote chromosome injuries in human leucocytes and can interfere with the reproductive system and normal development of animals and humans.[10] Dillingham et al. have reported that DMP exhibited teratogenicity, mutagenicity, and cellular toxicity.[11] Additionally, repeated inhalation of the vapor of DMP will cause irritation of the nasal mucous membrane and lead to noticeable kidney damage.[12]

Proteinases are a kind of important protein that can cleave the covalent peptide bond between amino acids and play an important role in many biologically relevant processes.[13] As a water-soluble globular protein, trypsin belongs to a serine protease that cleaves peptide bonds at the carboxylic groups of lysine, arginine, and ornithine. This enzyme is excreted by the pancreas into the small intestine and takes part in the digestion of food proteins and other biological processes in vertebrates. Trypsin is a medium-sized protein owning 223 amino acid residues, with a molecular weight of 23.5 kDa,[14,15] and contains two domains of nearly equal size connected by six disulfide bonds. Every domain has six antiparallel β-foldings, and the active sites of trypsin are the catalytic triad, His 57, Asp 102, and Ser 195, located between the two domains.[16,17] Trypsin is often used as an important model of the digestive proteases to investigate the interactions of small molecules with proteins; it plays an essential role in digestion deconstruction of food. When DMP enters the human gastrointestinal tract, the digestive proteases may be the indirect binding targets, and there might be interaction between DMP and trypsin. The binding of some exogenous environmental pollutants with

Received: September 24, 2014
Revised: December 11, 2014
Accepted: December 11, 2014
Published: December 11, 2014

ACS Publications © 2014 American Chemical Society

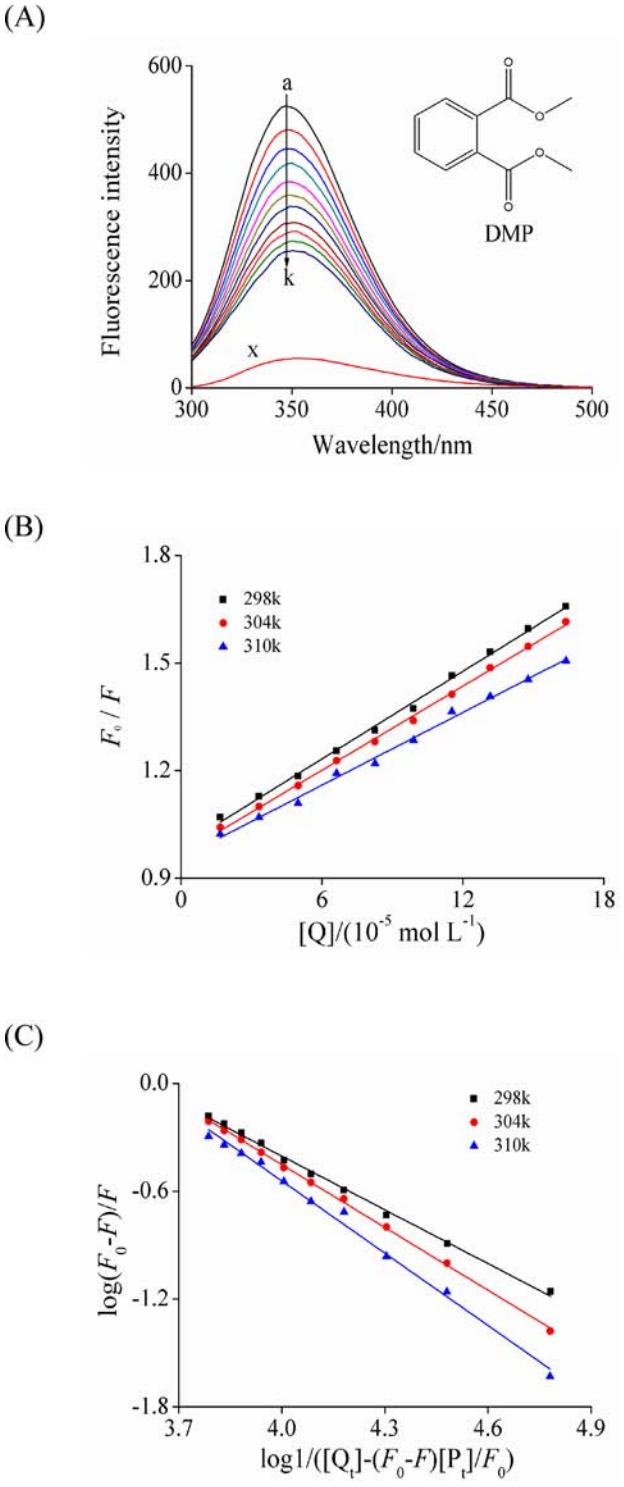

Figure 1. (A) Effect of DMP on the fluorescence spectra of trypsin (pH 7.4, T = 298 K, λ_{ex} = 280 nm, λ_{em} = 347 nm); c(trypsin) = 1.5 × 10^{-6} mol L^{-1}; c(DMP) = 0, 1.66, 3.32, 4.98, 6.62, 8.26, 9.90, 11.53, 13.16, 14.78, and 16.39 × 10^{-5} mol L^{-1} for curves a → k, respectively. Curve x shows the emission spectrum of DMP only, c(DMP) = 1.66 × 10^{-5} mol L^{-1}. Inset shows the molecular structure of DMP. (B) The Stern–Volmer plots for the fluorescence quenching of trypsin by DMP at three different temperatures. (C) log ($F_0 - F$)/F against log1/([Q_t] − ($F_0 - F$)[P_t]/F_0) plots of DMP–trypsin system.

trypsin can affect the conformation as well as the activity of trypsin and then cause the pathological changes in human body.

Wang et al. reported that the in vitro interaction of a widely used dye acid yellow 23 with trypsin induced the conformational changes of trypsin and led to the inhibition of enzyme activity.[18] To the best of our knowledge, no investigation on the interaction of DMP with trypsin has been previously reported; thus, exploring the DMP–trypsin interaction is significantly important because of the contribution to the understanding of the toxicity mechanism of DMP at the molecular level.

The present study was focused on the binding interaction between DMP and trypsin in physiological buffer (pH 7.4) with the use of a combination of spectroscopic, atomic force microscopy (AFM), cyclic voltammetric (CV), and molecular modeling approaches. The binding mode, binding site, and thermodynamic parameters of DMP with trypsin were characterized, and the conformational changes of trypsin induced by DMP were determined.

MATERIALS AND METHODS

Materials. Trypsin from bovine pancreas was purchased from Sigma Chemical Co., (St. Louis, MO); its stock solution (1.0 × 10^{-4} mol L^{-1}) was prepared by dissolving its crystals (11.8 mg) in 5 mL of Tris–HCl buffer (0.05 mol L^{-1} Tris base, 0.05 mol L^{-1} HCl, and 0.1 mol L^{-1} NaCl, pH 7.4) and then diluted to the required concentrations with the buffer. DMP (purity ≥99.5%) obtained from Aladdin Industrial Co. was prepared as a 1.0 × 10^{-2} mol L^{-1} solution in anhydrous methanol. *N*-α-Benzoyl-*L*-arginine ethyl ester (BAEE, from Aladdin Industrial Co., Shanghai, China) was dissolved in pH 7.4 Tris–HCl buffer to form a 6.0 × 10^{-3} mol L^{-1} solution. All other chemicals were of analytical reagent grade and used without further purification. Ultrapure water was used throughout the experiment.

Fluorescence Measurements. Fluorescence measurements were performed on a Hitachi spectrofluorimeter (Model F-7000, Hitachi, Japan) using a 1.0 cm path length quartz cuvette placed in a thermostat bath. A 3.0 mL solution containing 1.5 × 10^{-6} mol L^{-1} trypsin was titrated by successive additions of 1.0 × 10^{-2} mol L^{-1} DMP stock solution. After the solutions were mixed thoroughly and kept for 5 min, the fluorescence spectra of the solutions were measured in the wavelength range of 300–500 nm upon exciting the samples at 280 nm using 2.5/2.5 nm slit widths. The corresponding emission spectra of free DMP were measured as blanks (i.e., successive addition of DMP solutions into 3.0 mL Tris–HCl buffer) to eliminate background signal. Additionally, fluorescence intensities were corrected for the inner-filter effect before analysis of the binding and quenching data using the relationship[19]

$$F_c = F_m e^{(A_1+A_2)/2} \quad (1)$$

where A_1 and A_2 are the absorbance of DMP at excitation and emission wavelengths, and F_c and F_m represent the corrected and measured fluorescence, respectively. The intensity of fluorescence used in this paper was the corrected fluorescence intensity.

Synchronous fluorescence spectra of trypsin in the absence and presence of DMP were measured by setting the excitation and emission wavelength interval ($\Delta\lambda$) at 15 and 60 nm. The appropriate blank corresponding to the free DMP and buffer was subtracted to correct for background fluorescence.

UV–vis Absorption Measurements. The UV–vis absorbance spectra of trypsin, DMP, and DMP–trypsin mixtures were recorded at room temperature on a Shimadzu UV–2450 spectrophotometer (Shimadzu, Japan) at wavelengths between 200 and 320 nm.

The enzyme activity was measured spectrophotometrically by continuously measuring *N*-α-benzoyl-*L*-arginine (BA) formation at a wavelength of 253 nm with BAEE as the substrate.[20] A series of assay solutions dissolved in 0.05 mol L^{-1} Tris–HCl buffer (pH 7.4) containing different concentrations of DMP and a fixed concentration of trypsin (1.5 × 10^{-6} mol L^{-1}) was prepared and incubated for 3 h at

dx.doi.org/10.1021/jf5046359 | J. Agric. Food Chem. 2015, 63, 75–84

Table 1. Quenching Constants (K_{SV}), Binding Constants (K), and Relative Thermodynamic Parameters of the DMP−Trypsin System

T (K)	K_{SV} (× 10^3 L mol^{-1})	R^a	K (× 10^3 L mol^{-1})	n	R^b	$\Delta H°$ (kJ mol^{-1})	$\Delta G°$ (kJ mol^{-1})	$\Delta S°$ (J mol^{-1} K^{-1})
298	4.07	0.9988	3.92	1.00	0.9986		−20.51	
304	3.90	0.9992	4.08	1.16	0.9996	4.16	−21.01	82.80
310	3.37	0.9976	4.19	1.33	0.9969		−21.51	

^aR is the correlation coefficient for the K_{SV} values. ^bR is the correlation coefficient for the K values.

37 °C (the concentration of methanol was less than 0.03% in the total reaction volume). The assay was initiated by adding the DMP−trypsin complex solution to the substrate (BAEE, 7.0 × 10^{-4} mol L^{-1}), and the absorbance of the mixture at 253 nm was then determined every 20 s at room temperature. The enzymatic activity without DMP was defined as 100%. Relative enzymatic activity (%) = (slope of reaction kinetics equation obtained by reaction with inhibitor)/(slope of reaction kinetics equation obtained by reaction without inhibitor) × 100.[21]

Molecular Simulation. Molecular modeling of the DMP−trypsin complexation was performed using AutoDock 4.2 and AutoDockTools 1.5.6 (ADT). The crystal structure of trypsin (PDB code 2ZQ1) was taken from the Protein Data Bank (http://www.rcsb.org/pdb).[22] Water molecules were removed, polar hydrogens were added, and Kollman united atom partial charges were assigned during protein preparation. The 3D structure of DMP was constructed in Sybyl ×1.1 (Tripos Inc., St. Louis, U.S.), and its energy-minimized conformation was obtained with the help of the MMFF94 force field using MMFF94 charges. During the docking study, a grid box defined to enclose the entire binding site of trypsin with dimensions of 126 Å × 126 Å × 126 Å and a grid spacing of 0.375 Å was used. The Lamarckian genetic algorithm (LGA) was applied to search binding conformations, and a total of 100 runs were carried out during docking simulation.

Atomic Force Microscopy (AFM) Measurements. AFM measurements were carried out in tapping mode using an Asylum Research atomic force microscope (MFP-3D SA) at room temperature. Silicon nitride probes from Olympus (USA) with spring constants of 0.3−4.8 N m^{-1} were used. The tip radius of the probes was 9 ± 2 nm, and rectangular cantilevers with a length of 240 μm were used. The scanning rate was set at 1 Hz. Samples imaged in air were prepared by a drop 5 μL of the trypsin solution in the absence and presence of DMP on freshly cleaved mica at the required concentrations and dried overnight. Images were processed with the Igor Pro 6.3 software package and were presented unfiltered.

Cyclic Voltammetric (CV) Experiments. CV experiments were carried out on a CHI-660B electrochemical workstation (Chenhua Instrumental Company, Shanghai) with a three-electrode system. The working electrode was a glassy carbon disk electrode; an Ag/AgCl electrode was selected as the reference electrode with a Pt wire as the counter electrode. The concentration of DMP was kept at 1.0 × 10^{-5} mol L^{-1}, and the trypsin solution was added at different concentrations in the range of 0−1.5 × 10^{-6} mol L^{-1}. All test solutions were thoroughly deoxygenated by bubbling high-purity nitrogen for 10 min. A stream of nitrogen was blown gently across the surface of the solution in order to maintain the solution anaerobic throughout all the experiments.

Circular Dichroism (CD) Spectra. CD spectra in the far-UV region (190−250 nm) were recorded at room temperature on a Bio-Logic MOS 450 CD spectrometer (Bio-Logic, Claix, France) using a quartz cell with 1 mm path length in pH 7.4 Tris−HCl buffer under constant nitrogen flush. The concentration of trypsin was kept at 1.5 × 10^{-5} mol L^{-1}, while the DMP concentration was varied by keeping the molar ratios of DMP to trypsin as 0:1, 2:1, and 5:1. All of the obtained CD spectra were corrected for buffer signal. The online SELCON3 program (http://dichroweb.cryst.bbk.ac.uk/html/home.shtml) was used to analyze the CD spectroscopic data to obtain the contents of different secondary structures of trypsin.

Fourier Transform Infrared (FT-IR) Measurements. FT-IR spectra were performed on a Thermo Nicolet-5700 FT-IR spectrometer (Thermo Nicolet Co., USA) equipped with a germanium attenuated total reflection (ATR) accessory and a DTGS KBr detector. All spectra were taken via the ATR method with resolution of 4 cm^{-1} and 60 scans. The FT-IR spectra of free trypsin (1.5 × 10^{-5} mol L^{-1}) and DMP−trypsin complex (the molar ratio of DMP to trypsin was kept at 5:1) were recorded in the range of 1800−1400 cm^{-1} at room temperature. The corresponding absorbance contributions of buffer and free DMP solutions were recorded and subtracted with the same instrumental parameters.

RESULTS AND DISCUSSION

Fluorescence Quenching of Trypsin by DMP. Fluorescence quenching of protein usually attributed to a variety of molecular interactions including excited-state reactions, energy transfer, ground-state complex formation, and collisional quenching.[23] As shown in Figure 1, panel A, trypsin displayed a strong emission peak at 347 nm on excitation at 280 nm, and the peak intensity of trypsin decreased gradually with increased amounts of DMP. When the added concentration of DMP reached 1.64 × 10^{-4} mol L^{-1}, nearly 51.7% decrease in the fluorescence intensity of the peak accompanied by a 4 nm red shift was observed, which suggests that DMP interacted with trypsin, and the microenvironment of the fluorescence chromophore of trypsin was altered upon binding with DMP.

Quenching of protein fluorescence induced by a quencher can be classified as either dynamic quenching or static quenching, and the quenching mechanism can be distinguished based on their temperature dependence.[24] To speculate the fluorescence quenching mechanism, the fluorescence titration experiments were carried out at 298, 304, and 310 K, and the data were analyzed by the well-known Stern−Volmer equation:

$$\frac{F_0}{F} = 1 + K_{SV}[Q] = 1 + K_q\tau_0[Q] \quad (2)$$

where F_0 and F represent the fluorescence intensities in the absence and presence of DMP, K_{SV} is the Stern−Volmer dynamic quenching constant, and its value can be determined by linear regression of a plot of F_0/F against $[Q]$. K_q is the quenching rate constant of the biomolecule, $K_q = K_{SV}/\tau_0$. τ_0 is the average lifetime of the fluorophore without quencher (τ_0 = 2.80 × 10^{-9} s),[25] and $[Q]$ is the concentration of DMP.

The Stern−Volmer plots (Figure 1B) obtained at different temperatures showed a good linear relationship, which suggests a single quenching procedure between DMP and trypsin occurred, and the corresponding K_{SV} values for the DMP−trypsin complex are listed in Table 1. An inverse correlation between K_{SV} and temperature (decrease tendency of K_{SV} with increasing temperatures) was observed, which indicates that the probable fluorescence quenching mechanism of trypsin by DMP was initiated by complex formation, namely, static quenching.[26] Moreover, larger K_q values (1.45 × 10^{12}, 1.39 × 10^{12}, and 1.20 × 10^{12} L mol^{-1} s^{-1} at 298 K, 304 K, and 310 K, respectively) for the DMP−tryspin complexation compared to the reported maximum scatter collision quenching constant (2

dx.doi.org/10.1021/jf5046359 | J. Agric. Food Chem. 2015, 63, 75−84

$\times 10^{10}$ mol L^{-1} s^{-1}) also indicated that the quenching process was mainly governed by a static quenching procedure.[27]

Binding Constants and Number of Binding Sites. To further characterize the binding properties of DMP with trypsin, the binding constant K and the number of binding sites n for the DMP−trypsin complex were determined using the following equation:[28]

$$\log \frac{F_0 - F}{F} = n \log K - n \log \frac{1}{[Q_t] - \frac{(F_0 - F)[P_t]}{F_0}} \quad (3)$$

where F_0 and F are the same as in eq 2. $[Q_t]$ and $[P_t]$ stand for the total concentration of the ligand and the protein, respectively. From the intercept and slope of the regression curve of $\log (F_0 - F)/F$ versus $\log 1/([Q_t] - (F_0 - F)[P_t]/F_0)$ (Figure 1C), the values of K and n at the three temperatures were calculated (Table 1). Because of the n values approximately equal to 1, it can be inferred that there was a single class of binding sites on trypsin for DMP. The increasing trend of K with rising temperature suggested that the DMP−tryspin interaction was an endothermic reaction and that the increasing temperature was in favor of this binding.[29] The K value at 298 K was 3.92×10^3 L mol^{-1}, which was similar to that of a previous report on DMP interaction with HSA.[30]

Prediction of Binding Site of DMP on Trypsin. As a serine protease, the enzymatic mechanism of trypsin is similar to that of other serine proteases, with a catalytic triad (His57, Asp102, and Ser195).[31] Trypsin contains the primary substrate-binding pocket (S1 binding pocket) formed by amino acid residues 189−195, 214−220, and 225−228.[32] To predict the binding site of DMP on trypsin, the molecular modeling was employed to simulate the binding mode between DMP and trypsin.

Cluster analysis of 100 docking runs showed a total of nine multimember conformational clusters at a root−mean−square deviation (rmsd) tolerance of 2.0 Å (Figure 2A). The cluster with the lowest binding energy (red histogram in Figure 2A) was found to contain the highest number of the analyzed conformations (38 out of 100), which was the most energetically favorable. Thus, the cluster possessed the lowest energy (−5.12 kcal mol^{-1}), and the most frequent locus was used for binding orientation analysis; the obtained energy information is given in Table 2. The calculated binding Gibbs free energy ($\Delta G_{binding}$ = intermolecular energy + torsional energy) was −5.12 kcal mol^{-1}, which was equal to the predicted binding energy (−5.12 kcal mol^{-1}), which indicates that the docking result was credible.

As shown in Figure 2, panel B, DMP did not bind into the S1 binding pocket of trypsin, while it had a high affinity very close to the active site pocket, especially adjacent to the catalytic residues (His 57, Asp 102, and Ser 195). It was observed that DMP was surrounded by the amino acid residues including Phe41, Cys42, Ala56, His57, Tyr59, Asp102, Met104, Gly193, and Ser195. Moreover, two hydrogen bonds were formed between the oxygen atoms of DMP and the hydrogen atoms on Ser195 and Gly193 of trypsin, and their bond lengths were 1.712 and 2.187 Å, respectively, which suggested the involvement of hydrogen bonding in the DMP−tryspin interaction. The docking results indicated that DMP actually interacted with the catalytic residues located in the region close to the S1 binding pocket of trypsin, and the binding may affect the enzymatic activity.

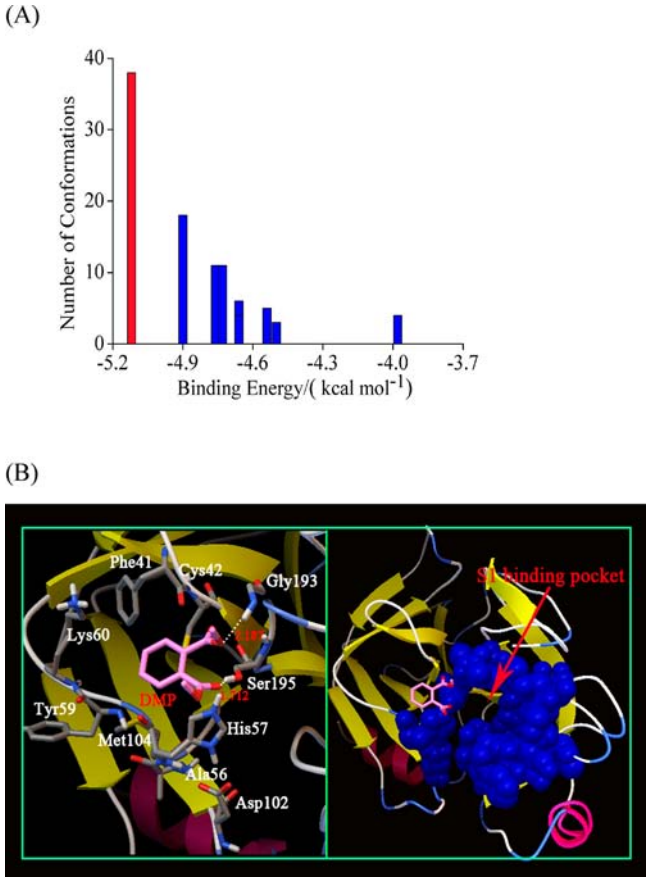

Figure 2. (A) Cluster analysis of the AutoDock docking runs of DMP with trypsin. (B) The interaction site between DMP (showing stick representation) and trypsin (ribbon form). The white dashed lines stand for hydrogen bonds.

Thermodynamic Parameters and Binding Forces. A thermodynamic process was considered to be responsible for the formation of a complex considered from the dependence of binding constant on temperature.[33] Therefore, the thermodynamic parameters including enthalpy change ($\Delta H°$), entropy change ($\Delta S°$), and free energy change ($\Delta G°$) of the interaction were analyzed to further characterize the bonding force between DMP and trypsin using the following equations:

$$\log K = -\frac{\Delta H°}{2.303RT} + \frac{\Delta S°}{2.303R} \quad (4)$$

$$\Delta G° = \Delta H° - T\Delta S° \quad (5)$$

where R is the gas constant (8.314 J mol^{-1} K^{-1}), T is the experimental temperature (298, 304, and 310 K), and K is the binding constant at the corresponding temperature. The calculated values of $\Delta H°$, $\Delta S°$, and $\Delta G°$ are summarized in Table 1. The negative signal for $\Delta G°$ showed that the interaction process was spontaneous. The positive $\Delta H°$ and $\Delta S°$ values indicated that hydrophobic interactions played a major role in the binding of DMP to trypsin based on the rule generalized by Ross and Subramanian.[34] It was obvious that the $\Delta G°$ value (−4.91 kcal mol^{-1}) at 298 K was a little larger than the calculated $\Delta G°$ value from molecular modeling. This difference could be explained by the fact that X-ray structure of the protein from crystals was different from that of the aqueous system used in this study.[35]

dx.doi.org/10.1021/jf5046359 | J. Agric. Food Chem. 2015, 63, 75−84

Table 2. Binding Free Energies of DMP−Trypsin Interaction with the Most Favorable Docking Gesture

complex	intermol energy (kcal mol^{-1})	internal energy (kcal mol^{-1})	torsional energy (kcal mol^{-1})	binding energy (kcal mol^{-1})	$\Delta G_{binding}$ (kcal mol^{-1})
DMP−trypsin	−6.31	−0.53	1.19	−5.12	−5.12

Effect of DMP on Trypsin Activity. As shown in Figure 3, trypsin activity decreased with the incremental addition of DMP, and the enzymatic activity decreased to 62.3% of the initial level when the concentration of DMP reached to 1.0×10^{-4} mol L^{-1}, which indicates that the interaction of DMP with trypsin can inhibit the enzymatic activity. There are two fundamental characteristics about the active site region of trypsin: (i) the catalytic triad composed of amino acid residues His 57, Asp 102, and Ser 195; (ii) the S1 binding pocket was near Ser 195, which can define the cut position of the peptidic bond.[36] If a ligand enters into the hydrophobic pocket or locates near this pocket, the enzymatic activity could be affected.[37] This experimental result further supported the molecular docking studies.

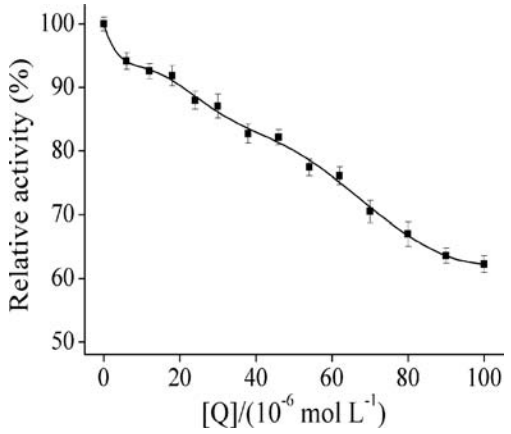

Figure 3. Trypsin activity in the absence and presence of DMP at different concentrations. c(trypsin) = 1.5×10^{-6} mol L^{-1}, and c(BAEE) = 7.0×10^{-4} mol L^{-1}.

Changes in Trypsin Topography. AFM is a very useful imaging technique in visualizing the interaction between small molecules and protein owing to its high resolution. To study the changes in trypsin topography following by the addition of DMP, AFM was performed on the free trypsin and the DMP−trypsin complex in pH 7.4 Tris−HCl buffer.

As shown in Figure 4, panel A, the trypsin was adsorbed evenly on the mica surfaces, and its topography image can be clearly observed. Cross-sectional images of two single trypsin molecules are given. After the widths of 50 single trypsin molecules were averaged, 5.0 nm was obtained for the mean width. The mean height of the individual trypsin molecules adsorbed on mica was determined to be 0.8 nm. This average width was larger than the reported data (3.8 nm) based on X-ray diffraction studies.[38] Upon complexation with DMP, trypsin molecules appeared to be more swollen on the mica substrate (Figure 4B), and the mean width and height of the individual trypsin molecules reached 12.0 and 2.5 nm, respectively. The increase in the size indicated that DMP interacted with trypsin and that a DMP−trypsin complex was formed. After binding with DMP, the stable dispersion of the protein aggregation became more evident in the AFM photograph, which suggests that the formation of the DMP−trypsin complex may cause a major destabilization of the native conformation of trypsin. From the three-dimensional graph of free trypsin and the DMP−trypsin complex (Figure 4C,D), it was clearly observed that the interaction between DMP and trypsin induced the topography image changes of trypsin and aggregation, which may be due to the changes of microenvironment around the trypsin molecule and the enzyme molecule exposing to a more hydrophobic environment after interaction with DMP. To minimize the number of unfavorable factors to form a stable structure, the trypsin molecule reduced its surface area in contact with water by molecular aggregation. The results suggested that hydrophobic interactions existed between trypsin and DMP, which was consistent with that of above thermodynamic analysis.

Electrochemical Behavior of DMP in the Presence of Trypsin. The cyclic voltammograms of DMP in the absence and presence of trypsin are shown in Figure 5. DMP exhibited a deoxidization peak at −0.98 V in pH 7.4 Tris−HCl buffer, which was the characteristic of the electroactive moiety of DMP. When trypsin was added to the DMP solution, a positive shift of the deoxidization peak along with a decrease in peak current was found, and no new peak was observed in the same scan potential range. These results indicated that the binding interaction between DMP and trypsin occurred and the electro−inactive complex was formed.[39] It was difficult for DMP in the complex to make contact with the electrode surface, and the free DMP concentration on the electrode surface was reduced after bonding with trypsin; thus, the peak current was decreased.[40]

Effect of DMP on the Conformation of Trypsin. UV−vis absorbance spectroscopy is widely used to explore the conformational changes of protein and to investigate ligand−protein complex formation. Figure 6 shows the difference of absorption spectra of trypsin after interaction with DMP, which were obtained by subtracting the corresponding absorption spectra of free DMP from those of DMP−trypsin complex. Trypsin has two main absorption peaks located at 205 and 280 nm. The stronger absorption peak at 205 nm reflects the peptide bond absorption peak that is due to the $\pi \rightarrow \pi^*$ transition of trypsin's characteristic polypeptide backbone structure C═O, and the weaker one at 280 nm appears to be due to the absorption of aromatic amino acids.[41] With the addition of DMP to trypsin solution, the peak at 205 nm shifted obviously toward the longer wavelength, and the intensity decreased sharply, which suggests that the binding of DMP to trypsin may cause the conformational change of trypsin. Moreover, decrease in the peak intensity at 280 nm also suggested that the polarity of the microenvironment around Trp and Tyr residues of trypsin was affected by the interaction with DMP.

Alteration in the microenvironment around the fluorophores (Tyr and Trp) of trypsin was further explored by synchronous fluorescence spectra. Figure 7, panels A and B display the effect of the increasing concentrations of DMP on the synchronous fluorescence spectra of trypsin when the scanning interval $\Delta\lambda$ was fixed at 15 and 60 nm, respectively. Upon the addition of DMP, the maximum emission wavelength of Tyr residue at $\Delta\lambda$

dx.doi.org/10.1021/jf5046359 | J. Agric. Food Chem. 2015, 63, 75−84

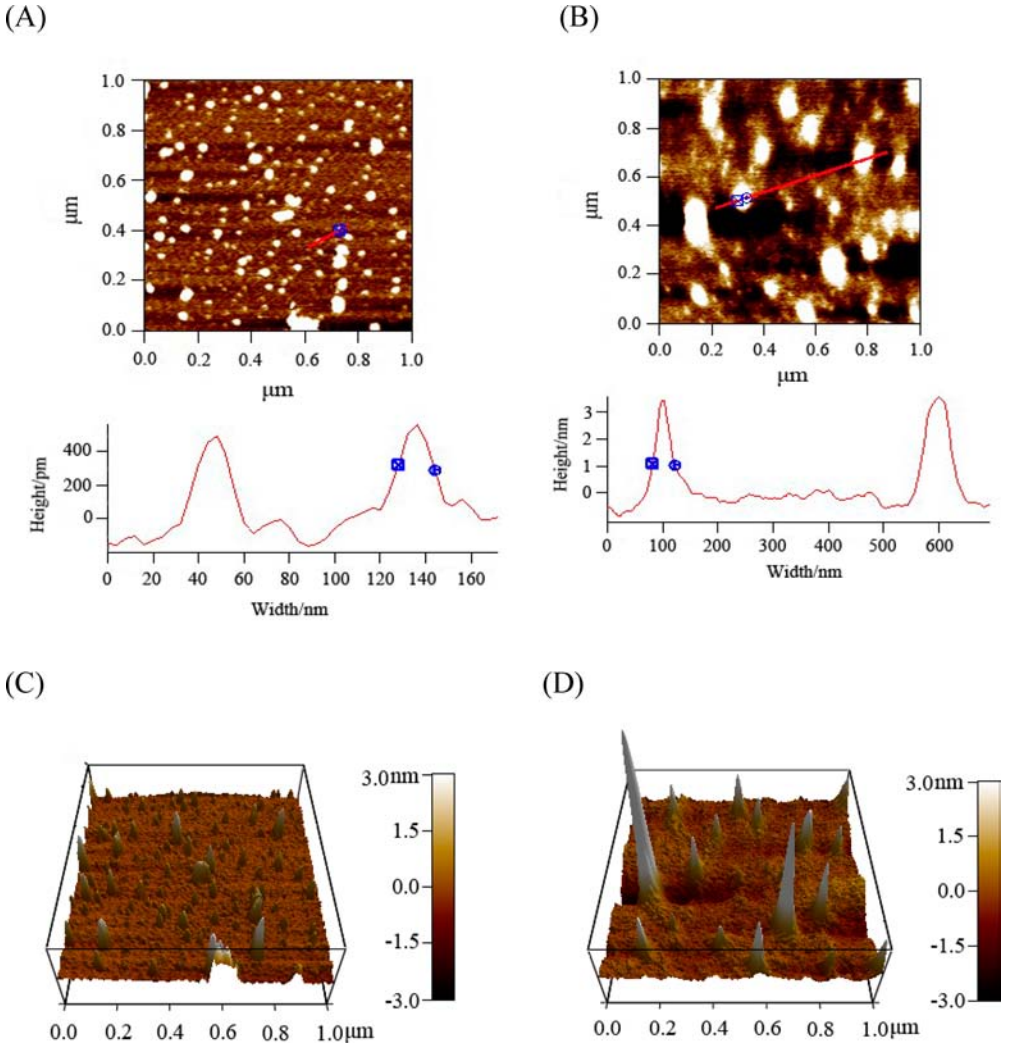

Figure 4. AFM topography image of (A) trypsin and the (B) DMP−trypsin complex adsorbed onto mica with tapping mode in air, and the scan size of the image is 1.0 μm × 1.0 μm. Panels C and D are the three-dimensional graphs for panels A and B, respectively. c(trypsin) = 1.5 × 10^{-9} mol L^{-1}, c(DMP) = 1.5 × 10^{-8} mol L^{-1}.

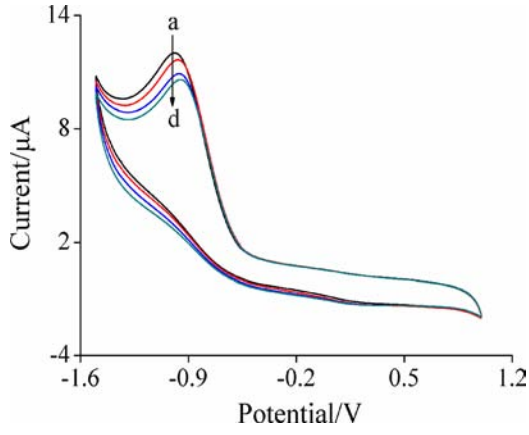

Figure 5. Cyclic voltammograms of DMP and DMP treated with different concentrations of trypsin. c(DMP) = 1.0 × 10^{-5} mol L^{-1}; c(trypsin) = 0, 5.0, 10.0, and 15.0 × 10^{-7} mol L^{-1} for curves a → d, respectively.

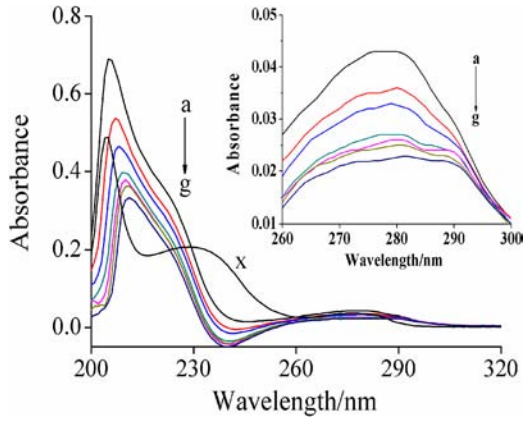

Figure 6. UV−vis absorption spectra of trypsin in the presence of DMP at different concentrations. c(trypsin) = 1.5 × 10^{-6} mol L^{-1}; c(DMP) = 0, 1.66, 3.32, 4.98, 6.62, 8.26, and 9.90 × 10^{-5} mol L^{-1} for curves a → g, respectively. Curve x shows the absorption spectrum of DMP only. c(DMP) = 1.66 × 10^{-5} mol L^{-1}. (inset) The UV spectra of the DMP−trypsin system in the wavelength range of 260−300 nm.

= 15 nm showed inconspicuous shift (Figure 7A), which indicates that DMP had little effect on the microenvironment of the Tyr residue, while the emission peak of the Trp residue at

dx.doi.org/10.1021/jf5046359 | J. Agric. Food Chem. 2015, 63, 75−84

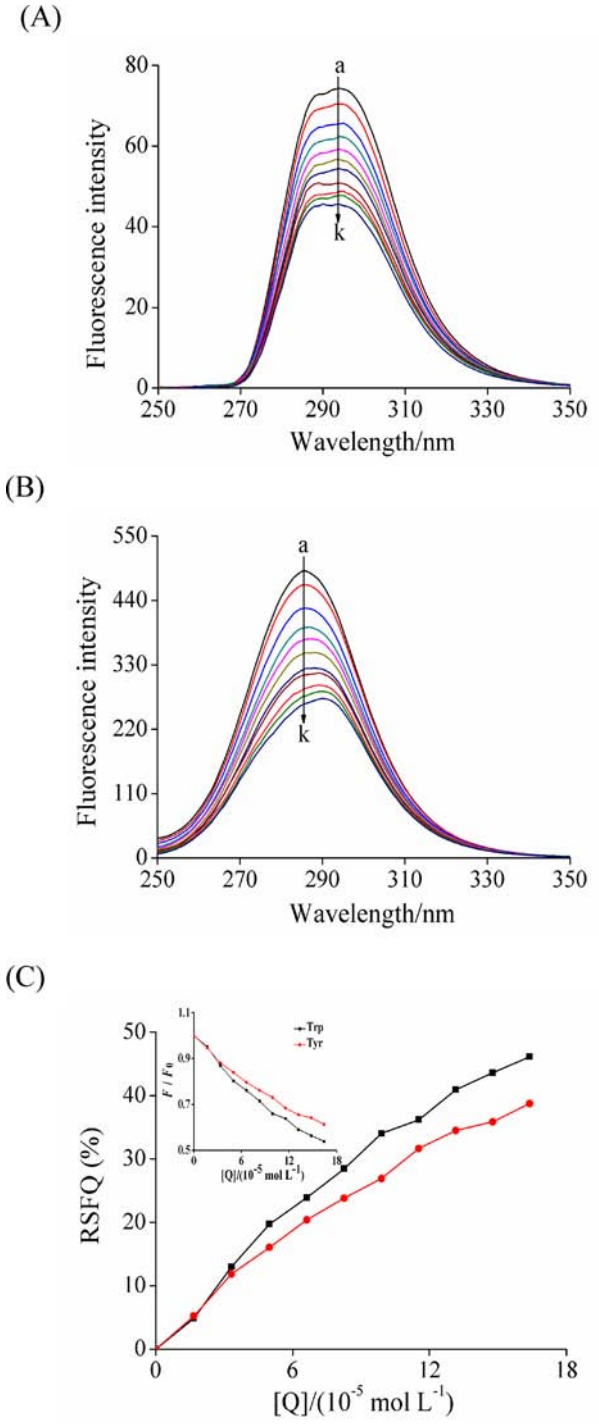

Figure 7. Synchronous fluorescence spectra of trypsin with different concentrations of DMP at (A) $\Delta\lambda$ = 15 nm and (B) $\Delta\lambda$ = 60 nm. c(trypsin) = 1.5 × 10^{-6} mol L^{-1}; c(DMP) = 0, 1.66, 3.32, 4.98, 6.62, 8.26, 9.90, 11.53, 13.16, 14.78, and 16.39 × 10^{-5} mol L^{-1} for curves a → k, respectively. (C) Comparative evaluation of DMP effect on the ratios of synchronous fluorescence quenching (RSFQ) of trypsin.

$\Delta\lambda$ = 60 nm displayed an obvious red shift (from 286−290 nm, shown in Figure 7B), which suggests that the hydrophobicity decreased and the polarity increased around the Trp residue.[42]

The RSFQ were calculated by using the equation RSFQ = 1 − F/F_0 (F_0 and F are the fluorescence intensities of trypsin in the absence and presence of DMP, respectively).[29] As shown in Figure 7, panel C, the data of RFSQ at $\Delta\lambda$ = 60 nm were a little higher than the corresponding ones at $\Delta\lambda$ = 15 nm at the same DMP concentrations, which may be due to more contribution of Trp residue to the quenching of the intrinsic fluorescence, and DMP was closer to Trp compared to Tyr residue.

To detect the possible influence of DMP binding on the secondary structure of trypsin, CD measurements were performed in the absence and presence of different amounts of DMP (Figure 8). The CD spectrum of trypsin exhibited only

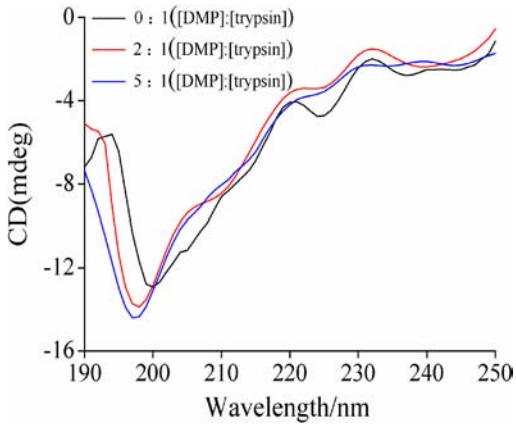

Figure 8. CD spectra of trypsin in the presence of increasing amounts of DMP. c(trypsin) = 1.5 × 10^{-5} mol L^{-1}; the molar ratios of DMP to trypsin were (a) 0:1, (b) 2:1, and (c) 5:1, respectively.

one negative band at 200 nm. Generally, the β-sheet shows a CD band at 210−220 nm; however, the irregular strands in trypsin structure may cause the negative CD band shift from the ideal β-sheet position toward the 200 nm region.[43] With the addition of DMP, the intensity of the negative peak increased with obvious blue shift; similar findings have been reported for the interactions of oxytetracycline and tetracycline with trypsin.[14,44] Then, the CD spectra data were analyzed by the online SELCON3 software, and the contents of different secondary structure of trypsin were obtained and listed in Table 3. The results showed that the β-sheet structure was predominant with a high percentage in trypsin, which was identical to the literature.[45] When the molar ratios of DMP to trypsin increased, a decreasing tendency of the β-sheet and β-turn contents were observed, while the α-helix and random coil contents tended to increase, which indicated that DMP induced the secondary structure changes of trypsin and thus may influence the function of the enzyme.

Infrared spectroscopy is a powerful means for investigating the secondary structures of proteins. The amide I band (1600−1700 cm^{-1}, mainly C═O stretch) and the amide II band (1600−1500 cm^{-1}, C−N stretch coupled with N−H bending mode) are main vibrational bands of the peptide moiety associated with the secondary structure of proteins,[46] and the amide I band is more sensitive to the change of secondary structure of protein than the amide II band.[47] Upon DMP interaction, the FT-IR difference spectra of trypsin [(DMP−trypsin solution) − DMP solution] were obtained to monitor the variation of these vibrations (Figure 9A). It was apparent that the peak position of amide I of trypsin moved from 1640−1646 cm^{-1}, and the one of amide II shifted from 1550−1552 cm^{-1} after addition of DMP, which suggests that DMP interacted with the C═O and C−N groups in the protein polypeptides and caused the rearrangement of the polypeptide carbonyl hydrogen bonding network.[48]

dx.doi.org/10.1021/jf5046359 | J. Agric. Food Chem. 2015, 63, 75−84

Table 3. Secondary Structural Analysis of Free Trypsin and DMP−Trypsin Systems from CD Data

molar ratio [DMP]:[trypsin]	α-helix (%)	β-sheet (%)	β-turn (%)	random coil (%)
0:1	13.8	43.8	20.6	21.8
2:1	15.9	40.9	20.1	23.1
5:1	17.1	39.1	19.8	24.0

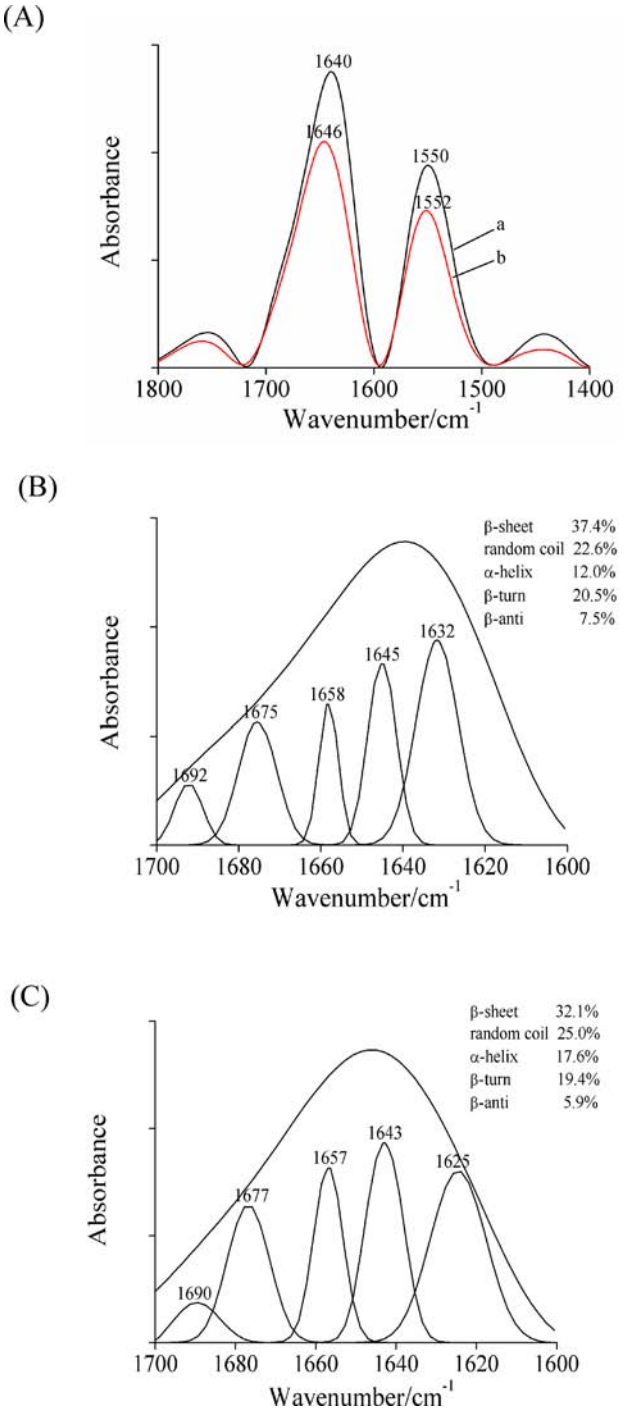

Figure 9. (A) The FT-IR spectra of (a) free trypsin and (b) difference spectra [(DMP−trypsin solution) − DMP solution] at pH 7.4 in the region of 1800−1400 cm^{-1}. c(trypsin) = 1.5 × 10^{-5} mol L^{-1}, c(DMP) = 7.5 × 10^{-5} mol L^{-1}. The curve-fitted amide I region of (B) free trypsin and its (C) DMP complex.

The curve-fitted spectra of trypsin infrared amide I bands before and after the binding with DMP were analyzed to further characterize the secondary structure change of trypsin according to the literature.[49] As shown in Figure 9, panel B, the free trypsin contained β-sheet 37.4% (1632 cm^{-1}), random coil 22.6% (1645 cm^{-1}), α-helix 12.0% (1658 cm^{-1}), β-turn 20.5% (1675 cm^{-1}), and β-antiparallel 7.5% (1692 cm^{-1}). After interaction with DMP ([DMP]:[trypsin] = 5:1), the contents of β-sheet, β-turn, and β-antiparallel reduced from 37.4−32.1%, from 20.5−19.4%, and from 7.5−5.9%, respectively, while the α-helix structure and random coil increased from 12.0−17.6% and from 22.6−25.0%, respectively (Figure 9C). The results indicated that the binding of DMP to trypsin led to the conformational changes of trypsin with an increase of α-helix and random coil stability and loss of β-structure content.

In summary, humans are exposed to thousands of different chemicals each day, and the chemicals may gather in organisms through the food chain and induce acute and chronic toxicity. The contaminants may show their toxicity by interacting with the biological macromolecules and affecting the structure as well as the function of the macromolecules after entering organisms. Hence, exploring the toxic effects and mechanism of contaminants at a molecular level is helpful to perfect the toxicity evaluation system of the contaminants and forecast the related effects on macroorganisms or populations. Also, it will be useful to provide reference and technical support for formulating a reasonable standard to protect human health. Investigation of DMP−trypsin interaction by a combination of fluorescence, UV−vis absorption, circular dichroism, Fourier transform infrared spectroscopic and atomic force microscopy, and cyclic voltammetric and molecular docking approaches revealed that DMP can bind with trypsin to form the DMP−trypsin complex. DMP actually interacted with the catalytic residues (His 57, Asp 102, and Ser 195) located within the region close to the S1 binding pocket of trypsin and resulted in the inhibition of the enzymatic activity. The binding process was primarily driven by hydrophobic interactions, as the values of $\Delta H°$ and $\Delta S°$ were found to be 4.16 kJ mol^{-1} and 82.80 J mol^{-1} K^{-1}, respectively. The binding of DMP to trypsin induced an increase in α-helix and random coil contents and a decrease in β-sheet and β-turn structure and caused the change of surface morphology of trypsin and its molecular aggregation. Additionally, the DMP binding to trypsin weakened the electrochemical signal of DMP to some extent, which confirmed the formation of the DMP−trypsin complex.

Park et al. have reported that exposure of *C. riparius* to a most commonly used plasticizer Di-(2-ethylhexyl) phthalate (DEHP) induced the decrease of the serine-type endopeptidase (SP) gene expression, and the *C. riparius* SP was putatively classified as a chymotrypsin-like protein that was primarily expressed in the gut where pollutants are frequently encountered.[50] Since trypsin belongs to the chymotrypsin superfamily of serine endopeptidases, the changes in gene expression might cause some adverse effects on trypsin by DEHP. Our experimental results indicated that DMP, an analogue of DEHP, can bind to trypsin and affect the structure and function of the enzyme under simulative physiological conditions. Although in vitro results could not completely

dx.doi.org/10.1021/jf5046359 | J. Agric. Food Chem. 2015, 63, 75−84

represent what happens in vivo and the fully biochemical properties of DMP, this study will be helpful to comprehensively understand the mechanism of DMP that affects the conformation and activity of trypsin in biological processes and its toxicity assessment in the environment.

AUTHOR INFORMATION

Corresponding Author

*E-mail: gwzhang@ncu.edu.cn. Phone: +8679188305234. Fax: +8679188304347.

Funding

The authors gratefully acknowledge the financial support of this study by the National Natural Science Foundation of China (31460422 and 21167013), the Natural Science Foundation of Jiangxi Province (20143ACB20006 and 20142BAB204001), the Joint Specialized Research Fund for the Doctoral Program of Higher Education (20123601110005), the Program of Jiangxi Provincial Department of Science and Technology (20141BBG70092), and the Research Program of State Key Laboratory of Food Science and Technology of Nanchang University (SKLF−ZZB−201305, SKLF−ZZA−201302, and SKLF−KF−201203).

Notes

The authors declare no competing financial interest.

REFERENCES

(1) Bauer, M. J.; Herrmann, R. Estimation of the environmental contamination by phthalic acid esters leaching from household wastes. *Sci. Total Environ.* **1997**, *208*, 49−57.

(2) Howdeshell, K. L.; Wilson, V. S.; Furr, J.; Lambright, C. R.; Rider, C. V.; Blystone, C. R.; Hotchkiss, A. K.; Gray, L. E. A mixture of five phthalate esters inhibits fetal testicular testosterone production in the sprague-dawley rat in a cumulative, dose-additive manner. *Toxicol. Sci.* **2008**, *105*, 153−165.

(3) Ikonomou, M. G.; Kelly, B. C.; Blair, J. D.; Gobas, F. A. P. C. An interlaboratory comparison study for the determination of dialkyl phthalate esters in environmental and biological samples. *Environ. Toxicol. Chem.* **2012**, *31*, 1948−1956.

(4) Serrano, S. E.; Braun, J.; Trasande, L.; Dills, R.; Sathyanarayana, S. Phthalates and diet: A review of the food monitoring and epidemiology data. *Environ. Health* **2014**, *13*, 43.

(5) Romani, F.; Tropea, A.; Scarinci, E.; Federico, A.; Russo, C. D.; Lisi, L.; Catino, S.; Lanzone, A.; Apa, R. Endocrine disruptors and human reproductive failure: The in vitro effect of phthalates on human luteal cells. *Fertil. Steril.* **2014**, *102*, 831−837.

(6) Miodovnik, A.; Edwards, A.; Bellinger, D. C.; Hauser, R. Developmental neurotoxicity of ortho-phthalate diesters: Review of human and experimental evidence. *Neurotoxicology* **2014**, *41*, 112−122.

(7) Heudorf, U.; Mersch-Sundermann, V.; Angerer, J. Phthalates: Toxicology and exposure. *Int. J. Hyg. Environ. Health* **2007**, *210*, 623−634.

(8) Xu, B.; Gao, N. Y.; Cheng, H. F.; Xia, S. J.; Rui, M.; Zhao, D. D. Oxidative degradation of dimethyl phthalate (DMP) by UV/H_2O_2 process. *J. Hazard. Mater.* **2009**, *162*, 954−959.

(9) Yuan, B. L.; Li, X. Z.; Graham, N. Aqueous oxidation of dimethyl phthalate in a Fe(VI)-TiO_2-UV reaction system. *Water Res.* **2008**, *42*, 1413−1420.

(10) Li, J. X.; Gu, J. D.; Pan, L. Transformation of dimethyl phthalate, dimethyl isophthalate, and dimethyl terephthalate by Rhodococcus rubber Sa and modeling the processes using the modified Gompertz model. *Int. Biodeterior. Biodegrad.* **2005**, *55*, 223−232.

(11) Dillingham, E. O.; Autian, J. Teratogenicity, mutagenicity, and cellular toxicity of phthalate esters. *Environ. Health Perspect.* **1973**, *3*, 81−89.

(12) Autian, J. Toxicity and health threats of phthalate esters: Review of the literature. *Environ. Health Perspect.* **1973**, *4*, 3−26.

(13) Chai, J.; Xu, Q. F.; Dai, J. P.; Liu, R. T. Investigation on potential enzyme toxicity of clenbuterol to trypsin. *Spectrochim. Acta, Part A* **2013**, *105*, 200−206.

(14) Chi, Z. X.; Liu, R. T.; Zhang, H. Noncovalent interaction of oxytetracycline with the enzyme trypsin. *Biomacromolecules* **2010**, *11*, 2454−2459.

(15) Zhang, H. M.; Zhou, Q. H.; Wang, Y. Q. Studies on the interactions of 2,4-dinitrophenol and 2,4-dichlorphenol with trypsin. *J. Fluoresc.* **2010**, *20*, 507−516.

(16) Hu, X. X.; Yu, Z. H.; Liu, R. T. Spectroscopic investigations on the interactions between isopropanol and trypsin at molecular level. *Spectrochim. Acta, Part A* **2013**, *108*, 50−54.

(17) He, W.; Dou, H. J.; Zhang, L.; Wang, L. J.; Wang, R. Y.; Chang, J. B. Spectroscopic study on the interaction of trypsin with bicyclol and analogs. *Spectrochim. Acta, Part A* **2014**, *118*, 510−519.

(18) Wang, J.; Liu, R. T.; Qin, P. F. Toxic interaction between acid yellow 23 and trypsin: Spectroscopic methods coupled with molecular docking. *J. Biochem. Mol. Toxicol.* **2012**, *26*, 360−367.

(19) Bi, S. Y.; Sun, Y. T.; Qiao, C. Y.; Zhang, H. Q.; Liu, C. M. Binding of several anti-tumor drugs to bovine serum albumin: Fluorescence study. *J. Lumin.* **2009**, *129*, 541−547.

(20) Mu, Y.; Lin, J.; Liu, R. T. Interaction of sodium benzoate with trypsin by spectroscopic techniques. *Spectrochim. Acta, Part A* **2011**, *83*, 130−135.

(21) Yan, J. K.; Zhang, G. W.; Hu, Y. T.; Ma, Y. D. Effect of luteolin on xanthine oxidase: Inhibition kinetics and interaction mechanism merging with docking simulation. *Food Chem.* **2013**, *141*, 3766−3773.

(22) Dhar, S.; Rana, D. K.; Pal, A.; Bhattacharya, S. C. Photobehavior and docking simulations of drug within macromolecules: Binding of an antioxidative isoquinolindione to a serine protease and albumin proteins. *J. Photochem. Photobiol., B* **2013**, *129*, 69−77.

(23) Chen, J. B.; Zhou, X. F.; Zhang, Y. L.; Gao, H. P. Potential toxicity of sulfanilamide antibiotic: Binding of sulfamethazine to human serum albumin. *Sci. Total Environ.* **2012**, *432*, 269−274.

(24) Shahabadi, N.; Maghsudi, M.; Kiani, Z.; Pourfoulad, M. Multispectroscopic studies on the interaction of 2-*tert*-butylhydroquinone (TBHQ), a food additive, with bovine serum albumin. *Food Chem.* **2011**, *124*, 1063−1068.

(25) Lakowicz, J. R.; Weber, G. Quenching of fluorescence by oxygen. Probe for structural fluctuations in macromolecules. *Biochemistry* **1973**, *12*, 4161−4170.

(26) Lu, Y.; Wang, G. K.; Lu, X. M.; Lv, J.; Xu, M. H.; Zhang, W. W. Molecular mechanism of interaction between norfloxacin and trypsin studied by molecular spectroscopy and modeling. *Spectrochim. Acta, Part A* **2010**, *75*, 261−266.

(27) Wu, X. L.; He, W. Y.; Wang, W. P.; Luo, X. P.; Cao, H. Y.; Lin, L. X.; Feng, K. Q.; Liu, Z. G. Investigation of the interaction between (−)-epigallocatechin-3-gallate with trypsin and α-chymotrypsin. *Int. J. Food Sci. Technol.* **2013**, *48*, 2340−2347.

(28) Wang, Y. Q.; Zhang, H. M. Comparative studies of the binding of six phthalate plasticizers to pepsin by multispectroscopic approach and molecular modeling. *J. Agric. Food Chem.* **2013**, *61*, 11191−11200.

(29) Bijari, N.; Shokoohinia, Y.; Ashrafi-Kooshk, M. R.; Ranjbar, S.; Parvaneh, S.; Moieni-Arya, M.; Khodarahmi, R. Spectroscopic study of interaction between osthole and human serum albumin: Identification of possible binding site of the compound. *J. Lumin.* **2013**, *143*, 328−336.

(30) Xie, X. Y.; Wang, Z. W.; Zhou, X. M.; Wang, X. R.; Chen, X. G. Study on the interaction of phthalate esters to human serum albumin by steady-state and time-resolved fluorescence and circular dichroism spectroscopy. *J. Hazard. Mater.* **2011**, *192*, 1291−1298.

(31) Polgar, L. The catalytic triad of serine peptidases. *Cell. Mol. Life Sci.* **2005**, *62*, 2161−2172.

(32) Ma, W. Z.; Tang, C.; Lai, L. H. Specificity of trypsin and chymotrypsin: Loop-motion-controlled dynamic correlation as a determinant. *Biophys. J.* **2005**, *89*, 1183−1193.

(33) Kandagal, P. B.; Ashoka, S.; Seetharamappa, J.; Shaikh, S. M. T.; Jadegoud, Y.; Ijare, O. B. Study of the interaction of an anticancer drug with human and bovine serum albumin: Spectroscopic approach. *J. Pharm. Biomed. Anal.* **2006**, *4*, 393−399.
(34) Ross, P. D.; Subramanian, S. Thermodynamics of protein association reactions: Forces contributing to stability. *Biochemistry* **1981**, *20*, 3096−3102.
(35) Sharma, S. A.; Anandakumar, S.; Ilanchelian, M. A combined spectroscopic and molecular docking study on site selective binding interaction of Toluidine blue O with human and bovine serum albumins. *J. Lumin.* **2014**, *151*, 206−218.
(36) Zhang, H. M.; Zhou, Q. H.; Cao, J.; Wang, Y. Q. Mechanism of cinnamic acid-induced trypsin inhibition: A multitechnique approach. *Spectrochim. Acta, Part A* **2013**, *116*, 251−257.
(37) Wang, Y. Q.; Zhang, H. M.; Cao, J.; Zhou, Q. H. Interaction of methotrexate with trypsin analyzed by spectroscopic and molecular modeling methods. *J. Mol. Struct.* **2013**, *1051*, 78−85.
(38) Diaz, J. F.; Balkus, K. J., Jr. Enzyme immobilization in MCM-41 molecular sieve. *J. Mol. Catal. B* **1996**, *2*, 115−126.
(39) Zhao, J.; Zheng, X. F.; Xing, W.; Huang, J. Y.; Li, G. X. Electrochemical studies of camptothecin and its interaction with human serum albumin. *Int. J. Mol. Sci.* **2007**, *8*, 42−50.
(40) Wen, W.; Tan, Y. M.; Xiong, H. Y.; Wang, S. F. Voltammetric and spectroscopic investigations of the interaction between colchicine and bovine serum albumin. *Int. J. Electrochem. Sci.* **2010**, *5*, 232−241.
(41) Yang, B. J.; Liu, R. T.; Hao, X. P.; Wu, Y. Z.; Du, J. The interactions of glutathione-capped CdTe quantum dots with trypsin. *Biol. Trace Elem. Res.* **2012**, *146*, 396−401.
(42) Ge, F.; Chen, C. Y.; Liu, D. Q.; Han, B. Y.; Xiong, X. F.; Zhao, S. L. Study on the interaction between theasinesin and human serum albumin by fluorescence spectroscopy. *J. Lumin.* **2010**, *130*, 168−173.
(43) Gonçalves, R.; Mateus, N.; De Freitas, V. Biological relevance of the interaction between procyanidins and trypsin: A multitechnique approach. *J. Agric. Food Chem.* **2010**, *58*, 11924−11931.
(44) Chi, Z. X.; Liu, R. T.; Yang, H. X.; Shen, H. M.; Wang, J. Binding of tetracycline and chlortetracycline to the enzyme trypsin: Spectroscopic and molecular modeling investigations. *PLoS One* **2011**, *6*, e28361.
(45) Manavalan, P.; Johnson, W. C. Sensitivity of circular dichroism to protein tertiary structure class. *Nature* **1983**, *305*, 831−832.
(46) Surewicz, W. K.; Mantsch, H. H.; Chapman, D. Determination of protein secondary structure by Fourier transform infrared spectroscopy: A critical assessment. *Biochemistry* **1993**, *32*, 389−394.
(47) Sandhya, B.; Hegde, A. H.; Kalanur, S. S.; Katrahalli, U.; Seetharamappa, J. Interaction of triprolidine hydrochloride with serum albumins: Thermodynamic and binding characteristics and influence of site probes. *J. Pharm. Biomed. Anal.* **2011**, *54*, 1180−1186.
(48) Li, Y.; Yao, X. J.; Jin, J.; Chen, X. G.; Hu, Z. D. Interaction of rhein with human serum albumin investigation by optical spectroscopic technique and modeling studies. *BBA, Proteins Proteomics* **2007**, *1774*, 51−58.
(49) Zhang, G. W.; Wang, L.; Pan, J. H. Probing the binding of the flavonoid diosmetin to human serum albumin by multispectroscopic techniques. *J. Agric. Food Chem.* **2012**, *60*, 2721−2729.
(50) Park, K.; Kwak, I. S. Expression of *Chironomus riparius* serine-type endopeptidase gene under di-(2-ethylhexyl)-phthalate (DEHP) exposure. *Comp. Biochem. Physiol., Part B* **2008**, *151*, 349−354.

JOURNAL OF AGRICULTURAL AND FOOD CHEMISTRY

Article

pubs.acs.org/JAFC

Proteomics Investigation Reveals Cell Death-Associated Proteins of Basidiomycete Fungus *Trametes versicolor* Treated with Ferruginol

Yu-Han Chen,[†] Ting-Feng Yeh,[†] Fang-Hua Chu,[†] Fu-Lan Hsu,[‡] and Shang-Tzen Chang*[,†]

[†]School of Forestry and Resource Conservation, National Taiwan University, No. 1, Section 4, Roosevelt Road, Taipei 106, Taiwan

[‡]Taiwan Forestry Research Institute, Council of Agriculture, Executive Yuan, 53 Nan-Hai Road, Taipei 100, Taiwan

Supporting Information

ABSTRACT: Ferruginol has antifungal activity against wood-rot fungi (basidiomycetes). However, specific research on the antifungal mechanisms of ferruginol is scarce. Two-dimensional gel electrophoresis and fluorescent image analysis were employed to evaluate the differential protein expression of wood-rot fungus *Trametes versicolor* treated with or without ferruginol. Results from protein identification of tryptic peptides via liquid chromatography−electrospray ionization tandem mass spectrometry (LC−ESI-MS/MS) analyses revealed 17 protein assignments with differential expression. Downregulation of cytoskeleton *β*-tubulin 3 indicates that ferruginol has potential to be used as a microtubule-disrupting agent. Downregulation of major facilitator superfamily (MFS)−multiple drug resistance (MDR) transporter and peroxiredoxin TSA1 were observed, suggesting reduction in self-defensive capabilities of *T. versicolor*. In addition, the proteins involved in polypeptide sorting and DNA repair were also downregulated, while heat shock proteins and autophagy-related protein 7 were upregulated. These observations reveal that such cellular dysfunction and damage caused by ferruginol lead to growth inhibition and autophagic cell death of fungi.

KEYWORDS: *antifungal activity, autophagy, basidiomycete, ferruginol, proteomics, Trametes versicolor*

INTRODUCTION

Ferruginol, a phenolic diterpene, is present in resins/exudates and heartwood of many plants, particularly coniferous trees such as *Calocedrus macrolepis* var. *formosana*,[1] *Cryptomeria japonica*,[2] *Taiwania cryptomerioides*,[3] and *Thuja plicata*.[4] In addition, an increasing number of reports revealed that ferruginol has excellent antifungal activities against fungi belonging to the family of basidiomycetes.[3,5,6] The general mechanisms of antifungal actions reviewed by Odds et al.[7] indicated that antifungal agents interfered with the cellular integrity of fungi via several targets including cell wall, cell membrane, microtubule assembly, sterol synthesis, protein synthesis, and DNA/RNA synthesis. Moreover, Ramsdale[8] reported that antifungals/fungicides can induce cell death via programmed cell death (PCD) pathways in pathogenic fungi. These findings revealed that antifungal agents can target specific cellular molecules and further mediate cell-death pathways to inhibit the growth of fungi. Chang et al.[3] examined the antifungal activities of five compounds—ferruginol, helioxanthin, savinin, taiwanin C, and hinokiol—isolated from *T. cryptomerioides* heartwood. They reported that ferruginol has the best antifungal performance against the basidiomycete fungus *Trametes versicolor*. However, specific study on the antifungal actions of ferruginol against basidiomycete fungus is limited.

Proteomics is a research tool for surveying comprehensive information on molecular networks within the living cells. Fungal proteomics has been intensively studied in the last 10 years, and many fungal genomes have been sequenced.[9,10] This tool can be further employed to identify the proteins that participate in regulation networks upon treatment with antifungal reagents or stress conditions.[11] Cagas et al.[12] investigated the proteomic response of an antifungal agent (caspofungin) against ascomycete fungus *Aspergillus fumigatus*. Shimizu et al.[13] used a proteomic differential display technique to identify the responses of basidiomycete fungus *Phanerochaete chrysosporium* to the addition of vanillin. These findings revealed that many cellular enzymes and metabolic shifts were regulated by specific stimulation. The objective of this study is to assess the regulation of cellular molecules at the proteome level of basidiomycete fungus *T. versicolor* upon addition of ferruginol. A proteomic differential display technique using two-dimensional electrophoresis (2DE) was adopted to profile the mechanism.

MATERIALS AND METHODS

Compound and Fungal Strain. Ferruginol was isolated from ethanolic heartwood extracts of a 40-year-old *Taiwania cryptomerioides* Hayata. The wood samples were harvested from the Experimental Forest of National Taiwan University in Nan-Tou County. Air-dried heartwood samples were soaked in 95% ethanol for 7 days. Crude extract was filtered, concentrated, and then lyophilized (yield 6.3%, based on dry weight of heartwood). The ethanolic extracts were fractionated by liquid−liquid partition to yield *n*-hexane-soluble fraction (50.8%), ethyl acetate-soluble fraction (27.0%), *n*-butanol-soluble fraction (1.6%), and water-soluble fraction (9.5%). The *n*-hexane-soluble fraction was divided into nine subfractions (H1−H9) by open-column chromatography (230−400-mesh silica gel; Merck, Darmstadt, Germany) and then eluted with a stepwise gradient of ethyl acetate/*n*-hexane from 0% to 100% (v/v). According to our previous study,[14] ferruginol was purified from subfraction H2 via a HPLC system equipped with a semipreparative silica column (mobile

Received: September 29, 2014
Revised: November 26, 2014
Accepted: December 1, 2014
Published: December 8, 2014

 © 2014 American Chemical Society

phase ethyl acetate/*n*-hexane = 5/95; flow rate 4 mL/min; retention time = 9.8 min).

Trametes versicolor (Linnaeus: Fries) Pilat (BCRC 35253), a wood-rot test strain in JIS K 1517, ASTM D1413, and EN113, was obtained from the Bioresource Collection and Research Center (BCRC) of Food Industry Research and Development Institute in Taiwan.

Antifungal Assay. Agar dilution test was employed to evaluate the antifungal activity of ferruginol. Ferruginol was dissolved in 150 μL of 99.5% methanol and added into sterilized potato dextrose agar (PDA, 15 mL) in a 9 cm Petri dish with final concentrations of 25, 50, 100, 200, and 400 μg/mL. Methanol served as a control treatment. A 3 mm plug of mycelium was transferred to tested dishes and then incubated at 25 ± 2 °C and 70% relative humidity (RH). When the mycelia of the control group reached the border of the plate, the growth diameter was recorded to calculate the antifungal index (AI) as a percentage:

$$\mathrm{AI} = (1 - D_t/D_c) \times 100$$

D_t is the mycelium diameter of test groups, and D_c is the mycelium diameter of the control.

Liquid Culture of Fungal Cells for Proteomic Analysis. For proteomic analysis, *T. versicolor* was incubated in a liquid medium [700 mL of potato dextrose broth (PDB) in a 1-L Erlenmeyer flask] at 25 ± 2 °C under air. Cultures were incubated on an orbital shaker at 100*g* in darkness. After a 7-day preincubation, ferruginol in ethanol (1500 μL) and Tween 20 (350 μL) was added into the liquid medium with a final concentration of 100 μg/mL. For the control, only ethanol (1500 μL) and Tween 20 (350 μL) were added in the culture. At the 11th incubation day, cultured mycelia were filtered and weighed (100 °C dry weight).

Extraction and Quantification of Fungal Proteins. *T. versicolor* was treated with ferruginol for 4 days, and its mycelia were filtered, washed with chilled ultrapure water, and frozen in liquid nitrogen. The frozen mycelia (2 g, fresh weight) were ground into a fine powder in liquid nitrogen with a mortar and pestle and extracted with precooled (−20 °C) buffer containing 10% trichloroacetic acid and 20 mM dithiothreitol (DTT) in acetone. The mixture was precipitated at −20 °C for 50 min and centrifuged at 6000*g* (4 °C) for 30 min. Pellets were washed with precooled acetone containing 20 mM DTT, washed twice with 100% precooled acetone, and then dried in a freeze-dryer.

The lyophilized pellets (500 mg) were solubilized by urea buffer containing 7 M urea, 2 M thiourea, 4% (w/v) 3-[(3-cholamidopropyl)-dimethylammonio]-1-propanesulfonic acid (CHAPS), and 1% (w/v) DTT, and the supernatant was collected by centrifugation at 12000*g* (25 °C) for 10 min. The protein concentration was quantified by the Bradford method[15] with bovine serum albumin (BSA) and protein assay dye reagent (Bio-Rad Laboratories, Inc.).

Two-Dimensional Electrophoresis. Figure 1 illustrates the experimental process of proteomic differential analysis. Proteins from *T. versicolor* were separated by two-dimensional electrophoresis (2DE) and stained with fluorescent dye (SYPRO Ruby), and the gel images were analyzed with ImageMaster software. For all tested groups, 300 μg of protein was mixed with rehydration solution (urea buffer, 2% ampholyte, and trace bromophenol blue) and then rehydrated with immobilized pH gradient (IPG) strips (17 cm, nonlinear gradient, Bio-Rad) for 12 h. The voltage of the isoelectric focusing (IEF) was programed from 100 to 8000 V to reach a total of 40000 V·h (50 μA for each strip). After IEF, the strips were immediately equilibrated with reduction solution [2% (w/v) DTT in equilibration buffer containing 50 mM Tris-HCl (pH 8.8), 6 M urea, 30% (v/v) glycerol, 2% (w/v) sodium dodecyl sulfate (SDS), and a trace of bromophenol blue] for 15 min, followed by the alkylation solution [2.5% (w/v) iodoacetamide (IAA) in equilibration buffer] for 15 min.

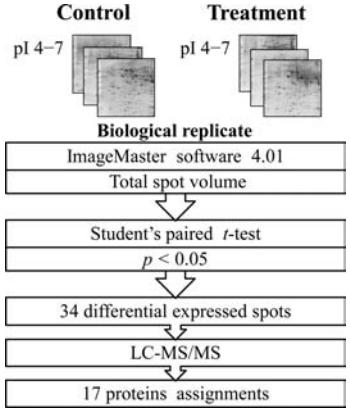

Figure 1. Workflow for studying differential protein expression of *T. versicolor* treated with or without ferruginol (100 μg/mL).

The second-dimension separation was performed by SDS−12% polyacrylamide gel electrophoresis (PAGE). After the 2DE separation, all gels were washed three times with deionized water to remove the residue of SDS. Gels were stained with SYPRO Ruby (Invitrogen) and digitalized with Typhoon 9400 scanner (Amersham Bioscience) at 200 μm pixel size. The images were analyzed with ImageMaster Platinum software v4.01 (Amersham Bioscience). Spot detection, matching, background subtraction (average on boundary), and image normalization were performed by this software. Only spots present in at least two biological replicates were taken as true signals. The volume of spots was normalized to the total volume of all spots in the analysis to compensate for slight differences in sample loading and gel staining. Protein spots with significantly changed levels (*t*-test, $p < 0.05$) were selected for protein identification.

Identification of Proteins and Database Search. Selected spots from both control and treatment gels were excised manually and washed three times with double-distilled H_2O. Gels were destained with 50% acetonitrile (ACN)/25 mM ammonium bicarbonate (37 °C), reduced with 10 mM DTT/25 mM ammonium bicarbonate (56 °C, 1 h in dark), and alkylated with 55 mM IAA/25 mM ammonium bicarbonate (room temperature, 45 min in dark). Gels were dehydrated with 100% ACN and rehydrated with trypsin (Promega, Madison, WI) (37 °C, 16 h). Oligopeptides were extracted twice in 5% formic acid (FA)/50% ACN with agitation (on ice, 20 min) and then dried via a centrifugal evaporator. Tryptic peptides were analyzed on a nano-HPLC system (LC Packing, Netherlands) with a 75-μm inner-diameter/15 cm C_{18} microcapillary column (Agilent Technologies). The HPLC system was connected with an ion-trap mass spectrometer (LCQ DECA XP plus, Thermo Finnigan, San Jose, CA) equipped with an electrospray ionization source (spraying voltage 1.8 kV). Elution conditions included a 40 min linear gradient from 100% to 40% buffer A (buffer A, 5% ACN/0.1% formic acid; buffer B, 80% ACN/0.1% formic acid; flow rate, 0.2 mL/min). Spectra were acquired by a full scan (m/z 450−2000).

Mascot software (www.matrixscience.com) was used for protein identification and comparison with the National Center for Biotechnology Information (NCBI) nonredundant protein sequence database and Swiss-Prot database against fungi taxonomy. Two missed tryptic cleavages per peptide and variable modification of carboxymethylation on cysteine and lysine, oxidation on methionine, and deamidation on asparagine or glutamine residues were permitted during the identification process. The identified proteins whose MOWSE (molecular weight search) scores exceeded 51 (NCBI) or 35 (Swiss-Prot) were taken as significant hits ($p < 0.05$). Sequences of identified proteins are listed in Tables S1 and S2 in Supporting Information.

RESULTS AND DISCUSSION

Antifungal Ability of Ferruginol. An agar dilution test was performed to assess the antifungal activity of ferruginol against *Trametes versicolor* (white-rot fungus) at concentrations of 25, 50, 100, 200, and 400 μg/mL. Results (Figure 2A) show that the antifungal indexes were 26%, 34%, 41%, 42%, and 43%, respectively. The antifungal activity of ferruginol reached a maximum at the dosage of 100 μg/mL and then leveled off.

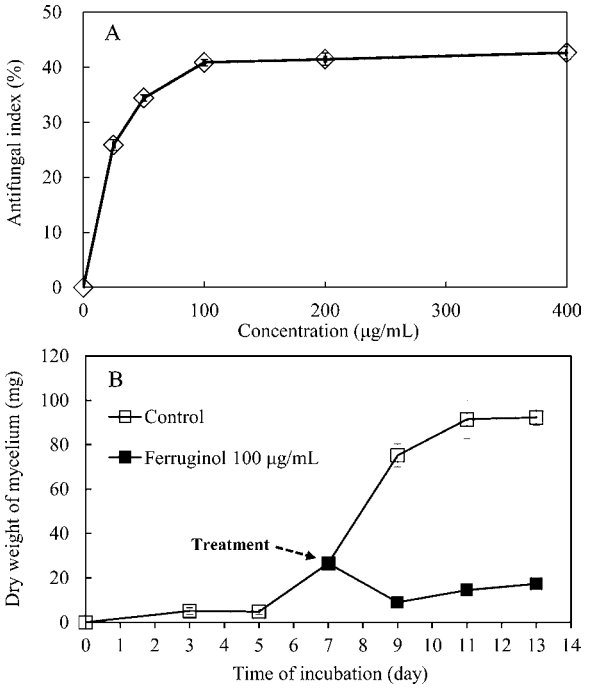

Figure 2. (A) Antifungal activity of ferruginol against *T. versicolor* on agar plate tests. (B) Dry weight of mycelium of *T. versicolor* on liquid culture test treated with (■) or without (□) ferruginol (100 μg/mL). Results are mean ± SD (n = 4).

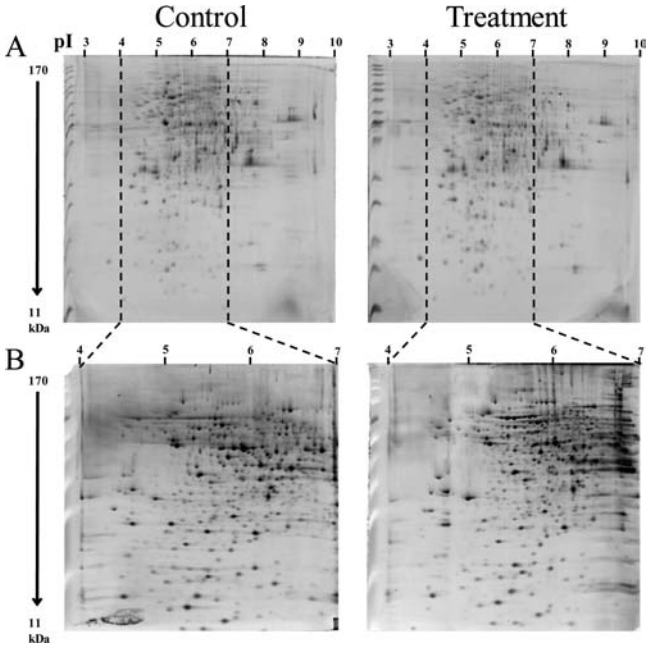

Figure 3. Two-dimensional electrophoretic analysis of *T. versicolor* proteins (300 μg) extracted from control and ferruginol-treated (100 μg/mL) groups. Proteomics analysis was carried out with (A) wide-range (pH 3−10) IPG strips and (B) narrow-range (pH 4−7) IPG strips. p*I*, isoelectric point.

To investigate the mechanisms of ferruginol on inhibition of *T. versicolor* growth, a liquid culture test was performed at the concentration of 100 μg/mL (Figure 2B). The dry weights of nontreated mycelia (control) increased slightly for 5 incubation days (lag phase, about 5 mg), increased linearly from the fifth to the 11th day of incubation (log phase), and exhibited stationary-phase fungal growth after the 11th day of incubation (about 90 mg). However, the dry weights of treated-mycelia decreased to lower than 20 mg after treatment with ferruginol at the seventh day. To analyze the protein expression patterns of ferruginol-treated *T. versicolor*, the mycelia were harvested at the end of the growth log phase (11th day) for further electrophoretic analysis.

Two-Dimensional Electrophoresis and Differential Display Analysis. Total proteins were extracted from mycelia with or without ferruginol treatments and used for quantitative comparison in the 2DE analysis (Figure 3). The average fluorescence intensity of each protein spot was measured to determine the protein expression level. The gels showed major spots between pH 4 and 7 in the wide-range (pH 3−10) immobilized pH gradient (IPG) strips (Figure 3A). To further separate the overlapping spots, narrow-range (pH 4−7) IPG strips were used, and the results revealed more detectable spots on a 2D gel (Figure 3B).

Approximately 360 spots were visualized in each 2D gel separated from the pH 4−7 IPG strip. The protein spot volumes from the control and treatment groups were statistically compared (t-test). A total of 34 protein spots, including 19 spots from nontreated (control) samples and 15 spots from ferruginol-treated samples, showed differential protein expression levels ($p < 0.05$) (Figure 4). A total of 17 nonredundant proteins and two not-identified proteins were identified among these proteins: 12 were downregulated (Table 1) and 7 were upregulated (Table 2) upon ferruginol treatment.

Downregulated Proteins upon Ferruginol Treatment. Exposure of *T. versicolor* cells to ferruginol showed decreased expression volumes in manganese ion homeostasis-related protein (spot 473) (Figure 5 and Table 1). Manganese homeostasis in the budding yeast *Saccharomyces cerevisiae* is under intensive investigation.[16,17] Reports indicated that manganese is both an essential trace element to living cells and a cofactor for metalloproteins. These findings suggest that an array of metalloproteins, such as oxidoreductases, DNA/RNA polymerases, peptidases, kinases, decarboxylases, and sugar transferases, of *T. versicolor* may function abnormally in transcription, glycolysis, and sugar transformation regulation upon ferruginol treatment.

To survive in natural environments, microorganisms possess two major transporter proteins, ATP-binding cassette (ABC) and major facilitator superfamily (MFS), for active secretion of endogenous and exogenous toxicants. Nelissen et al.[18] carried out a computer-aided genome analysis of 186 MFS transporters from the budding yeast *S. cerevisiae*, and their results showed that a total of 28 proteins confer a role in multidrug-efflux pumps with multiple drug resistance (MDR) function. Remarkably, the potential MFS−MDR transporter (spot 584) of *T. versicolor* was downregulated after ferruginol treatment (Figure 5 and Table 1). Thus, it was hypothesized that the first-line defense barrier, active secretion of toxins, of *T. versicolor* cells was reduced or dysfunctional. This might cause further damage within *T. versicolor* cells. Del Sorbo et al.[19] also suggested that the inhibitory activity of the two types of transporters (ABC and MFS) could be developed as an antifungal strategy. Taken together, these results suggest that downregulation of MFS−MDR transporter is an antifungal strategy of ferruginol against *T. versicolor*.

Removal of hydrogen peroxide, alkyl hydroperoxides, and various oxidative stresses by peroxiredoxin TSA1 (spot 503), a thiol-specific antioxidant enzyme (thioredoxin peroxidase), had

dx.doi.org/10.1021/jf504717x | J. Agric. Food Chem. 2015, 63, 85−91

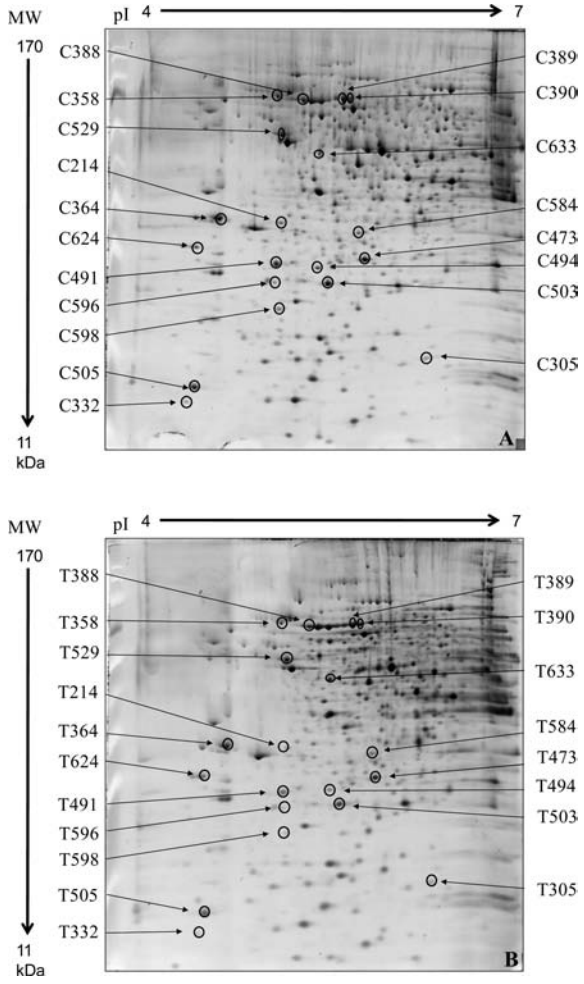

Figure 4. Two-dimensional gel images of (A) nontreated (control) and (B) ferruginol-treated *T. versicolor* protein expression patterns.

been demonstrated.[20,21] Iraqui et al.[22] further indicated that TSA1 maintains genome stability and avoids cell death of *S. cerevisiae*. Taken together, the downregulations of MFS−MDR transporter and peroxiredoxin TSA1 suggested that ferruginol reduced the defensive capabilities of *T. versicolor* cells. This may further result in the nonintegrity of *T. versicolor* cellular molecules such as cytoskeleton, polypeptide, and DNA.

The downregulated DNA polymerase ζ catalytic subunit (spot 494) of ferruginol-treated *T. versicolor* cells also corroborates the aforementioned damage situations. DNA polymerase ζ is an error-prone polymerase and comprises both Rev3 (catalytic subunit) and Rev7 (accessory subunit) in *S. cerevisiae*.[23] Downregulation of DNA polymerase ζ catalytic subunit (Figure 5 and Table 1) might result in dysfunction of DNA polymerase ζ. Lawrence[24] reviewed that the cellular functions of DNA polymerase ζ are participating in an extension step as a mismatch extender in translesion synthesis (TLS). For severe injuries caused by DNA damage, TLS is an important damage tolerance system and rescues cells for survival.[25−27] Hence, these findings suggest that the damage tolerance system of *T. versicolor* cannot function normally to assist cells in recovery from DNA damage caused by ferruginol.

In this study, β-tubulin 3 (spot 529) of *T. versicolor* was identified with a decrease in expression volume (Figure 5 and Table 1), suggesting that the ferruginol-treated *T. versicolor* cells might reduce cell motility, arrest the cell cycle, and inhibit cell growth/division.[28−30] Kiso et al.[31] screened antifungal agents and their results revealed that 2,5-dihydrophenylalanine (DHPA), a phenylalanine analogue, induced selective loss of both α- and β-tubulins in the filamentous fungus *Aspergillus nidulans*. According to the liquid culture test of *T. versicolor* treated with ferruginol, the growth of *T. versicolor* cells was inhibited. Average dry weights of treated mycelia were significantly lower than that of nontreated one (control) (Figure 2B). These findings suggest that ferruginol may be a type of microtubule-disrupting antifungal agent.

In addition, this study identified two downregulated proteins with uncertain functions, including hypothetical protein NCER_101469 (spot 491) and protein kinase C substrate (spot 305) of ferruginol-treated *T. versicolor* cells. The ratios of expression volumes (treatment/control) are 0.4 and 0.1, respectively (Table 1). Their functions await further investigation.

Among the 12 downregulated proteins, spots 596, 332, 598, and 214 were identified as phosphoenolpyruvate carboxykinase AcuF, nascent polypeptide-associated complex subunit β, mitochondrial protein involved in sorting of proteins in the mitochondria, and DNA damage checkpoint protein Rad24,

Table 1. Downregulated Proteins Identified in *T. versicolor* Mycelia as Differentially Expressed in Response to Ferruginol

spot no.[a]	expression ratio[b]	protein name	accession no.	Mowse score	cov (%)/pep[c]	theor mol mass (kDa)	pI
473	0.7	Mn ion homeostasis-related protein	XP_569373	70	3/2	46.9	9.44
584	0.6	potential MFS−MDR transporter	XP_719316	75	2/2	61.8	8.25
503	0.6	peroxiredoxin TSA1	XP_001382622	126	9/2	21.8	4.92
494	0.6	DNA polymerase ζ catalytic subunit	XP_754928	52	1/2	188.1	6.64
529	0.5	β-tubulin 3	AAM92170	629	27/10	43.1	5.81
491	0.4	hypothetical protein NCER_101469	EEQ81917	61	4/2	32.9	8.50
505	0.3	*d*	*d*				
305	0.1	protein kinase C substrate	EEQ92115	65	2/2	62.8	5.20
596	ctrl only	phosphoenolpyruvate carboxykinase AcuF	XP_002375147	51	2/2	66.5	5.87
332	ctrl only	nascent polypeptide-associated complex subunit β	A5DF06	36	7/2	16.5	5.54
598	ctrl only	mitochondrial protein involved in sorting of proteins in the mitochondria	XP_002493683	53	2/1	39.6	7.66
214	ctrl only	DNA damage checkpoint protein Rad24	XP_001837506	125	16/4	28.9	4.76

[a]Protein identified against NCBI, except spot 332 against Swiss-Prot. [b]Ratio of treatment/control upon addition of ferruginol. [c]Coverage of protein sequence/matched peptide number. [d]Not identified.

dx.doi.org/10.1021/jf504717x | J. Agric. Food Chem. 2015, 63, 85−91

Table 2. Upregulated Proteins Identified in *T. versicolor* Mycelia as Differentially Expressed in Response to Ferruginol

spot no.[a]	expression ratio[b]	protein name	accession no.	Mowse score	cov (%)/pep[c]	theor mol mass (kDa)	pI
624	1.6	*d*	*d*				
633	2.0	ATP-dependent RNA helicase eIF4A	Q2UPY3	106	6/2	47.3	5.39
389	2.2	heat shock protein	XP_567978	117	3/2	71.4	5.57
388	2.5	heat shock protein HSS1	Q01877	1017	25/16	70.5	5.13
364	2.7	tpis_emeni triosephosphate isomerase	XP_664504	62	5/2	27.1	5.89
358	3.0	autophagy-related protein 7	Q5AWA2	41	1/2	73.4	6.74
390	3.8	heat shock protein 70	ACT22525	534	8/5	72.1	5.63

[a]Protein identified against NCBI, except spots 633 and 358 against Swiss-Prot. [b]Ratio of treatment/control upon addition of ferruginol. [c]Coverage of protein sequence/matched peptide number. [d]Not identified.

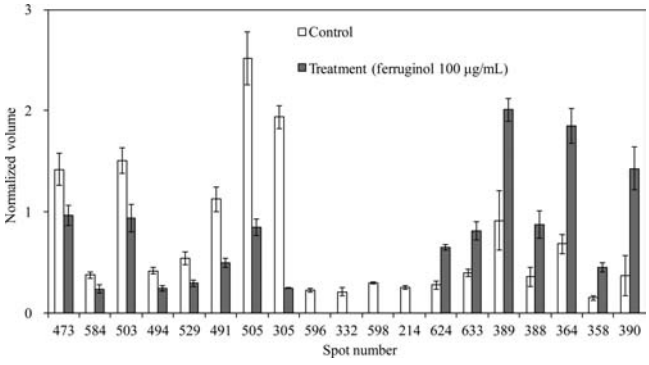

Figure 5. Comparison of expression patterns from nontreated (control) and ferruginol-treated *T. versicolor* protein by statistical analysis. Results are mean ± SE (n = 3). Protein expressions are significantly different at the level of $p < 0.05$ according to the student's paired t-test.

respectively. They were detected in nontreated (control) *T. versicolor* cells only. Phosphoenolpyruvate carboxykinase AcuF (spot 596) is a key enzyme associated with gluconeogenesis for producing hexose sugars of filamentous fungi via the tricarboxylic acid cycle to metabolize carbon sources.[32] This result suggests that ferruginol-treated *T. versicolor* cells cannot regulate glucose content normally via the processes of gluconeogenesis and tricarboxylic acid cycle.

Simultaneous observations of a drastic decrease in nascent polypeptide-associated complex subunit β (spot 332) and mitochondrial protein involved in sorting of proteins in the mitochondria (spot 598) (Figure 5 and Table 1) suggested that ferruginol-treated *T. versicolor* cells diminished the flux of nascent polypeptides and the capacity for correct translation. Nascent polypeptide-associated complex (NAC) is a heterodimer composed of α- and β-subunits and has a chaperone role in cells.[33,34] It also has a central role as a proteostasis sensor to control the folding state of the cellular proteome.[35] These results suggest that the proteostasis of ferruginol-treated *T. versicolor* cells is not under control.

In this study, expression of the DNA damage checkpoint protein Rad24 (spot 214) of *T. versicolor* cells was observed only in nontreated control (Figure 5 and Table 1). This finding supports the idea that ferruginol-treated *T. versicolor* cells might arrest the processing of the cell cycle and result in functionally defective DNA replication. Hartwell and Weinert[36] reported that eliminating the checkpoint control functions of eukaryotic cells may result in chromosome transmission infidelity. Aylon and Kupiec[37] further indicated that Rad24 plays a critical role in coordination of the response to repair chromosomal damage in *S. cerevisiae*. Taken together, the downregulation of peroxiredoxin TSA1, DNA polymerase ζ catalytic subunit, and DNA damage checkpoint protein Rad24 of *T. versicolor* cells strongly suggest that ferruginol is potentially involved in DNA damage or mutation, which might account for DNA nonintegrity and further cell death.

Upregulated Proteins upon Ferruginol Treatment. Six proteins are upregulated, including ATP-dependent RNA helicase eIF4A (spot 633), heat shock protein (spot 389), heat shock protein HSS1 (spot 388), tpis_emeni triosephosphate isomerase (spot 364), autophagy-related protein 7 (spot 358), and heat shock protein 70 (spot 390, Table 2). Eukaryotic translation factor 4A (eIF4A) participates in the initial step of mRNA translation. This ATP-dependent RNA helicase can unwind the secondary structure of mRNA at the 5′ untranslated region (UTR).[38] It is a critical stage of translational control. Upregulation of eIF4A suggests that *T. versicolor* cells appear to rescue cells by increasing their protein synthesis ability. However, the correct folding structure of protein is essential to such function. In this study, the nascent polypeptide-associated complex subunit β (spot 332, Table 1) and mitochondrial protein involved in sorting of proteins in the mitochondria (spot 598, Table 1) of *T. versicolor* cells were downregulated. These findings suggest that *T. versicolor* cells attempt to enhance the translation processes but the actions of protein sorting and folding cannot function normally. Taken together, *T. versicolor* cells might produce dysfunctional proteins and cause a massive stress.

Among these upregulated proteins, there are three heat shock proteins (HSPs). The ratios of expression volumes (treatment/control) of HSP (spot 389), HSS1 (spot 388), and HSP70 (spot 390) are 2.2, 2.5, and 3.8, respectively (Table 2). HSPs are highly conserved from bacteria to animals and function as molecular chaperones against stress. Jolly and Morimoto[39] reviewed the functions of HSPs and indicated that HSPs may control signal transduction at multiple checkpoints in the apoptosis pathways (type I programmed cell death, PCD). Moreover, among these HSPs, the small HSPs and HSP70 possess antiapoptotic activity for promoting cell survival. Matsuzaki et al.[40] investigated the proteomic responses of the white-rot fungus *Phanerochaete chrysosporium* to exogenous benzoic acid, and their results exhibited a similar stress response that the HSP70 was upregulated. These findings suggest that exposure of *T. versicolor* cells to ferruginol activates a defensive response via induction of HSPs.

Triosephosphate isomerase (spot 364) regulates the equilibrium of triosephosphates between dihydroxyacetone phosphate and D-glyceraldehyde 3-phosphate in glycolysis metabolism. Organisms convert glucose into pyruvate via glycolysis and release high-energy compounds, including ATP and NADH. In this study, the ratio of expression volumes (treatment/control) of triosephosphate isomerase was 2.7

(Figure 5 and Table 2). This upregulation of glycolytic protein suggests that *T. versicolor* cells appear to enhance energy production against stress conditions. Parente et al.[41] investigated the proteomic responses of dimorphic fungus *Paracoccidoides brasiliensis* under iron deprivation, and their results exhibited a similar response that glycolytic proteins were upregulated against stress. Upregulation of these proteins seems to indicate that *T. versicolor* cells can activate defense and rescue responses against ferruginol. However, the current results showed upregulation of a key autophagy-related protein (Atg7, spot 358, Table 2) of *T. versicolor* cells upon addition of ferruginol, inferring that those rescue reactions may be insufficient to reduce the toxic effects caused by ferruginol. This idea is consistent with the liquid culture test result of *T. versicolor* that the growth of mycelium was inhibited after treatment with ferruginol (Figure 2B).

Autophagy (self-eating, type II PCD) leads aberrant organelles and misfolded proteins for breakdown in autophagosomes, and the cells recycle these molecules for energy generation in response to aging or starvation conditions.[42] Nevertheless, excessive autophagy will induce a total collapse of cellular functions due to autophagic-type cell death. In this study, the ratio of expression volumes (treatment/control) of Atg7 is 3.0 (Figure 5 and Table 2). Atg7 is a unique ubiquitin-activating enzyme involved in the ubiquitin-like conjugation systems for processing the formation of autophagosomes.[43] This evidence demonstrates that *T. versicolor* cells had massive autophagy. Garrido et al.[44] further indicated that HSP70 is a decisive regulator that blocks the mitochondrial apoptotic pathway (type I PCD). In summary, upregulation of both HSP70 and Atg7 supports the idea that ferruginol induces *T. versicolor* cells toward cellular demise via type II PCD.

In this study, the downregulation of DNA damage checkpoint protein Rad24 (spot 214, Table 1) and DNA polymerase ζ catalytic subunit (spot 494, Table 1) suggests that the cell cycle of *T. versicolor* was arrested and the DNA damage cannot be completely repaired. In addition, the downregulation of peroxiredoxin TSA1 (Table 1) also suggests that *T. versicolor* cells suffered an abnormal accumulation of reactive oxygen species, contributing to irreversible damage that might cause cell death. Similar evidence that catalase, a key antioxidant enzyme, was selectively eliminated during autophagic cell death was reported.[45] Hence, ferruginol caused *T. versicolor* cells to move toward autophagic cell death in the current study.

In conclusion, antifungal processes of ferruginol against the basidiomycete *T. versicolor* at the proteome level were investigated. Results indicated that the defensive capabilities of *T. versicolor* cells were reduced. DNA and nascent polypeptides of *T. versicolor* cells might be attacked. The current results suggest that ferruginol induced destruction of vital cell organelles or proteins and caused cellular dysfunction. This process may further contribute to cell death of *T. versicolor*.

■ ASSOCIATED CONTENT

Supporting Information

Two tables listing sequences of identified down- and upregulated proteins. This material is available free of charge via the Internet at http://pubs.acs.org.

■ AUTHOR INFORMATION

Corresponding Author

* Phone +886-2-33664626; fax +886-2-23654520; e-mail peter@ntu.edu.tw.

Funding

This work was financed by the Ministry of Science and Technology from Taiwan (NSC 96-2628-B-002-023-MY3).

Notes

The authors declare no competing financial interest.

■ ACKNOWLEDGMENTS

We thank Dr. Keng-Hao Hsu for technical assistance and suggestions. We thank the Experimental Forest of National Taiwan University for providing experimental materials. We appreciate the excellent technical assistance of Technology Commons, College of Life Science, National Taiwan University, with the image analyzer (Typhoon 9400), and we thank the Instrument Center of National Cheng Kung University, National Science Council of Taiwan, for LC-MS/MS analyses.

■ REFERENCES

(1) Chang, S. T.; Wang, S. Y.; Wu, C. L. Identification of exudates from the bark of *Calocedrus macrolepis* var. *formosana* (Florin). *For. Prod. Ind.* **2000**, *19*, 59−65 (in Chinese).

(2) Imai, T.; Tanabe, K.; Kato, T.; Fukushima, K. Localization of ferruginol, a diterpene phenol, in *Cryptomeria japonica* heartwood by time-of-flight secondary ion mass spectrometry. *Planta* **2005**, *221*, 549−556.

(3) Chang, S. T.; Wang, S. Y.; Wu, C. L.; Su, Y. C.; Kuo, Y. H. Antifungal compounds in the ethyl acetate soluble fraction of the extractives of Taiwania (*Taiwania cryptomerioides* Hayata) heartwood. *Holzforschung* **1999**, *53*, 487−490.

(4) Sharp, H.; Latif, Z.; Bartholomew, B.; Bright, C.; Jones, C. D.; Sarker, S. D.; Nash, R. J. Totarol, totaradiol and ferruginol: three diterpenes from *Thuja plicata* (Cupressaceae). *Biochem. Syst. Ecol.* **2001**, *29*, 215−217.

(5) Kusumoto, N.; Ashitani, T.; Murayama, T.; Ogiyama, K.; Takahashi, K. Antifungal abietane-type diterpenes from the cones of *Taxodium distichum* Rich. *J. Chem. Ecol.* **2010**, *36*, 1381−1386.

(6) Ho, C. L.; Yang, S. S.; Chang, T. M.; Su, Y. C. Composition, antioxidant, antimicrobial and anti-wood-decay fungal activities of the twig essential oil of *Taiwania cryptomerioides* from Taiwan. *Nat. Prod. Commun.* **2012**, *7*, 261−264.

(7) Odds, F. C.; Brown, A. J. P.; Gow, N. A. R. Antifungal agents: Mechanisms of action. *Trends Microbiol.* **2003**, *11*, 272−279.

(8) Ramsdale, M. Programmed cell death in pathogenic fungi. *Biochim. Biophys. Acta, Mol. Cell Res.* **2008**, *1783*, 1369−1380.

(9) Martin, F.; Cullen, D.; Hibbett, D.; Pisabarro, A.; Spatafora, J. W.; Baker, S. E.; Grigoriev, I. V. Sequencing the fungal tree of life. *New Phytol.* **2011**, *190*, 818−821.

(10) Martinez, D.; Larrondo, L. F.; Putnam, N.; Gelpke, M. D. S.; Huang, K.; Chapman, J.; Helfenbein, K. G.; Ramaiya, P.; Detter, J. C.; Larimer, F.; Coutinho, P. M.; Henrissat, B.; Berka, R.; Cullen, D.; Rokhsar, D. Genome sequence of the lignocellulose degrading fungus *Phanerochaete chrysosporium* strain RP78. *Nat. Biotechnol.* **2004**, *22*, 695−700.

(11) Kroll, K.; Pähtz, V.; Kniemeyer, O. Elucidating the fungal stress response by proteomics. *J. Proteomics* **2014**, *97*, 151−163.

(12) Cagas, S. E.; Jain, M. R.; Li, H.; Perlin, D. S. Profiling the *Aspergillus fumigatus* proteome in response to caspofungin. *Antimicrob. Agents Chemother.* **2011**, *55*, 146−154.

(13) Shimizu, M.; Yuda, N.; Nakamura, T.; Tanaka, H.; Wariishi, H. Metabolic regulation at the tricarboxylic acid and glyoxylate cycles of the lignin-degrading basidiomycete *Phanerochaete chrysosporium* against exogenous addition of vanillin. *Proteomics* **2005**, *5*, 3919−3931.

(14) Wang, S. Y.; Wu, J. H.; Shyur, L. F.; Kuo, Y. H.; Chang, S. T. Antioxidant activity of abietane-type diterpenes from heartwood of *Taiwania cryptomerioides* Hayata. *Holzforschung* **2002**, *56*, 487−492.
(15) Bradford, M. M. A rapid and sensitive method for the quantitation of microgram quantities of protein utilizing the principle of protein-dye binding. *Anal. Biochem.* **1976**, *72*, 248−254.
(16) Reddi, A. R.; Jensen, L. T.; Culotta, V. C. Manganese homeostasis in *Saccharomyces cerevisiae*. *Chem. Rev.* **2009**, *109*, 4722−4732.
(17) Luk, E.; Jensen, L. T.; Culotta, V. C. The many highways for intracellular trafficking of metals. *J. Biol. Inorg. Chem.* **2003**, *8*, 803−809.
(18) Nelissen, B.; De Wachter, R.; Goffeau, A. Classification of all putative permeases and other membrane plurispanners of the major facilitator superfamily encoded by the complete genome of *Saccharomyces cerevisiae*. *FEMS Microbiol. Rev.* **1997**, *21*, 113−134.
(19) Del Sorbo, G.; Schoonbeek, H. J.; De Waard, M. A. Fungal transporters involved in efflux of natural toxic compounds and fungicides. *Fungal Genet. Biol.* **2000**, *30* (1), 1−15.
(20) Netto, L. E. S.; Chae, H. Z.; Kang, S. W.; Rhee, S. G.; Stadtman, E. R. Removal of hydrogen peroxide by thiol-specific antioxidant enzyme (TSA) is involved with its antioxidant properties: TSA possesses thiol peroxidase activity. *J. Biol. Chem.* **1996**, *271*, 15315−15321.
(21) Park, S. G.; Cha, M. K.; Jeong, W.; Kim, I. H. Distinct physiological functions of thiol peroxidase isoenzymes in *Saccharomyces cerevisiae*. *J. Biol. Chem.* **2000**, *275*, 5723−5732.
(22) Iraqui, I.; Kienda, G.; Soeur, J.; Faye, G.; Baldacci, G.; Kolodner, R. D.; Huang, M.-E. Peroxiredoxin Tsa1 is the key peroxidase suppressing genome instability and protecting against cell death in *Saccharomyces cerevisiae*. *PLoS Genet.* **2009**, *5*, No. e1000524.
(23) Nelson, J. R.; Lawrence, C. W.; Hinkle, D. C. Thymine-thymine dimer bypass by yeast DNA polymerase zeta. *Science* **1996**, *272*, 1646−1649.
(24) Lawrence, C. W. Cellular roles of DNA polymerase zeta and Rev1 protein. *DNA Repair* **2002**, *1*, 425−435.
(25) Prakash, S.; Johnson, R. E.; Prakash, L. Eukaryotic translesion synthesis DNA polymerases: Specificity of structure and function. *Annu. Rev. Biochem.* **2005**, *74*, 317−353.
(26) Murakumo, Y. The property of DNA polymerase zeta: REV7 is a putative protein involved in translesion DNA synthesis and cell cycle control. *Mutat. Res., Fundam. Mol. Mech. Mutagen.* **2002**, *510*, 37−44.
(27) Broomfield, S.; Hryciw, T.; Xiao, W. DNA postreplication repair and mutagenesis in *Saccharomyces cerevisiae*. *DNA Repair* **2001**, *486*, 167−184.
(28) Xiang, X.; Plamann, M. Cytoskeleton and motor proteins in filamentous fungi. *Curr. Opin. Microbiol.* **2003**, *6*, 628−633.
(29) Dumontet, C.; Durán, G. E.; Steger, K. A.; Murphy, G. L.; Sussman, H. H.; Sikic, B. I. Differential expression of tubulin isotypes during the cell cycle. *Cell Motil. Cytoskeleton* **1996**, *35*, 49−58.
(30) Nogales, E.; Wolf, S. G.; Downing, K. H. Structure of the alpha beta tubulin dimer by electron crystallography. *Nature* **1998**, *391*, 199−203.
(31) Kiso, T.; Fujita, K. I.; Ping, X.; Tanaka, T.; Taniguchi, M. Screening for microtubule-disrupting antifungal agents by using a mitotic-arrest mutant of *Aspergillus nidulans* and novel action of phenylalanine derivatives accompanying tubulin loss. *Antimicrob. Agents Chemother.* **2004**, *48*, 1739−1748.
(32) Hynes, M. J.; Draht, O. W.; Davis, M. A. Regulation of the *acuF* gene, encoding phosphoenolpyruvate carboxykinase in the filamentous fungus *Aspergillus nidulans*. *J. Bacteriol.* **2002**, *184*, 183−190.
(33) Beatrix, B.; Sakai, H.; Wiedmann, M. The alpha and beta subunit of the nascent polypeptide-associated complex have distinct functions. *J. Biol. Chem.* **2000**, *275*, 37838−37845.
(34) Wegrzyn, R. D.; Deuerling, E. Molecular guardians for newborn proteins: Ribosome-associated chaperones and their role in protein folding. *Cell. Mol. Life Sci.* **2005**, *62*, 2727−2738.
(35) Kirstein-Miles, J.; Scior, A.; Deuerling, E.; Morimoto, R. I. The nascent polypeptide-associated complex is a key regulator of proteostasis. *EMBO J.* **2013**, *32*, 1451−1468.
(36) Hartwell, L. H.; Weinert, T. A. Checkpoints: Controls that ensure the order of cell cycle events. *Science* **1989**, *246*, 629−634.
(37) Aylon, Y.; Kupiec, M. The checkpoint protein Rad24 of *Saccharomyces cerevisiae* is involved in processing double-strand break ends and in recombination partner choice. *Mol. Cell. Biol.* **2003**, *23*, 6585−6596.
(38) Rogers, G. W.; Komar, A. A.; Merrick, W. C. eIF4A: The godfather of the DEAD box helicases. *Prog. Nucleic Acid Res. Mol. Biol.* **2002**, *72*, 307−331.
(39) Jolly, C.; Morimoto, R. I. Role of the heat shock response and molecular chaperones in oncogenesis and cell death. *JNCI, J. Natl. Cancer Inst.* **2000**, *92*, 1564−1572.
(40) Matsuzaki, F.; Shimizu, M.; Wariishi, H. Proteomic and metabolomic analyses of the white-rot fungus *Phanerochaete chrysosporium* exposed to exogenous benzoic acid. *J. Proteome Res.* **2008**, *7*, 2342−2350.
(41) Parente, A. F. A.; Bailão, A. M.; Borges, C. L.; Parente, J. A.; Magalhães, A. D.; Ricart, C. A. O.; Soares, C. M. A. Proteomic analysis reveals that iron availability alters the metabolic status of the pathogenic fungus *Paracoccidioides brasiliensis*. *PLoS One* **2011**, *6*, No. e22810.
(42) Gozuacik, D.; Kimchi, A.; Gerald, P. S. Autophagy and cell death. *Curr. Top. Dev. Biol.* **2007**, *78*, 217−245.
(43) Tsujimoto, Y.; Shimizu, S. Another way to die: Autophagic programmed cell death. *Cell Death Differ.* **2005**, *12*, 1528−1534.
(44) Garrido, C.; Galluzzi, L.; Brunet, M.; Puig, P. E.; Didelot, C.; Kroemer, G. Mechanisms of cytochrome *c* release from mitochondria. *Cell Death Differ.* **2006**, *13*, 1423−1433.
(45) Yu, L.; Wan, F. Y.; Dutta, S.; Welsh, S.; Liu, Z. H.; Freundt, E.; Baehrecke, E. H.; Lenardo, M. Autophagic programmed cell death by selective catalase degradation. *Proc. Natl. Acad. Sci. U.S.A.* **2006**, *103*, 4952−4957.

JOURNAL OF AGRICULTURAL AND FOOD CHEMISTRY

Article

pubs.acs.org/JAFC

Enhanced Degradation of Herbicide Isoproturon in Wheat Rhizosphere by Salicylic Acid

Yi Chen Lu,[†,‡] Shuang Zhang,[§] Shan Shan Miao,[†,‡] Chen Jiang,[†,‡] Meng Tian Huang,[†] Ying Liu,[†] and Hong Yang*[,†]

[†]Jiangsu Key Laboratory of Pesticide Science, College of Sciences, Nanjing Agricultural University, Nanjing 210095, China

[‡]Key Laboratory of Monitoring and Management of Crop Diseases and Pest Insects, Ministry of Agriculture, Nanjing Agricultural University, Nanjing 210095, China

[§]State Key Laboratory of Food Science and Technology, Jiangnan University, Wuxi 214122, China

Supporting Information

ABSTRACT: This study investigated the herbicide isoproturon (IPU) residues in soil, where wheat was cultivated and sprayed with salicylic acid (SA). Provision of SA led to a lower level of IPU residues in rhizosphere soil compared to IPU treatment alone. Root exudation of tartaric acid, malic acid, and oxalic acids was enhanced in rhizosphere soil with SA-treated wheat. We examined the microbial population (e.g., biomass and phospholipid fatty acid), microbial structure, and soil enzyme (catalase, phenol oxidase, and dehydrogenase) activities, all of which are associated with soil activity and were activated in rhizosphere soil of SA-treated wheat roots. We further assessed the correlation matrix and principal component to figure out the association between the IPU degradation and soil activity. Finally, six IPU degraded products (derivatives) in rhizosphere soil were characterized using ultraperformance liquid chromatography with a quadrupole-time-of-flight tandem mass spectrometer (UPLC/Q-TOF-MS/MS). A relatively higher level of IPU derivatives was identified in soil with SA-treated wheat than in soil without SA-treated wheat plants.

KEYWORDS: *isoproturon, soil, salicylic acid, organic acids, microbial degradation*

INTRODUCTION

Isoproturon [3-(4-isopropylphenyl)-1,1-dimethylurea] (IPU) is a phenylurea herbicide widely used for controlling pre- and postemergence weed in soils with cultivation of various food crops.[1] While in agronomic practice IPU is applied to crop fields, not all administrated herbicide is absorbed by its targets. Instead, the left herbicide (or residue) may accumulate in soils, crops, or runoff into the adjacent ecosystems. Due to its high water solubility, IPU has been on the list of the 33 priority substances that have great potential to contaminate surface and groundwater.[2,3] As IPU is moderately hydrophobic and weakly absorbed by soils, it tends to accumulate in plants and consequently risks crop production and food safety.[4,5]

Soil is considered as a major sink for the bulk globally used herbicides, because more than 80% of the chemicals reside in soils after field administration.[6] The fate of soil herbicides is determined by chemical, physical, and biological processes, each of which individually or coordinately influences degradation, sediment, or transformation of herbicide within soils or soil-crop systems.[7,8] Among these, degradation is a fundamental process for soil herbicides.[9] Soil microbes are thought of as a dominant contribution to dissipation of organic contaminants.[10] IPU degradation involves biotic and abiotic processes, but bacterium-facilitated biodegradation in soil is of particular interest, because it undergoes a complete mineralization to harmless inorganic products.[11] Microorganism-based decay of IPU is possibly promoted by plant root growth in rhizosphere soil, because plants provide favorable conditions for soil microorganisms to live. The rhizo-degradation of IPU may depend on plant−soil microbe interactions. Recently, many efforts have been made to investigate the degradation of herbicides in plant and soil.[12−16] The efficiency of herbicide degradation in soil relies on environmental factors such as dissolved organic matter (including low-molecular-weight organic acids, LMWOAs), microbial community, soil enzyme activity, and soil structure.[17−19] Several bacterial strains have been isolated from soils with the capability of mineralizing IPU.[1,11] This makes it possible that IPU can be potentially decayed under an appropriate condition. To date, only a few documents are available on the rhizo-degradation of IPU.

Salicylic acid (SA) is a signal molecule involved in regulation of a wide range of plant growth, development, and responses to biotic and environmental stresses.[20−22] Our recent studies have shown that IPU-induced toxicity in wheat plants could be attenuated by external SA.[22] However, whether SA-regulated low accumulation of IPU in plants is associated with the IPU degradation in soils is unknown. Wheat (*Triticum aestivum*) is one of the most important crops, as it provides a staple food for more than half of the world population. As an essential crop, wheat is one of the targets of herbicide contamination.[23] Understanding the mechanisms for herbicide degradation in wheat and its surrounding soils is critical to minimize the environmental risk and ensure the safety of crop production. In

Received: October 22, 2014
Revised: December 7, 2014
Accepted: December 15, 2014
Published: December 15, 2014

ACS Publications © 2014 American Chemical Society

DOI: 10.1021/jf505117j
J. Agric. Food Chem. 2015, 63, 92−103

this study, we examined whether exogenous provision of SA stimulated LWMOAs efflux from wheat roots when exposed to IPU. We also investigated the effects of SA on soil microbial activities (microbial community and soil enzyme activities), which might be responsible for accelerating the degradation of IPU in soil. Using ultraperformance liquid chromatography−tandem mass spectrometry (UPLC-MS/MS), we further characterized the degraded products of IPU in rhizosphere soil. Our analysis provided evidence that IPU degradation in rhizosphere soil was enhanced by SA application on wheat plants. With cultivation of SA-treated wheat, the soil microbial population, enzyme activity, and microbial metabolites (e.g., phosphplipid fatty acids, as biomarkers) in rhizosphere soil were greatly improved. Thus, the aims of the study were to identify whether provision of SA affected the degradation of IPU residue in soil in which wheat plants were cultivated and to support the hypothesis that SA-accelerating IPU degradation in the soil rhizosphere fractions was through stimulation of root exudation of organic acids and enhancement of microbial population and activity. This study will help uncover a role of SA in modulating the IPU catabolism in wheat-planted soil and the intrinsic relationship between root exudation, microbial activity, and IPU degradation.

MATERIALS AND METHODS

Materials and treatments. Isoproturon (purity of 96.9%) and wheat seeds (*Triticum aestivum*, cv. Yangmai 13) were provided by the Academy of Agriculture Science in Jiang Su, Nanjing, China. IPU-free soil (organic carbon, 2.13%; total N, 1.26 g kg^{-1}; available P, 34.3 mg kg^{-1} and available K, 91.5 mg kg^{-1}; pH 7.6) was collected from the Experimental Station of Nanjing Agricultural University, Nanjing, China (Euric Gleysols, N 32.03°; E 118.84°). The soil was sampled from the surface layer (0−20 cm depth), air-dried, and sieved through a 3 mm mesh.[14]

Sterilized wheat seeds were germinated, and the uniformly germinating seeds were transferred to a plastic pot (1 L) containing 1,120 g of prepared soil. Seedlings were grown in a growth chamber (PGX-350D, SAFE Co.) under a light intensity of 200 μmol m^{-2} s^{-1} with a light/dark cycle of 14/10 h at 25/20 °C and watered to keep 70% relative water content in soils. Wheat was planted in the soil mixed with IPU at 4 mg kg^{-1} dry soil. For SA treatment, wheat leaves were sprayed with 5 mg L^{-1} SA and the SA treatment was undertaken once a day and lasted for 6 days. Water was sprayed for control seedlings. Soils adhered tightly to roots were collected as rhizosphere soil, while those shaken off from roots were collected as nonrhizosphere soil.[14,15] The bulk soil was the mixture of rhizosphere and nonrhizosphere soils.[16] When harvested, fine root fragments were carefully teased out to avoid any influence of cutoff roots. The fresh samples were used for measuring enzyme activities and phospholipid fatty acids (PLFAs), microbial population, and other parameters.

Determination of IPU and its degradation products. Isoproturon and its metabolites in soil were analyzed based on the method of Liang et al.[22] with slight modification. Samples in the soil (10 g) were ultrasonically extracted three times with mixed acetone−water (3:1, *v*/*v*) (each time 10 mL extraction solution for 30 min), followed by centrifugation at 4,000*g* for 10 min and filtration. The filtrate was pooled and concentrated to remove acetone with a rotary vacuum evaporator at 40 °C. The residual water was loaded onto an LC-C_{18} solid phase extraction (SPE) column (Supelclean, 300 mg). The elute was discarded, and the column was washed with 4 mL of high performance liquid chromatography (HPLC) grade methanol. The methanol solution was collected for analysis.

Fresh plant tissues (1.0 g) were homogenized with 15 mL of extraction solvent (acetone/water, 3:1, *v*/*v*) and ultrasonicated for 30 min. The homogenate was centrifuged at 5000*g* for 10 min and filtrated. The process was repeated in triplicate. The supernatant was concentrated to remove acetone by rotary vacuum evaporator at 40 °C. The residual water was extracted by petroleum ether for three times (each time with 10 mL). The organic phase was collected, dried on anhydrous sodium sulfate, and evaporated to dryness. The residue was redissovled in 10 mL of distilled water. The dissolved solution was transferred to an LC-C_{18} SPE column. The elute was discarded. Then, 2 mL of petroleum ether-diethyl ether (98:2, *v*/*v*) was passed through the column at 2.5 mL min^{-1}, and the eluted solution was removed. The residue in the column was washed with 4 mL of chromatographic grade methanol, and the washing solution was collected and quantified by HPLC. As seen in Supporting Information Table S1, the recoveries for the spiked soil and plant samples were in the range of 89.8−117.3%, with the relative standard deviations (RSDs) (n = 3) from 1.9% to 4.8%, confirming a convenient performance of analytic technique for determination of IPU in soil and plant tissues.

Liquid chromatography/mass spectrometer (LC/MS) analysis of soil extracts was performed with an ultraperformance liquid chromatography (UPLC) apparatus equipped with a Waters Acquity photodiode array (PDA) detector (Waters, USA) connected to a Waters SYNAPT SYNAPT Quadrupole-time-of-flight (Q-TOF) Mass Spectrometer (Waters, USA) (UPLC/Q-TOF-MS/MS). Chromatographic operation was set under conditions as follows: XBridge C_{18} columns (2.1 × 100 mm, granulation of 3.5 μm, Waters); injection volume, 4 μL; mobile phase with two solvents: A (100% Acetonitrile) and B (99.9% H_2O/0.1% formic acid, *v*/*v*) at a 0.3 mL min^{-1} flow rate. The elution steps were followed: 0−0.1 min linear gradient from 0 to 15% of A, 0.1−15 min linear gradient from 15 to 35% of A, 15−25 min linear gradient from 35 to 100% of A and 25−27 min isocratic at 100% of A. After returning to the initial conditions, the equilibration was achieved within 3 min.

The electrospray (ESI) in positive mode and TOF-MS parameters were optimized to reach the best sensibility on isoproturon and its metabolites ion $[M + H]^+$ for the m/z range from 50 to 1,000. The ESI source was operated at 50 °C with the desolvation temperature of 400 °C. The desolvation gas flew at the rate of 500 L h^{-1}. A capillary voltage was set at 3.5 kV. The cone voltage was set at 30 V. In order to achieve high fragmentation of protonated and deprotonated molecules ($[M + H]^+$), the collision energy was between 6 and 15 eV. IPU-derived metabolites were detected by comparison of the exact molecular masses and fragmentation pathway of the precursor $[M + H]^+$ ions recorded during LC-MS experiments. The targeted MS/MS experiments were performed using a collision energy ramp of 8 to 18 eV (positive ion mode).

Leucine enkephaline at the concentration of 2 ng μL^{-1} (exact mass of 556.2771 Da $[M + H]^+$) was infused at the flow rate of 10 μL min^{-1} in the lock spray channel. A spectrum of 0.3 s was acquired every 15 s and allowed exact mass determination during UPLC-MS and UPLC-MS/MS experiments. All acquisition and analysis of data were controlled by MassLynx V 4.1 software.

Assaying of soil enzyme activity. Catalase (CAT, E.C. 1.11.1.6) activity was measured by back-titrating residual H_2O_2 with $KMnO_4$.[24] Soil samples (2 g) were weighted into a 100 mL conical flask, which was added with 40 mL of distilled water and 5 mL of 3% hydrogen peroxide solution. The mixture was shaken at 120 rpm for 30 min at 30 °C, and 5 mL of 3 M H_2SO_4 was introduced immediately after shaking to end the reaction. The filtrate (25 mL) was titrated with 0.02 M $KMnO_4$ consumed g^{-1} dry matter.[25]

Dehydrogenase (DHA, EC 1.1.1.1) activity was determined using the reduction of 2,3,5-triphenylteterazolium chloride (TTC) method.[26] Samples of 5 g of soil and 50 mg of $CaCO_3$ were mixed thoroughly and transferred into three test tubes (1.6 × 15 cm). To each tube with stopper, 2 mL of 1% TTC and 2.5 mL of deionized water were added. The samples were mixed on a vortex and incubated at 30 °C. After 20 h, trephenylformanzan, a product from the reduction of TTC, was extracted by adding 25 mL of methanol and shaken in an orbital shaker (150 rev min^{-1}) under dark conditions for 15 min. The samples were collected in a volumetric flask. The tube was washed with methanol until the red color disappeared. The filtrate was diluted with additional methanol to a final volume of 100 mL. The color intensity was measured at 485 nm with methanol as a blank.

DOI: 10.1021/jf505117j
J. Agric. Food Chem. 2015, 63, 92−103

Table 1. Isoproturon Accumulation in Soil (RS, BS, and NRS) with Wheat Planted for 10 d, and Its Bioconcentration Factors (BCFs) and Translocation Factors (TFs) in Shoots and Roots of Wheat[a]

	IPU concentration (mg kg^{-1})					BCF		
	Soil							
treatment	RS	BS	NRS	Shoot	Root	Shoot	Root	TF
Control	–	3.18 ± 0.051a	–	–	–	–	–	–
IPU	2.63 ± 0.052c	2.83 ± 0.039b	3.07 ± 0.053a	3.56 ± 0.012	0.74 ± 0.015	1.26 ± 0.016	0.26 ± 0.006	4.82 ± 0.079
IPU+SA	2.17 ± 0.037e	2.44 ± 0.051d	2.82 ± 0.088b	2.74 ± 0.016*	0.45 ± 0.042*	1.13 ± 0.017*	0.18 ± 0.013*	6.12 ± 0.540*

[a]Control, unplanted soil; RS, rhizosphere soil; BS, bulk soil; NRS, nonrhizosphere soil; BCF: fresh weight ratio of isoproturon concentration in plant to the bulk soil; TF: ratio of shoot BCF to root BCF. Seedlings grew in soils with IPU (4 mg kg^{-1}) for 4 d. After that, the leaves were sprayed with 5 mg L^{-1} SA once a day for 6 d. The control soil also contained 4 mg kg^{-1} isoproturon. Values are the means ± standard deviations (n = 3). Data of soil with different letters are significantly different ($p < 0.05$, Turkey's test). Asterisks indicate the significant differences between IPU and IPU+SA ($p < 0.05$).

Activities of phenol oxidase (PO, EC 1.10.3.2) were determined according to the method of Carine et al.[27] with some modifications. The PO activity was assayed by adding 5 mL of modified universal buffer (MUB) solution (pH 2.0) and 200 μL of a 0.01 M ABTS solution to the mixture. The mixture was incubated at 30 °C for 5 min and centrifuged at 11,300g at 4 °C for 2 min. The oxidation rate of ABTS to ABTS$^{\bullet+}$ released in the supernatant was measured at 420 nm (ε = 18460 M^{-1} cm^{-1}).

Analysis of organic acids. Root exudates in rhizosphere soil were collected according to the methods of Tuason and Arocena[28] and Gao[29] with minor modification. Fresh soil samples (10 g on dry-weight basis) were packed in a 50 mL plastic centrifuge tube, followed by addition of 10 mL of 0.1% H_3PO_4 (v/v) and shaken in a thermostat reciprocating shaker at 25 ± 0.5 °C for 2 h. Soil suspensions were mixed with 10 mL of 0.1 M NaOH and shaken again at 4 ± 0.5 °C for 10 min. The suspension was centrifuged at 10,000g for 30 min, acidified with 1 M HCl, and filtrated to remove precipitated humic acids. The filtrates were extracted three times with 10 mL of ethyl acetate. The organic phase containing organic acids was obtained by evaporation of the solvent in a rotary evaporator at 35 °C and redissolution of the residue in 1 mL of double-distilled water. The solution was filtered through a 0.45 μm filter (Millex-HV, Millipore). The quantitative determination of organic acids was carried out using a HPLC (Supporting Information Table S2).

Measurement of soil microbial biomass C and N in soil. The fumigation extraction method was used for determining soil microbial biomass carbon (SMBC) and nitrogen (SMBN).[30] Ten grams of soil was fumigated with alcohol-free chloroform at 25 °C for 24 h. Excess chloroform was removed by repeated evacuation. Samples were extracted by 60 mL of 0.5 M K_2SO_4 on a rotary shaker at 220 rpm for 60 min and filtered through Whatman qualitative filter paper. The samples from each treatment were placed for 24 h at 25 °C without fumigation and immediately extracted and filtered as described above. Soil filtrates were stored at −20 °C prior to analysis for SMBC and SMBN.[31] The concentrations of soluble organic carbon (SOC) in soil fractions were determined according to Gao et al.[29] SMBN was determined at 280 nm using a UV-1700 spectrophotometer (Shimadzu, Japan) by the method of Turner et al.[32] and Guo et al.[18]

Extraction and analysis of phospholipid fatty acids. PLFAs were determined based on the method of Hammesfahr et al.[33] The details of PLFAs extraction, esterification reaction, and quantification were presented in Supporting Information Table S3.

Statistic analysis. All the experiments were performed at least three repetitive independent treatments. The values were expressed as means ± standard deviation. Statistical analysis of the results was performed using SPSS statistics 20 for Windows. The statistical significance of the results was determined through analyses of variance post hoc test (ANOVA, Tukey's test) at the 95% confidence level ($p < 0.05$). Principal component analysis (PCA) was used to classify treatments according to their PLFAs using SIMCA-P 13.03 software.

RESULTS

Effect of SA on IPU degradation in soil. Compared to the soil without wheat planting (unplanted soil), the wheat-planted soil accumulated a lower level of IPU (Table 1). The concentration of IPU was always higher in nonrhizosphere soil (NRS) than in rhizosphere soil (RS). The bulk soil (BS) had a moderate concentration of IPU. When the wheat plants were exposed to IPU and/or treated with SA, the IPU residues in RS, BS, and NRS with IPU treatment alone were 1.21-, 1.16-, and 8.14-fold higher than that of IPU+SA treatment, indicating that SA application was able to reduce IPU residues in wheat-planted soil.

SA provision to plants gave rise to much less accumulation of IPU in roots and aerial parts (64.4% down in roots and 29.9% down in shoots) relative to the control (IPU treatment alone) (Table 1). To get an insight into the effect of SA on IPU accumulation, we analyzed the bioconcentration factor (BCF) and translocation factor (TF) for wheat under IPU-exposure. The BCF refers to the quotient between the organism and medium substance concentrations.[14] In the absence or presence of SA, the value of BCF_{shoot} was always higher than that of BCF_{root}, pointing out that more IPU was accumulated in the above-ground than in the root. Surprisingly, both BCF_{shoot} and BCF_{root} with IPU+SA treatment were found to be lower than those with IPU treatment alone. We further assessed the translocation factor (TF), the ratio of IPU concentration in aerial part to root, which is often used to evaluate the plant capability of translocating xenobiotics from root to shoot.[14] Although TF_{IPU} and TF_{IPU+SA} were above one (implying a potential for IPU accumulation in the above-ground of wheat), the TF value was higher for IPU+SA treatment than that for IPU treatment, pointing to the fact that IPU moved more rapidly in the IPU+SA-treated wheat than in the IPU-treated wheat.

Effect of SA on exudation of organic acids in wheat roots. Because SA provision led to more IPU degradation in wheat-planted soil, we inferred that root exudation might be altered. The extractable tartaric, malic, and oxalic acids are important organic acids liberated from roots to the rhizosphere.[20] Analysis of the organic acids in roots and planted soils showed a large variation under different conditions. Tartaric and malic acids were only detected in root tissue and rhizosphere soil (Figure 1). In rhizosphere soil, exudation of tartaric acid was drastically promoted by SA and IPU+SA treatment, which were 1.69- and 1.95-fold higher than the control; in contrast, no significant increase in tartaric acid was found in the IPU-exposed rhizosphere soil as compared to the

DOI: 10.1021/jf505117j
J. Agric. Food Chem. 2015, 63, 92−103

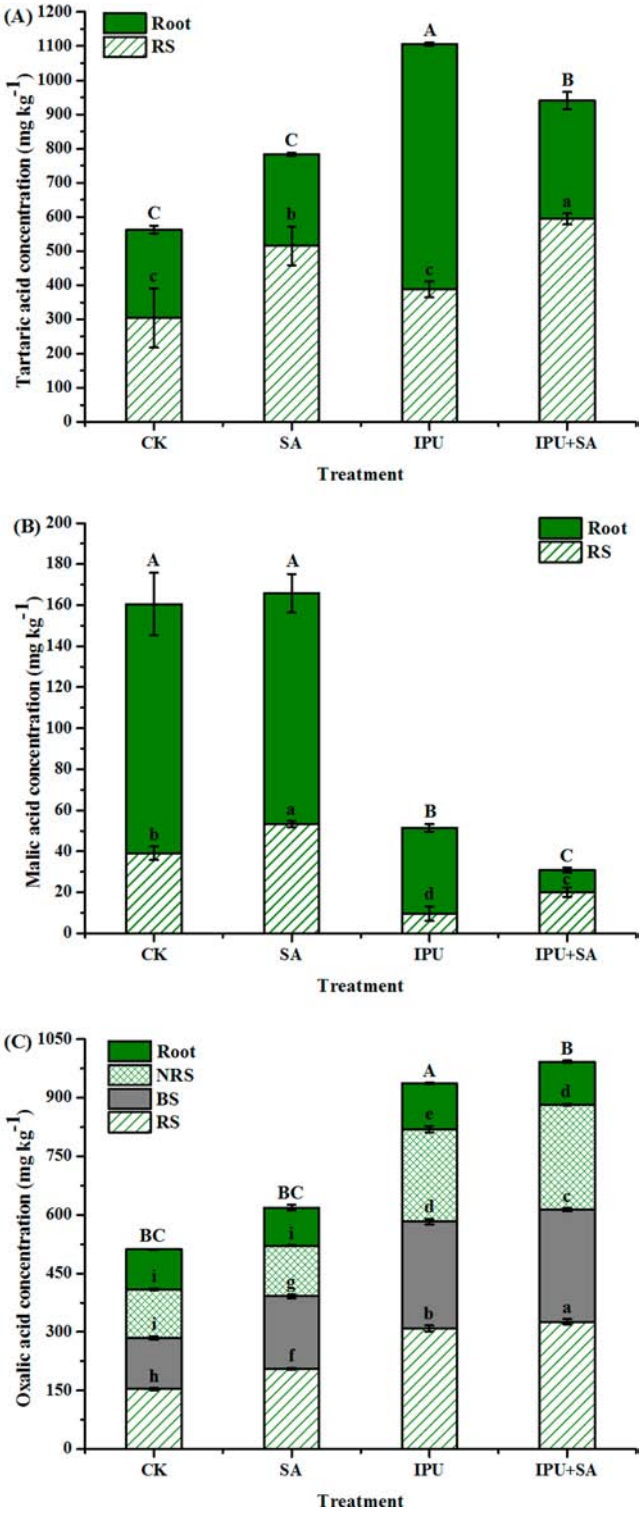

Figure 1. Concentrations of tartaric acid (A), malic acid (B), and oxalic acid (C) in rhizosphere (RS), nonrhizosphere (NRS), and bulk soils (BS) and wheat roots. Seedlings grew in soils with IPU (4 mg kg^{-1}) and without IPU (CK, control) for 4 d. After that, the leaves were sprayed with 5 mg L^{-1} SA once a day for 6 d. Values are the means ± standard deviations (n = 3). Data with different capital letters (wheat root) and lower case letters (soil) are significantly different (p < 0.05, Turkey's test).

control; however, more tartaric acid appeared to accumulate in IPU-treated roots (Figure 1A).

IPU treatment inhibited accumulation of malic acid in roots and rhizosphere soil (Figure 1B). While SA application stimulated the secretion of malic acids to soil with IPU, much less malate was accumulated in the root. The tartaric and malic acids in NRS and BS were assessed but undetectable. For oxalic acid, it could be detected in any of the compartments. Compared to control, provision of SA increased the levels of oxalic acid in BS and RS (Figure 1C). Treatment with IPU enhanced the content of oxalic acid in the BS and RS. In addition, oxalic acid in the NRS was also found to accumulate. Under the IPU exposure, the SA-regulated increase in oxalic acid was limited.

Effect of SA on soil enzyme activities in IPU-polluted soil. Catalase (CAT) is an intracellular enzyme involved in microbiological redox capacity.[34] Its activity in RS, BS, and NRS appeared to change slightly with all treatments (Figure 2A). Soil dehydrogenase activity (DHA) serves as an effective parameter for assessing the side effect of herbicide treatments on the soil microbial biomass.[35] Compared to the control, provision of SA alone did not affect DHA in rhizosphere soil (or BS), but IPU exposure resulted in the significant decrease in DHA (Figure 2B). For IPU+SA treatment, the DHA was largely recovered in rhizosphere soil. The DHA in BS and NRS was reduced with IPU relative to the control, and application of SA could hardly affect the DHA in the presence of IPU. We finally determined the activity of phenol oxidase (PO), a soil microoganism excreted enzyme catalyzing the oxidation of recalcitrant aromatic compounds.[27] In the three compartments, treatment with IPU led to the lower activity of PO compared to the control or SA alone; however, the rebound of PO activity was displayed in the presence of SA (Figure 2C).

Effect of SA on soil microbial nutrition in the presence of IPU. Soil microbial biomass carbon (SMBC), microbial quotient, and soil microbial biomass N (SMBN) are crucial biological indexes, representative of soil quality, deterioration, and correlation with degradation of herbicides.[36] Under all circumstances, concentrations of SMBC, microbial quotient, and SMBN progressively decreased in the following order: RS > BS > NRS (Table 2). The content of SMBC was drastically increased in the soil with IPU compared to control. Unexpectedly, much higher SMBC contents were examined with IPU+SA treatment. The change of microbial quotient demonstrated a similar trend to the change of SMBC (Table 2).

Effects of SA on the microbial community. PLFA is a group of phosphorus-containing fatty acids, which are frequently used for monitoring soil microbial community structure and their relative abundance under a certain environmental condition.[37,38] To investigate the microbial population and microbial biomass in the soil fractions, we determined phospholipid fatty acids from various microbial communities including $Gram^+$ bacteria, $Gram^-$ bacteria, actinomycetes, fungi, arbuscular mycorrhizal fungi (AM fungi), and eukaryotes. Soil with wheat-cultivation usually had a higher level of PLFA than that of the control (CK, soil with no wheat-cultivation) (Table 3). RS usually had the highest level of PLFA, whereas NRS had the lowest level of PLFA. SA had a potent effect on PLFA accumulation in the microbial community, particularly in RS. For example, SA provision significantly increased PLFA contents in Gram-negative (7.41) and -positive (7.26) bacteria compared to the controls (5.24 and 5.69, respectively). The enhancement of PLFA contents by SA could be found in the presence of IPU. Similarly, SA provision alone and IPU+SA treatment increased the PLFA

DOI: 10.1021/jf505117j
J. Agric. Food Chem. 2015, 63, 92−103

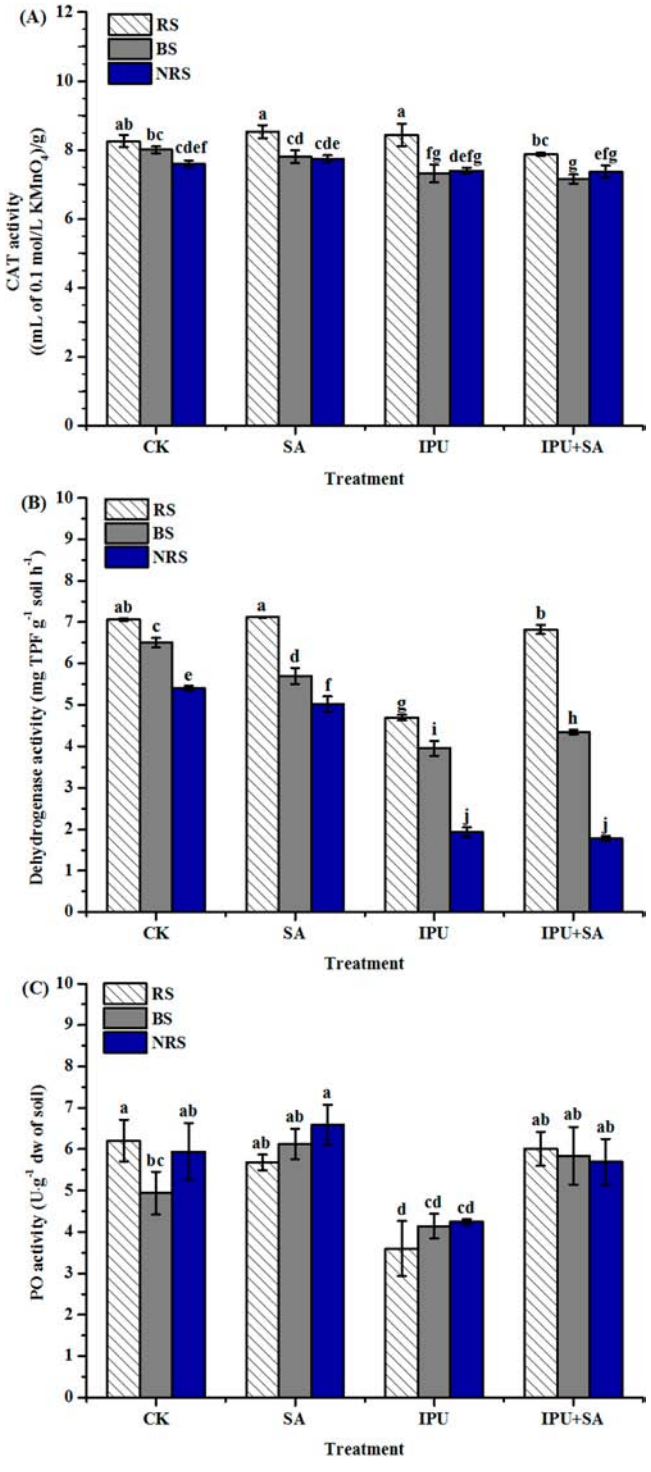

Figure 2. Effect of isoproturon (IPU) on catalase (CAT), dehydrogenase, and phenol oxdase (PO) activities in rhizosphere (RS), nonrhizopheric (NRS), and bulk (BS) soils with wheat planted for 10 d. Seedlings grew in soils with IPU (4 mg kg^{-1}) for 4 d. After that, the leaves were sprayed with 5 mg L^{-1} SA once a day for 6 d. Values are the means ± standard deviations (n = 3). Data with different letters are significantly different (p < 0.05, Turkey's test).

contents in fungi by 3.84- and 3.12-fold over the controls, respectively. The SA-promoted increase in PLFA accumulation was also detected in actinomycetes and eukaryotic microorganisms. These results suggest that SA application prompted the root exudates (e.g., organic acids), leading to the increase of soil microbial population. However, in the most bacteria, treatment with IPU did not induce accumulation of PLFA, except for eukaryote that had a positive response to IPU stress.

More than 70 PLFAs were assessed in this study. Microbial biomass, represented by the total PLFA, ranged from 8.48 to 22.01 nmol g^{-1} and was typically higher in RS than other soil fractions in all treatments (Figure 3A). The change of PLFA is indicative of a stressful environment for the soil microorganisms.[39] The major shifts in the microbial community under the IPU and/or SA treatment could be ascertained using the percentage of stress indicator (the ratios of bacterial to fungal PLFAs and Gram-negative to Gram-positive bacteria). The stress level of microbes in the unplanted and IPU-treated soils was significantly higher than that in the control samples (Figure 3B). The RS had a marginally lower stress compared to the IPU-free plant soils, while the stress was lower than that in both BS and NRS. Remarkably, the stress was increased by IPU treatment alone, especially in RS, BS, and NRS.

IPU treatment increased the ratio of bacterial to fungal PLFA (B/F), but the ratio decreased significantly in the presence of SA. No significant difference in B/F PLFAs was observed between the unplanted soil and planted soil (RS, BS, and NRS) without SA and IPU treatment (Figure 3C). Interestingly, the B/F PLFAs in the presence of SA progressively declined in the following sequence: NRS > BS > RS; meanwhile, the opposite trend was observed in samples without SA application (Figure 3C). Lower B/F ratios are considered to be indicative for a more sustainable agro-ecosystem, in which organic matter decomposition dominates the provision of plant nutrients.[40,41] The SA treatment had a stimulatory effect on the content of fungal PLFA in both the IPU-free and IPU-treated soils (Table 3).

The ratio of Gram-negative bacteria/Gram-positive bacteria (GN/GP) in the IPU-exposed unplanted soil was lower than that of the unplanted control (decreased by 27.4%) (Figure 3D). Meanwhile, the ratio of GN/GP was increased by application of SA in RS of SA and IPU+SA treatment. Additionally, the SA application also increased the amount of specific microbial PLFAs to some extent (Table 3). The content of $Gram^+$ PLFAs was higher than that of $Gram^-$ PLFAs in RS and NRS soils, revealing that $Gram^+$ was more resistant to the IPU toxicity. Taken together, although PLFAs in different microbial community and soil fractions varied under IPU exposure, provision of SA could promote accumulation of PLFAs in bacteria with or without IPU.

Principal component analysis and correlation matrix of multivariate. Using principal component analysis (PCA), the experimental data can be transformed into a new coordinate system by analyzing the variance. As shown in Figure 4, the first two principal components explained 0.747 of the total variance (R^2), with 50.8% and 23.9% for the first (PC1) and the second (PC2) components, respectively. The model can be considered valid, because the prediction goodness parameter (cum Q^2) was 0.475 (Supporting Information Table S4) and R^2 was not more than 2 units of cum Q^2.[42]

Soil samples with IPU were on the positive side of PC2, and samples without IPU were on the negative side of PC2 (Supporting Information Figure S1A), indicating a remarkable difference between the two treatments and that PC2 was markedly influenced by IPU exposure. The SA- and IPU+SA-treated RS was clearly distinguished by positive PC1 values, indicating that provision of SA had the largest effect on the first

DOI: 10.1021/jf505117j
J. Agric. Food Chem. 2015, 63, 92−103

Table 2. Effect of IPU and/or SA on Soil Microbial Biomass Carbon (SMBC), Microbial Quotient, and Microbial Biomass Nitrogen in the Wheat-Planted Soil[a]

properties	location	treatment			
		CK	SA	IPU	IPU+SA
C_{mic} (μg C/g dry soil)	RS	117.24 ± 5.90Ad	157.10 ± 14.67Ac	302.62 ± 2.00Ab	584.60 ± 7.58Aa
	BS	97.26 ± 11.00Bc	109.67 ± 9.04Bc	285.43 ± 2.12Bb	342.85 ± 3.88Ba
	NRS	76.81 ± 7.00Cd	99.80 ± 0.99Bc	218.13 ± 3.42Cb	321.14 ± 26.41Ba
Microbial quotient (μg/g)	RS	0.01 ± 0.00052Ad	0.014 ± 0.0013Ac	0.027 ± 0.00018Ab	0.052 ± 0.00670Aa
	BS	0.0086 ± 0.00098Bc	0.0097 ± 0.00080Bc	0.025 ± 0.00019Bb	0.030 ± 0.00034Ba
	NRS	0.0068 ± 0.00062Cd	0.0089 ± 0.00088Bc	0.019 ± 0.00030Cb	0.028 ± 0.00230Ba
Δ absorbance (abs 10/g dry soil)	RS	0.115 ± 0.020 Ac	0.290 ± 0.012 Aa	0.113 ± 0.003 Ac	0.173 ± 0.005 Ab
	BS	0.097 ± 0.016 Ab	0.143 ± 0.003 Ba	0.097 ± 0.002 Bb	0.097 ± 0.003 Bb
	NRS	0.091 ± 0.009Aab	0.109 ± 0.021 Ca	0.084 ± 0.008 Bb	0.090 ± 0.013 Bab

[a]RS, rhizosphere soil; BS, bulk soil; NRS, nonrhizosphere soil; Δ absorbance, increment in absorbance. Values are the means ± standard deviations (n = 3). Different lower case letters indicate the significant differences between the different treatments ($p < 0.05$). Means followed by different capital letters are significantly different between different soil samplings ($p < 0.05$).

Table 3. Variations of Specific PLFAs in the Three Soil Fractions of RS, BS, and NRS[a]

location	treatment	PLFA concentration (nmol g^{-1})					
		Gram negative	Gram positive	fungi	AM fungi	actinomycetes	eukaryote
RS	CK	5.24 ± 0.300de	5.69 ± 0.510bcde	0.43 ± 0.026ef	0.62 ± 0.020c	2.56 ± 0.042cde	0.48 ± 0.025 cd
	SA	7.41 ± 0.660a	7.26 ± 0.380a	1.65 ± 0.073a	0.88 ± 0.002a	3.79 ± 0.140a	0.63 ± 0.009b
	IPU	5.24 ± 0.240de	6.31 ± 0.500bc	0.39 ± 0.046ef	0.63 ± 0.009c	2.77 ± 0.210def	0.75 ± 0.028a
	IPU+SA	6.51 ± 0.230b	6.58 ± 0.400b	1.34 ± 0.042b	0.76 ± 0.017b	3.16 ± 0.037bc	0.51 ± 0.007c
BS	CK	5.19 ± 0.030de	5.60 ± 0.120def	0.46 ± 0.077def	0.61 ± 0.039c	2.49 ± 0.048fg	0.47 ± 0.022 cd
	SA	6.31 ± 0.360bc	6.34 ± 0.710cde	1.28 ± 0.068b	0.77 ± 0.070b	3.21 ± 0.047b	0.51 ± 0.055c
	IPU	5.37 ± 0.360de	5.64 ± 0.290def	0.38 ± 0.081f	0.63 ± 0.027c	2.82 ± 0.140de	0.62 ± 0.016b
	IPU+SA	5.77 ± 0.380 cd	6.14 ± 0.250bcd	0.60 ± 0.010d	0.66 ± 0.006c	2.82 ± 0.012de	0.50 ± 0.060c
NRS	CK	3.90 ± 0.530f	4.29 ± 0.710h	0.45 ± 0.010def	0.50 ± 0.002ef	2.06 ± 0.160h	0.38 ± 0.044ef
	SA	4.13 ± 0.012f	4.57 ± 0.085gh	0.54 ± 0.018de	0.55 ± 0.034d	2.27 ± 0.110gh	0.37 ± 0.006f
	IPU	4.36 ± 0.150f	5.15 ± 0.190fg	0.40 ± 0.037ef	0.54 ± 0.040de	2.61 ± 0.150ef	0.41 ± 0.003def
	IPU+SA	5.26 ± 0.015de	5.79 ± 0.470cde	0.42 ± 0.057ef	0.66 ± 0.019c	2.95 ± 0.120bcd	0.47 ± 0.009 cd
CK-free plant		4.96 ± 0.033e	4.62 ± 0.130gh	0.78 ± 0.012c	0.48 ± 0.007f	0.48 ± 0.007f	0.41 ± 0.008def
IPU-free plant		4.26 ± 0.067f	5.46 ± 0.240ef	0.30 ± 0.032f	0.39 ± 0.013g	0.39 ± 0.013g	0.46 ± 0.002cde

[a]Different letters within a row indicate different levels of significance ($p < 0.05$).

principal component. Within RS, samples associated with IPU treatment alone and IPU+SA were significantly different.

The loading scatter plot showed the contribution of each variation to the first two principal components, which disclosed the dominating correlation structure among the variables. The plot can be divided into four colored regions, where the variables in the same tinctorial region are positively correlated (Supporting Information Figure S1B). The total PLFA had the highest contribution to PC1 and was positively correlated with variables in the red region as well as the yellow and blue regions, but negatively correlated with the stress indicator, the concentration of IPU (C_{IPU}), and the ratio of bacteria/fungi (B/F). This observation suggests that the soil microbial biomass had an important role in IPU degradation and was facilitated by release of organic acids. Likewise, the soil enzyme activities were located in the diagonal direction of the green zone, illustrating that the enzyme activities were negatively associated with the IPU (C_{IPU}) concentration and the ratio of bacteria/fungi (B/F) (Supporting Information Figure S1B).

The biplot indicated the effect of variables on the observations (Figure 4), showing that the soil microbial biomass and IPU concentration had the main contribution to the discrimination among the differently treated samples. The RS with SA and IPU+SA treatments was close to the variables of soil microbes and organic acids, but situated on the opposite side of the concentration of IPU. This indicated that application of SA prompted the soil microbial biomass, secretion of organic acids from wheat root, and degradation of IPU.

The correlation matrix was additionally used to assess the inner relationship among variables. The activities of soil enzymes were positively related to the tartaric and malic acids and some soil microbes (G^-, G^+, fungi, and AM fungi) but were negatively related to the stress indicator and concentration of IPU (Table 4). These results indicated that SA-promoted organic acids stimulated the growth of bacteria and fungi following the enhancement of soil enzyme activities and leading to the accelerated degradation of IPU.

Analysis of IPU residues and derivatives in rhizosphere soil. In the positive mode, $[M + H]^+$ ions of IPU and its metabolites in the rhizosphere sample were identified by high resolution/full-scan MS detection, and the registration of mass spectra was allowed to achieve a mass accuracy better than 5 ppm error (ppm) for all protonated $[M + H]^+$ molecules from a single analysis. LC-MS/MS spectra of IPU metabolites were obtained via fragmentation of molecular ions. The fragmentation pattern of IPU was subsequently used for the confident structural identification of metabolites. The full scan mass spectra of fragment ions of rhizosphere soil treated with IPU were compared to those of the blank soil to find out the potential metabolites. The parent herbicide and its main five

DOI: 10.1021/jf505117j
J. Agric. Food Chem. 2015, 63, 92−103

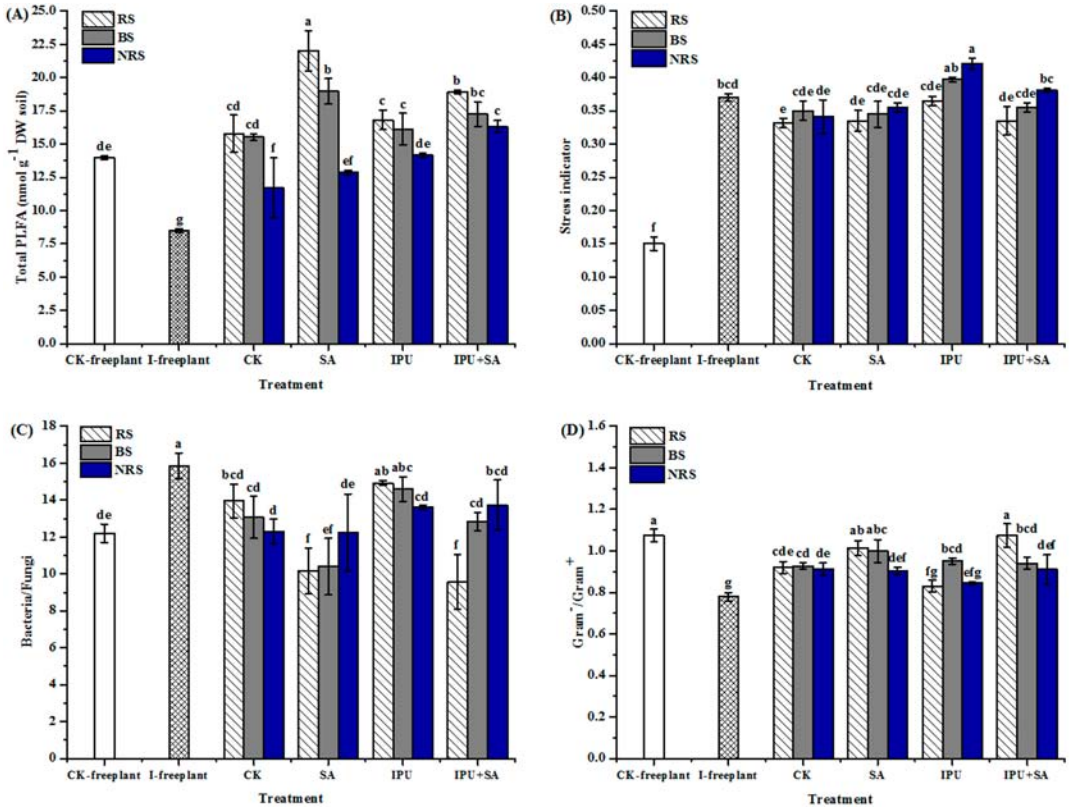

Figure 3. Total PLFA concentration (A), stress indicator (B), bacteria/fungi (C), and $Gram^{-}/Gram^{+}$ (D) of rhizosphere (RS), nonrhizosphere (NRS), and bulk soils (BS) with or without IPU and/or SA exposure. PLFA, the phospholipid fatty acid; $Gram^{-}/Gram^{+}$, Gram-negative bacteria/Gram-positive bacteria. Values are the means ± standard deviations (n = 3). Data with different letters are significantly different ($p < 0.05$, Turkey's test).

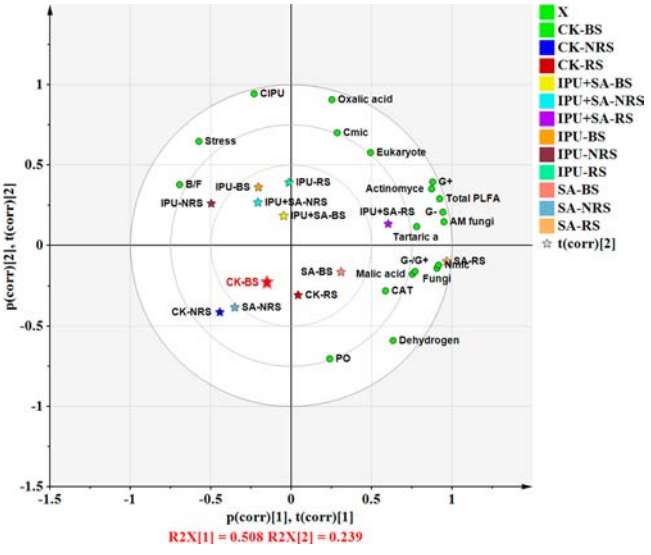

Figure 4. Biplot of 19 detected indexes of three parts of rhizosphere (RS), nonrhizosphere (NRS), and bulk soils (BS) with wheat planted for 10 d. Seedlings grew in soils with IPU (4 mg kg^{-1}) for 4 d. After that, the leaves were sprayed with 5 mg L^{-1} SA once a day for 6 d. PCA axes explained 50.8% and 23.9% of the total variation for sediment 1 and 2 microcosms, respectively.

metabolites (2# to 6#) were detected, and the mass data of IPU and its 5 metabolites of IPU were summarized in Table 5.

The extract MS^2 spectra of the molecular ion of m/z 207 occurred at the retention time of 8.07 min (Supporting Information Figure S2A). Fragmentation of IPU led to two product ions at m/z 165 and 134. The most abundant product ion at m/z 165 was generated by the loss of an isopropyl group (42 Da). The product ions at m/z 134 was 31 Da less than m/z 165, indicating the loss of a $-N(CH_3)_2$ group (Supporting Information Figure S3A). These characteristic product ions above were important for identification of IPU-metabolites.

The mass spectrum of metabolite 2# peaked at 5.76 min, and the fragment ion of m/z 223 was produced by addition of 17 Da (hydroxy group) from IPU (Supporting Information Figure S2B). Its main product ions were m/z 205 and 165, which were the same as the two fragment ions of IPU. Thus, metabolite 2# was identified as hydroxylated IPU (2-OH-isopropyl-IPU) with the addition of a hydroxyl group (Supporting Information Figure S3B; Table 5).

2-OH-Monodemethyl-IPU (metabolite 3#) was eluted at 5.32 min with protonated molecular ion $[M + H]^+$ of m/z 209 in the full-scan MS (Supporting Information Figure S2C). In the MS^2 spectrum, it had the typical and most abundant fragment ion at m/z 191 (loss of a hydroxy group), which further lost a neutral moiety of $O{=}C{-}NH{-}CH_3$ to form ion at m/z 134 (Supporting Information Figure S3C; Table 5).

Metabolite 4# peaked at 6.92 min and had a protonated molecular ion $[M + H]^+$ at m/z 195 (Supporting Information Figure S2D). The MS/MS spectra gave prominent ions at m/z 178 and 150, which were produced by the loss of $-NH_2$ via doffing-amidogen and further loss of $C{=}O$, respectively (Supporting Information Figure S3D; Table 5). Thus, we tentatively elucidated metabolite 4# to be formed by N-dealkylation of metabolite 2#.

DOI: 10.1021/jf505117j
J. Agric. Food Chem. 2015, 63, 92−103

Table 4. Correlation Coefficient Matrix between the Soil Enzymatic, Chemical, and Microbiological Properties[a]

Variables	CAT	Dehydrogenase	PO	Tartaric acid	Malic acid	Oxalic acid	Total PLFA	Stress indicator	B/F	G^-/G^+	G^-	G^+	Eukaryote	Fungi	Actinomycetes	AM fungi	C_{mic}	N_{mic}	C_{IPU}
CAT	1.000	0.689	-0.023	0.717	0.730	-0.186	0.415	-0.560	-0.206	0.108	0.390	0.446	0.475	0.400	0.319	0.414	-0.211	0.619	-0.491
Dehydrogenase		1.000	0.399	0.569	0.617	-0.345	0.367	-0.874	-0.529	0.573	0.452	0.333	0.150	0.541	0.203	0.425	-0.166	0.574	-0.724
PO			1.000	0.011	0.208	-0.436	0.024	-0.658	-0.611	0.506	0.113	-0.092	-0.586	0.386	0.003	0.185	-0.171	0.228	-0.604
Tartaric acid				1.000	0.793	0.376	0.618	-0.473	-0.397	0.445	0.619	0.664	0.527	0.587	0.557	0.603	0.457	0.719	-0.025
Malic acid					1.000	-0.020	0.597	-0.511	-0.338	0.396	0.607	0.579	0.351	0.562	0.560	0.606	0.000	0.803	-0.333
Oxalic acid						1.000	0.447	0.332	0.087	0.129	0.398	0.545	0.575	0.112	0.470	0.337	0.902	0.064	0.857
Total PLFA							1.000	-0.305	-0.506	0.646	0.988	0.980	0.622	0.799	0.969	0.978	0.361	0.794	0.027
Stress indicator								1.000	0.572	-0.544	-0.391	-0.273	-0.005	-0.511	-0.152	-0.400	0.130	-0.485	0.727
B/F									1.000	-0.826	-0.575	-0.384	0.169	-0.904	-0.510	-0.637	-0.122	-0.690	0.435
G^-/G^+										1.000	0.744	0.543	0.052	0.823	0.615	0.744	0.345	0.642	-0.258
G^-											1.000	0.955	0.560	0.833	0.945	0.983	0.364	0.807	-0.041
G^+												1.000	0.708	0.700	0.926	0.924	0.442	0.717	0.131
Eukaryote													1.000	0.217	0.566	0.512	0.318	0.393	0.306
Fungi														1.000	0.804	0.882	0.183	0.891	-0.316
Actinomycetes															1.000	0.962	0.362	0.803	0.108
AM fungi																1.000	0.301	0.850	-0.102
C_{mic}																	1.000	0.070	0.725
N_{mic}																		1.000	-0.334
C_{IPU}																			1.000

[a]CAT, catalase activity; Dehydrogenase, dehydrogenase activity; PO, phenol oxidase; B/F, bacteria/fungi; G^-/G^+, Gram-negative bacteria/Gram-positive bacteria; G^-, Gram-negative bacteria; G^+, Gram-positive bacteria; C_{mic}, microbial biomass carbon; AM fungi, arbuscular mycorrhizal fungi; N_{mic}, microbial biomass nitrogen; C_{IPU}, the concentration of IPU. SIMCA uses a coloring scheme in ten levels (from dark color to white) to assist in the interpretation of the correlation matrix. The darker the color, the higher the absolute correlation.

Table 5. Isoproturon and Their Degradation Products Identified in Rhizosphere Soil with Wheat Planted for 10 d in the Presence of SA

								MS^2 m/z[b]	
no.	metabolites	ion mode	R_t[a] (min)	calcd m/z $[M + H]^+$	exptl m/z $[M + H]^+$	ppm error	chemical formula	precursor ion	main fragment ions
1	Isoproturon, IPU	$[M + H]^+$	8.07	207.1497	207.1496	−0.48	$C_{12}H_{18}N_2O$	207	165, 134
2	2-OH-isopropyl-IPU	$[M + H]^+$	5.76	223.1447	223.1452	2.24	$C_{12}H_{18}N_2O_2$	223	205, 165
3	2-OH-monodemethyl-IPU	$[M + H]^+$	5.32	209.1290	209.1286	−1.91	$C_{11}H_{16}N_2O_2$	209	191, 149, 134
4	2-OH-didemethyl-IPU	$[M + H]^+$	6.92	195.1134	195.1139	2.56	$C_{10}H_{14}N_2O_2$	195	178, 150
5	Monodemethyl-IPU	$[M + H]^+$	7.91	193.1341	193.1347	3.11	$C_{11}H_{16}N_2O$	193	151, 136, 94
6	Didesmethyl-IPU	$[M + H]^+$	7.56	179.1184	179.1187	1.67	$C_{10}H_{14}N_2O$	179	137, 120, 94

[a]R_t: retention time. [b]MS^2 m/z: Base peaks of MS^2 fragment ions are shown in the table.

Metabolite 5# eluted at 7.91 min with a protonated molecular ion $[M + H]^+$ at m/z 193 and was 14 Da less than its parent IPU and formed by a loss of methyl group (Supporting Information Figure S2E). The corresponding fragment ions at m/z 151 were generated by loss of the isopropyl group and m/z 136 through cleaving of an amino C−N bond. The fragment ion of m/z 136 further lost an isopropyl group and gave rise to the ions at m/z 94, which represented the rest anilin moiety (Supporting Information Figure S3E; Table 5). Thus, metabolite 5# could be characterized as *N*-dealkylation products of parent IPU.

The molecular ion at m/z 179 (metabolite 6#) was eluted at 7.56 min (Supporting Information Figure S2F). The MS/MS spectra showed that elimination of C_3H_7, NH_2, and O═C-NH_2 groups led to occurrence of fragment ions at m/z 137, 120, and 94, from which Metabolite 6# was defined as didesmethyl-IPU (Supporting Information Figure S3F; Table 5).

The residual concentration of parent IPU and IPU-derived metabolites in the presence and absence of SA was determined. The concentrations of IPU in rhizosphere soil with SA application were moderately decreased by 14.5% compared to those without SA application (Figure 5). Furthermore, the relative intensities of IPU-metabolites in rhizosphere soil were much greater in the presence of SA than those in the absence of SA. IPU-metabolites with m/z 195, 193, and 179 under the IPU +SA treatment were increased by 52.7%, 9.1%, and 31.8% compared to the IPU treatment alone, respectively. The other two IPU-derivatives (m/z 223 and 209) were slightly increased by SA application but were not significantly different with IPU treatment alone (Figure 5).

DISCUSSION

Our recent study has demonstrated that SA was able to reduce the accumulation of IPU and improve the antitoxic capacity against IPU in wheat plants.[22] Such an observation allowed for the assumption that SA-regulated low levels of IPU in wheat plants are most likely associated with the degradation of IPU in soils, although the chemical and biological mechanisms for SA

DOI: 10.1021/jf505117j
J. Agric. Food Chem. 2015, 63, 92−103

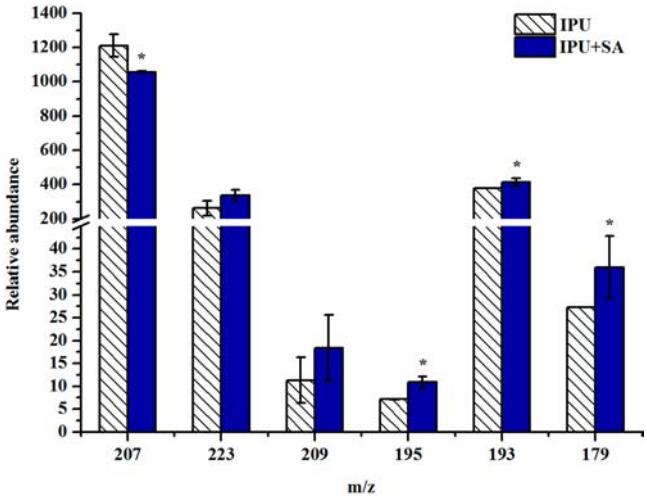

Figure 5. IPU-derived degradation products extracted from IPU-treated rhizosphere soil planted with wheat for 10 d under SA treatment or untreatment. Seedlings grew in soils with IPU (4 mg kg^{-1}) for 4 d. After that, the leaves were sprayed with 5 mg L^{-1} SA once per day for 6 d. Vertical bars represent three replicate measurements ± standard deviations. Asterisks indicate the significant differences between the treatments of SA+IPU and IPU ($p < 0.05$).

action in the plant are largely unknown. To investigate the role of SA in regulating IPU degradation in plants, we in detail characterized the IPU residues and their degradation products in wheat using UPLC-TOF-MS/MS.[43] Most detected IPU-derivatives were sugar-conjugated. Degradation and glycosylation of IPU-derivatives could be enhanced by applying salicylic acid (SA). While more sugar-conjugated IPU-derivatives were identified in wheat with SA application, lower levels of IPU were detected, indicating that SA is able to accelerate intracellular IPU catabolism. Because SA can promote IPU decay in wheat plants, this prompted us to assume that SA could also affect IPU degradation in soil through cultivation of wheat plants. Thus, we located the IPU residues in three soil fractions including RS, BS, and NRS, and we chemically characterized IPU degradation products in the major region of rhizosphere soil. Using UPLC/Q-TOF-MS/MS, more IPU-derivatives have been detected in the soil with SA-treated plants, indicating that SA can also enhance IPU catabolism in soil. To figure out the process of IPU degradation, we performed a comprehensive study by analyzing exudation of three major organic acids in roots and examining soil microbial population, biomass, nutrition, enzyme activities, group-specific PLFAs, and their correlations, all of which are closely associated with degradation of IPU. SA provision could promote the IPU degradation in soil because IPU concentrations with SA in RS, BS, and NRS were much lower that those without SA treatment (Table 1). SA-improved IPU degradation in the soil was most likely through enhancement of exudation of organic acids from roots, soil microbial population, and consequently acceleration of removal of IPU. To our knowledge, this is the first report on the comprehensive analysis of IPU degradation in soil fractions promoted by SA.

It is well-known that degradation of organic compounds in soils is mainly executed by microorganisms, but the efficacy of the degradation relies on the activity of the microbial community. Many environmental factors influence the processes, including root exudates, soil structure, nutrient conditions, and others.[19,44,45] One of the most active sites for organic compound degradation is the rhizosphere, where many root exudates are liberated from plants. In this study, only three organic acids, tartaric, malic, and oxalic acids, were detected in wheat, although we simultaneously examined several other organic acids, such as citric and succinic acids, but all of them were undetectable. This could be the result of different plant species that secrete only some kinds of dominant organic acids, particularly under toxic substances. For example, buckwheat (*Fagopyrum esculentum*), a monocot, predominantly secretes oxalic acids when challenged by excess aluminum (Al).[46] By contrast, *Cassia tora*, a dicot, tends to release citric acids when exposed to Al.[20] Root exudation of organic acids such as oxalate and malate induced by toxic organic compounds was also reported in several crops, such as maize, wheat, ryegrss, and *Cucurbita pepo*.[47,48] However, tartaric and malic acids were only detected in root tissue and rhizosphere soil, while oxalic acid occurred in root tissue and rhizosphere soil, nonrhizosphere, and bulk soil. One of the possible reasons is that both tartaric and malic acids were more favorably degraded in rhizosphere soil than oxalic acid, making less tartaric and malic acids accumulated in nonrhizosphere and bulk soils. Meanwhile, a large amount of oxalate could efflux to the rhizosphere that possibly diffused to nonrhizosphere and bulk soil. Alternatively, oxalate can also be generated by some microorganisms because some types of microbes are able to use soil-existing organic compounds (e.g., DOM) to release oxalate.[49]

The negative correlation between the exudation of organic acids and the concentration of IPU in the presence of SA indicated that the organic acids affected the IPU degradation by a biological process. Recent studies have demonstrated that dissolved organic matter (DOM) or organic acids in soil were observed to enhance the dissolution of prometryn,[50] chlorotoluron,[12] and isoproturon.[51] Therefore, the biodegradation of IPU could be promoted by the organic acids. In fact, organic acids released from plant roots provide the necessary nutrition and energy for survival and proliferation of rhizosphere microbes.[52] For instance, malate secreted from *Arabidopsis* roots selectively signaled and recruited the beneficial rhizobacterium *Bacillus subtilis* FB17.[53] The present study showed that exudation of tartaric and malic acids in the presence of SA increased soil microbial PLFA concentrations in rhizosphere soil, consistent with the evidence that soil microbial carbon (C_{mic}), nitrogen (N_{mic}), and microbial quotient were improved. Thus, the wheat growth may influence the soil microbial biomass by altering the spatial distribution and content of available substrates from rhizodeposition in the presence of SA.

Soil microbes play an important role in soil formation, nutrient cycling, and contaminant degradation, and the rate of herbicide metabolism was directly related to the microbial biomass.[10] In our case, total PLFAs concentration, as a biomarker of soil microbial biomass, showed a negative correlation with IPU residues (Figure 3A; Table 1). Moreover, soil microbes are sensitive to the changing environment.[54] It was found that the ratio of B/F was higher at IPU than that at IPU+SA, suggesting that a higher proportion of fungi occurred in the presence of SA. The proportion of fungi prompted by SA in soil was conducive to accelerate the degradation of IPU. $Gram^-$ bacteria were known to be sensitive to the utilizable carbon[55] and generally stimulated by plant root exudation in soil.[56,57] It was also found that the proportion of $Gram^-$ bacteria with IPU+SA was significantly higher than that with IPU, implying that a more utilizable carbon source was available

DOI: 10.1021/jf505117j
J. Agric. Food Chem. 2015, 63, 92−103

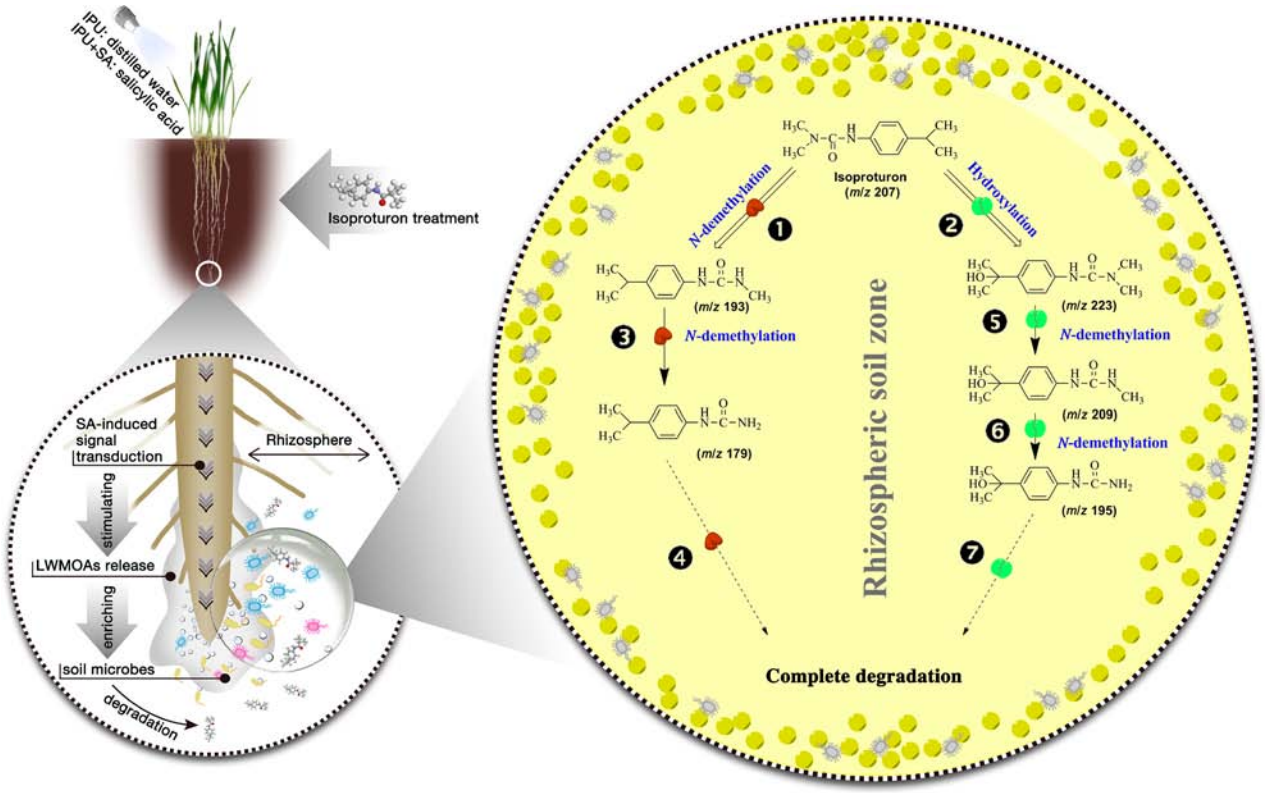

Figure 6. Proposed pathway of degradation in soil with wheat planted for 10 d.

in the presence of SA. Taken together, the SA-responsive release of organic acids promoted microorganism growth by improving C_{mic}, N_{mic}, and microbial quotient, thus making more IPU degraded.

Soil enzyme activities are also thought of as sensitive to pollutants and have been proposed as biomarkers for soil organic pollution degradation.[16,18] Herbicide residues disturb soil microbial communities by negatively affecting soil enzyme activities.[35] The activities of DHA were inhibited by IPU as a result of IPU toxicity to soil microbes (Figure 2) but were recovered in the presence of SA, pointing to the role of SA in alleviating the toxicity of IPU. PO is an extracellular enzyme and is also involved in biodegradation and detoxification of some aromatic xenobiotics such as organochlorinated compounds or polycyclic aromatic hydrocarbons (PAH).[27] By examination of PO, we found that its activity changed similarly to DHA in RS. However, the activity of CAT with IPU+SA was lower than that with IPU in RS. CAT is an intracellular enzyme found in most bacteria and can split hydrogen peroxide into molecular oxygen for preventing cells from damage by reactive oxygen species (ROS).[23,58] Notably, SA was well demonstrated to suppress the ROS production under environmental stresses.[59,60] The CAT activity was down-regulated, possibly due to the SA-induced decrease in ROS production.

The pathway of IPU degradation in rhizosphere soil was investigated by identifying intermediate metabolites. UPLC-TOF-MS/MS analysis resulted in characterization of five intermediate metabolites, including 2-OH-isopropyl-IPU (Metabolite 2#), 2-OH-monodemethyl-IPU (Metabolite 3#), 2-OH-didemethyl-IPU (Metabolite 4#), monodemethyl-IPU (Metabolite 5#), and didemethyl-IPU (Metabolite 6#). Unlike detoxified herbicide derivatives by means of conjugation with polar donor metabolic molecules,[61] microbial-meditated decay of IPU was associated with the catabolic pathway, leading to the direct degradation. Based on the finding, we proposed two main catabolic pathways of IPU in the present study. As shown in Figure 6 (Step 1, 3), one of the IPU-degradation pathways proceeds by consecutive *N*-demethylation to monodemethyl-IPU (Metabolite 5#) and didesmethyl-IPU (Metabolite 6#). This pathway has been studied mainly in bacterial cultures.[62,63] The other parallel pathway was initiated by hydroxylation of the isopropyl side chain of IPU to 2-OH-isopropyl-IPU (Metabolite 2#), which was subsequently *N*-demethylated to 2-OH-monodemethyl-IPU (Metabolite 3#) and 2-OH-didemethyl-IPU (Metabolite 4#) (Figure 6; Step 2, 5, 6). These IPU hydroxylated derivatives were commonly produced by soil fungi.[11] The detected intermediates can be further broken down by aerobic microbes, of which the process was divided into three stages—ring hydroxylation, cleavage of aromatic ring, and oxidation of the aliphatic moiety to Krebs cycle intermediates—and could be finally broken down to CO_2 and H_2O (Figure 6; Step 4, 7).[64] In a nutshell, provision of SA stimulated exudation of organic acids in rhizosphere soil. The increased organic acids enriched the soil microbial communities, modified the soil enzyme activity, and consequently accelerated the degradation of IPU (Figure 6).

■ ASSOCIATED CONTENT

Supporting Information

Tables of spiked recoveries of isoproturon in soil, wheat shoots, and roots; calibration of organic acids; marker PLFA in various organisms; and results of PLS-Class model; detailed methods; loading scatter plot (A) and score scatter plot (B); LC-MS/MS analysis of isoproturon (IPU) degradation products in IPU-treated rhizosphere soil; and product ion MS/MS spectra. This

DOI: 10.1021/jf505117j
J. Agric. Food Chem. 2015, 63, 92−103

material is available free of charge via the Internet at http://pubs.acs.org.

AUTHOR INFORMATION

Corresponding Author

*Telephone number: +86-25-84395207. E-mail: hongyang@njau.edu.cn.

Funding

The authors acknowledge the financial support of the National Natural Science Foundation of China (No. 21077055) and Special Fund for Agro-scientific Research in the Public Interest (No. 201203022) from the Ministry of Agriculture of China.

Notes

The authors declare no competing financial interest.

REFERENCES

(1) Sørensen, S. R.; Ronen, Z.; Aamand, J. Isolation from agricultural soil and characterization of a *Sphingomonas* sp. able to mineralize the phenylurea herbicide isoproturon. *Appl. Environ. Microbiol.* **2001**, *67*, 5403−5409.

(2) Directive 2000/60/EC of the European Parliament and of the Council establishing a framework for Community action in the field of water policy. CELEX-EUR Official Journal L 327, 1−72, 22 December 2000. URL (http://ec.europa.eu/food/plant/protection/evaluation/legal_en.htm).

(3) Johnson, A. C.; Besien, T. J.; Bhardwaj, C. L.; Dixon, A.; Gooddy, D. C.; Haria, A. H.; White, C. Penetration of herbicides to groundwater in an unconfined chalk aquifer following normal soil applications. *J. Contam. Hydrol.* **2001**, *53*, 101−117.

(4) Chauhan, L. K.; Kumar, M.; Paul, B. N.; Goel, S. K.; Gupta, S. K. Cytogenetic effects of commercial formulations of deltamethrin and/or isoproturon on human peripheral lymphocytes and mouse bone marrow cells. *Environ. Mol. Mutagen.* **2007**, *48*, 636−643.

(5) Bi, Y. F.; Miao, S. S.; Lu, Y. C.; Qiu, C. B.; Zhou, Y.; Yang, H. Phytotoxicity, bioaccumulation and degradation of isoproturon in green algae. *J. Hazard. Mater.* **2012**, *243*, 242−249.

(6) Fang, H.; Yu, Y. L.; Chu, X. Q.; Wang, X. G.; Yang, X. E.; Yu, J. Q. Degradation of chorpyrifos in laboratory soil and its impact on soil microbial functional diversity. *J. Environ. Sci.* **2009**, *21*, 380−386.

(7) Arias-Estévez, M.; López-Periago, E.; Martínez-Carballo, E.; Simal-Gándara, J.; Mejuto, J. C.; García-Río, L. The mobility and degradation of pesticides in soil and the pollution of groundwater resources. *Agric. Ecosyst. Environ.* **2008**, *123*, 247−260.

(8) Wang, H. Z.; Zuo, H. G.; Ding, Y. J.; Miao, S. S.; Jiang, C.; Yang, H. Biotic and abiotic degradation of pesticide Dufulin in soils. *Environ. Sci. Pollut. Res.* **2014**, *21* (6), 4331−4342.

(9) Pateiro-Moure, M.; Arias-Estévez, M.; López-Periago, E.; Martínez-Carballo, E.; Simal-Gándara, J. Occurrence and downslope mobilization of quaternary herbicide residues in vineyard-devoted soils. *Bull. Environ. Contam. Toxicol.* **2008**, *80* (5), 407−411.

(10) Spaczyński, M.; Seta-Koselska, A.; Patrzylas, P.; Betlej, A.; Skórzyńska-Polit, E. Phytodegradation and biodegradation in rhizosphere as efficient methods of reclamation. *Acta Agrophys.* **2012**, *19* (1), 155−169.

(11) Rønhede, S.; Sørensen, S. R.; Jensen, B.; Aamand, J. Mineralization of hydroxylated isoproturon metabolites produced by fungi. *Soil Biol. Biochem.* **2007**, *39*, 1751−1758.

(12) Song, N. H.; Chen, L.; Yang, H. Effect of dissolved organic matter on mobility and activation of chlorotuluron in soil and wheat. *Geoderma* **2008**, *146*, 344−352.

(13) Cui, J.; Zhang, R.; Wu, G. L.; Zhu, H. M.; Yang, H. Salicylic acid reduces napropamide toxicity by preventing its accumulation in rapeseed (*Brassica napus* L.). *Arch. Environ. Contam. Toxicol.* **2010**, *59*, 100−108.

(14) Cui, L. E.; Yang, H. Accumulation and residue of napropamide in alfalfa (*Medicago sativa*) and soil involved in toxic response. *J. Hazard. Mater.* **2011**, *190*, 81−86.

(15) Li, Y. Y.; Yang, H. Bioaccumulation and degradation of pentachloronitrobenzene and in *Medicago sativa*. *J. Environ. Manage.* **2013**, *119*, 143−150.

(16) Sui, Y.; Yang, H. Bioaccumulation and degradation of atrazine in several Chinese ryegrass genotypes. *Environ. Sci.: Processes Impacts* **2013**, *15* (12), 2338−2344.

(17) Jiang, L.; Huang, J.; Liang, L.; Zheng, P. Y.; Yang, H. Mobility of prometryne in soil as affected by dissolved organic matter. *J. Agric. Food Chem.* **2008**, *56*, 11933−11940.

(18) Guo, H.; Chen, G. F.; Lv, Z. P.; Zhao, H.; Yang, H. Alteration of microbial properties and community structure in soils exposed to napropamide. *J. Environ. Sci.* **2009**, *21*, 494−502.

(19) Ma, B.; He, Y.; Chen, H. H.; Xu, J. M.; Rengel, Z. Dissipation of polycyclic aromatic hydrocarbons (PAHs) in the rhizosphere: synthesis through meta-analysis. *Environ. Pollut.* **2010**, *158*, 855−861.

(20) Yang, Z. M.; Wang, J.; Wang, S. H.; Xu, L. L. Salicylic acid-induced aluminum tolerance by modulation of citrate efflux from roots of *Cassia tora* L. *Planta* **2003**, *217*, 168−174.

(21) Horváth, E.; Szalai, G.; Janda, T. Induction of abiotic stress tolerance by salicylic acid signaling. *J. Plant Growth Regul.* **2007**, *26*, 290−300.

(22) Liang, L.; Lu, Y. L.; Yang, H. Toxicology of isoproturon to the food crop wheat as affected by salicylic acid. *Environ. Sci. Pollut. Res.* **2012**, *19*, 2044−2054.

(23) Yin, X. L.; Jiang, L.; Song, N. H.; Yang, H. Toxic reactivity of wheat (*Triticum aestivum*) plants to herbicide isoproturon. *J. Agric. Food Chem.* **2008**, *56*, 4825−4831.

(24) Stępniewska, Z.; Wolińska, A.; Ziomek, J. Response of soil catalase activity to chromium contamination. *J. Environ. Sci.* **2009**, *21*, 1142−1147.

(25) Ma, Y.; Zhang, J. Y.; Wong, M. H. Microbial activity during composting of anthracene-contaminated soil. *Chemosphere* **2003**, *52*, 1505−1513.

(26) Gu, Y.; Wang, P.; Kong, C. H. Urease, invertase, dehydrogenase and polyphenoloxidase activities in paddy soil influenced by allelopathic rice variety. *Eur. J. Soil Biol.* **2009**, *45*, 436−441.

(27) Carine, F.; Enrique, A. G.; Stéven, C. Metal effects on phenol oxidase activities of soils. *Ecotox. Environ. Safe.* **2009**, *72*, 108−114.

(28) Tuason, M. M. S.; Arocena, J. M. Root organic acid exudates and properties of rhizosphere soils of white spruce (*Picea glauca*) and subalpine fir (*Abies lasiocarpa*). *Can. J. Soil Sci.* **2009**, *89* (3), 287−300.

(29) Gao, Y. Z. Gradient distribution of root exudates and polycyclic aromatic hydrocarbons in rhizosphere soil. *Soil Sci. Soc. Am. J.* **2011**, *72*, 1694−1703.

(30) Brookes, P. C.; Landman, A.; Pruden, G.; Jenkinson, D. S. Chloroform fumigation and the release of soil nitrogen: a rapid direct extraction method to measure microbial biomass nitrogen in soil. *Soil Biol. Biochem.* **1985**, *17* (6), 837−842.

(31) Liang, B.; Yang, X. Y.; He, X. H.; Zhou, J. B. Effects of 17-year fertilization on soil microbial biomass C and N and soluble organic C and N in loessial soil during maize growth. *Biol. Fertil. Soils* **2011**, *47*, 121−128.

(32) Turner, B. L.; Bristow, A. W.; Haygarth, P. M. Rapid estimation of microbial biomass in grassland soils by ultra-violet absorbance. *Soil Biol. Biochem.* **2001**, *33*, 913−919.

(33) Hammesfahr, U.; Heuer, H.; Manzke, B.; Smalla, K.; Bruhn, S. T. Impact of the antibiotic sulfadiazine and pig manure on the microbial community structure in agricultural soils. *Soil Biol. Biochem.* **2008**, *40*, 1583−1591.

(34) Perucci, P.; Scarponi, L. Effects of the herbicide imazethapyr on soil microbial biomass and various soil enzyme activities. *Biol. Fertil. Soils* **1994**, *17*, 237−240.

(35) Cycoń, M.; Wójcik, M.; Borymski, S.; Piotrowska-Seget, Z. Short-term effects of the herbicide napropamide on the activity and structure of the soil microbial community assessed by the multi-approach analysis. *Appl. Soil Ecol.* **2013**, *66*, 8−18.

(36) Xie, X. M.; Liao, M.; Yang, J.; Chai, J. J.; Fang, S.; Wang, R. H. Influence of root-exudates concentration on pyrene degradation and

DOI: 10.1021/jf505117j
J. Agric. Food Chem. 2015, 63, 92−103

soil microbial characteristics in pyrene contaminated soil. *Chemosphere* **2012**, *88*, 1190−1195.
(37) Amir, S.; Merlina, G.; Pinelli, E.; Winterton, P.; Revel, J. C.; Hafidi, M. Microbial community dynamics during composting of sewage sludge and straw studied through phospholipid and neutral lipid analysis. *J. Hazard. Mater.* **2008**, *159* (2−3), 593−601.
(38) Zhao, C. H.; Xing, M. Y.; Yang, J.; Lu, Y. S.; Lv, B. Y. Microbial community structure and metabolic property of biofilms in vermifiltration for liquid-state sludge stabilization using PLFA profiles. *Bioresour. Technol.* **2014**, *151*, 340−346.
(39) Zhang, X. Y.; Liu, X. Y.; Liu, S. S.; Liu, F. H.; Chen, L. S.; Xu, G.; Zhong, C. L.; Su, P. C.; Cao, Z. N. Response of *Scirpus triqueter*, soil enzymes and microbial community during phytoremediation of pyrene contaminated soil in simulated wetland. *J. Hazard. Mater.* **2011**, *193*, 45−51.
(40) de Vries, F. T.; Hoffland, E.; van Eekeren, N.; Brussaard, L.; Bloem, J. Fungal/bacterial ratios in grasslands with contrasting nitrogen management. *Soil Biol. Biochem.* **2006**, *38*, 2092−2103.
(41) Qin, H.; Brookes, P. C.; Xu, J. M. *Cucurbita spp.* and Cucumis sativus enhance the dissipation of polychlorinated biphenyl congeners by stimulating soil microbial community development. *Environ. Pollut.* **2014**, *184*, 306−312.
(42) Farag, M. A.; Mohsen, M.; Heinke, R.; Wessjohann, L. A. Metabolomic fingerprints of 21 date palm fruit varieties from Egypt using UPLC/PDA/ESI-qTOF-MS and GC-MS analyzed by chemometrics. *Food Res. Int.* **2014**, *64*, 218−226.
(43) Lu, Y. C.; Zhang, S.; Yang, H. Acceleration of the herbicide isoproturon degradation in wheat by glycosyltransferases and salicylic acid. *J. Hazard. Mater.* **2015**, *283*, 806−814.
(44) Chaudhry, Q.; Blom-Zandstra, M.; Gupta, S.; Joner, E. J. Utilising the synergy between plants and rhizosphere microorganisms to enhance breakdown of organic pollutants in the Environment. *Environ. Sci. Pollut. Res.* **2005**, *12* (1), 34−48.
(45) Gerhardt, K. E.; Huang, X. D.; Glick, B. R.; Greenberg, B. M. Phytoremediation and rhizoremediation of organic soil contaminants: Potential and challenges. *Plant Sci.* **2009**, *176*, 20−30.
(46) Yang, J. L.; Zheng, S. J.; He, Y. F.; You, J. F.; Zhang, L.; Yu, X. H. Comparative studies on the effect of a protein-synthesis inhibitor on aluminium-induced secretion of organic acids from *Fagopyrum esculentum* Moench and *Cassia tora* L. roots. *Plant Cell Environ.* **2006**, *29*, 240−246.
(47) White, J. C.; Mattina, M. I.; Lee, W. Y.; Eitzer, B. D.; Iannucci-Berger, W. Role of organic acids in enhancing the desorption and uptake of weathered *p, p′*-DDE by *Cucurbita pepo*. *Environ. Pollut.* **2003**, *124* (1), 71−80.
(48) Luo, L.; Zhang, S.; Shan, X. Q.; Zhu, Y. G. Oxalate and root exudates enhance the desorption of *p, p′*-DDT from soils. *Chemosphere* **2006**, *63* (8), 1273−1279.
(49) Dutton, M. V.; Evans, C. S. Oxalate production by fungi: its role in pathogenicity and ecology in the soil environment. *Can. J. Microbiol.* **1996**, *42*, 881−895.
(50) Chen, G.; Lin, C.; Chen, L.; Yang, H. Effect of polar-dissolved organic matter fractions on the mobility of prometryne in soil. *J. Soil. Sediment.* **2011**, *11*, 395−405.
(51) Ding, Q.; Wu, H. L.; Xu, Y.; Guo, L. J.; Liu, K.; Gao, H. M.; Yang, H. Impact of low molecular weight organic acids and dissolved organic matter on sorption and mobility of isoproturon in two soils. *J. Hazard. Mater.* **2011**, *190* (1−3), 823−832.
(52) Joner, E. J.; Leyval, C. Rhizosphere gradients of polycyclic aromatic hydrocarbon (PAH) dissipation in two industrial soils and the impact of arbuscular mycorrhiza. *Environ. Sci. Technol.* **2003**, *37*, 2371−2375.
(53) Rudrappa, T.; Czymmek, K. J.; Pare, P. W.; Bais, H. P. Root-secreted malic acid recruits beneficial soil bacteria. *Plant Physiol.* **2008**, *148*, 1547−1556.
(54) Fierer, N.; Schimel, J. P.; Holden, P. A. Variations in microbial community composition through two soil depth profiles. *Soil Biol. Biochem.* **2003**, *35*, 167−176.
(55) Byss, M.; Elhottova, D.; Triska, J.; Baldrian, P. Fungal bioremediation of the creosote-contaminated soil: Influence of *Pleurotus ostreatus* and *Irpex lacteus* on polycyclic aromatic hydrocarbons removal and soil microbial community composition in the laboratory-scale study. *Chemosphere* **2008**, *73*, 1518−1523.
(56) Söderberg, K. H.; Probanza, A.; Jumpponen, A.; Bååth, E. The microbial community in the rhizosphere determined by community-level physiological profiles (CLPP) and direct soil- and cfu-PLFA techniques. *Appl. Soil Ecol.* **2004**, *25*, 135−145.
(57) Johansen, A.; Olsson, S. Using phospholipid fatty acid technique to study short-term effects of the biological control agent *Pseudomonas fluorescens* DR54 on the microbial microbiota in barley rhizosphere. *Microb. Ecol.* **2005**, *49*, 272−281.
(58) Yao, X. H.; Min, H.; Lu, Z. H.; Yuan, H. Influence of acetamprid on soil enzymatic activities and respiration. *Eur. J. Soil. Biol.* **2006**, *42*, 120−126.
(59) Mutlu, S.; Atici, O.; Nalbantoglu, B. Effects of salicylic acid and salinity on apoplastic antioxidant enzymes in two wheat cultivars differing in salt tolerance. *Biol. Plant* **2009**, *53*, 334−338.
(60) Zhou, Z. S.; Guo, K.; Elbaz, A. A.; Yang, Z. M. Salicylic acid alleviates mercury toxicity by preventing oxidative stress in roots of *Medicago sativa*. *Environ. Exp. Bot.* **2009**, *65*, 27−34.
(61) Zhang, J. J.; Lu, Y. C.; Yang, H. Chemical modification and degradation of atrazine in Medicago sativa through multiple pathways. *J. Agric. Food Chem.* **2014**, *62*, 9657−9668.
(62) Bending, G. D.; Lincolin, S. D.; Sørensen, S. R.; Morgan, J. A. W.; Aamand, J.; Walker, A. In-field spatial variability in the degradation of the phenyl-urea herbicide isoproturon is the result of interactions between degradative *Sphingomonas spp.* and soil pH. *Appl. Environ. Microbiol.* **2003**, *69*, 827−834.
(63) Sebai, T. E.; Lagacherie, B.; Soulas, G.; Martin-Laurent, F. Isolation and characterisation of an isoproturon-mineralising Methylopila sp. TES from French agricultural soil. *FEMS Microbiol. Lett.* **2004**, *239*, 103−110.
(64) Greń, I.; Guzik, U.; Wojcieszyńska, D.; Łabużek, S. Molekularne podstawy rozkładu ksenobiotycznych związków aromatycznych. *Biotechnologia* **2008**, *2*, 58−67.

DOI: 10.1021/jf505117j
J. Agric. Food Chem. 2015, 63, 92−103

JOURNAL OF AGRICULTURAL AND FOOD CHEMISTRY

Article

pubs.acs.org/JAFC

Are Odorant Constituents of Herbal Tea Transferred into Human Milk?

Melanie Y. Denzer,[†] Frauke Kirsch,[†] and Andrea Buettner*[,†,§]

[†]Department of Chemistry and Pharmacy, Institute of Food Chemistry, Friedrich-Alexander-University Erlangen-Nürnberg, 91054 Erlangen, Germany

[§]Fraunhofer Institute for Process Engineering and Packaging (IVV), 85354 Freising, Germany

Supporting Information

ABSTRACT: The present study investigates aroma transfer from commercial nursing tea, consumed in the maternal diet, into human milk by correlating sensory assessments with quantitative analytical data. The target terpenes were quantified in milk (expressed before and after tea consumption) and tea samples via gas chromatography−mass spectrometry (GC-MS) using stable isotope dilution assays (volunteer donors $n = 5$). Sensory analyses were carried out on different milk samples from a single donor, sampled before (blank) and at different times after tea ingestion. Quantitative analysis revealed that no significant odorant transfer into milk was observed after lactating women drank the tea. The comparative sensorial analysis of milk samples expressed before and after tea consumption confirmed that tea ingestion had no significant influence on the odor profile of human milk.

KEYWORDS: *human milk, odorant transfer, herbal tea, SAFE (solvent-assisted flavor evaporation), sensory*

INTRODUCTION

The potential transfer of odorants into breast milk attracts increasing attention in scientific research. There are several indications that odorants are transferred from the maternal diet into mother's milk and may influence the nursing behavior and later dietary habits of infants. As one example, infants whose mothers consumed carrot juice during pregnancy or nursing accepted carrot-flavored cereals better than babies without this prior exposure.[1] Thus, breast-fed children may perceive an array of different flavor impressions with the odor of human milk consecutively changing due to variable maternal nutrition. This assumption is supported by a study from Hausner et al., who showed that breast-fed infants, in contrast to formula-fed children, have high initial acceptance of caraway-flavored purée irrespective of whether previously exposed to *d*-carvone through mother's milk or not, suggesting that the process of breastfeeding itself facilitates acceptance of novel flavors.[2] There are many studies focusing the research on sensorial effects of odorants transferred into human milk.[2−5] Mennella et al. evaluated the odor change of human milk after lactating women ingested garlic,[3] beer,[4] or carrot juice[5] but did not characterize the alteration either by description of the smell or by chemical analysis of the milk's odorants. Studies aimed at investigating the molecular aspects of odorant transfer into human milk are thus few. Hausner et al. demonstrated the transfer of d-carvone from the maternal diet into breast milk.[2] These authors observed that several orally ingested volatiles are transferred according to specific time profiles and in relatively low percentages into mother's milk.[6] Similar results were obtained by Kirsch et al. for the orally ingested odorant 1,8-cineole.[7] Contrarily, Sandgruber et al. observed that the sensory profile of breast milk from women consuming fish oil capsules remained unmodified in relation to the control human milk with regard to their content of specific fish oil marker substances.[8]

Overall, odorant transfer from the maternal diet into human milk is not yet fully understood. The general problem of studies in this field is that investigators either are dealing with complex food matrices with often variable natural odorant values that are mostly in very low concentration ranges or perform highly controlled studies with odorant model applications that are, at times, difficult to relate to general real-life situations. Food containing naturally concentrated components may be represented by nursing tea, which is often consumed during pregnancy and nursing as the herbal constituents are traditionally known to foster lactation. The main ingredients of this product are fennel, anise, and caraway. Previous analyses of our group have shown that the main aroma compounds of fennel−anise−caraway tea (Meßmer) are limonene, 1,8-cineole, fenchone, estragole, d-carvone, *trans*-anethole, *p*-anisaldehyde, and anisketone. Accordingly, the focus of this study was on the investigation of odorant transfer of these selected terpenes from nursing tea into human milk. Specifically, the aim was to elucidate if characteristic and potent odorants in nursing tea are transmitted into the milk, on both qualitative and quantitative bases, and to relate this molecular analytical data to the respective sensory impact of nursing tea consumption on breast milk aroma profiles.

MATERIALS AND METHODS

Chemicals. Unlabeled (*R*)-(+)-limonene, 1,8-cineole, (1*R*)-(−)-fenchone, estragole, (*S*)-(+)-carvone, *trans*-anethole, *p*-anisaldehyde, anisketone, methyl octanoate, and $NaHCO_3$ were purchased from Aldrich (Steinheim, Germany). Dichloromethane (DCM) was obtained from ACROS Organics (Geel, Belgium). Na_2SO_4 was

Received: August 26, 2014
Revised: November 21, 2014
Accepted: December 1, 2014
Published: December 1, 2014

 © 2014 American Chemical Society

purchased from VWR International BDH PROLABO (Lutterworth, UK). Deuterium-labeled limonene-d_2, 1,8-cineole-d_3, estragole-d_4, carvone-d_4, *trans*-anethole-d_3, *p*-anisaldehyde-d_3, and anisketone-d_3 were provided by aromaLAB AG (Freising, Germany).

Human Milk Samples. Human milk samples were provided by volunteer donors (A−E) who gave written informed agreement to participate in the experiment, which was obtained prior to sample collection and analysis after a full explanation of the intent and nature of the test procedure. Withdrawing from the experiment was possible at any time. The experiment was approved by the Ethical Committee of the Medical Faculty, Friedrich-Alexander-University Erlangen-Nürnberg. Five lactating women, one multiparous, four primiparous, were recruited for the aroma transfer experiment. They ranged in age from 22 to 35 years (mean 29.8 years), and their infants ranged from 6 to 55 weeks of age (mean 33.4 weeks). None of the mothers was allergic to any of the tea ingredients. The subjects had no acute medical complaints during the experiment, normal breast milk production, and no breast infection. All mothers produced milk in excess of their baby's needs. The sampling took place according to each mother's preference and with their own systems, by manual expression or the usage of either a mechanical or electrical breast pump. Sample volumes ranged from approximately 10 to 80 mL. The fresh milk samples were analyzed within 4 h after expression, with samples stored in a refrigerator in the meantime, or after a maximum of 4 days of storage at −20 °C.

Human Milk Samples for the Odorant Transfer Experiment. The experimental setup consisted of three different blocks, each of which comprised a period of 6 days. During these days the subjects were not allowed to consume herbs, aliments including herbs, and especially fennel, anise, or caraway. They also were advised not to use cosmetic or sanitary products containing herbal ingredients. The first 4 days of each block were used as wash-out days. At the fourth day of each block, the women had to collect a milk sample, the control sample. On day 5, the mothers were instructed to drink 950 mL of customary fennel−anise−caraway tea (Meßmer, Ostfriesische Tee Gesellschaft Laurens Spethmann GmbH & Co. KG, Seevetal, Germany) within 30 min. The preparation of the tea was according to the following instructions: the mothers had to incubate four tea bags with exactly 1 L of boiling water for 6 min. Then the tea bags had to be removed without squeezing them. A smallish leftover (about 70 mL) should be cooled to room temperature, and then 50 mL thereof was bottled for analysis. The remaining cool tea should be drunk. The participants were required to express milk 30 min (first block), 1 h (second block), and 2 h (third block) after total tea ingestion. In each case, control samples were taken as blanks prior to tea ingestion; these samples are, accordingly, named blank 0.5 h, blank 1 h, and blank 2 h. Due to various degrees of lactation, not all subjects participated in every block and some mothers repeated single blocks.

Human Milk Samples for Sensorial Analyses. To examine if adults could discriminate differences in odor of mother's milk as a function of fennel−anise−caraway tea ingestion, a sensory panel orthonasally evaluated the respective human milk samples. These samples were from a donor who expressed several small milk samples (25−40 mL) directly before and 30, 105, 155, and 225 min after tea ingestion and stored them in the refrigerator until sample collection. Time points of sampling were, on the one hand, dictated by the breastfeeding regimens and, on the other hand, defined according to previous evidence on systemic bioavailability of odorants after ingestion obtained from a range of studies from our and other groups as monitored via blood, breath, and urine.[9−12] All in all, the sum of these studies clearly shows systemic appearance of odorants to take place roughly between 30 and 120 min. Sample collection took place immediately after expression of the last sample, followed by immediate sensory analysis, thereby ensuring that the samples were stored for no longer than 5 h in total. For sensory evaluation, samples were adjusted to room temperature directly before testing.

Extraction of Milk Sample Odorants by Solvent-Assisted Flavor Evaporation (SAFE). For a fast and careful isolation of the volatiles from human milk (12.31−81.00 g), in this case potential nursing tea terpenes, SAFE[13] was used. Each milk sample was thawed if necessary, weighed in a flask, spiked with the respective internal standards (range of the concentrations of the labeled substances in the internal standard solutions for milk in DCM: limonene-d_2, 5.61−7.30 μg/mL; 1,8-cineole-d_3, 1.30−2.39 μg/mL; estragole-d_4, 0.45−0.64 μg/mL; (*R*)-(−)-carvone-d_4, 1.06−1.55 μg/mL; *trans*-anethole-d_3, 0.58−7.73 μg/mL; *p*-anisaldehyde-d_3, 1.45−2.36 μg/mL; anisketone-d_3, 7.64−11.17 μg/mL) according to the sample volume (approximately 1−2 μL of each internal standard solution per gram of milk), and stirred at room temperature for 10 min to homogenize with the standard. Subsequently, DCM (50% v/v) was added to the respective milk sample, and the solutions were equilibrated by stirring for 30 min until a stable phase had formed. These emulsions were immediately distilled using the SAFE apparatus at 50 °C and approximately 1×10^{-4} mbar. Evaporated volatiles were frozen with liquid nitrogen, and after thawing, the two distillate phases (DCM and water from the sample) were extracted three times with 25 mL of DCM. The combined DCM phases were dried over anhydrous Na_2SO_4 and concentrated by means of Vigreux distillation at 50 °C. Subsequently, the concentrate was extracted twice with $NaHCO_3$ solution (50% v/v) to remove carboxylic acids, dried over Na_2SO_4, and finally concentrated to a total volume of approximately 100 μL at 50 °C by means of microdistillation. The prepared sample extracts were stored at −20 °C until measurement, but no longer than 4 days.

Extraction of the Tea Samples by Liquid−Liquid Extraction. For each time-dependent odorant transition experiment, samples of the consumed tea were analyzed. Compared to the other terpenes, the contents of *trans*-anethole and carvone in the tea beverage were very high; thus, these compounds had to be determined separately in diluted tea. Therefore, 0.5 mL of tea beverage was placed in a 100 mL measuring flask that was then filled with water; 150 μL of the internal standard solution in DCM, containing carvone-d_4 (c = 3.83−92.79 μg/mL) and *trans*-anethole-d_3 (c = 4.07−22.79 μg/mL), was added to 10 mL of this solution, and subsequently the sample was stirred at room temperature for 10 min to homogenize with the standard. Afterward, the diluted tea was extracted three times with 30 mL of dichloromethane. The combined organic phases were dried over anhydrous Na_2SO_4 and concentrated by means of Vigreux distillation and microdistillation. For analysis of the undiluted tea, 25 mL of the beverage was spiked with 50 μL of the internal standard solution in DCM comprising 1,8-cineole-d_3 (c = 2.00−2.37 μg/mL), estragole-d_4 (c = 40.84−50.27 μg/mL), *p*-anisaldehyde-d_3 (c = 18.02−294.64 μg/mL), and anisketone-d_3 (c = 2.91−50.27 μg/mL) and with 25 μL of the internal standard solution containing limonene-d_2 (c = 1.87−2.36 g/mL). The tea was stirred for 10 min at room temperature, then the sample was extracted three times with 75 mL of DCM, and the further preparation was as described for the diluted tea. The prepared tea extracts were stored at −20 °C until measurement, but no longer than 4 days.

Quantification by Stable Isotope Dilution Assay (SIDA). The quantification of the terpenes in human milk and tea was carried out by means of stable isotope dilution assays.[14] SIDA is the most precise quantification technique at hand in modern aroma analytics and is the optimum methodology that can rule out potential losses of target odorants during isolation, workup, and analysis.[15] During this procedure, defined amounts of the respective stable isotope-labeled analytes were added prior to sample preparation to act as internal standard. This quantification technique has the advantage that the added labeled analytes behave similarly to the unlabeled analytes in the sample; both, analyte and labeled standard, experience the same losses or other changes during sample preparation, so that errors from such processes are automatically compensated. According to the analytical requirements, pentane solutions containing the respective labeled analytes were diluted in DCM. The resulting concentrations of the labeled analytes, limonene-d_2, 1,8-cineole-d_3, estragole-d_4, carvone-d_4, *trans*-anethole-d_3, *p*-anisaldehyde-d_3, and anisketone-d_3, were subsequently confirmed using methyl octanoate as an internal standard and solutions of the respective unlabeled analytes to establish a three-point calibration curve.[7] The measurements were performed using a gas chromatograph with flame ionization detector (GC-FID) system. Because the concentrations of the labeled substances might change

dx.doi.org/10.1021/jf504073d | J. Agric. Food Chem. 2015, 63, 104−111

over time, for example, because of partial evaporation of the solvent when the bottles are opened for usage, determination of the concentrations was repeated approximately every 4 weeks. Different calibration solutions for the quantification of the analytes in human milk and tea samples were prepared in DCM, comprising various concentrations of all unlabeled analytes but always the same concentrations of the respective isotopically labeled analytes. The concentrations of analytes in the samples were calculated by inserting the signal ratio from gas chromatography−mass spectrometry (GC-MS) analysis of the unlabeled to labeled molecules in the resulting calibration equations. The concentration of fenchone in the samples was determined using carvone-d_4 as respective labeled standard. For each calibration curve (X, ratio of concentrations; Y, ratio of areas) several weighting factors were evaluated to find the one that matched best.[16] The coefficient of determination of all calibration curves was always >0.99.

Gas Chromatography. *GC-FID.* For the determination of the concentrations of the labeled analyte solutions, a GC-FID system (Trace GC Ultra, Thermo Scientific, Dreieich, Germany) was used together with a DB-FFAP (30 m length, 0.32 mm inner diameter, and 0.25 μm film thickness; Agilent J&W GC columns, Munich, Germany) as analytical capillary. An uncoated, deactivated fused silica capillary was used as a precolumn (0.32 mm inner diameter, 0.5−3.5 m length) and changed regularly to avoid accumulation of any contaminants. Helium was used as a carrier gas, and a constant flow of 2.80 mL/min was applied. The temperature program started with an oven temperature of 40 °C that was held for 2 min followed by an 8 °C/min increase to 170 °C and a 40 °C/min increase to 230 °C, which were held for 5 min. Injections were carried out manually with an injection volume of 1 μL.

GC-MS. The GC-MS with a quadrupole system (GC 7890A with MSD 5975C, Agilent Technologies, Waldbronn, Germany) was used together with a DB-FFAP (30 m length, 0.25 mm inner diameter, and 0.25 μm film thickness; Agilent J&W GC columns, Munich, Germany) for the measurement of milk and tea sample extracts and for the respective calibration solutions. The mass spectrometer was operated in electron ionization mode at 70 eV. Helium was used as carrier gas, and a constant flow of 1.3 mL/min was applied. The temperature program started with an oven temperature of 40 °C that was held for 2 min followed by a 4 °C/min temperature increase to 170 °C and a 40 °C/min temperature increase to 230 °C; the end temperature was held for 10 min. The injection volume was 2 μL. Temperatures used were 200 °C for the MS transfer line, 200 °C for the ion source, and 150 °C for the quadrupole. The analytes in milk and tea samples were identified by comparison of the mass spectra and retention indices according to the method of Van den Dool and Kratz[17] with those of the commercially available substances.

Sensory Analysis. A trained sensory panel evaluated fennel−anise−caraway tea and the respective human milk samples orthonasally to assess if the odor of breast milk changed after the woman consumed fennel−anise−caraway tea. Before the sensory analysis of the samples, a trained panel (eight females, two males; 24−39 years of age, mean = 27.64 years) established in a preliminary test the attributes for milk and fennel−anise−caraway tea with the help of exemplary samples of tea and human milk. For the evaluation of the samples, the panelists were subsequently asked to score the intensities of these attributes on a scale from 0 (no perception) to 3 (strong perception); intermediate steps of 0.5 were allowed. The sensory analysis of the nursing tea was performed by a trained panel of 12 females and 3 males (24−40 years of age, mean = 28.33 years); the evaluation of the human milk samples took place on another day by a slightly different panel of 12 females and 1 male (22−39 years of age, mean = 27.46 years).

Method Validation and Investigation of Potential Storage Effects on the Investigated Terpenoid Substances in Human Milk. Detailed information about the method validation and the investigation of potential storage effects on the investigated terpenoide substances in human milk can be found in Appendix A of the Supporting Information.

Statistical Analyses. By means of a Mandel test, the calibration curves were tested for linearity. Few curves were linear; the other curves were found to be quadratic. However, differences in linear and quadratic curves were extremely low, so that for all calibrations the linear regression was chosen. Outliers were detected by the Nalimov test. For the comparison of different means, Student's t test was used. The results of the sensorial experiments were tested by two-way analysis of variance (ANOVA) followed by Fisher's least significant difference (LSD) test in the case of normally distributed values or by the Scheirer−Ray−Hare test, followed by the Schaich−Hamerle test, if values were not normally distributed.

RESULTS

Quantification of Odorants in Fennel−Anise−Caraway Tea. The results of the analyzed tea samples demonstrated that the mean concentrations of limonene (8.36 ± 4.83 μg/L) and 1,8-cineole (1.24 ± 0.53 μg/L) were low compared to the concentrations of the other terpenes (range ∼ 30−200 μg/L), especially carvone (238 ± 308 μg/L) and *trans*-anethole (858 ± 1973 μg/L), which showed relatively high concentrations (Table 1). There were also significant differences between the concentrations of the single tea preparations as shown by the large standard deviations and wide ranges (Table 1).

Table 1. Mean and Range of the Content of the Analyzed Terpenes of 16 Tea Samples

substance	mean content (μg/L)	range of content (μg/L)
limonene	8.4 ± 4.8	1.8−19.2
1,8-cineole	1.2 ± 0.53	0.60−3.0
fenchone	39.6 ± 30.6	7.2−141.8
estragole	26.6 ± 17.5	4.0−76.7
carvone	238.4 ± 308.4	12.6−1208.3
trans-anethole	858.1 ± 1973.2	83.2−7266.4
p-anisaldehyde	187.5 ± 187.5	75.0−454.3
anisketone	39.7 ± 17.9	16.7−80.2

Concentrations of Selected Terpenes in Human Milk before and after the Ingestion of Fennel−Anise−Caraway Tea. The mean concentrations of the terpenes limonene, 1,8-cineole, fenchone, estragole, carvone, *trans*-anethole, *p*-anisaldehyde, and anisketone in each group of analyzed human milk samples, that is, expressed before (blanks) and at different times after ingestion of fennel−anise−caraway tea, are shown in Figure 1. The mean concentrations of all analyzed terpenes of the milk samples, collected after tea ingestion, were comparable to those of the blank samples. Overall, the concentrations were very low, irrespective of whether the samples belonged to the blank or the tea ingestion group; furthermore, quite pronounced variation was present within each group (Figure 1). There were no significant differences between the mean values of samples obtained before or at different times after tea consumption ($p > 0.05$). Because averaging the data might obscure significant changes in individual participants, the obtained quantitative data were also analyzed on an individual basis (data of mother C are shown in Table 2; for the data of mothers A, B, D, and E see Table B2b-2e in the Supporting Information). Here it can be seen that the variation of the terpene content in all blank samples of one mother is quite large; for example, the concentration of 1,8-cineole in samples from mother C ranged from 1.07 to 54.2 μg/kg. Furthermore, changes in concentrations after tea ingestion did not follow a time-dependent

dx.doi.org/10.1021/jf504073d | J. Agric. Food Chem. 2015, 63, 104−111

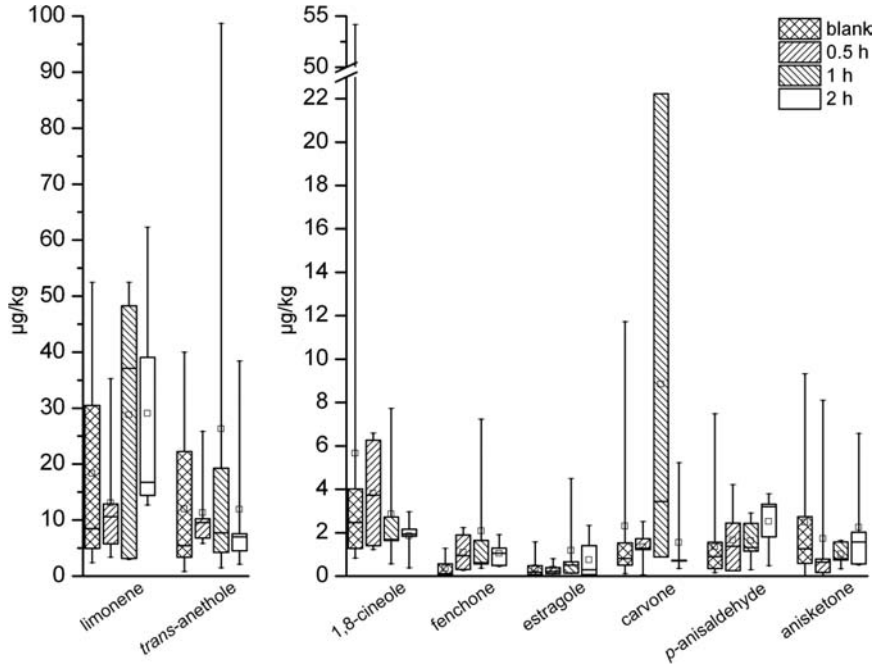

Figure 1. Terpene content in 19 blank human milk samples and in samples 0.5 h (6), 1.0 h (5), and 2.0 h (5) after tea ingestion, respectively.

Table 2. Single Values of the Content of the Analyzed Terpenes in Milk Samples of Mother C and the Respective Concentrations of the Ingested Tea Samples[a]

		µg/kg or µg/L									
		blank, 0.5 h	0.5 h after tea ingestion	blank, 0.5 h repetition	0.5 h after tea ingestion repetition	blank, 1 h	1 h after tea ingestion	blank, 2 h	2 h after tea ingestion	blank, 2 h repetition	2 h after tea ingestion repetition
limonene	in ingested tea		19.2		8.78		9.21		5.79		12.9
limonene	in human milk	4.95	5.74 (30%)	28.5	35.2 (401%)	2.48	37.1 (403%)	52.5	14.4 (248%)	13.2	16.8 (130%)
1,8-cineole	in ingested tea		1.20		1.22		0.92		1.15		1.27
1,8-cineole	in human milk	2.23	2.58 (216%)	10.8	4.89 (401%)	1.07	2.72 (272%)	54.2	1.94 (194%)	2.48	2.96 (234%)
fenchone	in ingested tea		11.0		46.9		35.4		37.6		38.5
fenchone	in human milk	0.02	1.90 (17%)	0.09	2.23 (5%)	0.02	1.65 (5%)	0.07	0.50 (1%)	0.26	1.06 (3%)
estragole	in ingested tea		36.5		32.5		15.1		18.4		43.2
estragole	in human milk	0.05	0.11 (<0.005%)	0.24	0.23 (1%)	0.04	0.13 (1%)	0.13	0.05 (<0.005%)	0.14	0.11 (<0.005%)
carvone	in ingested tea		69.9		199		71.5		158		392
carvone	in human milk	0.51	1.73 (2%)	0.82	1.29 (1%)	0.20	0.89 (1%)	0.43	0.35 (<0.005%)	1.37	0.71 (<0.005%)
trans-anethole	in ingested tea		259		247		83.2		84.8		2347
trans-anethole	in human milk	2.05	9.09 (4%)	11.2	10.2 (4%)	0.79	4.23 (5%)	32.5	2.11 (2%)	5.89	4.49 (2%)
p-anisaldehyde	in ingested tea		192		400		123		168		454
p-anisaldehyde	in human milk	0.17	0.25 (<0.005%)	0.44	4.22 (1%)	0.16	2.43 (2%)	7.48	3.31 (2%)	0.90	3.20 (1%)
anisketone	in ingested tea		52.8		68.4		29.7		41.2		80.2
anisketone	in human milk	0.11	0.17 (<0.005%)	0.55	0.79 (1%)	0.60	0.80 (3%)	2.74	0.57 (1%)	0.59	0.52 (1%)

[a]Percentages of concentrations in human milk relative to the amount in the corresponding tea samples are given in parentheses.

dx.doi.org/10.1021/jf504073d | J. Agric. Food Chem. 2015, 63, 104−111

pattern. In some samples after tea ingestion the concentrations of the respective odorants were even lower than in the blanks (e.g., the *trans*-anethole content in human milk samples of mother C was 32.5 μg/kg for the blank sample compared to 2.11 μg/kg at 2 h after tea ingestion; Table 2). In other samples the content of some terpenes, for example, limonene, was higher after tea ingestion than in the blanks (e.g., the limonene content in human milk samples of mother C was 2.48 μg/kg for the blank sample compared to 37.1 μg/kg at 1 h after tea ingestion; Table 2). Some mothers repeated parts of the experiment; thus, for some times and participants, duplicate samples were available. The repetition experiments, especially those of the 1 h sample of mother B and the 0.5 h sample of woman C, showed that the concentrations of at least some odorants varied strongly in the samples from different days (Table 2, Table B2c). Comparing the *trans*-anethole content of the milk sample from mother C 0.5 h after tea ingestion (9.09 μg/kg) with the respective blank sample (2.05 μg/kg) (Table 2), one might suppose the transfer of the odorant from consumed tea into human milk. However, a repetition of this experiment shows in contrast that there was no odorant transfer (blank milk sample, 11.2 μg/kg; milk sample, 0.5 h after tea ingestion, 10.2 μg/kg) (Table 2). Although the participants were advised to drink a distinct amount of tea infusion prepared in a defined way, the absolute intake of terpenes was highly different for every woman and every sampling day, because the exact composition of the final beverage varied due to natural variations in the plant raw material and the influence of even small changes in the preparation process (Table 1). To compare human milk samples after tea consumption depending on the time of expression, the quantified values were additionally normalized to the absolute amount of each terpene ingested via the infusion; these normalized values are listed in Table 2 and Table B2b-2e. Also for these normalized values, no significant differences were present between the groups of human milk samples from different sampling times after tea consumption ($p > 0.05$). For fenchone, estragole, carvone, *trans*-anethole, *p*-anisaldehyde, and anisketone, the concentrations in the tea beverage, ranging from 4.02 μg/L to >7.27 mg/L, were much higher than in the milk samples, whereas for limonene and 1,8-cineole, with concentrations in the tea sample from 0.60 to 19.2 μg/L, the milk samples showed higher contents. Table 3 illustrates this by giving the mean percentual amount of terpenes in milk, calculated under the assumption that all terpenes in milk result from tea intake. The values for *p*-anisaldehyde demonstrate that only a negligible amount of 1−2% (Table 3) could be theoretically transferred from herbal tea into human milk, whereas in part >700% (Table 3) of limonene could be theoretically transferred from the beverage into breast milk; this is impossible and shows that the high limonene content has to originate from other sources.

Table 3. Percentual Amounts of Terpenes in Milk, on the Assumption That All Terpenes in Milk Result from Tea Intake[a]

substance	0.5 h	1.0 h	2.0 h
limonene	205	758	318
1,8-cineole	262	290	163
fenchone	5	19	3
estragole	1	8	3
carvone	1	32	2
trans-anethole	3	30	10
p-anisaldehyde	1	2	1
anisketone	3	5	7

[a]The percentual values of the terpene contents in human milk dependent on tea ingestion were calculated from the of six milk samples 0.5 h after tea consumption, five milk samples 1.0 h after tea ingestion, and five milk samples 2.0 h after tea ingestion compared to the average terpene content of the corresponding tea samples.

Sensory Analysis of Fennel−Anise−Caraway Tea and of Human Milk Samples Expressed before and after Tea Ingestion. In the pretest of the tea beverage, the sensory panel rated the following odor qualities with intensities above 1, which means that these attributes were perceived at least with a weak or clearly perceivable odor impression: fennel (2.41), anise (2.09)/licorice (1.23), caraway (1.50), chamomile (1.32), and sweet (1.14). These attributes together with the characteristic milk odor attributes,[18] hay-like, fatty, like boiled milk, metallic, fishy, rancid, like butter, and like egg white, were thus chosen to evaluate the fresh human milk samples. Due to a similar odor impression of anise and licorice, these attributes were combined for the sensorial analysis of the milk. Figure 2 shows the results displayed as sensory profiles of the five different samples. The odor qualities sweet (0.54−0.77), fatty (0.46−0.65), like boiled milk (0.69−1.00), and like butter (0.35−0.58) were perceived as very weak for all five breast milk samples. The intensities of the other nine attributes were even lower than 0.5, which means that these odors were practically unnoticeable. Thus, the panel detected only characteristic milk odors, and none of the tea attributes was distinctly perceived. Statistical analyses demonstrated for all odor qualities that the slight differences in intensity ratings between all samples and panelists, respectively, were not significant ($p > 0.05$).

Method Validation and Investigation of Potential Storage Effects on the Investigated Terpenoid Substances in Human Milk. The limit of decision, limit of determination, and recovery for each of the analytes in human milk are listed in Table A1 in Appendix A (Supporting Information). Quantification of odorants in human milk dependent on storage time under freeze-storage conditions could successfully rule out any degradations or losses under the given experimental conditions (Table A3). Details are provided in Appendix A.

DISCUSSION

Concentrations of Selected Terpenes in Human Milk before and after Ingestion of Fennel−Anise−Caraway Tea. The tea was chosen as this product represents an example of a beverage often consumed by breastfeeding women. In comparison to other transfer studies based on relatively high dosages of single odorants (e.g., 30−100 mg of *d*-carvone and 100 mg of *trans*-anethole, respectively[2,6]), the consumed odorant concentrations in the present study were relatively low (approximately 1−1000 μg) and the odorant profile was rather complex. The study design was thus targeted at real-life conditions and is of special relevance for the topic of odorant transfer into human milk. The analysis of the blank human milk samples demonstrated that nearly all analyzed milk samples contained each of the analyzed volatiles in trace amounts (approximately 0.35−20 μg/kg). Large inter- and intra-individual variations in odorant content were observed. Likely explanations are that milk is a biological matrix with constantly varying composition, for example, with regard to fat content.[19] The monitored terpenes are ubiquitous in everyday cuisine and sanitary and cosmetic products, so it can be assumed that these

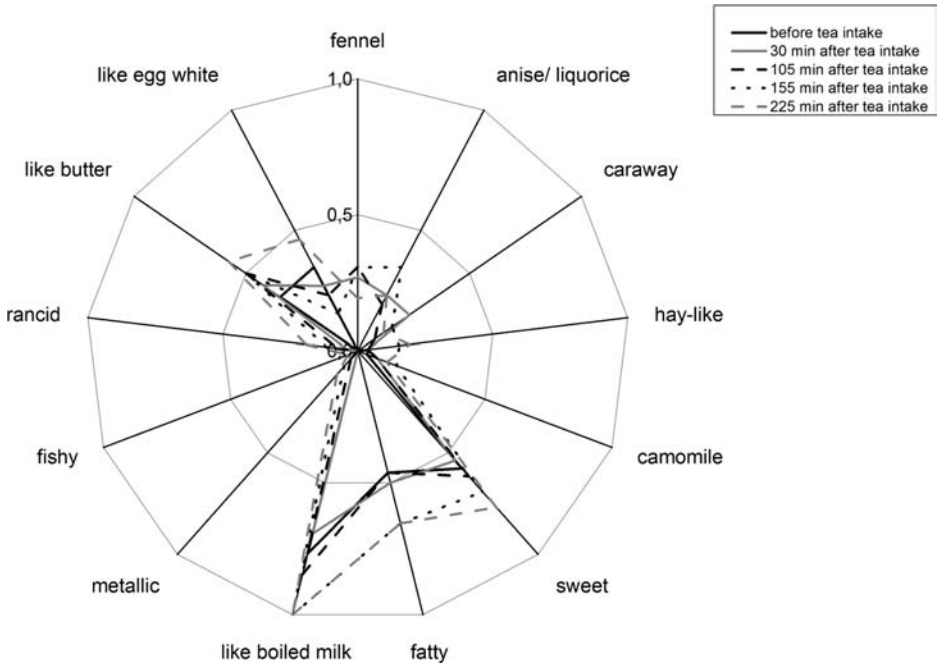

Figure 2. Orthonasal odor profile of fresh human milk samples before and after ingestion of fennel–anise–caraway tea.

terpenes are regularly consumed and absorbed in detectable amounts.[20] With regard to this observation, the present study is accordingly well in line with previous findings. Traces of terpenes have been reported in milk samples several times.[21,22] The present results of the comparison of the respective odor concentrations in tea and in the related human milk samples demonstrate that the ingestion of a typically consumed amount of fennel–anise–caraway tea had no significant influence on the concentrations of the analyzed odorants in human milk samples. Thus, it can be concluded that there was either no transfer of the analyzed odorants from ingested tea into the human milk or that the transferred amounts were so low that the basic terpene content, as monitored in the blanks, was predominant and the small transferred amount was negligible. The obtained data were also analyzed on an individual basis: On the one hand, the concentrations of some terpenes in the blanks were in some cases higher than in the respective milk samples expressed after tea ingestion, and on the other hand the comparison of all blanks of the same participant showed high variations in the respective terpene concentrations. Taking these variations into consideration, a slightly higher content of an odorant in a single measurement of a milk sample expressed after tea ingestion compared to the blank must be deemed as insignificant. This is especially true in view of the fact that the respective odorants were present in the milk samples independent of tea ingestion, as shown by the blank measurements. With regard to the above-said, one might deduce that significant odorant transfer into human milk might occur only either (I) if sufficient concentrations of the respective odorants are consumed, (II) if the substances are relatively stable and are not prone to strong biotransformation under physiological conditions as discussed in more detail in Buettner,[23] or (III) if the represented substances are not commonly found in human milk as a kind of "background profile". This might directly relate to the observations of Hausner et al.,[6] who reported in a study involving higher odorant dosages that the transfer of orally ingested odorants into human milk seemed to be dependent on the chemical structures of the molecules and that relatively low amounts were transferred into the milk despite the relatively high intake. Compared to the average contents of d-carvone and *trans*-anethole in milk samples after odorant ingestion from the studies of Hausner et al., the average concentrations of the terpenes in the milk samples of the present study after tea ingestion were only slightly lower. However, in the studies by Hausner et al. the blank values were lower than in the present study, and thus the differences between blanks and samples after odorant ingestion were much more pronounced. The reason for these low blank values probably was the strict diet that the subjects of the Hausner studies had to follow. In contrast, the mothers that participated in the present experiments were instructed to stay with their normal diet and to avoid overdoses of food that contained the analyzed terpenes. Summarizing both studies, the concentrations of potentially transferred substances detected in the milk samples was about a factor 1000 lower than in the ingested supplement or food. Consequently, when considering common odorant concentrations in foods, the likelihood of odorant transmission into human milk with association to sensory relevance seems to be at least limited with regard to many common food flavors (see also Buettner[23]).

Sensory Analysis of Fennel–Anise–Caraway Tea and of Human Milk Samples Expressed before and after Tea Ingestion. A further objective of our study was to characterize potential sensorial changes of the breast milk in relation to the tea consumption. Therefore, the sensorial analysis was arranged with milk samples of one mother with various expression times. The results of the sensorial experiment demonstrated that the ingestion of normal quantities of commercial fennel–anise–caraway tea showed no significant influence on the odor profile of human milk. Different results concerning a sensorially relevant odorant transfer into human milk were provided by the studies from the working group of Mennella and Beauchamp. These authors reported that the consumption of garlic capsules (1.5 g of garlic extract), alcohol (0.3 g/kg body weight), or carrot juice (500 mL) slightly altered the aroma profile of

dx.doi.org/10.1021/jf504073d | J. Agric. Food Chem. 2015, 63, 104–111

human milk. In the respective samples, the odor intensity peaked 2 h after the intake of garlic capsules and carrot juice and 1 h after alcohol consumption.[3−5] However, it is not clear if the panel only perceived a sensory difference with a rather diffuse character that might also have been induced by other parameters such as short periods of storage during the experiments or could actually smell the specific flavor in the human milk. Apart from that, with the only exception of the alcohol study, no chemical-analytical parameters were analyzed to monitor a potential odorant transfer into human milk. Overall, the occurrence of an odor change of human milk due to the transfer of flavors from the diet appears to be important not only concerning immediate reactions of the nursling to the altered flavor but also with regard to later associative effects, specifically related to possible influences on food preferences. However, the presumably much more prevalent influence of smells that nurslings encounter while being associated with their mothers in everyday life have to the best of our knowledge been basically neglected. The odor dosages from such "external" sources may drastically exceed what is delivered via the milk. This aspect might be another promising area of research for future studies into the field of odorant learning.

Method Validation and Investigation of Potential Storage Effects on the Investigated Terpenoid Substances in Human Milk. A detailed discussion of the method validation as well as the investigation of potential storage effects on terpenoid substances in human milk samples is provided in Appendix A (Supporting Information).

■ ASSOCIATED CONTENT

Ⓢ Supporting Information

Method validation and investigation of potential storage effects on the investigated terpenoid substances in human milk and tables of the single values of the content of the analyzed terpenes in milk samples of mothers A, B, D, and E and the respective concentrations of the ingested tea samples; tables include also the normalized data; terpene content in milk 0.5, 1.0, and 2.0 h, respectively, after tea ingestion was normalized on the corresponding terpene concentration in tea. This material is available free of charge via the Internet at http://pubs.acs.org.

■ AUTHOR INFORMATION

Corresponding Author

*(A.B.) Mail: Henkestraße 9, 91054 Erlangen, Germany. Phone: ++49-9131-8522739. Fax: ++49-9131-8522587. E-mail: Andrea.Buettner@fau.de.

Funding

This work was supported by the German Federal Ministry of Education and Research (BMBF). The study sponsor had no involvement in the design and accomplishment of the study or in the process of publication. The authors are exclusively responsible for the contents of this publication.

Notes

The authors declare no competing financial interest.

■ ACKNOWLEDGMENTS

We are grateful to the mothers who voluntarily provided samples of their milk. We thank Prof. Horst-Christian Langowski and Fraunhofer IVV, Freising, Germany, for supporting our scientific work.

■ ABBREVIATIONS USED

DCM, dichloromethane; GC-MS, gas chromatography−mass spectrometry; SAFE, solvent-assisted flavor evaporation; SIDA, stable isotope dilution assays; GC-FID, gas chromatography−flame ionization detector; LSD, least significant difference

■ REFERENCES

(1) Mennella, J. A.; Jagnow, C. P.; Beauchamp, G. K. Prenatal and postnatal flavor learning by human infants. *Pediatrics* **2001**, *107*, e88.

(2) Hausner, H.; Nicklaus, S.; Issanchou, S.; Mølgaard, C.; Møller, P. Breastfeeding facilitates acceptance of a novel dietary flavour compound. *Clin. Nutr.* **2010**, *29*, 141−148.

(3) Mennella, J. A.; Beauchamp, G. K. Maternal diet alters the sensory qualities of human milk and the nursling's behavior. *Pediatrics* **1991**, *88*, 737−744.

(4) Mennella, J. A.; Beauchamp, G. K. Beer breast feeding and folklore. *Dev. Psychobiol.* **1993**, *26*, 459−466.

(5) Mennella, J. A.; Beauchamp, G. K. Experience with a flavor in mother's milk modifies the infant's acceptance of flavored cereal. *Dev. Psychobiol.* **1999**, *35*, 197−203.

(6) Hausner, H.; Bredie, W. L. P.; Mølgaard, C.; Petersen, M. A.; Møller, P. Differential transfer of dietary flavour compounds into human breast milk. *Physiol. Behav.* **2008**, *95*, 118−124.

(7) Kirsch, F.; Beauchamp, J.; Buettner, A. Time-dependent aroma changes in breast milk after oral intake of a pharmacological preparation containing 1,8-cineole. *Clin. Nutr.* **2012**, *31*, 682−692.

(8) Sandgruber, S.; Much, D.; Amann-Gassner, U.; Hauner, H.; Buettner, A. Sensory and molecular characterisation of human milk odour profiles after maternal fish oil supplementation during pregnancy and breastfeeding. *Food Chem.* **2011**, *128*, 485−494.

(9) Beauchamp, J.; Kirsch, F.; Buettner, A. Real-time breath gas analysis for pharmacokinetics: monitoring exhaled breath by on-line proton-transfer-reaction mass spectrometry after ingestion of eucalyptol-containing capsules. *J. Breath Res.* **2010**, DOI: 10.1088/1752−7155/4/2/026006.

(10) Wagenstaller, M.; Buettner, A. Coffee aroma constituents and odorant metabolites in human urine. *Metabolomics* **2013**, *10* (2), 225−240.

(11) Wagenstaller, M.; Buettner, A. Quantitative determination of odorants and their glucuronide conjugates in human urine. *Metabolites* **2013**, *3*, 637−657.

(12) Zeller, A.; Horst, K.; Rychlik, M. Study of the metabolism of estragole in humans consuming fennel tea. *Chem. Res. Toxicol.* **2009**, *22* (12), 1929−1937.

(13) Engel, W.; Bahr, W.; Schieberle, P. Solvent assisted flavour evaporation − a new and versatile technique for the careful and direct isolation of aroma compounds from complex food matrices. *Eur. Food Res. Technol.* **1999**, *209*, 237−241.

(14) Schieberle, P.; Grosch, W. Quantitative analysis of aroma compounds in wheat and rye bread crusts using a stable isotope dilution assay. *J. Agric. Food Chem.* **1987**, *35*, 252−257.

(15) Grosch, W. Evaluation of the key odorants of foods by dilution experiments, aroma models and omission. *Chem. Senses* **2001**, *26* (5), 533−545.

(16) Almeida, A. M.; Castel-Branco, M. M.; Falcao, A. C. Linear regression for calibration lines revisited: weighting schemes for bioanalytical methods. *J. Chromatogr., B: Anal. Technol. Biomed. Life Sci.* **2002**, *774*, 215−222.

(17) Van den Dool, H.; Kratz, P. D. A generalization of the retention index system including linear temperature programmed gas-liquid partition chromatography. *J. Chromatogr.* **1963**, *11*, 463−471.

(18) Spitzer, J.; Doucet, S.; Buettner, A. The influence of storage conditions on flavour changes in human milk. *Food Qual. Pref.* **2010**, *21*, 998−1007.

(19) Szabo, E.; Boehm, G.; Beermann, C.; Weyermann, M.; Brenner, H.; et al. Fatty acid profile comparisons in human milk sampled from the same mothers at the sixth week and the sixth month of lactation. *J. Pediatr. Gastroenterol. Nutr.* **2010**, *50*, 316−320.

(20) Krzysztof, C. Skin penetration of terpenes from essential oils and topical vehicles. *Planta Med.* **2006**, *72*, 311−316.
(21) Shimoda, M.; Yoshimura, T.; Ishikawa, B.; Hayakawa, I.; Osajima, Y. Volatile compounds in human milk. *J. Fac. Agric. Kyushu Univ.* **2000**, *45*, 199−206.
(22) Hausner, H.; Philipsen, M.; Skov, T. H.; Petersen, M. A.; Bredie, W. L. P. Characterization of the volatile composition and variations between infant formulas and mother's milk. *Chem. Percept.* **2009**, *2*, 79−93.
(23) Büttner, A. Human milk odour profiles. In *Dietary and Nutritional Aspects of Human Breast Milk*; Preedy, E., Ed.; Kings College: London, UK, 2012.

JOURNAL OF AGRICULTURAL AND FOOD CHEMISTRY

Article

pubs.acs.org/JAFC

Flavor Chemistry of Lemon-Lime Carbonated Beverages

Bethany J. Hausch,[†] Yaowapa Lorjaroenphon,[§] and Keith R. Cadwallader*[,†]

[†]Department of Food Science and Human Nutrition, University of Illinois at Urbana−Champaign, 1302 West Pennsylvania Avenue, Urbana, Illinois 61801, United States

[§]Department of Food Science and Technology, Faculty of Agro-Industry, Kasetsart University, 50 Ngamwongwan Road, Bangkok 10900, Thailand

Supporting Information

ABSTRACT: The most potent aroma-active components of Sprite (SP), Sierra Mist (SM), and 7UP (7UP) were identified. Aroma extracts were prepared by liquid−liquid continuous extraction/solvent-assisted flavor evaporation (LLCE/SAFE). Twenty-eight compounds were detected by gas chromatography−olfactometry (GC-O) with linalool (floral, lavender), octanal (pungent orange), and 2,3-dehydro-1,8-cineole (minty) determined to be predominant aroma compounds based on their high flavor dilution (FD) factors by aroma extract dilution analysis (AEDA). The data indicate that lemon-lime flavor is composed of a small number of compounds (22 at the most in SM), and only a subset of these may be important because many compounds were detected only at low FD factors. Predominant aroma compounds (23) were quantified using static headspace solid phase microextraction (SPME) combined with stable isotope dilution assays (SIDA). In contrast to FD factors, the calculated odor-activity values (OAVs) indicate that octanal and limonene make the greatest contribution to the overall aroma of lemon-lime carbonated beverages, followed by nonanal, decanal, linalool, 1,8-cineole, and geranyl acetate. The results demonstrate that lemon-lime carbonated beverages share many of the same compounds but the relative abundance of these compounds varies by brand.

KEYWORDS: *lemon-lime, flavor chemistry, carbonated beverage, aroma extract dilution analysis (AEDA), stable isotope dilution assay (SIDA), odor-activity value (OAV), linalool, octanal, 2,3-dehydro-1,8-cineole, limonene*

INTRODUCTION

The first carbonated beverages came from natural sources in the form of effervescent mineral springs and yeast fermentation.[1] Early scientific investigations of carbon dioxide in water date back to 1741, when carbonated water was produced using bicarbonate salts, and by the late the 1760s and 1770s, scientists had developed ways of dissolving carbon dioxide in water under pressure.[1] The first commercial manufacture of carbonated water occurred in the late 1770s when Thomas Henry, a chemist and apothecary in Manchester, England, designed an apparatus that could carbonate up to 12 gal per batch and sold the product in corked glass bottles.[1,2]

The intended use of carbonated water changed as new carbonation technologies were developing. Although artificially carbonated mineral water was originally used for medicinal purposes and was required to contain sodium bicarbonate, it became a source of refreshment; soda was eliminated, and flavorings were added.[2] The early flavorings used in carbonated water for refreshment were largely from fruits and included sarsaparilla, lemon, pineapple, orange, strawberry, vanilla, peach, grape, almond, ginger, and cloves, among others.[2]

The volume of carbonated beverage sales has been declining since 2003. Yet, despite this trend, carbonated beverages accounted for $76.3 billion in 2013 sales for the United States.[3] Lemon-lime was among the top 10 carbonated beverage types in 2013, with Sprite taking the sixth largest market share.[3] Considering the market value of this product, it is important to understand the flavor profile and chemistry of lemon-lime flavor. Current details regarding the composition and chemistry of lemon-lime flavor in a beverage system are limited.

A review of the literature on essential oils indicates that certain oils from *Aloysia citriodora* Palau (lemon verbena)[4] and *Citrus aurantifolia* (Christm.) Swingle (lime) are important to the food industry.[5] Much work has been done to identify and quantify the composition of various oils for the purposes of detecting oil adulteration[6] or determining the antimicrobial activity of the oil.[7] It is also well-known that terpenes, the largest class of compounds in lemon oils, are unstable in acidic environments and undergo rearrangements.[8−12] Acid-catalyzed reactions of terpenes can occur at even mildly acidic pH (pH < ∼6).[8]

Numerous citrus varieties exist, and there is subsequently variation in the most abundant compounds in citrus. However, limonene is most abundant in lime oils on a percent by weight basis.[4,8,13] Neral and geranial (citral isomers) have been found to be very abundant in some varieties of lemon verbena.[4] Although acid-catalyzed reactions have been extensively studied, particularly in the case of citral, it is interesting to look at a real food system, namely, lemon-lime carbonated beverages, and find out which flavor compounds are important. Due to the large commercial value of lemon-lime carbonated beverages, this research has great potential to benefit the

Received: October 7, 2014
Revised: December 10, 2014
Accepted: December 12, 2014
Published: December 12, 2014

ACS Publications © 2014 American Chemical Society

DOI: 10.1021/jf504852z
J. Agric. Food Chem. 2015, 63, 112−119

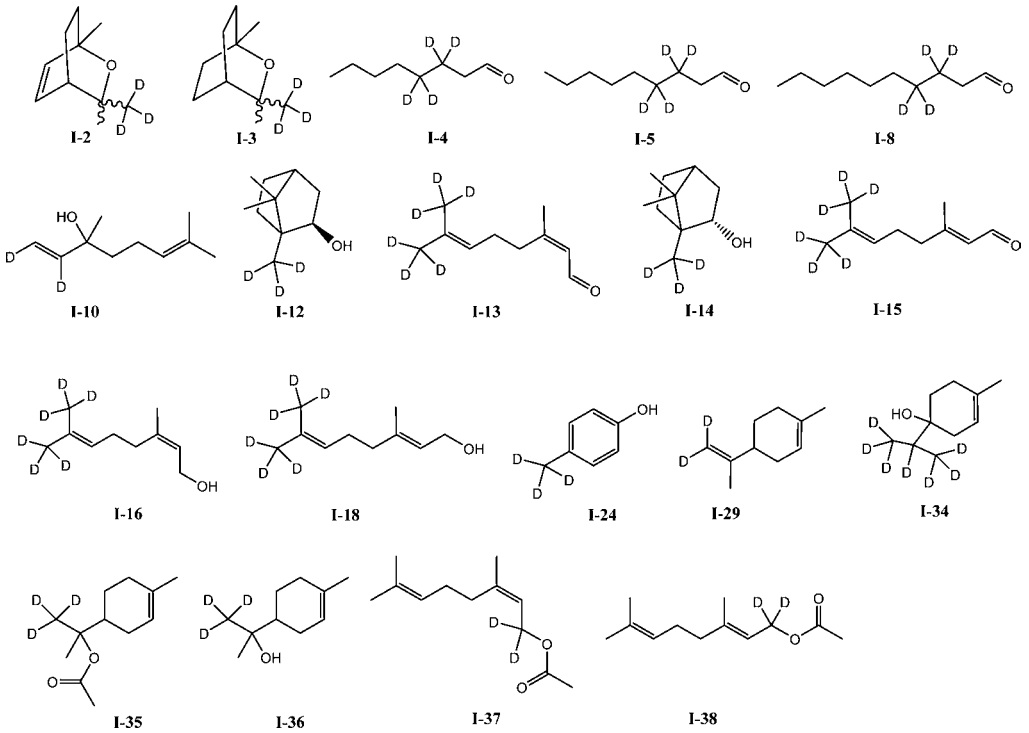

Figure 1. Structures of isotopically labeled compounds used for quantification (compound numbers correspond to those in Table 2).

beverage industry. When a consumer reaches for their favorite lemon-lime beverage, the flavor of the product they drink is distinctly different from that which was manufactured at the plant. Our ultimate goal is to understand the changes that take place as a result of the dynamic nature of the complex lemon-lime beverage system. Furthermore, this research aims to identify the key flavor compounds common to lemon-lime.

MATERIALS AND METHODS

Materials. Sprite (Coca-Cola Co., Atlanta, GA, USA), Sierra Mist (PepsiCo, Inc., Purchase, NY, USA), and 7UP (Dr. Pepper/Seven Up, Inc., Plano, TX, USA) were purchased in January 2009 and June 2010 at a local grocer (Urbana, IL, USA).

Chemicals. Unless otherwise stated, chemicals and reagents were obtained from Sigma-Aldrich Co. (St. Louis, MO, USA) for unlabeled standards. Nerol and geraniol were obtained from Bedoukian Research, Inc. (Danbury, CT, USA), and acetic acid was obtained from Fisher Scientific (Fair Lawn, NJ, USA). The isotope 4-([$^2H_3$]-methyl)-phenol was purchased from C/D/N Isotopes Inc. (Quebec, Canada). Published methods were used for the synthesis of (*E*)-4,5-epoxy-(*E*)-2-decenal,[14] 2,3-dihydro-5-hydroxy-6-methyl-4(*H*)-pyran-4-one (dihydromaltol),[15] [$^2H_2$]-limonene,[16] and [$^2H_2$]-linalool.[17] The Supporting Information provides synthetic procedures or references with modified procedures for the following compounds: 2,3-dehydro-1,8-cineole, [$^2H_3$]-2,3-dehydro-1,8-cineole, [$^2H_3$]-1,8-cineole, [$^2H_4$]-octanal, [$^2H_4$]-nonanal, [$^2H_4$]-decanal, [$^2H_3$]-isoborneol, [$^2H_6$]-neral, [$^2H_3$]-borneol, [$^2H_6$]-geranial, [$^2H_6$]-nerol, [$^2H_6$]-geraniol, [$^2H_7$]-4-terpineol, [$^2H_3$]-α-terpinyl acetate, [$^2H_3$]-α-terpineol, [$^2H_2$]-neryl acetate, and [$^2H_2$]-geranyl acetate. The structures of all isotope standards used can be found in Figure 1. All unlabeled compound purities were >90% (neat, hot split, 250 °C, GC-FID) except in the case of the isotope mixtures listed here: neral and geranial, 35.8 and 59.9%, respectively; [$^2H_6$]-neral and [$^2H_6$]-geranial, 21.8 and 52.3%, respectively; [$^2H_6$]-nerol and [$^2H_6$]-geraniol, 32.8 and 59.3%, respectively; and [$^2H_3$]-isoborneol and [$^2H_3$]-borneol, 48.3 and 47.0%, respectively.

Preparation of Aroma Extracts. Volatile components were isolated by liquid–liquid continuous extraction (LLCE). For each extraction, 500 mL of a carbonated beverage, 100 mL of deodorized deionized–distilled water, and 20 μL of an internal standard solution (417 μg/mL of 6-undecanone in methanol) were placed in the LLCE apparatus (Z101567, Sigma-Aldrich Co.). The device was connected to a 250 mL round-bottom flask containing the extraction solvent (200 mL of diethyl ether), which was subsequently refluxed by heating the flask in a 47 °C water bath, whereas the condenser of the LLCE apparatus was held at 5 °C. After extraction for 18 h at ambient temperature (~23 °C) with constant stirring in the sample chamber, the ether layers were recovered and concentrated to 50 mL using a Vigreux column at 43 °C. Solvent-assisted flavor evaporation (SAFE) was performed for 2 h according to the method described by Rotsatchakul et al.[18] The resulting aroma extract was further concentrated to 10 mL using a Vigruex column at 43 °C, dried over anhydrous sodium sulfate, and concentrated to a final volume of 500 μL using a gentle stream of nitrogen. Each aroma extract was stored in a 2 mL vial equipped with a PTFE-lined screw cap at −70 °C until analysis.

Gas Chromatography–Olfactometry (GC-O) and Aroma Extract Dilution Analysis (AEDA). The relative potency of individual odorants was determined using AEDA according to the method previously described.[19] Serial dilutions (1:3, v/v) of each aroma extract were prepared in diethyl ether and stored in a 2 mL vial equipped with a PTFE-lined screw cap at −70 °C until analysis. The GC-O system consisted of a 6890 GC (Agilent Technologies Inc., Palo Alto, CA, USA) equipped with a FID, an on-column injector (3 °C temperature tracking mode), and an olfactory detection port (DATU Technology Transfer, Geneva, NY, USA). Dilutions and concentrated extracts were analyzed on a polar capillary column (RTX-Wax, 15 m × 0.32 mm i.d.; 0.5 μm film; Restek, Bellefonte, PA, USA). Concentrated aroma extracts were also analyzed using a nonpolar capillary column (RTX-5MS, 15 m × 0.32 mm i.d.; 0.5 μm film; Restek) for calculation of retention indices (RI). For GC-O, column effluent was split 1:5 between the FID and olfactory detection port using deactivated fused silica tubing (1 m × 0.25 mm i.d.; Restek), with both detector temperatures held at 250 °C. The GC oven temperature was programmed from 40 to 225 °C at a rate of 10 °C/min with initial and final hold times of 5 and 30 min, respectively. Helium was used as

DOI: 10.1021/jf504852z
J. Agric. Food Chem. 2015, 63, 112–119

Table 1. Predominant Aroma-Active Components of Three Commercial Brands of Lemon-Lime Carbonated Beverages

		RI[a]			FD factor[b]		
no.[c]	compound	WAX	RTX-5	odor description[d]	SP	7UP	SM
1	unknown	1155	–[e]	piney, terpiney	3	–	–
2	2,3-dehydro-1,8-cineole[f]	1196	985	minty, pine needles	81	81	81
3	1,8-cineole[f]	1211	1024	minty/eucalyptus	–	–	3
4	octanal[f]	1297	1002	pungent orange	81	81	243
5	nonanal[f]	1406	1103	orange, sweet, pungent	3	9	27
6	acetic acid[g]	1450	–	vinegar	–	9	–
7	unknown	1451	–	fresh, melony	9	9	27
8	decanal[f]	1511	1205	pungent, green, cilantro	9	9	27
9	unknown	1534	–	stale, burnt sugar	3	9	–
10	linalool[f]	1545	1099	floral, lavender	243	2187	729
11	butanoic acid[h]	1638	–	cheesy	<3	3	–
12	isoborneol[f]	1692	1160	camphorous	9	<3	<3
13	neral[f]	1701	1240	lemony	3	–	3
14	borneol[f]	1725	1168	earthy, camphorous	81	3	3
15	geranial[f]	1753	1271	lemon oil, lemon cleaner	3	–	9
16	nerol[f]	1771	1229	lemon cleaner	3	3	<3
17	unknown	1812	–	sweet, fruity	–	3	–
18	geraniol[f]	1854	1254	lemon cleaner	9	9	9
19	2,3-dihydro-5-hydroxy-6-methyl-4(*H*)-pyran-4-one (dihydromaltol)[h]	1884	–	burnt sugar	–	–	3
20	3-hydroxy-2-methyl-4(*H*)-pyran-4-one (maltol)[h]	2000	–	burnt sugar	–	9	–
21	unknown	2026	–	inky, phenolic	–	3	<3
22	(*E*)-4,5-epoxy-(*E*)-2-decenal[i]	2029	1381	unripe	–	–	3
23	4-hydroxy-2,5-dimethyl-3(2*H*)-furanone (HDMF)[i]	2046	1088	burnt sugar	81	27	9
24	4-methylphenol (*p*-cresol)[f]	2096	1083	dung, stable	81	81	<3
25	eugenol[h]	2148	–	cloves	–	–	3
26	3-hydroxy-4,5-dimethyl-2(5*H*)-furanone (sotolon)[i]	2225	1111	curry	3	27	<3
27	unknown	2346	–	waxy, liver-like	3	<3	<3
28	benzoic acid[f]	2449	1306	sweet, candy	27	–	81

[a]Retention index determined from GC-O data. [b]Flavor dilution factor determined on RTX-Wax column (SM, Sierra Mist; SP, Sprite). [c]Compound numbers correspond to peak numbers in Tables 2 and 3 and Figure 2. [d]Odor property as perceived during GC-O. [e]Odor not detected. [f]Compound positively identified based on odor property, mass spectral data, and RIs on both RTX-Wax and RTX-5 columns. [g]Compound tentatively identified based on odor property, mass spectral data, and RI on RTX-Wax column. [h]Compound tentatively identified based on odor property on RTX-Wax column. [i]Compound tentatively identified based on odor property and RI on RTX-Wax and RTX-5 columns.

a carrier gas at a constant flow rate of 2.2 mL/min. Other conditions of GC-O have been previously described.[20]

Gas Chromatography–Mass Spectrometry (GC-MS). The GC-MS system consisted of a 6890 GC/5973N MSD (Agilent Technologies Inc.) equipped with a cool on-column injector (3 °C temperature tracking mode). Separations were performed on 1 μL injections of each extract using either a polar capillary column (RTX-Wax, 30 m × 0.25 mm i.d.; 0.5 μm film; Restek) or a nonpolar column (RTX-5SLIM, 30 m × 0.25 mm i.d.; 0.5 μm film; Restek). The oven temperature was programmed from 35 to 225 °C at a rate of 4 °C/min with initial and final hold times of 5 and 20 min, respectively. Helium was used as carrier gas at a constant rate of 1.0 mL/min. The MSD conditions were as follows: capillary direct interface temperature, 280 °C; ionization energy, 70 eV; mass range, 35–300 amu; electron multiplier voltage (Autotune +200 V); scan rate, 5.27 scans/s.

Compound Identification. Compound identification was based on matching retention indices (on two different GC column phases), odor descriptions, and mass spectra of unknowns with those of authentic standards. Tentative identifications were based on one or more, but not all, of the above criteria. A homologous series of *n*-alkanes was used for the determination of retention indices according to the method of van Den Dool and Kratz.[21]

Quantification of Aroma-Active Compounds. *Stable Isotope Dilution Analysis (SIDA).* The aroma compounds presented in Tables 2 and 3 were categorized into three groups for quantification purposes.

(1) Compounds **3**–**5**, **8**, **12**, **14**, **16**, **18**, **24**, **30**–**35**, **37**, and **38**: The lemon-lime carbonated beverage (~5 mL) was poured into the 20 mL screw-top headspace (HS) vial equipped with a Teflon-coated stir bar and Teflon-lined silicon cap. The exact weight of sample was calculated by weight difference. The appropriate amounts of isotopically labeled standards used as internal standards were individually spiked through the septum. The sample was vigorously stirred by vortex, and then sodium chloride (1 g) was added. The vial was recapped with a new cap before analysis by solid phase microextraction (SPME). The sample vial was agitated at 250 rpm and incubated at 40 °C for 10 min. The HS volatiles were then extracted at the same temperature for 20 min using 50/30 μm DVB/Carboxen/PDMS StableFlex fiber (Supelco, Bellefonte, PA, USA). The aroma compounds were desorbed at 260 °C in the hot splitless injector of the GC-MS and separated on a Stabilwax column using the GC oven program described above.

(2) Compounds **29** and **36** (high concentration): Each isotope compound was spiked into 1 mL of lemon-lime carbonated beverage prepared in the HS vial. Odor-free water (9 mL) was added and stirred using vortex. The diluted sample (0.5 mL) was transferred to the new HS vial containing 4.5 mL of odor-free water and 1 g of sodium chloride. The concentrations of limonene (**29**) and α-terpineol (**36**) were then analyzed by SPME as described above.

(3) Compounds **2**, **10**, **13**, and **15** (pH-dependent stability): Approximately 150 mL of lemon-lime carbonated beverage was poured through a condenser at 0 °C into a three-neck flask, equipped with a pH meter and stir bar. The pH of the sample was adjusted to 7 with 2 M aqueous sodium hydroxide solution. The weight differences of carbonated beverage and sodium hydroxide solution were recorded to calculate the exact ratio. Approximately 5 mL of the mixture was prepared in the HS vial. The labeled standards were individually

DOI: 10.1021/jf504852z
J. Agric. Food Chem. 2015, 63, 112–119

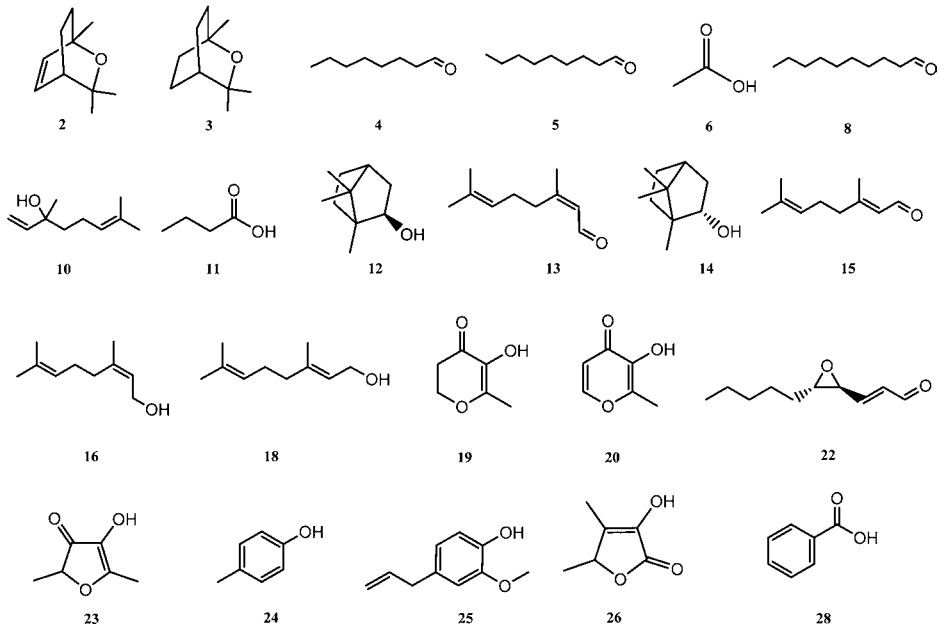

Figure 2. Structures of the aroma-active compounds identified in three commercial brands of lemon-lime carbonated beverages (compound numbers correspond to those in Tables 1−3).

spiked, and then 1 g of sodium chloride was added before quantification by SPME as before.

Calculations. The concentration of each odorant was calculated from the response factor (R_f), mass ratio, and area ratio of the selected ions presented in Table 2. The response factor was determined by plotting the area ratio of the unlabeled to labeled standard against the mass ratio and taking the inverse of the slope. The mass ratios chosen were 10:1, 5:1, 1:1, 1:5, and 1:10. The equation used to calculate the concentration of selected aroma compounds is

$$C = A_{\text{unlabeled}}/A_{\text{isotope}} \times R_f \times M_{\text{isotope}}/(M_{\text{soda}} \times B)$$

where C = concentration of aroma compound in the decarbonated soda (ng/g), $A_{\text{unlabeled}}$ = area of the extracted ion chromatogram for the unlabeled compound, A_{isotope} = area of the extracted ion chromatogram for the isotope compound, R_f = response factor, the inverse of the slope when the area ratio versus mass ratio are plotted, M_{isotope} = mass of the isotopically labeled standard (ng), M_{soda} = mass of the just-out-of-the-can carbonated beverage (g), and B = correction factor to convert the mass to a decarbonated basis. The correction factors B can be found in Table S1 of the Supporting Information.

Statistical Analysis. Quantifications of aroma compounds were run in triplicate. The analysis of variance (ANOVA) was performed by SAS program (SAS institute Inc., Cary, NC, USA). The least significant difference (LSD) was then tested if there was a significant difference (p value < 0.05) among the lemon-lime carbonated samples.

Determination of Odor Threshold. The odor detection threshold in water of a compound was determined orthonasally following published procedures.[22,23] All test samples (50 mL each) were presented in 125 mL Teflon sniff bottles (Nalge Nunc International, Rochester, NY, USA) in an ascending concentration series consisting of six samples (1:3 dilution series). The number of panelists for evaluation of odor threshold of 2,3-dehydro-1,8-cineole (**2**) and isoborneol (**12**) was 12 (7 females and 5 males; 22−52 years) and 12 (8 females and 4 males; 22−47 years), respectively. It is also important to note that the isoborneol (**12**) standard consisted of a racemic mixture of the two enantiomers (*d*- and *l*-).

Calculation of Odor Activity Values (OAVs). The OAV of a compound was calculated as the ratio of its concentration in lemon-lime carbonated beverage to its odor threshold in water, which was obtained from the literature or determined in our laboratory.

RESULTS

Aroma Extraction Dilution Analysis (AEDA). A combined total of 28 aroma-active compounds were detected in the three brands using gas chromatography-olfactometry (GC-O), as shown in Table 1 and Figure 2. The identification data for the aroma-active compounds in SP, SM, and 7UP indicated that linalool (no. **10**) was the single most potent aroma compound in lemon-lime carbonated beverages, while octanal (no. **4**) and 2,3-dehydro-1,8-cineole (no. **2**) were moderately potent aroma-active compounds. The data indicate that lemon-lime is composed of a small number of compounds (22 at the most, in SM) and only a subset of these may be important since many compounds have low FD factors.

Notably, lemon-lime carbonated beverages contain several groups of compounds with both similar odor properties and close retention indices on the polar GC column, as evidenced in Table 1. Specifically, these include 2,3-dehydro-1,8-cineole (**2**) and 1,8-cineole (**3**) with piney and eucalyptus notes; isoborneol (**12**) and borneol (**14**) with camphorous notes; neral (**13**), geranial (**15**), nerol (**16**), and geraniol (**18**) with lemony/lemon cleaner notes. Three aliphatic, straight-chain (*n*-) aldehydes, octanal (**4**), nonanal (**5**), and decanal (**8**), with similar pungent citrusy notes were also detected. The compounds in each group are structurally similar to one another, which provides a strong indication that compounds have undergone reactions and rearrangements. The original flavoring is derived from lemon oil, and it is well-known that terpenes undergo acid-catalyzed reactions.[8,24]

Linalool, determined to be the single most potent aroma compound by FD factor, is commonly found in lemon and lime oils,[4,25] as well as other citrus oils.[26,27] Furthermore, it can also be produced by structural rearrangements of other compounds (e.g., geraniol and nerol) frequently found in lemon/lime oils.[8] In an acidic model (pH 2.9) geraniol and nerol have been found to rearrange to form linalool in only 1 or 2 h, respectively, at 25 °C.[28] Furthermore, linalool itself is not stable in an acidic environment, converting into α-terpineol after only 2 h at pH 2.9.[28]

DOI: 10.1021/jf504852z
J. Agric. Food Chem. 2015, 63, 112−119

Table 2. Isotope-Labeled Internal Standards, Selected Ions, and Response Factors for Quantification

unlabeled compound			labeled compound			
no.[a]	compound	ion[b]	no.[c]	compound	ion[b]	R_f[d]
2	2,3-dehydro-1,8-cineole	124	**I-2**	[$^2H_3$]-2,3-dehydro-1,8-cineole	127	1.19
3	1,8-cineole	154	**I-3**	[$^2H_3$]-1,8-cineole	157	0.97
4	octanal	110	**I-4**	[$^2H_4$]-octanal	114	0.49
5	nonanal	114	**I-5**	[$^2H_4$]-nonanal	116	0.44
8	decanal	128	**I-8**	[$^2H_4$]-decanal	130	1.92
10	linalool	121	**I-10**	[$^2H_2$]-linalool	123	1.01
12	isoborneol	110	**I-12**	[$^2H_3$]-isoborneol	113	1.07
13	neral	69	**I-13**	[$^2H_6$]-neral	75	0.68
14	borneol	110	**I-14**	[$^2H_3$]-borneol	113	0.83
15	geranial	69	**I-15**	[$^2H_6$]-geranial	75	0.69
16	nerol	69	**I-16**	[$^2H_6$]-nerol	75	0.68
18	geraniol	69	**I-18**	[$^2H_6$]-geraniol	75	0.96
24	*p*-cresol	108	**I-24**	[$^2H_3$]-*p*-cresol	111	1.27
29	limonene	136	**I-29**	[$^2H_2$]-limonene	138	0.98
30	γ-terpinene	136	**I-29**[e]	[$^2H_2$]-limonene	138	0.34
31	*p*-cymene	134	**I-29**[e]	[$^2H_2$]-limonene	138	0.22
32	α-terpinolene	136	**I-29**[e]	[$^2H_2$]-limonene	138	0.25
33	fenchol	81	**I-14**[e]	[$^2H_3$]-borneol	98	1.10
34	4-terpineol	71	**I-34**	[$^2H_7$]-4-terpineol	75	0.68
35	α-terpinyl acetate	136	**I-35**	[$^2H_3$]-α-terpinyl acetate	139	1.36
36	α-terpineol	59	**I-36**	[$^2H_3$]-α-terpineol	62	0.91
37	neryl acetate	121	**I-37**	[$^2H_2$]-neryl acetate	123	0.89
38	geranyl acetate	121	**I-38**	[$^2H_2$]-geranyl acetate	123	0.96

[a]Compound numbers correspond to peak numbers in Tables 1 and 3 and Figure 2. [b]Selected ion. [c]The letter "I" means isotopically labeled compound followed by the compound number. [d]Response factor. [e]A structurally similar compound was selected as the internal standard.

The three aliphatic straight-chain (*n*-) aldehydes, octanal (**4**), nonanal (**5**), and decanal (**8**), are present in the original citrus oil used to produce the lemon-lime flavorings.[29−31] On the basis of the results of AEDA, octanal is the second most potent odorant in SM with an FD factor of 243, whereas it is also important in SP and 7UP with FD factors of 81 in both beverages. The odor properties of *n*-aldehyrdes change slightly as a function of increasing chain length. Sensory work on carbon chain length shows that subjects were able to distinguish between pairs of *n*-aldehydes of differing chain lengths; however, octanal could not be distinguished from nonanal, nor could nonanal be distinguished from decanal.[32] This indicates that the *n*-aldehydes are important to the overall aroma of lemon-lime carbonated beverages collectively but not necessarily individually.

Another important potent odorant identified in lemon-lime carbonated beverages was 2,3-dehydro-1,8-cineole (dehydrocineol, **2**). This minty, eucalyptus-smelling compound had an FD factor of 81 in all three products. Dehydrocineol has been reported as a degradation product of citral.[8,11,33,34] Kimura et al.[33] monitored citral degradation in a citric acid solution and reported dehydrocineol as a degradation product of *p*-mentha-1,5-dien-8-ol and *p*-mentha-1(7),2-dien-8-ol. Results from our previous study[34] confirmed the above to be true and further demonstrated that dehydrocineole is highly unstable under acidic conditions. Dehydrocineole has been reported in numerous essential oils, including lemon grass,[35] lime,[5] licorice root,[36] and garden lovage,[37] among others. This compound may be present in the essential oil used for making the lemon-lime flavorings as well as formed from citral in the acidic environment of the carbonated beverage.

As expected, the citral isomers, geranial (**14**) and neral (**12**), were among the aroma-active components in the lemon-lime carbonated beverages. The levels of these isomers can be quite high in lemon oil; for example, 29.0% geranial and 20.0% neral were reported in lemon verbena oil.[4] The presence of high levels of citral can be used as a measure of essential oil quality.[4,38] Yet, although these aldehydes are clearly important in lemon and lime oils, they did not emerge as predominant aroma components in lemon-lime carbonated beverages, as indicated by their relatively low FD factors. This can be explained by their tendency to readily undergo acid-catalyzed rearrangements. A study that followed the degradation of citral over 2 weeks in an acidic buffer solution (pH 3.0; stored in the dark at 40 °C) demonstrated that nearly all of the geranial and neral was transformed into other compounds in only 3 days.[10]

An unknown compound (**7**) with a retention index (RI) of 1451 (wax) and contributing a fresh, melony aroma was detected at FD factors of 27 in SM and 9 in both SP and 7UP. It is hypothesized that this compound is a low threshold nonenal isomer. A number of the unsaturated C_9 aldehydes have green, cucumber-like ((*Z*)-3- and (*Z*)-4-nonenal) or melon-like odors ((*Z*)-5-, (*E*)-6-, (*Z*)-6-, (*E*)-7-, and (*Z*)-7-nonenal).[39] Some of these compounds have odor detection threshold values in the low parts per billion (ppb) range, such as (*Z*)-4-nonenal with an odor threshold of 80 ppb and (*E*)-6-nonenal with an odor threshold of 4.6 ppb (thresholds determined in paraffin oil).[39] In the present study, no mass spectral data were available for this compound because it was below the GC-MS detection limits. This further supports the hypothesis that the unknown has a very low threshold. In the identification work done up until this point, two unsaturated nonenal isomers were eliminated, specifically (*Z*)-6-nonenal or 8-nonenal, as neither compound had the same odor properties or RI values when compared to the unknown. Further

DOI: 10.1021/jf504852z
J. Agric. Food Chem. 2015, 63, 112−119

Table 3. Concentrations, Odor Thresholds, and Odor Activity Values of Selected Odorants Identified in Lemon-Lime-Flavored Carbonated Beverages

		concentration[c] (ppb; ng/g)					OAV[b]		
no.[a]	compound	SP	7UP	SM	threshold[d] (ppb)		SP	7UP	SM
2	2,3-dehydro-1,8-cineole	5.2 c	10.1 b	12.2 a	17.2	*e*	0.3	0.6	0.7
3	1,8-cineole	30.4 a	19.0 b	14.4 b	1.3	Buttery et al., 1987[43]	23.4	14.6	11.0
4	octanal	192 b	585 a	146 c	0.7	Buttery et al., 1988[47]	274	836	209
5	nonanal	48.3 c	61.5 b	108 a	1	Buttery et al., 1988[47]	48.3	61.5	108.1
8	decanal	109 c	341 a	200 b	2	Buttery et al., 1988[47]	54.6	171	99.9
10	linalool	195 c	483 a	390 b	6	Buttery et al., 1987[43]	32.5	80.4	65.0
12	isoborneol	56.9 a	14.6 c	47.2 b	16.4[f]	*e*	3.5	0.9	2.9
13	neral	215 b	508 a	71.5 c	30	Buttery, 1993[48]	7.2	16.9	2.4
14	borneol	210 a	96.0 b	43.2 c	180/80[g]	Padrayuttawat et al., 1997[49]	1.2/2.6	0.5/1.2	0.2/0.5
15	geranial	359 b	874 a	129 c	32	Buttery et al., 1990[50]	11.2	27.3	4.0
16	nerol	57.5 c	132 a	103 b	300	Ohloff, 1978[44]	0.2	0.4	0.3
18	geraniol	64.5 c	321 a	133 b	40	Buttery et al., 1987[43]	1.6	8.0	3.3
24	*p*-cresol	15.2 a	19.3 a	14.0 a	55	Buttery et al., 1988[47]	0.3	0.4	0.3
29	limonene	1200 b	3220 a	2980a	10	Buttery et al., 1974[51]	120	322	298
30	γ-terpinene	94.4 b	143 b	867 a	1000	Tamura et al., 1996[52]	0.1	0.1	0.9
31	*p*-cymene	160 a	84.8 b	140 a	150	Buttery et al., 1974[51]	1.1	0.6	0.9
32	α-terpinolene	44.3 b	128 a	155 a	200	Buttery et al., 1968[53]	0.2	0.6	0.8
33	fenchol	523 a	259 b	110 c					
34	4-terpineol	666 a	224 b	253 b	340	Buttery et al., 1974[51]	2.0	0.7	0.7
35	α-terpinyl acetate	5.3 b	10.8 a	5.0 b	2500	Tamura et al., 1993[29]	0.0	0.0	0.0
36	α-terpineol	6980 a	2500 b	1480 c	350	Buttery et al., 1974[51]	19.9	7.1	4.2
37	neryl acetate	201 b	165 c	262 a	2000	Tamura et al., 1993[29]	0.1	0.1	0.1
38	geranyl acetate	178 c	248 b	272 a	9	Buttery et al., 1988[47]	19.8	27.6	30.2

[a]Compound numbers correspond to peak numbers in Tables 1 and 2 and Figure 2. [b]Odor activity value. [c]Means, averaged from three replications; different letters indicate significant difference (p value < 0.05). [d]Odor detection threshold in water. [e]Determined in our laboratory, as described under Materials and Methods. [f]Racemic mixture. [g]Enantiomers of (1*R*,2*S*)-(+)- and (1*S*,2*R*)-(−)-borneol, respectively.

investigation of the other possible isomers of nonenal could lead to the identification of this compound.

Odor Activity Values (OAVs). OAVs are an alternative method to AEDA for determining the importance of aroma compounds and have the advantage of taking some matrix effects into account, that is, flavor release from water. Agreement between AEDA and OAVs gives confidence to ranking of odorant importance. In this study, both aroma-active compounds and high-abundance volatiles were quantified; the latter were chosen due to their potential to affect flavor release. All volatiles quantified are given in Table 2, along with the isotope standard used for quantitation, ion choice, and response factor.

The concentrations and OAVs of aroma compounds in lemon-lime carbonated beverages are shown in Table 3. To the greatest extent possible, the thresholds used were determined using similar methodology (Teflon sniff bottles) to reduce variation caused by methodology. Among 23 aroma compounds, octanal (**4**) and limonene (**29**) had the highest OAVs in all three brands. Notably, the OAV of octanal is 836 in 7UP, much higher than the corresponding values for octanal in SP and SM (274 and 209, respectively). Due to its relatively high FD factor in all brands and because of distinct brand differences in octanal concentration, it is likely that octanal is one of the main distinguishing compounds among the brands.

The OAVs for limonene are high in 7UP and SM, at 322 and 298, respectively (OAV of 120 for SP). Limonene was considered to have high potency by means of its OAV, but it was not even detected by GC-O. Limonene, as well as α-terpineol (**36**), is present at approximately 1 order of magnitude higher concentration that the other volatiles quantified. The high abundance and moderately low odor detection threshold in water account for limonene's importance. Limonene is a major compound in lemon and lime oils.[4,13,40,41] It also emerged as an important aroma-active compound in sensory-directed research of fresh lemon oil.[12]

In addition, the OAVs of 1,8-cineole (**3**), nonanal (**5**), decanal (**8**), linalool (**10**), and geranyl acetate (**38**) in all lemon-lime carbonated beverages were >10. Linalool was determined to be the most potent aroma compound on the basis of its high FD factor. Differences in odor potency, as determined by FD factor and OAV, can be related to the difference of thresholds in air and water. FD factors depend on each compound's odor threshold in air, whereas the calculated OAVs depend on each compound's threshold in water, which is a better indication of the perceived flavor, taking the matrix into account. A compound's threshold may be different in water and in air, as observed with linalool. The threshold of linalool in air is 0.4−0.8 ng/L (ppt),[42] whereas linalool's threshold in water is 6 μg/L (ppb).[43] Thus, the higher threshold in water helps explain why linalool appears to be less significant.

Notably, two of the most important aroma-active compounds, limonene and linalool, are chiral. In the case of both of these compounds, the odor property remains the same, regardless of the enantiomer.[44] For limonene, the published thresholds in air are similar for both the (*R*) and (*S*) enantiomers, 135 and 270 ppb, respectively. However, the threshold in air is significantly different for the linalool enantiomers, with a threshold 80 times lower for the (*R*) isomer, 0.036 ppb, compared to 2.9 ppb for the (*S*) isomer. (*R*)-Linalool has previously been reported to be in 13.6% enantiomeric excess in lemon oil.[45] Certainly, chiral analysis of

DOI: 10.1021/jf504852z
J. Agric. Food Chem. 2015, 63, 112−119

these aroma-active compounds, with linalool in particular, would refine the estimates provided by OAV. The thresholds available for comparison of enantiomers were in air, whereas those used for the calculation of OAVs in Table 3 are in water.

The quantitative data indicate that low levels of citral (neral and geranial) remained in the lemon-lime carbonated beverages. Geranial is the more abundant isomer present at levels of 359, 874, and 129 ng/g in SP, 7UP, and SM, respectively. The lemon-lime carbonated beverage was neutralized before analysis of these compounds to prevent the labeled standards from rearranging. Much lower concentrations of the citral isomers were found when the pH was not controlled in an earlier study in our laboratory.[46] These compounds likely do not play an important role in the overall aroma of lemon-lime carbonated beverages due to their low abundance. This result is intriguing given the importance of citral in fresh lemon oil.[12]

GC-O data culminating in FD factors for compounds by brand were determined for beverages from different lots used for quantification, and reasonable agreement in trends is seen from these two data sets. Neither FD factors nor OAVs are able to account for compound interactions that may affect flavor release. Furthermore, despite the relatively simple matrix of carbonated beverages, the acid, carbonation, and sugar could also affect release. Aroma reconstitution models can verify the predictions made by these analytical tools and would be an important area for future work.

Conclusion. The popularity of lemon-lime carbonated beverages, along with the complex chemistry arising from acid-catalyzed rearrangements of terpenes, makes this an important system to study. By investigating the three most popular brands of lemon-lime carbonated beverages, octanal and limonene were determined to be the most important aroma-active compounds by considering the OAVs, whereas linalool, 1,8-cineole, nonanal, decanal, and geranyl acetate were also moderately important. Meanwhile, the aroma contribution of citral was limited.

■ ASSOCIATED CONTENT

Supporting Information

Procedures for all compound syntheses and a table showing the beverage weight loss from decarbonation. This material is available free of charge via the Internet at http://pubs.acs.org.

■ AUTHOR INFORMATION

Corresponding Author

*(K.R.C.) Phone: (217) 333-5803. Fax: (217) 333-1875. E-mail: cadwlldr@illinois.edu.

Funding

Partial support for this project was provided by the National Institute of Food and Agriculture, U.S. Department of Agriculture, under Project ILLU-698-366.

Notes

The authors declare no competing financial interest.

■ ABBREVIATIONS USED

SP, Sprite; SM, Sierra Mist; 7UP, 7UP; LLCE, liquid−liquid continuous extraction; SAFE, solvent-assisted flavor evaporation; GC-O, gas chromatography−olfactometry; FD, flavor dilution; AEDA, aroma extract dilution analysis; SPME, solid phase microextraction; SIDA, stable isotope dilution assays; OAVs, odor-activity values; GC-MS, gas chromatography−mass spectrometry

■ REFERENCES

(1) Hargitt, B. Introduction. In *Carbonated Soft Drinks: Formulation and Manufacture*; Steen, D. P., Ashurst, P. R., Eds.; Blackwell Publishing: Oxford, UK, 2006; pp 1−14.

(2) Riley, J. J. *A History of the American Soft Drink Industry*; American Bottlers of Carbonated Beverages: Washington, DC, USA, 1958.

(3) *Special Issue: U.S. Beverage Results for 2013*; *Beverage-Digest*; Beverage Digest Co.: Bedford Hills, NY, USA, March 31, 2014; pp 1−3.

(4) Lira, P.; van Baren, C. M.; Retta, D.; Bandoni, A. L.; Gil, A.; Gattuso, M.; Gattuso, S. Characterization of lemon verbena (*Aloysia cirtriodora* Palau) from Argentina by the essential oil. *J. Essent. Oil Res.* **2008**, *20*, 350−353.

(5) Patil, J. R.; Jayaprakasha, G. K.; Murthy, K. N. C.; Tichy, S. E.; Chetti, M. B.; Patil, B. S. Apoptosis-mediated proliferation inhibition of human colon cancer cells by volatile principles of *Citrus aurantifolia*. *Food Chem.* **2009**, *114*, 1351−1358.

(6) Lifshitz, A.; Stepak, Y.; Basker, H. B. Characterization of Isreal lemon oil and detection of its adulteration. *J. Food Sci.* **1969**, *34*, 254−257.

(7) Thavanapong, N.; Wetwitayaklung, P.; Charoenteeraboon, J. Comparison of essential oils compositions of *Citrus maxima* Merr. peel obtained by cold press and vacuum steam distillation methods and of its peel and flower extract obtained by supercritical carbon dioxide extraction method and their antimicrobial activity. *J. Essent. Oil Res.* **2010**, *22*, 71−77.

(8) Clark, B. C., Jr.; Chamblee, T. S. Acid-catalyzed reactions of citrus oils and other terpene-containing flavors. In *Off-Flavours in Foods and Beverages*; Charalambous, G., Ed.; Elsevier Science Publishers: Amsterdam, The Netherlands, 1992; pp 229−285.

(9) Baxter, R. L.; Laurie, W. A.; McHale, D. Transformations of monoterpenoids in aqueous acids − reactions of linalool, geraniol, nerol and their acetates in aqueous citric acid. *Tetrahedron* **1978**, *34*, 2195−2199.

(10) Ueno, T.; Masuda, H.; Ho, C. Formation mechanism of *p*-methylacetophenone from citral via a *tert*-alkoxy radical intermediate. *J. Agric. Food Chem.* **2004**, *52*, 5677−5684.

(11) Peacock, V. E.; Kuneman, D. W. Inhibition of the formation of α-*p*-dimethylstyrene and *p*-cymen-8-ol in a carbonated citral-containing beverage system. *J. Agric. Food Chem.* **1985**, *33*, 330−335.

(12) Schieberle, P.; Grosch, W. Identification of potent flavor compounds formed in an aqueous lemon oil citric-acid emulsion. *J. Agric. Food Chem.* **1988**, *36*, 797−800.

(13) Chisholm, M. G.; Wilson, M. A.; Gaskey, G. M. Characterization of aroma volatiles in key lime essential oils (*Citrus aurantifolia* Swingle). *Flavour Fragrance J.* **2003**, *18*, 106−115.

(14) Lin, J.; Fay, L. B.; Welti, D. H.; Blank, I. Synthesis of *trans*-4,5-epoxy-(*E*)-2-decenal and its deuterated analog used for the development of a sensitive and selective quantification method based on isotope dilution assay with negative ion chemical ionization. *Lipids* **1999**, *34*, 1117−1126.

(15) Mills, F. D. Synthesis of acetoxydihydromaltol acetate and dihydromaltol. *Carbohydr. Res.* **1972**, *23*, 433−436.

(16) Chen, H.; Chan, K. K.; Budd, T. Pharmacokinetics of *d*-limonene in the rat by GC-MS assay. *J. Pharm. Biomed. Anal.* **1998**, 631−640.

(17) Steinhaus, M.; Fritsch, H.; Schieberle, P. Quantitation of (*R*)- and (*S*)-linalool in beer using solid phase microextraction (SPME) in combination with a stable isotope dilution assay (SIDA). *J. Agric. Food Chem.* **2003**, *51*, 7100−7105.

(18) Rotsatchakul, P.; Chaiseri, S.; Cadwallader, K. R. Identification of characteristic aroma components of Thai fried chili paste. *J. Agric. Food Chem.* **2008**, *56*, 528−536.

(19) Grosch, W. Detection of potent odorants in food by aroma extraction dilution analysis. *Trends Food Sci. Technol.* **1993**, *17*, 142−144.

DOI: 10.1021/jf504852z
J. Agric. Food Chem. 2015, 63, 112−119

(20) Zhou, Q.; Wintersteen, C. L.; Cadwallader, K. R. Identification and quantification of aroma-active components that contribute to the distinct malty flavor of buckwheat honey. *J. Agric. Food Chem.* **2002**, *50*, 2016−2021.
(21) van Den Dool, H.; Kratz, P. D. A generalization of the retention index system including linear temperature programmed gas-liquid partition chromatography. *J. Chromatogr.* **1963**, *11*, 463−471.
(22) ASTM International. Standard practice for determination of odor and taste thresholds by a forced-choice ascending concentration series method of limits. ASTM Standard E679-04, 2004.
(23) Watcharananun, W.; Cadwallader, K. R.; Huangrak, K.; Kim, H.; Lorjaroenphon, Y. Identification of predominant odorants in Thai desserts flavored by smoking with "Tian Op," a traditional Thai scented candle. *J. Agric. Food Chem.* **2009**, *57*, 996−1005.
(24) Freeburg, E. J.; Mistry, B. S.; Reineccius, G. A.; Scire, J. Stability of citral-containing and citralless lemon oils in flavor emulsions and beverages. *Perfum. Flavor.* **1994**, *19*, 23−32.
(25) Veriotti, T.; Sacks, R. High-speed GC and GC/time-of-flight MS of lemon and lime oil samples. *Anal. Chem.* **2001**, *73*, 4395−4402.
(26) Song, H. S.; Phi, N. T. L.; Sawamura, M. Volatile profile of the peel oil of Kiyomi (*Citrus unshiu* Marcov. × *C. sinensis* Osbeck), a new hybrid sweet citrus fruit. *J. Essent. Oil Res.* **2009**, *21*, 26−30.
(27) Choi, H.-S.; Kondo, Y.; Sawamura, M. Characterization of the odor-active volatiles in Citrus Hyuganatsu (*Citrus tamurana* Hort. ex Tanaka). *J. Agric. Food Chem.* **2001**, *49*, 2404−2408.
(28) Pedersen, D. S.; Capone, D. L.; Skouroumounis, G. K.; Pollnitz, A. P.; Sefton, M. A. Quantitative analysis of geraniol, nerol, linalool, and α-terpineol in wine. *Anal. Bioanal. Chem.* **2003**, *375*, 517−522.
(29) Tamura, H.; Yang, R.; Sugisawa, H. Aroma profiles of peel oils of acid citrus. In *Bioactive Volatile Compounds from Plants*; Teranishi, R., Buttery, R. G., Sugisawa, H., Eds.; American Chemical Society: Washington, DC, USA, 1993; pp 121−136.
(30) Gabriele, B.; Fazio, A.; Dugo, P.; Costa, R.; Mondello, L. Essential oil composition of *Citrus medica* L. cv. Diamante (Diamante citron) determined after using different extraction methods. *J. Sep. Sci.* **2009**, *32*, 99−108.
(31) Miyazawa, N.; Tomita, N.; Kurobayashi, Y.; Nakanishi, A.; Ohkubo, Y.; Maeda, T.; Fujita, A. Novel character impact compounds in yuzu (*Citrus junos* Sieb. ex Tanaka) peel oil. *J. Agric. Food Chem.* **2009**, *57*, 1990−1996.
(32) Laska, M.; Teubner, P. Olfactory discrimination ability for homologous series of aliphatic alcohols and aldehydes. *Chem. Senses* **1999**, *24*, 263−270.
(33) Kimura, K.; Nishimura, H.; Iwata, I.; Mizutani, J. Deterioration mechanism of lemon flavor. 2. Formation mechanism of off-odor substances arising from citral. *J. Agric. Food Chem.* **1983**, *31*, 801−804.
(34) Lorjaroenphon, Y.; Hausch, B. J.; Cadwallader, K. R. Formation and stability of 2,3-dehydro-1,8-cineol in a model carbonated beverage system. In *Flavour Science*; Ferreira, V., Lopez, R., Eds.; Elsevier: San Diego, CA, USA, 2014; pp 231−235.
(35) Leimann, F. V.; Goncalves, O. H.; Machado, R. A. F.; Bolzan, A. Antimicrobial activity of microencapsulated lemongrass essential oil and the effect of experimental parameters on microcapsules size and morphology. *Mater. Sci. Eng. C−Biomimetic Supramol. Syst.* **2009**, *29*, 430−436.
(36) Tanaka, A.; Horiuchi, M.; Umano, K.; Shibamoto, T. Antioxidant and anti-inflammatory activities of water distillate and its dichloromethane extract from licorice root (*Glycyrrhiza uralensis*) and chemical composition of dichloromethane extract. *J. Sci. Food Agric.* **2008**, *88*, 1158−1165.
(37) Raal, A.; Arak, E.; Orav, A.; Kailas, T.; Muurisepp, M. Composition of the essential oil of *Levisticum officinale* W.D.J. Koch from some European countries. *J. Essent. Oil Res.* **2008**, *20*, 318−322.
(38) Vekiari, S. A.; Protopapadakis, E. E.; Papadopoulou, P.; Papanicolaou, D.; Panou, C.; Vamvakias, M. Composition and seasonal variation of the essential oil from leaves and peel of a Cretan lemon variety. *J. Agric. Food Chem.* **2002**, *50*, 147−153.
(39) Meijboom, P. W.; Jongenotter, G. A. Flavor perceptibility of straight chain, unsaturated aldehydes as a function of double-bond position and geometry. *J. Am. Oil Chem. Soc.* **1981**, *58*, 680−682.
(40) Njoroge, S. M.; Ukeda, H.; Kusunose, H.; Sawamura, M. Volatile components of Japanese yuzu and lemon oils. *Flavour Fragrance J.* **1994**, *9*, 159−166.
(41) Minh Tu, N. T.; Thanh, L. X.; Une, A.; Ukeda, H.; Sawamura, M. Volatile constituents of Vietnamese pummelo, orange, tangerine and lime peel oils. *Flavour Fragr. J.* **2002**, 169−174.
(42) Blank, I.; Fischer, K.-H.; Grosch, W. Intensive neutral odourants of linden honey: differences from honeys of other botanical origin. *Z. Lebensm.-Unters. Forsch.* **1989**, *189*, 426−433.
(43) Buttery, R. G.; Ling, L. C.; Light, D. M. Tomato leaf volatile aroma components. *J. Agric. Food Chem.* **1987**, *35*, 1039−1042.
(44) Rychlik, M.; Schieberle, P.; Grosch, W. *Compilation of Odor Thresholds, Odor Qualitities and Retention Indices of Key Food Odorants*; Deutsche Forschungsanstalt für Lebensmittelchemie and Institut für Lebensmittelchemie der Technischen Universität München: Garching, Germany, 1998; pp 1−63.
(45) Bicchi, C.; D'Amato, A.; Manzin, V. Cyclodextrin derivatives in the gas chromatographic separation of racemic mixtures of volatile compounds VII. The use of 2,6-di-*O*-methyl-3-*O*-pentyl-β-cyclodextrin diluted in phases with different polarity in the separation of racemates in complex mixtures. *J. Chromatogr., A* **1994**, *666*, 137−146.
(46) Hausch, B. J. Flavor chemistry of lemon-lime carbonated beverages. M.S. thesis, University of Illinois, 2010.
(47) Buttery, R. G.; Turnbaugh, J. G.; Ling, L. C. Contribution of volatiles to rice aroma. *J. Agric. Food Chem.* **1988**, *36*, 1006−1009.
(48) Buttery, R. G. Quantitative and sensory aspects of flavor of tomato and other vegetables and fruits. In *Flavor Science: Sensible Principles and Techniques*; Acree, T. E., Teranishi, R., Eds.; American Chemical Society: Washington, DC, USA, 1993; pp 259−286.
(49) Padrayuttawat, A.; Yoshizawa, T.; Tamura, H.; Tokunaga, T. Optical isomers and odor thresholds of volatile constituents in *Citrus sudachi*. *Food Sci. Technol. Int. Tokyo* **1997**, *3*, 402−408.
(50) Buttery, R. G.; Teranishi, R.; Ling, L. C.; Turnbaugh, J. G. Quantitative and sensory studies on tomato paste volatiles. *J. Agric. Food Chem.* **1990**, *38*, 336−340.
(51) Buttery, R. G.; Black, D. R.; Guadagni, D. G.; Ling, L. C.; Connolly, G.; Teranishi, R. California bay oil. I. Constituents, odor properties. *J. Agric. Food Chem.* **1974**, *22*, 773−777.
(52) Tamura, H.; Fukuda, Y.; Padrayuttawat, A. Characterization of citrus aroma quality by odor threshold values. In *Biotechnology for Improved Foods and Flavors*; American Chemical Society: Washington, DC, USA, 1996; pp 282−294.
(53) Buttery, R. G.; Seifert, R. M.; Guadagni, D. G.; Black, D. R.; Ling, L. Characterization of some volatile constituents of carrots. *J. Agric. Food Chem.* **1968**, *16*, 1009−1015.

DOI: 10.1021/jf504852z
J. Agric. Food Chem. 2015, 63, 112−119

JOURNAL OF AGRICULTURAL AND FOOD CHEMISTRY

Article

pubs.acs.org/JAFC

Preparation and Characterization of a Laboratory Scale Selenomethionine-Enriched Bread. Selenium Bioaccessibility

María Sánchez-Martínez, Teresa Pérez-Corona, Carmen Cámara, and Yolanda Madrid*

Department of Analytical Chemistry, Faculty of Chemical Science, Complutense University of Madrid. Avenida Complutense s/n, 28040, Madrid, Spain

ABSTRACT: This study focuses on the preparation at lab scale of selenomethionine-enriched white and wholemeal bread. Selenium was supplemented either by adding selenite directly to the dough or by using lab-made selenium-enriched yeast. The best results were obtained when using fresh selenium-enriched yeast. The optimum incubation time for selenomethionine-enriched yeast preparation, while keeping formation of selenium byproducts to a minimum, was 96 h. Selenium content measured by isotope dilution analysis (IDA)-ICP-MS in Se-white and Se-wholemeal bread was 1.28 ± 0.02 $\mu g\ g^{-1}$ and 1.16 ± 0.02 $\mu g\ g^{-1}$ (expressed as mean ± SE, 3 replicates), respectively. HPLC postcolumn IDA-ICP-MS measurements revealed that selenomethionine was the main Se species found in Se-enriched bread, which accounted for ca. 80% of total selenium. In vitro gastrointestinal digestion assay provided selenium bioaccessibility values of 100 ± 3% and 40 ± 1% for white and wholemeal Se-enriched bread, respectively, being selenomethionine the main bioaccessible Se species in white bread, while in wholemeal bread this compound was undetectable.

KEYWORDS: *selenium, selenium-enriched bread, yeast, biotransformation, bioaccessibility*

INTRODUCTION

Selenium (Se) is an essential trace element for humans. Supplementation of Se at supranutritional doses, in a population with low selenium status, may help to prevent or reduce different types of tumors,[1] e.g., lung, kidney, pancreas, or prostate cancer. However, the role of selenium in cancer prevention is not well understood yet and should be carefully examined to establish whether supplementation is advisible for treatment or prevention of a specific disease. Se deficiency can affect immune and reproductive systems and thyroid function, and it has been also associated with the occurrence of Keshan and Kaschin−Beck diseases.[2] The recommended dietary allowance (RDA) of this element has not been clearly established yet, because its requirement is highly dependent on several factors such as age, gender, eating patterns, country, etc.[3] The United Kingdom Expert Group on Vitamins and Minerals[4] set the RDA at 60 and 70 μg/day for women and men, respectively, while the Spanish Agency of Food Security and Nutrition[5] set it at 55 μg/day for women and 70 μg/day for men.

In areas where Se concentration in soil is low, its content in cereals and vegetables is also low and consequently the intake by the population is below the RDA.[6,7] With the aim of preventing Se deficiency, two main strategies have been applied: development of Se-enriched foods and agronomic biofortification of crops by using Se-fertilizers. Several Se-enriched food products such as wine,[8] beer,[9] yogurt,[10] or sauerkraut[11] have been developed in recent years. However, biofortification of crops with selenium through foliar and soil application has been the most widely used technique,[12−18] wheat being the main cereal selected when performing this agronomic practice. Although bread intake has decreased in recent years as a result of changing eating patterns,[5,19] it is still the main component of the diet in countries such as Spain, Italy, and Greece[20] and an important source of Se in the United States[21] with selenomethionine (SeMet) as the predominant selenium species.[22,23] Wheat from North America and Canada, with high Se concentrations,[24] was imported to Europe until the mid-1970s,[25] but nowadays, since regional wheat is being used to a higher extent, a decrease of Se intake has been observed among the general population.

Since biofortification is a laborious and expensive process, the aim of this work was to prepare lab-scale Se-enriched breads by using laboratory-made selenized yeast as source of selenium. Evaluation of Se biotransformation and stability of selenium species during baking was carried out by using HPLC postcolumn isotope dilution analysis (IDA)-ICP-MS.[26] Homogeneity studies were also performed to select the most suitable technology for preparing Se-enriched breads with a homogeneous distribution of selenium. Finally, Se bioaccessibility in the resulting Se-enriched white and wholemeal breads was assessed by applying an in vitro digestion assay. The main novelty of the current study involves a rigorous control of all the variables affecting the preparation of Se-enriched bread with the aim of scaling up the process from the laboratory to the industrial or commercial field. The results obtained on selenium bioaccessibility in white and whole bread are also of great interest from the nutritional point of view.

MATERIALS AND METHODS

Chemicals. Chemicals and reagents were of analytical grade, and solutions were prepared with deionized water (18 MΩ cm) from a Milli-Q water purification system unit (Millipore, USA). Stock

Received: March 28, 2014
Revised: December 19, 2014
Accepted: December 19, 2014
Published: January 2, 2015

ACS Publications © 2015 American Chemical Society

DOI: 10.1021/jf505069d
J. Agric. Food Chem. 2015, 63, 120−127

standard solutions of selenomethionine (SeMet), selenomethylselenocysteine (MeSeCys), and selenocystine ($SeCys_2$) purchased from Sigma-Aldrich (Germany) were prepared by dissolving each in 3% hydrochloric acid (37%, Merck, Germany). Inorganic Se solutions were prepared by dissolving sodium selenite (Na_2SeO_3) and selenate (Na_2SeO_4), purchased from Merck (Germany), in 2% HNO_3 (60%, Sharlau, Spain). Stock solutions were stored at 4 °C, and working solutions were prepared daily by dilution. Selenomethionine-Se-oxide (SeMetO) was obtained by oxidation of a SeMet standard using hydrogen peroxide (35%, Panreac, Spain).

Culture medium for yeast growth was "yeast extract peptone dextrose" (YEPD), composed of 1% of yeast extract (Sigma, Germany), 2% glucose (Fluka, Germany), and 2% peptone water (10 mM peptone from Sigma, Germany; 5 M NaCl from Merck, Germany; at pH 7.2).

Acid digestion of samples was carried out with HNO_3 and H_2O_2. For gastrointestinal simulated digestion, α-amilase (Merck, Germany), $NaHCO_3$ (Sigma, Germany), and intestinal solution (consisting of 1.5% of porcine pancreatin from Merck, Germany; 0.15% of biliary salts from Sigma, Germany; and 0.15 M NaCl) and gastric solution (consisting of 6% porcine pepsin from Merck, Germany; 0.15 M NaCl at pH 1.8 adjusted with 2 M HCl) were used.

Enzymatic hydrolysis was performed by using a nonspecific enzyme, protease XIV, from *Streptomyces griseus* (Sigma, Germany). Tris-HCl solution was prepared with Trizma base (Fluka, Germany) dissolved in water, and the pH was adjusted to 7.5 with HCl.

The ^{77}Se-enriched standard (Cambridge Isotope Laboratories, USA) was purchased as a powder, dissolved in a minimum volume of sub-boiled HCl, and diluted to the corresponding final volume with Milli-Q water. The resulting ^{77}Se-enriched solution was used for quantifying total Se and Se-species concentration.

Selenium species separation by anionic-exchange chromatography was achieved by using 10 mM citric acid (Sigma, Germany) in 2% MeOH (99.9%, Scharlau, Spain) adjusted to pH 5 with ammonium hydroxide (Fluka, Germany) as the mobile phase. The mobile phase used for reversed-phase chromatography was 0.1% trifluoroacetic acid, TFA (Sigma-Aldrich, Germany), in 2% MeOH. The mobile phase employed for size exclusion chromatography (SEC) was 50 mM Tris-HCl and 0.05 mM KCl (Fluka, Germany) at pH 6.8.

The ingredients (white flour, whole-meal flour, and yeast) for baking were purchased from a traditional bakery in Madrid, Spain. Se-enriched yeast certified reference material (CRM) SELM-1 (NRCC, Canada) was used to validate the method.

Instrumentation. For bread-making, dough was fermented in an incubator (Heraeus D-6450, Germany) followed by baking in a thermostatic oven (Digitronic, JP Selecta, Spain). Yeast selenization was performed in an Optic Ivymen System provided with a constant temperature incubator shaker (Comecta S.A., Spain). For homogeneity studies ingredients were mixed in a V-shaped laboratory mixer with dimensions of 415 × 400 × 415 mm (Venus FTLMV, Filtra, Spain).

For total selenium analysis, samples were digested in an analytical microwave oven (CEM, Matthews, USA). For the selenium species extraction, enzymatic hydrolysis was performed by using a Sonoplus ultrasonic homogenizer (Bandenlin, Germany) fitted with a titanium 3 mm diameter microtip and a GM200 HF generator. Extracts from enzymatic hydrolysis were centrifuged in an Eppendorf centrifuge 5804 R F34-6-38 (Germany).

Elemental detection was carried out by using an ICP-MS (Agilent HP-7700 series, USA) equipped with an octopole reaction cell for monitoring ^{76}Se, ^{77}Se, ^{78}Se, ^{79}Br, ^{80}Se, ^{81}Br, ^{82}Se and ^{83}Kr isotopes. Argon-based polyatomic interferences were reduced using H_2 as cell gas at an optimized flow rate of 4.5 mL min^{-1}. A commercial Meinhard nebulizer was used as sample introduction system device for the ICP-MS

Chromatographic separation was performed with a high-pressure pump (Jasco PU-2089, Italy) fitted with a six-port sample injection valve (Rheodyne 7725i, Rohnert Park, CA, USA) with a 100 μL loop. Different columns were coupled to ICP-MS for selenium speciation analysis: anionic exchange PRP-X100 (250 × 4.1 mm, 10 μm) (Hamilton, Switzerland); reversed-phase ion pairing C8 Zorbax R_x-C_8 (250 × 3.0 mm, 5 μm) (Agilent, USA); and SEC BioBasic-Sep 60 from 0.1 to 6 kDa (300 × 7.8 mm, 5 μm) (Thermo Fisher, Spain).

Methods. *Preparation of Se-Enriched Bread.* Bread pieces of around 3 × 3 × 3 cm were prepared. For that purpose, 5.00 g of wheat flour (with 13% moisture content and 10.3% of protein) or wholemeal flour (with 11% moisture content and 9.6% of protein), 0.10 g of sodium chloride, yeast (0.15 g of fresh yeast or 0.05 g of lyophilized yeast), and 2.5 mL of deionized water were used, as described in the literature.[13,27] With the aim of preparing bread with approximately 1 μg g^{-1} of Se, 5 μg of selenium was added. Selenium was supplemented either by adding selenite directly to the dough or by using lab-made Se-enriched yeast. The dough was first mechanically mixed during 5 min and then hand-kneaded during five more minutes. Parameters such as temperature and time of fermentation for dough rising and baking were optimized; the optimal conditions were 20 min of dough fermentation at 30 °C in an incubator, followed by baking at 200 °C during 25 min in a thermostatic oven. When using selenite for baking, selenium was incorporated into the water and mixed with all the ingredients. In this case, fermentation times from 20 min to 24 h were assayed in order to allow the complete transformation of selenium by yeast. Once the baking process was finished, bread was cooled at room temperature. Se-enriched bread was lyophilized, minced, and kept at −80 °C until analysis. Control bread was prepared similarly to Se-enriched bread but without adding Se.

Saccharomyces cerevisiae was growth in an incubator shaker under sterile conditions and by using a volume of 2.5 mL of YEPD and 5 μg of sodium selenite at 28 °C Different incubation times (16, 17, 96 h) were tested with the aim of achieving the highest yield of the selenization process.[8,28,29]

Total Se Determination by IDA-ICP-MS. Total Se content in the samples was determined by IDA-ICP-MS. For this purpose, an appropriate amount of ^{77}Se spike solution, 1.00 mL of nitric acid, and 0.25 mL of hydrogen peroxide were added to 0.15 g of yeast and 0.10 g of bread, dough, or flour. Afterward samples were digested in an analytical microwave oven at 130 °C for 15 min with a ramp temperature of 10 min, following the conditions described elsewhere.[30] The resulting solutions were diluted to 10.00 mL with Milli-Q water, and measurements were performed by IDA-ICP-MS

To apply IDA-ICP-MS, isotope intensities were corrected by using a detector dead time of 30 ns. The interferences caused by SeH^+ were corrected with a Se factor (f_{Se}) ranging between 2.2 and 2.4% of the Se signal, which is in agreement with data reported by other authors.[31,32] Next, mass bias in ^{78}Se/^{77}Se and ^{80}Se/^{77}Se isotope ratio was corrected by the exponential model.[32] Mass bias discrimination was computed every five analyses, and a mass bias factor (K) of ca. −4% per mass unit, similar to those reported before,[14,31] was obtained. Se concentration was calculated using the IDA equation described by García-Alonso et al.[26]

Determination of Se Species by HPLC Coupled to Postcolumn IDA-ICP-MS. Se speciation in the proteolytic extracts of the raw ingredients and baking products was carried out by HPLC-IDA-ICP-MS by using species-unspecific mode. Selenium species were extracted by means of applying enzymatic hydrolysis by adding 30 mg of protease XIV and 3.0 mL of 30 mM Tris-HCl solution (pH 7.5) to 0.15 g of yeast and 0.10 g of bread, dough, or flour. The resulting extracts were centrifuged for 20 min at 10000 rpm, and supernatants were filtered through a 0.22 μm nylon filter. A comparative study of Se-species extraction methodologies was performed by using microwave-assisted extraction (MAE) (37 °C, 30 min), incubation in a thermostatic bath (37 °C, 24 h), and ultrasonic probe sonication (37 °C, 2 min). In addition, acid hydrolysis with diluted HCl was used as an alternative to enzymatic hydrolysis.[33] Different chromatographic separation mechanisms, anionic exchange PRP-X100, reversed-phase ion pairing C8 Zorbax R_x-C_8, and SEC BioBasic-Sep 60 from 0.1 to 6 kDa were used for performing Se speciation. Identification of Se species was achieved by matching retention times and by spiking experiments. The analytical methodology used was validated by analyzing a reference material certified for SeMet (SELM-1).

DOI: 10.1021/jf505069d
J. Agric. Food Chem. 2015, 63, 120−127

Table 1. Total Se and SeMet Content in Raw Ingredients and Baked Products[a]

	total Se (μg of Se/g d.m.)	extracted Se (μg of Se/g d.m.)	% recovery	SeMet (μg of Se/g d.m.)	% recovery
control					
white wheat flour	0.28 ± 0.01	0.26 ± 0.02	93 ± 1	0.22 ± 0.01	84 ± 3
white dough	0.28 ± 0.02	0.28 ± 0.02	100 ± 2	0.23 ± 0.02	83 ± 3
white bread	0.28 ± 0.03	0.28 ± 0.02	102 ± 2	0.22 ± 0.01	80 ± 4
whole meal flour	0.10 ± 0.01	0.10 ± 0.01	100 ± 2	<LOD	<LOD
wholemeal bread	0.10 ± 0.01	0.10 ± 0.01	100 ± 2	<LOD	<LOD
Se-enriched					
fresh yeast	34.0 ± 0.1	35.0 ± 0.1	103 ± 5	24.1 ± 0.1	71 ± 2
dried yeast	28.0 ± 0.1	9.52 ± 0.05	34 ± 4	6.47 ± 0.03	68 ± 1
white dough[b]	1.29 ± 0.03	1.29 ± 0.06	100 ± 5	0.95 ± 0.03	74 ± 3
white bread[b]	1.28 ± 0.02	1.29 ± 0.02	101 ± 2	1.04 ± 0.02	81 ± 3
wholemeal bread[b]	1.16 ± 0.02	1.10 ± 0.02	95 ± 2	0.86 ± 0.05	78 ± 4

[a]Mean ± SE/ $N = 3$ replicates. LOD determined by analyzing ten solutions of the lowest point of calibration ($N = 3$), calculated from 3σ of the signal, and then referred to the regression line. [b]Samples were prepared by dosing selenium as selenized fresh yeast.

Extraction efficiency was calculated as the amount of selenium extracted relative to the total selenium concentration obtained after acid digestion. Blank analysis was also performed for estimating the occurrence of selenocompounds in the protease used for performing enzymatic hydrolysis.

Quantification of Se species was carried out by postcolumn IDA-ICP-MS. For this purpose, a ^{77}Se-enriched standard solution of the appropriate known concentration was added, at a constant rate (0.1 mL min^{-1}), through a T piece placed at the end of the column; afterward the resulting mixture was nebulized into the plasma for ICP-MS measurements. The conventional intensity chromatograms (counts s^{-1}) were converted into mass flow chromatograms (ng min^{-1}) by applying the online isotope dilution equation. Peak area measurements were performed to obtain the amount of Se.

In Vitro Gastrointestinal Digestion Assay. The in vitro gastrointestinal digestion method employed was based on that described by Luten et al.[34] Briefly, approximately 1.00 g of the dried sample and 5.0 mL of water containing 5 mg of α-amylase were mixed by shaking for 1 min and incubated for 15 min at 37 °C. Next, 3.0 mL of gastric juice (see Chemicals) was added, and the resulting mixture was shaken for 1 min before incubation at 37 °C for 4 h. Subsequently, the pH was adjusted to 6.8 with saturated sodium bicarbonate to stop the gastric process. After that, 2.0 mL of intestinal juice (see Chemicals) was added, and the mixture was energetically shaken for 1 min and left at 37 °C for 4 h, with periodical stirring. Then, samples were centrifuged at 6000 rpm for 30 min at 4 °C. The supernatant was filtered through a 0.22 μm nylon filter and was kept at 4 °C until analysis. Blanks of gastrointestinal digestion were prepared in parallel.

Se Homogeneity in the Bread Rolls. The homogeneous distribution of Se in bread was assessed by simulating an industrial baking process. For that purpose, dough of 100.0 g of wheat flour, 2.0 g of NaCl, 50.0 mL of distilled water, and 3.0 g of selenized fresh yeast was prepared, and then it was divided into 20 pieces of approximately 5.0 g each. The ingredients used to prepare the dough were mixed both by hand kneading and by mechanical mixing in a V-shaped laboratory mixer to compare selenium distribution in terms of homogeneity. Total Se concentration was determined in each piece (3 replicates for each) by using ICP-MS following the above-mentioned procedure.

RESULTS AND DISCUSSION

Method Validation. Detection (LOD) and quantification limits (LOQ) were determined by analyzing, in triplicate, ten solutions of the lowest point of calibration. They were calculated from 3σ and 10σ, respectively, of the signal and then referred to the regression line. Reproducibility was calculated as % RSD (relative standard deviation) from five measurements of two independent standard solutions of 20 and 100 μg L^{-1} of Se(IV), carried out on three nonconsecutive days. A LOD and LOQ of 0.001 μg L^{-1} and 0.004 μg L$^{-1,}$ respectively, were achieved for total selenium for ICP-MS. For SeMet, LOD was 0.7 μg L^{-1} and LOQ was 2.2 μg L^{-1}. Precision was determined in terms of repeatability and reproducibility, which were better than 2% RSD for ICP-MS.

The analytical methodology used was validated by analyzing a reference material certified for SeMet (SELM-1). Since at 95% confidence no significant differences were observed between the certified value (3448 ± 146 mg kg^{1-}) and the experimental value (3215 ± 122 mg kg^{1-}), the method was considered accurate for performing speciation.

Selenium Accumulation and Biotransformation during Baking. With the aim of optimizing baking conditions, ingredients were mixed at different ratios and were kneaded until elastic doughs were attained. In addition, different times of fermentation (from 15 min to 24 h) at a temperature of 30 °C were tested. Different baking times (from 5 to 30 min) and temperatures (from 180 to 200 °C) were also assayed in order to achieve a browned crust and spongy crumb, avoiding overbaking. All conditions were optimized in terms of obtaining breads with taste, flavor, texture, and color appropriate for human consumption. As a result, 20 min of dough fermentation at 30 °C, followed by baking at 200 °C for 25 min, was selected as optimal conditions for baking.

ICP-MS methodology was employed to determine total selenium concentration in flour (wheat flour or wholemeal flour), yeast (fresh and lyophilized), and bread samples. The results are shown in Table 1. Se levels in control white and wholemeal bread were 0.28 ± 0.03 μg g^{-1} and 0.10 ± 0.01 μg g^{-1}, respectively. Se content in the yeast used for baking was negligible, which means that Se found in control samples comes from the flour used for baking. Data in Table 1 also suggest that selenium remains unaltered under the high temperature conditions used during baking, as has been pointed out by other authors.[13,35] Se levels were clearly higher in control white bread than in control wholemeal bread. However, studies from biofortification of crops by using Se-rich fertilizers have reported lower Se content in white flour than in wholemeal flour because selenium is preferentially accumulated in embryo,[36] which is partially lost during milling. However, the provenance of the flour (wholemeal and white) used in this work cannot be assigned to the same wheat since they were purchased in a local store. Therefore, differences in Se levels between white and wholemeal control breads cannot be linked to a single factor. Wholemeal and white bread enriched with 1

DOI: 10.1021/jf505069d
J. Agric. Food Chem. 2015, 63, 120−127

μg of Se g^{-1}, as Se-enriched yeast, contained 1.16 ± 0.02 and 1.28 ± 0.02 μg g^{-1} of Se, respectively. Considering the concentration of Se present in control bread, the recovery of the added Se was over 99%. Similar results were obtained when selenium was directly added as selenite. Thus, it can be assumed that selenium was incorporated into the bread regardless of the method of supplementation used (either by adding selenite directly to the dough or by using a Se-enriched yeast for rising the dough).

Determination and quantification of Se species in the proteolytic extracts was performed by HPLC coupled to postcolumn IDA-ICP-MS. The extraction of Se species in food samples is usually carried out by enzymatic hydrolysis using protease XIV.[8,9,31,37] Conventionally enzymatic hydrolysis required incubation times of 17−24 h.[8,31,37,38] In recent years, the use of ultrasound and microwave energy[11,31,39] has been proposed as alternative methods to speed up sample treatment procedures.

In the present work, Se-species extraction in Se-enriched bread was carried out with and without enzymes. The extraction of species without enzymes resulted in low recovery values: only 17 ± 1% of the total Se was extracted while quantitative extraction (101 ± 2%) was achieved by using enzymatic hydrolysis with protease in Tris-HCl. In order to speed up the sample treatment process, ultrasonic probe sonication (USP) and microwave assisted extraction (MAE) were used. Regarding the amount of Se extracted, no significant differences were observed between the use of MAE (103 ± 3%), incubation (101 ± 2%), and USP (105 ± 3%). However, the methodology based on the use of ultrasonic probe was chosen for further experiments because it significantly reduces the extraction time (2 min in comparison with 30 min and 24 h for MAE and incubation, respectively). As a result, enzymatic hydrolysis with protease XIV in 30 mM Tris-HCl buffer by USP was chosen to perform Se extraction from both raw ingredients and baking products.

Figure 1 shows that SeMet is the main Se species detected in bread samples by LC-ICP-MS, using both anionic exchange and reversed-phase separation columns. Due to the lack of Se-labeled standards, quantification of the Se species was performed by using postcolumn IDA-ICP-MS, by means of continuous mixing of ^{77}Se spike solution with the effluent coming out of the column. SeMet concentration in Se-enriched white and wholemeal bread represents around 80% of total Se level present in the sample. On the other hand, the similarity between SeMet values obtained in Se-enriched bread and in the Se-enriched white dough (Table 1) indicates that SeMet integrity is not affected by baking. This finding is in agreement with data reported by Hart et al.[13] Contrarily, Warburton and Goenaga-Infante[22] observed a decrease in SeMet content after bread processing and production, although this could be due to differences in the recipe used for baking.

Despite the good results obtained using protease, the presence of Se species in the enzyme[40] employed to extract Se compounds may have a negative impact on the detection limit, and therefore, special control of the blanks is required. The use of acid hydrolysis as an alternative to enzymatic hydrolysis[33] was tested by using incubation bath, USP, and MAE; unfortunately only ca. 7% of the total Se content was extracted. The success of acid hydrolysis in releasing selenoamino acids is highly dependent on the sample matrix. D'Ulivo[41] reported that SeMet and SeCys standards were broken down and remained stable up to 22 h, whereas the

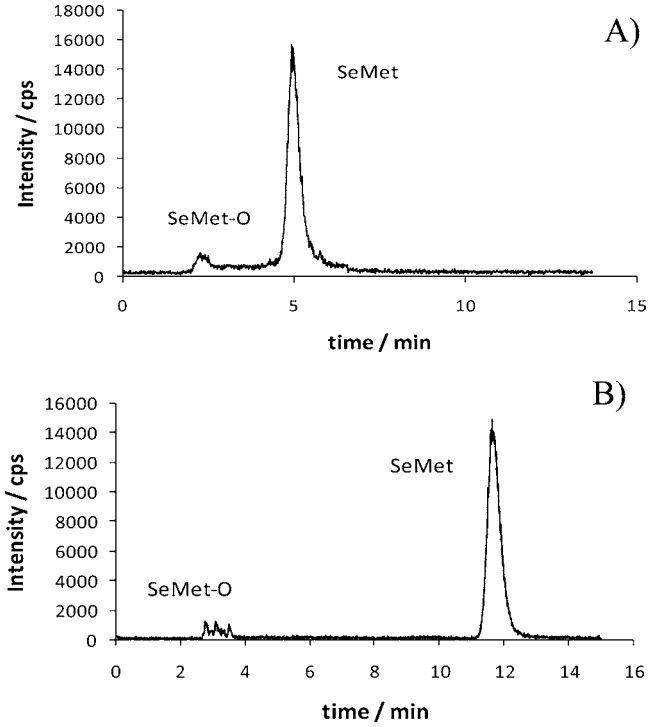

Figure 1. Typical chromatograms of Se-enriched bread prepared using Se-yeast after enzymatic hydrolysis achieved at m/z 78 by (A) anionic exchange PRP-X100 column and (B) reversed-phase C8 Zorbax column, coupled to ICP-MS.

extraction efficiency observed by Montes-Bayón et al.[42] for SeMet in *Brassica juncea* was very low. Acid hydrolysis is a harsh treatment that can lead to degradation of Se species or to some matrix degradation, which can hinder the determination of the species of interest. Therefore, since acid hydrolysis did not provide a reasonable recovery of SeMet, the optimized enzymatic hydrolysis was selected for all the experiments. However, protease blank analysis was always performed because selenium level in the enzyme could vary between batches.

The supplementation of Se for making Se-enriched bread was achieved either by adding selenite directly to the dough or by using laboratory-made selenized yeast. When dosing selenite directly to the dough, Se was quantitatively incorporated into the bread; however, the content of SeMet found was similar to that present in the flour (Table 1). The low amount of SeMet found could be attributed to an incomplete transformation of selenite into SeMet during fermentation. As was evidenced by size exclusion chromatography-ICP-MS (Figure 2), Se was biotransformed into low molecular weight (<5 kDa) Se species, which were not detected when using anion exchange or reversed-phase HPLC-ICP-MS. The results obtained are in disagreement with those published by other authors. Lazo-Vélez et al.[43] reported a complete transformation of selenite into selenomethionine when adding selenite directly. The differences could be explained by differences in the baking process used. Lazo-Velez et al. include sugar as an ingredient, which may help yeast to grow and, therefore, improve the biotransformation of selenium.

Se-enriched bread was successfully obtained by using selenized yeast, which was made in the lab following the protocol described in Methods. Selenized yeast preparation requires a careful control of experimental conditions[44]

DOI: 10.1021/jf505069d
J. Agric. Food Chem. 2015, 63, 120−127

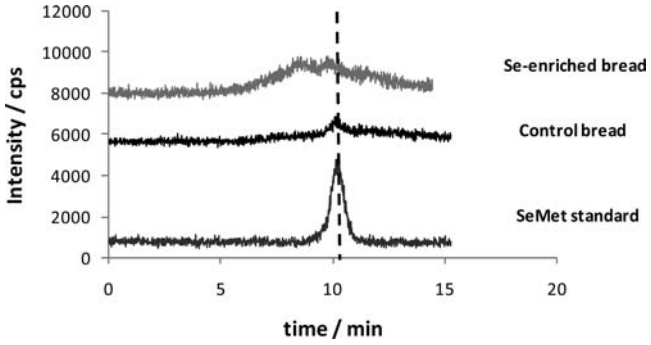

Figure 2. Size exclusion chromatograms achieved at m/z 78 by using BioBacic-Sep 60 column after enzymatic hydrolysis of control and Se-enriched bread obtained by direct addition of Se in the dough before kneading.

(temperature control, stirring, ventilation, and incubation time) to ensure that SeMet is the primary selenium species produced. In this study, selenized yeast (*Saccharomyces cerevisiae*) was prepared in YEPD culture medium in the presence of 5 μg of selenite. The resulting selenium species were monitored by HPLC-ICP-MS over 96 h of incubation (at 3 different time points, 12, 24, and 96 h). After 96 h, selenomethionine accounted for approximately 70% of the added Se (Table 1). A typical anion exchange-ICP-MS chromatogram of Se-enriched yeast at different incubation times is shown in Figure 3.

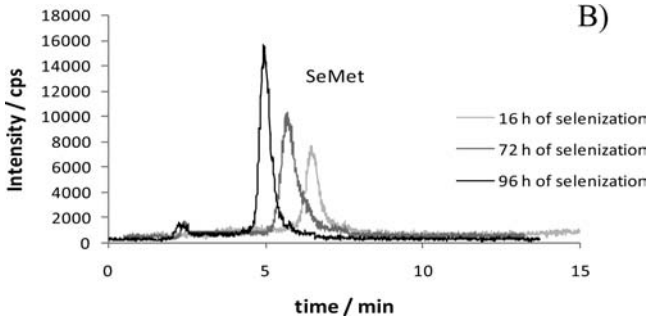

Figure 3. HPLC-ICP-MS chromatogram achieved at m/z 78 by anionic exchange column of Se-enriched yeast produced under controlled conditions of temperature (28 °C), stirring (280 rpm), and different times of incubation (16, 72, and 96 h).

During the experiments, it was observed that the use of fresh baker's yeast after it has been stored for 2 weeks leads to problems associated with variations in flavor, odor, and rate of fermentation, originating bread with bad flavor. It is well-known that one of the most satisfactory methods for preserving yeast is the use of dried yeast. So, in the current work the preparation of Se-enriched yeast was also performed by using dried yeast commercially available. Thus, dried yeast, acquired from a local market, was rehydrated and then cultured in the presence of 5 μg of selenite (in order to have 1 μg g^{-1} in the resulting bread) following the procedure already described when using fresh yeast. Analysis of total Se concentration in the resulting selenized yeast provided concentration values accounting for 103% and 34% of the added Se, when using fresh and dried yeast, respectively (Table 1). Either dried or fresh yeast is able to accumulate and biotransform selenium; however, fresh yeast accumulates higher amounts of Se than dried yeast. Therefore, we decided to prepare Se-enriched bread by using fresh yeast but keeping in mind that it should not be stored longer than 2 weeks. With the aim of overcoming this difficulty, one approach to be tested in the future could be to grow the yeast under the selected conditions to get SeMet, and then drying and using it like normal dry yeast.

From results obtained, selenium was added to the dough through the yeast, which is about 3% of the total weight of bread; therefore a homogeneous distribution of this ingredient is crucial to get selenium uniformly distributed in the resulting bread. Common baking practices consist of preparing the dough and then dividing it into small dough rolls. With the aim of scaling up the process from the lab scale to the pilot scale, dough preparation was carried out by mixing the ingredients either by hand (for up to 20 min) or mechanically (first mechanically mixed during 5 min and then hand-kneaded during five more minutes) following the procedure described in Methods. The resulting dough was divided into 20 pieces of approximately 5 g each and baked. The resulting bread pieces underwent microwave assisted acid digestion for Se concentration determination by IDA-ICP-MS. Figure 4 illustrates that the distribution of Se in the resulting pieces prepared by hand kneading is less homogeneous, and therefore, it provides higher standard deviation values than those prepared by mechanical mixing of the ingredients.

Bioaccessibility of Se in Se-Enriched Bread and Estimated Human Intake. Results from in vitro simulated gastrointestinal digestion of Se-enriched bread (white and

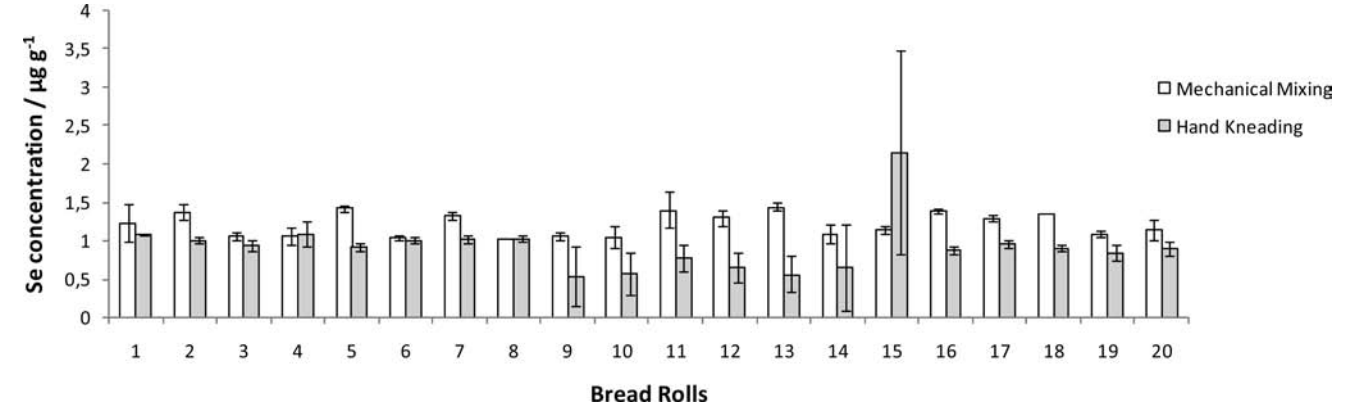

Figure 4. Selenium distribution in Se-enriched bread prepared with Se-yeast and combining the ingredients by hand kneading versus mechanical mixing. Results are given as mean ± SE (N = 3 replicates).

DOI: 10.1021/jf505069d
J. Agric. Food Chem. 2015, 63, 120−127

Table 2. Total Selenium and SeMet Concentrations in Gastric and Gastrointestinal-Simulated Extracts[a]

	digestion (μg/g d.m.)			
	gastric		gastrointestinal	
	Se	SeMet	Se	SeMet
control white bread	0.21 ± 0.02	<LOD	0.25 ± 0.01	<LOD
Se-enriched white bread[b]	0.89 ± 0.01	0.85 ± 0.03	1.25 ± 0.02	1.21 ± 0.02
control wholemeal bread	0.04 ± 0.01	<LOD	0.04 ± 0.01	<LOD
Se-enriched wholemeal bread[b]	0.44 ± 0.01	<LOD	0.42 ± 0.01	<LOD

[a]Mean ± SE. $N = 3$ replicates. LOD determined by analyzing ten solutions of the lowest point of calibration ($N = 3$), calculated from 3σ of the signal, and then referred to the regression line. [b]Samples were prepared by dosing selenium as selenized fresh yeast.

wholemeal) are shown in Table 2. Soluble Se fractions after simulated gastric and gastrointestinal digestion in Se-enriched white bread were 75% and 89% of total Se, respectively, whereas in Se-enriched wholemeal bread the amount of extracted Se was much lower (ca. 40%). Selenium species in the bioaccessible fractions were determined by HPLC-IDA-ICP-MS (Table 2). SeMet was the main selenium species found in the bioaccessible fraction of Se-enriched white bread. Se species in the bioaccessible fraction of Se-wholemeal bread were below the LOD. Differences in Se bioaccessibility between white and wholemeal bread could be attributed to the presence of dietary fiber, an unavailable carbohydrate[17] present in higher amounts in wholemeal than in white bread. High contents of fiber can lower both protein and starch digestibility[45] and, therefore, decrease the capability of enzymes to release Se from those compounds. These results highlight the low bioaccessibility of SeMet found in whole bread, which is of interest from the nutritional point of view because of the relatively high consumption of whole wheat products.

Based on these results, an estimation of Se intake was carried out. A daily consumption of approximately 60 g of Se-enriched white bread, following the Guidelines for Healthy Nutrition,[46] would provide 70 μg of Se per day, which is within the recommended range (RDA is 55−70 μg day^{-1}), although the amount of selenium supplied by other food sources should be also taken into consideration. However, according to the World Health Organization,[47] an intake of 400 μg day^{-1} is considered safe.

To the best of our knowledge, this is the first time that homogeneous Se-enriched bread is obtained by using selenized fresh yeast, with good recoveries of SeMet. The simple, cheap, and fast procedure used could be considered as an alternative to the more expensive and more extended procedure of agronomic biofortification of crops using Se-fertilizers. A scale-up development for Se-enriched bread is also proposed. Almost all (99%) of the added Se by using selenized fresh yeast was incorporated in the bread with SeMet accounting for 80% of total Se. Se-enriched bread, with SeMet as the main species, can be a suitable source of this element for people with Se deficiency. The bioaccessibility of selenium in Se-enriched bread was 100 ± 3% and 40 ± 1% for white and wholemeal bread, respectively.

AUTHOR INFORMATION

Corresponding Author

*E-mail: ymadrid@ucm.es. Phone: 34 91 3945145. Fax: 34 91 3944321.

Funding

The Complutense University Group of Trace and Speciation Analysis would like to thank the Spanish Commission of Science and Technology (CTQ2011-22732), the Community of Madrid, (Spain), and the European Community for funding the FEDER program (S2013/ABI-3028, AVANSECAL-CM). M.S.-M. would also like to thank the Spanish Government for her doctoral fellowship (CTQ2008-05925).

Notes

The authors declare no competing financial interest.

REFERENCES

(1) Jackson, M. I.; Combs, G. F., Jr. Selenium and anticarcinogenesis: underlying mechanisms. *Curr. Opin. Clin. Nutr. Metab. Care* **2008**, *11* (6), 718−726.

(2) Rayman, M. P. The importance of selenium to human health. *Lancet* **2000**, *356* (9225), 233−241.

(3) Rayman, M. P. The use of high-selenium yeast to raise selenium status: how does it measure up? *Br. J. Nutr.* **2004**, *92* (4), 557−573.

(4) UK EGVM (United Kingdom Expert Group on Vitamins and Minerals). *Revised review of selenium (EVM/99/17.REVISE-DAUG2002)*; UK EGVM: United Kingdom, 2002.

(5) AESAN (Spanish Agency of Food Security and Nutrition). *Nutritional evaluation of Spanish diet II. Micronutrients. National Survey of Dietetic Intake (ENIDE)*; Ministry of Health: Spain, 2001.

(6) Dumont, E.; Vanhaeck, F.; Cornelis, R. Selenium speciation from food source to metabolites: a critical review. *Anal. Bioanal. Chem.* **2006**, *385* (7), 1304−1323.

(7) Combs, G. F. Selenium in global foods systems. *Br. J. Nutr.* **2001**, *85* (5), 517−547.

(8) Pérez-Corona, M. T.; Sánchez-Martínez, M.; Valderrama, M. J.; Rodríguez, M. E.; Cámara, C.; Madrid, Y. Selenium biotransformation by *Saccharomyces cerevisiae* and *Saccharomyces bayanus* during white wine manufacture: Laboratory-scale experiments. *Food Chem.* **2011**, *124* (3), 1050−1055.

(9) Sánchez-Martínez, M.; Galvao, P.; da Silva, E.; Pérez-Corona, T.; Cámara, C.; Ferreira, S. L. C.; Madrid, Y. Selenite biotransformation during brewing. Evaluation by HPLC-ICP-MS. *Talanta* **2012**, *88*, 272−276.

(10) Alzate, A.; Fernández-Fernández, A.; Pérez-Conde, C.; Gutiérrez, A. M.; Cámara, C. Comparison of biotransformation of inorganic selenium by *Lactobacillus* and *Saccharomyces* in lactic fermentation process of yogurt and kefir. *J. Agric. Food Chem.* **2008**, *56* (18), 8728−8736.

(11) Peñas, E.; Martínez-Villaluenga, C.; Frías, J.; Sánchez-Martínez, M. J.; Pérez-Corona, M. T.; Madrid, Y.; Cámara, C.; Vidal-Valverde, C. Se improves indole glucosinolate hydrolysis products content, Se-methylselenocysteine content, antioxidant capacity and potential anti-inflammatory properties of sauerkraut. *Food Chem.* **2012**, *132* (2), 907−914.

(12) Galinha, C.; Freitas, M. C.; Pacheco, A. M. G.; Countinho, J.; Maças, B.; Almeida, A. S. Determination of selenium in bread-wheat samples grown under a Se-supplementation regime in actual field conditions. *J. Radioanal. Nucl. Chem.* **2012**, *291* (1), 231−235.

(13) Hart, D. J.; Fairweather-Tait, S. J.; Broadley, M. R.; Dickinson, S. J.; Foot, I.; Knott, P.; McGrath, S. P.; Mowat, H.; Norman, K.; Scott, P. R.; Stroud, J. L.; Tucker, M.; White, P. J.; Zhao, F. J.; Hurst, R.

DOI: 10.1021/jf505069d
J. Agric. Food Chem. 2015, 63, 120−127

Selenium concentration and speciation in biofortified flour and bread: Retention of selenium during grain biofortification, processing and production of Se-enriched food. *Food Chem.* **2011**, *126* (4), 1771−1778.
(14) Kirby, J. K.; Lyons, G. H.; Karkkainen, M. P. Selenium speciation and bioavailability in biofortified products using species-unspecific isotope dilution and revered phase ion pairing-inductively coupled plasma-mass spectrometry. *J. Agric. Food Chem.* **2008**, *56* (5), 1772−1779.
(15) Bryszewska, M. A.; Ambroziak, W.; Diowksz, A.; Baxter, M. J.; Langford, N. J.; Lewis, D. J. Changes in the chemical form of selenium observed during the manufacture of a selenium-enriched sourdough bread for use in a human nutrition study. *Food Addit. Contam.* **2005**, *22* (2), 135−140.
(16) Welch, R. M.; Graham, R. D. Agriculture: the real nexus for enhancing bioavailable micronutrients in food crops. *J. Trace Elem. Med. Biol.* **2005**, *18* (4), 299−307.
(17) Dewettinck, K.; Van Bockstaele, F.; Kühne, B.; Van de Walle, D.; Courtens, T. M.; Gellynck, X. Nutritional value of bread: Influence of processing, food interaction and consumer perception. *J. Cereal Sci.* **2008**, *48* (2), 243−257.
(18) Zhao, F.; López-Bellido, F. J.; Gray, C. W.; Whalley, W. R.; Clark, L. J.; McGrath, S. P. Effects of soil compaction and irrigation on the concentrations of selenium and arsenic in wheat grains. *Sci. Total Environ.* **2007**, *372* (2−3), 433−439.
(19) Siega-Riz, A. M.; Popkin, B. M.; Carson, T. Differences in food patterns at breakfast by sociodemographic characteristics among a nationally representative sample of adults in the United States. *Prev. Med.* **2000**, *30* (5), 415−424.
(20) González-Turmo, I. The Mediterranean diet: Consumption, cuisine and food habits. In *Mediterra. The Mediterranean diet for sustainable regional development*; Mombiela, F., Ed.; Presses de Sciences Po: Paris, 2012; pp 115−132.
(21) Barret, J.; Patterson, C.; Reilly, C.; Tinggi, U. Selenium in the diet of children with phenylketonuria. In *Nutrient Availability: Chemical and Biological Aspects*; Southgate, D. A. T., Johnson, I. T., Fenwick, G. F., Eds.; Royal Society of Chemistry: London, U.K., 1989; pp 281−283.
(22) Warburton, E.; Goenaga-Infante, H. Methane mixed plasma-improved sensitivity of inductively coupled plasma mass spectrometry detection for selenium speciation analysis wheat-based food. *J. Anal. At. Spectrom.* **2007**, *22*, 370−376.
(23) Cubadda, F.; Aureli, F.; Ciardullo, S.; D'Amato, M.; Raggi, A.; Acharya, R.; Reddy, R. A. V.; Prakash, N. T. Changes in selenium speciation associated with increasing tissue concentrations of selenium in wheat grain. *J. Agric. Food Chem.* **2010**, *58* (4), 2295−2301.
(24) Gerrior, S.; Bente, L.; Hiza, H. *Nutrient content of the US food supply, 1909−2000*; Department of Agriculture, Center for Nutrition Policy and Promotion: US, 2004.
(25) MacPherson, A.; Barclay, M. N. I..; Scott, R.; Yates, R. W. S. Loss of Canadian wheat imports lowers selenium intake and status of Scottish population. In *Trace Elements in Man and Animals*; Fischer, P. W. F., L'Abbé, M. R., Cockell, K. A., Gibson, R. S., Eds.; NCR Press: Ottawa, Canada, 1997; pp 203−205.
(26) García-Alonso, J. I.; Rodríguez, P. La dilución isotópica en el análisis de trazas. In *Análisis químico de trazas*; Cámara, C., Pérez-Conde, C., Eds.; Editorial Síntesis S.A.: Spain, 2001; pp 223−278.
(27) Rosell, C. M.; Santos, E.; Sanz-Penella, J. M.; Haros, M. Wholemeal wheat bread: A comparison of different breadmaking processes and fungal phytase addition. *J. Cereal Sci.* **2009**, *50* (2), 272−277.
(28) Martínez-Sierra, J. G.; Moreno-Sanz, F.; Herrero-Espílez, P.; Marchante-Gayón, J. M.; García-Alonso, J. I. Biosynthesis of sulfur-34 labelled yeast and its characterisation by multicollector-ICP-MS. *J. Anal. At. Spectrom.* **2007**, *22*, 1105−1112.
(29) Ponce de León, C. A.; Bayón, M. M.; Paquin, C.; Caruso, J. A. Selenium incorporation into *Saccharomyces cerevisiae* cells: a study of different incorporation methods. *J. Appl. Microbiol.* **2002**, *92* (4), 602−610.
(30) Cabañero, A. I.; Madrid, Y.; Cámara, C. Selenium and mercury bioaccessibility in fish samples: an in vitro digestion method. *Anal. Chim. Acta* **2004**, *526* (1), 51−61.
(31) Pedrero, Z.; Ruiz−Encinar, J.; Madrid, Y.; Cámara, C. Application of species-specific isotope dilution analysis to the correction for selenomethionine oxidation in Se-enriched yeast simple extracts during storage. *J. Anal. At. Spectrom.* **2007**, *22*, 1061−1066.
(32) Hinojosa-Reyes, L.; Marchante-Gayón, J. M.; García-Alonso, J. I.; Sanz-Medel, A. Determination of selenium in biological materials by isotope dilution analysis with an octapole reaction system ICP-MS. *J. Anal. At. Spectrom.* **2003**, *18*, 11−16.
(33) Aitken, A.; Learmonth, M. Quantitation of Tryptophan in Proteins. In *The Protein Protocols Handbook*, 2nd ed.; Walker, J. M., Ed.; Humana Press: New Jersey, USA, 2002: pp 41−44.
(34) Luten, J.; Crews, H.; Flynn, A.; Van-Dael, P.; Kastenmayer, P.; Hurrell, R.; Deelstra, H.; Shen, L.; Fairweather-Tait, S.; Hickson, K.; Farré, R.; Schlemmer, U.; Frohlich, W. Interlaboratory trial on the determination of the *in vitro* iron dialysability from food. *J. Sci. Food Agric.* **1996**, *72* (4), 415−424.
(35) Garvin, D. F.; Hareland, G.; Gregoire, B. R.; Finley, J. W. Impact of wheat grain selenium content variation on milling and bread baking. *Cereal Chem.* **2011**, *88*, 195−200.
(36) Moore, K. L.; Shröder, M.; Lombi, E.; Zhao, F.; McGrath, S. P.; Hawkesford, M. J.; Shewry, P. R.; Grovenor, R. M. NanoSIMS analysis of arsenic and selenium in cereal grain. *New Phytol.* **2010**, *185* (2), 434−445.
(37) Goenaga-Infante, H.; Sturgeon, R.; Turner, J.; Hearn, R.; Sargent, M.; Maxwell, P.; Yang, L.; Barzev, A.; Pedrero, Z.; Cámara, C.; Díaz-Huerta, V.; Férnandez-Sánchez, M. L.; Sanz-Medel, A.; Emese, K.; Fodor, P.; Wolf, W.; Goldschmidt, R.; Vacchina, V.; Szpunar, J.; Valiente, L.; Huertas, R.; Labarraque, G.; Davis, C.; Zeisler, R.; Turk, G.; Rizzio, E.; Mackay, L. G.; Myors, R. B.; Saxby, D. L.; Askew, S.; Chao, W.; Jun, W. Total selenium and selenomethionine in pharmaceutical yeast tablets: assessment of the state of the art of measurement capabilities through international intercomparison CCQM-P86. *Anal. Bional. Chem.* **2008**, *390* (2), 629−642.
(38) Cabañero, A. I.; Madrid, Y.; Cámara, C. Enzymatic probe sonication extraction of Se in animal-based food samples: a new perspective on sample preparation for total and Se speciation analysis. *Anal. Bioanal. Chem.* **2005**, *381* (2), 373−379.
(39) Peachey, E.; McCarthy, N.; Goenaga-Infante, H. Acceleration of enzymatic hydrolysis of protein-bound selenium by focused microwave energy. *J. Anal. At. Spectrom.* **2008**, *23*, 487−492.
(40) Cuderman, P.; Sitbilj, V. How critical is the use of commercially available enzymes for selenium speciation? *Anal. Bioanal. Chem.* **2009**, *393* (3), 1007−1013.
(41) D'Ulivo, A. Determination of selenium and tellurium in environmental samples. Critical Review. *Analyst* **1997**, *122*, 117R−144R.
(42) Montes-Bayón, M.; Yanes, E. G.; Ponce de León, C.; Jayasimhulu, K.; Stalcup, A.; Shann, J.; Caruso, A. Initial studies of selenium speciation in *Brassica juncea* by LC with ICPMS and ES-MS detection: an approach for phytoremediation studies. *Anal. Chem.* **2002**, *74*, 107−113.
(43) Lazo-Vélez, M. A.; Gutiérrez-Díaz, V. A.; Ramírez-Medrano, A.; Serna-Saldívar, S. O. Effect of sodium selenite addition and sponge dough fermentation on selenomethionine generation during production of yeast-leavened breads. *J. Cereal Sci.* **2013**, *58* (1), 164−169.
(44) Rampler, E.; Rose, S.; Wieder, D.; Ganner, A.; Dohnal, I.; Dalik, T.; Hann, S.; Koellensperger, G. Monitoring the production process of selenized yeast by elemental speciation analysis. *Metallomics* **2012**, *4* (11), 1176−1184.
(45) FAO/WHO (Food and Agriculture Organization/World Health Organization). *Protein quality evaluation report of a joint FAO/WHO expert consulation*; Food and Agriculture Organization: Rome, Italy, 1991.
(46) SENC (Spanish Society of Communitary Nutrition). *Guidelines for Healthy Nutrition*; Spanish Society of Communitary Nutrition: Madrid, Spain, 2007.

DOI: 10.1021/jf505069d
J. Agric. Food Chem. 2015, 63, 120−127

(47) WHO (World Health Organization). *Trace element in human nutrition and health*; World Health Organization: Geneva, Switzerland, 1996.

DOI: 10.1021/jf505069d
J. Agric. Food Chem. 2015, 63, 120−127

JOURNAL OF AGRICULTURAL AND FOOD CHEMISTRY

Article

pubs.acs.org/JAFC

The Problem of 2,4,6-Trichloroanisole in Cork Planks Studied by Attenuated Total Reflection Infrared Spectroscopy: Proof of Concept

Ana R. Garcia,[†,§] Luís F. Lopes,[†] Ricardo Brito de Barros,[†] and Laura M. Ilharco*[,†]

[†]Centro de Química-Física Molecular and IN − Institute of Nanoscience and Nanotechnology, Complexo I, Instituto Superior Técnico, Universidade de Lisboa, Av. Rovisco Pais 1, 1049-001 Lisboa, Portugal

[§]Departamento de Química e Farmácia, FCT, Universidade do Algarve, Campus de Gambelas, 8005-139 Faro, Portugal

Supporting Information

ABSTRACT: Attenuated total reflection infrared spectroscopy (ATR-IR) proved to be a promising detection technique for 2,4,6-trichloroanisole (TCA), which confers organoleptic defects to bottled alcoholic beverages, allowing the proposal of a criterion for cork plank acceptance when meant for stopper production. By analysis of a significant number of samples, it was proved that the presence of TCA, even in very low concentrations, imparts subtle changes to the cork spectra, namely, the growth of two new bands at ∼1417 (νC═C of TCA ring) and 1314 cm^{-1} (a shifted νCC of TCA) and an increase in the relative intensities of the bands at ∼1039 cm^{-1} (δCO of polysaccharides) and ∼813 cm^{-1} (τCH of suberin), the latter by overlapping with intense bands of TCA. These relative intensities were evaluated in comparison to a fingerprint of suberin (ν_{as}C−O−C), at 1161 cm^{-1}. On the basis of those spectral variables, a multivariate statistics linear analysis (LDA) was performed to obtain a discriminant function that allows classifying the samples according to whether they contain or not TCA. The methodology proposed consists of a demanding acceptance criterion for cork planks destined for stopper production (with the guarantee of nonexistence of TCA) that results from combining the quantitative results with the absence of the two TCA correlated bands. ATR infrared spectroscopy is a nondestructive and easy to apply technique, both on cork planks and on stoppers, and has proven more restrictive than other techniques used in the cork industry that analyze the cleaning solutions. At the level of proof of concept, the method here proposed is appealing for high-value stopper applications.

KEYWORDS: *cork, trichloroanisole, infrared spectroscopy, ATR-IR, wine stoppers*

INTRODUCTION

Cork is a natural, renewable, and biodegradable raw material; its unique physical properties have stimulated the broadening of application fields.[1,2] This is particularly true in Portugal, which is the largest worldwide producer.[3,4] Cork has a very complex composition, but the main constituent is suberin, defined as a glycerolipid polyester, or a mixture of fatty acids and heavy organic alcohols that form a macromolecular network, insoluble in all common solvents.[5] Another important constituent is lignin, with a less known structure than other natural and synthetic polymers, built by phenylpropane units randomly organized, having characteristic side chains with para-substituted phenolic hydroxyl groups, either free or etherified.[6,7] The 2D representations of proposed structures for suberin and lignin are schematized in Figure 1.

Recent studies on the chemical composition of cork from *Quercus suber* L. (oak), the main natural source of cork, point out that the determining variation factor is the individual tree rather than the geographical origin.[8] The average chemical composition of natural cork from *Q. suber* L. is approximately suberin 40%, lignin 22%, polysaccharides 18%, total extractives 15%, and ash below 1%.[9] The oak cork natural variability with location is mainly reflected in the amounts of extractives and polysaccharides, whereas the relative contents in suberin and lignin are not much affected.[9]

Traditionally, the growth of filamentous fungi in cork was considered beneficial, but currently the detection of volatile compounds, namely, chloroanisoles and chlorophenols, is associated with the incidence of some fungi.[10,11] Those volatiles can also be produced by different sources of phenol and

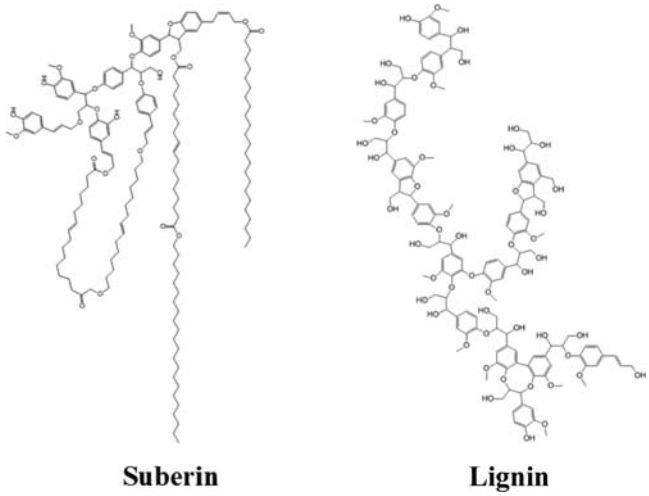

Figure 1. Schematic 2D representations of suberin and lignin, obtained with ChemDraw Ultra 12.0.

Received: July 11, 2014
Revised: December 1, 2014
Accepted: December 9, 2014
Published: December 9, 2014

ACS Publications © 2014 American Chemical Society

chlorine, such as some cleaning products and sanitizers (that contaminate surface waters). The honeycomb-type structure can provide adequate reservoirs for holding these volatile compounds in the cork core.[1,12]

The presence of volatiles is a critical problem in the food industry, because chloroanisoles and chlorophenols are associated with "musty" off-flavors and odors. Because cork materials are widely used to seal bottles of alcoholic beverages, the migration of chloroanisoles from the stoppers may result in those undesirable odors or tastes.[13] In fact, the production of chloroanisoles by fungi in cork slabs is considered the most frequent cause of organoleptic defects of wines.[14,15] The strongest chloroanisole is 2,4,6-trichloroanisole (TCA),[16] formed mainly due to the microflora associated with corks.[15,17] It is usually considered to be primarily responsible for economical losses in the wine industry, due to the increase of cork taint in bottled wine.[18] Several analytical techniques can now be employed to detect the presence of TCA, and numerous processes have been developed to reduce its quantity in cork.[19−24] Bleaching is the most used, but it does not remove all of the TCA. Moreover, when chlorinated products are used in the process, the formation of chlorophenols can be induced.[3]

The sensitivity of the olfactory receptor cells to TCA is extremely high: the threshold in wine can be low as 1.4−4.6 ng/L (or parts per trillion, ppt),[25] which is a detection limit difficult to match by analytical methods. Given the dimension of this problem, it is now settled that a preventive action is a main priority, starting with the detection of these compounds in the cork planks before stoppers are produced.

In the present work, a systematic analysis of attenuated total reflection infrared spectroscopy (ATR-IR) spectra of a substantial number of natural cork stoppers was performed to establish a safe criterion for TCA absence that may eventually be used for acceptance of cork planks intended for stoppers production.

EXPERIMENTAL PROCEDURES

Samples. Natural cork stoppers for wines that need to age in the bottle, from the *Q. suber* L. variety, were obtained from one manufacturer (the name is undisclosed for confidentiality reasons). The information provided consisted of whether the corks came from batches containing detectable traces of TCA in the last cleaning solution or not. No particular information was specified about the detection method, except that it was by chromatography. The stoppers, cut out directly from natural cork planks, were cylindrical single pieces, a total of 50. Two series of samples were provided: series A (15), from batches in which TCA was not detected in the last cleaning solution and, therefore, allegedly without TCA; and series R (30 five), from batches in which TCA was detected in the last cleaning solution and therefore expected to have TCA.

A 0.01 M solution of 2,4,6-trichloroanisol (Sigma-Aldrich, 99%) in ethanol (absolute, ≥99.8%, Sigma-Aldrich) was prepared to artificially embed TCA onto clean cork. Different amounts were deposited onto the cork surface to obtain a variety of low TCA concentrations upon solvent evaporation.

Infrared Characterization. All of the infrared spectra were scanned in a Mattson FTIR spectrometer RS1, equipped with a wide band MCT detector (400−4000 cm^{-1}). The spectra, with 4 cm^{-1} resolution, are presented without baseline or smooth corrections.

For analyzing pure TCA and cork powder from different regions of the same stopper, diffuse reflectance infrared Fourier transform (DRIFT) spectra were recorded using a Graseby/Specac selector. The samples were diluted in KBr (from Aldrich, FTIR grade) in a weight proportion of 1:4. The spectra were the ratio of 500 single-beam scans for the sample to the same number of scans for pure KBr, used as background. The spectra were transformed to Kubelka−Munk units using FIRST software.

The external surfaces of the stoppers were analyzed by infrared attenuated total reflection (IR-ATR) spectra, with a horizontal Pike Technologies (HATR) accessory. A slim slice of the stopper external surface was cut and placed on a SeZn ATR crystal (4 mm thick and 80 mm long) with 10 reflections and an incidence angle of 45°. Conditions for an "ideal contact" between the sample and the crystal were guaranteed, so that the band intensities remained constant as contact slightly changed.[26] The spectra were also obtained as a ratio of 500 single-beam scans of the sample to the same number of background (clean ATR crystal) scans. The spectra were transformed to $\log_{10}(1/R)$ using FIRST software.

A Bruker Hyperion 2000 microscope coupled to a Vertex 70 FTIR spectrometer was used to map the distribution of TCA in some of the samples. The spectra of very thin cork slices were acquired in transmission mode, with a spatial resolution of 15 μm.

RESULTS AND DISCUSSION

Infrared Spectrum of TCA. The infrared spectrum of 2,4,6-trichloroanisole is known, but the detailed analysis has not been published so far. It is shown in Figure 2, in DRIFT.

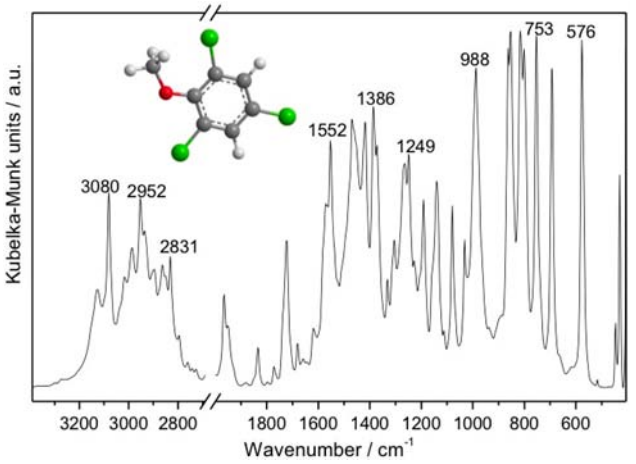

Figure 2. DRIFT spectrum of pure 2,4,6-trichloroanisole.

Two groups of very strong bands are observed, in the ∼1600−1370 and ∼1000−600 cm^{-1} regions, respectively, plus a number of strong ones in the 2900−3200 cm^{-1} region. A detailed assignment was made mainly by comparison with the parent molecules 2,4,6-trichlorophenol and anisole[27,28] and is presented in Table 1.

Cork Infrared Characterization. In general, the cork stoppers have a light color and, after bleaching, the external surface becomes more whitish. Both the heterogeneities of natural cork and the bleaching process may lead to differences in the infrared absorption bands. To assess these possibilities, several regions of a bleached cork stopper from a batch where no TCA was detected in the cleaning solution (sample A1) were characterized by DRIFTS. The spectra are compared in Figure 3.

The spectra in Figure 3, normalized to the strongest suberin band (ν_{as}COC, at 1161 cm^{-1}), show only changes in the bands' relative intensities, confirming some variability in the chemical components' proportions. The differences associated with the presence or absence of spots (sites a and b) are very small, whereas those related to the influence of bleaching (mostly site d) are clearer, pointing to bleaching as the main cause for adjustments in chemical proportions: the intensities of the

dx.doi.org/10.1021/jf503309a | J. Agric. Food Chem. 2015, 63, 128−135

Table 1. Band Assignment of the DRIFT Spectrum of 2,4,6-Trichloroanisole[a]

$\tilde{\nu}$ (cm^{-1})	assignment	$\tilde{\nu}$ (cm^{-1})	assignment
$3127_{(sh,m)}$		$1331_{(w)}$	νCC
$3080_{(m)}$	νCH	$1304_{(m)}$	
$3017_{(sh,m)}$		$1265/1249_{(db,S)}$	δCH
$2987_{(sh,m)}$	$\nu_{as}CH_3$	$1227_{(sh,m)}$	δCH
$2952_{(m)}$	$\nu_{as}CH_3$	$1192_{(m)}$	
$2936_{(sh,m)}$		$1140_{(m)}$	δCH
$2897_{(m)}$		$1080_{(m)}$	ν_{ring} (breathing)
$2863_{(m)}$	ν_sCH_3	$1032_{(m)}$	νC−O−C
$2831_{(m)}$	ν_sCH_3	$988_{(VS)}$	ν_{ring} (breathing)
2800−1700	overtone and combination bands	$861/853_{(db,VS)}$	γCH
$1570_{(sh,m)}$	νC=C (ring)	$815/801_{(db,VS)}$	νCCl
$1552_{(S)}$	νC=C (ring)	$753_{(VS)}$	γCH (oop)
$1469_{(S)}$	$\delta_{as}CH_3$	$693_{(VS)}$	γCH (oop)
$1418_{(S)}$	νC=C (ring)	$576_{(VS)}$	δ_{ring}(oop)
$1386_{(S)}/1372_{(sh)}$	δ_sCH_3	$446_{(m)}$	δCOC

[a]w, weak; m, medium; S, strong; VS, very strong; sh, shoulder; db, doublet; oop, out of plane.

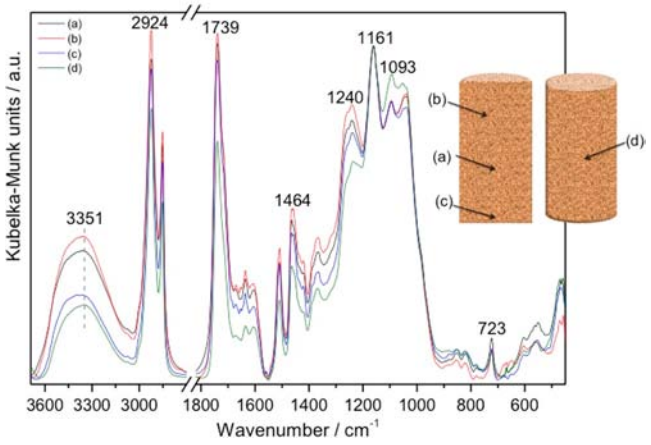

Figure 3. DRIFT spectra of different regions of a bleached cork stopper: inner surface without defects (a), with spots (b), and close to the edge (c); outer surface (d). The spectra are normalized to the maximum.

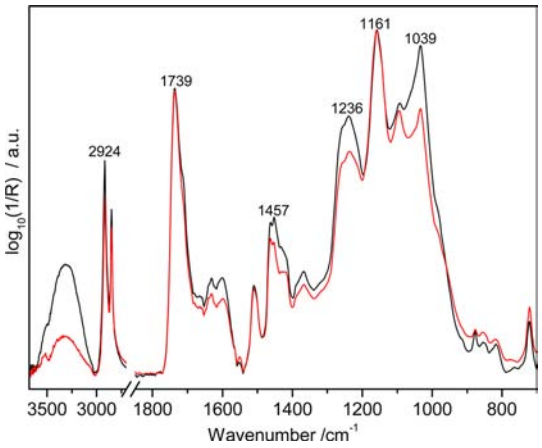

Figure 4. ATR infrared spectra of slides of two cork stoppers (sample A1, black line; and sample A4, red line) after being submitted to the bleaching process.

Table 2. Band Assignment of the Infrared ATR Spectrum of Bleached Cork[a]

$\tilde{\nu}$ (cm^{-1})	assignment	cork component
$\sim3350_{(S)}$	νO−H	suberin, lignin and adsorbed water
$2924_{(S)}$	$\nu_{as}CH_2$	suberin alkyl chains
$2853_{(S)}$	$\nu_{as}CH_2$	suberin alkyl chains
$1739_{(VS)}$	νC=O	suberin ester groups
$1714_{(sh)}$	νC=O	lignin
$1635_{(m)}$	νC=C	suberin and lignin aliphatic groups
$1606_{(m)}$	νC=C	suberin aliphatic groups
$1509_{(m)}$	νC=C	lignin aromatic rings (fingerprint)
$1457_{(S)}$	δ_sCH_2	suberin aliphatic groups (fingerprint)
$1420_{(sh)}$	$\delta_s(O)CH_3$	lignin
$1364_{(m)}$	δ_sCH_3	suberin (fingerprint)
$1236_{(VS)}$	νCO	suberin (fingerprint)
$1161_{(VS)}$	ν_{as}COC	suberin (fingerprint)
$1094_{(VS)}$	δCH	polysaccharides
$1039_{(VS)}$	δCO	polysaccharides
$852_{(m)}$	τCH (oop)	suberin
$818_{(m)}$	ρCH_3	suberin/lignin
$723_{(m)}$	τCH (oop)	suberin

[a]w, weak; m, medium; S, strong; VS, very strong; sh, shoulder; oop, out of plane.

bands at 2924, 1739, 1464, and 1240 cm^{-1} decrease in comparison to the suberin fingerprint, at 1161 cm^{-1}, whereas those at 1093 and 1039 cm^{-1} appear to increase. For the systematic study that follows, the inner surfaces of cork stoppers will be analyzed.

The ATR spectra of two slides of stoppers from a bleached batch (A1 and A4) were used to establish the standard "clean" cork and are shown in Figure 4.

The spectra in Figure 4 were also normalized to the characteristic suberin band ν_{as}COC, at 1161 cm^{-1}, and correlate well with ATR infrared spectra of cork stoppers in the literature.[29−31] The assignment of the main bands is summarized in Table 2.[6,32−34]

The band shifts observed between the two samples are within the spectral resolution, and the changes in relative intensities are probably due to heterogeneities, as expected in natural samples. In fact, the amount of lignin in natural cork can vary from 19 to 24%, probably being the chemical component with less variability. In the case of suberin, its content varies from ~30 to almost 50%.[8]

Cork with TCA Embedded in Situ. The objective of characterizing cork samples with TCA embedded in the laboratory was to establish spectral regions unambiguously assignable to TCA on cork. The ATR infrared spectra were obtained only after complete evaporation of the solvent. The spectra of the same stopper, clean and with embedded TCA, are compared in Figure 5.

The presence of TCA induces the appearance of new bands at 3078, 1550, 1417, 1383, 987, 796, and 752 cm^{-1}, which can be considered as fingerprints of TCA in cork. Other strong modes of TCA can alter the band shape of the cork spectrum due to overlapping, as in the case of the bands at 1138, 1080, 854, and 692 cm^{-1}. Moreover, in the region between 1470 and 1415 cm^{-1}, the shoulder at 1468 cm^{-1} and the maximum at 1452 cm^{-1} invert their relative intensities, and the cork band at 1236 cm^{-1} splits into two components (1259 and 1248 cm^{-1}),

dx.doi.org/10.1021/jf503309a | J. Agric. Food Chem. 2015, 63, 128−135

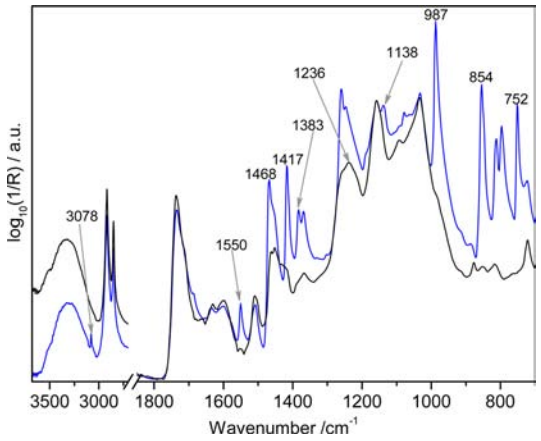

Figure 5. ATR infrared spectra of a clean cork stopper (black line) and the same sample after incorporation of TCA (blue line). The spectra were not baseline corrected and were normalized to the suberin band at 1161 cm^{-1}.

the first shifted from the maximum observed for the pure TCA doublet (1265 and 1249 cm^{-1}).

Evaluation of the Presence of TCA in Stoppers from Natural Cork. Taking into account that the natural amount of TCA expected in stoppers is very low, we are aware that only the very strong vibrational bands of TCA will probably be observed in the tainted samples. On the other hand, because TCA is formed within natural cork, it is possible that the interactions with the medium lead to conformational changes and thus to spectral differences regarding pure or artificially added TCA and also that a heterogeneous spatial distribution throughout the sample occurs. This effect is well illustrated in Figure 6A, which refers to one stopper of series R (from a batch in which TCA was detected in the last cleaning solution): the honeycomb-like cork structure is observed over an area of 0.02 mm^2, as well as the corresponding 3D mapping of the integrated intensity of the band at 1417 cm^{-1} (the strong νC=C of TCA). The ATR spectra of seven cork stopper slices of series R are presented in Figure 6B. Only the region 1800−700 cm^{-1} is shown, because the main differences are observed in this wavenumber region.

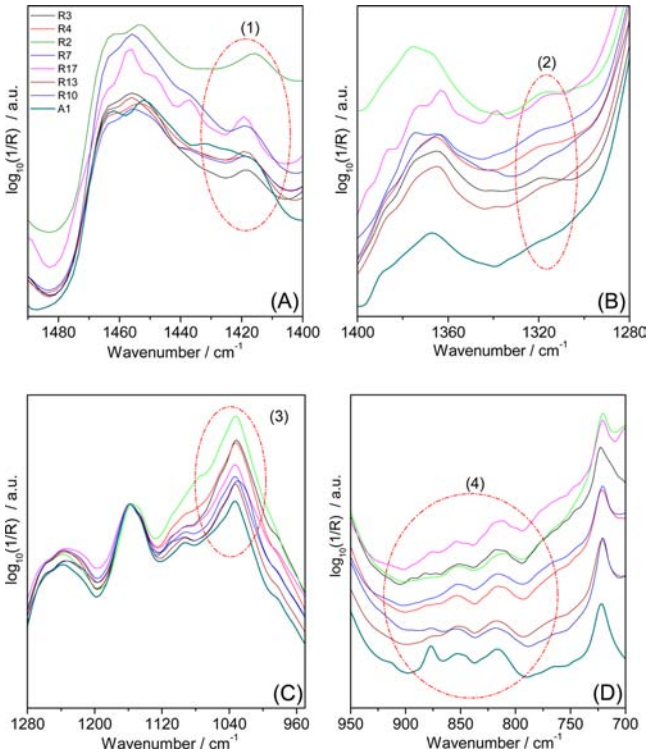

Figure 7. Details of the ATR infrared spectra of cork stopper slices in which TCA was detected in the cleaning solution, compared to a "clean" sample (A1). The spectra are baseline corrected and normalized at 1161 cm^{-1}.

As expected, the changes in the overall spectral shape are much more subtle than when TCA was embedded in situ. However, some effects are clear, and the corresponding regions are labeled (1−4) in Figure 6B. These spectral regions are enhanced in Figure 7, where the same samples are compared with one from a "TCA clean" stopper (A1).

Analysis of Figure 7 establishes spectral characteristics inherent to corks with TCA:

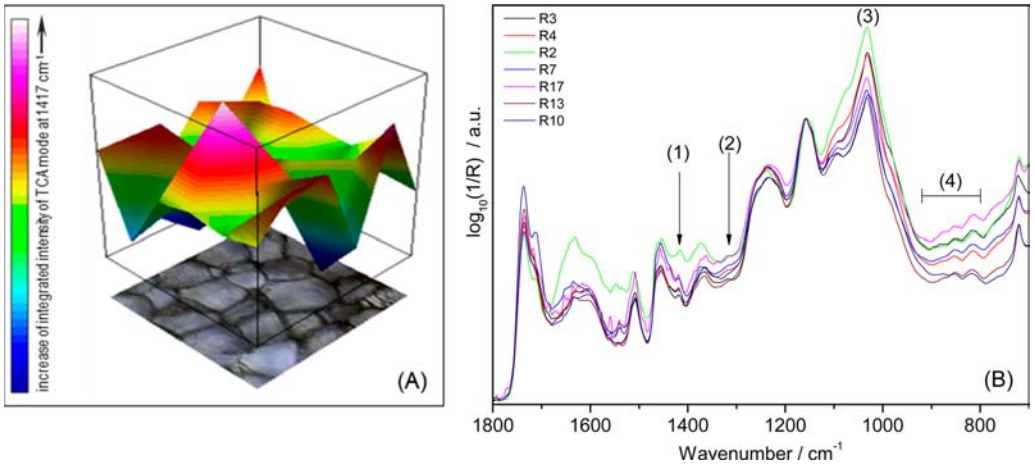

Figure 6. (A) Image of a 0.02 mm^2 area of a stopper slice in which TCA was detected in the cleaning solution (sample R2) and corresponding 3D distribution of the integrated intensity of the TCA mode at 1417 cm^{-1}. (B) ATR infrared spectra of cork stoppers in which TCA was detected in the cleaning solution (series R): highlighted bands at 1417 cm^{-1} (1), ∼1314 cm^{-1} (2), and ∼1039 cm^{-1} (3) and the spectral region between 950 and 800 cm^{-1} (4). The spectra are baseline corrected and normalized at 1161 cm^{-1}.

dx.doi.org/10.1021/jf503309a | J. Agric. Food Chem. 2015, 63, 128−135

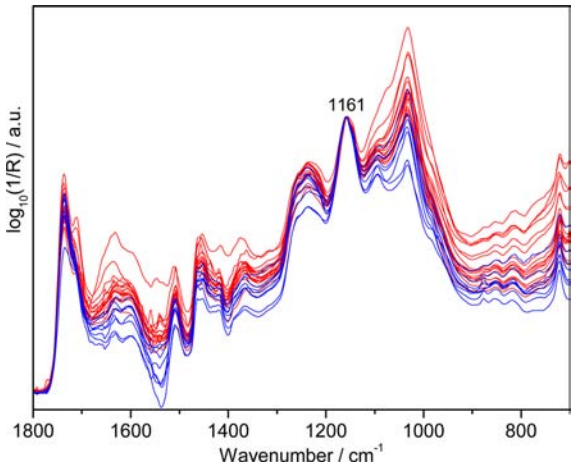

Figure 8. ATR infrared spectra of cork stopper slices: series A, from batches in which TCA was not detected (blue spectra); series R, from batches in which TCA was detected (red spectra). The spectra were baseline corrected and normalized at 1161 cm^{-1}.

In region 1, the TCA band near 1417 cm^{-1} grows, coincident with the observed for the sample with TCA embedded in the laboratory.

In region 2, a very small band at ∼1314 cm^{-1} (almost a shoulder) is present; this new band was neither observed in the spectra of cork with incorporated TCA nor does it corresponds to a pure TCA band, but it may result from $\pi-\pi$ interactions between the aromatic ring of TCA formed in situ and those of the suberin or lignin molecules.

In region 3, the relative intensity of the band at ∼1039 cm^{-1} (δCO of polysaccharides) is much higher than in the spectrum of the sample without TCA. As referred to above, these polysaccharides may originate from natural cork or from fungi cells walls. Because TCA can be synthesized by cork fungi, this band may be an indirect indication of contamination.

In region 4, the spectra between 950 and 800 cm^{-1} have a higher relative intensity that can be easily related with the presence of TCA, because its spectrum has very strong bands in this region, namely, the νCCl mode (that appears as a doublet at 815 and 801 cm^{-1} in pure TCA).

In summary, the appearance of bands at ∼1417 and ∼1314 cm^{-1} and the intensity increase of the spectral region 950−800 cm^{-1} are direct indications of the presence of TCA in a cork stopper. The relative increase of the polysaccharide band at ∼1039 cm^{-1} in comparison to the suberin fingerprint at 1161 cm^{-1} can be an indirect sign.

The observation of these four effects, although subtle, attests to the presence of TCA in cork, even in low concentrations, and ATR appears as a good candidate method for TCA detection. However, the purpose of the present work is to use this technique to establish criteria for guaranteeing the absence of TCA in cork, consequently allowing the approval of cork planks intended for the manufacture of high-value wine stoppers. To establish these criteria, further spectra were analyzed for the two complete series of samples provided (A and R). The ATR spectra are shown in Figure 8.

In the regions named above as 3 and 4, the TCA effects were tentatively quantified by the ratio between the intensity of a particular band to that of the 1161 cm^{-1} band: I_{1039}/I_{1161} and I_{813}/I_{1161}, respectively. About 50 specimens (of the two series of samples A and R) were considered an acceptable number to carry out an analysis of variance (ANOVA) of those two intensity ratios. The extreme points were excluded from the statistical analysis, based on the modified Thompson Tau test for outlier determination.[35] The Tukey test proved that the means difference between A and R series is significant at the 0.05 level, and the confirmation of equal variance for the two populations was obtained by using the Brown−Forsythe test. The samples used in the calculations, the results of the Brown−Forsythe test and ANOVA, are summarized in Table S1 in the Supporting Information. Because the two populations' means are significantly different, the ratios I_{1039}/I_{1161} and I_{813}/I_{1161}, the mean values, and corresponding confidence intervals are shown in Figure 9. The average intensity ratio I_{1039}/I_{1161} is 0.96 ± 0.06 for the samples allegedly without TCA and 1.15 ± 0.06 for the samples with TCA, and the average ratio I_{813}/I_{1161} is 0.42 ± 0.03 and 0.50 ± 0.04, respectively (95% confidence level). Accordingly, cork samples definitely not contaminated with TCA are expected to present simultaneously a I_{1039}/I_{1161} ratio below 0.96 ± 0.06 and a I_{813}/I_{1161} ratio below 0.42 ± 0.03.

Cork being a natural product, the ideal sampling would consist of a larger number of specimens, identified by production region and pretreatments. The limitations of the previous statistical analysis on the data from spectral regions 3 and 4 may be partially overcome by complementing with the information from regions 1 and 2. A complete evaluation of the spectral effects of TCA is indispensable to establish the final criteria for deciding on the acceptance of a cork plank. The four effects are combined in Figure 10A.

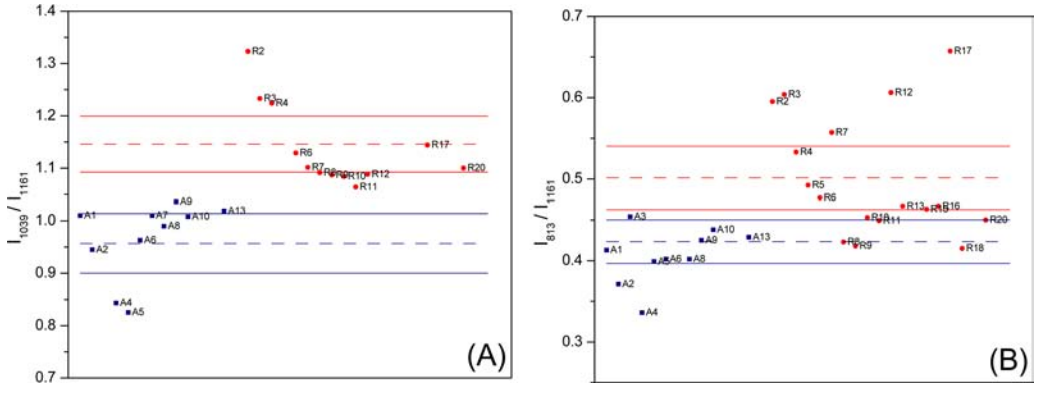

Figure 9. Band intensity ratios for the samples used in the statistical analysis, ratio mean value (dashed line), and limits of the confidence interval (solid lines): (A) I_{1039}/I_{1161}; (B) I_{813}/I_{1161}; (blue squares) series A (allegedly without TCA); (red circles) series R (with TCA).

dx.doi.org/10.1021/jf503309a | J. Agric. Food Chem. 2015, 63, 128−135

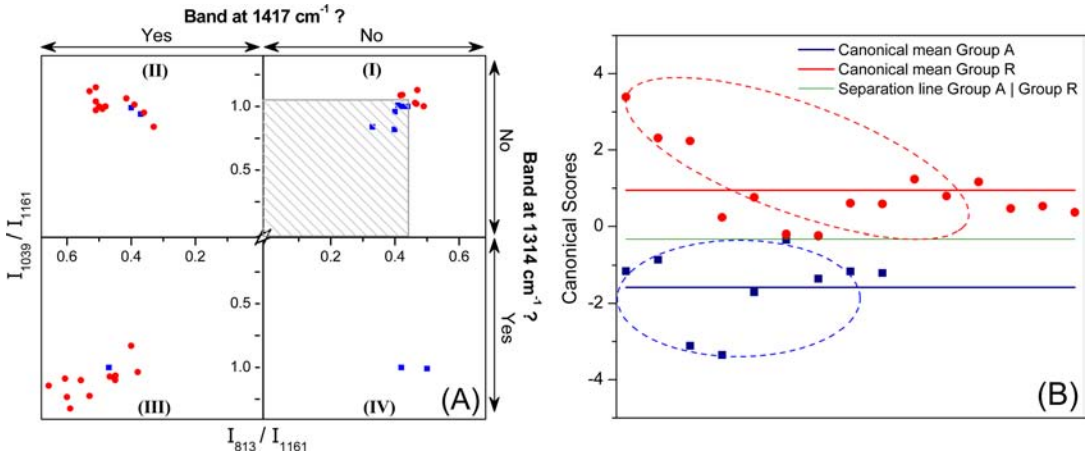

Figure 10. (A) Combined evaluation of the four effects of TCA on the ATR spectra of cork stoppers; (B) canonical scores for group A and R training data (TD) and corresponding canonical means: (blue squares) series A (allegedly without TCA); (red circles) series R (with TCA).

Table 3. Multivariate Statistics Linear Discriminant (LDA) Results Obtained for ATR Infrared Training Data of Samples A and R

Equality test of covariance matrices

LOG of determinants

Group A	Group R	pooled
-16.07151	-14.94561	-14.68797

Likelihood-ratio test

Statistic	df	p-value
11.49966	10	0.31994

Canonical discriminant analysis

Eigenvalue	% variance	cumulative	Canonical correlation
1.63764	100.00	100.00	0.78796

Wilks' Lambda test

Wilks' Lambda	χ^2	df	p-value
0.37913	19.39772	4	6.5641×10^{-4}

Standardized canonical coefficients

	Canonical variable 1
A	0.88636
B	-0.02822
C	0.44731
D	-0.07619

Unstandardized canonical coefficients

	Canonical variable 1
Constant	-13.0017
A	11.89704
B	-0.40931
C	1.05491
D	-0.16162

Classification summary for training data

	Predicted group		
	Group A	Group R	Total
Group A	9	0	9
	100.00 %	0.00 %	100.00 %
Group R	0	15	15
	0.00 %	100.00 %	100.00 %

Error rate for classification is 0.00 %

In the absence of the bands at 1417 and 1341 cm^{-1} (quadrant I) and only within the shaded area (limited by $I_{1039}/I_{1161} \leq 1.02$ and $I_{813}/I_{1161} \leq 0.45$), all of the spectral observations point to safely concluding the nonexistence of TCA in the cork stoppers. In line with this conclusion, all of the samples within the shaded area come from batches in which TCA was not detected in the last cleaning solution. When the bands at 1417 and 1341 cm^{-1} are both present (quadrant III), the cork stoppers are probably contaminated with TCA. Clearly, most of the samples included in this quadrant also present high values of the band ratios I_{1039}/I_{1161} and I_{813}/I_{1161} and therefore have a high possibility of TCA presence. Indeed, only one sample within this quadrant comes from A batches. If only the band at 1314 cm^{-1} is observed (quadrant IV), the

dx.doi.org/10.1021/jf503309a | J. Agric. Food Chem. 2015, 63, 128−135

conclusions can be more difficult. Only two samples are in these conditions, and both come from A batches. However, because the I_{1039}/I_{1161} and I_{813}/I_{1161} band ratios are high, the possibility of contamination in those cork stoppers may not be excluded. When only the band at 1417 cm^{-1} is observed (quadrant II), it is so unequivocal that it constitutes a strong enough indication of the presence of TCA in the cork. In this case, even if the band ratios do not support this hypothesis, the cork stoppers should be considered contaminated.

To further discriminate samples with and without TCA, a multivariate statistics linear discriminant analysis (LDA) was applied to the ATR infrared data. The two data categories A and R were used, as previously, and the four spectral effects were considered as independent variables: X_1 (the ratio I_{1039}/I_{1161}), X_2 (the ratio I_{813}/I_{1161}), X_3 (the TCA band at 1417 cm^{-1}), and X_4 (the TCA band at 1314 cm^{-1}). The dummy variables X_3 and X_4 were assigned either as 1 or 0, to account for the presence or absence of the bands, respectively. The output results (OriginPro 9.1) are summarized in Table 3, and the training data are reported in Table S2 in the Supporting Information. Equality of covariance matrices within groups is attested by similar log determinants and p value (0.319) of the likelihood-ratio test. Only one discriminant function and one eigenvalue accounting for 100% of the variance in the relationship are obtained, along with good canonical correlation between the discriminant function and the dependent variables. Statistical significance of the discriminant function is withdrawn from the low p value of the Wilks' lambda test. According to the LDA analysis, the intensity ratio X_1 (I_{1039}/I_{1161}) is the most relevant variable for the discrimination (canonical coefficient 0.886), followed by X_3, X_4, and X_2 (I_{813}/I_{1161}). Strong validity of the variables chosen to distinguish between R and A samples is given by the absence of error in the classification (Table 3) and corresponding post probabilities obtained for the training data. Cross-validation (Table S2 in the Supporting Iinformation) evidences a higher error rate, most probably due to misclassification of some observations, namely those of group A that contain the relevant band at 1417 cm^{-1} (X_3), pointing to a better allocation in group R. This corroborates the previous analysis, with the possibility of exclusion of some A samples. The canonical scores obtained for the ATR data along with the group centroids for A and R and the corresponding separation boarder line are represented in Figure 10B, confirming good quality of the discrimination attained. On the basis of this LDA, cork planks or stoppers can be safely rejected whenever they are allocated in the centroid region of group R. For acceptance of cork samples (guarantee of inexistence of TCA), however, the strong physical meaning of the bands at 1417 and 1341 cm^{-1} must be taken into account: the allocation in the centroid region of group A should be combined with the absence of both bands directly related with TCA. This leads to rejecting all of the samples already rejected by other methods, usually performed on the cleaning solutions, plus some accepted by those methods. Thus, the result is a more restrictive method in terms of acceptance of cork planks for stopper manufacture, especially adequate for cases when the economical damage for TCA-contaminated stoppers is more significant, namely, when high-value wines are at stake. Besides, it is a direct method, nondestructive, simple, rapid, and applicable both on the cork planks and on the cork stoppers.

Although the application of the proposed method renders valuable information, it is a proof of concept, and, prior to implementation, we are aware that a significantly larger number of samples should be tested.

■ ASSOCIATED CONTENT

Supporting Information

Tables S1 and S2. This material is available free of charge via the Internet at http://pubs.acs.org.

■ AUTHOR INFORMATION

Funding

This work was supported by Fundação para a Ciência e a Tecnologia (partly by Project RECI/CTM-POL/0342/2012).

Notes

The authors declare no competing financial interest.

■ ACKNOWLEDGMENTS

We acknowledge the undisclosed stopper manufacturer for kindly providing the samples.

■ REFERENCES

(1) Gibson, L. J.; Easterling, K. E.; Ashby, M. F. The structure and mechanics of cork. *Proc. R. Soc. London A* **1981**, *377*, 99−117.

(2) Silva, S. P.; Sabino, M. A.; Fernandes, E. M.; Correlo, V. M.; Boesel, L. F.; Reis, R. L. Cork: properties, capabilities and applications. *Int. Mater. Rev.* **2005**, *50*, 345−365.

(3) Pereira, H. *Cork: Biology, Production and Uses*, 1st ed.; Elsevier: Amsterdam, The Netherlands, 2007; pp 320−322.

(4) Lopes, M. H.; Barros, A. S.; Pascoal Neto, C.; Rutledge, D.; Delgadillo, I.; Gil, A. M. Variability of cork from portuguese *Quercus suber* studied by solid-state ^{13}C-NMR and FTIR spectroscopies. *Biopolymers* **2001**, *62*, 268−277.

(5) Cordeiro, N.; Belgacem, M. N.; Silvestre, A. J. D.; Pascoal Neto, C.; Gandini, A. Cork suberin as a new source of chemicals. 1. Isolation and chemical characterization of its composition. *Int. J. Biol. Macromol.* **1998**, *22*, 71−80.

(6) Shabaka, A. A.; Nada, A. M. A.; Fadly, M. Infrared spectroscopic study of thermally treated lignin. *J. Mater. Sci.* **1990**, *25*, 2925−2928.

(7) Hatakeyama, H.; Hatakeyama, T. Lignin structure, properties, and applications. *Adv. Polym. Sci.* **2010**, *232*, 1−63.

(8) Pereira, H. Cork chemical variability. *BioResources* **2013**, *8*, 2246−2256.

(9) Pereira, H. Chemical composition and variability of cork from *Quercus suber* L. *Wood Sci. Technol.* **1988**, *22*, 211−218.

(10) Álvarez-Rodríguez, M. L.; López-Ocaña, L.; López-Coronado, J. M.; Rodríguez, E.; Martínez, M. J.; Larriba, G.; Coque, J.-J. R. Cork taint of wines: role of the filamentous fungi isolated from cork in the formation of 2,4,6-trichloroanisole by O methylation of 2,4,6-trichlorophenol. *Appl. Environ. Microbiol.* **2002**, *68*, 5860−5869.

(11) Tindale, C. R.; Whitfield, F. B.; Levingston, S. D.; Ly Nguyen, T. H. Fungi Isolated from packaging materials: their role in the production of 2,4,6-trichloroanisole. *J. Sci. Food Agric.* **1989**, *49*, 437−447.

(12) Miranda, I.; Gominho, J.; Pereira, H. Cellular structure and chemical composition of cork from the Chinese cork oak (*Quercus* variabilis). *J. Wood Sci.* **2013**, *59*, 1−9.

(13) Rocha, S.; Delgadillo, I.; Ferrer Correia, A. J.; Barros, A.; Wells, P. Application of an electronic aroma sensing system to cork stopper quality control. *J. Agric. Food Chem.* **1998**, *46*, 145−151.

(14) Barreto, M. C.; Vilas Boas, L.; Carneiro, L. C.; San Romão, M. V. Volatile compounds in samples of cork and also produced by selected fungi. *J. Agric. Food Chem.* **2011**, *59*, 6568−6574.

(15) Simpson, R. F.; Sefton, M. A. Origin and fate of 2,4,6-trichloroanisole in cork bark and wine corks. *Aust. J. Grape Wine Res.* **2007**, *13*, 106−116.

(16) Daniels-Lake, B. J.; Prange, R. K.; Gaul, S. O.; McRae, K. B.; de Antueno, R.; McLachlan, D. Musty "off" flavor in Nova Scotia potatoes

is associated with 2,4,6-trichloroanisole released from pesticide-treated soils and high soil temperature. *J. Am. Soc. Hortic. Sci.* **2007**, *132*, 112−119.
(17) Olivella, M. A.; Caixach, J.; Planas, C.; Oliveras, A.; Jové, P. Concentrations of organochlorine pesticides and 2,4,6-trichloroanisole in cork bark. *Chemosphere* **2012**, *86*, 754−758.
(18) Juanola, R.; Subirá, D.; Salvadó, V.; Garcia Regueiro, J. A.; Anticó, E. Migration of 2,4,6-trichloroanisole from cork stoppers to wine. *Eur. Food Res. Technol.* **2005**, *220*, 347−352.
(19) Rocha, S.; Delgadillo, I.; Ferrer Correia, A. J. Improvement of the volatile components of cork from *Quercus suber* L. by an autoclaving procedure. *J. Agric. Food Chem.* **1996**, *44*, 872−876.
(20) Taylor, M. K.; Young, T. M.; Butzke, C. E.; Ebeler, S. E. Supercritical fluid extraction of 2,4,6-trichloroanisole from cork stoppers. *J. Agric. Food Chem.* **2000**, *48*, 2208−2211.
(21) Recio, E.; Álvarez-Rodríguez, M. L.; Rumbero, A.; Garzón, E.; Coque, J. J. R. Destruction of chloroanisoles by using a hydrogen peroxide activated method and its application to remove chloroanisoles from cork stoppers. *J. Agric. Food Chem.* **2011**, *59*, 12589−12597.
(22) Pereira, C.; Gil, L.; Carriço, L. Reduction of the 2,4,6-trichloroanisole content in cork stoppers using gamma radiation. *Radiat. Phys. Chem.* **2007**, *76*, 729−732.
(23) Garde-Cerdán, T.; Lorenzo, C.; Zalacain, A.; Alonso, G. L.; Salinas, M. R. Using near infrared spectroscopy to determine haloanisoles and halophenols in barrel aged red wines. *LWT−Food Sci. Technol.* **2012**, *46*, 401−405.
(24) Boudaoud, N.; Eveleigh, L. A new approach to the characterization of volatile signatures of cork wine stoppers. *J. Agric. Food Chem.* **2003**, *51*, 1530−1533.
(25) Sefton, M. A.; Simpson, R. F. Compounds causing cork taint and the factors affecting their transfer from natural cork closures to wine − a review. *Aust. J. Grape Wine Res.* **2005**, *11*, 226−240.
(26) Buffeteau, T.; Desbat, B.; Eyquem, D. Attenuated total reflection Fourier transform infrared microspectroscopy: theory and application to polymer samples. *Vib. Spectrosc.* **1996**, *11*, 29−36.
(27) Faniran, J. A.; Shurvell, H. F. Raman and infrared spectra of 2,4,6-trichlorophenol and 2,4,6-tribromophenol. *J. Raman Spectrosc.* **1980**, *9*, 73−75.
(28) Hoffmann, L. J. H.; Marquardt, S.; Gemechu, A. S.; Baumgärtel, H. The absorption spectra of anisole-h8, anisole-d3 and anisole-d8. The assignment of fundamental vibrations in the S_0 and the S_1 states. *Phys. Chem. Chem. Phys.* **2006**, *8*, 2360−2377.
(29) Ortega-Fernández, C.; González-Adrados, J. R.; García-Vallejo, M. C.; Calvo-Haro, R.; Cáceres-Esteban, M. J. Characterization of surface treatments of cork stoppers by FTIR-ATR. *J. Agric. Food Chem.* **2006**, *54*, 4932−4936.
(30) González-Adrados, J. R.; Garcia-Vallejo, M. C.; Caceres-Esteban, M. J.; Garcia de Ceca, J. L.; Gonzalez-Hernandez, F.; Calvo-Haro, R. Control by ATR-FTIR of surface treatment of cork stoppers and its effect on their mechanical performance. *Wood Sci. Technol.* **2012**, *46*, 349−360.
(31) González-Gaitano, G.; Ferrer, M. A. C. Definition of QC parameters for the practical use of FTIR-ATR spectroscopy in the analysis of surface treatment of cork stoppers. *J. Wood Chem. Technol.* **2013**, *33*, 217−233.
(32) Rocha, S. M.; Goodfellow, B. J.; Delgadillo, I.; Neto, C. P.; Gil, A. M. Enzymatic isolation and structural characterisation of polymeric suberin of cork from *Quercus suber* L. *Int. J. Biol. Macromol.* **2001**, *28*, 107−119.
(33) Olivella, M. À.; Fernández, I.; Cano, L.; Jové, P.; Oliveras, A. Role of chemical components of cork on sorption of aqueous polycyclic aromatic hydrocarbons. *Int. J. Environ. Res.* **2013**, *7*, 225−234.
(34) Oliveira, L.; Evtuguin, D. V.; Cordeiro, N.; Silvestre, A. J. D.; Silva, A. M. S.; Torres, I. C. Structural characterization of lignin from leaf sheaths of "Dwarf Cavendish" banana plant. *J. Agric. Food Chem.* **2006**, *54*, 2598−2605.
(35) Anbarasi, M. S.; Ghaayathri, S.; Kamaleswari, R.; Abirami, I. Outlier detection for multidimensional medical data. *Int. J. Comput. Ssci. Inf. Technol.* **2011**, *2*, 512−516.

JOURNAL OF AGRICULTURAL AND FOOD CHEMISTRY

Article

pubs.acs.org/JAFC

Screening of Single-Stranded DNA (ssDNA) Aptamers against a Zearalenone Monoclonal Antibody and Development of a ssDNA-Based Enzyme-Linked Oligonucleotide Assay for Determination of Zearalenone in Corn

Yuan-Kai Wang,[†,‡] Qi Zou,[†,‡] Jian-He Sun,[*,‡] Heng-an Wang,[‡] Xingmin Sun,[§] Zhi-Fei Chen,[∥] and Ya-Xian Yan[*,‡]

[‡]Shanghai Key Laboratory of Veterinary Biotechnology, School of Agriculture and Biology, Shanghai Jiao Tong University, Shanghai 200240, People's Republic of China

[§]Department of Infectious Disease and Global Health, Tufts University, Cummings School of Veterinary Medicine, 200 Westboro Road, North Grafton, Massachusetts 01536, United States

[∥]Shanghai Entry-Exit Inspection and Quarantine Bureau, Shanghai 200135, People's Republic of China

Supporting Information

ABSTRACT: A hypotoxic immunosorbent assay for the detection of zearalenone (ZEN) was developed, by identifying a single-stranded DNA (ssDNA) aptamer with high specificity and affinity for a ZEN monoclonal antibody (mAb-ZEN). ssDNA aptamers, which could mimic ZEN epitopes, were identified using the modified systematic evolution of ligands by an exponential enrichment (SELEX) technique. The purified mAb-ZEN was coated on microtiter plates as a target recognized by the random oligonucleotide ssDNA library. The binding affinity between the aptamers and mAb-ZEN during each round was measured by the biotin−streptavidin−horseradish peroxidase system. During 15 rounds of screening, an increasing binding affinity was observed. The enriched ssDNA library binding to mAb-ZEN with high affinity was cloned, sequenced, and analyzed. One aptamer (number 46), which displays the highest affinity and specificity for the mAb-ZEN, was used to establish an indirect competition enzyme-linked oligonucleotide assay (ELONA) to measure the ZEN concentration in corn. Under optimal conditions, the regression equation for quantification of ZEN was $y = -0.0778x + 0.713$ ($R^2 = 0.9981$). The detection limit and IC_{50} were 0.01 and 0.2 ng/mL, respectively, with a working range of 0.03−2.5 ng/mL. The recovery rates of the spiked samples in the ELONA ranged from 95 to 105%. Aptamers, which can mimic many types of low-weight analytes in agricultural products, could serve as surrogates for the development of hypotoxic, environmentally friendly immunological detection methods.

KEYWORDS: *aptamer, zearalenone, monoclonal antibody, affinity, ELONA*

INTRODUCTION

Zearalenone (ZEN) is a secondary metabolite produced by fungi belonging to the genus *Fusarium*, including *Fusarium graminearum* and *Fusarium roseum*, and a mycotoxin that contaminates various agricultural products worldwide.[1,2] ZEN is estrogenic and carcinogenic, causes DNA damage, and is reproductively toxic to humans and animals.[3] Infants and children are reported more vulnerable to the effects of ZEN than adults.[4] To decrease the incidence of ZEN-based toxicity in infants and children, the European Commission regulations specify a maximum ZEN level of 20 μg/kg in cereal-based foods manufactured for consumption by children.[5] This upper limit is considerably lower than the maximum amount permitted in cereals (100 μg/kg) for adults. The need for more stringent limits of ZEN levels in the foods of infants and young children has necessitated more sensitive measures. To this end, highly sensitive, rapid, and simple methods to monitor the ZEN content in food and feed products have been recently developed.

Currently, low-molecular-weight analytes (both free and conjugates) are widely used in quantitative chromatographic and immunologic assays to detect mycotoxin in agriculture commodities for production of food and feed products. However, some low-molecular-weight analytes are quite toxic (such as pesticides and mycotoxins), and the use of an analyte and/or it is conjugate in an assay may be harmful to the operator and/or environment. Furthermore, analytes are expensive to produce, and the efficiency of chemical conjugation between low-molecular-weight analytes and a carrier, such as a protein or enzyme, is low.[6] To improve the analytical methods, anti-idiotypic antibodies[7] and phage-displayed peptides[8] have been developed to mimic antigenic epitopes on analyte surfaces. However, screening of anti-idiotypic antibodies is costly and time-consuming. In addition, phage-displayed peptides can fail because of their inherent cytotoxicity. The systematic evolution of ligands by exponential enrichment (SELEX) technology was developed in the 1990s[9] to generate highly specific nucleic acid sequences (aptamers) with high affinity for various ligands. Recently, aptamers have

Received: August 6, 2014
Revised: December 4, 2014
Accepted: December 8, 2014
Published: December 8, 2014

ACS Publications © 2014 American Chemical Society

been widely used in diagnosis, detection, and chemical analysis of various substances, such as thrombin,[10] *Mycobacterium tuberculosis*,[11] and cocaine.[12] Aptamers have also been employed to mimic antibodies for detection of mycotoxins, such as ochratoxin A,[13,14] fumonisin B1 (FB1),[15] and ZEN.[16] In light of less expensive screening procedures, aptamers can now be used to mimic analytes and are more suitable than phage-displayed peptides and anti-idiotypic antibodies for hypotoxic analysis. To date, however, there have been no studies to develop aptamers as specific binding antibodies for the detection of low-molecular-weight analytes in agricultural products. In this study, we identified and charactierzed a single-stranded DNA (ssDNA) aptamer, which recognizes a monoclonal antibody against ZEN with high specificity and affinity. A hypotoxic immunoassay to detect ZEN was developed using this ssDNA aptamer to replace the ZEN conjugation, thereby avoiding environmental and operator exposure to toxin. Multiple low-molecular-weight analytes can be analyzed simultaneously using aptamers and an enzyme-linked oligonucleotide assay (ELONA) in the future, which offers several advantages over other methods, such as high sensitivity, rapidity, and safety.

MATERIALS AND METHODS

Materials. ZEN and FB1 were purchased from Sigma Chemical (St. Louis, MO). Monoclonal antibodies (mAb) against ZEN (2C9, mAb-ZEN) and FB1 (6H3, mAb-FB1) were generated in our laboratory.[17,18] Aflatoxin B1 (AFB1), deoxynivalenol (DON), and mAbs against DON (mAb-DON) or AFB1 (mAb-AFB1) were obtained from Huaan Megnech (Beijing, China). EasyTaq PCR MasterMix and a 50 base pair (bp) DNA ladder were purchased from CWbio (Beijing, China). A 20 bp DNA ladder was purchased from Thermo Scientific (Bremen, Germany). A UNIQ-10 column polyacrylamide gel electrophoresis (PAGE) gel extraction kit was purchased from Sangon Biotech (Shanghai) Co., Ltd. (Shanghai, China). Dynabeads M-280 streptavidin was purchased from Invitrogen (Grand Island, NY). Horseradish peroxidase (HRP)-conjugated streptavidin was purchased from AnaSpec (Fremont, CA), and the pMD18-T vector was purchased from TaKaRa Bio, Inc. (Tokyo, Japan). A plasmid extraction kit was purchased from Omega Bio-Tek (Norcross, GA). A random ssDNA library with strands of an overall length of 71 nucleotides (nt) containing a 35 nt random sequence flanked by two 18 nt constant sequences (5′-CGGAATTCTT-GATGTTGC-[35 nt]-CAACTTAGTAGGATCCCG-3′), a forward primer (P1, 5′-CGGAATTCTTGATGTTGC-3′), a reverse primer (P2, 5′-CGGGATCCTACTAAGTTG-3′), and a biotin-labeled forward primer (biotin-P1, 5′-biotin-CGGAATTCTTGATGTTGC-3′) used for amplification of double-stranded DNA (dsDNA) were synthesized by Sangon Biotech (Shanghai, China). The ZEN-free corn samples were provided by the Shanghai Entry−Exit Inspection and Quarantine Bureau (Shanghai, China).

Equipment. A NanoDrop 1000 spectrophotometer and 37 °C incubator were purchased from Thermo Scientific (Bremen, Germany); microtiter plates were purchased from Greiner Bio-One GmbH (Frickenhausen, Germany); and a microplate reader was purchased from BioTek Instruments, Inc. (Winooski, VT).

SELEX Screening Procedure. The purified anti-ZEN mAb (mAb-ZEN) was diluted to 10 μg/mL with coating buffer (50 mM carbonate buffer at pH 9.6). Three antibodies (mAb-FB1, mAb-AFB1, and mAb-DON) were mixed with equal concentrations and volumes and diluted to 10 μg/mL with coating buffer. Antibody solution (100 μL) was added to each microtiter plate well, followed by incubation at 4 °C overnight. The antigen-coated microtiter plate was washed 3 times with 10 mM phosphate-buffered saline (PBS) containing 0.05% Tween-20 (PBST) then blocked with 3% bovine serum albumin (BSA) at 37 °C for 2 h, followed by washing with PBST 3 times. The 20 μL original random ssDNA pool was dissolved in 500 μL of binding buffer (pH 7.4, containing 20 mM Tris−HCl, 100 mM NaCl, 5 mM KCl, 1 mM $CaCl_2$, and 2 mM $MgCl_2$), denatured at 94 °C for 10 min, and immediately cooled on ice for 10 min, followed by incubation at room temperature for 10 min. The denatured 100 μL ssDNA pool solution was added to blank wells coated with 3% BSA only as a negative control and incubated at 37 °C for 1 h to remove residual ssDNA bound to the BSA. Then, 100 μL of the counter BSA-treated ssDNA solution was added to the antibody mixture wells and incubated at 37 °C for 1 h to further subtract the residual ssDNA bound to the three antibodies (mAb-FB1, mAb-AFB1, and mAb-DON) as a second counter selection to increase the specificity and affinity of the selected ssDNA pool. Thereafter, the counter BSA and three antibody-selected ssDNA solution was moved to the mAb-ZEN-coated wells and incubated at 37 °C for 1 h. After washing with washing buffer (0.02−0.05% Tween in binding buffer) 5 times to remove unbound ssDNA, 100 μL of elution buffer (20 mM Tris-HCl, 4 M guanidine thiocyanate, and 1 mM dithiothreitol) was added to the wells and the plates were incubated at 80 °C for 10 min to dissociate the ssDNA from the antibodies. The eluted ssDNA was extracted using phenol/chloroform/isoamyl alcohol and precipitated with ethanol. Finally, the selected ssDNA was dissolved in 20 μL of TE buffer (10 mM Tris-HCl and 1 mM ethylenediaminetetraacetic acid at pH 8.0) and stored at −20 °C for future use. To improve the specificity and affinity of the selected ssDNA pool, the amounts of ssDNA and mAb-ZEN, incubation time of the ssDNA with the target IgG, and Tween concentration in the washing buffer were changed in subsequent selection rounds, as shown in Supplementary Table 1 of the Supporting Information.

Optimization of Symmetry and Asymmetry Polymerase Chain Reaction (PCR). To enrich the eluted ssDNA pool of each round of selection, dsDNA was generated by PCR in 25 μL reactions consisting of 12.5 μL of 2× EasyTaq PCR MasterMix, 1.0 μL of eluted ssDNA as a template, 1.0 μL of forward primer (biotin-P1), 1.0 μL of reverse primer (P2), and 9.5 μL of deionized water. Amplification consisted of a pre-denaturation cycle at 94 °C for 5 min, followed by denaturation at 94 °C for 30 s, annealing at 50 °C for 30 s, and extension at 72 °C for 20 s. One sample was taken out at each 5, 8, 12, 16, 20, and 25 cycle for amplification analysis. All remaining samples underwent a final extension cycle at 72 °C for 2 min. The PCR products were then separated by 12% PAGE and stained with silver nitrate.[19]

After generation of the dsDNA via symmetry PCR, asymmetry PCR was employed to produce a sufficient amount of ssDNA for affinity assays. The asymmetry PCR was performed in a 25 μL reaction volume consisting of 12.5 μL of 2× EasyTaq PCR MasterMix, 1.0 μL of dsDNA as a template, 1.0 μL of forward primer (biotin-P1), 1.0 μL of reverse primer (P2), and 9.5 μL of deionized water. To optimize the yield of ssDNA, the ratios of forward and reverse primers were tested at 1:0, 10:1, 30:1, 50:1, 80:1, and 100:1. The amplification conditions for the asymmetry PCR were performed as described above for the symmetry PCR. All PCR samples were separated on denaturing 8% PAGE containing 7 M urea, and the ssDNA band was extracted from the gel using the UNIQ-10 spin column DNA gel extraction kit as described in the manual. Purified ssDNA was stored at −20 °C until use in the ELONA to determine the optical density (OD) in 450 nm.

OD Values in ELONA and Specificity Assay of ssDNA in Each Screening Round. Each well of the microtiter plate was coated with 100 μL (1 μg/mL) of mAb-ZEN and incubated at 4 °C overnight. After washing with PBST 3 times, the coated wells were blocked with 3% BSA. Then, 50 μL of biotinylated ssDNA aptamer (100 pM), which was generated in the asymmetry PCR assay, was mixed with 50 μL of binding buffer, added to the antibody-coated wells, and incubated at 37 °C for 1 h. After washing, 100 μL of 1 μg/mL HRP-conjugated streptavidin was added to the wells and the plate was incubated at 37 °C for 1 h. After washing 3 times, 100 μL of substrate solution [3,3′,5,5′-tetramethylbenzidine (TMB)] was added to the wells and the plates were incubated at 37 °C for 10 min. Finally, 50 μL of 2 M H_2SO_4 was added to stop the reaction, and the absorbance of the wells was determined using a microplate reader at 450 nm. The ELONA was performed in triplicate.

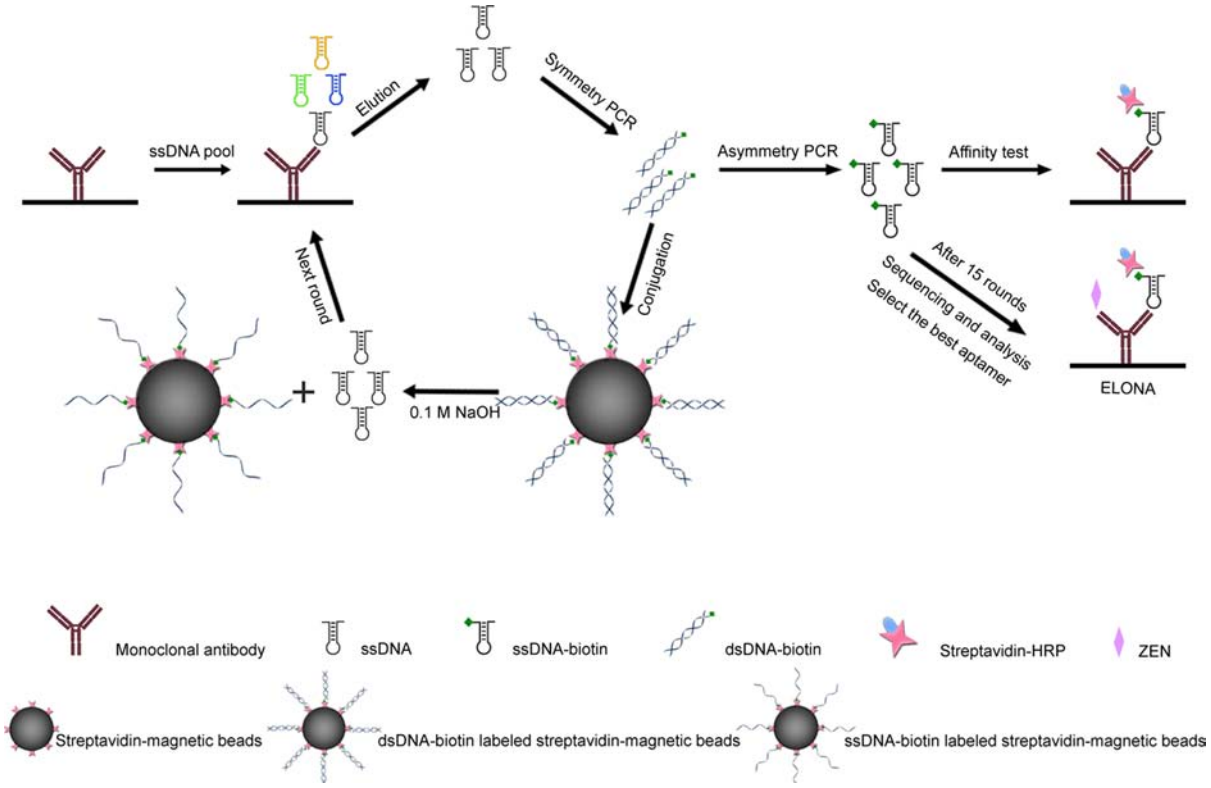

Figure 1. Schematic illustration of ssDNA screening and ELONA.

Preparation of a ssDNA Library Using Streptavidin-Coated Magnetic Beads. To yield a sufficient quantity of ssDNA for use as a seed pool in the next screening round, the selected ssDNA pool from each round of screening was used as a PCR template to generate dsDNA with primer pair biotin-P1 and P2 under the PCR reaction conditions as described above. Two strands of the PCR products were separated and the non-biotinlated ssDNA was recovered using streptavidin-coated magnetic beads. Briefly, the magnetic beads (100 μL containing about 6−7 × 10^7 Dynabeads) were separated from the storage buffer (PBS at pH 7.4 with 0.1% BSA and 0.02% sodium azide, v/v) in a magnetic field and washed 3 times with 2× binding and washing buffer (BW buffer, 10 mM Tris-HCl at pH 7.5 with 1 mM ethylenediaminetetraacetic acid and 2 M NaCl). A total of 200 μL of dsDNA was mixed with the magnetic beads and shaked gently for 20 min at room temperature. Then, the tube containing the mixture was placed under a magnetic field; the supernatant was removed; and the beads were washed 3 times in BW buffer. A total of 50 μL of 0.1 M NaOH was added to the tube containing beads and incubated at 37 °C for 30 min to uncoil the dsDNA. After the tube was placed in a magnetic field, non-biotinylated ssDNA was separated, while biotinylated ssDNA remained bound to the streptavidin beads. The supernatant containing the non-biotinylated ssDNA was recovered.

Aptamer Sequence Analysis. After the final selection round, the eluted ssDNA aptamer was used as a template to generate dsDNA by PCR amplification. The purified dsDNA was cloned into the pMD-18T. A total of 96 clones was randomly selected and sequenced by Sangon Biotech (Shanghai, China). The sequences were analyzed for homology and secondary structures using DNAMAN software (Lynnon Corporation, Pointe-Claire, Quebec, Canada). The clones with the correct sequences were used to prepare biotinylated ssDNA via asymmetry PCR amplification. The affinity and specificity of the ssDNA were also detected as described above.

The binding of the selected ssDNA to mAB-ZEN was determined in a way similar to that used in the SELEX screening procedure. Briefly, the plate was coated with 100 μL per well of diluted mAb-ZEN and blocked with 3% BSA. Then, different concentrations of ssDNA aptamer (from 0 to 1000 nM) were added in the wells and incubated at 37 °C for 1 h. After washing with washing buffer 5 times, 100 μL of elution buffer was added to the wells and the plates were incubated at 80 °C for 10 min to dissociate the ssDNA from mAb-ZEN. The eluted ssDNA was quantified using a NanoDrop 1000 spectrophotometer. Each concentration of ssDNA was determined in triplicate. The data were analyzed by GraphPad Prism 5 to fit the nonlinear specific binding curve, and the equilibrium dissociation constant (K_d) was calculated.

ELONA Development To Determine the ZEN Content. The ELONA was developed on the basis of the selected ssDNA aptamer, which had a relatively higher specificity and affinity. The concentrations of coating antibody, aptamer, and HRP-conjugated streptavidin were optimized by chessboard titration. The optimal ELONA contitions were as follows: a 100 μL aliquot of mAb-ZEN diluted to 1 μg/mL was added to each well of a microtiter plate and incubated at 4 °C overnight. After washing, 3% BSA was added to each well and the plate was incubated at 37 °C for 2 h. ZEN standard solutions (50 μL; 50, 10, 1, 0.1, 0.01, 0.001, 0.0001, and 0 ng/mL) were mixed with an equal volume of biotinylated ssDNA aptamer (100 pM). Each concentration of the standard was added to the plate in triplicate, which was incubated at 37 °C for 1 h and then washed 3 times. Afterward, 100 μL of HRP-conjugated streptavidin (1 μg/mL) was added to each well, and the plate was incubated at 37 °C for 1 h. After washing, 100 μL of TMB buffer was added to each well and the plate was incubated at 37 °C for 10 min. To stop the reaction, 50 μL of 2 M H_2SO_4 was added. The OD of the wells at 450 nm was recorded in a microplate reader. The standard curves were prepared using Origin 8.0 software (Northampton, MA). The log-transformed ZEN concentration was used as the x axis of the standard curve, and the y axis (B/B_0) represents the OD value of the standard solutions divided by the OD value at 0 ng/mL.

A schematic of ssDNA screening and the principle of ELONA is shown in Figure 1.

Specificity Study of the ELONA. To evaluate the specificity of the ssDNA-based ELONA, cross-reactivity of other mycotoxins (AFB1, FB1, and deoxynivalenol) with the anti-ZEN mAb was

dx.doi.org/10.1021/jf503733g | J. Agric. Food Chem. 2015, 63, 136−141

determined using the following formula (IC_{50} indicates the 50% inhibiton):

$$\text{cross-reactivity (\%)} = \frac{IC_{50} \text{ for ZEN}}{IC_{50} \text{ for other mycotoxins}} \times 100\%$$

Recovery Study. The extracts of corn samples were prepared as described previously,[20−25] and ZEN concentrations in the spiked samples were determined using a mAb-2C9-based enzyme-linked immunosorbent assay (ELISA)[17] and ssDNA-based ELONA. ZEN-free corn samples were ground and dried in a 60 °C incubator overnight. Standard ZEN solution was added to 10 g corn samples (1, 10, and 50 μg/kg for the ELONA and 50, 100, and 150 μg/kg for the ELISA) and allowed to incubate at room temperature overnight. Then, 40 mL of methanol/water (70:30, v/v) was added to each sample and shaken vigorously for 30 min at room temperature on a horizontal shaker. After an additional 10 min incubation period, the supernatant was centrifuged at 4000*g* for 20 min. For the 2C9-based ELISA, the supernatant was diluted 5-fold with 10 mM PBS, and for the ELONA, the supernatant was diluted 5-fold with binding buffer before analysis. Then, the extracts of the spiked samples were analyzed by ELISA and ELONA to determine the ZEN recovery rates. All spiked samples were analyzed in triplicate.

RESULTS AND DISCUSSION

Optimization of PCR Reaction Conditions. For the symmetry PCR, after 5, 8, 12, 16, 20, and 25 cycles of amplification, the dsDNA was analyzed by 12% PAGE. The results showed that, after 20 cycles, the yield of dsDNA reached a maximum and, after 25 cycles, the amount of non-specific DNA was greatest. Thus, 20 cycles were chosen for subsequent amplifications. Meanwhile, the annealing temperature (50−60 °C) had no effect on PCR amplification.

For the asymmetry PCR, different ratios of forward and reverse primers (1:0, 10:1, 30:1, 50:1, 80:1, and 100:1) were evaluated to generate higher amounts of ssDNA. As shown in Supplementary Figure 1 of the Supporting Information, the optimal ratio of forward and reverse primers was 80:1, giving the highest yield of ssDNA. The cycles of the asymmetry PCR were also optimized, and 30−35 cycles were the optimal amplification cycles to produce the highest amount of specific ssDNA (see Supplementary Figure 2 of the Supporting Information).

Selection of the ssDNA Aptamer Recognizing the Monoclonal Antibody. The affinity of each round of ssDNA for the anti-ZEN mAb was evaluated using a biotin−streptavidin−HRP-based ELISA. The OD values from rounds 1−15 are shown in Figure 2. The results indicate that affinity increased more than 5-fold after 15 rounds of screening, with OD values reaching a maximum after round 12.

Aptamer Sequence Analysis, Affinity, and Specificity. After 15 rounds of selection, the enriched ssRNA pool was amplified by PCR and cloned into the pMD-18T vector. A total of 96 clones were selected for sequencing. Of these, 63 clones had a complete genome length of 71 nt covering a 35 nt random sequence flanked by two 18 nt constant sequences.

Biotin-conjugated ssDNA aptamers were generated by asymmetric PCR using the 63 clones as templates. The affinities and specificities of 63 ssDNA aptarmers for mAb-ZEN as well as mAb-AFB1, mAb-FB1, and mAb-deoxynivalenol were determined by ELONAs using $OD_{450\ nm}$ values as readouts. All 63 aptamers show no specific binding to mAb-AFB1, mAb-FB1, and mAb-deoxynivalenol (data not shown), and 10 ssDNA aptamers with higher affinity in ELONA are listed in Table 1. The free energy (ΔG), which indicates the stability of the ssDNA, was predicted using DNAMAN software, and the results are also shown in Table 1.

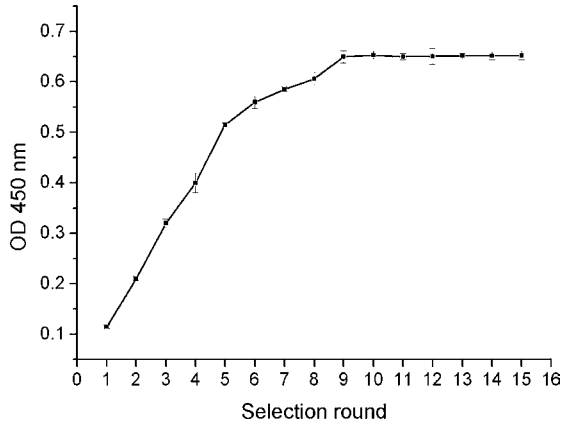

Figure 2. OD value of each round of ssDNA library screening using the biotin−streptavidin−HRP-based ELISA. The error bars indicate the interday standard deviation.

The putative secondary structures of these 10 aptamers were predicted using DNAMAN software and are shown in Supplementary Figure 3 of the Supporting Information. The main structure was a stem loop, which may bind antibody using this specific structure or through additional folding.

Development of an ELONA To Determine the ZEN Content Based on the Selected Aptamer. On the basis of sequence structure, affinity, and specificity analyses in ELONA, aptamers 46, 54, and 72 were used to develop the ELONAs to determine the ZEN concentration in samples. Aptamer 46, which shows better sensitivity and detection limit, was chosen for further studies and optimization of the ELONA. The K_d between aptamer number 46 and mAb-ZEN was 50.5 ± 5.4 nM. The binding saturation curve is shown in Supplementary Figure 4 of the Supporting Information. The optimal concentrations of coating antibody and HRP-conjugated streptavidin were 1 and 3 μg/mL, respectively, and the optimal dilution ratio of the aptamers was 1:10 (100 pM). The standard curve of this ELONA is shown in Figure 3. The regression equation for ZEN quantification was $y = -0.0778x + 0.713$ ($R^2 = 0.9981$). The detection limit and half maximal inhibitory concentration (IC_{50}) were 0.01 and 0.2 ng/mL, respectively, with a working range of 0.03−2.5 ng/mL. The intra- and interday standard deviations were 7.6 and 9.3% (data not shown), respectively, which indicates that this method had good reproducibility. Moreover, there were no competitive combining abilities of AFB1, FB1, and DON with the anti-ZEN mAb (cross-reactivity < 0.01%) in the ELONA using ssDNA aptamer number 46. These results indicate that this method has good specificity for ZEN. Thus, the best aptamer should be considered with the comprehensive factors, such as K_d values, OD values in ELONA, free energy, and detection sensitivity.

Recovery Rates of the ZEN Content in ELONA and ELISA. Previously, we showed that the limit of detection and IC_{50} are 0.051 and 1.9 ng/mL in ELISA, respectively.[17] Thus, the sensitivity of the ELONA (0.01 and 0.2 ng/mL for detection limit and IC_{50}, respectively) is greater than that of ELISA (Table 2). The 1, 10, and 50 μg/kg spiked corn samples were analyzed by ELONA, while 50, 100, and 150 μg/kg were determined by ELISA. As shown in Table 2, the recovery rates of the spiked samples in the ELONA ranged from 95 to 105%. Both the ELONA and ELISA could accurately detect ZEN

dx.doi.org/10.1021/jf503733g | J. Agric. Food Chem. 2015, 63, 136−141

Table 1. Sequences, Free Energy, and Affinity of Selected Aptamers

number	sequence (5′−3′)	free energy, ΔG (kcal/M)	OD at 450 nm
11	GGGATCCTACTAAGTTGACACAACAACCGAAATAACCTATACGCGCACACCAGCAACATCAAGAATTCCGAA	−2.85	0.61
33	GGGATCCTACTAAGTTGACAAGACACAACGCAGAGAAAGAAGCGTCGGAGGCAACATCAAGAATTCCGAA	−0.96	0.604
39	GGAATTCTTGATGTTGCAGCCTCCCGTAGTTTGCGTGTTTGTTGTGTGTGTGCAACTTAGTAGGATCCCGAA	−2.45	0.606
40	GGAATTCTTGATGTTGCTGGCTCGGCGGGTATTTCCAATGCGCGGGGGGTTTCAACTTAGTAGGATCCCGAA	−3.47	0.614
41	TTATTCTTGATGTTGCTCGACGACACACGCCTTATTTAGATGAAACTTCTGCAACTTAGTAGGATCCCGAA	−0.60	0.617
46	GGAATTCTTGATGTTGCCTGGGATTGTTTGGGCCTTGTGTTTTCTTCCGTTCCAACTTAGTAGGATCCCGAA	−2.34	0.756
47	GGAATTCTTGATGTTGCATTCTTGTACACCTCTCTCTGTGTCTCTCTTCTATCAACTTAGTAGGATCCCGAA	−0.99	0.64
54	GGGATCCTACTAAGTTGACAGCACCGGAATACACTCCACTCACGCGTCGACTGCAACATCAAGAATTCCGAA	−3.93	0.617
72	GGGATCCTACTAAGTTGGGAATAAAACTAACAAACGAACTCCGCTCAAGCCGGCAACATCAAGAATTCCGAA	−5.30	0.63
77	GGAATTCTTGATGTTGCATCTTGTGGCTTTTCTCTTTTTCGCGTCATATGGGCAACTTAGTAGGATCCCGAA	−2.34	0.663

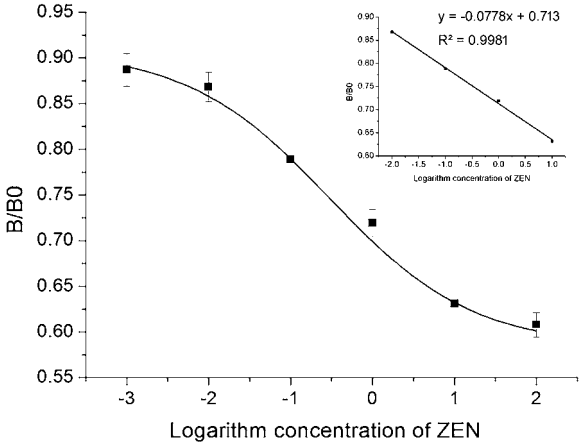

Figure 3. Standard curve of the DNA aptamer-based ELISA. The error bars indicate the interday standard deviation. The log-transformed ZEN concentration was used as the x axis of the standard curve, and the y axis (B/B_0) represents the OD value of the standard solutions divided by the OD value at 0 ng/mL.

Table 2. Recovery Rates of Spiked Samples by ELONA and ELISA

	ELONA		ELISA	
spiked (μg/kg)	found (μg/kg) (mean ± SD[a])	recovery rate (%)	found (μg/kg) (mean ± SD[a])	recovery rate (%)
1	0.97 ± 0.03	97	*b*	*b*
10	10.5 ± 0.42	105	*b*	*b*
50	47.7 ± 1.56	95	48.4 ± 1.43	97
100	*b*	*b*	96.1 ± 3.56	96
150	*b*	*b*	137 ± 7.14	91

[a]SD = standard deviation (n = 3). [b]Not detected.

from the spiked samples and showed similar sensitivity in determining the ZEN content in the 50 μg/kg spiked sample.

As shown in Supplementary Table 2 of the Supporting Information, many highly sensitive analytical methods have been proposed to detect mycotoxins in agricultural products. Because the ELONA is an easy, rapid, and hypotoxic method, it is a significant improvement in detecting mycotoxins compared to other highly sensitive methods, including electrochemical sensor, immunoassay, and surface plasmon resonance. In addition, the ssDNA aptamer method has several advantages over the phage-displayed peptide technology, which can also mimic an antigenic epitope in a hypotoxic method,[8] including no requirement for bacterial transformation and protein expression.[12,13] Preparation of ssDNA aptamers is relatively easier, less expensive, and less time-consuming than phage-displayed peptides, and aptamers usually have greater specificity and affinity for their targets.

In conclusion, in this study, ssDNA aptamers against ZEN mAb were selected and identified. Aptamer number 46, which had a lower ΔG and higher affinity, specificity, and sensitivity than other aptamers, was chosen as a ZEN substitute to develop an ELONA for determination of the ZEN content in corn. This ELONA is less expensive and has greater sensitivity than previous hypotoxic screening technologies. The sensitivity and stability may be improved further by new detection platforms and optimization. Other aptamer-based hypotoxic analytical methods, such as fluorescent strip sensors,[14] electrochemical immunoassays, and chemiluminescence immunoassays could be developed in the future.

■ ASSOCIATED CONTENT

Supporting Information

product of asymmetric PCR with different ratios of forward and reverse primer (Supplementary Figure 1), product of different asymmetric PCR cycles (Supplementary Figure 2). secondary structure of the selected aptamers (Supplementary Figure 3), binding saturation curve of number 46 aptamer to a mAb-ZEN-coated plate (Supplementary Figure 4), protocol of aptamer screening in different rounds (Supplementary Table 1), and comparison of high sensitivity and hypotoxic analytical methods for detection of ZEN (Supplementary Table 2). This material is available free of charge via the Internet at http://pubs.acs.org.

■ AUTHOR INFORMATION

Corresponding Authors

*Telephone: +86-2134206926. E-mail: sunjhe@sjtu.edu.cn.
*Telephone: +86-2134206003. E-mail: yanyaxian@sjtu.edu.cn.

Author Contributions

†Yuan-Kai Wang and Qi Zou contributed equally to this work.

Funding

This work was financially supported by the Chinese National Programs for High Technology Research and Development (2007AA10Z424).

Notes

The authors declare no competing financial interest.

■ ACKNOWLEDGMENTS

The authors thank Dr. Diane Schmidt (Tufts University) for critical review of the manuscript.

REFERENCES

(1) Placinta, C. M.; D'Mello, J. P. F.; Macdonald, A. M. C. A review of worldwide contamination of cereal grains and animal feed with *Fusarium* mycotoxins. *Anim. Feed Sci. Technol.* **1999**, *78*, 21−37.

(2) Tanaka, K.; Sago, Y.; Zheng, Y.; Nakagawa, H.; Kushiro, M. Mycotoxins in rice. *Int. J. Food Microbiol.* **2007**, *119*, 59−66.

(3) Kim, I. H.; Son, H. Y.; Cho, S. W.; Ha, C. S.; Kang, B. H. Zearalenone induces male germ cell apoptosis in rats. *Toxicol. Lett.* **2003**, *138*, 185−192.

(4) European Food Safety Authority (EFSA).. Scientific opinion on the risks for public health related to the presence of zearalenone in food. *EFSA J.* **2011**, *9*, 2197−2321.

(5) European Commission.. European Commission Regulation (EC) no. 856/2005 of 6th June 2005, amending Regulation (EC) no. 466/2001 as regards *Fusarium* toxins. *Off. J. Eur. Union* **2005**, *143*, 3−8.

(6) Xiao, H.; Clarke, J. R.; Marquardt, R. R.; Frohlich, A. A. Improved methods for conjugating selected mycotoxins to carrier proteins and dextran for immunoassays. *J. Agric. Food Chem.* **1995**, *43*, 2092−2097.

(7) Yu, F. Y.; Chu, F. S. Production and characterization of a monoclonal anti-anti-idiotype antibody against fumonisin B1. *J. Agric. Food Chem.* **1999**, *47*, 4815−4820.

(8) He, Q. H.; Xu, Y.; Huang, Y. H.; Liu, R. R.; Huang, Z. B.; Li, Y. P. Phage-displayed peptides that mimic zearalenone and its application in immunoassay. *Food Chem.* **2011**, *126*, 1312−1315.

(9) Ellington, A. D.; Szostak, J. W. *In vitro* selection of RNA molecules that bind specific ligands. *Nature* **1990**, *346*, 818−822.

(10) White, R.; Rusconi, C.; Scardino, E.; Wolberg, A.; Lawson, J.; Hoffman, M.; Sullenger, B. Generation of species cross-reactive aptamers using "Toggle" SELEX. *Mol. Ther.* **2001**, *4*, 567−573.

(11) Chen, F.; Zhou, J.; Luo, F.; Mohammed, A.-B.; Zhang, X.-L. Aptamer from whole-bacterium SELEX as new therapeutic reagent against virulent *Mycobacterium tuberculosis*. *Biochem. Biophys. Res. Commun.* **2007**, *357*, 743−748.

(12) Stojanovic, M. N.; de Prada, P.; Landry, D. W. Aptamer-based folding fluorescent sensor for cocaine. *J. Am. Chem. Soc.* **2001**, *123*, 4928−4931.

(13) Cruz-Aguado, J. A.; Penner, G. Determination of ochratoxin a with a DNA aptamer. *J. Agric. Food Chem.* **2008**, *56*, 10456−10461.

(14) Wang, L.; Chen, W.; Ma, W.; Liu, L.; Zhao, Y.; Zhu, Y.; Xu, L.; Kuang, H.; Xu, C. Fluorescent strip sensor for rapid determination of toxins. *Chem. Commun. (Cambridge, U. K.)* **2011**, *47*, 1574−1576.

(15) McKeague, M.; Bradley, C. R.; Girolamo, A. D.; Visconti, A.; Miller, J. D.; DeRosa, M. C. Screening and initial binding assessment of fumonisin B1 aptamers. *Int. J. Mol. Sci.* **2010**, *11*, 4864−4881.

(16) Chen, X.; Huang, Y.; Duan, N.; Wu, S.; Ma, X.; Xia, Y.; Zhu, C.; Jiang, Y.; Wang, Z. Selection and identification of ssDNA aptamers recognizing zearalenone. *Anal. Bioanal. Chem.* **2013**, *405*, 6573−6581.

(17) Wang, Y. K.; Wang, J.; Wang, Y. C.; Chen, Z. F.; Yan, Y. X.; Hao, Q. W.; Li, S. Q.; Yu, C.; Yang, C. Y.; He, S. J. Preparation of anti-zearalenone monoclonal antibodies and development of an indirect competitive ELISA for zearalenone. *Microbiol. China* **2011**, *38*, 1793−1800.

(18) Wang, Y. C.; Wang, J.; Wang, Y. K.; Yan, Y. X. Preparation of monoclonal antibodies and development of an indirect competitive ELISA for fumonisin B-1 detection. *J. Shanghai Jiaotong Univ., Agric. Sci.* **2011**, *29*, 69−74.

(19) Morrissey, J. H. Silver stain for proteins in polyacrylamide gels: A modified procedure with enhanced uniform sensitivity. *Anal. Biochem.* **1981**, *117*, 307−310.

(20) Chen, J.; Fang, Z.; Liu, J.; Zeng, L. A simple and rapid biosensor for ochratoxin A based on a structure-switching signaling aptamer. *Food Control* **2012**, *25*, 555−560.

(21) Wang, Y. K.; Shi, Y. B.; Zou, Q.; Sun, J. H.; Chen, Z. F.; Wang, H. a.; Li, S. Q.; Yan, Y. X. Development of a rapid and simultaneous immunochromatographic assay for the determination of zearalenone and fumonisin B1 in corn, wheat and feedstuff samples. *Food Control* **2013**, *31*, 180−188.

(22) Hervás, M.; López, M. Á.; Escarpa, A. Electrochemical immunoassay using magnetic beads for the determination of zearalenone in baby food: An anticipated analytical tool for food safety. *Anal. Chim. Acta* **2009**, *653*, 167−172.

(23) Wang, Y. K.; Yan, Y. X.; Mao, Z. W.; Wang, H. a.; Zou, Q.; Hao, Q. W.; Ji, W. H.; Sun, J. H. Highly sensitive electrochemical immunoassay for zearalenone in grain and grain-based food. *Microchim. Acta* **2013**, *180*, 187−193.

(24) Wang, Y. K.; Yan, Y. X.; Ji, W. H.; Wang, H. A.; Zou, Q.; Sun, J. H. Novel chemiluminescence immunoassay for the determination of zearalenone in food samples using gold nanoparticles labeled with streptavidin−horseradish peroxidase. *J. Agric. Food Chem.* **2013**, *61*, 4250−4256.

(25) Choi, S. W.; Chang, H. J.; Lee, N.; Kim, J. H.; Chun, H. S. Detection of mycoestrogen zearalenone by a molecularly imprinted polypyrrole-based surface plasmon resonance (SPR) sensor. *J. Agric. Food Chem.* **2009**, *57*, 1113−1118.

JOURNAL OF AGRICULTURAL AND FOOD CHEMISTRY

Article

pubs.acs.org/JAFC

Straightforward Method To Quantify GSH, GSSG, GRP, and Hydroxycinnamic Acids in Wines by UPLC-MRM-MS

Anna Vallverdú-Queralt,*[,†,‡,§] Arnaud Verbaere,[§] Emmanuelle Meudec,[§] Veronique Cheynier,[§] and Nicolas Sommerer[§]

[†]Nutrition and Food Science Department, XaRTA, INSA, Pharmacy School, Av Joan XXIII s/n, University of Barcelona, Barcelona, 08028 Spain

[‡]CIBER Fisiopatología de la Obesidad y la Nutrición (CIBERobn), Instituto de Salud Carlos III, 28029 Madrid, Spain

[§]INRA, UMR1083 Sciences pour l'œnologie, Plateforme Polyphénols, 2, place Viala, Montpellier Cedex, 34060, France

ABSTRACT: A novel, robust and fast ultrahigh performance liquid chromatography−multiple reaction monitoring mass spectrometry method has been developed for the simultaneous quantification of reduced glutathione (GSH), oxidized glutathione (GSSG), grape reaction product (GRP) and hydroxycinnamic acids in wine. The method was evaluated in terms of linearity, precision, accuracy, limits of detection and quantification, stability and matrix effects. Quantitative recovery (74−110%) and satisfactory interday precision (RSD <14%) were achieved for all target compounds. No significant matrix-dependent suppression/enhancement effects were observed. To demonstrate the method applicability, white, rosé and red wine samples with different levels of oxidation were analyzed. Levels of GSH and GSSG varied from 1.63 to 9.91 mg/L and from 0.32 to 3.33 mg/L, respectively. Levels of caftaric acid ranged from 2.57 to 293.07 mg/L. Levels of GRP were between 28.35 and 114.20 mg/L.

KEYWORDS: *glutathione, hydroxycinnamic acids, UPLC-MRM-MS, method validation*

INTRODUCTION

Wine phenolics have been recently gaining interest because of their biological effects, including free-radical scavenging, metal chelation, inhibition of cellular proliferation, and modulation of enzymatic activity and signal transduction pathways.[1] Hydroxycinnamic acids, and especially the tartaric esters of caffeic acid (caftaric acid) and of *p*-coumaric acid (coutaric acid), are the major phenolic compounds in grape flesh and consequently in juices and wines made with minimal skin contact.[2] During crushing and pressing, both of these molecules are oxidized to caftaric acid *O*-quinone under the action of grape polyphenoloxidase unless care is taken to avoid oxidation. The discovery of Grape Reaction Product (GRP),[3] identified as 2-S glutathionyl caftaric acid,[4] has provided evidence that grape also contains large amounts of glutathione (L-γ-glutamyl-L-cysteinyl-glycine, GSH), as GRP results from nucleophilic addition of glutathione onto caftaric acid quinone. Glutathione in plants is maintained in the reduced form by the ascorbate−glutathione cycle, and it is involved in the cell redox balance.[5−7] The ratio of caftaric and coutaric acids relative to GSH is a varietal characteristic and determines must susceptibility to oxidative browning. Glutathione, originating from the grape berry or from yeast metabolism, is also found in wines, where it occurs in both the reduced (GSH) and oxidized (GSSG) forms. Glutathione is attracting increasing interest because of its role as antioxidant in wine, limiting browning and protecting aroma compounds, as recently reviewed.[8] This role can be exerted through reduction of quinones and formation of GSSG, or via nucleophilic addition of glutathione on quinones, on aldehydes and/or on aldehyde condensation products with flavan-3-ols.[9]

Despite substantial interest in GSH and GSSG determination, the best protocol for sample preparation and analysis and quantification of these molecules is still investigated. Previously reported methods for the analyses of GSH and GSSG in wine musts include enzymatic assay,[10,11] high performance liquid chromatography (HPLC) with electrochemical detection,[12] without sample derivatization, and thiol derivatization followed by HPLC with UV detection[13−15] or fluorimetric detection.[16,17] Fluorimetric detection has been proved to be a fast and accurate method[18] but gives access only to GSH (or total glutathione after reduction of GSSG). Simultaneous detection of GSH and GSSG can be achieved by HPLC after derivatization of free amino groups.[19] In general, these methods are relatively complex and time-consuming and provide additional sources of variability and bias.[20] More recent methods involving mass spectrometry (MS) detection after HPLC separation of GSSG and GSH have been developed and applied to analyze both forms of glutathione in wine.[20,21] However, to the best of our knowledge, no method is available to analyze GSH, GSSG and hydroxycinnamic acids simultaneously. Therefore, the aim of this study is to provide a single, sensitive and rapid ultrahigh performance liquid chromatography-multiple reaction monitoring mass spectrometry (UPLC-MRM-MS) method without glutathione derivatization for the analysis of GSH, GSSG, GRP and hydroxycinnamic acids (ferulic, *p*-coumaric, caffeic, coutaric, fertaric and caftaric acids)

Received: September 12, 2014
Revised: November 21, 2014
Accepted: December 2, 2014
Published: December 2, 2014

ACS Publications © 2014 American Chemical Society

DOI: 10.1021/jf504383g
J. Agric. Food Chem. 2015, 63, 142−149

in white, rosé and red wines. The UPLC-MRM-MS method offers improved sensitivity, speed and resolution for analytical determinations, and it combines the advantage of high resolution chromatography and specific detection.

MATERIALS AND METHODS

Standards and Reagents. Methanol and formic acids were purchased from VWR Prolabo (Fontenay sous Bois. France). Caffeic, caftaric, ferulic and *p*-coumaric acids, GSH and GSSG were purchased from Sigma (Saint-Louis, MO, USA). Purified p-deionized water was used (Milli-Q purification system, Millipore, France) for the preparation of all solutions. All the standards were prepared with 1% formic acid in water.

Samples. The wines were provided by the INRA experimental winery at Pech Rouge (Gruissan, France). All selected wines were made from grapes harvested at commercial maturity, in September 2013, from the INRA Pech Rouge vineyard. The white and rosé wines were made from Viognier and Syrah varieties, respectively, using three processes differing in the extent of must oxidation. For each variety, the grapes were machine-harvested in two lots (1000 kg), either protected from oxidation (i.e., maintained under dry ice pellets from harvest through all the must processing stages) or nonprotected. After crushing and destemming, each grape lot was pressed by a 10 hL pneumatic press (Bucher Vaslin SA, Chalonnes sur Loire, France), to yield 60−65% must. The musts obtained by pressing each grape lot were supplemented with pectolytic enzymes (Rapidase clear, La Littorale, Montpellier, France) (2g h/L) and allowed to decant overnight at 10 °C in stainless steel tanks. A subsample (100 L) of the musts protected from oxidation was submitted to flash pasteurization (20 s, at 84 °C) to inhibit grape polyphenoloxidase (PPO). The six must samples (3 whites/3 rosés, without oxygen protection/with oxygen protection/with oxygen protection and flash pasteurized) were then inoculated with Fermicru rosé and Fermicru LVCB yeasts (Oenobrands SAS, Montpellier, France) (20g h/L) for rosé and white musts, respectively, and fermented to dryness.

The red wines were obtained from the same mechanically harvested Grenache noir grapes by traditional soaking (control) or flash détente, as described earlier.[22]

Characterization and Quantification of GSH, GSSG, GRP and Hydroxycinnamic Compounds. UPLC-MRM-MS analyses were carried out using an Acquity UPLC system (Waters, Saint-Quentin-en-Yvelines, France) hyphenated to a triple quadrupole (QqQ) TQD mass spectrometer (Waters, Saint-Quentin-en-Yvelines, France) operating in MRM mode with electrospray ionization (ESI) either in positive or negative ionization modes. The spectrometer was operated in the negative ion mode for the hydroxycinnamic acids and GRP and in the positive ion mode for the GSH and GSSG. The diode array detection (DAD) spectra were recorded in the range of 210−600 nm (resolution 1.2 nm).

The UPLC system included a binary pump, a cooled autosampler maintained at 7 °C and equipped with a 5-μL sample loop, a 100-μL syringe and a 30-μL needle, and a DAD. MassLynx software was used to control the instruments and to acquire the data and TargetLynx software was used to process the data. The column used for chromatographic separation was a reversed-phase Acquity HSS T3 1.8 μm 1.0 × 100 mm (Waters, Saint-Quentin-en-Yvelines, France) protected by a 0.2 μm in-line filter and maintained at 40 °C. The mobile phase consisted of 1% (v/v) formic acid in Milli-Q water (solvent A) and 1% (v/v) formic acid in methanol (solvent B). The elution program was as follows: isocratic for 8 min with 0% B, 0−35% B (2 min), 35−99% B (4 min) followed by washing and reconditioning of the column. The source and desolvation temperatures were respectively set at 120 and 450 °C. Nitrogen was used as desolvation (500 L/h) and cone (50 L/h) gas. Argon was used as collision gas at a flow rate of 0.16 mL/min. Capillary voltage was set at 3.5 kV in positive mode and 2.8 kV in negative mode.

Samples were diluted 2:3 (v/v) with 1% formic acid in water, filtered through a 0.22 μm PTFE filter (Waters) and injected into the column by using the Partial Loop with Needle Overfill injection mode with an injection volume of 1 μL. The flow rate was 0.170 mL/min and the oven temperature maintained at 40 °C. Two detectors were used: DAD and the QqQ detector. Validation of the method was carried out through standard addition method. GRP, coutaric and fertaric acids were quantified as mg equivalent caftaric acid.

Analytical Method Performances. The method was validated following the "Bioanalytical Method Validation" of the U.S. Department of Health and Human Services (Food and Drug Administration).[23] Validation assays were performed by means of standard-addition method in one red wine, one rosé wine and one white wine. The analytical method was checked for linearity, limit of detection (LOD), limit of quantification (LOQ), recovery, precision, stability and matrix effects.

Statistical Analysis. Statistical calculations were made using the GraphPad Prism version 5.0 package (GraphPad Software, San Diego, CA). Wine samples were analyzed in triplicate. Unless otherwise specified, data are presented as the mean ± SD. Statistical comparisons were performed using paired two-tailed Student's *t* test with the level of significance set at $p < 0.05$.

RESULTS AND DISCUSSION

Optimization and Validation of an UPLC-MRM-MS Method for the Analysis of GSH, GSSG, GRP and Hydroxycinnamic Acids. The main objective of the present work was to develop a rapid and simple method based on UPLC-MRM-MS for simultaneous determination of GSH, GSSG, GRP, and hydroxycinnamic acids in wine. Therefore, experiments were carried out in order to optimize their chromatographic separation and also their MRM detection. MRM is the method of choice for quantification in MS; it is both very sensitive and highly specific because it is based on the analysis of parent and fragment ions that are characteristic of each target molecule.[24]

The polar nature of GSH and GSSG requires the use of highly aqueous mobile phases to obtain a suitable retention under reversed-phase conditions. However, the loss in retention time may occur over time as a consequence of pore dewetting when using the conventional reversed-phase columns at 100% aqueous conditions. The selected column HSS T3 uses a trifunctional C_{18} phase bound at an intermediate ligand density, specially designed to be used with 100% aqueous mobile phases. Moreover, it was necessary to use an acidic mobile phase to improve the chromatographic behavior of the targeted compounds. Therefore, formic acid was selected because of its compatibility and volatility with ESI sources.[24] Two different proportions were tested (0.1% and 1%), and the best results were obtained using 1% formic acid in water. The optimized chromatographic conditions are detailed in the Materials and Methods.

For all target compounds, separation was achieved in less than 12 min. The UPLC-MRM-MS profiles obtained for all target compounds after injection of a white wine are presented in Figure 1 and Table 1. Direct infusion of standards in water 1% formic acid provided the fragmentation pattern and collision energy suitable for the sensitive detection of target analytes. For the compounds that are not available as standards, additional experiments have been performed by injecting the wines. ESI provided singly charged positive $[M + H]^+$ precursor ions for GSH and GSSG and singly charged negative $[M - H]^-$ ions for GRP and hydroxycinnamic acids. Two MRM ion transitions were selected for each compound (Table 1); the most intense transition was used for quantification, while the other one was employed for identification. For hydroxycinnamic acids, the main observed transition corresponded to a neutral loss of 44 u, i.e. CO_2, which is typical of compounds

DOI: 10.1021/jf504383g
J. Agric. Food Chem. 2015, 63, 142−149

Figure 1. UPLC-MS/MS chromatogram of a white wine with oxygen protection for GSH, GSSG, GRP and hydroxycinnamic acids.

having a carboxylic acid moiety. For hydroxycinnamic esters and for GRP, the main fragment ion corresponds to tartaric acid (m/z 149). Consequently, caftaric acid was used for calibration of coutaric acid, fertaric acid and GRP. For GSH and GSSG, the main transitions are neutral losses of 129 u, which is characteristic of glutathione (loss of glutamate).[25] Identifications were achieved by comparing the retention times and UV−visible and MS spectra with those of available standards

Method Validation. In order to assess the performance of the proposed method, the main analytical method performances were thoroughly evaluated (Table 2). The linearity of the method was tested using standard solutions at seven concentration levels from 0.5 to 100 mg/L for GSH, GSSG, caffeic, *p*-coumaric and ferulic acids. For caftaric acid, the linearity was checked from 0.5 to 500 mg/L. The method yielded linear responses up to 100 mg/L for GSH, GSSG, caffeic, *p*-coumaric and ferulic acids and up to 500 mg/L for caftaric acid. These are improved concentration ranges compared with those previously reported.[18,26,27] The weighted $(1/x)$ calibration curves $(y = ax + b)$ were found to be linear in the studied range with determination coefficients (R^2) ≥0.9889 and RSDs $(n = 3) \leq 5\%$.

Recovery and Precision. Recovery pertains to the efficiency of an analytical method within the limits of variability. Analyte recoveries were assessed by analyzing the percentage of recovery of each compound in wines. The samples were spiked at three concentration levels (2, 10, and 50 mg/L) of each compound before analysis. The spiked samples were prepared in triplicate and analyzed under the previously established optimal conditions. The percentage of recovery was calculated for each compound, while the corresponding relative standard deviation (R.S.D.) was representative for intraday precision. The interday precision (intermediate precision) was calculated from analyses performed in triplicate over three consecutive days, with five replicates per day. Each day, samples were prepared. The prepared concentration ranges were in accordance with the concentration ranges established in the linearity.

Quantitative recoveries at all three concentration levels tested in white, rosé and red wines ranged from 72% to 110% (Table 2). Both intra- and interday precision studies presented satisfactory results for all compounds in the three matrices tested, with RSDs below 7% and 13%, respectively, for white wine; below 12% and 14% for rosé wine, and below 9% and 14% for red wine (Table 2). For the values analyzed, recovery and precision were within the accepted values for the Bioanalytical Method Validation.[23]

Table 1. UPLC-DAD-MRM-MS Parameters for GSH, GSSG, GRP and Hydroxycinnamic Acids

Analytes	rt[a] (min)	ESI MODE	MRM transitions[b]	Collision energy (V)	Cone voltage (V)	UV−visible spectrum (max. wavelength)
GSH	0.97	Positive	308 → 179	12	22	
			308 → 76	26	22	
GSSG	1.84	Positive	613 → 355	20	36	
			613 → 177	34	36	
Caftaric acid	8.01	Negative	311 → 149	10	22	326
			311 → 179	16	22	
GRP	10.11	Negative	616 → 149	40	40	329
			616 → 167	40	50	
Coutaric acid	10.14	Negative	295 → 149	24	10	327
			295 → 163	24	10	
Caffeic acid	10.50	Negative	179 → 135	24	26	323
			179 → 79	14	26	
Fertaric acid	10.71	Negative	325 → 149	28	10	321
			325 → 193	28	10	
***p*-Coumaric acid**	11.12	Negative	163 → 119	14	26	309
			163 → 93	26	26	
Ferulic acid	11.38	Negative	193 → 178	14	26	323
			193 → 149	14	26	

[a]rt: retention time. [b]The first line reports the quantifier MRM transition and the second line the qualifier transition.

DOI: 10.1021/jf504383g
J. Agric. Food Chem. 2015, 63, 142−149

Table 2. Method Validation Parameters: Correlation Coefficients (R^2), Limits of Detection (LOD) and Quantification (LOQ), Recovery and Precisions Intra and Inter-day in White, Rosé and Red Wines

	GSH	GSSG	ferulic acid	caffeic acid	*p*-coumaric acid	caftaric acid
Red Wine						
r2	0.9902	0.9956	0.9953	0.9899	0.9913	0.9906
LOD (mg/L)	0.0045	0.0042	0.0203	0.0105	0.0095	0.0246
LOQ (mg/L)	0.0149	0.0139	0.0677	0.0350	0.0317	0.0821
Recovery (%)						
50 mg/L	98 ± 1	102 ± 2	97 ± 2	96 ± 5	95 ± 3	98 ± 1
10 mg/L	86 ± 1	83 ± 2	107 ± 5	108 ± 2	110 ± 5	90 ± 8
2 mg/L	106 ± 3	107 ± 3	75 ± 2	103 ± 3	101 ± 5	72 ± 1
precision intraday (RSD %)						
50 mg/L	1	2	2	1	2	2
10 mg/L	6	2	9	3	6	7
2 mg/L	1	3	2	6	4	3
precision interday (RSD %)						
50 mg/L	3	6	6	3	2	2
10 mg/L	13	9	12	7	10	10
2 mg/L	14	10	11	13	13	13
suppression/enhancement effect (%)	93 ± 4	92 ± 3	95 ± 2	104 ± 3	106 ± 2	104 ± 3
Rosé Wine						
r2	0.9901	0.9889	0.9952	0.9906	0.9903	0.9902
LOD (mg/L)	0.0018	0.0054	0.0294	0.0022	0.0007	0.0051
LOQ (mg/L)	0.0062	0.0180	0.0981	0.0075	0.0024	0.0170
Recovery (%)						
50 mg/L	103 ± 2	97 ± 3	99 ± 2	90 ± 6	95 ± 2	95 ± 1
10 mg/L	94 ± 2	101 ± 8	94 ± 4	92 ± 4	102 ± 1	95 ± 8
2 mg/L	89 ± 7	110 ± 4	75 ± 2	92 ± 2	83 ± 1	74 ± 1
precision intraday (RSD %)						
50 mg/L	2	4	8	9	3	4
10 mg/L	5	7	11	3	5	6
2 mg/L	9	12	7	11	8	10
precision interday (RSD %)						
50 mg/L	3	4	5	5	3	6
10 mg/L	6	11	7	6	4	5
2 mg/L	12	13	11	10	9	14
suppression/enhancement effect (%)	95 ± 3	93 ± 4	92 ± 4	102 ± 4	101 ± 3	103 ± 3
White Wine						
r2	0.9938	0.9915	0.9911	0.9911	0.9932	0.9919
LOD (mg/L)	0.0014	0.0038	0.0029	0.0014	0.0027	0.0037
LOQ (mg/L)	0.0046	0.0128	0.0096	0.0046	0.0093	0.0123
Recovery (%)						
50 mg/L	100 ± 4	95 ± 5	98 ± 3	96 ± 1	95 ± 2	94 ± 3
10 mg/L	91 ± 5	101 ± 7	98 ± 6	104 ± 5	97 ± 5	94 ± 4
2 mg/L	85 ± 2	97 ± 6	89 ± 2	92 ± 7	109 ± 6	110 ± 5
precision intraday (RSD %)						
50 mg/L	5	6	3	1	5	2
10 mg/L	5	6	5	7	6	4
2 mg/L	1	5	4	7	1	5
precision interday (RSD %)						
50 mg/L	4	10	6	7	6	7
10 mg/L	12	7	9	10	8	10
2 mg/L	12	6	13	12	13	13
suppression/enhancement effect (%)	98 ± 2	94 ± 4	93 ± 3	103 ± 3	97 ± 3	99 ± 2

Limits of Detection and Quantification. The sensitivity of the method was evaluated determining the LODs and LOQs. Regarding the two MRM transitions, the quantifier transition was used for quantitative purposes, while the confirmation transition was used for qualitative analysis and for the method limits. The LOD was calculated as the quantity of analyte able to produce a chromatographic peak three times higher than the noise of the baseline in a chromatogram (S/N = 3) of a sample. The LOQ was set at ten times higher than the noise of the baseline in a chromatogram (S/N = 10).[23] The LOD for GSH was 0.0014 and 0.0018 mg/L in white and rosé wines, respectively, whereas in red wines it was 0.0045 mg/L. For GSSG, the LOD ranged from 0.0038 to 0.0054 mg/L in white, rosé and red wines. The values of LOD and LOQ obtained in

DOI: 10.1021/jf504383g
J. Agric. Food Chem. 2015, 63, 142−149

our method are lower than those reported by other authors using MRM-MS. Du Toit et al.[21] reported a LOD of 0.2 mg/L in grape juice and wine for GSSG, while Mattivi et al.[20] reported LODs of 0.05 and 0.03 mg/L for GSH and GSSG, respectively. Our LODs and LOQs values are also lower than those reported using fluorescence detection after derivatization.[27,28] Marchand and de Revel[27] reported a LOD of 2.45 mg/L in white wine and 3.06 mg/L in red wine for GSSG. Janes et al.[28] reported a LOD and LOQ of 0.06 and 0.2 mg/L, respectively, in white grape juice and wine for GSH. However, Kritzinger et al.[29] reported similar LODs in white and red grape juice and wine to our method. For GSH, the LOD was 0.002 mg/L, and for GSSG, it was 0.001 mg/L.

The LODs for hydroxycinnamic acids in white wine ranged from 0.0014 mg/L for caffeic acid to 0.0037 mg/L for caftaric acid. In rosé and red wines, LODs were higher. The highest values were obtained for ferulic and caftaric acids. The LOD for ferulic acid was 0.0294 mg/L and 0.0203 mg/L in rosé and red wines, respectively. For caftaric acid, LODs were 0.0051 mg/L and 0.0246 mg/L in rosé and red wines, respectively, and similar to those reported by other authors.[30,31]

Stability. The chemical stability of an analyte under specific conditions for given time intervals can be assessed in several ways. Stability evaluations should cover the expected sample handling and storage conditions during the study. The stabilities studied were freeze and thaw stability and sample stability.

For the freeze/thaw stability, three freeze−thaw cycles were assessed in a mixture of the standards and on two wine samples (one rose and one white) used for the validation. No significant reduction of analyte concentrations in the standards or in wine samples was observed after the cycles.

The stability of the processed sample was studied from the moment the standards were prepared until the time the samples were analyzed in the autosampler, in this case about 24 h. There was a slight decrease in GSH (13%) and GSSG (7%) levels, while hydroxycinnamic acids remained stable over 24 h at 4 °C. Thus, it is recommended to prepare standards daily, at least for GSH and GSSG.

One area of concern in sample analysis is the introduction of relatively large amounts of salts or nonvolatile pollutants into the ion source, which may degrade the performance of the instrument. However, no deterioration in absolute sensitivity was observed over the course of each batch or between batches, and other assays run on the same instrument were unaffected after injection of wine samples. Moreover, no significant ($P > 0.05$) shift (±0.02 min) in retention times was observed over the course of the method development, validation, and subsequent application to real wine samples.

Matrix Effects. Finally, suppression/enhancement effects were also evaluated by calculating the ratio of the peak area of the analytes recorded for the sample spiked with the standards and the peak area of analytes recorded for the standard solution (expressed in percentage). Analyses were carried out in triplicate. In our study, no significant matrix-dependent suppression/enhancement effects were observed in the three matrices under the proposed UPLC-MRM-MS conditions (Table 2). In the evaluation of matrix effects, values lower than 100% indicate that matrix-dependent signal suppression occurs, while values higher than 100% indicate matrix-dependent signal enhancement. The eventual suppression and enhancement effects are generally matrix, analyte, method, and ion source dependent.[32]

Application to Wine Samples. The applicability of the proposed method was demonstrated by analyzing eight different wine samples: two red, three rosé and three whites wines. The three wines in the white and rosé series differed by the must preparation: nonprotected from oxygen exposure, protected from oxygen, protected from oxygen, and flash pasteurized to inhibit grape PPO. The two red wines were prepared from the same grapes by fermentation on pomace, respectively after destemming and crushing (control) or after flash détente. The latter process, which consists of rapidly heating the grapes in a closed tank and suddenly applying strong vacuum to induce fragilization of the grape cell walls and instant cooling of the grapes, enhances phenolic extraction. Two to 14-fold increases in hydroxycinnamic acid contents have been reported in wines obtained using this technique compared to the corresponding control wines.[22]

Results are reported in Table 3. GSH ranged from 1.63 mg/L in the control red wine to 9.91 mg/L in rosé wine made from must protected from oxidation and treated with flash pasteurization. Significant differences ($p < 0.05$) in GSH levels were found among the three types of wine and the different treatments. Marchand and de Revel[27] reported levels of GSH between 1.1 and 7.1 mg/L in white wines and between 0.3 and 0.7 mg/L in red wines whereas Fracasseti et al.[26] described that the content of GSH in wines varied from not detected to 27.4 mg/L. GSH levels strongly depend on the variety,[15] type of wine, exposure to oxygen, tyrosinase activity, grape skin maceration, yeast strain and fermentation conditions.[21,33,34] In the case of GSSG, significant differences between the three types of wine were also found. The highest content, 3.33 mg/L, was found in white wine made without protection from oxidation and the lowest, 0.32 mg/L, in rosé wine made from musts treated with flash pasteurization. Mattivi et al.[20] reported GSSG levels in wines to range from not detected to 16.2 mg/L.

Differences in GSH and GSSG contents within the rosé wine series can be attributed to different levels of must oxidation. Indeed, must protection against oxidation resulted in higher concentration of GSH and lower concentration of GSSG, as described earlier.[21] However, in our study, the concentrations of GSSG, ranging from 0.32 to 1.77 mg/L, represented only a few percent of the loss of GSH. This suggests that, during must oxidation, GSH was predominantly converted to nucleophilic addition products, including GRP, rather than oxidized to GSSG, as shown earlier.[3] In contrast, in the white wines series, the GSH level was not correlated with that of oxygen protection and no significant difference ($p > 0.05$) was found for GSSG levels. This is likely due to the different grape variety, yeast strains, and wine-making conditions used for the white and rosé wines.[21,33,34] Moreover, GSH has been shown to react with other compounds, such as aldehydes and their condensation products with catechin in wine.[35] The flash détente red wine contained significantly higher ($p < 0.05$) levels of both GSH and GSSG than the control, suggesting increased extraction of glutathione in the flash detente process.

Large variations were also observed in the wine phenolic composition. Wines prepared from musts that were not protected from oxidation presented higher GRP values and lower caftaric and coutaric acid levels in both the rosé and white wine series. The ratio of caftaric acid to GRP was much higher in the white wines, probably reflecting a much higher ratio of caftaric acid to glutathione in Viognier than in Syrah. Red wines contained higher levels of hydroxycinnamic esters than the white and rosé wines, owing to both the particularly high

DOI: 10.1021/jf504383g
J. Agric. Food Chem. 2015, 63, 142−149

Table 3. Levels of GSH, GSSG, GRP and Hydroxycinnamic Acids[a]

samples	GSH (mg/L)	GSSG (mg/L)	GRP (mg/L)	Ferulic acid (mg/L)	Caftaric acid (mg/L)	Coumaric acid (mg/L)	Caffeic acid (mg/L)	Coutaric acid (mg/L)	Fertaric acid (mg/L)
Rosé wine with oxygen protection and flash pasteurization	9.91 ± 0.18^{a}	0.32 ± 0.02^{a}	78.96 ± 1.49^{a}	0.49 ± 0.01^{a}	23.16 ± 0.49^{a}	0.13 ± 0.01^{a}	1.22 ± 0.06^{a}	32.34 ± 3.46^{a}	13.05 ± 0.91^{a}
Rosé wine with oxygen protection	5.79 ± 0.07^{b}	0.52 ± 0.04^{b}	81.29 ± 1.21^{a}	0.56 ± 0.07^{a}	9.83 ± 0.19^{b}	1.33 ± 0.09^{b}	4.28 ± 0.14^{b}	25.25 ± 1.23^{b}	10.87 ± 0.21^{b}
Rosé wine without oxygen protection	5.43 ± 0.05^{b}	1.77 ± 0.04^{c}	114.20 ± 0.86^{b}	0.55 ± 0.01^{a}	2.57 ± 0.18^{c}	0.87 ± 0.05^{c}	1.87 ± 0.03^{c}	16.96 ± 0.23^{c}	11.63 ± 0.12^{b}
White wine with oxygen protection and flash pasteurization	4.29 ± 0.05^{c}	3.22 ± 0.04^{d}	65.26 ± 2.51^{c}	0.60 ± 0.06^{a}	114.91 ± 2.57^{d}	0.24 ± 0.04^{a}	2.39 ± 0.15^{d}	84.93 ± 6.50^{d}	21.06 ± 0.23^{c}
White wine with oxygen protection	3.94 ± 0.12^{d}	3.22 ± 0.07^{d}	61.09 ± 1.11^{c}	0.70 ± 0.11^{a}	107.29 ± 2.80^{d}	0.66 ± 0.01^{d}	5.21 ± 0.06^{e}	77.93 ± 1.05^{e}	19.48 ± 0.58^{c}
White wine without oxygen protection	5.80 ± 0.12^{b}	3.33 ± 0.08^{d}	84.75 ± 3.60^{a}	0.63 ± 0.07^{a}	69.16 ± 1.59^{e}	0.54 ± 0.03^{e}	4.04 ± 0.14^{b}	75.24 ± 3.46^{e}	20.12 ± 0.53^{c}
Red wine with flash detente	2.54 ± 0.05^{e}	3.13 ± 0.06^{d}	61.49 ± 1.79^{c}	0.92 ± 0.08^{b}	293.07 ± 6.28^{f}	0.60 ± 0.01^{d}	3.80 ± 0.15^{f}	263.98 ± 5.48^{f}	58.03 ± 1.83^{d}
Red wine control	1.63 ± 0.04^{f}	2.93 ± 0.02^{e}	28.35 ± 1.70^{d}	0.90 ± 0.09^{b}	232.33 ± 8.51^{g}	1.17 ± 0.04^{f}	4.23 ± 0.31^{b}	200.87 ± 6.87^{g}	64.12 ± 1.63^{d}

[a]Superscript letters in the columns represent significant statistical differences ($P < 0.05$).

content of the Grenache grape variety and extraction from skins in the red wine-making process. They also showed lower amounts of GRP, which is in agreement with the low ratio of GSH to hydroxycinnamic (i.e., caftaric and coutaric) acids in the Grenache grapes and limited extent of oxidation in the red wine-making process.[36] Flash détente also resulted in higher levels of caftaric acid, coutaric acid and GRP, indicating that this process increases the extraction rate of both hydroxycinnamic esters and glutathione. Martinez-Pinilla et al.[37] reported levels of caftaric acid between 33.93 and 42.96 mg/L whereas Mattivi et al.[20] reported values in the range 42.5−316.8 mg/L. The fertaric acid levels were significantly higher ($p < 0.05$) in the red wines than in the whites and lower in the rosé wines and showed no difference ($p < 0.05$) within each series, meaning that they depended on the variety and increased with maceration but were unaffected by oxidation.

Free hydroxycinnamic acids were present in low amounts. The highest values for ferulic were found in red wines (0.90−0.92 mg/L) due to the increase of extraction. Levels in white and rosé wines were not significantly different ($p > 0.05$) between wines without oxygen protection, wines protected from oxidation, and wines with oxygen protection and flash pasteurization. The concentrations of *p*-coumaric and caffeic acid were higher in the wines protected from oxidation but lower after flash pasteurization. They were also significantly lower ($p < 0.05$) in the red wine obtained by flash détente than in the control. The values are within the range reported for white wines by other researchers.[37−40]

In this work, a simple and single run UPLC-MRM-MS approach was developed for the analysis of GSH, GSSG, GRP and hydroxycinnamic acids in wines. The method was completely validated providing a sensitive analysis for compound detection and showing satisfactory data for all parameters tested. Good results were obtained with respect to linearity and recovery as well as an excellent level of precision. The proposed method minimized sample preparation and solvent consumption and increased sample throughput. The applicability of the proposed method was assessed through the analysis of real wines.

AUTHOR INFORMATION

Corresponding Author

*E-mail: avallverdu@ub.edu,; vallverd@supagro.inra.fr.

Funding

Funding for this work was provided by the Ministry of Education and Culture for International mobility of professors and researchers to foreign centers of higher education and research (José Castillejo), the Instituto de Salud Carlos III, ISCIII (CIBERobn), the Quality Group from Generalitat de Catalunya (GC) 2014 SGR 773 and also financial support of GIS IBiSA (Infrastructures en Biologie Santé et Agronomie) and from Région Languedoc Roussillon for funding of the UPLC-MS equipment.

Notes

The authors declare no competing financial interest.

ACKNOWLEDGMENTS

We thank Julien Perret and Mathias Lacrois, graduate students, for their initial help and Alain Samson (UE Pech Rouge) for providing the wine samples and description.

DOI: 10.1021/jf504383g
J. Agric. Food Chem. 2015, 63, 142−149

REFERENCES

(1) Crozier, A.; Jaganath, I. B.; Clifford, M. N. Dietary phenolics: chemistry, bioavailability and effects on health. *Nat. Prod. Rep.* **2009**, *26*, 1001−1043.

(2) Singleton, V. L.; Timberlake, C. F.; Lea, A. G. H. The phenolic cinnamates of white grapes and wine. *J. Sci. Food Agric.* **1978**, *29*, 403−410.

(3) Singleton, V. L.; Salgues, M.; Zaya, J.; Trousdale, E. Caftaric acid disappearance and conversion to products of enzymic oxidation in grape must and wine. *Am. J. Enol. Vitic.* **1985**, *36*, 50−56.

(4) Cheynier, V.; Trousdale, E.; Singleton, V. L.; Salgues, M.; Wylde, R. Characterization of 2-*S*-glutathionylcaftaric acid and its hydrolysis in relation to grape wines. *J. Agric. Food Chem.* **1986**, *34*, 217−221.

(5) Foyer, C. H.; Halliwell, B. The presence of glutathioneand glutathione reductase in chloroplasts: a proposedrole in ascorbic acid metabolism. *Planta* **1976**, *133*, 21−25.

(6) Alscher, R. G. Biosynthesis and antioxidant function of glutathione in plants. *Physiol. Plant* **1989**, *77*, 457−464.

(7) Noctor, G.; Foyer, C. H. Ascorbate and glutathione: keeping active oxygen under control. *Annu. Rev. Plant Physiol. Plant Mol. Biol.* **1998**, *49*, 249−279.

(8) Kritzinger, E. C.; Bauer, F. F.; Du Toit, W. J. Role of glutathione in wine: A review. *J. Agric. Food Chem.* **2013**, *61*, 269−277.

(9) Sonni, F.; Moore, E. G.; Clark, A. C.; Chinnici, F.; Riponi, C.; Scollary, G. R. Impact of glutathione on the formation of methylmethine- and carboxymethine-bridged (+)-catechin dimers in a model wine system. *J. Agric. Food Chem.* **2011**, *59*, 7410−7418.

(10) Adams, D. O.; Liyanage, C. Glutathione increases in grape berries at the onset of ripening. *Am. J. Enol. Vitic.* **1993**, *44*, 333−338.

(11) Cassol, T.; Adams, D. O. Detection of glutathione in white wines using an enzymatic analytical method. *Am. J. Enol. Vitic.* **1995**, *46*, 410.

(12) Rabenstein, D. L.; Saetre, R. Mercury-based electrochemical detector for liquid chromatography for the detection of glutathione and other sulfur-containing compounds. *Anal. Chem.* **1977**, *49*, 1036−1039.

(13) Giustarini, D.; Dalle-Donne, I.; Colombo, R.; Milzani, A.; Rossi, R. An improved HPLC measurement for GSH and GSSG in human blood. *Free Radic. Biol. Med.* **2003**, *35*, 1365−1372.

(14) Cheynier, V.; Basire, N.; Rigaud, J. Mechanism of trans-caffeoyltartaric acid and catechin oxidation in model solutions containing grape polyphenoloxidase. *J. Agric. Food Chem.* **1989**, *37*, 1069−1071.

(15) Cheynier, V.; Souquet, J. M.; Moutounet, M. Glutathione content and glutathione to hydroxycinnamic acid ratio in Vitis vinifera grapes and musts. *Am. J. Enol. Vitic.* **1989**, *40*, 320−324.

(16) Toyooka, T.; Suzuki, T.; Saito, Y. Fluorogenic reagent for thiols: 4-(N,N-dimethylaminosulphonyl)-7-fluoro-2,1,3-benzoxadiazole. *Analyst* **1989**, *114*, 413−419.

(17) Chin, C. C.; Wold, F. The use of tributylphosphine and 4-(aminosulfonyl)-7-fluoro-2,1,3-benzoxadiazole in the study of protein sulfhydryls and disulfides. *Anal. Biochem.* **1993**, *214*, 128−134.

(18) Park, S. K.; Boulton, R.; Noble, A. Automated HPLC analysis of glutathione and other volatile thiols in grape musts and wine using pre-column derivatization with fluorescence detection. *Food Chem.* **2000**, *69*, 475−480.

(19) Dalle-Donne, I.; Rossi, R.; Colombo, R.; Giustarini, D.; Milzani, A. Biomarkers of oxidative damage in human disease. *Clin. Chem.* **2006**, *52*, 601−623.

(20) Mattivi, F.; Fedrizzi, B.; Zenato, A.; Tiefenthaler, P.; Tempesta, S.; Perenzoni, D.; Cantarella, P.; Simeoni, F.; Vrhovsek, U. Development of reliable analytical tools for evaluating the influence of reductive winemaking on the quality of Lugana wines. *Anal. Chim. Acta* **2012**, *732*, 194−202.

(21) Du Toit, W.; Lisjak, K.; Stander, M.; Prevoo, D. Using LC-MSMS To Assess Glutathione Levels in South African White Grape Juices and Wines Made with Different Levels of Oxygen. *J. Agric. Food Chem.* **2007**, *55*, 2765−2769.

(22) Wirth, J.; Morel-Salmi, C.; Souquet, J. M. The impact of oxygen exposure before and after bottling on the polyphenolic composition of red wines. *Food Chem.* **2010**, *123*, 107−116.

(23) FDA. 2013. USD of H and HSF and DAS. Bioanalytical Method Validation. Available at: http://www.fda.gov/downloads/drugs/guidancecomplianceregulatoryinformation/guidances/ucm368107.pdf. Accessed March 21, 2014.

(24) Vallverdú-Queralt, A.; Odriozola-Serrano, I.; Oms-Oliu, G.; Lamuela-Raventós, R. M.; Elez-Martínez, P. Changes in the polyphenol profile of tomato juices processed by pulsed electric fields. *J. Agric. Food Chem.* **2012**, *60*, 9667−9672.

(25) Li, J.; Yue, Y.; Michael, C.; Denino, P.; ÒConnell, N.; Cornelis ECA. Hop identification of a novel glutathione adduct of diclofenac, 4-hydroxy-2-glutathion-deschloro-diclofenac, upon incubation with human liver microsomes. *Drug Metab. Dispos.* **2005**, *33*, 484−489.

(26) Fracassetti, D.; Lawrence, N.; Tredoux, A. G. L.; Tirelli, A.; Nieuwoudt, H. H.; Du Toit, W. J. Quantification of glutathione, catechin and caffeic acid in grape juice and wine by a novel ultra-performance liquid chromatography method. *Food Chem.* **2011**, *128*, 1136−1142.

(27) Marchand, S.; de Revel, G. A HPLC fluorescence-based method for glutathione derivatives quantification in must and wine. *Anal. Chim. Acta* **2010**, *660*, 158−163.

(28) Janes, L.; Lisjak, K.; Vanzo, A. Determination of glutathione content in grape juice and wine by high-performance liquid chromatography with fluorescence detection. *Anal. Chim. Acta* **2010**, *674*, 239−242.

(29) Kritzinger, E.; Stander, M.; Du Toit, W. J. Assessment of glutathione levels in model solution and grape ferments supplemented with glutathione-enriched inactive dry yeast preparations using a novel UPLC-MS/MS method. *Food Addit. Contam., Part A* **2012**, *30*, 80−92.

(30) Gonçalves, J.; Mendes, B.; Silva, C. L.; Câmara, J. S. Development of a novel microextraction by packed sorbent-based approach followed by ultrahigh pressure liquid chromatography as a powerful technique for quantification phenolic constituents of biological interest in wines. *J. Chromatogr., A* **2012**, *1229*, 13−23.

(31) Sáenz-Navajasa, M. P.; Ferreira, V.; Dizya, M.; Fernández-Zurbano, P. Characterization of taste-active fractions in red wine combining HPLC fractionation, sensory analysis and ultra performance liquid chromatography coupled with mass spectrometry detection. *Anal. Chim. Acta* **2010**, *673*, 151−9.

(32) Gosetti, F.; Mazzucco, E.; Zampieri, D.; Gennaro, M. C. Signal suppression/enhancement in high-performance liquid chromatography tandem mass spectrometry. *J. Chromatogr., A* **2010**, *1217*, 3929−3937.

(33) Maggu, M.; Winz, R.; Kilmartin, P. A.; Trought, M. C. T.; Nicolau, L. Effect of skin contact and pressure on the composition of Sauvignon Blanc must. *J. Agric. Food Chem.* **2007**, *55*, 10281−10288.

(34) Patel, P.; Herbst Johnstone, M.; Lee, S. A.; Gardner, R. C.; Weaver, R.; Nicolau, L.; Kilmartin, P. A. Influence of juice pressing conditions on polyphenols, antioxidants and varietal aroma of Sauvignon blanc microferments. *J. Agric. Food Chem.* **2010**, *58*, 7280−7288.

(35) Sonni, F.; Moore, E. G.; Clark, A. C.; Chinnici, F.; Riponi, C.; Scollary, R. Impact of Glutathione on the Formation of Methylmethine- and Carboxymethine-Bridged (+)-Catechin Dimers in a Model Wine System. *J. Agric. Food Chem.* **2011**, *59*, 7410−7418.

(36) Cheynier, V.; Hidalgo-Arellano, I.; Souquet, J. M.; Moutounet, M. Estimation of the oxidative changes in phenolic compounds of Carignane during wine making. *Am. J. Enol. Vitic.* **1997**, *48*, 225−228.

(37) Martínez-Pinilla, O.; Martínez-Lapuente, L.; Guadalupe, Z.; Ayestarán, B. Sensory profiling and changes in colour and phenolic composition produced by malolactic fermentation in red minority varieties. *Food Res. Int.* **2012**, *46*, 286−293.

(38) Recamales, A.; Sayago, A.; Gonzalez-Miret, M. L.; Hernanz, D. The effect of storage conditions on the phenolic composition and color of white wine. *Food Res. Int.* **2006**, *39*, 220−229.

(39) Sioumis, N.; Kallithraka, S.; Makris, D.; Kefalas, P. Kinetics of browning onset in white wines: Influence of principal redox-active

DOI: 10.1021/jf504383g
J. Agric. Food Chem. 2015, 63, 142−149

polyphenols and impact on the reducing capacity. *Food Chem.* **2006**, *94*, 98−104.
(40) Kallithraka, S.; Salacha, M. I.; Tzourou, I. Changes in phenolic composition and antioxidant activity of white wine during bottle storage: Accelerated browning test versus bottle storage. *Food Chem.* **2009**, *113*, 500−505.

DOI: 10.1021/jf504383g
J. Agric. Food Chem. 2015, 63, 142−149

JOURNAL OF AGRICULTURAL AND FOOD CHEMISTRY

Article

pubs.acs.org/JAFC

Water Stress Proteins from *Nostoc commune* Vauch. Exhibit Anti-Colon Cancer Activities in Vitro and in Vivo

Songjia Guo,[†,§] Shuhua Shan,[†,∥] Xiaoting Jin,[†] Zongwei Li,[†] Zhuoyu Li,*[,†,‡] Liangqi Zhao,[†] Quan An,[⊥] and Wei Zhang[⊥]

[†]Institute of Biotechnology, Key Laboratory of Chemical Biology and Molecular Engineering of National Ministry of Education, Institute of Biotechnology, Shanxi University, Taiyuan 030006, China

[‡]College of Life Science, Zhejiang Chinese Medical University, Hangzhou 310053, China

[§]Department of Medical Laboratory, Fenyang College of Shanxi Medical University, Fenyang 032200, China

[∥]Department of Biology, Taiyuan Normal University, Taiyuan 030031, China

[⊥]China Institute for Radiation Protection, Taiyuan 030031, China

Supporting Information

ABSTRACT: *Nostoc commune* has been traditionally used in China as a health food and medicine. The water stress proteins (WSP) of *Nostoc commune* are the major component of the extracellular matrix. This study purified and identified the water stress proteins (WSP1) from *Nostoc commune* Vauch., which could inhibit the proliferation of human colon cancer cell lines. The IC_{50} values of WSP1 against DLD1, HCT116, HT29, and SW480 cells were 0.19 ± 0.02, 0.21 ± 0.03, 0.39 ± 0.05, and 0.41 ± 0.01 μg/μL, respectively. Notably, it displayed very little effect on the normal human intestinal epithelial FHC cell line. The IC_{50} value of WSP1 against FHC cells was 0.67 ± 0.05 μg/μL. Moreover, the growth of DLD1 xenografted tumors in nude mice were significantly suppressed in the WSP1 treated group. Mechanistically, the cell-cycle analysis revealed that WSP1 induced growth inhibition by G1/S arrest. Meanwhile, Western blotting and immunohistochemistry assays showed WSP1 could activate caspase-8, -9, and -3, along with subsequent PARP cleavage. Furthermore, the pan-caspase inhibitor, z-VAD-FMK, partly reversed the effect caused by WSP1, confirming that WSP1 induced cell apoptosis through caspase-dependent pathway. Collectively, WSP1 has targeted inhibition for colon cancer proliferation both in vitro and in vivo and it is valuable for future exploitation and utilization as an antitumor agent.

KEYWORDS: *Nostoc commune Vauch, water stress protein 1 (WSP1), colorectal cancer (CRC), apoptosis, nude mice*

INTRODUCTION

Colorectal cancer (CRC) is a worldwide disease with an annual incidence of 1 million cases. It is the second most common cause of cancer mortality and comprises 9% of the cancer burden globally.[1] In China, CRC ranks fourth among the most common cancers and the mortality rate is 57.5%.[2] Chemotherapy is used in the treatment of cancer with one or more antineoplastic drugs. Patients often receive the combination of chemotherapy with various chemical agents.[3] However, the toxicity and side effects greatly restrict the application of chemotherapeutic agents.[4] Efforts have focused on developing effective therapeutic regimens to combat colon cancer with low toxicity and side effects.

A large number of previous studies have shown that many extracts from plants or microorganisms have exhibited strong inhibitory properties on several types of cancers, especially on colon epithelial tumors.[5] For example, compounds from color-fleshed potatoes have shown pro-apoptotic properties in human colon cancer cells,[6] major metabolites of 6-gingerol had cytotoxic effects on human cancer cells,[7] and dietary black and brown rice bran displayed antitumor effects in tumor-bearing mice.[8] *Nostoc commune* Vauch. (NCV) is an edible terrestrial cyanobacterium and is a photosynthetic prokaryote. In China, NCV is a popular food and is rich in protein, calcium, iron, vitamin C, and other nutrients.[9,10] Accumulated evidence indicates that substances from NCV could prevent fatty liver, kidney stones, and heart diseases.[11,12] The bioactive fractions from NCV showed multiantioxidant and antitumor activities;[13,14] however, the molecular mechanisms remain poorly understood.

In the present study, we purified active proteins from NCV, which had remarkable inhibitory effects on cell proliferation of colon cancer. Mass spectrometry analysis indicated that the protein belonged to the water stress proteins (WSP). *Nostoc commune* typically synthesizes water stress proteins when they are subjected to acute water stress in nature. WSP is a group of acidic polypeptides with cryptic functions and PI values between 4.3 and 4.8. WSP is a major extracellular matrix protein, which maintains the structure and function of the extracellular matrix.[15] The WspA from *Nostoc commune* possesses β-D-galactosidase activity[16] and is associated with 1,4-β-D-xylanxylanohydrolase activity.[17] Previous reports have shown that *wspA* is a single copy gene,[18] while WspA has microheterogeneity characterized by two or more proteins of 30−40 kDa but with identical N-terminal sequence.[19] These

Received: July 11, 2014
Revised: December 18, 2014
Accepted: December 19, 2014
Published: December 19, 2014

ACS Publications © 2014 American Chemical Society

DOI: 10.1021/jf503208p
J. Agric. Food Chem. 2015, 63, 150−159

isoforms may arise from deamidation, covalent modification, protease degradation, etc. In this study, we purified three predominate proteins (39, 37, and 35 kDa). They were all identified as WSP by MALDI-TOF analysis and were named WSP1. On the basis of the above data, the single copy gene (accession KF003026) that encoded the water stress protein (WSP1) was cloned into pET28a, and the recombinant protein of WSP1 (GI: 530891432) was obtained by genetic engineering technology.[20] The molecular weight of the recombinant WSP1 was found to be 39 kDa and could significantly inhibit the proliferation of human colon cancer cells.[20]

We report that WSP1 possessed potent antitumor effects on human colon cancer cell lines (DLD1, HCT-116, HT-29, and SW480). More importantly, WSP1 could suppress DLD1 xenografted tumors in nude mice. The results further indicated that the WSP1 treatment induced colon cancer cell apoptosis by triggering the caspase-dependent pathway and suppressed cell growth by G1/S arrest. Interestingly, WSP1 specifically suppressed proliferation and induced apoptosis in colon cancer cells in vitro and in vivo but not in normal human colon epithelial cells. The data presented in this study provides evidence for the potential of WSP1 as an antitumor agent against colon cancer.

MATERIALS AND METHODS

Chemicals. RPMI-1640 medium and fetal bovine serum (FBS) were obtained from GIBCO (Grand Island, NY). 3-4,5-Dimethylthiazol-2-yl-2,5-diphenyltetrazolium bromide (MTT) and DAPI (4′,6′-diamidino-2-phenylindole) were obtained from Sigma (St. Louis, MO). 5,5′,6,6′-Tetrachloro-1,1′,3,3′-tetraethyl-imidacarbocyanine iodide (JC-1) and the pan-caspase inhibitor (z-VAD-FMK) were provided by Beyotime Institute of Biotechnology (Haimen, China). The annexin V-FITC apoptosis detection kit was purchased from Oncogene (San Diego, CA). The antibodies used in this study were as follows: GAPDH and β-actin antibodies were purchased from Abmart (Arlington, MA); pRb was obtained from Cell Signaling Technology (Danvers, MA); c-Myc, cyclineD1, and cyclineE1 antibodies were obtained from Bioworld Technology (Minneapolis, MN); AIF, Bax, Bcl-2, caspase-3, -8, and -9, and polymerase (PARP) antibodies were obtained from the Beyotime Institute of Biotechnology (Haimen, China).

Isolation and Purification of WSP1 Polypeptides from *Nostoc commune* Vauch. Desiccated colonies of NCV were collected from Shanxi, China, in 2012. Then 20 g of desiccated colonies (unground) were cleaned with double distilled water, then suspended in 1000 mL of PBS (phosphate-buffered saline, pH 7.4, containing 1 mM PMSF) for 48 h, followed by centrifugation at 12000 rpm for 25 min at 4 °C. Then, the supernatant was precipitated with acetone (V/V = 1:2) at −20 °C for 2 h. The obtained precipitation was dissolved with appropriate volumes of PBS and subjected to ammonium sulfate fractionation. The precipitation from 30−60% ammonium sulfate was resuspended in PBS, dialyzed, and concentrated by ultrafiltration through a 10 kDa MWCO hollow fiber membrane (Millipore, USA). Proteins were analyzed with a 10% SDS-PAGE and a 10% nondenature PAGE. The collected active fractions showed three bands on both the SDS-PAGE and nondenature PAGE gels. Gels were stained using CBB R-250. The relative gray value of WSP1 was calculated using Image-J software.

Mass Spectrometry Analysis and Protein Identification. The purified target proteins were resolved using a 10% SDS-polyacrylamide gel. The SDS-PAGE was performed using standard methods on a Mini-Protean II system 3 (Bio-Rad, USA). The target protein band was cut from the SDS-PAGE gel and sent to Shanghai Applied Protein Technology Co. Ltd., China, for protein identification. Protein identification was performed using a matrix-assisted laser desorption/ionization-time-of-flight method (MALDI-TOF, Applied Biosystems USA), a peptide mass fingerprint (PMF), and the NCBI database.

Cloning of the WSP1 Gene. Specific primers for PCR amplification of the full-length *WSP1* gene in NCV were designed according to the *wspA* gene sequence of *Nostoc commune* (accession no. AB518000). The primer sequences were as follows:

Forward: 5′-CGCGGATCCATGGCTCTTTACGGCT-3′.

Reverse: 5′-CCGCTCGAG TTATTCATTAACAATCGT-3′.

PCR was performed under the following conditions: initial denaturation at 95 °C for 3 min, followed by 30 cycles of 95 °C for 1 min, 60 °C for 1 min, 72 °C for 1 min, and a final extension step at 72 °C for 10 min.

Cell Culture. Human colon cancer cell lines (DLD1, SW480, HT-29, and HCT116) and a normal colonic epithelial cell line (FHC) were obtained from the Chinese Type Culture Collection. Human colon cancer cell lines were cultured in RPMI 1640 medium supplemented with 10% (v/v) heat-inactivated FBS. The FHC was cultured in F12 medium with 10% FBS. All media were supplemented with 100 U/mL penicillin (Sigma, Germany) and 100 mg/mL streptomycin (Sigma, Germany). All cultures were incubated at 37 °C with 5% fully humidified CO_2.

MTT Assay. Growth inhibitory effects of WSP1 on DLD1, HCT116, SW480, HT-29, and FHC were determined using a MTT assay. Cells (1×10^4) were seeded into 96-well plates and allowed to grow for 24 h for acclimatization. The cells were then incubated with treatments of 0, 0.05, 0.15, and 0.25 μg/μL WSP1 for 48 h. Then 20 μL of MTT (5 mg/mL) was added to each well and further incubated for 4 h. The blue formazan produced was dissolved by DMSO, and the absorbance was measured at 570 nm with an ELISA plate reader. The percentage of cell growth inhibition was calculated with the formula: (A570 Control − A570 Experiment/A570 Control) × 100%. After the preliminary screening, in order to determine the time-dependent manner of WSP1 induced cell growth inhibition, DLD1 was treated with 0.05, 0.15, and 0.25 μg/μL WSP1 for 24 and 48 h. Assays were performed in triplicate independent experiments. The 50% inhibitory concentration (IC_{50}) of 48 h was determined as the anticancer drug concentration, causing a 50% reduction in cell viability and calculated by regression analysis.

Clonogenic Survival Assay. DLD1 cells were counted and plated onto 6-well tissue culture plates (1000 cells/well) in 1640 medium supplemented with 10% FBS. After attachment, the cells were treated with 0.15 μg/μL WSP1 for 10 days. The cells were then fixed with immune dye fixative and stained with 0.1% crystal violet. The results were observed under a stereomicroscope (OLYMPUS SZX16, Japan). The number of clones (more than 50 cells each) counted in 10 different microscopic fields were used to calculate the colon formation rate: Colon Formation Rate = (Clones/Seeded Cells) × 100%.

DAPI Staining and Quantification of Apoptotic Cells. To examine the effects of WPS1 on cancer cell apoptosis, a DAPI nuclear staining assay was performed. DLD1, HCT116, and FHC cells were plated in 6-well plates with glass slides (1×10^6 cells/well). After treatment with 0.15 μg/μL WSP1 for 48 h, the cells were fixed with immunostaining fixative for 60 min at 4 °C. Fixed cells were washed twice with PBS and incubated with DAPI for 1 h at 4 °C in the dark. Then the slides were washed with PBS to remove the excess DAPI and the cell nuclei were observed under a laser confocal scanning microscope (LCSM; OLYMPUS FV1000, Japan). The apoptosis rate of colon cancer cells treated with WSP1 was determined by scoring the number of cells with nucleus phenotypic changes in 20 different microscopic fields under LCSM.

Analysis of Cell Apoptosis and Cell Cycle by Flow Cytometry. WSP1 induced apoptosis in DLD1 was analyzed by flow cytometry using the Annexin V-FITC and propidium iodide (PI) double staining method. Briefly, after incubation with 0.15 μg/μL WSP1 for 48 h, cells were trypsinized and washed with PBS. Cells were then stained with 200 μL of Annexin V solution (10 μL of Annexin V + 200 μL of binding buffer) and 300 μL of PI (5 μL PI + 300 μL binding buffer) in the dark (RT) for 30 min. The population of Annexin V positive cells was examined using a FACSort flow cytometer. The cell cycle of DLD1 cells was assessed with a cell

DOI: 10.1021/jf503208p
J. Agric. Food Chem. 2015, 63, 150−159

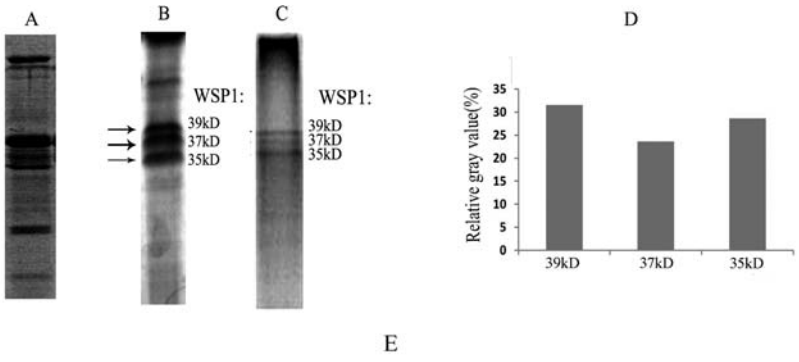

E

MALYGYTIGEDRDDNDSNGKELDVYRFLIPSAPGGTIITPTLVGTVNVAGTVTNADLEGLGTNPSTQRVS
AVNEARASGTTTPIDPTVTVVNNVDQPFAPATTSPTRTPSDLRRFGFESGADFGGTPTALYNISGNPTT
QNGVPVGSSLYRITTANPGTISLVDTFGPATTAAQRQGTQPTNPGKYADGLAIDNLNPGSTRAFASDFE
NRDEIASDNTKNNLYKVDLLTGELSAPIVLRTPSGQALNVTRGSGSNPEFGLDSGLAFTNSGSQRLLAL
LQNGAVYEITGYQDELAASGLGLGSATGSNGAGFATATLLNTVNLPTAAGQEYEGFTIVNE↵

Figure 1. Purification of WSP1 from *Nostoc commune* Vauch. (A) Total proteins precipitated from 100% ammonium sulfate analyzed by 10% SDS-PAGE. (B) Precipitation from 30−60% ammonium sulfate analyzed by 10% SDS-PAGE. (C) Precipitation from 30−60% ammonium sulfate analyzed by 10% nondenaturing PAGE. (D) Relative gray values of three bands of WSP1 based in (B). (E) Amino acid sequence of WSP1 protein of 39 kDa.

cycle detection kit by FACScan. DLD1 cells were plated into 60 mm dishes (1×10^6 cells/dish) and incubated overnight. Cells were treated with 0.15 μg/μL WSP1 for 48 h and then trypsinized. These cells were washed with PBS and fixed in 70% ethanol at −20 °C for 12 h. The ethanol was removed after centrifugation, and the cells were resuspended in 1 mL of PBS, 100 μL of ribonuclease A (100 μg/mL PBS), and 400 μL of propidium iodide (400 μg/mL PBS) in the dark (RT) for 30 min. The percentages of cells in different cell cycle phases were analyzed using FACScan, and experiments were performed in triplicate.

Measurement of Changes of Mitochondrial ($\Delta\psi m$). Measurement of mitochondrial transmembrane potential was performed with DLD1 cells. First, 5×10^5 cells/well were seeded into 6-well plates. After treatment with WSP1 (0.15 μg/μL) for 48 h, the cells were then harvested and stained with 10 mg/mL JC-1 at 37 °C for 10 min. Then, the stained cells were washed, resuspended with PBS, and analyzed for their red and green fluorescence from JC-1 using a flow cytometer. Data are reported as the percentage of cells with depolarized mitochondrial membranes, and experiments were performed in triplicate.

Western Blotting Analysis. The human colon cancer cell line DLD1 (1×10^6) was treated with 0.15 μg/μL WSP1 for 24 and 48 h. After the treatment, cells were incubated with lysis buffer for 30 min on ice and then centrifuged for 10 min at 13000 rpm. Protein concentrations were measured with Bradford reagent (Bio-Rad, USA), and an equal amount of protein (60 μg) from each sample was separated by 10% SDS-PAGE and then transferred to PVDF membranes. The membranes were blocked using Tris-buffered saline with 0.1% Tween-20 and 5% skimmed milk for 1.5 h at room temperature. The membranes were probed with primary antibodies at 4 °C overnight. The membranes were then washed three times with Tris-buffered saline containing 0.1% Tween-20 and probed for 2 h at room temperature with HRP conjugated secondary antibodies. Protein bands were visualized using enhanced chemiluminescence, and experiments were performed in triplicate.

In Vivo Studies in Nude Mice. All animal experiments were carried out following procedures approved by the Institutional Animal Care and Use Committee of China Institute for Radiation Protection. The review board and ethics committee of the institution specifically approved this study.

Sixteen BALB/c nude mice (five-week old, female, weighing between 18 and 21 g) were purchased from the Institute of Zoology, Chinese Academy of Sciences. The nude mice were maintained under specified-pathogen free (SPF) conditions in the laboratory animal service center of the China Institute for Radiation Protection. DLD1 cells in 0.2 mL of PBS (5×10^6) were injected subcutaneously into the right oxter of each nude mouse. Fourteen days later, solid tumors were apparent in all injected nude mice and the 16 nude mice were randomly divided into two groups (each group with 8 nude mice) with no significant difference of tumor volumes between the groups. Mice in the WSP1 group received an intraperitoneal injection of 60 μg WSP1/g body weight every 3 days (total six injections), and the control mice were treated with PBS. The body weight and tumor diameters of nude mice were measured twice a week. Tumor volumes were calculated using the formula: tumor volume (cm^3) = 0.5 tumor length (cm) × tumor width^2 (cm^2). Then 21 days later, all mice were sacrificed according to ethical demands and tumors were excised, weighed, and frozen at −80 °C for further Western blotting and immunohistochemical analysis.

Immunohistochemical Analysis. Tumors were fixed in 10% formalin, embedded in paraffin wax, and used for immunohistochemical analysis. The paraffin sections were dewaxed in xylene and dehydrated in serially diluted ethanol. Antigen retrieval was carried out using citrate buffer (pH 6.0). All sections were stained with antihuman K_i-67, activated-caspase-8, activated-caspase-9, and PARP. Staining was performed using a universally labeled streptavidin−biotin kit according to the standard protocol. The percentage of cells was calculated by Imagepro-Plus 6.0 software.

Statistical Analysis. Data analysis was carried out using SPSS 17.0 software. Results were expressed as mean ± SD. IC_{50} values were calculated by regression analysis. Differences in means between the control and treatment groups were determined using a two-tailed unpaired Student's t test or a One-Way ANOVA followed by Tukey's multiple comparison tests. Values of less than 0.05 ($p < 0.05$) and 0.01 ($p < 0.01$) were considered statistically significant and highly significant, respectively.

RESULTS

Purification and Identification of WSP1. Total extracellular matrix proteins of NCV were prepared by 100% (m/v) ammonium sulfate precipitation (Figure 1A). After ammonium sulfate grading precipitation, three proteins (39, 37, and 35 kDa) dominated in both the SDS-PAGE (Figure 1B) and the nondenaturing PAGE gels (Figure 1C). The three proteins were all identified as WSP1 by MALDI-TOF analysis

DOI: 10.1021/jf503208p
J. Agric. Food Chem. 2015, 63, 150−159

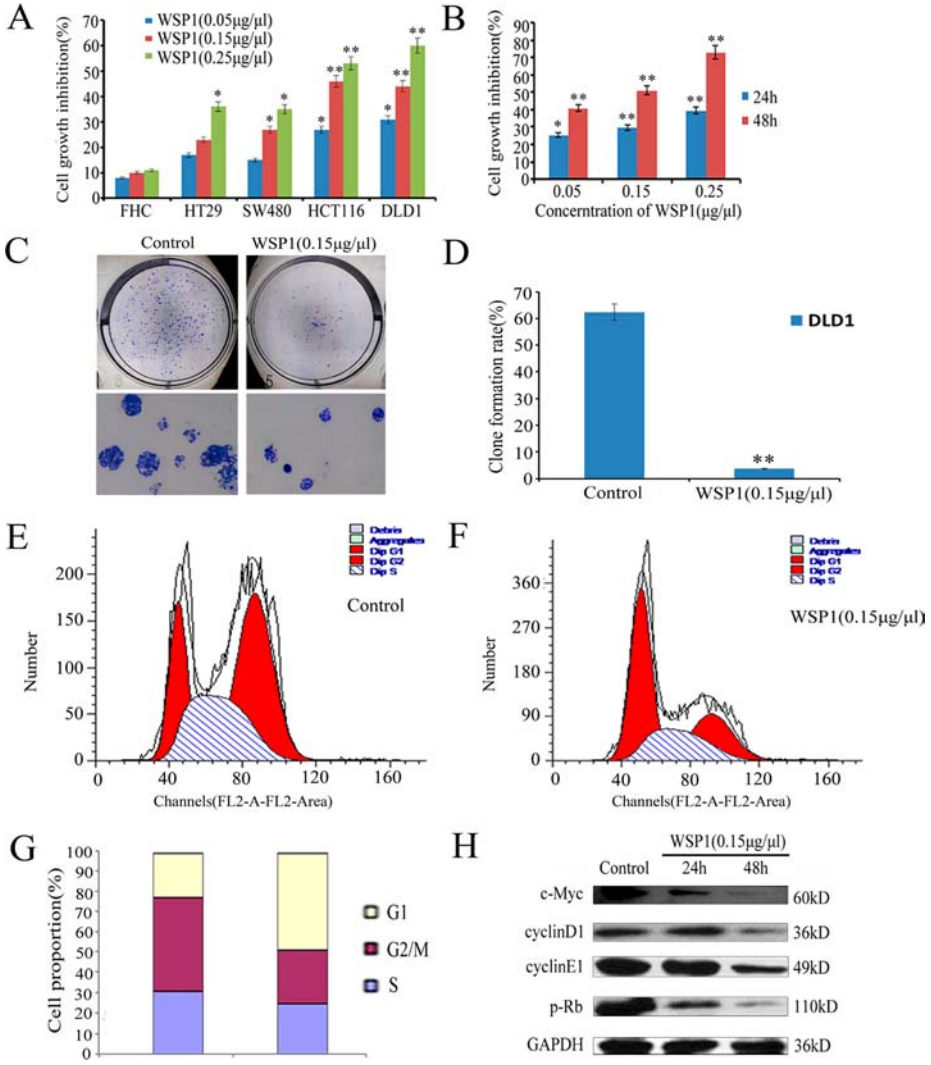

Figure 2. WSP1 antiproliferative activities. (A) Dose-dependent cell proliferation assays. FHC, HT29, SW480, HCT116, and DLD1 cells were treated with different doses (0, 0.05, 0.15, and 0.25 $\mu g/\mu L$) of WSP1 for 48 h, and cell proliferation was measured by MTT assay. (B) Time-dependent cell proliferation assays. DLD1 cells were seeded in the presence of WSP1 for 24 and 48 h. (C) Clonogenic survival assays. DLD1 cells (1000/well) were seeded in 6-well plates in the absence or presence of WSP1 for 10 d, then the clonogenic assay was carried out. (D) Colon Formation Rate = (Clones/Seeded Cells) × 100%. (E,F) Effects of WSP1 on cell cycle distribution in DLD1 cells. Cells were treated with WSP1 (0.15 $\mu g/\mu L$) for 48 h. DNA content was analyzed by cytometry. Accumulated cells in the G1 phase were compared with the control. (G) The percent of cell population in G0/G1, G1, S, and G2/M phases of the cell cycle. (H) Effects of WSP1 treatment on cell cycle proteins as shown by Western blotting. Antibodies were used against cyclin D1, cyclin E1, c-Myc, and pRb. GAPDH antibody was used as an internal control. The results represent mean ± SD of three independent experiments. $^*p < 0.05$, $^{**}p < 0.01$ compared with untreated cells.

(Supporting Information, Figure S1), and the three peptide fragments with identical amino acid sequences were detected at 55.8% (39 kDa), 45.3% (37 kDa), and 42.8% (35 kDa) coverage to WSP1 (GI: 530891431) of NCV (Supporting Information, Figure S1). The microheterogeneity of WSP1 was consistent with previous reports.[18,19] On the basis of the band intensity analysis, the three bands of WSP1 in Figure 1B were estimated to account for 31.5% (39 kDa), 23.6% (37 kDa), and 28.6% (35 kDa) of the total purified protein (Figure 1D). Additionally, the amino acid sequence of WSP1 protein of 39 kDa is shown in Figure 1E.

Cloning of WSP1 Gene. The full-length coding sequence of *WSP1* gene was amplified by PCR from the total cDNA of NCV. The identified *WSP1* gene sequence has been submitted to GenBank under accession number KF003026. It encoded a polypeptide of 337 amino acids (GI: 530891431) with an 83% sequence identity to WspA of *N. commune* KU002 (accession no. AB518000).

WSP1 Suppresses Cell Growth of Human Colon Cancer. This study investigated the sensitivity of colon cancer cells (HT29, SW480, DLD1, and HCT116) and normal colon epithelial cells (FHC) to WSP1. The proliferation of those cells treated with various concentrations of WSP1 for 24 or 48 h was monitored using a MTT assay. As shown in Figure 2A,B, WSP1 markedly suppressed colon cancer cells growth in a time- or dose-dependent manner; however, it displayed less effect on FHC cell proliferation. The IC_{50} values of WSP1 for DLD1, HCT116, HT29, and SW480 cells were 0.19 ± 0.02, 0.21 ± 0.03, 0.39 ± 0.05, and 0.41 ± 0.01 $\mu g/\mu L$, respectively, and the IC_{50} against FHC was 0.67 ± 0.05 $\mu g/\mu L$ (Table 1). The ability of individual cells to aggregate into viable colony clusters can be measured by a clonogenic survival assay; therefore, this assay was performed with DLD1 cells to evaluate the long-term

DOI: 10.1021/jf503208p
J. Agric. Food Chem. 2015, 63, 150−159

Table 1. Cytotoxic Activity of WSP1 against Various Human Cell Lines

cell lines	IC_{50} ($\mu g/\mu L$) ± SD
DLD1 (colon cancer cell)	0.19 ± 0.02
HCT116 (colon cancer cell)	0.21 ± 0.03
HT29 (colon cancer cell)	0.39 ± 0.05
SW480 (colon cancer cell)	0.41 ± 0.01
FHC (colon epithelial cell)	0.67 ± 0.05

effects of WSP1 on cell survival. The results showed that the clone formation rate of each group was 62.2 ± 5.1% in control group of 10 days, 2.8 ± 0.1% in WSP1-treated group of 10 days (Figure 2D). The data showed that the cell clone formation inhibiting effect of all the WSP1-treated groups were extremely significantly different from the control groups ($p < 0.01$). The result showed that clonogenicity was significantly inhibited in colon cancer cells cultured in the presence of WSP1 (Figure 2C).

WSP1 Inhibits Colon Cancer Cell Growth by G1-Phase Arrest. To determine the mechanisms by which WSP1 inhibits the proliferation of colon cancer cells, analysis of cell cycle by flow cytometry was applied with WSP1 treated DLD1 cells. As shown in Figure 2E,F, DLD1 exposed to WSP1 resulted in a time-dependent cell percentage reduction in the S-phase and accumulation in the G1-phase. The percentage of cells in different phases is shown in Figure 2G.

The expression levels of cell cycle associated proteins were analyzed by Western blotting. Compared with the control, the levels of c-Myc, cyclin D1, cyclin E1, and p-Rb decreased in DLD1 cells with the WSP1 treatment (Figure 2H), suggesting that the induced G1 phase arrest was attributed to the inhibition of c-Myc expression, followed by decreased cyclin D1, cyclin E1, and Rb phosphorylation expression.

Treatment of WSP1 Induces the Apoptosis of Human Colon Cancer Cells. Because many chemotherapeutic drugs have been used to treat tumors by inducing apoptosis,[21,22] we questioned whether WSP1 inhibited the colon cancer cell proliferation by inducing apoptosis. DLD1, HCT116, and FHC cells were treated with 0.15 $\mu g/\mu L$ WSP1 for 48 h, and apoptotic bodies were detected by DAPI staining. The results showed WSP1-treated cells exhibited the apoptotic characteristics of chromatin condensation with typical apoptotic bodies. The number of apoptotic nuclei significantly increased in the group of colon cancer cells with the WSP1 treatment. In contrast, the WSP1-treated FHC cells did not display any obvious apoptotic bodies (Figure 3A,B).

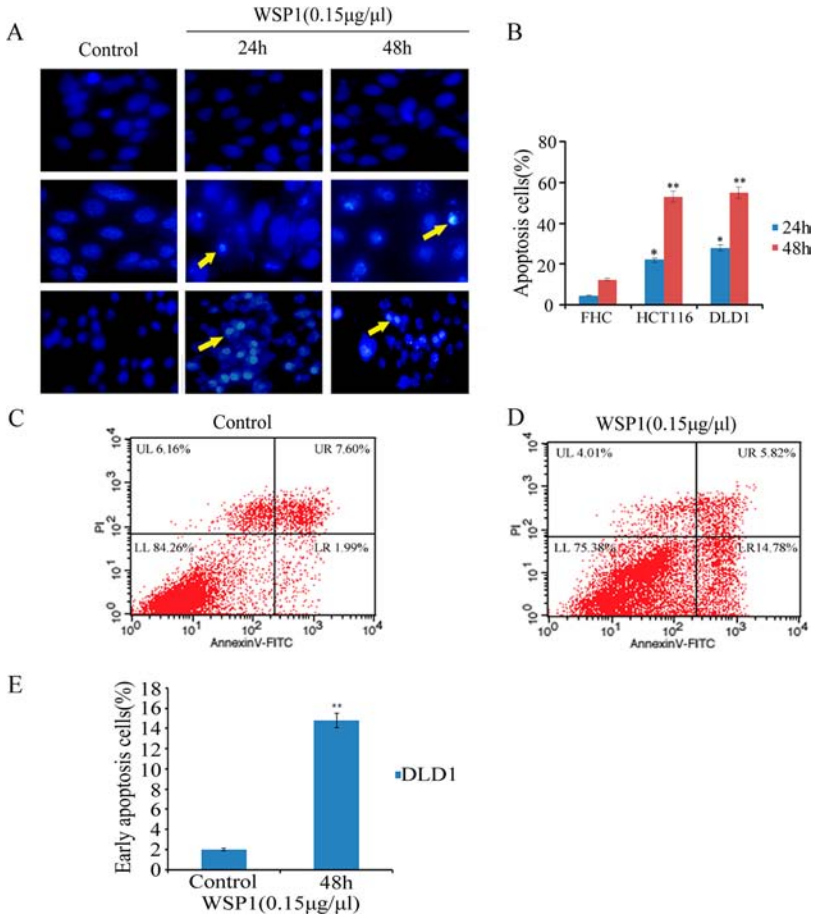

Figure 3. Effects of WSP1 on apoptosis. (A) DLD1 and HCT116 were treated with WSP1 (0.15 $\mu g/\mu L$) for 24 or 48 h, and monolayer cultures were stained with DAPI to reveal apoptotic changes in the cell nuclei. Apoptotic bodies were pointed out by arrows. (B) Apoptotic cells of DLD1 and HCT116 were calculated. (C,D) DLD1 cells were either untreated or treated with WSP1 (0.15 $\mu g/\mu L$) for 48 h. Effects of WSP1 on cell apoptosis induction assessed by Annexin V/PI method using flow cytometry. The bottom right quadrant represented cells stained mainly by Annexin V (early apoptotic cells). (E) The early apoptosis ratio of DLD1 was shown in the bar graph. All experiments were performed at least three times in independent cell culture. *$p < 0.05$, **$p < 0.01$ compared cells untreated with WSP1.

DOI: 10.1021/jf503208p
J. Agric. Food Chem. 2015, 63, 150−159

The degree of apoptosis was further determined by monitoring Annexin V-stained cells. DLD1 cells were treated with WSP1 for 48 h and then subjected to a flow cytometry analysis using Annexin V/propidium iodide double-staining. Compared to the control group, the ratio of Annexin V-stained cells was significantly increased in the group in the WSP1 treatment (Figure 3C,D). The early apoptotic cell percentage increased from 1.99 ± 0.38% to 14.78 ± 1.37% for DLD1 cells in the WSP1 treatment (Figure 3E).

WSP1 Alters Mitochondrial Membrane Potential and Induces Cell Apoptosis. Mitochondrial membrane depolarization[23] usually occurs in the stage of cell apoptosis. The collapse of mitochondrial membrane potential ($\Delta\psi m$), which reflects changes in mitochondrial membrane permeability, plays a vital role in the apoptotic process. Next, the changes of mitochondrial membrane potential were measured using JC-1 by flow cytometry. Under normal circumstances, JC-1 accumulates in active mitochondria in which it fluoresces red. A reduction in mitochondrial membrane potential results in the replacement of red fluorescence by green JC-1 monomers. The result indicated that there was an elevated percentage of DLD1 cells with depolarized mitochondrial membranes (time-dependently) after treatment with WSP1 for 48 h (Figure 4A). The fluorescent intensity ratio of red and green is shown in Figure 4B.

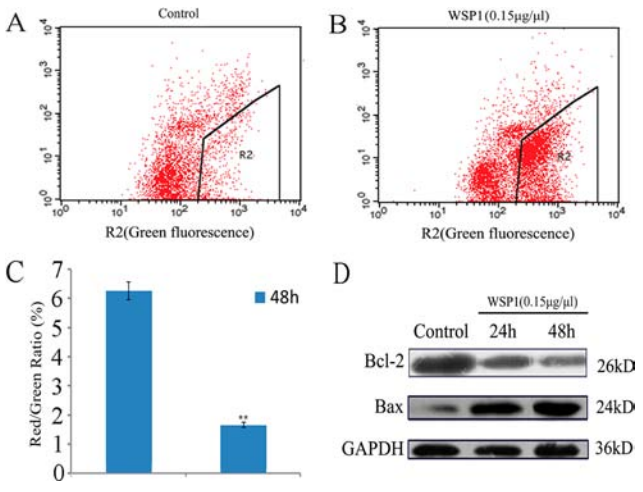

Figure 4. WSP1 induced mitochondrial membrane depolarization and releases of apoptotic factors in DLD1 cells. (A,B) Cells treated with WSP1 (0.15 $\mu g/\mu L$) for 48 h were harvested and subjected to flow cytometric analysis of mitochondrial membrane potential by JC-1 staining. Results were shown as mean values from three independent experiments. Treatment caused significant increases in the percentage of cells with depolarized mitochondrial membrane compared with the control (*$p < 0.05$, **$p < 0.01$). (C) Red and green fluorescence ratio of DLD1 cells treated and untreated by flow cytometric analysis. (D) Expressions of Bax and Bcl-2 were analyzed by Western blotting. GAPDH was used as the loading control. Representative Western blotting from two independent experiments was shown.

It is recognized that Bcl-2 family proteins regulate the mitochondrial membrane potential and the Bax/Bcl-2 ratio determines the cellular survival or apoptotic cell death.[24] The results showed that WSP1 could inhibit the antiapoptotic Bcl-2 protein and elevate the pro-apoptotic Bax protein (Figure 4D). With this, the Bax/Bcl-2 ratio was significantly increased (Figure 4D) and there was a subsequent reduction of mitochondrial membrane potential (Figure 4B,C). These data suggested that WSP1 caused mitochondrial dysfunction and the alteration of the Bax/Bcl-2 ratio that accounted for the WSP1-induced decline of $\Delta\psi m$.

WSP1 Treatment Induces the Caspase-Dependent Apoptosis in DLD1 Cells. To further explore the molecular mechanisms of WSP1 to induce cell apoptosis, the detection of PARP cleavage[25] was performed using Western blotting. The result showed WSP1 induced proteolytic inactivation of PARP and the extent of cleavage was elevated time-dependently (Figure 5A). Because PARP is a substrate of executioner caspases, its cleavage indicates that caspases might be activated during the cell death process. It is been known that caspase activation is involved in the cleavage of its pro-caspase.[26] After the WSP1 treatment, there were more pro-caspases-8 and -9 cleaved into caspases-8 and -9 (Figure 5A). In addition, the caspase-3 was further activated and led to apoptosis in DLD1 cells with the WSP1 treatment (Figure 5A). Moreover, the pan-caspase inhibitor, z-VAD-FMK, could partially reverse WSP1-inhibited cell proliferation in a dose dependent manner (Figure 5B); 20 μM z-VAD-FMK had inhibitory effects on the activation of caspase-9 (Figure 5C). These results confirmed that WSP1 induced apoptosis can be at least partially attributed to the activation of the caspase signaling pathway.

WSP1 Inhibits DLD1 Xenografted Tumor Growth in Nude Mice. To determine the anticolon cancer effects of WSP1 in vivo, we performed xenograft studies with DLD1-bearing nude mice. The nude mice received intraperitoneal injections of 60 μg WSP1/g body weight every 3 days. As shown in Figure 6, the WSP1-treatment for five injections resulted in a significantly reduced tumor volume and mass compared with the untreated group ($p < 0.01$). This phenomenon achieved a higher significance ($p < 0.01$) after six times injections. Furthermore, histology analyses revealed that WSP1-treated tumors had massive growth inhibition and apoptosis, as indicated by the significant reduction of K_i-67 and increase of actived-caspase-8, -9, and PARP (Figure 7). In addition, no mice died during the experiment. The body weights of the control group and the experimental group had no obvious difference (Figure 6A).

DISCUSSION

Studies have revealed that microorganisms serve as rich sources of anticancer therapeutics.[27−30] Previous studies have shown that *Nostoc commune* Vauch. contains various nutritional ingredients and has been used as food and medicine for centuries in China.[12] In this study, we found that the WSP1 from *Nostoc commune* Vauch. has anticolon cancer activity both in vitro and in vivo.

To prepare WSP1, *Nostoc commune* Vauch. does not need to be ground because water stress protein is the major component of the extracellular matrix.[16,18] The proteins obtained in this study had a relatively high purity. As shown in Figure 1D, WSP1 accounted for 83.6% of the total extracellular matrix protein. The three proteins of different molecular weights in the SDS-PAGE were all identified as WSP1 by mass spectrum. These isoforms may arise from deamidation, covalent modification, protease degradation, etc.[19] On the basis of our previous studies,[20] the WSP1 of 39 kDa was the main anticolon cancer protein and its amino acid sequence is shown in Figure 1E.

Malignant tumor growth is due to the abnormality of cell proliferation or regulation defects of cell death. Cell cycle arrest and apoptosis induction are concurrent.[31] The occurrence of

DOI: 10.1021/jf503208p
J. Agric. Food Chem. 2015, 63, 150−159

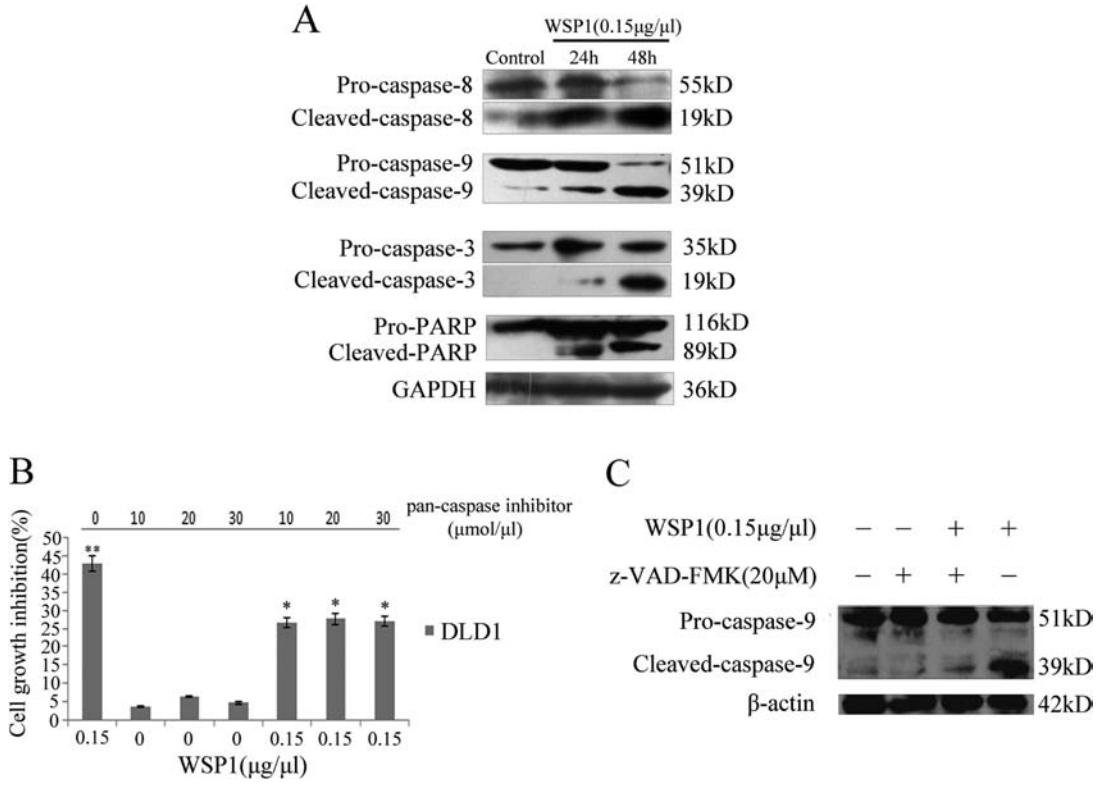

Figure 5. WSP1 induced caspase-dependent apoptosis in DLD1 cells. (A) Caspases and PARP were determined by Western blotting after treatment with WSP1 (0.15 μg/μL). GAPDH was used as the loading control. (B,C) The pan-caspase inhibitor reversed WSP1-suppressed cell proliferation. DLD1 cells were preincubated for 1 h in the absence or presence of 20 μM pan-caspase inhibitor, z-VAD-fmk, and were treated with WSP1 (0.15 μg/μL) for 48 h. Proliferation inhibitions of DLD1 cells were calculated by MTT, and the expression of caspase-9 was analyzed by Western blotting. $^{**}p < 0.01$ vs cells untreated with WSP1.

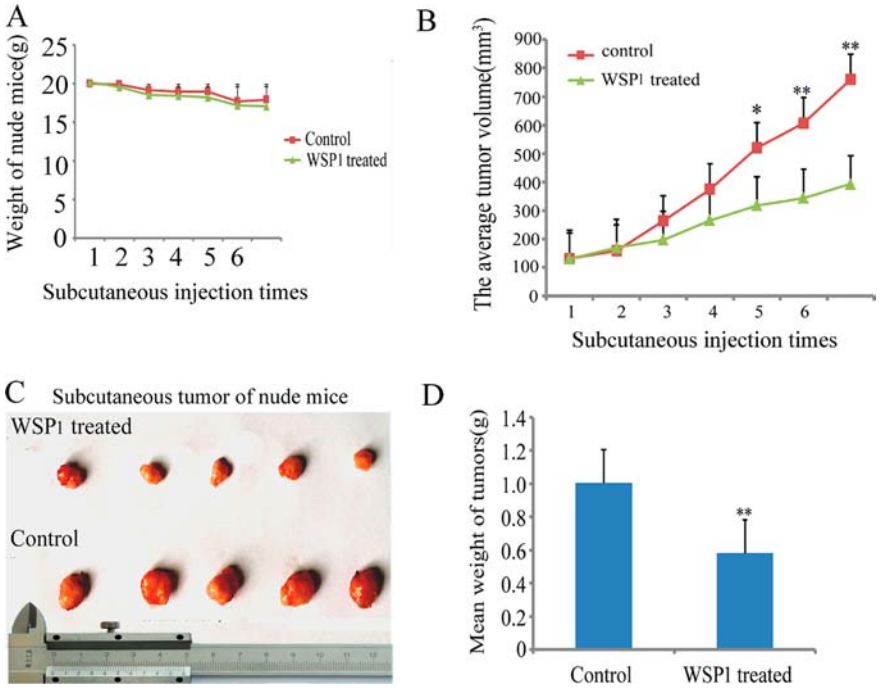

Figure 6. Effects of WSP1 on the growth of xenografted tumor in nude mice. DLD1 cells (5×10^6) were injected subcutaneously into the right oxter of the nude mice. After tumor formation, the mice were divided into two groups and treated with WSP1 (60 μg/g body weight) every 3 days or with PBS as control. (A) Curve of average body weight in two groups within 21 days. (B) Tumor volumes of both groups were calculated. (C) After six treatments with WSP1, mice were sacrificed and five representative tumors of each group were shown. (D) Mass of dissected tumors was excised. Results represent mean ± SD (n = 8). $^{**}p < 0.01$ vs control group.

DOI: 10.1021/jf503208p
J. Agric. Food Chem. 2015, 63, 150−159

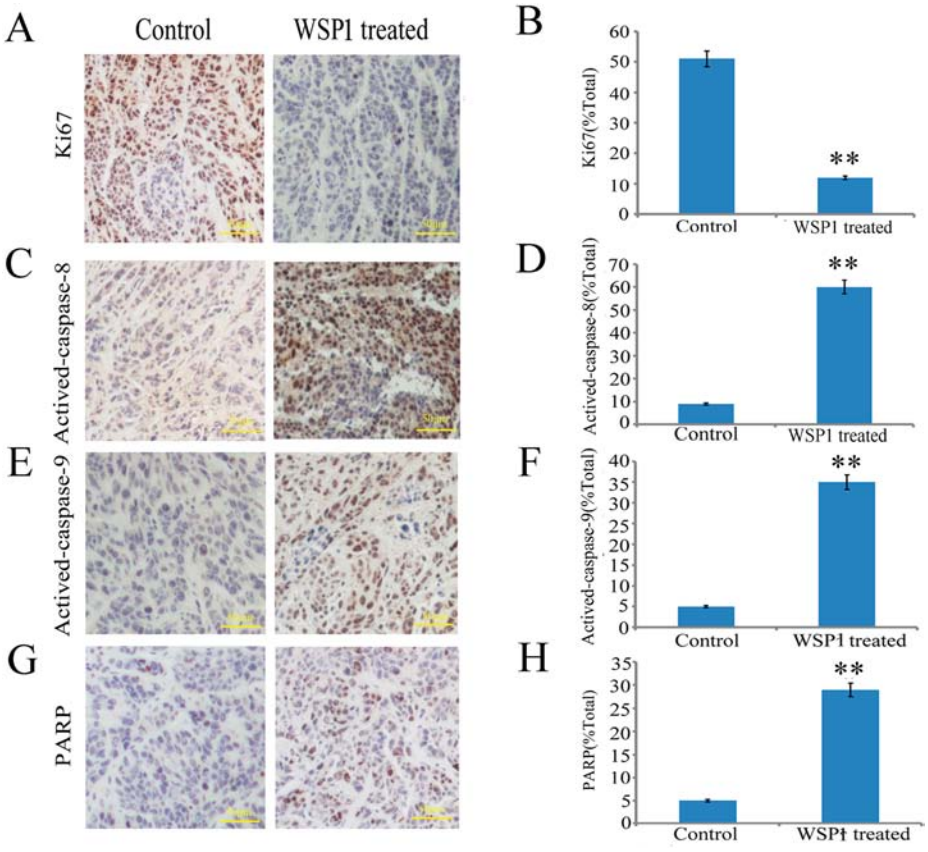

Figure 7. Immunohistochemical analysis of the expression of K_i-67, activated-caspase-8, activated-caspase-9, and PARP in the dissected tumor tissues by WSP1 treatment or control. There were significant differences between control and WSP1-treated group (**$p < 0.01$).

cell death is not caused by biochemical abnormalities but rather to completely split cell cycle events. Morphological change is considered the most reliable standard of apoptosis. The results showed that WSP1 dramatically inhibited proliferation of CRC cells in vitro, and the typical morphological changes of apoptosis were observed with WSP1 treatment (Figure 3A). Especially, WSP1 could induce the cell cycle arrest and apoptosis significantly. Moreover, it exerted obvious negative effects on normal colonic epithelial cell FHC, suggesting WSP1 has targeted antitumor effects on colon cancer cells.

It is known that c-Myc plays an important role in the cell cycle by activating cyclin D1 and cyclin E1, which in turn lead to phosphorylation of the retinoblastoma protein (Rb) and facilitate the cells entering the G1 phase.[32] Here, WSP1 induced cell cycle arrest at the G1/S phase in DLD1 cells. The corresponding Western blotting demonstrated that c-Myc expression was reduced, followed by the down regulations of cyclin D1, cyclin E1, and pRb expression. Thus, WSP1 could induce cell growth inhibition through the induction of G1-arrest in colon cancer cells (Figure 8).

Tumor formation often results from an increase in cell proliferation and a decrease in cell apoptosis.[33] The ability to induce apoptosis in tumor cells is as important as antitumor drugs.[34] Apoptosis usually initiated by caspase activation, even though not all cell apoptosis is linked to caspase activation.[35] Furthermore, PARP, a nuclear enzyme involved in DNA repair, is a well-known substrate for caspase-3 cleavage during apoptosis. Studies showed that PARP cleavage reduced DNA repair function and is considered to be a hallmark of apoptosis.[36] In the process of identifying the pathways by

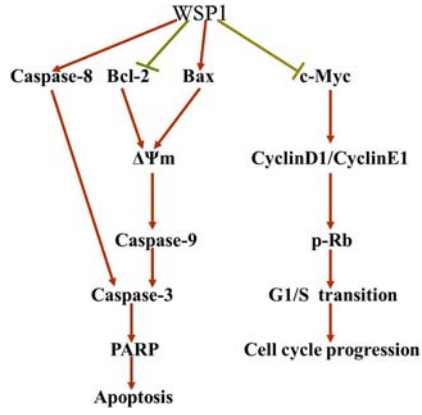

Figure 8. Proposed the possible signal pathway for growth inhibition and apoptosis induced by WSP1 in DLD1 cells.

which WSP1 induced colon cancer cell apoptosis, PARP was found to be cleaved and mediated by a cascade of caspases, including caspase-8 of the extrinsic apoptosis pathway and caspase-9 of the intrinsic pathway. These initiator caspases then lead to the activation of capsase-3. The present study showed that caspase-8, -9, and -3 in DLD1 cells were all activated with the WSP1 treatment. Consistently, WSP1-induced DLD1 cell apoptosis was partially suppressed and the cleavage of pro-caspase-9 was reversed by the addition of the pan-caspase inhibitor. The immunohistochemistry of DLD1 xenografted nude mice further confirmed that actived-caspase-8, -9, and PARP had strong expression in the cells treated with WSP1. These data confirmed that the caspase-dependent pathway was

DOI: 10.1021/jf503208p
J. Agric. Food Chem. 2015, 63, 150−159

responsible for the apoptotic process caused by WSP1 (Figure 8).

Cell survival depends on the maintenance of mitochondrial membrane potential.[37] The Bcl-2 family members consist of pro- and antiapoptotic proteins, which work together with other proteins to maintain a dynamic balance between the survival and death of cells by regulating the function of mitochondria. In human tumors, the expressions of Bcl-2, Bcl-xL, or other antiapoptotic homologues are up-regulated and the expression of pro-apoptotic protein Bax or Bak is down-regulated.[38] This study showed that WSP1 induced precocious apoptosis in DLD1 cells, as evidenced by a decrease in the expression of Bcl-2 and an increase in Bax, accompanied by a decrease in $\Delta\psi m$ (Figure 8).

The water stress protein, WSP1 from *Nostoc commune* Vauch. was prepared and studied in the present investigation. It indicated that WSP1 could suppress the growth of colon cancer cells by inducing cell cycle G1-phase arrest. Its apoptosis-promoting activity is attributed to the activation of caspase-dependent pathway. In agreement with the in vitro data, WSP1 could also suppress the growth of xenografted DLD1 tumors in vivo, indicating that it may be developed as an effective therapeutic agent for patients with colon cancers.

Intraperitoneal injection was applied in vivo in our study. It is an effective administration method for protein drugs in mice models. However, although it has good clinical characteristics such as a good curative effect and low side effects, the bioavailability of protein drugs is only a small percentage of their short half-life, they have large molecular weights and poor trans-membrane ability using methods other than injection. In contrast, using intravenous injection, protein drugs easily cause an immune response. Therefore, it has been an urgent task for scientists to research and develop protein drugs that are stable, have a long half-life, and have good biocompatibility and easy absorption. Studies[39−41] have shown that a chemical modification or a prodrug, such as an enzyme inhibitor, working as an absorption accelerator, could improve the absorption and reduce the immune response of protein drugs delivered via intravenous injection. For example, PEG (polyethylene glycol) is often used to carry modified protein structures and it could prolong the half-life of protein drugs and control their velocity into the blood. In addition, the injectable microspheres can achieve slow-release effects. Other non-injection methods such as nasal and pulmonary routes of administration can also improve the absorption and utilization of protein drugs. To improve the bioavailability of protein drugs, new biotechnology such as nanoliposomes are being used as oral and transdermal protein drug delivery carriers.

Collectively, WSP1 has specific antitumor activities on colon cancer and may have great potential for medicinal applications.

■ ASSOCIATED CONTENT

Ⓢ Supporting Information

Summary of WSP1 identification by MALDI-TOF analysis. This material is available free of charge via the Internet at http://pubs.acs.org.

■ AUTHOR INFORMATION

Corresponding Author

*For Zhuoyu Li: phone, 86-351-7018268; fax, 86-351-7018268; E-mail, lzy@sxu.edu.cn.

Funding

This study was supported by the National Natural Science Foundation of China (nos. 31271516 and 31201072), the Shanxi Province Science Foundation for Youths (2012021028-4), the Oversea Scientists' Funds (20111009/10), and the Research Fund for the Doctoral Program of Higher Education of China (20111401110011).

Notes

The authors declare no competing financial interest.

■ ACKNOWLEDGMENTS

We thank Dr. Enmin Zou of the Department of Biological Sciences of Nicholls State University, USA, for improving the readability of the paper.

■ REFERENCES

(1) Herszenyi, L.; Tulassay, Z. Epidemiology of gastrointestinal and liver tumors. *Eur. Rev. Med. Pharmacol. Sci.* **2010**, *14*, 249−258.

(2) Ling, Y.; Lian-di, L.; Yu-de, C. Cancer incidence and mortality estimates and prediction for year 2000 and 2005 in China. *Chin. J. Health Stat.* **2005**, *22*, 218−221.

(3) Bang, Y.-J.; Van Cutsem, E.; Feyereislova, A.; Chung, H. C.; Shen, L.; Sawaki, A.; Lordick, F.; Ohtsu, A.; Omuro, Y.; Satoh, T. Trastuzumab in combination with chemotherapy versus chemotherapy alone for treatment of HER2-positive advanced gastric or gastro-oesophageal junction cancer (ToGA): a phase 3, open-label, randomised controlled trial. *Lancet* **2010**, *376*, 687−697.

(4) Fernandez-Rozadilla, C.; Cazier, J.; Moreno, V.; Crous-Bou, M.; Guinó, E.; Durán, G.; Lamas, M.; López, R.; Candamio, S.; Gallardo, E. Pharmacogenomics in colorectal cancer: a genome-wide association study to predict toxicity after 5-fluorouracil or FOLFOX administration. *Pharmacogenomics J.* **2012**, *13*, 209−217.

(5) Harlev, E.; Nevo, E.; Lansky, E. P.; Lansky, S.; Bishayee, A. Anticancer attributes of desert plants: a review. *Anti-Cancer Drugs* **2012**, *23*, 255−271.

(6) Madiwale, G. P.; Reddivari, L.; Stone, M.; Holm, D. G.; Vanamala, J. Combined effects of storage and processing on the bioactive compounds and pro-apoptotic properties of color-fleshed potatoes in human colon cancer cells. *J. Agric. Food Chem.* **2012**, *60*, 11088−11096.

(7) Lv, L.; Chen, H.; Soroka, D.; Chen, X.; Leung, T.; Sang, S. 6-Gingerdiols as the major metabolites of 6-gingerol in cancer cells and in mice and their cytotoxic effects on human cancer cells. *J. Agric. Food Chem.* **2012**, *60*, 11372−7.

(8) Choi, S. P.; Kim, S. P.; Nam, S. H.; Friedman, M. Antitumor effects of dietary black and brown rice brans in tumor-bearing mice: relationship to composition. *Mol. Nutr. Food Res.* **2013**, *57*, 390−400.

(9) FAN, Q.-y.; WU, X.-y.; YANG, L.-q.; ZHU, X.-h.; MAO, G.-h. Research Progress of Nostoc commune vauch. *J. Changshu Inst. Technol.* **2007**, *4*, 012.

(10) Watanabe, F.; Yabuta, Y.; Tanioka, Y.; Bito, T. Biologically active vitamin B12 compounds in foods for preventing deficiency among vegetarians and elderly subjects. *J. Agric. Food Chem.* **2013**, *61*, 6769−6775.

(11) Ku, C. S.; Yang, Y.; Park, Y.; Lee, J. Health Benefits of Blue-Green Algae: Prevention of Cardiovascular Disease and Nonalcoholic Fatty Liver Disease. *J. Med. Food* **2013**, *16*, 103−111.

(12) MostafaS.Microalgal biotechnology: prospects and applications. In *Agricultural and Biological Sciences "Plant Science"*; Dhal, N. K., Sahu, S. C., Eds.; InTech: Rijeka, Croatia, 2012; Chapter 12.

(13) Kovač, D. J.; Simeunović, J. B.; Babić, O. B.; Mišan, A. Č.; Milovanović, I. L. Algae in food and feed. *Food Feed Res.* **2013**, *40*, 21−32.

(14) Ken, C.-F.; Hsiung, T.-M.; Huang, Z.-X.; Juang, R.-H.; Lin, C.-T. Characterization of Fe/Mn-superoxide dismutase from diatom Thallassiosira weissflogii: cloning, expression, and property. *J. Agric. Food Chem.* **2005**, *53*, 1470−1474.

DOI: 10.1021/jf503208p
J. Agric. Food Chem. 2015, 63, 150−159

(15) Scherer, S.; Potts, M. Novel water stress protein from a desiccation-tolerant cyanobacterium. Purification and partial characterization. *J. Biol. Chem.* **1989**, *264*, 12546−12553.
(16) Mohamed Morsy, F.; Kuzuha, S.; Takani, Y.; Sakamoto, T. Novel thermostable glycosidases in the extracellular matrix of the terrestrial cyanobacterium *Nostoc commune*. *J. Gen. Appl. Microbiol.* **2008**, *54*, 243−252.
(17) Hill, D.; Hladun, S.; Scherer, S.; Potts, M. Water stress proteins of *Nostoc commune* (Cyanobacteria) are secreted with UV-A/B-absorbing pigments and associate with 1,4-beta-D-xylanxylanohydrolase activity. *J. Biol. Chem.* **1994**, *269*, 7726−7734.
(18) Wright, D. J.; Smith, S. C.; Joardar, V.; Scherer, S.; Jervis, J.; Warren, A.; Helm, R. F.; Potts, M. UV irradiation and desiccation modulate the three-dimensional extracellular matrix of *Nostoc commune* (Cyanobacteria). *J. Biol. Chem.* **2005**, *280*, 40271−40281.
(19) Sakamoto, T.; Kumihashi, K.; Kunita, S.; Masaura, T.; Inoue-Sakamoto, K.; Yamaguchi, M. The extracellular-matrix-retaining cyanobacterium *Nostoc verrucosum* accumulates trehalose, but is sensitive to desiccation. *FEMS Microbiol. Ecol.* **2011**, *77*, 385−394.
(20) Guo, S.-j.; Shan, S.-h.; Jin, X.-t.; Li, Z.-w.; Song, L.; Li, Z.-y. Cloning and Expression of a Novel Water Stress Protein from *Nostoc commune* Vauch. and Its Inhibitory Effect on the Proliferation of Human Colon Cancer SW480 Cells. *Food Sci.* **2014**, *35*, 151−155.
(21) Johnstone, R. W.; Ruefli, A. A.; Lowe, S. W. Apoptosis: a link between cancer genetics and chemotherapy. *Cell* **2002**, *108*, 153−164.
(22) Fulda, S.; Debatin, K. Extrinsic versus intrinsic apoptosis pathways in anticancer chemotherapy. *Oncogene* **2006**, *25*, 4798−4811.
(23) Parlato, M.; Souza-Fonseca-Guimaraes, F.; Philippart, F.; Misset, B.; Adib-Conquy, M.; Cavaillon, J.-M.; Jacqmin, S.; Journois, D.; Lagrange, A.; de Villechenon, G. P. CD24-Triggered Caspase-Dependent Apoptosis via Mitochondrial Membrane Depolarization and Reactive Oxygen Species Production of Human Neutrophils Is Impaired in Sepsis. *J. Immunol.* **2014**, *192*, 2449−2459.
(24) Singh, N.; Sarkar, J.; Sashidhara, K. V.; Ali, S.; Sinha, S. Anti-tumour activity of a novel coumarin−chalcone hybrid is mediated through intrinsic apoptotic pathway by inducing PUMA and altering Bax/Bcl-2 ratio. *Apoptosis* **2014**, 1−12.
(25) Yu, S.-W.; Wang, H.; Poitras, M. F.; Coombs, C.; Bowers, W. J.; Federoff, H. J.; Poirier, G. G.; Dawson, T. M.; Dawson, V. L. Mediation of poly (ADP-ribose) polymerase-1-dependent cell death by apoptosis-inducing factor. *Science* **2002**, *297*, 259−263.
(26) Shi, Y. Mechanisms of caspase activation and inhibition during apoptosis. *Mol. Cell* **2002**, *9*, 459−470.
(27) Garay, L. A.; Boundy-Mills, K. L.; German, J. B. Accumulation of high-value lipids in single-cell microorganisms: a mechanistic approach and future perspectives. *J. Agric. Food Chem.* **2014**, *62*, 2709−2727.
(28) Cragg, G.; Newman, D. Nature: a vital source of leads for anticancer drug development. *Phytochem. Rev.* **2009**, *8*, 313−331.
(29) Pagano, A.; Honore, S.; Mohan, R.; Berges, R.; Akhmanova, A.; Braguer, D. Epothilone B inhibits migration of glioblastoma cells by inducing microtubule catastrophes and affecting EB1 accumulation at microtubule plus ends. *Biochem. Pharmacol.* **2012**, *84*, 432−443.
(30) Chang, Y. C.; Hsiao, Y. M.; Wu, M. F.; Ou, C. C.; Lin, Y. W.; Lue, K. H.; Ko, J. L. Interruption of lung cancer cell migration and proliferation by fungal immunomodulatory protein FIP-fve from Flammulina velutipes. *J. Agric. Food Chem.* **2013**, *61*, 12044−52.
(31) Tewari-Singh, N.; Gu, M.; Agarwal, C.; White, C. W.; Agarwal, R. Biological and molecular mechanisms of sulfur mustard analogue-induced toxicity in JB6 and HaCaT cells: possible role of ataxia telangiectasia-mutated/ataxia telangiectasia-Rad3-related cell cycle checkpoint pathway. *Chemical Res. Toxicol.* **2010**, *23*, 1034−1044.
(32) Butt, A. J.; McNeil, C. M.; Musgrove, E. A.; Sutherland, R. L. Downstream targets of growth factor and oestrogen signalling and endocrine resistance: the potential roles of c-Myc, cyclin D1 and cyclin E. *Endocr.-Relat. Cancer* **2005**, *12*, S47−S59.
(33) Evan, G. I.; Vousden, K. H. Proliferation, cell cycle and apoptosis in cancer. *Nature* **2001**, *411*, 342−348.
(34) Brown, J. M.; Attardi, L. D. The role of apoptosis in cancer development and treatment response. *Nature Rev. Cancer* **2005**, *5*, 231−237.
(35) Hengartner, M. O. The biochemistry of apoptosis. *Nature* **2000**, *407*, 770−776.
(36) Tewari, M.; Quan, L. T.; O'Rourke, K.; Desnoyers, S.; Zeng, Z.; Beidler, D. R.; Poirier, G. G.; Salvesen, G. S.; Dixit, V. M. Yama/CPP32β, a mammalian homolog of CED-3, is a CrmA-inhibitable protease that cleaves the death substrate poly (ADP-ribose) polymerase. *Cell* **1995**, *81*, 801−809.
(37) Wang, Y. L.; Frauwirth, K. A.; Rangwala, S. M.; Lazar, M. A.; Thompson, C. B. Thiazolidinedione activation of peroxisome proliferator-activated receptor γ can enhance mitochondrial potential and promote cell survival. *J. Biol. Chem.* **2002**, *277*, 31781−31788.
(38) Zangemeister-Wittke, U.; Leech, S. H.; Olie, R. A.; Simões-Wüst, A. P.; Gautschi, O.; Luedke, G. H.; Natt, F.; Häner, R.; Martin, P.; Hall, J. A novel bispecific antisense oligonucleotide inhibiting both bcl-2 and bcl-xL expression efficiently induces apoptosis in tumor cells. *Clin. Cancer Res.* **2000**, *6*, 2547−2555.
(39) Almeida, A. J.; Souto, E. Solid lipid nanoparticles as a drug delivery system for peptides and proteins. *Adv. Drug Delivery Rev.* **2007**, *59*, 478−490.
(40) De, A.; Bose, R.; Kumar, A.; Mozumdar, S., Nanoparticulate Delivery Systems. In *Targeted Delivery of Pesticides Using Biodegradable Polymeric Nanoparticles*; Springer: New York, 2014; pp 37−57.
(41) Wulff-Pérez, M.; de Vicente, J.; Martín-Rodríguez, A.; Gálvez-Ruiz, M. J. Controlling lipolysis through steric surfactants: new insights on the controlled degradation of submicron emulsions after oral and intravenous administration. *Int. J. Pharm.* **2012**, *423*, 161−166.

DOI: 10.1021/jf503208p
J. Agric. Food Chem. 2015, 63, 150−159

JOURNAL OF AGRICULTURAL AND FOOD CHEMISTRY

Article

pubs.acs.org/JAFC

Anti-inflammatory Activity of Guluronate Oligosaccharides Obtained by Oxidative Degradation from Alginate in Lipopolysaccharide-Activated Murine Macrophage RAW 264.7 Cells

Rui Zhou,[†,∥] Xuyang Shi,[‡,∥] Yan Gao,[§] Nan Cai,[†] Zedong Jiang,[#] and Xu Xu*[,†]

[†]College of Life Science, Shenzhen Key Laboratory of Marine Bioresources and Ecology, Shenzhen University, Shenzhen 518060, China [‡]College of Life Science, Shenzhen Key Laboratory of Microbial Genetic Engineering, Shenzhen University, Shenzhen 518060, China

[§]National Oceanographic Center of Qingdao, Qingdao 266071, China

[#]Fujian Provincial Key Laboratory of Food Microbiology and Enzyme Engineering, Xiamen 361021, China

ABSTRACT: Alginate has notably diverse pharmacological activities. The present study investigated the anti-inflammatory activity of the guluronate oligosaccharides prepared by oxidative degradation (GOS-OD) from alginate. GOS-OD significantly attenuated the production of nitric oxide (NO), prostaglandin E_2 (PGE_2), and reactive oxygen species (ROS), the expression of inducible nitric oxide synthase (iNOS) and cyclooxygenase (COX)-2, and the secretion of pro-inflammatory cytokines in lipopolysaccharide (LPS)-activated murine macrophage RAW 264.7 cells. Moreover, GOS-OD potently decreased the binding of LPS to the cell surface and LPS-induced Toll-like receptor 4 (TLR4) and cluster of differentiation (CD) 14 expression. Additionally, GOS-OD could remarkably inhibit the LPS-induced activation of nuclear factor (NF)-κB and mitogen-activated protein (MAP) kinase pathways in RAW 264.7 cells. These results indicate that GOS-OD may reduce the LPS-stimulated inflammatory responses through blocking the activation of NF-κB and MAP kinases, suggesting that GOS-OD may be considered as a potential nutraceutical for inflammation.

KEYWORDS: *alginate oligosaccharides, lipopolysaccharide, Toll-like receptor 4, nuclear factor-κB, mitogen-activated protein kinases*

INTRODUCTION

Increasing evidence has confirmed that inflammation is associated with various diseases, such as cancer, obesity, and cardiovascular diseases.[1,2] Hence, the study of anti-inflammatory pathways is crucial to the development of new nutraceuticals or drugs for the treatment of inflammatory-mediated diseases. Lipopolysaccharide (LPS)-stimulated inflammatory models have been widely used to study the anti-inflammatory activity of various naturally derived substances.[3,4] Toll-like receptors (TLRs) play important roles in the molecular mechanisms of inflammation, particularly TLR4.[5] TLR4 has been shown to be the predominant modulator of the pro-inflammatory responses induced by LPS.[6] Cluster of differentiation (CD) 14 acts as an important cofactor for the binding of LPS to TLR4, an interaction that plays a critical role in the innate immune system response.[7] Recent works have demonstrated that LPS-stimulated inflammation is mainly mediated by TLR4 and CD14.[8] TLR4 signaling triggers a cascade of pro-inflammatory events that lead to the activation of the transcription factor, nuclear factor (NF)-κB, cellular kinases, such as mitogen-activated protein (MAP) kinases, protein kinase B (Akt), and phosphoinositide 3-kinase (PI3K), and the induction of the overexpression of inflammatory-related mediators, including nitric oxide (NO), prostaglandin E_2 (PGE_2), reactive oxygen species (ROS), pro-inflammatory proteins, such as inducible nitric oxide synthase (iNOS) and cyclooxygenase (COX)-2, and pro-inflammatory cytokines.[9,10] Therefore, naturally derived extracts/compounds that can efficiently reduce the LPS-induced activation of NF-κB and MAP kinase pathways should be considered as potential nutraceuticals or drugs for the treatment of inflammatory diseases.[11,12]

Although the anti-inflammatory activity of natural polysaccharides has been widely investigated to find anti-inflammatory agents that work through suppressing the production of NO and PGE_2 and down-regulating the expression of iNOS and COX-2,[11−13] wide application of those polysaccharides is difficult due to their high molecular weights and low solubilities. Therefore, the depolymerization of polymers may possibly overcome the limitation. The anti-inflammatory activity of naturally derived oligosaccharides, such as lactulose oligosaccharides,[14] mannan oligosaccharides,[15] and chitosan oligosaccharides,[16] have been widely investigated in recent years using in vitro and in vivo models of inflammation. Alginates are natural polysaccharides found in brown seaweed and are copolymerized alternatively by the two monomers α-1,4-L-guluronic acid (G) and β-1,4-D-mannuronic acid (M). They are used in a wide variety of industries, such as the food, textile, and pharmaceutical industries.[17] Alginate oligosaccharides (AOS) depolymerized by different methods from polymers show various phamacological activities. In previous works, we have reported that the different bioactivities of AOS can be attributed to the different structures. Unsaturated AOS that have been prepared by enzyme degradation possess various

Received: July 24, 2014
Revised: December 7, 2014
Accepted: December 8, 2014
Published: December 8, 2014

ACS Publications © 2014 American Chemical Society

bioactivities such as the induction of cytokine production,[18] neuroprotective activities,[19,20] macrophage bactericidal activity, and immunostimulatory activity,[21,22] whereas the saturated AOS prepared by acid hydrolysis have low bioactivities. AOS produced by the oxidative degradation method have been used as tissue engineering agents.[23] However, to the best of our knowledge, the anti-inflammatory activities of AOS prepared by oxidative degradation have not been reported.

In this study, we investigated the effect of AOS produced by different degradation methods on LPS-induced NO production in RAW 264.7 cells and found that only GOS-OD significantly reduced the LPS-induced excessive secretion of NO. Next, we provide key insights into potential mechanisms for the anti-inflammatory activity of GOS-OD in LPS-activated RAW 264.7 cells.

MATERIALS AND METHODS

Chemicals and Reagents. Alginates (1000 cps grade) were obtained from Nuotai (Shanghai, China). Fetal bovine serum (FBS) was purchased from Biontex (Planegg, Germany). RPMI-1640 culture medium was from Thermo Scientific (Hudson, NH, USA). Anti-mouse iNOS antibody, anti-mouse COX-2 antibody, anti-mouse NF-κB antibody, and antibodies for MAP kinases including p38, JNK, and ERK were all obtained from Cell Signaling Technology (Beverly, MA, USA). Anti-mouse TLR4 antibody and anti-CD14 were purchased from Abcam (Cambridge, UK). 2′,7′-Dichlorofluorescein diacetate (DCF-DA) was provided by Beyotime Inst. Biotech. (Jiangsu, China). NG-nitro-L-arginine methyl ester (L-NAME) and FITC-conjugated LPS were obtained from Sigma-Aldrich (St. Louis, MO, USA). The other reagents were all commercially available.

Preparation of Alginate Oligosaccharides. First, we prepared polyguluronate (PG) and polymannuronate (PM) (DP = 20−24) using methods previously described.[24] Second, AOS (GOS-OD, MOS-OD, GOS-AH, MOS-AH, GOS-ED, and MOS-ED) were obtained from PG and PM by oxidative degradation,[25] acid hydrolysis,[26] and enzymatic degradation,[27] respectively. Finally, alginate saccharide samples were sterilized by filtration using 0.22 μm filter membranes (Millipore Co., Billerica, MA, YSA) prior to the experiments.

Cell Culture and Viability Assays. Murine RAW 264.7 cells were purchased from the Shanghai cell bank of the Chinese Academy of Sciences (Shanghai, China). These cells were incubated in RPMI-1640 medium plus 10% FBS, 100 U/mL penicillin, and 100 μg/mL streptomycin sulfate in a humidified incubator with 5% CO_2. Cell viability was examined by a WST-8 assay (Beyotime Inst. Biotech.) according to the manufacturer's instructions. In brief, the cells were seeded onto 96-well plates (2×10^5 cells/well) and incubated with all various saccharide samples (GOS-OD, MOS-OD, GOS-AH, MOS-AH, GOS-ED, MOS-ED, PG, and PM) or GOS-OD (0.1−2 mg/mL) for 24 h. One hundred microliters of CCK-8 reagent (0.5 mg/mL) was added to the wells. The absorbance was examined at 540 nm by a Spectra Max microplate reader (Molecular Devices, LLC, Sunnyvale, CA, USA).

Measurement of NO, PGE_2, and ROS. For NO and PGE_2 measurements, RAW 264.7 cells were seeded onto 96-well plates (2×10^5 cells/well). Then, the cells were incubated with saccharide samples (1 mg/mL) or GOS-OD (0.1−2 mg/mL) for 2 h and treated with or without 1 μg/mL LPS for 24 h. The nitrite concentration was detected as an indicator of NO secretion via the Griess reaction.[28] Fifty microliters of supernatant was mixed with 50 μL of Griess reagent. The absorbance of the mixture was detected by a microplate reader (Molecular Devices, LLC). Levels of PGE_2 in the supernatant were quantified by an enzyme-linked immunosorbent assay (ELISA) kit (Cayman Chemical Co., Ann Arbor, MI, USA) according to the manufacturer's instructions.

The fluorescent probe DCFH-DA (Beyotime Inst. Biotech.) was used to measure ROS. RAW 264.7 cells (5×10^5 cells/well) were treated with GOS-OD (0.1−2 mg/mL) for 2 h and then incubated with or without LPS (1 μg/mL) for 24 h. Then, the cells were washed twice with PBS and incubated with a 10 μM DCFH-DA solution at 37 °C for 30 min. After three washings with PBS, the cells were harvested. The fluorescence intensity of the cell suspensions was measured using a fluorescence-activated cell sorting (FACS) system (Becton Deckinson, San Jose, CA, USA).

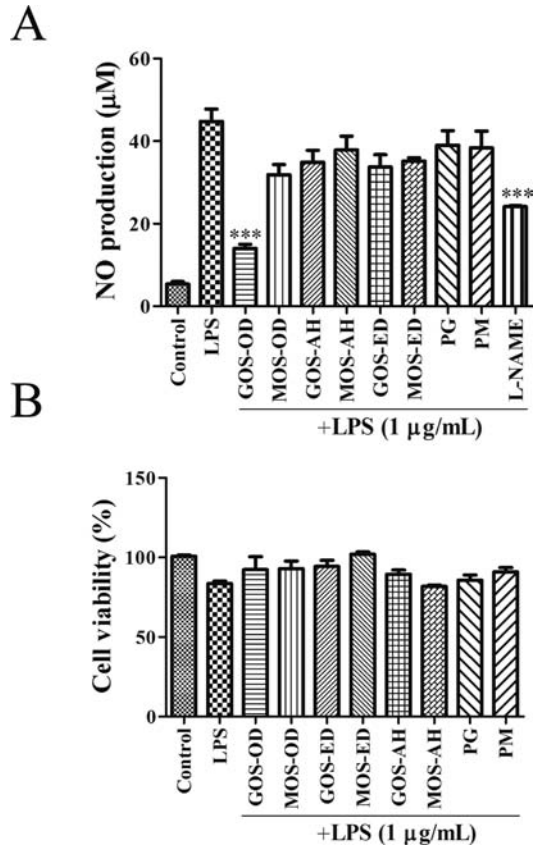

Figure 1. Effects of GOS-OD, MOS-OD, GOS-AH, MOS-AH, GOS-ED, MOS-ED, PG, and PM on NO production and cell viability in LPS-activated RAW 264.7 cells. (A) RAW 264.7 cells preincubated with 1 mg/mL saccharides for 2 h were treated with 1 μg/mL LPS for 24 h. The nitrite concentration in the culture supernatant was detected to indicate NO production. L-NAME (1 mM), a NOS inhibitor, was used as a positive control. (B) Cells preincubated with 1 mg/mL saccharides for 2 h were treated with 1 μg/mL LPS for 24 h. The cell viability was measured using a CCK-8 assay. Values are the mean ± SD of three independent experiments. (***) $p < 0.001$ indicates significant differences compared to the LPS-treated group.

Measurement of TNF-α, IL-1β, and IL-6. RAW 264.7 cells were seeded onto 96-well plates (2×10^5 cells/well). Then, the cells were preincubated with 0.1−2 mg/mL GOS-OD for 2 h and treated with or without LPS (1 μg/mL) for 24 h. Levels of TNF-α, IL-1β, and IL-6 in the supernatant were quantified by an ELISA kit (NeoBioscience Technology Co., Ltd., Shenzhen, China) according to the manufacturer's instructions.

Reverse Transcription Polymerase Chain Reaction (RT-PCR). RAW 264.7 cells (1×10^6 cells/well) pretreated with 0.1−2 mg/mL GOS-OD were stimulated with or without 1 μg/mL LPS for 12 h. Total RNA was extracted from the treated cells using Trizol reagent ($RNA_{fast200}$, Fastagen, China). For each sample, 1 μg of RNA was used for reverse transcription. The PCR primers are as follows: forward strand iNOS, 5′-CAA CCA GTA TTA TGG CTC CT-3′; reverse strand iNOS, 5′-GTG ACA GCC CGG TCT TTC CA-3′; forward strand COX-2, 5′-CCA CTT CAA GGG AGT CTG GA-3′; reverse strand COX-2, 5′-AGT CAT CTG CTA CGG GAG GA-3′; forward strand β-actin, 5′-GGA GAA GAT CTG GCA CCA CAC C-3′; reverse strand β-actin, 5′-CCT GCT TGC TGA TCC ACA TCT GCT GG-3′. β-Actin was used as an internal standard.

dx.doi.org/10.1021/jf503548a | J. Agric. Food Chem. 2015, 63, 160−168

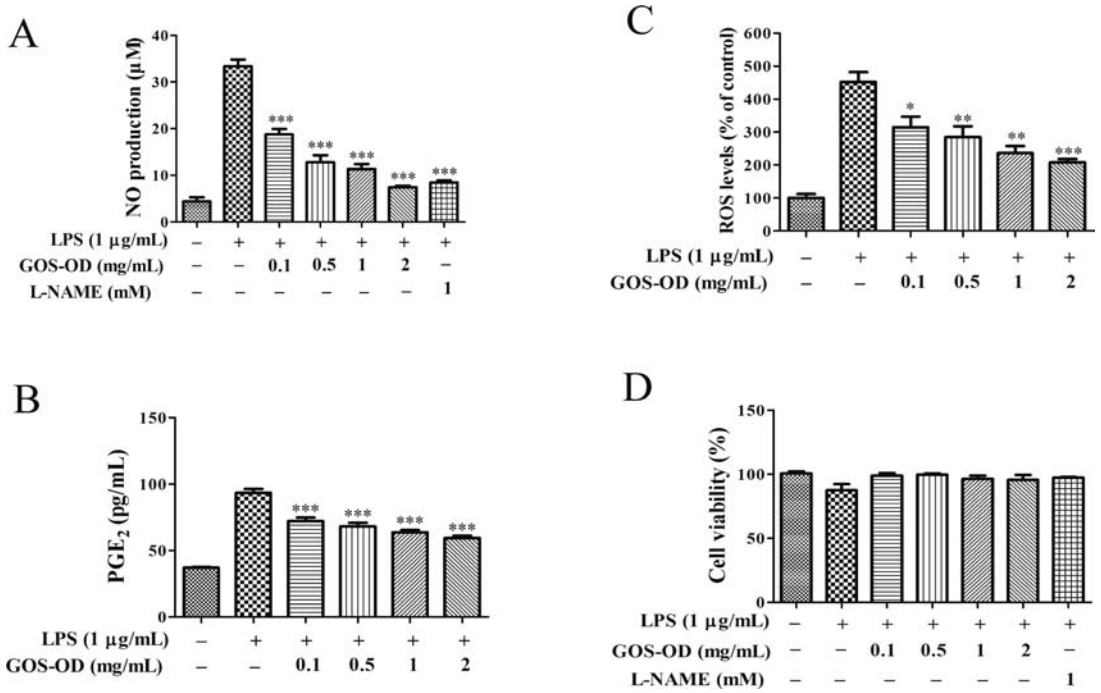

Figure 2. Effects of GOS-OD on the production of NO, PGE_2, and ROS in LPS-activated RAW 264.7 cells. Cells preincubated with 0.1−2 mg/mL GOS-OD for 2 h were treated with 1 μg/mL LPS for 24 h. NO (A) and PGE_2 production (B) in the culture supernatant was detected by ELISA. ROS production was measured by FACS analysis (C). The viability of cells preincubated with 0.1−2 mg/mL GOS-OD and treated with LPS was measured by the CCK-8 assay (D). L-NAME (1 mM) was used as a positive control. Values are the mean ± SD of the three independent experiments. (∗) $p < 0.05$, (∗∗) $p < 0.01$, and (∗∗∗) $p < 0.001$ indicate significant differences compared to the LPS-treated group.

Western Blot Analysis. RAW 264.7 cells were seeded onto 6-well plates (1×10^6 cells/well). Then, the cells were pretreated with GOS-OD (0.1−2 mg/mL) for 2 h and incubated with or without 1 μg/mL LPS for 24 h. Next, the cells were washed three times with ice-cold PBS. Cellular lysates were prepared in lysis buffer (Biocolors, Shanghai, China) at 4 °C for 30 min and centrifuged at 12000 rpm. After the quantification of proteins by a bicinchoninic acid (BCA) protein assay kit (Auragene Bioscience Corp. Inc., Changsha, China), 50 μg of cellular proteins was resolved using a 12.5% sodium dodecyl sulfate−polyacrylamide gel electrophoresis (SDS-PAGE) and transferred onto a polyvinylidene difluoride (PVDF) membrane (Amersham Pharmacia Biotech., UK). The membranes were treated with 10% skimmed milk in Tris-buffered saline containing 0.1% Tween 20 (TBST) to block the nonspecific binding. Thereafter, the membranes were washed adequately and hybridized with anti-mouse iNOS antibody (dilution 1:1000) or anti-mouse COX-2 antibody (dilution 1:1000) in 5% skimmed milk in TBST overnight at 4 °C. After three washings with TBST, the membranes were incubated with a horseradish peroxidase-conjugated secondary antibody at 37 °C for 2 h. The expression levels of iNOS and COX-2 proteins were observed by an LAS3000 luminescent image analyzer (Fujifilm Life Science, Tokyo, Japan). The density of the Western blot bands was analyzed using Quantity One software (Bio-Rad).

To analysis the expression of TLR4 and CD14, RAW 264.7 cells (1×10^6 cells/well) were preincubated with 2 mg/mL GOS-OD for 2 h and treated with or without 1 μg/mL LPS at 37 °C for 24 h. After protein preparation, the Western blot analysis was carried out using anti-TLR4 and anti-CD14 antibodies.

To test NF-κB/p65 expressions, RAW 264.7 cells (1×10^6 cells/well) pretreated with 2 mg/mL GOS-OD for 2 h were incubated with 1 μg/mL LPS for 30 min. Then, the nuclear and cytoplasmic proteins were extracted by a KeyGEN Nuclear and Cytoplasmic Protein Extraction Kit (KeyGen Biotech., Nanjing, China). After protein quantitation, the Western blot analysis was performed using an anti-NF-κB/p65 antibody, similar to the method described above.

To determine the expression levels of MAP kinases, RAW 264.7 cells (1×10^6 cells/well) were preincubated with 2 mg/mL of GOS-OD for 2 h and stimulated with or without LPS (1 μg/mL) at 37 °C for 10 min. After the suitable proteins were obtained, the Western blot analysis was carried out as described above using corresponding antibodies, including phosphorylated and nonphosphorylated p38, JNK, and ERK MAP kinases.

Fluorescence Analysis. To observe the effect of GOS-OD on the binding of FITC-conjugated LPS (FITC-LPS) to RAW 264.7 cell surfaces, cells were seeded onto glass coverslips (Corning Inc. Life Sciences, MA, USA) in 6-well plates for 24 h. The cells were preincubated with 2 mg/mL GOS-OD for 2 h and then stimulated with 10 μg/mL FITC-LPS for 1 h. Finally, the cells were washed three times with PBS and fixed in 4.0% (w/v) paraformaldehyde for 15 min at room temperature. The samples were observed using a Fluoview FV1000 laser scanning confocal microscope (Olympus, Tokyo, Japan).

Flow Cytometry Analysis. To further verify the effect of GOS-OD on the binding of FITC-LPS to RAW 264.7 cell surfaces, the cells were preincubated with 2 mg/mL GOS-OD for 2 h and treated with 10 μg/mL FITC-LPS for 30 min. Then, the cells were harvested and resuspended in RPMI-1640 medium and subjected to FACS for analysis.

Immunofluorescence Analysis. To examine TLR4 expression and nuclear NF-κB in RAW 264.7 cells, cells were seeded onto glass coverslips in 6-well plates for 24 h. Then, the cells were pretreated with 2 mg/mL GOS-OD for 2 h and treated with LPS (1 μg/mL) for 1 h. Thereafter, the cells were fixed with 4.0% (w/v) paraformaldehyde at room temperature for 15 min. After three washes with PBS, the cells were permeabilized in 0.2% (v/v) Triton X-100 for 30 min and washed three times. Next, the cells were blocked in 1% (w/v) goat serum in PBS for 60 min. Then, the cells were treated with mouse monoclonal anti-TLR4 antibody or anti-NF-κB/p65 antibody diluted in 1% goat serum/PBS (1:400) overnight at 4 °C. After removal of the primary antibodies and three washings, the cells were treated with Alexa Fluor 488-conjugated secondary anti-mouse antibody/PBS (1:200) for 2 h at 37 °C. Finally, the nuclei were stained with DAPI (5 μg/mL).

dx.doi.org/10.1021/jf503548a | J. Agric. Food Chem. 2015, 63, 160−168

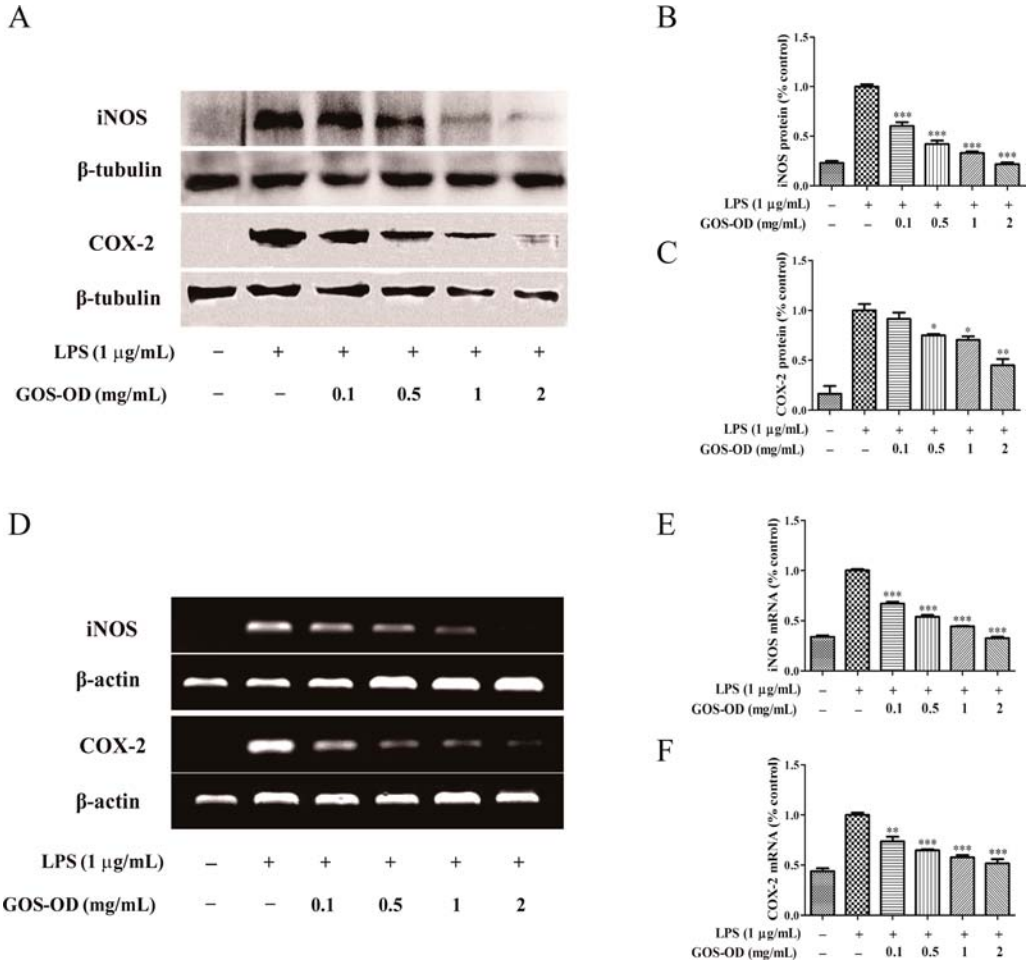

Figure 3. Effects of GOS-OD on iNOS and COX-2 expressions in LPS-activated RAW 264.7 cells. (A) Cells preincubated with 0.1−2 mg/mL GOS-OD for 2 h were treated with 1 μg/mL LPS for 24 h. The expressions of iNOS, COX-2, and β-tubulin proteins were detected by Western blot analysis. Relative iNOS (B) and COX-2 (C) protein levels were calculated with reference to the LPS-treated group. (D) Cells preincubated with 0.1−2 mg/mL GOS-OD for 2 h were treated with 1 μg/mL LPS for 12 h. Then, whole RNA was extracted for RT-PCR. Relative iNOS (E) and COX-2 (F) mRNA levels were calculated with reference to the LPS-treated group. Values are the mean ± SD of three independent experiments. (*) $p < 0.05$, (**) $p < 0.01$, and (***) $p < 0.001$ indicate significant differences compared to the LPS-treated group.

The immunofluorescence analysis was performed using a Fluoview FV1000 laser scanning confocal microscope (Olympus).

Cell Morphology of RAW 264.7 Cells. Dark field microscopy was performed on an upright optical microscope Olympus BX51. RAW 264.7 cells (4×10^5 cells/well) were cultured on a coverglass placed in a plastic culture dish and were pretreated with GOS-OD (1−2 mg/mL) for 2 h. After 24 h of incubation without or with LPS (1 μg/mL), the cell morphology of RAW 264.7 cells was monitored by dark field microscopy. Cell morphology was observed using a 40× objective and then captured by a color CCD camera (DP70, Olympus). The images were processed by ImageJ software.

Statistical Analysis. The data were processed as the mean ± standard deviation (SD). One-way analysis of variance (ANOVA) and Student's t tests were performed to determine any significant differences. p values <0.05 were considered to be significant.

RESULTS

Effect of Alginate Polysaccharides and Oligosaccharides on the Production of NO. We measured the effect of different types of saccharides on LPS-stimulated production of NO in RAW 264.7 cells. L-NAME is an analogue of arginine that inhibits NO production and was used as a positive control. Figure 1A shows that NO production was increased significantly by LPS treatment compared with control. Among all of the tested alginate saccharides, GOS-OD remarkably reduced the LPS-stimulated overproduction of NO as well as L-NAME treatment, whereas all other saccharides showed no statistically significant decreases. Figure 1B shows that none of the AOS, polysaccharides, or other reagents had a cytotoxic effect on RAW 264.7 cells. Thus, it is suggested that the changes in NO production may not be due to the cellular toxicity of AOS. NO-inhibitory effects have been commonly used as an indicator of the effectiveness of anti-inflammatory agents.[11,12] Thus, we focused on exploring the anti-inflammatory activity and molecular mechanisms of GOS-OD in subsequent studies.

Effect of GOS-OD on the Production of Inflammatory Mediators (NO, PGE_2, and ROS). The effect of GOS-OD on the LPS-activated secretion of NO, PGE_2, and ROS was examined. Panels A−C of Figure 2 show that GOS-OD notably suppressed the LPS-induced secretion of NO, PGE_2, and ROS at concentrations of 0.1−2 mg/mL. Cell viability results show that GOS-OD treatment with LPS stimulation did not have any cytotoxicity (Figure 2D). These results demonstrate that the inhibitory activity of GOS-OD on LPS-induced NO, PGE_2, and ROS productions cannot be induced by cytotoxic effects.

dx.doi.org/10.1021/jf503548a | J. Agric. Food Chem. 2015, 63, 160−168

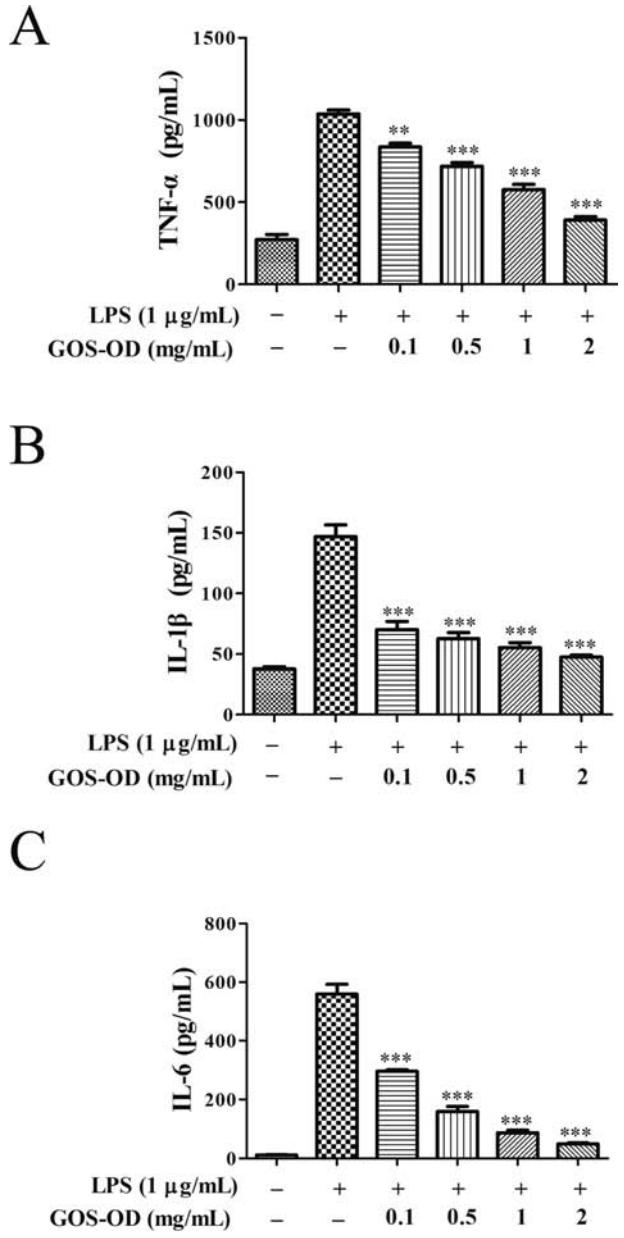

Figure 4. Effects of GOS-OD on pro-inflammatory cytokine productions in LPS-activated RAW 264.7 cells. Cells preincubated with 0.1−2 mg/mL GOS-OD for 2 h were treated with 1 μg/mL LPS for 24 h. Using an ELISA kit, TNF-α (A), IL-1β (B), and IL-6 (C) in the supernatant were detected. Values are the mean ± SD of three independent experiments. (**) $p < 0.01$ and (***) $p < 0.001$ indicate significant differences compared to the LPS-treated group.

Effect of GOS-OD on the Expression of iNOS and COX-2. It is well-established that iNOS and COX-2 are the most important enzymes for the synthesis of NO and PGE_2, respectively. Thus, the protein and gene expressions of iNOS and COX-2 were detected in LPS-activated cells. According to Western blot analysis and RT-PCR, LPS activation clearly increased the protein (Figure 3A) and mRNA (Figure 3D) expressions of iNOS and COX-2 when compared with controls in RAW 264.7 cells. However, GOS-OD prominently inhibited LPS-induced iNOS and COX-2 protein (Figure 3B,C) and mRNA (Figure 3E,F) expressions in a concentration-dependent manner.

Effect of GOS-OD on the Production of TNF-α, IL-1β, and IL-6. The effects of GOS-OD on the secretion of inflammatory cytokines, such as TNF-α, IL-1β, and IL-6, were evaluated in LPS-activated RAW 264.7 cells. As shown in Figure 4, the production of TNF-α (Figure 4A), IL-1β (Figure 4B), and IL-6 (Figure 4C) was significantly increased with LPS stimulation. However, the overproduction of TNF-α, IL-1β, and IL-6 was considerably reduced by 0.1−2 mg/mL GOS-OD treatment, indicating that GOS-OD is able to suppress the LPS-induced production of inflammatory cytokines in RAW 264.7 cells.

Effect of GOS-OD on the Binding of LPS and the Expression of TLR4 and CD14. The effect of GOS-OD on the binding of LPS to the surface of RAW 264.7 cells was examined by FITC-LPS. As shown in Figure 5A, LPS fluorescence was observed outside the cell membrane in RAW 264.7 cells when cells were stimulated with FITC-LPS alone. However, treatment with LPS in the presence of GOS-OD significantly prevented the binding of LPS to the RAW 264.7 cell surface. This phenomenon was further confirmed by FACS analysis (Figure 5B). These results indicate that GOS-OD exerts an antagonistic effect of GOS-OD against LPS binding to receptors on the cell surface, such as TLR4 and CD14. Therefore, the effect of GOS-OD on LPS-activated TLR4 and CD14 expressions was further evaluated. According to immunofluorescence results, GOS-OD pretreatment significantly blocked the LPS-induced expression of TLR4 (Figure 5C). Panels D and E of Figure 5 show that GOS-OD effectively decreased LPS-stimulated overexpression of TLR4 and CD14 proteins, respectively. Our results suggest that GOS-OD may suppress the initiation phase of LPS-activated intercellular signaling pathways by inhibiting the binding of LPS to cell surface receptors and the expressions of TLR4/CD14 on RAW 264.7 cells.

Effect of GOS-OD on the Activation of NF-κB. NF-κB is one of the crucial transcription factors that control the expression of inflammatory enzymes and inflammatory mediators.[29] Thus, the effect of GOS-OD on the activation of NF-κB was measured in LPS-activated cells using immunofluorescence microscopy and Western blot analysis. Figure 6A shows that LPS stimulation obviously induced the translocation of the NF-κB/p65 subunit from the cytosol to the nucleus, whereas GOS-OD treatment noticeably inhibited the nuclear translocation of NF-κB/p65. Similar results were found by Western blot analysis (Figure 6B).

Effect of GOS-OD on the Activation of MAP Kinases. The critical roles of MAP kinase signaling pathways in LPS-activated RAW 264.7 cells have been well established.[4] Therefore, the effect of GOS-OD on the phosphorylation levels of p38, ERK, and JNK MAP kinases was determined in LPS-activated cells (Figure 7). As expected, the LPS-induced phosphorylation of p38, ERK, and JNK MAP kinases was effectively suppressed with GOS-OD treatment. These results suggest that the LPS-stimulated activation of MAP kinases might be blocked by GOS-OD.

Reduction of LPS-Stimulated Irregular Cell Morphology by GOS-OD. We observed the effect of GOS-OD on the morphology of RAW 264.7 cells without or with LPS treatment using dark field microscopy. The control RAW 264.7 cells (Figure 8A) showed a round shape and smooth cell membrane, as did those subjected to GOS-OD treatment alone (1 and 2 mg/mL) (Figure 8B,C). However, the LPS-stimulated cells exhibited an irregular and rough form with enhanced spreading

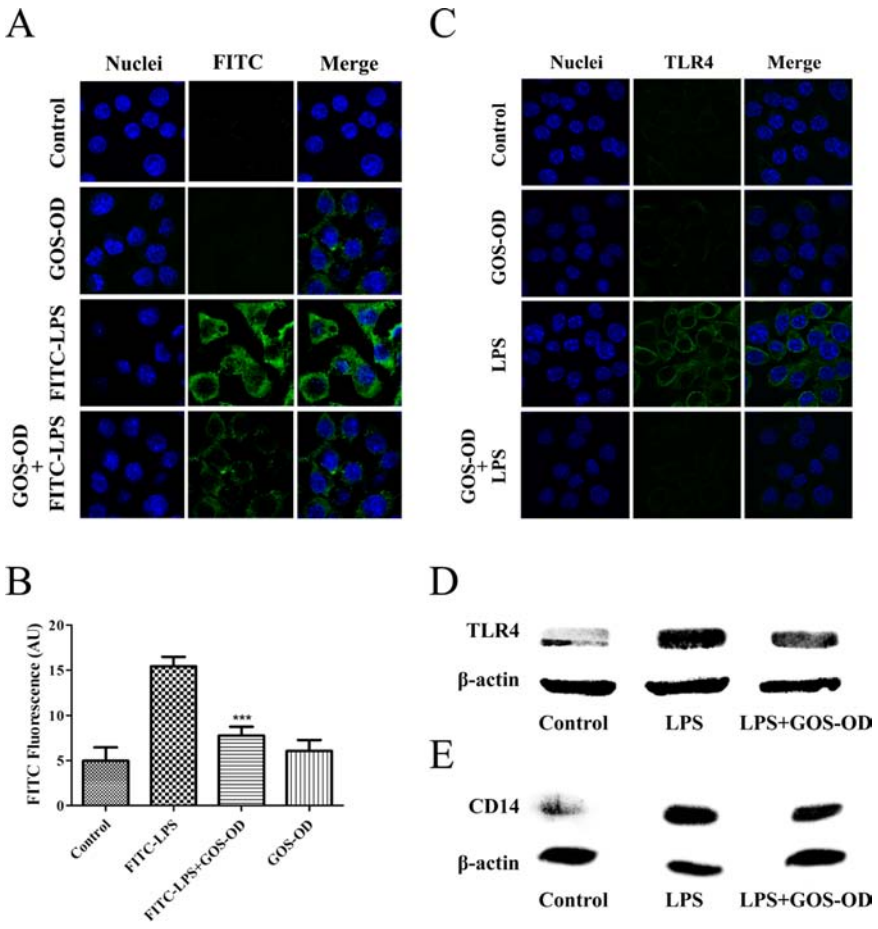

Figure 5. Effects of GOS-OD on the binding of LPS on RAW 264.7 cell surfaces and TLR4 and CD14 expressions in LPS-activated RAW 264.7 cells. (A) RAW 264.7 cells preincubated with 2 mg/mL GOS-OD for 2 h were treated with 10 μg/mL FITC-LPS for 1 h, and then the binding of LPS was detected by confocal microscopy. (B) RAW 264.7 cells preincubated with 2 mg/mL GOS-OD for 2 h were treated with 10 μg/mL FITC-LPS for 30 min, and then the binding of LPS was measured by FACS analysis. (C) RAW 264.7 cells were preincubated with 2 mg/mL GOS-OD for 2 h and then treated with 1 μg/mL LPS for 1 h. The immunofluorescence analysis was performed with anti-TLR4 antibody. DAPI was used to label the nuclei. The images were observed by confocal microscopy (60×). RAW 264.7 cells were preincubated with 2 mg/mL GOS-OD for 2 h and then treated with 1 μg/mL LPS for 24 h. TLR4 (D) and CD14 (E) protein expressions were detected by Western blot analysis. The representative images and results from three independent experiments are shown here. (***) $p < 0.001$ indicates significant differences compared to the LPS-treated group.

and reduced cell number (Figure 8D) in comparison with the control (Figure 8A). It is clear that 1 mg/mL GOS-OD pretreatment can reduce the LPS-stimulated cell morphology change (Figure 8E), with a higher inhibition effect at 2 mg/mL (Figure 8F). The cell numbers in average images were measured by using ImageJ software. We observed that LPS decreased macrophage proliferation by 50% compared with the proliferation of macrophages in control group (Figure 8G). GOS-OD did not have any effect on macrophage morphology but may act as a promoter to macrophage proliferation (Figure 8G), suggesting that GOS-OD specifically affects macrophage functions. Quantification revealed that 81.8 ± 8.7% of cells exhibited activated morphology (larger nuclei, cytoplasm with increased granularity, accelerated spreading, and forming pseudopodia) upon LPS induction and 49 ± 8.3 and 29 ± 8.3% upon GOS-OD treatment with LPS stimulation, compared to 1.2 ± 0.7% of untreated cells (Figure 8H). These results have demonstrated that GOS-OD pretreatment could reduce the LPS-stimulated irregular cell morphology.

DISCUSSION

In recent years, the anti-inflammatory activities of natural oligosaccharides have been widely studied. Chitosan oligosaccharides were found to be effective in the treatment of LPS-simulated inflammatory mediators in RAW 264.7 cells and intestinal inflammation in a mouse model through inhibition of NF-κB signaling.[16,30] Lactulose oligosaccharides showed excellent inhibition effect on pro-inflammatory cytokines such as interleukins (IL) 1, 6, and 12 in rat colitis.[14] Alginates are natural polysaccharides derived from brown seaweed.[17] AOS that are depolymerized by different methods display a wide variety of pharmacological activities; however, the anti-inflammatory activities of AOS remain uncertain. We believe this is the first work to investigate the anti-inflammatory activities of AOS depolymerized by oxidative degradation in LPS-stimulated inflammation model.

LPS-activated macrophage produces redundant inflammatory mediators (NO, PGE_2, and ROS) and pro-inflammatory cytokines (TNF-α, IL-1β, and IL-6) and serves as a general inflammation model for evaluating the anti-inflammatory activities of agents in vitro.[4,11,12] In the present work, we

dx.doi.org/10.1021/jf503548a | J. Agric. Food Chem. 2015, 63, 160−168

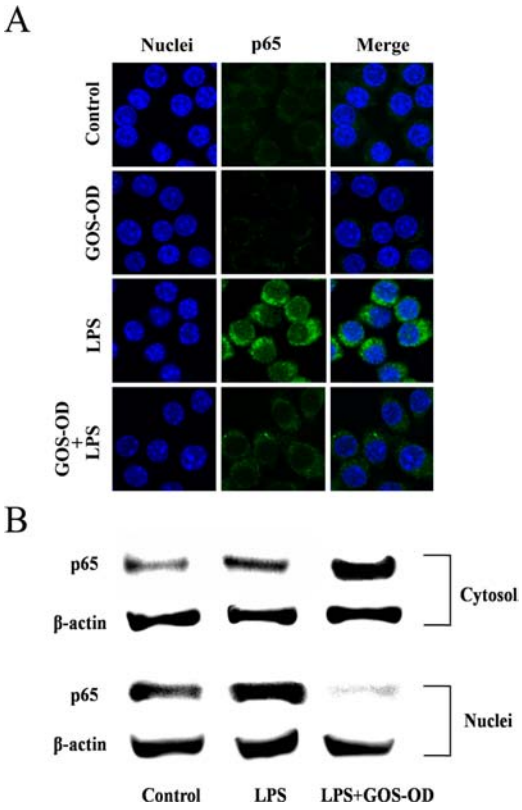

Figure 6. Effect of GOS-OD on the activation of NF-κB in LPS-activated RAW 264.7 cells. (A) Cells preincubated with 2 mg/mL GOS-OD for 2 h were treated with 1 μg/mL LPS for 1 h. The immunofluorescence analysis was performed with anti-NF-κB/p65 antibody. DAPI was used to label the nuclei. The images were captured by confocal microscopy (60×). The representative images from three independent experiments are shown here. (B) Cells preincubated with 2 mg/mL GOS-OD for 2 h were treated with 1 μg/mL of LPS for 30 min. Expression of NF-κB/p65 protein was detected by Western blot analysis. The representative Western blot bands from three independent experiments are shown here.

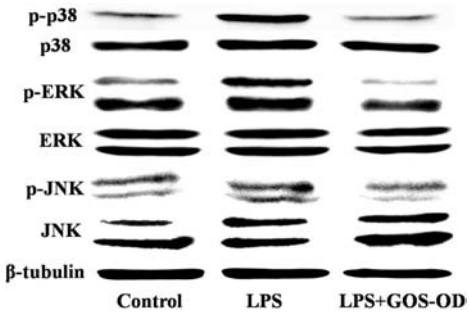

Figure 7. Effects of GOS-OD on the phosphorylation of MAP kinases. (A) Cells were preincubated with 2 mg/mL GOS-OD for 2 h and then treated with 1 μg/mL LPS for 10 min. For the detection of phosphorylated and nonphosphorylated MAP kinases, total cell lysates were extracted and measured by Western blot analysis. The representative Western blot bands from three independent experiments are shown here.

found that GOS-OD effectively suppressed the overproduction of inflammatory mediators in LPS-activated RAW 264.7 cells. In addition, the LPS-induced expression of iNOS and COX-2 mRNA was notably inhibited by GOS-OD treatment, indicating that the inhibitory activity of GOS-OD on the expression of iNOS and COX-2 proteins occurs at the pretranslational or transcriptional level.

Previous works have demonstrated that TLRs, especially TLR4, play a critical role in innate immune responses by activating the downstream signaling pathways of inflammatory responses.[5,31] CD14 is an important cofactor for TLR4-mediated signal transduction.[10] Upon binding of LPS to TLR4/CD14, the complex leads to downstream signal transduction through the NF-κB-mediated inflammatory cascade.[6] Here, we found that pretreatment with GOS-OD markedly inhibited LPS binding to the cell surface (Figure 5A,B). Then, GOS-OD was found to effectively attenuate LPS-induced TLR4 and CD14 expressions (Figure 5C−E), demonstrating that GOS-OD may inhibit the initial steps of signal transduction cascades through preventing the binding of LPS to the cell surface receptors and suppressing TLR4 and CD14 expressions in LPS-activated RAW 264.7 cells.

NF-κB and MAP kinase are the most important signaling pathways in LPS-stimulated inflammatory responses.[4,32,33] NF-κB transcription factor is retained in an inactive form in the cytoplasm by interaction with IκB proteins. Activation of NF-κB leads to phosphorylation of IκB proteins and induces the nuclear translocation of NF-κB/p65 units and transcription of target genes.[29] In this work, we observed that preincubation with GOS-OD could effectively reverse the LPS activated nuclear translocation of NF-κB/p65 (Figure 6), indicating that GOS-OD may affect the degradation and phosphorylation of IκB proteins. Furthermore, evidence has shown that MAP kinase signaling pathways are involved in the production of inflammatory mediators and the expression of iNOS and COX-2 proteins in LPS-activated RAW 264.7 cells through NF-κB activation.[34,35] Thus, the inhibitory activity of MAP kinases may be another important molecular mechanism to study in anti-inflammation. Western blot analysis shows that the phosphorylation of p38, ERK, and JNK MAP kinases induced by LPS was remarkably attenuated with GOS-OD treatment (Figure 7). These findings suggest that the inhibitory activity of GOS-OD on the activation of the MAP kinase signaling pathway may involve the GOS-OD-mediated suppression of NF-κB signaling pathway in LPS-induced RAW 264.7 cells.

Our previous study found that GOS-ED effectively induced NO production and that other AOS showed very low or no such activities.[21] However, we found that GOS-OD was a stronger inhibitor of NO production than other AOS in this work. These results indicate that the structure of AOS plays an important role in their activities. GOS-OD, which has a carboxyl group at the 1-position of the reducing end,[25] differs in structure from AOS-ED and AOS-AH. The existence of the carboxyl group may play an important role in the inhibitory effect of GOS-OD on LPS-stimulated NO production. In conclusion, GOS-OD was found to effectively suppress the overproduction of inflammatory mediators (NO, PGE_2, and ROS), inflammatory proteins (iNOS and COX-2), and pro-inflammatory cytokines (TNF-α, IL-1β, and IL-6) in a dose-dependent manner in LPS-activated RAW 264.7 cells. Additionally, GOS-OD inhibited the binding of LPS to the cell surface and attenuated LPS-induced TLR4 and CD14 expressions. Finally, we demonstrated that the anti-inflammatory activity of GOS-OD may be attributed to the suppressed activation of NF-κB and MAP kinase signaling pathways. Therefore, in the future, GOS-OD may be developed as a potential nutraceutical for inflammatory-mediated diseases.

dx.doi.org/10.1021/jf503548a | J. Agric. Food Chem. 2015, 63, 160−168

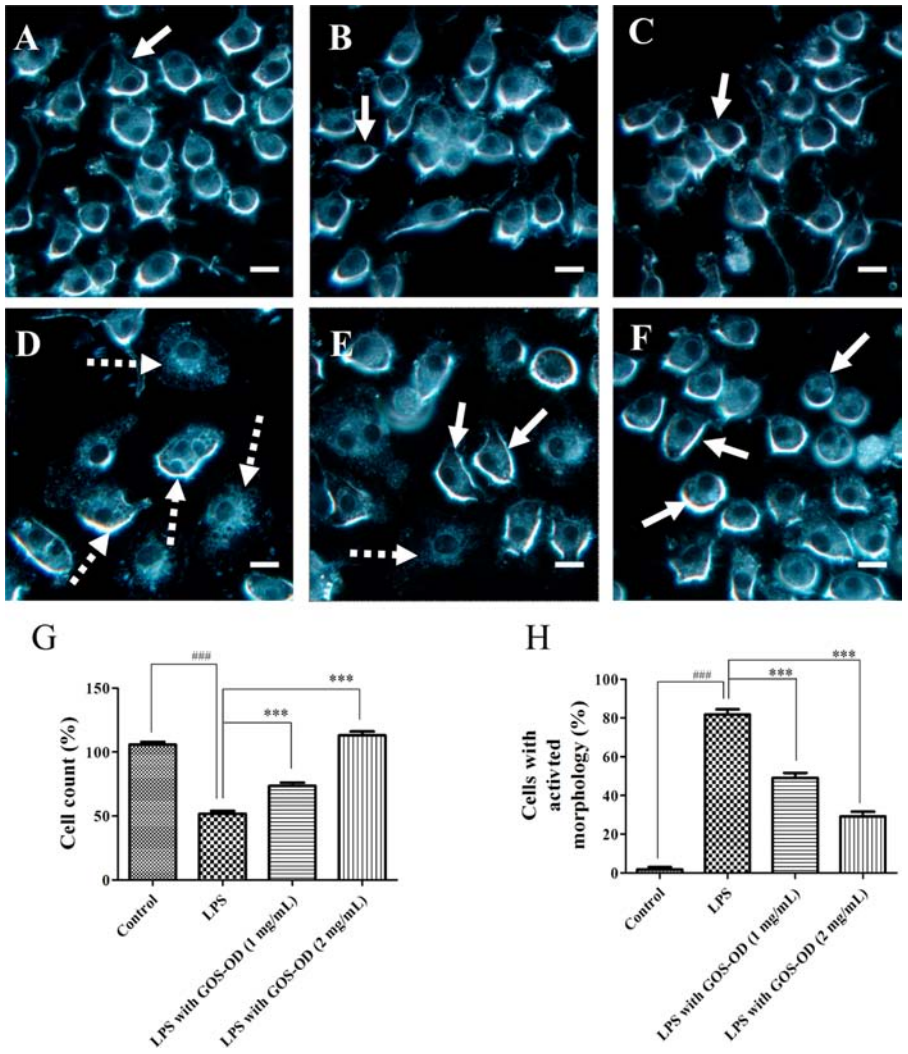

Figure 8. Effects of GOS-OD on the LPS-stimulated morphological changes of RAW 264.7 cells. (A) control; (B) 1 mg/mL GOS-OD; (C) 2 mg/mL GOS-OD; (D) 1 μg/mL LPS-treated group; (E) LPS-treated with 1 mg/mL GOS-OD; (F) 1 μg/mL LPS-treated with 2 mg/mL GOS-OD. The cells were pretreated with GOS-OD for 2 h before incubation with LPS for 24 h. Morphology of RAW 264.7 macrophage cells was visualized by dark field microscopy (40×). Normal cell morphology is indicated by white arrows, and the activated cell morphology is indicated by white dot arrows. Scale bar = 20 μm. Cell count in an average area (G) and percentage of cells with activated morphology (H) were analyzed by ImageJ software. (###) $p < 0.001$ indicates significant differences between the control group and the LPS-treated group; (***) $p < 0.001$ indicates significant differences between the LPS-treated group and the LPS with GOS-OD treated group.

AUTHOR INFORMATION

Corresponding Author

*(X.X.) Phone: 86-755-26534977. Fax: 86-755-26534274. E-mail: xuxu@szu.edu.cn.

Author Contributions

‖R.Z. and X.S. contributed equally to this work.

Funding

This work was financially supported by the National Natural Science Foundation of China (Grant 31000770), the China Postdoctoral Science Foundation (Grant 2013M540664, Grant 2014T70825), the Knowledge Innovation Program in Shenzhen Scientific Research and Development Funding Program (Grant JCYJ20130329111455027), and the Shenzhen Bureau of Science, Technology and Information (Grant JCYJ20130408172946974).

Notes

The authors declare no competing financial interest.

ACKNOWLEDGMENTS

We are grateful to Dr. Jiazuan Ni, Dr. Deming Gou, and Qingguo Han from Shenzhen University, and Dr. Min Wan from Karolinska Institute, Sweden, for their technical assistance and kind help.

ABBREVIATIONS USED

AOS, alginate oligosaccharides; AH, acid hydrolysis; CD14, cluster of differentiation 14; COX-2, cyclooxygenase-2; ED, enzyme degradation; ELISA, enzyme linked immunosorbent assay; GOS, guluronate oligosaccharide; IL, interleukin; iNOS, inducible nitric oxide; LPS, lipopolysaccharide; MOS, mannuronate oligosaccharide; MAPK, mitogen activated protein kinase; NF-κB, nuclear factor-kapppa B; NO, nitric oxide; OD, oxidative degradation; PG, polyguluronate; PM, polymannuronate; PGE_2, prostaglandin E_2; ROS, reactive oxygen species; TLR4, Toll-like receptor 4; TNF, tumor necrosis factor

REFERENCES

(1) Calder, P. C.; Albers, R.; Antoine, J. M.; Blum, S.; Bourdet-Sicard, R.; Ferns, G. A.; Folkerts, G.; Friedmann, P. S.; Frost, G. S.; Guarner, F.; Lovik, M.; Macfarlane, S.; Meyer, P. D.; M'Rabet, L.; Serafini, M.; Van, E. W.; Van, L. J.; Dias, W. V.; Vidry, S.; Winklhofer-Roob, B. M.; Zhao, J. Inflammatory disease processes and interactions with nutrition. *Br. J. Nutr.* **2009**, *101*, S1−S45.

(2) Pawelec, G.; Goldeck, D.; Derhovanessian, E. Inflammation, ageing and chronic disease. *Curr. Opin. Immunol.* **2014**, *29*, 23−28.

(3) Zhong, Y.; Chiou, Y. S.; Pan, M.-H.; Shahidi, F. Anti-inflammatory activity of lipophilic epigallocatechin gallate (EGCG) derivatives in LPS-stimulated murine macrophages. *Food Chem.* **2012**, *134*, 742−748.

(4) Lee, M. S.; Kwon, M. S.; Choi, J. W.; Shin, T.; No, H. K.; Choi, J. S.; Byun, D. S.; Kim, J. I.; Kim, H. R. Anti-inflammatory activities of an ethanol extract of *Ecklonia stolonifera* in lipopolysaccharide-stimulated RAW 264.7 murine macrophage cells. *J. Agric. Food Chem.* **2012**, *60*, 9120−9129.

(5) Mcinturff, J. E.; Modlin, R. L.; Kim, J. The role of Toll-like receptors in the pathogenesis and treatment of dermatological disease. *J. Invest. Dermatol.* **2005**, *125*, 1−8.

(6) Chow, J. C.; Young, D. W.; Golenbock, D. T.; Christ, W. J.; Gusovsky, F. Toll-like receptor-4 mediates lipopolysaccharide-induced signal transduction. *J. Biol. Chem.* **1999**, *274*, 10689−10692.

(7) Kim, D.; Kim, J. Y. Anti-CD14 antibody reduces LPS responsiveness via TLR4 internalization in human monocytes. *Mol. Immunol.* **2014**, *57*, 210−215.

(8) Wu, J. F.; Zhou, J. M.; Chen, X. H.; Fortenbery, N.; Eksioglu, E. A.; Wei, S.; Dong, J. C. Attenuation of LPS-induced inflammation by ICT, a derivate of icariin, via inhibition of the CD14/TLR4 signaling pathway in human monocytes. *Int. Immunopharmacol.* **2012**, *12*, 74−79.

(9) Bianchi, M. E.; Manfredi, A. A. How macrophages ring the inflammation alarm. *Proc. Natl. Acad. Sci. U.S.A.* **2014**, *111*, 2866−2867.

(10) Levy, E.; Xanthou, G.; Petrakou, E.; Zacharioudaki, V.; Tsatsanis, C.; Fotopoulos, S.; Xanthou, M. Distinct roles of TLR4 and CD14 in LPS-induced inflammatory responses of neonates. *Pediatr. Res.* **2009**, *66*, 179−184.

(11) Jiang, Z.; Hama, Y.; Yamaguchi, K.; Oda, T. Inhibitory effect of sulphated polysaccharide porphyran on nitric oxide production in lipopolysaccharide-stimulated RAW264.7 macrophages. *J. Biochem.* **2012**, *151*, 65−74.

(12) Hwang, P. A.; Chien, S. Y.; Chan, Y. L.; Lu, M. K.; Wu, C. H.; Kong, Z. L.; Wu, C. J. Inhibition of lipopolysaccharide (LPS)-induced inflammatory responses by *Sargassum hemiphyllum* sulfated polysaccharide extract in RAW 264.7 macrophage cells. *J. Agric. Food Chem.* **2011**, *59*, 2062−2068.

(13) Niu, Y. G.; Shang, P. P.; Chen, L.; Zhang, H.; Gong, L.; Zhang, X. W.; Yu, W. J.; Xu, Y. H.; Wang, Q.; Yu, L. L. Characterization of a novel alkali-soluble heteropolysaccharide from tetraploid *Gynostemma pentaphyllum* makino and its potential anti-inflammatory and antioxidant properties. *J. Agric. Food Chem.* **2014**, *62*, 3783−3790.

(14) Algieri, F.; Rodriguez-Nogales, A.; Garrido-Mesa, N.; Vezza, T.; Garrido-Mesa, J.; Utrilla, M. P.; Montilla, A.; Cardelle-Cobas, A.; Olano, A.; Corzo, N.; Guerra-Hernandez, E.; Zarzuelo, A.; Rodriguez-Cabezas, M. E.; Galvez, J. Intestinal anti-inflammatory effects of oligosaccharides derived from lactulose in the trinitrobenzenesulfonic acid model of rat colitis. *J. Agric. Food Chem.* **2014**, *62*, 4285−4297.

(15) Che, T. M.; Johnson, R. W.; Kelley, K. W.; Dawson, K. A.; Moran, C. A.; Pettigrew, J. E. Effects of mannan oligosaccharide on cytokine secretions by porcine alveolar macrophages and serum cytokine concentrations in nursery pigs. *J. Anim. Sci.* **2012**, *90*, 657−668.

(16) Yousef, M.; Pichyangkura, R.; Soodvilai, S.; Chatsudthipong, V.; Muanprasat, C. Chitosan oligosaccharide as potential therapy of inflammatory bowel disease: therapeutic efficacy and possible mechanisms of action. *Pharmacol. Res.* **2012**, *66*, 66−79.

(17) Lee, K. Y.; Mooney, D. J. Alginate: Properties and biomedical applications. *Prog. Polym. Sci.* **2012**, *37*, 106−126.

(18) Iwamoto, M.; Kurachi, M.; Nakashima, T.; Kim, D.; Yamaguchi, K.; Oda, T.; Iwamoto, Y.; Muramatsu, T. Structure−activity relationship of alginate oligosaccharides in the induction of cytokine production from RAW264.7 cells. *FEBS Lett.* **2005**, *579*, 4423−4429.

(19) Eftekharzadeh, B.; Khodagholi, F.; Abdi, A.; Maghsoudi, N. Alginate protects NT2 neurons against H_2O_2-induced neurotoxicity. *Carbohydr. Polym.* **2010**, *79*, 1063−1072.

(20) Tusi, S. K.; Khalaj, L.; Ashabi, G.; Kiaei, M.; Khodagholi, F. Alginate oligosaccharide protects against endoplasmic reticulum- and mitochondrial-mediated apoptotic cell death and oxidative stress. *Biomaterials* **2011**, *32*, 5438−5458.

(21) Xu, X.; Wu, X.; Wang, Q.; Cai, N.; Zhang, H.; Jiang, Z.; Wan, M.; Oda, T. Immunomodulatory effects of alginate oligosaccharides on murine macrophage RAW264.7 cells and their structure−activity relationships. *J. Agric. Food Chem.* **2014**, *62*, 3168−3176.

(22) Xu, X.; Bi, D.; Wu, X.; Wang, Q.; Wei, G.; Chi, L.; Jiang, Z.; Oda, T.; Wan, M. Unsaturated guluronate oligosaccharide enhances the antibacterial activities of macrophages. *FASEB J.* **2014**, *28*, 1−10.

(23) Bouhadir, K. H.; Lee, K. Y.; Alsberg, E.; Damm, K. L.; Anderson, K. W.; Mooney, D. J. Degradation of partially oxidized alginate and its potential application for tissue engineering. *Biotechnol. Prog.* **2001**, *17*, 945−950.

(24) Haug, A.; Larsen, B.; Smidsrod, O. A study of the constitution of alginic acid by partial acid hydrolysis. *Acta Chem. Scand.* **1996**, *20*, 183−190.

(25) Yang, Z.; Li, J.; Guan, H. Preparation and characterization of oligomannuronates from alginate degraded by hydrogen peroxide. *Carbohydr. Polym.* **2004**, *58*, 115−121.

(26) Yamasaki, Y.; Yokose, T.; Nishikawa, T.; Kim, D.; Jiang, Z.; Yamaguchi, K.; Oda, T. Effects of alginate oligosaccharide mixtures on the growth and fatty acid composition of the green alga *Chlamydomonas reinhardtii*. *J. Biosci. Bioeng.* **2012**, *113*, 112−116.

(27) Xu, X.; Iwamoto, Y.; Kitamura, Y.; Oda, T.; Muramatsu, T. Root growth-promoting activity of unsaturated oligomeric uronates from alginate on carrot and rice plants. *Biosci., Biotechnol., Biochem.* **2003**, *67*, 2022−2025.

(28) Jiang, Z.; Okimura, T.; Yamaguchi, K.; Oda, T. The potent activity of sulfated polysaccharide, ascophyllan, isolated from *Ascophyllum nodosum* to induce nitric oxide and cytokine production from mouse macrophage RAW264.7 cells: comparison between ascophyllan and fucoidan. *Nitric Oxide* **2011**, *25*, 407−415.

(29) Pateras, I.; Giaginis, C.; Tsigris, C.; Patsouris, E.; Theocharis, S. NF-κB signaling at the crossroads of inflammation and atherogenesis: searching for new therapeutic links. *Expert Opin. Ther. Targets* **2014**, *18*, 1089−1101.

(30) Yang, E. J.; Kim, J. G.; Kim, J. Y.; Kim, S. C.; Lee, N. H.; Hyun, C. G. Anti-inflammatory effect of chitosan oligosaccharides in RAW 264.7 cells. *Cent. Eur. J. Biol.* **2010**, *5*, 95−102.

(31) Siegemund, S.; Sauer, K. Balancing pro- and anti-inflammatory TLR4 signaling. *Nat. Immunol.* **2012**, *13*, 1031−1033.

(32) Park, H. Y.; Han, M. H.; Park, C.; Jin, C. Y.; Kim, G. Y.; Choi, I. W.; Kim, N. D.; Nam, T. J.; Kwon, T. K.; Choi, Y. H. Anti-inflammatory effects of fucoidan through inhibition of NF-κB, MAPK and Akt activation in lipopolysaccharide-induced BV2 microglia cells. *Food Chem. Toxicol.* **2011**, *49*, 1745−1752.

(33) Dong, X. Q.; Du, Q.; Yu, W. H.; Zhang, Z. Y.; Zhu, Q.; Che, Z. H.; Chen, F.; Wang, H.; Chen, J. Anti-inflammatory effects of oxymatrine through inhibition of nuclear factor-kappa B and mitogen-activated protein kinase activation in lipopolysaccharide-induced BV2 microglia cells. *Iran. J. Pharm. Res.* **2013**, *12*, 165−174.

(34) Vallabhapurapu, S.; Karin, M. Regulation and function of NF-kappa B transcription factors in the immune system. *Annu. Rev. Immunol.* **2009**, *27*, 693−733.

(35) Chao, W. W.; Kuo, Y. H.; Lin, B. F. Anti-inflammatory activity of new compounds from *Andrographis paniculata* by NF-κB transactivation inhibition. *J. Agric. Food Chem.* **2010**, *58*, 2505−2512.

JOURNAL OF AGRICULTURAL AND FOOD CHEMISTRY

Article

pubs.acs.org/JAFC

Phytochemical Profiles and Antioxidant Activity of Different Varieties of *Adinandra* Tea (*Adinandra* Jack)

Yongsheng Chen,[†] Gu Chen,*[,†] Xiong Fu,[†] and Rui-Hai Liu*[,†,‡]

[†]College of Light Industry and Food Sciences, South China University of Technology, 381 Wushan Road, Guangzhou, Guangdong 510641, People's Republic of China

[‡]Department of Food Science, Cornell University, Ithaca, New York 14853, United States

ABSTRACT: Consumption of plant foods has been negatively associated with the risk of developing chronic diseases, which is partly attributed to their rich and diverse phytochemicals. To promote the rational and effective application of *Adinandra* tea (*Adinandra* Jack), a traditional Chinese tea (Shiyacha) widely consumed as a health beverage, the complete phytochemical profile and antioxidant activity of four varieties of *Adinandra* tea were analyzed. They were rich in phenolics and flavonoids, ranging from 71.29 to 140.54 mg of gallic acid equivalent/g and from 19.13 to 88.72 mg of catechin equivalent/g, respectively. Their antioxidant capacities were high, as revealed by oxygen radical absorbance capacity, peroxyl radical scavenging capacity, and cellular antioxidant activity (CAA) assays. An obvious antiproliferation effect was observed in HepG2 and MCF-7 cells, with EC_{50} ranging from 1.05 to 6.44 mg/mL and from 2.26 to 8.02 mg/mL, respectively. Among the four varieties compared, Nitida and Millettii had a higher CAA value and antiproliferation activity, while Latifolia contained considerable bound phenolics.

KEYWORDS: *Adinandra tea, phytochemicals, phenolics, flavonoids, antioxidant activity, antiproliferation activity*

INTRODUCTION

Epidemiological and interventional studies have shown that regular consumption of fruits, vegetables, whole grain, and other plant foods is negatively associated with the risk of developing chronic diseases.[1−3] The health benefits of plant foods are partly attributed to their rich and diverse phytochemicals, such as phenolics, carotenoids, alkaloids, etc.[4,5] Therefore, consumers are suggested to obtain nutrients and bioactive compounds from a wide variety of plant foods for optimal nutrition and health benefits.[2,4] Tea beverage rich in phytochemicals is a good source for dietary phytochemicals.[6]

Adinandra tea, famous as Shiyacha in Chinese, is a traditional Chinese tea consumed widely in south China. Different from tea of the tropical evergreen plant *Camellia sinensis*, *Adinandra* tea is an infusion made from leaves picked from plants belonging to *Adinandra* Jack. *Adinandra* tea has been consumed as a health tea beverage in China for hundreds of years and is reported to have many curative effects, such as reduction of blood pressure, anti-inflammatory, antibacterial, antitumor, antitoxic, and analgesic effects.[7,8] Over the past few decades, limited reports have been published about *Adinandra* tea. Chemical analysis of *Adinandra nitida* revealed that it was rich in flavonoids, such as camellianin A, camellianin B, and apigenin,[9−14] with high 1,1-diphenyl-2-picrylhydrazyl (DPPH) radical scavenging activity.[10] An antiproliferative effect of camellianin A, camellianin B, and apigenin from *A. nitida* was reported in cancer cell lines, such as A431,[15] HepG2, and MCF-7[16] cells, although their mechanism remained elusive. However, thus far, there is no report on the phytochemical profiles and antioxidant activity of different varieties of *Adinandra*. Therefore, we performed the following studies to (1) determine the phytochemical profiles of four *Adinandra* varieties, namely, *Adinandra nitida* Merr. ex H. L. Li, *Adinandra glischroloma* Hand.-Mazz. var. *jubata* (H. L. Li) Kobuski, *Adinandra millettii* (Hook. & Arn.) Benth. & Hook. f. ex Hance, and *Adinandra latifolia* L. K. Ling, hereafter as Nitida, Jubata, Millettii, and Latifolia, respectively, (2) analyze the total antioxidant activity of four varieties *in vitro* and *in vivo*, and (3) compare the antiproliferation activity of four varieties on HepG2 and MCF-7 cells. Results here may contribute to the more rational and effective application and use of *Adinandra* tea.

MATERIALS AND METHODS

Chemicals and Reagents. Catechin, 2,6-dichloroindophenol sodium salt hydrate, chloranil, 2,2′-azobis-amidinopropane (ABAP), Folin−Ciocalteu reagent, gallic acid, and dichlorofluorescin diacetate (DCFH-DA) were purchased from Sigma (St. Louis, MO). Vanillin was purchased from Aladdin (Shanghai, China). Williams' medium E (WME), insulin, and other cell culture reagents were purchased from Gibco U.S. Biotechnology Co. The other chemicals were purchased from Sangon (Shanghai, China).

***Adinandra* Samples and Sample Preparation.** Four *Adinandra* varieties used are described in Table 1. Samples of Nitida and Jubata were obtained from Shiwandashan and authenticated by the Guangxi Institute of Chinese Medicine and Pharmaceutical Science. Samples of Latifolia and Millettii were supplied by the Kunming Institute of Botany, Chinese Academy of Sciences, and the Institute of Environmental Protection and Design, Huaqiao University, respectively. Samples were collected in autumn of 2013 and stored at −25 °C until use.

Extraction of Free Phenolic Compounds. Free phenolic compounds in *Adinandra* samples were extracted using the method reported previously.[17,18] Briefly, 2 g of samples were blended with 150 mL of 80% chilled acetone for 5 min and then homogenized for 5 min. After centrifugation at 4500 rpm for 10 min, residue was extracted 2

Received: August 1, 2014
Revised: December 5, 2014
Accepted: December 10, 2014
Published: December 10, 2014

ACS Publications © 2014 American Chemical Society

dx.doi.org/10.1021/jf503700v | J. Agric. Food Chem. 2015, 63, 169−176

Table 1. Descriptions of the Four *Adinandra* Varieties Used in This Study

variety	description	moisture content (%)
Nitida	no hair, normal size leaves, long pedicel (10−20 cm)	12.64
Jubata	stem and leaves densely covered with long and bristle-like hairs, normal size leaves	11.59
Millettii	no hair, normal size leaves, short pedicel (2 cm)	16.55
Latifolia	no hair, large leaves, short pedicel (1 cm)	19.08

more times. Pooled supernatants were filtered through filter paper and evaporated at 45 °C. The extract was finally reconstituted with water to 10 mL and stored at −40 °C until use.

Extraction of Bound Phenolic Compounds. Bound phenolics in *Adinandra* samples were extracted using the method reported previously.[18,19] Briefly, the residue of the free phenolic compound extraction were flushed with nitrogen gas, sealed, and digested with 20 mL of 4 M sodium hydroxide at room temperature for 90 min with shaking. The mixture was acidified with hydrochloric acid to pH 2.0 and extracted 10 times with ethyl acetate. Pooled ethyl acetate fractions were evaporated at 45 °C to dryness. The extract were reconstituted in 10 mL of water and stored at −40 °C until use.

Determination of the Phenolic Content. The total phenolic content in extract was determined using the modified Folin−Ciocalteu colorimetric method.[20,21] Gallic acid was used as a standard, and the total phenolic content was expressed as milligrams of gallic acid equivalent per gram of dry weight (DW). Briefly, diluted extracts or standard were mixed with Folin−Ciocalteu reagent for 6 min and then neutralized by sodium carbonate. The absorbance of the resulting solution was measured at 760 nm after 90 min of incubation.

Determination of the Flavonoid Content. The total flavonoid content was determined using the sodium borohydride/chloranil protocol (SBC) developed by our group.[22] Catechin was used as a standard, and the total flavonoid content was expressed as milligrams of catechin equivalent per gram of DW. Briefly, extracts were dried under nitrogen gas and reconstituted in 1 mL of terahydrofuran/ethanol (THF/EtOH, 1:1, v/v). Catechin hydrate standard was prepared fresh in 1 mL of THF/EtOH (1:1, v/v). Extracts or standard were mixed with 0.5 mL of 50 mM $NaBH_4$ solution and 0.5 mL of 74.6 mM $AlCl_3$ solution. Then, they were shaken in an orbital shaker at 180 rpm at room temperature for 30 min. An additional 0.5 mL of 50.0 mM $NaBH_4$ solution was added with shaking continued for another 30 min. Chilled 2.0 mL of 0.8 M acetic acid solution was added and kept in the dark for 15 min after being thoroughly mixed. Then, 1 mL of 20.0 mM chloranil was added and heated at 99 °C with shaking for 60 min. The reaction solutions were cooled using tap water, and the volume was brought to 4 mL using methanol. Then, 1 mL of 16% (w/v) vanillin was added and mixed. A total of 2 mL of 12 M HCl was added and kept in the dark for 15 min after a thorough mix. After centrifugation at 2500 rpm for 10 min, the absorbance of the supernatant was immediately measured at 490 nm.

Quantification of the Total Antioxidant Activity by the Oxygen Radical Absorbance Capacity (ORAC) Assay. The total antioxidant activity was determined using the ORAC assay described by Huang et al. and modified by our group.[23,24] Briefly, 20 μL extracts or Trolox were mixed with 200 μL of fluorescein (final concentration of 0.96 μM) and incubated at 37 °C for 20 min. Then, 20 μL of freshly prepared 119.4 mM ABAP was added to each well using an eight-channel pipetter. The fluorescence was measured immediately at 485 nm excitation and 535 nm emission for 35 cycles every 4.5 min using a Fluoroskan Ascent fluorescent spectrophotometer (Molecular Devices, Sunnyvale, CA) at 37 °C. Using a standard curve of Trolox, ORAC values were presented as micromoles of Trolox equivalent (TE) per gram of DW of the sample.

Determination of the Total Antioxidant Activity by the Peroxyl Radical Scavenging Capacity (PSC) Assay. The total antioxidant activity was measured using the PSC assay.[25] Peroxyl radicals generated by thermal degradation of ABAP can oxidize non-fluorescent DCFH to fluorescent dichlorofluorescein (DCF). The antioxidant activity of antioxidants to scavenge peroxyl radicals was calculated on the basis of the reduction of DCF fluorescence in the reaction. DCFH-DA was prehydrolyzed with 1 mM KOH to remove the diacetate moiety just prior to use. Fluorescence was monitored at 485 nm excitation and 535 nm emission with a Fluoroskan Ascent fluorescent spectrophotometer (Molecular Devices, Sunnyvale, CA). Vitamin C was used as a standard, and results were presented as micromoles of vitamin C equivalent per gram of sample.

Cell Culture. Human liver cancer cells HepG2, grown in WME [supplemented with 5% fetal bovine serum (FBS), 10 mM *N*-2-hydroxyethylpiperazine-*N*′-2-ethanesulfonic acid (HEPES), 2 mM L-glutamine, 5 μg/mL insulin, 0.05 μg/mL hydrocortisone, 50 units/mL penicillin, 50 μg/mL streptomycin, and 100 μg/mL gentamycin], were maintained at 37 °C and 5% CO_2. Human breast cancer cells MCF-7 were maintained in Dulbecco's modified Eagle's medium (DMEM) supplemented with 50 units/mL penicillin, 50 μg/mL streptomycin, 100 μg/mL gentamicin, and 10% FBS at 37 °C and 5% CO_2.

Cellular Antioxidant Activity (CAA) of *Adinandra* Extracts and CAA Quantification. The CAA assay was performed as previously described.[26] Briefly, HepG2 cells were seeded at a density of 6×10^4 cells/well in a 96 well microplate. At 24 h after seeding, the growth medium was removed and the wells were washed with PBS. Then, the cells were treated for 1 h with 100 μL of medium containing *Adinandra* extracts plus 50 μM DCFH-DA. Certain wells were washed with 100 μL of phosphate-buffered saline (PBS) (PBS wash protocol), and certain wells were not washed (no PBS wash protocol). ABAP (600 μM) in 100 μL of Hanks' Balanced Salt Solution (HBSS) was added to the cells. PBS wash protocol indicated that cells were pretreated with *Adinandra* extracts before ABAP was added, and no PBS wash indicated that cells were co-treated with *Adinandra* extracts and ABAP. Fluorescence was monitored at 485 nm excitation and 535 nm emission every 5 min for 13 circles using a Fluoroskan Ascent fluorescent spectrophotometer (Molecular Devices, Sunnyvale, CA) at 37 °C. It was calculated as CAA (units) = $1 - (\int SA/\int CA)$, where $\int SA$ is the integrated area under the fluorescence versus time curve of the sample and $\int CA$ is the integrated area under the fluorescence versus time curve of the control. The median effective dose (EC_{50}) of the *Adinandra* extracts was calculated from the median effect plot of $\log(f_a/f_u)$ versus log(dose), where f_a is the fraction affected by the treatment (CAA unit) and f_u is the fraction unaffected by the treatment (1 − CAA unit). The EC_{50} values were expressed as the mean ± standard deviation (SD) of triplicate data obtained from the same experiment. EC_{50} values were converted to CAA values, which were expressed as micromoles of quercetin equivalent (QE) per 100 g of *Adinandra* extracts, using the mean EC_{50} value for quercetin from three separate experiments.

Antiproliferation Test. The antiproliferative effects of *Adinandra* extracts were assessed as previously described.[27] Briefly, cells were seeded at a density of 2.5×10^4 calls/well in the central wells of the 96 well microplate. After 4−6 h of incubation to allow for sufficient attachment, growth medium was changed to 100 μL of fresh medium containing different concentrations of *Adinandra* extracts. The wells receiving fresh medium without extracts served as the control. After 72 h of incubation, the number of the viable cells were counted by the methylene blue assay.[28] The antiproliferative effects were assessed by the EC_{50} values, which were expressed as milligrams of *Adinandra* extracts per milliliter.

High-Performance Liquid Chromatography (HPLC) Analysis. On the basis of the method reported previously,[29] phenolic compounds of *Adinandra* extracts were separated in a Waters C_{18} column (5 μm, 250 × 4.6 mm) on a Waters HPLC system (Waters Corp., Milford, MA). The binary mobile phase consisted of solvents A (acidified water at pH 2 and trifluoroacetic acid) and B (methanol).

The mobile-phase gradient used was 0−10 min, 35% B; 10−11 min, 35−45% B; 11−26 min, 45−55% B; 26−27 min, 55−72% B; 27−40 min, 72−100% B; 40−44 min, 100−35% B; and 44−50 min, 35% B. The injection volume was 20 μL for each sample, and the flow rate was 1.0 mL/min. The peaks were identified by their retention times by comparing the ultraviolet−visible (UV−vis) spectra. Pure standards used for the identification were quercitrin, camellianin A, camellianin B, and apigenin. The recovery rates of camellianin B, quercitrin, camellianin A, and apigenin were 108.16 ± 7.19, 92.68 ± 6.17, 97.56 ± 2.54, and 102.30 ± 2.00% from the extracts, respectively. The contents of quercitrin, camellianin A, camellianin B, and apigenin were determined and expressed as milligrams per gram of DW according to the standard curve.

Statistical Analysis. Data were presented as the mean ± SD from at least three replicates per samples. Analysis of variation (ANOVA) and Tukey's test were performed using SPSS (SPSS, Inc., Chicago, IL), and dose−effect analysis was performed using Calcusyn software, version 2.0 (Biosoft, Cambridge, U.K.). Statistical significance was set at $p < 0.05$.

RESULTS AND DISCUSSION

Phenolic Content of *Adinandra* Varieties. Expressed as milligrams of gallic acid equivalent per gram of sample on a DW basis, the free, bound, and total phenolic contents of four *Adinandra* varieties are shown in Figure 1. The highest free

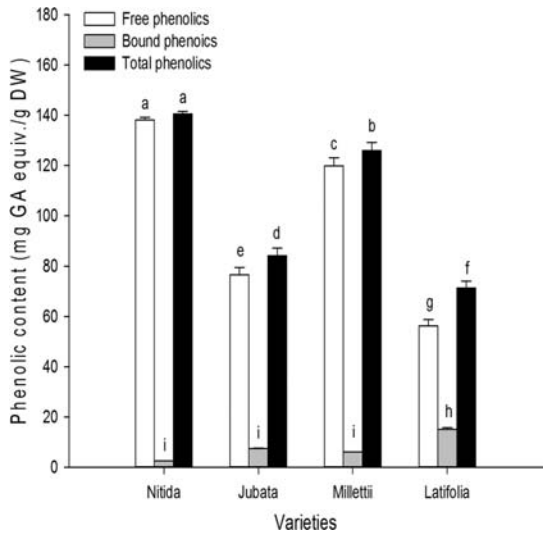

Figure 1. Free, bound, and total phenolic contents of the four *Adinandra* varieties. Bars with different letters differ significantly at $p < 0.05$.

phenolic content was found in Nitida (138.09 ± 1.08 mg/g), followed by Millettii (119.89 ± 3.14 mg/g), and then Jubata (76.62 ± 2.89 mg/g). Latifolia had the lowest free phenolic content (56.25 ± 2.52 mg/g). There were significant differences in the free phenolic contents among the four *Adinandra* varieties ($p < 0.05$). The highest bound phenolic content was observed in Latifolia (15.04 ± 0.65 mg/g), followed by Jubata (7.52 ± 0.08 mg/g), and then Millettii (6.07 ± 0.05 mg/g). Nitida had the lowest bound phenolic content (2.45 ± 0.05 mg/g). Overall, the bound phenolic content was significantly lower than the free phenolics. Therefore, the highest total phenolics were found in Nitida (140.54 ± 1.04 mg/g), followed by Millettii (125.96 ± 3.19 mg/g), and then Jubata (84.14 ± 2.97 mg/g). Latifolia had the lowest total phenolic content (71.29 ± 2.69 mg/g). The differences of total phenolics were significant among the four varieties ($p < 0.05$).

Although the contribution of bound phenolics to total phenolics might be ignored in Nitida (1.74%) and quite small in Millettii (4.82%) and Jubata (8.94%), it accounted for about one-fifth of the total phenolics in Latifolia (21.09%). It is suggested that the bound phytochemicals are resistant to digestion in the stomach and small intestine, and they may reach and be released in the colon after fermented by gut micribiota.[30] Here, the relatively high percentage of bound phenolics in Latifolia might have similar application.

Flavonoid Content of *Adinandra* Varieties. Expressed as milligrams of catechin equivalent per gram of samples on a DW basis, the free, bound, and total flavonoid contents of *Adinandra* varieties were shown in Figure 2. The free flavonoid content of

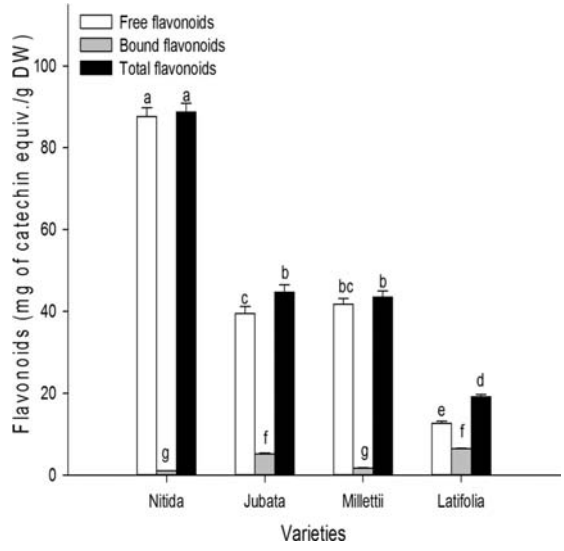

Figure 2. Free, bound, and total flavonoid contents of the four *Adinandra* varieties. Bars with different letters differ significantly at $p < 0.05$.

Nitida (87.66 ± 2.17 mg/g) was higher ($p < 0.01$) than those of the other varieties. The free flavonoid contents of Jubata (39.54 ± 1.66 mg/g) and Millettii (41.85 ± 1.43 mg/g) were similar ($p > 0.05$) and higher ($p < 0.05$) than that of Latifolia (12.64 ± 0.54 mg/g). For the bound flavonoid content, both Jubata (5.20 ± 0.25 mg/g) and Latifolia (6.49 ± 0.10 mg/g) had higher contents ($p < 0.05$) than Nitida (1.06 ± 0.05 mg/g) and Millettii (1.72 ± 0.08 mg/g). There was no significant difference in bound flavonoid contents between Jubata and Latifolia or between Nitida and Millettii. The contribution of bound flavonoid to total flavonoid contents was ignorable in Nitida (1.19%) and Millettii (3.95%), but it was 11.62% in Jubata and 33.92% in Latifolia. The total flavonoid content was highest ($p < 0.01$) in Nitida (88.72 ± 2.13 mg/g). The total flavonoid contents of Jubata (44.74 ± 1.79 mg/g) and Millettii (43.54 ± 1.48 mg/g) were similar ($p > 0.05$) and both higher ($p < 0.05$) than that of Latifolia (19.13 ± 0.54 mg/g).

Percentage Contribution of Flavonoids to Phenolics. On the basis of a micromole basis, the percentage contribution of flavonoids to phenolics was calculated and presented in Figure 3. The contributions of free flavonoids to free phenolics and bound flavonoids to bound phenolics ranged from 13.2 to 37.21% and from 16.6 to 40.51%, respectively. Total flavonoids accounted for 15.75 to 37% of the total phenolics, indicating flavonoids were one of the major phenolics in *Adinandra*. The contribution of free flavonoids to free phenolics was the highest

dx.doi.org/10.1021/jf503700v | J. Agric. Food Chem. 2015, 63, 169−176

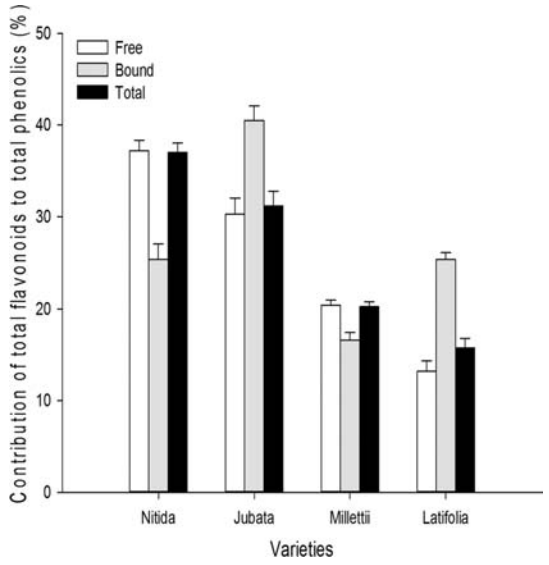

Figure 3. Percent contribution of flavonoids to phenolics (mean ± SD; n = 3).

in Nitida (37.21%), followed by Jubata (30.28%), and then Millettii (20.44%), while it was lowest in Latifolia (13.2%). The contribution of bound flavonoids to bound phenolics was highest in Jubata (40.51%), followed by Nitida (25.32%), and Latifolia (25.31%), while it was lowest in Millettii (16.6%). The contribution of total flavonoids to total phenolics was highest in Nitida (37%), followed by Jubata (31.19%), and then Millettii (20.26%), while it was lowest in Latifolia (15.75%).

***In Vitro* Antioxidant Activity Measured by ORAC and PSC.** The *in vitro* antioxidant activities were evaluated by ORAC and PSC assays. Expressed as micromoles of TE per gram of sample DW, the ORAC values of *Adinandra* are shown in Figure 4. Free phenolic extracts of Nitida had the highest ORAC value (2170.1 ± 197.22 μM TE/g of DW), followed by Latifolia (585.76 ± 53.21 μM TE/g of DW), Millettii (452.46 ± 72.38 μM TE/g of DW), and then Jubata (358.63 ± 25.18 μM TE/g of DW). The ORAC value of bound phenolic extract was highest in Latifolia (156.75 ± 11.34 μM TE/g of DW),

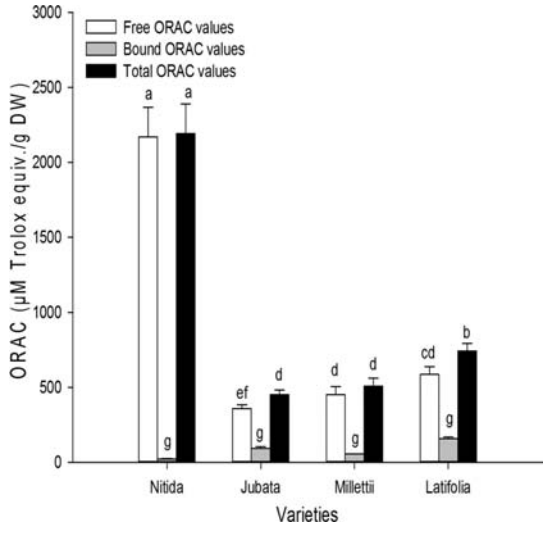

Figure 4. ORAC values of the four *Adinandra* varieties (mean ± SD; n = 3). Bars with different letters differ significantly at $p < 0.05$.

followed by Jubata (93.00 ± 11.59 μM TE/g of DW), Millettii (54.96 ± 1.04 μM TE/g of DW), and then Nitida (21.25 ± 3.53 μM TE/g of DW). Although the bound ORAC value accounted for only 0.97% of the total ORAC value in Nitida, their contributions should not be ignored in the total ORAC value of Millettii (10.83%), Jubata (20.59%), and Latifolia (21.11%). The total ORAC value of Nitida (2191.4 ± 199.43 μM TE/g of DW) was the highest ($p < 0.01$) of the varieties tested. The total ORAC values of Jubata (451.64 ± 30.63 μM TE/g of DW) and Millettii (507.42 ± 54.41 μM TE/g of DW) were similar ($p > 0.05$) but lower ($p < 0.05$) than that of Latifolia (742.51 ± 51.36 μM TE/g of DW).

The PSC value was expressed as micromoles of vitamin C equivalent per gram of sample DW. The PSC values of *Adinandra* varieties were presented in Figure 5. Free phenolic

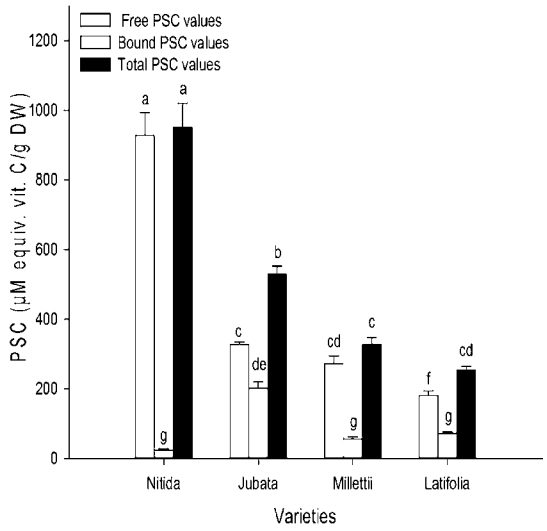

Figure 5. PSC values of the four *Adinandra* varieties (mean ± SD; n = 3). Bars with different letters differ significantly at $p < 0.05$.

extracts of Nitida had the highest PSC value (927.23 ± 66.93 μM vitamin C/g of DW), followed by Jubata (327.57 ± 6.65 μM vitamin C/g of DW), Millettii (272.19 ± 22.36 μM vitamin C/g of DW), and then Latifolia (181.44 ± 12.34 μM vitamin C/g of DW). The PSC value of bound phenolic extract was highest in Jubata (201.20 ± 18.50 μM vitamin C/g of DW), followed by Latifolia (71.75 ± 4.60 μM vitamin C/g of DW), Millettii (55.85 ± 5.82 μM vitamin C/g of DW), and then Nitida (24.05 ± 3.21 μM vitamin C/g of DW). The contribution of the bound PSC value to the total PSC value in Nitida was as small as 2.53%. However, the contribution of bound PSC values to the total PSC value in Millettii (17.03%), Latifolia (28.34%), and Jubata (38.05%) should not be underestimated. The total PSC value of Nitida (951.28 ± 70.13 μM vitamin C/g of DW) was the highest ($p < 0.01$) of the varieties tested. The total PSC values of Latifolia (253.19 ± 10.82 μM vitamin C/g of DW) and Millettii (328.04 ± 19.73 μM vitamin C/g of DW) were similar ($p > 0.05$) but lower ($p < 0.05$) than that of Jubata (528.77 ± 22.60 μM vitamin C/g of DW). The highest total PSC value was found in Nitida (Figure 5), which was consistent with the highest total phenolics, flavonoids, and total ORAC values observed in Nitida (Figures 1, 2, and 4). There were significant correlations between PSC values and total phenolics (R^2 = 0.800; $p < 0.05$) and between PSC values and total flavonoids (R^2 = 1.000; $p < 0.01$). This

dx.doi.org/10.1021/jf503700v | J. Agric. Food Chem. 2015, 63, 169−176

Table 2. Average Phytochemical Content, ORAC, and PSC Values of the Four *Adinandra* Varieties

	free	bound	total
phenolics (mg of gallic acid equiv./g of DW)	97.71 ± 34.26	7.77 ± 4.80	105.48 ± 29.96
flavonoids (mg of catechin equiv./g of DW)	45.42 ± 28.19	3.62 ± 2.39	49.03 ± 26.24
ORAC (μmol of TE/g of DW)	891.74 ± 780.77	81.49 ± 53.04	973.24 ± 749.01
PSC (μmol of vitamin C equiv./g of DW)	427.11 ± 308.0	88.21 ± 70.98	515.32 ± 285.08

revealed that total phenolics and flavonoids had significant contribution to the PSC values of the samples tested.

The average phenolic and flavonoid content, ORAC, and PSC values of the four *Adinandra* varieties were analyzed and presented as the mean ± SD in Table 2. On average, *Adinandra* varieties had high phenolic content (105.48 ± 29.96 mg of gallic acid equiv./g of DW) and flavonoid content (49.03 ± 26.24 mg of catechin equiv./g of DW). Their antioxidant activities were also high in the ORAC value (973.24 ± 749.01 μmol of TE/g of DW) and the PSC value (515.32 ± 285.08 μmol of vitamin C equiv./g of DW). However, the big standard deviations indicated the diversity among these four varieties.

***In Vivo* Antioxidant Activity Measured by CAA.** The antioxidant activity of free phenolic extracts was further measured *in vivo* by the CAA assay. *Adinandra* extracts inhibited the increase in fluorescence from the formation of DCF in a dose-dependent manner, whether the cells had been washed with PBS or not between the antioxidant and the ABAP treatments. As shown in Figure 6, the EC_{50} values of four

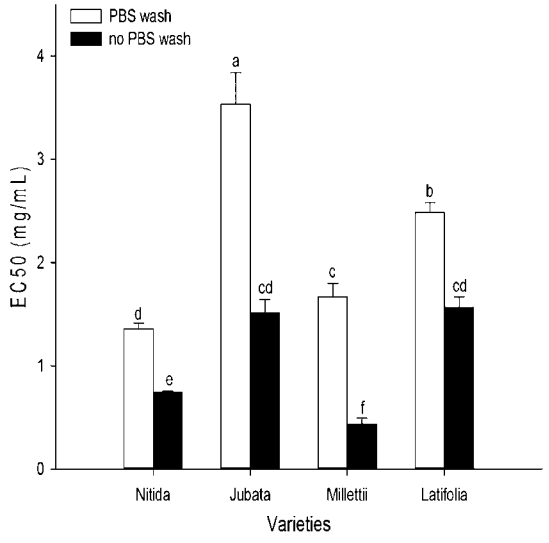

Figure 6. EC_{50} of free phenolic extracts from four *Adinandra* varieties (mean ± SD; $n = 3$). Bars with different letters differ significantly at $p < 0.05$.

varieties ranged from 0.43 to 1.56 mg/mL in the no PBS wash protocol and from 1.35 to 3.53 mg/mL in the PBS wash protocol. In the no PBS wash protocol, Millettii had the lowest EC_{50} values (430.87 ± 62.57 μg/mL), followed by Nitida (744.58 ± 10.65 μg/mL), Jubata (1509.4 ± 135.20 μg/mL), and then Latifolia (1562.8 ± 106.32 μg/mL). In the PBS wash protocol, which focused more on the intracellular antioxidant activity, Nitida had the lowest EC_{50} values (1359.3 ± 56.75 μg/mL), followed by Millettii (1668.2 ± 132.97 μg/mL), and then Latifolia (2482.2 ± 97.11 μg/mL). Jubata had the highest EC_{50} values (3533.2 ± 304.85 μg/mL).

On the basis of the comparison of EC_{50} values of samples and quercetin, the CAA value was expressed as micromoles of QE per 100 g of *Adinandra* and shown in Figure 7. CAA values

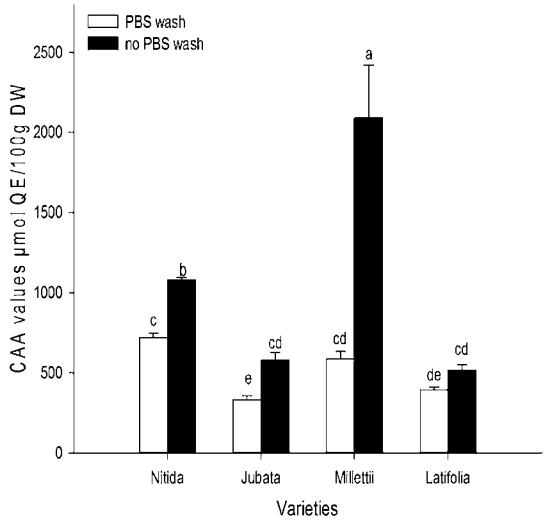

Figure 7. CAA values of the free phenolic extracts from four *Adinandra* varieties (mean ± SD; $n = 3$). Bars with different letters differ significantly at $p < 0.05$.

ranged from 516.06 to 2090.0 μmol of QE/100 g in the no PBS wash protocol and from 331.13 to 722.29 μmol of QE/100 g in the PBS wash protocol. In the no PBS wash protocol, Millettii had the highest CAA value (2090.0 ± 330.95 μmol of QE/100 g), followed by Nitida (1080.1 ± 15.36 μmol of QE/100 g). Jubata (580.31 ± 50.06 μmol of QE/100 g) and Latifolia (516.06 ± 33.89 μmol of QE/100 g) had lower CAA values. In the PBS wash protocol, Nitida (722.29 ± 29.71 μmol of QE/100 g) had the highest CAA value, followed by Millettii (587.26 ± 45.77 μmol of QE/100 g), Latifolia (395.49 ± 15.83 μmol of QE/100 g), and then Jubata (331.13 ± 27.64 μmol of QE/100 g).

The CAA assay reflects the absorption, metabolism, and distribution of antioxidants at the cellular level, and it is more accurate in evaluation of cellular antioxidant activity.[26,31] The CAA values were negatively correlated with EC_{50} values. Regardless of the protocol and expression method used, Nitida and Millettii showed higher antioxidant activity, which was consistent with higher phenolic contents in Nitida and Millettii (Figure 1).

The cellular antioxidant quality of free phenolic extracts was calculated from their CAA values, phenolic contents, and flavonoid contents and expressed as micromoles of QE per 100 μmol of flavonoids or phenolics. In the no PBS wash protocol, Millettii had the highest CAA value relative to the free phenolics (2.97 ± 0.47 μmol of QE/100 μmol of free phenolics), followed by Latifolia (1.56 ± 0.10 μmol of QE/100 μmol of free phenolics), Nitida (1.33 ± 0.019 μmol of QE/100 μmol of free phenolics), and Jubata (1.29 ± 0.11 μmol of

dx.doi.org/10.1021/jf503700v | J. Agric. Food Chem. 2015, 63, 169−176

Table 3. Cellular Antioxidant Quality of the Four *Adinandra* Varieties

variety	CAA quality of free phenolics (μmol of QE/100 μmol of phenolics)		CAA quality of free flavonoids (μmol of QE/100 μmol of flavonoids)	
	no PBS wash	PBS wash	no PBS wash	PBS wash
Nitida	1.33 ± 0.019	0.89 ± 0.037	3.58 ± 0.051	2.39 ± 0.098
Jubata	1.29 ± 0.11	0.74 ± 0.061	4.26 ± 0.37	2.43 ± 0.20
Millettii	2.97 ± 0.47	0.83 ± 0.065	14.50 ± 2.30	4.08 ± 0.32
Latifolia	1.56 ± 0.10	1.20 ± 0.048	11.84 ± 0.78	9.07 ± 0.36

QE/100 μmol of free phenolics). Millettii also had the highest CAA value relative to the free flavonoids (14.50 ± 2.30 μmol of QE/100 μmol of free flavonoids), followed by Latifolia (11.84 ± 0.78 μmol of QE/100 μmol of free flavonoids), Jubata (4.26 ± 0.37 μmol of QE/100 μmol of free flavonoids), and Nitida (3.58 ± 0.051 μmol of QE/100 μmol of free flavonoids). In the PBS wash protocol, Latifolia had the highest CAA value relative to the free phenolics (1.20 ± 0.048 μmol of QE/100 μmol of free phenolics), followed by Nitida (0.89 ± 0.037 μmol of QE/100 μmol of free phenolics), Millettii (2.97 ± 0.47 μmol of QE/100 μmol of free phenolics), and Jubata (0.74 ± 0.061 μmol of QE/100 μmol of free phenolics). Latifolia also had the highest CAA value relative to the free flavonoids (9.07 ± 0.36 μmol of QE/100 μmol of free flavonoids), followed by Millettii (4.08 ± 0.32 μmol of QE/100 μmol of free flavonoids), Jubata (2.43 ± 0.20 μmol of QE/100 μmol of free flavonoids), and Nitida (2.39 ± 0.098 μmol of QE/100 μmol of free flavonoids).

Inhibition of Proliferation in Human Cancer Cells. The antiproliferation effects of free phenolic extract from four varieties were tested against liver cancer cell HepG2 and breast cancer cell MCF-7. The *Adinandra* free phenolic extract effectively inhibited the cancer cell proliferation dose-dependently. Their inhibition of EC_{50} ranged from 1.05 to 6.44 mg/mL for HepG2 cells and from 2.26 to 8.02 mg/mL for MCF-7 cells (Table 4). For the HepG2 cells, Millettii extracts had the strongest inhibitory effect and the lowest EC_{50} (1.05 ± 0.089 mg/mL), followed by Nitida (1.49 ± 0.023 mg/mL), Jubata (1.85 ± 0.056 mg/mL), and finally Latifolia (6.44 ± 0.46 mg/mL). For the MCF-7 cells, Nitida (2.26 ± 0.19 mg/mL) and Millettii (2.43 ± 0.23 mg/mL) had a similar inhibitory effect, both stronger than Latifolia (4.01 ± 0.12 mg/mL). Jubata had the weakest effect and highest EC_{50} value (8.02 ± 0.32 mg/mL). Similar to the comparison in antioxidant activity by EC_{50} of CAA and CAA values (Figures 6 and 7), a higher antiproliferative effect was found in Nitida and Millettii (Table 3), which was consistent with and could be explained by their higher phenolic contents (Figure 1). Further investigation of individual phenolic compounds will shed light on the contribution and mechanism of their antiproliferative activities.

Table 4. Antiproliferative Activities of the Free Phenolic Extract from Four *Adinandra* Varieties toward Cancer Cells[a]

variety	antiproliferative capacity to HepG2 EC_{50} (mg/mL)	antiproliferative capacity to MCF-7 EC_{50} (mg/mL)
Nitida	1.49 ± 0.023 bc	2.26 ± 0.19 c
Jubata	1.85 ± 0.056 b	8.02 ± 0.32 a
Millettii	1.05 ± 0.089 c	2.43 ± 0.23 c
Latifolia	6.44 ± 0.46 a	4.01 ± 0.12 b

[a]Values in the same rows with different letters differ significantly at $p < 0.05$.

HPLC Analysis. The phenolic compounds of *Adinandra* varieties were further analyzed by HPLC (Figure 8). Camellianin B, quercitrin, camellianin A, and apigenin were reported to be the main components of Nitida;[9−12] therefore, their contents were determined using standards and presented in Table 5. In Nitida, camellianin B, quercitrin, and camellianin A were mainly detected in the free phenolic extracts, while apigenin was found in bound phenolic extracts. These four compounds in total were about 183 mg/g of DW and might account for most of the phenolics in Nitida. The recrystallized camellianin A extract from Nitida was reported to inhibit 33.8 and 8.7% of MCF-7 and HepG2 cells at 200 μM.[16] Here, a relatively higher antiproliferative effect was observed in the Nitida extract in MCF-7 and HepG2 cells (Table 4), which suggested that its antiproliferative effect might be attributed to the synergy or interactions of different phenolic compounds.

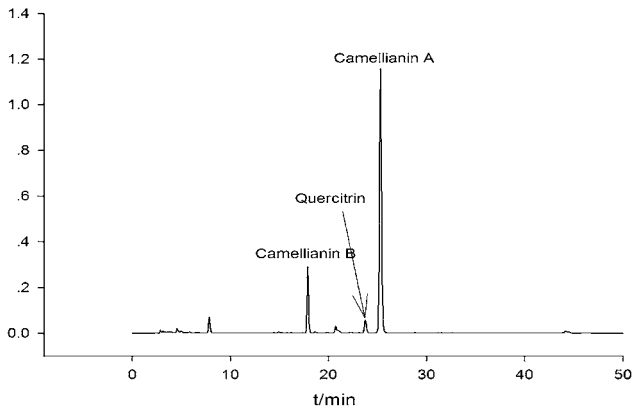

Figure 8. HPLC for Nitida free extracts.

In Latifolia, quercitrin and camellianin A were mainly detected in the free phenolic extracts, while camellianin B in the bound phenolic extract contributed more than 50% to the total camellianin B, which was consistent with its high content of bound phenolics (Figure 1). Among the four components quantified, only little amounts of camellianin B (3.89 ± 0.17 mg/g of DW) and quercitrin (1.99 ± 0.30 mg/g of DW) were detected in Jubata. Trace levels of camellianin B (0.58 ± 0.05 mg/g of DW) and quercitrin (0.18 ± 0.02 mg/g of DW) were detected in Millettii. These results suggest that phenolics other than these four components contribute to the total phenolics and antioxidant and antiproliferation activities of Jubata and Millettii, which deserved further investigation.

In summary, results here have revealed that four *Adinandra* varieties are rich in phytochemicals and have high antioxidant and antiproliferation activities. Thus, they are good source of natural antioxidants and antiproliferative compounds with further application in food and pharmaceutical industries. Among the four varieties compared, higher antioxidant and

Table 5. Contents of Camellianin B, Quercitrin, Camellianin A, and Apigenin in *Adinandra* Varieties (Milligrams Per Gram of DW) Revealed by HPLC

variety		camellianin B (mg/g of DW)	quercitrin (mg/g of DW)	camellianin A (mg/g of DW)	apigenin (mg/g of DW)
Nitida	free	34.11 ± 4.97	6.43 ± 0.48	142.71 ± 21.20	ND
	bound	0.22 ± 0.00	0.43 ± 0.00	ND	0.01 ± 0.00
	total	34.33 ± 4.97	6.86 ± 0.48	142.71 ± 21.20	0.01 ± 0.00
Jubata	free	3.53 ± 0.17	1.99 ± 0.30	ND	ND
	bound	0.35 ± 0.00	ND	ND	ND
	total	3.89 ± 0.17	1.99 ± 0.30	ND	ND
Millettii	free	ND	0.18 ± 0.02	ND	ND
	bound	0.58 ± 0.05	ND	ND	ND
	total	0.58 ± 0.05	0.18 ± 0.02	ND	ND
Latifolia	free	3.27 ± 0.09	0.32 ± 0.02	5.17 ± 0.001	ND
	bound	3.98 ± 0.16	0.04 ± 0.00	ND	ND
	total	7.25 ± 0.18	0.36 ± 0.02	5.17 ± 0.001	ND

antiproliferation activities were found in Nitida and Millettii, which was consistent with and could be explained by their higher phenolic contents. The main phenolic components in Nitida were camellianin A, camellianin B, quercitrin, and apigenin, while the main phenolics in Millettii await further identification. Nitida contained ignorable bound phenolics, but the bound phenolics in other varieties, especially Latifolia, should not be underestimated and can be used in the future to provide additional health benefits.

AUTHOR INFORMATION

Corresponding Authors

*Telephone: 86-13660887090. Fax: 86-20-87113849. E-mail: chengu@scut.edu.cn.

*Telephone: 607-255-6235. Fax: 607-254-4868. E-mail: rl23@cornell.edu.

Funding

The authors are grateful to the Guangdong Province Government (China) for its support through the program "Leading Talent of Guangdong Province" to Rui-Hai Liu.

Notes

The authors declare no competing financial interest.

REFERENCES

(1) Liu, R. H. Health benefits of fruit and vegetables are from additive and synergistic combinations of phytochemicals. *Am. J. Clin. Nutr.* **2003**, *78*, 517S−520S.

(2) Liu, R. H. Dietary bioactive compounds and their health implications. *J. Food Sci.* **2013**, *78*, A18−A25.

(3) Willett, W. C. Balancing life-style and genomics research for disease prevention. *Science* **2002**, *296*, 695−698.

(4) Liu, R. H. Health-promoting components of fruits and vegetables in the diet. *Adv. Nutr.* **2013**, *4*, 384S−392S.

(5) Liu, R. H. Potential synergy of phytochemicals in cancer prevention: Mechanism of action. *J. Nutr.* **2004**, *134*, 3479S−3485S.

(6) Higdon, J. V.; Frei, B. Tea catechins and polyphenols: Health effects, metabolism, and antioxidant functions. *Crit. Rev. Food Sci. Nutr.* **2003**, *43*, 89−143.

(7) Chen, Y.; She, G.; Chen, H. Study on antitumor activities of substances extracted from *Adinadra nitida* Merr. ex H. Li. *J. Shantou Univ., Nat. Sci.* **1997**, *12*, 43−45.

(8) Yu, J.; Chen, M. Studies on flavonoids extraction from *Adinandra nitida* Merr. ex H. L. Li. and on their antioxidative and bacteriostatic bioactivities. *J. Shantou Univ., Nat. Sci.* **1997**, *12*, 52−56.

(9) Liu, B.; Ning, Z.; Zhan, Y.; Xu, K.; Gao, J. Chracterization and 1,1-diphenyl-2-picrylhydrazyl radical scavenging activity of methanol and supercritical carbon dioxide extracts from leaves of *Adinandra nitida*. *J. Food Biochem.* **2008**, *32*, 431−442.

(10) Liu, B.; Ma, Y.; Liu, Y.; Yang, Z.; Zhang, L. Ultrasonic-assisted extraction and antioxidant activity of flavonoids from *Adinandra nitida* leaves. *Trop. J. Pharm. Res.* **2013**, *12*, 1045−1051.

(11) Zhang, J.; Tao, D.; Duan, J.; Liang, Z.; Zhang, W.; Zhang, L.; Huo, Y.; Zhang, Y. Separation and identification of compounds in *Adinandra nitida* by comprehensive two-dimensional liquid chromatography coupled to atmospheric pressure chemical ionization source ion trap tandem mass spectrometry. *Anal. Bioanal. Chem.* **2006**, *386*, 586−593.

(12) Zhang, L. Y.; Zhang, J.; Wang, H.; Zhang, L. H.; Zhang, W. B.; Zhang, Y. K. Analysis of flavonoids in leaves of *Adinandra nitida* by capillary electrochromatography on monolithic columns with stepwise gradient elution. *J. Sep. Sci.* **2005**, *28*, 774−779.

(13) Zhang, J.; Yang, J.; Duan, J. C.; Liang, Z.; Zhang, L. H.; Huo, Y. S.; Zhang, Y. K. Quantitative and qualitative analysis of flavonoids in leaves of *Adinandra nitida* by high performance liquid chromatography with UV and electrospray ionization tandem mass spectrometry detection. *Anal. Chim. Acta* **2005**, *532*, 97−104.

(14) Zhang, J.; Tao, D.; Duan, J.; Liang, Z.; Zhang, W.; Zhang, L.; Huo, Y.; Zhang, Y. Separation and identification of compounds in *Adinandra nitida* by comprehensive two-dimensional liquid chromatography coupled to atmospheric pressure chemical ionization source ion trap tandem mass spectrometry. *Anal. Bioanal. Chem.* **2006**, *386*, 586−593.

(15) Yuan, E.; Liu, B.; Ning, Z.; Chen, C. Preparative separation of flavonoids in *Adinandra nitida* leaves by high-speed counter-current chromatography and their effects on human epidermal carcinoma cancer cells. *Food Chem.* **2009**, *115*, 1158−1163.

(16) Gao, H.; Liu, B.; Liu, F.; Chen, Y. Anti-proliferative effect of camellianin A in *Adinandra nitida* leaves and its apoptotic induction in human HepG2 and MCF-7 cells. *Molecules* **2010**, *15*, 3878−3886.

(17) Sun, J.; Chu, Y. F.; Wu, X. Z.; Liu, R. H. Antioxidant and antiproliferative activities of common fruits. *J. Agric. Food Chem.* **2002**, *50*, 7449−7454.

(18) Guo, X.; Li, T.; Tang, K.; Liu, R. H. Effect of germination on phytochemical profiles and antioxidant activity of mung bean sprouts (*Vigna radiata*). *J. Agric. Food Chem.* **2012**, *60*, 11050−11055.

(19) Adom, K. K.; Liu, R. H. Antioxidant activity of grains. *J. Agric. Food Chem.* **2002**, *50*, 6182−6187.

(20) Singleton, V. L.; Orthofer, R.; Lamuela-Raventos, R. M. Analysis of total phenols and other oxidation substrates and antioxidants by means of Folin−Ciocalteu reagent. In *Methods in Enzymology, Oxidants and Antioxidants, Part A*; Packer, L., Ed.; Academic Press: San Diego, CA, 1999; Vol. *299*, pp 152−178.

(21) Liu, R. H.; Sun, J. Antiproliferative activity of apples is not due to phenolic-induced hydrogen peroxide formation. *J. Agric. Food Chem.* **2003**, *51*, 1718−1723.

(22) He, X.; Liu, D.; Liu, R. H. Sodium borohydride/chloranil-based assay for quantifying total flavonoids. *J. Agric. Food Chem.* **2008**, *56*, 9337−9344.

(23) Huang, D. J.; Ou, B. X.; Hampsch-Woodill, M.; Flanagan, J. A.; Prior, R. L. High-throughput assay of oxygen radical absorbance capacity (ORAC) using a multichannel liquid handling system coupled with a microplate flourescence reader in 96-well format. *J. Agric. Food Chem.* **2002**, *50*, 4437−4444.
(24) Zhang, M. W.; Zhang, R. F.; Zhang, F. X.; Liu, R. H. Phenolic profiles and antioxidant activity of black rice bran of different commercially available varieties. *J. Agric. Food Chem.* **2010**, *58*, 7580−7587.
(25) Adom, K. K.; Liu, R. H. Rapid peroxyl radical scavenging capacity (PSC) assay for assessing both hydrophilic and lipophilic antioxidants. *J. Agric. Food Chem.* **2005**, *53*, 6572−6580.
(26) Wolfe, K. L.; Liu, R. H. Cellular antioxidant activity (CAA) assay for assessing antioxidants, foods, and dietary supplements. *J. Agric. Food Chem.* **2007**, *55*, 8896−8907.
(27) Yoon, H.; Liu, R. H. Effect of 2α-hydroxyursolic acid on NF-κB activation induced by TNF-α in human breast cancer MCF-7 cells. *J. Agric. Food Chem.* **2008**, *56*, 8412−8417.
(28) Felice, D. L.; Sun, J.; Liu, R. H. A modified methylene blue assay for accurate cell counting. *J. Funct. Foods* **2009**, *1*, 109−118.
(29) Zuo, W.; Xu, J.; Zhou, C.; Gan, L. Simultaneous determination of five flavonoid compounds in leaves of *Adinandra nitida* by HPLC−PAD. *China J. Chin. Mater. Med.* **2010**, *35*, 2406−2409.
(30) Liu, R. H. Whole grain phytochemicals and health. *J. Cereal Sci.* **2007**, *46*, 207−219.
(31) Wolfe, K. L.; Kang, X.; He, X.; Dong, M.; Zhang, Q.; Liu, R. H. Cellular antioxidant activity of common fruits. *J. Agric. Food Chem.* **2008**, *56*, 8418−8426.

JOURNAL OF AGRICULTURAL AND FOOD CHEMISTRY

Article

pubs.acs.org/JAFC

Characterization of Immunomodulatory Activities of Honey Glycoproteins and Glycopeptides

M. Ahmed Mesaik,[†,§,∥] Nida Dastagir,[†,∥] Nazim Uddin,[†] Khalid Rehman,[†] and M. Kamran Azim*[,†]

[†]Dr. Panjwani Center for Molecular Medicine and Drug Research, International Center for Chemical and Biological Sciences, University of Karachi, Karachi 75270, Pakistan

[§]Faculty of Pharmacy, Universiti Kebangsaan Malaysia, Jalan Raja Muda Abdul Aziz, 50300 Kuala Lumpur, Malaysia

Supporting Information

ABSTRACT: Recent evidence suggests an important role for natural honey in modulating immune response. To identify active components responsible, this study investigated the immunomodulatory properties of glycoproteins and glycopeptides fractionated from *Ziziphus* honey. Honey proteins/peptides were fractionated by size exclusion chromatography into five peaks with molecular masses in the range of 2−450 kDa. The fractionated proteins exhibited potent, concentration-dependent inhibition of reactive oxygen species production in zymosan-activated human neutrophils (IC_{50} = 6−14 ng/mL) and murine macrophages (IC_{50} = 2−9 ng/mL). Honey proteins significantly suppressed the nitric oxide production by LPS-activated murine macrophages (IC_{50} = 96−450 ng/mL). Moreover, honey proteins inhibited the phagocytosis latex bead macrophages. The production of pro-inflammatory cytokines IL-1β and TNF-α by human monocytic cell line in the presence of honey proteins was analyzed. Honey proteins did not affect the production of IL-1β; however, TNF-α production was significantly suppressed. These findings indicated that honey glycoproteins and glycopeptides significantly interfere with molecules of the innate immune system.

KEYWORDS: *honey, glycoprotiens, immunomodulatory, phagocytosis, oxidative burst*

INTRODUCTION

Natural honey is a well-known neutraceutical that is mainly composed of fructose, glucose, sucrose, and maltose. Small amounts of oligosaccharides, proteins, amino acids, minerals, trace elements, vitamins, aroma compounds, and polyphenols are also present (reviewed in ref 1). Honey exerts a number of pharmacological effects including antimicrobial, immunomodulatory, prebiotic, antinematodal, anti-inflammatory, and antinociceptive activities.[1−9] It showed both bacteriostatic and bactericidal potentials against pathogenic bacteria including drug-resistant strains.[5] Honey was found to exert anti-inflammatory effects via inhibiting (a) thrombin-induced reactive oxygen species (ROS) production[6] and (b) myeloperoxidase-dependent oxidative burst by professional phagocytes.[7] It inhibited nitric oxide (NO) production in a carrageenen-induced inflammatory rat model.[10] In addition, manuka, pasture, and jellybush honeys were found to reduce ROS production[11] and stimulate monocytes (MonoMac-6 cell line) to produce tumor necrosis factor-α (TNF-α), interleukin (IL)-1β, and IL-6, which are known to play vital roles in tissue repair.[12] The effect of honey on cytokine production was found to be associated with a 5.8 kDa component isolated from manuka honey, which interacted with TLR-4.[13] Natural honey exhibited antitumor activity by inhibiting the growth of Lewis lung carcinoma/2 cells.[14] An immunostimulatory effect of honey on antibody production against thymus-dependent (sheep red blood cells) and thymus-independent (*Escherichia coli*) antigens in mice has also been observed.[15] Likewise, honey also inhibited mitogen-activated T cell proliferation in vitro.[16] Moreover, honey regulates homeostasis by inhibiting human platelet aggregation and blood coagulation proteins.[17]

Natural honeys have a low protein content, which varies from type to type. Characterization of honey proteins from various sources was found to be valuable in determining the floral and geographical origin.[18] A number of studies pointed out the immunomodulatory potential of honey proteins. Four immunologically characterized IgE-binding glycoproteins (belonging to the major royal jelly protein-1 (MRJP-1) family) were identified in honey, and N-linked glycosylation in these proteins played an important role in binding of IgE.[19,21] Ultracentrifugation of royal jelly (RJ) revealed that the MRJP1 was the most abundant protein of RJ present in monomeric (55 kDa) as well as oligomeric (ca. 450 kDa) forms.[20] Honey contains MRJP1 protein as well, which exerts its immunostimulatory effect by stimulating TNF-α production in murine peritoneal macrophages, and the protein moiety of this glycoprotein was found be responsible for this property.[22] Recently, highly glycosylated arabinogalactan proteins (AGPs) with molecular masses of ∼110 kDa have been characterized from New Zealand kanuka honey.[23] AGPs are proteoglycans that contain type II arabinogalatans and 2−10% covalently attached protein that is typically rich in hydroxyproline and serine. AGPs are compact molecules consisting of a protein core to which highly branched polysaccharide chains are attached.[24] AGPs are found in the female sexual tissues of flowers and thus could be a potential source of AGPs in honey. AGPs and type II arabinogalactans from different sources have been shown to exert immunomodulatory properties.[25] As a

Received: August 1, 2014
Revised: December 7, 2014
Accepted: December 12, 2014
Published: December 12, 2014

ACS Publications © 2014 American Chemical Society

continuation of our research, we have elaborated the role(s) of honey glycoproteins and glycopeptides in the modulation of innate immune systems.

MATERIALS AND METHODS

Fractionation and Characterization of Honey Proteins. *Honey Samples.* Monofloral *Ziziphus* species honey samples produced by *Apis mellifera* in bee farms located in Himalayan and Pothohar plateau regions in northern Pakistan were used during this study.

Ammonium Sulfate Precipitation. Honey samples were diluted in buffer A (20 mM Tris-HCl, 150 mM NaCl, and 0.05% sodium azide, pH 7.4) and centrifuged at 2500*g* for 20 min at 4 °C to remove particulates, particularly pollens. The supernatants were collected and processed for ammonium sulfate precipitation at 4 °C with 80% saturation. The solution was kept on a stirrer for 1−2 h followed by centrifugation at 8300*g* at 4 °C. The pellets were dissolved in buffer and stored at −20 °C until use.

Gel Filtration Chromatography (GFC). GFC of crude honey proteins was carried out by using a Hiload 16/60 Superdex 200 Prep grade column (GE Healthcare, Uppsala, Sweden) with buffer A as mobile phase. Chromatography was done using an AKTA FPLC system (GE Healthcare) at the flow rate of 1 mL/min, and fractions of 2 mL were collected. The resultant five chromatographic peaks were termed GFC-P1−GFC-P5. Fractions containing a high molecular mass peak, GFC-P1, were pooled and treated with 8 M urea (Sigma-Aldrich, Steinheim, Germany) followed by rechromatography in the same conditions. Peaks GFC-P1−GFC-P3 were concentrated by ultrafiltration (MWCO 10 kDa, Millipore, Darmstadt, Germany), whereas peaks GFC-P4 and GFC-P5 were freeze-dried (Alpha 1-2/LD plus, Suarlee, Belgium) and resuspended in buffer A. Protein estimation was carried out by using a modified Lowry's protein assay kit (Thermo Scientific, Rockford, IL, USA).[26] The molecular masses of proteins were estimated by using a Gel Filtration Calibration Kit HMW (GE Healthcare BioSciences AB, Uppsala, Sweden), which contains five proteins and Blue dextran 2000 (ovalbumin M_r 43000; conalbumin M_r 75000; aldolase M_r 158,000; ferritin M_r 440,000; thyroglobulin M_r 669,000; and Blue dextran 2000 M_r 2,000,000).

Reverse Phase HPLC of GFC Peaks. The gel chromatography peaks GFC-P1 and GFC-P5 were subjected to reverse phase HPLC using a C-18 column (Purospher STAR, RP-18 end-capped (5 μm, 150-4.6, Merck, Darmstadt, Germany). The column was equilibrated with 0.1% TFA, and 100 μL of filtered protein sample was applied with a flow rate of 1.0 mL/min. Gradient elutions were made with acetonitrile as 5 min/0%, 40 min/70%, and 45 min/0%. Peaks were collected, concentrated, and stored at −20 °C until next use.

Mass Spectrometry. MALDI-TOF analysis of peaks obtained by RPLC was carried out as follows. Half a microliter of peptide suspension was mixed with 0.5 μL of matrix solution (sinapinic acid in 1:1 0.1% TFA/acetonitrile). The matrix/analyte solution was applied to the sample plate. Mass spectra were recorded on a Bruker Ultraflex III TOF/TOF spectrometer. Two hundered shots of light from a smart beam laser were irradiated to record mass spectra. Bioinformatics analysis of mass spectrometric data was done by using Glycosuite Database and GlycoMod tool of ExPASy server (www.expasy.org).

Immunomodulatory Activity Assays. *Isolation of Phagocytic Cells.* Polymorph nuclear leukocytes (PMNLs) were collected from human blood by using Ficoll paque gradient centrifugation. For this purpose, blood was drawn from healthy human volunteers (36−45 years old) who had not received any medication for 1 week. Blood was mixed with equal volumes of lymphocyte separation medium (MP Biomedical, Inc., Kaysersberg, France) and Hank's balanced salt solution (HBSS) without calcium and magnesium (Sigma-Aldrich, Steinheim, Germany). The diluted blood was kept undisturbed at room temperature for 30−45 min. When red blood cells (RBCs) settled, supernatant was layered onto 5 mL of LSM in a separate centrifuge tube and centrifuged at 400*g* for 20 min at 4 °C. Supernatant was discarded, and pellet was resuspended in HBSS free from calcium and magnesium and washed at 300*g* for 15 min at 4 °C. In the presence of RBCs contamination, RBCs were lysed with sterile distilled water; finally, pellet was resuspended in HBSS containing calcium and magnesium. Cell viability was determined using trypan blue dye, and cell count was adjusted to 1,000,000 cells per milliliter.

In addition, murine peritoneal macrophages were collected after the injection of 10 mL of sterile phosphate buffer saline (PBS) into mouse peritoneum (immunized with 1 mL of sterile fetal bovine serum 72 h earlier). Cells were spun at 300*g* for 15 min at 4 °C. Pellet was resuspended in 1 mL of sterile PBS, viability was checked with trypan blue exclusion method (cells were >95% viable), and count was adjusted as 1,000,000 cells per milliliter.

Chemiluminescence Assay for Oxidative Burst. The effect of honey protein fractions on ROS production was measured on PMNLs and mouse peritoneal macrophages. In brief, cells were plated in flat-bottomed 96-well plates and activated by serum opsonized zymosan-A (Sigma-Aldrich) at 250 μg/mL final concentration. Protein/peptide/glypeptide samples added at various concentrations (0.125−2.0 μg/mL) and plates were incubated for 20 min at room temperature. Luminol (3-aminophthalhydrazide) (Alfa Aesar, Karlsruhe, Germany) was added at 1.5 μg/mL final concentration. Plates were immediately kept in the thermostated chamber of a Luminoskan, and chemluminescence kinetics of ROS production was monitored as relative light units (RLUs) for 50 min in the Luminoskan (Labsystem, Helsinki, Finland) with repeated scans.[27]

Nitric Oxide Assay. The murine macrophage cells (J774.2 cell line) were purchased from the European Collection of Cell Cultures (Salisbury, UK). Cells were cultured in complete DMEM (Sigma-Aldrich) supplemented with 10% heat-inactivated fetal bovine serum (FBS), 100 U/mL penicillin, and 100 μg/mL streptomycin. The effect of honey proteins on NO production was monitored according to the method of Inoue et al.[28] Briefly, cells were seeded in a 96-well plate as 1.8×10^5 cells/well and activated by 30 μg/mL of LPS (*Escherichia coli* serotype 0111:B4, DIFCO Laboratories, Detroit, MI, USA) for the production of nitric oxide. Protein samples were added at various concentrations, and the plate was incubated at 37 °C for 48 h. Supernatants (50 μL) from each well were mixed with an equal amount of Griess reagent (0.1% naphthylethylenediamine dihydrochloride in distilled water and 1% sulfanilic acid in 5% H_3PO_4 in 1:1 ratio) (Fisher Scientific, Leicestershire, UK), and absorbance was recorded at 550 nm using a Spectra Max plus 340 (Molecular Devices, Synnyvale, CA, USA).

Phagocytosis Assay. Phagocytosis assay was performed according to the method of Foukas et al. with some modifications.[29] The murine macrophage cells (J774.2 cell line) were cultured in complete DMEM and seeded into a 96-well tissue culture-treated plate with 5×10^4 cells/well. Culture reaction plate was incubated in CO_2 environment at 37 °C with 5% CO_2 for 24 h. The next day, latex beads (fluorescent coated carboxylated modified polystyrene beads, 1 μm, Sigma-Aldrich) were added as 100 beads/cell. Protein samples were added as 800 ng/mL final concentration, and the plate was further incubated for 24 h at 37 °C in a CO_2 environment. Afterward, supernatant was removed and wells were washed twice by gently inverting the plate with 1× PBS. Trypan blue (1×, 50 μL) was added to each well, and the plate was kept at room temperature for 1 min. The trypan blue was removed, and fluorescence was recorded at 575−610 nm using a fluorescence reader (Molecular Devices).

Cytokine (TNF-α and IL-1β) Production Assay. THP-1 cell line (human monocytic leukemia cells) was purchased from the European Collection of Cell Cultures. Cells were cultured in a 75 mm^2 tissue culture flask with complete RPMI-1640 medium (MP Biomedical, Solon, OH, USA) supplemented with 10% FBS, 10 mM HEPES, 1 mM sodium pyruvate, 2 mM L-glutamine, 5.5 mM D-glucose, 50 μM β-mercaptoethanol, and 1% penicillin and streptomycin. Cells were seeded into a 24-well polystyrene sterile culture plate with 20 ng/mL PMA (SERVA, Heidelberg, Germany), which causes differentiation of monocytes to macrophages. The culture plate was incubated at 37 °C for 24 h. The next day, cells were activated with 50 ng/mL LPS, protein samples were added in various concentrations, and the plate was incubated at 37 °C with 5% CO_2. Supernatants were collected after 6 h, and levels of TNF-α and IL-1β were estimated using an

ELISA kit (R&D System, Minneapolis, MN, USA). Absorbance was recorded at 450 nm using a microplate reader (DIA Reader, Gmblt, Wr. Neudorf, Austria).[30]

Statistical Analysis. All experiments were run in triplicates, and data are presented as the statistical mean ± standard deviation (STD). A one-way analysis of variance (ANOVA) was applied to measure the significant difference between the results of test proteins and controls. Significance level was set as $P < 0.05$, $P < 0.01$, and $P < 0.005$.

RESULTS AND DISCUSSION

Separation and Characterization of Honey Glycoproteins and Glycopeptides. Previously, we have reported

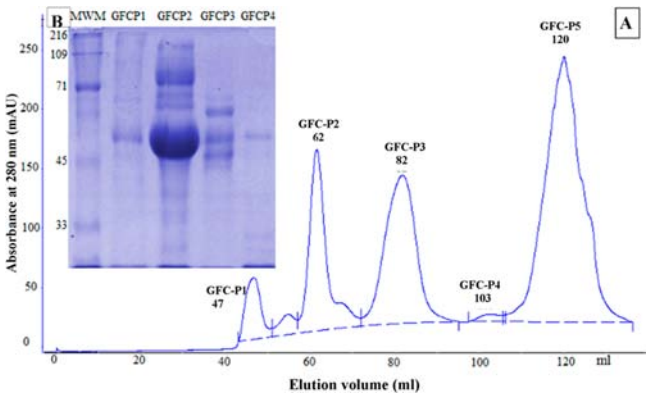

Figure 1. (A) Gel filtration chromatogram of *Ziziphus* honey proteins and peptides using AKTA FPLC system and Hiload 16/60 Superdex 200 prep grade column. Peak names and elution volumes (mL) are given. (B) SDS-PAGE of gel filtration peaks 1−4 designated GFC-P1, GFC-P2, GFC-P3, and GFC-P4 (MWM, protein molecular weight marker).

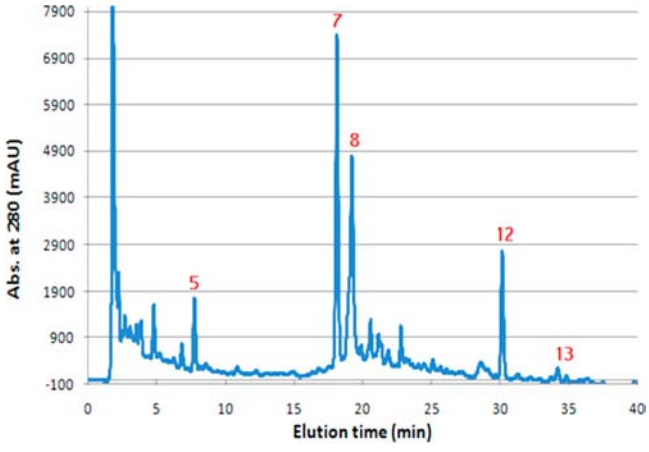

Figure 2. Reverse phase HPLC chromatogram of peak GFC-P5 using a C18 column. Prominent peak numbers are noted.

immunomodulatory activity of honey.[6,8] In the present study, we characterized immunomodulatory properties of proteoglycans, glycoproteins, and glypeptides from *Ziziphus* honey. We and others have already reported that honey proteins can be separated into five or six peaks by size exclusion chromatography.[19,31,32] Here, we report the role of fractionated honey proteins on the innate immune response. For this purpose, crude proteins extracted from *Ziziphus* honeys (produced by *A. mellifera* in bee farms located in northern Pakistan) were subjected to size exclusion chromatography using a Hiload Superdex 200 prep grade column and AKTA FPLC system. Consistent with previous findings, size exclusion chromatography separated honey proteins and peptides into five peaks (namely, GFC-P1−GFC-P5) (Figure 1A). In agreement with previous results,[19,31] we found an array of proteins with molecular masses in the range from 10 to ∼450 kDa in peaks GFC-P1−GFC-P4 as revealed by nondenaturing (i.e., GFC) as well as reducing/denaturing (SDS-PAGE) conditions (Figure 1B), whereas peak GFC-P5 contained low molecular mass peptides/glycopeptides (2−5 kDa).

The high molecular mass protein peak GFC-P1 was treated with 8 M urea followed by rechromatography with the same column (Hiload Superdex 200 prep grade). Untreated and 8 M urea treated peak GFC-P1 eluted at the same time (Supporting Information, supplementary Figure 1), whereas SDS-PAGE of this peak (Figure 1B) showed a band at 55 kDa, which indicated that high molecular mass proteins in the peak were dissociated into smaller subunits. Reverse phase liquid chromatography (RPLC) of GFC-P1 showed two distinct peaks (Supporting Information, supplementary Figure 2). These peaks were eluted during the start of the gradient, which indicated their hydrophilic nature. Typically, proteins show λ_{max} at 280 nm, whereas the UV spectra of RPLC peaks determined by diode array detector showed λ_{max} at 266 nm (Supporting Information, supplementary Figure 2). These observations pointed out covalently attached glycans, polyphenols, and other natural products to the protein core. Manuka, kanuka, and clover honeys have been reported to contain type II arabinogalactan proteins with molecular masses of >100 kDa.[23−25] Hence, high molecular mass protein peak (GFC-P1) presumably contained MRJP1 proteins. Molecular masses of proteins in peaks GFC-P2−GFC-P4 were found to be in the range of 10−200 kDa.[19] SDS-PAGE of GFC-P2 showed multiple bands with an intense band of 50−55 kDa, whereas GFC-P3 contained proteins of 45−70 kDa masses.

Peptides and glypeptides in peak GFC-P5 were further separated by RPLC, which resulted in 13 fractions (Figure 2). Peaks 8, 12, and 13 of RPLC were found to possess potent ROS production inhibitory activity (see below). MALDI mass spectrometric analysis of these peaks was carried out (Figure 3 and Supporting Information, supplementary Figure 3). Mass spectra were analyzed using the GlycoMod tool (www.expasy.org), which showed that peak 8 contained highly glycosylated peptide(s) with a molecular mass of 1157 Da (Figure 3A). A number of possible structures of O-linked glycopeptides(s) were found. This glycopeptide was characterized as O-linked glypeptide with a glycan structure of (Hex)3 (HexNAc)1 (Deoxyhexose)2 (Sulph)1 (HexA)1 (Figure 3A). Peak 12 was found to be a hybrid type N-linked glycoconjugate with the core region consisting of two *N*-acetylglucosamine residues and three mannose residues (Figure 3B). The peptide mass was calculated as 1066 Da, whereas the mass of the glycosylated peptide was 3086 (Figure 3B). The MALDI MS spectrum of relatively nonpolar peak 13 showed a single mass peak corresponding to peptide mass 1939 Da (Supporting Information, supplementary Figure 3). $[M + H]^+$, $[M + Na]^+$, and $[M + NH_4]^+$ adducts were expected to form during mass spectrometry; therefore, possible structures of these adducts were considered using GlycoMod. We used proteins and peptides fractionated by gel filtration chromatography for immunomodulatory assays.

Effect of Honey Glycoproteins/Glycopeptides on ROS Production. Activation of immune cells by any antigen induces the respiratory burst that results in ROS release. The

dx.doi.org/10.1021/jf505131p | J. Agric. Food Chem. 2015, 63, 177−184

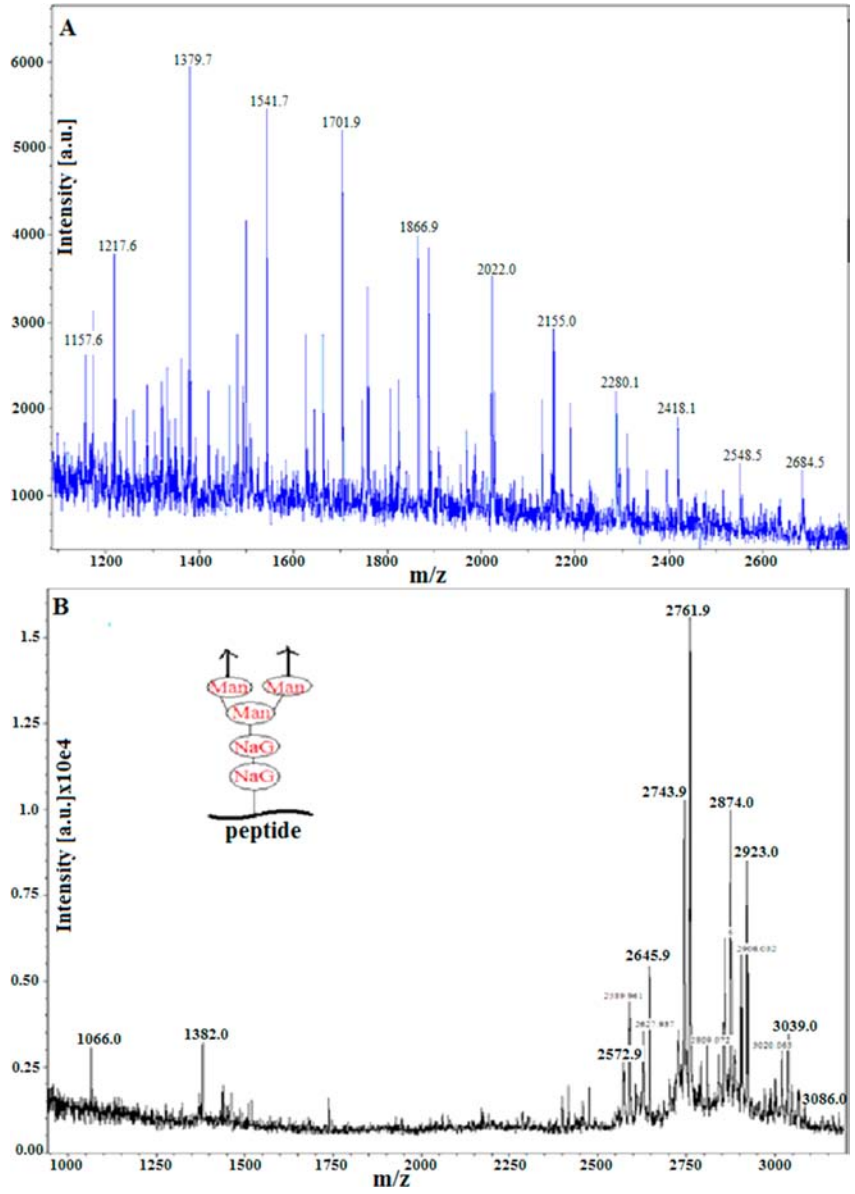

Figure 3. MALDI-MS spectra of peaks 8 (A) and 12 (B) from Figure 2.

ROS are known to play a crucial role in the pathogenesis of various inflammatory diseases including cardiovascular diseases, rheumatoid arthritis, and other inflammatory diseases. The manuka and pasture honeys were reported to have potential to reduce the production of ROS in MM-6 cells.[11] We previously reported the ability of natural honey to inhibit thrombin-induced ROS production[6] as well as myeloperoxidase-dependent oxidative burst of professional phagocytes.[7] The current experiments revealed that ROS production by human polymorph nuclear cells and mouse peritoneal macrophages was significantly suppressed by honey proteins/peptides of different molecular masses, that is, peaks GFC-P1−GFC-P5 (Figure 4; Table 1). Production and level of ROS were detected by luminol probe, which captures intracellular ROS (mainly HOCl besides the H_2O_2 and OH^- species) and converts them into a luminescent product, which was detected and recorded by luminoskan in the form of RLUs. All protein peaks showed potent inhibition of ROS production by neutrophils (IC_{50} = 6−14 ng/mL) and macrophages (IC_{50} = 2−9 ng/mL) stimulated with serum opsonized zymosan (SOZ). Zymosan is a fungal cell wall component, when coated with serum; it binds to cell surface phagocytosis receptors and serves as a potent activator of NADPH oxidase. The activation of NADPH oxidase results in the production of superoxide ($O_2^{\bullet-}$), which is a major player of host defense against bacteria and fungi. However, superoxide and other ROS must be controlled, and their continuous and excessive production can lead to inflammation.[33] The SOZ elicits phagocytosis through the Fcγ receptors on phagocytic cells.[34] Therefore, inhibition of ROS by honey proteins can be linked to the interference with or down-regulation of Fcγ receptors.

Among different fractions of peak GFC-P5 that were separated by RPLC, peaks RP-8, RP-12, and RP-13 suppressed ROS generation by neutrophils. These peptides showed significant inhibition of ROS production with IC_{50} values of 120 nM (RP-8), 50 nM (RP-12), and 150 nM (RP-13) (Figure 5). These results revealed that the proteins and peptides of honey play vital roles in ROS inhibition.

Effect of Honey Glycoproteins and Glycopeptides on Phagocytosis. Phagocytosis is the foremost mechanism of

dx.doi.org/10.1021/jf505131p | J. Agric. Food Chem. 2015, 63, 177−184

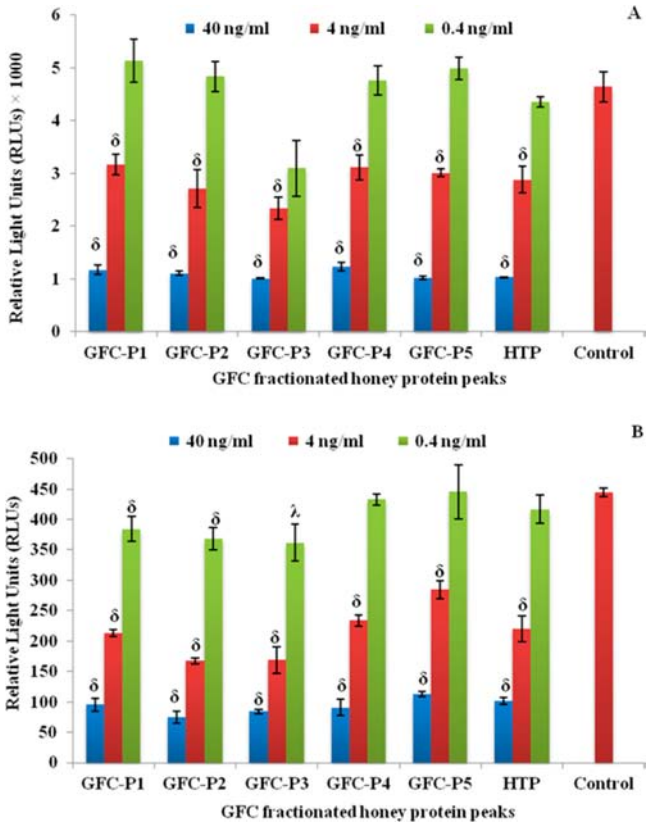

Figure 4. Effect of honey protein fractions on reactive oxygen species production. (A) Human polymorph nuclear leukocytes and (B) mouse peritoneal macrophages were activated with serum opsonized zymosan (SOZ) for ROS production. Effects of honey proteins at different concentrations were evaluated by chemiluminescence measurement using luminol probe. GFC-P1−GFC-P5 represent different protein peaks; HTP refers to honey total proteins. Control represents the cells activated with serum opsonized Zymosan. Bar graph corresponds to the statistical mean ± standard deviation. Statistical analysis was applied using one-way ANOVA with significance levels of <0.005, <0.01, and 0.05, represented as δ, λ, and ε respectively.

Table 1. Effect of Honey Protein Fractions on the Production of Recative Oxygen Species (ROS), Nitric Oxide (NO), and Phagocytosis

	IC_{50} (ng/mL ± standard deviation)		
	ROS inhibition		NO inhibition
GFC fractionated honey protein peaks	PMNLs	peritoneal macrophages	j774.2 macrophages
GFC-P1	13.3 ± 1	3.5 ± 0.32	96.2 ± 4.7
GFC-P2	12.4 ± 0.1	2.1 ± 0.1	114.7 ± 2.3
GFC-P3	6.6 ± 0.1	2.2 ± 0.6	175.4 ± 21
GFC-P4	14.7 ± 1.1	4.8 ± 0.6	452 ± 3.6
GFC-P5	12.2 ± 0.2	9.2 ± 1.0	417.2 ± 24.2
crude honey protein	11.3 ± 2.1	4.5 ± 0.4	288.4 ± 25
ibuprofen[a]	2.5 ± 0.6	16.9 ± 2.5	
N^G-monomethyl L-arginine acetate[b]			24.2 ± 0.8

[a]An anti-inflammatory drug used as standard for ROS inhibition (expressed in μg/mL). [b]A standard drug for NO inhibition (expressed in μg/mL).

immune system to fight invading microorganisms and a key feature of innate immune response. Macrophages are the most

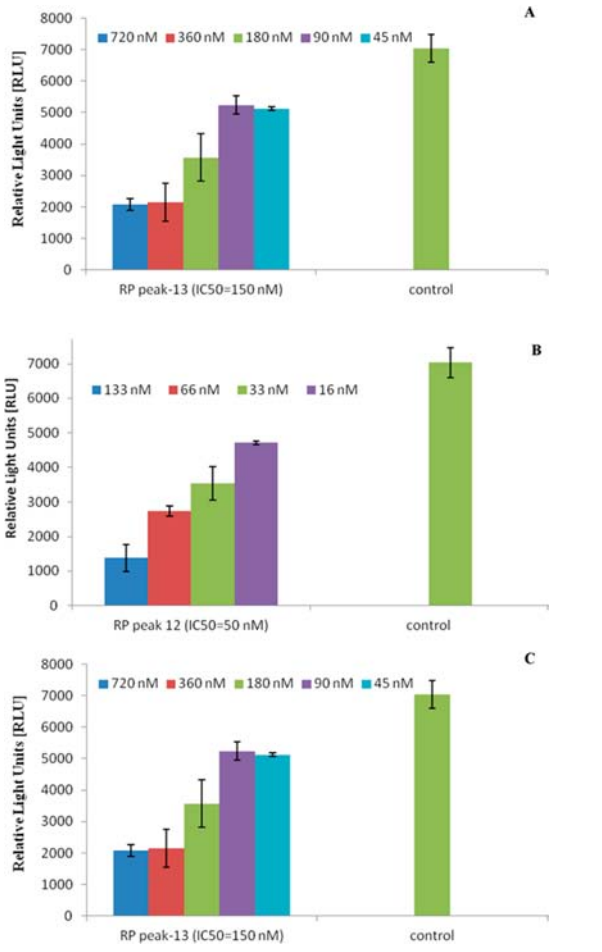

Figure 5. Effect of RPLC peaks RP-8 (A), RP-12 (B), and RP-13 (C) on reactive oxygen species production by human polymorph nuclear leukocytes. Control represents the cells activated with serum opsonized zymosan. Statistical analysis was applied using one-way ANOVA with significance levels <0.005, <0.01, and 0.05.

proficient phagocytes. The binding of bacterial molecules to receptors on phagocyte surface elicits them to engulf and wipe out the invaders through the professional killing mechanism that includes respiratory burst process. In the current study, we investigated the effect of honey proteins on receptor-mediated phagocytosis of red fluorescent coated polystyrene modified unopsonized latex beads by J774.2 mouse macrophage cells. Honey proteins/peptides exhibited significant inhibitory effect at 800 ng/mL (Figure 6A; Table 1). Peaks GFC-P3 and GFC-P4 presented the highest degree of inhibition on phagocytosis (70%), whereas the other honey protein peaks showed moderate inhibitory effects.

Phagocytosis of unopsonized particles involves a number of cell surface receptors including scavenger receptors (MARCO, SR-A, SR-B, SR-C, LOX-1, etc.) and nonscavenger receptors (β-integrin, mannose, CD-48, β-glucan, asialoglycoproteins receptors, etc.).[35] Among these macrophage receptors, MARCO has been extensively studied for its role in latex beads and other inert and unopsonized environmental particles phagocytosis.[36,37] In the present study, honey proteins might inhibit phagocytosis through interfering with one or more of these receptors. Hence, honey proteins exerted their anti-inflammatory potential by interfering with phagocytotic process.

dx.doi.org/10.1021/jf505131p | J. Agric. Food Chem. 2015, 63, 177−184

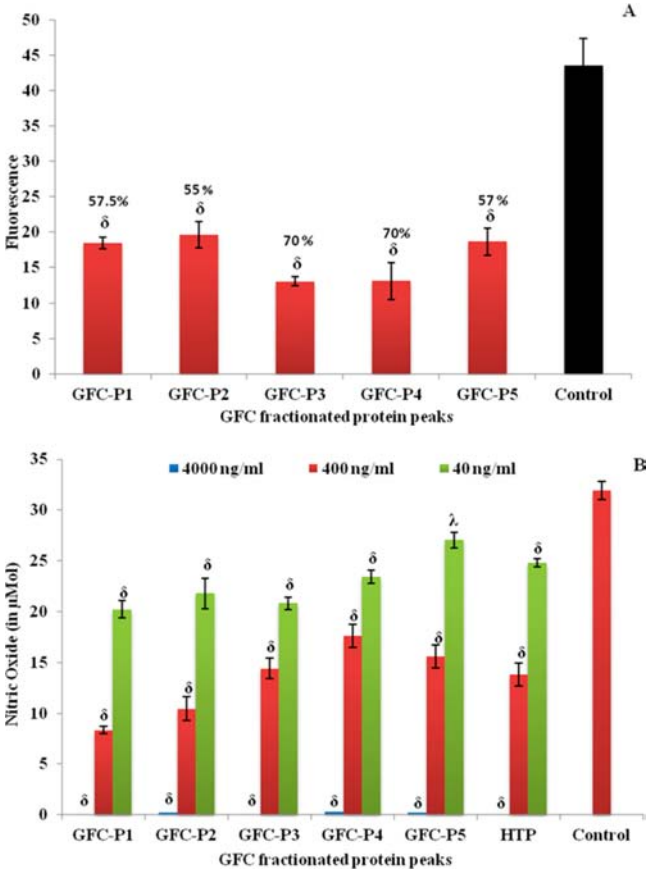

Figure 6. (A) Effect of honey protein fractions on phagocytosis. Macrophage phagocytosis was performed by using carboxylated modified latex beads and murine macrophage cell line J774.2. Control represents the cells with latex beads. The values on the bars show the percent inhibition of the phagocytosis by the respective protein fraction. Bar graph represents the statistical mean ± standard deviation. (B) Effect of honey protein fractions on NO production by J774.2 macrophages. Cells were activated by bacterial LPS for NO production. Control represents cells treated with LPS. Bar graph represents the statistical mean ± standard deviation. HTP referred as honey total proteins. One-way ANOVA was applied with significance levels <0.005, <0.01, and 0.05, which are represented as δ, λ, and ε, respectively.

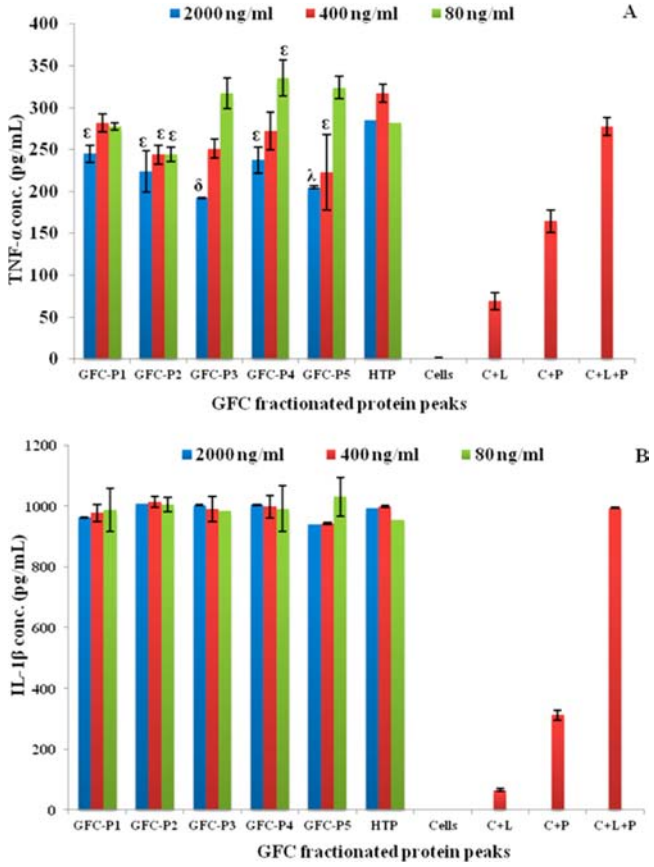

Figure 7. Effects of honey protein fractions on pro-inflammatory cytokine IL-1β (A) and TNF-α (B) production by human monocytic cells (THP-1 cells). Controls used during these assays were (a) cells only, (b) cells treated with LPS (C+L), (c) cells treated with PMA (C+P), and (d) cells treated with both LPS and PMA (C+L+P), which served as positive control. Bar graphs represent the statistical mean ± standard deviation. One-way ANOVA was applied with significance levels <0.005, <0.01, and 0.05, which are represented as δ, λ, and ε, respectively.

Effect of Honey Glycoproteins and Glycopeptides on Nitric Oxide Production. Effect of honey proteins on NO production by macrophages was also evaluated. Nitric oxide, the product of inducibe nitric oxide synthase, is a key modulator of immune response. The increase in NO production results in inflammation and progression of various chronic inflammatory diseases including rheumatoid arthritis, septic shock, inflammatory bowel disease, cardiovascular diseases, and several autoimmune disorders.[38] Nitric oxide inhibition is required in the treatment of many inflammatory disorders. Natural honey was reported to inhibit NO production in carrageenen-induced inflammatory rat model.[10,39] In the current study, the inhibitory effect of honey proteins on NO production was investigated using murine macrophage cells J774.2 that generate the inducible form of nitric oxide (Figure 6B; Table 1). All protein peaks showed a significant inhibition of NO production (IC_{50} = 130−450 ng/mL) by murine macrophage cells J774.2, which were stimulated with bacterial LPS. As a component of bacterial outer cell membrane, LPS serves as a potent activator of macrophage immune response. It binds to the macrophages through the CD14 and Toll-like receptors, which in turn activate NF-κB transcription factor. The NF-κB regulates a large number of genes involved in inflammation, cell proliferation, cell survival, and apoptosis.[40,41] Honey proteins might inhibit NO production by either binding to these receptor(s) or down-regulating the NF-κB gene expression.[42,43]

Effect of Honey Proteins and Peptides on Pro-inflammatory Cytokine Production. We further investigated the effect of honey proteins on pro-inflammatory cytokine production using THP-1 human monocytic cells. Pro-inflammatory cytokines, mainly TNF-α and IL-1β, play a central role in the establishment of inflammatory processes. Honey has been shown to stimulate the production of TNF-α, IL-1β, TGF-β, and matrix metalloproteinases (MMP-9) by human monocytes[12] and keratinocytes.[44] Moreover, the protein content of the honey glycoproteins was found to be responsible for stimulation of pro-inflammatory cytokine production.[22] In the current study, honey proteins were tested at different concentrations for their effects on the production of TNF-α and IL-1β by human monocyte cell line (THP-1 cells). For cytokine production, these cells were first differentiated into macrophages by PMA and then activated by LPS for the

dx.doi.org/10.1021/jf505131p | J. Agric. Food Chem. 2015, 63, 177−184

production of cytokines. In our experiments, honey proteins did not affect the production of IL-1β at the concentrations tested (Figure 7B) but exerted significant effects on TNF-α production (Figure 7A). We found that the production of pro-inflammatory cytokine TNF-α production was 10−20% down-regulated by peak GFC-P2. Peaks GFC-P3−GFC-P5 showed suppression of TNF-α production at higher protein concentration (2000 ng/mL) and stimulation at lower concentration (80 ng/mL). These results pointed out the involvement of TNF-α in the immunomodulatory activity of honey proteins and peptides. The high molecular mass glycoproteins/proteoglycans of honey might exert their effects by binding with cell surface receptors followed by activation of signaling pathway(s), whereas (glyco)peptides in peak GFC-P5 might be effective by interaction with intracellular receptor(s) after an internalization mechanism.

■ ASSOCIATED CONTENT

Ⓢ Supporting Information

Supplementary Figures 1−3. This material is available free of charge via the Internet at http://pubs.acs.org.

■ AUTHOR INFORMATION

Corresponding Author

*(M.K.A.) Mail: International Center for Chemical and Biological Sciences, University of Karachi, Karachi 75270, Pakistan. Phone: +9221-111222292, ext. 236. Fax: +9221-3498018. E-mail: kamran.azim@iccs.edu or mkamranazim@yahoo.co.uk.

Author Contributions

‖M.A.M. and N.D. contributed equally.

Funding

We are grateful to the Higher Education Commission, Islamabad, Pakistan, for financial support.

Notes

The authors declare no competing financial interest.

■ REFERENCES

(1) Bogdanov, S.; Jurendic, T.; Sieber, R.; Gallmann, P. Honey for nutrition and health: a review. *J. Am. Coll. Nutr.* **2007**, *27*, 677−689.

(2) Molan, P. Why honey is effective as a medicine. 2. The scientific explanation of its effects. *Bee World* **2001**, *82*, 22−40.

(3) Azim, M. K.; Sajid, M. Evaluation of nematocidal activity in natural honey. *Pak. J. Bot.* **2009**, *41*, 3261−3264.

(4) Sajid, M.; Azim, M. K. Characterization of the nematicidal activity of natural honey. *J. Agric. Food Chem.* **2012**, *60*, 7428−7434.

(5) Ahmed, A.; Azim, M. K.; Mesaik, M. A.; Nazimuddin; Khan, R. A. Natural honey modulates physiological glycemic response compare to stimulated honey and D-glucose. *J. Food Sci.* **2008**, *73*, 165−167.

(6) Ahmed, A.; Khan, R. A.; Mesaik, M. A. Anti inflammatory effect of natural honey on bovine thrombin induced oxidative burst in phagocytes. *Phytother. Res.* **2009**, *23*, 801−808.

(7) Molan, P. C. Honey as an antimicrobial agent. In *Bee Products: Properties, Applications and Apitherapy*; Mizrahi, A, Lensky, Y., Eds.; Plenum Press: New York, 1997; pp 27−37.

(8) Mesaik, M. A.; Azim, M. K.; Mohiuddine, S. Honey modulates oxidative burst in professional phagocytes. *Phytother. Res.* **2008**, *22*, 1404−1408.

(9) Azim, M. K.; Perveen, H.; Mesaik, M. A.; Simjee, S. U. Antinociceptive activity of natural honey in thermal-nociception in mice. *Phytother. Res.* **2007**, *21*, 194−197.

(10) Owoyele, B. V.; Adenekan, O. T.; Soladoye, A. O. Effect of honey on inflammation and nitric oxide production in Wistar rats. *J. Chinese Integr. Med.* **2011**, *9*, 447−452.

(11) Tonka, A.; Cooper, R. A.; Price, A. J.; Molan, P. C.; Jones, K. P. Stimulation of TNF-α release in monocytes by honey. *Cytokines* **2001**, *14*, 240−242.

(12) Tonks, A. J.; Cooper, R. A.; Jones, K. P.; Blair, S.; Parton, J.; Tonks, A. Honey stimulates inflammatory cytokine production from monocytes. *Cytokines* **2003**, *21*, 242−247.

(13) Tonks, A. J.; Dudley, E.; Porter, N. G.; Parton, J.; Brazier, J.; Smith, E. L.; Tonks, A. 5.8-kDa component of manuka honey stimulate immune cells via TLR4. *J. Leukocyte Biol.* **2007**, *82*, 1147−1155.

(14) Fukuda, M.; Kobayashi, K.; Hirono, Y.; Miyagawa, M.; Ishada, T.; Ejiogu, E. C.; Sawai, M.; Pinkerton, K. E.; Takeuchi, M. Jungle honey enhances immune function and antitumor activity. *Evidece-Based Complement. Altern. Med.* **2011**, No. 908743, DOI: 10.1093/ecam/nen086.

(15) Al-Waili, N. S.; Haq, A. Effect of honey on antibody production against thymus-dependent and thymus-independent antigens in primary and secondary immune responses. *J. Med. Food* **2004**, *7*, 491−494.

(16) Duddukuri, G. R.; Rao, D. N.; Rao, A. R. Suppressive effect of honey on antigen/mitogen stimulated murine T cell proliferation. *Pharm. Biol.* **2002**, *40*, 39−44.

(17) Ahmed, A.; Khan, R. A.; Azim, M. K.; Saeed, S. A.; Mesaik, M. A.; Ahmed, S.; Imran, I. Effect of natural honey on human platelets and blood coagulation proteins. *Pak. J. Pharm. Sci.* **2011**, *24*, 389−397.

(18) Mohammed, S. E. A.; Azim, M. K. Characterization of natural honey protein: Implication for the floral and geographical origin of honey. *Int. J. Food Sci. Technol.* **2012**, *47*, 362−368.

(19) Won, S.; Li, C. Y.; Kim, J.; Rhee, H. Immunological characterization of honey major proteins and its application. *Food Chem.* **2009**, *113*, 1334−1338.

(20) Slimúth, J. Some properties of the main protein of honeybee (*Apis mellifera*) royal jelly. *Apidologie* **2001**, *32*, 69−80.

(21) Hayashi, T.; Takamatsu, N.; Nakashma, T.; Arita, T. Immunological characterization of honey proteins and identification of MRJP 1 as an IgE-binding protein. *Biosci., Biotechnol., Biochem.* **2011**, *75*, 556−560.

(22) Majtan, J.; Kovacova, E.; Bilikova, K.; Simuth, J. The immunostimulatory effect of the recombinant apalbumin-1 major honeybee royal jelly protein on TNF-α release. *Int. Immunopharmacol.* **2006**, *6*, 269−278.

(23) Steinhorn, G.; Sims, I. M.; Carnachan, S. M.; Carr, A. J.; Schlothauer, R. Isolation and characterisation of arabinogalactan-proteins from New Zealand kanuka honey. *Food Chem.* **2011**, *128*, 949−956.

(24) Showalter, A. M. Arabinogalactan-proteins: structure, expression and function. *CMLS, Cell. Mol. Life Sci.* **2001**, *58*, 1399−1417.

(25) Gronhaug, T. E.; Ghildyal, P.; Barsett, H.; Michaelsen, T. E.; Morris, G.; Diallo, D.; Inngjerdingen, M.; Paulsen, B. S. Bioactive arabinogalactans from the leaves of *Opilia celtidifolia* Endl. ex Walp. (Opiliaceae). *Glycobiology* **2010**, *20*, 1654−1664.

(26) Lowry, O. H.; Rosebrough, N. J.; Farr, A. L.; Randall, R. J. Protein measurement with the Folin phenol reagent. *J. Biol. Chem.* **1951**, *193*, 265−275.

(27) Mesaik, M. A.; Rahat, S.; Khan, K. M.; Zia-Ullah; Choudhary, M. I.; Murad, S.; Ismail, Z.; Atta-ur-Rehman; Ahmed, A. Synthesis and immunomodulatory properties of selected oxozolon derivative. *Bioorg. Med. Chem.* **2004**, *12*, 2049−2057.

(28) Inoue, S.; Itagaki, S. I.; Amano, F. Intracellular killing of *Listeria monocytogenes* in the J774.1 macrophage-like cell line and the lipopolysaccharide (LPS)-resistant mutant LPS1916 cell line defective in the generation of reactive oxygen intermediates after LPS treatment. *Infect. Immun.* **1995**, *63*, 1876−1886.

(29) Foukas, L. C.; Katsoulas, H. L.; Paraskevopoulou, N.; Metheniti, A.; Lambropoulou, M.; Marmaras, V. J. Phagocytosis of *Escherichia coli* by insect hemocytes requires both activation of the ras/mitogen-activated protein kinase signal transduction pathway for attachment and b3 integrin for internalization. *J. Biol. Chem.* **1998**, *273*, 14813−14818.

(30) Mesaik, M. A.; Jabeen, A.; Halim, S. A.; Begum, A.; Khalid, A. S.; Asif, M.; Choudhary, M. I. In silico and in vitro immunomodulatory studies on compounds of *Lindelofia stylosa*. *Chem. Biol. Drug Design* **2012**, *79*, 290−299.
(31) Iglesias, M. T.; Martin-Alvarez, P. J.; Polo, M. C.; Lorenzo, C. D.; Pueyo, E. Protein analysis of honey by fast protein liquid chromatography: application to differentiate floral and honeydew honeys. *J. Agric. Food Chem.* **2006**, *21*, 8322−8327.
(32) Mohammed, S. E. A.; Sajid, M.; Azim, M. K. Isolation of 62 kDa protein with antioxidant properties from natural honey. *J. Chem. Soc. Pak.* **2014**, *36*, 453−456.
(33) Guzik, T.; Korbut, R.; Adamek-Guzik, T. Nitric oxide and superoxide in inflammation. *J. Physiol. Pharmacol.* **2003**, *54*, 469−487.
(34) Nordenfelt, P.; Tapper, H. Phagosome dynamics during phagocytosis by neutrophils. *J. Leukocyte Biol.* **2011**, *90*, 271−284.
(35) Palecanda, A.; Kobzik, L. Receptors for unopsonized particles: the role of alveolar macrophage scavenger receptors. *Curr. Mol. Med.* **2001**, *1*, 589−595.
(36) Arredouani, M. S.; Palecanda, A.; Koziel, H.; Huang, Y. C.; Imrich, A.; Sulahian, T. H.; Kobzik, L. MARCO is the major binding receptor for unopsonized particles and bacteria on human alveolar macrophages. *J. Immunol.* **2005**, *175*, 6058−6064.
(37) Arredouani, M.; Yang, Z.; Ning, Y.; Qin, G.; Soininen, R.; Tryggvason, K.; Kobzik, L. The scavenger receptor MARCO is required for lung defense against pneumococcal pneumonia and inhaled particles. *J. Exp. Med.* **2004**, *200*, 267−272.
(38) Grisham, M. B.; Jourd'heuil, D.; Wink, D. A. Physiological chemistry of nitric oxide and its metabolites: implication in inflammation. *Am. J. Physiol. Gastrointest. Liver Physiol.* **1999**, *274*, G315−G321.
(39) Kassim, M.; Yusoff, K. M.; Ong, G.; Sekaran, S.; Yusof, M. Y.; Mansor, B. M. Gelam honey inhibits lipopolysaccharide-induced endotoxemia in rats through the induction of heme oxygenase-1 and the inhibition of cytokines, nitric oxide, and high-mobility group protein B1. *Fitoterapia* **2012**, *83*, 1054−1059.
(40) Meng, F.; Lowell, C. A. Lipopolysaccharide (LPS)-induced macrophage activation and signal transduction in the absence of Src-family kinases Hck, Fgr, and Lyn. *J. Exp. Med.* **1997**, *185*, 1661−1670.
(41) Sharif, O.; Bolshakov, V. N.; Raines, S.; Newham, P.; Perkins, N. D. Transcriptional profiling of the LPS induced NF-κB response in macrophages. *BMC Immunol.* **2007**, *8*, 1.
(42) Garg, A.; Agarwal, B. B. Nuclear transcription factor-κB as a target for cancer drug development. *Leukemia* **2002**, *16*, 1053−1068.
(43) Morgan, M. J.; Liu, Z. G. Crosstalk of reactive oxygen species and NF-κB signaling. *Cell Res.* **2010**, *21*, 103−115.
(44) Majtan, J.; Kumar, P.; Majtan, T.; Walls, A. F.; Klaudiny, J. Effect of honey and its major royal jelly protein 1 on cytokine and MMP-9 mRNA transcript in human keratinocytes. *Exp. Dermatol.* **2010**, *19*, e73−e79.

JOURNAL OF AGRICULTURAL AND FOOD CHEMISTRY

Article

pubs.acs.org/JAFC

A Novel Triterpenoid Isolated from Apple Functions as an Anti-mammary Tumor Agent via a Mitochondrial and Caspase-Independent Apoptosis Pathway

Aimin Qiao,[†] Yihai Wang,[§] Limin Xiang,[§] Chunhua Wang,[§] and Xiangjiu He*[,§]

[†]School of Biosciences and Biopharmaceuticals and [§]School of Pharmacy, Guangdong Pharmaceutical University, Guangzhou 510006, China

ABSTRACT: A novel triterpenoid, named 3β-*trans*-cinnamoyloxy-2α-hydroxy-urs-12-en-28-oic acid (CHUA), was one of the main components of apple peels and showed potent in vitro antitumor activity against human tumor cells. In vivo antitumor experiments showed that CHUA could significantly inhibit the growth of mammary tumor in a nude mouse xenograft model at a dose of 50 mg/kg/day without body weight loss and mortality. In vitro, CHUA could induce apoptosis in MDA-MB-231 cells through the detection of DNA fragments and LDH activity. Simultaneously, mitochondrial transmembrane potential was markedly reduced and the release of cytochrome *c* was increased after CHUA treatment. It also up-regulated the expression ratio of mitochondrial Bax/Bcl-2 regulated by SIRT1 and p53. Interestingly, z-VAD-fmk and z-DEVD-fmk augmented cell death after CHUA treatment. Other protease(s) different from caspase-3 might be responsible for the degradation of PARP. These results suggested that the pro-apoptotic activity of CHUA may be adjusted by mitochondrial and caspase-independent pathways.

KEYWORDS: *apple, caspase-3-independent apoptosis, MDA-MB-231 cells, 3β-trans-cinnamoyloxy-2α-hydroxy-urs-12-en-28-oic acid*

INTRODUCTION

Apple (*Malus pumila*) is one of the most widely cultivated tree fruits. Epidemiological studies have shown that the consumption of apples may be related to a significantly reduced risk of many diseases such as carcinogenesis,[1,2] cardiovascular disease,[3] cognitive impairment,[4] acute inflammatory disease,[5] and diabetes.[6] Moreover, apple extracts have been shown to protect against gastrointestinal mucosa alterations[7] and have antitumor activity. Therefore, apples as an important part of consumption of plant foods could be beneficial for human health.

The bioactive compounds and antitumor activities of apple were investigated in our previous study. Twenty-two triterpenoids, including eight novels, have been purified from the peels of Red Delicious apple. It was found that the triterpenoids of apples exhibited pronounced in vitro antitumor activities and may be responsible for the antitumor activities of whole apples.[8,9] The total triterpenoids (ATT) of apples showed antitumor activity and could initiate apoptosis of breast cancer cells through mitochondrial pathway.[10]

Apoptosis is a fundamental cellular response, which plays a crucial role in regulating tissue homeostasis by removing unused cells. It is a well conserved cell death pathway executed by caspases including initiator and executioner. Caspases, a family of cysteine proteases, have the main function as central regulators of cell death during apoptosis.[11,12]

Cell apoptosis is mainly induced by intrinsic and extrinsic pathways involving either mitochondria or death receptors. The mitochondria-dependent apoptosis pathway is mainly regulated by pro-apoptotic factor Bax and the anti-apoptotic factor Bcl-2 family. The balance between Bax and Bcl-2 or Bcl-xL in the mitochondrial may determine cell survival or death. These proteins can also promote mitochondrial outer membrane permeabilization by regulating Mfn1, a GTPase involved in mitochondrial fusion.[13,14]

p53, a known tumor suppressor, induces cell cycle arrest and apoptosis related to DNA damage. It can also activate its downstream target genes, including Bcl-2 and Bax, for apoptosis. SIRT1 is a highly conserved nicotinamide adenine dinucleotide (NAD)-dependent histone deacetylase that plays an important role in promoting cell survival through regulating p53 in response to DNA damage.[15,16]

A new compound named 3β-*trans*-cinnamoyloxy-2α-hydroxy-urs-12-en-28-oic acid (CHUA) was isolated and identified from apple in our previous study.[8] CHUA is the one of main triterpenoids of apple and has been shown to significantly inhibit the growth of a number of malignant cell lines in a former preliminary study, especially breast cancer cells. In the present work, CHUA was extracted and purified from red apple, and its antitumor activities in vivo were investigated using the nude mouse xenograft model. The proposed mechanisms of CHUA-induced MDA-MB-231 cell apoptosis were studied through mitochondrial and caspase-independent pathways in vitro.

MATERIALS AND METHODS

Plant Material and Reagents. Red Fuji apples, which were harvested in October 2009, were bought from Wuhan Shahu Fruits Market (Wuhan, China).

All analytical and HPLC grade chemicals were purchased from Mallinckrodt Chemicals (Phillipsburg, NJ, USA). D101 macroporus resin was purchased from Xi'an Lanxiao Resin Corp. Ltd. (Xi'an,

Received: August 4, 2014
Revised: December 18, 2014
Accepted: December 18, 2014
Published: December 18, 2014

ACS Publications © 2014 American Chemical Society

DOI: 10.1021/jf5053546
J. Agric. Food Chem. 2015, 63, 185−191

China). Cell culture medium, Dulbecco's modified Eagle medium (DMEM), and fetal bovine serum (FBS) were products of Gibco Life Technologies (Grand Island, NY, USA). Bax, ICAD, PARP, cytochrome *c*, p53, Bcl-2, Bcl-X_L, SIRT1, and secondary antibody were bought from Santa Cruz Biotechnology (Santa Cruz, CA, USA). Z-Ile-Glu-Thr-Asp-FMK (Z-IETD-FMK) and Z-Leu-Glu(OMe)-His-Asp(OMe)-FMC (Z-LEHD-FMK) were purchased from ICN (Aurora, OH, USA). Z-Asp(O-Me)-Glu(O-Me)-Val-Asp(O-Me) fluoromethyl ketone (Z-DEVD-FMK) and benzylocarbonyl-Val-Ala-Asp-fluoromethyl ketone (Z-VAD-FMK) were purchased from Calbiochem (Gibbstown, NJ, USA). RNase A, rhodamine 123, proteinase K, and MTT were purchased from Sigma-Aldrich Chemical Co. (St. Louis, MO, USA).

Extraction and Purification of CHUA from Apples. The fresh apple peels of red Fuji variety (20 kg) were dried under vacuum at 60 °C and then smashed into powder, which was refluxed using 10 volumes of 95% ethanol for 2 h twice. The solvent was recovered under vacuum at 45 °C, and the residue was suspended in 2 L of water and subjected to a D101 macroporus resin column (100 × 1500 mm). The column was eluted with 10 L of 60% ethanol and then with 10 L of 95% ethanol, respectively. The fraction of 95% ethanol elution was concentrated and dried, getting the total triterpenoids (96.0 g). The total triterpenoids (92.0 g) was subjected to a silica gel column (230–400 mesh, 420 × 80 mm), gradiently eluted with CH_2Cl_2/MeOH (the CH_2Cl_2/MeOH ratios were from 100:0 to 0:100). The CH_2Cl_2/MeOH (50:1) elution (5.1 g) was purified by a Sephadex LH-20, followed by a HPLC (250 × 22 mm, 5 μm, Alltima C_{18}) using 82% methanol (adding 0.1% CF_3COOH, pH 2.0) as mobile phase, and CHUA (810.2 mg) were obtained.

The purity of CHUA was determined according to a HPLC method using a Waters HPLC system (equipped with a 600 pump and PDA detector) (Milford, MA, USA). The column was LiChrospher 100 RP-100e 5 μm (4.6 × 250 mm), and detection was at 210 nm. The mobile phase was $CH_3CN/H_2O/CF_3COOH$ (80:20:0.1) with a flow rate at 1.0 mL/min. The column temperature was set at 40 °C.

Nude Mouse Xenograft Model. Six-week old female nude mice (Balb/c-nu/nu) were bought from Guangdong Medical Experimental Animal Center. All animal experiment protocols were confirmed by the Animal Ethics Committee of Wuhan University. CHUA was dissolved in DMSO. Mice were randomly allocated to two groups with 10 animals per group. One hundred microliters of exponential MDA-MB-231 cells (3×10^6 cells) was injected subcutaneously into the backs of mice. When tumors become apparent after 9 days, 100 μL of DMSO containing CHUA was administered intraperitonelly to the therapy group at a dose of 50 mg/kg/day; the vehicle group was treated by only 100 μL of DMSO in the same way. Mice were sacrificed on day 10 post-CHUA treatment, and the tumor tissues were collected and weighed. The length and width of the tumors were measured, and the tumor volume was calculated using the following equation: volume = (length × width^2)/2.

Antiproliferative Effects of CHUA against Cancer Cell Line. Human breast cancer (MDA-MB-231, MCF-7), human liver cancer (HepG2), human colon cancer (Caco-2), human cervical cancer (HeLa), and human lung adenocarcinoma (A549) cell lines were purchased from ATCC. The MTT method was utilized to evaluate the bioactivity of CHUA. Briefly, tumor cells were cultured in DMEM with 10% FBS and maintained at 37 °C in 5% CO_2. A total of 2.5×10^4 cells were seeded in each well of a 96-well plate before the experiment day. After incubation overnight, the cells were treated by various concentrations of CHUA for 48 h. Cell viability was determined by the MTT assay. Experiments were performed in triplicate for each sample.

DNA Ladder Assay. DNA extraction and electrophoresis were performed as described previously.[17] Briefly, MDA-MB-231 cells (2×10^5) were seeded into a 100 cm dish for 24 h before the experimental day, and then the cells treated by 3.5 μM CHUA at indicated times were incubated with 0.25% trypsin for 10 min at 37 °C. The enzymatic digestion was terminated by mixing the suspension with an equal volume of DMEM supplemented with 10% FBS. Then floating cells were collected by centrifugation at 1000*g* for 10 min. The cell pellet was washed twice in ice-cold PBS. To detect the DNA fragments, an apoptotic DNA Laddering Kit (Shanghai Xinle Institute of Biotechnology, China) was used according to the manufacturer's protocol. The DNA fragments were separated by 2% agarose gel containing 0.2 mg/mL EB. The gel was photographed using an ultraviolet gel documentation system (UVI Tec Ltd., Cambridge, UK).

Lactate Dehydrogenase (LDH) Activity-Based Cytotoxicity Assays.[17] The MDA-MB-231 cells (2×10^5) were seeded into a 6-well plate for 24 h before CHUA was added. On the next day, the prepared cells were treated by 3.5 μM CHUA at different time courses or the cells were treated with or without z-VAD-fmk, z-DEVD-fmk, z-IETD-fmk, z-LEHD-fmk at given concentrations for 1 h and then treated with CHUA for 24 h. After treatment, floating cells were collected from cultured medium by centrifugation at 4 °C for 5 min. The LDH released in the cultured supernatant was used as an index of necrotic death, the LDH content in the cell pellets lysis was used for the apoptotic death, and the LDH present in the adherent viable cells was used as intracellular LDH. The LDH activities of the cell lysis and the cultured supernatant were measured according to the reference with a slight modification.

Measurement of Mitochondrial Transmembrane Potential ($_\Delta\Psi_m$). To measure the mitochondrial transmembrane potential ($_\Delta\Psi_m$), MDA-MB-231 cells (2×10^5) were seeded into a 100 cm dish for 24 h before the experimental day, and then the cells treated by 3.5 μM CHUA at the indicated time were incubated with 0.25% trypsin for 10 min at 37 °C. The enzymatic digestion was terminated by mixing the suspension with an equal volume of DMEM. The cells were collected by centrifugation (240*g*) at 4 °C for 5 min, then the cells were gently washed with 1 mL of cold PBS one time, and the cells were resuspended in rhodamine 123 staining solution (1 μg/mL) in the dark for 30 min. The samples were analyzed by flow cytometry.

Effects of Caspase Inhibitor on MDA-MB-231 Cells Treated by CHUA. The effects of caspase inhibitor on MDA-MB-231 cells were measured by MTT assay described above. The cultured cells were seeded in a 96-well plate with a density of 2.5×10^4 cells/well without or with z-VAD-fmk, z-DEVD-fmk, z-LEHD-fmk, and z-IETD-fmk at given concentrations for 1 h and then treated with 3.5 μM CHUA for another 24 h. After the treatment, the cell viability was measured by MTT assay.

Western Blot Analysis. MDA-MB-231 cells were treated with 3.5 μM CHUA for different time courses as indicated. All of the cells were harvested according to the method described by Laetitia et al.[18] Briefly, the cells were gently washed with ice-cold PBS and lysated by RIRA buffer containing proteinase inhibitor. Protein concentrations were determined by the Bio-Rad DC protein assay. Fifteen mirograms of proteins for each channel was separated by 12% SDS-PAGE and transferred to a nitrocellulose membrane. The membranes were incubated with appropriately diluted primary antibodies, followed by horseradish peroxidase-conjugated secondary antibodies against the corresponding species. Labeling was detected using the ECL system (Amersham Biosciences).

Statistical Analysis. Experimental values were expressed as the mean ± SEM. The differences between groups were assessed by one way-analysis of variance followed by multiple comparisons. Statistical significance is expressed as follows: *, $p < 0.05$; **, $p < 0.01$.

RESULTS AND DISCUSSION

Structure Identification of CHUA. CHUA was a white powder. The ESI-MS gave the $[M - H]^-$ ion at *m/z* 601, and its molecular formula was drawn as $C_{39}H_{54}O_5$ from HR-MS and ^{13}C NMR. In its ^1H NMR, there were three groups of characteristic signals of monosubstituted benzene, which showed at 8.12 (2H, br d, *J* = 8.6 Hz), 7.53 (2H, br t, *J* = 8.6 Hz), and 7.17 ppm (H, br t, *J* = 8.6 Hz), respectively. There was a pair of *trans*-conjugated olefinic protons, which appeared at 8.00 (H, d, *J* = 16.0 Hz) and 6.65 ppm (H, d, *J* = 16.0 Hz). There were 12 sp^2-hybrid carbons in the lower field of ^{13}C NMR, which included 2 carbonyl carbons. From its ^1H and ^{13}C

DOI: 10.1021/jf5053546
J. Agric. Food Chem. 2015, 63, 185–191

NMR and DEPT spectra, a *trans*-cinnamic acid part could be deduced. In the ^{13}C NMR spectra, there were a carbonyl signal at 180.1 ppm and two olefinic carbons at 139.7 and 126.1 ppm, which implied there was a carbon−carbon double bond in the molecule. The results showed that CHUA was a triterpene possessing an ursane skeleton. Compared with our former study,[8] the triterpenoid was identified as 3β-*trans*-cinnamoyloxy-2α-hydroxy-urs-12-en-28-oic acid (CHUA), which was a novel triterpenoid isolated from apple. The chemical structure of CHUA is shown in Figure 1.

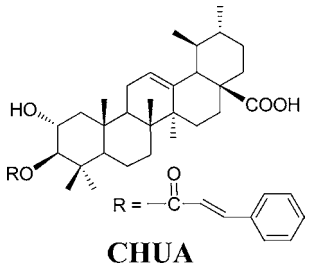

Figure 1. Chemical structure of CHUA.

The purity of CHUA was 97.3 ± 5.1%, determined by HPLC method. CHUA was used for in vivo and in vitro antitumor studies. It was dissolved in DMSO, and the stock solution was diluted with cell culture medium to keep the concentration of DMSO <0.1%.

Effect of CHUA on Cell Growth and Proliferation of Human Tumor Cells. To examine the in vitro antitumor effects of CHUA, a series of human tumor cell lines were treated with various doses of CHUA (1, 2, 4, 8, 16, and 32 μM) for 48 h, and cell viability was assayed by MTT method. The inhibitory rates of CHUA against human tumor cell lines are shown in Figure 2A. The results suggested that CHUA significantly inhibited the cell growth and proliferation of MDA-MB-231, MCF-7, and A549 cell lines with IC_{50} values of 2.57 ± 0.11, 5.45 ± 0.23, and 6.37 ± 0.29 μM, respectively. In particular, it should be noted that CHUA achieved the best inhibitory effect for MDA-MB-231 cell lines among the six tumor cell lines. On the basis of these results, MDA-MB-231 was selected to investigate the in vivo antitumor effects and mechanisms of CHUA in subsequent research.

In Vivo Antitumor Activity. CHUA was tested for anti-mammary tumor activity in nude mice on the basis of its potent inhibitory activity against the MDA-MB-231 cell line in vitro. To evaluate the in vivo antitumor effect of CHUA, growth inhibition of MDA-MB-231 xenografts in nude mice was further investigated. Administration of CHUA resulted in significant growth suppression of MDA-MB-231 xenografts compared to the control group. As shown in Figure 2B, tumor growth in the CHUA-treated group was significantly inhibited compared to the control group. The average tumor weight in the CHUA-treated group was significantly lighter than that in the control group ($p < 0.01$) at the end of the experiment (Figure 2C). Also, there were no statistical significant differences in body weights between the CHUA-treated and control groups, indicating a low general toxicity of CHUA.

Characterization of CHUA-Induced Cell Death in MDA-MB-231 Cells. To determine the characteristics of CHUA-induced MDA-MB-231 cell death, DNA fragmentation was examined. DNA fragmentation was obviously observed in CHUA-treated MDA-MB-231 cells (Figure 3).

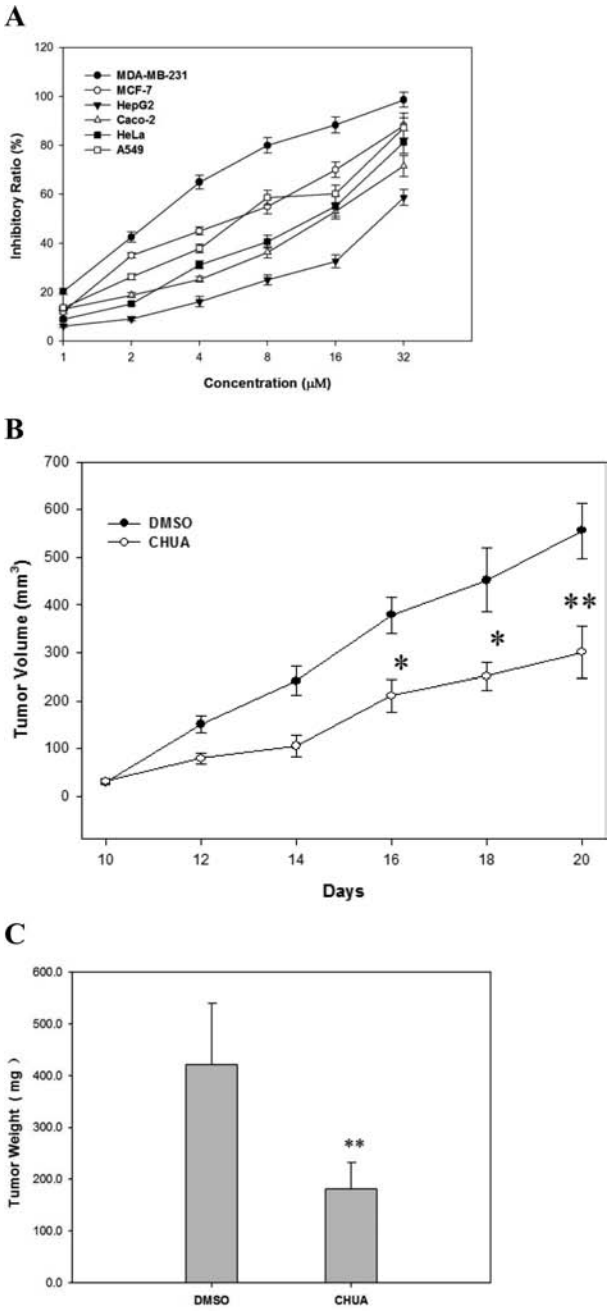

Figure 2. In vitro and in vivo antitumor effects of CHUA. (A) Antiproliferative effects of CHUA against human tumor cell lines. Different tumor cells were treated by various concentrations of CHUA for 48 h, and then the MTT method was used to evaluate the cell viability. The values presented are the mean ± SEM (n = 3). (B) Growth curves of subcutaneous tumors in mice treated with CHUA or DMSO. After succeeding in making this model, the mice were treated with 50 mg/kg/day CHUA 100 μL or the same volume of DMSO. Tumor size was measured every day after treatment. The values presented are the mean ± SEM (n = 10 in each group). (*) $p < 0.05$; (**) $p < 0.01$. (C) Weights of tumors in mice after 10 days of drug treatments. (**) $p < 0.01$. After the last day's drug treatment, the mice were sacrificed and the burdened tumors were removed carefully, and weighed. The values presented are the mean ± SEM (n = 10 in each group).

In the LDH activity assay, the ratio of apoptotic MDA-MB-231 cells increased from 12.0 to 41.1% in a time-dependent manner. The maximal apoptosis happened at 36 h and then

DOI: 10.1021/jf5053546
J. Agric. Food Chem. 2015, 63, 185−191

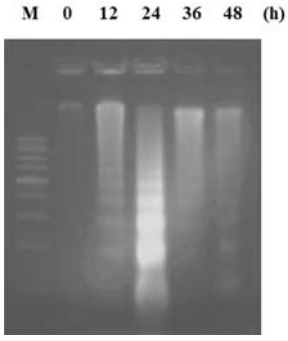

Figure 3. CHUA-induced DNA fragmentation of MDA-MB-231 cells. The cells were treated with 3.5 μM CHUA at the indicated time. The DNA purified from each sample was separated by 2% agarose gel electrophoresis to detect the DNA ladder after drug treatment.

reduced quickly; however, the necrosis ratio continued to increase (Figure 4).

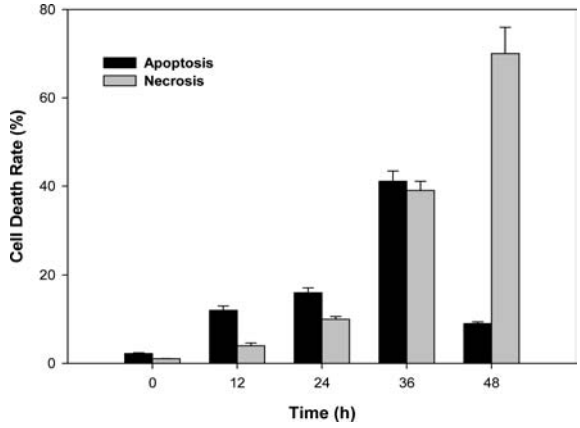

Figure 4. Apoptotic and necrotic ratios in CHUA-treated MDA-MB-231 cells. The cells were treated with 3.5 μM CHUA at the indicated time. The ratios of LDH released from floating dead cells and the culture medium were used to distinguish the proportion of apoptotic and necrotic cells. Results are represented as the mean ± SEM (n = 3).

Mitochondrial Transmembrane Potential ($\Delta\Psi_m$) Was Markedly Reduced by CHUA Treatment in MDA-MB-231 Cells. Lots of apoptotic signals are initiated by mitochondria to transduce cell death. Depletion of the mitochondria membrane potential ($\Delta\Psi_m$) is an early marker of the apoptotic process. Changes in the mitochondrial transmembrane potential in CHUA treated with MDA-MB-231 cells were analyzed by flow cytometry using the dye rhodamine 123, a specific fluorescent probe for analysis of mitochondrial transmembrane potential. Compared with the control group, the mitochondrial transmembrane potential was reduced after CHUA treatment correlated with time increasing, and the maximal decrease happened at 36 h (Figure 5), implying that CHUA-induced MDA-MB-231 cell apoptosis through mitochondrial pathway.

Enhanced Bax/Bcl-2 Expression Ratio in CHUA-Treated MDA-MB-231 Cells. It is well-known that the mitochondrial pathway is regulated by Bcl-2 family members to trigger downstream signaling. To understand the potential antitumor mechanism, the apoptosis-related proteins were detected using Western blot method. The data showed that the expression of pro-apoptotic Bax and the release of cytochrome c began to increase in response to CHUA treatment, whereas the expression levels of anti-apoptotic Bcl-2 and Bcl-X_L were down-regulated after 12 h of treatment. These results indicated that CHUA induced apoptosis, resulting in an increased ratio of Bax/Bcl-X_L, accompanied the translocation of cytochrome c from the mitochondria (Figure 6).

Expressions of SIRT1 and p53 in CHUA-Induced MDA-MB-231 Cell Death. SIRT1 can bind p53 and deacetylates its C-terminus, resulting in inhibition of p53- or Bax-mediated apoptosis. To test whether SIRT1 and p53 take part in CHUA-induced MDA-MB-231 cell death, Western blot analysis was used to detect the expressions of SIRT1 and p53. As shown in Figure 6, the expression level of SIRT1 began to attenuate after CHUA treatment for 24 h. As expected, p53 expression was up-regulated in a time-dependent manner.

Caspase Protected against CHUA-Induced MDA-MB-231 Cell Death. Many studies have shown that caspases are required in apoptosis. In this study, it was found that the inhibitor of pan-caspase (z-VAD-fmk) and the inhibitor of

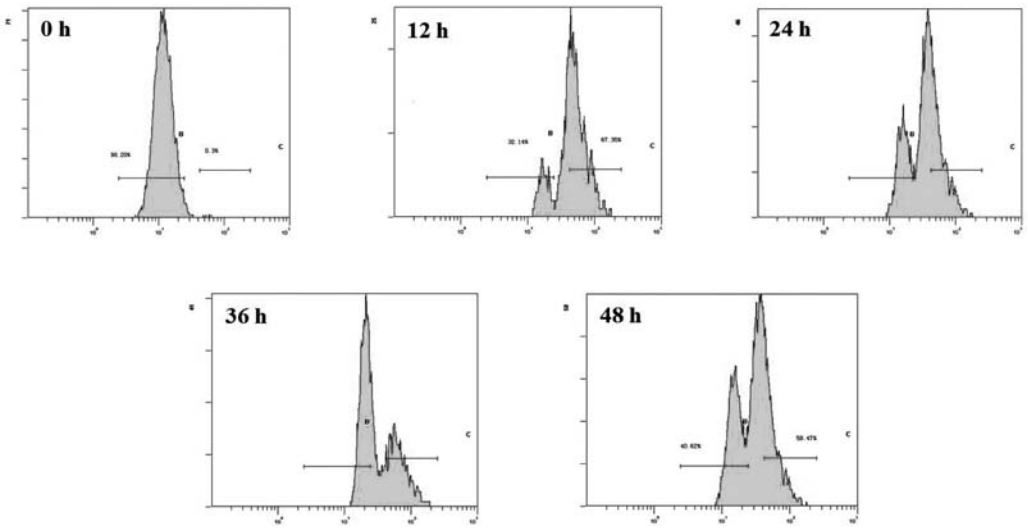

Figure 5. Effect of CHUA on the loss mitochondrial membrane potential on MDA-MB-231 cells. The cells were treated with 3.5 μM CHUA at the indicated time. Both adherent and floating cells were collected and incubated with PBS containing 1 μg/mL rhodamine 123. The mitochondrial membrane potential was detected by FCM.

DOI: 10.1021/jf5053546
J. Agric. Food Chem. 2015, 63, 185−191

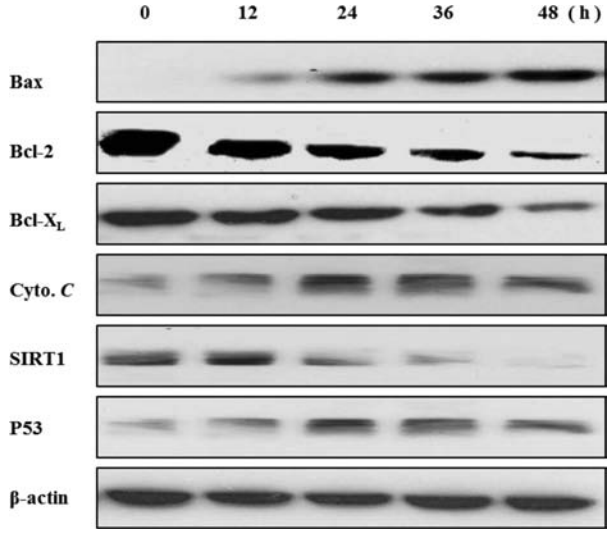

Figure 6. Release of cytochrome *c* and expressions of Bax, Bcl-2, Bcl-X, p53, and SIRT1 in CHUA-induced MDA-MB-231 cells. Cells were treated with 3.5 μM CHUA for 0, 12, 24, 36, or 48 h, the cell lysates (15 μg of protein for each channel) were separated by 12% SDS-PAGE, and the protein expressions were detected by Western blot analysis.

caspase-3 (z-DEVD-fmk) augmented the cell death to a significant difference. However, the inhibitor of caspase-8 (z-IETD-fmk) and the inhibitor of caspase-9 (z-LEHD-fmk) had no effect on the MDA-MB-231 cell death (Figure 7A).

In the LDH-based assay, it was found that the inhibitor of pan-caspase can significantly increase apoptosis; however, the caspase-3 inhibitor significantly increased necrosis on CHUA-treated MDA-MB-231 cells (Figure 7B). These results suggested that caspase-3 plays a protective role against CHUA-treated MDA-MB-231 cells.

Expressions of Caspase-3, ICAD, and PARP in CHUA-Induced MDA-MB-231 Cell Death. Caspase exists in normal cells as an inactive enzyme and is activated by removal of an aspartic acid residue. Activated caspase exerts the function related with apoptosis. Among them, caspase-3 is a common downstream apoptosis effector, which is processed and activated by caspase-9 or -8. To further investigate the influence of caspase on cells, apoptosis was challenged by CHUA. Western blot analysis was carried out to detect whether or not the participation of caspase-3 was involved in this process. As we expected, the 32 kDa band of procaspase-3 remained with no significant change after treatment with CHUA; also, no active form of caspase-3 was found. Moreover, ICAD is a classical substrate of caspase-3 and executes the characteristic fragmentation of DNA. ICAD is expressed as two isoforms, one is 45 kDa (ICAD-L/DFF45) and another is 35 kDa (ICAD/DFF35). The two isoforms have been reported to bind and inhibit CAD, but only ICAD-L/DFF45 has been reported to be functional.[19,20] Thus, the ICAD-L/DFF45 expression in MDA-MB-231 cells was examined. Interestingly, after exposure to CHUA for different time courses, the expression of ICAD-L remained with no change, too. Another characteristic associated with the execution phase of the apoptosis pathway is the specific PARP cleavage by the caspase. This cleavage leads to inactivation of the enzyme, thus preventing futile DNA repair cycle. It has been reported that caspase-3 is the most efficient processing enzyme for PARP.[21] Cleavage of PARP was examined after treatment with CHUA.

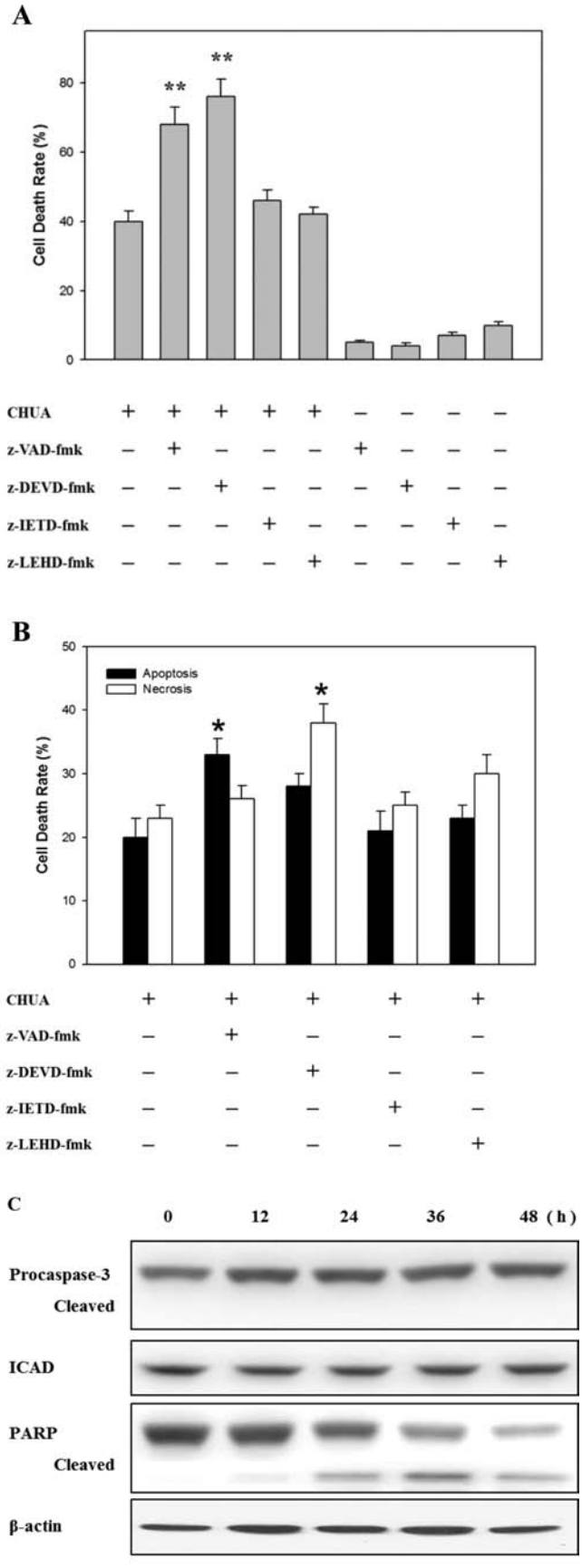

Figure 7. Effects of caspase on CHUA-induced MDA-MB-231 cell death. (A) Cells were pretreated without or with z-VAD-fmk 10 μM, z-DEVD-fmk 20 μM, z-IETD-fmk 20 μM, or z-LEHD-fmk 20 μM for 1

DOI: 10.1021/jf5053546
J. Agric. Food Chem. 2015, 63, 185−191

Figure 7. continued

h and then treated with 10 μM CHUA for another 24 h, and the cell death rate was measured by MTT assay. Mean ± SEM (n = 5). (**) p < 0.01. (B) Cells were treated as in (A), and then the characteristics of cell death were determined by LDH activity-based assay. Mean ± SEM (n = 5). (*) p < 0.05. (C) Involvement of caspase-3 independent pathway during CHUA-induced apoptosis in MDA-MB-231 cells. The cells were treated with 3.5 μM CHUA for the indicated times. The substrates of caspase-3, ICAD, and PARP were detected using Western blot analysis.

Surprisingly, PARP was activated and formed the 85 kDa isoform, which was digested from its 116 kDa precursor in a time-dependent manner, indicating that other enzyme(s) activated PARP (Figure 7C).

CHUA is a novel triterpenoid isolated from apple, which has showed potential antitumor activity against many types of tumors, especially breast cancer cells.[10] The aim of this study was to investigate the effects of CHUA as a chemopreventive agent in a nude mouse xenograft model and in vitro experiment. Although CHUA and other plant-derived triterpenoids have attracted a lot of interest for cancer study, there has, so far, been no study published about CHUA as a dietary supplementation for chemopreventive purposes. In this study, CHUA significantly inhibited the cell growth and proliferation of different tumor cell lines. In particular, it should be noted that CHUA achieved best inhibitory effect for MDA-MB-231 cell lines with the IC_{50} value of 2.57 ± 0.11 μM. In vivo antitumor experiments showed that CHUA could substantially reduce the occurrence and growth of mammary tumor in a nude mouse xenograft model at a dose of 50 mg/kg/day without body weight loss and mortality. The inhibition of CHUA on solid tumor may be stronger than HBA (natural triterpenoid analogue) with the same dose and the same treatment method.[22] As we know, apples are the most common fruit in our daily life, and apple peels are a waste product of apple sauce and canned apple manufacture. Rich in triterpenoids, they could be of benefit to our health. Triterpenoids form 3 kg of apple peels could contribute a sufficient amount of CHUA for chemoprevention for a 100 lb human according to animal experiments in vivo. Therefore, CHUA should undergo drug special preparations before use as a potential drug.

The antitumor mechanism of CHUA in MDA-MB-231 cells was further investigated. Apoptosis is characterized by a fragmentation of nuclear chromatin and dilatation of the endoplasmic reticulum. Results of DNA fragmentation and LDH activity assay suggested that CHUA-induced MDA-MB-231 cell death involved a mechanism of apoptosis. The mitochondrial transmembrane potential is a characteristic feature of apoptosis. Normally, mitochondria play the central role in supplying cells with ATP for survival. Dysfunction of mitochondria has been frequently reported in human cancera related with apoptosis because of the changes in membrane integrity that resulted in the disruption of the mitochondrial transmembrane potential.[23] In this research, the mitochondrial transmembrane potential on MDA-MB-231 cells treated by CHUA was decreased in a time-dependent manner. This result implied that the mitochondrial pathway might be involved in MDA-MB-231 cell apoptosis.

As we know, the collapse of the mitochondrial membrane potential correlates with an increased expression of Bax/Bcl-2 ratio, which is followed by cytochrome c release. Therefore, the ratio between Bcl-2 and Bax or Bcl-XL and Bax is a decisive factor to activate cell death.[13,24,25] Were these proteins involved or not in this apoptotic process? The results showed that MDA-MB-231 cells treated with CHUA exhibited the elevated ratio between Bax and Bcl-2 or Bcl-XL. Meanwhile, the release of cytochrome c was obviously up-regulated followed by the increased ratios. These results strongly suggested that the mitochondrial pathway was activated in CHUA-induced apoptosis on MDA-MB-231 cells.

p53 is a major regulator of apoptosis through different points. It may transcriptionally activate genes that are essential to growth arrest and DNA damage. It can also activate the pro-apoptotic Bcl-2 family number Bax.[26,27] As Bax expression increased, our attention was drawn to p53 because Bax is a gene promoter containing a p53-binding domain and is up-regulated by p53 in response to DNA damage. Moreover, Bax links p53 with apoptotic machinery of mitochondia, which results in the release of cytochrome c and activation of caspases. In this study, CHUA induced rapid accumulation of p53, which was positively correlated with subsequent up-regulation of Bax. These results indicate that p53 plays a pivotal role in the initiation phase of CHUA-induced MDA-MB-231 cell apoptosis.

SIRT1 has been proposed to promote tumor development and progression; also, SIRT1-mediated deacetylation suppresses the functions of several tumor suppressors, including p53. It also inhibits apoptotic cell death by deacetylating the DNA repair factor Ku70 that is tightly associated with Bax, resulting in the change of the mitochondrial permeability.[28] In this study, CHUA attenuated SIRT1 expression and triggered the activation of p53 and Bax, suggesting that SIRT1 inactivation was associated with p53- and Bax-mediated cell death by CHUA.

UV irradiation and some chemotherapeutic agents cause release of mitochondrial cytochrome c, which binds to Apaf-1, and the complex mediates recruitment of procaspase-9 and activates caspase-3. Caspases, a family of proteases, are one of the essential executioners of apoptosis, and their cleavage and subsequent activation are considered the primary hallmarks of apoptosis; however, there have been other reports that cell death is increased even when its function is shut down.[29,30] To further confirm the participation of caspase in cell death, different caspase inhibitors were used in the experiment. Interestingly, the results of this study showed that pretreatment with the caspase inhibitors z-VAD-fmk (pan-caspase inhibitor) and z-DEVD-fmk (caspase-3 inhibitor) significantly enhanced CHUA-induced MDA-MB-231 cell death, but the z-IETD-fmk (caspase-8 inhibitor) and z-LEAD-fmk (caspase-9 inhibitor) had almost no effect on cell viability, which implied that caspase-independent apoptosis happened. In the LDH assay, pretreatment with z-DEVD-fmk (caspase-3 inhibitor) significantly enhanced CHUA-induced MDA-MB-231 cell death after CHUA treatment. With this special question, we further examined the protein expression of caspase-3 and its substrates of ICAD and PARP. ICAD was left unaffected because no active form of caspase-3 was detected after CHUA treatment; however, cleaved PARP was detected, indicating that other proteins contribute to cell death and PARP activation in part. All data here allowed us to speculate that other enzymes existed to induce the apoptotic signals on MDA-MB-231 cells treated by CHUA.

DOI: 10.1021/jf5053546
J. Agric. Food Chem. 2015, 63, 185−191

Taken together, CHUA induced apoptosis in MDA-MB-231 cells via mitochondrial pathways, and some proteases different from caspase-3 might be responsible for the degradation of PARP. A more detailed mechanism of CHUA-induced MDA-MB-231 cell apoptosis remains to be elucidated.

AUTHOR INFORMATION

Corresponding Author

*(X.H.) Phone/fax: 86-20-3935-2132. E-mail: hexiangjiu@163.com.

Funding

This research was funded by the National Natural Science Foundation of China (No. U1203103).

Notes

The authors declare no competing financial interest.

REFERENCES

(1) Charde, M.; Chakole, R. D.; Ahmed, A. Apple phytochemicals for human benefits. *Int. J. Pharmacol. Res.* **2011**, *1*, 40−55.

(2) Liu, R. H.; Liu, J. R.; Chen, B. Apples prevent mammary tumors in rats. *J. Agric. Food Chem.* **2005**, *53*, 2341−2343.

(3) Knekt, P.; Jarvinen, R.; Reunanen, A.; Maatela, J. Flavonoid intake and coronary mortality in Finland: a cohort study. *Br. Med. J.* **1996**, *312*, 478−481.

(4) Cheng, D.; Xi, Y.; Cao, J.; Cao, D.; Ma, Y.; Jiang, W. Protective effect of apple (Ralls) polyphenol extract against aluminum-induced cognitive impairment and oxidative damage in rat. *Neurotoxicity* **2014**, *17*, 111−120.

(5) Sekhon-Loodu, S.; Catalli, A.; Kulka, M.; Wang, Y.; Shahidi, F.; Rupasinghe, H. P. Apple flavonols and n-3 polyunsaturated fatty acid-rich fish oil lowers blood C-reactive protein in rats with hypercholesterolemia and acute inflammation. *Nutr. Res. (N.Y.)* **2014**, *34*, 535−543.

(6) Schulze, C.; Bangert, A.; Kottra, G.; Geillinger, K. E.; Schwanck, B.; Vollert, H.; Blaschek, W.; Daniel, H. Inhibition of the intestinal sodium-coupled glucose transporter 1 (SGLT1) by extracts and polyphenols from apple reduces postprandial blood glucose levels in mice and humans. *Mol. Nutr. Food Res.* **2014**, *58*, 1795−1808.

(7) Carrasco-Pozo, C.; Speisky, H.; Brunser, O.; Pastene, E.; Gotteland, M. Apple peel polyphenols protect against gastrointestinal mucosa alterations induced by indomethacin in rats. *J. Agric. Food Chem.* **2011**, *59*, 6459−6466.

(8) He, X. J.; Liu, R. H. Triterpenoids isolated from apple peels have potent antiproliferative activity and may be partially responsible for apple's anticancer activity. *J. Agric. Food Chem.* **2007**, *55*, 4366−4370.

(9) He, X. J.; Liu, R. H. Phytochemicals of apple peels: isolation, structure elucidation, and their antiproliferative and antioxidant activities. *J. Agric. Food Chem.* **2008**, *56*, 9905−9910.

(10) He, X. J.; Wang, Y. H.; Hu, H.; Zhang, Z. X. In vitro and in vivo antimammary tumor activities and mechanisms of the apple total triterpenoids. *J. Agric. Food Chem.* **2012**, *60*, 9430−9436.

(11) Kim, S. O.; Han, J. Pan-caspase inhibitor zVAD enhances cell death in RAW 246.7 macrophages. *J. Endotoxin Res.* **2001**, *7*, 292−296.

(12) Zhao, X.; Wang, R.; Qian, Y.; Li, G.; Zhou, Y.; Sun, P. *In vivo* preventive effects of insect tea on buccal mucosa cancer in ICR mice. *J. Cancer Res. Ther.* **2014**, *10*, 651−657.

(13) Lin, M. L.; Chen, S. S.; Huang, R. Y.; Lu, Y. C.; Liao, Y. R.; Reddy, M. V.; Lee, C. C.; Wu, T. S. Suppression of PI3K/Akt signaling by synthetic bichalcone analog TSWU-CD4 induces ER stress- and Bax/Bak-mediated apoptosis of cancer cells. *Apoptosis* **2014**, *19*, 1637−1653.

(14) Hunt, A.; Evan, G. Till death us do part. *Science* **2001**, *293*, 1784−1785.

(15) Wood, J. G.; Rogina, R.; Lavu, S.; Howitz, K.; Helfand, S. L.; Tatar, M.; Sinclair, D. Sirtuin activators mimic caloric restriction and delay aging in metazoans. *Nature* **2004**, *430*, 686−689.

(16) Brazil, D. P.; Hemmings, B. A. Ten years of protein kinase B signalling: a hard Akt to follow. *Trends Biochem. Sci.* **2001**, *26*, 657−664.

(17) Fei, X. F.; Wang, B. X.; Tashiro, S.; Li, T. J.; Ma, J. S.; Ikejima, T. Apoptotic effects of ginsenoside Rh2 on human malignant melanoma A375-S2 cells. *Acta Pharmacol. Sin.* **2002**, *23*, 315−322.

(18) Laetitia, C.; Anne, J.; Claire, T.; Chantal, B. H.; Chedorge, M.; Denis, M.; Vallette, G.; Laboisse, C. L. Growth phase-dependent expression of ICAD-L/DFF45 modulates the pattern of apoptosis in human colonic cancer cells. *Cancer Res.* **2002**, *62*, 2169−2174.

(19) Brain, D. L.; Lynn, A. M. Directing caspase-3/CAD induced DNA strand breaks to coordinate changes in gene expression. *Cell Cycle* **2010**, *9*, 2940−2945.

(20) Sakahira, H.; Enari, M.; Nagata, S. Cleavage of CAD inhibitor in CAD activation and DNA degradation during apoptosis. *Nature* **1998**, *391*, 96−99.

(21) Katebi, S. N.; Razavi, Y.; Zeighamy, A. S.; Khodagholi, F.; Haghparast, A. Morphine could increase apoptotic factors in the nucleus accumbens and prefrontal cortex of rat brains reward circuitry. *Brain Res.* **2013**, *1540*, 1−8.

(22) Majeed, R.; Hamid, A.; Sangwan, P. L.; Chinthakindi, P. K.; Koul, S.; Rayees, S.; Singh, G.; Mondhe, D. M.; Mintoo, M. J.; Singh, S. K.; Rath, S. K.; Saxena, A. K. Inhibition of phosphotidylinositol-3 kinase pathway by a novel naphthol derivative of betulinic acid induces cell cycle arrest and apoptosisincancer cells of different origin. *Cell Death Dis.* **2014**, *5*, 1−19.

(23) Hamzeloo-Moghadam, M.; Aghaei, M.; Fallahian, F.; Jafari, S. M.; Dolati, M.; Abdolmohammadi, M. H.; Hajiahmadi, S.; Esmaeili, S. Britannin, a sesquiterpene lactone, inhibits proliferation and induce sapoptosis through the mitochondrial signaling pathway in human breast cancer cells. *Tumour Biol.* **2014**, DOI: 10.1007/s13277-014-2744-9.

(24) Zhang, Y. J.; Xing, D.; Liu, L. PUMA promotes Bax translocation by both directly interacting with Bax and by competitive binding to Bcl-XL during UV-induced apoptosis. *Mol. Biol. Cell* **2009**, *20*, 3077−3087.

(25) Kluck, R. M.; Bossy, W. E.; Green, D. R.; Newmeyer, D. D. The release of cytochrome *c* from mitochondria: a primary site for Bcl-2 regulation of apoptosis. *Science* **1997**, *275*, 1132−1136.

(26) Miyashita, T.; Reed, J. C. Tumor suppressor p53 is a direct transcriptional activator of the human bax gene. *Cell* **1995**, *80*, 293−299.

(27) Nakano, K.; Vousden, K. H. PUMA, a novel proapoptotic gene, is induced by p53. *Mol. Cell* **2001**, *7*, 683−694.

(28) Cardone, M. H.; Roy, N.; Stennicke, H. R.; Salvesen, G. S.; Franke, T. F.; Stanbridge, E.; Frisch, S.; Reed, J. C. Regulation of cell death protease caspase-9 by phosphorylation. *Science* **1998**, *282*, 1318−1321.

(29) Vercau, L. D.; Beyaert, R.; Denecker, G.; Goossens, V.; Van Loo, G.; Declercq, W.; Grooten, J.; Fiers, W.; Vandenabeele, P. Inhibition of caspases increases the sensitivity of L929 cells to necrosis mediated by tumor necrosis factor. *J. Exp. Med.* **1998**, *187*, 1477−1485.

(30) Cui, Q.; Yu, J. H.; Wu, J. N.; Tashiro, S. I.; Satoshi, O. S.; Minami, M.; Ikejima, T. P53-mediated cell cycle arrest and apoptosis through a caspase-3-independent, but caspase-9-dependent pathway in oridonin-treated MCF-7 human breast cancer cells. *Acta Pharmacol. Sin.* **2007**, *28*, 1057−1066.

DOI: 10.1021/jf5053546
J. Agric. Food Chem. 2015, 63, 185−191

JOURNAL OF AGRICULTURAL AND FOOD CHEMISTRY

Article

pubs.acs.org/JAFC

Monascus Secondary Metabolites Monascin and Ankaflavin Inhibit Activation of RBL-2H3 Cells

Yu-Ying Chang, Wei-Hsuan Hsu, and Tzu-Ming Pan*

Department of Biochemical Science and Technology, College of Life Science, National Taiwan University, No. 1, Sec. 4, Roosevelt Road, Taipei 10617, Taiwan

ABSTRACT: *Monascus*-fermented products have been used as dietary food and traditional medicine due to their beneficial effects on circulation and digestive systems in Asia for thousands of years. Besides, monascin and ankaflavin, secondary metabolites from *Monascus*-fermented products, have proven anti-inflammatory and immunomodulatory effects. In previous research, monascin and ankaflavin ameliorated ovalbumin-induced airway allergic reaction often used as a type I allergy asthma model. Additionally, mast cells play critical roles in type I allergy. Therefore, RBL-2H3 cells were used as the mast cell model to determine whether the improving effects on asthma of monascin and ankaflavin came from influencing mast cells. PMA and ionomycin are common activators of mast cells because they stimulate the main signaling molecules during mast cell activation. Forty micromolar monascin and ankaflavin inhibited PMA/ionomycin-induced mast cell degranulation and TNF-α secretion through suppressing the phosphorylation of PKC and MAPK family ERK, JNK, and p38. Consequently, monascin and ankaflavin affected the activation of mast cells and may have the potential to improve type I allergy.

KEYWORDS: *mast cell, monascin, ankaflavin, allergy, PPARγ*

INTRODUCTION

Allergy is defined as the over-reaction that some people show toward nontoxic substances such as peanuts and pollens.[1] On the basis of the mechanism of allergy and the mainly participative cells, allergies are classified into four types. Type I allergy includes asthma, allergic rhinitis, food allergy, and so forth. Its mechanism begins with antigen presenting cells (APCs) contacting allergens, and then APCs recognize, engulf, and present antigens to naïve T cells, which make T cells activated and differentiated. In allergic patients, T cells tend to differentiate into T helper 2 (Th2) cells. Th2 cells release cytokines including interleukin-4 (IL-4), IL-5, and IL-13 that turn B cells into IgE-releasing plasma cells. The produced IgE bind to IgE receptors on mast cells. As a result, the next time allergy patients contact the same allergen, the allergen would cross-link with IgE previously bound on mast cells, followed by triggering biochemical reactions including activation of tyrosine kinase, PKC, mitogen-activated protein kinase (MAPK), calcium influx, and cytoskeleton remodeling.[2] After this signaling process, the mast cells activate and secrete inflammatory mediators with different effects on human. For instance, mast cells degranulate and release histamine, which would increase cell permeability, promote mucus production, and boost smooth muscle constriction.[1,3] TNF-α induces adhesion molecules expressed on endothelial cells and then recruits more immune cells to exaggerate the inflammatory reaction. The process of TNF-α release is also induced by PKC activation, calcium elevation, and MAPK phosphorylation. Furthermore, there are two forms that secrete TNF-α. One is the same as histamine, which is previously stored in the mast cell granules and is released upon exocytosis. The other is that MAPK phosphorylation induces the translocation of transcription factors into cell nucleus, and then TNF-α is transcribed and newly synthesized.[4] Finally, these mediators lead to patients displaying symptoms of bronchial constriction, diarrhea, and wheal-and-flare reaction.[1,3]

The prevalence of type I allergy increases with modernized and industrialized lifestyles (WAO), but there is no effective medicine with low side effects. Therefore, more and more groups investigate relative research to resolve the problems. *Monascus*-fermented products are natural and have been consumed for more than a thousand years, so their side effects may be less. Monascin and ankaflavin isolated from *Monascus* are secondary metabolites and have been determined to have antioxidative,[5−8] anti-inflammatory,[9,10] antidiabetes,[11−13] and immunomodulatory effects.[14,15] Additionally, monascin and ankaflavin have been proven to improved ovalbumin-treated BALB/c mice airway inflammation, which is a commonly used model of asthma.[10,16] Our previous study further examined whether monascin and ankaflavin affect participative cells in allergy. We found that monascin inhibited the maturation of dendritic cells, which belong to APCs. Without full maturation, dendritic cells could not present antigens to downstream T cells, and then allergy may be ameliorated. Monascin also interfered with EL4 T cells releasing Th2 cytokines, which are critical factors in allergic reaction.[14] However, the effects of monascin and ankaflavin on the activation of mast cells have not been studied.

Peroxisome proliferator-activated receptor γ (PPARγ) is a member of the nuclear receptor superfamily. After binding with its ligands, PPARγ translocates from cytoplasm into nucleus and recruits coactivators to modulate the expression of target gene.[17] PPARγ ligands have been shown to repress the

Received: August 21, 2014
Revised: December 19, 2014
Accepted: December 19, 2014
Published: December 19, 2014

ACS Publications © 2014 American Chemical Society

DOI: 10.1021/jf504013n
J. Agric. Food Chem. 2015, 63, 192−199

activation of mast cells.[18] In addition, monascin and ankaflavin both are PPARγ ligands.[5,19] They may have the same effect as other ligands.

In this study, we tested whether monascin and ankaflavin have beneficial effects on RBL-2H3 cells, which are often seen as mast cells. The RBL-2H3 cell is activated by PMA and ionomycin, which would induce protein kinase C phosphorylation and calcium concentration elevation, respectively.[20,21] These two responses are principal signaling molecules during the activation of mast cells.[22] We demonstrated that both monascin and ankaflavin suppressed the degranulation and TNF-α release of RBL-2H3 mast cells and that they achieved the effects through inhibiting the phosphorylation of the significant signaling molecules PKC, MAPK family ERK, JNK, and p38. Therefore, monascin and ankaflavin may possess the ability to be applied to the treatment of type I allergy patients.

MATERIALS AND METHODS

Chemicals and Reagents. Phorbol 12-myristate 13-acetate (PMA), ionomycin, PPAR-γ antagonist GW9662, rosiglitazone, bovine serum albumin (BSA), sodium dodecyl sulfate (SDS), dimethyl sulfoxide (DMSO), 4-nitrophenyl *N*-acetyl-β-D-glucosaminide (pNAG), Triton X-100, and dichlorodihydrofluorescein diacetate (DCFH-DA) were purchased from Sigma Chemical Co. (St. Louis, MO, USA). Minimum essential medium (MEM), fetal bovine serum (FBS), trypsin−EDTA,and nonessential amino acids were purchased from HyClone Laboratories (Logan, UT, USA). Sodium bicarbonate and sodium pyruvate were purchased from Caisson Laboratories (North Logan, UT, USA). Polyvinyldiene difluoride (PVDF) was purchased from Pall Corp. (Port Washington, NY, USA). Enhanced chemiluminescent (ECL) reagent was purchased from Advansta Inc. (Menlo Park, CA, USA). Anti-GAPDH antibody, anti-PKC, anti-p-PKC, anti-p-JNK, and anti-p-p38 were purchased from Abcam Co. (Cambridge, UK). Anti-p-p44/42 MAPK antibody and anti-COX-2 were purchased from Cell Signaling Technology (Beverly, MA, USA). Anti-rabbit antibody (secondary antibody) was purchased from GeneTex (San Antonio, TX, USA). Fura-2-acetoxymethyl ester (Fura-2 AM) was purchased from Invitrogen (Carlsbad, CA, USA). TNF-α ELISA kit was purchased from BioLegend Inc. (San Diego, CA, USA). Protein extraction solution was purchased from iNtRON Biotechnology, Inc. (Sangdaewon-Dong, Korea). The Bio-Rad protein assay dye was from Bio-Rad Laboratories (Hercules, CA, USA). Monascin and ankaflavin were isolated from *Monascus*-fermented rice (red mold rice) by SunWay Biotechnology Co. (Taipei, Taiwan).

RBL-2H3 Cell Culture. Rat basophilic leukemia (RBL)-2H3 cells were purchased from the Bioresource Collection and Research Center (Hsinchu, Taiwan). RBL-2H3 cells were cultured in MEM supplemented with 15 g/L sodium bicarbonate, 0.1 mM nonessential amino acids, 1.0 mM sodium pyruvate, and 15% heat-inactivated FBS. Cells were cultured at 37 °C in a humidified atmosphere of 5% CO_2.

Cell Viability Assay. The toxicity of monascin and ankaflavin to RBL-2H3 cells was evaluated with the crystal violet assay. After seeding into a 24-well plate overnight, the cells were cultured with different concentrations of tested samples for 24 h. Cells were washed with PBS and incubated with 0.5% crystal violet dye (dissolved in PBS solution) for 30 min. The cells were rinsed to remove the excess of dye and then air-dried overnight. Finally, 2% SDS was used to dissolve the dye, and the dye intensity was monitored at the wavelength of 600 nm.

β-Hexosaminidase Assay. The β-hexosaminidase assay was performed as described previously with some modification.[23] Treated with monascin, ankaflavin, and rosiglitazone for 24 h, the RBL-2H3 cells were cultured with Tyrode's buffer (135 mM NaCl, 5 mM KCl, 1 mM $MgCl_2$, 1.8 mM $CaCl_2$, 5.6 mM glucose, 20 mM HEPES, and 0.1% BSA, pH 7.4) with 10 μM ionomycin for 30 min. After collection of cell supernatants for the released form of β-hexosaminidase, Tyrode's buffer with 0.5% Triton X-100 was added to destroy cell membrane and collect the β-hexosaminidase, which is inside the cells. For quantitation, to 5 μL samples was added 50 μL of 0.1 M citrate buffer (pH 4.5) with β-hexosaminidase substrate 4-nitrophenyl pNAG at 37 °C for 90 min. Finally, treatment with 150 μL of 0.1 M carbonate buffer (pH 9.0) stopped the reaction, and the intensity of absorption at 405 and 630 nm was measured. Before calculation with the following equation, subtract the background intensity of 630 nm from the intensity of 405 nm: (absorption of supernatant of the stimulated cells − absorption of supernatant of control)/(absorption of total amount of β-hexosaminidase in the cells − absorption of supernatant of control) × 100.

Quantification of TNF-α by ELISA. Before cells were induced with 50 nM PMA and 500 nM ionomycin for 3 h, they were treated with 40 μM monascin, ankaflavin, and rosiglitazone for 24 h. The cell medium was collected and stored at −80 °C until tested. The levels of TNF-α released into culture medium were determined with ELISA kits from BioLegend.

Immunoblot Analysis. After cell collection and extraction with the protein extraction solution (iNtRON Biotechnology, Inc.), the protein samples were subjected to 10% SDS−polyacrylamide gel electrophoresis (PAGE). The protein spots were electrotransferred to a PVDF membrane, and then the membrane was incubated with blocking buffer (phosphate-buffered saline (PBS) containing 0.05% Tween-20 and 5% w/v nonfat dry milk) for 1 h and washed with PBST (PBS containing 0.05% Tween-20) three times, each time for 5 min, followed by a diluted solution of anti-p-PKC, anti-PKC, anti-p-p38, and anti-p-JNK antibodies (Abcam) and anti-p-ERK, anti-COX-2 antibodies (Cell Signaling Technology) overnight at 4 °C. In addition, the blots probed with a 1:1000 diluted solution of anti-GAPDH (Abcam) antibody were used as internal control to keep each well loading with the same amount of protein. The membrane was washed three times, each time for 5 min in PBST, shaken in a solution of horseradish peroxidase (HRP)-linked anti-rabbit or anti-mouse IgG secondary antibody, and washed three more times, each time for 5 min in PBST. The expressions of proteins were detected by enhanced chemiluminescent (ECL) reagent (Advansta Inc.A) and image reader (ProteinSimple FluorChem M, ProteinSimple, Santa Clara, CA, USA). The intensity of blots were analyzed and quantitated with ImageJ software.

Measurement of Intracellular Calcium Level. Investigating intracellular calcium used a calcium-sensitive fluorescent Fura-2 AM, and the assay was as described previously with some change.[24] The cells were seeded in 12-well plates (1×10^5/mL) and cultured with samples for 24 h. After incubation with 2 μM Fura-2 AM for 1 h, the cells were washed two times with Tyrode's buffer and then cleaved by trypsin. Cells were collected and loaded into 96-well black-bottom, black-wall microplates. The cells were induced with PMA/ionomycin for 15 min. Finally, the fluorescent ratio of Fura-2 AM fluorescent (emission 490 nm) was monitored by 340 and 380 nm excitation, respectively. The intensity of wavelengths was calculated as a percentage compared to that of control and PMA/ionomycin groups: intracellular calcium level (%) = (Fura-2 AM fluorescence of samples − Fura-2 AM fluorescence of control)/(Fura-2 AM fluorescence of group PMA/ionomycin − Fura-2 AM fluorescence of control) × 100.

Measurement of Intracellular ROS Level. Intracellular ROS amount was investigated with ROS reactive fluorescent DCFH-DA. The cells were seeded into 6 cm plates (1×10^5/mL) overnight, treated with samples for 24 h, and then stimulated with PMA/ionomycin for 1 h. Cleavage by trypsin and three washings with Tyrode's buffer were followed by incubation with 45 μM DCFH-DA for 45 min at 37 °C. After that, the cells were washed three times with Tyrode's buffer to remove the fluorescence that did not penetrate into cells. After suspending cells in the buffer, cells were assayed by flow cytometer (BD, FACSCanto II, Becton-Dickinson Bioscience, San Jose, CA, USA).

Statistical Analysis. Each experiment was determined at least three times. Results are expressed as the mean ± standard deviation (SD). Data were compared by one-way analysis of variance (ANOVA) using the general linear model procedure of SPSS software (SPSS Institute, Inc., Chicago, IL, USA) followed by ANOVA with Duncan's test. The value of $p < 0.05$ was considered statistically significant.

DOI: 10.1021/jf504013n
J. Agric. Food Chem. 2015, 63, 192−199

RESULTS

Effects of Monascin and Ankaflavin on Degranulation and TNF-α Release. First, we examined the cytotoxic effects of monascin and ankaflavin on RBL-2H3 cells by using the crystal violet stain assay. As shown in Figure 1A, 10, 20, and 40 μM monascin and ankaflavin did not cause significant cytotoxicity to cells. Therefore, we further investigated whether monascin and ankaflavin under this concentration could influence the activation of RBL-2H3 mast cells. After activation, mast cells would degranulate and secrete lots of pro-inflammatory cytokines such as TNF-α and IL-4. Mast cells would release histamine, β-hexosaminidase, protease, and so on, which were previously stored in the granules before degranulation. Thus, the β-hexosaminidase release assay is commonly used as a marker of mast cell degranulation.[23] Cells were pretreated with monascin, ankaflavin, and PPARγ ligand rosiglitazone for 24 h, and then they were induced with PMA/ionomycin. As shown in Figure 1B, the effects of monascin and ankaflavin on RBL-2H3 degranulation are dose-dependent. Twenty micromolar monascin and 40 μM monascin, ankaflavin, and rosiglitazone significantly ameliorated mast cell degranulation. On the other hand, 20 μM monascin and ankaflavin and 40 μM monascin, ankaflavin, and rosiglitazone remarkably decreased the TNF-α secretion of RBL-2H3 cells (Figure 1C).

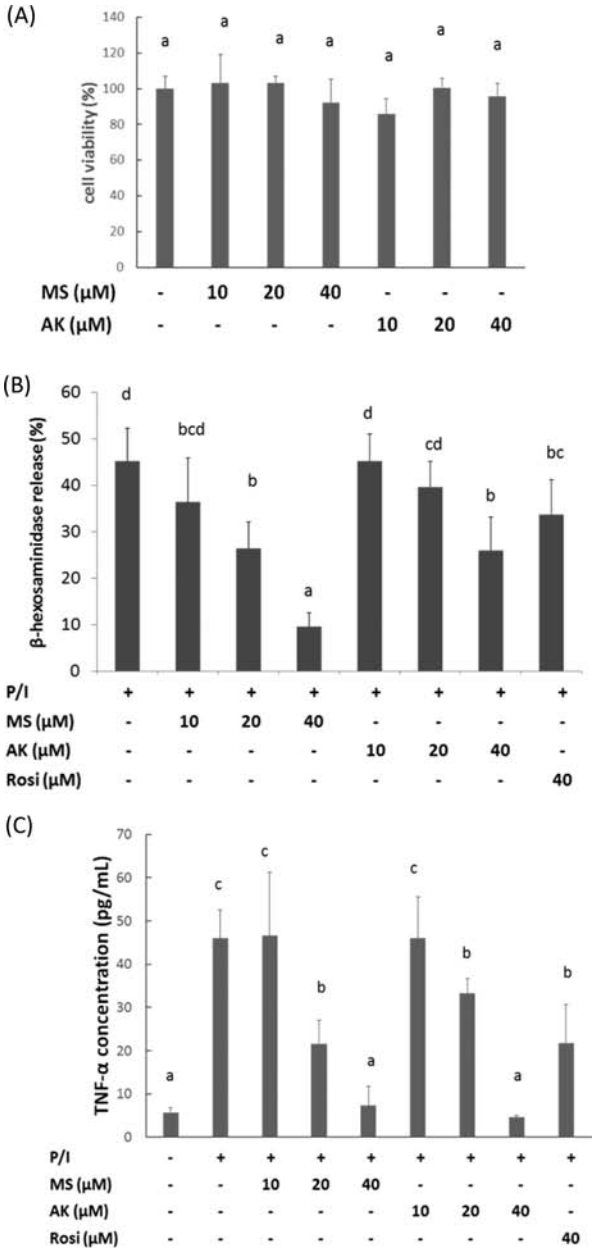

Figure 1. Effects of monascin and ankaflavin on (A) cell viability, (B) degranulation, and (C) TNF-α release in RBL-2H3 cells. Different letters above the bars indicate significant difference at $p < 0.05$ level. MS, monascin; AK, ankaflavin; Rosi, rosiglitazone; GW, GW9662 (PPARγ antagonist); P/I, PMA/ionomycin.

Roles of PPARγ, Monascin, and Ankaflavin on the Activation of Mast Cells. Monascin, ankaflavin, and rosiglitazone are PPARγ ligands.[16] In addition, many PPARγ agonists have been proven to possess an improving effect on the activation of mast cells.[18] To verify whether the ameliorative expressions of monascin, ankaflavin, and rosiglitazone on activation are achieved by PPARγ activation, we added the PPARγ antagonist GW9662 with samples to the cells for 24 h, and then we stimulated cells with PMA/ionomycin. As shown in Figure 2, degranulation and TNF-α secretion of RBL-2H3 had no effect after the addition of GW9662. These represented that even if PPARγ binds with GW9662, which would block PPARγ activation, inhibition effects of monascin, ankaflavin, and rosiglitazone on RBL-2H3 cell activation were still exhibited. Therefore, monascin, ankaflain, and rosiglitazone influenced the activation RBL-2H3 cells in a PPARγ-independent pathway.

Effects of Monascin and Ankaflavin on the Phosphorylation of MAPK. Because monascin, ankaflavin, and rosiglitazone achieved the inhibition of mast cell activation through a PPAR-unrelated mechanism, there would be some other mechanism to fulfill the amelioration effects. To elucidate that, we first investigated the phosphorylation of the MAPK family, which is critical during cytokine formation, such as TNF-α;[24] we examined the phosphorylation of MAPK family ERK, JNK, and p38 after sample treatments for 24 h and PMA/ionomycin induction for 10 min. As shown in Figures 3A−C, after stimulation with PMA/ionomycin, ERK, JNK, and p38 phosphorylations were apparently up-regulated. Incubation with monascin, ankaflavin, and rosiglitazone down-regulated the phosphorylation level of ERK, JNK, and p38 in RBL-2H3 cells. COX-2, the essential role during inflammatory mediator prostaglandins, has been reported to be regulated by p38 activation.[25] As shown in Figure 3D, we found a similar effect between p38 phosphorylation and COX-2 expression. Monascin, ankaflavin, and rosiglitazone all reduced the phosphorylation of p38 and the expression of COX-2 at the same time.

Effect of Monascin and Ankaflavin on the Phosphorylation of PKC, Intracellular Calcium, and ROS Level. We have investigated the alternation of monascin and ankaflavin on MAPK phosphorylation, and we further wondered whether samples could vary the upstream signaling molecules PKC activated by stimulant PMA.[20] As shown in Figure 4A, monascin and ankaflavin reduced the phosphorylation states of PKC. This indicated that samples influenced the activation of PKC. Furthermore, ionomycin is an ionophore, which increases intracellular calcium level. It is vital during mast cell activation.[21] The calcium-reactive fluorescent Fura-2 AM was used to detect intracellular level after culture with monascin, ankaflavin, and rosiglitazone for 24 h and then the incubation with PMA/ionomycin for 15 min. As shown in Figure 4B, monascin, ankaflavin, and rosiglitazone were ineffective on

DOI: 10.1021/jf504013n
J. Agric. Food Chem. 2015, 63, 192−199

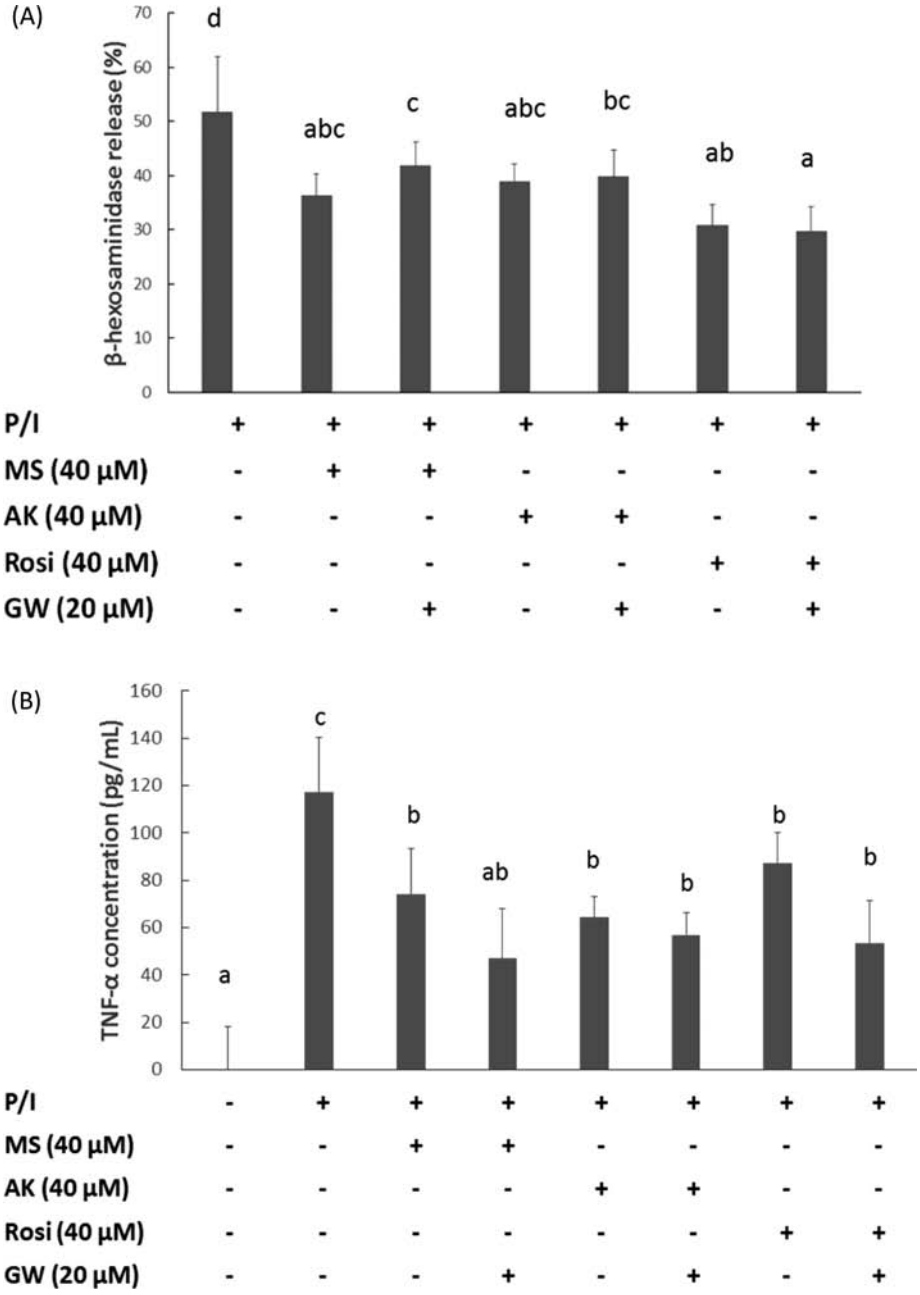

Figure 2. Relationships of the reducing effects of MS and AK with PPARγ on the (A) degranulation and (B) TNF-α release of RBL-2H3 mast cells. Different letters above the bars indicate significant difference at $p < 0.05$ level. MS, monascin; AK, ankaflavin; Rosi, rosiglitazone; GW, GW9662 (PPARγ antagonist); P/I, PMA/ionomycin.

intracellular calcium amount. Additionally, it has been reported that reactive oxygen species (ROS) are not only upstream but also downstream of calcium influx. In the beginning of mast cell activation, ROS induced an elevated calcium concentration through activation of NADPH oxidase. Later, the increased calcium level stimulated ROS by mitochondria.[26] Because there is no influence on calcium level, we investigated whether samples also had no effects on intracellular ROS level. The ROS amount was observed by ROS-sensitive fluorescent DCFH-DA. We found that monascin, ankaflavin, and rosiglitazone did not affect the intracellular ROS level (Figure 4C).

DISCUSSION

The activation of mast cells is a prominent process in type I allergic reaction. In addition, mast cells release a variety of pro-inflammatory substances including histamine, IL-4, TNF-α, prostaglandins, and leukotrienes, which are potent, multifunctional mediators. Finally, these mediators contribute to the allergic symptoms of patients.[1]

In this study, we verified that monascin, ankaflavin, and rosiglitazone improved degranulation and TNF-α release in RBL-2H3 mast cells in a PPARγ-independent mechanism. In fact, there are some improving effects of PPARγ ligands that are PPARγ independent. Okuyama et al. found that PPARγ agonist ciglitazone could inhibit inflammatory mediator leukotriene release in RBL-2H3 cells.[27] After incubation with GW9662, the

DOI: 10.1021/jf504013n
J. Agric. Food Chem. 2015, 63, 192−199

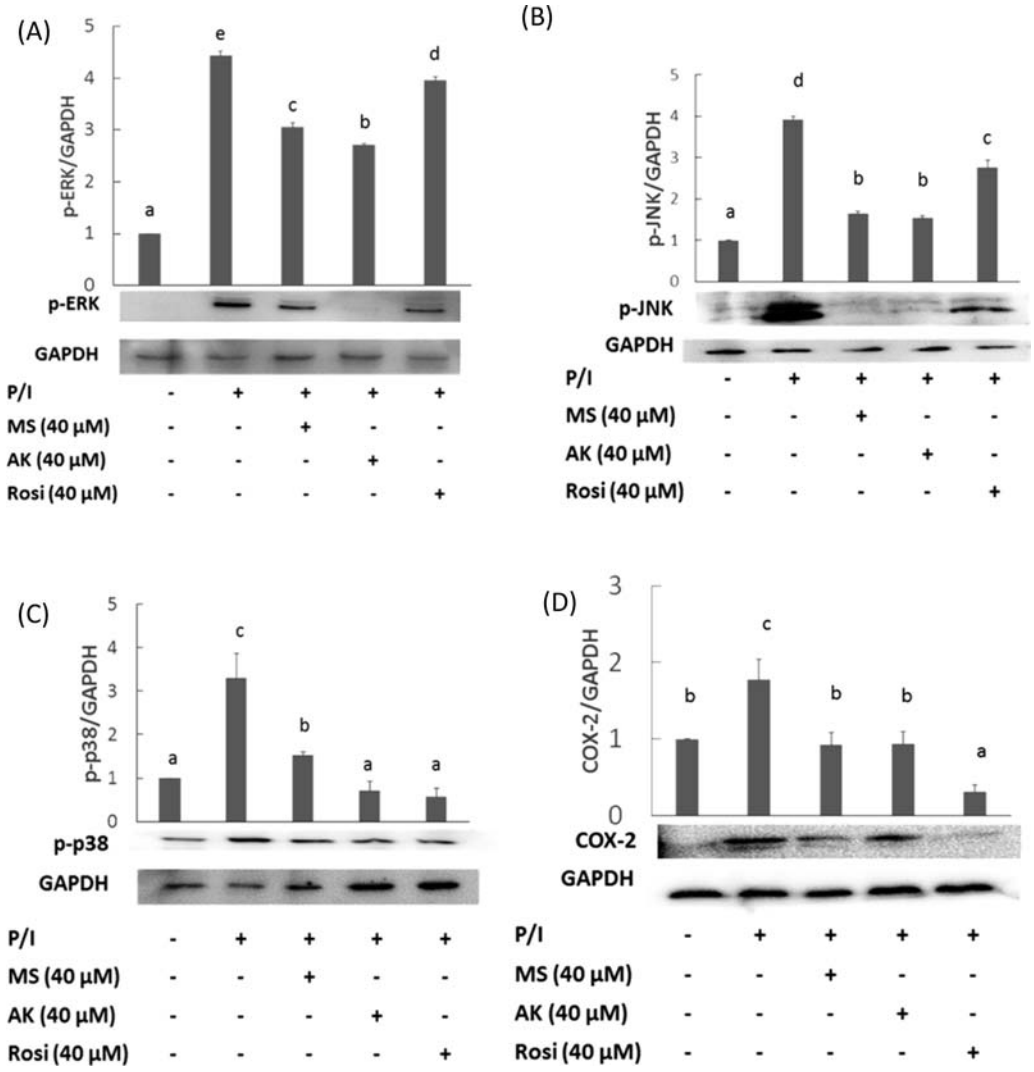

Figure 3. Effects of monascin and ankaflavin on the phosphorylation of (A) ERK, (B) JNK, (C) p38, and (D) COX-2 expression in RBL-2H3 mast cells. Different letters above the bars indicate significant difference at $p < 0.05$ level. MS, monascin; AK, ankaflavin; Rosi, rosiglitazone; GW, GW9662 (PPARγ antagonist); P/I, PMA/ionomycin.

reducing effect of ciglitazone on leukotriene secretion did not disappear. Additionally, the location of PPARγ still stayed at cytoplasm, indicating that the effect did not depend on the activation of PPARγ.[27] Besides, not all PPARγ ligands could influence mediator release in mast cells. For instance, in human cultured mast cells, histamine release was down-regulated by 15d-PGJ_2 but not down-regulated by troglitazone and ciglitazone.[28] The PPARγ-independent mechanism has also been reported in other kinds of cells. Furthermore, the concentration of PPARγ is much higher than the dissociation constant (K_d) of PPARγ. Therefore, there may still be other mechanisms to realize these phenomena.[18]

MAPK family ERK, JNK, and p38 are serine/threonine protein kinases and significant to cytokine and lipid mediator production in mast cells.[24,29] TNF-α formation is regulated by the activation of ERK.[30] Also, ERK controls the activity of phospholipase A_2 (PLA_2), which catalyzes the phospholipids in the membrane into arachidonic acid (AA). AA is the material needed in the manufacture of lipid mediators such as prostaglandins and leukotrienes.[30] We validated that monascin and ankaflavin diminished the phosphorylation level of ERK. Consequently, they may also have the potential to decrease the production of the lipid mediators, which would cause smooth muscle constriction, vasodilation, mucus overproduction, and nerve stimulation.[1]

PKC and intracellular calcium level are important to mast cell degranulation. We have found that monascin and ankaflavin inhibited the activation of PKC but did not affect the calcium concentration (Figure 4). These appearances could also be discovered in another study. Hide et al. determined that 10 μM azelastine had an effect on PKC phosphorylation but not on calcium level.[31] By comparison of their structures, monascin, ankaflavin, and azelastine are polycyclic. Therefore, this polycyclic structure may play a critical part in interfering with PKC activation. Now, azelastin has been developed into allergic rhinitis medicines in some counties, but it comes with some side effects such as nose burning, somnolence, and so on.[32,33] Monascin and ankaflavin had similar improving effects. Due to their natural properties, they would have lower side effects. Thus, they may be much safer to allergic patients.

In conclusion, PPARγ activators monascin, ankaflavin, and rosiglitazone ameliorated the pro-inflammatory mediator release of mast cells through a PPARγ-independent mechanism. As shown in Figure 5, monascin and ankaflavin influenced the

DOI: 10.1021/jf504013n
J. Agric. Food Chem. 2015, 63, 192−199

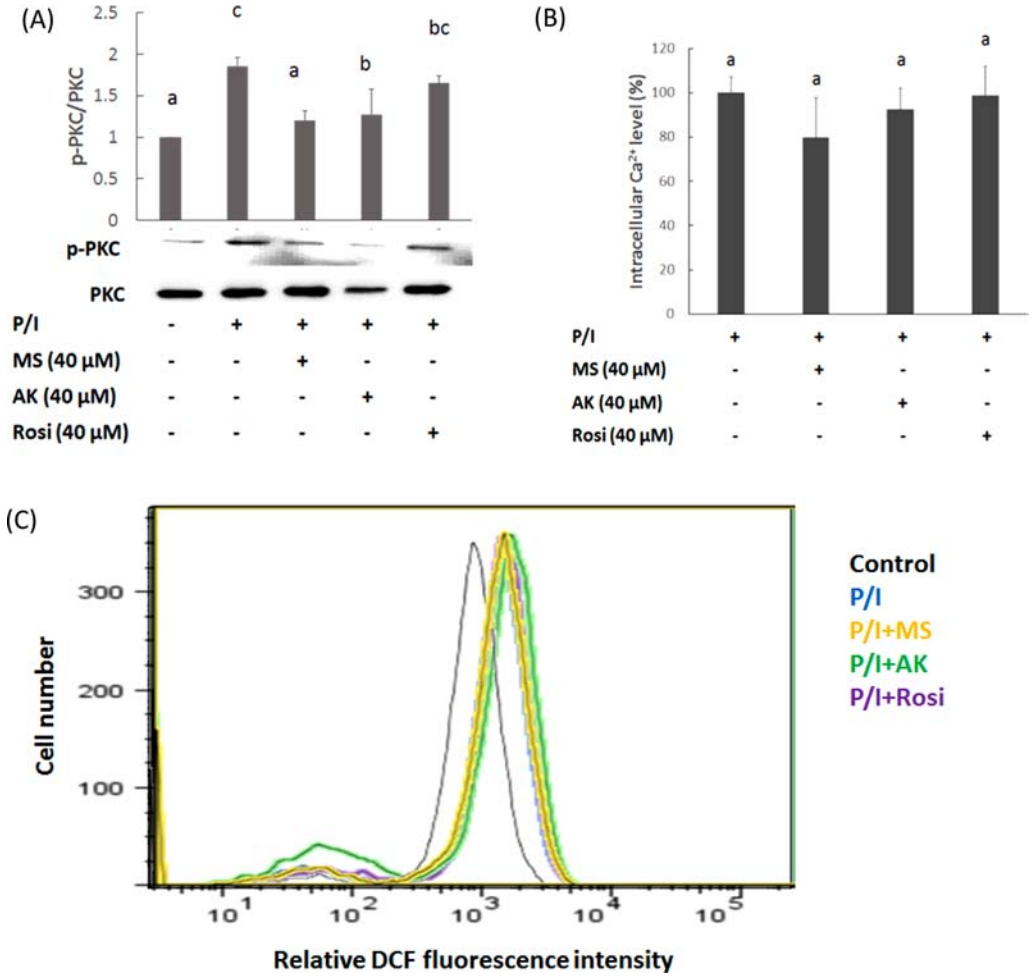

Figure 4. Effects of monascin and ankaflavin on (A) PKC phosphorylation, (B) intracellular calcium level, and (C) ROS level in RBL-2H3 mast cells. Different letters above the bars indicate significant difference at $p < 0.05$ level. MS, monascin; AK, ankaflavin; Rosi, rosiglitazone; GW, GW9662 (PPARγ antagonist); P/I, PMA/ionomycin.

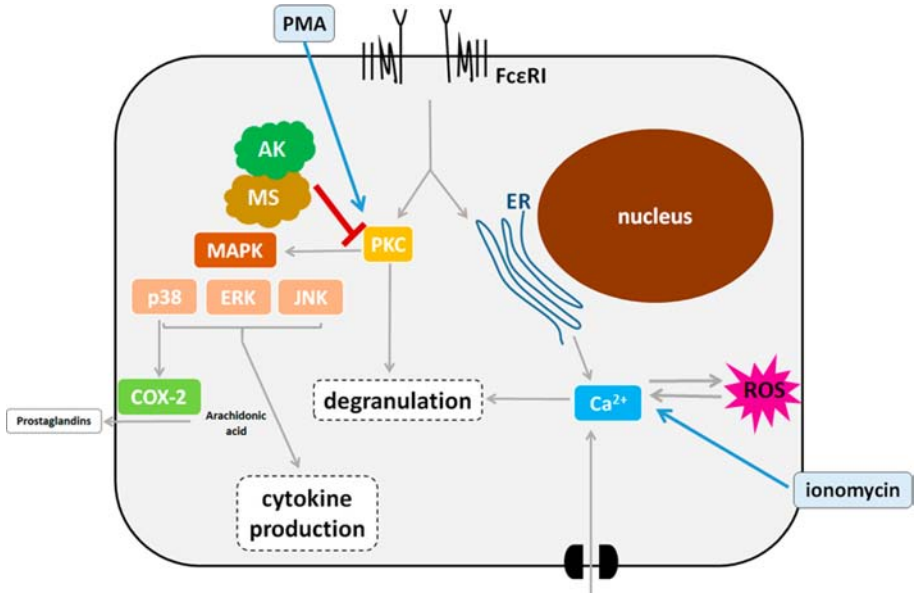

Figure 5. Proposed mechanism of monascin and ankaflavin on the inflammatory mediator release of mast cells.

activation of PKC and then affected downstream MAPK family ERK, JNK, and p38. On the other hand, rosiglitazone had no significant impact on the phosphorylation of PKC but still interfered with the activation of the MAPK family. In our

DOI: 10.1021/jf504013n
J. Agric. Food Chem. 2015, 63, 192−199

previous work, monascin and ankaflavin improved the ovalbumin-induced BALB/c airway allergic inflammation.[10,16] Monascin also down-regulated the maturation of dendritic cells and Th2 cytokine production.[16] We suggest that monascin and ankaflavin could suppress allergic reaction. To sum up these observations, monascin and ankaflavin may have a relieving effect on type I allergy patients and thus have potential for development into medicine s such as azelastine.

AUTHOR INFORMATION

Corresponding Author

*(T.-M.P.) Phone: +886-2-33664519, ext 10. Fax: +886-2-33663838. E-mail: tmpan@ntu.edu.tw.

Notes

The authors declare no competing financial interest.

ABBREVIATIONS USED

AK, ankaflavin; APC, antigen presenting cell; COX-2, cyclooxygenase-2; DCFH-DA, dichlorodihydrofluorescein diacetate; ERK, extracellular signal-regulated kinase; JNK, c-Jun N-terminal kinase; MAPK, mitogen-activated protein kinase; MS, monascin; PKC, protein kinase C; PMA, phorbol 12-myristate 13-acetate; PPARγ, peroxisome proliferator activated receptor γ; ROS, reactive oxygen species; Rosi, rosiglitazone; TNF-α, tumor necrosis factor-α

REFERENCES

(1) Parham, P. *Over-Reaction of the Immune System. The Immune System*, 3rd ed.; Garland Science, Taylor and Francis Group: London, UK, 2009; pp 366−385.

(2) Itoh, T.; Ohguchi, K.; Iinuma, M.; Nozawa, Y.; Akao, Y. Inhibitory effects of polymethoxy flavones isolated from *Citrus reticulate* on degranulation in rat basophilic leukemia RBL-2H3: enhanced inhibition by their combination. *Bioorg. Med. Chem.* **2008**, *16*, 7592−7598.

(3) Averbeck, M.; Gebhardt, C.; Emmrich, F.; Treudler, R.; Simon, J. C. Immunologic principles of allergic disease. *J. Dtsch. Dermatol. Ges.* **2007**, *5*, 1015−1028.

(4) Gordon, J. R.; Galli, S. J. Release of both preformed and newly synthesized tumor necrosis factor alpha (TNF-α)/cachectin by mouse mast cells stimulated via the FcεRI. A mechanism for the sustained action of mast cell-derived TNF-α during IgE-dependent biological responses. *J. Exp. Med.* **1991**, *174*, 103−107.

(5) Lee, B. H.; Hsu, W. H.; Chang, Y. Y.; Kuo, H. F.; Hsu, Y. W.; Pan, T. M. Ankaflavin: a natural novel PPARγ agonist upregulates Nrf2 to attenuate methylglyoxal-induced diabetes in vivo. *Free Radical Biol. Med.* **2012**, *53*, 2008−2016.

(6) C. P; Lin, Y. L.; Huang, P. H.; Tsai, H. S.; Chen, Y. H. Inhibition of endothelial adhesion molecule expression by *Monascus purpureus*-fermented rice metabolites, monacolin K, ankaflavin, and monascin. *J. Sci. Food Agric.* **2011**, *91*, 1751−1758.

(7) Hsu, W. H.; Lee, B. H.; Li, C. H.; Hsu, Y. W.; Pan, T. M. Monascin and AITC attenuate methylglyoxal-induced PPARγ phosphorylation and degradation through inhibition of the oxidative stress/PKC pathway depending on Nrf2 activation. *J. Agric. Food Chem.* **2013**, *61*, 5996−6006.

(8) Hsu, W. H.; Lee, B. H.; Chang, Y. Y.; Hsu, Y. W.; Pan, T. M. A novel natural Nrf2 activator with PPARγ-agonist (monascin) attenuates the toxicity of methylglyoxal and hyperglycemia. *Toxicol. Appl. Pharmacol.* **2013**, *272*, 842−851.

(9) Lee, B. H.; Hsu, W. H.; Huang, T.; Chang, Y. Y.; Hsu, Y. W.; Pan, T. M. Effects of monascin on anti-inflammation mediated by Nrf2 activation in advanced glycation end product-treated THP-1 monocytes and methylglyoxal-treated Wistar rats. *J. Agric. Food Chem.* **2013**, *61*, 1288−1298.

(10) Hsu, W. H.; Lee, B. H.; Huang, Y. C.; Hsu, Y. W.; Pan, T. M. Ankaflavin, a novel Nrf-2 activator for attenuating allergic airway inflammation. *Free Radical Biol. Med.* **2012**, *53*, 1643−1651.

(11) Lee, B. H.; Hsu, W. H.; Huang, T.; Chang, Y. Y.; Hsu, Y. W.; Pan, T. M. Monascin improves diabetes and dyslipidemia by regulating PPARγ and inhibiting lipogenesis in fructose-rich diet-induced C57BL/6 mice. *Food Funct.* **2013**, *4*, 950−959.

(12) Hsu, W. H.; Lee, B. H.; Chang, Y. Y.; Hsu, Y. W.; Pan, T. M. A novel natural Nrf2 activator with PPARγ-agonist (monascin) attenuates the toxicity of methylglyoxal and hyperglycemia. *Toxicol. Appl. Pharmacol.* **2013**, *272*, 842−851.

(13) Shi, Y. C.; Liao, V. H.; Pan, T. M. Monascin from red mold dioscorea as a novel antidiabetic and antioxidative stress agent in rats and *Caenorhabditis elegans*. *Free Radical Biol. Med.* **2012**, *52*, 109−117.

(14) Hsu, W. H.; Lee, B. H.; Hsu, Y. W.; Pan, T. M. Inhibition of Th2 cytokine production in T cells by monascin via PPAR-γ activation. *J. Agric. Food Chem.* **2013**, *61*, 8126−8133.

(15) Martinkova, L.; Patakova-Juzlova, P.; Krent, V.; Kucerova, Z.; Havlicek, V.; Olsovsky, P.; Hovorka, O.; Rihova, B.; Vesely, D.; Vesela, D.; Ulrichova, J.; Prikrylova, V. Biological activities of oligoketide pigments of *Monascus purpureus*. *Food Addit. Contam.* **1999**, *16*, 15−24.

(16) Hsu, W. H.; Lee, B. H.; Pan, T. M. Monascin attenuates oxidative stress-mediated lung inflammation via peroxisome proliferator-activated receptor-gamma (PPARγ) and nuclear factor-erythroid 2 related factor 2 (Nrf-2) modulation. *J. Agric. Food Chem.* **2014**, *62*, 5337−5344.

(17) Wagner, E. R.; He, B. C.; Chen, L.; Zuo, G. W.; Zhang, W.; Shi, Q.; Luo, Q.; Luo, X.; Liu, B.; Luo, J.; Rastegar, F.; He, C. J.; Hu, Y.; Boody, B.; Luu, H. H.; He, T. C.; Deng, Z. L.; Haydon, R. C. Therapeutic implications of PPAR in human osteosarcoma. *PPAR Res.* **2010**, 956427.

(18) Szeles, L.; Torocsik, D.; Nagy, L. PPARγ in immunity and inflammation: cell types and diseases. *Biochim. Biophys. Acta* **2007**, *1771*, 1014−1030.

(19) Hsu, W. H.; Lee, B. H.; Hsu, Y. W.; Pan, T. M. Peroxisome proliferator-activated receptor-γ activators monascin and rosiglitazone attenuate carboxymethyllysine-induced fibrosis in hepatic stellate cells through regulating the oxidative stress pathway but independent of the receptor for advanced glycation end products signaling. *J. Agric. Food Chem.* **2013**, *61*, 6873−6879.

(20) Slater, S. J.; Kelly, M. B.; Taddeo, F. J.; Rubin, E.; Stubbs, C. D. Evidence for discrete diacylglycerol and phorbol ester activator sites on protein kinase C. Differences in effects of 1-alkanol inhibition, activation by phosphatidylethanolamine and calcium chelation. *J. Biol. Chem.* **1994**, *269*, 17160−17165.

(21) Liu, C.; Hermann, T. E. Characterization of ionomycin as a calcium ionophore. *J. Biol. Chem.* **1978**, *253*, 5892−5894.

(22) Karra, L.; Levi-Schaffer, F. Down-regulation of mast cell responses through ITIM containing inhibitory receptors. *Adv. Exp. Med. Biol.* **2011**, *716*, 143−159.

(23) Blank, U.; Rivera, J. Assays for regulated exocytosis of mast cell granules. *Curr. Protoc. Cell Biol.***2006**, Chapter 15, Unit 15-11.

(24) Vo, T. S.; Kong, C. S.; Kim, S. K. Inhibitory effects of chitooligosaccharides on degranulation and cytokine generation in rat basophilic leukemia RBL-2H3 cells. *Carbohydr. Polym.* **2011**, *84*, 649−655.

(25) Han, E. H.; Hwang, Y. P.; Kim, H. G.; Park, J. H.; Choi, J. H.; Im, J. H.; Khanal, T.; Park, B. H.; Yang, J. H.; Choi, J. M.; Chun, S. S.; Seo, J. K.; Chung, Y. C.; Jeong, H. G. Ethyl acetate extract of *Psidium guajava* inhibits IgE-mediated allergic responses by blocking FcεRI signaling. *Food Chem. Toxicol.* **2011**, *49*, 100−108.

(26) Inoue, T.; Suzuki, Y.; Yoshimaru, T.; Ra, C. Reactive oxygen species produced up- or downstream of calcium influx regulate proinflammatory mediator release from mast cells: role of NADPH oxidase and mitochondria. *Biochim. Biophys. Acta* **2008**, *83*, 789−802.

(27) Okuyama, K.; Yamashita, M.; Kitabatake, Y.; Kawamura, S.; Takayanagi, M.; Ohno, I. Ciglitazone inhibits the antigen-induced

DOI: 10.1021/jf504013n
J. Agric. Food Chem. 2015, 63, 192−199

leukotrienes production independently of PPARγ in RBL-2H3 mast cells. *Eur. J. Pharmacol.* **2005**, *521*, 21−28.
(28) Sugiyama, H.; Nonaka, T.; Kishimoto, T.; Komoriya, K.; Tsuji, K.; Nakahata, T. Peroxisome proliferator-activated receptors are expressed in human cultured mast cells: a possible role of these receptors in negative regulation of mast cell activation. *Eur. J. Immunol.* **2000**, *30*, 3363−3370.
(29) Abdel-Raheem, I. T.; Hide, I.; Yanase, Y.; Shigemoto-Mogami, Y.; Sakai, N.; Shirai, Y.; Saito, N.; Hamada, F. M.; El-Mahdy, N. A.; El-Mahdy, N. A.; Sokar, S. S.; Nakata, Y. Protein kinase C-α mediates TNF release process in RBL-2H3 mast cells. *Br. J. Pharmacol.* **2005**, *145*, 415−423.
(30) Zhang, C.; Baumgartner, R. A.; Yamada, K.; Beaven, M. A. Mitogen-activated protein (MAP) kinase regulates production of tumor necrosis factor-alpha and release of arachidonic acid in mast cells. Indications of communication between p38 and p42 MAP kinases. *J. Biol. Chem.* **1997**, *272*, 13397−13402.
(31) Hide, I.; Toriu, N.; Nuibe, T.; Inoue, A.; Hide, M.; Yamamoto, S.; Nakata, Y. Suppression of TNF-alpha secretion by azelastine in a rat mast (RBL-2H3) cell line: evidence for differential regulation of TNF-α release, transcription, and degranulation. *J. Immunol.* **1997**, *159*, 2932−2940.
(32) Berger, W.; Hampel, F.; Bernstein, J.; Shah, S.; Sacks, H.; Meltzer, E. O. Impact of azelastine nasal spray on symptoms and quality of life compared with cetirizine oral tablets in patients with seasonal allergic rhinitis. *Ann. Allergy Asthma Immunol.* **2006**, *97*, 375−381.
(33) Corren, J.; Storms, W.; Bernstein, J.; Berger, W.; Nayak, A.; Sacks, H. Effectiveness of azelastine nasal spray compared with oral cetirizine in patients with seasonal allergic rhinitis. *Clin. Ther.* **2005**, *27*, 543−553.

DOI: 10.1021/jf504013n
J. Agric. Food Chem. 2015, 63, 192−199

JOURNAL OF AGRICULTURAL AND FOOD CHEMISTRY

Article

pubs.acs.org/JAFC

New Phenolic Compounds from *Coreopsis tinctoria* Nutt. and Their Antioxidant and Angiotensin I-Converting Enzyme Inhibitory Activities

Wei Wang,[†,∥] Wei Chen,[†,§,∥] Yingshi Yang,[†,§] Tianxing Liu,[†] Haiyan Yang,*[,§] and Zhihong Xin*[,†]

[†]Key Laboratory of Food Processing and Quality Control, College of Food Science and Technology, Nanjing Agricultural University, Nanjing 210095, People's Republic China

[§]College of Food Science and Pharmacy, Xinjiang Agricultural University, Urumqi, People's Republic China

ABSTRACT: Three new phenolic compounds, coretinphenol (**1**), coretincone (**2**), and coretinphencone (**3**), were isolated from the buds of *Coreopsis tinctoria* Nutt., together with nine known compounds, including butein (**4**), okanin (**5**), isoliquiritigenin (**6**), maritimetin (**7**), taxifolin (**8**), isookanin (**9**), marein (**10**), sachalinoside B (**11**), and 2-phenylethyl-β-D-glucoside (**12**). The chemical structures of these compounds were elucidated by extensive spectroscopic analysis and on the basis of their chemical reactivity. This work represents the first recorded example of the isolation of compounds **1**−**3**, **6**, **7**, **9**, **11**, and **12** from *C. tinctoria*. Compounds **5**−**9** showed strong diphenyl(2,4,6-trinitrophenyl)iminoazanium (DPPH) radical-scavenging activity, with IC_{50} values of 3.35 ± 0.45, 9.6 ± 2.32, 4.12 ± 0.21, 6.2 ± 0.43, and 7.9 ± 0.53 μM, respectively. Compounds **2** and **8** exhibited angiotensin I-converting enzyme inhibitory activity, with IC_{50} values of 228 ± 4.47 and 145.67 ± 3.45 μM, respectively. The activities of phenolic compounds isolated from *C. tinctoria* support the medicinal use of this plant in the prevention of cardiovascular diseases.

KEYWORDS: *Coreopsis tinctoria, structural identification, flavonoids, antioxidant activity, angiotensin I-converting enzyme inhibitory activity*

INTRODUCTION

Cardiovascular diseases (CVDs) are the leading cause of death worldwide, causing 17.3 million deaths per year.[1,2] It has been estimated that by 2030, there will be more than 23.6 million deaths annually resulting from CVDs all over the world.[2] Hypertension, one of the major risk factors related to CVDs, may be induced by many causes, for example, the imbalance of the renin angiotensin aldosterone system (RAAS), the kallikrein kinin system, and the sympathetic nervous system and genetic influences.[3] Among these causes, the angiotensin I-converting enzyme (ACE) plays a significant role in the RAAS, by converting the precursor angiotensin I into angiotensin II, a potent vasoconstrictor that is responsible for increasing blood pressure.[4] Therefore, finding potential ACE inhibitors from diverse natural resources has become a major target.[5] In particular, edible and medicinal plants have played important roles in functional food and drug development and continue to represent a promising source of new and interesting ACE inhibitors against hypertension.

Coreopsis tinctoria Nutt., which belongs to the Asteraceae/Compositae family, is a small, glabrous, aromatic annual plant distributed all over the world.[6,7] In China, it grows in the Karakorum Mountains at altitudes above 3000 m in southern Xinjiang. It is known as "snow chrysanthemum" or "snow tea" locally[8] and is traditionally used not only as a tea-like beverage but also as a folk medicine for the treatment of hypertension and hyperlipidemia in Uyghur folk medicine.[9] According to historical records, the decoction of *C. tinctoria* has been described by Huá Shòu as a traditional Chinese formula for diabetes as early as during the Yuan Dynasty (1271−1368 AD).[6] In North America and Romania, *C. tinctoria* was commonly cultivated in a variety of garden settings as an ornamental plant,[10] whereas the indigenous people of North America employed it as a therapeutic agent for several diseases, for example, diarrhea, internal pain, and bleeding, to strengthen blood, and as an emetic.[6] In Portugal, an infusion of two cups per day of *C. tinctoria* flowering tops, known as "Estrelas-do-Egipto", has been traditionally used to control diabetes.[10]

Previous studies have shown that *C. tinctoria* contains a diverse range of bioactive phytochemicals, including flavonoids,[6,11] phenolics,[12] phenylpropanoids,[13] polyacetylene glycosides,[8] and sterols,[14] with flavonoids being the major phytochemical present.[15] Although several investigations have been conducted on *C. tinctoria*, the precise nature of all of its bioactive components in antioxidant and antihypertensive activities remains unclear.

It is reported that the alcoholic extract of *C. tinctoria* buds showed the strongest antioxidant and antihypertensive effects.[9] Furthermore, in our preliminary studies, the methanol extract of *C. tinctoria* buds exhibited significant DPPH radical-scavenging activity and ACE inhibitory activity. It was for this reason that methanol was selected as an extraction solvent for the buds of *C. tinctoria*. An investigation of the chemical constituents in the bioactive extract led to the isolation of three new phenolic glycosides, together with nine other known compounds, and

Received: September 7, 2014
Revised: December 14, 2014
Accepted: December 17, 2014
Published: December 17, 2014

ACS Publications © 2014 American Chemical Society

DOI: 10.1021/jf504289g
J. Agric. Food Chem. 2015, 63, 200−207

evaluations of the antioxidant and ACE inhibitory activities of these compounds were performed.

Herein, we describe the experimental details of the separation process, as well as provide information pertaining to the elucidation of the structures of these compounds based on their spectroscopic properties and chemical reactivity.

MATERIALS AND METHODS

Chemicals. Dimethyl sulfoxide-d_6 (DMSO-d_6) and $CDCl_3$ were obtained from Merck (Darmstadt, Germany). Diphenyl(2,4,6-trinitrophenyl)iminoazanium (DPPH), ACE (EC 3.4.15.1), hippuric acid, and captopril were purchased from Sigma-Aldrich (St. Louis, MO, USA). All of the chemicals and solvents used in the current study were of analytical grade.

Materials. The aerial parts of *C. tinctoria* were purchased in September 2012 from the Beiyuanchun farmers market in Urumchi city of the Xinjiang Uygur Autonomous Region, China. The herbariums of *C. tinctoria* were deposited in the Key Laboratory of Food Processing and Quality Control, Nanjing Agricultural University, under number XJ8126. Thin-layer chromatography (TLC) analysis was performed on plates precoated with silica gel GF254 (10−40 μm). Column chromatography (CC) was performed over silica gel (300−400 mesh, Qingdao Marine Chemical Factory, Qingdao, China), reversed phase C18 (octadecylsilyl, ODS) silica gel (Silicycle, 50 μm, Canada), or Sephadex LH-20 (Sigma-Aldrich, St. Louis, MO, USA).

Instruments. UV spectra were recorded on a Beckman DU640 spectrophotometer (Beckman Coulter, Beijing, China). IR spectra were taken from KBr disks on a Nicolet Nexus 470 spectrophotometer (Thermo Scientific, Beijing, China). All of the ^1H and ^{13}C NMR spectra were recorded on Bruker Avance 300, 400, and 500 spectrometers (Bruker BioSpin GmbH, Beijing, China), using tetramethylsilane (TMS) as an internal standard. Two-dimensional NMR spectra include correlation spectroscopy (COSY), heteronuclear singular quantum correlation (HSQC), and heteronuclear multiple-bond correlation (HMBC). The chemical shifts in the NMR spectra were recorded as δ values. Electrospray ionization mass spectrometry (ESI-MS) analyses were measured on a Q-Tof Ultima Global GAA076 LC mass spectrometer (Waters Asia, Ltd., Singapore).

Extraction and Isolation. Dried buds of *C. tinctoria* (3 kg) were homogenized using a Polytron homogenizer prior to extracting three times with 80% acetone (1:6, v/v) at ambient temperature for 24 h. The resulting solution was then filtered, and the filtrate was combined and concentrated under vacuum at 30 °C until approximately 90% of the solvent had been evaporated. The remaining solution was then extracted sequentially with equal volumes of ethyl acetate (EtOAc) and methanol (three times), and the methanol solution was collected and concentrated under vacuum to give the methanol extract (15.8 g).

The methanol extract was separated into five fractions (A−E) by normal-phase silica gel column chromatography (CC) (100 g of silica gel, 300−400 mesh) using a stepwise gradient elution of cyclohexane/EtOAc/MeOH (from 100:0:0 to 0:100:0 to 0:0:100, v/v/v).

Fracton A (2.1 g) was separated into two subfractions (A-1 and A-2) on a normal-phase silica gel column using a stepwise gradient elution of petroleum ether/acetone (from 100:0 to 0:100, v/v). Fraction A-1 was then passed through a Sephadex LH-20 column with a $CHCl_3$/MeOH eluent (1:1, v/v) to yield compound **1** (3.5 mg). Fraction A-2 was purified on a silica gel column with a cyclohexane/EtOAc eluent (50:1, v/v) to produce compound **2** (3.7 mg).

Fraction B (3.4 g) was also purified by silica gel column chromatography with a cyclohexane/EtOAc eluent (50:1, v/v) to give three subfractions, B-1, B-2, and B-3. Fraction B-1 was passed through a Sephadex LH-20 column using a $CHCl_3$/MeOH eluent (1:1, v/v) to yield compound **3** (3.6 mg). Fraction B-2 was purified by silica gel column chromatography with a cyclohexane/EtOAc eluent (95:1, v/v) to give fraction B-2-1, which was separated through a Sephadex LH-20 column using a $CHCl_3$/MeOH eluent (1:1, v/v) to produce compound **4** (8.3 mg). Fraction B-3 was purified by column chromatography over silica gel with a cyclohexane/EtOAc eluent (200:1, v/v) to afford compound **5** (12.3 mg).

Fraction C (2.5 g) was separated into two subfractions (C-1 and C-2) by silica gel CC using petroleum ether/acetone (100:1, v/v) as an eluent. Fraction C-1 was subsequently purified by silica gel CC using petroleum ether/acetone (50:1, v/v) as an eluent to afford compound **6** (9.3 mg). Purification of fraction C-2 by silica gel CC eluting with a cyclohexane/EtOAc (10:1, v/v) gave compound **7** (11.3 mg).

Fraction D (5.8 g) was purified by normal-phase CC over silica gel, eluting with a petroleum ether/acetone eluent (15:1, v/v), to produce two subfractions, D-1 and D-2. Fraction D-1 was subjected to CC over silica gel with a petroleum ether/acetone eluent (100:1, v/v) to give compound **8** (10.5 mg), and fraction D-1-1. Fraction D-1-1 was subsequently purified over a Sephadex LH-20 column with a $CHCl_3$/MeOH eluent (1:1, v/v) to give compound **9** (13.4 mg). Fraction D-2 was purified by reversed-phase chromatography over silica gel using a stepwise gradient elution of MeOH/H_2O (80:20−0:100, v/v) to give fraction D-2-1, which was further purified using a Sephadex LH-20 column with a $CHCl_3$/MeOH eluent (1:1, v/v) to give compound **10** (51.9 mg).

Fraction E (2.0 g) was subjected to CC over silica gel using a stepwise gradient elution of petroleum ether/acetone (100:1 to 0:100, v/v) to provide two subfractions, E-1 and E-2. Fraction E-1 was subsequently purified by CC over a silica gel column using a petroleum ether/acetone eluent (10:1, v/v) to afford faction E-1-1, which was purified using a Sephadex LH-20 column with a $CHCl_3$/MeOH eluent (1:1, v/v) to give compound **11** (8.9 mg). Fraction E-2 was purified by silica gel CC, eluting with petroleum ether/acetone (60:1, v/v) to give compound **12** (21.5 mg).

Acid Hydrolysis of the Saponins and Determination of the Absolute Configuration of the Monosaccharides. The assay used to determine the absolute configuration of the monosaccharides was performed as described in the literature with minor modifications.[15] Briefly, a solution of the pure compound (2 mg) in 2 M HCl (2 mL) was heated at 85 °C for 15 h, and the resulting mixture was then evaporated under vacuum to give a residue, which was repeatedly distilled to dryness from H_2O under vacuum to produce a neutral residue. Then, the residue obtained and 2 mg of L-cysteine methyl ester hydrochloride were dissolved in 1 mL of anhydrous pyridine, and the resulting mixture was stirred at 60 °C for 1 h. A 3:1 mixture of HMDS−TMCS (hexamethyldisilazane−trimethylchlorosilane) was then added (300 μL), and the solution was stirred for 30 min. Hexane (3 mL) and water (1 mL) were then added to the solution. The hexane layer was dried over anhydrous Na_2SO_4 and subjected to GC-MS analysis under the following conditions: capillary column, HP-5MSi (30 m × 0.25 mm, with a 0.25 μm film, Agilent, USA); detection, FID; injection temperature, 250 °C; initial temperature, 160 °C, raised to 250 °C at 15 °C/min; final temperature maintained at 250 °C for 10 min.

Assay of DPPH Radical Scavenging. The DPPH radical-scavenging assay was performed according to the method described by Rivero-Pérez et al.[16] with slight modifications. Briefly, 1 mL of 0.2 mM DPPH ethanol solution was added to 2.5 mL of the sample solutions at different concentrations, and the resulting mixtures were shaken vigorously in the absence of light for 30 min. The absorbance values were then measured at 517 nm. Vitamin E (VE) was employed as a positive control. The antioxidant activity of the test compounds was expressed as IC_{50}, with the IC_{50} being defined as the concentration of test compounds required to inhibit the formation of DPPH radicals by 50%. All of the samples were analyzed in triplicate.

Measurement of Inhibitory Activity toward ACE. The measurement of inhibitory activity toward ACE was performed according to the method described by Cushman and Cheung,[17] which was slightly modified. The enzyme was added last to initiate the reaction, and tubes were incubated, usually for 10 min at 37 °C. One milliliter of ethyl acetate was added to the tubes and mixed by vortex for 15 s to extract hippuric acid from the acidified solution. The hippuric acid was redissolved in 3 mL of water, and the amount formed was determined by its absorbance at 228 nm. Captopril was employed as a positive control. The inhibitory activity of the test compounds was expressed as IC_{50}, with the IC_{50} being defined as the concentration of test compounds required to inhibit the ACE activity by 50%. All of the samples were analyzed in triplicate.

DOI: 10.1021/jf504289g
J. Agric. Food Chem. 2015, 63, 200−207

Table 1. NMR Spectral Data for Compound 1 in DMSO-d_6 at 400 (^{1}H) and 100 MHz (^{13}C)

position	H (J, Hz)	HSQC	HMBC (H→C)	^{1}H−^{1}H COSY
1		137.0		
2		148.4		
3		108.7		
3-CH_3	2.50 (s, 3H)	8.0	C-2, C-3, C-4	
4		152.8		
5	6.70 (s, 1H)	102.1	C-3, C-4, C-6, C-2′	
6		138.1		
1′	1.59 (d, J = 6.84 Hz, 3H)	21.8	C-2′, C-3′, C-6	
2′	4.07 (m, 1H)	30.2	C-5, C-6	H-1′, H-3′
3′	1.95 (dd, J = 7.68 Hz, 15.32 Hz, 2H)	37.8	C-1′, C-2′, C-4′, C-5′, C-6	
4′	2.35 (m, 2H)	25.4		H-3′
5′	5.84 (t, J = 7.24 Hz, 1H)	124.6		H-4′
6′		135.0		
6′-CH_3	1.98 (s, 3H)	12.8	C-5′, C-6′, C-7′	
7′	4.34 (s, 2H)	67.6	C-4′, C-5′	
1″	4.89 (d, J = 7.08 Hz, 1H)	106.7	C-1	H-2″
2″	3.99 (m, 1H)	70.3		
3″	3.99 (m, 1H)	76.9		H-2″
4″	3.99 (m, 1H)	74.4		H-3″, H-5″
5″	3.80 (m, 1H)	76.9		
6″	4.30 (m, 1H), 4.22 (m, 1H)	61.6		H-5″

Statistical Analysis. All of the assay results reported in the present work were analyzed according to Duncan's multiple-comparison test ($p < 0.05$), using version 18.0 of the SPSS software package. The resulting data were presented as the mean ± standard deviation.

RESULTS AND DISCUSSION

Elucidation of the Structures of the New Phenolics. Compound **1** was isolated as a yellow amorphous powder. Its molecular formula was determined to be $C_{21}H_{32}O_9$ on the basis of HRESIMS analysis of the pseudomolecular ion peak at m/z 451.1952 $[M + Na]^+$ (calculated as 451.1944), indicating six degrees of unsaturation. The UV spectrum of compound **1** revealed three strong absorption bands at 207, 230, and 280 nm. The IR spectrum displayed strong absorption bands at 3421, 1650, 1399, and 1047 cm^{-1}, corresponding to hydroxyl, olefinic, alkyl, and glycosidic functionalities, respectively. The ^{1}H NMR and ^{13}C NMR spectra of compound **1** revealed the presence of one benzene ring, one double bond, and one sugar unit in the molecule. Analysis of the ^{1}H−^{1}H COSY, HSQC, and HMBC spectra of compound **1** allowed for the complete assignment of the ^{1}H and ^{13}C NMR spectral data (Table 1). The sugar unit sequence from an anomeric proton H-1″ to oxymethylene proton H-6″ through oxymethine protons H-2″, H-3″, H-4″, and H-5″, as well as H-1′ to H-5′, was established by ^{1}H−^{1}H COSY. HMBC analysis of compound **1** displayed several key correlations, including the 3-CH_3 group with the C-2, C-3, and C-4 carbons, H-1′ with the C-2′, C-3′, and C-6 carbons, H-2′ with the C-5 and C-6 carbons, and the 6′-CH_3 group with the C-5′, C-6′, and C-7′ carbons. Key correlations from H-1″ to C-1 were observed in the HMBC experiments, indicating that the sugar moiety was connected directly to the C-1 position of the benzene ring. The anomeric configuration of the pyranosyl sugar unit was identified as a β-glucopyranosyl group on the basis of its $^3J_{\text{H-1″, H-2″}}$ coupling constant of 7.08 Hz. Acid hydrolysis of compound **1** with 2 M HCl liberated aglycone and D-glucose, which were identified by gas chromatography−mass spectrometry (GC-MS) analysis of the corresponding trimethylsilyl L-cysteine derivative and a direct comparison with an authentic sample of the same material that had been prepared in the same manner. The results revealed that the acid hydrolysate of pure compound **1** contained a D-glucose derivative. This result was confirmed through a comparison of the retention time of this derivative with that of the authentic D- (t_R, 20.254) and L-glucose derivatives (t_R, 20.705), respectively, with both samples providing a retention time of 20.254 min. Consequently, the structure of compound **1** was determined to be 2,4-dihydroxy-3-methyl-6-(7-hydroxy-6-methylhep-5-en-2-yl)-β-D-glucopyranoside and informally named coretinphenol (Figure 1).

Compound **2** was isolated as a yellow amorphous powder, and its molecular formula was determined to be $C_{21}H_{22}O_{10}$ on the basis of HRESIMS analysis of the pseudomolecular ion peak at m/z 433.1142 $[M - H]^-$ (calculated as 433.1135). The UV spectrum of compound **2** revealed strong absorption bands at 212, 267, and 383 nm. The IR spectrum displayed strong absorption bands at 3421, 3254, 1656, 1399, and 1062 cm^{-1}, which are characteristic of flavonoid-glycoside type structures. Analysis of its 1D NMR data suggested the presence of an aglycone moiety and a sugar unit (Table 2). The aglycone resonances showed a β-unsaturated ketone olefinic proton at δ 7.78 (d, J = 8.88 Hz, 1H, H-β), an ABX spin system at δ 6.60 (d, J = 2.44 Hz, 1H, H-3′), 6.65 (dd, J = 2.44 Hz, 8.92 Hz, 1H, H-5′), and 8.22 (d, J = 8.96 Hz, 1H, H-6′), and an ABCX spin system at δ 7.40 (d, J = 2.08 Hz, 1H, H-2), 7.78 (d, J = 8.88 Hz, 1H, H-4), 6.93 (d, J = 8.20 Hz, 1H, H-5), and 7.26 (dd, J = 2.08 Hz, 8.16 Hz, 1H, H-6), as well as a broad proton singlet at δ 13.50 (s, 1H) attributable to 2′-OH. The ^{13}C NMR of compound **2** revealed the presence of 21 carbon signals, with 6 of these being assigned to the sugar moieties, 15 to the aglycone including 12 aromatic ring carbons, 2 olefinic carbons, and a characteristic carbonyl group at δ 192.3. These data revealed that the structure of compound **2** closely resembled that of compound **4**, which has been previously isolated from this plant.[18] A direct comparison of the ^{1}H and ^{13}C NMR data of these two compounds revealed that they share the same skeleton. The ^{1}H NMR spectrum of compound **2** revealed that the resonance signals corresponding to the H-4 at δ 7.78 and α-OH protons in compound **2** had been

DOI: 10.1021/jf504289g
J. Agric. Food Chem. 2015, 63, 200−207

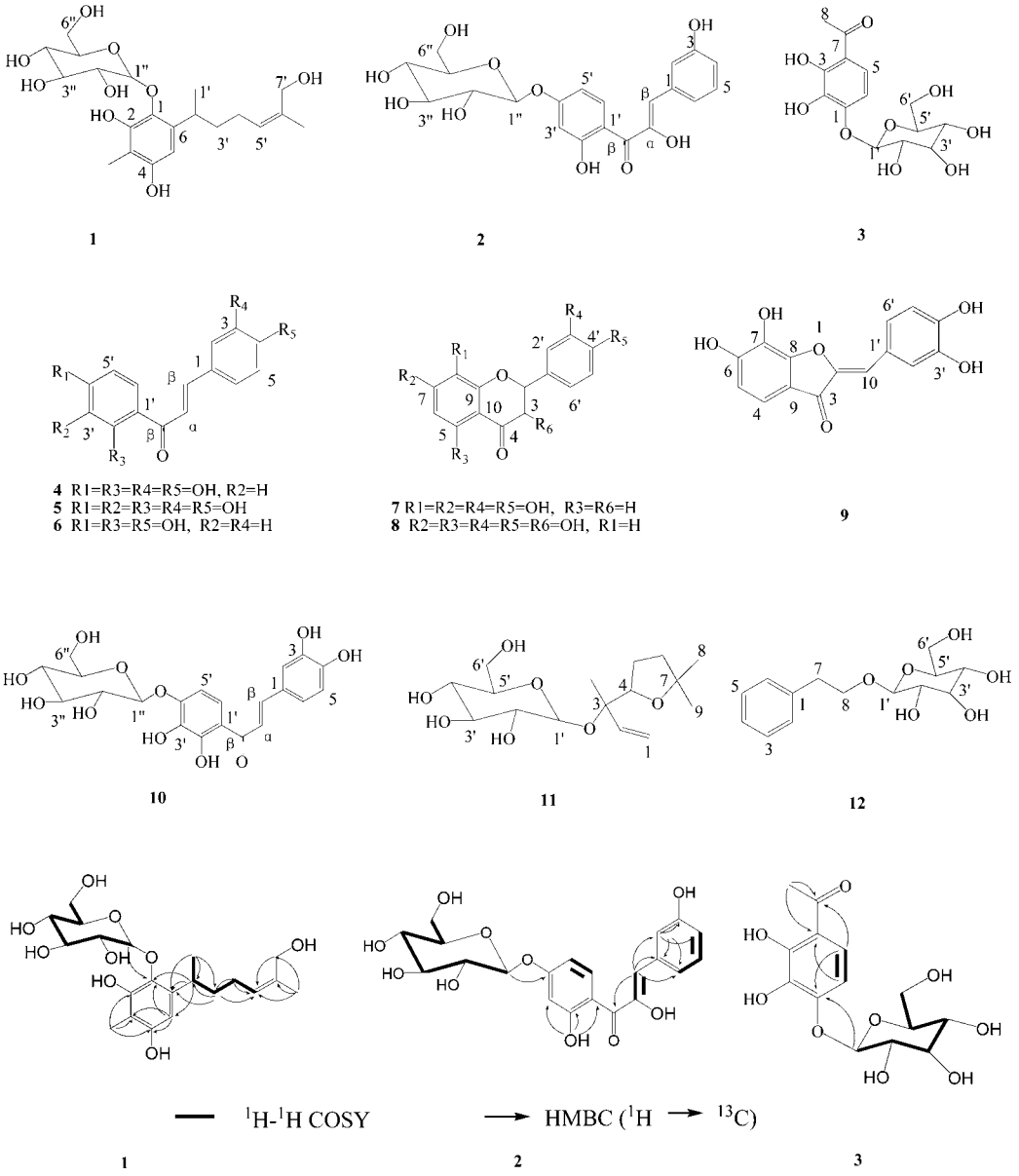

Figure 1. Chemical structures of the 12 compounds isolated from the methanol extract of *C. tinctoria*: **1**, coretinphenol; **2**, coretincone; **3**, coretinphencone; **4**, butein; **5**, okanin; **6**, isoliquiritigenin; **7**, maritimetin; **8**, taxifolin; **9**, isookanin; **10**, marein; **11**, sachalinoside B; **12**, 2-phenylethyl-*β*-D-glucoside. Key ^{1}H−^{1}H COSY and HMBC correlations for compounds **1**, **2**, and **3** are also shown.

replaced by a hydroxyl group and one olefinic proton at δ 7.65 in compound **4**. This difference was also supported by the presence of a methine carbon at δ 117.3 (C-4) and a quaternary carbon at δ 145.5 (C-α) in the ^{13}C NMR spectrum of compound **2**. These signals were replaced by the carbon signals at δ 148.8 and 117.3 in the spectrum of compound **4**, respectively. This assignment was further supported by HMBC correlations from the 2′-OH to C-1′, C-2′, and C-3′ and H-β to C-1, C-2, C-6, and C-β′. The full structure of compound **2** was further confirmed by ^{1}H−^{1}H COSY, HSQC, and HMBC experiments (Table 2). The anomeric proton of the glucopyranosyl sugar moiety at δ 5.15 (d, J = 7.52 Hz, 1H, H-1″) coupling to the C-4′ at δ 163.9 suggested the sugar moiety connected directly to C-4′ of aglycone. The anomeric configuration of the sugar unit was determined as a β-glucopyranosyl group from its $^{3}J_{\text{H-1″, H-2″}}$ coupling constant of 7.52 Hz. Following the hydrolysis of compound **2** with 2 M HCl and its subsequent trimethylsilylation for GC-MS analysis, the retention time of the sugar was found to be the same as that of an authentic sample of D-glucose. On the basis of this evidence, the structure of compound **2** was characterized as α,3,2′-trihydroxy-4′-*O*-β-D-glucopyranosylchalcone and informally named coretincone (Figure 1).

Compound **3** was isolated as a colorless amorphous powder. Its molecular formula was established as $C_{14}H_{18}O_9$ on the basis of HRESIMS analysis of the pseudomolecular ion peak at m/z 329.0881 $[M - H]^-$ (calculated as 329.0873), indicating six degrees of unsaturation. The UV spectrum showed strong absorption bands at 217, 283, and 343 nm. The IR spectrum displayed strong absorption bands at 3415, 1638, 1508, and 1074 cm^{-1}, corresponding to hydroxyl, carbonyl, aromatic, and glycosidic functionalities, respectively. The ^{1}H and ^{13}C NMR spectra were typical of a glycosidic type compound. The ^{1}H NMR spectrum revealed the presence of an AB spin system at δ 7.39 (d, J = 9.05 Hz, 1H) and 6.75 (d, J = 8.95 Hz, 1H), an

DOI: 10.1021/jf504289g
J. Agric. Food Chem. 2015, 63, 200−207

Table 2. NMR Spectral Data for Compound 2 in DMSO-d_6 at 400 (^{1}H) and 100 MHz (^{13}C)

position	*H* (*J*, Hz)	HSQC	HMBC (H→C)	^{1}H−^{1}H COSY
1		127.2		
2	7.40 (d, *J* = 2.08 Hz, 1H)	115.2	C-3, C-6, C-*β*	
3		148.5		
4	7.78 (d, *J* = 8.88 Hz, 1H)	117.3	C-2, C-5, C-6	
5	6.93 (d, *J* = 8.20 Hz, 1H)	115.5	C-1, C-3	
6	7.26 (dd, *J* = 2.08 Hz, 8.16 Hz, 1H)	122.7		H-5
1′		115.0		
2′		166.1		
2′-OH	13.50 (s, 1H)		C-1′, C-2′, C-3′	
3′	6.60 (d, *J* = 2.44 Hz, 1H)	103.8	C-1′, C-5′	
4′		163.9		
5′	6.65 (dd, *J* = 2.44 Hz, 8.92 Hz, 1H)	108.1	C-1′, C-4′	
6′	8.22 (d, *J* = 8.96 Hz, 1H)	131.9	C-2′, C-4′, C-*β*′	H-5′
α		145.5		
β	7.78 (d, *J* = 8.88 Hz, 1H)	145.3	C-1, C-2, C-6, C-*β*′	
β′		192.3		
1″	5.15 (d, *J* = 7.52 Hz, 1H)	100.1	C-4′	H-2″
2″	3.51 (m, 1H)	73.6		
2″-OH	4.76 (d, *J* = 4.08 Hz, 1H)		C-1″, C-3″	H-2″
3″	3.57 (m, 1H)	77.1		H-2″, H-4″
3″-OH	4.48 (d, *J* = 3.92 Hz, 1H)			H-3″
4″	3.49 (m, 1H)	70.3		
4″-OH	4.40 (d, *J* = 4.32 Hz, 1H)			H-4″
5″	3.57 (m, 1H)	76.9		H-4″
6″	3.74 (m, 1H), 3.97 (m, 1H)	61.6		H-5″

anomeric proton at *δ* 4.87 (d, *J* = 7.15 Hz, 1H), and a methyl at *δ* 2.57 (s, 3H). The ^{13}C NMR spectrum of compound **3** revealed the presence of 14 carbon signals, with 8 of these signals being assigned to the aglycone and 6 to the sugar moieties. The signals at *δ* 150.5, 134.2, and 151.1, connecting to three oxygen atoms, were attributed to the C-1, C-2, and C-3 carbons, respectively, and a signal at *δ* 203.8, corresponding to a carbonyl group, was assigned to the C-7 carbon. This assignment was further confirmed by HMBC correlations from H-5 to C-1, C-3, and C-7, from H-6 to C-1, C-2, and C-4, and from H-8 to C-4 and C-7. The full structure of compound **3** was further confirmed by ^{1}H−^{1}H COSY, HSQC, and HMBC experiments (Table 3). Key correlations from H-1′ to C-1 were observed in the HMBC experiments, indicating that the sugar unit was connected directly to the C-1 position of the aromatic ring. The anomeric configuration of the sugar unit was determined as a *β*-glucopyranosyl group from its $^3J_{\text{H-1′, H-2′}}$ coupling constant of 7.15 Hz. The *β*-glucopyranosyl group for compound **3** was also identified as D-glucose by the same procedures as for compounds **1** and **2**. Consequently, the structure of compound **3** was characterized as 2,3-dihydroxy-4-formoxyl-1-*O*-*β*-D-glucopyranoside and informally named coretinphencone (Figure 1).

Nine known compounds (Figure 1) were identified as butein (**4**),[18] okanin (**5**),[19] isoliquiritigenin (**6**),[18] maritimetin (**7**),[20] taxifolin (**8**),[21] isookanin (**9**),[22] marein (**10**),[11] sachalinoside B (**11**),[23] and 2-phenylethyl-*β*-D-glucoside (**12**),[24] respectively, by comparing their physical and spectroscopic data with those reported in the literature.

Antioxidant Activity of the Pure Compounds Isolated from *C. tinctoria*. The antioxidant activities of the 12 pure compounds were tested using the DPPH radical-scavenging assay. The results of these experiments are shown in Figure 2A. DPPH radical-scavenging activity of compounds **1**−**12** ranged from 13.2 to 89.4% at the concentration of 100 *μ*M. Compounds **5**−**9** displayed powerful DPPH radical-scavenging activity compared with the positive control vitamin E, followed by compounds **1**−**4** and **10**, whereas compounds **11** and **12** had the lowest activity. These compounds were further tested to calculate their IC_{50} values at different concentrations ranging from 1 to 100 *μ*M, and the results are shown in Table 4. The IC_{50} values of compounds **5**−**9** were 3.35 ± 0.45, 9.6 ± 2.32, 4.12 ± 0.21, 6.2 ± 0.43, and 7.9 ± 0.53 *μ*M, respectively, and were much lower than

Table 3. NMR Spectral Data for Compound 3 in DMSO-d_6 at 400 (^{1}H) and 100 MHz (^{13}C)

position	*H* (*J*, Hz)	HSQC	HMBC (H→C)	^{1}H−^{1}H COSY
1		150.5		
2		134.2		
3		151.1		
4		115.4		
5	7.39 (d, *J* = 9.05 Hz, 1H)	122.0	C-1, C-3, C-7	H-6
6	6.75 (d, *J* = 8.95 Hz, 1H)	106.5	C-1, C-2, C-4	
7		203.8		
8	2.57 (s, 3H)	26.8	C-4, C-7	
1′	4.87 (d, *J* = 7.15 Hz, 1H)	100.9	C-1	H-2′
2′	3.34 (m, 1H)	73.1	C-1′	
3′	3.36 (m, 1H)	77.2		H-2′, H-4′
4′	3.17 (t, *J* = 8.95 Hz, 1H)	69.6		
5′	3.30 (m, 1H)	75.8		H-4′
6′	3.47 (m, 2H)	60.6		H-5′
	3.71 (d, *J* = 11.75 Hz, 1H)	60.6		

DOI: 10.1021/jf504289g
J. Agric. Food Chem. 2015, 63, 200−207

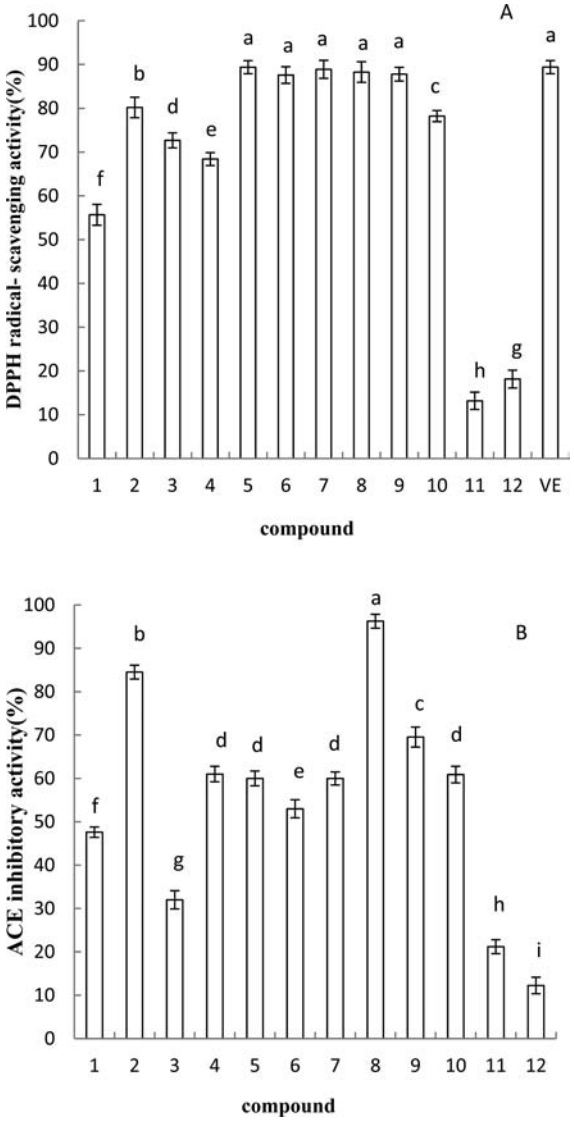

Figure 2. DPPH radical-scavenging activity (A) and ACE inhibitory activity (B) of the isolated compounds at concentrations of 100 and 400 μM, respectively. Coretinphenol (**1**), coretincone (**2**), coretinphencone (**3**), butein (**4**), okanin (**5**), isoliquiritigenin (**6**), maritimetin (**7**), taxifolin (**8**), isookanin (**9**), marein (**10**), sachalinoside B (**11**), and 2-phenylethyl-β-D-glucoside (**12**). Each value has been presented as the mean ± standard deviation of three experiments. (a–i) Results with a different letter differ significantly ($p < 0.05$).

those of vitamin E; these results are consistent with the values previously reported.[22,25−28]

ACE Inhibitory Activity of the Pure Compounds Isolated from *C. tinctoria*. The ACE inhibitory activities of the 12 pure compounds at the concentration of 400 μM were assessed, and the results are reported in Figure 2B. Among the pure compounds isolated from *C. tinctoria*, compound **8** exhibited strong ACE inhibitory activity, followed by compounds **2**, **4**−**7**, **9**, and **10**, whereas other compounds had weak ACE inhibitory activity. To further characterize the ACE inhibitory effect of these compounds, all of the compounds at different concentrations, ranging from 10 to 400 μM, were tested. Compounds **2** and **8** in particular possessed ACE inhibitory activity with IC_{50} values of 228 ± 4.47 and 145.67 ± 3.45 μM, respectively, whereas other compounds exhibited no inhibitory effect on ACE (Table 4). The IC_{50} value of captopril was

Table 4. IC_{50} Values of the 12 Compounds Isolated from the Methanol Extract of *C. tinctoria* and Positive Control for DPPH Radical-Scavenging Activity and ACE Inhibitory Activity

	IC_{50} (μM)	
compd	DPPH assay	ACE inhibitory assay
1	92.51 ± 1.17	>300
2	33.49 ± 0.47	228 ± 4.47
3	51.25 ± 0.51	>300
4	61.24 ± 0.41	>300
5	3.35 ± 0.45	>300
6	9.6 ± 2.32	>300
7	4.12 ± 0.21	>300
8	6.2 ± 0.43	145.67 ± 3.45
9	7.9 ± 0.53	>300
10	48.35 ± 0.36	>300
11	>100	>300
12	>100	>300
VE[a]	24.73 ± 0.97	>300
captopril		0.009 ± 2.32

[a]VE, vitamin E.

determined to be 0.009 ± 2.32 μM, similar to the value previously reported in the literature.[29] Previous studies have demonstrated that flavonoids have the potential to inhibit ACE activity in vitro by developing complexes with metal ions, which is an active center of ACE. Therefore, the metal ions of ACE are reduced and ACE activity decreases.[30,31] It has been reported that the ability of flavonoids to chelate metal ions varies depending on the position of the hydroxyl group in the molecular structure, where a hydroxyl group attached to the 3,5- and 3′,4′-positions are crucial to the inhibition of ACE activity.[32,33] The structure of compound **8** is consistent with this characteristic; therefore, compound **8** showed potent ACE inhibitory activity.

NMR and ESI-MS Spectroscopic Data. Coretinphenol (1): yellow amorphous powder; ^{1}H NMR and ^{13}C NMR data, see Table 1; ESI-MS m/z 451.1952 $[M + Na]^+$.

Coretincone (2): yellow amorphous powder; ^{1}H NMR and ^{13}C NMR data, see Table 2; ESI-MS m/z 433.1142 $[M - H]^-$.

Coretinphencone (3): colorless amorphous powder; ^{1}H NMR and ^{13}C NMR data, see Table 3; ESI-MS m/z 329.0881 $[M - H]^-$.

Butein (4): yellow amorphous powder; ^{1}H NMR (300 MHz, acetone-d_6, TMS) δ 7.27 (d, J = 1.71 Hz, 1H, H-2), 6.82 (d, J = 8.13 Hz, 1H, H-5), 7.20 (dd, J = 1.74, 8.19 Hz, 1H, H-6), 6.27 (d, J = 2.22 Hz, 1H, H-3′), 6.40 (d, J = 2.16, 8.82 Hz, 1H, H-5′), 8.14 (d, J = 8.91 Hz, 1H, H-6′), 7.65 (s, 2H, H-α, β); ^{13}C NMR δ 126.6 (C-1), 115.7 (C-2), 145.5 (C-3), 148.8 (C-4), 115.7 (C-5), 122.3 (C-6), 113.0 (C-1′), 164.8 (C-2′), 102.5 (C-3′), 165.6 (C-4′), 108.0 (C-5′), 132.7 (C-6′), 117.3 (C-α), 144.6 (C-β), 191.4 (C-β′); ESI-MS m/z 271.1 $[M - H]^-$.

Okanin (5): yellow amorphous powder; ^{1}H NMR (400 MHz, DMSO-d_6, TMS) δ 7.26 (d, J = 1.95 Hz, 1H, H-2), 6.82 (d, J = 8.13 Hz, 1H, H-5), 7.20 (dd, J = 2.01, 8.22 Hz, 1H, H-6), 6.44 (d, J = 8.88 Hz, 1H, H-5′), 7.68 (d, J = 8.22 Hz, 1H, H-6′), 7.65(s, 2H, H-α, β); ^{13}C NMR δ 126.2 (C-1), 115.7 (C-2), 145.5 (C-3), 148.8 (C-4), 115.6 (C-5), 122.2 (C-6), 113.3 (C-1′), 153.5 (C-2′), 132.4 (C-3′), 152.5 (C-4′), 107.6 (C-5′), 117.3 (C-6′), 122.2 (C-α), 144.4 (C-β), 191.9 (C-β′); ESI-MS m/z 287.1 $[M - H]^-$.

Isoliquiritigenin (6): yellow amorphous powder; ^{1}H NMR (400 MHz, acetone-d_6, TMS) δ 7.77 (dd, J = 2.44, 6.64 Hz, 2H, H-2, 6), 6.96 (d, J = 8.64 Hz, 2H, H-3, 5), 6.50 (dd, J = 2.44, 8.88

DOI: 10.1021/jf504289g
J. Agric. Food Chem. 2015, 63, 200−207

Hz, 1H, H-3′), 6.38 (dd, J = 2.24, 8.88 Hz, 1H, H-5′), 8.16 (d, J = 8.80 Hz, 1H, H-6′), 7.84 (d, J = 11.96 Hz, 2H, H-α, β); ^{13}C NMR δ 126.6 (C-1), 130.9 (C-2, 6), 115.8 (C-3, 5), 160.1 (C-4), 113.6 (C-1′), 164.7 (C-2′), 102.8 (C-3′), 166.7 (C-4′), 107.7 (C-5′), 132.4 (C-6′), 117.3 (C-α), 144.2 (C-β), 191.9 (C-β′); ESI-MS m/z 255.1 $[M - H]^-$.

Maritimetin (7): yellow amorphous powder; ^{1}H NMR (500 MHz, acetone-d_6, TMS) δ 5.42 (dd, J = 2.84, 12.88 Hz, 1H, H-2), 2.67 (dd, J = 2.88, 16.80 Hz, 1H, H-3), 3.04 (dd, J = 12.88, 16.76 Hz, 1H, H-3), 7.33 (d, J = 8.60 Hz, 1H, H-5), 6.62 (d, J = 8.64 Hz, 1H, H-6), 7.06 (d, J = 1.80 Hz, 1H, H-2′), 6.88 (d, J = 8.80 Hz, 1H, H-5′), 6.89 (dd, J = 1.76, 8.80 Hz, 1H, H-6′); ^{13}C NMR δ 145.9 (C-2), 182.4 (C-3), 116.4 (C-4), 112.2 (C-5), 155.4 (C-6), 130.6 (C-7), 154.6 (C-8), 115.0 (C-9), 113.0 (C-10), 123.9 (C-1′), 118.8 (C-2′), 146.3 (C-3′), 148.3 (C-4′), 115.6 (C-5′), 124.9 (C-6′); ESI-MS m/z 287.1 $[M - H]^-$.

Taxifolin (8): yellow amorphous powder; ^{1}H NMR (400 MHz, acetone-d_6, TMS) δ 5.05 (d, J = 11.44 Hz, 1H, H-2), 4.64 (d, J = 11.44 Hz, 1H, H-3), 5.96 (d, J = 2.16 Hz, 1H, H-6), 6.00 (d, J = 2.16 Hz, 1H, H-8), 7.08 (d, J = 2.08 Hz, 1H, H-2′), 6.88 (d, J = 8.08 Hz, 1H, H-5′), 6.94 (dd, J = 2.08, 8.16 Hz, 1H, H-6′); ^{13}C NMR δ 83.6 (C-2), 72.2 (C-3), 197.3 (C-4), 166.9 (C-5), 96.1 (C-6), 164.1 (C-7), 95.1 (C-8), 163.8 (C-9), 100.6 (C-10), 128.8 (C-1′), 114.8 (C-2′), 144.8 (C-3′), 145.6 (C-4′), 114.8 (C-5′), 119.9 (C-6′); ESI-MS m/z 303.1 $[M - H]^-$.

Isookanin (9): yellow amorphous powder; ^{1}H NMR (300 MHz, DMSO-d_6, TMS) δ 7.41 (s, 1H, H-2′), 7.36 (d, J = 8.46 Hz, 1H, H-6′), 7.10 (d, J = 8.46 Hz, 1H, H-4), 6.84 (d, J = 8.34 Hz, 1H, H-5′), 6.72 (d, J = 8.10 Hz, 1H, H-5), 6.58 (s, 1H, H-10); ^{13}C NMR δ 145.9 (C-2), 182.4 (C-3), 116.4 (C-4), 112.2 (C-5), 155.4 (C-6), 130.6 (C-7), 154.6 (C-8), 115.0 (C-9), 113.0 (C-10), 123.9 (C-1′), 124.9 (C-2′), 115.6 (C-3′), 148.3 (C-4′), 146.3 (C-5′), 118.8 (C-6′); ESI-MS m/z 285.1 $[M - H]^-$.

Marein (10): yellow amorphous powder; ^{1}H NMR (500 MHz, DMSO-d_6, TMS) δ 7.29 (d, J = 2.05 Hz, 1H, H-2), 6.81 (d, J = 8.15 Hz, 1H, H-5), 7.22 (dd, J = 2.10, 8.25 Hz, 1H, H-6), 6.77 (d, J = 9.20 Hz, 1H, H-5′), 7.73 (d, J = 9.20 Hz, 1H, H-6′), 13.12 (s, 1H, 2′-OH), 4.90 (d, J = 7.30 Hz, 1H, H-1″), 3.33 (m, 1H, H-2″), 3.20 (m, 1H, H-3″), 3.39 (m, 1H, H-4″), 3.50 (dd, J = 5.95, 11.85 Hz, 1H, H-5″), 3.49 (dd, J = 5.95, 11.85 Hz, H, H-6″), 3.73 (dd, J = 2.00, 11.85 Hz, 1H, H-6″), 7.66(s, 2H, H-α, β); ^{13}C NMR δ 126.1 (C-1), 115.7 (C-2), 145.5 (C-3), 148.9 (C-4), 115.8 (C-5), 122.5 (C-6), 115.9 (C-1′), 152.4 (C-2′), 134.4 (C-3′), 150.4 (C-4′), 106.3 (C-5′), 121.4 (C-6′), 101.0 (C-1″), 73.2 (C-2″), 69.8 (C-3″), 75.8 (C-4″), 77.3 (C-5″), 60.5 (C-6″), 145.9 (C-α), 117.4 (C-β), 192.6 (C-β′); ESI-MS m/z 449.0 $[M - H]^-$.

Sachalinoside B (11): colorless amorphous powder; ^{1}H NMR (500 MHz, acetone-d_6, TMS) δ 4.94 (dd, J = 1.60, 10.80 Hz, 1H, H-1α), 5.21 (dd, J = 1.28, 17.40 Hz, 1H, H-1β), 6.01 (dd, J = 10.80, 17.40 Hz, 1H, H-2), 1.24 (s, 3H, 3-CH_3), 4.06 (t, J = 7.00 Hz, 1H, H-4), 1.77 (m, 2H, H-5), 1.85 (m, 1H, H-6α), 1.99 (m, 1H, H-6β), 1.23 (s, 3H, H-8), 1.20 (s, 3H, H-9), 4.60 (d, J = 7.70 Hz, 1H, H-1′), 3.10 (t, J = 8.40 Hz, 1H, H-2′), 3.39 (d, J = 8.35 Hz, 1H, H-3′), 3.29 (m, 1H, H-4′), 3.29 (m, 1H, H-5′), 3.64 (m, 1H, H-6′α), 3.80 (m, 1H, H-6′β); ^{13}C NMR δ 111.3 (C-1), 145.5 (C-2), 79.0 (C-3), 84.2 (C-4), 38.3 (C-5), 27.5 (C-6), 83.5 (C-7), 23.8 (C-8), 22.4 (C-9), 97.9 (C-1′), 75.2 (C-2′), 78.1 (C-3′), 71.8 (C-4′), 77.2 (C-5′), 63.1 (C-6′); ESI-MS m/z 331.2 $[M - H]^-$.

2-Phenylethyl-β-D-glucoside (12): colorless amorphous powder; ^{1}H NMR (500 MHz, acetone-d_6, TMS) δ 7.18−7.30 (m, 5H, H-2, 3, 4, 5, 6), 3.23 (t, J = 8.56 Hz, 2H, H-7), 4.06 (m, 2H, H-8), 4.36 (d, J = 7.72 Hz, 1H, H-1′), 2.95 (m, 1H, H-2′), 3.39 (m, 1H, H-3′), 3.40 (m, 1H, H-4′), 3.41 (m, 1H, H-5′), 3.68 (m, 1H, H-6′α), 3.85 (m, 1H, H-6′β); ^{13}C NMR δ 139.0 (C-1), 128.2 (C-2, 6), 128.9 (C-3, 5), 126.0 (C-4), 36.0 (C-7), 70.0 (C-8), 103.5 (C-1′), 73.9 (C-2′), 76.6 (C-3′), 70.8 (C-4′), 77.0 (C-5′), 62.1 (C-6′); ESI-MS m/z 283.3 $[M - H]^-$.

Purification of the methanol extract of *C. tinctoria* allowed for the isolation of three new phenolics, coretinphenol (**1**), coretincone (**2**), and coretinphencone (**3**), and nine known compounds, including butein (**4**), okanin (**5**), isoliquiritigenin (**6**), maritimetin (**7**), taxifolin (**8**), isookanin (**9**), marein (**10**), sachalinoside B (**11**), and 2-phenylethyl-β-D-glucoside (**12**). The structures of these compounds were elucidated using a combination of spectroscopic methods and chemical analysis. To the best of our knowledge, this is the first report concerning the isolation of compounds **1**−**3**, **6**, **7**, **9**, **11**, and **12** from *C. tinctoria*. Compounds **5**−**9** exhibited strong antioxidant activity against DPPH radical, and compounds **2** and **8** showed ACE inhibitory activity. It is worth mentioning, however, the bioactivities of these compounds in vitro are not necessarily equal to their actual beneficial effects in vivo. These mainly depend on the bioaccessibility and bioavailability in vivo, where they are mostly mixed with biomacromolecule such as carbohydrates, lipids, and proteins to form the complex matrix. Several factors interfere with the real effects of a compound, such as food source and chemical interactions with other phytochemicals and biomolecules present in the food matrix.[34] Further studies should be carried out to assess the bioactivities of these compounds in animal experiments, as well as to validate their real effects in the human body in the future.

In conclusion, 12 compounds have been identified from the buds of *C. tinctoria*, and 8 of these compounds have been isolated for the first time. In particular, three of these compounds have been identified as novel phenolics: coretinphenol (**1**), coretincone (**2**), and coretinphencone (**3**). The findings in the current research may explain, in part, the antioxidant function and antihypertensive effect of *C. tinctoria* as a tea beverage and a folk medicine. Further studies are warranted to confirm the antihypertensive effect of *C. tinctoria* in vivo and elucidate the mechanism of ACE inhibition.

AUTHOR INFORMATION

Corresponding Authors

*(H.Y.) E-mail: yanghaiyan@163.com.

*(Z.X.) Phone/fax: +86 25 8439 5618. E-mail: xzhfood@njau.edu.cn.

Author Contributions

‖W.W. and W.C. contributed equally to this work and should be considered co-first authors.

Funding

This work was financially supported by the Chinese National Natural Science Fund (Grant 31260377), the science and technology program of Urumqi city (Grant Y121120008), the Fundamental Research Funds for the Central Universities (Grant KYZ201118), the project funded by special funds of agro-product quality safety risk assessment of Ministry of Agriculture of the People's Republic of China (GJFP2014011), and a project funded by the Priority Academic Program Development of Jiangsu Higher Education Institutions.

Notes

The authors declare no competing financial interest.

DOI: 10.1021/jf504289g
J. Agric. Food Chem. 2015, 63, 200−207

REFERENCES

(1) Wang, X.; Ouyang, Y.; Liu, J.; Zhu, M.; Zhao, G.; Bao, W.; Hu, F. B. Fruit and vegetable consumption and mortality from all causes, cardiovascular disease, and cancer: systematic review and dose-response meta-analysis of prospective cohort studies. *BMJ* **2014**, *349*, 1−14.

(2) Smith, S. C.; Collins, A.; Ferrari, R.; Holmes, D. R.; Logstrup, S.; McGhie, D. V.; Ralston, J.; Sacco, R. L.; Stam, H.; Taubert, K.; Wood, D. A.; Zoghbi, W. A. Our time: a call to save preventable death from cardiovascular disease (heart disease and stroke). *J. Am. Coll. Cardiol.* **2012**, *60*, 2343−2348.

(3) Oparil, S.; Zaman, M. A.; Calhoun, D. A. Pathogenesis of hypertension. *Ann. Intern. Med.* **2003**, *139*, 761−776.

(4) Danilczyk, U.; Penninger, J. M. Angiotensin-converting enzyme II in the heart and the kidney. *Circ. Res.* **2006**, *98*, 463−471.

(5) Wijesekara, I.; Kim, S. K. Angiotensin-I-converting enzyme (ACE) inhibitors from marine resources: prospects in the pharmaceutical industry. *Mar. Drugs* **2010**, *8*, 1080−1093.

(6) Dias, T.; Bronze, M. R.; Houghton, P. J.; Mota-Filipe, H.; Paulo, A. The flavonoid-rich fraction of *Coreopsis tinctoria* promotes glucose tolerance regain through pancreatic function recovery in streptozotocin-induced glucose-intolerant rats. *J. Ethnopharmacol.* **2010**, *132*, 483−490.

(7) Gaspar, L.; Oliveira, A. P.; Silva, L. R.; Andrade, P. B.; Pinho, P. G. d.; Botelho, J.; Valentão, P. Metabolic and biological prospecting of *Coreopsis tinctoria*. *Rev. Bras. Farmacogn.* **2012**, *22*, 350−358.

(8) Zhang, Y.; Shi, S.; Zhao, M.; Chai, X.; Tu, P. Coreosides A−D, C14-polyacetylene glycosides from the capitula of *Coreopsis tinctoria* and its anti-inflammatory activity against COX-2. *Fitoterapia* **2013**, *87*, 93−97.

(9) Sun, Y.-H.; Zhao, J.; Jin, H.-T.; Cao, Y.; Ming, T.; Zhang, L.-L.; Hu, M.-Y.; Hamlati, H.; Pang, S.-B.; Ma, X.-P. Vasorelaxant effects of the extracts and some flavonoids from the buds of *Coreopsis tinctoria*. *Pharm. Biol.* **2013**, *51*, 1158−1164.

(10) Zălaru, C.; Crişan, C.; Călinescu, I.; Moldovan, Z.; Ţârcomnicu, I.; Litescu, S.; Tatia, R.; Moldovan, L.; Boda, D.; Iovu, M. Polyphenols in *Coreopsis tinctoria* Nutt. fruits and the plant extracts antioxidant capacity evaluation. *Cent. Eur. J. Chem.* **2014**, *12*, 858−867.

(11) Zhang, Y.; Shi, S.; Zhao, M.; Jiang, Y.; Tu, P. A novel chalcone from *Coreopsis tinctoria* Nutt. *Biochem. Syst. Ecol.* **2006**, *34*, 766−769.

(12) Shimokoriyama, M. Anthochlor pigments of *Coreopsis tinctoria*. *J. Am. Chem. Soc.* **1957**, *79*, 214−220.

(13) Reichling, J.; Thron, U. Accumulation of rare phenylpropanoids in *Agrobacterium rhizogenes* transformed root cultures of *Coreopsis tinctoria*. *Planta Med.* **1990**, *56*, 488−490.

(14) Zhang, Y.; Tu, P. F. Chemical constituents of *Coreopsis tinctoria*. *China J. Chin. Mater. Med.* **2012**, *37*, 3581−3584.

(15) Deyrup, S. T.; Gloer, J. B.; O'Donnell, K.; Wicklow, D. T. Kolokosides A−D: triterpenoid glycosides from a Hawaiian isolate of *Xylaria* sp. *J. Nat. Prod.* **2007**, *70*, 378−382.

(16) Rivero-Perez, M. D.; Muniz, P.; Gonzalez-Sanjose, M. L. Antioxidant profile of red wines evaluated by total antioxidant capacity, scavenger activity, and biomarkers of oxidative stress methodologies. *J. Agric. Food Chem.* **2007**, *55*, 5476−5483.

(17) Cushman, D. W.; Cheung, H. S. Spectrophotometric assay and properties of the angiotensin-converting enzyme of rabbit lung. *Biochem. Pharmacol.* **1971**, *20*, 1637−1648.

(18) Prachayasittikul, S.; Buraparuangsang, P.; Worachartcheewan, A.; Isarankura-Na-Ayudhya, C.; Ruchirawat, S.; Prachayasittikul, V. Antimicrobial and antioxidative activities of bioactive constituents from *Hydnophytum formicarum* Jack. *Molecules* **2008**, *13*, 904−921.

(19) Zhao, J.; Sun, Y.; Xu, F.; Li, C.; Hu, M.; Zhang, L.; Pang, S. Study on flavonoids of *Coreopsis tinctoria* Nutt. *Nat. Prod. Res. Dev.* **2013**, *25*, 50−52.

(20) Xiang, Z.-b.; Chen, H.-s.; Jin, Y.-s.; Wang, G.-l.; Xiang, L.-x.; Chen, W. Phenolic constituents of *Canarium album*. *Chem. Nat. Compd.* **2010**, *46*, 119−120.

(21) Inada, A.; Murata, H.; Somekawa, M.; Nakanishi, T. Phytochemical studies of seeds of medicinal plants. II. A new dihydroflavonol glycoside and a new 3-methyl-1-butanol glycoside from seeds of *Platycodon grandiflorum* A. De Candolle. *Chem. Pharm. Bull.* **1992**, *40*, 3081−3083.

(22) Venkateswarlu, S.; Panchagnula, G. K.; Subbaraju, G. V. Synthesis and antioxidative activity of 3′,4′,6,7-tetrahydroxyaurone, a metabolite of *Bidens frondosa*. *Biosci., Biotechnol., Biochem.* **2004**, *68*, 2183−2185.

(23) Fan, W.; Tezuka, Y.; Komatsu, K.; Namba, T.; Kadota, S. Prolyl endopeptidase inhibitors from the underground part of *Rhodiola sacra* SH Fu. *Biol. Pharm. Bull.* **1999**, *22*, 157−161.

(24) Piao, M. S.; Kim, M. R.; Lee, D. G.; Park, Y.; Hahm, K. S.; Moon, Y. H.; Woo, E. R. Antioxidative constituents from *Buddleia officinalis*. *Arch. Pharmacal Res.* **2003**, *26*, 453−457.

(25) Lin, H. Y.; Chang, S. T. Antioxidant potency of phenolic phytochemicals from the root extract of *Acacia confusa*. *Ind. Crops Prod.* **2013**, *49*, 871−878.

(26) Chin, Y. W.; Jung, H. A.; Liu, Y.; Su, B. N.; Castoro, J. A.; Keller, W. J.; Pereira, M. A.; Kinghorn, A. D. Anti-oxidant constituents of the roots and stolons of licorice (*Glycyrrhiza glabra*). *J. Agric. Food Chem.* **2007**, *55*, 4691−4697.

(27) Brighente, I. M. C.; Dias, M.; Verdi, L. G.; Pizzolatti, M. G. Antioxidant activity and total phenolic content of some Brazilian species. *Pharm. Biol.* **2007**, *45*, 156−161.

(28) Jung, M. J.; Kang, S. S.; Jung, H. A.; Kim, G. J.; Choi, J. S. Isolation of flavonoids and a cerebroside from the stem bark of *Albizzia julibrissin*. *Arch. Pharmacal Res.* **2004**, *27*, 593−599.

(29) Vermeirssen, V.; Van Camp, J.; Verstraete, W. Optimisation and validation of an angiotensin-converting enzyme inhibition assay for the screening of bioactive peptides. *J. Biochem. Biophys. Methods* **2002**, *51*, 75−87.

(30) Smyk, B.; Pliszka, B.; Drabent, R. Interaction between cyanidin 3-glucoside and Cu(II) ions. *Food Chem.* **2008**, *107*, 1616−1622.

(31) Balasuriya, B. N.; Rupasinghe, H. V. Plant flavonoids as angiotensin converting enzyme inhibitors in regulation of hypertension. *Funct. Foods Health Dis.* **2011**, *5*, 172−188.

(32) Kwon, E.-K.; Lee, D.-Y.; Lee, H.; Kim, D.-O.; Baek, N.-I.; Kim, Y.-E.; Kim, H.-Y. Flavonoids from the buds of *Rosa damascena* inhibit the activity of 3-hydroxy-3-methylglutaryl-coenzyme a reductase and angiotensin I-converting enzyme. *J. Agric. Food Chem.* **2009**, *58*, 882−886.

(33) Guerrero, L.; Castillo, J.; Quinones, M.; Garcia-Vallve, S.; Arola, L.; Pujadas, G.; Muguerza, B. Inhibition of angiotensin-converting enzyme activity by flavonoids: structure-activity relationship studies. *PLoS One* **2012**, *7*, No. e49493.

(34) Palafox-Carlos, H.; Ayala-Zavala, J. F.; Gonzalez-Aguilar, G. A. The role of dietary fiber in the bioaccessibility and bioavailability of fruit and vegetable antioxidants. *J. Food Sci.* **2011**, *76*, R6−R15.

DOI: 10.1021/jf504289g
J. Agric. Food Chem. 2015, 63, 200−207

JOURNAL OF AGRICULTURAL AND FOOD CHEMISTRY

Article

pubs.acs.org/JAFC

4-Acetylantroquinonol B Suppresses Tumor Growth and Metastasis of Hepatoma Cells via Blockade of Translation-Dependent Signaling Pathway and VEGF Production

Chien-Hsin Chang,[†] Tur-Fu Huang,[†] Kung-Tin Lin,[†] Chun-Chieh Hsu,[†] Wei-Luen Chang,[†] Shih-Wei Wang,[§] Feng-Nien Ko,[#] Hui-Chin Peng,[†] and Ching-Hu Chung*[,§]

[†]Institute of Pharmacology, College of Medicine, National Taiwan University, Taipei, Taiwan

[§]Department of Medicine, Mackay Medical College, New Taipei City, Taiwan

[#]Oneness Biotech Company, Ltd., Taipei, Taiwan

Supporting Information

ABSTRACT: Hepatocellular carcinoma (HCC) has become one of most common malignancies and a leading cause of cancer mortality worldwide. Previous study has shown that 4-acetylantroquinonol B (4AAQB) isolated from *Antrodia cinnamomea* (or niu-chang-chih) was observed to inhibit HepG2 cell proliferation via affecting cell cycle. However, the in vivo effects and antimetastatic activity of 4AAQB have not yet been addressed. This study found that 4AAQB inhibited HepG2 and HuH-7 hepatoma cell growth in both in vitro and in vivo models and exhibited pronounced inhibitory effects on HuH-7 tumor growth in xenograft and orthotopic models. 4AAQB efficiently inhibited the phosphorylation of mTOR and its upstream kinases and the downstream effectors and decreased the production of VEGF and activity of Rho GTPases in HuH-7 cells. Furthermore, 4AAQB inhibited in vitro HuH-7 cell migration and in vivo pulmonary metastasis. The results suggested that 4AAQB is a potential candidate for HCC therapy.

KEYWORDS: *hepatocellular carcinoma, Antrodia cinnamomea, 4AAQB, RhoGTPase, mTOR, metastasis, VEGF*

INTRODUCTION

Hepatocellular carcinoma (HCC) has become one of the most common malignancies and a leading cause of cancer mortality worldwide. It causes more than a million fatalities each year worldwide, and it is prevalent in Asia, including Taiwan; however, the increasing incidence of HCC has also been reported in Western countries.[1,2] The predominant risk factor in Asia and Africa is chronic hepatitis B viral (HBV), which, however, in Western countries and Japan is chronic hepatitis C viral (HCV) infection.[3,4] Although surgery is the most effective therapeutic approach for HCC, tumor invasiveness, intrahepatic spread, and extrahepatic metastasis are the key factors affecting HCC prognosis.[5] Therefore, it is important to elucidate the molecular pathogenesis of HCC to develop new strategies against this devastating disease.

There are many signaling pathways involved in tumor cell growth and metastasis.[6] The phosphatidylinositol 3-kinase (PI3K)/Akt pathway was demonstrated to play a major role in these processes. PI3K can then activate Akt that subsequently phosphorylates several other cytoplasmic proteins and mammalian target of rapamycin (mTOR). mTOR phosphorylates the translational regulators p70S6 kinase (p70S6K) and eukaryotic initiation factor (eIF) 4E-binding protein 1 (4E-BP1), resulting in cell growth promotion and cell cycle progression.[3,7] The PI3K/Akt/mTOR signaling pathway has recently become a promising target owing to its frequent activation and dysregulation in HCC. The mTOR pathway is activated in >50% patients with HCC, and phosphorylation of Akt has also been detected in up to 71% of HCC samples. This aberrant signaling is associated with invasion and metastasis of HCC and correlated with poor outcome.[8]

Antrodia cinnamomea (niu-chang-chih) is a well-known medicinal mushroom and grows naturally only in Taiwan. It has been applied in traditional Chinese medicine for the treatment of diarrhea, food poisoning, drug intoxication, abdominal pain, itchy skin, hypertension, and cancer therapy.[9,10] The biological activities of *A. cinnamomea* have been described, including antioxidant, anti-inflammatory, hepatoprotective, and antitumor activities.[11−13] *A. cinnamomea* has recently become more popular as a therapeutic agent for several human cancers.[9,11,14]

Several pure compounds in the fruiting body and mycelium of *A. cinnamomea* with antitumor activity have been isolated and identified,[12] particularly for hepatoma via the inhibition of cell growth and induction of apoptosis in human liver cancer cell lines.[15,16] Lin et al. isolated 4-acetylantroquinonol B (4AAQB) from the mycelium of *A. cinnamomea*, which potently inhibited the proliferation and growth of the hepatocellular carcinoma cell line (IC_{50} = 0.1 μg/mL).[17] A previous study showed that 4AAQB exerted an inhibitory effect on tumor growth by decreasing the expression of CDK2 and CDK4 and increasing the expression of p27, p53, and p21, resulting in cell cycle arrest.[18] However, to the best of our knowledge, there

Received: September 15, 2014
Revised: November 25, 2014
Accepted: December 10, 2014
Published: December 10, 2014

ACS Publications © 2014 American Chemical Society

DOI: 10.1021/jf504434v
J. Agric. Food Chem. 2015, 63, 208−215

have been no studies reporting that 4AAQB and other related antroquinonol compounds exhibit anticancer efficacy in in vivo models. In this study, we found that 4AAQB inhibited the PI3K/Akt/mTOR pathways in the human hepatocellular carcinoma cell line HuH-7. In addition, 4AAQB displayed prominent antitumor and antimetastatic effects in xenograft and lung metastasis models.

MATERIALS AND METHODS

Materials. 4-Acetylantroquinonol B was isolated from the mycelium of *A. cinnamomea* as described previously.[17] Lactate dehydrogenase (LDH) assay reagents were purchased from Promega (Madison, WI, USA). Antibodies to phospho-Akt (Ser473), phospho-mTOR (Ser2448), were purchased from Epitomics (Burlingame, CA, USA). Antibody to phospho-ERK1/2 (Thr202/Tyr204), ERK1/2, phospho-p70S6K (Thr389), and β-actin were purchased from Cell Signaling Technologies (Boston, MA, USA).

Cell Culture. Human hepatocellular carcinoma cell lines HepG2 and HuH-7 were obtained from the American Type Culture Collection. HepG2 and HuH-7 cells were cultured at 37 °C in HEPES-buffered Dulbecco's modified Eagle's medium (DMEM), containing 10% fetal bovine serum (Gibco) supplemented with $NaHCO_3$, glutamax I (Gibco), 100 IU/mL penicillin G (sodium salt), 100 μg/mL streptomycin, and 0.25 μg/mL amphotericin B (antibiotic−antimitotic solution, Gibco).

Cell Viability Assay. Hepatoma cells (HepG2 and HuH-7, 5×10^3 cells/well) were subcultured onto 96-well plates and starved with serum-free DMEM for 48 h. Then hepatoma cells were incubated in DMEM with 10% FBS in the absence or presence of various concentrations of 4AAQB (0.1, 0.3, 1, 3, and 10 μg/mL) for 48 h. After treatment, the medium was discarded first. To fix the adherent cells, 100 μL of trichloroacetic acid (10% (w/v)) was added to each well and incubated at 4 °C for 1 h. Then the plates were washed with deionized water and dried in the air. To each well was added 50 μL of sulforhodamine B (SRB) solution (0.4% w/v in 1% acetic acid) and incubated for 5 min at room temperature. To remove unbound SRB in the plates, the plates were washed with 1% acetic acid and then air-dried. The residual bound SRB was solubilized with 100 μL of 10 mM Tris base buffer (pH 10.5) and then read using a microtiter plate reader at 495 nm.

Cell Cycle Analysis. HuH-7 cells were pretreated with vehicle and different concentrations of 4AAQB for 24 h. Cell cycle experiments were performed with HuH-7 cells treated with vehicle as a control. According to the manufacturer's protocol (Apoptosis and Cell Proliferation Kit; BD Biosciences, San Jose, CA, USA), the experiment was conducted and analyzed by flow cytometry.

Oligonucleotide Microarray Analysis. HuH-7 cells were pretreated with vehicle or 4AAQB (3 μg/mL) for 24 h. Microarray experiments were performed with HuH-7 cells treated with vehicle as a control. According to the manufacturer's guidelines, the synthesized cDNA was synthesized and hybridized onto Human OneArray microarrays (Phanlanx Biotech Group, Hsinchu, Taiwan). Data analysis was conducted also according to the manufacturer's guidelines. Target preparation was performed using an Eberwine-based amplification method with an Amino Allyl Message Amp II aRNA Amplification Kit (Ambion, AM1753) to generate amino-allyl antisense RNA. Labeled aRNA coupled with NHS-CyDye was prepared and purified prior to hybridization. Purified coupled aRNA was quantified using a NanoDrop ND-1000. All array results were verified by the CyDye incorporation efficiency at >10 dye molecules/1000 nt. After duplicate sample analysis, there were 1177 up-regulated genes and 791 down-regulated genes.

Western Blotting. Western blotting was performed as previously described.[19] HuH-7 cells were pretreated with vehicle of various concentrations of 4AAQB (0.3, 1, 3, and 10 μg/mL) for 12 h. For the Rho/Rac1 pull-down assay, cells were harvested as described above and processed according to the manufacturer's protocol (Rho/Rac1 Activation Assay kit; Millipore, Billerica, MA, USA). The binding active Rho/Rac1 proteins were detected by Western blotting.

ELISA. HuH-7 cells (10^5 cells/well in 96 wells) were treated with various concentrations of 4AAQB or vehicle for 24 h, and then the supernatant was collected to examine the amount of vascular endothelial growth factor (VEGF) protein. A VEGF Human ELISA Kit (Novex, Invitrogen) was used according to the manufacturer's instructions.

Migration Assay. Migration assay of HuH-7 cells was measured by Coaster Transwells (polycarbonate filter, 8 μm pore size), which were coated with 0.2% gelatin. HuH-7 cells (5×10^4 cells/well) were treated with vehicle or different concentrations of 4AAQB (1, 3, ad 10 μg/mL), and then cells were seeded into the upper chamber. To the bottom chamber was added DMEM supplemented with 10% FBS. After incubation at 37 °C for 16 h, all nonmigrant cells were removed from the upper face of the Transwell membrane with a cotton swab, and the HuH-7 cells that had transmigrated through the micropore and that were still bound to the membrane were fixed with 4% paraformaldehyde in PBS solution and stained with 0.5% toluidine blue in 4% paraformadehyde. Migration was quantified by counting the number of stained cells on the membrane under a light microscope (Nikon, Japan) at a magnification of 200× in three random fields and then photographed. All determinations were obtained by replication in at least three independent experiments.

Animals. Male NOD SCID mice (8−10 weeks old) were used in all studies. All of the experimental protocols regarding animal study have been approved by the Institutional Animal Care and Use Committee at College of Medicine, Tzu-Chi University.

Subcutaneous Xenograft Models. HepG2 or HuH-7 (2×10^6) cells in a volume of 100 μL were injected subcutaneously into the right flank of the male NOD SCID mice. After 9 days, when tumors reached 2 mm in diameter, the mice were randomly given vehicle or 4AAQB at a dosage of 0.2 or 2 mg/kg for the HepG2 model and at a dosage of 0.5 or 2 mg/kg for the HuH-7 model once daily by intraperitoneal injection. Tumor size and body weight were measured every day. The tumor volume was calculated according to the following formula: $V = (\text{length} \times \text{width}^2/2)$. In accordance with the Animal Ethics Committee, the experiments should be stopped when an unbearable situation appeared in animals.

Immunohistochemistry Study. Paraffin embedded tumor were cut in 25 μm sections and then immunolocalized with ROCK1. The sections were incubated with 1% H_2O_2 and washed three times in PBS containing Triton X-100 (0.4%) and 2% BSA. Blocking was performed with 10% BSA and then incubated on a rocking table with Rock1 monoclonal antibody at 4 °C overnight. Sections were washed with PBS, incubated with the biotinylated anti-mouse IgG, washed with PBS again, and then incubated with 0.2% ABC solution (Vector Laboratories, Burlingame, CA, USA). After a washing with PBS, sections were treated with DAB (Sigma) for 15 min. Sections were mounted on gelatinized slides, air-dried overnight, and coverslipped.

Orthotopic Tumor Models. An orthotopic tumor model was created by intrahepatically injecting 2×10^6 HuH-7 cells in a volume of 100 μL into 8−10-week-old male NOD SCID mice. Seven days after implantation, mice were randomly divided into two groups (vehicle and 4AAQB). 4AAQB-treated groups received 2 mg/kg by intraperitoneal injection every day. The tumor-bearing mice were sacrificed by CO_2 asphyxiation on day 25 after administration of 4AAQB, and the livers were excised. Tumor-bearing liver lobes were fixed in formalin (10%). The orthotopic hepatocarcinoma area of liver surface was white and the background was dark red. White area was quantified using ImageJ software.

Experimental Metastasis Analysis. Metastasis analysis was performed as previously described.[20] Briefly, HuH-7 cells (2×10^6 cells) were slowly injected into the lateral tail vein of NOD SCID mice to initiate tumor metastasis. 4AAQB (0.5 or 2 mg/kg) was intraperitoneally administered to mice everyday from 3 days before tumor cell injection to 21 days after tumor cell injection (the day sacrificed).

Statistical Analysis. All values are presented as the mean ± SEM. Differences between groups were assessed by one-way ANOVA and Newman−Keuls multiple-comparison test when appropriate. p values <0.05 ($p < 0.05$) were considered to be significantly different.

DOI: 10.1021/jf504434v
J. Agric. Food Chem. 2015, 63, 208−215

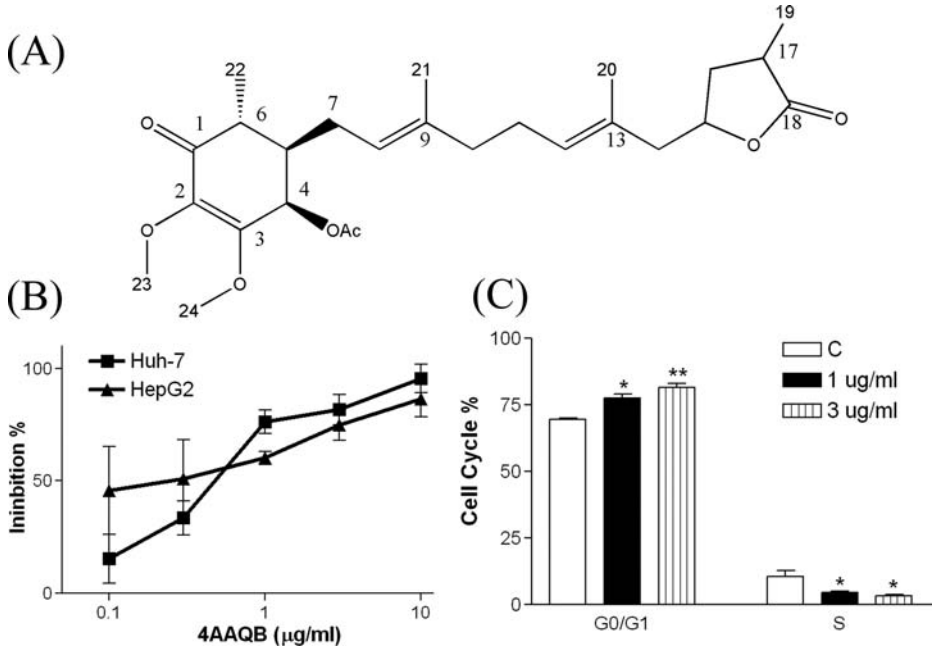

Figure 1. Structure of 4AAQB and its effect on hepatoma cell viability and cell cycle. The structure of 4AAQB is shown in panel A. HepG2 (B) and HuH-7 (C) cells were seeded onto plates for 24 h and starved for another 48 h with serum-free DMEM. Quiescent cells were cultivated with DMEM containing 10% FBS in the absence or presence of various concentrations of 4AAQB. After 48 h, cell viability was detected by the SRB assay. The results are presented as percentages of inhibition (mean ± SEM, $n = 4$). (D) HuH-7 cells were treated with vehicle or 4AAQB (1 and 3 μg/mL) for 24 h and analyzed by flow cytometry. Cell cycle distribution is shown as percentage in cell cycle phase.

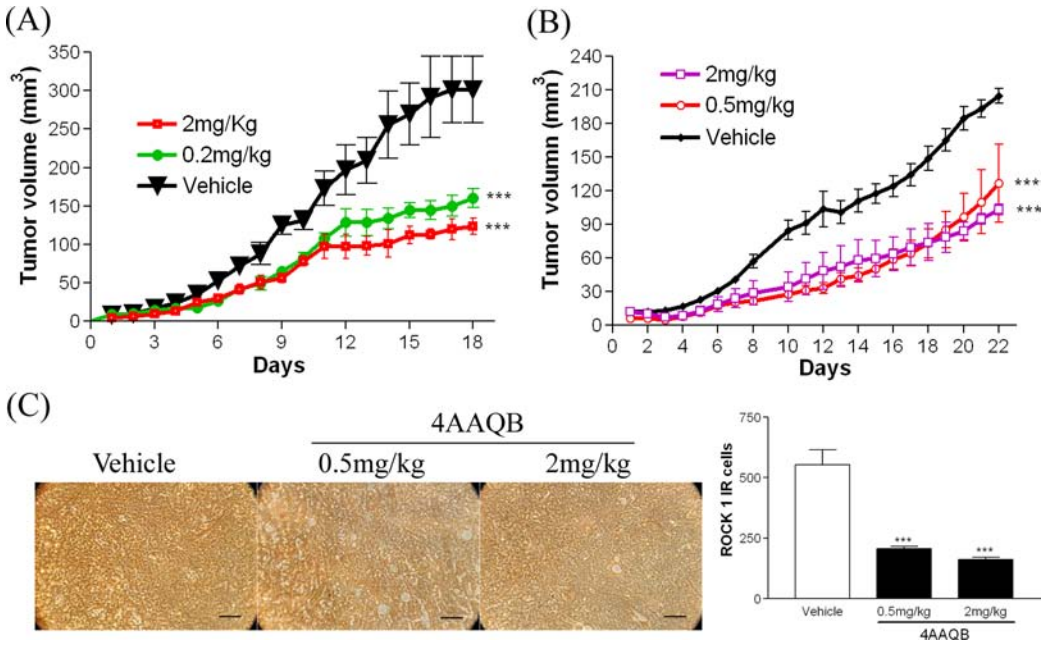

Figure 2. Effect of 4AAQB on HepG2 and HuH-7 tumor xenograft in vivo. SCID mice were sc inoculated with 2×10^6 cells of HepG2 (A) or HuH-7 (B). When tumors reached 2 mm in diameter, mice were administered vehicle or indicated dosage of 4AAQB by intraperitoneal injection once daily (QD). The tumor volumes of HepG2 and HuH-7 xenograft models were measured and plotted daily in 4AAQB-treated or control mice: points, mean tumor volume (mm^3). (C) Expression of ROCK1 in HuH-7 tumor xenograft was studied, and the ROCK 1 immunoreactive (IR) cells were counted. Scale bar = 10 μm, SE; (*) $p < 0.05$ and (***) $p < 0.001$.

RESULTS

Effects of 4AAQB on the Inhibition of HepG2 and HuH-7 Hepatoma Cell Proliferation. The structure of 4AAQB is shown in Figure 1A. A previous study reported that 4AAQB displayed a great growth inhibitory effect on HepG2 cells.[17] Because hepatocellular carcinoma is the major type in hepatoma and HepG2 is a hepatoblastoma, we used another hepatocellular carcinoma cell line, HuH-7, to examine the inhibitory effects of 4AAQB in this study. We first determined the effect of 4AAQB on hepatoma cell proliferation. HepG2 and HuH-7 cells were treated with 4AAQB for 48 h, followed by SRB assay. As shown in Figure 1B,C, 4AAQB inhibited the

DOI: 10.1021/jf504434v
J. Agric. Food Chem. 2015, 63, 208−215

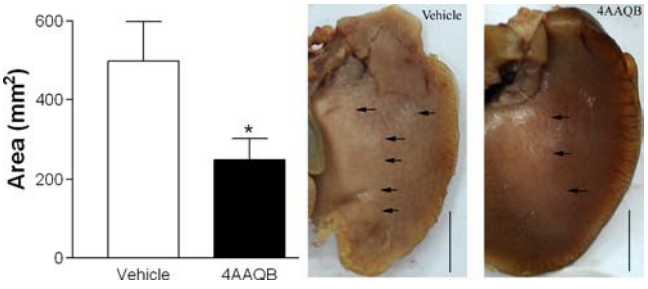

Figure 3. In vivo effect of 4AAQB on human hepatocellular carcinoma (HCC) growth in orthotopic xenograft models. SCID mice were intrahepatically inoculated with 2×10^6 cells of HuH-7. After 7 days, the mice were treated intraperitoneally with 4AAQB or vehicle once daily. Arrow bar is used to point out the orthotopic hepatocarcinoma area, which was quantified using ImageJ software. Scale bar = 2.5 mm.

proliferation of HuH-7 cells in a concentration-dependent manner, with a similar potency in HepG2 cells (IC_{50} = 0.57 μg/mL, ≈1.9 μM, in HuH-7 and 0.365 μg/mL, ≈1.22 μM, in HepG2).

Effects of 4AAQB on HuH-7 Cell Cycle. In light of a previous study showing that 4AAQB causes cell cycle arrest in HepG2 cells, we further examined the effects of 4AAQB on cell cycle and apoptosis in HuH-7 cells. Here we found that after treating the cells with 4AAQB, the proportion of cells in the G0/G1 phase is increased and that in the S phase decreased (Figure 1D). However, 4AAQB did not induce cell apoptosis in HuH-7 cells (data not shown).

Antitumor Effects of 4AAQB in in Vivo Models. To assess the antitumor effects of 4AAQB in vivo, HepG2 and HuH-7 cells were subcutaneously injected into the right flanks of NOD/SCID mice to establish a xenograft model. Tumor-bearing mice were intraperitoneally administered 4AAQB at a dosage of 0.2 or 2 mg/kg/day for the HepG2 model and at a dosage of 0.5 or 2 mg/kg/day for the HuH-7 model. Tumor volume rapidly increased in the vehicle group in both models. The administration of 4AAQB significantly suppressed tumor growth in a dose-dependent manner in both models (Figure 2). In addition, ROCK-1 expression was studied by DAB staining. The 4AAQB-treated group significantly decreased ROCK1 expression in the HuH-7 tumor cell (Figure 2C). Therefore, we examined whether 4AAQB elicits antitumor activity when HuH-7 tumor cells are orthotopically transplanted. Seven days after tumor transplantation, mice were intraperitoneally administered vehicle or 4AAQB at a dosage of 2 mg/kg/day. In this intrahepatic model, 4AAQB also exhibited a pronounced inhibitory effect on tumor growth (Figure 3). These results clearly showed that 4AAQB displayed antitumor activity in vivo.

Effects of 4AAQB on mRNA Expression. To determine whether 4AAQB treatment induces transcriptomic changes, a microarray using the Human OneArray system were performed. The top 10 enrichment pathway terms from gene set enrichment analysis are shown in Supplementary Table 1 in the Supporting Information. The top-scoring network was linked with the ECM pathway. In this pathway, there were six genes that were significantly down- or up-regulated (MAPK1, TGB1, RAF1, ROCK1, ARHGAP5, and GSN). These genes are known to be associated with cell shape changes during cell spreading or migration, in which both ERK and PI3K are known to be important. In addition, we found that the expression of epithelial-mesenchymal transition (EMT)-asso-

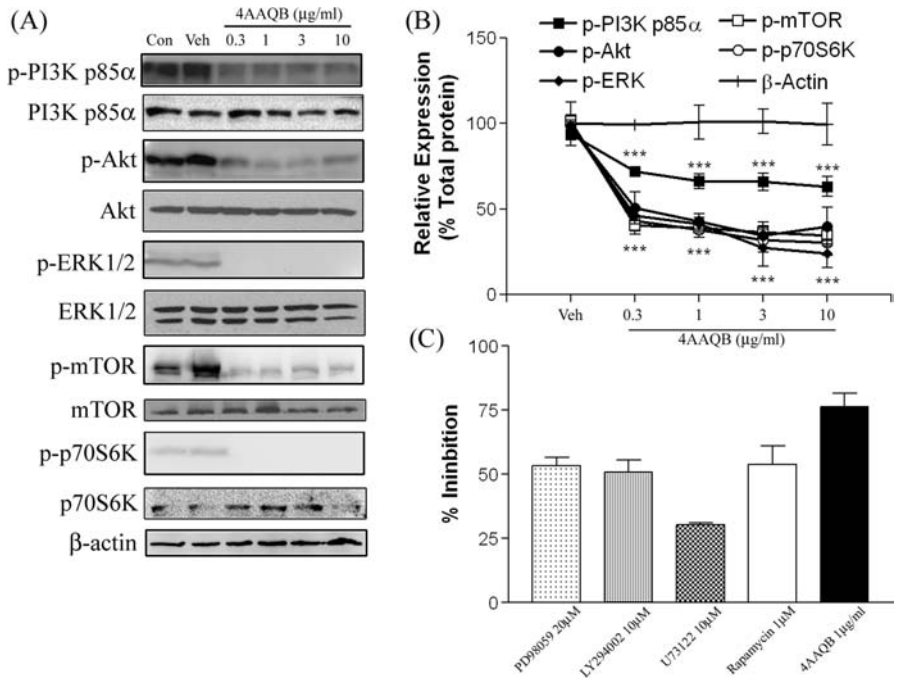

Figure 4. Effect of 4AAQB on PI3K/Akt/mTOR and ERK pathways. (A) HuH-7 cells were incubated in the absence or presence of 4AAQB (0.3−1 μg/mL) for 30 min. Then, the cells were harvested and lysed for the detection of the PI3K/Akt/mTOR and ERK pathway activation by Western blot. β-Actin expression is protein loading control. (B) Quantitative densitometry of the relative level of protein was performed with Image-Pro Plus and is shown at the right. Data are expressed as mean ± SEM of five independent experiments. (***) $p < 0.001$ compared with the control (Veh) group. (C) HuH-7 cells were treated with various kinase inhibitors and 4AAQB. After 48 h, cell viability was detected by SRB assay. The results are presented as percentages of inhibition (mean ± SEM, n = 4).

DOI: 10.1021/jf504434v
J. Agric. Food Chem. 2015, 63, 208−215

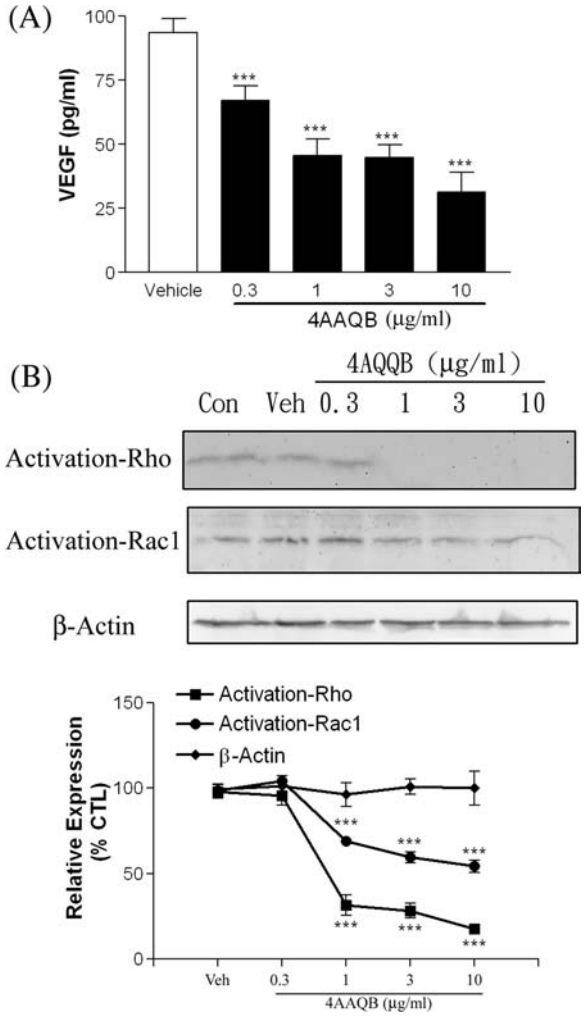

Figure 5. Effects of 4AAQB on VEGF production and Rho GTPase activity in hepatocellular carcinoma cells, HuH-7. (A) VEGF protein expression was evaluated by ELISA in conditioned medium of HuH-7 in the presence or absence of 4AAQB at the indicated concentrations. Data are represented as mean ± SEM (n = 6). (***) $p < 0.001$ indicates significant differences from the vehicle control. (B) Activated Rho and Rac1 assays were performed according to the manufacturer's protocol. β-Actin expression is protein loading control. Quantitative densitometry of the relative level of protein was performed with Image-Pro Plus and is shown at the right. Data are expressed as mean ± SEM of five independent experiments. (***) $p < 0.001$ compared with the vehicle (CTL) group.

ciated genes was altered after 4AAQB treatment (Supplementary Table 2).

4AAQB Inhibits the PI3K/Akt/mTOR and ERK Pathways in HCC Cells. Given that the cell cycle was partly affected by 4AAQB and that the microarray data showed that the expression of EMT-associated genes was altered after 4AAQB treatment, we validated this observation to further understand the underlying mechanism of action of 4AAQB. The PI3K/Akt/mTOR and RAS/RAF/MAPK pathways, well-known signaling pathways, are important in HCC development. Thus, followup experiments to determine whether 4AAQB affects the phosphorylation of these proteins in HuH-7 cells were performed. Western blot experiments showed that 4AAQB suppressed the phosphorylation of PI3K, Akt, mTOR, p70S6K, and ERK (Figure 4). However, the total expression of these proteins was not affected after 4AAQB treatment. These results indicated that the anticancer activity of 4AAQB against HuH-7 cells is associated with the PI3K/Akt/mTOR and ERK pathways. We further compared 4AAQB's inhibitory activity on cell proliferation with the well-characterized inhibitors of these pathways to determine their correlation in HuH-7 cells. HuH-7 cells were treated with either 20 μM PD98059 (ERK-specific inhibitor), 10 μM LY294002 (PI3K-specific inhibitor), 10 μMU73122 (PLC inhibitor), or 1 μM rapamycin (mTOR inhibitor), followed by SRB assays. As shown in Figure 4B, PD98059, LY294002, and rapamycin resulted in approximately 50% inhibition of cell growth, indicating that ERK, PI3K, and mTOR are involved in HuH-7 cell growth, whereas 4AAQB (1 μg/mL) resulted in an inhibition to a greater extent. However, U73122 resulted in only a 25−30% inhibition.

4AAQB Inhibits VEGF Release. As per previous study, high VEGF expression is associated with hepatocellular carcinoma progression.[21] The PI3K/Akt/mTOR pathway increases the synthesis of transcript factors to regulate the expression and production of VEGF. Therefore, we examined the effect of 4AAQB on VEGF release in HuH-7 cells. After a 24 h treatment with various concentrations of 4AAQB, the supernatant was collected for analysis. 4AAQB was observed to suppress VEGF release in a concentration-dependent manner in HuH-7 cells (Figure 5A).

Effects of 4AAQB on Rho and Rac1 Activation. The Rho GTPase signaling cascade, including Rho and Rac which are activated by VEGF, is a key regulator of cytoskeletal dynamics and affects various cellular processes such as vesicle trafficking, cytoskeleton regulation, and migration.[22] As shown in Figure 5B, we found that 4AAQB inhibited the activation of Rho and Rac1 in a concentration-dependent manner, indicating that Rho GTPases are involved in the inhibitory actions of 4AAQB.

4AAQB Inhibits in Vitro Cell Migration and in Vivo Pulmonary Metastasis in HuH-7 Cells. Because of the EMT-associated genes that were altered after 4AAQB treatment (Supporting Information, Supplementary Table 2), we further examined whether 4AAQB affects cell migration in HuH-7 cells. As shown in Figure 6A, HuH-7 cell migration was inhibited by 4AAQB in a concentration-dependent manner. Finally, we investigated the effect of 4AAQB in the HuH-7 lung metastasis model in NOD/SCID mice. In this model, a single intravenous bolus injection of 2×10^6 HuH-7 cells resulted in lung metastases. 4AAQB (0.5 or 2 mg/kg) was intraperitoneally administered to the mice from 3 days before tumor cell injection. Twenty-one days later, the mice were sacrificed, and lungs were removed. Mice treated with 4AAQB result in a significant dose-dependent reduction in lung metastases (Figure 6B).

■ DISCUSSION

A. cinnamonea has been widely used to treat cancer and inflammation. Various components isolated from the fruiting bodies and mycelia of *A. cinnamomea* have been reported to exhibit some biological activity.[23] Antroquinonol, a ubiquinone derivative isolated from the mycelia of *A. cinnamomea*, shows potent anticancer activity against various human malignant carcinoma cell lines; it is particularly potent against Hep3B (IC_{50} = 0.13 ± 0.02 μM).[24] Morever, it has been reported to display hepatoprotective effects both in vitro and in vivo.[25] Lin and Chiang further investigated the mechanism of action of 4AAQB and found that it potently inhibits HepG2 cell

DOI: 10.1021/jf504434v
J. Agric. Food Chem. 2015, 63, 208−215

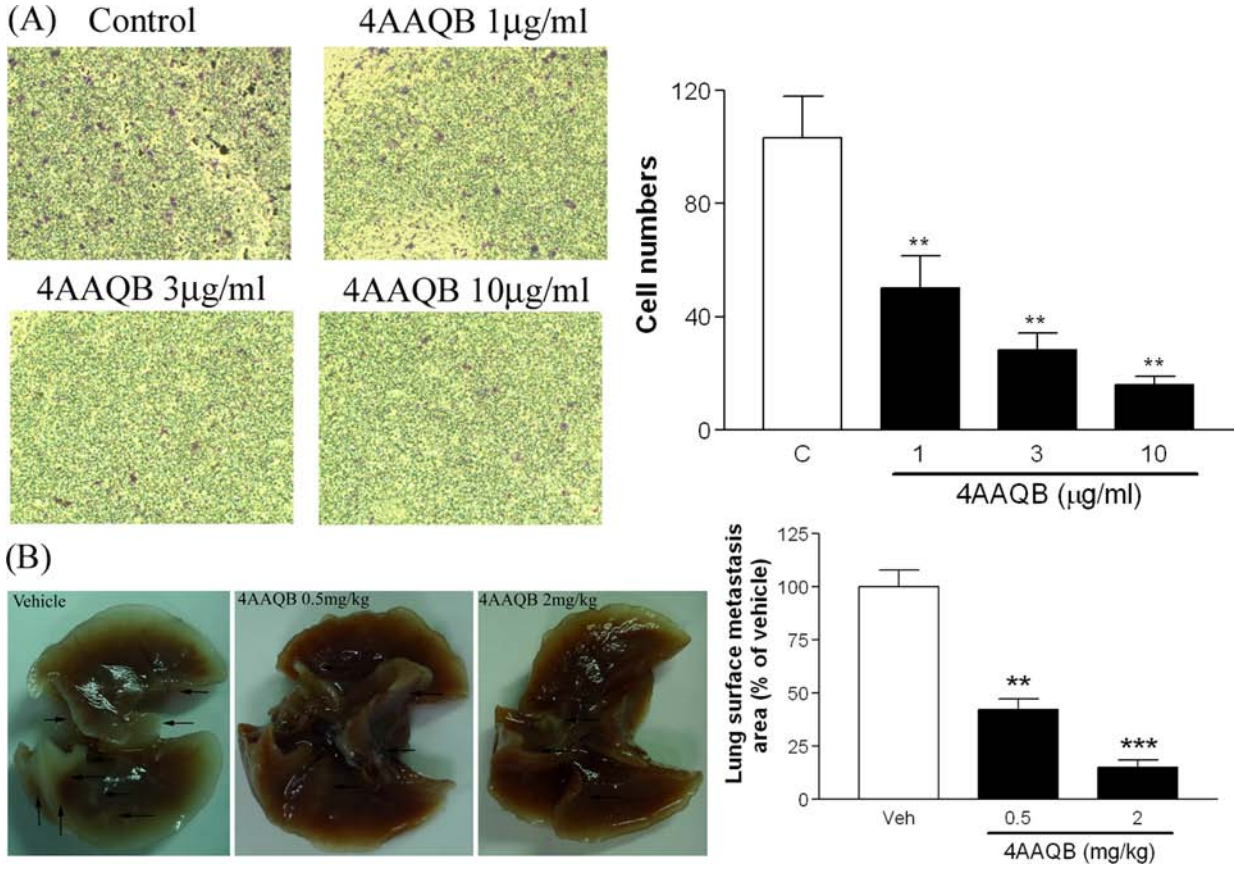

Figure 6. Effects of 4AAQB on cell migration and experimental lung metastasis. (A) HuH-7 cells were treated with various concentrations of 4AAQB and migrated through gelatin-coated transwell for 16 h. The migrated cells were counted, and data are expressed as the mean ± SEM of three independent experiments. (**)$p < 0.01$ compared with control (CTL) group. (B) HuH-7 hepatocellular carcinoma cells (10^6) were injected into the lateral tail vein of a SCID mouse. Twenty-one days later, the lungs were removed, and surface-visible tumors were counted in the absence and presence of 4AAQB treatment. The hepatocarcinoma metastasis area of lung surface is white and the background is dark red. The white area was quantified using ImageJ software. A corresponding bar graph is expressed as percentage of vehicle ($n = 8$).

proliferation by exerting various effects on cell cycle regulators.[18] The present study reveals that 4AAQB significantly suppresses HuH-7 cell proliferation, with a similar inhibitory effect on HepG2 cells, and exhibits potent antitumor effects in vivo. To the best of our knowledge, this is the first study to demonstrate the antitumor effect of 4AAQB in vivo.

Aberrant activation and deregulation of the PI3K/Akt/mTOR pathway occurs in various human cancers. This pathway has become one of the most important therapeutic targets for anticancer drug development because of its integral role in the regulation of various important cellular processes.[3,7,26] Currently, targeting mTOR signaling pathways for chemotherapy for cancer, including HCC, is investigated because of its aberrant activation in approximately 50% patients.[27] Microarray data also showed that various genes were affected by 4AAQB treatment, especially linking with the ECM pathway (Supporting Information, Supplementary Table 1), indicating that the effect of 4AAQB may be associated with this pathway. We further found that 4AAQB effectively inhibited the phosphorylation of mTOR and its upstream kinases, PI3K and Akt, and the downstream effectors (p70S6K) in HuH-7 cells (Figure 4). It has been shown that p70S6K activity is essential for G1 progression.[28] This result may be supported by the fact that 4AAQB induced G1 arrest in HepG2 cell in a previous study[18] and in HuH-7 cells in our study. However, 4AAQB did not induce apoptosis in HuH-7 cells, indicating that its antiproliferative activity excluded an apoptotic effect. The mTOR signaling pathway is also regulated by a PI3K/Akt-independent pathway, such as ERK, p38 MAPK, and AMPK[29] (Figure 4). We also use these kinase inhibitors to evaluate the importance of these protein kinases involved in cancer cell growth. Because 4AAQB significantly inhibited the phosphorylation of the ERK/PI3K/mTOR signaling pathway and ERK/PI3K/mTOR inhibition is correlated with cancer cell growth inhibition, the anticancer effect of 4AAQB may dependent on PI3K/Akt/mTOR pathway blockage.

In addition, mTOR plays a key role in angiogenesis, that is, the formation of new blood vessels to provide oxygen and nutrients to growing and dividing cells. mTOR activation through the PI3K/Akt pathway is associated with increased translation of hypoxia-inducible factor (HIF)-1α, therefore driving the expression of angiogenic growth factors.[30] VEGF is spontaneously produced by hepatoma cells; after a 24 h treatment with 4AAQB, VEGF production decreased in concentration-dependently in HuH-7 cells (Figure 5A), indicating that a downstream effector of mTOR was also inhibited by 4AAQB. VEGF, acting directly through the VEGF receptor (VEGFR), leads to the activation of a downstream signaling pathway and phenotypic changes such as an increase in cell migration and invasion.[31] A growing body of evidence indicates that one of the signaling cascades activated by VEGF, Rho GTPases including Rho, Rac1, and Cdc42, plays a crucial

DOI: 10.1021/jf504434v
J. Agric. Food Chem. 2015, 63, 208−215

role in controlling a variety of cellular processes such as cell proliferation, actin cytoskeleton reorganization, and gene expression.[32,33] The aberrant activity of GTPases has been implicated in cancers and other diseases.[34,35] In the present study, 4AAQB inhibited the activation of Rho and Rac1 in a concentration-dependent manner (Figure 5B).

Various therapeutic approaches, including resection, hepatic artery injection sclerotherapy, ethanol injections, and ablation therapy, have had remarkable effects on primary lesions in HCC. However, HCC prognosis remains poor because of tumor invasiveness, intrahepatic spread, and extrahepatic metastase.[36] Pulmonary lesions are the most common extrahepatic HCC metastases, accounting for 50−60% of the total metastases that occur.[37,38] Therefore, more aggressive treatments for extrahepatic metastases need to be considered. In the in vivo pulmonary metastasis model, 4AAQB dose-dependently reduced lung metastasis foci (Figure 6B), indicating that 4AQQB exhibited not only antitumor but also antimetastatic activities toward HCC.

In conclusion, we demonstrated that 4AAQB inhibited tumor growth in vitro by inducing cell cycle arrest and blocking the PI3K/Akt/mTOR and ERK pathways. The production of VEGF and activity of Rho GTPase were also decreased after 4AAQB treatment. More importantly, 4AAQB exhibited antitumor activity in vivo, including xenograft and orthotopic tumor models in addition to pulmonary metastasis. Taken together, our results suggest that 4AAQB is a potential anticancer agent for treating HCC. Although no clinical studies have been conducted with 4AQQB, two studies with *A. cinnamomea* have been approved. One study was aimed to determine the MTD/DLTs and safety/tolerability profiles of antroquinonol (pure compound purified from *A. cinnamomea*); no treatment-emergent adverse events (TEAEs) were reported as determined.[39] There are only mild side effects including stomach upset, dry mouth, and diarrhea, which can be alleviated by stopping use or taking the supplement with meals to relieve stomach upset and diarrhea. Further clinical trials are required for a full evaluation of this valuable medicinal mushroom for potential clinical applications.

■ ASSOCIATED CONTENT

Supporting Information

Supplementary Tables 1 and 2. This material is available free of charge via the Internet at http://pubs.acs.org.

■ AUTHOR INFORMATION

Corresponding Author

*(C.-H. Chung) Mail: Department of Medicine, Mackay Medical College, No. 46, Sec. 3, Jhong-Jheng Road, Sanzhi District, New Taipei City, Taiwan. Phone: 886-2-26360303. Fax: 886-2-26361295. E-mail: chchung@mmc.edu.tw.

Author Contributions

T.-F. Huang and C.-H. Chung conceived of and designed the experiments. C.-H. Chang, K.-T. Lin, H.-C. Peng, and C.-H. Chung performed the experiments. C.-H. Chang, C.-C. Hsu, S.-W. Wang, and C.-H. Chung analyzed the data. W.-L. Chang and F.-N. Ko contributed purified materials/analysis tools. C.-H. Chang and C.-H. Chung wrote the manuscript.

Funding

This study was supported by research grants from the Ministry of Science and Technology of Taiwan (102-2320-B-715-002-MY2) and Mackay Medical College (MMC-1031A02 and 1031B17) awarded to C.-H. Chung.

Notes

The authors declare no competing financial interest.

■ ABBREVIATIONS USED

HCC, hepatocellular carcinoma; 4AAQB, 4-acetylantroquinonol B; PI3K, phosphatidylinositol 3-kinase; mTOR, mammalian target of rapamycin; p70S6K, p70S6 kinase; SRB, sulforhodamine B; VEGF, vascular endothelial growth factor

■ REFERENCES

(1) El-Serag, H. B.; Mason, A. C. Rising incidence of hepatocellular carcinoma in the United States. *N. Engl. J. Med.* **1999**, *340*, 745−750.

(2) Gomaa, A. I.; Khan, S. A.; Toledano, M. B.; Waked, I.; Taylor-Robinson, S. D. Hepatocellular carcinoma: epidemiology, risk factors and pathogenesis. *World J. Gastroenterol.* **2008**, *14*, 4300−4308.

(3) Lee, J. H.; Lee, H.; Yun, S. M.; Jung, K. H.; Jeong, Y.; Yan, H. H.; Hong, S.; Hong, S. S. IPD-196, a novel phosphatidylinositol 3-kinase inhibitor with potent anticancer activity against hepatocellular carcinoma. *Cancer Lett.* **2013**, *329*, 99−108.

(4) Llovet, J. M.; Burroughs, A.; Bruix, J. Hepatocellular carcinoma. *Lancet* **2003**, *362*, 1907−1917.

(5) Yang, M. H.; Chen, C. L.; Chau, G. Y.; Chiou, S. H.; Su, C. W.; Chou, T. Y.; Peng, W. L.; Wu, J. C. Comprehensive analysis of the independent effect of twist and snail in promoting metastasis of hepatocellular carcinoma. *Hepatology* **2009**, *50*, 1464−1474.

(6) Villanueva, A.; Newell, P.; Chiang, D. Y.; Friedman, S. L.; Llovet, J. M. Genomics and signaling pathways in hepatocellular carcinoma. *Semin. Liver Dis.* **2007**, *27*, 55−76.

(7) Bhaskar, P. T.; Hay, N. The two TORCs and Akt. *Dev. Cell* **2007**, *12*, 487−502.

(8) Chen, J. S.; Wang, Q.; Fu, X. H.; Huang, X. H.; Chen, X. L.; Cao, L. Q.; Chen, L. Z.; Tan, H. X.; Li, W.; Bi, J.; Zhang, L. J. Involvement of PI3K/PTEN/AKT/mTOR pathway in invasion and metastasis in hepatocellular carcinoma: association with MMP-9. *Hepatol. Res.* **2009**, *39*, 177−186.

(9) Lee, C. C.; Yang, H. L.; Way, T. D.; Kumar, K. J.; Juan, Y. C.; Cho, H. J.; Lin, K. Y.; Hsu, L. S.; Chen, S. C.; Hseu, Y. C. Inhibition of cell growth and induction of apoptosis by *Antrodia camphorata* in HER-2/neu-overexpressing breast cancer cells through the induction of ROS, depletion of HER-2/neu, and disruption of the PI3K/Akt signaling pathway. *Evidence-Based Complement. Altern. Med.* **2012**, *2012*, No. 702857.

(10) Wu, M. D.; Cheng, M. J.; Wang, W. Y.; Huang, H. C.; Yuan, G. F.; Chen, J. J.; Chen, I. S.; Wang, B. C. Antioxidant activities of extracts and metabolites isolated from the fungus *Antrodia cinnamomea*. *Nat. Prod. Res.* **2011**, *25*, 1488−1496.

(11) Ao, Z. H.; Xu, Z. H.; Lu, Z. M.; Xu, H. Y.; Zhang, X. M.; Dou, W. F. Niuchangchih (*Antrodia camphorata*) and its potential in treating liver diseases. *J. Ethnopharmacol.* **2009**, *121*, 194−212.

(12) Geethangili, M.; Tzeng, Y. M. Review of pharmacological effects of *Antrodia camphorata* and its bioactive compounds. *Evidence-Based Complement. Altern. Med.* **2011**, *2011*, No. 212641.

(13) Wen, C. L.; Chang, C. C.; Huang, S. S.; Kuo, C. L.; Hsu, S. L.; Deng, J. S.; Huang, G. J. Anti-inflammatory effects of methanol extract of *Antrodia cinnamomea* mycelia both in vitro and in vivo. *J. Ethnopharmacol.* **2011**, *137*, 575−584.

(14) Hseu, Y. C.; Tsou, H. T.; Kumar, K. J.; Lin, K. Y.; Chang, H. W.; Yang, H. L. The antitumor activity of *Antrodia camphorata* in melanoma cells: modulation of Wnt/β-catenin signaling pathways. *Evidence-Based Complement. Altern. Med.* **2012**, *2012*, No. 197309.

(15) Hsu, Y. L.; Kuo, Y. C.; Kuo, P. L.; Ng, L. T.; Kuo, Y. H.; Lin, C. C. Apoptotic effects of extract from *Antrodia camphorata* fruiting bodies in human hepatocellular carcinoma cell lines. *Cancer Lett.* **2005**, *221*, 77−89.

DOI: 10.1021/jf504434v
J. Agric. Food Chem. 2015, 63, 208−215

(16) Song, T. Y.; Hsu, S. L.; Yen, G. C. Induction of apoptosis in human hepatoma cells by mycelia of *Antrodia camphorata* in submerged culture. *J. Ethnopharmacol.* **2005**, *100*, 158−167.
(17) Lin, Y. W.; Pan, J. H.; Liu, R. H.; Kuo, Y. H.; Sheen, L. Y.; Chiang, B. H. The 4-acetylantroquinonol B isolated from mycelium of *Antrodia cinnamomea* inhibits proliferation of hepatoma cells. *J. Sci. Food Agric.* **2010**, *90*, 1739−1744.
(18) Lin, Y. W.; Chiang, B. H. 4-Acetylantroquinonol B isolated from *Antrodia cinnamomea* arrests proliferation of human hepatocellular carcinoma HepG2 cell by affecting p53, p21 and p27 levels. *J. Agric. Food Chem.* **2011**, *59*, 8625−8631.
(19) Lin, K. T.; Lien, J. C.; Chung, C. H.; Kuo, S. C.; Huang, T. F. Bp5250 inhibits vascular endothelial growth factor-induced angiogenesis and HIF-1α expression on endothelial cells. *Naunyn Schmiedebergs Arch. Pharmacol.* **2012**, *385*, 39−49.
(20) Chang, C. H.; Chung, C. H.; Hsu, C. C.; Peng, H. C.; Huang, T. F. Inhibitory effects of polypeptides derived from a snake venom C-type lectin, aggretin, on tumor cell-induced platelet aggregation. *J. Thromb. Haemost.* **2014**, *12*, 540−549.
(21) Yamaguchi, R.; Yano, H.; Iemura, A.; Ogasawara, S.; Haramaki, M.; Kojiro, M. Expression of vascular endothelial growth factor in human hepatocellular carcinoma. *Hepatology* **1998**, *28*, 68−77.
(22) Heasman, S. J.; Ridley, A. J. Mammalian Rho GTPases: new insights into their functions from in vivo studies. *Nat. Rev. Mol. Cell Biol.* **2008**, *9*, 690−701.
(23) Lu, M. C.; El-Shazly, M.; Wu, T. Y.; Du, Y. C.; Chang, T. T.; Chen, C. F.; Hsu, Y. M.; Lai, K. H.; Chiu, C. P.; Chang, F. R.; Wu, Y. C. Recent research and development of *Antrodia cinnamomea*. *Pharmacol. Ther.* **2013**, *139*, 124−156.
(24) Lee, T. H.; Lee, C. K.; Tsou, W. L.; Liu, S. Y.; Kuo, M. T.; Wen, W. C. A new cytotoxic agent from solid-state fermented mycelium of *Antrodia camphorata*. *Planta Med.* **2007**, *73*, 1412−1415.
(25) Kumar, K. J.; Chu, F. H.; Hsieh, H. W.; Liao, J. W.; Li, W. H.; Lin, J. C.; Shaw, J. F.; Wang, S. Y. Antroquinonol from ethanolic extract of mycelium of *Antrodia cinnamomea* protects hepatic cells from ethanol-induced oxidative stress through Nrf-2 activation. *J. Ethnopharmacol.* **2011**, *136*, 168−177.
(26) Vivanco, I.; Sawyers, C. L. The phosphatidylinositol 3-kinase AKT pathway in human cancer. *Nat. Rev. Cancer* **2002**, *2*, 489−501.
(27) Villanueva, A.; Chiang, D. Y.; Newell, P.; Peix, J.; Thung, S.; Alsinet, C.; Tovar, V.; Roayaie, S.; Minguez, B.; Sole, M.; Battiston, C.; Van Laarhoven, S.; Fiel, M. I.; Di Feo, A.; Hoshida, Y.; Yea, S.; Toffanin, S.; Ramos, A.; Martignetti, J. A.; Mazzaferro, V.; Bruix, J.; Waxman, S.; Schwartz, M.; Meyerson, M.; Friedman, S. L.; Llovet, J. M. Pivotal role of mTOR signaling in hepatocellular carcinoma. *Gastroenterology* **2008**, *135*, 1972−1983.
(28) Lane, H. A.; Fernandez, A.; Lamb, N. J.; Thomas, G. p70s6k function is essential for G1 progression. *Nature* **1993**, *363*, 170−172.
(29) Memmott, R. M.; Dennis, P. A. Akt-dependent and -independent mechanisms of mTOR regulation in cancer. *Cell Signal.* **2009**, *21*, 656−664.
(30) Del Bufalo, D.; Ciuffreda, L.; Trisciuoglio, D.; Desideri, M.; Cognetti, F.; Zupi, G.; Milella, M. Antiangiogenic potential of the mammalian target of rapamycin inhibitor temsirolimus. *Cancer Res.* **2006**, *66*, 5549−5554.
(31) Fan, F.; Wey, J. S.; McCarty, M. F.; Belcheva, A.; Liu, W.; Bauer, T. W.; Somcio, R. J.; Wu, Y.; Hooper, A.; Hicklin, D. J.; Ellis, L. M. Expression and function of vascular endothelial growth factor receptor-1 on human colorectal cancer cells. *Oncogene* **2005**, *24*, 2647−2653.
(32) Bryan, B. A.; D'Amore, P. A. What tangled webs they weave: Rho-GTPase control of angiogenesis. *Cell. Mol. Life Sci.* **2007**, *64*, 2053−2065.
(33) Jaffe, A. B.; Hall, A. Rho GTPases: biochemistry and biology. *Annu. Rev. Cell Dev. Biol.* **2005**, *21*, 247−269.
(34) Ridley, A. J. Rho proteins and cancer. *Breast Cancer Res. Treat.* **2004**, *84*, 13−19.
(35) Sahai, E.; Marshall, C. J. RHO-GTPases and cancer. *Nat. Rev. Cancer* **2002**, *2*, 133−142.
(36) Huo, T. I.; Lin, H. C.; Huang, Y. H.; Wu, J. C.; Chiang, J. H.; Lee, P. C.; Lee, S. D. The model for end-stage liver disease-based Japan Integrated Scoring system may have a better predictive ability for patients with hepatocellular carcinoma undergoing locoregional therapy. *Cancer* **2006**, *107*, 141−148.
(37) Kawamura, M.; Nakajima, J.; Matsuguma, H.; Horio, H.; Miyoshi, S.; Nakagawa, K.; Fujisawa, T.; Kobayashi, K. Surgical outcomes for pulmonary metastases from hepatocellular carcinoma. *Eur. J. Cardiothorac. Surg.* **2008**, *34*, 196−199.
(38) Natsuizaka, M.; Omura, T.; Akaike, T.; Kuwata, Y.; Yamazaki, K.; Sato, T.; Karino, Y.; Toyota, J.; Suga, T.; Asaka, M. Clinical features of hepatocellular carcinoma with extrahepatic metastases. *J. Gastroenterol. Hepatol.* **2005**, *20*, 1781−1787.
(39) http://clinicaltrials.gov/ct2/show/study/NCT01134016?term=Antroquinonol&rank=1&sect=X4370156&view=results.

DOI: 10.1021/jf504434v
J. Agric. Food Chem. 2015, 63, 208−215

JOURNAL OF AGRICULTURAL AND FOOD CHEMISTRY

Article

pubs.acs.org/JAFC

Structure, Morphology, and Assembly Behavior of Kafirin

Jie Xiao,[†] Yunqi Li,[‡] Ji Li,[†] Alejandro Perez Gonzalez,[†] Qiuyang Xia,[†] and Qingrong Huang*[,†]

[†]Department of Food Science, Rutgers University, 65 Dudley Road, New Brunswick, New Jersey 08901, United States

[‡]Key Laboratory of Low Carbon Chemical Power of Jilin Province, Changchun Institute of Applied Chemistry, Changchun 130022, People's Republic of China

Supporting Information

ABSTRACT: Prolamins from grains have attracted intensive attention in recent years due to their potential in satisfying the demand for environmentally friendly (biodegradable), abundantly available (sustainable), and cost-effective biomaterials. However, for kafirin, the prolamin from sorghum, its composition, structure, morphology, and self-assembly behaviors have not been fully characterized. In this paper, kafirin was extracted from the whole sorghum grain and found to contain 68, 14, 6, and 12% of α-, β-, and γ-fractions and cross-linked kafirin, respectively. Freeze-dried kafirin contained ~49% α-helix in the solid state. When dissolved in 65% (v/v) isopropanol, 60% (v/v) *tert*-butanol, and 85% (v/v) ethanol aqueous solvents, the relative α-helix content in kafirin increased with the decrease of solvent polarity. Structural analysis using small-angle X-ray scattering (SAXS) indicated that kafirin (2 mg/mL) took stretched and extended conformations with dimensions of 118 × 15 × 15 and 100 × 11 × 11 Å in 60% *tert*-butanol and 65% isopropanol, respectively. More elongated conformation of individual kafirin with high-order assembly was observed in 85% ethanol. Protein aggregation occurred as protein concentration increased in its good solvent. The morphology of kafirin assemblies captured by atomic force microscopy (AFM) revealed that kafirin protein took uniform particle morphology at low concentration, and disk-like or rod-like structures resulting from solvent evaporation induced particle interactions emerged at high concentrations. These results suggest that both protein concentration and solvent polarity can effectively regulate kafirin assemblies from thick rod-like to slim rod-like structures, a convenient way to tune the fibrillation of prolamin-based biomaterials.

KEYWORDS: *kafirin, SDS-PAGE, secondary structure, morphology, self-assembly, SAXS*

INTRODUCTION

Growing research interest in protein-based biomaterials has been stimulated by the demand for alternatives to traditional synthetic polymers that have expanded functional properties to accommodate a broader spectrum of applications.[1] Among various protein candidates, zein, the prolamin protein in maize, has received increasing research attention.[2,3] The composition, structure, dissolution, and gelation behavior of zein have been extensively studied.[4−7] Due to its unique properties, such as its solubility in aqueous alcohol, highly hydrophobic and non-allergenic nature, excellent oxygen barrier property, reduced susceptibility to proteolytic degradation, and ability to withstand gastric pH, zein is considered superior to other proteins, especially in the food packaging and drug delivery applications. Currently, research projects intended to explore its applications in tissue scaffolding, active ingredient encapsulation, and drug delivery are in full swing.[8−10]

Kafirin, the sorghum prolamin protein, resembles zein in its solubility, molecular weight, amino acid composition, and structure of polypeptides.[11,12] Compared to zein, kafirin is relatively more hydrophobic and less digestible,[13,14] which enables more stable films with superior gas and water vapor barrier characteristics. It is a more effective encapsulation vehicle with stronger protective function.[15] Therefore, kafirin has the potential to be an alternative to zein in biomaterial applications. Nevertheless, the effort to fulfill its potential is still seriously lacking. Of all the available research papers, only a few report kafirin's satisfying performance in film casting application.[16−19]

Many factors, such as protein composition, purity, concentration, secondary and tertiary structures, morphology, and self-assembly behavior, are known to affect the processing performance and functional properties of protein-based biomaterials.[20] To develop biomaterials from kafirin, it is necessary to understand the physical properties of kafirin in the first place. Although extraction methods and digestibility of kafirin received adequate research attentions, a clear view of the secondary structure, morphology, and self-assembly phenomena of kafirin and their relationship with processing properties is still absent.

In this presented work, we carried out a detailed investigation of kafirin on its composition, structure, morphology, and self-assembly behavior. The components of kafirin extracted from sorghum grain using 60% *tert*-butanol were identified on the basis of sodium dodecyl sulfate−polyacrylamide gel electrophoresis (SDS-PAGE). The secondary structure was characterized using Fourier transform infrared (FTIR) and circular dichroism (CD) in solid and liquid states. The morphology and self-assembly behavior of kafirin in different alcohol solutions were studied by synchrotron small-angle X-ray scattering

Received: September 26, 2014
Revised: December 4, 2014
Accepted: December 15, 2014
Published: December 15, 2014

ACS Publications © 2014 American Chemical Society

DOI: 10.1021/jf504674z
J. Agric. Food Chem. 2015, 63, 216−224

(SAXS) and atomic force microscopy (AFM). Key parameters affecting kafirin structure based on these measurements were obtained, and the results are very relevant in guiding future investigation of kafirin-based biomaterials with designed quality.

MATERIALS AND METHODS

Materials. Whole food-grade retail sorghum grain (*Sorghum bicolor* Moench) was purchased from Northern Food Inc. (Hicksville, NY, USA). Commercial zein (260-01283) was purchased from Wako Pure Chemical Industries, Ltd. (New York, NY, USA). Tris-alkali, sodium dodecyl sulfate (SDS), *N*,*N*,*N*′,*N*′-tetramethylethylenediamine (TEMED), 2-mercaptoethanol (2-ME), bromophenol blue, Coomassie brilliant blue G-250, and prestained protein markers (broad range protein maker) were purchased from Bio-Rad Laboratories, Inc. (Hercules, CA, USA). Milli-Q water was used throughout the experiments.

Preparation of Kafirin by Ultrasound-Assisted *tert*-Butanol Extraction. Whole sorghum grain was milled to 40 mesh, and lipid was first removed from milled grain with *n*-hexane. The defatted flour was then extracted at room temperature with water followed by 0.5 M NaCl (the ratio of raw material to extract solution is 1:10) three times each (1 h each). At the end of each extraction cycle, the dispersion was centrifuged at 8000 rpm for 10 min and the supernatant was discarded to fully separate out the albumin and globulin proteins. The residue was then washed with distilled water three times in a similar way to remove salt. The remnants were then extracted by using 60% *tert*-butanol twice for 2 h each and 10 min of ultrasonication using an FS-28 solid-state ultrasonicator (bath type with sonic power, 225 W; sweep frequency, 40 kHz) (Fisher Scientific, Pittsburgh, PA, USA) at the interval of 30 min. The extract fraction was then centrifuged at 8000 rpm for 15 min, and the supernatant was then freeze-dried directly. Because the first extraction fraction contains pink color due to the coextraction of alcohol-soluble impurities, only the second extraction fraction was kept for further analysis. The second extract fraction powder has a white color, and the protein content was determined as 87% by combustion method with a nitrogen analyzer (FP-428, Leco Corp., St. Joseph, MI, USA) calibrated with analytical reagent grade EDTA (a factor of 6.25 was used to convert the nitrogen to protein).

Sodium Dodecyl Sulfate−Polyacrylamide Gel Electrophoresis (SDS-PAGE). Three milligrams of protein was denatured and reduced by heating samples at 95 °C for 5 min in 1 mL of loading buffer containing 0.01 mol/L Tris-HCl buffer (pH 6.8), 2% (w/v) SDS, 10%(v/v) glycerol, and 5% (v/v) β-mercaptoethanol (2-ME). The prestained protein marker (molecular weights ranging from 6.5 to 110.3 kDa) was used. Commercial zein was run under reducing condition as a control. Each sample solution (10 μL) or protein marker was loaded onto discontinuous sodium dodecyl sulfate polyacrylamide gel with 4% stacking gel and 12% separating gel. Migration was done in a Bio-Rad Mini-Protean II system under 90 V for 2 h. Gel was stained with 0.1% Coomassie brilliant blue G 250 in 45% methanol and 10% acetic acid and destained in solution with the composition ratio of methanol/acetic acid/water = 1:1:8, v/v/v. Gel was scanned by Bio-Rad Universal Hood II gel imaging system, and densitometry analysis was performed using Image J 2.1.4.7 software.

Amino Acid Composition Analysis. Seventy-five milligrams of kafirin was placed in a 20 mL ampule and mixed with 10 mL of 6 M HCl. After sealing, the protein was hydrolyzed at 110 °C for 22 h under vacuum. The hydrolysate was then dried under vacuum at 60 °C. The dried sample was dissolved in 3−5 mL of 0.2 M sodium citrate buffer (pH 2.2) to yield an amino acid concentration of 50−250 nmol/mL. The protein solution was filtered through a 0.2 μm syringe filter and loaded onto a Hitachi L-8800 amino acid analyzer (Tokyo, Japan) equipped with a Hitachi 2622SC ion-exchange column for amino acid composition analysis.

Attenuated Total Reflectance Fourier Transform Infrared (ATR-FTIR) Spectroscopy. ATR-FTIR spectra were collected by a Thermal Nicolet Nexus 670 FTIR spectrometer (Thermo Electron Corp., Madison, WI, USA). Kafirin protein powder was wrapped in aluminum foil and pressed into a flat pellet by hand to ensure good contact with the ATR crystal. Each spectrum was collected at wavenumber range from 4000 to 600 cm^{-1} and averaged over 256 scans with 4 cm^{-1} resolution. With the aid of OMNIC 7.2 software, the original FTIR spectrum was then smoothed with smoothing points (11, 21.213 cm^{-1}). Second-derivative (Savitsky−Golay derivative) analysis in the wavenumber ranging from 1700 to 1520 cm^{-1}, which covered the typical amide I and amide II peaks, was then conducted to identify positions of individual component peaks. With the assistance of Origin 9.0 software, multiple-peak fitting was conducted by fitting peak positions obtained from second-derivative to Gaussian functions. On the basis of the attribution relationship between component peaks and types of secondary structure, the ratio of secondary structure was determined by calculating the peak area ratio.

Circular Dichroism (CD) Spectroscopy. CD spectra were collected at 25 °C using an AVIV model 400 circular dichroism spectrometer equipped with 0.1 cm path length quartz cuvettes (model 110-OS, Hellma, USA). Wavelength scans were conducted from 190 to 260 nm with a bandwidth of 1 nm. Samples, with protein concentration of 0.2 mg/mL, were filtered by 0.45 μm membrane (Millipore, Ireland) before testing. Three scanning acquisitions were gathered, and one representative set of spectra was collected. For each spectrum, the medium baseline was subtracted and mean residue ellipticity (MRE) (mdeg·cm^2/dmol) versus wavelength was plotted.[21] It was calculated as $[\theta]\lambda = \mathrm{MRW}\theta\lambda/10dc$, where the average molecular weight of an amino acid residue is 109.867 g/mol, $\theta\lambda$ is the measured ellipticity at the specific wavelength in mdeg, c is the concentration of protein in g/mL, and d is the path length in cm. Secondary structure estimation was processed by curve fitting with reference CD curves of α-helix, β-sheet, random coil, and β-turn conformations.

Synchrotron Small-Angle X-ray Scattering. SAXS data were collected at Bio-CAT, 18-ID beam line section, at the Advanced Photon Source, Argonne National Laboratory. Freshly prepared kafirin (2 mg/mL) in 60% (v/v) *tert*-butanol, 65% isopropanol, and 85% ethanol aqueous solutions was examined. The X-ray wavelength was 1.033 Å, and the experimental setup included a 3 m sample-to-detector length camera and another 0.3 m sample-to-detector length camera with the high-sensitivity CCD detector. A quartz capillary flow cell of 1.5 mm diameter was fitted to a brass block; this sample holder was maintained at 25 °C in all experiments. A Microlab 500 Hamilton pump was used to load samples into the flow cell at a constant rate (10 mL/s) during X-ray exposure to minimize radiation damage. A single exposure of 1 s was used to acquire the scattering data, 15 curves were collected for each sample, and their averaged curves were utilized for further analysis. Identical measurement configurations were used for solvent backgrounds and sample solutions for proper background subtraction.

Small-Angle X-ray Scattering Data Analysis. The total scattering intensity, $I(Q)$, for a monodisperse protein can be expressed as[22]

$$I(Q) = n_p(\Delta\rho)^2 v^2 P(Q) S(Q) \quad (1)$$

where n_p is the number density of colloidal particles per unit volume in the solution, v is the specific volume of protein that can be predicted through the empirical equation proposed by Fischer et al.,[23] $Q = (4\pi/\lambda)\sin(\theta/2)$ is the scattering vector, where λ is the wavelength of the X-ray beam, θ is the scattering angle, and $\Delta\rho$ is the contrast of electron densities between proteins and solvent, $P(Q)$ is the form factor of a given protein that reflects the shape of individual protein, and $S(Q)$ is the structure factor that probes the structure of proteins in the solution. For an ellipsoidal particle with a parallel radius a and a perpendicular radius b of the equivalent ellipsoid of protein, the form factor can be expressed as[24,25]

$$P(Q) = \int_0^1 \left[\frac{3(\sin u - u\cos u)}{u^3}\right]^2 \mathrm{d}x \quad \text{with} \quad u = Qb\left[\frac{ax}{b} + (1-x)^2\right] \quad (2)$$

DOI: 10.1021/jf504674z
J. Agric. Food Chem. 2015, 63, 216−224

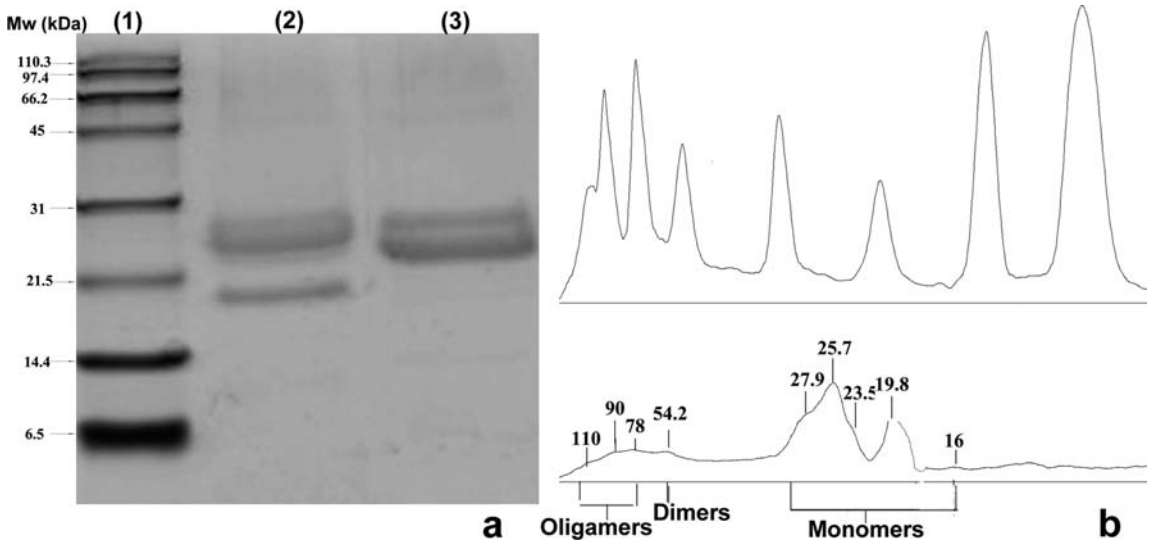

Figure 1. (a) Electrophoretic pattern of kafirin and zein under reducing conditions. Lanes: 1, protein marker; 2, kafirin under reducing condition; 3, commercial zein under reducing condition. (b) Plot fit curves for protein standard (upper) and kafirin (lower) under reducing conditions.

The protein aggregation and protein−protein interaction upon concentration increase in solutions can be described by using the effective structure factor $S(Q,C)$:[26]

$$S(Q, C) = \frac{C_0 I(Q, C)}{C I(Q, C_0)} \quad (3)$$

Here $I(Q,C)$ is the scattering intensity profile from a protein solution with concentration C, and C_0 corresponds to dilute solution in which protein aggregation is negligible.

Guinier analysis and pair distribution function (PDF) were used to obtain the radius of gyration R_g, cross-section radius of gyration (R_c), and size distribution, respectively. The Guinier approximation was given by

$$I(Q) = \alpha\pi Q^{-\alpha} A \exp\left(-\frac{R_\alpha^2 Q^2}{3-\alpha}\right) \quad (4)$$

where $\alpha = 0$ for a solid sphere, $\alpha = 1$ for a rod-like object, and $\alpha = 2$ for a sheet-like object. When the classic Guinier fit ($\alpha = 0$) was performed, A was equal to $I(0)$, the scattering intensity at $Q = 0$, and R_g equaled R_α. When rod-like Guinier fit was performed, R_c was equivalent to $\sqrt{2}R_\alpha$. When sheet-like Guinier fit was performed, T, the thickness, was equivalent to $(12)^{1/2}R_\alpha$.

GNOM package was used to generate the PDF $P(r)$, which displayed the probability of finding one point within the particle dimension D_m at a distance r from a given point.[27] The low-resolution structures (2−3 nm^{-1}) of kafirin in aqueous medium were restored by using the algorithm DAMMIN.[28,29] The program DAMMIN produced the model as an ensemble of densely packed beads inside a spherical search volume with a diameter D_{max}. The simulated annealing was utilized to find a compact conformation that had a minimum discrepancy between the experimental and calculated scattering curves. For each model body, five independent DAMMIN restorations were performed. Then, the program DAMAVER was used to generate the averaged model that represented the common features of all restorations at low resolution.

Atomic Force Microscopy (AFM). Tapping mode AFM images were collected with a NanoScope IIIA Multimode AFM (Veeco Instruments Inc., Santa Barbara, CA, USA) equipped with a silicon-etched RTESP7 cantilever (Veeco Nanoprobe, Camarillo, CA, USA). A silicon tip with nominal spring constant of 40 N/m was used. Before tip engagement, the drive frequency of the silicon tip was tuned to a frequency range of 300−320 kHz. Kafirin solutions (0.2 mL, dissolved in 60% butanol) with different initial concentrations of 0.1, 0.2, and 0.5 mg/mL were dripped onto a freshly cleaved mica surface; after 30 min of absorption, samples were dried under a stream of nitrogen gas. All of the collected images were flattened before further analysis. Section and bearing analyses, which were incorporated in the Nanoscope 5.30 software, were utilized to obtain the quantitative information of kafirin protein self-assembly morphology.

RESULTS AND DISCUSSION

Kafirin Composition. Kafirin and zein showed typical electrophoretic patterns as described by previous researchers[30,31] (Figure 1a). Under reducing conditions, kafirin showed major bands with M_r of 23.8 and 25.1 kDa, indicating the presence of α1-, α2-kafirin polypeptides. Bands at 19.8 and 27.9 kDa were identified as β- and γ-kafirin polypeptides. In addition, one light band was found at 54.2 kDa, suggesting the presence of stable dimers. A few faint bands of higher molecular weight were also present, indicating soluble oligomers. As a comparison, commercial zein showed predominately α1- and α2-zein bands at M_w of 22.1 and 25.4 kDa.

According to the calculated peak areas from the gel run under reducing conditions (Figure 1b), α-, β-, and γ-fractions and cross-linked kafirin (dimer and oligomers) account for 68, 14, 6, and 12% of the total detected kafirin, respectively. As a percent of total monomers this is equivalent to 77, 16, and 7% of α-, β-, and γ-fractions, respectively. Previous studies indicated that α-kafirin comprised 80−84%, whereas β- and γ-kafirin constituted 7−8 and 9−12% of the total monomers, respectively.[32−34] The main differences in the results, namely, decreased proportion in α- and γ-kafirin fractions and increased presence of β-kafirin, may have been due to the higher extraction yield of oligomers, which were composed of γ- and α- kafirins linked together by disulfide bonds.[35] Because γ- and β-kafirins and protein oligomers encapsulated α-kafirin in a disulfide-bound polymeric network in the protein body,[36] the ultrasound treatment with intense agitation and friction forces may effectively disrupt the cross-linked matrix, leading to a higher dissolution yield of cross-linked kafirin and soluble oligomers.[37]

Amino acid compositions of the extracted kafirin protein together with previously reported results of kafirin obtained by similar extraction procedures[38,39] are presented in Table 1.

DOI: 10.1021/jf504674z
J. Agric. Food Chem. 2015, 63, 216−224

Table 1. Amino Acid Composition (g/100 g Protein) of Kafirin

amino acid	I[a]	II[b]	III[c]
aspartic	6.0	6.5	7.3
threonine	2.9	2.6	2.8
serine	4.3	4.1	3.9
glutamic acid	28.2	30.0	30.5
glycine	1.4	1.1	1.2
alanine	11.8	12.4	12.5
half-cysteine	3.2	0.4	0.7
valine	3.8	5.0	5.1
methionine	2.1	1.0	1.1
leucine	17.5	19.2	18.8
tyrosine	3.6	5.5	5.3
phenylalanine	6.6	6.4	4.6
lysine	0.1	0.1	0.3
proline	10.2	10.0	10.1
histidine	1.6	0.9	1.3
arginine	3.8	1.0	2
isoleucine	3.0	4.8	4.2

[a]Analysis results reported by work of our laboratory. [b]Analysis results reported by work of R. W. Jones [c]Analysis results reported by work of R. Jambunathan.

Paired two-tail t tests showed p values of 0.88 and 0.78 compared with Jones's and Jambunathan's papers, respectively, indicating our sample has no significant difference with those reported samples. The uncharged or nonpolar neutral amino acids, namely, glycine, alanine, valine, methionine, leucine, tyrosine, phenylalanine, proline, and isoleucine, made up 60.1% of the total amino acids, which contributed to the highly hydrophobic nature of prolamin. Glutamic acid, leucine, alanine, and proline were the most abundant amino acids, accounting for about 28.2, 17.5, 11.8, and 10.2%, respectively, of the total amino acids. The protein contained low levels of lysine, glycine, and histidine. Although most of the amino acid contents of our extracted kafirin were consistent with previous results, the contents of methionine and cysteine were found to be much higher than their counterparts. These differences may be related to the higher fractions of β- and γ- kafirins and their disulfide cross-linked oligomers, all containing rich amounts of cysteine and methionine.[40,41] Therefore, this peculiar property could render a greater propensity to form intermolecular disulfide cross-linking and possibly additional protein aggregates.[42]

Secondary Structure of Kafirin. Because changes in secondary structure affect the properties of kafirin, such as surface hydrophobicity and film-forming properties,[43] the FTIR spectrum of kafirin in solid state (Figure 2a) was collected and analyzed. Typical amide I and amide II absorption peaks appeared at 1653 and 1541 cm^{-1}, respectively. Stretching vibrations of the C═O bond of the amide together with the weakly coupled in-plane N−H bending and C−N stretching contribute to the amide I absorption.[44] Because both C═O and N—H bonds were involved in the hydrogen bonding between different elements contributing to secondary structure, amide I bond was an ideal wavenumber range for secondary structure analysis of protein. Previous studies have systematically correlated proteins of known secondary structure with the shape of the amide I band, and the following secondary structure in this band has been suggested:[45,46] β-turn, 1678−1682 cm^{-1}; α-helix, 1648−1659 cm^{-1}; random coil, 1638−1640 cm^{-1}; and β-sheet, 1625−1635 cm^{-1}. Figure 2b shows the second-derivative plot of the amide I peak of kafirin. Four major components of kafirin were identified in the amide I region at 1681, 1658, 1644, and 1627 cm^{-1}, respectively. The most prominent bands at 1658 and 1644 cm^{-1} originated from α-helical structures, followed by those in the 1681 and 1627 cm^{-1} regions, which correspond to β-turn and β-sheets, respectively. Figure 2c shows the multiple peak fitting at the four wavelengths using Gaussian function. By calculation of the individual component peak areas, the composition of kafirin secondary structure was determined as 49% α-helix, 27% β-turn, and 24% β-sheet, respectively.

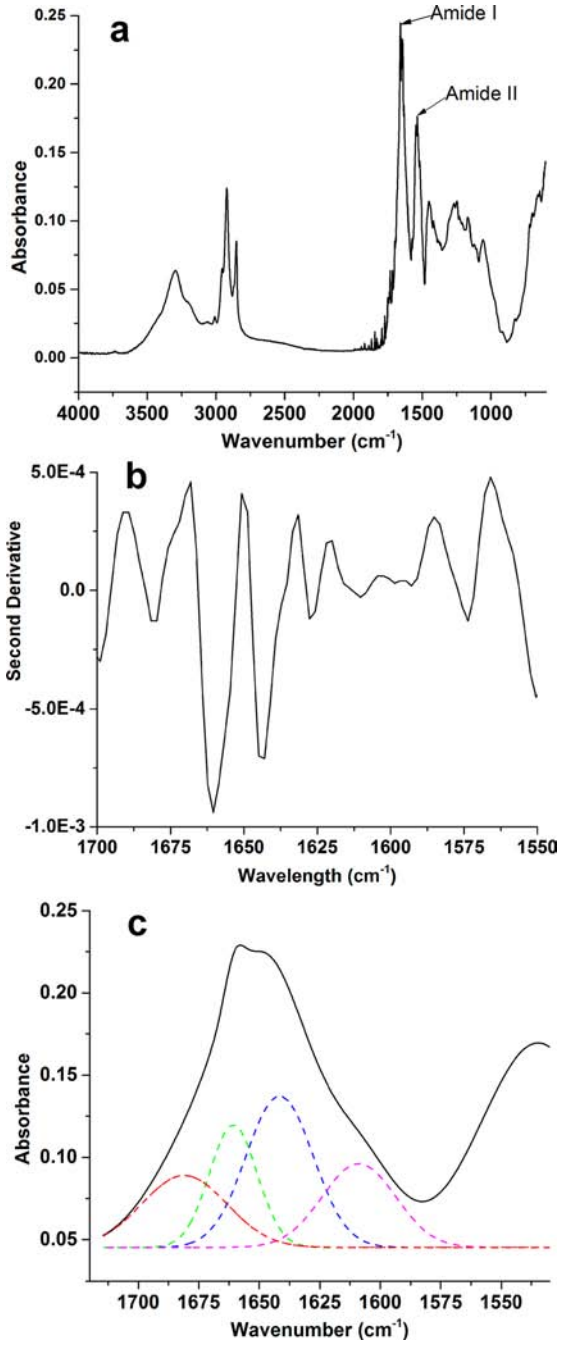

Figure 2. (a) FTIR spectrum of kafirin; (b) second-derivative FTIR spectrum of amide I and II bands of kafirin; (c) best fit for the FTIR spectrum using Gaussian multiple peaking fitting analysis for the peaks associated with protein secondary structure.

DOI: 10.1021/jf504674z
J. Agric. Food Chem. 2015, 63, 216−224

The secondary structure contents of kafirin in liquid solutions with different polarities were then determined via far-UV CD spectra. The CD profiles of kafirin in 60% *tert*-butanol, 65% isopropanol, and 85% ethanol are shown in Figure 3. In all cases, the CD spectra of kafirin exhibited the characteristics of α-helix with two strong negative ellipticity values at 208 and 222 nm. CD ellipticity at 222 nm has been widely used to estimate α-helix content in proteins.[47] The CD profiles of kafirin in different solvents show that the unshifted band at 222 nm has noticeable changes in the ellipticity. Consensus values of the relative α-helix content in 65% isopropanol, 60% *tert*-butanol, and 85% ethanol are 53.1, 57.9, and 68.4%, respectively. The change in α-helix content suggested that kafirin underwent solvent-induced conformational transformations as a combination result of differences in polarity index and proton-accepting ability of different solvents. Dielectric constants of these solvents were then calculated as 40.0, 39.5, and 32.7 by linear combination of dielectric constants of organic solvents and water (dielectric constants of *tert*-butanol, isopropanol, ethanol, and water are 12.4, 18.3, 24.3, and 80.1, respectively, under ambient condition). Because the polarity of a solvent is proportional to the value of the dielectric constant, it can be seen that the α-helix content increases as solvent polarity decreases. Furthermore, the α-helix content is in agreement with early study that reported the α-helix content of native kafirin to be 50−60%.[42] Compared with the value measured in dry state, the α-helix contents were higher in solutions. This result may be either due to the difference in sensitivities to α-helix structures under different analyzing techniques or further evidence of the solvent polarity induced conformational changes. Dry powder form is the extreme circumstance of polarity changes: the *tert*-butanol evaporated before water during the lyophilization process, causing kafirn to undergo a media change from a highly hydrophobic to a highly hydrophilic environment. Because water is more polar than *tert*-butanol, it, again, suggested that

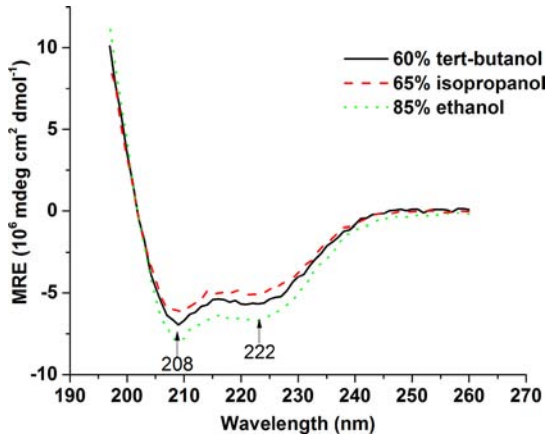

Figure 3. Far-UV CD spectra of kafirin in 60% *tert*-butanol, 65% isopropanol, and 85% ethanol.

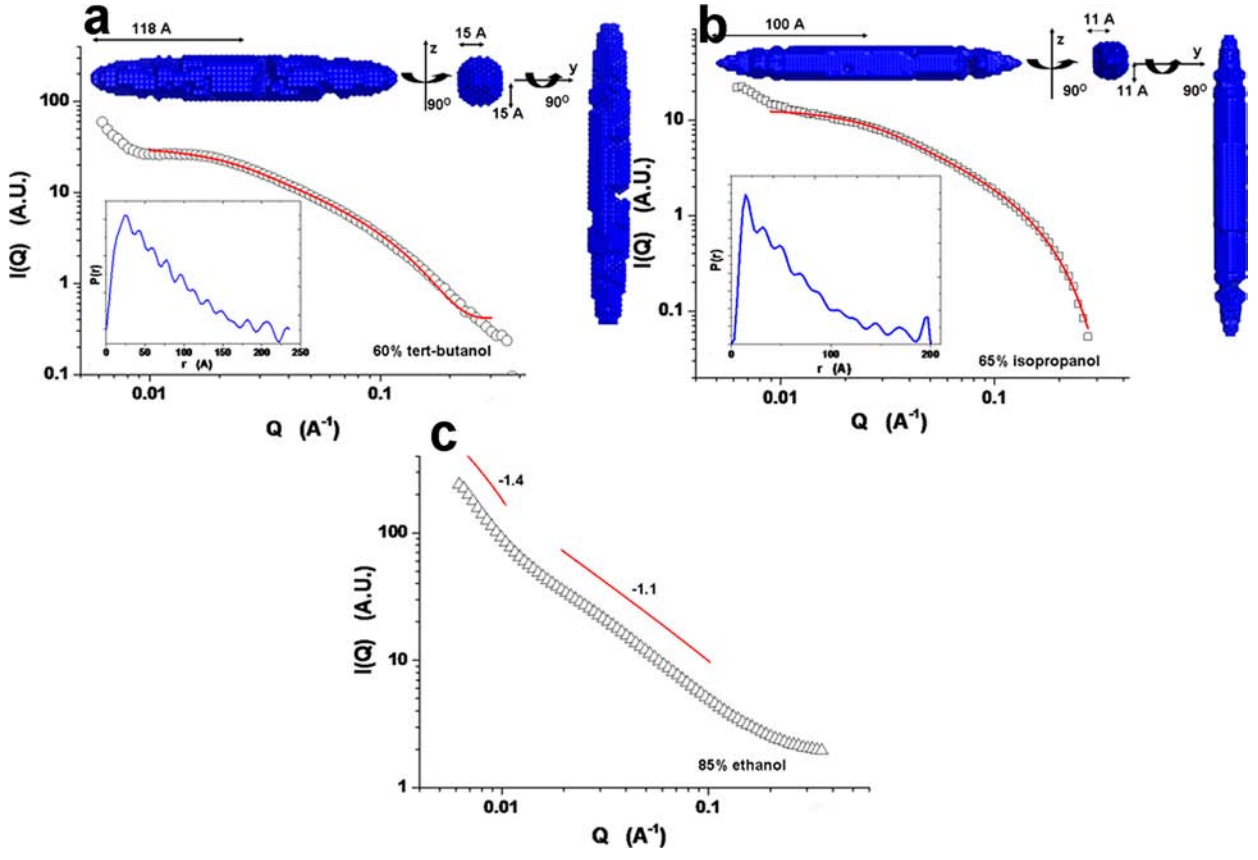

Figure 4. Small-angle X-ray scattering (SAXS) profiles of 2 mg/mL kafirin in (a) 60% *tert*-butanol, (b) 65% isopropanol, and (c) 85% ethanol. The SAXS data of kafirin in (a) 60% *tert*-butanol and (b) 65% isopropanol were best fitted with ellipsoidal form factor. The insets of panels a and b are corresponding pair distribution function (PDF) curve (below) and ab initio modeling performed by DAMMIN. Power law was used to fit both the low and intermediate Q regions of (c) kafirin in 85% ethanol.

DOI: 10.1021/jf504674z
J. Agric. Food Chem. 2015, 63, 216−224

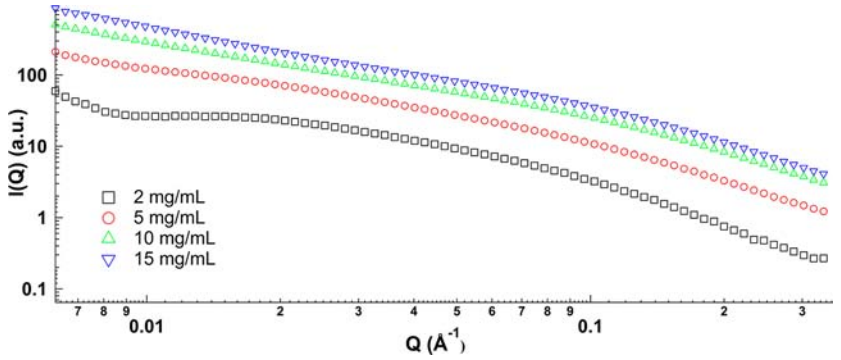

Figure 5. SAXS profiles of kafirin in aqueous 60% *tert*-butanol at different concentrations.

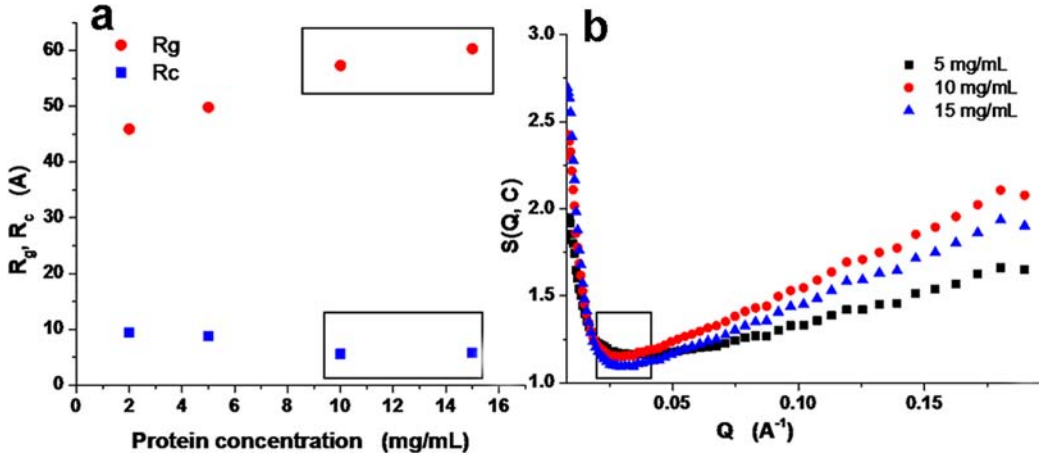

Figure 6. (a) Radius of gyration (R_g) and cross-section radius of gyration (R_c) of kafirin in 60% *tert*-butanol; (b) effective structure factor of 5−15 mg/mL kafirin in 60% *tert*-butanol.

increasing the polarity of kafirin surrounding media could decrease the α-helix content. In-depth understanding of changes in the secondary structure of kafirin with processing conditions can help develop new methodologies to optimize properties of kafirin-based materials.

Structure and Self-Assembly Behavior of Kafirin in Solutions. The shape and size of kafirin in different solvents were extracted on the basis of the SAXS data via form factor fitting, pair distribution function, and ab initio modeling. Figure 4 presents the SAXS profiles of 2 mg/mL kafirin in 60% *tert*-butanol, 65% isopropanol, and 85% ethanol aqueous solutions, respectively. Among the fittings using solid sphere, cylinder, and ellipsoid models, the last delivered the best fit, and we only discuss it later. Kafirin in 60% *tert*-butanol and 65% isopropanol showed prolate ellipsoid, with dimensions of 118 × 15 × 15 and 100 × 11 × 11 Å, respectively (Figure 4a,b). The slightly skewed PDF curve also verified this elongated conformation with a typical fingerprint of a maximum at small distance, and the location of the maximum is corresponding to the radius of the cross-section (insets, below).[26] On the basis of the PDF curve, ab initio modeling of kafirin showed a stretched and extended conformation (insets, above). Compared with 60% *tert*-butanol, kafirin in 65% isopropanol aqueous solution exhibited a more compact structure with a smoother surface (insets, above). Different from 60% *tert*-butanol and 65% isopropanol, kafirin in 85% ethanol showed a straighter profile (Figure 4c). Thus, only the power-law relationship was used to fit the low and intermediate Q regions. The exponents of −1.4 at low Q region and −1.1 at intermediate Q region suggested that either the individual kafirin or its assembly has extended conformation with a high-order elongated structure.

Figure 5 shows the scattering profile of kafirin in 60% *tert*-butanol at concentrations of 2, 5, 10, and 15 mg/mL, respectively. On the basis of Guinier plots of globular and rod-like particles (Supporting Information, Figures S1 and S2), the radius of gyration (R_g) and cross-section radius of gyration (R_c) of kafirin in 60% *tert*-butanol were extracted and plotted against kafirin concentration in Figure 6a. As protein concentration increased from 2 to 5 mg/mL, R_g increased from 46 to 50 Å and R_c slightly decreased from 9.4 to 8.8 Å. Further increase of kafirin concentration to 15 mg/mL resulted in R_g increase to 60.3 Å, and R_c slightly decreased to 5.8 Å, respectively. The increase of R_g and decrease of R_c resulted in a dramatic increase of axial ratio [calculated by $4/3(R_g/R_c)^3$] from 155.2 to 1498.3 upon protein concentration increasing from 2 to 15 mg/mL, which clearly indicated the aggregation of kafirin at high concentration with an elongated format.

The aggregation behavior of kafirin in 60% *tert*-butanol upon concentration increase was further analyzed via effective structure factor. The effective structure factors $S(Q,C)$ of kafirin in 60% *tert*-butanol, calculated on the basis of eq 3, are shown in Figure 6b by taking the scattering intensity profile at C_0 = 2 mg/mL as dilute condition. The values of $S(Q,C)$ in the entire Q region were >1, suggesting an aggregation of kafirin in a given correlation length range. An inverted peak was found at low Q region, which reciprocally corresponded to correlation length ($d = 2\pi/Q^*$, the average separation of proteins). When kafirin concentration increased from 5 to 10 mg/mL, the

DOI: 10.1021/jf504674z
J. Agric. Food Chem. 2015, 63, 216−224

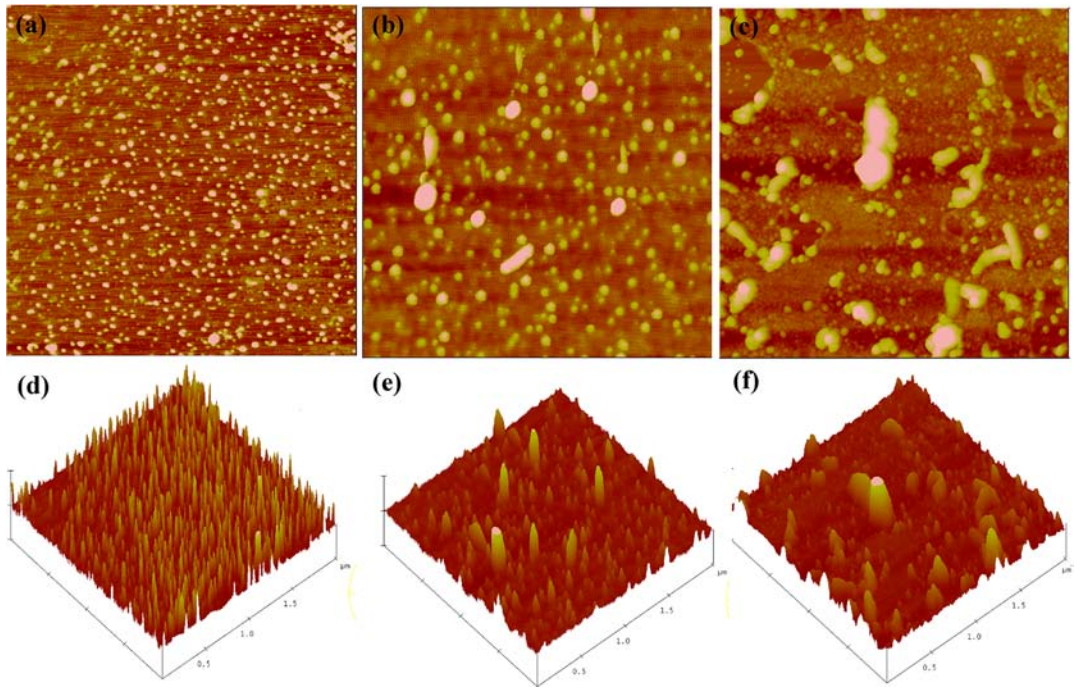

Figure 7. Morphology of kafirin on mica using tapping mode−atomic force microscopy (AFM) height images with casting solutions of 0.1 mg/mL (a), 0.2 mg/mL (b) and 0.5 mg/mL (c) and their corresponding 3D images in panels d, e, and f. The scale size is 2 μm × 2 μm, and the z scales for each concentration are 10, 20, and 80 nm, respectively.

correlation length was kept at 249 Å. However, further increase of kafirin concentration to 15 mg/mL resulted in a decrease of correlation length to 213 Å due to the concentration-dependent aggregation of kafirin. It is unlike concentration-independent correlation length of zein in aqueous ethanol solution,[48] but similar to the case of zein in acetic acid,[49] which indicates this solvent is good enough to fully dissolve karfirin.

Morphology and Solvent Evaporation Induced Self-Assembly of Kafirin. AFM is an effective tool to capture the morphology and self-assembly of either individual proteins or their aggregates. Figure 7 exhibits the height and 3D images of kafirin casting from 60% *tert*-butanol solution with different initial protein concentrations. During solvent evaporation, kafirin concentration in solution increased dramatically, and the remaining solvent became increasingly hydrophilic due to the lower boiling temperature of *tert*-butanol. Protein particles were expected as results of the intramolecular contact of individual proteins, and butanol evaporation triggered hydrophobic protein−protein interactions.

It was observed that kafirin dispersed well in forms of either ellipsoidal or disk-like particles at initial protein concentrations of 0.1 mg/mL, as shown in Figure 7a,d. On the basis of section analysis and statistical bearing analysis, most of individual proteins self-assembled into uniform particles with vertical size between 12 and 17 nm and horizontal size between 20 and 40 nm. Further dilution did not change the particle size (data not shown), which indicated that kafirin presented a rather stable aggregation state when prepared from dilute alcohol solution. This finding is analogous to the observation reported by Yamada et al [50] in the case of zein. The uniformly distributed protein aggregates had also been reported by McMaster et al.[51] using AFM. When the initial protein concentration was increased to 0.2 mg/mL, apart from the presence of individual spherical particles, large disk-like and rod-like particles began to emerge as shown in Figure 7b,e. Under section analysis, a typical disk-like particle had the three axis lengths of 115 nm (x-axis), 106 nm (y-axis), 13 nm (z-axis), and a typical rod-like particle had three axis lengths of 246 nm (x-axis), 86 nm (y-axis), 12 nm (z-axis), respectively. Significant protein aggregation continued, and even larger disk or rod-like structures were formed when the initial protein concentration was further increased to 0.5 mg/mL, as shown in Figure 7c,f. Additionally, the standard deviation for particle size was much larger at 0.5 mg/mL than at 0.2 mg/mL, indicating a more heterogeneous distribution of kafirin aggregates. Combining the results of both SAXS and AFM, the observed morphology of kafirin in dry state may be explained as individual protein with quite prolate dimension in the dilute solution aggregated into stable ellipsoid particles as the concentration increased and the hydrophobicity of the solvent decreased during the solvent evaporation process. As the initial protein concentration continued to increase, chances for individual prolate protein to interact with neighboring proteins enhanced, and small aggregates grew into disk or rod-like aggregates in a larger scale.

Key parameters affecting kafirin structure based on our investigations included the chemical compositions, solvent polarity, protein concentration, and solvent-induced evaporation process. Results gained in this work are relevant in guiding the development of kafirin-based biomaterials. The high propensity of protein aggregation due to the higher proportion of β- and γ-fractions and cross-linked kafirin is the basis for understanding its physical nature and rheological property in solution state. Clarification of the conformational changes of kafirin protein along with changes in protein concentration and solvent polarity is vital for designing the sample preparation and formulation process for kafirin-based biomaterials. The self-assembly behavior of kafirin under solvent-induced evaporation process lays the foundation for the understanding of its film-forming properties and the preparation of kafirin-based fibrillar materials.

DOI: 10.1021/jf504674z
J. Agric. Food Chem. 2015, 63, 216−224

■ ASSOCIATED CONTENT

Supporting Information

Guinier plots for compact spherical particles and rod-like-particles for the scattering intensity profiles of 2, 5, 10, and 15 mg/mL kafirin in 60% *tert*-butanol solution. This material is available free of charge via the Internet at http://pubs.acs.org.

■ AUTHOR INFORMATION

Corresponding Author

*(Q.H.) Phone: (848) 932-5514. Fax (732) 932-6776. E-mail:qhuang@aesop.rutgers.edu.

Funding

This research used resources of the Advanced Photon Source, a U.S. Department of Energy (DOE) Office of Science User Facility operated for the DOE Office of Science by Argonne National Laboratory under Contract DE-AC02-06CH11357. This project was supported by Grant 9 P41 GM103622 from the National Institute of General Medical Sciences of the National Institutes of Health. The content is solely the responsibility of the authors and does not necessarily reflect the official views of the National Institute of General Medical Sciences or the National Institutes of Health.

Notes

The authors declare no competing financial interest.

■ ACKNOWLEDGMENTS

We thank Drs. Avanish Parmarand and Fei Xu at CABM, Rutgers University, for their assistance in using CD.

■ REFERENCES

(1) Krochta, J. M. Proteins as raw materials for films and coatings: definitions, current status and opportunities. In *Protein-Based Films and Coatings*; Gennadios, A., Ed.; CRC Press: Boca Raton, FL, USA, 2002.

(2) Anderson, T. J.; Lamsal, B. P. Zein extraction from corn, corn products, and coproducts and modifications for various applications: a review. *Cereal Chem.* **2011**, *88*, 159−173.

(3) Lawton, J. W. Zein: a history of processing and use. *Cereal Chem.* **2002**, *79*, 1−18.

(4) Anderson, T. J.; Lamsal, B. P. Development of new method for extraction of α-zein from corn gluten meal using different solvents. *Cereal Chem.* **2011**, *88*, 356−362.

(5) Nonthanum, P.; Lee, Y.; Padua, G. W. Effect of γ-zein on the rheological behavior of concentrated zein solutions. *J. Agric. Food Chem.* **2012**, *60*, 1742−1747.

(6) Selling, G. W.; Hamaker, S. A. H.; Sessa, D. J. Effect of solvent and temperature on secondary and tertiary structure of zein by circular dichroism. *Cereal Chem.* **2007**, *84*, 265−270.

(7) Argos, P.; Pedersen, K.; Marks, M. S.; Larkins, B. A. A structural model for maize zein proteins. *J. Biol. Chem.* **1982**, *257*, 9984−9990.

(8) Wang, Q.; Padua, G. W. Controlled self-organization of zein nanostructures for encapsulation of active food ingredients. *Abstr. Pap. Am. Chem. Soc.* **2007**, *233*, 46−46.

(9) Luo, Y. C.; Teng, Z.; Wang, Q. Development of zein nanoparticles coated with carboxymethyl chitosan for encapsulation and controlled release of vitamin D3. *J. Agric. Food Chem.* **2012**, *60*, 836−843.

(10) Kayaci, F.; Uyar, T. Electrospun zein nanofibers incorporating cyclodextrins. *Carbohydr. Polym.* **2012**, *90*, 558−568.

(11) Shull, J. M.; Watterson, J. J.; Kirleis, A. W. Proposed nomenclature for the alcohol-soluble proteins (kafirins) of sorghum-bicolor (L Moench) based on molecular-weight, solubility, and structure. *J. Agric. Food Chem.* **1991**, *39*, 83−87.

(12) Derose, R. T.; Ma, D. P.; Kwon, I. S.; Hasnain, S. E.; Klassy, R. C.; Hall, T. C. Characterization of the kafirin gene family from sorghum reveals extensive homology with zein from maize. *Plant Mol. Biol.* **1989**, *12*, 245−256.

(13) Taylor, J. R. N.; Schober, T. J.; Bean, S. R. Novel food and non-food uses for sorghum and millets. *J. Cereal Sci.* **2006**, *44*, 252−271.

(14) Duodu, K. G.; Taylor, J. R. N.; Belton, P. S.; Hamaker, B. R. Factors affecting sorghum protein digestibility. *J. Cereal Sci.* **2003**, *38*, 117−131.

(15) Taylor, J.; Taylor, J. R. N.; Dutton, M. F.; de Kock, S. Identification of kafirin film casting solvents. *Food Chem.* **2005**, *90*, 401−408.

(16) Buffo, R. A.; Weller, C. L.; Gennadios, A. Films from laboratory-extracted sorghum kafirin. *Cereal Chem.* **1997**, *74*, 473−475.

(17) Emmambux, M. N.; Stading, M.; Taylor, J. R. N. Sorghum kafirin film property modification with hydrolysable and condensed tannins. *J. Cereal. Sci.* **2004**, *40*, 127−135.

(18) Taylor, J.; Taylor, J. R. N.; Belton, P. S.; Minnaar, A. Preparation of free-standing films from kafirin protein microparticles: mechanism of formation and functional properties. *J. Agric. Food Chem.* **2009**, *57*, 6729−6735.

(19) da Silva, L. S.; Taylor, J. R. N. Physical, mechanical, and barrier properties of kafirin films from red and white sorghum milling fractions. *Cereal Chem.* **2005**, *82*, 9−14.

(20) Musigakun, P.; Thongngam, M. Characteristics and functional properties of sorghum protein (kafirin). *Kasetsart J. (Nat. Sci.)* **2007**, 313−318.

(21) Petrella, E. C.; Machesky, L. M.; Kaiser, D. A.; Pollard, T. D. Structural requirements and thermodynamics of the interaction of proline peptides with profilin. *Biochemistry* **1996**, *35*, 16535−16543.

(22) Huang, Q. R.; Dubin, P. L.; Lal, J.; Moorefield, C. N.; Newkome, G. R. Small-angle neutron scattering studies of charged carboxyl-terminated dendrimers in solutions. *Langmuir* **2005**, *21*, 2737−2742.

(23) Fischer, H.; Polikarpov, I.; Craievich, A. F. Average protein density is a molecular-weight-dependent function. *Protein Sci.* **2004**, *13*, 2825−2828.

(24) Li, Y.; Li, J.; Xia, Q.; Zhang, B.; Wang, Q.; Huang, Q. Understanding the dissolution of α-zein in aqueous ethanol and acetic acid solutions. *J. Phys. Chem. B* **2012**, *116*, 12057−12064.

(25) Zhang, F.; Skoda, M. W. A.; Jacobs, R. M. J.; Martin, R. A.; Martin, C. M.; Schreiber, F. Protein interactions studied by SAXS: effect of ionic strength and protein concentration for BSA in aqueous solutions. *J. Phys. Chem. B.* **2006**, *111*, 251−259.

(26) Svergun, D. I.; Koch, M. H. J. Small-angle scattering studies of biological macromolecules in solution. *Rep. Prog. Phys.* **2003**, *66*, 1735−1782.

(27) Semenyuk, A. V.; Svergun, D. I. GNOM − a program package for small-angle scattering data-processing. *J. Appl. Crystallogr.* **1991**, *24*, 537−540.

(28) Volkov, V. V.; Svergun, D. I. Uniqueness of ab initio shape determination in small-angle scattering. *J. Appl. Crystallogr.* **2003**, *36*, 860−864.

(29) Svergun, D. I. Restoring low resolution structure of biological macromolecules from solution scattering using simulated annealing. *Biophys. J.* **1999**, *76*, 2879−2886.

(30) Beckwith, A. C.; Jones, R. M. Physical chemical properties of grain sorghum prolamine fractions and components. *J. Agric. Food Chem.* **1972**, *20*, 259−261.

(31) Nunes, A.; Correia, I.; Barros, A.; Delgadillo, I. Characterization of kafirin and zein oligomers by preparative sodium dodecyl sulfate−polyacrylamide gel electrophoresis. *J. Agric. Food Chem.* **2005**, *53*, 639−643.

(32) Hamaker, B. R.; Mohamed, A. A.; Habben, J. E.; Huang, C. P.; Larkins, B. A. Efficient procedure for extracting maize and sorghum kernel proteins reveals higher prolamin contents than the conventional method. *Cereal Chem.* **1995**, *72*, 583−588.

(33) Watterson, J. J.; Shull, J. M.; Kirleis, A. W. Quantitation of α-karafins, β-karafins, and γ-kafirins in vitreous and opaque endosperm of sorghum-bicolor. *Cereal Chem.* **1993**, *70*, 452−457.

DOI: 10.1021/jf504674z
J. Agric. Food Chem. 2015, 63, 216−224

(34) De Mesa-Stonestreet, N. J.; Alavi, S.; Bean, S. R. Sorghum proteins: the concentration, isolation, modification, and food applications of kafirins. *J. Food Sci.* **2010**, *75*, R90−R104.
(35) El Nour, I. N. A.; Peruffo, A. D. B.; Curioni, A. Characterisation of sorghum kafirins in relation to their cross-linking behaviour. *J. Cereal Sci.* **1998**, *28*, 197−207.
(36) Bean, S. R.; Loerger, B. P.; Smith, B. M.; Blackwell, D. L. Sorghum protein structure and chemistry: implications for nutrition and functionality. In *Advances in Cereal Science: Implications to Food Processing and Health Promotion*; Awika1, M. J., Piironen, V., Bean, S., Eds.; American Chemical Society: Washington, DC, USA, 2011; Vol. 1089, pp 131−147.
(37) Bean, S. R.; Ioerger, B. P.; Park, S. H.; Singh, H. Interaction between sorghum protein extraction and precipitation conditions on yield, purity, and composition of purified protein fractions. *Cereal Chem.* **2006**, *83*, 99−107.
(38) Jones, R. W.; Beckwith, A. C. Proximate composition and proteins of three grain sorghum hybrids and their dry-mill fractions. *J. Agric. Food Chem.* **1970**, 33−36.
(39) Jambunathan, R.; Mertz, E. T. Amino acid compositions of whole kernel and endosperm protein fractions of sorghum. In *Research Progress Report on Inheritance and Improvement of Protein Quality in Sorghum bicolor L. Moench.*; Axtell, J. D., Oswalt, D. L., Eds.; Purdue University: West Lafeyette, IN, USA, 1972; p 43.
(40) Chamba, E. B.; Halford, N. G.; Forsyth, J.; Wilkinson, M.; Shewry, P. R. Molecular cloning of β-kafirin, a methionine-rich protein of sorghum grain. *J. Cereal Sci.* **2005**, *41*, 381−383.
(41) Shull, J. M.; Watterson, J. J.; Kirleis, A. W. Purification and immunocytochemical localization of kafirins in *Sorghum bicolor* (L. Moench) endosperm. *Protoplasma* **1992**, *171*, 64−74.
(42) Belton, P. S.; Delgadillo, I.; Halford, N. G.; Shewry, P. R. Kafirin structure and functionality. *J. Cereal Sci.* **2006**, *44*, 272−286.
(43) Gao, C. L.; Taylor, J.; Wellner, N.; Byaruhanga, Y. B.; Parker, M. L.; Mills, E. N. C.; Belton, P. S. Effect of preparation conditions on protein secondary structure and biofilm formation of kafirin. *J. Agric. Food Chem.* **2005**, *53*, 306−312.
(44) Renugopalakrishnan, V.; Chandrakasan, G.; Moore, S.; Hutson, T. B.; Berney, C. V.; Bhatnagar, R. S. Bound water in collagen: evidence from Fourier-transform infrared and Fourier-transform infrared photoacoustic spectroscopic study. *Macromolecules* **1989**, *22*, 4121−4124.
(45) Zhang, B. C.; Luo, Y. C.; Wang, Q. Effect of acid and base treatments on structural, rheological, and antioxidant properties of α-zein. *Food Chem.* **2011**, *124*, 210−220.
(46) Singh, N.; Georget, D. M. R.; Belton, P. S.; Barker, S. A. Zein-iodine complex studied by FTIR spectroscopy and dielectric and dynamic rheometry in films and precipitates. *J. Agric. Food Chem.* **2009**, *57*, 4334−4341.
(47) Wang, Y.; Padua, G. W. Nanoscale characterization of zein self-assembly. *Langmuir* **2012**, *28*, 2429−2435.
(48) Li, Y.; Li, J.; Xia, Q.; Zhang, B.; Wang, Q.; Huang, Q. Understanding the dissolution of α-zein in aqueous ethanol and acetic acid solutions. *J. Phys. Chem. B* **2012**, *116*, 12057−12064.
(49) Li, Y. Q.; Xia, Q. Y.; Shi, K.; Huang, Q. R. Scaling behaviors of α-zein in acetic acid solutions. *J. Phys. Chem. B* **2011**, *115*, 9695−9702.
(50) Yamada, K.; Takahashi, H.; Noguchi, A. Improved water resistance in edible zein films and composites for biodegradable food packaging. *Int. J. Food Sci. Technol.* **1995**, *30*, 599−608.
(51) McMaster, T. J.; Miles, M. J.; Wannerberger, L.; Eliasson, A. C.; Shewry, P. R.; Tatham, A. S. Identification of microphases in mixed α- and ω-gliadin protein films investigated by atomic force microscopy. *J. Agric. Food Chem.* **1999**, *47*, 5093−5099.

DOI: 10.1021/jf504674z
J. Agric. Food Chem. 2015, 63, 216−224

JOURNAL OF AGRICULTURAL AND FOOD CHEMISTRY

Article

pubs.acs.org/JAFC

Structural Characterization of Two Water-Soluble Polysaccharides from Black Soybean (*Glycine max* (L.) Merr.)

Jun Liu,* Xiao-yuan Wen, Juan Kan, and Chang-hai Jin*

College of Food Science and Engineering, Yangzhou University, Yangzhou 225127, Jiangsu, China

ABSTRACT: Black soybeans (*Glycine max* (L.) Merr.) have been widely used as a health food and medicinal herb in oriental medicine. In the present study, the chemical structures of two water-soluble polysaccharides (black soybean polysaccharide 1 (BSPS-1) and black soybean polysaccharide 3 (BSPS-3)) isolated from black soybeans were characterized by high performance size-exclusion chromatography (HPSEC), methylation analysis, and 1D (^{1}H, ^{13}C) and 2D (COSY, TOCSY, HSQC, NOESY, and HMBC) NMR spectra. The molecular weights of BSPS-1 and BSPS-3 were 1.95×10^5 and 1.88×10^5 Da, respectively. Methylation analysis and NMR spectra indicate that BSPS-1 is composed of 1,6-α-D-glucopyranosyl residues. By contrast, BSPS-3 is mainly composed of a 1,3-β-D-galactopyranosyl residue backbone with side chains substituted at the O-6 position consisting of large content of T-α-L-Ara*f*-(1→ residues, and small contents of →5)-α-L-Ara*f*-(1→, →2)-α-L-Rha*p*-(1→, and 4-*O*-Me-β-D-GlcA*p*-(1→ residues. Our results suggest that BSPS-1 is a linear (1→6)-α-D-glucan, whereas BSPS-3 is a type II arabinogalactan. The unique structures of BSPS-1 and BSPS-3 indicate that they might have wide applications in food and pharmaceutical industries.

KEYWORDS: *black soybean, NMR, structural characterization, polysaccharides*

INTRODUCTION

Black soybeans (*Glycine max* (L.) Merr.) are soybeans with black seed coats, which have been widely used as a health food and medicinal herb in oriental medicine. The pigmentation on the black soybeans is due to the abundance of anthocyanins in the seed coat.[1] Several studies suggest that black soybeans comprise various classes of bioactive compounds, including oil, isoflavones, anthocyanins, saponins, polysaccharides, and proteins.[2−5] Among these compounds, anthocyanins have been demonstrated to have a wide range of beneficial health effects, such as antioxidant, anti-inflammatory, antiobesity, antidiabetic, and antimutagenicity properties.[6−11]

Although polysaccharides have been reported as one of the secondary metabolites of black soybeans, information on the structure characterization and biological activities of black soybean polysaccharides (BSPS) is still limited. Liao et al. revealed that (1,6)-α-D-glucan might be the major component of BSPS. The polysaccharide component could inhibit proliferation and induce differentiation in human leukemic U937 cells by activating the immune response of mononuclear cells.[12] Moreover, BSPS could promote myelopoiesis activity in the bone marrow, stimulate production of various hematopoietic growth factors from spleen cells, and reconstitute bone marrow that has been myelosuppressed by irradiation and 5-fluorouracil.[13] Wu et al. reported that BSPS could stimulate granulocyte colony-stimulated factor production in peripheral blood mononuclear cells.[14] Recently, we reported the extraction, preliminary characterization, and in vitro antioxidant activity of BSPS.[15] Two main water-soluble polysaccharide fractions (black soybean polysaccharide 1 (BSPS-1) and black soybean polysaccharide 3 (BSPS-3)) were obtained. These two fractions have been demonstrated to be composed of different monosaccharides and possess potential superoxide anion and DPPH radical scavenging activities.

In order to establish the structure−function relationships of BSPS and further facilitate its applications in food and pharmaceutical industries, the main objective of this study was to characterize the detailed structure features of BSPS-1 and BSPS-3 by high performance size-exclusion chromatography (HPSEC), methylation analysis, and nuclear magnetic resonance (NMR) spectra.

MATERIALS AND METHODS

Materials and Reagents. Black soybean (*G. max* (L.) merr.) seeds were obtained from Heilongjiang Beizhen Food Co., Ltd. (Heilongjiang, China). Crude polysaccharides were isolated from black soybean flour and further purified on chromatography of DEAE-52 and Sepharose CL-4B.[15] Two main purified fractions of BSPS-1 and BSPS-3 were used in this study. Deuterium oxide (D_2O) was purchased from Sigma Chemical Co. (St. Louis, MO, USA). All other reagents were of analytical grade.

Monosaccharide Composition Analysis. The monosaccharide compositions of BSPS-1 and BSPS-3 were determined as described previously.[15] The trimethylsilyl derivatives of polysaccharide hydrolyzate were analyzed on a Trace GC Ultra gas chromatograph (Thermo Fisher Scientific, Waltham, MA, USA) equipped with flame ionization detector (FID) and a CP-Sil5 capillary column (30 m × 0.25 mm × 0.25 μm). Nitrogen gas was used as the carrier gas. Temperature-programmed GC measurements were carried out from 100 °C (held for 5 min), to 150 °C (held for 5 min) at a rate of 5 °C/min, and then to 240 °C (held for 2 min) at a rate of 5 °C/min.

Determination of Purity and Molecular Weight. The purity and molecular weight (MW) of BSPS-1 and BSPS-3 were determined by HPSEC on an Agilent 1200 system (Agilent Technologies, Palo Alto, CA, USA) equipped with a TSK gel G4000 PW_{XL} column (30

Received: October 27, 2014
Revised: December 13, 2014
Accepted: December 14, 2014
Published: December 15, 2014

ACS Publications © 2014 American Chemical Society

DOI: 10.1021/jf505172m
J. Agric. Food Chem. 2015, 63, 225−234

cm × 7.8 mm × 10 μm, Tosoh Corp., Tokyo, Japan) and an evaporative light scattering detector (ELSD). Sample solution (20 μL) was injected and eluted with distilled water at 50 °C with a flow rate of 0.7 mL/min. The molecular weights of polysaccharide samples were calculated from the calibration curve of T-series dextran standards (T-500, T-200, T-100, T-50, and T-10).

Methylation and GC−MS Analysis. For glycosyl linkage analysis, uronic acid residues of BSPS-1 and BSPS-3 were first reduced as described previously.[16] Then, methylation of BSPS-1 and BSPS-3 was carried out according to the method of Ciucanu and Kerek.[17] The complete methylation was confirmed by the lack of hydroxyl peak on a Varian 670 FT-IR spectrometer (Varian Inc., Palo Alto, CA, USA). The permethylated polysaccharide was then hydrolyzed with trifluoroacetic acid at 120 °C for 2 h, reduced with $NaBH_4$, and acetylated with acetic anhydride. The resulting partially methylated alditol acetate derivatives were analyzed on a Thermo Trace DSQ II GC-MS (Thermo Fisher Scientific, Waltham, MA, USA) equipped with a TR-5MS capillary column (30 m × 0.25 mm × 0.25 μm). The initial column temperature was set at 100 °C, and programmed to 250 °C (held for 5 min) at 6 °C/min. Helium was used as the carrier gas at the rate of 1 mL/min. The partially methylated alditol acetates were identified by their retention times and electron ionization spectra.

NMR Analysis. The fine chemical structures of BSPS-1 and BSPS-3 were analyzed by an AVANCE-600 NMR spectrometer (Bruker Inc., Rheinstetten, Germany). For NMR measurements, the dried sample (20 mg) was dissolved in 0.5 mL of D_2O and kept at room temperature for 3 h. ^1H (600 Hz) and ^{13}C (150 Hz) NMR spectra were recorded at 25 °C. Then, the 2D NMR spectra including $^1H/^1H$ homonuclear correlation spectroscopy (COSY), total correlation spectroscopy (TOCSY), heteronuclear single quantum coherence (HSQC), heteronuclear multiple-bond coherence (HMBC), and nuclear Overhauser enhancement spectroscopy (NOESY) were recorded.

RESULTS AND DISCUSSION

Structural Characterization of BSPS-1. Monosaccharide composition analysis showed that BSPS-1 was made up of arabinose, rhamnose, galactose, glucose, and mannose in the molar ratio of 1.79:1.00:2.59:26.54:1.01.[15] Thus, BSPS-1 can be mainly regarded as a glucan. To determine the monosaccharide linkages, BSPS-1 was methylated and converted into the corresponding alditol acetates for GC−MS analysis. As shown in Table 1, the major derivative of BSPS-1 was 1,5,6-tri-*O*-acetyl-2,3,4-tri-*O*-methyl-D-glucitol, indicating that BSPS-1 is mainly composed of (1→6)-linked glucopyranosyl residues. The purity and molecular weight of BSPS-1 was measured by HPSEC system. As shown in Figure 1a, BSPS-1 exhibited only one symmetrical sharp peak, indicating that this fraction was a homogeneous polysaccharide. According to the calibration curve of standards, the molecular weight of BSPS-1 was determined as 1.95×10^5 Da.

Table 1. Partial Methylated Alditol Acetates and Deduced Glycosidic Linkages of BSPS-1 and BSPS-3

partial methylated alditol acetates	deduced glycosidic linkages	molar ratio (%) BSPS-1	BSPS-3
2,3,5-Me_3-Ara[a]	T-Ara*f*-(1→	4.5	16.9
2,3-Me_2-Ara	→5)-Ara*f*-(1→	nd[b]	6.7
3,4-Me_2-Rha	→2)-Rha*p*(1→	3.4	3.8
2,4,6-Me_3-Gal	→3)-Gal*p*-(1→	7.9	38.3
2,4-Me_2-Gal	→3,6)-Gal*p*-(1→	nd	16.6
2,3,4,6-Me_4-GlcA*p*	T-GlcA*p*-(1→	nd	8.4
2,3,4-Me_3-Glc	→6)-Glc*p*-(1→	84.2	9.3

[a]2,3,5-Me_3-Ara =2,3,5-tri-*O*-methyl-1,4-di-*O*-acetyl-arabinitol, etc. [b]Not detected.

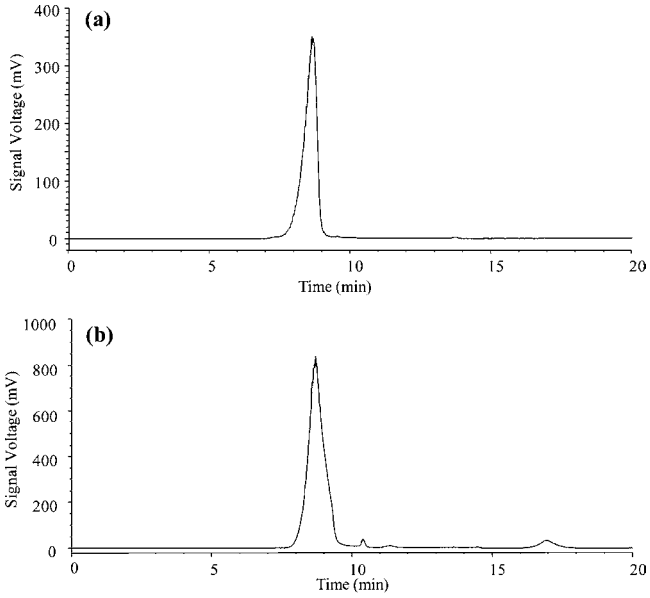

Figure 1. HPSEC elution profile of purified fractions BSPS-1 (a) and BSPS-3 (b).

As shown in Figure 2a, the ^1H NMR spectrum of BSPS-1 shows only one dominant peak at δ 4.92 ppm in the anomeric region, indicating that these glucosyl residues are α-glycosidically linked. Combining the result of methylation analysis and literature data,[18−22] this peak is assigned to the H-1 of →6)-α-D-Glc*p*-(1→. The chemical shift of H-2 can be assigned from the COSY spectrum based on the principle that H-2 correlates with H-1 (Figure 2b). Similarly, H-3 to H-6 can also be assigned. Therefore, the chemical shifts at 3.53, 3.66, 3.45, 3.85, 3.70, and 3.93 ppm can be attributed to H-2, H-3, H-4, H-5, H-6, and H-6′ of the glucosyl residues, respectively. All the proton chemical shifts can also be confirmed by TOCSY spectrum (Figure 2c). In the high field region of the ^1H NMR spectrum, a small methyl signal at 1.24 ppm should be assigned to the H-6 of rhamnose residue. However, the signals of sugar residues such as arabinose, galactose, and mannose are not clearly detected in the ^1H NMR spectrum of BSPS-1, which is probably due to the low contents of these residues.

The ^{13}C NMR spectrum of BSPS-1 is shown in Figure 3a. The chemical shift at 97.65 ppm is attributed to the anomeric carbon atoms of →6)-α-D-Glc*p*-(1→. The other carbon signals (C-2 to C-6) are identified from cross peaks in the HSQC spectrum (Figure 3b) as well as the literature data.[18,19,22] Accordingly, the carbon chemical shifts at 71.29, 73.40, 69.53, 70.23, and 65.66 ppm can be assigned to C-2, C-3, C-4, C-5, and C-6 of glucosyl residue. However, no typical signal is observed for uronic acid groups, which is in agreement with the result of the *m*-hydroxydiphenyl colorimetric method.[15] All the ^1H and ^{13}C chemical shifts for BSPS-1 are listed in Table 2 and are consistent with previous reports.[18−24] To confirm the sequence of glucosyl residues in the polysaccharide, HMBC and NOESY experiments were carried out. The cross peaks of H1−C6 and H6′−C1 are observed in the HMBC spectrum (Figure 3c). In the NOESY spectrum (Figure 3d), the cross peaks of H1−H6′ and H1−H6 are detected. These results all suggest that the glucosyl residues are linked by α-(1→6) glycosidic linkage.

DOI: 10.1021/jf505172m
J. Agric. Food Chem. 2015, 63, 225−234

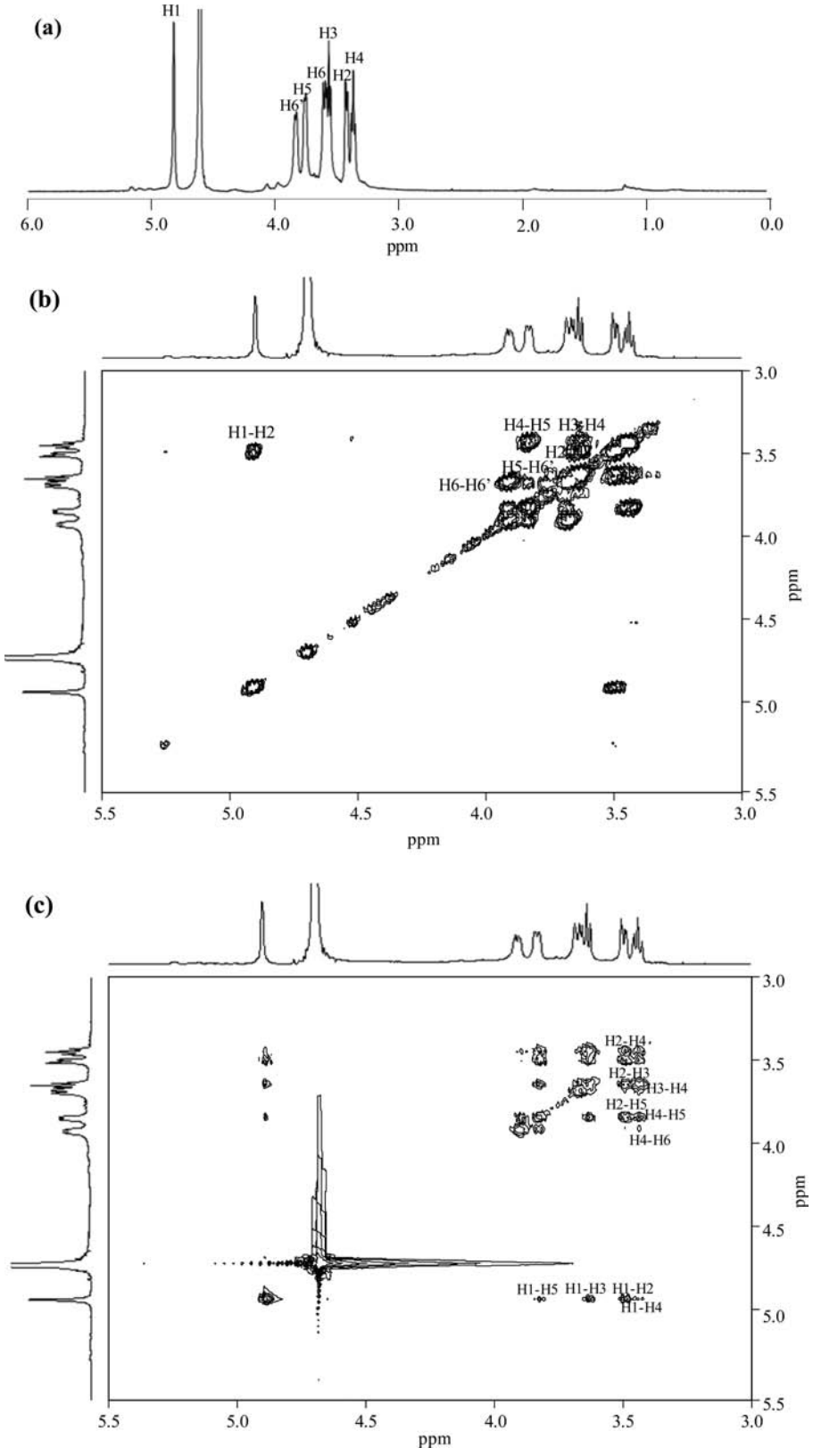

Figure 2. ^{1}H NMR (a), ^{1}H/^{1}H-COSY (b), and TOCSY (c) spectra of BSPS-1. In ^{1}H/^{1}H-COSY and TOCSY spectra, H1−H2 represents correlation between H-1 and H-2 of →6)-*α*-D-Glc*p*-(1→ residue, etc.

On the basis of above results, BSPS-1 is determined as a linear (1→6)-*α*-D-glucan. Until now, only few plants including *Ipomoea batatas*, *Cistanche deserticola*, *Angelica sinensis*, *Pueraria lobata*, *Panax ginseng*, and *Dimocarpus longan* have been reported to produce (1→6)-*α*-D-glucan. Zhao et al. reported that the (1→6)-*α*-D-glucan isolated from the root of *Ipomoea batatas* had strong immunostimulatory activity in a mouse model.[24] Wu et al. found that three polysaccharides from the

DOI: 10.1021/jf505172m
J. Agric. Food Chem. 2015, 63, 225−234

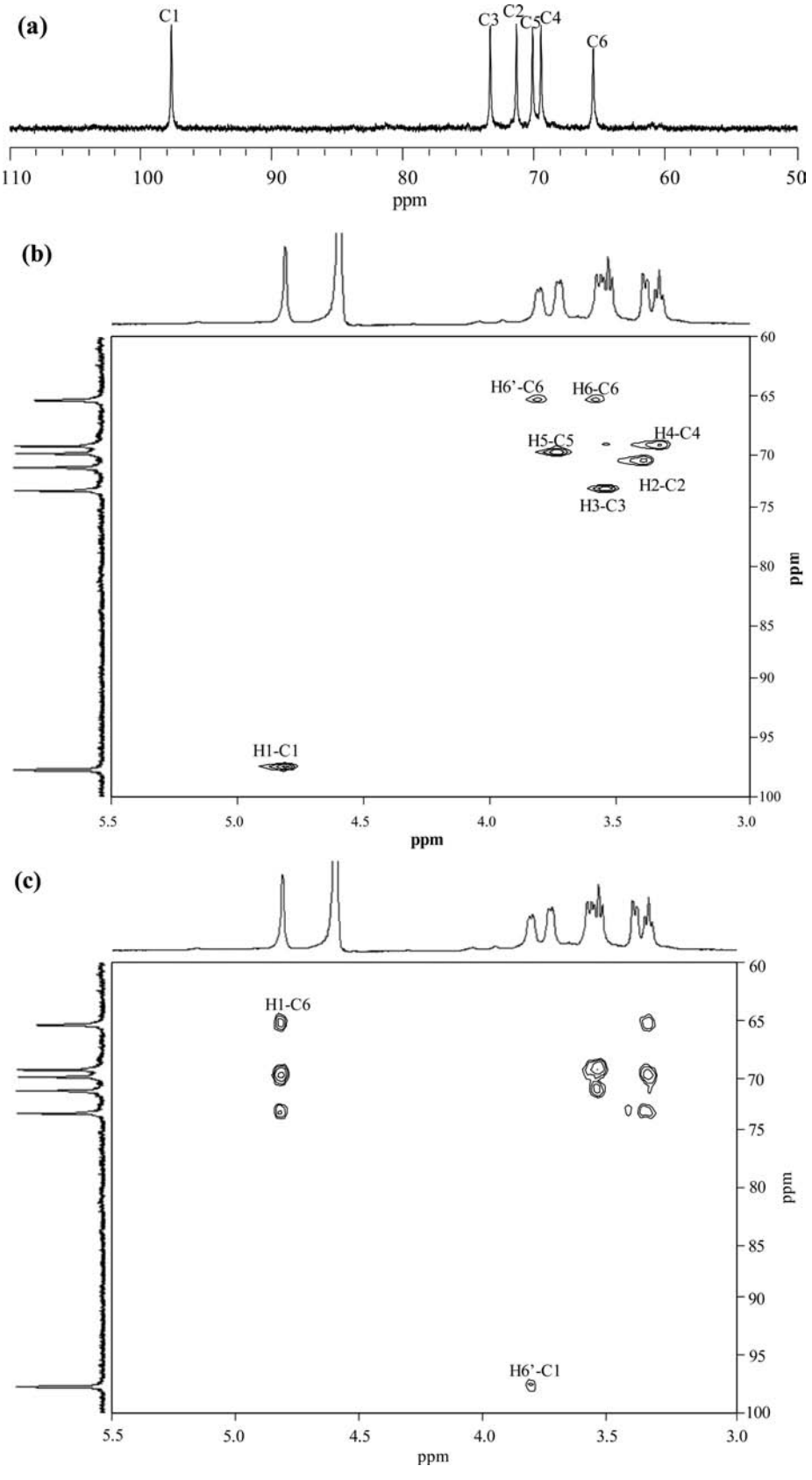

Figure 3. continued

DOI: 10.1021/jf505172m
J. Agric. Food Chem. 2015, 63, 225−234

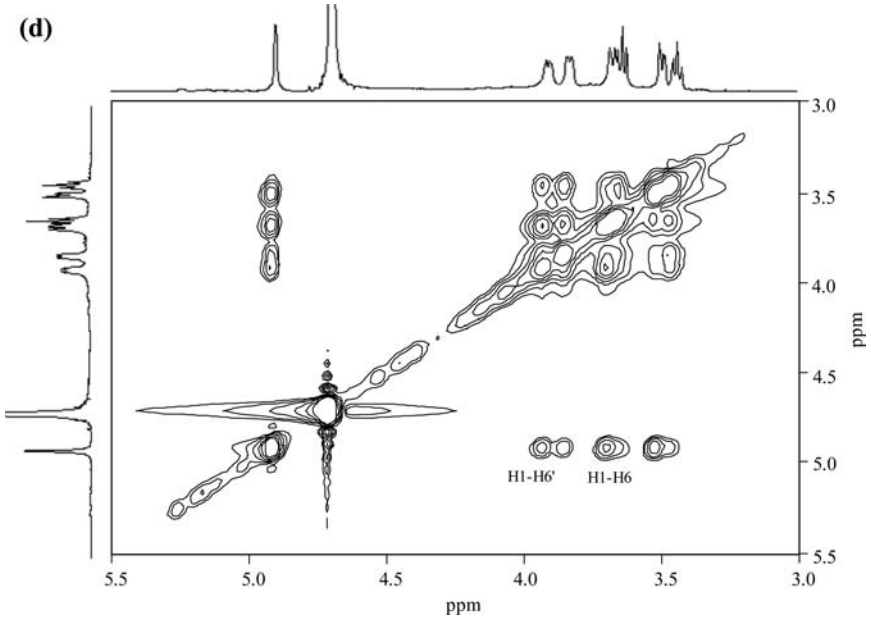

Figure 3. ^{13}C NMR (a), HSQC (b), HMBC (c), and NOESY (d) spectra of BSPS-1 in D_2O at 25 °C. In the HSQC spectrum, H1−C1 represents the cross peak between H-1 and C-1 of →6)-α-D-Glc*p*-(1→ residue, etc. In the HMBC spectrum, H1−C6 represents the heteronuclear coherence between H-1 and C-6 of adjacent →6)-α-D-Glc*p*-(1→ residues. In the NOESY spectrum, H1−H6′ represents the NOE contacts between H-1 and H6′ of adjacent →6)-α-D-Glc*p*-(1→ residues.

Table 2. Summary of ^{1}H and ^{13}C Chemical Shifts for BSPS-1

glycosidic linkage	H1/ C1	H2/ C2	H3/ C3	H4/ C4	H5/ C5	H6,H6′/ C6
→6)-α-D-Glc*p*-(1→	4.92	3.53	3.66	3.45	3.85	3.70, 3.90
	97.65	71.29	73.40	69.53	70.23	65.66

stem of *Cistanche deserticola* had a backbone of (1→6)-α-D-glucan with different molecular weights.[21] Cao et al. characterized a (1→6)-α-D-glucan from the root of *Angelica sinensis* (Oliv.) Diels.[18] Cui et al. extracted (1→6)-α-D-glucan from the root of *Pueraria lobata* (Willd.) Ohwi, and found that the sulfated derivative of glucan could significantly attenuate PC12 cell damage caused by hydrogen peroxide.[19] Sun et al. reported the structural characterization and immunostimulatory activity of a linear (1→6)-α-D-glucan isolated from *Panax ginseng* C. A. Meyer.[20] Recently, Zhu et al. isolated a (1→6)-α-D-glucan from flesh tissues of *Dimocarpus longan* Lour and demonstrated that the polysaccharide had anticancer activity against the growth of HepG2 cells.[22] In our previous study, BSPS-1 as a novel resource of (1→6)-α-D-glucan has been demonstrated to have potential superoxide anion and DPPH radical scavenging activities.[15] From the above literature, it could be concluded that (1→6)-α-D-glucan could be a health beneficial polysaccharide and might have wide applications in food and pharmaceutical industries.

Structural Characterization of BSPS-3. In our previous study, GC analysis showed that BSPS-3 was composed of arabinose, rhamnose, galactose, and mannose in the molar ratio of 16.80:3.60:33.66:1.00.[15] This indicated that BSPS-3 was probably an arabinogalactan. Methylation analysis (Table 1) further showed that the dominant linkage types of BSPS-3 were T-α-L-Ara*f* -(1→, →3,6)-β-D-Gal*p*-(1→, and →3)-β-D-Gal*p*-(1→, accompanied by small amounts of →5)-α-L-Araf-(1→, GlcA*p*-(1→, →2)-α-L-Rha*p*-(1→, and →6)-α-D-Glc*p*-(1→. As shown in Figure 1b, the molecular weight determination of BSPS-3 exhibited one major symmetrical sharp peak and another two small peaks. The molecular weight of main peak in BSPS-3 was determined to be 1.88×10^5 Da.

In the ^{1}H NMR spectrum of BSPS-3 (Figure 4a), the chemical shift at 5.18 ppm should be assigned to an α-linked residue (residue A). The corresponding chemical shift of this residue at 109.26 ppm in ^{13}C NMR spectrum (Figure 4b) can be confirmed by the HSQC spectrum (Figure 4c). According to the results of methylation analysis and literature data,[25−28] this residue can be identified as T-α-L-Ara*f* -(1→. From the TOCSY spectrum (Figure 5a), H-2 can be assigned at 4.16 ppm which correlates with H-1. H-3, H-4, H-5, and H-5′ can be assigned to the shifts at 3.88, 4.07, 3.80, and 3.67 ppm as shown in the COSY spectrum (Figure 5b). The corresponding ^{13}C chemical shifts of T-α-L-Ara*f* -(1→ can be assigned from the HSQC spectrum (Figure 4c) and are listed in Table 3. The assignments are consistent with the literature.[25−31]

From the ^{1}H NMR spectrum of BSPS-3 (Figure 4a) and the literature,[26−28] the H-1 signal at 5.02 ppm can be assigned as →5)-α-L-Araf-(1→ (residue B). The assignment of H-2 for →5)-α-L-Araf-(1→ at 4.05 ppm can be obtained by its correlation with H-1 in the TOCSY spectrum (Figure 5a). However, the other proton signals for →5)-α-L-Araf-(1→ are not detected in both TCOSY and COSY spectra, which is due to the low content of this residue. By comparing with literature data,[26−28] all the ^{1}H and ^{13}C chemical shifts of →5)-α-L-Araf-(1→ are identified from the cross peaks in the HSQC spectrum (Figure 4c).

As shown in Figure 4a, the H-1 signal at 4.62 ppm can be assigned to →3,6)-β-D-Gal*p*-(1→ (residue C), which is consistent with literature.[25,26,28,32] The assignment of H-2 (3.64 ppm) can be confirmed by its correlation with the H-1 signal in COSY and TOCSY spectra (Figure 5). The chemical shift of H-3 can be attributed to 3.83 ppm from its correlation with H-2. Comparing HSQC spectrum with the literature[25,26,28,30,32] allows the signals of H-4, H-5, and H-6 to be

DOI: 10.1021/jf505172m
J. Agric. Food Chem. 2015, 63, 225−234

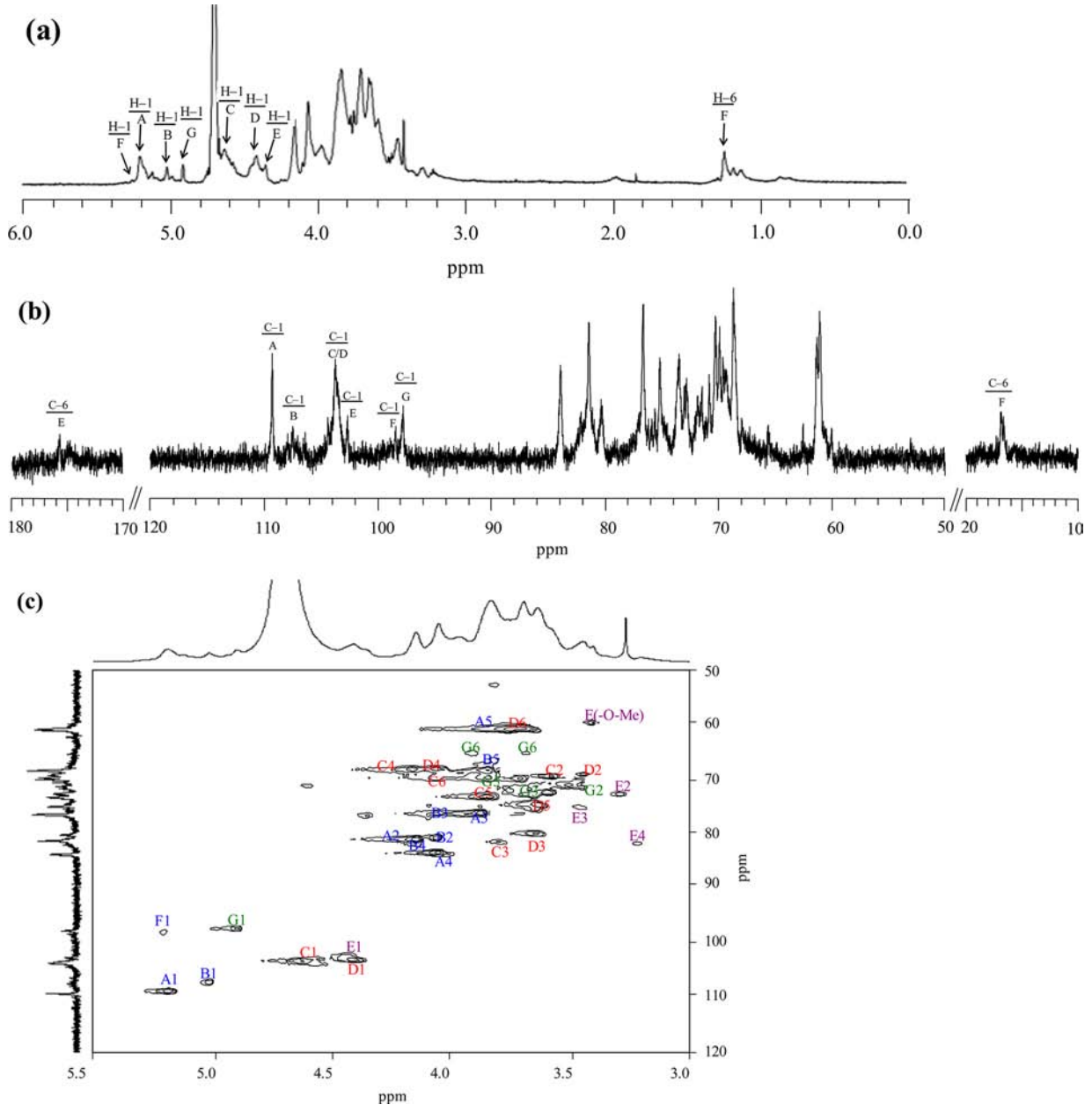

Figure 4. ^{1}H NMR (a), ^{13}C NMR (b), and HSQC (c) spectra of BSPS-3 in D_2O at 25 °C. A, B, C, D, E, F, and G represent the residues of *α*-L-Ara*f*-(1→, →5)-*α*-L-Ara*f*-(1→, →3,6)-*β*-D-Gal*p*-(1→, →3)-*β*-D-Gal*p*-(1→, 4-*O*-Me-*β*-D-GlcA*p*-(1→, →2)-*α*-L-Rha*p*(1→, and →6)-*α*-D-Glc*p*-(1→, respectively. In the HSQC spectrum, A1 represents the cross peak between H-1 and C-1 of residue A, etc.

assigned to chemical shifts at 4.18, 3.90, and 3.99 ppm, respectively. In addition, all the ^{13}C chemical shifts of →3,6)-*β*-D-Gal*p*-(1→ can also be identified from the cross peaks of HSQC spectrum (Figure 4c). Similarly, the H-1 signal at 4.38 ppm can be assigned to →3)-*β*-D-Gal*p*-(1→ (residue D). The ^{1}H and ^{13}C chemical shifts of this residue can be identified from COSY, TOCSY, and HSQC spectra. The corresponding chemical shifts are listed in Table 3 and are also consistent with previous reports.[29−32]

The signal at *δ* 102.6 ppm in the ^{13}C NMR spectrum can be attributed to C-1 of 4-*O*-Me-*β*-D-GlcA*p*-(1→ (residue E) according to the literature.[33,34] A small peak observed at 175.30 ppm is a typical signal of carboxyl group from uronic acid. A cross peak at 3.40/59.90 ppm is shown in the HSQC spectrum (Figure 4c), which is assigned to the $-OCH_3$ group of this residue. The other ^{1}H and ^{13}C chemical shifts of 4-*O*-Me-*β*-D-GlcA*p* are identified from the cross peaks in the COSY (Figure 5b) and HSQC spectra (Figure 4c). The chemical shifts identified are also consistent with literature data.[33,34] In addition, the small anomeric signal at 5.21 ppm can be assigned to the H-1 of →2)-*α*-L-Rha*p*-(1→ (residue F) according to the literature.[26,27,35,36] The signal at 1.24 ppm should be attributed to H-6 (exocyclic $-CH_3$ group) of →2)-*α*-L-Rha*p*-(1→in the ^{1}H NMR spectrum (Figure 4a). In the ^{13}C NMR spectrum, signals at 16.54 and 98.30 ppm belong to the $-CH_3$ and C-1 of →2)-*α*-L-Rha*p*-(1→, respectively (Figure 4b). These chemical shifts can be confirmed by the HSQC spectrum (Figure 4c). Other chemical shifts are assigned acorrding to the ^{13}C NMR spectrum and literature data.[26,27,36] Notably, BSPS-3 also contains a small amount of →6)-*α*-D-Glc*p*-(1→ (residue G) as confirmed by the ^{13}C NMR and

DOI: 10.1021/jf505172m
J. Agric. Food Chem. 2015, 63, 225−234

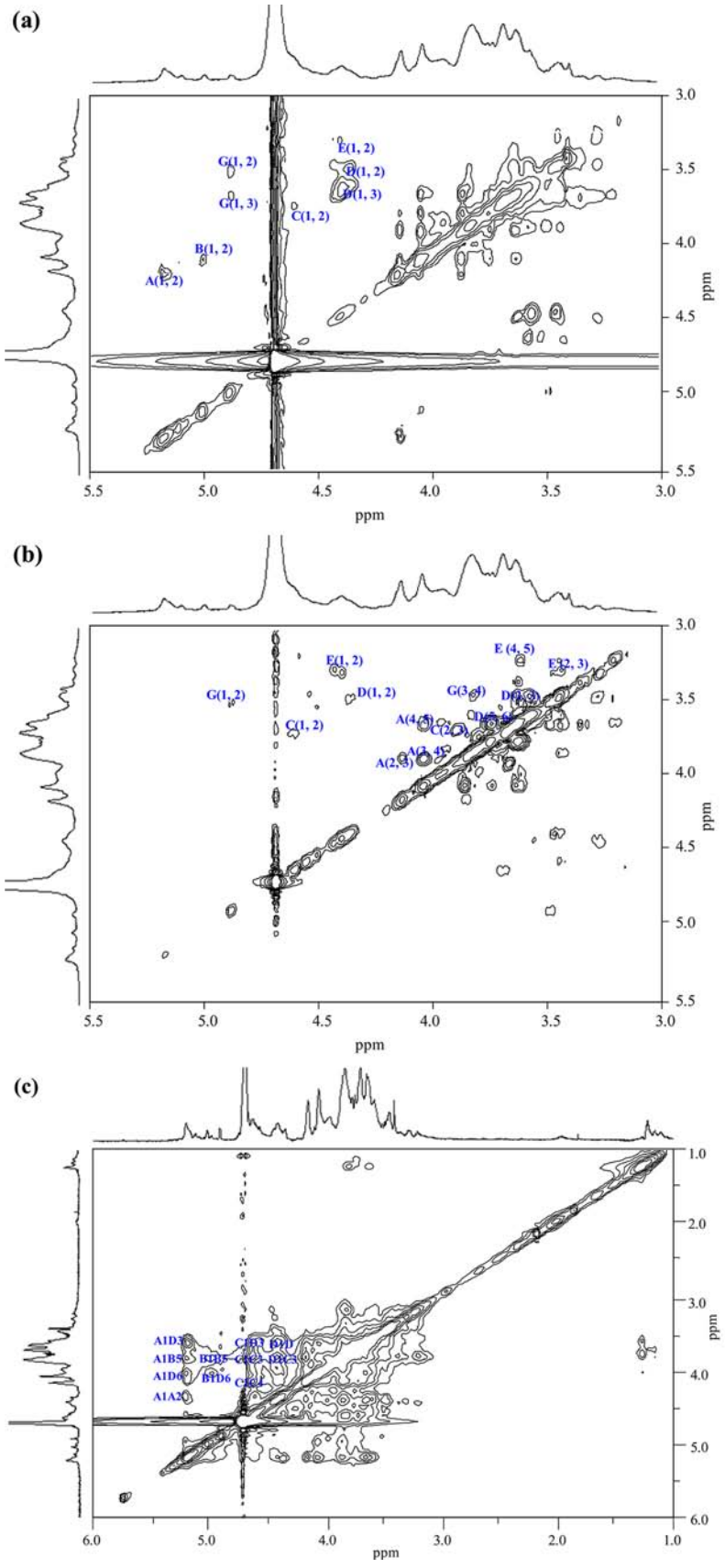

Figure 5. TOCSY (a), $^{1}H/^{1}H$-COSY (b), and NOESY (c) spectra of BSPS-3 in D_2O at 25 °C. In the TOCSY and $^{1}H/^{1}H$-COSY spectra, A(1, 2) represents correlation between H-1 and H-2 of residue A, etc. In the NOESY spectrum, A1D3 represents the NOE contacts between H-1 of residue A and H-3 of residue D, etc.

DOI: 10.1021/jf505172m
J. Agric. Food Chem. 2015, 63, 225−234

Table 3. Summary of ^{1}H and ^{13}C Chemical Shifts for BSPS-3

glycosidic linkage	H1/C1	H2/C2	H3/C3	H4/C4	H5/C5	H6,H6′/C6	−OCH_3
A: α-L-Ara*f*-(1→	5.18	4.16	3.88	4.07	3.80/3.67		
	109.26	81.48	76.56	83.95	61.09		
B: →5)-α-L-Ara*f*-(1→	5.02	4.05	3.92	4.15	3.85		
	107.50	81.39	76.57	82.07	67.92		
C: →3,6)-β-D-Gal*p*-(1→	4.62	3.64	3.83	4.18	3.90	3.99	
	103.70	69.89	81.43	68.48	73.42	69.41	
D: →3)-β-D-Gal*p*-(1→	4.38	3.45	3.65	4.06	3.64	3.73	
	103.63	69.85	80.18	68.48	75.16	61.09	
E: 4-*O*-Me-β-D-GlcA*p*-(1→	4.40	3.31	3.42	3.24	3.60	−	3.40
	102.60	72.75	75.21	82.02	75.34	175.30	59.90
F: →2)-α-L-Rha*p*(1→	5.21	4.09	3.87	3.34	3.78	1.24	
	98.3	77.6	69.30	73.70	69.80	16.54	
G: →6)-α-D-Glc*p*-(1→	4.92	3.53	3.66	3.45	3.85	3.70, 3.90	
	97.65	71.29	73.40	69.53	70.23	65.66	

HSQC spectra. The chemical shifts of this residue are identical with that of BSPS-1.

The sequence of glycosyl residues for BSPS-3 was determined by NOESY experiment. As shown in Figure 5c, H-1 of T-α-L-Ara*f* -(1→ and →5)-α-L-Araf-(1→ have strong NOE contacts with H-6 of →3,6)-β-D-Gal*p*-(1→, indicating that these two residues are linked to the O-6 position of →3,6)-β-D-Gal*p*-(1→. Similarly, T-α-L-Ara*f* -(1→ is also linked to the O-5 position of →5)-α-L-Araf-(1→, →3,6)-β-D-Gal*p*-(1→ is linked to the O-3 position of →3)-β-D-Gal*p*-(1→, and →3)-β-D-Gal*p*-(1→ is linked to the O-3 position of →3,6)-β-D-Gal*p*-(1→ as assigned from the NOESY spectrum. However, →6)-α-D-Glc*p*-(1→ has no significant NOE contact with other residues. This suggests that BSPS-1 is not absolutely separated from BSPS-3 in the purification step, thus, a small amount of BSPS-1 is contained in BSPS-3. The NOE contacts of →2)-α-L-Rha*p*-(1→ and 4-*O*-Me-β-D-GlcA*p*-(1→ with other residues are not observed in the NOESY spectrum due to their low contents.

Combining all the information obtained above, the complete assignments of all the linkage patterns can be determined as listed in Table 3. The backbone of BSPS-3 is mainly composed of 1,3-β-D-galactopyranosyl residues with side chains substituted at the O-6 position consisting of large content of T-α-L-Ara*f* -(1→ residues, and lesser contents of →5)-α-L-Araf-(1→, →2)-α-L-Rha*p*-(1→ and 4-*O*-Me-β-D-GlcA*p*-(1→ residues. Therefore, BSPS-3 can be considered as a type II arabinogalactan. Till now, type II arabinogalactan has been isolated from various plants including *Andrographis paniculata*, *Anogeissus latifolia*, *Chrysanthemum morifolium*, *Centella asiatica*, *Endopleura uchi*, *Plantago major*, *Stevia rebaudiana*, *Viscum album*, etc., and demonstrated to possess many valuable bioactivities such as antitussive, antitumor, anticomplementary, antiviral, antioxidative, and immunological activities.[16,28,30,31,37−41]

In conclusion, our results suggest that BSPS-1 is a linear (1→6)-α-D-glucan, whereas BSPS-3 is a type II arabinogalactan. On the basis of methylation and NMR spectra analysis, the possible structural schemes for BSPS-1 and BSPS-3 are proposed in Figure 6. Notably, the unique structures of BSPS-1 and BSPS-3 indicated that they might possess many valuable bioactivities and have wide applications in food or pharmaceutical industries. Further works on the biological activities of these two polysaccharides are in progress.

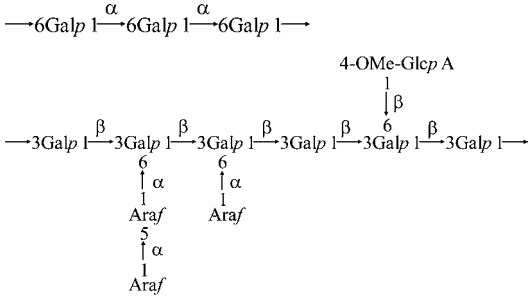

Figure 6. Propsed stuctures of BSPS-1 and BSPS-3.

AUTHOR INFORMATION

Corresponding Authors

*(J.L.) Tel: +86-514-87978158. Fax: +86-514-87313372. E-mail: junliu@yzu.edu.cn.

*(C.-h.J.) Tel: +86-514-87978158. Fax: +86-514-87313372. E-mail: chjin@yzu.edu.cn.

Funding

This work was partly supported by Grants-in-Aid for scientific research from the National Natural Science Foundation of China (No. 31101216), Natural Science Foundation of the Education Committee of Jiangsu province (No. 11KJB550006), Postgraduate Innovation Project of Jiangsu Province (No. SJLX_0610), Scientific and Technological Development Program of Jiangsu Province (No. BC2013408), and New Century Talents Project of Yangzhou University.

Notes

The authors declare no competing financial interest.

ACKNOWLEDGMENTS

The authors thank the testing center of Yangzhou University for NMR measurements.

REFERENCES

(1) Todd, J. J.; Vodkin, L. O. Pigmented soybean (*Glycine max*) seed coats accumulate proanthocyanidins during development. *Plant Physiol.* **1993**, *102*, 663−670.

(2) Song, J.; Liu, C.; Li, D.; Gu, Z. Evaluation of sugar, free amino acid, and organic acid compositions of different varieties of vegetable soybean (*Glycine max* [L.] Merr). *Ind. Crops Prod.* **2013**, *50*, 743−749.

(3) Correa, C. R.; Li, L.; Aldini, G.; Carimi, M.; Chen, C. Y. O.; Chun, H. K.; Cho, S. M.; Park, K. M.; Russell, R. M.; Blumberg, J. B.; Yeum, K. J. Composition and stability of phytochemicals in five

DOI: 10.1021/jf505172m
J. Agric. Food Chem. 2015, 63, 225−234

varieties of black soybeans (*Glycine max*). *Food Chem.* **2010**, *123*, 1176−1184.
(4) Xu, B.; Chang, S. K. Total phenolics, phenolic acids, isoflavones, and anthocyanins and antioxidant properties of yellow and black soybeans as affected by thermal processing. *J. Agric. Food Chem.* **2008**, *56*, 7165−7175.
(5) Zhang, R. F.; Zhang, F. X.; Zhang, M. W.; Wei, Z. C.; Yang, C. Y.; Zhang, Y.; Tang, X. J.; Deng, Y. Y.; Chi, J. W. Phenolic composition and antioxidant activity in seed coats of 60 Chinese black soybean (*Glycine max* L. Merr.) varieties. *J. Agric. Food Chem.* **2011**, *59*, 5935−5944.
(6) Takahashi, R.; Ohmori, R.; Kiyose, C.; Momiyama, Y.; Ohsuzu, F.; Kondo, K. Antioxidant activities of black and yellow soybeans against low density lipoprotein oxidation. *J. Agric. Food Chem.* **2005**, *53*, 4578−4582.
(7) Wang, Y. I.; Sheen, L. Y.; Chou, C. C. Storage effects on the content of anthocyanin, mutagenicity, and antimutagenicity of black soybean koji. *LWT—Food Sci. Technol.* **2010**, *43*, 702−707.
(8) Kim, J. M.; Kim, J. S.; Yoo, H.; Choung, M. G.; Sung, M. K. Effects of black soybean [*Glycine max* (L.) Merr.] seed coats and its anthocyanidins on colonic inflammation and cell proliferation *in vitro* and *in vivo*. *J. Agric. Food Chem.* **2008**, *56*, 8427−8433.
(9) Astadi, I. R.; Astuti, M.; Santoso, U.; Nugraheni, P. S. *In vitro* antioxidant activity of anthocyanins of black soybean seed coat in human low density lipoprotein (LDL). *Food Chem.* **2009**, *112*, 659−663.
(10) Kurimoto, Y.; Shibayama, Y.; Inoue, S.; Soga, M.; Takikawa, M.; Ito, C.; Nanba, F.; Yoshida, T.; Yamashita, Y.; Ashida, H.; Tsuda, T. Black soybean seed coat extract ameliorates hyperglycemia and insulin sensitivity via the activation of AMP-activated protein kinase in diabetic mice. *J. Agric. Food Chem.* **2013**, *61*, 5558−5564.
(11) Kanamoto, Y.; Yamashita, Y.; Nanba, F.; Yoshida, T.; Tsuda, T.; Fukuda, I.; Nakamura-Tsuruta, S.; Ashida, H. A black soybean seed coat extract prevents obesity and glucose intolerance by up-regulating uncoupling proteins and down-regulating inflammatory cytokines in high-fat diet-fed mice. *J. Agric. Food Chem.* **2011**, *59*, 8985−8993.
(12) Liao, H. F.; Chou, C. J.; Wu, S. H.; Khoo, K. H.; Chen, C. F.; Wang, S. Y. Isolation and characterization of an active compound from black soybean [*Glycine max* (L.) Merr.] and its effect on proliferation and differentiation of human leukemic U937 cells. *Anti-Cancer Drugs* **2001**, *12*, 841−846.
(13) Liao, H. F.; Chen, Y. J.; Yang, Y. C. A novel polysaccharide of black soybean promotes myelopoiesis and reconstitutes bone marrow after 5-flurouracil- and irradiation-induced myelosuppression. *Life Sci.* **2005**, *77*, 400−413.
(14) Wu, M. H.; Lee, Y. C.; Tsai, W. J.; Yang, W. B.; Chen, Y. C.; Chuang, K. A.; Liao, J. F.; Wang, C. C.; Kuo, Y. C. Characterized polysaccharides from black soybean induce granulocyte colony-stimulated factor gene expression in a phosphoinositide 3-kinase-dependent manner. *Immunol. Invest.* **2011**, *40*, 39−61.
(15) Liu, J.; Wen, X.; Zhang, X.; Pu, H.; Kan, J.; Jin, C. Extraction, characterization and *in vitro* antioxidant activity of polysaccharides from black soybean. *Int. J. Biol. Macromol.* **2015**, *72*, 1182−1190.
(16) Kang, J.; Cui, S. W.; Phillips, G. O.; Chen, J.; Guo, Q.; Wang, Q. New studies on gum ghatti (*Anogeissus latifolia*) part II. Structure characterization of an arabinogalactan from the gum by 1D, 2D NMR spectroscopy and methylation analysis. *Food Hydrocolloids* **2011**, *25*, 1991−1998.
(17) Ciucanu, I.; Kerek, F. A simple and rapid method for the permethylation of carbohydrates. *Carbohydr. Res.* **1984**, *131*, 209−217.
(18) Cao, W.; Li, X. Q.; Liu, L.; Wang, M.; Fan, H. T.; Li, C.; Lv, Z.; Wang, X.; Mei, Q. Structural analysis of water-soluble glucans from the root of *Angelica sinensis* (Oliv.) Diels. *Carbohydr. Res.* **2006**, *341*, 1870−1877.
(19) Cui, H.; Liu, Q.; Tao, Y.; Zhang, H.; Zhang, L.; Ding, K. Structure and chain conformation of a (1→6)-a-D-glucan from the root of *Pueraria lobata* (Willd.) Ohwi and the antioxidant activity of its sulfated derivative. *Carbohydr. Polym.* **2008**, *74*, 771−778.
(20) Sun, L.; Peng, X.; Sun, P.; Shi, J.; Yuan, X.; Zhu, J.; Tai, G.; Zhou, Y. Structural characterization and immunostimulatory activity of a novel linear a-(1→6)-D-glucan isolated from *Panax ginseng* C.A. Meyer. *Glycoconjugate J.* **2012**, *29*, 357−364.
(21) Wu, X. M.; Tu, P. F. (2005). Isolation and characterization of a-(1→6)-glucans from *Cistanche deserticola*. *J. Asian Nat. Prod. Res.* **2005**, No. 7, 823−828.
(22) Zhu, Q.; Jiang, Y.; Lin, S.; Wen, L.; Wu, D.; Zhao, M.; Chen, F.; Jia, Y.; Yang, B. Structural identification of (1→6)-a-D-glucan, a key responsible for the health benefits of longan, and evaluation of anticancer activity. *Biomacromolecules* **2013**, *14*, 1999−2003.
(23) Luo, X.; Xu, X.; Yu, M.; Yang, Z.; Zheng, L. Characterisation and immunostimulatory activity of an a-(1→6)-D-glucan from the cultured *Armillariella tabescens* mycelia. *Food Chem.* **2008**, *111*, 357−363.
(24) Zhao, G.; Kan, J.; Li, Z.; Chen, Z. Characterization and immunostimulatory activity of an (1→6)-a-D-glucan from the root of *Ipomoea batatas*. *Int. Immunopharmacol.* **2005**, *5*, 1436−1445.
(25) Gane, A. M.; Craik, D.; Munro, S. L.; Howlett, G. J.; Clarke, A. E.; Bacic, A. Structural analysis of the carbohydrate moiety of arabinogalactan-proteins from stigmas and styles of *Nicotiana alata*. *Carbohydr. Res.* **1995**, *277*, 67−85.
(26) Golovchenko, V. V.; Khramova, D. S.; Ovodova, R. G.; Shashkov, A. S.; Ovodov, Y. S. Structure of pectic polysaccharides isolated from onion *Allium cepa* L. using a simulated gastric medium and their effect on intestinal absorption. *Food Chem.* **2012**, *134*, 1813−1822.
(27) Habibi, Y.; Heyraud, A.; Mahrouz, M.; Vignon, M. R. Structural features of pectic polysaccharides from the skin of *Opuntia ficus-indica* prickly pear fruits. *Carbohydr. Res.* **2004**, *339*, 1119−1127.
(28) Liang, F.; Hu, C.; He, Z.; Pan, Y. An arabinogalactan from flowers of *Chrysanthemum morifolium*: structural and bioactivity studies. *Carbohydr. Res.* **2014**, *387*, 37−41.
(29) Goellner, E. M.; Utermoehlen, J.; Kramer, R.; Classen, B. Structure of arabinogalactan from *Larix laricina* and its reactivity with antibodies directed against type-II-arabinogalactans. *Carbohydr. Polym.* **2011**, *86*, 1739−1744.
(30) Samuelsen, A. B.; Paulsen, B. S.; Wold, J. K.; Knutsen, S. H.; Yamada, H. Characterization of a biologically active arabinogalactan from the leaves of *Plantago major* L. *Carbohydr. Polym.* **1998**, *35*, 145−153.
(31) Wagner, H.; Jordan, E. An immunologically active arabinogalactan from *Viscum album* 'berries'. *Phytochemistry* **1988**, *27*, 2511−2517.
(32) Matulová, M.; Capek, P.; Kaneko, S.; Navarini, L.; Liverani, F. S. Structure of arabinogalactan oligosaccharides derived from arabinogalactan-protein of *Coffea arabica* instant coffee powder. *Carbohydr. Res.* **2011**, *346*, 1029−1036.
(33) Brecker, L.; Wicklein, D.; Moll, H.; Fuchs, E. C.; Becker, W. M.; Petersen, A. Structural and immunological properties of arabinogalactan polysaccharides from pollen of timothy grass (*Phleum pratense* L.). *Carbohydr. Res.* **2005**, *340*, 657−663.
(34) Shakhmatov, E. G.; Toukach, P. V.; Kuznetsov, S. P.; Makarova, E. N. Structural characteristics of water-soluble polysaccharides from *Heracleum sosnowskyi* Manden. *Carbohydr. Polym.* **2014**, *102*, 521−528.
(35) Linnerborg, M.; Weintraub, A.; Widmalm, G. Structural studies of the O-antigen polysaccharide from *Escherichia coli* O138. *Eur. J. Biochem.* **1997**, *247*, 567−571.
(36) Zhang, X.; Liu, L.; Lin, C. Structural features, antioxidant and immunological activity of a new polysaccharide (SP1) from sisal residue. *Int. J. Biol. Macromol.* **2013**, *59*, 184−191.
(37) Bento, J. F.; Noleto, G. R.; de Oliveira Petkowicz, C. L. Isolation of an arabinogalactan from *Endopleura uchi* bark decoction and its effect on HeLa cells. *Carbohydr. Polym.* **2014**, *101*, 871−877.
(38) Chatterjee, U. R.; Ray, S.; Micard, V.; Ghosh, D.; Ghosh, K.; Bandyopadhyay, S. S.; Ray, B. Interaction with bovine serum albumin of an anti-oxidative pectic arabinogalactan from *Andrographis paniculata*. *Carbohydr. Polym.* **2014**, *101*, 342−348.

DOI: 10.1021/jf505172m
J. Agric. Food Chem. 2015, 63, 225−234

(39) Oliveira, A. J. B.; Cordeiro, L. M. C.; Gonçalves, R. A. C.; Ceole, L. F.; Ueda-Nakamura, T.; Iacomini, M. Structure and antiviral activity of arabinogalactan with (1→6)-b-D-galactan core from *Stevia rebaudiana* leaves. *Carbohydr. Polym.* **2013**, *94*, 179−184.
(40) Nosál'ová, G.; Majee, S. K.; Ghosh, K.; Raja, W.; Chatterjee, U. R.; Jureček, L.; Ray, B. Antitussive arabinogalactan of *Andrographis paniculata* demonstrates synergistic effect with andrographolide. *Int. J. Biol. Macromol.* **2014**, *69*, 151−157.
(41) Wang, X.; Zheng, Y.; Zuo, J.; Fang, J. Structural features of an immunoactive acidic arabinogalactan from *Centella asiatica*. *Carbohydr. Polym.* **2005**, *59*, 281−288.

DOI: 10.1021/jf505172m
J. Agric. Food Chem. 2015, 63, 225−234

JOURNAL OF AGRICULTURAL AND FOOD CHEMISTRY

Article

pubs.acs.org/JAFC

Protocatechuic Acid Inhibits Oleic Acid-Induced Vascular Smooth Muscle Cell Proliferation through Activation of AMP-Activated Protein Kinase and Cell Cycle Arrest in G0/G1 Phase

Ming-Cheng Lin,[†,‡] Ting-Tsz Ou,[#] Chun-Hua Chang,[#] Kuei-Chuan Chan,*[,†,‡] and Chau-Jong Wang*[,#,⊥]

[†]Department of Internal Medicine, Chung-Shan Medical University Hospital, No. 110, Sec. 1, Jianguo N. Road, Taichung 402, Taiwan

[‡]School of Medicine, Institute of Medicine, Chung-Shan Medical University, No. 110, Sec. 1, Jianguo N. Road, Taichung 402, Taiwan

[#]Institute of Biochemistry and Biotechnology, Chung Shan Medical University, No. 110, Sec. 1, Jianguo N. Road, Taichung 402, Taiwan

[⊥]Department of Medical Research, Chung Shan Medical University Hospital, No. 110, Sec. 1, Jianguo N. Road, Taichung 402, Taiwan

ABSTRACT: Protocatechuic acid (PCA) has been implicated in the progression of atherosclerosis. The proliferation of vascular smooth muscle cells (VSMC) may play a crucial role in the pathogenesis of atherosclerosis. Adenosine 5′-monophosphate-activated protein kinase (AMPK) additionally exerts several beneficial effects on vascular function and improves vascular abnormalities. The current study sought to determine whether PCA has an inhibitory effect on VSMC proliferation under oleic acid (OA) treatment. A7r5 cells were treated with OA (150 μM) or cotreated with OA and PCA (150 μg/mL) for 24 and 48 h. PCA-treated cells were found to cause an increase in G0/G1 cell cycle arrest. Western blotting showed that PCA increased the expressions of p53 and $p21^{Cip1}$, subsequently decreasing the expression of cyclin E1 and Cdk2. In addition, PCA induced phosphorylation of AMPK and inhibited the expression of fatty acid synthase, Akt-p, and Skp2 after stimulation with OA. After treatment with AMPK inhibitor, the effects of PCA mentioned above were reversed. Taken together, PCA inhibited OA-induced VSMC proliferation through AMPK activation and down-regulation of FAS and AKT signals, which then blocks G0/G1 phase cell cycle progression. These findings provide a new insight into the protective properties of PCA on VSMC, which may constitute a novel effective antiatherosclerosis agent.

KEYWORDS: *Akt, AMP-activated protein kinase, cell cycle, protocatechuic acid, vascular smooth muscle cell proliferation*

INTRODUCTION

Atherosclerosis is a chronic inflammation and proliferative process of the arteries. The abnormal proliferation of vascular smooth muscle cells (VSMCs) is the key pathological factor in the initiation and progression of vascular disorders, including arteriosclerosis.[1] VSMC activation promotes a synthetic phenotype that underlies vessel growth disorders causing in-stent restenosis, transplant vasculopathy, and vein bypass graft failure.[2] The best way to control the proliferation of VSMCs has been a major focus in the development of new therapeutic strategies. Recently, adenosine 5′-monophosphate-activated protein kinase (AMPK), a cellular fuel sensor, has emerged as a therapeutic target for atherosclerosis.[3]

AMPK, a physiological sensor of cellular energy, has been reported to play a key role in energy metabolism and to exert a cardiovascular protective function under physiological conditions and diseases of the vascular system.[4] It has also been reported that AMPK activation by 5-aminoimidazole-4-carboxamide ribonucleoside inhibits PDGF-BB-induced human VSMC proliferation.[5] In addition, AMPK activation has been reported to lead to improved endothelial function,[6] attenuation of myocardial ischemia injury in mice,[7] and suppression of neointimal formation in a balloon injury rat model.[8] In particular, the deletion of AMPK has been reported to reduce the level of p21, probably through S-phase kinase-associated protein 2 (Skp2)-mediated degradation, thereby causing neointimal hyperplasia.[9] Recently, it has been reported that AMPK plays a significant role in cell growth arrest,[10,11] making it an ideal candidate for studies targeted at reducing VSMC growth.

Protocatechuic acid (PCA) is chemically known as 3,4-dihydroxybenzoic acid and is widely distributed and present in most edible plants.[12] It is also commonly found in the human diet including in bran, brown rice, and onions.[13] PCA is also found in many fruits such as plums, gooseberries, and grapes[14] and plants including Sudan mallow (*Hibiscus sabdariffa* L.)[15] and Japanese ginkgo.[16] Its pharmacological effects have been reported including antioxidant,[17] antibacterial,[18] anticancer,[19] antidiabetic,[20] antiaging,[21] and anti-inflammation[22] activities. Natural and synthetic polyphenols that stimulate AMPK have shown protective and antiatherogenic properties in aortic atherosclerotic lesions.[23] In the present study, we hypothesized that PCA would attenuate oleic acid (OA)-induced VSMC proliferation, and we attempted to explore the molecular mechanisms underlying the protective effect of PCA.

Received: November 3, 2014
Revised: December 15, 2014
Accepted: December 16, 2014
Published: December 16, 2014

ACS Publications © 2014 American Chemical Society

DOI: 10.1021/jf505303s
J. Agric. Food Chem. 2015, 63, 235−241

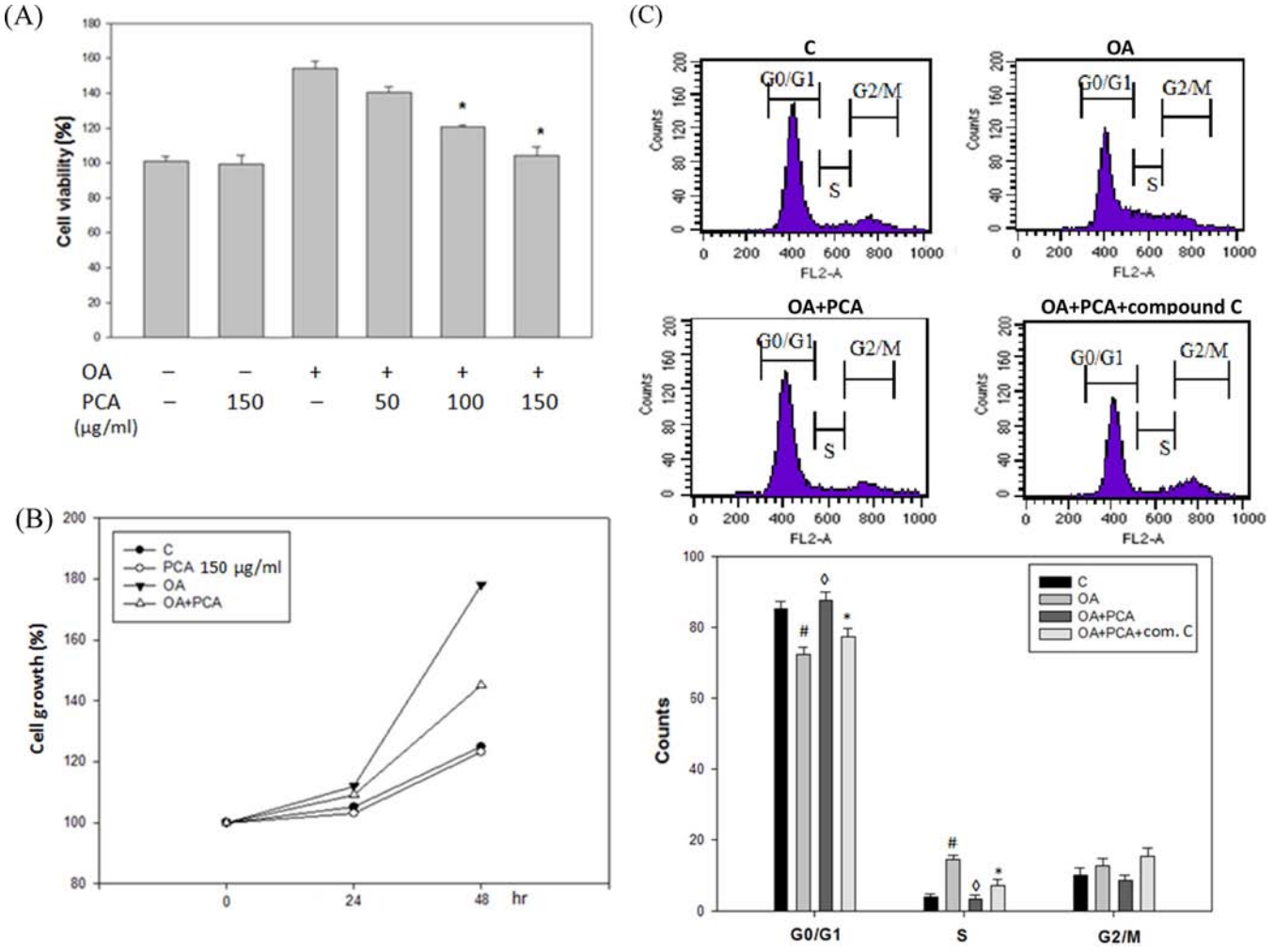

Figure 1. Effect of OA, PCA, and compound **C** (AMPK inhibitor) on growth of VSMCs. (A) A7r5 cells were cotreated with OA (150 μM) and various concentrations (50, 100, and 150 μg/mL) of PCA for 48 h. (B) A7r5 cells were cotreated with OA (150 μM) and PCA (150 μg/mL) for the indicated times (0, 24, and 48 h). Cell viability was assayed using MTT. (C) A7r5 cells were pretreated with compound **C** (10 μM) for 30 min and then treated with OA (150 μM), PCA (150 μg/mL), and compound **C** for 48 h. C, control; com. C, compound **C**; G0/G1, the diploid population in the G0/G1 phase of the cell cycle; S, the cell population in the S phase; G2/M, the tetraploid population in the M phase. Data are represented as the mean ± SD (n = 3). (#) $p < 0.05$ versus the control group; (◊) $p < 0.05$ versus the OA group; (∗) $p < 0.05$ versus the OA+PCA group.

MATERIALS AND METHODS

Cell Culture. The cell line A7r5, a smooth muscle cell line derived from rat thoracic aorta, was obtained from the American Type Culture Collection (ATCC no. CRL-1444; Manassas, VA, USA). The A7r5 cells were cultured in DMEM supplemented with 10% fetal bovine serum (FBS), 2 mmol/L glutamine, 1% penicillin−streptomycin, and 1.5 g/L sodium bicarbonate (all from Gibco/BRL, Gaithersburg, MD, USA). All cell cultures were maintained at 37 °C in a humidified atmosphere of 5% CO_2.

Cell Growth and MTT Assay. The effect of OA (Sigma, St. Louis, MO, USA) on cell growth was determined in the A7r5 cells. The A7r5 cells were seeded in 24-well culture plates at a density of 4×10^4 cells/well, incubated for 48 h, treated with OA (150 μM) bound to BSA to stimulate cell growth as the control, or cotreated with OA and PCA (50−150 μg/mL) (Alfa Aesar, Ward Hill, MA, USA) for 48 h and 150 μg/mL of PCA for the indicated time. To measure cell viability, 0.2 mg/mL MTT (Sigma) was added to each well and incubated at 37 °C in a humidified atmosphere of 5% CO_2 for another 4 h and solubilized with isopropanol. The viable number of cells was directly proportional to the production of formazan measured spectrophotometrically at 563 nm. Cell viability was determined using an MTT assay.[24]

Cell Cycle Analysis Using Flow Cytometry. A7r5 cells were seeded in 6-well plates, treated with compound **C** (10 μM), OA (150 μM) alone, or cotreated with OA and PCA (150 μg/mL) for 48 h. The OA-treated cells were harvested with trypsin−EDTA, washed with cold PBS, and fixed with cold 70% alcohol for 4 h at −20 °C. The fixed cells were then removed from the alcohol and stained with 50 μg/mL propidium iodide (Sigma) solution containing 10 μg/mL RNase A in darkness for at least 30 min on ice. The distribution of cells in different cell cycle phases characterized by specific amounts of DNA (G0/G1 = diploid, S = DNA synthesis between diploid and tetraploid, and G2/M = tetraploid, preceding cell division) was determined using flow cytometry (FACS Calibur; BD Biosciences). A minimum of 10000 cells per sample was counted, and DNA histograms were analyzed using CellQuest software (BD Biosciences) for cell cycle analysis.[25]

Western Blot. Following appropriate treatment, A7r5 cells were lysed and equal amounts of cell lysates (50 μg of protein) were separated by electrophoresis on 8−12% SDS polyacrylamide gel and transferred to nitrocellulose membranes (Millipore, Bedford, MA, USA). The membranes were incubated with Tris-buffered saline containing 1% (w/v) nonfat milk and 0.1% (v/v) Tween-20 for 1 h to block nonspecific binding, washed with Tween-20 for 30 min, and then incubated with the appropriate primary antibody at 4 °C overnight. Specific antibodies were used to evaluate the expressions of p-AMPK, fatty acid synthase (FAS), Cip1/p21, cyclin E1, cyclin-dependent kinase 2 (Cdk2), p-Akt,p53,p-p53, and skp2 (all from Santa

DOI: 10.1021/jf505303s
J. Agric. Food Chem. 2015, 63, 235−241

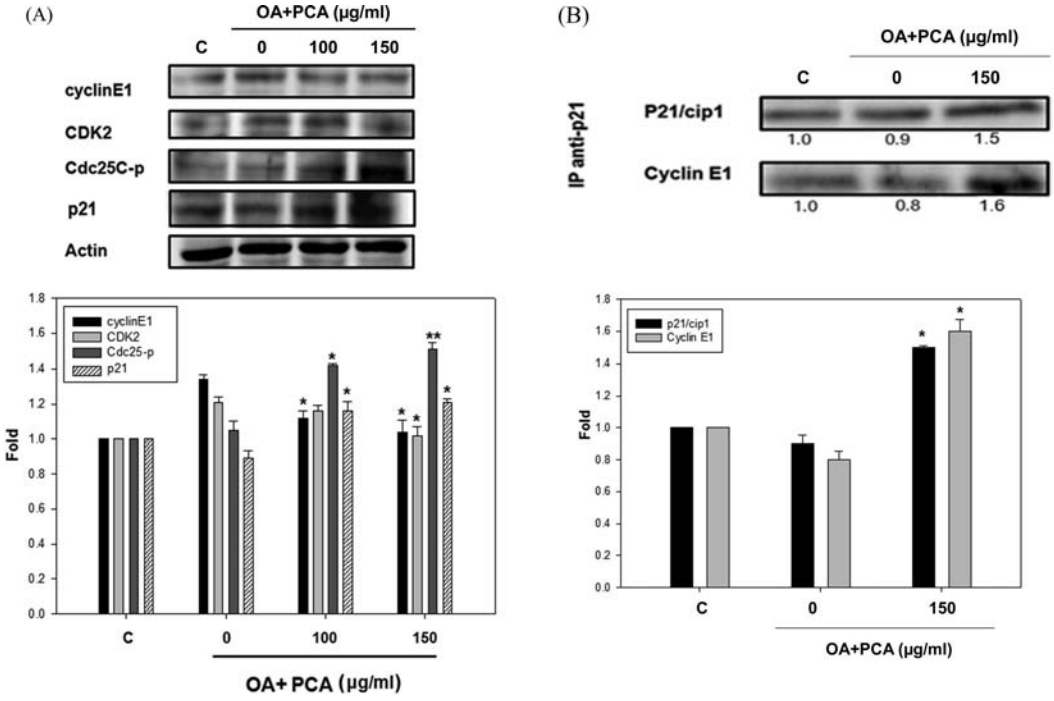

Figure 2. Inhibition of cell cycle related protein in VSMCs by PCA. A7r5 cells were cotreated with OA (150 μM) and PCA (100 and 150 μg/mL) or vehicle-treated control. (A) After treatment, the cell lysates for protein extraction were prepared and adjusted for Western blot analysis. Proteins were detected by specific antibodies (cyclin E1, CdK2, Cdc25C-p, p21), and β-actin was used as a loading control. (B) After treatment of cells with PCA 150 μg/mL, the formation of the cyclin E1−p21 complex was assayed by immunoprecipitation analysis. Each mean value is the average of three independent experiments ± SD. (*) $p < 0.05$ versus the OA group.

Cruz Biotechnology, Santa Cruz, CA, USA), Cdc25 (Cell Signaling, Beverly, MA, USA), and β-actin (Sigma). The membranes were then incubated with horseradish peroxidase-conjugated second antibody (Sigma) for 1 h and developed using ECL chemiluminescence (Millipore), and the densitometry was analyzed using AlphaImager Series 2200 software.[26] The results were representative of at least three independent experiments.

Immunoprecipitation Analysis. A7r5 (4×10^4/mL) cells were seeded into 10 cm plates and treated with OA (150 μM) alone or cotreated with OA and PCA (150 μg/mL) for 48 h. The A7r5 cells were then lysed and transferred to a new tube, followed by the addition of 25 μL of protein A/G plus agarose, incubation for 30 min on ice, and centrifugation. The supernatant was removed, and the protein quantity was determined. Eight micrograms of Cip1/p21 antibody was added per 0.5 mg of protein, and the samples were incubated for 2 h before the addition of 20 μL of Ultralink immobilized A/G bead slurry (Pierce, Rockford, IL, USA) for another 2 h. The samples were centrifuged, and the precipitate was washed more than five times. The remaining steps were the same as for the Western blot analysis.

AMPK Inhibitor. Compound **C**, an AMPK inhibitor, was purchased from Sigma. The cells were treated with 10 μmol of compound **C** for 30 min, followed by treatment with PCA. Specific antibodies were used to evaluate the expressions of AMPK-p, FAS, Akt-p, p53-p, p21, and skp2

Statistical Analysis. All data are expressed as the mean ± SD of three independent experiments, and statistical comparisons were evaluated using one-way analysis of variance (ANOVA). A p value <0.05 was considered to be statistically significant.

RESULTS

Effect of OA, PCA, and AMPK Inhibitor on VSMC Proliferation. Several studies have shown that OA is the active component of free fatty acid and that it can induce VSMC proliferation. Treatment with OA (150 uM) was found to lead to induction of the proliferation of VSMCs compared with the controls by MTT assay (Figure 1A). The proliferative potency of OA was inhibited by PCA ($p < 0.05$). Treatment with PCA (150 μg/mL) alone did not cause cytotoxicity in the cells. In addition, the cotreatment of OA and PCA (150 μg/mL) caused a time-dependent inhibition of the growth of VSMCs (24 to 48 h) (Figure 1B).

To investigate whether PCA treatment imparts an antiproliferative effect against A7r5 cells, the effect of PCA cotreatment with OA on cell cycle distribution was determined by flow cytometry. Stimulation of VSMCs with PCA (150 μg/mL) was characterized by an increase in the percentage of the G0/G1 phase and reduced S phase in comparison with the control cells. Thus, cells treated with PCA had a delay in cell cycle progression. After treatment with compound **C** (AMPK inhibitor), the stimulatory effect of PCA on VSMCs was reversed (Figure 1C).

Effect of PCA on Cell Cycle-Related Protein Expression. The cyclin E/Cdk2 complex performs an important role in controlling the G0/G1 phase. Western blot analysis showed that OA treatment for 48 h caused a moderate increase in the protein levels of cyclin E and Cdk2. Cells cotreated with OA and PCA (100 and 150 μg/mL) had decreased expressions of cyclin E and Cdk2 ($p < 0.05$). In addition, the treatment of cells with PCA significantly increased the phosphorylation of Cdc25C compared with OA at 48 h (Figure 2A). We further investigated the effect of PCA on the Cdk inhibitor (CDKI) $p21^{Kip1}$; PCA treatment dose-dependently increased the protein levels of $p21^{Cip1}$ compared with OA treatment. We then assessed whether PCA causes an increased interaction between induced p21 and cyclin E1. To assess the effect of PCA on binding, the cell extracts were subjected to immunoprecipitation, and the results indicated an increased binding of $p21^{Cip1}$

DOI: 10.1021/jf505303s
J. Agric. Food Chem. 2015, 63, 235−241

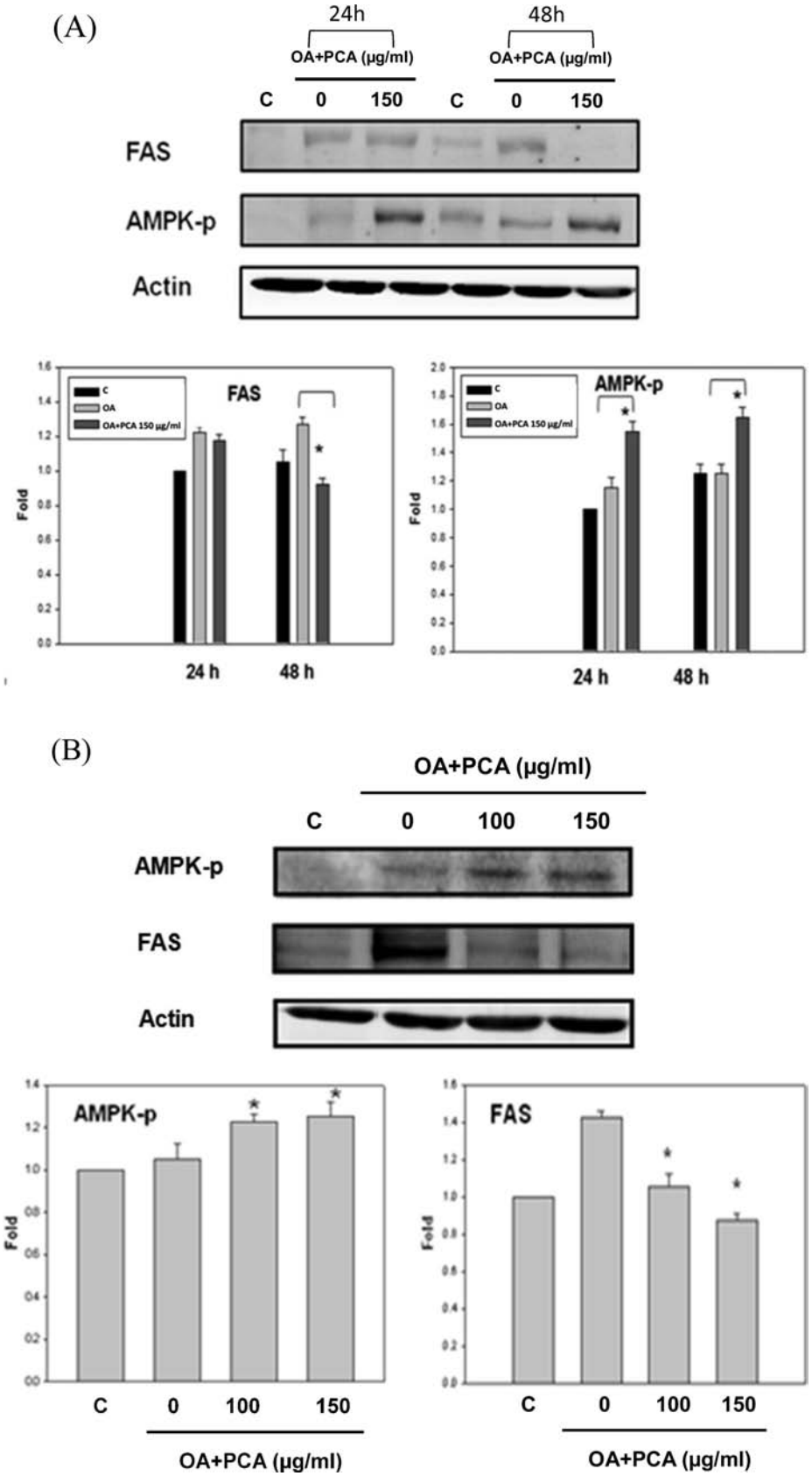

Figure 3. PCA enhanced the activation of AMPK and decreased the expression of FAS. (A) A7r5 cells were cotreated with OA (150 μM) and PCA (150 μg/mL) for various times (24, 48 h). (B) Cells were cotreated with OA (150 μM) and PCA (100 and 150 μg/mL) for 48 h. The cell lysates for protein extraction were prepared and adjusted for Western blot analysis. Proteins were detected by specific antibodies (AMPK-p and FAS), and β-actin was used as a loading control. Each mean value is the average of three independent experiments ± SD. (*) $p < 0.05$ versus the OA group.

DOI: 10.1021/jf505303s
J. Agric. Food Chem. 2015, 63, 235−241

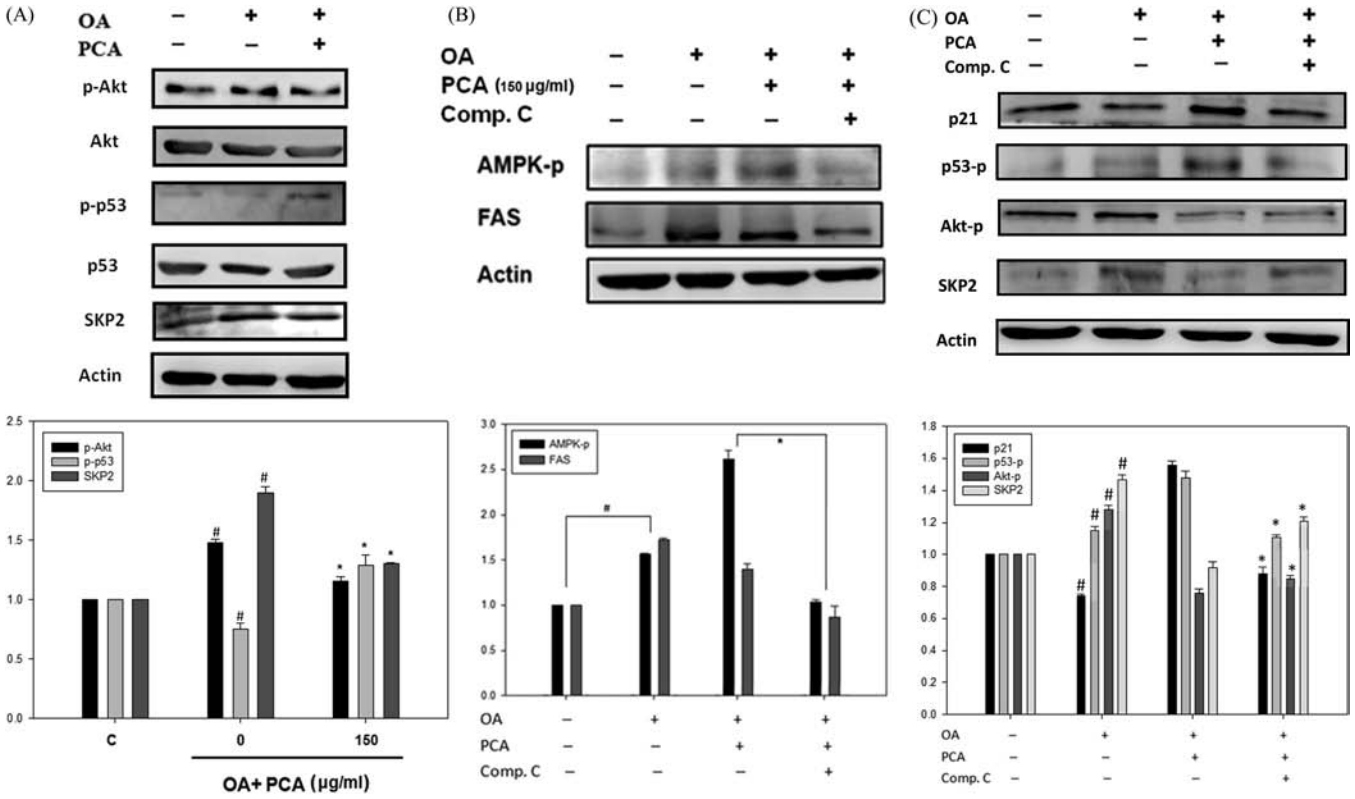

Figure 4. Effects of compound **C** (AMPK inhibitor) on the expressions of AMPK-p, FAS, and downstream proteins. (A) Cells were treated with OA (150 μM) and PCA (150 μg/mL) for 48 h. The cell lysates for protein extraction were prepared and adjusted for Western blot analysis. Proteins were detected by specific antibodies (p-Akt, p-p53, SKP2). (B, C) Cells were pretreated with compound **C** (10 μM) for 30 min and then with OA (150 μM) and PCA (150 μg/mL) for 48 h. The cell lysates for protein extraction were prepared and adjusted for Western blot analysis. Proteins were detected by specific antibodies (AMPK-p, FAS, p21, p53, Akt-p, and SKP2). Comp. C, compound **C**. Each mean value is the average of three independent experiments ± SD. (#) $p < 0.05$ versus the control group; (*) $p < 0.05$ versus the OA+PCA group.

and cyclin E in PCA-treated A7r5 cells compared with the OA group (Figure 2B).

Effect of PCA on AMPK Phosphorylation. Several physiological and pharmacological stimuli can activate AMPK, such as shear stress, statins, and adiponectin.[27] The effect of PCA stimuli on the phosphorylation of AMPK Thr-172 with the cotreatment with OA in the VSMCs was determined first. Cotreatment with OA and PCA (150 μg/mL) increased the phosphorylation of AMPK Thr-172 at 24 and 48 h and decreased the protein level of FAS until 48 h (Figure 3A). In addition, the protein level of FAS was decreased and phosphorylation of AMPK (Thr-172) was increased in a dose-dependent manner after PCA treatment for 48 h (Figure 3B). We further determined whether the AMPK pathway is involved in the process by which PCA causes Skp2, p-Akt, and p-p53 expression. The OA-induced increased expression of Skp2 was inhibited by PCA. The phosphorylation of Akt was markedly increased by incubation of the cells with OA. This effect was attenuated by treatment with PCA. In contrast, the phosphorylation of p53 was increased by treatment with PCA (Figure 4A). To clarify the role of AMPK phosphorylation in PCA-treated VSMCs, we used an AMPK inhibitor (compound **C**) to reduce the phosphorylation of AMPK. The PCA-stimulated expression of FAS was impaired in VSMCs pretreated with compound **C** (Figure 4B). After treatment with AMPK inhibitor, the PCA-induced increased expressions of p21 and p53-p were significantly reduced. Besides, the PCA-induced decreased expressions of Akt-p and Skp2 were increased significantly (Figure 4C).

DISCUSSION

It is well-known that nutrition plays a vital role in some chronic diseases. Epidemiological evidence has shown that dietary intake of vegetables and fruits rich in polyphenols is associated with a reduction in coronary heart disease.[28] Increasing interest has been paid to the phenolic acid, PCA, due to the recognition of a variety of biological effects. PCA was reported to inhibit monocyte adhesion/infiltration and reduces atherosclerosis in apolipoprotein E-deficient mice.[29,30] Besides, PCA was also reported to have an inhibitory effect on oxidation of low-density of lipoprotein (LDL).[31] In this study, we demonstrate for the first time that PCA suppresses A7r5 cell proliferation through the activation of AMPK-induced pathways including inhibition of protein synthesis (FAS, Akt-p, Skp2) and regulation of the cell cycle in VSMCs. Our findings also suggest that AMPK inhibits VSMC proliferation through the induction of a p53/p21^{Cip1} pathway or through a Skp2 pathway, which then blocks G0/G1 phase cell cycle progression.

AMPK activation has been shown to inhibit neointimal formation.[32] However, to the best of our knowledge, no studies have yet clarified the effects of PCA on AMPK in A7r5 cells. In the present study, we focused on the effects of PCA on AMPK and the subsequent consequences in A7r5 cells. Persistent activation of AMPK has been shown to accelerate p53-dependent senescence in mammalian cells,[33] and p53 is a well-recognized tumor suppressor protein, which regulates the cell cycle and apoptosis.[34] p21^{Cip1}, a CDKI, has been reported to bind and inhibit the activity of cyclin−Cdk complexes and to be

DOI: 10.1021/jf505303s
J. Agric. Food Chem. 2015, 63, 235−241

required for efficient G1 arrest.[34] The Akt family of serine threonine kinases is of critical importance with regard to growth factor signaling, cell proliferation, survival, and oncogenesis.[35] Park et al. reported an analogue of resveratrol-inhibited rat aortic VSMC proliferation by blocking Akt signaling.[36] OA was thought to be the active component of free fatty acid that induces VSMC proliferation,[37,38] and it has been also reported that OA can enhance VSMC proliferation via PI3K/Akt signaling pathway, thus inducing atherosclerosis.[39] Akt can phosphorylate MDM2 on S166 and S186, thus promoting translocation of MDM2 to the nucleus, where it negatively regulates p53 function.[40] In this study, we found that the inhibition of Akt phosphorylation by PCA was involved in blocking OA-induced VSMC proliferation. Besides, cell cycle regulation by PCA-induced AMPK was mediated via up-regulation of the p53- $p21^{Cip1}$ axis.

AMPK activators have been shown to suppress VSMC proliferation through the induction of $p53/p21^{Cip1}$, subsequently causing cell cycle arrest.[8,41] This is consistent with our results, which showed that PCA significantly activated AMPK Thr-172 phosphorylation and its downstream targets p53 and $p21^{Cip1}$ in A7r5 cells. These findings suggest that PCA exerts an antiproliferative effect, at least in part, via an AMPK-p53-$p21^{Cip1}$ signaling pathway.

AMPK was also reported to inhibit the glucose-activated expression of FAS gene in rat hepatocytes.[42] Metformin, an oral antidiabetic drug, was reported to inhibit hepatic gene expression of FAS, thus reducing hepatic free acid production, via activation of AMPK.[43] Previous study has showed that mulberry leaf polyphenol extracts can reduce hepatic lipid accumulation through activation of the AMPK and suppression of FAS.[44] Skp2, a well-characterized E3 ubiquitin ligase, has been reported to play important roles in cell proliferation,[45] differentiation,[46] senescence,[47] and cancer metastasis.[48] Blockade of FAS was reported to induce tumor cell cycle arrest by down-regulation of Skp2.[49] Song et al. demonstrated that AMPK2 deletion causes aberrant VSMC migration by increasing Skp2-mediated E-cadherin down-regulation.[50] In addition, Skp2-mediated p21 reduction has also been shown to regulate VSMC proliferation.[9] In the present study, we found that AMPK activation by PCA increased the expression of p21 through disruption of the p21−Skp2 complex.

In conclusion, this is the first study to show that PCA effectively suppressed cell proliferation and cell cycle progression of VSMCs through activation of AMPK. The growth suppression effect may be attributed to the activation of AMPK−p53−$p21^{Cip1}$ signaling and the inhibitory effect on cell cycle progression by AMPK−FAS−Skp2 signaling. Our results provide preliminary evidence that PCA exerts an inhibitory effect on OA-induced A7r5 cell proliferation.

AUTHOR INFORMATION

Corresponding Author

*(C.-J.W.) Phone: 886-4-24730022, ext. 11670. Fax: 886-4-23248167. E- mail: wcj@csmu.edu.tw.

Funding

This work was supported by a grant from the Ministry of Science and Technology (NSC 99-2632-B-040-001-MY3), Taiwan.

Notes

The authors declare no competing financial interest.

ABBREVIATIONS USED

VSMC, vascular smooth muscle cells; PCA, protocatechuic acid; OA, oleic acid; CcdK2, cyclin-dependent kinase 2; CDKI, cyclin-dependent kinase inhibitors; Cdc25C, cell division cycle 25 homologue C; AMPK, adenosine 5′-monophosphate-activated protein kinase; FAS, fatty acid synthase

REFERENCES

(1) Dzau, V. J.; Braun-Dullaeus, R. C.; Sedding, D. G. Vascular proliferation and atherosclerosis: new perspectives and therapeutic strategies. *Nat, Med.* **2002**, *8*, 1249−1256.

(2) Cai, Y.; Knight, W. E.; Guo, S.; Li, J. D.; Knight, P. A.; Yan, C. Vinpocetine suppresses pathological vascular remodeling by inhibiting vascular smooth muscle cell proliferation and migration. *J. Pharmacol. Exp. Ther.* **2012**, *343*, 479−488.

(3) Motoshima, H.; Goldstein, B. J.; Igata, M.; Araki, E. AMPK and cell proliferation−AMPK as a therapeutic target for atherosclerosis and cancer. *J. Physiol.* **2006**, *574*, 63−71.

(4) Song, P.; Zou, M. H. Regulation of NAD(P)H oxidases by AMPK in cardiovascular systems. *Free Radical Biol. Med.* **2012**, *52*, 1607−1619.

(5) Igata, M.; Motoshima, H.; Tsuruzoe, K.; Kojima, K.; Matsumura, T.; Kondo, T.; Taguchi, T.; Nakamaru, K.; Yano, M.; Kukidome, D. Adenosine monophosphate-activated protein kinase suppresses vascular smooth muscle cell proliferation through the inhibition of cell cycle progression. *Circ. Res.* **2005**, *97*, 837−844.

(6) Lee, W. J.; Lee, I. K.; Kim, H. S.; Kim, Y. M.; Koh, E. H.; Won, J. C.; Han, S. M.; Kim, M. S.; Jo, I.; Oh, G. T. α-Lipoic acid prevents endothelial dysfunction in obese rats via activation of AMP-activated protein kinase. *Arterioscler., Thromb., Vasc. Biol.* **2005**, *25*, 2488−2494.

(7) Pan, C.; Lou, L.; Huo, Y.; Singh, G.; Chen, M.; Zhang, D.; Wu, A.; Zhao, M.; Wang, S.; Li, J. Salvianolic acid B and tanshinone IIA attenuate myocardial ischemia injury in mice by NO production through multiple pathways. *Ther. Adv. Cardiovasc. Dis.* **2011**, DOI: 1753944710396538.

(8) Liang, K. W.; Yin, S. C.; Ting, C. T.; Lin, S. J.; Hsueh, C. M.; Chen, C. Y.; Hsu, S. L. Berberine inhibits platelet-derived growth factor-induced growth and migration partly through an AMPK-dependent pathway in vascular smooth muscle cells. *Eur. J. Pharmacol.* **2008**, *590*, 343−354.

(9) Song, P.; Wang, S.; He, C.; Wang, S.; Liang, B.; Viollet, B.; Zou, M. H. AMPKα2 deletion exacerbates neointima formation by upregulating Skp2 in vascular smooth muscle cells. *Circ. Res.* **2011**, *109*, 1230−1239.

(10) Stone, J. D.; Narine, A.; Tulis, D. A. Inhibition of vascular smooth muscle growth via signaling crosstalk between AMP-activated protein kinase and cAMP-dependent protein kinase. *Front. Physiol.* **2012**, *3*, DOI: 10.3389/fphys.2012.00409.

(11) Mihaylova, M. M.; Shaw, R. J. The AMPK signalling pathway coordinates cell growth, autophagy and metabolism. *Nat. Cell Biol.* **2011**, *13*, 1016−1023.

(12) Liu, R. H. Potential synergy of phytochemicals in cancer prevention: mechanism of action. *J. Nutr.* **2004**, *134*, 3479S−3485S.

(13) Herrmann, K.; Nagel, C. W. Occurrence and content of hydroxycinnamic and hydroxybenzoic acid compounds in foods. *Crit. Rev. Food Sci. Nutr.* **1989**, *28*, 315−347.

(14) Li, P.; Wang, X.; Wang, H.; Wu, Y. High performance liquid chromatographic determination of phenolic acids in fruits and vegetables. *Biomed. Environ. Sci.* **1993**, *6*, 389−398.

(15) Tseng, T. H.; Hsu, J. D.; Lo, M. H.; Chu, C. Y.; Chou, F. P.; Huang, C. L.; Wang, C. J. Inhibitory effect of hibiscus protocatechuic acid on tumor promotion in mouse skin. *Cancer Lett.* **1998**, *126*, 199−207.

(16) Ellnain-Wojtaszek, M. Phenolic acids from *Ginkgo biloba* L. Part II. Quantitative analysis of free and liberated by hydrolysis phenolic acids. *Acta Pol. Pharm.* **1997**, *54*, 229.

DOI: 10.1021/jf505303s
J. Agric. Food Chem. 2015, 63, 235−241

(17) Li, X.; Wang, X.; Li, X.; Chen, S.; Chen, D.; Wang, X.; Chen, S.; Chen, D. Antioxidant activity and mechanism of protocatechuic acid in vitro. *Funct. Foods Health Dis.* **2011**, *7*, 232−244.
(18) Chao, C. Y.; Yin, M. C. Antibacterial effects of roselle calyx extracts and protocatechuic acid in ground beef and apple juice. *Foodborne Pathogens Dis.* **2009**, *6*, 201−206.
(19) Tanaka, T.; Tanaka, T.; Tanaka, M. Potential cancer chemopreventive activity of protocatechuic acid. *J. Exp. Clin. Med.* **2011**, *3*, 27−33.
(20) Scazzocchio, B.; Varì, R.; Filesi, C.; D'Archivio, M.; Santangelo, C.; Giovannini, C.; Iacovelli, A.; Silecchia, G.; Volti, G. L.; Galvano, F. Cyanidin-3-*O*-*β*-glucoside and protocatechuic acid exert insulin-like effects by upregulating PPAR*γ* activity in human omental adipocytes. *Diabetes* **2011**, *60*, 2234−2244.
(21) Shi, G. F.; An, L. J.; Jiang, B.; Guan, S.; Bao, Y.-M. Alpinia protocatechuic acid protects against oxidative damage in vitro and reduces oxidative stress in vivo. *Neurosci. Lett.* **2006**, *403*, 206−210.
(22) Lende, A. B.; Kshirsagar, A. D.; Deshpande, A. D.; Muley, M. M.; Patil, R. R.; Bafna, P. A.; Naik, S. R. Anti-inflammatory and analgesic activity of protocatechuic acid in rats and mice. *Inflammopharmacology* **2011**, *19*, 255−263.
(23) Kim, E. J.; Choi, Y. K.; Han, Y. H.; Kim, H. J.; Lee, I. K.; Lee, M. O. ROR*α* suppresses proliferation of vascular smooth muscle cells through activation of AMP-activated protein kinase. *Int. J. Cardiol.* **2014**, *175*, 515−521.
(24) Sargent, J.; Taylor, C. Appraisal of the MTT assay as a rapid test of chemosensitivity in acute myeloid leukaemia. *Br. J. Cancer* **1989**, *60*, 206.
(25) Penna, G.; Sozzani, S.; Adorini, L. Cutting edge: selective usage of chemokine receptors by plasmacytoid dendritic cells. *J. Immunol.* **2001**, *167*, 1862−1866.
(26) Fanton, C. P.; McMahon, M.; Pieper, R. O. Dual growth arrest pathways in astrocytes and astrocytic tumors in response to Raf-1 activation. *J. Biol. Chem.* **2001**, *276*, 18871−18877.
(27) Sun, W.; Lee, T. S.; Zhu, M.; Gu, C.; Wang, Y.; Zhu, Y.; Shyy, J. Y. Statins activate AMP-activated protein kinase in vitro and in vivo. *Circulation* **2006**, *114*, 2655−2662.
(28) Masella, R.; Santangelo, C.; D'Archivio, M.; LiVolti, G.; Giovannini, C.; Galvano, F. Protocatechuic acid and human disease prevention: biological activities and molecular mechanisms. *Curr. Med. Chem.* **2012**, *19*, 2901−2917.
(29) Wang, D.; Wei, X.; Yan, X.; Jin, T.; Ling, W. Protocatechuic acid, a metabolite of anthocyanins, inhibits monocyte adhesion and reduces atherosclerosis in apolipoprotein E-deficient mice. *J. Agric. Food Chem.* **2010**, *58*, 12722−12728.
(30) Wang, D.; Zou, T.; Yang, Y.; Yan, X.; Ling, W. Cyanidin-3-*O*-*β*-glucoside with the aid of its metabolite protocatechuic acid, reduces monocyte infiltration in apolipoprotein E-deficient mice. *Biochem. Pharmacol.* **2011**, *82*, 713−719.
(31) Lee, M. J.; Chou, F. P.; Tseng, T. H.; Hsieh, M. H.; Lin, M. C.; Wang, C. J. Hibiscus protocatechuic acid or esculetin can inhibit oxidative LDL induced by either copper ion or nitric oxide donor. *J. Agric. Food Chem.* **2002**, *50*, 2130−2136.
(32) Ki, S. H.; Lee, J. W.; Lim, S. C.; Hien, T. T.; Im, J. H.; Oh, W. K.; Lee, M. Y.; Ji, Y. H.; Kim, Y. G.; Kang, K. W. Protective effect of nectandrin B, a potent AMPK activator on neointima formation: inhibition of Pin1 expression through AMPK activation. *Br. J. Pharmacol.* **2013**, *168*, 932−945.
(33) Jones, R. G.; Plas, D. R.; Kubek, S.; Buzzai, M.; Mu, J.; Xu, Y.; Birnbaum, M. J.; Thompson, C. B. AMP-activated protein kinase induces a p53-dependent metabolic checkpoint. *Mol. Cell* **2005**, *18*, 283−293.
(34) Giono, L. E.; Manfredi, J. J. The p53 tumor suppressor participates in multiple cell cycle checkpoints. *J. Cell. Physiol.* **2006**, *209*, 13−20.
(35) Altomare, D.; Khaled, A. Homeostasis and the importance for a balance between AKT/mTOR activity and intracellular signaling. *Curr. Med. Chem.* **2012**, *19*, 3748.
(36) Park, E. S.; Lim, Y.; Hong, J. T.; Yoo, H. S.; Lee, C. K.; Pyo, M. Y.; Yun, Y. P. Pterostilbene, a natural dimethylated analog of resveratrol, inhibits rat aortic vascular smooth muscle cell proliferation by blocking Akt-dependent pathway. *Vasc. Pharmacol.* **2010**, *53*, 61−67.
(37) Egan, B.; Lu, G.; Greene, E. Vascular effects of non-esterified fatty acids: implications for the cardiovascular risk factor cluster. *Prostaglandins, Leukotrienes Essent. Fatty Acids* **1999**, *60*, 411−420.
(38) Greene, E. L.; Lu, G.; Zhang, D.; Egan, B. M. Signaling events mediating the additive effects of oleic acid and angiotensin II on vascular smooth muscle cell migration. *Hypertension* **2001**, *37*, 308−312.
(39) Yun, M. R.; Lee, J. Y.; Park, H. S.; Heo, H. J.; Park, J. Y.; Bae, S. S.; Hong, K. W.; Sung, S. M.; Kim, C. D. Oleic acid enhances vascular smooth muscle cell proliferation via phosphatidylinositol 3-kinase/Akt signaling pathway. *Pharmacol. Res.* **2006**, *54*, 97−102.
(40) Manning, B. D.; Cantley, L. C. AKT/PKB signaling: navigating downstream. *Cell* **2007**, *129*, 1261−1274.
(41) Sung, J. Y.; Choi, H. C. Aspirin-induced AMP-activated protein kinase activation regulates the proliferation of vascular smooth muscle cells from spontaneously hypertensive rats. *Biochem. Biophys. Res. Commun.* **2011**, *408*, 312−317.
(42) Foretz, M.; Carling, D.; Guichard, C.; Ferré, P.; Foufelle, F. AMP-activated protein kinase inhibits the glucose-activated expression of fatty acid synthase gene in rat hepatocytes. *J. Biol. Chem.* **1998**, *273*, 14767−14771.
(43) Zhou, G.; Myers, R.; Li, Y.; Chen, Y.; Shen, X.; Fenyk-Melody, J.; Wu, M.; Ventre, J.; Doebber, T.; Fujii, N. Role of AMP-activated protein kinase in mechanism of metformin action. *J. Clin. Invest.* **2001**, *108*, 1167−1174.
(44) Wu, C. H.; Chen, S. C.; Ou, T. T.; Chyau, C. C.; Chang, Y. C.; Wang, C. J. Mulberry leaf polyphenol extracts reduced hepatic lipid accumulation involving regulation of adenosine monophosphate activated protein kinase and lipogenic enzymes. *J. Funct. Foods* **2013**, *5*, 1620−1632.
(45) Wu, Y. J.; Bond, M.; Sala-Newby, G. B.; Newby, A. C. Altered S-phase kinase-associated protein-2 levels are a major mediator of cyclic nucleotide-induced inhibition of vascular smooth muscle cell proliferation. *Circ. Res.* **2006**, *98*, 1141−1150.
(46) Rodriguez, S.; Wang, L.; Mumaw, C.; Srour, E. F.; Celso, C. L.; Nakayama, K. i.; Carlesso, N. The SKP2 E3 ligase regulates basal homeostasis and stress-induced regeneration of HSCs. *Blood* **2011**, *117*, 6509−6519.
(47) Lin, H. K.; Chen, Z.; Wang, G.; Nardella, C.; Lee, S. W.; Chan, C. H.; Yang, W. L.; Wang, J.; Egia, A.; Nakayama, K. I. Skp2 targeting suppresses tumorigenesis by Arf-p53-independent cellular senescence. *Nature* **2010**, *464*, 374−379.
(48) Onder, T. T.; Gupta, P. B.; Mani, S. A.; Yang, J.; Lander, E. S.; Weinberg, R. A. Loss of E-cadherin promotes metastasis via multiple downstream transcriptional pathways. *Cancer Res.* **2008**, *68*, 3645−3654.
(49) Knowles, L. M.; Axelrod, F.; Browne, C. D.; Smith, J. W. A fatty acid synthase blockade induces tumor cell-cycle arrest by down-regulating Skp2. *J. Biol. Chem.* **2004**, *279*, 30540−30545.
(50) Song, P.; Zhou, Y.; Coughlan, K. A.; Dai, X.; Xu, H.; Viollet, B.; Zou, M. H. Adenosine monophosphate−activated protein kinase-*α*2 deficiency promotes vascular smooth muscle cell migration via S-phase kinase−associated protein. 2. Upregulation and E-cadherin down-regulation. *Arterioscler., Thromb., Vasc. Biol.* **2013**, *33*, 2800−2809.

DOI: 10.1021/jf505303s
J. Agric. Food Chem. 2015, 63, 235−241

JOURNAL OF AGRICULTURAL AND FOOD CHEMISTRY

Article

pubs.acs.org/JAFC

Protective Effects of Selenium-Enriched Probiotics on Carbon Tetrachloride-Induced Liver Fibrosis in Rats

Yunhuan Liu, Qing Liu, Gengping Ye, Alamzeb Khan, Jin Liu, Fang Gan, Xian Zhang, Shahnawaz Kumbhar, and Kehe Huang*

Institute of Nutritional and Metabolic Disorders in Domestic Animals and Fowl, Nanjing Agricultural University, Nanjing 210095, People's Republic of China

ABSTRACT: This study aimed to investigate the effects of Se-enriched probiotics (SP) on the liver fibrosis induced by CCl_4 in rats. The results showed that SP significantly decreased serum alanine aminotransferase (87.0 ± 1.96 U/L), aspartate aminotransferase (101 ± 3.13 U/L), hepatic hydroxyproline (898 ± 72.5 μg/g), and malondialdehyde (2.39 ± 0.34 nmol/mg) levels, but increased glutathione peroxidase (37.2 ± 3.19 U/mg), superoxide dismutase (201 ± 19.2 U/mg), and glutathione levels (3.32 ± 0.25 mg/g) ($P < 0.05$) in rats treated by CCl_4. SP suppressed hepatic inflammation and necrosis induced by CCl_4. Moreover, SP significantly reduced the expression of α-smooth muscle actin, collagen, TGF-β1, TIMP-1, and inflammation-related gene and induced apoptosis of activated hepatic stellate cells ($P < 0.05$) in rats treated by CCl_4. Our results suggest that SP could protect the liver from fibrosis by attenuating hepatic oxidative stress, suppressing hepatic inflammation, and inducing apoptosis of hepatic stellate cells.

KEYWORDS: *liver fibrosis, selenium-enriched probiotics (SP), oxidative stress, inflammation, apoptosis*

INTRODUCTION

Hepatic fibrosis is a general pathological basis for hepatic cirrhosis and liver cancer, which is induced by a variety of etiological factors.[1] So, prevention and treatment of fibrosis is one of the crucial therapeutic goals in hepatology. Some studies have shown that reduction of oxidative stress is beneficial to ameliorate liver fibrosis.[2] Therefore, radical scavengers and antioxidants have emerged as effective antifibrotic agents to prevent liver fibrosis. It was generally believed that inflammation could initiate a series of events which lead to liver fibrosis.[3] The activated hepatic stellate cells (HSCs) are major targets for antifibrotic therapy. It has been shown that inducing the apoptosis of activated HSCs was an effective method to treat established experimental fibrosis.[4]

Selenium (Se) is an essential element for human and animals.[5] It is an essential component of some antioxidant enzymes and plays a pivotal role in the antioxidant defense system.[6] There is evidence that indicates that Se was decreased in chronic liver diseases.[7] Probiotics have also been considered as possible additive therapy in treating liver diseases caused by viral infection, alcoholism, and metabolic disorders.[8−10] In addition, probiotics such as *Lactobacillus* and *S. cerevisiae* could prevent oxidative stress induced liver injury.[11,12]

In our labratory, a newly developed Se-enriched probiotics (SP) product was produced by culturing *Lactobacillus acidophilus* (*L. acidophilus*) and *Saccharomyces cerevisiae* (*S. cerevisiae*) with sodium selenite being added into the culture medium under suitable conditions of the microenvironment. Both strains have a strong ability to convert sodium selenite into organic Se. Previous studies of dietary SP supplementation for livestock, poultry, and mice showed that the SP has the combined effects of selenium and probiotics.[13−15]

Until now, there have not been any reports concerning the effects of SP on liver injury in rats. CCl_4 is one of the classic hepatotoxicants used to induce liver injury. Long-term treatment of CCl_4 can cause chronic liver damage and is also a commonly recognized model for inducing hepatic fibrosis.[16] The aim of the current study was to investigate the effect of SP on CCl_4-induced liver fibrosis and further explore the underlying mechanisms.

MATERIALS AND METHODS

Chemicals. GSH-Px, SOD, GSH, MDA, and hydroxyproline assay kit was obtained from the institute of Jiancheng Biotechnology (Nanjing, China). The kit of assay total protein was purchased from the Biyuntian company (Nanjing, China). α-SMA monoclonal antibody were purchased from Abcam (Cambridge, U.K.). CCl_4 was purchased from the institute of Shoude (Nanjing, China).

Selenium-Enriched Probiotics and Probiotics. Both the Se-enriched probiotics (SP) and probiotics (P) products consist of two probiotic strains, *L. acidophilus* and *S. cerevisiae*. The colony-forming units (CFU) of *L. acidophilus* and *S. cerevisiae* in both products was about 10^{11}/mL and 10^9/mL, respectively. The content of total Se in the SP is 10.0 mg/L, with >90% being organic Se and >75% being selenomethionine, which were detected by AF-610A atomic fluorescence spectrometer.[17]

Animals and Feeding. The study was carried out according to protocols approved by the Animal Care and Use Committee of Nanjing Agricultural University, (Certification No.: SYXK (Su) 2011-0036).

Forty male Wistar rats weighing (200 ± 20g) were purchased from the Center of Laboratory Animals, Yangzhou University (Yangzhou, China). The rats were housed in a controlled condition at 25 ± 2 °C and a 12 h light/dark cycle. The rats were acclimatized for more than 1 week to use. The content of selenium in the basal diet was 0.05 mg/kg. The sodium selenite (SS), probiotics (P), and Se-enriched probiotics (SP) diets were made by grinding the basal diet into powder, which was then

Received: August 14, 2014
Revised: December 11, 2014
Accepted: December 16, 2014
Published: December 16, 2014

ACS Publications © 2014 American Chemical Society

DOI: 10.1021/jf5039184
J. Agric. Food Chem. 2015, 63, 242−249

mixed with SS, P, and SP. The doses of SS, P, and SP were calculated and mixed with the basal diet to obtain three different kinds of new diets and then supplied to the rats.

Experimental Procedure. Forty male Wistar rats were randomly divided into five groups of 8. Each group had 4 replicates, with 2 rats per replicate. The groups were as follows: (A) control group, (B) CCl_4 group, (C) CCl_4 + P group, (D) CCl_4 + SS group, and (E) CCl_4 + SP group. Group (A) received an intraperitoneal injection of olive oil (2 mL/kg body weight) twice weekly for 7 weeks. Groups (B−E) received intraperitoneal injection with CCl_4 (2 mL/kg body weight, 1:1 in olive oil) twice weekly for 7 weeks. Groups (A−B) were fed the basal diet containing 0.05 μg/g of Se per day. Groups (C−E) were fed the P diet, SS diet, SP diet per day, respectively. The number of viable microbial cells was approximately 10^9 CFU/g in the SP and P diets. The final total Se concentration was 0.3 μg/g in the SS and SP diets. During the experimental period, no rats died. Blood and liver samples were collected at the end of 7 weeks and immediately stored at −70 °C.

Biochemical Analysis of Serum Enzymes. Serum was obtained from blood by centrifugation at 5000*g* for 5 min at 4 °C. Serum ALT and AST were measured using an automated chemistry analyzer.

Measurement of GSH, GSH-Px, SOD, and MDA in Liver Tissue. Liver samples were weighed and homogenized with nine volumes of ice-cold buffer (1 mmol/L EDTA, 0.32 mol/L sucrose and 10 nmol/L Tris-HCl, pH = 7.4). The homogenates were centrifuged at 5000*g* for 5 min. The activities of GSH-Px and SOD and the levels of GSH and MDA in liver tissues were determined using a commercial assay kit, according to the instructions.

Assay of Hepatic Hydroxyproline in Liver Tissue. Hepatic hydroxyproline was detected using a commercial assay kit. The content of hepatic hydroxyproline was represented as μg of hydroxyproline per g of wet liver tissues.

Histopathological Examination and Immunohistochemical Staining. Liver samples from rats were fixed in 10% formalin. Hematoxylin-eosin (H&E) and Sirius red stains were performed using standard procedures. The Sirius red staining was used for analysis of hepatic fibrosis. A computerized image-analysis system was used to quantifiy the liver fibrosis (Image-Pro Plus version 6.0; Media Cybernetics, MD, U.S.A.). Data for liver fibrosis were shown as the mean percentage of the total hepatic area in the liver sections. For immunohistochemical examination, the liver tissues were incubated with monoclonal antibody of α-SMA and then incubated with streptavidin−peroxidase complex. The peroxidase conjugates were subsequently visualized using diaminobenzidine (DAB) solution. The liver sections were counterstained using hematoxylin, and then the liver sections were mounted on a coverslip.

RNA Extraction and Real-Time Polymerase Chain Reaction (Real-Time PCR) Assay. The mRNA expression levels of Collagen I, α-SMA, TNF-α, IL-6, MCP-1, TGF-β, Bcl-2, Bcl-xL, Bax, and TIMP1 were determined by real-time PCR. The primers were designed by Primer 5.0 online software and shown in Table 1. The isolation of RNA and synthesis of cDNA were carried out as previously reported.[15] Quantitative real-time PCR was performed on an ABI Prism 7300 Detection System (Applied Biosystems, U.S.A.). Relative gene expression was determined by the $\Delta\Delta C_T$ method using β-actin as an internal control. All reactions were performed in duplicate.

Statistical Analysis. Data were analyzed statistically using SPSS 19.0 for Windows. Experimental results were expressed as mean ± SD. Statistical significance was tested with one-way ANOVA followed by the Student−Newman−Keuls post hoc test. *P*-values <0.05 were considered statistically significant.

RESULTS

Effects of SP on General Features and Liver Function. The changes in the body and liver weight, liver index, food intake, and biochemical parameters of control and treatment groups during experimental period are given in Table 2. Treatment with CCl_4 caused a significant decrease in the body weight compared with control group ($P < 0.05$). The body weight in the P, SS, or SP group was significantly increased ($P < 0.05$) compared with the CCl_4-treated group. However, there was no significant difference in the body weight between the SS and P groups. The SP group showed a significant increase ($P < 0.05$) in the body weight compared with the SS or P group.

There was a significant increase in liver weight in the CCl_4-treated group compared with the control group ($P < 0.05$). The liver weight in the P, SS, or SP group was significantly decreased ($P < 0.05$) compared with the CCl_4-treated group. However, there was no significant difference in the liver weight of the P, SS and SP groups. As shown in Table 2, there was a significant increase in liver index of CCl_4-treated group compared with control group ($P < 0.05$). The liver index in the P, SS, or SP group was significantly decreased ($P < 0.05$) compared with the CCl_4-treated group. However, there was no significant difference in the liver index between the SS and P groups. The SP group showed a significant decrease ($P < 0.05$) in the liver index compared with the SS or P group. P, SS, and SP supplementation did not affect the food intake in the CCl_4-administered rats (Table 2). In addition, there was a significant increase in the level of serum ALT and AST in the CCl_4-treated group compared with control group ($P < 0.05$). The serum level of ALT and AST in the P, SS, or SP group was significantly decreased ($P < 0.05$) compared with the CCl_4-treated group. However, there was no significant difference in the level of serum ALT and AST between the SS and P groups. The SP group showed a significant decrease ($P < 0.05$) in the level of ALT and AST compared with the SS or P group.

Table 1. Primer Sequences for Real-Time PCR

target genes		sequences
collagen I	forward	5′-TGCCGTGACCTCAAGATGTGCC-3′
	reverse	5′-CATCCACAAGCGTGCTGTAGGTG-3′
α-SMA	forward	5′-CTGGAGAAGAGCTACGAACTGC-3′
	reverse	5′-CTGATCCACATCTGCTGGAAGG-3′
TGF-β1	forward	5′-CTTCAGCTCCACAGAGAAGAACTGC-3′
	reverse	5′-CACGATCATGTTGGACAACTGCTCC-3′
TNF-α	forward	5′-ATGAGCACAGAAAGCATGATC-3′
	reverse	5′-TACAGGCTTGTCACTCGAATT-3′
IL-6	forward	5′-CTTCCAGCCAGTTGCCTTCTTG-3′
	reverse	5′-TGGTCTGTTGTGGGTGGTATCC-3′
MCP-1	forward	5′-GTCACG CTT CTG GGC CTG T-3′
	reverse	5′-GTG CTTGAG GTG GTT GTG GA-3′
Bcl-2	forward	5′- CTGGCATCTTCTCCTTCCAG-3′
	reverse	5′- CATGCTGGGGCCATATAGTT-3′
Bcl-xL	forward	5′- AGCCATTGAGTGAGGTGCTT-3′
	reverse	5′- AGCTCTGGGGCACCTATCTT-3′
Bax	forward	5′- CCTTTTTGCTACAGGGTTTCAT-3′
	reverse	5′- CAAAGTAGAAGAGGGCAACCAC-3′
TIMP1	forward	5′-GCATCTGGCATCCTCTTGTT-3′
	reverse	5′-AAGAAGCTGCAGGCATTGAT-3′
β-actin	forward	5′-CTATCGGCAATGAGCGGTTCC-3′
	reverse	5′-TGTGTTGGCATAGAGGTCTTTACG-3′

Effects of SP on Histopathologic Change in Liver Tissues. In the control group, liver sections showed normal lobular architecture and cell structure (Figure 1A). In CCl_4-treated group, there were many micro nodules separated by fibrous septa, necrosis, inflammation, and hepatocyte ballooning, indicated by HE staining (Figure 1B). P and SS groups showed moderate inflammation and necrosis (Figure 1C,D). However, treatment with SP markedly reduced liver inflammation and necrosis induced by CCl_4. (Figure 1E).

Effects of SP on Collagen Accumulation in Liver Tissues. To assess the impact of P, SS, and SP on liver fibrosis

DOI: 10.1021/jf5039184
J. Agric. Food Chem. 2015, 63, 242−249

Table 2. Effects of SP on the Body Weight, Food Intake, Liver Weight, Liver Index (Liver Weight/Body Weight × 100%) and Biochemical Parameters of Rat[a]

	control	CCl_4	CCl_4–+P	CCl_4+SS	CCl_4+SP
initial body weight (g)	195 ± 6.21	198 ± 3.32	195 ± 5.36	194 ± 2.83	200 ± 6.75
final body weight (g)	338^{a} ± 2.61	302^{d} ± 9.94	320^{c} ± 4.89	322^{c} ± 3.47	328^{b} ± 3.79
liver weight (g)	13.6^{c} ± 0.63	16.9^{a} ± 1.28	15.7^{b} ± 0.41	15.7^{b} ± 0.57	15.4^{b} ± 0.61
liver index (%)	4.02^{d} ± 0.16	5.58^{a} ± 0.25	4.90^{b} ± 0.18	4.87^{b} ± 0.13	4.67^{c} ± 0.14
food intake (g/day)	20.5 ± 0.22	18.4 ± 0.13	19.4 ± 0.24	19.8 ± 0.16	20.4 ± 0.38
ALT (U/L)	42.6^{d} ± 2.03	168^{a} ± 5.75	106^{b} ± 3.91	113^{b} ± 4.19	87.0^{c} ± 1.96
AST (U/L)	71.3^{d} ± 1.08	138^{a} ± 5.86	113^{b} ± 5.32	116^{b} ± 4.31	101^{c} ± 3.13

[a]Data are represented as mean ± SD (n = 8). Different letters above the values within each test parameter indicate significant differences between groups (P < 0.05).

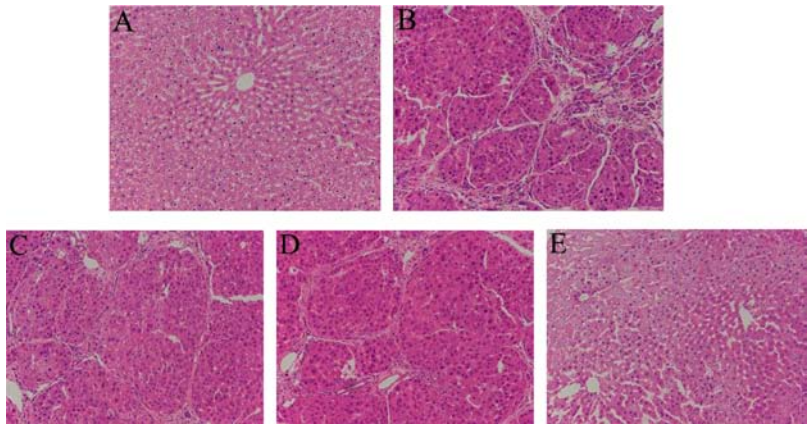

Figure 1. Liver sections were stained with H&E (original magnification 100×). (A) Control group, (B) CCl_4 group, (C) CCl_4 + P group, (D) CCl_4 + SS group, and (E) CCl_4 + SP group.

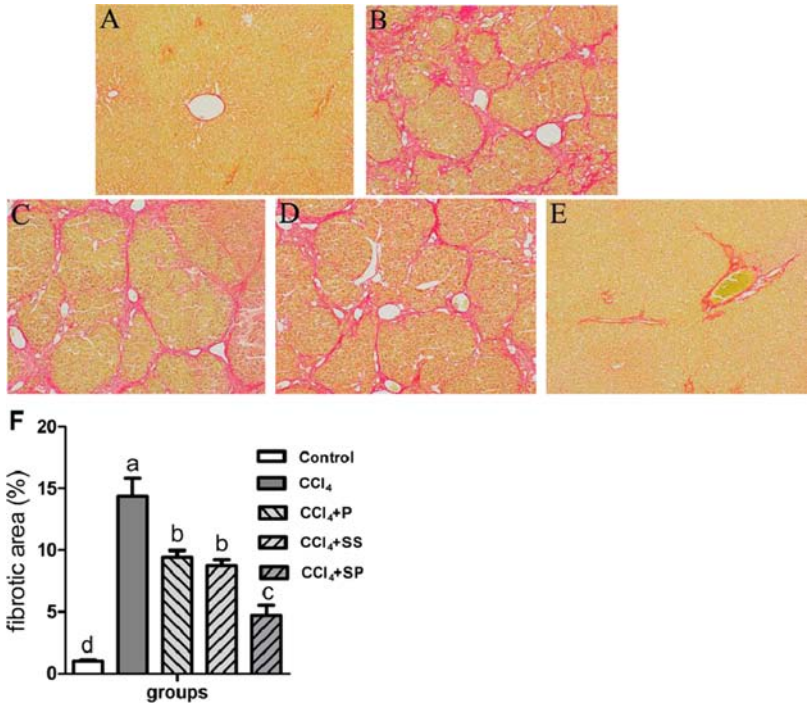

Figure 2. Liver sections were stained with Sirius red (original magnification 100×). (A) Control group, (B) CCl_4 group, (C) CCl_4 + P group, (D) CCl_4 + SS group, and (E) CCl_4 + SP group. Area ratio of stained collagen was quantified and shown in (F). Values of each bar are means ± SD (n = 8). Columns with different letters differ significantly (P < 0.05).

induced by CCl_4, liver samples were stained with Sirius red to determine the deposition of collagen. Liver sections from CCl_4 groups showed obvious red staining in the fibrotic septa compared with the control group. In P and SS groups (Figure 2C,D), liver fibrosis was mildly diminished. However, treatment with SP markedly reduced the degree of liver fibrosis (Figure 2E).

DOI: 10.1021/jf5039184
J. Agric. Food Chem. 2015, 63, 242−249

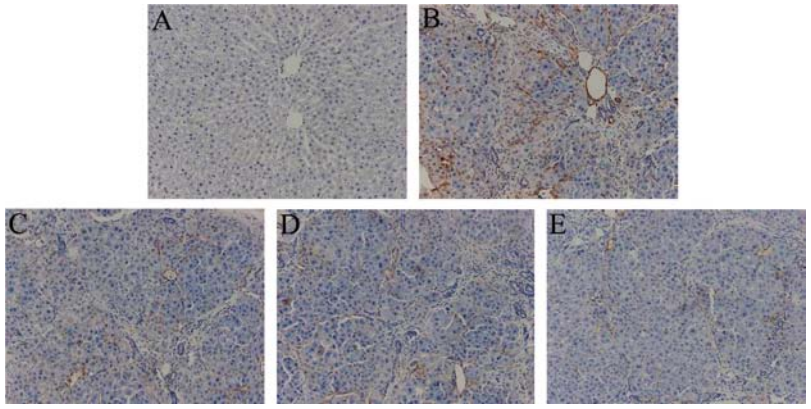

Figure 3. Immunohistochemical staining for activated HSC in liver sections (original magnification 200×). (A) Control group, (B) CCl_4 group, (C) CCl_4 + P group (D) CCl_4+SS group, and (E) CCl_4+SP group.

These results were consistent with the fibrosis area shown in Figure 2F. P, SS, and SP decreased fibrosis area to different extent.

Effects of SP on HSC Activation in Liver Tissues. We detected the activation degree of HSCs in the livers using immunohistochemical staining for α-SMA (Figure 3), a marker of activated HSCs. α-SMA expressions were more distinctly observed in the portal tracts, fibrous septa, and sinusoids in the livers from CCl_4-treated group compared with the control group (Figure 3A). Less α-SMA-positive HSCs were seen in P and SS groups compared with the CCl_4-treated group (Figure 3C,D). However, treatment with SP markedly ameliorated α-SMA expression in the fibrous areas (Figure 3E).

Effects of SP on Hydroxyproline Content in Liver Tissues. The content of hepatic hydroxyproline was an important indicator of liver fibrosis. After CCl_4 administration, The hydroxyproline content was significantly increased compared with control group (P < 0.05, Figure 4). The

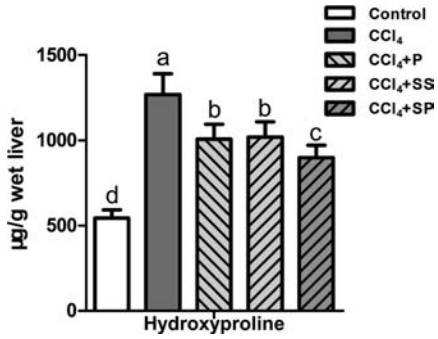

Figure 4. Effects of SP on hepatic hydroxyproline content. Data are represented as mean ± SD (n = 8). Columns with different letters differ significantly (P < 0.05).

hydroxyproline content in the P, SS, or SP groups was significantly decreased compared with the CCl_4-treated group (P < 0.05, Figure 4). However, there was no difference in the hydroxyproline content between the SS and P groups. The SP group showed a further decrease in the hydroxyproline content compared with the SS or P group (P < 0.05, Figure 4).

Effects of SP on GSH and MDA Levels, GSH-Px, and SOD Activities in Liver Tissues. The levels of GSH, the activities of GSH-Px and SOD were decreased highly in the CCl_4-treated group compared with the control group (P < 0.05, Figure 5). The antioxidant activity of GSH-Px in the P group was not higher than that in the CCl_4-treated group, but there was a significant increase in the SS and SP groups compared with the CCl_4-treated group (P < 0.05, Figure 5A). However, the SP group showed a further increase in the activity of GSH-Px compared with the SS group (P < 0.05, Figure 5A). After CCl_4 administration, the SOD activities were significantly decreased compared with the control group (P < 0.05, Figure 5B). The SOD activities in the P, SS, or SP groups were increased compared with the CCl_4-treated group (P < 0.05, Figure 5B). There were no significant differences in SOD activities between the SS and P groups. However, the SP group showed a further increase compared with the P group (P < 0.05, Figure 5B). After CCl_4 administration, the GSH level was significantly decreased compared with control group (P < 0.05, Figure 5C). The GSH level in the P, SS, or SP group was significantly enhanced compared with CCl_4-treated group (P < 0.05, Figure 5C). However, there was no difference in the GSH level between the P and the SS groups. The SP group showed a further increase compared with the P group (P < 0.05, Figure 5C). Treatment with CCl_4 caused a significant increase in the MDA contents compared with control group (P < 0.05). The MDA contents in the P, SS, or SP groups significantly decreased compared with the CCl_4-treated group (P < 0.05, Figure 5D). However, there was no difference in the MDA contents between the SS and P groups. The SP group showed a further decrease in the MDA content compared with the SS or P group (P < 0.05, Figure 5D).

Effects of SP on the Expression of α-SMA, Collagen-I, and Profibrogenic Markers in Liver Tissues. The mRNA expression levels of α-SMA, collagen-I, TGF-β1, and TIMP-1 genes were significantly increased in the CCl_4-treated group compared with control group (P < 0.05, Figure 6). These genes in the P, SS, or SP groups were significantly decreased compared with the CCl_4-treated group (P < 0.05, Figure 6). However, there was no difference in the mRNA expression levels of these pro-fibrogenic markers between the SS and P groups. The SP group showed a further decrease in the mRNA expression levels of these pro-fibrogenic markers compared with the SS or P group (P < 0.05, Figure 6).

Effects of SP on the Expression of Inflammation-Related Genes in Liver Tissues. To determine whether SP could suppress inflammation induced by CCl_4, we detected the expression of TNF-α, IL-6, and MCP-1 genes in the liver. The mRNA levels of TNF-α, IL-6, and MCP-1 were highly increased in the CCl_4-treated group compared with the control group (P < 0.05, Figure 7). But the mRNA expression levels of these

DOI: 10.1021/jf5039184
J. Agric. Food Chem. 2015, 63, 242−249

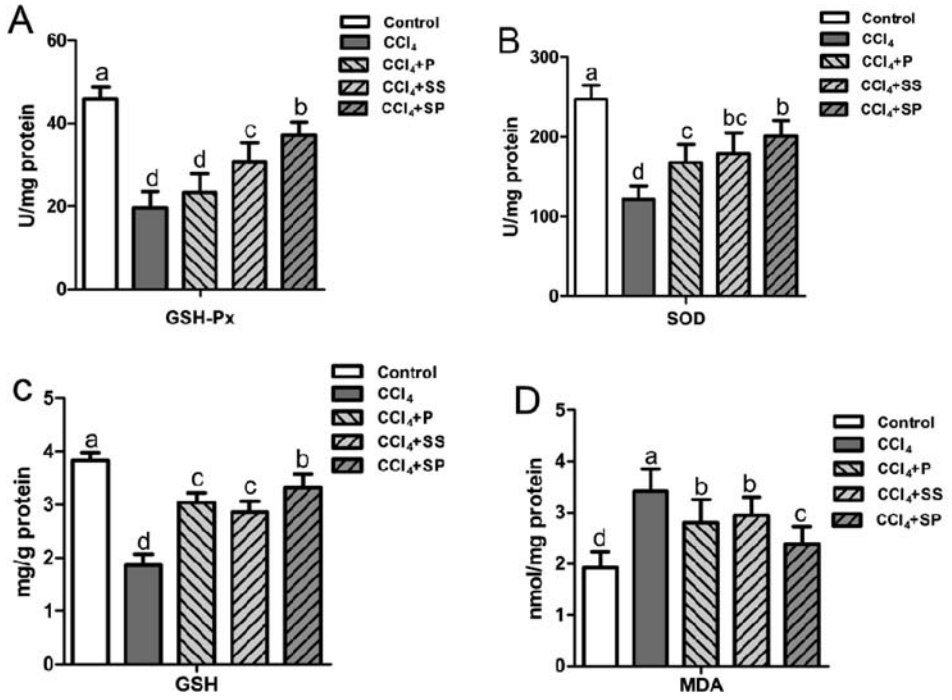

Figure 5. Effects of SP on hepatic oxidative stress parameters. (A) the activities of GSH-Px; (B) the activities of SOD; (C) the levels of GSH; and (D) the levels of MDA. Data are represented as mean ± SD (n = 8). Columns with different letters differ significantly (P < 0.05).

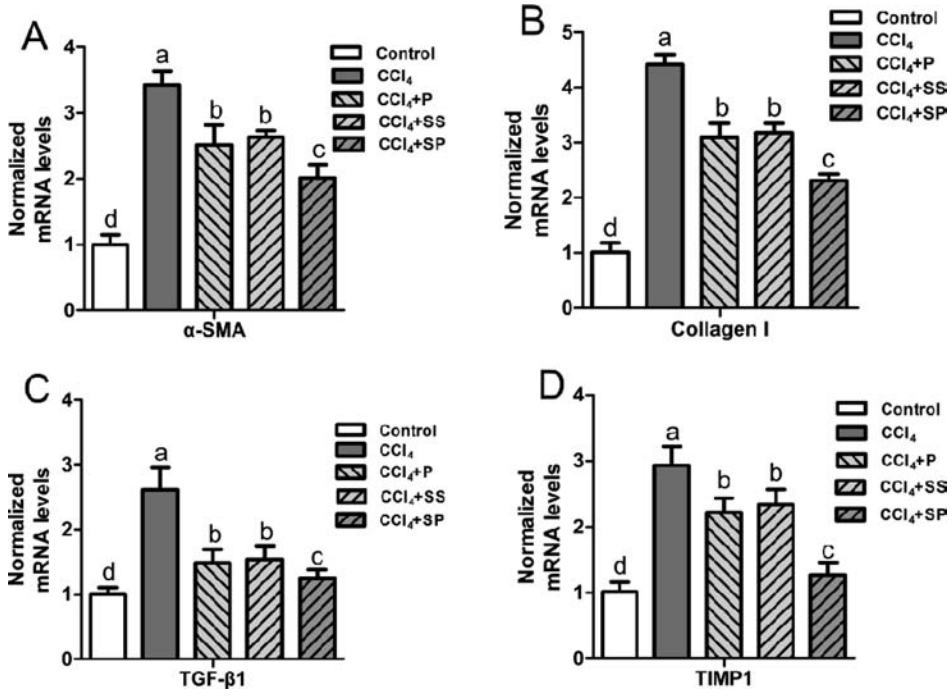

Figure 6. Effects of SP on fibrosis-related gene expressions. Real-time PCR analysis detected the mRNA expression levels of (A) α-SMA, (B) pro-collagen-I, (C) TGF-β1, and (D) TIMP-1 in liver. β-actin served as an internal control. Data are represented as mean ± SD (n = 8). Columns with different letters differ significantly (P < 0.05).

inflammation-related genes in the P, SS, or SP groups were significantly reduced compared with the CCl_4-treated group (P < 0.05, Figure 7). However, there was no difference in the mRNA expression levels of these inflammation-related genes between the SS and P groups. The SP group showed a further decrease in the mRNA expression levels of these inflammation-related genes compared with the SS or P group (P < 0.05, Figure 7).

Effects of SP on the Expression of Apoptosis-Related Genes in Liver Tissues. To further investigate the possible mechanisms by which SP induced apoptosis of activated HSCs, the mRNA levels of apoptosis regulating genes were analyzed. As shown in Figure 8, the mRNA levels of the antiapoptosis genes Bcl-2 and Bcl-xL were highly increased in the CCl_4-treated group compared with the control group (P < 0.05). The mRNA levels of these antiapoptosis genes in the P, SS, and SP groups were

DOI: 10.1021/jf5039184
J. Agric. Food Chem. 2015, 63, 242−249

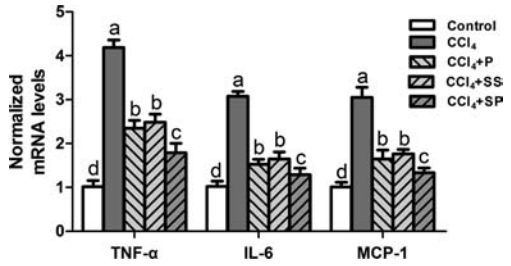

Figure 7. Effects of SP on inflammation-related gene expressions. Real-time PCR analysis detected the mRNA expression levels of TNF-α, IL-6, and MCP-1 in liver. β-actin served as an internal control. Data are represented as mean ± SD (n = 8). Columns with different letters differ significantly (P < 0.05).

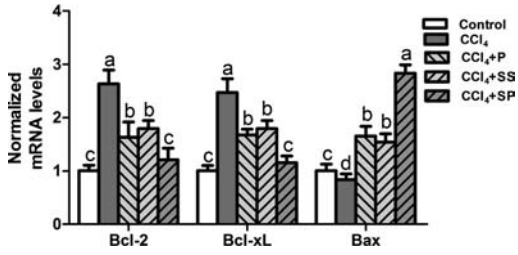

Figure 8. Effects of SP on apoptosis-related gene expressions. Real-time PCR analysis detected the mRNA expression levels of Bcl-2, Bcl-xl, and Bax in liver. β-actin served as an internal control. Data are represented as mean ± SD (n = 8). Columns with different letters differ significantly (P < 0.05).

significantly decreased (P < 0.05) compared with the CCl_4-treated group. However, there was no difference in the mRNA levels of these apoptosis-regulating genes between the SS and P groups. The SP group showed a further decrease in the mRNA expression levels of these antiapoptosis genes compared with the SS or P group (P < 0.05). As shown in Figure 8, the mRNA level of pro-apoptotic gene Bax was decreased highly in CCl_4-treated group compared with control group (P < 0.05). The mRNA expression level of the pro-apoptotic gene Bax in the P, SS, and SP groups was significantly increased compared with the CCl_4-treated group (P < 0.05, Figure 8). However, there was no difference in the mRNA expression levels of the pro-apoptotic gene Bax between the SS and P groups. The SP group showed a further increase in the mRNA levels of the pro-apoptotic gene Bax compared with the SS or P group (P < 0.05, Figure 8).

DISCUSSION

Liver fibrosis is a general consequence of chronic liver injury induced by different mechanisms, including viral infection, xenobiotics damage, and some genetic diseases.[18,19] However, the treatment programs to reverse liver fibrosis have not yet been well established. Currently, the urgent need in hepatic fibrosis management is to find some effective products related to low-toxicity.[20,21] Some studies have demonstrated that hepatic fibrosis induced by CCl_4 was ameliorated by dietary supplementation of Se.[22,23] A recent study showed that probiotics were beneficial in treating chronic liver diseases.[24] In our laboratory, we developed an SP product that has the combined effects of selenium and probiotics. The present study showed that treatment of SP was effective in reducing CCl_4-induced liver injury. This research is the first to investigate the effect of SP on CCl_4-induced liver fibrosis in rats and explore the underlying mechanisms.

Serum marker enzymes, such as ALT and AST, are generally recognized indicators of liver damage, and they are elevated in hepatocellular necrosis. The present study showed that the activities of ALT and AST were increased in CCl_4-treated rats, suggesting serious hepatocellular injury. Supplementation of SP significantly attenuated the increased activities of the serum enzymes. The histological results also demonstrated that the normal lobular architecture was damaged and pseudolobules were formed in CCl_4-treated rats. Collagen and hydroxyproline contents were also obviously increased in CCl_4-treated rats. Liver fibrosis is the progressive accumulation of ECM in the liver.[25] Collagen is a main component of ECM in fibrotic tissue. Hydroxyproline is a main component of the collagen and plays a key role in collagen stability.[26] SP could effectively reduce the content of these biomarkers. The result suggested that SP could ameliorate liver fibrosis induced by CCl_4.

Oxidative stress was a main contributor in the pathophysiologic process of liver fibrosis.[27] To verify the effect of SP on oxidative stress in hepatic fibrogenesis, some oxidative stress indicators were determined, including GSH, GSH-Px, SOD, and MDA. Consistent with the earlier studies, decreased liver GSH level, GSH-Px, and SOD activities and increased liver MDA levels were shown in the CCl_4-treated rats.[28,29] Our previous studies demonstrated that dietary SP supplementation for livestock, poultry, and mice could increase the activities of GSH-Px and SOD and the level of GSH.[14,15,17] In our study, we found that SP supplementation could significantly increase the GSH level and the activities of GSH-Px and SOD and markedly decrease the MDA level in livers, compared with that in CCl_4-treated rats. In addition, oxidative stress, especially lipid peroxidation, could induce collagen synthesis to exacerbate liver fibrosis.[30] Thus, the reduction of the extracellular matrix in the SP group may be attributed to its antioxidant activity.

It has been demonstrated that HSCs play a key role in the development of liver fibrosis.[31] In response to liver injury, HSCs undergo a process of activation by the accumulation of extracellular matrix (ECM) proteins.[32] Hence, liver fibrosis could be resolved by inducing apoptosis of HSCs, reducing the in-liver collagen and decreasing the expression of tissue inhibitors of metallo-proteinases (TIMPs).[33] In the current study, the mRNA expession levels of collagen I, α-SMA, and TIMP-1were increased in the CCl_4-treated group compared to the control group, but the administration of SP significantly decreased them. The present data showed that the inhibition of HSC activation contributed to a decrease in the excess accumulation of extracellular matrix (ECM) in the SP-treated rats.

Inflammation plays a critical role in the initiation and progression of liver fibrosis.[32] Kuppfer cells and monocytes could produce many pro-inflammatory cytokines, including TNF-α and IL-6, in response to stimuli.[34] In addition, the infiltration of inflammation could regulate the HSC activation and ECM deposition by secretion of growth factors and cytokines, especially MCP-1 and TGF-β1.[35,36] The expression level of MCP-1 is high in activated HSCs. MCP-1 also plays a pivotal role in activation of inflammatory cells, while TGF-β1 has been characterized as a key cytokine that mediates hepatic fibrogenesis.[35,37] Previous work showed that probiotics had a protective role in LPS/D-GalN-induced-induced liver damage, which contributed to their anti-inflammatory property.[24] Selenium-enriched lactobacillus could also decrease the plasma TNF-α level compared with CCl_4-treated rats.[38] Indeed, our results showed that SP supplementation could significantly decrease the gene expression of pro-inflammatory cytokines in

DOI: 10.1021/jf5039184
J. Agric. Food Chem. 2015, 63, 242−249

livers, compared with those of CCl_4-treated rats. Accordingly, the potential mechanism of SP in protecting CCl_4-induced hepatotoxicity could be related to a suppression of inflammatory responses.

Inducing apoptosis of activated HSCs is an emerging therapy for hepatic fibrosis.[39] Survival of cells is regulated by pro-apoptotic and anti-apoptotic Bcl-2/Bad family proteins.[40] Previous work showed that selenium supplementation could decrease CCl_4-induced hepatic fibrosis in mice by inducing apoptosis of activated HSCs.[23] Our results showed that the expression of Bcl-2 and Bcl-xL was significantly decreased, and the expression of Bax in the SP group compared with that of the CCl_4 group. Our study suggested that SP could ameliorate liver fibrosis by inducing the apoptosis of activated HSCs.

The protective effect of probiotics against CCl_4-induced liver injury has also been reported.[12] The combination of different probiotics has a significant effect in modulating the intestinal flora and decreasing the level of endotoxins in the liver compared with single probiotics.[41,42] So, in our study, SP and P products containing two probiotic strains, *L. acidophilus* and *S. cerevisia* were used. The dosages of probiotics ranged from 10^9 CFU/day to 10^{11} CFU/day in each rat in the related studies.[43−46] In our experiment, the dosage of probiotics was approximately 10^{10} CFU/day. Some studies used the probiotics by gavage,[11,45] others by food supplement.[46] In our study, we mixed probiotics with the basal diet and administered them by food supplement, for the sake of operational ease and because of the lower risk of damage to the rats. Our results indicated that administrating probiotics by food supplement is viable.

In conclusion, the present study showed that administration of SP was effective in attenuating CCl_4-induced liver injury and fibrosis. The primary mechanisms of this effect could be due to attenuating hepatic oxidative stress, suppressing hepatic inflammation, and inducing apoptosis of activated HSCs. Our study suggested that SP might be a potential dietary agent for prevention of hepatic fibrosis.

AUTHOR INFORMATION

Corresponding Author

*Tel: +86-25-84395507; fax: +86-25-84398669; e-mail: khhuang@njau.edu.cn.

Notes

The authors declare no competing financial interest.

ACKNOWLEDGMENTS

This work was funded by the National Natural Science Foundation of China (31272627), the Research Fund for Doctoral Program of Higher Education in China (20110097110014 and 20120097130002), and the Priority Academic Program Development of Jiangsu Higher Education Institutions (Jiangsu, China).

ABBREVIATIONS:

SP, Selenium-enriched probiotics; Se, selenium; P, probiotics; CCl_4, carbon tetrachloride; ALT, alanine aminotransferase; AST, aspartate aminotransferase; GSH-Px, glutathione peroxidase; GSH, glutathione; MDA, malondialdehyde; SOD, superoxide dismutase; α-SMA, α-smooth muscle actin; HSC, hepatic stellate cell; TNF-α, tumor necrosis factor-α; IL-6, interleukin-6; TGF-β1, transforming growth factor β1; MCP-1, monocyte chemotactic protein 1

REFERENCES

(1) Jiao, J.; Friedman, S. L.; Aloman, C. Hepatic fibrosis. *Curr. Opin. Gastroenterol.* **2009**, *25*, 223−229.

(2) Nieto, N.; Friedman, S. L.; Greenwel, P.; Cederbaum, A. I. CYP2E1-mediated oxidative stress induces collagen type I expression in rat hepatic stellate cells. *Hepatology* **1999**, *30*, 987−996.

(3) Marra, F. Chemokines in liver inflammation and fibrosis. *Front. Biosci.* **2002**, *7*, 1899−1914.

(4) Wang, X.; Ikejima, K.; Kon, K.; Arai, K.; Aoyama, T.; Okumura, K.; Abe, W.; Sato, N.; Watanabe, S. Ursolic acid ameliorates hepatic fibrosis in the rat by specific induction of apoptosis in hepatic stellate cells. *J. Hepatol.* **2011**, *55*, 379−387.

(5) Rayman, M. P. The importance of selenium to human health. *Lancet* **2000**, *356*, 233−241.

(6) Arthur, J. R.; McKenzie, R. C.; Beckett, G. J. Selenium in the immune system. *J. Nutr.* **2003**, *133*, 1457S−1459S.

(7) Thuluvath, P.; Triger, D. Selenium in chronic liver disease. *J. Hepatol.* **1992**, *14*, 176−182.

(8) Loguercio, C.; Federico, A.; Tuccillo, C.; Terracciano, F.; D'Auria, M. V.; Blanco, C. D. V. Beneficial effects of a probiotic *VSL# 3* on parameters of liver dysfunction in chronic liver diseases. *J. Clin. Gastroenterol.* **2005**, *39*, 540−543.

(9) Cesaro, C.; Tiso, A.; Del Prete, A.; Cariello, R.; Tuccillo, C.; Cotticelli, G.; del Vecchio Blanco, C.; Loguercio, C. Gut microbiota and probiotics in chronic liver diseases. *Dig Liver Dis.* **2011**, *43*, 431−438.

(10) Wang, Y.; Kirpich, I.; Liu, Y.; Ma, Z.; Barve, S.; McClain, C. J.; Feng, W. *Lactobacillus rhamnosus GG* treatment potentiates intestinal hypoxia-inducible factor, promotes intestinal integrity and ameliorates alcohol-induced liver injury. *Am. J. Pathol.* **2011**, *179*, 2866−2875.

(11) Rishi, P.; Mavi, S. K.; Bharrhan, S.; Shukla, G.; Tewari, R. Protective efficacy of probiotic alone or in conjunction with a prebiotic in Salmonella-induced liver damage. *FEMS Microbiol. Ecol.* **2009**, *69*, 222−230.

(12) Lai, J. T.; Hsieh, W. T.; Fang, H. L.; Lin, W. C. The protective effects of a fermented substance from *Saccharomyces cerevisiae* on carbon tetrachloride-induced liver damage in rats. *Clin Nutr.* **2009**, *28*, 338−345.

(13) Pan, C.; Zhao, Y.; Liao, S. F.; Chen, F.; Qin, S.; Wu, X.; Zhou, H.; Huang, K. Effect of selenium-enriched probiotics on laying performance, egg quality, egg selenium content, and egg glutathione peroxidase activity. *J. Agric. Food Chem.* **2011**, *59*, 11424−11431.

(14) Ibrahim, H. A.; Zhu, Y.; Wu, C.; Lu, C.; Ezekwe, M. O.; Liao, S. F.; Huang, K. Selenium-enriched probiotics improves murine male fertility compromised by high fat diet. *Biol. Trace Elem. Res.* **2012**, *147*, 251−60.

(15) Gan, F.; Ren, F.; Chen, X.; Lv, C.; Pan, C.; Ye, G.; Shi, J.; Shi, X.; Zhou, H.; Shituleni, S. A.; Huang, K. Effects of selenium-enriched probiotics on heat shock protein mRNA levels in piglet under heat stress conditions. *J. Agric. Food Chem.* **2013**, *61*, 2385−2391.

(16) Hernandez-Munoz, R.; Diaz-Munoz, M.; Suarez, J.; Chagoya de Sanchez, V. Adenosine partially prevents cirrhosis induced by carbon tetrachloride in rats. *Hepatology* **1990**, *12*, 242−248.

(17) Ran, L.; Wu, X.; Shen, X.; Zhang, K.; Ren, F.; Huang, K. Effects of selenium form on blood and milk selenium concentrations, milk component and milk fatty acid composition in dairy cows. *J. Sci. Food Agric.* **2010**, *90*, 2214−2219.

(18) Yi, X.; Long, L.; Yang, C.; Lu, Y.; Cheng, M. Maotai ameliorates Diethylnitrosamine-Initiated hepatocellular carcinoma formation in mice. *PLoS One* **2014**, *9*, e93599.

(19) Flier, J. S.; Underhill, L. H.; Friedman, S. L. The cellular basis of hepatic fibrosis-mechanisms and treatment strategies. *N. Engl. J. Med.* **1993**, *328*, 1828−1835.

(20) Dossey, A. T. Insects and their chemical weaponry: new potential for drug discovery. *Nat. Prod Rep.* **2010**, *27*, 1737−1757.

(21) Teichert, R. W.; Olivera, B. M. Natural products and ion channel pharmacology. *Future Med. Chem.* **2010**, *2*, 731−744.

(22) Shen, X. H.; Cheng, W. F.; Li, X. H.; Sun, J. Q.; Li, F.; Ma, L.; Xie, L. M. Effects of dietary supplementation with vitamin E and selenium on rat hepatic stellate cell apoptosis. *World J. Gastroenterol.* **2005**, *11*, 4957−4961.

DOI: 10.1021/jf5039184
J. Agric. Food Chem. 2015, 63, 242−249

(23) Ding, M.; Potter, J. J.; Liu, X.; Torbenson, M. S.; Mezey, E. Selenium supplementation decreases hepatic fibrosis in mice after chronic carbon tetrachloride administration. *Biol. Trace Elem Res.* **2010**, *133*, 83−97.
(24) Wang, Y.; Li, Y.; Xie, J.; Zhang, Y.; Wang, J.; Sun, X.; Zhang, H. Protective effects of probiotic *Lactobacillus casei* Zhang against endotoxin-and D-galactosamine-induced liver injury in rats via anti-oxidative and anti-inflammatory capacities. *Int. Immunopharmacol.* **2013**, *15*, 30−7.
(25) Kisseleva, T.; Brenner, D. A. Mechanisms of fibrogenesis. *Exp. Biol. Med.* **2008**, *233*, 109−122.
(26) Fallowfield, J. A.; Hayden, A. L.; Snowdon, V. K.; Aucott, R. L.; Stutchfield, B. M.; Mole, D. J.; Pellicoro, A.; Henke, A.; Schrader, J. Relaxin modulates human and rat hepatic myofibroblast function and ameliorates portal hypertension in vivo. *Hepatology* **2014**, *59*, 1492−1504.
(27) Parola, M.; Robino, G. Oxidative stress-related molecules and liver fibrosis. *J. Hepatol.* **2001**, *35*, 297−306.
(28) Park, C. M.; Youn, H. J.; Chang, H. K.; Song, Y. S. TOP1 and 2, polysaccharides from *Taraxacum officinale*, attenuate CCl_4-induced hepatic damage through the modulation of NF-kB and its regulatory mediators. *Food Chem. Toxicol.* **2010**, *48*, 1255−1261.
(29) Naik, S. R.; Panda, V. S. Antioxidant and hepatoprotective effects of Ginkgo biloba phytosomes in carbon tetrachloride-induced liver injury in rodents. *Liver Int.* **2007**, *27*, 393−399.
(30) Lee, K. S.; Buck, M.; Houglum, K.; Chojkier, M. Activation of hepatic stellate cells by TGF alpha and collagen type I is mediated by oxidative stress through c-myb expression. *J. Clin. Invest.* **1995**, *96*, 2461.
(31) Bataller, R.; Brenner, D. A. Liver fibrosis. *J. Clin. Invest.* **2005**, *115*, 209−218.
(32) Friedman, S. L. Mechanisms of hepatic fibrogenesis. *Gastroenterology* **2008**, *134*, 1655−1669.
(33) Iredale, J.; Benyon, R.; Pickering, J.; McCullen, M.; Northrop, M.; Pawley, S.; Hovell, C.; Arthur, M. Mechanisms of spontaneous resolution of rat liver fibrosis. Hepatic stellate cell apoptosis and reduced hepatic expression of metalloproteinase inhibitors. *J. Clin. Invest.* **1998**, *102*, 538−549.
(34) Yogalakshmi, B.; Viswanathan, P.; Anuradha, C. V. Investigation of antioxidant, anti-inflammatory and DNA-protective properties of eugenol in thioacetamide induced liver injury in rats. *Toxicology* **2010**, *268*, 204−212.
(35) Wallace, K.; Burt, A.; Wright, M. Liver fibrosis. *Biochem. J.* **2008**, *411*, 1−18.
(36) Seki, E.; De Minicis, S.; Österreicher, C. H.; Kluwe, J.; Osawa, Y.; Brenner, D. A.; Schwabe, R. F. TLR4 enhances TGF-β signaling and hepatic fibrosis. *Nat. Med.* **2007**, *13*, 1324−1332.
(37) Choi, S. S.; Omenetti, A.; Witek, R. P.; Moylan, C. A.; Syn, W.-K.; Jung, Y.; Yang, L.; Sudan, D. L.; Sicklick, J. K.; Michelotti, G. A. Hedgehog pathway activation and epithelial-to-mesenchymal transitions during myofibroblastic transformation of rat hepatic cells in culture and cirrhosis. *Am. J. Physiol. Gastrointest. Liver Physiol.* **2009**, *297*, G1093−G1106.
(38) Chen, L.; Pan, D. D.; Zhou, J.; Jiang, Y. Z. Protective effect of selenium-enriched Lactobacillus on CCl4-induced liver injury in mice and its possible mechanisms. *World J. Gastroenterol.* **2005**, *11*, 5795−5800.
(39) Wright, M. C.; Issa, R.; Smart, D. E.; Trim, N. Gliotoxin stimulates the apoptosis of human and rat hepatic stellate cells and enhances the resolution of liver fibrosis in rats. *Gastroenterology.* **2001**, *121*, 685−698.
(40) Kakkar, P.; Singh, B. K. Mitochondria: a hub of redox activities and cellular distress control. *Mol. Cell. Biochem.* **2007**, *305*, 235−253.
(41) Jonkers, D.; Stockbrugger, R. Review article: Probiotics in gastrointestinal and liver diseases. *Aliment. Pharmacol. Ther.* **2007**, *26*, 133−148.
(42) Kirpich, I. A.; McClain, C. J. Probiotics in the treatment of the liver diseases. *J. Am. Coll Nutr.* **2012**, *31*, 14−23.
(43) Bauer, T. M.; Fernandez, J.; Navasa, M.; Vila, J.; Rodes, J. Failure of *Lactobacillus* spp. to prevent bacterial translocation in a rat model of experimental cirrhosis. *J. Hepatol.* **2002**, *36*, 501−506.
(44) Soriano, G.; Sanchez, E.; Guarner, C.; Schiffrin, E. J. *Lactobacillus johnsonii* La1 without antioxidants does not decrease bacterial translocation in rats with carbon tetrachloride-induced cirrhosis. *J. Hepatol.* **2012**, *57*, 1395−1396.
(45) Chiva, M.; Soriano, G.; Rochat, I.; Peralta, C.; Rochat, F.; Llovet, T.; Mirelis, B.; Schiffrin, E. J.; Guarner, C.; Balanzo, J. Effect of *Lactobacillus johnsonii* La1 and antioxidants on intestinal flora and bacterial translocation in rats with experimental cirrhosis. *J. Hepatol.* **2002**, *37*, 456−462.
(46) Stadlbauer, V.; Mookerjee, R. P.; Hodges, S.; Wright, G. A.; Davies, N. A.; Jalan, R. Effect of probiotic treatment on deranged neutrophil function and cytokine responses in patients with compensated alcoholic cirrhosis. *J. Hepatol.* **2008**, *48*, 945−951.

DOI: 10.1021/jf5039184
J. Agric. Food Chem. 2015, 63, 242−249

JOURNAL OF AGRICULTURAL AND FOOD CHEMISTRY

Article

pubs.acs.org/JAFC

Effect of Cooking on *in Vitro* Digestion of Pork Proteins: A Peptidomic Perspective

Siying Wen, Guanghong Zhou, Li Li, Xinglian Xu, Xiaobo Yu, Yun Bai, and Chunbao Li*

Key Laboratory of Meat Processing and Quality Control, Ministry of Education, Synergetic Innovation Center of Food Safety and Nutrition, Jiangsu Innovation Center of Meat Production and Processing, Key Laboratory of Animal Products Processing, Ministry of Agriculture, Synergetic Innovation Center of Meat Processing and Quality Control, Nanjing Agricultural University, Nanjing 210095, P.R. China

Supporting Information

ABSTRACT: This study was designed to investigate the effect of cooking on *in vitro* digestibility and peptide profiling of pork protein. We simulated gastrointestinal digestion of cooked pork that was treated with pepsin alone or followed by trypsin treatment. Digested products were identified using matrix-assisted laser desorption/ionization−time-of-flight mass spectrometry and liquid chromatography−mass spectrometry analyses. Cooking led to a reduction ($p < 0.05$) in digestibility and band intensities on sodium dodecyl sulfate−polyacrylamide gel electrophoresis gels. Peptide profiling and identification analyses also showed significant difference ($p < 0.05$) in the m/z ranges and number of peptides from the pepsin-digested products between raw (4 °C) and very well done samples (100 °C). Peptides sequenced from pepsin-digested samples under lower degrees of doneness disappeared as the temperature increased. Meanwhile, the trypsin cleavages appeared more consistent among different degrees of cooking. Further work may be needed to evaluate the bioavailability of the digested products under different cooking temperatures.

KEYWORDS: *cooking, in vitro digestibility, peptidomics, sequencing*

INTRODUCTION

Cooking is the way to convert raw meat into edible meat. The degree of cooking affects palatability and consumer acceptability differing with primal cuts and cooking methods.[1−4] Generally speaking, people in western countries prefer roasting and grilling with medium doneness, but Asian people prefer stewing and stir-frying with very well doneness. In recent years, the degree of doneness has been associated with the production of heterocyclic aromatic amines and the risk of colorectal cancer in the clinic.[5,6] However, meat has played and will continue to play a crucial role in the supply of high-quality protein, vitamins, and minerals.[7] Notably, it should be paid more attention to how cooking affects the bioavailability of nutrients in meat, especially proteins. However, few data are available.

A French group have performed much work on the effect of cooking on *in vitro* digestibility of meat, and they found that heat-induced oxidation and increased surface hydrophobicity of myofibrillar proteins could result in protein aggregation, which further decreased the pepsin digestion rate.[8−11] However, the nutritional quality of meat proteins should not only be associated with digestibility or amino acid composition but also with peptide size and sequences,[12−14] which may affect protein digestibility after cooking. It is known that oligopeptides can be degraded by the brush border peptide hydrolases and taken up into intestinal epithelial cells where the size of oligopeptides may be critical.[15] It is crucial to characterize the digested products from meat proteins when they go through the stomach and the gut to evaluate the effect of cooking on meat protein bioavailability.[16]

The objective of the present study was to characterize the *in vitro* digested products with pepsin and trypsin from cooked pork under different cooking temperatures by mimicking gastrointestinal digestion in the human body.

MATERIALS AND METHODS

Samples and Cooking Procedure. Pork longissimus dorsi muscles ($n = 8$; muscle pH 5.83 ± 0.18) were obtained at 36 h postmortem from a commercial meat packing company. After all visible fat and connective tissue were removed, each pork muscle was cut vertically into five 2 cm thick pieces (weighing 90−110 g each). Three of these pieces were packed in retort pouch and cooked in a 72 °C water bath (Julabo, TW 20, Germany) to different center temperatures, i.e., 60 °C (cooking time of 12−16 min), 65 °C (cooking time of 21−29 min), and 70 °C (cooking time of 33−37 min), individually. The fourth piece was packed in retort pouch and cooked in a 100 °C water bath (Julabo, TW 20, Germany) to the center temperature of nearest to 100 °C (cooking time of 3 h). The fifth piece was not cooked (4 °C) as the control (raw). During cooking, the center temperature of the samples was monitored using a digital, hand-held thermometer (Testo108, Testo AG, Germany). After cooking, the samples were cooled to the room temperature (20 ± 2 °C). Eight repeats were applied for each temperature point.

***In Vitro* Digestion.** Cooked meat was *in-vitro*-digested according to the procedure by Escudero et al., with some modifications.[14] Briefly, meat samples (0.5 g, each) were homogenized in 2 mL of double-distilled water for 2 × 30 s at 9500 rpm and 2 × 30 s at 13 500 rpm with 30 s cooling between bursts. The homogenate was adjusted to pH 2.0 with 1 mol/L HCl, and pepsin (≥400 units/mg of protein, from porcine gastric mucosa, product number P7125, Sigma-Aldrich, St. Louis, MO) was added 0.016 g each at a ratio of 1:31.25 of the substrate based on the weight of meat. The mixture was incubated at 37 °C for 2 h with continuous shaking, and then the enzyme was inactivated by adjusting the pH to 7.5 with 1 mol/L NaOH on ice. A total of 1 mL of the resulting

Received: August 24, 2014
Revised: November 21, 2014
Accepted: November 24, 2014
Published: November 24, 2014

 © 2014 American Chemical Society

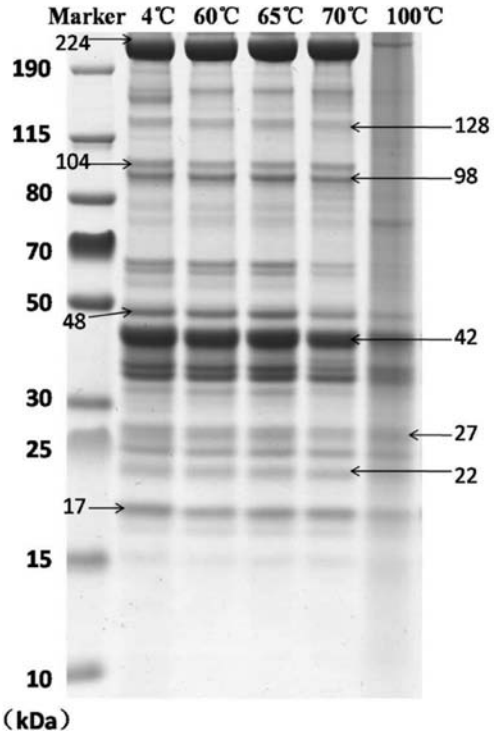

Figure 1. SDS−PAGE profiling of total proteins from cooked pork under different cooking temperatures. Proteins of bands with different numbers on the right five lanes were quantified and identified, with more details seen in Table 1.

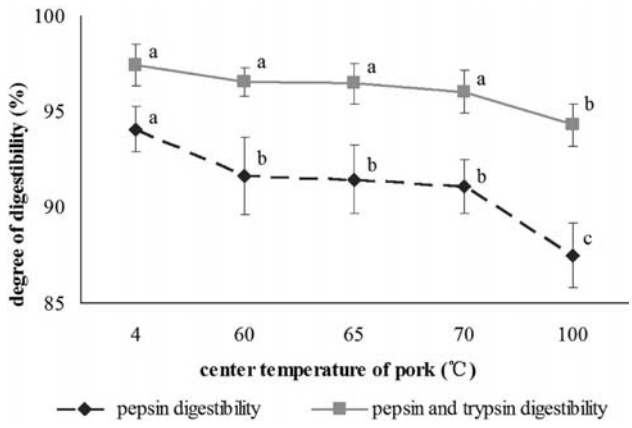

Figure 2. *In vitro* digestibility of pork under different cooking temperatures. Diamond, samples were treated with pepsin; black box, samples were treated with pepsin followed by trypsin. Different letters indicate statistically significant difference among the values.

digestion mixture was removed for peptide profiling, and the remaining (approximately 1.5 mL) was kept at 37 °C for trypsin digestion. Trypsin (1645 units/mg of protein, from porcine pancreas, lyophilized powder, type II-S, product number T7409, Sigma-Aldrich, St. Louis, MO) was added 0.006 g each at a ratio of 1:50 substrate based on the mass of meat left. The reaction mixture was maintained under the same conditions as above. After 2 h of trypsin digestion, enzyme activity was terminated by heating at 95 °C for 5 min and then 1 mL of the resulting digestion mixture was taken out for peptide profiling. Both the pepsin digests and pepsin/trypsin digests were deproteinized by adding three volumes of ethanol and storing for 12 h at 4 °C. The samples were then centrifuged at 10000*g* for 20 min at 4 °C. The supernatant and precipitate were separated and stored at −18 °C.

***In Vitro* Digestibility.** Two portions of meat sample weighing 1 g were taken from each piece. One portion was only treated with pepsin, and the other one was treated with pepsin, followed by trypsin. The digestion procedures were the same as above. After digestion, the digest was centrifuged at 10000*g* for 20 min at 4 °C and the supernatant was discarded. The precipitate was dried until the weight was constant. The degree of digestibility was calculated by the weight change of insoluble protein as the following equation:

$$DT = \left(1 - \frac{W_i}{W_t}\right) \times 100\%$$

where DT is the digestibility, W_i is the weight of dried insoluble protein, and W_t is the total weight of meat before digestion.

Table 1. Identified Proteins and Relative Band Intensities on SDS−PAGE Gels (Mean ± Standard Deviation)[a]

protein name	M_{re}[b] (kDa)	M_{rt}[c] (kDa)	4 °C	60 °C	65 °C	70 °C	100 °C	accession number	sequence coverage (%)	score
myosin-1	220	224	6.32 ± 0.89 a	5.82 ± 0.80 ab	5.27 ± 0.96 b	4.14 ± 1.17 c	0.12 ± 0.07 d	NP_001098421	3	429
myosin-2		224						NP_999301	3	429
myosin-binding protein C, fast type	137	128	0.71 ± 0.26 a	0.63 ± 0.09 a	0.62 ± 0.11 a	0.51 ± 0.11 b	nd	XP_003127419	4	121
α-actinin-3-like isoform 1	98	104	0.59 ± 0.10 a	0.48 ± 0.09 b	0.46 ± 0.07 b	0.30 ± 0.10 c	nd	XP_003122525	4	127
glycogen phosphorylase, muscle form isoform 1	90	98	1.12 ± 0.21 a	1.08 ± 0.14 a	1.01 ± 0.15 a	0.63 ± 0.32 b	nd	XP_003122636	9	352
β-enolase	48	48	2.20 ± 1.26 a	1.45 ± 0.14 b	1.43 ± 0.15 b	1.46 ± 0.20 b	0.37 ± 0.13 c	NP_001037992	7	138
actin, α skeletal muscle	42	42	3.67 ± 0.63 a	3.98 ± 0.39 a	3.85 ± 0.66 a	2.74 ± 0.94 b	0.78 ± 0.52 c	NP_776650	15	357
creatine kinase M type		43						NP_001123421	3	107
triosephosphate isomerase	27	27	0.72 ± 0.16 a	0.71 ± 0.09 a	0.70 ± 0.17 a	0.64 ± 0.16 a	0.51 ± 0.10 b	-	-	-
myosin light chain 3	22	22	0.80 ± 0.22 a	0.84 ± 0.14 a	0.83 ± 0.14 a	0.71 ± 0.12 ab	0.60 ± 0.24 b	-	-	-
myoglobin	18	17	1.71 ± 0.28 a	1.51 ± 0.21 ab	1.44 ± 0.38 bc	1.29 ± 0.30 c	0.56 ± 0.31 d	-	-	-

[a]Means with different letters in the same row differ significantly ($p < 0.05$). nd = not detectable. Proteins marked with "-" are bands that could not be identified by the MALDI−ToF−ToF method but matched with Swiss-Prot. [b]Estimated molecular weights of the proteins. [c]Theoretical molecular weights of the identified proteins.

dx.doi.org/10.1021/jf505323g | J. Agric. Food Chem. 2015, 63, 250−261

Gel Electrophoresis and Protein Identification. Sodium dodecyl sulfate−polyacrylamide gel electrophoresis (SDS−PAGE) was performed to characterize the total protein profiles before and after cooking to different center temperatures.

A total of 1 g of cooked meat was homogenized in 4 mL of extraction buffer (2% SDS and 0.01 mol/mL sodium phosphate buffer at pH 7.0) with an Ultra Turrax homogenizer (IKA T25 Digital, Germany). The homogenate was centrifuged (Allegra 64R, Beckman Coulter, Brea, CA) at 1500*g* for 15 min at 4 °C. The protein concentration of the supernatant was determined with a BCA protein assay kit (catalog number 23225, Thermo Scientific, Waltham, MA).

Appropriate volumes of protein samples were mixed with 12.5 μL of XT sample buffer (Bio-Rad, Hercules, CA) and made up to a total volume of 50 μL with ultrapure water to a final protein concentration of 0.5 μg/μL. Protein samples were denatured by heating at 95 °C for 5 min. A total of 10 μL of each sample was loaded on 4−12% Bis-Tris Criterion precast gels (catalog number 345-0125, Bio-Rad, Hercules, CA). The gels were run in 900 mL of XT MES running buffer (Bio-Rad, Hercules, CA) at 150 V for approximately 1 h, until the bromophenol blue dye front just disappeared. After electrophoresis, proteins were stained with Coomassie Blue R250 for 3 h and destained until the bands were clear.

Gel images were captured using an image scanner (GE Healthcare, Little Chalfont, U.K.), and the band intensities were quantified with the Quantity One software (Bio-Rad, Hercules, CA). The intensity of each band was calculated as its actual intensity relative to the intensity of the 190 kDa band in the prestained calibration marker (catalog number 161-0377, Bio-Rad, Hercules, CA).

A total of 12 different bands were picked up and further identified by matrix-assisted laser desorption/ionization−time-of-flight tandem mass spectrometry (MALDI−ToF MS−MS, ultrafleXtreme Bruker, Germany).[17] In brief, protein bands were destained, cleaned, and digested in gel with trypsin (Promega, Madison, WI). The extracted peptide mixtures were analyzed by MALDI−ToF−ToF MS. All peptide spectra were matched with the online MASCOT program (http://www.matrixscience.com) against the Swiss-Prot databases. The data matching was performed with a peptide mass tolerance of 0.12 Da and ToF−ToF fragment ion mass tolerance of 0.6 Da. Carbamidomethyl of Cys was chosen as fixed modification; oxidation of Met and pyro-Glu formation of N-terminal Gln were chosen as dynamic modifications; and one missing tryptic cleavage was allowed. Hits were applied only if their MASCOT probability were less than 0.05.

Characterization of the Digested Products. *MALDI−ToF MS Analysis.* The ethanol-soluble fractions from the pepsin-treated and the pepsin/trypsin-treated samples were characterized by MALDI−ToF MS in duplicate. An aliquot (1 μL) of each sample was spotted on the target plate with an equal volume of matrix solution [α-cyano-4-hydroxycinnamic acid (CHCA), 0.005 g/mL prepared in 50% acetonitrile (ACN)/0.1% trifluoroacetic acid (TFA)]. The mixture was dried before analysis. Positive-ion (MH^+) spectra were acquired in the linear MALDI−ToF MS mode (ultrafleXtreme Bruker, Germany). The *m*/*z* signals were recorded between 200 and 1500 for peptide identification.

The peak data of the MS spectra were subjected to hierarchical clustering using the ClinProTools 2.2 software (Bruker Daltonics, Germany). Principal component analysis (PCA) was performed using the unsupervised clustering mode.

Liquid Chromatography−Mass Spectrometry (LC−MS) Analysis. The ethanol-soluble fractions from the pepsin-treated and pepsin/trypsin-treated samples were also analyzed with hybrid quadrupole orbitrap mass spectrometer equipped with a nanoelectrospray ionization source with an online nano-LC system (Nano LC-Q-Exactive-MS-MS, Thermo Fisher Scientific, Waltham, MA). The ethanol-soluble fractions were filtered through ultra-0.5 mL centrifugal filter units with ultracel-3 membrane (Amicon Ultra, Millipore, Ireland) under centrifugation at 15000*g* for 15 min. Peptide mixtures were then fractionated on an online nano-LC system (EASY-nLC 1000, Thermo Scientific, Waltham, MA). Samples were loaded onto a C_{18} column (2 cm long, 100 μm inner diameter, and 5 μm particle size) at a maximum pressure of 500 bar.

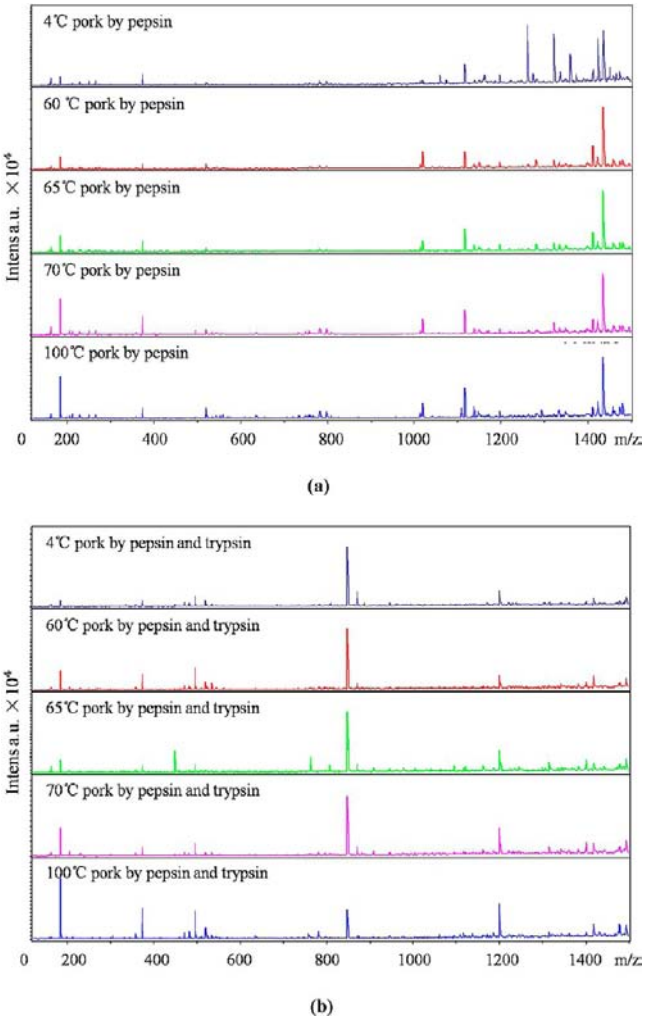

Figure 3. MALDI−ToF MS spectra of ethanol-soluble fragments from pork under different cooking temperatures. Each panel includes five spectra from 4, 60, 65, 70, and 100 °C samples: (a) pepsin treated and (b) pepsin and trypsin treated.

Peptides were separated using a mobile phase changing from 0.1% formic acid (FA) in water (buffer A) to 0.1% FA in ACN (buffer B). A step-gradient elution at a flow rate of 350 nL/min was applied with an increasing concentration of buffer B: (1) 10 min from 0 to 8%, (2) 25 min from 8 to 20%, (3) 15 min from 20 to 30%, (4) 5 min from 30 to 90%, and finally kept at 90% until the procedure completed. The hybrid quadrupole orbitrap mass spectrometer was operated in a data-dependent mode, and a scan cycle was initiated with a full-scan MS spectrum (from *m*/*z* 100 to 1500). The top 20 abundant ions were selected for collision-induced dissociation (CID) fragmentation in the linear ion trap, and the exclusion time was set as 60 s.

MS/MS spectra of peptides were matched using Proteome Discoverer (Thermo Fisher Scientific, Waltham, MA) against the Swiss-Prot *Sus scrofa* database (http://www.uniprot.org/taxonomy/complete-proteomes). Data matching was performed with a fragment ion mass tolerance of 0.8 Da and a parent ion tolerance of 10 ppm. Oxidation of Met and pyro-Glu formation of N-terminal Gln were chosen as dynamic modifications, and two missing cleavages were allowed. Unspecific enzyme was used in the peptic peptide database search, while both unspecific enzyme and trypsin were used in the peptide search for pepsin/trypsin-treated samples. Peptide identification was accepted if they could be established at a PeptideProphet probability of greater than 95%. Protein matching was accepted if they could be established at the probability of greater than 95% and contained at least two identified spectra.

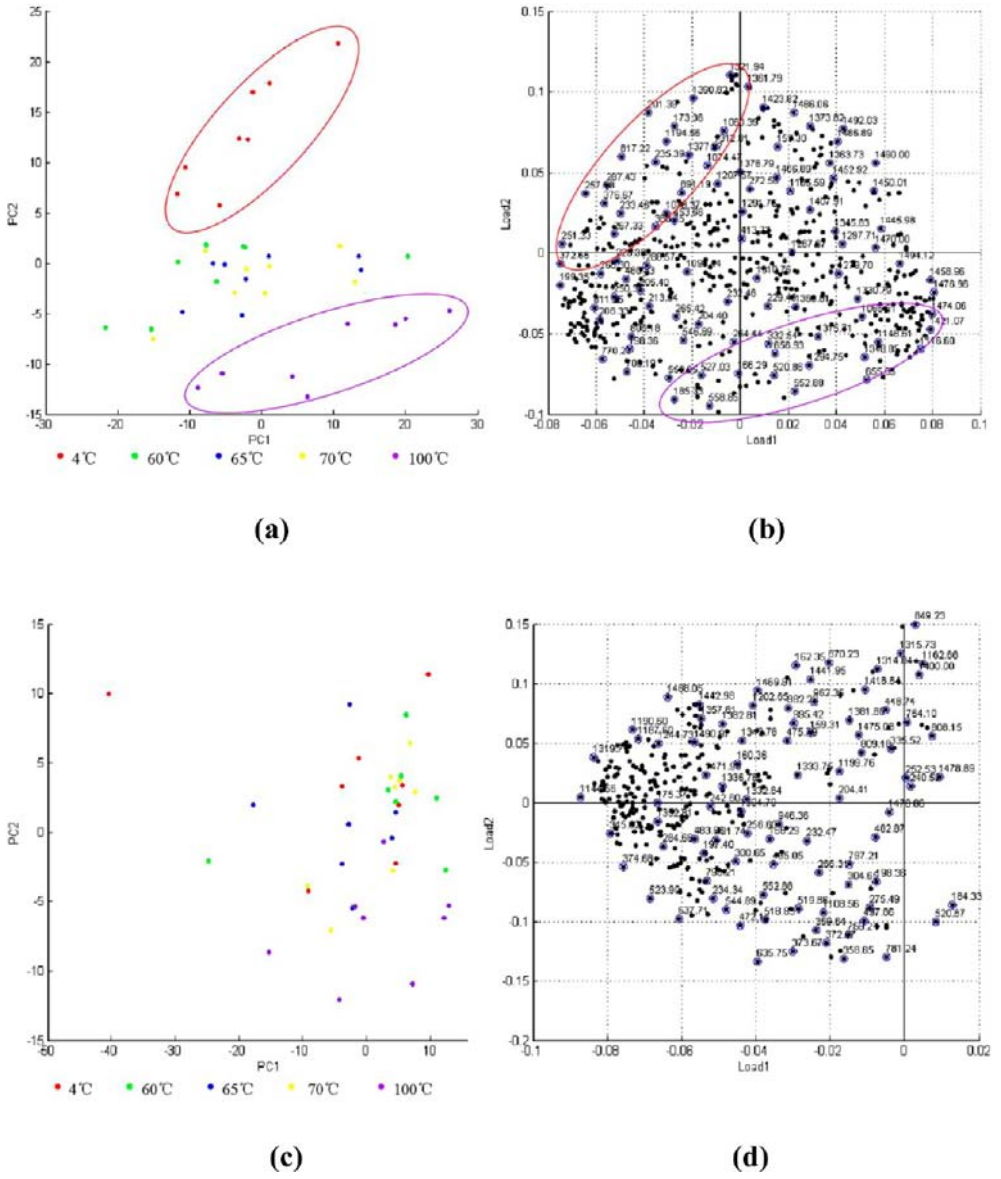

Figure 4. PCA plots of the peptides from cooked pork treated with pepsin and trypsin: (a and c) scores plot, treated with pepsin and pepsin/trypsin, respectively (red, green, blue, yellow, and purple plots represent 4, 60, 65, 70, and 100 °C treatment samples) and (b) and (d) loadings plot, treated with pepsin and pepsin/trypsin, respectively.

Statistical Analysis. The effects of cooking on *in vitro* digestibility and SDS−PAGE band intensities were evaluated by one-way analysis of variance and the Duncan's multiple-range test using the SAS program (SAS Institute, Inc., Cary, NC). PCA on spectral data was described in the MALDI−ToF MS Analysis section.

RESULTS AND DISCUSSION

Effect of Cooking on Pork Protein Profiling and *In Vitro* Digestibility. Generally, band intensities on SDS−PAGE gels decreased as the center temperature increased, especially for 100 °C samples (Figure 1). A possible explanation for the decrease in band intensities is the aggregation of meat proteins. Previous studies indicated that a high cooking temperature led to increased oxidation and protein surface hydrophobicity of myofibrillar proteins[8,9] and, as a result, increased protein aggregation. Sarcoplasmic proteins, which contain various types of enzymes, pigments, and regulatory proteins, may aggregate between 40 and 60 °C.[18] The heat-induced protein aggregation normally appeared with the decreased equivalent circle diameter and number of particles.[11,19]

In details, muscle proteins showed different responses to cooking ($p < 0.05$) in terms of band intensities on SDS−PAGE gels (Figure 1 and Table 1). Myosin heavy chain (224 kDa), α-actinin (104 kDa), β-enolase (48 kDa), and myoglobin (18 kDa) showed a distinct intolerance to heating in that their band intensities dropped at 60 °C ($p < 0.05$). Myosin-binding protein C (128 kDa), glycogen phosphorylase (98 kDa), and actin/creatine kinase (42 kDa) had a bit stronger heat tolerance, and the band intensities decreased significantly at 70 °C ($p < 0.05$). A previous study has confirmed that myosin has endothermic transitions at 54 °C, with a transition temperature of 77 °C for actin.[20] However, triosephosphate isomerase and myosin light chain 3 (22 kDa) were more tolerant to high-temperature cooking (100 °C). Kajak-Siemaszko et al. showed a similar SDS−PAGE pattern of meat proteins during cooking, but they did not show qualitative and quantitative data.[21] Our data suggest that the

dx.doi.org/10.1021/jf505323g | J. Agric. Food Chem. 2015, 63, 250−261

different responses of meat proteins to cooking could be indicative of different digestibilities.

Cooking had a significant effect ($p < 0.05$; Figure 2) on *in vitro* digestibility of pork treated with pepsin and trypsin. When pork was treated only with pepsin, cooking led to a distinct decrease ($p < 0.05$) in digestibility between 60 °C and raw meat and between 70 and 100 °C but there was no significant difference ($p > 0.05$) between 60 and 70 °C. For pork treated with pepsin followed by trypsin, only a high temperature (100 °C) resulted in a significant decrease in digestibility. These results are in accordance with previous studies in which the digestion rate was applied to evaluate *in vitro* digestibility.[11,19] In those studies, the decrease in protein digestibility was associated with protein aggregation. It is notable that the values of digestibility are quite different from those by Santé-Lhoutellier et al.[8] mainly because of the different methodologies in which the OD_{280} value was applied to quantify peptides in that previous study, while we calculated it on a dry weight basis.

Effect of Cooking on Peptide Profiling after Digestion. As described above, cooking affected the extent of *in vitro* digestion. However, to our knowledge, peptides in the digested products under different cooking temperatures have never been characterized. Therefore, two types of high-throughput methods, including MALDI−ToF MS and nano-LC−MS−MS, were applied to characterize the composition of digested products.

MALDI−ToF MS analysis revealed different peptide profiles for the ethanol-soluble fractions from the samples with different degrees of cooking (Figure 3). Meat cooked at higher temperatures had relatively less abundant peptides with a m/z range between 200 and 1200 after pepsin treatment (Figure 3a), but the difference became weak after pepsin/trypsin treatment (Figure 3b). This is in accordance with the changes of *in vitro* digestibility.

PCA revealed significant differences in peptide composition and abundance under different cooking temperatures. Again, peptides from raw (4 °C) and very well done (100 °C) pork were well-separated from the other three groups after pepsin digestion (Figure 4a; scores plot) in that fragments from raw meat had relatively smaller mass than the other groups (Figure 4b; loadings plot). Peptides from 60, 65, and 70 °C samples could not be well separated (Figure 4b). However, peptides from all of the groups could not be separated at all after pepsin/trysin digestion (panels c and d of Figure 4). It is notable that the sensitivity of MALDI−ToF MS seems not good enough to characterize low-abundance peptides.

LC−MS analysis was performed to characterize peptides more sensitively. According to a previous study, the size of peptides from pepsin/pancratin-digested pork ranges from 6 to 16 amino acids,[14] and in the present study, the m/z search range was set between 800 and 2000. A total of 1000 peptides were identified from the pepsin-treated samples, and 1203 peptides were identified from the pepsin/trypsin-treated samples. Of these peptides, 554, 466, 484, 329, and 376 peptides were sequenced from pepsin-digested samples for 4, 60, 65, 70, and 100 °C groups, individually, and 662, 549, 520, 431, and 549 peptides were sequenced from pepsin/trypsin-digested samples (Figure 5a) from 4, 60, 65, 70, and 100 °C groups, respectively. When peptides were categorized by m/z into three groups, 800−1000, 1000−1500 and 1500−2000, the majority of peptides have a m/z of 1000−1500 or 1500−2000. The 70 °C samples had the least peptides across three mass to charge ranges whether the samples were treated with pepsin alone or followed by trypsin (panels b and c of Figure 5). This could be due to the protein

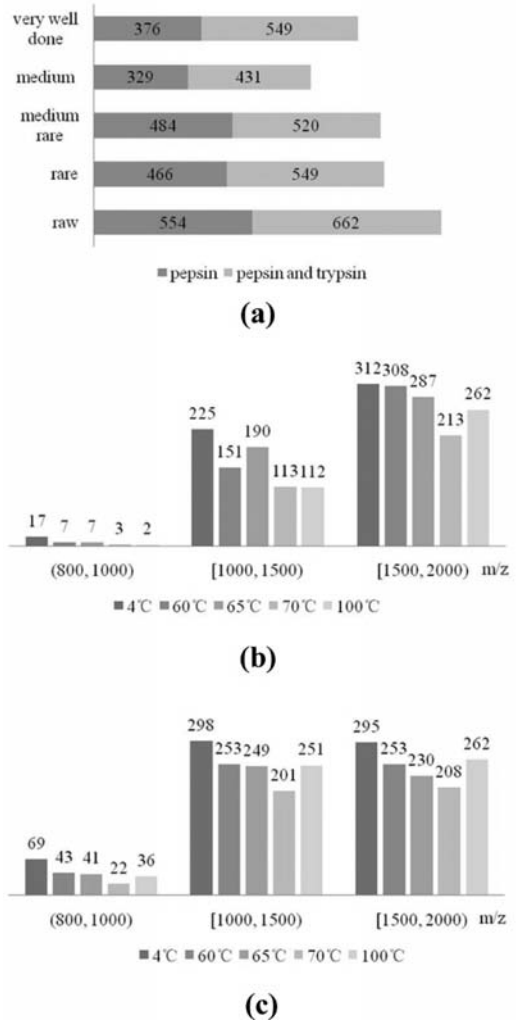

Figure 5. Number of identified peptides from cooked pork treated with pepsin and trypsin: (a) total number of identified peptides between 800 to 2000 Da, (b) number of the peptides from pepsin-digested samples categorized by size, and (c) number of the peptides from pepsin/trypsin-digested samples categorized by size.

aggregation associated with the resistance to the proteolysis of digestive enzymes.[9,11,19] We also found that peptide sequences from pepsin-treated samples were different from those from pepsin/trypsin-treated samples (see the Supporting Information), which could be attributed to the stochasticity of active sites of pepsin.[22]

Peptides were matched with porcine muscle proteins against the Swiss-Prot *S. scrofa* database. High-abundance peptides were mainly from several myofibrillar proteins (myosin, actin, tropomyosin, and titin) and sarcoplasmic proteins (phosphorylase, glyceraldehyde-3-phosphate dehydrogenase, creatine kinase, 6-phosphofructokinase, etc.). Notably, 16−21% of identified peptides came from myosin heavy chain. This gives a good explanation for the decrease in band intensities on SDS−PAGE gels (Figure 1). To explore the effect of cooking on the digestion pattern of these proteins, we localized identified sequences to the intact protein sequence chains. Figure 6 is an example of myosin heavy chain (myosin-4). Generally, peptides identified from pepsin-digested samples under lower temperature disappeared as the temperature increased. Meanwhile, in comparison to the pepsin cleavages (a1−a3 of Figure 6), the pepsin/trypsin cleavages appeared more consistent among samples under

dx.doi.org/10.1021/jf505323g | J. Agric. Food Chem. 2015, 63, 250−261

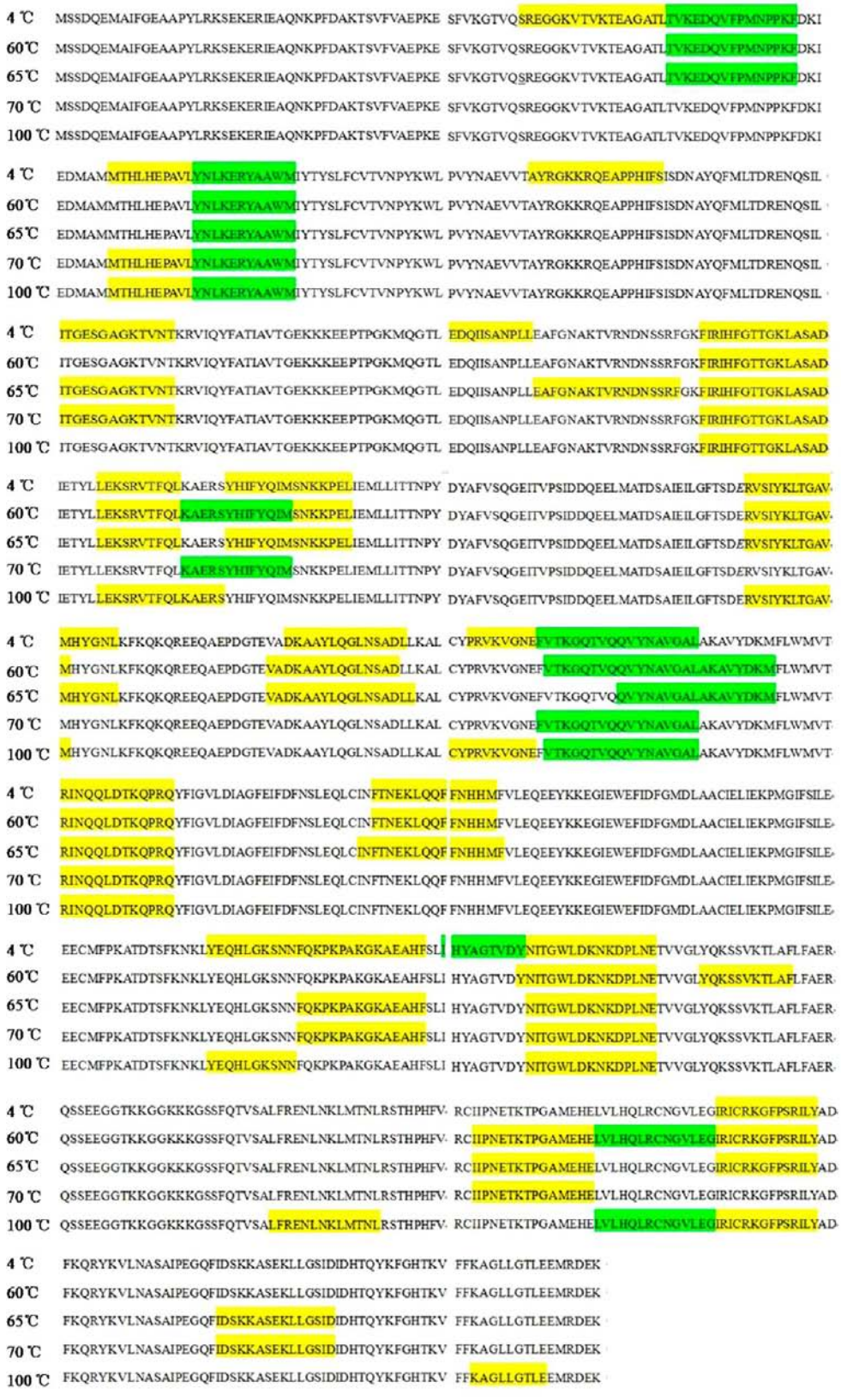

(a1)

Figure 6. continued

dx.doi.org/10.1021/jf505323g | J. Agric. Food Chem. 2015, 63, 250−261

(a2)

Figure 6. continued

dx.doi.org/10.1021/jf505323g | J. Agric. Food Chem. 2015, 63, 250−261

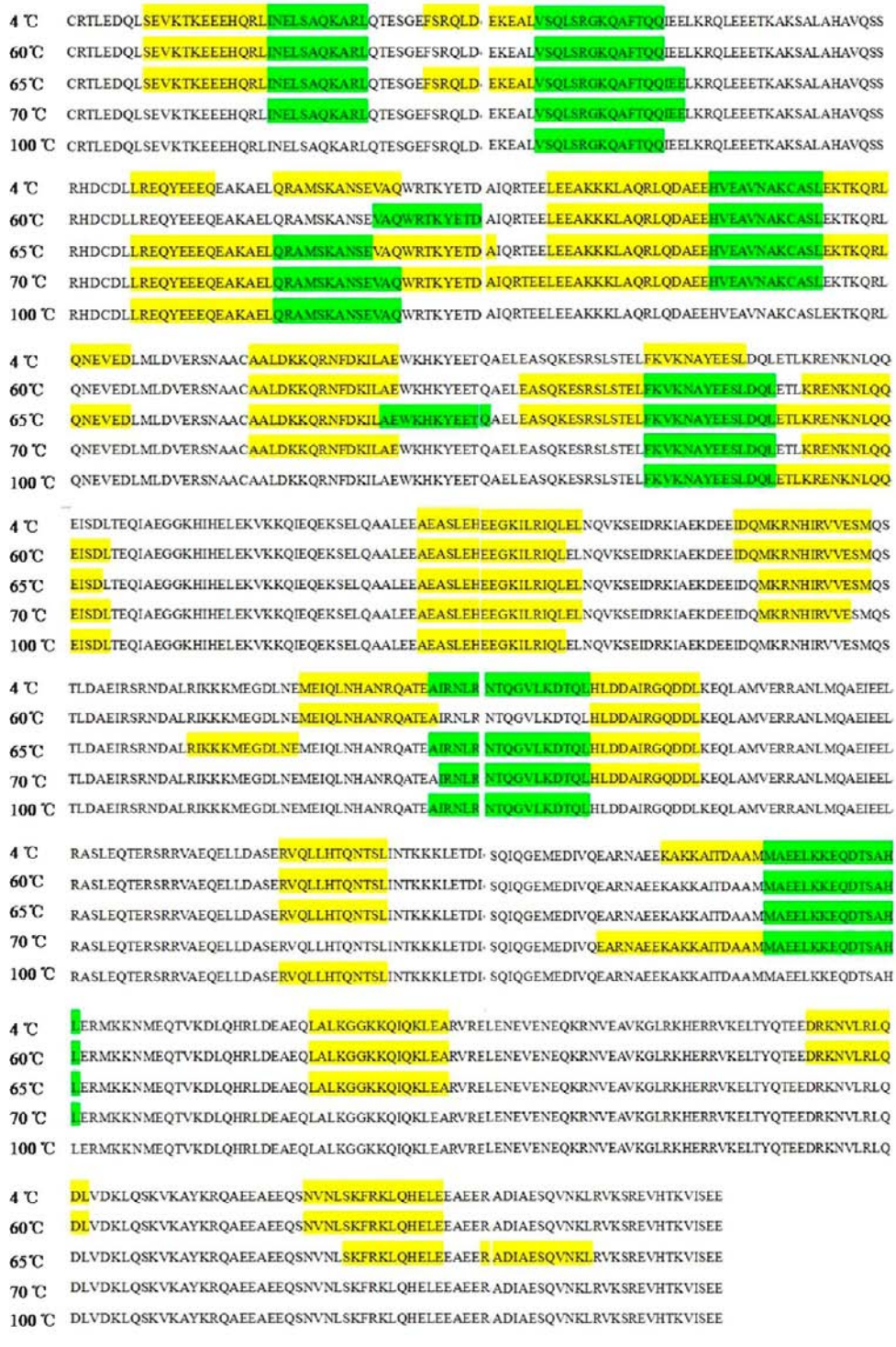

(a3)

Figure 6. continued

dx.doi.org/10.1021/jf505323g | J. Agric. Food Chem. 2015, 63, 250−261

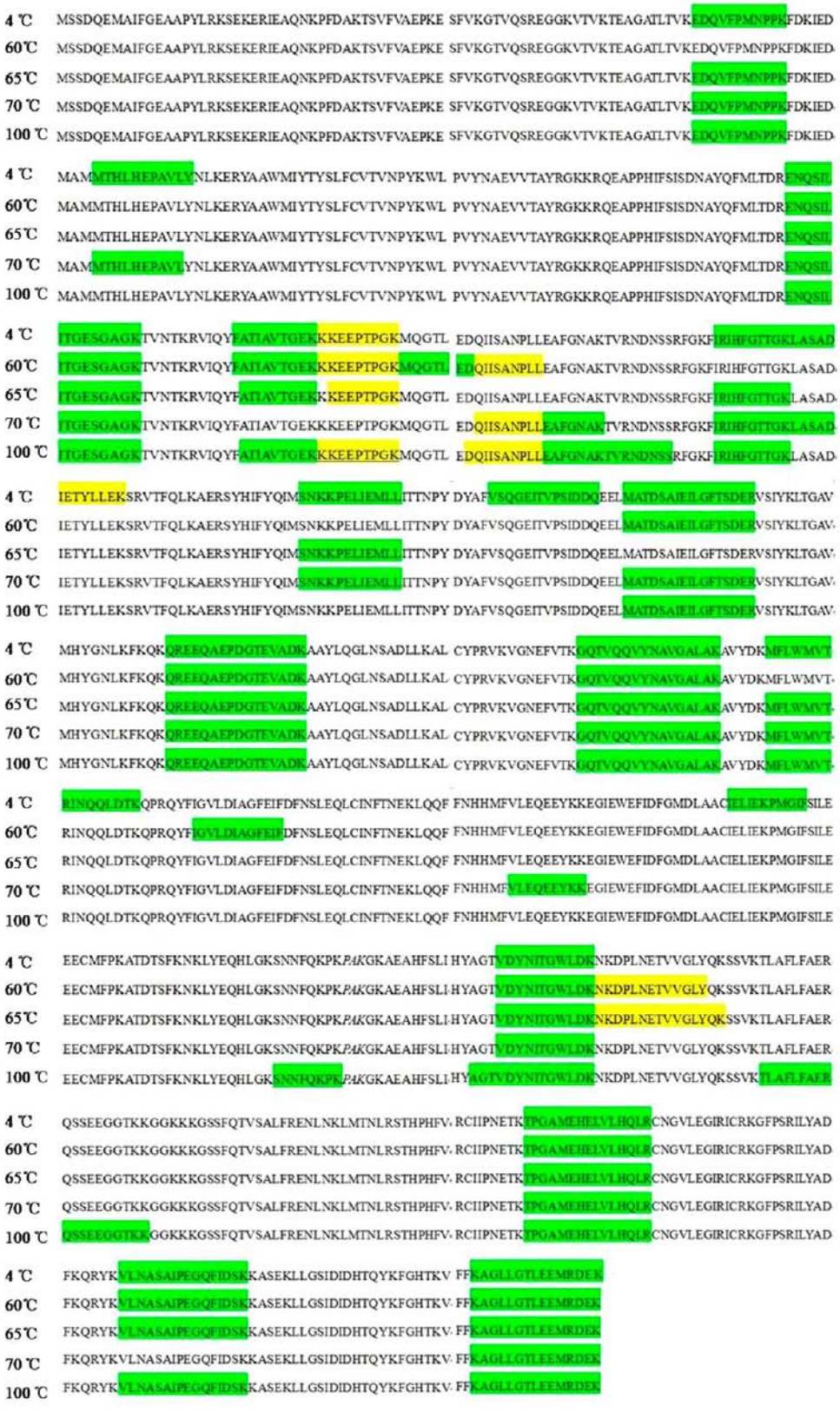

(b1)

Figure 6. continued

dx.doi.org/10.1021/jf505323g | J. Agric. Food Chem. 2015, 63, 250−261

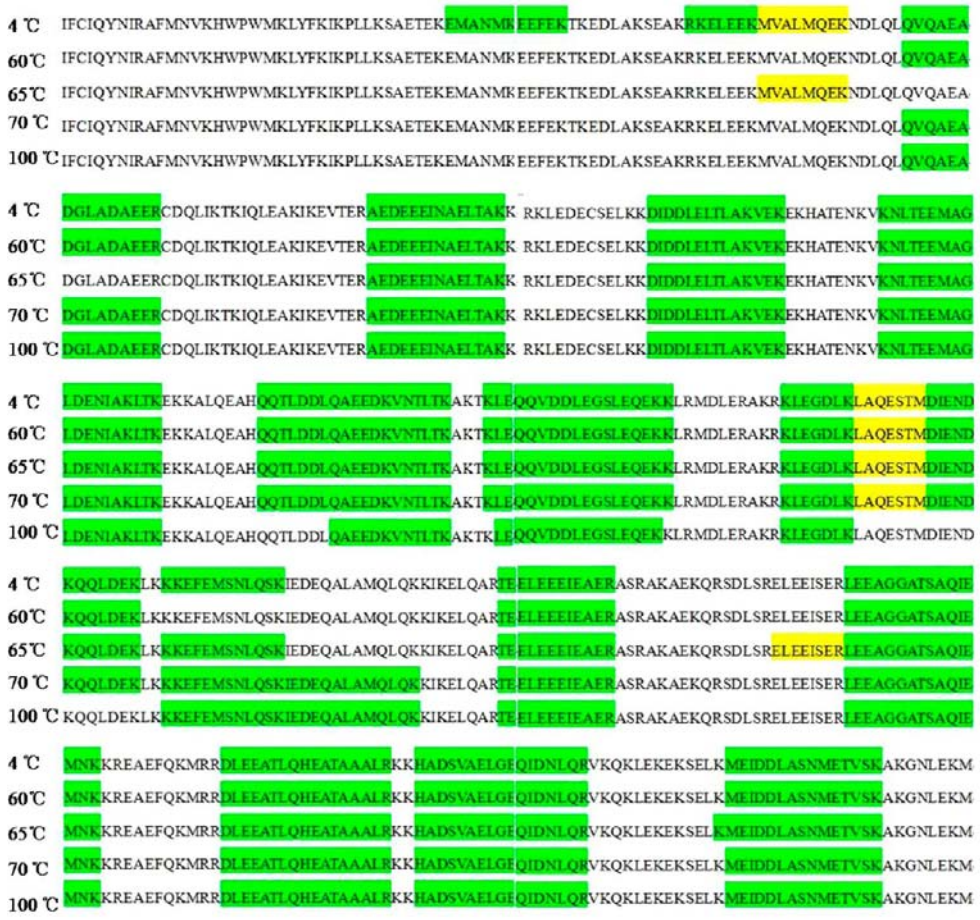

(b2)

Figure 6. continued

dx.doi.org/10.1021/jf505323g | J. Agric. Food Chem. 2015, 63, 250−261

(b3)

Figure 6. Localization of peptides from myosin-4 in response to cooking: (a1) peptides from pepsin-digested samples located at myosin head-like domain (positions 1−781), (a2) peptides from pepsin-digested samples located at myosin coiled tail domain (positions 812−1250), (a3) peptides from pepsin-digested samples located at myosin coiled tail domain (positions 1251−1937), (b1) peptides from pepsin/trypsin-digested samples located at myosin head-like domain (positions 1−781), (b2) peptides from pepsin/trypsin-digested samples located at myosin coiled tail domain (positions 812−1250), and (b3) peptides from pepsin/trypsin-digested samples located at myosin coiled tail domain (positions 1251−1937). Different colors of highlights were used to distinguish the peptides just next to each other.

different cooking temperatures (b1−b3 of Figure 6). For pepsin-digested samples, 10 peptides appeared in all five groups, while 33 peptides appeared in trypsin digestion with the carbon-terminal cleavage sites as Lys and Arg. Although it could be due to the trypsin peptides better identified in the database search than pepsin, this indicates that cooking may

dx.doi.org/10.1021/jf505323g | J. Agric. Food Chem. 2015, 63, 250−261

change the conformation of proteins but the cleavage sites of digestive enzymes change little.

In summary, cooking had a significant effect on *in vitro* digestibility and pepsin digestion but not for pepsin/trypsin digestion. Characterized peptides showed the stochasticity of pepsin cleavage and the stability of trypsin cleavage. Although there was no significant difference in peptide profiles after two-step digestion, it could be significant for absorption and bioavailability in the live body, and additionally, some of the peptides could have bioactive functions.

■ ASSOCIATED CONTENT

Supporting Information

LC−MS information on peptide sequences from pepsin-treated and pepsin/trypsin-treated samples. This material is available free of charge via the Internet at http://pubs.acs.org.

■ AUTHOR INFORMATION

Corresponding Author

*Telephone: 86-25-84395679. E-mail: chunbao.li@njau.edu.cn.

Funding

This work was funded by Grants 31471600, NCET-11-0668, 20110097110024, and KYZ201119.

Notes

The authors declare no competing financial interest.

■ ACKNOWLEDGMENTS

The authors gratefully acknowledge Dr. Peiming Gu from Thermo Fisher Scientific for assisting in LC−MS analysis and Dr. Hongyu Ma from College of Plant Protection, Nanjing Agricultural University, for assisting in MALDI−ToF MS analysis.

■ ABBREVIATIONS USED

SDS−PAGE, sodium dodecyl sulfate−polyacrylamide gel electrophoresis; MALDI−ToF MS, matrix-assisted laser desorption/ionization−time-of-flight mass spectrometry; Nano LC-Q-Exactive-MS-MS, hybrid quadrupole orbitrap mass spectrometer equipped with a nanoelectrospray ionization source with an online nano-LC system

■ REFERENCES

(1) Wulf, D. M.; Morgan, J. B.; Tatum, J. D.; Smith, G. C. Effects of animal age, marbling score, calpastatin activity, subprimal cut, calcium injection, and degree of doneness on the palatability of steaks from limousin steers. *J. Agric. Food Chem.* **1996**, *74* (3), 569−576.

(2) Lorenzen, C. L.; Neely, T. R.; Miller, R. K.; Tatum, J. D.; Wise, J. W.; Taylor, J. F.; Buyck, M. J.; Reagan, J. O.; Savell, J. W. Beef customer satisfaction: Cooking method and degree of doneness effects on the top loin steak. *J. Anim. Sci.* **1999**, *77* (3), 637−644.

(3) Savell, J. W.; Lorenzen, C. L.; Neely, T. R.; Miller, R. K.; Tatum, J. D.; Wise, J. W.; Taylor, J. F.; Buyck, M. J.; Reagan, J. O. Beef customer satisfaction: Cooking method and degree of doneness effects on the top sirloin steak. *J. Anim. Sci.* **1999**, *77* (3), 645−652.

(4) Neely, T. R.; Lorenzen, C. L.; Miller, R. K.; Tatum, J. D.; Wise, J. W.; Taylor, J. F.; Buyck, M. J.; Reagan, J. O.; Savell, J. W. Beef customer satisfaction: Cooking method and degree of doneness effects on the top round steak. *J. Anim. Sci.* **1999**, *77* (3), 653−660.

(5) Jinap, S.; Mohd-Mokhtar, M. S.; Farhadian, A.; Hasnol, N. D. S.; Jaafar, S. N.; Hajeb, P. Effects of varying degrees of doneness on the formation of heterocyclic aromatic amines in chicken and beef satay. *Meat Sci.* **2013**, *94* (2), 202−207.

(6) Cotterchio, M.; Boucher, B. A.; Manno, M.; Gallinger, S.; Okey, A. B.; Harper, P. A. Red meat intake, doneness, polymorphisms in genes that encode carcinogen-metabolizing enzymes, and colorectal cancer risk. *Cancer Epidemiol., Biomarkers Prev.* **2008**, *17* (11), 3098−3107.

(7) Pereira, P. M.; Vicente, A. F. Meat nutritional composition and nutritive role in the human diet. *Meat Sci.* **2013**, *93*, 586−592.

(8) Santé-Lhoutellier, V.; Astruc, T.; Marinova, P.; Greve, E.; Gatellier, P. Effect of meat cooking on physicochemical state and *in vitro* digestibility of myofibrillar proteins. *J. Agric. Food Chem.* **2008**, *56* (4), 1488−1494.

(9) Bax, M. L.; Aubry, L.; Ferreira, C.; Daudin, J. D.; Gatellier, P.; Rémond, D.; Santé-Lhoutellier, V. Cooking temperature is a key determinant of *in vitro* meat protein digestion rate: Investigation of underlying mechanisms. *J. Agric. Food Chem.* **2012**, *60* (10), 2569−2576.

(10) Bax, M. L.; Sayd, T.; Aubry, L.; Ferreira, C.; Viala, D.; Chambon, C.; Rémond, D.; Santé-Lhoutellier, V. Muscle composition slightly affects *in vitro* digestion of aged and cooked meat: Identification of associated proteomic markers. *Food Chem.* **2013**, *136* (3), 1249−1262.

(11) Promeyrat, A.; Bax, M. L.; Traoré, S.; Aubry, L.; Santé-Lhoutellier, V.; Gatellier, P. Changed dynamics in myofibrillar protein aggregation as a consequence of heating time and temperature. *Meat Sci.* **2010**, *85* (4), 625−631.

(12) Davila, A. M.; Blachier, F.; Gotteland, M.; Andriamihaja, M.; Benetti, P. H.; Sanz, Y.; Tomé, D. Intestinal luminal nitrogen metabolism: role of the gut microbiota and consequences for the host. *Pharmacol. Res.* **2013**, *68* (1), 95−107.

(13) Guerra, A.; Etienne-Mesmin, L.; Livrelli, V.; Denis, S.; Blanquet-Diot, S.; Alric, M. Relevance and challenges in modeling human gastric and small intestinal digestion. *Trends Biotechnol.* **2012**, *30* (11), 591−600.

(14) Escudero, E.; Sentandreu, M. A.; Toldrá, F. Characterization of peptides released by *in vitro* digestion of pork meat. *J. Agric. Food Chem.* **2010**, *58* (8), 5160−5165.

(15) Daniel, H. Molecular and integrative physiology of intestinal peptide transport. *Annu. Rev. Physiol.* **2004**, *66*, 361−384.

(16) Dangin, M.; Guillet, C.; Garcia-Rodenas, C.; Gachon, P.; Bouteloup-Demange, C.; Reiffers-Magnani, K.; Fauquant, J.; Ballèvre, O.; Beaufrère, B. The rate of protein digestion affects protein gain differently during aging in humans. *J. Physiol.* **2003**, *549* (2), 635−644.

(17) Lametsch, R.; Kristensen, L.; Larsen, M. R.; Therkildsen, M.; Oksbjerg, N.; Ertbjerg, P. Changes in the muscle proteome after compensatory growth in pigs. *J. Anim. Sci.* **2006**, *84* (4), 918−924.

(18) Tornberg, E. Effects of heat on meat proteins—Implications on structure and quality of meat products. *Meat Sci.* **2005**, *70* (3), 493−508.

(19) Promeyrat, A.; Gatellier, P.; Lebret, B.; Kajak-Siemaszko, K.; Aubry, L.; Santé-Lhoutellier, V. Evaluation of protein aggregation in cooked meat. *Food Chem.* **2010**, *121*, 412−417.

(20) Bertram, H. C.; Wu, Z. Y.; Berg, F.; Andersen, H. J. NMR relaxometry and differential scanning calorimetry during meat cooking. *Meat Sci.* **2006**, *74* (4), 684−689.

(21) Kajak-Siemaszko, K.; Aubry, L.; Peyrin, F.; Bax, M. L.; Gatellier, P.; Astruc, T.; Przybylski, W.; Jaworska, D.; Gaillard-Martinie, B.; Santé-Lhoutellier, V. Characterization of protein aggregates following a heating and freezing process. *Food Res. Int.* **2011**, *44*, 3160−3166.

(22) Kaur, L.; Maudens, E.; Haisman, D. R.; Boland, M. J.; Singh, H. Microstructure and protein digestibility of beef: the effect of cooking conditions as used in stews and curries. *LWT—Food Sci. Technol.* **2014**, *55* (2), 612−620.

JOURNAL OF AGRICULTURAL AND FOOD CHEMISTRY

Article

pubs.acs.org/JAFC

Production of Chlorogenic Acid and Its Derivatives in Hairy Root Cultures of *Stevia rebaudiana*

Xiao Fu,[†,‡] Zhong-Ping Yin,[*,†,‡] Ji-Guang Chen,[†,‡] Xin-Chen Shangguan,[†] Xiaoqiang Wang,[†,§] Qing-Feng Zhang,[†,‡] and Da-Yong Peng[†]

[†]Jiangxi Key Laboratory of Natural Products and Functional Food and [‡]College of Food Science and Engineering, Jiangxi Agricultural University, Nanchang 330045, China

[§]Department of Biological Sciences, University of North Texas, Denton, Texas 76203, United States

ABSTRACT: Chlorogenic acid and its derivatives (CADs) are valuable bioactive plant secondary metabolites with many health benefits. In the present study, *Stevia rebaudiana* hairy root cultures were established, and the culture conditions for the production of CADs were optimized. The hairy roots were induced by coculture of *S. rebaudiana* leaves and *Agrobacterium rhizogenes* (C58C1) after infection, which were further verified by PCR detection of *rol*B and *rol*C genes. HPLC-MS and HPLC analysis showed that chlorogenic acid (3-caffeoylquinic acid, 3-CQA), 3,5-dicaffeoylquinic acid (3,5-CQA), and 4,5-dicaffeoylquinic acid (4,5-CQA) were the major CADs in the hairy roots. Eight single roots with rapid growth rate were selected. Among them, T3 had the highest yield of CADs. B5 medium supplemented with 40 g/L sucrose was more suitable for the production of CADs than others. Under optimal culture conditions, the total content of these three compounds reached 105.58 mg/g and total yield was 234.40 mg/100 mL.

KEYWORDS: *Stevia rebaudiana, hairy root, Agrobacterium rhizogenes, chlorogenic acid, phenylpropanoid*

INTRODUCTION

Stevia rebaudiana is a perennial herbaceous plant first found in South America.[1] The leaves of *S. rebaudiana* contain large amounts of sweet diterpenoid secondary metabolites, named steviol glycosides. Stevioside and rebaudioside A are the main sweet components of *S. rebaudiana* leaf.[2,3] With the increase of public concern with diabetes and obesity, *S. rebaudiana* has gradually become a main resource of commercial natural zero-calorie sweetener and is cultivated in many countries such as China, Korea, Brazil, the United States, Indonesia, and Canada.[4,5] Besides steviol glycosides, secondary metabolites such as polyphenols,[6,7] alkaloids,[8] sterols,[9] flavonoids,[10] triterpenoids,[9] and cardiac glycosides[11] are also found in *S. rebaudiana*. Compared with the high content of steviol glycosides, the amount of these bioactive components is much lower. Karaköse et al. identified 24 hydroxycinnamic acid derivatives of quinic and shikimic acid in *S. rebaudiana* leaves by LC-MS^n, and the contents of 3-caffeoylquinic acid (3-CQA), 3,5-dicaffeoylquinic acid (3,5-CQA), and 4,5-dicaffeoylquinic acid (4,5-CQA) were 35.5, 145.6, and 37.2 μg/g, respectively.[6]

Compared to conventional plant cultivation, which suffers from the limitation of cultivated land and climate, tissue culture (e.g., hairy root and cell suspension culture) is a promising approach to produce high-value plant secondary metabolites.[12] Hairy root cultures are genetically and biologically stable compared with cell suspension cultures and, furthermore, show vigorous growth in phytohormone-free medium.[13−15] Moreover, hairy root cultures often have greater capacity to produce secondary metabolites compared to their parent plants.[16] According to the research of Liu et al., *Echinacea purpurea* hairy root cultures were a possible way to produce caffeic acid derivatives, and the contents of cichoric acid, caftaric acid, and chlorogenic acid in these hairy roots were 19.21, 3.56, and 0.93 mg/g dry biomass, respectively.[17] It has been reported that overexpression of the AtPAP1 gene in *Platycodon grandiflorum* hairy roots caused significant increase of chlorogenic acid accumulation; the chlorogenic acid content was 421.31 μg/100 mg dry weight, which was 9.89 times higher than that of the control hairy root (42.60 μg/100 mg).[18]

In the present work, we establish *S. rebaudiana* hairy root cultures. HPLC-MS analysis of hairy root extracts was carried out, and three compounds, namely, 3-CQA, 3,5-CQA, and 4,5-CQA, were detected (Table 1). It was reported that these compounds have various bioactivities. Shin et al. examined the in vivo anti-inflammatory effects of 3-CQA using dextran sulfate sodium induced colitis in mice and found that 3-CQA dramatically improved colitis histological scores and thus might be used in the diet to prevent intestinal inflammation.[19] Cho et al. showed that 3-CQA was a potential bioactive compound for body weight reduction and lipid metabolism regulation in vivo.[20] Watanabe et al. investigated the blood pressure-lowering effect and safety of CADs through a randomized clinical trial, and their results suggested that these compounds were effective in decreasing blood pressure and safe for patients with mild hypertension.[21] According to Robinson et al., dicaffeoylquinic acids inhibited HIV-1 replication by inhibiting the integrase activity.[22] Xiong et al. reported that 3-CQA, 3,5-CQA. and 4,5-CQA all significantly suppressed the growth of *Staphylococcus aureus* and *Escherichia coli*.[23] To the best of our knowledge, there is no literature on the production of CADs by *S. rebaudiana* hairy root cultures.

Received: August 31, 2014
Revised: December 17, 2014
Accepted: December 18, 2014
Published: December 18, 2014

ACS Publications © 2014 American Chemical Society

DOI: 10.1021/jf504176r
J. Agric. Food Chem. 2015, 63, 262−268

Table 1. Linear Relationships of HPLC Analysis of Chlorogenic Acids and Its Derivatives

compound	regression eq	linearity range (μg/mL)	correlation factor (R^2)
3-caffeoylquinic acid	$Y = 28.052X - 121.540$	9.50−285.00	0.9997
3,5-dicaffeoylquinic acid	$Y = 24.989X - 82.588$	9.25−277.50	0.9995
4,5-dicaffeoylquinic acid	$Y = 27.167X - 162.680$	9.75−292.50	0.9992

Our results indicated that hairy root cultures of *S. rebaudiana* would be a promising approach to produce these bioactive compounds.

MATERIALS AND METHODS

Chemicals and Reagents. 3-CQA (HPLC grade, ≥98%), 3,5-CQA (HPLC grade, ≥97%), and 4,5-CQA (HPLC grade, ≥97%) were purchased from Tautobiotech (Shanghai, China). An *EasyPure* Plant Genomic DNA Kit, an *EasyPure* Plasmid MiniPrep Kit, and 2× TransTaq High Fidelity PCR SuperMix were purchased from TransGen Biotech (Beijing, China). The HPLC grade methanol (MeOH) was purchased from TEDIA (Fairfield, OH, USA).

***Stevia rebaudiana*.** The seeds of *S. rebaudiana* var. FengNong 3 were purchased from Suzhou, Anhui, China. The seeds were successively surface-sterilized with 70% ethanol for 30 s and 0.1% (w/v) mercuric chloride for 20 min. The sterile seeds were placed on 1/2MS medium (with 3% sucrose and 0.6% agar, pH 5.8 ± 0.2) and incubated under a 12/12 h (light/dark) photoperiod at 25 ± 1 °C. After 2−3 weeks of incubation, the aseptic seedlings were obtained.

***Agrobacterium rhizogenes*.** *A. rhizogenes* strain C58C1 was kindly provided by Prof. Guo-Yin Kai of Shanghai Normal University. *A. rhizogenes* was inoculated on solid YEB medium, which contained 50 mg/L of kanamycin (Kan) and incubated at 28 °C. Single colonies were picked up and transplanted into YEB liquid medium (supplemented with 50 mg/L of Kan) and then cultured in a shaker (Sukun, Shanghai, China) at 180 rpm and 28 °C for 24 h. *A. rhizogenes* culture was transferred into fresh medium and recultured for another 10 h. The cultured *A. rhizogenes* was collected by centrifugation at 5000 rpm for 10 min and then resuspended in 1/2MS liquid medium. The *A. rhizogenes* was precultured under the above-mentioned conditions for 30 min before use.

Induction of *Stevia rebaudiana* Hairy Root Cultures. The young leaves of aseptic *Stevia* seedlings were collected and precultured on the surface of 1/2MS solid medium containing 100 μmol/L acetosyringone (AS) for 2 days. These precultured explants were immersed in the culture medium of *A. rhizogenes* for 20 min, and then the surface bacteria and moisture were removed with sterile filter paper. The infected explants were placed on the surface of 1/2MS solid medium containing 100 μmol/L AS and cultured at 28 °C in the dark. After 2 days of cocultivation, the explants were transferred to 1/2MS solid medium supplemented with 500 mg/L cefotaxime sodium (Cef) to eliminate the residual bacteria. Adventitious roots appeared in the wound sites of explants in 3 weeks after infection. A single root was excised and cultured on the 1/2MS solid medium containing Cef (500 mg/L). After bacteria were eliminated, hairy roots were transferred into 1/2MS liquid medium for subculture.

Screening of Hairy Roots. Hairy roots with high growth rate were selected for further studies. Half a gram of hairy roots was inoculated in a 250 mL Erlenmeyer flask containing 100 mL of 1/2MS liquid medium (with 3% sucrose, pH 5.8 ± 0.2) and then cultured in a shaker at 115 rpm and 28 ± 2 °C in the dark for 24 days. The hairy roots were collected after 24 days of culture, and the fresh weight (FW) was determined after the hairy roots were rinsed with tap water and the excessive water was removed with filter paper. The hairy roots were dried at 60 °C until a constant dry weight (DW) was obtained. CAD content was determined by HPLC. Hairy root lines that contained more TP-CADs (total production of chlorgenic acid and its derivatives in 100 mL of medium, which was calculated by multiplying the content sum of 3-CQA, 3,5-CQA, and 4,5-CQA with the dry biomass weight) were selected for further experiments.

Confirmation of Hairy Roots. Plasmid DNA of *A. rhizogenes*, total DNA of hairy roots, and total DNA of untransformed roots were extracted with SDS reagent by following the manufacturer's instructions (TransGen Biotech, Beijing, China). PCR amplification was performed in a 50 μL reaction mixture containing 50 ng of templates DNA, 0.4 μM of each primer, and 25 μL of 2× *EasyTaq* PCR SuperMix (containing Taq DNA polymerase, $MgCl_2$, and dNTP). The forward and reverse primer sequences for *rol*B gene amplification were 5′-GCTCTTGCAGTGCTAGATTT-3′ and 5′-GAAGGTGCAAGCTACCTCTC-3′, and those for *rol*C gene amplification were 5′-CTCCTGACATCAAACTCGTC-3′ and 5′-TGCTTCGAGTTATGGGTACA-3′, respectively. The procedure of PCR was as follows: the first cycle was performed at 94 °C for 5 min, followed by 35 cycles of 94 °C for 45 s, 60 °C for 45 s, 72 °C for 60 s, and the final extension was 10 min at 72 °C. PCR products were analyzed by electrophoresis separation.

Extraction of CADs. Hairy roots were ground into fine powder after drying. Two hundred milligrams of hairy root powder was extracted by ultrasonic method in 4 mL of 70% ethanol twice. The supernatant was collected and combined after centrifugation for 10 min at 5000 rpm. Its volume was accurately adjusted to 10 mL with distilled water. After filtering through 0.22 mm pore size filter, the sample solution was used for HPLC and HPLC-ESI-MS analysis.

Qualitative and Quantitative Analysis of CADs. CADs in the hairy roots were identified by HPLC-ESI-MS (6430 HPLC-MS system; Aglient Technologies, Santa Clara, CA, USA) and quantified by HPLC (1260 HPLC system; Aglient Technologies). The HPLC parameters were as follows: chromatographic column, Waters Symmetry C_{18} column (4.6 mm × 250 mm, 5 μm; Waters, Milford, MA, USA); mobile phase, 0.2% acetic acid (A) and methanol (B); flow rate, 1 mL/min; elution procedure, 0−10 min, 70% A; 10−15 min, 70−45% A; 15−25 min, 45% A; 25−26 min, 45−70% A; 26−30 min, 70% A; detection wavelength, 327 nm; column temperature, 40 °C; volume of sample injection, 10 μL. Authentic compounds (3-CQA, 3,5-CQA, and 4,5-CQA) were dissolved in MeOH; the concentrations were adjusted to 9.50−285.00, 9.25−277.50, and 9.75−292.50 μg/mL, respectively, and the calibration curves were established under the same determination conditions. HPLC-ESI-MS analysis was performed in negative mode according to the method of Sun et al.[24]

Optimization of Culture Conditions. Half a gram of T3 hairy roots was inoculated into 250 mL Erlenmeyer flasks that contained 100 mL of 1/2MS liquid medium supplemented with 30 g/L of different sugars (maltose, glucose, sucrose, or fructose) or 100 mL of different media (MS 1/2MS, B5, 1/2B5, WPM, or 1/2WPM) supplemented with 30 g/L of sucrose, or 100 mL of B5 liquid medium supplemented with different concentrations of sucrose (10, 20, 30, 40, 50, or 60 g/L), respectively. All of the hairy roots were cultured under the same conditions described above, and FW, DW, and CAD content were determined.

Dynamic Characteristics of Hairy Root Growth and CAD Accumulation. The growth curve and CAD accumulation curve of T3 hairy root were established according to the change of FW, DW, and CAD content during a growth cycle. Half a gram of T3 hairy roots was inoculated in a 250 mL Erlenmeyer flask that contained 100 mL of B5 liquid medium supplemented with 40 g/L sucrose and then cultured for 36 days under the aforementioned conditions. FW, DW, and CAD content were determined every 3 days during the growth cycle.

Data Statistics and Analysis. The results were given as mean values ± standard deviations (SD). Data were analyzed by the DPS 6.55 statistical software, and statistical analysis was performed using the ANOVA followed by Tukey's test (at $P \leq 0.01$).

DOI: 10.1021/jf504176r
J. Agric. Food Chem. 2015, 63, 262−268

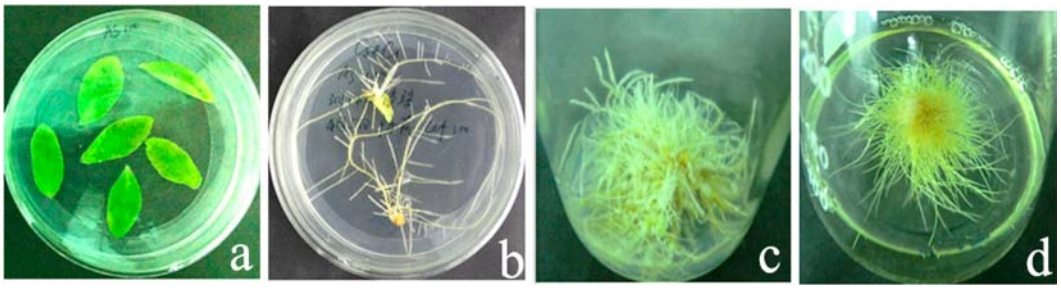

Figure 1. Establishment of *Stevia rebaudiana* hairy root cultures: (a) preculture of *S. rebaudiana* leaves on 1/2MS medium supplemented with 100 μmol/L of AS; (b) hairy roots grew from infected explants (1/2MS medium supplemented with 100 mg/L of Cef); (c) hairy roots cultured on 1/2MS solid medium; (d) hairy roots cultured in 1/2MS liquid medium.

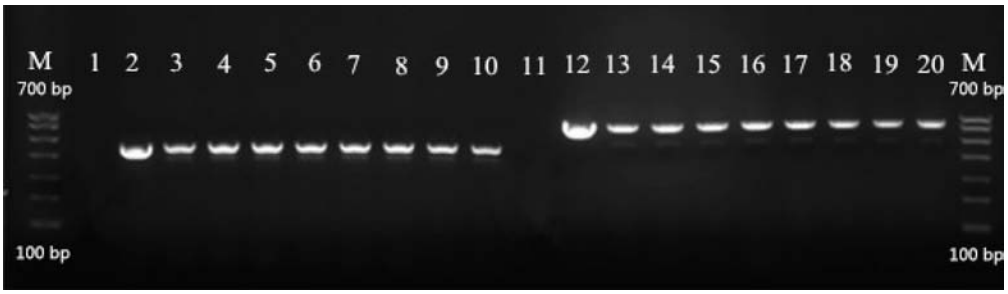

Figure 2. PCR analysis of the *rol*B and *rol*C genes in the hairy root lines of *Stevia rebaudiana*. Lanes: M, marker (from 100 to 700 bp); 1 and 11, DNA from nontransformed roots (negative control); 2 and 12, Ri plasmid DNA (positive control); 3−10 and 13−20, DNA from T1, T3, T4, T5, T9, T14, T16, and T17 strains induced by *Agrobacterium rhizogenes*. *RolB* genes are shown in lanes 1−10, and *rolC* genes are shown in lanes 11−20.

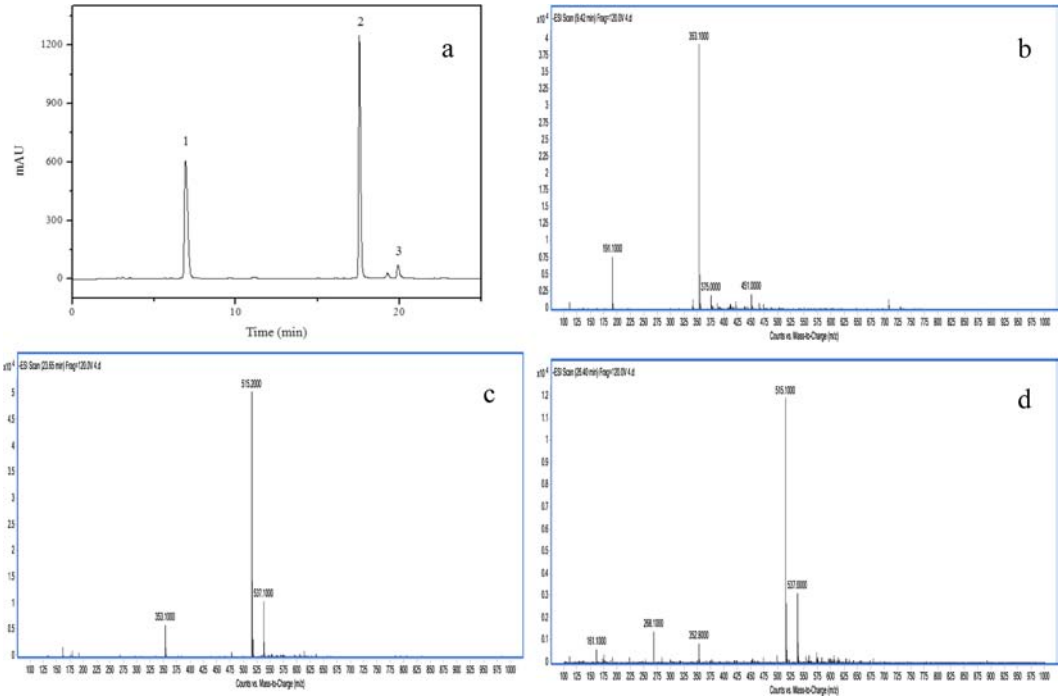

Figure 3. HPLC chromatograms and mass spectra of hairy root extracts: (a) HPLC chromatogram of hairy root extracts; (b) mass spectrum of peak 1 shown in the HPLC chromatogram; (c) mass spectum of peak 2 shown in the HPLC picture; (d) mass spectrum of peak 3 shown in the HPLC picture. Peaks 1 (6.877 min, *m*/*z* 353.1) was identified as 3-CQA ($C_{16}H_{18}O_9$), peak 2 (17.553 min, *m*/*z* 515.2) was identified as 3,5-CQA ($C_{25}H_{24}O_{12}$), and peak 3 (19.908 min, *m*/*z* 515.1) was identified as 4,5-CQA ($C_{25}H_{24}O_{12}$). HPLC chromatogram was obtained at 327 nm.

RESULTS AND DISCUSSION

Establishment of Transgenic Hairy Root Lines. Coculture is a method commonly used to induce hairy roots, by which hairy roots are induced from wounded explants when they were cocultured with *A. rhizogenes*. The sterilized *S. rebaudiana* explants (young leaves) were infected by *A. rhizogenes* C58C1 after 2 days of preculture. Hairy root cultures were generated from the wounds of infected explants in the third week after infection, which showed high branching and no geotropism (Figure 1b). No similar root was observed in the

DOI: 10.1021/jf504176r
J. Agric. Food Chem. 2015, 63, 262−268

control. Sujatha et al. reported that *Artemisia vulgaris* hairy roots were generated in 2 weeks after cocultivation, and no hairy roots appeared in the control group.[25] According to Kúzma's investigation, hairy roots grew from the wounded and infected sites of *Salvia austriaca* explants in 2 weeks after infection and continued to grow to the fourth week.[26] Single root tips (2−3 cm long) were excised and cultured on 1/2MS hormone-free solid medium. The root tips grew rapidly (as shown in Figure 1c). After several successive subcultures, there was no visible bacterium on the surface of medium, indicating that the residual bacteria had been clearly removed. The bacterium-free root tips were transferred into 1/2MS liquid medium for suspension culture (Figure 1d).

Confirmation of Hairy Roots by PCR. *Rol* genes are the important Ri plasmid genes of *A. rhizogenes* and play a vital role in hairy root induction. Therefore, *rol* genes are commonly used as reference genes to confirm the hairy roots. In the present paper, eight hairy root samples, Ri plasmid (positive control), and uninduced root (negative control, from germ-free *S. rebaudiana* seedling) were analyzed by PCR. The results (Figure 2) showed that *rol*B (lanes 3−10 in Figure 2) and *rol*C (lanes 13−20) were present in all eight hairy root samples, as well as in the positive control (lanes 2 and 12). However, these genes were absent in the roots excised from nontransformed plants (lanes 1 and 11). The results indicated that the *rol* genes were successfully inserted into the genome of *S. rebaudiana*.

Qualitative Analysis of CADs. The extracts of *S. rebaudiana* hairy roots were analyzed by HPLC-ESI-MS and HPLC. The results indicated that there were three major compounds in the extracts (Figure 3a). These compounds were identified as chlorgenic acid (peak 1) and dicaffeoylquinic acid (peaks 2 and 3) by their pseudomolecular ions at m/z 353 $[M - H]^-$, 515 $[M - H]^-$, and 515 $[M - H]^-$, respectively. We further confirmed that the three compounds were 3-CQA (peak 1), 3,5-CQA (peak 2), and 4,5-CQA (peak 3), respectively, by standard addition of authentic standards.

It has been reported that the biosynthesis of steviol glycosides is limited to green tissues in *S. rebaudiana*. Steviol is produced in the plastids and endoplasmic reticulum and glycosylated by UDP-glucosyltransferases in the cytoplasm; the steviol glycosides are then stored in vacuoles.[27] It is not surprising that no steviol glycoside was detected in the hairy root cultures because the biosynthetic genes were probably not expressed in roots. To overcome such problems, we will need to overexpress key genes of the biosynthetic pathway in the hairy roots. Certainly other parameters may also play roles for producing secondary metabolites, such as the available oxygen, nutrients, light, water, and pH. These growth conditions in the shake flask culture of hairy roots were dramatically different from those of field growth, and the notable difference may cause the silence of the critical genes of steviol glycoside synthesis. The insert of exogenous gene(s) from *A. rhizogenes* may also result in the change of gene expressing and thus lead to the absence of steviol glycoside.

Screening of High-Producing Hairy Root Lines. Eight hairy root lines with typical phenotype and high growth rate were selected from the induced hairy roots at the beginning. These hairy root lines were further confirmed by PCR detection of *rol*B and *rol*C genes. To get the lines with high production of CADs, the eight roots were further screened by the determination of FW, DW, and CAD content after 24 days of culture (Figure4). Among the eight roots, T3 exhibited the highest growth rate, followed by T17. The FW and DW of T3

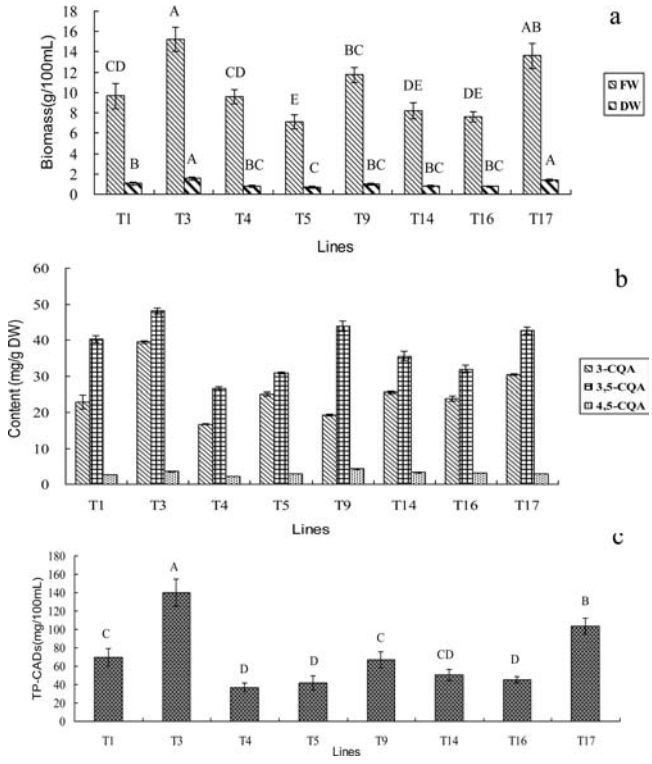

Figure 4. Biomass accumulation and CAD production of eight hairy root lines: (a) biomass accumulation of eight hairy root strains; (b) content of 3-CQA, 3,5-CQA, and 4,5-CQA in eight hairy root strains; (c) TP-CADs of eight hairy root strains. Half a gram of hairy roots was inoculated in 250 mL Erlenmeyer flasks containing 100 mL of 1/2MS liquid medium supplemented with 30 g/L sucrose. Each experiment was repeated five times. TP-CADs is the summation production of 3-CQA, 3,5-CQA, and 4,5-CQA.

were 15.23 and 1.54 g/100 mL, respectively, which increased over 30 times after 24 days of culture. According to the results of HPLC analysis, T3 hairy roots had the highest contents of 3-CQA (39.41 mg/g) and 3,5-CQA (48.10 mg/g), whereas T9 contained more 4,5-CQA (4.29 mg/g). For each line, 3,5-CQA was the most abundant compound, followed by 3-CQA. The content of 4,5-CQA was much lower than those of 3,5-CQA and 3-CQA. In terms of TP-CADs, T3 was the optimal line. Its TP-CADs (140.36 mg/100 mL) is significantly higher than that of other lines. Therefore, T3 was selected as the optimal one for further experiments.

Optimization of Culture Conditions on Biomass Accumulation and TP-CADs. It is widely believed that sucrose is a suitable carbon source for the biosynthesis of secondary metabolites in the cultivation of plant in vitro systems.[28] In the present paper, the effects of maltose, glucose, sucrose, and fructose on biomass accumulation and TP-CADs of T3 hairy root were compared. Our results confirmed that sucrose was the most suitable carbon source.

Furthermore, the effect of sucrose concentration (10−60 g/L) on biomass accumulation and TP-CADs of T3 hairy roots was also investigated. The highest biomass accumulation was achieved in 40 g/L of sucrose, and the FW and DW were 17.93 and 2.34 g/100 mL, respectively (Figure 5a). The slow growth of hairy roots in the medium with sucrose lower than 40 g/L might be caused by the lack of energy substance. However, the inhibition of growth in higher concentration of sucrose might result from the high osmotic stress. Similar to our study, the

DOI: 10.1021/jf504176r
J. Agric. Food Chem. 2015, 63, 262−268

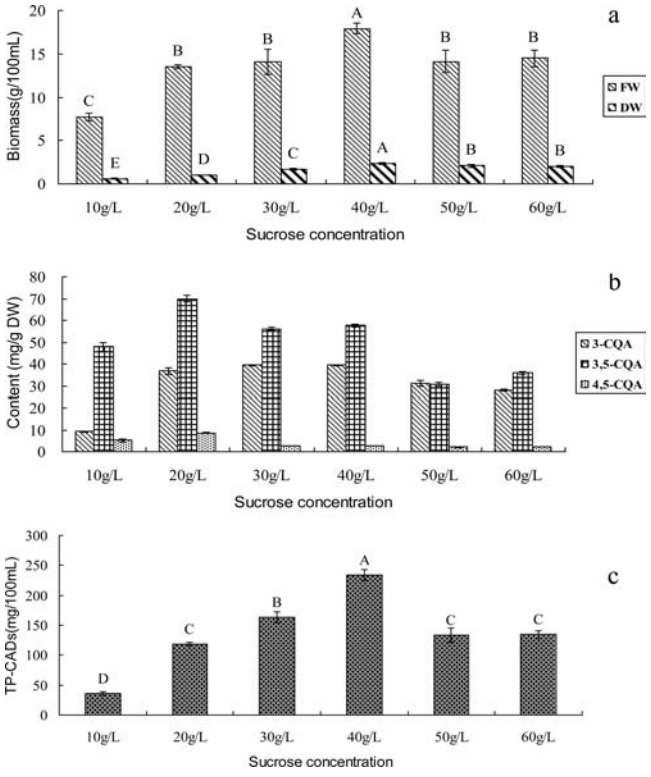

Figure 5. Effect of sucrose concentrations on biomass and CAD accumulation of T3: (a) biomass accumulation of T3 cultured in medium supplemented with 10, 20, 30, 40, 50, or 60 g/L sucrose, respectively; (b) content of 3-CQA, 3,5-CQA, and 4,5-CQA of T3 cultured in medium supplemented with 10, 20, 30, 40, 50, or 60 g/L sucrose, respectively; (c) TP-CADs of T3 cultured in medium supplemented with 10, 20, 30, 40, 50, or 60 g/L sucrose, respectively. Half a gram of hairy roots was inoculated in 250 mL Erlenmeyer flasks containing 100 mL of B5 liquid medium, which were supplemented with 10, 20, 30, 40, 50, or 60 g/L sucrose, respectively. Each experiment was repeated five times.

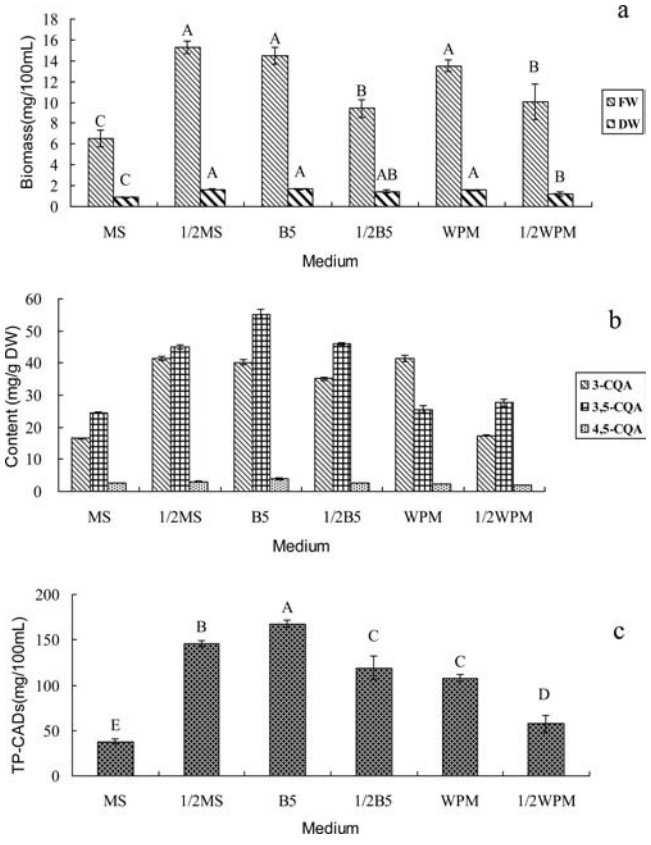

Figure 6. Effect of medium on biomass and CAD accumulation of T3: (a) biomass accumulation of T3 cultured in different media; (b) content of 3-CQA, 3,5-CQA, and 4,5-CQA of T3 cultured in different media; (c) TP-CADs of T3 cultured in different media. Half a gram of hairy roots was inoculated in 250 mL Erlenmeyer flasks containing 100 mL of MS, 1/2MS, B5, 1/2B5, WPM, or 1/2WPM liquid medium, respectively. All of the media were supplemented with 30 g/L sucrose. Each experiment was repeated five times.

highest biomass accumulation of *A. vulgaris* hairy roots was obtained in 1/2MS medium supplemented with 40 g/L sucrose.[25] The highest content of 3-CQA (39.45 mg/g) was achieved in B5 medium with 30 g/L sucrose. However, for 3,5-CQA and 4,5-CQA, the highest contents were obtained with 20 g/L sucrose, which were 69.45 and 8.63 mg/g, respectively (Figure 5b). In consideration of both biomass and metabolite content, the highest TP-CADs (233.54 mg/100 mL) were achieved in 40 g/L sucrose (Figure 5c). The results indicated that 40 g/L sucrose was the optimal concentration for both growth and TP-CADs of *S. rebaudiana* hairy roots. It has been reported that high content of caffeic acid derivatives was obtained in MS medium supplemented with 30 g/L sucrose by *E. purpurea* hairy root cultures.[17] Wu et al. used 1/2MS medium with 50 g/L sucrose to cultivate adventitious roots of *E. purpurea* in a 1000 L airlift bioreactor and obtained 5 mg of chlorogenic acid, 22 mg of chichoric acid, and 4 mg of caftaric acids per gram of roots (DW).[29]

Culture medium was one of the most important factors in the accumulation of secondary metabolites of in vitro cultures.[28,30] In the present study, the effects of three commonly used media with two different concentrations on the production of CADs were compared (Figure 6). The results showed that 1/2MS, B_5, and WPM were all suitable for T3 hairy root growth; although the highest DW (1.69 g/100 mL) was obtained in B5 medium, no significant difference was observed among these three media (Figure 6a). The highest contents of 3-CQA, 3,5-CQA, and 4,5-CQA were obtained in 1/2MS (41.33 mg/g), B5 (55.24 mg/g), and B5 medium (3.88 mg/g), respectively (Figure 6b). For TP-CADs, B5 was the most suitable culture medium with production of 167.78 mg/100 mL (Figure 6c). Therefore, B5 was selected as the optimal culture medium for *S. rebaudiana* hairy root growth and CAD production. Similar to our study, B5 medium was found to be fit for *Scutellaria baicalensis* hairy root growth, and the baicalin content of dry root cultured in this medium was 14.1−30.0%, which was significantly higher than that of the control (field-grown roots).[31]

Growth Kinetics of Hairy Root Cultures and TP-CADs. The time course of *S. rebaudiana* hairy root growth in B5 liquid medium is shown in Figure 7a. The whole growth cycle could be divided into four stages: adaptive phase (0−6th day), exponential phase (6−24th day), stationary phase (24−30th day), and decline phase (after the 30th day). The highest biomass accumulation appeared in the 24−27th days, and the DW reached 2.22 g/100 mL, which was over 48 times that in inoculation. The hairy roots changed to brown, and the liquid culture medium gradually darkened after 30 days. Similar results were reported by Cesar et al., and they obtained the highest DW of muscadine grape hairy roots at the 21st day with

DOI: 10.1021/jf504176r
J. Agric. Food Chem. 2015, 63, 262−268

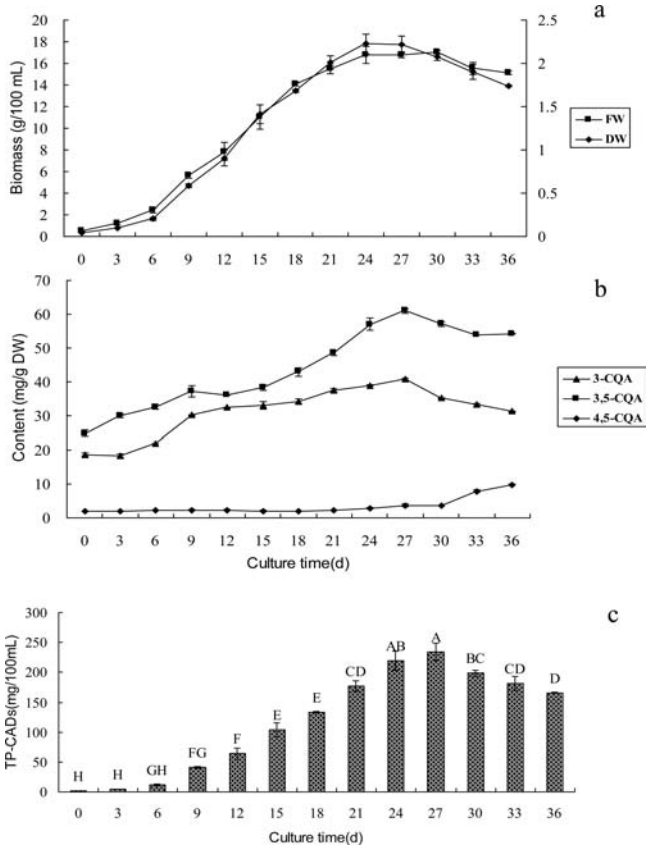

Figure 7. Time course of growth and CAD production of *Stevia rebaudiana* hairy roots: (a) time course of growth of hairy roots; (b) time course of the contents of 3-CQA, 3,5-CQA, and 4,5-CQA of hairy roots; (c) time course of TP-CADs of hairy roots. Half a gram of hairy roots was inoculated in 250 mL Erlenmeyer flasks containing 100 mL of B5 liquid medium supplemented with 40 g/L sucrose. Hairy roots were collected every 3 days. Each experiment was repeated three times.

BDS medium and at the 27th day with BDS+GR medium.[32] The highest contents of 3-CQA (40.85 mg/g) and 3,5-CQA (61.03 mg/g) were achieved at the 27th day after inoculation. However, the highest 4,5-CQA content (9.81 mg/g) was achieved at the 36th day (Figure 7b). We obtained the highest TP-CADs at the 27th day after inoculation (Figure 7c), which was 234.40 mg/100 mL. Therefore, hairy root cultures of *S. rebaudiana* provide an attractive alternative and sustainable approach to produce CADs.

In conclusion, the hairy root cultures of *S. rebaudiana* for the production of CADs were first reported. Three secondary metabolites, 3-CQA, 3,5-CQA, and 4,5-CQA, were identified and quantified in the hairy roots. B5 medium supplemented with 40 g/L sucrose was the best culture condition for CAD production, and the best harvest date of hairy root was the 27th day after inoculation. Our results suggest that the hairy root cultures of *S. rebaudiana* are promising for the large-scale production of CADs.

AUTHOR INFORMATION

Corresponding Author

*(Z.-P.Y.) E-mail: yin_zhongping@163.com. Phone/fax: +86 791 83813863.

Funding

We are grateful for the financial support of research projects from the Natural Science Foundation of PR China (No. 31260368), Natural Science Foundation of Jiangxi Province of China (No. 20132BAB204004), and Graduate Innovation Fund of Jiangxi Agricultural University (NDYC2013-S003).

Notes

The authors declare no competing financial interest.

ACKNOWLEDGMENTS

We acknowledge the HPLC-ESI-MS technical assistance of Sun Yong, University of Nanchang, Jiangxi, China.

ABBREVIATIONS USED

MS, Murashige Skoog medium; B5, B5 medium; WPM, woody plant medium; 1/2MS, 1/2B5 and 1/2WPM media were macroelement in half compared to MS, B5, and WPM media; AS, acetosyringone; Cef, cefotaxime sodium; 3-CQA, 3-caffeoylquinic acid; 3,5-CQA, 3,5-dicaffeoylquinic acid; 4,5-CQA, 4,5-dicaffeoylquinic acid; CADs, chlorogenic acid and its derivatives; TP-CADs, total production of chlorogenic acid and its derivatives

REFERENCES

(1) Brandle, J. E.; Starratt, A. N.; Gijzen, M. *Stevia rebaudiana*: its agricultural, biological, and chemical properties. *Can. J. Plant Sci.* **1998**, *78*, 527−536.

(2) Crammer, B.; Ikan, R. Sweet glycosides from the *Stevia* plant. *Chem. Br.* **1986**, *22*, 915−916.

(3) Montoro, P.; Molfetta, I.; Maldini, M.; Ceccarini, L.; Piacente, S.; Pizza, C.; Macchia, M. Determination of six steviol glycosides of *Stevia rebaudiana* (Bertoni) from different geographical origin by LC−ESI−MS/MS. *Food Chem.* **2013**, *141*, 745−753.

(4) Yadav, S. K.; Guleria, P. Steviol glycosides from *Stevia*: biosynthesis pathway review and their application in foods and medicine. *Crit. Rev. Food Sci. Nutr.* **2012**, *52*, 988−998.

(5) Megeji, N. W.; Kumar, J. K.; Singh, V.; Kaul, V. K.; Ahuja, P. S. Introducing *Stevia rebaudiana*, a natural zero-calorie sweetener. *Curr. Sci.* **2005**, *88*, 801−804.

(6) Karaköse, H.; Jaiswal, R.; Kuhnert, N. Characterization and quantification of hydroxycinnamate derivatives in *Stevia rebaudiana* leaves by LC-MS^n. *J. Agric. Food Chem.* **2011**, *59*, 10143−10150.

(7) Kim, I. S.; Yang, M.; Lee, O. H.; Kang, S. N. The antioxidant activity and the bioactive compound content of *Stevia rebaudiana* water extracts. *LWT−Food Sci. Technol.* **2011**, *44*, 1328−1332.

(8) Michalika, A.; Hollinsheada, J.; Jones, L.; Fleet, G. W. J.; Yu, C. Y.; Hu, X. G.; Well, R. V.; Horne, G.; Wilson, F. X.; Kato, A.; Jenkinson, S. F.; Nash, R. J. Steviamine, a new indolizidine alkaloid from *Stevia rebaudiana*. *Phytochem. Lett.* **2010**, *3*, 136−138.

(9) Ibrahim, N. A.; El-Gengaihi, S.; Motawe, H.; Riad, S. A. Phytochemical and biological investigation of *Stevia rebaudiana* Bertoni; 1-labdane-type diterpene. *Eur. Food Res. Technol.* **2007**, *224*, 483−488.

(10) Amriteswori, R.; Margaret, F. R. The flavonoids of *Stevia rebaudiana*. *J. Nat. Prod.* **1983**, *46*, 194−195.

(11) Manish, T.; Subhash, R. Preliminary studies on *Stevia rebaudiana* leaves: proximal composition, mineral analysis and phytochemical screening. *J. Med. Sci.* **2006**, *6*, 321−326.

(12) Srivastava, S.; Srivastava, A. K. Hairy root culture for mass-production of high-value secondary metabolites. *Crit. Rev. Biotechnol.* **2007**, *27*, 29−43.

(13) Srivastava, V.; Kaur, R.; Chattopadhyay, S. K.; Banerjee, S. Production of indus-trially important cosmaceutical and pharmaceutical derivatives of betuligenol by *Atropa belladonna* hairy root mediated biotransformation. *Ind. Crops Prod.* **2013**, *44*, 171−175.

(14) Giri, A.; Narasu, M. L. Transgenic hairy roots: recent trends and applications. *Biotechnol. Adv.* **2000**, *18*, 1−22.

DOI: 10.1021/jf504176r
J. Agric. Food Chem. 2015, 63, 262−268

(15) Washida, D.; Shimomura, K.; Takido, M.; Kitanaka, S. Auxins affected ginsenoside production and growth of hairy roots in *Panax hybrid*. *Biol. Pharm. Bull.* **2004**, *27*, 657−660.
(16) Kim, Y. J.; Wyslouzil, B. E.; Weathers, P. J. Secondary metabolism of hairy root cultures in bioreactors. *In Vitro Cell. Dev. Biol.: Plant* **2002**, *38*, 1−10.
(17) Liu, C. Z.; Abbasi, B. H.; Gao, M.; Murch, S. J.; Saxena, P. K. Caffeic acid derivatives production by hairy root cultures of *Echinacea purpurea*. *J. Agric. Food Chem.* **2006**, *54*, 8456−8460.
(18) Tuan, P. A.; Kwon, D. Y.; Lee, S.; Arasu, M. V.; Al-Dhabi, N. A.; Park, N.; Park, S. U. Enhancement of chlorogenic acid production in hairy roots of *Platycodon grandiflorum* by over-expression of an *Arabidopsis thaliana* transcription factor AtPAP1. *Int. J. Mol. Sci.* **2014**, *15*, 14743−14752.
(19) Shin, H. S.; Satsu, H.; Bae, M. J.; Zhao, Z.; Ogiwara, H.; Totsuka, M.; Shimizu, M. Anti-inflammatory effect of chlorogenic acid on the IL-8 production in Caco-2 cells and the dextran sulphate sodium-induced colitis symptoms in C57BL/6 mice. *Food Chem.* **2015**, *168*, 167−175.
(20) Cho, A. S.; Jeon, S. M.; Kim, M. J.; Yeo, J.; Seo, K. I.; Choi, M. S.; Lee, M. K. Chlorogenic acid exhibits anti-obesity property and improves lipid metabolism in high-fat diet-induced-obese mice. *Food Chem. Toxicol.* **2010**, *48*, 937−943.
(21) Watanabe, T.; Arai, Y.; Mitsui, Y.; Kusaura, T.; Okawa, W.; Kajihara, Y.; Saito, I. The blood pressure-lowering effect and safety of chlorogenic acid from green coffee bean extract in essential hypertension. *Clin. Exp. Hypertens.* **2006**, *28*, 439−449.
(22) Robinson, W. E., Jr.; Reinecke, M. G.; Abdel-Malek, S.; Jia, Q.; Chow, S. A. Inhibitors of HIV-1 replication that inhibit HIV integrase. *Proc. Natl. Acad. Sci. U.S.A.* **1996**, *93*, 6326−6331.
(23) Xiong, J.; Li, S.; Wang, W.; Hong, Y.; Tang, K.; Luo, Q. Screening and identification of the antibacterial bioactive compounds from *Lonicera japonica* Thunb. leaves. *Food Chem.* **2013**, *138*, 327−333.
(24) Sun, Y.; Li, H. Y.; Hu, J. N.; Li, J.; Fan, Y. W.; Liu, X. R.; Deng, Z. Y. Qualitative and quantitative analysis of phenolics in *Tetrastigma hemsleyanum* and their antioxidant and antiproliferative activities. *J. Agric. Food Chem.* **2013**, *61*, 10507−10515.
(25) Sujatha, G.; Zdravković-Korać, S.; Ćaliać, D.; Flamini, G.; Ranjitha Kumari, B. D. High-efficiency *Agrobacterium rhizogenes*-mediated genetic transformation in *Artemisia vulgaris*: hairy root production and essential oil analysis. *Ind. Crops Prod.* **2013**, *44*, 643−652.
(26) Kúzma, Ł.; Kisiel, W.; Królicka, A.; Wysokínska, H. Genetic transformation of *Salvia austriaca* by *Agrobacterium rhizogenes* and diterpenoid isolation. *Pharmazie* **2011**, *66*, 904−907.
(27) Brandle, J. E.; Telmer, P. G. Steviol glycoside biosynthesis. *Phytochemistry* **2007**, *68*, 1855−1863.
(28) Thiruvengadam, M.; Praveen, N.; Kim, E. H.; Kim, S. H.; Chung, I. M. Production of anthraquinones, phenolic compounds and biological activities from hairy root cultures of *Polygonum multiflorum* Thunb. *Protoplasma* **2014**, *251*, 555−566.
(29) Wu, C. H.; Murthy, H. N.; Hahn, E. J.; Paek, K. Y. Large-scale cultivation of adventitious roots of *Echinacea purpurea* in airlift bioreactors for the production of chichoric acid, chlorogenic acid and caftaric acid. *Biotechnol. Lett.* **2007**, *29*, 1179−1182.
(30) Rao, S. R.; Ravishankar, G. A. Plant cell cultures: chemical factories of secondary metabolites. *Biotechnol. Adv.* **2002**, *20*, 101−153.
(31) Tiwari, R. K.; Trivedi, M.; Guang, Z. C.; Guo, G. Q.; Zheng, G. C. *Agrobacterium rhizogenes* mediated transformation of *Scutellaria baicalensis* and production of flavonoids in hairy roots. *Biol. Plant.* **2008**, *52*, 26−35.
(32) Nopo-Olazabal, C.; Hubstenberger, J.; Nopo-Olazabal, L.; Medina-Bolivar, F. Antioxidant activity of selected stilbenoids and their bioproduction in hairy root cultures of muscadine grape (*Vitis rotundifolia* Michx.). *J. Agric. Food Chem.* **2013**, *61*, 11744−11758.

DOI: 10.1021/jf504176r
J. Agric. Food Chem. 2015, 63, 262−268

JOURNAL OF AGRICULTURAL AND FOOD CHEMISTRY

Article

pubs.acs.org/JAFC

β-(1 → 3)-Glucanolytic Yeasts from Brazilian Grape Microbiota: Production and Characterization of β-Glucanolytic Enzymes by *Aureobasidium pullulans* 1WA1 Cultivated on Fungal Mycelium

Anelize Bauermeister,[†] Ismael R. Amador,[†] Carla P. Pretti,[†] Ellen C. Giese,[‡,§] André L. M. Oliveira,[†] Mário A. Alves da Cunha,[∥] Maria Inês Rezende,[†] Robert F. H. Dekker,*[,‡,⊥] and Aneli M. Barbosa*[,†,‡]

[†]Departamento de Bioquímica e Biotecnologia, Centro de Ciências Exatas (CCE), Universidade Estadual de Londrina, Londrina, Paraná 86051-990, Brazil

[‡]Biorefining Research Institute, Lakehead University, Thunder Bay, Ontario, Canada P7B 5E1

[∥]Departamento de Química, Universidade Tecnológica Federal do Paraná, Bairro Fraron, Pato Branco, Paraná 85503-390, Brazil

[⊥]Biorefining and Biotechnology Consultancy, Rua João Huss 200, Gleba Palhano, Londrina, Paraná 86050-490, Brazil

Supporting Information

ABSTRACT: A total of 95 yeast strains were isolated from the microbiota of different grapes collected at vineyards in southern Brazil. The yeasts were screened for β-(1 → 3)-glucanases using a newly developed zymogram method that relies upon the appearance of clearance zones around growing colonies cultured on agar−botryosphaeran medium and also by submerged fermentation on nutrient medium containing botryosphaeran, a (1 → 3),(1 → 6)-β-D-glucan. Among 14 β-(1 → 3)-glucanase-positive yeasts identified, four strains produced the highest β-glucanolytic activities and were evaluated for enzyme production on cellobiose, botryosphaeran, and mycelial biomass from *Botryosphaeria rhodina* (MAMB-05). Yeast strain 1WA1 produced the highest β-(1 → 3)-glucanase and β-glucosidase activities and was identified by molecular characterization as *Aureobasidium pullulans*. The physicochemical properties of the crude β-glucanolytic enzyme preparation were characterized, and the preparation was used to hydrolyze several β-D-glucans (laminarin, botryosphaeran, lasiodiplodan, pustulan, and curdlan). The production and physicochemical properties of the β-glucanolytic preparation enable its potential applications in wine enology and production of prebiotics through hydrolysis of β-D-glucans.

KEYWORDS: *grape microbiota yeasts, Aureobasidium pullulans, Botryosphaeria rhodina, β-D-glucans, β-(1 → 3)-glucanases, β-glucosidases, botryosphaeran*

INTRODUCTION

The fruiting body of grapes constitutes a biôme (phytophyllosphere) of complex microbiota colonizing the skin of the grape berry that includes bacteria and filamentous fungi, among which are yeasts. Their presence in grape must used to make wine can exert sensorial features on the wines produced.[1] These microbial consortia may constitute an important source of enzymes that can be applied to wine oenology and food and beverage processing. In this special category are the β-glucosidases that have been demonstrated in playing a role in releasing flavors and aromas in wines through their cleavage of monoterpene glucosides into monoterpenes.[2] Wines left to age on the lees (*sur lie*) result in autolysis of the sedimented yeast cells as a consequence of enzymatic hydrolysis of the cell wall (1 → 3),(1 → 6)-β-D-glucans by yeast β-(1 → 3)-glucanases that release mannoproteins, which impart organoleptic characteristics to the wine and improve its quality.[3] Some of the enzymes produced by yeasts of grape biota have distinct benefits of operating at low acid pH values and can tolerate high alcohol levels, conditions that occur during vinification.[4]

The enzymes capable of hydrolyzing the (1 → 3)-β-D-glucans that may carry (1 → 6)-β-linked D-glucosyl appendages are active on substrates, such as (1 → 3),(1 → 6)-β-D-glucans found in yeast and fungal cell walls, fungal exopolysaccharides (EPS), e.g., botryosphaeran and scleroglucan, laminarin [a low branched algal (1 → 3)-β-D-glucan], paramylon [an unbranched algal (1 → 3)-β-D-glucan], and curdlan [an insoluble, unbranched bacterial (1 → 3)-β-D-glucan],[5] include β-(1 → 3)-glucanases of the *exo* and *endo* types and unspecific β-glucosidases, and have been found in yeasts as well as bacteria, fungi, algae, and higher plants.[6]

Botryosphaeria rhodina MAMB-05 secretes an EPS of the (1 → 3),(1 → 6)-β-D-glucan type named botryosphaeran by submerged fermentation (SmF) when cultivated on glucose or sucrose, concomitantly producing large amounts of mycelial biomass.[7] Three types of D-glucans [(1 → 3),(1 → 6)-β-D-glucan, a (1 → 4),(1 → 6)-α-D-glucan, and a (1 → 6)-β-D-glucan] are present in the mycelium from *B. rhodina* MAMB-05.[8] This material constitutes a rich source of β-D-glucans and can serve as a suitable and cheap fermentation substrate to induce specific β-(1 → 3)- and β-(1 → 6)-glucanases rather than using more expensive isolated (1 → 3)-β-D-glucans for this purpose.[9]

Received: September 11, 2014
Revised: December 2, 2014
Accepted: December 19, 2014
Published: December 19, 2014

ACS Publications © 2014 American Chemical Society

DOI: 10.1021/jf504333h
J. Agric. Food Chem. 2015, 63, 269−278

In this paper, we describe the isolation of yeasts from different cultivars of grapes and wine musts collected in vineyards within the southern states of Brazil. The yeast isolates were screened for β-(1 → 3)-glucanase activities using a newly developed zymogram method and also by SmF when grown on botryosphaeran and mycelial biomass obtained from *B. rhodina* (MAMB-05). The best enzyme-producing yeast strain (1WA1) was identified by molecular characterization as *Aureobasidium pullulans*. Production of β-(1 → 3)-glucanases and β-glucosidases by *A. pullulans* 1WA1 on mycelial biomass was examined, and the crude β-glucanolytic enzyme preparation characterized and used in the hydrolysis of several β-D-glucans.

MATERIALS AND METHODS

Materials. Botryosphaeran was produced by *B. rhodina* MAMB-05 [Microbiological Culture Collection at Universidade Estadual de Londrina (UEL), Brazil] grown on glucose.[10] Fungal mycelium was collected by centrifugation (1500*g* for 15 min at 4 °C) and freeze-dried without prewashing the mycelium. The lyophilized fungal mycelium (LFM) was pulverized to a powder, stored dry in sealed plastic bags at −20 °C, and referred to as LFM *in natura*. A portion of the fungal mycelium collected was also sterilized in an autoclave (121 °C for 20 min), followed by lyophilization, and used for comparative purposes. Lasiodiplodan [an exocellular soluble (1 → 6)-β-D-glucan] was produced by *Lasiodiplodia theobromae* MMPI grown on glucose.[11] Curdlan [a (1 → 3)-β-D-glucan from *Alcaligenes faecalis*] was purchased from Megazyme International (Bray, Ireland). Pustulan [a (1 → 6)-β-D-glucan isolated from the lichen *Actinogyra muehlenbergii*] was a kind gift from Dr. Philip A. J. Gorin (Universidade Federal do Paraná, Curitiba, Paraná, Brazil). Laminarin [a (1 → 3),(1 → 6)-β-D-glucan from the alga *Laminaria digitata*], laminaribiose, laminaritriose, gentiobiose, and *p*-nitrophenyl-β-D-glucopyranoside (*p*-NPG) were purchased from Sigma-Aldrich (St. Louis, MO).

Isolation of Yeast Species from Grape Microbiota. Nine different table/wine grape varieties common to southern Brazil (Isabel, Bordô, Rubi, Vênus, Itália, Benitaka, Takasumi, Brasil, and Moscato-Bailey) and the must from Isabel and Bordô grapes were collected from vineyards in the states of Paraná and Rio Grande do Sul. The grape berries were collected in the field and placed in sterile cotton sacks. Three whole, undamaged berries from each grape variety were aseptically transferred to flasks containing 25 mL of 0.9% (w/v) NaCl and left stationary at room temperature (28 ± 2 °C). After 48 h, aliquots were transferred to YEPD solid medium [1% (w/v) yeast extract, 2% (w/v) peptone, 2% (w/v) glucose, and 2% (w/v) agar, containing 0.05% (w/v) amoxicillin] and left at 28 °C for 3 days. A total of 95 yeast strains were isolated and purified by the streak-plate method. Yeast colonies were replated repeatedly on YEPD plates until pure. The purified yeast isolates were maintained in YEPD tubes at 4 °C and subcultured at 3 monthly intervals.

Screening Yeast Isolates for β-(1 → 3)-Glucanases. In the screening program, two methods were employed; the isolated yeast strains were grown in SmF on botryosphaeran and on agar medium (zymogram; see below). From this combinatory approach, yeasts were identified that were β-glucanolytic through the observation that botryosphaeran was hydrolyzed and supported cell growth. Yeast isolates were cultivated in 50 mL Erlenmeyer flasks containing 10 mL of nutrient medium comprising Vogel minimum salts medium (VMSM)[12] and botryosphaeran (0.6 g/L) at 28 °C under shaking conditions (180 rpm) for 96 h. β-(1 → 3)-Glucanase activity was assayed against laminarin; see below. The extracellular fluid (ECF) was recovered by centrifugation (3000*g* for 15 min at 4 °C) and used as the source of enzyme.

Zymogram Method for Detecting β-(1 → 3)-Glucanase Activity. The yeast isolates were cultured on agar media in Petri dishes containing agar (2%, w/v), VMSM, and 0.8 g/L botryosphaeran as the sole carbon (C) source. Cultures were incubated at 28 °C for up to 120 h. β-(1 → 3)-Glucanase activity was visualized on the agar plates as a transparent halo around the yeast colonies, following the flooding of the plates with absolute ethanol (~15 mL). The intensity of transparency of the developed halo observed after 1 h (Figure 1) indicated the presence of strong β-(1 → 3)-glucanase activity as a consequence of the yeasts producing enzymes capable of hydrolyzing botryosphaeran.

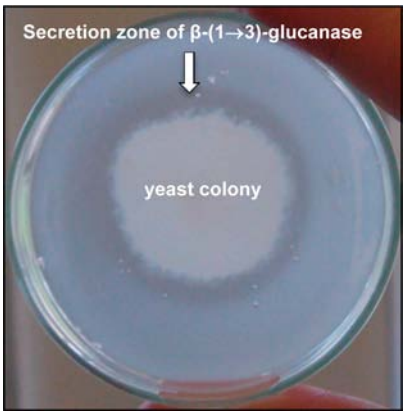

Figure 1. Zymogram showing a halo displaying β-(1 → 3)-glucanase activity around a growing colony of *A. pullulans* 1WA1. Cells were grown on agar−botryosphaeran media in Petri dishes for up to 120 h, and then the plates were flooded with absolute ethanol and left for 1 h to develop the clearance zone.

Molecular Identification of Yeast Strain 1WA1 from Grape Microbiota. Of the 14 β-(1 → 3)-glucanase-positive yeast strains isolated in the screening program, strain 1WA1 produced the highest enzyme activity and was selected for identification and phylogenetic positioning by sequencing of the internal transcribed spacer (ITS) ITS1−5.8S−ITS2 region of the nuclear ribosomal gene complex. Strain 1WA1 was grown in liquid YEPD medium for 48 h, and total DNA was extracted.[13] Polymerase chain reaction (PCR) amplification reactions were carried out,[14] and the amplification products were purified using PureLink Quick Gel Extraction and PCR Purification Combo Kit (Life Technologies, Carlsbad, CA). Sequencing reactions were performed on an ABI 3500 automated sequencer (Applied Biosystems, Germany) using a BigDye Terminator v3.1 Cycle Sequencing Kit (Life Technologies, Carlsbad, CA) with the same primers used for PCR amplifications. The new 5.8S-ITS sequence of strain 1WA1 was deposited in GenBank (accession number HM855956). The identity of the sequenced strain was determined by BLASTN comparison using the National Center for Biotechnology Information (NCBI) database, assuming the best hit to confirm the identity of the selected strain at the species level when sequences showed at least 98% identity to the best hit, a procedure considered robust for fungal species identification. The identity of the sequenced strain 1WA1 was further confirmed through the Fungal Barcoding Pairwise Sequence Alignment tool using the default parameters (http://www.fungalbarcoding.org/BioloMICSSequences.aspx?file=all) and submitted to multiple alignment with 25 closely related taxa retrieved from GenBank. The multiple alignment was accomplished using the ClustalX2 program,[15] with the resulting multiple sequence alignment manually adjusted using BioEdit software.[16] Phylogenetic inference was conducted using MEGA6;[17] the evolutionary history was inferred using the neighbor-joining method; and the evolutionary distances were computed using the Jukes−Cantor method. The strength of internal branches of the final phylogenetic tree was tested with bootstrap (BS) analysis with 1000 replications, and the sequences were employed in the molecular data sets that ranged from 470 to 575 base pairs (bp) in length prior to the elimination of ambiguous or unalignable data, with a total of 430 positions in the final data set. BS values of 50% or higher are shown at the tree branches. The ITS region of *Dothichiza pithyophila* (FJ150969) was used as an outgroup.

Cultivation of *A. pullulans* 1WA1 and Production of β-Glucanolytic Enzymes. Cells of *A. pullulans* 1WA1 (deposited at

DOI: 10.1021/jf504333h
J. Agric. Food Chem. 2015, 63, 269−278

the Microbiological Culture Collection at UEL) were grown on YEPD plates for 96 h. Inoculum was prepared by taking a loopful of yeast cells and added to isotonic saline to a final concentration of 1×10^7 cells. A total of 1 mL was used to inoculate 25 mL of nutrient medium (VMSM and 0.6 g/L botryosphaeran at pH 6.0) in 125 mL Erlenmeyer flasks. Enzyme production was also examined using cellobiose (10 g/L) as the sole C source and in separate experiments, sterilized (autoclaved) and unsterilized (*in natura*) LFM (10 g/L). The effect of the concentration of *in natura* LFM (0.5−3.0%, w/v) on the production of β-(1 → 3)-glucanase and β-glucosidase was performed in Erlenmeyer flasks (125 mL) comprising VMSM. Cultures were incubated at 28 °C (180 rpm) for 96 h. The profiles of growth and β-glucanolytic enzyme production of *A. pullulans* 1WA1 were examined by cultivating the yeast strain on *in natura* LFM (10 g/L) for 168 h. At the following time intervals: 0, 6, 12, 24, 36, 48, 60, 72, 96, 120, 144, and 168 h, three Erlenmeyer flasks were removed for analyses. All experiments were carried out in triplicate, and the results represent the means ± standard deviation (SD).

Analytical Methods. *Enzyme Assays.* The ECF obtained after centrifuging the yeast-grown cultures was used as the source of enzyme. β-(1 → 3)-Glucanase activity was measured against laminarin,[18] followed by measuring the reducing sugars produced by the cuproarsenate method.[19] β-Glucosidase activity was measured against *p*-NPG.[18] β-Glucosidase activity was determined by measuring the amount of *p*-nitrophenol (*p*-NP) liberated (A_{410}; extinction coefficient, 18 300 M^{-1} cm^{-1}). Units of enzyme activity were defined as the number of micromoles of product per minute per milliliter under the standard assay conditions.

Sugars. Total sugars were determined by the phenol−sulfuric acid method,[20] and reducing sugars were determined by the cuproarsenate method.[19] D-Glucose was used as the standard.

Proteins. Soluble proteins were determined by a modified Lowry method[21] using bovine serum albumin as the standard.

Physicochemical Properties of the Crude β-Glucanolytic Enzyme Preparation. To evaluate the effect of pH and temperature on enzyme activity, the ECF was incubated with substrate (laminarin or *p*-NPG) at 35 °C in buffers of different pH (pH 2.5−3.5, 0.2 M glycine/HCl; pH 4−5.5.0, 0.2 M sodium acetate; pH 3.5−6.0, 0.2 M sodium citrate; and pH 3.0−6.5, 0.2 M sodium citrate−sodium phosphate) and at various temperatures (30−90 °C) at the optimum pH for 20 min. Temperature stability of β-(1 → 3)-glucanase activity was determined by incubating the enzyme solution without substrate at 30−60 °C for times ranging from 10 min to 24 h and then adding substrate and assaying for enzyme activity. Kinetic parameters were determined by incubating the ECF at different concentrations of laminarin (0.02−1.20 mg/mL) in 0.2 M citrate−phosphate buffer (pH 4.5) for 20 min at 60 °C for β-(1 → 3)-glucanase and, for β-glucosidase, *p*-NPG (0.016−0.48 mg/mL) in 0.2 M sodium acetate buffer (pH 4.0) and incubated for 20 min at 75 °C. K_m and V_{max} values were determined from Lineweaver−Burk plots.

Enzymatic Hydrolysis of β-D-Glucans by the Crude β-Glucanolytic Enzyme Preparation. Enzymatic hydrolysis of the β-D-glucans, botryosphaeran, laminarin, lasiodiplodan, pustulan, and curdlan (1 g/L), was conducted in 50 mL volumes in 0.025 M sodium acetate buffer (pH 4.5) using 0.5 units of β-(1 → 3)-glucanase (activity assayed against laminarin) in the crude enzyme preparation and incubated at 40 °C. Aliquot samples (1.0 mL) were withdrawn at various intervals (0 min, 5 min, 10 min, 15 min, 30 min, 45 min, 60 min, 120 min, and 24 h) and heated for 10 min at 100 °C to inactivate enzyme activity. The degree of β-D-glucan hydrolysis was measured by the reducing sugar method.[19] Glucose in the hydrolyzates was measured by the glucose oxidase method (Glucose Assay Kit, Sigma). Enzymatic hydrolysis products were analyzed by high-performance anion-exchange chromatography with pulsed amperometric detection (HPAEC/PAD; see below).

Enzymatic hydrolysis of cellobiose, gentiobiose, and laminariobiose (1 g/L) was conducted in a final volume of 0.5 mL consisting of 0.025 M sodium acetate buffer (pH 4.5) using 0.1 units of β-glucosidase (activity assayed against *p*-NPG) in the crude enzyme preparations from *A. pullulans* 1WA1, *Trichoderma harzianum* Rifai, and *B. rhodina* MAMB-05. The latter two enzyme preparations were produced according to Giese et al.[18] The reactions were performed at 50 °C for 20 min and then heated for 10 min at 100 °C to arrest enzyme activity. The hydrolysis products were measured as glucose by the glucose oxidase method.

HPAEC/PAD Analysis of β-D-Glucan Enzymatic Hydrolyzates. Unhydrolyzed polymeric material in the enzymatic digests was precipitated with ethanol (3 vol) and removed by centrifugation (7000*g* for 15 min). The supernatant was evaporated under reduced pressure, and the resulting syrup was redissolved in 0.4 mL of deionized water. Samples of 0.025 mL were used for sugar analysis by HPAEC/PAD on a Dionex ICS 3000 instrument (Dionex, Sunnyvale, CA). Mono- and oligosaccharides were separated on a CarboPac PA200 (Dionex) column (4 × 250 mm) at a flow rate of 1.0 mL/min. The column was equilibrated in 0.10 M NaOH (97%) and 0.50 M sodium acetate (3%). After 15 min, a linear 0−0.25 M concentration gradient of sodium acetate was applied over a 70 min interval, while the concentration of NaOH remained at 0.10 M. Sugar quantification was carried out from peak area measurements using response factors obtained from standard sugars.

RESULTS AND DISCUSSION

Screening Grape Yeasts for β-(1 → 3)-Glucanase and β-Glucosidase Activities. The microbial biodiversity of grape berries are complex, and their population varies according to environmental conditions.[1] Among the filamentous fungi dominating grape microflora is the yeast-like fungus, *A. pullulans*.[22] A strain of *A. pullulans* isolated from Brazilian grape ecosystems was reported to produce β-glucosidases.[23] Non-*Saccharomyces* β-glucosidases have been applied commercially in wine oenology to augment aroma and taste of wines, and β-(1 → 3)-glucanases too have found applications in vinification.[24]

The streak-plate method was used to isolate yeasts from the microbiota of nine grape varieties from vineyards in the southern states of Brazil and some grape musts. The grape berries were left in contact with isotonic saline solution to facilitate detachment of the microbial species from the grape skin, which comprises a waxy, cuticular layer that affects the adherence of microbial cells colonizing the surface.[25] The dislodgement of microbes from the grape berry appears to depend upon the extraction methods employed.[26] Saline water extracts of the grape berries were plated onto agar medium containing amoxicillin (antibiotic) and left to grow, resulting in a mixture of different filamentous fungi, including yeasts colonizing the surface of the agar. The microorganisms growing on the agar plates displayed various morphological characteristics: color (white, yellow, pink, but not black), superficial colony features, such as smooth or rough surfaces, and brightness or opaqueness of the colony. A total of 95 yeasts were isolated: 85 yeast strains from grapes taken from vineyards in the state of Paraná located at Marialva (designated by the letter M) and Warta (W) and 10 yeasts from the Isabel grape variety (*Vitisla brusca*) taken from a vineyard in the southern state of Rio Grande do Sul in Brazil.

The isolated yeast colonies were screened for β-glucanolytic activity [β-(1 → 3)-glucanase and β-glucosidase] by growing them on agar medium containing botryosphaeran and employing a specific zymogram procedure developed in this work (see below). The yeasts were evaluated according to their ability to produce exocellular enzymes that formed a transparent halo around the growing colony when plated on agar. To determine quantitative enzyme activities of each of the isolated yeasts, it was necessary to cultivate the yeast strains on liquid nutrient medium containing botryosphaeran and evaluate the

DOI: 10.1021/jf504333h
J. Agric. Food Chem. 2015, 63, 269−278

Table 1. Comparison of β-(1 → 3)-Glucanase and β-Glucosidase Production in Submerged Fermentation by Yeast Strains 1WA1, 1WA2, 2WS2, and 3WS5 Grown on Different Substrates [Botryosphaeran, Cellobiose, and the Mycelium (LFM) Obtained from *B. rhodina* MAMB-05]

	enzyme activity (units/mL)					
	substrate					
			mycelium (LFM) (10 g/L)			
	botryosphaeran (0.6 g/L)	cellobiose (10 g/L)	*in natura*		autoclaved	
yeast isolate[a]	(units/mL)	(units/mL)	(units/mL)	(units/mg)[b]	(units/mL)	(units/mg)[b]
			β-(1→3)-Glucanase[c]			
1WA1[d]	0.145 ± 0.001	1.047 ± 0.024	0.917 ± 0.04	3.380 ± 0.17	0.930 ± 0.01	4.010 ± 0.13
1WA2	0.128 ± 0.002	0.475 ± 0.026	0.780 ± 0.03	2.835 ± 0.11	0.730 ± 0.09	3.100 ± 0.31
2WS2	0.105 ± 0.003	0.519 ± 0.053	0.765 ± 0.16	2.848 ± 0.64	0.498 ± 0.025	2.175 ± 0.10
3WS5	0.112 ± 0.002	0.491 ± 0.08	0.818 ± 0.05	3.028 ± 0.10	0.265 ± 0.032	1.103 ± 0.12
			β-Glucosidase[e]			
1WA1[d]	0.003 ± 0.001	0.027 ± 7 × 10^{-4}	0.030 ± 0.001	0.101 ± 0.003	0.024 ± 0.00	0.103 ± 0.003
1WA2	0.002 ± 0.000	0.028 ± 7 × 10^{-4}	0.024 ± 0.001	0.085 ± 0.002	0.021 ± 0.001	0.085 ± 0.005
2WS2	0.001 ± 0.000	0.030 ± 0.001	0.024 ± 0.001	0.087 ± 0.003	0.019 ± 0.001	0.081 ± 0.002
3WS5	0.002 ± 0.001	0.026 ± 0.002	0.027 ± 0.001	0.102 ± 0.003	0.012 ± 0.001	0.048 ± 0.002

[a]Grown for 96 h. [b]Specific activity (units/mg of protein). [c]Assayed against laminarin as the substrate. [d]Molecularly characterized as *A. pullulans*. [e]Assayed using *p*-NPG.

β-(1 → 3)-glucanase and β-glucosidase activities produced through specific assays against the substrates, laminarin and *p*-NPG, respectively.

The developed zymograms allowed for rapid screening of large numbers of yeast strains for β-glucanolytic activity, which, in turn, were used for further study by SmF on nutrient medium containing botryosphaeran as the sole C source under shaking conditions. Through this combined approach (zymogram and SmF), 14 yeast strains were identified as showing β-glucanolytic activity. Yeasts that could grow on botryosphaeran included strains 4MA3 and 4MA5 (isolated from Takassumi grapes) and 6MS1 and 6MA2 (Benitaka grapes) taken from grapes in a vineyard at Marialva (Paraná) and 1WA1, 1WA2, and 2WS2 (Moscato-Bailey grapes) and 3WS2, 3WS3, 3WS5, 3WS6, 3WS10, 3WS13, and 3WA10 (Isabel grapes) from a vineyard in Warta (Paraná).

Among the Marialva yeasts isolated, strains 4MA3, 4MA5, 6MS1, and 6MA2 produced low enzyme titers that ranged from 1 to 6 milliunits/mL for β-(1 → 3)-glucanase and from 0 to 4.3 milliunits/mL for β-glucosidase when grown by SmF on nutrient media containing botryosphaeran. Yeasts isolated from grapes collected in Warta, in contrast, produced higher enzyme titers that ranged from 1.5 to 113 milliunits/mL for β-(1 → 3)-glucanase and from 2.7 to 12.6 milliunits/mL for β-glucosidase.

Among the yeast strains examined by SmF when grown on botryosphaeran, the best four producers of β-(1 → 3)-glucanases were strains 1WA1, 1WA2 and 2WS2 (Moscato-Bailey grapes) and 3WS5 (Isabel grapes), all isolated from grapes collected at the Warta vineyard and evaluated for enzyme production by SmF when grown on different substrates.

Zymogram for Screening β-(1 → 3)-Glucanase Activity. Screening by SmF was slow and costly on the use of media, including botryosphaeran, and could not conveniently process large numbers of yeasts for screening. A more rapid screening method was sought that was cheaper on polysaccharide use, and a new zymogram procedure was developed. The two methods, nevertheless, demonstrated that the same yeast strains showed β-glucanolytic activities. The zymogram method allowed for a specific assay procedure to rapidly detect β-(1 → 3)-glucanase activity for screening large numbers of yeasts on agar plates. The zymogram procedure was fine-tuned using the yeast strain 1WA1 (molecularly characterized as *A. pullulans*; see below), which was found to be the best producer of β-(1 → 3)-glucanases through SmF (Table 1). The yeasts were grown on agar medium containing botryosphaeran, and afterward, the plates were irrigated with absolute ethanol, which after 1 h, developed clear halos (transparent zones) around the yeast colony (Figure 1). The halo diameters were greater than the diameters of the yeast colony, indicating that β-(1 → 3)-glucanase was secreted exocellularly and diffused through the agar medium to hydrolyze the substrate. Botryosphaeran was hydrolyzed to degraded products (mixed linked gluco-oligosaccharides) that resulted in a clear zone on the agar plates, because these sugars were soluble in alcohol. The unhydrolyzed areas of botryosphaeran on the agar plates remained opaque because of the β-D-glucan not being soluble in ethanol. The novelty of this method was that alcohol was used to distinguish areas between hydrolyzed and unhydrolyzed botryosphaeran on the agar plates, which allowed for rapid detection of yeast β-(1 → 3)-glucanase activities. A bacterial β-(1 → 3)-glucanase has been detected by a zymogram method employing laminarin and using calcofluor white to detect the hydrolysis zones when visualized under ultraviolet (UV) light.[24]

Production of β-Glucanolytic Enzymes by Selected Yeast Strains Grown on Different Substrates. Commercially available laminarin has commonly been used to induce the microbial synthesis of β-(1 → 3)-glucanases by SmF[6] but is an expensive substrate for this purpose. Botryosphaeran, as used in this work, is also considered expensive to produce, but in producing botryosphaeran by *B. rhodina* MAMB-05, large amounts of mycelial biomass are produced.[7] Studies from our laboratory have shown[8] that the mycelium is a rich source of β-D-glucans and a more convenient and less expensive substrate for the microbial production of β-(1 → 3)-glucanases by SmF.[9]

Table 1 shows the production of β-(1 → 3)-glucanases and β-glucosidases by four selected yeast strains (1WA1, 1WA2, 2WS2, and 3WS5) grown on different substrates: cellobiose, botryosphaeran, and LFM (*B. rhodina* MAMB-05 cultivated on glucose and prepared and treated as described under the

DOI: 10.1021/jf504333h
J. Agric. Food Chem. 2015, 63, 269−278

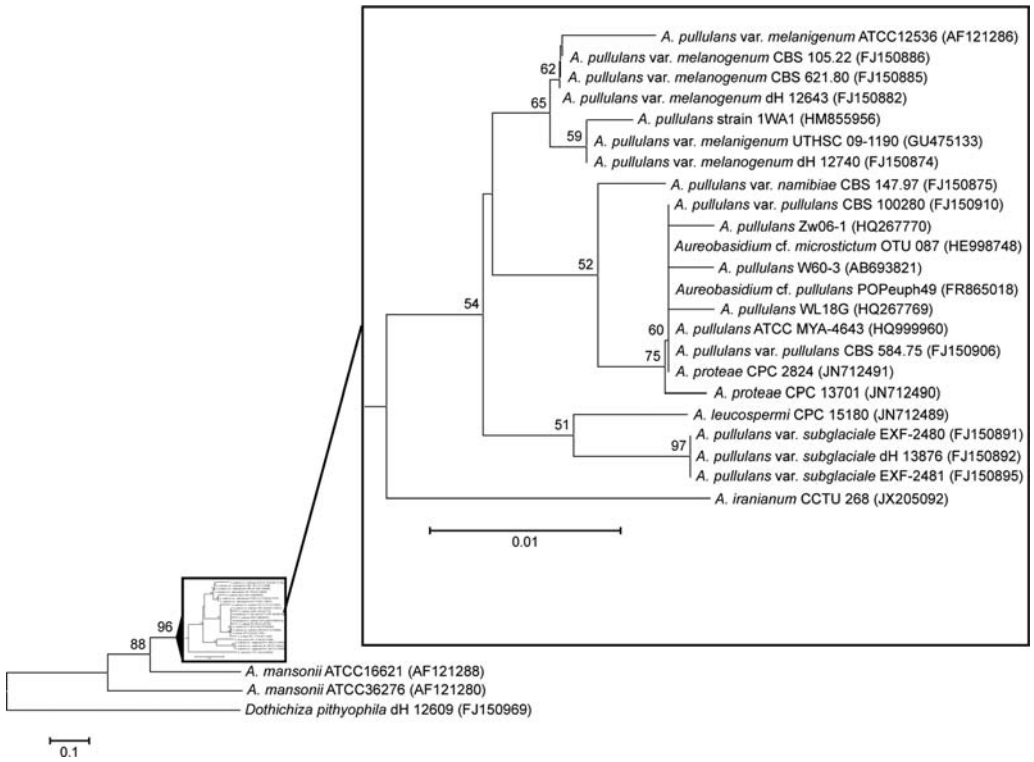

Figure 2. Phylogenetic tree of *A. pullulans* strain 1WA1. The evolutionary history was inferred using the neighbor-joining method. The percentage of replicate trees in which the associated taxa clustered together in the BS test (1000 replicates) is shown above the branches when higher than 50%. The evolutionary distances were computed using the Kimura two-parameter method and are in the units of the number of base substitutions per site. All positions with less than 95% site coverage were eliminated; that is, fewer than 5% alignment gaps, missing data, and ambiguous bases were allowed at any position. There were a total of 430 positions in the final data set. Evolutionary analyses were conducted using MEGA6.

Materials and Methods). The highest activity for both enzymes occurred with strain 1WA1. Cellobiose resulted in the highest β-(1 → 3)-glucanase titers (1.047 units/mL) for 1WA1, while the other yeast strains exhibited lower enzyme activities. *Candida wickerhamii*, a yeast fermenting cellobiose into ethanol, was reported to produce high intracellular β-glucosidase activity (13.7 units/mg) when grown on cellobiose[27] but has not been described as an inducer of β-(1 → 3)-glucanases. Botryosphaeran proved to be a poor substrate for the production of both enzymes compared to the fungal mycelium. The two LFM preparations (*in natura* and autoclaved) did not produce significant differences between them in terms of enzyme titers (units/mL) and specific activities (units/mg of protein), but the β-(1 → 3)-glucanase and β-glucosidase activities produced on both substrates were higher compared to the other substrates tested (Table 1). *B. rhodina* MAMB-05 mycelium contains both (1 → 3),(1 → 6)- and (1 → 6)-linked β-D-glucans,[8] and these components were possibly responsible for inducing the higher β-(1 → 3)-glucanase activities obtained. *T. harzianum*, has also been reported to produce β-(1 → 3)-glucanases when cultivated on the mycelium of *Botrytis cinerea* (1.04 units/mg) and *Saccharomyces cerevisiae* (1.0 units/mg) cells.[28] β-(1 → 3)-Glucanase production by *T. harzianum* Rifai and *B. rhodina* MAMB-05 cultivated on mycelium from *B. rhodina* MAMB-05 resulted in enzyme titers of 0.80 and 0.67 units/mL obtained over 5 and 10 days growth for the respective fungi.[18] Yeasts, in contrast, produce these enzymes in lesser times than the fungi, e.g., in 3 days for *Pichia anomala* YF07b,[29] while our yeast strain 1WA1 reached maximal β-(1 → 3)-glucanase activity after 2−3 days of growth on LFM (*in natura*; see below). Of the four yeast strains evaluated, strain 1WA1 resulted in the highest β-(1 → 3)-glucanase activity and was selected for molecular identification, with a further study on β-glucanolytic enzyme production.

Molecular Identification of Yeast Strain 1WA1. The identification of fungal isolates is largely facilitated by the sequencing of the ITS region of the nuclear ribosomal operon and is supported by the large data set available in public databanks and recently proposed for use as a primary barcode marker for fungi phylogeny.[30] The sequence analysis of yeast strain 1WA1 isolated from the grape berries led to the identification at the species level as being *A. pullulans*, through the use of both the BlastN and the Fungal Barcoding tools. The fungus-like yeast *A. pullulans* and filamentous fungi dominate the microflora of grape berries.[22] The phylogenetic analysis of yeast strain 1WA1 plus 25 of the closest relative *Aureobasidium* species and *A. pullulans* varieties confirmed their close phylogenetic relatedness with *A. pullulans* with BS of 96% and clustering close to *A. pullulans* var. *melanogenum* with BS of 59%, as presented in Figure 2. Cultures of *A. pullulans* var. *melanogenum* form characteristically melanized, dark-colored colonies and are found colonizing environments with nutritional limitations.[31] This contrasts with the characteristically white colonies formed by strain 1WA1 described here. Although the use of ITS sequences to identify new fungal isolates is supported by the literature and widely used as a phylogenetic marker, the unequivocal attributes of a species must be supported by different sets of gene sequences. In addition, as observed in Figure 2, the variability of the *Aureobasidium* ITS sequences observed by most of the data available is narrow and the possible occurrence of a new species is not discarded.

DOI: 10.1021/jf504333h
J. Agric. Food Chem. 2015, 63, 269−278

Table 2. Effect of the Concentration of Mycelial Biomass from *B. rhodina* MAMB-05 on the Production of β-(1 → 3)-Glucanase and β-Glucosidase by *A. pullulans* Strain 1WA1

	total sugars[a]		reducing sugars[b]			enzyme activity			
						β-(1→3)-glucanase		β-glucosidase	
LFM[c] (%, w/v)	initial (g/L)	residual (g/L)	initial (g/L)	residual (g/L)	protein[d] (mg/mL)	(units/mL)	(units/mg)[e]	(units/mL)	(units/mg)[e]
0.5	0.841	0.493 ± 0.016	0.351	0.002 ± 0.001	0.239 ± 0.002	0.227 ± 0.009	0.950 ± 0.043	0.010 ± 0.001	0.042 ± 0.004
1.0	1.530	0.886 ± 0.047	0.717	0.009 ± 0.001	0.386 ± 0.003	0.332 ± 0.007	0.860 ± 0.024	0.016 ± 0.001	0.042 ± 0.003
1.5	2.256	1.232 ± 0.070	1.006	0.009 ± 0.001	0.529 ± 0.013	0.426 ± 0.012	0.805 ± 0.044	0.023 ± 0.001	0.044 ± 0.003
2.0	2.756	1.586 ± 0.075	1.508	0.017 ± 0.003	0.730 ± 0.003	0.465 ± 0.007	0.637 ± 0.012	0.031 ± 0.001	0.043 ± 0.001
3.0	4.105	2.131 ± 0.035	2.127	0.019 ± 0.001	0.974 ± 0.010	0.546 ± 0.014	0.561 ± 0.019	0.035 ± 0.001	0.036 ± 0.000

[a]Measured by the phenol−sulfuric acid method.[20] [b]Measured by the cuproarsenate method.[19] [c]LFM = lyophilized fungal mycelium (*in natura*). [d]Soluble protein concentration (measured by the Hartree[21] method) in the culture medium after 96 h of growth. [e]Specific activity (units/mg of protein). The initial soluble protein concentrations were 0.58, 1.01, 1.35, 1.85, and 1.92 mg/mL for the respective LFM concentrations.

Production of β-Glucanolytic Enzymes by *A. pullulans* 1WA1 Cultivated on Mycelial Biomass. The effect of the concentration of mycelial biomass (LFM, *in natura*) on the production of β-(1 → 3)-glucanases and β-glucosidases by *A. pullulans* 1WA1 is shown in Table 2. β-(1 → 3)-Glucanase titers (units/mL) increased, while the specific activity (units/mg of protein) inversely decreased as the concentration of LFM in the nutrient medium increased. The amount of soluble protein in the culture fluid was high at 96 h of cultivation and increased as the LFM concentration in the nutrient medium increased (Table 2), despite no exogenous protein being added to the nutrient formulation. The protein arises through its solubilization by autoclaving of the LFM as well as from the disruption of the fungal mycelium during SmF through the action of the cell-wall-degrading enzymes, resulting in the release of soluble proteins (measured by a modified Lowry method[21]) into the culture medium, hence, the decrease in the specific activity as the amount of LFM increased. β-Glucosidase titers similarly increased but did not appear to significantly affect the specific activity of this enzyme (Table 2).

The initial sugars content (total and reducing sugars) in the nutrient media following autoclaving and prior to inoculation was rather high for each of the amounts of LFM added (Table 2). LFM was isolated following the harvesting of the fungal mycelium and was deliberately not prewashed. This procedure allowed for the LFM preparation to retain residual botryosphaeran in the mycelial fraction that could, in turn, induce β-glucanolytic enzymes. EPS retained and polysaccharides from fragmented cell wall material released to the medium upon autoclaving will present high initial total sugars content as measured by the phenol−sulfuric acid method.[20] The initial reducing sugars content too was high and may arise from the action of β-glucanases present in the LFM preparation during time of harvesting and lyophilization. Cell-wall-bound β-glucanases have been observed in the mycelium from another *B. rhodina* strain, DABAC-P82.[32]

The residual reducing sugars (RRS) content in the medium decreased at all of the concentrations of LFM examined, indicating that the yeast totally consumed these sugars (Table 2). The RRS concentration decreased during growth of the yeast at each of the levels of LFM added. However, in contrast to the RRS, only between 41 and 48% of the total soluble sugars were consumed by the yeast at 96 h within the range of LFM added to the nutrient medium. The remaining total sugars content (52−59%) may have been attributable to the presence of EPS produced by *A. pullulans* 1WA1 (see also the profile of sugar use in Figure 3B), because *A. pullulans* is well-known to produce exocellular pullulan[33] and, recently, a (1 → 3),(1 → 6)-β-D-glucan.[34] The presence of EPS in the culture medium would contribute to the total sugars concentration as measured by the phenol−sulfuric acid method.

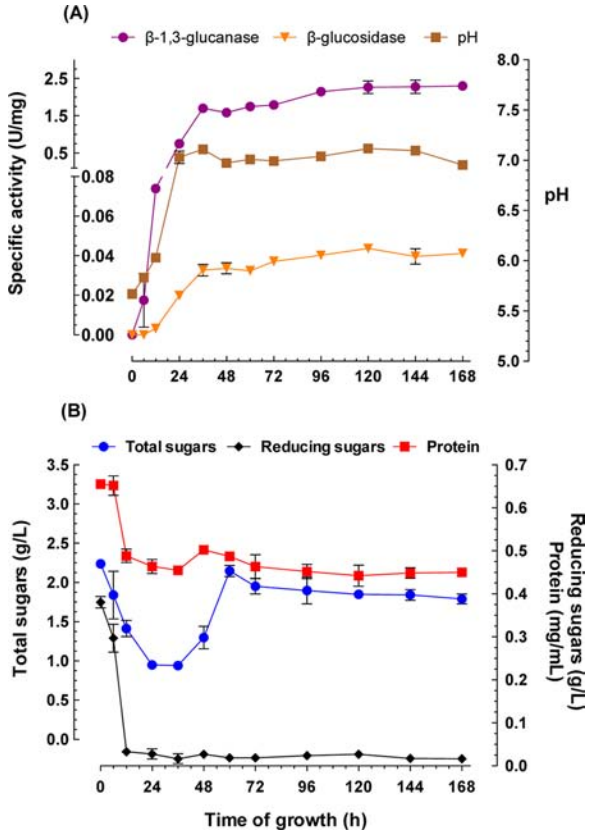

Figure 3. Profile for the production of β-(1 → 3)-glucanases and β-glucosidases by *A. pullulans* 1WA1 cultivated on the mycelium of *B. rhodina* MAMB-05. β-(1 → 3)-Glucanase activity was measured against laminarin as a substrate. Yeast biomass could not be determined during the fermentation run, because undegraded fungal mycelium (LFM) still remained in the culture fluid, and this interfered with yeast biomass determination by the gravimetric procedure.

The profile for enzyme production is shown in Figure 3 when the yeast strain was grown on nutrient medium containing LFM (*in natura*) over a period of 168 h. A substrate loading of 1% (w/v) of LFM was chosen as at higher loadings, SmF on this substrate becomes impractical because of the high solids consistency of the culture medium. β-(1 → 3)-Glucanase production plateaued after 48 h (1.10−1.20 units/mg), while β-

DOI: 10.1021/jf504333h
J. Agric. Food Chem. 2015, 63, 269−278

glucosidase also leveled-off after 48 h (0.03−0.04 units/mg). About 31% of the soluble protein liberated from the LFM was consumed by the yeast over the time course of fermentation, with most of this occurring within the first 36 h of growth. The total sugars concentration in the culture medium decreased for the first 36 h (from an initial 2.238 g/L), as the yeast consumed the LFM. Thereafter, the total sugars concentration commenced to increase until 60 h and then leveled-off to a final concentration of 1.791 g/L at 168 h (Figure 3). The reason for the increase was most likely due to the secretion of EPS, as discussed above. During the 168 h period, there was no increase in the RRS level, indicating that the yeast consumed all RRS. Both yeast enzymes, however, remained remarkably stable over the 168 h fermentation period. Optimization of both enzymes by statistical design when *A. pullulans* 1WA1 was cultivated on fungal mycelium has resulted in specific activities of 5.96 units/mg [β-(1 → 3)-glucanase] and 1.77 units/mg (β-glucosidase) (unpublished results).

Physicochemical Properties of the Crude β-Glucanolytic Enzyme Preparation. Considering that *A. pullulans* 1WA1 produced β-glucanolytic enzymes, it may find application to aid wine maturation to improve the sensorial characteristics of wines. It was therefore of interest to assess whether the β-(1 → 3)-glucanases and β-glucosidases could tolerate and survive under the conditions of winemaking: low pH (3.3−3.7 for table wines) and high ethanol content (9−15% by volume). The crude β-glucanolytic enzyme preparation from *A. pullulans* 1WA1 grown on LFM was examined for its stability at pH 3.5 (0.20 M citrate−phosphate buffer; control) in the presence of 15% (v/v) ethanol at this pH when exposed at ambient temperature for 72 h. The yeast crude enzyme preparation was found to be remarkably stable under this condition. β-(1 → 3)-Glucanase retained ∼80% of its original activity in the presence of 15% ethanol, while β-glucosidase retained full activity under the same conditions. A bacterial β-(1 → 3)-glucanase grown on yeast cell walls as the C source has been found to be stable to 17.5% (v/v) ethanol and was used in vinification.[24] Both β-(1 → 3)-glucanases and β-glucosidases in the crude enzyme preparation from *A. pullulans* 1WA1 were remarkably stable at low pH, high ethanol content, and 30−40 °C, a requirement for functioning during vinification.

The physicochemical properties of the crude β-glucanolytic preparation from *A. pullulans* 1WA1 are summarized in Table 3. The optimum pH and temperature of β-(1 → 3)-glucanase and β-glucosidase was 4.5 and 60 °C and 4.0 and 75 °C, respectively, which agreed with the literature for yeast species.[29,35] High-temperature optima were also reported for the β-glucosidases from a commercial preparation from *Aspergillus niger* (62 °C),[36] and the wine yeast *Debaryomyces vanrijiae* (40 °C).[37] β-(1 → 3)-Glucanase from *A. pullulans* 1WA1 was stable at 30−40 °C for up to 24 h. The apparent K_m of β-(1 → 3)-glucanase and β-glucosidase was evaluated using laminarin and *p*-NPG, respectively, as substrates. The respective apparent K_m values were 0.09 and 0.04 mg/mL, with V_{max} of 1.07 and 0.011 μmol min^{-1} mg^{-1}. The apparent K_m values were relatively low and show that these enzymes have high affinities for their substrates, laminarin and *p*-NPG, respectively. The apparent K_m of a β-(1 → 3)-glucanase from *Pichia pastoris* was reported to be 3.5 mg/mL,[38] while that for β-glucosidase from *P. anomala* was 0.47 mM.[36]

Enzymatic Hydrolysis of β-D-Glucans and β-Glucodisaccharides by the Crude β-Glucanolytic Enzyme Preparation. β-(1 → 3)-Glucanases have been used to obtain laminari-oligosaccharides through the enzymatic hydrolysis of various (1 → 3)-β-D-glucans.[39,40] Gluco-oligosaccharides find commercial applications as prebiotics in formulating physiological functional foods because of their health benefits, including immunostimulation.[41]

Laminarin [algal (1 → 3),(1 → 6)-β-D-glucan], botryosphaeran [fungal (1 → 3),(1 → 6)-β-D-glucan], lasiodiplodan [fungal (1 → 6)-β-D-glucan], pustulan [lichen (1 → 6)-β-D-glucan], and curdlan [bacterial (1 → 3)-β-D-glucan] were hydrolyzed using the crude β-glucanolytic enzyme preparation of *A. pullulans* 1WA1 grown on LFM.

Although laminarin[42] and botryosphaeran[10] are both (1 → 3),(1 → 6)-β-glucans, they possess different degrees of branching, 10 and 22%, respectively, and the nature of the appendages at C-6 along the (1 → 3)-β-D-glucan chain also differs: glucose as compared to glucose and gentiobiose, respectively. Both (1 → 3)-β-D-glucans exist in solution in a triple helix conformation.[43] The crude β-glucanolytic enzyme preparation hydrolyzed the two polysaccharides differently and reflects a difference in the molecular structure between these (1 → 3)-β-D-glucan types (see Supplementary Table 1 of the Supporting Information). At 24 h, laminarin was almost totally hydrolyzed (∼95%), while botryosphaeran was hydrolyzed to the extent of ∼7.6%. HPAEC/PAD analysis of the enzymatic hydrolyzates of the two β-D-glucans revealed an array of gluco-oligosaccharides of the (1 → 3)-β-D-linked kind [degree of polymerization (DP) of 2−4] as well as gentiobiose. Products of DP > 4 were also observed but could not be resolved during the chromatographic run in all of the enzymatic hydrolyzates of the β-glucans examined. At 120 min, laminarin was hydrolyzed to the extent of ∼66% and the enzymatic hydrolyzates contained the following products as percent relative amounts: glucose as the chief product (71%), with lesser amounts of gentiobiose (18.5%), laminaribiose (8.3%), laminaritriose (1.4%), and laminaritetraose (1%). During the same time (120 min), botryosphaeran was poorly hydrolyzed (5.4%) and the product array was somewhat similar to glucose (74.1%), the major hydrolysis product, but gentiobiose was present in lower amounts (7.9%) compared to laminaribiose (15.6%). Laminaritetraose was not detected. The presence of large amounts of

Table 3. Physicochemical Properties of the Crude β-Glucanolytic Enzyme Preparation from *A. pullulans* 1WA1 Grown on Mycelial Biomass (LFM)

property	β-(1→3)-glucanase	β-glucosidase
winemaking conditions (pH 3.5, 15% ethanol)	80% retained at 72 h	100% retained at 72 h
pH optimum	4.5[a]	4.0[a]
temperature optimum	60 °C[b]	75 °C[c]
temperature stability[b]	30−40 °C: 100% retained at 24 h	30−40 °C: 100% retained at 24 h
	45 °C: 50% retained at 24 h	ND[d]
	50 °C: 55% retained at 1 h	ND
	55 °C: 12% retained at 1 h	ND
	60 °C: <10% retained at 1 h	ND
apparent K_m (mg/mL)	0.09[e]	0.04[f]
V_{max} (μmol min^{-1} mg^{-1})	1.07	0.011

[a]Citrate−phosphate buffer. [b]Conducted at pH 4.5. [c]pH 4.0. [d]ND = not determined. [e]Laminarin. [f]*p*-NPG (substrate inhibition at >0.20 mg/mL).

DOI: 10.1021/jf504333h
J. Agric. Food Chem. 2015, 63, 269−278

glucose in both hydrolyzates was a consequence of the action of β-glucosidases, which act as accessory enzymes in synergy with the β-(1 → 3)-glucanases in degrading the (1 → 3),(1 → 6)-β-D-glucans into glucose. Similar profiles of hydrolysis products have been observed when crude β-(1 → 3)-glucanase preparations from *T. harzianum* Rifai and *B. rhodina* MAMB-05 degraded laminarin.[41] In contrast, the crude β-(1 → 3)-glucanase preparations of *T. harzianum* Rifai and *B. rhodina* MAMB-05 were reported to degrade botryosphaeran more extensively, ∼100 and ∼50%, respectively, within 24 h.[40]

Lasiodiplodan consists of a non-ramified chain of β-(1 → 6)-linked D-glucose units.[44] Pustulan from lichen is also a linear (1 → 6)-β-D-glucan but contains an *O*-acetyl group at every 8−9 glucose units along the chain.[45] The hydrolysis of the two (1 → 6)-β-D-glucans by the crude β-glucanolytic enzyme preparation from *A. pullulans* 1WA1 resulted in different degrees of hydrolysis. Lasiodiplodan was hydrolyzed to the extent of 20% over 24 h, while that of pustulan resulted in 4.4% hydrolysis within the same time interval (see Supplementary Table 1 of the Supporting Information). Hydrolysis of the (1 → 6)-β-D-glucan chain is only possible through the action of the β-(1 → 6)-glucanases, which were present in the crude enzyme preparation. HPAEC/PAD analysis of 120 min hydrolyzates of lasiodiplodan and pustulan showed that glucose represented 85.6 and 91.8%, respectively, of the total hydrolysis sugars released. Both enzymatic hydrolyzates also revealed the presence of gentiobiose (14.4% from lasiodiplodan and 8.2% from pustulan) as well as gentio-oligosaccharides of DP > 4. The reason why the two (1 → 6)-β-D-glucan preparations from different genetic sources were hydrolyzed differently is not known, but the presence of *O*-acetyl groups along the (1 → 6)-β-D-glucan chain of pustulan may have influenced the mode of enzymatic attack. The crude β-glucanolytic enzyme preparation from *Acremonium persicinum* was also reported to degrade pustulan to very small extents.[46]

Curdlan, an unbranched, linear bacterial (1 → 3)-linked β-D-glucan,[47] was hydrolyzed by the crude β-glucanolytic enzyme preparation to the extent of ∼40% within 24 h (see Supplementary Table 1 of the Supporting Information). HPAEC/PAD analysis of 120 min hydrolyzates of curdlan revealed that 68% of the liberated products were glucose, together with laminaribiose (20%) and laminaritriose (11.6%). Laminaritetraose was not detected. A crude β-(1 → 3)-glucanase preparation from *T. harzianum* was reported to hydrolyze curdlan and resulted in 80% saccharification,[48] while β-(1 → 3)-glucanases from *Streptomyces* sp. selectively hydrolyzed curdlan to laminaribiose.[49]

Table 4 shows that non-specific β-glucosidase activity was observed in the crude β-glucanolytic enzyme preparation from *A. pullulans* 1WA1, with preference for the disaccharides, cellobiose and laminaribiose. The specificities of the β-glucosidases present in the crude β-glucanolytic enzyme preparations from the three microorganisms examined varied considerably (Table 4). The β-glucosidases from *B. rhodina* MAMB-05 showed the highest preference toward laminaribiose and lower preferences for cellobiose and gentiobiose, whereas the crude enzyme showed equal preference for (1 → 4)- and (1 → 3)-β-D-glucosidic linkages. In contrast, the β-glucosidase from *T. harzianum* Rifai showed low preference for all three D-glucosidic linkages (Table 4). The crude β-glucanolytic enzyme preparations from *B. rhodina* MAMB-05 and *T. harzianum* Rifai grown on botryosphaeran were reported to have similar preferences for cellobiose and gentiobiose.[18]

Table 4. Comparison of the Specificities of β-Glucosidases from the Crude β-Glucanolytic Enzyme Preparations of *A. pullulans* 1WA1, *T. harzianum* Rifai, and *B. rhodina* MAMB-05 toward Different Gluco-disaccharides

	disaccharide conversion (%)[a]		
source of β-glucosidase	cellobiose[b]	gentiobiose	laminaribiose
A. pullulans 1WA1	68.76	21.96	62.87
B. rhodina MAMB-05[c]	70.28	78.66	98.76
T. harzianum Rifai[c]	18.36	23.85	22.03

[a]Glucose measured by the glucose oxidase method. [b]Cellobiose, β-D-glucopyranosyl-(1 → 4)-β-D-glucopyranose; gentiobiose, β-D-glucopyranosyl-(1 → 6)-β-D-glucopyranose; and laminaribiose, β-D-glucopyranosyl-(1 → 3)-β-D-glucopyranose. [c]*B. rhodina* MAMB-05 and *T. harzianum* Rifai were grown on nutrient medium containing botryosphaeran as the sole C source.[18]

In summary, 95 yeast strains were isolated from the microbiota of nine grape varieties taken from vineyards in Brazil. The yeast isolates were screened for β-(1 → 3)-glucanase activity by SmF and a novel zymogram procedure when cultivated on botryosphaeran. Among the 14 β-(1 → 3)-glucanase-positive yeasts isolated, yeast strain 1WA1 (identified as *A. pullulans*) produced the highest β-glucanolytic activities. The crude enzyme preparation was used to hydrolyze several β-D-glucans. These enzymes find application in wine oenology, food and beverage processing, and the production of (1 → 3)- and (1 → 6)-linked β-gluco-oligosaccharides for use as prebiotics.

■ ASSOCIATED CONTENT

Supporting Information

Hydrolysis of different β-glucans by the crude β-glucanolytic enzyme preparation from *A. pullulans* 1WA1 grown on LFM. This material is available free of charge via the Internet at http://pubs.acs.org.

■ AUTHOR INFORMATION

Corresponding Authors

*E-mail: xylanase@gmail.com.

*Telephone: +55-43-3371-4276. Fax: +55-43-3371-4286. E-mail: anelibarbosa@gmail.com.

Present Address

§Ellen C. Giese: Coordenação de Processos Metalúrgicos e Ambientais, Centro de Tecnologia Mineral (CETEM), Avenida Pedro Calmon 900, Rio de Janeiro, Rio de Janeiro 21941-908, Brazil.

Funding

Grants from Coordenação de Aperfeiçoamento de Pessoal de Nível Superior (CAPES), (DGU 153/08), Brazil (DGU 153/08), Fundação Araucária do Paraná, Brazil (13056 Chamada 02/2008) (to Aneli M. Barbosa), and the Natural Science and Engineering Council of Canada (NSERC)−Research Capacity Development (to Robert F. H. Dekker) supported this work. The Department of Foreign Affairs and International Trade−Canada/Brazil funded a postdoctoral research fellowship to Ellen C. Giese.

Notes

The authors declare no competing financial interest.

DOI: 10.1021/jf504333h
J. Agric. Food Chem. 2015, 63, 269−278

ABBREVIATIONS USED

BS, bootstrap; DP, degree of polymerization; ECF, extracellular fluid; EPS, exopolysaccharide; HPAEC/PAD, high-performance anion-exchange chromatography with pulsed amperometric detection; ITS, internal transcribed spacer; LFM, lyophilized fungal mycelium; *p*-NP, *p*-nitrophenol; *p*-NPG, *p*-nitrophenyl-β-D-glucopyanoside; RRS, residual reducing sugars; SmF, submerged fermentation; VMSM, Vogel minimum salts medium; YEPD, yeast extract−peptone−dextrose

REFERENCES

(1) Barata, A.; Malfeito-Ferreira, M.; Loureiro, V. The microbial ecology of wine grape berries. *Int. J. Food Microbiol.* **2012**, *153*, 243−259.

(2) Gonzalez-Pombo, P.; Farina, L.; Carrau, F.; Batista-Viera, F.; Brena, B. M. A novel extracellular β-glucosidase from *Issatchenkia terricola*: Isolation, immobilization and application for aroma enhancement of white Muscat wine. *Process Biochem.* **2011**, *46*, 385−389.

(3) Ribéreau-Gayon, P.; Glories, Y.; Maujean, A.; Dubourdieu, D. Carbohydrates. In *Handbook of Enology*, 2nd ed.; Ribéreau-Gayon, P., Glories, Y., Maujean, A., Dubourdieu, D., Eds.; John Wiley & Sons, Ltd.: Hoboken, NJ, 2006; Vol. *2*, Chapter 3, pp 65−90.

(4) Strauss, M. L. A.; Jolly, N. P.; Lambrechts, M. G.; van Rensburg, P. Screening for the production of extracellular hydrolytic enzymes by non-*Saccharomyces* wine yeasts. *J. Appl. Microbiol.* **2001**, *91*, 182−190.

(5) Martin, K.; McDougall, B. M.; McIlroy, S.; Jayus; Chen, J. Z.; Seviour, R. J. Biochemistry and molecular biology of exocellular fungal β-(1,3)- and β-(1,6)-glucanases. *FEMS Microbiol. Rev.* **2007**, *31*, 168−192.

(6) Pitson, S. M.; Seviour, R. J.; Mcdougall, B. M. Noncellulolytic fungal β-glucanases—Their physiology and regulation. *Enzyme Microb. Technol.* **1993**, *15*, 178−192.

(7) Steluti, R. M.; Giese, E. C.; Piggato, M. M.; Sumiya, A. F. G.; Covizzi, L. G.; Job, A. E.; Cardoso, M. S.; Da Silva, M. D.; Dekker, R. F. H.; Barbosa, A. M. Comparison of Botryosphaeran production by the ascomyceteous fungus *Botryosphaeria* sp., grown on different carbohydrate carbon sources, and their partial structural features. *J. Basic Microbiol.* **2004**, *44*, 480−486.

(8) Corradi da Silva, M. L.; Fukuda, E. K.; Vasconcelos, A. F. D.; Dekker, R. F. H.; Matias, A. C.; Monteiro, N. K.; Cardoso, M. S.; Barbosa, A. M.; Silveira, J. L. M.; Sassaki, G. L.; Carbonero, E. R. Structural characterization of the cell wall D-glucans isolated from the mycelium of *Botryosphaeria rhodina* MAMB-05. *Carbohydr. Res.* **2008**, *343*, 793−798.

(9) Giese, E. C.; Dekker, R. F. H.; Scarminio, I. S.; Barbosa, A. M.; da Silva, R. Comparison of β-1,3-glucanase production by *Botryosphaeria rhodina* MAMB-05 and *Trichoderma harzianum* Rifai and its optimization using a statistical mixture design. *Biochem. Eng. J.* **2011**, *53*, 239−243.

(10) Barbosa, A. M.; Steluti, R. M.; Dekker, R. F. H.; Cardoso, M. S.; da Silva, M. L. C. Structural characterization of Botryosphaeran: A (1 → 3;1 → 6)-β-D-glucan produced by the ascomyceteous fungus, *Botryosphaeria* sp. *Carbohydr. Res.* **2003**, *338*, 1691−1698.

(11) Cunha, M. A. A.; Turmina, J. A.; Ivanov, R. C.; Barroso, R. R.; Marques, P. T.; Fonseca, E. A. I.; Fortes, Z. B.; Dekker, R. F. H.; Khaper, N.; Barbosa, A. M. Lasiodiplodan, an exocellular (1→6)-β-D-glucan from *Lasiodiplodia theobromae* MMPI: Production on glucose, fermentation kinetics, rheology and anti-proliferative activity. *J. Ind. Microbiol. Biotechnol.* **2012**, *39*, 1179−1188.

(12) Vogel, H. J. A convenient growth medium for *Neurospora crassa*. *Microb. Genet. Bull.* **1956**, *13*, 42−43.

(13) Harju, S.; Fedosyuk, H.; Peterson, K. R. Rapid isolation of yeast genomic DNA: Bust n' grab. *BMC Biotechnol.* **2004**, *4*, 8.

(14) Esteve-Zarzoso, B.; Belloch, C.; Uruburu, F.; Querol, A. Identification of yeasts by RFLP analysis of the 5.8S rRNA gene and the two ribosomal internal transcribed spacers. *Int. J. Syst. Bacteriol.* **1999**, *49*, 329−337.

(15) Larkin, M. A.; Blackshields, G.; Brown, N. P.; Chenna, R.; McGettigan, P. A.; McWilliam, H.; Valentin, F.; Wallace, I. M.; Wilm, A.; Lopez, R.; Thompson, J. D.; Gibson, T. J.; Higgins, D. G. Clustal W and Clustal X version 2.0. *Bioinformatics* **2007**, *23*, 2947−2948.

(16) Hall, T. A. BioEdit: A user-friendly biological sequence alignment editor and analysis program for Windows 95/98/NT. *Nucleic Acids Symp. Ser.* **1999**, *41*, 95−98.

(17) Tamura, K.; Stecher, G.; Peterson, D.; Filipski, A.; Kumar, S. MEGA6: Molecular evolutionary genetics analysis version 6.0. *Mol. Biol. Evol.* **2013**, *30*, 2725−2729.

(18) Giese, E. C.; Covizzi, L. G.; Borsato, D.; Dekker, R. F. H.; da Silva, M. D.; Barbosa, A. M. Botryosphaeran, a new substrate for the production of β-1,3-glucanases by *Botryosphaeria rhodina* and *Trichoderma harzianum* Rifai. *Process Biochem.* **2005**, *40*, 3783−3788.

(19) Somogyi, M. A new reagent for the determination of sugars. *J. Biol. Chem.* **1945**, *160*, 61−68.

(20) Dubois, M.; Gilles, K. A.; Hamilton, J. K.; Rebers, P. A.; Smith, F. Colorimetric method for determination of sugars and related substances. *Anal. Chem.* **1956**, *28*, 350−356.

(21) Hartree, E. F. Determination of protein: A modification of the lowry method that gives a linear photometric response. *Anal. Biochem.* **1972**, *48*, 422−427.

(22) Fleet, G. H. Yeast interactions and wine flavour. *Int. J. Food Microbiol.* **2003**, *86*, 11−22.

(23) Baffi, M. A.; Tobal, T.; Lago, J. H. G.; Boscolo, M.; Gomes, E.; Da-Silva, R. Wine aroma improvement using a β-glucosidase preparation from *Aureobasidium pullulans*. *Appl. Biochem. Biotechnol.* **2013**, *169*, 493−501.

(24) Blättel, V.; Larisika, M.; Pfeiffer, P.; Nowak, C.; Eich, A.; Eckelt, J.; Konig, H. β-1,3-Glucanase from *Delftia tsuruhatensis* strain MV01 and its potential application in vinification. *Appl. Environ. Microbiol.* **2011**, *77*, 983−990.

(25) Hardie, W. J.; O'Brien, T. P.; Jaudzems, V. G. Morphology, anatomy and development of the pericarp after anthesis in grape, *Vitis vinifera* L. *Aust. J. Grape Wine Res.* **1996**, *2*, 97−142.

(26) Combina, M.; Mercado, L.; Borgo, P.; Elia, A.; Jofre, V.; Ganga, A.; Martinez, C.; Catania, C. Yeasts associated to Malbec grape berries from Mendoza, Argentina. *J. Appl. Microbiol.* **2005**, *98*, 1055−1061.

(27) Skory, C. D.; Freer, S. N.; Bothast, R. J. Properties of an intracellular β-glucosidase purified from the cellobiose-fermenting yeast *Candida wickerhamii*. *Appl. Microbiol. Biotechnol.* **1996**, *46*, 353−359.

(28) Delacruz, J.; Rey, M.; Lora, J. M.; Hidalgogallego, A.; Dominguez, F.; Pintortoro, J. A.; Llobell, A.; Benitez, T. Carbon source control on β-glucanases, chitobiase and chitinase from *Trichoderma harzianum*. *Arch. Microbiol.* **1993**, *159*, 316−322.

(29) Wang, X.; Chi, Z.; Yue, L.; Li, J. Purification and characterization of killer toxin from a marine yeast *Pichia anomala* YF07b against the pathogenic yeast in crab. *Curr. Microbiol.* **2007**, *55*, 396−401.

(30) Schoch, C. L.; Seifert, K. A.; Huhndorf, S.; Robert, V.; Spouge, J. L.; Levesque, C. A.; Chen, W. Nuclear ribosomal internal transcribed spacer (ITS) region as a universal DNA barcode marker for Fungi. *Proc. Natl. Acad. Sci. U. S. A.* **2012**, *109*, 6241−6246.

(31) Gostincar, C.; Ohm, R.; Kogej, T.; Sonjak, S.; Turk, M.; Zajc, J.; Zalar, P.; Grube, M.; Sun, H.; Han, J.; Sharma, A.; Chiniquy, J.; Ngan, C.; Lipzen, A.; Barry, K.; Grigoriev, I.; Gunde-Cimerman, N. Genome sequencing of four *Aureobasidium pullulans* varieties: Biotechnological potential, stress tolerance, and description of new species. *BMC Genomics* **2014**, *15*, 549.

(32) Crognale, S.; Bruno, M.; Fidaleo, M.; Moresi, M.; Petruccioli, M. Production of β-glucan and related glucan-hydrolases by *Botryosphaeria rhodina*. *J. Appl. Microbiol.* **2007**, *102*, 860−871.

(33) Chi, Z. M.; Wang, F.; Chi, Z.; Yue, L. X.; Liu, G. L.; Zhang, T. Bioproducts from *Aureobasidium pullulans*, a biotechnologically important yeast. *Appl. Microbiol. Biotechnol.* **2009**, *82*, 793−804.

(34) Muramatsu, D.; Iwai, A.; Aoki, S.; Uchiyama, H.; Kawata, K.; Nakayama, Y.; Nikawa, Y.; Kusano, K.; Okabe, M.; Miyazaki, T. β-

DOI: 10.1021/jf504333h
J. Agric. Food Chem. 2015, 63, 269−278

Glucan derived from *Aureobasidium pullulans* is effective for the prevention of influenza in mice. *PLoS One* **2012**, *7* (7), No. e41399.
(35) Rodriguez, M. E.; Lopes, C.; Valles, S.; Giraudo, M. R.; Caballero, A. Selection and preliminary characterization of β-glycosidases producer Patagonian wild yeasts. *Enzyme Microb. Technol.* **2007**, *41*, 812−820.
(36) Barbagallo, R. N.; Spagna, G.; Palmeri, R.; Restuccia, C.; Giudici, P. Selection, characterization and comparison of β-glucosidase from mould and yeasts employable for enological applications. *Enzyme Microb. Technol.* **2004**, *35*, 58−66.
(37) Belancic, A.; Gunata, Z.; Vallier, M. J.; Agosin, E. Beta-glucosidase from the grape native yeast *Debaryomyces vanrijiae*: Purification, characterization, and its effect on monoterpene content of a Muscat grape juice. *J. Agric. Food Chem.* **2003**, *51*, 1453−1459.
(38) Xu, Z. W.; Shih, M. C.; Poulton, J. E. An extracellular exo-β-(1,3)-glucanase from *Pichia pastoris*: Purification, characterization, molecular cloning, and functional expression. *Protein Expression Purif.* **2006**, *47*, 118−127.
(39) Barbosa, A. M.; Dekker, R. F. H.; Giese, E. C. *Bioactive Oligosaccharides: Production, Biological Functions and Potential Commercial Applications*; Nova Science Publishers, Inc.: Hauppauge, NY, 2010.
(40) Giese, E. C.; Covizzi, L. G.; Dekker, R. F. H.; Monteiro, N. K.; da Silva, M. D. C.; Barbosa, A. M. Enzymatic hydrolysis of botryosphaeran and laminarin by β-1,3-glucanases produced by *Botryosphaeria rhodina* and *Trichoderma harzianum* Rifai. *Process Biochem.* **2006**, *41*, 1265−1271.
(41) Otaka, K. Functional oligosaccharide and its new aspect as immune modulation. *J. Biol. Macromol.* **2006**, *6*, 3−9.
(42) Barsanti, L.; Vismara, R.; Passarelli, V.; Gualtieri, P. Paramylon (β-1,3-glucan) content in wild type and WZSL mutant of *Euglena gracilis*. Effects of growth conditions. *J. Appl. Phycol.* **2001**, *13*, 59−65.
(43) Giese, E. C.; Dekker, R. F. H.; Barbosa, A. M.; da Silva, R. Triple helix conformation of botryosphaeran, a (1 → 3;1 → 6)-β-D-glucan produced by *Botryosphaeria rhodina* MAMB-05. *Carbohydr. Polym.* **2008**, *74*, 953−956.
(44) Vasconcelos, A. F. D.; Monteiro, N. K.; Dekker, R. F. H.; Barbosa, A. M.; Carbonero, E. R.; Silveira, J. L. M.; Sassaki, G. L.; da Silva, R.; da Silva, M. D. C. Three exopolysaccharides of the β-(1 → 6)-D-glucan type and a β-(1 → 3;1 → 6)-D-glucan produced by strains of *Botryosphaeria rhodina* isolated from rotting tropical fruit. *Carbohydr. Res.* **2008**, *343*, 2481−2485.
(45) Iacomini, M.; Gorin, P. A. J.; Baron, M.; Tulloch, A. P.; Mazurek, M. Novel D-glucans obtained by dimethyl-sulfoxide extraction of the lichens *Letharia vulpina*, *Actinogyra muehlenbergii*, and an *Usnea* sp. *Carbohydr. Res.* **1988**, *176*, 117−126.
(46) Pitson, S. M.; Seviour, R. J.; McDougall, B. M. Effect of carbon source on extracellular (1 → 3)- and (1 → 6)-β-glucanase production by *Acremonium persicinum*. *Can. J. Microbiol.* **1997**, *43*, 432−439.
(47) Zhang, R.; Edgar, K. J. Properties, chemistry, and applications of the bioactive polysaccharide curdlan. *Biomacromolecules* **2014**, *15*, 1079−1096.
(48) Grandpierre, C.; Janssen, H. G.; Laroche, C.; Michaud, P.; Warrand, J. Enzymatic and chemical degradation of curdlan targeting the production of β-(1→3) oligoglucans. *Carbohydr. Polym.* **2008**, *71*, 277−286.
(49) Kurakake, M.; Yamanouchi, Y.; Kinohara, K.; Moriyama, S. Enzymatic properties of β-1,3-glucanase from *Streptomyces* sp. Mo. *J. Food Sci.* **2013**, *78*, C502−C506.

NOTE ADDED AFTER ASAP PUBLICATION

This article published January 5, 2015 with an error in the total number of aligned positions in the final dataset of the Materials and Methods Section; and an incorrect BS value in the Results Section. The corrected version posted January 5, 2015.

DOI: 10.1021/jf504333h
J. Agric. Food Chem. 2015, 63, 269−278

JOURNAL OF AGRICULTURAL AND FOOD CHEMISTRY

Article

pubs.acs.org/JAFC

Identification of Edible Bird's Nest with Amino Acid and Monosaccharide Analysis

Yong Guan Chua,[‡] Sheot Harn Chan,[†] Bosco Chen Bloodworth,[†] Sam Fong Yau Li,[‡] and Lai Peng Leong*[,‡]

[†]Food Laboratory, Centre of Analytical Sciences, Health Sciences Authority, 11 Outram Road, Singapore 169078

[‡]Department of Chemistry, National University of Singapore, 3 Science Drive 3, Singapore 117543

Supporting Information

ABSTRACT: This study describes the approach of amino acid and monosaccharide combined with Hotelling T2 range plot to identify edible bird nests (EBN) and non-EBN. Prior to the approach, an analytical method was developed and validated to quantify monosaccharides in EBN. Hotelling T2 range plots of both compounds were successful in predicting the different types of EBN and differentiating EBN and non-EBN. This outcome suggests EBN contains a group of glycoproteins which is not affected by the EBN's coloration, country of origin, and/or the processing method of the food item. In addition, the glycoproteins were shown to be unique to EBN. EBN were revealed to be rich in protein and essential amino acids as well as contain a wider variety of monosaccharides than most food items. The overall findings suggest that amino acid and monosaccharide provide information not only on the detected compounds and also insights into the glycoproteins of EBN.

KEYWORDS: *edible bird's nest, amino acid, monosaccharide, Hotelling T2 range plot*

INTRODUCTION

Edible bird's nests (EBN) are known to be a invaluable food made from the salivary secretion of the *Aerodramus* genus (commonly known as swiftlets) located mainly in the South East Asian countries or regions within this geographical range.[1] It is a highly esteemed food item, especially among the Chinese, as it has been shown to have an inhibitory effect toward the flu virus and helps maintain a youthful, radiant complexion.[3] These therapeutic effects are due to the sialyl-sugar chains and epidermal growth factor in EBN, respectively.[5,6] In spite of the long history of EBN consumption dating back to 618 AD, the first scientific study on EBN was conducted only in the early 20th century to determine the proximate protein and carbohydrate content.[7] It was revealed that the largest compositional fraction of EBN is protein followed by carbohydrate. As such, many new analytical methods have been developed, especially in the past decade, to understand the characteristic structure of the protein and carbohydrate in EBN. These analytical methods can be divided into 2 categories: molecular biological methods and chemical methods.

Molecular biological based methods, such as electrophoresis, are some of the earliest methods used to study the major biological macromolecule in EBN, protein. In the study by Roussel et al., it was demonstrated that electrophoresis was capable of isolating the proteins in EBN.[7] In addition, the authors further deduced that the proteins were rich in serine, threonine, and proline. This study laid the foundation for future work on EBN's protein. Recently, Yang et al. demonstrated the use of SDS-PAGE to isolate two major protein molecules in EBN (106 kDa and 128 kDa).[11] They also performed a detailed analysis on the proteomic profile of EBN using two-dimensional electrophoresis.[2] Though the use of molecular biology based methods in isolating distinguishing and quantifying protein molecules in EBN is achievable, the protein molecules must still be intact, which is often not feasible in the case of a heavily processed food item like EBN.

Chemical methods used for characterization of EBN are generally based on chromatographic techniques such as gas chromatography (GC) and liquid chromatography (LC) coupled to different types of detectors. The applications of the GC and LC based analytical platforms have been reported in several research studies to be able to determine structure of the glycans and also a diverse class of compounds such as amino acids, monosaccharides, fatty acids, and hormones in EBN.[8−13] While the use of chemical analytical methods is a useful tool in identifying EBN, the major problem of employing these methods lies in the inadequate number of samples to represent the entire spectrum of EBN. In view of the limitations and drawbacks on current studies, it is important to develop a new approach to identify EBN and non-EBN.

Amino acid and monosaccharide are promising candidates for the identification of EBN as they are the monomeric constituents of protein and carbohydrate in EBN.[18,19] Although determination of both amino acids and monosaccharides is a relatively complex process, amino acids and monosaccharides are preferred over their polymers.[23] This is because EBN is a food item that is cleaned by soaking it in water and drying under high temperature for a long period of time.[8] These cleaning processes are likely to trigger the denaturation and breakdown of the polymers, protein and carbohydrate, which would cause inaccuracy in quantification of the polymers. On

Received: July 4, 2014
Revised: November 11, 2014
Accepted: November 13, 2014
Published: November 13, 2014

ACS Publications © 2014 American Chemical Society

the other hand, amino acid and monosaccharide are relatively stable even when the samples are soaked in water and/or subjected to heat.[24,25] Additional information on the type of protein and carbohydrate could also be provided by the analysis of amino acid and monosaccharide. Hence, amino acid and monosaccharide analysis are selected for this study.

The aim of this study is to demonstrate the potential of amino acid and monosaccharide analysis, combined with Hotelling T2 range plot, to identify EBN and non-EBN. Hotelling T2 range plot is a chemometrics plot which reduces the amino acids and monosaccharides into a T2 value. This plot simplifies the data analysis process and, more importantly, combines multiple variables to create a unique fingerprint for the sample. Its application is often found in quality control of products.[20−22] In this study, Hotelling T2 range plot is used to determine whether the sample is an EBN by comparing the T2 value against the T2 critical value, corresponding to 95% confidence interval. The practical applicability of the plot was evaluated with different types of EBN and samples suspected to possess a similar matrix to EBN (non-EBN). Furthermore, EBN will be compared with other food items rich in protein and/carbohydrate to assess the nutrition value of the former. This comprehensive study will, we hope, be able to not only create a new approach in identifying EBN, but also offer insightful information on the monomers (amino acid and monosaccharide) and polymers (protein and carbohydrate) of EBN.

MATERIALS AND METHODS

Information on the Samples and Chemical Reagents. All EBNs used in this Article had been processed by soaking, physical removal of birds' feathers and drying prior to the analysis. The EBN samples are labeled by a number to represent the biological replicate followed by a letter to indicate the different technical replicate in Supporting Information Table 1 (e.g., EBN 1A). The non-EBN samples, cow's milk, chicken egg yolk, chicken egg white, quail egg yolk, and quail egg white, were obtained from the local retailers. The rest of the non-EBN samples (fetuin, infant formula, and human saliva) were obtained from various sources. Fetuin from fetal bovine serum was purchased from Sigma-Aldrich (St Louis, MO) while the standard reference material infant formula, T2562, was purchased from FAPAS. The human saliva was obtained from a male human volunteer. Amino acid standards and the amino acid derivatization kit (EZ: faast GC-FID amino acid analysis kit) were purchased from Phenomenex. The standard used consists of the following 17 amino acids: alanine (1), glycine (2), valine (3), leucine (4), isoleucine (5), threonine (6), serine (7), proline (8), aspartic acid (9), methionine (10), 4-hydroxyproline (11), glutamic acid (12), phenylalanine (13), lysine (14), hydroxylysine (15), tyrosine (16), and cystine (17). The internal standard for amino acid analysis is norvaline. The chemicals 1-phenyl-3-methyl-5-pyrazolone (PMP) and trifluoroacetic acid were obtained from Aldrich (St. Louis, MO). The 7 monosaccharides, mannose (1), glucose (2), galactose (3), rhamnose (4), fucose (5), ribose (6), and xylose (7), used in the standards were purchased from Sigma-Aldrich (St. Louis, MO). The internal standard (D-glucose-$^{13}C_6$) was purchased from Cambridge Isotope Laboratories. All the other reagents utilized were of analytical grade.

Amino Acid Analysis. EBN (0.2 g) was hydrolyzed with concentrated HCl (6 N) for 24 h. The hydrolyzed sample was filtered and dried using a rotary evaporator. The dried extract was reconstituted with 10 mL of hydrochloric acid (0.1 N) The reconstituted sample was further diluted 20 times prior to mixing 100 μL of the diluted solution with 100 μL of internal standard. A 1.5 mL syringe with a sorbent tip was then immersed into the mixture solution, and the mixture solution was drawn up the sorbent tip. Next, 200 μL of deionized water was added and was drawn up the sorbent tip. Subsequently, the 1.5 mL syringe was replaced with a 0.6 mL syringe. A mixture solution of sodium hydroxide and n-propanol, consisting of 1 portion of n-propanol to 1.5 portion of sodium hydroxide, was prepared. A 200 μL portion of the mixture solution of sodium hydroxide and n-propanol was pipetted into the sample preparation vial. The mixture solution was drawn up the 0.6 mL syringe, and all the liquid and sorbent particles were ejected into the sample preparation vial. Next, 50 μL of the derivatizing agent was added to the mixture followed by 100 μL of iso-octane and then 100 μL of hydrochloric acid solution. The mixture was vortexed for 0.5 min after each chemical reagent was added into the preparation vial. The emulsion was allowed to stand for 1 min so that two distinct layers would appear. The upper layer is then transfer into a 1 mL vial for the analysis with a Hewlett-Packard 6890 Series GC system coupled to an Aligent Technologies 7683 series injector and flame ionization detector (FID). The Zebron ZBAAA (10 m × 0.25 mm capillary GC column) was used for the GC separation. The carrier gas (helium) had a flow rate of 1.5 mL/min. The column oven temperature was programmed to start at 110 °C and to increase at 32 °C per min to 320 °C. The FID detector temperature was set at 320 °C. A 2 μL portion was injected by an autosampler at an injection temperature of 250 °C and a split level of 1:2. The software Chemstation was used to analyze the results.

Monosaccharides Analysis. A 2 μg portion of EBN was hydrolyzed in 2.0 mL of trifluoroacetic acid (2 M) at 120 °C for 4 h. After that, the hydrolyzed solution was cooled to room temperature prior to filtration into a round-bottom flask with a 0.45 μm PTFE filter. Next, the hydrolyzed solution was evaporated to dryness, and the dried extract was reconstituted with 3 mL of water. Two solutions, 0.75 M of PMP dissolved in methanol and 50:50, v/v ammonium hydroxide/deionized water, were prepared for the derivatization reaction. A 750 μL portion of PMP solution, 450 μL of ammonia hydroxide, and 10 μL of the internal standard (100 mg/L) were added to 150 μL of the reconstituted monosaccharide solution. The mixture solution was then vortexed and incubated in a heating block at 70 °C for 2 h to permit derivatization to occur. Then, the mixture solution was evaporated to dryness using a gentle stream of nitrogen gas. Finally, the mixture solution was reconstituted with 150 μL of ACN and 850 μL of water prior to sending it to an Agilent 1100 LC system coupled to an API 3000 Q-Trap liquid chromatography tandem mass spectrometer (LC/MSMS) with Turbolon Spray source (Applied Biosystems, Foster City, CA) for analysis. The analytical column Inertsil HPLC column (ODS-3, 3 μm particle size, 3 mm i.d. × 100 mm) produced by G.L. Sciences, Tokyo, Japan, was used for the separation of the monosaccharides. The injection volume was 10 μL. Elution was carried out with a flow rate of 0.35 mL/min at 25 °C. The mobile phase consisted of 100 mM ammonia acetate (pH 6.9) with (A) 0% of acetonitrile and (B) 60% acetonitrile. The condition of the mobile phase is follows: 30−35% B (0.0−25.0 min), isocratic at 35% B (25.0−30.0 min), 35−55% B (30.0−50.0 min), 55−30% B (50.0−50.1 min), isocratic at 30% B (50.1−55.0 min). The mass spectrometer (MS) was equipped with an electrospray ionization interface operating in the positive mode. The MS parameters are stated in Supporting Information Table 2. The software Analyst Software 1.4.2 was utilized to analyze the results obtained from the samples.

Statistical Analysis. The normalized data from both analyses were exported to SIMCAP+ software package version 13 (Umetrics, Umea, Sweden) for chemometrics analysis. Significance calculation was based on a two-tailed Student's t test performed with Microsoft Excel software (Microsoft Corporation). Compounds with $p > 0.05$ are considered to have no significant difference. The data was divided into model set and prediction set. The model set comprises genuine EBNs, and it is used to establish the Hotelling T2 range plot. EBN for the model set were collected at random by the authors from an EBN farm located in Johor Bahru, Malaysia, to ensure the integrity and quality of the food item from farm to fork. In the model set, each EBN has three technical replicates to factor in the variation of the analytical method. The prediction set consists of EBNs to account for variation in color and country origin of the food item. Each EBN is also analyzed three times in the prediction set. The prediction set is utilized to determine

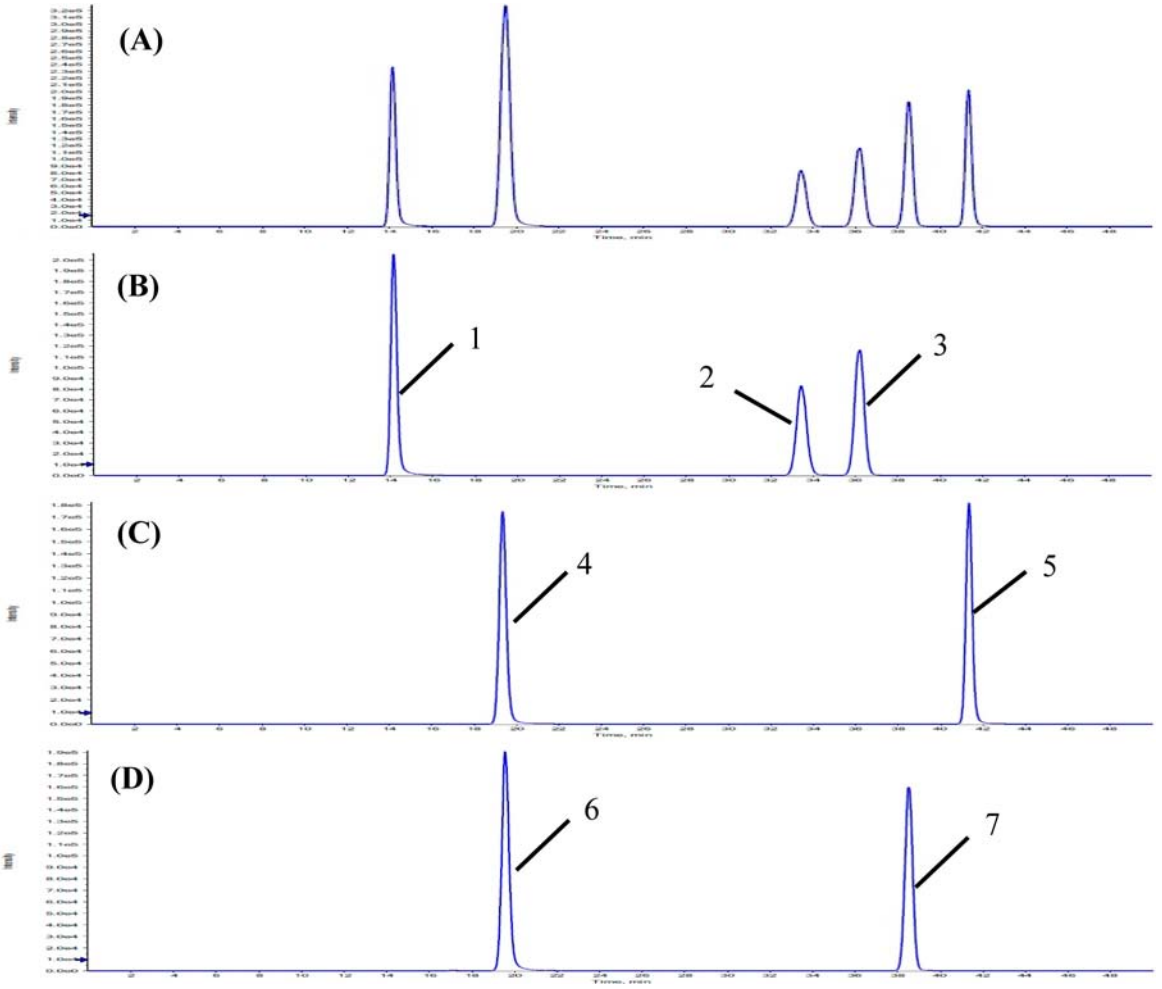

Figure 1. Chromatograms of a 10 000 ppm monosaccharide standard. (A) Total ion chromatogram. (B) Extracted ion chromatogram for mannose, glucose, and galactose (m/z 511.4 → 175.1). (C) Extracted ion chromatogram for rhamnose and fucose (m/z 495.3 → 175.1). (D) Extracted ion chromatogram for ribose and xylose (m/z 481.2 → 175.0). The monosaccharides are labeled on the basis of the Information on the Samples and Chemical Reagents section.

the optimal scaling method and to serve as an independent group of EBN for validation.

RESULTS AND DISCUSSION

Development and Validation of an Analytical Method for the Monosaccharide Analysis of EBNs. In this study, the amino acid and monosaccharide content of EBN was analyzed. The analytical method used to determine amino acids is a well-established one. It has been demonstrated by Ruiz et al. that the accurate quantification of amino acids could be performed within a short analysis time of 10 min with GC-FID.[29] Hence, this analytical method was employed in the study for the quantification of the amino acid content in EBN. On the other hand, the analysis of monosaccharides is not as straightforward. Studies have revealed that the monosaccharides originated mainly from the glycans of EBNs.[12,30] As such, it is expected that the monosaccharides' concentration may differ by a few orders of magnitude due to the minute presence of some monosaccharides in the glycans.[31] Thus, the analytical method employed to analyze the monosaccharides requires a large dynamic range to take into account this fact. However, at the moment, most analytical methods do not possess the required dynamic range to quantify the monosaccharides in EBN.[32] In addition, low resolution and long analysis time often hinder the accuracy and efficiency of the available analytical methods.[33] Hence, a new analytical method would have to be developed and validated.

Acid hydrolysis is performed to release the monosaccharides in this study. This is an indiscriminating method which implies that monosaccharides would be released from all the oligosaccharides and/or polysaccharides in EBN.[34] Hence, besides the quantification of common neutral monosaccharides in glycans, mannose, glucose, galactose, fucose, and xylose, it is also important to include monosaccharides like rhamnose and ribose as they exhibit a high possibility to be in polysaccharide.[35] After the liberation of monosaccharides, LC/MSMS in MRM mode was utilized to analyze the monosaccharides. This is because the analytical platform is able to make use of the advantages provided by both the gradient flow of the mobile phase and the MRM mode to improve the resolution and sensitivity of the analysis.

However, it has reported that MS detection would not be able to achieve the dynamic range for monosaccharide analysis as monosaccharides have poor MS/MS fragmentation.[36] Thus, a derivatization step is incorporated into the analytical method. The derivatizing agent chosen was PMP because the monosaccharide PMP derivative possesses excellent fragmentation efficiency for MS detection.[37] In addition, the derivatiza-

dx.doi.org/10.1021/jf503157n | J. Agric. Food Chem. 2015, 63, 279−289

tion reaction could be conducted under mild conditions, and no isomerization of the derivatized monosaccharides would occur.[38] Referring to Figure 1, it is observed that chromatographic separation of mannose, glucose and galactose, rhamnose and fucose, ribose and xylose was achieved with the gradient flow of the mobile phase while coeluting monosaccharides are differentiated with the MRM mode.

The optimized analytical method was also applied onto monosaccharide standards with concentration range 50−10 000 ppb. The linearity of all 7 monosaccharides was evaluated by inspecting the peak area as a function of concentration. Excellent correlation coefficients (>0.99) were obtained from the calibration curves of the monosaccharaides. The retention time, limits of detection (LODs), and limits of quantification (LOQs) were tabulated in Table 1. The LODs and LOQs are observed to be lower than the reported literature values.[37] Moreover, the small fluctuation in retention times and high correlation coefficient provided confidence for the quantification of the 7 monosaccharides using the developed analytical method.

Table 1. Retention Time, Linearity, LOQ, and LOD for Seven Monosaccharides (n = 6)

compd name	equation	linearity	LOQ (ppb)	LOD (ppb)
mannose	$y = 2.30x - 0.0634$	1.000	10	5
glucose	$y = 1.35x + 0.0033$	0.990	20	10
galactose	$y = 0.25x + 0.0011$	1.000	20	10
rhamnose	$y = 2.19x - 0.0696$	0.990	10	5
fucose	$y = 2.07x + 0.0180$	1.000	10	5
ribose	$y = 2.47x - 0.0474$	1.000	10	5
xylose	$y = 2.20x + 0.015$	1.000	10	5

The reference material, fetuin, was used to validate the monosaccharide analysis. Fetuin was utilized because similarly to EBN, it is a matrix rich in glycoproteins.[39] Besides, fetuin is a well-established glycoprotein that has been used in the validation of analytical methods involved in the quantification of monosaccharides from carbohydrate.[33] An intra- and interday study was conducted on the reference material. Results of the validation were in good agreement with the stated literature range of the reference material (Table 2).[25,33,40,41] Excellent RSDs for the monosaccharides were achieved utilizing the analytical method (RSD < 5%). Interestingly, several monosaccharides like glucose, rhamnose, and xylose were noted to be present in the fetuin even though they are not part of the glycoprotein in fetuin. This is possibly due to monosaccharides attaching to the glycoprotein through glycation.[40]

Although the amino acid analysis has been established, an intra- and interday study was conducted with infant formula to verify the accuracy and precision of the analytical method. The results were in agreement with the state values of the reference material and the RSDs were below 6% (Supporting Information Table 3).

Establishing the Hotelling T2 Range Plot To Identify EBN. The amino acid and monosaccharide chromatograms representing the EBN were illustrated in Figure 2. Visual inspection of the amino acid chromatograms reveals that 17 amino acids were detected in the EBN. It was noted that several amino acids such as tryptophan, asparagine, and glutamine are not detected in EBN. This is due to the utilization of acid hydrolysis to liberate the amino acids before the chromatographic analysis. This approach would result in the hydrolysis of tryptophan and the deamidation of asparagine and glutamine into aspartic acid and glutamic acid, respectively.[42] It was also observed from the amino acid chromatogram that there are no obvious differences between the EBNs from the model and prediction set. On the other hand, 7 monosaccharides were detected in EBN, and there was no clear distinction between the EBNs from the model and prediction set. This provides the confidence that it is viable to establish a Hotelling T2 range plot with both types of analysis to identify EBN.

Amino acids and monosaccharides have been used in the past to differentiate food items that are suspected to have a similar matrix.[43,44] Such studies rely on the fact that the polymers of amino acids and monosaccharides, protein and carbohydrate, would exhibit variation if they are produced from different species. However, in this study, the authors utilized a different approach: the homogeneity of amino acids and monosaccharides. EBN is a food item that is known to be produced by *Aerodramus* genus. Thus, EBNs are expected to exhibit a homogeneous amino acid and monosaccharide signature as they originate from the same species.

In this study, the data from amino acid and monosaccharide analysis was combined with PCA to identify the EBN. PCA is known to be capable of reducing the complex data from individual amino acid and monosaccharide chromatogram into a single score on the score plot. The scores are then utilized to deduce the confidence region known as Hotelling T2 ellipse. Studies have shown that the scaling method has a direct impact on the prediction ability of the score plot as it changes the weights of the variables. As such, three different scaling methods, uv scaling, par scaling, and no scaling, were performed to determine the ideal scaling method to be employed to identify EBN. The PCA score plots for the different scaling methods are displayed in Supporting Information Figures 1 and 2. It was observed that no score was found located beyond the

Table 2. Validation Result on the Monosaccharide Analysis of Fetuin (n = 6)[a]

		intraday			interday		
compd name	assigned range (mg/g sample)	mean (mg/g sample)	SD	RSD (%)	mean (mg/g sample)	SD	RSD (%)
mannose	25.15 ± 2.15	23.41	0.70	2.99	24.09	0.69	2.87
galactose	39.45 ± 6.45	43.11	1.39	3.22	43.17	0.36	0.84
fucose	1.00 ± 1.00	0.83	0.03	4.15	0.87	0.03	3.99
glucose	N.A.	10.30	0.34	3.27	10.33	0.03	0.26
rhamnose	N.A.	0.13	0.00	3.08	0.13	0.00	0.77
ribose	N.A.	0.00	0.00	0.00	0.00	0.00	0.00
xylose	N.A.	2.11	0.10	4.94	2.22	0.09	4.24

[a]SD represents standard deviation. N.A. represents not available.

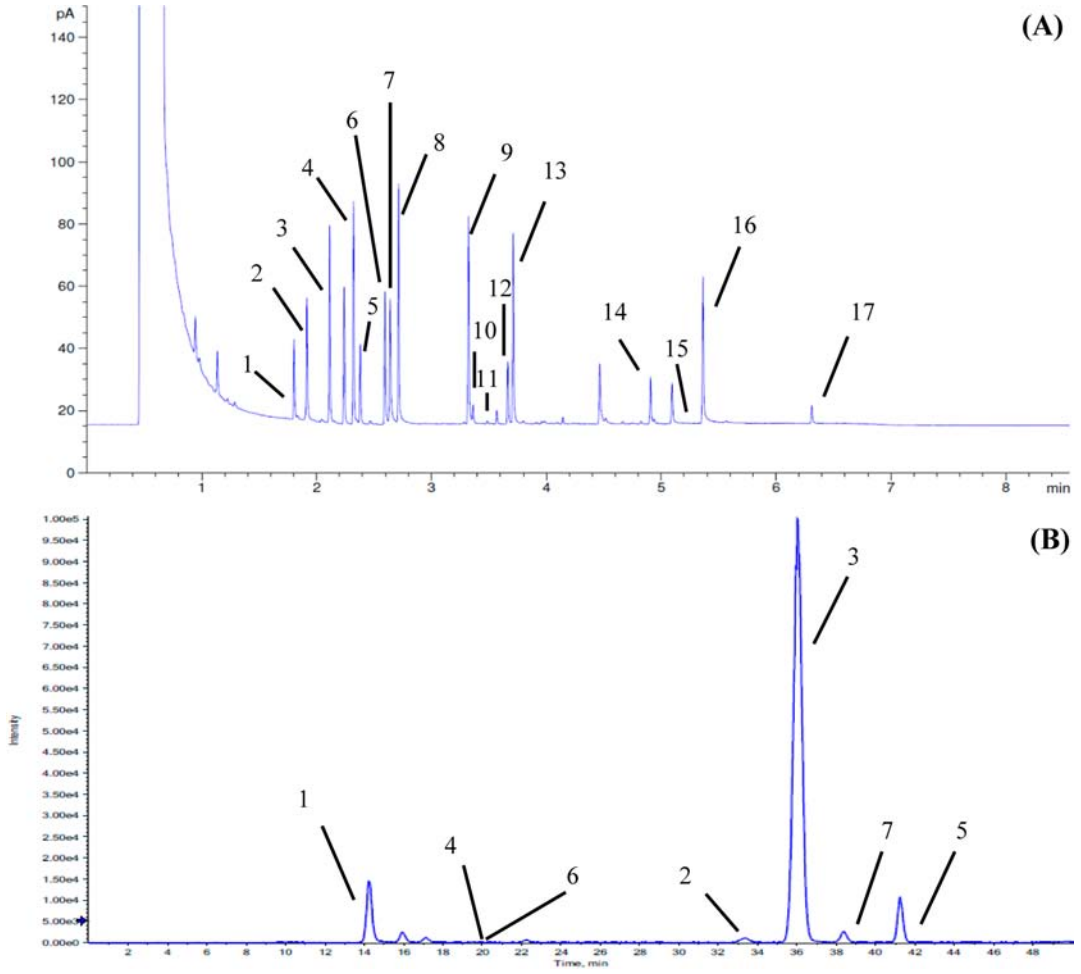

Figure 2. Chromatogram of EBN from the (A) amino acid data and (B) monosaccharide data. The amino acids and monosaccharides are labeled on the basis of the Information on the Samples and Chemical Reagents section.

Hotelling T2 ellipse, at 95% confidence level. In addition, the PCA score plots exhibited satisfactory goodness of fit (R^2) and goodness of prediction (Q^2) that were generally greater than the level of 0.5 (Table 3).

The Hotelling T2 range plots of the respective PCA score plots were plotted to visualize the graphical display in their numerical form. It was evident from the T2 range plots that none of samples from the model set has a T2 range value greater than the T2 critical value (Table 3). Thus, the prediction set would be used to evaluate the different scaled score plots. The result from the amino acid data shows that application of uv scaling (Figure 3A) would result in a Hotelling T2 range plot that could accurately predict all the EBN while par and no scaling would create score plots with low prediction ability (Table 3). Similarly, the score plots based on the monosaccharide data also demonstrated that uv scaling is the ideal scaling method (Figure 3B). Uv scaling involves the division of each variable by its standard deviation. Upon scaling, the variables would have the same weight, thus preventing the dominance of variables with high fluctuations.[47] This indicates that the Hotelling T2 range plots from both data sets have to be unbiased to all the input variables to be able to predict EBN.

The amino acid and monosaccharide content of EBN could be significantly affected by the difference in EBN: coloration, country of origin, and/or type of cleaning method applied to the EBN.[48] Thus, the optimized Hotelling T2 range plots from both data sets were used to perform a study on the different types of EBN. The prediction ability results in Table 3 show that different types of EBN could be accurately predicted by the plots from both data sets, thereby pointing out the feasibility of identifying EBN with amino acid and monosaccharide combined with Hotelling T2 range plot. The success of predicting the different types of EBN also demonstrated that amino acid and monosaccharide content is not significantly

Table 3. Model Performance Parameters and Prediction Ability of Hotelling T2 Range Plots Using Different Types of Scaling Methods

	amino acid			monosaccharide		
	uv scaling	par scaling	no scaling	uv scaling	par scaling	no scaling
Model Parameters						
no. of PCs	3	3	3	2	2	2
$R^2(X)$	0.791	0.824	0.999	0.826	0.906	0.999
$Q^2(X)$	0.524	0.456	0.995	0.560	0.711	0.248
T2 critical value	9.779	9.779	9.779	7.041	7.041	7.041
Prediction Ability						
model set (%)	100	100	100	100	100	100
prediction set (%)	100	98.2	75.7	100	88.3	83.8

dx.doi.org/10.1021/jf503157n | J. Agric. Food Chem. 2015, 63, 279−289

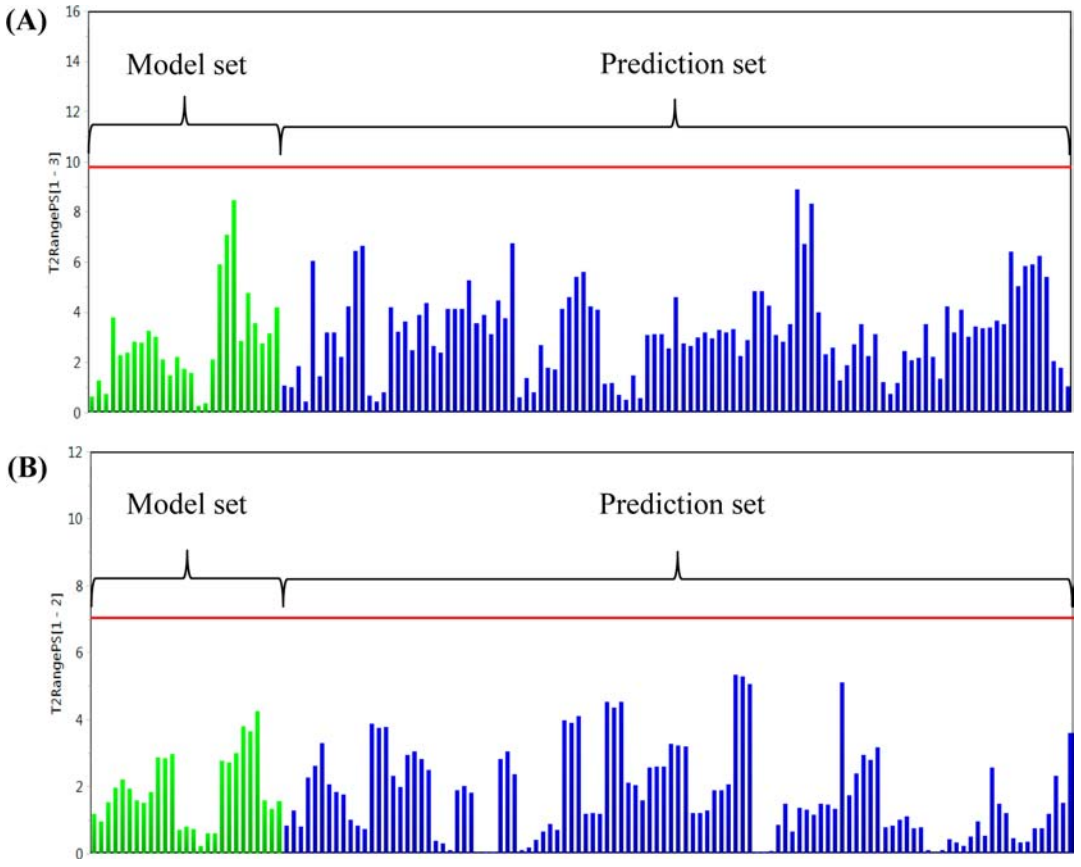

Figure 3. Hotelling T2 range plot of the model set (green) and prediction set (blue). Plot A constructed on the basis of amino acid data subjected to uv scaling. Plot B constructed on the basis of monosaccharide data subjected to uv scaling. Both plots A and B contain a red line representing the critical value.

affected by variation in the coloration, country of origin, and/or type of cleaning method applied to the food item.

Recently, several research studies have demonstrated the existence of common glycoproteins among the EBN with different coloration or country of origin.[3,2] Thus, since the amino acid and monosaccharide originated mainly from the protein and carbohydrate portion of EBN, the similarity in amino acid and monosaccharide could be attributed to the glycoproteins in EBN. In addition, it is suggested the quantity of these glycoproteins is not significantly affected by factors such as coloration, country of origin, and/or type of cleaning method applied to the EBN.

Evaluation of Hotelling T2 Range Plot with Non-EBN. The Hotelling T2 range plots from the amino acid and monosaccharide data were established with 17 amino acids and 7 monosaccharides, respectively. These amino acids and monosaccharides are known to be common building blocks for protein and carbohydrate. As such, it is possible that there are samples which contain similar amino acid and monosaccharide content as EBN. Thus, non-EBN samples are utilized to determine the differentiating capabilities of the Hotelling T2 range plots. These samples were selected because they are known to contain a high quantity of amino acid and monosaccharide or they were being produced in a similar manner as EBN.[43,49,50]

From the examination of the Hotelling T2 range plot in Figure 4, it was observed that the T2 range values for all the non-EBN samples were larger than the T2 critical value for both amino acid and monosaccharide data, thereby affirming that the Hotelling T2 range plot from both data sets are objective parameters to identify EBN and non-EBN. Furthermore, the result suggests that the common glycoproteins in EBN do not exist in non-EBN.

Contribution plot is also applied to visualize the variable contribution difference between EBN and non-EBN.[51] On the basis of the contribution plots on both the amino acid and monosaccharide data, it was observed that the non-EBN would contain several variables which were clearly separated from EBN (Supporting Information Figures 3 and 4). Another interesting observation was that samples such as egg yolk and egg white from chicken and quail exhibited a similar variable profile for their respective data sets. This is not unexpected because these samples are similar products, originating from avian (Supporting Information Figures 3 and 4). However, in the case of milk and infant formula, both originating from cows, the contribution plots for the amino acid data illustrated a dissimilar profile while the opposite is exhibited in the plots based on monosaccharides (Figure 5). This could be attributed to the fact that infant formula is often enriched with amino acids to meet the needs of infant development.[4] Hence, the contribution plot reaffirms that only samples with a similar amino acid or monosaccharide content as EBN could be identified with the Hotelling T2 range plots.

Application of monosaccharide analysis to identify EBN has been reported. In these cases, identification of EBN is based on one or two monosaccharides.[9,45] Such an approach may lead to misinterpretation of samples with a similar matrix as EBN, since monosaccharides are commonly found in animals and plants.

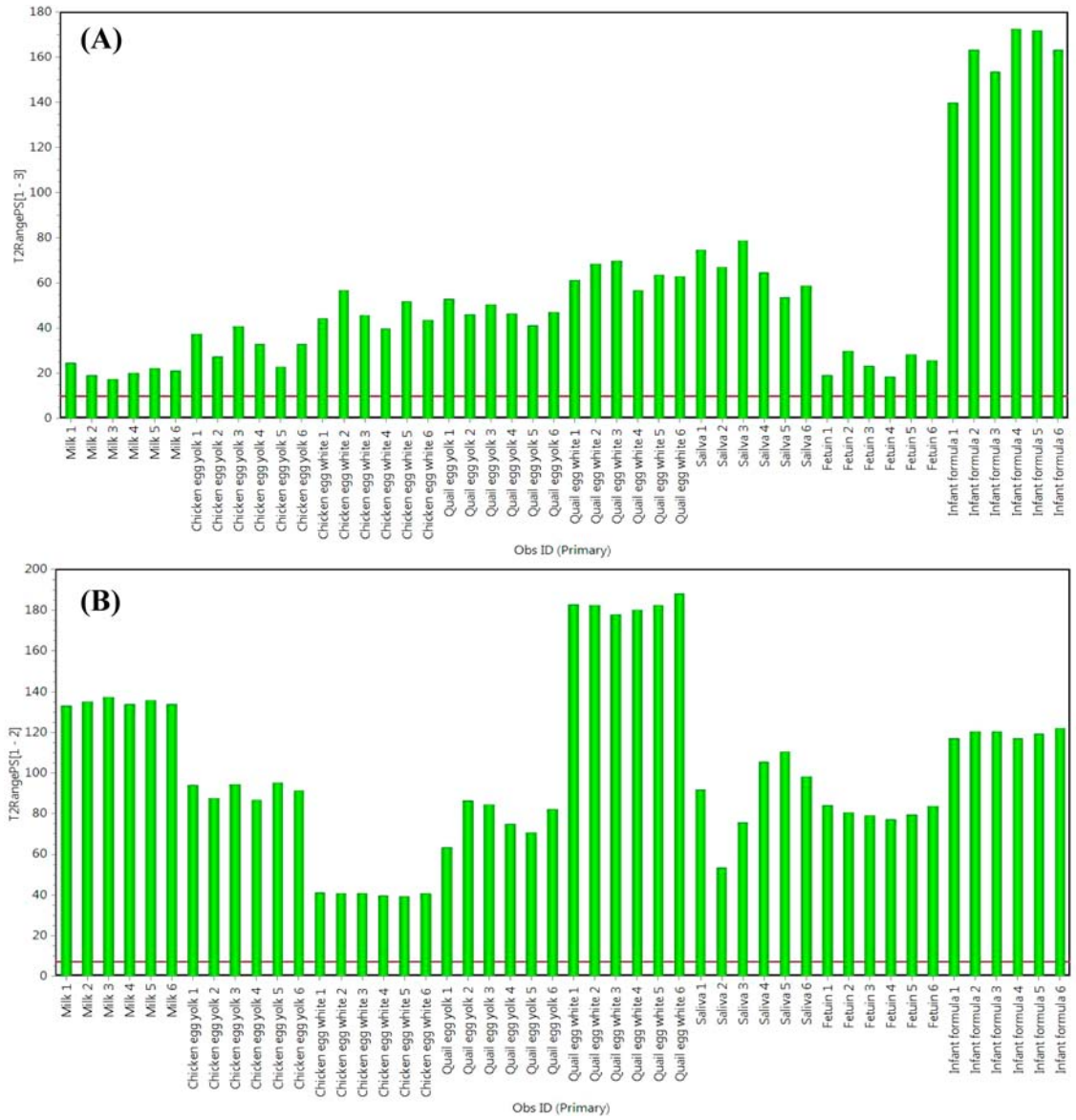

Figure 4. T2 range value of non-EBN from (A) amino acid data and (B) monosaccharide data.

Thus, in this study, identification of EBN is based on T2 range value. This would greatly increase the confidence level of the results as T2 range value is formulated from 7 monosaccharides.

In a comparison of the two types of analyses employed in this study, the amino acid analysis uses GC-FID while the monosaccharide analysis makes use of the LC/MSMS. Despite a difference in the type and monetary value of the analytical instruments utilized, both types of analyses were able to produce reliable results. The sample preparation in the amino acid analysis involves an extraction method taking up to 24 h and a number of steps to derivatize the amino acids. On the other hand, the monosaccharides are liberated using a hydrolysis method within 4 h and then derivatized using a one-step procedure prior to analyzing with LC/MSMS. This greatly reduces the complexity of the monosaccharide analysis. However, the analysis time taken to achieve chromatographic separation in the monosaccharide analysis was much longer than the amino acid analysis, which in turn leads to a lower throughput. As there is no single analysis method deemed to be more favorable than the other, the type of analysis method selected ultimately depends on the availability of the chemicals and machines, as both types of analysis are capable of producing Hotelling T2 range plots that are able to identify EBN and non-EBN.

Assessment of Amino Acid and Monosaccharide Content of EBN. In terms of the amino acid, aspartic acid, proline, and threonine were observed to have the highest concentration in EBN (Table 4). This result is in line with the findings published by Theng et al., and thus increases the reliability of the results on amino acids.[52] Aspartic acid (representing aspartic acid and asparagine) and proline are classified to be nonessential amino acids, implying that they could be synthesized by the human body. On the other hand, threonine is noted to be an essential amino acid (EAA); thus, the only way for humans to obtain this amino acid is through the consumption of food containing the amino acid. EAAs are vital to the well-being of human's health as EAAs are the precursors for protein synthesis and they are required as intermediates in various pathways of metabolism.[53] In fact, due

dx.doi.org/10.1021/jf503157n | J. Agric. Food Chem. 2015, 63, 279−289

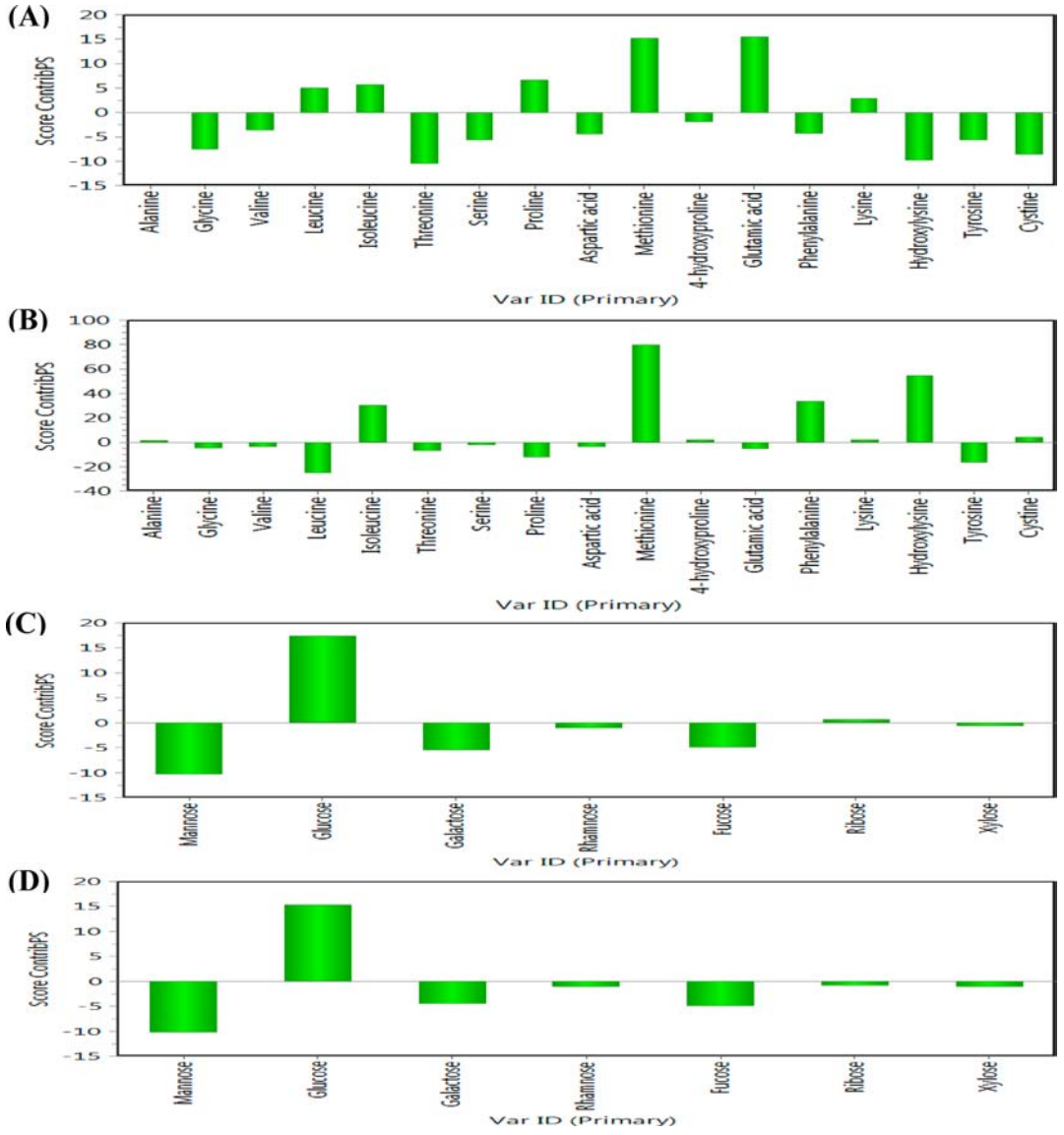

Figure 5. Contribution plots of milk and infant formula: (A) milk and (B) infant formula from amino acid data; (C) milk and (D) infant formula from monosaccharide data.

to the importance of EAA, the World Health Organization, Food and Agriculture Organization of the United Nations, and the United Nations University have set a recommended daily amount for EAAs.[15] The tabulation of amino acids also indicated the presence of two nonproteinogenic amino acids, namely, 4-hydroxyproline and hydroxylsine in EBN. These two amino acids are often used as indicators for the existence of collagen. Thus, it is proposed that the EBN contains collagen.[54,55]

The nutritional value of EBN was also assessed by comparing EBN with protein- and/or carbohydrate-rich food items such as milk, chicken egg yolk, chicken egg white, quail's egg yolk, quail's egg white, and infant formula (Table 4). Generally, the amino acid contents of all the amino acids are higher concentration in EBN than the rest of the food items with the exception of methionine in infant formula, thus illustrating that EBN is a better provider of amino acids than the protein rich food items. The total amino acid content was found to be larger in EBN. This indicates that protein constitutes a larger compositional fraction in the EBN matrix relative to the protein rich food items. EBN is also more enriched in EAAs than the protein and/or carbohydrate rich food items. Studies have shown that a higher EAA content would provide more building blocks for protein synthesis as well as increase the rate of the protein synthetic pathway.[51] As such, apart from the epidermal growth factor in EBN, the high EAA content is suggested to support the growth effects caused by the consumption of EBN.[6]

In the case for the monosaccharide data, the most prominent monosaccharide in EBN is galactose (111.85 μg/g of sample), which is likely to be derived from the glycans in EBN (Table 5). This deduction was made as several studies pointed out that galactose is the major neutral monosaccharide in the glycans of EBN.[13,9] Besides galactose, mannose, glucose, rhamnose fucose, and xylose were suggested to be derived from glycans as well. Ribose is the only monosaccharide that has not been demonstrated to be present in the glycans of EBN.[52] Its presence is most probably due to the DNA in EBN. It was noted from Table 4 that the monosaccharides have a much larger variation as compared to the amino acids; RSD of monosaccharide ranges from about 50% to 90% while it is less

dx.doi.org/10.1021/jf503157n | J. Agric. Food Chem. 2015, 63, 279−289

Table 4. Concentration of the Amino Acids of EBN and the Different Types of Food Items (n = 6)

		concentration of amino acid for different food items (mg/g of sample)						
no.	compd name	EBN	milk	chicken egg yolk	chicken egg white	quail egg yolk	quail egg white	infant formula
1	alanine	14.70 ± 0.93	0.97 ± 0.02	11.24 ± 0.93	7.15 ± 0.99	7.52 ± 0.80	6.67 ± 0.33	3.59 ± 0.15
2	glycine	19.95 ± 1.39	0.51 ± 0.03	6.38 ± 0.46	3.91 ± 0.38	4.73 ± 0.40	4.25 ± 0.11	2.72 ± 0.16
3	valine	36.43 ± 4.56	1.92 ± 0.04	12.08 ± 0.84	8.39 ± 0.82	9.03 ± 0.77	7.56 ± 0.08	6.25 ± 0.29
4	leucine	35.53 ± 2.30	2.86 ± 0.03	16.96 ± 1.26	10.17 ± 0.78	12.94 ± 1.04	9.27 ± 0.16	0.00 ± 0.00
5	isoleucine	15.23 ± 1.76	1.38 ± 0.04	9.97 ± 0.72	5.58 ± 0.50	7.35 ± 0.55	5.19 ± 0.11	10.18 ± 0.64
6	threonine	41.01 ± 2.96	1.01 ± 0.06	9.96 ± 1.81	4.47 ± 1.02	6.91 ± 1.35	6.34 ± 0.72	5.40 ± 0.26
7	serine	37.20 ± 4.16	0.94 ± 0.04	13.67 ± 3.90	5.83 ± 2.22	9.78 ± 2.33	6.60 ± 1.23	6.16 ± 0.35
8	proline	43.56 ± 3.74	3.58 ± 0.12	9.39 ± 0.85	3.91 ± 0.41	6.41 ± 0.53	3.62 ± 0.07	5.22 ± 0.30
9	aspartic acid	53.86 ± 5.09	2.53 ± 0.10	20.32 ± 2.82	13.65 ± 2.10	13.98 ± 2.37	13.32 ± 1.20	9.11 ± 0.33
10	methionine	3.86 ± 0.54	0.82 ± 0.03	2.91 ± 0.16	4.94 ± 0.41	4.19 ± 0.31[a]	3.69 ± 0.08[a]	10.51 ± 0.33
11	4-hydroxyproline	4.57 ± 2.86	0.00 ± 0.00	0.00 ± 0.00	0.00 ± 0.00	0.00 ± 0.00	0.00 ± 0.00	2.04 ± 0.13
12	glutamic acid	34.15 ± 2.73	8.28 ± 0.20	23.87 ± 4.04	19.08 ± 4.70	19.82 ± 4.01	19.68 ± 2.92	0.00 ± 0.00
13	phenylalanine	29.46 ± 2.34	1.52 ± 0.04	8.57 ± 0.76	7.89 ± 0.63	6.79 ± 0.69	6.59 ± 0.28	16.82 ± 0.60
14	lysine	16.22 ± 2.54	1.44 ± 0.09	9.74 ± 2.94	5.99 ± 0.94	7.04 ± 0.80	6.67 ± 1.28	4.60 ± 0.35
15	hydroxylysine	5.57 ± 0.57	0.00 ± 0.00	2.37 ± 0.25	4.59 ± 0.58	2.27 ± 0.19	2.46 ± 0.20	8.05 ± 0.52
16	tyrosine	31.41 ± 2.38	1.31 ± 0.07	7.27 ± 0.83	5.57 ± 0.85	6.05 ± 0.52	4.26 ± 0.27	0.00 ± 0.00
17	cystine	16.42 ± 1.93	0.00 ± 0.00	4.96 ± 0.82	6.77 ± 0.71	4.30 ± 0.51	4.74 ± 0.17	5.27 ± 0.47
	total EAA	177.75 ± 13.76	10.95 ± 0.67	70.21 ± 4.18	47.44 ± 2.09	54.26 ± 2.69	45.31 ± 1.75	53.76 ± 5.38
	total amino acid	439.15 ± 14.95	29.08 ± 1.96	169.69 ± 6.24	117.91 ± 4.29	129.11 ± 4.66	110.92 ± 4.46	95.93 ± 4.41

[a]No significance difference, $p > 0.05$.

Table 5. Concentration of the Monosaccharides of EBN and the Different Types of Food Items (n = 6)

		concentration of monosaccharide for different food items (mg/g of sample)						
no.	compd	EBN	milk	chicken egg yolk	chicken egg white	quail egg yolk	quail egg white	infant formula
1	mannose	10.53 ± 5.97	0.00 ± 0.00	1.59 ± 0.15	2.84 ± 0.18	2.01 ± 0.18	2.63 ± 0.26	0.53 ± 0.02
2	glucose	4.51 ± 3.89	57.29 ± 1.49	2.19 ± 0.19	7.25 ± 0.54	2.82 ± 0.26	57.49 ± 4.91	532.28 ± 26.56
3	galactose	111.85 ± 57.22	42.94 ± 0.80	0.82 ± 0.07	0.54 ± 0.04	1.07 ± 0.10	10.48 ± 1.13	520.51 ± 28.85
4	rhamnose	0.19 ± 0.15	0.00 ± 0.00	0.00 ± 0.00	0.00 ± 0.00	0.00 ± 0.00	0.00 ± 0.00	0.00 ± 0.00
5	fucose	11.39 ± 9.91	0.00 ± 0.00	0.00 ± 0.00	0.00 ± 0.00	0.00 ± 0.00	0.00 ± 0.00	0.00 ± 0.00
6	ribose	0.18 ± 0.12	0.26 ± 0.01	0.00 ± 0.00	0.00 ± 0.00	0.00 ± 0.00	0.00 ± 0.00	0.00 ± 0.00
7	xylose	2.13 ± 1.91	0.66 ± 0.03	0.00 ± 0.00	0.52 ± 0.06	0.11 ± 0.01	0.73 ± 0.06	1.19 ± 0.05
	total monosaccharide	140.77 ± 75.32	101.15 ± 2.11	4.60 ± 0.40	11.15 ± 0.71	6.01 ± 0.50	71.33 ± 6.18	1054.52 ± 53.53

than 20% in amino acids (Table 5). As mentioned earlier, monosaccharides are derived generally from the glycans. Glycans are linear or branched monosaccharide structures protruding out from the protein molecule. Thus, glycans might have been lost due to degradation during the cleaning process of EBN. In addition, Li et al. has demonstrated that proteoglycans of EBN could be extracted with water.[31] This implies that the loss of proteoglycans during the cleaning process of EBN could also have contributed to the larger RSD values in the monosaccharides.

Comparing the monosaccharides of EBN and the different types of food items, all 7 monosaccharides were detected in EBN while only certain monosaccharides were present in the rest of the food items (Table 5). This diversified monosaccharide profile in EBN could be attributed to the glycans detected in the food item mentioned previously. EBN has a significantly lower concentration of glucose than milk and infant formula. This is because both milk and infant formula contain a large amount of lactose.[49] This reasoning is further supported by the ratio of glucose and galactose in milk and infant formula, approximately 1:1 which coincides with lactose. Besides milk and infant formula, the glucose concentration in EBN is also found to be significantly lower than in chicken and quail egg white. Egg white of chicken and quail are known to be the source of energy for the avian embryonic growth.[53] As such, it was not surprising that the concentration of glucose is elevated in the chicken and quail egg white. Although the concentration of individual monosaccharide varies between the different types of samples, EBN generally has a higher overall monosaccharide content, with the exception of infant formula. This could be due to the presence of a rich lactose content in infant formula to satisfy the nutritional and energy requirements for infant growth.[54,55]

■ ASSOCIATED CONTENT

Supporting Information

Additional figures and tables, including PCA score plots, contribution plots, information on EBN, summary of MS data, and validation results. This material is available free of charge via the Internet at http://pubs.acs.org.

■ AUTHOR INFORMATION

Corresponding Author

*E-mail: laipeng@nus.edu.sg. Phone: +65 65162917. Fax: +65 6775 7895.

Notes

The authors declare no competing financial interest.

■ ACKNOWLEDGMENTS

The authors would like to acknowledge financial support from The Health Science Authority as well as National University of Singapore, National Research Foundation and Economic Development Board (SPORE, COY-15-EWI-RCFSA/N197-1), Ministry of Education (R-143-000-582-112 and R-143-000-519-112), and Environment and Water Industry Development Council Programme Office (EWI RFP 1301-IRIS-21 and EWI RFP 1301-IRIS-26). The authors would also like to thank the Shenzhen Development and Reform Commission (SZ DRC) for supporting this collaborative project with Peking University Shenzhen Graduate School. Special thanks to Kee Jiahui for her editorial assistance.

■ ABBREVIATIONS USED

EBN, edible bird's nests; EAA, essential amino acid; GC, gas chromatography; LC, liquid chromatography; PMP, 1-phenyl-3-methyl-5-pyrazolone; FID, flame ionization detector; MS, mass spectrometer; MRM, multireaction monitoring; PCA, principal component analysis; PC, principal components; uv, unit variance; par, pareto; R^2, goodness of fit; Q^2, goodness of prediction; LOQ, limits of quantification; LOD, limits of detection; DP, declustering potential; CE, collision energy; CXP, collision exit potential; EP, entrance potential; FP, focusing potential

■ REFERENCES

(1) Koon, L. C.; Cranbrook, E. o. *Swiftlets of Borneo—Builders of Edible Bird Nest*; Sabah Natural History Publication (Borneo): Borneo, Malaysia, 2002; pp 1−171.

(2) Marcone, M. F. Characterization of the edible bird's nest the "Caviar of the East". *Food Res. Int.* **2005**, *38*, 1125−1134.

(3) Guo, C. T.; Takahashi, T.; Bukawa, W.; Takahashi, N.; Yagi, H.; Kato, K.; Hidari, K.; Miyamoto, D.; Suzuki, T.; Suzuki, Y. Edible bird's nest extract inhibits influenza virus infection. *Antiviral Res.* **2006**, *70*, 140−146.

(4) Kong, Y. C.; Keung, W. M.; Yip, T. T.; Ko, K. M.; Tsao, S. W.; Ng, M. H. Evidence that epidermal growth factor is present in swiftlet's (Collocalia) nest. *Comp. Biochem. Physiol., Part B: Biochem. Mol. Biol.* **1987**, *87*, 221−226.

(5) Houdret, N.; Lhermitte, M.; Degand, P.; Roussel, P. Purification and chemical study of a glycoprotein from Collocalia. *Biochimie* **1975**, *57*, 603−608.

(6) Zhang, S. W.; Lai, X. T.; Liu, X. Q.; Li, Y.; Li, B. F.; Huang, X. L.; Zhang, Q. L.; Chen, W.; Lin, L.; Yang, G. W. Competitive enzyme-linked immunoassay for sialoglycoprotein of edible bird's nest in food and cosmetics. *J. Agric. Food Chem.* **2012**, *60*, 3580−3585.

(7) Liu, X. Q.; Lai, X. T.; Zhang, S. W.; Huang, X. L.; Lan, Q. X.; Li, Y.; Li, B. F.; Chen, W.; Zhang, Q. L.; Hong, D. Z.; Yang, G. W. Proteomic profile of edible bird's nest proteins. *J. Agric. Food Chem.* **2012**, *60*, 12477−12481.

(8) Yagi, H.; Yasukawa, N.; Yu, S. Y.; Guo, C. T.; Takahashi, N.; Takahashi, T.; Bukawa, W.; Suzuki, T.; Khoo, K. H.; Suzuki, Y.; Kato, K. The expression of sialylated high-antennary N-glyeans in edible bird's nest. *Carbohydr. Res.* **2008**, *343*, 1373−1377.

(9) Oda, M.; Ohta, S.; Suga, T.; Aoki, T. Study on food components: the structure of N-Linked asialo carbohydrate from the edible bird's nest built by collocalia fuciphaga. *J. Agric. Food Chem.* **1998**, *46*, 3047−3053.

(10) Pozsgay, V.; Jennings, H.; Kasper, D. L. 4,8-anhydro-N-acetylneuraminic acid. Isolation from edible bird's nest and structure determination. *Eur J Biochem* **1987**, *162*, 445−450.

(11) Saengkrajang, W.; Matan, N.; Matan, N. Nutritional composition of the farmed edible bird's nest (Collocalia fuciphaga) in Thailand. *J. Food Compos. Anal.* **2013**, *31*, 41−45.

(12) Ma, F.; Liu, D. Extraction and determination of hormones in the edible bird's nest. *Asian J. Chem.* **2012**, *24*, 117−120.

(13) Norhayati, M. K.; Azman, O.; Wan Nazaimoon, W. M. Preliminary study of the nutritional content of Malaysian edible bird's nest. *Malays. J. Nutr.* **2010**, *16*, 389−396.

(14) Ekeanyanwu, R. C. Evaluation of the crude protein and amino acid composition of Nigerian Monodora myristica (Ehuru). *Pak. J. Nutr.* **2013**, *12*, 219−223.

(15) Sun, Y.; Lige, B.; Van Huystee, R. B. HPLC determination of the sugar compositions of the glycans on the cationic peanut peroxidase. *J. Agric. Food Chem.* **1997**, *45*, 4196−4200.

(16) Fountoulakis, M.; Lahm, H. W. Hydrolysis and amino acid composition analysis of proteins. *J. Chromatogr.* **1998**, *826*, 109−134.

(17) Jong, C. H.; Tay, K. M.; Lim, C. P. Application of the fuzzy failure mode and effect analysis methodology to edible bird nest processing. *Comput. Electron Agric.* **2013**, *96*, 90−108.

(18) Weiss, M.; Manneberg, M.; Juranville, J. F.; Lahm, H. W.; Fountoulakis, M. Effect of the hydrolysis method on the determination of the amino acid composition of proteins. *J. Chromatogr.* **1998**, *795*, 263−275.

(19) Kwon, H.; Kim, J. Determination of monosaccharides in glycoproteins by reverse-phase high-performance liquid chromatography. *Anal. Biochem.* **1993**, *215*, 243−252.

(20) George, J. P.; Chen, Z.; Shaw, P. Fault detection of drinking water treatment process using PCA and hotelling's T2 chart. *World Acad. Sci., Eng. and Technol.* **2009**, *38*, 1061−1066.

(21) Gonzalez-De la Parra, M.; Rodríguez-Loaiza, P. Application of the Multivariate T2 Control Chart and the Mason-Tracy-Young Decomposition Procedure to the Study of the Consistency of Impurity Profiles of Drug Substances. *Quality Engineering* **2003**, *16*, 127−142.

(22) Eppe, G.; De Pauw, E. Advances in quality control for dioxins monitoring and evaluation of measurement uncertainty from quality control data. *J. Chromatogr. B: Anal. Technol. Biomed. Life Sci.* **2009**, *877*, 2380−2387.

(23) Nozal, M. J.; Bernal, J. L.; Toribio, M. L.; Diego, J. C.; Ruiz, A. Rapid and sensitive method for determining free amino acids in honey by gas chromatography with flame ionization or mass spectrometric detection. *J. Chromatogr.* **2004**, *1047*, 137−146.

(24) Wieruszeski, J. M.; Michalski, J. C.; Montreuil, J.; Strecker, G.; Peterkatalinic, J.; Egge, H.; Vanhalbeek, H.; Mutsaers, J.; Vliegenthart, J. F. G. Structure of the monosialyl oligosaccharides derived from salivary gland mucin glycoproteins of the Chinese swiftlet (genus collocalia) - characterization of novel types of extended core structure, Gal-Beta(1- 3) GlcNAc-Beta(1- 6) GalNAc-Alpha1- 3)GalNAc(1-OL), and of chain termination, Gal-Alpha(1- 4) 0−1 Gal-Beta(1- 4) 2GlcNAc-Beta(1- .)E. *J. Biol. Chem.* **1987**, *262*, 6650−6657.

(25) Nakagawa, H.; Hama, Y.; Sumi, T.; Li, S. C.; Maskos, K.; Kalayanamitra, K.; Mizumoto, S.; Sugahara, K.; Li, Y. T. Occurrence of a nonsulfated chondroitin proteoglycan in the dried saliva of Collocalia swiftlets (edible bird's-nest). *Glycobiology* **2007**, *17*, 157−164.

(26) Zhang, P.; Wang, Z.; Xie, M.; Nie, W.; Huang, L. Detection of carbohydrates using a pre-column derivatization reagent 1-(4-isopropyl) phenyl-3-methyl-5-pyrazolone by high-performance liquid chromatography coupled with electrospray ionization mass spectrometry. *J. Chromatogr. B: Anal. Technol. Biomed. Life Sci.* **2010**, *878*, 1135−1144.

(27) Honda, S.; Akao, E.; Suzuki, S.; Okuda, M.; Kakehi, K.; Nakamura, J. High performance liquid chromatography of reducing carbohydrates as strongly ultraviolet absorbing and electrochemically sensitive 1-phenyl-3-methyl-5-pyrazolone derivatives. *Anal. Biochem.* **1989**, *180*, 351−357.

(28) De Ruiter, G. A.; Schols, H. A.; Voragen, A. G. J.; Rombouts, F. M. Carbohydrate analysis of water-soluble uronic acid-containing polysaccharides with high-performance anion-exchange chromatography using methanolysis combined with TFA hydrolysis is superior to four other methods. *Anal. Biochem.* **1992**, *207*, 176−185.

(29) Lv, Y.; Yang, X.; Zhao, Y.; Ruan, Y.; Yang, Y.; Wang, Z. Separation and quantification of component monosaccharides of the

tea polysaccharides from Gynostemma pentaphyllum by HPLC with indirect UV detection. *Food Chem.* **2009**, *112*, 742−746.
(30) McRae, G.; Monreal, C. M. LC-MS/MS quantitative analysis of reducing carbohydrates in soil solutions extracted from crop rhizospheres. *Anal. Bioanal. Chem.* **2011**, *400*, 2205−2215.
(31) Rühmann, B.; Schmid, J.; Sieber, V. Fast carbohydrate analysis via liquid chromatography coupled with ultra violet and electrospray ionization ion trap detection in 96-well format. *J. Chromatogr. A* **2014**, *1350*, 44−50.
(32) Wu, X.; Jiang, W.; Lu, J.; Yu, Y.; Wu, B. Analysis of the monosaccharide composition of water-soluble polysaccharides from Sargassum fusiforme by high performance liquid chromatography/electrospray ionisation mass spectrometry. *Food Chem.* **2014**, *145*, 976−983.
(33) Yet, M. G.; Chin, C. C. Q.; Wold, F. The covalent structure of individual N-linked glycopeptides from ovomucoid and asialofetuin. *J. Biol. Chem.* **1988**, *263*, 111−117.
(34) Hammad, L. A.; Saleh, M. M.; Novotny, M. V.; Mechref, Y. Multiple-reaction monitoring liquid chromatography mass spectrometry for monosaccharide compositional analysis of glycoproteins. *J. Am. Soc. Mass Spectrom.* **2009**, *20*, 1224−1234.
(35) Wu, W.; Hamase, K.; Kigucki, M.; Yamamoto, K.; Zaitsu, K. Reversed-phase HPLC of monosaccharides in glycoproteins derivatized with aminopyrazine with fluorescence detection. *Anal. Sci.* **2000**, *16*, 919−922.
(36) Salchert, K.; Pompe, T.; Sperling, C.; Werner, C. Quantitative analysis of immobilized proteins and protein mixtures by amino acid analysis. *J. Chromatogr.* **2003**, *1005*, 113−122.
(37) Ceballos, L. S.; Morales, E. R.; Adarve, G. D. T.; Castro, J. D.; Martinez, L. P.; Sampelayo, M. R. S. Composition of goat and cow milk produced under similar conditions and analyzed by identical methodology. *J. Food Compos. Anal.* **2009**, *22*, 322−329.
(38) Salvador, L. D.; Suganuma, T.; Kitahara, K.; Tanoue, H.; Ichiki, M. Monosaccharide composition of sweetpotato fiber and cell wall polysaccharides from sweetpotato, cassava, and potato analyzed by the high-performance anion exchange chromatography with pulsed amperometric detection method. *J. Agric. Food Chem.* **2000**, *48*, 3448−3454.
(39) Craig, A.; Cloarec, O.; Holmes, E.; Nicholson, J. K.; Lindon, J. C. Scaling and normalization effects in NMR spectroscopic metabonomic data sets. *Anal. Chem.* **2006**, *78*, 2262−2267.
(40) Chua, Y. G.; Bloodworth, B. C.; Leong, L. P.; Li, S. F. Y. Metabolite profiling of edible bird's nest using gas chromatography/mass spectrometry and liquid chromatography/mass spectrometry. *Rapid Commun. Mass Spectrom.* **2014**, *28*, 1387−1400.
(41) Chaturvedi, P.; Warren, C. D.; RuizPalacios, G. M.; Pickering, L. K.; Newburg, D. S. Milk oligosaccharide profiles by reversed-phase HPLC of their perbenzoylated derivatives. *Anal. Biochem.* **1997**, *251*, 89−97.
(42) Lunven, P.; Le Clement De St Marcq, C.; Carnovale, E.; Fratoni, A. Amino acid composition of hen's egg. *Br. J. Nutr.* **1973**, *30*, 189−194.
(43) Liu, F.; Ong, E. S.; Li, S. F. Y. A green and effective approach for characterisation and quality control of Chrysanthemum by pressurized hot water extraction in combination with HPLC with UV absorbance detection. *Food Chem.* **2013**, *141*, 1807−1813.
(44) Agostoni, C.; Carratu, B.; Boniglia, C.; Riva, E.; Sanzini, E. Free amino acid content in standard infant formulas: Comparison with human milk. *J. Am. Coll. Nutr.* **2000**, *19*, 434−438.
(45) Yang, M.; Cheung, S. H.; Li, S. C.; Cheung, H. Y. Establishment of a holistic and scientific protocol for the authentication and quality assurance of edible bird's nest. *Food Chem.* **2014**, *151*, 271−278.
(46) Tung, C. H.; Pan, J. Q.; Chang, H. M.; Chou, S. S. Authentic determination of bird's nests by saccharides profile. *J. Food Drug Anal.* **2008**, *16*, 86−91.
(47) Ang, H. G.; Kwik, W. L.; Theng, C. Y. Total protein and amino acids contents of some common foods in South East Asia. *Food Chem.* **1984**, *15*, 243−255.
(48) Wu, G. Y. Amino acids: metabolism, functions, and nutrition. *Amino Acids* **2009**, *37*, 1−17.
(49) Shama, N.; Bai, S. W.; Chung, B. C.; Jung, B. H. Quantitative analysis of 17 amino acids in the connective tissue of patients with pelvic organ prolapse using capillary electrophoresis-tandem mass spectrometry. *J. Chromatogr. B: Anal. Technol. Biomed. Life Sci.* **2008**, *865*, 18−24.
(50) Neuman, R. E.; Logan, M. A. The determination of collagen and elastin in tissues. *J. Biol. Chem.* **1950**, *186*, 549−556.
(51) Katsanos, C. S.; Kobayashi, H.; Sheffield-Moore, M.; Aarsland, A.; Wolfe, R. R. A high proportion of leucine is required for optimal stimulation of the rate of muscle protein synthesis by essential amino acids in the elderly. *Am, J. Physiol.: Endocrinol. Metab.* **2006**, *291*, E381−E387.
(52) Wu, Y. J.; Chen, Y.; Wang, B.; Bai, L. Q.; Han, W. R.; Ge, Y. Q.; Yuan, F. Application of SYBRgreen PCR and 2DGE methods to authenticate edible bird's nest food. *Food Res. Int.* **2010**, *43*, 2020−2026.
(53) Foye, O. T.; Uni, Z.; Ferket, P. R. Effect of in ovo feeding egg white protein, beta-hydroxy-beta-methylbutyrate, and carbohydrates on glycogen status and neonatal growth of turkeys. *Poult. Sci.* **2006**, *85*, 1185−1192.
(54) Klein, C. J. Nutrient requirements for preterm infant formulas. *J. Nutr.* **2002**, *132*, 1395S−1577S.
(55) Hascoët, J. M.; Hubert, C.; Rochat, F.; Legagneur, H.; Gaga, S.; Emady-Azar, S.; Steenhout, P. G. Effect of formula composition on the development of infant gut microbiota. *J. Pediatr. Gastroenterol. Nutr.* **2011**, *52*, 756−762.

JOURNAL OF AGRICULTURAL AND FOOD CHEMISTRY

Article

pubs.acs.org/JAFC

Influence of Geosmin-Producing *Streptomyces* on the Growth and Volatile Metabolites of Yeasts during Chinese Liquor Fermentation

Hai Du, Hu Lu, and Yan Xu*

Synergetic Innovation Center of Food Safety and Nutrition, State Key Laboratory of Food Science and Technology, Key Laboratory of Industrial Biotechnology of Ministry of Education, School of Biotechnology, Jiangnan University, 1800 Lihu Avenue, Wuxi, Jiangsu 214122, People's Republic of China

ABSTRACT: Diverse *Streptomyces* species act as geosmin producers in the Chinese liquor-making process, causing an earthy, off-odor containment. Through microbiological and metabolite analyses, this paper investigates the influence of several geosmin-producing *Streptomyces* on the microbial community of a brewing system. The antifungal activity against functional liquor-brewing microbes was assayed by an agar diffusion method. Several *Streptomyces*, most notably *Streptomyces sampsonii* QC-2, inhibited the growth of the brewing functional yeasts and molds in pure culture. In a simulated coculture, *Streptomyces* spp. reduced the flavor compounds (alcohols and esters) contributed by yeasts. Nine components in *Streptomyces sampsonii* QC-2 broth were detected by ultraperformance liquid chromatography coupled with photo diode array (UPLC−PDA), with characteristic ultraviolet absorptions at 360, 380, and 400 nm. The main products of *Streptomyces sampsonii* QC-2 were identified by ultraperformance liquid chromatography−quadrupole time-of-flight mass spectrometry (UPLC/Q-TOF−MS/MS), and confirmed by standard mass spectrometry. The antifungal active components were revealed as a series of heptaene macrolide antibiotics.

KEYWORDS: *Streptomyces, geosmin, antifungal activity, heptaene macrolide antibiotics, Chinese liquor*

INTRODUCTION

Chinese liquor is fermented from grains (rice, sticky rice, sorghum, wheat, and corn) in multistrain solid-state culture. Liquor fermentation spontaneously occurs in pottery vats or mud pits over several months. The microbial counts and metabolite concentrations in heterogeneous natural liquor fermentations are widely variable, affecting the flavor and composition of Chinese liquor.[1] Successful Chinese liquor fermentation requires a succession of particular microbial activities. The main microbial source in Chinese liquor making is the fermentation starter *Daqu*, which provides nutrients for microbes that produce an array of enzymes with various biochemical properties. Therefore, the fermentation activities of yeasts, bacteria and filamentous fungi in *Daqu* largely determine the typical characteristics of the resulting fermented brans and fresh liquor.[2−5]

The *Daqu* fungi, including molds and yeasts, play an important role in the saccharification and alcoholic fermentation of Chinese liquor. Molds appear to influence the evolution of flavors and the activities of enzymes such as amylases and proteinases,[5,6] which are required for alcoholic fermentation of cooked sorghum. The predominant *Daqu* yeasts have been reported as *Saccharomyces cerevisiae*, *Pichia anomala*, and *Saccharomycopsis fibuligera*, which constitute the functional microbes in other fermented alcoholic beverages. *S. cerevisiae* and *P. anomala* mainly contribute flower-like and fruit-like volatile compounds, such as alcohols and esters, to the liquor flavor.[1,7] *S. fibuligera* secretes high-activity α-amylase and glucoamylase that can degrade raw starch.[8] Culture-independent methods have also identified non-*Saccharomyces* species (*Issatchenkia orientalis*, *Hanseniaspora guilliermondii*, and *Debaryomyces hansenii*),[5] which may potentially improve flavor diversity and reduce the alcohol content.[9,10]

When the fermented grains are removed from the opened fermenter, they become contaminated by a variety of microorganisms derived from the surrounding environment, many of which contribute to subsequent fermentation. In our previous studies, we found that if *Streptomyces*-sourced geosmin is introduced to the fermentation process, it becomes concentrated in the liquor after distillation.[2,11,12] Geosmin presence usually indicates that off-flavor producers have become well-established in the Chinese liquor-making process. Geosmin-producing *Streptomyces* have been identified in certain high- and low-temperature *Daqu*.[2]

Streptomyces spp. are ubiquitous soil bacteria noted for their ability to produce a vast array of antibiotics.[13] Indeed, 90% of *Streptomyces* produce antibiotics that inhibit the growth of other microbes.[13−15] Antibiotic-mediated species interactions are believed to enhance *Streptomyces* fitness and have been exploited as a plant disease biocontrol in soil.[16]

The present study investigates the extent to which introducing geosmin-producing *Streptomyces* affects the microbial community and flavor development in the fermentation processes of Chinese liquor. Adopting an analytical chemistry approach, it also proposes a mechanism by which geosmin-producing *Streptomyces* influences the brewing-functional microbes in the Chinese liquor-making process.

Received: July 15, 2014
Revised: November 27, 2014
Accepted: December 9, 2014
Published: December 9, 2014

ACS Publications © 2014 American Chemical Society

DOI: 10.1021/jf503351w
J. Agric. Food Chem. 2015, 63, 290−296

MATERIALS AND METHODS

Strains and Assays of Antifungal Activity. All strains in this study were isolated from the making process of *Daqu*-based Chinese light aromatic liquor. The isolated strains were identified by molecular taxonology based on their conservative rDNA sequences. Four geosmin-producing *Streptomyces* strains (*Streptomyces albus* FXJ, *Streptomyces fradiae* HX, *Streptomyces radiopugnans*QC-1, and *Streptomyces sampsonii* QC-2) were isolated from *Daqu*, and geosmin production was confirmed by gas chromatography−mass spectrometry (GC−MS). Antifungal activity was determined by the modified agar diffusion assay described in Coda et al.[17] Petri plates (90 mm diameter) containing 10 mL of potato dextrose agar (PDA) medium were inoculated with geosmin-producing strains. The plates were incubated at 30 °C for 72 h. Once the colony had developed, it was excised from the plate as an agar cylinder (9 mm diameter) and placed on a plate spread with functional liquor-brewing microbes at an appropriate concentration of cell suspension. The spread plates were then incubated at 30 °C for 72 h. All experiments were run in triplicate. The inhibitory activity of geosmin-producing strains was quantified as the diameter ratio of inhibition zone to agar cylinder ($R_{\text{inhibition zone}}/R_{\text{colony}}$).

The inhibitory effect of QC-2 broth sterilized by filtration was also assayed by modified agar diffusion assay. Strain QC-2 was inoculated in potato dextrose medium at 30 °C with shaking (250 rpm). At different incubation times, the QC-2 broths were filtered through a 0.22 μm membrane filter (Millipore Corporation, Bedford, MA). A plate inoculated with the test fungus (*S. fibuligera* FJ-4) at an optimal cell concentration was then dotted with 5 μL of the sterilized broth. All assays were performed in triplicate. The plate was incubated at 30 °C for 72 h, and the diameter (in mm) of the inhibition zone was measured.

Co-cultivation and Fermentation Experiments. The fermentation system of Chinese liquor was simulated as a cocultured system of the main brewing microorganisms. The solid-state fermentation medium was prepared as follows: 250 g sorghum was added to 350 mL hot water (70−80 °C), soaked for 24 h, and sterilized at 121 °C for 20 min. *Rhizopus oryzae* G4 (*R. oryzae* G4) was introduced to the simulated fermentation system at 10^4 CFU/g spore suspension, and incubated at 30 °C for 1 day to allow saccharification. The saccharified cultures were then inoculated with 10^5 CFU/g each of four yeast species (*S. cerevisiae* FJ-7, *P. anomala* FJ-3, *I. orientalis* FJ-2, and *S. fibuligera* FJ-4). Following 2-days of incubation at 30 °C, the spore or cell concentrations of the yeasts were adjusted to match the results of plate counts on PDA medium. *Streptomyces sampsonii* QC-2 (spore suspension 10^4 CFU/g) was inoculated into potato dextrose broth, and shaken at 250 rpm. The broths at different growth stages (lag phase (I), exponential phase (II), and stationary phase (III)) were sterilized by filtering through a 0.22 μm nylon membrane. Five-milliliters of the filtered QC-2 broths were added to the yeast cocultures. Medium without broth addition was prepared as a control reference sample.

Analysis of Yeast Growth. Yeast growth was measured by spread-plating onto Wallerstein Laboratory Nutrient (WLN) medium. Yeast cells from the simulation fermentation system were collected, 10-fold serially diluted in saline (0.85%, wt/vol, NaCl), and spread on triplicate WLN medium plates. Following incubation for 3 days at 30 °C, the yeast colony-forming units (CFUs) were identified by their morphological characteristics and counted.

Purifying Antifungal Active Compounds. The culture broth of strain QC-2 was prepared under the conditions of the cocultivation and fermentation experiments. The broth was incubated for 5 days, then centrifuged at 10 000 rpm for 15 min at 4 °C. The supernatant (approximately 40 mL) was purified and concentrated by a solid phase extraction (SPE) column (Welchrom C18E, Welch materials, Inc., MD, U.S.A.), and then successively eluted by 10 mL water, 50% acetonitrile/water, and 100% acetonitrile. The three eluents were separately collected and concentrated to 2 mL under a jet of nitrogen gas. After filtration through 0.22 μm membrane filters, 5 μL of each eluted fraction was retained for agar diffusion assay. Fractions showing antifungal activity were subjected to UPLC−PDA and ultra-performance liquid chromatography−quadrupole time-of-flight mass spectrometry (UPLC/Q-TOF−MS/MS) for compound identification.

Identifying Antifungal Active Substances. The active antifungal substances were identified by UPLC/Q-TOF−MS/MS. UPLC was performed in a Waters Acquity UPLC system (Milford, MA, U.S.A.) equipped with a binary solvent delivery system and an auto sampler. Chromatography was performed on a Waters Acquity C18 column (5 cm × 2.1 mm, 1.7-μm particles). The mobile phase was a gradient prepared from 0.1% formic acid (component A) and 100% acetonitrile (component B). Elution started with 5% B for 0.5 min; the proportion of A was then linearly increased to 100% over 10 min, reduced to 95% in the next 1 min and maintained isocratic for 2 min. Total run time, including conditioning of the column to the initial conditions, was 12 min. The flow rate of the eluting solvent was 0.3 mL/min. During the analyses, the column was maintained at 30 °C. The injection volume was 5 μL. Mass spectrometry was performed with a Waters Synapt Q-TOF system in positive and negative ion modes according to the manufacturer's instructions. The masses and compositions of the precursor and fragment ions were accurately calculated by the MassLynx 4.1 software supplied with the instrument, which calculates all possible elemental compositions consistent with the accurate mass. The relative concentrations of antifungal compounds to the external standard (amphotericin B 200 μg/L) were semiquantified on the basis of comparing their peak areas to that of the external standard on UPLC-PDA chromatograms at 380 nm.

Analysis of Volatile Metabolites. Analytes were extracted by solid-phase microextraction (SPME), using an automatic headspace sampling system (Multi Purpose Sample MPS 2 with an SPME adapter (GERSTEL Inc., Baltimore, MD, U.S.A.) equipped with a 50/30 μm DVB/CAR/PDMS fiber (2 cm, Supelco Inc., Bellefonte, PA, U.S.A.). Prior to analysis, the fiber was conditioned by insertion into the GC injector at 250 °C for 2 h to prevent contamination. A solid-state sample (3 g) was transferred to a screw-capped, straight-sided headspace vial (volume = 15 mL) and spiked with 10 μL of L-(−)-menthol (internal standard, IS), 4 mg/L in ethanol. After saturating the diluted solution with NaCl, the vial was tightly capped with a Teflon-faced silicone septum. The samples were equilibrated at 60 °C for 5 min and extracted for 45 min at the same temperature with stirring (250 rpm). Following extraction, the fiber was inserted into the injection port of the GC (250 °C) for 5 min to desorb the analytes.

The GC−MS analysis was performed in an Agilent 6890N GC coupled to an Agilent 5975 mass selective detector (MSD). The capillary column was a CP-Wax column (length = 60 m, i.d. = 0.25 mm, film thickness = 0.25 μm; Varian Inc., Palo Alto, CA, U.S.A.). The injector temperature was 250 °C, and the analysis was conducted in splitless mode. The operating conditions were as follows: temperature was started at 80 °C (holding for 2 min), then raised to 230 °C at 8 °C/min, and held at 230 °C for 10 min. The column carrier gas was helium (99.9995% purity) supplied at a constant flow rate of 2 mL/min. The electron impact energy was 70 eV, and the ion source temperature was set to 230 °C. The compounds were characterized by full-scan acquisition over an appropriate mass range (30−350 amu). The compounds were clearly identified by comparison to reference spectra (NIST05a.L, Agilent Technologies, Inc.) and pure standards.

The compounds were quantified by their main mass fragments. A calibration curve was derived by plotting the peak area ratios against the concentration ratios of main mass fragments to IS (m/z 81) as described in our previously published paper.[12] Each compound concentration in the sample was quantified by comparing the ratios of the peak areas with the calibration curve. Each determination was triplicated.

Statistical Analysis. To determine the effect of geosmin-producing strains on the flavors produced by the functional liquor-brewing fungus, the volatile metabolites were quantified. The obtained results were visualized on a heat map computed by R (version 3.0.2), in which cells were colored according to their Z scores (where Z = [observed value − mean]/standard deviation).

DOI: 10.1021/jf503351w
J. Agric. Food Chem. 2015, 63, 290−296

Table 1. Inhibition of Four Geosmin-Producing Strains on the Brewing Functional Microbes in a Chinese Liquor-Making Process

tested microorganisms			inhibition results[a] ($R_{inhibition\ zone}/R_{colony}$)[b]			
origin	strain	species	FXJ	HX	QC-1	QC-2
Qingcha Daqu from *Fenjiu*	FJ-4	*Saccharomycopsis fibuligera*	—[c]	1.22 ± 0.16	1.33 ± 0.07	1.39 ± 0.07
Gongan Daqu	Y4	*Saccharomycopsis fibuligera*	—	1.10 ± 0.03	1.11 ± 0.11	1.56 ± 0.21
Qingcha Daqu from *Fenjiu*	GS-1	*Hanseniaspora* sp.	—	—	1.88 ± 0.12	1.50 ± 0.19
Hongxin Daqu from *Fenjiu*	GS-2	*Saccharomyces cerevisiae*	—	—	1.13 ± 0.02	1.25 ± 0.08
Qingcha Daqu from *Fenjiu*	FJ-7	*Saccharomyces cerevisiae*	—	—	1.10 ± 0.06	1.44 ± 0.13
Qingcha Daqu from *Fenjiu*	FJ-2	*Issatchenkia orientalis*	—	—	1.11 ± 0.18	1.56 ± 0.17
Gongan Daqu	Y8m	*Issatchenkia orientalis*	—	—	1.01 ± 0.19	1.39 ± 0.11
Qingcha Daqu from *Fenjiu*	FJ-3	*Pichia anomala*	—	—	1.03 ± 0.06	1.01 ± 0.27
Gongan Daqu	Y6	*Pichia anomala*	—	—	1.02 ± 0.22	1.01 ± 0.14
Qingcha Daqu from *Fenjiu*	GS-4	*Bacillus amyloliquefaciens*	—	—	1.38 ± 0.11	1.13 ± 0.15
Qingcha Daqu from *Fenjiu*	GS-5	*Absidia corymbifera*	—	—	—	1.13 ± 0.11
Qingcha Daqu from *Fenjiu*	GS-6	*Mucor circinelloides*	—	1.63 ± 0.33	—	1.02 ± 0.07
Yangchun Daqu	G4	*Rhizopus oryzae*	—	—	1.38 ± 0.27	—
Qingcha Daqu from *Fenjiu*	GS-3	*Penicillium chrysogenum*	—	—	—	1.56 ± 0.26
Qingcha Daqu from *Laobaigan*	GS-7	*Trichoderma viride*	1.63 ± 0.09	2.50 ± 0.27	2.63 ± 0.15	2.25 ± 0.12

[a]Inhibition results are expressed as the mean diameter ratio of inhibition zone to agar cylinder in triplicate experiments. [b]R denotes the diameter of an inhibition zone or colony. [c]— indicates no inhibition zone.

RESULTS AND DISCUSSION

Influence of Geosmin-Producing *Streptomyces* On The Growth Of Microbes And Dynamics Of Yeast Populations Involved In Chinese Liquor Fermentation. Four *Streptomyces* strains (*Streptomyces albus* FXJ, *Streptomyces fradiae* HX, *Streptomyces radiopugnans* QC-1, and *Streptomyces sampsonii* QC-2) were identified as geosmin producers in our previous studies.[11] Communities of geosmin-producing *Streptomyces* have been studied by denaturing gradient gel electrophoresis (DGGE) and quantitative PCR.[2] In the present study, the antibacterial activity of geosmin-producing *Streptomyces* was determined by the agar diffusion method. Single-colony agar cylinders of the four geosmin-producing strains were placed on agar previously spread with functional brewing strains isolated from the liquor-making process, which provide flavor and enzymes. The inhibitions of geosmin-producing *Streptomyces* on the main functional strains were determined from the inhibition zones. As shown in Table 1, strain FXJ exerted a very weak antifungal activity, whereas strain HX inhibited only a portion of the fungus. Strain QC-1 inhibited a fraction of the bacteria, yeasts and molds. The strongest effect was exhibited by strain QC-2, which inhibited not only yeasts, molds and other fungi, but also (to some extent) bacteria under the same conditions. Importantly, the transparent inhibition zones around *S. fibuligera* FJ-4 and Y4 show that QC-2 strongly inhibits both of these strains. *S. fibuligera*, also known as *Endomycopsis fibuligera*, expresses liquefied raw starch enzyme and saccharifying enzyme. *S. fibuligera* ranks among the best yeast producers of starch decomposition enzymes.[21,22]

The sterilized potato dextrose broths, in which *S. sampsonii* QC-2 had been incubated up to different stages (QC-2 I (lag phase); QC-2 II (exponential phase), and QC-2 III (stationary phase)), were introduced to mixed cultures of the four yeasts, *S. cerevisiae* FJ-7, *P. anomala* FJ-3, *I. orientalis* FJ-2, and *S. fibuligera* FJ-4. According to Figure 1, the populations of the four yeasts were reduced by different degrees, reflecting their different inhibitions by strain QC-2. The QC-2 III results conspicuously differed from those of the controlled experiment, implying that *Streptomyces* can unbalance the microbial community of the brewing system. In contrast, the QC-2 I results varied only slightly from those of the control.

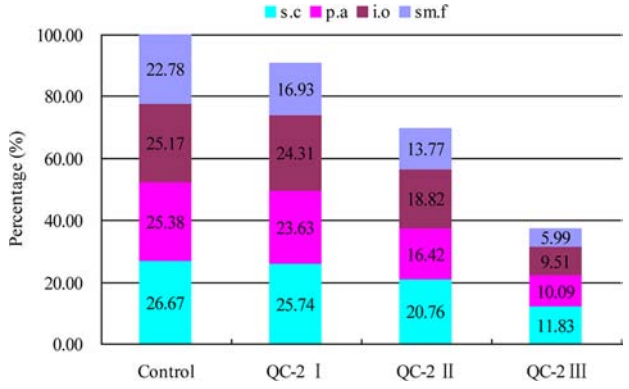

Figure 1. Populations of four brewing functional yeasts in a mixed-culture fermentation (s.c, *Saccharomyces cerevisiae* FJ-7; p.a, *Pichia anomala* FJ-3; i.o, *Issatchenkia orientalis* FJ-2; and sm.f, *Saccharomycopsis fibuligera* FJ-4) exposed to *Streptomyces sampsonii* QC-2 at different incubation stages (I, lag phase; II, exponential phase; and III, stationary phase). Numbers show the percentage of the yeast populations.

Kinetics of Biomass, Geosmin and Antifungal Activity during Strain QC-2 Fermentation. During fermentation in potato dextrose medium, strain QC-2 reached a maximum dry cell weight of 3.75 g/L after 5 days (stage II). The dry cell weight slightly decreased at later times, stabilizing at 2.65−3.68 g/L after prolonged fermentation (7−8 days; stage III). The concentration of the geosmin produced by strain QC-2 followed similar trends to the biomass (Figure 2). The activities of the sterile QC-2 broths were assayed against *S. fibuligera* FJ-4 from *Daqu*. Sterile broths of strain QC-2 incubated at different stages were pipetted onto PDA spread with *S. fibuligera* FJ-4, and the inhibition zone was measured after 3 days at 30 °C. As shown in Figure 3, the QC-2 broth of cells incubated for 2 days exerted no obvious antifungal effect. After 3−9 days, the inhibition zones became obvious and enlarged at later fermentation times.

DOI: 10.1021/jf503351w
J. Agric. Food Chem. 2015, 63, 290−296

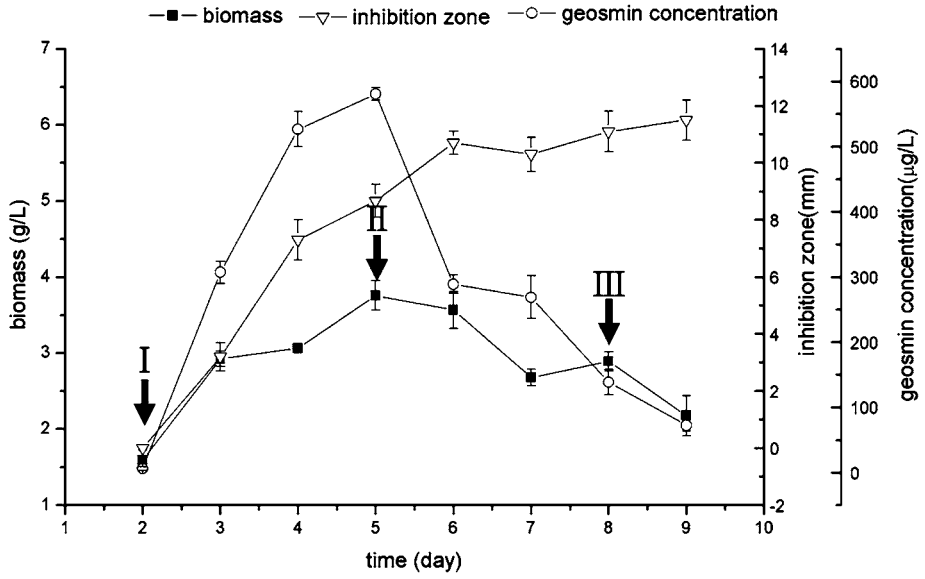

Figure 2. Biomasses, geosmin contents and antifungal activities of broths exposed to QC-2 at different fermentation stages. The test fungus is *Saccharomycopsis fibuligera* FJ-4.

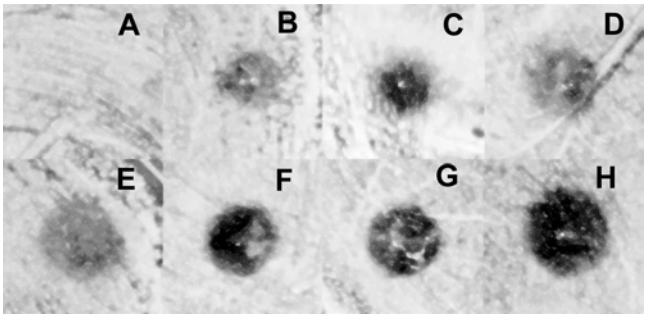

Figure 3. Antifungal activities of filter-sterilized broths of *Streptomyces sampsonii*QC-2 fermented for different periods. Shown are the inhibition zones against *Saccharomycopsis fibuligera* FJ-4 after 3 days of incubation at 30 °C. A, 2 days; B, 3 days; C, 4 days; D, 5 days; E, 6 days; F, 7 days; G, 8 days; and H, 9 days.

Influence of Strain QC-2 on the Volatile Metabolites in Mixed-Culture System. The mixed-culture system contained four brewing functional yeasts (*S. cerevisiae* FJ-7, *P. anomala* FJ-3, *I. orientalis* FJ-2, and *S. fibuligera* FJ-4) isolated from a Chinese liquor-making environment. The sterilized broths of geosmin-producing strain QC-2 at different incubation stages were introduced to the system. The volatile compounds in these experimental batches were quantified by HS−SPME−GC−MS, and a heat map of their Z scores was prepared. As shown in Figure 4, the main products of the mixed-yeast culture were esters, alcohols and acids. The geosmin concentration increased as the QC-2 incubation period lengthened before spiking into the mixed-culture system. The flavor of the mixed-culture brewing system was most obviously decreased by the QC-2 broth of cells incubated for 5 days (stage III). This decline was chiefly due to degradation of Group I and II alcohols and esters, such as 3-octanol, 3-methyl butanol, ethyl octanoate, and ethyl decanote. Meanwhile, the geosmin produced by *Streptomyces* has been recognized as an off-flavor volatile.[23,24] The results imply that geosmin-producing *Streptomyces* secretes antifungal compounds against the functional yeasts.

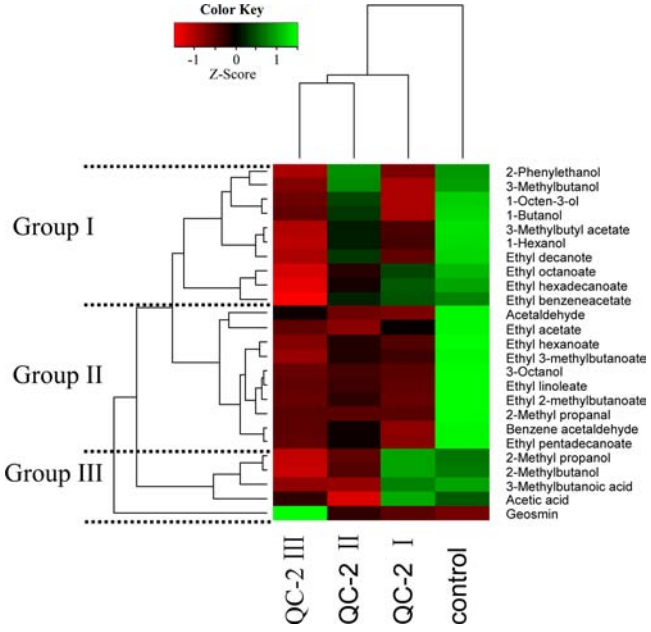

Figure 4. Volatile metabolites of four brewing functional yeasts in a mixed-culture fermentation (s.c, *Saccharomyces cerevisiae* FJ-7; p.a, *Pichia anomala* FJ-3; i.o, *Issatchenkia orientalis* FJ-2; sm.f, *Saccharomycopsis fibuligera* FJ-4) exposed to *Streptomyces sampsonii* QC-2 at different incubation stages (I, lag phase; II, exponential phase; and III, stationary phase).

Identifying the Antifungal Active Substances Produced by Strain QC-2. The QC-2 broth was purified and concentrated in a solid phase extraction (SPE) column. Three fractions were collected from three different eluents (see Materials and Methods). The ultraviolet absorption spectrum of the 50% acetonitrile/water fraction exhibited three characteristic peaks at 360, 380, and 400 nm. These peaks, detected by a photodiode array (PDA) detector at 6.5−7.6 min retention time (Figure 5B), characterize the chromophores of conjugate heptaene macrolides.[18,19] Nine peaks appeared in the spectrum of potato dextrose broth incubated with strain QC-2. However,

DOI: 10.1021/jf503351w
J. Agric. Food Chem. 2015, 63, 290−296

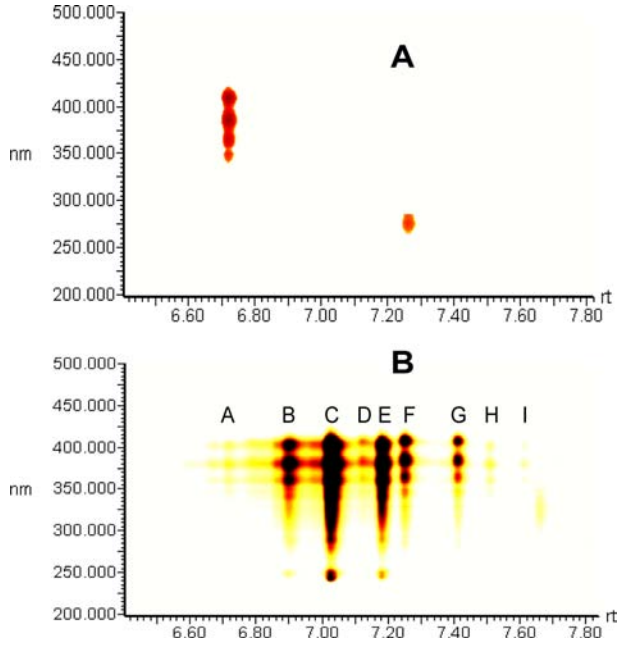

Figure 5. Photodiode array UV spectra of (A) standard sample amphotericin B and (B) peak A-I extracted from *Streptomyces sampsonii* QC-2 fermentation broth, precipitated on a C18 UPLC column (5 cm × 2.1 mm, 1.7-μm particles).

comparison with the retention time of amphotericin B in the PDA chromatogram reveals no amphotericin B production by strain QC-2 (Figure 5A).

The main components produced by strain QC-2 were identified and confirmed by UPLC−Q-TOF−MS/MS, standard spiking and mass spectrometry. The masses of these components were accurately determined by TOF−MS using negative electron spray ionization,[20] and the molecular ions are listed in Table 2. The approximate molecular weights of the main components in QC-2 broth were 1110.4, 1108.4, 1092.4, and 1176.4. This method also determines the abundances of the ion fragments. The molecular structures, derived from the mass spectrogram and compared with the PDA chromatogram, confirm the compounds as heptaene macrolide antibiotics. The number of double-bond equivalents (DBE) reported by the elemental composition tool were also consistent with the heptaene basic skeleton structure of the macrolide antibiotic class: C: 45, N: 1, O: 16, and DBE: 12. Error 0.1 Da. The ranges of possible elements and atomic numbers were as follows: C: 45−100, H: 0−100, N: 1−3, O: 16−20, and DBE: 16−25. The most likely formula was identified by analyzing the chemical element composition, based on the $[M - H]^-$ peak in negative ion mode. This analysis was performed by MassLynx application management software. The molecular formulas of the nine target compounds are listed in Table 2.

To confirm the structural formulas of these separate products, we directly imported the parent fragment ions from the raw data file, along with their structural formulas, into the Massfragment software, thus providing the fragment "soft spots". Finally, the proposed structural formulas were elucidated by Massfragment to assess their match to the corresponding fragment information. The formulas input to Massfragment were obtained from the accurate masses, which deviated from the theoretical values by 1.5 ppm at most. When the candicidin mixture standard was spiked into the broth of strain QC-2, the peaks of components B, C, E, and I were enhanced (see Figure 6A). The retention time of component C in QC-2 broth was similar to that of candicidin D, a heptaene macrolide of known chemical structure.[19] The contents of different components produced during fermentation were also quantified. Antifungal compound production in the QC-2 broth was maximized aat the seventh day of fermentation (Figure 6B), and was dominated by component C (whose concentration reached 504.83 μg/L). The changing trends of the antibiotics in the fermenting broth were consistent with those of the antifungal effect (inhibition zone diameter; see Figure 3). These results further confirm the active antifungal materials as heptaene macrolide antibiotics. Jørgensen and colleagues reported that most of their *Streptomyces* isolates produced candicidin, while all of them contained the *can* gene cluster responsible for candicidin biosynthesis.[19] The plasmid containing the genes can be conjugatively transferred to other streptomycetes.[19] Linear plasmids have also been identified as temperature-sensitive and easily lost,[25] and are commonly transferred to other species.[26] Although the *can* plasmid is not transferable to other *Streptomyces* strains in the laboratory, it may be responsible for spreading the candicidin biosynthesis gene cluster to other strains in natural environments such as Chinese liquor-making plants.

In conclusion, there were significant influences of diverse *Streptomyces* spp. acting as geosmin producers on the brewing functional microbials in a Chinese liquor making system. Some geosmin-producing *Streptomyces* could secrete antifungal compounds, heptaene macrolide antibiotics, against the normal fungi microbiota. In view of our results, the presence of *Streptomyces* may cause the imbalance of the microbial community of a brewing system. Accordingly, the contribution

Table 2. Antibiotic Contents in QC-2 Broth and Their Molecular Formulas, Hypothesized from Mass Spectrometry Information

			$[M - H]^-$			M	
component	retention time (min)	content (mg/L)	ion weight	formula	DBE[a]	formula	DBE[a]
A	6.60	0.06	1109.4296	$C_{57}H_{77}N_2O_{20}$	20.5	$C_{57}H_{78}N_2O_{20}$	20
B	6.72	0.12	1107.4186	$C_{57}H_{75}N_2O_{20}$	21.5	$C_{57}H_{76}N_2O_{20}$	21
C	6.90	1.43	1109.4172	$C_{57}H_{77}N_2O_{20}$	20.5	$C_{57}H_{78}N_2O_{20}$	20
D	7.03	3.77	1107.4064	$C_{57}H_{75}N2O_{20}$	21.5	$C_{57}H_{76}N_2O_{20}$	21
E	7.18	1.60	1091.4081	$C_{57}H_{75}N_2O_{19}$	20.5	$C_{57}H_{76}N_2O_{19}$	20
F	7.25	0.56	1107.4064	$C_{57}H_{75}N_2O_{20}$	21.5	$C_{57}H_{76}N_2O_{20}$	21
G	7.41	0.54	1091.4203	$C_{57}H_{75}N_2O_{19}$	21.5	$C_{57}H_{76}N_2O_{19}$	21
H	7.51	0.15	1075.4175	$C_{57}H_{75}N_2O_{18}$	21.5	$C_{57}H_{76}N_2O_{18}$	21
I	7.61	0.08	1107.4064	$C_{57}H_{75}N_2O_{20}$	21.5	$C_{57}H_{76}N_2O_{20}$	21

[a]DBE = double-bond equivalents.

DOI: 10.1021/jf503351w
J. Agric. Food Chem. 2015, 63, 290−296

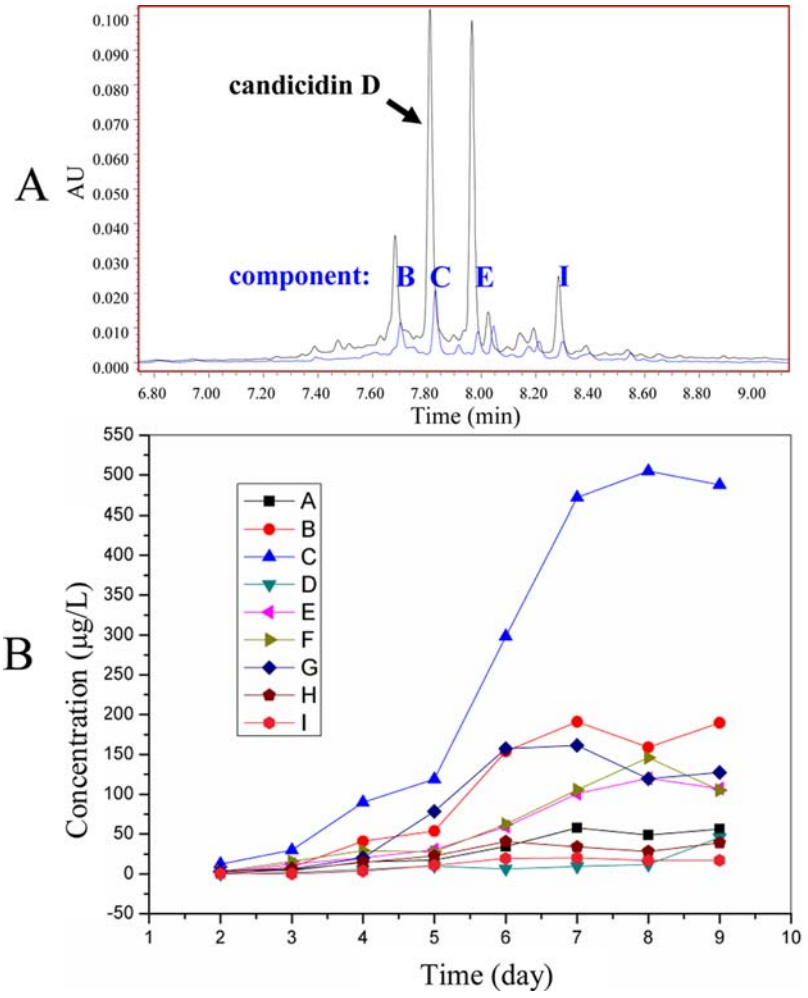

Figure 6. (A) Comparison of UV chromatogram (at 380 nm) of QC-2-produced antifungal active substances and that spiked with candicidin standard, precipitated on a C18 UPLC column (10 cm × 2.1 mm, 1.7-μm particles) and (B) concentrations of antibiotic component A-I produced by *Streptomyces sampsonii* QC-2 at different fermentation stages.

of yeasts to liquor flavor were decreased, such as alcohols and esters. Therefore, liquor makers should keep a close eye on the geosmin-producing *Streptomyces.*

AUTHOR INFORMATION

Corresponding Author

*Tel: +86 510 85918197; fax: +86 510 85918201; e-mail: yxu@jiangnan.edu.cn.

Notes

The authors declare no competing financial interest.

ACKNOWLEDGMENTS

We are grateful to the National High Technology Research and Development Program of China (2013AA102108, 2012AA021301), the National Natural Science Foundation of China (31371822, 31271921), the Program of Introducing Talents of Discipline to Universities (111 Project) (111-2-06), the Cooperation Project of Jiangsu Province among Industries, Universities, and Institutes (BY2010116) and the Fundamental Research Funds for the Central Universities (JUDCF10016). Special thanks also go to the "169" plan of Chinese liquor for its financial support and supply of *Daqu* samples.

REFERENCES

(1) Zhang, W. X.; Wu, Z. Y.; Zhang, Q. S.; Wang, R.; Li, H. Combination of newly developed high quality Fuqu with traditional Daqu for Luzhou-flavor liquor brewing. *World J. Microb. Biot.* **2009**, *25*, 1721−1726.

(2) Du, H.; Lu, H.; Xu, Y.; Du, X. Community of environmental *Streptomyces* related to geosmin development in Chinese liquors. *J. Agric. Food Chem.* **2013**, *61*, 1343−1348.

(3) Zheng, X. W.; Tabrizi, M. R.; Nout, M. J. R.; Han, B. Z. Daqu—A traditional Chinese liquor fermentation starter. *J. I. Brewing* **2011**, *117*, 82−90.

(4) Wu, Z. Y.; Zhang, W. X.; Zhang, Q. S.; Hu, C.; Wang, R.; Liu, Z. H. Developing new sacchariferous starters for liquor production based on functional strains isolated from the pits of several famous Luzhou-flavor liquor brewers. *J. I. Brewing* **2009**, *115*, 111−115.

(5) Wang, H. Y.; Gao, Y. B.; Fan, Q. W.; Xu, Y. Characterization and comparison of microbial community of different typical Chinese liquor Daqus by PCR-DGGE. *Lett. Appl. Microbiol.* **2011**, *53*, 134−140.

(6) Zheng, X.-W.; Yan, Z.; Han, B.-Z.; Zwietering, M. H.; Samson, R. A.; Boekhout, T.; Nout, M. J. R. Complex microbiota of a Chinese "Fen" liquor fermentation starter (Fen-Daqu), revealed by culture-dependent and culture-independent methods. *Food Microbiol.* **2012**, *31*, 293−300.

(7) Li, X.-R.; Ma, E.-B.; Yan, L.-Z.; Meng, H.; Du, X.-W.; Zhang, S.-W.; Quan, Z.-X. Bacterial and fungal diversity in the traditional Chinese liquor fermentation process. *Int. J. Food Microbiol.* **2011**, *146*, 31−37.

DOI: 10.1021/jf503351w
J. Agric. Food Chem. 2015, 63, 290−296

(8) Van Rensburg, P.; Van Zyl, W. H.; Pretorius, I. S. Engineering yeast for efficient cellulose degradation. *Yeast* **1998**, *14*, 67−76.
(9) Medina, K.; Boido, E.; Farina, L.; Gioia, O.; Gomez, M. E.; Barquet, M.; Gaggero, C.; Dellacassa, E.; Carrau, F. Increased flavour diversity of Chardonnay wines by spontaneous fermentation and co-fermentation with *Hanseniaspora vineae*. *Food Chem.* **2013**, *141*, 2513−2521.
(10) Contreras, A.; Hidalgo, C.; Henschke, P. A.; Chambers, P. J.; Curtin, C.; Varela, C. Evaluation of non-*Saccharomyces* yeasts for the reduction of alcohol content in wine. *Appl. Environ. Microb.* **2014**, *80*, 1670−1678.
(11) Du, H.; Xu, Y. Determination of the microbial origin of geosmin in Chinese liquor. *J. Agric. Food Chem.* **2012**, *60*, 2288−2292.
(12) Du, H.; Fan, W.; Xu, Y. Characterization of geosmin as source of earthy odor in different aroma type Chinese liquors. *J. Agric. Food Chem.* **2011**, *59*, 8331−8337.
(13) Schrempf, H. *Streptomycetaceae: Life Style, Genome, Metabolism and Habitats*; John Wiley & Sons, Ltd: New York, 2001.
(14) Li, Q. L.; Ning, P.; Zheng, L.; Huang, J. B.; Li, G. Q.; Hsiang, T. Fumigant activity of volatiles of *Streptomyces globisporus* JK-1 against *Penicillium italicum* on *Citrus microcarpa*. *Postharvest. Biol. Tec.* **2010**, *58*, 157−165.
(15) Jain, P. K.; Jain, P. C. Isolation, characterization and antifungal activity of *Streptomyces sampsonii* GS 1322. *Indian J. Exp. Biol.* **2007**, *45*, 203−206.
(16) McNeal, K. S.; Herbert, B. E. Volatile organic metabolites as indicators of soil microbial activity and community composition shifts. *Soil Sci. Soc. Am. J.* **2009**, *73*, 579−588.
(17) Coda, R.; Cassone, A.; Rizzello, C. G.; Nionelli, L.; Cardinali, G.; Gobbetti, M. Antifungal activity of *Wickerhamomyces anomalus* and *Lactobacillus plantarum* during sourdough fermentation: Identification of novel compounds and long-term effect during storage of wheat bread. *Appl. Environ. Microb.* **2011**, *77*, 3484−3492.
(18) Parekh, A. C.; Dave, C. V. Hamycin—Separation of toxicity and antifungal activity in mice. *Life Sci.* **1976**, *19*, 1737−1742.
(19) Jørgensen, H.; Fjaervik, E.; Hakvag, S.; Bruheim, P.; Bredholt, H.; Klinkenberg, G.; Ellingsen, T. E.; Zotchev, S. B. Candicidin biosynthesis gene cluster is widely distributed among *Streptomyces* spp. isolated from the sediments and the neuston layer of the Trondheim fjord, Norway. *Appl. Environ. Microb.* **2009**, *75*, 3296−303.
(20) Cao, W.; Zhang, K.; Tao, G.; Wang, X.; Liu, Y. Identification of the fatty acyl residues composition and molecular species of phosphatidylcholines in soy lecithin powder by UPLC−ESI-MS/MS. *Chromatographia* **2012**, *75*, 1271−1278.
(21) Lv, X.-C.; Huang, X.-L.; Zhang, W.; Rao, P.-F.; Ni, L. Yeast diversity of traditional alcohol fermentation starters for Hong Qu glutinous rice wine brewing, revealed by culture-dependent and culture-independent methods. *Food Control* **2013**, *34*, 183−190.
(22) Ismaya, W. T.; Hasan, K.; Kardi, I.; Zainuri, A.; Rahmawaty, R. I.; Permanahadi, S.; El Viera, B. V.; Harinanto, G.; Gaffar, S.; Natalia, D.; Subroto, T.; Soemitro, S. Chemical modification of *Saccharomycopsis fibuligera* R64 α-Amylase to improve its stability against thermal, chelator, and proteolytic inactivation. *Appl. Biochem. Biotechnol.* **2013**, *170*, 44−57.
(23) Jachymova, J.; Votruba, J.; Viden, I.; Rezanka, T. Identification of *Streptomyces* odor spectrum. *Folia Microbiol.* **2002**, *47*, 37−41.
(24) Scholler, C. E. G.; Gurtler, H.; Pedersen, R.; Molin, S.; Wilkins, K. Volatile metabolites from actinomycetes. *J. Agric. Food Chem.* **2002**, *50*, 2615−2621.
(25) Pang, X.; Sun, Y.; Liu, J.; Zhou, X.; Deng, Z. A linear plasmid temperature-sensitive for replication in *Streptomyces hygroscopicus* 10−22. *FEMS Microbiol. Lett.* **2002**, *208*, 25−28.
(26) Ravel, J.; Wellington, E. M. H.; Hill, R. T. Interspecific transfer of *Streptomyces*giant linear plasmids in sterile amended soil microcosms. *Appl. Environ. Microb.* **2000**, *66*, 529−534.

DOI: 10.1021/jf503351w
J. Agric. Food Chem. 2015, 63, 290−296

JOURNAL OF AGRICULTURAL AND FOOD CHEMISTRY

Article

pubs.acs.org/JAFC

Beta-Carotene Chemical Stability in Nanoemulsions Was Improved by Stabilized with Beta-Lactoglobulin−Catechin Conjugates through Free Radical Method

Jiang Yi,[†,‡] Yuzhu Zhang,[‡] Rong Liang,[§] Fang Zhong,*[,†] and Jianguo Ma[†]

[†]Key Laboratory of Food Colloids and Biotechnology, Ministry of Education, School of Food Science and Technology, Jiangnan University, Wuxi 214122, P.R. China

[‡]Western Regional Research Center, ARS, USDA, Albany, California 94710, United States

[§]Key Laboratory of Food Colloids and Biotechnology, Ministry of Education, School of Chemical and Material Engineering, Jiangnan University, Wuxi 214122, P.R. China

ABSTRACT: Beta-lactoglobulin (BLG)−catechin conjugates were prepared by a free radical method and investigated with sodium dodecyl sulfate polyacrylamide gel electrophoresis (SDS-PAGE), electrospray ionization−mass spectrometry (ESI-MS), and far-UV circular dichroism (CD). Covalent binding between BLG and catechin were confirmed with SDS-PAGE and ESI-MS. About 93% of beta-lactoglobulin was conjugated with catechin or catecin fragments according to the gel intensity analysis software. Far-UV CD results showed that the content of β-sheet decreased with a corresponding increase in unordered structures after grafting. Both nanoemulsions with mean particle size between 160 and 170 nm were prepared. Both the rate of particle growth and the total beta-carotene (BC) loss at 50 °C were significantly greater than at 4 and 25 °C. The retention rates of BC in nanoemulsions were 27.8% and 48.6% for BLG and BLG−catechin conjugates, respectively, after 30 days of storage at 50 °C. The BC retention encapsulated in nanoemulsion was significantly improved using BLG−catechin conjugates, compared with BLG alone. The increase of BC retention in nanoemulsions encapsulated with BLG−catechin conjugates was due to the significant improvement of antioxidative properties (reducing power, free radical scavenging activity, and hydroxyl radical scavenging activity) of BLG after covalent binding with catechin. The results indicated that the proteins modified with polyphenols can be widely used in a labile bioactive compounds encapsulation delivery system.

KEYWORDS: *beta-lactoglobulin, beta-carotene, catechin, antioxidant activities, ESI-MS, nanoemulsion*

INTRODUCTION

High previtamin A activity and strong antioxidant activity make beta-carotene (BC) an important carotenoid for human nutrition.[1,2] BC is, however, highly susceptible to isomerization, oxidation, and degradation due to the polyunsaturated structure (11 double bonds),[3] and its application in food systems was strictly limited. Oil-in-water nanoemulsion delivery systems encapsulated by biomacromolecules have been developed recently to encapsulate and protect BC from oxidation. The advantages of such a system include high stability against flocculation or aggregation, high optical clarity, and increased bioavailability of lipophilic bioactive molecules.[4−6]

Compared to conventional emulsions (1−10 μm), the nanoemulsion delivery systems loaded with lipophilic bioactives (BC) may have much higher bioavailability (bioaccessibility). However, due to the small droplet diameter (D < 200 nm) and the high surface area-to-volume ratio, protection of BC with nanoemulsions may be less effective compared with conventional emulsion.[6] We recently reported that there is an inverse relationship between the chemical stability of incorporated BC and the particle diameter.[6] Tan and Nakajima also reported that small particle size with large interfacial surface led to more loss of BC.[7] To increase the stability of BC in nanoemulsions without decreasing bioavailability, new emulsifiers with strong antioxidant activity are needed.

It was reported that a free radical grafting approach, which employed a hydrogen peroxide−ascorbic acid pair as the radical initiator system, may be used to prepare biopolymer−polyphenol conjugates.[8,9] Compared with biopolymers alone, biopolymer−polyphenol conjugates may provide better protection of easily oxidized lipophilic bioactive compounds used in food delivery systems. However, the binding mechanism and the effects of polyphenol on biomacromolecules structure have not been clearly explained.

Generally, proteins exhibit lower toxicity and were more biocompatible compared with small surfactants and synthesized polymers.[10] Bovine beta-lactoglobulin (BLG), the major component of whey protein, is a common food addictive, used especially as an emulsifier due to the excellent emulsification properties. What's more, compared to surfactants (Tween), BLG showed protective activity of encapsulated bioactive compounds against degradation, as well as controlled release capacity for the resistance digestion properties against pepsin but not trypsin.[11,12]

Catechin is one of the natural polyphenols found in tea and fruits with strong antioxidant activities.[13−15] Noncovalent

Received: September 2, 2014
Revised: December 16, 2014
Accepted: December 16, 2014
Published: December 16, 2014

ACS Publications © 2014 American Chemical Society

DOI: 10.1021/jf5056024
J. Agric. Food Chem. 2015, 63, 297−303

interactions between proteins and catechins have been documented,[16,17] and covalent conjugation between biopolymers and catechin has been proposed to enhance their antioxidant activities.[8,18,19] The objective of this study was to obtain covalent BLG−catechin conjugates with improved antioxidant activities, which were characterized by SDS-PAGE, ESI-MS, and far-UV CD. Also, the potential applications in oil-in-water nanoemulsion delivery systems as emulsifier were analyzed.

MATERIALS AND METHODS

Materials. Beta-lactoglobulin (≥90%), beta-carotene (≥97%, UV), (+)-catechin (≥98% high-performance liquid chromatography (HPLC)-grade), L-ascorbic acid, hydrogen peroxide (30%, w/w), 2,2-diphenyl-1-picrylhydrazil (DPPH), potassium ferricyanide, and 1,10-phenanthroline were obtained from Sigma-Aldrich (St. Louis, MO). Corn oil was purchased from a local market (Albany, CA, U.S.A.). All solvents used for ESI-MS were Optima liquid chromatography/mass spectrometry (LC/MS)-grade (Fisher Scientific, PA). All other chemicals and reagents used were HPLC-grade and obtained from Sigma-Aldrich (St. Louis, MO). Ultrapure water (18.2 MΩ) was supplied by a Milli-Q apparatus (Millipore Corporation).

Conjugation of BLG with Catechin. The conjugation of BLG−catechin was prepared with a method similar to that reported in the literature.[9] Briefly, 0.5 g of BLG was dissolved in 50 mL of ultrapure water in a 125 mL glass flask, then 0.5 mL of 10.0 M H_2O_2 and 0.25 g of L-ascorbic acid were added and incubated for 2 h at room temperature with stirring. After that, 0.35 mmol of catechin was added and the reaction was allowed to proceed for 24 h at room temperature. Unreacted catechin was removed by dialysis against ultrapure water to 30 times the volume of the reaction solution using Slide-A-Lyzer Dialysis Cassettes, 2K MWCO (Thermo-Scientific, Waltham, MA, U.S.A.) for 48 h at 4 °C. The water was changed 10 times at approximately equal intervals. No free catechin was detectable in the dialyzed conjugates solution by HPLC analysis. The resulting BLG−catechin solution was lyophilized for further use. Blank BLG (control) was prepared with the same method without catechin.

Sodium Dodecyl Sulfate Polyacrylamide Gel Electrophoresis. A 4−20% gradient polyacrylamide gel prepared in-house was used for SDS-PAGE analysis. Five μL of BLG and BLG−catechin conjugates (protein content was ∼5 mg/mL) were mixed with 5 μL of ultrapure water and 10 μL of 2X SDS sample buffer (100 mM Tris-HCl, pH 6.8, 4% SDS, 0.2% bromophenol blue, 20% glycerol, and 200 mM 2-mercaptoethanol) and then heated for 5 min at 95 °C. Fifteen μL of each sample was loaded to a designated well for electrophoresis at 120 V with a Tris-HEPES-SDS running buffer (100 mM Tris, 100 mM (4-(2-hydroxyethyl)-1-piperazineethanesulfonic acid) (HEPES), 3 mM sodium dodecyl sulfate (SDS), pH 8.0). The gel was stained using the Colloidal Coomassie G-250 Staining protocols.[20] The stained gel was scanned with an ImageQuant LAS 4000 digital imaging system (GE Healthcare, Piscataway, NJ, U.S.A.).

Circular Dichroism. A J-815 circular dichroism (CD) spectrometer (Jasco, Tokyo, Japan) was used to analyze the conformational changes of the protein after grafting in the wavelength range of 195−260 nm using a cell with a 2.0 mm path length as described previously.[21] Samples were prepared with 10 mM phosphate buffer (PB) (pH 7.0) at a protein concentration of 0.2 mg/mL. Scanning was performed at 50 nm/min at 20 °C. CD spectra were collected 10 times for each sample and displayed as mean residue ellipicity (degrees × cm^2/dmol) using 113 for the average number of amino acid residues per molecule of BLG.

Electrospray Ionization−Mass Spectrometry. A Thermo Easy Nano-II (Thermo Fisher Scientific, Waltham, MA, U.S.A.) HPLC was used to inject samples in the LC-MS system. After filtered with a 0.22 μm filter, 1 mg/mL blank BLG or BLG−catechin conjugates dissolved in ultrapure water were diluted 1:10 with 0.1% formic acid in water. Solvent A was 0.1% formic acid in water. Solvent B was 0.1% formic acid in acetonitrile. For each injection, 2 μL of the sample was applied at 100 bar backed with 8 μL of solvent A onto a reverse-phase trap cartridge (100 μm i.d. with 3 cm of Vydac Everest C18 5 μM/200 Å) (Precision Capillary Columns, CA, U.S.A.). Gradient elution of the sample was accomplished at 200 nL/min with the gradient 2−16% B for 7 min, 16−35% B for 20 min, and 35−80% B for 4 min. The analytical column was a New Objectives PicoChip column with 10 cm Reprosil-PUR C18-AQ, 3 μm, 120 Å packing (New Objectives Inc., MA, U.S.A.). Electrospray ionization−mass spectrometry (ESI-MS) data were collected on a Thermo Orbitrap Elite. Heated capillary was set to 250 °C. ESI voltage was 2.7 KV. Full scans (300−2000 Da) were collected in the Orbitrap with resolution set to 30 000. MS−MS scans were collected, but only full scan data were used for deconvolution and calculation of molecular mass of BLG and the conjugates. The program MagTran was used to deconvolute the electrospray data to determine the molecular masses for the samples.[22] Positive-ion mode was used in this study.

Preparation of Beta-Carotene Emulsions. Blank BLG or BLG−catechin conjugates were dissolved in ultrapure water and stirred for 3 h to form a 1% (w/w) solution. Beta-carotene (BC, 0.1%) was dissolved in carrier oils (corn oil) by stirring for 5 min at 50 °C, and stirring continued for 1 h at room temperature to ensure complete solubilization under nitrogen. A crude emulsion of 10% (wt) of the BC corn oil solution in the 1% protein solution at a mass ratio of 1:9 (oil phase/aqueous phase) was formed by high-speed homogenization for 2 min (PT10/35, Kinematica GmbH, Eschbach, Germany). The crude emulsion was then further homogenized through a high-pressure microfluidizer (M-110L, Microfluidics, MA, U.S.A.) seven times at 15 000 psi (103.4 MPa) at 25 °C. The homogenized samples were stored at 4 °C for further use.

Particle Diameter and Zeta-Potential Analysis. The mean particle diameter, particle size distribution (PDI), and zeta-potential of BC nanoparticles were determined by dynamic light scattering technique using a Malvern Zetasizer (Nano-ZS; Malvern Instruments, Worcestershire, U.K.). Refractive indices of 1.45 for BC oil droplet and 1.33 for ultrapure water were used. To reduce multiple scattering effects, the nanoparticles were diluted 100 times prior to the measurements. The tests were performed in triplicate.

Storage Stability of BC Emulsions. The nanoemulsion samples prepared freshly were transferred into screw-capped glass vials immediately after preparation. The samples were stored at 4, 25, and 50 °C in the dark for 30 days, and the same aliquots were removed at day 0, 2, 4, 6, 9, 16, 23, and 30 for particle size and BC content analysis. The BC was extracted from the nanoemulsions with 3 mL of ethanol/*n*-hexane (1:2, v:v) three times. The hexane fractions were combined and brought up to 10 mL for HPLC analysis to assay the stabilization of BC by BLG and BLG−catechin conjugates in the BC-loaded nanoemulsions.[6]

HPLC quantification of BC was performed using an Agilent 1100 HPLC system with diode array UV−vis absorption detector (DAD; Agilent, Santa Clara, CA, U.S.A.) as previously described,[23] and the BC quantitation range (0.1−100 μg mL^{-1}) was established for HPLC analysis of BC in nanoemulsions. A polymeric C_{30} reverse-phase analytical column (250 × 4.6 mm i.d., 5 μm, YMC, Inc., Wilmington, NC, U.S.A.) was used to separate BC with a flow rate of 1 mL min^{-1} at room temperature. The guard column was a reverse-phase C_{18} column (50 × 3.0 mm i.d., 5 μm, YMC, Inc.). The injection volume was 20 μL, and the detection wavelength was 450 nm. The chromatography conditions were as follows: solvent A, methanol/acetonitrile/water (84:14:2, v/v/v); solvent B, dichloromethane. The solvent gradient program was 80% A/20% B at 0 min and was changed linearly to 45% A/55% B in 15 min, maintained for 5 min, and followed by a linear return to 80% A/20% B at 25 min.

Chemical Antioxidant Activities. *Ferric Reducing Power.* The reducing power of blank BLG, BLG−catechin conjugates, and catechin was measured as described by Siddhuraju and Becker[24] with slight modifications. One mL of the blank BLG, BLG−catechin, and free catechin as a control at 1 mg/mL (w/v) was diluted in phosphate buffer (PB) (0.2 M, pH 7.0), mixed with 1 mL potassium ferricyanide (1% w/v) and incubated at 50 °C for 20 min. Next, 1 mL of trichloroacetic acid (TCA) (10% w/v) was added, and the mixture was centrifuged at 4000 rpm for 10 min (Beckman Coulter, Pasadena, CA,

DOI: 10.1021/jf5056024
J. Agric. Food Chem. 2015, 63, 297−303

U.S.A.). One mL of distilled water and 0.5 mL of ferric chloride (0.1% w/v) was added to the supernatant and blended for 10 s. The absorbance was detected at 700 nm by Nanodrop 2000c (Thermo Scientific, Wilmington, DE, U.S.A.) after 10 min. The antioxidant activity of free catechin was measured and used as a control.

DPPH Radical Scavenging Activity. The 2,2-diphenyl-1-picrylhydrazil (DPPH) radical scavenging activity was determined according to the method of Gülçin et al.[25] Two mL of the sample (blank BLG, BLG−catechin conjugate, or catechin) at 1 mg/mL (w/v) was added to 2 mL of 0.1 mM DPPH dissolved in ethanol and was agitated for 10 s, and then kept for 30 min at room temperature. The absorbance was read at 517 nm. The radical scavenging activity (AA_D) was calculated according to the following equation,

$$AA_D(\%) = 100 \times (A_C - (A_S - A_B))/A_C$$

where A_C represents the absorbance of control, A_S represents the absorbance of the solution after the sample solution was added, and A_B represents the absorbance of the sample solution alone.

Hydroxyl Radical Scavenging Activity. With slight modification, the method described by Li et al.[26] was used to measure the hydroxyl radical scavenging activity of blank BLG, BLG−catechin conjugate, and catechin at 1 mg/mL (w/v). 1,10-Phenanthroline (5 mM) was dissolved in PB (0.2 M, pH 7.4) and was mixed with $FeSO_4$ (5 mM) solution. 0.1% H_2O_2 was added, and the mixture was incubated at 37 °C for 60 min. The absorbance at 536 nm was recorded with a Nanodrop 2000c (Thermo Scientific, U.S.A.). The hydroxyl radical scavenging activity of the sample was calculated using the following equation,

$$AA_H(\%) = 100 \times (A_S - A_C)/(A_B - A_C)$$

where A_S is the absorbance of the sample, A_C is the absorbance of control solution that sample solution was replaced with the same amount of distilled water, and A_B is the absorbance of solution without the samples or H_2O_2.

Statistics. All experiments were performed at least three times and were reported as mean ± standard deviation. The data were analyzed by the analysis of variance (ANOVA) using the SPSS 17.0 package (IBM, New York, U.S.A.). Duncan's multiple range test was used to determine the significant differences of the mean values ($P < 0.05$).

RESULTS AND DISCUSSION

BLG−Catechin Conjugation. The molecular weight of native BLG, blank BLG, and BLG−catechin conjugates was determined by SDS-PAGE. The bands corresponding to native BLG, blank BLG, and BLG conjugation with catechin under reducing conditions are shown in Figure 1. Different isoforms of BLG were found at ~18 kDa. Small amounts of BLG dimers are observed at ~40 kDa. Almost no changes occurred after beta-lactoglobulin reacted with L-ascorbic acid (free radical method without catechin), indicating no L-ascorbic acid was conjugated on BLG. The slight decrease of the mobility of BLG after grafting with catechin in SDS gel indicated the increase of molecular weight of BLG. The SDS-PAGE results showed that catechin was covalently binding to BLG. This is consistent with the apparent increase in the molecular weight of other proteins after covalent grafting. The molecular weight of bovine milk proteins was also increased after covalent grafting with flavonoid by laccase-catalyzed method,[19] and You et al. reported that the molecular weight of ovotransferrin was increased after covalent binding with catechin.[27] According to the SDS-PAGE results and the gel intensity analysis software, about 93% of beta-lactoglobulin was conjugated with catechin or catecin fragments.

The molecular weight changes after conjugation were further investigated with ESI-MS (Figure 2). Two main peaks, 18 361.5 and 18 277.6 Da, were found in the BLG purchased from Sigma, corresponding to BLG A and BLG B, respectively. After conjugation, the BLG−catechin conjugates were found to contain mainly two components with molecular weights of 18 474.4 and 18 390.6 Da, respectively. The differences in the molecular mass of the components in blank and catechin-conjugated BLG (increase by 113 Da) were consistent with the successful covalent attachment of possible parts of catechin molecules, which gave several fragments peaks when analyzed with ESI-MS. The ESI-MS results further confirmed the conjugation of catechin with BLG.

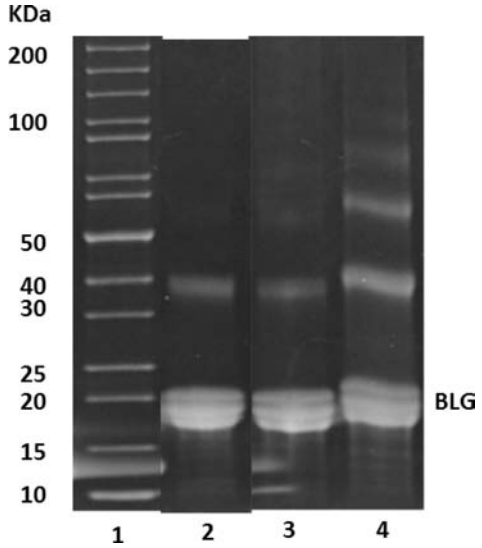

Figure 1. SDS-PAGE results under reducing conditions of BLG and BLG−catechin conjugates. Lanes: 1, protein markers; 2, native BLG; 3, blank BLG (control); 4, BLG−catechin conjugates.

Catechin Conjugation Effect on BLG Secondary Structure. After covalent conjugation with catechins, changes in the secondary structure of BLG were determined by far-UV CD spectroscopy (Figure 3). The negative peak at 216 nm indicates that BLG is rich in β-sheet secondary structure. However, the catechin-grafting reaction resulted in marked shifts in wavelength of negative peak from 216 to 206 nm, indicating changes occurred in BLG's secondary structure. The secondary structure compositions of BLG and BLG−catechin conjugates were calculated with DichroWeb online (Table 1). The composition of blank BLG in this study was as follows: α-helix, 12.8%; β-sheet, 38.8%; turn, 21.7%; and unordered, 25.5%, similar to the result reported in a recent publication.[21] After conjugation, the β-sheet structure decreased from 38.8% to 30.0%, while the unordered structure increased from 25.5% to 31.9%, indicating that BLG became more unordered, which was consistent with the results reported by Ali et al.[28] Rawel et al.[29] also found that covalent attachment of chlorogenic acid to bovine serum albumin led to the decrease of ordered structure with a parallel increase in unordered structures. The increase of unordered secondary structure of BLG may lead to the exposure of an interior hydrophobic amino acid, such as tryptophan and tyrosine, which is mainly responsible for the antioxidant activities of proteins, resulting in improvement of antioxidant activities. The exposure of the hydrophobic amino acid may also lead to the increase of emulsifying activities.

Physical Stability of BC Nanoemulsions. The particle diameters of BC nanoemulsions prepared with BLG and BLG−catechin are shown in Table 2. No significant differences in

DOI: 10.1021/jf5056024
J. Agric. Food Chem. 2015, 63, 297−303

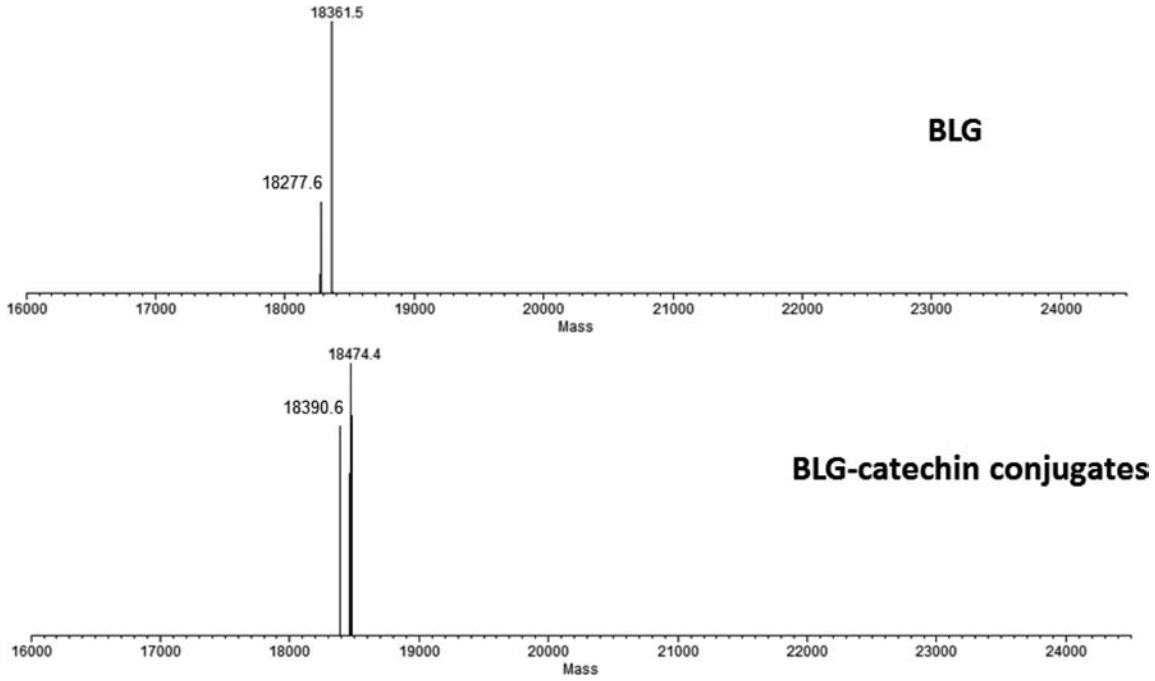

Figure 2. Electrospray ionization−mass spectrometry of blank BLG (control) and BLG−catechin conjugates.

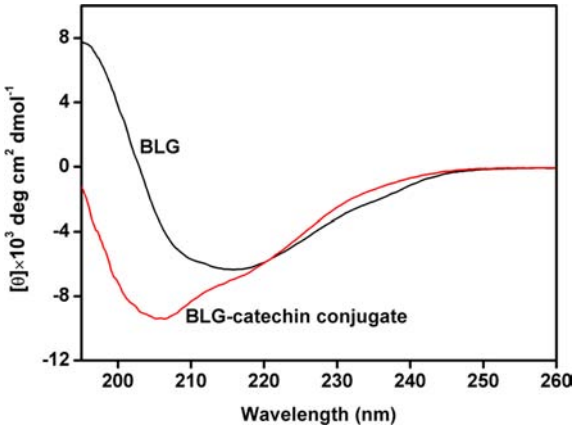

Figure 3. Far-UV CD spectra (195−260 nm) of blank BLG (control) and BLG−catechin conjugates.

Table 1. Secondary Structure Composition of Blank BLG and BLG−Catechin Conjugates[a]

samples	α-helix (%)	β-sheet (%)	turns (%)	unordered (%)
blank BLG	12.8	38.8	21.7	25.5
BLG−catechin	15.2	30.0	21.6	31.9

[a]The secondary structure composition was calculated from far-UV CD spectra data using DichroWeb online (http://dichroweb.cryst.bbk.ac.uk/html/home.shtml).

particles size were found, indicating the emulsifying properties of BLG were not affected by grafting catechin.

Particle diameter profiles were used to evaluate the physical stability of BC-loaded nanoemulsions over 30 days at 4, 25, and 50 °C (Figure 4). Heat treatment is inevitable in the food industry. To simulate food process parameters and to show the great ability of BLG−catechin conjugates in improving BC's storage stability, 4, 25, and 50 °C were chosen as storage temperature. The initial mean particle diameters were 161.7 and 167.6 nm for BLG and BLG−catechin conjugates, respectively. However, due to the large difference in density between the oil-emulsified droplet and the aqueous continuous phase, gravitational forces may cause the emulsion particles to rise and concentrate at the surface. The reduction in the interparticle distances may result in flocculation or aggregation. During the 30-day testing period at 4 °C, both BC nanoemulsions were kept relatively stable and the diameters showed <5 nm increase. At 25 °C, the diameters of the particles in both samples showed a slight increase (~5−15 nm). In contrast, the particle diameters of emulsions at 50 °C showed a higher increment of 25−35 nm for high-motion velocity and the particle size distribution was broadened, compared to the initial droplet diameters. The exposure of the nonpolar amino acid group of BLG increased the hydrophobic attraction between droplets, and this may lead to the increase in the particle size and particle aggregation.[30] Even though a larger particle size increase occurred at high temperature, no phase separation or creaming were observed during the 30-day period at the three temperatures for the samples, suggesting both BLG and BLG−catechin conjugate-stabilized nanoemulsions possessed high kinetic stability.

Table 2. Mean Particle Diameter (Z-average, nm), Polydispersity Index (PDI), and Zeta-Potential of BC Nanoemulsions Encapsulated with Blank BLG and BLG−Catechin Conjugates

characteristics	blank BLG	BLG−catechin conjugates
Z-average (nm)	161.7 ± 1.7	167.6 ± 1.3
PDI	0.101 ± 0.021	0.104 ± 0.018
zeta-potential	−57.2 ± 1.3	−62.9 ± 1.5

Retention of BC in Nanoemulsions. BC retention in both samples decreased with the increase of storage time in the dark at three different incubation temperatures. At 4 °C, after 30 days, the BC retentions were 89.8% and 94.0% for BLG- and BLG−catechin-stabilized BC nanoemulsions, respectively.

DOI: 10.1021/jf5056024
J. Agric. Food Chem. 2015, 63, 297−303

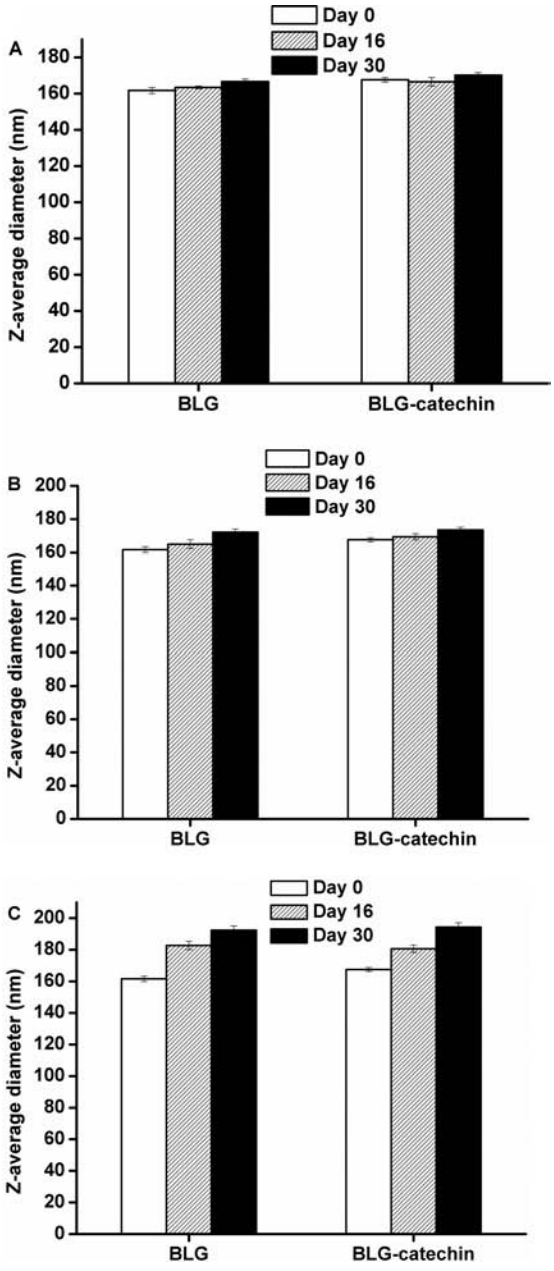

Figure 4. Change of Z-average diameters of blank BLG and BLG−catechin conjugate-stabilized BC nanoemulsions over time (30 days) at 4 (A), 25 (B), and 50 °C (C). Data are represented as the mean ± standard deviation (n = 3).

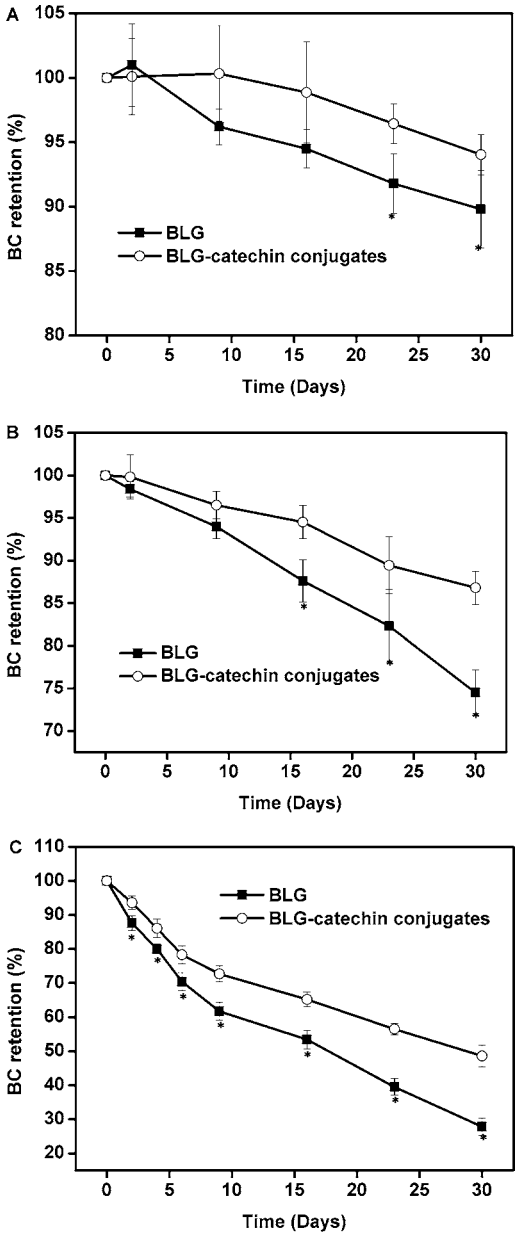

Figure 5. Retention of BC in blank BLG and BLG−catechin conjugate-stabilized nanoemulsions over time (30 days) at 4 (A), 25 (B), and 50 °C (C). Data are represented as the mean ± standard deviation (n = 3). *Significant (P < 0.05) difference.

Stored at 25 °C for 30 days, 74.5% and 86.8% of BC was retained in the emulsions when stabilized with BLG and BLG−catechin conjugates, respectively; BC retention decreased to 27.8% and 48.6% for BLG and BLG−catechin conjugate nanoemulsions, respectively, at 50 °C after 30 days (Figure 5). Similar to particle diameter growth, the total BC loss was greater at 50 °C than at 4 and 25 °C (Figure 5), demonstrating that temperature is an important factor in impacting the stability of encapsulated bioactive compounds. Compared to blank BLG, BC stabilized with BLG−catechin conjugate nanoemulsions exhibited significantly improved chemical stability and higher retentions (Figure 5), indicating the great capability of BLG−catechin conjugates in enhancing the chemical stability of encapsulated lipophilic molecules. Ali et al.[28] also reported that, compared with the unmodified protein, whey protein modified by coffee-specific phenolics showed an increase in lutein ester remaining in conventional emulsions when exposed to UV light. BC oxidation and degradation were mostly likely due to the dissolved oxygen, transition metal (Fe^{3+}) in aqueous phase, and free radicals in oil phase.[3,31] The improvement of reducing power, DPPH radical scavenging activity, and hydroxyl radical scavenging activity (Table 3) may be among the factors that led to the increase of BC chemical stability encapsulated by BLG−catechin conjugates.

Chemical Antioxidant Activities. The effects of catechin conjugation on BLG antioxidant activities were analyzed. The reducing power, DPPH radical scavenging activity, and hydroxyl radical scavenging activity (OH·) at 1 mg/mL of protein concentration are shown in Table 3. The reducing

DOI: 10.1021/jf5056024
J. Agric. Food Chem. 2015, 63, 297−303

Table 3. Reducing Power, AA_D Free Radical Scavenging Activities, and AA_H Free Radical Scavenging Activities of Blank BLG, BLG−Catechin Conjugates, and Catechin[a,b]

antioxidant activities	blank BLG	BLG−catechin conjugates	catechin
reducing power (Abs)	0.008 ± 0.002 a	0.032 ± 0.003 b	0.222 ± 0.026 c
DPPH AA_D scavenging activity (%)	7.6 ± 0.4 a	87.4 ± 2.6b	85.9 ± 2.9 b
hydroxyl AA_H scavenging activity (%)	7.3 ± 0.8 a	66.5 ± 2.0 c	21.9 ± 1.5 b

[a]BLG, BLG−catechin conjugates, and catechin concentrations were 1 mg/mL (w/v). [b]Different letters in the same row indicate significant difference ($P < 0.05$) (Duncan analysis).

power measurement was quantified by calculating the inhibition of the conversion of Fe^{3+} to Fe^{2+} by the samples. Compared to the reducing power of BLG (0.008), that of BLG−catechin conjugate quadrupled to 0.032. Compared to control BLG, the DPPH radical and hydroxyl radical scavenging activities of BLG after catechin conjugation were markedly improved 11.5 and 9.1 times (to 87.4% and 66.5%), respectively. These results indicated BLG's chemical antioxidant activities were sharply improved after grafting with catechin. It is worth noting that the hydroxyl radical scavenging activity of BLG−catechin conjugates was greater than those of both free BLG and catechin, indicating strong synergistic antioxidant effects existed between BLG and catechin.

The antioxidant activities of other proteins were also reported to have significant improvement, e.g., in gallic acid or catechin−gelatin conjugates and catechin−ovotransferrin conjugates.[9,27] The outstanding antioxidant activity of polyphenols has been attributed to the higher number of hydroxyl group substituents.[32−34] The hydroxyl groups of catechin added to BLG may lead to improved antioxidant activities of BLG−catechin conjugates.

In summary, BLG−catechin conjugates were obtained using hydrogen peroxide−ascorbic acid pair by radical method. The covalent binding of catechin to BLG was confirmed by SDS-PAGE and ESI-MS and the impact of the conjugation on BLG secondary structure was analyzed by far-UV CD. BC retention in nanoemulsions encapsulated by conjugates was higher than that in BLG alone. Chemical antioxidant activities of conjugates were appreciably improved, compared to BLG alone. High antioxidant activities suggested that BLG−catechin conjugates can be used in functional food and delivery food systems.

AUTHOR INFORMATION

Corresponding Author

*Phone: +86-510-85197876; Fax:+86-510-85197876; E-mail: fzhong@jiangnan.edu.cn.

Funding

This work was financially supported by National 125 Program 2011BAD23B02, 2013AA1022207; NSFC 31171686, 31401533; NSF-Jiangsu-BK2012556; 111 Project B07029; PCSIRT0627 and JUSRP11422.

Notes

The authors declare no competing financial interest.

REFERENCES

(1) Borel, P.; Lietz, G.; Goncalves, A.; Szabo de Edelenyi, F.; Lecompte, S.; Curtis, P.; Goumidi, L.; Caslake, M. J.; Miles, E. A.; Packard, C.; Calder, P. C.; Mathers, J. C.; Minihane, A. M.; Tourniaire, F.; Kesse-Guyot, E.; Galan, P.; Hercberg, S.; Breidenassel, C.; González Gross, M.; Moussa, M.; Meirhaeghe, A.; Reboul, E. CD36 and SR-BI Are Involved in Cellular Uptake of Provitamin A Carotenoids by Caco-2 and HEK Cells, and Some of Their Genetic Variants Are Associated with Plasma Concentrations of These Micronutrients in Humans. *J. Nutr.* **2013**, *143*, 448−456.

(2) Paiva, S. A. R.; Russell, R. M. Beta-carotene and other carotenoids as antioxidants. *J. Am. Coll. Nutr.* **1999**, *18*, 426−433.

(3) Boon, C. S.; McClements, D. J.; Weiss, J.; Decker, E. A. Factors Influencing the Chemical Stability of Carotenoids in Foods. *Crit. Rev. Food Sci. Nutr.* **2010**, *50*, 515−532.

(4) Liang, R.; Shoemaker, C. F.; Yang, X.; Zhong, F.; Huang, Q. Stability and Bioaccessibility of β-Carotene in Nanoemulsions Stabilized by Modified Starches. *J. Agric. Food Chem.* **2013**, *61*, 1249−1257.

(5) McClements, D. J.; Xiao, H. Potential biological fate of ingested nanoemulsions: Influence of particle characteristics. *Food Funct.* **2012**, *3*, 202−220.

(6) Yi, J.; Li, Y.; Zhong, F.; Yokoyama, W. The physicochemical stability and in vitro bioaccessibility of beta-carotene in oil-in-water sodium caseinate emulsions. *Food Hydrocolloids* **2014**, *35*, 19−27.

(7) Tan, C. P.; Nakajima, M. β-Carotene nanodispersions: Preparation, characterization and stability evaluation. *Food Chem.* **2005**, *92*, 661−671.

(8) Curcio, M.; Puoci, F.; Iemma, F.; Parisi, O. I.; Cirillo, G.; Spizzirri, U. G.; Picci, N. Covalent Insertion of Antioxidant Molecules on Chitosan by a Free Radical Grafting Procedure. *J. Agric. Food Chem.* **2009**, *57*, 5933−5938.

(9) Spizzirri, U. G.; Iemma, F.; Puoci, F.; Cirillo, G.; Curcio, M.; Parisi, O. I.; Picci, N. Synthesis of Antioxidant Polymers by Grafting of Gallic Acid and Catechin on Gelatin. *Biomacromolecules* **2009**, *10*, 1923−1930.

(10) He, W.; Tan, Y. N.; Tian, Z. Q.; Chen, L. Y.; Hu, F. Q.; Wu, W. Food protein-stabilized nanoemulsions as potential delivery systems for poorly water-soluble drugs: Preparation, in vitro characterization, and pharmacokinetics in rats. *Int. J. Nanomed.* **2011**, *6*, 521−533.

(11) Qian, C.; Decker, E. A.; Xiao, H.; McClements, D. J. Physical and chemical stability of β-carotene-enriched nanoemulsions: Influence of pH, ionic strength, temperature, and emulsifier type. *Food Chem.* **2012**, *132*, 1221−1229.

(12) Yi, J.; Lam, T. I.; Yokoyama, W.; Cheng, L. W.; Zhong, F., Beta-carotene encapsulated in food protein nanoparticles reduces peroxyl radical oxidation in Caco-2 cells. *Food Hydrocolloids* **2014**, *43*, 31−40.

(13) Higdon, J. V.; Frei, B. Tea Catechins and Polyphenols: Health Effects, Metabolism, and Antioxidant Functions. *Crit. Rev. Food Sci. Nutr.* **2003**, *43*, 89−143.

(14) Meyer, A. S.; Heinonen, M.; Frankel, E. N. Antioxidant interactions of catechin, cyanidin, caffeic acid, quercetin, and ellagic acid on human LDL oxidation. *Food Chem.* **1998**, *61*, 71−75.

(15) Morel, I.; Lescoat, G.; Cogrel, P.; Sergent, O.; Pasdeloup, N.; Brissot, P.; Cillard, P.; Cillard, J. Antioxidant and iron-chelating activities of the flavonoids catechin, quercetin and diosmetin on iron-loaded rat hepatocyte cultures. *Biochem. Pharmacol.* **1993**, *45*, 13−19.

(16) Bandyopadhyay, P.; Ghosh, A. K.; Ghosh, C. Recent developments on polyphenol−protein interactions: Effects on tea and coffee taste, antioxidant properties and the digestive system. *Food Funct.* **2012**, *3*, 592−605.

(17) Hasni, I.; Bourassa, P.; Hamdani, S.; Samson, G.; Carpentier, R.; Tajmir-Riahi, H.-A. Interaction of milk α- and β-caseins with tea polyphenols. *Food Chem.* **2011**, *126*, 630−639.

(18) Ishii, T.; Mori, T.; Tanaka, T.; Mizuno, D.; Yamaji, R.; Kumazawa, S.; Nakayama, T.; Akagawa, M. Covalent modification of proteins by green tea polyphenol (−)-epigallocatechin-3-gallate through autoxidation. *Free Radical Biol. Med.* **2008**, *45*, 1384−1394.

DOI: 10.1021/jf5056024
J. Agric. Food Chem. 2015, 63, 297−303

(19) Kim, S.; Cavaco-Paulo, A. Laccase-catalysed protein−flavonoid conjugates for flax fibre modification. *Appl. Microbiol. Biotechnol.* **2012**, *93*, 585−600.
(20) Dyballa, N.; Metzger, S. Fast and Sensitive Colloidal Coomassie G-250 Staining for Proteins in Polyacrylamide Gels. *J. Vis. Exp.* **2009**, e1431.
(21) Yi, J.; Lam, T. I.; Yokoyama, W.; Cheng, L. W.; Zhong, F. Controlled Release of β-Carotene in β-Lactoglobulin−Dextran-Conjugated Nanoparticles' In Vitro Digestion and Transport with Caco-2 Monolayers. *J. Agric. Food Chem.* **2014**, *62*, 8900−8907.
(22) Zhang, Z.; Marshall, A. A universal algorithm for fast and automated charge state deconvolution of electrospray mass-to-charge ratio spectra. *J. Am. Soc. Mass Spectrom.* **1998**, *9*, 225−233.
(23) Yi, J.; Lam, T. I.; Yokoyama, W.; Cheng, L. W.; Zhong, F. Cellular Uptake of β-Carotene from Protein Stabilized Solid Lipid Nanoparticles Prepared by Homogenization−Evaporation Method. *J. Agric. Food Chem.* **2014**, *62*, 1096−1104.
(24) Siddhuraju, P.; Becker, K. Antioxidant Properties of Various Solvent Extracts of Total Phenolic Constituents from Three Different Agroclimatic Origins of Drumstick Tree (*Moringa oleifera* Lam.) Leaves. *J. Agric. Food Chem.* **2003**, *51*, 2144−2155.
(25) Gülçin, İ.; Küfrevioğlu, Ö. İ.; Oktay, M.; Büyükokuroğlu, M. E. Antioxidant, antimicrobial, antiulcer and analgesic activities of nettle (*Urtica dioica* L.). *J. Ethnopharmacol.* **2004**, *90*, 205−215.
(26) Li, Y.; Jiang, B.; Zhang, T.; Mu, W.; Liu, J. Antioxidant and free radical-scavenging activities of chickpea protein hydrolysate (CPH). *Food Chem.* **2008**, *106*, 444−450.
(27) You, J.; Luo, Y.; Wu, J. Conjugation of Ovotransferrin with Catechin Shows Improved Antioxidant Activity. *J. Agric. Food Chem.* **2014**, *62*, 2581−2587.
(28) Ali, M.; Homann, T.; Khalil, M.; Kruse, H.-P.; Rawel, H. Milk Whey Protein Modification by Coffee-Specific Phenolics: Effect on Structural and Functional Properties. *J. Agric. Food Chem.* **2013**, *61*, 6911−6920.
(29) Rawel, H. M.; Rohn, S.; Kruse, H.-P.; Kroll, J. Structural changes induced in bovine serum albumin by covalent attachment of chlorogenic acid. *Food Chem.* **2002**, *78*, 443−455.
(30) Kim, H. J.; Decker, E. A.; McClements, D. J. Impact of Protein Surface Denaturation on Droplet Flocculation in Hexadecane Oil-in-Water Emulsions Stabilized by β-Lactoglobulin. *J. Agric. Food Chem.* **2002**, *50*, 7131−7137.
(31) Takahashi, A.; Suzuki, J.-i.; Shibasaki-Kitakawa, N.; Yonemoto, T. A kinetic model for co-oxidation of β-carotene with oleic acid. *J. Am. Oil Chem. Soc.* **2001**, *78*, 1203−1207.
(32) Amic, D.; Davidovic-Amic, D.; Beslo, D.; Trinajstic, N. Structure−radical scavenging activity relationships of flavonoids. *Croat. Chem. Acta* **2003**, *76*, 55−61.
(33) Heijnen, C. G. M.; Haenen, G. R. M. M.; van Acker, F. A. A.; van der Vijgh, W. J. F.; Bast, A. Flavonoids as peroxynitrite scavengers: The role of the hydroxyl groups. *Toxicol. In Vitro* **2001**, *15*, 3−6.
(34) Rice-Evans, C.; Miller, N.; Paganga, G. Antioxidant properties of phenolic compounds. *Trends Plant Sci.* **1997**, *2*, 152−159.

DOI: 10.1021/jf5056024
J. Agric. Food Chem. 2015, 63, 297−303

JOURNAL OF AGRICULTURAL AND FOOD CHEMISTRY

Article

pubs.acs.org/JAFC

Fermentative Conditions Modulating Sweetness in Dry Wines: Genetics and Environmental Factors Influencing the Expression Level of the *Saccharomyces cerevisiae HSP12* Gene

Axel Marchal,[*,†,‡,∥] Philippe Marullo,[†,§,∥] Cécile Durand,[†,§] Virginie Moine,[§] and Denis Dubourdieu[†,‡]

[†]Universite de Bordeaux, ISVV, EA 4577, Unité de recherche Oenologie, F-33882 Villenave d'Ornon, France

[‡]INRA, ISVV, USC 1366 Oenologie, 33882 Villenave d'Ornon, France

[§]BIOLAFFORT, 126 quai de la Souys, F-33100 Bordeaux, France

ABSTRACT: Yeast lees influence the organoleptic properties of wines by increasing their sweet taste. This effect is in part due to the protein Hsp12p, which is regulated by different stress response pathways in *Saccharomyces cerevisiae*. This work investigated the genetics and environmental factors influencing the expression level of the *HSP12* gene in an enological context. RT-qPCR confirmed that the *HSP12* expression level is regulated by temperature change and ethanol content during the alcoholic fermentation but not by the sugar content. Moreover, this gene shows an important variation according to the yeast strain used. For the first time yeast strain is demonstrated to play an important role in the perception of sweetness in red wine due to post-fermentation lees autolysis. Interestingly, a correlation between the expression level of *HSP12* and the sweetness perception was found using yeast strains of different origins. All of the findings provide new insights on the contribution of yeast to wine taste.

KEYWORDS: *HSP12, wine sweetness, expression level, protein, strain, Saccharomyces cerevisiae, taste*

INTRODUCTION

Wine quality depends on both its complexity of odors and its harmony of flavors. This taste balance is mainly due to interactions between sweet, sour, and bitter tastes. In particular, sweetness plays a decisive role in wine perception and is likely to contribute to the pleasure of the tasters.[1] Dry wines containing <2 g/L (below the perception threshold) of residual sugar exhibit paradoxically a subtle sweet taste.[2] Previous works have established that ethanol, glycerol,[3−5] polysaccharides,[4] and nucleotides[6] have no direct influence on sweetness perception in the concentration ranges at which they are found in dry wines. However, sensory studies have shown that wine sweetness increases during yeast lees autolysis[5] and oak wood aging;[7] therefore, the molecular determinants explaining these phenomena have been, at least in part, elucidated.[5,8]

In particular, we demonstrated in a previous work that *HSP12* has a direct or an indirect role in the increase of wine sweetness observed during yeast lees autolysis.[5] Biochemical and sensory experiments suggested that a peptide fraction of Hsp12p causes the sweet perception. We also demonstrated that sweetness intensity was linked to the amount of yeast lees in contact with wine during autolysis. All of these findings suggest that Hsp12p is involved in the gain of sweetness conferred by yeast lees.

The *HSP12* gene encodes a small heat-shock protein described as a LEA-like protein in *Saccharomyces cerevisiae*.[9] This protein is crucial for the survival of a variety of stress conditions including heat shock,[10] osmotic[11] and oxidative stresses,[10] freezing,[12] or desiccation.[13] Hsp12p protein is also implied in the extension of lifespan in dietary restriction[14] as well as in biofilm formation.[15] Despite numerous studies, the molecular function of this protein was not completely elucidated. Unlike other small heat shock proteins, *HSP12* displays a negligible molecular chaperone activity regarding protein aggregation.[14] In contrast, structural and biochemical studies suggested that *HSP12* interacts with lipid molecules and has a membrane-stabilizing role acting as a "lipid chaperone".[10,14,16] The expression level of this gene has been widely investigated due to its important response to a wide set of environmental stresses.[17] Many studies reported an induction of *HSP12* expression related to stress in both laboratory[18] and biotechnological contexts.[12,19] In the wine alcoholic fermentation context, *HSP12* appears to be highly expressed[20] despite the high sugar concentration found in wine, which is supposed to down-regulate its expression.[21,22] The high expression level of *HSP12* in the enological context is likely due to high ethanol concentration[23] and the stationary growth phase of fermenting yeast. Moreover, important physicochemical parameters in wine fermentation can modulate the expression level of this gene, including low and high temperatures,[24,25] nitrogen content,[26] and lipid concentration.[27] Besides the impact of environmental conditions, an important variability in global gene expression can be found within yeast strains[28,29] and species.[30] For *HSP12*, this general trend is verified both for the mRNA expression[31,32] and for the protein production level.[30]

These previous works emphasize that the great range of *HSP12* expression variation and the subsequent amount of protein may be linked to the resulting sweetness perception in wine.[5] However, these experiments were carried out in many

Received: September 12, 2014
Revised: December 15, 2014
Accepted: December 19, 2014
Published: December 19, 2014

ACS Publications © 2014 American Chemical Society

DOI: 10.1021/jf504408t
J. Agric. Food Chem. 2015, 63, 304−311

Table 1. Yeast Strains Used

name	genotype	origin	comment	reference
Zymaflore Fx10	diploid, HO/HO	Laffort	red wine specialized starter	Marullo et al., 2009
Δ°hsp12	diploid, *HO/HO*, *hsp12*Δ°/*hsp12*Δ°	lab collection		Marchal et al., 2011
D2	diploid, *HO/HO*	lab collection	derived from the distillery yeast alcotech 24	Blein et al., 2013
W1	diploid, *HO/HO*	lab collection	derived from the natural isolate YSP128	Blein et al., 2013
B1	diploid, *HO/HO*	lab collection	derived from the brewery yeast	Blein et al., 2013
Zymaflore VL3	diploid, *HO/HO*	Laffort	white wine specialized starter	
Actiflore F33	diploid, *HO/HO*	Laffort	generic starter	
XMC30	diploid, *HO/HO*	Laffort	red wine specialized starter	

different conditions (media, strain), impairing the elucidation of the main factors modulating the *Hsp12p* expression in wine context. This study proposes to investigate the effect of some genetic and environmental factors affecting *HSP12* expression.

MATERIALS AND METHODS

Yeast Strains and Growth Media Used. The *S. cerevisiae* strains used are listed in Table 1. The construction of the strain Δ°*hsp12* was described in Marchal et al.[5] This strain is isogenic to the commercial starter Zymaflore Fx10 (Laffort, France) referenced as H4-1D in a previous work.[33] The other strains are commercial starters form Laffort or homothallic monosporic clones previously referenced by Blein-Nicolas et al.[30] Yeast strains were propagated at 28 °C on YPD medium (1% yeast extract, 2% peptone, dextrose 2%) containing 2% agar to prepare a solid medium.

Fermentation on KP Medium. Fermentations were carried out using the model synthetic medium (KP medium) buffered at pH 3.30 and containing 190 mg(N)/L of assimilable nitrogen.[34] Fermenting sugars are constituted by an equimolar mix of glucose and fructose and were set to 240 g/L. Other concentrations of sugars were used (120, 160, or 300 g/L) for one experiment as specified in the text. Precultures were run for 24 h at 24 °C under orbital agitation (150 rpm) in the fermentation media filtered through a 0.45 μm nitrate cellulose membrane (Millipore, Molsheim, France) and diluted 1:1 with Milli-Q water. The inoculum concentration was 10^6 viable cells/mL. Fermentations were run in closed 350 mL glass reactors, locked to maintain anaerobiosis, with permanent stirring (300 rpm). Fermentations were carried out at 26 °C, but other temperatures (12, 18, 22, or 31 °C) were used for an experiment as specified in the text.

The amount of CO_2 released (g/L) was monitored daily by the weight loss of the bioreactors. The raw fermentation kinetics data were smoothed by a Loess function and plotted using the R program as previously described.[35] All fermentations were done in triplicate.

Yeast Cell Collection and Quantification. Cells were collected from fermenting KP medium at nearly 46 g/L of CO_2 produced for analyzed cell expression. In the expression monitoring experiment, samples were collected at different fermentation points (30, 46, 55, 66, or 76 g/L of CO_2 produced). The cell concentration was quantified using a flow cytometer (QuantaSC MPL, Beckman Coulter, Fullerton, CA, USA), equipped with a 488 nm laser (22 mW) and a 670 nm long-pass filter. Samples were diluted in McIlvaine buffer, pH 4.0 (0.1 M citric acid, 0.2 M sodium phosphate dibasic), and propidium iodide was added (0.3% v/v) to stain dead cells (FL3 channel).

Quantification of *HSP12* Expression Level. Extractions of mRNA and cDNA synthesis were carried out as previously described (Thibon et al. 2008).[36] Briefly, 1×10^7 cells were harvested, washed, and lysed using a Fastprep FP120 apparatus (MP Biomedicals, Solon, OH, USA). RNA was extracted using Tri reagent (Sigma, L'Isle d'Abeau Chesnes, France), and DNA contamination was treated using a DNA-free Kit (Ambion Inc., Austin, TX, USA); RNAs were retrotranscribed into cDNAs using the iScriptTM cDNA Synthesis Kit (Bio-Rad, Hercules, CA, USA). The extracted RNA was quantified using the ND-1000 UV−visible light spectrophotometer (NanoDrop Technologies, Wilmington, DE, USA). The absence of contaminant genomic DNA in RNA preparations was verified using RNA as a template in real-time PCR assays. Each cDNA sample was analyzed two times independently by quantitative real-time PCR using iCycler iQ (Bio-Rad). Gene transcripts were amplified by using the following primers: *HSP12* p321, GGGTGTCTTCCAAGGTGTC; p322, TTGGCGGCTCCCATGTAATC (151 bp); *ALG9* p605, CACGGATAGTGGCTTTGGTGAACAATTAC; p606, TATGATTATCTGGCAGCAGGAAAGAACTTGGG (163 bp); *ACT1* p323, TACCGGCCAAATCGATTCTC; p904, TACTGGTATTGTTTTGGATTCC (123 bp). The *ALG9* gene was used as a second reference gene as proposed previously.[37] Real-time quantitative PCRs (qPCRs) were carried out using the iQ SYBR Green Super Mix (Bio-Rad). Primers were added at a concentration of 0.3 mM each. The PCR program used was as follows: 3 min at 95 °C for initial denaturation, then 40 cycles of 10 s at 95 °C, 30 s at TM, and 30 s at 72 °C. A final melt curve was carried out for control specific amplification by 36 cycles of 10 s starting at 65 °C, with increasing steps of 0.5 °C at each cycle. The PCR efficiencies were 80.2, 89.7, and 88.7% for *HSP12*, *ACT1*, and *ALG9*, respectively. A standard curve was determined for each gene using genomic DNA as template, where x is the threshold cycle and y is the log value of the starting quantity (ng): *HSP12* ($y = -3.90x + 21.44$, adjusted $R^2 = 0.995$); *ACT1* ($y = -3.62x + 22.44$, adjusted $R_2 = 0.985$); *ALG9* ($y = -3.65x + 23.81$, adjusted $R_2 = 0.994$). Standard curves were obtained from eight points in triplicate, and linearity was observed from 0.0366 to 183 ng of DNA. A threshold value for the fluorescence of all samples was set manually to adjust the Ct value of standard samples in each experiment. The relative amounts of *HSP12* with respect to each reference gene were calculated from the standard curve. Expression levels obtained from both reference genes were highly correlated (Pearson correlation test $r = 0.99$, $p_{val} = 1 \times 10^{-8}$); consequently, only the *HSP12/ACT1* ratios are graphically presented.

Production of Wine without *Hsp12p*. A red grape juice of Merlot (Bordeaux) harvested in 2011 was used for this study. This grape must obtained by thermoextraction was supplemented with ammonium sulfate and glucose plus fructose to obtain a final concentration of 210 mg(N)/L of assimilable nitrogen and 210 g/L of sugar. A batch of 6 L of this grape must was fermented with the strain Δ°hsp12 at 24 °C until completion of the fermentation. The final amount of residual sugar at the end of alcoholic fermentation was <2 g/L. This wine was then dispatched in 1 L glass vessel and supplemented with the biomass of different strains freshly harvested by centrifugation (5 min, 8000*g*) and washed two times with sterile water (4 °C). The concentration of the added biomass in wine was adjusted to 2×10^8 cells/mL to remain close to the yeast concentration usually found in enology.[35] After 24 h, the viability of the cell was controlled by platting 1 mL of wine on YPD. Fewer than 10^3 viable cells/mL were recovered.

Yeast Autolysis. Yeast autolysis of the different strains (Fx10, Δ°hsp12, D2, W1, B1, VL3, F33, and XMC30) took place at 32 °C during 10 days without light or stirring. At the end of this period, the wines were centrifuged (4000 rpm, 15 min) to eliminate yeast lees and kept at 4 °C for 24 h in sterilized glass bottles inerted with CO_2 until tasting.

Wine Tasting. All of the tasting sessions took place in a specific room equipped with individual booths and air-conditioned at 20 °C. The samples (20 mL) were presented at 18 °C in normalized dark glasses coded with random numbers. All of the panelists (17 tasters aged from 21 to 64 years) were wine-tasting specialists or winemakers and had been previously informed of the nature and risks associated

DOI: 10.1021/jf504408t
J. Agric. Food Chem. 2015, 63, 304−311

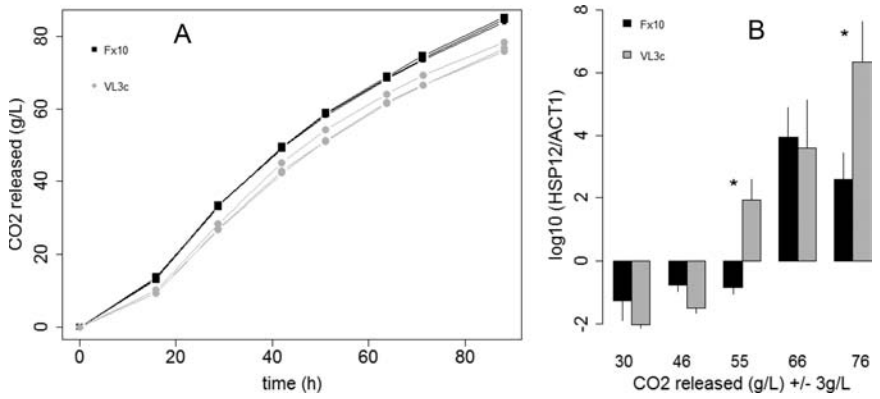

Figure 1. *HSP12* expression monitoring during alcoholic fermentation at 26 °C. (A) Yeast strains were cultivated in a synthetic medium containing 240 g/L sugar and fermented at 26 °C. The time course of CO_2 production is shown for each strain replicate. The black squares and gray circles represent the strains Fx10 and VL3, respectively. (B) Cell samples were collected at different fermentation points when the CO_2 produced reached 30, 46, 55, 66, and 76 g/L. The average of the *HSP12* expression at each time point is shown on the bar plot (expressed as the logarithm of *HSP12*/*ACT1* ratio). Bar errors indicate the standard error of the three replicates. Statistically relevant differences between strains were indicated for each collecting point by a (∗) Wilcoxon test ($\alpha = 0.05$).

with the investigation. The presentation order of the glasses was randomly changed between each taster.

Prior to the formal evaluation of wines, the panelists performed training sessions. In a first session, a hydroethanolic solution (12% alcohol by vol, 3 g/L of tartaric acid, pH adjusted to 3.5) with sucrose adjusted at different concentrations (0, 3, 6, and 12 g/L) was presented to the tasters. In a second session, a red wine (Bordeaux 2011, 12.9% alcohol by vol, 0.3 g/L glucose + fructose) was used for a similar test. For both sessions, tasters were asked to classify the wines following the intensity of sweetness. A Page test was used to interpret these results.[38]

For the formal evaluation of the yeast strain impact on sweetness, the wines were tasted the day after centrifugation. The tasters were asked to rate the wines on a scale from 0 to 7. The statistical interpretation was based on an analysis of variance (ANOVA) according to the recommendations of the International Organization for Standardization.[39]

Statistical and Graphical Analyses. All of the statistical and graphical analyses were carried out using the R program version 2.15.1.[40] The variation of each trait analyzed was estimated by an analysis of variance (ANOVA) according to the model in figure captions. For each variable, the homogeneity of the variance was assessed using a Levene test by means of R's car package, as well as the normality of residues distribution using a Shapiro test. Duncan's multiple comparison was used to determine which means differ significantly (Duncan's multiple comparison, $\alpha = 0.05$) using the *agricolae* package. When required, a Wilcoxon test was used with at least three independent repetitions.

RESULTS AND DISCUSSION

***HSP12* Expression Correlates with the Progression of Alcoholic Fermentation.** Our study investigated the genetic and environmental factors affecting the expression level of *HSP12* during the alcoholic fermentation. First, we monitored by quantitative PCR the *HSP12* mRNA level of two commercial starters (Zymaflore VL3 and Fx10) during the alcoholic fermentation carried out at 26 °C in a synthetic grape juice containing 240 g/L of sugar. The expression level of both strains was compared nearly at the same fermentation advancement (30, 46, 55, 66, and 76 g/L of CO_2 produced) to compare the strains at the same physiological stage (Figure 1A). As shown in panel B, the expression level of *HSP12* steadily increased during the fermentation process. For both strains, significant changes were observed between the earliest and latest stages (Table 2). At 55 and 76 g/L of CO_2 produced,

Table 2. Multiple Test Comparison of the *HSP12* Expression during Alcoholic Fermentation[a]

	CO_2 produced in				
strain	30 g/L	46 g/L	55 g/L	66 g/L	76 g/L
Fx10	−1.25 cd	−0.75 bcd	−0.84 bcd	3.93 ab	2.58 bcd
VL3	−2.02 c	−1.50 bc	1.92 abc	3.59 ab	6.34 a

[a]Data presented are the mean of *HSP12* expression levels expressed in log 10(*HSP12*/*ACT1*) at different moments of alcoholic fermentation (CO_2 produced). For each strain, a one-way analysis of variance was carried out to estimate the sampling point effect ($Y = \mu + CO_2 i + \varepsilon(i)$). The letters beside each strain value indicate groups with a statistical difference according to the linear model used (Duncan test, $\alpha = 0.05$).

the *HSP12* expression level differs between VL3 and Fx10 (pairwise Wilcoxon test, $\alpha = 0.05$), indicating that the strains do not respond at the same time to their changing environment (pairwise Wilcoxon test $\alpha = 0.05$).

This first experiment confirms previous studies showing the steady increase of *HSP12* expression during the alcoholic fermentation.[20] Indeed, a linear correlation between CO_2 produced and *HSP12* expression was found (Spearman $\rho = 0.71$, $p_{val} = 2.89 \times 10^{-6}$), suggesting that ethanol concentration and fermentation progression might trigger in part *HSP12* expression. The strain VL3 seems to be generally more stressed than Fx10 with an earlier induction of *HSP12* expression. Accordingly, the strain VL3 showed a longer CO_2 production kinetics, finishing 3 days after Fx10 (data not shown). This first experiment suggested that the expression level of *HSP12* is concomitant with the increasing level of ethanol in wine, corroborating the results obtained in previous studies.[23]

In aqueous solution, ethanol exhibits a sweet taste but also an antagonist bitterness.[41,42] Previous works have showed that this compound has no significant effect on wine sweetness.[3,4] In accordance with these results, we have recently demonstrated that the addition of 1.5% v/v ethanol to a wine does not increase its sweet taste.[5] These data suggest that ethanol has no direct impact on wine sweet taste. Nevertheless, some tasters frequently point out that wines with high levels of alcohol often exhibit an intense sweet taste.[2] Consequently, this empirical relationship between ethanol level and sweetness intensity could be indirect and interpreted through the effect of Hsp12p. Indeed, a higher level of ethanol could lead to an increased

DOI: 10.1021/jf504408t
J. Agric. Food Chem. 2015, 63, 304−311

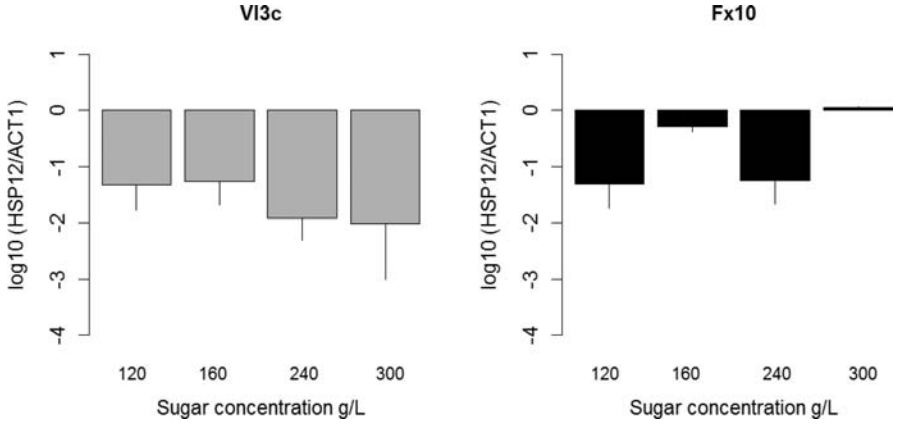

Figure 2. Sugar concentration does not affect the *HSP12* expression level at 26 °C. Fermenting biomass samples were collected at mid fermentation (46 g/L of CO_2 produced) from different synthetic musts containing 120, 160, 240 and 300 g/L initial sugar and fermented at 26 °C. The average of the *HSP12* expression is shown on the bar plot (expressed as the logarithm of *HSP12/ACT1* ratio). Bar errors indicate the standard error of the three replicates.

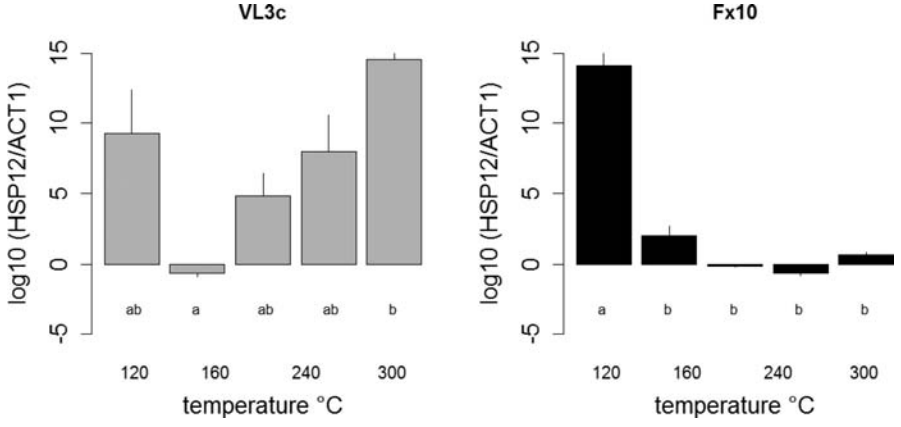

Figure 3. Temperature has a strong effect on *HSP12* expression level. Fermenting biomass samples was collected at mid fermentation (46 g/L of CO_2 produced) from a synthetic must containing 240 g/L initial sugar and fermented at different temperatures of 12, 18, 22, 26, and 31 °C. The average of the *HSP12* expression is shown on the bar plot (expressed as the logarithm of *HSP12/ACT1* ratio). Bar errors indicate the standard error of the three replicates. A two-way analysis of variance was carried out to estimate the strain and temperature and their interaction ($Y = \mu + \text{strain}^{i} + \text{temperature}^{j} + \varepsilon^{ij}$). A significant effect was found for yeast strains and temperature × strain interaction. The letters below the bar plot indicate groups with a statistical difference according to the linear model used (Duncan test, $\alpha = 0.05$).

expression of this protein at the end of alcoholic fermentation, thus increasing the sweet taste of wine.

Temperature and Sugar Concentration Differentially Influenced *HSP12* Expression. In this section, the transcriptional response of the *HSP12* gene for osmotic pressure and temperature was investigated using the same two yeast starters (VL3 and Fx10) in a synthetic grape must. For the osmotic stress response, fermentations were carried out at 26 °C with initial sugar amount varying from 120 to 300 g/L. Fermenting yeast was sampled when the CO_2 produced reached 46 g/L. In fact, at this fermentation point, both strains showed a similar expression level (Figure 1), allowing comparison of other factors. Therefore, this point was chosen to measure the specific effect of sugar concentration by dissociating it from ethanol impact. As expected, sugar content has a strong impact on the successful completion of fermentation. Strains Fx10 and VL3 left, respectively, 9 and 43 g/L of residual sugars in the highest sugar conditions (data not shown). In contrast, we did not detect any significant changes between *HSP12* expression fold for both strains. This result suggested that sugar content in must did not affect per se the expression of this gene (Figure 2). Although the *HSP12* gene is activated by the HOG pathway,[43] this lack of expression induction due to high sugar concentration has been previously described in industrial conditions.[21]

To analyze the *HSP12* response to temperature, isothermal fermentations (12, 18, 22, 26, or 31 °C) were carried out in a synthetic must containing 240 g/L sugars. Samples of both Fx10 and VL3 were taken when the CO_2 produced reached 46 g/L. Contrary to sugar content, the temperature drastically modified the expression level of *HSP12* (Figure 3). For both strains, high *HSP12* expression values were found at low temperature (12 °C), confirming the strong induction of this gene in cold conditions.[24] With warmer temperatures, strains responded in a different manner. At 18 °C, VL3 and Fx10 showed similar expression profiles. However, when fermentation temperature was higher, the *HSP12* expression level strongly increased for VL3 (>10-fold). These findings confirmed that the white wine starter VL3 is quite sensitive to temperature as previously shown for heat shock resistance.[31] In contrast, Fx10 showed a steady expression level of *HSP12* between 18 and 31 °C, which corroborates the good adaptation of this strain to high temperatures and its use for red grape fermentation.[33] The strong strain × temperature effect found

DOI: 10.1021/jf504408t
J. Agric. Food Chem. 2015, 63, 304−311

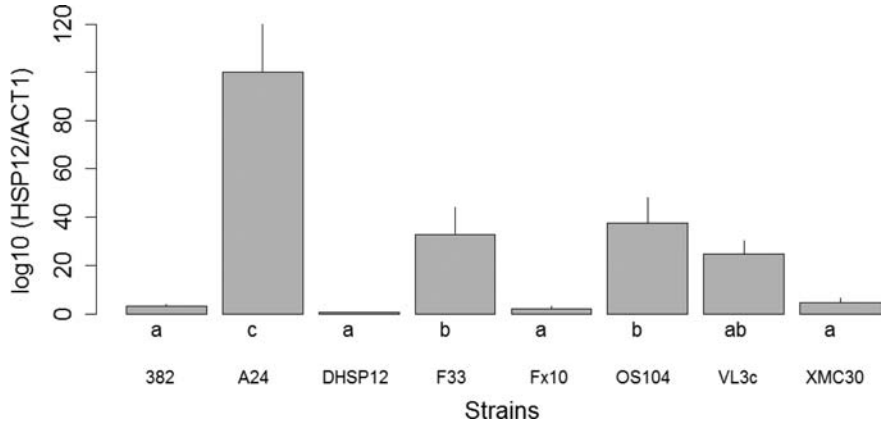

Figure 4. The *HSP12* expression level differs according to the strains at mid fermentation. Fermenting biomass of eight yeast strains was collected at mid fermentation (46 g/L of CO_2 produced) from a synthetic must containing 240 g/L initial sugar and fermented at 26 °C. The average of the *HSP12* expression is shown on the bar plot (expressed as the logarithm of *HSP12/ACT1* ratio). Bar errors indicate the standard error of three replicates. A one-way analysis of variance was carried out to estimate the strain effect ($Y = \mu + \text{gene}^i + \varepsilon^i$). The letters below the bar plot indicate groups with a statistical difference according to the linear model used (Duncan test, $\alpha = 0.05$).

(24% of total variance explained) by analysis of variance highlighted that yeast strains and fermentation temperature might affect drastically both the expression level of *HSP12* mRNA and its related protein amount.

Even if fermentation temperature significantly influences the *HSP12* expression, this parameter does not appear to be really relevant as a possible tool to modulate the sweetness intensity in enological conditions. In fact, fermentation temperature deeply affects the overall organoleptic profile,[44,45] and high temperatures (>30 °C) are detrimental to completion of fermentation.[33] In white winemaking, the temperature must be controlled when fermentation is run in high-capacity fermenting tanks to avoid these risks. Furthermore, low temperatures (<18 °C) drastically affect the aromatic expression of wine due to the increase of ester synthesis by yeast.[44] Thus, low temperatures are not recommended for the elaboration of complex white wines.[46] In the case of white winemaking in oak barrels, the fermentation temperatures remain close to the cellar temperature and are most of the time not controlled. Therefore, they are often higher than in stainless steel tank fermentation (from 22 to 25 °C).[46] Such a winemaking process could therefore result in higher *HSP12* expression and, combined with the release of sweet compounds from oak wood,[8] may produce a more intense sweetness in the final product.

In red winemaking, whereas the wine temperature should be maintained at 26−28 °C to avoid stuck fermentation, post-fermentation maceration is sometimes achieved at higher temperatures (30−32 °C).[46] During this period, part of the yeast biomass is still metabolically active and may have a *HSP12* expression shift that could increase the concentration of the related protein.

Yeast Strain Background Affects *HSP12* Expression during Alcoholic Fermentation. The impact of yeast strains on the expression of *HSP12* was then assayed during alcoholic fermentation. For these studies we used four commercial starters (VL3, Fx10, XMC30, and F33), the Δ°hsp12 strains (isogenic to Fx10), and three yeast strains from other biotopes (brewery = B1, distillery = D2, and oak exudate = W1). These three last strains showed sluggish CO_2 kinetics and were unable to ferment the totality of the synthetic must (data not shown). As *HSP12* expression is linked to the relative amount of produced ethanol, all of the fermenting yeasts were sampled when the accumulative produced CO_2 was close to 46 g/L. At this sampling point, all of the strains showed a high viability (>85%) and were fermenting actively. As shown in Figure 4, the *HSP12* expression ranged about 34-fold between extreme individuals. Four distinct groups were statistically determined (Duncan test, $\alpha = 0.05$). The nonenological strains D2 and W1 expressed the highest quantity of *HSP12* mRNA, whereas some wine starters F10, Fx10, and XMC30 showed the lowest values. Nevertheless, no significant correlations were found between fermentation phenotypes and *HSP12* expression level (data not shown), which was likely due to the small set of strains studied in this work. To our knowledge, few studies investigated the expression level of several strains during the wine alcoholic fermentation. In previous studies, similar variations were found between unrelated strains.[31] However, the *HSP12* expression level was estimated after the application of a heat shock situation not frequently found in controlled enological conditions. Our results confirmed that the mRNA expression level of *HSP12* is strongly affected by the strain used.

Impact of the Yeast Strain on the Sweetness Perception after Lees Aging. Our data confirmed a strong variability for *HSP12* gene expression within yeast strains. The role of this gene product on sweetness perception suggested that yeast strain may affect the sweetness of wine during lees aging. Because yeast strains affected wine taste for many factors (i.e., acetic acid, residual sugars, esters...[47]), the direct comparison of wines fermented with different strains does not allow verifying rigorously this hypothesis. To overcome this problem, we fermented a Merlot grape juice with the strain Δ°hsp12 to obtain a red wine exempted of Hsp12p protein and related peptides. Yeast biomass of eight different strains was added to this wine, and a post-fermentative maceration was carried out for 10 days as described under Materials and Methods. The biomass was harvested at the mRNA quantification point (46 g/L CO_2) from the eight strains previously described. Because of the small quantities of residual sugars (<2 g/L), yeasts were not able to develop and were degraded following autolysis mechanisms.

The application of Page methodology (Table 3) showed that the sensory training tests were significant at 1% in both matrices. The implementation of this methodology resulted in

DOI: 10.1021/jf504408t
J. Agric. Food Chem. 2015, 63, 304−311

Table 3. Results of the Panel Training to Sweetness Perception[a]

matrix	R_1	R_2	R_3	R_4	L	L'[b]
model solution	30	36	47	57	471	3.86**
red wine	26	34	46	64	488	5.29**

[a] R_1, R_2, R_3, and R_4 are the sums of ranks for addition of, respectively, 0, 3, 6, and 12 g/L of sucrose. L and L′ were calculated as described in ISO 8587:2006[38] for the Page test: $L = \sum_{i=1}^{p} iR_i$ and $L' = (12L - 3np(p+1)^2)/(p(p+1)(n(p-1))^{1/2})$ (n is the number of panelists and p the number of modalities/treatments). [b] Significance: ns, nonsignificant ($L' < 1.645$); *, significant at 5% ($L' \geq 1.645$); **, significant at 1% ($L' \geq 2.326$)

the successful creation of a panel trained to perceive differences of sweetness intensity in both a model solution and a red wine. The results demonstrate their ability to classify wines following sweet intensity even in a matrix such as red wine containing numerous sapid compounds that are likely to interact with sweetness perception.

The eight resulting wines obtained after the post-fermentation maceration were submitted to sensory analysis to assay their sweetness intensity. Panelists were asked to rate sweetness on a scale from 0 to 7. A two-way analysis of variance was used (Figure 5) and demonstrated that there was no "panelist effect". In contrast, the results showed a strong "yeast strain effect", allowing the discrimination of five distinct groups of sweetness intensity among the eight modalities (Duncan's test, $\alpha = 0.05$). The base wine was the same for all of these modalities, and the only difference was the yeast strain used for lees aging. Consequently, this sensory study clearly establishes that yeast strain influences the sweet taste of wine. Previous works showed that yeast strain has a strong influence on white wine aroma,[48,49] and a recent study suggests a similar effect for fruity red wine aroma revelation.[50] Here, we demonstrated for the first time that the taste of wine was also affected by the yeast strain during autolysis. This parameter appears as an effective factor to modulate wine sweetness and such sweetening effect could therefore be taken into consideration as an additional relevant criterion to select industrial yeast strains.

Moreover, the wine aged with the strain Δ°hsp12 received the lowest rate (Figure 5), whereas the one aged with W1 was perceived as the sweetest. Among the commercial starters used for red winemaking, Fx10 and XMC30 provided more sweetness to wine than F33. More generally, we observed a weak correlation between *HSP12* expression and sweetness intensity (Kendall correlation test, $T = 22$, p value = 0.0601), suggesting that Hsp12p might contribute to the sweetness modulation consecutive to yeast autolysis. The imperfect correlation observed can be due to different causes. First, the correlation was established with yeast samples collected at mid fermentation, which does not reflect exactly the final expression level of this gene. In fact, as shown in Figure 1, the *HSP12* expression level can vary drastically during the alcoholic fermentation. However, we chose this sampling point to compare strains with an active fermentation and showing the same viability level (>85%). As some strains (W1, D2) used were unable to finish the alcoholic fermentation, a sampling point at mid fermentation was the most relevant choice. This correlation should be also much clearer using more strains or by measuring directly the expression level of Hsp12p protein instead of quantifying the mRNA level. However, independent

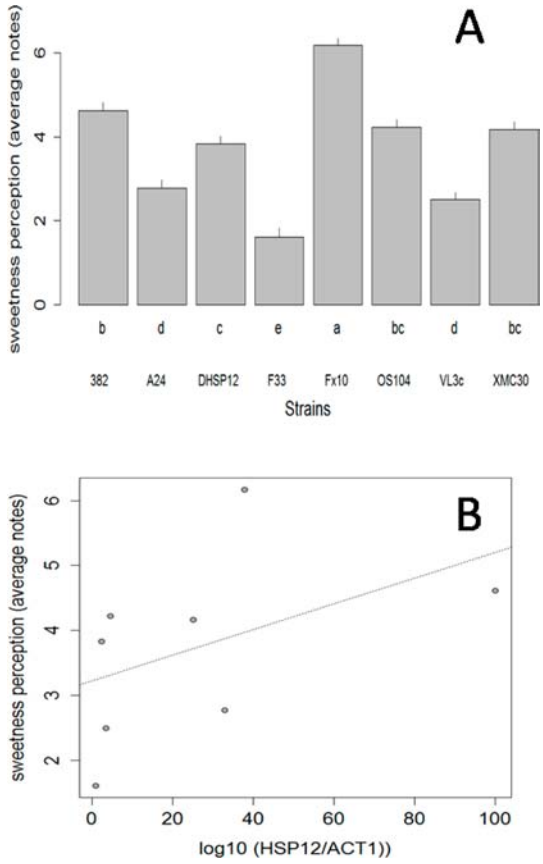

Figure 5. Wine in contact with lees obtained from different yeast strains showed marked differences in sweetness perception. (A) A wine without Hsp12p was obtained by fermenting a Merlot juice with Δ°hsp12. Yeast biomass of eight different strains was added to this wine, and aging on lees was carried out at 32 °C for 10 days. This biomass was collected from fermenting cells at 46 g/L of CO_2 produced. After wine centrifugation, a panel tasted the modalities, and the sweetness intensity was rated on a scale from 0 to 7. Bar errors indicate the standard error of 17 notes. A two-way analysis of variance was used to estimate the strain effect ($Y = \mu + \text{strain}^i + \text{panel}^j + \varepsilon^{ij}$). The letters below the bar plot indicate groups with a statistical difference according to the linear model used (Duncan test, $\alpha = 0.05$). (B) Relationship between sweetness perception and expression level of *HSP12* (Kendall correlation test, $T = 22$, p value = 0.0601).

experimental data suggest that in the case of the *HSP12* gene, the mRNA and protein expression are well correlated.[51] Moreover, in a previous work we quantified by shotgun proteomics the relative abundance of Hsp12p for some strains used in this study.[30] For example, strains W1 and D2 exhibited a high expression level of Hsp12p, whereas strain B1 showed a much lower expression; these results sustain the results found in the present study.

This work provides new insights concerning the fermentative parameters modulating wine sweetness by means of *HSP12* expression. The exact implication of the Hsp12p protein and the factors influencing its release in wine need further investigations to better control and rationalize the post-fermentative processes.

AUTHOR INFORMATION

Corresponding Author

*(A.M.) E-mail: axel.marchal@u-bordeaux.fr. Phone: (33) 5 57 57 58 67. Fax: (33) 5 57 57 58 13.

DOI: 10.1021/jf504408t
J. Agric. Food Chem. 2015, 63, 304−311

Author Contributions

‖A.M. and P.M. contributed equally to this work.

Funding

This article has emanated from research conducted with the financial support of the Conseil Interprofessionnel des Vins de Bordeaux and France AgriMer.

Notes

The authors declare no competing financial interest.

■ ACKNOWLEDGMENTS

We thank Maria Martí Raga for her correction that helped to improve the manuscript and Lauriane Sindt for graphical assistance.

■ REFERENCES

(1) Williamson, P. O.; Robichaud, J.; Francis, I. L. Comparison of Chinese and Australian consumers' liking responses for red wines. *Aust. J. Grape Wine Res.* **2012**, *18*, 256−267.

(2) Peynaud, E. In *Le Goût du Vin*; Dunod: Paris, France, 1980.

(3) Gawel, R.; Van Sluyter, S.; Waters, E. J. The effects of ethanol and glycerol on the body and other sensory characteristics of Riesling wines. *Aust. J. Grape Wine Res.* **2007**, *13*, 38−45.

(4) Jones, P. R.; Gawel, R.; Francis, I. L.; Waters, E. J. The influence of interactions between major white wine components on the aroma, flavour and texture of model white wine. *Food Qual. Pref.* **2008**, *19*, 596−607.

(5) Marchal, A.; Marullo, P.; Moine, V.; Dubourdieu, D. Influence of yeast macromolecules on sweetness in dry wines: role of the *Saccharomyces cerevisiae* protein Hsp12. *J. Agric. Food Chem.* **2011**, *59*, 2004−2010.

(6) Charpentier, C.; Aussenac, J.; Charpentier, M.; Prome, J. C.; Duteurtre, B.; Feuillat, M. Release of nucleotides and nucleosides during yeast autolysis: kinetics and potential impact on flavor. *J. Agric. Food Chem.* **2005**, *53*, 3000−3007.

(7) Marchal, A.; Pons, A.; Lavigne, V.; Dubourdieu, D. Contribution of oak wood ageing to the sweet perception of dry wines. *Aust. J. Grape Wine Res.* **2013**, *19*, 11−19.

(8) Marchal, A.; Waffo-Téguo, P.; Génin, E.; Mérillon, J. M.; Dubourdieu, D. Identification of new natural sweet compounds in wine using centrifugal partition chromatography-gustatometry and Fourier transform mass spectrometry. *Anal. Chem.* **2011**, *83*, 9629−9637.

(9) Mtwisha, L.; Brandt, W.; McCready, S.; Lindsey, G. G. HSP 12 is a LEA-like protein in *Saccharomyces cerevisiae*. *Plant Mol. Biol.* **1998**, *37*, 513−521.

(10) Welker, S.; Rudolph, B.; Frenzel, E.; Hagn, F.; Liebisch, G.; Schmitz, G.; Scheuring, J.; Kerth, A.; Blume, A.; Weinkauf, S.; Haslbeck, M.; Kessler, H.; Buchner, J. Hsp12 is an intrinsically unstructured stress protein that folds upon membrane association and modulates membrane function. *Mol. Cell* **2010**, *39*, 507−520.

(11) Siderius, M.; Rots, E.; Mager, W. H. High-osmolarity signalling in *Saccharomyces cerevisiae* is modulated in a carbon-source-dependent fashion. *Microbiology* **1997**, *143*, 3241−3250.

(12) Pacheco, A.; Pereira, C.; Almeida, M. J.; Sousa, M. J. Small heat-shock protein Hsp12 contributes to yeast tolerance to freezing stress. *Microbiology* **2009**, *155*, 2021−2028.

(13) Sales, K.; Brandt, W.; Rumbak, E.; Lindsey, G. The LEA-like protein HSP 12 in *Saccharomyces cerevisiae* has a plasma membrane location and protects membranes against desiccation and ethanol-induced stress. *Biochim. Biophys. Acta* **2000**, *1463*, 267−278.

(14) Herbert, A. P.; Riesen, M.; Bloxam, L.; Kosmidou, E.; Wareing, B. M.; Johnson, J. R.; Phelan, M. M.; Pennington, S. R.; Lian, L. Y.; Morgan, A. NMR structure of Hsp12, a protein induced by and required for dietary restriction-induced lifespan extension in yeast. *PLoS One* **2012**, *7*, No. e41975.

(15) Zara, S.; Antonio Farris, G.; Budroni, M.; Bakalinsky, A. T. HSP12 is essential for biofilm formation by a Sardinian wine strain of *S. cerevisiae*. *Yeast* **2002**, *19*, 269−276.

(16) Singarapu, K. K.; Tonelli, M.; Chow, D. C.; Frederick, R. O.; Westler, W. M.; Markley, J. L. Structural characterization of Hsp12, the heat shock protein from *Saccharomyces cerevisiae*, in aqueous solution where it is intrinsically disordered and in detergent micelles where it is locally α-helical. *J. Biol. Chem.* **2011**, *286*, 43447−43453.

(17) Gash, A. Yeast stress responses. In *Yeast Stress Responses*; Hohmann, S., Mager, W., Eds.; Springer: Berlin, Germany, 2003; Vol. 1, pp 11−57.

(18) Rep, M.; Reiser, V.; Gartner, U.; Thevelein, J. M.; Hohmann, S.; Ammerer, G.; Ruis, H. Osmotic stress-induced gene expression in *Saccharomyces cerevisiae* requires Msn1p and the novel nuclear factor Hot1p. *Mol. Cell. Biol.* **1999**, *19*, 5474−5485.

(19) Perez-Torrado, R.; Bruno-Barcena, J. M.; Matallana, E. Monitoring stress-related genes during the process of biomass propagation of *Saccharomyces cerevisiae* strains used for wine making. *Appl. Environ. Microbiol.* **2005**, *71*, 6831−6837.

(20) Rossignol, T.; Dulau, L.; Julien, A.; Blondin, B. Genome-wide monitoring of wine yeast gene expression during alcoholic fermentation. *Yeast* **2003**, *20*, 1369−1385.

(21) Kim, N. R.; Yang, J.; Kwon, H.; An, J.; Choi, W.; Kim, W. Mutations of the TATA-binding protein confer enhanced tolerance to hyperosmotic stress in *Saccharomyces cerevisiae*. *Appl. Microbiol. Biotechnol.* **2013**, *97*, 8227−8238.

(22) de Groot, E.; Bebelman, J. P.; Mager, W. H.; Planta, R. J. Very low amounts of glucose cause repression of the stress-responsive gene HSP12 in *Saccharomyces cerevisiae*. *Microbiology* **2000**, *146*, 367−375.

(23) Aranda, A.; Querol, A.; del Olmo, M. Correlation between acetaldehyde and ethanol resistance and expression of HSP genes in yeast strains isolated during biological aing in sherry wines. *Arch. Microbiol.* **2002**, *177*, 304−312.

(24) Schade, B.; Jansen, G.; Whiteway, M.; Entian, K. D.; Thomas, D. Y. Cold adaptation in budding yeast. *Mol. Biol. Cell* **2004**, *15*, 5492−5502.

(25) Pizarro, F. J.; Jewett, M. C.; Nielsen, J.; Agosin, E. Growth temperature exerts a differential physiological and transcriptional response in laboratory and wine strains of *Saccharomyces cerevisiae*. *Appl. Environ. Microbiol.* **2008**, *74*, 6358−6368.

(26) Backhus, L. E.; DeRisi, J.; Brown, P. O.; Bisson, L. F. Functional genomic analysis of a commercial wine strain of *Saccharomyces cerevisiae* under differing nitrogen conditions. *FEMS Yeast Res.* **2001**, *1*, 111−125.

(27) Tesniere, C.; Delobel, P.; Pradal, M.; Blondin, B. Impact of nutrient imbalance on wine alcoholic fermentations: nitrogen excess enhances yeast cell death in lipid-limited must. *PLoS One* **2013**, *8*, No. e61645.

(28) Brem, R. B.; Yvert, G.; Clinton, R.; Kruglyak, L. Genetic dissection of transcriptional regulation in budding yeast. *Science* **2002**, *296*, 752−755.

(29) Ambroset, C.; Petit, M.; Brion, C.; Sanchez, I.; Delobel, P.; Guerin, C.; Chiapello, H.; Nicolas, P.; Bigey, F.; Dequin, S.; Blondin, B. Deciphering the molecular basis of wine yeast fermentation traits using a combined genetic and genomic approach. *G3 (Bethesda)* **2011**, *1*, 263−281.

(30) Blein-Nicolas, M.; Albertin, W.; Valot, B.; Marullo, P.; Sicard, D.; Giraud, C.; Huet, S.; Bourgais, A.; Dillmann, C.; de Vienne, D.; Zivy, M. Yeast proteome variations reveal different adaptive responses to grape must fermentation. *Mol. Biol. Evol.* **2013**, *30*, 1368−1383.

(31) Carrasco, P.; Querol, A.; del Olmo, M. Analysis of the stress resistance of commercial wine yeast strains. *Arch. Microbiol.* **2001**, *175*, 450−457.

(32) Watanabe, M.; Tamura, K.; Magbanua, J. P.; Takano, K.; Kitamoto, K.; Kitagaki, H.; Akao, T.; Shimoi, H. Elevated expression of genes under the control of stress response element (STRE) and Msn2p in an ethanol-tolerance sake yeast Kyokai no. 11. *J. Biosci. Bioeng.* **2007**, *104*, 163−170.

DOI: 10.1021/jf504408t
J. Agric. Food Chem. 2015, 63, 304−311

(33) Marullo, P.; Mansour, C.; Dufour, M.; Albertin, W.; Sicard, D.; Bely, M.; Dubourdieu, D. Genetic improvement of thermo-tolerance in wine *Saccharomyces cerevisiae* strains by a backcross approach. *FEMS Yeast Res.* **2009**, *9*, 1148−1160.
(34) Marullo, P.; Bely, M.; Masneuf-Pomarede, I.; Pons, M.; Aigle, M.; Dubourdieu, D. Breeding strategies for combining fermentative qualities and reducing off-flavor production in a wine yeast model. *FEMS Yeast Res.* **2006**, *6*, 268−279.
(35) Albertin, W.; Marullo, P.; Aigle, M.; Dillmann, C.; de Vienne, D.; Bely, M.; Sicard, D. Population size drives industrial Saccharomyces cerevisiae alcoholic fermentation and is under genetic control. *Appl. Environ. Microbiol.* **2011**, *77*, 2772−2784.
(36) Thibon, C.; Marullo, P.; Claisse, O.; Cullin, C.; Dubourdieu, D.; Tominaga, T. Nitrogen catabolic repression controls the release of volatile thiols by *Saccharomyces cerevisiae* during wine fermentation. *FEMS Yeast Res.* **2008**, *8* (7), 1076−1086.
(37) Teste, M. A.; Duquenne, M.; Francois, J. M.; Parrou, J. L. Validation of reference genes for quantitative expression analysis by real-time RT-PCR in *Saccharomyces cerevisiae*. *BMC Mol. Biol.* **2009**, *10*, 99.
(38) International Organization for Standardization. *Sensory Analysis. Methodology. Ranking*; ISO 8587:2006; International Organization for Standardization: Geneva, Switzerland, 2006.
(39) International Organization for Standardization. *Sensory Analysis. Methodology. Magnitude Estimation Method*; ISO 11056:1999; International Organization for Standardization: Geneva, Switzerland, 1999.
(40) R Development Core Team. *R; A Language and Environment for Statistical Computing*; R Foundation for Statistical Computing: Vienna, Austria, 2010.
(41) Blizard, D. A. Sweet and bitter taste of ethanol in C57BL/6J and DBA2/J mouse strains. *Behav. Genet.* **2007**, *37*, 146−159.
(42) Scinska, A.; Koros, E.; Habrat, B.; Kukwa, A.; Kostowski, W.; Bienkowski, P. Bitter and sweet components of ethanol taste in humans. *Drug Alcohol Depend.* **2000**, *60*, 199−206.
(43) Martinez-Pastor, M. T.; Marchler, G.; Schuller, C.; Marchler-Bauer, A.; Ruis, H.; Estruch, F. The *Saccharomyces cerevisiae* zinc finger proteins Msn2p and Msn4p are required for transcriptional induction through the stress response element (STRE). *EMBO J.* **1996**, *15*, 2227−2235.
(44) Torija, M. J.; Beltran, G.; Novo, M.; Poblet, M.; Guillamón, J. M.; Mas, A.; Rozès, N. Effects of fermentation temperature and *Saccharomyces* species on the cell fatty acid composition and presence of volatile compounds in wine. *Int. J. Food Microbiol.* **2003**, *85*, 127−136.
(45) Sumby, K. M.; Grbin, P. R.; Jiranek, V. Microbial modulation of aromatic esters in wine: current knowledge and future prospects. *Food Chem.* **2010**, *121*, 1−16.
(46) Ribéreau-Gayon, P.; Glories, Y.; Maujean, A.; Dubourdieu, D. *Handbook of Enology, Volume 1: The Microbiology of Wine and Vinifications*; Wiley: New York, 2000.
(47) Marullo, P.; Dubourdieu, D., Yeast selection for wine flavour modulation. In *Managing Wine Quality. Volume 2. Oenology and Wine Quality*; Reynolds, A., Ed.; Woodhead Publishing: Cambridge, UK, 2010; pp 293−345.
(48) Dubourdieu, D.; Tominaga, T.; Masneuf, I.; Des Gachons, C. P.; Murat, M. L. The role of yeasts in grape flavor development during fermentation: the example of Sauvignon blanc. *Am. J. Enol. Vitic.* **2006**, *57*, 81−88.
(49) Egli, C. M.; Edinger, W. D.; Mitrakul, C. M.; Henick-Kling, T. Dynamics of indigenous and inoculated yeast populations and their effect on the sensory character of Riesling and Chardonnay wines. *J. Appl. Microbiol.* **1998**, *85*, 779−789.
(50) Gammacurta, M.; Marchand, S.; Albertin, W.; Moine, V.; De Revel, G. Impact of yeast strain on ester levels and fruity aroma persistence during aging of bordeaux red wines. *J. Agric. Food Chem.* **2014**, *62*, 5378−5389.
(51) Schwanhäusser, B.; Busse, D.; Li, N.; Dittmar, G.; Schuchhardt, J.; Wolf, J.; Chen, W.; Selbach, M. Global quantification of mammalian gene expression control. *Nature* **2011**, *473*, 337−342.

DOI: 10.1021/jf504408t
J. Agric. Food Chem. 2015, 63, 304−311

JOURNAL OF AGRICULTURAL AND FOOD CHEMISTRY

Article

pubs.acs.org/JAFC

Contribution of Phenolic Compounds to Food Flavors: Strecker-Type Degradation of Amines and Amino Acids Produced by *o*- and *p*-Diphenols

Rosa M. Delgado, Rosario Zamora, and Francisco J. Hidalgo*

Instituto de la Grasa, Consejo Superior de Investigaciones Científicas, Avenida Padre García Tejero 4, 41012 Seville, Spain

ABSTRACT: The ability of 20 phenolic derivatives to produce the Strecker-type degradation of phenylalanine and phenylglycine methyl ester was studied to investigate both the direct degradation of amino acids and amines by phenolic compounds in the absence of added oxidants and the effect of the number and positions of hydroxyl groups in the aromatic ring of the phenolic compound in relation to its ability to produce carbonyl derivatives from amino compounds. The obtained results showed that polyphenols can produce the Strecker degradation of amino acids and amines in the absence of added oxidants. The only requisite for producing the reaction is the presence of two hydroxyl groups in ortho or para positions. However, the presence of two hydroxyl groups in meta position in an additional aromatic ring can inhibit the Strecker-degrading ability of the hydroxyl groups in ortho or para positions. A reaction pathway that explains all of these findings is proposed. In addition, the effect of reaction conditions on the obtained reaction yields was studied. Activation energies (E_a) for phenylacetaldehyde formation from phenylalanine in the presence of hydroquinone, 1,2,4-trihydroxybenzene, and benzoquinone were 32.9, 31.5, and 28.8 kJ/mol, respectively.

KEYWORDS: *amine degradation, amino acid degradation, phenols, quinones, Strecker-type degradation*

INTRODUCTION

Phenolic compounds contribute to food flavors in multiple ways. Thus, and because of their bitterness or astringency, phenolic compounds have a significant role in the flavor of foods and drinks such as beer, wine, tree nuts, chocolate, coffee, tea, fruit-based products, and soy products.[1−3] In addition, and because of their antioxidant properties, they participate in the lipid oxidation process that takes place in many foods upon processing. In these foods they play a major role in the inhibition of the production of lipid-derived off-flavors.[4−6] Furthermore, because some phenols are able to react with carbonyl compounds, they are able to modify the flavor-generating reactions in which these carbonyl compounds are involved. This occurs, for example, in the flavor and off-flavor development via Maillard chemistry.[7−9] Moreover, phenolic compounds are able to scavenge lipid-derived carbonyl compounds that play a significant role in the flavor of foods.[10]

In addition to all of these roles, phenolic compounds can also be transformed either enzymatically or nonenzymatically into quinones, and quinones are able to degrade amino acids with major consequences in the flavor of foods.[11,12] Thus, for example, Rizzi[13] converted catechol moieties into *o*-quinones by using ferricyanide ion as the oxidant at 22 °C in pH 7.17 phosphate buffer, and these quinones were able to convert amino acids into their corresponding Strecker aldehydes.

Although different studies have shown that amino acids can be degraded by quinones, to the best of our knowledge the direct degradation of amino acids by phenolic compounds in the absence of added oxidants has not been described. Furthermore, the effect of the number and positions of hydroxyl groups in the aromatic ring of the phenolic compound in relation to its potential for degrading amino acids is not known.

In an attempt to understand the structural characteristics of phenolic compounds that favor their ability to degrade amino acids, this study analyzes the role of 20 phenolic compounds on phenylalanine degradation in a buffered model system analogous to that employed previously in the study of amino acid degradation by lipid oxidation products.[14] Phenylalanine was selected as model amino acid because its Strecker aldehyde phenylacetaldehyde has a high boiling point (195 °C), can be easily determined by gas chromatography−mass spectrometry (GC-MS), and is a very powerful odorant.[15]

MATERIALS AND METHODS

Chemicals. Twenty phenolic compounds were employed in this study. They were simple phenolic compounds having two or three hydroxyl groups, phenolic derivatives having also alkyl, methoxy, or carboxylic groups, and complex phenolic compounds having more than one aromatic ring (Figure 1). To facilitate their study, they were classified into five groups: *o*-diphenols, *m*-diphenols, *p*-diphenols, trihydroxy derivatives, and complex phenols. These groups also included some analogues for comparison purposes. All of these phenolic compounds as well as the other employed chemicals were purchased from Aldrich (Milwaukee, WI, USA), Sigma (St. Louis, MO, USA), Fluka (Buchs, Switzerland), or Merck (Darmstadt, Germany) and were of analytical grade.

Formation of Phenylacetaldehyde in Phenylalanine/Phenol Reaction Mixtures. Mixtures of phenylalanine (25 μmol) and the phenolic compound (0−30 μmol) in 500 μL of 0.3 M buffer were introduced in closed test tubes and heated in a heater block at 120−180 °C for 0−1 h. The following buffers were employed: sodium

Received: September 30, 2014
Revised: December 16, 2014
Accepted: December 22, 2014
Published: December 22, 2014

ACS Publications © 2014 American Chemical Society

DOI: 10.1021/jf5047317
J. Agric. Food Chem. 2015, 63, 312−318

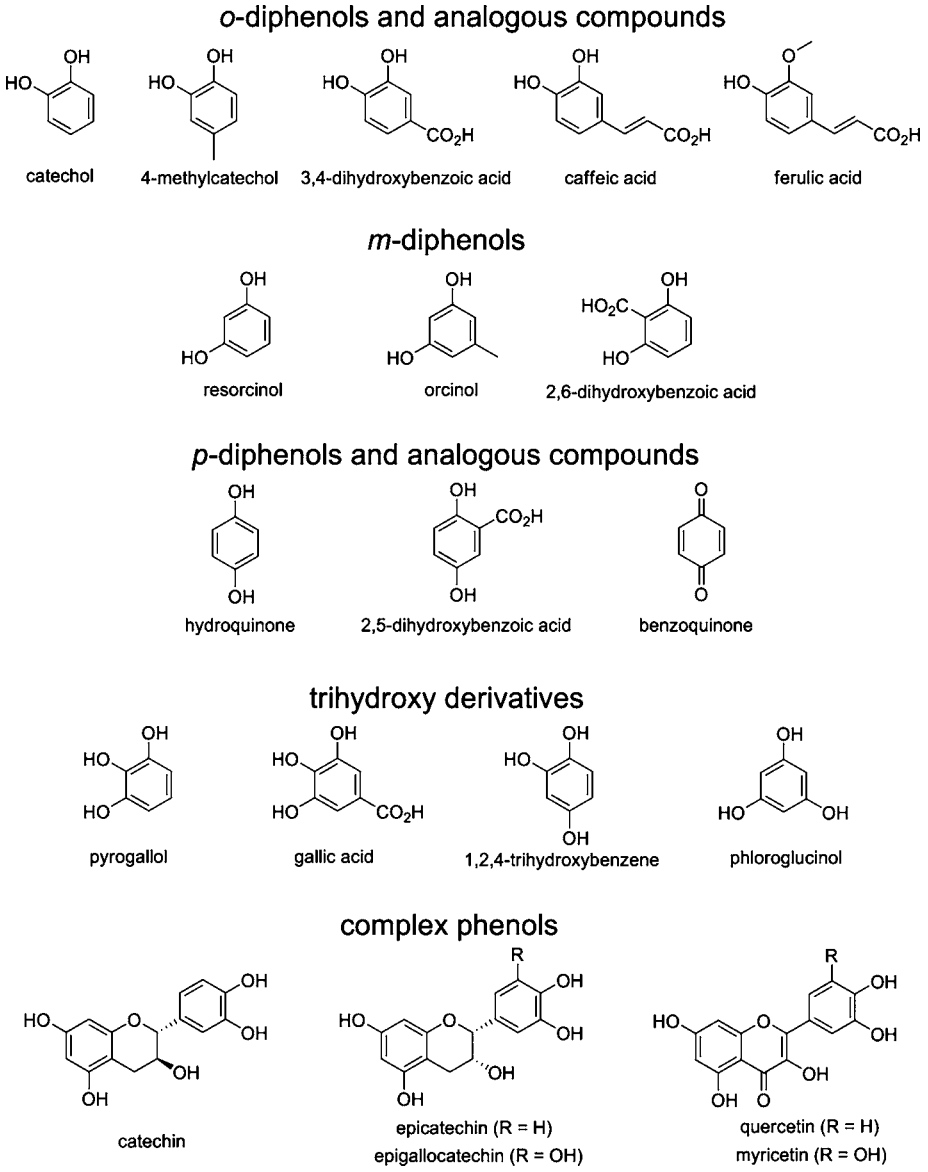

Figure 1. Phenolic compounds employed in this study.

citrate for pH 3−6 and sodium phosphate for pH 6−8. After cooling (10 min at room temperature), reaction mixtures were diluted with 1 mL of acetonitrile and 50 μL of internal standard solution (54.8 mg of methyl heptanoate in 25 mL of ethanol). Phenylacetaldehyde was determined by GC-MS.

Formation of Methyl 2-Oxo-2-phenylacetate, Benzaldehyde, Benzoic Acid, and Methyl Benzoate in Phenylglycine Methyl Ester/Phenol Reaction Mixtures. Equimolecular mixtures of phenylglycine methyl ester and either hydroquinone or benzoquinone (10 μmol of each) in 500 μL of 0.3 M sodium citrate buffer, pH 3, were introduced in closed test tubes and heated at 180 °C for 1 h. After cooling (10 min at room temperature), reaction mixtures were studied by GC-MS to determine the formed reaction products.

GC-MS Analyses. GC-MS analyses were conducted with a Hewlett-Packard 6890 GC Plus coupled with an Agilent 5973 MSD (mass selective detector, quadrupole type). A fused-silica HP5-MS capillary column (30 m × 0.25 i.d.; coating thickness, 0.25 μm) was used, and 1 μL of sample was injected in the pulsed splitless mode. Working conditions were as follows: carrier gas, helium (1 mL/min at constant flow); injector, 250 °C; oven temperature programmed from 40 °C (1 min) to 240 °C at 5 °C/min and then to 300 °C at 10 °C/min; transfer line to MSD, 280 °C; ionization EI, 70 eV; ion source temperature, 230 °C; mass range, 28−550 amu.

Determination of Phenylacetaldehyde Content. Quantification of phenylacetaldehyde was carried out as described previously[14] by preparing standard curves of phenylacetaldehyde in the 1.55 mL of solution prepared for GC-MS injection. Ten different concentration levels of phenylacetaldehyde were used. Phenylacetaldehyde content was directly proportional to the aldehyde/internal standard area ratio (r = 0.999, p < 0.0001). The coefficients of variation were <10%.

Statistical Analysis. All data given are mean ± SD values of, at least, three independent experiments. Statistical comparisons among different groups were made using analysis of variance. When significant F values were obtained, group differences were evaluated by the Tukey test.[16] Statistical comparisons were carried out using Origin v. 7.0 (OriginLab Corp., Northampton, MA, USA). The significance level is p < 0.05 unless otherwise indicated.

RESULTS

Formation of Phenylcetaldehyde in Phenylalanine/Phenol Reaction Mixtures. The ability of 20 phenolic compounds to convert phenylalanine into phenylacetaldehyde was investigated by heating 10 μmol of the phenol and 25 μmol

DOI: 10.1021/jf5047317
J. Agric. Food Chem. 2015, 63, 312−318

of the amino acid in sodium citrate buffer, pH 3, for 1 h at 180 °C. The obtained results (Table 1) showed that there was a relationship between the structure of the assayed phenol and its ability to produce phenylacetaldehyde.

Table 1. Formation of Phenylacetaldehyde in Mixtures of Phenylalanine and Phenols[a]

phenol tested	phenylacetaldehyde formed (μmol/mmol of phenylalanine)
none	10.7 ± 2.2 a
catechol	30.3 ± 2.4 b,c
4-methylcatechol	36.7 ± 4.2 b,d
3,4-dihydroxybenzoic acid	19.2 ± 5.5 e,f
caffeic acid	22.0 ± 1.7 e,g
ferulic acid	8.5 ± 0.8 a
resorcinol	11.1 ± 1.0 a
orcinol	11.5 ± 1.1 a
2,6-dihydroxybenzoic acid	10.6 ± 2.1 a
hydroquinone	29.5 ± 1.9 b,c
2,5-dihydroxybenzoic acid	24.9 ± 5.7 c,e,g
benzoquinone	66.1 ± 2.0 h
pyrogallol	43.2 ± 4.5 d,i
gallic acid	27.5 ± 1.5 c,g
1,2,4-trihydroxybenzene	46.0 ± 1.5 i
phloroglucinol	9.2 ± 1.5 a
catechin	10.9 ± 1.8 a
epicatechin	11.2 ± 1.8 a
epigallocatechin	11.9 ± 2.4 a,f
quercetin	11.9 ± 0.4 a
myricetin	12.9 ± 1.9 a,f

[a]Values with the same letter in the same column are not significantly different ($p < 0.05$).

For polyphenols having two hydroxyl groups at the aromatic ring, only those having these groups in ortho or para positions were able to produce the Strecker degradation of the amino acid to a higher extent than the control phenylalanine. For that reason, neither resorcinol, orcinol, nor 2,6-dihydroxybenzoic acid produced more phenylacetaldehyde than the control (Table 1). In addition, the presence of the two hydroxyl groups is needed, and one hydroxyl group cannot be replaced by a methoxy group. For that reason, ferulic acid did not produce more phenylacetaldehyde than the control. On the contrary, caffeic acid was able to increase phenylacetaldehyde formation by 106%.

There was not any difference between the Strecker degradation ability of *o*- and *p*-diphenols. Thus, catechol and hydroquinone increased the phenylacetaldehyde produced by the control by about 180%. However, the presence of other groups in the ring and the relative positions of all groups determined either an increase or a decrease in the phenylacetaldehyde produced. Thus, a methyl group at position 4 (4-methylcatechol) increased the formation of phenylacetaldehyde by 33% with respect to that formed by catechol. On the contrary, the presence of a carboxylic group at the same position (3,4-dihydroxybenzoic acid) reduced the formation of phenylacetaldehyde by 57% with respect to that formed by catechol. Curiously, the same carboxylic group only reduced by 24% the formation of phenylacetaldehyde with respect to that formed by hydroquinone in 2,5-dihydroxybenzoic acid. Finally, the presence of a conjugated carbon−carbon double bond at position 4 (such in caffeic acid) also reduced the phenylacetaldehyde formed by catechol by 42%.

When three hydroxyl groups were present, the relative positions of the hydroxyl groups determined the activity. Thus, the presence of two hydroxyl groups at ortho or para positions was required to observe an increased phenylacetaldehyde formation. For that reason, phloroglucinol did not increase phenylacetaldehyde formation in comparison to the control. On the contrary, both pyrogallol and 1,2,4-trihydroxybenzene increased phenylacetaldehyde formation. This increase was higher than that exhibited by catechol and hydroquinone, more likely because the number of hydroxyl groups in ortho or para positions was higher in these trihydroxy derivatives than in the dihydroxy derivatives. The increases in phenylacetaldehyde formation with respect to control were 304 and 330% for pyrogallol and 1,2,4-trihydroxybenzene, respectively. The introduction of a carboxylic group in the ring, such as in gallic acid, decreased the amount of phenylacetaldehyde formed by 48% with respect to that produced by pyrogallol.

Complex phenols, such as those shown in Figure 1, usually have several aromatic rings with different substitutions. Thus, they may have two hydroxyl groups in meta position at the A-ring, which according to the above results did not seem to contribute to phenylacetaldehyde formation. In addition, they may have several hydroxyl groups, usually in ortho positions at the B-ring, which should be contributing to phenylacetaldehyde formation, also according to the above results. Despite these hydroxyl groups in ortho positions at the B-ring, the assayed complex phenols did not increase phenylacetaldehyde formation (Table 1).

When benzoquinone was tested in place of a phenolic derivative, this compound produced more phenylacetaldehyde than any of the assayed phenolic compounds (Table 1). In fact, it produced 195% more phenylacetaldehyde than its phenol analogue hydroquinone.

1,2,4-Trihydroxybenzene and hydroquinone, as models of tri- and dihydroxy derivatives, respectively, were selected for the rest of this study because of their ability to degrade phenylalanine to a high extent. In addition, parallel studies were also carried out with benzoquinone for comparison purposes.

Effect of Reaction Conditions (pH, Concentration of the Phenolic Compound, Time, and Temperature) on the Phenylacetaldehyde Produced in Phenylalanine/Phenol Reaction Mixtures. The formation of phenylacetaldehyde depended on the pH of the reaction (Figure 2), although this dependence was smaller than that observed in the Strecker-type degradation of amino acids produced by lipid oxidation products.[14] Thus, the formation of phenylacetaldehyde was more or less constant at pH values ≤5 and decreased at higher pH values. Because previous studies involving the Strecker degradation of amino acids were carried out at pH 3,[14] this pH was also selected for this study.

Phenylacetaldehyde formation also depended on the amount of phenol added (Figure 3). In fact, there was a linear correlation ($r > 0.99$, $p < 0.01$) between the amount of phenol added and the phenylacetaldehyde produced at low concentrations of phenol. The maximum concentrations of phenylacetaldehyde were achieved when 25 μmol of phenylalanine was treated with either 10 μmol of hydroquinone, 7.5 μmol of benzoquinone, or 5 μmol of 1,2,4-trihydroxybenzene. Addition

DOI: 10.1021/jf5047317
J. Agric. Food Chem. 2015, 63, 312−318

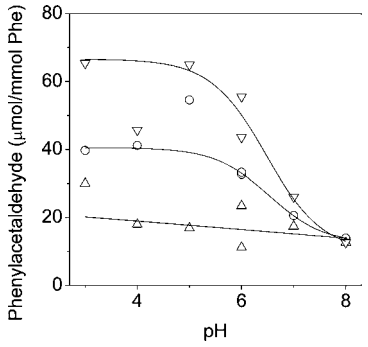

Figure 2. Effect of reaction pH on the phenylacetaldehyde produced in the reaction of phenylalanine with hydroquinone (△), 1,2,4-trihydroxybenzene (○), and benzoquinone (▽). Equimolecular mixtures of the amino acid and the phenol were heated at 180 °C for 1 h.

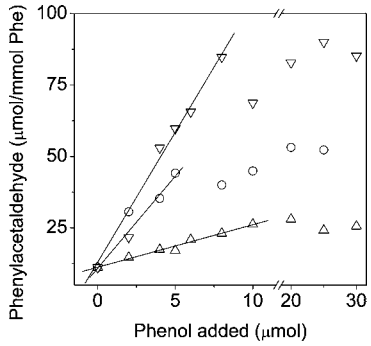

Figure 3. Effect of the concentration of the phenol on the phenylacetaldehyde produced in the reaction of phenylalanine with hydroquinone (△), 1,2,4-trihydroxybenzene (○), and benzoquinone (▽). Mixtures of the phenylalanine (25 μmol) and the phenol in 0.3 M sodium citrate buffer were heated at 180 °C for 1 h.

of higher amounts of phenolic compound did not produce significant increases in the phenylacetaldehyde produced.

Phenylacetaldehyde formation also depended on the incubation time and temperature (Figure 4). Thus, the amount of phenylacetaldehyde produced increased linearly ($r > 0.93$, $p < 0.02$) as a function of time at the different assayed temperatures when phenylalanine was heated in the presence of hydroquinone (Figure 4A). Similar behavior was observed in the case of the other two derivatives assayed: 1,2,4-trihydroxybenzene ($r > 0.97$, $p < 0.03$; Figure 4B) and benzoquinone ($r > 0.97$, $p < 0.002$; Figure 4C).

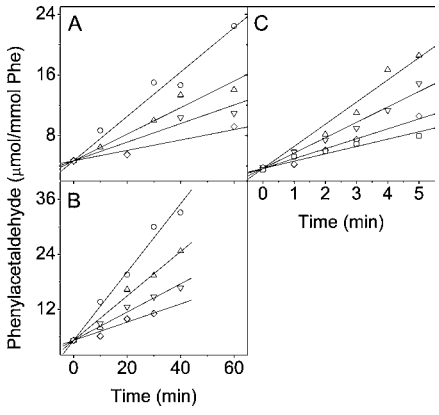

Figure 4. Time course of phenylacetaldehyde produced in the reaction of phenylalanine with (A) hydroquinone, (B) 1,2,4-trihydroxybenzene, and (C) benzoquinone. Equimolecular mixtures of phenylalanine and the phenol in 0.3 M sodium citrate buffer were heated at the indicated times and temperatures. The temperatures assayed were 180 (○), 160 (△), 140 (▽), 120 (◇), and 100 °C (□).

Reaction rates at the different assayed temperatures were calculated using the equation

$$[\text{phenylacetaldehyde}] = [\text{phenylacetaldehyde}]_0 + kt$$

where $[\text{phenylacetaldehyde}]_0$ represents the intercept, k is the rate constant, and t is the time. These rate constants were used in an Arrhenius plot (Figure 5) for calculation of the activation

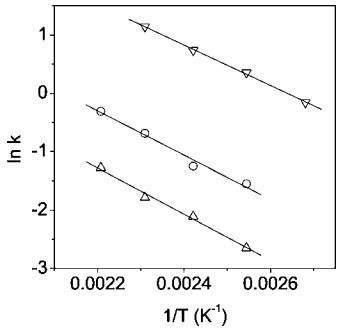

Figure 5. Arrhenius plot for phenylacetaldehyde production in the reaction of phenylalanine with hydroquinone (△), 1,2,4-trihydroxybenzene (○), and benzoquinone (▽).

energy (E_a) of phenylacetaldehyde formation from phenylalanine in the presence of phenolic compounds. The values obtained for E_a were 32.9 kJ/mol for hydroquinone, 31.5 kJ/mol for 1,2,4-trihydroxybenzene, and 28.8 kJ/mol for benzoquinone.

Strecker-Type Degradation of Phenylglycine Methyl Ester. In an attempt to clarify the mechanism of the reaction and to investigate if amines were also able to suffer Strecker-type degradation, the reaction of phenylglycine methyl ester with both hydroquinone and benzoquinone was studied under the same reaction conditions above-described for phenylalanine. Phenylglycine methyl ester was selected for this study because it has several substituents at the α-carbon that can favor the exit of the proton at this carbon.

Figure 6A shows the chromatogram obtained after 1 h of heating at 180 °C of an equimolecular mixture of hydroquinone and phenylglycine methyl ester. As observed in the figure, the initial phenylglycine methyl ester was absent after 1 h of heating, but a significant amount of hydroquinone was still present. The main reaction product was benzaldehyde, although other degradation products of phenylglycine methyl ester could be easily identified. These were the Strecker-type degradation products methyl 2-oxo-2-phenylacetate, benzoic acid, benzoic acid methyl ester, and benzaldehyde dimethyl acetal. Products derived from hydroquinone were 4-methoxyphenol and trace amounts of benzoquinone, which was unambiguously identified. 4-Aminophenol could also be present in trace amounts, but it appeared under the hydroquinone peak and could not be unambiguously identified.

When the reaction was carried out between benzoquinone and phenylglycine methyl ester, the same products as in the reaction with hydroquinone were identified in the reaction mixture, although proportions among them were slightly

DOI: 10.1021/jf5047317
J. Agric. Food Chem. 2015, 63, 312−318

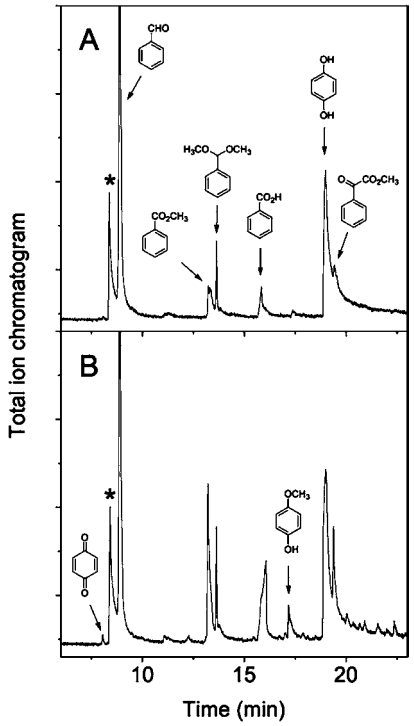

Figure 6. Total ion chromatograms obtained for reaction mixtures of phenylglycine methyl ester with (A) hydroquinone and (B) benzoquinone. Samples were heated for 1 h at 180 °C in sodium citrate buffer, pH 3. Identified compounds are indicated in the figure. Peaks marked with ∗ corresponded to the buffer.

different (Figure 6B). Thus, phenylglycine methyl ester disappeared completely after 1 h of heating at 180 °C in the presence of benzoquinone, and a part of benzoquinone was converted into hydroquinone. In addition, the residual presence of benzoquinone was detected to a higher extent than when hydroquinone was the reactant (see Figure 6A). Analogously to the hydroquinone/phenylglycine methyl ester reaction mixture, the main reaction product was benzaldehyde. Other reaction products were methyl 2-oxo-2-phenylacetate, benzoic acid, benzoic acid methyl ester, and benzaldehyde dimethyl acetal. Analogously to hydroquinone/phenylglycine reaction mixtures, the products derived from benzoquinone were 4-methoxyphenol and hydroquinone. 4-Aminophenol could also be present in trace amounts, but it appeared under the hydroquinone peak and could not be unambiguously identified.

DISCUSSION

Since its discovery more than 150 years ago,[17] the Strecker degradation of amino acids has emerged as an almost endless source of flavor-significant compounds.[12,18] Although it was considered for many years as a part of Maillard chemistry produced by carbohydrates, nowadays Strecker-type reactions are known to be also produced in the course of nonenzymatic browning reactions by other food components such as lipid oxidation products,[19,20] amines,[21] and polyphenol-derived quinones,[13] among others. The results obtained in the present study extend the number of food components able to produce the Strecker degradation of amino acids also to polyphenols in the absence of added oxidants. Nevertheless, not all polyphenols were able to produce the Strecker degradation of amino acids. Only polyphenols having some structural characteristics produced this reaction. Thus, only polyphenols having at least two hydroxyl groups in ortho or para positions were able to degrade phenylalanine. However, the presence in the same molecule of other aromatic ring with two hydroxyl groups in meta position canceled the ability of these complex phenols to degrade phenylalanine.

This behavior should be a consequence of the mechanism of the reaction. Thus, the fact that two hydroxyl groups in ortho or para positions are needed suggests that the polyphenol has to be converted into the corresponding quinone to produce the reaction. This was observed when the reaction between hydroquinone and phenylglycine methyl ester was studied by GC-MS (Figure 6A). The presence of trace amounts of benzoquinone was observed in the chromatogram, although no oxidant was added. These oxidations of *o*- and *p*-dihydroxy derivatives to the corresponding quinones have been described by different authors.[22,23] According to these findings, the reaction pathway shown in Figure 7 is proposed for the

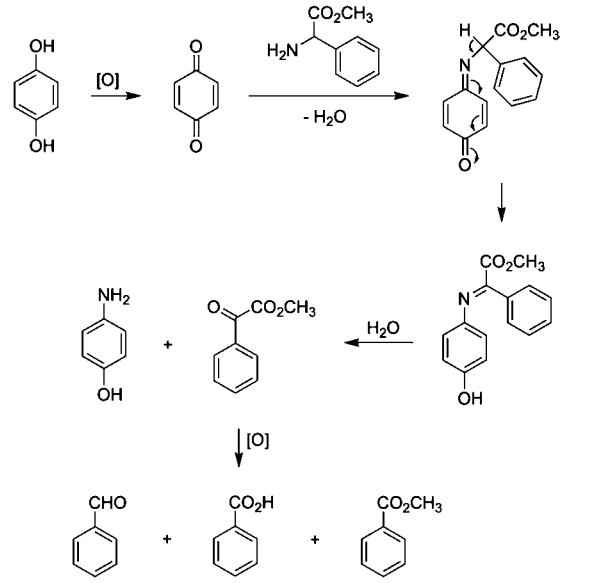

Figure 7. Proposed pathway for the reaction of phenylglycine methyl ester with hydroquinone and benzoquinone.

phenylglycine methyl ester degradation in the presence of hydroquinone. In the presence of amino compounds and air, *o*- and *p*-diphenols are able to produce the corresponding quinones to some extent. These quinones form then the corresponding imines with the amino group of the amino compound. Finally, tautomerism converts the ketoimine into the corresponding α-imino ester, the driving force being conjugation. The hydrolysis of the α-ketoimine is the origin of the Strecker-type carbonyl compound (methyl 2-oxo-2-phenylacetate) detected in the reaction and of 4-aminophenol, which was not unambiguously identified. This 4-aminophenol might be the origin of the detected 4-methoxyphenol. Methyl 2-oxo-2-phenylacetate was not stable under the employed reaction conditions as it degraded to benzaldehyde, which was the major reaction product. Benzaldehyde oxidation is likely the origin of benzoic acid and its methyl ester, although benzoic acid can also be produced directly in the cleavage of methyl 2-oxo-2-phenylacetate.

A similar pathway is likely taking place with phenylalanine (Figure 8). In this case, the produced α-iminocarboxylic acid intermediate decarboxylates to the corresponding *N*-(4-

DOI: 10.1021/jf5047317
J. Agric. Food Chem. 2015, 63, 312−318

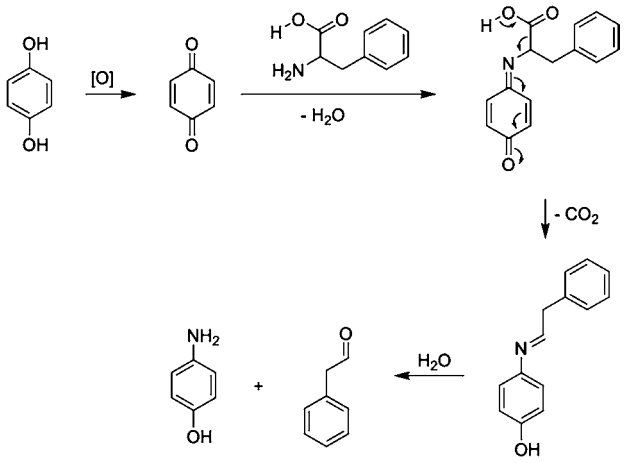

Figure 8. Proposed pathway for the reaction of phenylalanine with hydroquinone and benzoquinone.

hydroxyphenyl)aldimine. After hydrolysis of the latter aldimine, phenylacetaldehyde is produced.

These pathways explain the relative activities of simple di- and trihydroxy derivatives, which are related to their relative facility to be converted into quinones. In addition, the electronic effects of other substituents in the ring will also play a role in the overall reaction yield. On the contrary, it does not explain the low yields of phenylacetaldehyde obtained with complex phenols. These last results are likely a consequence of two opposite effects. On the one hand, the above results demonstrate that *o*- and *p*-diphenols are easily transformed into quinones, and these derivatives are able to convert amino acids and amines into their corresponding carbonyl derivatives. On the other, *m*-diphenols have been shown to be very efficient carbonyl scavengers.[10,24,25] The obtained results seem to suggest that the carbonyl-scavenging ability of the A-ring is higher than the Strecker-inducer capacity of the B-ring. Only myricetin, which has a pyrogallol moiety in the B-ring, seemed to increase slightly the phenylacetaldehyde produced in comparison to control, although this increase was not significant.

A further proof of this pathway was obtained when the reaction between benzoquinone and phenylglycine methyl ester was studied. The reaction not only produced compounds identical to those of the hydroquinone/phenylglycine methyl ester reaction mixtures but significant amounts of hydroquinone were found, therefore confirming the existence of redox processes in these mixtures that would facilitate the conversion of benzoquinone into hydroquinone and vice versa. For the same reason, the appearance of benzoic acid as an oxidation product of benzaldehyde is not surprising. The only differences between benzoquinone and hydroquinone for these reactions are the reaction yield, which was higher for benzoquinone (Table 1 and Figure 3), and the lower reaction time needed for benzoquinone to produce phenylacetaldehyde (Figure 4). Both results are in agreement with the conversion of hydroquinone into benzoquinone as a previous step for the Strecker degradation. Nevertheless, E_a for phenylacetaldehyde formation in benzoquinone/phenylalanine reaction mixtures was only slightly lower than E_a for phenylacetaldehyde formation in hydroquinone/phenylalanine reaction mixtures, therefore indicating that conversion of hydroquinone into benzoquinone is not an energetically difficult process, although it does not seem to be very favored kinetically.

All of these results confirm that polyphenols can produce the Strecker degradation of amino acids in the absence of added oxidants. In addition, analogous reactions can also be produced in amines, therefore demonstrating that the presence of the carboxylic group might be desirable but not essential. The only requisite for polyphenols to produce Strecker-type degradations is the presence of two hydroxyl groups in ortho or para positions. On the other hand, the presence of two hydroxyl groups in meta position in another part of the molecule can inhibit the Strecker-degrading ability of the hydroxyl groups in ortho or para positions.

AUTHOR INFORMATION

Corresponding Author

*(F.J.H.) Phone: +34 954 611 550. Fax: +34 954 616 790. E-mail: fhidalgo@ig.csic.es.

Funding

This study was supported in part by the European Union (FEDER funds) and the Plan Nacional de I + D of the Ministerio de Economía y Competitividad of Spain (Project AGL2012-35627).

Notes

The authors declare no competing financial interest.

ACKNOWLEDGMENTS

We are indebted to José L. Navarro for technical assistance.

REFERENCES

(1) Soto-Vaca, A.; Gutierrez, A.; Losso, J. N.; Xu, Z.; Finley, J. W. Evolution of phenolic compounds from color to flavor problems to health benefits. *J. Agric. Food Chem.* **2012**, *60*, 6658−6677.

(2) Maga, J. A.; Katz, I. Simple phenol and phenolic compounds in food flavor. *CRC Crit. Rev. Food Sci. Nutr.* **1978**, *4*, 323−372.

(3) Casassa, L. F.; Harbertson, J. F. Extraction, evolution, and sensory impact of phenolic compounds during red wine maceration. *Annu. Rev. Food Sci. Technol.* **2014**, *5*, 83−109.

(4) Plaza, M.; Pozzo, T.; Liu, J. Y.; Ara, K. Z. G.; Turner, C.; Karlsson, E. N. Substituent effects on in vitro antioxidizing properties, stability, and solubility in flavonoids. *J. Agric. Food Chem.* **2014**, *62*, 3321−3333.

(5) Gobert, M.; Remond, D.; Loonis, M.; Buffiere, C.; Sante-Lhoutellier, V.; Dufour, C. Fruits, vegetables and their polyphenols protect dietary lipids from oxidation during gastric digestion. *Food Funct.* **2014**, *5*, 2166−2174.

(6) Contini, C.; Alvarez, R.; O'Sullivan, M.; Dowling, D. P.; Gargan, S. O.; Monahan, F. J. Effect of an active packaging with citrus extract on lipid oxidation and sensory quality of cooked turkey meat. *Meat Sci.* **2014**, *96*, 1171−1176.

(7) Kokkinidou, S.; Peterson, D. G. Control of Maillard-type off-flavor development in ultrahigh-temperature-processed bovine milk by phenolic chemistry. *J. Agric. Food Chem.* **2014**, *62*, 8023−8033.

(8) Tressl, R.; Bahri, D.; Holzet, M.; Kossa, T. Formation of flavor components in asparagus. 2. Formation of flavor components in cooked asparagus. *J. Agric. Food Chem.* **1977**, *25*, 459−463.

(9) Totlani, V. M.; Peterson, D. G. Reactivity of epicatechin in aqueous glycine and glucose Maillard reaction models: quenching of C_2, C_3, and C_4 sugar fragments. *J. Agric. Food Chem.* **2005**, *53*, 4130−4135.

(10) Hidalgo, F. J.; Zamora, R. 2-Alkenal-scavenging ability of *m*-diphenols. *Food Chem.* **2014**, *160*, 118−126.

(11) Bittner, S. When quinones meet amino acids: chemical, physical and biological properties. *Amino Acids* **2006**, *30*, 205−224.

(12) Rizzi, G. P. The Strecker degradation of amino acids: newer avenues for flavor formation. *Food Rev. Int.* **2008**, *24*, 416−435.

DOI: 10.1021/jf5047317
J. Agric. Food Chem. 2015, 63, 312−318

(13) Rizzi, G. P. Formation of Strecker aldehydes from polyphenol-derived quinones and α-amino acids in a nonenzymic model system. *J. Agric. Food Chem.* **2006**, *54*, 1893−1897.
(14) Zamora, R.; Gallardo, E.; Hidalgo, F. J. Strecker degradation of phenylalanine initiated by 2,4-decadienal or methyl 13-oxooctadeca-9,11-dienoate in model systems. *J. Agric. Food Chem.* **2007**, *55*, 1308−1314.
(15) Fors, S. Sensory properties of volatile Maillard reaction products and related compounds. In *The Maillard Reaction in Foods and Nutrition*; Waller, G. R., Feather, M. S., Eds.; American Chemical Society: Washington, DC, USA, 1983; pp 185−286.
(16) Snedecor, G. W.; Cochran, W. G. *Statistical Methods*, 7th ed.; Iowa State University Press: Ames, IA, USA, 1980.
(17) Strecker, A. Note on a peculiar oxidation by alloxan. *Justus Liebigs Ann. Chem.* **1862**, *123*, 363−365.
(18) Adams, A.; De Kimpe, N. Chemistry of 2-acetyl-1-pyrroline, 6-acetyl-1,2,3,4-tetrahydropyridine, 2-acetyl-2-thiazolidine, and 5-acetyl-2,3-dihydro-4*H*-thiazine: extraordinary Maillard flavor compounds. *Chem. Rev.* **2006**, *106*, 2299−2319.
(19) Hidalgo, F. J.; Zamora, R. Strecker-type degradation produced by the lipid oxidation products 4,5-epoxy-2-alkenals. *J. Agric. Food Chem.* **2004**, *52*, 7126−7131.
(20) Adams, A.; Bouchaert, C.; Van Lancker, F.; De Meulenaer, B.; De Kimpe, N. Amino acid catalysis of 2-alkylfuran formation from lipid oxidation-derived α,β-unsaturated aldehydes. *J. Agric. Food Chem.* **2011**, *59*, 11058−11062.
(21) Zamora, R.; Gallardo, E.; Hidalgo, F. J. Amine degradation by 4,5-epoxy-2-decenal in model systems. *J. Agric. Food Chem.* **2006**, *54*, 2398−2404.
(22) Jacobs, J.; Tehrani, K. A.; De Kimpe, N. A survey of synthetic routes towards 2-azaanthraquinones. *Tetrahedron* **2011**, *67*, 9459−9471.
(23) Hodge, J. E. Dehydrated foods. Chemistry of browning reactions in model systems. *J. Agric. Food Chem.* **1953**, *1*, 928−943.
(24) Cheng, K. W.; Wong, C. C.; Cho, C. K.; Chu, I. K.; Sze, K. H.; Lo, C.; Chen, F.; Wang, M. Trapping of phenylacetaldehyde as a key mechanism responsible for Naringerin's inhibitory activity in mutagenic 2-amino-1-methyl-6-phenylimidazo[4,5-*b*]pyridine formation. *Chem. Res. Toxicol.* **2008**, *21*, 2026−2034.
(25) Salazar, R.; Arámbula-Villa, G.; Hidalgo, F. J.; Zamora, R. Structural characteristics that determine the inhibitory role of phenolic compounds on 2-amino-1-methyl-6-phenylimidazo[4,5-*b*]pyridine (PhIP) formation. *Food Chem.* **2014**, *151*, 480−486.

DOI: 10.1021/jf5047317
J. Agric. Food Chem. 2015, 63, 312−318

This is an open access article published under a Creative Commons Attribution (CC-BY) License, which permits unrestricted use, distribution and reproduction in any medium, provided the author and source are cited.

JOURNAL OF AGRICULTURAL AND FOOD CHEMISTRY

Article

pubs.acs.org/JAFC

Application of High-Intensity Ultrasound to Palm Oil in a Continuous System

Yubin Ye and Silvana Martini*

Department of Nutrition, Dietetics, and Food Sciences, Utah State University, 8700 Old Main Hill, Logan, Utah 84322-8700, United States

Supporting Information

ABSTRACT: High-intensity ultrasound (HIU) was used in a continuous system to change the crystallization behavior of palm oil. Different power levels (75, 110, and 180 W) and pulse durations (continuous application and 5, 10, and 15 s pulses) were used to optimize sonication conditions. Results showed that HIU applied at low power level (75 W) was the most efficient condition in inducing palm oil crystallization at 35 °C, generating a crystalline network with higher solid fat content (SFC), higher elasticity, and sharper melting profile after 60 min of crystallization. Changes in elasticity observed as a consequence of sonication were maintained after tempering the samples at 25 °C for 24 h, but were lost after tempering at 5 °C. No significant differences (α = 0.05) were observed in SFC values of the sonicated and nonsonicated samples after tempering, whereas the sharper melting behavior observed in the sonicated sample was maintained after tempering.

KEYWORDS: *high-intensity ultrasound, flow cell, power level, crystallization, palm oil, polymorphism*

INTRODUCTION

Power ultrasound, or high-intensity ultrasound (HIU), is an invasive technique that uses acoustic waves operating at low frequency (20−100 kHz) and high power (10−10000 W cm^{-2}) levels. These acoustic waves travel through the material and induce the formation of cavities.[1] Cavitation is associated with high localized temperatures, high shear forces, and high pressures that lead to several physicochemical changes in the material.[2] Some of these changes include the generation of chemical reactions (sonochemistry),[3,4] changes in crystallization behavior (sonocrystallization),[5,6] and changes in physical properties of materials.[7−9] In particular, sonocrystallization is defined as the phenomenon associated with the induction or modification of the crystallization behavior of different materials without generating any chemical changes.[10] Sonocrystallization techniques have been used in food applications since the early 2000s. Chow et al. used HIU to modify the primary and secondary nucleation of ice and sucrose,[11,12] whereas Patel et al. showed that power ultrasound can be used to control the crystallization process of lactose during the nucleation phase.[13] Early studies in lipid systems were performed by Patrick et al., who evaluated the effect of ultrasonic intensity on palm oil crystalline structures.[14] Sato and co-workers used HIU in cocoa butter and pure triacylglycerols[15,16] and showed that HIU induces lipid crystallization as evidenced by shorter induction times in sonicated samples. In addition, these authors showed that HIU promotes the formation of a stable polymorphic form, especially at high crystallization temperatures.

Previous work in our laboratory[17−20] and by other research groups[21] indicates that HIU can be used as a novel processing tool to modify the functional properties of lipids. HIU has the ability to change the crystallization behavior of lipids and therefore their functional properties such as texture, thermal behavior, solid/liquid ratio, and crystal size.

All previous studies about lipid sonocrystallization have been performed in a batch with volumes between 5 and 100 mL.[16−21] The effect of HIU on the crystallization of lipids in a continuous system has never been investigated.

The purpose of this research is to evaluate the use of HIU in a continuous system, which is a more realistic representation of an industrial setting. The overall objective of this research is to optimize the processing conditions (power level and irradiation pulse) needed to use HIU in a continuous system to modify the physical properties (microstructure, melting profiles, polymorphism, and viscoelasticity) of palm oil.

MATERIALS AND METHODS

Materials. Refined, bleached, and deodorized palm oil provided by Archer Daniels Midland (ADM Oils, Oils Division, Chicago, IL, USA) was used in this experiment. The melting point of the palm oil is 37.2 ± 0.4 °C (AOCS Official Method Cc 1-25). The chemical composition of the sample consisted of 48% of saturated fatty acids, 40% of monounsaturated fatty acids, 10% of polyunsaturated fatty acids, and 2% of *trans*-fatty acids according to the product data sheet provided by ADM.

Sample Preparation and Continuous System. The continuous system consisted of a flow cell connected to a sonicator and an external water bath (Figure 1). Five liters of palm oil was placed in a 6 L Erlenmeyer flask and melted in a 70 °C water bath to completely erase crystal memory. The flask was then placed in a 40 °C water bath to allow for temperature stabilization. Once the sample reached approximately 42 °C, it was pumped into the flow cell at 7.3 mL/s using a peristaltic pump (261 mL; the retention of the sample in the cell is around 36 s) and collected in NMR tubes and beakers. The flow cell was connected to a water bath filled with an ethylene glycol water mixture (3:1 v/v) and set at −18 °C. This low temperature in the

Received: October 17, 2014
Revised: December 16, 2014
Accepted: December 17, 2014
Published: December 17, 2014

 © 2014 American Chemical Society

DOI: 10.1021/jf505041s
J. Agric. Food Chem. 2015, 63, 319−327

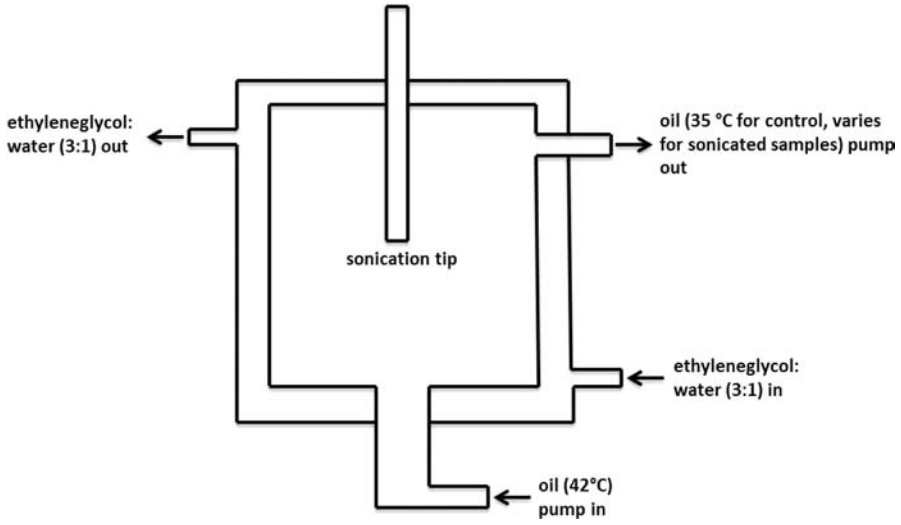

Figure 1. Flow cell system used to evaluate the effect of HIU on the crystallization behavior of palm oil.

water bath was necessary to cool the sample in the flow cell from 42 to 35 °C. A diagram of the flow cell used is shown in Figure 1.

Ultrasound Application. HIU (20 ± 1 kHz operation frequency) was generated using UIP1500hd equipment (Hielscher Ultrasound Technology, Ringwood, NJ, USA) with a 3.8 cm^2 frontal area sonication tip. HIU was applied 1 min after pumping of the sample had been started to ensure that the cell was completely filled with the sample and to stabilize the temperature of the sample. Previous research in our laboratory[17,19] and by other research groups[21] showed that the effect of HIU is more significant when samples are crystallized at low supercoolings. Because the melting point of our sample is 37.2 ± 0.4 °C, a crystallization temperature of 35 °C was chosen for our experiments. The effects of ultrasound using different power levels were evaluated in this study using 75 W (the lowest power setting that can be achieved by our ultrasound generator), 110 W (middle setting), and 180 W (safety maximum power setting recommended by the manufacturer of the sonicator). Sonication was applied in a continuous manner and using 5, 10, and 15 s pulse durations. A continuous duration indicates sonication continuously for 5 min, whereas sonication using an X s pulse duration means that HIU was applied every X s for a duration of X s. For example, a 5 s pulse duration means HIU was applied every 5 s with the duration of 5 s. Sample was pumped into the system for 5 min from the start of the sonication. Control samples (samples crystallized without the use of HIU) were collected at the beginning of the experiment before the application of HIU. Samples were collected every minute during the crystallization process in different tubes (one tube per minute). The first tube always consisted of nonsonicated sample (control). Solid fat content and crystal morphology were monitored in these samples as a function of storage time at 35 °C. Samples were kept at 35 °C in an incubator for 60 min to allow complete crystallization and then rapidly cooled to 25 and 5 °C and tempered for 24 h at these temperatures. The objective of this step is to evaluate if the effect of sonication is maintained through the tempering process.

Solid Fat Content (SFC). SFC values of palm oil during and after crystallization at 35 °C were measured using a NMR 120 minispec NMR analyzer (Bruker, Germany) following AOCS direct method Cd 16b-93. Samples were collected at the exit of the flow cell and loaded into the NMR tube every minute and kept at 35 °C to allow complete crystallization. SFC was measured as soon as the sample was taken out of the flow cell (time zero) and every 5 min for 30 min and every 10 min until the end of crystallization (60 min). The crystallization curves were fitted to the Avrami equation (eq 1) by least-squares nonlinear regression.[22]

$$SFC_{(t)}/SFC_{(\infty)} = 1 - \exp(-kt^n) \quad (1)$$

$SFC(t)$ and SFC_∞ are the SFC (%) at time t and the maximum SFC after crystallization is completed, respectively. The SFC data fitted to this model were used to determine the rate constant of crystallization (k) at a particular temperature and the mechanism of nucleation and crystal growth through the exponent, n.[23]

Microstructure. Crystal morphology was recorded during crystallization using a polarized light microscope (PLM-Olympus BX 41 America Inc., Melville, NY, USA) with a digital camera (Lumenera Scientific, Infinity 2, Ottawa, Ontario, Canada) attached and a thermostated stage to allow for temperature control during the measurement. The pipet, slides, and slide covers were tempered at 35 °C in the incubator. A 20× magnification objective was used.

Crystal Polymorphism by X-ray Diffraction (XRD). After 60 min of crystallization, samples were filtered under vacuum for 2 min, and crystals were collected to perform XRD measurement. The same filtration treatment was performed in samples tempered at 25 and 5 °C for 24 h. Samples were filtered to separate as many crystals as possible from the liquid phase, minimize the signal of the liquid fat in the XRD, and therefore obtain a better resolution. The polymorphic forms of fat crystals were determined by using a Philips Analytical X'Pert Pro X-ray Diffraction system (PW 3040/60 Console). The X-ray generator used a high-power ceramic diffraction X-ray tube with copper anode (PW 3373/00 ceramic tube Cu LFF), with voltage at 45 kV and current at 40 mA. Samples were scanned from 3° to 30° (2θ scale) at a rate of 1°/min at ambient temperature. The data were collected using X'Pert Data Collector and analyzed by X'Pert HighScore PANalytical software.

Melting Profile. The thermal behavior of the crystallized material was evaluated using a differential scanning calorimeter (DSC-TA Instruments Q20). The crystallized material (5−15 mg) was placed in a hermetic aluminum pan and heated from T_c (35, 25, or 5 °C) to 80 °C at 5 °C/min to evaluate its melting behavior. Melting parameters such as onset temperature (T_{on}; temperature at which the sample starts melting), peak temperature (T_p; temperature at which the melting peak reaches its maximum), and melting enthalpy (energy required for melting) were recorded. The melting enthalpy was used to evaluate the amount of crystallized material and the solid/liquid ratio in the lipid network. These analyses provided information about (a) the amount of solids generated as a consequence of HIU (induction or delay of the crystallization) through the melting enthalpy values, (b) the solid/liquid ratio of the crystal network formed as a function of temperature during melting, and (c) the melting range of the lipid network (through T_p and T_{on}).

Viscoelastic Properties. A TA Instruments AR-G2 magnetic bearing rheometer was used to evaluate the viscoelastic properties of the material. Oscillatory tests were performed by strain sweep step to obtain viscoelastic parameters such as the storage modulus (G'). The

DOI: 10.1021/jf505041s
J. Agric. Food Chem. 2015, 63, 319−327

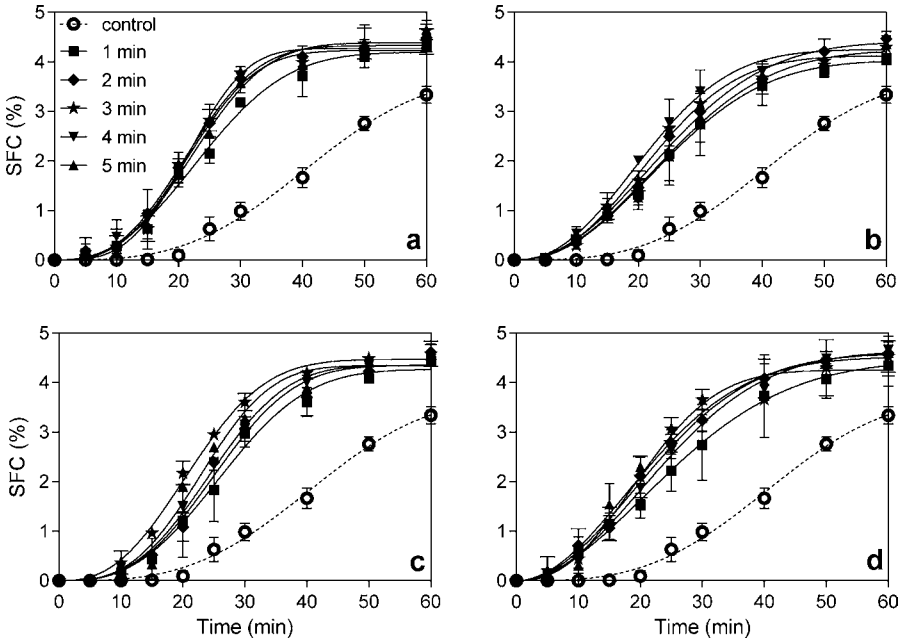

Figure 2. SFC of palm oil without (control, open circles) and with (solid symbols) HIU during the first 60 min of the crystallization process at 35 °C. A 75 W power level was used in a continuous manner (a) and using pulses of different durations (5, 10, and 15 s; b, c, and d, respectively).

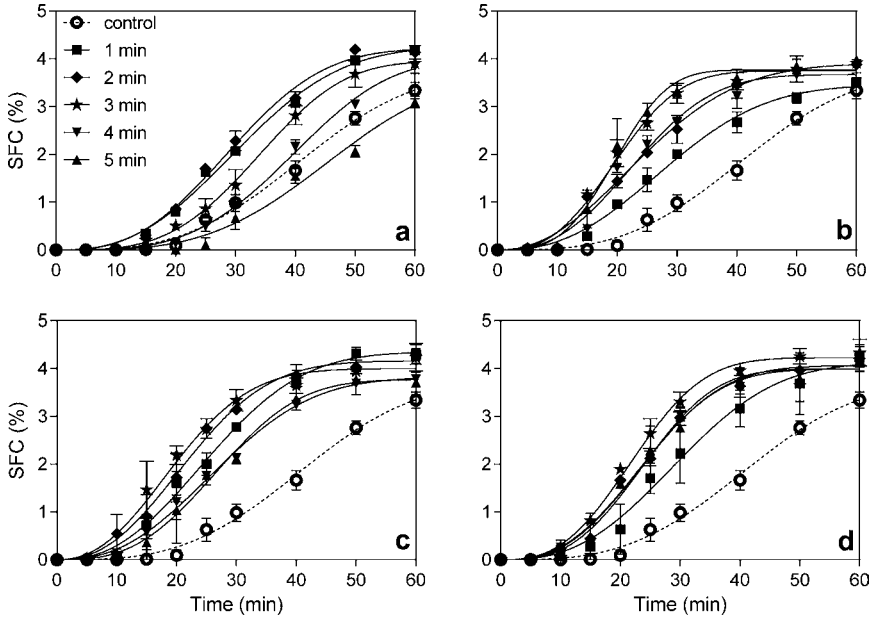

Figure 3. SFC of palm oil without (control, open circles) and with (solid symbols) HIU during the first 60 min of the crystallization process at 35 °C. A 110 W power level was used in a continuous manner (a) and using pulses of different durations (5, 10, and 15 s; b, c, and d, respectively).

experiments were carried out using a parallel plate geometry (40 mm diameter) with a temperature-controlled Peltier plate. The temperature of the plate was set at 35, 25, or 5 °C. For the strain sweep step, a constant frequency of 1 Hz (6.28 rad/s) was used, and strain values were set from 0.0008 to 10%.

Statistical Analysis. Crystallization experiments were performed in duplicate, and physical properties were measured in duplicate. Significant differences (α = 0.05) were evaluated using two-way ANOVA using GraphPad Prism software, version 6.00 for Windows (GraphPad Software, San Diego, CA, USA).

RESULTS AND DISCUSSION

Optimizing the Process Condition. Figures 2−4 show the crystallization behavior of palm oil measured by SFC as a function of time when different power levels of ultrasound were applied using different pulse types. Figure 2 shows SFC changes when samples were sonicated using 75 W power using a continuous sonication (Figure 2a), a 5 s pulse (Figure 2b), a 10 s pulse (Figure 2c), and a 15 s pulse (Figure 2d). When HIU is applied in a continuous manner, SFC values increased rapidly after 10 min, whereas SFC values increased after 20 min in the control samples (Figure 2a). Panels a−d of Figure 2 show no difference in crystallization between the modes of sonication (continuous vs pulses) with onset of crystallization observed at 20 min for the nonsonicated samples and at 10 min for the sonicated ones and final SFC values of 3.3 and 4.3% on average, respectively. Avrami analysis (R^2 values between 0.96 and 0.99)

DOI: 10.1021/jf505041s
J. Agric. Food Chem. 2015, 63, 319−327

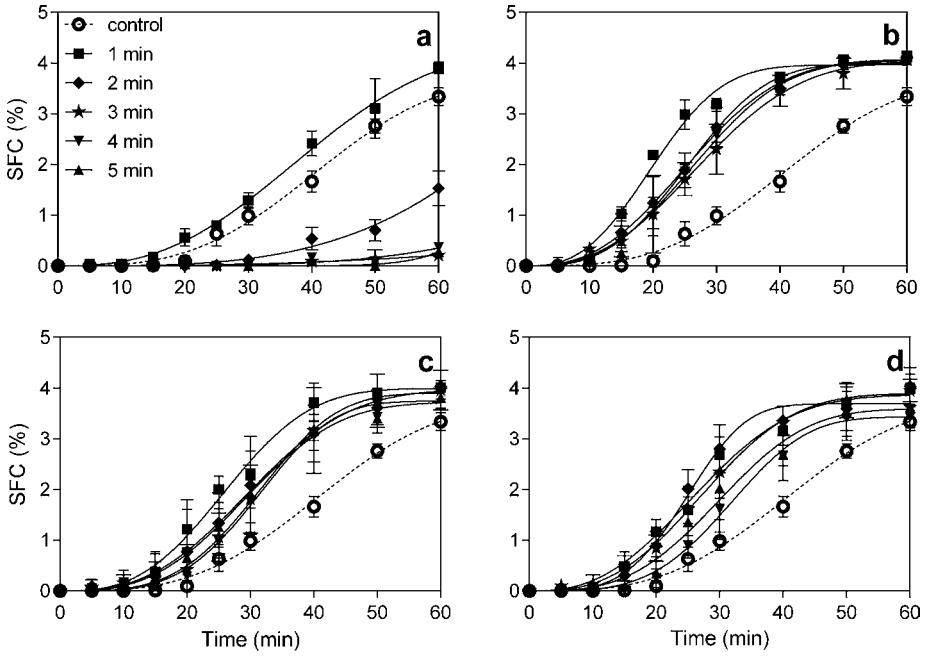

Figure 4. SFC of palm oil without (control, open circles) and with (solid symbols) HIU during the first 60 min of the crystallization process at 35 °C. A 180 W power level was used in a continuous manner (a) and using pulses of different durations (5, 10, and 15 s; b, c, and d, respectively).

showed 2 orders of magnitude higher k values for the sonicated samples compared to the nonsonicated ones with very little change in n values (Table 1). These data show that sonication indeed increased the crystallization rate of palm oil. Figure 3a shows SFC values obtained when samples were sonicated at 110 W in a continuous manner. This sonication condition did not induce lipid crystallization as shown by the similar SFC obtained between tubes at 1−5 min and the control tube and the similar values of k (Table 1). However, when sonication was applied using 5, 10, and 15 s pulses, sonication seems to be somehow efficient at inducing crystallization (Figure 3b−d) and k values were 1 or 2 orders of magnitude higher in the sonicated samples compared to the nonsonicated ones. R^2 values obtained from the Avrami fitting for these samples ranged between 0.96 and 0.99. When samples were sonicated using 180 W of power in a continuous manner (Figure 4a), HIU delayed crystallization after 2 min of sonication (see data in Figure 4a, tube 2 to 5 min). This delay in crystallization was so significant that data obtained for tubes 2−5 did not converge to the Avrami equation. Similar to the data discussed in Figure 3, HIU was able to induce crystallization when applied at 180 W using 5, 10, and 15 s pulses (Figure 4b−d), but higher k values were consistently obtained only for samples sonicated using 5 s pulses (Table 1). Avrami R^2 values ranged from 0.93 and 0.99.

Data obtained from the Avrami analysis show some variation in n values between the sonicated and nonsonicated samples (Table 1). n reflects details regarding nucleation and crystal growth mechanisms. Many studies discussed the values of n for various types of nucleation and growth of crystals.[24,25] For example, an n value of 3 indicates plate-like growth from sporadic nuclei or spherulitic growth from instantaneous nuclei, whereas an n of 2 corresponds to needle-like growth from sporadic nuclei or plate-like growth from instantaneous nuclei. For the control samples, n values were close to 3, whereas after sonication, the n values decreased to close to 2. This suggests a change in the type of nucleation and growth of crystals after HIU was applied. As discussed by Meng et al., lower values of n and higher values of k are associated with an increased rate of crystallization and a more instantaneous nucleation process with a shorter induction time.[25] Table 1 also shows the SFC_∞ calculated using the Avrami fit with significantly ($P > 0.05$) higher SFC_∞ values obtained for the samples sonicated using 75 W of power.

It is very likely that the lower efficiency of HIU observed at higher power levels is due to temperature increases obtained during sonication. When samples were sonicated in a continuous manner, a linear temperature increase was observed as a function of time with values of 0.6491 °C/min (R^2 = 0.8879) for 75 W, 1.463 °C/min (R^2 = 0.9671) for 110 W, and 1.847 °C/min (R^2 = 0.9869) for 180 W. The total temperature increases after 5 min of sonication are 3.2, 7.3, and 9.2 °C for 75, 110, and 180 W, respectively. The above results indicate that even though higher power levels of ultrasound can generate more cavitation in the system and therefore more positive effects on crystallization as described in previous research,[19−21] they can also generate higher temperatures, which contrast the cavitation events by melting the crystals that are being formed. In this experimental setup, the thermal effect of higher power levels of HIU played an important role in delaying lipid crystallization (Figures 3a and 4a). In addition, greater temperature increases were obtained for the continuous application compared to the pulsed ones for samples sonicated at higher power levels (110 and 180 W). Temperature increases observed over the 5 min sonication using 110 W for 5, 10, and 15 s were 6.1, 4.9, and 6.2 °C, respectively, whereas temperature increases observed for the 180 W sonication condition were 5.8, 6.1, and 4.9 °C for the 5, 10, and 15 s pulses, respectively. The lower temperature increase for pulse irradiation types with higher power levels explains the induction in crystallization when pulse sonication was applied in Figures 3b−d and 4b−d. In summary, higher power levels of HIU generate more heat, and when the temperature is high enough, a delay in crystallization might occur. To overcome this

DOI: 10.1021/jf505041s
J. Agric. Food Chem. 2015, 63, 319−327

Table 1. Avrami Constant (k,[a] min^{-n}), Avrami Exponent (n[a]), and Equilibrium or Maximum SFC (SFC_∞,[a] %) Obtained from the Avrami Fitting for Samples Crystallized without and with Different Power Levels (75, 110, and 180 W) of Ultrasound

power	HIU	k_c	k_1	k_2	k_3	k_4	k_5
75 W	continuous	6.05×10^{-6}	2.3×10^{-4}	1.1×10^{-4}	1.6×10^{-4}	2.0×10^{-4}	1.8×10^{-4}
	5 s		5.8×10^{-4}	6.8×10^{-4}	4.8×10^{-4}	7.0×10^{-4}	6.0×10^{-4}
	10 s		7.4×10^{-5}	5.4×10^{-5}	2.6×10^{-4}	5.6×10^{-5}	5.0×10^{-5}
	15 s		1.3×10^{-3}	8.9×10^{-4}	2.0×10^{-4}	9.7×10^{-4}	8.7×10^{-4}
110 W	continuous		8.9×10^{-5}	6.2×10^{-5}	3.9×10^{-6}	1.6×10^{-6}	1.4×10^{-6}
	5 s		1.7×10^{-4}	6.4×10^{-4}	1.8×10^{-4}	1.9×10^{-4}	4.2×10^{-5}
	10 s		2.6×10^{-4}	4.8×10^{-4}	7.3×10^{-4}	1.9×10^{-4}	5.0×10^{-5}
	15 s		8.1×10^{-5}	1.5×10^{-4}	1.3×10^{-4}	5.8×10^{-5}	1.2×10^{-4}
180 W	continuous		4.4×10^{-5}				
	5 s		2.1×10^{-4}	1.5×10^{-4}	1.3×10^{-4}	7.3×10^{-5}	3.9×10^{-5}
	10 s		5.5×10^{-5}	5.0×10^{-5}	2.6×10^{-6}	1.4×10^{-6}	3.0×10^{-5}
	15 s		1.3×10^{-4}	3.4×10^{-6}	5.3×10^{-5}	1.6×10^{-6}	1.5×10^{-5}
power	HIU	n_c	n_1	n_2	n_3	n_4	n_5
75 W	continuous	3.14	2.53	2.84	2.75	2.66	2.65
	5 s		2.22	2.17	2.35	2.26	2.19
	10 s		2.80	2.93	2.58	2.95	3.04
	15 s		1.97	2.17	2.72	2.09	2.18
110 W	continuous		2.62	2.76	3.43	3.53	3.44
	5 s		2.49	2.19	2.75	2.61	3.25
	10 s		2.43	2.36	2.30	2.49	2.90
	15 s		2.67	2.66	2.77	2.95	2.73
180 W	continuous		2.65				
	5 s		2.71	2.61	2.59	2.79	3.02
	10 s		2.89	2.80	3.63	3.80	2.97
	15 s		2.61	3.81	2.86	3.77	3.16
power	HIU	$SFC_{\infty c}$	$SFC_{\infty 1}$	$SFC_{\infty 2}$	$SFC_{\infty 3}$	$SFC_{\infty 4}$	$SFC_{\infty 5}$
75 W	continuous	3.70	4.20[b]	4.33[b]	4.31[b]	4.26[b]	4.41[b]
	5 s		4.04	4.41[b]	4.12	4.25[b]	4.24[b]
	10 s		4.26[b]	4.35[b]	4.47[b]	4.35[b]	4.34[b]
	15 s		4.31[b]	4.41[b]	4.10	4.57[b]	4.41[b]
110 W	continuous		4.26[b]	4.22	3.95	3.99	3.59
	5 s		3.45	3.91	3.75	3.67	3.77
	10 s		4.35[b]	4.16	4.00	3.81	3.77
	15 s		4.12	4.06	4.23	3.99	3.99
180 W	continuous		4.34[b]				
	5 s		3.96	4.07	4.04	4.05	4.00
	10 s		4.00	3.97	3.90	3.75	3.72
	15 s		3.87	3.69	3.90	3.43	3.60

[a]Subscript "c" indicates the control sample, subscripts "1−5" indicate the samples collected at each minute during sonication. R^2 values for Avrami fitting were all above 0.96, except for the samples collected from 2 to 5 min under 180 W sonication in a continuous manner, where data did not fit the Avrami model, [b]SFC_∞ values are significantly different ($P < 0.05$) from the control sample.

disadvantage, pulse irradiation of sonication can be applied to induce crystallization by generating less heat. Temperature increases as a function of time can be found in Figure 1 of the Supporting Information.

Physical Properties of Sonicated Samples (75 W Continuous). Results described in the previous section demonstrate the sonication using 75 W is the most efficient at inducing crystallization and at generating more solids in the crystalline network formed. Becausee no differences were found in SFC values as a function of sonication mode (continuous vs pulse), the continuous mode was chosen to continue our experiments of physical characterization of the sonicated samples. The continuous condition was chosen over the pulse ones because it would be an easier method to implement in a processing plant. To perform the physical characterization, samples were collected at the exit of the flow cell as described before and mixed together as the "sample with HIU". A control sample was always taken before the sonication. Physical properties such as crystal microstructure, viscoelasticity, melting profile, and polymorphism were evaluated on these samples.

Microstructure of the Crystals. Figure 5 shows the microstructure of the palm oil samples crystallized in the flow

DOI: 10.1021/jf505041s
J. Agric. Food Chem. 2015, 63, 319−327

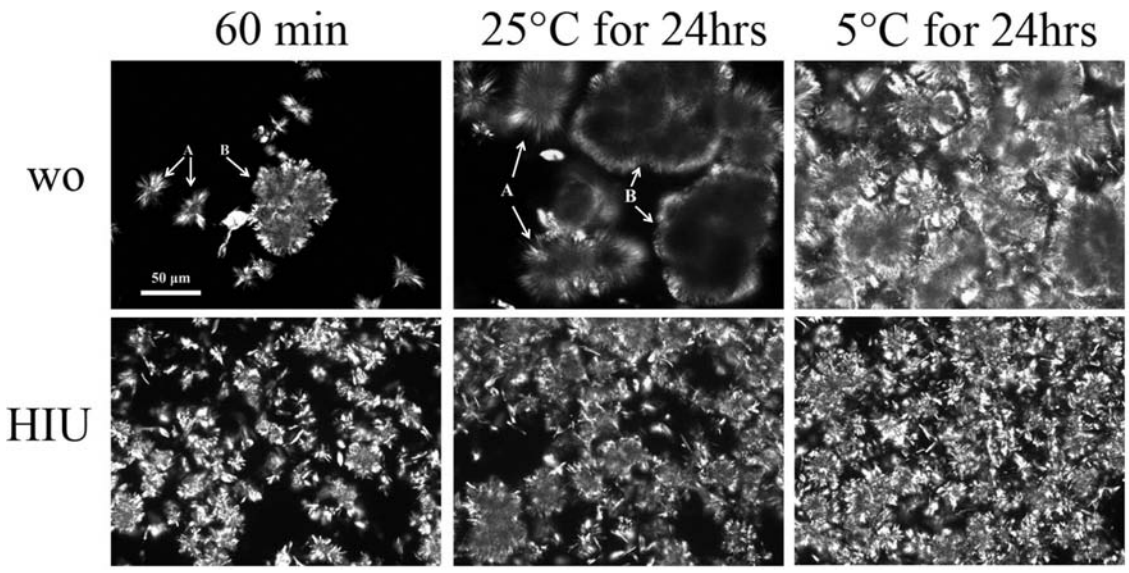

Figure 5. Microstructure of palm oil crystallized without and with HIU at 35 °C for 60 min and tempered at 25 °C for 24 h and at 5 °C for 24 h. In the pictures for samples without HIU for 60 min and at 25 °C for 24 h, two different morphologies are indicated (A and B).

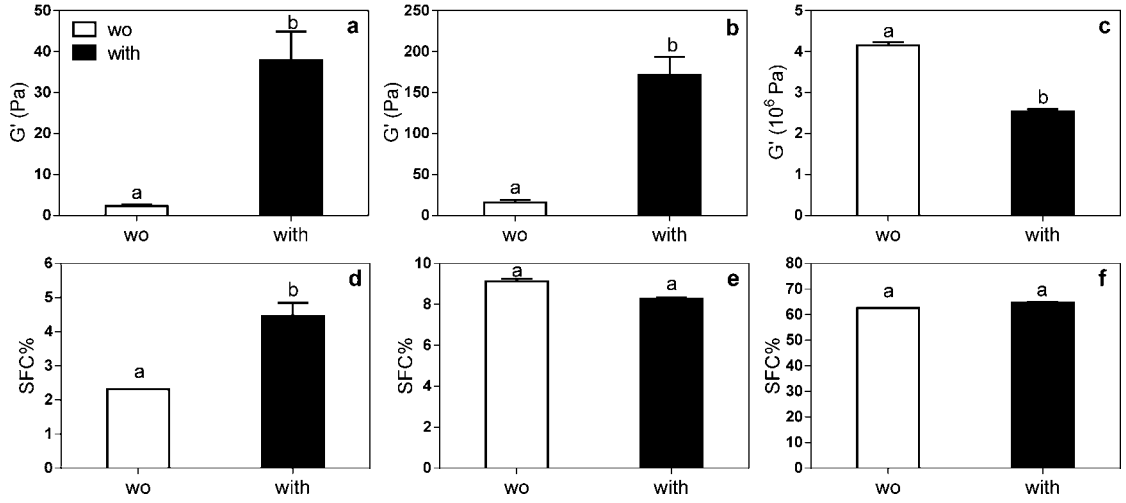

Figure 6. Storage modulus (G') and corresponding SFC values of palm oil crystallized without and with HIU at 35 °C for 60 min (a, d) and after tempering at 25 °C for 24 h (b, e) and 5 °C for 24 h (c, f).

cell with and without HIU using 75 W of power in a continuous manner. After crystallization had been induced in the flow cell, samples were kept at 35 °C in an incubator for 60 min to allow for complete crystallization and tempered for 24 h at 25 and 5 °C. PLM pictures shown in Figure 5 demonstrate that HIU significantly affects the formation of crystals in different sizes and shapes compared to the nonsonicated samples. Big round crystals (indicated with arrow B in the picture wo_60 min) were observed after 60 min at 35 °C in samples crystallized without HIU. A continuous growth of size for this big round crystal was observed after 24 h of tempering at 25 °C (approximately 80 μm in diameter). Arrow A in the picture shows an example of a crystal with a different morphology characterized by needle-like spherulites, which are usually associated with β' crystals.[26] Crystals continued to grow and formed an interconnected crystalline network of big spherulites after tempering at 5 °C for 24 h, which makes the identification of individual crystals or clusters very difficult. When HIU was applied to the samples, the amount of crystal clusters increased and the crystal aggregates generated a more uniform size distribution with smaller crystals, especially after 24 h of tempering. Similar results were found in the research on palm oil by Chen et al.,[21] who showed different crystal morphologies of palm oil crystallized with and without sonication. It is also interesting to observe that crystal size and morphology did not change substantially in the sonicated samples as a function of tempering. There might be several reasons that can cause this phenomenon: (a) the greater number of crystals generated after HIU application act as nuclei for the secondary crystallization to occur, and therefore the solid mass deposited over each crystal is lower compared to the nonsonicated samples were fewer crystals are present and therefore more solid mass is deposited in each crystal, resulting in crystal growth; (b) the solid/liquid ratio for sonicated samples is higher than that of nonsonicated samples, which means less liquid oil could be used to crystallize in sonicated samples during tempering; and (c) high pressures and high shear forces generated during sonication destroyed the regular shape of the crystal clusters and irregular or rough cluster shape might prevent the orderly arrangement of TAG molecules into the crystalline lattice.

DOI: 10.1021/jf505041s
J. Agric. Food Chem. 2015, 63, 319−327

Changes observed in crystal morphology as a consequence of sonication can be attributed to the formation of different molecular compounds or to the presence of different polymorphic forms. Therefore, XRD measurements were performed to evaluate the polymorphic forms generated during sonication and tempering.

Crystal Polymorphism. The polymorphism of crystals obtained after crystallization of the samples with and without HIU at 35 °C for 60 min was determined with X-ray. This measurement was also performed in the same samples tempered for 24 h at 25 and 5 °C. Signals at short spacings of 3.7, 3.8, 3.9, 4.45, and 4.6 Å were identified. All conditions tested showed a strong signal at 4.6 Å, indicating the presence of β crystals. No strong peaks were observed at 4.2 Å, indicating that β' crystals were not present in these samples[27−30] (X-ray diffractograms can be found in Figure 2 of the Supporting Information).

Viscoelastic Properties. Figure 6 shows the comparison of the storage modulus (G') and the corresponding SFC measurements between samples crystallized with and without HIU application. Samples were taken after 60 min of crystallization at 35 °C and after 24 h of tempering at 25 and 5 °C. As expected, sonicated samples crystallized for 60 min at 35 °C had significantly ($P < 0.05$) higher G' and SFC values than those of nonsonicated ones. After 24 h of tempering at 25 °C, G' values for both samples (sonicated and nonsonicated ones) increased as a result of ongoing crystallization during tempering (Figure 5) due to the exposure to a higher supercooling. Sonicated samples maintained a higher G' after tempering ($P < 0.05$), whereas SFC values showed no statistical difference ($P > 0.05$). Changes observed in G' and SFC values after tempering at 25 °C might be due to different phenomena: (a) increased interaction between crystal clusters in smaller crystals (Figure 5), leading to a higher G'; (b) SFC of the nonsonicated samples increased from 2.4 to 9.1% on average during tempering, whereas SFC of the sonicated samples increased only from 4.5 to 8.3%; this means that HIU induced the crystallization during the first 60 min and therefore there is not much left to crystallize during the tempering as the sample reached the thermodynamic equilibrium. When samples were tempered at 5 °C for 24 h, SFC values for both samples increased dramatically to the same level, and it is very interesting to observe that the G' values obtained for samples without HIU application are significantly higher than the ones obtained for the sonicated samples. The difference in crystal size and shape (Figure 5) and cluster interconnections might contribute to the different G' values observed after tempering at 5 °C for 24 h.

Melting Profile. The melting profiles of palm oil crystallized with and without HIU at 35 °C and stored at different tempering conditions (25 and 5 °C for 24 h) are shown in Figure 7. Only one melting peak was observed for both samples (with and without HIU) crystallized at 35 °C for 60 min (Figure 7a). Samples crystallized with HIU showed a sharper and deeper but narrower melting curve as compared to the nonsonicated sample. The peak temperature of the sample decreased from 48.4 ± 3.1 to 41.2 ± 0.1 °C when HIU was applied (Table 2). As expected, after tempering at 25 °C for 24 h (Figure 7b), two melting peaks were observed for both samples (with and without HIU). The melting peak observed at lower temperatures can be attributed to the secondary crystallization that occurred during tempering. Three peaks were observed for samples tempered at 5 °C for 24 h (Figure 7c), of which the two lower melting peaks can be attributed to the secondary crystallization that occurs during the tempering at 5 °C. Table 2 shows the melting parameters of palm oil crystallized with and without HIU application. Melting parameters reported for the tempered samples correspond to the highest melting peak because this peak represents the crystals formed during the sonication experiment. The peak temperature (T_p) for the nonsonicated samples crystallized for 60 min at 35 °C was significantly ($P < 0.05$) higher than the sonicated samples. The same results were maintained after tempering at 25 and 5 °C for 24 h. The reason for the shift to lower peak temperature after sonication might be due to the different crystal microstructure and to different particle size distribution of the crystals. Enthalpy (ΔH) values of samples crystallized with HIU and kept for 60 min at 35 °C were significantly ($P < 0.05$) higher than the ones obtained in the nonsonicated samples. After tempering at 25 and 5 °C, no difference was found for the enthalpy between HIU samples with and without HIU for the highest melting fraction. These results are in accordance with previously discussed data related to SFC values (Figure 6).

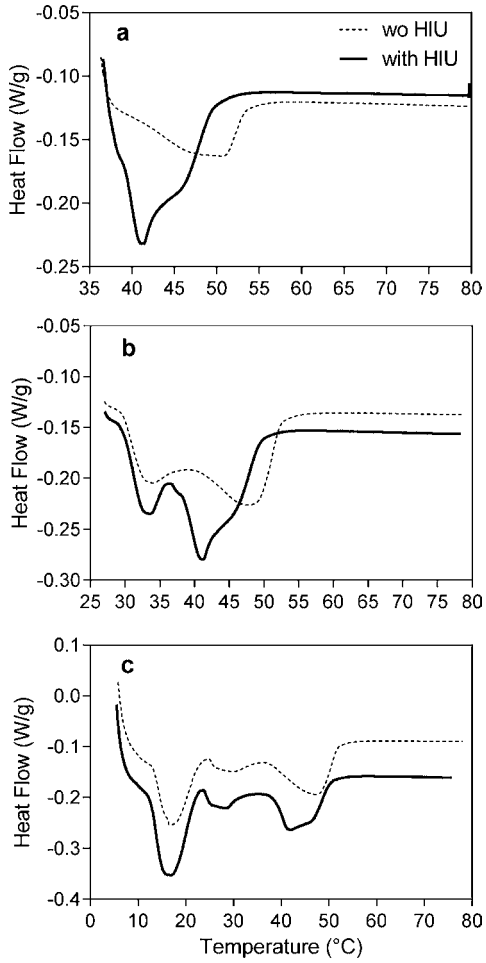

Figure 7. Melting profile of palm oil crystalline network obtained after crystallization without (dotted line) and with (solid line) HIU at 35 °C for 60 min (a) and after tempering at 25 °C (b) and 5 °C (c) for 24 h.

Figure 8 shows the melting profile of the crystalline networks generated in this study. The melting profile is reported as the amount of solids remaining at a specific temperature (% solid) as the sample is being heated in the DSC. Only the highest

DOI: 10.1021/jf505041s
J. Agric. Food Chem. 2015, 63, 319−327

Table 2. Melting Parameters of Palm Oil Crystallized with and without Sonication[a]

	60 min		25 °C, 24 h		5 °C, 24 h	
melting parameter	without HIU	with HIU	without HIU	with HIU	without HIU	with HIU
T_{on} (°C)	N/A	N/A	39.4 ± 0.9A	38.3 ± 0.5A	39.0 ± 1.6A	38.4 ± 0.0A
T_p (°C)	48.4 ± 3.1A	41.2 ± 0.1B	47.6 ± 1.5A	41.4 ± 0.1B	48.5 ± 1.1A	42.5 ± 0.3B
ΔH (J/g)	4.8 ± 0.4A	11.1 ± 0.6B	5.8 ± 0.3AC	6.8 ± 0.9AC	7.2 ± 1.9AC	9.4 ± 1.1BC

[a]The data were collected at 60 min and after tempering for 24 h at 25 and 5 °C. Data reported are mean values and standard deviations of two independent runs. The same upper case letters in a row indicate that values are not significantly different (α = 0.05). N/A indicates that the value could not be calculated because it fell outside the temperature range of the DSC run.

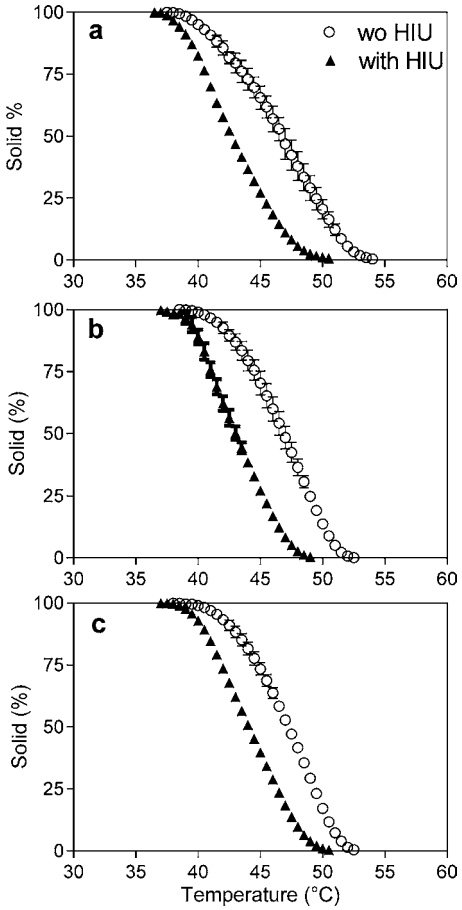

Figure 8. Melting profile of palm oil samples expressed as the percentage of solids remaining at a specific temperature during DSC melting. Melting profiles of sonicated and nonsonicated samples are indicated with solid and open symbols, respectively. Samples were crystallized at (a) 35 °C for 60 min and tempered at (b) 25 °C for 24 h and (c) 5 °C for 24 h.

melting fractionation was studied. Palm oil crystallized with HIU showed a lower percentage of solid at any given temperature when crystallized at 35 °C. The same results were maintained after tempering at 25 and 5 °C. The sonicated sample showed a steeper and sharper melting profile, which can be explained by the smaller size of crystals generated by HIU and as a consequence of a faster melting rate. Similar results were reported by Suzuki et al.[18] and Ye et al.[19] in other lipid systems such as anhydrous milk fat and interesterified soybean oil.

This study showed that HIU can be used in a continuous system to promote the crystallization of palm oil and to change its functional properties. Results obtained in this study provide scientific support to implement HIU as an additional processing tool in the edible oil industry. The importance of optimizing the sonication conditions is highlighted in this research noting that the amount of heat generated during sonication can contrast the effect of cavitation. Future work in this area to support the hypothesis that HIU can be used as an additional processing tool to modify the functional properties of edible lipids in industrial settings could include changing the flow rate of the pumped oil and the crystallization temperature in the system. The goal of implementing this additional tool in the edible oil industry is not only to change the physical properties of the lipid but also to induce lipid crystallization, reduce processing times, and ultimately reducing processing costs.

■ ASSOCIATED CONTENT

Supporting Information

Figures 1 and 2. This material is available free of charge via the Internet at http://pubs.acs.org.

■ AUTHOR INFORMATION

Corresponding Author

*(S.M.) E-mail: silvana.martini@usu.edu. Phone: (435) 797-8136. Fax: (435) 797-2179.

Funding

We thank the Utah Agricultural Experiment Station (UAES) (UTAO 1171 NC 1023) for funding support. This paper was approved by the UAES as Paper 8745.

Notes

The authors declare no competing financial interest.

■ ABBREVIATIONS USED

HIU, high-intensity ultrasound; AOCS, American Oil Chemists' Society; ADM, Archer Daniels Midland; NMR, nuclear magnetic resonance; SFC, solid fat content; PLM, polarized light microscopy; XRD, X-ray diffraction; DSC, differential scanning calorimetry; T_c, crystallization temperature; T_{on}, onset temperature; T_p, peak temperature; ΔH, enthalpy variation; G', storage modulus; ANOVA, analysis of variance; n, Avrami exponent; k, Avrami constant; SFC_∞, equilibrium solid fat content; TAG, triacylglycerol

■ REFERENCES

(1) Rastogui, N. K. Opportunity and challenges in application of ultrasound in food processing. *CRC Crit. Rev. Food Sci.* **2011**, *51*, 705–772.

(2) Soria, A. C.; Villamiel, M. Effect of ultrasound on the technological properties and bioactivity of food: a review. *Trends Food Sci. Technol.* **2010**, *21*, 323–331.

(3) Mason, T. J. Sonochemistry: current uses and future prospects in the chemical and processing industries. *Philos. Trans. R. Soc. London, A* **1999**, *357*, 355–369.

DOI: 10.1021/jf505041s
J. Agric. Food Chem. 2015, 63, 319–327

(4) Suslick, K. S.; Mdleleni, M. M.; Ries, J. T. Chemistry induced by hydrodynamic cavitation. *J. Am. Chem. Soc.* **1997**, *119*, 9303−9304.
(5) de Castro, M. D. L.; Priego-Capote, F. Ultrasound-assisted crystallization (sonocrystallization). *Ultrason. Sonochem.* **2007**, *14*, 717−724.
(6) Li, H.; Li, H. R.; Guo, Z. C.; Liu, Y. The application of power ultrasound to reaction crystallization. *Ultrason. Sonochem.* **2006**, *13*, 359−363.
(7) Kresic, G.; Lelas, V.; Jambrak, A. R.; Herceg, Z.; Brncic, S. R. Influence of novel food processing technologies on the rheological and thermophysical properties of whey proteins. *J. Food Eng.* **2008**, *87*, 64−73.
(8) Martini, S.; Potter, R.; Walsh, M. K. Optimizing the use of power ultrasound to decrease turbidity in whey protein suspensions. *Food Res. Int.* **2010**, *43*, 2444−2451.
(9) Villamiel, M.; de Jong, P. Influence of high-intensity ultrasound and heat treatment in continuous flow on fat, proteins, and native enzymes of milk. *J. Agric. Food Chem.* **2000**, *48*, 472−478.
(10) Martini, S. Chapter 2: An overview of ultrasound. In *Sonocrystallization of Fats*; SpringerBriefs in Food, Health, and Nutrition: Berlin, Germany, 2013; p 12.
(11) Chow, R.; Blindt, R.; Chivers, R.; Povey, M. The sonocrystallisation of ice in sucrose solutions: primary and secondary nucleation. *Ultrasonics* **2003**, *41*, 595−604.
(12) Chow, R.; Blindt, R.; Chivers, R.; Povey, M. A study on the primary and secondary nucleation of ice by power ultrasound. *Ultrasonics* **2005**, *43*, 227−230.
(13) Patel, S. R.; Murthy, Z. V. P. Ultrasound assisted crystallization for the recovery of lactose in an anti-solvent acetone. *Cryst. Res. Technol.* **2009**, *44*, 889−896.
(14) Patrick, M.; Blindt, R.; Janssen, J. The effect of ultrasonic intensity on the crystal structure of palm oil. *Ultrason. Sonochem.* **2004**, *11*, 251−255.
(15) Higaki, K.; Ueno, S.; Koyano, T.; Sato, K. Effects of ultrasonic irradiation on crystallization behavior of tripalmitoylglycerol and cocoa butter. *J. Am. Oil Chem. Soc.* **2001**, *78*, 513−518.
(16) Ueno, S.; Ristic, R. I.; Higaki, K.; Sato, K. In situ studies of ultrasound-stimulated fat crystallization using synchrotron radiation. *J. Phys. Chem. B* **2003**, *107*, 4927−4935.
(17) Martini, S.; Suzuki, A. H.; Hartel, R. W. Effect of high intensity ultrasound on crystallization behavior of anhydrous milk fat. *J. Am. Oil Chem. Soc.* **2008**, *85*, 621−628.
(18) Suzuki, A. H.; Lee, J.; Padilla, S. G.; Martini, S. Altering functional properties of fats using power ultrasound. *J. Food Sci.* **2010**, *75*, E208−E214.
(19) Ye, Y. B.; Wagh, A.; Martini, S. Using high intensity ultrasound as a tool to change the functional properties of interesterified soybean oil. *J. Agric. Food Chem.* **2011**, *59*, 10712−10722.
(20) Ye, Y.; Tan, C. Y.; Kim, D. A.; Martini, S. Application of high intensity ultrasound to a zero-trans shortening during temperature cycling at different cooling rates. *J. Am. Oil Chem. Soc.* **2014**, *91*, 1155−1169.
(21) Chen, F. F.; Zhang, H.; Sun, X. Y.; Wang, X. G.; Xu, X. B. Effects of ultrasonic parameters on the crystallization behavior of palm oil. *J. Am. Oil Chem. Soc.* **2013**, *90*, 941−949.
(22) Marangoni, A. G. On the use and misuse of the Avrami equation in characterization of the kinetics of fat crystallization. *J. Am. Oil Chem. Soc.* **1998**, *75*, 1465−1467.
(23) Wright, A. J.; Hartel, R. W.; Narine, S. S.; Marangoni, A. G. The effect of minor components on milk fat crystallization. *J. Am. Oil Chem. Soc.* **2000**, *77*, 463−475.
(24) Cheong, L. Z.; Zhang, H.; Xu, Y.; Xu, X. B. Physical characterization of lard partial acylglycerols and their effects on melting and crystallization properties of blends with rapeseed oil. *J. Agric. Food Chem.* **2009**, *57*, 5020−5027.
(25) Meng, Z.; Liu, Y. F.; Jin, Q. Z.; Huang, J. H.; Song, Z. H.; Wang, F. Y.; Wang, X. G. Comparative analysis of lipid composition and thermal, polymorphic, and crystallization behaviors of granular crystals formed in beef tallow and palm oil. *J. Agric. Food Chem.* **2011**, *59*, 1432−1441.
(26) Martini, S.; Herrera, M. L.; Hartel, R. W. Effect of cooling rate on crystallization behavior of milk fat fraction/sunflower oil blends. *J. Am. Oil Chem. Soc.* **2002**, *79*, 1055−1062.
(27) Ishikawa, H.; Shiota, M.; Murakami, M.; Nakajima, I. Polymorphic behavior of palm oil and modified palm oils. *Food Sci. Technol. Int. Tokyo* **1997**, *3*, 77−81.
(28) Sato, K.; Arishima, T.; Wang, Z. H.; Ojima, K.; Sagi, N.; Mori, H. Polymorphism of POP and SOS. I. Occurrence and polymorphic transformation. *J. Am. Oil Chem. Soc.* **1989**, *66*, 664−674.
(29) Bayes-Garcia, L.; Calvet, T.; Cuevas-Diarte, M. A.; Ueno, S.; Sato, K. In situ observation of transformation pathways of polymorphic forms of 1,3-dipalmitoyl-2-oleoyl glycerol (POP) examined with synchrotron radiation X-ray diffraction and DSC. *CrystEngComm* **2013**, *15*, 302−314.
(30) Zhang, X.; Li, L.; Xie, H.; Liang, Z.; Su, J.; Liu, G.; Li, B. Effect of temperature on the crystalline form and fat crystal network of two model palm oil-based shortenings during storage. *Food Bioprocess. Technol.* **2014**, *7*, 887−900.

DOI: 10.1021/jf505041s
J. Agric. Food Chem. 2015, 63, 319−327

JOURNAL OF AGRICULTURAL AND FOOD CHEMISTRY

Article

pubs.acs.org/JAFC

De Novo Synthesis of Amino Acids during the Maillard Reaction: qTOF/ESI Mass Spectrometric Evidence for the Mechanism of Akabori Transformation

Ossanna Nashalian and Varoujan A. Yaylayan*

Department of Food Science and Agricultural Chemistry, McGill University, 21,111 Lakeshore, Ste. Anne de Bellevue, Quebec, Canada H9X 3V9

ABSTRACT: The transformation of α-amino acids into their hydroxymethyl derivatives during the Maillard reaction is an intriguing possibility for catalysis by metal salts in the presence of Strecker aldehydes; the process is commonly known as the Akabori reaction. The mechanism of this reaction was studied in the presence of glucose, using glycine copper complex and paraformaldehyde as Akabori model system in aqueous mixtures heated at 110 °C for 2 h and subsequently analyzed by qTOF/ESI/MS. Isotope-labeling studies of the various products identified have provided for the first time mass spectrometric evidence for the detailed mechanism of Akabori transformation, particularly the formation of Schiff base adducts prior to the final conversion into serine and hydroxymethyl-serine. Furthermore, the results have indicated that sugars do not interfere with such transformations and, on the contrary, the presence of glycine−copper complexes in the Maillard model systems can enhance the production of Maillard reaction intermediates.

KEYWORDS: *mechanism of Akabori reaction, glycine−copper complexes, Maillard reaction, serine, hydroxymethyl-serine*

INTRODUCTION

Contrary to the reaction of α-amino groups of amino acids with carbonyl moieties, which has been studied for over a century, the interaction of α-carbons of α-amino acids with aldehydes such as Strecker aldehyde has not been examined in detail in the context of the Maillard reaction. Akabori et al. first reported the chemical synthesis of serine or threonine from glycine in the presence of two common Strecker aldehydes, formaldehyde and acetaldehyde.[1] This transformation of one amino acid into another was catalyzed by metal salts such as copper and iron and is commonly referred to as the Akabori reaction.[2] The generality of this reaction was later extended to different amino acids (serine, glycine, and alanine) and different metal complexes (Ni, Co, and Cu) and using various aldehydes (acetaldehyde, formaldehyde, pyruvic acid, and benzaldehyde).[3,4] The transformation of the α-amino acids into their corresponding β-hydroxy amino acids required relatively mild conditions; heating at 100 °C for 1 h in water generated both serine and threonine with average yields of 30%[1] and 32−80%,[3−5] respectively. The initial mechanism proposed by Akabori et al.[1] attributed the activation of the α-carbon to the formation of the amino acid metal complexes. William and Busch[6] demonstrated through NMR studies the enhanced acidity and lability of α-methylene hydrogens in such complexes due to the electron-withdrawing action of the metal ions. Under alkaline conditions, the formed carbanion would serve as a nucleophile that can condense with a carbonyl moiety such as formaldehyde or acetaldehyde.[1,4] However, it was later proposed that the amino acid metal complexes first undergo Schiff base formation with the aldehyde followed by the subsequent activation of the α-carbon to generate carbanion.[3,7] The formation of the Schiff base adducts was assumed to enhance even more the acidity of the α-carbon, allowing the reaction to proceed at milder pH conditions and with higher yields.[3] The formation of Schiff base intermediates was further confirmed in polarimetric studies involving serine−copper complexes and formaldehyde[8] and glycine−copper complex and acetaldehyde through observation of their subsequent intramolecular cyclization products initiated by the newly formed serine hydroxyl groups to generate 1,3-oxazolidine moieties as reported by the two research groups of Aune et al.[9] and Teo and O'Connor.[8]

Although the Akabori reaction was initially intended for chemical synthesis to generate β-hydroxy amino acids, the conditions needed for its formation are readily available in food. Many foods are heated under conditions similar to those of the Akabori reaction, and the needed precursors the amino acids, Strecker aldehydes, and metals are either present or generated during processing. In fact, a variant of this reaction has been observed under pyrolytic conditions,[10] where the α-carbons of amino acids were activated toward nucleophilic addition with aldehydes. However, such activation was initiated through decarboxylation (Figure 1, pathway A) rather than through metal catalysis as in the case of the Akabori reaction, and consequently the resulting adduct after deamination step constituted a chain elongation process of the aldehyde rather than the formation of a new amino acid as in the case of Akabori reaction (Figure 1, pathway B). If Akabori transformation can be demonstrated to be a feasible pathway in the Maillard reaction, it can generate hitherto unknown amino acid structures or enhance the concentration of serine and threonine levels that are known to generate sugar-like reactive intermediates upon thermal degradation.[11] Considering the fact that the occurrence of this reaction could influence the aroma profile and may even generate potentially unknown amino acid structures, we have studied its

Received: October 28, 2014
Revised: December 12, 2014
Accepted: December 16, 2014
Published: December 16, 2014

ACS Publications © 2014 American Chemical Society

DOI: 10.1021/jf5051975
J. Agric. Food Chem. 2015, 63, 328−334

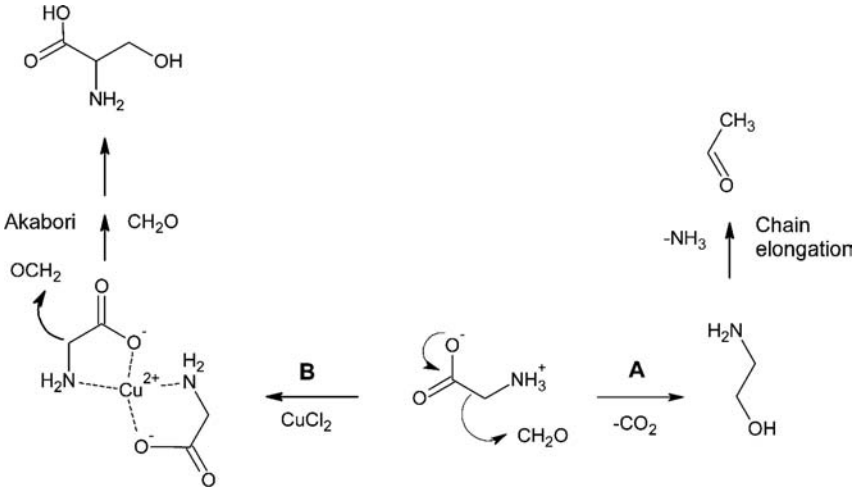

Figure 1. Activation of the α-carbon of glycine as nucleophile (A) through thermal decarboxylation with subsequent chain elongation of formaldehyde and (B) through metal complex formation (Akabori reaction) in the presence of formaldehyde (see Figure 2 for details).

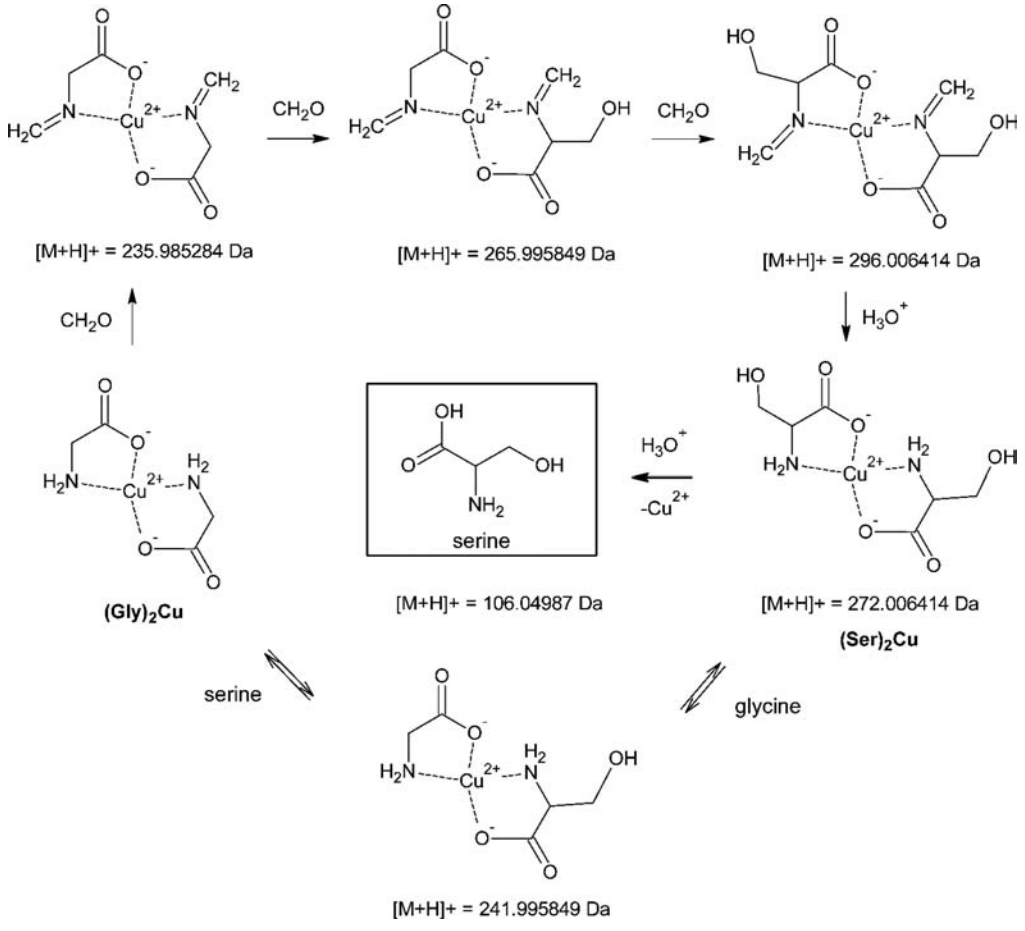

Figure 2. Mechanism of the Akabori reaction in the presence of formaldehyde and generation of serine. $[M + 1]^+$ values represent theoretical masses (corresponding observed masses are shown in Table 2).

role in Maillard model systems using glucose, glycine, and paraformaldehyde aqueous mixtures heated at 110 °C for 2 h and subsequently analyzed by qTOF/ESI/MS.

MATERIALS AND METHODS

Materials and Reagents. L-Glycine (98%), L-alanine (99%), L-serine (99%), D-glucose, paraformaldehyde, potassium hydroxide (KOH), and copper(II) chloride ($CuCl_2$) (99.9%) were purchased from Sigma-Aldrich Chemical Co. (Oakville, ON, Canada). [^{13}C-1,^{13}C-2,^{15}N]glycine (98%) and [U_6-^{13}C]glucose (99%) were purchased from Cambridge Isotope Laboratories (Andover, MA, USA). LC-MS grade water and methanol (OmniSolv, >99%) were obtained from VWR International (Mississauga, ON, Canada).

Synthesis of Amino Acid–Metal Complexes. $(Ala)_2Cu$, $(Gly)_2Cu$, and $(Ser)_2Cu$ complexes were prepared by dissolving alanine (0.89 g), glycine (0.75 g), and serine (1.05 g) in methanol (10 mL) in the presence of KOH (0.05 g) followed by the addition of 0.5 mol of

DOI: 10.1021/jf5051975
J. Agric. Food Chem. 2015, 63, 328−334

$CuCl_2$. The dark blue precipitates were washed with methanol, filtered, and dried. The amino acid adducts were confirmed by obtaining their elemental composition from their accurate masses determined by qTOF/ESI/MS analysis (alanine−copper complex at m/z 261.9985 $[M + Na]^+$ (calculated for $C_6H_{12}CuN_2NaO_4$ with an error of −1.4 ppm, glycine−copper complex at m/z 233.9665 $[M + Na]^+$ (calculated for $C_4H_8CuN_2NaO_4$ with an error of 5.4 ppm), and serine−copper complex at m/z 272.0059 $[M + H]^+$ (calculated for $C_6H_{13}CuN_2O_6$ with an error of 3.9 ppm). Isotope-labeled precursors were prepared similarly.

Sample Preparation. Model systems (6.0 mg) consisting of amino acid metal complexes were mixed with glucose (equimolar amounts) and excess paraformaldehyde (20 mg), dissolved in water (2 mL), and heated on a sand bath in an open vial (5 mL capacity) at 110 °C for 2 h until dry. Controls such as serine and $(Ser)_2Cu$ were also similarly heated and analyzed generating ions at m/z 106.0492 and 272.0059, respectively. To generate some of the observed intermediates, mixtures comprising $(Ser)_2Cu$/glycine and $(Gly)_2Cu$/excess serine were similarly heated and analyzed, generating the ions at m/z 241.9956 and 272.0045, respectively (see Figure 2). In addition, $(Ser)_2Cu$ was heated in the presence of excess paraformaldehyde and analyzed as control (see Table 1). Selected dry residues were then analyzed for their volatile components using pyrolysis gas chromatography−mass spectrometry (Py-GC/MS), and for their nonvolatile components using electrospray ionization mass spectrometry (qTOF/ESI/MS). All samples were analyzed in duplicates.

Table 1. Composition of the Model Systems

control model system[a]	model system[a]
paraformaldehyde/$CuCl_2$	$(Gly)_2Cu$/paraformaldehyde
glycine/paraformaldehyde	(^{13}C-1 Gly)$_2$Cu/paraformaldehyde
$(Gly)_2Cu$*	(^{13}C-2 Gly)$_2$Cu/paraformaldehyde
$(Gly)_2Cu$/serine*	(^{15}N Gly)$_2$Cu/paraformaldehyde
glycine/serine*	$(Gly)_2Cu$/glucose−paraformaldehyde
glycine/serine/ paraformaldehyde	$(Gly)_2Cu/U_6$-^{13}C glucose− paraformaldehyde
glycine	$(Ala)_2Cu$/paraformaldehyde
serine	$(Ser)_2Cu$
	$(Ser)_2Cu$/glycine

[a]Heated (110 °C for 2 h in water) and dried model systems were first analyzed by qTOF/ESI/MS for nonvolatiles, and some model systems (indicated by asterix) were also thermally desorbed by Py-GC/MS for volatile analysis.

Quadrupole Time of Flight/Electrospray Ionization/Mass Spectrometric (qTOF/ESI/MS) Analysis. The dry reaction residues or synthetic samples were dissolved in water to a concentration of 1 mL/mg. The sample was then diluted 10-fold in 10% methanol prior to analysis by qTOF/ESI/MS. The qTOF/ESI/MS system was composed of a Bruker Maxis Impact quadrupole time-of-flight mass spectrometer (Bruker Daltonics, Bremen, Germany) operated in positive ion mode. Samples (1 μL) were injected directly into the LC-MS. Instrument calibration was done using sodium formate clusters. The electrospray interface settings were the following: nebulizer pressure, 1.0 bar; drying gas, 8 L/min, 200 °C; capillary voltage, 4500 V. Scan range was from m/z 100 to 1000. The data were analyzed using Bruker Compass Data Analysis software version 4.1. Tandem mass spectrometry (MS/MS) was carried out in MRM mode using 20.0 eV collision energy for the ion at m/z 272.

Thermal Desorption by Pyrolysis Gas Chromatography−Mass Spectrometry (Py-GC-MS). A Varian CP-3800 gas chromatograph coupled to a Saturn 2000 ion trap detector interfaced to a CDS Pyroprobe 2000 unit through a valved interface (CDS 1500) was used for the desorption of the volatiles from the dried residues. The residues from selected dry and heated model systems shown in Table 1 were weighed (0.5 mg) into quartz tubes (0.3 mm thickness), plugged at both ends with glass wool (Supelco, Bellefonte, PA, USA) inserted inside a coil probe and pyrolyzed at 250 °C for 20 s under a helium atmosphere (Table 1).The separation was performed using a fused silica DB-5MS column (50 m length × 0.2 mm i.d. × 33 μm film thickness). The GC method used for the analysis of the volatiles was as follows: GC column flow rate was regulated by an electronic flow controller (EFC) and set at a pressure pulse of 55 psi for first 3 min and then decreased to 32 psi at the rate of 300 psi/min and finally increased to 70 psi at a rate of 1.23 psi/min for the rest of the run. The GC oven temperature was set at −5 °C for the first 5 min using CO_2 as the cryogenic cooling source and then increased to 50 °C at a rate of 50 °C/min. Then, the oven temperature was again increased to 270 °C at a rate of 8 °C/min and kept at 270 °C for 5 min. The samples were detected by using an ion trap mass spectrometer. The MS transfer line temperature was set at 250 °C, manifold temperature was set at 50 °C, and ion trap temperature was set at 175 °C. The ionization voltage of 70 eV was used, and EMV was set at 1600 V. The generated data were analyzed using the AMDIS_32 version 2.69 computer software, and peak identification was done using the NIST version 2.0 mass spectral research program.

Structural Identification. Evidence for the proposed structures of nonvolatile reaction intermediates were provided through qTOF/ESI MS analysis of their elemental composition and isotope-labeling studies or by the use of synthetic intermediates or standards. Furthermore, the incorporation of copper in the identified complexes was confirmed by the isotopic signature of copper through detection of M + 2 peaks at 30% relative intensity. Volatile reaction products were identified by comparison of their retention times and mass spectra with commercial or in situ generated standards in addition to NIST library matches and stable isotope labeling data.

RESULTS AND DISCUSSION

Amino acids are one of the primary reactants required for the Maillard reaction. The type and distribution of various amino acids contribute significantly to the nutritive value and aroma profile of foods.[12,13] Although free amino acids are usually formed in processed food through hydrolysis of proteins, the notion that some amino acids may be also generated de novo during processing from already existing precursors has not been explored in the context of the Maillard reaction. The chemical transformation known as the Akabori reaction provides this opportunity because it requires precursors that are generally found in food and reaction parameters encountered under food-processing conditions. As detailed above, the Akabori reaction transforms existing amino acids into their β-hydroxyl counterparts (Figure 1, pathway B), of which only two amino acids, serine and threonine, are naturally found in food proteins. The Akabori modification of amino acids has not been explored within the context of the Maillard reaction or in the presence of

Table 2. Elemental Composition[a] of the Common Products Generated in $(Gly)_2Cu$/Paraformaldehyde Model System without[b] and with[c] Glucose and Shown in Figures 2 and 3

$[M + H]^+$ (m/z)	elemental composition	error (ppm)
106.0500	$C_3H_8NO_3$	3.9
136.0603	$C_4H_{10}NO_4$	5.0
235.9840/237.9830[b]	$C_6H_9CuN_2O_4$	7.8
241.9943/243.9924[b]	$C_5H_{11}CuN_2O_5$	8.7
265.9949/267.9934[b]	$C_7H_{11}CuN_2O_5$	5.6
272.0044/274.0033	$C_6H_{13}CuN_2O_6$	9.4
296.0054/298.0050[b]	$C_8H_{13}CuN_2O_6$	5.3
238.0930[c]	$C_8H_{16}NO_7$	1.3
325.1369[c]	$C_{11}H_{21}N_2O_9$	37.0
342.1407[c]	$C_{12}H_{24}NO_{10}$	1.9

[a]The two masses shown represent copper isotopes $^{63}Cu/^{65}Cu$. [b]Ions observed only in $(Gly)_2Cu$/paraformaldehyde model system. [c]Ions observed only in $(Gly)_2Cu$/paraformaldehyde/glucose model system.

DOI: 10.1021/jf5051975
J. Agric. Food Chem. 2015, 63, 328−334

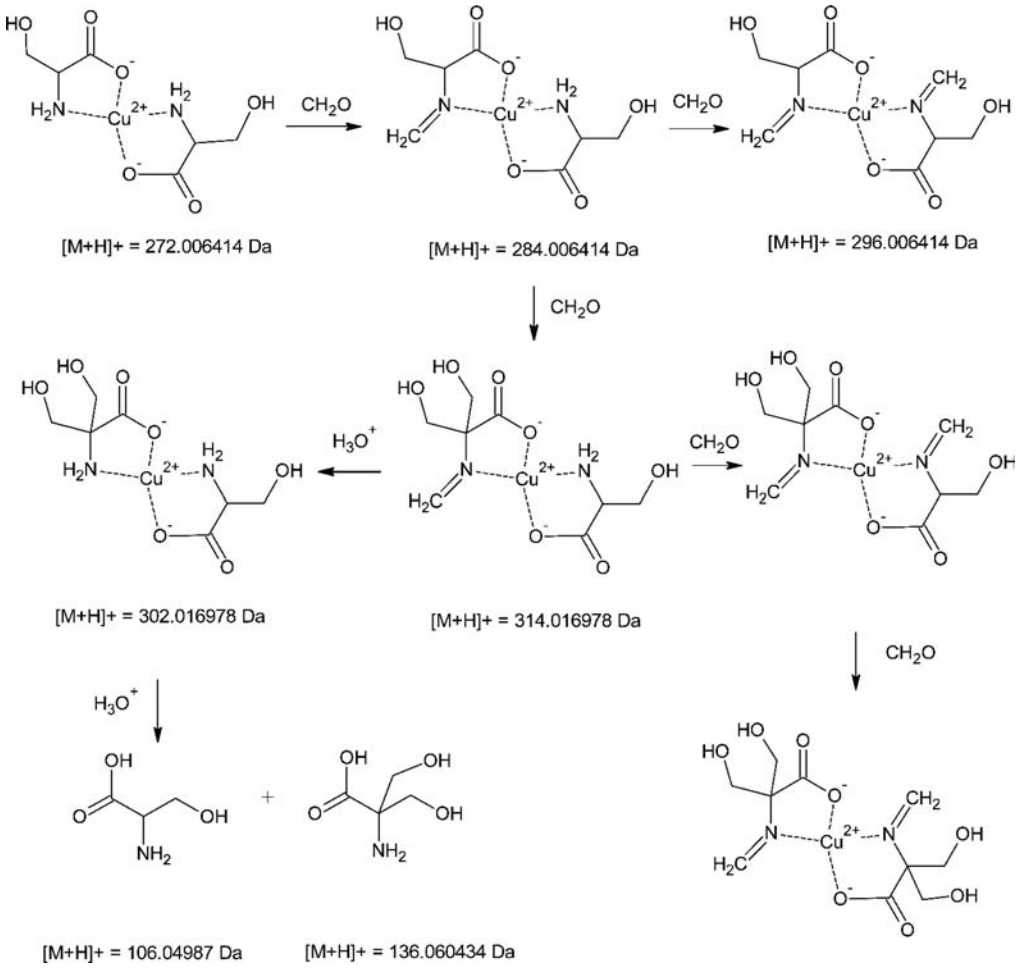

Figure 3. Intermediates identified in the reaction model of $(Ser)_2Cu/CH_2O$ heated in water at 110 °C for 2 h. $[M + 1]^+$ values represent theoretical masses (corresponding observed masses are shown in Table 3).

Table 3. Elemental Composition of Copper-Containing Intermediates in $(Ser)_2Cu$/Paraformaldehyde Model System Shown in Figure 3

$[M + H]^{+a}$ (m/z)	elemental composition	error (ppm)
296.0038/298.0048	$C_8H_{13}CuN_2O_6$	10.7
272.0056/274.0088	$C_6H_{13}CuN_2O_6$	5.0
284.0056/286.0035	$C_7H_{13}CuN_2O_6$	4.8
296.0038/298.0048	$C_8H_{13}CuN_2O_6$	10.7
314.0157/316.0144	$C_8H_{15}CuN_2O_7$	5.8
326.0153/328.0149	$C_9H_{15}CuN_2O_7$	6.8
356.0273/358.0323	$C_{10}H_{17}CuN_2O_8$	2.2
136.0607	$C_4H_{10}NO_4$	2.1
106.0500	$C_3H_8NO_3$	3.9

[a]The two masses shown represent copper isotopes $^{63}Cu/^{65}Cu$.

Table 4. Incorporation of Labeled Glycine Atoms into the Products of Heated $(Gly)_2Cu/CH_2O$ Model System (See Figure 2)

$[M + H]^+$ (m/z)	elemental composition	label incorporation from glycine[a]
106.0500	$C_3H_8NO_3$	1x C-1, 1x C-2, 1x N-15
136.0603	$C_4H_{10}NO_4$	1x C-1, 1x C-2, 1x N-15
235.9840	$C_6H_9CuN_2O_4$	2x C-1*, 2x C-2, 2x N-15
241.9943	$C_5H_{11}CuN_2O_5$	2x C-1, 2x C-2, 2x N-15
265.9949	$C_7H_{11}CuN_2O_5$	2x C-1, 2x C-2*, 2x N-15
272.0044	$C_6H_{13}CuN_2O_6$	2x C-1, 2x C-2, 2x N-15
296.0054	$C_8H_{13}CuN_2O_6$	2x C-1, 2x C-2, 2x N-15*

[a]The calculated error (in ppm) in all of the reported ions ranged between 0.23 and 15.5 ppm except ions indicated by asterisks, for which the error ranged between 17.3 and 28 ppm.

reducing sugars. Detailed understanding of the role of Akabori transformation within the Maillard reaction system can reveal not only the possible formation of new amino acid structures but also its possible influence on the mechanism and the general outcome of the Maillard reaction itself. Isotope-labeling studies were performed to confirm the formation of serine, the Akabori amino acid in heated (110 °C) aqueous model systems of glucose, glycine–copper complex [$(Gly)_2Cu$], and formaldehyde, and to investigate the role of glycine copper complex in modifying the Maillard reaction profile.

The various model systems listed in Table 1 were heated at 110 °C for 2 h, and the resulting dry residues were analyzed by qTOF/ESI/MS for nonvolatiles, and selected model systems were also analyzed by Py-GC/MS to thermally desorb and characterize the volatile reaction products already formed under aqueous heating conditions. Heating $(Gly)_2Cu$ alone mainly causes oxidative decarboxylation of glycine and formation of its corresponding Strecker aldehyde;[14,15] however, when heated in the presence of excess formaldehyde with or without glucose, the reaction mixtures generated many products and intermediates that supported the proposed formation of serine, the Akabori

DOI: 10.1021/jf5051975
J. Agric. Food Chem. 2015, 63, 328–334

Table 5. Comparison of Elemental Composition[a] and Accurate Masses of Product Ions at *m/z* 272.0059 [Generated from Synthetic $(Ser)_2Cu$] and That of the Ion at *m/z* 272.0044 Generated in the $(Gly)_2Cu/CH_2O$ Reaction Mixture

product ion of *m/z* 272.0059 $[M + H]^+$	product ion of *m/z* 272.0044 $[M + H]^+$
241.9947 ($C_5H_{11}CuN_2O_5$)	241.9956 ($C_5H_{11}CuN_2O_5$)
210.0053 ($C_5H_{11}CuN_2O_3$)	210.0061 ($C_5H_{11}CuN_2O_3$)
185.9814 ($C_3H_9CuNO_4$)	185.9826 ($C_3H_9CuNO_4$)
123.9809 (C_2H_7CuNO)	123.9843 (C_2H_7CuNO)
106.0530 ($C_3H_8NO_3$)	106.0532 ($C_3H_8NO_3$)

[a]The calculated error (in ppm) in all of the reported ions ranged between 3 and 26 ppm.

amino acid of glycine observed at *m/z* 106.0500 (see Table 2 and Figure 2) and α-hydroxymethyl-serine at *m/z* 136.0603, which was predicted to be formed through two consecutive Akarbori transformations of glycine[16] and can be considered as the Akabori amino acid of serine under the Maillard reaction conditions. Furthermore, as shown in Figures 2 and 3 and Tables 2 and 3, many of the copper-containing intermediate complexes identified in the reaction medium provided, for the first time, high-resolution mass spectral evidence (qTOF/ESI/MS) for their formation supported by the presence of isotopic peaks of copper and the isotopic incorporation patterns from the specifically labeled precursors, thus further confirming the mechanistic details of Akabori transformation of glycine. Furthermore, the model system that included glucose also showed, in addition to the above-mentioned ions, additional major ions at *m/z* 238.0930, 325.1369, and 342.1392, which were absent when the glycine−copper complex was replaced with glycine. The first two ions incorporated 6 carbon atoms from U_6-^{13}C-glucose, and their elemental compositions indicated sugar amino acid(s) adducts, whereas the third ion incorporated 12 carbon atoms from U_6-^{13}C-glucose that can be assigned to a diglycosylated ammonia. (The details of the role of glucose during the Akabori reaction will be published elsewhere.)

Mass Spectrometric and Isotope-Labeling Evidence for the Formation of Schiff Bases of Amino Acid−Metal Complexes with Aldehydes Prior to Akabori Transformation. The Akabori modification of amino acids is a stepwise transformation involving several consecutive reactions. Much like the Maillard reaction, a key initial step proposed in the Akabori reaction is the formation of imine between the amino groups of the metal complex and the excess aldehyde in the reaction mixture.[2] This step is considered critical for the activation of the α-carbon. Although there is indirect evidence for the formation of this intermediate, no mass spectrometric evidence is presented so far. Analysis of the heated reaction mixture of $(Gly)_2Cu$ and formaldehyde indicated the formation of several copper complexes and the free serine as shown in Figure 2 and listed in Table 2. According to the intermediates identified in Figure 2, the glycine−copper complex undergoes double Schiff base formation with formaldehyde to generate the ion at *m/z* 235.9840. The activated complex then can react with two formaldehyde molecules to generate the ion at *m/z* 296.0054 followed by hydrolysis of the Schiff bases resulting in the formation of a $(Ser)_2Cu$ complex at *m/z* 272.0044. Depending on the pH, the amino acid−metal complexes can either undergo ligand exchange[17] in the presence of free amino acids to generate the mixed complex (Gly)Cu(Ser) at *m/z* 241.9943 or decompose at lower pH values to release free amino acid serine at *m/z* 106.0500. As shown in Table 4, all of the listed intermediates display the expected isotope label incorporation patterns from C-1, C-2, and the nitrogen atom of glycine. Furthermore, each of the intermediate copper complexes also exhibited the isotopic signature of copper through detection of its M + 2 peaks at 30% relative intensity (Table 2). To confirm the formation of serine complex at *m/z* 272.0044 in the reaction

Table 6. Elemental Composition of the Reaction Products[a] in the $(Ala)_2Cu$/Paraformaldehyde Model System Shown in Figure 4

$[M + H]^+$ (*m/z*)	elemental composition	error (ppm)
120.0650	$C_4H_{10}NO_3$	8.9
132.0645	$C_5H_{10}NO_3$	11.9
264.0144/266.0120[a]	$C_8H_{13}CuN_2O_4$	10.3

[a]The two masses shown represent copper isotopes $^{63}Cu/^{65}Cu$.

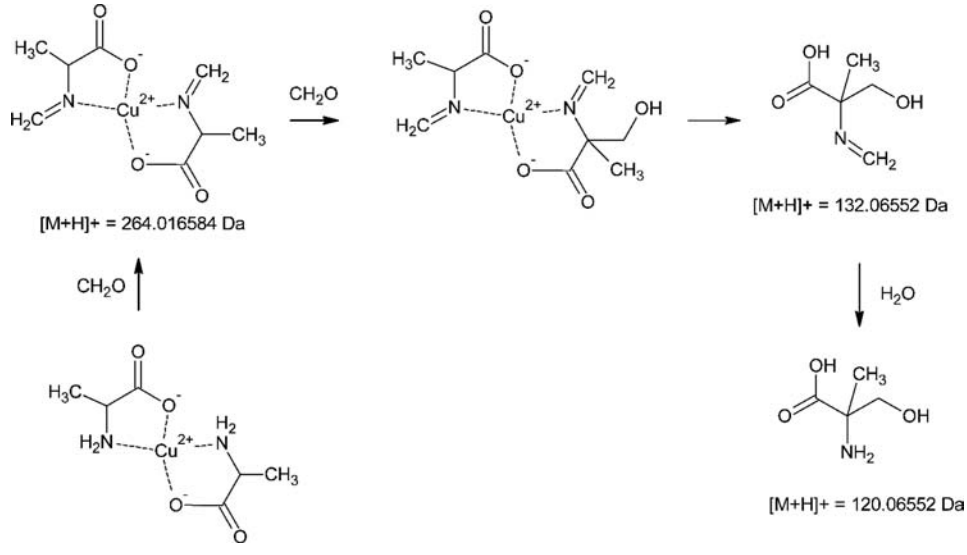

Figure 4. Formation of Akabori amino acid from $(Ala)_2Cu$ and CH_2O. $[M + 1]^+$ values represent theoretical masses (corresponding observed masses are shown in Table 6).

DOI: 10.1021/jf5051975
J. Agric. Food Chem. 2015, 63, 328−334

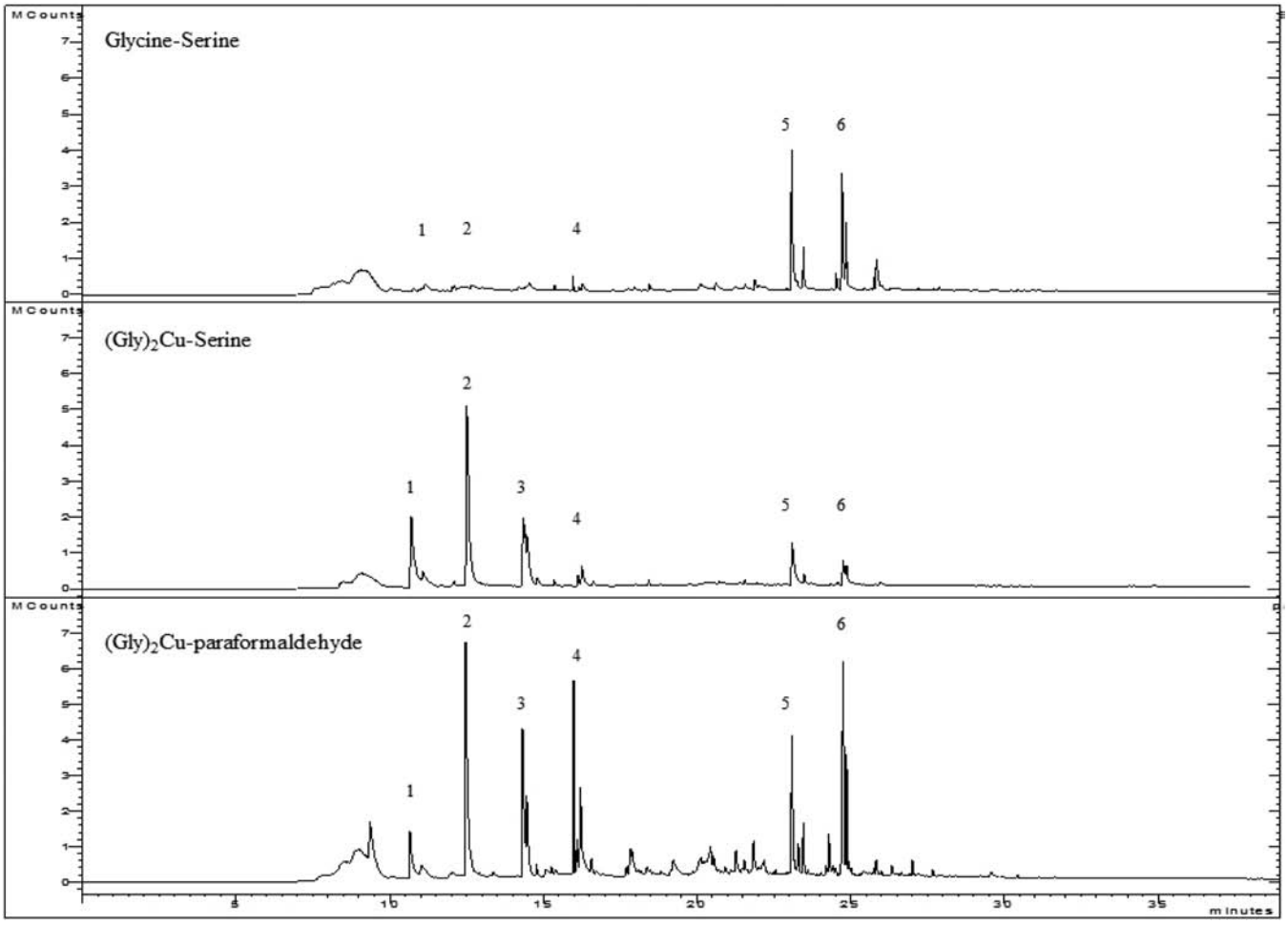

Figure 5. Comparison of the major volatile compounds thermally desorbed from the heated (in water at 110 °C) residues of glycine/serine, $(Gly)_2Cu$/serine, and $(Gly)_2Cu$/paraformaldehyde model systems: (1) 2-methyl-(1*H*)-pyrrole; (2) 2-methylpyrazine; (3) 2,6-dimethylpyrazine; (4) 1,3,5-trimethylhexahydrotriazine; (5) 1,5-dimethyl-2(1*H*)-pyrazinone; (6) 1,5,6-trimethyl-2(1*H*)-pyrazinone.

mixture of $(Gly)_2Cu$ and formaldehyde, MS/MS analysis of synthetic $(Ser)_2Cu$ was performed and the product ions were compared with the daughter ions of m/z 272.0044 detected in the reaction mixture. The MS/MS fragments of this adduct matched exactly that of the synthetic standard (see Table 5). Furthermore, the synthetic $(Ser)_2Cu$ complex was reacted with formaldehyde to identify many of the other copper-containing complexes observed in the original reaction mixture of $(Gly)_2Cu$ and formaldehyde, which were thought to arise from the in situ formed $(Ser)_2Cu$ complex and the already present formaldehyde. Table 3 and Figure 3 show the observed and predicted complexes of copper that could be formed by the interaction of formaldehyde with serine−copper complex. These ions were also detected in the original reaction mixture of $(Gly)_2Cu$ and formaldehyde. The serine−copper complex, similar to the glycine−copper complex, can undergo Akabori transformation as shown in Figure 3 through Schiff base formation and similarly generate its corresponding Akabori amino acid hydroxymethyl-serine observed at m/z 136.0603, which was originally identified by Akabori et al.[1] as an unknown compound but later characterized as α-hydroxymethyl-serine by Otani and Winitz.[16] The two key intermediates identified at m/z 314.0143 and 302.0151 (Figure 3) not only support the formation of α-hydroxymethyl-serine but provide further evidence for the importance of formation of Schiff base−metal complexes in the Akabori reaction. None of the above products were detected in the absence of copper complex of glycine or when free glycine was reacted with formaldehyde. The formation of α-hydroxymethyl-serine in this model system is noteworthy because it indicates the possibility of formation of unusual amino acids during the Maillard reaction. In addition, the reaction of alanine−copper complex with formaldehyde similarly generated the Schiff base adduct observed at m/z 264.0144, further supporting the importance and generality of Schiff base formation in the mechanism of Akabori reaction (see Figure 4; Table 6). These observations are not surprising and are consistent with the theoretical considerations regarding the ease of Schiff base formation on the amino groups of metal complexes due to the extra stabilization gained through hyperconjugation of its π-system with the metal[7] and, consequently, further enhancing the acidity of the α-carbon due to additional delocalization of the negative charge over the newly formed imminium moiety,[18] giving rise to a more reactive α-carbanion intermediate capable of being alkylated more readily by formaldehyde.

Implications of the Akabori Transformation to the Volatile Profile of the Maillard Reaction. Considering that $(Gly)_2Cu$ when heated will generate serine in the presence of formaldehyde, it was expected that volatiles generated in this model system should resemble the volatiles generated in a glycine/serine system. Indeed, when the dried residues of the

DOI: 10.1021/jf5051975
J. Agric. Food Chem. 2015, 63, 328−334

above heated model systems (unheated samples when pyrolyzed did not generate any volatiles) were thermally desorbed, five of the six major peaks shown in Figure 5 were found to be in common. Similarly, the $(Gly)_2Cu$/serine model system also shared these common peaks as shown in Figure 5. More importantly, the intensities of these peaks in the Akabori model system of $(Gly)_2Cu$/formaldehyde were significantly enhanced, indicating the ability of $(Gly)_2Cu$ to sustain the transformation of glycine into serine through stabilization of the important precursors shown in Figures 2 and 3 that can act as a reservoir for the continuous generation of volatiles.

AUTHOR INFORMATION

Corresponding Author

*(V.A.Y.) Phone: (514) 398-7918. Fax: (514) 398-7977. E-mail: varoujan.yaylayan@mcgill.ca.

Funding

We acknowledge funding for this research from the Natural Sciences and Engineering Research Council of Canada (NSERC).

Notes

The authors declare no competing financial interest.

REFERENCES

(1) Akabori, S.; Otani, T. T.; Marshall, R.; Winitz, M.; Greenstein, J. P. A synthesis and resolution of dl-serine. *Arch. Biochem. Biophys.* **1959**, *83*, 1−9.

(2) Beck, W. Metal complexes of biologically important ligands, CLXXII [1]. Metal ions and metal complexes as protective groups of amino acids and peptides − reactions at coordinated amino acids. *Z. Naturforsch.* **2009**, *64B*, 1221−1245.

(3) Ichikawa, T.; Maeda, S.; Araki, Y.; Ishido, Y. Synthetic studies of amino acids by the use of the copper complex. I. Syntheses of β-hydroxy DL-amino acids by the use of the complex of copper(II) with the Schiff base derived from glycine and pyruvic acid. *J. Am. Chem. Soc.* **1970**, *92*, 5514−5516.

(4) Sato, M.; Okawa, K.; Akabori, S. A new synthesis of threonine. *Bull. Chem. Soc. Jpn.* **1957**, *30*, 937−938.

(5) Ikutani, Y.; Okuda, T.; Sato, M.; Akabori, S. The reaction of glycine cobalt complex with acetaldehyde. *Bull. Chem. Soc. Jpn.* **1959**, *32*, 203−204.

(6) Williams, D. H.; Busch, D. H. Selective labilizing of α-hydrogen atoms by chelation of α-aminocarboxylic acids. *J. Am. Chem. Soc.* **1965**, *87*, 4644−4645.

(7) Belikov, V. M.; Vitt, S. V.; Kuznetsova, N. I.; Bezrukov, M. G.; Saporovskaya, M. B. Reaction of the copper complex of L-alanine with acetaldehyde and the mechanism of the Akabori reaction. *Russ. Chem. Bull.* **1969**, *18*, 2371−2375.

(8) Teo, S.-B.; O'Connor, M. J. A polarimetric study of the reaction of bis(L-serinato)copper(II) with formaldehyde. *Inorg. Chim. Acta* **1984**, *92*, 57−60.

(9) Aune, J. P.; Maldonado, P.; Larcheres, G.; Pierrot, M. The crystal and molecular structure of copper(II) bis-2,5-dimethyloxazolidine-4-carboxylate dihydrate. Relation between the structure of the complex and the synthesis of DL-threonine. *J. Chem. Soc. D, Chem. Comm.* **1970**, 1351−1352.

(10) Yaylayan, V. A.; Keyhani, A. Origin of 2,3-pentanedione and 2,3-butanedione in D-glucose/L-alanine Maillard model systems. *J. Agric. Food Chem.* **1999**, *47*, 3280−3284.

(11) Shu, C.-K. Pyrazine formation from serine and threonine. *J. Agric. Food Chem.* **1999**, *47*, 4332−4335.

(12) Friedman, M. Nutritional value of proteins from different food sources. A review. *J. Agric. Food Chem.* **1996**, *44*, 6−29.

(13) Wong, K. H.; Abdul Aziz, S.; Mohamed, S. Sensory aroma from Maillard reaction of individual and combinations of amino acids with glucose in acidic conditions. *Int. J. Food Sci. Technol.* **2008**, *43*, 1512−1519.

(14) Nashalian, O.; Yaylayan, V. A. Thermally induced oxidative decarboxylation of copper complexes of amino acids and formation of Strecker aldehyde. *J. Agric. Food Chem.* **2014**, *62*, 8518−8523.

(15) Yablokov, V. A.; Smeltsova, I. L.; Faerman, V. I. Kinetics of heat-induced transformation of copper complexes with amino acids. *Russ. J. Gen. Chem.* **2014**, *84*, 568−570.

(16) Otani, T. T.; Winitz, M. Studies on hydroxyamino acids. I. Synthesis of some α-alkylated serines. *Arch. Biochem. Biophys.* **1960**, *90*, 254−259.

(17) Pearson, R. G.; Lanier, R. D. Rates of rapid ligand exchange reactions by nuclear magnetic resonance line broadening studies. *J. Am. Chem. Soc.* **1964**, *86*, 765−771.

(18) Crugeiras, J.; Rios, A.; Riveiros, E.; Richard, J. P. Substituent effects on electrophilic catalysis by the carbonyl group: anatomy of the rate acceleration for PLP-catalyzed deprotonation of glycine. *J. Am. Chem. Soc.* **2011**, *133*, 3173−3183.

DOI: 10.1021/jf5051975
J. Agric. Food Chem. 2015, 63, 328−334

JOURNAL OF AGRICULTURAL AND FOOD CHEMISTRY

Article

pubs.acs.org/JAFC

Toxic Ipomeamarone Accumulation in Healthy Parts of Sweetpotato (*Ipomoea batatas* L. Lam) Storage Roots upon Infection by *Rhizopus stolonifer*

Lydia N. Wamalwa,[†,⊥] Xavier Cheseto,[‡] Elizabeth Ouna,[‡] Fatma Kaplan,[§,¶] Nguya K. Maniania,[‡] Jesse Machuka,[⊥] Baldwyn Torto,[‡] and Marc Ghislain*[,†]

[†]International Potato Centre, P.O. Box 25171-00603, Nairobi, Kenya

[‡]International Centre of Insect Physiology and Ecology (ICIPE)-African Insect Science for Food and Health, P.O. Box 30772-00100, Nairobi, Kenya

[§]Department of Biology, University of Florida, Gainesville, Florida 32611, United States

[⊥]Kenyatta University, P.O. Box 43844-00100, Nairobi, Kenya

[¶]Kaplan Schiller Research, LLC., Gainesville, Florida 32604, United States

Supporting Information

ABSTRACT: Furanoterpenoid accumulation in response to microbial attack in rotting sweetpotatoes has long been linked to deaths and lung edema of cattle in the world. However, it is not known whether furanoterpenoid ipomeamarone accumulates in the healthy-looking parts of infected sweetpotato storage roots. This is critical for effective utilization as animal feed and assessment of the potential negative impact on human health. Therefore, we first identified the fungus from infected sweetpotatoes as a *Rhizopus stolonifer* strain and then used it to infect healthy sweetpotato storage roots for characterization of furanoterpenoid content. Ipomeamarone and its precursor, dehydroipomeamarone, were identified through spectroscopic analyses, and detected in all samples and controls at varying concentrations. Ipomeamarone concentration was at toxic levels in healthy-looking parts of some samples. Our study provides fundamental information on furanoterpenoids in relation to high levels reported that could subsequently affect cattle on consumption and high ipomeamarone levels in healthy-looking parts.

KEYWORDS: *sweetpotato, furanoterpenoids, ipomeamarone, animal and human health safety, Rhizopus stolonifer*

INTRODUCTION

Despite the prevalence of respiratory infections and deaths relating to furanoterpenoids on global health of cattle and possibly humans, the concentration levels of these compounds in diseased and healthy-looking parts of infected sweetpotatoes is poorly understood and insufficiently documented. Phytoalexins are inducible metabolites elicited by biotic and abiotic factors. Sweetpotato contains several phytoalexins, collectively known as furanoterpenoids, including ipomeamarone, **1**; dehydroipomeamarone, **2**; 4-ipomeanol, **3**; and 1,4-ipomeadiol, **4** (Figure 1).[1,2] Biotic factors such as fungi are reported to elicit varying levels of furanoterpenoids,[2] which cause hepatoxicity, pneumonia, lung edema,[3−5] and cattle deaths.[6] Although information on furanoterpenoids is available concerning isolation methods[7] and presence in sweetpotatoes,[2,8] there is no documented or accessible information on variation of the concentrations from inoculation point on toward healthy-looking parts of an infected sample. This is important because in sub-Saharan Africa (SSA), sweetpotato is a food crop for many rural poor families whereby both healthy and infected sweetpotato storage roots are harvested together. The infected parts are usually removed and fed to farm animals, while the remaining apparently healthy parts are consumed by the farm households, typically in western Kenya (Dr. Robert Mwanga, sweetpotato breeder, personal communication).

Sweetpotato is ranked the third most important root and tuber crop after potato and cassava in SSA. As a food crop, sweetpotato is used by many poor families because of the higher yield in dry matter content per unit area compared to cereal cultivation on an equivalent piece of land.[9] In addition, sweetpotatoes are particularly important during dry periods of the year when cereal crops are unavailable.[9] Unfortunately, it is during the same dry period that the crop is attacked by insects and microbes.[10,11] It is also known that farmers in SSA practice piece-meal harvesting, which exposes the storage roots left in the soil during dry seasons to insects and microbes.[12] Farmers who harvest sweetpotato storage roots for sale are faced with postharvest infection because microbes attack the storage roots owing to the favorable warm conditions and bruising caused by handling.[13] Storage roots respond to attack by eliciting production of furanoterpenoids to fight off the infection within the sweetpotato tissues. The total furanoterpenoid level of three compounds was documented between 25 and 67,000 mg/kg in harvested storage root samples irrespective of the microbe that elicited their accumulation.[1,2] The use of radioactivity to analyze ipomeamarone levels has been done, but more sensitive

Received: May 6, 2014
Revised: November 13, 2014
Accepted: November 24, 2014
Published: November 24, 2014

ACS Publications © 2014 American Chemical Society

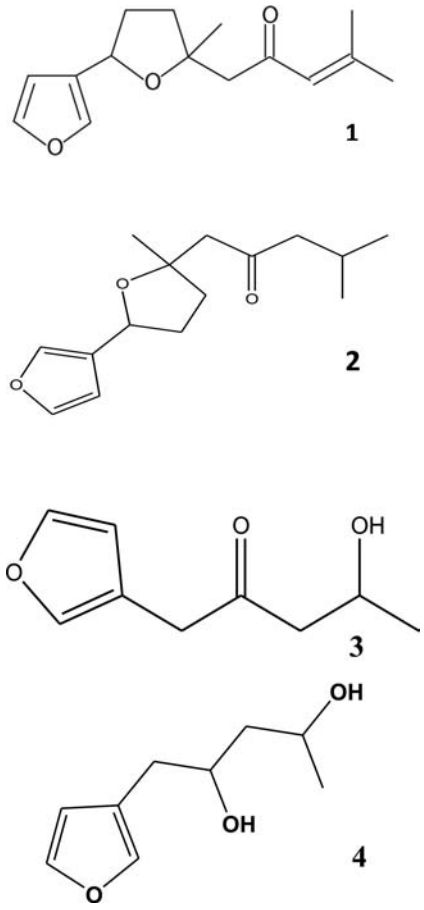

Figure 1. Furanoterpenoids in sweetpotatoes: ipomeamarone, **1**; dehydroipomeamarone, **2**; 4-ipomeanol, **3**; and 1,4-ipomeadiol, **4**.

techniques, such as coupled liquid chromatography-quadruple time-of-flight mass spectrometry (LC−QToF−MS) and coupled gas chromatography−mass spectrometry (GC−MS), are needed.[14]

It is not known how far into the healthy-looking storage root samples that these furanoterpenoids are found and at what levels. Since this could potentially expose both humans and farm animals to either chronic or acute toxicity, we (i) isolated and identified a fungus from field samples that elicited furanoterpenoid production; (ii) characterized the furanoterpenoids using GC−MS and LC−QToF−MS; (iii) evaluated the furanoterpenoid concentration levels produced for different sweetpotato cultivars after infection by the isolated fungus; and (iv) determined the furanoterpenoid levels within the apparently healthy part of infected storage roots.

MATERIALS AND METHODS

Plant Materials. Two types of sweetpotato (*Ipomoea batatas* L. Lam) samples were used to analyze for ipomeamarone concentrations: weevil-infected sweetpotatoes for fungal isolation and healthy sweetpotatoes for inoculation experiments with the isolated fungus. Healthy sweetpotatoes were purchased from markets in Nairobi, Kenya and were classified by the vendors as Kemb, Naspot, Bungoma, and Nyawo cultivars. Weevil-infested sweetpotato storage roots were sampled from a farm at the Kenya Agricultural Research Institute (KARI), Marigat, Kenya during the dry season when infestation was high. Sampled storage roots were carefully placed in covered but aerated plastic jars (20.5 cm × 10.5 cm) immediately after harvest and then incubated at 25−28 °C for 5 days to promote growth of microbes.

Isolation and Identification of Fungus from Weevil-Infested Sweetpotatoes. Isolation was carried out from fully infected storage roots in jars by using a pin and plated on potato dextrose agar (PDA) (Oxoid, Hampshire, England) media supplemented with 50 μg/mL streptomycin sulfate (Sigma, St. Louis, MO) and chloramphenicol (25 μg/mL) (Sigma, St. Louis, MO) to inhibit bacterial growth. Plates were incubated overnight at 25 °C during which several colonies emerged. Single colonies were isolated and subcultured on PDA without antibiotics. There was a colony that was consistently found on all the PDA plates, and then named Marigat isolate-1 (MI-1). It was identified using both morphological and molecular characterization. For morphological identification, a fungal isolation technique previously described was used.[15] The PDA plate was inoculated using a sterile needle. A sterile glass coverslip was placed in an oblique position on the culture, and plates were incubated at 25 °C for 4−6 days. From day two onward, coverslips were removed daily and mounted on a slide stained with lactophenol aniline blue (Sigma-Aldrich, St. Louis, MO). The coverslips were examined using a light microscope (Leica, Wetzlar, Germany) at the magnifications ×8 and ×40.

Molecular characterization of MI-1 was initiated by isolation of genomic DNA using CTAB method from mycelia grown on PDA plates.[16] Polymerase chain reaction (PCR) was conducted using internal transcribed spacers (ITS) primer pairs.[17] Nonspecific PCR products generated were further eliminated by band-stab PCR.[18] The PCR comprised a 25 μL reaction that consisted of PCR buffer (1*x*), ITS1 primer (0.2 μM), ITS4 primer (0.2 μM), dNTPs (0.06 mM), $MgCl_2$ (2 mM), and Taq polymerase (0.5 unit) (Thermo Scientific, Wyman, MA). The primer sequences for ITS1 and ITS4 were 5′ TCCGTAGGTGAACCTGCGG 3′ and 5′ TCCTCCGCTTATTGATATGC 3′, respectively.[17] This reaction mix was subjected to the following PCR program: initial denaturation 94 °C for 5 min, followed by 40 cycles of denaturation 94 °C for 45 s, annealing temperature 60 °C for 30 s, elongation 72 °C for 90 s, and a final elongation 72 °C for 6 min. PCR was conducted on several other microbes to verify that the amplicon generated from MI-1 was not present in other microbes or if present, it was not of a similar size. The microbes included were as follows: MI-1; *Metarhizium anisopliae* IC30 from ICIPE; *Ceratocystis fimbriata* f. sp. *platani* (CBS 127659); *Clavibacter michiganensis* ssp. *michiganensis*; *Catharanthus roseus* containing Udinese-Stolbur phytoplasma from CBS-KNAW Fungal Biodiversity Centre (Utrecht, The Netherlands); and an unknown fungus culture collected from potato fields and were grown on PDA media containing streptomycin sulfate. PCR products were resolved on 1% agarose gel in TBE for 1 h at 100 V. PCR products were purified using QIAquick PCR Purification kit (Qiagen, Hilden, Germany) and Gel Extraction kit (Qiagen, Hilden, Germany). Purified PCR products were sequenced using GS-FLX 454 platform (454 Life Sciences/Roche, Bradford, CT).

Extraction and Identification of Furanoterpenoids from Fungal-Infected Sweetpotatoes. The storage root samples were prepared using a previously described method[2] with few modifications. Healthy storage roots from sweetpotato cultivars namely Kemb, Naspot, Nyawo, and Bungoma were washed, surface sterilized for 5 min using 0.5% sodium hypochlorite, and rinsed three times in sterile distilled water in a laminar flow hood. In the first experiment, the storage root samples were cut into halves and placed in clean sterile plastic containers and then inoculated with actively growing fungal isolate (MI-1) from agar plugs, while the controls were not inoculated. The sweetpotato samples (both inoculated and noninoculated) were replicated three times for each cultivar. The second experiment consisted of inoculating Kemb and Naspot cultivars using MI-1, and storage roots tied with polythene and elastic bags to restrict growth of the fungus. The storage roots were incubated at 25 °C for 7−14 days for infection. This second experiment consisted of two cultivars, Kemb and Naspot, with seven samples. Each sample was chopped into 1 cm slices to analyze furanoterpenoid levels from infection point to the healthy-looking tissue. Differences between means were estimated using a Student−Newman−Keuls test.

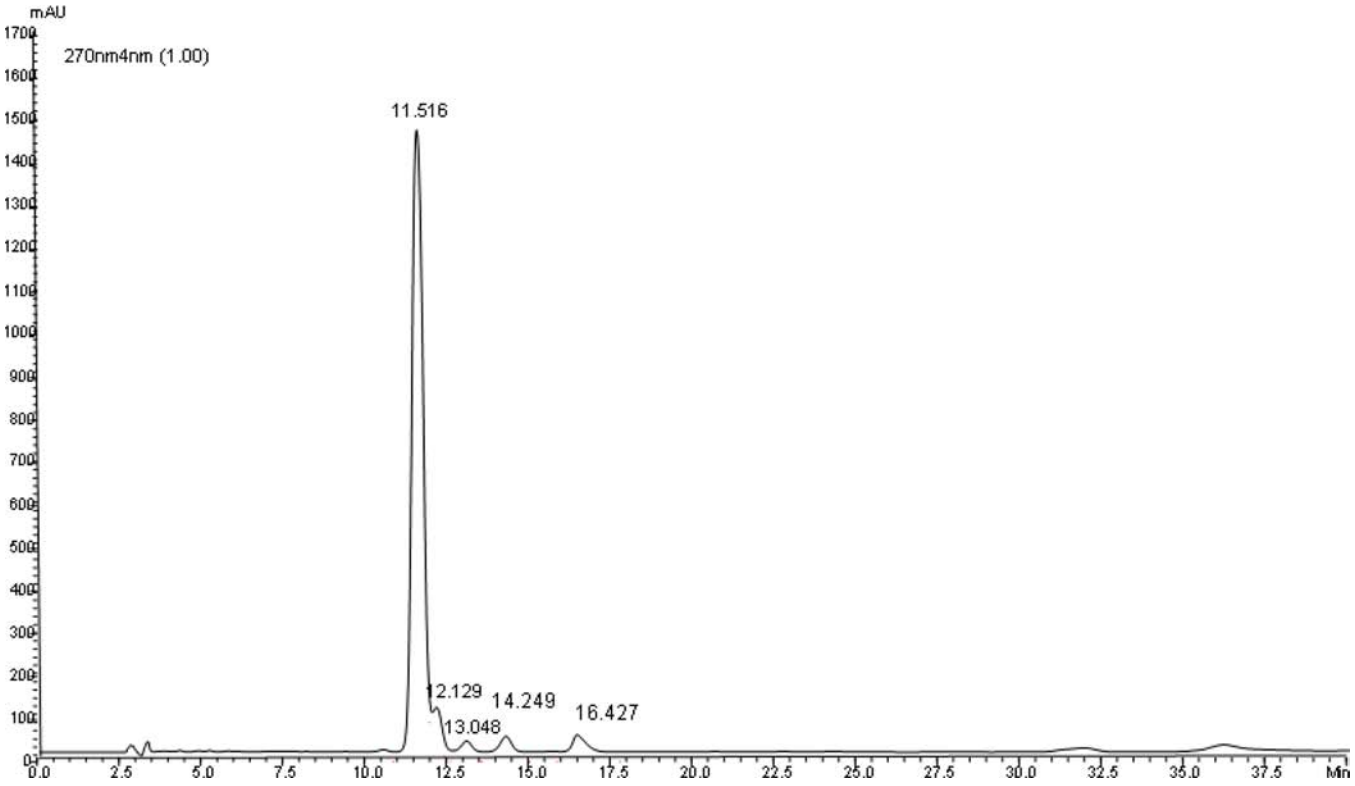

Figure 2. HPLC profile of the furanoterpenoid mix isolated from column chromatography with ipomeamarone and dehydroipomeamarone indicated as 16.43 min and 11.52 min, respectively.

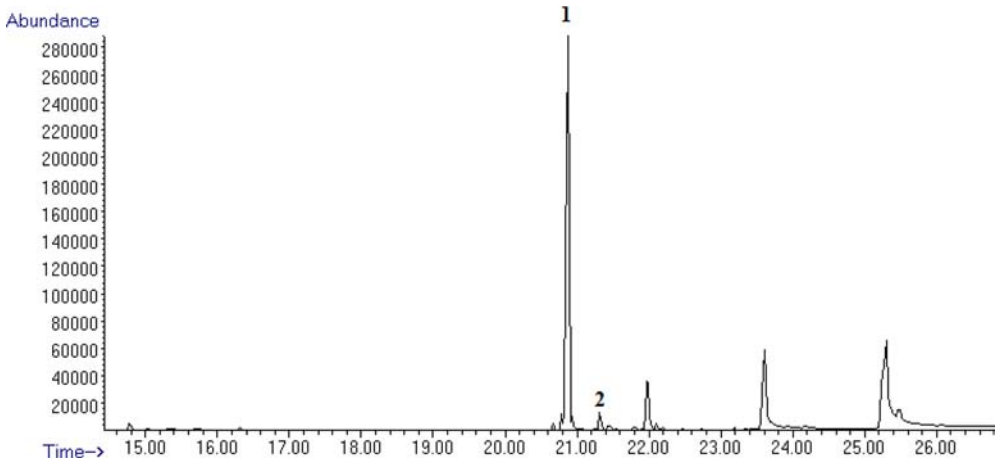

Figure 3. Representative GC−MS total ion chromatogram of purified furanoterpenoids: ipomeamarone, **1**; and dehydroipomeamarone, **2**.

The fungus covering the sweetpotato was scraped off. The storage roots were then weighed and blended in 100 mL of methanol and 3 g of NaCl for 3 min. For isolation and purification of dehydroipomeamarone and ipomeamarone, 268 g of infected sweetpotato was extracted with 550 mL of methanol. The extracts were filtered using Whatman filter paper No. 4, poured in conical flasks, and then concentrated in a rotary evaporator to remove methanol and water. The volume of concentrated crude extract was estimated as 10 mL, and the same volume of 10 mL of dichloromethane (Sigma, St. Louis, MO) was added to effectively double the volume of the extract for each flask. The organic phases were combined, concentrated to dryness in a rotary evaporator to remove any remaining solvents from the crude extract, weighed, and then purified by chromatography.

Fifteen grams of the extracted materials was chromatographed on 32−63 μm silica gel (Riedel-de Haen, Seelze, Germany) using a hexane−ethyl acetate gradient. The furanoterpenoids fraction was eluted with 90% hexane:ethyl acetate, which was further cleaned by column chromatography using a hexane−acetone gradient to yield ipomeamarone mix (1 g). Further purification of the eluent was carried out on a Shimadzu VP series using a 205 mm × 10 mm i.d., 5 μM ACE Q C-18 column (ACE, Aberdeen, Scotland). The mobile phase used an isocratic program (A:B), 60:40 with a flow rate of 1 mL/min, and run time was 20 min. Detection was by UV absorption at 270 nm to obtain 18 mg of ipomeamarone and 15 mg of dehydroipomeamarone with percentage yield being 0.12% and 0.10%, respectively (Figure 2). Structures of the isolated furanoterpenoids were determined by means of chromatographic and spectroscopic techniques (LC−QToF−MS, GC−MS, and 1- and 2-D NMR) and by comparison with spectroscopic literature data.[1,19]

For GC−MS analyses, the furanoterpenoids fractions was analyzed by split/splitless injection using a model 7890 gas chromatograph coupled to a 5975C inert XL EI/CI mass spectrometer (Agilent

dx.doi.org/10.1021/jf504702z | J. Agric. Food Chem. 2015, 63, 335−342

Technologies, Palo Alto, CA) (GC−MS) equipped with a 30 m × 0.25 mm i.d. × 0.25 μm film thickness HP-5 column (El 70 eV) (Agilent Technologies, Palo Alto, CA). Helium was used as the carrier gas at a flow rate of 1.2 mL/min. The oven temperature was held at 35 °C for 3 min and then programmed to increase at 10 °C/min to 280 °C and maintain this temperature for 10 min. The target peaks were identified through comparison of their mass spectra with Adams2.L, Chemecol.L, and NIST05a.L library data (Figure 3).

For LC−QToF−MS analyses, the crude extract was concentrated in vacuo to dryness, redissolved in 3 mL of LC−MS grade CHROMASOLV methanol (Sigma-Aldrich, St. Louis, MO), and centrifuged at 14,000 rpm for 5 min, after which 0.5 μL was automatically injected into LC−QToF−MS. The chromatographic separation was achieved on a Waters ACQUITY UPLC (ultra-performance liquid chromatography) I-class system (Waters Corporation, Maple Street, MA) fitted with a 2.1 mm × 100 mm, 1.7-μm particle size Waters ACQUITY UPLC BEH C18 column (Waters Corporation, Dublin, Ireland) heated to 40 °C and an autosampler tray cooled to 15 °C. Mobile phases of water (A) and acetonitrile (B), each with 0.01% formic acid were employed. The following gradient was used: 0−1.5 min, 10% B; 1.5−2 min, 10−50% B; 2−6 min, 50−100% B; 6−9 min, 100% B; 9−10 min, 90−10% B; 10−12 min, 10% B. The flow rate was held constant at 0.4 mL/min. The UPLC system was interfaced by electrospray ionization (ESI) to a Waters Xevo QToF−MS operated in full scan MS^E in positive mode. Data were acquired in resolution mode over the m/z range of 100−1200 with a scan time of 1 s using a capillary voltage of 0.5 kV, sampling cone voltage of 40 V, source temperature of 100 °C, and desolvation temperature of 350 °C. The nitrogen desolvation flow rate was 500 L/h. For the high-energy scan function, a collision energy ramp of 25−45 eV was applied in the T-wave collision cell using ultrahigh purity argon (≥99.999%) as the collision gas. A continuous lock spray reference compound (leucine enkephalin; $[M + H]^+ = 556.2766$) was sampled at 10 s intervals for centroid data mass correction. The mass spectrometer was calibrated across the 50−1200 Da mass range using a 0.5 mM sodium formate solution prepared in 90:10 2-propanol/water (v/v). MassLynx version 4.1 SCN 712 (Waters Corporation, Maple Street, MA) was used for data acquisition and processing. The elemental composition was generated for every analyte. Potential assignments were calculated using monoisotopic masses with specifications of a tolerance of 10 ppm deviation and both odd- and even-electron states possible. The number and types of expected atoms were set as follows: carbon, ≤100; hydrogen, ≤100; oxygen, ≤50; nitrogen, ≤6; sulfur, ≤6. The LC−QToF−MS data acquisition and analysis were based on the following defined parameters: mass accuracy (ppm) = 1,000,000 × (calculated mass − accurate mass)/calculated mass; fit conf % is the confidence with which accurate mass (measured data) matches the theoretical isotope models of the elemental composition in the list; elemental composition is a suggested formula for the specified mass. This is a summation of the quantities of elements, isotopes, or superatoms that can compose the measured data, calculated using the following atomic masses of the most abundant isotope of the elements: C = 12.0000000, H = 1.0078250, N = 14.0030740, O = 15.9949146, and S = 31.9720718. The empirical formula generated was used to predict structures that were proposed based on the online database, fragmentation pattern, and literature.

To verify the identity of these peaks, nuclear magnetic resonance (NMR) was done. The isolated and purified ipomeamarone and dehydroipomeamarone samples (5 mg each) were each dissolved in $CDCl_3$ (Cambridge Isotope Laboratories, Tewksbury, MA) and placed in 2.5 mm × 100 mm MATCH NMR tubes (Norell, Landisville, NJ). 1D and 2D ^1H and ^{13}C NMR spectroscopy, including correlation spectroscopy (COSY), heteronuclear single-quantum coherence (HSQC), and heteronuclear multiple-bond correlation (HMBC) spectroscopy, were used for verification. For the dehydroipomeamarone, 2D nuclear Overhauser effect spectroscopy (NOESY) data were collected and analyzed for additional structural verification (see Supporting Information). All NMR spectra were acquired at 22 °C using a 5 mm TXI CryoProbe (Bruker Corporation, Billerica, MA) and a Bruker Avance II 600 console (600 MHz for ^1H and 151 MHz for ^{13}C) except for 2D NOESY data, which was collected at 25 °C. Residual $CHCl_3$ was used to reference chemical shifts to δ 7.26 ppm for ^1H, and δ C1 of ipomeamarone is referenced to 72.6 ppm for ^{13}C in the HSQC spectrum by a previous report for consistency with the literature.[20] We also checked the residual $CHCl_3$ in $CDCl_3$ for ^{13}C in the HSQC spectra to confirm that it was properly referenced according to a previous study.[21] NMR spectra were processed using Bruker Topspin 2.0 and MestReNova (Mestrelab Research) software packages.

Quantitation of Furanoterpenoids in Sweetpotato Samples. LC−QToF−MS in full scan MS^E in positive mode was used to detect furanoterpenoids in extracts based on accurate mass measurement, retention time, fragmentation pattern, and reference spectra database published online of isolated dehydroipomeamarone and ipomeamarone (standards).[22] Dehydroipomeamarone and ipomeamarone were quantitated using generated standard calibration curves prepared from the isolated compounds. Serially diluted solutions of isolated standards (0.01−200 μg/μL) were analyzed by LC−QToF−MS to generate linear calibration curves (peak area vs concentration) for ipomeamarone [$y = 583{,}064x + 642{,}221$ ($R^2 = 0.9991$)] and dehydroipomeamarone [$y = 324{,}980x + 177{,}617$ ($R^2 = 0.9995$)], which served as the bases for external quantitation.

RESULTS AND DISCUSSION

Identification of MI-1 as *Rhizopus stolonifer*. Identification of MI-1 fungus isolated from the field-collected sweetpotato storage roots was conducted because different microbes elicit varying furanoterpenoid responses.[2] On the basis of morphological features (sporangia, sporangiophores, spores, collumella, rhizoids, and stolons); sporangiophores that arise from intersections with rhizoids and stolons; the dome-shaped columella; and not falling off when the sporangium dried out, MI-1 was identified as belonging to the genus *Rhizopus*. Morphological features of MI-1 had similarities to previously reported *R. stolonifer*.[23,24] The major finding was the collumella being dome-shaped, which differed from other *Rhizopus* species as previously reported as follows: *R. oryzae* has an ellipsoidal collumella; *R. sexualis*, a conical-cylindrical shape; and *R. microspores*, a subglobose to conical shape.[25] From these observations, it was appropriate to suggest that MI-1 fungus was *R. stolonifer*.

The morphological features of *Rhizopus* further confirmed by molecular evidence enabled us identify the species. The ITS primer pair generated an amplicon of 950 bp for MI-1 fungus; none of the other species in this study had a similar band size to MI-1. *Metarhizium anisopliae* IC30 had a band of 600 bp. Sequencing generated a number of reads, but searches were conducted using sequences longer than 200 bp, based on nonredundant database of NCBI, and produced 100 hits. These hits were mainly ITS1, ITS2, 5.8S, 18S, and 28S fragments with partial or complete length sequences; the top 19 hits based on *e*-value were *Rhizopus stolonifer*. Sequence similarity was of 91−99% with *e*-values between 0 and 9×10^{-162}. The best alignment to MI-1 was isolate AM933546.1, which had a sequence identity of 98% and an *e*-level of 0. The *R. stolonifer* isolate had a partial sequence of 18S rRNA gene, ITS1; 5.8S rRNA gene, ITS2; and partial sequence of 28S rRNA gene. Molecular characterization using ITS primers confirmed that MI-1 fungus was *R. stolonifer*; such primers have previously been used in *R. stolonifer* identification.[16]

Chromatographic and Spectroscopic Techniques Confirmed Presence of Furanoterpenoids. The furanoterpenoids ipomeamarone and dehydroipomeamarone were successfully identified using HPLC, GC−MS, LC−QToF−MS,

Table 1. Furanoterpenoids-Present and Concentrations in Sweetpotato Extracts from Four Cultivars for Both Inoculated Samples and Their Respective Controls[a]

cultivar samples inoculated with MI-1 and respective controls with no inoculation	phytolaexin present	mean concentration levels (μg/g) ± s.e.
kemb samples	ipomeamarone	1476.2 ± 278.7 a
kemb samples	dehydroipomeamarone	2914.2 ± 420.8 a
control	ipomeamarone	95.9 ± 8.2 c
control	dehydroipomeamarone	56.2 ± 9.3 c
nyawo samples	ipomeamarone	1089.9 ± 269.5 ab
nyawo samples	dehydroipomeamarone	1459.7 ± 339.9 b
control	ipomeamarone	96.0 ± 8.2 c
control	dehydroipomeamarone	61.8 ± 9.3 c
naspot samples	ipomeamarone	833.7 ± 245.4 ab
naspot samples	dehydroipomeamarone	1153.2 ± 223.9 b
control	ipomeamarone	56.1 ± 8.2 c
control	dehydroipomeamarone	61.8 ± 9.3 c
bungoma samples	ipomeamarone	676.5 ± 132.2 bc
bungoma samples	dehydroipomeamarone	910.0 ± 208.7 bc
control	ipomeamarone	105.1 ± 8.2 c
control	dehydroipomeamarone	92.6 ± 9.3 c

[a]Means with the same letter are not significantly different from each other.

and 1D and 2D NMR techniques by comparing their resonances to published data.[20,21,26,27] The HPLC analysis (Figure 2) showed six peaks with ipomeamarone and dehydroipomeamarone eluting at 16.4 and 11.6 min, respectively. GC−MS analysis also revealed six peaks and tentatively identified two of these peaks as ipomeamarone, **1**, at a retention time (R_t) of 20.8 min and dehydroipomeamarone, **2**, at an R_t of 21.4 min (Figure 3). LC−QToF−MS analysis also identified the two peaks as ipomeamarone (with elemental composition, $C_{15}H_{23}O_3$; m/z 251.1647, 0.0 ppm error to theoretical value; and a fit conf % of 99.96) at a R_t of 2.87 min and dehydroipomeamarone (with elemental composition, $C_{15}H_{21}O_3$; m/z 249.1491, 2.0 ppm error to theoretical value; and a fit conf % of 98.78) at a R_t of 3.04 min. These results were consistent with the GC−MS analysis.

The HPLC purified peaks analyzed by NMR confirmed the presence of ipomeamarone and dehydroipomeamarone. ^{1}H chemical shifts of ipomeamarone were in agreement with literature, while dehydroipomeamarone was a mixture based on LC−QToF−MS and NMR data.[20,27] For dehydroipomeamarone, we observed the ^{1}H chemical shifts at positions C-7 as 6.15 ppm (1H), C-9 as 2.13 ppm (3H), and C-10 as 1.85 ppm (3H), which were the only ^{1}H chemical shifts as provided by previous workers.[27] These workers reported the ^{1}H chemical shifts for positions C-7 as 6.11 ppm (1H), C-9 as 2.09 ppm (3H), C-10 as 1.81 ppm (3H), and all of the other ^{1}H chemical shifts were similar to those of ipomeamarone.[27] Unfortunately, these three ^{1}H chemical shifts differed 0.04 ppm between our spectrum and previously reported data.[27] Since the dehydroipomeamarone sample was a mixture, having just ^{1}H 1D NMR was not satisfactory to confirm the presence of dehydroipomeamarone. Unfortunately, previous workers did not provide any information about NMR solvent or ^{13}C chemical shift data for the synthetic dehydroipomeamarone.[27] Therefore, we acquired a 2D NMR (COSY, HSQC, HMBC, NOESY) spectrum for dehydroipomeamarone and ipomeamarone samples to compare the ^{13}C chemical shifts, since dehydroipomeamarone is a derivative of ipomeamarone, which we confirmed using ^{1}H NMR. Ipomeamarone 2D NMR data was used for comparison. Both ^{1}H and ^{13}C chemical shifts of dehydroipomeamarone were similar to ipomeamarone for carbon positions from 1′−4′ and from 1−6, but differed at positions 7, 8, 9, and 10: consistent with the structure. NOESY data for dehydroipomeamarone provided us additional evidence to confirm its correct identification.

Variations in Ipomeamarone Concentrations between and within Cultivars. The main furanoterpenoids produced were ipomeamarone, **1**, and dehydroipomeamarone, **2**, found in all samples and noninoculated controls. The concentration of furanoterpenoid ranged between 50.6 and 2,330 mg/kg for inoculated samples and 12.4−144.5 mg/kg for the controls. These high levels exceeded those reported previously for *R. stolonifer* of 200−1,100 mg/kg but were comparable to high ipomeamarone elicitors such as *C. fimbriata* and *Fusarium solani* with levels from 1,100−9,300 mg/kg.[2] Similar results have been reported on noninfected sweetpotatoes with low ipomeamarone concentrations between 40 and 325 mg/kg for cultivars in the United Kingdom.[8] Generally, mechanical injury or damaged but noninfected sweetpotato is reported to elicit low furanoterpenoid levels, while infected samples have high levels due to the increase in enzyme activity, which correlates to furanoterpenoid production.[28,29] The low ipomeamarone levels in storage roots of negative control samples from this study confirm that injury or bruising of sweetpotato roots occurs, but the ipomeamarone levels are low.

Concentration levels for ipomeamarone ranged between 50.6 and 2,126.7 mg/kg, while they ranged from 39.3−2,230.4 mg/kg for dehydroipomeamarone. The higher dehydroipomeamarone levels could possibly be because it is a precursor of ipomeamarone, which means that it was yet to be enzymatically converted to ipomeamarone, or dehydroipomeamarone might have inhibited production of ipomeamarone to some extent as reported previously.[1] In preliminary experiments (not shown), ipomeamarone levels were high in inoculated samples, probably due to long incubation time of 28 days compared to the current study where inoculation ranged between 7 and 14 days. More research needs to be conducted to verify this.

Variations in mean ipomeamarone levels by cultivar were as follows: Kemb had the highest mean of 1,476.2 mg/kg, followed by Nyawo with 1,089.9 mg/kg; Naspot had a mean of 833.7 mg/kg, while Bungoma had a mean of 676.5 mg/kg (Table 1). High concentrations of dehydroipomeamarone were

dx.doi.org/10.1021/jf504702z | J. Agric. Food Chem. 2015, 63, 335−342

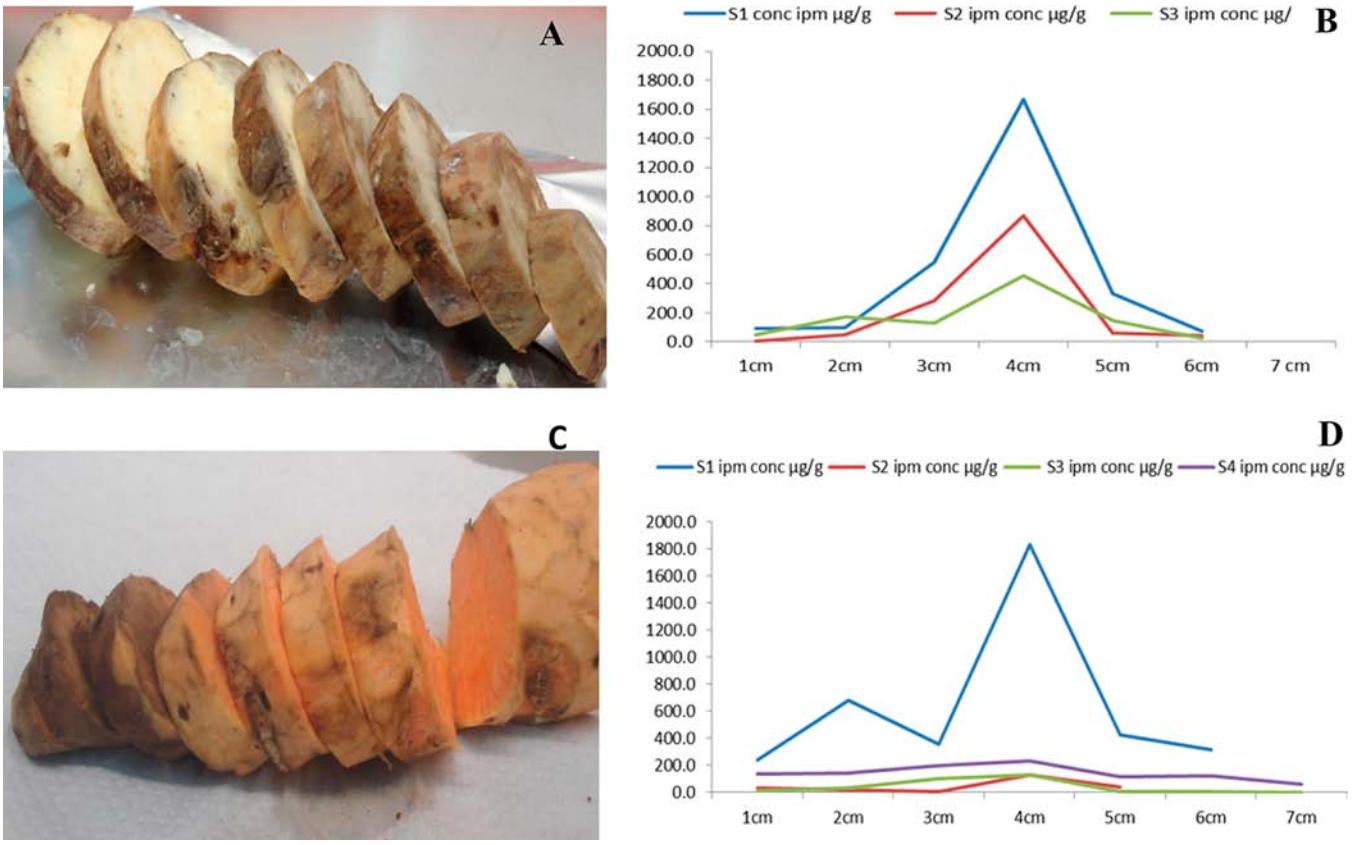

Figure 4. Controlled infection of sweetpotato samples by *Rhizopus stolonifer* that enabled ipomeamarone analysis of 1 cm slices for Kemb (A, B) and Naspot (C, D) cultivar samples.

also observed in almost all samples in this study: Kemb had the highest with 1,462.6 mg/kg, Nyawo had 1,459.7 mg/kg, Naspot had 1,153.2 mg/kg, and Bungoma had 910 mg/kg (Table 1). There were significant ($p < 0.05$) differences between cultivars. In addition, there were differences in ipomeamarone levels within the same cultivar, for example, Nyawo had 602 mg/kg in one sample, while the other had 2,126 mg/kg. Similar variations were observed for different cultivars for ipomeamarone in other studies ranging from 11−2,000 mg/kg.[2,8] Such variations have been speculated to be associated with moisture loss, root maturity, and susceptibility or resistance to fungal infection.[30] Other causes of variation include environmental factors such as postharvest practices by different farmers before arrival at the markets. These variations could have affected the concentrations in the current study. Differences in concentrations for these cultivars also suggest that they vary in resistance to *R. stolonifer* attack with Kemb being the most resistant, followed by Nyawo, Naspot, and Bungoma. These results concur with reports from other studies where the differences in ipomeamarone levels were attributed to *Rhizopus* soft rot resistance.[31]

Higher Ipomeamarone Concentrations in Healthy Parts Away from the Infection Site. We were successful in confining MI-1 fungus in the controlled infection experiment of Naspot and Kemb cultivars. We observed visually the infection to be high at the inoculation place while decreasing progressively with increased distance from the inoculation site (Figure 4). By contrast, evaluation of the 1 cm slices recorded high ipomeamarone levels for regions with visibly low infection, while low levels were observed for regions with visibly high infection (Figure 4). This trend was observed for all samples evaluated, which showed high ipomeamarone levels at the border between the visibly infected and the healthy-looking site. Similar results have been reported that phytoalexins are produced in healthy tissues surrounding wounded parts but terminate in the necrotic tissue.[32] The highest levels of ipomeamarone were observed in both Kemb and Naspot samples of 1,671.2 and 1,708.4 mg/kg, respectively, at the border between the visible infection and healthy-looking tissues (Figure 4). We also observed differences in ipomeamarone levels in some samples, which could have been due to variations in infection on the fungus along the storage root (Figure 4). There were significant ($p < 0.05$) differences between the samples. In another study, it was reported that elimination of 3−10 mm of disease portions beyond infected regions and also cooking removes most ipomeamarone.[33] This could be true for root samples with high levels only at the border, but in the current study, some samples had high levels even in subsequent layers. This suggests that removal of 1 cm from the infection area will still leave behind most of ipomeamarone depending on how much the subsequent layers had accumulated. In other studies, cooking was reported to destroy about 80% of ipomeamarone, but this depends on the initial concentration level found in the storage root before cooking.[34,35]

Since rural poor farmers in SSA keep 1−2 cows, and these farm animals contribute 30−80% of farm income,[36] if they feed them with diseased sweetpotatoes with exceeding toxicity, their fragile revenues will be at threatened by high costs of treatment or even total low of the intoxicated cow. This information is important for farmers' knowledge since they harvest infected roots, cut off the infected part to feed the farm animals, and then consume the healthy-looking parts (Dr. Robert Mwanga,

dx.doi.org/10.1021/jf504702z | J. Agric. Food Chem. 2015, 63, 335−342

sweetpotato breeder, personal communication). Although there are no reports on how far into the visibly healthy-looking part the farmers cut off these storage roots, either the farmers' household consume the parts with high ipomeamarone concentration, or the animals are fed with it. Results drawn from this study suggest that at least 2−3 cm away from the border between the healthy-looking and the infected part of the damaged sweetpotato storage root should be cut off and disposed of, and the infected part should not be fed to the farm animals because of the presence of toxic phytoalexins.

In conclusion, ipomeamarone accumulation in the apparently healthy parts of damaged sweetpotato storage roots should be considered as a potential economic problem and health threat to both the rural poor farm families and large-scale farmers worldwide. Our results reveal the importance of this problem, but more research should be directed to obtaining information on (i) furanoterpenoids present in infested and infected sweetpotatoes harvested from the sweetpotato fields; (ii) furanoterpenoid levels in sweetpotatoes from farmers' households; (iii) varietal response to fungal infection resulting in ipomeamarone accumulation; (iv) degradation of ipomeamarone after processing infested roots and accumulation in metabolism in animal and human organisms; and (v) management of the problem by the rural poor.

■ ASSOCIATED CONTENT

Supporting Information

HMBC and NOESY NMR spectroscopic data in $CDCl_3$ for ipomeamarone and dehydroipomeamarone. This material is available free of charge via the Internet at http://pubs.acs.org.

■ AUTHOR INFORMATION

Corresponding Author

*E-mail: M.Ghislain@cgiar.org. Phone: 254 (020) 4223641. Fax: 254 (020 4223600).

Notes

The authors declare no competing financial interest.

■ ACKNOWLEDGMENTS

This study was financially supported by the Rockefeller Foundation, United States Agency for International Development, and the Bill and Melinda Gates Foundation. We are grateful to Daisy Salifu from ICIPE for guidance on statistical analysis. We are also grateful to George Michuki for the sequencing work using the 454-sequencer. NMR experiments were performed in the McKnight Brain Institute at the National High Magnetic Field Laboratory's AMRIS Facility, which is supported by National Science Foundation Cooperative Agreement No. DMR-1157490 and the State of Florida, in part by an NIH award No. S10RR031637, for magnetic resonance instrumentation; we thank J. Rocca for assistance. James Woodhall and Neil Boonham of the Food and Environment Research Agency (FERA), United Kingdom, gave advice on mycology, and Marcel Westenberg of the National Plant Protection Organisation, The Netherlands, provided the genomic DNA of some microbes, and we are thankful.

■ REFERENCES

(1) Oguni, I.; Uritani, I. Dehydroipomeamarone as an intermediate in biosynthesis of ipomeamarone, a phytoalexin from sweetpotato root infected with *Ceratocystis fimbriata*. *Plant Physiol.* **1974**, *53*, 649−652.

(2) Clark, C. A.; Lawrence, A.; Martin, F. A. Accumulation of furanoterpenoids in sweetpotato tissue following inoculation with different pathogens. *Phytopathology* **1981**, *71*, 708−711.

(3) Beier, C. Natural pesticides and bioactive components in foods. *Rev. Environ. Contam. Toxicol.* **1990**, *113*, 47−137.

(4) Shen, Y. Determination of furanoterpenoid toxins from sweetpotato by thin-layer chromatography. *Chin. J. Chromatogr.* **1997**, *15* (4), 328−330.

(5) Moss, M. O. Fungi, quality and safety issues in fresh fruits and vegetables. *J. Appl. Microbiol.* **2008**, *104*, 1239−1243.

(6) Fighera, R. A.; Rozza, D. B.; Piazer, J. V.; Copetti, M. V.; Irigoyen, L. F.; Barros, C. S. L. Interstitial pneumonia in cattle fed moldy sweetpotatoes (*Ipomoea batatas* L. Lam). *Pesq. Vet. Bras.* **2003**, *23* (4), 1−5.

(7) Smith, R. A.; Drummond, S.; Haines, A.; Porter, J. R.; Hock, R. S. Induction of umbelliferone in sweetpotato cell suspension culture using mercuric chloride. *Biotechnol. Lett.* **2001**, *23*, 1397−1400.

(8) Coxon, D. T.; Curtis, R. F.; Howard, B. Ipomeamarone, a toxic furanoterpenoid in sweetpotato (*Ipomoea batatas*) in the United Kingdom. *Food Cosmet. Toxicol.* **1975**, *13*, 87−90.

(9) Low, J.; Lynam, J.; Lemaga, B.; Crissman, C.; Barker, I.; Thiele, G.; Namanda, S.; Wheatley, C.; Andrade, M. Sweetpotato in Sub-Saharan Africa. In *The Sweetpotato*; Loebenstein, G., Thottappilly, G., Eds.; Springer: ARO, Israel, 2009; pp 359−390.

(10) Akazawa, T.; Uritani, L.; Kubota, H. Isolation of ipomeamarone and two coumarin derivatives from sweetpotato roots injured by the weevil *Cylas formicarius elegantulus*. *Arch. Biochem. Biophys.* **1960**, *88*, 150−156.

(11) Mwanga, R. O. M.; p'Obwoya, O.; Odongo, B.; Turyamureeba, G. M. Sweetpotatoes (*Ipomoea batatas* L. Lam.). In *Agriculture in Uganda. Vol. II Crops. National Agricultural Research Organization (NARO) and Technical Centre for Agricultural and Rural Cooperation (CTA)*; Mukiibi, J. K., Ed.; Fountain Publishers: Kampala, Uganda, 2001; pp 233−251.

(12) Ebregt, E.; Struik, P. C.; Odongo, B.; Abidin, P. E. Piecemeal versus one-time harvesting of sweetpotato in north-eastern Uganda with special reference to pest damage. *Wageningen J. Life Sci.* **2007**, *55-1*, 75−92.

(13) Ray, R. C.; Ravi, V. Post-harvest spoilage of sweetpotato in tropics and control measures. *Crit. Rev. Food Sci. Nutr.* **2005**, *45*, 623−644.

(14) Akazawa, T. Biosynthesis of ipomeamarone. II Synthetic mechanism. *Arch. Biochem. Biophys.* **1964**, *105*, 512−516.

(15) Humberqq, R. A. Fungi: Identification. In *Manual of Techniques in Insect Pathology*; Lacey, L., Ed.; Academic Press: San Diego, CA, 1997; pp 153−186.

(16) Gherbawy, Y. A.; Hussein, N. A. Molecular characterization of *Mucor circinelloides* and *Rhizopus stolonifer* strains isolated from some Saudi fruits. *Foodborne Pathog. Dis.* **2010**, *7* (2), 137−142.

(17) White, T. J.; Bruns, T.; Lee, S.; Taylor, J. W. Amplification and direct sequencing of fungal ribosomal RNA genes for phylogenetics. In *PCR Protocols: A Guide to Methods and Applications*; Innis, M. A., Gelfand, D. H., Sninsky, J. J., White, T. J., Eds.; Academic Press: New York, 1990; pp 315−322.

(18) Bjourson, A. J.; Cooper, J. E. Band-stab PCR: A simple technique for the purification of individual PCR products. *Nucleic Acids Res.* **1992**, *20* (17), 4675.

(19) Boyd, M. R.; Wilson, B. J. Preparative and analytical gas chromatography of ipomeamarone, a toxic metabolite of sweetpotatoes (*Ipomoea batatas*). *J. Agric. Food Chem.* **1971**, *19* (3), 547−550.

(20) Sugimura, T.; Tai, A. Total syntheses of (+)-ipomeamarone and (−)-ngaione via novel intramolecular hydrogen abstraction. *Tetrahedron* **1994**, *50* (40), 11647−11658.

(21) Gottlieb, H. E.; Kotlyar, V.; Nudelman, A. NMR chemical shifts of common laboratory solvents as trace impurities. *J. Org. Chem.* **1997**, *62*, 7512−7515.

(22) *ChemSpider*; Royal Society of Chemistry: Cambridge, U.K.. http://www.chemspider.com/Chemical-Structure.1906.html (accessed September 2014).

(23) Ho, H.; Chen, Z. Post-cleavage transformation of columella of *Rhizopus stolonifer* (Mucoraceae). *Bot. Bull. Acad. Sin.* **1994**, *35*, 249−259.
(24) Kwon, J. H.; Kang, S. W.; Kim, J. S.; Park, C. S. *Rhizopus* soft rot on cherry tomato caused by *Rhizopus stolonifer* in Korea. *Mycobiology* **2001**, *29* (3), 176−178.
(25) Schippers, M. A. A. A revision of the genus *Rhizopus* I: The *Rhizopus stolonifer*-group and *Rhizopus oryzae*. *Stud. Mycol.* **1984**, *25*, 1−19.
(26) Schneider, J. A.; Lee, C. J.; Naya, Y.; Nakanishi, K.; Oba, K.; Uritani, I. The fate of the phytoalexin ipomeamarone: Furanoterpenes and butenolides from *Ceratocystis fimbriata*-infected sweetpotatoes. *Phytochemistry* **1984**, *23* (4), 759−764.
(27) Oguni, I.; Uritani, I. Isolation of dehydroipomeamarone, a new sesqui-terpenoid from the black-rot fungus infected sweetpotato root tissue and its relation to the biosynthesis of ipomeamarone. *Agric. Biol. Chem.* **1973**, *37*, 2443−2444.
(28) Uritani, I. Biochemistry on postharvest metabolism and deterioration of some tropical tuberous crops. *Bot. Bull. Acad. Sin.* **1999**, *40*, 177−183.
(29) Vidhyasekaran, P. *Molecular Biology and Host Defense Mechanisms*, 2nd ed.; Taylor and Francis: Boca Raton, FL, 2008; pp 427.
(30) Jenkins, P. D. Differences in susceptibility of sweetpotato (*Ipomoea batatas*) to infection by storage fungi in Bangladesh. *Phytopathology* **1981**, *102*, 247−256.
(31) Clark, C. A.; Hoy, M. W. Identification of resistance in sweetpotato to *Rhizopus* soft rot using two inoculation methods. *Plant Dis.* **1994**, *78* (11), 1078−1082.
(32) Agrios, G. N. *Plant Pathology*, 5th ed.; Elsevier: Burlington, MA, 2005; pp 235−236.
(33) Catalano, E. A.; Hasling, V. C.; Dupung, H. P.; Constantin, R. J. Ipomeamarone in blemished and diseased sweetpotatoes. *J. Agric. Food Chem.* **1977**, *25*, 94−96.
(34) Wilson, B. J.; Yang, D. T. C.; Boyd, M. R. Toxicity of mold-damaged sweetpotatoes (*Ipomoea batatas*). *Nature* **1970**, *227* (5257), 521−522.
(35) Cody, M.; Haard, N. F. Influence of cooking on toxic stress metabolites in sweetpotato root. *J. Food Sci.* **1976**, *41* (2), 469−470.
(36) *Cattle and Small Ruminant Production Systems in Sub-Saharan Africa. A Systematic Review*; Otte, M. J., Chilonda, P., Eds.; Food and Agricultural Organization: Rome, 2002; pp 36.

JOURNAL OF AGRICULTURAL AND FOOD CHEMISTRY

Article

pubs.acs.org/JAFC

Natural Occurrence of Four *Alternaria* Mycotoxins in Tomato- and Citrus-Based Foods in China

Kai Zhao,[†,‡] Bing Shao,[§] Dajin Yang,[‡] and Fengqin Li*[,‡]

[†]Institute for Nutrition and Food Safety, Chinese Center for Disease Control and Prevention, 7 Panjiayuan Nanli, Chaoyang District, Beijing 100021, People's Republic of China

[‡]Key Laboratory of Food Safety Risk Assessment, Ministry Health, China National Center for Food Safety Risk Assessment, 7 Panjiayuan Nanli, Chaoyang District, Beijing 100021, People's Republic of China

[§]Beijing Center for Disease Control and Prevention, 16 Hepingli Middle Street, Dongcheng District, Beijing 100013, People's Republic of China

Supporting Information

ABSTRACT: A total of 70 tomato-based and 86 citrus-based products collected in China were analyzed for alternariol, alternariol monomethyl ether, tentoxin, and tenuazonic acid by ultraperformance liquid chromatography−electrospray ionization−tandem mass spectrometry. No toxins were found in any fresh tomato or citrus fruit samples. Tenuazonic acid was the predominant toxin detected in all tomato ketchup (10.2−1787 μg/kg) and tomato juice samples (7.4−278 μg/kg). Alternariol was quantitated at higher level than alternariol monomethyl ether with the ratio of alternariol/alternariol monomethyl ether ranging from 0.37 to 104 in 14 alternariol-positive tomato ketchup samples. Tentoxin was detected at much lower levels in all samples analyzed. Some citrus juice samples were positive for tenuazonic acid and alternariol monomethyl ether. It is necessary to conduct a systemic surveillance of *Alternaria* toxins in raw and processed foods to provide the scientific basis for risk assessment of dietary exposure to these toxins in Chinese populations.

KEYWORDS: *Alternaria toxins, tomato-based products, citrus-based products, China, UPLC-MS/MS*

INTRODUCTION

Alternaria toxins are produced by *Alternaria* species that are saprophytic and pathogenic on many plants. These species of fungi produce more than 70 secondary metabolites, but a small proportion of these toxins have been chemically characterized and documented to act as mycotoxins to humans and animals.[1,2] The most important *Alternaria* toxins with toxicological significance reported to occur in cereals, oilseeds,[3] vegetables (especially tomato),[4,5] and fruits (apples,[6] citrus fruits[7] etc.) are alternariol, **1**; alternariol monomethyl ether, **2**; tentoxin, **3**; and tenuazonic acid, **4** (Figure 1).

Limited in vivo study showed that alternariol monomethyl ether poses fetotoxicity and teratogenicity to hamsters.[8] Moreover, alternariol and alternariol monomethyl ether are mutagenic and genotoxic in various in vitro systems, and there is also some evidence for carcinogenic properties in unconventional assays.[9,10] In addition, it has been suggested that the contamination of *Alternaria* toxins in small grains, especially in wheat grains, is much heavier in the high-incidence areas for human esophageal cancer than in the low-incidence areas.[11] The production of these toxins is affected by interactions among the *Alternaria* strain, the growing substrate, and the environmental conditions.[2] Fresh plant products affected by *Alternaria* regularly present visible rotten areas, and the *Alternaria* toxins can be transferred from the rotten part to the surrounding tissues.[6] Hence, *Alternaria* toxins are also present in processed plant products due to the limitations of the current industrial procedures to eliminate the rotting tissues completely.[12] The occurrence of *Alternaria* mycotoxins in processed foodstuffs is becoming an increasing concern for public health. The analytical methods for the analysis of these toxins have focused on liquid chromatography coupled to single mass spectrometry (MS) or tandem MS.[7,10,13−17] Stable isotope dilution assays have been employed in the determination of *Alternaria* toxins, in which labeled internal standards were used to compensate for analyte losses during sample preparation and ion suppression in the ESI interface in current methodology.[16,18,19]

Tomatoes and citrus fruits can easily be infected by fungi of *Alternaria*, and their products such as tomato ketchups and citrus juice are frequently contaminated with *Alternaria* mycotoxins.[7] Although only a limited number of papers describe the contamination of *Alternaria* toxins in local agricultural crops in China, the natural occurrence of these mycotoxins in tomato and tomato products, citrus, and citrus products have not been reported so far. On the other hand, risk assessments relating to food safety in China are frequently hampered by the lack of quantitative data. According to the European Food Safety Authority (EFSA),[10] the contribution to dietary exposure to *Alternaria* toxins is mainly made by grain and grain-based products, vegetables and vegetable products, and fruits and fruit products, depending on the toxin and the food consumption pattern in different countries. To the present

Received: July 18, 2014
Revised: December 12, 2014
Accepted: December 18, 2014
Published: December 18, 2014

ACS Publications © 2014 American Chemical Society

DOI: 10.1021/jf5052738
J. Agric. Food Chem. 2015, 63, 343−348

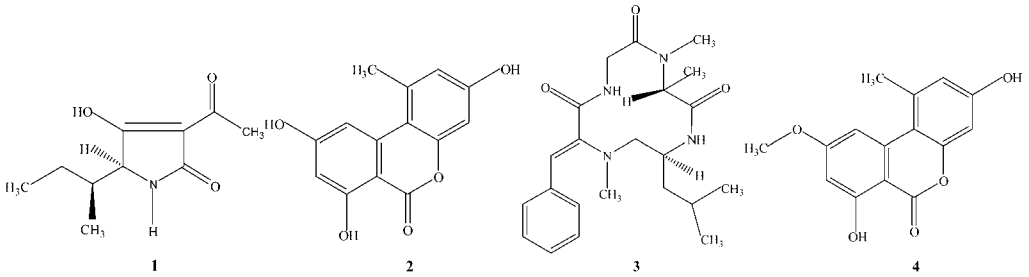

Figure 1. Chemical structures of tenuazonic acid, **1**; alternariol, **2**; tentoxin, **3**; and alternariol monomethyl ether, **4**.

time, however, no study has been carried out for *Alternaria* toxin contamination in tomato and citrus products at the national level in China. Therefore, no data on risk assessment of dietary exposure to *Alternaria* toxins in the Chinese population is available so far. To provide the scientific data for assessing the impact of *Alternaria* toxins on Chinese public health, the purpose of this study was to evaluate the natural occurrence of associated *Alternaria* mycotoxins in Chinese fresh tomato, tomato ketchup, and fresh citrus, and citrus juice. The results obtained will be expected to contribute to either the development of strategies to reduce risk from these contaminants or the ongoing research on the relationship between the consumption of tomato and citrus products contaminated with *Alternaria* toxins and human disease.

MATERIALS AND METHODS

Reagents and Chemicals. Methanol and acetonitrile used for sample extraction and toxin separation were of HPLC grade (Dikma Pure, Richmond Hill, GA, USA). Both ammonium bicarbonate (Sigma-Aldrich, St. Louis, MO, USA) and formic acid (≥95% purity) (Fluka, Steinheim, Germany) were of analytical grade. Pure water was obtained from a Millipore Milli-Q System (Millipore, Bedford, MA, USA). Standards for alternariol (purity > 98%), alternariol monomethyl ether (purity > 98%), tentoxin (purity > 99%), and tenuazonic acid (purity > 99%) were purchased from Fermenteck Ltd. (Jerusalem, Israel). All experimental practice followed Environmental Health Safety Guidelines for the use of chemicals authorized by China National Center for Food Safety Risk Assessment. In addition, sample collection and solvent extracts should be handled with care.

Samples. A total of 30 fresh tomato and 40 tomato-based products including tomato ketchup (n = 31) and tomato juice (n = 9) samples as well as 50 fresh citrus and 36 citrus juice samples were randomly collected from supermarkets and agricultural trade markets in Beijing. The fresh tomatoes covered the main cultivars in China such as common tomato and cherry tomato that came from the main vegetable-producing regions including Beijing, Shandong, Hebei, Jiangsu, Tianjin, Fujian, Zhejiang, and Guangdong provinces. Tomato ketchup and tomato juice samples covered the main brands available in markets in China; the nine tomato ketchup samples were imported from Bulgaria (two samples), Italy (two samples), Japan, Turkey, Australia, the United States, and Spain, respectively. All samples were stored at 4 °C until analysis.

Toxin Extraction. The extraction of *Alternaria* toxins from samples was modified on the basis of the methods described by Kocher[20] and Rheinhold et al.[21] with a minor modification. In brief, both fresh tomatoes and citrus fruits were fully ground, whereas tomato- and citrus-based products were blended or shaken thoroughly. A test portion of 5 g of sample was homogenized with 20 mL of acetonitrile/water/methanol (45:45:10, v/v/v) and sonicated in an ultrasonic cleaner for 30 min, followed by centrifuging for 10 min at 7000 rpm. A portion of 5 mL of supernatant was diluted 5 times with distilled water, adjusted to pH 3−4 with formic acid, and passed through a HLB solid phase extraction (SPE) cartridge (Waters, Rupperswil, Switzerland) preconditioned with 5 mL of methanol followed by 5 mL of water. The cartridge was washed with 5 mL of water followed by 5 mL of methanol−water (20:80, v/v). *Alternaria* toxins were eluted with 5 mL of methanol and 5 mL of acetonitrile sequentially. The organic phase elutes were combined, evaporated to dryness, and dissolved in 1 mL of methanol/water (10:90, v/v) containing 0.5 mmol/L ammonium bicarbonate and centrifuged for 5 min at 10000 rpm. An aliquot of 10 μL of the extract was injected for *Alternaria* toxins analysis by UPLC-MS/MS.

UPLC Conditions. Detection and quantitation of the four target mycotoxins were performed on a Micromass Quattro Premier XE ultra performance liquid chromatography−tandem mass spectrometry (UPLC-MS/MS) system (Waters, Milford, MA, USA). The column used was a 100 mm × 2.1 mm i.d., 1.7 μm, BEH C_{18} (Waters) thermostated at 40 °C. The mobile phase included 0.5 mmol/L ammonium bicarbonate solution (solvent A) and methanol (solvent B). A binary gradient at a flow rate of 0.3 mL/min was programmed starting at 90% A, reached 100% B in 5 min, and was maintained there for 2 min. Afterward, B was linearly decreased to 10% B within 0.1 min and maintained at this composition of mobile phase for 2 min. The retention times of the four toxins were 1.69 min for tenuazonic acid, 3.79 min for alternariol, 4.38 min for tentoxin, and 4.94 min for alternariol monomethyl ether.

Preparation of Standard Solutions. Stock *Alternaria* toxin standard solutions at the concentration of 100 mg/L were prepared by dissolving appropriate amounts of alternariol, alternariol monomethyl ether, tentoxin, and tenuazonic acid standard powder in methanol, respectively, and stored in amber vessels at −18 °C for up to 1 year. Working standard solutions were made by diluting the stock standard solutions with *Alternaria* toxin-free sample extract prepared following the toxin extraction procedure.

MS/MS Conditions. MS/MS was performed on a Waters Aquity Quattro Premier XE triple-quadrupole mass spectrometer equipped with electrospray ionization (ESI) source. The source block temperature was 100 °C, and desolvation temperature was 350 °C. Nitrogen (purity = 99.9%) was used as both the cone gas and desolvation gas at flow rates of 1 and 552 L/h, respectively, whereas high-purity argon was used as the collision gas at a flow rate of 0.2 mL/min. The mass spectrometer was operated in negative electrospray ionization (ESI^-) mode for quantitation of the four toxins. Data acquisition and evaluation were performed by Masslynx software (Micromass, Manchester, UK).

Method Validation. To evaluate the performance of UPLC-MS/MS conditions for analysis of the four mycotoxins, the matrix-matched calibration curve was made to compensate for matrix effect. Standard solutions of the four mycotoxins at concentrations ranging from 5 to 100 μg/L for tenuazonic acid, from 20 to 400 μg/L for alternariol, from 2 to 40 μg/L for tentoxin, and from 0.4 to 8 μg/L for alternariol monomethyl ether were added to the final extract solution of mycotoxin-free fresh tomato, tomato ketchup, fresh citrus, and citrus juice and processed for analysis by LC-MS/MS. To determine the method recoveries and the relative standard deviation (RSD), analyses of the spiked four matrix samples at spiking levels between 5 and 50 μg/kg (six repetitions for each) for the four mycotoxins were carried out. The limit of detection (LOD) and the limit of quantification (LOQ) for these four mycotoxins were determined with signal-to-noise ratios of 3:1 and 10:1, respectively. Reproducibility was evaluated over five consecutive days at three nominal tenuazonic acid concentrations (50, 500, and 5000 μg/kg) by spiking the

DOI: 10.1021/jf5052738
J. Agric. Food Chem. 2015, 63, 343−348

uncontaminated matrix. For each concentration and day, the standard addition scheme described above was conducted. For determination of intralaboratory reproducibility, two tomato ketchup samples naturally contaminated with tenuazonic acid, alternariol, tentoxin, and alternariol monomethyl ether at levels of 370, 37, 3.3, and 10 μg/kg and two citrus juice samples naturally contaminated with tenuazonic acid, alternariol, tentoxin, and alternariol monomethyl ether at concentrations of 370, 37, 3.3, and 10 μg/kg, respectively, were analyzed three times within 2 weeks, and duplicate analyses were conducted for each sample each time.

RESULTS AND DISCUSSION

Method Optimization. For the four toxins cleanup from a HLB SPE cartridge, methanol/water in different ratios (20:80, 30:70, and 40:60, v/v) and acetonitrile/water/methanol (45:45:10, v/v/v), respectively, were studied. Better cleanup efficiency of the analytes was obtained when methanol/water (20:80, v/v) was selected. Additionally, the choice of mobile phase should be based on the consideration of ionization efficiency before the analytes enter the MS/MS system to obtain good resolution and high sensitivity. In terms of additives in the mobile phase, aqueous ammonia, ammonium formate, and ammonium bicarbonate were studied. Responses and peak shape were greatly improved when 0.5 mmol/L of aqueous solution of bicarbonate was used as solvent A. Results indicated that when acetonitrile was chosen as the mobile phase, the ionization of all the selected analytes was significantly suppressed, and the abundance and sensitivity were thus reduced. Conversely, very positive results were observed when methanol was used as the mobile phase. Therefore, methanol was selected as the strong elution mobile phase in the present study.

Method Validation. Matrix-matched standards were used for calibration to compensate for the matrix effect. The concentrations used for making calibration curves ranged from 5 to 100 μg/L for **1**, from 20 to 400 μg/L for **2**, from 2 to 40 μg/L for **3**, and from 0.4 to 8 μg/L for **4** with linear coefficients better than 0.999. The method showed an excellent linearity over the ranges of 16−320 μg/kg for **1**, 0.3−6 μg/kg for **2**, 1.6−32 μg/kg for **3**, and 4−80 μg/kg for **4** expressed by the coefficients (r^2) of >0.99 for all curves. The validation results demonstrated high sensitivity, repeatability, and linearity of the method. The LODs of tenuazonic acid, alternariol, tentoxin, and alternariol monomethyl ether were 1, 5, 0.5, and 0.1 μg/kg in tomato-based products and 1, 6, 0.7, and 0.1 μg/kg in citrus-based samples, respectively, which were the same as or lower than those reported by Noser et al.[5] but higher than those obtained with the stable isotope method.[14,16,19]

To extract the four mycotoxins rapidly from the tested matrix and to eliminate coextraction of potentially interfering matrix components as much as possible, absolute recoveries of the four toxins from four matrices were assessed. The recovery of tenuazonic acid from tomato ketchup was performed with a naturally tenuazonic acid-contaminated sample because no tenuazonic acid-free tomato ketchup samples were found in this study. For each analyte/matrix combination, the recoveries at three spiking levels ranged from 73.4 to 111.2% for all four toxins in tomato- and citrus-based product samples; values fall within the range of 70−120% as recommended by the European Commission.[22] On the other hand, RSDs for all four toxins were <20% with the range 2.5−20.0%, which was compatible with the general requirement of the analytical method. With regard to intralaboratory repeatability, the coefficients of variation (CV) were 4.2% for tenuazonic acid in tomato ketchup and 4.2% in citrus juice, 14.6% for alternariol in tomato ketchup and 14.6% in citrus juice, 12.3% for tentoxin in tomato ketchup and 12.3% in citrus juice, and 9.8% for alternariol monomethyl ether in tomato ketchup and 9.8% in citrus juice. On the basis of these results, we conclude that the extraction efficiencies achieved by the method used in the present study were high and consistent. Under LC-MS/MS conditions, very good resolution for the four mycotoxins in tomato samples was observed and their spectra were similar to those of the corresponding standards.

Natural Occurrence of the Four *Alternaria* Toxins in Fresh Tomato and Tomato-Based Products. Contamination levels of the four *Alternaria* toxins in Chinese tomato and tomato-based product samples are given in Table 1. No toxins were detected in all of the fresh tomato samples. In terms of tomato ketchup, alternariol and alternariol monomethyl ether were detected in 14 (45.2%) samples at levels ranging from 2.5 to 300 μg/kg (mean = 80 μg/kg) and in 28 (90.3%) samples within a range of 0.32−38 μg/kg (mean = 8.0 μg/kg), respectively. Alternariol was quantitated at higher levels than alternariol monomethyl ether with the ratio of alternariol/alternariol monomethyl ether ranging from 0.37 to 104 (average = 17) in 14 alternariol positive samples, among which 21.4% (3/14) were <1. Thus, the concentration of alternariol was higher than that of alternariol monomethyl ether in these alternariol-positive samples. All tomato juice samples were negative for alternariol but 7 (7/9, 77.8%) were positive for alternariol monomethyl ether with the level up to 5.8 μg/kg (average = 1.4 μg/kg). Tentoxin was less frequently detected than alternariol monomethyl ether and tenuazonic acid. Alternariol was negative in tomato juice samples.

Table 1. Concentrations of the Four *Alternaria* Toxins in Tomato and Tomato-Based Products

			toxin concn (μg/kg)		
sample	toxin	positive (%)	range	mean	median
fresh tomato (n = 30)	**1**	0			
	2	0			
	3	0			
	4	0			
tomato ketchup (n = 31)	**1**	31 (100)	10.2−1787	338	186
	2	14 (45.2)	2.5−300	80	29
	3	26 (83.9)	1.53−15.8	4.9	5.0
	4	28 (90.3)	0.32−38	8.0	6.6
tomato juice (n = 9)	**1**	9 (100)	7.4−278	87	72
	2	0			
	3	3 (33.3)	1.85−5.7	3.7	3.6
	4	7 (77.8)	0.20−5.8	1.42	0.62

Tenuazonic acid was the predominant toxin quantitatively as shown in Table 1. It was detected at average concentrations of 338 μg/kg in tomato ketchup and 87 μg/kg in tomato juice samples. A total of 2 (6.4%) tomato ketchup samples were contaminated with tenuazonic acid at >1000 μg/kg with a maximum of 1786 μg/kg, 4 samples (12.9%) between 500 and 1000 μg/kg, 15 samples (48.4%) between 100 and 500 μg/kg, and 18 samples below 100 μg/kg. The maximum concentration of tenuazonic acid was higher than the result reported by Noser,[5] but lower than that reported by Terminiello et al.[4]

DOI: 10.1021/jf5052738
J. Agric. Food Chem. 2015, 63, 343−348

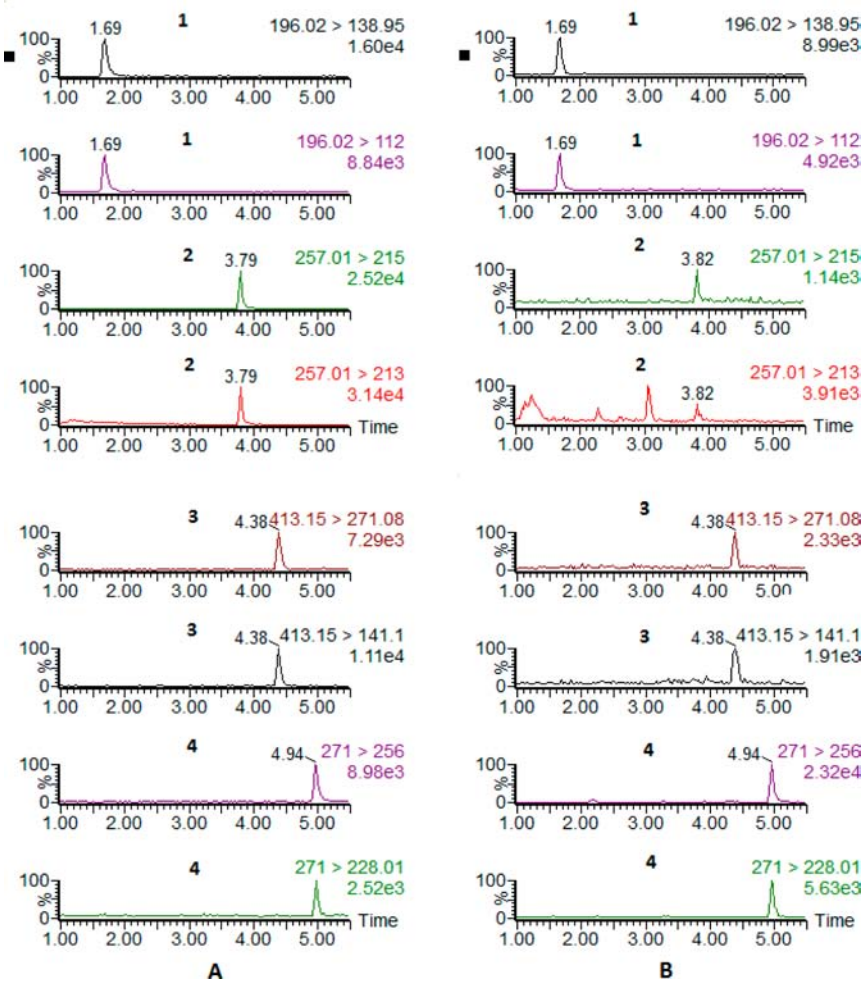

Figure 2. MRM chromatograms of (A) tenuazonic acid, **1**; alternariol, **2**; tentoxin, **3**; and alternariol monomethyl ether, **4** standards in 25, 100, 5, and 1.2 μg/kg; and (B) a naturally contaminated tomato ketchup sample in 89 μg/kg for tenuazonic acid, **1**; 11 μg/kg for alternariol, **2**; 6.2 μg/kg for tentoxin, **3**; and 12 μg/kg for alternariol monomethyl ether, **4**, respectively.

With regard to tenuazonic acid concentration in tomato juice, six samples were contaminated with tenuazonic acid at a level of <100 μg/kg and three samples with tenuazonic acid at >100 μg/kg. It should be pointed out that 10 imported tomato ketchup samples were heavily contaminated by tenuazonic acid with the average concentration of 558 μg/kg, much higher than those of domestic origin (Mann−Whitney U test, $Z = -2.155$, $P < 0.05$). Among these, the top three concentrations of tenuazonic acid (1787, 1464, and 939 μg/kg) were found in samples imported from Italy, Spain, and Australia, respectively. Tentoxin was found in 26 (26/31, 83.9%) tomato ketchup and 3 (3/9, 33.3%) tomato juice samples up to 15.8 and 5.7 μg/kg, respectively. Therefore, tentoxin was the toxin with the lowest contamination level in tomato products. With regard to the co-occurrence of four *Alternaria* toxins in tomato ketchup, all of the toxins were simultaneously detected in 14 alternariol-positive samples (45.2%), whereas alternariol monomethyl ether, tentoxin, and tenuazonic acid were in 28 alternariol monomethyl ether-positive samples (90.3%). The MRM chromatograms of a naturally contaminated ketchup sample as well as the corresponding standards are given in Figure 2.

Natural Occurrence of the Four *Alternaria* Toxins in Citrus Fruit and Citrus Juice. None of the four *Alternaria* toxins were detected in 50 fresh citrus samples without any spoilage (shown as Table 2). Tenuazonic acid was also the main *Alternaria* toxin detected in 9 of 36 (25.0%) citrus juice samples at a level between 1.21 and 4.3 μg/kg (mean = 1.80 μg/kg and median of 1.28 μg/kg), whereas alternariol monomethyl ether was found in 4 of 36 samples (11.1%) at levels up to 0.2 μg/kg. However, neither alternariol nor tentoxin was detected in citrus juice samples. Tenuazonic acid and alternariol monomethyl ether were simultaneously detected in only one citrus juice. These results were consistent with those reported by Asam et al.[14]

Table 2. Concentrations of the Four *Alternaria* Toxins in Fresh Citrus Fruit and Citrus Juice

			toxin concn (μg/kg)		
sample	toxins	positive (%)	range	mean	median
fresh citrus fruit (n = 50)	**1**	0			
	2	0			
	3	0			
	4	0			
citrus juice (n = 36)	**1**	9 (25.0)	1.21−4.3	1.80	1.28
	2	0			
	3	0			
	4	4 (11.1)	0.11−0.20	0.14	0.12

DOI: 10.1021/jf5052738
J. Agric. Food Chem. 2015, 63, 343−348

To the best of our knowledge, this is the first report on the natural co-occurrence of alternariol, alternariol monomethyl ether, tentoxin, and tenuazonic acid in Chinese retail fresh tomato, tomato ketchup, fresh citrus, and citrus juice. The levels of four *Alternaria* toxins in citrus and citrus juice were quite low and might not be of any health risk for human beings. In terms of each toxin that occurred and the level in tomato ketchup samples, our findings correspond with those of Swiss samples: tenuazonic acid > alternariol > alternariol monomethyl ether > tentoxin.[7] In particular, alternariol was quantitated at higher levels than alternariol monomethyl ether with the ratio of alternariol/alternariol monomethyl ether up to 104 (average = 17) in 14 alternariol-positive samples. These results tended to be different from those in wheat reported previously in China.[23] Additionally, a positive correlation between alternariol and alternariol monomethyl ether (r^2 = 0.850, $P < 0.001$) and also the total dibenzopyrone derivatives (alternariol + alternariol monomethyl ether) and tenuazonic acid (r^2 = 0.796, $P < 0.001$) in wheat samples has been demonstrated by Li et al.,[23] indicating the coproduction of these toxins on wheat grains by *Alternaria* species in fields. However, no significant correlations were found in concentrations between alternariol and alternariol monomethyl ether (r^2 = 0.070) and total dibenzopyrone derivatives and tenuazonic acid (r^2 = 0.035) in tomato ketchup samples. Invasion of tomato and wheat by different species of *Alternaria* may mainly contribute to the difference in toxin levels in the same area.

In contrast, alternariol was found at levels of 1 and 13 μg/kg with high frequency in apple (67% of 44 samples) and tomato (93% of 44 samples) products, respectively, reported by Ackermann et al.[24] A survey conducted in Brazil revealed that neither alternariol monomethyl ether nor alternariol was detected in 80 samples, but tenuazonic acid was found in 7 tomato pulp (39−111 μg/kg) and 4 tomato puree (29−76 ng/g) samples.[25] Low mean levels of alternariol (up to 25 μg/kg) and alternariol monomethyl ether (up to 0.7 μg/kg) were measured in vegetables, mainly tomato paste.[16] Tenuazonic acid at levels between 15 and 195 μg/kg, between 363 and 909 μg/kg, and between 8 and 242 μg/kg were found in commercial tomato ketchup, tomato paste, and pureed tomato samples analyzed by stable isotope dilution assays, respectively.[16] All results mentioned above are much lower than ours. However, about 60% of Argentinian tomato pulp samples were contaminated with tenuazonic acid, alternariol monomethyl ether, and alternariol at levels up to 4021 μg/kg (29% of 80 samples), 1734 μg/kg (26% of 80 samples), and 8756 μg/kg (6% of 80 samples),[4] respectively, with the maximum levels of tenuazonic acid, alternariol, and alternariol monomethyl ether higher than those obtained in the present study.

Alternaria mycotoxins in tomato and citrus products are most likely to come from the contaminated raw material. Tomato ketchup was made from tomatoes through a series of steps including washing, heating, pulping, condensing, etc. It is well-known that *Alternaria* rapidly colonizes tomatoes and produces mycotoxins under favorable conditions. It was speculated that *Alternaria* mycotoxins in tomato ketchup probably came from decayed tomatoes or from the steps contaminated with *Alternaria* species during the production line.[4] *Alternaria* mycotoxins detected at higher concentrations in tomato ketchup than in fresh tomatoes were partly due to the former being concentrated after production.

EFSA has given a scientific opinion on the risks for animal and public health related to dietary exposure to seven *Alternaria* mycotoxins.[10] The estimated chronic dietary exposures for the four toxins were much lower than the corresponding threshold of toxicological concern (TTC), indicating no human health concern according to the in vitro model for intestinal absorption and consumption data in China (data not shown).[26,27] However, alternariol and alternariol monomethyl ether were genotoxic and bound to the DNA of esophageal epithelium of the human fetus, activated oncogenes in the human fetal epithelium, and induced epithelial proliferation of human fetal esophagus in vitro.[28] Although *Alternaria* spp. are the most frequent fungal species invading tomatoes,[2,12] there are no specific regulations for any of the *Alternaria* toxins in foods in China so far. Therefore, systemic long-term surveillance of *Alternaria* toxins in raw and processed foods all over China, especially in the area with high incidence of esophageal cancer, as well as a thorough assessment of dietary exposure to these toxins in Chinese populations should be intensified to evaluate consumers' health risk.

■ ASSOCIATED CONTENT

Ⓢ Supporting Information

Tables A−C (MRM parameters, LODs and LOQs, and recoveries and RSDs of the four toxins in samples). This material is available free of charge via the Internet at http://pubs.acs.org.

■ AUTHOR INFORMATION

Corresponding Author

*(F.L.) Phone/fax: 86-10-67776356. E-mail: lifengqin@cfsa.net.cn.

Funding

This study was financially supported by the National High-tech R&D Program (863 Program) and the Ministry of Science and Technology of the People's Republic of China (Grant 2012AA101603).

Notes

The authors declare no competing financial interest.

■ REFERENCES

(1) Bottalico, A.; Logrieco, A. *Alternaria* plant diseases in Mediterranean countries and associated mycotoxins. In *Alternaria Biology, Plant Diseases and Metabolites*; Chełkovski, J., Visconti, A., Eds.; Elsevier Science: New York, 1992; pp 209−232.

(2) Barkai-Golan, R. *Alternaria* mycotoxins. In *Mycotoxins in Fruits and Vegetables*; Barkai-Golan, R., Nachman, P., Eds.; Academic Press: San Diego, CA, USA, 2008; 185 pp.

(3) Králová, J.; Hajšlová, J.; Poustka, J.; Hochman, M.; Bjelková, M.; Odstrčilová, L. Occurrence of *Alternaria* toxins in fibre flax, linseed, and peas grown in organic and conventional farms: monitoring pilot study. *Czech J. Food Sci.* **2006**, *24*, 288−296.

(4) Terminiello, L.; Patriarca, A.; Pose, G.; Fernandez Pinto, V. Occurrence of alternariol, alternariol monomethyl ether and tenuazonic acid in Argentinean tomato puree. *Mycotoxin Res.* **2006**, *22*, 236−240.

(5) Noser, J.; Schneider, P.; Rother, M.; Schmutz, H. Determination of six *Alternaria* toxins with UPLC-MS/MS and their occurrence in tomatoes and tomato products from the Swiss market. *Mycotoxin Res.* **2011**, *27*, 265−271.

(6) Robiglio, A. L.; Lopez, S. E. Mycotoxin production by *Alternaria alternata* strains isolated from red delicious apples in Argentina. *Int. J. Food Microbiol.* **1995**, *24*, 413−417.

DOI: 10.1021/jf5052738
J. Agric. Food Chem. 2015, 63, 343−348

(7) Magnani, R. F.; De Souza, G. D.; Rodrigues-Filho, E. Analysis of alternariol and alternariol monomethyl ether on flavedo and albedo tissues of tangerines (*Citrus reticulata*) with symptoms of *Alternaria* brown spot. *J. Agric. Food Chem.* **2007**, *55*, 4980−4986.
(8) Pollock, G. A.; DiSabatino, C. E.; Heimsch, R. C.; Hilbelink, D. R. The subchronic toxicity and teratogenicity of alternariol monomethyl ether produced by *Alternaria solani*. *Food Chem. Toxicol.* **1982**, *20*, 899−902.
(9) Ostry, V. *Alternaria* mycotoxins: an overview of chemical characterization, producers, toxicity, analysis and occurrence in foodstuffs. *World Mycotoxin J.* **2008**, *1*, 175−188.
(10) EFSA on Contaminants in the Food Chain (CONTAM). Scientific opinion on the risks for animal and public health related to the presence of *Alternaria* toxins in feed and food. *EFSA J.* **2011**, *9*, 2407, DOI:10.2903/j.efsa.2011.2407.
(11) Zhang, X. H.; Wang, F. R.; Xie, T. X.; Wang, J. L. Incidence of various species of fungi in cereals for human consumption in areas with high incidence of esophageal cancer in Ci county. *J. Hyg. Res.* **1996**, *25*, 166−168.
(12) Logrieco, A.; Moretti, A.; Solfrizzo, M. *Alternaria* toxins and plant diseases: an overview of origin, occurrence and risks. *World Mycotoxin J.* **2009**, *2*, 129−140.
(13) Lau, B. P.; Scott, P. M.; Lewis, D. A.; Shriniwas, R. K.; Cléroux, C.; Roscoe, V. A. Liquid chromatography−mass spectrometry and liquid chromatography−tandem mass spectrometry of the *Alternaria* mycotoxins alternariol and alternariol monomethyl ether in fruit juices and beverages. *J. Chromatogr., A* **2003**, *998*, 119−131.
(14) Asam, S.; Konitzer, K.; Schieberle, P.; Rychlik, M. Stable isotope dilution assays of alternariol and alternariol monomethyl ether in beverages. *J. Agric. Food Chem.* **2009**, *57*, 5152−5160.
(15) Siegel, D.; Feist, M.; Proske, M.; Koch, M.; Nehls, I. Degradation of the *Alternaria* mycotoxins alternariol, alternariol monomethyl ether, and altenuene upon bread baking. *J. Agric. Food Chem.* **2010**, *58*, 9622−9630.
(16) Asam, S.; Konitzer, K.; Rychlik, M. Precise determination of the *Alternaria* mycotoxins alternariol and alternariol monomethyl ether in cereal, fruit and vegetable products using stable isotope dilution assays. *Mycotoxin Res.* **2011**, *27*, 23−28.
(17) Prelle, A.; Spadaro, D.; Garibaldi, A.; Lodovica, M. G. A new method for detection of five *Alternaria* toxins in food matrices based on LC-APCI-MS. *Food Chem.* **2013**, *140*, 161−167.
(18) Asam, S.; Liu, Y.; Konitzer, K.; Rychlik, M. Development of a stable isotope dilution assay for tenuazonic acid. *J. Agric. Food Chem.* **2009**, *59*, 2980−2987.
(19) Liu, Y.; Rychlik, M. Development of a stable isotope dilution LC-MS/MS method for the *Alternaria* toxins tentoxin, dihydrotentoxin, and isotentoxin. *J. Agric. Food Chem.* **2013**, *61*, 2970−2978.
(20) Kocher, U. Determination of 7 *Alternaria*-toxins in edible oil and oilseeds by LC-MS/MS. In *Gesellschaft für Mykotoxin Forschung*, Proceedings of the 29th Mycotoxin Workshop, Fellbach, Germany, May 14−16, 2007; p 72.
(21) Rheinhold, L.; Bartels, I. *Alternaria*-Toxine mit Festphasenextraktion und LC-MS/MS bestimmen. *Labor-Praxis* **2007**, *10*, 62−65.
(22) European Commission. SANCO/12571/2013. Guidance document on analytical quality control and validation procedures for pesticide residues analysis in food and feed; available at http://ec.europa.eu/food/plant/plant_protection_products/guidance_documents/docs/qualcontrol_en.pdf (accessed Dec 5, 2014).
(23) Li, F. Q.; Yoshizawa, T. *Alternaria* mycotoxins in weathered wheat from China. *J. Agric. Food Chem.* **2000**, *48*, 2920−2924.
(24) Ackermann, Y.; Curtui, V.; Dietrich, R.; Gross, M.; Latif, H.; Määrtlbauer, E.; Usleber, E. Widespread occurrence of low levels of alternariol in apple and tomato products, as determined by comparative immunochemical assessment using monoclonal and polyclonal antibodies. *J. Agric. Food Chem.* **2011**, *59*, 6360−6368.
(25) Da Motta, S.; Valente Soares, L. M. Survey of Brazilian tomato products for alternariol, alternariol monomethyl ether, tenuazonic acid, and cyclopiazonic acid. *Food Addit. Contam.* **2001**, *18*, 630−634.
(26) Kroes, R.; Renwick, A. G.; Cheeseman, M.; Kleiner, J.; Mangelsdorf, I.; Piersma, A.; Chilter, B.; Schlatter, J.; van Schoothorst, F.; Vos, J. G.; Würtzen, G. Structure-based thresholds of toxicological concern (TTC): guidance for application to substances at low levels in the diet. *Food Chem. Toxicol.* **2004**, *42*, 65−83.
(27) Burkhardt, B.; Pfeiffer, E.; Metzler, M. Absorption and metabolism of the mycotoxins alternariol and alternariol-9-methyl ether in Caco-2 cells *in vitro*. *Mycotoxin Res.* **2009**, *25*, 149−157.
(28) Liu, G.; Qian, Y.; Zhang, P.; Dong, W.; Qi, Y.; Guo, H. Etiological role of *Alternaria alternata* in human esophageal cancer. *Chin. Med. J.* **1992**, *105*, 394−400.

DOI: 10.1021/jf5052738
J. Agric. Food Chem. 2015, 63, 343−348

JOURNAL OF AGRICULTURAL AND FOOD CHEMISTRY

Article

pubs.acs.org/JAFC

Brown Alga *Ecklonia cava* Polyphenol Extract Ameliorates Hepatic Lipogenesis, Oxidative Stress, and Inflammation by Activation of AMPK and SIRT1 in High-Fat Diet-Induced Obese Mice

Hyeyoon Eo,[†] You-jin Jeon,[§] Myoungsook Lee,[#] and Yunsook Lim*[,†]

[†]Department of Food and Nutrition, Kyung Hee University, 26 Kyunghee-daero, Dongdaemun-gu, Seoul 130-701, Republic of Korea

[§]Department of Marine Life Sciences, Jeju National University, Jeju 690-756, Republic of Korea

[#]Department of Food and Nutrition, Sungshin Women's University and Research Institute of Obesity Sciences, Sungshin Women's University, Seoul 136-742, Republic of Korea

ABSTRACT: Obesity is considered to be a metaflammatory condition. *Ecklonia cava*, brown algae rich in polyphenols, has shown strong antioxidant activity in vitro. This study investigated the effect of *E. cava* polyphenol extract (ECPE) on the regulation of fat metabolism, inflammation, and the antioxidant defense system in high fat diet-induced obese mice. After obesity was induced by a high-fat diet (HFD), the mice were administered ECPE by gavage for 5 days/12 weeks. ECPE supplementation reduced body weight gain, adipose tissue mass, plasma lipid profiles, hepatic fat deposition, insulin resistance, and the plasma leptin/adiponectin ratio derived from HFD-induced obesity. Moreover, ECPE supplementation selectively ameliorated hepatic protein levels associated with lipogenesis, inflammation, and the antioxidant defense system as well as activation of AMPK and SIRT1. Collectively, ECPE supplement might have potential antiobesity effects via regulation of AMPK and SIRT1 in HFD-induced obesity.

KEYWORDS: *Ecklonia cava polyphenol extract, obesity, AMPK, SIRT1, hepatic lipid metabolism, inflammation*

INTRODUCTION

Recently, obesity has been recognized as a chronic metabolic disorder.[1] Under an obese condition, there are several abnormalities in lipid metabolism, the antioxidant defense system, and inflammatory responses. As the storage of triglyceride (TG) in adipose tissue exceeds its limit, it is likely to encourage the release of free fatty acids (FFA) into circulation, and released FFA could be brought into nonadipose tissues such as the liver.[2] Obese subjects might undergo nonalcoholic fatty liver disease (NAFLD) characterized by an increase in fat accumulation in the liver caused by abnormalities, including reduced fatty acid (FA) oxidation or TG secretion and increased FA uptake or de novo lipogenesis.[3] Moreover, the TG overload in liver could cause hepatic damage and increase reactive oxygen species (ROS), which induce lipid peroxidation and inflammation.[4]

At the molecular level, AMP-activated protein kinase (AMPK) and Sirtuin 1 (SIRT1) are regarded as key fuel sensors or metabolic modulators. It is well-documented in detail that AMPK plays a key role in hepatic lipid metabolism, through inactivation of several metabolic enzymes, in switching on catabolic pathways such as β-oxidation as well as switching off anabolic pathways involving lipid metabolism in the liver.[5,6] SIRT1, an NAD^+-dependent protein deacetylase, is involved in several metabolic pathways in various tissues.[7] Especially, SIRT1 is involved in lipid and glucose metabolism, inflammatory response, and oxidative stress in hepatic tissue.[8] Furthermore, it has been reported that SIRT1 modulates fatty acid β-oxidation and cholesterol/bile homeostasis through the peroxisome proliferator-activated receptor alpha (PPARα)/peroxisome proliferator-activated receptor gamma coactivator 1 (PGC1) pathway and liver X receptor (LXR)/farnesoid X receptor (FXR) signaling, respectively.[9,10] SIRT1 might also regulate lipid metabolism by deacetylation of sterol regulatory element binding proteins (SREBPs), which are pivotal modulators of lipogenesis and cholesterolgenesis[11,12] and inflammatory responses such as tumor necrosis factor alpha (TNFα) and interleukin 1 beta (IL-1β).[9] Thereby, inactive or reduced levels of SIRT1 increased susceptibility to dyslipidemia, hepatic steatosis, inflammation, and endoplasmic reticulum stress.[7,9] Recently, a partnership between AMPK and SIRT1 has been well-documented in a previous study.[13] Briefly, when SIRT1 is stimulated by certain activators such as NAD^+, SIRT1 regulates AMPK by deacetylation of liver kinase B1 (LKB1). According to previous studies, the mechanism provides a comprehensive explanation in hepatic lipid metabolism and NAFLD by suggesting an SIRT1/AMPK cycle.[14] Therefore, partnership between AMPK and SIRT1 could be considered as a crucial target to regulate hepatic lipid metabolism related to NAFLD in obesity.

Brown alga *Ecklonia cava* is produced in bountiful amounts on the coast of Jeju Island, Korea. *E. cava* contains copious polysaccharides such as fucoidans as well as polyphenols including dieckol, eckol, phloroglucinol, 6,6′-bieckol, and eckstolonol.[15] In the previous study, *E. cava* ethanolic extracts suppressed the lipopolysaccharide (LPS)-induced cytokines such as TNFα and IL-1β and reduced the inducible nitric oxide

Received: June 17, 2014
Revised: November 14, 2014
Accepted: December 5, 2014
Published: December 5, 2014

ACS Publications © 2014 American Chemical Society

synthase (iNOS) and the cyclooxygenase-2 (COX-2) expression by blocking transcription factors of the nuclear factor kappa B (NFκB) and the mitogen-activated protein kinase (MAPK) activation in BV2 microglia.[16] Among the polyphenols of *E. cava*, dieckol is the most ample compound in *E. cava*, and it has been reported for having some beneficial potential such as antioxidative effects and antithrombotic activity.[17,18] A recent study reported that dieckol, which was isolated from *E. cava*, inhibited adipogenesis by activating AMPK and suppressing adipocyte differentiation in 3T3-L1 preadipocytes.[19] However, little research has focused on the molecular mechanisms by which *E. cava* polyphenol extract (ECPE) regulates hepatic lipid metabolism in an obese animal model.

We investigated how ECPE ameliorates hepatic lipid metabolism, oxidative stress, and inflammation through modulation of AMPK and SIRT-1 in high-fat diet (HFD)-induced obese mice.

MATERIALS AND METHODS

Preparation of ECPE. ECPE used in this study was provided from Aqua Green Tech., Jeju, Korea. The preparation of dieckol-rich polyphenols from *E. cava* was described previously.[20] In brief, the *E. cava* was collected from the coast of Jeju Island, Korea. The powdery *E. cava* (500 g) was suspended in 10 L of 70% ethanol and stirred for 24 h at room temperature. The solution was filtered and then concentrated under reduced pressure to give the oily extract. Then, the organic soluble fraction was taken by treatment with ethyl acetate (47.85 g), and the extract was evaporated under vacuum.

Quantification of Total Phenol and Major Compounds in ECPE. The total phenol content in the polyphenol extract was measured by using the protocol described by Kim et al.[21] The quantitative analysis in the major compounds in the polyphenol extract from *E. cava* was performed by their HPLC analysis and quantitative standard curve. The quantitative standard curves of the main compounds were calculated by their area (%) in high-performance liquid chromatography (HPLC) under concentrations between 25 and 400 μg/mL.

Identification of Major Compounds in ECPE and Chemical Structure of Dieckol. The structural identification of the major compounds in the polyphenol extract from *E. cava* was performed by using the method described in a previous paper.[22] The major compounds in the extract were confirmed by LC-DAD-ESI/MS and 1D NMR spectrum. To operate LC-DAD-ESI/MS, 10 μL of 5 mg/mL sample solution was directly injected on an Atlantis T3 column (3 μm 3.0 × 150 mm column) (Waters, Milford, MA, USA). The mobile phase comprised acetonitrile/water in gradient mode as follows: acetonitrile with 0.1% formic acid/water with 0.1% formic acid (0−40 min, 10:90−40:60 v/v; 40−50 min, ∼50:50 v/v; and 50−60 min, ∼100:0 v/v). The flow rate was 0.2 mL/min, and the UV absorbance was detected at 290 nm. The source voltage was set to 4.5 kV and the capillary temperature to 250 °C. The other conditions were as follows: capillary voltage, −36.5 V; interoctapole lens voltage, 10 V; sheath gas, 80 psi (551.6 kPa); auxiliary gas, 20 psi (137.9 kPa). The major compounds were confirmed as dieckol, 2,7″-phloroglucinol-6,6′-bieckol, pyrogallol-phloroglucinol-6,6′-bieckol, and phlorofucofuroeckol-A, respectively. After purification of the compounds from the *E. cava* extract, their ^{1}H NMR and ^{13}C NMR spectra were measured with a JEOL JNM-LA 300 spectrometer (JEOL Ltd., Tokyo, Japan), and the mass spectra (FAB-MS and EIMS) were recorded on a JEOL JMS 700 spectrometer.

Dieckol: amorphous powder; ^{1}H NMR (400 MHz, methanol-d_4) δ 6.15 (1H, s), 6.13 (1H, s), 6.09 (1H, δ, 2.9 Hz), 6.06 (1H, δ, 2.9 Hz), 6.05 (1H, δ, 2.9 Hz), 5.98 (1H, δ, 2.8 Hz), 5.95 (1H, δ, 2.8 Hz), 5.92 (3H, m); ^{13}C NMR (100 MHz, methanol-d_4) δ 161.8, 160.1, 157.8, 155.9, 154.5, 152.4, 147.3, 147.2, 147.1, 146.9, 144.3, 144.1, 143.4, 143.3, 138.6, 138.5, 126.5, 126.2, 125.6, 125.5, 124.9, 124.6, 124.5, 99.9, 99.7, 99.5, 99.4, 97.6, 96.2, 95.8, 95.7, 95.3; ESI-MS $[M - H]^-$ at m/z 741.11.

2,7″-Phloroglucinol-6,6′-bieckol: amorphous powder; ^{1}H NMR (400 MHz, methanol-d_4) δ 5.57 (1H, s), 5.89 (1H, s), 5.74 (1H, m), 5.84 (1H, m), 5.74 (1H, m), 6.25 (1H, s), 6.14 (1H, s), 5.84 (1H, m), 5.89 (1H, m), 5.84 (1H, m), 6.52 (1H, s), 6.14 (1H, m), 6.44 (1H, m), 6.77 (1H, s), 6.72 (1H, s), 8.93 (1H, s), 8.93 (1H, s), 9.19 (1H, s), 9.19 (1H, s), 9.19 (1H, s), 9.04 (1H, s), 8.26 (1H, s), 9.94 (1H, s), 8.59 (1H, s), 9.88 (1H, s), 9.86 (1H, s), 9.25 (1H, s), 9.75 (1H, s), 9.21 (1H, s); ^{13}C NMR (100 MHz, methanol-d_6) δ 127.6, 143.0, 93.0, 137.1, 125.6, 147.2, 106.5, 152.2, 95.5, 152.4, 127.6, 137.1, 162.0, 98.7, 160.3, 95.5, 160.3, 98.8, 124.3, 147.2, 94.5, 144.1, 124.3, 147.2, 110.0, 144.1, 101.5, 151.8, 137.2, 144.1, 159.7, 96.7, 157.1, 95.5, 157.1, 96.7, 159.8, 97.8, 159.3, 95.2, 159.2, 97.9, 122.5, 153.9, 99.8, 156.8, 99.9, 152.8; ESI-MS $[M - H]^-$ at m/z 973.37.

Pyrogallol-phloroglucinol-6,6′-bieckol: amorphous powder; ^{1}H NMR (400 MHz, methanol-d_4) δ 6.10 (1H, s), 5.99 (1H, s), 5.72 (1H, m), 5.75 (1H, m), 5.72 (1H, m), 6.25 (1H, s), 6.14 (1H, s), 5.88 (1H, δ, 2.21 Hz), 5.88 (1H, δ, 2.21 Hz), 5.85 (1H, δ, 2.21 Hz), 6.72 (1H, δ, 2.2 Hz), 6.08 (1H, δ, 2.2 Hz), 5.89 (1H, δ, 2.01 Hz), 5.54 (1H, δ, 2.01 Hz), 5.89 (1H, δ, 2.01 Hz), 9.116 (1H, s), 9.03 (1H, s), 8.92 (1H, s), 9.27 (1H, s), 9.20 (1H, s), 9.20 (1H, s), 9.18 (1H, s), 9.03 (1H, s), 8.92 (1H, s), 8.25 (1H, s), 9.94 (1H, s), 9.87 (1H, s), 9.87 (1H, s), 9.20 (1H, s), 9.20 (1H, s); ^{13}C NMR (100 MHz, methanol-d_4) δ 125.2, 145.9, 95.5, 145.9, 125.1, 147.9, 105.5, 148.4, 95.4, 151.9, 127.8, 135.3, 161.9, 97.9, 160.3, 95.5, 160.3, 97.8, 124.4, 144.4, 94.4, 144.4, 124.5, 147.9, 105.4, 148.4, 95.5, 151.4, 127.8, 138.3, 159.2, 100.2, 156.9, 99.5, 159.3, 96.3, 154.0, 96.6, 152.1, 122.5, 153.5, 96.6, 159.9, 99.0, 159.8, 94.6, 159.8, 98.6; ESI-MS $[M - H]^-$ at m/z 973.03.

Phlorofucofuroeckol-A: amorphous powder; ^{1}H NMR (400 MHz, methanol-d_4) δ 6.63 (1H, s, H-7), 6.40 (1H, s, H-11), 6.26 (1H, s, H-2), 5.97 (2H, δ, J = 2.1 Hz, H-200, 600), 5.94 (1H, t, J = 1.9 Hz, H-40), 5.92 (1H, t, J = 2.0 Hz, H-400), 5.88 (2H, δ, J = 2.1 Hz, H-20, 60); ^{13}C NMR (100 MHz, CD_3OD) δ 162.7, 162.6, 161.0, 161.0, 154.0, 152.5, 152.0, 149.1, 149.0, 146.7, 144.7, 139.2, 136.2, 128.9, 125.9, 125.6, 123.2, 106.2, 106.1, 100.8, 100.2, 98.6, 98.5, 97.0, 96.2, 96.2; ESI-MS $[M - H]^-$ at m/z 601.36.

Animals and Experimental Design. Male C57BL/6 mice (n = 40; 4 weeks old) were obtained from Orient Bio (Gyeonggi-do, South Korea) and were housed two or three per cage in a room (temperature, 21−23 °C; relative humidity, 45−55%; 12 h dark/light cycle). After acclimation for 1 week, mice were then randomly divided into two groups: the normal control diet group (CD; n = 10) and the high-fat diet group (HFD; n = 30). CD was provided with regular diet (D12450B, 10% kcal fat, Research Diets, New Brunswick, NJ, USA), whereas HFD was provided with high-fat diet (D12451, 45% kcal fat, Research Diets) for 10 weeks. Food and distilled water were supplied ad libitum.

After obesity was induced by the high-fat diet, the animals were divided into four groups, 10 mice in each group and supplemented as follows: CON, nonobese control group mice fed CD were gavaged with distilled water; HF, obese mice fed HFD were gavaged with distilled water; LE, obese mice fed HFD were gavaged ECPE at a (low) dose of 100 mg/kg/day; HE, obese mice fed HFD were gavaged with ECPE at a (high) dose of 500 mg/kg/day. The identical volume of gavage with either distilled water or ECPE was administrated by oral gavage 5 times a week for 12 weeks. ECPE was freshly suspended in distilled water. The body weight and food intake were measured twice a week.

Mice were fasted for 15 h after the last treatment and then euthanized by inhalation with isoflurane (Baxter, Deerfield, IL, USA). Blood was collected by cardiac puncture using a heparin (Sigma-Aldrich, St. Louis, MO, USA) coated syringe. Plasma was obtained by centrifugation at 3000 rpm for 15 min. Tissues such as the liver and adipose pads were removed after cardiac puncture, washed of blood or foreign materials by saline, weighed, and immediately frozen in liquid nitrogen. All of the samples were stored at −80 °C until they were used for experiments. Experimental protocol was approved by the Institutional Animal Care and Use Committee of the Kyung Hee University.

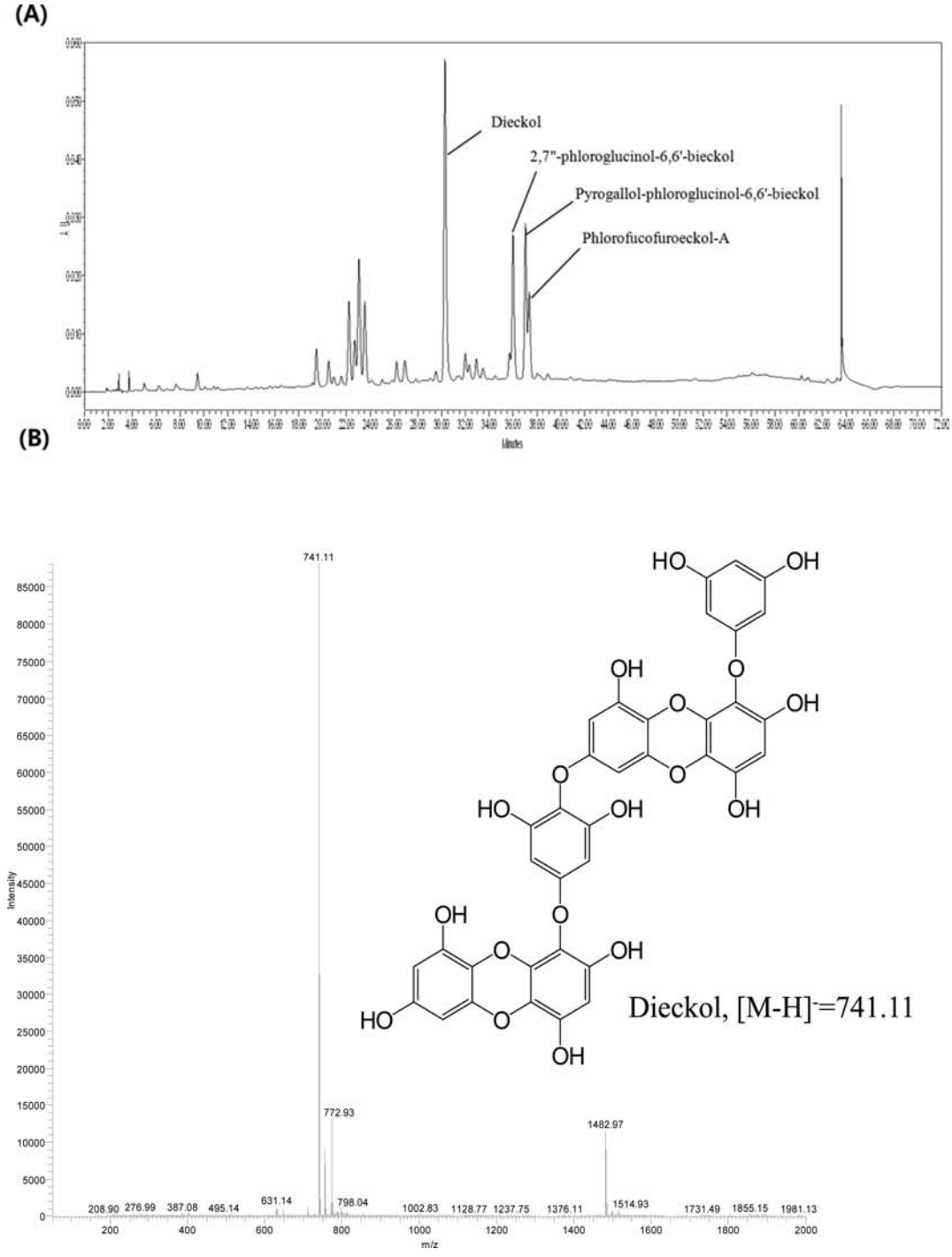

Figure 1. Quantification and identification of *E. cava* polyphenol extract (ECPE): (A) polyphenol contents in ECPE quantified by HPLC analysis; (B) electrospray ionization mass spectrometry (ESI/MS) of ECPE and chemical structure of dieckol.

Intraperitoneal Glucose Tolerance Test (IPGTT). A week before the end point, the animals were fasted overnight for 16 h prior to the IPGTT test. The 50% glucose solution (2 g/kg) was injected intraperitoneally. Blood glucose level was measured with a glucometer (NOCODING1, Seoul, Korea) at 0 (as basal fasting blood glucose level, FBG), 15, 30, 60, 90, and 120 min after injection of glucose solution. The area under the curve (AUC) was calculated using the trapezoidal rule as follows: $AUC_i = [(\text{blood glucose})_i + (\text{blood glucose})_{i-1}] \times [(\text{time})_i - (\text{time})_{i-1}]/2$.

Plasma Biomarker Analysis. The contents of plasma triglyceride (TG), total cholesterol (TC), and high-density lipoprotein cholesterol (HDL-C) were determined using commercial kits (Bio-Clinical System, Gyeonggi-do, South Korea). The atherogenic index (AI) was estimated as follows: AI = ([TC] − [HDL-C])/[HDL-C]. Plasma glutamic oxaloacetic transaminase (GOT) and glutamic pyruvic transaminase (GPT) were determined by enzymatic assays with commercial kits (Bio-Clinical System). The plasma concentrations of leptin, adiponectin, and insulin were determined using enzyme-linked immuosorbent assay (ELISA) commercial kits (RayBiotech, Inc., Norcross, GA, USA). The homeostasis model assessment of insulin resistance (HOMA-IR) was calculated as follows: fasting insulin (μU/mL) × fasting glucose (mmol/L)/22.5. All of the commercial kits were performed according to the manufacturer's instructions, respectively.

dx.doi.org/10.1021/jf502830b | J. Agric. Food Chem. 2015, 63, 349−359

Table 1. Effects of ECPE on Body Weight, Food Intake, Liver Weight, and Adipose Tissue Weight[a]

	group[b]			
	CON	HF	LE	HE
body weight (g)				
before supplementation	30.35 ± 0.58 a	38.56 ± 1.09 b	39.23 ± 0.74 b	38.01 ± 0.61 b
after supplementation	37.31 ± 0.80 a	48.51 ± 0.73 c	48.07 ± 0.70 c	44.96 ± 0.78 b
gain	6.95 ± 0.44 a	9.96 ± 0.79 b	8.84 ± 0.65 ab	6.94 ± 0.62 a
food intake (g/day)	3.17 ± 0.06 c	2.84 ± 0.05 ab	2.97 ± 0.05 b	2.78 ± 0.05 a
food efficiency ratio (%)	2.84 ± 0.16 a	4.59 ± 0.39 c	3.87 ± 0.28 bc	3.23 ± 0.26 ab
liver (g)	1.23 ± 0.07 ab	1.30 ± 0.13 ab	1.48 ± 0.15 b	1.08 ± 0.05 a
total adipose tissue (g)	3.88 ± 0.28 a	8.88 ± 0.48 c	8.31 ± 0.35 bc	7.67 ± 0.32 b
visceral fat (g)	2.71 ± 0.19 a	5.65 ± 0.26 c	4.91 ± 0.13 b	5.03 ± 0.15 b
epididymal	1.43 ± 0.10 a	2.08 ± 0.09 c	1.77 ± 0.11 b	2.34 ± 0.10 c
mesenteric	0.66 ± 0.07 a	1.94 ± 0.17 c	1.55 ± 0.11 b	1.32 ± 0.10 b
retroperitoneal	0.62 ± 0.03 a	1.63 ± 0.08 c	1.59 ± 0.08 c	1.37 ± 0.05 b
subcutaneous fat (g)	1.17 ± 0.11 a	3.24 ± 0.26 b	3.39 ± 0.29 b	2.64 ± 0.23 b
inguinal	0.98 ± 0.07 a	2.83 ± 0.25 b	3.04 ± 0.28 b	2.36 ± 0.23 b
brown	0.20 ± 0.04 a	0.41 ± 0.05 c	0.35 ± 0.04 bc	0.28 ± 0.03 ab

[a]Values are means ± SEM. Mean values with unlike letters are significantly different ($p < 0.05$). [b]CON, mice fed the control diet (negative control); HF, mice fed the high-fat diet (positive control); LE, mice supplemented with low dose (100 mg/kg/day) of ECPE; HE, mice supplemented with high dose (500 mg/kg/day) of ECPE.

Histological Observation of Hepatic Tissue. Liver tissue was isolated and immediately fixed in 10% neutral buffered formalin. The tissues were dehydrated and then embedded in paraffin wax. Histological sections (5 μm thickness) of the tissues were cut, deparaffinized in xylene, rehydrated in alcohol gradients, and then stained with hematoxylin and eosin (H&E). The stained sections were mounted with histological mounting medium (Histomount, GA, USA) after drying. All images were observed using an optical microscope (Olympus BX51; Olympus Optical, Tokyo, Japan).

Western Blot Analysis. Liver was homogenized at 4 °C in the lysis buffer (20 mM Tri-HCl, 150 mM $NaCl_2$, pH 7.5, 1% NP40, 0.5% sodium deoxycholate stock, 1 mM EDTA, 0.1% sodium dodecyl sulfate (SDS)) and then centrifuged at 14000 rpm at 4 °C for 30 min. The supernatants were used for Western blot analysis. The total protein concentrations of the fraction were measured by Bio-Rad protein assay (Bio-Rad, Hercules, CA, USA). A total of 40 g of protein samples was separated with SDS-PAGE and then transferred onto polyvinylidene fluoride (PVDF) membranes (Millipore, Marlborough, MA, USA). The membranes were blocked with 3% bovine serum albumin in phosphate-buffered saline−0.1% Tween 20 (PBS-T) and incubated overnight with primary antibodies at 4 °C. The primary antibodies were directed against AMPK, phosphorylated AMPK (p-AMPK; Thr172), acetyl CoA carboxylase (ACC), phosphorylated ACC (p-ACC; Ser79), monocyte chemoattractant protein-1 (MCP-1), catalase, and nuclear factor kappa B (NFκB) (Cell Signaling Technology, Inc., Danvers, MA, USA); carnitine palmitoyltransferase I A (CPT1A), SIRT1, C-reactive protein (CRP), glutathione peroxidases (GPx), and Lamin B1 (Abcam, Cambridge, MA, USA); SREBP1c, PPARα, fatty acid synthase (FAS), lipoprotein lipase (LPL), PPARγ coactivator 1 (PGC1), interleukin 6 (IL-6), IL-1β, TNFα, COX-2, and copper−zinc superoxide dismutase (CuZnSOD) (Santa Cruz Biotechnology, Inc., Santa Cruz, CA, USA); hemeoxygenase 1 (HO-1) and manganese superoxide dismutase (MnSOD) (Stressgen, Victoria, Canada); and α-tubulin (Sigma-Aldrich, St. Louis, MO, USA). Then, the blots were washed four times for 10 min with PBS-T. Thereafter, the membranes were incubated with respective secondary antibodies for 1 h and washed with PBS-T again. Signals were then developed using the ECL luminol reagent (Santa Cruz Biotechnology, Inc.) and then recorded and quantified with the Syngene G box (Syngene, Cambridge, UK, USA).

Measurement of Lipid Peroxidation. As a marker of lipid peroxidation, levels of malondialdehyde (MDA) were measured by using the thiobarbituric acid (TBA) method.[23] Mixtures of 10% (w/v) tissue homogenate with 0.15 M KCl, 8.1% SDS, and a 20% acetic acid−0.8% TBA mixture were heated in a water bath at 95 °C for 60 min. After cooling with tap water, distilled water and a mixture of *n*-butanol and pyridine (15:1 v/v) were added and then centrifuged at 4000 rpm for 10 min to obtain a clear supernatant. The absorbance of the supernatant was measured at 532 nm.

Statistical Analysis. The results are expressed as means ± standard error of mean (SEM). Significant differences among the groups were determined by one-way ANOVA using SPSS (version 20.0 for Windows, SPSS Inc., Chicago, IL, USA). Duncan's multiple-range tests was followed when differences were identified among the groups at p values of <0.05.

RESULTS

Quantification and Identification of Major Polyphenol Compounds in ECPE. Total phenol content exhibited 28.20 ± 0.58% in the extract; therefore, we named it the polyphenol extract for this study. The contents of the main compounds shown, respectively, in 5 mg of ECPE were as follows: dieckol, 235.54 μg (4.70%); 2,7″-phloroglucinol-6,6′-bieckol, 125.7 μg (2.51%); pyrogallol-phloroglucinol-6,6′-bieckol, 42.12 μg (0.84%); and phlorofucofuroeckol-A, 48.22 μg (0.96%) (Figure 1A).

In addition, identification of major polyphenol compounds in ECPE was performed by LC-MS, and the chemical structure of dieckol, which was at the highest peak of Figure 1A, is also indicated in Figure 1B.

Effect of ECPE on Food Intake and Body Weights. The mice fed HFD gained more weight compared to the mice fed CD during the obesity induction period. For the 12 weeks of supplementation, the HF group still gained more weight (9.96 ± 0.79) compared to CON (6.95 ± 0.44 g) (Table 1). At the same time, the mice supplemented with ECPE were affected in body weight, and especially a high dose of ECPE significantly lowered body weight gain (6.94 ± 0.62 g). Body weight gain in HE was similar to that of CON. In addition, the food intake of the HFD-fed groups was lower than CON regardless of ECPE supplementation. Accordingly, the food efficiency ratio (FER) of ECPE supplementation was lower than that of HF dose-dependently (Table 1).

dx.doi.org/10.1021/jf502830b | J. Agric. Food Chem. 2015, 63, 349−359

Table 2. Effect of ECPE on Plasma Lipid Profiles, Liver Toxicity, Adipokines, and Insulin Resistance[a]

	group[b]			
	CON	HF	LE	HE
lipid profiles[c]				
TG (mg/dL)	126.48 ± 8.29 a	211.79 ± 19.28 b	119.33 ± 9.74 a	130.00 ± 9.68 a
TC (mg/dL)	154.87 ± 2.97 a	192.50 ± 6.69 b	158.35 ± 6.59 a	139.09 ± 7.08 a
HDL-C (mg/dL)	92.63 ± 3.81	100.17 ± 4.69	103.63 ± 3.05	90.95 ± 3.98
AI	0.69 ± 0.07 a	0.94 ± 0.06 b	0.54 ± 0.08 a	0.55 ± 0.09 a
liver toxicity[d]				
GOT (Karmen/mL)	115.12 ± 5.90 b	178.84 ± 7.18 c	71.14 ± 5.33 a	69.66 ± 8.46 a
GPT (Karmen/mL)	6.60 ± 1.56 a	17.352 ± 4.12 b	8.21 ± 2.14 a	6.70 ± 1.66 a
adipokines				
leptin (ng/mL)	11.10 ± 0.64 a	36.02 ± 11.09 b	33.44 ± 3.71 b	22.55 ± 2.56 ab
adiponectin (ng/mL)	17.34 ± 0.82	17.21 ± 1.17	16.92 ± 1.22	19.86 ± 1.71
leptin/adiponectin	0.65 ± 0.05 a	2.06 ± 0.55 b	2.08 ± 0.32 b	1.16 ± 0.14 a
insulin resistance[e]				
FBG (mmol/L)	8.07 ± 0.31 a	11.00 ± 0.18 b	10.65 ± 0.18 b	10.28 ± 0.25 b
insulin (μU/mL)	8.74 ± 1.08 ab	12.64 ± 1.85 b	10.06 ± 2.27 ab	5.24 ± 0.41 a
HOMA-IR	3.13 ± 0.40 ab	6.24 ± 0.97 c	4.67 ± 0.99 bc	2.38 ± 0.17 a

[a]Values are means ± SEM. Mean values with unlike letters are significantly different ($p < 0.05$). [b]CON, mice fed the control diet (negative control); HF, mice fed the high-fat diet (positive control); LE, mice supplemented with low dose (100 mg/kg/day) of ECPE; HE, mice supplemented with high dose (500 mg/kg/day) of ECPE. [c]TG, plasma triglyceride; TC, total cholesterol; HDL-C, high-density lipoprotein cholesterol; AI, atherogenic index. [d]GOT, glutamic oxaloacetic transaminase; GPT, glutamic pyruvic transaminase. [e]FBG, fasting blood glucose level; HOMA-IR, homeostasis model assessment of insulin resistance.

Effect of ECPE on Liver and Adipose Tissue Weights. The liver weight was not significantly different among HFD-fed groups or between CON and HF as shown in Table 1.

To demonstrate the effect of ECPE on body fat accumulation, we measured adipose pad weight of five sites (epididymal, mesenteric, retroperitoneal, inguinal, and brown adipose tissue) and total body fat mass. The weights of adipose tissues in HF were higher than those in CON. However, the weight of visceral adipose tissues (VAT), except epididymal fat, in HE was slightly decreased compared to the HF group. In addition, the weight of brown adipose fat in HE was significantly lower than that in HF. Thus, the body weight and the gross weight of adipose tissue were decreased in HE compared to HF (Table 1).

Effect of ECPE on Plasma Biomarkers. Plasma lipid profiles are shown in Table 2. The concentrations of the plasma TG and total cholesterol were significantly increased in HF compared to CON. However, TG and TC levels of the ECPE-supplemented group regardless of dose showed significant decreases compared to those of HF. The AI related to cardiovascular disease in LE and HE was lower than that in HF, whereas there were no significant differences in high-density lipoprotein cholesterol (HDL-C) among all groups.

To verify the potential toxic effects of ECPE supplementation, plasma GOT and GPT levels were measured as markers of hepatic function and liver injury (Table 2). Both GOT and GPT in HF levels were higher than those of CON, whereas LE and HE showed lower levels of GOT and GPT compared to HF.

As shown in Table 2, there was an increase in plasma leptin in HF compared to CON and there was a slight decrease in plasma leptin in HG compared to HF. There were no significant differences among all groups in plasma adiponectin levels. As a useful inflammatory and obesity biomarker, we calculated the leptin and adiponectin ratio (LAR). LAR in HF was significantly higher than that in CON, but HE showed a significant decrease in LAR compared to HF.

Effect of ECPE on Glucose Tolerance and Insulin Resistance. An IPGTT was performed to evaluate glucose tolerance and insulin resistance (Figure 2A). The data showed that HFD induced glucose tolerance compared to CD. On the other hand, the levels of blood glucose in ECPE-supplemented groups were lower than those of HF an hour after injection. To quantify the effectiveness of supplementation, we also calculated the area under the curve (AUC) of the IPGTT (Figure 2B). FBG in HF were higher than those of CON, but the IPGTT levels between the HF group and ECPE-supplemented groups were not significantly different. However, AUC was significantly reduced in both LE and HE compared to HF (Figure 2B).

To examine insulin resistance, FBG and plasma insulin levels were measured and HOMA-IR values were calculated (Table 2). There was an increase in FBG level in HF contrary to CON, but *E. cava* supplementation regardless of dose did not show any beneficial effect on FBG level. However, plasma insulin levels in HE were significantly lower than those in HF. HOMA-IR in HF was higher than that in CON, but HE showed a significant decrease in HOMA-IR compared to HF.

Histological Analysis of Liver. The fat deposition in the liver was increased in HF contrary to CON. However, the ECPE-supplemented group showed dose-dependently decreased fat accumulation in hepatic tissue compared to HF (Figure 3).

Effect of ECPE on Protein Levels of Hepatic AMPK and Its Downstream Genes in the HFD-Induced Obese Mice. To investigate whether ECPE supplementation activates AMPK and its downstream genes, we measured protein levels of AMPK and phosphorylated AMPK (p-AMPK) in the liver (Figure 4A). The protein levels of AMPK were not different among the groups. However, protein levels of the phosphorylation of AMPK in HE were significantly increased compared to other groups.

Effect of ECPE on Protein Levels of Hepatic Lipogenesis and Energy Metabolism Related Genes in the

dx.doi.org/10.1021/jf502830b | J. Agric. Food Chem. 2015, 63, 349−359

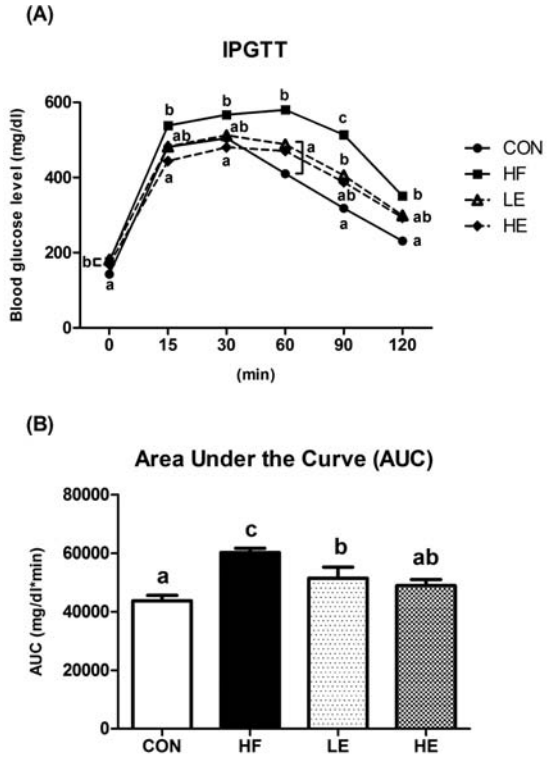

Figure 2. Effect of ECPE on (A) glucose tolerance and (B) glucose area under the curve (AUC) in high-fat diet induced obese mice. Values are means ± SEM. Mean values with unlike letters are significantly different ($p < 0.05$). CON, mice fed the control diet (negative control); HF, mice fed the high-fat diet (positive control); LE, mice supplemented with low dose (100 mg/kg/day) of ECPE; HE, mice supplemented with high dose (500 mg/kg/day) of ECPE.

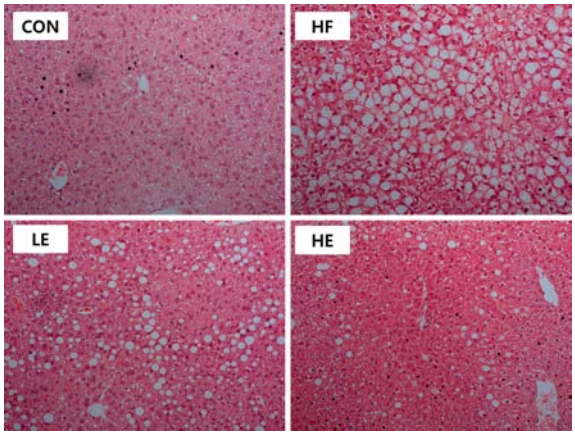

Figure 3. Effect of ECPE on liver morphology (magnification ×100) in high-fat diet induced obese mice. CON, mice fed the control diet (negative control); HF, mice fed the high-fat diet (positive control); LE, mice supplemented with low dose (100 mg/kg/day) of ECPE; HE, mice supplemented with high dose (500 mg/kg/day) of ECPE.

HFD-Induced Obese Mice. We examined protein levels of hepatic lipogenesis (Figure 4B) and fatty acid β-oxidation (Figure 4C). HF group was characterized by increased levels of SREBP1c and decreased levels of PPARα compared to CON, but ECPE-supplemented groups showed a reversed tendency. The FAS and LPL levels were increased in HF compared to CON. On the other hand, ECPE supplementation reduced the protein levels of FAS and LPL regardless of dose (Figure 4B). At the same time, the protein levels of fatty acid β-oxidation, including p-ACC and CPT1A, were decreased in HF compared to those of CON, but ECPE supplementation regardless of dose increased the protein levels of those markers (Figure 4C).

Effect of ECPE on Protein Levels of Hepatic SIRT1 and PGC1α in the HFD-Induced Obese Mice. The protein levels of SIRT1 and PGC1α were measured in the liver. SIRT1 was decreased under the obese condition. However, the ECPE-supplemented groups showed an increased pattern of SIRT1 levels compared to HF dose-dependently. In addition, the protein level of PGC1α in cytosol was not significantly different among all groups. Although the protein level of PGC1α in the nucleus was significantly decreased in HF compared to those of CON, LE and HE presented increased levels of PGC1α in the nucleus (Figure 5A).

Effect of ECPE on Protein Levels of Hepatic Inflammatory Response Related Genes in the HFD-Induced Obese Mice. The protein levels of inflammatory markers, including MCP1, TNFα, IL-1β, and IL-6, were increased under the obese condition. However, the protein levels of those markers were significantly decreased in HE, except IL-6. In addition, the protein levels of nuclear factor kappa B (NFκB) were increased in HF compared to CON. On the other hand, the levels of nuclear NFκB were significantly decreased in both LE and HE compared to HF. The protein levels of COX-2 were increased in HF compared to CON, but the levels were slightly decreased in both LE and HE (Figure 5B).

Effect of ECPE on Hepatic Lipid Peroxidation and Hepatic Antioxidant Defense System Related Proteins in the HFD-Induced Obese Mice. The level of MDA was checked for explaining lipid peroxidation as an indicator of hepatic oxidative stress (Figure 6A). HFD has an adverse effect on the liver through oxidative stress compared to CD. Despite the high oxidative stress in HF, the MDA level of ECPE-supplemented groups was decreased. In addition, we measured the protein involved in the antioxidant defense system at the molecular level. The protein levels of CuZnSOD were not significantly different among the groups. However, the protein levels of GPx and catalase were significantly increased in HE among the groups. At the same time, the protein levels of HO-1 were significantly increased in HF compared to CON, but the levels in LE and HE were not changed compared to HF (Figure 6B).

DISCUSSION

In this study, we investigated whether ECPE could have antiobesity and anti-inflammatory effects and mechanisms in which regulate hepatic lipid metabolism in HFD-induced obese mice for the first time. Our results demonstrated that supplementation of ECPE regardless of dose reduced further weight gain, improved glucose tolerance and dyslipidemia, attenuated TG accumulation, and stimulated hepatic β-oxidation in hepatic tissue. Furthermore, our data showed that supplementation of ECPE is beneficial in regulation of the antioxidant defense system and in improvement of the inflammatory status of HFD-induced obesity. ECPE used in the study contains various polyphenols including diekol, 2,7″-phloroglucinol-6,6′-bieckol, pyrogallol-phloroglucinol-6,6′-bieckol, and phlorofucofuroeckol-A. Although dieckol is the major bioactive component in ECPE, the beneficial effect of ECPE might be derived from combination of dieckol and/or other polyphenol components in ECPE.

dx.doi.org/10.1021/jf502830b | J. Agric. Food Chem. 2015, 63, 349−359

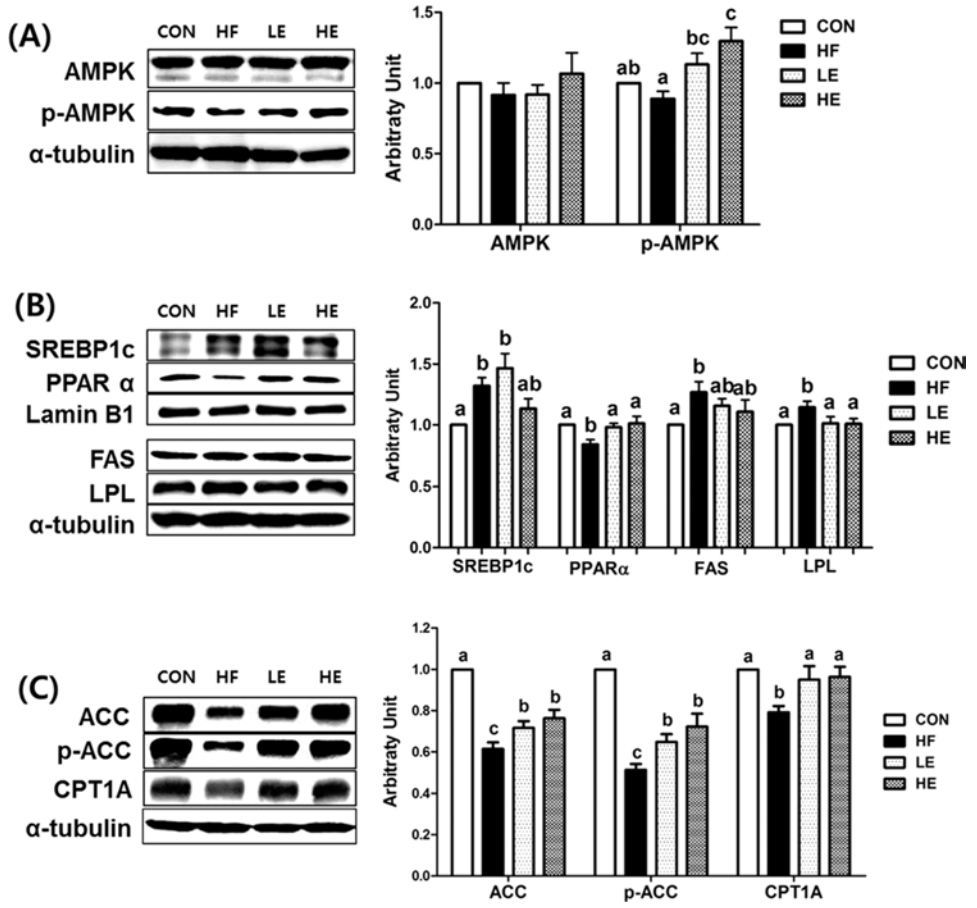

Figure 4. Effect of ECPE on expression of (A) AMPK (AMPK and p-AMPK), (B) lipogenesis (SREBP1c, PPARα, FAS, and LPL), and (C) fatty acid β-oxidation (ACC, p-ACC, and CPT1A). The protein samples measured by Western blot were pooled from six mice per group. A representative image of repeated experiments is shown in the left panel. The bands show the intensity of the bands that were densitometrically measured and normalized to the band levels of α-tubulin (cytosol) or Lamin B1 (nucleus). Values are means ± SEM (n = 6). Mean values with unlike letters are significantly different ($p < 0.05$). CON, mice fed the control diet (negative control); HF, mice fed the high-fat diet (positive control); LE, mice supplemented with low dose (100 mg/kg/day) of ECPE; HE, mice supplemented with high dose (500 mg/kg/day) of ECPE.

The body weight gain at the end-point of this study was significantly lower in HE than that of HF without food intake change. In addition, the visceral fat weights, particularly in mesenteric and retroperitoneal fat pads, were decreased in HE, which led to a reduction of total adipose tissue weight (Table 1). However, the epididymal fat weight did not show a significant difference between CON and HF regardless of ECPE supplementation.

It is also well-known that obesity, particularly increased visceral adipose tissue mass, is one of the major risk factors in developing type 2 diabetes.[24] In other words, individuals with obesity show increased FBG levels or insulin resistances. Our current study showed the beneficial effect of ECPE, especially at high dose, on impaired glucose metabolism demonstrated by AUC levels for glucose tolerance and HOMA-IR for insulin resistance. HE, high dose of ECPE supplementation (500 mg/kg), reduced plasma insulin levels but did not lower the fasting blood glucose level under obese condition. Thus, it can be inferred that HE improves glucose tolerance and insulin resistance, represented by HOMA-IR, under obese condition.

Furthermore, plasma levels of adipokines are distinguished biomarkers for insulin resistance as well as adiposity. Al-Hamodi et al. reported that alterations in plasma adiponectin or leptin might be associated with adiposity and insulin resistance and suggested that the leptin/adiponectin ratio would be a better indicator of insulin resistance as well as adiposity than the singular level of leptin or adiponectin.[24] In addition, plasma leptin has a stronger correlation with obese parameters such as body mass index (BMI) and lipid profiles than plasma adiponectin.[24] In the current study, we observed that plasma leptin in HF was increased compared to CON and HF showed a higher leptin/adiponectin ratio than CON. At the same time, we found that the high-dose ECPE supplementation reduced the leptin/adiponectin ratio compared to HF. This tendency was comparable with the plasma insulin and HOMA-IR data that we presented above. The results suggest that *E. cava* might have a beneficial effect on impaired glucose metabolism by ameliorating glucose intolerance and insulin resistance in HFD-induced obesity, especially with respect to type 2 diabetes.

Dyslipidemia is another well-known complication of obesity. The archetypal dyslipidemia in obesity includes increases in TG and free fatty acids (FFA) as well as an imbalance between HDL-C and LDL-C.[25] In a previous study, extract of *E. cava* reduced levels of plasma TG and total cholesterol and increased levels of HDL-C in db/db mice.[26] Our results similarly showed that ECPE supplementation significantly reduced the plasma TG levels in HFD-fed mice regardless of dose. Moreover, ECPE supplementation regardless of dose group showed decreases in TC levels, whereas there were no significant differences in HDL-C levels among the groups. Eventually, all

dx.doi.org/10.1021/jf502830b | J. Agric. Food Chem. 2015, 63, 349−359

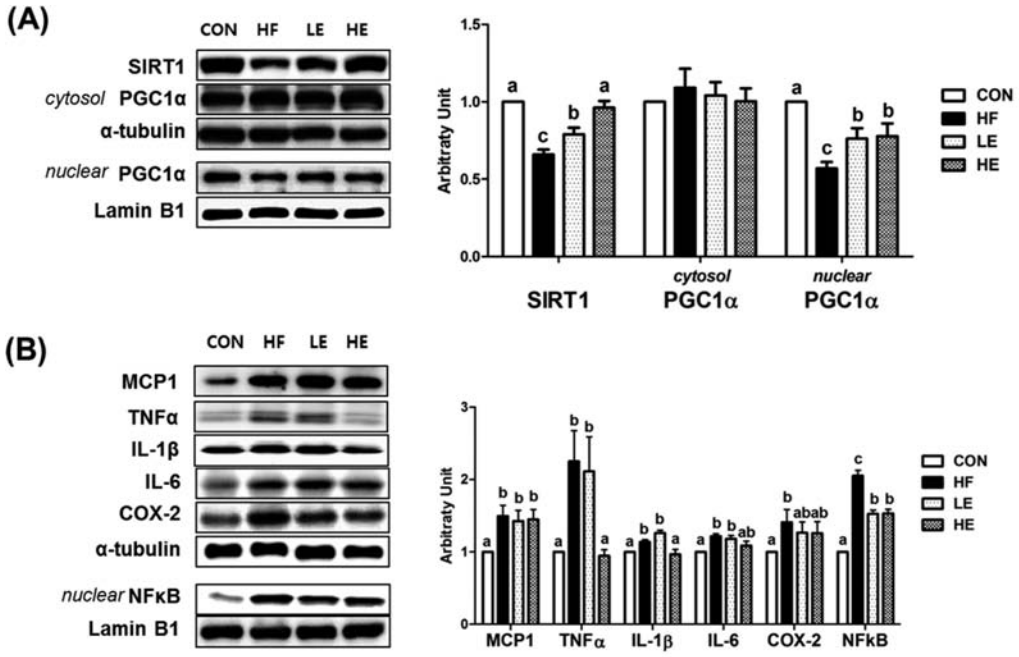

Figure 5. Effect of ECPE on (A) SIRT1 signaling and (B) inflammatory response. The protein samples measured by Western blot were pooled from six mice per group. A representative image of repeated experiments is shown in the upper panel. The bands show the intensity of the bands that were densitometrically measured and normalized to the band levels of Lamin B (nuclear) or α-tubulin (cytosol). Values are means ± SEM (n = 6). Mean values with unlike letters are significantly different ($p < 0.05$). CON, mice fed the control diet (negative control); HF, mice fed the high-fat diet (positive control); LE, mice supplemented with low dose (100 mg/kg/day) of ECPE; HE, mice supplemented with high dose (500 mg/kg/day) of ECPE.

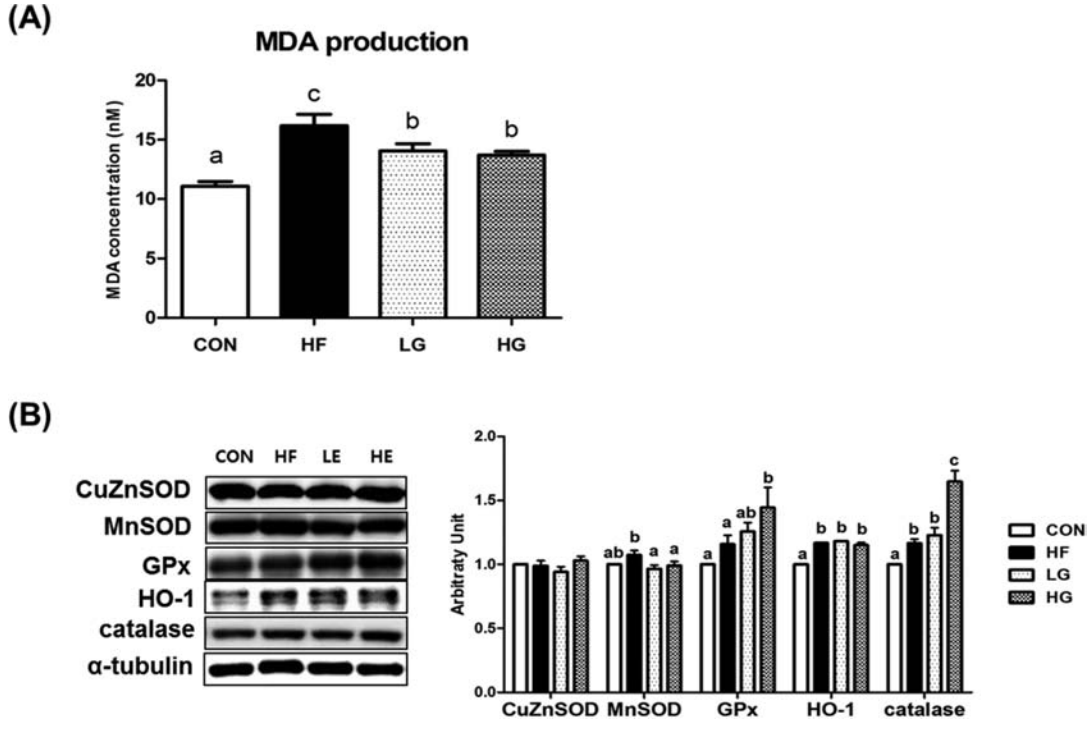

Figure 6. Effect of ECPE on (A) lipid peroxidation and (B) antioxidant defense system. (A) Lipid peroxidation was quantified as a level of malondialdehyde. (B) The protein samples measured by Western blot were pooled from six mice per group. A representative image of repeated experiments is shown in the upper panel. The bands show the intensity of the bands that were densitometrically measured and normalized to the band levels of α-tubulin. Values are means ± SEM (n = 6). Mean values with unlike letters are significantly different ($p < 0.05$). CON, mice fed the control diet (negative control); HF, mice fed the high-fat diet (positive control); LE, mice supplemented with low dose (100 mg/kg/day) of ECPE; HE, mice supplemented with high dose (500 mg/kg/day) of ECPE.

dx.doi.org/10.1021/jf502830b | J. Agric. Food Chem. 2015, 63, 349−359

ECPE supplemented groups showed an improvement in the A) compared to HF. These results suggest that ECPE supplementation might have a beneficial effect on improving circulating TG and TC levels and thus have potential in the prevention of dyslipidemia-induced atherogenesis in obese mice.

We examined how ECPE influences the HFD-induced abnormal hepatic lipid metabolism as well. Previous studies showed that fatty liver disease was caused by an increased fatty acid influx into the liver, which leads to ectopic fat accumulation in hepatocytes in obese subjects.[27,28] Furthermore, recent studies reported that HFD-fed animals showed a higher hepatic expression of genes related to lipogenesis, whereas they showed lower levels of hepatic proteins related to fatty acid β-oxidation.[29,30] At the molecular level, our results showed that ECPE supplementation regulated hepatic lipid metabolism by stimulating phosphorylation of AMPK. Previous studies reported that activated AMPK negatively regulates SREBP, a major transcription factor of fatty acid synthesis. Particularly, the level of SREBP is higher in subjects with NAFLD.[31,32] An overexpression of SREBP1c, one of SREBP isoforms, allows expression of lipogenic enzymes, including acetyl-CoA carboxylase 1 (ACC1) and FAS.[33,34] The primary downstream targets for AMPK are 3-hydroxy-3-methylglutaryl-coenzyme A reductase (HMG-CoA reductase) and ACC, which are rate-controlling enzymes of cholesterol and malonyl-CoA synthesis, respectively. Because malonyl-CoA is a material of fatty acid synthesis and an allosteric regulator of carnitine palmitoyltracsferase-1 (CPT1), which takes up long-chain fatty acyl-CoA into mitochondria, inactivation of ACC leads to reducing lipogenesis as well as fatty acid β-oxidation.[35] A previous study showed that dieckol isolated from *E. cava* activated AMPK and inhibited adipogenesis in 3T3-L1 preadipocytes.[19] Similarly, this study demonstrated that ECPE supplementation in HFD-induced obese mice had higher levels of proteins involving β-oxidation and lower levels of proteins associated with lipogenesis than the HF group, as shown in Figure 4B. In detail, a high dose of ECPE supplementation decreased the protein level of SREBP1c in the nucleus, and this led to a decreased protein level of FAS. At the same time, both a low and a high dose of ECPE supplementation increased the protein level of PPARα, and this increase resulted in decreased LPL production. In addition, ECPE supplementation inactivated ACC and thus increased the protein level of CPT1A, which is a rate-limiting enzyme of lipid oxidation.[36] Taken together, we suggest that ECPE supplementation suppressed hepatic lipid accumulation by reducing lipogenesis and stimulating fatty acid β-oxidation. The results are well in accordance with our histological observation of hepatic tissue, as shown in Figure 3. HF had a large amount of fat droplets in liver compared to CON. However, ECPE supplementation ameliorated hepatic lipid accumulation, particularly in the high dose ECPE-supplemented group.

A previous study reported that the increase in fatty acid β-oxidation through AMPK activation changed the NAD^+/NADH ratio and consequently stimulated SIRT1 expression in hepatocytes.[37] SIRT1 plays crucial roles in glucose homeostasis, lipid metabolism, oxidative stress, and inflammation.[8] In particular, SIRT1 activation results in an increase in fatty acid β-oxidation via PPARα and peroxisome proliferator-activated receptor gamma coactivator 1-alpha (PGC1α)[8] as well as an improvement of inflammatory response via NFκB activation.[38] In a previous study, rats with NAFLD showed significantly low levels of hepatic SIRT1, but caloric restriction restored hepatic SIRT1 levels to that in nonobese subjects.[39] In addition, Puigserver mentioned that PGC1α in hepatocytes interacts with liver-enriched transcription factors, including hepatocyte nuclear factor 4 alpha (HNF4α), forkhead box protein O1 (FOXO1), and PPARα, and these factors are associated with gluconeogenesis.[40] Taken together, activation of AMPK by decreased cells' energy status, accompanied by exercise or caloric restriction, stimulates SIRT1 in response to NAD^+ ratio, subsequently increases PGC1α and consequently enhances mitochondrial biogenesis and its function.[13] The present study showed that the protein levels of cytosolic SIRT1, as well as the nuclear levels of both PGC1α and PPARα, were increased in the ECPE-supplemented groups, whereas those were decreased in obese control group (HF). In addition, the nuclear protein levels of both PGC1α and PPARα are in accordance with insulin resistance demonstrated by AUC levels, as mentioned earlier. These results suggest that activated AMPK by ECPE supplementation might consequently increase NAD^+ by fatty acid β-oxidation and lead to activated hepatic SIRT1 in HFD-induced obese mice. Thus, increased SIRT1 by ECPE supplementation might ameliorate impaired glucose metabolism as well as up-regulate lipolysis through increased fatty acid β-oxidation, as demonstrated by PGC1α and PPARα in HFD-induced obesity.

As stated above, obesity is also recognized as a systemic low-grade chronic inflammation, which is induced by inflammatory mediators such as TNFα, IL-6, and CRP secreted from excessive adipose tissue and some improperly activated immune cells.[41] Our results similarly showed that HFD increased pro-inflammatory cytokines, such as TNFα, IL-1β, and IL-6, and the increases in those markers activated NFκB, which produced much more TNFα and IL-1β and also resulted in the production of other inflammatory mediators, such as COX-2, in the liver. At the same time, our data showed that a particularly high dose of ECPE supplementation reduced the levels of pro-inflammatory markers, including TNFα and IL-1β. In addition, whereas NFκB translocation into the nucleus was increased in the HF group compared to CON, ECPE supplementation at both low and high doses decreased the NFκB translocation into the nucleus (Figure 5B). Consequently, the increase in COX-2 resulting from NFκB activation was decreased in the ECPE-supplemented groups. Previous studies had demonstrated a similar tendency that *E. cava* inhibited lipopolysaccharide-induced COX-2, TNFα, and IL-1β via the NFκB pathway in BV2 microglia.[16]

Elevated oxidative stress is another factor for obesity-linked inflammation.[42] In this study, we measured lipid peroxidation, as demonstrated by MDA, one of the valid biomarkers of oxidative stress[43,44] in the liver. Our data showed that the MDA level was significantly increased in the HF group compared to CON, whereas the level was decreased in all ECPE-supplemented groups regardless of its dose. The results suggest that ECPE suppresses overproduction of ROS induced by obesity. In addition, the current study demonstrated that antioxidant defense enzymes, including GPx and catalase in the liver, were significantly increased in HE compared to the other groups. Both GPx and catalase are involved in the conversion of H_2O_2 into H_2O and molecular O_2. Increased levels of GPx and catalase may be associated with decreased lipid peroxidation demonstrated by MDA levels. Therefore, it is fairly easy to understand why ECPE supplementation significantly reduced the plasma levels of GOT and GPT compared to nontreated

HF groups. As plasma activities of GOT and GPT are sensitive clinical markers of hepatic damage including NAFLD,[45] our data suggest that ECPE supplementation, especially at high dose, plays a beneficial role in protection against liver damage via regulation of oxidative stress under an obese condition. However, some previous studies had documented that *E. cava* increased the hepatic activity of SOD against ethanol-induced liver damaged mice[20] and phlorotannins isolated from *E. cava* have neuro-protective effects by regulating ROS scavenging activity in HT22 cells.[46] Several studies have tried to establish the mechanisms of the antioxidant defense enzymes such as SODs, GPx, catalase, and HO-1 but, unfortunately, the patterns in expression of endogenous antioxidants between healthy normal status and disease state have not shown consistency so far.[47] Therefore, further experiments are required for examination of the activation of key markers such as the nuclear factor (erythroid-derived 2)-like 2 (Nrf2) and the activities of antioxidant enzymes in other tissues.

Collectively, ECPE has beneficial effects on hepatic lipid metabolism, inflammation, and oxidative stress through activation of AMPK and regulation of its downstream genes in HFD-induced obese mice. In other words, ECPE might be involved in a partnership between AMPK and SIRT1, which reduces hepatic lipogenesis in HFD-induced obesity. Moreover, ECPE reduced the protein levels that are related to inflammatory response such as TNFα, IL-1β, and NFκB. Furthermore, ECPE activated GPx and catalase and consequently reduced hepatic lipid peroxidation. These results suggest that *E. cava* might be a potential nutraceutical to treat not only impaired hepatic lipid metabolism but also inflammation and oxidative stress via regulation of AMPK and SIRT1 in obesity.

AUTHOR INFORMATION

Corresponding Author

*(Y.L.) Phone: +82 2 961 0262. Fax: +82 2 961 0261. E-mail: ylim@khu.ac.kr.

Funding

This work was supported by Korea Institute of Planning and Evaluation for Technology in Food, Agriculture, Forestry and Fisheries (811003-03-2-SB240).

Notes

The authors declare no competing financial interest.

ABBREVIATIONS USED

ACC, acetyl CoA carboxylase; AI, atherogenic index; AMPK, AMP-activated protein kinase; ANOVA, one-way analysis of variance; AUC, area under the curve; CPT1A, carnitine palmitoyltransferase I A; COX-2, cyclooxygenase 2; ECPE, *Ecklonia cava* polyphenol extract; FA, fatty acid; FAS, fatty acid synthase; FER, food efficiency ratio; FFA, free fatty acid; GOT, glutamic oxaloacetic transaminase; GPT, glutamic pyruvic transaminase; GPx, glutathione peroxidases; H&E, hematoxylin and eosin; HDL-C, high-density lipoprotein cholesterol; IL-1β, interleukin 1 beta; IL-6, interleukin 6; IPGTT, intraperitoneal glucose tolerance test; LC-MS, liquid chromatography−mass spectrometry; LPL, lipoprotein lipase; MCP-1, monocyte chemoattractant protein-1; MDA, malondialdehyde; NAFLD, nonalcoholic fatty liver disease; NF-κB(p65), nuclear factor κ B; PGC1, peroxisome proliferator-activated receptor gamma coactivator 1; PPARα, peroxisome proliferator-activated receptor alpha; ROS, reactive oxygen species; SAT, subcutaneous adipose tissue; SEM, standard error of the mean; SIRT1, sirtuin 1; SOD, superoxide dismutase; SREBP1c, sterol regulatory element binding protein 1c; TC, total cholesterol; TG, triglyceride; TNFα, tumor necrosis factor alpha; WAT, white adipose tissue

REFERENCES

(1) Jang, W. S.; Choung, S. Y. Antiobesity effects of the ethanol extract of *Laminaria japonica* Areshoung in high-fat-diet-induced obese rat. *Evidence-Based Complement. Altern. Medicine: eCAM* **2013**, No. 492807.

(2) Voshol, P. J.; Rensen, P. C.; van Dijk, K. W.; Romijn, J. A.; Havekes, L. M. Effect of plasma triglyceride metabolism on lipid storage in adipose tissue: studies using genetically engineered mouse models. *Biochim. Biophys. Acta* **2009**, *1791*, 479−485.

(3) Koo, S. H. Nonalcoholic fatty liver disease: molecular mechanisms for the hepatic steatosis. *Clin. Mol. Hepatol.* **2013**, *19*, 210−215.

(4) Tessari, P.; Coracina, A.; Cosma, A.; Tiengo, A. Hepatic lipid metabolism and non-alcoholic fatty liver disease. *Nutr., Metab., Cardiovasc. Dis.* **2009**, *19*, 291−302.

(5) Viollet, B.; Guigas, B.; Leclerc, J.; Hebrard, S.; Lantier, L.; Mounier, R.; Andreelli, F.; Foretz, M. AMP-activated protein kinase in the regulation of hepatic energy metabolism: from physiology to therapeutic perspectives. *Acta Physiol.* **2009**, *196*, 81−98.

(6) Hardie, D. G. Sensing of energy and nutrients by AMP-activated protein kinase. *Am. J. Clin. Nutr.* **2011**, *93*, 891S−896S.

(7) Li, X. SIRT1 and energy metabolism. *Acta Biochim. Biophys. Sinica* **2013**, *45*, 51−60.

(8) Colak, Y.; Ozturk, O.; Senates, E.; Tuncer, I.; Yorulmaz, E.; Adali, G.; Doganay, L.; Enc, F. Y. SIRT1 as a potential therapeutic target for treatment of nonalcoholic fatty liver disease. *Med. Sci. Monit.: Int. Med. J. Exp. Clin. Res.* **2011**, *17*, HY5−HY9.

(9) Purushotham, A.; Schug, T. T.; Xu, Q.; Surapureddi, S.; Guo, X.; Li, X. Hepatocyte-specific deletion of SIRT1 alters fatty acid metabolism and results in hepatic steatosis and inflammation. *Cell Metab.* **2009**, *9*, 327−338.

(10) Li, X.; Zhang, S.; Blander, G.; Tse, J. G.; Krieger, M.; Guarente, L. SIRT1 deacetylates and positively regulates the nuclear receptor LXR. *Mol. Cell* **2007**, *28*, 91−106.

(11) Walker, A. K.; Yang, F.; Jiang, K.; Ji, J. Y.; Watts, J. L.; Purushotham, A.; Boss, O.; Hirsch, M. L.; Ribich, S.; Smith, J. J.; Israelian, K.; Westphal, C. H.; Rodgers, J. T.; Shioda, T.; Elson, S. L.; Mulligan, P.; Najafi-Shoushtari, H.; Black, J. C.; Thakur, J. K.; Kadyk, L. C.; Whetstine, J. R.; Mostoslavsky, R.; Puigserver, P.; Li, X.; Dyson, N. J.; Hart, A. C.; Naar, A. M. Conserved role of SIRT1 orthologs in fasting-dependent inhibition of the lipid/cholesterol regulator SREBP. *Genes Dev.* **2010**, *24*, 1403−1417.

(12) Ponugoti, B.; Kim, D. H.; Xiao, Z.; Smith, Z.; Miao, J.; Zang, M.; Wu, S. Y.; Chiang, C. M.; Veenstra, T. D.; Kemper, J. K. SIRT1 deacetylates and inhibits SREBP-1C activity in regulation of hepatic lipid metabolism. *J. Biol. Chem.* **2010**, *285*, 33959−33970.

(13) Ruderman, N. B.; Xu, X. J.; Nelson, L.; Cacicedo, J. M.; Saha, A. K.; Lan, F.; Ido, Y. AMPK and SIRT1: a long-standing partnership? *Am. J. Physiol. Endocrinol. Metab.* **2010**, *298*, E751−E760.

(14) Shen, Z.; Liang, X.; Rogers, C. Q.; Rideout, D.; You, M. Involvement of adiponectin-SIRT1-AMPK signaling in the protective action of rosiglitazone against alcoholic fatty liver in mice. *Am. J. Physiol. Gastrointest. Liver Physiol.* **2010**, *298*, G364−G374.

(15) Li, Y.; Qian, Z. J.; Ryu, B.; Lee, S. H.; Kim, M. M.; Kim, S. K. Chemical components and its antioxidant properties in vitro: an edible marine brown alga, *Ecklonia cava*. *Bioorg. Med. Chem.* **2009**, *17*, 1963−1973.

(16) Jung, W. K.; Ahn, Y. W.; Lee, S. H.; Choi, Y. H.; Kim, S. K.; Yea, S. S.; Choi, I.; Park, S. G.; Seo, S. K.; Lee, S. W.; Choi, I. W. *Ecklonia cava* ethanolic extracts inhibit lipopolysaccharide-induced cyclo-oxygenase-2 and inducible nitric oxide synthase expression in BV2

microglia via the MAP kinase and NF-kappaB pathways. *Food Chem. Toxicol.* **2009**, *47*, 410−417.
(17) Park, S. J.; Kim, Y. T.; Jeon, Y. J. Antioxidant dieckol downregulates the Rac1/ROS signaling pathway and inhibits Wiskott-Aldrich syndrome protein (WASP)-family verprolin-homologous protein 2 (WAVE2)-mediated invasive migration of B16 mouse melanoma cells. *Mol. Cells* **2012**, *33*, 363−369.
(18) Kim, T. H.; Ku, S. K.; Bae, J. S. Antithrombotic and profibrinolytic activities of eckol and dieckol. *J. Cell. Biochem.* **2012**, *113*, 2877−2883.
(19) Ko, S. C.; Lee, M.; Lee, J. H.; Lee, S. H.; Lim, Y.; Jeon, Y. J. Dieckol, a phlorotannin isolated from a brown seaweed, *Ecklonia cava*, inhibits adipogenesis through AMP-activated protein kinase (AMPK) activation in 3T3-L1 preadipocytes. *Environ. Toxicol. Pharmacol.* **2013**, *36*, 1253−1260.
(20) Kang, M. C.; Ahn, G.; Yang, X.; Kim, K. N.; Kang, S. M.; Lee, S. H.; Ko, S. C.; Ko, J. Y.; Kim, D.; Kim, Y. T.; Jee, Y.; Park, S. J.; Jeon, Y. J. Hepatoprotective effects of dieckol-rich phlorotannins from *Ecklonia cava*, a brown seaweed, against ethanol induced liver damage in BALB/c mice. *Food Chem. Toxicol.* **2012**, *50*, 1986−1991.
(21) Kim, S. Y.; Kim, E. A.; Kang, M. C.; Lee, J. H.; Yang, H. W.; Lee, J. S.; Lim, T. I.; Jeon, Y. J. Polyphenol-rich fraction from *Ecklonia cava* (a brown alga) processing by-product reduces LPS-induced inflammation in vitro and in vivo in a zebrafish model. *Algae* **2014**, *29*, 165−174.
(22) Lee, J. H.; Ko, J. Y.; Oh, J. Y.; Kim, C. Y.; Lee, H. J.; Kim, J.; Jeon, Y. J. Preparative isolation and purification of phlorotannins from *Ecklonia cava* using centrifugal partition chromatography by one-step. *Food Chem.* **2014**, *158*, 433−437.
(23) Zhao, G.; Souers, A. J.; Voorbach, M.; Falls, H. D.; Droz, B.; Brodjian, S.; Lau, Y. Y.; Iyengar, R. R.; Gao, J.; Judd, A. S.; Wagaw, S. H.; Ravn, M. M.; Engstrom, K. M.; Lynch, J. K.; Mulhern, M. M.; Freeman, J.; Dayton, B. D.; Wang, X.; Grihalde, N.; Fry, D.; Beno, D. W.; Marsh, K. C.; Su, Z.; Diaz, G. J.; Collins, C. A.; Sham, H.; Reilly, R. M.; Brune, M. E.; Kym, P. R. Validation of diacyl glycerolacyltransferase I as a novel target for the treatment of obesity and dyslipidemia using a potent and selective small molecule inhibitor. *J. Med. Chem.* **2008**, *51*, 380−383.
(24) Al-Hamodi, Z.; Al-Habori, M.; Al-Meeri, A.; Saif-Ali, R. Association of adipokines, leptin/adiponectin ratio and C-reactive protein with obesity and type 2 diabetes mellitus. *Diabetol. Metab. Syndrome* **2014**, *6*, 99.
(25) Klop, B.; Elte, J. W.; Cabezas, M. C. Dyslipidemia in obesity: mechanisms and potential targets. *Nutrients* **2013**, *5*, 1218−1240.
(26) Lee, S. H.; Min, K. H.; Han, J. S.; Lee, D. H.; Park, D. B.; Jung, W. K.; Park, P. J.; Jeon, B. T.; Kim, S. K.; Jeon, Y. J. Effects of brown alga, *Ecklonia cava* on glucose and lipid metabolism in C57BL/KsJ-db/db mice, a model of type 2 diabetes mellitus. *Food Chem. Toxicol.* **2012**, *50*, 575−582.
(27) Gaemers, I. C.; Stallen, J. M.; Kunne, C.; Wallner, C.; van Werven, J.; Nederveen, A.; Lamers, W. H. Lipotoxicity and steatohepatitis in an overfed mouse model for non-alcoholic fatty liver disease. *Biochim. Biophys. Acta* **2011**, *1812*, 447−458.
(28) Trauner, M.; Arrese, M.; Wagner, M. Fatty liver and lipotoxicity. *Biochim. Biophys. Acta* **2010**, *1801*, 299−310.
(29) Liao, C. C.; Ou, T. T.; Wu, C. H.; Wang, C. J. Prevention of diet-induced hyperlipidemia and obesity by caffeic acid in C57BL/6 mice through regulation of hepatic lipogenesis gene expression. *J. Agric. Food Chem.* **2013**, *61*, 11082−11088.
(30) Kim, S.; Jin, Y.; Choi, Y.; Park, T. Resveratrol exerts anti-obesity effects via mechanisms involving down-regulation of adipogenic and inflammatory processes in mice. *Biochem. Pharmacol.* **2011**, *81*, 1343−1351.
(31) Shimano, H. Sterol regulatory element-binding proteins (SREBPs): transcriptional regulators of lipid synthetic genes. *Prog. Lipid Res.* **2001**, *40*, 439−452.
(32) Kohjima, M.; Higuchi, N.; Kato, M.; Kotoh, K.; Yoshimoto, T.; Fujino, T.; Yada, M.; Yada, R.; Harada, N.; Enjoji, M.; Takayanagi, R.; Nakamuta, M. SREBP-1c, regulated by the insulin and AMPK signaling pathways, plays a role in nonalcoholic fatty liver disease. *Int. J. Mol. Med.* **2008**, *21*, 507−511.
(33) Horton, J. D. Sterol regulatory element-binding proteins: transcriptional activators of lipid synthesis. *Biochem. Soc. Trans.* **2002**, *30*, 1091−1095.
(34) Um, M. Y.; Hwang, K. H.; Ahn, J.; Ha, T. Y. Curcumin attenuates diet-induced hepatic steatosis by activating AMP-activated protein kinase. *Basic Clin. Pharmacol. Toxicol.* **2013**, *113*, 152−157.
(35) Viollet, B.; Foretz, M.; Guigas, B.; Horman, S.; Dentin, R.; Bertrand, L.; Hue, L.; Andreelli, F. Activation of AMP-activated protein kinase in the liver: a new strategy for the management of metabolic hepatic disorders. *J. Physiol.* **2006**, *574*, 41−53.
(36) Gower, B. A.; Nagy, T. R.; Blaylock, M. L.; Wang, C.; Nyman, L. Estradiol may limit lipid oxidation via Cpt 1 expression and hormonal mechanisms. *Obes. Res.* **2002**, *10*, 167−172.
(37) Hou, X.; Xu, S.; Maitland-Toolan, K. A.; Sato, K.; Jiang, B.; Ido, Y.; Lan, F.; Walsh, K.; Wierzbicki, M.; Verbeuren, T. J.; Cohen, R. A.; Zang, M. SIRT1 regulates hepatocyte lipid metabolism through activating AMP-activated protein kinase. *J. Biol. Chem.* **2008**, *283*, 20015−20026.
(38) Salminen, A.; Hyttinen, J. M.; Kaarniranta, K. AMP-activated protein kinase inhibits NF-kappaB signaling and inflammation: impact on healthspan and lifespan. *J. Mol. Med.* **2011**, *89*, 667−676.
(39) Cohen, H. Y.; Miller, C.; Bitterman, K. J.; Wall, N. R.; Hekking, B.; Kessler, B.; Howitz, K. T.; Gorospe, M.; de Cabo, R.; Sinclair, D. A. Calorie restriction promotes mammalian cell survival by inducing the SIRT1 deacetylase. *Science* **2004**, *305*, 390−392.
(40) Puigserver, P. Tissue-specific regulation of metabolic pathways through the transcriptional coactivator PGC1-alpha. *Int. J. Obes.* **2005**, *29* (Suppl. 1), S5−S9.
(41) Vachharajani, V.; Granger, D. N. Adipose tissue: a motor for the inflammation associated with obesity. *IUBMB Life* **2009**, *61*, 424−430.
(42) Itabe, H. Oxidized low-density lipoprotein as a biomarker of in vivo oxidative stress: from atherosclerosis to periodontitis. *J. Clin. Biochem. Nutr.* **2012**, *51*, 1−8.
(43) Chirico, S.; Smith, C.; Marchant, C.; Mitchinson, M. J.; Halliwell, B. Lipid peroxidation in hyperlipidaemic patients. A study of plasma using an HPLC-based thiobarbituric acid test. *Free Radical Res. Commun.* **1993**, *19*, 51−57.
(44) Serafini-Cessi, F.; Cessi, C. Thiobarbituric acid test as an index of phospholipid peroxidation. *Sperimentale* **1968**, *118*, 371−378.
(45) Ma, Y. Y.; Li, L.; Yu, C. H.; Shen, Z.; Chen, L. H.; Li, Y. M. Effects of probiotics on nonalcoholic fatty liver disease: a meta-analysis. *World J. Gastroenterol.* **2013**, *19*, 6911−6918.
(46) Kang, S. M.; Cha, S. H.; Ko, J. Y.; Kang, M. C.; Kim, D.; Heo, S. J.; Kim, J. S.; Heu, M. S.; Kim, Y. T.; Jung, W. K.; Jeon, Y. J. Neuroprotective effects of phlorotannins isolated from a brown alga, *Ecklonia cava*, against H_2O_2-induced oxidative stress in murine hippocampal HT22 cells. *Environ. Toxicol. Pharmacol.* **2012**, *34*, 96−105.
(47) Lim, H. H.; Yang, S. J.; Kim, Y.; Lee, M.; Lim, Y. Combined treatment of mulberry leaf and fruit extract ameliorates obesity-related inflammation and oxidative stress in high fat diet-induced obese mice. *J. Med. Food* **2013**, *16*, 673−680.

JOURNAL OF AGRICULTURAL AND FOOD CHEMISTRY

Article

pubs.acs.org/JAFC

Effect of Gibberellin on the Biosynthesis of Tocopherols in Oilseed Rape (*Brassica napus* L.) and *Arabidopsis*

Xue Du,[†] Nazim Hussain,*[,†] Zhilan Li,[†] Xiaoyang Chen,[‡] Shuijin Hua,[§] Dongqing Zhang,[§] and Lixi Jiang*[,†]

[†]Institute of Crop Science, College of Agriculture and Biotechnology, Zhejiang University, 866 Yu-Hang-Tang Road, Hangzhou 310058, P.R. China

[‡]Institute of Crop Science, Jinhua Academy of Agricultural Sciences, 828 Shuanglong Nan, Jinhua 321017, P.R. China

[§]Institute of Crop and Nuclear Agricultural Sciences, Zhejiang Academy of Agricultural Sciences, 198 Shiqiao Road, Hangzhou 310021, P.R. China

Supporting Information

ABSTRACT: Elevating the yield and altering the composition of seed tocopherols (Toc's) are important to rapeseed breeding and production. However, little is known about the biosynthesis of Toc's in response to environmental signals. In this study, we investigated the effects of exogenous gibberellin (GA_3) and paclobutrazol (PAC) on Toc biosynthesis. We also explored the interactive effects between the two plant growth regulators (PGRs) and other factors, such as PGR treatment duration, genotype, and growing location on the total Toc yield and composition in oilseed rape seed. GA_3 significantly enhanced the production of Toc's and elevated the α-/γ-Toc ratio in a time- and genotype-dependent manner. By contrast, PAC significantly reduced Toc yield. Genotypic differences were observed in the effects of GA_3 on Toc yield and composition in the seeds. GA_3 significantly increased the Toc yield and α-/γ-Toc ratio in Zheyou-50, a genotype with a low proportion of very long chain fatty acids (VLCFAs). However, GA_3 did not significantly influence these parameters in Jiu-Er-13Xi, a genotype with a high VLCFA proportion. The increased Toc yield induced by GA_3 was mediated by the upregulation of genes (*BnPDS1* and *BnVTE1*) that catalyze the production of Toc precursors. Therefore, applying GA_3 can improve rapeseed quality by increasing Toc yield and improving Toc composition.

KEYWORDS: *Brassica, Arabidopsis, gibberellin (GA_3), paclobutrazol (PAC), tocopherol content, tocopherol composition, gene expression*

INTRODUCTION

Oilseed rape (*Brassica napus* L., AACC, $2n$ = 38) in the Brassicaceae family has a high economic importance worldwide.[1,2] Oilseed rape oil is a vital dietary source of vitamin E in China, particularly in the Yangtze River valley region.[3,4] Tocopherols (Toc's) constitute a family of vital lipid-soluble antioxidants with several health benefits.[5−8] Protection of the photosynthetic apparatus from oxygen toxicity and lipid peroxidation in plants is attributed to α-tocopherol (α-Toc) enrichment in the chloroplast membrane,[9] whereas the prevention of polyunsaturated fatty acids from oxidation in seeds is enhanced by γ-tocopherol (γ-Toc).[10] The biological activities of the vitamin E components α-Toc, β-tocopherol (β-Toc), γ-tocopherol (γ-Toc), and δ-tocopherol (δ-Toc) are 100%, 30%, 15%, and 5%, respectively.[11] Canola oil, on the average, contains a high amount of vitamin E, with ∼64% γ-Toc, ∼35% α-Toc, and <1% δ-Toc.[1,12,13]

Plant growth regulators (PGRs) play important roles in various aspects of plant growth and development, including seed maturation and the accumulation of seed storage reserves.[14] Gibberellins (GAs) constitute a large group of tetracyclic diterpenoids that regulate seed germination, leaf expansion, stem and root extension, flower induction and development, and fruit expansion.[15−18] GA signals are received and transduced via the GID1 GA receptor/DELLA repressor pathway. *Arabidopsis* has five functionally overlapping DELLA proteins,[19−22] namely, GAI, RGA, RGL1, RGL2, and RGL3, that are nuclear negative regulators in the GA signaling pathway.[20,23,24] Paclobutrazol (PAC) or (2*RS*,3*RS*)-1-(4-chlorophenyl)-4,4-dimethyl-2-(1*H*-1,2,4-triazol-1-yl)pentan-3-ol interacts antagonistically with GA by inhibiting its synthesis by blocking conversion of *ent*-kaurene to *ent*-kaurenoic acid. Exogenous PAC suppresses shoot growth, leading to reduced plant height, internode elongation, and leaf area as well as to increased lodging resistance, branch number, and seed yield in oilseed rape.[25,26]

Increasing the total Toc and/or altering the Toc composition (α-/γ-Toc ratio) are important to rapeseed breeding and commercial production. Previous studies on vegetable and maize seeds revealed interactive effects between genotypes and environmental factors on seed Toc's.[27−31] However, little is known about the response of seed Toc's to exogenous PGRs. Therefore, we conducted a field experiment to investigate the effects of gibberellic acid (GA_3) and its synthesis inhibitor PAC on seed Toc's. We also analyzed the expression levels of the

Received: August 4, 2014
Revised: December 16, 2014
Accepted: December 16, 2014
Published: December 16, 2014

ACS Publications © 2014 American Chemical Society

DOI: 10.1021/jf505312c
J. Agric. Food Chem. 2015, 63, 360−369

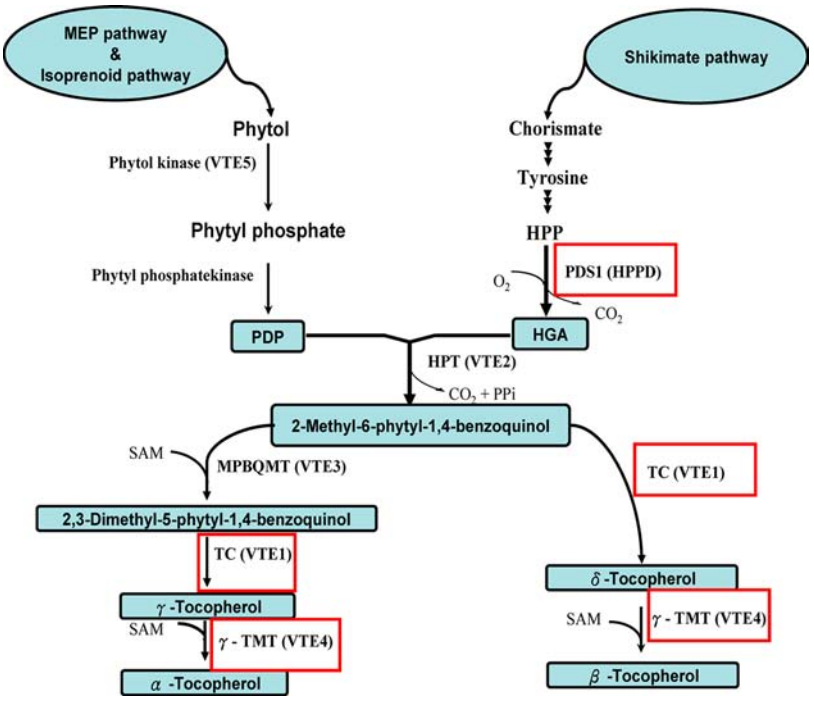

Figure 1. Tocopherol biosynthesis pathway in plants; a model from *Arabidopsis* adapted from Hussain et al.[8] HPP, *p*-hydroxyphenylpyruvate; HGA, homogentisic acid/homogentisate; PDP, phytyldiphosphate; HPPD (PDS1), HPP dioxygenase; HPT (VTE2), homogentisate phytyltransferase; MPBQMT (VTE3), 2-methyl-6-phytyl-1,4-benzoquinol methyltransferase; TC (VTE1), tocopherol cyclase; γ-TMT (VTE4), γ-tocopherol methyltransferase. Genes highlighted and closed in red boxes were selected to study expression in response to exogenous GA_3 and/or PAC.

Table 1. Timing of PGR Applications to Rapeseed Plants (Year 2013)[a]

		Year 2013								
Location	PGRs Spray Timings	March 1	March 11	March 18	March 25	April 4	April 12	April 17	April 24	May 1
Hangzhou	S1									
	S2									
	S3									
	PGRs Spray Timings	Feb 29	March 9	March 14	March 22	March 27	April 2	April 12	April 20	April 24
Jinhua	S1									
	S2									
	S3									

[a]S1 = PGRs spray from bud formation to seed maturity; S2 = from flowering initiation to seed maturity; S3 = from flowering completion to seed maturity stage. Shaded boxes show the timings of PGRs spray.

PDS1, *VTE1*, and *VTE4* genes to monitor the synthesis of Toc precursors. *PDS1* plays a critical role in the conversion of *p*-hydroxyphenylpyruvate (HPP) to homogentisic acid (HGA). *VTE1* encodes a Toc cyclase that directly converts 2-methyl-6-phytyl-1,4-benzoquinol (MPBQ) into δ-Toc or 2,3-dimethyl-5-phytyl-1,4-benzoquinol (DMPBQ) into γ-Toc.[32] *VTE4* is a transmethylase that catalyzes the production of α-Toc from γ-Toc and β-Toc from δ-Toc [33] (Figure 1). We also aim to understand the interactive effects between the PGRs and other factors, such as PGR treatment duration, genotype, and growing location.

MATERIALS AND METHODS

Plant Materials and Growth Conditions of *Arabidopsis*. The *Arabidopsis thaliana* ecotype Langdsberg *erecta* (L*er*) (wild-type (WT)), the quadruple mutant (*gai-t6 rga-t2 rgl1-1 rgl2-1*) of wild-type background (*q-della/WT*), and the penta mutant (*ga1-3 gai-t6 rga-t2 rgl1-1 rgl2-1*) of *ga1-3* background (*p-della*), were used to evaluate the effects of GA_3 application on Toc's in *Arabidopsis* seeds.[24] The *q-della/WT* mutant was donated by Prof. Fu Xiangdong of the Institute of Genetics and Developmental Biology, Chinese Academy of Sciences. The *p-della* mutant was provided by Prof. Jinrong Peng of the College of Life Science, Zhejiang University. All plants were grown under the same conditions (16 h light/8 h darkness) and harvested almost simultaneously. Seeds were stored in a dry cabinet (15% moisture level) until used.

Plant Material and Growth Conditions of Rapeseed. Field experiments were conducted during the winter canola growing season (2012−2013) at Hangzhou (location 1, L1) and Jinhua (L2). Both cities are in Eastern China, and are ∼250 km apart. Zheyou-50 (genotype 1, G1), a canola type with a high seed oil content of ∼50%, and Jiu-Er-13Xi (G2), a high erucic acid type with a low seed oil content of only 40%, were used. Pesticides and herbicides were applied following local cultivation management. One-month-old seedlings of uniform height were selected and transplanted from the nursery to the respective fields. The soil type of the fields at both locations was loamy clay. Before transplanting from nursery to field, urea at a rate of 150 kg ha^{-1} was applied as a basal dose fertilizer. At the end of January 2013, a second dose of urea was applied as topdressing at a rate of 75 kg ha^{-1}.

DOI: 10.1021/jf505312c
J. Agric. Food Chem. 2015, 63, 360−369

The fields at both sites were not irrigated because rainfall was sufficient in Hangzhou (738.4 mm) and Jinhua (868.5 mm) during the rapeseed growth season. Plants were spaced 0.35 m apart between rows and 0.30 m within rows. The field experiment at both locations was performed following a randomized complete block design with three replications (blocks).

Application of PGRs to the Plants. GA_3 (plant growth regulator 1, P1) at 150 μmol L^{-1} and PAC (P3) at 150 mg L^{-1} were applied to rapeseed plants. Both PGRs were purchased from Sangon Company (Shanghai, China). Water was used as a control (P2). All PGRs were sprayed at 7−9 day intervals (no spraying on raining days) during one of the following stages: S1 (from bud formation to seed maturity), S2 (from flowering initiation to seed maturity), or S3 (from flowering completion to seed maturity). Timing and duration of PGR applications are listed in Table 1. S1, S2, and S3 included 9, 7, and 5 PGR spray events, respectively. Colored threads were tied to the main branch of rapeseed plants to tag the flowering initiation dates.

Analysis of Tocopherols. Toc's were extracted and analyzed as previously described with slight modifications.[2,34] In brief, ~75 mg of seeds were weighed and transferred into a 2 mL skirted screw-cap microtube containing 1.3 mL of *n*-hexane. The seeds were pulverized with a bead mill homogenizer (Bead Ruptor-24, Omni, Kennesaw, Georgia, U.S.A.) at 8 m s^{-1} for 30 s. The samples were stored in the dark for 15 h to extract Toc's. A 20 μL aliquot of the supernatant was analyzed on a normal-phase high-performance liquid chromatography (HPLC) apparatus (model 600, Waters, Milford, Massachusetts, U.S.A.) equipped with a Zorbax Rx-SIL column (4.6 mm × 250 mm × 5 μm; Agilent, Englewood, Colorado, U.S.A.) and a fluorescence detector (λ_{ex} = 295 nm; λ_{em} = 330 nm). The mobile phase of hexane/*tert*-butyl methyl ether (94:6, v/v) was delivered isocratically at 1 mL min^{-1}. Calibration curves of pure standards were used to quantify the Toc isoforms. References for α- (purity 99.90%, cat. no. 47783), β- (purity 99.00%, cat. no. 46401), γ- (purity 99.10%, cat. no. 47785), and δ-Toc (purity 95.50%, cat. no. 47784) were analytical standards and were obtained from Supelco (Bellefonte, Pennsylvania, U.S.A.). Liquid chromatography-grade hexane (Sigma−Aldrich, Shanghai, China) was used as the solvent. The peaks of the Toc standards (α-, β, γ-, and δ-Toc) were distinguished by their retention times. The standard curve for the quantification of the experimental samples was calibrated according to the corresponding peaks of individual Toc derivatives. The contents of Toc's were expressed in mg per kg of seed, and the total amount of Toc's was calculated as the sum of α- and γ-Toc.

Analysis of Gene Expression by Reverse Transcription Quantitative Polymerase Chain Reaction. Flowers were tagged with different colored threads to indicate days after pollination (DAP). Only seeds from the siliques on main inflorescences were harvested for RNA extraction. The RNA samples were isolated with the Invisorb Spin Plant RNA Mini Kit (Invitek, Berlin, Germany) following the manufacturer's instructions. Reverse transcription quantitative polymerase chain reaction (RT-qPCR) amplification was performed as previously described.[35] All primer pairs used in the RT-qPCR analyses of *Arabidopsis* and rapeseed are listed in Supporting Information, Tables S1 and S2, respectively.

Statistical Analysis. For the analysis of gene expression, baseline and threshold cycles (CT value) were determined automatically by using Bio-Rad iQ Software (version 3.0; Hercules, California, U.S.A.). Relative amounts of RNA transcripts were calculated as previously described.[36] Field experimental data were classified with Win-Excel and subjected to ANOVA with the MStatc statistical package (version 7.05). Treatment means were compared for least significant differences at $P \leq 0.05$ or $P \leq 0.01$ (Table 2).

RESULTS

Response of Total Toc and Its Components to Exogenous PGRs and the Interactions between PGRs and Other Factors. ANOVA reveals that genotype (G), PGR (P), and number of PGR applications (S) significantly affected the total Toc and its composition. Growth location (L) only significantly affected α-Toc and the α-/γ-Toc ratio. Most of the interactions among these factors significantly affected the variation in total Toc and its components. However, the interaction between L × S and L × P × G exerted no significant effects on the α-Toc content, and the interaction between P × G exhibited no significant effect on the γ-Toc content (Table 2).

Table 2. ANOVA Showing the Effects of Location, PGR Type, Duration of PGR Treatment, and Genotype on Seed Tocopherol in Rapeseed[a]

factor	α-Toc	γ-Toc	total Toc	α-/γ-Toc ratio
location (L)	**	ns	ns	**
PGRs (P)	**	**	**	**
L × P	**	**	**	**
duration of PGR effect (or total spray times) (S)	**	**	**	**
L × S	ns	**	*	**
P × S	**	**	**	**
P × L × S	**	**	**	*
genotype (G)	**	**	**	**
L × G	**	**	**	*
P × G	**	ns	**	**
P × G × L	ns	**	*	**
S × G	**	**	**	**
L × S × G	**	*	*	**
P × S × G	**	**	**	**
L × P × S × G	**	**	**	**
error MS	229.411	341.067	974.096	0.001
CV (%)	7.10	5.93	6.10	4.07

[a]P, plant growth regulators (PGRs); G, genotype; L, location; S, duration of PGR effect (or total spray times); details are available in the Materials and Methods section. *Indicates significance at $P \leq 0.05$; **indicates significance at $P \leq 0.01$; ns = nonsignificant.

Effect of PGRs on Toc Content and Composition. Compared with the water control, GA_3 significantly increased the total Toc, α-Toc, and γ-Toc contents as well as the α-/γ-Toc ratio ($P \leq 0.01$). Meanwhile, PAC significantly reduced the total Toc but did not significantly influence the α-Toc and γ-Toc contents or the α-/γ-Toc ratio (Table 3).

Effect of the Interaction between PGR and Genotype on Seed Toc's. Highly significant variations in the seed total Toc, α-Toc, and α-/γ-Toc ratio ($P \leq 0.01$) were observed in response to the interaction between PGR and genotype (G), whereas no significant differences were observed in the seed γ-Toc (Table 3). Zheyou-50 plants treated with GA_3 produced higher total Toc (667.22 mg kg^{-1} seeds) and α-Toc (282.54 mg kg^{-1} seeds) than those treated with PAC or water. The lowest total Toc (380.74 mg kg^{-1} seeds) and α-Toc contents (160.00 mg kg^{-1} seeds) were observed in the Jiu-Er-13Xi plants untreated with PGR (Table 3). The Jiu-Er-13Xi plants treated with GA_3 had the highest α-/γ-Toc ratio (0.80), whereas the Zheyou-50 plants treated with PAC had the lowest α-/γ-Toc ratio (0.66) (Table 3).

Effect of the Interactions between PGR and Location on Seed Toc's. The interaction between PGR and location caused highly significant variations in the total Toc, α-Toc, and γ-Toc contents as well as in the α-/γ-Toc ratio ($P \leq 0.01$) (Table 2). The highest total Toc (538.35 mg kg^{-1} seed) and γ-Toc (315.32 mg kg^{-1} seed) contents were obtained after applying GA_3 at the Hangzhou site (L1). Conversely, the highest α-Toc content (238.38 mg kg^{-1} seed) and α-/γ-Toc ratio (0.82) were

DOI: 10.1021/jf505312c
J. Agric. Food Chem. 2015, 63, 360−369

Table 3. Responses of Seed Toc Yield and Composition to PGR and the Interactive Effects between PGR and Location, Genotype, and Duration of PGR Effect (or Total Spray Times) In Rapeseed[a]

	Factors	Total-Toc	α-Toc	γ-Toc	α-/γ-Toc ratio
PGRs (P)	P1	536.03 a	230.71 a	305.32 a	0.77 a
	P2	507.60 b	207.39 b	300.21 ab	0.70 b
	P3	491.62 c	201.62 b	289.99 b	0.71 b
	Sig. Level	**	**	**	**
P x G interaction	P1G1	667.22 a	282.54 a	384.69	0.74 bc
	P1G2	404.83 d	178.87 d	225.96	0.80 a
	P2G1	634.47 b	254.78 b	379.69	0.67 d
	P2G2	380.74 d	160.00 e	220.74	0.73 c
	P3G1	597.08 c	236.64 c	360.43	0.66 d
	P3G2	386.16 d	166.60 de	219.56	0.76 b
	Sig. Level	**	**	ns	**
P x L interaction	P1L1	538.35 a	223.03 b	315.32 a	0.73 b
	P1L2	533.71 a	238.38 a	295.33 bc	0.82 a
	P2L1	515.02 ab	207.89 c	307.14 ab	0.68 c
	P2L2	500.18 ab	206.90 c	293.29 bc	0.72 b
	P3L1	471.44 b	188.59 d	282.85 c	0.69 c
	P3L2	511.80 ab	214.66 bc	297.14bc	0.73 b
	Sig. Level	**	**	**	**

	Factors	Total-Toc	α-Toc	γ-Toc	α-/γ-Toc ratio
P x S interaction	P1S1	625.50 a	263.62 a	361.88 a	0.74 bc
	P1S2	461.47 d	199.07 de	262.41 f	0.77 b
	P1S3	521.12 c	229.44 b	291.68 de	0.81 a
	P2S1	527.36 bc	213.22 b-d	314.14 bc	0.68 e
	P2S2	476.78 d	197.72 de	279.06 ef	0.72 cd
	P2S3	518.68 c	211.24 cd	307.44 cd	0.70 de
	P3S1	556.99 b	225.51 bc	331.49 b	0.70 de
	P3S2	459.42 d	191.91 e	267.50 f	0.74 bc
	P3S3	458.44 d	187.45 e	270.99 f	0.69 de
	Sig. Level	**	**	**	**

[a]Sig. level shows the level of significance. The values of Toc content and composition are the means of three replications. P, plant growth regulators (PGRs); G, genotype; L, location; S, duration of PGR effect (or total spray times); details are available in the Materials and Methods section. Different letters to the figures in the same column following each category indicate significant differences at $P \leq 0.01$ (**) or 0.05 (*) as per ANOVA results.

Table 4. Responses of Seed Toc Yield and Composition to the Interactive Effects of PGR and Location, Genotype, and Duration of PGR Effect (Or Total Spray Times) In Rapeseed[a]

	Factors	Total-Toc	α-Toc	γ-Toc	α-/γ-Toc ratio
P x L x S interaction	P1L1S1	673.9 a	269.79 a	404.12 a	0.69 f-h
	P1L1S2	452.15 ij	192.73 d	259.42 h	0.75 c
	P1L1S3	489.01f-j	206.57 b-d	282.43 e-h	0.74 cd
	P1L2S1	577.09 bc	257.45 a	319.65 cd	0.80 b
	P1L2S2	470.80 g-j	205.40 b-d	265.40 h	0.79 b
	P1L2S3	553.24 c-e	252.31 a	300.93 d-f	0.88 a
	P2L1S1	555.90 cd	223.12 b	332.77 bc	0.67 g-i
	P2L1S2	479.87 g-j	197.78 cd	282.08 e-h	0.71 d-f
	P2L1S3	509.31 d-g	202.75 b-d	306.56 c-e	0.66 hi
	P2L2S1	498.82 f-i	203.32 b-d	295.51 d-g	0.70 e-g
	P2L2S2	473.69 g-j	197.65 cd	276.04 f-h	0.73 c-e
	P2L2S3	528.04 d-f	219.72 bc	308.33 c-e	0.73 c-e
	P3L1S1	506.31 e-h	192.17 d	314.15 cd	0.64 i
	P3L1S2	449.73 j	188.46 d	261.28 h	0.74 cd
	P3L1S3	458.27 ij	185.14 d	273.13 f-h	0.68 f-h
	P3L2S1	607.67 b	258.84 a	348.83 b	0.75 c
	P3L2S2	469.10 g-j	195.37 d	273.73 f-h	0.74 c-e
	P3L2S3	458.62 h-j	189.76 d	268.86 gh	0.70 e-g
	Sig. Level	**	**	**	*
P x G x L interaction	P1G1L1	635.78 bc	259.65	376.13 ab	0.72 c-e
	P1G2L1	440.92 e	186.40	254.51 d	0.73 b-d
	P1G1L2	698.67 a	305.42	393.24 a	0.77 b
	P1G2L2	368.75 gh	171.34	197.41 f	0.87 a
	P2G1L1	614.23 c	246.2	368.03 bc	0.67 f
	P2G2L1	415.82 ef	169.58	246.25 d	0.69 ef
	Sig. Level	*	ns	**	**

	Factors	Total-Toc	α-Toc	γ-Toc	α-/γ-Toc ratio
P x S x G interaction	P1SIG1	832.14 a	345.46 a	486.67 a	0.72 cd
	P1SIG2	418.86 e	181.77 e	237.09 fg	0.77 bc
	P1S2G1	494.32 d	212.76 cd	281.56 e	0.76 bc
	P1S2G2	428.63 e	185.37 e	243.23 f	0.78 b
	P1S3G1	675.23 b	289.40 b	385.83 c	0.75 bc
	P1S3G2	367.01 fg	169.48 e-g	197.53 i	0.87 a
	P2SIG1	668.09 b	270.62 b	397.47 bc	0.68 d-f
	P2SIG2	386.63 e-g	155.82 f-h	230.81 f-h	0.69 d-f
	P2S2G1	558.18 c	222.82 cd	335.36 d	0.67 e-g
	P2S2G2	395.38 ef	172.62 e-g	222.77 f-i	0.78 b
	P2S3G1	677.14 b	270.90 b	406.24 bc	0.67 e-g
	P2S3G2	360.21 fg	151.57 gh	208.64 hi	0.73 b-d
	P3SIG1	688.31 b	266.66 b	421.65 b	0.63 g
	P3SIG2	425.68 e	184.35 e	241.33 f	0.77 bc
	P3S2G1	532.04 cd	208.58 d	323.46 d	0.65 fg
	P3S2G2	386.80 e-g	175.25 ef	211.55 g-i	0.83 a
	P3S3G1	570.89 c	234.70 c	336.19 d	0.70 de
	P3S3G2	345.99 g	140.20 h	205.79 hi	0.68 d-f
	Sig. Level	**	**	**	**
P x G x L interaction	P2G1L2	654.71 b	263.36	391.35 a	0.67 f
	P2G2L2	345.66 h	150.43	195.23 f	0.77 b
	P3G1L1	561.59 d	213.28	348.31 c	0.62 g
	P3G2L1	381.29 g	163.89	217.39 ef	0.76 bc
	P3G1L2	632.57 bc	260.01	372.56 ab	0.70 d-f
	P3G2L2	391.03 fg	169.31	221.72 e	0.76 b
	Sig. Level	*	ns	**	**

[a]Sig. level shows the level of significance. The values of Toc yield and composition are the means of three replications. P, plant growth regulators (PGRs); G, genotype; L, location; S, duration of PGR effect (or total spray times); details are available in the Materials and Methods section. Different letters to the figures in the same column following each category indicate significant differences at $P \leq 0.01$ (**) or 0.05 (*) as per ANOVA results.

achieved after applying GA_3 at the Jinhua site (L2). Application of PAC at the Hangzhou site (L1) produced the lowest total Toc, α-Toc, and γ-Toc contents as well as the lowest α-/γ-Toc ratio (Table 3).

DOI: 10.1021/jf505312c
J. Agric. Food Chem. 2015, 63, 360−369

Table 5. Responses of Seed Toc Yield and Composition to the Four Factors Interactive Effects of PGR and Location, Genotype, and Duration of PGR Effect (or Total Spray Times) In Rapeseed[a]

	Factors	Total-Toc	α-Toc	γ-Toc	α-/γ-Toc ratio	Factors	Total-Toc	α-Toc	γ-Toc	α-/γ-Toc ratio
P x G x L x S interaction	P1G1L1S1	875.01 a	334.73 a	540.28 a	0.62 n	P2G2L1S1	448.62 j-l	174.44 k-o	274.20 g	0.64 mn
	P1G1L1S2	453.52 jk	205.73 g-k	247.79 gh	0.83 bc	P2G2L1S2	415.49 j-n	178.89 j-n	236.60 g-j	0.75 e-j
	P1G1L1S3	578.82 gh	238.50 d-g	340.32 f	0.70 h-m	P2G2L1S3	383.35 l-q	155.39 m-p	227.96 h-k	0.68 k-n
	P1G1L2S1	789.25 b	356.19 a	433.06 bc	0.82 b-e	P2G2L2S1	324.64 q	137.20 p	187.44 lm	0.73 f-k
	P1G1L2S2	535.11 hi	219.79 e-i	315.33 f	0.70 i-m	P2G2L2S2	375.27 m-q	166.34 l-p	208.93 h-m	0.80 c-f
	P1G1L2S3	771.63 bc	340.30 a	431.34 bc	0.79 c-g	P2G2L2S3	337.08 o-q	147.75 n-p	189.33 k-m	0.78 c-g
	P1G2L1S1	472.79 ij	204.84 h-k	267.95 g	0.76 d-i	P3G1L1S1	596.02 f-h	205.35 h-k	390.66 de	0.52 o
	P1G2L1S2	450.78 j-l	179.73 j-n	271.05 g	0.67 k-n	P3G1L1S2	529.83 hi	209.60 g-j	320.23 f	0.65 mn
	P1G2L1S3	399.19 k-p	174.64 k-o	224.54 h-l	0.78 c-g	P3G1L1S3	558.92 h	224.88 e-h	334.03 f	0.67 k-n
	P1G2L2S1	364.93 n-q	158.70 l-p	206.23 i-m	0.77 c-h	P3G1L2S1	780.60 bc	327.96 a	452.64 b	0.73 f-l
	P1G2L2S2	406.48 j-n	191.01 i-l	215.47 h-l	0.89 b	P3G1L2S2	534.24 hi	207.55 g-j	326.69 f	0.64 mn
	P1G2L2S3	334.84 pq	164.32 l-p	170.52 m	0.96 a	P3G1L2S3	582.86 gh	244.51 c-f	338.35 f	0.72 g-l
	P2G1L1S1	663.17 d-f	271.80 bc	391.37 de	0.70 i-m	P3G2L1S1	416.61 j-n	178.98 j-n	237.63 g-j	0.76 e-i
	P2G1L1S2	544.24 h	216.68 f-i	327.56 f	0.66 l-n	P3G2L1S2	369.64 m-q	167.31 l-p	202.32 j-m	0.83 b-d
	P2G1L1S3	635.27 e-g	250.11 c-e	385.16 e	0.65 mn	P3G2L1S3	357.62 n-q	145.39 op	212.23 h-l	0.69 j-n
	P2G1L2S1	673.00 de	269.43 b-d	403.57 c-e	0.67 k-n	P3G2L2S1	434.75 j-m	189.72 i-l	245.03 g-i	0.77 c-g
	P2G1L2S2	572.11 gh	228.96 e-h	343.15 f	0.67 k-n	P3G2L2S2	403.97 k-o	183.19 j-m	220.77 h-l	0.83 bc
	P2G1L2S3	719.01 cd	291.70 b	427.32 b-d	0.69 j-n	P3G2L2S3	334.37 pq	135.00 p	199.36 j-m	0.68 k-n
	Sig. Level	**	**	**	**	Sig. Level	**	**	**	**

[a]Sig. level shows the level of significance. The values of Toc yield and composition are the means of three replications. P, plant growth regulators (PGRs); G, genotype; L, location; S, duration of PGR effect (or total spray times); details are available in the Materials and Methods section. Different letters to the figures in the same column following each category indicate significant differences at $P \leq 0.01$ (**) or 0.05 (*) as per ANOVA results.

Effect of the Interaction between PGR and PGR Treatment Duration on Seed Toc's. The interaction between PGR and PGR treatment duration led to significant variations in the total Toc, α-Toc, and γ-Toc contents and in the α-/γ-Toc ratio ($P \leq 0.01$) (Table 2). The application of GA_3 (P1) from the green floral bud stage to seed maturity (S1) resulted in the highest total Toc (625.50 mg kg^{-1} seed), α-Toc (263.62 mg kg^{-1} seed), and γ-Toc (361.88 mg kg^{-1} seed) contents, whereas the application of GA_3 from flowering completion to seed maturity (S3) produced the highest α-/γ-Toc ratio (0.81). The application of PAC from flowering completion to seed maturity caused the lowest total Toc (458.44 mg kg^{-1} seed), α-Toc (187.45 mg kg^{-1} seed), and γ-Toc (270.99 mg kg^{-1} seed) contents and the α-/γ-Toc ratio (0.69) made statistic sense (Table 3).

Effect of the Interaction among PGR, Location, and PGR Treatment Duration on Seed Toc's. The interaction among PGR, location, and PGR treatment duration caused significant variations in the total Toc, α-Toc, and γ-Toc contents ($P \leq 0.01$) and a significant variation in the α-/γ-Toc ratio ($P \leq 0.05$) (Table 2). Among the 18 treatment combinations, the application of GA_3 from the green floral bud stage to seed maturity at the Hangzhou site (P1L1S1) resulted in the highest total Toc (673.90 mg kg^{-1} seed), α-Toc (269.79 mg kg^{-1} seed), and γ-Toc (404.12 mg kg^{-1} seed) contents. Conversely, the application of PAC from flowering initiation to seed maturity at the Hangzhou site (P3L1S2) led to the lowest total Toc (449.73 mg kg^{-1} seed) and γ-Toc (261.28 mg kg^{-1} seed) contents. The lowest α-Toc content (185.14 mg kg^{-1} seed) appeared following the P3L1S3 treatment combination. The highest α-/γ-Toc (0.88) was achieved by the P1L2S3 treatment combination, whereas the lowest α-/γ-Toc value (0.64) was obtained by the P3L1S1 treatment combination (Table 4).

Effect of the Interaction among PGR, PGR Treatment Duration, And Genotype on Seed Toc's. The interaction among PGR, genotype, and PGR treatment duration (PGS) gave rise to significant variations in the total Toc, α-Toc, and γ-Toc contents and the α-/γ-Toc ratio ($P \leq 0.01$) (Table 2). Among the 18 treatment combinations, GA_3 treatment from flowering initiation to seed maturity (P1S1G1) produced the highest total Toc (832.14 mg kg^{-1} seed), α-Toc (345.46 mg kg^{-1} seed), and γ-Toc (486.67 mg kg^{-1} seed) contents in the Zheyou-50 plants. The Jiu-Er-13Xi plants treated with PAC from flowering completion to seed maturity (P3S3G2) had the lowest total Toc (345.99 mg kg^{-1} seed), α-Toc (140.20 mg kg^{-1} seed), and γ-Toc (205.79 mg kg^{-1} seed) contents. The highest (0.83) and lowest (0.63) α-/γ-Toc ratios were produced by the P3S2G2 and P3S1G1 treatment combinations, respectively (Table 4).

Effect of the Interaction among PGR, Genotype, And Location on Seed Toc's. The interaction among the PGR, genotype, and location (PGL) caused a significant variation in the total Toc yield ($P \leq 0.05$) as well as significant variations in the γ-Toc content and α-/γ-Toc ratio ($P \leq 0.01$). However, the interaction did not produce a significant variation in the α-Toc content (Table 2). Among the 12 treatment combinations, GA_3 treatment at the Jinhua site (P1G1L2) produced the highest total Toc (698.67 mg kg^{-1} seed) and γ-Toc (393.24 mg kg^{-1} seed) yields in the Zheyou-50 plants. Conversely, the Jiu-Er-13Xi plants treated with PAC at Hangzhou (P3G2L1) resulted in the lowest total Toc (381.29 mg kg^{-1} seed) and γ-Toc (217.39 mg kg^{-1} seed) yields. The highest (0.87) and lowest (0.62) values of α-/γ-Toc were caused by the P1G2L2 and P3G1L1 treatment combinations, respectively (Table 4).

Effect of the Interactions among PGR, Location, PGR Treatment Duration, And Genotype on Seed Toc's. The interaction among all the four factors significantly influenced amount of Toc and composition ($P \leq 0.01$, Table 2). Among the 36 treatment combinations, GA_3 treatment from bud formation to seed maturity at the Hangzhou site (P1G1L1S1) produced the highest total Toc (875.01 mg kg^{-1} seed), α-Toc (334.73 mg kg^{-1} seed), and γ-Toc (540.28 mg kg^{-1} seed)

DOI: 10.1021/jf505312c
J. Agric. Food Chem. 2015, 63, 360−369

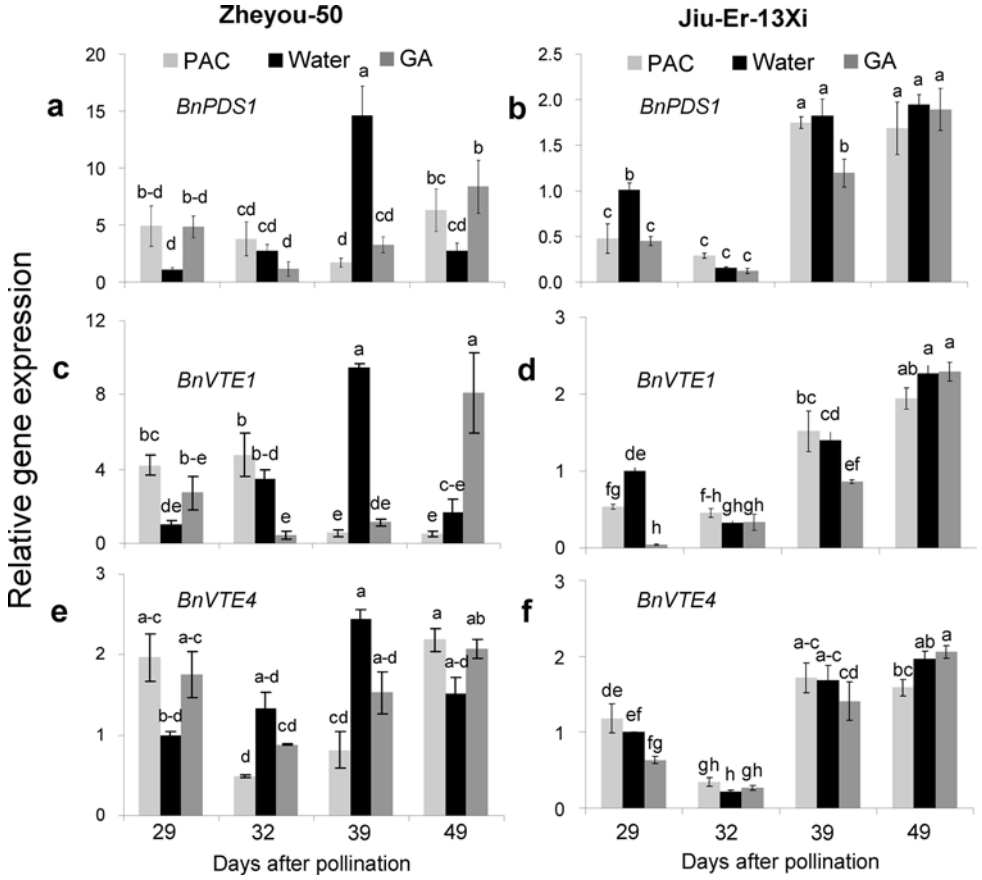

Figure 2. Relative transcription levels of tocopherol biosynthesis genes in GA_3, PAC, and water treated (control) plants of oilseed rape genotypes treated for different durations of GA_3 (or total spray times). Water, untreated/control plants; PAC, paclobutrazol. Bars on graphs show ±standard error.

contents in the Zheyou-50 plants. The Jiu-Er-13Xi plants untreated with PGR from flowering completion to seed maturity at the Jinhua site (P2G2L2S1) produced the lowest total Toc (324.64 mg kg^{-1} seed), and α-Toc (137.20 mg kg^{-1} seed) that was statistically at par to α-Toc content obtained with P3G2L2S3 treatment combination. The lowest γ-Toc (170.52 mg kg^{-1} seed) contents were produced by P1G2L2S3 treatment combination. The highest (0.96) and lowest (0.52) α-/γ-Toc ratios were obtained from the P1G2L2S3 and P3G1L1S1 treatment combinations, respectively (Table 5).

Transcriptional Changes in the Genes Regulating Toc Biosynthesis in Response to PGR Application. We investigated the effects of exogenous GA_3 and PAC on the expression levels of *BnPDS1*, *BnVTE1*, and *BnVTE4*, which are important in the Toc biosynthetic pathway (Figures 1 and 2). The RNA samples were harvested at 29, 32, 39, and 49 DAP, 7, 3, 4, and 1 day(s) after the sixth, seven, eighth, and ninth PGR applications, respectively. The result of RT-qPCR based on the RNA samples collected at 49 DAP, 1 day after the ninth application, indicated that GA_3 significantly upregulated the expression of *BnPDS1* and *BnVTE1* in Zheyou-50 (Figure 2a and c). No significant differences in gene expression were observed between the plants treated with GA_3 and water at 49 DAP in Jiu-Er-13Xi (Figure 2b, d, and f). The RT-qPCR results based on the RNAs collected at other time points (29, 32, and 39 DAP) from both genotypes did not show that GA_3 significantly upregulated the expression levels of *BnPDS1*, *BnVTE1*, and *BnVTE4*. Moreover, at 39 DAP striking inhibitory responses were observed in the expression of all three genes to PGRs in Zheyou-50 and to GA_3 in Jiu-Er-13Xi (Figure 2a–f).

Response of Toc Synthesis to GA Enhancement in *Arabidopsis*. To confirm whether or not GA enhancement can increase *PDS1*, *VTE1*, and *VTE4* expression and seed Toc content, we compared the expression levels of *VTE1*, *VTE4*, and *PDS1* between the WT (L*er*) and *q-della/WT* mutant (Figure 3d–f) as well as the seed Toc yield among the WT (L*er*), *q-della*, *p-della*, and wild-type plants treated with GA_3 (WT + GA_3) in *Arabidopsis* (Figure 3a–c).

The enhanced GA signaling in the *q-della/WT* mutant induced the upregulation of *VTE1*, *VTE4*, and *PDS1* at 4, 8, 12, and 16 DAP (Figure 3d–f). The expression levels of all three genes peaked at 12 DAP. *PDS1* expression showed the greatest difference between WT and the mutant. The transcript level of *PDS1* was 2-fold higher in the *q-della/WT* mutant than in the WT (Figure 3d).

The *q-della/WT* mutant, *p-della* mutant, and WT + GA_3 plants had considerably higher seed Toc yields than the WT plants (Figures 3a). Each 1 kg of *q-della/WT*, *p-della*, and WT + GA_3 seeds contained 412, 413, and 402 mg of Toc's, respectively, which were 11.9%, 12.2%, and 9.2% higher than the Toc in WT. The differences in the total Toc content between the genotypes were derived from the differences in γ-Toc content. No significant differences in seed α-Toc content were observed among the WT, *q-della/WT*, *p-della*, and WT + GA_3 plants, but the γ-Toc content was significantly higher in the *q-della*, *p-della*, and WT + GA_3 plants than in the WT plants (Figure 3a–c).

DOI: 10.1021/jf505312c
J. Agric. Food Chem. 2015, 63, 360–369

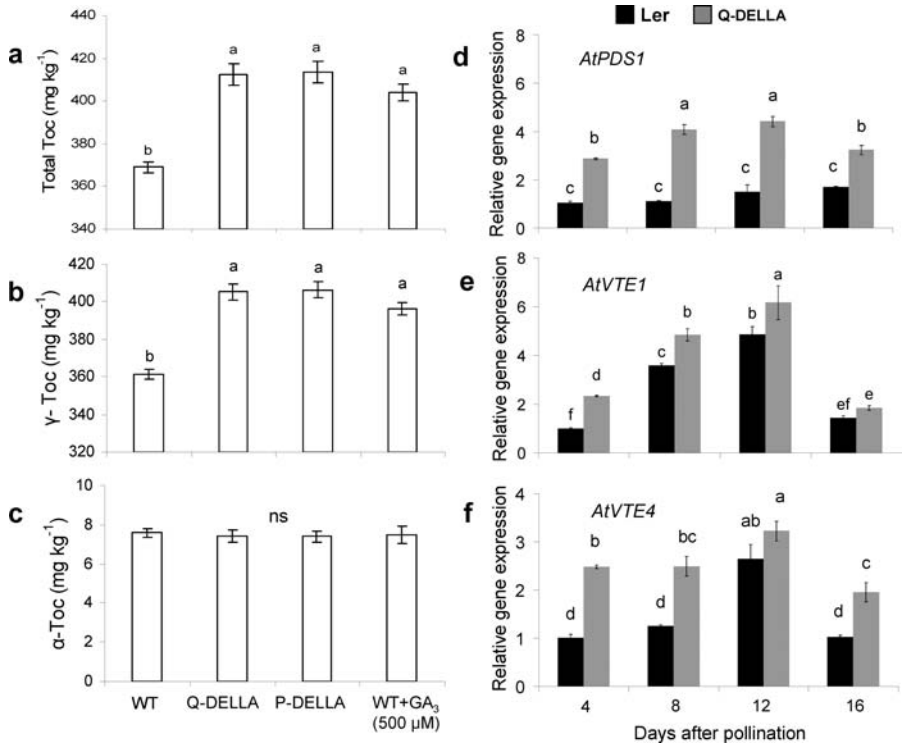

Figure 3. Comparison of α-Toc (a), γ-Toc (b), and total Toc (c) content among *Arabidopsis thaliana* WT, *q-della/WT*, *p-della* mutants and WT + GA_3 plants. Letters on the bars shows the comparison among treatment being significant at $P \leq 0.01$; ns = nonsignificant. Comparison of relative transcription levels of tocopherol biosynthesis genes (*AtVTE1*, *AtVTE4*, and *AtPDS1*) among *Arabidopsis* ecotype Langdsberg *erecta* [WT(*Ler*)] and *q-della/WT* mutant are shown in (d), (e), and (f), respectively, at different seed developmental stages. Bars on graphs show ±standard error.

DISCUSSION

GA signaling regulates a number of genes that are important for plant development processes, including seed germination, stem elongation, trichome, flower and fruit formation, and seed maturation.[15−18,37,38] We have reported recently that GA signaling promotes the expression of a group of GDSL-type genes that hydrolyze lipids.[24] We also observed that GA affects total Toc yield and the major Toc components in *Arabidopsis*. We postulated that a similar mechanism might exist in rapeseed, a major source of edible oil worldwide. Given that PAC is an inhibitor of GA synthesis and functionally antagonistic to GA,[39,40] we assumed that exogenous GA_3 and PAC may reversely affect seed Toc's in rapeseed. To test this hypothesis, we designed a field experiment and analyzed the PGR effects as well as any interactive effects between the PGR and factors such as genotype, PGR treatment duration, and planting location. Regardless of other factors, GA_3 increased total Toc yield 5.6% compared with the control. By contrast, the GA inhibitor PAC reduced the total Toc yield 3.3% compared with the control. Although the α-Toc and γ-Toc contents were both increased by exogenous GA_3, the increased α-Toc content (11.24%) was much higher than that for γ-Toc content (1.7%). Consequently, the value of α-/γ-Toc was significantly increased following GA_3 treatment (Table 3). In general, α-Toc is the predominant form of Toc in photosynthetic tissues, whereas γ-Toc is predominant in most plant seeds. A high α-/γ-Toc ratio is desired by rapeseed breeders because α-Toc has the highest vitamin E activity (100%), whereas γ-Toc has merely 8−19% relative activity.[41,42]

PGR treatment duration affected Toc production. The seed Toc yield increased as the PGR treatment duration was prolonged. The longest duration (S1) of GA_3 application (P1S1) caused the highest total Toc yield (625.5 mg kg^{-1} seed), whereas the shortest PAC duration (P3S3) led to the lowest total Toc yield (458.44 mg kg^{-1} seed) (Table 3, section P × S interaction). GA_3 signaling affects various processes of plant growth.[25,26] In the present study, early application of GA_3 (S1) caused undesirable changes in various agronomic traits, including increased plant height, reduced numbers of branches and pods per plant, and reduced seed yield (data not shown). However, late application of GA_3 (P1S3) did not significantly influence Toc yield compared with the control (P2S3). This dilemma can be overcome under some circumstances through particular genotype and location combinations. For example, the effect of GA_3 in elevating Toc yield was significantly greater than that for the control (P2G2L1S3) when GA_3 was applied during S3 to Jiu-Er-13Xi plants at the Hangzhou site (P1G2L1S3) (Table 5, section P × G × L × S interaction).

Genotype and PGR interaction significantly influenced the total Toc and Toc composition of the seeds. In general, the application of GA_3 to Zheyou-50 plants (P1G1) significantly increased Toc yield compared with the control (P2G1). However, the application of GA_3 to Jiu-Er-13Xi plants (P1G2 combination) did not significantly increase the total Toc yield as compared with the control (P2G2 combination) (Table 3, section P × G interaction). These results indicate the presence of genotypic differences in the response to exogenous GA_3. Zheyou-50 is a canola-type winter cultivar with a low content of erucic acid (<1%) but a high proportion of C_{18} fatty acids in seeds. By contrast, Jiu-Er-13Xi is a traditional Chinese "double high" cultivar with a high content of erucic acid (>40%) in seeds. Erucic acid (C22:1) is a very long chain fatty acid (VLCFA). In our previous study, we concluded that the amount of Toc, in particular α-Toc, significantly and negatively

DOI: 10.1021/jf505312c
J. Agric. Food Chem. 2015, 63, 360−369

correlates with VLCFA in seeds.[2] Given such a correlation, we speculate that the increase in the Toc content of Jiu-Er-13Xi seeds as promoted by GA signaling enhancement is considerably limited.

The mechanism by which GA increases seed Toc yield can be partially explained by analyzing the transcriptional levels of the genes that are important to the Toc biosynthetic pathway (Figure 1). At the first day after the ninth application, the expression levels of *BnPDS1* and *BnVTE1* were 3-fold and 4-fold upregulated, respectively, by exogenous GA_3, which may account for the increased total Toc yield. *PDS1* is responsible for the synthesis of HGA, an upstream precursor of Toc, from HPP, whereas *VTE1* participates in the synthesis of γ-Toc from DMPBQ.[43−48] However, the upregulation of these two genes was observed only in Zheyou-50, which coincided with the finding that the Zheyou-50 plants treated with GA_3 exhibited increased total Toc (Table 3, section P × G interaction). Moreover, the genes were only upregulated at day one after the ninth application of GA_3 (Figure 2). The upregulation of genes in response to PGRs was not detected by RT-qPCR at other time points (29, 32, and 39 DAP). This might be due to (i) the long interval between PGR applications in terms of DAP and (ii) the delayed harvesting of seed samples for RNA extraction after PGR applications. To demonstrate the effect of endogenous GA_3 enhancement, we used the *Arabidopsis q-della/WT* mutant, in which most DELLA genes have lost their function and GA signaling is genetically enhanced. Under the given conditions, *AtPDS1* and *AtVTE4* were upregulated at all time points, whereas *AtVTE1* was upregulated at all time points except at 16 DAP. The upregulation of these genes increased the total Toc and γ-Toc contents but not the α-Toc content in the *Arabidopsis* mutants and WT + GA_3 plants (Figure 3a and b). This result was partially contradictory to that of rapeseed, where the upregulation of *BnPDS1* and *BnVTE1* was also associated with a greater amount of total Toc but was mainly due to the increase in α-Toc content (Table 3, section P sole effect and P × G interaction). Normally, in *Arabidopsis* seed, Toc composition predominately consists of γ-Toc (≥95%), δ-Toc (≤5%), and very small amounts of α-Toc (≤1%).[49−51] On the other hand, the most abundant types of seed Toc's on average in rapeseed are γ-Toc (46%) and α-Toc (35%), with a small proportion of δ-Toc (1%).[52,53,2,4,34] The difference between the α-Toc contents in both the species could be explained in terms of lower γ-tocopherol methyltransferase (γ-TMT) activity in *Arabidopsis*. Previously, Shintani and DellaPenna made an attempt to overexpress the γ-TMT in *Arabidopsis* seeds that led to the conversion of more than 95% of the γ-Toc to α-Toc, showing that the activity of γ-TMT could be the possible rate-limiting factor in the conversion of γ-Toc to α-Toc in *Arabidopsis*.[49]

In conclusion, exogenous GA_3 elevated total Toc yield, particularly the α-Toc content, in seeds of oilseed rape. However, the increased total Toc was dependent on the duration of GA_3 treatment, genotype, and planting location. Rapeseed plants responded to longer durations of GA_3 treatment with higher Toc yield. The genotype with a low VLCFA proportion responded to GA_3 with significantly higher Toc yield and α-/γ-Toc ratio, whereas the genotype with a high VLCFA proportion did not show a significant response to GA_3 in terms of the overall Toc yield or Toc composition. However, the molecular mechanisms by which GA signaling increases α-Toc content in rapeseed but increases γ-Toc content in *Arabidopsis* have yet to be elucidated.

■ ASSOCIATED CONTENT

Supporting Information

List of primer pairs used for RT-qPCR to amplify fragments of *VTE1*, *VTE4*, *PDS1*, and *ACTIN2* in *Arabidopsis* and list of primer pairs used for RT-qPCR to amplify fragments of *VTE1*, *VTE4*, *PDS1*, and *ACTIN7* in *Brassica napus* L. This material is available free of charge via the Internet at http://pubs.acs.org.

■ AUTHOR INFORMATION

Corresponding Authors

*E-mail: hussain138@yahoo.com. Tel.: 86 571 88982905. Fax: +86 571 88982905.

*E-mail: jianglx@zju.edu.cn. Tel.: +86 571 88982905. Fax: +86 571 88982905.

Funding

The work of our lab was sponsored by the National Key Basic Research Project (abbreviated as 973 project, Code no. 2015CB150205) and Jiangsu Collaborative Innovation Center for Modern Crop Production.

Notes

The authors declare no competing financial interest.

■ ACKNOWLEDGMENTS

We thank Mei Li for her technical assistance.

■ REFERENCES

(1) Fritsche, S.; Wang, X.; Li, J.; Stich, B.; Kopisch-Obuch, F. J.; Endrigkeit, J.; Leckband, G.; Dreyer, F.; Friedt, W.; Meng, J.; Jung, C. A candidate gene-based association study of Tocopherol content and composition in rapeseed (*Brassica napus*). *Front. Plant Sci.* **2012**, *3*, 129.

(2) Li, Y. L.; Hussain, N.; Zhang, L. M.; Chen, X. Y.; Ali, E.; Jiang, L. X. Correlations between tocopherol and fatty acid components in germplasm collections of *Brassica* oilseeds. *J. Agric. Food Chem.* **2013**, *61*, 34−40.

(3) Zhou, W. J.; Zhang, G. Q.; Tuvesson, S.; Dayteg, C.; Gertsson, B. Genetic survey of Chinese and Swedish oilseed rape (*Brassica napus* L.) by simple sequence repeats (SSRs). *Genet. Resour. Crop Evol.* **2006**, *53*, 443−447.

(4) Hussain, N.; Jabeen, Z.; Li, Y. L.; Chen, M. X.; Li, Z. L.; Guo, W. L.; Shamsi, I. H.; Chen, X. Y.; Jiang, L. X. Detection of tocopherol in rapeseed (*Brassica napus* L.) using gas chromatography with flame ionization detector. *J. Integr. Agric.* **2013**, *5*, 803−814.

(5) Pryor, W. A. Vitamin E and heart disease: Basic science to clinical intervention trials. *Free Radical Biol. Med.* **2000**, *28*, 141−164.

(6) Bell, S. J.; Grochoski, G. T. How safe is vitamin E supplementation? *Crit. Rev. Food Sci.* **2008**, *48*, 760−774.

(7) Zhang, W.; Shu, X. O.; Li, H.; Yang, G.; Cai, H.; Ji, B. T.; Gao, J.; Gao, Y. T.; Zheng, W.; Xiang, Y. B. Vitamin intake and liver cancer risk: A report from two cohort studies in China. *J. Natl. Cancer Inst.* **2012**, *104*, 1174−1182.

(8) Hussain, N.; Irshad, F.; Jabeen, Z.; Imran, H. S.; Li, Z. L.; Jiang, L. X. Biosynthesis, structural, and functional attributes of tocopherols in planta: Past, present, and future perspectives. *J. Agric. Food Chem.* **2013**, *61*, 6137−6149.

(9) Munne-Bosch, S.; Weiler, E. W.; Alegre, L.; Muller, M.; Duechting, P.; Falk, J. alpha-Tocopherol may influence cellular signaling by modulating jasmonic acid levels in plants. *Planta* **2007**, *225*, 681−691.

(10) Fachechi, C.; Nisi, R.; Gala, R.; Leone, A.; Caretto, S. Tocopherol biosynthesis is enhanced in photomixotrophic sunflower cell cultures. *Plant Cell Rep.* **2007**, *26*, 525−530.

(11) Traber, M. G. Vitamin E. In *Modern Nutrition in Health and Disease*, 10th ed.; Shils, M. E., Shike, M., Ross, A. C., Caballero B.,

DOI: 10.1021/jf505312c
J. Agric. Food Chem. 2015, 63, 360−369

Cousins R. J., Eds.; Lippincott Williams & Wilkins: Baltimore, MD, 2006; pp 396−411.
(12) Goffman, F. D.; Becker, H. C. Genetic analysis of tocopherol content and composition in winter rapeseed. *Plant Breed.* **2001**, *120*, 182−184.
(13) Goffman, F. D; Becker, H. C. Genetic variation of tocopherol content in a germplasm collection of *Brassica napus* L. *Euphytica* **2002**, *125*, 189−196.
(14) Chen, M. X.; Du, X.; Zhu, Y.; Wang, Z.; Hua, S. J.; Li, Z. L.; Guo, W. L.; Zhang, G. P.; Peng, J. R.; Jiang, L. X. Seed fatty acid reducer acts downstream of gibberellin signalling pathway to lower seed fatty acid storage in *Arabidopsis*. *Plant Cell Environ.* **2012**, *35*, 2155−2169.
(15) Sasaki, A.; Itoh, H.; Gomi, K.; Akie, S.; Hironori, I.; Kenji, G.; Miyako, U. T.; Kanako, I.; Masatomo, K.; Dong-Hoon, J.; Gynheung, A.; Hidemi, K.; Motoyuki, A.; Makoto, M. Accumulation of phosphorylated repressor for gibberellin signaling in an F-box mutant. *Science* **2003**, *299*, 1896−1898.
(16) Cheng, H.; Qin, L. J.; Lee, S. C.; Fu, X. D.; Richards, D. E.; Cao, D. N.; Luo, D.; Harberd, N. P.; Peng, J. R. Gibberellin regulates *Arabidopsis* floral development via suppression of DELLA protein-function. *Development* **2004**, *131*, 1055−1064.
(17) Sun, M. H.; Zhang, M. H.; Liu, H. Y.; Li, L. G.; Yu, X.; Su, W. A.; Tang, Z. C. Distribution of water channel protein RWC3 and its regulation by GA and sucrose in rice (*Oryza sativa*). *Acta Bot. Sin.* **2004**, *46*, 1056−1064.
(18) Fleet, C. M.; Sun, T. P. A DELLAcate balance: The role of gibberellin in plant morphogenesis. *Curr. Opin. Plant Biol.* **2005**, *8*, 77−85.
(19) Ueguchi-Tanaka, M.; Nakajima, M.; Katoh, E.; Ohmiya, H.; Asano, K.; Saji, S.; Hongyuc, X.; Ashikari, M.; Kitano, H.; Yamaguchi, I. Molecular interactions of a soluble gibberellin receptor, GID1, with a rice DELLA protein, SLR1, and gibberellin. *Plant Cell.* **2007**, *19*, 2140−2155.
(20) Silverstone, A. L.; Ciampaglio, C. N.; Sun, T. The *Arabidopsis* RGA gene encodes a transcriptional regulator repressing the gibberellin signal transduction pathway. *Plant Cell.* **1998**, *10*, 155−169.
(21) Lee, S.; Cheng, H.; King, K. E.; Wang, W.; He, Y.; Hussain, A.; Lo, J.; Harberd, N. P.; Peng, J. R. Gibberellin regulates Arabidopsis seed germination via RGL2, a GAI/RGA-like gene whose expression is up-regulated following imbibition. *Gene Dev.* **2002**, *16*, 646−658.
(22) Jiang, C.; Fu, X. GA action: Turning on de-DELLA repressing signaling. *Curr. Opin. Plant Biol.* **2007**, *10*, 461−465.
(23) Yu, H.; Ito, T.; Zhao, Y. X.; Peng, J. R.; Kumar, P. P.; Meyerowitz, E. M. Floral homeotic genes are targets of gibberellin signaling in flower development. *Proc. Natl. Acad. Sci. U.S.A.* **2004**, *101*, 7827−7832.
(24) Chen, M. X.; Du, X.; Zhu, Y.; Wang, Z.; Hua, S. J.; Li, Z. L.; Guo, W. L.; Zhang, G. P.; Peng, J. R.; Jiang, L. X. Seed fatty acid reducer acts downstream of gibberellin signalling pathway to lower seed fatty acid storage in *Arabidopsis*. *Plant Cell Environ.* **2012**, *35*, 2155−2169.
(25) Baylis, A. D.; Wright, I. T. J. The effects of lodging and a paclobutrazol−chlormequat chloride mixture on the yield and quality of oilseed rape. *Ann. Appl. Biol.* **1990**, *116*, 287−295.
(26) Downey, R. K.; Robbelen, G. Brassica species. In *Oil crops of the world*; Robbelen, G., Downey, R. K., Ashri, A., Eds.; McGraw Hill: New York, 1989; pp 339−362.
(27) Kamal-Eldin, A.; Andersson, R. A multivariate study of the correlation between tocopherol content and fatty acid composition in vegetable oils. *J. Am. Oil Chem. Soc.* **1997**, *74*, 375−380.
(28) Dolde, D.; Vlahakis, C.; Hazebroek, J. Tocopherols in breeding lines and effects of planting location, fatty acid composition, and temperature during development. *J. Am. Oil Chem. Soc.* **1999**, *76*, 349−355.
(29) Goffman, F. D.; Bohme, T. Relationship between fatty acid profile and vitamin E content in maize hybrids (*Zea mays* L.). *J. Agric. Food Chem.* **2001**, *49*, 4990−4994.
(30) Richards, A.; Wijesundera, C.; Salisbury, P. Genotype and growing environment effects on the tocopherols and fatty acids of *Brassica napus* and *B. juncea*. *J. Am. Oil Chem. Soc.* **2008**, *85*, 159−168.
(31) Egesel, C. O.; Gul, M. K.; Kahriman, F.; Ozer, I.; Turk, F. The effect of nitrogen fertilization on tocopherols in rapeseed genotypes. *Eur. Food Res. Technol.* **2008**, *227*, 871−880.
(32) Porfirova, S.; Bergmuller, E.; Tropf, S.; Lemke, R.; Dormann, P. Isolation of an *Arabidopsis* mutant lacking vitamin E and identification of a cyclase essential for all tocopherol biosynthesis. *Proc. Natl. Acad. Sci. U.S.A.* **2002**, *99*, 12495−12500.
(33) Bergmüll, E.; Porfirova, S.; Dörmann, P. Characterization of an *Arabidopsis* mutant deficient in γ-tocopherol methyltransferase. *Plant Mol. Biol.* **2003**, *52*, 1181−1190.
(34) Hussain, N.; Li, H.; Jiang, Y. X.; Jabeen, Z.; Shamsi, I. H.; Ali, E.; Jiang, L. X. Response of seed tocopherols in oilseed rape to nitrogen fertilizer sources and application rates. *J. Zhejiang Univ., Sci., B* **2014**, *15*, 181−193.
(35) Pak, H. S.; Guo, Y.; Chen, M. X.; Chen, K. M.; Li, Y. L.; Hua, S. J.; Shamsi, I.; Meng, H. B.; Shi, C. G.; Jiang, L. X. The effect of exogenous methyl jasmonate on the flowering time, floral organ morphology, and transcript levels of a group of genes implicated in the development of oilseed rape flowers (*Brassica napus* L.). *Planta.* **2009**, *231*, 79−91.
(36) Livak, K. J.; Schmittgen, T. D. Analysis of relative gene expression data using real-time quantitative PCR and the $2^{-\Delta\Delta C_T}$ method. *Methods* **2001**, *25*, 402−408.
(37) Swain, S. M.; Reid, J. B.; Kamiya, Y. Gibberellins are required for embryo growth and seed development in pea. *Plant J.* **1997**, *12*, 1329−1338.
(38) King, R. W.; Moritz, T.; Junttila, O.; Evans, L. T. Long-day induction of flowering in *Lolium temulentum* involves sequential increases in specific gibberellins at the shoot apex. *Plant Physiol.* **2001**, *127*, 624−632.
(39) Karssen, C. M.; Zagórski, S.; Kepczynski, J.; Groot, S. P. C. Key role for endogenous gibberellins in the control of seed germination. *Ann. Bot. (London, U. K.)* **1989**, *63*, 71−80.
(40) Rademacher, W. Growth retardants: Effects on gibberellin biosynthesis and other metabolic pathways. *Annu. Rev. Plant Physiol. Plant Mol. Biol.* **2000**, *51*, 501−531.
(41) Kamaleldin, A; Appelqvist, L. A. The chemistry and antioxidant properties of tocopherols and tocotrienols. *Lipids* **1996**, *31*, 671−701.
(42) Pongracz, G.; Weiser, H.; Matzinger, D. Tocopherols—Antioxidants in nature. *Fat Sci. Technol.* **1995**, *97*, 90−104.
(43) Hedden, G.; Thomas, S. Gibberellin biosynthesis and its regulation. *Biochem. J.* **2012**, *444*, 11−25.
(44) Kaneko, M.; Itoh, H.; Inukai, Y.; Sakamoto, T.; Ueguchi-Tanaka, M.; Ashikari, M.; Matsuoka, M. Where do gibberellin biosynthesis and gibberellin signaling occur in rice plants? *Plant J.* **2003**, *35*, 104−115.
(45) Itoh, H.; Tanaka-Ueguchi, M.; Kawaide, H.; Chen, X. B.; Kamiya, Y.; Matsuoka, M. The gene encoding tobacco gibberellin 3 β-hydroxylase is expressed at the site of GA action during stem elongation and flower organ development. *Plant J.* **1999**, *20*, 15−24.
(46) Mene-Saffrane, L.; DellaPenna, D. Biosynthesis, regulation and functions of tocochromanols in plants. *Plant Physiol. Biochem.* **2010**, *48*, 301−309.
(47) Hedden, P.; Phillips, A. L. Gibberellin metabolism: New insights revealed by the genes. *Trends Plant Sci.* **2000**, *5*, 523−530.
(48) Olszewski, N.; Sun, T. P.; Gubler, F. Gibberellin signaling: Biosynthesis, catabolism, and response pathways. *Plant Cell.* **2002**, *14*, S61−80.
(49) Shintani, D.; DellaPenna, D. Elevating the vitamin E content of plants through metabolic engineering. *Science* **1998**, *282*, 2098−2100.
(50) Van, E. A. L.; Lincoln, K.; Durrett, T. P.; Valentin, H. E.; Shewmaker, C. K.; Thorne, G. M.; Jiang, J.; Baszis, S. R.; Levering, C. K.; Aasen, E. D.; Hao, M.; Stein, J. C.; Norris, S. R.; Last, R. L. Engineering vitamin E content: From Arabidopsis mutant to soy oil. *Plant Cell.* **2003**, *15*, 3007−3019.

DOI: 10.1021/jf505312c
J. Agric. Food Chem. 2015, 63, 360−369

(51) Sattler, S. E.; Cheng, Z.; DellaPenna, D. From *Arabidopsis* to agriculture: Engineering improved vitamin E content in soybean. *Trends Plant Sci.* **2004**, *9*, 365−367.
(52) Marwede, V.; Schierholt, A.; Möllers, C.; Becker, H. C. Genotype × Environment interactions and heritability of tocopherol contents in Canola. *Crop Sci.* **2004**, *44*, 728−731.
(53) Goffman, F. D.; Velasco, L.; Becker, H. C. Tocopherols accumulation in developing seeds and pods of rapeseed (*Brassica napus* L.). *Fett/Lipid* **1999**, *101*, 400−403.

DOI: 10.1021/jf505312c
J. Agric. Food Chem. 2015, 63, 360−369

JOURNAL OF AGRICULTURAL AND FOOD CHEMISTRY

Article

pubs.acs.org/JAFC

Evaluation of the Discriminative Potential of a Novel Biomarker for Estradiol Treatments in Bovine Animals

Patricia Regal,*[,†,§] Marco H. Blokland,[†] Cristina A. Fente,[§] Saskia S. Sterk,[†] Alberto Cepeda,[§] and Leen A. van Ginkel[†]

[†]RIKILT – Part of Wageningen UR, P.O. Box 230, 6700 AE Wageningen, The Netherlands

[§]Department of Analytical Chemistry, Nutrition and Bromatology, Faculty of Veterinary Science, University of Santiago de Compostela, 27002 Lugo, Spain

ABSTRACT: The endogenous occurrence of natural hormones obstructs the application of classical targeted methods as confirmatory options. In the case of estradiol, the ultimate confirmation of its exogenous administration relies on gas chromatography coupled to combustion/isotope ratio mass spectrometry (GC-C/IRMS). A serum dipeptide composed of pyroglutamic acid and phenylalanine was identified as a potential biomarker of estradiol treatments in adult cows. To evaluate its potential to pinpoint suspicious samples, samples from prepubertal females under different estrogenic treatments have been analyzed. The results confirmed the up-regulation of the dipeptide in adult bovines. The 2-week-old females exhibited short-lasting responses only in a few animals. The 6-month-old female showed a delayed but clear increase on the biomarker level. The composition of the anabolic preparations, the dose, and/or the administration route are possible additional reasons for the reduced response in young animals. A comparison to previous results reported by various researchers is included.

KEYWORDS: *biomarker, estradiol, serum, cattle, age*

INTRODUCTION

Natural hormones and compounds with hormonal activities are widely applied in veterinary medicine. Anabolic steroids have been effective in increasing feed conversion and promoting growth in farm animals.[1] On the other hand, some steroids and hormones influencing sexual functions have been administered to females to induce and/or synchronize estrus. The low cost and high effectiveness of protocols based on a combination of estradiol with progestagens have led to the widespread application of hormones in reproductive control programs for timed artificial insemination in cattle.[2,3] Despite all these prima facie benefits, the administration of hormones and substances having a hormonal action in livestock farming has been forbidden in the European Union (EU) since the 1980s,[4−7] aiming at protecting consumers. This ban has resulted in controversial disputes among different countries.[8] With respect to the use of estradiol-17β with the aim of promoting animal growth, the Scientific Committee on Veterinary Measures relating to Public Health evaluated recent evidence suggesting that it had to be considered as a complete carcinogen (http://ec.europa.eu/food/fs/sc/scv/out50_en.pdf), and its opinion was accordingly reflected in a European Directive.[9] As other options for estrus synchronization exist and are already implemented in the European market,[10] estradiol and its ester-like derivatives were also forbidden as reproductive tools in the EU with the Directive 2003/74/EC.[9] The use of estradiol in farm animals has been limited to strict veterinary prescription and always for non-growth-promoting purposes (treatment of fetus maceration or mummification or treatment of pyometra in cattle). However, the large profit obtained with anabolic and hormonal preparations through both kinds of applications may cause, illegal, continued use by some veterinary practitioners and farmers.

The administration of anabolic xenobiotic compounds can be relatively easily detected using targeted methods.[11] However, the administration of synthetic natural hormones such as estradiol or testosterone largely remains an unsolved issue for European authorities. These compounds are endogenous to the animal, and the establishment of acceptable threshold levels to detect an exogenous administration is a quite limited approach.[12,13] The hormone levels for a population cannot be easily defined due to the wide animal diversity and the great influence of many physiological and environmental factors. In addition, natural hormones such as estradiol and/or testosterone are frequently administered as esterified forms to obtain a slow release of the hormones. Even though steroid esters have been detected in hair,[14−16] their detection and quantification are not always possible in every treated animal.[15,17] The confirmation of intact steroid esters in body fluids or tissue would provide unequivocal evidence of an illegal administration of an endogenous compound. However, their detection presents a number of analytical challenges such as a rapid metabolism to nature-identical steroids and their low concentration in the animal body.[15,18,19] As a result of all these facts, a deeper insight and additional research on natural hormones administration in farm animals are relevant and necessary.

Innovative in vivo methods that may be useful in the future control of the abuse or misuse of natural hormones in cattle include targeted and untargeted profiling methods, metabolic pathways analyses, the "omics" technologies, and gas chromatography coupled to combustion/isotope ratio mass

Received: August 6, 2014
Revised: November 29, 2014
Accepted: December 8, 2014
Published: December 8, 2014

ACS Publications © 2014 American Chemical Society

dx.doi.org/10.1021/jf503773u | J. Agric. Food Chem. 2015, 63, 370−378

spectrometry (GC-C/IRMS). In the past few years, the pattern recognition of steroid profiles, including phase II metabolites, has emerged as a promising approach for tracing the abuse of natural hormones.[20,21] Researchers have suggested the study of untreated and/or control animals to provide a reference threshold value on hormone levels.[13] However, the levels of these natural compounds are highly variable among animals, and it is hard to confidently define the endogenous levels of a specific population.[22,23] In these cases, the inspection of the overall steroid profile is also required as an additional check, as well as further confirmation with alternative methods. On the other hand, a few "omic" studies have been reported as promising strategies to detect the administration of exogenous estradiol in cattle[24−29] and also for other anabolic compounds in different species.[30−32] These methods based on high-dimensional data sets are very useful tools to find candidate biomarkers for a specific biological situation. Biomarkers in general, and in particular blood biomarkers, have found several applications in the veterinary analytical field.[33] The potential of biomarker profiling to screen for the use of steroids administration, including estradiol, has been already highlighted. Specific combinations of plasma proteins were studied and their profiles proposed as future screening methods of steroids administration in cattle, mainly in calves.[34,35] However, additional validation studies covering both treated and untreated animals are required to confidently apply these approaches in monitoring strategies. Basically, all of the previously mentioned methods can be used to pinpoint suspect samples that should be confirmed with, preferably, GC-C/IRMS. This technique has offered a unique method for the unambiguous differentiation between natural hormones and homologous synthetic compounds in cattle.[36] However, the costly instrumentation and the time-consuming and complex sample preparation reduce the applicability of this method to only a few laboratories. Besides, no criterion devoted to the interpretation of GC-C/IRMS analytical data are available in any official analytical document such as the 2002/657/EC decision. Recently, Janssens et al. applied a threshold value of $|\Delta\ ^{13}C| > 3‰$, used by the World Anti-Doping Agency for doping control purposes, illustrating the capability of the method and the validity of the threshold for food safety as well.[37] The selection of suspicious samples through the application of more accessible methods would limit the number of samples that would require further GC-C/IRMS.

Most likely in the near future the detection of the administration of a natural hormone, more precisely estradiol-17β, in cattle will be based on the measurement and profiling of other compounds, directly or indirectly related with this estrogen. In this regard, the investigation and study of novel biomarkers that could be applied alone or combined with other similar ones is necessary. In a previous metabolomics study performed on serum from estradiol-treated female animals, a dipeptide, composed by pyroglutamic acid and phenylalanine, that is, L-Pyr-L-Phe, was highlighted as a potential biomarker candidate for these hormonal treatments. This compound is up-regulated in cows treated with estradiol-17β or estradiol benzoate. The usefulness of this biomarker was tested and confirmed in several serum samples from adult (2−5 years) female animals, using a targeted HPLC-MS/MS method.[38] The biomarker proved to be useful for a specific population composed of adult female Holstein-Friesian bovine animals, from a certain geographical area (northwestern Spain). However, for the validation of these promising candidates, the evaluation of their performance using more animal trials and applying different estradiol preparations is mandatory. In this research, plasma samples from prepubertal females (2−24 weeks) treated with estradiol-based preparations and under different conditions have been analyzed.

MATERIALS AND METHODS

Chemicals. Estradiol benzoate, testosterone decanoate, and testosterone cypionate were obtained from Sigma-Aldrich (Zwijndrecht, The Netherlands). Ivomec, dimethyl sulfoxide (DMSO), Mygliol 840, diethylene glycol monobutyl ether (DEGMBE), and arachide oil were purchased at Spruyt Hillen (IJsselstein, The Netherlands). Estradiol benzoate, methyl prednisone acetate, dromostanolone (5α-androstane-2α-methyl-17β-ol-3-one), and 1-dehydroandrostanolone (1,(5α)-androstene-17β-ol-3-one) for the treatment of the 6-month-old animal were obtained from Steraloids Inc. Ltd. (London, UK). L-Pyroglutamyl-L-phenylalanine (L-Pyr-L-Phe) was purchased from Bachem Distribution Services GmbH (Weil am Rhein, Germany). LC-MS grade acetonitrile, water, and methanol were obtained from Biosolve (Valkenswaard, The Netherlands). Formic acid was obtained from Merck (Darmstadt, Germany). All other chemicals used were of analytical reagent grade.

Experimental Animals. The serum and plasma samples used in this study were selected from previous animal experiments, collected at different times, but analyzed now during the same time frame.

The serum samples were obtained from 13 Holstein-Friesian cows aged between 24 months and 5 years, from different dairy farms in Galicia (Spain). Animals were fed a diet usually employed in the animal husbandry practice and had ad libitum access to water. Blood samples were collected from (a) three cows treated with an intramuscular injection of a veterinary drug containing 5 mg of estradiol benzoate (EB) and 1.250 IU of chorionic gonadotropin; (b) one animal treated with an intramuscular injection of a veterinary drug consisting of 2 mg of estradiol-17β (E_2) and 8 mg of vitamin E; and (c) three cows treated with an intravaginal device composed of a progesterone-releasing spiral (1.55 g) plus a capsule containing 10 mg of EB. Samples were collected (a and b) 3 days and (c) 6 days after administration. The day of sample collection was based on the veterinary purpose of these drugs (estrus control). Four nontreated cows were used as control animals. In addition, two samples from bovine females treated with an intravaginal progesterone-releasing spiral (not containing estradiol) were analyzed and expected to behave as control samples. Samples from progesterone-treated animals were collected 8 days after administration. Immediately after blood clotting and 10 min of centrifugation at 1300*g*, serum samples were frozen at −20 °C. The veterinary treatments took place under a veterinary reproductive control program before October 2006.

Some of the plasma samples were obtained from a previous animal trial conducted at the Physiology Weihenstephan, Technical University of Münich (Germany).[39] The protocol was approved by the ethical committee of the "Regierung von Oberbayern". Twenty prepubertal female Holstein-Friesian calves were obtained from identified sources at an age of 2 weeks, and the four different groups (control, control carrier-only, treated once, treated three times) were housed in separate pens. The animals were fed according to veal calf practice, using milk replacer and roughage, and had drinking water ad libitum. Five animals were not treated and were used as reference group. Pour-on experiments were carried out using hormone cocktails containing three steroid esters: 25 mg of estradiol benzoate (EB), 60 mg of testosterone decanoate (TD), and 60 mg of testosterone cypionate (TC). Prior to the application, the animals were shaved on the back from neck to tail. There, they were treated with 10 mL of pour-on cocktail, using four different carrier solvents (ivermectin 1% pour-on preparation Ivomec; DMSO; propylenglycol dicaprylate Miglyol 840; and DEGMBE). Four animals were treated only once, at day 1, with 10 mL of hormone cocktail, but each animal was treated with a different carrier solvent. Four animals were treated three times, on days 1, 7, and 14 (repeated treatment), with 10 mL of hormone cocktail and also different carrier. Four animals were treated three times, on days 1, 7, and 14 (repeated treatment), with 10 mL of a different carrier solvent for each animal.

dx.doi.org/10.1021/jf503773u | J. Agric. Food Chem. 2015, 63, 370−378

Additionally, one animal was injected intramuscularly in the neck on day 1 with a cocktail of 35 mg of EB, 60 mg of TD, and 60 mg of TC, and one animal was injected on days 1, 7, and 14 with the hormone cocktail. For the injection, arachide oil was used as the carrier. One animal was injected three times (days 1, 7, and 14) only with arachide oil. Samples of blood were collected at different points after the first treatment (considered as day 1), up to 70 days after. Samples were collected in EDTA blood collection tubes and centrifuged, and the plasma was stored at −20 °C and used for the analysis.

Lastly, plasma samples from a Holstein-Friesian female treated by intramuscular injection with four substances suspended in vegetable oil were also analyzed. The experiment was performed at the facilities of ASG (Animal Sciences Group of Wageningen UR), Lelystad, The Netherlands, starting at 6 months of age. The animal was treated weekly, twice with each steroid, in the following order: 1-dehydroandrostanolone, methyl prednisone acetate, estradiol benzoate, and dromostanolone, 25 mL per injection (12.5 mL in each side of the neck). The total dose of each steroid was 250 mg per 50 mL of solution in vegetable-based oil. Pretreatment control samples were collected 29, 30, 31, and 32 days before the first EB administration (considered as day 1). The injections of 1-dehydroandrostanolone were administered 28 and 21 days before the first EB dose and those of medroxy prednisone acetate 14 and 7 days before. Then, estradiol benzoate was administered at days 1 and 8 (repeated treatment). Afterward, dromostanolone was injected at days 14 and 21. Blood samples were collected daily (except 2 days every 5 days) starting at day 1, up to day 25. Samples were collected in EDTA blood collection tubes and centrifuged, and the plasma was stored at −20 °C and used for the analysis.

Table 1 presents a summary of all samples analyzed during this study. All of the samples were stored at −20 °C until analysis.

Sample Preparation. All serum and plasma samples were prepared using a very simple and straightforward protocol. Briefly, samples were defrosted at room temperature and homogenized. An amount of 100 μL of serum/plasma was filtered on centrifugal devices (cutoff at 10 kDa, 8600*g*, 4 °C, 30 min) to remove high molecular weight proteins. After transferring the filtrates to injection vials, 5 μL of each sample was injected into the chromatographic system.

LC-MS/MS Method. The analysis of the dipeptide Pyr-Phe was performed with an ultraperformance liquid chromatographic (UPLC) system, consisting of vacuum degasser, refrigerated autosampler, and binary pump (Acquity UPLC system; Waters, Milford, MA, USA) equipped with a reversed phase Waters Acquity UPLC CSH C18 analytical column of 2.1 × 10 mm and 1.7 μm particle size. The gradient (solvent A, water 0.1% formic acid; solvent B, acetonitrile 0.1% formic acid) was as follows: 0 min, 0% B; 0−4 min, linear increase to 50% B; 4−4.5 min, 99% B; 4.5−5 min, isocratic; 5−5.1 min, return to initial conditions 0% B; total run time = 6 min. The flow was 600 μL min^{-1}, with the column oven at 60 °C. The UPLC system was connected to a triple-quadrupole mass spectrometer model XEVO TQ-S (Waters) equipped with an electrospray interface operating in the positive ion mode. The MRM transitions acquired for Pyr-Phe were obtained from the infusion of the dipeptide standard in acetonitrile/water 10:90 (v/v): 277.1 → 120.2, 277.1 → 166.2, 277.1 → 231.1. The collision energy for each MRM transition was set at 20, 10, and 10 eV, respectively. Capillary voltage was set at 3.20 kV, cone voltage at 40 V, source temperature at 150 °C, and desolvation temperature at 650 °C.

A targeted method was developed to confirm the presence of Pyr-Phe in the serum and plasma samples. The performance of the analytical method was evaluated by checking the performance criteria in samples: the S/N ratio ≥3 for all of the monitored MRM transitions and the retention time of the analyte within the tolerance limit of 2.5%. The analyte area of the samples was normalized every day by using the mean peak area of a standard solution of Pyr-Phe at a level of 10 μg L^{-1} (peak area in the sample/peak area of standard solution), injected at the beginning and the end of the series of samples. Hence, the abundance of Pyr-Phe in the serum/plasma was expressed as area ratio. Additionally, linearity was checked by constructing standard calibration curves and calibration curves using spiked serum samples (bovine serum from Sigma), at concentration levels in the range between 0.25 and 10 μg L^{-1}. Calibration curves were calculated daily by least-squares linear regression analysis of the peak area of the dipeptide.

Statistical Analysis. All descriptive statistical analysis and calculations were carried out using the Microsoft Excel software package version 2010 (Microsoft Corp.). Mean and standard deviation of peptide levels in samples from estradiol-treated animals and from nontreated animals were calculated to evaluate the biomarker effect in different age groups.

RESULTS AND DISCUSSION

Recent studies have focused on the measurement of various biomarkers that may be able to indicate treatments with estrogenic hormones in cattle.[34,35,38−41] In this research area, samples collected in vivo, on farms, appear convenient options for biomarker determination. The major advantage of samples as urine, blood, or hair is that routine controls may be performed while the animal is still at the farm. Some researchers have highlighted the superiority of serum in comparison to plasma for mass spectrometry-based metabolomics and biomarker discovery, due to the higher metabolite concentrations in serum.[42,43] For the present work, both kinds of matrices have been used. As long as the same sample preparation is used, either matrix should generate similar results when using targeted analysis.

Animal Age. The up-regulation of the biomarker in estradiol-treated adult females can be seen in Figure 1. The box plot summarizes the data obtained for these 13 animals. A clear age effect was observed when the levels of the biomarker in adult cows were compared with those obtained for prepubertal females. In the older animals the area ratios of Pyr-Phe were 0.5 ± 0.1 for control and/or progesterone-treated females and 2.8 ± 1.1 in treated animals. The basal serum concentrations in cows resulted in almost twice the plasmatic levels found in young animals. This group showed plasmatic levels below or at 0.4, except in the case of samples from treated individuals. Figure 2 shows a box plot of the plasma levels of Pyr-Phe in young females. The 2-week-old females exhibited inconsistent and short-lasting responses in some cases, whereas the 6-month-old female showed a delayed but clear increase on the biomarker level 2 weeks after the first EB dose. A possible reason for the missing and/or reduced response in young females could be the age and sexual development of the animals. The age of the animal plays an important role in the establishment of acceptable reference thresholds of biomarkers, as it influences the endogenous levels of the sex steroids.[44] Even though puberty onset will differ between animals, rather accurate age ranges may be established for a specific species and breed. In a study performed with 39 Holstein-Friesian heifers, the puberty onset was detected in a range of 38−55 weeks of age.[44] These data indicate that the young females included in this work can be considered as prepubertal animals. The latter was expected to be more responsive as it was closer to puberty onset.

It has already been suggested that prepubertal animals behave differently from adult animals in their response to anabolic treatments. In 2011, Becker et al. conducted two transcriptomics studies in parallel, one with postpubertal 24-month-old Nguni heifers and other one with prepubertal female 2−4-week-old Holstein-Friesian calves.[39] The animals were administered combinations of estrogenic and androgenic compounds. No successful results were obtained for prepubertal heifers. In a study by Cacciatore et al. female and

Table 1. Characteristics of the Different Holstein-Friesian Females Used for Evaluating the Potential of Pyr-Phe as Biomaker for Estradiol Treatments

							sample characteristics				additional information		
class	animal no.	initial age	sex	admin route[a]	drug[b]		days after treatment	collection time	matrix	origin	feed	breed	environment
control	1, 2	2−5 years	♀	IVa	P_4		8	2006	serum	Spain	diet typically used in dairy practice	Holstein	dairy farm
	3, 4, 5, 6	2−5 years											
treated	7, 8, 13	2−5 years		IM	EB		3						
	9, 10, 11	2−5 years		IVa	P_4 + EB		6						
	12	2−5 years		IM	E_2		3						
control	3956	6 months	♀				29, 30, 31, and 32 before first EB	2007	plasma	Netherlands	milk replacer, roughage, drinking water ad libitum	Holstein	experimental conditions
treated	3956	6 months	♀	IM	DHA (at days −28 and −21), MPA (at days −14 and −7), EB (at days 0 and 7), DROM (at days 14 and 21)		0.5, 1, 2, 3, 4, 7, 8, 9, 10, 11, 14, 15, 16, 17, 18, 21, 22, 23, 24, 25 after first EB (considered day 0)						
control	175	2 weeks	♀				1, 42	2008	plasma	Germany	milk replacer, roughage, drinking water ad libitum	Holstein	experimental conditions
	182						1, 21,						
	185						4						
	191						1, 56						
	193						21						
control (carriers)	172	2 weeks	♀	IM	carrier only		1, 14, 21						
	173			pour-on	carrier only	DEGMBE	5						
	177					DMSO	1, 14, 28						
	181					Ivomec	4						
	184					Miglyol	1, 14, 56						
treated (×1)	174	2 weeks	♀	IM	EB + TD + TC (×1)		1, 5, 7, 28						
	178		♀	pour-on	EB + TD + TC (×1)	DEGMBE	7, 21						
	180					DMSO	1, 6, 14						
	183					Ivomec	1, 5, 21						
	188					Miglyol	56						
treated (×3)	171	2 weeks	♀	IM	EB + TD + TC (×3)		1, 6, 14, 28, 70						
	179		♀	pour-on	EB + TD + TC (×3)	DEGMBE	0 (predose), 21, 42, 56						
	187					DMSO	6						
	190					Ivomec	1, 14, 21, 28						
	192					Miglyol	42, 70						

[a]IVa, intravaginal; IM, intramuscular; pour-on, different carrier solvent per animal (DEGMBE, DMSO, Ivomec, Miglyol). [b]DROM: dromostanolone; DHA, 1-dehydroandrostanolone; E2:,estradiol; EB, estradiol benzoate; MPRED, methy prednisone acetate; P4, progesterone; TC, testosterone cypionate; TD, testosterone decanoate.

dx.doi.org/10.1021/jf503773u | J. Agric. Food Chem. 2015, 63, 370−378

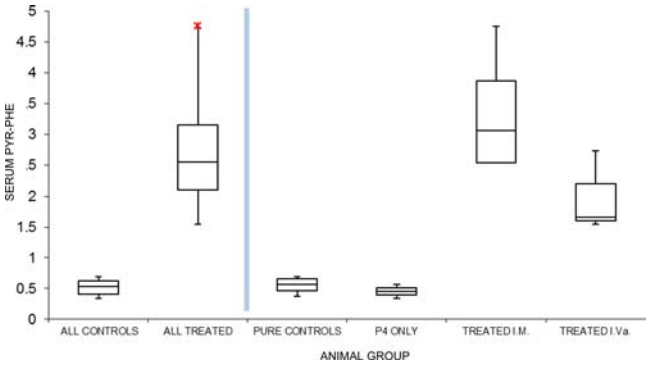

Figure 1. Overview of the presence of Pyr-Phe in the serum of adult cows treated or not with estradiol preparations (P_4, progesterone; IM, intramuscular; IVa, intravaginal). Box plot shows serum levels of the marker; the box limits are in the 25th and 75th percentiles, and the band in the middle of the box is the median; the whiskers are in the 1.5 interquartile range. Data not included between the whiskers are plotted as an outlier with a small cross.

male crossbred Holstein-Friesian × Fries-Hollands calves at an age of 10 weeks[34] were treated with a combination of EB and 19-nortestosterone decanoate intramuscularly. Among the nine plasma potential biomarkers measured, only one of the analytes (ir-inhibin) was down-regulated in males under hormonal treatment, but unaffected in females.

Administration Route, Dose, and Other Anabolic Compounds. The treatments applied in this study included several carrier solvents, anabolic combinations, doses, and routes of administration (see Table 1). All of the adult animals were treated with relatively low doses of estradiol, but a clear effect was observed in the levels of the selected biomarker, regardless of the route of administration and the drug (free estradiol or benzoate) (Figure 1). A smaller effect was noted for the intravaginal treatment. However, the mechanism of diffusion via vaginal mucosa is different and slower, and also the simultaneous administration of progesterone may have influenced the expression of the marker. A recent study by Wasowska and Krzymowska indicated that exogenous progesterone in porcine females affected the secretion of androgens and estrogens, resulting in a negative feedback for estradiol.[45] This feedback could lead to an altered response of the biomarker. The most evident up-regulation of Pyr-Phe was observed in the animal treated with estradiol-17β (lowest dose of estrogen), suggesting a stronger response to the free form. A possible reason is that esters need to be hydrolyzed before binding to receptors. Females under treatments with only progesterone (no estrogens) showed no significant differences in the levels of the dipeptide in comparison to "pure" control females.

For the 2-week-old heifers, the levels of Pyr-Phe in the control group, including the animals treated with carriers only, were measured at different points. No significant modifications could be observed, suggesting no influence of the carriers on the biomarker. The detected levels in plasma had an area ratio below 0.4 (0.2−0.4). For the treated animals, both pour-on and intramuscular administrations yielded inconsistent results, with short-term peaks in the levels of the dipeptide in some of the cases. In the pour-on group, a mild response of the marker could be observed only in one animal (Figure 3). A noticeable up-regulation (ratio 0.5) was expressed around day 21 in animal 179, treated three times (Figure 3C). The increase corresponds to 7 days after the last administration (of three consecutive doses), when some degree of steroid accumulation in the subcutaneous fat may be expected. The levels of the marker rapidly decreased to basal/control conditions. A mild effect was observed in animal 183, also around day 21 (Figure 3B). In this case, it was still in the range of the control animals. This animal received only one dose, and the initial basal levels of the dipeptide were very low (below 0.3) in comparison to the rest of the group. Pour-on formulations cannot be considered a topical route of administration in cattle under normal husbandry conditions.[46] In a natural environment, cattle lick themselves (allolicking) and lick other cattle (heterolicking). Thus, part of the drug may pass through the digestive tract, and not only in the treated animal but also in animals from the same herd or group. Additionally, different carrier solvents were applied per animal, possibly leading to different administration efficiencies. The highest levels of Pyr-Phe after treatment were observed for DEGMBE preparations, matching the results for hair analysis reported by Stolker et al.[15] At day 7, animal 178 (treated once) showed a response of 0.6 in the same range as animal 179 (treated three times) at day 21, both treated with formulas based on DEGMBE. In the intramuscular treatments, a clearer effect was observed in both females, even though the response was different in each animal (Figure 4). A single administration resulted in a late effect on the biomarker, reaching the maximum (measured) level almost 1 month after the administration (Figure 4A). The animal injected three times showed the same level after the second dose, suggesting some kind of accumulative effect (Figure 4B). Unfortunately, plasma from every time point was not available for analysis to obtain a complete pattern of the biomarker throughout the treatment.

Figure 2. Overview of the presence of Pyr-Phe in the plasma from young bovine females, grouped by age and treatment (IM, intramuscular; EB, estradiol benzoate; DROM, dromostanolone). Box plot shows plasma levels of the marker; the box limits are in the 25th and 75th percentiles, and the band in the middle of the box is the median; the whiskers are in the 1.5 interquartile range. Data not included between the whiskers are plotted as an outlier with a small cross.

dx.doi.org/10.1021/jf503773u | J. Agric. Food Chem. 2015, 63, 370−378

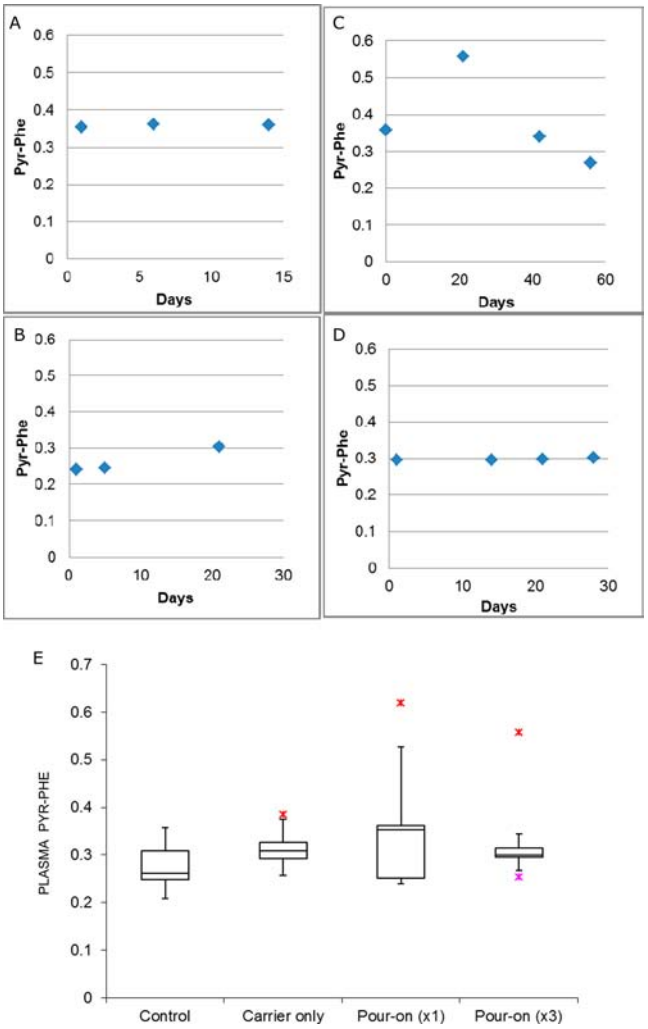

Figure 3. Evaluation of Pyr-Phe levels in the 2-week-old control females treated via pour-on and comparison to their respective control animals. The four upper plots represent the evolution of the marker in four individual animals treated once (A, B) or three times (C, D). The box plot (E) shows the serum levels of the marker in all the pour-on and control cases; the box limits are in the 25th and 75th percentiles, and the band in the middle of the box is the median; the whiskers are

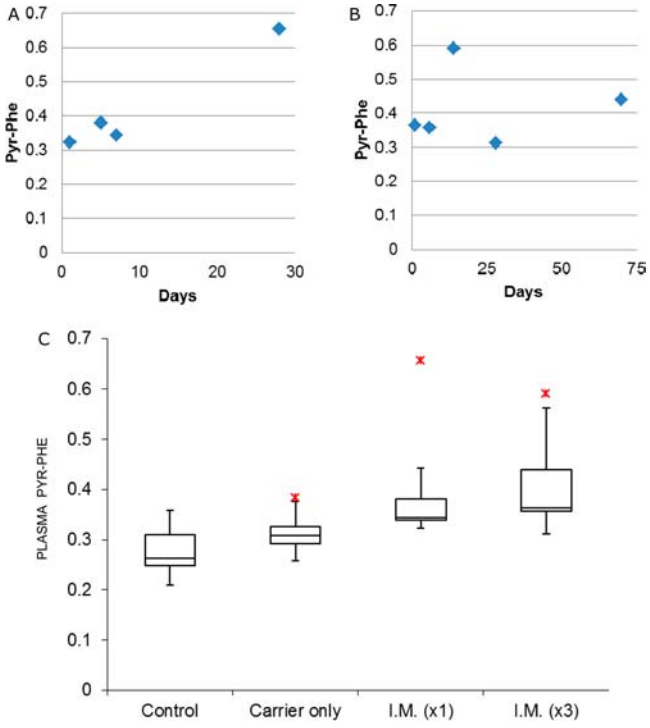

Figure 4. Evaluation of Pyr-Phe levels in the 2-week-old control females treated intramuscularly (IM) and comparison to their respective control animals. The two upper plots represent the evolution of the marker in two individual animals treated once (A) or three times (B). The box plot (C) shows the serum levels of the marker in all the IM samples and in control cases; the box limits are in the 25th and 75th percentiles, and the band in the middle of the box is the median; the whiskers are in the 1.5 interquartile range. Data not included between the whiskers are plotted as an outlier with a small cross.

Although it is difficult to draw conclusions, it is pertinent to make a few remarks. On the one hand, the doses applied may not have been high enough to raise an effect in the biomarker, especially in the case of pour-on treatments. On the other hand, the possibility exists for the androgenic compounds (TD and TC) to have an antagonistic effect on this biomarker. Hemmer et al. selected four peptides in the plasma of male and gravid female fish, as potential estrogenic biomarkers.[47] Afterward, they performed experiments with 17β-trenbolone to investigate possible effects of the synthetic androgen. All four peptide biomarkers were significantly reduced in females exposed at the highest treatment level, which corresponded with significant reductions in fecundity and changes in ovarian morphology. Other researchers have reported similar problems when using a combination of estrogenic and androgenic drugs in bovine animals.[34,39]

For the 6-month-old female, four different steroids were administered (DHA, MPA, EB, and DROM), reaching a total dose per compound of 250 mg. Whether due to the higher estrogenic dose or the difference of age, the changes in the peptide concentration were clearer in this prepubertal animal (Figure 5). The samples collected before the first injection appeared within basal levels, similar to those found in the 2-week-old animals. The first two samples collected (12 and 24 h) after the first EB injection showed decreased levels in comparison to the initial control samples (1 month earlier). However, the effects and/or feedback that the previous administration of DHA and MPA may have on the response of this biomarker remain unknown. DHA is a potent androgen with anabolic properties, and MPA is a synthetic glucocorticoid or corticosteroid. The possible interference of androgenic drugs has been previously discussed. Additionally, glucocorticoids can also inhibit endogenous production of sex steroids and can affect protein synthesis within the liver.[48,49] This last fact is especially relevant when one is working with protein or peptide makers. Unfortunately, no samples were collected during DHA and MPA administration. In the days following first EB injection, the biomarker came back to initial concentrations and exceeded them 2 weeks later, reaching levels closer to those found in treated adult females (Figure 5A). The last compound administered was DROM, a less potent synthetic derivative of dihydrotestosterone with enhanced anabolic activity and with certain antiestrogenic activity. Its administration did not lower the expression of the marker. It is difficult to draw tight conclusions for this range of age as there was only one animal.

Other Factors. The results suggest that both the protocol of administration and sampling and the variability of farm animals could affect the reliability of the method. However,

dx.doi.org/10.1021/jf503773u | J. Agric. Food Chem. 2015, 63, 370−378

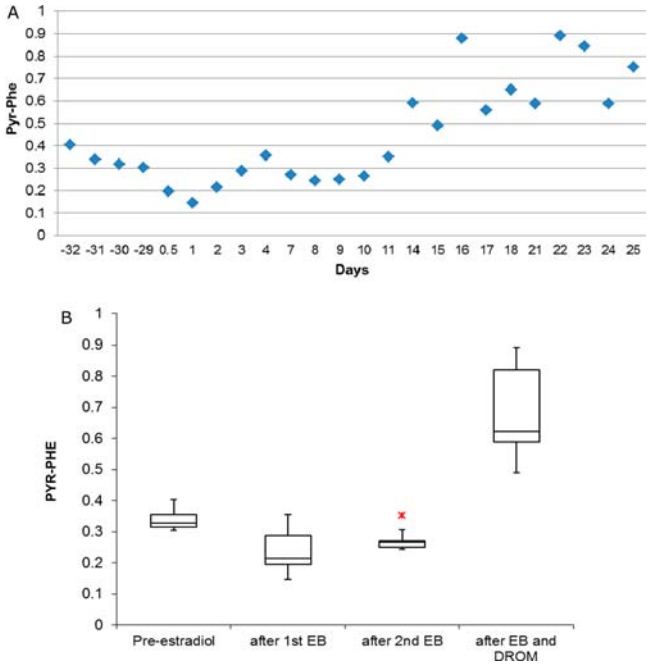

Figure 5. Evaluation of Pyr-Phe levels in the 6-month-old female treated intramuscularly with EB and other drugs. The point-to-point graph (A) shows the evolution of Pyr-Phe during the animal experiment, day 0 being the day of the first injection of EB. The box plot (B) shows the serum levels of the marker at different stages of the experiment; the box limits are in the 25th and 75th percentiles, and the band in the middle of the box is the median; the whiskers are in the 1.5 interquartile range. Data not included between the whiskers are plotted as an outlier with a small cross.

other factors such as origin, gender, breed, health status, and feed may also influence the expression of Pyr-Phe in estradiol-treated animals. In addition, it is essential to differentiate between genders when one is dealing with biomarkers and profiling methods for the detection of hormonal treatments.[13,21,34] In future studies, the presence of this dipeptide should be assessed in adult and prepubertal males. The feeding should not be excluded as a source of variability. In the present study, the prepubertal population followed a diet completely different from adult cows. On the other hand, experimental animals may not give the same results as animals living on real farms due to stress factors and differences in the management and environmental conditions. Finally, the possible classification of this biomarker as a marker of effect instead of exposure should not be excluded. That would mean that its presence is correlated to an estrogenic effect rather than to an administration or exposure to a specific compound (estradiol). Therefore, observational data about its presence and amount in bovine animals exposed to estrogen-like substances, such as mycotoxins and phytosterols, should be considered and explored soon as it would enhance the significance of this work. Also, these kinds of studies are necessary to facilitate the translation of this biomarker into practice.

No definitive solution has been found yet to solve the problem of the illegal administration of estradiol in cattle. A strong influence of age in effect-based detection approaches has been reported,[35,50] as well as a potential contribution of other drugs and individual variations. Results reported suggest that it is necessary to establish different biomarkers for specific treatment regimens and different age/gender classes of animals. The capability of Pyr-Phe to identify adult cows that are "highly suspicious" of estradiol treatments was proven. A potential threshold is established at a ratio of 1.0 because all of the samples from treated cows were above it. In the case of prepubertal animals, a threshold of 0.4 may be concluded from this study and proposed, but the screening ability would be clearly lower for these animals.

The introduction of new powerful tests is still required for prepubertal heifers. Combining multiple biomarkers in a panel might be beneficial, along with other options such as hair analysis or steroid profiling. The ultimate confirmation would rely on GC-C/IRMS. The matrix of choice for this powerful technique is urine. The use of different matrices for screening and confirmation is an obstacle to their implementation into routine. For this reason, the ultimate screening tool would preferably be urine-based. Moreover, the detection frame of screening and confirmation needs to be compatible.

AUTHOR INFORMATION

Corresponding Author

*(P.R.) Phone: +31(0)317480256. Fax: +31(0)317417717. E-mail: patricia.regallopez@wur.nl or patricia.regal@usc.es.

Notes

The authors declare no competing financial interest.

ABBREVIATIONS USED

DEGMBE, diethylene glycol monobutyl ether; DHA, 1-dehydroandrostanolone; DMSO, dimethyl sulfoxide; DROM, dromostanolone; E_2, estradiol; EB, estradiol benzoate; GC-C/IRMS, gas chromatography coupled to combustion/isotope ratio mass spectrometry; HPLC-MS/MS, high-performance liquid chromatography coupled to tandem mass spectrometry; MPA, methyl prednisone acetate; TC, testosterone cypionate; TD, testosterone decanoate

REFERENCES

(1) Dikeman, M. E. Effects of metabolic modifiers on carcass traits and meat quality. *Meat Sci.* **2007**, *77*, 121−135.

(2) Fernandes, P.; Teixeira, A. B.; Crocci, A. J.; Barros, C. M. Timed artificial insemination in beef cattle using Gn RH agonist, PGF2α and estradiol benzoate (EB). *Theriogenology* **2001**, *55*, 1521−1532.

(3) Sales, J. N. S.; Carvalho, J. B. P.; Crepaldi, G. A.; Cipriano, R. S.; Jacomini, J. O.; Maio, J. R. G.; Souza, J. C.; Nogueira, G. P.; Baruselli, P. S. Effects of two estradiol esters (benzoate and cypionate) on the induction of synchronized ovulations in *Bos indicus* cows submitted to a timed artificial insemination protocol. *Theriogenology* **2012**, *78*, 510−516.

(4) Council Directive 81/602/EEC of 31 July 1981 concerning the prohibition of certain substances having a hormonal action and of any substances having a thyrostatic action. *Off. J. Eur. Communities* **1981**, *L222*, 32−33.

(5) Council Directive 85/649/EEC of 31 December 1985 prohibiting the use in livestock farming of certain substances having a hormonal action. *Off. J. Eur. Communities* **1985**, *L 382*, 228−231.

(6) Council Directive 88/146/EEC of 7 March 1988 prohibiting the use in livestock farming of certain substances having a hormonal action. *Off. J. Eur. Communities* **1988**, *L70*, 16−18.

(7) Council Directive 96/22/EC of 29 April 1996 concerning the prohibition on the use in stockfarming of certain substances having a hormonal or thyrostatic action and of beta-agonists, and repealing Directives 81/602/EEC, 88/146/EEC and 88/299/EEC. *Off. J. Eur. Communities* **1996**, *L125*, 3−9.

(8) Regal, P.; Cepeda, A.; Fente, C. A. Natural hormones in food-producing animals: legal measurements and analytical implications. In

Food Production − Approaches, Challenges and Tasks, 1st ed.; Aladjadjiyan, A., Ed.; In Tech: Rijeka, Croatia, 2012; pp 205−230.
(9) Directive 2003/74/EC of the European Parliament and of the Council of 22 September 2003, amending Council Directive 96/22/EC concerning the prohibition on the use in stockfarming of certain substances having a hormonal or thyrostatic action and of beta-agonists. *Off. J. Eur. Union* **2003**, *L262*, 17−21.
(10) Lane, E. A.; Austin, E. J.; Crowe, M. A. Oestrous synchronisation in cattle − current options following the EU regulations restricting use of oestrogenic compounds in food-producing animals: a review. *Anim. Reprod. Sci.* **2008**, *109*, 1−16.
(11) Malone, E.; Elliott, C. T.; Kennedy, D. G.; Regan, L. Development of a rapid method for the analysis of synthetic growth promoters in bovine muscle using liquid chromatography tamdem mass spectrometry. *Anal. Chim. Acta* **2009**, *637*, 112−120.
(12) Scarth, J.; Akre, C.; van Ginkel, L.; le Bizec, B.; de Brabander, H.; Korth, W.; Points, J.; Teale, P.; Kay, J. Presence and metabolism of endogenous androgenic-anabolic steroid hormones in meat-producing animals: a review. *Food Addit. Contam., Part A* **2009**, *26*, 640−671.
(13) Scarth, J. P.; Clarke, A.; Teale, P.; Mill, A.; Macarthur, R.; Kay, J. Detection of endogenous steroid abuse in cattle: results from population studies in the UK. *Food Addit. Contam., Part A* **2011**, *28*, 44−61.
(14) Regal, P.; Vázquez, B. I.; Franco, C. M.; Cepeda, A.; Fente, C. A. Development of a rapid and confirmatory procedure to detect 17β-estradiol 3-benzoate treatments in bovine hair. *J. Agric. Food Chem.* **2008**, *56*, 11607−11611.
(15) Stolker, A. A. M.; Groot, M. J.; Lasaroms, J. J. P.; Nijrolder, A. W. J. M.; Blokland, M. H.; Riedmaier, I.; Becker, C.; Meyer, H. H. D.; Nielen, M. W. F. Detectability of testosterone esters and estradiol benzoate in bovine hair and plasma following pour-on treatment. *Anal. Bioanal. Chem.* **2009**, *395*, 1075−1087.
(16) Bichon, E.; Béasse, A.; Prevost, S.; Christien, S.; Courant, F.; Monteau, F.; Le Bizec, B. Improvement of estradiol esters monitoring in bovine hair by dansylation and liquid chromatography/tandem mass spectrometry analysis in multiple reaction monitoring and precursor ion scan modes. *Rapid Commun. Mass Spectrom.* **2012**, *26*, 819−827.
(17) Duffy, E.; Mooney, M. H.; Elliott, C. T.; O'Keeffe, M. Studies on the persistence of estradiol benzoate and nortestosterone decanoate in hair of cattle following treatment with growth promoters, determined by ultra-high-performance liquid chromatography−tandem mass spectrometry. *J. Chromatogr., A* **2009**, *1216*, 8090−8095.
(18) Gray, B. P.; Teale, P.; Pearce, C. M. Analysis of methyloxime derivatives of intact esters of testosterone and boldenone in equine plasma using ultra high performance liquid chromatography tandem mass spectrometry. *Drug Test. Anal.* **2011**, *3*, 206−213.
(19) Kaabia, Z.; Dervilly-Pinel, G.; Hanganu, F.; Cesbron, N.; Bichon, E.; Popot, M. A.; Bonnaire, Y.; Le Bizec, B. Ultra high performance liquid chromatography/tandem mass spectrometry based identification of steroid esters in serum and plasma: an efficient strategy to detect natural steroids abuse in breeding and racing animals. *J. Chromatogr., A* **2013**, *1284*, 126−140.
(20) Regal, P.; Nebot, C.; Díaz-Bao, M.; Barreiro, R.; Cepeda, A.; Fente, C. Disturbance in sex-steroid serum profiles of cattle in response to exogenous estradiol: a screening approach to detect forbidden treatments. *Steroids* **2011**, *76*, 365−375.
(21) Blokland, M. H.; Van Tricht, E. F.; Van Rossum, H. J.; Sterk, S. S.; Nielen, M. W. F. Endogenous steroid profiling by gas chromatography-tandem mass spectrometry and multivariate statistics for the detection of natural hormone abuse in cattle. *Food Addit. Contam., Part A* **2012**, *29*, 1030−1045.
(22) Nielen, M. W. F.; Lasaroms, J. J. P.; Essers, M. L.; Sanders, M. B.; Heskamp, H. H.; Bovee, T. F. H.; van Rhijn, J.; Groot, M. J. The ultimate veal calf reference experiment: hormone residue analysis data obtained by gas and liquid chromatography tandem mass spectrometry. *Anal. Chim. Acta* **2007**, *586*, 30−34.
(23) Vascellari, M.; Capello, K.; Stefani, A.; Biancotto, G.; Moro, L.; Stella, R.; Pozza, G.; Mutinelli, F. Evaluation of thymus morphology and serum cortisol concentration as indirect biomarkers to detect low-dose dexamethasone illegal treatment in beef cattle. *BMC Vet. Res.* **2012**, *8*, 129.
(24) Dumas, M. E.; Canlet, C.; Vercauteren, J.; André, F.; Paris, A. Homeostatic signature of anabolic steroids in cattle using $^{1}H-^{13}C$ HMBC NMR metabonomics. *J. Proteome Res.* **2005**, *4*, 1493−1502.
(25) Gardini, G.; Del Boccio, P.; Colombatto, S.; Testore, G.; Corpillo, D.; Di Ilio, C.; Urbani, A.; Nebbia, C. Proteomic investigation in the detection of the illicit treatment of calves with growth-promoting agents. *Proteomics* **2006**, *6*, 2813−2822.
(26) Dervilly-Pinel, G.; Weigel, S.; Lommen, A.; Chereau, S.; Rambaud, L.; Essers, M.; Antignac, J.; Nielen, M. W. F.; Le Bizec, B. Assessment of two complementary liquid chromatography coupled to high resolution mass spectrometry metabolomics strategies for the screening of anabolic steroid treatment in calves. *Anal. Chim. Acta* **2011**, *700*, 144−154.
(27) Regal, P.; Anizan, S.; Antignac, J.; Le Bizec, B.; Cepeda, A.; Fente, C. Metabolomic approach based on liquid chromatography coupled to high resolution mass spectrometry to screen for the illegal use of estradiol and progesterone in cattle. *Anal. Chim. Acta* **2011**, *700*, 16−25.
(28) Riedmaier, I.; Benes, V.; Blake, J.; Bretschneider, N.; Zinser, C.; Becker, C.; Meyer, H. H. D.; Pfaffl, M. W. RNA-sequencing as useful screening tool in the combat against the misuse of anabolic agents. *Anal. Chem.* **2012**, *84*, 6863−6868.
(29) Divari, S.; Pregel, P.; Cannizzo, F. T.; Starvaggi Cucuzza, L.; Brina, N.; Biolatti, B. Oxytocin precursor gene expression in bovine skeletal muscle is regulated by 17β-oestradiol and dexamethasone. *Food Chem.* **2013**, *141*, 4358−4366.
(30) Kieken, F.; Pinel, G.; Antignac, J. P.; Paris, A.; Garcia, P.; Popot, M. G.; Grall, M.; Mercadier, V.; Toutain, P. L.; Bonnaire, Y.; Le Bizec, B. Generation and processing of urinary and plasmatic metabolomic fingerprints to reveal an illegal administration of recombinant equine growth hormone from LC-HRMS measurements. *Metabolomics* **2011**, *7*, 84−93.
(31) Anizan, S.; Bichon, E.; Duval, T.; Monteau, F.; Cesbron, N.; Antignac, J. P.; Le Bizec, B. Gas chromatography coupled to mass spectrometry-based metabolomic to screen for anabolic practices in cattle: identification of 5α-androst-2-en-17-one as new biomarker of 4-androstenedione misuse. *J. Mass Spectrom.* **2012**, *47*, 131−140.
(32) Cannizzo, F. T.; Pegolo, S.; Starvaggi Cucuzza, L.; Bargelloni, L.; Divari, S.; Franch, R.; Castagnaro, M.; Biolatti, B. Gene expression profiling of thymus in beef cattle treated with prednisolone. *Res. Vet. Sci.* **2013**, *95*, 540−547.
(33) Ludwig, S. K. J.; van Ginkel, L. A.; Nielen, M. W. F. Screening of protein biomarkers for sports doping and veterinary control. *TrAC−Trends Anal. Chem.* **2014**, *57*, 47−63.
(34) Cacciatore, G.; Eisenberg, S. W. F.; Situ, C.; Mooney, M. H.; Delahaut, P.; Klarenbeek, S.; Huet, A.; Bergwerff, A. A.; Elliott, C. T. Effect of growth-promoting 17β-estradiol, 19-nortestosterone and dexamethasone on circulating levels of nine potential biomarker candidates in veal calves. *Anal. Chim. Acta* **2009**, *637*, 351−359.
(35) Ludwig, S. K. J.; Smits, N. G. E.; Cannizzo, F. T.; Nielen, M. W. F. Potential of treatment-specific protein biomarker profiles for detection of hormone abuse in cattle. *J. Agric. Food Chem.* **2013**, *61*, 4514−4519.
(36) Janssens, G.; Courtheyn, D.; Mangelinckx, S.; Prévost, S.; Bichon, E.; Monteau, F.; De Poorter, G.; De Kimpe, N.; Le Bizec, B. Use of isotope ratio mass spectrometry to differentiate between endogenous steroids and synthetic homologues in cattle: a review. *Anal. Chim. Acta* **2013**, *772*, 1−15.
(37) Janssens, G.; Mangelinckx, S.; Courtheyn, D.; Prévost, S.; De Poorter, G.; De Kimpe, N.; Le Bizec, B. Application of gas chromatography−mass spectrometry/combustion/isotope ratio mass spectrometry (GC-MS/C/IRMS) to detect the abuse of 17β-estradiol in cattle. *J. Agric. Food Chem.* **2013**, *61*, 7242−7249.
(38) Regal, P.; Seijas, J. A.; Cepeda, A.; Fente, C. Structure elucidation and HPLC-MS/MS determination of a potential biomarker for estradiol administration in cattle. *Anal. Bioanal. Chem.* **2013**, *405*, 9537−9546.

(39) Becker, C.; Riedmaier, I.; Reiter, M.; Tichopad, A.; Groot, M. J.; Stolker, A. A. M.; Pfaffl, M. W.; Nielen, M. F. W.; Meyer, H. H. D. Influence of anabolic combinations of an androgen plus an estrogen on biochemical pathways in bovine uterine endometrium and ovary. *J. Steroid Biochem. Mol. Biol.* **2011**, *125*, 192−201.
(40) Mooney, M. H.; Situ, C.; Cacciatore, G.; Hutchinson, T.; Elliott, C.; Bergwerff, A. A. Plasma biomarker profiling in the detection of growth promoter use in calves. *Biomarkers* **2008**, *13*, 246−256.
(41) Cunningham, R. T.; Mooney, M. H.; Xia, X.; Crooks, S.; Matthews, D.; O'Keeffe, M.; Li, K.; Elliott, C. T. Feasibility of a clinical chemical analysis approach to predict misuse of growth promoting hormones in cattle. *Anal. Chem.* **2009**, *81*, 977−983.
(42) Liu, L.; Aa, J.; Wang, G.; Yan, B.; Zhang, Y.; Wang, X.; Zhao, C.; Cao, B.; Shi, J.; Li, M.; Zheng, T.; Zheng, Y.; Hao, G.; Zhou, F.; Sun, J.; Wu, Z. Differences in metabolite profile between blood plasma and serum. *Anal. Biochem.* **2010**, *406*, 105−112.
(43) Yu, Z.; Kastenmüller, G.; He, Y.; Belcredi, P.; Möller, G.; Prehn, C.; Mendes, J.; Wahl, S.; Roemisch-Margl, W.; Ceglarek, U.; Polonikov, A.; Dahmen, N.; Prokisch, H.; Xie, L.; Li, Y.; Wichmann, H. E.; Peters, A.; Kronenberg, F.; Suhre, K.; Adamski, J.; Illig, T.; Wang-Sattler, R. Differences between human plasma and serum metabolite profiles. *PLoS One* **2011**, *6*, No. e21230.
(44) Nakada, K.; Moriyoshi, M.; Nakao, T.; Watanabe, G.; Taya, K. Changes in concentrations of plasma immunoreactive follicle-stimulating hormone, luteinizing hormone, estradiol-17β, testosterone, progesterone, and inhibin in heifers from birth to puberty. *Domest. Anim. Endocrinol.* **2000**, *18*, 57−69.
(45) Wąsowska, B.; Stefańczyk-Krzymowska, S. Local effect of progesterone infusion into the porcine ovarian artery on androgen and estrogen secretion during the middle luteal phase. *Reprod. Biol.* **2009**, *9*, 161−179.
(46) Toutain, P. L.; Ferran, A.; Bousquet-Mélou, A. Species differences in pharmacokinetics and pharmacodynamics. *Handb. Exp. Pharmacol.* **2010**, *199*, 19−48.
(47) Hemmer, M. J.; Cripe, G. M.; Hemmer, B. L.; Goodman, L. R.; Salinas, K. A.; Fournie, J. W.; Walker, C. C. Comparison of estrogen-responsive plasma protein biomarkers and reproductive endpoints in sheepshead minnows exposed to 17β-trenbolone. *Acuat. Toxicol.* **2008**, *88*, 128−136.
(48) van Staa, T. P. The pathogenesis, epidemiology and management of glucocorticoid-induced osteoporosis. *Calcif. Tissue Int.* **2006**, *79*, 129−137.
(49) Gong, H.; Jarzynka, M. J.; Cole, T. J.; Lee, J. H.; Wada, T.; Zhang, B.; Gao, J.; Song, W. C.; DeFranco, D. B.; Cheng, S. Y.; Xie, W. Glucocorticoids antagonize estrogens by glucocorticoid receptor-mediated activation of estrogen sulfotransferase. *Cancer Res.* **2008**, *68*, 7386−7393.
(50) Snoj, T.; Dolenc, J.; Kobal, S. Sex steroid levels in urine of cattle of different ages: evaluation of abuse control procedures. *Food Addit. Contam., Part A* **2014**, *31*, 614−620.

JOURNAL OF AGRICULTURAL AND FOOD CHEMISTRY

Letter

pubs.acs.org/JAFC

Critical Evaluation of Changes in the Ratio of Insoluble Bound to Soluble Phenolics on Antioxidant Activity of Lentils during Germination

ABSTRACT: A new indicator, the ratio of insoluble bound phenolics (IBPs) to soluble phenolics (SPs), is suggested as an effective means to monitor changes in the antioxidant activity of lentils during germination. This indicator may be used to monitor other process-induced changes in antioxidant potential of food phenolics in other foods. The antioxidant activity of SPs, IBPs, and total value, the sum of both free and esterified phenolics, of germinated CDC Richlea lentil variety was evaluated for 4 days. Total phenolic content (TPC), total flavonoid content (TFC), 2,2-diphenyl-1-picrylhydrazyl (DPPH) radical, and 2,2′-azinobis(3-ethylbenzothiazoline-6-sulfonic acid) (ABTS) radical cation scavenging ability were employed to record antioxidant activities. An incremental increase in IBPs was found in TPC, TFC, DPPH, and ABTS radical cation scavenging ability, whereas SPs showed a declining trend in TFC, DPPH, and ABTS, except TPC during 4 days of germination. The ratio of IBPs to SPs increased using most methods, and this may be possibly due to the changes of phenolic compound formation from soluble into insoluble bound form during germination process. The ratio can be used as a novel method for monitoring process-induced changes in the antioxidant activity of foods.

KEYWORDS: *lentil, germination, insoluble bound phenolics, antioxidant activity*

INTRODUCTION

Lentils have attracted much interest from food scientists and consumers alike as they serve as an excellent dietary source of legumes that are rich in dietary fiber, carbohydrates, protein, various vitamins, minerals, and several health-beneficial fatty acids.[1] Some epidemiological studies have reported their effects in lowering cholesterol and reducing colon cancer, heart diseases, and type-2 diabetes.[2]

Germination is an efficient and economical bioprocess for improving the nutritional quality and functionality of seeds and legumes and is well-studied in the plant physiology area. Reactive oxygen species (ROS) play a key role in seed development, dormancy breaking ability, and regulation of germination processes such as signaling molecules.[3] Meanwhile, phenolic compounds are responsible for controlling ROS that stimulate production of phenolic compounds by activating enzymatic or nonenzymatic pathways.[4] This complex reaction process affects the composition and quantity of phenolic compounds, leading to changes in nutritional and functional quality of seeds.

The reason for alteration of antioxidant activity of soluble phenolics (SPs) and insoluble bound phenolics (IBPs) induced by germination has not been fully explored. For this reason, we tested the ratio of IBPs to SPs to see if it would provide a useful tool for better understanding and monitoring of changes in antioxidant activity by predicting the localization and molecular transportation mechanism of phenolic compounds in plant cells during germination. Most phenolic compounds are synthesized in the intracellular space, especially in the endoplasmic reticulum, and are stored in vacuoles as SPs.[5] On the other hand, IBPs are transported from intracellular space and localized in cell walls by forming covalent bonds with insoluble macromolecules such as cellulose, arabinoglycan, and proteins or by self-polymerization. Therefore, changes in the ratio of these phenolics may provide a useful tool for predicting localization and transportation mechanisms of phenolic compounds and alteration of antioxidant activity upon processing, as exemplified for germination of lentils in this study. Thus, we monitored changes of antioxidant activity of SPs and IBPs procured from germinated lentils and used the ratio of IBPs to SPs to explain the results.

MATERIALS AND METHODS

Germination of Lentils. Fifty grams of CDC (Crop Development Center) Richlea lentils was washed thoroughly with distilled water and then placed on aluminum plates covered with a wet paper towel and allowed sufficient oxygen at 24.5 ± 0.8 °C. The germination process was followed on days 1, 2, 3, and 4. Water was supplied every 12 h to sustain adequate humidity. After germination, samples were dried in a forced air oven at 55 °C for 24 h and then stored at 4 ± 1 °C.

Extraction of Soluble Phenolics and Insoluble Bound Phenolics. Extraction of SPs from germinated lentils was followed as described by Wettasinghe and Shahidi with slight modification,[6] and IBPs were extracted as described by Naczk and Shahidi.[7]

Total Phenolic Content (TPC). TPC of germinated lentils was determined as described by Singleton and co-workers and as explained by Chandrasekara and Shahidi.[8,9]

Total Flavonoid Content (TFC). TFC was measured as described by Chandrasekara and Shahidi.[9]

2,2-Diphenyl-1-picrylhydrazyl (DPPH) Radical Scavenging Ability. DPPH radical scavenging ability was conducted as described as Sekhon-Loodu with slight modification.[10] Briefly, 1.9 mL of DPPH solution (0.1 mM) was mixed with 0.1 mL of sample, which was then allowed to react for 30 min at room temperature in the dark; the absorbance was then read at 517 nm.

2,2′-Azinobis(3-ethylbenzothiazoline-6-sulfonic acid) (ABTS) Radical Cation Scavenging Ability. ABTS radical cation was produced as described by Miller and Rice-Evans using ABTS and potassium persulfate.[11]

Statistical Analysis. Statistical analysis was conducted using IBM statistics version 21 (IBM Corp., Armonk, NY, USA). Duncan's test

Received: November 25, 2014
Revised: December 23, 2014
Accepted: January 5, 2015
Published: January 5, 2015

ACS Publications © 2015 American Chemical Society

DOI: 10.1021/jf505632p
J. Agric. Food Chem. 2015, 63, 379−381

Table 1. Total Phenolics and Total Flavonoid Contents of Soluble and Insoluble Bound Phenolics of Germinated Lentils as Gallic Acid Equivalent (GAE) or Catechin Equivalent (CE)[a]

germination time (days)	soluble phenolics	bound phenolics	total (soluble + bound)	ratio (bound/soluble)
Total Phenolic Content (GAE mg/g)				
0	3.35 ± 0.02b	4.78 ± 0.03a	8.13 ± 0.05a	1.43 ± 0.00a
1	3.13 ± 0.04a	5.18 ± 0.08b	8.31 ± 0.10a	1.66 ± 0.03c
2	3.84 ± 0.06c	5.71 ± 0.01d	9.55 ± 0.06c	1.49 ± 0.02b
3	3.83 ± 0.06c	5.33 ± 0.11c	9.16 ± 0.07b	1.39 ± 0.05a
4	4.25 ± 0.06d	6.45 ± 0.08e	10.69 ± 0.14d	1.52 ± 0.00b
Total Flavonoid Contents (CE mg/g)				
0	2.49 ± 0.03c	2.98 ± 0.18a	5.47 ± 0.21b	1.19 ± 0.06a
1	2.13 ± 0.05b	3.16 ± 0.01a	5.29 ± 0.05ab	1.49 ± 0.03b
2	2.17 ± 0.00b	3.56 ± 0.09b	5.73 ± 0.09c	1.64 ± 0.04c
3	2.01 ± 0.02a	3.16 ± 0.01a	5.17 ± 0.01a	1.58 ± 0.02c
4	1.96 ± 0.02a	3.85 ± 0.10c	5.82 ± 0.10c	1.96 ± 0.06d

[a]Values in each column having the same letter are not significantly different ($p > 0.05$).

Table 2. DPPH and ABTS Cation Radical Scavenging Abilities of Soluble and Insoluble Bound Phenolics of Germinated Lentils[a]

germination time (days)	soluble phenolics	bound phenolics	total (soluble + bound)	ratio (bound/soluble)
DPPH Radical Scavenging Ability (%)				
0	61.3 ± 1.6d	47.7 ± 0.1a	109.0 ± 1.6a	0.78 ± 0.02a
1	55.0 ± 0.4b	53.2 ± 1.3b	108.2 ± 1.6a	0.97 ± 0.02b
2	58.4 ± 0.3c	65.8 ± 1.6d	124.2 ± 1.4c	1.13 ± 0.03c
3	53.1 ± 0.4a	62.9 ± 0.1c	116.1 ± 0.5b	1.19 ± 0.01d
4	53.5 ± 0.2a	76.1 ± 1.3e	129.7 ± 1.5d	1.42 ± 0.02e
ABTS Cation Radical Scavenging Ability (%)				
0	63.3 ± 0.6c	48.2 ± 0.7a	111.5 ± 1.2b	0.76 ± 0.00a
1	56.7 ± 1.7a	49.9 ± 1.1a	106.6 ± 2.2a	0.88 ± 0.03b
2	60.9 ± 1.2b	58.5 ± 1.9c	119.4 ± 3.1c	0.96 ± 0.01c
3	57.8 ± 0.1a	53.3 ± 1.2b	111.1 ± 1.3b	0.92 ± 0.02d
4	57.6 ± 0.3a	65.3 ± 0.5d	122.8 ± 0.7c	1.13 ± 0.01e

[a]Values in each column having the same letter are not significantly different ($p > 0.05$).

was employed when the one-way ANOVA showed significant differences ($p < 0.05$).

RESULTS AND DISCUSSION

Total Phenolic Content. TPCs of SPs and IBPs in germinated lentils were determined using Folin−Ciocalteu's assay, and results are shown in Table 1. The germination process led to increase of TPC in both SPs (from 3.35 to 4.25 mg gallic acid equivalents (GAE)/g of defatted weight (DW)) and IBPs (from 4.78 to 6.45 mg GAE/g of DW). In agreement with this result, TPC of SPs isolated from germinated green lentils (*Lens esculenta*) showed increase of TPC during 7 days.[12]

The sum of SPs and IBPs, expressed as total value, showed an increasing pattern from 8.13 to 10.69 mg/g, and this result might indicate gradual synthesis of phenolic compounds during the germination process. In addition, the ratio of IBPs to SPs increased from 1.43 to 1.52.

Total Flavonoid Content. The influence of germination on changes in TFC in SPs and IBPs is presented Table 1. TFC of SPs decreased from 2.49 to 1.96 mg catechin equivalents (CE)/g of DW during the 4 days of germination, whereas that of IBPs increased from 2.98 to 3.85 CE mg/g. Decrease of TFC in SPs may be related to the degradation of flavonoids by oxidants such as ROS, which are produced in cells, especially in the mitochondria, during electron transfer chain reaction.[13,14] ROS play a key role as signaling molecules and affect cell division and growth. In doing so, the concentration of ROS is controlled by phenolic compounds, which act as regulators in plant metabolism by scavenging ROS, resulting in degradation of phenolic compounds. On the other hand, decrease of SPs can also be caused by their transport from intracellular space to cell wall and transformation from SPs into IBPs. This argument gains support from the previous findings of Strack et al.,[15] who reported that the increase in cell wall flavonoids during aging of Scots pine leaf paralleled a decrease in soluble flavonoids. They concluded that vacuolar efflux of these metabolites and deposition in the cell wall had occurred and that quercetin and kaempferol derivatives were also found in the cell wall of epidermal cells in lisianthus flowers petals.[16] Phenylpropanoids, particularly hydroxycinnamic acid derivatives, contribute to cell wall formation through esterification with complex carbohydrates.[17] These endoplasmic reticulum synthesized compounds were reported to be released in small vesicles that fuse in larger bodies and migrate to cell wall, after fusion with the plasma membrane.[18]

The ratio between IBPs and SPs is also shown Table 1. The ratio was increased significantly from 1.19 to 1.96 ($p < 0.05$), and this indicates that the decrease of SPs is more likely due to transportation of flavonoids from intracellular to cell walls rather than degradation by ROS. This is because the decreased value (0.53) of SPs from 2.49 to 1.96 is comparable with the increased value in IBPs (0.87), and the difference (0.34) is similar to the increase of total value (0.35) from 5.47 to 5.82, which might be related to the synthesis of phenolic compounds

DOI: 10.1021/jf505632p
J. Agric. Food Chem. 2015, 63, 379−381

during germination. Thus, both transportation and synthesis of flavonoids may occur at the same time during germination; further confirmation of this would benefit from more detailed study using HPLC methodology.

DPPH Radical Scavenging Ability. The DPPH radical scavenging ability of SPs and IBPs in germinated lentils is presented in Table 2. The germination process decreased the DPPH radical scavenging ability of SPs from 61.3 to 53.5%, whereas an increase from 47.1 to 76.1% was found for IBPs.

The continuous increase of total values induced by germination process was from 111.5 to 122.8%, and this increment may be associated with the synthesis of phenolic compounds during the germination process. The ratio of IBPs to SPs significantly increased by approximately 2-fold from 0.78 to 1.42. This is most likely related to the enhancement of IBPs, possibly due to transportation of SPs into cell wall as discussed in the case of total flavonoids.

ABTS Radical Cation Scavenging Ability. The ABTS radical cation scavenging ability of SPs and IBPs of germinated lentils is shown in Table 2. Enhancement of ABTS radical cation scavenging ability of IBPs was observed in germinated lentils compared to the control (from 48.2 to 65.3%); a decreasing trend was found in SPs from 63.3 to 57.6% during 4 days of germination. A moderate increase in the total and ratio of IBPs to SPs was found in germinated lentils from 111.5 to 122.8% and from 0.76 to 1.13, respectively. The reason for this change may be the same as that discussed for TPC, TFC, and DPPH results.

In short, a novel indicator, the ratio of IBPs to SPs, was proposed for the reasoning on the alteration of phenolic formation in lentils during the germination process. In all measurements tested, the ratio showed increasing trends, allowing speculation such as transportation of phenolic compounds from vacuole into cell wall followed transformation into insoluble bound phenolics by forming covalent bond with insoluble macromolecules. Although only one type of processing was given in this study, the ratio can be applied to many other types of process-induced phenolic changes in foods for the fundamental reasoning.

JuDong Yeo
Fereidoon Shahidi*

Department of Biochemistry, Memorial University of Newfoundland, St. John's, Newfoundland, Canada A1B 3X9

AUTHOR INFORMATION

Corresponding Author

*(F.S.) Phone: (709) 864-8552. E-mail: fshahidi@gmail.com.

Funding

We are grateful to the Natural Science and Engineering Council (NSERC) of Canada in the form of a Discovery Grant to FS.

Notes

The authors declare no competing financial interest.

REFERENCES

(1) Adsule, R. N. Lentil (*Lens culinaris* Medik.). In *Food and Feed from Legumes and Oilseeds*; Nwoloko, E., Smartt, J., Eds.; Chapman & Hall: Boca Raton, FL, USA, 1996; pp 84−110.

(2) Agriculture & Agri-Food Canada. Lentils: Situation and outlook; http://www.agr.gc.ca.

(3) Apel, K.; Hirt, H. Reactive oxygen species: metabolism, oxidative stress, and signal transduction. *Plant Biol. Annu. Rev.* **2004**, *55*, 373−399.

(4) Świeca, M.; Baraniak, B. Nutritional and antioxidant potential of lentil sprouts affected by elicitation with temperature stress. *J. Agric. Food Chem.* **2014**, *62*, 3306−3313.

(5) Agati, G.; Azzarello, E.; Pollastri, S.; Tattini, M. Flavonoids as antioxidants in plants: location and functional significance. *Plant Sci.* **2012**, *196*, 67−76.

(6) Wettasinghe, M.; Shahidi, F. Antioxidant and free radical-scavenging properties of ethanolic extracts of defatted borage (*Borago officinalis* L.) seeds. *Food Chem.* **1999**, *67*, 399−414.

(7) Naczk, M.; Shahidi, F. The effect of methanol-ammonia-water treatment on the content of phenolic acids of canola. *Food Chem.* **1989**, *31*, 159−164.

(8) Singleton, V. L.; Rossi, J. A. Colorimetry of total phenolics with phosphomolybdic-phosphotungstic acid reagents. *Am. J. Enol. Vitic.* **1965**, *16*, 144−158.

(9) Chandrasekara, A.; Shahidi, F. The content of insoluble bound phenolics in millets and their contribution to antioxidant capacity. *J. Agric. Food Chem.* **2010**, *58*, 6706−6714.

(10) Sekhon-Loodu, S.; Warnakulasuriya, S. N.; Rupasinghe, H. P. V.; Shahidi, F. Antioxidant ability of fractionated apple peel phenolics to inhibit fish oxidation. *Food Chem.* **2013**, *140*, 189−196.

(11) Miller, N. J.; Rice-Evans, C. A. The relative contributions of ascorbic acid and phenolic antioxidants to the total antioxidant activity of orange and apple fruit juices and blackcurrant drink. *Food Chem.* **1997**, *60*, 331−337.

(12) Cevallos-Casals, B. A.; Cisneros-Zevallos, L. Impact of germination on phenolic content and antioxidant activity of 13 edible seed species. *Food Chem.* **2010**, *119*, 1485−1490.

(13) Nohl, H.; Gille, L.; Kozlov, A. V. Antioxidant-derived prooxidant formation from ubiquinol. *Free Radical Biol. Med.* **1998**, *25*, 666−675.

(14) Chance, B.; Sies, H.; Boveris, A. Hydrogen peroxide metabolism in mammalian organs. *Physiol. Rev.* **1979**, *59*, 527−593.

(15) Strack, D.; Heilemann, J.; Mömken, M.; Wray, V. Cell wall-conjugated phenolics from Coniferae leaves. *Phytochemistry* **1988**, *27*, 3517−3521.

(16) Markham, K. R.; Ryan, K. G.; Gould, K. S.; Richards, G. K. Cell wall sited flavonoids in lisianthus flower petals. *Phytochemistry* **2000**, *54*, 681−687.

(17) McLusky, S. R.; Bennet, M. H.; Beale, M. H.; Lewis, M. J.; Gaskin, P.; Mansfield, J. W. Cell wall alterations and localized accumulation of feruoyl-3′-methoxytyramine in onion epidermis at sites of attempted penetration of *Botrytis allii* are associated with actin polarization, peroxidase activity and suppression of flavonoid biosynthesis. *Plant J.* **1999**, *17*, 523−534.

(18) Meyer, D.; Pajonk, S.; Micali, C.; O'Connell, R.; Schulze-Lefert, P. Extracellular transport and integration of plant secretory proteins into pathogen-induced cell wall compartments. *Plant J.* **2009**, *57*, 986−999.

DOI: 10.1021/jf505632p
J. Agric. Food Chem. 2015, 63, 379−381

JOURNAL OF AGRICULTURAL AND FOOD CHEMISTRY

Article

pubs.acs.org/JAFC

Uptake and Accumulation of Bulk and Nanosized Cerium Oxide Particles and Ionic Cerium by Radish (*Raphanus sativus* L.)

Weilan Zhang,[†,⊥] Stephen D. Ebbs,[‡] Craig Musante,[§] Jason C. White,[§] Cunmei Gao,[†,#] and Xingmao Ma*[,†]

[†]Department of Civil and Environmental Engineering and [‡]Department of Plant Biology and Center for Ecology, Southern Illinois University, Carbondale, Illinois 62901, United States

[§]Department of Analytical Chemistry, The Connecticut Agricultural Experiment Station, 123 Huntington Street, New Haven, Connecticut 06504, United States

[#]College of Marine Sciences, Shanghai Ocean University, Shanghai 201306, China

Supporting Information

ABSTRACT: The potential toxicity and accumulation of engineered nanomaterials (ENMs) in agricultural crops has become an area of great concern and intense investigation. Interestingly, although below-ground vegetables are most likely to accumulate the highest concentrations of ENMs, little work has been done investigating the potential uptake and accumulation of ENMs for this plant group. The overall objective of this study was to evaluate how different forms of cerium (bulk cerium oxide, cerium oxide nanoparticles, and the cerium ion) affected the growth of radish (*Raphanus sativus* L.) and accumulation of cerium in radish tissues. Ionic cerium (Ce^{3+}) had a negative effect on radish growth at 10 mg $CeCl_3$/L, whereas bulk cerium oxide (CeO_2) enhanced plant biomass at the same concentration. Treatment with 10 mg/L cerium oxide nanoparticles (CeO_2 NPs) had no significant effect on radish growth. Exposure to all forms of cerium resulted in the accumulation of this element in radish tissues, including the edible storage root. However, the accumulation patterns and their effect on plant growth and physiological processes varied with the characteristics of cerium. This study provides a critical frame of reference on the effects of CeO_2 NPs versus their bulk and ionic counterparts on radish growth.

KEYWORDS: *cerium oxide, nanomaterials, nanoparticles, radish, phytotoxicity, plant uptake*

INTRODUCTION

Nanotechnology is a rapidly expanding global industry. Engineered nanomaterials (ENMs) with their size smaller than 100 nm in at least two dimensions are increasingly found in commercial products. Due to their small size and large specific surface area, ENMs exhibit novel and different physical, chemical, and biological properties from their bulk or ionic counterparts. These unique properties provide new opportunities to fight diseases, enhance energy efficiency, and improve the environment.[1−3]

Although the synthesis of ENMs adds desirable physical and/or chemical properties over the bulk or ionic forms, the potential environmental health and safety implications of ENM use have become a serious concern. Previous research has shown that some ENMs used in consumer products are released into the environment, and many of these materials are detected in wastewater streams.[4−6] As one of the most commonly employed nanomaterials, cerium oxide nanoparticles (CeO_2 NPs) have attracted great attention. The potential toxicity of CeO_2 NPs (6−40 nm, unmodified) to bacteria, fish, and mammalian cells has been reported.[7,8] Plants play a critical role in maintaining ecosystem health and function and as a food source for humans. Plant uptake of ENMs represents an important pathway for human exposure to these nanoparticles through food consumption.[9] Consequently, investigation of the uptake and accumulation of ENMs by agricultural crops is not only warranted but also critical to food safety and human health. However, there are only a small number of studies in the literature that have addressed the interactions of CeO_2 NPs with terrestrial plants.[10−16] In one study, Wang et al.[10] found that uncoated CeO_2 NPs (<25 nm) at 0.1−10 mg/L had a slightly positive effect on tomato (*Solanum lycopersicum* L.) growth and yield (e.g., increased production of tomato fruit at 10 mg/L). However, cerium was reportedly transported from roots to shoots and accumulated in edible tissues, although the chemical form of Ce was not determined. These authors further investigated the transgenerational effect of CeO_2 NPs and found that second-generation seedlings grown with seeds from parental plants treated with 10 mg/L CeO_2 NPs were significantly smaller and accumulated more cerium as compared to seedlings generated from control plants.[11] Ma et al.[12] studied how rare earth oxide NPs affected root elongation and found that bare CeO_2 NPs with an average diameter of 7.2 ± 0.7 nm had no effects on rape (*Brassica napus* L.), radish (*Raphanus sativus* L.), wheat (*Triticum aestivum* L.), cabbage (*Brassica oleracea* L.), tomato (*Lycopersicon esculentum* L.), and cucumber (*Cucumis sativus* L.) at 2000 mg/L. Rico et al.[13] demonstrated that exposing rice seedlings to bare CeO_2 NPs with an average size of 231 ± 16 nm up to 500 mg/L for 10 days caused no visible signs of toxicity. However, CeO_2 NPs induced a

Received: June 18, 2014
Accepted: December 22, 2014
Published: December 22, 2014

ACS Publications © 2014 American Chemical Society

DOI: 10.1021/jf5052442
J. Agric. Food Chem. 2015, 63, 382−390

concentration-dependent modification of the oxidative stress and antioxidant defense system in the rice seedlings. Several studies have reported the uptake and accumulation of CeO_2 NPs by agricultural crops. For instance, Zhang and colleagues[14] showed that 7 and 25 nm bare CeO_2 NPs were detected in cucumber tissues, but the transport of cerium from roots to shoots was limited. Zhao et al.[15] investigated the effects of bare and alginate-coated CeO_2 NPs on corn plants and reported that surface coating and soil organic matter could promote the translocation of cerium in higher plants. A recent study demonstrated that intact CeO_2 NPs (7 nm) were taken up by soybean roots.[16] In summary, CeO_2 NPs can be taken up by plants and accumulated in plant tissues, but the majority of the NPs appeared to remain in the root tissues, raising concerns on the heightened accumulation of ENMs by root vegetables.[17]

Interestingly, even though the edible tissues of below-ground vegetables often have direct contact with soilborne ENMs and present the highest potential for ENM accumulation in food crops, little attention has been paid to this important group of food plants. In this study, radish (*R. sativus* L.) was adopted as a model plant in that it is a popular vegetable with high global consumption. In addition, radishes mature rapidly in full sun and light and can be harvested in 3−4 weeks, making it an ideal plant to study the fate and impact of environmental chemicals on the development of below-ground vegetables. The objectives of this study were twofold: (1) How does cerium in different chemical forms (e.g., ionic cerium vs cerium particles) and physical sizes affect the growth of radish? (2) How extensively and differently will the radish tissues take up and accumulate cerium in different forms and sizes? With these two objectives, we aimed to fill some of the current knowledge gap on the possible differential accumulation of cerium with different forms and particle sizes by plants. Even though detailed studies on the cerium effect of essential physiological and biochemical processes are not the concern of this study, their interactions are important for mechanistic understanding of the interactions of plants and nanoparticles and warrant further investigations.

MATERIALS AND METHODS

Chemicals. Dispersions of CeO_2 NPs (10 wt % in H_2O) and cerium chloride powder were purchased from Sigma-Aldrich (St. Louis, MO, USA). The bulk powder of CeO_2 was obtained from Strem Chemicals, Inc. (Newburyport, MA, USA). Hoagland solution (one-fourth strength) was prepared by dissolving an appropriate amount of the modified Hoagland basal salt mixture (Phytotechnology Laboratories, Lenexa, KS, USA) with deionized water. The size and morphology of CeO_2 NPs and the bulk suspensions were characterized by transmission electron microscopy (TEM). The hydrodynamic size and zeta potential of CeO_2 NPs in one-fourth strength Hoagland solution were measured with a dynamic light scattering instrument (Malvern Zetasizer Nano-ZS90, NY, USA).

Seed Germination and Growth Conditions. The radish seeds [Cherriette (F1)] were obtained from Johnny's Selected Seeds (Winslow, ME, USA). Seeds were surface sterilized with 1.25% sodium hypochlorite solution for 10 min and then rinsed with deionized water three times. The sterilized seeds were germinated on moist filter paper in a Petri dish for 7 days. Healthy young seedlings of similar size (7.5−8 cm in height from the root tip to the tip of cotyledons) and stage of development were transferred to 50 mL polypropylene centrifuge tubes containing one-fourth strength Hoagland solution and were incubated in a growth cart with a 16 h light/8 h dark cycle (28 °C) to allow the seedlings to further develop. The growth cart was equipped with four T5 fluorescent tubes, providing a light intensity of approximately 104 μmol m^{-2} s^{-1} of visible light (400−700 nm) at the height of plant leaves. After 7 days, the seedlings were transferred from the centrifuge tubes to 100 mL glass jars containing 10 mg/L of bulk or nanosized cerium oxide (CeO_2) or cerium chloride ($CeCl_3$). Each jar had a floating lid made by Hareline 2 mm thin fly foam (Fishwest, Sandy, UT, USA) so that the plant roots were constantly submerged in the treatment solutions. Due to the scarcity of information on the potential adsorption of cerium on foam surface, it was assumed that the potential impact of foam on cerium bioavailability was insignificant in this study. Four treatments were prepared, all in one-fourth strength Hoagland solution: (1) control (no cerium treatment); (2) 10 mg/L CeO_2 NPs; (3) 10 mg/L CeO_2 bulk; and (4) 10 mg/L $CeCl_3$. The concentration of 10 mg/L was chosen because this value is considered environmentally relevant[18] and our previous studies also showed that CeO_2 NPs at this concentration slightly enhanced plant growth.[10,11] Each treatment had 12 replicates. The solutions in the jars were replenished every other day with the same treatment solution to compensate for evapotranspiration, with the assumption that Ce would be taken up concurrently with water by plants. However, if plants preferably take up water, it is possible that cerium would accumulate in the growing solution. Plants were harvested 35 days after germination (i.e., 21 days after treatment). Additionally, a separate set of radish plants were grown and treated exactly as above. The harvested tissues from these plants were used to determine the distribution of cerium across the fine root tips and storage roots microscopically (see below for details).

Plant Physiological Responses. For the first batch of plants, daily transpiration rate was recorded for each seedling after it was transferred to 100 mL glass jars by measuring the water surface drop before the solution replenishment. The cumulative transpiration of each treatment was then calculated by summing the daily transpiration over the 21 day treatment period. Relative chlorophyll content was measured with a SPAD 502 Plus Chlorophyll Meter (Spectrum Technologies, Inc. Aurora, IL, USA) 1 day prior to harvest and was expressed as a percent of control. An OS 1p chlorophyll fluorometer (Opti-sciences, Inc., Hudson, NH, USA) was used to measure the yield of quantum efficiency of PSII (light-adapted Y(II)) and the photochemical efficiency of PSII (dark-adapted F_V/F_M) on the same day the relative chlorophyll was measured. Five of the 12 replicates from each treatment were used in a leakage test to assess root membrane integrity. The leakage test followed the published procedures with some modifications.[19] Briefly, the entire fine root system was submerged in 50 mL of deionized water and the initial conductivity C_w was measured immediately (Orion ROSS Ultra pH/ATC Triode Orion Star A325 Thermo Fisher Scientific, Waltham, MA, USA). The conductivity of the solution was measured again as C_0 after 3 h of incubation at room temperature. The entire fine roots were then autoclaved at 121 °C for 20 min with a Tuttnauer Brinkman 3850 M autoclave to release all electrolytes. The final conductivity C_t was measured after the samples cooled to room temperature. The percentage of electrolyte leakage was calculated as $EL = (C_0 - C_w)/(C_t - C_w) \times 100$.

Uptake, Accumulation, and Distribution of Cerium. At harvest, radish plants were separated into fine roots, storage roots (the edible radish bulb), and shoots. The tissues were then dried in an oven at 75 °C for 7 days and their dry weights determined. For each treatment, the 12 storage roots and 12 shoot tissues were divided into four groups, respectively. The shoot and storage root tissues in each group were then ground together into fine powders, from which 0.25 g of the ground tissues was weighed and digested in 4 mL of 70% nitric acid and swirled to mix. For the fine roots, the remaining seven replicates (five replicates used for the electrolyte leakage test were excluded) were divided into three groups, and each group contained either two or three of the fine root systems. Due to the smaller biomass of the fine roots, all ground tissues from each group were used for the digestion. The nitric acid digest was heated at 95 °C for 20 min and then at 45 °C for 4 min, and the cycle was repeated five times until all of the dry tissues were dissolved. Afterward, 2 mL of hydrogen peroxide was added to the mixture and heated using the same temperature cycle until the solution was clear. The digest solution was

DOI: 10.1021/jf5052442
J. Agric. Food Chem. 2015, 63, 382−390

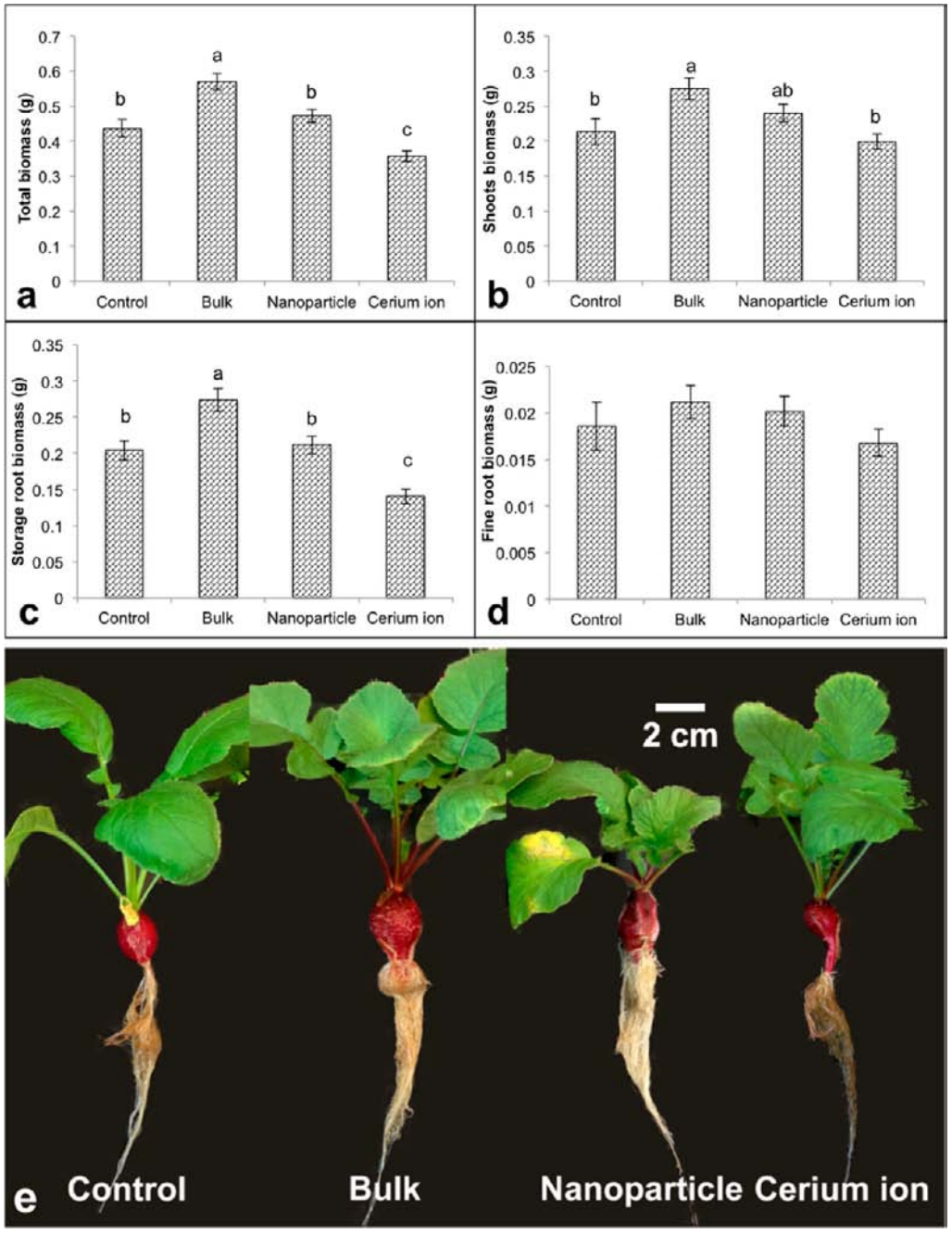

Figure 1. Dry biomass of total radish and different radish tissues treated with 10 mg/L of different forms of cerium (a–d). The reported values are the mean of 12 replicates, and the error bars represent standard error. Different letters represent significant differences between the treatments ($p < 0.05$). (e) Images of typical radish plants from the different treatments.

then analyzed by inductively coupled plasma–mass spectrometry (ICP-MS) to obtain the concentration of cerium in each sample.

The radish roots used to determine the localization and distribution of cerium in their fine roots and storage roots were harvested at day 21 after treatment. To obtain a reference for the anatomy of the radish storage root, a cross section of the radish storage root taken at the equator was cut with a razor blade and observed under a Kruss MBL3000 light microscope (A.KRÜSS Optronic, Hamburg, Germany) (Supporting Information, Supplementary Figure 1). The radish fine root tips and sections of the storage roots from each treatment were also examined using a Zeiss LSM 510 META confocal microscope. A laser excitation wavelength of 543 nm was used, and an emission filter band-pass was set between 530 and 590 nm to collect both the laser reflection and autofluorescence in this region. To image the storage root, the root was first cut in half horizontally from the thickest point, and then a thin slice (~1 mm) of the storage root was cut from the bottom half of the storage root. That slice was then divided into four pieces and one of the pieces was randomly selected to determine the radial distribution of cerium toward the midpoint of the storage root. A schematic illustration of the slices preparation is shown in Supplementary Figure 1 in the Supporting Information. For each sample, a serial scanning along the z-axis of the sample was conducted, and the numbers of scanning planes varied from 8 to 11. The distance between two optical planes was approximately 10.2 μm.

Data Analysis. A one-way ANOVA was performed in this study for data analysis. The Duncan test was conducted for post hoc comparisons.

DOI: 10.1021/jf5052442
J. Agric. Food Chem. 2015, 63, 382–390

RESULTS

Characterization of CeO_2 NPs and the Bulk. Supplementary Figure 2 in the Supporting Information shows the TEM images of CeO_2 NPs and bulk CeO_2 in one-fourth strength Hoagland solution. The nanoparticles displayed variable shapes and sizes. Individual nanoparticles possessed triangular, rectangular, and other irregular shapes. The images indicate that the average diameter of individual CeO_2 NPs ranged from 10 to 30 nm. The nanoparticles aggregated considerably in the Hoagland solution, due to the high ionic strength. The hydrodynamic diameter of the nanoparticle aggregates was ~600 nm as measured by DLS. The zeta potential of CeO_2 NPs in the Hoagland solution was approximately −11.9 mV, suggesting that the nanoparticles were not stable. Bulk CeO_2 NPs were mostly at the micrometer scale, but the sizes were not uniform. Particles at the nanoscale were also detected in the bulk solutions. The sizes of bulk CeO_2 NPs ranged approximately from 100 to 4000 nm.

Plant Physiological Status. The radish exposed to CeO_2 bulk had the highest total dry biomass, which was significantly greater than all other treatments (Figure 1a). The biomass of the nanoparticle treated plants was not significantly different from the control plants. The plant biomass exposed to cerium ions was significantly lower than that of all other treatments. When the plant tissues were examined separately, the bulk cerium treated radishes, which had similar shoot biomasses as CeO_2 NPs treated radishes, had significantly higher dry shoot biomass than control and cerium ion treatment (Figure 1b). The dry weight of storage roots across the treatments exhibited patterns similar to those of the total dry biomass (Figure 1c), but the dry biomass of fine roots did not differ significantly as a function of treatment (Figure 1d). In addition to the total biomass, the distribution of the biomass between the root (fine + storage root) and shoot compartments was significantly different in response to treatment. The shoot/root ratio of dry biomass of cerium ion treated radish (1.34 ± 0.11) was significantly higher ($p < 0.05$) than all other treatments, which had similar ratios (control, 1.00 ± 0.10; bulk CeO_2, 0.95 ± 0.06; CeO_2 NPs, 1.07 ± 0.07). Visually, there was no apparent adverse effect of any of the cerium treatments on the growth and development of the radish plants except for the size differences (Figure 1e).

In addition to the root biomass, the fine root membrane integrity was significantly affected by different forms of cerium. Figure 2 indicates that 10 mg/L of CeO_2 NPs and ionic cerium resulted in significantly greater electrolyte leakage when compared to the control roots. Leakage from bulk cerium treated roots was not significantly different from control roots. The accumulative transpiration of radish for all treatments was comparable until day 21, then the accumulative transpiration of cerium ion treated radish became significantly lower than for other treatment groups (Supporting Information, Supplementary Figure 3). The relative chlorophyll content expressed in percentage is shown in Table 1. Although all treated radishes had lower chlorophyll content, only the bulk CeO_2 and CeO_2 NPs treated leaves had significantly lower chlorophyll content compared to the controls. The average quantum yield of photosystem II (Y(II)) and the F_V/F_M ratio for plants from different treatments are also shown in Table 1. The results indicated that the Y(II) was unaffected by the treatments. In contrast, only bulk CeO_2 treated radishes displayed an F_V/F_M ratio significantly lower value than the control. No significant differences were observed between the other cerium treatments.

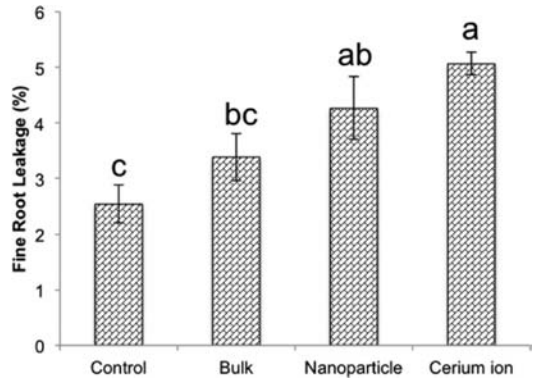

Figure 2. Electrolyte leakage from radish fine roots grown hydroponically in different solutions. The reported values are the average of five replicates in each treatment, and the error bars represent standard error. Different letters represent significant differences between the treatments ($p < 0.05$).

Cerium Uptake and Accumulation. Not surprisingly, exposure to cerium resulted in significantly greater concentrations of this element in plant tissues. For the treated plants, the cerium concentration and content were significantly higher in the fine roots than in other tissues (Figure 3). Among different treatments, the concentration of cerium in the storage root was not significantly different between cerium treatments (Figure 3A). In the shoot tissues, cerium ion treated radish had highest cerium concentration, followed by bulk cerium and then CeO_2 NPs treated radish (Figure 3A). The fine roots of CeO_2 NPs treated radish had significantly higher concentration of cerium than the bulk and ion treated radish (Figure 3B). When the cerium content rather than the concentration in different tissues was compared, cerium content in the storage roots of different treatments was still similar. The shoot cerium content of bulk and ion treated radishes was not significantly different but was markedly higher than that of nanoparticle treated radishes (Figure 3D). In the fine roots, the cerium content demonstrated patterns similar to the cerium concentration for different treatments (Figure 3D).

Cerium Localization and Distribution in Radish Root and Storage Root. For the fine root tips, the confocal microscopic images were captured both on the surface and at different depths from the surface. The control had some weak signals either from the cerium content in control tissues or from background excitation (Figure 4a). In contrast, plant roots from treated plants all generated stronger signals (Figure 4b–f). However, the signal patterns were noticeably different. On the bulk CeO_2 treated root, the signals were only detected from the mucilage surrounding the root tip in both surface and deeper scanning images (Figure 4b,c). CeO_2 NPs were detected on larger areas of the root surface as well as the mucilage on the root tip of the nanoparticle treated plants (Figure 4d). The signal was even more prominent in the deeper scanning planes (Figure 4e). For cerium ion treated radish root, the signals were predominantly detected in the surrounding areas. Neither the surface scan nor the deep scan detected significantly stronger signals than the controls within the root itself (Figure 4f).

Figure 5 shows the confocal images of cut slices of radish storage roots. The control storage root showed little signal (Figure 5a). In comparison, storage roots from treated plants had strong signals. For bulk CeO_2 treated radish, all signals

DOI: 10.1021/jf5052442
J. Agric. Food Chem. 2015, 63, 382−390

Table 1. Relative Chlorophyll Content Expressed as a Percentage of Control of Each Treatment, Average $Y(II)$, and F_V/F_M Ratio, $n = 12$[a]

treatment	relative chlorophyll (%)	standard error	$Y(II)$	standard error	F_V/F_M	standard error
control	100.00 a	2.67	0.774	0.007	0.830 a	0.003
bulk	87.22 b	3.84	0.728	0.022	0.757 b	0.026
nanoparticle	83.69 b	4.24	0.731	0.020	0.780 ab	0.016
cerium ion	91.51 ab	4.68	0.697	0.060	0.797 ab	0.020

[a]Different letters in the table represent significant differences between treatments ($p < 0.05$).

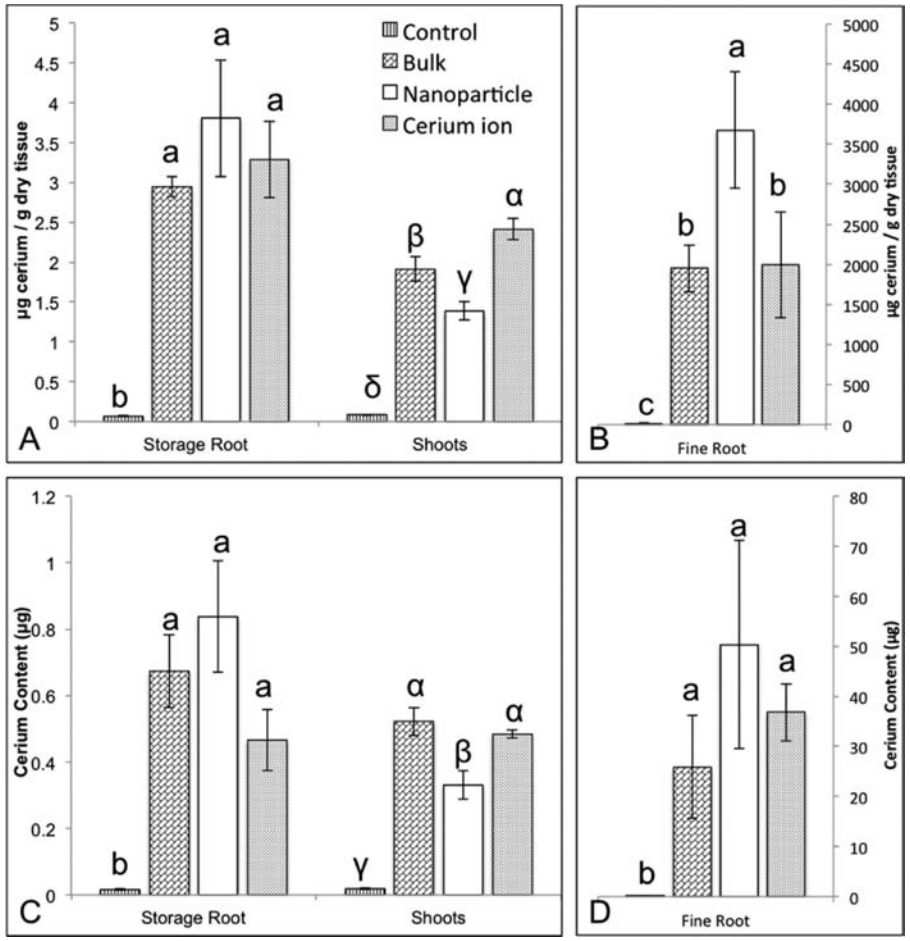

Figure 3. Cerium concentration (A, B) and mass (C, D) in different radish tissues. The reported values in panels A and C are the average of four measurements. The reported values in panels B and D are the average of two or three measurements. Errors bars represent standard error. Letters above bars reflect their statistical grouping. Different letters and Greek symbols represent significant differences between the treatments ($p < 0.05$).

came from the pigmented periderm with a random pattern (Figure 5b). For CeO_2 NPs treated radish, stronger signals were observed in the pigmented periderm. In addition, the nanoparticles appeared to penetrate further into the storage root (Figure 5c). Cerium was detected not only in the periderm but also in the secondary vascular tissues in the storage root of cerium ion treated radish (Figure 5d,e).

DISCUSSION

Accompanying the ever-expanding applications of engineered nanomaterials are the increasing concerns about their toxicity to humans and the environment. A major question scientists are trying to ascertain is whether the reduction of microsized particles to nanosized particles will significantly increase their toxicity. Several previous studies have shown that nanoparticles typically exhibit stronger effects on plants than their bulk counterparts.[20,21] For example, following a 15 day hydroponic exposure, the biomass of zucchini plant exposed to silver nanoparticles was 75% less than that of plants treated with the same concentrations of bulk silver powder.[21] For CeO_2 particles, it is well accepted that the presence of highly mobile lattice oxygen on the surface will cause oxygen vacancy on the surface.[22] With the decrease of nanoparticle size, the specific surface area and consequently the density of the oxygen vacancy increase. The separation of oxygen from the lattice structure generates electrons, which can be used to reduce Ce^{4+} to Ce^{3+}. With increasing oxygen vacancy, the ratio of Ce^{3+}/Ce^{4+} will increase on the surface of nanoparticles.[23] Because Ce^{3+} is about 14% larger than Ce^{4+},[22] the conversion of Ce^{4+} to Ce^{3+} will strain the lattice structure and increase the reactivity and uperoxide dismutase (SOD) mimetic activity of the CeO_2 particles.[24] Therefore, particle size is an important consid-

DOI: 10.1021/jf5052442
J. Agric. Food Chem. 2015, 63, 382−390

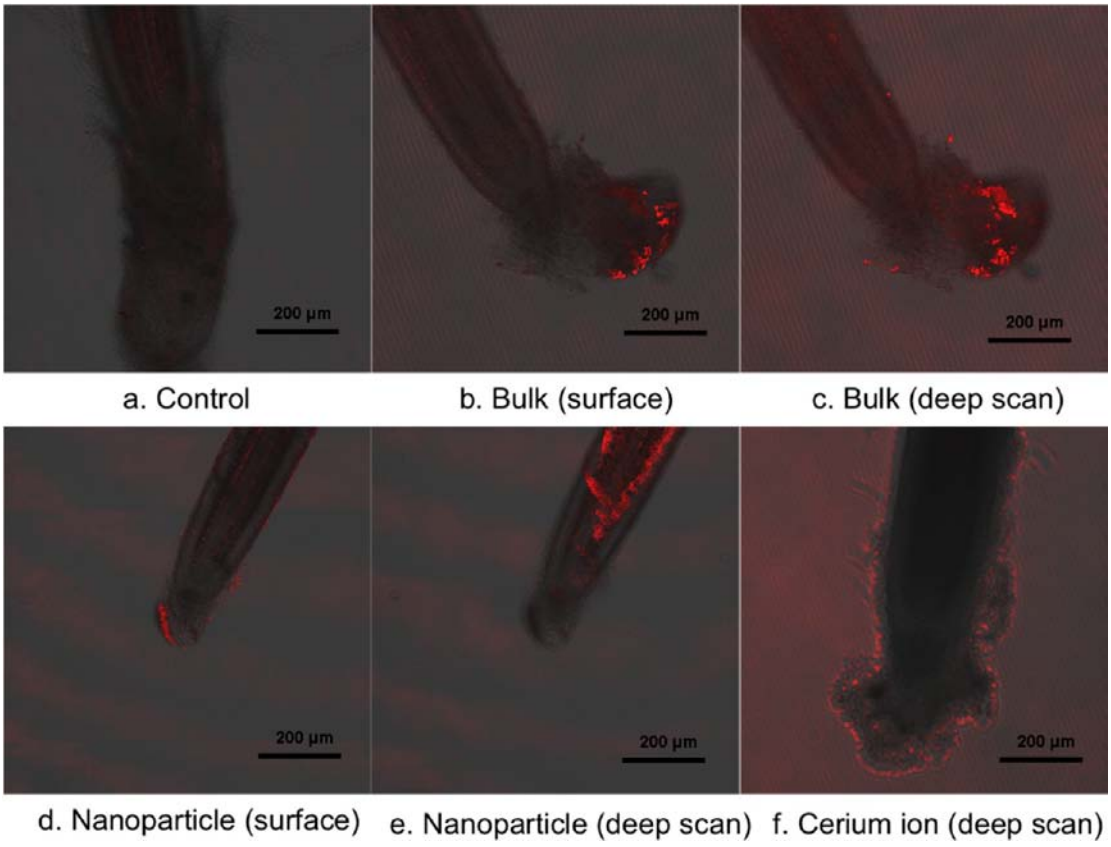

Figure 4. Confocal microscopic images depicting the accumulation of cerium in the fine roots of radish: (a) control root showing weak signals; (b, c) surface and representative deeper scan of fine roots treated by bulk CeO_2; (d, e) surface and representative deeper scan of fine roots exposed to CeO_2 NPs; (f) deeper scan image of fine roots exposed to cerium ion. The deeper scan images shown were selected from a stack of deep scan images for different roots.

eration in the assessment of the environmental toxicity of CeO_2. Unfortunately, information on the size effect of CeO_2 particles on plant development in the literature is very limited.

Due to the potential dissolution of some metallic nanoparticles, another major question actively investigated in the scientific community of nanotoxicology is the comparative toxicity of nanoparticles and the ionic form of the particles. Because of the general acceptance that CeO_2 NPs are stable in liquid solutions, ionic cerium was generally not included in the treatment paradigms.[13−16] However, the broad applications of different forms and sizes of cerium require a comprehensive understanding and comparison of their fate and phytotoxicity. Our investigation provides an assessment of the differential fate and phytotoxicity of cerium in its ionic, nanoscale, and bulk particle forms. Several physiological parameters including the root membrane integrity photosynthesis-related measurements, and biomass parameters were affected by certain forms of cerium at the tested concentration.

Whereas the specific mechanisms by which cerium compounds may compromise membrane integrity are not known and may differ, all forms and sizes of cerium resulted in some damage to root membrane integrity as indicated by an increase in electrolyte leakage. However, the effect was significant only for the nanoparticle and ionic forms. The changes in the integrity of root membrane could also alter the membrane potential and potentially the function of the membrane.[24] It has been reported that altered plasma membrane integrity and potential are associated with changes in the ion fluxes into plant roots.[25] Whether this alteration of membrane integrity influenced the concentration of any essential macronutrients or micronutrients in radish was not examined, but would be a reasonable question for future studies. For the bulk CeO_2 and CeO_2 NPs, in addition to their impact on the membrane, physical adsorption on root surface and blockage of nutrient uptake by plant roots may also occur. It is possible that such impacts on the roots may have affected the uptake of elements such as magnesium or iron, two nutrients associated with the synthesis of chlorophyll. A decrease in the concentration of either of these essential nutrients might have contributed to the decrease in relative chlorophyll content observed in some treatments. Other aspects of chlorophyll synthesis or degradation could have been affected as well, and a more detailed study will be required to understand the extent or severity of effects of cerium on chlorophyll metabolism. The significantly lower F_V/F_M values observed for the bulk cerium treatment as compared to the control plants suggested that photosynthetic electron transport associated with photosystem II was stressed in those plants, but not for the other cerium treatments. These results differ from a study with plantlets of *Medicago arborea* in which nanoceria was found to have a more negative effect on the F_V/F_M ratio than the same concentrations of bulk cerium.[25] Other studies have shown that the influence of cerium compounds on plant photochemistry differs depending on factors such as plant Mn status[26] and the presence of salt stress.[27] Definitive conclusions about the comparative phytotoxicity of the cerium ion and nanoceria cannot be made without further investigation. Even so, the overall effects of all treatments on the two photo-

DOI: 10.1021/jf5052442
J. Agric. Food Chem. 2015, 63, 382−390

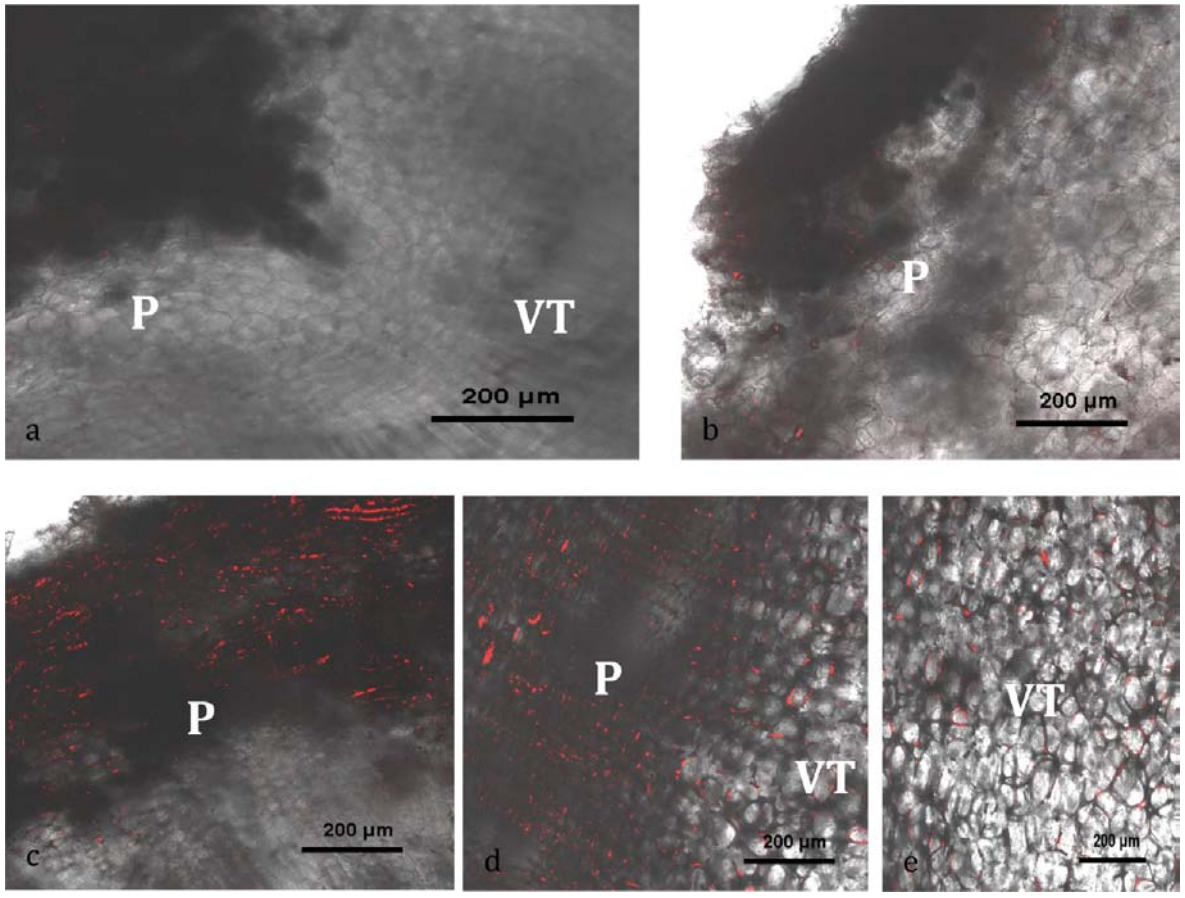

Figure 5. (a) Confocal images of the horizontal slices of radish storage root treated with different types of cerium: (a) control; (b) bulk CeO_2 treated radish; (c) CeO_2 NPs treated radish; (d, e) ionic cerium treated radish. P, periderm; VT, vascular tissues.

synthetic parameters measured were modest and perhaps not indicative of a significant stress imposed on the plants, particularly given that there were no overt visible effects observed for any treatments, including the ionic cerium and the CeO_2 NPs treatments. The only other indication of a negative effect of treatment with cerium was the decrease in biomass observed for the cerium ion treatment.

The shoot/root ratio of radish was also affected by cerium, primarily through the change of the biomass of the storage roots. Because the root thickening is a result of the combined cell division and enlargement of secondary xylem and phloem cells that depends on the activity of the vascular cambium,[28] it is possible that different forms cerium of have different impacts on the activity of the vascular cambium. One could speculate that the bulk CeO_2 might have enhanced the activity of the vascular cambium, whereas ionic Ce inhibited it. Metabolically, according to the "sink capacity" theory, the storage root represents a major reservoir for radish, and sucrose transported within radish is the main carbohydrate for the growth of sinks. As such, photosynthate distribution into different tissues is heavily affected by the activity of sucrose synthase (SuSy).[29−33] If future studies examined the expression of SuSy genes and/or measured the activity of this enzyme in the radish hypocotyl in response to different forms of cerium, it might be possible to ascertain whether the changes in the mass of the storage root in response to bulk or ionic cerium treated radish plants were due to changes in sink strength. The specific mechanisms by which these cerium compounds influence the biomass of radish storage roots have implications for the agricultural production of radish and related vegetable species and are therefore worth further attention.

It should be pointed out that the concentration of $CeCl_3$ used in this study was very low, and the impact of chloride ion is not expected to be substantial. Parida and Das[34] investigated plant salt tolerance and salinity effects on plant growth and reported that under 100 mM NaCl (3.55 g/L Cl^-), chloride demonstrated limited influence on the osmotic adjustment of cell membrane. Scialabba and Melati[35] also reported that sodium chloride up to a concentration of 0.1% positively affected radish growth. The Cl^- in the ionic cerium solution used in this study was significantly lower than those reported values and was not expected to significantly contribute to the negative effect observed in the ionic treatment group. Consequently, the negative effect observed in the ionic treatment should be attributed to the ionic cerium. Another caveat about the results is that 10 mg/L was the concentration of the compounds of CeO_2 and $CeCl_3$, not the concentration of cerium as an element. Due to the different molecular weight percentage of cerium in CeO_2 and $CeCl_3$, the actual concentration of cerium as an element was 8.14 mg Ce/L in CeO_2 NPs and the bulk and was only 5.68 mg Ce/L in the ionic form. Cerium in CeO_2 was 43.5% higher than in the ionic form. If the equivalent concentration of cerium as an element was used, the ionic cerium may display an even stronger effect on plant physiology.

In addition to the yield of edible storage root, the potential accumulation of cerium was examined. Exposed plants had detectable cerium in all plant tissues, including the edible

DOI: 10.1021/jf5052442
J. Agric. Food Chem. 2015, 63, 382−390

storage roots and leaves, even though the forms of cerium in these tissues are unknown. However, the forms of cerium in plant tissues may affect both their toxicity and potential availability to humans, and they deserve detailed investigation in future studies. In the current study, the significantly higher cerium detected in the shoot tissues of exposed plants indicated that cerium translocation from roots to shoot had occurred. The upward transport of bulk cerium to radish shoots was unexpected given the size of the particles and the low dissolution rate of bulk CeO_2. It is most likely that the cerium content detected from the bulk treated shoot tissues was from the nanoscale particles present in the bulk mixture (Supporting Information, Supplementary Figure 2). The upward transport of CeO_2 NPs and ionic cerium from roots to shoots was expected and has been reported in the literature.[10,14,35,36] Interestingly, however, when the cerium localization in the storage root was investigated with the confocal microscope, signals of cerium in the vascular tissues were observed only in cerium ion treatment, suggesting that active transport may function as an important pathway of cerium accumulation only for ion treated radishes. In contrast, signals from the CeO_2 NPs and bulk treated radish roots were mainly located on the periderms. The results suggest that adsorption and diffusion of particulate cerium along the radial direction might be a more important pathway for CeO_2 NPs and bulk accumulation in radish storage roots. The diffusion may possibly occur from the lenticels on the periderm, but more precise techniques are needed to confirm this assumption. From the food safety point of view, the cerium accumulation in the edible storage root is more concerning, and our results showed that although cerium concentration and content were similar across the cerium treatment, the distribution of cerium in the storage roots varied and, consequently, its availability to humans would vary. For example, the majority of particulate cerium accumulated in the edible tissue could be removed in the food preparation process, whereas ionic cerium in the storage roots is more likely to be consumed by humans with the storage root.

In closing, our results suggested that 10 mg/L cerium as cerium oxide or cerium chloride could affect the growth of radish and could accumulate in the edible storage root and shoot tissues. However, the impacts and accumulation patterns varied significantly by the size and chemical form of cerium. Ionic cerium displayed the strongest impact on radish root membrane integrity and growth, followed by CeO_2 NPs and then the bulk. Whereas different forms cerium of all accumulate in radish tissues, their accumulation potential and distribution patterns varied greatly. As a result, potential exposure and risk to human health through diet exposure to different sizes and forms of cerium may vary, and these differences should be considered when the food safety of cerium in the environment is evaluated.

■ ASSOCIATED CONTENT

Supporting Information

Transmission electron microscopic images of bulk CeO_2 and CeO_2 NPs, accumulative transpiration of radish plants, and anatomy of radish storage root. This material is available free of charge via the Internet at http://pubs.acs.org.

■ AUTHOR INFORMATION

Corresponding Author

*(Dr. Xingmao Ma) Present address: Zachry Department of Civil Engineering, Texas A&M University, College Station, TX 77843-3136. Phone: 979-845-3011. Fax: 979-862-1542. E-mail: xma@civil.tamu.edu.

Present Address

⊥(W.Z.) Texas A & M University, College Station, TX.

Funding

We acknowledge the financial support of the USDA-AFRI (2012-67005-19585) and USDA-AFRI (2011-67006-30181).

Notes

The authors declare no competing financial interest.

■ REFERENCES

(1) Tiede, K.; Hassellöv, M.; Breitbarth, E.; Chaudhry, Q.; Boxall, A. Considerations for environmental fate and ecotoxicity testing to support environmental risk assessments for engineered nanoparticles. *J. Chromatogr., A* **2009**, *1216* (3), 503−509.

(2) Nowack, B.; Bucheli, T. D. Occurrence, behavior and effects of nanoparticles in the environment. *Environ. Pollut.* **2007**, *150* (1), 5−22.

(3) Bystrzejewska-Piotrowska, G.; Golimowski, J.; Urban, P. L. Nanoparticles: their potential toxicity, waste and environmental management. *Waste Manage.* **2009**, *29* (9), 2587−2595.

(4) Brar, K.; Verma, M.; Tyagi, R. D.; Surampalli, R. Y. Engineered nanoparticles in wastewater and wastewater sludge − evidence and impacts. *Waste Manage.* **2010**, *30* (3), 504−520.

(5) Been, T. M.; Westerhoff, P. Nanoparticle silver released into water from commercially available sock fabrics. *Environ. Sci. Technol.* **2008**, *42* (11), 4133−4139.

(6) Limbach, L. K.; Bereiter, R.; Müller, E.; Krebs, R.; Gälli, R.; Stark, W. J. Removal of oxide nanoparticles in a model wastewater treatment plant: influence of agglomeration and surfactants on clearing efficiency. *Environ. Sci. Technol.* **2008**, *42* (15), 5828−5833.

(7) Pelletier, D. A.; Suresh, A. K.; Holton, G. A.; McKeown, C. K.; Wang, W.; Gu, B.; Mortensen, N. P.; Allison, D. P.; Joy, D. C.; Allison, M. R.; Brown, S. D.; Phelps, T. J.; Doktycz, M. J. Effects of engineered cerium oxide nanoparticles on bacterial growth and viability. *Appl. Environ. Microbiol.* **2010**, *76* (24), 7981−7989.

(8) Rosenkranz, P.; Fernández-Cruz, M. L.; Conde, E.; Ramírez-Fernández, M. B.; Flores, J. C.; Fernández, M.; Navas, J. M. Effects of cerium oxide nanoparticles to fish and mammalian cell lines: an assessment of cytotoxicity and methodology. *Toxicol. in Vitro* **2012**, *26* (6), 888−896.

(9) Zhu, H.; Han, J.; Xiao, J. Q.; Jin, Y. Uptake, translocation, and accumulation of manufactured iron oxide nanoparticles by pumpkin plants. *J. Environ. Monit.* **2008**, *10* (6), 713−717.

(10) Wang, Q.; Ma, X.; Zhang, W.; Pei, H.; Chen, Y. The impact of cerium oxide nanoparticles on tomato (*Solanum lycopersicum* L.) and its implications for food safety. *Metallomics* **2012**, *4* (10), 1105−1112.

(11) Wang, Q.; Ebbs, S. D.; Chen, Y.; Ma, X. Trans-generational impact of cerium oxide nanoparticles on tomato plants. *Metallomics* **2013**, *5* (6), 753−759.

(12) Ma, Y.; Kuang, L.; He, X.; Bai, W.; Ding, Y.; Zhang, Z.; Zhao, Y.; Chai, Z. Effects of rare earth oxide nanoparticles on root elongation of plants. *Chemosphere* **2010**, *78* (3), 273−279.

(13) Rico, C. M.; Hong, J.; Morales, M. I.; Zhao, L.; Barrios, A. C.; Zhang, J. Y.; Peralta-Videa, J. R.; Gardea-Torresdey, J. L. Effect of cerium oxide nanoparticles on rice: a study involving the antioxidant defense system and in vivo fluorescence imaging. *Environ. Sci. Technol.* **2013**, *47* (11), 5635−5642.

(14) Zhang, Z.; He, X.; Zhang, H.; Ma, Y.; Zhang, P.; Ding, Y.; Zhao, Y. Uptake and distribution of ceria nanoparticles in cucumber plants. *Metallomics* **2011**, *3* (8), 816−822.

(15) Zhao, L.; Peralta-Videa, J. R.; Varela-Ramirez, A.; Castillo-Michel, H.; Li, C.; Zhang, J.; Aguilera, R. J.; Keller, A. A.; Gardea-Torresdey, J. L. Effect of surface coating and organic matter on the uptake of CeO_2 NPs by corn plants grown in soil: insight into the uptake mechanism. *J. Hazard. Mater.* **2012**, *225*, 131−138.

(16) Lopez-Moreno, M. L.; de la Rosa, G.; Hernandez-Viezcas, J.; Castillo-Michel, H.; Botez, C.; Peralta-Videa, J. R.; Gardea-Torresdey,

DOI: 10.1021/jf5052442
J. Agric. Food Chem. 2015, 63, 382−390

J. L. Evidence of the differential biotransformation and genotoxicity of ZnO and CeO_2 nanoparticles on soybean (*Glycine max*) plants. *Environ. Sci. Technol.* **2010**, *44* (19), 7315−7320.
(17) Boxall, A.; Chaudhry, Q.; Sinclair, C.; Jones, A.; Aitken, R.; Jefferson, B.; Watts, C. *Current and Future Predicted Environmental Exposure to Engineered Nanoparticles*; Central Science Laboratory, Department of the Environment and Rural Affairs, London, UK, 2007.
(18) Sanchez-Viveros, G.; Gonzalez-Mendoza, D.; Alarcon, A.; Ferrera-Cerrato, R. Copper effects on photosynthetic activity and membrane leakage of *Azolla filiculoides* and *A. caroliniana*. *Int. J. Agric. Biol.* **2010**, *12* (3), 365−368.
(19) Feizi, H.; Moghaddam, P. R.; Shahtahmassebi, N.; Fotovat, A. Impact of bulk and nanosized titanium dioxide (TiO_2) on wheat seed germination and seedling growth. *Biol. Trace Elem. Res.* **2012**, *146* (1), 101−106.
(20) Stampoulis, D.; Sinha, S. K.; White, J. C. Assay-dependent phytotoxicity of nanoparticles to plants. *Environ. Sci. Technol.* **2009**, *43* (24), 9473−9479.
(21) Dutta, P.; Pal, S.; Seehra, M. S.; Shi, Y.; Eyring, M.; Ernst, R. D. Concentration of Ce^{3+} and oxygen vacancies in cerium oxide nanoparticles. *Chem. Mater.* **2006**, *18*, 5144−5146.
(22) Deshpande, S.; Patil, S.; Kuchibhatla, S. T.; Seal, S. Size dependency variation in lattice parameter and valency states in nanocrystalline cerium oxide. *Appl. Phys. Lett.* **2005**, *87* (13), No. 133113.
(23) Heckert, E. G.; Karakoti, A. S.; Seal, S.; Self, W. T. The role of cerium oxide state in the SOD mimetic activity of nanoceria. *Biomaterials* **2008**, *29* (18), 2705−2709.
(24) Lindberg, S.; Strid, H. Aluminium induces rapid changes in cytoplasmic pH and free calcium and potassium concentrations in root protoplast of wheat (*Triticum aestivum*). *Physiol. Plant.* **1997**, *99* (3), 405−414.
(25) Gomez-Garay, A.; Pintos, B.; Manzanera, J. A.; Lobo, C.; Villalobos, N.; Martin, L. Uptake of CeO_2 nanoparticles and its effect on growth of *Medicago arborea* in vitro plantlets. *Biol. Trace Elem. Res.* **2014**, *161*, 143−150.
(26) Qu, C.; Liu, C.; Guo, F.; Hu, C.; Ze, Y.; Li, C.; Zhou, Q.; Hong, F. Improvement of cerium on photosynthesis of maize seedlings under a combination of potassium deficiency and salt stress. *Biol. Trace Elem. Res.* **2014**, *155*, 104−113.
(27) Qu, C.; Gong, X.; Liu, C.; Hong, M.; Wang, L.; Hong, F. Effects of manganese deficiency and added cerium on photochemical efficiency of maize chloroplasts. *Biol. Trace Elem. Res.* **2012**, *146*, 94−100.
(28) Wherrett, T.; Ryan, P. R.; Delhaize, E.; Shabala, S. Effect of aluminum on membrane potential and ion fluxes at the apices of wheat roots. *Funct. Plant Biol.* **2005**, *32* (3), 199−208.
(29) Zaki, H. E. M.; Takahata, Y.; Yokoi, S. Analysis of the morphological and anatomical characteristics of roots in three radish (*Raphanus sativus*) cultivars that differ in root shape. *J. Hortic. Sci. Biotechnol.* **2012**, *87* (2), 172−178.
(30) Farrar, J. F. Regulation of shoot-root ratio is mediated by sucrose. *Plant Soil.* **1996**, *185* (1), 13−19.
(31) Rouhier, H.; Usuda, H. Spatial and temporal distribution of sucrose synthase in the radish hypocotyl in relation to thickening growth. *Plant Cell Physiol.* **2001**, *42* (6), 583−593.
(32) Usuda, H.; Demura, T.; Shimogawara, K.; Fukuda, H. Development of sink capacity of the "storage root" in a radish cultivar with a high ratio of "storage root" to shoot. *Plant Cell Physiol.* **1999**, *40* (4), 369−377.
(33) Wardlaw, I. F. The control and pattern of movement of carbohydrates in plants. *Bot. Rev.* **1968**, *34* (1), 79−105.
(34) Parida, A. K.; Das, A. B. Salt tolerance and salinity effects on plants: a review. *Ecotoxicol. Environ. Saf.* **2005**, *60* (3), 324−349.
(35) Scialabba, A.; Melati, M. R. The effect of NaCl on growth and xylem differentiation of radish seedlings. *Bot. Gaz.* **1990**, *151* (4), 516−521.
(36) Hu, X.; Ding, Z.; Chen, Y.; Wang, X.; Dai, L. Bioaccumulation of lanthanum and cerium and their effects on the growth of wheat (*Triticum aestivum* L.) seedlings. *Chemosphere* **2002**, *48* (6), 621−629.

DOI: 10.1021/jf5052442
J. Agric. Food Chem. 2015, 63, 382−390

JOURNAL OF AGRICULTURAL AND FOOD CHEMISTRY

Article

pubs.acs.org/JAFC

Combined Photo-Fenton–SBR Processes for the Treatment of Wastewater from the Citrus Processing Industry

José Guzmán,*[,†,‡] Rosa Mosteo,[†] María P. Ormad,[†] and José L. Ovelleiro[†]

[†]Department of Chemical Engineering and Environmental Technologies, University of Zaragoza, C/María de Luna 3, 50018 Zaragoza, Spain

[‡]Institute on Tropical Fruit Research, Ave 7ma no. 3005 e/30 and 32 Miramar, La Habana, Cuba

ABSTRACT: In this study, the photo-Fenton process was combined with a sequencing batch reactor (SBR) for the treatment of synthetic samples of citrus wastewater (CWW). An experimental design based on the surface response methodology was applied to assess the individual and combined effects of several operating parameters ($COD_{initial}$, Fe_3^+ concentration and H_2O_2 concentration) on the photo-Fenton treatment efficiency (DOC removal) with the aim of optimizing the process. The experimental results obtained under optimal conditions for CWW with high $COD_{initial}$ (10000 mgO_2/L) showed a partial degradation of organic matter of around of 61% (measured as DOC). Thereafter, the photo-Fenton effluent was neutralized and clarified before being subjected to the SBR reactor. The results show degradation yields up to 93% of the initial DOC removal without producing undesired side effects, using a hydraulic retention time (HRT) of 1.59 d. The final effluent contained a concentration of organic matter (measured as COD) of 120 mg O_2/L.

KEYWORDS: *citrus, wastewater, photo-Fenton, SBR*

INTRODUCTION

Citrus cultivation (mainly oranges) is a major industry and a significant economic sector in the United States, Brazil, Mexico, China, India, Iran, and most Mediterranean countries including Spain and Greece.[1] According to the Statistical Database of the Food and Agriculture Organization of the United Nations (FAOSTAT), world orange production in 2012 was estimated to be 68.2 million tons. For the fiscal year 2011, FAOSTAT estimated a citrus production of 0.27 million tons in Cuba. A high percentage of this produce (~84%) is used to manufacture products such as juice and essential oils, among others byproducts.

The citrus processing industry generates significant quantities of wastewaters, waste, and atmospheric emissions. Appropriate technology is therefore required to ensure the efficient management of all the resources involved. Citrus processing plants require large amounts of water and consequently produce large volumes of wastewater,[2] generating around 1.96 m^3 of wastewater/t of fruit.

Citrus wastewater derives from the production of citrus juice, the extraction of essential oils as byproduct, and the cleaning operations of equipment and industrial installations.[3] The organic load of this effluent can reach 26000 mgO_2/L (measured as COD) and suspended solids (TSS) 700−1000 mg/L. Furthermore, they usually present high conductivity and an acidic pH. The organic matter present in the effluent is composed by carbohydrates, organic acids, pectin, cellulose, hemicellulose, proteins, and traces of essential oils, which are inhibitors and toxics of biological treatments (the main process used to treat these effluents). The toxicity of citrus wastewater can be due to the high concentration of organic compounds, including the terpenes, the major constituents of essential oils.[4] The most important terpene present in essential oil from citrus is *R*-(+)limonene (90% of the total) and is found in high concentrations in actual industrial effluents. It is known that values of 0.008% (v/v) *R*-(+)limonene are toxic and have an inhibitory effect.[5]

The processes commonly used to treat this wastewater are biological processes such as activated sludge treatment. The main difficulties in the implementation of these processes are associated with space required, high hydraulic retention times, and the economic costs due to the high demand for energy in the process of aeration if the process is aerobic. Moreover, as in other food industries,[6] the majority of these treatments operate unsatisfactorily because of seasonal variability, the composition, and the high organic matter concentration of these effluents.

Previous studies carried out by our research group with citrus wastewater show that when the activated sludge process is directly fed with citrus effluents containing a concentration of organic matter higher than 2150 mg O_2/L, the proliferation of filamentous bacteria appears within a few hours. This growth produces undesirable side effects such as foams and bulking phenomena, which interfere with the treatment efficiency. These operational problems are very common in food industry plants, given the high content of colloidal and dissolved organic matter of low molecular weight which is easily biodegradable and which creates a situation of nutritional stress that leads to bulking.[7]

A possible alternative could be the application of advanced oxidation processes (AOPs) as a pretreatment in order to produce a partial degradation of the organic matter and to decrease the concentration of inhibitor compounds in aerobic biological treatments. In recent years, AOPs have been used to treat refractory wastewaters because they are effective for the

Received: July 10, 2014
Accepted: December 22, 2014
Published: December 22, 2014

ACS Publications © 2014 American Chemical Society

DOI: 10.1021/jf505377a
J. Agric. Food Chem. 2015, 63, 391−397

degradation of most of the pollutants.[8] However, there are few references to the treatment of effluents generated in citrus industries with advanced oxidation processes. Caudo et al.[9] tested copper-pillared clays in wet hydrogen peroxide catalysts oxidation of citrus wastewaters. After 4 h of oxidation reaction, the total organic carbon (TOC) decreased 50% and the biodegradability of the effluent (BOD_5/COD) increased from 0.05 to 0.4.

Among the different AOPs, the Fenton process is a promising alternative wastewater treatment. The Fenton oxidation process is based on the use of a combination of hydrogen peroxide and ferrous ion to form active hydroxyl radicals in acidic solutions.[10] This technique is highly effective for removing organic substances and color from wastewater.[11] In the photo-Fenton process (FF), additional reactions occur in the presence of light that produce hydroxyl radicals or increase the production rate of hydroxyl radicals,[12] thus increasing the efficiency of the process.

The combination of photo-Fenton processes and biological treatments for wastewater decontamination has attracted more attention in recent years as a result of various studies.[13] The photo-Fenton process is usually applied as a pretreatment to increase biodegradability and/or to decrease concentration of organic matter in order to improve the degradation of effluents by a biological process. Previous studies carried out by our research group[6,14,15] show that the application of photo-Fenton−biological processes is appropriate for the treatment of effluents in the wine industry.

The sequencing batch reactor (SBR), based on the principles of the activated sludge process, is typically used in combined systems owing to its simplicity, flexibility of operation, small floor space requirements, and good removal efficiency.[16] The SBR operation treatment cycle can be divided into the following five stages: filling, reaction, settling, decantation, and idle. All these stages occur in a single reactor.[17] In addition, the hydraulic retention time (HRT) can be adjusted by varying the decanted volumes after a settling period.[18]

In recent years, the combined Fenton−SBR process has been used to treat refractory wastewaters such as dyestuff,[19] landfill leachate,[20] textile effluent,[21] antibiotic wastewater,[11] agro-industrial effluents,[22] and other types of recalcitrant wastewater.[23] However, citrus wastewater treatment with this combined process has not been reported to date.

The aim of this study is to examine the degradation of synthetic samples of citrus wastewater by means of the photo-Fenton process combined with the SBR system. Furthermore, the effects of different factors such as the concentrations of Fe, H_2O_2, and initial organic matter on DOC removal by the photo-Fenton treatment are investigated. A three-level factorial statistical experimental design and surface response methodology were used in the experimental study. Optimal reagent doses maximizing DOC removal was determined.

MATERIALS AND METHODS

Wastewater. Owing to the seasonal character of citrus juice production, which generates wastewaters for about 6 months of the year, it was necessary to reproduce citrus effluents by means of synthetic samples of citrus wastewater (CWW). These samples were prepared by diluting natural orange juice in distilled water, taking into account the characteristic of real effluent generated in a citrus industry from Cuba (Table 1). The natural orange juice was obtained from fresh fruits: oranges (*Citrus sinensis* L.) var. Valencia, selected in a state of optimum ripeness, uniform size, and without apparent physical damage. The oranges were washed with water at room temperature and symmetrically cut in half to obtain the juice by manual squeezing in the laboratory.

Table 1. Physicochemical Characterization of Citrus Wastewater (Mean Values)

parameter	real citrus effluents[a]	CWW
pH	3.8	3.5
conductivity (μS/cm 20 °C)	998	460
TSS (mg/L)	777	275
turbidity (NTU)	669	140
COD (mg/L)	10019	10000
BOD_5 (mg/L)	6619	4710
DOC (mg/L)		4238
biodegradability (BOD_5/COD)	0.66	0.47
fats and oil (mg/L)	0.009	0.005

[a]*Monitoring report and characterization of wastewater, Citrus Industrial Company "Héroes de Girón" Jagüey Grande*; National Company for Analysis and Technical Services UEB Matanzas (ENAST): Matanzas, Cuba, 2009.

The physicochemical characterization of CWW is presented in Table 1. This shows a low pH, high biodegradability, and a high concentration of organic matter, suspended solids, and turbidity. Table 2 shows the methodology used in the analysis of the different parameters.

Table 2. Analytical Methodology

parameters	method	reference
pH	4500-HB	standard methods
conductivity	27888:1995	UNE-EN ISO
TSS	2540-D	standard methods
VSS	2540-E	standard methods
turbidity	70127:1999	ISO
COD	410.4	EPA
BOD_5	5210 B	standard methods
DOC	5310B	standard methods
iron concentration	3500-B	EPA
H_2O_2 concentration	semiquantitative metavanadate method	Nogueira et al., 2005
ammonia nitrogen (NH_3-N and NH_3 or NH_4^+)	4500-NH_3	standard methods
phosphorus (Pt, PO_4^{3-}, and P_2O_5)	4500-PC	standard methods
volatile acidity	34229:1981	UNE-EN
fats and Oil	968.20, 9392.12, and 947.13	AOAC

Photo-Fenton Process. The reagents used for the photo-Fenton experiments were iron salt ($FeCl_3{\cdot}6H_2O$, Probus) and commercial hydrogen peroxide (30% (v/v), Carlo Erba). Predetermined amounts of commercial H_2O_2 and $FeCl_3$ were added to the sample in the reactor at the beginning of each experiment. The iron salt was mixed with the synthetic sample before the addition of hydrogen peroxide.

The photo-Fenton experiments were carried out using 100 mL flasks placed inside an ATLAS SUNTEST CPS+ solar chamber air-cooled at 35 °C. A xenon lamp emitted 5−6% of the photons in the 290−400 nm spectral range. The profile of the photons emitted between 400 and 800 nm followed the solar spectrum with a light intensity of 500 W/m^2, corresponding to 50% of AM1 (AM1 representing the light intensity of midday equatorial solar radiation).[24,25] The aqueous solutions were magnetically stirred (45 rpm). All experiments were conducted at the natural pH of the synthetic samples during 30 min, which ensured total consumption of the H_2O_2 concentration employed.

DOI: 10.1021/jf505377a
J. Agric. Food Chem. 2015, 63, 391−397

To detect possible interferences, a control sample without the addition of H_2O_2 and iron salt was used in each photo-Fenton experiment to quantify losses by volatilization and other causes. Each experiment was carried out in triplicate.

A three-level factorial statistical experimental design and the response surface methodology (RSM)[26] were used to investigate the effects of the three independent variables on the response factor and to determine the optimal conditions for maximizing the yield of the removal of organic matter (measured as DOC), defined as $Y_{DOC} = [(DOC_i - DOC_f)/DOC_i] \times 100$, where DOC_f is DOC in the sample after treatment and DOC_i is the initial value of DOC in the sample. The independent variables were the H_2O_2 concentration (established as a percentage of the stoichiometric weight ratio between the H_2O_2 and the COD, $R = H_2O_2/COD = 2.125$), the Fe^{3+}concentration (as mass ratio $[Fe^{3+}/H_2O_2] = 0.02-2.0$), and the organic matter concentration (1000−10000 mgO_2/L, measured as COD) present in the sample. The levels chosen for these variables followed those given in the bibliographic references.[5,27] The low, center, and high levels of each variable are designated as −1, 0, and +1, respectively, as shown in Table 3. A total of 27 experiments were carried out.

Table 3. Levels of Variables in Three-Level Factorial Statistical Experiment Design

		code variable level		
		low	center	high
parameter	variable	−1	0	+1
X_1	Fe^{3+} (mg/L)	85	510	850
X_2	H_2O_2 (mg/L)	425	2550	4250
X_3	$COD_{initial}$ (mg/L)	1000	6000	10000

The program used was the Windows version of Statgraphics Plus 5.1. This is a statistical software package both for the design of experiments as well as for obtaining graphs and statistical parameters, reduced models, and the tools necessary for data processing in general such as optimization tools.

After the different assays, the samples were filtered by means of 0.45 μm cellulose filters (Millipore) to remove suspended particulates before the analytical measurements. The DOC analysis was performed with a Shimadzu TOC-VCSH analyzer (detection limit: 5 mg C/L), carried out by method 5310B.[28] The concentration of H_2O_2 was monitored with Merckoquant peroxide analytical test strips (0−25 mgH_2O_2/L, 0−100 mgH_2O_2/L, and 0−1000 mgH_2O_2/L) and using the metavanadate method.[29] The concentration of total and dissolved iron was analyzed with the phenanthroline method 3500-B[28] using a multiparameter Hanna HI 83099 photometer in order to check the iron precipitation.

SBR Experimental Process. The aerobic degradation process was conducted in a SBR reactor. The reactor (4 L) was equipped with an air pump and air diffuser to guarantee the necessary dissolved oxygen for the degradation process and mixing. The cycle procedure was divided into four stages as follows: filling (0.25 h), aerobic reaction, settling (1 h), and idle (0.5 h). The seeding sludge was taken from the secondary sedimentation tank of a municipal wastewater treatment plant.

Aerobic degradation experiments of pretreated citrus wastewaters by the photo-Fenton process were performed with the synthetic samples that contained the highest concentration of organic matter (10000 mg/L, measured as COD). Sodium hydroxide 25% (w/v) ($CaOH_2$, Panreac) was added to pretreated samples to neutralize the pH; the sludge produced in the reaction was allowed to settle for approximately 0.5 h.

The citrus wastewaters showed a low content of nutrients (phosphorus, 4.5 mg/L; total nitrogen, 17.7 mg/L). The specialized literature reports that a stoichiometric nutrient ratio of COD:N:P

Table 4. Design Matrix and Results

	variable levels (codified values)			DOC removal (Y_{DOC})	
experiment no.	Fe^{3+} (mg/L)	H_2O_2 (mg/L)	$COD_{initial}$ (mg/L)	predicted value	observed value
1	850 (+1)	2550 (0)	1000 (−1)	40.6	45.5
2	510 (0)	2550 (0)	6000 (0)	22.5	21.7
3	510 (0)	425 (−1)	10000 (+1)	8.3	8.5
4	850 (+1)	4250 (+1)	1000 (−1)	52.2	44.6
5	85 (−1)	4250 (+1)	6000 (0)	29.7	11.7
6	510 (0)	425 (−1)	6000 (0)	3.5	12.9
7	850 (+1)	4250 (+1)	6000 (0)	18.3	23.7
8	85 (−1)	425 (−1)	1000 (−1)	32.8	15.9
9	510 (0)	425 (−1)	1000 (−1)	26.9	19.8
10	85 (−1)	2550 (0)	10000 (+1)	4.3	1.0
11	85 (−1)	425 (−1)	6000 (0)	−1.4	1.1
12	85 (−1)	2550 (0)	1000 (−1)	66.3	94.1
13	850 (+1)	4250 (+1)	10000 (+1)	12.4	17.8
14	85 (−1)	425 (−1)	10000 (+1)	−7.7	1.7
15	510 (0)	4250 (+1)	1000 (−1)	71.9	60.9
16	85 (−1)	2550 (0)	6000 (0)	21.3	6.1
17	850 (+1)	425 (−1)	10000 (+1)	18.1	10.1
18	510 (0)	2550 (0)	1000 (−1)	56.6	59.3
19	510 (0)	4250 (+1)	10000 (+1)	10.3	15.9
20	850 (+1)	425 (−1)	1000 (−1)	14.8	13.9
21	85 (−1)	4250 (+1)	10000 (+1)	1.9	7.2
22	850 (+1)	2550 (0)	6000 (0)	17.5	16.2
23	850 (+1)	425 (−1)	6000 (0)	2.4	13.8
24	510 (0)	2550 (0)	10000 (+1)	16.5	11.0
25	850 (+1)	2550 (0)	10000 (+1)	22.4	13.3
26	510 (0)	4250 (+1)	6000 (0)	27.1	33.8
27	85 (−1)	4250 (+1)	1000 (−1)	85.5	94.0

DOI: 10.1021/jf505377a
J. Agric. Food Chem. 2015, 63, 391−397

equal to 100:5:1 is required in order to give a suitable growth of microorganisms.[30] Therefore, the nutrient content was increased by dosing appropriate amounts of phosphate (KH_2PO_4, Panreac) and urea ($(NH_2)_2CO$, Panreac) salts in the influent prior to being fed to the SBR.

The treated synthetic sample was added to the SBR. The microorganisms were previously acclimatized, using diluted photo-treated samples as a feed, during a period of 30 days. The biomass concentration in the reactor was maintained in the range 3−4 g/L (measured as volatile suspended solids (VSS)), and the sludge retention time (SRT) was selected at 20 d with the aim of maintaining a high biomass concentration within the reactor. In addition, the dissolved oxygen concentration (DO) was maintained at values higher than 2 mg/L during the aerobic stage. For each batch performed in this work, the bioreactor continued operating until the %COD removal did not vary notably with time. The cycle was repeated 6−9 times in order to obtain repetitive results. The reactor was maintained at 25 °C (laboratory temperature) during the operation period.

The COD, DOC, volatile acidity, ammonium nitrogen (NH_3-N), phosphorus, dissolved iron, SST, turbidity, and color of the effluents were measured at the end of each process. In addition, during each cycle of the SBR, the sludge volume index (SVI) and settled sludge volume (V30) were measured according to the standard methods for the examination of water and wastewater (methods 2710D and 2710C). The microorganisms were observed with an optical microscope (Axiostar Plus Zeiss) using fresh preparations.

RESULTS AND DISCUSSION

Influence of Concentration of Organic Matter, Fe^{3+}, and H_2O_2 in the Photo-Fenton Process. Table 4 shows the RSM design matrix applied in this study, the measured values, and the responses predicted by the model for the DOC removal for each experiment. It can be seen that for the majority of experiments carried out with CWW with $COD_{initial}$ 10000 mgO_2/L (higher concentration of organic matter content) achieved lower DOC removal values (Y_{DOC}) than samples with $COD_{initial}$ in the range of 1000−6000 mgO_2/L. Degradation maxima of 94% is achieved for CWW with 1000 mgO_2/L (measured as COD) and 18% for CWW with 10000 mgO_2/L (measured as COD). This indicates that the initial composition of the samples has an important influence on the degradation performance.

Increasing the initial concentration of H_2O_2 produces higher degree of degradation. However, increasing the Fe^{3+} concentration results in a decrease in the degradation yields, except for treatment of samples with highest organic matter concentration (Table 4). Finally, the same percentage of the stoichiometric weight ratio between the H_2O_2 and the $COD_{initial}$ produces similar average values of yields of organic matter (Y_{DOC} = 16−22).

Figure 1 (main effect plot) and Figure 2 (Pareto diagram) show a statistical analysis of the results obtained in this research

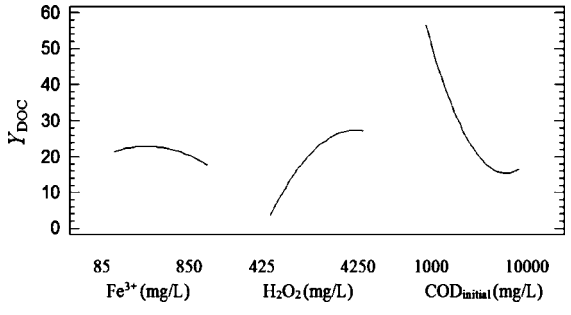

Figure 1. Main effects plot for photo-Fenton process.

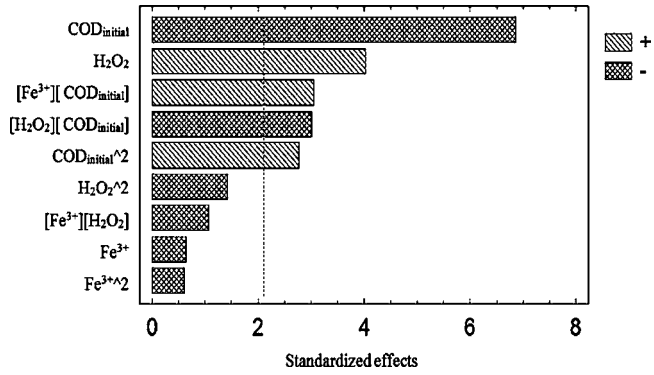

Figure 2. Pareto chart for synthetic samples of citrus wastewater.

to see the influence of the variables on the response factor (Y_{DOC}). The main effects plot in Figure 1 represents the effect of each variable on the response factor. As can be observed, an increase in both the initial concentration of the organic matter (measured as COD) and the iron concentration leads to a decrease in the degree of degradation of the organic matter. However, an increase in the H_2O_2 concentration has a positive effect on the degree of degradation of the organic matter. The slope of the plot is indicative of the importance of the variable on the response factor. It can be observed that the most influential variables are the initial concentration of organic matter in the CWW and the H_2O_2 concentration.

A Pareto graphic is used to draw conclusions about which of these variables and interactions are most significant. This graphic shows both the magnitude and the importance of the effects (variables and interactions). All the standardized effects were given in absolute values, and those which overpass the significance line (vertical line) exert a statistically significant influence on the response factor. The Pareto chart for CWW (Figure 2) shows that the variables and interactions that can be considered important in photo-Fenton processes are $COD_{initial}$, H_2O_2, and the interactions $[Fe^{3+}][COD_{initial}]$ and $[H_2O_2]$-$[COD_{initial}]$.

The application of RSM offers an empirical relationship between the response function and the independent variables. The mathematical relationship between the response factor and the variables can be approximated by a quadratic polynomial equation and represented by contour plots. Response surface plots provide a method for predicting the optimum conditions for treatment of CWW by the photo-Fenton process.

The coefficient of the response function for selected variables was determined by correlating the experimental results with the response factor by using the Windows version of Statgraphics Plus 5.1. The study was done for a confidence interval of 95%. The response function with the determined coefficients for DOC removal (Y_{DOC}) is presented by eq 1. The response factor predictions were in good agreement with the experimental data ($R^2 > 0.85$). This can be seen by comparing the measured values against the responses predicted by the model for Y_{DOC} (Table 4).

$$Y_{DOC} = 22.49 - 1.88X_1 + 11.77X_2 - 20.07X_3 - 3.83X_1X_2 + 10.94X_1X_3 - 10.77X_2X_3 - 3.08X_1^2 - 7.17X_2^2 + 14.03X_3^2 \quad (1)$$

Figure 3 shows the contour plots of the response factor (Y_{COD}) for CWW with 1000, 6000, and 10000 mgO_2/L of

DOI: 10.1021/jf505377a
J. Agric. Food Chem. 2015, 63, 391−397

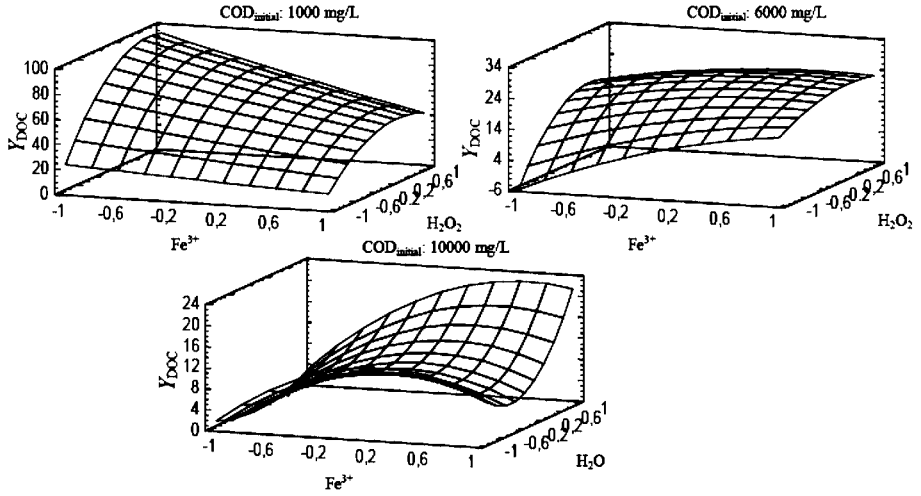

Figure 3. Contour plots for synthetic samples of citrus wastewater.

$COD_{initial}$. For the treatment of CWW with 1000 mgO_2/L, it can be seen that the operating conditions employed to achieve the maximum value in the response factor (i.e., values close to 100% organic matter removal (DOC removal)) come within the region of the experimental design.

On the other hand, samples with an organic matter concentration of 6000−10000 mgO_2/L show an optimum of Fe^{3+} concentration using a H_2O_2 concentration in the range of 425−4250 mg/L, in which the response factor reaches a maximum value. For these conditions, the maximum H_2O_2 concentration needed to reach values close to 100% of DOC removal falls outside the region of the experimental design. While it is true that this region should be considered with caution, the results suggest that there would be a higher response factor with the use of higher H_2O_2 concentrations than those considered in the study (obtained from an increase in the percentage of the stoichiometric ratio H_2O_2/COD) and intermediate values of Fe^{3+}.

Using the model reflected in eq 1, the most suitable conditions for decreasing the concentration of organic matter present in CWW with $COD_{initial}$ of 10000 mgO_2/L were calculated by considering the photo-Fenton process as a previous stage to the SBR process. The selected doses were as follows: $[H_2O_2]$ = 15938 mg/L (75% of stoichiometric value) and $[Fe^{3+}]$ = 510 mg/L for 61% COD removal.

The CWW ($COD_{initial}$ of 10000 mg/L) was treated by the photo-Fenton process using the following reagent doses: $[H_2O_2]$ = 15938 mg/L and $[Fe^{3+}]$ = 510 mg/L. The results are shown in Table 5. It can be observed that under these operating conditions a good level of degradation of organic matter was achieved. After 30 min of treatment, the final concentration of organic matter was 1818 mgC/L (measured as DOC) and 2225 mgO_2/L (measured as COD). Therefore, the photo-Fenton process is a technique capable of partially decreasing the concentration of organic matter present in citrus wastewaters with high organic load.

The evolution of the pH during the treatment shows a decrease mainly due to the formation of intermediate compounds such as organic acids (acetic acid, malic acid, etc.) which are difficult to oxidize. In the presence of these organic ligands, the Fe(III) can form stable complexes or associated ion pairs which exhibit charge transfer bands of ligand to metal in the UV−visible spectrum that are photochemically active and generate Fe(II) by irradiation. The irradiations of these complexes improve the photocatalytic properties for degrading organic compounds.[31] Consequently, approximately 63.5% of the catalyst remains in solution after the treatment. However, in these pH conditions (pH < 2), the absorption coefficient of the iron complexes decreases and Fe^{3+} appears as $Fe(H_2O)_6^{3+}$,[32] which is much less effective at absorbing light and in the production $^{\bullet}OH$,[33] resulting in an inefficient use of the peroxide.[31,34,35]

Table 5. Physicochemical Parameters of Treated Effluent by Photo-Fenton Process (Mean Values)

parameter	value	removal efficiency (%)
pH	1.6	
conductivity (μS/cm 20 °C)	7.5	
TSS (mg/L)	81	68
turbidity (NTU)	45	69
COD (mg/L)	2225	78
BOD_5 (mg/L)	1165	80
DOC (mg/L)	1818	61
biodegradability (BOD_5/COD)	0.52	
apparent color (CPU)	1560	
real color (CPU)	286	
total Fe (mg/L)	324	
NH_4^+ (mg/L)	1.4	97
total *P* (mg/L)	1.4	69
volatile acidity (g/L)	2.5	
fats and Oil (mg/L)	<DL	

Degradation of Pretreated CWW by the SBR Process. The synthetic samples used to study the viability of the combined photo-Fenton/SBR process for the treatment of wastewater from the citrus industry were those samples with the highest concentration of organic matter (10000 mg/L of $COD_{initial}$). First, the CWW was treated by the photo-Fenton process using the previously selected conditions.

After the photo-Fenton process, the pretreated samples were conditioned by neutralization and sedimentation. In this stage, dissolved iron was mainly precipitated because the concentration in the clarified effluent was 0.7 mg/L and the pH was adjusted to 7−8. The concentration of organic matter decreased until 1000 mgC/L (measured as DOC) or 1634 mgO_2/L (measured as COD), amounts which can be

DOI: 10.1021/jf505377a
J. Agric. Food Chem. 2015, 63, 391−397

Table 6. Effect of Photo-Fenton Oxidation on SBR Treatment

	SBR operation conditions			SBR effluent			
samples	COD (mg/L)	THR (d)	F/M (d^{-1})	COD (mg/L)	DOC (mg/L)	V30 (mL/L)	SVI (mL/g)
pretreated CWW	1634	1.59	0.3	120	71	310	115

assimilated by the microorganisms present in the biological reactor.[6,14,15]

After the acclimatization process, the pretreated CWW were treated by SBR. Table 6 shows the control parameters and the features of the final effluent.

A yield of 93% in the degradation of organic matter (measured as DOC) was achieved by the SBR process. The average organic matter concentration in the final effluent was 120 mg O_2/L (measured as COD). The total yield of organic matter degradation by the combined photo-Fenton process and biological treatment was 96% (measured as COD). Furthermore, the concentration of SST, turbidity, and color in the final effluent were 111 mg/L, 59 NTU, and 116 CPU, respectively. According to the Cuban legislation currently in force concerning wastewater discharge, the effluents of the citrus industry treated by this sequence of processes can be discharged into the wastewater collecting system.[36]

For these operating conditions in the SBR process, a significant decrease in the concentration of volatile acids (24%) measured as acetic acid was obtained during the first half hour of treatment. At the same time, a significant reduction in COD and DOC and an important consumption of nutrients was observed. The presence of a significant fraction of readily biodegradable compounds in the effluent, mainly organic acids of low molecular weight, accelerates the efficiency of the aerobic metabolism of biomass.

Furthermore, the analyses of NH_3^+-N, P_{total} and volatile acidity in the final effluent showed a concentration of 2.6, 2.9, and 370 mg/L, respectively. The high concentrations of volatile acids indicate the presence of a fraction of volatile organic compound which is more complex to degrade. These results are obtained for hydraulic retention times (HRT) of 1.59 d. For complete elimination of these compounds, a higher HRT is required, around 3 d of biological treatment.

Microbiological analyses showed a balance between the different types of microorganisms detected in the biological reactor (bacterium, protozoes, filamentous microorganisms, etc.), producing a correct flocculation and a good settleability of sludge. During the SBR process, the settleability and compactibility of sludge were very good. This is due, among other factors, to an appropriate F/M ratio.[30,37] The average values of the sludge volume index (SVI) and settled sludge volume (V30) parameters were 115 mL/g and 310 mL/L, respectively.

The results suggest that a combined system composed of the photo-Fenton process and biological treatment based on the SBR process is an effective and attractive alternative for the treatment of citrus processing wastewater, particularly during the period when effluents with a higher organic load are generated, although more studies on how system characteristics enhance or limit the individual and global efficiencies, and eventually, the overall treatment cost, must be performed.[13]

AUTHOR INFORMATION

Corresponding Author

*Phone: + 34 876555039. Fax: + 34 976762142. E-mail: 662175@celes.unizar.es.

Funding

We acknowledge financial support for this work from the DGA-FSE Research Team T33, Department of Chemical Engineering and Environmental Technologies of the University of Zaragoza. We thank the University of Zaragoza and Santander Bank for a Ph.D. grant awarded to José Guzmán Hidalgo. "Proyecto financiado por el Ministerio de Educación en el marco del Programa Campus de Excelencia Internacional", Campus Iberus (CEF11-0017).

Notes

The authors declare no competing financial interest.

REFERENCES

(1) Martin, M. A.; Siles, J. A.; Chica, A. F.; Martin, A. Biomethanization of orange peel waste. *Bioresour. Technol.* **2010**, *101*, 8993−8999.

(2) Thevendiraraj, S.; Klemes, J.; Paz, D.; Aso, G.; Cardenas, G. L. Water and wastewater minimisation study of a citrus plant. *Resour. Conserv. Recycl.* **2003**, *37*, 227−250.

(3) Guzmán, J.; Prévez, L.; Abreu, S.; Fernández, C. M.; Moya, R.; Bello, M.; Menéndez, C.; Mesa, J.; Oliva, M.; Olivera, L. A. Sostenibilidad del proceso de obtención de aceite esencial cítrico: aplicación de la producción más limpia (PML). *Ing. Quim.* **2011**, *499*, 52−57.

(4) Karaouzas, I.; Cotou, E.; Albanis, T. A.; Kamarianos, A.; Skoulikidis, N. T.; Giannakou, U. Bioassays and biochemical biomarkers for assessing olive mill and citrus processing wastewater toxicity. *Environ. Toxicol.* **2011**, *26*, 669−676.

(5) Valdés, P.; Guerrero, B.; Nieves, G.; De la Torre, V. Tratamiento de aguas residuales cítricas por vía anaerobia. *Rev. Int. Contam. Ambiental* **1994**, *10*, 69−75.

(6) Mosteo, R. *Characterization and treatment of winery wastewater by advanced oxidation processes and biological treatment*. Doctoral Thesis. University of Zaragoza, Spain, 2006.

(7) Rodríguez, E.; Isac, L.; Fernández, N.; Zornoza, A.; Mas, M. Identificación de bacterias filamentosas en EDAR industriales. *Tecnol. agua* **2008**, *303*, 56−64.

(8) Pera-Titus, M.; García-Molina, V.; Baños, M. A.; Gimenéz, J.; Esplugas, S. Degradation of chlorophenols by means of advanced oxidation processes: a general review. *Appl. Catal., B* **2004**, *47*, 219−256.

(9) Caudo, S.; Genovese, C.; Perathoner, S.; Centi, G. Copper-pillared clays (Cu-PILC) for agro-food wastewater purification with H_2O_2. *Microporous Mesoporous Mater.* **2008**, *107*, 46−57.

(10) Chamarro, E.; Marco, A.; Esplugas, S. Use of Fenton reagent to improve organic chemical biodegradability. *Water Res.* **2001**, *35*, 1047−1051.

(11) Elmolla, E. S.; Chaudhuri, M. Combined photo-Fenton−SBR process for antibiotic wastewater treatment. *J. Hazard. Mater.* **2011**, *192*, 1418−1426.

(12) Pignatello, J. J.; Liu, D.; Huston, P. Evidence for an additional oxidant in the photo assisted Fenton reaction. *Environ. Sci. Technol.* **1999**, *33*, 1832−1839.

(13) Oller, I.; Malato, S.; Sánchez-Pérez, J. A. Combination of Advanced Oxidation Processes and biological treatments for wastewater decontamination—a review. *Sci. Total Environ.* **2011**, *409*, 4141−4166.

(14) Mosteo, R.; Ormad, M. P.; Ovelleiro, J. L. Photo-Fenton processes assisted by solar light used as previous step to biological treatment applied to winery wastewaters. *Water Sci. Technol.* **2007**, *56*, 89−94.

DOI: 10.1021/jf505377a
J. Agric. Food Chem. 2015, 63, 391−397

(15) Mosteo, R.; Sarasa, J.; Ormad, M. P.; Ovelleiro, J. L. Sequential Solar Photo-Fenton–Biological System for the Treatment of Winery Wastewaters. *J. Agric. Food Chem.* **2008**, *56*, 7333–7338.
(16) Zhang, H.; Choi, H. J.; Huang, C. P. Optimization of Fenton process for the treatment of landfill leachate. *J. Hazard. Mater.* **2005**, *125*, 166–174.
(17) Mace, S.; Mata-Alvarez, J. Utilization of SBR technology for wastewater treatment: an overview. *Ind. Eng. Chem. Res.* **2002**, *41*, 5539–5553.
(18) Rodriguez, D. C.; Pino, N.; Penuela, G. Monitoring the removal of nitrogen by applying a nitrification–denitrification process in a sequencing batch reactor (SBR). *Bioresour. Technol.* **2011**, *102*, 2316–2321.
(19) Garcia-Montano, J.; Torrades, F.; Garcia-Hortal, J. A.; Domenech, X.; Peral, J. Combining photo-Fenton process with aerobic sequencing batch reactor for commercial hetero-bireactive dye removal. *Appl. Catal., B* **2006**, *67*, 86–92.
(20) Guo, J. S.; Abbas, A. A.; Chen, Y. P.; Liu, Z. P.; Fang, F.; Chen, P. Treatment of landfill leachate using a combined stripping, Fenton, SBR, and coagulation process. *J. Hazard. Mater.* **2010**, *178*, 699–705.
(21) Blanco, J.; Torrades, F.; De la Varga, M.; Garcia-Montano, J. Fenton and biological-Fenton coupled processes for textile wastewater treatment and reuse. *Desalination* **2012**, *286*, 394–399.
(22) Wu, D. L.; Wang, W.; Guo, Q. W.; Shen, Y. H. Combined Fenton–SBR process for bamboo industry wastewater treatment. *Chem. Eng. J.* **2013**, *214*, 278–284.
(23) Christensen, A.; Gurol, M. D.; Garoma, T. Treatment of persistent organic compounds by integrated advanced oxidation processes and sequential batch reactor. *Water Res.* **2009**, *43*, 3910–3921.
(24) Yuranova, T.; Mosteo, R.; Bandara, J.; Laub, D.; Kiwi, J. Self-cleaning cotton textiles surfaces modified by photoactive SiO_2/TiO_2 coating. *J. Mol. Catal. A: Chem.* **2006**, *244*, 160–167.
(25) Mosteo, R.; Ormad, M. P.; Mozas, E.; Sarasa, J.; Ovelleiro, J. L. Factorial experimental design of winery wastewaters treatment by heterogeneous photo-Fenton process. *Water Res.* **2006**, *40*, 1561–1568.
(26) Charles, R. H.; Kennneth, V. T. *Fundamental Concepts in the Design of Experiments*; University Press: Oxford, 1999.
(27) Lucas, M. S.; Peres, J. A. Removal of COD from olive mill wastewater by Fenton's reagent: kinetic study. *J. Hazard. Mater.* **2009**, *168*, 1253–1259.
(28) Eaton, A. D.; Clesceri, L. S.; Rice, E. W.; Greenberg, A. E.; Franson, M. A. H. *Standard Methods for the Examination of Water and Wastewater*, 21st ed.; ;American Public Health Association–American Water Works Assoication–Water Environment Federation (APHA-AWWA-WEF): Washington, DC, 2005.
(29) Nogueira, R. F. P.; Oliveira, M. C.; Paterlini, W. C. Simple and fast spectrophotometric determination of H_2O_2 in photo-Fenton reactions using metavanadate. *Talanta* **2005**, *66*, 86–91.
(30) Tchobanoglous, G.; Burton, F. L.; Stensel, H. D. *Metcalf & Eddy Inc. Wastewater Engineering: Treatment and Reuse*, 4th ed.; McGraw-Hill Inc.: New York, NY, 2003.
(31) Safarzadeh-Amiri, A.; Bolton, J. R.; Cater, S. R. The use of iron in advanced oxidation processes. *J. Adv. Oxid. Technol.* **1996**, *1*, 18–26.
(32) Flynn, C. M., Jr. Hydrolysis of inorganic iron (III) salts. *Chem. Rev.* **1984**, *84*, 31–41.
(33) Feng, W.; Nansheng, D. Photochemistry of hydrolytic iron(III) species and photoinduced degradation of organic compounds. A minireview. *Chemosphere* **2000**, *41*, 1137–1147.
(34) Wells, C. F.; Salam, M. A. The effect of pH on the kinetics of the reaction of iron(II) with hydrogen peroxide in perchlorate media. *J. Chem. Soc., A* **1968**, 24–29.
(35) Neyens, E.; Baeyens, J. A review of classic Fenton's peroxidation as an advanced oxidation technique. *J. Hazard. Mater.* **2003**, *98*, 33–50.
(36) *Vertimiento de Aguas Residuales a las Aguas Terrestres y al alcantarillado. Especificaciones*, NC 27:1999; Oficina Nacional de Normalización (NC), 1999.
(37) Ramalho, R. S. *Tratamiento de aguas residuales*, 2nd ed.; Ed.ial Reverté, SA: Barcelona, España, 2003; pp 253–409.

DOI: 10.1021/jf505377a
J. Agric. Food Chem. 2015, 63, 391–397

JOURNAL OF AGRICULTURAL AND FOOD CHEMISTRY

Article

pubs.acs.org/JAFC

Distribution and Accumulative Pattern of Tetracyclines and Sulfonamides in Edible Vegetables of Cucumber, Tomato, and Lettuce

Mohamed Bedair M. Ahmed,[†,§] Anushka Upamali Rajapaksha,[†] Jung Eun Lim,[†] Ngoc Thang Vu,[‡] Il Seop Kim,[‡] Ho Min Kang,[‡] Sang Soo Lee,*[,†] and Yong Sik Ok*[,†]

[†]Department of Biological Environment and [‡]Department of Horticulture Science, Kangwon National University, Chuncheon 200-701, Korea

[§]Department of Food Toxicology and Contaminants, National Research Centre, Cairo, Egypt

Supporting Information

ABSTRACT: Veterinary antibiotics can be released to environment by the animals' excretions, which thereby poses human health and ecological risks. Six antibiotics (tetracycline, oxytetracycline, chlortetracycline, sulfamethazine, sulfamethoxazole, and sulfadimethoxine) at three concentrations (5, 10, and 20 mg kg^{-1} soil) were employed in pots filled with a loamy sand upland soil. Three types of vegetable seedlings, including cucumber (*Cucumis sativus*), cherry tomato (*Solanum lycopersicum*), and lettuce (*Lactuca sativa*), were also cultivated during 45 d in the greenhouse. All antibiotics taken up by tested plants showed negative effects on growth. Relatively high levels of tetracyclines and sulfonamides (SAs) were detected in the nonedible parts, roots, and leaves of cucumber and tomato, but fruit parts accumulated them lower than acceptable daily intake. Indeed, cucumber roots accumulated SAs by up to 94.6% of total addition (at 5 mg kg^{-1} soil).

KEYWORDS: *bioaccumulation, emerging contaminant, pharmaceuticals, phytoavailability, risk assessment, veterinary antibiotics*

INTRODUCTION

Contamination of agricultural soils with agrochemicals, such as pesticides and fertilizers, and its potential accumulation in the crop tissues are well investigated. Adamo et al.[1] studied the uptakes of Zn, Cr, Cu, and Pb by lettuce plant from metals-contaminated soils and reported the order of transfer factor from soil to vegetables, Zn > Cu > Cr ≥ Pb. They revealed that the Pb contents in all collected samples were below the maximum levels of Pb in edible vegetables set by the European Union.[2] Babu et al.[3] also studied the uptake of organochlorine pesticides (DDT and HCH) by Basmati rice (*Oryza sativa*) from the soil. Residues of both pesticides were found in all soil and plant samples except for a few grain samples. Maximum and minimum levels of residue were observed in husk and grains, respectively, and the levels of DDT and CHC in grains were quite below the regulation by the government of India and WHO/FAO. Similarly, Waliszewski et al.[4] investigated DDT and HCH isomer levels in soil and carrot root and leaf. Their results revealed the organochlorine pesticide diffusion from agricultural soils to growing carrot plants and its vapor-adsorption by leaves.

Residues and metabolites of antibiotics are very important organic pollutants in our surrounding environments. Antibiotics are widely used for therapeutic purposes to treat or control infectious diseases in humans and animals. Antibiotics in veterinary practice are also used to increase feed efficiency and to promote growth in food producing animals at subtherapeutic levels.[5−7] Tetracyclines (TCs) and sulfonamides (SAs) as the most popular antibiotics groups that are active against a broad spectrum of Gram-positive/negative bacteria, some obligate anaerobes, protozoa, parasites, and fungi.[8,9] In Korea, TCs and SAs antibiotics are most commonly used in veterinary medicine, where the Korean Food and Drug Administration[10] reported that TCs have been used the most among antimicrobials in veterinary medicine (470.9 t) followed by penicillins (170.7 t) and SAs (157.4 t).[11−13] In European countries, including Spain, France, Germany, United Kingdom, Poland, and Italy, TCs are also most commonly used in veterinary medicine followed by penicillins and SAs and show the annual consumptions of 205−658 t of TCs, 83−567 t of penicillins, and 45−174 t of SAs.[14] The overuse of antibiotics in the field of livestock industry may lead to occurrence of antibiotics' residue due to animal excretions and animal products having a high concentration of antibiotics.[7,12,15−17] Excretion is the major means by which human and veterinary antibiotics are introduced into the environment. The application of manure to agricultural soils mainly leads to the release of residual antibiotics into soils through leaching and runoff, which thereby threatens groundwater and surface water quality.[12] Some leftover livestock feeds that contain therapeutic agents may also be discarded as waste or lost along with the runoff during watering and rainfall episodes.[18,19] In addition, significant amounts of antibiotics are discharged into the environment from wastewater treatment facilities, septic systems, and agricultural waste storage structures. Awad et al.[11] comprehensively monitored the occurrence and seasonal variations of TCs and SAs in water, sediment, and soil. They

Received: July 24, 2014
Revised: December 8, 2014
Accepted: December 15, 2014
Published: December 15, 2014

ACS Publications © 2014 American Chemical Society

DOI: 10.1021/jf5034637
J. Agric. Food Chem. 2015, 63, 398−405

observed higher levels of TCs and SAs in water, sediment, and soil during winter than summer season due to lower degradation rate in winter season. Ok et al.[13] also found the highest concentration of TCs and SAs in water, sediment, and soil at a site adjacent to the composting facility than at a site far away from that facility. As a result, the residual antibiotics in soil and water can be taken up by plants.[18,20−22]

Few studies investigated the uptake of antibiotics by plants. Sulfadimethoxine was found in root and leaves of barley with concentrations of 1.2 and 1.1 mg g^{-1}, respectively (on dry weight basis), when the barley was cultivated in soils treated with 300 mg L^{-1} sulfadimethoxine.[23] Kumar et al.[22] reported that the maximum amount of chlortetracycline recovered in plant tops was found in corn followed by cabbage and green onion. The amount of accumulated chlortetracycline in plant tissues was small (0.002−0.017 mg kg^{-1} fresh weight), but it increased with increased rate of chlortetracycline into the manure. Dolliver et al.[21] reported that the highest amount of sulfamethazine was detected in lettuce followed by potato and corn. Michelini et al.[24] also evaluated the effects of sulfadiazine on willow (*Salix fragilis* L.) and maize (*Zea mays* L.) plants. They found that the high concentration of sulfadiazine caused serious stress in willow (e.g., reduced C/N ratio and total chlorophyll content) and the death of maize, which thereby shows a strong potential to impair plant performance and biomass.

Because of consumption of agricultural products containing antibiotics' residues, public health could be threatened. Especially, continuous exposure to antibiotics could lead to allergic reactions and chemical poisoning by the development of resistant bacterial strains.[25,26] Several regulatory authorities had set maximum residue limits (MRLs) for antibiotics in foods of animal origin, for example, the European Union set MRLs for TCs that ranged between 0.1 mg kg^{-1} in milk and meat and 0.6 mg kg^{-1} in kidney, while it was set at 0.1 mg kg^{-1} for SAs in all livestock products.[27] However, no limit was set for food crops.

Previous studies focused on the presence and prevalence of antibiotics in environmental compartments as well as the impact of antibiotics on seed germination and plant growth. Some studies focused on the uptake of antibiotics by edible and nonedible plants and calculated the antibiotics contents in the different parts of nonripened plants. However, no study was found related to the accumulation and distribution patterns of antibiotics in the ripened plants' parts, especially the edible parts, through the exposure to different concentrations of antibiotics. Moreover, the previous studies did not focus on the safety assessment of those edible parts for human consumption with the successive increasing of antibiotics' dosage. Therefore, in this study, we hypothesized that the antibiotics of TCs and SAs accumulated in different parts of cucumber, tomato, and lettuce plants. In addition, the accumulation or plant uptake of antibiotics may show different distribution or patterns depending on the antibiotics' types or plant species. Consequently, this study was conducted (i) to reveal the effect of TCs and SAs on the growth of cucumber, tomato, and lettuce plants by measuring growth parameters including plant height, number of leaves, chlorophyll content, shoot weight, root weight, total root surface area, and fruit weight; (ii) to quantify the absorbed antibiotics in the different plant parts for food safety assessment; and (iii) to trace the distribution and cumulative patterns of various antibiotics.

MATERIALS AND METHODS

Antibiotics. Target antibiotic compounds were selected based on frequency of use in Korea.[10] Target antibiotic standards, including 97.5% tetracycline hydrochloride (referred to as TC in this study), 97% oxytetracycline hydrochloride (OTC), 97% chlortetracycline hydrochloride (CTC), 99% sulfamethazine (SMT), 99.7% sulfamethoxazole (SMX), and 98.5% sulfadimethoxine (SDM), were obtained from Sigma-Aldrich (St. Louis, MO, USA). The physicochemical characteristics of these antibiotics are shown in Table S1 of the Supporting Information. Acetonitrile, methanol, acetone, hexane, formic acid, and water of HPLC-grade were also obtained from LiChrosolv Co. (Merck, Germany). The solid-phase extraction (SPE) cartridges and 3 mL/60 mg of HLB (hydrophilic−lipophillic−balanced) were purchased from Waters Oasis Co. (Milford, MA, USA).

Stock solutions of antibiotics were prepared at a concentration of 100 mg L^{-1} as follows: 10 mg of individual standard (corrected by purity) was accurately weighed, dissolved in small amount of methanol, diluted to 100 mL with deionized water, and then stored at −20 °C.

Experimental Procedure. Each of 36 plastic pots (200 mm diameter × 190 mm tall) was filled with a loamy sand upland soil obtained from experimental field at Kangwon National University, Chuncheon, Korea. Each pot contained 3.7 kg of dry soil. Three kinds of plant seedlings, including cucumber (*Cucumis sativus*, 45 d old), tomatoes (*Solanum lycopersicum*, 45 d old), and lettuce (*Lactuca sativa*, 30 d old), were used for the cultivation experiment. Each of 12 pots was used for each cultivation of cucumber, tomato, and lettuce plants. The plants were individually transplanted as one plant in each pot and then irrigated by antibiotics' free water and kept for 2 weeks for adaptation before the addition of subjected antibiotics. Antibiotics, including TCs and SAs at the levels of 5, 10, and 20 mg kg^{-1} soil, were collectively spiked through the irrigation water at four doses (one dose per week) along with no antibiotics' addition as the control. All pots were irrigated twice a week with 50 mL of water containing antibiotics and 100 mL of water containing fertilizers, in order. To ensure the effects of antibiotics on plant growth only, the essential fertilizers of common plants were provided except phosphate fertilizer because of its negative effect on TCs adsorption by plants.[28] Plant seedlings were grown in a greenhouse, which was completely controlled at 25 °C and 70% humidity for 45 d of cultivation period. During cultivation, the growth parameters, such as plant height (cm), number of leaves, and leaf chlorophyll content by a chlorophyll meter (Minolta, SPAD-502, Japan), were measured weekly, and other parameters, such as weights of root, shoot, and fruit, and total root surface area, were determined after harvest (or 45 d of cultivation).

Plant Samples Preparation. After 45 d of cultivation, all seedlings had completely become ripened. The harvested shoots of each plant were washed with tap water and dried using an adsorbent paper for weighing. The fruits of each plant were also weighed. To remove the moisture completely, the harvested leaves and fruits were chopped and then subjected to a freeze-drier (OPERON, FDB-5503, Korea). For the measurement of root's surface area, the adhered soil was removed carefully, washed using the tap water, and then dried using an adsorbent paper. The Epson 10000XL scanner equipped with the WIN MAC RHIZO V 2009c program (Regent Instruments Inc., Canada) was employed for the morphological characterization of roots.[29] Briefly, the roots were placed in a tray (300 mm width × 400 mm length × 20 mm thickness) with water for separating out roots and moisturizing, and then the surface area of roots was determined.

Antibiotics' Uptake by Plants. The antibiotics' extraction from plant samples was done using the modified procedures of Migliore et al.[23] and Dolliver et al.[21] Specifically, 500 mg of dried and crushed plant sample was extracted with 8 mL of methanol:HCl (95:5), mixed for 30 s using a vortex (Vortex-2 genie, Scientific Industries, USA), sonicated for 10 min using an ultrasonic (JAC−1505, Korea), and centrifuged for 10 min at 4500 rpm, and then the supernatant was collected. The residue was extracted again with 5 mL of acetone using the same procedure. The supernatants were mixed and dried under N_2

DOI: 10.1021/jf5034637
J. Agric. Food Chem. 2015, 63, 398−405

Table 1. Differences between Growth Parameters for Control and Antibiotics' Treated Plants

plants	treatments (mg kg^{-1})	plant height (cm)	number of leaves	chlorophyll content (SPAD)	shoot weight (g)	root weight (g)	total root surface area (cm^2)	fruit weight (g)
tomato	control	54.33 a[a]	25.00 a	53.14 a	98.67 a	12.68 a	839.88 a	39.83 a
	5	30.00 b	17.33 bc	49.74 b	68.83 bc	6.32 c	683.90 c	40.33 a
	10	50.33 a	19.33 b	51.08 ab	80.17 b	8.92 b	778.35 b	40.83 a
	20	30.00 b	15.33 c	46.42 c	63.00 c	4.36 c	382.00 d	37.67 a
cucumber	control	66.00 a	8.00 a	59.12 a	72.50 a	10.81 a	919.04 a	70.36 a
	5	41.33 b	8.33 a	55.21 b	40.93 b	7.77 b	789.12 b	55.57 ab
	10	52.33 ab	8.33 a	58.30 a	46.17 b	9.47 a	855.52 ab	77.35 a
	20	40.67 b	8.00 a	54.94 b	32.50 b	7.32 b	685.78 c	38.67 b
lettuce	control	19.67 a	11.33 a	40.77 a	42.23 a	5.36 a	138.94 a	
	5	15.33 bc	9.00 b	35.96 b	17.09 c	1.81 c	97.67 b	
	10	18.00 ab	10.67 a	38.14 ab	23.76 b	3.36 b	126.18 a	
	20	14.33 c	8.67 b	32.60 c	13.69 c	1.62 c	82.16 b	

[a]Mean separation within columns by Duncan's multiple range test at $P = 0.05$, $n = 3$.

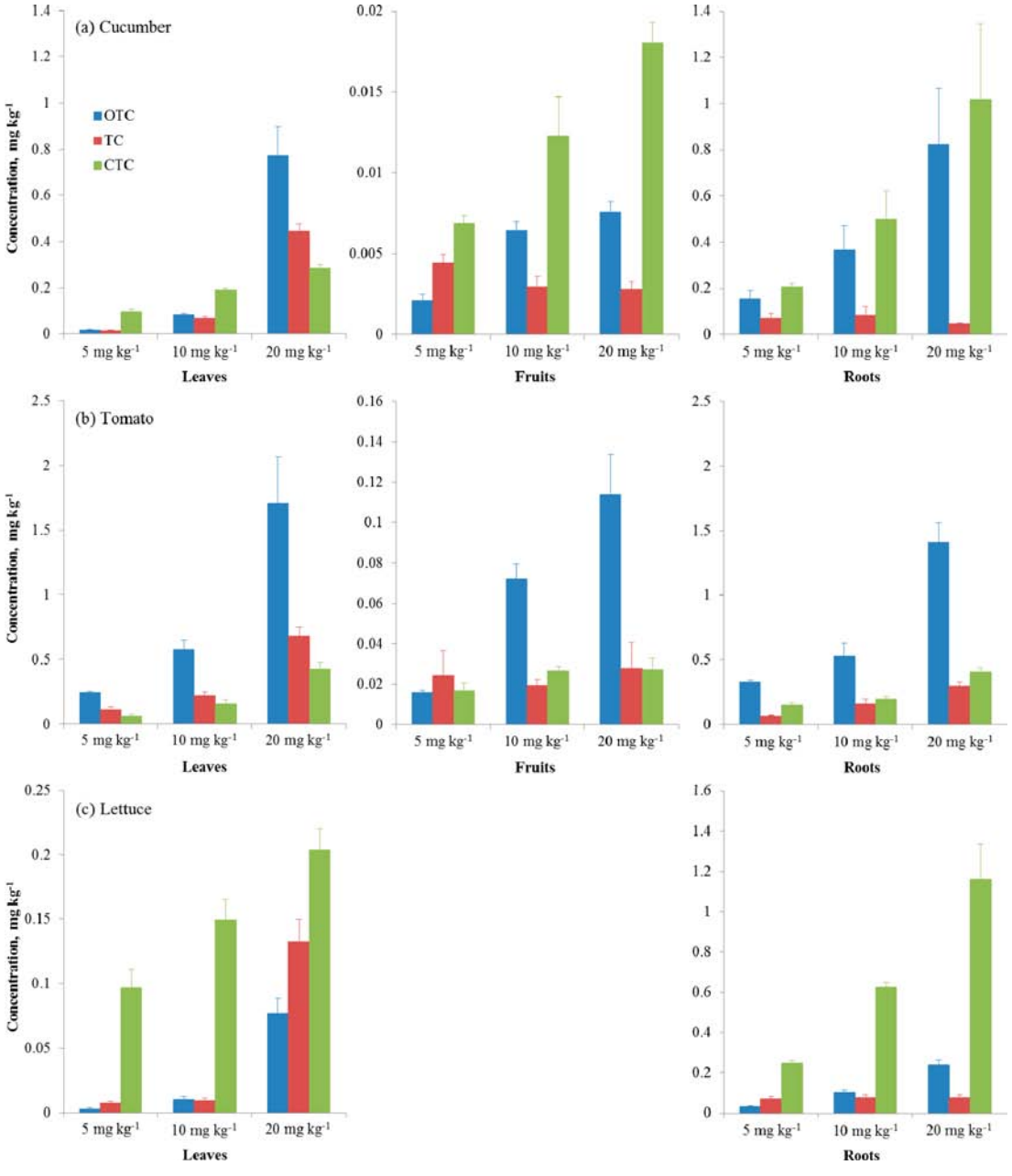

Figure 1. Tetracyclines (TCs) uptake by (a) cucumber, (b) tomato, and (c) lettuce at 5, 10, and 20 mg kg^{-1} treatments.

DOI: 10.1021/jf5034637
J. Agric. Food Chem. 2015, 63, 398−405

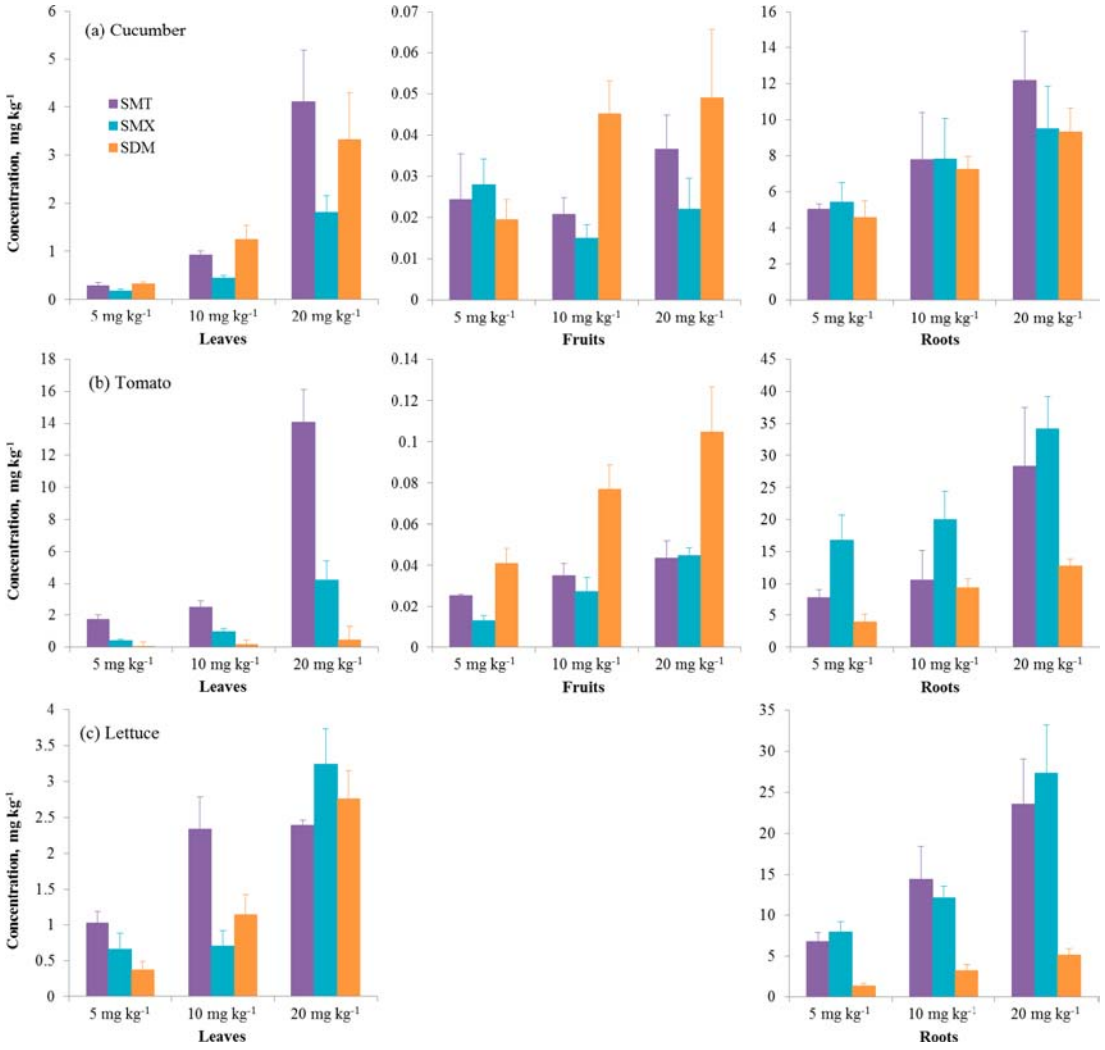

Figure 2. Sulfonamides (SAs) uptake by (a) cucumber, (b) tomato, and (c) lettuce at 5, 10, and 20 mg kg^{-1} treatments.

gas at 40 °C. The residue was resuspended in 5 mL of methanol:nanopure water (50:50) and defatted with 5 mL of hexane three times. Hexane (the upper layer) was removed each time after the liquid–liquid partitioning. The remaining liquid extract was dried under N_2 gas at 40 °C up to 2.5 mL, which was subjected to the cleanup step using SPE.

The SPE cleanup procedure was performed according to Kim and Carlson[30] using an OASIS HLB 60 mg cartridge (Waters Corp., Milford, MA, USA). The cartridge was preconditioned with 3 mL of methanol, 3 mL of 0.5 N HCl, and 3 mL of nanopure water. The sample was passed through the cartridge at a flow rate of 2 mL min^{-1}, and then the SPE cartridge was washed twice with 3 mL of nanopure water and dried under depression for 5 min. The antibiotics were then eluted from the cartridge twice with 2.5 mL of methanol. The methanol extract was dried under N_2 gas at 40 °C until the volume reached ~150 μL and was then transferred to a 500-μL degraded Eppendorf tube. The final volume of eluate was completed to 400 μL using the mobile phase A solution (0.1% formic acid in HPLC-grade water, pH 2.6) and then mixed and filtered through a 0.22-μm cellulose acetate filter. The eluate was transferred into an amber vial equipped with 250 μL of a glass insert vial for HPLC–MS analysis.

The concentration of antibiotics was determined by the procedures of Kim and Carlson[30] using a HPLC–MS (Agilent 1260 series, Agilent Technologies, Palo Alto, CA, USA) equipped with a variable wavelength UV detector. Electrospray ionization (ESI) was used to detect the target antibiotic, and a positive mode was adapted. For the chromatographic separation of antibiotics, the same mobile phases (A, 0.1% formic acid in HPLC-grade water, pH 2.6; and B, 0.1% formic acid in HPLC-grade acetonitrile) of a study by Kim and Carlson[30] were used; however, a different HPLC column and pump program for the gradient elution of the mobile phases were employed. The used column was a YMC-Pack Pro C18 RS reversed-phase column (150 mm long × 2.0 mm i.d., 3-μm pore size) instead of an Xterra C18 column (50 mm long × 2.1 mm i.d., 2.5-μm pore size). A C18 guard column (Phenomenex, Torrance, CA, USA) was used to filter any particulates from the sample. The gradient program for the mobile phases started by a volume of 96:4 (A:B), which ramped to 88:12 (A:B) in 15 min and to 80:20 (A:B) in 10 min and then went back to the initial conditions in 5 min and remained isocratic for 5 min. The column temperature was maintained at 25 °C. Injection volume was 20 μL with a flow rate of 0.2 mL min^{-1}.

A Thermo Finnigan LCQ Duo ion traps mass spectrometer (Thermo, Woburn, MA, USA), equipped with a heated capillary interface and ESI, was used to perform the mass spectrometric analysis. Ultrapure N_2 gas was used for drying and nebulizing. Spray voltage was set to 4.5 kV, and the capillary voltage was autotuned to 3.5 kV. Drying gas temperature was set to 350 °C, and a flow rate was 10.0 L min^{-1}. Average concentration in triplicate of the individual antibiotics was calculated. Calibration curves established for the six antibiotics ranged from 100–5000 μg L^{-1}. When sample concentration exceeded the highest calibration point, the injection volume was reduced.

DOI: 10.1021/jf5034637
J. Agric. Food Chem. 2015, 63, 398–405

Statistics. Data were analyzed using SAS v.9.3 software (SAS Institute Inc., Cary, NC, USA). Mean separations were calculated using Duncan's multiple range test at a 0.05 significance level.

RESULTS AND DISCUSSION

Analysis of Antibiotics. Calibration was done for the six antibiotics and showed excellent linearity in the concentration ranges of 100−5,000 μg L^{-1}, with $R^2 \geq 0.996$ (Table S2 and Figure S1, Supporting Information). The extraction method and HPLC−MS conditions proved to enable a good simultaneous separation for the six antibiotics without neither overlapping between antibiotics nor interfering with the plant matrix as shown in the HPLC−MS chromatograms (Figure S2, Supporting Information).

Antibiotics Effects on Plant Growth. The growth parameters, including plant height, number of leaves, leaf chlorophyll content, shoot weight, fruit weight, root weight, and total root surface area, were determined to evaluate the effects of TCs and SAs on plant growth (Table 1). The results revealed that the antibiotics negatively affected all growth parameters for tomato except the fruit weight, which was no different with the control. This result may be due to the low retained quantities of antibiotics in tomato's fruits, which did not affect the fruit weight of treated plants; meanwhile, the other negatively affected growth parameters concerning roots and leaves of tomato may be due to their high contents of antibiotics as seen in the following results of Figures 1 and 2. The highest level of antibiotics (20 mg kg^{-1} soil) had the worst effects on the growth parameters of tomato. For cucumber, the antibiotics showed the negative effects on the growth parameters except the values of leaves' number, because the negative effect for antibiotics on cucumber's leaves was not observed in leaves' number but in the leaves sizes, which were reduced compared to the control (leaf size data not shown). Interestingly, the antibiotics' concentrations of 5 and 20 mg kg^{-1} had similar and negative effects on the plants' growth parameters compared to those of 10 mg kg^{-1}. Generally, our results showed that the antibiotics of TCs and SAs had negative effects on the plant growth of cucumber, tomato, and lettuce.

Different toxic effects between antibiotic compounds are due to their different behavior in the soil via sorption, degradation, and chelating with metals.[35] SAs have been known as antibiotics with higher bioavailability for plants than TCs because of their higher mobility in soils.[31−34] Furthermore, SMX and SMT in the SAs group were found to be toxic to plant growth in the soil as reported by Liu et al.[35] whereas CTC and OTC in the TCs group enhanced the growth of radish and wheat and also reported no negative effects on the growth of corn.[36] Those previous findings support our results concerning the growth negative effects for antibiotics on the three treated plants at the levels of 5 and 20 mg kg^{-1}; this negative effect could be due to the fact that the negative impact of SAs on plants was higher than the enhancing impact for TCs at those levels (5 and 20 mg kg^{-1}). Meanwhile, at the level of 10 mg kg^{-1}, the absorbed amount of TCs may have had a growth enhancing effect equivalent to the growth inhibiting effect for the absorbed amount of SAs. Therefore, some growth parameters for the 10 mg kg^{-1} treated plants were not negatively affected and statistically equal to those of the control plants. We believe that those obtained results are very important and considered a very interesting phenomenon; however, our data and analysis were limited to explain this phenomenon. Further work should be done to reveal the possible mechanism using more various levels of antibiotics.

Antibiotics Uptake by Cucumber, Tomato, and Lettuce. *Tetracyclines (TCs).* Accumulations of TCs were found in parts of leaves, fruits, and roots for each cucumber, tomato, and lettuce, as shown in Figure 1. For the cucumber, the increasing levels from 5−20 mg kg^{-1} of OTC, TC, and CTC led to the higher uptake by leaves, fruits, and roots (Figure 1). The accumulation of OTC and CTC was higher in the fruits and roots of cucumber than that of TC in the same parts, whereas the OTC showed the highest accumulation in leaves at 20 mg kg^{-1}. All TCs were highly accumulated in parts of leaves and roots rather than in parts of fruits.

The accumulation of OTC was the highest in all parts of tomato over all levels of OTC (Figure 1). Moreover, as the level of OTC increased, its accumulation by tomato was accelerated. No difference in accumulation was found between TC and CTC, and the accumulation of TC and CTC was much less than that of OTC.

For the lettuce, CTC showed the highest accumulation in all parts compared to other TCs over all levels of addition (Figure 1). In particular, the roots of lettuce accumulated the highest concentrations of CTC over all levels of addition, which were 0.249, 0.624, and 1.160 mg kg^{-1} fresh weight at 5, 10, and 20 mg kg^{-1}, respectively. These values of accumulation in the roots indicated up to 5.6-times higher than those in the leaves when the same level of CTC was treated. No difference of TC accumulation in the roots was found, and the OTC accumulation was fluctuated over all levels of addition. In brief summary, the accumulations of TCs by the subjected plants were higher in leaves and roots than in fruits and were gradually increased as the level of addition increased. The accumulations of OTC and CTC were generally higher than that of TC and maximized in tomato and lettuce, respectively. These obtained results were in accordance with Kumar et al.[22] who stated that the absorbed level of CTC by corn, cabbage, and green onion increased as the level of CTC increased in the manure−soil mixture. Hu et al.[37] also reported that the applied groups of antibiotics, including TCs and SAs, to the cultivated vegetables of radish, rape, celery, and coriander were biologically accumulated in vegetables through water transport and passive absorption.

Sulfonamides (SAs). With increasing level of SAs, the accumulating trend was very similar to that of TCs in all parts of tested plants including cucumber, tomato, and lettuce; however, the levels of accumulation were much higher than TCs (Figure 2). For cucumber and tomato, the accumulation of all SAs in leaves and roots was generally higher than that in their fruits, and it was increased as levels of SAs increased to 20 mg kg^{-1}. Especially, the accumulation of SMT was the highest in the leaves of cucumber and tomato over all levels. For the roots of cucumber, no difference of accumulation was found at the same level of SAs; however, as the level of SAs increased, the accumulation was gradually increased. At the level of 5 mg kg^{-1}, the accumulations of SAs in all parts of cucumber were not different, and those were relatively lower than at the higher additive level of SAs. For the fruits of tomato, the accumulation of SDM was the most, and that of SMX was the lowest at all the levels of addition. In other words, the accumulation of SDM was 68.9, 64.7, and 57.2% higher than that of SMX at 5, 10, and 20 mg kg^{-1}, respectively. For lettuce, all types of SAs were highly accumulated in roots rather than leaves. The accumulations of SMT in leaves of lettuce indicated the

DOI: 10.1021/jf5034637
J. Agric. Food Chem. 2015, 63, 398−405

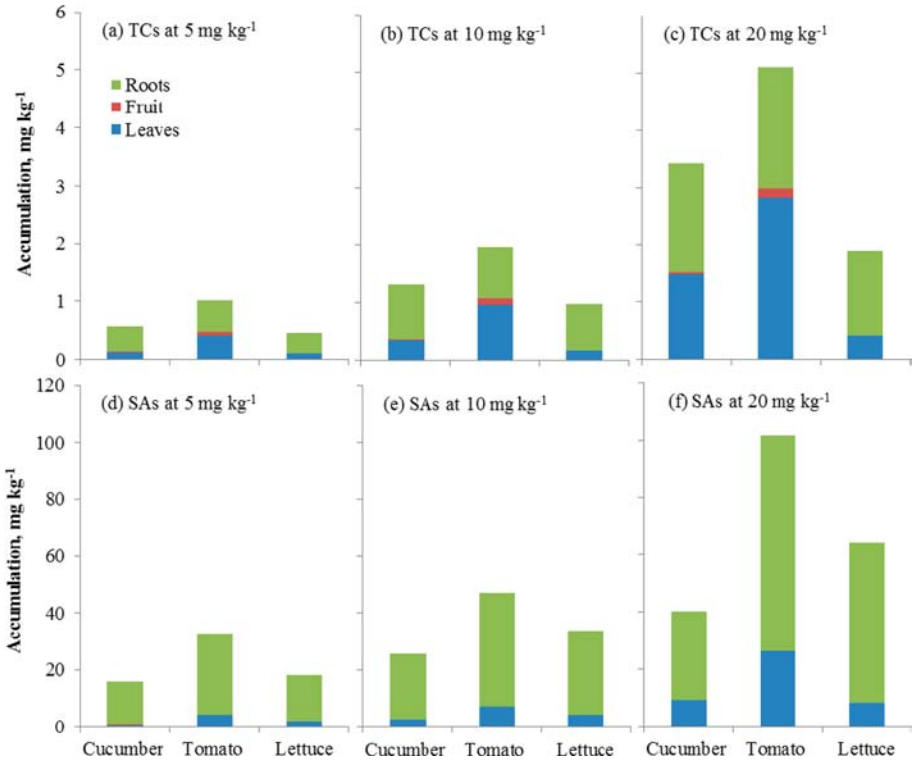

Figure 3. Distributed ratios of absorbed tetracyclines (TCs) and sulfonamides (SAs) between the different plant parts of roots, fruit, and leaves.

highest values of 1.02 and 2.34 mg kg^{-1} at 5 and 10 mg kg^{-1}, respectively, among SAs; however, the accumulation of SMT was not extended at 20 mg kg^{-1} compared to at 10 mg kg^{-1}. SMT and SMX showed rapid and linear increases of their accumulation by adding higher levels in the roots of lettuce, whereas SDM was slightly increased as its level increased. In general, the amounts of accumulated SAs were increased as the levels of each SA increased, and the accumulations of SAs were the least in the fruits for cucumber and tomato in this study.

Migliore et al.[23] reported that relatively high concentrations of 1.234 and 1.063 mg g^{-1} SDM were detected in the root and leaves of barley, respectively, grown in the soils treated with 300 mg L^{-1} of SDM. Dolliver et al.[21] found that the highest amount of SMT was taken up by lettuce, followed by potato and corn. On the basis of the results of TCs and SAs uptake by cucumber, tomato, and lettuce in this study, the accumulation of SAs was markedly higher than that of TCs. It can be explained with the low molecular weights of SAs, which are water-soluble and not strongly sorbed to soil particles; therefore, SAs may facilitate the uptake or accumulation by plant tissues.[21,31,37,38] On the contrary, because TCs have opposite characteristics to SAs, TCs are relatively stable and strongly sorbed to soil particles and thus not easily taken up by plants from the soil.[37,39]

Safety Assessment. The acceptable daily intake (ADI) values for TCs and SAs had been established by JECFA[40] and are defined as 0–30 μg kg^{-1} body-weight d^{-1} for TCs and 0–50 μg kg^{-1} body-weight d^{-1} for SAs. Because body weight is typically assumed to be 60 kg as an adult, the ADI values of TCs and SAs are 1.8 and 3.0 mg d^{-1}, respectively. In this study, the concentrations of TCs in edible parts of all plants were between 0.002 mg kg^{-1} (OTC in cucumber fruit at 5 mg kg^{-1}) and 0.204 mg kg^{-1} (CTC in lettuce leaves at 20 mg kg^{-1}). For the SAs, the concentrations in edible parts of all plants were between 0.013 mg kg^{-1} (SMX in tomato fruits at 5 mg kg^{-1}) and 3.240 mg kg^{-1} (SMX in lettuce leaves at 20 mg kg^{-1}). On the basis of the report estimated by WHO,[41] a typical adult in the eastern countries consumes fresh vegetables about 233 g d^{-1} including 81.5, 4.8, and 2.3 g d^{-1} of tomato, cucumber, and lettuce, respectively. Therefore, the amounts of TCs and SAs accumulated from the edible parts of tested plants were in the safe limit.

Distribution of TCs and SAs in Different Parts of Plants. Figure 3 shows the distribution of TCs and SAs in roots, fruits, and leaves of cucumber, tomato, and lettuce. For the cucumber, the total amounts of accumulated TCs to plant bodies (including leaves, fruits, and roots) were 0.574, 1.309, and 3.418 mg kg^{-1} at the concentrations of 5, 10, and 20 mg kg^{-1}, respectively (Table 2). It was linearly increased as the concentration of TCs into soils increased (Figure S3, Supporting Information). The amount of accumulated TCs in the leaves of cucumber at 5 mg kg^{-1} was 22.1% of the total accumulated TCs in all parts of plant body, but it was sharply increased to 43.9% at 20 mg kg^{-1}. On the contrary, the

Table 2. Total Absorbed Amounts of Tetracyclines by Plants

		total absorbed amounts (fresh weight basis; mg kg^{-1})			
plants	treatments (mg kg^{-1})	TC	OTC	CTC	total
cucumber	5	0.089	0.175	0.310	0.574
	10	0.151	0.452	0.705	1.309
	20	0.496	1.603	1.320	3.418
tomato	5	0.199	0.590	0.231	1.021
	10	0.400	1.178	0.381	1.959
	20	1.009	3.231	0.864	5.104
lettuce	5	0.077	0.035	0.346	0.459
	10	0.088	0.112	0.773	0.972
	20	0.211	0.318	1.364	1.892

DOI: 10.1021/jf5034637
J. Agric. Food Chem. 2015, 63, 398–405

amounts of accumulated TCs in the fruits and roots of cucumber were decreased as the level of TCs addition increased (2.3 to 0.8% for fruits and 75.5 to 55.3% for roots). In the case of SAs for the cucumber, the total concentrations of SAs were also linearly increased as the concentrations of SAs into soils increased (Table 3; Figure S4, Supporting Information).

Table 3. Total Absorbed Amounts of Sulfonamides by Plants

		total absorbed amounts (fresh weight basis; mg kg^{-1})			
plants	treatments (mg kg^{-1})	SMT	SMX	SDM	total
cucumber	5	5.359	5.633	4.924	15.916
	10	8.725	8.295	8.546	25.566
	20	16.319	11.330	12.692	40.341
tomato	5	9.573	17.193	6.113	32.879
	10	13.106	20.963	13.011	47.080
	20	42.445	38.467	20.887	101.799
lettuce	5	7.813	8.582	1.773	18.169
	10	16.776	12.790	4.377	33.943
	20	25.993	30.589	7.876	64.458

Moreover, the highest accumulation of SAs was detected in the roots up to 94.6% (at 5 mg kg^{-1}) compared to other parts of plant body. Interestingly, the smallest accumulation of SAs was found in the fruits of cucumber (<0.5%) compared to other parts of the plant body.

For the tomato, the total amounts of TCs were 1.021, 1.959, and 5.104 mg kg^{-1} at the concentrations of 5, 10, and 20 mg kg^{-1}, respectively (Table 2). The accumulation of TCs increased as the level of TCs addition increased (Figure S3, Supporting Information). The proportions of TCs accumulation in the leaves and roots were similar, which ranged from 40.2−55.2% of total accumulation of TCs in the all parts of plant body, and the accumulation of TCs in the fruits was the smallest, which ranged from 5.5% out of 1.02 mg kg^{-1} (the total content of TCs at 5 mg kg^{-1} spiking) to 3.3% out of 5.10 mg kg^{-1} (the total content of TCs at 20 mg kg^{-1} spiking) compared to other parts (Table 2). For the SAs, the roots of tomato accumulated the SAs the highest (up to 86.8% of total amount of SAs accumulated) compared to the leaves and fruits. Especially, the accumulation of SAs in the fruits of tomato as an edible part was less than 0.3% of the total amount of SAs accumulated.

For the lettuce, each TCs/SAs accumulation was not altered as the level of their addition increased from 5−20 mg kg^{-1} (Tables 2 and 3). The values of accumulation of TCs and SAs in the leaves were 0.413 and 8.392 mg kg^{-1} at 20 mg kg^{-1} spiked and equal to 21.8 and 13.0% occupied of total amount of TCs and SAs accumulation in the plant body, respectively.

Our results of TCs and SAs accumulated in plant bodies showed that the distributions of TCs and SAs were roots > leaves > fruits in general. These results agree with a study by Migliore et al.[23] who stated that the concentration of antibiotics in the roots was higher than other parts of wheat and corn. Similarly, Liu et al.[42] concluded that the distribution of all antibiotics in the wetland plant (*Phragmites australis*) followed the sequence root > leaf > stem. On the other hand, Hu et al.[37] found that the distribution of antibiotics in various tissues of the vegetables was leaves > stems > roots. They also insisted that the types and growth stages of vegetables would affect the distribution of antibiotics. The differences of antibiotics uptake and the distribution on plant, which occurred in the different studies, are due to the limited understanding of the interactions of antibiotic concentrations in manure/soil, antibiotic chemical characteristics, specific crops, plant growth stage, and plant physiology.[21]

We conclude that the growth of cucumber, tomato, and lettuce was relatively inhibited by the TCs and SAs accumulated from soils spiked at the levels of 5, 10, and 20 mg kg^{-1}. The accumulation of OTC was the highest in the cucumber and tomato, while CTC was the highest accumulated among TCs in the lettuce. The accumulation of SAs was the smallest in a part of fruits for cucumber and tomato that equals < 0.5% and 0.3%, respectively, from the total absorbed amounts of SAs. Moreover, the total amounts of TCs and SAs accumulated in the plant bodies were significantly increased as the level of their additions increased . Adding to that, the descending order for the total TCs contents in plants was tomato > cucumber > lettuce, while for SAs, it was tomato > lettuce > cucumber. In general, the relatively high level of TCs and SAs was detected in the nonedible parts (roots and leaves) of cucumber and tomato, and the fruits of these plants also contained a lower level than the ADI of antibiotics.

■ ASSOCIATED CONTENT

Supporting Information

Properties of antibiotics used in the study, analytical performance of the method, calibration graphs of TCs and SAs, chromatograms for antibiotics in positive samples, and total accumulated amounts of TCs and SAs in plants at different treatments. This material is available free of charge via the Internet at http://pubs.acs.org.

■ AUTHOR INFORMATION

Corresponding Authors

*E-mail: sslee97@kangwon.ac.kr.

*E-mail: soilok@kangwon.ac.kr.

Funding

This work was supported by the Korea Ministry of Environment as a Geo-Advanced Innovative Action Project (G112-00056-0004-0) and by the Ministry of Education, Science and Technology as the Basic Science Research Program through the National Research Foundation of Korea (NRF) (2012R1A1B3001409). Instrumental analyses were supported by the Korea Basic Science Institute, the Environmental Research Institute, and the Central Laboratory of Kangwon National University, Korea.

Notes

The authors declare no competing financial interest.

■ REFERENCES

(1) Adamo, P.; Iavazzo, P.; Albanese, S.; Agrelli, D.; De Vivo, B.; Lima, A. Bioavailability and soil-to-plant transfer factors as indicators of potentially toxic element contamination in agricultural soils. *Sci. Total Environ.* **2014**, *500−501*, 11−22.

(2) Commission Regulation (EC). *No 1881/2006 of 19 December 2006 Setting Maximum Levels for Certain Contaminants in Foodstuffs*; European Commission: Brussels, Belgium, 2006.

(3) Babu, G. S.; Farooq, M.; Ray, R. S.; Joshi, P. C.; Viswanathan, P. N.; Hans, R. K. DDT and HCH residues in Basmati rice (*Oryza sativa*) cultivated in Dehradun (India). *Water, Air, Soil Pollut.* **2003**, *144*, 149−157.

(4) Waliszewski, S. M.; Carvajal, O.; Gomez-Arroyo, S.; Amador-Munoz, O.; Villalobos-Pietrini, R.; Hayward-Jones, P. M.; Valencia-

DOI: 10.1021/jf5034637
J. Agric. Food Chem. 2015, 63, 398−405

Quintana, R. DDT and HCH isomer levels in soils, carrot root, and carrot leaf samples. *Bull. Environ. Contam. Toxicol.* **2008**, *81*, 343−347.
(5) Lim, J. E.; Kim, H. W.; Jeong, S. H.; Lee, S. S.; Yang, J.; Kim, K. H.; Ok, Y. S. Characterization of burcucumber biochar and its potential as an adsorbent for veterinary antibiotics in water. *J. Appl. Biol. Chem.* **2014**, *57*, 65−72.
(6) Schwarz, S.; Kehrenberg, C.; Walsh, T. R. Use of antimicrobial agents in veterinary medicine and food animal production. *Int. J. Antimicrob. Agents* **2001**, *17*, 431−437.
(7) Wassenaar, T. M. Use of antimicrobial agents in veterinary medicine and implications for human health. *Crit. Rev. Microbiol.* **2005**, *31*, 155−169.
(8) Baran, W.; Adamek, E.; Ziemianska, J.; Sobczak, A. Effects of the presence of sulfonamides in the environment and their influence on human health. *J. Hazard. Mater.* **2001**, *196*, 1−15.
(9) Oka, H.; Ito, Y.; Matsumoto, H. Chromatographic analysis of tetracycline antibiotics in foods. *J. Chromatogr., A* **2000**, *882*, 109−133.
(10) Monitoring of antimicrobial resistance on the food-animals and meats. *National Antimicrobial Resistance Management Program: 2009, Final Report*; KFDA, Korean Food and Drug Administration: Chungcheongbuk-do, Korea, 2009.
(11) Awad, Y. M.; Kim, S. C.; Abd El-Azeem, S. A. M.; Kim, K. H.; Kim, K. R.; Kim, K.; Jeon, C.; Lee, S. S.; Ok, Y. S. Veterinary antibiotics contamination in water, sediment, and soil near a swine manure composting facility. *Environ. Earth Sci.* **2014**, *71*, 1433−1440.
(12) Kim, K. R.; Owens, G.; Kwon, S. I.; So, K. H.; Lee, D. B.; Ok, Y. S. Occurrence and environmental fate of veterinary antibiotics in the terrestrial environment. *Water, Air, Soil Pollut.* **2011**, *214*, 163−174.
(13) Ok, Y. S.; Kim, S. C.; Kim, K. R.; Lee, S. S.; Moon, D. H.; Lim, K. J.; Sung, J. K.; Hur, S. O.; Yang, J. E. Monitoring of selected veterinary antibiotics in environmental compartments near a composting facility in Gangwon Province, Korea. *Environ. Monit. Assess.* **2011**, *174*, 693−701.
(14) Sales of veterinary antimicrobial agents in 26 EU/EEA countries in 2012 (EMA/333921/2014). *European Surveillance of Veterinary Antimicrobial Consumption, 2014*; European Medicines Agency: London, 2014. www.ema.europa.eu/docs/en_GB/document_library/Report/2014/10/WC500175671.pdf (accessed November 22, 2014).
(15) Anadon, A.; Martinez-Larranaga, M. R. Residues of antimicrobial drugs and feed additives in animal products: Regulatory aspects. *Livest. Prod. Sci.* **1999**, *59*, 183−198.
(16) Kim, K. R.; Owens, G.; Ok, Y. S.; Park, W. K.; Lee, D. B.; Kwon, S. I. Decline in extractable antibiotics in manure-based composts during composting. *Waste Manage.* **2012**, *32*, 110−116.
(17) Kwon, S. I.; Owens, G.; Ok, Y. S.; Lee, D. B.; Jeon, W. T.; Kim, J. G.; Kim, K. R. Applicability of the Charm II system for monitoring antibiotic residues in manure-based composts. *Waste Manage.* **2011**, *31*, 39−44.
(18) Jjemba, P. K. The potential impact of veterinary and human therapeutic agents in manure and biosolids on plants grown on arable land: A review. *Agric., Ecosyst. Environ.* **2002**, *93*, 267−278.
(19) Sarmah, A. K.; Meyer, M. T.; Boxall, A. B. A. A global perspective on the use, sales, exposure pathways, occurrence, fate, and effects of veterinary antibiotics (VAs) in the environment. *Chemosphere* **2006**, *65*, 725−759.
(20) Boxall, A. B. A.; Johnson, P.; Smith, E. J.; Sinclair, C. J.; Stutt, E.; Levy, L. S. Uptake of veterinary medicines from soils into plants. *J. Agric. Food. Chem.* **2006**, *54*, 2288−2297.
(21) Dolliver, H.; Kumar, K.; Gupta, S. Sulfamethazine uptake by plants from manure-amended soil. *J. Environ. Qual.* **2007**, *36*, 1224−1230.
(22) Kumar, K.; Gupta, S. C.; Baidoo, S. K.; Chander, Y.; Rosen, C. J. Antibiotic uptake by plants from soil fertilized with animal manure. *J. Environ. Qual.* **2005**, *34*, 2082−2085.
(23) Migliore, L.; Brambilla, G.; Casoria, P.; Civitareale, C.; Cozzolino, S.; Gaudio, L. Effect of sulphadimethoxine contamination on barley (*Hordeum distichum* L., Poaceae, Liliopsida). *Agric. Ecosyst. Environ.* **1996**, *60*, 121−128.
(24) Michelini, L.; Reichel, R.; Werner, W.; Ghisi, R.; Thiele-Bruhn, S. Sulfadiazine uptake and effects on *Salix fragilis* L. and *Zea mays* L. plants. *Water, Air, Soil Pollut.* **2012**, *223*, 5243−5257.
(25) Ferguson, J.; Baxtera, A.; Youngb, P.; Kennedyb, G.; Elliottb, C.; Weigelc, S.; Gatermannc, R.; Ashwind, H.; Steadd, S.; Sharmand, M. Detection of chloramphenicol and chloramphenicol glucuronide residues in poultry muscle, honey, prawn, and milk using a surface plasmon resonance biosensor and Qflex® kit chloramphenicol. *Anal. Chim. Acta* **2005**, *529*, 109−113.
(26) Kim, S. C.; Yang, J. E.; Ok, Y. S.; Carlson, K. Dissolved and colloidal fraction transport of antibiotics in soil under biotic and abiotic conditions. *Water Qual. Res. J. Can.* **2010**, *45*, 275−285.
(27) Commission Regulation (EEC) No. 37/2010. on pharmacologically active substances and their classification regarding maximum residue limits in foodstuffs of animal origin. *Off. J. Eur. Union* **2010**, 15.
(28) Wang, Y. J.; Sun, R. J.; Xiao, A. Y.; Wang, S. Q.; Zhou, D. M. Phosphate affects the adsorption of tetracycline on two soils with different characteristics. *Geoderma* **2010**, *156*, 237−242.
(29) Arsenault, J. L.; Pouleur, S.; Messier, C.; Guay, R. WinRHIZO, a root-measuring system with a unique overlap correction method. *Hortic. Sci.* **1995**, *30*, 906.
(30) Kim, S. C.; Carlson, K. Quantification of human and veterinary antibiotics in water and sediment using SPE/LC/MS/MS. *Anal. Bioanal. Chem.* **2007**, *387*, 1301−1315.
(31) Boxall, A. B. A.; Blackwell, P.; Cavallo, R.; Kay, P.; Tolls, J. The sorption and transport of a sulphonamide antibiotic in soil systems. *Toxicol. Lett.* **2002**, *131*, 19−28.
(32) Figueroa, R. A.; Leonard, A.; Mackay, A. A. Modeling tetracycline antibiotic sorption to clays. *Environ. Sci. Technol.* **2004**, *38*, 476−483.
(33) Mackay, A. A.; Canterbury, B. Oxytetracycline sorption to organic matter by metal-bridging. *J. Environ. Qual.* **2005**, *34*, 1964−1971.
(34) Tolls, J. Sorption of veterinary pharmaceuticals in soils: A review. *Environ. Sci. Technol.* **2001**, *35*, 3397−3406.
(35) Liu, F.; Ying, G.; Tao, R.; Zhao, J.; Yang, J.; Zhao, L. Effects of six selected antibiotics on plant growth and soil microbial and enzymatic activities. *Environ. Pollut.* **2009**, *157*, 1636−1642.
(36) Batchelder, A. R. Chlortetracycline and oxytetracycline effects on plant growth and development in soil systems. *J. Environ. Qual.* **1982**, *11*, 675−678.
(37) Hu, X.; Zhou, Q.; Luo, Y. Occurrence and source analysis of typical veterinary antibiotics in manure, soil, vegetables, and groundwater from organic vegetable bases, northern China. *Environ. Pollut. Control* **2010**, *158*, 2992−2998.
(38) Rajapaksha, A. U.; Vithanage, M.; Lim, J. E.; Ahmed, M. B. M.; Zhang, M.; Lee, S. S.; Ok, Y. S. Invasive plant-derived biochar inhibits sulfamethazine uptake by lettuce in soil. *Chemosphere* **2014**, *111*, 500−504.
(39) Lunestad, B. T.; Goksayr, J. Reduction in the antibacterial effect of oxytetracycline in sea water by complex formation with magnesium and calcium. *Dis. Aquat. Org.* **1990**, *9*, 67−72.
(40) Joint FAO/WHO Expert Committee on Food Additives. Residue Evaluation of Certain Veterinary Drugs, Meeting 2010—Evaluation of data on ractopamine residues in pig tissues. *FAO JECFA Monographs*; Food and Agriculture Organization of the United Nations: Rome, 2010. www.fao.org/docrep/012/i1618e/i1618e00.pdf (accessed November 24, 2013).
(41) WHO. GEMS/Food regional diets: Regional per capita consumption of raw and semi-processed agricultural commodities. *Global Environment Monitoring System/Food Contamination Monitoring and Assessment Programme*; World Health Organization: Geneva, Switzerland, 2003. http://www.who.int/foodsafety/chem/gems_regional_diet.pdf (accessed November 24, 2013).
(42) Liu, L.; Yu-Hong, L.; Chao-Xiang, L.; Wang, Z.; Dong, J.; Ge-Fu, Z.; Huang, X. Potential effect and accumulation of veterinary antibiotics in *Phragmites australis* under hydroponic conditions. *Ecol. Eng.* **2013**, *53*, 138−143.

DOI: 10.1021/jf5034637
J. Agric. Food Chem. 2015, 63, 398−405

JOURNAL OF AGRICULTURAL AND FOOD CHEMISTRY

Article

pubs.acs.org/JAFC

Interrelations between Herbage Yield, α-Tocopherol, β-Carotene, Lutein, Protein, and Fiber in Non-Leguminous Forbs, Forage Legumes, and a Grass−Clover Mixture as Affected by Harvest Date

Anjo Elgersma,*[,†] Karen Søegaard,[‡] and Søren Krogh Jensen[§]

[†]Independent Scientist, P.O. Box 323, 6700 AH Wageningen, The Netherlands

[‡]Department of Agroecology and Environment, Faculty of Agricultural Science, Aarhus University, Blichers Allé 20, P.O. Box 50, 8830 Tjele, Denmark

[§]Department of Animal Sciences, Faculty of Agricultural Science, Aarhus University, Blichers Allé 20, P.O. Box 50, 8830 Tjele, Denmark

ABSTRACT: Pastures with diverse botanical composition may enhance animal-derived product quality. A recent study demonstrated high vitamin concentrations and yields in some forb species. The objectives of the present study were to investigate interrelations between herbage yields, vitamin concentrations, protein and fiber contents and analyze the effect of harvest date. We hypothesized that interrelations would be similar across investigated forage species. Four nonleguminous forbs: salad burnet (*Sanguisorba minor*), caraway (*Carum carvi*), chicory (*Cichorium intybus*), and ribwort plantain (*Plantago lanceolata*), three legumes: yellow sweet clover (*Melilotus officinalis*), lucerne (*Medicago sativa*), and birdsfoot trefoil (*Lotus corniculatus*) and a perennial ryegrass (*Lolium perenne*)−white clover (*Trifolium repens*) mixture were sown in a field trial with two replicated and randomized blocks. Forage in 1.5 m × 9 m plots was grown in two consecutive years and cut four times per year (May−October). Analyses of variance were performed. In most herbages, α-tocopherol and β-carotene were positively correlated as were β-carotene and lutein; all vitamins were negatively correlated with fiber content and herbage yield. β-Carotene was positively correlated with protein content. α-Tocopherol and β-carotene contents were generally highest in October and lowest in July. Our results showed similar interrelationships in most investigated species, and we suggest that these species may be mixed when designing novel biodiverse mixtures for particular product quality characteristics.

KEYWORDS: *herb, forb, forage legume, vitamin, α-tocopherol, β-carotene, lutein, seasonal pattern*

INTRODUCTION

Change is needed in the design and management of our food systems in order to enhance natural resource use. Fresh herbage is an important natural source of protein, fiber, fatty acids (FA), and vitamins in ruminant diets. Although synthetic vitamins are cheap and widely used in animal production, there is interest in naturally occurring vitamins, particularly in organic farming systems where use of synthetic or nonorganic feed and supplements has to be minimized. Fresh forage contains fat-soluble vitamins with antioxidative properties, e.g., α-tocopherol and β-carotene (pro-vitamin A),[1] and antioxidants like lutein. Tocopherols (vitamin E) and carotenoids, such as lutein and β-carotene, can be directly transferred from fresh grass into milk.[2] Vitamins in forage species are thus important for the vitamin concentration as well as the oxidative stability of animal-derived foods such as dairy[3] and meat products.[4] Several factors affect concentrations of α-tocopherol and β-carotene in plant species.[1,5]

Both α-tocopherol and β-carotene are quenching singlet oxygen and thereby protecting against photo-oxidative stress, but they act at different locations. The β-carotene counteracts the chlorophyl-photosensitized formation of singlet oxigen, whereas α-tocopherol captures free radicals and protects the membranes.[6] Excessive concentrations of α-tocopherol may be harmful to the plant because it increases the rigidity of membranes. However, this may be counteracted by changes in the FA profile of the membranes and elevated concentrations of β-carotene and other antioxidants.[7]

Concentrations of vitamins and FA in plants depend on factors such as regrowth stage, nitrogen (N) availability, temperature, day length, and leaf proportion in the harvested herbage.[8,9] Tocopherols are located in the photosynthetic parts of plants, in the chloroplasts.[7] Thus, leaves contain more tocopherol than stems.[10]

Herbaceous species of grasslands in temperate-climate zones mainly comprise three broad plant functional groups: grasses, forage legumes and nonleguminous forbs; the latter are generally not included in seeds mixtures for agricultural grasslands, except for special situations such as for organic farms.[11]

In many forb species, antioxidant properties have been reported.[12,13] Pastures with a more diverse botanical composition, including forbs, may enhance oxidative stability of milk. However, there is an agronomic knowledge gap in terms of quantitative data on the yield and quality of forbs in lowland regions with intensive systems. Few studies on vitamin concentrations in forages have been carried out with grass-

Received: July 30, 2014
Revised: December 22, 2014
Accepted: December 22, 2014
Published: December 22, 2014

ACS Publications © 2014 American Chemical Society

DOI: 10.1021/jf503658n
J. Agric. Food Chem. 2015, 63, 406−414

Table 1. Minimum (min), Average (avg), and Maximum (max) Air Temperatures, Accumulated Precipitation and Global Radiation during Growth Intervals (Days of Year; 40 d before Initial Harvest and between Successive Harvests of Herbage) during 2009 and 2010

2009	primary growth	1st regrowth	2nd regrowth	3rd regrowth
growth interval	19/4−28/5	29/5−8/7	9/7−20/8	21/8−22/10
duration (d)	40[a]	41	43	63
min. temp. (°C)	5.7	9.3	11.8	7.9
avg. temp. (°C)	10.3	14.6	16.2	11.5
max. temp. (°C)	15.0	19.1	20.6	15.2
precipitation (mm)	54	73	109	105
radiation (MJ m^{-2})	742	921	692	598
2010	primary growth	1st regrowth	2nd regrowth	3rd regrowth
growth interval	21/4−30/5	31/5−12/7	13/7−18/8	19/8−20/10
duration (d)	40[a]	43	37	63
min. temp. (°C)	4.9	10.6	12.5	7.4
avg. temp. (°C)	8.4	14.7	17.0	11.2
max. temp. (°C)	12.3	19.0	21.3	14.8
precipitation (mm)	53	77	136	118
radiation (MJ m^{-2})	635	880	569	602

[a]Defined value.

legume mixtures (e.g., ref 14). Data on vitamins, yield, dry matter (DM) content, FA, protein, and fiber content in nonleguminous forb species are scarce, however, data from a field experiment with nonleguminous forbs, legumes, and a perennial ryegrass−white clover mixture has been recently published by us.[11,15]

Insight into the relationship between agro-ecological and environmental aspects for these traits that are important for food quality is lacking and could help to develop management guidelines and design novel biodiverse pastures for particular product quality characteristics such as higher unsaturated FA contents or flavours (e.g., refs 16 and 17). The aims of this study were to examine interrelations between herbage yield, vitamin concentrations, and protein and fiber contents as affected by harvest date during the growing season. We hypothesized that those interrelations would be similar for the investigated forages.

MATERIALS AND METHODS

Experimental Design, Plant Material, and Sward Management. The experiment was established in spring 2008 at the Research Farm Foulumgaard, Aarhus University, Denmark on a loamy sandy soil with pH (KCl) 5.9. Experimental details on establishment were reported earlier.[11] Pure stands were sown of four nonleguminous forb species, three legumes, and a mixture of perennial ryegrass (*Lolium perenne* L.) and white clover (*Trifolium repens* L.). The nonleguminous forbs were: salad burnet (*Sanguisorba minor* Scop.), caraway (*Carum carvi* L.), chicory (*Cichorium intybus* L.), and ribwort plantain (*Plantago lanceolata* L.). The legumes were yellow sweet clover (*Melilotus officinalis* (L.) Pall.), lucerne (*Medicago sativa* L.), and birdsfoot trefoil (*Lotus corniculatus* L.). The experimental design was a randomized block with two replications. Net plot size was 1.5 m × 9 m and there were 8 plots in each block.

Agronomic Management. One replicate was fertilized with cattle slurry which was applied with hoses in spring (17 April 2009 and 15 April 2010) and after the second cut (10 July 2009 and 15 July 2010) at 40.5 and 30.8, 23.9, and 20.5 t ha^{-1}, respectively. These dates and amounts reflect typical slurry applications on nonorganic farms in the region. The other replicate received only potassium sulfate in amounts that provided K comparable to that in the slurry: 200 kg ha^{-1} K was applied on 10 July 2009, and 100 kg ha^{-1} K on 7 April 2010 and 16 July 2010 (after the second cut). As P was not limiting, no P was applied. Thus, the main difference between this and the slurry-treated plots was additional N in slurry (ca. 190 kg ha^{-1} y^{-1} total N in slurry, of which ca. 114 kg ha^{-1} was NH_4−N). As replicate was confounded with slurry, a model was chosen with replicate (slurry) as fixed effect.

In this experiment, which was carried out on agricultural soils with high fertility, amounts of available N, P, and K were apparently not limiting.[11] The N-delivery capacity of the experimental site was at least 200 kg N ha^{-1} in 2009 and 140 kg N ha^{-1} in 2010, approaching the amounts of total N provided in slurry (185 and 195 kg N ha^{-1} of which 60% was NH_4−N). The loss of slurry N due to ammonia volatilization may explain the absence of a response to the additional N provided in slurry. Yields were presented earlier[11] and were similar in slurry-fertilized and mineral-K fertilized replicates, as were CP contents and other compounds in the harvested herbage. Replicate plots had generally similar digestibility values and there were no significant block differences for any of the measured traits.

Swards were cut with a forage harvester (J Haldrup A/S, Løgstør, Denmark) to a residual stubble height of 7 cm. Prior to cutting, visual observations were made on species development and leaf proportion but no phenological data were recorded.

Harvest Dates and Weather. Cutting dates in 2009 were 29 May, 9 July, 21 August, and 23 October, and in 2010, 31 May, 13 July, 19 August, and 21 October. These dates corresponded with standard dates for grass harvesting of typical 4-cut systems in Denmark, which are based on calendar date. The duration of the regrowth intervals of the herbages that were cut in harvests two to four (July 9/13, August 21/19 and October 23/21 in 2009/2010) was rather similar in both years: 41, 43, and 61 days in 2009 and 43, 37, and 61 days in 2010, respectively. Irrigation was applied on 9 and 29 June 2009 (38 and 54 mm respectively) and on 15 July 2010 after the second cut (15 mm following slurry application) to prevent drought stress.

Weather data were recorded daily at the Foulumgaard weather station within 500 m of the plot area. The winter of 2009/2010 was characterized by low temperatures and late frosts, and spring growth started late. The average temperature in April 2010 was only 6.5 °C whereas in April 2009 it was 9.4 °C (Table 1). Means of monthly air temperatures from April to October varied between 7.0 and 16.5 °C in 2009 and between 6.5 and 17.8 °C in 2010. On average, temperatures were higher in 2009 than in 2010, except during July and October. Means of monthly rainfall from April to October varied between 0 and 82 mm in 2009 and between 21 and 113 mm in 2010; total growing season rainfall was 367 and 445 mm, respectively. April 2009 was very dry (0 mm) and also in later months the rainfall in 2009 was lower than in 2010, except in June. There was a dry period though in 2009 from June 21 until July 7, with high temperatures. The total global radiation was much higher in 2009 than in 2010: from April to August,

DOI: 10.1021/jf503658n
J. Agric. Food Chem. 2015, 63, 406−414

total growing season radiation was 3252 and 2970 MJ m^{-2}, respectively.

Sample Processing and Chemical Analyses. After cutting, the herbage was weighed and samples were taken. One *ca.* 200 g sample was dried at 60 °C for 48 h in an air-forced oven, and used to determine DM content and for all chemical analyses. Ash was determined after combustion for 6 h at 525 °C, and N content was determined.[18] A Fiber-Tec system was used to determine neutral detergent fiber (NDF),[19] acid detergent fiber (ADF), and acid detergent lignin (ADL).[20] A second sample of ca. 500 g was taken from each cut in both years, immediately frozen in a plastic bag at −20 °C, freeze-dried and subsequently stored in an airtight plastic bag at −20 °C until analysis. Samples were later lyophilized and milled through a 1 mm screen. Of this material, 2 g was saponified in alcohol and the vitamins were subsequently extracted into heptane, analyzed by HPLC and quantified for α-tocopherol, ß-carotene (the sum of all isomers) and lutein.[21] Fatty acids were extracted in a mixture of chloroform, methanol, and water[22] after acidification by boiling in 3 mol L^{-1} of HCl for 1 h. Methyl esters were synthesized from alkaline methanol with BF_3 as catalyst and analyzed on gas liquid chromatography as methyl esters with C17 as internal standard. Unsown species (that comprised <5% of herbage DM) were excluded from the samples used for chemical analyses. In the October harvest of 2010, no herbage samples could be collected of salad burnet and yellow sweet clover due to low yields; in the latter species also one replicate sample was lacking in three other harvests.[11] In addition to absence of data in 5 plots, in 4 herbage samples no vitamins could be measured for yellow sweet clover because low yields prevented taking a 500 g sample, so vitamin data were only available in 7 out of 16 potential samples.

Statistical Analysis. Analysis of variance procedures were applied using the MIXED procedures of SAS (Version 9).[23,24] There were eight "species" (the seven forb species plus the mixture) and four harvests per year. Crude protein (CP) was calculated as 6.25 × N. The category "other compounds" was calculated as 1,000 − (NDF + CP + FA + Ash), lignin as ADL, cellulose as ADF − ADL and hemicellulose as NDF − ADF. For each species, mean, standard deviation and coefficient of variation were calculated for each parameter. The experimental design was a randomized block with two replications that were, however, confounded with management; hence statistically, sample size was n=1. Therefore,[25] yield and quality parameters were evaluated with a model that included fixed main effects of species, cut and replicate (block = slurry) (λ_b) to account for differences in fertilization regime and possible effects of N and P on yield and quality:

$$Y_{bscy} = \mu + \alpha_s + \beta_c + (\alpha\beta)_{sc} + \delta_b + A_y + B_{bs} + C_{bsc} + D_{sy} + F_{bsy} + E_{bscy}$$

where Y_{bscy} = the recorded value for species s in cut c of replicate (block) b in year y.

Greek letters denote fixed effects. Capital Latin letters denote random effects. Lower case Latin letters identify the effects and observations. E_{bscy} represents the random error.

The following effects were considered to be random effects: year (A_y), replicate × species (B_{bs}), replicate × species × cut (C_{bsc}), species × year (D_{sy}) and replicate × species × year (F_{bsy}). Because in an earlier model[11] the year × replicate effect $(\delta\lambda)_{yb}$ was not significant for any of the parameters, this interaction term was not included. The interaction species × cut $(\alpha\beta)_{sc}$ was significant and was kept in the model as a fixed effect. Interactions including replicate were generally small and kept in the model as random effects in order to take into account the random variation between plots and to take into account certain correlations that must be expected because of the design structure (e.g., same plot measured in both years). When analyzing experiments with a sample size n=1, ANOVA can be performed if some relevant interaction terms are random or absent and assuming that those random or absent terms have no true fixed effect.[25] These assumptions were met.

Differences detected among main effects and interactions were assessed using the PDIFF option in the least-squares means statement. All tests of significance were made at $P = 0.05$. First, overall covariance analyses were carried out to test the effect of species. Then, for each species simple regression analyses were conducted between vitamin concentrations and 1) yield, 2) NDF, and 3) CP, as well as among vitamin concentrations. Finally, multiple regression analyses were conducted with α-tocopherol, β-carotene, or lutein as dependent variables, and yield, concentrations of chemical compounds and weather parameters as independent variables. Starting with the full model, nonsignificant variables were successively dropped from the model until only significant variables remained. Temperature, rainfall and radiation were calculated for each regrowth interval (Table 1) and also for periods of 10, 7, 5, and 2 days before cutting.

Earlier Findings. Yield and concentrations of vitamins and other compounds differed among species[11,15] as summarized in Table 2.

Table 2. Significance of Main Effects of Species (S) and Cut (C), Their Interaction (S × C) and of Year (Y) for Concentrations of α-Tocopherol, β-Carotene, and Lutein, DM Yield, Concentrations of Neutral Detergent Fiber (NDF), Acid Detergent Fibrer (ADF), Acid Detergent Lignin (ADL), Crude Protein (CP), Fatty Acids (FA), "Other Compounds" and Ash, and Cell Wall Composition for Eight Species (Four Non-Leguminous Forbs, Three Forage Legumes and a Perennial Ryegrass−White Clover Mixture), Based on Four Cuts in 2009 and 2010: *** P < 0.001; ** P < 0.01; * P < 0.05; NS Not Significant[a]

	sign			
trait	S	C	S × C	Y
vitamins (mg kg^{-1} DM)				
α-tocopherol	**	*	NS	NS
β-carotene	*	***	***	NS
lutein	**	***	**	***
yield (kg DM ha^{-1} yr^{-1})	*	***	NS	NS
DM composition (g kg DM^{-1})				
NDF	**	***	NS	NS
ADF	**	***	NS	NS
ADL	***	***	NS	*
CP	***	***	*	NS
FA	**	*	***	**
other compounds[b]	***	***	NS	NS
ash	***	***	*	NS
cell wall composition (%)				
cellulose[c]	NS	NS	NS	NS
hemicellulose[d]	NS	***	**	NS

[a]Data summarized from Elgersma et al.[11,15]. [b]Other =100 − (NDF + CP + Ash) − mainly water-soluble carbohydrates and other components. [c]100(ADF-ADL)/NDF. [d]100(NDF-ADF)/NDF.

Averaged across harvests and years, yields were lower in yellow sweet clover, salad burnet and caraway (3.9, 4.6, and 5.6 t DM ha^{-1} $year^{-1}$, respectively) than in the grass−clover mixture and lucerne (12.5 and 15.4 t DM ha^{-1} $year^{-1}$, respectively). Lucerne, chicory, ribwort plantain, and birdsfoot trefoil had similar DM yields to the perennial ryegrass−white clover mixture. Ribwort plantain and lucerne had the highest concentrations of NDF (402 and 383 g kg DM^{-1}, respectively), ADF (339 and 321 g kg DM^{-1}, respectively), and ADL (78 and 67 g kg DM^{-1}, respectively). Birdsfoot trefoil had low NDF (328 g kg DM^{-1}) and ADF (272 g kg DM^{-1}) concentrations but a high ADL concentration (62 g kg DM^{-1}), as well as a low ash content (91 g kg DM^{-1}). The highest ash concentration was found in chicory (143 g kg DM^{-1}). CP concentrations were highest in legume

DOI: 10.1021/jf503658n
J. Agric. Food Chem. 2015, 63, 406−414

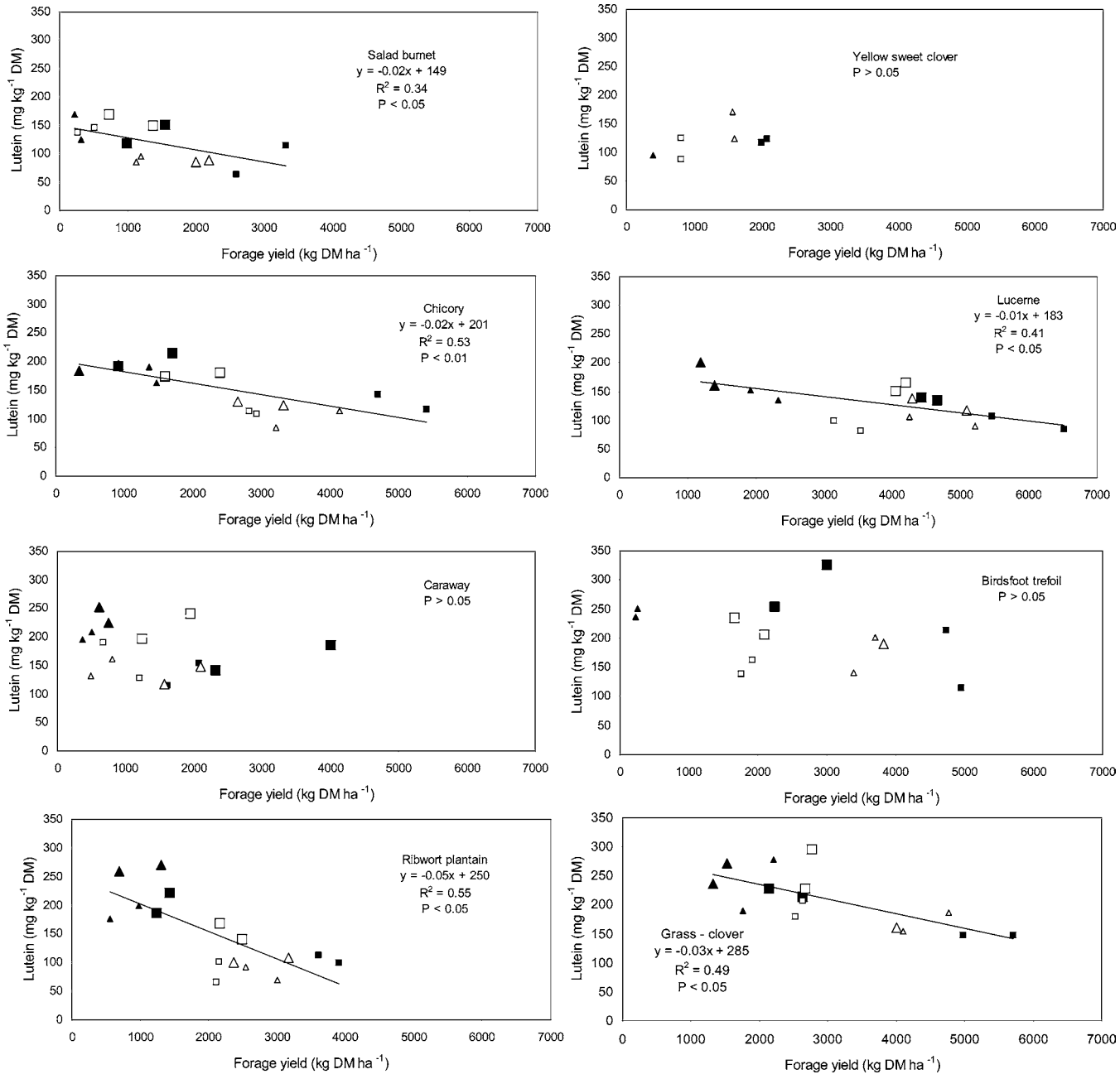

Figure 1. Relationships between concentrations of lutein and dry matter yield during four harvests (■ late May, Δ early July, □ mid/late August, ▲ mid/late October) in 2009 (small symbols) and 2010 (large symbols) yield in (left) salad burnet, chicory, caraway, and ribwort plantain, and (right:) yellow sweet clover, lucerne, birdsfoot trefoil, and a perennial ryegrass−white clover mixture.

species (198−206 g kg DM^{-1}) and in the grass−clover mixture (199 g kg DM^{-1}), and lowest in chicory and ribwort plantain (102 and 115 g kg DM^{-1}, respectively). The concentration of "other compounds" (i.e., not being ash, CP, fiber, or FA) including water-soluble carbohydrates, was significantly higher in salad burnet (452 g kg DM^{-1}) than in all other species; it was also higher in chicory and caraway (406 and 400 g kg DM^{-1}, respectively) than in the legume species (306−349 g kg DM^{-1}) and the mixture (320 g kg DM^{-1}).[11] Fatty acid concentrations were lowest in lucerne, ribwort plantain, chicory and yellow sweet clover (15.9, 17.1, 19.2, and 19.3 g kg^{-1} DM, respectively) and highest in birdsfoot trefoil and caraway (24.5 and 27.0 g kg^{-1} DM, respectively)[15]

α-Tocopherol concentrations were on average lowest in lucerne and yellow sweet clover (21 and 23 mg kg^{-1} DM) and highest (and exceeding those of the grass - clover mixture) in ribwort plantain and salad burnet (77 and 85 mg kg^{-1} DM, respectively). β-Carotene concentrations were lowest in lucerne, salad burnet and yellow sweet clover (26, 30, and 33 mg kg^{-1} DM) and highest in grass-clover, ribwort plantain, birdsfoot trefoil and caraway (48, 56, 59, and 61 mg kg^{-1} DM, respectively). Lutein concentrations were lowest in lucerne, salad burnet, yellow sweet clover, ribwort plantain and chicory (129, 129, 131, 149, and 152 mg kg^{-1} DM) and highest in birdsfoot trefoil, the grass−clover mixture, and caraway (206, 195, and 174 mg kg^{-1} DM, respectively).

Species × cut interactions were not significant for yield and most chemical compounds (Table 2), except for concentrations of CP and ash ($P < 0.05$),[11] β-carotene ($P < 0.001$), and total FA ($P < 0.01$).[15] Species × cut interactions that were significant were relatively small compared to main effects. There was no effect of year, except for concentrations of lignin ($P < 0.05$), FA ($P < 0.01$), and lutein ($P < 0.001$) (Table 2).

DOI: 10.1021/jf503658n
J. Agric. Food Chem. 2015, 63, 406−414

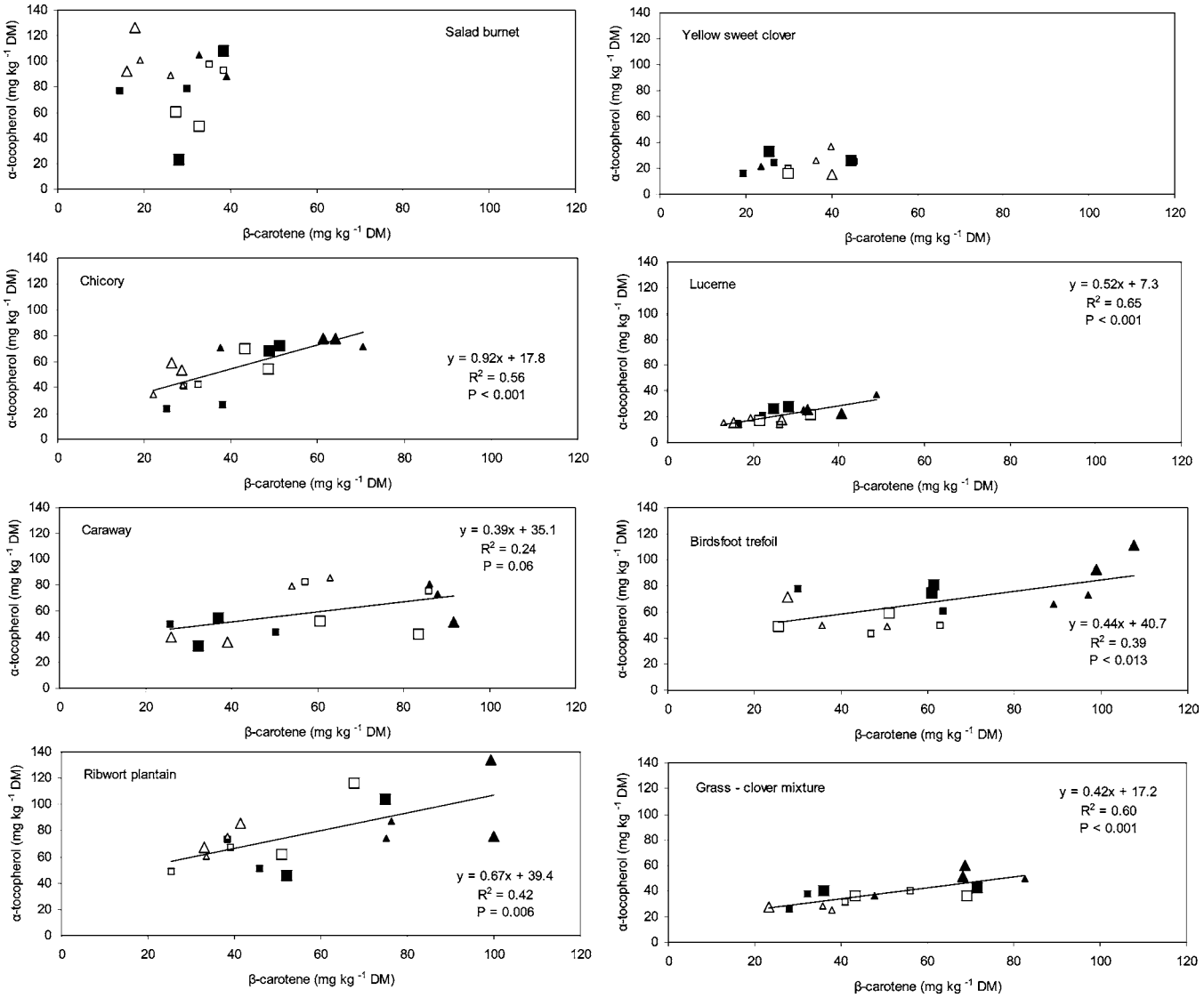

Figure 2. Relationships between concentrations of α-tocopherol and of β-carotene at four cuts (■ late May, Δ early July, □ mid/late August, ▲ mid/late October) in 2009 (small symbols) and 2010 (large symbols) in (left) salad burnet, chicory, caraway, and ribwort plantain, and (right) yellow sweet clover, lucerne, birdsfoot trefoil, and a perennial ryegrass−white clover mixture.

RESULTS

Seasonal Variation in Herbage Dry Matter Yield, Chemical Composition of the Forage, and Vitamin Contents. Lutein concentrations are shown in relation to DM yield in Figure 1. Herbage yields were generally lowest in the fourth harvest ($P < 0.001$) as can be seen in Figure 1. The seasonal growth patterns differed between years: in 2009, the first cut yielded most whereas in 2010, the second cut was most productive, except for caraway. During the fourth cut, yields were comparable in both years (caraway, ribwort plantain) or slightly higher in 2009 (chicory, lucerne, grass−clover mixture). Annual yields were numerically lower in 2010 than in 2009 for most species except caraway but averaged across species, there was no statistically significant effect of year (Table 2). For most species, the DM yield of the first cut was much higher in 2009 than in 2010: e.g., that of grass−clover produced 5.3 and 2.4 t DM ha^{-1} and birdsfoot trefoil yielded 4.8 and 2.6 t DM ha^{-1}, respectively. Leaf proportions of all species (not shown) were highest in the fourth harvest when all species were in the vegetative stage. Lucerne, yellow sweet clover, and chicory had a high proportion of stems during summer. Stems in birdsfoot trefoil were small, thin and green in both years, in contrast to stems of other forb species. Caraway had few stems that occurred already early May when other forbs were still vegetative; they started flowering after the first cut. Grass was in the heading stage at the time of the May harvests. Caraway had in the first cut of 2009 more stems and flowers than in the first cut of 2010.

Averaged across all species, large differences were found for ash and CP contents between harvest dates (Table 2). Ash concentrations were lower ($P < 0.001$) in cuts 1 and 2 than in cuts 3 and 4, whereas CP concentrations were higher ($P < 0.001$) in the first than in the second cut and then increased to become highest in cuts 3 and 4 (not shown). There were large differences ($P < 0.001$) between harvest dates in the concentration of "other compounds" including water-soluble carbohydrates, which were highest in the first cut and lowest in the third cut. The fiber contents (i.e., concentrations of NDF, ADF and ADL) differed between harvests ($P < 0.001$) and were lowest in the fourth harvest for all species, coinciding with low

DOI: 10.1021/jf503658n
J. Agric. Food Chem. 2015, 63, 406−414

Table 3. Regression Coefficients (b) and R^2 of Regression Lines for Relationships between α-Tocopherol or β-Carotene Concentrations (mg kg^{-1} DM) and Dry Matter (DM) Yield, Neutral Detergent Fiber (NDF) and Nitrogen (N) Content, Across 8 Harvests (n = 16), for 8 Species[a]

	yield (t DM ha^{-1})				NDF (g kg DM^{-1})				N (g kg DM^{-1})			
	α-tocopherol		β-carotene		α-tocopherol		β-carotene		α-tocopherol		β-carotene	
	b	R^2	b	R^2	b	R^2	b	R^2	b	R^2	b	R^2
salad burnet	NS		−5.4	0.35	NS		−0.11	0.52	NS		0.14	0.56
caraway	−14.6	0.57	−16.7	0.43	NS		NS		NS		0.49	0.53
chicory	−11.9	0.87	−7.7	0.55	NS		−0.16	0.56	0.57	0.38	0.58	0.59
ribwort plantain	NS		−17.5	0.56	NS		−0.18	0.29	NS		NS	
yellow sweet clover	NS		NS		−0.08	0.62	NS		NS		NS	
lucerne	−2.1	0.25	−1.0	0.58	−0.08	0.50	−0.11	0.44	NS		0.27	0.39
birdsfoot trefoil	NS		−9.4	0.36	−0.18	0.47	−0.30	0.64	NS		0.75	0.51
grass−clover	−4.5	0.31	−10.1	0.53	NS		NS		NS		0.38	0.27

[a]Only values are shown with $P < 0.05$.

Table 4. Regression Coefficients for Herbage Yield (b) and Mean Air Temperature of the 7 Days before Harvest (T7) (c) with P Values and R^2 of Multiple Regression Analyses for Relationships of Explanatory Variables for Variation in Concentrations of β-Carotene, α-Tocopherol, and Lutein, Respectively, in Four Non-Leguminous Forbs, 3 Forage Legumes, a Perennial Ryegrass−White Clover Mixture (n = 16), and Across All Species (n = 128)

	β-carotene					α-tocopherol					lutein				
	yield		T7			yield		T7			yield		T7		
	(t DM/ha)		(°C)			(t DM/ha)		(°C)			(t DM/ha)		(°C)		
species	b	P	c	P	R^2	b	P	c	P	R^2	b	P	c	P	R^2
salad burnet	−5.0	0.03		NS	0.49		NS		NS	NS	−20.1	0.04		NS	(0.39)
caraway	−16.3	0.00		NS	0.54	−14.6	0.00		NS	0.57		NS		NS	NS
chicory	−4.8	0.02	−1.5		0.72	−11.4	<.00		NS	0.88	−13.3	0.03	−3.4	0.04	0.66
ribwort plantain	(−8.8)[a]	(0.06)	−2.7		0.74		NS		NS	NS		NS	−7.9	0.01	0.76
yellow sweet clover		NS	1.8		NS		NS		NS	NS		NS		NS	NS
lucerne	−3.6	0.01		NS	0.67		NS	−0.8		0.54		NS		NS	0.44
birdsfoot trefoil	−6.3	0.05	−3.1		0.71		NS	−2.7		0.57		NS		NS	NS
grass−clover	−8.7	0.02		NS	0.56		NS		NS	0.40	−25.3	0.01		NS	0.50
all species	−5.8	<0.00	−1.6	<0.00	0.36	−9.2	<0.00		NS	0.25		NS	−4.6	<0.00	0.22

[a]Values in brackets have a P value of 0.06.

yields. The concentrations of ADF and its components (hemicellulose and lignin) were generally higher in 2010 than in 2009 ($P < 0.05$).

Vitamin concentrations differed significantly ($P < 0.001$) among harvests (Table 2) and were generally lowest in the second cut, and highest in the fourth cut (Figure 2). The fourth cut showed high vitamin concentrations in both years, but α-tocopherol levels were higher in 2010 than in 2009. Interactions between species and cut were not significant for α-tocopherol (Table 2).

The ranking order for coefficients of variation of the species differed for the various parameters. The extent of variability in relation to the mean was generally highest for herbage yield, followed by contents of β-carotene, ADL, hemicellulose, α-tocopherol, cellulose and lutein; ash had the lowest value (not shown). The coefficients of variation for β-carotene ranged from 27 to 44%, for α-tocopherol from 27 to 33% and for lutein from 22 to 29% with ribwort plantain (44%) as outlier.

Relations between α-Tocopherol and β-Carotene, Lutein, Herbage Dry Matter Yield, and Chemical Composition. Covariance analyses of all data with vitamin contents as dependent variables showed large effects of species ($P < 0.001$) and yield ($P < 0.001$), therefore analyses were carried out for each species to investigate interrelations among vitamins contents, and between vitamins, yield, chemical compounds and weather parameters.

Figure 2 shows the relationship between α-tocopherol and β-carotene across harvest dates (four cuts in two years) for all species. Seasonal and annual fluctuations in vitamin contents can also be seen in Figures 1 and 2; harvests in May when most and October when all herbage was in the vegetative stage are depicted in black symbols and harvests during summer, when most species were in the generative stage, with open symbols. There was a positive correlation between α-tocopherol and β-carotene concentration in all species, except in salad burnet and yellow sweet clover where no relationship was found. Both vitamins were negatively correlated with yield in the non-leguminous forbs caraway, ribwort plantain ($P = 0.08$ for α-tocopherol), and to a lesser extent chicory; in salad burnet, β-carotene showed a negative relation with yield but there was no relation between α-tocopherol and yield (Table 3). In the grass−clover mixture, the negative relation between yield and β-carotene was stronger than that for α-tocopherol; in lucerne a similar pattern was found. Correlations in lucerne were less strongly negative than in grass−clover. In yellow sweet clover, no relations between yield and vitamin concentrations were found. In birdsfoot trefoil, only β-carotene was negatively correlated with yield. The correlation between β-carotene and yield was generally more negative than that between α-

DOI: 10.1021/jf503658n
J. Agric. Food Chem. 2015, 63, 406−414

tocopherol and yield, except in chicory. Salad burnet, caraway, birdsfoot trefoil and chicory had a low NDF content relative to grass−clover. Negative correlations between NDF and β-carotene were found in most forb species and with α-tocopherol in the legumes (Table 3).

In most herbages, lutein and β-carotene were positively correlated (not shown) but lutein and α-tocopherol were not correlated. Lutein was neither correlated with protein or NDF content (not shown). There was a negative correlation between lutein and herbage yield in salad burnet, chicory, ribwort plantain, lucerne, and the grass−clover mixture (Figure 1).

Multiple regression analyses (Table 4) revealed that across all species (n = 128), the variation in β-carotene was in part explained (R^2 = 0.36) by yield and temperature (mean of 7 days before cutting); the variation in α-tocopherol by yield (R^2 = 0.25); and the variation in lutein by temperature (R^2 = 0.22). The average temperature of 10, 7, or 5-day intervals prior to harvest had stronger correlations in the regressions than temperature during the entire growth interval (Table 1). Therefore, we chose the 7-day interval. Radiation and rainfall did not have significant effects; therefore, only temperature was included in the models.

In most species, temperature had more effect on β-carotene than on α-tocopherol (Table 4). Adding chemical compounds to the model did not improve the outcome. For example, there were significant simple correlations (Table 3) between β-carotene and NDF or CP but significance of those compounds was lost when temperature or yield were included in the models (Table 4).

DISCUSSION

Main Variation Factors of Vitamin Contents; Effect of Harvest Date. Concentrations of vitamins and FA in plants depend on factors such as regrowth stage, N availability, temperature, day length, and leaf proportion in the harvested herbage.[8,9] The main variation factors of vitamin contents are species c.q. botanical composition,[26] stage of maturity,[26,27] point in the growing season,[27] leaf/stem ratio,[10] and environmental factors.[28]

The stage of maturity of a species at harvest is determined by the duration of the preceding regrowth period, the daylength and weather conditions during the regrowth period. In this experiment, all species were cut at similar dates. The primary growth period may have differed according to species-specific temperature thresholds for growth. From the second harvest onward (July until October), regrowth periods, and associated temperature sums and radiation during each of these periods, were the same for all species. Radiation had no effect and temperature only explained part of the variation in β-carotene and lutein concentrations. In most species, temperature had more effect on β-carotene than on α-tocopherol.

In this experiment, leaf proportions of species were highest in October, which coincided with generally high concentrations of vitamins. This is in line with Brown[30] who found four times more α-tocopherol in grass leaves than in stems, and three times more α-tocopherol in clover leaves than in petioles. As tocopherols are located in the photosynthetic parts of plants, in the chloroplasts,[7] leaves contain more tocopherol than stems.[10] Higher contents of β-carotene have also been found in plants containing a higher proportion of leaves.[9] Unfortunately, in this study grass and clover leaves and stems were not separated; levels of α-tocopherol in mixed grass-clover herbage were 35, 48, and 35% higher in October (when both species were in the vegetative stage) than in May (when grass was heading), July, and August (when white clover had most flowers), respectively, and β-carotene levels were 70, 140, and 30% higher (Figure 2). Vitamin concentrations were thus generally lowest in July, which is in line with results from another Danish findings[31] reporting that β-carotene contents in grasslands with red clover (*Trifolium pratense* L.), white clover, lucerne and chicory, were lower in July than in May.[14] We also found 1.2−1.7 times higher contents of β-carotene in May than in July for all species except caraway and yellow sweet clover. Lucerne and yellow sweet clover had 1.3, and birdsfoot trefoil 1.5 times more α-tocopherol in May than in July (Figure 2).

Legumes flower most abundantly in summer. Levels of α-tocopherol were 71 and 69% higher in birdfoot trefoil, and 61 and 74% higher in lucerne in October than in July and August, respectively; figures for β-carotene were 195 and 220%, and 111 and 61%. Also chicory, salad burnet and ribwort plantain showed this pattern (Figure 2). In general, the concentration of β-carotene fluctuated more within each species than that of α-tocopherol, while lutein showed least variation. Lutein and β-carotene are found in association and the reason for the lower variation in lutein concentrations across the various harvest dates is not clear.

In pastures, species are mixed but here single-species stands of forbs were studied. Caution should be taken when intrapolating yield and chemical composition data, as plant species can interact differently with each other when grown in a mixture than when grown in monoculture. Interspecific interaction can affect canopy structure and leaf/stem ratio of species. Stress factors such as pests may cause increased α-tocopherol levels;[7] however, no pests or diseases were observed in our study.

Differences between Species; Relationships with Chemical Compounds. In this experiment, species differences were significant: α-tocopherol concentrations were on average lowest in lucerne and yellow sweet clover and highest in ribwort plantain and salad burnet; β-carotene concentrations were lowest in lucerne, salad burnet and yellow sweet clover and highest in grass-clover, ribwort plantain, birdsfoot trefoil and caraway; and lutein concentrations were lowest in lucerne, salad burnet, yellow sweet clover, ribwort plantain and chicory and highest in birdsfoot trefoil, the grass−clover mixture and caraway. Concentrations in pure stands of ribwort plantain and salad burnet (on average 77 and 85 mg α-tocopherol kg^{-1} DM, respectively), grass-clover and ribwort plantain (48 and 56 mg β-carotene kg^{-1} DM, respectively), and grass−clover and birdsfoot trefoil (195 and 206 mg lutein kg^{-1} DM, respectively) were comparable with reported data[29] from Southern Norway of 76−83 mg kg^{-1} DM α-tocopherol, 44−48 mg kg^{-1} DM β-carotene, and 193−244 mg lutein kg^{-1} DM in two mixed pastures with similar herbage proportions of nonleguminous forbs; however, these were mainly annual and biannual weeds.

This study demonstrated in a range of forb species a negative correlation between herbage yield and concentrations of β-carotene (6 out of 7 forbs), lutein (4 out of 7 forbs) and α-tocopherol (3 out of 7 forbs). In a perennial ryegrass−white clover mixture, negative correlations between herbage yield and all 3 vitamins were found; this was also the case in lucerne and chicory. Yellow sweet clover was the only forb where no correlation between herbage yield and vitamin contents occurred which may in part have been caused by missing values for this species.[11]

DOI: 10.1021/jf503658n
J. Agric. Food Chem. 2015, 63, 406−414

In all forbs except yellow sweet clover the β-carotene content was negatively correlated with NDF and positively with N contents; both correlations were significant for salad burnet, chicory, lucerne and birdsfoot trefoil. In caraway, there was a numerically negative correlation with NDF and a significant positive correlation with N content and in ribwort plantain, there was a significant negative correlation with NDF and a numerically positive correlation with N content; both numerical trends were not significant due to outliers. These correlations are in line with our expectation because herbage in a vegetative stage, i.e., in the October harvests, has a high leaf proportion which is associated with lower fiber and higher protein contents compared with herbage in a generative stage. Indeed, in autumn the yields were lowest and herbage contained most protein, least fiber (lignin, cellulose, hemicellulose), had a high ash content[11] and the highest concentrations of vitamins.[15] Correlations between α-tocopherol and NDF were only present in the 3 legumes, and between α-tocopherol and N only in chicory (Table 3); for this we do not have an explanation. There was no indication that interrelations of herbage yield, NDF and N with vitamin contents differed among legumes and nonleguminous forbs; however, numbers of species were rather low which hampers a general comparison of functional groups. Within most species, concentrations of α-tocopherol and β-carotene were positively correlated. In line with our results, positive correlations between chlorophyll and carotenoid pigments have been reported for several species.[32,33] With exception of salad burnet and yellow sweet clover, this study confirmed our hypothesis that interrelations between vitamins, yield, and quality compounds were rather similar for the investigated species.

Effect of Weather. The weather may provide an explanation for the fact that in 2010, vitamin concentrations in the first harvest were much higher than in 2009, which was very evident in e.g. chicory. The winter of 2009/2010 was severe and spring growth started late (Table 1). During the 20 days preceding the date of the first cut, the average air temperature was 9.6 °C in 2010 compared to 10.6 °C in 2009[11] which implies that in 2010 the forage was less mature during the first harvest. There was also a cold period after the third cut in 2010, which might have caused a delay in regrowth resulting in physiologically younger forage in the fourth cut compared to 2009. However, the higher vitamin concentrations in October of 2010 might also partly reflect differences between first-year swards and second-year swards, in combination with different daily mean temperatures and solar radiation during the growth intervals.

As in October daylength is shorter than in May, July, and August, yield levels in autumn were confounded with low radiation (Table 1). However, radiation did not explain variation in yield or vitamins when included in models. Concentrations of α-tocopherol and β-carotene in forage species grown in Southern Sweden generally had higher concentrations than from plants grown in Northern Sweden[14] but differences in daylength and temperature were confounded with other factors. In a controlled environment, β-carotene concentration in leaves increased with temperature after 3 to 4 weeks in kale (*Brassica oleracea* L.) and decreased in spinach (*Spinacea oleracea* L.) on a fresh mass basis,[32] but no temperature effects on caroteinoid contents were found when expressed on a dry matter basis. Similarly, in our study no direct relationship was found between mean air temperature during regrowth and concentrations of α-tocopherol, β-carotene, and lutein in herbage of the various forage species. Temperature during the last week before harvest did have an effect, which was greater than that of temperature during the last 2 days before harvest. This knowledge may be used in prediction models.

Relevance to Practice and Future Perspectives. The increasing interest of consumers in environment, animal welfare and the origin and method of food production is reflected in growing preference for food products of, i.e., pasture-based systems of production. For example, in the USA organic dairy markets are growing and the demand for milk and dairy products from pasture-fed cows has increased in recent years.[34,35] A substantial body of information is now available on the differences in composition and sensory properties of products from pasture-based and concentrate-based production systems. For milk, there has been less focus on grassland than for beef, presumably because in many regions forage represents a smaller proportion in feed rations of lactating compared to growing animals. Emerging data indicate that milk and meat produced from botanically diverse pastures have higher concentrations of specific (groups of) FA such as CLA and n-3 FA and antioxidants, which may be benefial for human health.[17] Our results indicate that yield and high temperature both had a negative effect on β-carotene and lutein concentrations. These compounds would be prone to decline in view of possible higher temperatures due to climate change. In our study, α-tocopherol content was not affected by variables other than yield. In the summer period the vitamin content is lower due to higher temperature. This knowledge can be included in decision support systems, when trying to reach specific goals for herbage quality; this is especially important for high producing dairy cows or for production of special products. Taking early cuts in spring and autumn, when the temperature is lower, would be a cultivation strategy when aiming for forage with high contents of β-carotene and unsaturated FA[15] and a high nutritive value, but is associated with a lower yield. Cutting at a greater stubble height or taking off animals before the sward is grazed down could be another way to increase leaf proportion and thus enhance vitamin contents in animal diets. Choice of species combination for a mixture when establishing a new sward is another issue that warrants further research and preferably on-farm testing. The high vitamin concentrations in most nonleguminous forbs in our study compared to those in major forages such as grass−clover and particularly lucerne, may encourage adoption of these species by farmers but would in practice require a number of challenges to be overcome, including development of optimal seed mixtures and management practices that can increase persistency of forbs in mixed swards under cutting and/or grazing.[36]

AUTHOR INFORMATION

Corresponding Author

*E-mail: anjo.elgersma@hotmail.com. Tel: +31 633871347.

Notes

The authors declare no competing financial interest.

ACKNOWLEDGMENTS

The project was funded by the Danish "Fund for organic farming". We thank M. Würtz Reeh and E. Lyng Pedersen for performing the lab work and Dr. K. Kristensen for statistical advice. Financial support of A. Elgersma by EU-COST FA0802

DOI: 10.1021/jf503658n
J. Agric. Food Chem. 2015, 63, 406−414

Feed for Health, by granting her short-term scientific missions in 2012 to Denmark, is gratefully acknowledged.

REFERENCES

(1) Ballet, N.; Robert, J. D.; Williams, P. E. V. *Vitamins in forages*; CABI Publishing: Wallingford, U.K., 2000.
(2) Morand-Fehr, P.; Fedele, V.; Decandia, M.; Le Frileux, Y. Influence of farming and feeding systems on composition and quality of goat and sheep milk. *Small Ruminant Res.* **2007**, *68*, 20−34.
(3) Havemose, M. S.; Weisbjerg, M. R.; Bredie, W. L. P.; Nielsen, J. H. Influence of feeding different types of roughage on the oxidative stability of milk. *Int. Dairy J.* **2004**, *14*, 563−570.
(4) Mercier, Y.; Gatellier, P.; Renerre, M. Lipid and protein oxidation in vitro, and antioxidant potential in meat from Charolais cows finished on pasture or mixed diet. *Meat Sci.* **2004**, *66*, 467−473.
(5) Höjer, A.; Nadeau, E.; Jensen, S. K.; Gustavsson, A.-M. Fatty acid concentrations in grasses and legumes in mixed leys as affected by cutting time, site and year. In: Höjer, A., 2012. *Phytoestrogens and fatty acids in forage and bovine milk*. Doct. thesis, Swedish Univ. Agric. Sci.: Umeå, Sweden. *List of Publ., II*, pp 1−24.
(6) Asensi-Fabado, A. M.; Munné-Bosch, S. Vitamins in plants:occurrence, biosynthesis and antioxidant function. *Trends Plant Sci.* **2010**, *15*, 582−592.
(7) Munné-Bosch, S.; Alegre, L. The function of tocopherols and tocotrienols in plants. *Critical Rev. Plant Sci.* **2002**, *21*, 31−57.
(8) Booth, V. H. Alpha-tocopherol content of forage crops. *J. Sci. Food Agric.* **1964**, *15*, 342−344.
(9) Livingston, A.; Smith, D.; Carnahan, H. L.; Knowles, R. E.; Nelson, J. W.; Kohler, G. O. Variation in xanthophyll and carotene content of lucerne, clovers and grasses. *J. Sci. Food Agric.* **1968**, *19*, 632−636.
(10) McDonald, P.; Edwards, R. A.; Greenhalgh, J. F. D.; Morgan, C. A. *Animal Nutrition*, 6th ed.; Pearson Education Ltd.: Essex U.K., 2002.
(11) Elgersma, A.; Søegaard, K.; Jensen, S. K. Herbage dry matter production and forage quality of three legumes and four non-leguminous forbs in single-species stands. *Grass Forage Sci.* **2014**, *69*, 705−716.
(12) Al-Mamum, M.; Yamaki, K.; Masumizu, T.; Nakai, Y.; Saito, K.; Sano, H.; Tamura, Y. Superoxide anion radical scavenging activities of herbs and pastures in northern Japan determined using electron spin resonance spectrometry. *Int. J. Biol. Sci.* **2007**, *3*, 349−355.
(13) Xu, B. J.; Chang, S. K. C. A comparative study on phenolic profiles and antioxidant activities of legumes as affected by extraction solvents. *J. Food Sci.* **2007**, *72*, S159−S166.
(14) Lindqvist, H.; Nadeau, E.; Jensen, S. K. Alpha-tocopherol and β-carotene in legume-grass mixtures as influenced by wilting, ensiling and type of silage additive. *Grass Forage Sci.* **2012**, *67*, 119−128.
(15) Elgersma, A.; Søegaard, K.; Jensen, S. K. Fatty acids, α-tocopherol, β-carotene and lutein contents in forage legumes, forbs and a grass − clover mixture. *J. Agric. Food Chem.* **2013**, *61*, 11913−11920.
(16) Larsen, M. K.; Kidmose, U.; Kristensen, T.; Beaumont, P.; Mortensen, G. Chemical composition and sensory quality of bovine milk as affected by type of forage and proportion of concentrate in the feed ration. *J. Sci. Food Agric.* **2013**, *93*, 93−99.
(17) Moloney, A. P.; Monahan, F. J.; Schmidt, O. Quality and authenticity of grassland products. *Grassland Sci. Eur.* **2014**, *19*, 600−602.
(18) Hansen, B. Determination of nitrogen as elementary N, an alternative to Kjeldahl. *Acta Agric. Scand.* **1989**, *39*, 113−118.
(19) Mertens, D. R. Gravimetric determination of amylase-treated neutral detergent fiber in feeds with refluxing in beakers or crucibles: Collaborative study. *J. AOAC Int.* **2002**, *85*, 1217−1240.
(20) Van Soest, P. J. Use of detergents in the analysis of fibrous feeds. *J. AOAC* **1963**, *46*, 825−835.
(21) Jensen, S. K. Improved Bligh and Dyer extraction procedure. *Lipid Techn.* **2008**, *20*, 280−281.
(22) Bligh, E. G.; Dyer, W. J. A rapid method of total lipid extraction and purification. *Can. J. Biochem. Phyisol.* **1959**, *37*, 911−917.
(23) SAS Release 9.3 for Windows; SAS Institute Inc.: Cary, NC, USA, 2011.
(24) Littell, R.C.l; Milliken, G. A.; Stroup, W. W.; Wolfinger, R. D. *SAS_Systems for Mixed Models*; SAS Inst. Inc.: Cary, NC, USA, 2006.
(25) Cochran, W. G.; Cox, G. M. *Experimental Designs*; Wiley: New York, 1957.
(26) Danielsson, H.; Nadeau, E.; Gustavsson, A..-M.; Jensen, S. K.; Søegaard, K.; Nilsdotter-Linde, N. Contents of alpha-tocopherol and beta-carotene in grasses and legumes harvested at different maturities. *Grassland Sci. Eur.* **2008**, *13*, 432−434.
(27) Nozière, P.; Graulet, B.; Lucas, A.; Martin, B.; Grolier, P.; Doreau, M. Carotenoids for ruminants: From forages to dairy products. *An. Feed Sci. Technol.* **2006**, *152*, 204−218.
(28) Hjarde, W.; Hellström, V.; Åkerberg, E. The contents of tocopherol and carotene in red clover as dependent on variety, conditions of variety, conditions of cultivation and stage of development. *Acta Agric. Scand.* **1963**, *13*, 3−16.
(29) Adler, S. A.; Dahl, A. V.; Jensen, S. K.; Thuen, E.; Gustavsson, A.-M.; Steinshamn, H. Fatty acid composition, fat-soluble vitamin concentrations and oxidative stability in bovine milk produced on two pastures with different botanical composition. *Livest. Sci.* **2013**, *154*, 93−102.
(30) Brown, F. The tocopherol content of farm feeding-stuffs. *J. Sci. Food Agric.* **1953**, *4*, 161−165.
(31) Larsen, M. K.; Fretté, X. C.; Kristensen, T.; Eriksen, J.; Søegaard, K.; Nielsen, J. H. Fatty acid, tocopherol and carotenoid content in herbage and milk affected by sward composition and season of grazing. *J. Sci. Food Agric.* **2012**, *92*, 2891−2898.
(32) Lefsrud, M. G.; Kopsell, D. A.; Kopsell, D. E.; Curran-Celentano, J. Air temperature affects biomass and carotenoid pigment accumulation in kale and spinach grown in a controlled environment. *HortSci.* **2005**, *40*, 2026−2030.
(33) Terry, N.; Abadia, J. Function of iron in chloroplasts. *J. Plant Nutr.* **1986**, *9*, 609−649.
(34) Washburn, S. P. Pasture-based dairy production systems in the United States. Book of Abstracts of the 65th Annual Meeting of the European Federation of Animal Science, *No. 20*, Copenhagen, Denmark, 25−29 August 2014; p. 138.
(35) Haugen, V. J. Grass based pasture dairy systems in the Mid-West: an overview. Book of Abstracts of the 65th Annual Meeting of the European Federation of Animal Science, *No. 20*, Copenhagen, Denmark, 25−29 August 2014; p. 139.
(36) Søegaard, K.; Mortensen, T. B.; Eriksen, J. Designing high-yielding, high-diversity and low-input temporary grasslands. In: Proc. 22th Int. Grassl. Congress, Sydney, Australia, 2013; pp 474−475.

DOI: 10.1021/jf503658n
J. Agric. Food Chem. 2015, 63, 406−414

JOURNAL OF AGRICULTURAL AND FOOD CHEMISTRY

Article

pubs.acs.org/JAFC

Effect of Co-formulation of 1,3-Dichloropropene and Chloropicrin on Evaporative Emissions from Soil

Daniel J. Ashworth,*[,†,§] Scott R. Yates,[§] Ian J. Van Wesenbeeck,[#] and Mike Stanghellini[⊥]

[†]Department of Environmental Sciences, University of California, Riverside, California 92521, United States

[§]U.S. Salinity Laboratory, Agricultural Research Service, U.S. Department of Agriculture, 450 West Big Springs Road, Riverside, California 92507, United States

[#]Dow AgroSciences, 9330 Zionsville Road, Indianapolis, Indiana 46268, United States

[⊥]TriCal Inc., P.O. Box 1327, Hollister, California 95024, United States

ABSTRACT: Co-formulations of 1,3-dichloropropene (1,3-D) and chloropicrin (CP) are commonly used for preplant fumigation in the production of high-value crops. Various ratios of 1,3-D to CP are available in these co-formulations. Collation of previous field data suggested that when the two fumigants were co-applied, the emissions of CP were significantly lower than when CP was applied singly. However, none of these previous studies had a control treatment with CP applied alone, alongside a treatment where CP was co-applied with 1,3-D under the same climatic and edaphic conditions. This work aimed to address this issue by measuring emission fluxes from soil columns maintained under controlled conditions in which 1,3-D and CP were applied alone and as four commercial co-formulations with various 1,3-D:CP ratios. A strong positive relationship between CP emissions and CP percentage in the formulation was observed. Furthermore, strong positive relationships between CP degradation half-life and CP percentage in the formulation and between CP degradation half-life and total column emissions suggested that the lower emissions were due to faster CP degradation when the CP percentage (and hence initial application mass) in the formulation was low. The presence of 1,3-D did not significantly affect the degradation rate of CP, and, therefore, it is hypothesized that co-application was, in itself, not a significant factor in emission losses from the columns. The findings have implications for the accurate modeling of CP because the effect of initial mass applied on CP degradation rate is not usually considered.

KEYWORDS: *fumigants, degradation, half-life, soil columns, Telone II, Tri-Clor, Telone C-17, Telone C-35, Pic-Clor 60, Pic-Clor 80*

INTRODUCTION

The use of chemical fumigants is critical in agricultural areas of states such as California and Florida, where high-value crops, requiring efficacious pest control, are commonly grown.[1] Although they provide excellent plant pest control, fumigants are highly volatile, making them prone to evaporation into the atmosphere. In addition to the toxic nature of these volatile chemicals, they also have the potential to contribute to the formation of near-surface ozone if sufficient NO_x is available for reaction. Therefore, degradation of air quality and associated inhalation health risks in agricultural workers and local populations are potential hazards associated with fumigant application[2] that warrant management via mitigation strategies such as emission reduction (e.g., tarps and irrigation) and buffer zones. The ban on the use of methyl bromide, together with the recent withdrawal of methyl iodide in the United States, has limited the options for growers requiring the high degree of pest control offered by soil fumigants. 1,3-Dichloropropene (1,3-D) and chloropicrin (CP) are broad-spectrum fumigants with fungicidal, herbicidal, insecticidal, and nematicidal properties; however, weed control with these products is limited.[3,4] Often, 1,3-D and CP are applied together to enhance pest control. For example, commercial products of 1,3-D are often combined with CP to enhance the control of fungi.[5] These fumigants can be applied using shank injection or drip application, with or without tarps. The aerobic soil half-life of 1,3-D is given as 1.7−53 days.[3] For CP, half-life is reported as a few hours to several days[6] but is commonly considered to be approximately 4.5 days in sandy loam soil.[7]

In California, fumigant use is increasing. Pesticide Use Reports published annually by California Department of Pesticide Regulations (CDPR)[8] indicate that CP use increased from 2.49×10^6 kg in 2007 to 4.09×10^6 kg in 2012, and that 1,3-D use increased from 4.35×10^6 kg in 2007 to 5.57×10^6 kg in 2012. Indeed, 1,3-D and CP were ranked the first and third most used fumigants (based on mass applied) in California in 2012, respectively. In the same year, they were ranked the third and fifth most used pesticides (based on mass applied), respectively. Strawberry production is an important, and increasing, user of fumigants. According to CDPR[9] the fumigated land area for this commodity increased by 16% from 2011 to 2012. The majority of the 2011−2012 increase in fumigant use in strawberry production was due to the fumigants metam sodium (72% increase), 1,3-D (24% increase), and CP (11% increase).

Given their increasing use and importance, it is necessary to consider the emissions behavior of 1,3-D and CP. These fumigants can be applied separately or as co-formulations with

Received: August 11, 2014
Accepted: December 22, 2014
Published: December 22, 2014

ACS Publications © 2014 American Chemical Society

DOI: 10.1021/jf506010b
J. Agric. Food Chem. 2015, 63, 415−421

Table 1. Total Emissions and Maximum Fluxes of Chloropicrin (CP) in Collated Field Study Data Where either Co-formulations (C-17, C-35, or Inline) of CP and 1,3-Dichloropropene (1,3-D), or CP Alone, Have Been Applied

	chloropicrin +1,3-D					chloropicrin only				
	CP emissions					CP emissions				
	total (%)	max flux[a] (μg m^2 s^{-1})	application	tarp?	ref	total (%)	max flux[a] (μg m^2 s^{-1})	application	tarp?	ref
	11	14	S	Y	22	46	21	S	Y	26
	17	8	S	Y	18	49	23	S	Y	26
	8	3	S	Y	18	63	64	S	Y	27[b]
	3	3	S	Y	17	69	75	S	Y	27[b]
	1	2	S	Y	17	37	17	S	Y	27[b]
	9	10	S	Y	17	34	21	S	Y	27[b]
	30	23	S	N	18	51	37	S	N	26
	9	6	S	N	18	50	23	S	N	26
	7	9	S	N	17	65	106	S	N	27[b]
	8	7	S	N	17	61	133	S	N	27[b]
	3	5	S	N	17	22	47	D	Y	24
	8	19	D	Y	23	17	28	D	Y	24
	11	11	D	Y	10	15	24	D	Y	24
	8	6	D	Y	24	12	15	D	Y	24
	6	5	D	Y	24	22	39	D	Y	24
	5	4	D	Y	24	9	13	D	Y	24
	2	2	D	Y	18	14	28	D	Y	24
	10	19	D	Y	25	3	6	D	Y	24
	9	18	D	Y	25					
	9	13	D	Y	25					
	5	7	D	Y	25					
	3	1	D	N	[18]					
av (all)	8	9				36	40			
SD (all)	6	6				22	34			
n (all)	22	22				18	18			
av (shank)	10	8				53	52			
SD (shank)	8	6				12	41			
n (shank)	11	11				10	10			
av (drip)	7	10				14	25			
SD (drip)	3	7				6	14			
n (drip)	11	11				8	8			
av (tarped)	8	9				29	30			
SD (tarped)	4	6				21	20			
n (tarped)	16	16				14	14			
av (nontarped)	10	9				57	75			
SD (nontarped)	10	8				7	53			
n (nontarped)	6	6				4	4			

[a]Maximum CP flux normalized to an application rate of 112 kg ha^{-1} (100 lb acre^{-1}). Application types were either shank (S) or drip (D). [b]Data from Chloropicrin Manufacturers Task Force (CMTF) study, reported by Cryer and Van Wesenbeeck.[27]

various 1,3-D:CP ratios. However, there appears to be an effect of using co-formulations on the total emission losses of CP measured. We collated data (Table 1) from several field experiments in which CP was applied either alone or as the 1,3-D:CP co-formulations Telone C-17 (~17% CP, 83% 1,3-D), Telone C-35 (~35% CP, 65% 1,3-D), and Inline (~33% CP, 61% 1,3-D). Meta-analysis of these data showed that, on average, total CP emissions (% of applied) were ~4.5 times lower when CP was applied as a co-formulation with 1,3-D compared to being applied singly. Such observations have not been made for 1,3-D. These data are discussed in more detail later in this paper, but ostensibly suggest that when added as a co-formulation with 1,3-D, percentage emissions of CP are significantly lower than when it is applied singly. In fact, in some field studies, zero, or an extremely low amount of, detectable CP was emitted from the soil.[10] A possible explanation for these findings is that the presence of 1,3-D enhances the degradation of CP. There is evidence in the literature[11] showing that the degradation rate of CP increased by approximately 15% in soil containing 1,3-D compared to that in soil with no 1,3-D.

A major limitation of this collated emissions data, as it is used for this comparison, is that these previous studies were not designed specifically to test the effect of co-application of 1,3-D

DOI: 10.1021/jf506010b
J. Agric. Food Chem. 2015, 63, 415−421

and CP on CP emissions. Therefore, none of these studies had a control treatment with CP applied alone alongside a treatment in which CP was co-applied with 1,3-D under the exact same climatic and edaphic conditions. The goal of this work was to address this issue by measuring emission fluxes from soil columns maintained under controlled conditions in which 1,3-D and CP were applied alone and at various 1,3-D:CP ratios. Our hypothesis was that co-application of 1,3-D and CP would result in lower total emissions of CP than when CP was applied alone due to increased (or changes in) fumigant degradation kinetics when CP concentrations in soil are reduced.

MATERIALS AND METHODS

Chemicals, Sampling Tubes, and Soil. The commercially available 1,3-D and CP formulations used in this study were Telone II (1,3-D only), Tri-Clor (CP only), Telone C-17 (~17% CP, 83% 1,3-D), Telone C-35 (~35% CP, 65% 1,3-D), Pic-Clor 60 (~60% CP, 40% 1,3-D), and Pic-Clor 80 (~80% CP, 20% 1,3-D). Telone II, C-17, and C-35 were donated by Dow Agrosciences (Indianapolis, IN, USA) and Tri-Clor, PC-60, and PC-80 by TriCal Inc. (Hollister, CA, USA).

Sodium sulfate (anhydrous), *n*-hexane, and ethyl acetate were obtained from Fisher Scientific (Fair Lawn, NJ, USA). Acetone was obtained from Burdick and Jackson (Muskegon, MI, USA). XAD-4 (2 section 400/200 mg) and Anasorb CSC charcoal (2 section 400/200 mg) sorbent tubes were purchased from SKC Inc. (Eighty Four, PA, USA). Deionized water was used in the preparation of solutions.

Sandy loam soil (75% sand, 18% silt, 7% clay; 0.92% organic matter; Arlington soil series) was collected from the plowed, upper 30 cm of field 2B of the University of California Riverside Agricultural Station. This field has been used in numerous field and laboratory fumigant emission studies performed by the U.S. Salinity Laboratory (see, e.g., refs 12−14); however, the soil for this study was collected from an area of the field that had not been previously fumigated. The soil was sieved to 5 mm and stored in sealed plastic bags in a cool environment. The gravimetric moisture content of the soil used in the experiments was between 4 and 5%.

Soil Column Study. Stainless steel soil columns (12 cm diameter × 150 cm length) were used to study the surface emissions of co-formulations of 1,3-D and CP, following a simulated shank injection at 46 cm soil depth. The general design and setup of the columns has been described previously.[15,16] Soils were packed into the columns in 5 cm intervals to a dry bulk density of 1.5 g cm^{-3}. The top of each column was sealed with a stainless steel flux chamber. The columns were housed in a controlled temperature room where the ambient temperature was maintained at 25 °C.

Approximately 177 mg of a fumigant formulation was injected into the center of a soil column at 46 cm depth (equivalent field application rate of approximately 156 kg ha^{-1}). Specifically, the amounts of 1,3-D and CP applied for each formulation were as follows: Telone II, 177.1 mg of 1,3-D, 0 mg of CP; Telone C-17, 143.1 mg of 1,3-D, 29.0 mg of CP; Telone C-35, 115.2 mg of 1,3-D, 62.8 mg of CP; Pic-Clor 60, 71.4 mg of 1,3-D, 106.6 mg of CP; Pic-Clor 80, 35.1 mg of 1,3-D, 142.9 mg of CP; and Tri-Clor, 0 mg of 1,3-D, 176.4 mg of CP. Immediately after application, a vacuum (100 mL min^{-1}) was applied to the outlet of the flux chamber to sweep clean air across the soil surface. In this way, headspace gas vapors were collected on in-line sorbent tubes (XAD-4 filter media) that were sampled every 4 h throughout the experiment. Backup sorbent tubes were used to check for fumigant breakthrough. All sampled tubes were capped on both ends and stored in a freezer at −19 °C. Background air within the controlled column environment was sampled daily by pulling the air through an XAD-4 sorbent tube for 24 h periods. In addition, at the start of the experiment, blank XAD-4 and charcoal tubes were placed in the sample storage freezer (i.e., storage blanks). Analysis of all storage blank and background air sampling tubes yielded nondetectable levels of each fumigant, and so no correction was required for these potential sources of contamination. At the end of the experiment (10 days), XAD-4 tubes were cut into their A and B sections and each was placed into separate glass vials. After the addition of 4 mL of *n*-hexane, the vials were immediately capped and shaken for 1 h, and then 1 mL of supernatant solvent was removed for gas chromatography (GC) analysis. For the charcoal backup tubes, the procedure was the same except that the entire charcoal medium was removed into a glass vial, and 4 mL of acetone was used for the extraction.

Each co-formulation treatment was performed in triplicate, although for the PC-80 treatment, one of the three replicates yielded data that were deemed unreliable since they were very different from the other two replicates and also outside the trend observed across the experimental data set as a whole. This replicate was therefore excluded. When appropriate, one-way analysis of variance (ANOVA) was used to statistically compare emission losses between treatments at the 95% confidence level. This analysis was performed in Microsoft Office Excel 2007.

Degradation Study. Degradation kinetics of 1,3-D and CP in each formulation were also determined for the Arlington soil. Moist (5% gravimetric moisture content) soil (10 g) was placed into a 20 mL glass vial and 200 μg of fumigant added (total amount of 1,3-D plus CP) for each treatment/replicate. The vials were immediately capped (Teflon-faced butyl caps) and placed at 25 °C. At times 0 (immediately after adding fumigant), 2, 4, 8, 24, 48, 72, 144, and 240 h triplicate vials were removed and placed at −19 °C. At the end of the experiment, 10 g of anhydrous sodium sulfate and 10 mL of ethyl acetate were quickly added to each frozen vial before immediate recapping, shaking for 1 h, and subsequent removal of 1 mL of supernatant to an amber GC vial for GC analysis. Extraction efficiencies were determined as ~80% for both chemicals. Degradation loss of 1,3-D and CP from the soil was fitted with a first-order kinetic model to calculate the degradation rate constant and half-life for each chemical in each treatment.

Analysis. Analysis of sorbent tube and soil solvent extracts was carried out using an Agilent Technologies 7890C GC, equipped with a microelectron capture detector. The column was a DB-VRX 122-1534 with dimensions of 30 m × 0.25 mm × 1.4 μm (Agilent Technologies) running at a flow rate of 1.4 mL min^{-1} and with He as the carrier gas. The inlet temperature was 240 °C and the detector temperature, 290 °C. The GC oven temperature was maintained at 45 °C for 1 min after sample injection, increasing to 80 °C at a rate of 2.5 °C min^{-1} and then to 120 °C at a rate of 30 °C min^{-1}, before being held at this temperature for 2 min. Under these conditions, retention times of *cis*-1,3-D, *trans*-1,3-D, and CP were 11.0, 12.3, and 13.8 min, respectively. Sets of eight standards encompassing the range of concentrations of the samples were prepared from the Telone II (1,3-D only) and TriClor (CP only) formulations. Standards were prepared in the same solvent as the samples. 1,3-D data are reported as total 1,3-D (i.e., the sum of the *cis* and *trans* isomers).

RESULTS AND DISCUSSION

Figure 1 shows total emission losses of 1,3-D and CP (as a percentage of the amounts added) for each formulation. Total emissions of 1,3-D (~30−35% across all treatments) were broadly consistent with previously published values for both field[17−19] and laboratory[15,16] studies. One-way ANOVA testing showed no statistically significant differences ($p > 0.05$) in 1,3-D emissions across the treatments. The relative consistency of 1,3-D total emissions across the treatments indicates that co-formulation of this fumigant with CP did not affect 1,3-D emission behavior from the columns, consistent with previously published work (Table 1). Conversely, total CP emissions varied widely across the treatments, increasing monotonically from 0.018 to 14% as the amount of CP in the formulation increased (Figure 1).

In general, emission flux curves followed the expected trend of a peak in emissions shortly after application, followed by a gradual decline and tailing of the curve over time (data not

DOI: 10.1021/jf506010b
J. Agric. Food Chem. 2015, 63, 415−421

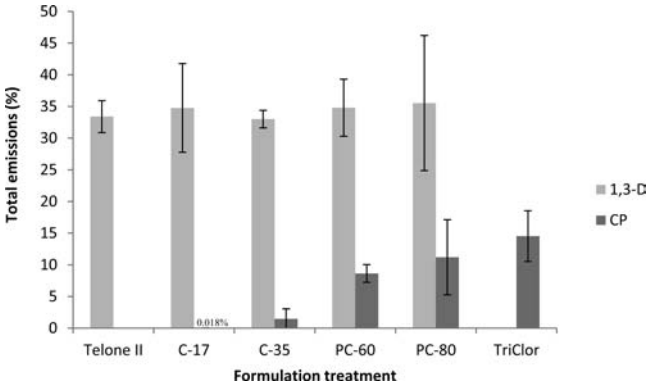

Figure 1. Total 1,3-D and CP emission losses (as percentage of amount added) for each treatment. Average CP emissions for the C-17 treatment were 0.018% (standard deviation = 0.018%).

shown). For formulations containing both 1,3-D and CP, this tailing occurred over a longer period for 1,3-D than for CP, probably due to the longer degradation half-life of the former.[15] Of significance in the assessment of the effects on air quality and risk assessment of fumigant operations is the maximum flux, in terms of both its magnitude and its timing. For each treatment, these variables are shown in Table 2. Peak emission flux generally occurred very rapidly after fumigant application, typically within 12 h. Compared to each fumigant applied singly, peak fluxes across the treatments generally declined in response to decreasing percentage (or mass) of each fumigant in the treatment. However, this relationship was not proportional as is particularly noticeable for the treatments with low CP levels. For example, the peak CP flux in the C-17 treatment was only 0.07% of the peak flux in the CP-only treatment despite containing 17% of the total CP level of this treatment. Similarly, the value for the C-35 treatment was just 6.3%, despite containing 35% of the CP amount in the CP-only treatment. Such dramatically disproportional differences were not observed across the 1,3-D treatments. Overall, CP again showed very different emission flux behavior from 1,3-D.

These experiments were conducted in an attempt to elucidate observations made during a meta-analysis of a number of published field studies in which co-application of 1,3-D and CP as the commercial product C-17, C-35, or Inline (a commercial drip application product with 33% CP and 61% 1,3-D), or as CP applied singly, was performed (Table 1). This meta-analysis, where the data from a number of independent studies were combined in a weight-of-evidence approach, suggested a hypothesis that chloropicrin emissions are reduced in the presence of 1,3-D. For example, on average, for this data set as a whole, co-application across 22 studies yielded approximately 4.5 times lower CP emissions (8% total emissions) than single CP application across 18 independent studies (36% total emissions). If only shank applications are considered (the same as emulated in the present study), the difference in CP emissions between co-formulation (10% total CP emissions) and single application (53% total CP emissions) is even greater. For drip applications, the difference in total CP emissions is lower but still marked (7% for co-application and 14% for single CP application). Clearly, emission reduction strategies, such as tarping, may be an important factor affecting emission levels across the collated studies, some of which were tarped whereas some were not. However, large differences in CP emissions between co-application and single CP application are similarly observed if tarping is removed as a potential factor. For example, for tarped shank applications, CP emissions averaged 8% with co-application and 50% with single application. With nontarped shank applications the values were 11 and 57%, respectively. In addition to an apparent effect on total CP emissions, the maximum emission flux of CP also seemed to be affected by co-formulation of CP with 1,3-D across these studies (Table 1). The maximum CP emission flux (normalized to an effective application rate of 112 kg ha^{-1} (100 lb acre^{-1})) for shank applications was reduced by >5 times from 52 μg m^2 s^{-1} with a single application to 8 μg m^2 s^{-1} with co-application. On the basis of anecdotal evidence, these results are also consistent with the experience of growers and applicators in the field, who have observed that chloropicrin is rarely detected (by olfactory sense or lachrimation) in Telone C-17 applications in the Pacific Northwest.

Overall, these collated field data broadly concur with our soil column studies in suggesting that when CP is co-applied with 1,3-D, total CP emissions and emission fluxes are reduced compared with CP applied alone. However, our column studies allow for a more detailed analysis of the relationship between the percentage of CP in a co-formulation and CP emissions. Indeed, for the column data, one-way ANOVA testing revealed that CP percentage in the formulation was statistically a highly significant (p = 0.008) factor affecting total CP emissions. We further observed a strong positive relationship (R^2 = 0.99) between CP percentage in a formulation and CP emissions (Figure 2), indicating that as CP levels decreased (and, consequently, 1,3-D levels increased) in the co-formulation, a process occurred to limit CP emissions from the soil. However, this relationship was not linear, but was rather best fitted with a

Table 2. Average Peak Emission Flux and Its Timing, Degradation Rate Constant, and Half-Life for 1,3-Dichloropropene (1,3-D) and Chloropicrin (CP) across All Treatments

	1,3-D				CP			
	emissions		degradation		emissions		degradation	
	peak flux (μg m^2 s^{-1})	peak flux time (h)	k (h^{-1})	$t_{1/2}$ (h)	peak flux (μg m^2 s^{-1})	peak flux time (h)	k (h^{-1})	$t_{1/2}$ (h)
Telone II (1,3-D)[a]	80.4	4−8	0.0038	182.4				
C-17	29.8	8−12	0.0048	144.4	0.016	8−12	0.280	2.5
C-35	22.3	8−12	0.0033	210.0		8−12	0.047	14.7
PC-60	13.1	12−16	0.0030	231.0	9.5	12−16	0.020	35.4
PC-80		8−12	0.0031	223.5	16.6		0.012	59.7
TriClor (CP)					23.5	8−12	0.010	66.6

[a]Emission flux of 1,3-D for the Telone II treatment showed a relatively high degree of variation due to one of the three replicates exhibiting a relatively rapid and high peak emission flux.

DOI: 10.1021/jf506010b
J. Agric. Food Chem. 2015, 63, 415−421

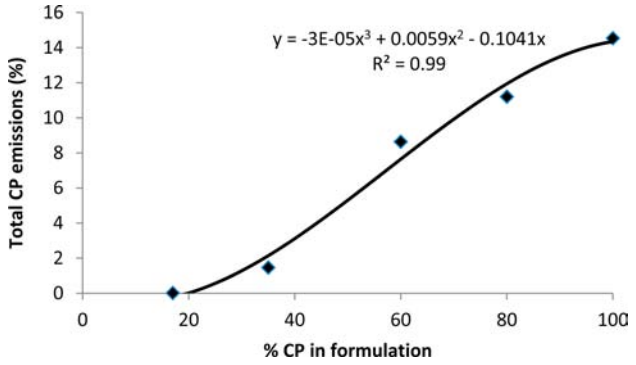

Figure 2. Relationship between percentage CP in the formulation and total CP emissions (percentage of amount added). Fitted line is a third-order polynomial.

third-order polynomial equation, which suggested a disproportional relationship between total CP emissions and CP percentage in the formulation (similar to the CP emission flux data). We are not aware of any previously published data that report this relationship.

In the column system, two processes are considered to dominate fumigant fate and transport, emissions and degradation. Because determining in situ degradation rates within the column is not possible, a separate degradation study was performed to quantify this parameter for each formulation product. In this degradation study, the total fumigant mass (1,3-D + CP) addition at the start of the experiment was the same for each formulation treatment. Subsequent loss of fumigant was attributed to soil degradation. Fitting a first-order kinetic model to the loss of fumigant over time yielded the degradation rate constants and half-lives shown in Table 2. At the lowest level of CP addition (C-17), CP half-life was just 2.5 h and at the highest level (CP only), was 66.6 h. As shown in Figure 3, a

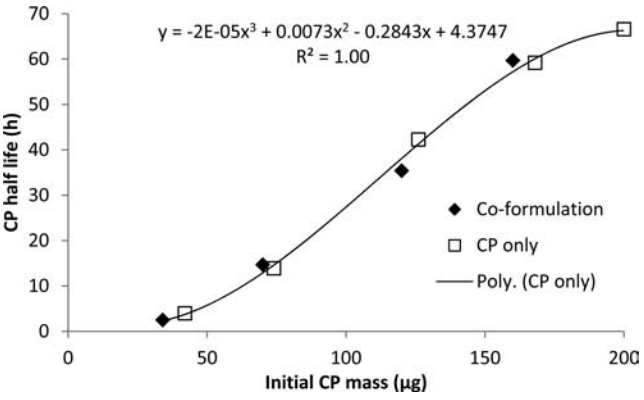

Figure 3. Relationship between initial CP mass added and CP degradation half-life in the presence (co-formulation data points) and absence (CP-only data points) of 1,3-D. The co-formulation data points are, from left to right, C-17, C-35, PC-60, and PC-80. Fitted line is third-order polynomial.

strong positive relationship between initial CP mass added in the formulation and CP half-life was observed across all treatments. For 1,3-D, across the six formulation products, half-lives ranged from 144 to 231 h, and no consistent relationship between half-life and percentage of 1,3-D in the formulation was observed. Therefore, in contrast to CP, it was concluded that the initial mass of 1,3-D was not significant in dictating the half-life of this fumigant. To determine whether the degradation of CP was related to the co-presence of 1,3-D, half-lives for various initial CP masses were determined in a separate degradation study in which approximately equivalent initial amounts of TriClor (CP only) were added to soils (i.e., in the absence of 1,3-D). The strong overlap between the data sets for CP degradation both in the presence and in the absence of 1,3-D (Figure 3) indicates that CP degradation rate was not affected by the presence of 1,3-D.

Because the total amount of fumigant (1,3-D + CP) added to each treatment of the degradation study was the same, the amounts of applied CP varied across the treatments. As shown in Figure 3, the initial CP mass controlled its degradation rate within the soil, with smaller masses degrading more rapidly. The dependency of fumigant degradation upon initial mass or concentration has been previously observed,[20,21] and rapid degradation (half-life of 2.9 h) of CP in sandy loam soil has also been reported when the initial concentration was low (10 μg^{-1}).[15] With a lower initial concentration, the number of biological and chemical sites available for degradation is greater per unit mass of fumigant. At higher initial concentrations, competition for such sites is likely greater, leading to a lower degree of degradation. Although this process may explain the degradation behavior of CP, it does not explain why 1,3-D was not affected in a similar way. However, Zheng et al.[11] noted that for soil collected from the same field as the current study, autoclave sterilization led to a >6 times increase in CP half-life from 9 days to 57 days when compared to control soil, demonstrating the significant influence microbial populations have on CP degradation rates. For 1,3-D, however, the increase due to sterilization was much less marked, from 139 to 193 days (averages of *cis* and *trans* isomers). This apparently strong dependence upon biological processes suggests that the suppression or death of soil microbes at high CP concentrations may induce slower CP degradation. The observed differences in CP degradation rate across the formulations provide a highly probable explanation for the observed trend in column CP total emissions and emission fluxes. A positive linear relationship (R^2 = 0.97) was observed between CP half-life and total emissions across the formulations. This strongly suggests that dramatically faster degradation in formulations with lower levels of CP resulted in relatively low amounts of CP available for emission to air. The degradation studies further suggested that this effect occurred irrespective of 1,3-D presence. Therefore, although there were significant differences in CP emissions across the formulations, this cannot be attributed to a 1,3-D/CP co-formulation effect. This suggests that we would expect the same CP emissions as those observed in the current column experiment if it was carried out using equivalent initial application masses of CP alone.

From an air quality perspective, the low CP emissions from certain co-formulations are clearly beneficial. The results have implications for volatility and environmental fate modeling of CP because its degradation rate is not often considered in relation to its initial application mass. The calculation of buffer zone sizes around fumigated fields is based on a linear scaling of empirically derived emission losses from studies utilizing the maximum labeled application rates. Therefore, the relationship between emission flux and application rate is assumed to be linear and have a slope of 1; that is, doubling the application rate would double the emission flux. Translating the current work into this broader context can be achieved by regressing maximum CP flux (commonly used as the primary indicator of fumigant impact on local air quality) against CP application rate

DOI: 10.1021/jf506010b
J. Agric. Food Chem. 2015, 63, 415−421

(Figure 4). In this case, although the relationship is linear, the slope is <1 (i.e., 0.22), indicating a disproportional effect of

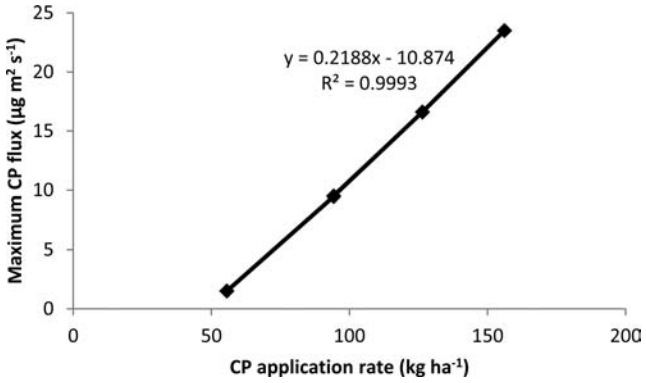

Figure 4. Relationship between CP application rate and CP peak emission flux from soil columns. The data points are, from left to right, C-35, PC-60, PC-80, and TriClor (CP only). The data point for C-17 did not fit the linear trend.

application rate on emission flux within this range of application rates. For example, Table 1 indicates that with C-35 application to the soil columns (CP application rate equivalent to 55.6 kg ha^{-1}) the peak flux was 1.5 $\mu g\ m^2\ s^{-1}$, whereas Figure 4 indicates that with a doubling of this application rate, the peak flux would more than double to 13.5 $\mu g\ m^2\ s^{-1}$, that is, a 9 times increase. Overall, this work suggests that at low CP application rates, smaller buffer zones may be adequate to protect public health because, due to more rapid degradation of CP in the soil, emissions would be disproportionately lower than suggested by a linear scaling approach. The observations presented in this paper may help to more accurately predict such emissions.

AUTHOR INFORMATION

Corresponding Author

*(D.J.A.) E-mail: Daniel.Ashworth@ars.usda.gov. Phone: (951) 369-4802. Fax: (951) 342-4964.

Funding

This work was carried out at the USDA-ARS U.S. Salinity Laboratory, Riverside, CA, under funding from TriCal Inc, Hollister, CA, the receipt of which is gratefully acknowledged. The statements and conclusions in this report are those of the contractors and not necessarily those of TriCal Inc. The mention of commercial products, their source, or their use in connection with material reported herein is not to be construed as actual or implied endorsement of such products. The use of trade, firm, or corporation names in this document is for the information and convenience of the reader. Such use does not constitute an official endorsement or approval by the U.S. Department of Agriculture or the Agricultural Research Service of any product or service to the exclusion of others that may be suitable.

Notes

The authors declare no competing financial interest.

ACKNOWLEDGMENTS

We thank Qiaoping Zhang for technical assistance throughout the study.

REFERENCES

(1) Ruzo, L. O. Physical, chemical and environmental properties of selected chemical alternatives for the pre-plant use of methyl bromide as soil fumigant. *Pest Manage. Sci.* **2006**, *62*, 99−113.

(2) CDPR. *Volatile Organic Compound (VOC) Emissions from Pesticides*; Sacramento, CA, USA, 2013; available at http://www.cdpr.ca.gov/docs/emon/vocs/vocproj/vocmenu.htm.

(3) Dow Agrosciences. *1,3-Dichloropropene: a profile*; Indianapolis, IN, 1996.

(4) U.S. Environmental Protection Agency. *Reregistration Eligibility Decision for Chloropicrin*; Sacramento, CA, USA, 2008; available at http://www.epa.gov/oppsrrd1/REDs/chloropicrin-red.pdf.

(5) Noling, J. W.; Becker, J. O. The challenge of research and extension to define and implement alternatives to methyl bromide. *J. Nematol.* **1994**, *26*, 573−586.

(6) CDPR. *Evaluation of Chloropicrin as a Toxic Air Contaminant*; Sacramento, CA, USA, 2010; available at http://www.cdpr.ca.gov/docs/emon/pubs/tac/exec_sum_0210.pdf.

(7) Wilhelm, S. N.; Shepler, K.; Lawrence, L. J.; Lee, H. Environmental fate of chloropicrin. In *Fumigants: Environmental Fate, Exposure, and Analysis*; Sieber, J. N., Knuteson, J. A., Woodrow, J. E., Wolfe, N. L., Yates, M. V., Yates, S. R., Eds.; American Chemical Society: Washington, DC, USA, 1996.

(8) CDPR. *Summary of Pesticide Use Report Data 2012 Indexed by Chemical*; Sacramento, CA, USA, 2014; available at http://www.cdpr.ca.gov/docs/pur/pur12rep/chmrpt12.pdf.

(9) CDPR. *Summary of Pesticide Use Report Data 2012 Indexed by Commodity*; Sacramento, CA, USA, 2014; available at http://www.cdpr.ca.gov/docs/pur/pur12rep/comrpt12.pdf.

(10) Van Wesenbeeck, I. J.; Knuteson, J. A.; Barnekow, D. E.; Phillips, A. Measuring flux of soil fumigants using the aerodynamic and dynamic flux chamber methods. *J. Environ. Qual.* **2007**, *36*, 613−620.

(11) Zheng, W.; Papiernik, S. K.; Guo, M.; Yates, S. R. Competitive degradation between the fumigants chloropicrin and 1,3-dichloropropene in unamended and amended soils. *J. Environ. Qual.* **2003**, *32*, 1735−1742.

(12) Gan, J.; Yates, S. R.; Ohr, H. D.; Sims, J. J. Volatilization and distribution of methyl iodide and methyl bromide after subsoil application. *J. Environ. Qual.* **1997**, *26*, 1107−1115.

(13) Zheng, W.; Papiernik, S. K.; Guo, M.; Yates, S. R. Accelerated degradation of methyl iodide by agrochemicals. *J. Agric. Food Chem.* **2003**, *51*, 673−679.

(14) Ashworth, D. J.; Yates, S. R.; Luo, L.; Xuan, R. Coupling of soil solarization and reduced rate fumigation: effects on methyl iodide emissions from raised beds under field conditions. *J. Agric. Food Chem.* **2013**, *61*, 12510−12515.

(15) Ashworth, D. J.; Yates, S. R. Surface irrigation reduces the emission of volatile 1,3-dichloropropene from agricultural soils. *Environ. Sci. Technol.* **2007**, *41*, 2231−2236.

(16) Ashworth, D. J.; Ernst, F. F.; Xuan, R.; Yates, S. R. Laboratory assessment of emission reduction strategies for the agricultural fumigants 1,3-dichloropropene and chloropicrin. *Environ. Sci. Technol.* **2009**, *43*, 5073−5078.

(17) Gao, S.; Trout, T. J. Surface seals reduce 1,3-dichloropropene and chloropicrin emissions in field tests. *J. Environ. Qual.* **2007**, *36*, 110−119.

(18) Gao, S.; Trout, T. J.; Schneider, S. Evaluation of fumigation and surface seal methods on fumigant emissions in an orchard replant field. *J. Environ. Qual.* **2008**, *37*, 369−377.

(19) Luo, L.; Yates, S. R.; Ashworth, D. J.; Xuan, R.; Becker, J. O. Effect of films on 1,3-dichloropropene and chloropicrin emissions, soil concentration and root knot nematode control in a raised bed. *J. Agric. Food Chem.* **2013**, *61*, 2400−2406.

(20) Ma, Q. A.; Gan, J.; Papiernik, S. K.; Becker, J. O.; Yates, S. R. Degradation of soil fumigants as affected by initial concentration and temperature. *J. Environ. Qual.* **2001**, *30*, 1278−1286.

(21) Zhang, Y.; Spokas, K.; Wang, D. Degradation of methyl isothiocyanate and chloropicrin in forest nursery soils. *J. Environ. Qual.* **2005**, *34*, 1566−1572.

DOI: 10.1021/jf506010b
J. Agric. Food Chem. 2015, 63, 415−421

(22) Knuteson, J. A.; Dolder, S.; Carver, L. *Air, Surface Water, And Ground Water Field Study of 1,3-Dichloropropene in a South Florida Vegetable Production System*; Final Report GH-C 4550; Dow AgroSciences: Indianapolis, IN, USA, 1997.
(23) Knuteson, J. A.; Dolder, S. C.; Meuller, J. P. *Field Volatility of 1,3-D and Chloropicrin from Shallow Drip Irrigation Application of Telone C-35 EC to Strawberry Beds with VIF Tarp*; Interim Report GH-C4918; Dow Agrosciences: Indianapolis, IN, USA, 1999.
(24) California Strawberry Commission (CSC). *Reducing Fumigant Emissions using Impermeable Films and Water Seal in Pre-Plant Strawberry Raised Beds*; Progress Report for the CSC, 2006.
(25) California Strawberry Commission (CSC). *Reducing Fumigant Emissions using Impermeable Films and Water Seal in Pre-Plant Strawberry Raised Beds*; Progress Report for the CSC, 2007.
(26) Ajwa, H. A.; Sullivan, D. *Monitoring of Chloropicrin Field Emission From Shank Applications at Shallow and Deep Injection Depths*; Final Report for the Chloropicrin Manufacturers Task Force, 2008
(27) Cryer, S. A.; van Wesenbeeck, I. J. Estimating field volatility of soil fumigants using CHAIN_2D: mitigation methods and comparison against chloropicrin and 1,3-dichloropropene field observations. *Environ. Model. Assess.* **2010**, *15*, 309−318.

DOI: 10.1021/jf506010b
J. Agric. Food Chem. 2015, 63, 415−421

JOURNAL OF AGRICULTURAL AND FOOD CHEMISTRY

Article

pubs.acs.org/JAFC

Solid Lipid Nanoparticles Co-loaded with Simazine and Atrazine: Preparation, Characterization, and Evaluation of Herbicidal Activity

Jhones Luiz de Oliveira,[†] Estefânia Vangelie Ramos Campos,[†,‡] Camila Morais Gonçalves da Silva,[‡] Tatiane Pasquoto,[§] Renata Lima,[§] and Leonardo Fernandes Fraceto*[,†,‡]

[†]Department of Environmental Engineering, São Paulo State University, Sorocaba, Brazil

[‡]Department of Biochemistry, Institute of Biology, State University of Campinas, Cidade Universitária Zeferino Vaz, Campinas, Brazil

[§]Department of Biotechnology, University of Sorocaba, Sorocaba, Brazil

ABSTRACT: Solid lipid nanoparticles (SLN) containing the herbicides atrazine and simazine were prepared and characterized, and in vitro evaluation was made of the release kinetics, herbicidal activity, and cytotoxicity. The stability of the nanoparticles was investigated over a period of 120 days, via analyses of particle size, ζ potential, polydispersion, pH, and encapsulation efficiency. SLN showed good physicochemical stability and high encapsulation efficiencies. Release kinetics tests showed that use of SLN modified the release profiles of the herbicides in water. Herbicidal activity assays performed with pre- and postemergence treatment of the target species *Raphanus raphanistrum* showed the effectiveness of the formulations of nanoparticles containing herbicides. Assays with nontarget organisms (*Zea mays*) showed that the formulations did not affect plant growth. The results of cytotoxicity assays indicated that the presence of SLN acted to reduce the toxicity of the herbicides. The new nanoparticle formulations enable the use of smaller quantities of herbicide and therefore offer a more environmentally friendly method of controlling weeds in agriculture.

KEYWORDS: *environmental nanotechnology, herbicides, nanoparticles, herbicidal activity*

INTRODUCTION

The growing demand for food to sustain the global population has resulted in increased efforts to maximize agricultural production.[1] However, the presence of weeds that directly compete with crops for light, water, and nutrients can adversely affect productivity.[2] Herbicides that are widely used to control weeds offer advantages such as rapid action, flexibility in terms of the timing of application, and the ability to treat extensive areas.[3] Atrazine (2-chloro-4-ethylamine-6-isopropylamine-*s*-triazine) and simazine [2-chloro-4,6-bis(*s*-ethylaminotriazine)] are members of the triazine family of herbicides that have low solubility in water (30 and 5 mg/L, respectively) and a mechanism of action based on the inhibition of photosynthesis (due to their action on photosystem II); they are used in the pre- and postemergence control of weeds.[4]

A disadvantage associated with the use of herbicides lies in the fact that these substances have a wide range of different molecular structures and properties, which influences their behavior in the environment in terms of persistence, mobility, and toxicity.[5] Repeated applications are often required in order to achieve the desired results, which can increase adverse effects on the environment and nontarget organisms.[6]

The use of nanotechnology in agriculture has received increasing attention, with the development of new formulations containing active compounds.[6−8] The main objectives of these formulations are to (i) increase the solubility of active compounds, (ii) provide slow release, and (iii) provide protection against premature degradation. The use of carrier systems offers advantages, compared to conventional systems, because they can increase the biological activity of active substances, reduce the quantities necessary, and diminish the risk of contamination of hydric resources due to leaching.[9,10]

A wide range of different particles can be used, obtained from a variety of matrices and preparation procedures.[11] Solid lipid nanoparticles, whose matrices consist of lipids that are solid at ambient temperature, are particularly useful as carrier systems for nonpolar substances. They possess good physicochemical stability, promote sustained release of the active principle from the solid matrix, and can be metabolized by a variety of organisms.[12,13]

Many different types of carriers have been developed for the modified release of agricultural pesticides, including cyclodextrins,[14,15] clays,[16,17] silica,[18] lignin,[19] polymeric microparticles,[20−24] and nanoparticles.[25−27] Recent review articles have described advances in the use of modified release systems for active agents of interest in the agricultural sector.[28,29]

In a previous study,[26] nanoparticles of poly(ε-caprolactone) were developed as a carrier system for atrazine, and the results obtained with target organisms (*Brassica* sp.) showed the effectiveness of these formulations of nanospheres and nanocapsules, compared to a commercial formulation.

The objective of the present work was to prepare and characterize solid lipid nanoparticles used as a carrier system for a combination of the two herbicides atrazine and simazine. The use of a combination of two herbicides is a technique widely used in weed control, and in association with other procedures is an effective strategy for the control of vegetation. The

Received: August 18, 2014
Accepted: December 23, 2014
Published: December 23, 2014

ACS Publications © 2014 American Chemical Society

DOI: 10.1021/jf5059045
J. Agric. Food Chem. 2015, 63, 422−432

presence of more than one herbicide can broaden the range of target weeds, reduce costs, and help to prevent the emergence of plants resistant to the herbicides.

The advantage of using solid lipid nanoparticles loaded with two different herbicides lies in improved efficiency of the formulation, while at the same time helping to reduce toxicity to nontarget organisms and the wider environment. Concerning the use of polymeric nanoparticles,[26] lipid nanoparticles were selected for use in the present work, because they offer high colloidal stability as well as competitive production costs and ease of scale-up.

Evaluation of the characteristics and stability of the nanoparticles was performed by measurements of particle size (by means of dynamic light scattering), ζ potential, pH, polydispersion index, and encapsulation efficiency, as a function of time (up to 120 days). Particle morphology was investigated by transmission electron microscopy (TEM), and nanoparticle tracking analysis (NTA) was employed to measure the concentration and size distribution of the particles. The profiles of release of the herbicides from the SLN were investigated, and cytotoxicity of the formulations was evaluated via cellular viability assays with 3T3 cells. The effectiveness of the formulation was determined in herbicidal activity assays with pre- and postemergence treatment of the target species *Raphanus raphanistrum*. The same assays were repeated with *Zea mays* in order to determine the effects of the formulation on a nontarget organism. The goal was to develop a formulation suitable for future use in agriculture that provided increased effectiveness, while using smaller quantities of herbicides and reducing possible adverse impacts on the environment and human health.

MATERIALS AND METHODS

Materials. The reagents atrazine, simazine, poly(vinyl alcohol) (PVA; 30−70 kDa), and glycerol tripalmitate were obtained from Sigma−Aldrich. The solvents chloroform and acetone were acquired from Labsynth. Acetonitrile and methanol (HPLC-grade) were obtained from J. T. Baker. Seeds of *Raphanus raphanistrum* and *Zea mays* were purchased from ISLA Sementes. The substrate used to cultivate the plants was obtained from Hortaliça Mix.

Production of Solid Lipid Nanoparticles Containing Herbicides. SLN were prepared according to the method of emulsification with solvent evaporation, described in a previous report.[30] The lipid phase was prepared from 5 mL of chloroform, 250 mg of glycerol tripalmitate, and 5 mg each of atrazine (ATZ) and simazine (SMZ). After preparation, the lipid phase was inserted into an aqueous phase composed of 1.25% (m/v) PVA and the mixture was sonicated (Unique DES500) for 4 min at a power of 40 W. The pre-emulsion formed was then submitted to high-speed Ultraturrax homogenization (Tecnal TE-102) at 14 000 rpm for 7 min. After this step, the chloroform was removed by evaporation in a rotary evaporator and the sample was concentrated to obtain final concentrations of ATZ and SMZ of 0.5% (m/v).

Quantification of Atrazine and Simazine and Determination of Encapsulation Efficiency. The herbicides were quantified by high-performance liquid chromatography (HPLC) employing a Varian ProStar instrument (Agilent Technologies) fitted with a model PS 210 pump, a UV−vis detector operated at a wavelength of 225 nm, and a Phenomenex Gemini C^{18} reverse-phase column (5 μm, 250 × 4.6 mm) kept at a temperature of 25 °C. The mobile phase was composed of acetonitrile and deionized water (50:50 v/v), at a flow rate of 0.8 mL/min. Both herbicides were quantified in the same chromatographic run. The limits of detection and quantification, respectively, were 0.21 μg/mL and 0.71 μg/mL (atrazine) and 0.18 μg/mL and 0.60 μg/mL (simazine).

Determination of the efficiency of encapsulation of herbicides in nanoparticles was performed by the ultrafiltration/centrifugation technique, employing ultrafiltration devices containing a cellulose membrane with a molecular exclusion pore size of 10 kDa (Microcon, Millipore). The filtrate was collected, and the concentrations of the nonencapsulated herbicides were quantified by HPLC. The encapsulation efficiencies could then be determined by the difference between total amounts (100%) of the herbicides and the amounts found in the filtrate. The measurements were performed in triplicate after 0, 15, 30, 60, and 90 days.

CHARACTERIZATION OF NANOPARTICLES

Measurements of Size Distribution (by Dynamic Light Scattering) and ζ Potential. Hydrodynamic diameter and polydispersion of the particles were determined by the dynamic light scattering technique, on a Zetasizer ZS 90 instrument (Malvern Instruments). The ζ potential was determined by microelectrophoresis, on the Zetasizer ZS 90. Nanoparticles (with and without herbicides) were diluted in deionized water (1:1000 v/v) and analyzed at 25 °C, with the detector at a fixed angle of 90°. Results were expressed as the average of three determinations. In order to determine the stability of the system as a function of time, the samples were analyzed after 0, 15, 30, 60, and 90 days.

Nanoparticle Morphology Determined by Transmission Electron Microscopy. SLN morphology was evaluated by use of a Zeiss-LEO microscope (Model 906). The samples were prepared from droplets of a suspension of nanoparticles (with or without herbicides), which were deposited onto 200-mesh copper grids and allowed to dry for 15 min. After this period, a droplet of uranyl acetate solution (2%) was added to each grid, as a contrast agent, and the excess solution was removed with tissue paper. After drying, the samples were analyzed by use of the microscope operated at a voltage of 80 kV.[31]

Determination of Particle Size Distribution and Concentration by Nanoparticle Tracking Analysis. Concentration and size distribution of the solid lipid nanoparticles was investigated by the nanoparticle tracking analysis technique. Equipment comprised a NanoSight LM 10 cell (green laser, 532 nm) and a sCMOS camera controlled via NanoSight v.2.3 software. The SLN suspensions were diluted 11 000 times, and each sample was analyzed in triplicate. In order to ensure that different particles were analyzed, each replicate used 1 mL of sample suspension injected into the volumetric cell in order to displace the contents that had been measured previously. Each repetition consisted of five measurements, with approximately 2000 particles counted in each analysis. The final result was the size-distributed number concentration of the particles.[32]

Evaluation of Interaction of Herbicides with Nanoparticles by Differential Scanning Calorimetry and Fourier Transform Infrared Spectroscopy. In differential scanning calorimetry (DSC) analyses, 5 mg portions of each sample (herbicides, nanoparticles, and lipids) were weighed on an analytical balance, placed in sealed aluminum pans, and analyzed on a model Q20 instrument (TA Instruments). The thermal program consisted of a heating ramp from 5 to 250 °C, at a rate of 10 °C/min, under a flow of nitrogen (50 mL/min). An empty pan was used as a reference. These measurements were performed for all the sample materials (atrazine, simazine, tripalmitin, a tripalmitin/atrazine/simazine physical mixture, SLN alone, and SLN containing atrazine and simazine).

DOI: 10.1021/jf5059045
J. Agric. Food Chem. 2015, 63, 422−432

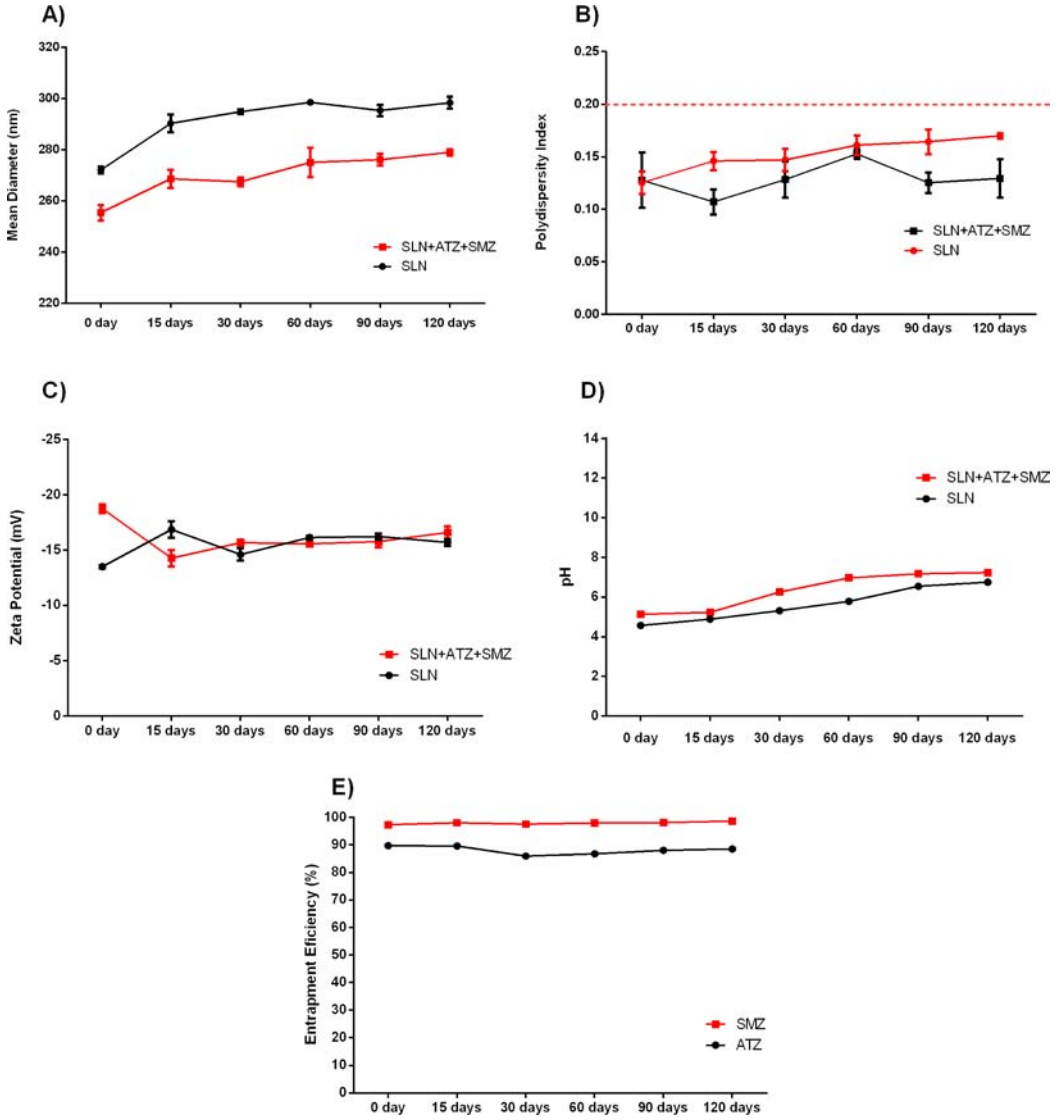

Figure 1. Stability of nanoparticles over a period of 120 days. SLN, solid lipid nanoparticles; SLN + ATZ + SMZ, solid lipid nanoparticles containing atrazine and simazine. (A) Hydrodynamic diameter of nanoparticles; (B) polydispersity index; (C) ζ potential; (D) pH; (E) encapsulation efficiency.

Fourier transform infrared (FTIR) analyses were performed on a Model 660 (Varian) spectrometer fitted with an attenuated total reflectance accessory (GladiATR, Pike Technologies) equipped with a diamond crystal (2.2 × 3.0 mm). The wavenumber range used was from 4000 to 400 cm^{-1}, the incidence angle was 45°, and 32 scans were collected for each sample, at a resolution of 8 cm^{-1}. The types of samples analyzed were the same as those used in the DSC analyses.

Release Kinetics Assays and Mathematical Modeling of the Data. Kinetics of release of ATZ and SMZ, free or encapsulated in SLN, was investigated in a two-compartment system with donor and acceptor compartments. The donor compartment contained 2 mL of the formulation and was separated from the acceptor compartment by a Spectrapore cellulose membrane with a molecular exclusion pore size of 1 kDa. The system was constantly agitated under "sink" conditions. Aliquots of 1 mL were collected at intervals of 15, 30, and 60 min during the first 7 h, after which a further two aliquots were collected at 24 h intervals, up to a maximum time of 55 h. The analyte concentrations were determined by HPLC and used to determine the percentage release of the herbicides. The experiments were performed in triplicate.[26]

The results of the release experiments were used to calculate the apparent flux values (J_{app}), according to Fick's first law (eq 1), using the slope of the linear section of the plot of the values:

$$M_t = M_0 - SJt \quad (1)$$

where M_t is the cumulative amount of the active agent released through the membrane of area S, as a function of time t, and M_0 is the total quantity of the active agent.[33,34]

The type of mechanism governing the release of herbicides from nanoparticles was elucidated by use of the Korsmeyer–Peppas model (also known as the power law).[35,36]

Evaluation of Cytotoxicity of Nanoparticles Containing Herbicides. Assessment of cytotoxicity was performed by the 3-(4,5-dimethylthiazol-2-yl)-2,5-diphenyltetrazolium bromide (MTT) assay. Balb-c 3T3 mouse fibroblast cells were kept in continuous culture at 37 °C, under a humid atmosphere containing 5% CO_2. The culture medium used was Dulbecco's modified Eagle's medium (DMEM) supplemented with 10% fetal bovine serum, 100 units/mL penicillin, and 100 μL of

DOI: 10.1021/jf5059045
J. Agric. Food Chem. 2015, 63, 422–432

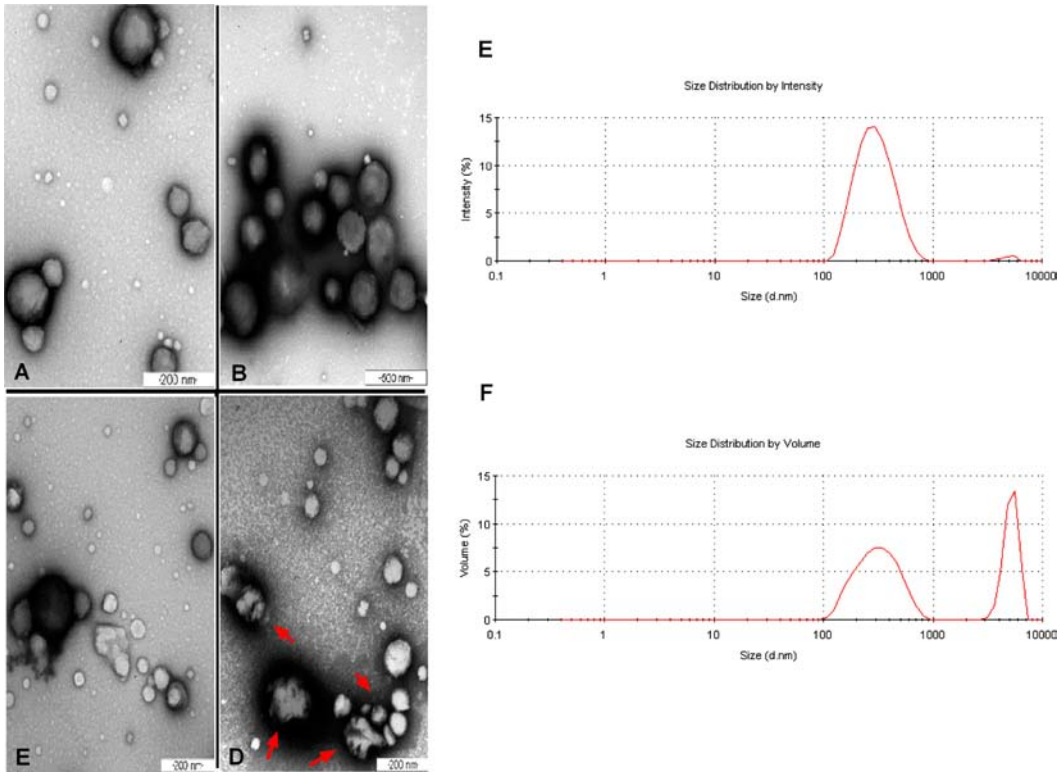

Figure 2. Analysis of SLN morphology immediately after preparation (day 0) and following 120 days of storage: (A) SLN, day 0, 27800× magnification; (B) SLN + ATZ + SMZ, day 0, 21560× magnification; (C) SLN, 120 days, 27800× magnification; (D) SLN + ATZ + SMZ, 120 days, 21560× magnification (red arrows indicate particle deformations); (E) size distribution after 120 days, according to intensity (SLN + ATZ + SMZ); (F) size distribution after 120 days, according to volume (SLN + ATZ + SMZ).

streptomycin sulfate. The cells were plated out and, after a period of 48 h, were exposed for 24 h to a commercial formulation of herbicides (Primatop, Syngenta) and to nanoparticle suspensions (with and without herbicides). The herbicide concentrations tested were 0, 15.6, 31.25, and 62.5 μg/mL. Cellular viability was determined by the mitochondrial reductase activity of live cells, which causes conversion of the yellow tetrazolium salt to blue/purple crystals of formazan. After the 24 h period, the cells were incubated with MTT (0.5 mg/mL) for 3 h at 37 °C, followed by dissolution of the formazan crystals by agitation for 30 min in ethanol. The number of viable cells was then determined by colorimetric analysis (at a wavelength of 570 nm) employing a microplate reader (Multiskan MS, Labsystems).[37,38]

Herbicidal Activity Assays. Herbicidal activity was evaluated by means of pre- and postemergence treatments employing the target species *Raphanus raphanistrum* (wild radish) and nontarget species *Zea mays* (maize). Applications were made of commercial formulation (Primatop, Syngenta) and SLN containing herbicides, at concentrations equivalent to the recommended dosage (3 kg/ha). Control treatments consisted of nanoparticles without herbicides, applied at the same dilutions as the suspensions of nanoparticles containing herbicides, as well as water alone. The plants were cultivated in containers with a height of 17 cm and an upper diameter of 5.2 cm, which were completely filled with the substrate (Hortaliça Mix). One seed was planted in each container. For the preemergence treatment, the formulations were applied to the substrates by spraying soon after planting the seeds. After 13 days, the plants were collected and washed, and measurements were made of the fresh aerial parts and roots. For the postemergence treatment, the formulations were applied in the form of a spray 7 days after planting, and measurements of the aerial and root parts were made after a further 7 days of cultivation. The treatments were repeated for 1:10 (v/v) dilutions of the formulations (equivalent to application of herbicides at a rate of 0.3 kg/ha). Each test (pre- and postemergence) was performed with triplicates of five containers. The values obtained for the masses of the plants were calculated as means and standard deviations, and statistical evaluation employed analysis of variance (ANOVA) with the Tukey–Kramer test. These analyses were performed with GraphPad Prism v6 software.

RESULTS AND DISCUSSION

The purpose of this work was to develop solid lipid nanoparticles as a carrier system for the two herbicides (simazine and atrazine), offering an alternative technique for weed control. In earlier work by our research group,[26] polymeric carrier systems were developed for atrazine, and good results were obtained in terms of effectiveness of formulations. Meanwhile, in the present work, we use the strategy of associating two different herbicides in order to achieve more effective weed control, reducing costs, and helping to avoid the development of plant resistance.[39,40] Combinations of the herbicides atrazine and simazine are available commercially under various brand names (Controller 500 SC, Extrazin SC, Herbimix SC, Primatop SC, and Triamex 500 SC), and all are specifically registered for use in maize cultivations. The products are indicated for use at the preemergence stage, or after emergence, with weeds at the stage of 2–4 leaves, at dosages varying from 1.75 to 3.5 kg/ha^{-1}

DOI: 10.1021/jf5059045
J. Agric. Food Chem. 2015, 63, 422–432

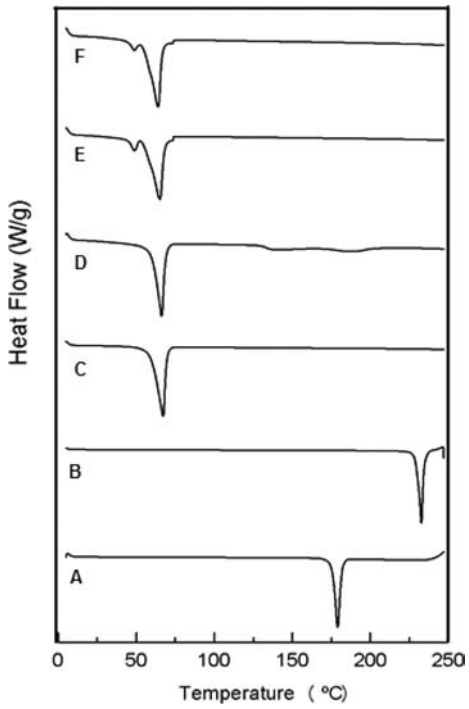

Figure 3. Differential scanning calorimetry evaluation of interaction between herbicides and components of the SLN formulation: Thermograms for (A) ATZ, (B) SMZ, (C) tripalmitin, (D) physical mixture, (E) SLN, and (F) SLN + ATZ + SMZ.

(equivalent to 3.5−7.0 L/ha of the commercial products). The dosage applied varies according to manufacturer and soil type, with smaller quantities used in the case of light soils, and greater quantities with clay soils or in the presence of high levels of organic matter.[41]

When the relative merits of solid lipid nanoparticles and polymeric nanoparticles of poly(ε-caprolactone) are considered, the great advantage of the former lies in their lower production costs, which makes them commercially attractive for use in agricultural applications. The following discussion describes the results obtained for this new formulation containing two herbicides.

Stability of Solid Lipid Nanoparticles. The stability of the nanoparticles was investigated over a period of 120 days, by measurements of hydrodynamic diameter, ζ potential, polydispersion index, pH, and encapsulation efficiency (Figure 1). At the beginning of the period, the hydrodynamic diameter of SLN without herbicides was 272.2 ± 1.35 nm, while nanoparticles loaded with herbicides showed a hydrodynamic diameter of 255.43 ± 3.01 nm. Hydrodynamic diameters of all the formulations increased significantly after 15 days of storage (Figure 1A). After this period, the SLN without the herbicides then remained stable up to the end of the trial (120 days).

The polydispersity index provides an indication of the homogeneity of size distribution of the particles. Values below 0.2 are considered to be indicative of good stability, with the particles present within a narrow size range.[42] Soon after preparation, the formulations showed polydispersity index values below 0.15 (Figure 1B). The values then increased

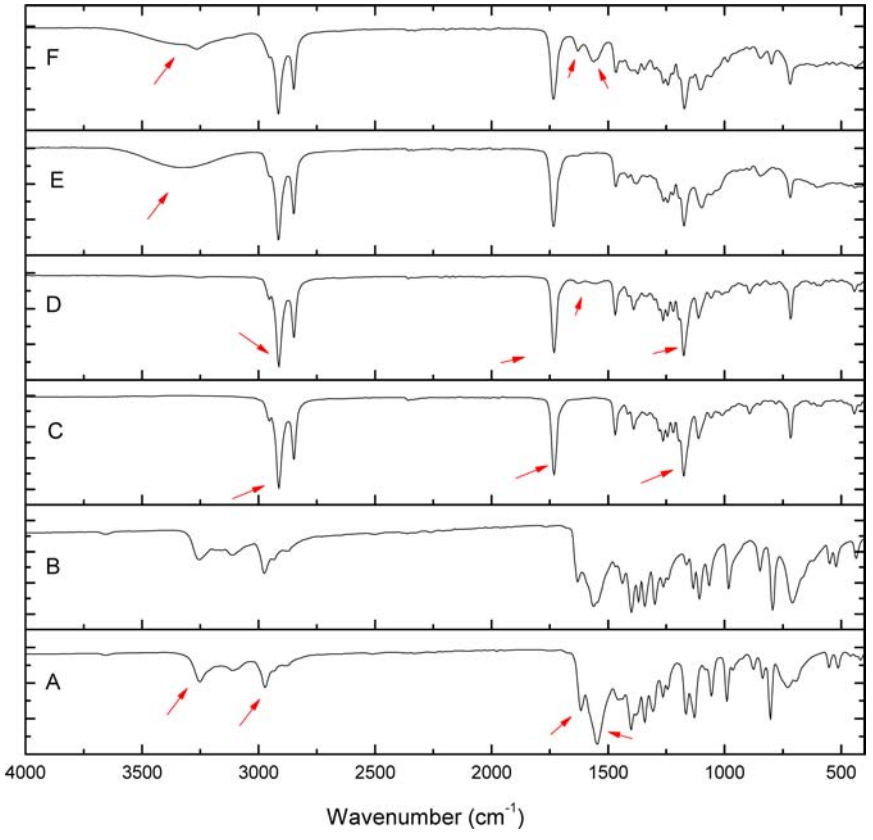

Figure 4. Infrared spectroscopic evaluation of interaction between herbicides and components of the SLN formulation: FTIR spectra for (A) ATZ, (B) SMZ, (C) tripalmitin, (D) physical mixture, (E) SLN, and (F) SLN + ATZ + SMZ. Arrows indicate the main characteristic absorption bands in each spectrum.

DOI: 10.1021/jf5059045
J. Agric. Food Chem. 2015, 63, 422−432

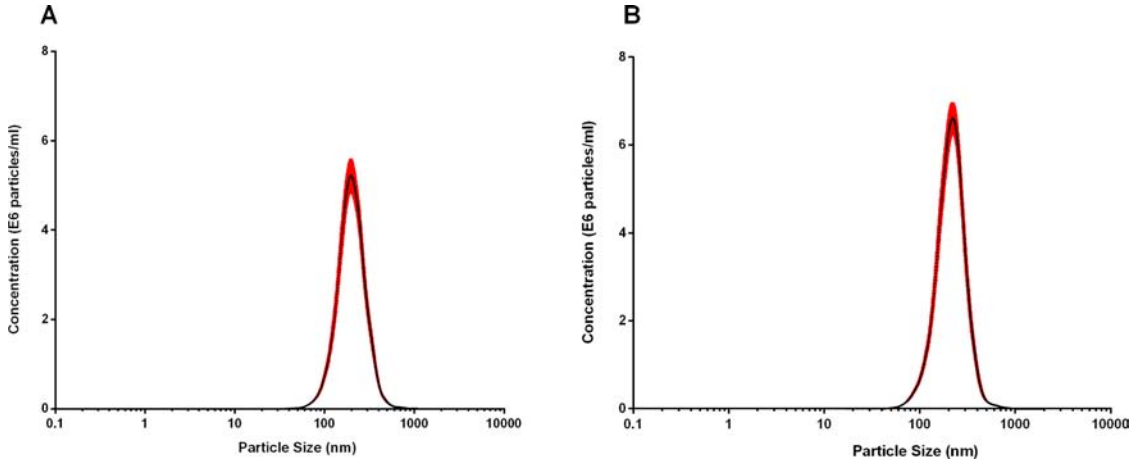

Figure 5. Nanoparticle number concentration as a function of particle size: (A) SLN; (B) SLN + ATZ + SMZ. Analyses were performed at 25 °C (n = 15). Red shading corresponds to the standard deviation of the analyses.

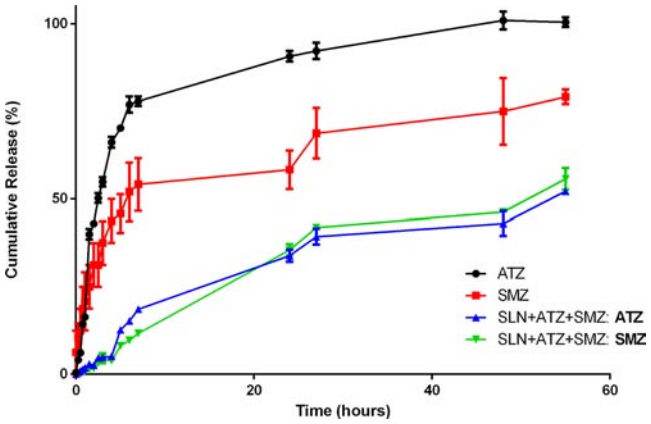

Figure 6. In vitro release kinetics profiles for atrazine and simazine, free or associated with SLN, determined in triplicate (n = 3) at 25 °C by use of the two-compartment system.

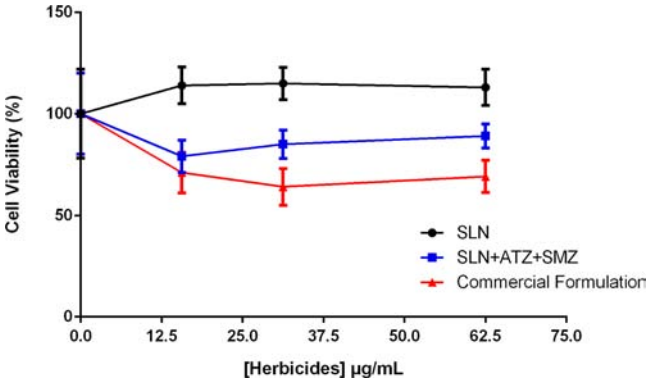

Figure 7. Evaluation of cytotoxicity of SLN (with and without herbicides) and commercial formulation, for herbicide concentrations of 0, 15.6, 31.25, and 62.5 μg/mL.

Table 1. Apparent Flux Values for Free and Encapsulated Herbicides

formulation	F_{app} (mg·m^{-2}·h^{-1})
ATZ	428.0 ± 43.74
SMZ	322.8 ± 31.5
SLN + ATZ + SMZ: ATZ	50.9 ± 0.69
SLN + ATZ + SMZ: SMZ	13.8 ± 1.04

Table 2. Values of Release Constant k, Release Exponent n, and Correlation Coefficient r Obtained by Mathematical Modeling

formulation	k (min^{-1})	n	r
SLN + ATZ + SMZ: ATZ	0.40 ± 0.03	0.76	0.9829
SLN + ATZ + SMZ: SMZ	0.31 ± 0.05	0.83	0.9814

over the period of the trial, but remained below 0.2, indicating satisfactory stability of the formulations as a function of time.

The ζ potential is a parameter that can be used to evaluate the stability of colloidal systems. However, in the present work, the PVA surfactant used during preparation of the formulations was adsorbed on the surface of the particles, creating a layer that provided steric stabilization. Hence, the measured ζ potential values reflected the charges on the particles, while here the stability of the particles was related to steric hindrance caused by the presence of PVA molecules on the surfaces of nanoparticles and not by the surface charge, as reported previously.[43] The SLN formulations showed negative ζ potential values that were not affected by encapsulation of the herbicides (Figure 1C). After 30 days of storage, an average value of −15 mV was obtained, which remained stable up to the end of the trial.

Figure 1D shows the profile of variation of pH as a function of time, for all the formulations. The observed changes were the same for all the particles, probably due to the occurrence of hydrolytic processes in the medium (such as the hydrolysis of tripalmitin), as well as modification of the lipid matrix of the particles, including phenomena such as crystallization or recrystallization, which altered the ionic equilibrium of species present in the medium.[44] Another possible contributing factor was the degradation of PVA by hydrolytic processes, which could cause changes in the medium leading to an increase in pH. However, further work will be needed in order to obtain a better understanding of these phenomena.

Joint encapsulation of the herbicides resulted in encapsulation efficiencies of 89.7% ± 0.02% (atrazine) and 97.3% ± 0.05% (simazine), which remained stable over time. This indicated the effectiveness of SLN for encapsulation of herbicides, because despite the variations in particle size, pH, and ζ potential, the encapsulation efficiency remained

DOI: 10.1021/jf5059045
J. Agric. Food Chem. 2015, 63, 422−432

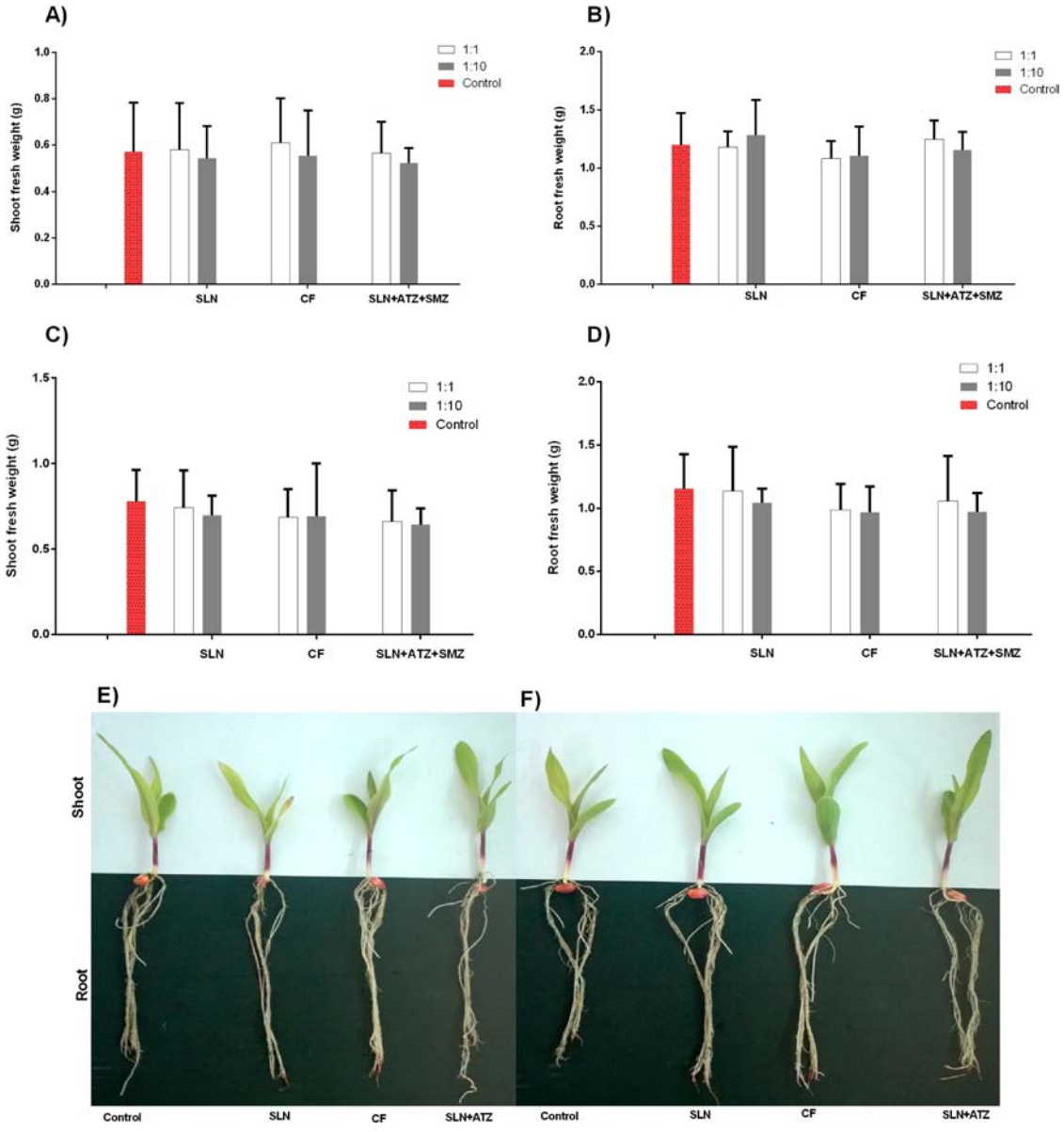

Figure 8. Effects of solid lipid nanoparticles (SLN), commercial formulation (CF), and solid lipid nanoparticles loaded with herbicides (SLN + ATZ + SMZ) on plant growth (nontarget species), at dosages equivalent to 3 and 0.3 kg/ha: (A) fresh masses of aerial parts after pre-emergence treatment; (B) fresh masses of roots after pre-emergence treatment; (C) fresh masses of aerial parts after postemergence treatment; and (D) fresh masses of roots after postemergence treatment. (E, F) Images of *Zea mays* plants after pre-emergence treatment at dosages equivalent to 3 and 0.3 kg/ha, respectively.

unaffected. The high values obtained can be explained by solubility of the herbicides in the lipid matrix, which is supported by their low solubility in water (30 mg/L for atrazine and 5 mg/L for simazine).[45]

Nanoparticle Morphology (Transmission Electron Microscopy). TEM micrographs of the SLN are shown in Figure 2. The particles obtained immediately after preparation were spherical, with average sizes of 111 ± 2.3 nm and 178 ± 3.1 nm in the presence and absence of herbicides, respectively (Figure 2A,B). These values were smaller than those obtained by photon correlation spectroscopy (PCS), which can be explained by the fact that the PCS technique measured the hydrodynamic diameter of the particles, while the TEM analyses employed dried samples.[27] Microscopic analyses performed at the end of the storage period showed that in the absence of herbicides, SLN remained spherical (Figure 2C), while SLN containing herbicides showed deformations (indicated by arrows in Figure 2D). This was reflected in the appearance of a new particle population with low intensity (Figure 2E) but high volume (Figure 2F), which corroborated the results obtained for hydrodynamic diameter, where a significant increase in particle size was observed after 120 days.

Interaction between Herbicides and Nanoparticles. Analyses employing differential scanning calorimetry (Figure 3) and infrared spectroscopy (Figure 4) were used to investigate the interactions of herbicides with SLN, as well as to determine whether the preparation process caused any changes in the components of the formulations.

DSC results revealed the presence of two narrow endothermic peaks, at 179 and 232 °C (Figure 3A,B), corresponding to the fusion points of atrazine and simazine, respectively. Figure 3C shows a peak at 64 °C, corresponding

DOI: 10.1021/jf5059045
J. Agric. Food Chem. 2015, 63, 422−432

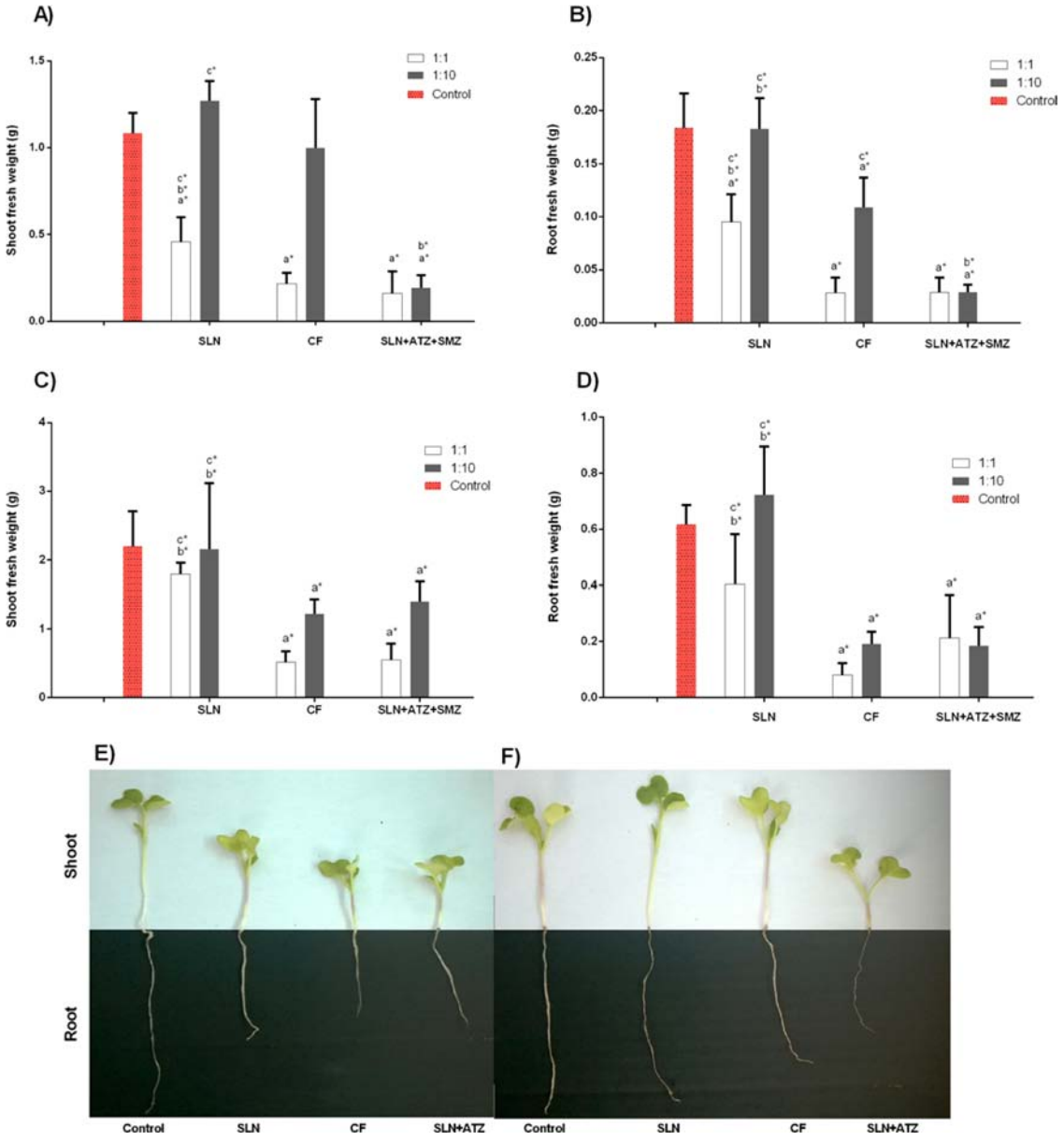

Figure 9. Effects of solid lipid nanoparticles (SLN), commercial formulation (CF), and solid lipid nanoparticles loaded with herbicides (SLN + ATZ + SMZ) on plant growth (target species), at dosages equivalent to 3 and 0.3 kg/ha: (A) fresh masses of aerial parts after pre-emergence treatment; (B) fresh masses of roots after pre-emergence treatment; (C) fresh masses of aerial parts after postemergence treatment; and (D) fresh masses of roots after postemergence treatment. (E, F) Images of *Raphanus raphanistrum* plants after pre-emergence treatment at dosages equivalent to 3 and 0.3 kg/ha, respectively. A significance level of $p < 0.05$ was considered for the differences obtained between groups, at the same application level, where a* indicates significant difference relative to the control; b* indicates significant difference relative to the commercial formulation; and c* indicates significant difference relative to SLN loaded with herbicides.

to the fusion point of the β form of pure tripalmitin lipid.[46] Results for the physical mixture of the components (Figure 3D) revealed two broad herbicide peaks, which were shifted due to interaction with tripalmitin. Analysis of SLN without herbicides (Figure 3E) showed a symmetrical peak at 64 °C, due to fusion of the β form of tripalmitin, and another peak at 48 °C, corresponding to recrystallization of the α form of tripalmitin.[47] In colloidal suspensions, lipids can show changes in crystallization and polymorphism, which consequently affect the fusion point.[47,48] In the case of SLN containing herbicides (Figure 3F), peaks characteristic of the fusion of forms α and β of tripalmitin were observed, but there were no symmetrical herbicide peaks at around 179 and 232 °C, indicating that the herbicides were dispersed throughout the nanoparticle matrix and were not present in the form of crystals.

The infrared spectra obtained for atrazine and simazine are shown in Figure 4 panels A and B, respectively. Similarities can be seen in the spectra, because both compounds belong to the triazine herbicide family, with specific bands at 3251 cm^{-1} corresponding to symmetrical and asymmetrical axial deformation of N−H, at 2972 cm^{-1} due to aliphatic C−H stretching and at 1616 and 1546 cm^{-1} due to deformation of C═C and C═N bonds, respectively. The spectrum of tripalmitin (Figure 4C) shows specific bands at 2914 cm^{-1} corresponding to stretching of alkyl group C−H, at 1733 cm^{-1} corresponding to stretching of ester C═O, and at 1173 cm^{-1} due to angular

DOI: 10.1021/jf5059045
J. Agric. Food Chem. 2015, 63, 422−432

deformation of C−O. The spectrum for the physical mixture (Figure 4D) shows the characteristic bands of tripalmitin, together with deformation of the C═C and C═N bonds of the herbicides. The spectrum for SLN without herbicides (Figure 4E) shows most of the bands corresponding to tripalmitin, together with a band at around 3340 cm^{-1} indicative of the presence of the −O-H group in the structure, which probably resulted from the use of the water and poly(vinyl alcohol) as stabilizers during preparation of the nanoparticles. Another characteristic −O-H deformation band of water can be seen at 1640 cm^{-1} in this spectrum. Figure 4F shows the spectrum for SLN loaded with atrazine and simazine, with the presence of characteristic bands corresponding to poly(vinyl alcohol), tripalmitin, and (indicated by the arrows) shifted lower intensity bands at 1629 and 1561 cm^{-1} associated with deformation of C═C and C═N bonds of the herbicides. These features indicate that the herbicides were encapsulated and/or had interacted with the nanoparticles. In previous work, de Melo et al.[49] used changes in FTIR spectra to show that the bioactive compound articaine interacted with nanospheres of alginate/chitosan, as well as with nanocapsules of PCL/PEG, confirming that both types of nanoparticle were suitable for loading with articaine.

Nanoparticle Tracking Analysis. The nanoparticle tracking analysis technique was used to characterize SLN suspensions immediately after their preparation. Figure 5 shows the concentrations of nanoparticles as a function of particle size. For SLN without herbicides, the particle number concentration was $(9.09 \pm 0.70) \times 10^{12}$ particles/mL and the average hydrodynamic diameter was 240.37 ± 95.54 nm. Encapsulation of the herbicides resulted in a concentration of $(11.75 \pm 0.64) \times 10^{12}$ particles/mL and an average hydrodynamic diameter of 252.18 ± 91.56 nm. It can be seen that use of DLS and NTA techniques resulted in similar average hydrodynamic diameter values, as well as particle number concentrations that were in the same range, evidencing the satisfactory conditions used to prepare the formulations. An important point is that the formulations showed the monomodal size distributions associated with only one population of particles. This type of homogeneity is desirable in modified release formulations, because there are therefore likely to be fewer interferences in the process of release of the active agents.[50]

Release Kinetics Assays and Mathematical Modeling. Release kinetics assays were conducted in order to obtain further information concerning the interactions between herbicides and nanoparticles, as well as the mechanisms involved in herbicide release. Figure 6 shows the curves obtained for cumulative release of the herbicides as a function of time. In these experiments, the herbicide molecules were able to traverse the 1 kDa pores of the cellulose membrane separating the donor and acceptor compartments, enabling observation of the progressive release of herbicide into solution. The results (Figure 6) showed that the presence of SLN modified the release profiles, which were slower compared to those of the free herbicides. For the free herbicides, 50% release was obtained in 2.5 h (ATZ) and 5.3 h (SMZ). When the compounds were encapsulated together in SLN, 50% release of the same quantities of the herbicides was obtained in 52.9 h (ATZ) and 51.1 h (SMZ).

The apparent fluxes (F_{app}) for the free and encapsulated herbicides are listed in Table 1. The data showed that the mass flux of simazine was lower than that of atrazine, for both free and encapsulated forms. When the herbicides were encapsulated, atrazine showed an initial release that was faster than that of simazine. This can be explained by the lower encapsulation efficiency obtained for atrazine, with initial fast release of the fraction of the herbicide that was not encapsulated. However, after the initial release, the release profiles for the two herbicides were very similar, indicating that the compounds had interacted in similar ways with the hydrophobic cores of the nanoparticles.

Release profiles of the herbicides were analyzed by use of the Korsmeyer−Peppas mathematical model. Linear regression was used to calculate the values of release exponent n, release constant k, and correlation coefficient r (Table 2).

Use of the Korsmeyer−Peppas model enables prediction of the mechanism of release of active compounds from nanostructured systems, which can essentially be by either Fickian diffusion and/or case II transport.[36] Here, the values obtained for the release exponent were in the range $0.45 > n > 0.85$, indicating that the kinetics could be described by anomalous transport, which involves a combination of the two different mechanisms. The values of the release constants k showed that atrazine was released faster than simazine, in agreement with the results obtained in kinetics and apparent flux experiments. Grillo et al.[25] also obtained higher release constant values for atrazine when the Korsmeyer−Peppas model was used to investigate the mechanisms of release of the herbicides atrazine, simazine, and ametryn from nanocapsules composed of poly(ε-caprolactone).

In Vitro Cytotoxicity Assays. The MTT reduction test employing 3T3 fibroblast cells was used to determine whether encapsulation of the herbicides altered their cytotoxicity. The results (Figure 7) showed that in the absence of herbicides, SLN were not cytotoxic in the concentration range tested, since cellular viability remained at around 100%. When herbicides were incorporated into SLN, cellular viability of 80% was obtained for the highest concentration tested, while greater cytotoxicity was observed for the commercial formulation, with a value of 64% obtained at the same concentration. These findings confirmed that encapsulation of the herbicides in the solid lipid nanoparticles resulted in a decrease in cytotoxicity.

Herbicidal Activity Assays. Effects of nanoparticle formulations, with and without herbicides, as well as the commercial formulation, were investigated for pre- and postemergence treatments applied to a target species (*Raphanus raphanistrum*) and a nontarget species (*Zea mays*), at concentrations equivalent to 0.3 and 3 kg/ha.

Atrazine and simazine are used together to increase the spectrum of action in controlling weeds in maize plantations. Maize is resistant to these herbicides because of the presence in this species of a soluble enzyme, glutathione S-transferase, that detoxifies both atrazine and simazine.[1,4] For the nontarget species (for pre- and postemergence treatments), none of the formulations showed any phytotoxic effects on the aerial and root parts of plants when compared with the control (Figure 8).

For the target species, in the case of pre-emergence treatments, all the formulations showed effects on both the aerial and root parts of plants, compared to the control treatment (Figure 9). At the 3 kg/ha concentration level, effects of the commercial formulation and herbicides encapsulated in SLN were significantly greater, compared to SLN without herbicides, which could be attributed to the presence of the active agents. However, when the formulations were diluted 10 times (0.3 kg/ha), SLN without herbicides showed no

DOI: 10.1021/jf5059045
J. Agric. Food Chem. 2015, 63, 422−432

phytotoxicity, compared to the control, and the commercial formulation showed a significant effect only on the roots. On the other hand, SLN containing herbicides caused greater effects on both the aerial parts and roots of plants, compared to the commercial formulation. This provided evidence of the effectiveness and agricultural potential of SLN containing herbicides, since when applications were performed at the recommended concentrations, all the formulations caused inhibition of growth, while at 10 times lower concentrations, the effect of the commercial formulation decreased, while SLN containing herbicides remained effective (Figure 9E).

In the case of postemergence treatment, SLN without herbicides showed no phytotoxic effects on aerial parts or roots, at either concentration, compared to the control. However, the commercial formulation and SLN loaded with herbicides showed phytotoxic effects on aerial parts and roots at both concentrations. No significant differences were observed between these phytotoxic effects.

The phytotoxic effects of SLN in pre- and postemergence assays could have been due to interactions of SLN with roots of *R. raphanistrum*, resulting in changes in the processes of absorption of water and/or nutrients. It is also possible that absorption of nanoparticles by the roots caused toxic effects and reduced growth rates. There have been several reports of interactions between nanoparticles and plants.[51−53] Meanwhile, it should be highlighted that the interaction of SLN with *R. raphanistrum* (Figure 9E,F) appeared to be species-specific, because no toxic effects of SLN were observed in assays with *Z. mays*, at the same concentration range (Figure 8E,F).

The greater effectiveness of SLN containing herbicides could be explained by reduced soil sorption of the active agents, as well as physicochemical and microbiological protection provided by encapsulation and sustained release of herbicides provided by the nanoparticles. Similar findings were reported previously[26] for encapsulation of atrazine in PCL nanoparticles (nanocapsules and nanopheres) and evaluation of the effects on mustard plants (*Brassica* sp.).

In conclusion, the herbicides atrazine and simazine were successfully incorporated into solid lipid nanoparticles, with encapsulation efficiencies of around 90% for atrazine and 98% for simazine. SLN showed hydrodynamic diameters between 255 and 300 nm and remained stable over a period of 120 days. DSC and FTIR analyses confirmed that the herbicides were encapsulated and interacted with the lipid matrix. The use of TEM and NTA techniques demonstrated that the nanoparticles were spherical, with an average concentration of 12×10^{12} particles/mL. Encapsulation resulted in modification of the herbicide release profiles, with slower and more sustained release compared to the free forms of the herbicides. Evaluation of cytotoxicity by the MTT test showed that SLN provided a protective effect and acted to decrease the toxicity of the active agents. In herbicidal activity assays, postemergence treatment with SLN containing the two herbicides was as effective as use of the commercial formulation. In the case of pre-emergence treatment, SLN loaded with herbicides were more effective, compared to the commercial product, indicating the potential of these formulations for use in agriculture. An important finding was that the formulations of SLN containing two active agents were more effective, compared to the commercial formulation, and caused no toxicity in nontarget organisms (*Z. mays* plants and mouse fibroblast cells). The findings illustrate one of the ways in which nanotechnology can be used to develop effective systems for modified release of herbicides, providing greater efficiency in weed control, reducing the quantities of active agents required, and at the same time decreasing toxicity toward nontarget organisms.

AUTHOR INFORMATION

Corresponding Author

*Telephone 55 15 3238-3400, ext 3456; fax 55 15 3228-2842; e-mail leonardo@sorocaba.unesp.br.

Funding

We are grateful for the financial support provided by the São Paulo State Research Foundation (FAPESP, Grant 2012/20076-9), CNPq, and FUNDUNESP.

Notes

The authors declare no competing financial interest.

REFERENCES

(1) Weis, M.; Gutjahr, C.; Rueda Ayala, V.; Gerhards, R.; Ritter, C.; Schölderle, F. Precision farming for weed management: Techniques. *Gesunde Pflanz.* **2008**, *60*, 171−181.

(2) Brighenti, A. M.; de Oliveira, M. F. Biologia de plantas daninhas. In *Biologia e Manejo de plantas daninhas*; Omnipax: Curitiba, Brazil, 2011; pp 1−36.

(3) de Oliveira, R. S., Jr. Introdução ao Controle Químico. In *Biologia e Manejo de plantas daninhas*; Omnipax: Curitiba, Brazil, 2011; pp 125−140.

(4) Breckenridge, C. B.; Werner, C.; Stevens, J. T.; Summer, D. D. Hazard assessment for selected symmetrical and asymmetrical triazine herbicides. *Triazine Herbic.* **2008**, 346−358.

(5) Beckie, H. J.; Tardif, F. J. Herbicide cross resistance in weeds. *Crop Prot.* **2012**, *35*, 15−28.

(6) Nair, R.; Varghese, S. H.; Nair, B. G.; Maekawa, T.; Yoshida, Y.; Kumar, D. S. Nanoparticulate material delivery to plants. *Plant Sci.* **2010**, *179*, 154−163.

(7) Chen, H.; Yada, R. Nanotechnologies in agriculture: New tools for sustainable development. *Trends Food Sci. Technol.* **2011**, *22*, 585−594.

(8) Gruère, G. P. Implications of nanotechnology growth in food and agriculture in OECD countries. *Food Policy* **2012**, *37*, 191−198.

(9) Kah, M.; Hofmann, T. Nanopesticide research: Current trends and future priorities. *Environ. Int.* **2014**, *63*, 224−235.

(10) Kah, M.; Beulke, S.; Tiede, K.; Hofmann, T. Nanopesticides: State of knowledge, environmental fate, and exposure modeling. *Crit. Rev. Environ. Sci. Technol.* **2013**, *43*, 1823−1867.

(11) Mousavi, S. R.; Rezaei, M. Nanotechnology in agriculture and food production. *J. Appl. Environ. Biol. Sci.* **2011**, *1*, 414−419.

(12) Joshi, M. D.; Müller, R. H. Lipid nanoparticles for parenteral delivery of actives. *Eur. J. Pharm. Biopharm.* **2009**, *71*, 161−172.

(13) Mehnert, W.; Mäder, K. Solid lipid nanoparticles. *Adv. Drug Delivery Rev.* **2012**, *64*, 83−101.

(14) Guo, H.; Zhang, J.; Liu, Z.; Yang, S.; Sun, C. Effect of Tween80 and β-cyclodextrin on the distribution of herbicide mefenacet in soil−water system. *J. Hazard. Mater.* **2010**, *177*, 1039−1045.

(15) Villaverde, J.; Maqueda, C.; Morillo, E. Effect of the simultaneous addition of β-cyclodextrin and the herbicide norflurazon on its adsorption and movement in soils. *J. Agric. Food Chem.* **2006**, *54*, 4766−4772.

(16) Cornejo, L.; Celis, R.; Domínguez, C.; Hermosín, M. C.; Cornejo, J. Use of modified montmorillonites to reduce herbicide leaching in sports turf surfaces: Laboratory and field experiments. *Appl. Clay Sci.* **2008**, *42*, 284−291.

(17) Maqueda, C.; Villaverde, J.; Sopeña, F.; Undabeytia, T.; Morillo, E. Effects of soil characteristics on metribuzin dissipation using clay−gel-based formulations. *J. Agric. Food Chem.* **2009**, *57*, 3273−3278.

(18) Barik, T. K.; Sahu, B.; Swain, V. Nanosilica—from medicine to pest control. *Parasitol. Res.* **2008**, *103*, 253−258.

DOI: 10.1021/jf5059045
J. Agric. Food Chem. 2015, 63, 422−432

(19) Garrido-Herrera, F. J.; Daza-Fernández, I.; González-Pradas, E.; Fernández-Pérez, M. Lignin-based formulations to prevent pesticides pollution. *J. Hazard. Mater.* **2009**, *168*, 220−225.
(20) El Bahri, Z.; Taverdet, J.-L. Elaboration and characterisation of microparticles loaded by pesticide model. *Powder Technol.* **2007**, *172*, 30−40.
(21) Grillo, R.; Melo, N. F. S.; Lima, R.; Lourenço, R. W.; Rosa, A. H.; Fraceto, L. F. Characterization of atrazine-loaded biodegradable poly(hydroxybutyrate-*co*-hydroxyvalerate) microspheres. *J. Polym. Environ.* **2010**, *18*, 26−32.
(22) Grillo, R.; Pereira, A. do E. S.; de Melo, N. F. S.; Porto, R. M.; Feitosa, L. O.; Tonello, P. S.; Filho, N. L. D.; Rosa, A. H.; Lima, R.; Fraceto, L. F. Controlled release system for ametryn using polymer microspheres: Preparation, characterization and release kinetics in water. *J. Hazard. Mater.* **2011**, *186*, 1645−1651.
(23) Sopeña, F.; Maqueda, C.; Morillo, E. Controlled release formulations of herbicides based on micro-encapsulation. *Cienc. Invest. Agrar.* **2009**, *36*, 27−42.
(24) Suave, J.; Dall'Agnol, E. C.; Pezzin, A. P. T.; Meier, M. M.; Silva, D. A. K. Biodegradable microspheres of poly(3-hydroxybutyrate)/poly(ε-caprolactone) loaded with malathion pesticide: Preparation, characterization, and in vitro controlled release testing. *J. Appl. Polym. Sci.* **2010**, *117*, 3419−3426.
(25) Grillo, R.; dos Santos, N. Z. P.; Maruyama, C. R.; Rosa, A. H.; de Lima, R.; Fraceto, L. F. Poly(ε-caprolactone)nanocapsules as carrier systems for herbicides: Physico-chemical characterization and genotoxicity evaluation. *J. Hazard. Mater.* **2012**, *231*−*232*, 1−9.
(26) Pereira, A. E. S.; Grillo, R.; Mello, N. F. S.; Rosa, A. H.; Fraceto, L. F. Application of poly(epsilon-caprolactone) nanoparticles containing atrazine herbicide as an alternative technique to control weeds and reduce damage to the environment. *J. Hazard. Mater.* **2014**, *268*, 207−215.
(27) Silva, M. dos S.; Cocenza, D. S.; Grillo, R.; Melo, N. F. S.; Tonello, P. S.; de Oliveira, L. C.; Cassimiro, D. L.; Rosa, A. H.; Fraceto, L. F. Paraquat-loaded alginate/chitosan nanoparticles: Preparation, characterization and soil sorption studies. *J. Hazard. Mater.* **2011**, *190*, 366−374.
(28) Campos, E. V. R.; de Oliveira, J. L.; Fraceto, L. F. Applications of controlled release systems for fungicides, herbicides, acaricides, nutrients, and plant growth hormones: A review. *Adv. Sci. Eng. Med.* **2014**, *6*, 373−387.
(29) Ghormade, V.; Deshpande, M. V.; Paknikar, K. M. Perspectives for nano-biotechnology enabled protection and nutrition of plants. *Biotechnol. Adv.* **2011**, *29*, 792−803.
(30) Vitorino, C.; Carvalho, F. A.; Almeida, A. J.; Sousa, J. J.; Pais, A. A. C. C. The size of solid lipid nanoparticles: An interpretation from experimental design. *Colloids Surf., B* **2011**, *84*, 117−130.
(31) Jores, K.; Mehnert, W.; Drechsler, M.; Bunjes, H.; Johann, C.; Mäder, K. Investigations on the structure of solid lipid nanoparticles (SLN) and oil-loaded solid lipid nanoparticles by photon correlation spectroscopy, field-flow fractionation and transmission electron microscopy. *J. Controlled Release* **2004**, *95*, 217−227.
(32) Anderson, W.; Kozak, D.; Coleman, V. A.; Jämting, Å. K.; Trau, M. A comparative study of submicron particle sizing platforms: Accuracy, precision and resolution analysis of polydisperse particle size distributions. *J. Colloid Interface Sci.* **2013**, *405*, 322−330.
(33) Fiel, L. A.; Paese, K.; Rizzi, M.; Guterres, S. S.; Pohlmann, A. R. A strategy to estimate the intrinsic flux of a poorly water soluble substance for comparison with its release from lipid-core nanocapsules. *Colloids Surf., A* **2014**, *441*, 716−724.
(34) Guterres, S. S.; Poletto, F. S.; Colomé, L. M.; Raffin, R. P.; Pohlmann, A. R. Polymeric nanocapsules for drug delivery. In *Colloids in Drug Delivery*; CRC Press: Boca Raton, FL, 2010; pp 71−98.
(35) Soppimath, K. S.; Aminabhavi, T. M.; Kulkarni, A. R.; Rudzinski, W. E. Biodegradable polymeric nanoparticles as drug delivery devices. *J. Controlled Release* **2001**, *70*, 1−20.
(36) Peppas, N. A.; Sahlin, J. J. A simple equation for the description of solute release. III. Coupling of diffusion and relaxation. *Int. J. Pharm.* **1989**, *57*, 169−172.
(37) De Lima, R.; Feitosa, L.; Pereira, A. do E. S.; De Moura, M. R.; Aouada, F. A.; Mattoso, L. H. C.; Fraceto, L. F. Evaluation of the genotoxicity of chitosan nanoparticles for use in food packaging films. *J. Food Sci.* **2010**, *75*, N89−N96.
(38) De Lima, R.; Feitosa, L. O.; Grillo, R.; Pereira, A. E.; Fraceto, L. F. Evaluation of the genotoxicity of polymeric microparticles containing ametryn herbicide. *J. of Environ. Sci. Eng.* **2012**, *4A*, 553−565.
(39) Gressel, J. Synergizing herbicides. *Rev. Weed Sci.* **1990**, *5*, 49−82.
(40) Damalas, C. A.; Eleftherohorinos, I. G. Dicamba and atrazine antagonism on sulfonylurea herbicides used for johnsongrass (*Sorghum halepense*) control in corn (*Zea mays*). *Weed Technol.* **2001**, *15*, 62−67.
(41) Rodrigues, B. N.; Almeida, F. L. S. *Guia de Herbicidas*, 6th ed.; Livroceres: Piracicaba, Brazil, 2011.
(42) Mohanraj, V. J.; Chen, Y. Nanoparticles: A review. *Trop. J. Pharm. Res.* **2007**, *5*, 561−573.
(43) Schaffazick, S. R.; Guterres, S. S.; Freitas, L. de L.; Pohlmann, A. R. Caracterização e estabilidade físico-química de sistemas poliméricos nanoparticulados para administração de fármacos. *Quím. Nova* **2003**, *26*, 726−737.
(44) Choi, K.-O.; Aditya, N. P.; Ko, S. Effect of aqueous pH and electrolyte concentration on structure, stability and flow behavior of non-ionic surfactant based solid lipid nanoparticles. *Food Chem.* **2014**, *147*, 239−244.
(45) EXTONET. Pesticide information profiles, 2014.
(46) Awad, T. S.; Helgason, T.; Weiss, J.; Decker, E. A.; McClements, D. J. Effect of Omega-3 fatty acids on crystallization, polymorphic transformation and stability of tripalmitin solid lipid nanoparticle suspensions. *Cryst. Growth Des.* **2009**, *9*, 3405−3411.
(47) Heurtault, B. Physico-chemical stability of colloidal lipid particles. *Biomaterials* **2003**, *24*, 4283−4300.
(48) Bunjes, H. Structural properties of solid lipid based colloidal drug delivery systems. *Curr. Opin. Colloid Interface Sci.* **2011**, *16*, 405−411.
(49) de Melo, N. F. S.; Campos, E. V. R.; Gonçalves, C. M.; de Paula, E.; Pasquoto, T.; de Lima, R.; Rosa, A. H.; Fraceto, L. F. Development of hydrophilic nanocarriers for the charged form of the local anesthetic articaine. *Colloids Surf., B* **2014**, *121*, 66−73.
(50) Marcato, P. D. Preparação, caracterização e aplicações em fármacos e cosméticos de nanopartículas lipídicas sólidas. *Rev. Eletronica Farm.* **2009**, *6*, 1.
(51) Roy, A.; Singh, S. K.; Bajpai, J.; Bajpai, A. K. Controlled pesticide release from biodegradable polymers. *Centr. Eur. J. Chem.* **2014**, *12*, 453−469.
(52) Rico, C. M.; Majumdar, S.; Duarte-Gardea, M.; Peralta-Videa, J. R.; Gardea-Torresdey, J. L. Interaction of nanoparticles with edible plants and their possible implications in the food chain. *J. Agric. Food Chem.* **2011**, *59*, 3485−3498.
(53) Remedios, C.; Rosário, F.; Bastos, V. Environmental nanoparticles interactions with plants: morphological, physiological, and genotoxic aspects. *J. Bot.* **2012**, *2*, 1−8.

DOI: 10.1021/jf5059045
J. Agric. Food Chem. 2015, 63, 422−432

JOURNAL OF AGRICULTURAL AND FOOD CHEMISTRY

Article

pubs.acs.org/JAFC

Dosage Effect of High-Amylose Modifier Gene(s) on the Starch Structure of Maize *amylose-extender* Mutant

Hongxin Jiang,[†] Mark Campbell,[‡] Yusheng Wu,[§] Shuangkui Du,[⊥] Sathaporn Srichuwong,[†] and Jay-lin Jane*[,†]

[†]Department of Food Science and Human Nutrition, Iowa State University, Ames, Iowa 50011, United States

[‡]Division of Science, Truman State University, Kirksville, Missouri 63501, United States

[§]School of Arts and Sciences, University of the Southwest, Hobbs, New Mexico 88240, United States

[⊥]College of Food Science and Engineering, Northwest A&F University, Yangling, Shanxi 712100, China

ABSTRACT: The objective of this study was to investigate how dosages of high-amylose modifier (HAM) gene(s) affected the structure of maize *amylose extender* (*ae*) mutant starch. GEMS-0067 (G), a homozygous mutant of *ae* and the HAM gene(s), and H99*ae* (H), an *ae* single mutant, were self-pollinated or inter-crossed to produce maize endosperms of G/G, G/H, H/G, and H/H with 3, 2, 1, and 0 doses of HAM gene(s), respectively. Endosperm starch was fractionated into amylopectin, amylose, and intermediate component (IC) of large and small molecular weights using 1-butanol precipitation of amylose followed by gel-permeation chromatography. Increases in the dosage of HAM gene(s) from 0 to 3 decreased the amylopectin content. The HAM-gene dosage significantly changed the branch chain-length of small-molecular-weight IC, but had little effect on the branch chain-length distributions of amylopectin and large-molecular-weight IC and the molecular structure of amylose.

KEYWORDS: *high-amylose maize starch, high-amylose modifier gene, starch structure, resistant starch*

INTRODUCTION

Starch is the major energy reserve of green plants and widely exists in seeds, tubers, roots, stems, leaves, and fruits.[1] Starch is composed of mainly amylopectin and amylose molecules. Amylopectin molecules consist of chains of (α1→4)-linked D-glucopyranose units, which are connected by (α1→6) glycosidic branch linkages. Amylose molecules are primarily linear chains of (α1→4)-linked D-glucopyranose units; amylose molecules with large molecular weight possess a few branches.[2−5] In addition to amylose and amylopectin, high-amylose maize starch also consists of intermediate components (IC) that have branched structures with branch chains longer than amylopectin but molecular weights smaller than amylopectin and similar to amylose.[6−11]

Amylopectin molecules are synthesized through cooperative reactions catalyzed by enzymes including starch synthases, starch branching enzymes (SBEs), and starch debranching enzymes.[12−16] SBEs include SBEI and SBEII. SBEII prefers to cleave, transfer, and form shorter branch-chains, whereas SBEI prefers to transfer and form longer branch-chains.[17] There are two isoforms of SBEII identified in maize endosperm, SBEIIa and SBEIIb. SBEIIb plays a major role in the biosynthesis of amylopectin molecules in maize endosperm.[14] Maize *ae* mutants, deficient of SBEIIb activity in the endosperm, produce high-amylose maize starch with greater contents of amylose and IC and longer branch chain-lengths of amylopectin than the normal maize starch.[3,11,18,19]

A public high-amylose maize line registered as GEMS-0067 has been developed from USDA-ARS Germplasm Enhancement of Maize (GEM) Project by selectively crossing the exotic line of GUAT209:S13 to a hybrid OH43*ae*×H99*ae*.[20] The GEMS-0067 maize line is a homozygous mutant of *amylose-extender* (*ae*) and high-amylose modifier (HAM) gene(s).[20] Preliminary results showed that the HAM gene(s) in the GEMS-0067 included the *sbeI* allele.[21] Starch of the GEMS-0067 maize consists of 39.4−43.2% resistant starch (RS) determined using the AOAC Method 991.43 for total dietary fiber, which is much greater than that of maize *ae* single mutants of H99*ae*, OH43*ae*, B89*ae*, and B84*ae* (11.5−19.1%).[11] Structures of the RS have been characterized as long-chain double-helical crystallites of amylose and IC, which maintain the B-type semicrystalline structures at 95−100 °C and, thus, are highly resistant to enzymatic hydrolysis.[6,11,22,23]

The gene-dosage effects, non-allelic interactions, and heritability of high amylose content of the GEMS-0067 maize were studied using maize samples grown in two locations (Kirksville, Missouri, and Brookings, South Dakota) and two years (2005 and 2006).[24] Results showed that the dosage of HAM gene(s) had an additive effect on the amylose content of starch produced by maize *ae* mutant. On the basis of the results reported by Wu et al.,[24] we selected two sets of the maize samples with different HAM gene(s) dosages grown in Kirksville, MO and Brookings, SD in summer of 2006 to characterize fine structures of the starches. In this study, we aimed to investigate effects of HAM gene(s) dosage present in maize *ae* mutants on the contents and structures of amylopectin, IC, and amylose and, in turn, the RS content of the starch.

Received: September 2, 2014
Revised: November 26, 2014
Accepted: December 15, 2014
Published: December 15, 2014

ACS Publications © 2014 American Chemical Society

DOI: 10.1021/jf504099x
J. Agric. Food Chem. 2015, 63, 433−439

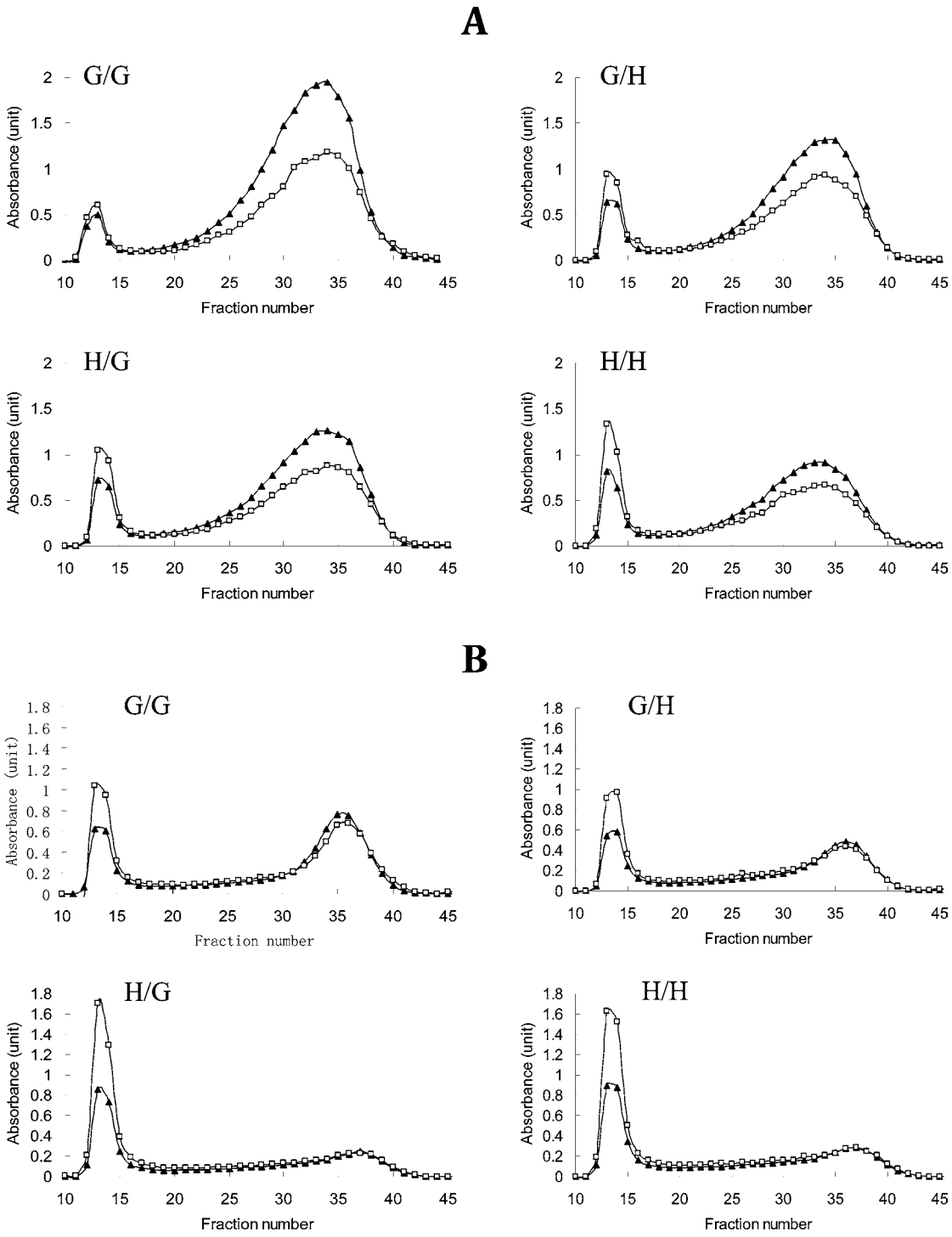

Figure 1. Sepharose CL-2B gel-permeation profiles of the whole starch samples (A) and amylopectin/IC mixtures (B). G/G, G/H, H/G, and H/H contained 3, 2, 1, and 0 doses of HAM gene(s), respectively. ▲, blue value; □, total carbohydrate.

MATERIALS AND METHODS

Materials. All the chemicals used for the study were reagent grade, used as received, and were purchased from Sigma-Aldrich Chemical Co. (St. Louis, MO) or Fisher Scientific (Pittsburgh, PA). Crystalline *Pseudomonas* isoamylase (EC 3.2.1.68) was purchased from Hayashibara Biochemical Laboratories, Inc. (Okayama, Japan) and used for debranching amylopectin and IC molecules.

Preparation of Maize Samples. GEMS-0067 and H99*ae* plants were grown in Kirksville, MO, and Brookings, SD, in summer 2006, and planted in a completely randomized design as described by Wu et al.[24] Each plot consisted of one row containing 20 individual plants of the same genotype. Rows were 4.5 m long and 0.75 m wide. There were six plots for each maize endosperm genotype. Through self-pollination and inter-crossing between GEMS-0067 (G) and H99*ae* (H), four maize endosperm genotypes, GEMS-0067×GEMS-0067 (G/G), GEMS-0067×H99*ae* (G/H), H99*ae*×GEMS-0067 (H/G), and H99*ae*×H99*ae* (H/H) with 3, 2, 1, and 0 doses of HAM gene(s), respectively, were produced. Individual samples were composed of 100 kernels from each ear in a genotype.

Starch Isolation. Endosperm starch was isolated from maize kernels using a wet milling method and protein present in the starch

DOI: 10.1021/jf504099x
J. Agric. Food Chem. 2015, 63, 433−439

was removed using an aqueous toluene solution as described by Li et al.[11]

Fractionation of Starch Components. Starch was fractionated into amylose and a mixture of amylopectin and IC using 1-butanol precipitation method.[11,13] Purity of the fractionated amylose and the mixture of amylopectin and IC was determined using Sepharose CL-2B gel-permeation chromatography (GPC),[11] and the collected fractions were analyzed for contents of total carbohydrate (phenol-sulfuric acid)[26] and amylose iodine blue staining.[27]

Amylopectin, IC, and Amylose Contents of Starch. Amylopectin, amylose, and IC contents of starch were determined using GPC and calculated on the basis of the total carbohydrate contents of the GPC peaks of native starch and the mixture of amylopectin and IC following the method of Li et al.[11]

RS Content of Starch. The RS content of starch was measured using AOAC Method 991.43 for total dietary fiber.[28]

Branch Chain-Length Distributions of Amylopectin and IC. Amylopectin and IC of different molecular weights were separated using a Sepharose CL-2B column as described by Li et al.[11] The collected fractions of amylopectin and IC of large and small molecular weights were each dispersed, debranched, and labeled with 8-aminopyrene-1,3,6-trisulfonic acid following the method of Morell et al.[29] with modification by Jiang et al.[6] Branch chain-length distributions of amylopectin and IC of large and small molecular weights were determined using a fluorophore-assisted capillary electrophoresis (FACE) (P/ACE MDQ, Beckman Coulter, Fullerton, CA) following the method of Morell et al.[29] with modification.[6]

Molecular-Size Distribution of Amylose. Molecular-size distributions of amylose molecules, before and after debranching, were determined using high-performance size-exclusion chromatography (HPSEC) following the method of Jiang et al.[6] with modifications. Shodex SB-804 and SB-803 analytical columns with a Shodex OH pak SB-G guard column (Showa Denko K.K., Tokyo, Japan) were used to analyze the molecular-size distribution of amylose. The amylose molecules were dispersed and debranched following the method of Li et al.[11] The debranched amylose was precipitated using absolute ethanol (20×). The collected debranched-amylose was dispersed in 90% DMSO in a boiling-water bath for 1 h, mechanically stirred at room temperature for 16 h, precipitated with absolute ethanol (20×), collected, and dispersed in hot water in a boiling-water bath for 30 min. The dispersed debranched-amylose (100 μL, 2 mg/mL) was filtered through a membrane (pore size of 5.0 μm) and injected into the HPSEC column as described earlier. Maltose, maltotriose, maltotetraose, maltoheptaose, and pullulan standards (P-5, P10, P20, P50, P100, P200, and P400, Showa Denko K.K., Tokyo, Japan) were used as reference standards for determining molecular size of amylose.

Statistical Analysis. All analyses were performed in duplicate. The mean values were analyzed using the method of Analysis of Variance (ANOVA) with the General Linear Model Procedure in SAS (Version 9.2, SAS Inst. Inc., Cary, NC). Differences between samples were evaluated by the *t*-test using Tukey's adjustment with the significance level set at $p < 0.05$.

RESULTS AND DISCUSSION

Contents of Amylopectin, Amylose, and IC. The GPC chromatograms of the starches isolated from maize *ae* mutants with different HAM-gene dosages are shown in Figure 1A. All the GPC profiles of the starches showed two peaks. The first peak (fractions 11−18) was amylopectin that had much larger molecular size, and the second peak (fractions 19−45) contained a mixture of amylose and IC (Figure 1A).

Amylopectin contents of the starches, calculated on the basis of the total carbohydrate content shown in the first peak of the GPC profile (Figure 1A), are shown in Table 1. Although the amylopectin contents of the starches harvested in Kirksville, MO, were higher than that of the starches harvested in Brookings, SD, the amylopectin content of the starch grown in the both locations increased with the decrease in the HAM-gene dosage (Table 1). The amylose and resistant starch contents of the starch samples, in general, decreased with the decrease in the HAM-gene dosage. The amylopectin contents were negatively correlated with the RS contents of the starches. These were consistent with previously reported results showing that amylose and IC contributed to the RS content of the maize *ae* mutant starch.[6] The G/H (2 doses of HAM gene) starch had moderately larger content of amylose and IC than the H/G (1 dose of HAM gene) starch; the G/H starch, however, displayed greater content of RS than the H/G starch (Table 1). This difference suggested that the HAM-gene dosage in the maize *ae* mutant not only increased the contents of amylose and IC but also altered the structures of IC, resulting in a substantially greater RS contents.

Table 1. Amylopectin, Amylose, and Intermediate Component (IC) Contents of Starches Isolated from Kernels of Self-Pollinated and Inter-crossed Lines of GEMS-0067 (G) and H99*ae* (H)

sample	amylopectin[a] (%)	amylose (%)	IC large[b] (%)	IC small[b] (%)	resistant starch[c] (%)
Kirksville, Missouri					
G/G[d]	11.8 ^{D}	63.7 ^{A}	7.8 ^{B}	16.7 ^{B}	35.0 ^{A}
G/H	18.3 ^{C}	54.3 ^{B}	7.5 ^{B}	19.9 ^{A}	28.1 ^{B}
H/G	22.1 ^{B}	55.8 ^{B}	7.5 ^{B}	14.6 ^{BC}	12.9 ^{D}
H/H	31.1 ^{A}	42.1 ^{C}	15.0 ^{A}	11.8 ^{C}	15.7 ^{C}
Brookings, South Dakota					
G/G	8.0 ^{D}	64.4 ^{A}	7.4 ^{C}	20.2 ^{B}	38.4 ^{A}
G/H	16.3 ^{C}	44.9 ^{B}	14.5 ^{B}	24.3 ^{A}	31.2 ^{B}
H/G	18.9 ^{B}	43.2 ^{B}	14.1 ^{B}	23.8 ^{A}	25.9 ^{C}
H/H	22.3 ^{A}	36.6 ^{C}	18.1 ^{A}	23.0 ^{A}	20.0 ^{D}

[a]Amylopectin, amylose, and IC contents were determined using normal butanol precipitation method and Sepharose Cl-2B gel-permeation chromatography followed by total carbohydrate content analysis. [b]Large-molecular-weight IC molecules were in fractions 19−30 (Figure 1B); small-molecular-weight IC molecules were in fractions 31−45 (Figure 1B). [c]Resistant starch content of the starch was measured using AOAC Method 991.43 for total dietary fiber. RS data of Kirksville, Missouri are adapted from Jiang et al. (2010d). [d]G/G, G/H, H/G, and H/H contained 3, 2, 1, and 0 doses of HAM gene(s), respectively. Data in the same column with different superscript letters are significantly different ($p < 0.05$).

The GPC chromatograms of the mixtures of amylopectin and IC after the amylose was removed using 1-butanol are shown in Figure 1B. The absence of amylose molecules in the mixture was evidenced with the reduced blue value between fractions 19 and 45 (Figure 1B). The contents of amylose, large-molecular-weight IC, and small-molecular-weight IC are summarized in Table 1. Although the amylose contents of the starches harvested in Kirksville, MO were higher (except G/G) than that of the starches harvested in Brookings, SD, the order of the changes were the same and the amylose contents of the G/H and H/G starches were similar. Variations were observed for the contents of the large- and small-molecular-weight IC between samples with different HAM-gene dosages, but there were no clear trends associated with the HAM-gene dosage. Because of the same order was observed in both locations, we only used the starch samples harvested in Kirksville, MO for fine structure analyses to understand the effect of HAM-gene dosage on starch structures.

Branch Chain-Length Distributions of Amylopectins. Branch chain-length distributions of amylopectin molecules of

DOI: 10.1021/jf504099x
J. Agric. Food Chem. 2015, 63, 433−439

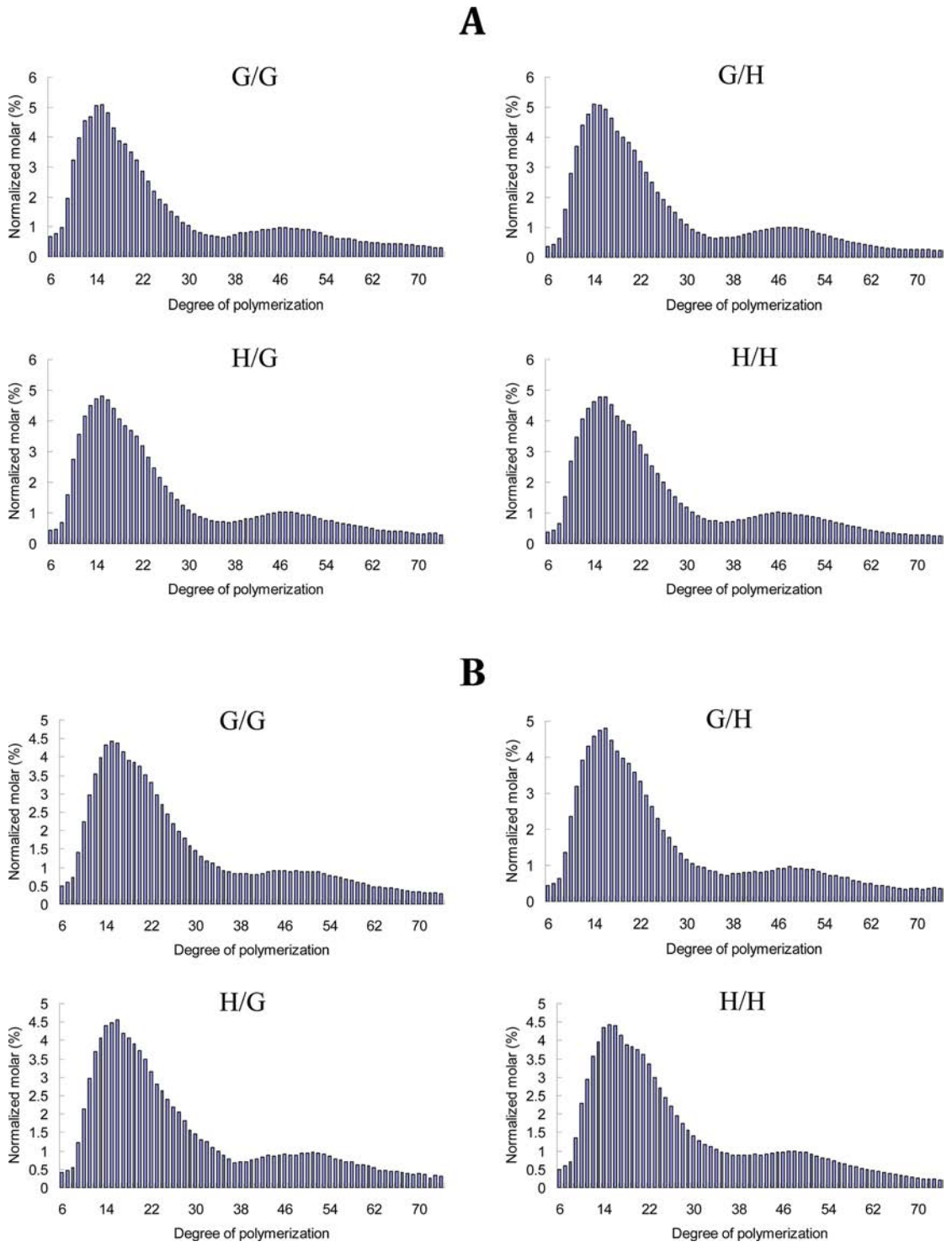

Figure 2. continued

DOI: 10.1021/jf504099x
J. Agric. Food Chem. 2015, 63, 433−439

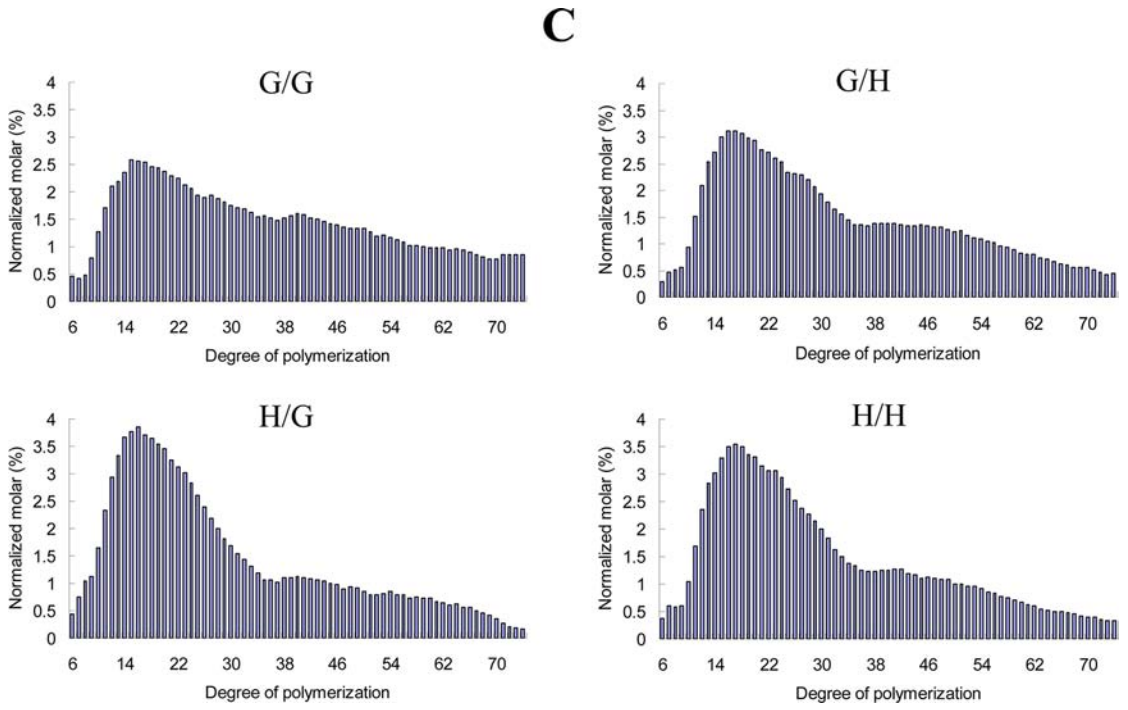

Figure 2. Branch chain-length distributions of amylopectins (A), large-molecular-weight IC (B), and small-molecular-weight IC (C). G/G, G/H, H/G, and H/H contained 3, 2, 1, and 0 doses of HAM gene(s), respectively. Fluorophore-assisted capillary electrophoresis was used for the analysis. The amylopectin, large-molecular-weight IC, and small-molecular-weight IC were collected from GPC fractions 11−18, 19−30, and 31−45, respectively (Figure 1B).

starches with different HAM-gene dosages are shown in Figure 2A. The branch chain-length profiles of the amylopectin molecules showed bimodal distributions with the peak chain-lengths at DP 14−15 and DP 46−49 (Figure 2A). The G/G amylopectin had slightly more short chains of DP ≤ 12 (16.2%) than other amylopectins (~13.5%). The percentages of branch chains with DP 13−24, DP 25−36, and DP ≥ 37 and average branch chain-lengths, however, were similar (data not shown). These results suggested that the HAM-gene dosage had little effect on the branch chain-length of amylopectin of the maize *ae* mutant starch.

Branch Chain-Length Distributions of Large-Molecular-Weight IC. Branch chain-length distributions of the large-molecular-weight IC of different HAM-gene dosages are shown in Figure 2B. The branch chain-length profiles of the large-molecular-weight IC also showed bimodal distributions (Figure 2B), similar to that of the amylopectins (Figure 2A). The large-molecular-weight IC of the starches having different HAM-gene dosages also displayed similar branch-chain-length distributions. These results showed that HAM-gene dosage also had little effect on the branch chain-length of large-molecular-weight IC of the *ae* mutant maize starch. The large-molecular-weight IC had average branch chain-lengths of DP 27.6, 27.3, 27.9, and 27.6 for G/G, G/H, H/G, and H/H, respectively, which were slightly longer than the amylopectin counterparts (DP 26.2, 26.3, 26.9, and 27.1 for G/G, G/H, H/G, and H/H, respectively). The similar branch-chain length distribution and average branch chain-length of amylopectin and large-molecular-weight IC of starch having different HAM gene dosage suggested that the large-molecular-weight IC and amylopectin had little or no contribution to the RS formation in maize *ae* mutant starch.

Branch Chain-Length Distributions of Small-Molecular-Weight IC. Branch chain-length distributions of the small-molecular-weight IC are shown in Figure 2C. The branch chain-length profiles of the small-molecular-weight IC showed a well-defined peak at chain-lengths of DP 15−17 and a shoulder at the chain-lengths of DP ≥37 (Figure 2C). The H/H sample (0 dosage) had a slightly larger percentage of long branch-chains (DP ≥ 37, 31.5%) and larger average branch chain-length (DP 30.8) but less percentage of branch-chains of DP 13−24 than the H/G counterpart (Table 2). As the HAM-gene dosage increased from 1 to 3, the percentages of branch-chains of DP ≥37 increased from 28.2 to 37.2 and 43.8% for the H/G, G/H, and G/G, respectively; and the average branch chain-lengths of the small-molecular-weight IC increased from DP 29.1 to DP 32.6, and DP 35.4 for the H/G, G/H, and G/G, respectively (Table 2); However, the percentages of branch-

Table 2. Molar-Based Branch Chain-Length Distributions of the Small-Molecular-Weight IC Separated from Starches of Self-Pollinated and Inter-crossed Lines of GEMS-0067 (G) and H99*ae* (H)[a]

sample	average CL (DP)[c]	DP ≤ 12 (%)	DP 13−24 (%)	DP 25−36 (%)	DP ≥ 37 (%)
G/G[d]	35.4 ^{A}	7.2 ^{B}	28.2 ^{D}	20.8 ^{C}	43.8 ^{A}
G/H	32.6 ^{B}	7.1 ^{B}	33.6 ^{C}	22.1 ^{B}	37.2 ^{B}
H/G	29.1 ^{D}	10.3 ^{A}	41.2 ^{A}	20.3 ^{D}	28.2 ^{D}
H/H	30.8 ^{C}	7.1 ^{B}	38.4 ^{B}	23.0 ^{A}	31.5 ^{C}

[a]The branch chain-length distribution of the small-molecular-weight IC was determined using a fluorophore-assisted capillary-electrophoresis. The small-molecular-weight IC was collected from GPC fractions 31−45 (Figure 1B). [c]CL = chain length; DP = degree of polymerization. [d]G/G, G/H, H/G, and H/H contained 3, 2, 1, and 0 doses of HAM gene(s), respectively. Data in the same column with different superscript letters are significantly different ($p < 0.05$).

DOI: 10.1021/jf504099x
J. Agric. Food Chem. 2015, 63, 433−439

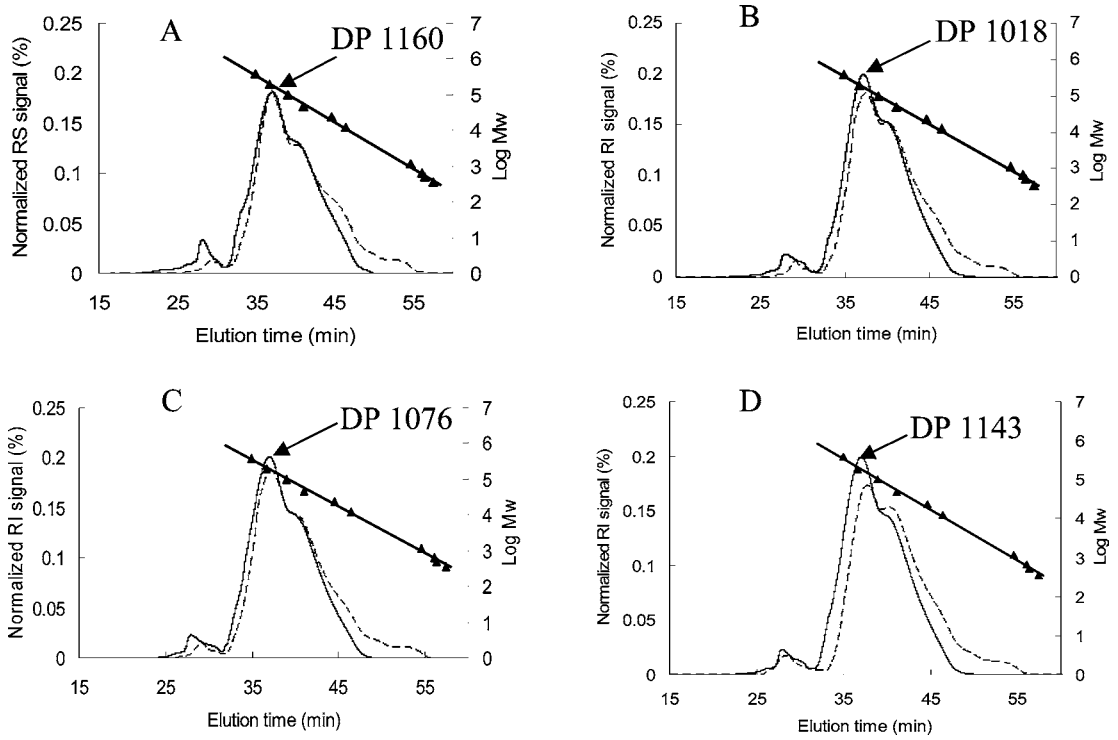

Figure 3. Molecular-weight distributions of amyloses separated from starches of self-pollinated and inter-crossed lines of GEMS-0067 (G) and H99*ae* (H). The separation was conducted using Shodex SB-804 and SB-803 analytical columns (Showa Denko K.K., Tokyo, Japan). (A) G/G with 3 doses of HAM gene(s); (B) G/H, 2 doses; (C) H/G, 1 dose; and (D) H/H, 0 dose. Solid lines, before isoamylase-debranching; dashed lines, after isoamylase-debranching; and linear line, a standard curve with molecular sizes of DP 2, 3, 4, 7, 75, 141, 292, 617, 1148, and 2346.

chains of DP 13−24 decreased from 41.2% to 33.6% and 28.2% for the H/G, G/H, and G/G, respectively. There were no clear trends observed for branches of DP ≤ 12 and DP 25−36 associating with the HAM-gene dosage (Table 2). The long branch-chains (DP ≥37, Table 2) increasing with the increase in the HAM-gene dosage facilitated the starch to develop more long-chain double-helical crystallites, which were resistant to enzymatic hydrolysis and resulted in the larger RS content of maize *ae* mutant starch (6). Small-molecular-weight IC of the H/G had a larger proportion of short chains with DP ≤ 24 (51.5%) than that of the H/H (45.5%, Table 2), which resulted in a lower resistant starch content of the H/G starch (12.9%) than that of the H/H starch (15.7%, Table 1). The greater concentration of short-branch chains of the H/G sample made the H/G sample more susceptible to enzymatic hydrolysis and resulted in less resistant starch content.

Molecular Structure of Amylose. The purity of the fractionated amylose was 98.6−99.8% examined using GPC. There was a very small amount of amylopectin shown at a peak between fractions 11 and 18, which displayed a typical low blue value of amylopectin (data not shown).

High-performance size-exclusion chromatograms of amylose molecules, before and after isoamylase-debranching, are shown in Figure 3. All the amyloses fractionated from starch samples of different HAM-gene dosages showed similar molecular weight distributions. There were three peaks shown on the chromatograms of amyloses, including a small peak (eluted between 25 and 32 min) with peak molecular sizes at DP 16502−17699, a major peak with peak molecular sizes at DP 1018−1160, and a shoulder-like peak with peak molecular sizes at DP ∼ 472 (Eluted at ∼40 min) (Figures 3A−D). The amyloses had average molecular sizes of DP 731−817 (Table 3), which were in agreement with the molecular sizes of amyloses isolated from high-amylose maize starches reported by Takeda et al.[30] After the amylose samples were subjected to an enzymatic debranching, similar molecular weight distributions were observed for all the debranched amylose samples obtained from starches of different HAM-gene dosages; the intensity of the small peak eluted between 25 and 32 min was reduced for the G/G, G/H, and H/G but not for the H/H (Figure 3A−D). These results suggested that the HAM-gene dosage of the maize *ae* mutant had little effect on the amylose molecular structure. There was no clear trend observed between the size of debranched amylose and the HAM-gene dosage (Table 3).

Table 3. Average Molecular Weights of Amyloses Separated from Starches of Self-Pollinated and Inter-crossed Lines of GEMS-0067 (G) and H99*ae* (H)

sample	before debranching (DP)[a]	after debranching (DP)
G/G[b]	817 ^{A}	452 ^{B}
G/H	731 ^{D}	445 ^{B}
H/G	795 ^{B}	487 ^{A}
H/H	756 ^{C}	417 ^{C}

[a]DP = degree of polymerization. [b]G/G, G/H, H/G, and H/H contained 3, 2, 1, and 0 doses of HAM gene(s), respectively. Data in the same column with different superscript letters are significantly different ($p < 0.05$).

In conclusion, the HAM-gene(s) dosage of *ae* mutant maize had little effect on the branch chain-length distributions of amylopectin and large-molecular-weight IC and on the molecular structure of amylose; but it increased the branch chain-length of small-molecular-weight IC and the content of

DOI: 10.1021/jf504099x
J. Agric. Food Chem. 2015, 63, 433−439

amylose and IC. The HAM-gene(s) dosage significantly altered the RS content of maize *ae* mutant starch.

AUTHOR INFORMATION

Corresponding Author

*Tel.: +1 515 294 9892. Fax: +1 515 294 8181. E-mail: jjane@iastate.edu.

Notes

The authors declare no competing financial interest.

REFERENCES

(1) Robyt, J. F. *Essentials of Carbohydrate Chemistry*; Springer-Verlag: New York, 1998.

(2) Hizukuri, S.; Takeda, Y.; Yasuda, M.; Suzuki, A. Multibranched nature of amylose and the action of debranching enzymes. *Carbohydr. Res.* **1981**, *94*, 205−213.

(3) Jane, J.; Chen, Y. Y.; Lee, L. F.; McPherson, A. E.; Wong, K. S.; Radosavljevic, M.; Kasemsuwan, T. Effects of amylopectin branch chain length and amylose content on the gelatinization and pasting properties of starch. *Cereal Chem.* **1999**, *76*, 629−637.

(4) Takeda, Y.; Shitaozono, T.; Hizukuri, S. Molecular-structure of corn starch. *Starch-Starke* **1988**, *40*, 51−54.

(5) French, D. Organization of starch granules. In *Starch: Chemistry and Technology*, 2 ed.; Whistler, R. L., Bemiller, J. N., Paschall, E. F., Eds.; Academic Press: New York, 1984; pp 183−247.

(6) Jiang, H.; Campbell, M.; Blanco, M.; Jane, J. Characterization of maize amylose-extender (*ae*) mutant starches. Part II: Structures and properties of starch residues remaining after enzymatic hydrolysis at boiling-water temperature. *Carbohydr. Polym.* **2010**, *80*, 1−12.

(7) Baba, T.; Arai, Y. Structural features of amylomaize starch. 3. Structural characterization of amylopectin and intermediate material in amylomaize starch granules. *Agric. Biol. Chem. Tokyo* **1984**, *48*, 1763−1775.

(8) Wang, Y. J.; White, P.; Pollak, L.; Jane, J. Amylopectin and intermediate materials in starches from mutant genotypes of the Oh43 inbred line. *Cereal Chem.* **1993**, *70*, 521−525.

(9) Kasemsuwan, T.; Jane, J.; Schnable, P.; Stinard, P.; Robertson, D. Characterization of the dominant mutant amylose-extender (Ae1−5180) maize starch. *Cereal Chem.* **1995**, *72*, 457−464.

(10) Klucinec, J. D.; Thompson, D. B. Fractionation of high-amylose maize starches by differential alcohol precipitation and chromatography of the fractions. *Cereal Chem.* **1998**, *75*, 887−896.

(11) Li, L.; Jiang, H.; Campbell, M.; Blanco, M.; Jane, J. Characterization of maize amylose-extender (*ae*) mutant starches: Part I. Relationship between resistant starch contents and molecular structures. *Carbohydr. Polym.* **2008**, *74*, 396−404.

(12) Smith, A. M. The biosynthesis of starch granules. *Biomacromolecules* **2001**, *2*, 335−341.

(13) Morell, M. K.; Myers, A. M. Towards the rational design of cereal starches. *Curr. Opin. Plant Biol.* **2005**, *8*, 204−210.

(14) James, M. G.; Denyer, K.; Myers, A. M. Starch synthesis in the cereal endosperm. *Curr. Opin. Plant Biol.* **2003**, *6*, 215−222.

(15) Wei, C.; Qin, F.; Zhou, W.; Chen, Y.; Xu, B.; Wang, Y.; Gu, M.; Liu, Q. Formation of semi-compound C-type starch granule in high-amylose rice developed by antisense RNA inhibition of starch-branching enzyme. *J. Agric. Food Chem.* **2010**, *58*, 11097−11104.

(16) Wei, C.; Xu, b.; Qin, F.; Yu, H.; Chen, C.; Meng, X.; Zhu, L.; Wang, Y.; Gu, M.; Liu, Q. C-type starch from high-amylose rice resistant starch granules modified by antisense RNA inhibition of starch branching enzyme. *J. Agric. Food Chem.* **2010**, *58*, 7383−7388.

(17) Guan, H. P.; Preiss, J. Differentiation of the properties of the branching isoenzymes from maize (Zea mays). *Plant Physiol.* **1993**, *102*, 1269−1273.

(18) Shi, Y.-C.; Seib, P. A. Fine structure of maize starches from four wx-containing genotypes of the W64A inbred line in relation to gelatinization and retrogradation. *Carbohydr. Polym.* **1995**, *26*, 141−147.

(19) Yuan, R. C.; Thompson, D. B.; Boyer, C. D. Fine structure of amylopectin in relation to gelatinization and retrogradation behavior of maize starches from three wx-containing genotypes in two inbred lines. *Cereal Chem.* **1993**, *70*, 81−89.

(20) Campbell, M. R.; Jane, J.; Pollak, L.; Blanco, M.; O'Brien, A. Registration of maize germplasm line GEMS-0067. *J. Plant Registra* **2007**, *1*, 60−61.

(21) Campbell, M.; Green, A.; Bell, J.; Jane, J.-l.; Jiang, H.; Wu, Y. Germplasm Enhancement of Maize report, http://www.public.iastate.edu/~usda-gem/Public_Reports/Yr_2007/GEMR_07_Campbell.pdf, 2007 (accessed date December 2014).

(22) Jiang, H.; Horner, H. T.; Pepper, T. M.; Blanco, M.; Campbell, M.; Jane, J. Formation of elongated starch granules in high-amylose maize. *Carbohydr. Polym.* **2010**, *80*, 534−539.

(23) Jiang, H.; Blanco, M.; Campbell, M.; Jane, J. Resistant-starch formation in high-amylose maize during kernel development. *J. Agric. Food Chem.* **2010**, *58*, 8043−8047.

(24) Wu, Y. S.; Campbell, M.; Yen, Y.; Wicks, Z., III; Ibrahim, A. M. H. Genetic analysis of high amylose content in maize (Zea mays L.) using a triploid endosperm model. *Euphytica* **2009**, *166*, 155−164.

(25) Schoch, T. J. Fractionation of starch by selective precipitation with butanol. *J. Am. Chem. Soc.* **1942**, *64*, 2957−261.

(26) Dubois, M.; Gilles, K. A.; Hamilton, J. K.; Rebers, P. A.; Smith, F. Colorimetric method for determination of sugars and related substances. *Anal. Chem.* **1956**, *28*, 350−356.

(27) Juliano, B. O. Asimplified assay for milled-rice amylose. *Cereal Sci. Today* **1971**, *16*, 334−340.

(28) AOAC. Association of Official Analytical Chemists (AOAC) Official Method 991.43. Total, soluble, and insoluble dietary fiber in foods. In *Official methods of analysis of the AOAC international*, 17th ed., rev. 2; Horwithz, W., Ed.; AOAC International: Gaithersburg, MD, 2003.

(29) Morell, M. K.; Samuel, M. S.; O'Shea, M. G. Analysis of starch structure using fluorophore-assisted carbohydrate electrophoresis. *Electrophoresis* **1998**, *19*, 2603−2611.

(30) Takeda, C.; Takeda, Y.; Hizukuri, S. Structure of amylomaize amylose. *Cereal Chem.* **1989**, *66*, 22−25.

DOI: 10.1021/jf504099x
J. Agric. Food Chem. 2015, 63, 433−439

JOURNAL OF AGRICULTURAL AND FOOD CHEMISTRY

Article

pubs.acs.org/JAFC

Changes in the Content of Free and Conjugated Polyamines during Lettuce (*Lactuca sativa*) Growth

Edgar Pinto* and Isabel M. P. L. V. O. Ferreira

REQUIMTE/Department of Chemical Sciences, Laboratory of Bromatology and Hydrology, Faculty of Pharmacy, University of Porto. R Jorge Viterbo Ferreira 228, 4050-313 Porto, Portugal

ABSTRACT: Polyamines (PAs) in plant foods are relevant due to the association of these bioactive nutrients with health and disease. The scope of the present study was to monitor the content of free, conjugated, and total (free + conjugated) putrescine (Put), spermidine (Spd), and spermine (Spm) at five stages of lettuce growth in three different greenhouses. The daily intake of PAs from lettuce consumption was estimated since its consumption represents about 7.2% of vegetables intake. Results showed that the content of free Put, Spd, and Spm decreased during plant growth, while the content of conjugated Put, Spd, and Spm increased. Nevertheless, the total PA content remained fairly constant. Significant differences were observed in the PAs content in lettuces grown in different greenhouses. The conjugated fraction of PAs in mature lettuces has an important contribution to the total PAs and will certainly influence the bioavailability and/or bioactivity of dietary polyamines.

KEYWORDS: *lettuce, polyamines, growth, daily intake, human health*

INTRODUCTION

Putrescine (Put), spermidine (Spd), and spermine (Spm) form a group of low molecular and aliphatic nitrogen polycations known as polyamines (PAs). These are commonly found in higher plants in free, soluble conjugated, and insoluble bound forms. Soluble conjugated PAs are mainly conjugated to small molecules such as phenolic compounds, whereas insoluble bound PAs are bound to macromolecules such as nucleic acids and proteins.[1] Put, Spd, and Spm usually have been included within the group of biogenic amines. However, due to their specific biological roles in plants they have become a peculiar group. In plants, PAs have been found in both the cytoplasm and other organelles (e.g., vacuoles, mitochondria, and chloroplasts).[2]

The biosynthetic pathways of PAs is highly conserved through evolution and starts from the two amino acid precursor molecules, L-arginine and L-methionine.[3] Two alternative biosynthetic pathways have been characterized. Put is synthesized through either arginine decarboxylase (ADC, EC 4.1.1.19) via agmatine (Agm) or ornithine decarboxylase (ODC, EC 4.1.1.17). Conversion of Agm into Put requires two distinct enzymes: *N*-carbamoylputrescine amidohydrolase (CPA, EC 3.5.1.53) and agmatine iminohydrolase (AIH, EC 3.5.3.12). Spd is synthesized by spermidine synthase (SPDS, EC 2.5.1.16) through the addition of an aminopropyl group, transferred from the decarboxylated *S*-adenosylmethionine (dcSAM), to Put. Spd can be aminopropylated at either Spm or thermospermine by the action of spermine synthase (SPMS, EC 2.5.1.22).[4,5] With regard to PAs catabolism, both Spd and Spm can be converted back to Put. Spermine oxidase (SMO, EC 1.5.3.16) mediates the back-conversion of Spm to Spd. Moreover, the enzyme polyamine oxidase (PAO, EC 1.5.3.11) catalyzes the conversion of Spd and Spm to 4-aminobutanal and *N*-(3-aminopropyl)-4-aminobutanal, respectively. Put is catabolized by diamine oxidases (DAOs) in a reaction that converts Put into Δ^1-pyrroline and generates NH_3 and H_2O_2 as byproducts.[3]

The amount of PAs present at a certain time within the human body is the result of three sources: (i) endogenous supply, (ii) through intestinal microorganisms, and (iii) exogenous supply through the diet.[6] The exogenous dietary source provides a much larger quantity of PAs than the other two sources. Thus, diet plays a key role controlling the body pool of these compounds and, consequently, in the regulation of several physiological mechanisms within the human body.[2] The dietary intake of PAs influences human health.[7] It has been suggested that a PA-rich diet could have several health benefits such as decreasing age-associated pathologies and increasing longevity.[8] However, a reduced intake of exogenous PAs through diet has also been proposed as an efficient nutritional strategy for several human conditions.[9−11]

In humans, PAs are involved in the regulation of many basic cellular processes, such as DNA replication, transcription, translation, cell proliferation, modulation of enzyme activities, cellular cation−anion balance, and membrane stability.[4,5] This occurs due to the inherent physicochemical properties of PAs that enable them to interact with negatively charged macromolecules such as nucleic acids, phospholipids, and proteins.[6] The importance of PAs in cellular growth and proliferation is well-established and has been related to their role in stabilizing the negative charges of DNA and of the chromatin structure, the regulation of several transcriptional factors, and protein synthesis.[7] PAs do not trigger cancer, but their increased availability enhances cell growth. However, it has been also documented that excessive accumulation of PAs induces apoptosis.[2] PAs play a vital role in the maintenance of intestinal

Received: September 19, 2014
Revised: December 24, 2014
Accepted: December 24, 2014
Published: December 24, 2014

ACS Publications © 2014 American Chemical Society

DOI: 10.1021/jf505453s
J. Agric. Food Chem. 2015, 63, 440−446

function and gut maturation. When damaged, the intestinal mucosa is able to repair itself, and PAs are essential for these repair processes. Moreover, PAs are widely described as essential growth factors for small intestinal and colonic mucosal growth and maturation.[6,7] PAs also show antioxidant activity and seem to be engaged in the reduction of cell membranes and DNA damage. At physiological levels, PAs can act as potent scavengers of reactive oxygen species (ROS).[2]

Although dietary PAs have been known as an important factor of health and disease, data on PA contents in foods are limited. Put, Spd, and Spm are present in variable amounts in various foods.[6,12] Regarding plant foods, very low levels, ranging from a few milligrams to less than a 100 mg/kg, are usually found.[2] Some work has been done in quantifying the PAs content in several plant foods.[13,14] However, no studies have addressed the PA content during the plant food growth period. Moreover, information concerning the content of conjugated PAs in food is scarce. Since in the last years an increased number of papers have been published encouraging the consumption of plant foods at their initial stages of growth (known as microgreens),[15,16] information regarding the PAs content of plant foods during their growth period is of great importance for consumers.

Lettuce is known to be an important source of mineral nutrients and phytochemicals that benefit human nutrition.[17] Additionally, it is one of the most consumed vegetables, accounting with a mean daily consumption in Europe of 23.4 g, which represents about 7.2% of the total dietary intake of vegetables.[18] Its global production was around 25 million tons in 2011.[19]

The aim of this study was to monitor the free and conjugated Put, Spd, and Spm content of a test plant food (*Lactuca sativa*) at five growth stages produced in three greenhouses as well as to estimate the daily intake of these compounds from lettuce consumption.

MATERIALS AND METHODS

Lettuce Cultivation, Sampling, and Sample Preparation. Lettuce (*Lactuca sativa*) plants (n = 100) with 2 weeks of growth were transferred on the same day to three different greenhouses: A_1 (41° 26.991 N, 8° 46.335 W), A_2 (41° 25.249 N, 8° 44.936 W), and A_3 (41° 27.435 N, 8° 45.377 W) located in NW Portugal, in a small region between Esposende and Vila do Conde. These three greenhouses were chosen because they were located in an intensive agriculture area, which is known to be the main supplier of vegetables to the city of Porto, Portugal. The experiments were conducted from December to February. All plants were exposed to the same conditions: light intensity, a total of 334 h of sunshine duration; photoperiod, on average 11.16 h; and temperature, average minimum temperature, 7.6 °C and average maximum temperature, 20.5 °C. Inorganic fertilizers were dissolved in 50 L water tanks and injected by an electric pump in long dripper pipes, from where the plants were fertigated. The nutrient elements provided (per plant and per fertigation) were as follows: 0.126 g N, 0.042 g K, 0.03 g P, 0.21 mg Fe, 0.051 mg Mn, and 0.013 mg Zn. The irrigation water used had the following characteristics: pH 6.91, electrical conductivity (EC) 401 mS/cm (at 25 °C), total dissolved solids (TDS) 201 mg/L, Ca^{2+} 70.2 mg/L, Mg^{2+} 19.2 mg/L, K^+ 5.2 mg/L, Na^+ 25.2 mg/L, Cl^- 83.4 mg/L, NO_3^- 37.4 mg/L, and SO_4^{2-} 66.8 mg/L.

Samples collection was always performed during the same period of the day (9–12 am). One kilogram (or at least 10 units) of lettuce was randomly harvested at five growth stages (2, 4, 6, 8, and 10 weeks hereinafter referred to as T_1, T_2, T_3, T_4, and T_5). After 10 weeks, lettuces reach their commercial maturity stage (T_5). Plant samples were placed into plastic containers, previously rinsed with diluted nitric acid (10% v/v) and deionized water, and kept at 4 °C on the way to the laboratory.

Soil was also sampled from the same locations using a stainless steel auger. In order to generate a representative sample, individual samples (n = 25) were combined to generate a composite sample.

At the laboratory, plant samples were cleaned and washed with deionized water to remove soil contamination. Afterward, inedible leaves were removed, and the remaining lettuce leaves were frozen at −80 °C and then freeze-dried. The dried samples were homogenized by grinding in a blender and sieved through a nylon sieve of 150 μm mesh size. Soil samples were spread in plastic trays, oven-dried for 24 h at 40 °C, crushed and sieved through a 2 mm nylon sieve, and stored at 4 °C until analysis.

Chemicals and Standard Solutions. Putrescine dihydrochloride, spermidine trihydrochloride, 1,7-diaminoheptane (internal standard, IS), spermine tetrahydrochloride, hydrochloric acid, acetonitrile, and 3,5-dinitrobenzoyl chloride (DNBZ-Cl) were purchased from Sigma–Aldrich (St. Louis, MO). Boric acid, sodium hydroxide, potassium chloride, ammonium nitrate and sodium chloride were from VWR (Radnor, PA). Perchloric acid ($HClO_4$) and carbon tetrachloride were both obtained from Merck (Darmstadt, Germany).

Standard stock solutions of PAs were prepared by dissolving each standard in 0.1 M HCl to provide a final concentration of 1000 mg/L. Working standard solutions (in the 0.5 to 10 mg/L interval range) were prepared daily from the stock solutions by adequate dilution with 0.1 M HCl. Sodium borate buffer was prepared from H_3BO_3 and KCl in water (0.5 M each) followed by titration with NaOH (0.5 M) to pH 10. DNBZ-Cl (56 mM) was prepared by dissolving a proper amount of the solid compound in acetonitrile.

Multielement calibration standards were prepared from 1000 mg/L single-element standard solutions (Sigma, MO) of Ca^{2+}, Mg^{2+}, K^+, and Na^+ for AAS and Cl^-, NO_3^-, PO_4^{3-}, and SO_4^{2-} for ion chromatography.

Instrumentation and Chromatographic Conditions. A Telstar (Terrassa, Spain) Cryodos-80 freeze-dry system was used to lyophilize lettuce samples. The moisture content was determined using HR73 Moisture Analyzer from Mettler Toledo (Greifensee, Switzerland). Water pH, electrical conductivity, and total dissolved solids were measured in situ by the IQ170 waterproof portable pH/conductivity/TDS meter (IQ Scientific Instruments, Carlsbad, CA). A PerkinElmer (Überlingen, Germany) 3100 flame (air-acetylene) atomic absorption spectrometer (AAS) was used for the determination of Ca^{2+}, Mg^{2+}, K^+, and Na^+. A PU-2089_{Plus} pump (Jasco, Tokyo, Japan) was used in conjunction with an IC-PAK anion-exchange column (10 μm, 50 × 4.6 mm) for Cl^-, NO_3^-, PO_4^{3-}, and SO_4^{2-} determination. Detection was done by a Waters Model 431 conductivity detector. The eluent was a 1.3-mM sodium gluconate/1.3-mM borax buffer solution adjusted to pH 8.5.

Chromatographic analysis of PAs was performed with an analytical HPLC unit (Jasco, Tokyo, Japan) equipped with Jasco PU-2080 HPLC pumps, Column Heater (Model 7981; Jones Chromatography, Hengoed, UK), and an MD-2010 Plus multiwavelength detector. The column was reversed-phase Ultracarb ODS (30) C18 (5 μm, 250 × 4.6 mm) (Phenomenex, Milford, MA). Borwin PDA Controller Software (JMBS Developments, Le Fontanil, France) was used for system control and data acquisition. Chromatographic separation was carried out by gradient elution with a mixture of two solvents and at a 1 mL/min flow rate. Solvent A consisted of 10 mM aqueous sodium formate/formic acid buffer at pH 3, and solvent B consisted of acetonitrile. The linear gradient program was as follows: 0–5 min, 40% B; 5–11 min, 58% B; 11–15 min, 58% B; 15–20 min, 65% B; 20–23 min, 65% B; 23–28 min, 95% B; 28–30 min, 95% B; 30–40 min, column rinse and re-equilibration. Column temperature was set at 35 °C. Detection was carried out at 250 nm.

Soil Analysis. Soil pH was measured in the supernatant of a 1:5 (w/v) suspension made up with ultrapure water. Organic matter content was determined based on its oxidation with a potassium dichromate (0.27 M) and sulfuric acid (98% v/v) mixture at 135 °C. CEC and particle size distribution were determined according to ISO methods.[20,21]

DOI: 10.1021/jf505453s
J. Agric. Food Chem. 2015, 63, 440–446

The extraction of Ca^{2+}, Mg^{2+}, K^+, and Na^+ from soil samples was performed following ISO 19730:2008.[22] Ten grams of air-dried soil and 25 mL of 1 M NH_4NO_3 solution were added to a 50 mL centrifuge tube and shaken for 2 h at 20 °C. Afterward, the solution was centrifuged at 5000*g* for 10 min and analyzed by AAS. The extraction of Cl^-, NO_3^-, PO_4^{3-}, and SO_4^{2-} from soil samples was conducted following ISO/TS 14256−1:2003[23] with some modifications. Briefly, soil samples were extracted with ultrapure water at a ratio 1:5 (w/v) at 20 °C. After 1 h of extraction, the solution was centrifuged at 5000*g* for 10 min. The above-mentioned anions were determined in the supernatant by ion chromatography.

Extraction and Analysis Of PAs. Lyophilized lettuce samples (100 mg) were homogenized in 2.5 mL of 5% (v/v) cold $HClO_4$ and incubated at 4 °C for 1 h. After centrifugation at 17000*g* for 30 min, the supernatant was collected and used as the sample extract to determine the content of free PAs.

In order to extract $HClO_4$-soluble conjugated PAs, a suitable portion of the previous extract was mixed with 12 M HCl (1:1, v/v) for 18 h at room temperature in centrifuge tubes as proposed by Fontaniella et al.[24] After acid hydrolysis, NaOH (10 M) was added to the centrifuge tubes to neutralize the HCl in excess, and the volume was made up to 2 mL with ultrapure water. This solution was used as a source of $HClO_4$-soluble conjugated PAs and free PAs.

PAs recovered from the nonhydrolyzed supernatant (free PAs) and the hydrolyzed supernatant (free + conjugated PAs) were quantified, after derivatization with DNBZ-Cl, by HPLC-DAD according to Pinto, Melo, and Ferreira.[14] Representative chromatograms of free and conjugated PAs are shown in Figures 1 and 2, respectively. Results are presented on a fresh weight (fw) basis. The detection limit (LOD) for Put, Spd, and Spm was 0.018, 0.034, and 0.042 μg/g, respectively, while the quantification limit (LOQ) was 0.062, 0.115, and 0.141 μg/g for Put, Spd, and Spm, respectively.

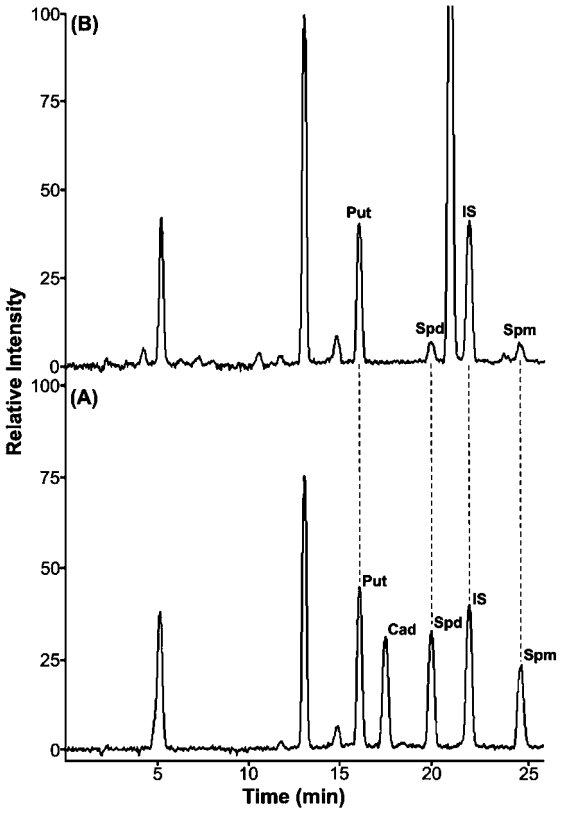

Figure 1. Representative chromatograms of free PAs: (A) mixed standard solution of 5 mg/L and (B) lettuce. Peaks: Put, putrescine; Cad, cadaverine; Spd, spermidine; IS, internal standard; and Spm, spermine.

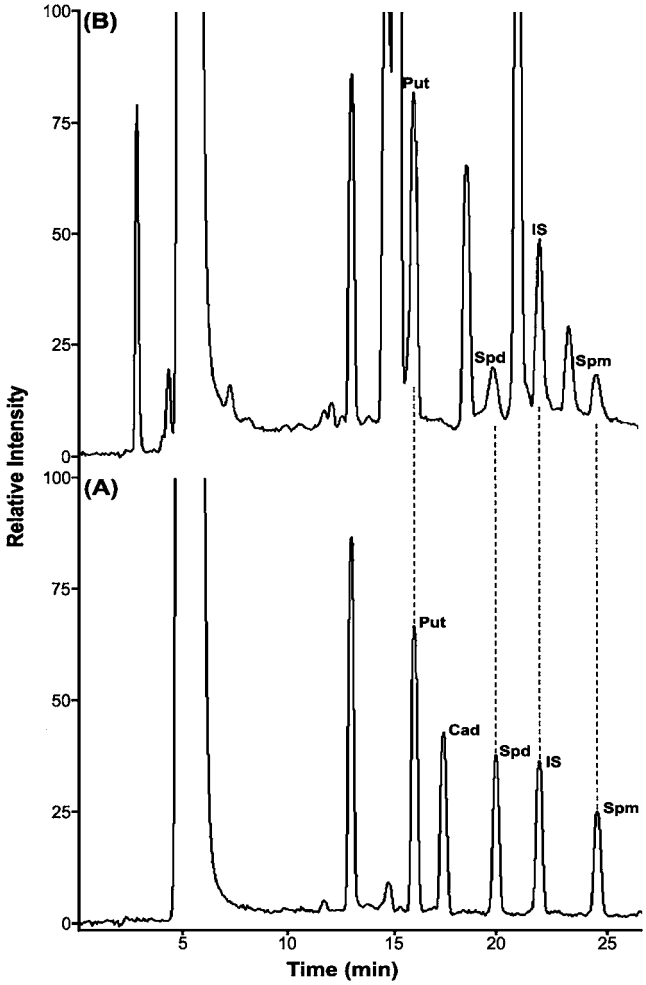

Figure 2. Representative chromatograms of conjugated PAs: (A) mixed standard solution of 5 mg/L and (B) lettuce. Peaks: Put, putrescine; Cad, cadaverine; Spd, spermidine; IS, internal standard; and Spm, spermine.

Estimated Daily Intake of PAs from Lettuce. The estimated daily intake (EDI) of Put, Spd, and Spm resulting from lettuce consumption was calculated. The EDI, which is dependent on both the PAs content of the edible part of the plants ($C_{polyamine}$; μg/g fw basis) and the average daily intake of lettuce ($DI_{lettuce}$), was calculated using the following formula:

$$EDI = DI_{lettuce} \times C_{polyamine}$$

where EDI is expressed as μmol/day, and DI was assumed to be 23.4 g/day for adults.[18]

Statistical Analysis. Data exploration, descriptive statistics calculation, and ANOVA were performed with IBM SPSS Statistics for Windows, version 22.0 (IBM Corp, Armonk, NY). Statistical significance was assumed for $p < 0.05$.

RESULTS AND DISCUSSION

Lettuce Leaf Biomass and Moisture Content. Lettuce leaf biomass at the 5 growth stages in the three greenhouses (A_1, A_2, and A_3) is shown in Table 1. A similar increase of leaf biomass was observed during lettuce growth in A_1, A_2, and A_3 greenhouses. No significant differences were observed between lettuce leaf biomass at T_1 and T_2. However, the increase of lettuce biomass was significant among T_3, T_4, and T_5 growth stages. Only at T_5 did A_2 lettuces show significantly higher biomass content compared to that of A_1 and A_3 lettuces.

DOI: 10.1021/jf505453s
J. Agric. Food Chem. 2015, 63, 440−446

Table 1. Lettuce Leaf Biomass (g FW/Plant) during the Five Stages of Lettuce Growth in the Three Greenhouses (A_1, A_2, and A_3)[a]

	lettuce ID		
growth stage	A_1	A_2	A_3
T_1	1.91 ± 0.04 a	1.85 ± 0.03 a	2.13 ± 0.09 a
T_2	6.69 ± 0.25 a	6.84 ± 0.31 a	8.23 ± 0.53 a
T_3	24.42 ± 1.45 b	24.08 ± 1.96 b	23.7 ± 1.75 b
T_4	56.68 ± 3.53 c	58.39 ± 4.36 c	59.54 ± 4.31 c
T_5	173.96 ± 6.94 d	186.85 ± 12.31 d	169.28 ± 8.17 d

[a]Data are presented as the mean ± SD (n = 5). In a column, different letters (a, b, c, and d) indicate significant differences between growth stages at $p < 0.05$.

No significant differences were found for the mean moisture content (94.3 ± 0.1%) of lettuces grown in the A_1, A_2, and A_3 greenhouses at the five growth stages.

Spatial Variation of Free and Conjugated PA Content in Lettuce Leaves. Significant differences were observed depending on the greenhouse where the lettuce was grown. A_1 lettuces showed significantly higher levels of all free PAs, while A_2 lettuces showed the lowest levels (Figures 3A, 4A, and 5A). For the conjugated PAs, this difference was not so clear for Put and Spd. However, A_2 lettuces showed a significantly higher level of conjugated Spm (Figures 3B, 4B, and 5B). For the total PAs, A_1 lettuces showed significantly higher levels of Put and Spd at all growth stages, whereas A_2 lettuces showed the lower levels of these PAs (Figures 3C and 4C).

A great body of evidence supports that abiotic stresses, such as metal toxicity, oxidative stress, drought, low temperature, and salinity, modulate the production of PAs in plants.[5] In order to understand the influence of soil properties in the PA content of lettuces, the analysis of soils from the three greenhouses was performed. A_2 soil showed a significantly higher pH, CEC, OM, and EC than the other two soils (A_1 and A_3). Moreover, A_2 soil was classified as a loamy sand soil, while A_1 and A_3 soils were sandy soils (Table 2). These characteristics are very important with regard to the bioavailability of essential and toxic elements to plants.[25] In Table 3 is shown the extractable content of Ca^{2+}, Mg^{2+}, K^+, Na^+, Cl^-, NO_3^-, PO_4^{3-}, and SO_4^{2-} of each of the three greenhouse soils. A_2 soil had the highest extractable content of Ca^{2+}, Mg^{2+}, K^+, NO_3^-, PO_4^{3-}, and SO_4^{2-} and the lowest extractable content of Na^+ and Cl^-. On the contrary, A_1 soil had the highest extractable content of Na^+ and Cl^- (Table 3). Given these results, it is hypothesized that the higher bioavailability of Na^+ and Cl^- in A_1 and A_3 soils is indicative of higher soil salinity. Since PAs are involved in salinity stress, these results can explain the highest amount of PAs (mainly in the free form) in A_1 and A_3 lettuces. The highest NO_3^- content in A_2 soil may have also influenced the PA content of lettuces, limiting the accumulation of Put in A_2 lettuces. Houdusse et al.[26] found that NO_3^- nutrition limited Put accumulation in wheat and pepper. The same authors also showed that the effect of salinity on PA content is highly dependent on nitrogen nutrition. Since the environmental conditions light intensity, temperature, photoperiod, and drought that can greatly influence the PAs content in plants were controlled in the present study, it seems that mineral nutrition and salinity were the factors responsible for the variation observed in the PA content among lettuces grown in different greenhouses.

Temporal Variation of Free and Conjugated PA Content in Lettuce Leaves. The free, conjugated, and total (free + conjugated) Put, Spd, and Spm contents at the five growth stages of lettuce (T_1, T_2, T_3, T_4, and T_5) in the three greenhouses (A_1, A_2, and A_3) are shown in Figures 3, 4, and 5. Regardless of the PA, a general trend was observed in all greenhouses: the content of free Put, Spd, and Spm decreased during plant growth (Figures 3A, 4A, and 5A), while the content of conjugated Put, Spd, and Spm increased (Figures 3B, 4B, and 5B). Despite the fluctuations observed in the content of free and conjugated PAs, total Put, Spd, and Spm content showed lower differences between different growth stages (Figure 5).

In plant foods, higher levels of free PAs are usually found in actively growing tissues.[5] Therefore, it is understandable that, in our study, higher levels of free Put, Spd, and Spm were obtained in the initial growth stages of all lettuces. Moreover, in plants, PAs are present not only as free molecules but also in the form of conjugates.[1] Similar to the free forms of PAs, conjugated PAs play key roles in plant survival, including cell division, flowering, and response to biotic and abiotic stresses. However, evidence suggests that these conjugates serve mainly as a reserve of PAs that can become available.[1,27] In the present study, higher levels of conjugated PAs were observed in the later stages of lettuce growth. This may be the reflex of a steady reduction of cell division during the lettuce growth period that results in an increase of the conjugated PA pool in plants. Sood and Nagar[28] also found an increase of conjugated Put, Spd, and

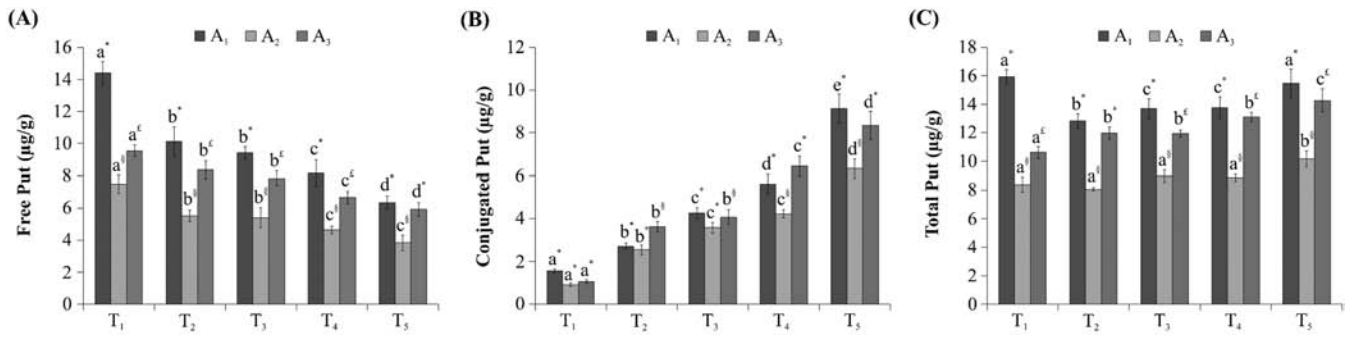

Figure 3. Free (A), conjugated (B), and total (C) putrescine (Put) content at five stages of lettuce growth (T_1, T_2, T_3, T_4, and T_5) in the three greenhouses (A_1, A_2, and A_3). Data are presented as the mean ± SD (n = 5). At a growth stage, different symbols (*, §, and £) indicate significant differences between greenhouses at $p < 0.05$. For a greenhouse, different letters (a, b, c, d, and e) indicate significant differences between growth stages at $p < 0.05$.

DOI: 10.1021/jf505453s
J. Agric. Food Chem. 2015, 63, 440−446

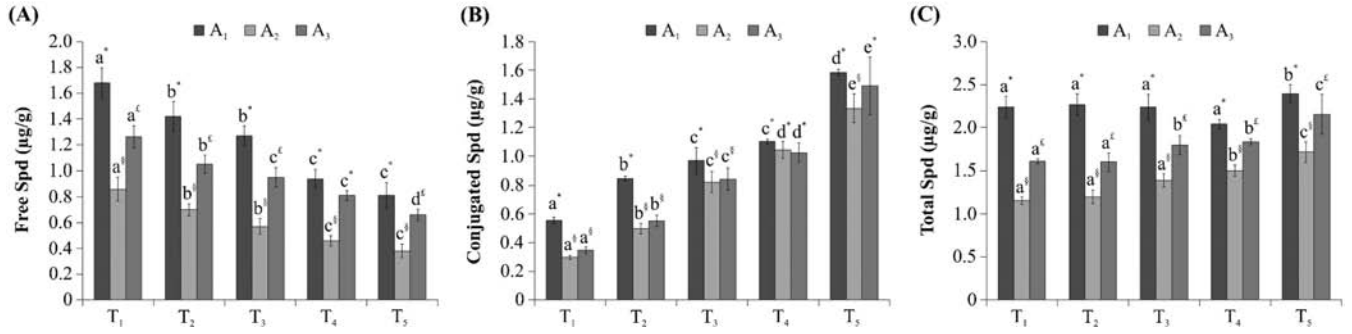

Figure 4. Free (A), conjugated (B), and total (C) spermidine (Spd) content at five stages of lettuce growth (T_1, T_2, T_3, T_4, and T_5) in the three greenhouses (A_1, A_2, and A_3). Data are presented as the mean ± SD (n = 5). At a growth stage, different symbols (*, §, and £) indicate significant differences between greenhouses at $p < 0.05$. For a greenhouse, different letters (a, b, c, d, and e) indicate significant differences between growth stages at $p < 0.05$.

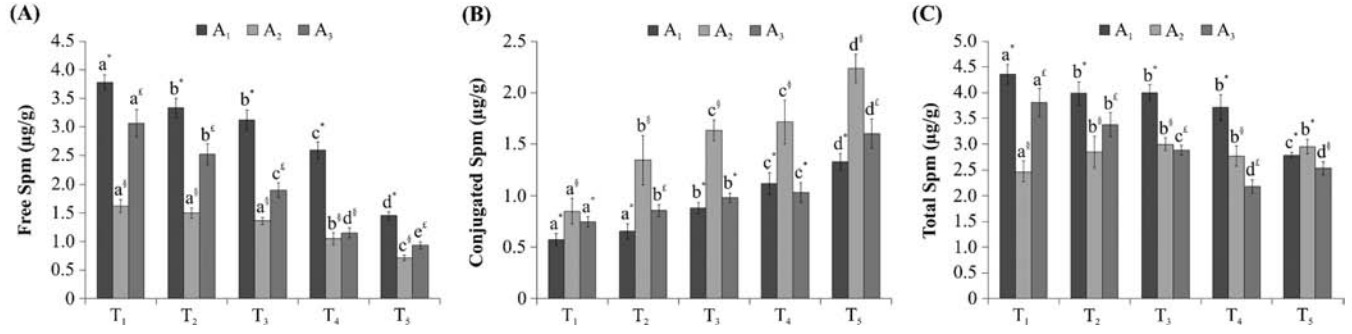

Figure 5. Free (A), conjugated (B), and total (C) spermine (Spm) content at five stages of lettuce growth (T_1, T_2, T_3, T_4, and T_5) in the three greenhouses (A_1, A_2, and A_3). Data are presented as the mean ± SD (n = 5). At a growth stage, different symbols (*, §, and £) indicate significant differences between greenhouse at $p < 0.05$. For a greenhouse, different letters (a, b, c, d, and e) indicate significant differences between growth stages at $p < 0.05$.

Table 2. Main Physicochemical Properties of the Three Greenhouse Soils (A_1, A_2, and A_3)[a]

	A_1	A_2	A_3
pH	6.5 ± 0.2 a	6.8 ± 0.1 b	6.6 ± 0.1 a
CEC (cmol/kg)	8.0 ± 0.5 a	18.1 ± 0.8 b	7.4 ± 0.6 a
OM (%)	53.1 ± 4.1 a	73.2 ± 2.8 b	21.3 ± 1.9 c
EC (μS/cm)	297 ± 49 a	645 ± 84 b	162 ± 19 c
clay (%)	1.9 ± 0.3 a	12.6 ± 0.4 b	2.3 ± 0.5 a
silt (%)	2.7 ± 0.4 a	12.8 ± 0.2 b	1.8 ± 0.3 a
sand (%)	94.9 ± 2.3 a	74.2 ± 2.0 b	95.4 ± 4.2 a
soil classification	sandy soil	loamy sand soil	sandy soil

[a]Data are presented as the mean ± SD (n = 15, i.e., triplicate analysis in each of the 5 sampling time points). Differences were tested according to ANOVA followed by Tukey's test. In a line, different letters (a, b, and c) indicate significant differences ($p < 0.05$) between the greenhouse soils.

Table 3. Extractable Content (mg/kg) of Chemical Species in the Three Greenhouses Soils (A_1, A_2, and A_3)[a]

	A_1	A_2	A_3
Ca^{2+}	784.0 ± 111.1 a	1285.3 ± 161.3 b	885.9 ± 99.5 c
Mg^{2+}	85.2 ± 11.9 a	199.8 ± 10.1 b	115 ± 20.2 c
K^+	167.1 ± 19.3 a	397.7 ± 35.7 b	109.8 ± 21.0 c
Na^+	194.4 ± 22.9 a	40.3 ± 13.7 b	76.5 ± 7.9 c
Cl^-	335.7 ± 50.9 a	16.2 ± 3.8 b	126.9 ± 27.4 c
NO_3^-	174.7 ± 44.0 a	411.0 ± 63.3 b	102.1 ± 31.5 c
PO_4^{3-}	50.9 ± 3.0 a	101.4 ± 3.1 b	63.5 ± 4.5 c
SO_4^{2-}	188.2 ± 27.7 a	485.3 ± 95.8 b	217.1 ± 64.6 a

[a]Data are presented as the mean ± SD (n = 15, i.e., triplicate analysis in each of the 5 sampling time points). Differences were tested according to ANOVA followed by Tukey's test. In a line, different letters (a, b, and c) indicate significant differences ($p < 0.05$) between greenhouses.

Spm during flower development of two species of rose (*Rosa damascena* and *Rosa bourboniana*).

Regardless of the greenhouse where lettuces were grown, free Put was always the most abundant PA, while free Spd was the least abundant. In particular, at T_5, free Put content was 6.4, 3.8, and 5.9 μg/g in A_1, A_2, and A_3 lettuces, respectively. These values are in close agreement with the 4 to 7.9 μg/g interval range described in the literature for lettuce.[2,13] For free Spd, the obtained levels in A_1, A_2, and A_3 lettuces at T_5 were 0.81, 0.38, and 0.66 μg/g, respectively. These values are significantly lower compared to the ones described by Ali et al.[13] in lettuces (6.2 to 9.1 μg/g). For free Spm, the obtained content at T_5 was 1.5, 0.7, and 0.9 in A_1, A_2, and A_3 lettuces, respectively, which are very similar to those reported in the literature (0.8 to 1.2 μg/g) for lettuce.[2,13] Similar to free Put, conjugated Put was the most abundant conjugated PA (9.1, 6.3, and 8.4 μg/g at T_5 in A_1, A_2, and A_3 lettuces, respectively), while conjugated Spd and Spm showed very similar contents. Since most studies carried out to date only determine the content of free Put, Spd, and Spm, data comparison between the content of conjugated PAs in our lettuces and other plant foods was impossible to perform.

Estimation of the PA Daily Intake from Lettuce Leaves. The EDI values of free, conjugated, and total (free + conjugated) PAs were calculated at each of the five growth

DOI: 10.1021/jf505453s
J. Agric. Food Chem. 2015, 63, 440−446

stages of A_1, A_2, and A_3 lettuces. Overall, the EDI values of free PAs were the highest in the first growth stage of lettuce (T_1), decreasing until the last growth stage (T_5). With regard to conjugated PAs, the inverse was observed: the first growth stage of lettuce (T_1) showed the lowest content, steadily increasing until the last growth stage (T_5).

Regarding the relative contribution of each PA for the dietary intake, Put was the most abundant PA (70% of the total PA fraction), followed by Spm (19%) and Spd (11%). Nishibori et al.[29] determined the content of PAs in several foods groups (e.g., vegetables, fruits, meat, cheese, cereals, nuts, eggs, and dairy) and estimated the daily intake of PAs from each food group. These authors found that vegetables are the main source of Put and Spd and that Put was responsible for almost half of the total PA intake considering all food groups. Other studies have also addressed the importance of vegetables as an important source of PAs in the human diet.[11,30,31]

Both free and conjugated PA content should be considered in the dietary intake estimation; thus, the total (free + conjugated) Put, Spd, and Spm mean content was calculated and discussed. A general trend was observed: A_1 lettuces contributed to the highest daily intake of PAs (3.81, 0.36, and 0.44 μmol/day for Put, Spd, and Spm, respectively), while A_2 lettuces contributed to the lowest daily intake of PAs (2.36, 0.22, and 0.32 μmol/day for Put, Spd, and Spm, respectively).

Several studies have estimated the daily intake of PAs; however, great variation is described depending on the type of food as well as on regional dietary habits. Among these studies, the lowest total PAs intake was obtained in Japan (200 μmol/day)[29] and the highest in European countries (316 μmol/day).[32] Considering this low and high total PA intake, it was observed that lettuce only contributes between 1.5 to 2.3% of the low total PA intake (200 μmol/day) and between 0.9 to 1.5% of the high total PA intake (316 μmol/day). It should be highlighted that most studies that deal with dietary PA intake consider only the free form of PAs present in foods.[2,13,31] Until now, it is not clear if the form in which PAs are present in foods influences their bioavailability and/or bioactivity. However, evidence suggests that this aspect is of major importance when studies are carried out with the aim of assessing the potential implications of dietary PA intake in human health since it is hypothesized that the toxicokinetics (absorption, distribution, metabolism, and excretion) of free, conjugated, and bound PAs will greatly differ among them.[6]

In recent years, increased consumption of plant foods at their initial growth stages (known as microgreens or baby leaf vegetables) has been observed due to their higher nutritional value, intense flavors, attractive colors, and tender textures.[16,17] According to our results, lettuce at the initial growth stages showed a higher content of free Put, Spd, and Spm than the conjugated form of these PAs. However, when lettuces are consumed in their mature stage (T_5), a higher contribution of conjugated Put, Spd, and Spm is observed. This information is very important considering the differences that are likely to exist between the bioavailability and/or bioactivity of free and conjugated PAs. Thus, it emphasized that due to the high contribution of the conjugated form of Put, Spd, Spm in the last stage of lettuces growth (maturity stage), conjugated PAs must be considered in studies evaluating the daily intake of PAs.

Until now, studies monitoring the PA content in plant foods have not detailed the form in which these compounds are present. This study describes relevant information about the evolution of free and conjugated Put, Spd, and Spm content during lettuce growth in three different greenhouses. Free PA content is significantly higher at the initial stages of lettuce growth, while at later growth stages conjugated PAs predominate. Despite these fluctuations, the total (free + conjugated) PA content remained fairly constant during the studied period. Data described here should be included in food databases to enable a reliable estimation of PA intake and how this intake can affect human health. The form in which a certain PA is present in foods will certainly influence its toxicokinetics. Thus, more studies in this field are required.

AUTHOR INFORMATION

Corresponding Author

*Tel: +351 220428642. Fax: +351 226093390. E-mail: ecp@estsp.ipp.pt.

Funding

Edgar Pinto thanks FCT (Portuguese Foundation for Science and Technology) for his Ph.D. grant (SFRH/BD/67042/2009). This work received financial support from the European Union (FEDER funds through COMPETE) and National Funds (FCT) through project Pest-C/EQB/LA0006/2013. This work also received financial support from the European Union (FEDER funds) under the framework of QREN through Project NORTE-07-0124-FEDER-000069. To all financing sources, we are greatly indebted.

Notes

The authors declare no competing financial interest.

REFERENCES

(1) Takahashi, T.; Kakehi, J. I. Polyamines: ubiquitous polycations with unique roles in growth and stress responses. *Ann. Bot. (Oxford, U. K.)* **2010**, *105*, 1−6.

(2) Kalač, P. Health effects and occurrence of dietary polyamines: A review for the period 2005−mid 2013. *Food Chem.* **2014**, *161*, 27−39.

(3) Fuell, C.; Elliott, K. A.; Hanfrey, C. C.; Franceschetti, M.; Michael, A. J. Polyamine biosynthetic diversity in plants and algae. *Plant Physiol. Biochem.* **2010**, *48*, 513−520.

(4) Kusano, T.; Berberich, T.; Tateda, C.; Takahashi, Y. Polyamines: essential factors for growth and survival. *Planta* **2008**, *228*, 367−381.

(5) Hussain, S. S.; Ali, M.; Ahmad, M.; Siddique, K. H. M. Polyamines: natural and engineered abiotic and biotic stress tolerance in plants. *Biotechnol. Adv.* **2011**, *29*, 300−311.

(6) Larque, E.; Sabater-Molina, M.; Zamora, S. Biological significance of dietary polyamines. *Nutrition* **2007**, *23*, 87−95.

(7) Moinard, C.; Cynober, L.; de Bandt, J. P. Polyamines: metabolism and implications in human diseases. *Clin. Nutr.* **2005**, *24*, 184−197.

(8) Soda, K. Polyamine intake, dietary pattern, and cardiovascular disease. *Med. Hypotheses* **2010**, *75*, 299−301.

(9) Rivat, C.; Richebe, P.; Laboureyras, E.; Laulin, J. P.; Havouis, R.; Noble, F.; Moulinoux, J. P.; Simonnet, G. Polyamine deficient diet to relieve pain hypersensitivity. *Pain* **2008**, *137*, 125−137.

(10) Bell, R. F.; Borzan, J.; Kalso, E.; Simonnet, G. Food, pain, and drugs: does it matter what pain patients eat? *Pain* **2012**, *153*, 1993−1996.

(11) Cipolla, B. G.; Havouis, R.; Moulinoux, J. P. Polyamine contents in current foods: a basis for polyamine reduced diet and a study of its long term observance and tolerance in prostate carcinoma patients. *Amino Acids* **2007**, *33*, 203−212.

(12) Kozova, M.; Kalac, P.; Pelikanova, T. Contents of biologically active polyamines in chicken meat, liver, heart and skin after slaughter and their changes during meat storage and cooking. *Food Chem.* **2009**, *116*, 419−425.

(13) Ali, M. A.; Poortvliet, E.; Stromberg, R.; Yngve, A. Polyamines in foods: development of a food database. *Food Nutr Res.* **2011**, *55*. DOI: 10.3402/fnr.v55i0.5572.

(14) Pinto, E.; Melo, A.; Ferreira, I. M. P. L. V. O. Sensitive quantitation of polyamines in plant foods by ultrasound-assisted benzoylation and dispersive liquid-liquid microextraction with the aid of experimental designs. *J. Agric. Food Chem.* **2014**, *62*, 4276−4284.
(15) Sun, J. H.; Xiao, Z. L.; Lin, L. Z.; Lester, G. E.; Wang, Q.; Harnly, J. M.; Chen, P. Profiling polyphenols in five *Brassica* species microgreens by UHPLC-PDA-ESI/HRMSn. *J. Agric. Food Chem.* **2013**, *61*, 10960−10970.
(16) Xiao, Z. L.; Lester, G. E.; Luo, Y. G.; Wang, Q. Assessment of vitamin and carotenoid concentrations of emerging food products: edible microgreens. *J. Agric. Food Chem.* **2012**, *60*, 7644−7651.
(17) Pinto, E.; Almeida, A. A.; Aguiar, A. A. R. M.; Ferreira, I. M. P. L. V. O. Changes in macrominerals, trace elements and pigments content during lettuce (*Lactuca sativa* L.) growth: influence of soil composition. *Food Chem.* **2014**, *152*, 603−611.
(18) WHO. *GEMS/Food Cluster Diets*; WHO: Geneva, Switzerland, 2013.
(19) FAOSTAT. *The FAO (Food and Agriculture Organization of the United Nations) Statistical Database*; FAO: Rome, Italy, 2011.
(20) ISO. *ISO 11260:1994: Soil Quality - Determination of Effective Cation Exchange Capacity and Base Saturation Level Using Barium Chloride Solution*; International Organization for Standardization: Geneva, Switzerland, 1994; p 10.
(21) ISO. *ISO 11277:1998: Soil Quality - Determination of Particle Size Distribution in Mineral Soil Material - Method by Sieving and Sedimentation*; International Organization for Standardization: Geneva, Switzerland, 1998; p 30.
(22) ISO. *ISO 19730:2008 - Soil Quality - Extraction of Trace Elements from Soil Using Ammonium Nitrate Solution*; International Organization for Standardization: Geneva, Switzerland, 2008; p 10.
(23) ISO/TS 14256−1:2003. *Soil Quality - Determination of Nitrate, Nitrite and Ammonium in Field-Moist Soils by Extraction with Potassium Chloride Solution - Part 1: Manual Method*; International Organization for Standardization: Geneva, Switzerland, 2003; pp 14.
(24) Fontaniella, B.; Mateos, J. L.; Vicente, C.; Legaz, M. E. Improvement of the analysis of dansylated derivatives of polyamines and their conjugates by high-performance liquid chromatography. *J. Chromatogr., A* **2001**, *919*, 283−288.
(25) Pinto, E.; Aguiar, A. A. R. M.; Ferreira, I. M. P. L. V. O. Influence of soil chemistry and plant physiology in the phytoremediation of Cu, Mn, and Zn. *Crit. Rev. Plant Sci.* **2014**, *33*, 351−373.
(26) Houdusse, F.; Garnica, M.; Zamarreno, A. M.; Yvin, J. C.; Garcia-Mina, J. Possible mechanism of the nitrate action regulating free-putrescine accumulation in ammonium fed plants. *Plant Sci.* **2008**, *175*, 731−739.
(27) Luo, J.; Fuell, C.; Parr, A.; Hill, L.; Bailey, P.; Elliott, K.; Fairhurst, S. A.; Martin, C.; Michael, A. J. A novel polyamine acyltransferase responsible for the accumulation of spermidine conjugates in *Arabidopsis* seed. *Plant Cell* **2009**, *21*, 318−333.
(28) Sood, S.; Nagar, P. K. Changes in endogenous polyamines during flower development in two diverse species of rose. *Plant Growth Regul.* **2004**, *44*, 117−123.
(29) Nishibori, N.; Fujihara, S.; Akatuki, T. Amounts of polyamines in foods in Japan and intake by Japanese. *Food Chem.* **2007**, *100*, 491−497.
(30) Bardocz, S.; Duguid, T. J.; Brown, D. S.; Grant, G.; Pusztai, A.; White, A.; Ralph, A. The importance of dietary polyamines in cell regeneration and growth. *Br. J. Nutr.* **1995**, *73*, 819−828.
(31) Zoumas-Morse, C.; Rock, C. L.; Quintana, E. L.; Neuhouser, M. L.; Gerner, E. W.; Meyskens, F. L. Development of a polyamine database for assessing dietary intake. *J. Am. Diet Assoc.* **2007**, *107*, 1024−1027.
(32) Ali, M. A.; Poortvliet, E.; Stromberg, R.; Yngve, A. Polyamines: total daily intake in adolescents compared to the intake estimated from the Swedish Nutrition Recommendations Objectified (SNO). *Food Nutr. Res.* **2011**, *55*. DOI: 10.3402/fnr.v55i0.5455

DOI: 10.1021/jf505453s
J. Agric. Food Chem. 2015, 63, 440−446

JOURNAL OF AGRICULTURAL AND FOOD CHEMISTRY

Article

pubs.acs.org/JAFC

Chemical Composition and Biological Activity of Four *Salvia* Essential Oils and Individual Compounds against Two Species of Mosquitoes

Abbas Ali,*[,†] Nurhayat Tabanca,[†] Betul Demirci,[§] Eugene K. Blythe,[#] Zulfiqar Ali,[†] K. Husnu Can Baser,[§,⊥] and Ikhlas A. Khan[†,‡,Δ]

[†]National Center for Natural Products Research, The University of Mississippi, University, Mississippi 38677, United States

[§]Department of Pharmacognosy, Anadolu University, Faculty of Pharmacy, 26470 Eskisehir, Turkey

[#]Coastal Research and Extension Center, Mississippi State University, South Mississippi Branch Experiment Station, Poplarville, Mississippi 39470, United States

[⊥]Botany and Microbiology Department, College of Science, King Saud University, Riyadh 11451, Saudi Arabia

[‡]Division of Pharmacognosy, Department of BioMolecular Sciences, School of Pharmacy, The University of Mississippi, University, Mississippi 38677, United States

[Δ]Department of Pharmacognosy, College of Pharmacy, King Saud University, Riyadh 11451, Saudi Arabia

Supporting Information

ABSTRACT: The chemical compositions of essential oils obtained from four species of genus *Salvia* were analyzed by gas chromatography with a flame ionization detector (GC-FID) and gas chromatography−mass spectrometry (GC-MS). The main compounds identified from *Salvia* species essential oils were as follows: 1,8-cineole (71.7%), α-pinene (5.1%), camphor (4.4%), and β-pinene (3.8%) in *Salvia apiana*; borneol (17.4%), β-eudesmol (10.4%), bornyl acetate (5%), and guaiol (4.8%) in *Salvia elegans*; bornyl acetate (11.4%), β-caryophyllene (6.5%), caryophyllene oxide (13.5%), and spathulenol (7.0%) in *Salvia leucantha*; α-thujene (25.8%), viridiflorol (20.4%), β-thujene (5.7%), and camphor (6.4%) in *Salvia officinalis*. In biting-deterrent bioassays, essential oils of *S. leucantha* and *S. elegans* at 10 μg/cm^2 showed activity similar to that of DEET (97%, *N*, *N*-diethyl-*m*-toluamide) in two species of mosquitoes, whereas the activities of *S. officinalis* and *S. apiana* essential oils were lower than those of the other oils or DEET. Pure compounds β-eudesmol and guaiol showed biting-deterrent activity similar to DEET at 25 nmol/cm^2, whereas the activity of 13-*epi*-manool, caryophyllene oxide, borneol, bornyl acetate, and β-caryophyllene was significantly lower than that of β-eudesmol, guaiol, or DEET. All essential oils showed larvicidal activity except that of *S. apiana*, which was inactive at the highest dose of 125 ppm against both mosquito species. On the basis of 95% CIs, all of the essential oils showed higher toxicity in *Anopheles quadrimaculatus* than in *Aedes aegypti*. The essential oil of *S. leucantha* with an LC_{50} value of 6.2 ppm showed highest toxicity in *An. quadrimaculatus*.

KEYWORDS: *Salvia species, β-eudesmol, guaiol, 13-epi-manool, biting deterrent, larvicide, Aedes aegypti, Anopheles quadrimaculatus*

INTRODUCTION

Mosquitoes are vectors for many pathogens that cause human diseases such as malaria, dengue fever, yellow fever, Rift Valley fever, and Chikungunya.[1] When significant levels of transmission occur, epidemics can result in high rates of human morbidity and mortality. Insecticides from various chemical groups are the basic tools used for management of mosquito populations. Due to extensive and indiscriminate use of insecticides, mosquitoes have developed resistance against these chemicals.[2] Plant essential oils have been suggested as alternative sources for insect control because they are selective, biodegrade to nontoxic products, and have minimal effects on nontarget organisms and the environment.[3] The search for new strategies for natural products to control vectors of these diseases is desirable because this can help in managing resistance to synthetic insecticides and reducing the use of toxic chemicals.[3] Much effort has, therefore, been focused to identify the effectiveness of plant essential oils against mosquito larvae because of their broad-spectrum activity against target insects, low mammalian toxicity, and biodegradability in the environment.[4−7]

The genus *Salvia* L. (Lamiaceae) contains more than 750 species of herbs, subshrubs, and shrubs of worldwide distribution, with many of the species commonly used in local folk medical practices and in cosmetics.[8−11] The name of the genus *Salvia* means "safe" or "well", from the Latin word *salvere*, referring to the curative properties of the known culinary and medicinal herb *Salvia officinalis* L.[12] Members of this genus are reported to produce many useful secondary metabolites including terpenes, phenolics, and their derivatives that have been central to the pharmacopoeias of many countries.[13] The healing reputation of *Salvia* species can be traced back to Roman times, and a well-known sage, *S. officinalis*, is particularly known for this.[14] *Salvia* species are

Received: October 14, 2014
Revised: December 13, 2014
Accepted: December 22, 2014
Published: December 22, 2014

ACS Publications © 2014 American Chemical Society

DOI: 10.1021/jf504976f
J. Agric. Food Chem. 2015, 63, 447−456

Table 1. Composition of the Essential Oils of *Salvia* Species

RRI[a]	compound	*S. apiana*[b] (%)	*S. elegans*[b] (%)	*S. leucantha*[b] (%)	*S. officinalis*[b] (%)	identification[c]
1014	tricyclene		0.1			t_R, MS
1032	α-pinene	5.1	1.4	0.8	1.9	t_R, MS
1076	camphene	0.5	3.5	0.3	1.0	t_R, MS
1118	β-pinene	3.8	2.4	0.2	1.0	t_R, MS
1159	δ-3-carene	2.4				MS
1174	myrcene	1.2				t_R, MS
1176	α-phellandrene	0.2				t_R, MS
1188	α-terpinene	0.3				t_R, MS
1203	limonene	1.5	0.4			t_R, MS
1213	1,8-cineole	71.7	3.5		4.4	t_R, MS
1246	(*Z*)-β-ocimene	1.1				MS
1255	γ-terpinene	0.5	0.3			t_R, MS
1266	(*E*)-β-ocimene	0.3				MS
1280	*p*-cymene	0.8	1.2			t_R, MS
1290	terpinolene	0.2	0.1			t_R, MS
1391	(*Z*)-3-hexenol		0.4			MS
1393	3-octanol		1.1			t_R, MS
1437	α-thujone				25.8	t_R, MS
1450	*trans*-linalool oxide (*furanoid*)		0.3	0.5		MS
1451	β-thujone				5.7	t_R, MS
1452	1-octen-3-ol		1.2	0.8		t_R, MS
1466	α-cubebene		0.4			t_R, MS
1478	*cis*-linalool oxide (*furanoid*)		0.1	0.5		MS
1492	cyclosativene		0.4			MS
1497	α-copaene	0.2	0.4			t_R, MS
1500	pentadecane			0.5		t_R, MS
1532	camphor	4.4	3.8		6.4	t_R, MS
1553	linalool	0.2	3.0	0.9		t_R, MS
1586	pinocarvone		0.5			t_R, MS
1591	bornyl acetate		5.0	11.4		t_R, MS
1600	β-elemene			0.2		t_R, MS
1611	terpinen-4-ol	0.5	2.4		0.4	t_R, MS
1612	β-caryophyllene	1.7		6.5	0.7	t_R, MS
1617	6,9-guaiadiene	0.2		4.9		MS
1628	aromadendrene		0.6			MS
1648	myrtenal		0.8			t_R, MS
1668	(*Z*)-β-farnesene		-	4.1		MS
1670	*trans*-pinocarveol		0.9	0.2		t_R, MS
1677	*epi*-zonarene			0.1		MS
1684	β-guaiaene			0.5		MS
1687	methylchavicol			0.7		t_R, MS
1687	α-humulene	0.1		0.6	2.1	t_R, MS
1704	γ-muurolene		0.4			MS
1706	α-terpineol	0.3	0.9	0.3		t_R, MS
1719	borneol	0.2	17.4	0.7	1.5	t_R, MS
1722	cabreuva oxide-II		0.6			MS
1725	verbenone		0.5			t_R, MS
1726	germacrene D			0.8		t_R, MS
1740	α-muurolene		0.8			MS
1741	β-bisabolene	0.4				t_R, MS
1755	bicyclogermacrene			0.3		t_R, MS
1768	cabreuva oxide-IV		0.6			MS
1773	δ-cadinene	0.4	2.1	0.5		MS
1776	γ-cadinene	0.2	0.6	1.1		MS
1804	myrtenol		0.6			t_R, MS
1823	cabreuva oxide-VI		0.3			MS
1838	(*E*)-β-damascenone		0.4	0.5		MS
1845	*trans*-carveol		0.1			t_R, MS
1849	calamenene	0.1	0.7	2.9		MS
1864	*p*-cymen-8-ol		0.5	0.2		t_R, MS
1868	(*E*)-geranyl acetone		0.5			MS

DOI: 10.1021/jf504976f
J. Agric. Food Chem. 2015, 63, 447−456

Table 1. continued

RRI[a]	compound	*S. apiana*[b] (%)	*S. elegans*[b] (%)	*S. leucantha*[b] (%)	*S. officinalis*[b] (%)	identification[c]
1898	1,11-oxidocalamenene			0.2		MS
1918	β-calacorene			1.4		MS
1941	α-calacorene		0.4	2.1		MS
1958	(*E*)-β-ionone		0.5			MS
1984	γ-calacorene		0.6	0.4		MS
1980	furopelargone A			3.2		MS
2008	caryophyllene oxide		1.7	13.5	0.8	t_R, MS
2045	humulene epoxide-I				1.1	MS
2071	humulene epoxide-II		0.2	0.6	4.5	MS
2174	fokienol		0.5			MS
2080	cubenol		0.5			MS
2088	1-*epi*-cubenol		0.8			MS
2098	globulol		0.5	0.6		MS
2103	guaiol		4.8			t_R, MS
2104	viridiflorol				20.4	t_R, MS, NMR
2105	furopelargone B			4.2		MS
2130	salviadienol			0.4		MS
2131	hexahydrofarnesyl acetone		0.6	1.5		MS
2144	spathulenol		1.3	7.0		t_R, MS
2192	nonanoic acid			0.5		t_R, MS
2185	γ-eudesmol		3.5			MS
2204	eremoligenol		0.7			MS
2209	T-muurolol		0.3			MS
2232	bulnesol		0.7			t_R, MS
2247	*trans*-α-bergamotol			0.5		MS
2250	α-eudesmol		3.7			t_R, MS
2256	cadalene			2.6		MS
2257	β-eudesmol		10.4		1.2	t_R, MS
2264	4,7-dimethyl-1-tetralone			2.6		MS
2298	decanoic acid			0.6		t_R, MS
2300	tricosane				3.2	t_R, MS
2324	caryophylla-2(12),6(13)-dien-5α-ol (=*caryophylladienol II*)			1.1		MS
2389	caryophylla-2(12),6-dien-5α-ol (=*caryophyllenol I*)			2.4		MS
2392	caryophylla-2(12),6-dien-5β-ol (=*Caryophyllenol II*)			2.7		MS
2500	pentacosane	0.1			3.7	t_R, MS
2600	hexacosane	0.2				t_R, MS
2622	phytol		0.6	0.3		MS
2679	13-*epi*-manool				1.8	t_R, MS, NMR
2700	heptacosane	0.2			4.4	t_R, MS
2900	nonacosane				5.7	t_R, MS
2931	hexadecanoic acid		tr	0.6	1.8	t_R, MS
	monoterpene hydrocarbons	17.9	9.4	1.3	3.9	
	oxygenated monoterpenes	77.3	40.3	14.7	44.2	
	sesquiterpene hydrocarbons	3.3	7.4	29.0	2.8	
	oxygenated sesquiterpenes		31.1	36.4	28	
	alkanes	0.5		0.5	17	
	fatty acids			1.7	1.8	
	diterpenes		0.6	0.3	1.8	
	others		4.7	6.1		
	total	99.0	93.5	90.0	99.5	

[a]RRI, relative retention indices calculated against *n*-alkanes on polar column. [b]Percent calculated from FID data for polar column; tr, trace (<0.1%). [c]Identification method: t_R, identification based on the retention times (t_R) of genuine compounds on the HP Innowax column; MS, identified on the basis of computer matching of the mass spectra with those of the Wiley and MassFinder libraries and comparison with literature data.

used to treat diarrhea, gonorrhea, hemorrhoids, and eye diseases and as an antiseptic, antispasmodic, and stomachic.[15] Phenolic compounds of this genus have also shown excellent antioxidant property.[16] Four *Salvia* species, *Salvia apiana* Jeps., *Salvia elegans* Vahl, *Salvia leucantha* Cav., and *Salvia officinalis* L., were investigated in the present study.

S. apiana (white sage, bee sage, sacred sage) is a coarsely branched shrub growing up to 1.5 m. This species is native to California. Silvery white leaves of *S. apiana* are highly aromatic,

DOI: 10.1021/jf504976f
J. Agric. Food Chem. 2015, 63, 447−456

stems are hollow, and the flower stalks rise 1 m above the foliage, producing white to pale lavender flowers.[8,17,18] Some California Indian tribes consider *S. apiana* to be sacred and burn the leaves as incense for purification ceremonies[17] A tea made from the leaves is reported to relieve colds and congestion and was used by Native Americans as a shampoo, dye, and hair straightener.[18,19] Seeds are sold as a natural food that are soaked and added to water, fruit juice, and cereals, whereas the leaves are used in cooking.[20]

S. elegans (pineapple sage; syn. *S. rutilans* Carrière) is a perennial subshrub native to the high mountains of central Mexico and Guatemala.[8,18,21] Plants grow to 1 m in height, produce bright red flowers in the fall and winter, and are grown either as summer annuals in cold regions or outdoors year-round in mild climates.[8,18] The aromatic leaves may be added to fruit salads, desserts, and cold drinks and used for making tea.[20]

S. leucantha (Mexican bush sage, velvet sage) originates in tropical and subtropical conifer forests of central and eastern Mexico. Flowers produced from summer until frost typically consist of a purple calyx and a purple or white corolla, both covered with fine, velvety hairs.[20] Leaves are aromatic with a slight roasted nut or chocolate scent, but are not used for culinary purposes.[22]

S. officinalis (common sage) originates from the northern shores of the Mediterranean and has been cultivated for centuries in Europe.[18] Sage has also been used in herbal medicine against acne, cancer, cramps, diabetes, diarrhea, flatulence, gingivitis, headache, inflammation of the mouth and throat, insect bites, upset stomach, and many other ailments.[23,24] Leaves have the highest content of essential oils just prior to bloom.[18]

Previous research indicates that some species of *Salvia* have larvicidal and repellent activity against mosquitoes. Amer and Mehlhorn[25] reported repellent activity of clary sage (*Salvia sclarea*) essential oil against *Aedes albopictus* Skuse and *Culex* species. Conti et al.[26] reported the repellent effect of *S. dorisiana*, *S. longifolia*, and *S. sclarea* essential oils against *Ae. albopictus*, whereas Mathew and Thoppil[27] reported larvicidal activity of the essential oils of *S. elegans* and *S. splendens* against *Ae. albopictus* larvae. Considering the diversity of compounds present in *Salvia* species and their potential to be used in integrated management of these disease vectors, it is important to study the chemical composition and biological activity of essential oils of different species of *Salvia*. This study reports the chemical composition and larvicidal and biting deterrent activities of essential oils of *S. leucantha*, *S. elegans*, *S. officinalis*, and *S. apiana* against yellow fever mosquito, *Ae. aegypti* L., and malaria mosquito, *Anopheles quadrimaculatus* Say.

MATERIALS AND METHODS

Chemicals and General Experimental Procedures. NMR spectra were obtained on a Bruker DRX-500 spectrometer (chemical shift values are in ppm, ^{1}H NMR at 500 MHz and ^{13}C NMR at 125 MHz). Optical rotations were measured at ambient temperature using a Rudolph Research Analytical Autopol IV. Thin layer chromatography (TLC) was carried out on aluminum-backed plates precoated with silica gel F_{254} (20 × 20 cm, 200 μm, Merck & Co. Inc., Whitehouse Station, NJ, USA). Visualization was made by spraying with vanillin–H_2SO_4 (1% ethanolic vanillin with 10% ethanolic H_2SO_4) followed by heating. Preparative TLC was conducted on glass-backed plates precoated with silica gel F_{254} (20 × 20 cm, 500 μm, Sorbent Technologies, Inc., Norcross, GA, USA). Authentic standards borneol (CAS Registry No. 464-45-9), bornyl acetate (CAS Registry No. 5655-61-8), guaiol (CAS Registry No. 489-86-1), β-eudesmol (CAS Registry No. 489-86-1), β-caryophyllene (CAS Registry No. 87-44-5), and caryophyllene oxide (CAS Registry No. 1139-30-6) were all purchased from Sigma-Aldrich Co., St. Louis, MO, USA.

Plant Material. Plants of *S. apiana* and *S. officinalis* 'Extrakta' used in this study were propagated from seed obtained from Johnny's Selected Seeds (Winslow, ME, USA). Plants of *S. elegans* and *S. leucantha* were propagated by cuttings obtained from stock plants originating from commercial nursery sources. Plants of *S. apiana* were grown in field rows in a sandy loam soil, and plants of *S. elegans*, *S. leucantha*, and *S. officinalis* 'Extrakta' were grown in 3 gal containers in a pine bark-based substrate in controlled-environment greenhouses at the South Mississippi Branch Experiment Station (SMBES) in Poplarville, MS, USA (30°50′26″ N, longitude 89°32′46″ W; USDA hardiness zone 8b). Voucher specimens 510 (*S. apiana*), 14 (*S. elegans*), 101 (*S. officinalis* 'Extrakta'), and 6 (*S. leucantha*) were deposited at the SMBES for future reference.

Aerial parts were harvested from 6-month-old plants of *S. elegans* and *S. leucantha* in April 2009, from 9-month-old plants of *S. apiana* in February and March 2010, and from 6-month-old plants of *S. officinalis* 'Extrakta' in March and May 2010. Harvested plant material was air-dried for 3 weeks inside an air-conditioned building (25 °C maximum). Dried plant material was packed loosely into cardboard boxes and stored in the same building until shipment to the National Center for Natural Products Research in Oxford, MS, USA, in September 2009 (*S. elegans* and *S. leucantha*), March 2011 (*S. officinalis* 'Extrakta'), and April 2011 (*S. apiana*).

Isolation of the Essential Oils. Aerial parts of *S. apiana*, *S. elegans*, *S. leucantha*, and *S. officinalis* were separately subjected to hydrodistillation for 3 h using a Clevenger-type apparatus according to the procedure published in European Pharmacopea. The oils were dried over anhydrous sodium sulfate and stored in sealed amber vials in a freezer. Essential oils were obtained from *S. apiana*, *S. elegans*, *S. leucantha*, and *S. officinalis* with 0.6, 0.04, 0.03, and 0.24% yields, respectively.

Gas Chromatography (GC) and Gas Chromatography–Mass Spectrometry (GC-MS) Analysis of Essential Oils. *Salvia* essential oils were analyzed by GC with a flame ionization detector (FID) and GC-MS using an Agilent GC–mass selective detector (MSD) system. The GC-MS analyses were done with an Agilent 5975 GC-MSD system. An Innowax fused silica capillary (FSC) column (60 m × 0.25 mm, 0.25 μm film thickness) was used with helium as the carrier gas (0.8 mL/min). The oven temperature was kept at 60 °C for 10 min, then programmed to 220 °C at a rate of 4 °C/min, then maintained constant at 220 °C for 10 min, and finally programmed to 240 °C at a rate of 1 °C/min. The injector temperature was set at 250 °C. The split flow was adjusted at 50:1. Mass spectra were recorded at 70 eV with the mass range m/z 35–450. The GC analyses were performed using an Agilent 6890N GC system. FID detector temperature was set to 300 °C, and the same operational conditions were applied to a duplicate of the same column used in GC-MS analyses. Simultaneous autoinjection was done to obtain equivalent retention times. Relative percentages of the separated compounds were calculated from integration of the peak areas in the GC-FID chromatograms (Table 1).

Individual components were identified by comparison of retention times with authentic samples or by comparison of their relative retention index (RRI) to a series of *n*-alkanes[28] and by computer matching with commercial mass spectral libraries (Wiley GC/MS Library, MassFinder 3 Library) and in-house "Baser Library of Essential Oil Constituents" built from authentic samples, known oils, and mass literature data.[29−32] These identifications were accomplished by comparison of retention times with authentic samples or by comparison of their RRI to a series of *n*-alkanes.[28]

Isolation of (+)-13-*epi*-Manool. *S. officinalis* (500 mg) essential oil was subjected to high-performance flash chromatography (HPFC) using a Biotage SI instrument with a 25 M silica column (flow rate = 5.0 mL/min) and eluted with hexanes (100%, 420 mL), hexanes/acetone mixtures (99:1 to 98:2, 210 mL; 98:2 to 93:7, 180 mL; 97:3 to 96:4, 180 mL; 96:4, 120 mL; 96:4 to 95:5, 120 mL; 95:5 to 90:10, 120 mL, 90:10 to 80:20, 90 mL; 80:20 to 70:30, 90 mL) and finally washed

DOI: 10.1021/jf504976f
J. Agric. Food Chem. 2015, 63, 447−456

with acetone (100%, 240 mL). Portions of 12 mL volume were collected in 16 × 100 mm test tubes. Fractions with similar TLC profiles (hexanes/acetone 98:2, 95:5, and 90:10 v/v) were combined to give three fractions. The last subfraction C (50 mg) was purified by preparative thin layer chromatography using hexanes/acetone (99:1, v/v) with R_f value 0.34 to afford (+)-13-*epi*-manool (>98%, 10 mg). $[\alpha]_D^{25}$ = +59.2 (*c* 1.0, $CHCl_3$); ^{1}H NMR (500 MHz, $CDCl_3$) δ 0.99 (td, *J* = 13.5, 4.2 Hz, H-1a), 1.72 (H-1b), 1.46 (tt-like, *J* = 13.5, 3.5 Hz, H-2a), 1.55 (H-2b), 1.14 (td, *J* = 13.5, 4.1 Hz, H-3a), 1.37 (H-3b), 1.05 (dd, *J* = 12.6, 2.7 Hz, H-5), 1.28 (H-6a), 1.68 (H-6b), 1.94 (td, *J* = 13.0, 5.2 Hz, H-7b), 2.35 (br d, *J* = 13.0 Hz, H-7a), 1.53 (H-9), 1.30 (H-11a), 1.51 (H-11b), 1.22 (H-12a), 1.71 (H-12b), 5.88 (dd, *J* = 17.4, 10.7 Hz, H-14), 5.02 (d, *J* = 10.7 Hz, H-15a), 5.17 (d, *J* = 17.4 Hz, H-15b), 1.27 (s, 3H, H-16), 4.49 (br s, H-17a), 4.79 (br s, H-17b), 0.84 (s, 3H, H-18), 0.77 (s, 3H, H-19), 0.65 (s, 3H, H-20); ^{13}C NMR (125 MHz, $CDCl_3$) δ 39.1 (t, C-1), 19.4 (t, C-2), 42.2 (t, C-3), 33.6 (s, C-4), 55.6 (d, C-5), 24.4 (t, C-6), 38.4 (t, C-7), 148.7 (s, C-8), 57.4 (d, C-9), 39.9 (s, C-10), 17.7 (t, C-11), 41.5 (t, C-12), 73.4 (s, C-13), 145.3 (d, C-14), 111.5 (t, C-15), 27.6 (q, C-16), 106.5 (t, C-17), 33.6 (q, C-18), 21.7 (q, C-19), 14.4 (q, C-20); EIMS, *m/z* 290 [M^+] $C_{20}H_{34}O$, 272 (7), 257 (43), 244 (9), 229 (6), 216 (6), 203 (11), 189 (19), 177 (20), 161 (16), 147 (15), 137 (87), 139 (23), 123 (45), 121 (41), 115 (6), 109 (52), 107 (54), 95 (92), 93 (68), 66 (45), 81 (100), 79 (69), 71 (40), 69 (71), 67 (49), 55 (59), 43 (42), 41 (61).

Gas Chromatography–Mass Spectrometry Analysis for Isolated Compound 13-*epi*-Manool. The purity of 13-*epi*-manool was analyzed using an HP 5890 series gas chromatograph linked to an HP 5970 mass spectrometer system using a DB-1 capillary column (20 m × 0.18 mm with 0.25 μm film thicknesses). Helium (1 mL/min) was used as carrier gas. The GC oven temperature was held at 50 °C for 2 min and then ramped to 280 °C at a rate of 5 °C/min. The scanned mass range was from *m/z* 40 to 550, and the ion source was operated in electron ionization (EI) mode with an electron energy set to 70 eV.

Mosquito Bioassays. *Insects.* *Ae. aegypti* and *An. quadrimaculatus* larvae and adults used in these studies were from a laboratory colony maintained at the Mosquito and Fly Research Unit at the Center for Medical, Agricultural and Veterinary Entomology, USDA-ARS, Gainesville, FL, USA. For biting-deterrence bioassays, eggs were hatched and the insects were reared to the adult stage in the laboratory and maintained at 27 ± 2 °C and 60 ± 10% relative humidity with a photoperiod regimen of 12:12 h (light/dark). Adult females (8–13 days old) were used. For larval bioassays, the eggs were hatched and the larvae were maintained at the above temperature.

Mosquito Biting Bioassays. Experiments were conducted by using a six-celled in vitro Klun and Debboun (K&D) module bioassay system developed by Klun et al.[33] for quantitative evaluation of biting-deterrent properties of candidate compounds. Briefly, the assay system consists of a six-well reservoir with each of the 3 × 4 cm wells containing 6 mL of blood. As described by Ali et al.,[34] a feeding solution consisting of CPDA-1 (citrate–phosphate–dextrose–adenine) and ATP was used instead of blood. Green fluorescent tracer dye (www.blacklightword.com) was used to determine feeding by the females. Essential oils of *S. leucantha*, *S. elegans*, *S. officinalis*, *S. apiana* and individual compounds were tested in this study. Essential oils were applied at concentrations of 10 μg/cm^2, pure compounds at 25 nmol/cm^2, and DEET (97%, *N*, *N*-diethyl-*m*-toluamide) (Sigma-Aldrich, St. Louis, MO, USA) at 25 nmol/cm^2 as positive control. All treatments were freshly prepared in molecular biology grade 100% ethanol (Fisher Scientific Chemical Co., Fair Lawn, NJ, USA) at the time of bioassay. The temperature of the solution in the reservoirs was maintained at 37 °C by continuously passing warm water through the reservoir using a circulatory bath. Reservoirs were covered with a layer of collagen membrane (Devro, Sandy Run, SC, USA). Test compounds were randomly applied to six 4 × 5 cm areas of organdy cloth and positioned over the membrane-covered CPDA-1 + ATP solution with a Teflon separator placed between the treated cloth and the six-celled module to prevent contamination of the module. A six-celled K&D module containing five female mosquitoes per cell was positioned over the cloth treatments covering the six CPDA-1 + ATP solution membrane wells, and trap doors were opened to expose the treatments to these females. The number of mosquitoes biting through cloth treatments in each cell was recorded after a 3 min exposure, and mosquitoes were prodded back into the cells to check the actual feeding. Mosquitoes were squashed and the presence or absence of green fluorescent tracer dye in the gut was used as an indicator of feeding. A replicate consisted of six treatments: four test materials, DEET (a standard biting deterrent), and ethanol-treated organdy as solvent control applied randomly. Two sets of five replications each with five females per treatment were conducted on two different days using a newly treated organdy and a new batch of females in each replication. Treatments were replicated 10 times.

Larval Bioassays. Bioassays were conducted to test essential oils of *S. leucantha*, *S. elegans*, *S. officinalis*, and *S. apiana* for their larvicidal activity against moquitoes by using the bioassay system described by Pridgeon et al.[35] Five 1-day-old *Ae. aegypti* and *An. quadrimaculatus* larvae were added in a droplet of water to each well of 24-well plates (BD Labware, Franklin Lakes, NJ, USA) by use of a disposable 22.5 cm Pasteur pipet. Fifty microliters of larval diet (2% slurry of 1:1 beef liver powder (Now Foods, Bloomingdale, IL, USA) and brewer's yeast (Lewis Laboratories Ltd., Westport, CT, USA) was added to each well by using a Finnpipette stepper (Thermo Fisher, Vantaa, Finland). All chemicals tested were diluted in ethanol. Eleven microliters of the test chemical was added to the labeled wells, whereas 11 μL of ethanol was added to control treatments. After the treatment application, the plates were swirled in clockwise and counterclockwise motions and front and back and side to side five times to ensure even mixing of the chemicals. Larval mortality was recorded 24 h after treatment. Larvae that showed no movement in the well after manual disturbance of the water were recorded as dead. A series of five concentrations ranging between 125 and 1.95 ppm were used in each treatment to obtain a range of mortality. Treatments were replicated 10 times for each essential oil.

Statistical Analyses. Proportion not biting was calculated as described by Ali et al.[34] As the K&D module bioassay system can handle only four treatments along with negative and positive controls, in order to make direct comparisons among more than four treatments and to compensate for variation in overall response among replicates, biting-deterrent activity was quantified as biting deterrence index (BDI). The BDIs were calculated using the formula

$$[\mathrm{BDI}_{i,j,k}] = \left[\frac{\mathrm{PNB}_{i,j,k} - \mathrm{PNB}_{c,j,k}}{\mathrm{PNB}_{d,j,k} - \mathrm{PNB}_{c,j,k}}\right]$$

where $\mathrm{PNB}_{i,j,k}$ denotes the proportion of females not biting when exposed to test compound *i* for replication *j* and day *k* (*i* = 1–4, *j* = 1–5, *k* = 1–2), $\mathrm{PNB}_{c,j,k}$ denotes the proportion of females not biting the solvent control "*c*" for replication *j* and day *k* (*j* = 1–5, *k* = 1–2), and $\mathrm{PNB}_{d,j,k}$ denotes the proportion of females not biting in response to DEET "*d*"(positive control) for replication *j* and day *k* (*j* = 1–5, *k* = 1–2). This formula makes an adjustment for interday variation in response and incorporates information from the solvent control as well as the positive control.

A BDI value of 0 indicates an effect similar to that of ethanol, whereas a value significantly greater than 0 indicates biting-deterrent effect relative to that of ethanol. BDI values not significantly different from 1 are statistically similar to DEET. BDI values were analyzed using the ANOVA procedure of SAS [single factor: test compound (fixed)] (SAS Institute, 2007), and means were separated using the Ryan–Einot–Gabriel–Welsch multiple-range test. To determine whether confidence intervals included the values of 0 or 1 for treatments, Scheffe's multiple-comparison procedure was used with the CLM option in SAS. LC_{50} values for larvicidal data were calculated by using the PROBIT procedure of SAS. Control mortality was corrected by using Abbott's formula.[36]

RESULTS AND DISCUSSION

The composition of four *Salvia* species was investigated in the present study. Identified compounds ranged between 90 and 99% (Table 1). *S. apiana* essential oil contained 1,8-cineole

DOI: 10.1021/jf504976f
J. Agric. Food Chem. 2015, 63, 447–456

(71.7%) as a major constituent followed by monoterpene hydrocarbons α-pinene (5.1%), camphor (4.4%), and β-pinene (3.8%). *S. elegans* essential oil had high content of borneol (17.4%), β-eudesmol (10.4%), bornyl acetate (5%), and guaiol (4.8%). Major constituents of *S. leucantha* oil were bornyl acetate (11.4%), caryophyllene oxide (13.5%), β-caryophyllene (6.5%), and spathulenol (7.0%). *S. officinalis* oil was rich in monoterpene hydrocarbon α-thujene (25.8%) and had high content of oxygenated sesquiterpene viridiflorol (20.4%).

Many studies have reported the composition of essential oils of these *Salvia* species. Chemical composition data on the essential oil of *S. apiana* showed 1,8-cineole as a major compound.[37,38] Mathew and Thoppil[27] reported spathulenol (38.73%) and β-caryophyllene (10.32%) as the major compounds of the *S. elegans* essential oil in samples extracted from the plant material collected from Ooth, southern India. Data on *S. elegans* essential oil differ from the above study where spathulenol (1.3%) is a minor compound and β-caryophyllene is totally absent. On the other hand, the *S. elegans* essential oil obtained from the cultivated species from Eboli, Italy, contained *cis*-thujone (38.7%), δ-cadinene (11.5%), geranyl acetate (6.9%), and geraniol (6.5%).[39] Data on the composition of *S. leucantha* essential oil corroborate the findings of Rondon et al.[40] Negi et al.,[41] and Upadhyaya et al.,[42,43] who reported bornyl acetate as the major compound followed by sesquiterpene hydrocarbons such as β-caryophyllene, α-guaiene, β-gurjunene, *cis*-muurola-3,5-diene, germacrene D, and bicyclogermacrene. In earlier investigations of the *Salvia* essential oils, we studied *S. leucantha* volatiles obtained by microdistillation technique, which showed limonene (34.6%), α-pinene (16.7%), and borneol (16.5%) as the major compounds, whereas β-caryophyllene (5.6%) and caryophyllene oxide (5.4%) were the major sesquiterpenes with low content of oxygened monterpenene bornyl acetate (0.1%).[44] These differences in chemical composition could be due to distillation technique used or growing conditions of the plants. The essential oil of *S. officinalis* was characterized by α-thujone (25.8%), β-thujone (5.7%), camphor (6.4%), and 1,8-cineole (4.4%) as major components, which also determine their chemotypes. The presence of thujone isomers in the essential oils is important because of their neurotoxic and hepatotoxic effects.[45] Thujone is banned as a food additive in the United States and Europe. The most common consumption of thujone is in dietary supplements such as sage-flavored products, teas, and drops and alcoholic beverages.[46] Oelschlagel at al.[46] found that *S. officinalis* 'Extrakta' contained the highest levels of α-thujone. They also reported low α-thujone in the essential oils of *S. officinalis* subsp. *major*, *S. officinalis* 'Berggarten', and *S. officinalis* 'Aurea'. In the present study, the 'Extrakta' variety of *S. officinalis* essential oil showed a high percentage (25.8%) of α-thujone and therefore cannot be recommended for use in the production of sage supplements. During the GC-MS analysis, the peak at RRI 2679 of the *S. officinalis* oil was not identified by the in-house "Baser Library of Essential Oil Constituents"; however, its mass spectrum was similar to that of 13-*epi*-manool according to the Wiley GC/MS Library and MassFinder 3 Library. To ensure its identity, this compound was isolated and characterized by 1D and 2D NMR spectroscopic data analyses (Figure 1). The chemical shift of H-17a (δ 4.50 for 13-*epi*-manool and δ 4.46 for manool) is the key to distinguish 13*S* and 13*R* isomers.[48] In our case, the ^{1}H NMR chemical shift of H-17a was observed at δ 4.49 and could be concluded for 13-*epi*-manool. Moreover, the specific rotation that we found in this study {$[\alpha]_D^{25}$ = +59.2 (*c* 1.0, $CHCl_3$)} also supported the identity as 13-*epi*-manool {$[\alpha]_D^{24}$ = +28 (*c* 1.5, $CHCl_3$ for manool.[49]

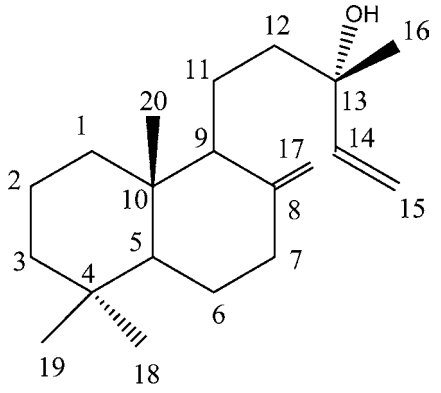

13-*epi*-manool

Figure 1. Structure of 13-*epi*-manool.

The in vitro K&D system used in this study specifically quantified the mosquito biting-deterrent properties of *Salvia* essential oils and the pure compounds. Essential oils of *S. leucantha* (BDI value = 1.01) and *S. elegans* (BDI value = 0.87) showed biting-deterrent activity similar to that of DEET, whereas the activity of essential oils of *S. officinalis* (BDI value = 0.63) and *S. apiana* (BDI value = 0.48) demonstrated low biting-deterrent activity against *Ae. aegypti* (Figure 2). The major compounds of the active oils *S. elegans* and *S. leucantha* were individually investigated. Among the pure compounds, (+)-β-eudesmol (BDI value = 0.81) and (−)-guaiol (BDI value = 0.82) showed the highest biting-deterrent activity, which was similar to that of DEET at 25 nmol/cm^2, whereas the activities of (−)-borneol (BDI value = 0.69) and (−)-borneol acetate (BDI value = 0.52) were significantly lower than that of DEET. The sesquiterpenes (−)-β-caryophyllene, (−)-caryophyllene oxide, and (+)-spathulenol were high in *S. leucantha* oil, and we previously reported their biting-deterrent activity with BDI values of 0.54 and 0.66 against *Ae. aegypti*, respectively.[50] Spathulenol has been reported to show good biting-deterrent activity against *Ae. aegypti* and *An. stepheni*,[51] and similar response of high biting-deterrent activity was observed in our laboratory against *Ae. aegypti* (A. Ali, unpublished data). The oxygenated diterpene 13-*epi*-manool was also investigated for mosquito activity in a search of new mosquito-deterrent agents. The biting-deterrent activity of (+)-13-*epi*-manool (BDI = 0.75) was lower than that of (+)-β-eudesmol and (−)-guaiol against *Ae. aegypti*. In *An. quadrimaculatus*, essential oils of *S. elegans* (BDI value = 0.9) and *S. leucantha* (BDI value = 0.86) also showed higher biting-deterrent activity that was similar to that of DEET, whereas the activities of essential oils of *S. officinalis* (BDI value = 0.6) and *S. apiana* (BDI value = 0.56) were lower than that of DEET (Figure 3). Pure compounds (+)-β-eudesmol (BDI value = 0.82) and (−)-guaiol (BDI value = 0.82) showed activity similar to that of DEET at 25 nmol/cm^2. (+)-13-*epi*-Manool demonstrated higher biting-deterrent activity than (−)-caryophyllene oxide, (−)-borneol, (−)-bornyl acetate, and (−)-β-caryophyllene; however, its activity was significantly lower than those of (+)-β-eudesmol, (−)-guaiol, or DEET in both species.

Previous research papers show repellent activity of essential oils of various *Salvia* species against different species of

DOI: 10.1021/jf504976f
J. Agric. Food Chem. 2015, 63, 447−456

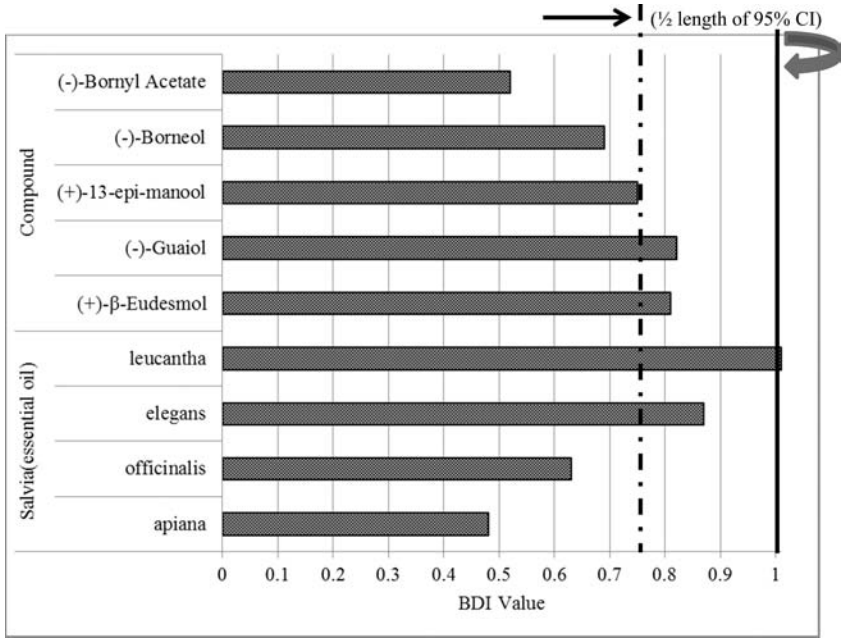

Figure 2. Biting-deterrent index (BDI) values of the essential oils extracted from samples of aerial parts of four species of *Salvia* and individual compounds against female *Ae. aegypti*. Essential oils were tested at 10 $\mu g/cm^2$ and the pure compounds were tested at 25 nmol/cm^2. Ethanol was the solvent control, and DEET at 25 nmol/cm^2 was used as positive control.

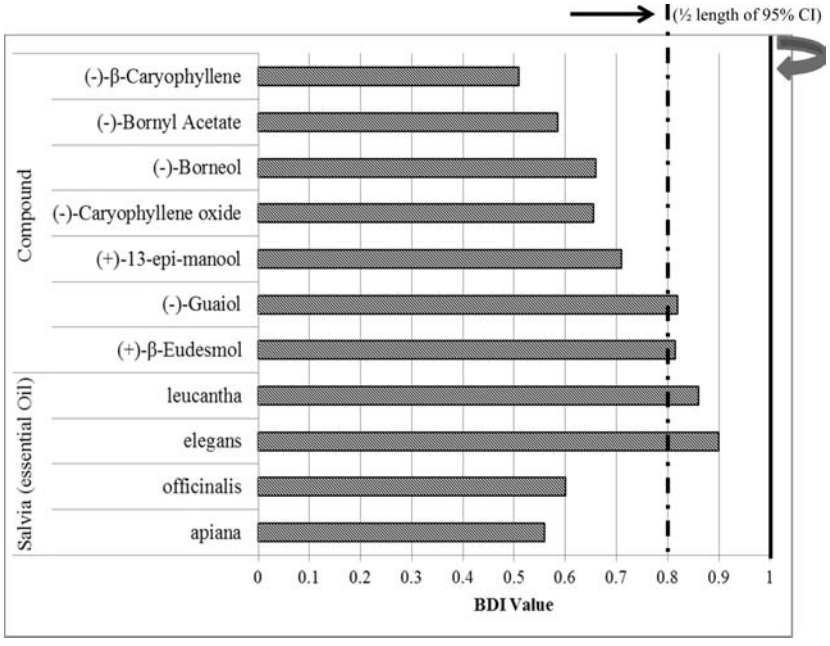

Figure 3. Biting-deterrent index (BDI) values of the essential oils extracted from samples of aerial parts of four species of *Salvia* and individual compounds against female *Anophelese quadrimaculatus*. Essential oils were tested at 10 $\mu g/cm^2$, and the pure compounds were tested at 25 nmol/cm^2. Ethanol was the solvent control, and DEET at 25 nmol/cm^2 was used as positive control.

mosquitoes. Conti et al.[26] reported that essential oils of *S. dorisiana*, *S. longifolia*, and *S. sclarea* have significant but variable repellent activity against *Ae. albopictus*. Essential oils of *S. dorisiana* with protection efficacy of 91−95% and protection times of 9.2 to 92.4 min were most active, whereas protection times of essential oils of *S. longifolia* and *S. sclarea* ranged between 3.2 and 60 min and between 3.6 and 64.2 min, respectively.[26] Amer and Melhorn[25] reported good repellent activity of essential oils of *S. sclarea* against mosquito species of *Ae. aegypti*, *An. stephensi*, and *Culex quinquefasciatus*. Kang et al.[52] showed low activity of essential oil of *S. officinalis* against *Culex pipens pallens* Cosquillett.

Ali et al.[50] reported significantly lower activity of (−)-*β*-caryophyllene and (−)-caryophyllene oxide than that of DEET against *Ae. aegypti*. Data of biting-deterrent activity of these compounds show a similar trend against *An. quadrimaculatus*. These data corroborate the finding of Paluch et al.,[53] who reported high repellent activity of (+)-*β*-eudesmol against *Ae. aegypti*.

DOI: 10.1021/jf504976f
J. Agric. Food Chem. 2015, 63, 447−456

Table 2. Toxicity of *Salvia* Species Essential Oils against 1-Day-Old Larvae of *Aedes aegypti* and *Anopheles quadrimaculatus* at 24 h after Treatment

	Aedes aegypti				*Anopheles quadrimaculatus*			
essential oil	LC_{50}, ppm (95% CI)[a]	LC_{90}, ppm (95% CI)	χ^2	df[b]	LC_{50}, ppm (95% CI)	LC_{90}, ppm (95% CI)	χ^2	df
S. *apiana*	NA*[c]	NA*			NA*	NA*		
S. *leucantha*	29.5 (26.1−33.1)	51.8 (44.5−64.6)	63.6	38	6.2 (5.3−7.2)	15.8 (12.8−21.1)	92.8	48
S. *elegans*	14.4 (12.7−16.3)	27.2 (23.1−34.3)	71.8	48	10.9 (9.4−12.8)	29.1 (23.0−40.4)	91.7	48
S. *officinalis*	56.9 (51.0−63.5)	92.4 (80.2−114.4)	57.9	38	14.1 (12.1−16.6)	35.8 (28.2−50.7)	77.9	48
(−)-borneol	NA**	NA**			NT**[d]	NT**		
(−)-bornyl acetate	NA**	NA**			NT**	NT**		
(−)-guaiol	NA**	NA**			NT**	NT**		
(+)-β-eudesmol	NA**	NA**			NT**	NT**		
(−)-β-caryophyllene	26.0 (22.5−30.3)[e]	64.8 (52.7−86.3)	95.7	48	NT**	NT**		
(−)-caryophyllene oxide	29.8 (25.7−34.7)[e]	74.1 (59.9−99.4)	95.6	48	NT**	NT**		
(+)-13-epi-manool	NA**	NA**			NT**	NT**		

[a]95% confidence interval. [b]df refers to degree of freedom. [c]NA (not active), showed <50% mortality at the highest screening dose of 125* ppm for essential oil and 100** ppm for pure compounds. [d]NT (not tested), ** compounds were not tested against *An. quadrimaculatus*. [e]Data from Ali et al.[47]

In larval screening bioassay, all of the essential oils showed larvicidal activity except *S. apiana*, which was inactive at the highest tested dose of 125 ppm against both mosquito species. Essential oil of *S. elegans* with LC_{50} and LC_{90} values of 14.4 and 27.2 ppm, respectively, showed the highest toxicity followed by the *S. leucantha* essential oil with LC_{50} and LC_{90} values of 29.5 and 51.8 ppm, respectively, against *Ae. aegypti* (Table 2). The toxicity of *S. officinalis* essential oil with LC_{50} and LC_{90} values of 56.9 and 92.4 ppm, respectively, was significantly lower than that of *S. leucantha* or *S. elegans* essential oils. In *An. quadrimaculatus*, essential oil of *S. leucantha* with LC_{50} and LC_{90} values of 6.2 and 15.8 ppm, respectively, showed the highest toxicity, which was significantly higher than those of *S. elegans* and *S. officinalis* essential oils (Table 2). The toxicity of *S. elegans* and *S. officinalis* essential oils was similar. In general, mortality was higher for *An. quadrimaculatus* with all of the oils tested than for *Ae. aegypti*. Of the tested pure compounds, only (−)-β-caryophyllene and (−)-caryophyllene oxide showed larvicidal acyivity with LD_{50} values of 26.0 and 29.8 ppm, respectively, against *Ae. aegypti*.[48] All other pure compounds tested in this study (borneol, bornyl acetate, guaiol, β-eudesmol, and 13-*epi*-manool) showed very weak or no activity at the highest dose of 100 ppm in the larvicidal screening bioassays against *Ae. aegypti* and *An. quadrimaculatus* larvae. Therefore, LD_{50} values were not calculated. The LD_{50} value of permethrin, which was used as positive control, was 0.0034 ppm.

Several studies have evaluated the toxicity of essential oils from various species of *Salvia* against mosquito larvae. Mathew and Thoppil[27] reported larvicidal toxicity of essential oils from aerial parts of *S. elegans*, *S. dorisiana*, *S. splendens* 'Blue Ribbon', and *S. splendens* 'Scarlet Sage Red' against larvae of *Ae. albopictus*. Essential oils of *S. elegans* and *S. splendens* 'Blue Ribbon' with LC_{50} values of 46.4 and 59.2 ppm, respectively, showed higher toxicity than *S. dorisiana* and *S. splendens* 'Scarlet Sage Red'. The essential oil of *S. dorisiana* showed insignificant toxicity against 4-day-old larvae of *Ae. albopictus*,[26] whereas the ethanol extract of *S. dorisiana* showed toxicity against the fourth-instar larvae of *C. pipiens* L. (LC_{50} = 62.7 ppm).[54] Pavela[55] reported larvicidal activity of essential oils from six species of *Salvia* against *C. quinquefasciatus* Say larvae. In addition, *S. sclarea* and *S. officinalis* essential oils showed larvicidal activity against *Spodoptera littoralis* Boisduval in both topical and fumigation trials,[56] whereas in topical and fumigation trials *S. officinalis* essential oil showed toxicity against *Musca domestica* L. adults.[57] Guaiol is reported to show larvicidal activity against larvae of *Mythimna separata* and *Plutella xylostella* and fumigant activity against larvae of *My. separata* and adult *Mu. domestica*.[58] However, this is the first report of larvicidal activity of guaiol against mosquitoes, and very low activity was found.

In conclusion, essential oils of *S. leucantha* and *S. elegans* showed biting-deterrent activity similar to that of DEET in both species of mosquitoes. *S. leucantha*, *S. elegans*, *S. officinalis*, and *S. apiana* essential oils contained 65.4, 38.5, 30.8, and 3.3% sesquiterpenes, respectively. Essential oils of *S. leucantha* and *S. elegans* were rich in sesquiterpenes. The biting-deterrent activity of these essential oils appears to follow the pattern of various sesquiterpene levels present in the individual oils. Essential oils of *S. leucantha* and *S. elegans*, with their high levels of sesquiterpenes, showed biting-deterrent activity similar to that of DEET. This is the first report on biting-deterrent activity of these oils against mosquitoes. Results indicate that essential oils of *S. leucantha* and *S. elegans* can be useful for preventing mosquito bites because of their demonstrated activity and, in general, most essential oils are considered to be minimum risk products. The diterpene 13-*epi*-manool was investigated for the first time against mosquitoes. The pure compounds β-eudesmol and guaiol show promise for development as mosquito deterrents. Essential oils of *S. leucantha*, *S. elegans*, and *S. officinalis* also showed larvicidal activity against both species of mosquitoes. Essential oils of these *Salvia* species are an important source of compounds that can be useful in developing selective, biodegradable, and naturally produced mosquito deterrents. However, further research is needed to identify activity of individual sesquiterpenes present in these oils and in mixtures of these sesquiterpenes to develop formulations for use as mosquito biting deterrents.

■ ASSOCIATED CONTENT

Supporting Information

Additional figures. This material is available free of charge via the Internet at http://pubs.acs.org.

DOI: 10.1021/jf504976f
J. Agric. Food Chem. 2015, 63, 447−456

AUTHOR INFORMATION

Corresponding Author

*(A.A.) E-mail: aali@olemiss.edu. Fax: (662) 915-6554.

Funding

This study was supported in part by USDA/ARS Grant 56-6402-1-612, Deployed War-Fighter Protection Research Program Grant, funded by the U.S. Department of Defense through the Armed Forces Pest Management Board, and a Special Research Initiative grant from the Mississippi Agricultural and Forestry Experiment Station.

Notes

The authors declare no competing financial interest.

ACKNOWLEDGMENTS

We thank Dr. James J. Becnel, USDA-ARS, Gainesville, FL, USA, for supplying mosquito eggs.

REFERENCES

(1) Becker, N. *Mosquitoes and Their Control*; Kluwer Academic/Plenum Publishers: New York, 2013.

(2) Roberts, D. R.; Andre, R. G. Insecticide resistance issues in vectors. *Am. J. Trop. Med. Hyg.* **1994**, *50* (Suppl.), 21−34.

(3) Isman, M. B. Botanical insecticides, deterrents, and repellents in modern agriculture and an increasingly regulated world. *Annu.. Rev. Entomol.* **2006**, *51*, 45−66.

(4) Jantan, I.; Yalvema, M. F.; Ahmad, N. W.; Jamal, J. A. Insecticidal activities of the leaf oils of eight *Cinnamomum* species against *Aedes aegypti* and *Aedes albopictus*. *Pharm. Biol.* **2005**, *43*, 526−532.

(5) Morais, S. M.; Facundo, V. A.; Bertini, L. M.; Cavalcanti, B. E. S.; Francisco, J. A.; Ferreira, S. A.; Brito, E. S.; Manoel, S. N. A. Chemical composition and larvicidal activity of essential oils from *Piper* species. *Biochem. Syst. Ecol.* **2007**, *35*, 670−675.

(6) Cheng, S. S.; Huang, C. G.; Chen, W. J.; Kuo, Y. H.; Chang, S. T. Larvicidal activity of tectoquinone isolated from red heartwood-type *Cryptomeria japonica* against two mosquito species. *Bioresour. Technol.* **2008**, *99*, 3617−3622.

(7) Silva, W. J.; Doria, G. A. A.; Maia, R. T.; Nunes, R. S.; Carvalho, G. A.; Blank, A. F.; Alves, P. B.; Marçal, R. M.; Cavalcanti, S. C. H. Effects of essential oils on *Aedes aegypti* larvae: alternatives to environmentally safe insecticides. *Bioresour. Technol.* **2008**, *99*, 3251−3255.

(8) Bailey, L. H.; Bailey, E. Z. Staff of L. H. Bailey Hortorium. *Hortus Third: A Concise Dictionary of Plants Cultivated in the United States and Canada*; Macmillan: New York, 1976.

(9) Tabanca, N.; Demirci, B.; Baser, K. H. C.; Aytac, Z.; Ekici, M.; Khan, I.; Jacob, M. R.; Wedge, D. E. Chemical composition and antifungal activity of *Salvia macrochlamys* and *Salvia recognita* essential oils. *J. Agric. Food Chem.* **2006**, *54*, 6593−6597.

(10) Kelen, M.; Tepe, B. Chemical composition, antioxidant and antimicrobial properties of the essential oils of three *Salvia* species from Turkish flora. *Bioresour. Technol.* **2005**, *99*, 4096−4104.

(11) Ozek, G.; Demirci, F.; Ozek, T.; Tabanca, N.; Wedge, D. E.; Khan, I.; Baser, K. H. C.; Duran, A.; Hamzaoglu, E. Gas chromatographic-mass spectrometric analysis of volatiles obtained by four different techniques from *Salvia rosifolia* Sm., and evaluation for biological activity. *J. Chromatogr.* **2010**, *1217*, 741−748.

(12) Dweck, A. C. The folklore and cosmetic use of various *Salvia* species. In *Sage: The Genus Salvia*; Kintzios, S. E., Ed.; Harwood Academic Publishers: Amsterdam, The Netherlands, 2005; pp 1−25.

(13) Tepe, B.; Eminagaoglu, O.; Akpulat, H. A.; Aydin, E. Antioxidant potentials and rosmarinic acid levels of the methanolic extracts of *Salvia verticillata* (L.) subsp. *verticillata* and *Salvia verticillata* (L.) subsp. *amasiaca* (Freyn & Bornm.). *Food Chem.* **2007**, *100*, 985−989.

(14) *Könemann. Botanica: The Illustrated A-Z. of Over 10,000 Garden Plants and How to Cultivate Them*; Gordon Cheers Publication: Hong Kong, 1999; pp 51−53.

(15) Rizk, A.; El-Ghazaly, G. *Medicinal and Poisonous Plants of Qatar*; Science and Applied Research Centre, University of Qatar, 1995; pp 140−141.

(16) Kosar, M.; Damien-Dorman, H. J.; Baser, K. H. C.; Hiltunen, R. *Salvia officinalis* L.: composition and antioxidant-related activities of a crude extract and selected sub-fractions. *Nat. Prod. Commun.* **2010**, *5*, 1453−1456.

(17) Bornstein, C.; Fross, D.; O'Brien, B. *California Native Plants for the Garden*; Cachuma Press: Los Olivos, CA, USA, 2005.

(18) Clebsch, B. *The New Book of Salvias: Sages for Every Garden*; Timber Press: Portland, OR, USA, 2003.

(19) Moerman, D. E. *Native American Ethnobotany*; Timber Press: Portland, OR, USA, 1998.

(20) Facciola, S. *Cornucopia II: A Source Book of Edible Plants*, 2nd ed.; Kampong Publications: Vista, CA, USA, 1998.

(21) Bryant, G.; Rodd, T. *Annuals and Perennials: A Gardener's Encyclopedia*; Firefly Books: Buffalo, NY, USA, 2011.

(22) Dufresne, R. F. *Why Salvias?*; Dufresne: Greensboro, NC, USA, 1997.

(23) Duke, J. A. *Handbook of Medicinal Herbs*, 2nd ed.; CRC Press: Boca Raton, FL, USA, 2002.

(24) van Wyk, B.; Wink, M. *Medicinal Plants of the World*; Timber Press: Portland, OR, USA, 2004.

(25) Amer, A.; Mehlhorn, H. Repellency effect of forty-one essential oils against *Aedes Anopheles* and *Culex* mosquitoes. *Parasitol. Res.* **2006**, *99*, 478−490.

(26) Conti, B.; Benelli, G.; Leonardi, M.; Afifi, F. U.; Cervelli, C.; Profeti, R.; Pistelli, L.; Canale, A. Repellent effect of *Salvia dorisiana, S. longifolia,* and *S. sclarea* (Lamiaceae) essential oils against the mosquito *Aedes albopictus* Skuse (Diptera: Culicidae). *Parasitol. Res.* **2012**, *111*, 291−299.

(27) Mathew, J.; Thoppil, J. E. Chemical composition and mosquito larvicidal activities of *Salvia* essential oils. *Pharm. Biol.* **2011**, *49*, 456−463.

(28) Curvers, J.; Rijks, J.; Cramers, C.; Knauss, K.; Larson, P. Temperature programmed retention indexes: calculation from isothermal data. Part 1, Theory. *J. High Resolut. Chromatogr.* **1985**, *8*, 607−610.

(29) McLafferty, F. W.; Stauffer, D. B. *The Wiley/NBS Registry of Mass Spectral Data*; Wiley: New York, 1989.

(30) Joulain, D.; König, W. A. *The Atlas of Spectra Data of Sesquiterpene Hydrocarbons*; EB-Verlag: Hamburg, Germany, 1998.

(31) ESO. *The Complete Database of Essential Oils*; Boelens Aroma Chemical Information Service: The Netherlands, 2000.

(32) König, W. A.; Joulain, D.; Hochmuth, D. H. Terpenoids and related constituents of essential oils. MassFinder 3. In *Convenient and Rapid Analysis of GCMS*; Hochmuth, D. H., Ed.; Hamburg, Germany, 2004.

(33) Klun, J. A.; Kramer, M.; Debboun, M. A new *in vitro* bioassay system for discovery of novel human-use mosquito repellents. *J. Am. Mosq. Control Assoc.* **2005**, *21*, 64−70.

(34) Ali, A.; Cantrell, C. L.; Bernier, U. R.; Duke, S. O.; Schneider, J. C.; Khan, I. *Aedes aegypti* (Diptera: Culicidae) biting deterrence: structure-activity relationship of saturated and unsaturated fatty acids. *J. Med. Entomol.* **2012**, *49*, 1370−1378.

(35) Pridgeon, J. W.; Becnel, J. J.; Clark, G. G.; Linthicum, K. J. A high-throughput screening method to identify potential pesticides for mosquito control. *J. Med. Entomol.* **2009**, *46*, 335−341.

(36) Abbott, W. S. A method of computing the effectiveness of an insecticide. *J. Econ. Entomol.* **1925**, *18*, 265−267.

(37) Borek, T. T.; Hochrien, J. M.; Irwin, A. N. Composition of the essential oil of white sage *Salvia apiana*. *Flavour Fragrance J.* **2006**, *21*, 571−572.

(38) Takeoka, G. R.; Hobbs, C.; Park, B. S. Volatile constituents of the aerial parts of *Salvia apiana* Jepson. *J. Essent. Oil Res.* **2010**, *22*, 241−244.

DOI: 10.1021/jf504976f
J. Agric. Food Chem. 2015, 63, 447−456

(39) De Martino, L.; Roscigno, G.; Mancini, E.; De Falco, E.; De Feo, V. Chemical composition and antigerminative activity of the essential oils from five *Salvia* species. *Molecules* **2010**, *15*, 735−746.
(40) Rondon, M.; Velasco, J.; Morales, A.; Rojas, J.; Carmona, J.; Gualtieri, M.; Hernandez, V. Composition and antibacterial activity of the essential oil of *Salvia leucantha* Cav. cultivated in Venezuela Andes. *Rev. Latinoam. Quim.* **2005**, *33*, 40−44.
(41) Negi, A.; Javed, M. S.; Melkani, A. B.; Dev, V.; Beauchamp, P. S. Steam volatile terpenoids from *Salvia leucantha*. *J. Essent. Oil Res.* **2007**, *19*, 463−465.
(42) Upadhyaya, K.; Dixit, V. K.; Padalia, R. C.; Mathela, C. S. Terpenoid composition and antioxidant activity of essential oil from leaves of *Salvia leucantha* Cav. *J. Essent. Oil Bearing Plants* **2009**, *12*, 551−556.
(43) Rojas, L. B.; Visbal, T.; Morillo, M.; De Rojas, Y. C.; Arzola, J. C.; Usubillaga, A. The volatile constituents of *Salvia leucantha*. *Nat. Prod. Commun.* **2010**, *5*, 937−938.
(44) Tabanca, N.; Demirci, B.; Turner, J. L.; Pounders, C.; Demirci, F.; Baser, K. H. C.; Wedge, D. E. Microdistillation and analysis of volatiles from eight ornamental *Salvia* taxa. *Nat. Prod. Commun.* **2010**, *5*, 1421−1426.
(45) Pinto, E.; Salguerio, L. R.; Cavaleiro, C.; Palmeira, A.; Goncalves, M. J. In vitro susceptibility of some species of yeast and filamentous fungi to essential oils of *Salvia officinalis*. *Ind. Crops Prod.* **2007**, *26*, 135−141.
(46) Waidyanatha, S.; Johnson, J. D.; Hong, S. P.; Robinson, V. G.; Gibbs, S.; Graves, S. W.; Hooth, M. J.; Smith, C. S. Toxicokinetics of α-thujone following intravenous and gavage administration of α-thujone or α- and β-thujone mixture in male and female F344/N rats and B6C3F1 mice. *Toxicol. Appl. Pharmacol.* **2013**, *271*, 216−228.
(47) Oelschlagel, S.; Quass, S.; Speer, K. The essential oil content and composition of selected *Salvia* species, sage teas and sage drops. *J. Food Sci. Eng.* **2012**, *2*, 427−436.
(48) Barrero, A. F.; Sanchez, J. F.; Alvarez-Manzaneda, E. J.; Munoz, D. M.; Haidour, A. Terpenoids and sterols from the wood of *Abies pinsapo*. *Phytochemistry* **1995**, *39*, 163−165.
(49) Villamizar, J. E.; Gamez, C.; Alcala, A.; Salazar, F.; Tropper, E.; Angarita, A.; Canus, N. Facile and simple synthesis of ring C aromatic diterpenes: synthesis of (+)-13-hydroxypodcarpa-8,11,13-triene and (+)-7-deoxynimbidiol. *Synth. Commun.* **2011**, *41*, 1733−1741.
(50) Ali, A.; Tabanca, N.; Kurkcuoglu, M.; Duran, A.; Blythe, E. K.; Khan, I. A.; Baser, K. H. C. Chemical composition, larvicidal and biting deterrent activity of essential oils of two subspecies of *Tanacetum argenteum* (Lam.) Willd and individual constituents against *Aedes aegypti* (L) (Diptera: Culicidae). *J. Med. Entomol.* **2014**, *51*, 824−830.
(51) Cantrell, C. L.; Klun, J. A.; Bryson, C. T.; Kobaisy, M.; Duke, S. O. Isolation and identification of mosquito bite deterrent terpenoids from leaves of American (*Callicarpa americana*) and Japanese (*Callicarpa japonica*) beautyberry. *J. Agric. Food Chem.* **2005**, *53*, 5948−5953.
(52) Kang, S. H.; Kim, M. K.; Seo, D. K.; Noh, D. J.; Yang, J. O.; Yoon, C.; Kim, G. H. Comparative repellency of essential oils against *Culex pipiens pallens* (Diptera: Culicidae). *J. Korean Soc. Appl. Biol. Chem.* **2009**, *52*, 353−359.
(53) Paluch, G.; Grodnitzky, J.; Bartholomay, L.; Coats, J. Quantitative structure-activity relationship of botanical sesquiterpenes: Spatial and contact repellency to the yellow fever mosquito *Aedes aegypti*. *J. Agric. Food Chem.* **2009**, *57*, 7618−7625.
(54) Cetin, H.; Cinbilgel, I.; Yanikoglu, A.; Gokceoglu, M. Larvicidal activity of some Labiatae (Lamiaceae) plant extracts from Turkey. *Phytother. Res.* **2006**, *20*, 1088−1090.
(55) Pavela, R. Larvicidal effects of various Euro-Asiatic plants against *Culex quinquefasciatus* Say larvae (Diptera: Culicidae). *Parasitol. Res.* **2008**, *102*, 555−559.
(56) Pavela, R. Insecticidal activity of some essential oils against larvae of *Spodoptera littoralis*. *Fitoterapia* **2005**, *76*, 691−696.
(57) Pavela, R. Insecticidal properties of several essential oils on the house fly (*Musca domestica* L.). *Phytother. Res.* **2008**, *22*, 274−78.
(58) Liu, T.; Wang, C.; Xie, H.; Mu, Q. Guaiol − a naturally occurring insecticidal sesquiterpene. *Nat. Prod. Comm.* **2013**, *8*, 1353−1354.

DOI: 10.1021/jf504976f
J. Agric. Food Chem. 2015, 63, 447−456

JOURNAL OF AGRICULTURAL AND FOOD CHEMISTRY

Article

pubs.acs.org/JAFC

HPLC-SPE-NMR Characterization of Major Metabolites in *Salvia fruticosa* Mill. Extract with Antifungal Potential: Relevance of Carnosic Acid, Carnosol, and Hispidulin

Vassiliki Exarchou,[†] Loukas Kanetis,[§] Zenovia Charalambous,[§] Sandra Apers,[†] Luc Pieters,[†] Vassilis Gekas,[§] and Vlasios Goulas*[,§]

[†]Laboratory of Natural Products and Food Research and Analysis (NatuRA), Department of Pharmaceutical Sciences, University of Antwerp, Universiteitsplein 1, 2610 Antwerp, Belgium

[§]Department of Agricultural Sciences, Biotechnology and Food Science, Cyprus University of Technology, 3603 Lemesos, Cyprus

ABSTRACT: Plant pathogenic fungi are considered of significant economic importance for adversely affecting both quantitatively and qualitatively fresh and processed produce. Extracts of *Salvia fruticosa* were initially screened for their antifungal activity, and the ethyl acetate fraction, being the most active, was further analyzed using HPLC-SPE-NMR hyphenation. The methoxylated flavones hispidulin, salvigenin, and cirsimaritin and the diterpenes carnosic acid, carnosol, and 12-methoxycarnosic acid were identified as the major components of the extract. In addition, the concentration levels of all identified components were determined using q-NMR. The antifungal activity of the crude extract and selected phytochemicals was estimated against the fungal species *Aspergillus tubingensis*, *Botrytis cinerea*, and *Penicillium digitatum*. The estimated MIC and MFC values of the ethyl acetate extract of *S. fruticosa*, as well as three of its major constituents, carnosic acid, carnosol, and hispidulin, support their antifungal activity, especially against *B. cinerea* and *P. digitatum*, suggesting their potential use in food and agricultural systems.

KEYWORDS: *Aspergillus tubingensis, Botrytis cinerea, diterpenes, flavonoids, Greek sage, Penicillium digitatum, phytochemicals, q-NMR*

INTRODUCTION

The genus *Salvia* is one of the largest genera in the Lamiaceae family. It comprises approximately 900 species that grow throughout the world, some of which are economically important considering their extensive use as spices, flavoring agents, and herbal drugs.[1,2] Ethnopharmacological studies reported that *Salvia* species have been used for more than 60 different ailments ranging from aches to epilepsy and mainly to treat colds, bronchitis, tuberculosis, hemorrhage, and menstrual disorders.[3] *Salvia officinalis* L. (sage), *Salvia miltiorrhiza* (red sage), *Salvia divinorum*, and *Salvia fruticosa* (Greek sage) are the most well-known and studied *Salvia* species.[3−6]

S. fruticosa is cultivated and/or grows wild in macquis and phrygana ecosystems in the Mediterranean basin.[4] Traditionally, aerial parts of *S. fruticosa* were used to treat many diseases such as malaria, fever, pneumonia, gastrointestinal tract disorders, cholera, plague, and common cold.[7] Numerous studies have revealed several physiological responses to *S. fruticosa*, which may be relevant to the promotion of health and the prevention or treatment of some chronic diseases. Antiproliferative activity against cancer cells,[8] cholinesterase inhibitory activity,[9] protection from oxidative damage of DNA,[10] and anti-inflammatory[11] and antimicrobial activities[1,2] of *S. fruticosa* have been highlighted. Furthermore, research has manifested the inhibitory effect of *S. fruticosa* against plant pathogenic fungi, such as *Aspergillus terreus*, *Fusarium oxysporum*, *Penicillium expansum*, *Verticillium dahliae*, *Botrytis cinerea*, *Alternaria solani*, *Rhizoctonia solani*, and *Sclerotinia sclerotiorum*. It is noteworthy that the antifungal potency of *S. fruticosa* has been mainly focused toward the efficacy of its essential oils, whereas their polar extracts have not been studied yet.[12−15]

Salvia species are known to be rich in a number of natural products such as essential oils, diterpenoids, triterpenoids, and flavonoids.[16] Phytochemical studies showed that *S. fruticosa* extracts are complex mixtures of diterpenes, phenolic acids, and flavonoids, but their phytochemical composition has not been studied thoroughly yet. Previous works on *Salvia* focused on targeted phytochemicals, using mainly chromatographic techniques highlighting the characteristic presence of carnosic acid, carnosol, and flavonoids.[17−21]

Direct crop losses caused by plant pathogenic fungi, as well as indirect product deterioration imposed by such contaminants, pose significant health and economic problems. In the agricultural sector, an array of approaches is employed to encounter the causal agents, with the use of conventional fungicides as the core component. However, concerns about environmental and human health risks associated with fungicide residues, in addition to issues regarding fungicide resistance due to their overuse, emphasize an increasing need to find and implement an alternative to synthetic fungicides approach, such as biofungicides.[22] Natural products, crude or isolated from aromatic and medicinal plants, can be envisaged as new antifungal ingredients.

Received: October 20, 2014
Revised: December 19, 2014
Accepted: December 23, 2014
Published: December 23, 2014

ACS Publications © 2014 American Chemical Society

DOI: 10.1021/jf5050734
J. Agric. Food Chem. 2015, 63, 457−463

In the search for naturally occurring antimicrobial agents, the antifungal activity of *S. fruticosa* extracts against the plant pathogenic fungi *Aspergillus tubingensis*, *B. cinerea*, and *P. digitatum* was assessed. The ethyl acetate extract of *S. fruticosa* was studied for the first time using HPLC-SPE-NMR set-up and q-NMR to reveal its phytochemical composition. Then, the antifungal activity of the major identified phytochemicals, namely, carnosic acid, carnosol, and hispidulin, was determined against plant pathogenic fungi using disk diffusion and broth microdilution assays because there are no data on their antifungal potency.

MATERIALS AND METHODS

Plant Material, Chemicals, and Fungal Microorganisms. *S. fruticosa* Mill. was collected from the Athalassa botanical gardens in Nicosia, Cyprus (Department of Agriculture, Ministry of Agriculture, Natural Resources and Environment) and was air-dried and pulverized into fine powder. Carnosic acid (≥91%), carnosol (≥98.0%), and hispidulin (≥98.0%) were obtained from Sigma-Aldrich to test their antifungal potency. Formulated fungicides containing the active ingredients fenhexamid (Teldor© 50WG; Bayer CropScience) and fludioxonil (Geoxe 50WG; Syngenta Crop Protection) were purchased from local authorized suppliers. Analytical grade solvents were obtained from Acros Organics. Water was prepared by reversed osmosis (Rios, Millipore), and for HPLC Milli-Q water (Millipore) was used. CH_3CN d_3, 99.8%, was purchased from Sigma-Aldrich.

Pure cultures of *A. tubingensis*, *B. cinerea*, and *P. digitatum* on Sabouraud agar, identified by molecular and standard microbiological methods, were used in the antimicrobial assays. Culture media, Sabouraud dextrose agar (SDA) and Sabouraud dextrose broth (SDB) were obtained from Oxoid.

Extraction and Sample Preparation. The extraction was carried out on a semi-automated Soxtec system 2055 (Foss Analytical, Hilleroed, Denmark) as described in previous work.[23] Three grams of plant material was placed into extraction thimbles, and 80 mL of ethyl acetate was transferred into each Soxtec extraction cup. Phytochemicals were extracted by setting the unit at the boiling position for 30 min and then at the rising position for 1 h. The ethyl acetate extracts were allowed to cool at room temperature and evaporated to dryness in a rotary evaporator at 45 °C. The dry extracts were stored at −20 °C until needed.

The ethyl acetate sage extract (27.2 mg) was dissolved in 1.5 mL of acetonitrile/water (2:1, v/v) and centrifuged. The supernatant was subjected to HPLC-SPE-NMR analysis.

HPLC-SPE-NMR. HPLC-SPE-NMR measurements were carried out on a chromatographic separation system consisting of an Agilent 1200 series HPLC with an in-line solvent degasser, quaternary pump, autosampler, column compartment with thermostat, and a diode array detector. The optimized HPLC-SPE-NMR parameters were used to analyze *S. fruticosa* extracts.[24] The Bruker/Spark Prospect 2 solid phase extraction unit (Bruker BioSpin and Spark, Emmen, The Netherlands) was used to trap the chromatographic peaks on Hysphere General Phase cartridges (2 mm i.d., 10−12 μm) after post-column addition of water by a Knauer K 120 HPLC pump (Berlin, Germany). The chromatographic peaks were multiply trapped from repeated HPLC injections on the same cartridge to increase their concentration, dried with dry nitrogen gas, and eluted with acetonitrile-d_3 into 3 mm NMR tubes using a Gilson Liquid Handler 215. 1D and 2D NMR spectra were recorded on a Bruker DRX-400 MHz instrument equipped with a 3 mm inverse broadband (BBI) probe using standard Bruker pulse sequences. The NMR system was controlled by software TopSpin 1.3 (Bruker BioSpin, Rheinstetten, Germany). Chemical shifts were expressed in parts per million (ppm) referenced to the solvent peak (1.94 ppm for CD_3CN).

The chromatographic separation was carried out a Luna C_{18}, 5 μm, analytical column (25 cm × 4.6 mm i.d., Phenomenex). The flow rate was 0.6 mL min^{-1}, and the injection volume was 50 μL. Gradient elution was performed using 0.1% formic acid (solvent A) and acetonitrile (solvent B) with the following linear gradient combination: at t = 0 min A = 90%, at t = 10 min A = 70%, at t = 20 min A = 50%, at t = 35 min A = 20%, at t = 50 min A = 0%, at t = 55 min A = 0%, and at t = 60 min A = 90%.

Quantitative NMR for Major Phytochemicals. For the quantitative analysis three independent samples were prepared by weighing 5 mg of the extract, adding 300 μL of acetonitrile-d_3, and transferring the mixture to 3 mm NMR tubes. All chemical shifts were measured with reference to the internal standard, 3-trimethylsilyl-2,2′,3′,3′-tetradeuteropropionic acid (TMSP-d_4) (δ_H = 0.000 ppm), of known concentration (0.3 mmol L^{-1}). NMR measurements were recorded on a Bruker DRX400 MHz instrument equipped with a 3 mm inverse broadband (BBI) probe (BrukerBiospin). The following acquisition parameters were used: $\pi/2$ excitation pulse; spectral width, 4006.4 Hz; 32K real data points; acquisition time, 4 s; relaxation delay, 15 s; number of transient accumulations, 256. Data were processed by using Topspin 1.3 (Bruker) software including manual phase correction and baseline correction over the entire spectral range.

Antifungal Properties. *Disk Diffusion Assay.* The inhibitory activity of the *S. fruticosa* extract and its main constituents on the mycelial growth of the plant pathogenic fungi *A. tubingensis*, *B. cinerea*, and *P. digitatum* was assessed by the disk diffusion assay.[25] The ethyl acetate extract of *S. fruticosa*, as well as its pure carnosic acid, carnosol, and hispidulin, was dissolved in 2 and 5% aqueous dimethyl sulfoxide (DMSO) solutions, respectively, and stock solutions of 1000 μg mL^{-1} were prepared. Conidial suspensions (10^6 conidia mL^{-1}) of each fungus were evenly distributed on the surface of SDA Petri dishes and were allowed to dry. Subsequently, sterile 6 mm in diameter Whatman filter paper disks were impregnated with 20 mL of each antimicrobial agent and were placed in the center of the inoculated Petri dishes. The natural products were tested at concentrations of 400 and 200 μg mL^{-1}, whereas aqueous solutions of synthetic fungicides were used as positive reference standards at the concentration of 10 μg mL^{-1}. More specifically, the hydroxyaniline fenhexamid was used as a reference botryticide, whereas the phenyllpyrole fludioxonil was used against *A. tubingensis* and *P. digitatum*. Negative controls were prepared using the solvents employed to dissolve the antimicrobial agents at their highest concentration. The plates were then sealed and incubated in the dark for 72 h at 25 °C. Mean inhibition zone diameters (IZD) were calculated against each microorganism by means of a ruler. Experiments were conducted three times, with two replicates per experiment.

Broth Microdilution Assay. A serial broth microdilution method was used to determine the minimum inhibitory concentrations (MIC) values of the ethyl acetate extract of *S. fruticosa* and its major constituents against the aforementioned plant pathogenic fungi.[25,26] Briefly, stock solutions of the natural antimicrobials were prepared in DMSO and serially diluted to obtain the desired final concentrations ranging from 300 to 10 μg mL^{-1}. The final DMSO content was 5% (v/v), and this solution was used as negative control. It is noteworthy that the DMSO controls did not show any inhibitory effects on the growth of the microorganisms tested (data not shown). One hundrend microliters of each tested concentration was added per well (96-well microplate) containing 80 μL of SDB and 20 μL of inoculum (10^6 conidia mL^{-1}). The final volume in each well was 200 μL. Aqueous solutions of fenhexamid and fludioxonil were used as standard fungicides for positive control (0.5, 0.1, 0.05, 0.01, 0.005, and 0.001 μg mL^{-1}). For each microorganism a sterility control that contained only the culture medium and a growth control for the respective conidial suspension without the tested antimicrobial agents were included. The plates were covered with a sterile plate sealer and incubated at 25 °C for 72 h in an orbital shaking incubator at 120 rpm. The assay was conducted three times, with two replicates per experiment. MIC was defined as the lowest concentrations of the compound that completely inhibited visible growth of the tested fungi. After the MICs were estimated, 20 mL samples from all of the optical clear wells, plus one negative control that showed growth, were spread onto the surface of SDB Petri dishes and incubated at 25 °C for a minimum of 72 h until mycelial growth was visible in the control plates. The minimum fungicidal concentration (MFC) value was determined as the lowest

DOI: 10.1021/jf5050734
J. Agric. Food Chem. 2015, 63, 457−463

concentration of the antimicrobial agent resulting in no growth on subculture, indicating 99.5% killing of the original inoculum.[26,27] Each experiment was repeated three times, and mean MFC values were calculated.

Statistical Analysis. The relative inhibition data for each fungal microorganism were compared using analysis of variance (ANOVA) and least significant difference (LSD) separation procedures of SAS version 9.1 (SAS Institute, Cary, NC, USA).

RESULTS AND DISCUSSION

Phytochemical Analysis of *S. fruticosa* Extract. Solvents of different polarities such as hexane, ethyl acetate, methanol, and water were used to prepare extracts of *S. fruticosa*. Preliminary data showed that ethyl acetate extract had the most potent antifungal potency among the tested extracts (data not shown). Therefore, the ethyl acetate extract of *S. fruticosa* was selected to be further analyzed. The chromatographic separation of the ethyl acetate extract of *S. fruticosa* was optimized and displayed six major peaks. The first three chromatographic peaks showed a UV spectrum (UV maxima at 260−270 and 340−350 nm) similar to those of flavonoids.[24] Their ^{1}H NMR spectra confirmed the flavonoid skeleton due to the presence of a deshielded signal in the region of 12−13 ppm attributed to hydroxyl proton OH-5 and the distinctive spin system in the aromatic region.[28] All three compounds exhibited an AA′XX′ pattern with two doublets resonating at the regions of ∼7.9 and 6.9 ppm, respectively, with a *J* coupling of 8.8 Hz and a number of singlets at the region of 3.7−3.9 ppm indicating the presence of methoxy groups. By comparison of the data obtained herein with those previously reported, compounds **1**, **2**, and **3** were identified as hispidulin (4′,5,7-trihydroxy-6-methoxyflavone), cirsimaritin (4′,5-dihydroxy-6,7-dimethoxyflavone), and salvigenin (5-hydroxy-6,7,4′-trimethoxyflavone).[29−31] The identified flavones differ in the degree of methylation of their hydroxyl groups. All compounds were unambiguously identified using 2D NMR experiments (COSY, HSQC, and HMBC), and their structures are described in Table 1 and Figure 1. Hispidulin and cirsimaritin were found for the first time in *S. fruticosa*, although they had been detected in other *Salvia* species.[32,33] The salvigenin in *S. fruticosa* has been recently identified.[34]

Compound **4** showed a methyl singlet at 0.85 integrating to six protons, two methyl doublets at 1.15 and 1.16 ppm, respectively, integrating to six protons, a 1H multiplet at 3.18 ppm, a 1H doublet at 5.39, and 1H singlet at 6.75 ppm. This combination of signals indicates a carnosol type diterpene. A comparison with literature NMR data allowed the identification of compound **4** as carnosol. The lack of signals in the region of 4−6 ppm and the similarity observed in almost all signals indicated the presence of carnosic acid (**5**). Compound **6** was easily attributed to 12-methoxycarnosic acid, due to the additional signal at 3.64 ppm integrating to three protons that suggested the presence of a methoxy group. All results are in agreement with previously reported NMR data and listed in Table 1 and Figure 1.[35,36] Carnosic acid and carnosol are the most well-known diterpenes in *Salvia* species, and they have been found in *S. fruticosa*.[19] The methoxy derivative of carnosic acid (compound **6**) is widely distributed in *Salvia* species,[37] but its presence in *S. fruticosa* has not been reported.

Quantitative ^{1}H NMR (q-NMR) is an extremely useful tool for the quantification of constituents in complex plant extracts without the need of laborious and time-consuming fractionation and isolation procedures. The area (referred to as the

Table 1. Retention Times, ^{1}H NMR Chemical Shifts, and Concentrations of the Chromatographic Peaks of *S. fruticosa* Ethyl Acetate Extract

peak	retention time (min)	compound	^{1}H NMR (400 MHz, CD_3CN), δ	concentration (mg g^{-1} extract)
1	26.1	hispidulin	δ 13.12 (s, 1, 5-OH), 7.86 (d, 2, *J* = 8.8 Hz, 2′,6′-CH), 6.96 (d, 2, *J* = 8.8 Hz, 3′,5′-CH), 6.59 (s, 2, overlapping of 8-CH and 3-CH), 3.87 (s, 3, 6-OCH_3)	8.0
2	29.8	cirsimaritin	δ 12.88 (s, 1, 5-OH), 7.88 (d, 2, *J* = 8.7 Hz, 2′,6′-CH), 6.97 (d, 2, *J* = 8.7 Hz, 3′,5′-CH), 6.77 (s, 1, 8-CH) 6.63(s, 1, 3-CH), 3.93 (s, 3, 7-OCH_3), 3.78 (s, 3, 6-OCH_3)	10.4
3	37.0	salvigenin	δ 12.86 (s, 1, 5-OH), 7.97 (d, 2, *J* = 9.0 Hz, 2′,6′-CH), 7.10 (d, 2, *J* = 9.0 Hz, 3′,5′-CH), 6.79 (s, 1, 8-CH) 6.67(s, 1, 3-CH), 3.94 (s, 3, 7-OCH_3), 3.88 (s, 3, 4′-OCH_3), 3.79 (s, 3, 6-OCH_3)	27.1
4	38.8	carnosol	δ 6.75 (s, 1, 14-CH), 5.39 (d, 1, *J* = 2.8 Hz, 7-CHOC), 3.18 (m, 1, 15−$CH(CH_3)_2$), 2.78 (d, 1, *J* = 13.5 Hz, 1α-CH_2), 2.69 (dd, 1, *J* = 14.1 and 3.5 Hz, 1β-CH_2), 2.18 (m, 1, 6β-CH_2), 1.87 (m, 1, 2α-CH_2), 1.84 (m, 1, 6α-CH_2), 1.69 (dd, 1, *J* = 10.6 and 5.0 Hz 5-CH), 1.60 (dt, 1, *J* = 13.6 Hz, 2β-CH_2), 1.50 (d, 1, *J* = 12.8 Hz, 3α-CH), 1.31 (ddd, 1, *J* = 12.0, 13.6, and 3.6 Hz, 3β-CH_2), 1.18 (d, 3, *J* = 6.8 Hz, 16-CH_3), 1.16 (d, 3, *J* = 6.7 Hz, 16-CH_3), 0.85 (s, 6, 17-CH_3 and 18-CH_3)	20.7
5	43.5	carnosic acid	δ 6.53 (s, 1, 14-CH), 3.36 (bd, 1, *J* = 11.6 Hz, 1β-CH_2), 3.14 (m, 1, 15-$CH(CH_3)_2$), 2.77 (m, 2, 7-CH_2), 2.27 (m, 1, 6β-CH_2), 2.08 (d, 1, *J* = 13.0 Hz, 2β-CH_2), 1.83 (bd, 1, *J* = 12 Hz, 6α-CH_2), 1.45−1.56 (m, 3, overlapping of 3α-CH_2, 2β-CH_2, and 5-CH), 1.32 (ddd, 1, *J* = 12.8, 13.2, and 4.0 Hz, 3β-CH_2), 1.17 (d, 3, *J* = 7.2 Hz, 17-CH_3), 1.15 (d, 3, *J* = 7.0 Hz, 16-CH_3), 1.08 (m, 1, 1α-CH_2), 0.98 (s, 3, 18-CH_3), 0.88 (s, 3, 19-CH_3)	257.2
6	45.8	12-methoxycarnosic acid	δ 6.53 (s, 1, 14-CH), 3.51 (m, 1, 1β-CH_2), 3.17 (m, 1, 15-$CH(CH_3)_2$), 2.79 (m, 2, 7-CH_2), 2.20 (m, 1, 6β-CH_2), 2.20 (m, 1, 2β-CH_2), 1.80 (bd, 1, 3*J* = 13.2 Hz, 6α-CH_2), 1.51 (m, 3, overlapping of 3α-CH_2, 2β-CH_2, and 5-CH), 1.30 (ddd, 1, *J* = 12.8, 13.6, and 4.8 Hz, 3β-CH_2), 1.18 (d, 3, *J* = 6.8 Hz, 17-CH_3), 1.15 (d, 3, *J* = 7.0 Hz, 16-CH_3), 1.05 (m, 1, 1α-CH_2), 0.96 (s, 3, 18-CH_3), 0.86 (s, 3, 19-CH_3), 3.64 (s, 3, 12-OCH_3)	103.4

DOI: 10.1021/jf5050734
J. Agric. Food Chem. 2015, 63, 457−463

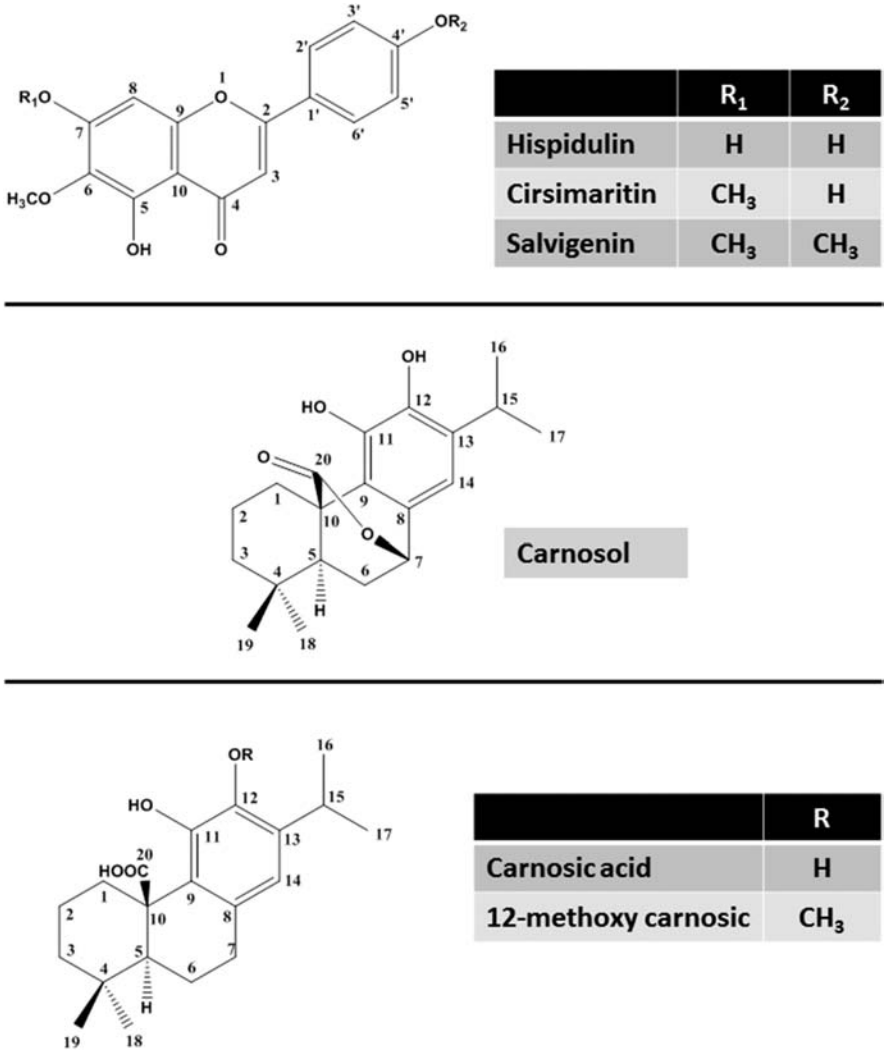

	R_1	R_2
Hispidulin	H	H
Cirsimaritin	CH_3	H
Salvigenin	CH_3	CH_3

	R
Carnosic acid	H
12-methoxy carnosic	CH_3

Figure 1. Structures of the major phytochemicals present in *Salvia fruticosa* Mill. extract.

Table 2. Antimicrobial Activity of *Salvia fruticosa* Ethyl Acetate Extract and Its Constituents by Measuring the Diameter of the Inhibition Zone (IZD) against the Tested Fungal Species, Using the Disk Diffusion Assay

		fungal microorganism					
		Aspergillus tubingensis		*Botrytis cinerea*		*Penicillium digitatum*	
antimicrobial agent	concentration (μg mL^{-1})	IZD[a] (mm)	% relative inhibition[b]	IZD (mm)	% relative inhibition	IZD (mm)	% relative inhibition
Salvia fruticosa[c]	400	8.1	49 B[h]	13.6	74.3 B	19.8	76.7 B
	200	NI[f]	NI	7.8	42.6 E	13.1	50.1 C
carnosic acid[d]	400	5.2	31.7 C	11.4	62.3 C	7.3	28.3 F
	200	NI	NI	1.8	9.8 G	1	3.9 I
carnosol[d]	400	NI	NI	7.9	43.2 E	8.8	34.1 E
	200	NI	NI	4.4	24 F	6.9	26.7 G
hispidulin[d]	400	NI	NI	10.1	54.3 D	10.7	41.5 D
	200	NI	NI	1.8	9.8 G	2.8	12.5 H
fludioxonil[e]	10	16.4	100 A	NA	NA	25.8	100 A
fenhexamid[e]	10	NA[g]	NA	18.3 A	100 A	NA	NA

[a]Antimicrobial activity was evaluated by measuring the diameter of the inhibition zone (IZD) against the tested fungal species, using the disk diffusion assay. The inoculated plates were incubated at 25 °C for 72 h. [b]Relative inhibition (%) was expressed as the quotient of the IZD of each antimicrobial agent of natural origin to that of the synthetic fungicide used per microorganism. The inhibition caused by the synthetic fungicides was considered 100%. [c]Ethyl acetate extract of *S. fruticosa* in 2% (v/v) DMSO. [d]Stock solutions of the pure compounds of the main constituents of *S. fruticosa* tested in 5% (v/v) DMSO. [e]Aqueous solutions of the synthetic fungicides fenhexamid and fludioxonil were used as positive controls. [f]NI, no inhibition zone was observed. [g]NA, the antimicrobial agent was not applied. [h]Relative inhibition values (%) followed by different letters within the same column were significantly different in least significant difference tests at $P = 0.01$.

DOI: 10.1021/jf5050734
J. Agric. Food Chem. 2015, 63, 457−463

Table 3. Minimum Inhibitory Concentration (MIC) and Minimum Fungicidal Concentration (MFC) of *Salvia fruticosa* Ethyl Acetate Extract and Its Constituents Evaluated Using the Broth Microdilution Method in Sabouraud Dextrose Broth

	fungal microorganism					
	Aspergillus tubingensis		*Botrytis cinerea*		*Penicillium digitatum*	
antimicrobial agent	MIC[a] (μg mL^{-1})	MFC[b] (μg mL^{-1})	MIC (μg mL^{-1})	MFC (μg mL^{-1})	MIC (μg mL^{-1})	MFC (μg mL^{-1})
Salvia fruticosa[c]	300	<300	100	162.5	150	212
carnosic acid[d]	200	300	150	200	200	285
carnosol[d]	300	<300	100	150	100	156
hispidulin[d]	300	<300	150	200	200	275
fenhexamid[e]	NA[f]	0.5	NA	NA	NA	NA
fludioxonil[e]	NA	NA	NA	0.5	NA	0.05

[a]The minimum inhibitory concentration (MIC) was evaluated using the broth microdilution method in Sabouraud dextrose broth. MICs were defined as the lowest concentrations causing no visible growth. Results were read after 72 h of incubation at 25 °C. [b]After the MIC values were determined, samples from all optically clear tubes (complete growth inhibition), plus a negative control showing growth, were subcultured on Sabouraud dextrose agar. The dishes were incubated at 25 °C for 3 days, until growth was clearly visible in the control, and the minimum fungicidal concentration (MFC) value was determined as the lowest concentration with no visible growth. [c]Ethyl acetate extract of *S. fruticosa* in 2% (v/v) DMSO. [d]Stock solutions of the pure compounds of the main constituents of *S. fruticosa* tested in 5% (v/v) DMSO. [e]Aqueous solutions of the synthetic fungicides fenhexamid and fludioxonil were used as positive controls. [f]NA, the antimicrobial agent was not applied.

intensity or the integral) of a NMR signal is directly proportional to the number of corresponding nuclei and thus, at variance with other techniques, the response factor is not dependent on the molecular structure. To date, q-NMR is considered to be at least as reliable and precise as the more commonly used chromatography-based techniques while providing several advantages such as simple method development, easy sample preparation, relatively short analysis time, and multiple calibration options without the need for identical reference materials.[38] The quantification of polyphenols and terpenes in complex plant extracts using q-NMR has been described comprehensively.[39,40] In Table 1, the concentration levels of the identified phytochemicals are displayed and show that carnosic acid and its 12-methoxy derivative were the main components of plant extract. Carnosol and hispidulin derivatives were found at lower concentrations ranging from 8.0 to 27.1 mg g^{-1}. Overall, the amount of diterpenes (381.3 mg g^{-1}) was significantly higher than that of flavonoids (45.6 mg g^{-1}) in *S. fruticosa* extract.

Antifungal Potential of *S. fruticosa* Extract and Its Constituents. It is difficult to correlate the antimicrobial activity of an extract to a specific compound due to their complexity and variability. Nevertheless, researchers have reported on the relationship between the chemical composition of the most abundant components of the extracts and their antimicrobial activity.[41] In addition, a structure−activity relationship for antimicrobial activity on a plethora of chemical classes is well documented.[42,43] Among the six major phytochemicals described in the present study, the selection of those that were further assessed for their antifungal activity was based on their abundance in the extract and their structural attributes. Thus, the diterpene carnosic acid was selected, because it was the predominant compound of the extract, and carnosol, for its structural dissimilarity among the other diterpenes found. With regard to the flavonoids, hispidulin was chosen because the other two, cirsimaritin and salvigenin, are hispidulin methoxy derivatives. The antifungal activity of *S. fruticosa* was initially qualitatively assessed against *A. tubingensis*, *B. cinerea*, and *P. digitatum*. The IZD was measured and the percent relative inhibition (RI) was estimated as the quotient of each antimicrobial agent of natural origin to that of the synthetic fungicide used per microorganism, considering the inhibition caused by each synthetic fungicide to be 100%. Overall, the inhibitory effect of all tested compounds was better at the concentration of 400 μg mL^{-1}, whereas among them the *S. fruticosa* extract was the most active against all fungal species, exhibiting moderate to high antifungal activity (Table 2). The least inhibited species by the extract was *A. tubingensis* with an RI of 49%, whereas for *B. cinerea* and *P. digitatum* the RI values were 74.3 and 76.7%, respectively. With regard to the natural compounds present in the extract, carnosic acid was the only one that caused inhibition across all tested microorganisms, ranging from the high 62.3% RI for *B. cinerea* to the lower 31.7% RI for *A. tubingensis*, whereas hispidulin performed the best against *P. digitatum*. Their antifungal potency was also quantitatively evaluated by means of MIC and MFC values (Table 3). The results confirmed that overall *A. tubingensis* was the least inhibited among the tested fungal species, as shown by the disk diffusion assay, with MIC values of 300 μg mL^{-1} for all *S. fruticosa* compounds, but carnosic acid had an MIC value of 200 μg m^{-1}. Similarly, MFC values recorded were ≥300 μg mL^{-1}. On the other hand, MIC values of *B. cinerea* and *P. digitatum* in the presence of the extract after 72 h were 100 and 150 μg mL^{-1}, respectively. On the basis of the MIC values of the pure phytochemicals, it can be suggested that overall *B. cinerea* was better inhibited (Table 3). *P. digitatum* MIC values were also in the same range. *B. cinerea* and *P. digitatum* exhibited the lowest MIC values in carnosol (100 μg mL^{-1}), followed by carnosic acid and hispidulin.

Cos et al. defined stringent end point criteria for "activity", suggesting that plant extracts should be considered efficacious if they exhibit IC_{50} values ≤100 μg mL^{-1}.[44] Considering that for the same active ingredient/microorganism system the MFC values, indicating 99.5% killing, should be by definition lower than its IC_{50} values, the ethyl acetate extract of *S. fruticosa* possesses antimicrobial properties worthy of further investigation, because the calculated MFC values for *B. cinerea* and *P. digitatum* were not far from the cutoff "activity" value.

The calculated MFC values for carnosic acid, carnosol, and hispidulin are in the same range as the extract itself, suggesting that probably its antifungal activity cannot be solely attributed to a single constituent. The antifungal potency of the extract also cannot be correlated with cirsirimatin, salvigenin, and 12-methoxycarnosic acid, because they were found at low concentrations and their chemical structures are closely similar to the tested phytochemicals.

DOI: 10.1021/jf5050734
J. Agric. Food Chem. 2015, 63, 457−463

A plethora of experimental studies have documented the promising biological activities of diterpenoids isolated from *Salvia* species, showing that most of them possess cytotoxic activity.[45] Carnosic acid and carnosol, as well as rosmanol and ferruginol, have been considered to be responsible for the biological activity of *Salvia* spp.[46] Collins and Charles manifest the significant inhibition of a range of food spoilage bacteria and yeasts by carnosol,[47] whereas carnosic acid and carnosol have been suggested to be responsible for the antimicrobial activity of *Rosmarinus officinalis* leaf extract against selected oral, cariogenic bacteria. The potent antifungal activity of carnosic acid against an array of yeast and molds was also documented by Gigante and co-workers.[48] With regard to hispidulin, no strong antimicrobial activity against *Staphylococcus aureus*, *Bacillus cereus*, *Escherichia coli*, *Salmonella typhimurium*, and *Candida albicans* was found because its MIC was >250 $\mu g\ mL^{-1}$.[49] The antifungal activity of cirsimaritin and salvigenin is maybe weaker than that of hispidulin as these compounds contain only one hydroxyl group on ring A, whereas a high antifungal activity of flavones is guaranteed by at least two hydroxyl groups on ring A.[50]

The action of different classes of natural products with diverse modes may be responsible for the antifungal activity of an extract. With regard to their mode of action, carnosic acid has exhibited the capacity to act as a natural free radical scavenger with a potential chemopreventive activity, whereas diterpenoids with antifungal activity on *B. cinerea* have been reported to induce permeabilization of the fungal cell membrane.[51,52] Flavonoids inhibit the growth of *Fusarium* spp. by different mechanisms, such as cross-linking of microbial enzymes; inhibition of microbial cellulases, xylanases, and pectinases; chelation of metals necessary for enzyme activity; and/or formation of a hard, almost crystalline, structure as a physical barrier against pathogen attack.[53]

Overall, the results obtained herein suggest the ability of the ethyl acetate extract of *S. fruticosa* to control a panel of fungal species, particularly responsible for postharvest fruit spoilage. In addition, MIC and MFC values of this extract meet the end point criteria for "activity". Research could be conducted toward the application of the extract alone or in combination with synthetic fungicides in the food industry, because it could be incorporated to edible coatings to control decay in organic production of horticultural crops. In addition, the documented antifungal activity of the *S. fruticosa* presented in this study should be explored also in other pathosystems to further elucidate its promising antimicrobial potential. HPLC-SPE-NMR and q-NMR experiments showed that diterpenes (carnosol, carnosic acid, 12-methoxycarnosic acid) and flavonoids (hispidulin, cirsimaritin, salvigenin) are the main constituents of the ethyl acetate extract. Although the antifungal potencies of carnosic acid, carnosol, and hispidulin could be characterized as moderate, they could be used as lead compounds toward the discovery of new antifungal agents.

AUTHOR INFORMATION

Corresponding Author

*(V. Goulas) Phone: +357 25 00 21 41. E-mail: vlasios.goulas@cut.ac.cy.

Notes

The authors declare no competing financial interest.

REFERENCES

(1) Delamare, A. P. L.; Moschen-Pistorello, I. T.; Artico, L.; Atti-Serafini, L.; Echeverrigaray, S. Antibacterial activity of essential oils of *Salvia officinalis* L. and *Salvia triloba* L. cultivated in South Brazil. *Food Chem.* **2007**, *100*, 603−608.

(2) Giwelli, A. A.; Dzamic, A. M.; Sokovic, M.; Ristic, M. S.; Janackovic, P.; Marin, P. D. The chemical composition, antimicrobial and antioxidant activities of the essential oil of *Salvia fruticosa* growing wild in Libya. *Arch. Biol. Sci.* **2013**, *65*, 321−329.

(3) Topcu, G. Bioactive triterpenoids from *Salvia* species. *J. Nat. Prod.* **2006**, *69*, 482−487.

(4) Papageorgiou, V.; Gardeli, C.; Mallouchos, A.; Papaioannou, M.; Komaitis, M. Variation of the chemical profile and antioxidant behavior of *Rosmarinis officinalis* L. and *Salvia fruticosa* Miller grown in Greece. *J. Agric. Food Chem.* **2008**, *56*, 7254−7264.

(5) De Palma, A.; Rossi, R.; Carai, M.; Cabras, C.; Colombo, G.; Arnoldi, L.; Riva, A.; Morazzoni, P.; Mauri, P. L. Pharmaceutical and biomedical analysis of terpene constituents in *Salvia miltiorrhiza*. *Cur. Pharm. Anal.* **2008**, *4*, 249−257.

(6) Casselman, I.; Nock, C. J.; Wohlmuth, H.; Weatherby, R. P. From local to global − fifty years of research on *Salvia divinorum*. *J. Ethnopharmacol.* **2014**, *151*, 768−783.

(7) Lardos, A. The botanical materia medica of the Iatrosophikon − a collection of prescriptions from a monastery in Cyprus. *J. Ethnopharmacol.* **2006**, *104*, 387−406.

(8) Xavier, C. P. R.; Fernandes-Ferreira, C. F. L. M.; Pereira-Wilson, C. *Salvia fruticosa*, *Salvia officinalis*, and rosmarinic acid induce apoptosis and inhibit proliferation of human colorectal cell lines: the role in MAPK/ERK pathway. *Nutr. Cancer* **2009**, *61*, 564−571.

(9) Senol, F. S.; Orhan, I. E.; Erdem, S. A.; Kartal, M.; Sener, B.; Kan, Y.; Celep, F.; Kahraman, A.; Dogan, M. Evaluation of cholinesterase inhibitory and antioxidant activities of wild and cultivated samples of sage (*Salvia fruticosa*) by activity-guided fractionation. *J. Med. Food* **2011**, *14*, 1476−1483.

(10) Ramos, A. A.; Pedro, D.; Collins, A. R.; Pereira-Wilson, C. Protection by *Salvia* extracts against oxidative and alkylation damage to DNA in human HCT115 and CO115 cells. *J. Toxicol. Environ. Health, Part A* **2012**, *75*, 765−775.

(11) Kaileh, M.; Berghe, W. V.; Bone, E.; Essawi, T.; Haegeman, G. Screening of indigenous Palestinian plants for potential anti-inflammatory and cytotoxic activity. *J. Ethnopharmacol.* **2007**, *113*, 510−516.

(12) Abou-Jawdah, Y.; Sobh, H.; Salameh, A. Antimycotic activities of selected plant flora, growing wild in Lebanon, against phytopathogenic fungi. *J. Agric. Food Chem.* **2002**, *50*, 3208−3213.

(13) Pitarokili, D.; Tzakou, O.; Loukis, A.; Harvala, C. Volatile metabolites from *Salvia fruticosa* as antifungals agents in soilborne pathogens. *J. Agric. Food Chem.* **2003**, *51*, 3294−3301.

(14) Goussous, S. J.; el-Samen, F. M. A.; Tahhan, R. A. Antifungal activity of several medicinal plants extracts against the early blight pathogen (*Alternaria solani*). *Arch. Phytopathol. Plant Prot.* **2010**, *43*, 1745−1757.

(15) Kadoglidou, K.; Lagopodi, A.; Karamanoli, K.; Vokou, D.; Bardas, G. A.; Menexes, G.; Constantinidou, H. I. A. Inhibitory and stimulatory effects of essential oils and individual monoterpenoids on growth and sporulation of four soil-borne fungal isolates of *Aspergillus terreus*, *Fusarium oxysporum*, *Penicillium expansum*, and *Verticillium dahlia*. *Eur. J. Plant Pathol.* **2011**, *130*, 297−309.

(16) Asku, T.; Tumen, G.; Satil, F.; Ates, M. Characterization of the phenolic composition and antimicrobial activities of Turkish medicinal plants. *Pharm. Biol.* **2009**, *47*, 563−571.

(17) Pizzale, L.; Bortolomeazzi, R.; Vichi, S.; Uberegger, E.; Conte, L. S. Antioxidant activity of sage (*Salvia officinalis* and *S. fruticosa*) and oregano (*Origanum onites* and *O. indercedens*) extracts related to their phenolic compound content. *J. Sci. Food Agric.* **2002**, *82*, 1645−1651.

(18) Exarchou, V.; Nenadis, N.; Tsimidou, M.; Gerothanassis, I. P.; Troganis, N.; Boskou, D. Antioxidant activities and phenolic composition of extracts from Greek oregano, Greek sage, and summer savory. *J. Agric. Food Chem.* **2002**, *50*, 5294−5299.

DOI: 10.1021/jf5050734
J. Agric. Food Chem. 2015, 63, 457−463

(19) Matsingou, T. C.; Petrakis, N.; Kapsokefalou, M.; Salifoglou, A. Antioxidant activity of organic extracts from aqueous infusions of sage. *J. Agric. Food Chem.* **2003**, *51*, 6696−6701.
(20) Dincer, C.; Topuz, A.; Sahin-Nadeem, H.; Ozdemir, K. S.; Cam, I. B.; Tontul, I.; Gokturk, R. S.; Ay, S. T. A comparative study on phenolic composition, antioxidant activity and essential oil content of wild and cultivated sage (*Salvia fruticosa* Miller) as influenced by storage. *Ind. Crop. Prod.* **2012**, *39*, 170−176.
(21) Cvetkovikj, I.; Stefkov, G.; Acevska, J.; Stanoeva, J. P.; Karapandzova, M.; Stefova, M.; Dimitrovska, A.; Kulevanova, S. Polyphenolic characterization and chromatographic methods for fast assessment of culinary *Salvia* species from South East Europe. *J. Chromatogr., A* **2013**, *1282*, 38−45.
(22) Mari, M.; Di Francesco, A.; Bertolini, P. Control of fruit postharvest diseases: old issues and innovative approaches. *Stewart Postharvest Rev.* **2014**, *10*, 1.
(23) Goulas, V.; Manganaris, G. A. Exploring the phytochemical content and the antioxidant potential of *Citrus* fruits grown in Cyprus. *Food Chem.* **2012**, *131*, 39−47.
(24) Goulas, V.; Exarchou, V.; Kanetis, L.; Gerothanassis, I. P. Evaluation of the phytochemical content, antioxidant activity and antimicrobial properties of mountain tea (*Sideritis syriaca*) decoction. *J. Funct. Foods* **2014**, *6*, 248−258.
(25) Gulluce, M.; Sahing, F.; Sokmend, M.; Ozer, H.; Daferera, D.; Sokmene, A.; Polissiou, M.; Adiguzel, A.; Ozkana, H. Antimicrobial and antioxidant properties of the essential oils and methanol extract from *Mentha longifolia* L. ssp. *longifolia*. *Food Chem.* **2007**, *103*, 1449−1456.
(26) Hammer, K. A.; Carson, C. F.; Riley, T. V. *In vitro* activity of *Melaleuca alternifolia* (tea tree) oil against dermatophytes and other filamentous fungi. *J. Antimicrob. Chemotherapy* **2002**, *50*, 195−199.
(27) Pinto, E.; Vale-Silva, L.; Cavaleiro, C.; Salgueiro, L. Antifungal activity of the clove essential oil from *Syzygium aromaticum* on *Candida*, *Aspergillus* and dermatophyte species. *J. Med. Microbiol.* **2009**, *58*, 1454−1462.
(28) Goulas, V.; Exarchou, V.; Troganis, A. N.; Psomiadou, E.; Fotsis, T.; Briasoulis, E.; Gerothanassis, I. P. Phytochemicals in olive-leaf extracts and their antiproliferative activity against cancer and endothelial cells. *Mol. Nutr. Food Res.* **2009**, *53*, 600−608.
(29) Hasrat, J. A.; Pieters, L.; Claeys, M.; Vlietinck, A. Adenosine-1 active ligands: cirsimarin, a flavone glycoside from *Microtea debilis*. *J. Nat. Prod.* **1997**, *60*, 638−641.
(30) Gu, L.; Weng, X. Antioxidant activity and components of *Salvia plebeia* R.Br. — a Chinese herb. *Food Chem.* **2001**, *73*, 299−305.
(31) Kolak, U.; Hacibekiroglou, I.; Ozturk, M.; Ozgokce, F.; Topcu, G.; Ulubelen, A. Antioxidant and anticholinesterase constituents of *Salvia poculata*. *Turk. J. Chem.* **2009**, *33*, 813−823.
(32) Areias, F.; Valentao, P.; Andrade, P. B.; Ferreres, F.; Seabra, R. M. Flavonoids and phenolic acids of sage: influence of some agricultural factors. *J. Agric. Food Chem.* **2000**, *48*, 6081−6084.
(33) Santos-Gomez, P. C.; Seabra, R. M.; Andrade, P. B.; Fernandes-Ferreira, M. Phenolic antioxidant compounds produced by *in vitro* shoots of sage (*Salvia officinalis* L.). *Plant Sci.* **2002**, *162*, 981−987.
(34) Topcu, G.; Ozturk, M.; Kusman, T.; Demirkoz, A. A. B. D.; Kolak, U.; Ulubelen, A. Terpenoids, essential oil composition, fatty acid profile, and biological activities of Anatolian *Salvia fruticosa* Mill. *Turk. J. Chem.* **2013**, *37*, 619−632.
(35) Pukalskas, A.; van Beek, T. A.; de Waard, P. Development of a triple hyphenated HPLC-radical scavenging detection-DAD-SPE-NMR system for the rapid identification of antioxidants in complex plant extracts. *J. Chromatogr., A* **2005**, *1074*, 81−88.
(36) Xiao, C.; Dai, H.; Liu, H.; Wang, L.; Tang, H. Revealing the metabonomic variation of rosemary extracts using ^{1}H NMR spectroscopy and multivariate data analysis. *J. Agric. Food Chem.* **2008**, *56*, 10142−10153.
(37) Wu, Y. B.; Ni, Z. Y.; Shi, Q. W.; Dong, M.; Kiyota, H.; Gu, Y. C.; Cong, B. Constituents from *Salvia* species and their biological activities. *Chem. Rev.* **2012**, *112*, 5967−6026.
(38) Simmler, C.; Napolitano, J. C.; McAlpine, J. B.; Chen, S. N.; Pauli, G. F. Universal quantitative NMR analysis of complex natural samples. *Curr. Opin. Biotechnol.* **2014**, *25*, 51−59.
(39) Kontogianni, V. G.; Exarchou, V.; Troganis, A. N.; Gerothanassis, I. P. Rapid and novel discrimination and quantification of oleanolic and ursolic acids in complex plant extracts using two-dimensional nuclear magnetic resonance spectroscopy − comparison with HPLC methods. *Anal. Chim. Acta* **2009**, *635*, 188−195.
(40) Charisiadis, P.; Tsiafoulis, C. G.; Exarchou, V.; Tzakos, A. G.; Gerothanassis, I. P. Rapid and direct low micromolar NMR method for the simultaneous detection of hydrogen peroxide and phenolics in plant extracts. *J. Agric. Food Chem.* **2012**, *60*, 4508−4513.
(41) Deans, S. G.; Svoboda, K. P. The antimicrobial properties of marjoram (*Origanum majorana* L.) volatile oil. *Flavour Fragrance J.* **1990**, *5*, 187−190.
(42) Moujir, L.; Gutierrez-Navarro, A. M.; Andres, L. S.; Luis, J.G. Structure-antimicrobial activity relationships of abietane diterpenes from *Salvia* species. *Phytochemistry* **1993**, *34*, 1493−1495.
(43) Manner, S.; Skogman, M.; Geores, D.; Vuorela, P.; Fallarero, A. Systematic exploration of natural and synthetic flavonoids for the inhibition of *Staphylococcus aureus* biofilm. *Int. J. Mol. Sci.* **2013**, *14*, 19434−19451.
(44) Cos, P.; Vlietinck, A. J.; Vanden Berghe, D.; Maes, L. Review: Anti-infective potential of natural products: how to develop a stronger in vitro 'proof-of-concept'. *J. Ethnopharmacol.* **2006**, *106*, 290−302.
(45) Bonito, M. C.; Cicala, C.; Marcotullio, M. C.; Maione, F.; Mascolo, N. Biological activity of bicyclic and tricyclic diterpenoids from *Salvia* species of immediate pharmacological and pharmaceutical interest. *Nat. Prod. Commun.* **2011**, *6*, 1205−1215.
(46) Matkowski, A. Plant *in vitro* culture for the production of antioxidants − a review. *Biotechnol. Adv.* **2008**, *26*, 548−560.
(47) Collins, M. A.; Charles, H. P. Antimicrobial activity of carnosol and ursolic acid: two anti-oxidant constituents of *Rosmarinus officinalis* L. *Food Microbiol.* **1987**, *4*, 311−315.
(48) Gigante, B.; Santos, C.; Silva, A. M.; Curto, M. J. M.; Nascimento, M. S. J.; Pinto, E.; Pedro, M.; Cerqueira, F.; Pinto, M. M.; Duarte, M. P.; Laires, A.; Rueff, J.; Goncalves, J.; Pegado, M. I.; Valdeira, M. L. Catechols from abietic acid: synthesis and evaluation as bioactive compounds. *Bioorg. Med. Chem.* **2003**, *11*, 1631−1638.
(49) Talib, W. H.; Abu Zarga, M. H.; Mahasneh, A. M. Antiproliferative, antimicrobial and apoptosis inducing effects of compounds isolated from *Inula viscosa*. *Molecules* **2012**, *17*, 3291−3303.
(50) Weidenbörner, M.; Hindorf, H.; Jha, H. C.; Tsotsonos, P. Antifungal activity of flavonoids against storage fungi of the genus *Aspergillus*. *Phytochemistry* **1990**, *29*, 1103−1105.
(51) Costa, S.; Utan, A.; Speroni, E.; Cervellati, R.; Piva, G.; Prandini, A.; Guerra, M. C. Carnosic acid from rosemary extracts: a potential chemoprotective agent against aflatoxin B1. An *in vitro* study. *J. Appl. Toxicol.* **2007**, *27*, 152−159.
(52) Cotoras, M.; Folch, C.; Mendoza, L. Characterization of the antifungal activity on *Botrytis cinerea* of the natural diterpenoids kaurenoic acid and 3β-hydroxy-kaurenoic acid. *J. Agric. Food Chem.* **2004**, *52*, 2821−2826.
(53) Treutter, D. Significance of flavonoids in plant resistance and enhancement of their biosynthesis. *Plant Biol.* **2005**, *7*, 581−591.

DOI: 10.1021/jf5050734
J. Agric. Food Chem. 2015, 63, 457−463

JOURNAL OF AGRICULTURAL AND FOOD CHEMISTRY

Article

pubs.acs.org/JAFC

Enantioselective Syntheses and Sensory Properties of 2-Methyl-tetrahydrofuran-3-thiol Acetates

Yifeng Dai, Junqiang Shao, Shaoxiang Yang, Baoguo Sun, Yongguo Liu, Ting Ning, and Hongyu Tian*

School of Food Chemistry, Beijing Key Laboratory of Flavor Chemistry, Beijing Technology and Business University, Beijing 100048, China

ABSTRACT: The enantioselective synthesis of four stereoisomers of 2-methyl-tetrahydrofuran-3-thiol acetate was achieved. The two enantiomers of the important intermediate *cis*-2-methyl-3-hydroxy-tetrahydrofuran were obtained by Sharpless asymmetric dihydroxylation (AD), whereas the two enantiomers of *trans*-2-methyl-3-hydroxy-tetrahydrofuran were derived from the corresponding optically active *cis*-isomers by Mitsunobu reaction. Each stereoisomer of 2-methyl-3-hydroxy-tetrahydrofuran went through mesylation and nucleophilic substitution to afford the corresponding product with specific configuration. (2*R*,3*S*)- and (2*R*,3*R*)-2-methyl-tetrahydrofuran-3-thiol acetate were obtained in 80% ee, whereas the (2*S*,3*R*)- and (2*S*,3*S*)-isomers were in 62% ee. The odor properties of the synthesized four stereoisomers were evaluated by gas chromatography−olfactometry (GC−O), which revealed perceptible differences among stereoisomers both in odor features and in intensities.

KEYWORDS: *2-methyl-tetrahydrofuran-3-thiol acetate, Sharpless AD, Mitsunobu reaction, enantioselective synthesis, sensory properties, GC−O*

INTRODUCTION

The olfactory properties of over 1400 enantiomers have been reported[1] since Rienäcker and Ohloff published the first data regarding the enantioselective perception of β-citronellol in 1961.[2] It is now well recognized that stereoisomers of many chiral chemical compounds are perceived differently as odorants by the human nose.[3] In addition to the differences in sensory properties, the stereoisomers of chiral odorants, such as Galaxolide and Tonalide, also have been found to be metabolized in living beings at different rates.[4] Therefore, it is significant to identify the desired odor-active isomers and further fulfill their commercial application from the prospective of improving odor qualities and reducing potential toxicological risks. Many research interests have been focused on the enantioselective preparation and organoleptic properties of chiral aroma compounds in recent years.[5−11]

Sulfur-containing compounds are an important category of flavor compounds due to their low odor thresholds and their unique odor features.[12,13] They are identified widely in volatile components of many foods and make significant contribution to food flavor,[14−18] especially to meat aroma.[19−23] 2-Methy-tetrahydrofuran-3-thiol is a representative sulfur-containing compound having meat aroma, which exists in four stereo-isomers due to the two chiral centers in the molecule. It is well-known that (±)-*trans*-isomer possesses stronger meaty and roasted notes while (±)-*cis*-isomer is weaker and has more sulfury and musty notes. Goeke prepared the four stereo-isomers by resolution and found their remarkable differences in odor features and intensities.[24] In comparison, the information about its acetylated form, 2-methyl-tetrahydrofuran-3-thiol acetate, is far more retarded, which was not been approved as a flavor compound in the United States by the Flavor Expert Panel (FEXPAN) before 2011 and appeared on the FEMA (Flavor and Extract Manufactures' Association) GRAS (generally recognized as safe) list 25 under no. 4686.[25] In our previous work, (±)-*trans*- and (±)-*cis*-isomers of 2-methyl-tetrahydrofuran-3-thiol acetate were prepared, and the odor properties were evaluated.[26] The results indicated that the diastereoisomers presented some organoleptic differences. However, as far as we know, the sensory properties of the four stereoisomers of 2-methyl-tetrahydrofuran-3-thiol acetate **1** (Figure 1) are still unknown. Therefore, the aim of this work

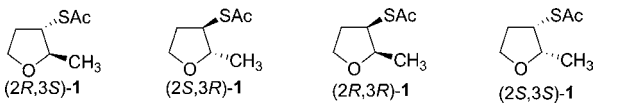

Figure 1. Four stereoisomers of 2-methyl-tetrahydrofuran-3-thiol acetate.

was to synthesize the four stereoisomers enantioselectively and investigate their sensory properties. In Goeke's work, the racemic diastereoisomers of 2-methyl-tetrahydrofuran-3-thiol were prepared by an iodocyclization approach starting from (3*Z*)- and (3*E*)-pent-3-en-1-ols, respectively. Also, (±)-*cis*-thiol was resolved via the camphanic acid thioesters to give the two enantiomers separately, whereas the two enantiomers of *trans*-thiol were produced via enzymatic resolution of *cis*-2-methyl-3-hydroxytetrafuran using the lipase *pseudomonas fluorescence*. Our present work tried a different way to prepare the four stereoisomers of **1** via chemical asymmetric catalytic approach (Figure 2).

Received: August 11, 2014
Revised: January 5, 2015
Accepted: January 5, 2015
Published: January 5, 2015

ACS Publications © 2015 American Chemical Society

DOI: 10.1021/jf503866x
J. Agric. Food Chem. 2015, 63, 464−468

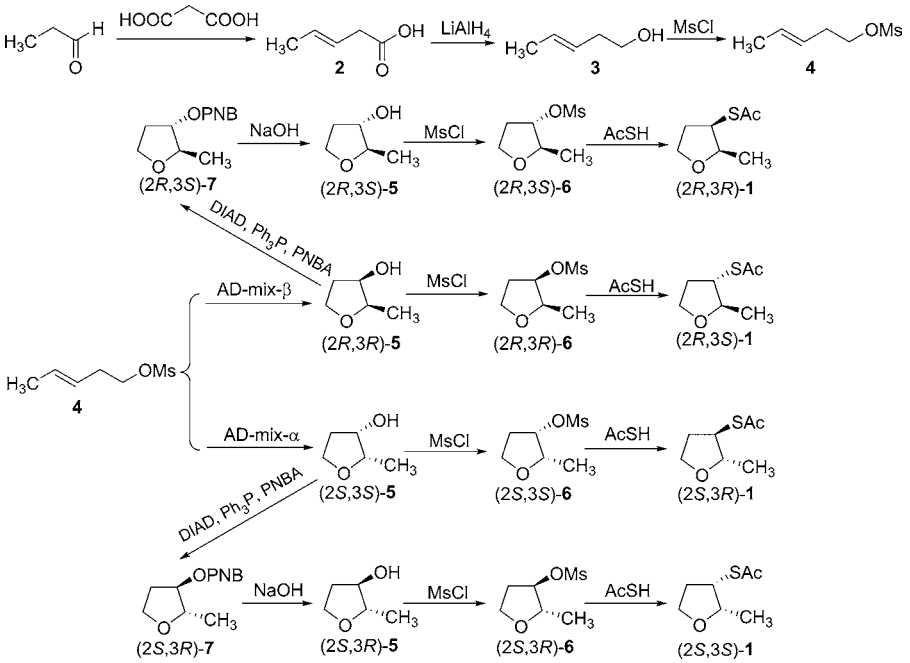

Figure 2. Synthetic routes leading to the optically active 2-methyl-tetrahydrofuran-3-thiol acetates.

MATERIALS AND METHODS

Chemicals. Triphenylphosphine (Ph_3P), diisopropyl azodicarboxylate (DIAD), and $LiAlH_4$ were purchased from Beijing Bailingwei Science and Technology Co. (Beijing, China), AD-mix-*α* and AD-mix-*β* were purchased from Sigma-Aldrich Chemical Co. (St. Louis, MO), and the others were purchased from Beijing Huaxue Shiji Co. (Beijing, China).

Syntheses. *(3E)-Pent-3-enoic Acid* ***2****.* The procedure for the preparation of **2** was adapted from the literature.[27] To a 1 L round bottomed flask equipped with a condenser and a bubbler connected to the exit of the condenser was added a solution of malonic acid (1 mol, 104 g), piperidinium acetate (from 0.85 g of piperidine and 0.6 g of acetic acid, 0.01 mol), and propionaldehyde (0.5 mol, 36.3 mL) in DMSO (400 mL). The reaction mixture was stirred at 40 °C for 2 h. Next, the solution was heated in an oil bath at 100 °C. A rapid evolution of carbon dioxide was observed. Heating was maintained until the evolution of carbon dioxide ceased. The solution was cooled to room temperature, poured into cold water (1 L), and extracted with diethyl ether. The combined extracts were washed with water, brine, dried over anhydrous $MgSO_4$, and evaporated under reduced pressure. The residue was distilled under vacuum (0.4 kPa, 60−65 °C) to give (3*E*)-pent-3-enoic acid **2** as a colorless oil (30 g, 60% yield). The product was used without further purification for the next step. ^{1}H NMR (300 MHz, $CDCl_3$): *δ* 1.68 (3H, d, *J* = 6.0 Hz, H-5), 3.05 (2H, d, *J* = 5.7 Hz, H-2), 5.54 (2H, m, H-3, H-4), 10−12 (1H, br, −COOH). ^{13}C NMR (75 MHz, $CDCl_3$): *δ* 17.9 (C-5), 37.8 (C-2), 121.9 (C-4), 130.0 (C-3), 179.0 (C-1). The spectral data of the obtained product were consistent with those as described by Thibonnet.[28]

(3E)-Pent-3-en-1-ol ***3*** *and (3E)-Pent-3-en-1-yl Mesylate* ***4****.* These two compounds were prepared according to our previously published procedures.[26] **3** was obtained by reduction of **2** with $LiAlH_4$ (88% yield), and then reacted with MsCl to give **4** (92% yield).

Data of **3**, ^{1}H NMR (300 MHz, $CDCl_3$): *δ* 1.65 (3H, d, *J* = 6.3 Hz, H-5), 2.22 (2H, m, H-2), 3.59 (2H, t, *J* = 6.3 Hz, H-1), 5.38 (1H, m, H-4), 5.57 (1H, m, H-3). ^{13}C NMR (75 MHz, $CDCl_3$): *δ* 18.0 (C-5), 35.9 (C-2), 62.0 (C-1), 127.2 (C-4), 128.1 (C-3).

Data of **4**, ^{1}H NMR (300 MHz, $CDCl_3$): *δ* 1.64 (3H, d, *J* = 6.3 Hz, H-5), 2.39 (2H, q, *J* = 6.9 Hz, H-2), 2.96 (3H, s, Me (mesyl)), 4.17 (2H, t, *J* = 6.9 Hz, H-1), 5.36 (1H, m, H-4), 5.57 (1H, m, H-3). ^{13}C NMR (75 MHz, $CDCl_3$): *δ* 17.5 (Me (C-5), 31.9 (C-2), 36.8 (Me (mesyl)), 69.4 (C-1), 124.5 (C-4), 128.7 (C-3).

(2R,3R)- or (2S,3S)-cis-2-Methyl-3-hydroxy-tetrahydrofuran ***5****.* The procedure for the Sharpless AD was adapted from the literature.[29] To a well-stirred mixture of AD-mix-*β* or AD-mix-*a* (11.05 g) in *t*-butyl alcohol−water (50 mL/50 mL) at room temperature was added **4** (1.312 g, 8 mmol). The reaction mixture was stirred at 5−10 °C overnight in the dark. Next, solid sodium sulfite (4 g) was added, and the mixture was stirred for an additional hour. Methylene chloride (30 mL) was added to the reaction mixture, and after separation of the layers, the aqueous phase (upper layer) was further extracted with CH_2Cl_2. The combined organic extracts were dried over anhydrous $MgSO_4$ and concentrated to give an oil, which was purified by column chromatography (silica gel, petroleum ether/ethyl acetate, 3/1) to afford (2*R*,3*R*)- or (2*S*,3*S*)-**5** as a light yellow oil.

*Data of (2R,3R)-****5*** *(from AD-mix-β).* 88% yield; purity, 95% by GC; 80% ee; $[\alpha]_D^{20}$ = −30.6° (*c* 4.80, $CHCl_3$). ^{1}H NMR (300 MHz, $CDCl_3$): *δ* 1.27 (3H, d, *J* = 6.3 Hz, Me), 1.93 (1H, m, H-4a), 2.22 (1H, m, H-4b), 3.73 (2H, m, H-3, H-5a), 4.03 (1H, dd, *J* = 15.9, 8.1 Hz, H-5b), 4.17 (1H, m, H-2). ^{13}C NMR (75 MHz, $CDCl_3$): *δ* 13.7 (Me), 35.4 (C-4), 65.5 (C-5), 72.8 (C-3), 78.6 (C-2).

*Data of (2S,3S)-****5*** *(from AD-mix-α).* 85% yield; purity, 96% by GC; 62% ee; $[\alpha]_D^{20}$ = +23.7° (*c* 4.50, $CHCl_3$). The ^{1}H NMR and ^{13}C NMR spectra of (2*S*,3*S*)-**5** were the same as those of the antipode.

(2R,3R)- or (2S,3S)-cis-2-Methyl-3-mesyloxy-tetrahydrofuran ***6****.* (2*R*,3*R*)- or (2*S*,3*S*)-**6** was prepared according to our previously published procedures.[26] (2*R*,3*R*)- or (2*S*,3*S*)-**5** reacted with MsCl to give (2*R*,3*R*)- or (2*S*,3*S*)-**6**.

*Data of (2R,3R)-****6****.* 89% yield; purity, 98% by GC; 80% ee; $[\alpha]_D^{20}$ = −19.7° (*c* 5.23, $CHCl_3$). ^{1}H NMR (300 MHz, $CDCl_3$): *δ* 1.33 (3H, d, *J* = 6.6 Hz, Me-2), 2.34 (2H, m, H-4), 3.05 (3H, s, Me (mesyl)), 3.80 (1H, td, *J* = 8.4, 5.4 Hz, H-5a), 4.08 (1H, q, *J* = 8.1 Hz, H-5b), 3.95 (1H, qd, *J* = 6.3, 3.6 Hz, H-2), 5.13 (1H, ddd, *J* = 5.4, 3.6, 2.1 Hz, H-3). ^{13}C NMR (75 MHz, $CDCl_3$): *δ* 14.4 (Me-2), 34.0 (C-4), 38.5 (Me (mesyl)), 65.8 (C-5), 77.2 (C-2), 81.9 (C-3).

*Data of (2S,3S)-****6****.* 90% yield; purity, 96% by GC; 62% ee; $[\alpha]_D^{20}$ = +15.5° (*c* 5.06, $CHCl_3$). The ^{1}H NMR and ^{13}C NMR spectra of (2*S*,3*S*)-**6** were in line with those of the antipode.

(2R,3S)- or (2S,3R)-trans-2-Methyl-tetrahydrofuran-3-thiol Acetate ***1****.* (2*R*,3*S*)- or (2*S*,3*R*)-**1** was prepared according to our previously published procedures.[26] (2*R*,3*R*)- or (2*S*,3*S*)-**6** reacted with AcSH to give (2*R*,3*S*)- or (2*S*,3*R*)-**1**.

DOI: 10.1021/jf503866x
J. Agric. Food Chem. 2015, 63, 464−468

*Data of (2R,3S)-**1***. 81% yield; purity, 97% by GC; 80% ee (t_R 21.540 min); $[\alpha]_D^{20}$ = +27.6° (*c* 4.63, $CHCl_3$). ^1H NMR (300 MHz, $CDCl_3$): δ 1.28 (3H, d, *J* = 6.0 Hz, Me-2), 1.85 (1H, m, H-4a), 2.49 (1H, m, H-4b), 2.34 (3H, s, Me (Ac)), 3.52 (1H, td, *J* = 8.7, 7.2 Hz, H-5), 3.96 (1H, td, *J* = 8.7, 5.7 Hz, H-5), 3.71−3.88 (2H, m, H-2, H-3). ^{13}C NMR (75 MHz, $CDCl_3$): δ 19.2 (Me-2), 30.6 (Me (Ac)), 33.2 (C-4), 46.6 (C-3), 66.7 (C-5), 79.9 (C-2), 195.3 (C═O).

*Data of (2S,3R)-**1***. 83% yield; purity, 98% by GC; 62% ee (t_R 20.694 min); $[\alpha]_D^{20}$ = −20.5° (*c* 4.49, $CHCl_3$). The ^1H NMR and ^{13}C NMR spectra of (2*S*,3*R*)-**1** were in line with those of the antipode.

*(2R,3S)- or (2S,3R)-trans-2-Methyl-3-p-nitrobenzoyloxy-tetrahydrofuran **7***. (2*R*,3*S*)- or (2*S*,3*R*)-7 was prepared according to our previously published procedures.[26] (2*R*,3*R*)- or (2*S*,3*S*)-**5** was treated with Ph_3P, DIAD, and *p*-nitrobenzoic acid to give (2*R*,3*S*)- or (2*S*,3*R*)-**7**.

*Data of (2R,3S)-**7***. 69% yield; mp 46−49 °C; $[\alpha]_D^{20}$ = +21.3° (*c* 4.80, $CHCl_3$). ^1H NMR (300 MHz, $CDCl_3$): δ 1.31 (3H, d, *J* = 6.3 Hz, Me-2), 2.10 (1H, m, H-4a), 2.35 (1H, m, H-4b), 3.83 (1H, m, H-5a), 4.06 (1H, m, H-5b), 4.14 (1H, m, H-2), 5.14 (1H, m, H-3), 8.18 (2H, d, *J* = 9 Hz, H-aryl), 8.27 (2H, d, *J* = 9 Hz, H-aryl). ^{13}C NMR (75 MHz, $CDCl_3$): δ 18.9 (Me-2), 32.0 (C-4), 66.6 (C-5), 79.9 (C-2), 81.1 (C-3), 123.0 (C-3′ and C-5′ (aryl)), 130.2 (C-2′ and C-6′ (aryl)), 134.9 (C-1′ (aryl)), 150.0 (C-4′ (aryl)), 164.2 (C═O).

*Data of (2S,3R)-**7***. 68% yield; mp 47−51 °C; $[\alpha]_D^{20}$ = −15.8° (*c* 4.80, $CHCl_3$). The ^1H NMR and ^{13}C NMR spectra of (2*S*,3*R*)-**7** were in line with those of the antipode.

*(2R,3S)- or (2S,3R)-trans-2-Methyl-3-hydroxy-tetrahydrofuran **5***. To a solution of NaOH (6.4 g, 160 mmol) in methanol/tetrahydrofuran (124 mL, 30:1) was added (2*R*,3*S*)- or (2*S*,3*R*)-**7** (12 g, 48 mmol) at room temperature. The mixture was stirred at room temperature for 5 h. The reaction mixture was concentrated under reduced pressure. The residue was diluted with water, and the mixture was extracted four times with diethyl ether. The combined organic phases were washed once with brine, dried over $MgSO_4$, and concentrated. The crude product was purified by column chromatography (petroleum ether/ethyl acetate, 6/1) to give (2*R*,3*S*)- or (2*S*,3*R*)-**5** as a light yellow oil.

*Data of (2R,3S)-**5***. 90% yield; purity, 97% by GC; 80% ee; $[\alpha]_D^{20}$ = +35.5° (*c* 2.74, MeOH) [lit.[30] $[\alpha]_D^{23}$ +11.7° (*c* 2.5, MeOH, 27% ee)]. ^1H NMR (300 MHz, $CDCl_3$): δ 1.76 (3H, d, *J* = 6.3 Hz, Me-2), 1.84 (1H, m, H-4a), 2.16 (1H, m, H-4b), 2.23 (1H, br, −OH), 3.82 (1H, m, H-3), 3.87−4.01 (3H, m, H-2, H-5). ^{13}C NMR (75 MHz, $CDCl_3$): δ 18.8 (Me-2), 34.3 (C-4), 66.0 (C-5), 76.7 (C-3), 81.7 (C-2).

*Data of (2S,3R)-**5***. 87% yield; purity, 96% by GC; 62% ee; $[\alpha]_D^{20}$ = −26.8° (*c* 4.28, MeOH) [lit.[30] $[\alpha]_D^{23}$ = −29.9° (*c* 2.5, MeOH, 70% ee)]. The NMR data were consistent with those of (2*R*,3*S*)-**5**.

*(2R,3S)- or (2S,3R)-trans-2-Methyl-3-mesyloxytetrahydrofuran **6***. (2*R*,3*S*)- or (2*S*,3*R*)-**5** was converted to the corresponding mesylate (2*R*,3*S*)- or (2*S*,3*R*)-**6** by the same procedure for (2*R*,3*R*)- or (2*S*,3*S*)-**6**.

*Data of (2R,3R)-**6***. 91% yield; purity, 97% by GC; 80% ee; $[\alpha]_D^{20}$ = +20.0° (*c* 6.00, $CHCl_3$). ^1H NMR (300 MHz, $CDCl_3$): δ 1.26 (3H, d, *J* = 6.6 Hz, Me-2), 2.18 (1H, m, H-4a), 2.24 (1H, m, H-4b), 3.04 (3H, s, Me (mesyl)), 3.89 (1H, td, *J* = 9.3, 6.6 Hz, H-5a), 4.01 (1H, td, *J* = 8.4, 3.3 Hz, H-5b), 4.12 (1H, m, H-2), 4.82 (1H, m, H-3). ^{13}C NMR (75 MHz, $CDCl_3$): δ 18.5 (Me-2), 32.5 (C-4), 38.4 (Me (mesyl)), 66.3 (C-5), 79.7 (C-2), 85.1 (C-3).

*Data of (2S,3S)-**6***. 92% yield; purity, 98% by GC; 62% ee; $[\alpha]_D^{20}$ = −14.5° (*c* 5.50, $CHCl_3$). The NMR data were consistent with those of (2*R*,3*R*)-**6**.

*(2R,3R)- or (2S,3S)-cis-2-Methyl-tetrahydrofuran-3-thiol Acetate **1***. (2*R*,3*S*)- or (2*S*,3*R*)-**6** was converted to the corresponding acetate (2*R*,3*R*)- or (2*S*,3*S*)-**1** by the same procedure for (2*R*,3*S*)- or (2*S*,3*R*)-**1**.

*Data of (2R,3R)-**1***. 85% yield; purity, 97% by GC; 80% ee (t_R 21.939 min); $[\alpha]_D^{20}$ = +10.7° (*c* 4.95, $CHCl_3$). ^1H NMR (300 MHz, $CDCl_3$): δ 1.19 (3H, d, *J* = 6.3 Hz, Me-2), 1.93 (1H, m, H-4a), 2.48 (1H, m, H-4b), 2.34 (3H, s, Me (Ac)), 3.75 (1H, td, *J* = 8.4, 6.3 Hz, H-5), 3.90 (1H, td, *J* = 8.4, 6.3 Hz, H-5), 4.13 (1H, m, H-2), 4.05 (1H, m, H-3). ^{13}C NMR (75 MHz, $CDCl_3$): δ 16.8 (Me-2), 30.6 (Me (Ac)), 33.5 (C-4), 46.3 (C-3), 65.9 (C-5), 76.5 (C-2), 195.4 (C═O).

*Data of (2S,3S)-**1***. 84% yield; purity, 98% by GC; 62% ee (t_R 22.265 min); $[\alpha]_D^{20}$ = −8.09° (*c* 4.37, $CHCl_3$). The NMR data were consistent with those of (2*R*,3*R*)-**1**.

Analytical Methods. *Enantioselective Analysis.* An Agilent 6890 GC with a flame ionization detector (FID) was used for GC analyses (Agilent Technologies, Santa Clara, CA). The columns used included a B-PM chiral capillary column (50 m × 0.25 mm × 0.25 μm), and a G-TA (50 m × 0.25 mm × 0.125 μm) from the ASTEC Co. (Chattanooga, TN). The analytical conditions for **1** and **5** (G-TA, 50 m) were as follows: injector temperature 250 °C, detector temperature 250 °C, N_2 as carrier gas, constant flow mode 0.8 mL/min, split ratio 50/1. The oven temperature was programmed from 50 to 170 °C at a rate of 5 °C/min, and held at 170 °C for 10 min. A different oven temperature program used for *cis*-**6** (B-PM, 50 m) was as follows: raised from 50 to 140 °C at a rate of 20 °C/min, and held at 140 °C for 2 min; raised to 155 °C at 0.2 °C/min, and was held at 155 °C for 5 min, then raised to 200 °C at 20 °C/min, and was held at 200 °C for 2 min. For *trans*-**6** (B-PM, 50 m), the conditions were as follows: raised from 50 to 120 °C at a rate of 5 °C/min, and held at 120 °C for 10 min; raised to 200 °C at 8 °C/min, and was held at 200 °C for 2 min. The concentration of samples was about 0.5 wt % in ethanol, and the injection volume was about 0.6 μL.

Chiral HPLC Analysis. HPLC analyses were conducted by an Agilent 1200 HPLC apparatus (column, Chiralcel OD-H or OB-H column (0.46 cm, ϕ × 15 cm) (Daicel, Japan); solvent, *n*-hexane-*i*-PrOH (9/1); flow rate, 0.5 mL/min; UV detection, 254 nm).

Chiral GC−O Analysis and Evaluation. Chiral GC−O analysis was carried out using an Agilent 6890N gas chromatograph installed with a chiral capillary column G-TA (50 m × 0.25 mm × 0.25 μm), a FID, and a sniffing port (Sniffer 9000; Brechbühler Scientific Analytical Solutions, Schlieren, Switzerland). The analytical conditions were the same as those in the determination of ee values by GC analysis. The column effluent was divided (ratio 1:1) between the FID detector and the sniffing port through one Y-shaped glass splitter. The effluent to the sniffing port was enclosed with a stream of humidified air of 16 mL/min and transferred to the glass detection cone by one length of capillary column at the temperature of 250 °C.

Sensory Panel. The panel consisted of 5 healthy, nonsmoking judges, 2 males and 3 females, aged 23−29. All panelists belong to the Beijing Key Laboratory of Flavor Chemistry, Beijing Technology and Business University. The judges were selected for their experience in assessing volatile flavor compounds of foods. A verbal description of the odor was obtained from the panelist when the peak appeared at the GC at the same time.

General Conditions for Odor Thresholds. Odor thresholds were determined according to the procedure described by Ullrich and Grosch.[31] The defined amounts of samples and the internal standard *trans*-2-decenal, the odor threshold of which in air is 2.7 ng/L,[32] were dissolved in EtOH and diluted stepwise by a factor of 1:1 (v/v). The aliquots were analyzed by GC−O until no odor was detectable.

NMR Spectroscopy. ^1H NMR and ^{13}C NMR spectra were recorded at 300 and 75 MHz, respectively, with an Avance 300 spectrometer. The experiments were done in full automation using standard parameter sets of the TOPSPIN 2.0 software package (Bruker). The compounds were dissolved in deuterated chloroform. The spectra were recorded at 25 °C.

Optical Rotations. Optical rotations were measured on an Autopol IV digital automatic polarimeter (Rudolph, Hackettstown, NJ).

RESULTS AND DISCUSSION

Preparation and Configuration Assignment of the Four Stereoisomers of 2-Methyl-tetrahydrofuran-3-thiol Acetate. The substrate for Sharpless AD, (3*E*)-pent-3-en-1-yl mesylate **4**, was easily prepared by the Knoevenagel condensation of propanal and malonic acid, followed by reduction with $LiAlH_4$ and mesylation. The procedure for Knoevenagel condensation was modified according to the

DOI: 10.1021/jf503866x
J. Agric. Food Chem. 2015, 63, 464−468

literature using DMSO as solvent instead of xylene,[27] which led to the remarkable improvements of both chemical selectivity and yield as compared to the results we published earlier.[26] (3*E*)-Pent-3-enoic acid **2** was obtained in about 60% yield with only 2% byproduct (2*E*)-pent-2-enoic acid.

The chiral centers of the four stereoisomers of 2-methyl-tetrahydrofuran-3-thiol acetate **1** were originated from Sharpless AD of (3*E*)-pent-3-en-1-yl mesylate **4**. 2-Methyl-3-hydroxy-tetrahydrofuran **5** was produced by Sharpless AD of **4** followed by an intramolecular S_N2 nucleophilic substitution in situ. The relative configuration of **5** was determined to be *cis* by comparing the ^{1}H NMR data with those of 2-methyl-3-hydroxy-tetrahydrofuran synthesized by oxidation of (3*E*)-pent-3-en-1-yl mesylate with H_2O_2/HCOOH or $KMnO_4$.[26] Also, the absolute configuration of **5** was tentatively assigned according to an empirical model developed by Sharpless et al.[33] (2*R*,3*R*)-*cis*-**5** was obtained using AD-mix-β as an oxidant, whereas (2*S*,3*S*)-*cis*-**5** was obtained from AD-mix-α. The specific rotation value of optically active (2*R*,3*S*)- or (2*S*,3*R*)-*trans*-**5** derived from the above obtained (2*R*,3*R*)- or (2*S*,3*S*)-*cis*-**5** by Mitsunobu reaction was consistent with the literature data,[30] which confirmed the aforementioned tentative assignment of absolute configuration. The chiral GC analysis of *cis*-**5** was carried out on G-TA (50 m × 0.25 mm × 0.125 μm) using trifluoroacetyl γ-cyclodextrin as chiral stationary phase, which enabled the separation of the two enantiomers of *cis*-**5**. (2*R*,3*R*)-**5** from AD-mix-β was obtained in 80% ee, whereas (2*S*,3*S*)-**5** was found in a relatively lower ee of 62%. (2*R*,3*R*)- or (2*S*,3*S*)-**5** was converted to the target compound (2*R*,3*S*)- or (2*S*,3*R*)-**1**, respectively, through S_N2 substitution of the corresponding mesylate by AcSH. The ee values of the intermediate mesylates were determined on B-PM (50 m × 0.25 mm × 0.125 μm), and the target compounds were analyzed by the same way as **5**. The obtained results of optical purity were consistent with those of **5**.

To obtain the two enantiomers of *cis*-**1**, (2*R*,3*R*)- or (2*S*,3*S*)-**5** produced by the Sharpless AD was subjected to Mitsunobu reaction, which gave (2*R*,3*S*)- or (2*S*,3*R*)-*trans*-2-methyl-3-*p*-nitrobenzoyloxy-tetrahydrofuran **7**. The determination of the ee values of the obtained benzoates failed by HPLC analyses on different columns, such as Chiralcel column OD-H and OB-H. The benzoates were then hydrolyzed to produce the two enantiomers of *trans*-**5**, respectively, which went through mesylation and nucleophilic substitution to afford the two enantiomers of *cis*-**1**, that is, (2*R*,3*R*)- and (2*S*,3*S*)-**1**. The ee values of (2*R*,3*R*)- and (2*S*,3*S*)-**1** were in accord with the starting material (2*R*,3*R*)- and (2*S*,3*S*)-**5**, which indicated no racemization occurred in Mitsunobu reaction, mesylation, and nucleophilic substitution.

Determination of Odor Properties. The enantiomers of *cis*- or *trans*-**1** were separated completely by a chiral GC column G-TA (50 m × 0.25 mm × 0.25 μm), on which the peak resolution R_s for two enantiomers of *cis*- or *trans*-**1** was 1.5 and 4.0, respectively. The odor properties of the four stereoisomers of 2-methyl-tetrahydrofuran-3-thiol acetate **1** were evaluated by the panel via chiral GC−O (Table 1). Among the four stereoisomers, both enantiomers of *trans*-**1** were found to possess meaty aroma as a top note, whereas the two enantiomers of *cis*-**1** were described to present mainly a top note of pungent smell of raw garlic and onion. In addition, the odor discrepancy between the two enantiomers of *trans*-**1** or *cis*-**1** also exited. For the enantiomers of *trans*-**1**, (2*S*,3*R*)-**1** smelled like roasted meat with an undernote of burnt and fried onion; in comparison, (2*R*,3*S*)-**1** smelled meaty with an undernote of sesame paste, fried onion and garlic, sweet, and sulfurous. Also, the former smelled more pleasant. For the enantiomers of *cis*-**1**, (2*R*,3*R*)-**1** presented additional savory and musty notes as compared to (2*S*,3*S*)-**1**.

Table 1. Odor Descriptions and Odor Thresholds of the Four Stereoisomers of 1

stereoisomers	odor description	odor thresholds in air[a] (ng/L)
(2*R*,3*S*)-**1**	meaty, sesame paste, fried onion and garlic, sweet, sulfurous	18.6
(2*S*,3*R*)-**1**	roasted meat, burnt, fried onion	7.3
(2*R*,3*R*)-**1**	raw garlic and onion-like, savory, musty, sulfurous	3.8
(2*S*,3*S*)-**1**	raw garlic and onion-like, sulfurous	5.7

[a]Mean values of duplicates, differing not more than ±10%.

Determination of Odor Thresholds. The odor thresholds of the four stereoisomers of 2-methyl-tetrahydrofuran-3-thiol acetate **1** were determined following the procedure described by Ullrich and Grosch.[31] Ethanol was used as solvent instead of diethyl ether because it was difficult to guarantee the accuracy of the sample concentration due to the high volatility of ether solution. For each stereoisomer, the sensory evaluations were performed in duplicate, and two stock solutions with similar concentration were prepared for each stereoisomer. The samples were evaluated by one judge, and the lowest concentration was double-checked by three consecutive GC−O runs. The odor thresholds of the two enantiomers of *trans*-**1**, that is, (2*R*,3*S*)- and (2*S*,3*R*)-**1**, were determined to be 18.6 and 7.3 ng/L air, respectively. In comparison, the odor thresholds of *cis*-**1**, that is, (2*R*,3*R*)- and (2*S*,3*S*)-**1**, were slightly lower, which were 3.8 and 5.7 ng/L air, respectively. The (2*R*,3*R*)-isomer was observed to have the lowest threshold, whereas the (2*R*,3*S*)-isomer had the highest threshold. Both isomers with relatively lower thresholds of *cis*- and *trans*-**1** were found to be (3*R*)-configuration. As compared to the odor thresholds of four stereoisomers of the corresponding thiol reported by Goeke,[24] the acetates had much higher thresholds. We tried to use the same procedure to determine the odor thresholds of the thiols prepared by hydrolysis of the corresponding stereoisomers of acetates. However, the separation of stereoisomers of thiols failed on chiral GC columns we have in our lab.

In conclusion, the four stereoisomers of 2-methyl-tetrahydrofuran-3-thiol acetate were prepared by application of Sharpless AD in conjunction with the Mitsunobu reaction. The GC−O data revealed that the four stereoisomers presented perceptible differences in odor properties. It looked as though the corresponding thiols had much lower odor thresholds. However, further work is needed, such as the preparation of enantiomerically pure stereoisomers, to determine the odor thresholds of these pure samples in water or air accurately.

AUTHOR INFORMATION

Corresponding Author

*Tel.: 86-10-68984545. Fax: 86-10-68985219. E-mail: tianhy@btbu.edu.cn.

Funding

This work was supported by the National Natural Science Foundation of China (no. 31271932), the National Key Technology R&D Program (2011BAD23B01), and the

DOI: 10.1021/jf503866x
J. Agric. Food Chem. 2015, 63, 464−468

Importation and Development of High-Caliber Talents Project of Beijing Municipal Institutions (CIT&TCD20140306).

Notes

The authors declare no competing financial interest.

■ ABBREVIATIONS USED

DIAD, diisopropyl azodicarboxylate; MsCl, methanesulfonyl chloride; AcSH, thiolacetic acid; AD, asymmetricdihyoxylation; HPLC, high-performance liquid chromatography; Ph_3P, triphenylphosphine; PNBA, *p*-nitrobenzoic acid; DMSO, dimethyl sulfoxide; GC−O, gas chromatography−olfactometry; FEMA, Flavor and Extract Manufacturers' Association; FEXPAN, Flavor Expert Panel; GRAS, generally recognized as safe; FID, flame ionization detector

■ REFERENCES

(1) Leffingwell, J. C. *Chirality & Odour Perception*, http://www.lefingwell.com/chirality/chirality.htm (accessed Dec. 12th, 2014).
(2) Rienäcker, R.; Ohloff, G. Optisch aktives *β*-citronellol aus (+)- oder (−)-pinan. *Angew. Chem.* **1961**, *73*, 240.
(3) Bentley, R. The nose as a stereochemist. Enantiomers and odor. *Chem. Rev.* **2006**, *106*, 4099−4112.
(4) Brenna, E.; Fuganti, C.; Serra, S. Enantioselective perception of chiral odorants. *Tetrahedron: Asymmetry* **2003**, *14*, 1−42.
(5) Brenna, E.; Fuganti, C.; Gatti, F. G.; Serra, S. Biocatalytic methods for the synthesis of enantioenriched odor active compounds. *Chem. Rev.* **2011**, *111*, 4036−4072.
(6) Norenberg, S.; Reichardt, B.; Andelfinger, V.; Eisenreich, W.; Engel, K. H. Influence of the stereochemistry on the sensory properties of 4-mercapto-2-heptanol and its acetyl-derivatives. *J. Agric. Food Chem.* **2013**, *61*, 2062−2069.
(7) Kraft, P.; Fráter, G. Enantioselectivity of the musk odor sensation. *Chirality* **2001**, *13*, 388−394.
(8) Aprotosoaie, A. C.; Hăncianu, M.; Costache, I.; Miron, A. Linalool: a review on a key odorant molecule with valuable biological properties. *Flavour Fragrance J.* **2014**, *29*, 193−219.
(9) Kirsch, F.; Buettner, A. Odor qualities and thresholds of physiological metabolites of 1,8-cineole as an example for structure activity relationships considering chirality aspects. *Chem. Biodiversity* **2013**, *10*, 1683−1695.
(10) Luntzel, C. S.; Widder, S.; Vossing, T.; Pickenhagen, W. Enantioselective syntheses and sensory properties of the 3-mercapto-2-methylpentanols. *J. Agric. Food Chem.* **2000**, *48*, 424−427.
(11) Liu, Y. G.; Chen, K.; Li, C.; Zhang, S.; Chen, H.; Tian, H. Y.; Sun, B. G. Preparation and characteristic odour of optically active 3-hydroxy-2-octanone. *Flavour Fragrance J.* **2012**, *27*, 393−396.
(12) McGorrin, R. J. The significance of volatile sulfur compounds in food flavors. In *Volatile Sulfur Compounds in Food*; Qian, M., Fan, X. T., Mahattanatawee, K., Eds.; ACS Symposium Series 1068; American Chemical Society: Washington, DC, 2011; pp 3−31.
(13) Goeke, A. Sulfur-containing odorants in fragrance chemistry. *Surfur Rep.* **2002**, *23*, 243−278.
(14) Blank, I. Sensory relevance of volatile organic sulfur compounds in food. In *Heteroatomic Aroma Compounds*; Reineccius, G. A., Reineccius, T. A., Eds.; ACS Symposium Series 826; American Chemical Society: Washington, DC, 2002; pp 25−53.
(15) Conde-Martinez, N.; Sinuco, D. C.; Osorio, C. Chemical studies on curuba (Passiflora mollissima (Kunth) L. H. Bailey) fruit flavour. *Food Chem.* **2014**, *157*, 356−363.
(16) Mahattanatawee, K.; Rouseff, R. L. Comparison of aroma active and sulfur volatiles in three fragrant rice cultivars using GC-Olfactometry and GC-PFPD. *Food Chem.* **2014**, *154*, 1−6.
(17) Starkenmann, C.; Niclass, Y. New cysteine-S-conjugate precursors of volatile sulfur compounds in bell peppers (Capsicum annuum L. Cultivar). *J. Agric. Food Chem.* **2011**, *59*, 3358−3365.
(18) Naef, R.; Velluz, A.; Jaquier, A. New volatile sulfur-containing constituents in a simultaneous distillation-extraction extract of red bell peppers (Capsicum annuum). *J. Agric. Food Chem.* **2008**, *56*, 517−527.
(19) Ruther, J.; Baltes, W. Sulfur-containing furans in commercial meat flavorings. *J. Agric. Food Chem.* **1994**, *42*, 2254−2259.
(20) Cano-Garcia, L.; Rivera-Jimenez, S.; Belloch, C.; Flores, M. Generation of aroma compounds in a fermented sausage meat model system by Debaryomyces hansenii strains. *Food Chem.* **2014**, *151*, 364−373.
(21) Thomas, C.; Mercier, F.; Tournayre, P.; Martin, J. L.; Berdague, J. L. Identification and origin of odorous sulfur compounds in cooked ham. *Food Chem.* **2014**, *155*, 207−213.
(22) Vermeulen, C.; Gijs, L.; Collin, S. Sensorial contribution and formation pathways of thiols in foods: A review. *Food Rev. Int.* **2005**, *21*, 69−137.
(23) Cerny, C. Origin of carbons in sulfur-containing aroma compounds from the Maillard reaction of xylose, cysteine and thiamine. *LWT-Food Sci. Technol.* **2007**, *40*, 1309−1315.
(24) Goeke, A. Diastereo-and enantioselective syntheses of 2-methyl-tetrahydrofuran-3-thiol. *Phosphorus, Sulfur Silicon Relat. Elem.* **1999**, *153*, 303−304.
(25) Smith, R. L.; Waddell, W. J.; Cohen, S. M.; Fukushima, S.; Gooderham, N. J.; Hecht, S. S.; Marnett, L. J.; Portoghese, P. S.; Rietjens, I. M. C. M.; Adams, T. B.; Gavin, C. L.; McGowen, M. M.; Taylor, S. V. Gras flavoring substances 25. *Food Technol.* **2011**, *65*, 44−55.
(26) Dai, Y. F.; Sun, B. G.; Tian, H. Y. Preparation and odour of cis- and trans-2-methyl tetrahydrofuran-3-thiolacetates. *J. Chem. Res.* **2014**, *38*, 236−239.
(27) Qin, C. G.; Davies, H. M. L. Rh_2(R-TPCP)$_4$-Catalyzed enantioselective [3+2]-cycloaddition between nitrones and vinyldiazoacetates. *J. Am. Chem. Soc.* **2013**, *135*, 14516−14519.
(28) Thibonnet, J.; Abarbri, M.; Parrain, J.-L.; Duchêne, A. Stereoselective access to functionalized *β*-*γ* unsaturated acids. *Tetrahedron* **2003**, *59*, 4433−4441.
(29) Hashiyama, T.; Morikawa, K.; Sharpless, K. B. a-Hydroxy ketones in high enantiomeric purity from asymmetric dihydroxylation of enol. *J. Org. Chem.* **1992**, *57*, 5067−5068.
(30) Brown, H. C.; Vara Prasad, J. V. N.; Zaidlewicz, M. Hydroboration. 82. Asymmetric hydroboration of representative cis disubstituted and heterocyclic olefins with dicaranylboranes of high enantiomeric purity. *J. Org. Chem.* **1988**, *53*, 2911−2916.
(31) Ullrich, F.; Grosch, W. Identification of the most intense volatile flavour compounds formed during autoxidation of linoleic acid. *Z. Lebensm.-Unters. Forsch.* **1987**, *184*, 277−282.
(32) Boelens, M. H.; van Gemert, L. J. Physiochemical parameters related to organoleptic properties of flavor components. In *Development in Food Flavours*; Birch, G., Lindley, M. G., Eds.; Elsevier Applied Science: London, UK, 1986; pp 23−49.
(33) Sharpless, K. B.; Amberg, W.; Bennani, Y. L.; Crispino, G. A.; Hartung, J.; Jeong, K. S.; Kwong, H. L.; Morikawa, K.; Wang, Z. M.; Xu, D.; Zhang, X.-L. The osmium-catalyzed asymmetric dihydroxylation: a new ligand class and a process improvement. *J. Org. Chem.* **1992**, *57*, 2768−2771.

DOI: 10.1021/jf503866x
J. Agric. Food Chem. 2015, 63, 464−468

JOURNAL OF AGRICULTURAL AND FOOD CHEMISTRY

Article

pubs.acs.org/JAFC

High Enantiomeric Excess of the Flavor Relevant 4-Alkyl-Branched Fatty Acids in Milk Fat and Subcutaneous Adipose Tissue of Sheep and Goat

Stefanie Kaffarnik, Carolina Heid, Yasemin Kayademir, Dorothee Eibler, and Walter Vetter*

University of Hohenheim, Institute of Food Chemistry (170b), Garbenstraße 28, 70593 Stuttgart, Germany

ABSTRACT: Volatile 4-alkyl-branched fatty acids are characteristic flavor compounds of sheep and goat. Due to the methyl branch, the carbon C-4 represents a stereogenic center with the possible presence of one or both enantiomers in the respective samples. In this study, we used enantioselective gas chromatography to study the enantiomeric composition of 4-methyloctanoic acid (4-Me-8:0) and 4-ethyloctanoic acid (4-Et-8:0) in milk and dairy products from sheep and goat as well as in goat subcutaneous tissue. Different columns coated with modified cyclodextrins were tested to resolve racemic 4-alkyl-branched fatty acid methyl ester standards. The best enantiomer resolution was obtained on 25% *octakis*(2,3,6-tri-*O*-ethyl)-γ-cyclodextrin (γ-TECD) diluted in OV-1701. For analysis of the food samples, the lipids were extracted and fatty acids in the extracts were converted into fatty acid methyl esters. Non-aqueous reversed-phase high-performance liquid chromatography was used to fractionate the samples in order to gain one solution enriched in 4-Me-8:0 methyl ester and one solution enriched with 4-Et-8:0 methyl ester. Subsequent analysis by enantioselective gas chromatography with mass spectrometry allowed only the detection of one enantiomer of 4-Me-8:0 and 4-Et-8:0 in the samples. By means of a non-racemic standard of 4-Me-8:0, it was found that the predominant enantiomer was (*R*)-4-Me-8:0.

KEYWORDS: *alkyl-branched-chain fatty acids, enantioselective analysis, modified cyclodextrins, goat, sheep, milk*

INTRODUCTION

The 4-alkyl-branched fatty acids, 4-methyloctanoic acid (4-Me-8:0), 4-ethyloctanoic acid (4-Et-8:0), and 4-methylnonanoic acid (4-Me-9:0), were found to be responsible for the characteristic sweet, goaty and sheepy aroma of sheep and goat.[1−4] The carbon at the branching point (i.e., C-4) represents a stereogenic center, due to its substitution with four chemically different moieties. Accordingly, 4-alkyl-branched fatty acids may occur in both *S*- and *R*-forms in nature. In such situations, enantioselective studies may contribute to the understanding of the impact because enantiomers of the same molecule may have different properties including flavor notes. In addition, enantioselective analyses can provide insights into the biosynthesis of chiral compounds.

Different modified cyclodextrins have been used for the enantiomer separation of chiral compounds by gas chromatography (GC). Cyclodextrins (CD) are cyclic oligosaccharides composed of six (α-cyclodextrin), seven (β-cyclodextrin), or eight (γ-cyclodextrin) (1,4)-linked α-glucopyranose units which have the three-dimensional shape of a hollow torus.[5−7] Each glucopyranose unit of the cyclodextrin has hydroxyl groups in the 2-, 3-, and 6-positions which need to be modified for their applicability in GC. Suitable substituents are alkyl groups, acetyl groups, or silyl groups (especially *tert*-butyldimethylsilyl substituents).[8,9] Unfortunately, the potential of a chiral stationary phase (CSP) for a successful enantiomer separation cannot be predicted and has to be tested individually. Previous research has shown that the enantiomer separation of chiral fatty acids becomes more difficult if the stereogenic center is remote from the functional carboxylic group. For instance, the food relevant *anteiso*-fatty acids (fatty acids with a methyl branch on the antepenultimate carbon which is the stereogenic center) 12-methyltetradecanoic acid (*a*15:0) and 14-methylhexadecanoic acid (*a*17:0) have 10 methylene groups or more between the headgroup and the methyl branch and are difficult to enantioseparate.[10] By contrast, the enantioseparation of racemic standards of free 2-, 3-, and 4-alkyl-branched fatty acids has been achieved on *heptakis*(2,3-di-*O*-methyl-6-*O*-*tert*-butyldimethylsilyl)-β-cyclodextrin (β-TBDM) as well as on *octakis*(2,3-di-*O*-methyl-6-*O*-*tert*-butyldimethylsilyl)-γ-cyclodextrin (γ-TBDM).[11−14]

The aim of this study was to analyze the enantiomer composition of 4-Me-8:0 and 4-Et-8:0 in sheep and goat samples. For the enantioselective analysis of racemic standards of 4-Me-8:0, 4-Et-8:0, and 4-Me-9:0 methyl esters, we tested four CSPs and finally applied a CSP consisting of 25% *octakis*(2,3,6-tri-*O*-ethyl)-γ-cyclodextrin (γ-TECD) diluted in OV-1701. For the analysis of samples, volatile fatty acids had to be enriched because they are present only as minor components in milk fat of goat and sheep as well as in sheep subcutaneous adipose tissue.[15−19] For this purpose, the lipid phase was isolated and the fatty acids in the fraction were transferred into fatty acid methyl esters which were fractionated by non-aqueous reversed-phase high-performance liquid chromatography (RP-HPLC) similarly to the method of Hauff et al.[10] Enriched fractions of the fatty acids were then analyzed by GC with mass spectrometry operated in the selected ion monitoring mode (GC/MS-SIM).

Received: July 29, 2014
Revised: December 22, 2014
Accepted: December 27, 2014
Published: December 27, 2014

ACS Publications © 2014 American Chemical Society

DOI: 10.1021/jf505452u
J. Agric. Food Chem. 2015, 63, 469−475

MATERIALS AND METHODS

Chemicals. Methanol (purity >95%), *n*-hexane (purity >95%), and acetonitrile (purity 99.9%) were from Th. Geyer (Renningen, Germany). Concentrated sulfuric acid (>98%) was from BASF (Ludwigshafen, Germany), whereas sodium chloride was from Carl Roth (Karlsruhe, Germany). Helium (purity 5.0) and nitrogen (purity 5.0) were from Westfalen (Münster, Germany). Racemic standards of 4-methyloctanoic acid (4-Me-8:0), 4-ethyloctanoic acid (4-Et-8:0), and 4-methylnonanoic acid (4-Me-9:0) were from Endeavor Specialty Chemicals Ltd. (Daventry, U.K.). Racemic 4-methylhexanoic acid (4-Me-6:0) was from Sigma-Aldrich (Steinheim, Germany). Two different standard mixtures were prepared and used in this study. The racemic standard mixture 1 consisted of the methyl esters of 4-Me-6:0, 4-Me-8:0, and 4-Me-9:0, whereas the racemic standard mixture 2 consisted of the methyl esters of 4-Me-8:0, 4-Me-9:0, and 4-Et-8:0. The concentration of each compound in the mixtures was 10 ng/μL. Because pure enantiomer standards were not commercially available, a non-racemic standard of free 4-methyloctanoic acid was produced as follows. Racemic 4-Me-8:0 was derivatized with (−)-menthol to give the corresponding 4-Me-8:0 (−)-menthyl ester (i.e., a mixture of two diastereomers). The diastereomers were separated by reversed-phase HPLC using four serially linked columns (similarly to the method shown below for the isolation of individual fatty acids) and 100% acetonitrile as the mobile phase.[20] From 80 to 100 min, 40 fractions were taken every 0.5 min and the (−)-menthyl esters were saponified with KOH, the solutions acidified with HCl, and the free 4-Me-8:0 extracted with *n*-hexane. Enantioselective analysis of the RP-HPLC fractions allowed selecting one solution showing a distinct non-racemic composition of 4-Me-8:0. Aliquots of this fraction were also transferred in the corresponding methyl ester.

Samples. In a recent study, we developed a method for the direct quantitation of volatile 4-alkyl-branched fatty acid methyl ester in sheep and goat samples.[18] The samples with quantitative data for 4-Me-8:0, 4-Et-8:0, and 4-Me-9:0 were used in the present study for enantioselective determinations.[18,19] In brief, we used two goat milk and two sheep milk samples and nine cheese samples made from goat or sheep milk. These samples were bought in retail stores close to Stuttgart (Germany) in 2013/2014. In addition, two samples of homogenized sheep subcutaneous adipose tissue were analyzed in this study. The milk and cheese samples were lyophilized and extracted by accelerated solvent extraction before transesterification, as previously described,[19] while the sheep subcutaneous adipose tissue was directly subjected to transesterification.[18]

Transesterification Procedure. An aliquot of 3 mL of the milk fat extract (fat content ∼1 g, solvent evaporated thereafter) or ∼1 g of subcutaneous adipose tissue and 50 mL of 1% sulfuric acid in methanol was placed in a 100 mL round flask. The sample solution was stirred and refluxed for 2 h at 80 °C. After cooling the mixture on ice, it followed the addition of 20 mL of distilled water, 30 mL of saturated aqueous sodium chloride solution, and 500 μL of *n*-hexane. The two-phase system was vigorously shaken, and the upper organic phase was separated for RP-HPLC enrichment.

Non-Aqueous Reversed-Phase High-Performance Liquid Chromatography (RP-HPLC). The fractionation was based on the method of Hauff et al.[10] developed for *anteiso*-fatty acids with modifications. About 0.2 mL of acetonitrile was placed in a 1.5 mL GC vial, and 0.2 mL of the sample extract in *n*-hexane was added. After shaking, the upper *n*-hexane phase was evaporated by a gentle stream of nitrogen at 30 °C. The fatty acid methyl esters remained in the more polar acetonitrile phase. This solution could directly be used for RP-HPLC analysis, because acetonitrile is miscible with the mobile phase methanol. Enrichment of 4-methyl-branched fatty acid methyl esters was performed with a Waters HPLC system (Milford, USA) consisting of a 717 plus auto sampler, a 616 pump, a 996 photodiode array detector (DAD), and a 600S controller. Sample solutions (20 μL) were injected at room temperature (24 °C). The flow rate of the mobile phase methanol was set to 0.5 mL/min. Three serially linked columns were used for separation, i.e., two Supelcosil LC-18-DB columns of 16 and 25 cm length, 4.6 mm inner diameter, and 5 μm particle size from Supelco (Taufkirchen, Germany) and one 25 cm length × 4.6 mm inner diameter C_{30}-RP-HPLC column with 5 μm particle size from Trentec (Gerlingen, Germany). Because methyl esters of saturated fatty acids do not provide a response in UV or fluorescence detectors, the samples were fractionated without a detector. For this reason, 14 fractions were collected in intervals of 4 min (corresponding to a 2 mL volume). Subsequently, 0.5 mL of water and 0.5 mL of saturated aqueous sodium chloride solution as well as 200 μL of *n*-hexane were added to each fraction for extraction. The organic phase containing the fatty acid methyl esters was separated and analyzed by GC/MS. Further concentration of fractions 5 and 6 by a factor of 2 was carried out as follows. In order to prevent loss of the volatile analytes, 15 μL of methanol was added to 40 μL of the sample and the resulting azeotropic mixture of *n*-hexane and methanol (72:28; v/v) was carefully evaporated with a slight stream of nitrogen until the final volume was 20 μL.

Column Testing by Gas Chromatography with Flame Ionization Detection (GC/FID). Enantioseparations of racemic standards of 4-methyl-branched fatty acid methyl esters on different CSPs were performed with a Hewlett-Packard 5890 series II GC equipped with a flame ionization detector (GC/FID), a 7673 auto sampler, and a split/splitless injector. The injection volume was set to 1 μL. Four columns with modified cyclodextrins were tested. The first two contained the same amount of the same modified cyclodextrin dissolved in two different polysiloxanes, i.e., 20% *heptakis*(6-*O*-*tert*-butyldimethylsilyl-2,3-di-*O*-methyl)-β-cyclodextrin (β-TBDM) in (i) SE-52 or (ii) PS086 (30 m length, 0.25 mm inner diameter, 0.1 μm film thickness, BGB Analytik, Adliswil, Switzerland). In addition, we used (iii) 66% *heptakis*(6-*O*-*tert*-butyldimethylsilyl-2,3-di-*O*-methyl)-β-cyclodextrin (β-TBDM) in OV-1701 (30 m length, 0.25 mm inner diameter, 0.1 μm film thickness, BGB Analytik, Adliswil, Switzerland) and (iv) 25% triethylated-γ-cyclodextrin (γ-TECD) in OV-1701 (12 m, 0.25 mm inner diameter, film thickness not specified). The γ-TECD column (Table 1) was prepared in the laboratories of Prof. Dr. Michael Oehme (University of Basel, Switzerland).[21−23]

Nitrogen was used as the carrier gas with a column head pressure of 10 psi (30 m columns) or 6 psi (12 m γ-TECD). For enantioselective analysis on the β-TBDM column, the oven program started at 60 °C for 10 min, ramped 0.5 °C/min to a final temperature of 80 °C (β-TBDM: method A). The performance on the γ-TECD column differed from that on the β-TBDM column. On γ-TECD, the isothermal temperature oven program was at 40 °C for 280 min (γ-TECD: method B).

Enantioselective GC/MS-SIM Analysis of 4-Alkyl-Branched Fatty Acids as Methyl Esters in Samples. Enantioselective analyses were performed with a CP-3800/1200 GC/MS system equipped with a CP-8410 auto sampler (Varian, Darmstadt, Germany). The split/splitless injector was heated to 250 °C and used in splitless mode (split opened after 2 min). The injection volume was 1, 2, or 3 μL, depending on the fatty acid concentration. Helium was used as the carrier gas with a flow rate of 1.2 mL/min. Electron ionization was carried out with 70 eV. The transfer line temperature was set at 40 °C, while the temperature of the ion source was 200 °C. The GC column (iv) (γ-TECD) was installed in the GC oven using a retention gap (1 m, 0.25 inner diameter). The analyses were performed isothermally at 40 °C. After the elution of the analytes, a second run was started for the elution of less volatile compounds in the sample solution. This run started for 8 min at 40 °C before the temperature was raised at 10 °C/min to 150 °C (hold time 1 min). The new injection also served to rinse the injector by the injection and volatilization of the solvent. This program was repeated three times in order to elute higher boiling compounds from the column. During the third run, we could not observe peaks anymore in the chromatogram. In the selected ion monitoring (SIM) mode, m/z 74, 87, 99, 115, 129, 141, and 172 (M^+ of 4-Me-8:0 methyl ester) were measured from 10 to 60 min followed by m/z 74, 87, 113, 115, 129, 155, and 186 (M^+ of 4-Me-9:0-ME and 4-Et-8:0-ME) from 60 to 90 min (method C). The limit of quantitation (LOQ) was determined to be 0.34 mg/g for 4-Me-8:0-ME as well as 0.78 mg/g for 4-Et-8:0-ME and 4-Me-9:0-ME. The limit of detection (LOD) was 0.10 mg/g for 4-Me-8:0-ME and 0.23 mg/g

DOI: 10.1021/jf505452u
J. Agric. Food Chem. 2015, 63, 469−475

Table 1. Enantioseparation Characteristics (Separation Factor α and Valley between the Peaks in %) of 4-Alkyl-Branched Fatty Acid Methyl Esters on Modified Cyclodextrin Columns

					α-value				valley between the enantiomer peaks (%)			
no.	column	solvent	length (m)	GC method	4-Me-6:0	4-Me-8:0	4-Et-8:0	4-Me-9:0	4-Me-6:0	4-Me-8:0	4-Et-8:0	4-Me-9:0
1 (i)	20% β-TBDM	SE-52	30	A	1.014	1.010	1.000	1.018	61	26		60
2 (ii)	20% β-TBDM	PS086	30	A	1.015	1.007	1.000	1.012	52	21		42
3 (iii)	66% β-TBDM	OV1701	30	A	1.023	1.014	1.000	1.010	58	26		35
4 (iv)	25% γ-TECD	OV1701	12	B	1.000	1.038	*a*	1.034	0	70	*a*	61
4[a] (iv)	25% γ-TECD	OV1701	12	C	*a*	1.029 ± 0.001	1.030 ± 0.001	1.028 ± 0.001	*a*	77 ± 2.8	81 ± 2.0	77 ± 2.9

[a]Analyzed by GC/MS (all other measurements were performed by GC/FID); mean values (racemic standard) $n = 10$.

for 4-Et-8:0-ME and 4-Me-9:0-ME. These concentrations were ∼100-fold higher compared to the nonchiral measurements.[18] This loss of sensitivity on the γ-TECD column was due to broader peaks at longer retention times as a consequence of the low isothermal oven temperature required for the resolution of the enantiomers. The quality of the enantiomer purity was expressed by the enantiomeric excess (ee) (eq 1):[10]

$$\text{ee} = (\text{E1} - \text{E2})/(\text{E1} + \text{E2}) \text{ in \%} \quad (1)$$

As will be shown later, in all cases, only one enantiomer could be detected in the samples. Due to the low concentrations of the 4-alkyl-branched fatty acids in the sample, we could not generally rule out the presence of trace amounts of the undetected enantiomer in the sample solutions (which would have been the requisite for ee = 100%). For this reason, the limit of detection (LOD) had to be determined and formed the basis to conclude on the minimum ee of the predominant enantiomer in the samples. Accordingly, ee was calculated by assigning the LOD to the nondetected enantiomer according to the literature.[24] Then, it was noted that the ee was larger than the resulting ee value.

Enantioselective GC/MS-SIM Analysis of Free 4-Alkyl-Branched Fatty Acids and the Corresponding Methyl Esters in a Non-Racemic Standard. Analyses were performed with a G1800B GCD-Plus system (Hewlett-Packard) equipped with a HP6890 autosampler and a split/splitless injector operated in splitless mode. Helium was used as the carrier gas with a constant flow of 1.0 mL/min. The temperatures of the injector and the transfer line were set to 250 °C and 280 °C, respectively. β-TBDM (ii) (see above) was used. The oven program for the enantioselective analysis of the free 4-Me-8:0 started at 50 °C for 1 min; then, the temperature was increased at 1 °C/min to 200 °C (10 min hold time). In the SIM mode, m/z 57, m/z 73, m/z 83, m/z 85, m/z 99, m/z 101, and m/z 158 (M^+) were recorded throughout the run. In addition, 4-Me-8:0-ME was analyzed with the following program: 50 °C for 1 min, then at 10 °C/min to 65 °C and after 150 min at 10 °C/min to 200 °C (10 min hold time). Seven ions (m/z 74, m/z 87, m/z 99, m/z 115, m/z 129, m/z 141, and m/z 172) were measured in SIM mode.

Analysis of the enantioenriched 4-Me-8:0 standard (see above) on the β-TBDM column (ii) showed an enantiomer ratio of the first to second enantiomer of 3:1 (ee = 50%). In a previous study of Dietrich et al., who synthesized both enantiomers, it was found that the (*R*)-enantiomer of 4-Me-8:0 eluted first from β-TBDM.[25] Transferred on our measurements on β-TBDM, the non-racemic standard showed an enantiomeric excess of (*R*)-4-Me-8:0. An aliquot of the non-racemic standard was converted into the corresponding methyl ester and used for the determination of the elution order of the methyl ester on the CSPs.

Determination of the Efficiency of the Enantiomer Separation and Statistical Analysis. The efficiency of the enantiomeric separation was evaluated by means of the separation factor α (eq 2) and the percentage valley between the two enantiomers (eq 3).

$$\alpha = t'_{R2}/t'_{R1} \quad (2)$$

with α = separation factor; t'_{R1} = reduced retention time of the first eluting enantiomer, and t'_{R2} = reduced retention time of the second eluting enantiomer.

$$V\ (\%) = \frac{\frac{1}{2}(H_{E1} + H_{E2}) - H_V}{\frac{1}{2}(H_{E1} + H_{E2})} * 100 \quad (3)$$

with V (%) = valley between the two enantiomers, H_{E1} = peak height of enantiomer 1, H_{E2} = peak height of enantiomer 2, and H_V = height of the valley between the two peaks.

The statistical analysis was performed by one-way analysis of variance (ANOVA), using $\alpha = 0.05$. Evaluation by means of the p-value which describes the level of significance was based on $p < 0.05$ for statistical significance and $p < 0.001$ for high statistical significance.

DOI: 10.1021/jf505452u
J. Agric. Food Chem. 2015, 63, 469−475

Table 2. Concentrations and Enantiomeric Excess of 4-Methyloctanoic Acid (4-Me-8:0), 4-Ethyloctanoic Acid (4-Et-8:0), and 4-Methylnonanoic Acid (4-Me-9:0) in Goat and Sheep Milk, Dairy Products, and Subcutaneous Adipose Tissue

			μg/g milk, cheese, and adipose fat[18,19] ± average deviation (n = 2)			first eluting enantiomer[a] ee (%)[b]		
no.	sample	type of milk	4-Me-8:0	4-Et-8:0	4-Me-9:0	4-Me-8:0	4-Et-8:0	4-Me-9:0
1	goat milk	goat milk	5.9 ± 0.08	3.9 ± 0.04	n.d.	>96.5	>87.8	
2	goat milk, organic	goat milk	6.9 ± 0.12	4 ± 0.06	n.d.	>96.5	>90.6	
3	goat, cream cheese	goat milk	15 ± 0.54	11 ± 0.41	n.d.	>95.9	>64.7	
4	goat, French soft cheese	goat milk	32 ± 0.11	23 ± 0.65	n.d.	>97.7	>93.4	
5	goat, organic butter cheese	goat milk	59 ± 0.59	24 ± 0.74	n.d.	>98.2	>80.6	
6	goat, hard cheese old	goat milk	185 ± 12	68 ± 4.5	n.d.	>98.0	>79.3	
7	sheep milk	sheep milk	6.2 ± 0.18	0.1 ± 0.02	n.d.	>95.7	<LOD	
8	sheep milk, organic	sheep milk	2.5 ± 0.04	0.2 ± 0.00	n.d.	>96.7	<LOD	
9	sheep, soft cheese	sheep milk	14 ± 0.00	0.9 ± 0.01	n.d.	>87.5	<LOD	
10	sheep, Pecorino hard cheese	sheep milk	21 ± 0.41	0.8 ± 0.24	n.d.	>93.3	<LOD	
11	sheep, semihard cheese	sheep milk	25 ± 0.61	1.5 ± 0.09	n.d.	>88.9	<LOD	
12	sheep, blue-veined cheese	sheep milk	29 ± 6.0	1.5 ± 0.21	n.d.	>91.8	<LOD	
13	sheep and goat, greek Feta cheese	sheep and sheep fat	15 ± 0.76	1.3 ± 0.11	n.d.	>91.6	>13	
14	subcutaneous adipose fat 1	sheep fat	48 ± 8.1	26 ± 3.5	5.6 ± 0.7	>93.8	<LOD	<LOD
15	subcutaneous adipose fat 2	sheep fat	23 ± 1.3	13 ± 1.7	2.9 ± 0.4[c]	>96.9	<LOD	<LOD

[a]Elution order on γ-TECD. [b]Minimum enantiomeric excess = (E1 − E2)/(E1 + E2) in %,[10] based on S/N = 3 for the enantiomer which could not be detected. Note that, in all occasions, the second enantiomer could not be detected. [c]Values close to or slightly below the detection limit.

RESULTS AND DISCUSSION

Enantioseparation of Racemic Volatile Branched-Chain Fatty Acid Methyl Esters on Modified Cyclodextrins. Three CSPs coated with β-TBDM were tested first because similar CSPs (15% β-TBDM or γ-TBDM in PS-268) were successfully used by Karl et al. for the enantiomer resolution of racemic standards of free alkyl-branched fatty acids.[13] Columns i and ii were coated with the same amount of the CSP dissolved in a nonpolar (SE-52) or medium polar (PS086) polysiloxane. Column i with the nonpolar polysiloxane showed slightly but not significantly better separation factors α and valleys between the peaks ($p > 0.05$) for the methyl esters of the three 4-methyl-branched fatty acids (Table 1). Similar observations were also made by Dietrich et al. for free 4-Me-BCFAs.[25,26] In contrast to *anteiso*-fatty acids,[10] the use of a high percentage of β-TBDM in the stationary phase could not really improve the enantioseparation of the 4-methyl-branched FAMEs (Table 1). Moreover, the enantiomers of the racemic 4-Et-8:0-ME standard could not be resolved on the β-TBDM columns (Table 1). For this reason, we also tested another CSP in form of a 12 m column coated with γ-TECD installed in the GC/MS system (Table 1). While a racemic standard of 4-Me-6:0-ME could not be enantioseparated on this column, separation factors α of >1.028 and valleys of >77% between the peaks were obtained for 4-Me-8:0-ME ($p < 0.01$ for the valley between the peaks; $p < 0.05$ for α) and 4-Me-9:0-ME ($p > 0.05$ for the valley between the peaks; $p > 0.05$ for α). Accordingly, the enantiomer resolution of 4-Me-8:0-ME was better than that on the β-TBDM columns (Table 1). Moreover, the enantioseparation of 4-Et-8:0-ME, i.e., the key-flavor compound for sheepy and goaty flavors,[2,3] was also resolved on the 25% γ-TECD column with similar success as for the 4-methyl-branched FAMEs (Table 1). Accordingly, the 12 m γ-TECD column was selected for studying the enantiomeric composition of the flavor relevant 4-Me-8:0, 4-Me-9:0, and 4-Et-8:0 as methyl esters in food samples.

Enrichment of 4-Alkyl-Branched Fatty Acid Methyl Esters from Sheep and Goat Samples by RP-HPLC Fractionation. Previous quantitation of the 4-alkyl-branched fatty acids in the samples resulted in concentrations of 0.1−185 μg/g fat in sheep and goat samples (Table 2).[18,19] These low levels were in agreement with data reported in the literature.[2,15−17,27] Due to the higher LOQ and LOD compared to nonchiral GC/MS measurements (see the Materials and Methods), these minor fatty acids were enriched by non-aqueous RP-HPLC by at least a factor of 20 prior to the enantioselective GC analysis. Nonchiral GC/MS analysis of the HPLC fractions verified that 4-Me-8:0-ME eluted into fraction 5 (16−20 min), while 4-Et-8:0-ME was detected in fraction 6 (20−24 min). In the samples with the highest amounts of 4-Et-8:0 (especially in goat samples), a share of 20−54% of this compound already eluted into fraction 5 (Figure 1). In agreement with the previous study, 4-Me-9:0 was only present in the sheep subcutaneous adipose tissue and could not be detected in milk and dairy products of goat and sheep.[18,19] In sheep subcutaneous adipose tissue, 4-Me-9:0-ME eluted into fraction 6, i.e., together with its isomer 4-Et-8:0-ME (Figure 2).

According to Hauff et al., this method eluted FAMEs mainly in dependence of length of the longest acyl chain while methyl branches had only a small effect on the retention.[10] Hence, the 4-alkyl-branched FAMEs could be completely separated from the major fatty acids in the samples (i.e., the methyl esters of 16:0, 18:0, 18:1*n*-9). However, the methyl esters of octanoic acid (8:0-ME), nonanoic acid (9:0-ME), as well as decanoic acid (10:0-ME) were also enriched by the procedure and presented the most abundant fatty acids in fraction 5 (Figure 1). The GC/MS chromatogram of fraction 6 was dominated by 9:0-ME, 10:0-ME, and undecanoic acid methyl ester (11:0-ME). However, this RP-HPLC enrichment step proved to be sufficient for enantioselective analysis of the 4-alkyl-branched fatty acids as methyl esters by GC/MS-SIM.

Enantiomeric Distribution of Volatile 4-Alkyl-Branched Fatty Acids in Sheep Subcutaneous Tissue and Ruminant Milk Fat. The GC/MS-SIM analysis of the RP-HPLC fractions 5 and 6 on γ-TECD resulted in the exclusive detection of a peak at the retention time of the first eluting enantiomer when compared to the racemic standard (Figure 2). This finding was in contrast to Karl et al., who

DOI: 10.1021/jf505452u
J. Agric. Food Chem. 2015, 63, 469−475

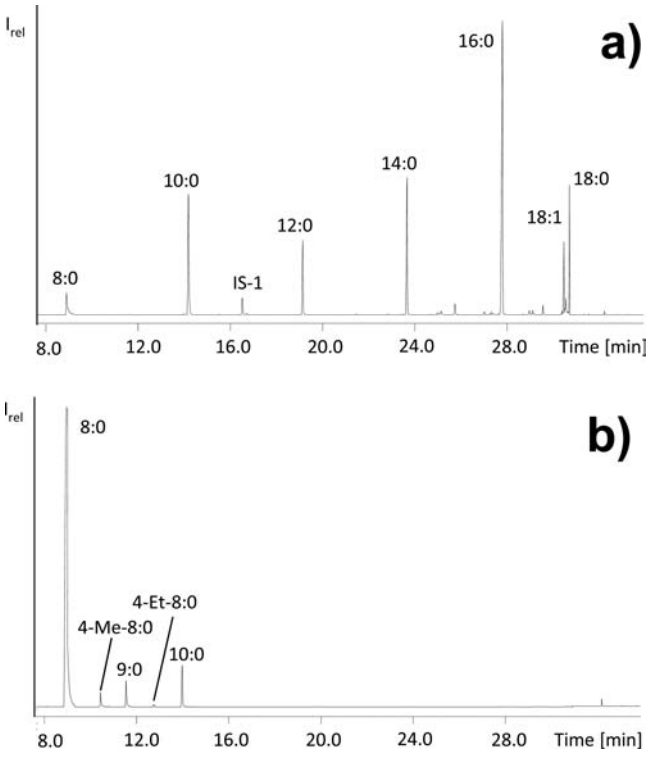

Figure 1. GC/MS chromatograms (HP-5ms column) of the fatty acid methyl esters (a) from the unfractionated goat milk sample and (b) in fraction 5 of the RP-HPLC fractionation.

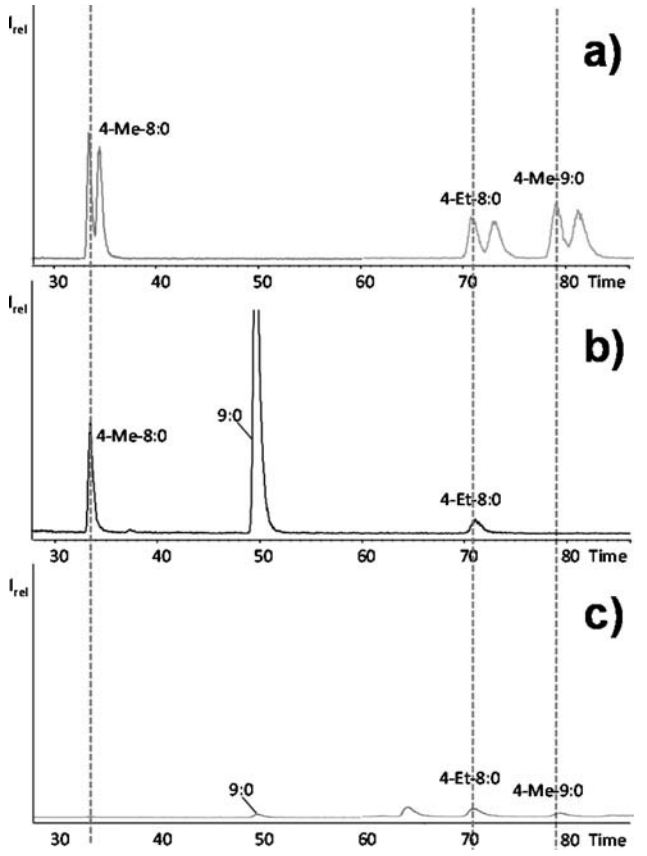

Figure 2. GC/MS chromatograms (25% γ-TECD in OV-1701) of the enantioseparations of (a) a racemic standard mixture of the methyl esters of 4-Me-8:0, 4-Et-8:0, and 4-Me-9:0, (b) RP-HPLC fraction 5 of a goat fresh cheese sample, and (c) RP-HPLC fraction 6 of a sheep subcutaneous adipose tissue sample.

reported a racemic distribution of 4-Me-8:0 in two sheep fat samples.[13] In order to exclude artifacts in our analysis, the results were verified by spiking the samples with similar amounts of racemic standards (methyl esters of 4-Me-8:0, 4-Et-8:0, and 4-Me-9:0) as present in the samples. After the standard addition, the peak height of the first eluted enantiomer (i.e., the one detected in the unspiked sample) had increased, while an additional peak was detected at the retention time of the second eluted enantiomer (Figure 3a). Moreover, the added amount in both nonchiral and chiral GC/MS chromatograms corresponded with the increase of peak area for the two peaks due to the spiking. This measure verified that the peaks detected in fact originated from the 4-alkyl-branched FAMEs and not from other FAMEs eluting at the same retention time from the γ-TECD column. Finally, normalization of the GC/MS-SIM ions m/z 74 and m/z 87 on the same height according to the method of Thurnhofer et al.[28] showed no difference in abundance for the two enantiomeric peaks in the spiked sample (Figure 3b). Thus, it was ultimately verified that for both 4-alkyl-branched fatty acids only one enantiomer could be detected in the sheep and goat samples.

By means of standards enriched in (*R*)-4-Me-8:0 and (*R*)-4-Me-8:0-ME (see the Materials and Methods), we could show that (*R*)-4-Me-8:0 (free acid) eluted first from β-TBDM (Figure 4a), while the elution order of the enantiomers was reversed for 4-Me-8:0-ME (Figure 4b). Moreover, (*R*)-4-Me-8:0-ME eluted first from γ-TECD, i.e., the reversed order as observed for the methyl ester on β-TBDM (compare Figures 3 and 4). Accordingly, the peak detected in all samples using the γ-TECD column originated from (*R*)-8-Me-8:0. For final verification, we also analyzed an HPLC fraction of a cheese sample on the β-TBDM column and this also verified the dominance of (*R*)-(4)-Me-8:0-ME, i.e., the second eluting enantiomer in our sample (Figure 4c).

Although only the (*R*)-enantiomer was detected in our sample, the LOD obtained for 4-Me-8:0 and 4-Et-8:0 did not allow enantiopurity to be verified. On the basis of an S/N ratio of 3 and by considering a concentration of the (*S*)-enantiomer corresponding to $S/N = 3$, the resulting ee of 4-Me-8:0 was between >98.2 and >87.5%. That means that the (*R*)-enantiomer represented in the worst case 93.25% and in the best case 99.1% of 4-Me-8:0 in the samples (Table 2). Note that these ee values should not be mixed up with identification of the (*S*)-enantiomer in our samples. Similarly, the ee of 4-Et-8:0 ranged from >93.4 to 82.35% (Table 2). In this case, the dominant enantiomer in the samples could not be identified.

Biosynthesis Pathway of 4-Me-8:0. Our measurements verified that 4-Me-8:0 was predominantly (if not enantiopure) present in the form of (*R*)-4-Me-8:0. This is remarkable because another class of chiral methyl-branched fatty acids, i.e., *anteiso*-fatty acids, were found with a clear dominance of the (*S*)-enantiomer in bovine milk fat (interestingly, *anteiso*-fatty acids eluted in reversed order, i.e., $R < S$, from the β-TBDM compared to 4-Me-8:0).[10,28] The different configurations of the predominant enantiomer indicated generally different biosynthetic pathways for both classes of compounds. While the *anteiso*-fatty acids are predominantly biosynthesized by using the amino acid isoleucine and malonyl-CoA as starters,[29,30] the primer for the biosynthesis of 4-alkyl-branched chain fatty acids is in all probability propionyl-CoA.[31] Propionyl-CoA, a

DOI: 10.1021/jf505452u
J. Agric. Food Chem. 2015, 63, 469−475

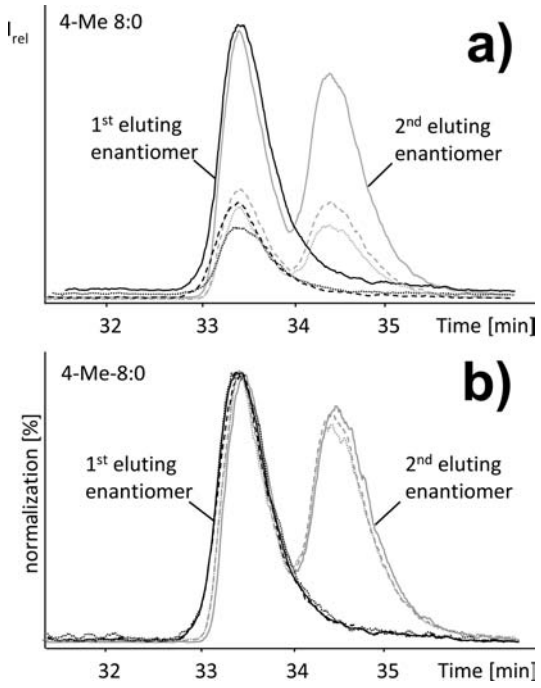

Figure 3. Overlay of the GC/MS-SIM chromatograms (25% γ-TECD in OV-1701) showing the total ion current (TIC) of the enantiomer separation of 4-Me-8:0-ME of sheep milk fat (fraction 5, black line) and a racemic standard of 4-Me-8:0-ME (gray line). Part a additionally shows the relative intensities of m/z 87 (dashed line) and m/z 74 (dotted line), whereas, in part b, the peaks of the TIC, m/z 87 and m/z 74, were normalized to the same abundance for the first eluted enantiomer.

degradation product of thymine and valine, is then carboxylated to give D-methylmalonyl-CoA (*S*-configuration). D-Methylmalonyl-CoA is then converted into L-methylmalonyl-CoA (*R*-configuration) by a methylmalonyl-epimerase. This step is important because only L-methylmalonyl-CoA can be reacted to succinyl-CoA, which is a component of the citrate-cyclus.[32]

In the biosynthesis of the 4-methyl-branched fatty acids, L-methylmalonyl-CoA is then activated by acetyl-carrier-protein (ACP)-transacylase into L-methylmalonyl-ACP which is merged with activated butyryl-ACP to give L-methyl-3-keto-hexanoyl-ACP. In the following, the keto function is reduced to give L-methyl-hexanoyl-ACP.[32] In the case of classic/common fatty acids, the ketone is reduced to the alcohol; then, water is eliminated, and the resulting double bond is hydrogenated.[32] For 4-Me-8:0, this step has not been investigated. However, our results verify that the conversion of L-methyl-3-keto-hexanoyl-ACP into L-methyl-hexanoyl-ACP is occurring enantioselectively, i.e., under maintenance of the *R*-configuration. Finally, (*R*)-4-Me-8:0 is formed by chain elongation with malonyl-CoA followed by elimination of the activation group. The biosynthesis of 4-Et-8:0 follows the same pathway except that butyryl-CoA is used as the primer instead of propionyl-CoA.[31] This also explains the formation of one enantiomer which is most likely the (*R*)-enantiomer.

Impact of the Enantiomeric Excess on the Flavor Perception. This pronounced enantiomeric excess of the chiral alkyl-branched fatty acids in the food samples resembles the one of other principal food compounds such as amino acids and monosaccharides.[33] Likewise, the high relevance of (*R*)-4-Me-8:0 in the goat and sheep samples could have an impact on the contribution of these compounds to the sheepy and goaty flavor because flavor thresholds had been previously determined with the help of racemic standards in different studies.[3,4] However, literature data on the flavor impression of the pure enantiomers of 4-Me-8:0 is equivocal. Karl et al. noted similar flavor impressions but a 2 times higher flavor intensity for the (*S*)-enantiomer of 4-Me-8:0 (and other 4-alkyl-branched fatty acids).[13] By contrast, Heinsman et al. reported that (*R*)-4-Me-8:0 showed the typical mutton smell and taste at a 5−10-fold higher intensity than the (*S*)-enantiomer.[34] The reasons for these differences in flavor perception of 4-Me-8:0 enantiomers remain unclear, and they had no practical relevance as long as it was thought that 4-Me-8:0 was racemic in sheep and goat samples. However, the new finding of the predominant presence of (*R*)-4-Me-8:0 in sheep and goat samples supports the relevance of enantioselective evaluation of the impact of this and further 4-alkyl-branched fatty acids on the sheepy and goaty flavor. It is noteworthy that two studies reported very similar sensorial qualities for the enantiomers of 4-Me-8:0.[13,34] In this context, it is worth noting that this similar impression of humans must not necessarily be valid as well for sheep and goats (which are bioproducing the compounds). In either case, the enantioselectivity of the 4-alkyl-branched fatty acids should be taken into account in the investigation of the characteristic flavor of goat and sheep samples.

AUTHOR INFORMATION

Corresponding Author

*E-mail: walter.vetter@uni-hohenheim.de. Phone: +49 711 459 24016.

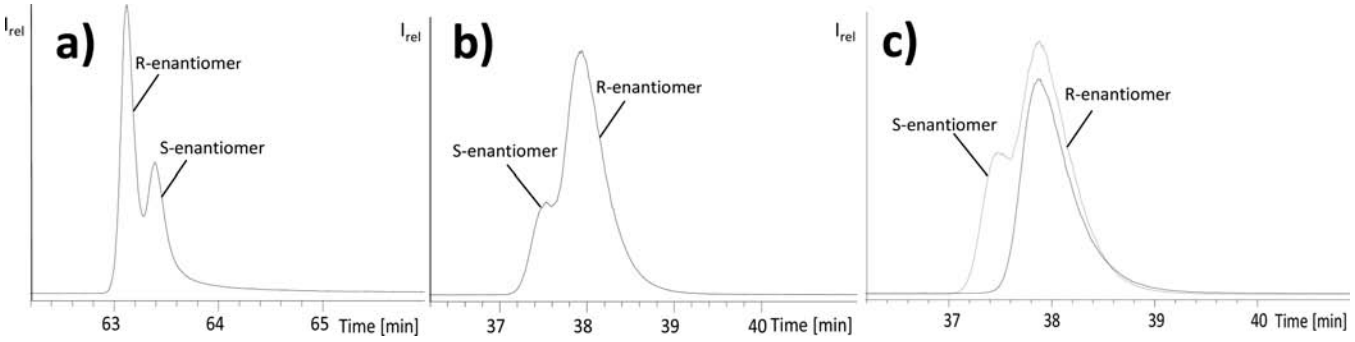

Figure 4. Partial GC/MS chromatogram (20% β-TBDM in PS086) of the enantiomer separation of the non-racemic standard of (a) free 4-Me-8:0 and (b) 4-Me-8:0-ME as well as (c) 4-Me-8:0-ME from goat soft cheese milk fat (RP-HPLC fraction 5, blue line) and a standard addition of this sample with 200 ng of 4-Me-8:0-ME (in sample solution 6.7 ng/μL).

DOI: 10.1021/jf505452u
J. Agric. Food Chem. 2015, 63, 469−475

Notes

The authors declare no competing financial interest.

■ ACKNOWLEDGMENTS

We are grateful to Prof. Michael Oehme (University of Basel, Switzerland) and Georg Hottinger (BGB Analytik, Adswil, Switzerland) for the preparation and supply of the modified cyclodextrin columns for enantioselective analysis.

■ REFERENCES

(1) Wong, E.; Nixon, L. N.; Johnson, C. B. Volatile medium chain fatty acids and mutton flavor. *J. Agric. Food Chem.* **1975**, *23*, 495−498.
(2) Wong, E.; Johnson, C. B.; Nixon, L. N. The contribution of 4-methyloctanoic (hircinoic) acid to mutton and goat meat flavour. *N. Z. J. Agric. Res.* **1975**, *18*, 261−266.
(3) Brennand, C. P.; Ha, J. K.; Lindsay, R. C. Aroma properties and thresholds of some branched-chain and other minor volatile fatty acids occuring in milk fat and milk lipids. *J. Sens. Stud.* **1989**, *4*, 105−120.
(4) Salles, C.; Sommerer, N.; Septier, C.; Issanchou, S.; Chabanet, C.; Garem, A.; Le Quéré, J.-H. Goat cheese flavor: Sensory evaluation of branched-chain fatty acids and small peptides. *J. Food Sci.* **2002**, *67*, 835−841.
(5) König, W. A. *Gas chromatographic enantiomer separation with modified cyclodextrins*; Hüthig Buch Verlag: Heidelberg, Germany, 1992; p 168.
(6) Schurig, V.; Nowotny, H.-P. Separation of enantiomers on diluted permethylated β-cyclodextrin by high-resolution gas chromatography. *J. Chromatogr. A* **1988**, *441*, 155−163.
(7) Allenmark, S.; Schurig, V. Chromatography on chiral stationary phases. *J. Mater. Chem.* **1997**, *7*, 1955−1963.
(8) Schurig, V. Enantiomer separation by gas chromatography on chiral stationary phases. *J. Chromatogr. A* **1994**, *666*, 111−129.
(9) Vetter, W.; Schurig, V. Enantioselective determination of chiral organochlorine compounds in biota by gas chromatograph on modified cyclodextrins. *J. Chromatogr. A* **1997**, *774*, 143−175.
(10) Hauff, S.; Hottinger, G.; Vetter, W. Enantioselective analysis of chiral *anteiso* fatty acids in the polar and neutral lipids of food. *Lipids* **2010**, *45*, 357−365.
(11) Dietrich, A.; Maas, B.; Messer, W.; Bruche, G.; Karl, V.; Kaunzinger, A.; Mosandl, A. Stereoisomeric flavor compounds, part LVIII: The use of *heptakis*(2,3-di-*O*-methyl-6-*O*-*tert*-butyldimethylsilyl)-β-cyclodextrin as a chiral stationary phase in flavor analysis. *J. High Resolut. Chromatogr.* **1992**, *15*, 590−593.
(12) Maas, B.; Dietrich, A.; Karl, V.; Kaunzinger, A.; Lehmann, D.; Köpke, T.; Mosandl, A. *tert*-Butyldimethylsilyl-substituted cyclodextrin derivatives as versatile chiral stationary phases in capillary GC. *J. Microcolumn Sep.* **1993**, *5*, 421−427.
(13) Karl, V.; Gutser, J.; Dietrich, A.; Maas, B.; Mosandl, A. Stereoisomeric flavour compounds LXVIII. 2-, 3-, and 4-alkyl-branched acids, part 2: Chirospecific analysis and sensory evaluation. *Chirality* **1994**, *6*, 427−434.
(14) Maas, B.; Dietrich, A.; Mosandl, A. Comparison of different 6-*tert*-butyldimethyl-silylated cyclodextrins as chiral stationary phases in GC. *J. Microcolumn Sep.* **1996**, *8*, 47−56.
(15) Alonso, L.; Fontecha, J.; Lozada, L.; Fraga, M. J.; Juárez, M. Fatty acid composition of caprine milk: Major, branched-chain, and *trans* fatty acids. *J. Dairy Sci.* **1999**, *82*, 878−884.
(16) Ha, J. K.; Lindsay, R. C. Volatile branched-chain fatty acids and phenolic compounds in aged Italian cheese flavors. *J. Food Sci.* **1991**, *56*, 1241−1247.
(17) Brennand, C. P.; Lindsay, R. C. Distribution of volatile branched-chain fatty acids in various lamb tissues. *Meat Sci.* **1992**, *31*, 411−421.
(18) Kaffarnik, S.; Preuß, S.; Vetter, W. Direct determination of flavor relevant and further branched-chain fatty acids from sheep subcutaneous adipose tissue by gas chromatography with mass spectrometry. *J. Chromatogr. A* **2014**, *1350*, 92−101.
(19) Kaffarnik, S.; Kayademir, Y.; Heid, C.; Vetter, W. Concentrations of volatile 4-alkyl-branched fatty acids in sheep and goat milk and dairy products. *J. Food Sci.* **2014**, *79*, C2209−C2214.
(20) Eibler, D.; Kaffarnik, S.; Tzschieter, C.; Heid, C.; Vetter, W. Manuscript in preperation, 2015.
(21) Jaus, A.; Oehme, M. Enantioselective behaviour of ethylated γ-cyclodextrins as GC stationary phases for chlorinated pesticides and phase characterisation by HPLC. *Chromatographia* **1999**, *50*, 299−304.
(22) Jaus, A.; Oehme, M. Enantioselective HRGC separation of toxaphene congeners by ethylated γ-cyclodextrins. *J. Sep. Sci.* **2000**, *23*, 304−308.
(23) Jaus, A.; Oehme, M. Gas chromatographic separation of atropisomeric polychlorinated biphenyls and methylsulfonylated derivatives with partially ethylated γ-cyclodextrin. *Chromatographia* **2000**, *52*, 242−244.
(24) Lebensmittelchemische Gesellschaft. Enantioselektive Analyse zur Natürlichkeitsbewertung von Aromastoffen. *Lebensmittelchemie* **2001**, *55*, 24−26.
(25) Dietrich, A.; Maas, B.; Brand, G.; Karl, V.; Kaunzinger, A.; Mosandl, A. Stereoisomeric flavor compounds, part LX: Diluted modified cyclodextrins as chiral stationary phases - the influence of the polysiloxane solvent. *J. High Resolut. Chromatogr.* **1992**, *15*, 769−772.
(26) Dietrich, A.; Maas, B.; Mosandl, A. Diluted modified cyclodextrins as chiral stationary phases - influence of the polysiloxane solvent: *Heptakis*(2,3-di-*O*-acetyl-6-*O*-*tert*-butyldimethylsilyl)-β-cyclodextrin. *J. High Resolut. Chromatogr.* **1995**, *18*, 152−156.
(27) Massart-Leen, A. M.; De Pooter, H.; Decloedt, M.; Schamp, N. Composition and variability of the branched-chain fatty acid fraction in the milk of goats and cows. *Lipids* **1981**, *16*, 286−292.
(28) Thurnhofer, S.; Hottinger, G.; Vetter, W. Enantioselective determination of *anteiso* fatty acids in food samples. *Anal. Chem.* **2007**, *79*, 4696−4701.
(29) Kaneda, T. Biosynthesis of branched-chain fatty acids V. Microbial stereospecific syntheses of D-12-methyltetradecanoic and D-14-methylhexadecanoic acids. *Biochim. Biophys. Acta* **1966**, *125*, 43−54.
(30) Kaneda, T. *Iso*- and *anteiso*-fatty acids in bacteria: Biosynthesis, function, and taxonomic significance. *Microbiol. Rev.* **1991**, *55*, 288−302.
(31) Ha, J. K.; Lindsay, R. C. Distribution of volatile branched-chain fatty acids in perinephric fats of various red meat species. *Lebensm.-Wiss. Technol.* **1990**, *23*, 433−440.
(32) Heinrich, P. C.; Müller, M.; Graeve, L. *Biochemie und Pathobiochemie*; Springer: Berlin, 2014; p 1073.
(33) Vollhardt, K. P. C.; Schore, N. E. *Organic Chemistry, Structure and Function*; W.H. Freeman and Company: New York and Basingstoke, U.K., 2003; p 1203.
(34) Heinsman, N. W. J. T.; Franssen, M. C. R.; Van Der Padt, A.; Boom, R. M.; Riet, K. V.; De Groot, A. Lipase-mediated resolution of branched chain fatty acids. *Biocatal. Biotransform.* **2002**, *20*, 297−309.

DOI: 10.1021/jf505452u
J. Agric. Food Chem. 2015, 63, 469−475

JOURNAL OF AGRICULTURAL AND FOOD CHEMISTRY

Article

pubs.acs.org/JAFC

Screening for Sulfate in Distillers Dried Grains and Solubles by FT−IR Spectroscopy

Thorben Nietner,[†,‡] Michael Pfister,[†] Barbara Brakowiecka-Sassy,[†] Marcus A. Glomb,[‡] and Carsten Fauhl-Hassek*[,†]

[†]Federal Institute for Risk Assessment, Max-Dohrn-Strasse 8-10, 10589 Berlin, Germany

[‡]Institute of Chemistry, Food Chemistry, Martin-Luther-University Halle-Wittenberg, Kurt-Mothes-Strasse 2, 06120 Halle (Saale), Germany

Supporting Information

ABSTRACT: Distillers Dried Grains and Solubles (DDGS) are an animal feed containing varying levels of sulfur. As ruminants are susceptible to high sulfur diets, sulfur content is of major interest to the parties involved. The variation in levels of sulfur in DDGS is mainly due to sulfate derived from the addition of sulfuric acid during the production. ATR/FT−IR spectroscopy was used to determine sulfate levels in 90 DDGS samples from various origins (Canada, China, EU, and U.S.A.). Specific absorption bands for sulfate at 615 and 1107 cm^{-1} enabled the analysis of sulfate in the DDGS matrix. Besides direct quantification (using band at 615 cm^{-1}), PLS regression was applied for the prediction of sulfate using FT−IR spectra and calibration with reference values analyzed by capillary electrophoresis. An extended calculation on the total sulfur estimated that 11% of the DDGS samples analyzed in this study featured sulfur contents higher than 0.80%.

KEYWORDS: *FTIR, capillary electrophoresis, bioethanol, DDGS, sulphate, feed safety, QSAFFE*

INTRODUCTION

The animal feed sector is affected more than ever by the rising lack of protein sources. The involved business has forced efforts to find alternative sources for animal nutrition, and novel feed materials are considered for entry into the market. Also, by- or coproducts from food production or industrial processes based on natural raw materials are considered and already used in the rearing of livestock. For example, Distillers Dried Grains and Solubles (DDGS) as byproducts of the bioethanol industry recently have gained importance in the animal feed sector. As such, the ethanol industry is primarily interested in the production of ethanol by fermentation of cereals (i.e., corn, wheat, barley, and sorghum), while at the same time obtaining a byproduct of high nutritional value (rich in proteins, raw fiber, fat, and minerals). However, it is of the utmost importance that animal feed materials derived from industrial processes or novel sources comply with legal requirements and that feed safety as well as food safety can be guaranteed in terms of the farm-to-fork principle.

With regard to DDGS, consistency in the nutritional value and quality of the feedstuff is particularly relevant, as sources of production are manifold and variation in the products composition is not only present among but also within production plants.[1,2] Besides the nutritional composition, one of the most important aspects regarding DDGS is its content of sulfur (S), which is strongly affected by the process of ethanol production. First, the concentration of sulfur-containing amino acids is increased by a factor of approximately three compared to the grain during the production process,[3] resulting in a content of S about 0.30 to 0.40 mass percent of endogenous origin depending on the raw material (corn or wheat). Second, sulfuric acid is used in many plants to control the pH of the cereal mash during fermentation and/or as a cleaning agent and can lead to high sulfate/sulfur levels in DDGS.[4] Many studies have already paid attention to the presence of S in DDGS and as Shurson, Tilstra, and Kerr (2012)[5] indicated, sulfur levels in DDGS can range from 0.31 to 1.93% (average 0.69%) on a dry matter (DM) basis. In addition, the sulfur content of Distillers Grains was reported to vary typically, showing a within-plant coefficient of variation from 6.4 to 40.8%[1] and 2.2 to 12.8%[6] respectively.

The particular interest in the sulfur content of DDGS is linked to the fact that ruminants are susceptible to high sulfur-containing diets. Although microbes present in the rumen require sulfur for their normal growth and metabolism, high S intake can decrease the bioavailability of trace minerals (e.g., copper, iron, zinc) and also lead to the production of H_2S by sulfate reducing bacteria (e.g., *Desulfovibrio* spp. and *Desulfotomaculum* spp.).[7] In ruminants, the major part of H_2S from the rumen will be eructated and inhaled during rumination and after entering the pulmonary vein in the lung, the H_2S consequently reaches the brain of the animal. As Schoonmaker and Beitz (2012) summarized, high concentrations of H_2S decrease cellular respiration and limit the rate of ATP generation causing necrosis of the cerebral cortex and softening of the brain tissue.[7] Severe cases of H_2S intoxication can result in polioencephalomalacia (PEM) and if not treated with thiamine, in the death of the animal.[7]

Received: August 1, 2014
Revised: December 19, 2014
Accepted: December 22, 2014
Published: December 22, 2014

ACS Publications © 2014 American Chemical Society

DOI: 10.1021/jf503704r
J. Agric. Food Chem. 2015, 63, 476−484

Risk for steers contracting PEM was reported to increase when the dietary S levels and the rumen available S levels in the diet increased; this was observed most clearly at dietary S levels above 0.6% and low levels of forage NDF in the diets.[8] However, Schoonmaker and Beitz (2012) mentioned that PEM incidence correlates not only with dietary S contents, but also with variation in the S content from day to day.[7] Therefore, consistency of the S content of DDGS but also of the whole diet must be regarded as a crucial factor in rearing of ruminants. According to the U.S. National Research Council,[9] the maximum tolerable dietary S level is 0.4% (DM basis) for beef cattle. For example, this dietary level could be exceeded if DDGS with sulfur content greater than 0.80% (DM basis) were fed to ruminants at high inclusion rates (DDGS: 40% of DM intake) in addition to corn and corn silage, assuming low sulfate levels in drinking water.[5,10]

In addition, inorganic forms of sulfur (i.e., sulfate) are described to be better available for ruminal bacteria.[7,8,11] In this context, Schoonmaker and Beitz (2012) mentioned that DDGS could show high sulfate levels of 0.5 to 1.7%, which can cause a dramatic increase in H_2S production in the rumen.[7] Moreover, Sarturi et al. (2013) observed greater ruminal H_2S concentrations for steers fed with Wet Distillers Grains with Solubles (WDGS) and sulfate-enriched diets compared with conventional or organic sulfur-enriched diets.[11] Therefore, great attention has to be devoted not only to sulfur levels, but also especially to sulfate levels in DDGS preventing ruminants of H_2S intoxication. Besides the risk of PEM, there is also a general interest in reducing sulfate levels (and sulfur levels) in DDGS because both ruminants and nonruminants show decreased feed intake and gain at high dietary S levels.[12,13] Sulfate levels in DDGS could be reduced most easily, if the use of sulfuric acid would be avoided and phosphoric acid or hydrochloric acid would be used instead for pH control in the production process.[14] Alternatively, the analysis of sulfate and/or sulfur levels in DDGS could enable the selection of feeds and batches of feed with acceptable S levels, and diets could also be kept to a more consistent S level in this way.[7]

Thus, the quantitative information on sulfur and/or sulfate in DDGS is of major interest to parties involved and certainly improves the quality and safety of DDGS. Traditionally, quantitative analysis of sulfur in animal feed has been performed by gravimetric analysis ($BaSO_4$) after oxidation of S-containing compounds to sulfate (e.g., AOAC Method 923.01).[15] Nowadays, X-ray fluorescence spectroscopy or inductively coupled plasma mass spectrometry (ICP-MS) are commonly used for this purpose. In the current study, the application of ATR/FT−IR spectroscopy for the determination of sulfate levels in DDGS as a rapid screening method is highlighted. The application targets the screening of sulfate levels in different batches of DDGS and was developed to easily preselect batches of DDGS with prominent sulfate levels. The technique itself could be used routinely in the field as laboratory expenses are limited and it could also serve as a process-oriented solution to control the sulfate content in DDGS on-site.

MATERIALS AND METHODS

DDGS Samples and Sample Preparation. 90 DDGS samples were collected in the frame of the EU project QSAFFE from reliable sources in the years 2011−2013. In this study, DDGS samples are defined as feed materials according to the numbering of the EU feed catalogue (Commission Regulation No. 68/2013):[16] either (a) number 1.12.10 (Distillers' dried grains) or (b) number 1.12.11 (Distillers' dried grains and solubles/Distillers' dark grains). The samples were produced from the bioethanol industry or the alcoholic beverage industry (whiskey, vodka) and were obtained from different geographical origins as stated by the provider. They were produced mainly from corn or wheat; details of the samples are provided as supplementary table (Supporting Information, SI). All samples were ground with a centrifugal mill (ZM 200, Retsch, Germany, mesh size 0.5 mm) and subsequently homogenized in plastic containers (filling level ∼2/3) for 6 h using a drum hoop mixer (RRM 100, Engelsmann, Germany). The DDGS samples were stored at 4 °C in the dark until analysis.

One preground DDGS sample without substantial sulfate level [#40, cf. SI], named sample A in this study, was spiked with different amounts of anhydrous sodium sulfate (analytical grade; ≥ 99.0%; Merck KGaA, Darmstadt, Germany) to levels of 1% to 5% sodium sulfate, in triplicates (each of 0.500 g) for FT−IR spectroscopy and in triplicates (each of 4.000 g) for capillary electrophoresis (CE). Also, one preground DDGS sample with medium sulfate content (1.44%) [#29, cf. SI], named sample B in this study, was analyzed to estimate precision of (1) FT−IR spectroscopy in the spectral range of interest, and (2) CE. In order to demonstrate the effect of Na_2SO_4-spiking to sulfate-containing DDGS, one further preground DDGS sample with medium sulfate content [#33, cf. SI], named sample C in this study, was spiked with 3% sodium sulfate.

FT−IR Spectroscopy. Prior to FT−IR spectroscopy, the preground DDGS samples were finely ground using a ball mill (MM 301, Retsch, Germany; 5 mL steel cylinders and 2 steel balls with 7 mm diameter, 30 Hz, 4 min) to achieve small-sized particles (more than 99% between 10 to 200 μm), as described before.[17] FT−IR spectra were collected with a Nicolet 6700 series spectroscope (Thermo Fisher Scientific, Waltham, MA, U.S.A.) equipped with a Smart Performer Accessory (single-bounce-ATR with diamond crystal), a micrometric pressure device enabling a standardized pressing force, a KBr beamsplitter, and a deuterated triglycine sulfate (DTGS) detector. In general, FT−IR spectroscopy of the DDGS samples was carried out as described in a previous study.[17] The spiked mixtures of sample A and sample C were ground with a ball mill (instrument setup specified above) for 4 × 1 min and mixed manually using a spatula after each grinding to improve homogeneous distribution of the sodium sulfate in the sample, which led to equal particle sizes as mentioned above. For estimation of precision, 10 replicates of sample B underwent fine grinding, triplicate FT−IR spectra of each replicate were collected, peak areas and sulfate contents (cf. following sections) were calculated. Then relative standard deviation (coefficient of variation) of the averaged sulfate contents of the triplicates (n = 10) was calculated.

Extraction of Sulfate and Capillary Electrophoresis. The extractable sulfate content of the DDGS samples was analyzed by capillary electrophoresis (CE). Sulfate was extracted out of the DDGS by weighing exactly 4.000 g of the preground sample material into a 50 mL Polypropylene Conical tube (30 × 115 mm; BD Biosciences, San Jose, U.S.A.) and adding 40.00 mL deionized water (18.2 MΩ; purified by Milli-Q Reference A+ System; Millipore, Schwalbach, Germany). The tube was capped and vigorously shaken until the sample material was dispersed in the water; then homogenized with an overhead shaker for 10 min, followed by 5 min supersonic wave treatment (35 kHz) and centrifugation for 10 min at an average of 7020g (8000 rpm, J2-HS Centrifuge with rotor JA-10, Beckman Coulter, U.S.A.). The supernatant was first filtered through an ashless filter paper (589/3, Whatman, Dassel, Germany) and subsequently through a 0.2 μm syringe filter (Perfect-flow Nylon membrane, WICOM, Heppenheim, Germany).

For capillary electrophoresis, 1000 μL of the filtered sample extract and 1000 μL of an internal standard solution of 2000 mg/L sodium chlorate (ACS reagent, ≥ 99.0%; Sigma-Aldrich, St. Louis, MO, U.S.A.) were diluted with deionized water to a final volume of 50 mL (using 50 mL glass flasks). Finally, 500 μL of this solution was pipetted to a 1 mL polypropylene vial and used for electrophoresis. Organic Acids Buffer (Agilent Technologies, Waldbronn, Germany) was used for electrophoretic separations. Three independent sulfate stock

DOI: 10.1021/jf503704r
J. Agric. Food Chem. 2015, 63, 476−484

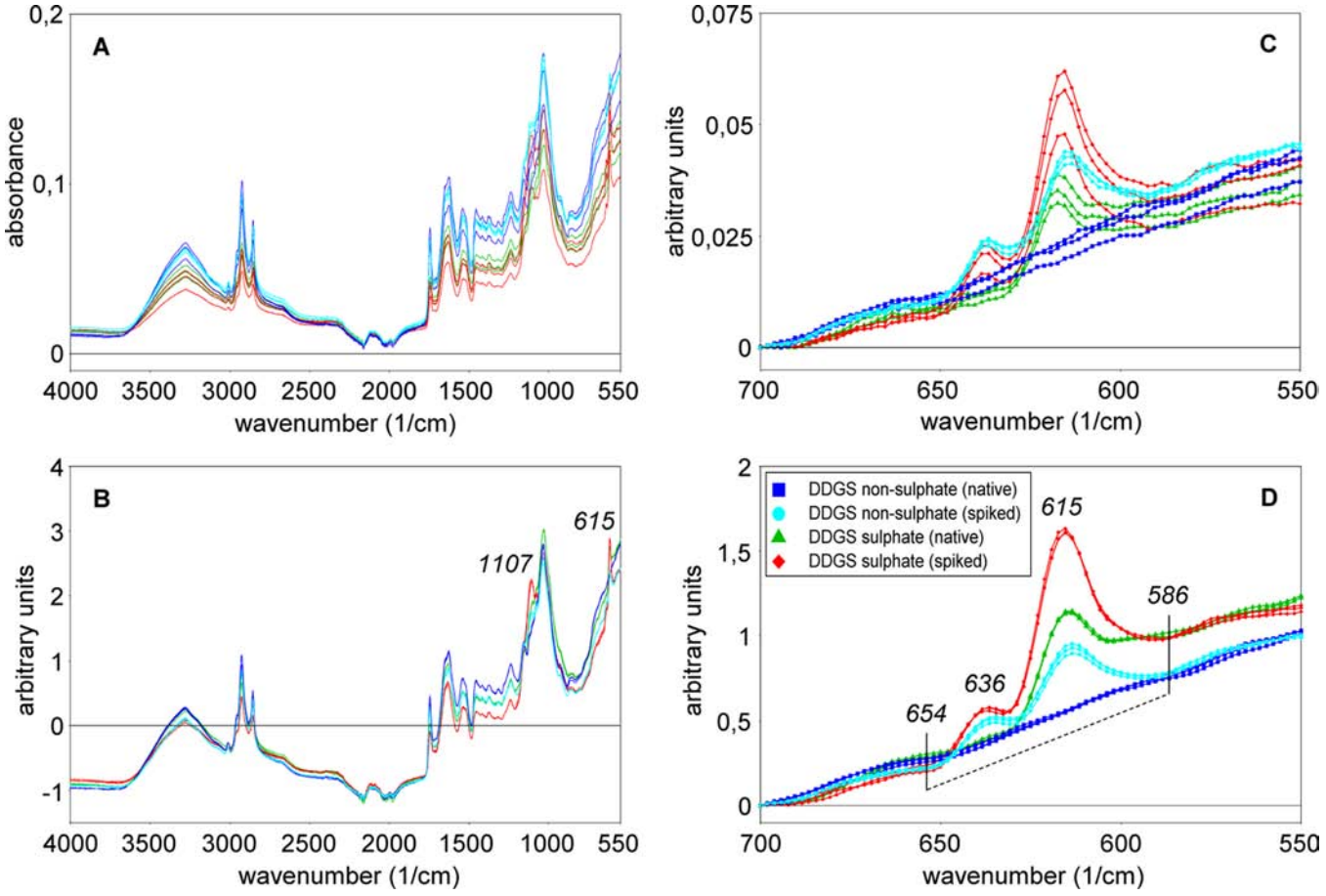

Figure 1. (A)+(C): FT−IR triplicate spectra of DDGS; (B)+(D): FT−IR spectra after preprocessing (SG smoothing and SNV transformation); exemplary shown for DDGS without natural sulfate content (sample A) and DDGS with natural sulfate content (sample C), both native and Na_2SO_4-spiked. (C)+(D): Spectra were zeroed to signal at 700 cm^{-1} for demonstration purposes (not conducted in actual data processing). (D): dashed line indicates wavenumber region for integration of bands; legend is representative for all single figures.

solutions of 500 mg/L were prepared by dissolving appropriate amounts of anhydrous sodium sulfate (analytical grade; ≥ 99.0%; Merck KGaA, Darmstadt, Germany) in deionized water to a volume of 1000 mL. Sulfate standard solutions (5, 20, 40, 60, and 80 mg/L) were prepared from these stock solutions for calibration and were run daily in the beginning, the middle and the end of each sample sequence. Calibration curves were calculated on the average results of the three independent sets of standard solutions and used for determination of the sulfate concentrations in the sample extracts. Also, sulfate concentrations in sample extracts (and in standard solutions) were corrected using the chlorate peak as internal standard in the respective electropherogram. Finally, sulfate contents in the solid DDGS samples were calculated from the sulfate concentrations of the sample extracts.

The CE system employed for the study was an Agilent 7100 system (Agilent Technologies, Waldbronn, Germany) equipped with a fused-silica capillary of 72 cm length and 75 μm I.D. and UV−vis detector (190−600 nm) for indirect detection of analytes. The capillary was initially activated with 0.1 mol/L $NaOH_{aq}$ and water, rinsed with buffer daily before analyses and for preconditioning (240 s) before each injection. Sample solutions were injected in the hydrodynamic mode for 2 s at 50 mbar and separations were performed at 30.0 °C and a constant voltage of −25 kV. Total run time (without preconditioning) was 10 min and detection was based on a wavelength of 254 nm using a reference wavelength of 200 nm. Fresh buffer solutions were used after every 6 samples, and the detector was autobalanced after 60 s.

The spiked mixtures of sample A were homogenized using a spatula and extracted as described above; extracts were analyzed by CE, and the results served for estimation of recovery. Sample B was extracted ten times and analyzed by CE accordingly for estimation of precision. Extraction of sample B was carried out consecutively during the extraction of the samples and CE analysis of the respective replicates went along with samples on the single days of measurement by means of quality control.

Data Analysis. *Univariate Calibration Using Corrected Peak Area.* FT−IR raw spectra were investigated using the OMNIC 7.4 software (Thermo Fisher Scientific). Raw spectra (triplicates) were imported into The Unscrambler X 10.2 software (CAMO Software, Oslo, Norway) and preprocessed by Savitzky-Golay smoothing (centered spectral window 11 points, third polynomial for fitting) followed by Standard Normal Variate (SNV) transformation. Preprocessed spectra were then exported to ASCII text files using semicolons as item delimiter, transcribed to csv-format using KNIME version 2.9.1 (KNIME, Zurich, Switzerland) and finally imported into the OMNIC software again. Here, a macro (written in the OMNIC Macros Basic 7.4) was used for the calculation of the corrected peak height and corrected peak area in the range of 653.750 and 586.246 cm^{-1} for all spectra and results were automatically saved as text file. Peak location for the calculation of the peak height was defined at 617 cm^{-1} (seek closest peak enabled) and a new linear baseline (in the range of 653.750 and 586.246 cm^{-1}) was used automatically to calculate the corrected values of height and area, respectively. The text file was finally imported into Excel 2010 (Microsoft, Redmond, WA, U.S.A.) to draw graphs and calculate regression equations.

Regression analysis was performed by fitting a linear model (least-squares approach) to the obtained data of DDGS sample A spiked with different amounts of sodium sulfate. The double sided confidence interval bands for prediction were calculated according to eq 1:

DOI: 10.1021/jf503704r
J. Agric. Food Chem. 2015, 63, 476−484

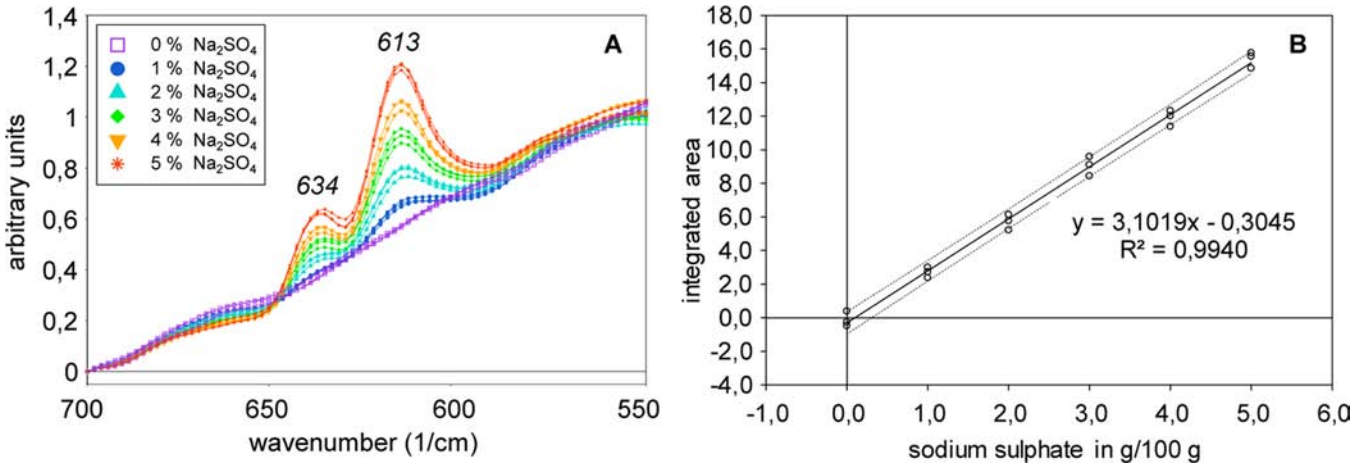

Figure 2. FT−IR triplicate spectra of DDGS sample A (SG smoothed, SNV transformed) spiked with different amounts of sulfate (A) and resulting calibration line with confidence intervals drawn by dashed lines (B). Spectra were zeroed to signal at 700 cm^{-1} in (A) for demonstration purposes (not conducted in actual data processing). Calibration was based on integration of bands between 654 and 586 cm^{-1}.

$$\hat{y} = (\hat{a} + \hat{b}x_i) \pm s_y t_{(p,df)} \sqrt{\frac{1}{m} + \frac{1}{n} + \frac{(x_i - \bar{x})^2}{Q_{xx}}} \quad (1)$$

where $\hat{a}$, $\hat{b}$, and x denote the intercept and slope estimated from calibration data and sulfate content respectively and s_y is the standard deviation of the residuals, calculated according to eq 2:

$$s_y = \sqrt{\frac{\sum (y_i - \hat{y}_i)^2}{n - 2}} \quad (2)$$

In eq 1, t is the student's t factor with p = 95% and degrees of freedom $df = n - 2$ are considering the number of samples (n) used for calibration. The number of replicates is indicated by m and Q_{xx} (sum of squared differences of contents) is calculated according to eq 3:

$$Q_{xx} = \sum (x_i - \bar{x})^2 \quad (3)$$

First, a calibration line was calculated for the sample spiked with different levels of sulfate and the respective corrected peak areas from the FT−IR spectra (matrix calibration). Then, this calibration was used to calculate the sulfate contents in all other samples analyzed in the study. Finally, these calculated sulfate contents were plotted against the sulfate contents analyzed by CE. The process coefficient of variation V_{x0}, based on the calibration using DDGS sample A, was calculated according to eq 4:

$$V_{x0} = \frac{s_y}{b \cdot \bar{x}} \quad (4)$$

Multivariate Calibration Using CE Reference Values (PLS Regression). For multivariate regression, FT−IR spectra were imported into The Unscrambler X 10.2 software, all sample triplicates were preprocessed by Savitzky-Golay smoothing (centered spectral window 11 points, third polynomial for fitting), then the triplicates were averaged, and finally SNV transformation was conducted. Partial least-squares regression (PLS regression) was calculated using the results from CE as reference values, based on NIPALS (Nonlinear Iterative Partial Least Squares) algorithm, mean centring and 7 requested latent variables (factors). Most important spectral variables of the calculated PLS models were consecutively selected three times (through the respective regression coefficients plot) and calculation of the new models with reduced number of variables was repeated accordingly. The PLS regression model was based on 2 latent variables (explaining 95.04% of the variance), a total number of 188 spectral variables (originally 1803, second step 568, third step 318, fourth step 188) and leave-one-out cross-validation was applied.

RESULTS AND DISCUSSION

Determining Sulfate by FT−IR Spectroscopy. FT−IR spectra of DDGS containing sulfate showed a unique band with local absorption maxima around 615 cm^{-1} (range: 640 cm^{-1} to 590 cm^{-1}) which were not present in DDGS without prominent sulfate levels (Figure 1). Also, a specific band around 1107 cm^{-1} was detectable in DDGS with high sulfate content (spiked with sodium sulfate). The band with the maximum around 615 cm^{-1} could be clearly attributed to one of the two fundamental IR active vibrations of the sulfate anion (SO_4^{2-}). In general, inorganic tetrahedral XY_4 molecules such as SO_4^{2-} show four normal modes of vibration; all are Raman-active, but only ν_3 and ν_4 are infrared-active.[18] For the sulfate anion in the free state, these vibrations appear at 1105 cm^{-1} (ν_3) and 611 cm^{-1} (ν_4) as it was described by Nakamoto.[18]

Addition of sodium sulfate to DDGS samples clearly increased the signal at 615 cm^{-1}, whereas the signal at 1107 cm^{-1} could only be detected at very high sulfate levels (Figure 1, red spectra: ∼4.2% sulfate) due to overlaying bands of compounds naturally present in the DDGS (e.g., C—O stretching vibrations of cellulose). In contrast to the maximum absorption signals reported in literature for pure sulfate salts,[18−20] the absorption maxima of ν_3 and ν_4 for sulfate in the matrix DDGS were sometimes found to be slightly shifted to lower or higher frequencies. The reason could possibly be the difference between the ATR technique and the transmission mode, as ATR generally introduces a shift to lower frequencies, or the DDGS matrix accounting for shifts in both directions of the frequency scale. Furthermore, the addition of sodium sulfate lead to an additional band at 636 cm^{-1} (Figure 1D) caused by the lowering of symmetry of the sulfate anion through coordination of the sodium cation. Possibly, coordination exists in the form of a bridged bidentate complex (C_{2v} instead of T_d), as it was previously reported for Na_2SO_4 and sulphato complexes.[21,22]

Recently, Zarrinbakhsh, Mohanty, and Misra (2013) reported on a water-soluble portion of DDGS which exhibits peaks at 1105 and 615 cm^{-1} only in the spectra of solid DDGS, but not in washed DDGS.[23] In consideration of the literature and our current study, their findings clearly indicate the presence of sulfate and their ascription of the major peak at

DOI: 10.1021/jf503704r
J. Agric. Food Chem. 2015, 63, 476−484

1105 cm^{-1} to the respective C—O vibrations of organic compounds should therefore be adjusted.

Quantification of Sulfate in DDGS by FT−IR Spectroscopy. In terms of quantification of sulfate, it was crucial to include both the signal of the normal sulfate anion at 615 cm^{-1} and the signal of the distorted sulfate anion at 636 cm^{-1}. Although for DDGS samples naturally containing sulfate simply the absorption at 615 cm^{-1} was noted, for all spiked DDGS samples linear relationship between band area and spiking level was only reached when integrating over both signals. This indicates that all distorted ions absorbing energy around the maximum of 636 cm^{-1} did not contribute to the absorption signal at 615 cm^{-1} anymore (due to band splitting). Hence, quantification of sulfate was based on the integration of the preprocessed FT−IR spectra of both spiked and nonspiked (native) DDGS samples between 654 and 586 cm^{-1} (Figure 1D). For calibration, DDGS sample A, derived from corn and without substantial sulfate level, was spiked with different amounts of sodium sulfate in levels of 1% to 5%, equal to 0.6% to 3.3% sulfate (Figure 2A). Integration of the respective preprocessed FT−IR spectra in the range of 654 cm^{-1} to 586 cm^{-1} resulted in a linear correlation of integrated area and sulfate content with superior confidence limits (Figure 2B). This matrix calibration was therefore used to calculate the sulfate contents in all other DDGS samples analyzed in the study. Generally, precision of FT−IR spectroscopic measurement in the spectral range of interest was good. Coefficient of variation of calculated sulfate contents (n = 10), based on DDGS sample B, was 2.4%, and the process coefficient of variation, based on the matrix calibration of sample A, was 5.6%.

It is also notable that the absorption maxima of the spiked DDGS (sample A) used for calibration (Figure 2A) compared to those of a spiked DDGS (sample C) with native sulfate content (cf. Figure 1D) were shifted two wavenumbers to lower frequency for both bands of the sodium sulfate vibrations (ν_3 and ν_4). However, this did not affect the integration, as the integration window was chosen broad enough to compensate for such shifts in the wavenumber scale. Furthermore, a quantification procedure aiming at the maximum height of the band around 615 cm^{-1} (using corrected absorbance values, data not shown), as it can generally be applied for quantitative IR spectroscopy,[24] was not as good as the approach by band/peak area demonstrated here. The procedure applied for calculation of the band/peak area included linear baseline correction of the spectra in the range of 654 to 586 cm^{-1}, before integration, and was carried out in the OMNIC Macros Basic 7.4 (Thermo Fisher Scientific). Although for the sample spectra, this resulted in slightly negative amplitudes around 640 cm^{-1} (Figure 3), the procedure was necessary in order to apply the calibration after addition of sodium sulfate using DDGS sample A (Figure 2) to the calculation of sulfate levels in all other samples. The main reason for choosing 654 cm^{-1} as the upper wavenumber for the baseline correction (Figure 3) was the additional signal of the distorted sulfate anion.

Comparison of FT−IR Spectroscopy and Capillary Electrophoresis. *Capillary Electrophoresis.* Sulfate content of DDGS samples was not only analyzed by the previously mentioned FT−IR approach, but also by the use of capillary electrophoresis (CE). The results served as reference values for comparison with FT−IR spectroscopy and also for multivariate calibration.

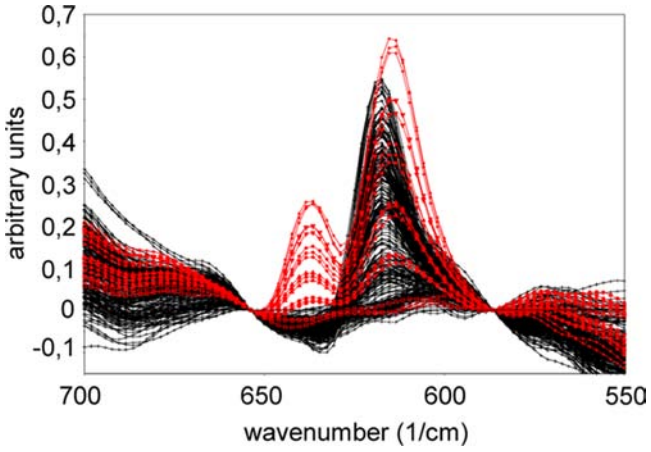

Figure 3. Linear baseline correction of preprocessed FT−IR spectra between 654 and 586 cm^{-1}. Shown are spectra of DDGS sample A, spiked with different amounts of sulfate (red) and spectra of all other DDGS analyzed in the study (black).

The vast majority of the sulfate present in DDGS is derived from sulfuric acid added in the production process and is probably not bound or located in the plant tissue, and therefore a preferably simple method for the extraction of sulfate out of the DDGS samples should work. In addition, several extraction methods for inorganic ions in plant materials had been reported before,[25−27] with sufficient extraction recoveries of sulfate and results indicating even quantitative extraction in comparison to reference methods.[28] Thus, extraction conditions and sample preparation procedure for CE were chosen in consideration of the methods for extraction of sulfate in these previous studies. Accordingly, the extractable sulfate contents analyzed in this study were considered to be capable to serve as reference values for comparison with the results achieved by FT−IR spectroscopy.

To support this assumption, DDGS sample A, without substantial sulfate content, was spiked with different amounts of sodium sulfate (1% to 5%) and analyzed for estimation of recovery. Also, DDGS sample B, with medium sulfate content (1.44%), was extracted ten times and accordingly analyzed by CE to underpin the precision of CE and its suitability as a reference method. Recovery ranged from 94% to 97% dependent on the amount of sulfate added to the sample, relative standard deviation of repetitive measurements (interday precision, n = 10) reached 1.7%. Sulfate was eluting about 3.5 min after the injection of the samples (Figure 4) and was identified by a separate standard addition procedure as well as all the identified peaks in the electropherogram (data not shown). Quantification of sulfate in all DDGS samples was based on correction of the peak area by an internal standard (chlorate) and calculation of the respective sulfate contents in the sample extracts using averaged calibration curves of the single working days.

Comparison of FT−IR and CE Based on Univariate Data. Regression of sulfate contents analyzed by FT−IR spectroscopy against the reference values determined by CE resulted in a linear relationship showing a slight overestimation of the sulfate content by FT−IR (Figure 5A). Although the results for DDGS samples which did not contain sulfate according to CE were leading to both positive and negative sulfate levels by FT−IR (e.g., due to integration of a negligible negative band), the offset in total was nearly zero indicating a good strategy for the

DOI: 10.1021/jf503704r
J. Agric. Food Chem. 2015, 63, 476−484

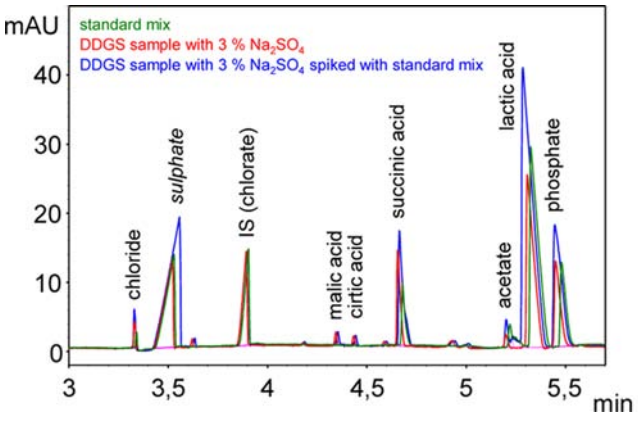

Figure 4. Analysis of sulfate in aqueous extracts of DDGS and in pure standard mix (containing different anions and organic acids) by capillary electrophoresis.

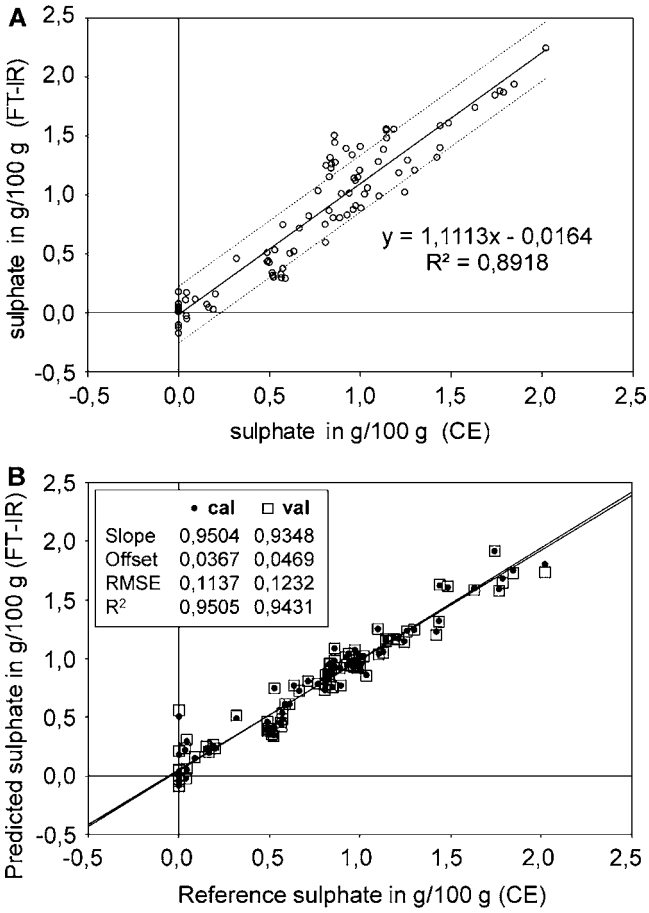

Figure 5. Capability of FT−IR spectroscopy for analysis of sulfate in DDGS. (A) based on integration of bands between 654 and 586 cm^{-1} with confidence intervals drawn by dashed lines; (B) based on PLS regression and 2 latent variables using CE results as reference values; RMSE stands for root mean squared error.

determination of sulfate by FT−IR. However, it was necessary to reintegrate 4 of the 90 samples that had been analyzed by FT−IR spectroscopy (by adjusting the right spectral wavenumber regions manually) as they were slightly shifted outside the region that had been selected for the automated calculation of the peak area (cf. above). In general, it was decided to include all DDGS samples that had been measured for the method comparison (elimination of outliers was omitted) to demonstrate the capability of the proposed strategy on a sample set of DDGS from various origins derived from corn and wheat (cf. SI).

Multivariate Calibration Using PLS Regression. The regression of the univariate results showed a rather high uncertainty for sulfate contents by FT−IR, especially for levels around 0.9% according to CE (cf. Figure 5A). In order to improve the significance of the approach and to overcome difficulties due to spectral window selection for peak area calculation, multivariate calibration was performed applying PLS regression. For this purpose, CE results were used as reference values and after subsequent selection of the most important spectral variables, PLS regression based on 2 latent variables (explained Y-variance: 95.0%) showed a reduced uncertainty with regards to the predictability of sulfate levels of DDGS using FT−IR spectra (Figure 5B). In this case, sulfate content was slightly underestimated by FT−IR spectroscopy, but was nearly unaffected when tested by leave-one-out cross-validation (explained Y-variance: 94.3%) indicating a robust calibration (Figure 5B). The most important finding with regard to the chemical information behind the data was, that the spectral variables used for the final PLS regression were consequentially correlated with the two fundamental IR active vibrations of the sulfate anion. The highest regression coefficients were found for the spectral regions from 1109 to 1088 cm^{-1} and from 623 to 599 cm^{-1} representing the S—O vibrations ν_3 (1105 cm^{-1}) and ν_4 (611 cm^{-1}) of the sulfate anion (Figure 6).

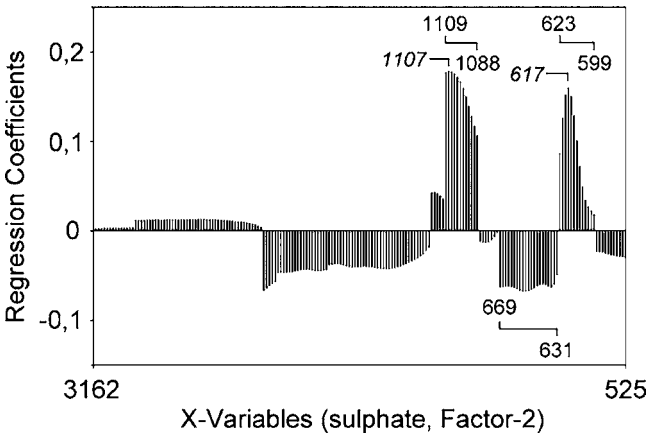

Figure 6. Most important spectral variables used for PLS regression and consistency with the fundamental S—O vibrations of the sulfate anion ν_3 (1105 cm^{-1}) and ν_4 (611 cm^{-1}). Scale of *X*-axis is not continuous.

Without a doubt, there is still a need to prove the robustness and validity of the calibration with an independent external sample set in the future. But in consideration of the sample set with a huge number of different origins included (cf. SI) and the strong correlation to the fundamental vibrations of the sulfate anion, the presented calibration is regarded as already solid at this stage. In general, improved specificity and the nonexisting influence of spectral window selection make the multivariate calibration advantageous, compared with the univariate procedure based on peak area calculation. First and foremost, the approach by FT−IR spectroscopy and subsequent multivariate data analysis could be used for the rapid

DOI: 10.1021/jf503704r
J. Agric. Food Chem. 2015, 63, 476−484

analysis of sulfate levels in DDGS (in terms of screening). By this, single batches of DDGS with high levels of sulfate could be identified and selected for further investigations. If the results indicate high sulfate levels, then verification of the results and analysis of the total sulfur levels (including sulfate) should consequently be carried out by reference methods, such as ICP-MS or X-ray fluorescence spectroscopy.

Estimation: Theoretical Calculation of Total Sulfur Contents. In general, quantitative information on sulfur and/or sulfate in DDGS is of interest to DDGS manufacturers, animal feed producers and farmers. Regarding DDGS, the total amount of sulfur (S) can be classified into S derived from organic compounds and S derived from inorganic compounds: S-rich organic compounds are mainly composed of amino acids containing S atoms or enzymes with S in the prosthetic group; inorganic compounds that contain S are mainly due to sulfate, derived mainly from sulfuric acid used in the production process of DDGS.

In the current study, it was shown that FT−IR spectroscopy could be used for estimation of sulfate levels in DDGS. However, organic forms of S, like S-containing amino acids and proteins, cannot be identified and thus will not be quantified by FT−IR spectroscopy. Nevertheless, the presented approach could be used for routine purposes, as the variability in the total S content of DDGS mainly depends on the inorganic form of S (i.e., sulfate) linked to the amount of sulfuric acid used in the production. In contrast, S-containing organic compounds mainly derive from the plant material (natural origin) and generally only a very low amount is added in the form of yeasts or nutrient salts during the production. Additionally, S derived from the plant material gives a relatively constant input to the production of DDGS, and the major part of it is organically bound with only about 10% of the S from natural origin being present in the form of sulfate.[29,30]

Bearing this in mind, the total S content of DDGS could be estimated, on the basis of a theoretical calculation, as the sum of: (1) the amount of S derived from sulfate (which could be determined by FT−IR spectroscopy) and (2) the amount of S derived from S-containing compounds which were already present in the natural plant material (and would in the main part be due to organic S-containing compounds). The amount of S naturally present in the plant material is dependent on the plant species but is well examined: based on the DM, corn contains an average of 0.12% S,[31] whereas for wheat, cultivated in the 1990s, a mean S content of 1.35 mg/g (0.14%) was reported.[30]

In the final product DDGS, all constituents are concentrated by a factor of approximately three compared to the grain and this would in theory, with regards to the above-mentioned mean S contents of the cereals, result in levels of 0.36% S for corn DDGS and 0.42% for wheat DDGS on a DM basis. However, for a final estimation of the total S contents in DDGS, one would have to consider the percentage of sulfate derived from the plant material, which is approximately 10% of the total S of plant-origin[29,30] and is already covered by the sulfate levels analyzed in this study. Therefore, the total S content of the DDGS samples was theoretically estimated as the sum of the sulfate content (based on the DM) and the "sulfate-corrected" mean S contents from the plant material (based on the DM) of 0.32% for corn DDGS and 0.38% for wheat DDGS (and DDGS of mixed origin). Finally, this resulted in estimated total S contents for the DDGS samples between 0.29% and 1.06% (median 0.63%) based on FT−IR spectroscopy using PLS regression, and consistently, in 0.32% to 1.08% (median 0.63%) when calculating with the reference values which have been analyzed by CE (Figure 7).

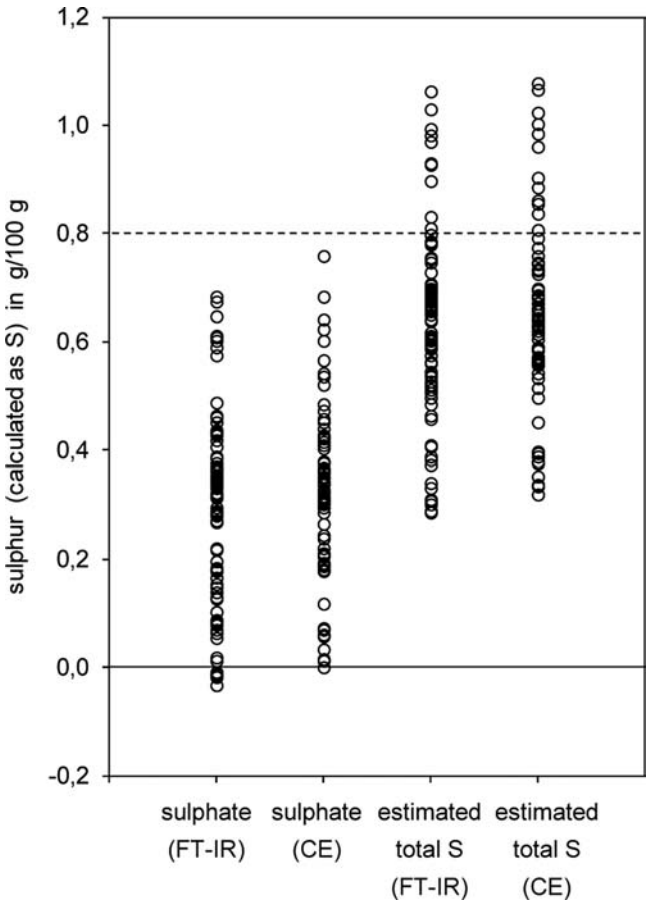

Figure 7. Distribution of sulfur contents of DDGS samples based on sulfate (from chemical analysis) and on estimation of total S contents (based on theoretical calculation). Sulfate (FT−IR) and sulfate (CE) are representing the sulfate levels (calculated as S) based on the DM of the samples; negative values are due to the multivariate calibration approach and should be regarded as zero/not detectable. Total S (FT−IR) and total S (CE) are estimated results of total S contents (calculated as S) additionally considering the theoretical input of plant-derived sulfur. The dashed line illustrates the maximum level of 0.8% S in DDGS discussed in literature.

With regards to the maximum tolerable dietary S level for beef cattle of 0.4% on a DM basis,[9] one has to consider that this dietary concentration could be exceeded if DDGS with a sulfur content greater than 0.80% (DM basis) were fed to ruminants at high inclusion rates (DDGS: 40% of DM intake), in addition to corn and corn silage assuming low sulfate levels in drinking water.[5,10] In such a scenario, 11% (based on FT−IR prediction), respectively 13% (based on CE results) of the DDGS samples analyzed in this study showed excessive sulfur levels on the basis of the theoretical calculation (Figure 7). However, such DDGS could still be fed at a lower inclusion rate or even mixed with batches of DDGS containing lower sulfur levels. This would not only protect ruminants of S toxicity and PEM, but could also show general advantages, because it has been reported that both ruminants and nonruminants show decreased feed intake and gain when feeding a high dietary S level.[12,13]

DOI: 10.1021/jf503704r
J. Agric. Food Chem. 2015, 63, 476−484

General Aspects and Future Perspectives. The study demonstrated that ATR/FT−IR spectroscopy can be applied to the determination of sulfate levels in the matrix DDGS. With regard to the maximum tolerable dietary S level for beef cattle of 0.4%, FT−IR spectroscopy could evaluate whether sulfate levels are low enough to use DDGS in high inclusion rates of the diet. It could serve as a prescreening method to select batches of DDGS with high sulfate levels before using techniques such as X-ray fluorescence spectroscopy or ICP-MS, especially if those are not affordable or FT−IR spectroscopy is already in use for other purposes. However, the final evaluation of sulfur levels in the study was based on an theoretical estimation combining the analyzed sulfate levels with the theoretical percentage of plant-derived sulfur in the form of organic S (as mean levels). Further investigation whether such an approach can be used in routine analysis should therefore be cross-validated with a complementary method (e.g., X-ray fluorescence spectroscopy) in the future. In conclusion, FT−IR spectroscopy can be applied for the comparison of DDGS batches regarding the sulfate content, which could be especially useful for blending of animal feed or adaption of process parameters in the production of DDGS.

■ ASSOCIATED CONTENT

Supporting Information

Detailed information on investigated DDGS samples (botanical origin, geographical origin, and method of production). This material is available free of charge via the Internet at http://pubs.acs.org.

■ AUTHOR INFORMATION

Corresponding Author

*Tel: +49-30-18412-3393; fax: +49-30-18412-3685; e-mail: Carsten.Fauhl-Hassek@bfr.bund.de.

Notes

The authors declare no competing financial interest.

■ ACKNOWLEDGMENTS

Alison Lowham from John Thompson & Sons Ltd. (Belfast, U.K.), Lujia Han from China Agricultural University (Beijing, China) and Patrick Hogrel from Cargill (Crevin, France) are acknowledged for supplying most of the DDGS samples. We thank Lars Valentin (BfR—Federal Institute for Risk Assessment, Berlin, Germany) for his help with transcription in KNIME and Philippe Vermeulen (CRA-W, Gembloux, Belgium) for providing the data for the moisture content of the DDGS samples. The QSAFFE project and research leading to these results received funding from the European Union Seventh Framework Programme (FP7/2007-2013) under grant agreement no. 265702.

■ REFERENCES

(1) Spiehs, M. J.; Whitney, M. H.; Shurson, G. C. Nutrients database for distiller's dried grains with solubles produced from new ethanol plants in Minnesota and South Dakota. *J. Anim. Sci.* **2002**, *80*, 2639−2645.

(2) Belyea, R. L.; Rausch, K. D.; Clevenger, T. E.; Singh, V.; Johnston, D. B.; Tumbleson, M. E. Sources of variation in composition of DDGS. *Anim. Feed Sci. Technol.* **2010**, *159*, 122−130.

(3) Liu, K. Chemical Composition of Distillers Grains, a Review. *J. Agric. Food Chem.* **2011**, *59*, 1508−1526.

(4) McAloon, A., Taylor, F., Yee, W., Ibsen, K., Wooley, R. *Determining the cost of producing ethanol from cornstarch and lignocellulosic feedstocks*. Technical Report NREL/TP-580−28893. National Renewable Energy Laboratory, Golden, CO, USA, 2000.

(5) Shurson, G. C., Tilstra, H., Kerr, B. J. Impact of the United States biofuels co-products on the feed industry. In *Biofuel Co-Products As Livestock Feed—Opportunities and Challenges*; Harinder, P. S., Ed.; Makkar FAO: Rome, 2012; pp 35−59.

(6) Buckner, C. D.; Wilken, M. F.; Benton, J. R.; Vanness, S. J.; Bremer, V. R.; Klopfenstein, T. J.; Kononoff, P. J.; Erickson, G. E. Nutrient variability for distillers grains plus solubles and dry matter determination of ethanol by-products. *Prof. Anim. Sci.* **2011**, *27*, 57−64.

(7) Schoonmaker, J. P., & Beitz, D. C. Hydrogen sulphide: synthesis, physiological roles and pathology associated with feeding cattle maize co-products of the ethanol industry. In *Biofuel Co-Products As Livestock Feed—Opportunities and Challenges*; Harinder, P. S., Ed.; Makkar FAO: Rome, 2012; pp 101−113.

(8) Nichols, C. A.; Bremer, V. A.; Watson, A. K.; Buckner, C. D.; Harding, J. L.; Erickson, G. E.; Klopfenstein, T. J.; Smith, D. R. The effect of sulfur as a model to predict incidence of polioencephalomalacia in feedlot cattle. *Bovine Pract.* **2013**, *47*, 47−53.

(9) NRC—National Research Council. *Nutrient Requirements of Beef Cattle*, 7th Ed.; National Academy Press: Washington, DC, U.S.A., 2000; pp 54−74.

(10) Boyles, S. *Distillers Grains with Solubles*. BEEF Cattle Letter No. 551, OSU Extension BEEF Team, Lancaster, USA, 2007.

(11) Sarturi, J. O.; Erickson, G. E.; Klopfenstein, T. J.; Rolfe, K. M.; Buckner, C. D.; Luebbe, M. K. Impact of source of sulfur on ruminal hydrogen sulfide and logic for the ruminal available sulfur for reduction concept. *J. Anim. Sci.* **2013**, *91*, 3352−3359.

(12) Erickson, G. E., Klopfenstein, T. J., Watson, A. K. Utilization of feed co-products from wet or dry milling for beef cattle. In *Biofuel Co-Products As Livestock Feed—Opportunities and Challenges*; Harinder, P. S., Ed.; Makkar FAO: Rome, 2012; pp 77−99.

(13) NRC—National Research Council. *Mineral Tolerance of Animals*, 2nd revised ed.; National Academy Press: Washington DC, U.S.A., 2005; pp 372−397.

(14) Vanness, S., Klopfenstein, T. J., Erickson, G. E., Karges, K. Sulfur in Distillers Grains. *Nebraska Beef Cattle Reports*, **2009**, Paper 538.

(15) AOAC Official Method 923.01. *Official Methods of Analysis of AOAC International*, 18th ed.; AOAC International: Gaithersburg, USA, 2005.

(16) Commission Regulation (EU) No 68/2013 of 16 January 2013 on the catalogue of feed materials. *Official Journal of the European Union* L 29/1, **2013**.

(17) Nietner, T.; Pfister, M.; Glomb, M. A.; Fauhl-Hassek, C. Authentication of the botanical and geographical origin of distillers dried grains and solubles (DDGS) by FT−IR spectroscopy. *J. Agric. Food Chem.* **2013**, *61*, 7225−7233.

(18) Nakamoto, K. *Infrared and Raman Spectra of Inorganic and Coordination Compounds − Part a: Theory and Applications in Inorganic Chemistry*, 6th ed.; John Wiley & Sons: Hoboken, NJ, 2009; pp 192 ff.

(19) Hunt, J. M.; Wisherd, M. P.; Bonham, L. C. Infrared absorption spectra of minerals and other inorganic compounds. *Anal. Chem.* **1950**, *22*, 1478−1497.

(20) Nyquist, R. A.; Putzig, C. L.; Leugers, M. A. Infrared and Raman spectral atlas of inorganic compounds and organic salts: Text and explanations. In *The Handbook of Infrared and Raman Spectra of Inorganic Compounds and Organic Salts*; Nyquist, R. A., Ed.; Academic Press: San Diego, CA, 1997; Vol. *1*, pp 9ff.

(21) Nyquist, R. A., Kagel, R. O. Infrared spectra of inorganic compounds. In *The Handbook of Infrared and Raman Spectra of Inorganic Compounds and Organic Salts*; Nyquist, R. A., Ed.; Academic Press: San Diego, CA, 1997; Vol. *4*, pp 1ff and 264ff.

(22) Nakamoto, K. *Infrared and Raman Spectra of Inorganic and Coordination Compounds—Part B: Applications in Coordination, Organometallic, And Bioinorganic Chemistry*, 6th Ed.; John Wiley & Sons: Hoboken, NJ, 2009; pp 84 ff.

(23) Zarrinbakhsh, N.; Mohanty, A. K.; Misra, M. Fundamental studies on water washing of the corn ethanol coproduct (DDGS) and

DOI: 10.1021/jf503704r
J. Agric. Food Chem. 2015, 63, 476−484

its characterization for biocomposite applications. *Biomass Bioenergy* **2013**, *55*, 251−259.
(24) Coates, J. Classical methods of quantitative analysis. In *Handbook of Vibrational Spectroscopy Vol. 3—Sample Characterization and Spectral Data Processing*; Chalmers, J. M. , Griffiths, P. R. , Eds.; John Wiley & Sons: Chichester, U.K., 2002; pp 2235−2257.
(25) Smolders, E.; Van Dael, M.; Merckx, R. Simultaneous determination of extractable sulphate and malate in plant extracts using ion chromatography. *J. Chromatogr.* **1990**, *514*, 371−376.
(26) Jimidar, M.; Hartmann, C.; Cousement, N.; Massart, D. L. Determination of nitrate and nitrite in vegetables by capillary electrophoresis with indirect detection. *J. Chromatogr. A* **1995**, *706*, 479−492.
(27) Zhou, M.; Guo, D. Simultaneous determination of chloride, nitrate and sulphate in vegetable samples by single-column ion chromatography. *Michrochem. J.* **2000**, *65*, 221−226.
(28) Kalbasi, M.; Tabatabai, M. A. Simultaneous determination of nitrate, chloride, sulfate and phosphate in plant materials by ion chromatography. *Commun. Soil Sci. Plant Anal.* **1985**, *16*, 787−800.
(29) Thomas, M. D.; Hendricks, R. H.; Bryner, L. C.; Hill, G. R. A study of the sulphur metabolism of wheat, barley and corn using radioactive sulphur. *Plant Physiology* **1944**, *19*, 227−244.
(30) Zhao, F. J.; Hawkesford, M. J.; McGrath, S. P. Sulphur assimilation and effects on yield and quality of wheat. *J. Cereal Sci.* **1999**, *30*, 1−17.
(31) Watson, S. A. Description, development, structure, and composition of the corn kernel. In *Corn: Chemistry and Technology*, 2nd ed.; White, P. J., Johnson, L. A., Eds.; American Association of Cereal Chemists: St. Paul, MN, 2003; pp 69−106.

DOI: 10.1021/jf503704r
J. Agric. Food Chem. 2015, 63, 476−484

JOURNAL OF AGRICULTURAL AND FOOD CHEMISTRY

Article

pubs.acs.org/JAFC

Novel Dispersive Micro-Solid-Phase Extraction Combined with Ultrahigh-Performance Liquid Chromatography–High-Resolution Mass Spectrometry To Determine Morpholine Residues in Citrus and Apples

Dawei Chen,[†] Hong Miao,[†] Jianhong Zou,[‡] Pei Cao,[†] Ning Ma,[†] Yunfeng Zhao,*[,†] and Yongning Wu[†]

[†]Key Laboratory of Food Safety Risk Assessment, Ministry of Health, China National Center for Food Safety Risk Assessment, Beijing 100021, People's Republic of China

[‡]Second Artillery General Hospital, Beijing 100088, People's Republic of China

Supporting Information

ABSTRACT: This paper presents a new analytical method for the determination of morpholine residues in citrus and apples using a novel dispersive micro-solid-phase extraction (DMSPE), followed by ultrahigh-performance liquid chromatography–high-resolution mass spectrometry (UHPLC–HRMS). Samples were extracted with 1% formic acid in acetonitrile/water (1:1, v/v) and then cleaned up using the DMSPE procedure. Morpholine from the extract was adsorbed to a polymer cation exchange sorbent and eluted with ammonium hydroxide/acetonitrile (3:97, v/v) through a 1 mL syringe with a 0.22 μm nylon syringe filter. All of the samples were analyzed by UHPLC–HRMS/MS on a Waters Acquity BEH hydrophilic interaction chromatography column using 0.1% formic acid and 4 mM ammonium formate in water/acetonitrile as the mobile phase with gradient elution. The method showed good linearity (R^2 > 0.999) in the range of 1–100 μg/L for the analyte. The limit of detection and limit of quantitation values of morpholine were 2 and 5 μg/kg, respectively. The average recoveries of morpholine from the citrus and apple samples spiked at three different concentrations (5, 20, and 100 μg/kg) were in a range from 78.4 to 102.7%.

KEYWORDS: *dispersive micro-solid-phase extraction, fruit, morpholine, high-resolution mass spectrometry, design of experiments*

INTRODUCTION

Morpholine, C_4H_9ON, has been widely used as an accelerant in rubber manufacturing, a sulfuration agent, a cleanser, a descaling agent, a surfactant, an agent in textile printing, and a fruit-preserving agent. It is added to some waxes as an emulsifier used in the preparation of wax coatings for fruits and vegetables.[1] In the presence of excess nitrite, morpholine can be chemically modified (nitrosated) to form *N*-nitrosomorpholine (NMOR), which has been proven to be a genotoxic carcinogen in rodents.[2]

Although morpholine as a component of the coating in fresh fruits is approved for use in China,[3] it is still under scrutiny by the European Union (EU) and has not been approved for use in the EU.[4] On the basis of a no observed adverse effect level [NOAEL, 96 mg kg^{-1} of body weight (bw) day^{-1}] in a chronic oral toxicity study for morpholine, an acceptable daily intake (ADI) of 0.48 mg kg^{-1} of bw day^{-1} was estimated by Health Canada.[2] However, there is no currently validated method to determine morpholine residues on waxed commodities, which caused residue data and estimated exposure for morpholine in citrus and apple fruits to not be obtained in China. It is well-known that gas chromatography–thermal conductivity detector (GC–TCD) and gas chromatography–mass spectrometry (GC–MS) or other methods [gas–liquid chromatography–thermal energy analyzer (GLC–TEA) and gas–liquid chromatography–mass spectrometry (GLC–MS)] could be used for analysis of morpholine residues in various matrix samples;[5−9] nevertheless, because of the high polarity and low molecular weight of morpholine, its response and sensitivity are not good enough for residue analysis in complex matrices. Recently, a liquid chromatography–mass spectrometry (LC–MS) method for the determination of morpholine in citrus and apples has been published,[10] but its affiliated extraction and no cleanup process resulted in a >20% ion suppression. The cleanup is considered to be a labor-intensive but effective process to overcome ion suppression. Currently, the cleanup methods, including solid-phase extraction (SPE) and dispersive solid-phase extraction (dSPE), are widely used to solve the matrix interferences in complex matrices for the residue analysis.[11−13] A dual SPE cartridge system was used as a pretreatment method for morpholine in pineapples by Gros et al., but it is time-consuming, laborious, and costly.[14] While a quick, easy, cheap, effective, rugged, and safe (QuEChERS)-based dSPE method for sample cleanup has been developed to improve sample throughput for residue analysis,[15,16] the purification effect is even worse than SPE.[17] On the contrary, dispersive micro-solid-phase extraction (DMSPE) can be categorized as a dSPE or SPE technique and exhibits some advantages over traditional dSPE (fewer matrix effects) and

Received: August 27, 2014
Revised: December 11, 2014
Accepted: December 24, 2014
Published: December 24, 2014

ACS Publications © 2014 American Chemical Society

DOI: 10.1021/jf5041178
J. Agric. Food Chem. 2015, 63, 485−492

SPE (such as without complex equipment, short time requirement, and less solvent consumption).[18−21] In the DMSPE cleanup technique, the solid sorbent is added directly to an extract and the cleanup procedure relies solely upon shaking and centrifugation. Graphene and carbon nanotubes (CNTs) are commonly used as solid sorbent materials for application in the sorbent phase of such processes. Polymer cation exchange (PCX), as a high molecular polymer, is a cation exchange sorbent material. PCX can adsorb the alkaline chemical substances directly and provide an effective separation. In the present study, all of those parameters that were supposed to affect the extraction efficiency in the DMSPE cleanup method, such as the amount of PCX, the adsorption time, and the type and volume of eluent, were carefully investigated and optimized. In analytical chemistry, optimization is a critical stage to find out the value that each factor could help to reach the best possible response.[22] Recently, the multivariate designs of experiments are accepted to obtain the optimal variable parameters.[23−26] The designs of experiments would not just significantly reduce the number of experiments, which can take less time, effort, and resources than the univariate studies, but also take the interactions between variables and nonlinear relations with the responses into account. Therefore, the central composite design (CCD) approach was used for studying the optimal variables in this DMSPE cleanup method.

MATERIALS AND METHODS

Chemicals and Reagents. Acetonitrile and methanol [high-performance liquid chromatography (HPLC) grade] were obtained from Fisher Scientific (Fair Lawn, NJ). Formic acid and ammonium formate (HPLC grade) was purchased from Tedia (Fairfield, OH). Ultrapure water was prepared from a Milli-Q reagent water system (Millipore, Bedford, MA). Cleanert PCX powder was obtained from Agela Technologies (Tianjing, China).

Morpholine was purchased from Supelco (Bellefonte, PA) and d_8−morpholine was obtained from Cambridge Isotope Laboratories (Tewksbury, MA). The purity of all of these standards was no less than 98.0%.

Standard stock solutions (1000 mg/L) were prepared by dissolving 10.0 mg of individual compounds in a 10 mL volumetric flask with methanol. The stock solutions were diluted in acetonitrile to prepare the intermediate standard solutions and the working standard solutions of 10 and 1 mg/L, respectively. All standard solutions were made in amber volumetric flasks and stored at −20 °C.

Sample Collection and Preparation. Apples and citrus were obtained from the local markets from Beijing, China. The apples were produced in Shandong and Gansu provinces in China as well as imported from Chile and the U.S.A. The citrus were transported from Jiangxi, Guangdong, Guangxi, Hubei, and Sichuan provinces in China as well as imported from South Africa and the U.S.A. All samples were cut into small pieces and homogenized using an electric grinder. One sample from 1 kg of apples/citrus was prepared and kept in 4 °C.

A total of 10 g of homogenized sample was weighed into a 50 mL polypropylene centrifuge tube, and a total of 40 μL of the internal standard (10 mg/L) was spiked into the sample. After 10 mL of 1% formic acid in acetonitrile/water (1:1 v/v) was added, the mixture was vortexed for 30 s, ultrasonicated for 10 min, and centrifuged at 8000 rpm for 5 min. The supernatant was poured off into a clean 50 mL polypropylene centrifuge tube and distilled to 20 mL with acetonitrile for the next purification. A total of 1 mL of the supernatant was transferred into a 2 mL eppendorf tube with 30 mg of PCX powder. The mixture was vortexed for 30 s for interaction between the analytes and PCX sorbent and then poured off into a 1 mL syringe with a 0.22 μm nylon syringe filter. The extracted solution was passed through the syringe and syringe filter manually and washed with 1 mL of acetonitrile again. Subsequently, the PCX enriched with the analytes was eluted with 2 mL of ammonium hydroxide/acetonitrile (3:97, v/v). The collected elution was prepared for ultrahigh-performance liquid chromatography−mass spectrometry (UHPLC−MS) analysis.

Chromatographic Conditions. UHPLC analysis was performed on a UHPLC Ultimate 3000 system (Dionex), using an Acquity BEH hydrophilic interaction chromatography (HILIC, 2.1 × 100 mm, 1.7 μm particle size) analytical column (Waters, Milford, MA) with the temperature maintained at 40 °C. The aqueous phase (A) consisted of a mixture of 0.1% formic acid and 4 mM ammonium formate in water, and the organic phase (B) was acetonitrile with 0.1% formic acid. The gradient started at 90% B for 2 min, reduced to 40% B in the next 4 min, followed by re-equilibration at 90% B for 3 min prior to the next injection. The flow rate was set to 300 μL/min, with a resulting overall runtime of 9 min. The injection volume was 10 μL.

Mass Spectrometry Conditions. A Q Exactive mass spectrometer (Thermo Fisher Scientific, Bremen, Germany) with heated electrospray ionization (HESI) was operated in the positive electrospray ionization (ESI^+) modes. The system was controlled by Xcalibur 2.2 (Thermo Fisher Scientific). The spray voltage was 3.5 kV for the positive mode. The temperature of ion transfer capillary, sheath gas, auxiliary gas, sweep gas, and S-lens radio frequency (RF) level were set to 325 °C, 30, 10, and 0 arbitrary units, and 55 V, respectively. The instrument was calibrated in the positive mode every 3 days using the calibration solutions, including caffeine, L-methionyl-arginyl-phenyl-alanylalanine acetate H_2O (MRFA), and a mixture of fluorinated phosphazines, Ultramark 1621, provided by the instrument manufacturer.

The Q Exactive detector was operated in targeted tandem mass spectrometry (tMS/MS) mode. The tMS/MS scan mode is similar to the SRM scan mode used in the triple quadrupole mass spectrometer. The mass spectrometer acquired a tMS/MS scan at a resolution of 70 000 full width at half maximum (fwhm) with 5.0×10^5 of automatic gain control (AGC) target (the number of ions to fill the C-trap) and 200 ms of maximum ion injection time (IT).

Design of Experiments. The software Design-Expert (version 8.0.5b, Stat-Ease, Inc., Minneapolis, MN) was used for experimental design, data analysis, and model building for response surface methodology (RSM).

The central composite design (CCD) approach was employed to identify optimum conditions in the DMSPE cleanup procedure. CCD requires an experiment number to meet $N = 2^k + 2k + c_p$, where k is the factor number and c_p is the replicate number of the central point.[22] In this study, the amount of PCX, the concentration of ammonium hydroxide in acetonitrile, and the volume of elute were set as three independent factors. A five-level three-parameter experimental design of the CCD approach was performed at random order with 20 run experiments, as shown in Table 1 and Table S1 of the Supporting Information. The full CCD was described as follows: (1) a full two-level (−1 and +1) factorial design, (2) center point (c_p = 5), and (3) two axial points on the axis of each design variable at a distance of α = 2.0 from the design center. The response Y (the efficiency of extraction) was established for the determination of optimum method conditions, and the recovery was selected as the indicator of the extraction efficiency. The optimal values of response Y were obtained by solving the regression equation and analyzing the three-dimensional response surface plot and contour plots.

Table 1. Variables and Levels Evaluated in the CCD

independent variable	unit	symbol	coded level				
			$-\alpha$	−1	0	+1	$+\alpha$
amount of PCX	mg	A	10	20	30	40	50
concentration of ammonium hydroxide	%	B	0.1	1.32	2.55	3.77	5
volume of eluent	mL	C	1	1.5	2	2.5	3

DOI: 10.1021/jf5041178
J. Agric. Food Chem. 2015, 63, 485−492

Table 2. Calibration Curve Equations, Correlation Coefficients (R^2), LOD, and LOQ for Morpholine

analyte	precursor ion (m/z)	fragment ion (m/z)	NCE (%)	linear range (μg/L)	linearity equation	R^2	LOD (μg/kg)	LOQ (μg/kg)
morpholine	88.0761	70.0658,[a] 68.0502	75	1−100	$Y = 0.10552X + 0.022816$	0.9997	2	5
d_8-morpholine	96.1259	78.1157,[a] 76.1035	75					

[a]Quantitative ion.

Method Validation. The selectivity of the method was performed by analyzing the blank samples, and matrix interferences were checked close to the elution zone of the analyte.

The calibration curve was constructed using working standard solutions and plotting the peak area ratio of the quantitative ion of the standard to the internal standard at concentrations of 1, 2, 5, 10, 25, 50, and 100 μg/L for morpholine. The concentration of the internal standard was 10 μg/L for d_8-morpholine.

The limit of detection (LOD) and limit of quantitation (LOQ) were estimated for the signal-to-noise (S/N) ratio of more than 3 and 10, respectively, from the chromatograms of samples spiked at the lowest concentration validated. Precision [intraday repeatability and interday reproducibility, in terms of percent relative standard deviation (RSD_r) and RSD_R, respectively] and recovery were estimated by spiked experiments in citrus and apple samples. Intraday repeatability of the method was evaluated by spiking the standard solutions to the six blank matrices at three different concentration levels (5, 20, and 100 μg/kg) and analyzing in the same run of the day on LC−MS. For interday reproducibility, the three concentrations were analyzed in three different days. Extraction recoveries of morpholine were measured in citrus and apples, which were fortified at three concentration levels (5, 20, and 100 μg/kg) with six replicates at each level. The recoveries were calculated from those measured in comparison to the expected concentrations.

The matrix effect (ME) was determined by constructing calibration curves in the blank extract and the pure solvent ($n = 3$). The effects were expressed in terms of signal suppression/enhancement (SSE) and calculated as follows: SSE = slope of spiked extract/slope of pure solvent standard.

Stability of the analyte in the matrix was determined by repeated analysis ($n = 3$) of spiked citrus and apple samples (5 and 20 μg/kg), which were stored at −20 °C. The samples were extracted and analyzed after 7, 14, and 21 days.

RESULTS AND DISCUSSION

Optimization of Chromatographic Conditions. The effects of different liquid chromatographic columns on the target compound separation and retention were initially studied. Three different types of analytical columns, namely, BEH C_{18} (2.1 × 100 mm, 1.7 μm), BEH HILIC (2.1 × 100 mm, 1.7 μm), and HSS T_3 (2.1 × 100 mm, 1.8 μm) were tested to their optimal elution conditions, which were shown in the Supporting Information. Figure S1 of the Supporting Information showed that morpholine had no good retention and weak MS response in C_{18} and T_3 columns because of its high polarity, which led to its co-elution with other impurities, while the HILIC column had a better retention effect and less interference from other impurities. As for the mobile phase, acetonitrile and water with a variety of modifiers were compared. A mixture of 4 mM ammonium formate and 0.1% formic acid solution was selected as the most suitable component for the mobile phase, in which a sufficiently good performance for ionization of morpholine was achieved with good peak symmetry under the optimized linear gradient mode.

MS/MS Optimization. *Optimization of Acquisition Modes.* Full-scan, targeted single ion monitoring (tSIM), and tMS/MS modes are three kinds of commonly used quantitative models for Q Exactive, and all were evaluated and optimized in the present study.

Full-scan mode is a full scan of all ions in the specified mass range. However, the precursor in the inclusion list (with retention times) can be selected in the quadrupole with a particular isolation width by tSIM mode. In tMS/MS mode, the precursor specified in the inclusion list is selected by quadrupole and fragmented in a higher energy collisional dissociation (HCD) cell with specific fragmentation energy. These three acquired modes were evaluated by the S/N ratios. The S/N ratios of morpholine (5 μg/L in a blank citrus extract) in different modes acquired within individual conditions are shown in Figure S2 of the Supporting Information. This figure highlights the fact that tMS/MS is more selective and specific than tSIM and full-scan modes because of complex matrices, which leads to better method detection limits. Therefore, the tMS/MS mode was selected as the quantitative model for morpholine in citrus and apples.

Optimization of the MS Condition in tMS/MS Mode. Using the Q Exactive tune application, the precursor ion was selected in the quadrupole and product ions were found by increasing the normalized collision energy (NCE) in tMS/MS mode. The actual HCD energy in electron volts is calculated on the basis of the chosen NCE, mass, and charge of the precursor ion.[27] After the product ions were chosen, fragmentation energy scans were carried out to obtain the optimal NCE for complete fragmentation of precursor ions. The optimal NCEs of the monitored ions are shown in Table 2.

MS Spectra of Morpholine and d_8-Morpholine. Using tMS/MS mode, the parent ions are selected in the quadruple (e.g., m/z 88.0761 for morpholine and m/z 96.1259 for d_8-morpholine) using a specified m/z window (4 Da) and subsequently fragmented in the HCD cell. A full scan of all fragmented ions originating from the parent ion was performed, and specific product ions were used for data analysis (m/z 70.0658 and 68.0502 for morpholine and m/z 78.1157 and 76.1035 for d_8-morpholine).

Optimization of the Extraction Procedure. Acidic methanol (1%) has been used to extract morpholine with water (0−2 mL), added for aid in the extraction.[10] Thus, the extraction efficiency was studied for the mixture of 1% acidic acetonitrile/water used as the extraction solution with different volumes in this study. Figure S3 of the Supporting Information showed that the extraction efficiency for morpholine was better at 1% formic acid than that at acetonitrile/water (1:1, v/v), and the 10 mL extraction solution was sufficient to extract morpholine completely. Moreover, ultrasound is of great help in the pretreatment of solid samples because it facilitates and accelerates the dissolution, fusion, and leaching.[28] Thus, the ultrasonic extraction was used to aid the extraction of morpholine from the citrus and apples.

During the DMSPE cleanup procedure, the parameters that affected the extraction efficiency, such as the amount of PCX, the adsorption time, and the type and volume of eluent were carefully studied. A one-factor analysis of the variable

DOI: 10.1021/jf5041178
J. Agric. Food Chem. 2015, 63, 485−492

Table 3. ANOVA for the Response Surface Quadratic Model

source	sum of squares	degree of freedom	mean square	F value	p value
model	4740.62	9	526.74	70.07	<0.0001
A	217.56	1	217.56	28.94	0.0003
B	2232.56	1	2232.56	296.98	<0.0001
C	1008.06	1	1008.06	134.09	<0.0001
AB	66.12	1	66.12	8.80	0.0141
AC	0.13	1	0.13	0.017	0.9000
BC	78.12	1	78.12	10.39	0.0091
A^2	292.21	1	292.21	38.87	<0.0001
B^2	953.78	1	953.78	126.87	<0.0001
C^2	271.17	1	271.17	36.07	0.0001
lack of fit	53.84	5	10.77	2.52	0.1663
pure error	21.33	5	4.27		
corrected total	4815.80	19			
standard deviation	2.74	R^2	0.9844		
coefficient of variation	3.57	adjusted R^2	0.9703		

preliminary experiment was performed first, and the preliminary study and results were shown in the Supporting Information. It was found that the adsorption of morpholine into PCX was a fast process, and the adsorption time greater than 30 s did not produce an extra enhancement of adsorption efficiency. As a result, a 30 s adsorption time was chosen for all subsequent experiments. As an analytical practice for SPE, it is well-known that alkaline substances are easily eluted from the strong cation exchange column in alkaline conditions. In addition, it is desirable to use a mobile phase for sample preparation to inject sample solutions into a LC system. Therefore, ammonium hydroxide in acetonitrile had been used to release morpholine from a PCX sorbent based on the ion exchange retention mechanism. Additionally, the detailed ion exchange retention mechanism including the structure of morpholine and PCX was provided in Figure S4 of the Supporting Information.

Design of Experiments. The one-factor analysis indicated that the amount of PCX, the concentration of ammonium hydroxide in acetonitrile, and the volume of eluent were the main effective factors for DMSPE but did not take into account interactions between factors. Therefore, the amount of PCX (10−50 mg, A), the concentration of ammonium hydroxide in acetonitrile (0.1−5%, B), and the volume of eluent (1−3 mL, C) were considered and optimized in CCD. After 20 run experiments described in Table S1 of the Supporting Information, the response Y was calculated on the basis of the efficiency of extraction for morpholine, and all statistical analysis were performed by Design-Expert software. The analysis of variance (ANOVA) for the response surface quadratic model showed that the model was significant, with a p value of less than 0.0001. The lack of fit of the model relative to its pure error showed a p value of 0.1663, which indicated that the fitted model was considered adequate to predict the efficiency of extraction under any set of the variable combination. Model coefficients for the response are shown in Table 3. The final equation in terms of coded factors was response = $87.18 + 3.69A + 11.81B + 7.94C - 2.87AB + 0.13AC - 3.12BC - 3.41A^2 - 6.16B^2 - 3.28C^2$. The three-dimensional (3D) surface response plots and their related counters, obtained using the fitted model, are shown in Figure 1. As shown in Figure 1, the concentration of ammonium hydroxide and the volume of eluent were two important factors that had a significant positive effect on the extraction efficiency. However, the amount of PCX affects the efficiency of the extraction process with the increasing of PCX from 20 to 30 mg, but it was almost unchanged above 30 mg. The optimum conditions were selected by the analysis data obtained from the response surface plots and the regression coefficient plots. The factor settings that maximize the efficiency of extraction were chosen in response optimization. Among these settings, the most desirable factor levels ranged as follows: 22−38 mg for the amount of PCX, 2.5−3.9% for the concentration of ammonium hydroxide, and 1.9−3 mL for the volume of eluent. To obtain the maximum response (Y = 90.7%; desirability = 0.994), the best combination was found to be 30 mg of PCX and 2 mL of 3% ammonium hydroxide in acetonitrile.

Under the above optimized PCX conditions for the DMSPE cleanup method, the pretreatment procedure was simple and fast and the cost of PCX for one sample is approximately 0.30 U.S. dollars. In addition, the total time required for the cleanup of one sample was only approximately 3 min.

Method Validation. *Selectivity.* With the high resolving power and accurate mass measurements of high-resolution mass spectrometry, no interfering peak at the retention time of morpholine was observed from citrus and apple samples. Extracted ion chromatograms for morpholine from the blank citrus, blank apple, and standard at 5 μg/L are shown in Figure 2.

Linearity, LOD, and LOQ. To obtain the internal calibration curves for the analyte, the peak area ratio of the quantitative ion of morpholine to d_8-morpholine was plotted at the concentration of 1−100 μg/L (Table 2). The coefficients of determination (R^2) of the calibration curve for morpholine were above 0.999, which indicated good linearity of the analytical range.

Here, the LOD and LOQ values of the complete method were calculated as 3 and 10 times the S/N ratio, which indicated 2 and 5 μg/kg, respectively.

Recovery and Precision. The results of the recovery, intraday repeatability, and interday reproducibility experiments are presented in Table 4. Overall, average recoveries, repeatability, and reproducibility varied from 78.4 to 96.2%, from 1.8 to 6.4% (RSD_r), and from 2.3 to 6.6% (RSD_R), respectively, for the citrus samples. However, the mean recoveries, repeatability, and reproducibility ranged from 85.4 to 102.7%, with RSD_r from 1.9 to 6.9% and RSD_R from 3.2 to 8.4% for the apple samples, which indicated that the established

DOI: 10.1021/jf5041178
J. Agric. Food Chem. 2015, 63, 485−492

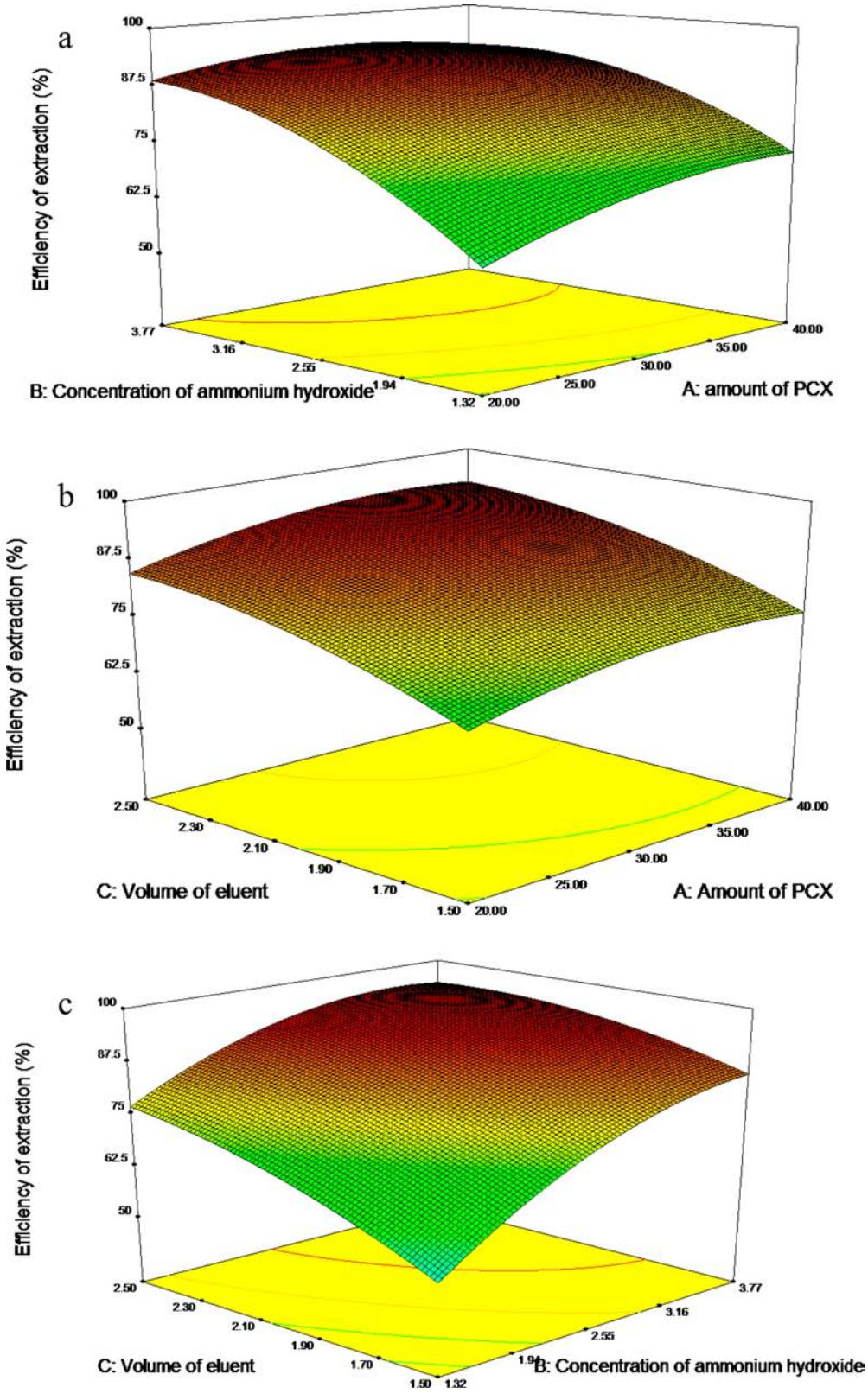

Figure 1. Three-dimensional graphs of the effects of the amount of PCX (A), the concentration of ammonium hydroxide (B) and the volume of elute (C) on efficiency of extraction: (a) fixed C = 2.0 mL, (b) fixed B = 2.55%, and (c) fixed A = 30 mg.

method was accurate enough and suitable for the determination of morpholine in citrus and apple.

Comparison on Matrix Effects. Removing the interference and minimization of the matrix effect in LC−MS is the key to have an accurate, robust, and sensitive quantitative assay.[29] In this study, matrix effects were evaluated by comparing slope ratios of matrix-matched standard calibration slopes with solvent standard calibration slopes (n = 3). It was found that

DOI: 10.1021/jf5041178
J. Agric. Food Chem. 2015, 63, 485−492

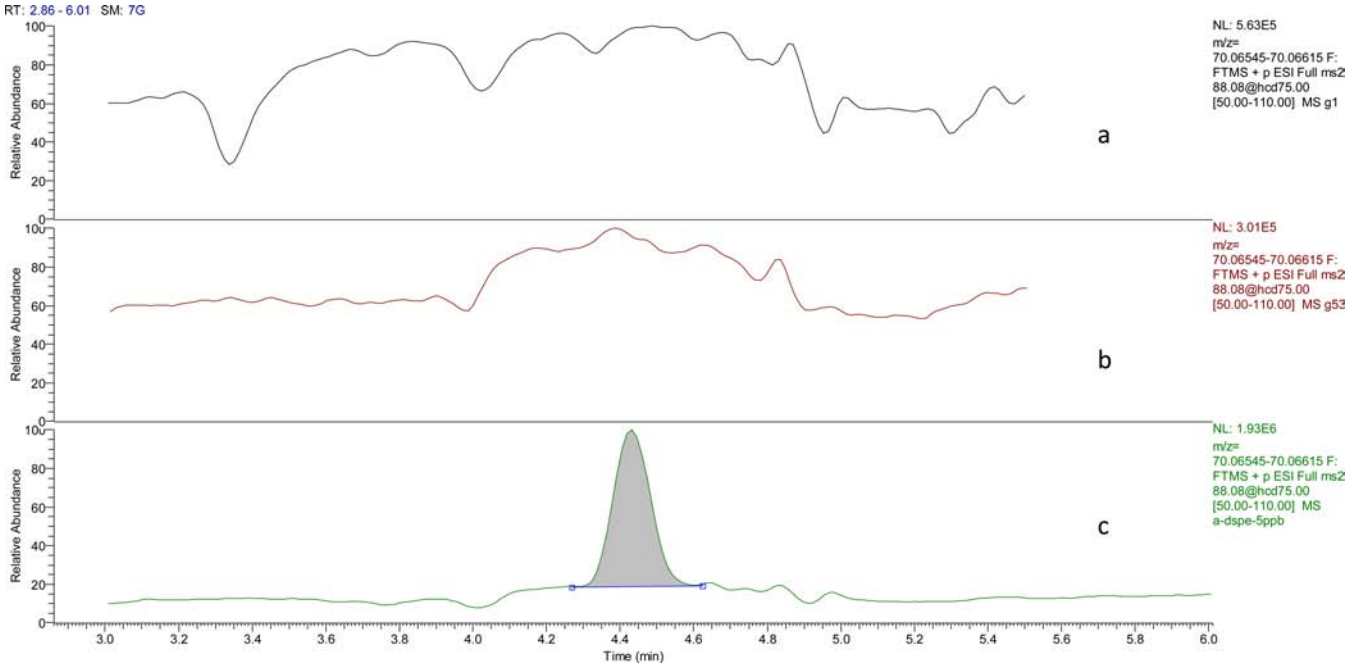

Figure 2. Extracted ion chromatograms for morpholine in the (a) blank citrus, (b) blank apple and (c) standard at 5 μg/L.

Table 4. Precision and Recovery of Morpholine

sample	fortified concentration (μg/kg)	average recovery (%, n = 6)	RSD_r (%)	RSD_R (%)	SSE (n = 3)
citrus	5	78.4	6.4	5.7	0.88 ± 0.03
	20	88.1	3.1	6.6	
	100	96.2	1.8	2.3	
apple	5	85.4	6.9	8.4	0.97 ± 0.02
	20	90.7	2.8	5.7	
	100	102.7	1.9	3.2	

slope ratios from the proposed method for citrus and apple samples were 0.88 ± 0.03 and 0.97 ± 0.02, which were in the range that Frenich et al. had put forward to consider tolerable if the value was between 0.8 and 1.2.[30] It was also observed that there was a slight matrix effect for morpholine in citrus and apple, and the citrus had a stronger matrix effect than the apple. To compensate for the matrix effects and quantify accurately for morpholine in different matrices, concentrations of morpholine in the samples should be calculated by the internal calibration curves.

Stability. The stability tests were performed among spiked samples (5 and 20 μg/kg) at different storage times (after 7, 14, and 21 days), and no obvious change for the recoveries (83.6−95.3%) were observed.

Application to Real Samples. A total of 10 citrus and 8 apples from local markets were analyzed for morpholine using the proposed method. A total of 5 citrus and 3 apples were positive for morpholine residues, with the concentrations of 80.5−598.7 μg/kg for citrus and 43.4−328.2 μg/kg for apples. Sen et al. had reported the contamination levels (0.25−7.7 mg/kg) of morpholine in 17 batches of apples coated with liquid waxes. They indicated that some citrus and apples from the local markets might have been processed with coating wax using morpholine. Further assessments should be conducted to determine whether the presence of contamination levels of morpholine in these samples pose a potential health hazard to humans based on the ADI (0.48 mg kg^{-1} of bw day^{-1}). Moreover, the proposed DMSPE method can be compared to other reported methods for the analysis of morpholine in citrus and apple samples. Table S2 of the Supporting Information compiles the comparison of the analytical features of the selected references. In comparison to the reported methods, fewer matrix effects with similar or better detection levels for the analysis of morpholine were achieved in this study.

In the present study, a new analytical method based on the DMSPE cleanup procedure was developed for the analysis of morpholine residues in citrus and apple samples. The proposed method was validated with fortified samples, and good recoveries were obtained. The LOD and LOQ were low enough to efficiently quantify morpholine in citrus and apple samples. To the best of our knowledge, this paper is the first to introduce application of PCX as a sorbent in DMSPE for sample preparations of alkaline substance and assumed to be widely used for alkaline contaminants at trace levels in the future.

■ ASSOCIATED CONTENT

Supporting Information

Chromatograms for morpholine at a concentration of 5 μg/L acquired with different columns (Figure S1), chromatograms for morpholine at a concentration of 5 μg/L acquired with different modes (Figure S2), effects of the mixture of 1% acidic acetonitrile/water used as the extraction solution with different volumes (Figure S3), adsorption mechanism of DMSPE based on the PCX sorbent (Figure S4), effects of the DMSPE cleanup variables for morpholine (Figure S5), efficiency of extraction as a function of three independent variables (Table S1), and comparison of selected analytical methods proposed for the determination of morpholine in citrus or apples (Table S2). This material is available free of charge via the Internet at http://pubs.acs.org.

DOI: 10.1021/jf5041178
J. Agric. Food Chem. 2015, 63, 485−492

AUTHOR INFORMATION

Corresponding Author

*Telephone: +86-10-67790051. Fax: +86-10-67770158. E-mail: zhaoyf703@126.com.

Funding

This work was financially supported by the International Science and Technology Cooperation Program of China (2011DFA-31770) and the National Support Program for Science and Technology (2012BAK01B01).

Notes

The authors declare no competing financial interest.

ACKNOWLEDGMENTS

The authors thank Thermo Fisher Scientific for technical support.

ABBREVIATIONS USED

DMSPE, dispersive micro-solid-phase extraction; UHPLC−HRMS, ultrahigh-performance liquid chromatography−high-resolution mass spectrometry; PCX, polymer cation exchange; HILIC, hydrophilic interaction chromatography; SPE, solid-phase extraction; dSPE, dispersive solid-phase extraction; LOD, limit of detection; LOQ, limit of quantification; RSD, relative standard deviation; NOAEL, no observed adverse effect level; ADI, acceptable daily intake; NMOR, *N*-nitrosomorpholine; CCD, central composite design; GC−TCD, gas chromatography−thermal conductivity detector; GLC−TEA, gas−liquid chromatography−thermal energy analyzer; GC−MS, gas chromatography−mass spectrometry; HESI, heated electrospray ionization; HCD, higher energy collisional dissociation; NCE, normalized collision energy

REFERENCES

(1) McGuire, R. G.; Dimitroglou, D. A. Evaluation of shellac and sucrose ester fruit coating formulations that support biological control of post-harvest grapefruit decay. *Biocontrol Sci. Technol.* **1999**, *9*, 53−65.

(2) Health Canada. *Archived—A Summary of Health Hazard Assessment of Morpholine in Wax Coatings of Apples*; Health Canada: Ottawa, Ontario, Canada, 2013.

(3) Ministry of Health of the People's Republic of China. *GB2760-2011, Standards for Use of Food Additives*; Ministry of Health of the People's Republic of China: Beijing, China, 2011.

(4) *European Union Food Additives Database*; https://webgate.ec.europa.eu/sanco_foods/main/index.cfm (accessed Sept 2013).

(5) Li, J.; Liu, Q.; Yu, L.; Zhang, C. Determination of morpholine in water by GC/MS. *Ind. Water Treatment* **2009**, *29*, 61−63.

(6) Sen, N. P.; Baddoo, P. A. An investigation on the possible presence of morpholine and *N*-nitrosomorpholine in wax-coated apples. *J. Food Sci.* **1988**, *53*, 183−191.

(7) Hotchkiss, J. H.; Vecchio, A. J. Analysis of direct contact paper and paperboard food packaging for *N*-nitrosomorpholine and morpholine. *J. Food Sci.* **1983**, *48*, 240−242.

(8) Sen, N. P.; Baddoo, P. A. Orgin of *N*-nitrosomorpholine contamination in margarine. *J. Food Sci.* **1986**, *51*, 216−217.

(9) Shi, Z. C.; Wang, S. Z.; Liu, Y. Determination of purity and impurities of morpholine by gas chromatography. *Sci. Technol. Chem. Ind.* **2013**, *21*, 41−47.

(10) Hengel, M. J.; Jordan, R.; Maguire, W. Development and validation of a standardized method for the determination of morpholine residues in fruit commodities by liquid chromatography−mass spectrometry. *J. Agric. Food Chem.* **2014**, *62*, 3697−3701.

(11) Li, Y.; Wang, M.; Yan, H.; Fu, S.; Dai, H. Simultaneous determination of multiresidual phenyl acetanilide pesticides in different food commodities by solid-phase extraction cleanup and gas chromatography−mass spectrometry. *J. Sep. Sci.* **2013**, *36*, 1061−1069.

(12) Kanrar, B.; Mandal, S.; Battacharya, A. Validation and uncertainty analysis of a multiresidue method for 42 pesticides in made tea, tea infusion and spent leaves using ethyl acetate extraction and liquid chromatography−tandem mass spectrometry. *J. Chromatogr. A* **2010**, *1217*, 1926−1933.

(13) Xie, W.; Han, C.; Qian, Y.; Ding, H. Y.; Chen, X. M.; Xi, J. Y. Determination of neonicotinoid pesticides residues in agricultural samples by solid-phase extraction combined with liquid chromatography−tandem mass spectrometry. *J. Chromatogr. A* **2011**, *1218*, 4426−4433.

(14) Gros, P.; Matignon, F.; Plonevez, S. Determination of morpholine in fruits using LC−MS/MS. *Ann. Falsif. Expert. Chim. Toxicol.* **2011**, *974*, 17−22.

(15) Yogendrarajah, P.; Poucke, C. V.; Meulenaer, B. D.; Saeger, S. D. Development and validation of a QuEChERS based liquid chromatography tandem mass spectrometry method for the determination of multiple mycotoxins in spices. *J. Chromatogr. A* **2013**, *1297*, 1−11.

(16) Bruzzoniti, M. C.; Checchini, L.; Carlo, R. M. D.; Orlandini, S.; Rivoira, L.; Bubba, M. D. QuEChERS sample preparation for the determination of pesticides and other organic residues in environmental matrices: A critical review. *Anal. Bioanal. Chem.* **2014**, *406*, 4089−4116.

(17) Perez-Burgos, R.; Grzelak, E. M.; Gokce, G.; Saurina, J.; Barbosa, J.; Barron, D. Quechers methodologies as an alternative to solid phase extraction (SPE) for the determination and characterization of residues of cephalosporins in beef muscle using LC−MS/MS. *J. Chromatogr. B: Anal. Technol. Biomed. Life Sci.* **2012**, *899*, 57−65.

(18) Farhadi, K.; Matin, A. A.; Amanzadeh, H.; Biparva, P.; Tajik, H.; Farshid, A. A.; Pirkharrati, H. A novel dispersive micro solid phase extraction using zein nanoparticles as the sorbent combined with headspace solid phase micro-extraction to determine chlorophenols in water and honey samples by GC−ECD. *Talanta* **2014**, *128*, 493−499.

(19) Asgharinezhad, A. A.; Moliazadeh, N.; Ebrahimzadeh, H.; Mirbabaei, F.; Shekari, N. Magnetic nanoparticles based dispersive micro-solid-phase extraction as a novel technique for coextraction of acidic and basic drugs from biological fluids and waste water. *J. Chromatogr. A* **2014**, *1338*, 1−8.

(20) Jimenez-Soto, J. M.; Cardenas, S.; Valcarcel, M. Dispersive micro solid-phase extraction of triazines from waters using oxidized single-walled carbon nanohorns as sorbent. *J. Chromatogr. A* **2012**, *1245*, 17−23.

(21) Mahpishanian, S.; Sereshti, H. Graphene oxide-based dispersive micro-solid phase extraction for separation and preconcentration of nicotine from biological and environmental water samples followed by gas chromatography−flame ionization detection. *Talanta* **2014**, *130*, 71−77.

(22) Candidoti, L. V.; De Zan, M. M.; Camara, M. S.; Goicoechea, H. C. Experimental design and multiple response optimization. Using the desirability function in analytical methods development. *Talanta* **2014**, *124*, 123−138.

(23) Khodadoust, S.; Ghaedi, M.; Hadjmohammadi, M. R. Dispersive nano solid material-ultrasound assisted microextraction as a novel method for extraction and determination and determination of bendiocarb and promecarb: Response surface methodology. *Talanta* **2013**, *116*, 637−646.

(24) Talebianpoor, M. S.; Khodadoust, S.; Rozbehi, A.; Akbartabar Toori, M.; Zoladl, M.; Ghaedi, M.; Mohammadi, R.; Hosseinzadeh, A. S. Application of optimized dispersive liquid−liquid microextraction for determination of melatonin by HPLC−UV in plasma samples. *J. Chromatogr. B: Anal. Technol. Biomed. Life Sci.* **2014**, *960*, 1−7.

(25) Khodadoust, S.; Talebianpoor, M. S.; Ghaedi, M. Application of an optimized dispersive nanomaterial ultrasound-assisted microextraction method for preconcentration of carbofuran and propoxur and their determination by high-performance liquid chromatography with UV detection. *J. Sep. Sci.* **2014**, *37*, 3117−3124.

DOI: 10.1021/jf5041178
J. Agric. Food Chem. 2015, 63, 485−492

(26) Khodadoust, S.; Ghaedi, M. Application of response surface methodology for determination of methyl red in water samples by spectrophotometry method. *Spectrochim. Acta, Part A* **2014**, *133*, 87−92.
(27) Kumar, P.; Rubies, A.; Centrich, F.; Granados, M.; Cortes-Francisco, N.; Caixach, J.; Companyo, R. Targeted analysis with benchtop quadrupole−orbitrap hybrid mass spectrometry: Application to determination of synthetic hormones in animal urine. *Anal. Chim. Acta* **2013**, *780*, 65−73.
(28) Luque de Castro, M. D.; da Silva, M. P. Strategies for solid sample treatment. *TrAC, Trends Anal. Chem.* **1997**, *16*, 16−24.
(29) Hajslova, J.; Zrostlikova, J. Matrix effects in (ultra) trace analysis of pesticide residues in food and biotic matrices. *J. Chromatogr. A* **2003**, *1000*, 181−197.
(30) Frenich, A. G.; Romero-Gonzalez, R.; Gomez-Perez, M. L.; Martinez Vidal, J. L. Multi-mycotoxin analysis in eggs using a QuEChERS-based extraction procedure and ultra-high-pressure liquid chromatography coupled to triple quadrupole mass spectrometry. *J. Chromatogr. A* **2011**, *1218*, 4349−4356.

DOI: 10.1021/jf5041178
J. Agric. Food Chem. 2015, 63, 485−492

JOURNAL OF AGRICULTURAL AND FOOD CHEMISTRY

Article

pubs.acs.org/JAFC

Ultratrace LC-MS/MS Analysis of Segmented Calf Hair for Retrospective Assessment of Time of Clenbuterol Administration in Agriforensics

Wilco F. Duvivier,[†] Teris A. van Beek,[†] Thijs Meijer,[‡] Ruth J. P. Peeters,[†] Maria J. Groot,[‡] Saskia S. Sterk,[‡] and Michel W. F. Nielen*[,†,‡]

[†]Laboratory of Organic Chemistry, Wageningen University, Dreijenplein 8, 6703 HB Wageningen, The Netherlands

[‡]RIKILT Wageningen UR, P.O. Box 230, 6700 AE Wageningen, The Netherlands

ABSTRACT: In agriforensics, time of administration is often debated when illegal drug residues, such as clenbuterol, are found in frequently traded cattle. In this proof-of-concept work, the feasibility of obtaining retrospective timeline information from segmented calf tail hair analyses has been studied. First, an ultraperformance liquid chromatography−tandem mass spectrometry (UPLC-MS/MS) hair analysis method was adapted to accommodate smaller sample sizes and in-house validated. Then, longitudinal 1 cm segments of calf tail hair were analyzed to obtain clenbuterol concentration profiles. The profiles found were in good agreement with calculated, theoretical positions of the clenbuterol residues along the hair. Following assessment of the average growth rate of calf tail hair, time of clenbuterol administration could be retrospectively determined from segmented hair analysis data. The data from the initial animal treatment study (n = 2) suggest that time of treatment can be retrospectively estimated with an error of 3−17 days.

KEYWORDS: *agriforensics, hair, β-agonist, mass spectrometry, liquid chromatography, veterinary control*

INTRODUCTION

Clenbuterol is a β-agonist approved for therapeutic use in some countries. However, it can also be used illegally, as a growth promoter for cattle. It increases the muscle-to-fat ratio and stimulates overall animal growth.[1−3] Clenbuterol-contaminated meat can cause food intoxication with severe consequences such as heart disorders,[4,5] and it has therefore been banned for use as a growth promoter in cattle in the European Union since 1988.[6] Many different methods for the analysis of clenbuterol and other β-agonist residues in different matrices have been published over the years.[1,2,7−24] Among these methods are approaches based on immunoassays,[7] receptor assays,[24] or biosensors,[1,8,9,21] but these methods lack either sensitivity or selectivity. To overcome these problems, gas chromatography−mass spectrometry (MS) and liquid chromatography (LC)−tandem MS (MS/MS) have been used to analyze a large range of β-agonists.[2,10−16,18−20,22,23] One of the difficulties that occurs when residues of a banned substance such as clenbuterol are found in animals, however, is the fact that animals are frequently traded. The owner can thus claim that a previous owner was responsible for the illegal administration of the detected substances. Current analysis methods are not sensitive enough to be used for estimated time of drug administration. To achieve this, human hair forensic techniques may be equally applicable in veterinary control and agriforensics.

Hair is a very interesting sample matrix because many compounds accumulate in hair via the bloodstream. Hair pigmentation can have an influence on the incorporation of compounds such as clenbuterol into the hair. Gleixner et al. found that more clenbuterol was accumulated into black hair compared to hair with less pigmentation; however, clenbuterol was detectable in hair samples regardless of the level of pigmentation.[25] The prolonged detectability of drugs in hair versus blood or urine makes it a powerful option for forensic investigations.[26,27] Because the average hair growth rate of human head hair is known, analysis of longitudinal segments can be applied to achieve a retrospective timeline of drug intake.[28,29] Longitudinal hair analysis enables correlation of, for example, drug-facilitated crime with the time of drug administration.[28] Typically, 1−3 cm longitudinal hair segments are used for drug analysis, corresponding to multiple months of hair growth.[30,31] Over the past 10 years, several attempts have been made to apply segmented hair analysis to animals, but primarily for horses.[32−40] Dunnett et al. published several papers describing segmented analysis of different drugs in horse hair, mainly focused on antibiotic residues. The distributions among tail hairs were consistent with the time of drug administration, although the used segment sizes (2.5−5 cm) were somewhat large compared to human forensic applications.[32−35] Similar approaches on horse hair have been reported by Anielski et al.[36] and Gray et al.[39] for the detection of anabolic steroids and related compounds. Furthermore, segmented hair analysis has also been used to retrospectively determine stress factors in the hair of bears[38] and orangutans.[40] The smallest segment length used in previous animal studies is 2 cm,[32−36,38−40] which does not allow a very accurate estimation of time of drug administration. Until now, segmented hair analysis has not been applied to bovine (calf) hair or to the illegal use of β-agonists such as clenbuterol.

Received: September 5, 2014
Revised: December 19, 2014
Accepted: December 24, 2014
Published: December 24, 2014

ACS Publications © 2014 American Chemical Society

DOI: 10.1021/jf5056437
J. Agric. Food Chem. 2015, 63, 493−499

In the current, preliminary, study, hair segments of approximately 10 mm were used to enable a more accurate retrospective timeline assessment, preferably with a margin of error on the order of weeks of hair growth (instead of months), which can be helpful in court cases when the time of illegal drug administration is critical in relation to animal ownership. For reliable retrospective timeline assessment, hair must be sampled following the forensic hair sampling protocol, as recommended by the Society of Hair Testing.[31] Sampling of a pencil-thick lock of hair by cutting as close to the skin as possible, in combination with the smaller segment sizes, results in much smaller amounts of hair, on the order of 25 mg instead of 50−1000 mg of hair, being available for analysis. Therefore, an ultratrace analysis method with a very low limit of detection was needed to be able to detect the very low residue levels in the much smaller samples. Apart from that, the average growth rate of bovine hair needed to be assessed, to convert the results of the segmented hair analysis to a retrospective timeline of drug administration. To this end, the analytical method of Nielen et al.[18] was adapted to achieve ultratrace detection of clenbuterol in segmented hair samples. Locks of bovine tail hair, obtained from a controlled treatment (n = 2) study, have been used to test the feasibility of the method and to obtain profiles of the clenbuterol distribution along locks of calf tail hair.

MATERIALS AND METHODS

Chemicals and Materials. All chemicals used were of (at least) analytical grade. Acetone, acetonitrile, ethyl acetate, and methanol were purchased from Actu-All Chemicals (Oss, The Netherlands). Acetic acid, ammonia, formic acid, hydrochloric acid, sodium acetate, and sodium hydroxide were purchased from Merck (Darmstadt, Germany). Chloroform was purchased from BioSolve (Valkenswaard, The Netherlands). Purified water was from a Milli-Q system (Millipore, Bedford, MA, USA). Clenbuterol hydrochloride was purchased from Sigma-Aldrich (St. Louis, MO, USA), and clenbuterol-d_6 internal standard was custom-synthesized previously at Wageningen University and Research Centre (Wageningen, The Netherlands).

Hair Samples. Blank hair samples were collected from the backs of different calves by shaving and were used for method development only. Incurred hair samples were collected from the tail of two male black-and-white Holstein Friesian calves of around 100 kg in a controlled treatment study performed at Ghent University (Ghent, Belgium). For ethical reasons, only two calves were dosed with clenbuterol, a banned substance, in this initial study. The calves were held in a separate stable, away from other cattle. The tails of the calves consisted of white hair only. During a 12 day acclimatization period, hair from the distal end of the tail of the two calves was sampled to obtain additional blank hair samples. Following the acclimatization period, the calves were treated for 14 days with clenbuterol. This animal study was approved by the Ethical Commission of Ghent University, under approval code EC2012/013, and took place from April until November. The treatment consisted of an oral dose of 1.2 μg clenbuterol (expressed as free base)/kg body weight dissolved in milk, once in the morning and once in the afternoon. Next, tail hair from the calves was sampled approximately once a month, for half a year. The detailed treatment and sampling schedule is shown in Figure 1A. At each sampling occasion, at least three pencil-thick hair samples were collected from the distal end of the tail of the calves, using the forensic hair sampling protocol recommended by the Society of Hair Testing.[31] Repeated sampling of the tail of the calves over the duration of the study caused differences in length of locks sampled on the same day, because some parts of the tail contained only shorter, newly grown, hairs due to previous sampling in that area. The resulting hair samples had a weight of approximately 30 mg/cm. For segmented analysis, hair samples were divided into 1 cm segments, starting from the proximal end.

Assessment of Hair Growth Rate. The average growth rate of calf tail hair was determined both for continued growth of existing hairs (length at start = 4.1 ± 0.5 cm), as well as for newly grown hair. Six female calves (black-and-white Holstein Friesian) were used, 1−3 weeks old (around 50 kg) at the start of the study. Continued hair growth was monitored by measuring the hair length of three locks of clearly marked tail hair during 8 weeks. To determine the average growth rate of newly grown hair, three other locks of tail hair from the same calves were cut as close to the skin as possible at the start of the study. The length of newly grown hair was also monitored during 8 weeks (one data point per week). From these results, average tail hair growth rates were determined per calf, which were then used to calculate the overall growth rate and standard deviation for the six calves. Finally, the average of the data from the first 26 days was used for all calculations regarding the theoretical position of the clenbuterol residues (see Results and Discussion).

Sample Preparation. The sample preparation of the hair samples was adopted from that of Nielen et al.[18] and adjusted to much smaller sample sizes. In short, 25 mg of hair were cut into small pieces (<3 mm), and 5.0 μL of internal standard was added (10 μg clenbuterol-d_6/L). One milliliter of 1.0 M sodium hydroxide was added, and the samples were heated for 2 h in a water bath at 65 °C. After the samples had cooled to room temperature, 1.0 mL of 1.0 M hydrochloric acid and 1.25 mL of 0.25 M sodium acetate buffer (pH 4.8) were added. Next, the samples were centrifuged for 10 min at 2000g, and the supernatant was transferred into a clean test tube. Prior to an additional centrifugation step, the pH of the supernatant was checked and, if necessary, adjusted to 4.8. The resulting supernatant was subjected to mixed-phase solid phase extraction (SPE) cleanup as described.[18] In short, the column was conditioned with 3 mL of methanol and 3 mL of sodium acetate buffer before the sample was introduced. After sequential washings with 1 mL of 1.0 M acetic acid, 6 mL of methanol, and 2 mL of acetone/chloroform (1:1), the retained compounds were eluted using 7.5 mL of 1% ammonia in ethyl acetate. After evaporation to dryness under a N_2 flow at 40 °C, the residue was reconstituted in 100.0 μL of 0.24% formic acid, and a 10.0 μL aliquot was injected in the LC-MS/MS system.

LC-MS/MS Method. The ultrahigh-performance liquid chromatography (UHPLC)-MS/MS analysis was carried out as follows. An Acquity UPLC system (Waters, Milford, MA, USA) was coupled to a Xevo TQ-S MS system (Waters), equipped with an electrospray ion source. The MS was used in positive ionization mode using the following conditions: capillary voltage, 3.0 kV; cone voltage, 20 and 25 V for clenbuterol and clenbuterol-d_6, respectively; source temperature, 150 °C; desolvation temperature, 400 °C; collision energy, 30 and 15 eV for clenbuterol and clenbuterol-d_6, respectively. Clenbuterol and clenbuterol-d_6 were analyzed in multiple reaction monitoring (MRM) mode using the following ion transitions: m/z 277.2 to m/z 132.1, 168.1, and 203.2 for clenbuterol and m/z 283.2 to m/z 204.1 for clenbuterol-d_6, respectively. Separation was achieved by using an Acquity BEH-C18 column (2.1 × 100 mm, 1.7 μm; Waters) at 40 °C and a flow rate of 0.4 mL/min. The mobile phases consisted of 25 mM formic acid in water (mobile phase A) and in acetonitrile (mobile phase B). The used gradient was as follows: isocratic elution for 1 min at 5% B, follwed by a gradient applied to 35% B in 8.5 min and then a steep gradient toward 100% B in 0.3 min. After 2.2 min at this condition, the system was re-equilibrated for 3 min at 5% B. Data analysis was performed using MassLynx V4.1 (Waters). Matrix-matched standards (MMS) were used for clenbuterol quantification in the hair samples. In short, clenbuterol standard was added to blank calf hair in concentrations ranging from 0.5 to 10 μg clenbuterol (expressed as free base)/kg hair. The resulting calibration curve was then used for concentration calculations in the hair samples. Throughout this work, all clenbuterol is expressed as the free-base basis.

Method Validation. The linearity of the MMS calibration curve was determined by analyzing the following clenbuterol concentrations in duplicate: 12.5, 25, 50, 100, and 250 pg per 25 mg of hair. The

DOI: 10.1021/jf5056437
J. Agric. Food Chem. 2015, 63, 493−499

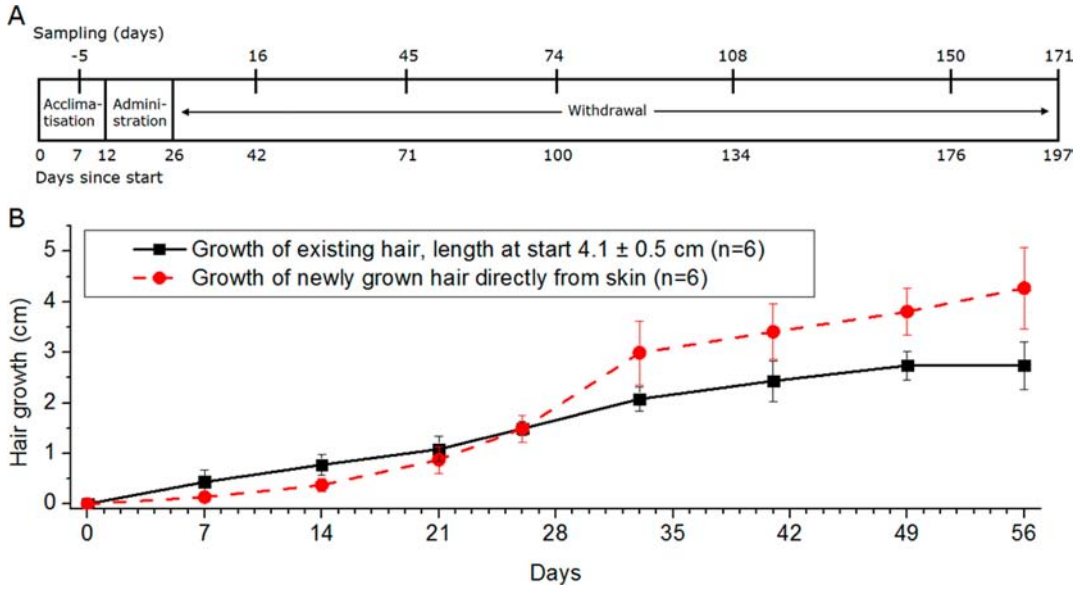

Figure 1. (A) Controlled animal treatment and sampling schedules. (B) Average hair growth rate of calf tail hair, both as continued growth from an existing lock and as new growth (after cutting as close to the skin as possible). Error bars represent intra-animal RSD (n = 6).

recovery was evaluated by spiking three blank hair samples with 50 pg clenbuterol/25 mg of hair. After sample pretreatment, 5.0 μL of internal standard was added just before injection instead of during spiking. Both experiments were executed on three different days. Further validation of the method regarding within-day repeatability, within-laboratory reproducibility, accuracy, decision limit (CCα), and detection capability (CCβ)[41] was performed using blank hair samples spiked at three concentration levels: 25, 50, and 100 pg per 25 mg of hair. A total set of 18 replicates for the 25 and 100 pg/25 mg concentration level and 21 replicates for the 50 pg/25 mg concentration level were analyzed on three different days. In addition, 21 blank hair samples were analyzed with the addition of internal standard only.

Data and Statistical Analysis. The hair growth data presented are mean values with corresponding relative standard deviations (RSD). Student's t test (two-sample assuming unequal variances) was used to assess significance of the difference between hair growth rates (P < 0.01). All validation data were evaluated using ANOVA. The analytical reproducibility of the method (10.6%) is shown as error bars in Figures 2−4.

RESULTS AND DISCUSSION

Ultratrace LC-MS/MS Method Development and Validation. The improved LC-MS/MS method for clenbuterol in hair allowed the analysis of hair samples as small as 25 mg, 2−40 times lower than in previously reported methods.[1,2,10,19,21,22] The within-day repeatability and within-laboratory reproducibility RSD were <9.6 and <10.6%, respectively, at all spike levels. Accuracy was 92−101% with an average recovery of 37%, which was slightly lower than the average recovery (49%) of the method by Nielen et al.[18] The incomplete recovery is possibly caused by incomplete reconstitution in only 100 μL, which volume is significantly lower than the 300 μL used by Nielen et al.[18] However, the lower reconstitution volume was necessary to obtain a final clenbuterol concentration high enough for LC-MS/MS analysis. Moreover, the added internal standard was capable of reproducibly correcting for the incomplete recovery, as shown by the accuracy and reproducibility data given above. Linearity of the MMS calibration curve was adequate in a range from 12.5 to 250 pg/25 mg hair (R^2 > 0.993). The resulting CCα and CCβ were 16.8 and 33.7 pg/25 mg hair, respectively. Compared to the CCβ reported in the previously described method[18] (<2500 pg/500 mg hair), we achieved a tremendous increase in absolute sensitivity, which was essential for the small sample amounts expected in this study. This sensitivity is similar to or better than that previously reported for clenbuterol in hair.[1,2,10,19,21,22]

Average Tail Hair Growth Rate. The average tail hair growth rate for calves has been determined for both continued growth on existing hairs and newly grown hair. For both types of hair, the locations were similar as used for sampling in the controlled treatment study. The length of three locks of tail hair and the length of newly grown hair on three other spots, after cutting as close to the skin as possible, were recorded over a period of 8 weeks. The resulting hair growth curves are shown in Figure 1. During the first 26 days, the growth rate was equal (P < 0.01) for both existing and new hair: 0.57 mm/day (± 0.05 and ± 0.10 mm/day for, respectively, continued and newly grown hair). After the first 26 days, the growth rate of existing hair plateaued, resulting in an average growth rate over 56 days of 0.49 ± 0.08 mm/day. During the 49 and 56 day time points, some of the locks became shorter or stayed the same length, indicating that the decreasing average growth rate was most likely caused by the breaking off of brittle tips of longer hairs. The latter hypothesis has been confirmed by dyeing tips of long tail hairs. After 2 weeks, the dyed part of the hair became shorter and new hair was formed at the proximal end of the hair, indicating that hair continued to grow, even though the total length did not increase. Hair zones containing drug residues will keep growing toward the distal end of the hair. The implications of breaking off brittle tips on the final retrospective timeline assessment should be investigated in more detail in future studies. The average growth rate at 26 days, 0.57 ± 0.08 mm/day, has been selected for further calculations, because both types of tail hair showed similar growth at this time point and later data points already showed plateauing of the hair growth rate for existing hairs (Figure 1). Few reference data on the hair growth rate of calves are available; the only data published report 0.20−0.23 mm/

DOI: 10.1021/jf5056437
J. Agric. Food Chem. 2015, 63, 493−499

day[42,43] but, unfortunately, these references do not provide experimental details, so it is unknown whether these reference data also relate to tail hair.

Segmented Hair Analysis for Retrospective Timeline Assessment of Clenbuterol Administration. The sampled locks of calf tail hair were analyzed after cutting into 1 cm segments. In view of the average hair growth rate as described above, each segment corresponded to approximately 17.5 days of hair growth. The resulting clenbuterol concentration profiles along the hair locks, prior to and up to 108 days after clenbuterol administration, are shown in Figure 2. Samples

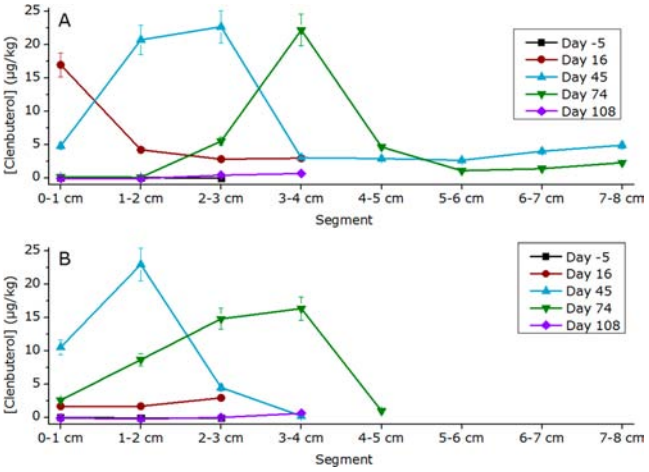

Figure 2. Clenbuterol concentration profiles versus hair segments from calf tail hair samples, taken at different time points (days before or after the end of the clenbuterol administration period of 14 days), of two different calves (A and B). Error bars represent the analytical reproducibility of the method (10.6%).

taken 108, 150, and 171 days after the end of the clenbuterol administration period did not contain clenbuterol in any hair segment. No clenbuterol was detected in the samples taken 5 days prior to clenbuterol administration (Figure 2), indicating that the calves did not come into contact with clenbuterol prior to the controlled administration and verifying once again that blank hair yields negative results. For the first calf (Figure 2A), peak clenbuterol concentrations were found in the 0−1 cm hair segment of the day 16 sample, in the 1−2 and 2−3 cm segments of the day 45 samples, and in the 3−4 cm segment of the day 74 samples. The longitudinal hair profiles from the samples obtained from the second calf (Figure 2B) showed peak clenbuterol concentrations in the 1−2 cm hair segment of the day 45 samples and in the 2−3 and 3−4 cm segments of the day 74 samples.

To establish the theoretical position of the clenbuterol residues in the hair lock samples, several issues have to be taken into account. First, clenbuterol was administered for 14 days (Figure 1A), theoretically resulting in incorporation into a longitudinal section of the hair of approximately 0.80 ± 0.11 cm, provided clenbuterol had been exclusively incorporated into hair via the hair root. The section in which clenbuterol was incorporated was, most likely, even larger because clenbuterol in cattle has a half-life time of 19 h during the distribution phase (first 3 days after administration) followed by a half-life time of 57 h during the elimination phase.[44] The majority (>95%) of the administered clenbuterol would have been metabolized or excreted from the body after 4 days. The additional days of unaltered clenbuterol in the blood circulation caused additional incorporation days in calf hair via the root. The prolonged presence of clenbuterol in the blood after withdrawal can add an extra 0.24 ± 0.03 cm to the length of the hair section containing clenbuterol. Furthermore, newly grown hair sections can be sampled only after clenbuterol reaches the skin surface. The skin thickness of calves is approximately 2.8 mm[42] and should be taken into account for the calculation of the theoretical position of the clenbuterol containing hair section. The theoretical positions of clenbuterol residues calculated using the average hair growth rate of 0.57 ± 0.08 mm/day and corrected for both the elimination time from the blood and the skin thickness are given in Table 1. The experimental data of hair segments containing clenbuterol peak concentrations were in good correlation with the calculated theoretical positions (Table 1). The theoretical position of the clenbuterol residues 108 days after administration would be around 5.5 cm, whereas the hair samples that could be taken at that time were of a maximum length of 4 cm. Thus, these 4 cm represent post-treatment hair only, in which clenbuterol could not have been incorporated. Besides the peak levels in the clenbuterol profiles along the hair segments, some segments showed some low residue levels of clenbuterol (e.g., day 16, 1−4 cm; day 45, 3−8 cm in Figure 2A). This is possibly caused by external contamination of hair via licking upon drinking the clenbuterol-containing milk[45] or by endogenous self-contamination via sweat, as described for human forensic practice by Henderson et al.[46] Another explanation for the low clenbuterol residue levels in segments not containing peak concentrations is

Table 1. Theoretical Position of Clenbuterol Residues in Calf Tail Hair, Calculated Using an Average Hair Growth Rate of 0.57 ± 0.08 mm/day, Experimental Position from Segmented Tail Hair Analysis, and Retrospective Assessment of the Time of Drug Administration

actual sample collection time after treatment	theor position of hair section containing clenbuterol residues (cm)	exptl position of clenbuterol peak concn in segmented tail hair samples (cm)	exptl retrospective time of clenbuterol admin (mean days ago and range)
day 16	0.28 ± 0.1 to 1.3 ± 0.2	0−1	13.5 4.8 ± 0.6 to 22.3 ± 3.0
day 45	1.9 ± 0.3 to 2.9 ± 0.4	1−3	39.7 22.3 ± 3.0 to 57.2 ± 7.7
day 74	3.5 ± 0.5 to 4.5 ± 0.6	2−4	57.2 39.7 ± 5.4 to 74.7 ± 10.1
day 108	5.5 ± 0.8 to 6.5 ± 0.9	not detected	not detected

DOI: 10.1021/jf5056437
J. Agric. Food Chem. 2015, 63, 493−499

axial diffusion of compounds along the hair, as described by Kintz et al.[47] However, both external contamination and axial diffusion will not interfere with the retrospective assessment of treatment time because in this preliminary trial only the position of the peak values in the clenbuterol concentration profiles along the hair segments was used. The peak values were much higher and could be easily distinguished from the slightly elevated levels caused by external contamination or axial diffusion. An initial attempt to remove external contamination by washing the hair segments with methanol prior to sample preparation did not reduce the detected traces of clenbuterol, in agreement with the findings of Hernández-Carrasquilla et al., who showed that methanol decontamination is insufficient to remove external β-agonist contamination from hair.[48] Because clenbuterol is a non-natural synthetic compound, residues in hair always indicate illegal use. Furthermore, the residue concentration following external contamination will be much lower compared to the peak concentration[45] and therefore not influence the assignment of the position of the clenbuterol peak along the hair.

In agriforensic practice, the time of drug administration will be unknown, and the segment of the hair in which the clenbuterol peak is detected must be converted to a timeline using an average hair growth rate. The skin thickness has been added to the start and end points of the segments, and the hair lengths have been converted to days of hair growth. The resulting retrospective estimations of time of clenbuterol treatment are included in Table 1. On the basis of this initial animal trial (n = 2), the retrospective estimations from segmented hair analysis were in good agreement with the actual period of clenbuterol administration. The accuracy of the retrospective estimation of the time of clenbuterol administration was 18 days when the clenbuterol peak concentration was detected in only one of the 1 cm long hair segments and approximately 35 days when detected equally in two subsequent hair segments (see, for example, the day 45 and 74 samples in panels A and B, respectively, of Figure 2). The experimental mean values for the retrospective time assessment show an error of only 3−17 days when compared to the actual time of clenbuterol administration (Table 1). It should be stressed that these results were obtained in a preliminary treatment (n = 2) study. Nevertheless, the results suggest that segmented hair analysis can be successfully used in agriforensics to obtain a retrospective estimation of the time of clenbuterol administration to calves.

Reproducibility of Longitudinal Clenbuterol Profiles. To test the reproducibility of the profiles, subsamples taken from the same lock of hair and duplicate locks of hair, sampled at the same time, were analyzed. A lock of tail hair sampled 45 days after the end of the clenbuterol administration period was divided into two subsamples, and 1 cm segments of these subsamples were analyzed. The conclusion with respect to the segments having the highest clenbuterol levels are comparable (Figure 3): both profiles show peak concentrations in the 1−2 cm segment, but for the second subsample, the peak clenbuterol concentration extended into the 2−3 cm segment. This may have been caused by uneven cutting of the hair due to bundling of the hair lock, which can result in slightly different sampling distances relative to the skin within a sampled lock. This phenomenon has been described in more detail by LeBeau et al.[49] and may result in two nonidentical subsamples after splitting of a lock of hair.

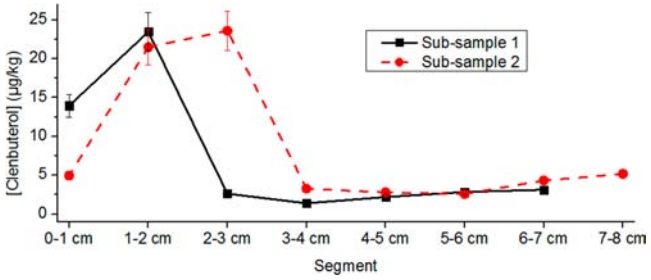

Figure 3. Clenbuterol concentration profiles versus hair segments from calf tail hair. Subsamples were obtained from a lock of hair sampled 45 days after the end of the clenbuterol administration period. Error bars represent the analytical reproducibility of the method (10.6%).

Figure 4 shows the concentration profiles of duplicate locks of hair, sampled at the same day. The duplicate samples, taken 45 days after administration (Figure 4A), show high clenbuterol

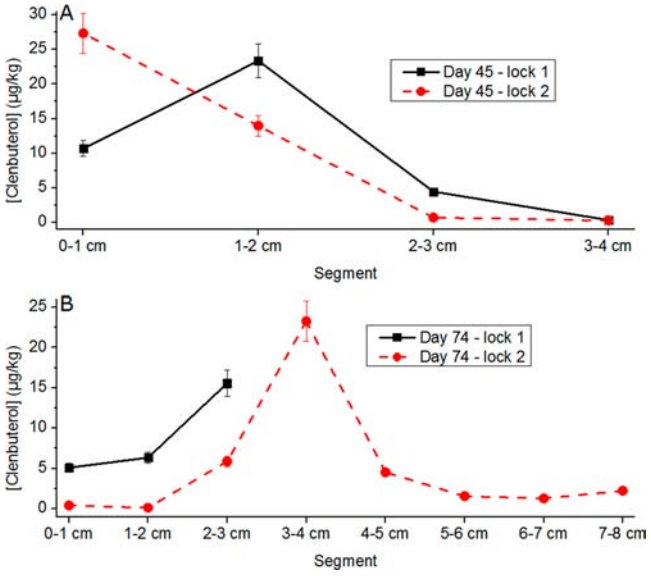

Figure 4. Clenbuterol concentration profiles versus hair segments from duplicate locks of calf tail hair, sampled (A) 45 and (B) 74 days after clenbuterol administration. Error bars represent the analytical reproducibility of the method (10.6%).

concentrations in the first two segments and lower in the distal segments, which is consistent with the calculated position of the clenbuterol residues (Table 1). For the analyzed duplicate samples collected 74 days after administration, a lock of 3 cm and a lock of 10 cm were analyzed (see Figure 4B). [Note: the difference in length of these locks is most likely caused by the repeated sampling of the tail of the calves. Some parts of the tail contained only shorter newly grown hairs, because those areas had been sampled before, whereas other parts still contained longer hairs on areas that had not been sampled before (see Materials and Methods).] An increase in clenbuterol concentration has been noted toward the 3−4 cm segment in both duplicate locks, and even though the length of the locks was not equal, the found trend is similar. A factor to be taken into account is the intra-animal variability: human hair forensics shows that the variation in residue concentrations between locks of hair from one person ranges from 14 to 62%. This can cause differences between and within locks of hair as also

DOI: 10.1021/jf5056437
J. Agric. Food Chem. 2015, 63, 493−499

observed in the present study (Figures 3 and 4). Note that the analytical variability of each data point is much lower (10.6%) according to the validation study. The position of the clenbuterol peak concentration, however, will not change by variation in the absolute concentration. In this respect, both samples showed comparable results: it can be stated that segmented hair analysis is reproducible in the assignment of the relevant segment position and, therefore, can result in a similar retrospective estimation of time of drug administration. It should be stressed, however, that inaccurate hair sampling can cause differences, even within a single lock of hair.[49] To reach the highest certainty about time of drug administration, multiple locks of hair should be sampled by cutting as close as possible to the skin and as straight as possible, in accordance with recommendations.[31]

FUTURE PERSPECTIVES

The LC-MS/MS method developed showed a CCβ value of 33.7 pg for as little as 25 mg of hair, which represents a major improvement compared to the previously described method (CCβ < 2500 pg for 500 mg of hair).[18] The resulting clenbuterol concentration profiles along the hair segments nicely shows the feasibility of retrospective estimation of the time of drug administration, with a mean error of 3−17 days, depending on the shape of the concentration profile of clenbuterol residues along the segments. To get a more precise retrospective estimation of the time of treatment, more reference profiles from different calves after controlled treatment should be analyzed and combined with more in-depth and longer lasting research toward differences in hair growth rates. In a follow-up study, both male and female calves and calves with different tail hair pigmentation should be included to gain more insight in the interanimal variation. Because many compounds accumulate in the hair of cattle, this method should be applicable to other banned substances as well, especially to other β-agonists. Extension of the scope can provide the agriforensics community with a powerful tool to estimate the time of illegal β-agonist administration. In many cases, an error on the order of a few weeks will be sufficient to support court cases in which (timelines of) illegal treatments are being challenged. Possibly, the retrospective timeline assessment could be improved further with trace analysis of even smaller segments. The latter may require entirely new analysis approaches such as longitudinal mass spectrometry imaging of intact hairs.[50]

AUTHOR INFORMATION

Corresponding Author

*(M.W.F.N.) Phone: +31 (0)317 480407. Fax: +31 (0)317 417717. E-mail: michel.nielen@wur.nl.

Funding

This research was funded by The Netherlands Organization for Scientific Research (NWO) within the framework of the Forensic Science program (Project 727.011.004).

Notes

The authors declare no competing financial interest.

ACKNOWLEDGMENTS

We are very thankful to Dr. Johan van Hende (Ghent University, Belgium) for assistance during hair sampling.

ABBREVIATIONS USED

LC, liquid chromatography; MMS, matrix-matched standards; MRM, multiple reaction monitoring; MS, mass spectrometry; MS/MS, tandem mass spectrometry; RSD, relative standard deviation; SPE, solid phase extraction

REFERENCES

(1) Johansson, M. A.; Hellenäs, K. E. Immunobiosensor analysis of clenbuterol in bovine hair. *Food Agric. Immunol.* **2003**, *15*, 197−205.

(2) Salquèbre, G.; Bresson, M.; Villain, M.; Cirimele, V.; Kintz, P. Clenbuterol determination in calf hair by UPLC-MS-MS: case report of a fraudulent use for cattle growth. *J. Anal. Toxicol.* **2007**, *31*, 114−118.

(3) Elliott, C. T.; Crooks, S. R. H.; McEvoy, J. G. D.; McCaughey, W. J.; Hewitt, S. A.; Patterson, D.; Kilpatrick, D. Observations on the effects of long-term withdrawal on carcass composition and residue concentrations in clenbuterol-medicated cattle. *Vet. Res. Commun.* **1993**, *17*, 459−468.

(4) Martínez-Navarro, J. F. Food poisoning related to consumption of illicit β-agonist in liver. *Lancet* **1990**, *336*, 1311.

(5) Maistro, S.; Chiesa, E.; Angeletti, R.; Brambilla, G. Beta blockers to prevent clenbuterol poisoning. *Lancet* **1995**, *346*, 180.

(6) Commission Decision 2003/74/EC. *Off. J. Eur. Communities* **2003**, *L262*, 17.

(7) Vanoosthuyze, K. E. I.; Arts, C. J. M.; Van Peteghem, C. H. Development of a fast and simple method for determination of β-agonists in urine by extraction on Empore membranes and detection by a test strip immunoassay. *J. Agric. Food Chem.* **1997**, *45*, 3129−3137.

(8) Haasnoot, W.; Kemmers-Voncken, A.; Samson, D. Immunofiltration as sample cleanup for the immunochemical detection of β-agonists in urine. *Analyst* **2002**, *127*, 87−92.

(9) Traynor, I. M.; Crooks, S. R. H.; Bowers, J.; Elliott, C. T. Detection of multi-β-agonist residues in liver matrix by use of a surface plasma resonance biosensor. *Anal. Chim. Acta* **2003**, *483*, 187−191.

(10) Schlupp, A.; Anielski, P.; Thieme, D.; Müller, R. K.; Meyer, H.; Ellendorff, F. The β-agonist clenbuterol in mane and tail hair of horses. *Equine Vet. J.* **2004**, *36*, 118−122.

(11) Dickson, L. C.; Macneil, J. D.; Lee, S.; Fesser, A. C. E. Determination of β-agonist residues in bovine urine using liquid chromatography-tandem mass spectrometry. *J. AOAC Int.* **2005**, *88*, 46−56.

(12) Fesser, A. C. E.; Dickson, L. C.; Macneil, J. D.; Patterson, J. R.; Lee, S.; Gedir, R. Determination of β-agonists in liver and retina by liquid chromatography-tandem mass spectrometry. *J. AOAC Int.* **2005**, *88*, 61−69.

(13) Van Hoof, N.; Courtheyn, D.; Antignac, J. P.; Van De Wiele, M.; Poelmans, S.; Noppe, H.; De Brabander, H. Multi-residue liquid chromatography/tandem mass spectrometric analysis of β-agonists in urine using molecular imprinted polymers. *Rapid Commun. Mass Spectrom.* **2005**, *19*, 2801−2808.

(14) Fiori, M.; Civitareale, C.; Mirante, S.; Magarò, E.; Brambilla, G. Evaluation of two different clean-up steps, to minimise ion suppression phenomena in ion trap liquid chromatography-tandem mass spectrometry for the multi-residue analysis of beta agonists in calves urine. *Anal. Chim. Acta* **2005**, *529*, 207−210.

(15) Zhang, J.; Xu, Y.; Di, X.; Wu, M. Quantitation of salbutamol in human urine by liquid chromatography-electrospray ionization mass spectrometry. *J. Chromatogr., B: Anal. Technol. Biomed. Life Sci.* **2006**, *831*, 328−332.

(16) Kang, M. J.; Yong, H. H.; Lee, W.; Kim, D. H. Validation and application of a screening method for β2-agonists, anti-estrogenic substances and mesocarb in human urine using liquid chromatography/tandem mass spectrometry. *Rapid Commun. Mass Spectrom.* **2007**, *21*, 252−264.

(17) Zhang, Y.; Zhang, Z.; Sun, Y.; Wei, Y. Development of an analytical method for the determination of β2-agonist residues in animal tissues by high-performance liquid chromatography with on-

DOI: 10.1021/jf5056437
J. Agric. Food Chem. 2015, 63, 493−499

line electrogenerated $[Cu(HIO_6)_2]_5^-$ luminol chemiluminescence detection. *J. Agric. Food Chem.* **2007**, *55*, 4949−4956.
(18) Nielen, M. W. F.; Lasaroms, J. J. P.; Essers, M. L.; Oosterink, J. E.; Meijer, T.; Sanders, M. B.; Zuidema, T.; Stolker, A. A. M. Multiresidue analysis of β-agonists in bovine and porcine urine, feed and hair using liquid chromatography electrospray ionisation tandem mass spectrometry. *Anal. Bioanal. Chem.* **2008**, *391*, 199−210.
(19) Ramos, F.; Baeta, M. L.; Reis, J.; Silveira, M. I. N. Evaluation of the illegal use of clenbuterol in Portuguese cattle farms from drinking water, urine, hair and feed samples. *Food Addit. Contam., Part A* **2009**, *26*, 814−820.
(20) Wang, L. Q.; Zeng, Z. L.; Su, Y. J.; Zhang, G. K.; Zhong, X. L.; Liang, Z. P.; He, L. M. Matrix effects in analysis of β-agonists with LC-MS/MS: influence of analyte concentration, sample source, and SPE type. *J. Agric. Food Chem.* **2012**, *60*, 6359−6363.
(21) Regiart, M.; Fernández-Baldo, M. A.; Spotorno, V. G.; Bertolino, F. A.; Raba, J. Ultra sensitive microfluidic immunosensor for determination of clenbuterol in bovine hair samples using electro-deposited gold nanoparticles and magnetic micro particles as bio-affinity platform. *Biosens. Bioelectron.* **2013**, *41*, 211−217.
(22) Jia, J. Y.; Zhang, L. N.; Lu, Y. L.; Zhang, M. Q.; Liu, G. Y.; Liu, Y. M.; Lu, C.; Li, S. J.; Lu, Y.; Zhang, R. W.; Yu, C. Hair analysis, a reliable and non-invasive method to evaluate the contamination by clenbuterol. *Ecotoxicol. Environ. Saf.* **2013**, *93*, 186−190.
(23) Wang, X.; Liu, Y.; Su, Y.; Yang, J.; Bian, K.; Wang, Z.; He, L. M. High-throughput screening and confirmation of 22 banned veterinary drugs in feedstuffs using LC-MS/MS and high-resolution orbitrap mass spectrometry. *J. Agric. Food Chem.* **2014**, *62*, 516−527.
(24) Boyd, S.; Heskamp, H. H.; Bovee, T. F. H.; Nielen, M. W. F.; Elliott, C. T. Development, validation and implementation of a receptor based bioassay capable of detecting a broad range of β-agonist drugs in animal feedingstuffs. *Anal. Chim. Acta* **2009**, *637*, 24−32.
(25) Gleixner, A.; Sauerwein, H.; Meyer, H. H. D. Accumulation of the β2-adrenoceptor agonist clenbuterol in calf hair of different pigmentation. *Arch. Lebensmittelhyg.* **1996**, *47*, 131−135.
(26) Boumba, V.; Ziavrou, K.; Vougiouklakis, T. Hair as a biological indicator of drug use, drug abuse or chronic exposure to environmental toxicants. *Int. J. Toxicol.* **2006**, *25*, 143−163.
(27) Kintz, P.; Villain, M.; Cirimele, V. Hair analysis for drug detection. *Ther. Drug Monit.* **2006**, *28*, 442−446.
(28) Kintz, P., Ed. *Analytical and Practical Aspects of Drug Testing in Hair*; CRC Press: New York, 2007; 382 pp.
(29) Vincenti, M.; Salomone, A.; Gerace, E.; Pirro, V. Application of mass spectrometry to hair analysis for forensic toxicological investigations. *Mass Spectrom. Rev.* **2013**, *32*, 312−332.
(30) Nakahara, Y. Hair analysis for abused and therapeutic drugs. *J. Chromatogr., B: Biomed. Sci. Appl.* **1999**, *733*, 161−180.
(31) Cooper, G. A. A.; Kronstrand, R.; Kintz, P. Society of Hair Testing guidelines for drug testing in hair. *Forensic Sci. Int.* **2012**, *218*, 20−24.
(32) Dunnett, M.; Lees, P. Trace element, toxin and drug elimination in hair with particular reference to the horse. *Res. Vet. Sci.* **2003**, *75*, 89−101.
(33) Dunnett, M.; Lees, P. Retrospective detection and deposition profiles of potentiated sulphonamides in equine hair by liquid chromatography. *Chromatographia* **2004**, *59*, S69−S78.
(34) Dunnett, M.; Lees, P. Hair analysis as a novel investigative tool for the detection of historical drug use/misuse in the horse: a pilot study. *Equine Vet. J.* **2004**, *36*, 113−117.
(35) Dunnett, M.; Richardson, D. W.; Lees, P. Detection of enrofloxacin and its metabolite ciprofloxacin in equine hair. *Res. Vet. Sci.* **2004**, *77*, 143−151.
(36) Anielski, P.; Thieme, D.; Schlupp, A.; Grosse, J.; Ellendorff, F.; Mueller, R. K. Detection of testosterone, nandrolone and precursors in horse hair. *Anal. Bioanal. Chem.* **2005**, *383*, 903−908.
(37) Gratacos-Cubarsi, M.; Castellari, M.; Valero, A.; Garcia-Regueiro, J. A. Hair analysis for veterinary drug monitoring in livestock production. *J. Chromatogr., B: Anal. Technol. Biomed. Life Sci.* **2006**, *834*, 14−25.
(38) Malcolm, K. D.; McShea, W. J.; Van Deelen, T. R.; Bacon, H. J.; Liu, F.; Putman, S.; Zhu, X.; Brown, J. L. Analyses of fecal and hair glucocorticoids to evaluate short- and long-term stress and recovery of Asiatic black bears (*Ursus thibetanus*) removed from bile farms in China. *Gen. Comp. Endocrinol.* **2013**, *185*, 97−106.
(39) Gray, B. P.; Viljanto, M.; Bright, J.; Pearce, C.; Maynard, S. Investigations into the feasibility of routine ultra high performance liquid chromatography-tandem mass spectrometry analysis of equine hair samples for detecting the misuse of anabolic steroids, anabolic steroid esters and related compounds. *Anal. Chim. Acta* **2013**, *787*, 163−172.
(40) Carlitz, E. H. D.; Kirschbaum, C.; Stalder, T.; van Schaik, C. P. Hair as a long-term retrospective cortisol calendar in orangutans (*Pongo* spp.): new perspectives for stress monitoring in captive management and conservation. *Gen. Comp. Endocrinol.* **2014**, *195*, 151−156.
(41) Commission Decision 2002/657/EC. *Off. J. Eur. Communities* **2002**, *L221*, 8−36.
(42) Gaillard, Y.; Balland, A.; Doucet, F.; Pépin, G. Detection of illegal clenbuterol use in calves using hair analysis. Application in meat quality control. *J. Chromatogr., B: Biomed. Sci. Appl.* **1997**, *703*, 85−95.
(43) Durant, A. A.; Fente, C. A.; Franco, C. M.; Vázquez, B. I.; Cepeda, A. Gas chromatography-tandem mass spectrometry determination of 17α-ethinylestradiol residue in the hair of cattle. Application to treated animals. *J. Agric. Food Chem.* **2002**, *50*, 436−440.
(44) Sauer, M. J.; Pickett, R. J. H.; Limer, S.; Dixon, S. N. Distribution and elimination of clenbuterol in tissues and fluids of calves following prolonged oral administration at a growth-promoting dose. *J. Vet. Pharmacol. Ther.* **1995**, *18*, 81−86.
(45) Groot, M. J.; Lasaroms, J. J. P.; van Bennekom, E. O.; Van Hende, J.; Nielen, M. W. F. Possible contamination with clenbuterol from treated veal calves to untreated pen mates. *Food Addit. Contam., Part A* **2013**, *30*, 1063−1067.
(46) Henderson, G. L. Mechanisms of drug incorporation into hair. *Forensic Sci. Int.* **1993**, *63*, 19−29.
(47) Kintz, P. Issues about axial diffusion during segmental hair analysis. *Ther. Drug Monit.* **2013**, *35*, 408−410.
(48) Hernández-Carrasquilla, M. External contamination of bovine hair with β2-agonist compounds: evaluation of decontamination strategies. *J. Chromatogr., B: Anal. Technol. Biomed. Life Sci.* **2002**, *767*, 235−243.
(49) LeBeau, M. A.; Montgomery, M. A.; Brewer, J. D. The role of variations in growth rate and sample collection on interpreting results of segmental analyses of hair. *Forensic Sci. Int.* **2011**, *210*, 110−116.
(50) Duvivier, W. F.; Van Beek, T. A.; Pennings, E. J. M.; Nielen, M. W. F. Rapid analysis of Δ-9-tetrahydrocannabinol in hair using direct analysis in real time ambient ionization orbitrap mass spectrometry. *Rapid Commun. Mass Spectrom.* **2014**, *28*, 682−690.

DOI: 10.1021/jf5056437
J. Agric. Food Chem. 2015, 63, 493−499

JOURNAL OF AGRICULTURAL AND FOOD CHEMISTRY

Article

pubs.acs.org/JAFC

High-Performance Liquid Chromatography Separation of *cis*−*trans* Anthocyanin Isomers from Wild *Lycium ruthenicum* Murr. Employing a Mixed-Mode Reversed-Phase/Strong Anion-Exchange Stationary Phase

Hongli Jin,[†,‡,§] Yanfang Liu,*[,‡] Zhimou Guo,[‡] Fan Yang,[∥] Jixia Wang,[‡,§] Xiaolong Li,[†,‡,§] Xiaojun Peng,[†] and Xinmiao Liang[‡]

[†]State Key Laboratory of Fine Chemicals, Dalian University of Technology, Dalian, Liaoning 116012, People's Republic of China

[‡]Key Laboratory of Separation Science for Analytical Chemistry, Dalian Institute of Chemical Physics, Chinese Academy of Sciences, Dalian, Liaoning 116023, People's Republic of China

[§]University of Chinese Academy of Sciences, Beijing 100039, People's Republic of China

[∥]Analytical Chemistry Service Center, Dalian Institute of Chemical Physics, Chinese Academy of Sciences, Dalian, Liaoning 116023, People's Republic of China

Supporting Information

ABSTRACT: The *cis*−*trans* isomerism is a common phenomenon for acylated anthocyanins. Nevertheless, few studies reported effective methods for the preparation of isomeric anthocyanins from natural products. In this work, a high-performance liquid chromatography (HPLC) method was developed to efficiently purify anthocyanin isomers from *Lycium ruthenicum* Murr. based on a mixed-mode reversed-phase/strong anion-exchange column (named XCharge C8SAX). Four commercially available columns were evaluated with a pair of isomeric anthocyanins, and the results demonstrated that the XCharge C8SAX column exhibited improved selectivity and column efficiency for the isomers. The chromatographic parameters, including pH, organic content, and ionic strength, were investigated. Optimal separation quality for the anthocyanin isomers was achieved on the XCharge C8SAX column. Six pure anthocyanins, including two pairs of *cis*−*trans* isomeric anthocyanins with one new anthocyanin, were purified from *L. ruthenicum* and identified. All of the results indicated that this method is an effective way to separate anthocyanins, especially for *cis*−*trans* isomers.

KEYWORDS: *anthocyanins, cis*−*trans anthocyanin isomer, Lycium ruthenicum Murr., mixed-mode stationary phase, HPLC*

INTRODUCTION

Anthocyanins, a group of phenolic compounds, confer the characteristic colors to most fruits and vegetables. Increased evidence have proven their possible heath benefits in preventing chronic and degradative diseases, including heart disease and cancer.[1] At present, although more than 600 naturally occurring anthocyanins have been characterized, only a limited number of pure anthocyanin standards are commercially available with a steep price. Most bioassays on anthocyanins have to be conducted with crude anthocyanin extracts, likely resulting in the ambiguous explanation of the bioactivity of anthocyanins.[2] Therefore, preparation of pure anthocyanins is demanded for their bioactivity investigation.

Lycium ruthenicum Murr. is a kind of widespread nutritional food in the salinized desert of the Qinghai−Tibet Plateau. It is also a famous traditional herb recorded in the Tibetan medical classic "Jing Zhu Ben Cao". *L. ruthenicum* has been applied to treat many diseases, such as heart disease, abnormal menstruation, and menopause. Besides, the pigments of *L. ruthenicum* are demonstrated to possess good antioxidant activity,[3,4] and thus, anthocyanins in this plant have aroused great interest to many researchers. Recently, Zheng et al.[5] characterized anthocyanins in *L. ruthenicum* by high-performance liquid chromatography (HPLC) with electrospray ionization−mass spectrometry (ESI−MS), suggesting that most of them are acylated anthocyanins. Chen et al.[6] had identified and quantified seven main anthocyanins in *L. ruthenicum*. The results showed that the anthocyanins were mainly acylated with coumaric acid in both *cis* and *trans* configurations. Nevertheless, few anthocyanins in this plant have been isolated and identified by nuclear magnetic resonance (NMR). Information on their chemical structures is still incomplete. The purification of anthocyanins with enough purity and amount for structural elucidation is of great importance.

Column chromatography (CC) has been used extensively in the separation of anthocyanins from natural products.[7−10] Different columns are able to offer different separation selectivities for anthocyanins, which provide significant contribution to the preparation of anthocyanins.[11] Unfortunately, this technique will suffer from laboriousness and low efficiency, owing to consecutive column separation. Poor reproducibility is another drawback that hampers the application of CC in the purification. Alternatively, HPLC, one of the most effective

Received: September 23, 2014
Revised: December 23, 2014
Accepted: December 24, 2014
Published: December 24, 2014

ACS Publications © 2014 American Chemical Society

DOI: 10.1021/jf504525w
J. Agric. Food Chem. 2015, 63, 500−508

techniques to isolate compounds from complex samples, provides many advantages over other techniques, such as high efficiency and good repeatability. It appears to be a practical method for anthocyanin preparation.[12,13] Nonetheless, owing to limited separation selectivity, this technique has to be used in combination with CC and taken as a final purification to yield pure anthocyanins.[8,11] Preparation of anthocyanins, especially for *cis*−*trans* isomers, by HPLC remains to be further improved.

Structurally, anthocyanins are heterosides of an aglycone unit (anthocyandin) with the aromatic carboxylates, such as *p*-coumaric acid, coffeic acid, etc., bonded to the sugar in the molecule. Therefore, the acylated unit of anthocyanin easily generates *cis*−*trans* isomers (Figure 1). These stereoisomers

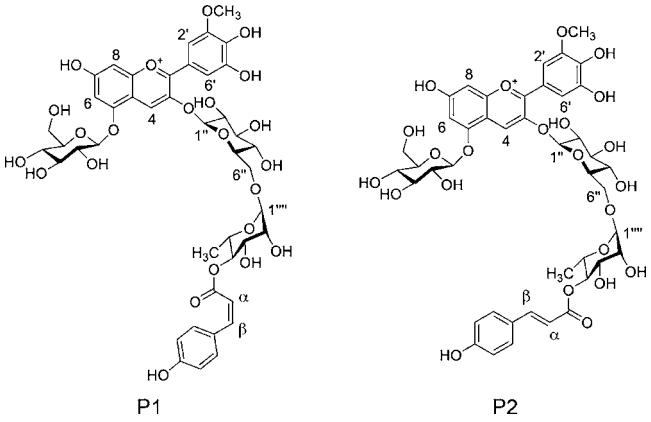

Figure 1. Structures of the *cis*−*trans* anthocyanin isomers from *L. ruthenicum*.

increase the difficulty in the isolation of anthocyanins from plants. The usual method for separating anthocyanins is almost exclusively performed on conventional C_{18} columns with aqueous acid/acetonitrile (ACN) as mobile phases.[14−16] This classic method shows good repeatability and efficiency for anthocyanin separation, but it has some limitations for isolating anthocyanin isomers. Multiple *p*-coumaric peaks for a given aglycone, attributed to the isomers, would occur, complicating the isolation and identification of anthocyanins.[17] In addition, the nearly co-eluted peaks are observed for some *cis*−*trans* anthocyanin isomers on reversed-phase (RP) columns, leading to difficulty in collecting compounds with good purity. Lately, Willemse et al.[18] have used hydrophilic interaction chromatography (HILIC) to separate anthocyanins for the first time. Co-elution of *cis*−*trans* acylated isomers, lower chromatographic efficiency, and higher organic solvent consumption restricted its application in the isomer purification. It is desirable to establish a HPLC method to achieve efficient preparation of isomeric anthocyanins.

The mixed-mode columns are capable of bringing interesting selectivity to separate complex mixtures and offer several advantages over conventional RP.[19−21] In recent years, Mccallum et al.[22] obtained improved separation of anthocyanins in grapes using a mixed-mode RP/anion-exchange column. Superior separation performance for acylated anthocanins was observed. Subsequently, Vergara et al.[23] published that different selectivities of the mixed-mode stationary phase were achieved in the separation of some wine anthocyanins probably based on the complex mechanisms of reverse chromatography and ion-exclusion chromatography. In the present work, we aimed to develop an efficient HPLC method to prepare *cis*−*trans* isomeric anthocyanins using a RP/strong anion-exchange column as well as to explore the effect of properties of stationary phases on selectivity toward the isomers. The potential of this approach will be demonstrated by the purification of anthocyanin isomers from *L. ruthenicum*.

MATERIALS AND METHODS

Plant Material. The fruits of *L. ruthenicum* were randomly sampled from Dulan (latitude, 36° 26′ N; longitude, 96° 31′ E; altitude, 2774 m). The fruits were ripe, hand-picked, and then preserved in 4 °C for subsequent experiments.

Apparatus and Reagents. Purification Factory is a preparative liquid chromatography (LC) system, which consists of two 2525 binary gradient modules (Waters, Milford, MA), an autosampler (Leap Technologies, Carrboro, NC), a 2498 ultraviolet (UV) detector (Waters), and MassLynx software (Waters, version 4.1).

Chromatographic separation and analysis were performed on an Alliance HPLC system consisting of a Waters 2695 HPLC pump and a 2489 UV−vis detector. Data acquisition and processing were conducted by Waters Empower software (Milford, MA).

Identification of pure compounds was carried out using mass spectrometry (MS) and NMR. MS was performed on a Q-TOF Premier (Waters MS Technologies, Manchester, U.K.). ^{1}H NMR and nuclear Overhauser effect spectrometry (NOESY) were measured on a Bruker DRX-400 spectrometer (^{1}H NMR at 600 MHz), with MeOH-d_4/TFA-*d* (95:5, v/v) as the solvent.

ACN was purchased from Merck of HPLC grade (Darmstadt, Germany) and from Yuwang Chemical Reagent Factory of industrial grade (Shandong, China). Methanol was purchased from Yuwang Chemical Reagent Factory of HPLC grade. Trifluoroacetic acid (TFA) and formic acid (FA) were purchased from J&K Chemical of HPLC grade (Hebei, China). Sodium biphosphate (NaH_2PO_4) was purchased from Sinopharm (Shanghai, China). Phosphoric acid was purchased from Tedia of HPLC grade (Fairfield, OH). Water for the HPLC mobile phase was reverse osmosis Milli-Q water (18.2 MΩ, Millipore, Billerica, MA). The references petunidin 3-*O*-[6-*O*-(4-*O*-(*cis*-*p*-coumaroyl)-*α*-L-rhamnopyranosyl)-*β*-D-glucopyranoside]-5-*O*-[*β*-D-glucopyranoside] (P1) and petunidin 3-*O*-[6-*O*-(4-*O*-(*trans*-*p*-coumaroyl)-*α*-L-rhamnopyranosyl)-*β*-D-glucopyranoside]-5-*O*-[*β*-D-glucopyranoside] (P2) were isolated in our laboratory. Their structures were characterized by MS and NMR. The structures of these two anthocyanins were displayed in Figure 1.

The columns used in this work are listed as follows: XTerra MS C_{18} (4.6 × 150 mm, 5 μm, Waters, Milford, MA), XUnion C_{18} (4.6 × 150 mm, 5 μm Acchrom, Beijing, China), XUnion C_8 (4.6 × 150 mm, 5 μm Acchrom, Beijing, China), and XCharge C8SAX (4.6 × 150 mm, 5 μm Acchrom, Beijing, China). The representative surface chemistry of the XCharge C8SAX stationary phase is shown in Figure 2. The detailed properties of the four columns are listed in Table 1.

Phosphate buffers were prepared using NaH_2PO_4 and adjusted to desired pH with H_3PO_4 solution at corresponding concentrations before the addition of organic solvent (pH values). The buffers were filtered through 0.22 μm membranes before use.

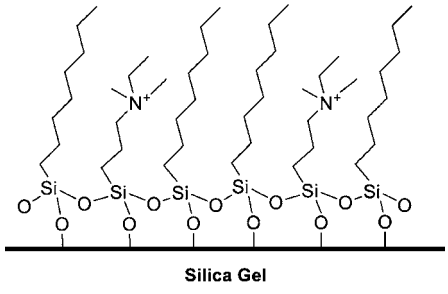

Figure 2. Representative surface chemistry of the XCharge C8SAX column.

DOI: 10.1021/jf504525w
J. Agric. Food Chem. 2015, 63, 500−508

Table 1. Physicochemical Properties of the Columns

column	ligand	specific surface area (m^2/g)	average pore size	total carbon (%)	column efficiency
XTerra MS C_{18}	C_{18}	175	125	15.5% C load	74000
XUnion C_{18}	C_{18}	320	100	20.3% C load	73000
XUnion C_8	C_8	320	100	12.4% C load	80000
XCharge C8SAX	C_8	320	100	9.57% C load	75000

The dead time (t_o) of the columns was measured by uracil. The column efficiency of all of the columns used in this work was determined by naphthalene with a similar retention factor (k). All results are the average of triplicate determinations. The resolution (R) and selectivity (α) were used for the evaluation of separation quality. These data could be calculated from the system suitability software of the ChemStation.

Chromatographic Conditions. HPLC experiments were performed at the flow rate of 1.0 mL/min. The column temperature was maintained at 30 °C throughout using a thermostat. Detection was carried out at 520 nm, unless otherwise specified.

For column selection, the mobile phase was composed of NaH_2PO_4 (10 mM, pH 1.5) and ACN (85:15, v/v).

The preparation of fractions 6, 8, and 9 was conducted on an XCharge C8SAX column (4.6 × 150 mm, 5 μm). The mobile phase A was 0.2% TFA (v/v) in water, and the mobile phase B was 0.2% TFA (v/v) in ACN. Different isocratic elution conditions were adopted to separate three fractions. Isocratic elution for fraction 6 was 12% B; isocratic elution for fraction 8 was 14% B; and isocratic elution for fraction 9 was 15% B.

HPLC analysis of pure compounds was performed on an XTerra MS C_{18} column (4.6 × 150 mm, 5 μm). The mobile phase A was 0.2% TFA (v/v) in water, and the mobile phase B was 0.2% TFA (v/v) in methanol. Gradient elution steps were as follows: 0−30 min, 15−50% B; 30−40 min, 90% B.

Extraction of Anthocyanins. The fruit of *L. ruthenicum* Murr. was extracted triply with 20-fold of 70% ethanol for 2 h at pH 2.5 (adjusted with hydrochloric acid). Subsequently, three filtrates were combined and concentrated by rotary evaporation at 50 °C in vacuum. Then, the aqueous extract was prepared on the AB-8 macroporous resin (50 × 520 mm, Chemical Plant of NanKai University, Tianjing, China). The strong polar constituents were removed with aqueous acid (0.5% FA, v/v). Then, the target constituent was eluted with 70% ethanol. It was concentrated by rotary evaporation at 50 °C in vacuum and, finally, lyophilized.

Sample Preparation. The anthocyanin sample obtained from extraction described above was dissolved in aqueous acid and subjected to a SCX solid-phase extraction (SPE) cartridge (40 mL, 20 g of sorbent, Acchrom), preconditioned successively with MeOH and distilled water (0.5% FA). Non-anthocyanin compositions were collected with 3 vol of 5% ACN (0.5% FA). Subsequently, anthocyanins were eluted with 3 vol of 30% ACN (1 M NaH_2PO_4 at pH 2.0). Anthocyanin solution was dried by rotary evaporation at 50 °C in vacuum to remove organic solvent as much as possible and then loaded on the AB-8 macroporous resin. Phosphate was washed out by distilled water (0.5% FA). Anthocyanins were eluted with 70% ethanol. They were concentrated by rotary evaporation at 50 °C in vacuum. Fractionation of anthochanin constitutions was carried out on an XTerra MS C_{18} column (50 × 150 mm, 5 μm, Waters, Milford, MA) using methanol/water (0.2% TFA) as mobile phases, and in total, 14 fractions were collected according to UV absorption intensity (shown in the Supporting Information). Fractions 6, 8, and 9 were selected in this work to conduct further separation. A total of 100 mg of each fraction (fractions 6, 8, and 9) was dissolved in 2.5 mL of acid water and filtered through 0.22 μm pore size membranes to obtain an anthocyanin sample with a concentration at about 40 mg/mL.

RESULTS AND DISCUSSION

Column Selection. Column selection is one of the first principal factors for better separation in LC. In this work, four commercially available columns with different solid phases but the same particle size, diameter, and column length were tested to separate a pair of *cis*−*trans* anthocyanin isomers. The chromatograms for four different columns are shown in Figure 3. The selectivity (a), resolution (R), and column efficiency (N) values for the tested anthocyanins on each column are listed in Table 2.

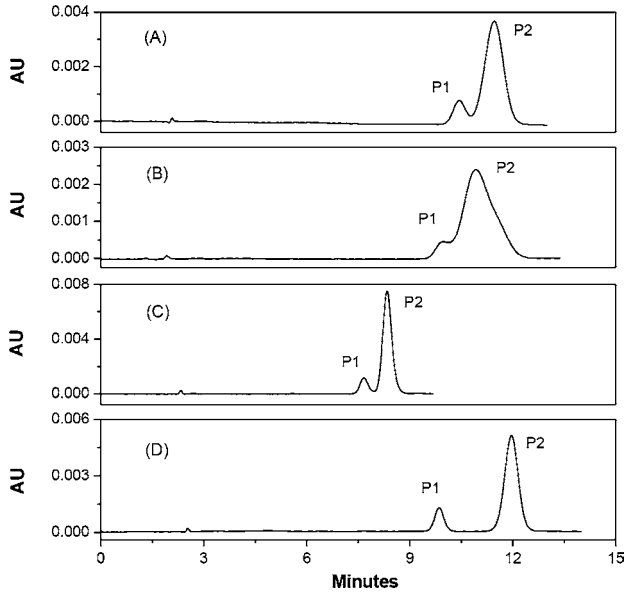

Figure 3. HPLC chromatograms of the anthocyanin isomers on (A) XTerra MS C_{18} (4.6 × 150 mm, 5 μm), (B) XUnion C_{18} (4.6 × 150 mm, 5 μm), (C) XUnion C_8 (4.6 × 150 mm, 5 μm), and (D) XCharge C8SAX (4.6 × 150 mm, 5 μm). Isocratic elution with NaH_2PO_4 (10 mM, pH 1.5) and ACN (85:15, v/v), with a flow rate of 1 mL/min, temperature of 30 °C, and wavelength of 520 nm.

Table 2. Column Parameters for the Separation of Isomeric Anthocyanins on the Four Columns

column	a	R	N
XTerra MS C_{18}	1.12	1.18	25000
XUnion C_{18}	1.12	*a*	*a*
XUnion C_8	1.11	1.43	30000
XCharge C8SAX	1.26	3.36	40000

[a]Could not be determined.

The XTerra MS C_{18} column, a hybrid-based C_{18} column, was chosen to separate the anthocyanin isomers for its good hydrophobic selectivity and excellent stability under high acidic conditions. The isomers were properly retained (P1 in Figure 1) with acceptable resolution for analytical purposes (R = 1.18; Table 2). Nonetheless, this analytical resolution seems inadequate for preparative application, because overlapping of the anthocyanin isomers might occur. It is necessary to separate them with satisfactory resolution. Selectivity has the greatest impact upon changing resolution, as compared to efficiency and retention (k). As a result, a column with better separation selectivity toward *cis*−*trans* anthocyanin isomers would be the

DOI: 10.1021/jf504525w
J. Agric. Food Chem. 2015, 63, 500−508

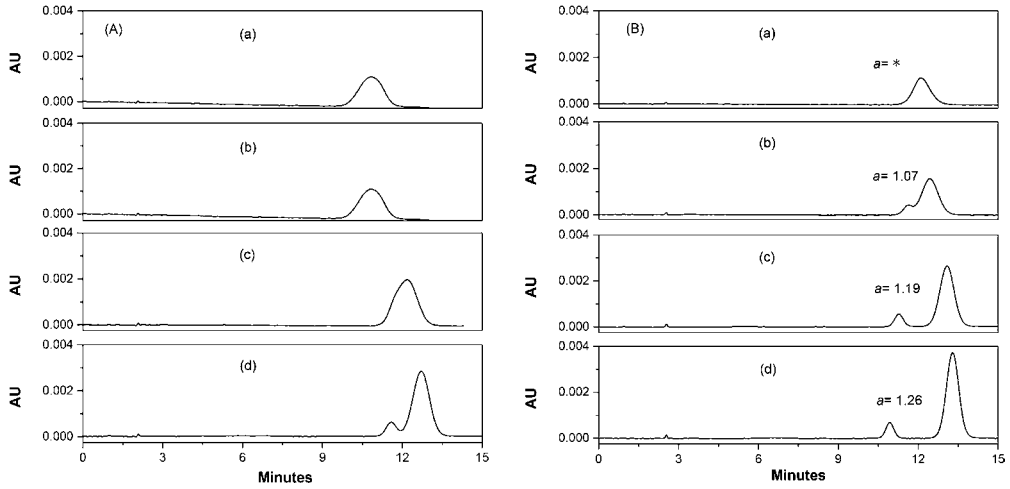

Figure 4. HPLC chromatograms of the anthocyanin isomers on the (A) XTerra MS C_{18} column and (B) XCharge C8SAX column with pH of the mobile phase at (a) 2.32, (b) 2.06, (c) 1.76, and (d) 1.56, with the mobile phase of 85:15 (v/v) phosphate buffer/ACN and ionic strength of 15 mM. Other conditions are the same as those in Figure 3.

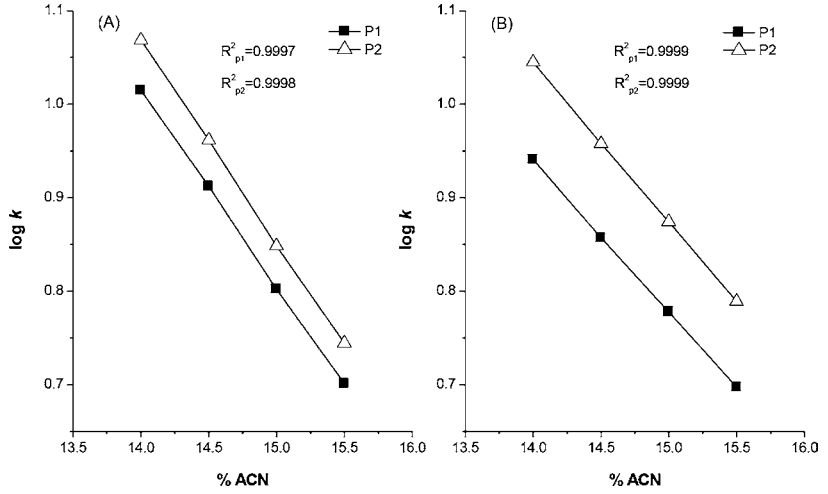

Figure 5. Plot of the log *k* versus volume fraction of ACN in the mobile phase: (A) XTerra MS C_{18} column and (B) XCharge C8SAX column, with the mobile phase from 86:14 to 84.5:15.5 (v/v) phosphate buffer at pH 1.5/ACN and ionic strength of 15 mM. Analytes: (■) P1 and (△) P2. Other conditions are the same as those in Figure 3.

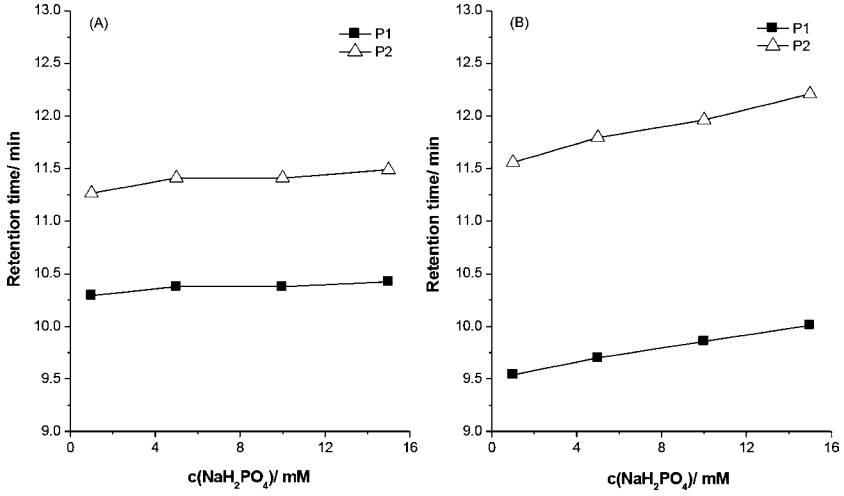

Figure 6. Plot of retention times of the anchoyanin isomers versus phosphate concentrations in the mobile phase from 1 to 15 mM: (A) XTerra MS C_{18} column and (B) XCharge C8SAX column, with the mobile phase of 85:15 (v/v) phosphate buffer at pH 1.5/ACN. Analytes: (■) P1 and (△) P2. Other conditions are the same as those in Figure 3.

DOI: 10.1021/jf504525w
J. Agric. Food Chem. 2015, 63, 500−508

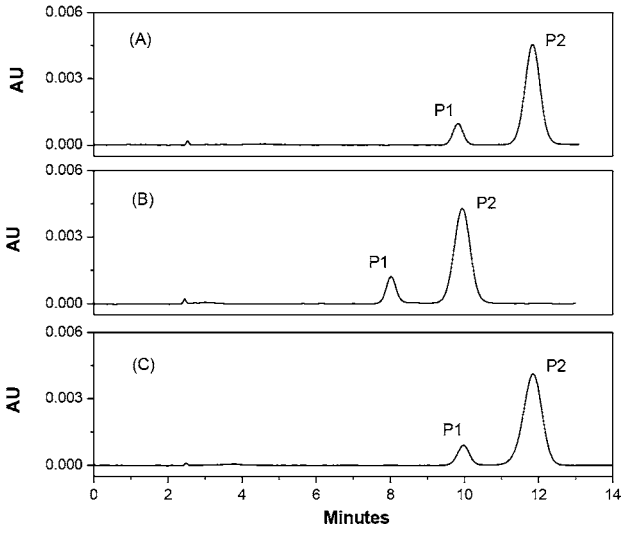

Figure 7. HPLC chromatograms of the anthocyanin isomers on the XCharge C8SAX column with (A) 85:15 phosphate buffer (ionic strength of 15 mM at pH 1.5)/ACN, (B) 86:14 (v/v) 5% (v/v) FA in water (pH 1.6−1.7)/5% (v/v) FA in ACN, and (C) 83:17 (v/v) 0.2% (v/v) TFA in water (pH 1.5−1.6)/0.2% (v/v) TFA in ACN. Other conditions are the same as those in Figure 3.

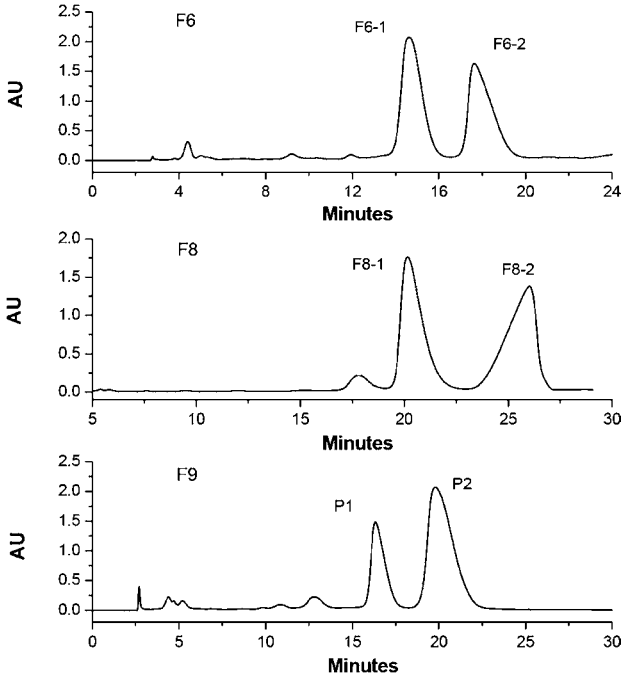

Figure 8. Preparative chromatograms of fractions 6, 8, and 9 under optimized conditions on the XCharge C8SAX column (4.6 × 150 mm, 5 μm). Conditions: mobile phase A, 0.2% TFA aqueous solution; mobile phase B, 0.2% TFA in ACN; and isocratic elution, 12% B for fraction 6, 14% B for fraction 8, and 15% B for fraction 9. Other conditions are the same as those in Figure 3.

optimal choice for their preparation. It appeared interesting that properties of stationary phases would influence the selectivity to the isomers.

For RP columns, the hydrophobic interaction was regarded as the most important contribution to retention. Its effect on the selectivity to the anthocyanin isomers was investigated. XUnion C_{18} and XUnion C_8, two conventional RP columns with alkyl C_{18} and C_8 ligands, respectively, were investigated for separation of

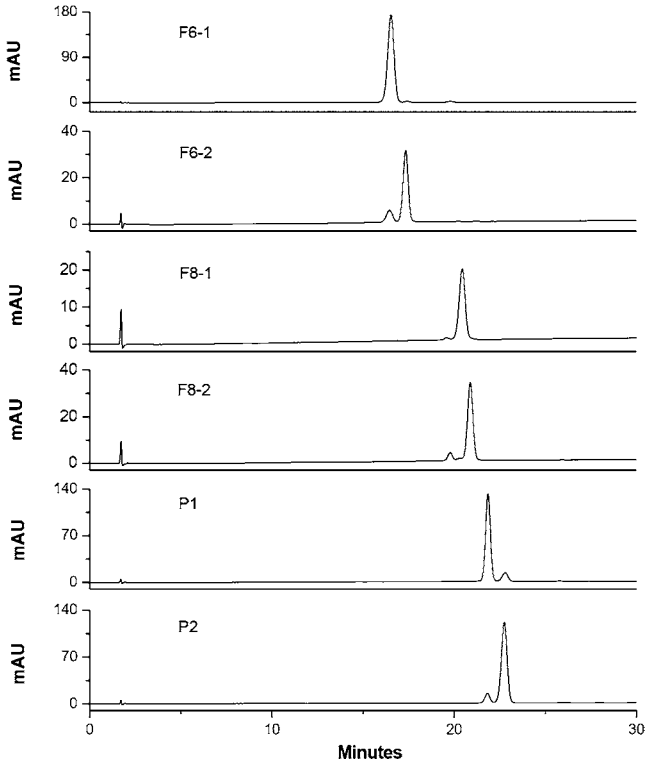

Figure 9. Purity evaluation of the isolated compounds on the XTerra MS C_{18} column (4.6 × 150 mm, 5 μm). F6-1 and F6-2 were isolated from fraction 6; F8-1 and F8-2 were isolated from the fraction 8; and P1 and P2 were isolated from fraction 9. Conditions: mobile phase A, 0.2% TFA aqueous solution; mobile phase B, 0.2% TFA in MeOH; gradient, from 15 to 50% B in 0−30 min. Other conditions are the same as those in Figure 3.

the anthocyanin isomers (panels B and C of Figure 3 for XUnion C_{18} and XUnion C_8, respectively). The results showed that the anthocyanins eluted earlier on XUnion C_8, indicating that the isomers experienced weaker hydrophobic interaction on XUnion C_8. However, selectivity values were similar on these two columns (a = 1.12 and 1.11 for XUnion C_{18} and XUnion C_8, respectively; Table 2). These data revealed that the contribution of the hydrophobic interaction to the selectivity for the *cis*−*trans* isomeric anthocyanins was quite limited. The XTerra MS C_{18} column, despite different bonding techniques, also had a similar selectivity value as either XUnion C_{18} or XUnion C_8. This phenomenon further confirmed the above deduction. The *cis*−*trans* isomerism is a form of stereoisomerism. Both of the isomers have exactly the same atoms joined up in exactly the same order. This means that their hydrophobicity might be analogical, and thus, conventional RP columns, which provided a single type of solute−sorbent hydrophobic interaction, would suffer from limited selectivity for the *cis*−*trans* anthocyanin isomers.

In addition, it was interesting to note that the XUnion C_8 column displayed much better resolution than XUnion C_{18}, as shown in Table 2. This could be primarily ascribed to the higher separation efficiency for the isomeric anthocyanins on XUnion C_8 than that on XUnion C_{18} (Table 2). It was reasonable to infer that stationary phases with C_8 alkyl ligands were more suitable for separation of the anthocyanin isomers.

In a highly acidic mobile phase, anthocyanins mainly exist in the falvylium cation form with a positive charge.[24,25] The *cis*−*trans* isomers of anthocyanin have a different spatial arrangement, probably resulting in a certain difference in electrostatic

DOI: 10.1021/jf504525w
J. Agric. Food Chem. 2015, 63, 500−508

Table 3. ^{1}H NMR Data for the Isolated Anthocyanins in CD_3OD/TFA-*d* (95:5, v/v)

H	F6-1	F6-2	F8-1	F8-2	P1	P2
			Anthocyandin			
4-H	8.96 s	8.95 s	8.97 s	8.92 s	8.90 s	8.96 s
6-H	7.03 s	7.02 s	7.03 s	7.03 s	7.01 s	7.03 s
8-H	7.05 s	7.03 s	7.04 s	7.03 s	7.01 s	7.06 s
2′-H	7.97 d (2.1)	7.97 d (2.1)	8.0 d (1.9)	7.82 s	7.93 s	7.99 d (1.5)
5′-H						
6′-H	7.80 d (2.1)	7.80 d (2.1)	7.85 d (2.0)	7.82 s	7.77 s	7.82 d (1.8)
3′-OCH_3	4.01 s	4.01 s	4.01 s		3.96 s	4.01 s
5′-OCH_3						
			3-*O*-Glucopyranoside			
1″	5.53 d (7.7)	5.54 d (7.8)	5.50 d (7.7)	5.49 d (7.8)	5.52 d (7.8)	5.53 d (7.8)
2″	3.50−3.80	3.2−4.1	3.45−3.86	3.46−4.07	3.43−3.92	3.84
3″						3.78
4″						3.70
5″						3.75
6a	3.96		3.97			3.98
6b	4.07		4.06			4.06
			5-*O*-Glucopyranoside			
1‴	5.22 d (7.8)	5.19 d (7.8)	5.20 d (7.8)	5.19 d (7.9)	5.20 d (7.8)	5.22 d (7.8)
2‴	3.50−3.80	3.2−4.1	3.36−4.06	3.46−4.07	3.43−3.92	3.82
3‴						3.76
4‴						3.72
5‴						3.73
6a	3.85					3.87
6b	3.86					3.96
			3-Glucosyl			
1⁗	5.00 d (7.2)	5.05 d (7.3)				
2⁗	3.50−3.80	3.2−4.1				
3⁗						
4⁗						
5⁗						
6a	3.84					
6b	3.94					
			6″-*O*-Rhamnopyranosyl			
1′′′′	4.75 s	4.68 s	4.72 s	4.72 s	4.66 s	4.74 s
2′′′′	3.50−3.80	3.50−3.80	3.50−3.80		3.43−3.92	3.61
3′′′′						3.59
4′′′′	4.93 t (9.7)	4.83 m	4.92 t (9.7)	4.92 t (9.8)	4.81 s	3.92 t (9.7)
5′′′′	3.50−3.80	3.50−3.80			3.43−3.92	3.58
−CH_3	1.0 d (6.2)	0.86 d (6.2)	1.03 d (6.3)	1.01 d (6.2)	0.86 d (6.2)	1.02 d (6.2)
			Hydroxycinnamic Acid			
2	7.50 d (8.6)	7.62 d (8.0)	7.08 s	7.43 d (8.6)	7.58 d (7.0)	7.44 d (8.5)
3	7.13 d (8.6)	7.10 d (8.0)		6.82 d (8.6)	6.69 d (6.9)	6.83 d (8.4)
5	7.13 d (8.6)	7.10 d (8.0)	6.79 d (8.2)	6.82 d (8.6)	6.69 d (6.9)	6.83 d (8.4)
6	7.50 d (8.6)	7.62 d (8.0)	6.93 d (8.2)	7.43 d (8.6)	7.58 d (7.0)	7.44 d (8.5)
α	6.29 d (16.0)	5.69 d (12.5)	6.22 d (15.9)	6.26 d (15.9)	5.56 d (12.7)	6.26 d (15.9)
β	7.58 d (16.0)	6.86 d (12.5)	7.52 d (15.9)	7.59 d (15.9)	6.77 d (12.7)	7.58 d (15.9)

interaction. Hence, the mixed-mode RP/ion-exchange stationary phase might be useful to provide improved selectivity. On the basis of the polar-copolymerized approach, the XCharge C8SAX column has both alkyl C_8 chains and quaternary ammonium groups on the silica surface, providing a hydrophobic interaction along with strong anion-exchange ability. As shown in Figure 3D, the anthocyanin isomers were completely separated on this mixed-mode column. Furthermore, XCharge C8SAX had better selectivity than the three other RP columns. It is possible that the presence of positively charged groups in the XCharge C8SAX column resulted in different extents of ionic repulsion with the isomeric anthocyanins and then provided a significant contribution to the improved selectivity. Accordingly, the resolution of the isomers on this mixed-mode column was superior to that on RP columns (Table 2).

Moreover, it is worth mentioning that, in previous papers, the mixed-mode column performed lower column efficiency and relatively longer analysis time for separation of anthocyanins in comparison to RP columns.[23] The XCharge C8SAX column exhibited high column efficiency to the anthocyanins, which was nearly twice as much as that on the XTerra MS C_{18} column (N = 40 000 and 25 000 for XCharge C8SAX and XTerra MS C_{18}, respectively; Table 2). Hypothetically, the strength of ionic

DOI: 10.1021/jf504525w
J. Agric. Food Chem. 2015, 63, 500−508

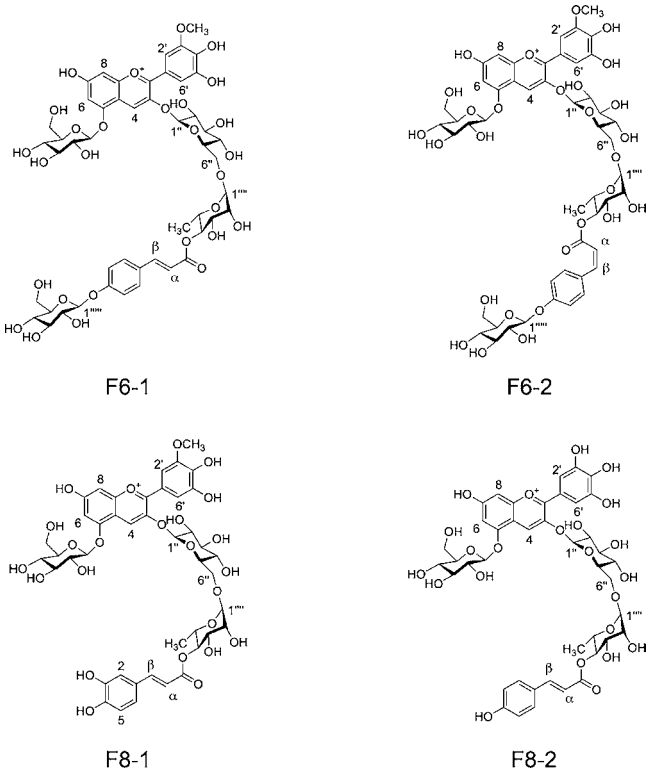

Figure 10. Chemical structures of the isolated anthocyanins.

repulsion between the positive charge on the stationary phase and falvylium cations could affect the separation efficiency.[21]

To summarize, benefiting from the presence of an appropriate level of positive charge on the surface of the solid phase, the XCharge C8SAX column displayed improved selectivity and better column efficiency for separation of the *cis*−*trans* anthocyanin isomers, which would be favorable for their preparation.

Mobile Phase Optimization. To obtain optimal separation performance on XCharge C8SAX, various mobile phase experimental factors, such as pH, organic content, and buffer concentration, were studied. The same experiments were also performed on the XTerra MS C_{18} column to further understand the retention mechanism of anthocyanins.

Effect of the pH. The pH value of elution has profound influence on the ionization of anthocyanins[25] and should be taken into consideration in the HPLC method development. As presented in Figure 4, separation of the anthocyanin isomers within the pH values of 2.32−1.56 was implemented on C_{18} and mixed-mode columns. The ionic strength and organic content were maintained constant at 15 mM and 15%, respectively.

On the XTerra MS C_{18} column (Figure 4A), the isomeric anthocyanins were co-eluted as one broad peak at pH ranging from 2.32 to 1.76 (panels a, b and c of Figure 4A). When pH decreased to 1.56 (panel d of Figure 4A), partial separation of the isomers was acquired. The secondary equilibria of anthocyanins, which would cause on-column band broadening,[26,27] was alleviated with a decreasing pH value. As a result, a highly acidic condition was of significance to ensure prevalence of the falvylium cations and improved chromatographic performance. However, the resolution for the isomers is still limited for preparative separation.

In contrast, the XCharge C8SAX column exhibited much better separation quality for the isomers than the XTerra C_{18} column. The resolution of the isomers was effectively improved on this mix-mode column with decreasing pH in the mobile phase (Figure 4B). At pH of 2.32, only one broad peak was observed (panel a of Figure 4B). When pH decreased to 2.06, a slight resolution of the isomers was achieved (panel b of Figure 4B). Baseline separation appeared at a pH value of 1.76 (panel c of Figure 4B), and better resolution as well as sharp peak shapes were obtained with pH of 1.56 (panel d of Figure 4B). This was due in part to the alleviation of the secondary equilibria effect by the decreased pH. More importantly, the electrostatic repulsion between the anthocyanin isomers and quaternary ammonium in the XCharge C8SAX column might provide remarkable contribution to the improvement of separation selectivity. The ionization of quaternary ammonium groups is barely changed within the studied pH values, whereas the charge of anthocyanins is pH-dependent. The percentage of flavylium cation species would increase with the decrease of pH. Meanwhile, the discrepancy in electrostatic force between the *cis*−*trans* isomeric anthocyanins became increasingly evident, leading to quite different strengths of ionic repulsion with positive charge in the XCharge C8SAX column. Thus, separation selectivity was improved constantly, as shown in Figure 4B.

Effect of the Organic Content. The XCharge C8SAX column has hydrophobic alkyl C_8 chains, and the anthocyanin isomers have some hydrophobic portions in the molecules. Two compounds could be retained through hydrophobic interaction. The linear solvent strength theory is often used to evaluate retention of a compound in reverse-phase liquid chromatography (RPLC)[28]

$$\log k = \log k_w - \frac{\phi_o}{2}(P_{H_2O} - P_o) \quad (1)$$

where P_{H_2O} is the polarity of water, P_o is the polarity of the organic solvent, Φ_o is the volume fraction of the organic solvent in percentage, and k_w is the retention factor of an analyte in water.

In this section, the influence of the organic modifier content in the mobile phase on the separation of the isomers was investigated under various ACN concentrations (from 14 to 15.5%). The ionic strength was kept constant at 15 mM, and the pH was fixed at 1.5. The log *k* versus the volume fraction of ACN was plotted in Figure 5. Obviously, the retention factor decreased linearly with the increase of the ACN content on these two columns. The correlation coefficients for the isomers were 0.9997/0.9998 on the XTerra MS C_{18} column and 0.9999/0.9999 on the XCharge C8SAX column. These results demonstrated that the anthocyanin isomers experienced RPLC retention behavior on both columns. The retention of the anthocyanins would be greatly susceptible to the change of the organic content on the XCharge C8SAX column.

Effect of the Buffer Ionic Strength. Given that the electrostatic repulsive interaction might be involved in the retention of anthocyanins on the XCharge C8SAX column, the influence of the ionic strength in the mobile phase on the separation of the isomers was further assessed under different buffer concentrations (from 1 to 15 mM). The organic content was kept at 15%, and the pH was fixed at 1.5. The plots of the retention time versus the ionic strength are presented in Figure 6. On the XTerra C_{18} column (Figure 6A), retention of the two isomers remained almost constant with the increase of the buffer concentration. Therefore, no obvious ion-exchange interaction existed. In comparison, the retention enhanced with an increasing buffer concentration on the XCharge C8SAX column

DOI: 10.1021/jf504525w
J. Agric. Food Chem. 2015, 63, 500−508

(Figure 6B), which is due to the reduction of Donnan exclusion between flavylium cations and positive quaternary ammonium groups in the stationary phase as a result of the electrostatic screen effect.[29]

From the above discussion, the XCharge C8SAX column provided a hydrophobic interaction along with an electrostatic repulsion for the separation of the anthocyanin isomers under the highly acidic conditions, which could be a reasonable explanation for its superior selectivity.

Effect of the Additive Types. Phosphate buffer has poor volatility and needs to be removed through the desalting process. Substitution of phosphate with other common acidic additives, including FA and TFA, was tested to separate the isomers on the XCharge C8SAX column. To maintain a pH value of the mobile phase around 1.5, 5% FA (pH 1.6−1.7) or 0.2% TFA (pH 1.5−1.6) was adopted. The organic content in the mobile phase was optimized to acquire a similar retention on the XCharge C8SAX column with different additives. As shown in Figure 7, FA and TFA could provide good chromatographic performance and, thus, were able to replace phosphate buffer. Moreover, as for preparative application, a satisfactory result was observed with TFA as the additive (as shown in the Supporting Information). The pH changed slightly for solutions containing TFA, even with large loading amounts, which could improve anthocyanin preparation. Hence, 0.2% TFA was recommended as mobile phase additives for separation of the isomers on the XCharge C8SAX column.

Purification of Anthocyanin Isomers from *L. ruthenicum* on the XCharge C8SAX Column. On the basis of the above results, a HPLC method was developed to separate the anthocyanin isomers using the XCharge C8SAX column. Three XTerra MS C_{18} purified fractions (fractions 6, 8, and 9) from *L. ruthenicum* were taken as examples for target purification. Chromatographic conditions for each fraction were optimized. The preparation chromatograms of fractions 6, 8, and 9 on the XCharge C8SAX column were presented in Figure 8.

Six compounds were yielded with sufficient amounts and dried by lyophilization. The purity of these compounds was checked by HPLC, which is shown in Figure 10. F6-2 is 85% pure, and other compounds are more than 90% pure. It was noticed that compounds F6-1 and F6-2 had close retention times on the XTerra MS C_{18} column (Figure 9). They were difficult to isolate and collect with favorable purity. However, these two compounds could be easily obtained with high purity on the XCharge C8SAX column. Similar results were observed for compounds F8-1 and F8-2 as well as compounds P1 and P2. These data demonstrated that this mixed-mode column could be used as the second-dimensional separation in anthocyanin preparation, because of its complementary separation selectivity.

Structure Elucidation. Identification of the pure compounds was performed by mass spectrum and NMR. The results of specific structural identification were as follows:

F6-1, red powder, $[M + H]^+$: m/z 1095.3169, calculated for $C_{49}H_{59}O_{28}$, m/z 1095.3187. ^{1}H NMR data are shown in Table 3. In comparison of the ^{1}H NMR and NOESY data to the literature,[8] F6-1 was identified as petunidin 3-*O*-[6-*O*-(4-*O*-(4-*O*-*trans*-(β-D-glucopyranoside)-*p*-coumaroyl)-α-L-rhamnopyranosyl)-β-D-glucopyranoside]-5-*O*-[β-D-glucopyranoside].

F6-2, red powder, $[M + H]^+$: m/z 1095.3169, calculated for $C_{49}H_{59}O_{28}$, m/z 1095.3187. ^{1}H NMR data are shown in Table 3. It was similar to F6-1. However, the olefinic proton signals of *p*-coumaric acids of F6-2 had smaller coupling constants (J = 12.5 Hz) than that of F6-1 (J = 16.0 Hz), indicating that its *p*-coumaric acid was *cis* configuration. In comparison of the ^{1}H NMR and NOESY data to F6-2 in the literature,[8] F6-2 was identified as petunidin 3-*O*-[6-*O*-(4-*O*-(4-*O*-*cis*-(β-D-glucopyranoside)-*p*-coumaroyl)-α-L-rhamnopyranosyl)-β-D-glucopyranoside]-5-*O*-[β-D-glucopyranoside]. To the best of our knowledge, it is a new anthocyanin.

F8-1, red powder, $[M + H]^+$: m/z 949.2598, calculated for $C_{43}H_{49}O_{24}$, m/z 949.2608. ^{1}H NMR data are shown in Table 3. In comparison of the ^{1}H NMR and NOESY data to the literature,[8] F8-1 was identified as petunidin 3-*O*-[6-*O*-(4-*O*-(*trans*-*p*-caffeoyl)-α-L-rhamnopyranosyl)-β-D-glucopyranoside]-5-*O*-[β-D-glucopyranoside].

F8-2, red powder, $[M + H]^+$: m/z 919.2469, calculated for $C_{42}H_{47}O_{23}$, m/z 919.2505. ^{1}H NMR data are shown in Table 3. In comparison of the ^{1}H NMR and NOESY data to the literature,[8] F8-2 was identified as delphinidin 3-*O*-[6-*O*-(4-*O*-(*trans*-*p*-coumaroyl)-α-L-rhamnopyranosyl)-β-D-glucopyranoside]-5-*O*-[β-D-glucopyranoside].

P1, red powder, $[M + H]^+$: m/z 933.2647, calculated for $C_{43}H_{49}O_{23}$, m/z 933.2659. ^{1}H NMR data are shown in Table 3. In comparison of the ^{1}H NMR and NOESY data to the literature,[8] P1 was identified as petunidin 3-*O*-[6-*O*-(4-*O*-(*cis*-*p*-coumaroyl)-α-L-rhamnopyranosyl)-β-D-glucopyranoside]-5-*O*-[β-D-glucopyranoside].

P2, red powder, $[M + H]^+$: m/z 933.2650, calculated for $C_{43}H_{49}O_{23}$, m/z 933.2659. ^{1}H NMR data are shown in Table 3. In comparison of the ^{1}H NMR and NOESY data to the literature,[8] P2 was identified as petunidin 3-*O*-[6-*O*-(4-*O*-(*trans*-*p*-coumaroyl)-α-L-rhamnopyranosyl)-β-D-glucopyranoside]-5-*O*-[β-D-glucopyranoside].

The chemical structures of P1 and P2 are shown in Figure 1, while others are shown in Figure 10. To the best of our knowledge, F6-2 is a new anthocyanin. Except for P2, all other anthocyanins were isolated from *L. ruthenicum* for the first time.

In summary, a HPLC method had been successfully developed to realize effective preparation of *cis*−*trans* isomeric anthocyanins from *L. ruthenicum* using the XCharge C8SAX column. Four commercially available columns were evaluated to separate a pair of anthocyanin isomers. The results indicated that the XCharge C8SAX column performed improved selectivity and better column efficiency in terms of separation of the isomers. Accordingly, discrimination of the isomers on this mix-mode column was superior to that on RP columns. Moreover, the mobile phases, including pH, organic content, and ionic strength, were investigated. The data explicitly demonstrated that combined mechanisms of the hydrophobic interaction and ionic repulsion were involved in anthocyanin retention on the mixed-mode column, which was a possible explanation for the improved selectivity to the isomers. On the basis of the established approach, six pure anthocyanins, containing two pairs of *cis*−*trans* anthocyanin isomers with one new anthocyanin, were isolated from *L. ruthenicum* and identified by MS and NMR. Five of them were purified from this plant for the first time. The overall results indicated that this method was feasible to efficiently separate anthocyanins, especially for *cis*−*trans* isomeric anthocyanins, benefiting from the improved separation selectivity.

■ ASSOCIATED CONTENT

Supporting Information

Fractionation of anthocyanin constitutions on a Prep XTerra MS C_{18} column (Figure S1) and preparation of fraction 9 on the XCharge C8SAX column with (A) 5% (v/v) FA and (B) 0.2%

DOI: 10.1021/jf504525w
J. Agric. Food Chem. 2015, 63, 500−508

(v/v) TFA (Figure S2). This material is available free of charge via the Internet at http://pubs.acs.org.

AUTHOR INFORMATION

Corresponding Author

*Telephone: +86-411-84379541. Fax: +86-411-84379539. E-mail: liuyanfang@dicp.ac.cn.

Funding

This work was supported by the Project of the National Science Foundation of China (21305138) and the External Cooperation Program of the Bureau of International Cooperation (BIC), Chinese Academy of Science (Grant 121421KYSB20130013).

Notes

The authors declare no competing financial interest.

REFERENCES

(1) Hou, D. X. Potential mechanisms of cancer chemoprevention by anthocyanins. *Curr. Mol. Med.* **2003**, *3*, 149−159.

(2) Seeram, N. P.; Adams, L. S.; Hardy, M. L.; Heber, D. Total cranberry extract versus its phytochemical constituents: Antiproliferative and synergistic effects against human tumor cell lines. *J. Agric. Food Chem.* **2004**, *52*, 2512−2517.

(3) Bai, H. J.; Wang, H. B.; Luo, F. Study on extracting and scavenging activity against DPPH free radical of pigment from *Lycium rethenicum*. *Acta Agric. Boreali-Occident. Sin.* **2007**, *16*, 190−192.

(4) Jin, L.; Weijing, Q.; Sujun, Z.; Haiying, L. Study on antioxidant activity of pigment of *Lycium ruthenicum*. *China J. Chin. Mater. Med.* **2006**, *31*, 1179−1183.

(5) Zheng, J.; Ding, C.; Wang, L.; Li, G.; Shi, J.; Li, H.; Wang, H.; Suo, Y. Anthocyanins composition and antioxidant activity of wild *Lycium ruthenicum* Murr. from Qinghai−Tibet Plateau. *Food Chem.* **2011**, *126*, 859−865.

(6) Chen, C.; Shao, Y.; Tao, Y. D.; Mei, L. J.; Shu, Q. Y.; Wang, L. S. Main anthocyanins compositions and corresponding H-ORAC assay for wild *Lycium ruthenicum* Murr. fruits from the Qaidam Basin. *J. Pharm. Technol. Drug Res.* **2013**, *2* (1/1−1/5), 5.

(7) Naito, K.; Umemura, Y.; Mori, M.; Sumida, T.; Okada, T.; Takamatsu, N.; Okawa, Y.; Hayashi, K.; Saito, N.; Honda, T. Acylated pelargonidin glycosides from a red potato. *Phytochemistry* **1998**, *47*, 109−112.

(8) Ando, T.; Saito, N.; Tatsuzawa, F.; Kakefuda, T.; Yamakage, K.; Ohtani, E.; Koshi-ishi, M.; Matsusake, Y.; Kokubun, H.; Watanabe, H.; Tsukamoto, T.; Ueda, Y.; Hashimoto, G.; Marchesi, E.; Asakura, K.; Hara, R.; Seki, H. Floral anthocyanins in wild taxa of *Petunia* (Solanaceae). *Biochem. Syst. Ecol.* **1999**, *27*, 623−650.

(9) Comeskey, D. J.; Montefiori, M.; Edwards, P. J. B.; McGhie, T. K. Isolation and structural identification of the anthocyanin components of red kiwifruit. *J. Agric. Food Chem.* **2009**, *57*, 2035−2039.

(10) Tamura, H.; Hayashi, Y.; Sugisawa, H.; Kondo, T. Structure determination of acylated anthocyanins in Muscat Bailey a grapes by homonuclear Hartmann−Hahn (HOHAHA) spectroscopy and liquid chromatography−mass spectrometry. *Phytochem. Anal.* **1994**, *5*, 190−196.

(11) Wang, E.; Yin, Y.; Xu, C.; Liu, J. Isolation of high-purity anthocyanin mixtures and monomers from blueberries using combined chromatographic techniques. *J. Chromatogr. A* **2014**, *1327*, 39−48.

(12) Kubota, M.; Ishikawa, C.; Sugiyama, Y.; Fukumoto, S.; Miyagi, T.; Kumazawa, S. Anthocyanins from the fruits of *Rubus croceacanthus* and *Rubus sieboldii*, wild berry plants from Okinawa, Japan. *J. Food Compos. Anal.* **2012**, *28*, 179−182.

(13) Takeoka, G. R.; Dao, L. T.; Full, G. H.; Wong, R. Y.; Harden, L. A.; Edwards, R. H.; Berrios, J. D. Characterization of black bean (*Phaseolus vulgaris* L.) anthocyanins. *J. Agric. Food Chem.* **1997**, *45*, 3395−3400.

(14) Tian, Q. G.; Giusti, M. M.; Stoner, G. D.; Schwartz, S. J. Screening for anthocyanins using high-performance liquid chromatography coupled to electrospray ionization tandem mass spectrometry with precursor-ion analysis, product-ion analysis, common-neutral-loss analysis, and selected reaction monitoring. *J. Chromatogr. A* **2005**, *1091*, 72−82.

(15) Wu, X. L.; Prior, R. L. Systematic identification and characterization of anthocyanins by HPLC−ESI−MS/MS in common foods in the United States: Fruits and berries. *J. Agric. Food Chem.* **2005**, *53*, 2589−2599.

(16) Nayak, C. A.; Srinivas, P.; Rastogi, N. K. Characterisation of anthocyanins from *Garcinia indica* Choisy. *Food Chem.* **2010**, *118*, 719−724.

(17) Valls, J.; Millan, S.; Pilar Marti, M.; Borras, E.; Arola, L. Advanced separation methods of food anthocyanins, isoflavones and flavanols. *J. Chromatogr. A* **2009**, *1216*, 7143−7172.

(18) Willemse, C. M.; Stander, M. A.; de Villiers, A. Hydrophilic interaction chromatographic analysis of anthocyanins. *J. Chromatogr. A* **2013**, *1319*, 127−140.

(19) Nogueira, R.; Lammerhofer, M.; Lindner, W. Alternative high-performance liquid chromatographic peptide separation and purification concept using a new mixed-mode reversed-phase/weak anion-exchange type stationary phase. *J. Chromatogr. A* **2005**, *1089*, 158−169.

(20) Li, J.; Shao, S.; Jaworsky, M. S.; Kurtulik, P. T. Simultaneous determination of cations, zwitterions and neutral compounds using mixed-mode reversed-phase and cation-exchange high-performance liquid chromatography. *J. Chromatogr. A* **2008**, *1185*, 185−193.

(21) Wei, J.; Guo, Z.; Zhang, P.; Zhang, F.; Yang, B.; Liang, X. A new reversed-phase/strong anion-exchange mixed-mode stationary phase based on polar-copolymerized approach and its application in the enrichment of aristolochic acids. *J. Chromatogr. A* **2012**, *1246*, 129−136.

(22) McCallum, J. L.; Yang, R.; Young, J. C.; Strommer, J. N.; Tsao, R. Improved high performance liquid chromatographic separation of anthocyanin compounds from grapes using a novel mixed-mode ion-exchange reversed-phase column. *J. Chromatogr. A* **2007**, *1148*, 38−45.

(23) Vergara, C.; Mardones, C.; Hermosin-Gutierrez, I.; von Baer, D. Comparison of high-performance liquid chromatography separation of red wine anthocyanins on a mixed-mode ion-exchange reversed-phase and on a reversed-phase column. *J. Chromatogr. A* **2010**, *1217*, 5710−5717.

(24) Fleschhut, J.; Kratzer, F.; Rechkemmer, G.; Kulling, S. E. Stability and biotransformation of various dietary anthocyanins *in vitro*. *Eur. J. Nutr.* **2006**, *45*, 7−18.

(25) Kennedy, J. A.; Waterhouse, A. L. Analysis of pigmented high-molecular-mass grape phenolics using ion-pair, normal-phase high-performance liquid chromatography. *J. Chromatogr. A* **2000**, *866*, 25−34.

(26) De Villiers, A.; Cabooter, D.; Lynen, F.; Desmet, G.; Sandra, P. High performance liquid chromatography analysis of wine anthocyanins revisited: Effect of particle size and temperature. *J. Chromatogr. A* **2009**, *1216*, 3270−3279.

(27) de Villiers, A.; Cabooter, D.; Lynen, F.; Desmet, G.; Sandra, P. High-efficiency high performance liquid chromatographic analysis of red wine anthocyanins. *J. Chromatogr. A* **2011**, *1218*, 4660−4670.

(28) Snyder, L. R.; Kirkland, J. J. *Introduction to Modern Liquid Chromatography*, 2nd ed.; Wiley: New York, 1979; p 260.

(29) Fallas, M. M.; Buckenmaier, S. M. C.; McCalley, D. V. A comparison of overload behaviour for some sub 2 μm totally porous and sub 3 μm shell particle columns with ionised solutes. *J. Chromatogr. A* **2012**, *1235*, 49−59.

DOI: 10.1021/jf504525w
J. Agric. Food Chem. 2015, 63, 500−508

JOURNAL OF AGRICULTURAL AND FOOD CHEMISTRY

Article

pubs.acs.org/JAFC

Analysis of 10 Metabolites of Polymethoxyflavones with High Sensitivity by Electrochemical Detection in High-Performance Liquid Chromatography

Jinkai Zheng,[†,§,∥] Jinfeng Bi,[†,∥] David Johnson,[§] Yue Sun,[§] Mingyue Song,[§] Peiju Qiu,[§] Ping Dong,[§] Eric Decker,[§] and Hang Xiao*[,§]

[†]Institute of Agro-Products Processing Science and Technology, Chinese Academy of Agricultural Sciences, Beijing 100193, People's Republic of China

[§]Department of Food Science, University of Massachusetts, Amherst, Massachusetts 01003, United States

ABSTRACT: Polymethoxyflavones (PMFs) have been known as a type of bioactive flavones that possess various beneficial biological functions. Accumulating evidence demonstrated that the metabolites of PMFs, that is, hydroxyl PMFs (OH-PMFs), had more potent beneficial biological effects than their corresponding parent PMFs. To facilitate the further identification and quantification of OH-PMFs in biological samples, the aim of this study was to develop a methodology for the simultaneous determination of 10 OH-PMFs using high-performance liquid chromatography (HPLC) coupled with electrochemistry detection. The HPLC profiles of these 10 OH-PMFs affected by different chromatographic parameters (different organic composition in mobile phases, the concentration of trifluoroacetic acid, and the concentration of ammonium acetate) are fully discussed in this study. The optimal condition was selected for the following validation studies. The linearity of calibration curves, accuracy, and precision (intra- and interday) at three concentration levels (low, middle, and high concentration range) were verified. The regression equations were linear ($r > 0.9992$) over the range of 0.005−10 μM. The limit of detection for 10 OH-PMFs was in the range of 0.8−3.7 ng/mL (S/N = 3, 10 μL injection). The recovery rates ranged from 86.6 to 108.7%. The precisions of intraday and interday analyses were less than 7.37 and 8.63% for relative standard deviation, respectively. This validated method was applied for the analysis of a variety of samples containing OH-PMFs. This paper also gives an example of analyzing the metabolites of nobiletin in mouse urine using the developed method. The transformation from nobiletin to traces of 5-hydroxyl metabolites has been discovered by this effective method, and this is the first paper to report such an association.

KEYWORDS: *hydroxyl polymethoxyflavones, HPLC, quantification, electrochemical detection, metabolites, nobiletin*

INTRODUCTION

Polymethoxyflavones (PMFs) are a unique class of bioactive flavonoids that are mainly found in citrus fruits such as sweet orange and tangerine, especially in their peels.[1] Increasing numbers of studies have demonstrated various beneficial biological functions of PMFs, for example, anti-inflammatory, anticarcinogenic, antiatherogenic, antiviral, and antioxidative effects.[2] We and others have identified several metabolites of PMFs after their oral administration in mice.[3−5] It was found that these metabolites are mainly hydroxyl PMFs (OH-PMFs). Interestingly, accumulating evidence has shown that OH-PMFs have potent biological activities,[6−13] and some of them were much stronger that those produced by their corresponding parent compounds.[3−5] OH-PMFs can be obtained by isolation from natural sources, such as citrus peels, and by chemical synthesis.[14] Several methods have been developed for the quantification of PMFs, including gas chromatography (GC),[15] supercritical liquid chromatography (SFC),[16] and high-performance liquid chromatography (HPLC) with UV detection.[17] However, there is no effective analytical method available for the simultaneous quantification of multiple OH-PMFs with quite similar chemical structures. With increasing interests in the beneficial bioactivities of PMFs, it is important to develop highly sensitive methods to analyze biological samples generated from animal and human studies that contain multiple OH-PMFs, for example, the metabolites of PMFs.

The electrochemical detection (ECD) is a powerful analytical method that can detect electric currents of less than nanoamps generated from oxidative or reductive reactions of test compounds.[18−20] OH-PMFs possess at least one phenolic group that is potentially reactive under electrical potential, which makes OH-PMFs good candidates for electrochemical detection. The aim of this study is to develop a fast, simple, and reliable HPLC coupled with ECD method for the assessment of 10 important OH-PMFs (Figure 1), namely, 4′-demethyltangeretin (**1**), 5-demethyltangeretin (**2**), 5,4′-didemethyltangeretin (**3**), 3′-demethylnobiletin (**4**), 4′-demethylnobiletin (**5**), 3′,4′-didemethylnobiletin (**6**), 5-demethylnobiletin (**7**), 5,3′-didemethylnobiletin (**8**), 5,4′-didemethylnobiletin (**9**), and 5,3′,4′-tridemethylnobiletin (**10**). Herein, we report a detailed validation of a HPLC-ECD method for the aforementioned 10 OH-PMFs, and we also successfully utilized this method to analyze urine samples containing multiple OH-PMFs and their metabolites generated from a mouse feeding study.

Received: November 17, 2014
Revised: December 30, 2014
Accepted: January 1, 2015
Published: January 1, 2015

ACS Publications © 2015 American Chemical Society

DOI: 10.1021/jf505545x
J. Agric. Food Chem. 2015, 63, 509−516

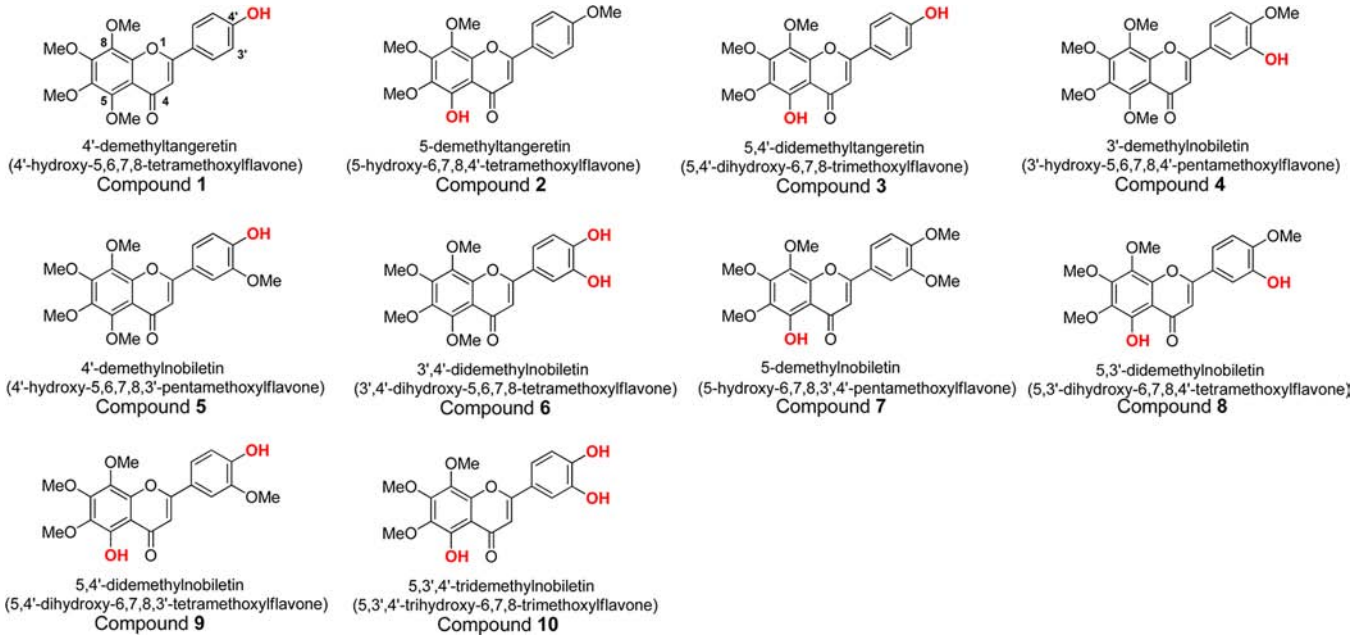

Figure 1. Chemical structures of 10 OH-PMF analogues.

MATERIALS AND METHODS

Reagents and Chemicals. Organic solvents, including methanol (MeOH), acetonitrile (ACN), tetrahydrofuran (THF), and trifluoroacetic acid (TFA), were of HPLC grade and obtained from Fisher Scientific. Ammonium acetate was a product of EMD Chemicals Inc. (Gibbstwon, NJ, USA). 4′-Demethyltangeretin (**1**), 5-demethyltangeretin (**2**), 5,4′-didemethyltangeretin (**3**), 3′-Demethylnobiletin (**4**), 4′-demethylnobiletin (**5**), 3′,4′-demethylnobiletin (**6**), 5-demethylnobiletin (**7**), 5,3′-didemethylnobiletin (**8**), 5,4′-didemethylnobiletin (**9**), and 5,3′,4′-tridemethylnobiletin (**10**) were synthesized following previously published methods.[3,4] The purity of these 10 OH-PMFs was >98%, and their chemical structures have been confirmed by MS and NMR.[3,4]

Instrumentation and Chromatographic Conditions. The CoulArray HPLC system (Chelmsford, MA, USA) consisted of a binary solvent delivery system (model 584), an autosampler (model 542), and a CoulArray Multi-Channel EC detector (model 6210) (Waters, Milford, MA, USA).[21] Instrument control and data processing were performed with CoulArray 3.06 software. An Ascentis RP-Amide reversed-phase HPLC column (15 cm × 4.6 mm id, 3 μm) (Sigma-Aldrich, St. Louis, MO, USA) was used. Flow rate was 1.0 mL/min. The temperature of the autosampler was set to 4 °C. The injection volumes were between 10 and 50 μL. The optimal elution conditions were as follows: mobile phase A, 75% water, 20% acetonitrile, 5% THF, and 50 mM ammonium acetate; mobile phase B, 50% water, 40% acetonitrile, 10% THF, and 50 mM ammonium acetate (pH values of both mobile phases were adjusted to 3.0). The linear solvent gradient consisted of 10% B at the beginning, 50% B at 5.0 min, 70% B at 15.0 min, 90% B at 25.0 min, 100% B at 25.1 min, and 100% B at 30.0 min. Re-equilibration duration was 5 min between individual runs. Two EC detection cells (each contains four channels) were used, and the detecting potentials were set at 100, 200, 300, 400, 500, 600, and 700 mV.

Optimization of Chromatographic Conditions. *Elution Conditions.* To obtain optimal resolution of 10 OH-PMFs simultaneously, two complex mobile phases A and B were used: A, 75% water, 20% acetonitrile, 5% THF, and 50 mM ammonium acetate; B, 50% water, 40% acetonitrile, 10% THF, and 50 mM ammonium acetate. Both mobile phases were adjusted to pH 3.0. Four different elution conditions were compared, that is, (i) isocratic elution with 40% A and 60% B; (ii) isocratic elution with 50% A and 50% B; (iii) isocratic elution with 60% A and 40% B; and (iv) gradient elution, 0 min (10% B), 5 min (50% B), 15 min (70% B), 25 min (90% B), 25.1 min (100% B), 30 min (100% B), 30.1 min (10% B), and 35 min (10% B).

pH Values of Mobile Phases. The pH values of mobile phases A and B were adjusted to different values in the range of 2.0−7.0 by adding different volumes of TFA. The effects of pH on the sensitivity, retention time, and peak resolution of 10 OH-PMFs were determined and compared.

Concentrations of Ammonium Acetate. In the mobile phases, ammonium acetate was used as a buffer system that can affect the sensitivity of the ECD. Five different concentrations of ammonium acetate (0, 25, 50, 75, and 100 mM) were used to determine their effects on the ECD of 10 OH-PMFs.

Validation of HPLC-ECD Method. The stock solutions (10 mM) of each standard compound were prepared in DMSO and stored at 4 °C, and the final test solutions with a series of concentrations were prepared by diluting the stock solution with 50% methanol just before every experiment. Linearity, limit of quantification (LOQ), and limit of detection (LOD), and precision of the current method were determined. To assess the linearity of the method, calibration curves were constructed with eight concentrations of each OH-PMF (0.005, 0.01, 0.05, 0.5, 5, 10, 20, and 50 μM) in the test solutions. Calibration curves were obtained by plotting the responses (peak areas) of 10 OH-PMF standards against their respective concentrations using a linear least-squares regression. The slope, intercept, and correlation coefficient (r^2) were calculated for each OH-PMFs using a regression equation. The sensitivity of the method was determined by the LOD and LOQ. LOD and LOQ were the lowest measured concentrations with signal-to-noise (S/N) ratios of of 3 and 10, respectively. A known amount of standard OH-PMFs (at low, medium, and high concentrations of 0.05, 0.5, and 5 μM, respectively) was added to mouse urine, and overall recoveries were determined by the standard addition method. Intraday and interday precisions were determined for both retention time and peak area at low (0.05 μM), medium (0.5 μM), and high (5 μM) concentrations of OH-PMFs.

Quantification of OH-PMFs in Biological Samples. The optimized HPLC-ECD method was utilized to quantify OH-PMFs in the urine of mice after they were fed nobiletin, a polymethoxyflavone found in citrus fruits. Fifteen CF-1 male mice (7 weeks of age) were fed nobiletin at 500 ppm in standard AIN-93G powder diet for 1 week. The urine was collected using Tecniplast metabolic cages (5 mice per cage) during the last 12 h of feeding. Two hundred microliters of collected urine sample was extracted with 500 μL of ethyl acetate three times. The combined ethyl acetate extracts were

DOI: 10.1021/jf505545x
J. Agric. Food Chem. 2015, 63, 509−516

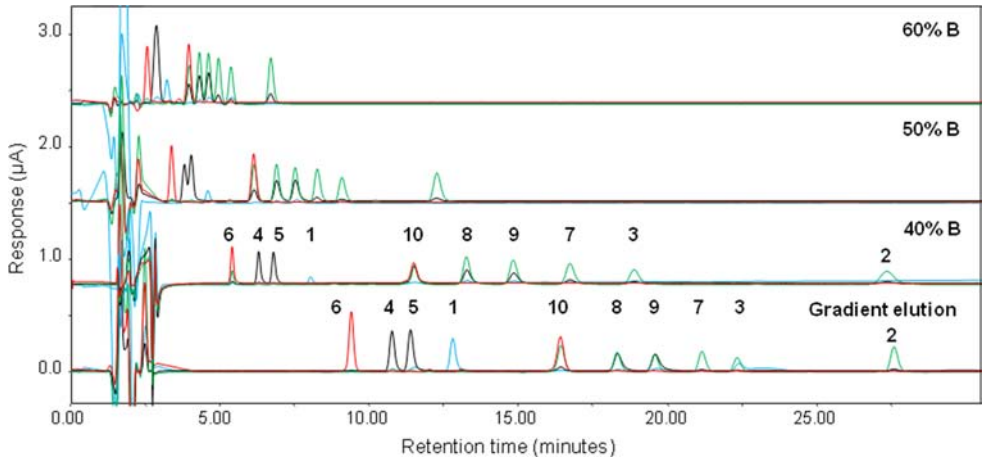

Figure 2. HPLC profiles of 10 OH-PMFs analyzed using four different elution conditions, that is, three isocratic elution conditions (i.e., 60, 50, and 40% mobile phase B) and one gradient elution condition (0 min, 10% B; 5 min, 50% B; 15 min, 70% B; 25 min, 90% B; 25.1 min, 100% B; 30 min, 100% B). The composition of mobile phase A was 75% water, 20% acetonitrile, 5% THF, and 50 mM ammonium acetate (pH 3.0); the composition of mobile phase B was 50% water, 40% acetonitrile, 10% THF, and 50 mM ammonium acetate (pH 3.0). Different EC potentials were used for detection (100 mV, in red; 300 mV, in green; 400 mV, in black; 600 mV, in blue). Each peak was labeled with corresponding OH-PMF **1**–**10** (injection volume = 10 μL; sample concentration = 0.5 μM).

Table 1. Retention Time (Minutes) of OH-PMFs 1–10 Eluted by Different Elution Conditions

elution condition	1	2	3	4	5	6	7	8	9	10
60% B	3.15[a]	6.58	5.25[a]	2.80[b]	2.80[b]	2.49[a]	4.84[a]	4.22[a]	4.51[a]	3.87[a]
50% B	4.51	12.07	8.91	3.74[a]	3.93[a]	3.30	8.10	6.78	7.37	6.01
40% B	7.88	26.91	18.52	6.16	6.63	5.28	16.42	13.01	14.56	11.29
gradient elution	12.95	27.65	22.90	10.70	11.35	9.46	21.20	18.50	19.80	16.90

[a]The peak cannot be separated with others from baseline. [b]The peak completely overlapped with another one.

dried under vacuum. Dried samples were dissolved in 1000 μL of 50% methanol for HPL-ECD analysis using the optimized method. The identities and concentrations of OH-PMFs (as metabolites of nobiletin) in mouse urine were determined by comparing the HPLC profiles of urine samples with those of OH-PMF standards and their corresponding standard curves.

Statistical Analysis. All analyses were performed in triplicate, and the results are presented as means ± standard deviation of three independent experiments.

RESULTS AND DISCUSSION

Optimization of HPLC-ECD Method. Different OH-PMFs may have different electrochemical reactivities and retention times under different chromatographical conditions. Therefore, it is necessary to determine the impact of multiple influencing factors (pH value, salt concentration, and polarity of eluents) to obtain optimal separation and sensitivity for all 10 OH-PMFs. The column was equilibrated for at least 2 h with new mobile phases when different mobile phases were used.

Optimization of Elution Condition. On the basis of our previous experience in analyzing PMFs by HPLC,[4,21] we developed two complex mobile phases A and B to optimize the elution conditions. Mobile phase A consisted of 75% water, 20% acetonitrile, 5% THF, and 50 mM ammonium acetate, and mobile phase B consisted of 50% water, 40% acetonitrile, 10% THF, and 50 mM ammonium acetate. In this section, the pH of mobile phases A and B was adjusted to 3.0. The effects of pH on the HPLC-ECD results are investigated in the following section. Four elution conditions were used to analyze a mixture of 10 OH-PMFs at 1 μM each. The HPLC profiles of 10 OH-PMFs under different elution conditions are shown in Figure 2, and the retentions times of OH-PMFs under different elution conditions are listed in Table 1. The isocratic elution with 60 or 50% of mobile phase B did not produce satisfactory separation of the 10 OH-PMFs, which was evidenced by overlapping peaks of different OH-PMFs, especially compounds **4** and **5**. In contrast, isocratic elution with 40% mobile phase B resulted in good separation of all 10 OH-PMFs. Nevertheless, the retention times of the 10 OH-PMFs were not evenly distributed, and compounds **1** and **4**–**6** were eluted within only 2.6 min when eluted with 40% mobile phase B. A potential drawback of the quick elution of compounds **1** and **4**–**6** is that any other compounds (e.g., contaminants or impurities) with similar retention times may have a good chance to interfere with one or more of them. The gradient elution (0 min, 10% B; 5 min, 50% B; 15 min, 70% B; 25 min, 90% B; 25.1 min, 100% B; 30 min, 100% B) produced the best separation of all 10 OH-PMFs within 30 min. Moreover, much better sensitivities can be obtained under gradient elution condition. For example, the sensitivity of compound **1** under gradient elution increased 8-fold in comparison with those under isocratic elution with 40% mobile phase B. Therefore, the gradient elution was selected as the optimal elution conditions.

Optimization of the pH of Mobile Phases. The pH of the mobile phase often significantly affects the nature of chromatograms, especially the sensitivity of ECD. In this section, we determine the effects of mobile phase pH on the retention time, sensitivity, and peak resolution of all OH-PMF. The initial pH values of mobile phases A and B were 7.15 and 7.34, respectively. Their pH values were adjusted to 2.0, 3.0, 4.0, 5.0, 6.0, and 7.0 by adding different volumes of TFA. The gradient elution condition was used in this section. As shown in Figure 3, varying pH values of the mobile phase had only

DOI: 10.1021/jf505545x
J. Agric. Food Chem. 2015, 63, 509–516

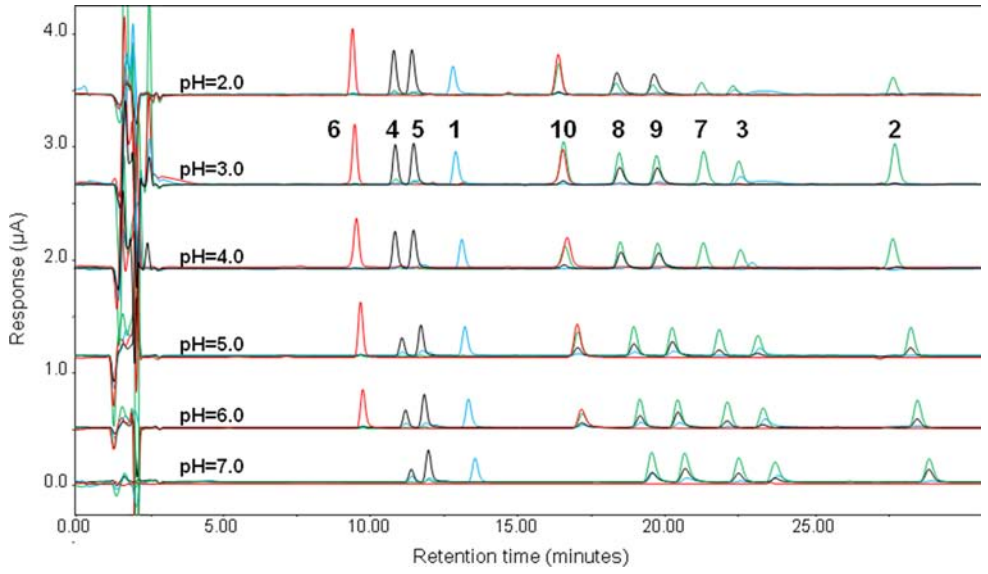

Figure 3. Effects of pH of mobile phases on HPLC profiles of 10 OH-PMFs. The pH values of both mobile phases A and B were adjusted to 2.0, 3.0, 4.0, 5.0, 6.0, or 7.0. Different EC potentials were used for detection (100 mV, in red; 300 mV, in green; 400 mV, in black; 600 mV, in blue). Each peak was labeled with corresponding OH-PMFs **1**−**10** (injection volume = 10 μL; sample concentration = 0.5 μM).

marginal effects on the retention times. To a certain extent, the peak symmetry and sharpness were improved when the pH decreased. Most importantly, the sensitivity of ECD was increased when the pH values of mobile phases were decreased. For example, as shown in Figure 4, at a potential of 400 mV,

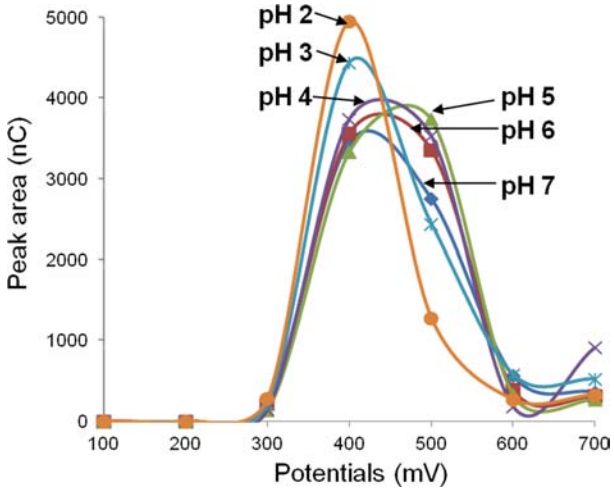

Figure 4. Effects of pH value on peak areas (nC) of compound **5** under different EC potentials (mV). The pH values of both mobile phases A and B were adjusted to 2.0, 3.0, 4.0, 5.0, 6.0, or 7.0. EC potentials were set at 100, 200, 300, 400, 500, 600, and 700 mV (injection volume = 10 μL; sample concentration = 0.5 μM; n = 3).

the mobile phase with pH 2.0 produced the highest sensitivity, followed by pH 3.0 and 4.0. A similar trend can be observed for other OH-PMFs. It is worth mentioning that at high pH, that is, pH 7.0, the sensitivity of ECD of compounds **6** and **10** became so low that they cannot be even detected at 1 μM concentration. Although pH 2.0 produced the highest overall sensitivity, we selected pH 3.0 as the optimal pH value for the mobile phases because high acidity of the mobile phase may cause damage to the stationary phase and therefore shorten the working life of the HPLC columns.

Optimization of Ammonium Acetate Concentration. For the mobile phase for use with EC detection, a buffered system that can provide ionic strength for good electron transfer is required in mobile phase.[22−24] In our study, ammonium acetate was used as a buffer system for EC detection.[25] The gradient elution condition was used in this section. Five different concentrations of ammonium acetate (0, 25, 50, 75, and 100 mM) were prepared in both mobile phases A and B with pH 3.0. As shown in Figure 5, the concentration of ammonium acetate did not have a significant effect on the retention times of OH-PMFs, but the addition of ammonium acetate greatly improved the symmetry and sharpness of peaks of OH-PMFs. Most interestingly, when the concentration of ammonium acetate increased from 0 to 25 mM and then to 50 mM, the sensitivity of EC detection was significantly enhanced. However, further increase of ammonium acetate concentration to 75 and 100 mM caused no further enhancement of sensitivity, and it even decreased sensitivity for some OH-PMFs. On the basis of these results, the optimal concentration of ammonium acetate was determined to be 50 mM, and this condition was used for the rest of the study described below.

Method Validation. Using the optimized chromatography conditions, we constructed the calibration curves for all 10 OH-PMFs by plotting the peak areas against a series of concentrations of prepared standards (0.005, 0.01, 0.05, 0.5, 5, 10, 20, and 50 μM, respectively; Figure 6). On the basis of the EC potential where the maximum sensitivities of different OH-PMFs were observed, we selected the potentials of 600, 300, 300, 400, 400, 100, 300, 300, 300, and 100 mV for analyzing OH-PMFs **1**−**10**, respectively. Satisfactory linearity was observed when the concentrations of OH-PMFs were within the range of 0.005−10 μM (Figure 6). The results on linear regression of standard curves of all 10 OH-PMFs (slope, intercept, correlation coefficient, and linear range) are reported in Table 2. The linearities of the standard curves for all 10 OH-PMFs were all >0.9992, suggesting good linearity within a relatively wide concentration range (0.005−10 μM, 2000-fold) for all 10 OH-PMFs. The limits of detection (LOD) and the limits of quantification (LOQ) were determined at signal-to-

DOI: 10.1021/jf505545x
J. Agric. Food Chem. 2015, 63, 509−516

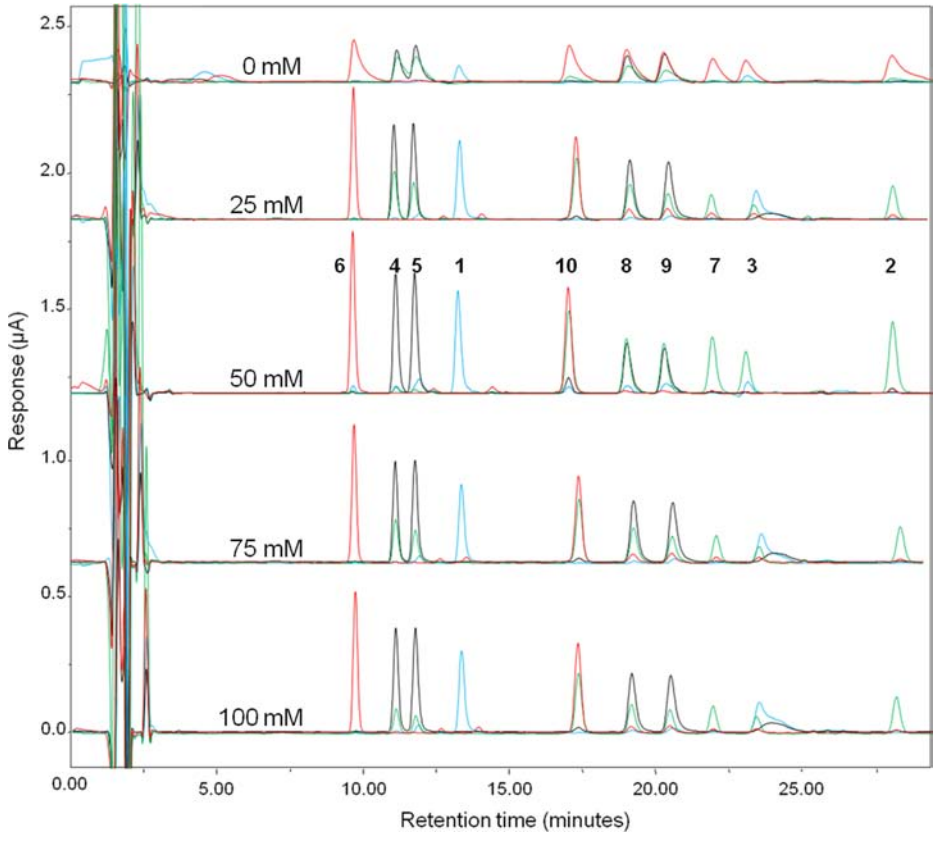

Figure 5. Effects of the concentrations of ammonium acetate (0, 25, 50, 75, and 100 mM) in the mobile phases on the HPLC profiles of 10 OH-PMFs. Different EC potentials were used for detection (100 mV, in red; 300 mV, in green; 400 mV, in black; 600 mV, in blue). Each peak was labeled with corresponding OH-PMFs **1**−**10** (injection volume = 10 μL; sample concentration = 0.5 μM).

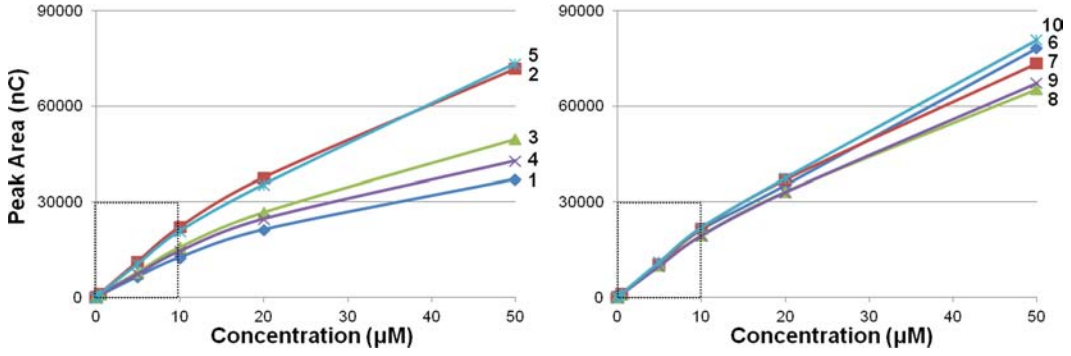

Figure 6. Calibration curves of OH-PMFs **1**−**10** (gradient elution; injection volume = 10 μL).

noise ratios (S/N) of 3 and 10, respectively. The results showed that the LODs of the 10 PMFs ranged from 8 to 37 pg per injection (10 μL) at a signal-to-noise ratio of 3:1, and the LODs ranged from 25 to 119 ng at a signal-to-noise ratio of 10:1.

Recovery rates of the extraction and detection method were obtained by analyzing the mouse urine samples that had been spiked with known amounts of OH-PMFs. As shown in Table 2, the recovery rates of different OH-PMFs ranged from 86.6 to 108.7% with the RSD (%, relative standard deviations) of <14.9% for all 10 OH-PMFs at 0.05, 0.5, and 5 μM that are representative of the low, medium, and high concentrations, respectively. Intraday and interday precisions (shown in Table 3) were determined at three different sample concentrations (0.05, 0.5, and 5 μM) by injecting the same sample solution three times a day for three consecutive days. Retention time and peak area were recorded and analyzed. Precision was expressed as RSD that was obtained from three repetitive injections of standard solutions of OH-PMFs. For intraday variation, the RSD of the retention time was between 0 and 0.88%, and the RSD of the peak area was between 1.03 and 7.37%. For the interday variation, the RSD of the retention time and the peak area were in the ranges of 0−1.46 and 0.70−8.63%, respectively. These results demonstrated that the method established in this study produced very good reproducibility. The RSD values for recovery and precision were the lowest at the concentration of 0.5 μM, which suggested that quantification of OH-PMFs by the method developed herein can produce the best repeatability when the concentrations of OH-PMFs are around 0.5 μM in the samples

DOI: 10.1021/jf505545x
J. Agric. Food Chem. 2015, 63, 509−516

Table 2. Linearity, Detection Limit, and Recovery Rate of 10 OH-PMFs[a]

	linearity			detection limit		recovery rate					
						0.05 μM		0.5 μM		5 μM	
compd no.	concn range (μM)	linear regression eq	r^2	LOD[b] (ng/mL)	LOQ[c] (ng/mL)	recovery rate (%)	RSD[d] (%)	recovery rate (%)	RSD (%)	recovery rate (%)	RSD (%)
1	0.005−10	$y = 1303.2x - 32.698$	0.9993	3.7	11.9	108.7	4.81	90.1	9.82	91.7	12.42
2	0.005−10	$y = 2245.9x + 7.2716$	0.999	2.4	7.1	86.6	3.32	96.7	3.11	93.7	6.04
3	0.005−10	$y = 1568.2x + 34.5$	0.9993	1.3	4.3	97.4	2.51	97.5	5.68	92.6	11.84
4	0.005−10	$y = 1444.9x + 88.864$	0.9993	1.8	5.4	102.7	5.40	99.9	4.68	98.9	14.91
5	0.005−10	$y = 2085.9x + 0.7716$	0.9995	2.0	6.1	105.9	6.25	96.3	5.97	95.7	8.77
6	0.005−10	$y = 2123.2x + 75.432$	0.9992	2.0	6.2	103.3	4.08	97.5	5.41	89.2	10.04
7	0.005−10	$y = 2082.6x + 79.259$	0.9996	0.8	2.5	92.3	3.70	90.8	4.57	92.8	4.78
8	0.005−10	$y = 1993.4x + 6.821$	0.9999	1.4	4.1	91.5	6.07	88.1	4.06	91.0	11.33
9	0.005−10	$y = 1968x + 1.9321$	0.9998	1.7	5.5	87.4	4.52	96.0	4.04	91.5	8.08
10	0.005−10	$y = 2228.3x + 37.222$	0.9996	2.0	6.2	103.6	2.04	97.7	5.05	96.7	9.86

[a]The potentials for analyzing OH-PMFs **1**−**10** were 600, 300, 300, 400, 400, 100, 300, 300, 300, and 100 mV, respectively; injection volume = 10 μL; $n = 3$). [b]LOD, limit of detection (S/N = 3). [c]LOQ, limit of quantification (S/N = 10). [d]RSD (%), relative standard deviations obtained from three replicates.

Table 3. Intraday and Interday Variation of 10 OH-PMFs on HPLC Coupled with EC Detector (Injection Volume = 10 μL; n = 3)

	0.05 μM				0.5 μM				5 μM			
comp. no.	Rt (min)	RSD (%)	peak area (nC)	RSD (%)	Rt (min)	RSD (%)	peak area (nC)	RSD (%)	Rt (min)	RSD (%)	peak area (nC)	RSD (%)
Intraday Repeatability												
1	12.93	0.45	54	3.88	12.93	0.55	489	1.03	12.99	0.09	6583	2.09
2	27.57	0.21	109	6.70	27.70	0.26	1157	2.00	27.53	0.21	10797	6.73
3	22.83	0.51	77	4.93	22.87	0.00	778	2.96	22.73	0.25	7727	3.12
4	10.77	0.77	94	4.71	10.67	0.00	927	1.63	10.67	0.54	7173	5.42
5	11.30	0.00	100	3.73	11.30	0.62	1057	2.19	11.30	0.88	10673	1.33
6	9.43	0.31	115	5.30	9.46	0.15	1237	2.03	9.48	0.18	10900	3.67
7	21.17	0.27	146	6.96	21.17	0.00	1110	3.25	21.13	0.27	9983	7.30
8	18.47	0.31	93	2.07	18.47	0.00	949	3.20	18.43	0.31	9713	1.79
9	19.77	0.29	89	7.37	19.77	0.00	907	3.86	19.70	0.51	9163	6.92
10	16.83	0.69	109	5.62	16.90	0.00	1133	1.84	16.83	0.69	10933	6.62
Interday Repeatability												
1	12.97	0.45	55	3.64	12.95	0.55	494	3.20	13.00	0.00	6486	3.57
2	27.73	1.46	119	8.63	27.65	0.26	1131	0.70	27.63	0.42	11237	3.67
3	23.00	1.26	82	6.20	22.90	0.00	853	3.80	22.83	0.51	7872	5.53
4	10.77	0.53	92	3.91	10.70	0.00	888	2.71	10.70	0.00	7307	2.33
5	11.43	1.34	102	1.91	11.35	0.62	1047	0.76	11.37	0.51	10430	1.98
6	9.50	0.73	121	5.24	9.46	0.15	1203	0.55	9.45	0.43	10686	2.17
7	21.30	0.63	151	3.81	21.20	0.00	1157	3.54	21.17	0.27	10489	4.23
8	18.60	0.86	99	7.23	18.50	0.00	1011	4.24	18.47	0.31	9973	5.42
9	19.93	1.03	94	5.26	19.80	0.00	993	4.13	19.77	0.29	9841	6.26
10	16.93	1.39	116	5.66	16.90	0.00	1188	1.83	16.83	0.69	11176	1.91

to be tested. The high precision and low LOD of the method indicated that the proposed method was sensitive and reliable for analyzing OH-PMFs.

Quantification of OH-PMFs in Mouse Urine. Using the optimized and validated method developed in the previous sections, we quantified OH-PMF metabolites in the urine of mice fed nobiletin, a permethoxylated PMFs. Three batches of urine samples were analyzed, and their HPLC profiles under different EC potentials are shown in Figure 7. We confirmed the identities of seven OH-PMF metabolites by comparing their retention times and characteristic EC responses at different potentials with those of the synthesized standard of OH-PMFs. The OH-PMF metabolites identified in the urine were OH-PMFs **4**−**10**. Previously, three OH-PMF metabolites (**4**−**6**) were identified in the urine of mice fed nobiletin.[14] Recently, we identified three OH-PMF metabolites (**8**−**10**) in the urine of mice fed OH-PMF **7**.[4] It is known that nobiletin can be converted to OH-PMF **7** by acid hydrolysis that removes the methyl group at the 5-position in the A-ring. We propose that nobiletin may be converted to OH-PMF **7** by the acid found in the stomach after oral consumption of nobiletin (Figure 8). Nobiletin and OH-PMF **7** are then metabolized to produce their OH-PMF metabolites as reported previously.[4,14]

Utilizing the standard curves generated from synthetic standards of OH-PMFs, the concentrations of OH-PMF metabolites in the urine were quantified, and the results are listed in Table 4. To ensure the accuracy of the quantification, proper dilutions were made to the urine samples so that the

DOI: 10.1021/jf505545x
J. Agric. Food Chem. 2015, 63, 509−516

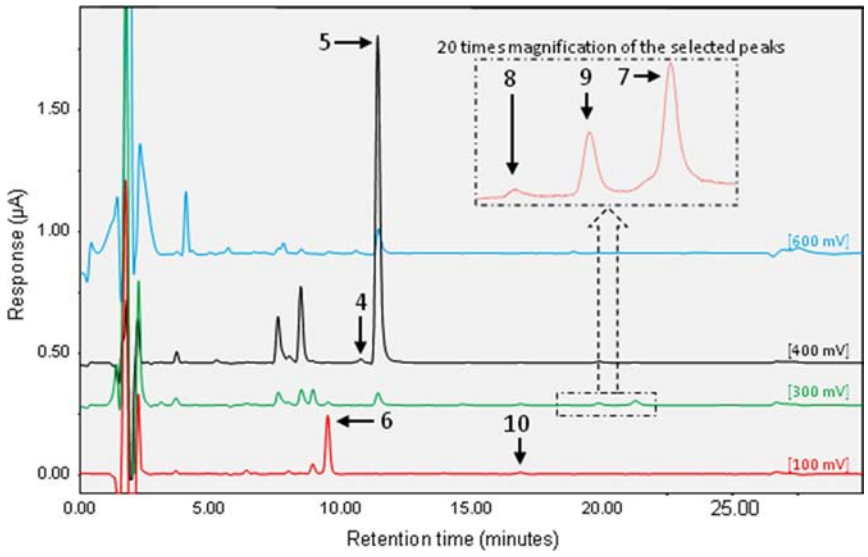

Figure 7. HPLC profiles of the OH-PMF metabolites of nobiletin in mouse urine. The urine samples were processed as described under Materials and Methods and then eluted with the optimized HPLC method. Different EC potential were used for detection (100 mV, in red; 300 mV, in green; 400 mV, in black; 600 mV, in blue). Each peak was labeled with corresponding OH-PMFs (injection volume = 10 μL; representative of three replicates).

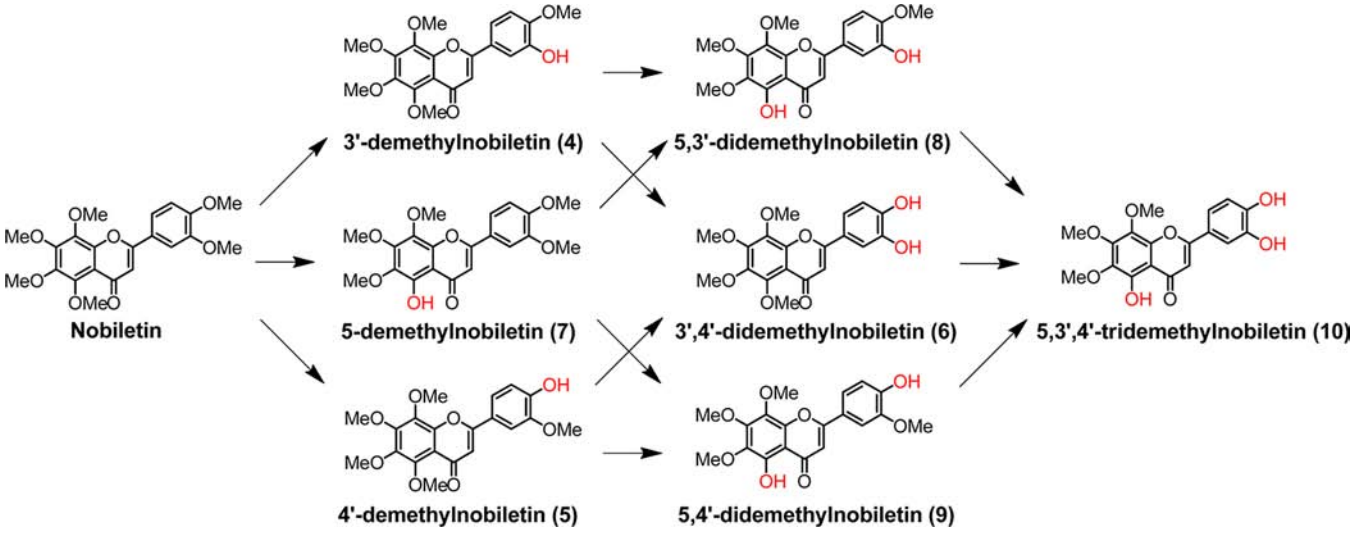

Figure 8. Proposed metabolism of nobiletin in mice.

Table 4. Concentrations (Nanomolar) of OH-PMF Metabolites of Nobiletin in Mouse Urine

batch	1	2	3	4	5	6	7	8	9	10
1				499	40988	6063	513	33	430	242
2				651	45063	6251	674	29	318	102
3				966	46021	6981	388	21	465	132

concentrations of OH-PMFs were within the linear range (0.005−10 μM) of the HPLC method. The results showed that OH-PMF **5** was the most abundant metabolite of nobiletin in mouse urine, followed by OH-PMF **6**. The concentrations of other metabolites (**4** and **7**−**10**) were much lower. Our results demonstrated that the HPLC-ECD method developed in this study can be used successfully to identify and quantify OH-PMFs in the biological sample (i.e., urine). Due to the high sensitivity and reproducibility of the method, it is expected that this method can be conveniently used to identify and quantify OH-PMFs in other biological samples such as blood, liver, kidney, and brain.

In conclusion, we have developed and validated a highly sensitive and reliable method for the simultaneous determination of 10 bioactive OH-PMFs by combining HPLC with EC detection. The HPLC profiles of these 10 OH-PMFs are significantly affected by different chromatographic parameters (i.e., organic solvent composition, pH, concentration of ammonium acetate of mobile phases). The optimal conditions were established to produce high sensitivity, linearity, accuracy, and recovery rate for 10 OH-PMFs within a wide concentration

DOI: 10.1021/jf505545x
J. Agric. Food Chem. 2015, 63, 509−516

range in a single HPLC run. The HPLC-ECD method established herein is expected to greatly facilitate the identification and quantification of OH-PMF metabolites in biological samples harvested from animal and human studies. The information on the bioactive metabolites in the biological samples will provide critical mechanistic insights into the molecular mechanism of PMFs and their metabolites.

AUTHOR INFORMATION

Corresponding Author

*(H.X.) Phone: (413) 545-2281. Fax: (413) 545-1262. E-mail: hangxiao@foodsci.umass.edu.

Author Contributions

‖J.Z. and J.B. contributed equally to this work.

Funding

This material is based upon work supported by a U.S. Department of Agriculture NRI grant (2014-67021), China National Science Foundation grants (31401581 and 31428017), the Massachusetts Agricultural Experiment Station, and the International Life Science Institute North America.

Notes

The authors declare no competing financial interest.

REFERENCES

(1) Li, S. M.; Lo, C. Y.; Ho, C. T. Hydroxylated polymethoxyflavones and methylated flavonoids in sweet orange (*Citrus sinensis*) peel. *J. Agric. Food Chem.* **2006**, *54*, 4176−4185.

(2) Li, S. M.; Pan, M. H.; Lo, C. Y.; Tan, D.; Wang, Y.; Shahidi, F.; Ho, C. T. Chemistry and health effects of polymethoxyflavones and hydroxylated polymethoxyflavones. *J. Funct. Foods* **2009**, *1*, 2−12.

(3) Li, S. M.; Wang, Z. Y.; Sang, S. M.; Huang, M. T.; Ho, C. T. Identification of nobiletin metabolites in mouse urine. *Mol. Nutr. Food Res.* **2006**, *50*, 291−299.

(4) Zheng, J. K.; Song, M. Y.; Dong, P.; Qiu, P. J.; Guo, S. S.; Zhong, Z. M.; Li, S. M.; Ho, C. T.; Xiao, H. Identification of novel bioactive metabolites of 5-demethylnobiletin in mice. *Mol. Nutr. Food Res.* **2013**, *57*, 1999−2007.

(5) Li, S. M.; Wang, H.; Guo, L. M.; Zhao, H.; Ho, C. T. Chemistry and bioactivity of nobiletin and its metabolites. *J. Funct. Foods* **2014**, *6*, 2−10.

(6) Lai, C. S.; Ho, M. H.; Tsai, M. L.; Li, S. M.; Badmaev, V.; Ho, C. T.; Pan, M. H. Suppression of adipogenesis and obesity in high-fat induced mouse model by hydroxylated polymethoxyflavones. *J. Agric. Food Chem.* **2013**, *61*, 10320−10328.

(7) Charoensinphon, N.; Qiu, P. J.; Dong, P.; Zheng, J. K.; Ngauv, P.; Cao, Y.; Li, S. M.; Ho, C. T.; Xiao, H. 5-Demethyltangeretin inhibits human nonsmall cell lung cancer cell growth by inducing G2/M cell cycle arrest and apoptosis. *Mol. Nutr. Food Res.* **2013**, *57*, 2103−2111.

(8) Lai, C. S.; Tsai, M. L.; Cheng, A. C.; Li, S. M.; Lo, C. Y.; Wang, Y.; Xiao, H.; Ho, C. T.; Wang, Y. J.; Pan, M. H. Chemoprevention of colonic tumorigenesis by dietary hydroxylated polymethoxyflavones in azoxymethane-treated mice. *Mol. Nutr. Food Res.* **2011**, *55*, 278−290.

(9) Qiu, P. J.; Guan, H. S.; Dong, P.; Li, S. M.; Ho, C. T.; Pan, M. H.; McClements, D. J.; Xiao, H. The p53-, Bax- and p21-dependent inhibition of colon cancer cell growth by 5-hydroxy polymethoxyflavones. *Mol. Nutr. Food Res.* **2011**, *55*, 613−622.

(10) Ko, H. C.; Jang, M. G.; Kang, C. H.; Lee, N. H.; Kang, S. I.; Lee, S. R.; Park, D. B.; Kim, S. J. Preparation of a polymethoxyflavone-rich fraction (PRF) of *Citrus sunki* Hort. ex Tanaka and its antiproliferative effects. *Food Chem.* **2010**, *123*, 484−488.

(11) Xiao, H.; Yang, C. S.; Li, S. M.; Jin, H. Y.; Ho, C. T.; Patel, T. Monodemethylated polymethoxyflavones from sweet orange (*Citrus sinensis*) peel inhibit growth of human lung cancer cells by apoptosis. *Mol. Nutr. Food Res.* **2009**, *53*, 398−406.

(12) Qiu, P. J.; Guan, H. S.; Dong, P.; Guo, S. S.; Zheng, J. K.; Li, S. M.; Chen, Y.; Ho, C. T. The inhibitory effects of 5-hydroxy-3,6,7,8,3′,4′-hexamethoxyflavone on human colon cancer cells. *Mol. Nutr. Food Res.* **2011**, *55*, 1523−1532.

(13) Qiu, P. J.; Dong, P.; Guan, H. S.; Li, S. M.; Ho, C. T.; Pan, M. H.; McClements, D. J.; Xiao, H. Inhibitory effects of 5-hydroxy polymethoxyflavones on colon cancer cells. *Mol. Nutr. Food Res.* **2010**, *54*, S244−S252.

(14) Li, S. M.; Pan, M. H.; Lai, C. S.; Lo, C. Y.; Dushenkov, S.; Ho, C. T. Isolation and syntheses of polymethoxyflavones and hydroxylated polymethoxyflavones as inhibitors of HL-60 cell lines. *Bioorg. Med. Chem.* **2007**, *15*, 3381−3389.

(15) Stremple, P. GC/MS analysis of polymethoxyflavones in citrus oils. *HRC−J. High Resolut. Chromatogr.* **1998**, *21*, 587−591.

(16) Dugo, P.; Mondello, L.; Dugo, G.; Heaton, D. M.; Bartle, K. D.; Clifford, A. A.; Myers, P. Rapid analysis of polymethoxylated flavones from citrus oils by supercritical fluid chromatography. *J. Agric. Food Chem.* **1996**, *44*, 3900−3905.

(17) Li, S. M.; Wang, Y.; Wang, Z. Y.; Xiao, H.; Lo, C. Y.; Rawson, N.; Ho, C. T. Quantitative analysis of hydroxylated polymethoxyflavones by high-performance liquid chromatography. *Biomed. Chromatogr.* **2010**, *24*, 838−845.

(18) Liang, Y.; Cao, W.; Chen, W. J.; Xiao, X. H.; Zheng, J. B. Simultaneous determination of four phenolic components in citrus honey by high performance liquid chromatography using electrochemical detection. *Food Chem.* **2009**, *114*, 1537−1541.

(19) Suzuki, K.; Katayama, M.; Takamatsu, K.; Kaneko, S.; Miyaji, K.; Ishikawa, H.; Matsuda, Y. Improvement of sensitivity and selectivity of high-performance liquid chromatography for anti-retroviral drugs (non-reverse transcriptase inhibitors) by diamond-electrode electrochemical and fluorescence detection. *J. Chromatogr., A* **2009**, *1216*, 3117−3121.

(20) Lebiedzinska, A.; Marszatt, M. L.; Kuta, J.; Szefer, P. Reversed-phase high-performance liquid chromatography method with coulometric electrochemical and ultraviolet detection for the quantification of vitamins B-1 (thiamine), B-6 (pyridoxamine, pyridoxal and pyridoxine) and B-12 in animal and plant foods. *J. Chromatogr., A* **2007**, *1173*, 71−80.

(21) Dong, P.; Qiu, P. J.; Zhu, Y.; Li, S. M.; Ho, C. T.; McClements, D. J.; Xiao, H. Simultaneous determination of four 5-hydroxy polymethoxyflavones by reversed-phase high performance liquid chromatography with electrochemical detection. *J. Chromatogr., A* **2010**, *1217*, 642−647.

(22) Prados, P.; Higashidate, S.; Imai, K.; Sato, Y.; Nagao, T. Sensitive determination of (−)-isoproterenol and (−)-(R)-1-(3,4-dihydroxyphenyl)-2-[(3,4-dimethoxyphenethyl) Amino] ethanol (T-0509), a cardiotonic agent, in rat plasma utilizing a fully automated catecholamine analyzer. *Biomed. Chromatogr.* **1994**, *8*, 49−51.

(23) Ranta, V. P.; Hamalainen, K. M.; Auriola, S.; Urtti, A. Gradient high-performance liquid chromatographic analysis of enkephalin peptides, their metabolites and enzyme inhibitors using combined ultraviolet and electrochemical detection. 1. Optimization of separation and detection. *J. Chromatogr., A* **1997**, *766*, 85−97.

(24) Raggi, M. A.; Bugamelli, F.; Sabbioni, C.; Ronchi, D. D.; Pinzauti, S.; Volterra, V. An improved HPLC-ED method for monitoring plasma levels of clozapine and its active metabolites in schizophrenic patients. *Chromatographia* **2000**, *51*, 147−153.

(25) Piazza, C.; Privitera, M. G.; Melilli, B.; Incognito, T.; Marano, M. R.; Leggio, G. M.; Roxas, M. A.; Drago, F. Influence of inulin on plasma isoflavone concentrations in healthy postmenopausal women. *Am. J. Clin. Nutr.* **2007**, *86*, 775−780.

DOI: 10.1021/jf505545x
J. Agric. Food Chem. 2015, 63, 509−516

JOURNAL OF AGRICULTURAL AND FOOD CHEMISTRY

Article

pubs.acs.org/JAFC

Toll-like Receptor 4 Mediates the Antitumor Host Response Induced by *Ganoderma atrum* Polysaccharide

Qiang Yu, Shao-Ping Nie,* Jun-Qiao Wang, Dan-Fei Huang, Wen-Juan Li, and Ming-Yong Xie*

State Key Laboratory of Food Science and Technology, Nanchang University, 235 Nanjing East Road, Nanchang 330047, China

ABSTRACT: The aim of this study is to investigate the role of Toll-like receptor (TLR) 4 in *Ganoderma atrum* polysaccharide (PSG-1)-induced antitumor activity. In vitro, the apoptosis rate of S-180 cells was increased in PSG-1-induced peritoneal macrophage derived from C3H/HeN (wild-type) mice, but not from C3H/HeJ (TLR4-deficient) mice. In the S-180 tumor model, phagocytosis, NO and ROS release, phosphorylation of MAPKs and Akt, and expression of NF-κB were increased by PSG-1 in peritoneal macrophage derived from C3H/HeN mice. Furthermore, PSG-1 elevated Th1 cytokine production and enhanced the cytotoxic activity of CTL and NK cells in C3H/HeN mice. In addition, PSG-1 decreased the tumor weight and increased the apoptosis rate and caspase-3 and caspase-9 activities of tumor derived from the C3H/HeN mice. However, none of these activities were observed in C3H/HeJ mice. In summary, these findings demonstrated that the antitumor activity of PSG-1 is mediated by TLR4.

KEYWORDS: *Toll-like receptor 4, Ganoderma atrum polysaccharide, antitumor, innate immunity, adaptive immunity*

INTRODUCTION

Great efforts have been made in therapeutic treatments, including surgery, radiation, and chemotherapy; however, due to severe adverse effects, cancer is still the leading cause of death.[1] Recently, cancer immunotherapy that recruits the host immune response to exert an antitumor effect without harming the host is of great interest.[2]

Toll-like receptors (TLRs) are mammalian homologues of the *Drosophila* Toll receptor.[3] Ten and twelve functional TLRs have been identified in humans and mice, respectively.[4] Among them, TLR4 is expressed by various immune cells, including macrophages, neutrophils, and dendritic cells. Binding of ligands to TLR4 initiates signal transduction via recruitment of the adaptor protein myeloid differentiation protein 88 (Myd88) and the interleukin receptor-associated kinase (IRAK), which in turn activate tumor necrosis factor receptor-associated factor 6 (TRAF6). This is followed by the activation of downstream signals, such as mitogen-activated protein kinase (MAPK) and nuclear factor-kB (NF-κB), and leads to the activation of a wide spectrum of target genes.[5]

Emerging studies have shown that TLR4 agonists can serve as immunomodulating agents and exhibit promising therapeutic potential for cancer immunotherapy.[6,7] It is worth noting that natural polysaccharides, which have been safely used as ingredients of traditional medicines and functional food for a long time in oriental countries, are attracting more and more attention since they trigger the response of innate immunity and in turn induce adaptive immunity via TLR4 signaling.[8,9]

Ganoderma atrum has been used as a Chinese traditional medicine and functional food for thousands of years. In recent years, it has become more and more popular in developed countries as a dietary supplement.[10] The polysaccharides are regarded as the major bioactive substances in *G. atrum*. We recently isolated and purified a polysaccharide from *G. atrum*, named PSG-1, with a purity of >99.8%, whose primary structural features and molecular weight were characterized.[11,12] Our in vitro study has demonstrated that TLR4 is the major receptor involved in specific binding of PSG-1 to macrophages, and PSG-1 induces macrophage activation through the TLR4 signaling pathway.[13]

Interestingly, my colleagues showed that oral administration of PSG-1 could inhibit S-180 tumor growth and enhance the host immune system through the TLR4-mediated signaling pathway.[14] However, the research results were carried out just by measuring the protein expression of TLR4 in peritoneal macrophage from BALB/c mice, and then they suggested PSG-1 may exert its antitumor effect through TLR4. Strictly speaking, the role of TLR4 in PSG-induced antitumor host response has still not been fully determined. Therefore, in this study, we investigated the antitumor activity of PSG-1 in C3H/HeN (wild-type) and C3H/HeJ (TLR4-deficient) mice, especially focused on the contribution of TLR4 in PSG-1-mediated innate and adaptive immune responses. To the best of our knowledge, this is the first time transgenic mice have been used to establish a tumor model for exploring the effect of TLR4 on the antitumor activity induced by PSG-1 in vivo. The results presented in our study could provide powerful evidence to support the vital role of TLR4 played in PSG-1-induced antitumor activity.

MATERIALS AND METHODS

Materials and Reagents. 3-(4,5-Dimethylthiazol-2-yl)-2,5-diphenyltetrazolium bromide (MTT) and fluorescein isothiocyanate (FITC)−dextran were purchased from Sigma (St. Louis, MO). The NO assay kit was obtained from Beyotime Biotech Inc. (Jiangsu, China), carboxyl-2′,7′-dichlorofluorescein diacetate (CM-DCFH) was from Molecular Probes (Eugene, OR). Antibodies against phospho-ERK1/2 (p-ERK1/2), phospho-JNK1/2 (p-JNK1/2), phospho-p38 (p-p38), phospho-Akt (p-Akt), and NF-κB were purchased from Cell Signaling

Received: August 27, 2014
Revised: December 30, 2014
Accepted: December 30, 2014
Published: December 30, 2014

ACS Publications © 2014 American Chemical Society

DOI: 10.1021/jf5041096
J. Agric. Food Chem. 2015, 63, 517−525

(Beverly, MA). ELISA kits were from R&D Systems (Minneapolis, MN). Annexin V−FITC apoptosis detection kits were obtained from Becton Dickinson Biosciences (San Jose, CA). Caspase-3 and caspase-9 colorimetric assay kits were purchased from BioVision, Inc. (Palo Alto, CA). Cell culture products were from Life Technologies (Paisley, Scotland, U.K.).

Cells and Animals. The murine S-180 cell line and YAC-1 cells were purchased from the Type Culture Collection of the Chinese Academy of Sciences, Shanghai, China. Cells were cultured in RPMI-1640 medium containing 10% fetal bovine serum and maintained in a humidified incubator at 37 °C in a 5% CO_2 atmosphere.

Female C3H/HeN and C3H/HeJ mice (6−8 weeks old) were obtained from the Shanghai Laboratory Animal Center, China. The mice were housed eight per cage at 25 °C with a 12 h/12 h light/dark cycle. All mice were cared for in accordance with the Guidelines for the Care and Use of Laboratory Animals published by the National Institutes of Health, Bethesda, MD (NIH Publication 85-23, 1996). All procedures were approved by the Animal Care Review Committee, Nanchang University, China.

Isolation of Mouse Peritoneal Macrophages. Each mouse was intraperitoneally injected with 5 mL of cold PBS, and peritoneal macrophages were aseptically harvested from peritoneal exudates by peritoneal lavage. Cells were resuspended in RPMI-1640 containing 10% heat-inactivated FBS. After 24 h of incubation, the cells were washed by PBS to remove nonadherent cells. The resultant cells were collected as peritoneal macrophages.

Macrophage Cytotoxicity Assay. After incubation with PSG-1 (20, 40, 80, and 160 μg/mL) for 48 h, the mouse peritoneal macrophages from C3H/HeN or C3H/HeJ were washed with fresh medium and coincubated with S-180 cells at a ratio of 25:1 for 48 h. The MTT method was performed to measure the growth inhibition of S-180 cells. Cytotoxicity was calculated as follows: cytotoxicity (%) = $(OD_T - (OD_S - OD_E))/OD_T \times 100$, where OD_T, OD_S, and OD_E are the optical density values of the target cell control, test sample, and effector cell control, respectively.

Establishment of the S-180 Model. After 1 week of acclimatization, C3H/HeN and C3H/HeJ mice were randomly divided into three experimental groups (n = 8 per group). (i) Normal group: healthy mice without tumor inoculation were gavaged with 0.2 mL of saline. The S-180 model was established as previously reported.[15] Briefly, the S-180 mouse sarcoma cells with ascites were harvested under sterile conditions. A total of 2×10^6 cells suspended in 0.2 mL of sterilized saline were subcutaneously inoculated into mice in the left axillary region. (ii) Control group: after the day of inoculation, the mice were gavaged with 0.2 mL of saline for 10 consecutive days. (iii) PSG-1 group: the mice were gavaged with 0.2 mL of PSG-1 (100 mg/kg body weight) for 10 consecutive days. Twenty-four hours after the last treatment, all the mice were sacrificed by cervical dislocation. Tumors and spleens were extirpated and weighed in germ-free conditions.

Neutral Red Uptake. Phagocytosis of macrophages was determined by the neutral red uptake method as described with minor modification.[16] Briefly, peritoneal macrophages isolated from mice were seeded at a density of 5×10^5 cells/well in the 24-well microplates and cultured for 24 h. After being washed by PBS twice, the cells were incubated with neutral red (50 mg/mL) for another 3 h and washed twice by PBS. The plate was blotted dry, and then 50% ethanol containing 1% glacial acetic acid was added to each well. The absorbance at 540 nm was measured by a microplate reader.

FITC−Dextran Internalization. The FITC−dextran internalization of peritoneal macrophages was determined by flow cytometry. Briefly, peritoneal macrophages (1×10^6 cells/well) were seeded in the 24-well plate, and 1 mg/mL FITC−dextran was added to each well. After incubation at 37 °C for 1 h, the cells were washed three times and resuspended in 500 μL of PBS for flow cytometric analysis.

Measurement of ROS Generation. Peritoneal macrophages were harvested and seeded at a density of 1×10^6 cells/well in the 24-well plate. After incubation with 10 mM CM-DCFH at 37 °C for 30 min in the dark, the cells were washed three times, resuspended in 500 μL of PBS, and then analyzed by flow cytometry.

Measurement of NO Production. NO production was measured according to the manufacturer's instruction. Briefly, peritoneal macrophages (5×10^5 cells/well) were placed in a 96-well plate. After incubation for 48 h, the supernatants were collected and incubated with an equal volume of Griess reagent for 10 min at 25 °C. Nitrite concentrations were calculated by a standard curve.

Western Blot Analysis. The whole-cell protein or nuclear protein was prepared from peritoneal macrophages using a cell lysis kit or nuclear and cytoplasmic extraction kit (Beyotime, Shanghai, China) according to the manufacturer's instructions. A 40 μg mass of denatured protein was loaded onto 10% SDS−polyacrylamide gel by electrophoresis and transferred to a nitrocellulose membrane. Nonfat milk (5%) (prepared in TBS containing 0.1% Tween 20 (TBST)) was used to block nonspecific binding for 1 h at 37 °C. Then the membrane was incubated with specific primary antibodies at 4 °C overnight. After being washed three times with TBST, the membrane was incubated at room temperature for 1 h with secondary antibody, and the signal was analyzed by using a BeyoECL Plus kit (Beyotime, Shanghai, China). Densitometry of the band was analyzed by Quantity One.

Preparation of Splenocytes. The extirpated spleens were minced into small pieces in germ-free conditions. A single-cell suspension was prepared by filtering the suspension through a sterile sieve mesh. The cells were treated with lysis buffer (0.15 M NH_4Cl, 0.01 M $KHCO_3$, and 0.1 mM Na_2EDTA, pH 7.4) to get rid of red blood cells, followed by washing twice with cold PBS. Then the cells were adjusted to a concentration of 5×10^6 cells/mL in RPMI-1640 medium supplemented with 10% fetal calf serum and incubated for 3 h in Petri dishes. The suspended cell populations were collected.

Cytotoxicity Assays of Natural Killer (NK) Cell Activity. Splenocytes were used as the effector cells for splenic NK cell activity assay as described.[17] Briefly, effector cells (5×10^5 cells/well) were cocultured with YAC-1 cells in 96-well microplates at a ratio of 50:1 at 37 °C for 20 h. A 20 μL volume of MTT (5 mg/mL) was added to each well, and then the MTT assay was employed after 4 h of incubation. NK cell activity was calculated via the following equation: cytotoxicity (%) = $(OD_T - (OD_S - OD_E))/OD_T \times 100$, where OD_T, OD_S, and OD_E are the optical density values of the target cell control, test samples, and effector cell control, respectively.

Cytotoxicity Assays of Cytotoxic T Lymphocyte (CTL) Activity. The CTL activity was measured using a method similar to that described above except that S-180 cells and splenocytes were used as target cells and effector cells, respectively, at a ratio of 50:1. CTL activity was calculated via the same equation as described above: cytotoxicity (%) = $(OD_T - (OD_S - OD_E))/OD_T \times 100$.

Cytokine Measurement by ELISA. Levels of IL-2, IFN-γ, and IL-12 were determined by the ELISA kits according to the manufacturer's instructions.

Analysis of Apoptotic Cells. The tumors harvested from S-180-bearing mice were minced into small pieces in germ-free conditions. A single-cell suspension was prepared by filtering the suspension through a sterile sieve mesh. The suspension was washed twice with cold PBS and adjusted to a concentration of 1×10^6 cells/mL. Then the cells were stained with Annexin V−FITC and propidium iodide (PI) for 15 min in the dark and analyzed by flow cytometry (FACS Calibur, Becton Dickinson, United States).

Measurement of Caspase Activities. Caspase-3 and caspase-9 colorimetric assay kits were used to measure the activities of caspase-3 and caspase-9 in S-180 cells. Briefly, 1×10^5 cells/mL were treated with cell lysis buffer for 10 min on ice and centrifuged at 10000g for 8 min. Then the supernatants were incubated with caspase substrate LEHD-AFC for caspase-9 and DEVD-AFC for caspase-3 at 37 °C for 1.5 h. Chromophore p-nitroanilide was measured by a microplate reader at 405 nm.

Statistical Analysis. Values are expressed as means ± SEM. One-way analysis of variance followed by the Student−Newman−Keuls test was used to determine the statistical significance between various groups. A value of $p < 0.05$ was considered to be statistically significant.

DOI: 10.1021/jf5041096
J. Agric. Food Chem. 2015, 63, 517−525

RESULTS

PSG-1-Induced Macrophage Cytotoxicity in Vitro Is TLR4-Dependent. To examine the macrophage cytotoxicity induced by PSG-1, peritoneal macrophages from C3H/HeN and C3H/HeJ mice were treated with PSG-1 in vitro and then cocultured with S-180 cells. Cytotoxicity was measured by the MTT method. The cytotoxicity of macrophages derived from C3H/HeN mice was dose-dependently enhanced by PSG-1 ($p < 0.05$), but there was no significant change in C3H/HeJ mice (Figure 1).

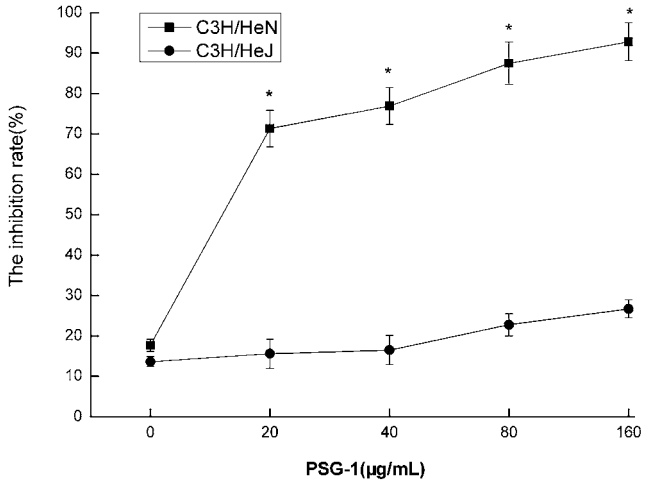

Figure 1. Effect of PSG-1 on macrophage-mediated cytotoxicity against tumor cells. Peritoneal macrophages were isolated from C3H/HeN (wild-type) or C3H/HeJ (TLR4-deficient) mice, cultured with various concentrations of PSG-1 in a 96-well plate for 48 h, and then cocultured with S-180 cells for another 48 h. The inhibition of S-180 cell proliferation was analyzed by the MTT method. These data are the means ± SEM of triplicate determinations. Key: *, $p < 0.05$ versus untreated cells.

Effect of PSG-1 on Macrophage Phagocytosis in TLR4-Deficient and Wild-Type Mice. Phagocytosis of peritoneal macrophages was measured by devouring neutral red. As shown in Figure 2A, there was a significant reduction in macrophage phagocytosis induced in both C3H/HeN and C3H/HeJ control groups compared with the normal groups. After PSG-1 administration, the phagocytic rate of the C3H/HeN mice was significantly increased compared to that of the control group ($p < 0.01$), but there was no significant increase in C3H/HeJ mice.

To confirm the effect of PSG-1 on the phagocytosis of peritoneal macrophages isolated from the S-180-tumor-bearing mice, flow cytometry was employed to analyze the FITC−dextran internalization. As shown in Figure 2B,C, PSG-1 markedly increased the phagocytosis of C3H/HeN mice ($p < 0.01$), but not that of C3H/HeJ mice, compared to that of the control groups.

Effect of PSG-1 on ROS and NO Production of Peritoneal Macrophage in TLR4-Deficient and Wild-Type Mice. As shown in Figure 3A,B the level of ROS in the control group was lower than that in the normal group. However, compared with that in the control group, ROS production was significantly increased in PSG-1-treated C3H/HeN mice. By contrast, no significant increase was recorded in C3H/HeJ mice. Moreover, peritoneal macrophages from C3H/HeN mice treated with PSG-1 exhibited an increase in NO production ($p < 0.01$), but the level of NO production in C3H/HeJ mice treated with PSG-1 showed no significant difference (Figure 3C).

Effect of PSG-1 on MAPK, PI3K/Akt, and NF-κB Pathways in TLR4-Deficient and Wild-Type Mice. To investigate whether the MAPK, PI3K/Akt, and NF-κB signaling pathways were involved in antitumor activity by PSG-1, we examined the effect of PSG-1 on the phosphorylation of ERK1/2, JNK1/2, p38, and Akt and expression of NF-κB in peritoneal macrophages by Western blotting. As shown in Figure 4, compared with those in the normal group, phosphorylation of ERK1/2, JNK1/2, p38, and Akt and expression of NF-κB were significantly decreased in the control group within both C3H/HeN and C3H/HeJ mice. However, significant enhancements in p-ERK1/2, p-JNK1/2, p-p38, p-Akt, and NF-κB levels were observed in C3H/HeN mice administrated with PSG-1, but not in C3H/HeJ mice.

Effect of PSG-1 on NK and CTL Activities in TLR4-Deficient and Wild-Type Mice. As shown in Figure 5A,B, compared with those of the normal group, NK and CTL activities of the control group were significantly decreased in C3H/HeN and C3H/HeJ mice. NK activity in the PSG-1-treated C3H/HeN mice was significantly higher than that in the control group ($p < 0.01$). However, the TLR4-defecient C3H/HeJ mice did not show any increase of NK activity. In addition, PSG-1 treatment enhanced CTL cytotoxicity in C3H/HeN mice compared with that in the control group, but not in C3H/HeJ mice.

Effect of PSG-1 on Cytokine Production of Spleen Lymphocytes in TLR4-Deficient and Wild-Type Mice. As compared to those in the normal group, IL-2, IFN-γ, and IL-12 levels were decreased in the control group in both C3H/HeN and C3H/HeJ mice. However, IL-2, IFN-γ, and IL-12 levels of PSG-1-treated C3H/HeN mice were significantly higher than those of the control group ($p < 0.01$) (Figure 5C). These data suggested that IL-2, IFN-γ, and IL-12 may contribute to the induction of antitumor activity mediated by PSG-1. Moreover, these treatments did not cause cytokine induction in C3H/HeJ mice.

Effect of PSG-1 on Tumor Weight and Apoptosis in TLR4-Deficient and Wild-Type Mice. The tumor weight of C3H/HeN mice treated with PSG-1 was significantly decreased compared to that of the control group ($p < 0.01$). However, no noticeable differences were found among the C3H/HeJ mice receiving different treatments (Figure 6A). Consistent with the above observation, the numbers of apoptotic cells were obviously increased in the tumors in PSG-1-treated C3H/HeN mice, but not in PSG-1-treated C3H/HeJ mice, compared to the control groups (Figure 6B).

Effect of PSG-1 on Caspase Activities in TLR4-Deficient and Wild-Type Mice. As shown in Figure 6C,D, both caspase-3 and caspase-9 activities increased after treatment with PSG-1 in the C3H/HeN mice ($p < 0.01$), but the activities of caspase-3 and caspase-9 were not significantly changed in C3H/HeJ mice.

DISCUSSION

Our previous studies have demonstrated that PSG-1 exerted an antitumor effect by boosting the host immune response.[18] However, the detailed underlying mechanism remains unclear. The present study first evaluated the effect of PSG-1 on macrophage-mediated cytotoxicity of S-180 cells by in vitro experiments using C3H/HeN (wild-type) and C3H/HeJ (TLR4-deficient) mouse-derived peritoneal macrophages. The macrophage cytotoxicity assay results showed that the percentage of apoptosis of S-180 cells was significantly increased

DOI: 10.1021/jf5041096
J. Agric. Food Chem. 2015, 63, 517−525

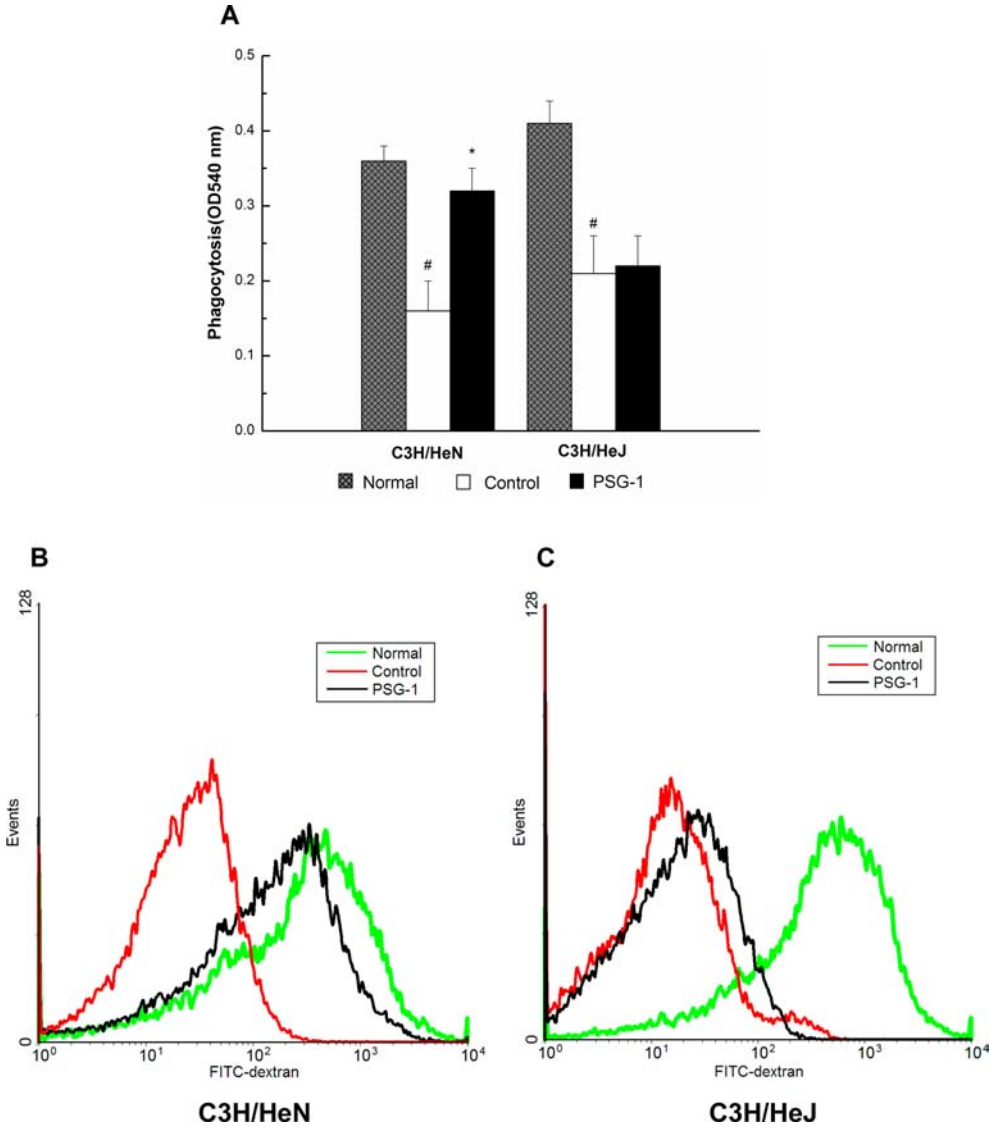

Figure 2. Effect of PSG-1 on macrophage phagocytosis in C3H/HeN (wild-type) and C3H/HeJ (TLR4-deficient) mice. (A) Phagocytosis of peritoneal macrophages was measured by devouring neutral red. Values are the means ± SEM of eight mice. Key: #, $p < 0.01$ versus normal group; *, $p < 0.01$ versus control group. (B, C) The extent of the phagocytic uptake of FITC−dextran was determined by flow cytometry.

in PSG-1-treated C3H/HeN mice but not in C3H/HeJ mice. On the basis of this observation, we hypothesized that TLR4 may be involved in the PSG-1-induced antitumor effect. To further elucidate the role of TLR4 in vivo, we established an S-180 tumor model in C3H/HeN and C3H/HeJ mice to explore the role of TLR4 in the antitumor immune response induced by PSG-1.

Macrophages play a vital role in host innate defense against microbial invaders and malignancies due to the nature of phagocytic, cytotoxic, and intracellular killing capacities.[19] Upon stimulation, the first reaction of macrophages is phagocytosis.[20] Meanwhile, as macrophages are highly secretory cells, they will produce large amounts of anticancer molecules such as NO and ROS, which can induce cytotoxicity of tumor cells.[21] Our data showed that the phagocytosis of peritoneal macrophages was markedly increased by PSG-1 in C3H/HeN mice, but not in C3H/HeJ mice, as evidenced by measuring neutral red uptake and FITC−dextran internalization. Similarly, the elevated release of NO and ROS was only detected in the peritoneal macrophages of C3H/HeN mice.

Given numerous studies have demonstrated that TLR4-mediated macrophage activation via a variety of intracellular signal transduction pathways,[22,23] we next sought to determine whether these pathways were also activated in vivo by PSG-1 administration. MAPKs are a family of serine/threonine protein kinases that include three major groups in mammalian cells, i.e., ERK1/2, JNK1/2, and p38.[24] PI3K and the downstream serine/threonine kinase Akt participate in mediating various cellular responses, such as cell growth, survival, and the trafficking of intracellular organelles.[25,26] Our previous study has demonstrated that MAPK and PI3K/Akt signaling pathways were simultaneously activated in PSG-1-stimulated macrophages. To study the putative effect of PSG-1 on MAPK and PI3K/Akt signaling pathways in S-180-tumor-bearing mice, we performed Western blot to detect the phosphorylation levels of total protein isolated from peritoneal macrophages. The results showed that the phophorylation levels of all three MAPKs and Akt were relatively high in C3H/HeN mice as compared to the control group, whereas no noticeable change was observed in C3H/HeJ mice. Furthermore, NF-κB is a universal transcription factor that regulates the transcription of numerous genes related to innate immunity.[27] Whether NF-κB was involved in the antitumor

DOI: 10.1021/jf5041096
J. Agric. Food Chem. 2015, 63, 517−525

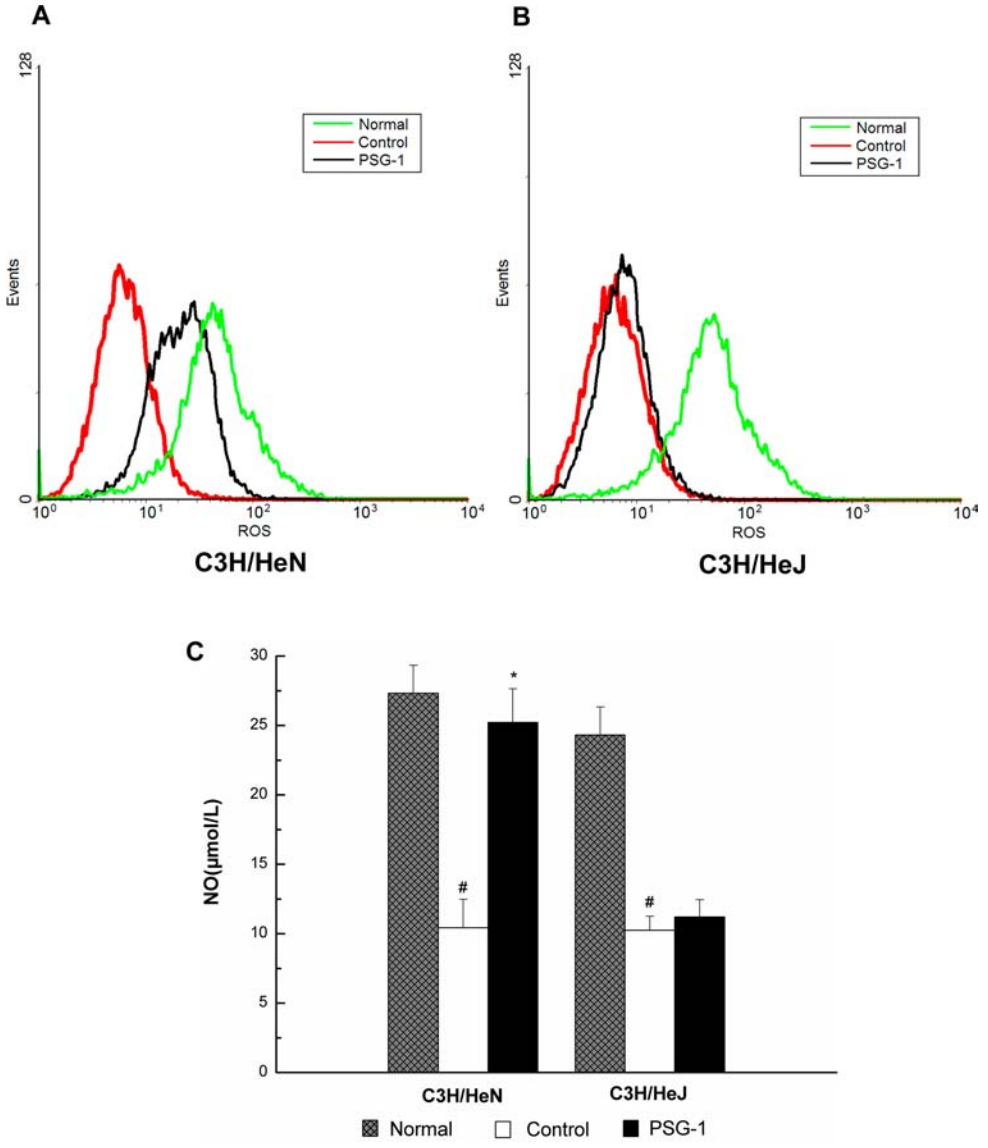

Figure 3. Effect of PSG-1 on ROS and NO production of peritoneal macrophages in C3H/HeN (wild-type) and C3H/HeJ (TLR4-deficient) mice. (A) The expression of fluorescence of 2′,7′-dichlorofluorescein (DCF) in peritoneal macrophages was analyzed by flow cytometry. (B) NO production was measured by the Griess method. Values are the means ± SEM of eight mice. Key: #, $p < 0.01$ versus normal group; *, $p < 0.01$ versus control group.

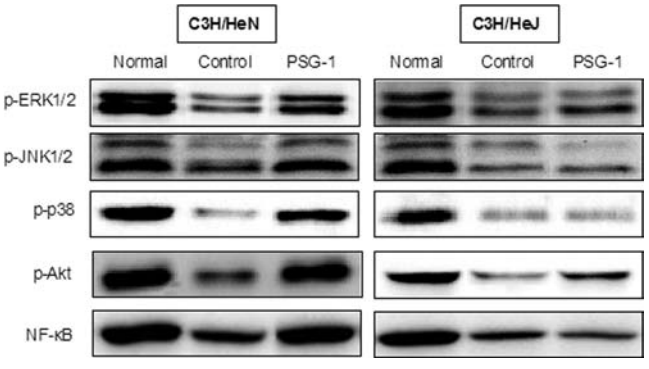

Figure 4. Effect of PSG-1 on the phosphorylation of ERK1/2, JNK1/2, p38, and Akt and expression of NF-κB in C3H/HeN (wild-type) and C3H/HeJ (TLR4-deficient) mice. The whole-cell and nuclear proteins isolated from peritoneal macrophages were analyzed by Western blot with anti-p-ERK1/2, anti-p-JNK1/2, anti-p-p38, anti-p-Akt, and anti-NF-κB antibodies.

immunity triggered by PSG-1 administration was investigated. As expected, enhanced NF-κB expression in the nucleus was detected in the peritoneal macrophage derived from C3H/HeN mice, but not C3H/HeJ mice. The above results indicated that PSG-1 elicited an antitumor effect by activating peritoneal macrophages and TLR4 was involved in antitumor innate immunity induced by PSG-1.

It is well documented that macrophages are the bridge cells between innate and adaptive immune responses.[28] After phagocytosis, macrophages will turn into antigen-presenting cells and then orchestrate the adaptive response by mediating lymphocytes.[29,30] Therefore, we focused on the effect of PSG-1 administration on spleen lymphocytes in S-180-tumor-bearing mice.

CTL and NK cells are known as two major populations of lymphocytes that are capable of killing tumor cells.[31] The cytotoxic activities of CTL and NK cells derived from spleen lymphocytes were analyzed. Although cytotoxic activities of C3H/HeN mouse-derived CTL against S-180 cells were

DOI: 10.1021/jf5041096
J. Agric. Food Chem. 2015, 63, 517−525

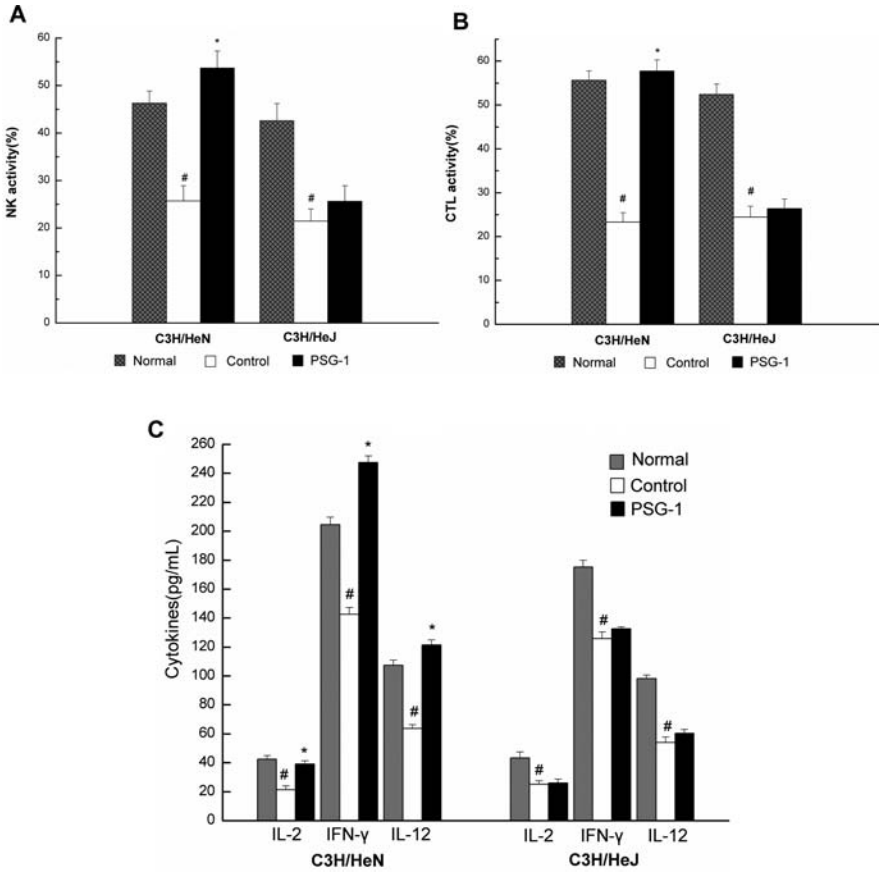

Figure 5. Effect of PSG-1 on NK and CTL activities and cytokine production of spleen lymphocytes in C3H/HeN (wild-type) and C3H/HeJ (TLR4-deficient) mice. (A, B) NK and CTL activities were evaluated by the cytotoxic activities of the spleen cells against YAC-1 cells (A) and S-180 tumor cells (B) ex vivo using the MTT method. (C) The production of cytokines was measured by ELISA. Values are the means ± SEM of eight mice. Key: #, $p < 0.01$ versus normal group; *, $p < 0.01$ versus control group.

significantly enhanced by PSG-1 treatment, the cytotoxic activities were not enhanced in C3H/HeJ mice. The function of NK cells is similar to that of CTL cells; however, unlike CTL, the killing by NK cells is nonspecific.[32] In the cytotoxic activities of NK cells, similar results were obtained. In nonspecific killing of the cells against YAC-1, cytolysis of C3H/HeN mouse-derived NK cells against YAC-1 was enhanced by PSG-1 treatment. Nonspecific killing activity of C3H/HeJ-derived NK cells was not increased by PSG-1 administration. These results displayed that NK and tumor-specific CTL activities were augmented by oral administration of PSG-1 via TLR4 stimulation.

Mounting evidence established that cytokines produced by T cells play an essential part in influencing the immune response toward protective antitumor immunity.[33] On the basis of the difference in secretion of cytokines, T helper (Th) lymphocytes are divided into Th1 and Th2 cells.[34] Hallmark Th1 cytokines, including IL-2, IFN-γ, and IL-12, are considered as characteristic of adaptive immunity.[35] The antitumor activities of IL-2, IFN-γ, and IL-12 have been extensively reported in murine tumor models.[36] Our present study showed that PSG-1 enhanced the production of IL-2, IFN-γ, and IL-12 and polarized the T-cell response to a Th1-dominant state in TLR4 wild-type mice, but not in TLR4-deficient mice, indicating that TLR4 plays an important role in the regulation of PSG-1-induced host antitumor adaptive immunity in tumor-bearing mice.

Apoptosis is the process of programmed cell death; it occurs normally as a homeostatic mechanism to maintain cell populations. Inappropriate apoptosis would promote carcinogenesis and tumor progression.[37] Caspases are a family of cysteine proteases that transduce the apoptotic signal cascade. Caspase-3 is known as a vital effector that is activated by caspase-9 via the mitochondrial pathway.[38] Our previous research has demonstrated that PSG-1 significantly inhibited tumor growth and promoted tumor apoptosis via mitochondrial pathways. Consistent with those findings, the current study found that C3H/HeN mice treated with PSG-1 had less tumor weight than the control mice. Moreover, the apoptosis rate and caspase-3 and caspase-9 activities of tumor derived from the C3H/HeN mice treated with PSG-1 were significantly increased compared with those of tumor derived from mice treated with vehicle. However, there were no significant differences in C3H/HeJ mice. We are therefore left with the important question of how TLR4 affects the tumor apoptosis triggered by PSG-1.

It is well-known that NO is a key effector molecule in macrophages.[39] However, there is accumulating evidence that NO not only plays a role in host defenses against tumor cells, but also is involved in the regulation of apoptosis. Apoptosis induced by NO occurs in diverse types of cells.[40−42] In addition, it has been demonstrated that caspase-3 and caspase-9 are central components in a cascade triggered by NO.[43] Considering our result has shown that PSG-1 induced NO release in peritoneal macrophages derived from the C3H/HeN mice, we speculated that NO released from PSG-1-activated macrophages may lead to an increase of caspase-3 and caspase-9 activities, resulting in

DOI: 10.1021/jf5041096
J. Agric. Food Chem. 2015, 63, 517−525

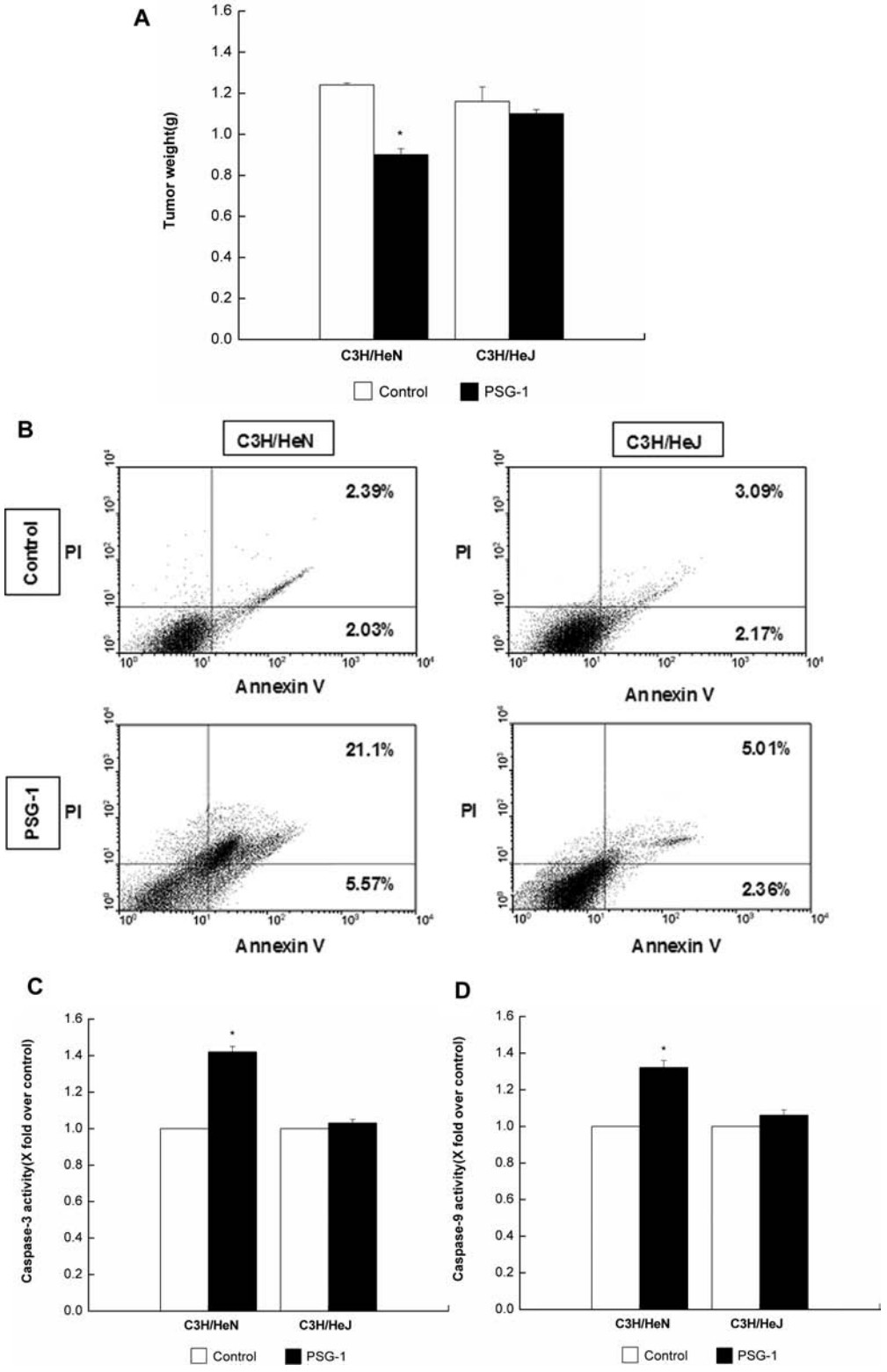

Figure 6. Effect of PSG-1 on the weight, apoptosis, and caspase activities of tumor derived from C3H/HeN (wild-type) and C3H/HeJ (TLR4-deficient) mice. (A) Tumor weight in S-180-bearing mice. (B) Detection of apoptotic cells by annexin V and PI double staining. S-180 tumor cells stained with annexin V−FITC and PI labeling and analyzed by flow cytometry. (C, D) Quantitative analysis of caspase-3 and caspase-9 activities in the tumor of S-180-bearing mice. Values are the means ± SEM of eight mice. Key: *, $p < 0.01$ versus control group.

apoptosis of tumor cells. However, the potential mechanisms may be complex, so more detailed investigation is needed.

Overall, the results presented in this paper displayed that PSG-1 elicited antitumor activity in vivo in a TLR4-dependent manner, and TLR4-mediated activation of innate and adaptive immunity was involved in antitumor immunity induced by PSG-1. These observations revealed the therapeutic potential of PSG-1 as a novel compound for cancer immunotherapy.

DOI: 10.1021/jf5041096
J. Agric. Food Chem. 2015, 63, 517−525

AUTHOR INFORMATION

Corresponding Authors

*Phone and fax: +86 791-88304452. E-mail: spnie@ncu.edu.cn.
*Phone and fax: +86 791-83969009. E-mail: myxie@ncu.edu.cn.

Funding

The financial support for this study by the National Key Technology R&D Program of China (Grant 2012BAD33B06), the Key Program of the National Natural Science Foundation of China (Grant 31130041), the Program for New Century Excellent Talents in University (Grant NCET-12-0749), the Research Program of the State Key Laboratory of Food Science and Technology (Grant SKLF-ZZA-201301), the Project of Science and Technology of the Jiangxi Provincial Education Department (Grant KJLD13004), and the Key Project of International Cooperation of the Jiangxi Provincial Department of Science and Technology (Grant 20141BDH80009) is gratefully acknowledged.

Notes

The authors declare no competing financial interest.

ABBREVIATIONS USED

CM-DCFH, carboxyl-2′,7′-dichlorofluorescein diacetate; CTL, cytotoxic T lymphocyte; FBS, fetal bovine serum; MAPKs, mitogen-activated protein kinases; NF-κB, nuclear factor-κB; NK cell, natural killer cell; NO, nitrite oxide; PI3K, phosphoinositide 3-kinase; ROS, reactive oxygen species; TLRs, Toll-like receptors; TLR4, Toll-like receptor 4

REFERENCES

(1) Sarkar, F. H.; Li, Y. Using chemopreventive agents to enhance the efficacy of cancer therapy. *Cancer Res.* **2006**, *66*, 3347−3350.

(2) Topalian, S. L.; Weiner, G. J.; Pardoll, D. M. Cancer immunotherapy comes of age. *J. Clin. Oncol.* **2011**, *29*, 4828−4836.

(3) Takeda, K.; Kaisho, T.; Akira, S. Toll-like receptors. *Annu. Rev. Immunol.* **2003**, *21*, 335−376.

(4) Medzhitov, R. Toll-like receptors and innate immunity. *Nat. Rev. Immunol.* **2001**, *1*, 135−145.

(5) Akira, S.; Takeda, K. Toll-like receptor signalling. *Nat. Rev. Immunol.* **2004**, *4*, 499−511.

(6) Apetoh, L.; Ghiringhelli, F.; Tesniere, A.; Obeid, M.; Ortiz, C.; Criollo, A.; Mignot, G.; Maiuri, M. C.; Ullrich, E.; Saulnier, P. Toll-like receptor 4-dependent contribution of the immune system to anticancer chemotherapy and radiotherapy. *Nat. Med.* **2007**, *13*, 1050−1059.

(7) Zhang, S.; Nie, S.; Huang, D.; Li, W.; Xie, M. Immunomodulatory effect of *Ganoderma atrum* polysaccharide on CT26 tumor-bearing mice. *Food Chem.* **2013**, *136*, 1213−1219.

(8) Hsu, H.-Y.; Jeyashoke, N.; Yeh, C.-H.; Song, Y.-J.; Hua, K.-F.; Chao, L. K. Immunostimulatory bioactivity of algal polysaccharides from *Chlorella pyrenoidosa* activates macrophages via Toll-like receptor 4. *J. Agric. Food Chem.* **2009**, *58*, 927−936.

(9) Liu, J.-Y.; Yang, F.-L.; Lu, C.-P.; Yang, Y.-L.; Wen, C.-L.; Hua, K.-F.; Wu, S.-H. Polysaccharides from *Dioscorea batatas* induce tumor necrosis factor-α secretion via Toll-like receptor 4-mediated protein kinase signaling pathways. *J. Agric. Food Chem.* **2008**, *56*, 9892−9898.

(10) Nie, S.; Zhang, H.; Li, W.; Xie, M. Current development of polysaccharides from *Ganoderma*: isolation, structure and bioactivities. *Bioact. Carbohydr. Diet. Fibre* **2013**, *1*, 10−20.

(11) Chen, Y.; Xie, M.-Y.; Nie, S.-P.; Li, C.; Wang, Y.-X. Purification, composition analysis and antioxidant activity of a polysaccharide from the fruiting bodies of *Ganoderma atrum*. *Food Chem.* **2008**, *107*, 231−241.

(12) Zhang, H.; Li, W.-J.; Nie, S.-P.; Chen, Y.; Wang, Y.-X.; Xie, M.-Y. Structural characterisation of a novel bioactive polysaccharide from *Ganoderma atrum*. *Carbohydr. Polym.* **2012**, *88*, 1047−1054.

(13) Yu, Q.; Nie, S.-P.; Wang, J.-Q.; Yin, P.-F.; Huang, D.-F.; Li, W.-J.; Xie, M.-Y. Toll-like receptor 4-mediated ROS signaling pathway involved in *Ganoderma atrum* polysaccharide-induced tumor necrosis factor-α secretion during macrophage activation. *Food Chem. Toxicol.* **2014**, *66*, 14−22.

(14) Zhang, S.; Nie, S.; Huang, D.; Huang, J.; Wang, Y.; Xie, M. Polysaccharide from *Ganoderma atrum* evokes antitumor activity via Toll-like receptor 4-mediated NF-κB and mitogen-activated protein kinase signaling pathways. *J. Agric. Food Chem.* **2013**, *61*, 3676−3682.

(15) Pal, A.; Bhattacharya, I.; Bhattacharya, K.; Mandal, C.; Ray, M. Methylglyoxal induced activation of murine peritoneal macrophages and surface markers of T lymphocytes in sarcoma-180 bearing mice: involvement of MAP kinase, NF-$\kappa\beta$ signal transduction pathway. *Mol. Immunol.* **2009**, *46*, 2039−2044.

(16) Weeks, B. A.; Keisler, A. S.; Myrvik, Q. N.; Warinner, J. E. Differential uptake of neutral red by macrophages from three species of estuarine fish. *Dev. Comp. Immunol.* **1988**, *11*, 117−124.

(17) Tsai, Y.-C.; Won, S.-J. Effects of tramadol on T lymphocyte proliferation and natural killer cell activity in rats with sciatic constriction injury. *Pain* **2001**, *92*, 63−69.

(18) Li, W. J.; Chen, Y.; Nie, S. P.; Xie, M. Y.; He, M.; Zhang, S. S.; Zhu, K. X. *Ganoderma atrum* polysaccharide induces anti-tumor activity via the mitochondrial apoptotic pathway related to activation of host immune response. *J. Cell Biochem.* **2011**, *112*, 860−871.

(19) Dunn, D. L.; Barke, R. A.; Ewald, D. C.; Simmons, R. L. Macrophages and translymphatic absorption represent the first line of host defense of the peritoneal cavity. *Arch. Surg. (Chicago, IL, U.S.)* **1987**, *122*, 105−110.

(20) Aderem, A.; Underhill, D. M. Mechanisms of phagocytosis in macrophages. *Annu. Rev. Immunol.* **1999**, *17*, 593−623.

(21) Adams, D. O.; Hamilton, T. A. The cell biology of macrophage activation. *Annu. Rev. Immunol.* **1984**, *2*, 283−318.

(22) Zhao, T.; Feng, Y.; Li, J.; Mao, R.; Zou, Y.; Feng, W.; Zheng, D.; Wang, W.; Chen, Y.; Yang, L. Schisandra polysaccharide evokes immunomodulatory activity through TLR 4-mediated activation of macrophages. *Int. J. Biol. Macromol.* **2014**, *65*, 33−40.

(23) Kim, H. S.; Kim, Y. J.; Lee, H. K.; Ryu, H. S.; Kim, J. S.; Yoon, M. J.; Kang, J. S.; Hong, J. T.; Kim, Y.; Han, S.-B. Activation of macrophages by polysaccharide isolated from *Paecilomyces cicadae* through toll-like receptor 4. *Food Chem. Toxicol.* **2012**, *50*, 3190−3197.

(24) Rao, K. M. K. MAP kinase activation in macrophages. *J. Leukocyte Biol.* **2001**, *69*, 3−10.

(25) Fruman, D. A.; Cantley, L. C. Phosphoinositide 3-kinase in immunological systems. *Semin. Immunol.* **2002**, *14*, 7−18.

(26) Fruman, D. A.; Meyers, R. E.; Cantley, L. C. Phosphoinositide kinases. *Annu. Rev. Biochem.* **1998**, *67*, 481−507.

(27) Baeuerle, P. A.; Henkel, T. Function and activation of NF-kappaB in the immune system. *Annu. Rev. Immunol.* **1994**, *12*, 141−179.

(28) Taylor, P. R.; Martinez-Pomares, L.; Stacey, M.; Lin, H.-H.; Brown, G. D.; Gordon, S. Macrophage receptors and immune recognition. *Annu. Rev. Immunol.* **2005**, *23*, 901−944.

(29) Fidler, I.; Kleinerman, E. Therapy of cancer metastasis by systemic activation of macrophages: from the bench to the clinic. *Res. Immunol.* **1993**, *144*, 284−287.

(30) Medzhitov, R.; Janeway, C. A., Jr Innate immunity: impact on the adaptive immune response. *Curr. Opin. Immunol.* **1997**, *9*, 4−9.

(31) Kos, F. J.; Engleman, E. G. Immune regulation: a critical link between NK cells and CTLs. *Immunol. Today* **1996**, *17*, 174−176.

(32) Cooper, M. A.; Fehniger, T. A.; Caligiuri, M. A. The biology of human natural killer-cell subsets. *Trends Immunol.* **2001**, *22*, 633−640.

(33) Parmiani, G.; Rivoltini, L.; Andreola, G.; Carrabba, M. Cytokines in cancer therapy. *Immunol. Lett.* **2000**, *74*, 41−44.

(34) Romagnani, S. T-cell subsets (Th1 versus Th2). *Ann. Allergy, Asthma, Immunol.* **2000**, *85*, 9−21.

(35) Szabo, S. J.; Sullivan, B. M.; Peng, S. L.; Glimcher, L. H. Molecular mechanisms regulating Th1 immune responses. *Annu. Rev. Immunol.* **2003**, *21*, 713−758.

(36) Dranoff, G. Cytokines in cancer pathogenesis and cancer therapy. *Nat. Rev. Cancer* **2004**, *4*, 11−22.

DOI: 10.1021/jf5041096
J. Agric. Food Chem. 2015, 63, 517−525

(37) Elmore, S. Apoptosis: a review of programmed cell death. *Toxicol. Pathol.* **2007**, *35*, 495−516.
(38) Riedl, S. J.; Shi, Y. Molecular mechanisms of caspase regulation during apoptosis. *Nat. Rev. Mol. Cell Biol.* **2004**, *5*, 897−907.
(39) Hibbs, J. B., Jr.; Taintor, R. R.; Vavrin, Z.; Rachlin, E. M. Nitric oxide: a cytotoxic activated macrophage effector molecule. *Biochem. Biophys. Res. Commun.* **1988**, *157*, 87−94.
(40) Brüne, B.; von Knethen, A.; Sandau, K. B. Nitric oxide (NO): an effector of apoptosis. *Cell Death Differ.* **1999**, *6*, 969−975.
(41) Brüne, B.; von Knethen, A.; Sandau, K. B. Nitric oxide and its role in apoptosis. *Eur. J. Pharmacol.* **1998**, *351*, 261−272.
(42) Chung, H.-T.; Pae, H.-O.; Choi, B.-M.; Billiar, T. R.; Kim, Y.-M. Nitric oxide as a bioregulator of apoptosis. *Biochem. Biophys. Res. Commun.* **2001**, *282*, 1075−1079.
(43) Brüne, B. Nitric oxide: NO apoptosis or turning it ON? *Cell Death Differ.* **2003**, *10*, 864−869.

DOI: 10.1021/jf5041096
J. Agric. Food Chem. 2015, 63, 517−525

JOURNAL OF AGRICULTURAL AND FOOD CHEMISTRY

Article

pubs.acs.org/JAFC

Novel Insights into the Inhibitory Mechanism of Kaempferol on Xanthine Oxidase

Yajie Wang,[†] Guowen Zhang,*[,†] Junhui Pan,[†] and Deming Gong[‡]

[†]State Key Laboratory of Food Science and Technology, Nanchang University, Nanchang 330047, China

[‡]School of Biological Sciences, The University of Auckland, Auckland 1142, New Zealand

ABSTRACT: Xanthine oxidase (XO), a key enzyme in purine catabolism, is widely distributed in human tissues. It can catalyze xanthine to generate uric acid and cause hyperuricemia and gout. Inhibition kinetics assay showed that kaempferol inhibited XO activity reversibly in a competitive manner. Strong fluorescence quenching and conformational changes of XO were found due to the formation of a kaempferol−XO complex, which was driven mainly by hydrophobic forces. The molecular docking further revealed that kaempferol inserted into the hydrophobic cavity of XO to interact with some amino acid residues. The main inhibition mechanism of kaempferol on XO activity may be due to the insertion of kaempferol into the active site of XO occupying the catalytic center of the enzyme to avoid the entrance of the substrate and inducing conformational changes of XO. In addition, luteolin exhibited a stronger synergistic effect with kaempferol than did morin at the lower concentration.

KEYWORDS: *xanthine oxidase, kaempferol, inhibition mechanism, spectroscopy, molecular simulation*

INTRODUCTION

Xanthine oxidase (XO), a key enzyme in purine metabolism, is widely distributed in mammalian tissues.[1] Structurally, XO is a 290 kDa homodimer with each of the monomers acting independently during catalysis. Each subunit is composed of one molybdopterin cofactor, one flavin adenine dinucleotide (FAD) cofactor, and two distinct [2Fe−2S] centers.[2] The oxidation of xanthine occurs at the molybdopterin center (Mo-pt), and the electrons thus introduced are rapidly distributed to the other centers by intramolecular electron transfer.[3] Previous studies have shown that milk can inhibit the metabolic activity of *Escherichia coli* depending on the presence of XO,[4] but the excess of XO will lead to the oxidation and rancidity of milk in the processing process of dairy products.[5] On the other hand, XO catalyzes the terminal two steps in purine catabolism (hypoxanthine → xanthine → uric acid) in the human body, and the overproduction or underexcretion of uric acid plays a vital role in disorders such as hyperuricemia, which is a key cause of gout.[6] In addition, hyperuricemia has become an independent risk of chronic kidney disease and cardiovascular disease.[7] Obviously, maintaining uric acid in normal levels is the important therapy for the prevention of gout and other disorders.

For most patients with primary gout, uric acid overproduction is one of the major factors of hyperuricemia.[7] Increasing the excretion of uric acid or reducing uric acid production is the major therapeutic pathway for hyperuricemia.[8] Because of uric acid production resulting from the oxidation of xanthine by XO, the inhibition of XO activity has been regarded as one of the promising targets for the treatment of hyperuricemia.[9] As a powerful XO inhibitor, allopurinol has been widely used in clinic, but it also exhibits serious side effects such as hypersensitivity syndrome, impaired liver function, and renal toxicity.[8,10] Thus, finding new XO inhibitors with minor side effects as alternatives to allopurinol is of great importance.

Flavonoids are a large group of polyphenolic natural products that are widely distributed in various foods and beverages of plant origin.[11] These compounds are increasingly recognized as possessing a broad spectrum of biological activities and important therapeutic effects.[12−14] Interestingly, many biologically active flavonoids appear to have effects on various proteins, including enzymes.[15] Because of the low toxicity, XO inhibitory activities of flavonoids have attracted extensive attention. Kaempferol (3,5,7,4′-pentahydroxyflavone, structure shown in Figure 1A), a major flavonoid compound in the diet that contributes 22−29% of total flavonoid intake,[16] widely existed in daily food such as vegetables (pumpkin, snake gourd, bunga kantan, etc.) and fruits (chokeberry, strawberry, etc.) as well as teas and Chinese herbal medicine.[17,18] Investigations have shown that kaempferol exhibits a wide range of biological activities including antioxidant, anti-inflammatory, anticoagulant, and cardiovascular-protective effects.[19] Previous studies have also found that kaempferol possesses significant XO inhibitory activity in vitro;[20] this provides the basis for the application research of kaempferol as a XO inhibitor and a food functional ingredient; however, to the best of our knowledge, its inhibitory mechanism on XO is still obscure.

The main goal of pharmacotherapy using a combination of different drugs with similar effects is to increase the efficacy of the treatment while decreasing its toxicity. Fernández et al.[21] have reported that hesperidin and diazepam showed the synergy in terms of sedative and sleeping; thus, the use of hesperidin may decrease the effective therapeutic doses of diazepam. Both morin and luteolin are flavonoid compounds with a similar structure as kaempferol, and previous studies have shown that they exerted a significant inhibitory action on

Received: September 21, 2014
Revised: December 18, 2014
Accepted: December 24, 2014
Published: December 24, 2014

ACS Publications © 2014 American Chemical Society

DOI: 10.1021/jf505584m
J. Agric. Food Chem. 2015, 63, 526−534

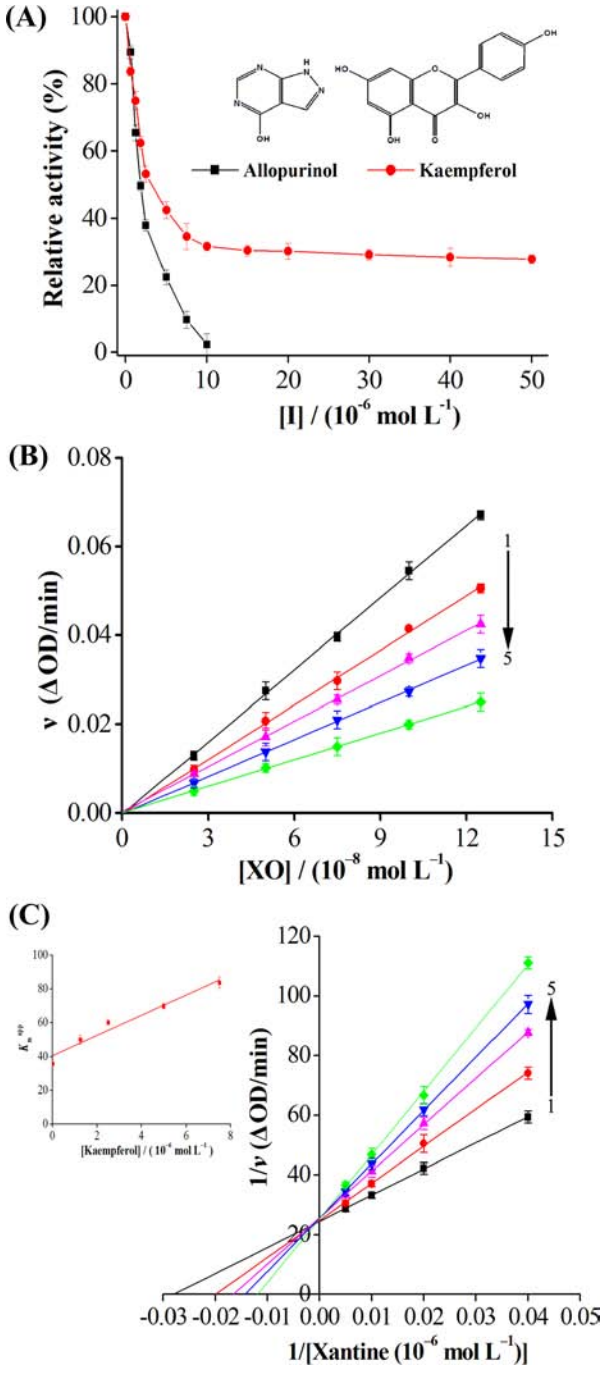

Figure 1. (A) Effect of kaempferol on XO activity (pH 7.5, T = 298 K). The inset shows the molecular structures of allopurinol and kaempferol. The final concentrations of xanthine and XO were 5.0 × 10^{-5} mol L^{-1} and 7.5 × 10^{-8} mol L^{-1}, respectively. (B) Plots of ν versus [XO]. c(xanthine) = 5.0 × 10^{-5} mol L^{-1}, c(kaempferol) = 0, 1.25, 2.5, 5.0, and 7.5 × 10^{-6} mol L^{-1} for curves 1 → 5, respectively. (C) Lineweaver–Burk plots. c(XO) = 7.5 × 10^{-8} mol L^{-1}, c(kaempferol) = 0, 1.25, 2.5, 5.0, and 7.5 × 10^{-6} mol L^{-1} for curves 1 → 5, respectively. The secondary plot represents the K_m^{app} versus [Kaempferol] (the upper left). Each value represents mean ± standard deviation (n = 3); $p < 0.05$ was considered to be statistically significant.

XO activity with a mixed type and a competitive manner, respectively.[22,23] Does each of them affect kaempferol inhibition on XO activity?

The aim of this work was to explore the inhibitory activity and type, explore the inhibitory mechanism of kaempferol on XO, and investigate the effects of morin or luteolin on kaempferol inhibiting XO activity in vitro using UV–vis absorption, fluorescence, circular dichroism (CD), and molecular docking methods. This study is expected to benefit further understanding of the inhibitory mechanism of kaempferol on XO and provide new insights into the applications of kaempferol as a XO inhibitor and a food functional ingredient.

MATERIALS AND METHODS

Materials. XO (EC 1.17.3.2, 35.7 units mL^{-1}) from bovine milk was obtained from Sigma-Aldrich Co. (St, Louis, USA). Xanthine was purchased from Sigma-Aldrich Co. (St, Louis, USA). Both of the stock solutions of XO (0.5 units mL^{-1}) and xanthine (5.0 × 10^{-4} mol L^{-1}) were prepared with 0.05 mol L^{-1} sodium phosphate buffer (pH 7.5). Kaempferol (analytical grade) was obtained from Aladdin Chemistry Co. (Shanghai, China), and its stock solution (5.0 × 10^{-3} mol L^{-1}) was prepared by dissolving its crystals in methanol and was diluted with the sodium phosphate buffer in the whole experiment process, but the contents of methanol were kept at less than 1% so that methanol had no effect on the activity and structure of XO. All stock solutions were stored at 0–4 °C and diluted to the required concentrations with the buffer. All other chemicals were of analytical reagent grade, and their aqueous solutions were prepared with freshly ultrapure water.

Enzyme Activity Assay. XO activity was measured by a UV–2450 spectrophotometer (Shimadzu, Japan) using a 1.0 cm quartz cell in a manner similar to that described by Tung et al.[24] with slight modifications. In the 2.0 mL reaction system, a series of assay solutions dissolved in 0.05 mol L^{-1} sodium phosphate buffer (pH 7.5) containing various amount of kaempferol and a fixed concentration of XO (7.5 × 10^{-8} mol L^{-1}) were incubated for 3 h at 37 °C to make the reaction equilibrium, and the assay was initiated by adding the substrate xanthine (the final concentration was 5.0 × 10^{-5} mol L^{-1}) to the complex solutions. The absorbance at 295 nm was then determined every 20 s at room temperature. Allopurinol was used as a positive control. The relative enzymatic activity was calculated as follows: the relative enzymatic activity (%) = (slope of reaction kinetics equation obtained by reaction with inhibitor)/(slope of reaction kinetics equation obtained by reaction without inhibitor) × 100.[25]

Kinetic Analysis for Inhibition Type. The assay was carried out in the absence and presence of kaempferol with varying concentrations of substrate xanthine using the same method as XO activity assay. The involved inhibition type was determined by the Lineweaver–Burk plot. For competitive inhibition, the Lineweaver–Burk equation can be written in double reciprocal form as follows:

$$\frac{1}{\nu} = \frac{K_m}{V_{max}}\left(1 + \frac{[I]}{K_i}\right)\frac{1}{[S]} + \frac{1}{V_{max}} \quad (1)$$

Secondary plot can be constructed from

$$K_m^{app} = \frac{K_m[I]}{K_i} + K_m \quad (2)$$

where ν is the enzyme reaction rate in the absence and presence of kaempferol. K_i and K_m represent the inhibition constant and Michaelis–Menten constant, respectively, and their values can be obtained from eqs 1 and 2. [I] and [S] are the concentrations of the inhibitor and substrate, respectively. K_m^{app} is the apparent Michaelis–Menten constant. The secondary plot of K_m^{app} versus [I] is linearly fitted, assuming a single inhibition site or a single class of inhibition site.[26]

Fluorometric Titration Experiments. A 2.0 mL sample of XO solution (4.0 × 10^{-7} mol L^{-1}) was added accurately to the quartz cell and then titrated by successive addition of 2.5 × 10^{-4} mol L^{-1} diluted kaempferol solution (to give a concentration range from 0–13.03 × 10^{-6} mol L^{-1}) with a microsyringe. Titrations were operated manually

DOI: 10.1021/jf505584m
J. Agric. Food Chem. 2015, 63, 526–534

and mixed moderately. These solutions were allowed to stand for 5 min to equilibrate, and then the fluorescence emission spectra were measured at 298, 304, and 310 K using a Hitachi spectrofluorimeter (Model F-7000, Hitachi, Japan) equipped with a 150 W xenon lamp and a thermostat bath. The excitation wavelength was 280 nm, and the excitation and emission bandwidths were both set at 2.5 nm. Appropriate blanks corresponding to the sodium phosphate buffer (pH 7.5) were subtracted to correct fluorescence background.

Synchronous fluorescence spectra were recorded by setting the excitation and emission wavelength interval ($\Delta\lambda$) at 15 and 60 nm over a wavelength range of 270−330 nm and 250−330 nm, respectively.

All the fluorescence data in this study were corrected for absorption of excitation light and reabsorption of emitted light according to the following relationship:[27]

$$F_c = F_m e^{(A_1+A_2)/2} \quad (3)$$

where F_c and F_m represent the corrected and measured fluorescence, respectively. A_1 and A_2 are the absorbance of kaempferol at excitation and emission wavelengths, respectively.

Circular Dichroism Analysis. The CD spectra of XO with increasing concentration of kaempferol were recorded at wavelengths between 190 and 250 nm on a Bio-Logic MOS 450 CD spectrometer (Bio-Logic, Claix, France) using a 1.0 mm quartz curet under constant nitrogen flush. The concentration of XO was kept at 1.0×10^{-6} mol L^{-1}, and the molar ratios of kaempferol to XO were varied as 0:1, 5:1, and 10:1. All observed CD spectra were measured in pH 7.5 sodium phosphate buffer at room temperature, and the buffer signal was subtracted. The online SELCON3 program was used to analyze the CD spectroscopic data to obtain the contents of different secondary structures of XO (http://dichroweb.cryst.bbk.ac.uk/html/home.shtml).

Molecular Simulation. The X-ray crystal structure of XO from bovine milk (PDB ID: 3ETR) was downloaded from the RCSB Protein Data Bank (http://www.rcsb.org/pdb).[28] The water molecules in XO were removed, whereas polar hydrogen atoms and Gasteiger charges were added to the macromolecule file for the preparation of docking running. The 3D structure of kaempferol was generated in Chem3D Ultra 8.0. The molecular docking studies were carried out by the MGL tools 1.5.6 with AutoGrid4 and AutoDock4. Docking calculations were performed using the default parameters, except for the number of GA runs (100 times) and the Lamarkian genetic algorithm with local search. To implement docking simulations, a grid box was defined with dimensions of 110 Å × 100 Å × 110 Å and a grid spacing of 0.403 Å. From the docking results, the best scoring docked model of a complex was chosen to represent its most favorable binding mode predicted by AutoDock. The outputs were further rendered with Pymol to obtain visible combination models.

Interaction Assay of Kaempferol with Morin or Luteolin on XO Activity. The interaction assay of kaempferol with morin or luteolin on XO activity was performed according to a previous report with slight modifications.[29] V_a and V_b are defined as the relative enzymatic activity in the presence of kaempferol and morin (or luteolin), respectively. V_{ab} represents the relative enzymatic activity in the presence of kaempferol and morin (or kaempferol and luteolin). If the inhibitory effect on XO of kaempferol with morin (or luteolin) is independent, the expected relative remnant activity of XO, V_c ($V_c = V_a \times V_b$) is equal to V_{ab}, and the combined effect is termed additive. In the data analysis for determining the type of interaction between kaempferol and morin or luteolin, only the values of $V_{ab} - V_c$ below −0.10 were regarded as synergistic (SY), and the values between −0.10 and +0.10 were considered as additive (AD).

Statistical Analysis. Data were analyzed using the SAS statistical package (version 8.1, SAS Institute, Cary, NC, USA). Obtained results including XO activity and inhibition type were expressed as means ± standard deviation (n = 3). One-way analysis of variance (ANOVA) was performed by using Origin 8.0 followed by multiple tests in order to determine the significant difference at $p < 0.05$.

RESULTS AND DISCUSSION

Inhibition of Kaempferol on XO Activity. As shown in Figure 1, panel A, the addition of kaempferol from 0−1.0×10^{-5} mol L^{-1} was found to dramatically decrease XO activity to approximately 30%, and then the decreasing tendency of XO activity was very slow with increasing amounts of the inhibitor. The concentration of kaempferol that resulted in a loss of 50% enzyme activity (IC_{50}) was determined to be $(2.18 \pm 0.02) \times 10^{-6}$ mol L^{-1} (allopurinol was $(1.79 \pm 0.02) \times 10^{-6}$ mol L^{-1}), which indicates that kaempferol was an effective XO inhibitor compared to allopurinol (positive control). This is due to the C-5 and C-7 hydroxyl groups in kaempferol that play an important role in inhibition.[30] As reported earlier, morin and luteolin with a similar structure as kaempferol have shown inhibition on XO activity with IC_{50} $(13.54 \pm 0.02) \times 10^{-6}$ mol L^{-1} and $(4.79 \pm 0.02) \times 10^{-6}$ mol L^{-1}, respectively.[22,23] It is likely that the meta-position hydroxyl groups on the B ring of flavonoid would decrease the electron cloud density of band I, which impacted the interaction of morin with XO negatively; thus, the inhibition of morin on XO was weaker than that of kaempferol. In contrast, the ortho-position hydroxyl groups on the B ring were in favor of the flavonoid−XO inteaction, which would enhance the inhibition of flavonoid on XO since luteolin showed better inhibition on XO than morin. The IC_{50} value of kaempferol was smaller than that of luteolin, this may be attributed to the 3-hydroxyl group of kaempferol, which was in favor of the distribution of the electron cloud and made the electronegativity of kaempferol increased.[31]

Reversibility. As shown in Figure 1, panel B, the plots of the ν versus [XO] at different kaempferol concentrations were constructed to confirm the reversibility of kaempferol mediated inhibition. The plots showed good linearity, and all passed the origin; moreover, the slope of the lines decreased with increased concentration of kaempferol, which indicates that the presence of kaempferol did not decrease the amount of efficient enzyme available, but it resulted in the inhibition of XO and an overall decrease of enzyme activity with respect to the oxidation of xanthine. These results suggested that the inhibition of kaempferol on XO was reversible and a noncovalent intermolecular interaction between kaempferol and XO.[32]

Inhibition Type. The Lineweaver−Burk double reciprocal plots were used to analyze the inhibition type of kaempferol on XO activity. The horizontal axis intercept ($-1/K_m$) increased and the vertical axis intercept ($1/V_{max}$) remained the same with increasing amounts of kaempferol (Figure 1C), which suggests that kaempferol caused a typical competitive inhibition[33] and that kaempferol may directly bind to the active site of XO competing with xanthine during catalysis. The inset of Figure 1, panel C showed the linear relationship between K_m^{app} and the concentration of kaempferol, which suggested that there was a single class of inhibition sites for kaempferol on XO. The value of inhibition constant (K_i) was calculated to be $(6.77 \pm 1.02) \times 10^{-6}$ mol L^{-1}.

Fluorescence Quenching of XO by Kaempferol. The above studies suggested that kaempferol may directly bind to the active site of XO to inhibit the enzyme activity. Therefore, fluorescence spectroscopy was further used to characterize the binding between kaempferol and XO. Figure 2, panel A shows the fluorescence emission spectra of XO with varying concentrations of kaempferol after being excited at a wavelength of 280 nm. The XO displayed a strong emission peak at

DOI: 10.1021/jf505584m
J. Agric. Food Chem. 2015, 63, 526−534

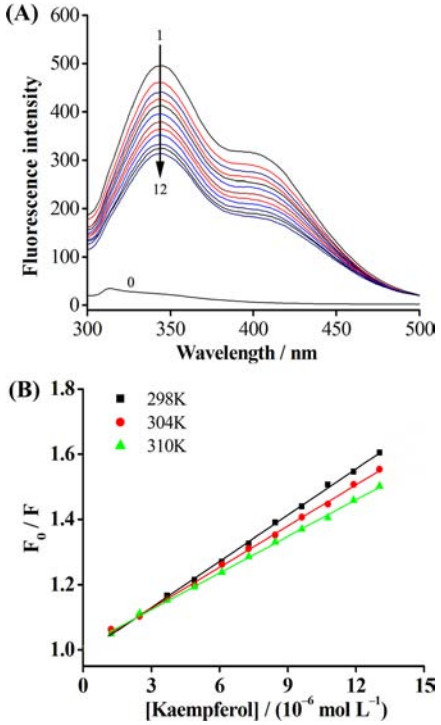

Figure 2. (A) Fluorescence spectra of XO in the absence and presence of kaempferol at different concentrations (pH 7.5, T = 298 K, λ_{ex} = 280 nm). c(XO) = 4.0 × 10^{-7} mol L^{-1}, and c(kaempferol) = 0, 1.24, 2.48, 3.69, 4.90, 6.10, 7.28, 8.45, 9.62, 10.77, 11.90, and 13.03 × 10^{-6} mol L^{-1} for curves 1 → 12, respectively. Curve 0 showed the emission spectrum of kaempfrol only, c(kaempferol) = 13.03 × 10^{-6} mol L^{-1}. (B) Stern−Volmer plots for the fluorescence quenching of XO by kaempferol at different temperatures.

342 nm, which resulted from the tryptophan and tyrosine residues of XO.[34] With increasing the amounts of kaempferol, the fluorescence emission peak of XO decreased significantly and regularly with no shift of the emission peak's position, which indicated that kaempferol interacted with XO and quenched the intrinsic fluorescence of XO.

Generally, fluorophore quenching can occur by different mechanisms, namely dynamic and static quenching processes. The static quenching is caused by the formation of the ground state complex, while the dynamic quenching is due to the collision between the fluorophore and the quencher. These two types of mechanisms can be distinguished by their different dependence on temperature or excited-state lifetime.[35] To determine the quenching mechanism of kaempferol binding to XO, the fluorescence quenching data were analyzed using the Stern−Volmer equation:[34]

$$\frac{F_0}{F} = 1 + K_{SV}[Q] = 1 + K_q\tau_0[Q] \quad (4)$$

where F_0 and F denote the steady-state fluorescence intensities of XO in the absence and presence of kaempferol, respectively. K_{SV} is the Stern−Volmer dynamic quenching constant, which was determined by linear regression of a plot of F_0/F against [Q]. K_q is the quenching rate constant of the biomolecule ($K_q = K_{SV}/\tau_0$). τ_0 is the average lifetime of the fluorophore without quencher, which is equal to 2.80 × 10^{-9} s.[36] [Q] is the concentration of kaempferol.

The plots of F_0/F versus [Q] at three different temperatures (298, 304, and 310 K) are shown in Figure 2, panel B, and the corresponding K_{SV} values for the complexation of kaempferol with XO are given in Table 1. A high linearity suggested that only one type of quenching process occurred, either static or dynamic quenching.[37] The K_{SV} values clearly displayed a decreasing tendency with increasing temperature, and the calculated K_q values at 298, 304, and 310 K were 1.69 × 10^{13}, 1.50 × 10^{13}, and 1.33 × 10^{13} L mol^{-1} s^{-1}, respectively, which were considerably greater than the maximum scatter collision quenching constant of various quenchers with biopolymers, 2.0 × 10^{10} L mol^{-1} s^{-1},[38] which indicates that the mechanism of the fluorescence quenching of XO was static and resulted from the formation of a kaempferol−XO complex.[39]

Then, the fluorescence titration data were further estimated to obtain the association constant (K_a) using the modified Stern−Volmer equation:[40]

$$\frac{F_0}{F_0 - F} = \frac{1}{f_a K_a[Q]} + \frac{1}{f_a} \quad (5)$$

where f_a is the fraction of accessible fluorescence. From the linear regression of $F_0/(F_0-F)$ versus $1/[Q]$, the values of K_a for the kaempferol−XO complex at three different temperatures are calculated (Table 1). The K_a values were in the order of 10^4 L mol^{-1}, which suggested that a moderate affinity existed between kaempferol and XO.

Thermodynamic Characteristics of Interactions. Generally, small ligands bind to biomolecules mainly through hydrogen bonds, van der Waals forces, hydrophobic interactions, and electrostatic forces. Determination of the thermodynamic parameters (enthalpy change $\Delta H°$, entropy change $\Delta S°$) can clarify the acting force of the binding interaction between kaempferol and XO, which was evaluated by the van't Hoff equation:

$$\log K_a = -\frac{\Delta H°}{2.303RT} + \frac{\Delta S°}{2.303R} \quad (6)$$

where R is the gas constant (8.314 J mol^{-1} K^{-1}), and T represents the experimental temperatures at 298, 304, and 310 K. By plotting log K_a versus $1/T$, $\Delta H°$ and $\Delta S°$ were determined. By knowing the $\Delta H°$ and $\Delta S°$ values, the free energy change ($\Delta G°$) can be calculated from the following equation:

$$\Delta G° = \Delta H° - T\Delta S° \quad (7)$$

Table 1. Quenching Constants K_{SV}, Modified Stern−Volmer Association Constants K_a, and Relative Thermodynamic Parameters for the Interaction between Kaempferol and XO at Different Temperatures

T (K)	K_{SV} (× 10^4 L mol^{-1})	R^a	K_a (× 10^4 L mol^{-1})	R^b	n	$\Delta H°$ (kJ mol^{-1})	$\Delta G°$ (kJ mol^{-1})	$\Delta S°$ (J mol^{-1} K^{-1})
298	4.72	0.9996	3.22	0.9992	1.04	49.45	−25.56	251.70
304	4.20	0.9993	3.90	0.9995	0.95		−27.07	
310	3.73	0.9994	6.99	0.9972	0.95		−28.58	

[a] R is the correlation coefficient for the K_{SV} values. [b] R is the correlation coefficient for the K_a values.

DOI: 10.1021/jf505584m
J. Agric. Food Chem. 2015, 63, 526−534

As shown in Table 1, the negative sign for ΔG° suggested that the kaempferol−XO binding interaction was spontaneous. The positive values of ΔH° and ΔS° indicated that the formation of kaempferol−XO complex was endothermic, and the values were frequently regarded as a typical evidence for hydrophobic interactions.[41] Thus, the kaempferol−XO complexation was driven mainly by hydrophobic forces.

Number of Binding Sites of Kaempferol on XO. For the static quenching interaction, when small molecules bind independently to a set of equivalent sites on a macromolecule, the number of binding sites (n) and binding constant (K_b) for the kaempferol−XO complex can be calculated from the slope and intercept of the regression curve of log $(F_0 - F)/F$ versus log$1/([Q_t] - (F_0 - F)[P_t]/F_0)$:[42]

$$\log \frac{F_0 - F}{F} = n \log K_b - n \log \frac{1}{[Q_t] - \frac{(F_0 - F)[P_t]}{F_0}} \quad (8)$$

where $[Q_t]$ and $[P_t]$ are the total concentrations of kaempferol and XO, respectively. As shown in Table 1, the values of n were approximately equal to 1, which suggested the existence of one binding site for kaempferol on XO, which was consistent with the results of inhibition-type studies. The K_b values of the kaempferol−XO complex were 4.79×10^4, 4.00×10^4, and 6.28×10^4 L mol^{-1} at 298, 304, and 310 K, respectivily, which were in accordance with the values of K_a at the corresponding temperatures.

Conformational Change of XO, Kaempferol Induced. Synchronous fluorescence spectroscopy can provide information about the alterations in the microenvironment around fluorophores of XO, which are related to the conformational changes of the enzyme. As shown in Figure 3, panels A and B, the maximum emission wavelength of both tyrosine and tryptophan residues had a slight red shift from 293−295 nm and from 285−286 nm, respectively, which suggest that the polarity around the tyrosine and tryptophan residues increased and the hydrophobicity decreased; namely, the fluorophores of XO were placed in a less hydrophobic environment and more exposed to the solvent with the addition of kaempferol.[43]

CD spectroscopy was performed to further monitor the conformational change of XO induced by kaempferol. As shown in Figure 3, panel C, the spectra of XO exhibited a negative band in the UV region at 216 nm, which is characteristic of β-sheet structure of protein.[44] The CD intensity of XO increased (shifting away from zero level) without any significant shift of peak's position upon increasing the concentration of kaempferol, which indicates that the secondary structure content of β-sheet increased and was also predominant in XO conformation after binding with kaempferol.[34] A similar phenomenon has been reported in the interaction of bixin with β-lactoglobulin.[45] The contents of different secondary structures of XO were analyzed with the use of the online SELCON3 program (Table 2). Compared with the free XO, it exhibited an increase in β-sheet and β-turn contents from 40.6% and 10.8% to 44.9% and 12.2%, respectively, and a decrease in α-helical and random coil structure contents from 13.2% and 35.4% to 9.5% and 33.4%, respectively, at a molar ratio of kaempferol to XO of 10:1. These results indicated that the binding of kaempferol to XO might have destroyed its hydrogen bonding networks[46] and induced minor unfolding of the polypeptides of the enzyme because of the loss of α-helical content.[27] It might be part of the mechanism of the enzymatic inhibition that the unfolding of

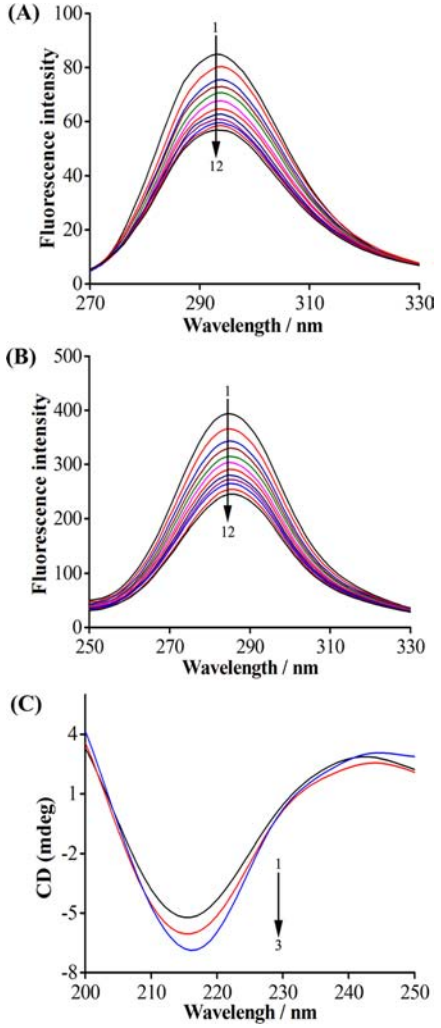

Figure 3. Synchronous fluorescence spectra of XO in the absence and presence of kaempferol (A) $\Delta\lambda$ = 15 nm, (B) $\Delta\lambda$ = 60 nm (pH 7.5, T = 298 K). c(XO) = 4.0×10^{-7} mol L^{-1}, and c(kaempferol) = 0, 1.24, 2.48, 3.69, 4.90, 6.10, 7.28, 8.45, 9.62, 10.77, 11.90, and 13.03×10^{-6} mol L^{-1} for curves 1 → 12, respectively. (C) The CD spectra of the kaempferol−XO system at pH 7.5. c(XO) = 1.0×10^{-6} mol L^{-1}, and the molar ratios of kaempferol to XO were 0:1(1), 5:1(2), and 10:1(3), respectively.

Table 2. Contents of Secondary Structures of Free XO and Kaempferol−XO Systems (CD Spectra) at pH 7.5

molar ratio [kaempferol]:[XO]	α-helix (%)	β-sheet (%)	β-turn (%)	random coil (%)
0:1	13.2	40.6	10.8	35.4
5:1	9.9	43.3	11.9	34.9
10:1	9.5	44.9	12.2	33.4

hydrophobic cavity was more conducive to kaempferol occupying the active site of XO. Moreover, since the helices are the most stable elements of secondary structure of protein, the decrease in α-helical content of XO induced by kaempferol probably led to a decline in its stability,[47] which thus resulted in a decrease in the catalytic activity of XO.

Computational Docking of the Kaempferol−XO Complex. Molecular docking was used to improve the understanding of the interaction between kaempferol and XO. The binding energy of conformational clusters was

DOI: 10.1021/jf505584m
J. Agric. Food Chem. 2015, 63, 526−534

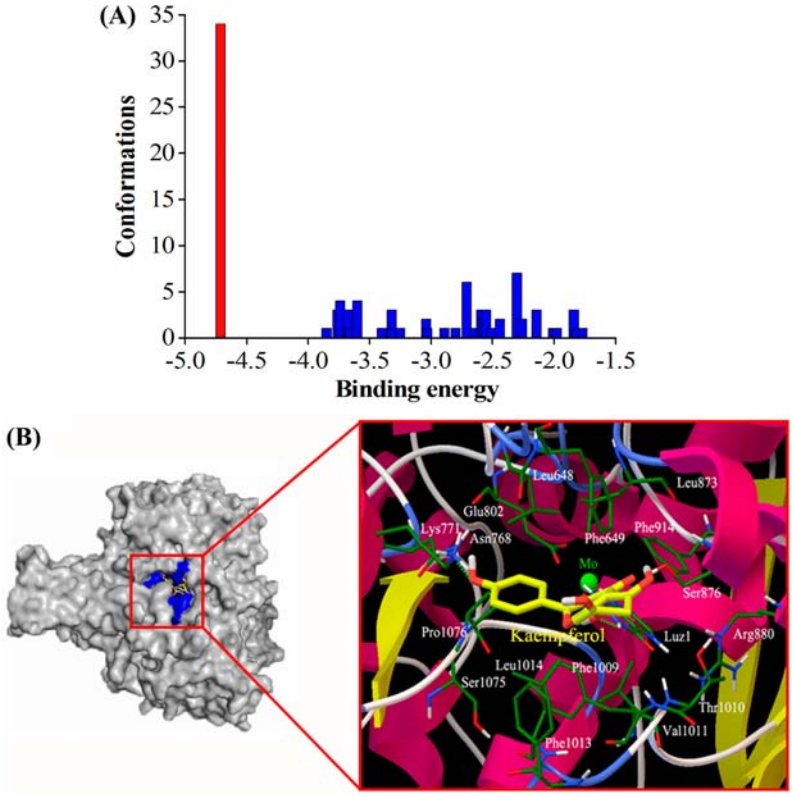

Figure 4. Molecular docking of kaempferol with XO. (A) Cluster analyses of the AutoDock docking runs of kaempferol with XO. (B) The corresponding docking mode of kaempferol into XO. In the surface structure, the coarser stick structure was used to represent kaempferol, which inserted into the hydrophobic cavity of XO (blue). The corresponding secondary structure of XO was displayed by ribbon form, and the main amino acid residues of XO in the active site were represented using thin stick. The green dashed line stands for hydrogen bonds.

Table 3. Interaction Effects of Kaempferol and Morin or Luteolin on the Inhibition of XO Activity at Different Concentrations

	kaempferol (0.5×10^{-6} mol L^{-1})			kaempferol (2.0×10^{-6} mol L^{-1})			kaempferol (8.0×10^{-6} mol L^{-1})		
	value		interaction	value		interaction	value		interaction
concentrations (mol L^{-1})	obsd (V_{ab})	expected (V_c)	$V_{ab} - V_c$	obsd (V_{ab})	expected (V_c)	$V_{ab} - V_c$	obsd (V_{ab})	expected (V_c)	$V_{ab} - V_c$
morin (2.0×10^{-6})	0.85	0.77	0.08AD[a]	0.30	0.55	−0.25SY[b]	0.25	0.39	−0.14SY
morin (1.4×10^{-5})	0.72	0.58	0.14AD	0.49	0.44	0.05AD	0.18	0.29	−0.11SY
morin (4.2×10^{-5})	0.34	0.35	0.01AD	0.24	0.29	−0.05AD	0.15	0.12	0.03AD
luteolin (1.0×10^{-6})	0.62	0.73	−0.11SY	0.35	0.46	−0.11SY	0.15	0.30	−0.15SY
luteolin (5.0×10^{-6})	0.22	0.40	−0.18SY	0.13	0.25	−0.12SY	0.10	0.16	−0.06AD
luteolin (1.0×10^{-5})	0.19	0.33	−0.14SY	0.14	0.21	−0.07AD	0.10	0.13	−0.03AD

[a]AD means additive interaction. [b]SY means synergistic interaction.

arranged according to the size of energy by performing the cluster analysis with the use of a root−mean−square deviation (rmsd) tolerance of 2.0 Å (Figure 4A). A total of 32 multimember conformational clusters was obtained from 100 docking runs. The cluster that possessed the most frequent locus (34 out of 100, the red bar in Figure 4A) and the lowest energy were the most optimal among all the clusters. The most energetically favorable binding gesture was selected for binding orientation analysis. From the docking results, the torsional energy and intermolecular energy were 1.49 kcal mol^{-1} and −6.20 kcal mol^{-1}, respectively; thus, the predicted binding energy ($\Delta G_{binding}$ = intermolecular energy + torsional energy) was obtained to be −4.71 kcal mol^{-1}, which was equal to the binding energy (−4.71 kcal mol^{-1}), which indicates that the docking result was credible.[48] The binding energy was slightly higher than $\Delta G°$ (−6.11 kcal mol^{-1}) obtained from above thermodynamic analysis at 298 K, which could be due to the lack of desolvation energy because the Autodock was performed under simulation of vacuum environment.

As shown in Figure 4, panel B, kaempferol inserted into the hydrophobic cavity of XO, the active site with molybdenum atomic (Mo) domain, and the only channel for the substrate xanthine to enter.[49] The bicyclic benzopyranone ring of kaempferol was sandwiched between amino acid residues Phe1009 and Phe914 and made aromatic interactions ($\pi-\pi$ effects) with the two phenylalanines, which were important for ligand−XO recognition.[24] Moreover, two hydrogen bonds were formed between kaempferol and several residues. One of the hydrogen bonds was constituted between the hydroxyl group in the B ring of kaempferol and Asn768, and the other was formed between the C3 hydroxyl group in the C ring of kaempferol and Luz1 (the coenzyme factor connecting with Mo atom), which suggests that weak hydrogen bond interaction between XO and kaempferol existed. In addition, it was found that the B ring of

DOI: 10.1021/jf505584m
J. Agric. Food Chem. 2015, 63, 526−534

kaempferol inserted into the hydrophobic region of XO interacted with residues Phe1013, Pro1076, Glu 802, Leu1014, Leu648, and Ser1075. The molecular docking supported and visualized the result that the binding of kaempferol with XO was driven mainly by hydrophobic interactions. These results suggested that the inhibitory mechanism of kaempferol on XO oxidation activity to xanthine may be due to the insertion of kaempferol into the active site of XO occupying the catalytic center of the enzyme, thus avoiding entrance of the substrate and causing conformational altertions in XO.

Effects of Morin or Luteolin on Kaempferol Inhibition of XO Activity. The XO inhibitory activities of kaempferol−morin and kaempferol−luteolin mixtures were determined to evaluate the possible synergistic effect. Synergistic effect means that the joint inhibitory ability of two inhibitors on the enzyme activity is greater than the sum of each inhibitor alone, which is different from the additive effect defined as the joint inhibitory effect of two inhibitors being equal to the sum of each inhibitor alone.[50] In this study, three different concentrations near the IC_{50} values of kaempferol, morin, and luteolin were selected. The obtained results are summarized in Table 3, where the remnant XO activity observed (V_{ab}) for kaempferol with morin or luteolin was compared to the remnant XO activity expected (V_c).

As shown in Table 3, the V_c value was calculated to be 0.55 when the remnant XO activity fractions were 0.61 (V_a) and 0.90 (V_b) (data not shown) at the individual added concentration of kaempferol and morin of 2.0×10^{-6} mol L^{-1}, respectively. However, the observed remnant of XO activity fraction (V_{ab}) was 0.30 when kaempferol and morin were added together. The ($V_{ab} - V_c$) value of −0.25 (<−0.10) suggested that these two flavonoids had a significant synergistic effect on the inhibition of XO activity. A similar phenomenon was observed when the concentrations of kaempferol and morin were 8.0×10^{-6} mol L^{-1} and 2.0×10^{-6} mol L^{-1} (or 1.4×10^{-5} mol L^{-1}), respectively. Because morin interacted with some amino acid residues located in the region near the hydrophobic cavity of XO,[22] while kaempferol bound to the active site, it can be thus deduced that the binding mode of the two flavonoids with XO strengthened the inhibition by occuping the entrance of the substrate xanthine and influencing the structure of XO. For the kaempferol−luteolin system, the concentration of luteolin was kept at 1.0×10^{-6} mol L^{-1}, and the different concentrations of kaempferol (0.5×10^{-6}, 2.0×10^{-6}, and 8.0×10^{-6} mol L^{-1}) were added to this solution. It was found that kaempferol and luteolin showed a synergistic effect on the inhibition of XO activity (Table 3). The synergistic inhibition of the kaempferol−luteolin mixture was also found when the concentration of luteolin was 5.0×10^{-6} mol L^{-1} and the concentration of kaempferol was 0.5×10^{-6} or 2.0×10^{-6} mol L^{-1}. These results indicated that luteolin may have a stronger synergistic effect with kaempferol on inhibiting XO activity than morin for the lower concentration required. The synergy mechanism could be conjectured that luteolin together with kaempferol bound to the active site of XO for its competetive manner by occupying the binding site of xanthine and inducing some conformational changes of XO.

In summary, the inhibitory mechanism of kaempferol on XO activity and its synergistic effect with morin or luteolin were investigated by multispectroscopic methods and molecular simulations. Taken together, the principal results of our study include the following: (i) kaempferol reversibly inhibited the catalytic activity of XO in a competetive manner with an IC_{50} value of $(2.18 \pm 0.02) \times 10^{-6}$ mol L^{-1} and K_i value of $(6.77 \pm 1.02) \times 10^{-6}$ mol L^{-1}; (ii) a strong fluorescence quenching of XO was observed due to the formation of a kaempferol−XO complex in a static procedure; (iii) the thermodynamic parameters, ΔH° and ΔS°, were calculated to be 49.45 kJ mol^{-1} and 251.70 J mol^{-1} K^{-1}, respectively, and ΔG° was negative, which suggests that the reaction between kaempferol and XO was a spontaneous process mainly driven by hydrophobic forces; (iv) there was a single class of binding site on XO for kaempferol, and the binding induced the conformational changes of XO; (v) it was predicted by molecular docking that kaempferol inserted into the hydrophobic cavity to interact with some amino acid residues Glu802, Leu873, Phe914, Arg880, Phe1009, Thr1010, Val1011, Leu1014, and Pro1076 located within the active site pocket; and (vi) kaempferol and luteolin or morin showed a significant synergistic effect on inhibiting the activity of XO, and luteolin exhibited a stronger synergistic effect with kaempferol at the lower concentration. As a consquence, the XO activity inhibited by kaempferol was probably due to the insertion of kaempferol into the active site of XO occupying the catalytic center of the enzyme to avoid entrance of xanthine and inducing conformational changes of XO. This study has provided new insights into the inhibition mechanism of kaempferol on XO and its joint effect with luteolin or morin. The results have shown that kaempferol could be a promising XO inhibitor, and the kaempferol−rich foods may be useful for the treatment of gout. Moreover, the ingestion of foods containing kaempferol and luteolin or morin may have a better therapeutic effect.

AUTHOR INFORMATION

Corresponding Author

*Phone: +8679188305234. Fax: +8679188304347. E-mail: gwzhang@ncu.edu.cn.

Funding

The authors are grateful for the financial support of this study by the National Natural Science Foundation of China (Nos. 21167013, 31460422, and 31060210), the Natural Science Foundation of Jiangxi Province (20142BAB204001 and 20143ACB20006), the Joint Specialized Research Fund for the Doctoral Program of Higher Education (20123601110005), the Program of Jiangxi Provincial Department of Science and Technology (20141BBG70092), and the Research Program of State Key Laboratory of Food Science and Technology of Nanchang University (SKLF−ZZB−201305, SKLF−ZZA−201302, and SKLF−KF−201203).

Notes

The authors declare no competing financial interest.

REFERENCES

(1) Chu, Y. H.; Chen, C. J.; Wu, S. H.; Hsieh, J. F. Inhibition of xanthine oxidase by *Rhodiola crenulata* extracts and their phytochemicals. *J. Agric. Food. Chem.* **2014**, *62*, 3742−3749.

(2) Enroth, C.; Eger, B. T.; Okamoto, K.; Nishino, T.; Pai, E. Crystal structures of bovine milk xanthine dehydrogenase and xanthine oxidase: Structure-based mechanism of conversion. *Proc. Natl. Acad. Sci. U.S.A.* **2000**, *97*, 10723−10728.

(3) Okamoto, K.; Matsumoto, K.; Hille, R.; Eger, B. T.; Pai, E. F.; Nishino, T.; Affiliations, A. The crystal structure of xanthine oxidoreductase during catalysis: Implications for reaction mechanism and enzyme inhibition. *Proc. Natl. Acad. Sci. U.S.A.* **2004**, *101*, 7931−7936.

DOI: 10.1021/jf505584m
J. Agric. Food Chem. 2015, 63, 526−534

(4) Hancock, J. T.; Salisbury, V.; Ovejero-Boglione, M. C.; Cherry, R.; Hoare, C.; Eisenthal, R.; Harrison, R. Antimicrobial properties of milk: Dependence on presence of xanthine oxidase and nitrite. *Antimicrob. Agents Chemother.* **2002**, *46*, 3308−3310.
(5) Zheng, S. M. The natural enzymes in milk. *China Dairy Industry* **1986**, *5*, 133−136.
(6) Ngoc, T. M.; Khoi, N. M.; Ha, D. T.; Nhiem, N. X.; Tai, B. H.; Dan, D. V.; Luong, H. V.; Son, D. C.; Bae, K. Xanthine oxidase inhibitory activity of constituents of *Cinnamomum cassia* twigs. *Bioorg. Med. Chem. Lett.* **2012**, *22*, 4625−4628.
(7) Niu, Y. F.; Zhu, H. J.; Liu, J.; Fan, H. F.; Sun, L.; Lu, W.; Liu, X.; Li, L. 3, 5, 2′, 4′-Tetrahydroxychalcone, a new non-purine xanthine oxidase inhibitor. *Chem.-Biol. Interact.* **2011**, *189*, 161−166.
(8) Zhao, M. M.; Zhu, D. S.; Sun-Waterhouse, D. X.; Su, G. W.; Lin, L. Z.; Wang, X.; Dong, Y. In vitro and in vivo studies on adlay-derived seed extracts: Phenolic profiles, antioxidant activities, serum uric acid suppression, and xanthine oxidase inhibitory effects. *J. Agric. Food. Chem.* **2014**, *62*, 7771−7778.
(9) Lü, J. M.; Yao, Q. Z.; Chen, C. Y. 3, 4-Dihydroxy-5-nitrobenzaldehyde (DHNB) is a potent inhibitor of xanthine oxidase: A potential therapeutic agent for treatment of hyperuricemia and gout. *Biochem. Pharmacol.* **2013**, *86*, 1328−1337.
(10) Murata, K.; Nakao, K.; Hirata, N.; Namba, K.; Nomi, T.; Kitamura, Y.; Moriyama, K.; Shintani, T.; Linuma, M.; Matsuda, H. Hydroxychavicol: A potent xanthine oxidase inhibitor obtained from the leaves of betel, *Piper betle*. *J. Nat. Med.* **2009**, *63*, 355−359.
(11) Romano, B.; Pagano, E.; Montanaro, V.; Fortunato, A.; Milic, N.; Borrelli, F. Novel insights into the pharmacology of flavonoids. *Phytother. Res.* **2013**, *27*, 1588−1596.
(12) Rasoulzadeh, F.; Jabary, H. N.; Naseri, A.; Rashidi, M. Fluorescence quenching study of quercetin interaction with bovine milk xanthine oxidase. *Spectrochim. Acta, Part A* **2009**, *72*, 190−193.
(13) Burda, S.; Oleszek, W. Antioxidant and antiradical activities of flavonoids. *J. Agric. Food. Chem.* **2001**, *49*, 2774−2779.
(14) González, R.; Ballester, I.; López-Posadas, R.; Suárez, M. D.; Zarzuelo, A.; Martínez-Augustin, O.; Sánchez De Medina, F. Effects of flavonoids and other polyphenols on inflammation. *Crit. Rev. Food Sci. Nutr.* **2011**, *51*, 331−362.
(15) Tian, J. N.; Liu, J. Q.; Tian, X.; Hu, Z. D.; Chen, X. G. Study of the interaction of kaempferol with bovine serum albumin. *J. Mol. Struct.* **2004**, *691*, 197−202.
(16) Niering, P.; Michels, G.; Wätjen, W.; Ohler, S.; Steffan, B.; Chovolou, Y.; Kampkötter, A.; Proksch, P.; Kahl, R. Protective and detrimental effects of kaempferol in rat H4IIE cells: Implication of oxidative stress and apoptosis. *Toxicol. Appl. Pharmacol.* **2005**, *209*, 114−122.
(17) Olszewska, M. Separation of quercetin, sexangularetin, kaempferol, and isorhamnetin for simultaneous HPLC determination of flavonoid aglycones in inflorescences, leaves, and fruits of three *Sorbus* species. *J. Pharm. Biomed. Anal.* **2008**, *48*, 629−635.
(18) Miean, K. H.; Mohamed, S. Flavonoid (myricetin, quercetin, kaempferol, luteolin, and apigenin) content of edible tropical plants. *J. Agric. Food. Chem.* **2001**, *49*, 3106−3112.
(19) Matei, I.; Hillebrand, M. Interaction of kaempferol with human serum albumin: A fluorescence and circular dichroism study. *J. Pharm. Biomed. Anal.* **2010**, *51*, 768−773.
(20) Nagao, A.; Seki, M.; Kobayashi, H. Inhibition of xanthine oxidase by flavonoids. *Biosci., Biotechnol., Biochem.* **1999**, *63*, 1787−1790.
(21) Fernández, S. P.; Wasowski, C.; Paladini, A. C.; Marder, M. Synergistic interaction between hesperidin, a natural flavonoid, and diazepam. *Eur. J. Pharmacol.* **2005**, *512*, 189−198.
(22) Yu, Z. F.; Fong, W. P.; Cheng, C. H. K. The dual actions of morin (3, 5, 7, 2′, 4′-pentahydroxyflavone) as a hypouricemic agent: Uricosuric effect and xanthine oxidase inhibitory activity. *J. Pharmacol. Exp. Ther.* **2006**, *316*, 169−175.
(23) Pauff, J. M.; Hille, R. Inhibition studies of bovine xanthine oxidase by luteolin, silibinin, quercetin, and curcumin. *J. Nat. Prod.* **2009**, *72*, 725−731.
(24) Tung, Y. T.; Chang, S. T. Inhibition of xanthine oxidase by *Acacia confusa* extracts and their phytochemicals. *J. Agric. Food. Chem.* **2010**, *58*, 781−786.
(25) Lin, L. Z.; Dong, Y.; Zhao, H. F.; Wen, L. R.; Yang, B.; Zhao, M. M. Comparative evaluation of rosmarinic acid, methyl rosmarinate, and pedalitin isolated from *Rabdosia serra* (MAXIM.) HARA as inhibitors of tyrosinase and α-glucosidase. *Food Chem.* **2011**, *129*, 884−889.
(26) Si, Y. X.; Yin, S. J.; Park, D.; Chung, H. Y.; Yan, L.; Lü, Z. R.; Zhou, H. M.; Yang, J. M.; Qian, G. Y.; Park, Y. D. Tyrosinase inhibition by isophthalic acid: Kinetics and computational simulation. *Int. J. Biol. Macromol.* **2011**, *48*, 700−704.
(27) Zhang, G. W.; Ma, Y. D. Mechanistic and conformational studies on the interaction of food dye amaranth with human serum albumin by multispectroscopic methods. *Food Chem.* **2013**, *136*, 442−449.
(28) Nongonierma, A. B.; Mooney, C.; Shields, D. C.; FitzGerald, R. J. Inhibition of dipeptidyl peptidase IV and xanthine oxidase by amino acids and dipeptides. *Food Chem.* **2013**, *141*, 644−653.
(29) Cai, S. B.; Wang, O.; Wang, M. Q.; He, J. F.; Wang, Y.; Zhang, D.; Zhou, F.; Ji, B. P. In vitro inhibitory effect on pancreatic lipase activity of subfractions from ethanol extracts of fermented oats (*Avena sativa* L.) and synergistic effect of three phenolic acids. *J. Agric. Food. Chem.* **2012**, *60*, 7245−7251.
(30) Takahama, U.; Koga, Y.; Hirota, S.; Yamauchi, R. Inhibition of xanthine oxidase activity by an oxathiolanone derivative of quercetin. *Food Chem.* **2011**, *126*, 1808−1811.
(31) Cos, P.; Ying, L.; Calomme, M.; Hu, J. P.; Cimange, K.; Poel, B. V.; Pieters, L.; Vlietinck, A. J.; Berghe, D. V. Structure−activity relationship and classification of flavonoids as inhibitors of xanthine oxidase and superoxide scavengers. *J. Nat. Prod.* **1998**, *61*, 71−76.
(32) Wang, Z. J.; Lee, J.; Si, Y. X.; Oh, S.; Yang, J. M.; Shen, D.; Qian, G. Y.; Yin, S. J. Toward the inhibitory effect of acetylsalicylic acid on tyrosinase: Integrating kinetics studies and computational simulations. *Process Biochem.* **2013**, *48*, 260−266.
(33) Lin, C. M.; Chen, C. S.; Chen, C. T.; Liang, Y. C.; Lin, J. K. Molecular modeling of flavonoids that inhibits xanthine oxidase. *Biochem. Biophys. Res. Commun.* **2002**, *294*, 167−172.
(34) Yan, J. K.; Zhang, G. W.; Hu, Y. T.; Ma, Y. D. Effect of luteolin on xanthine oxidase: Inhibition kinetics and interaction mechanism merging with docking simulation. *Food Chem.* **2013**, *141*, 3766−3773.
(35) Zhang, G. W.; Wang, L.; Pan, J. H. Probing the binding of the flavonoid diosmetin to human serum albumin by multispectroscopic techniques. *J. Agric. Food. Chem.* **2012**, *60*, 2721−2729.
(36) Lakowicz, J. R.; Weber, G. Quenching of fluorescence by oxygen. Probe for structural fluctuations in macromolecules. *Biochemistry* **1973**, *12*, 4161−4170.
(37) Cheng, Z. J. Studies on the interaction between scopoletin and two serum albumins by spectroscopic methods. *J. Lumin.* **2012**, *132*, 2719−2729.
(38) Lakowicz, J. R. *Principles of Fluorescence Spectroscopy*; Springer Publications: New York, 2009.
(39) Bi, S. Y.; Ding, L.; Tian, Y.; Song, D. Q.; Zhou, X.; Liu, X.; Zhang, H. Q. Investigation of the interaction between flavonoids and human serum albumin. *J. Mol. Struct.* **2004**, *703*, 37−45.
(40) Shuai, L.; Chen, Z.; Fei, P.; Wang, Q.; Yang, T. M. Spectroscopic analysis on the interaction of ferulic acid and tetramethylpyrazine with trypsin. *J. Lumin.* **2014**, *29*, 79−86.
(41) Ross, P. D.; Subramanian, S. Thermodynamics of protein association reactions: Forces contributing to stability. *Biochemistry* **1981**, *20*, 3096−3102.
(42) Wang, Y. Q.; Zhang, H. M.; Zhang, G. C.; Liu, S. X.; Zhou, Q. H.; Fei, Z. H.; Liu, Z. T. Studies of the interaction between paraquat and bovine hemoglobin. *Int. J. Biol. Macromol.* **2007**, *41*, 243−250.
(43) Lu, J. Q.; Jin, F.; Sun, T. Q.; Zhou, X. W. Multispectroscopic study on interaction of bovine serum albumin with lomefloxacin−copper (II) complex. *Int. J. Biol. Macromol.* **2007**, *40*, 299−304.

DOI: 10.1021/jf505584m
J. Agric. Food Chem. 2015, 63, 526−534

(44) Hadizadeh, M.; Keyhani, E.; Keyhani, J.; Khodadadi, C. Functional and structural alterations induced by copper in xanthine oxidase. *Acta Biochim. Biophys. Sin.* **2009**, *41*, 603−617.
(45) Zhang, Y.; Zhong, Q. X. Binding between bixin and whey protein at pH 7.4 studied by spectroscopy and isothermal titration calorimetry. *J. Agric. Food. Chem.* **2012**, *60*, 1880−1886.
(46) Guo, X. J.; Li, X. Z.; Jiang, Y. C.; Yi, L.; Wu, Q.; Chang, H. C.; Diao, X.; Sun, Y.; Pan, X. T.; Zhou, N. N. A spectroscopic study on the interaction between *p*-nitrophenol and bovine serum albumin. *J. Lumin.* **2014**, *149*, 353−360.
(47) Shen, Q.; Shao, J. L.; Peng, Q.; Zhang, W. J.; Ma, L.; Chan, A. S. C.; Gu, L. Q. Hydroxycoumarin derivatives: Novel and potent α-glucosidase inhibitors. *J. Med. Chem.* **2010**, *53*, 8252−8259.
(48) Ali, H. I.; Fujita, T.; Akaho, E.; Nagamatsu, T. A comparative study of AutoDock and PMF scoring performances and SAR of 2-substituted pyrazolotriazolopyrimidines and 4-substituted pyrazolopyrimidines as potent xanthine oxidase inhibitors. *J. Comput-Aided Mol. Des.* **2010**, *24*, 57−75.
(49) Gibson, E. A.; Duhme-Klair, A. K.; Perutz, R. N. Design and synthesis of water soluble (metallo) porphyrins with pendant arms: Studies of binding to xanthine oxidase. *New J. Chem.* **2010**, *34*, 1125−1134.
(50) Kartono, F.; Maibach, H. I. Irritants in combination with a synergistic or additive effect on the skin response: An overview of tandem irritation studies. *Contact Dermatitis* **2006**, *54*, 303−312.

DOI: 10.1021/jf505584m
J. Agric. Food Chem. 2015, 63, 526−534

JOURNAL OF AGRICULTURAL AND FOOD CHEMISTRY

Article

pubs.acs.org/JAFC

Structure Characterization of a Novel Polysaccharide from *Dictyophora indusiata* and Its Macrophage Immunomodulatory Activities

Wenzhen Liao,[†] Zhen Luo,[‡] Dan Liu,[†] Zhengxiang Ning,[†] Jiguo Yang,*[,†] and Jiaoyan Ren*[,†]

[†]College of Light Industry and Food Sciences, South China University of Technology, Guangzhou, Guangdong 510640, People's Republic of China

[‡]Research and Development Center, Infinitus (China) Company, Limited, Guangzhou, Guangdong 510665, People's Republic of China

ABSTRACT: A novel polysaccharide, here named DP1, was isolated from the fruiting body of *Dictyophora indusiata* using a water extraction method. Structure characterization revealed that DP1 had an average molecular weight of 1132 kDa and consisted of glucose (56.2%), galactose (14.1%), and mannose (29.7%). The main linkage type of DP1 were proven to be (1 → 3)-linked α-L-Man, (1 → 2,6)-linked α-D-Glc, (1 → 6)-linked β-D-Glc, (1 → 6)-linked β-D-Gal, and (1 → 6)-linked β-D-Man by periodate oxidation−Smith degradation and nuclear magnetic resonance analysis. The immunostimulating assay indicated that DP1 could significantly promote macrophage NO, TNF-α, and IL-6 secretion in murine RAW 264.7 cells involving complement receptor 3 (CR3). The immune activities of DP1 were quite stable under thermal processing (100, 121, and 145 °C). Besides, DP1 retained stability after acidic/alkline treatment (pH 4.0−10.0), which enabled it to be an ideal complementary medicine or functional food for therapeutics of hypoimmunity and immunodeficiency diseases.

KEYWORDS: *polysaccharide, Dictyophora indusiata, structure characterization, immunostimulating, complement receptor 3*

INTRODUCTION

Dictyophora indusiata, a member of the Phallaceae Corda family, is one of the most popular edible mushrooms consumed worldwide. Because of its attractive appearance, distinctive flavor, and high nutritive value, *D. indusiata* is also regarded as "queen of the mushrooms".[1] *D. indusiata* can also be used as a biopharmaceutical material with various therapeutic properties. In recent decades, many active compounds (e.g., polysaccharides, flavonoids, or proteins) from *D. indusiata* have been reported to possess immunoregulation, antioxidant, antityrosinase, anti-inflammatory, and neuroprotective activities.[2−4] Thereamong, the polysaccharides of *D. indusiata* received much more attention because of their multiple beneficial potency and relatively low toxicity.[5,6] To date, a couple of polysaccharides with various bioactivities have been purified from the fruiting body of *D. indusiata*, but rare information is available concerning their chemical structure and immunomodulatory activities.

Macrophage is one kind of the phagocyte that plays pivotal roles in the innate immune responses.[7,8] When the host is invaded by pathogenic organisms, macrophages can serve as antigen-presenting cells (APCs) that present antigen to T lymphocytes and, thus, induce the adaptive immune response.[9] Furthermore, macrophages also play important roles in embryogenesis, tumorigenesis, cutaneous wound healing, and hematopoiesis.[10−15] Thus, macrophages are usually used as ideal cell models to evaluate the immunomodulatory properties of bioactive compounds. Some botanical polysaccharides have been found to enhance the viability of macrophage against pathogenic microorganisms and tumorigenesis by increasing the secretion of nitric oxide (NO) and the production of cytokines, including tumor necrosis factor α (TNF-α) and interleukin (IL-1, IL-2, IL-6, IL-8, IL-10, and IL-12),[16−18] and it has been thought that polysaccharides can bind to specific membrane receptors of macrophage and activate the immune response through distinct signal transduction pathways.[19,20] However, the exact mechanisms involved in the activation of macrophages by polysaccharides are still not clear. For this sake, it is meaningful to explore the structural characterizations, biological functions, and molecular mechanisms of the polysaccharides from *D. indusiata*.

In the present study, a new polysaccharide, here called Dp1, with a purity of >97.5%, was separated from *D. indusiata*. The primary chemical structure and conformation of Dp1 were characterized. Also, its immunomodulatory activities and membrane receptors were examined using a murine RAW 264.7 macrophage model. The thermal stability of the Dp1 bioactivity against heat treatment was investigated, and its stability against acidic/alkali treatment at different pH conditions was studied as well. In addition, the possible signal transduction pathways involved in macrophage activation by Dp1 were discussed, and the results from this study might supply useful information to understand better the chemical structure and immunomodulatory activities of botanical polysaccharides.

MATERIALS AND METHODS

Materials and Reagents. *D. indusiata* was collected from Zhijin, Guizhou, China. The murine macrophage cell line RAW 264.7 was

Received: September 27, 2014
Revised: December 19, 2014
Accepted: December 19, 2014
Published: December 19, 2014

ACS Publications © 2014 American Chemical Society

DOI: 10.1021/jf504677r
J. Agric. Food Chem. 2015, 63, 535−544

obtained from American Type Culture Collection (ATCC, Rockville, MD). Dulbecco's modified Eagle's medium (DMEM), Fetal bovine serum (FBS), phosphate-buffered saline (PBS, pH 7.4), penicillin, and streptomycin were purchased from Gibco Life Technologies (Grand Island, NY). Anti-TLR2 antibody, anti-CR3 antibody, and anti-TLR4 antibody were obtained from Abcam, Inc. (Cambridge, MA). Laminarin and lipopolysaccharide (LPS) were obtained from Sigma Company (St. Louis, MO). Diethylaminoethyl (DEAE)-52 cellulose and Sephadex G-200 were purchased from GE Healthcare Life Science (Piscataway, NJ). A NO-detecting kit was purchased from Nanjing Jiancheng Institute of Biotechnology (Nanjing, China). Mouse IL-6 enzyme-linked immunosorbent assay (ELISA) kit and mouse TNF-α ELISA kit were acquired from Neobioscience Technology Co., Ltd. (Shenzhen, China). Standards of dextrans, uronic acid, phycite, glycerol, glycol reference, and monosaccharide references (e.g., glucose, galactose, xylose, mannose, and rhamnose) were purchased from Sigma Company (St. Louis, MO). The ultrapure water was obtained from a Milli-Q water purification system of Millipore (Bedford, MA). All of the other chemical reagents used in this study were of analytical grade.

Extraction and Purification of Polysaccharides from the Fruiting Body of *D. indusiata*. The fruiting body of *D. indusiata* was dried in a hot air-drying oven at 40 °C and crushed into powder using a tissue triturator. The powder of the fruiting body was extracted with boiling water at a ratio of 1:30 (w/w) for 2 h, and the obtained extract was centrifuged at 4000*g* for 15 min. The supernatant was then collected and concentrated at 60 °C. After that, the concentrated supernatant was deproteinated according to the Sevag method.[21] To remove the protein as much as possible, this deproteination process was repeated 10 times. The resulting solution was mixed with three volumes of absolute ethanol and kept overnight at 4 °C. The supernatant and precipitate were then separated by centrifugation at 5000*g* for 15 min. Finally, the precipitate was dried using vacuum freeze drying and collected as crude polysaccharides.

A total of 100 mg of crude polysaccharides was dissolved in 10 mL of ultrapure water and loaded onto a DEAE-52 anion-exchange chromatography column (2.5 × 60 cm). The elution was conducted using ultrapure water first and then by a series of NaCl solution in the sequence of 0.05, 0.1, 0.2, 0.3, and 0.5 M, at a flow rate of 0.5 mL/min. The eluent fractions were collected and analyzed by the phenol−sulfuric acid method.[22] Two fractions, DP1 (eluted by ultrapure water) and DP2 (eluted by 0.05 M NaCl) were obtained, dialyzed at 4 °C for 48 h, and lyophilized. In this study, we mainly focused the investigation on DP1, and the other fraction will be studied later.

After that, the DP1 fraction was further purified by Sephadex G-200 column chromatography. A total of 20 mg of DP1 was redissolved in 4 mL of ultrapure water and applied to a Sephadex G-200 column (2.5 × 60 cm). The sample was eluted with ultrapure water at a speed of 0.5 mL/min, and then the eluent was collected and detected using the phenol−sulfuric acid method for the determimation of 97.5% content.

Structure Characterization of DP1. *Molecular Weight Determination of DP1.* The weight-average molecular weight distribution of DP1 was analyzed by high-performance gel permeation chromatography (HPGPC, Waters, Milford, MA) on a Waters HPLC instrument with a TSK-GEL G-5000 PWXL column (300 × 7.8 mm inner diameter, 10 μm) and a TSK-GEL G-3000PWXL column (300 × 7.8 mm inner diameter, 6 μm, Tosoh Co., Ltd., Tokyo, Japan), using 0.01 mol/L KH_2PO_4 as the mobile phase at a flow rate of 0.6 mL/min.

Infrared (IR) Spectrum Analysis. The IR spectra of DP1 was analyzed according to the KBr disk method[23] using a Fourier transform infrared (FTIR) spectrophotometer (Bruker, Ettlingen, Germany) in the range of 400−4000 cm^{-1}.

Chemical Composition of DP1. A total of 20 mg of DP1 was hydrolyzed by 4 mL of trifluoroacetic acid (TFA) at 105 °C for 6 h. Excess of TFA was removed by rotary evaporation. Then, the residue was redissolved in methanol and dried by rotary evaporation. Finally, the residue was dissolved in ultrapure water and analyzed by ion-exchange chromatography (Dionex ICS-3000) equipped with an integrated amperometric detector and a Carbopac PA20 column (2 × 250 mm). The elution was conducted at a rate of 0.6 mL/min at a column temperature of 20 °C. Gradient elution was carried out according to the following process: 0−2 min, 100% 200 mmol/L NaOH; 2.1−20 min, 10% 20 mmol/L NaOH and 90% ultrapure water; and 20.1−40 min, 100% 200 mmol/L NaOH. The glucose, galactose, xylose, mannose, and rhamnose standards were derivatized as previously reported.[4] Acetyl inositol was used as the interior reference.

Periodate Oxidation−Smith Degradation. The periodate oxidation−Smith degradation method was taken out according to the report by Chi et al.,[24] with some modification. A total of 25 mg of DP1 sample was dissolved in 12.5 mL of ultrapure water and incubated with 12.5 mL of $NaIO_4$ (30 mmol/L) in the dark at room temperature. During the incubation period, 0.1 mL of the reaction liquid was taken out from the reaction system at different time intervals (0, 6, 12, 24, 36, 48, and 60 h), diluted into 100 mL with ultrapure water, and measured at 223 nm by an ultraviolet−visible (UV−vis) spectrophotometer (model UV-18000, Shimadzu, Japan) until the absorbance value became invariable. The process of periodate oxidation was stopped by the addition of 2 mL of glycol. Then, 2 mL of periodate product was titrated by 0.01 mol/L NaOH to quantify the production of formic acid. The rest of the periodate product was dialyzed in distilled water for 72 h and concentrated by rotary evaporation. Then, 70 mg of $NaBH_4$ was added to the residuary solution and kept in the dark for 24 h. The solution was adjusted to pH 5.0 with 0.1 mol/L acetic acid and dialyzed in distilled water for another 72 h. The solution was then concentrated and freeze-dried. A total of 10 mg of the residues was hydrolyzed by 4 mL of 2 mol/L TFA at 105 °C for 6 h. The lysate was acetylized with 1 mL of pyridine and 10 mg of hydroxylamine hydrochloride at 90 °C for 30 min. Then, 1 mL of acetic anhydride was added to the reaction system and continuously heating at 90 °C for another 30 min. The production of acetate derivative was analyzed by a gas chromatograph system (Aglient, 6890N, Agilent Technologies, Inc., Santa Clara, CA) with a DB-1701 capillary column (30 m × 0.25 mm × 0.25 μm, J&W Scientific, Fulsom, CA) and a flame ionization detector. The linearly heating program is from 80 to 220 °C at a speed of 2 °C/min, from 220 to 250 °C at a speed of 5 °C/min, and kept at 250 °C for 5 min. The temperature of the detector was set at 300 °C. Phycite, glycerol, glycol, rhamnose, arabinose, xylose, galactose, mannose, and glucose were used as standards.

Nuclear Magnetic Resonance (NMR). A total of 35 mg of DP1 was dissolved in 0.5 mL of D_2O in a NMR tube and then analyzed by a Bruker 600 MHz NMR apparatus (Bruker Corp., Fallanden, Switzerland).[25]

Thermogravimetric Analysis (TGA). The thermostability of DP1 was analyzed using TGA (Pyris Diamond TG−DTA, PerkinElmer Co., Waltham, MA). A total of 5 mg of DP1 sample was placed in the Al_2O_3 pan and heated from 60 to 600 °C with a heating rate of 10 °C/min. The analysis was conducted under a pure nitrogen gas atmosphere at a flow rate of 30 mL/min.

Immunomodulatory Activity and Stability Assay. *Cell Culture and Immunomodulatory Activity Test.* RAW 264.7 cells were cultured with DMEM plus 10% fetal bovine serum (FBS), 100 μg/mL streptomycin, and 100 units/mL penicillin and incubated at 37 °C with a 5% CO_2 humidified atmosphere in a carbon dioxide cell incubator. Cells were adjusted to a concentration of 1×10^6 cells/mL in the exponential phase, loaded onto the 96 well microplate (100 μL/well), and continuously incubated for 24 h. Then, the culture medium was changed to a new medium with DP1 samples and incubated for another 24 h. Antibodies (anti-TLR2, anti-CR3, and anti-TLR4, at a concentration of 5 μg/mL) and laminarin (500 μg/mL, the inhibitor of dectin-1) were added to cells to investigate the membrane receptors of DP1 on the RAW 264.7 cells. The cells were pretreated with antibodies and laminarin for 2 h prior to stimulation with different concentrations of DP1 (125, 250, 500, and 1000 μg/mL) and incubated for 24 h. LPS (50 μg/mL) was used as the positive control. After that, the supernatants of cells were collected and the levels of NO, TNF-α, and IL-6 were measured using a NO-detecting kit, mouse TNF-α ELISA kit, and mouse IL-6 ELISA kit, respectively, according to the instructions of the manufacturer.

Immunomodulatory Stability Assay. *Thermal Treatment.* DP1 was dissolved in PBS (pH 7.4) to make a final concentration of 500 μg/mL and subjected to different heat treatments (100 °C × 30 min, 121 °C

DOI: 10.1021/jf504677r
J. Agric. Food Chem. 2015, 63, 535−544

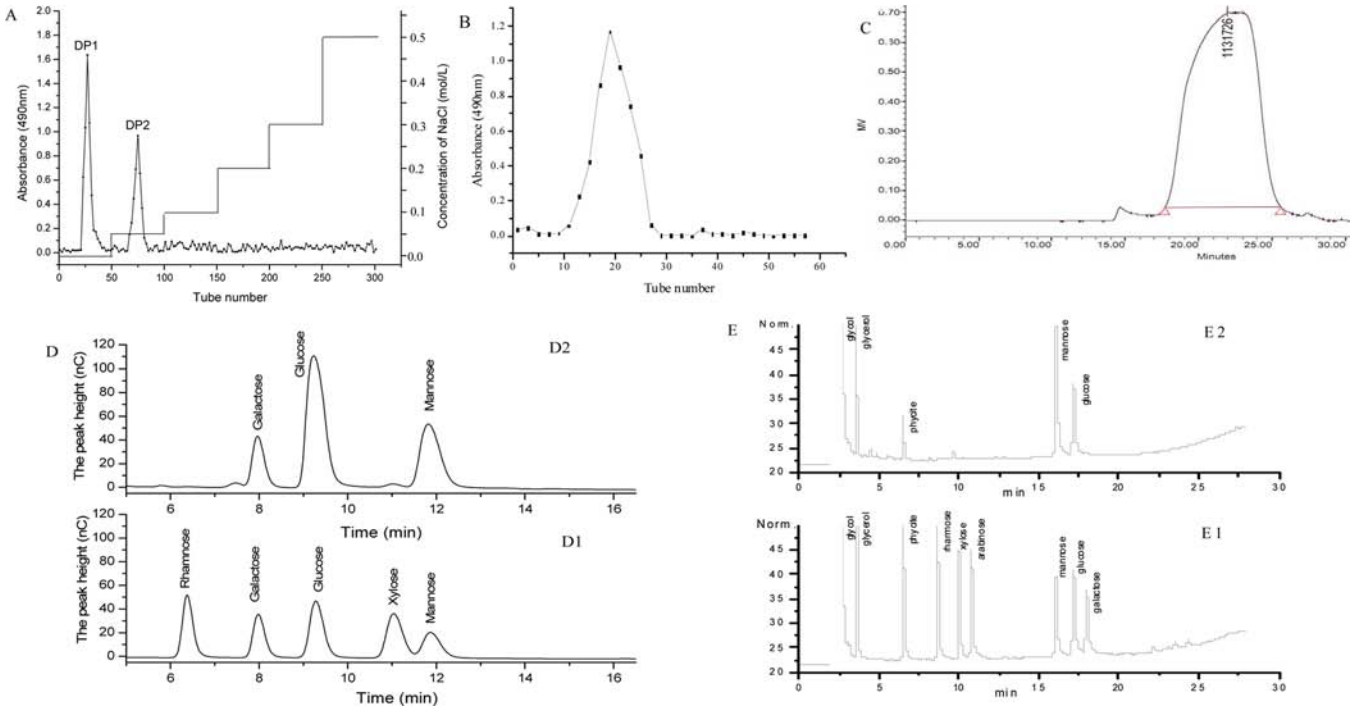

Figure 1. Chromatography of the polysaccharides from *D. indusiata* (DP1) by (A) DEAE-52 cellulose (DEAE-52), (B) Sephadex G-200, (C) HPGPC, (D) ion-exchange chromatography of the monosaccharide mixture (D1) and DP1 sample (D2), and (E) gas chromatography of the monosaccharide mixture (E1) and DP1 sample (E2).

× 30 min, and 145 °C × 30 min) and then cooled to room temperature. After that, DP1 was sterilized by a 0.22 μm microporous filtering film and then incubated with RAW 264.7 cells for 24 h. The changes of NO, TNF-α, and IL-6 levels were detected as described above.

Acidic/Alkaline Treatment. DP1 (500 μg/mL) was dissolved in different phosphate buffers to make final pH 2.0, 4.0, 6.0, 7.4, 8.0, and 10.0 and then kept overnight at room temperature. DP1 with different pH values was sterilized by 0.22 μm microporous filtering film and then incubated with RAW 264.7 cells for 24 h. The changes of NO, TNF-α, and IL-6 levels were detected as described above.

Combined Thermal Treatment and Acidic/Alkaline Treatment. DP1 (500 μg/mL) was dissolved in different phosphate buffers at pH 2.0, 4.0, 6.0, 7.4, 8.0, and 10.0. Then, the solution were heated at 121 °C for 30 min. All samples were sterilized by a 0.22 μm microporous filtering film and then incubated with RAW 264.7 cells for 24 h. The changes of NO, TNF-α, and IL-6 levels were detected as described above.

Statistical Analysis. Data were presented as the mean ± standard deviation (SD) for at least three replicates and analyzed by SPSS 16.0 (SPSS, Inc., Chicago, IL). Significance was determined at p values below 0.05 by analysis of variance (ANOVA). The difference between three or more groups was analyzed by one-way ANOVA multiple comparisons.

RESULTS AND DISCUSSION

Extraction and Purification of Polysaccharides from *D. indusiata*. Crude polysaccharides were isolated from the fruiting body of *D. indusiata* with a yield of 6.36%. The extracts were first purified by a DEAE-52 anion-exchange chromatography column (Figure 1A). Two independent peaks, DP1 (eluted by ultrapure water) and DP2 (eluted by 0.05 mol/L NaCl), were obtained. In the present study, we mainly focused on DP1, and the property of DP2 will be studied in our future work. The DP1 fraction was further purified by a Sephadex G-200 column. As shown in Figure 1B, a single peak of DP1 was observed. Finally, the DP1 fraction with a purity of >97.5% was obtained after dialysis and lyophilization.

Characterization of DP1. *Molecular Weight of DP1.* The weight-average molecular weight of DP1 was measured by HPGPC.[26] As shown in Figure 1C, a single peak was observed on the chromatogram and the molecular weight of DP1 was determined to be 1132 kDa. This result showed a great difference from the previous research by Hua et al.,[1] which indicated that the molecular weight of two polyacchrides from *D. indusiata* were 2100.99 and 18.16 kDa. The difference of the extraction method, the habitat, and the strain of *D. indusiata* may lead to the differences of molecular weights.

Monosaccharide Composition Assay. The monosaccharide composition of DP1 was analyzed using ion chromatography. As shown in Figure 1D, three monosaccharides, including galactose, glucose, and mannose, were identified according to the elution time of relative monosaccharide standards. The molar percentages of galactose, glucose, and mannose were 14.1, 56.2, and 29.7%, respectively. The results were different from that by Hua et al., who found that water-soluble polysaccharides from *D. indusiata* were composed of xylose, galactose, glucose, and mannose, with the molar percentages of 22.6, 18.6, 13.9, and 44.9%, respectively.[1]

Periodate Oxidation–Smith Degradation Analysis. The results for the periodate oxidation analysis of DP1 showed that 1.27 mol of periodate was consumed by every molar of sugar residues and 0.63 mol of acid was produced, indicating the existence of (1 → 2)- or (1 → 6)-linked glycosidic bonds. The periodate-oxidized DP1 sample was further analyzed by Smith degradation. Glycerol, erythritol, galactose, glucose, and mannose were observed after Smith degradation (Figure 1E). The presence of glycerol indicated the existence of (1 → 2)- or (1 → 6)-linked glycosidic bonds, while erythritol corresponded to the presence of (1 → 4)-linked glycosidic bonds. The presence of monosaccharides revealed the appearance of (1 → 3)-linked glycosidic bonds.

DOI: 10.1021/jf504677r
J. Agric. Food Chem. 2015, 63, 535−544

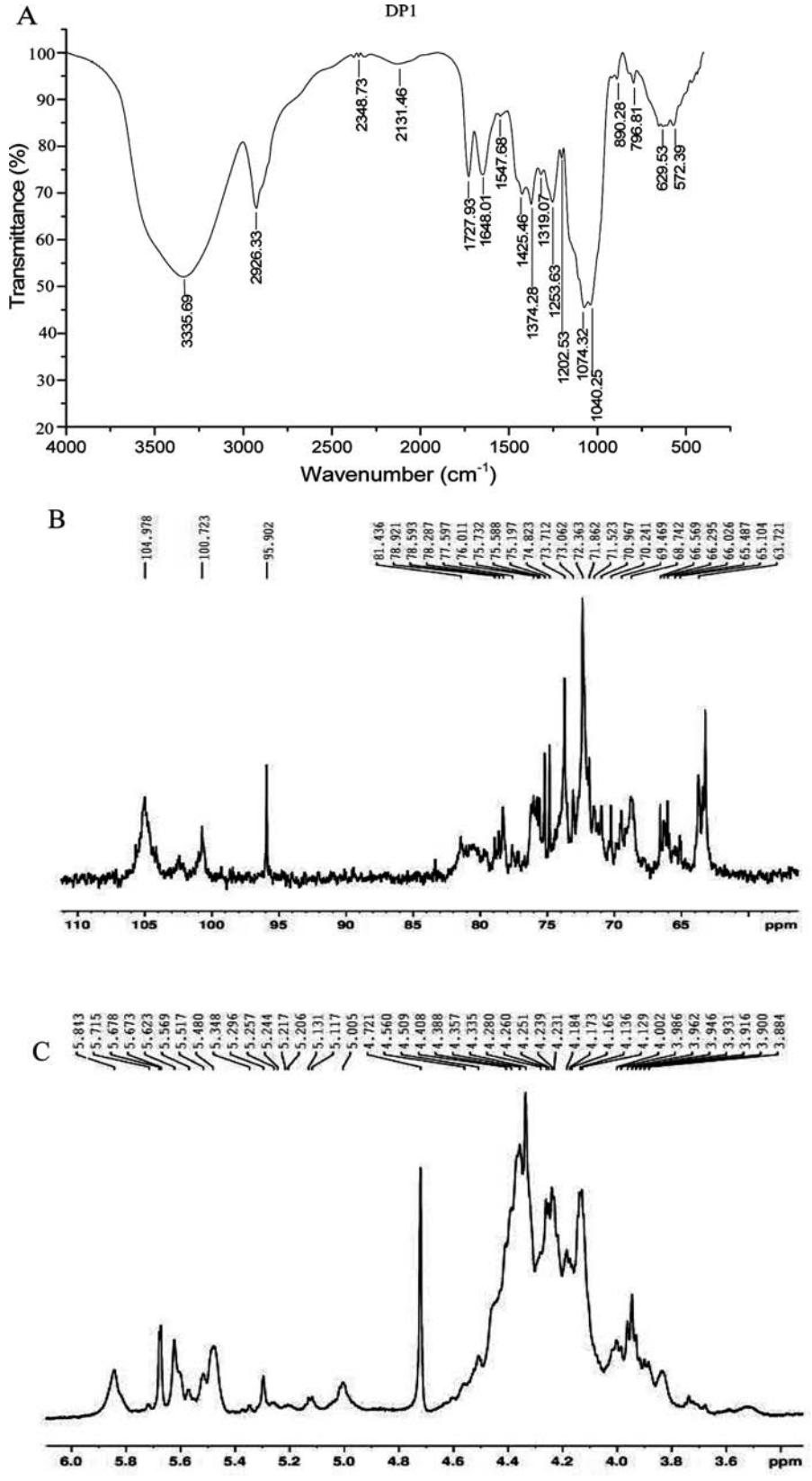

Figure 2. (A) FTIR spectrum, (B) ^{13}C NMR spectrum, and (C) ^{1}H NMR spectrum of the polysaccharides from *D. indusiata* (DP1).

IR Spectrum Analysis. The IR spectra of DP1 is shown in Figure 2A. The stretching intense characteristic peaks at 3335.69 cm^{-1} indicated the hydroxyl stretching vibration of the polysaccharide chains. The peak around 2926.33 cm^{-1} was attributed to the C−H stretching vibration.[27] The band at 1648.01 cm^{-1} may be due to the bound water. The absorption peaks between 1430 and 1200 cm^{-1} indicated the presence of the O−H deformation vibrations and C−O stretching vibrations,

DOI: 10.1021/jf504677r
J. Agric. Food Chem. 2015, 63, 535−544

respectively.[28] The bands at 1074.32 and 1040.25 cm^{-1} suggested that the skeletal modes of DP1 were pyranose rings. The absorption at 866 cm^{-1} indicated the β- pyranoside linkage in DP1. A characteristic peak at 796.81 cm^{-1} represented the presence of mannose.

NMR Analysis of DP1. The spectra of ^{1}H and ^{13}C NMR of DP1 are shown in panels B and C of Figure 2. The signals of DP1 in ^{1}H and ^{13}C NMR spectra were attributed on the basis of monosaccharide, glycosidic linkages, and chemical shifts.[29] The resonance signals of ^{13}C NMR between 95.0 and 110.0 ppm belonged to the anomeric carbon atoms of L-mannose, L-arabinose, D-galactose, D-glucose, and L-rhamnose.[29] The peak at 95.902 ppm suggested the presence of C-1 of a (1 → 3)-linked α-L-Man unit, and the peak at 100.723 ppm indicated the presence of C-1 of a (1 → 3)-linked α-D-Gal unit. Another peak at 104.978 ppm proved the presence of C-1 of a (1 → 2,6)-linked α-D-Glc unit, and the peak at 69.469 ppm corresponded to C-6 of a (1 → 6)-linked β-D-Glc unit. Besides, the peat at 68.742 ppm suggested the presence of C-6 of a (1 → 6)-linked β-D-Gal unit, and the peak at 66.569 ppm corresponded to the C-6 of a (1 → 6)-linked β-D-Man unit. The peaks in the region of 78.287−81.436 ppm (78.287, 78.593, 78.921, and 81.436 ppm) were attributed to the presence of (1 → 2)-, (1 → 3)-, or (1 → 4)-linked glycosidic bonds. The configuration of the glycosidic linkage of DP1 was analyzed by ^{1}H NMR spectra. The signals of ^{1}H NMR in the region of 5.400−5.843 ppm (5.483, 5.517, 5.569, 5.623, 5.673, 5.678, 5.715, and 5.843 ppm) indicated the presence of α-form furanose. The peaks at 5.000−5.400 ppm (5.005, 5.117, 5.131, 5.206, 5.217, 5.244, 5.257, 5.296, and 5.348 ppm) were attributed to the presence of α-form pyranose.

Immunomodulatory Activities of DP1. *Effects of DP1 on Macrophage NO, TNF-α, and IL-6 Production.* Modulation of the innate immune system can enhance the resistant ability of the host to exogenous pathogen threats.[30] It is thought that the stimulation of the immune system might be mainly through the activation of the macrophage and complement system.[31,32] Macrophage activation by immunomodulators is considered to be via the induction of NO expression and enhanced production of cytokines (TNF-a, IL-1, IL-6, IL-12, IL-10, etc.).[33] Thus, the effects of DP1 on macrophage NO, TNF-α, and IL-6 production were analyzed in this study. Untreated RAW 264.7 cells secreted very little NO, whereas the addition of DP1 in the medium significantly increased NO secretion in a dose-dependent manner (125−1000 μg/mL; Figure 3A). The concentration of NO reached 11.72 μmol/mL after treatment by 500 μg/mL DP1; this is higher than a polysaccharide from *Lentinula edodes* reported by Xu et al.[19] In the study by Xu et al., the concentration of NO was lower than 4 μmol/mL after treatment by 500 μg/mL of *L. edodes* polysaccharide. Meanwhile, DP1 had similar dose-dependent manner effects on macrophage TNF-α and IL-6 production (panels B and C of Figure 3). The macrophage IL-6 level (e.g., 1134 pg/mL IL-6 at 250 μg/mL DP1) treated by DP1 is higher than that of some polysaccharide fractions isolated from *Opuntia polyacantha*[14] (lower than 1000 pg/mL IL-6 at 250 μg/mL of some *O. polyacantha* fractions), whereas the TNF-α level (e.g., 588 pg/mL TNF-α at 250 μg/mL DP1) treated by DP1 is lower than that of a polysaccharide from *Ganoderma atrum* (over 1400 pg/mL TNF-α at 160 mg/mL *G. atrum* polysaccharide).[34] The results suggested that DP1 exhibited remarkable immunomodulatory activities by upregulation of NO, TNF-α, and IL-6 secretion in RAW 264.7 cells.

Roles of Complement Receptor 3 (CR3), Toll-Like Receptors (TLR2 and TLR4), and Dectin-1 on DP1-Induced Macrophage Immunomodulation. It has been proposed that macrophage activation is mediated primarily through the recognition of pathogen-associated molecular patterns (PAMPs) by pattern recognition receptors (PRRs) on the surface of macrophage cells. Stimulation of PRRs leads to the initiation of intracellular signaling pathways and eventually induces transcriptional activation and expression of cytokines. Recent evidence suggests that macrophages might bind polysaccharides and mediate immunomodulating effects mainly through CR3, TLR2, TLR4,

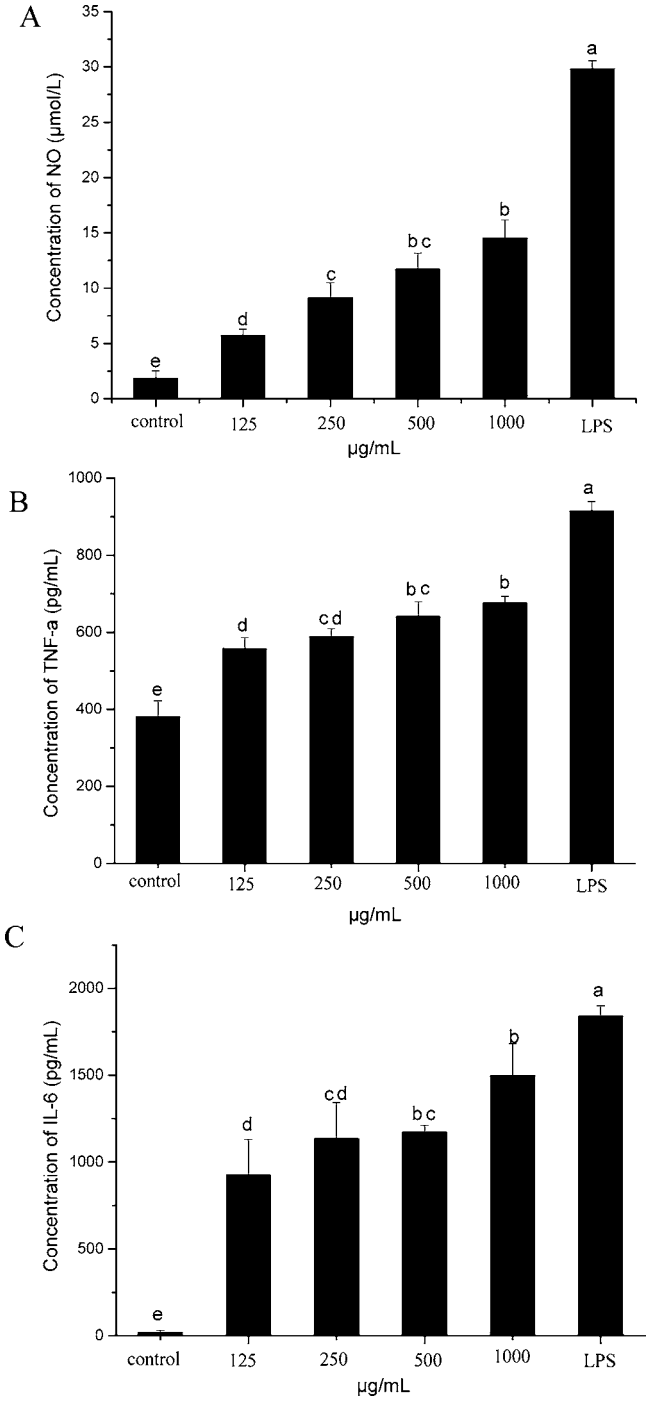

Figure 3. Effects of different concentrations of *D. indusiata* polysaccharides (DP1) on macrophage (A) NO, (B) TNF-α, and (C) IL-6 secretion in RAW 264.7 cells. The group without adding DP1 was used as the control, and LPS (50 μg/mL) was used as the positive control.

DOI: 10.1021/jf504677r
J. Agric. Food Chem. 2015, 63, 535−544

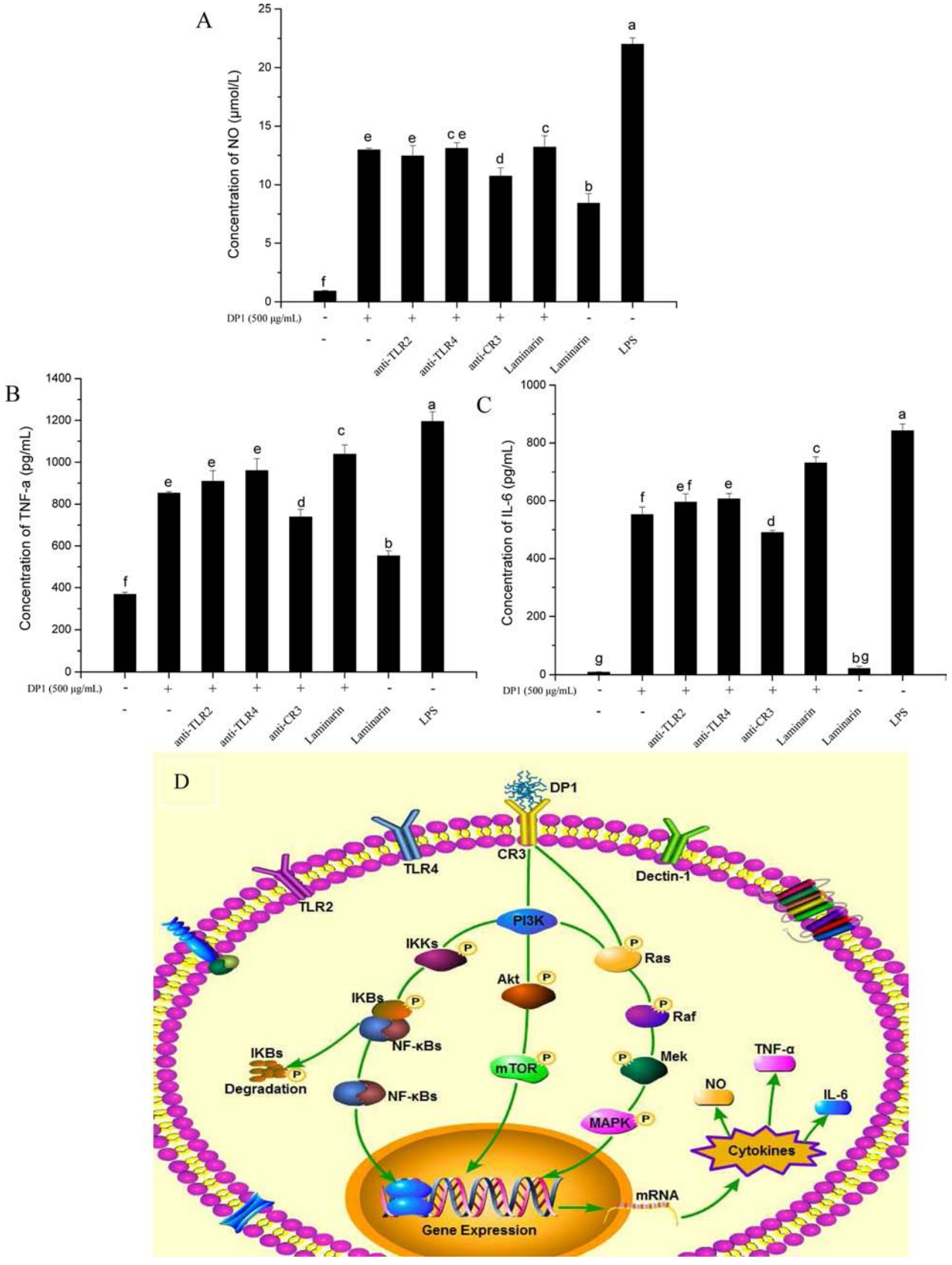

Figure 4. Roles of CR3, TLR2, TLR4, and dectin-1 on DP1 (the polysaccharides of *D. indusiata*)-induced (A) NO, (B) TNF-α, and (C) IL-6 secretion in RAW 264.7 cells. The cells were incubated with monoclonal antibodies (anti-TLR2, anti-CR3, and anti-TLR4) for 2 h and then washed with PBS 3 times before stimulating with DP1. For the dectin-1 group, cells were incubated with laminarin (inhibitor of dectin-1) for 2 h before stimulating with DP1 without washing with PBS. (D) Possible molecular mechanism of DP1-induced macrophage immunomodulation.

DOI: 10.1021/jf504677r
J. Agric. Food Chem. 2015, 63, 535−544

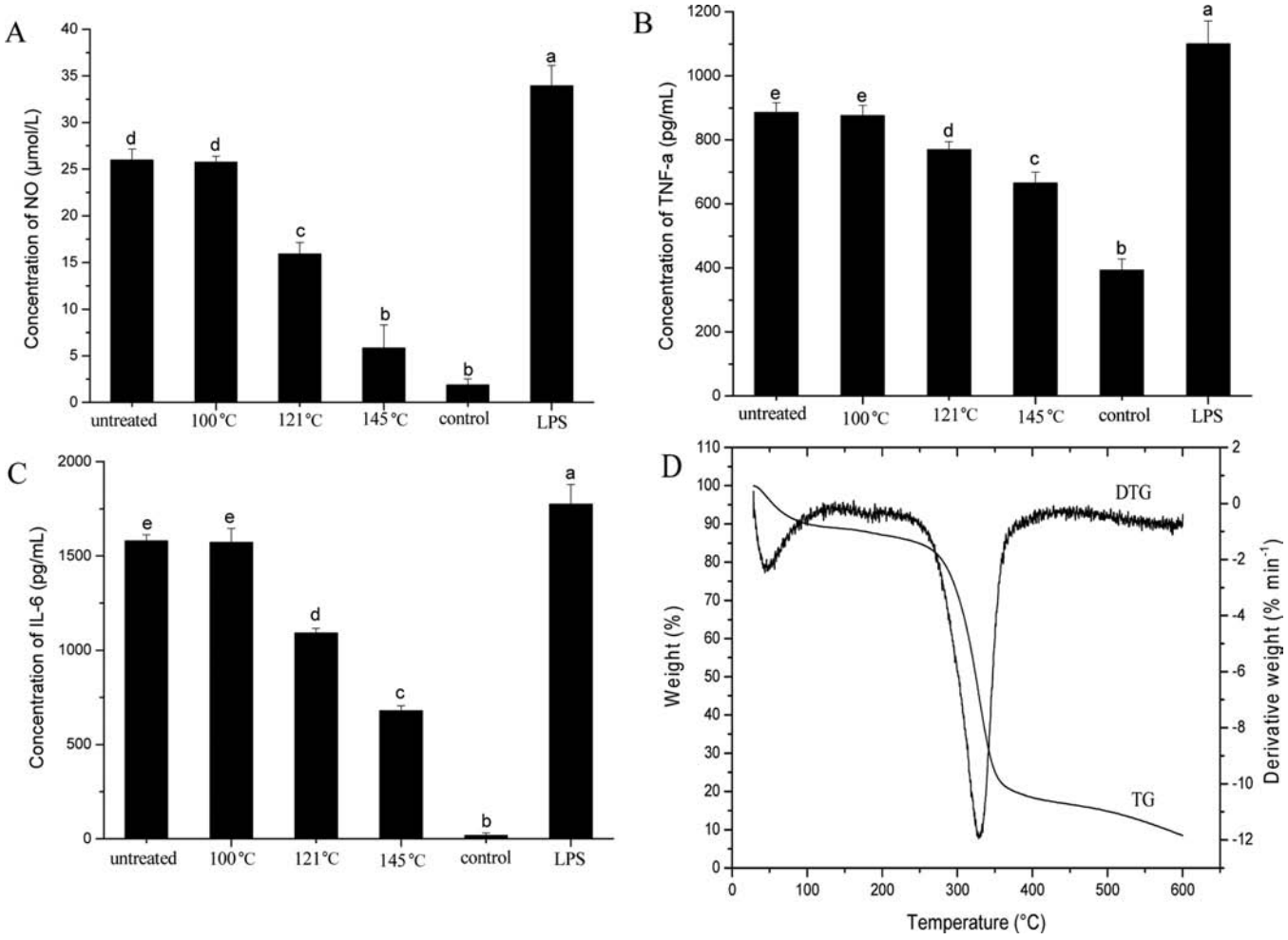

Figure 5. Effects of different temperature treatments on DP1 (the polysaccharides of *D. indusiata*)-induced (A) NO, (B) TNF-α, and (C) IL-6 secretion in RAW 264.7 cells. DP1 samples were divided into three groups and treated at 100, 121, and 145 °C for 30 min. Then, the cells were incubated with heat treatment DP1 samples for 24 h. (D) Thermogravimetry−differential therogravimetry (TG−DTG) curves of DP1.

or dectin-1.[35] In the present study, the roles of CR3, TLR2, TLR4, and dectin-1 on DP1-induced macrophage immunomodulation were investigated. Antibodies, including anti-CR3, anti-TLR2, anti-TLR4, and the inhibitor of dectin-1, laminarin, were preincubated with RAW 264.7 cells for 2 h and then incubated with DP1 for another 24 h. Laminarin is a β-glucan, which can specifically bind to dectin-1 and block the dectin-1-mediated immune responses.[36] The macrophage NO, TNF-α, and IL-6 productions were determined. As shown in panels A−C of Figure 4, after treatment of anti-CR3 and DP1, the levels of NO, TNF-α, and IL-6 were all visibly decreased in comparison to the group treated by DP1 only ($p < 0.05$). However, no decrease was found in the groups treated by anti-TLR2 and anti-TLR4. As for laminarin, it was even enhanced because of its own immunostimulating activity. These results indicated that CR3 was one of the receptors of DP1 on RAW 264.7. Previous studies have proven that CR3 possessed sugar specificity, and the polysaccharides containing *N*-acetyl-D-glucosamine or mannose in addition to glucose are most likely recognized by CR3.[34] Therefore, the mannose and glucose composition of DP1 may contribute to the specific binding of DP1 to CR3 on macrophage. Besides, there might be some other receptors of DP1 on the membrane of macrophage, because the NO level (Figure 4A), TNF-α level (Figure 4B), and IL-6 level (Figure 4C) in the treated group by anti-CR3 and DP1 were still higher than those in the group absent of DP1 treatment. CR3 has been proven to be involved in the activation of phosphoinositide-3-kinase (PI3K), phosphorylation of the downstream serine/threonine kinase Akt and mammalian target of rapamycin (mTOR), activation of the mitogen-activated protein kinase (MAPK), and nuclear factor-κB (NF-κB) signal transduction pathways. Activation of these signaling pathways ultimately leads to gene transcription and production of pro-inflammatory cytokines.[16] Therefore, we can infer that the possible molecular mechanism of DP1-induced macrophage immunomodulation was mainly through activation of the PI3K/Akt/MAPK/NF-κB signaling transduction pathways (Figure 4D), and these pathways will be characterized in our future study.

Effects of Thermal Treatment and Acidic/Alkali Treatment on DP1-Induced Macrophage Immunomodulation. It is well-established that severe environmental conditions, such as high tempreature, high pressure, and extreme pH, have great influence on the advanced structure of macromolecules.[37] In this study, the effects of different heat treatments and acidic/alkali treatments on the immunomodulation activity of DP1 were investigated. It was found that, with the increase of the temperature, DP1 exhibited a substantial decrease effect on macrophage NO, TNF-α, and IL-6 production, as shown in panels A, B, and C of Figure 5, respectively. It may be due to the fact that high temperatures (over 100 °C) can cause the breakdown of non-covalent bonds,

DOI: 10.1021/jf504677r
J. Agric. Food Chem. 2015, 63, 535−544

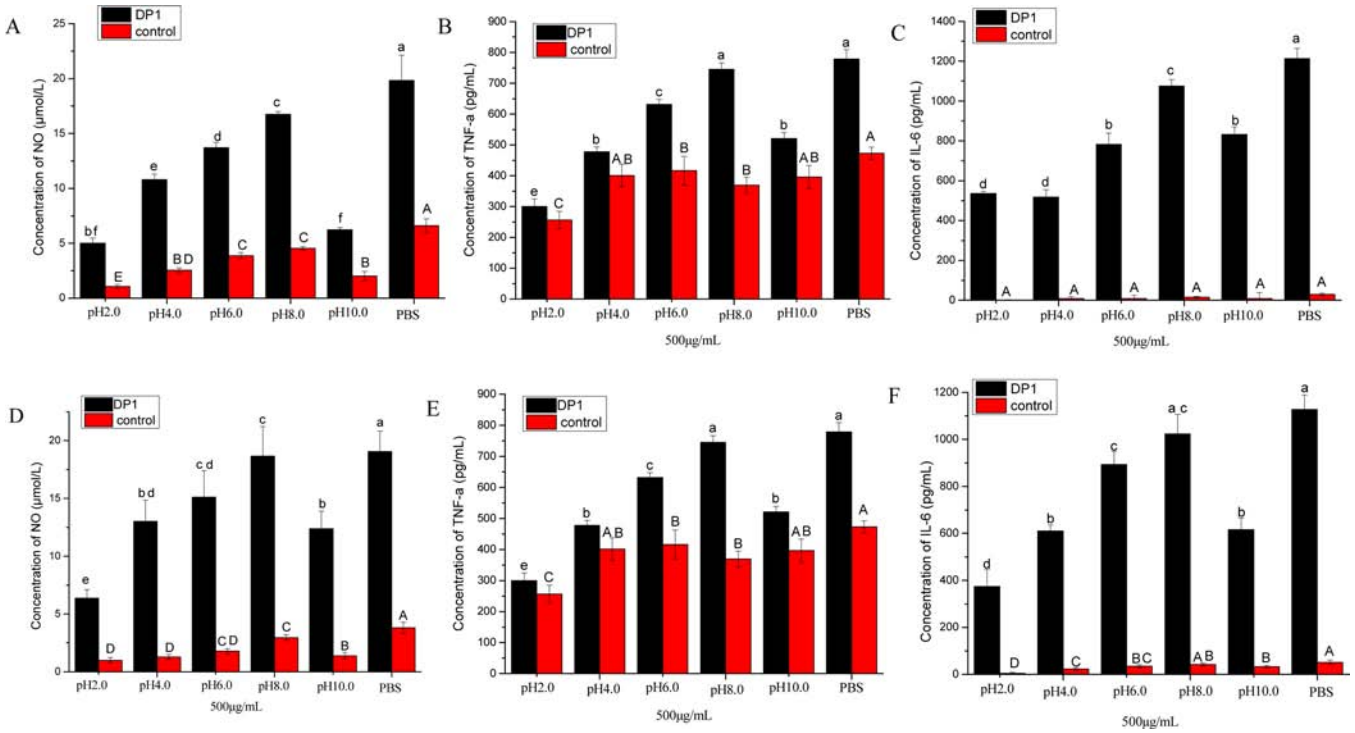

Figure 6. Effects of different pH treatments on DP1 (the polysaccharides of *D. indusiata*)-induced (A) NO, (B) TNF-α, and (C) IL-6 secretion in RAW 264.7 cells. Cells were incubated with DP1 at different pH values of phosphate buffers for 24 h. The cells of the control group were incubated at different pH values of phosphate buffers (without DP1) for 24 h. Co-effects of heat (121 °C) and different pH treatments on DP1-induced (D) NO, (E) TNF-α, and (F) IL-6 secretion in RAW 264.7 cells. Cells were incubated with heat treatment (121 °C) DP1 at different pH values of phosphate buffers for 24 h versus the control groups (without DP1).

such as ionic bonds, hydrogen bonds, and hydrophobic effects of DP1, and thus, in comparison to TNF-α and IL-6, the NO level was more sensitive to heat treatment and the 145 °C processing for 30 min destroyed 77.6% of its native activity. At this point, the immune activities of TNF-α and IL-6 were 24.9 and 57.0% of their native activities, respectively. Although being sensivity to heat treatment, DP1 was still able to upgrade the macrophage NO, TNF-α, and IL-6 levels after treatment at 145 °C. The reason for these results may be mainly because of the fact that thermal treatment just destroyed the higher structure (e.g., triple helical) of DP1. Recent evidence confirmed that the helix−coil transition of polysaccharide was induced by heat treatment at about 130−145 °C because of the breakage of hydrogen bonds.[38] The primary structure may not be damaged under the selected temperatures, although a higher structure may likely contribute much to the biological activity of DP1; the primary structure of DP1 also maintained a considerable part of its immune activity. The thermostability of DP1 was further analyzed using TGA. As shown in Figure 5D, neglecting the small weight loss at around 50 °C, attributed to the vaporization of retained moisture, the decomposition peak of DP1 was found at 329 °C. This degradation temperature of DP1 was much higher than that of the polysaccharides from haloalkalophilic *Bacillus* sp. I-450 (290 °C), as reported by Kumar et al.[39] These results further confirmed that DP1 exhibited good thermostability under extreme heat treatments.

Previous studies have also reported that the non-covalent bonds can also be destroyed in the strong acidic or alkline conditions.[40] Thus, the effects of pH changes on DP1 were investigated as well in the present study. The DP1 samples were pretreated by phosphate buffers with various pH (form 2.0 to 10.0) for 12 h. As shown in panels A−C of Figure 6, it was found that the cells without DP1 protection were very sensitive to different pH treatments, while the addition of DP1 remarkably enhanced the macrophage NO, TNF-α, and IL-6 secretion. Especially for IL-6, the protection effect of DP1 was more obvious. It turns out that, even at pH 4.0, DP1 could still protect the cells to recover 50% of their original NO, TNF-α, and IL-6 concentrations. It demonstrated that the structure of DP1 remained stable in a broad spectrum of pH levels. At alkline conditions (pH 10.0), DP1 showed less protection on the NO level of the cells but still contributed to the TNF-α and IL-6 secretion of macrophage.

The stability of DP1 against both heat treatment and acidic/alkline treatment was further explored. DP1 samples were dissolved in phosphate buffers with different pH values (from 2.0 to 10.0) and then heated at 121 °C for 30 min. The results demonstrated that DP1 still retained its immunomodulatory activities to enhance macrophage NO (Figure 6D), TNF-α (Figure 6E), and IL-6 (Figure 6F) secretion in RAW 264.7 cells. In this way, DP1 was proven to retain stable immunomodulatory activities, even undergoing combined heat treatment and acidic/alkline treatment. It was very interesting that, at pH 10.0, the results showed that the contribution of DP1 to the macrophage NO level was even enhanced after combined treatments (Figure 6D) than single alkline treatment (Figure 6A), and the reason was not yet clear. With the above results, we suggested the potential of DP1 as a novel immunomodulatory agent.

In this study, a new polysaccharide DP1 of 1132 kDa was purified from *D. indusiata*. DP1 consisted of (1 → 3)-linked α-L-Man, (1 → 2,6)-linked α-D-Glc, (1 → 6)-linked β-D-Glc, (1 → 6)-linked β-D-Gal, and (1 → 6)-linked β-D-Man. DP1 possessed significant immunomodulation activities by upregulating macrophage NO, TNF-α, and IL-6 secretion. One of the membrane

DOI: 10.1021/jf504677r
J. Agric. Food Chem. 2015, 63, 535−544

receptors of DP1 on RAW 264.7 was confirmed to be CR3. The PI3K/Akt/MAPK/NF-κB signaling pathways were thought to be involved in the immunomodulation function of DP1. DP1 retained stability across a broad spectrum of pH and thermal treatments. Thus, DP1 demonstrated the potential application as a complementary medicine for the hypoimmunity and immunodeficiency population.

AUTHOR INFORMATION

Corresponding Authors

*Telephone: +86-20-87112594. Fax: +86-20-38897117. E-mail: yangjg@scut.edu.cn.

*Telephone: +86-20-87112594. Fax: +86-20-38897117. E-mail: jyren@scut.edu.cn.

Funding

This study was supported by the National Key Technology Research and Development Program of China in the 12th Five-Year Period (2012BAD33B11), the Fundamental Research Funds for the Central Universities (2014ZZ0063 and 2013ZZ0061), and the Guangdong Natural Science Funds for Distinguished Young Scholars (S2013050013954).

Notes

The authors declare no competing financial interest.

REFERENCES

(1) Hua, Y.; Yang, B.; Tang, J.; Ma, Z.; Gao, Q.; Zhao, M. Structural analysis of water-soluble polysaccharides in the fruiting body of *Dictyophora indusiata* and their *in vivo* antioxidant activities. *Carbohydr. Polym.* **2012**, *87*, 343−347.

(2) Sharma, V. K.; Choi, J.; Sharma, N.; Choi, M.; Seo, S. Y. *In vitro* anti-tyrosinase activity of 5-(hydroxymethyl)-2-furfural isolated from *Dictyophora indusiata*. *Phytother. Res.* **2004**, *18*, 841−844.

(3) Geun Goo, B.; Baek, G.; Jin Choi, D.; Il Park, Y.; Synytsya, A.; Bleha, R.; Ho Seong, D.; Lee, C.; Kweon Park, J. Characterization of a renewable extracellular polysaccharide from defatted microalgae *Dunaliella tertiolecta*. *Bioresour. Technol.* **2013**, *129*, 343−350.

(4) Chen, H.; Yang, T.; Chen, M.; Chang, Y.; Lin, C.; Wang, E. I.; Ho, C.; Huang, K.; Yu, C.; Yang, F. Application of power plant flue gas in a photobioreactor to grow *Spirulina* algae, and a bioactivity analysis of the algal water-soluble polysaccharides. *Bioresour. Technol.* **2012**, *120*, 256−263.

(5) Kanmani, P.; Yuvaraj, N.; Paari, K. A.; Pattukumar, V.; Arul, V. Production and purification of a novel exopolysaccharide from lactic acid bacterium *Streptococcus phocae* PI80 and its functional characteristics activity *in vitro*. *Bioresour. Technol.* **2011**, *102*, 4827−4833.

(6) Tong, H.; Xia, F.; Feng, K.; Sun, G.; Gao, X.; Sun, L.; Jiang, R.; Tian, D.; Sun, X. Structural characterization and *in vitro* antitumor activity of a novel polysaccharide isolated from the fruiting bodies of *Pleurotus ostreatus*. *Bioresour. Technol.* **2009**, *100*, 1682−1686.

(7) Janeway, C. A., Jr.; Medzhitov, R. Innate immune recognition. *Annu. Rev. Immunol.* **2002**, *20*, 197−216.

(8) Uthaisangsook, S.; Day, N. K.; Bahna, S. L.; Good, R. A.; Haraguchi, S. Innate immunity and its role against infections. *Ann. Allergy, Asthma, Immunol.* **2002**, *88*, 253−265.

(9) Birk, R. W.; Gratchev, A.; Hakiy, N.; Politz, O.; Schledzewski, K.; Guillot, P.; Orfanos, C. E.; Goerdt, S. Alternative activation of antigen-presenting cells: Concepts and clinical relevance. *Hautarzt* **2001**, *52*, 193−200.

(10) Lingen, M. W. Role of leukocytes and endothelial cells in the development of angiogenesis in inflammation and wound healing. *Arch. Pathol. Lab. Med.* **2001**, *125*, 67−71.

(11) Klimp, A. H.; De Vries, E.; Scherphof, G. L.; Daemen, T. A potential role of macrophage activation in the treatment of cancer. *Crit. Rev. Oncol. Hematol.* **2002**, *44*, 143−161.

(12) Foo, N.; Ou Yang, H.; Chiu, H.; Chan, H.; Liao, C.; Yu, C.; Wang, Y. Probiotics prevent the development of 1,2-dimethylhydrazine (DMH)-induced colonic tumorigenesis through suppressed colonic mucosa cellular proliferation and increased stimulation of macrophages. *J. Agric. Food Chem.* **2011**, *59*, 13337−13345.

(13) Pan, M.; Chang, Y.; Tsai, M.; Lai, C.; Ho, S.; Badmaev, V.; Ho, C. Pterostilbene suppressed lipopolysaccharide-induced up-expression of iNOS and COX-2 in murine macrophages. *J. Agric. Food Chem.* **2008**, *56*, 7502−7509.

(14) Puangpraphant, S.; de Mejia, E. G. Saponins in yerba mate tea (*Ilex paraguariensis* A. St.-Hil) and quercetin synergistically inhibit iNOS and COX-2 in lipopolysaccharide-induced macrophages through NFκB pathways. *J. Agric. Food Chem.* **2009**, *57*, 8873−8883.

(15) Chiu, F.; Lin, J. HPLC analysis of naturally occurring methylated catechins, 3″-and 4″-methyl-epigallocatechin gallate, in various fresh tea leaves and commercial teas and their potent inhibitory effects on inducible nitric oxide synthase in macrophages. *J. Agric. Food Chem.* **2005**, *53*, 7035−7042.

(16) Schepetkin, I. A.; Quinn, M. T. Botanical polysaccharides: Macrophage immunomodulation and therapeutic potential. *Int. Immunopharmacol.* **2006**, *6*, 317−333.

(17) Lai, P. K. K.; Chan, J. Y. W.; Wu, S. B.; Cheng, L.; Ho, G. K. W.; Lau, C. P.; Kennelly, E. J.; Leung, P. C.; Fung, K. P.; Lau, C. B. S. Anti-inflammatory activities of an active fraction isolated from the root of *Astragalus membranaceus* in RAW 264.7 macrophages. *Phytother. Res.* **2014**, *28*, 395−404.

(18) Kulakowski, D. M.; Wu, S.; Balick, M. J.; Kennelly, E. J. Merging bioactivity with liquid chromatography−mass spectrometry-based chemometrics to identify minor immunomodulatory compounds from a Micronesian adaptogen, *Phaleria nisidai*. *J. Chromatogr. A* **2014**, *1364*, 74−82.

(19) Xu, X.; Yan, H.; Zhang, X. Structure and immuno-stimulating activities of a new heteropolysaccharide from *Lentinula edodes*. *J. Agric. Food Chem.* **2012**, *60*, 11560−11566.

(20) Gordon, S. Pattern recognition receptors: Doubling up for the innate immune response. *Cell* **2002**, *111*, 927−930.

(21) Staob, A. M. Removal of proteins from polysaccharides methods. *Carbohydr. Chem.* **1965**, *5*, 1−5.

(22) Dubois, M.; Gilles, K. A.; Hamilton, J. K.; Rebers, P.; Smith, F. Colorimetric method for determination of sugars and related substances. *Anal. Chem.* **1956**, *28*, 350−356.

(23) Liao, W.; Ning, Z.; Chen, L.; Wei, Q.; Yuan, E.; Yang, J.; Ren, J. Intracellular antioxidant detoxifying effects of diosmetin on 2,2-azobis(2-amidinopropane) dihydrochloride (AAPH)-induced oxidative stress through inhibition of reactive oxygen species generation. *J. Agric. Food Chem.* **2014**, *62*, 8648−8654.

(24) Chi, A.; Chen, J.; Wang, Z.; Xiong, Z.; Li, Q. Morphological and structural characterization of a polysaccharide from *Gynostemma pentaphyllum* Makino and its anti-exercise fatigue activity. *Carbohydr. Polym.* **2008**, *74*, 868−874.

(25) Wu, S.; Bao, Q.; Wang, W.; Zhao, Y.; Xia, G.; Zhao, Z.; Zeng, H.; Hu, J. Cytotoxic triterpenoids and steroids. *Planta Med.* **2011**, *77*, 922−928.

(26) Zhao, L.; Dong, Y.; Chen, G.; Hu, Q. Extraction, purification, characterization and antitumor activity of polysaccharides from *Ganoderma lucidum*. *Carbohydr. Polym.* **2010**, *80*, 783−789.

(27) Manrique, G. D.; Lajolo, F. M. FT-IR spectroscopy as a tool for measuring degree of methyl esterification in pectins isolated from ripening papaya fruit. *Postharvest Biol. Technol.* **2002**, *25*, 99−107.

(28) Kacurakova, M.; Capek, P.; Sasinkova, V.; Wellner, N.; Ebringerova, A. FT-IR study of plant cell wall model compounds: Pectic polysaccharides and hemicelluloses. *Carbohydr. Polym.* **2000**, *43*, 195−203.

(29) Jing, Y.; Huang, L.; Lv, W.; Tong, H.; Song, L.; Hu, X.; Yu, R. Structural characterization of a novel polysaccharide from pulp tissues of *Litchi chinensis* and its immunomodulatory activity. *J. Agric. Food Chem.* **2014**, *62*, 902−911.

(30) Schepetkin, I. A.; Xie, G.; Kirpotina, L. N.; Klein, R. A.; Jutila, M. A.; Quinn, M. T. Macrophage immunomodulatory activity of polysaccharides isolated from *Opuntia polyacantha*. *Int. Immunopharmacol.* **2008**, *8*, 1455−1466.

DOI: 10.1021/jf504677r
J. Agric. Food Chem. 2015, 63, 535−544

(31) Chihara, G. Recent progress in immunopharmacology and therapeutic effects of polysaccharides. *Dev. Biol. Stand.* **1991**, *77*, 191−197.
(32) Wang, S. Y.; Hsu, M. L.; Hsu, H. C.; Lee, S. S.; Shiao, M. S.; Ho, C. K. The anti-tumor effect of *Ganoderma lucidum* is mediated by cytokines released from activated macrophages and T lymphocytes. *Int. J. Cancer* **1997**, *70*, 699−705.
(33) Schepetkin, I. A.; Faulkner, C. L.; Nelson-Overton, L. K.; Wiley, J. A.; Quinn, M. T. Macrophage immunomodulatory activity of polysaccharides isolated from *Juniperus scopolorum*. *Int. Immunopharmacol.* **2005**, *5*, 1783−1799.
(34) Yu, Q.; Nie, S.; Wang, J.; Yin, P.; Li, W.; Xue, M. Polysaccharide from *Ganoderma atrum* induces tumor necrosis factor-α secretion via phosphoinositide 3-kinase/Akt, mitogen-activated protein kinase and nuclear factor-κB signaling pathways in RAW 264.7 cells. *Int. Immunopharmacol.* **2012**, *14*, 362−368.
(35) Bohn, J. A.; BeMiller, J. N. (1 → 3)-β-D-Glucans as biological response modifiers: A review of structure−functional activity relationships. *Carbohydr. Polym.* **1995**, *28*, 3−14.
(36) Gantner, B. N.; Simmons, R. M.; Canavera, S. J.; Akira, S.; Underhill, D. M. Collaborative induction of inflammatory responses by dectin-1 and toll-like receptor 2. *J. Exp. Med.* **2003**, *197*, 1107−1117.
(37) Thornton, B. P.; Větvicka, V.; Pitman, M.; Goldman, R. C.; Ross, G. D. Analysis of the sugar specificity and molecular location of the β-glucan-binding lectin site of complement receptor type 3 (CD11b/CD18). *J. Immunol.* **1996**, *156*, 1235−1246.
(38) Chen, Y.; Chiang, Y.; Hsu, F.; Tsai, L.; Cheng, H. Structural modeling and further improvement in pH stability and activity of a highly active xylanase from an uncultured rumen fungus. *Bioresour. Technol.* **2012**, *123*, 125−134.
(39) Kumar, C. G.; Joo, H.; Choi, J.; Koo, Y.; Chang, C. Purification and characterization of an extracellular polysaccharide from haloalkalophilic *Bacillus* sp. I-450. *Enzyme Microb. Technol.* **2004**, *34*, 673−681.
(40) Martínez-Felipe, A.; Cook, A. G.; Wallage, M. J.; Imrie, C. T. Hydrogen bonding and liquid crystallinity of low molar mass and polymeric mesogens containing benzoic acids: A variable temperature Fourier transform infrared spectroscopic study. *Phase Transitions* **2014**, *87*, 1191−1210.

DOI: 10.1021/jf504677r
J. Agric. Food Chem. 2015, 63, 535−544

JOURNAL OF AGRICULTURAL AND FOOD CHEMISTRY

Article

pubs.acs.org/JAFC

New Apoptosis-Inducing Sesquiterpenoids from the Mycelial Culture of Chinese Edible Fungus *Pleurotus cystidiosus*

Yongbiao Zheng,*[,†] Haiyue Pang,[†] Jifeng Wang,[‡] Guowei Shi,[‡] and Jianzhong Huang[†]

[†]Engineering Research Centre of Industrial Microbiology, Ministry of Education, College of Life Sciences, Fujian Normal University, Fuzhou, Fujian 350117, People's Republic of China

[‡]Fudan Institute of Urology, the Fifth People's Hospital of Shanghai, Fudan University, Shanghai 200240, People's Republic of China

Supporting Information

ABSTRACT: Two new bisabolane-type sesquiterpenoids, pleuroton A (**1**) and pleuroton B (**2**), and three clitocybulol derivatives, clitocybulol D (**3**), clitocybulol E (**4**), and clitocybulol F (**5**), were obtained from the mycelial culture of edible fungus *Pleurotus cystidiosus* O. K. Mill by repeated column chromatography over RP-18, Sephadex LH-20, and silica gel. Their structures were determined according to nuclear magnetic resonance data, high-resolution electron impact mass spectrometry, and circular dichroism spectra. These new sesquiterpenoids exhibited significant cytotoxicity against two human prostate cancer DU-145 and C42B cells in the 3-(4,5-dimethylthiazol-2-yl)-2,5-diphenyltetrazolium bromide assay. The median inhibitory concentration (IC_{50}) of compounds **1**, **2**, **3**, **4**, and **5** was 174, 28, 233, 162, and 179 nM, respectively, against the DU-145 cell and was 104, 52, 163, 120, and 119 nM, respectively, against the C42B cell. Especially, pleuroton B (**2**) exhibited the strongest cytotoxity among these sesquiterpenoids, which was confirmed by the colony formation assay. Furthermore, pleuroton B (**2**) could trigger the apoptosis of DU-145 cells through the detection of apoptosis cells using annexin V-FITC staining by flow cytometry, the observation of condensed nuclei in the apoptosis cells, and the western blot analysis for the expression of apoptosis-related proteins Bcl-2, Bak, and Bax. Analysis of structure−activity relationships of these sesquiterpenoids revealed that the unusual functional moiety of pleuroton B should contribute to its significant bioactivity. These results display the pharmacological potential of *P. cystidiosus*.

KEYWORDS: *edible fungus, Pleurotus cystidiosus, sesquiterpenoids, apoptosis inducing*

INTRODUCTION

Edible and medicinal fungi are a rich source of natural products with pharmacological potential; for example, davallialactone from *Inonotus xaranticus* could improve the aging process,[1] thelephantin O from *Thelephora aurantiotincta* could inhibit the proliferation of cancer cells,[2] etc. The genus *Pleurotus* is one of the major genera of edible fungi widely cultivated in China. Many different metabolites have been isolated from this genus. These include novel sesquiterpene pleurospiroketals[3] A−E and new monoterpenoids with inhibitory activity against nitric oxide production from *Pleurotus cornucopiae*,[4] diterpenoid eryngiolide A with cytotoxicity from *Pleurotus eryngii*,[5] ubiquinone-9 with an inhibitory effect on mammalian DNA topoisomerase I from *P. eryngii*,[6] and methane-type monoterpene pleurolactone from *P. eryngii*.[7]

Our recent experimental results indicated the ethyl acetate crude extracted from the mycelial culture of *Pleurotus cystidiosus* had shown significant inhibitory effects against prostate cancer DU-145 cells in the 3-(4,5-dimethylthiazol-2-yl)-2,5-diphenyltetrazolium bromide (MTT) assay. To investigate new pharmacological constituents, the strain *P. cystidiosus* was cultured in dishes laid with potato dextose agar media on a large scale. As a result, two new bisabolane-type sesquiterpenoids, pleuroton A (**1**) and pleuroton B (**2**), and three clitocybulol derivatives, clitocybulol D (**3**), clitocybulol E (**4**), and clitocybulol F (**5**), were obtained from the mycelial culture of *P. cystidiosus* by repeated column chromatography over RP-18, Sephadex LH-20, and silica gel.

MATERIALS AND METHODS

General Procedures. Ultraviolet (UV) spectra were measured on Shimadzu UV2401PC (Tokyo, Japan). Infrared (IR) spectra were recorded on a Bruker Tensor-27 FTIR spectrophotometer (Ettlingen, Germany). Optical rotations were measured with Jasco P-1020 automatic polarimeter (Tokyo, Japan). Nuclear magnetic resonance (NMR) spectra were recorded at 500 MHz for ^{1}H NMR and 150 MHz for ^{13}C NMR on a Bruker AMX-500 spectrometer (Bruker BioSpin Group, Zurich, Switzerland). High-resolution electron impact mass spectrometry (HREI−MS) spectra were recorded on AutoSpec Premier P776 mass spectrometer (Milford, MA). Circular dichroism spectra were measured on a Chirascan Plus spectroscope (Applied Photophysics, Leatherhead, Surrey, U.K.). Column chromatography was performed on silica gel (Qingdao Marine Chemical Company, Qingdao, China), reverse-phase octadecyl-silica RP-18 (Merck, Darmstadt, Germany), and Sephadex LH-20 (Amersham Biosciences, Piscataway, NJ). Thin-layer chromatography was performed on the precoated silica gel GF_{254} plates (Qingdao Marine Chemical Company, Qingdao, China). Organic solvents used were from Sinopharm Chemical Reagent Co., Ltd. (Shanghai, China). MTT, 4,6-diamidino-2-phenylindole (DAPI), RNaseA, and anti-β-actin were purchased from Sigma Chemical Co. (St. Louis, MO). Anti-Bcl-2, anti-Bax, and anti-Bak were purchased from Cell Signaling Technology (Danvers, MA). Annexin V-FITC Apoptosis Detection Kit was supplied by BD Biosciences, San Jose, CA.

Received: October 11, 2014
Revised: December 23, 2014
Accepted: December 23, 2014
Published: December 23, 2014

ACS Publications © 2014 American Chemical Society

DOI: 10.1021/jf504931n
J. Agric. Food Chem. 2015, 63, 545−551

Table 1. ^{1}H and ^{13}C NMR Spectral Data of Compounds 1 and 2, Recorded at 500 MHz in CD_3OD

	δ_H (multiplicity, J in Hz)		δ_C	
position	1	2	1	2
1	4.36 (t, J = 8.0, 1H)	4.28 (t, J = 8.2, 1H)	85.1 d	84.6 d
2	3.07 (d, J = 8.0, 1H)	3.47 (d, J = 8.2, 1H)	75.7 d	77.7 d
3			73.6 s	73.8 s
4α	1.49 (o, 2H)	1.51 (m, 2H)	33.8 t	33.8 t
4β	1.49 (o, 2H)			
5α	2.11 (m, 1H)	2.17 (o, 1H)	19.8 t	19.9 t
5β	1.79 (brd, 1H)	1.80 (brd, 1H)		
6	2.90 (brs, 1H)	3.14 (brs, 1H)	43.2 d	44.3 d
7			149.3 s	152.0 s
8	4.77 (d, J = 2.1, 1H)		86.4 d	105.8 s
9			199.8 s	196.8 s
10	6.44 (d, J = 1.1, 1H)	6.40 (d, J = 1.2, 1H)	120.4 d	119.7 d
11			161.0 s	161.6 s
12	1.96 (s, 3H)	1.95 (d, J = 1.0, 3H)	28.2 q	28.3 q
13	2.15 (s, 3H)	2.15 (d, J = 1.0, 3H)	21.4 q	21.4 q
14a	5.22 (t, J = 2.4, 1H)	5.24 (d, J = 3.1, 1H)	106.9 t	110.4 t
14b	5.05 (t, J = 2.4, 1H)	5.17 (t, J = 3.1, 1H)		
15	1.20 (s, 3H)	1.20 (s, 3H)	26.9 q	27.0 q

Table 2. ^{1}H and ^{13}C NMR Spectral Data of Compounds 3−5, Recorded at 500 MHz in CD_3OD

	δ_H (multiplicity, J in Hz)			δ_C		
position	3	4	5	3	4	5
1α	4.02 (s, 1H)	2.25 (dd, J = 16.2, 1.0, 1H)	1.86 (o, 1H)	88.5 d	45.9 t	45.9 t
1β		2.14 (dd, J = 16.2, 1.0, 1H)	2.49 (d, J = 16.15, 1H)			
2				136.1 s	131.5 s	132.1 s
3				77.7 s	77.7 s	77.8 s
4				150.7 s	151.0 s	151.3 s
5α	4.34 (dt, J = 2.1, 10.1, 1H)	4.26 (dt, J = 11.0, 2.1, 1H)	4.24 (dt, J = 12.9, 2.45, 1H)	68.4 t	68.4 t	67.9 t
5β	4.47 (dt, J = 2.1, 10.1, 1H)	4.47 (dt, J = 11.0, 2.1, 1H)	4.41 (dt, J = 12.9, 2,0, 1H)			
6				104.7 s	104.6 s	105.2 s
7α	3.66 (d, J = 2.4, 1H)	3.63 (d, J = 2.8, 1H)	2.06 (dd, 14.0, 7.0, 1H)	76.9 d	76.0 d	37.3 t
7β			1.82 (o, 1H)			
8	2.51 (m, 1H)	2.36 (m, 1H)	2.26 (o, 1H)	39.7 d	39.5 d	31.5 d
9				141.5 s	140.4 s	143.0 s
10α	2.24 (dt, J = 1.5, 14.0, 1H)	2.49 (m, 1H)	2.28 (o, 1H)	43.1 t	41.7 t	41.7 t
10β	2.18 (dt, J = 1.5, 14.0, 1H)	2.06 (dd, J = 15.7, 1.2, 1H)	2.15 (d, J = 15.4, 1H)			
11				43.3 s	43.6 s	43.5 s
12a	5.27 (t, J = 2.1, 1H)	5.27 (t, J = 2.1, 1H)	5.25 (t, J = 2.4, 1H)	107.9 t	107.8 t	107.5 t
12b	5.13 (t, J = 2.1, 1H)	5.13 (t, J = 2.1, 1H)	5.12 (t, J = 2.4, 1H)			
13	1.25 (d, J = 2.4, 3H)	1.11 (d, J = 7.5, 3H)	1.00 (o, 3H)	18.8 q	17.4 q	19.6 q
14	1.08 (s, 3H)	1.04 (s, 3H)	1.10 (o, 3H)	28.4 q	25.6 q	25.5 q
15	0.97 (s, 3H)	3.40 (o, 2H)	3.29 (o, 2H)	23.1 q	71.3 t	71.3 t

Fungus Material and Fermentation. The strain was isolated from the basidiocarp of *P. cystidiosus*, which grew in the Qingyun mountains in Yongtai, Fujian, China. Inferred from the comparison of internal transcribed spacer (ITS) DNA sequences (GenBank accession number KP164598; see Figure S1 of the Supporting Information), the strain was identified as *P. cystidiosus* O. K. Mill[8] and has been deposited in the China Center for Type Culture Collection (CCTCC number 2014256). The strain *P. cystidiosus* was cultured in 750 dishes each containing ca. 20 mL of potato dextose agar media with the total volume of 15 L. These dishes were incubated at 28 °C for 43 days.

Extraction and Isolation. The fermented mycelia, some of which have formed the synnematous anamorph in black (see Figure S2 of the Supporting Information), together with the cultured substrate in these dishes, were merged and extracted with AcOEt/MeOH/AcOH (80:15:5, v/v/v). The organic crude extract was partitioned with AcOEt and double-distilled water. The AcOEt phase was dried over sodium sulfate (anhydrous) and concentrated under reduced pressure to afford 4.41 g of a crude organic extract. The crude extract was subjected to medium-pressure liquid chromatography (MPLC) over RP-18 silica gel (170 g) using a stepwise gradient of 30, 50, 70, and 100% (v/v) MeOH in water and to afford fraction 1 (154.8 mg) obtained from 30% MeOH in water and fraction 2 (495.7 mg) obtained from 50% MeOH in water. Fraction 1 was then subjected to a Sephadex LH-20 column eluted with MeOH to afford fraction 11 (48.4 mg). Fraction 11 was separated to fraction 111 (4.6 mg) and fraction 112 (15.4 mg) by MPLC over RP-18 silica gel (30 g) (from 25% MeOH in water). Fraction 111 was subjected to silica gel (1.0 g) chromatography using a $CHCl_3$/MeOH solvent gradient to yield compound **3** (1.7 mg). Fraction 112 was further subjected to a Sephadex LH-20 column (100 g) eluted with MeOH to afford fraction 1121 (3.0 mg). Fraction 1121 was subjected to silica gel (1.0 g) chromatography using a $CHCl_3$/MeOH solvent gradient to yield compound **5** (2.3 mg). Fraction 2 was divided to fraction 21 (222.9 mg) (from 35% MeOH in water) and fraction 22 (134.1 mg) (from

DOI: 10.1021/jf504931n
J. Agric. Food Chem. 2015, 63, 545−551

45% MeOH in water) by MPLC over RP-18 silica gel (30 g). Fraction 21 was continuously subjected to a Sephadex LH-20 (120 g) column eluted with MeOH and to silica gel (2.0 g) chromatography using a $CHCl_3$/MeOH solvent gradient to yield compound **1** (6.1 mg). Fraction 22 was further subjected to a Sephadex LH-20 (120 g) column eluted with MeOH and to afford fraction 221 (16.6 mg) and fraction 222 (49.0 mg). Fraction 221 was subjected to silica gel (1.0 g) chromatography using a $CHCl_3$/MeOH solvent gradient (200:1) to yield compound **2** (3.0 mg). Fraction 222 was also subjected to silica gel (1.0 g) chromatography using a $CHCl_3$/MeOH solvent gradient (50:1) to yield compound **4** (23.5 mg). The physical properties and spectroscopic data of five new sesquiterpenoids are as follows:

Compound **1**: colorless oil. $[\alpha]_D^{25}$: +51.7 (*c* 0.23, methanol). UV (methanol) λ_{max}, nm: 216. HREI−MS, *m*/*z*: 266.1521 (calcd for $C_{15}H_{22}O_4$, 266.1518). IR (KBr) ν_{max}: 3441, 1749, 1623 cm^{-1}. ^1H and ^{13}C NMR spectral data are shown in Table 1.

Compound **2**: colorless oil. $[\alpha]_D^{25}$: +79.7 (*c* 0.32, methanol). UV (methanol) λ_{max}, nm: 247. HREI−MS, *m*/*z*: 282.1461 (calcd for $C_{15}H_{22}O_5$, 282.1467). IR (KBr) ν_{max}: 3443, 1758, 1684, 1622 cm^{-1}. ^1H and ^{13}C NMR spectral data are shown in Table 1.

Compound **3**: colorless oil. $[\alpha]_D^{25}$: −50.0 (*c* 0.17, methanol). UV (methanol) λ_{max}, nm: 209. HREI−MS, *m*/*z*: 282.1465 (calcd for $C_{15}H_{22}O_5$, 282.1467). IR (KBr) ν_{max}: 3426, 1630 cm^{-1}. ^1H and ^{13}C NMR spectral data are shown in Table 2.

Compound **4**: colorless oil. $[\alpha]_D^{25}$: −45.8 (*c* 0.20, methanol). UV (methanol) λ_{max}, nm: 207. HREI−MS, *m*/*z*: 282.1466 (calcd for $C_{15}H_{22}O_5$, 282.1467). IR (KBr) ν_{max}: 3423, 1631 cm^{-1}. ^1H and ^{13}C NMR spectral data are shown in Table 2.

Compound **5**: colorless oil. $[\alpha]_D^{25}$: −51.3 (*c* 0.07, methanol). UV (methanol) λ_{max}, nm: 207. HREI−MS, *m*/*z*: 266.1517 (calcd for $C_{15}H_{22}O_4$, 266.1518). IR (KBr) ν_{max}: 3418, 1631 cm^{-1}. ^1H and ^{13}C NMR spectral data are shown in Table 2.

MTT Cell Viability Assay. MTT cell viability assay was used to evaluate the inhibitory effect of these compounds on two human prostate cancer DU-145 and C42B cells. DU-145 and C42B cells were cultured in Dulbecco's modified Eagle's media (DMEM) complemented with 10% fetal bovine serum and 2 mM L-glutamine. The cells were maintained at 37 °C in a humidified atmosphere of 95% air and 5% CO_2. DU-145 and C42B cells (1×10^5/well) were cultured for 72 h in 96-well plates (Falcon, CA) in the presence of various concentrations of compounds. All wells (100 μL each) were incubated with 20 μL of 5 mg/mL MTT solution for 3 h at 37 °C. Then, 100 μL of "triplex solution" [10% sodium dodecyl sulfate (SDS), 5% isobutanol, and 12 mM hydrochloric acid (HCl)] was added to each well and incubated overnight at 37 °C. Absorbance was read at 595 nm on a microplate reader (M-3350, Bio-Rad) with 655 nm as a reference.

Colony Formation Assay. DU-145 cells were cultured in 6 well plates (1000/well) overnight and with new medium replaced in the presence of compound **2**, and the plates continued to incubate at 37 °C with 5% CO_2 for 10 days. On the last day, the medium was removed, and after washing with phosphate-buffered saline (PBS) and fixing with methanol, the colonies were stained with crystal violet solution for 3 h at room temperature. The images were acquired with a scanner, and visible colony numbers were counted after washing and air drying.

Assessing Apoptosis by Annexin-V/Propidium Iodide (PI) Staining. Cells were seeded in a 6 cm dish 1 day before compound treatment. After treatment with compound **2** at 35 nM for 24 h, DU-145 cells were stained with annexin V and PI following the protocol of the manufacturer. Subsequently, cells were analyzed by a FACSCalibur flow cytometer and BD CellQuest Pro software under the examination of FL1 channel for FITC and FL3 detector for PI, as described elsewhere.

Assessing Apoptosis Using DAPI Staining. After treatment with compound **2**, cells were collected and washed once with 2 mL of ice-cold PBS, fixed with 1 mL of 4% paraformaldehyde for 20 min, and washed once again with 2 mL of ice-cold PBS. The cells were incubated in 1 mL of DAPI at 50 μg/mL containing 100 μg/mL RNaseA. This mixture was incubated for 30 min at 37 °C. After washing with 2 mL of PBS 3 times, the cells were observed using fluorescence microscopy at 340 nm (excitation) and 488 nm (emission).

Western Blot Analysis. After treatment with or without a compound for different time courses, cells were harvested and lysed in ice-cold lysis buffer [20 mM Tris−HCl at pH 7.4, 150 mM NaCl, 1 mM ethylenediaminetetraacetic acid (EDTA), 1 mM ethylene glycol bis(2-aminoethyl ether)-*N*,*N*,*N*′,*N*′-tetraacetic acid (EGTA), 1% Triton, 2.5 mM sodium pyrophosphate, 1 mM β-glycerolphosphate, 1 mM sodium orthovanadate, 1 mg/mL leupeptin, and 1 mM phenylmethylsulfonyl fluoride]. The lysate was mixed with an equal volume of 2× loading buffer (4% SDS, 10% 2-mercaptoethanol, 20% glycerol, and 0.2 mg/mL bromophenol blue in 0.1 M Tris−HCl at pH 6.8) and boiled for 10 min immediately. The boiled lysates were subjected to 8−12% SDS−polyacrylamide gels, developed under 100 V, and then transferred to Immobilon-P membranes (Millipore). After blocking with 5% skim milk in phosphate-buffered saline with 0.1% Tween-20 for 1 h and incubation overnight with the corresponding primary antibodies in the blocking solution at 4 °C, primary antibodies were detected using either a peroxidase-conjugated immunopure goat anti-rabbit IgG (H + L) or peroxidase-conjugated immunopure goat anti-mouse IgG (H + L) secondary antibody and enhanced chemiluminescence.

RESULTS AND DISCUSSION

Identification of New Sesquiterpenoids. Compound **1** was obtained as a colorless oil. The molecular formula of compound **1** was found to be $C_{15}H_{22}O_4$ (five degrees of unsaturation) based on the HREI−MS peak at *m*/*z* 266.1521 $[M]^+$ and ^1H and ^{13}C NMR data (Table 1 and Figure S3 of the Supporting Information). In the IR spectra, the prominent absorptions indicated the presence of hydroxyl (3441 cm^{-1}), carbonyl (1749 cm^{-1}), and unsaturated double bond (1623 cm^{-1}) groups. NMR data [^1H, ^{13}C, and distortionless enhancement by polarization transfer (DEPT)] revealed resonances for three methyls, three methylenes, including one terminal sp^2 methylene (δ_H 5.22 and 5.05, δ_C 106.9), five methines, including three oxygenated methines (δ_H 4.36, δ_C 85.1; δ_H 3.07, δ_C 75.7; and δ_H 4.77, δ_C 86.4) and one sp^2 methine (δ_H 6.44, δ_C 120.4), and four quaternary carbons, including one oxygenated carbon (δ_C 73.6), one carbonyl carbon (δ_C 199.8), and two sp^2 quaternary carbons (δ_C 149.3 and 161.0). One sp^2 methylene, one sp^2 methine, one carbonyl carbon, and two sp^2 quaternary carbons represented three double bond equivalents. Therefore, compound **1** must be bicyclic to account for five double bond equivalents required by the molecular formula. The cross-peaks of H-1 and H-2, H-1 and H-6, H-5α/β and H-4α/β, and H-5α/β and H-6 in the $^1H-^1H$ correlation spectroscopy (COSY) spectrum showed the spin system of H-1, H-2, H-4α/β, H-5α/β, and H-6. Further, the heteronuclear multiple-bond correlations (HMBCs) from H_3-14 to C-2, C-3, and C-4, from H_2-14 to C-6 and C-8, from H-1 to C-2, C-7, and C-8, from H-6 to C-7, and from H-8 to C-7 could be observed and allowed for the establishment of the octahydrobenzofuran moiety of compound **1**, together with the oxygenated nature of C-1, C-2, C-3, and C-8. HMBC correlations from H_3-12/13 to C-11, C-10, and C-13/12 and from H-10 to C-9 and C-12/13, together with the chemical shift of C-9 (δ_C 199.8 s), allowed for the establishment of another moiety of the carbonyl-substituted isoprene in compound **1**, which was connected to C-8 according to the key HMBC from H-8 to C-9. On the basis of the above data, the planar structure of compound **1** was formed. The relative configuration of compound **1** was established by nuclear Overhauser effect spectrometry (NOESY) experiments. The presence of NOESY correlations of H-1 with H-6 and H-6 with

DOI: 10.1021/jf504931n
J. Agric. Food Chem. 2015, 63, 545−551

H-5α indicated the α orientation of these protons. Further, the NOESY cross-peaks between H-2 and H_3-15 and H-2 and H-8 established the relative configuration at C-2, C-3, and C-8 and the β orientation of these protons (Figure 1). Therefore, the structure of compound **1** was established as a derivative of bisabolane-type sesquiterpenoid cheimonophyllons[9,10] and named pleuroton A.

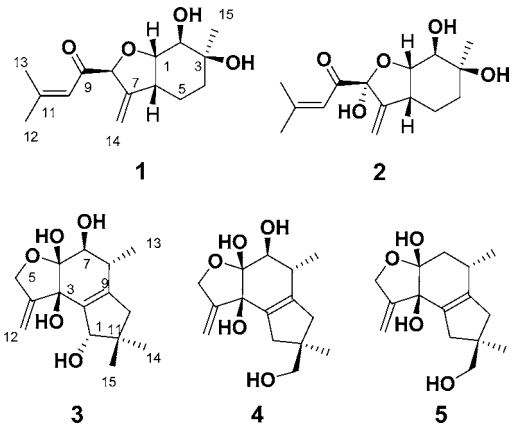

Figure 1. New sesquiterpenoids of *P. cystidiosus*.

Compound **2** was obtained as a colorless oil. The molecular formula of compound **2** was determined to be $C_{15}H_{22}O_5$ (five degrees of unsaturation) based on the HREI−MS peak at m/z 282.1461 $[M]^+$ and ^1H and ^{13}C NMR data (Table 1 and Figure S4 of the Supporting Information). NMR data (^1H, ^{13}C, and DEPT) displayed three methyls, three methylenes, including one terminal sp^2 methylene (δ_H 5.24 and 5.17, δ_C 110.4), four methines, including two oxygenated methines (δ_H 4.28, δ_C 84.6; δ_H 3.47, δ_C 77.7) and one sp^2 methine (δ_H 6.40, δ_C 119.7), and five quaternary carbons, including two oxygenated carbon (δ_C 73.8, 105.8), one carbonyl carbon (δ_C 196.8), and two sp^2 quaternary carbons (δ_C 152.0; δ_C 161.6). One sp^2 methylene, one sp^2 methine, one carbonyl carbon, and two sp^2 quaternary carbons represented three degrees of unsaturation. Thus, compound **2** must be bicyclic to account for five degrees of unsaturation required by the molecular formula. Comprehensive inspection of the NMR data [^1H, ^{13}C, heteronuclear single-quantum coherence (HSQC), HMBC, and $^1H-^1H$ COSY] revealed that compound **2** was similar to compound **1**, except that the oxygenated methine (δ_C 84.6) at C-8 in compound **1** was replaced by the dioxygenated quaternary carbon (δ_C 105.8) at the same position in compound **2** (Figure 1). The similar NOESY correlations of H-1 with H-6, H-6 with H-5α, H-2 with H_3-15, and H-2 with H-4β, established the relative configuration of compound **2**. Therefore, compound **2** was determined as an analogue of cheimonophyllons and named pleuroton B (**2**).

The molecular formula of compound **3** was assigned to $C_{15}H_{22}O_5$ based on the HREI−MS peak at m/z 282.1465 $[M]^+$ and NMR data (Table 2 and Figure S5 of the Supporting Information), requiring five degrees of unsaturation. The IR spectrum indicated the existence of hydroxyl (3426 cm^{-1}) and unsaturated double bond (1630 cm^{-1}) groups. Analysis of NMR data (^1H, ^{13}C, and DEPT) of compound **3** revealed 15 carbon signals attributed to three methyls, three methylenes, including one terminal sp^2 methylene (δ_H 5.27 and 5.13, δ_C 107.9) and one oxygenated methylene (δ_H 4.34 and 4.47, δ_C 68.4), three methines, including two oxygenated methines (δ_H 4.02, δ_C 88.5; δ_H 3.66, δ_C 76.9), and six quaternary carbons, including two oxygenated carbon (δ_C 77.7, 104.7 s) and three sp^2 quaternary carbons (δ_C 136.1, 150.7, and 141.5), indicating a tricyclic sesquiterpene backbone. HMBC correlations from the protons of two methyl groups at 0.97 (s, H-15) and 1.08 (s, H-14) to the corresponding carbons (C-1, C-11, and C-10) indicated the presence of *gem*-dimethyl groups and deduced the one 5-carbon moiety, including C-1, C-11, C-10, C-14, and C-15. According to HMBCs from H_3-13 to C-7, C-8, and C-9, from H-8 to C-6, C-7, C-9, and C-13, and from H-7 to C-3, C-6, C-8, C-9, and C-13, together with the $^1H-^1H$ COSYs of H-8 and H-7 and H-8 and H-13, and the consideration of the chemical shift of C-6 (δ_C 104.7 s), C-2 (δ_C 136.1 s), and C-9 (δ_C 141.5 s), a moiety of three hydroxy-substituted cyclohexenes could be recognized in compound **3**. Additionally, a furan moiety fusing with terminal alkene was assigned by analyzing the HMBC from H_2-12 to C-3, C-4, and C-5 and from H_2-5 to C-3, C-4, C-6, and C-12. Therefore, the planar structure of compound **3** was established (Figure 1).

Following a similar strategy, compounds **4** and **5** were recognized. Compound **4** has the molecular formula of $C_{15}H_{22}O_5$ based on the HREI−MS peak at m/z 282.1466 $[M]^+$ and NMR data (Table 2 and Figure S6 of the Supporting Information), requiring five degrees of unsaturation. The IR spectrum indicated the existence of hydroxyl (3423 cm^{-1}) and unsaturated double bond (1631 cm^{-1}) groups. Analysis of NMR data of compound **4** revealed 15 carbon signals attributed to two methyls, five methylenes, including one terminal sp^2 methylene (δ_H 5.27 and 5.13, δ_C 107.8) and two oxygenated methylene (δ_H 4.47 and 4.26, δ_C 68.4; δ_H 3.40, δ_C 71.3), two methines, including one oxygenated methine (δ_H 3.63, δ_C 76.0), and six quaternary carbons, including two oxygenated carbon (δ_C 77.7 and 104.6) and three sp^2 quaternary carbons (δ_C 131.5, 151.0, and 140.4). Compound **5** has the molecular formula of $C_{15}H_{22}O_4$ based on the HREI−MS peak at m/z 266.1517 $[M]^+$ and NMR data (Table 2 and Figure S7 of the Supporting Information), requiring five degrees of unsaturation. The IR spectrum indicated the existence of hydroxyl (3418 cm^{-1}) and unsaturated double bond (1631 cm^{-1}) groups. Analysis of NMR data of compound **5** revealed 15 carbon signals attributed to two methyls, six methylenes, including one terminal sp^2 methylene (δ_H 5.25 and 5.12, δ_C 107.5) and two oxygenated methylenes (δ_H 4.41 and 4.24, δ_C 67.9; δ_H 3.29, δ_C 71.3), one methine, and six quaternary carbons, including two oxygenated carbon (δ_C 77.8 and 105.2) and three sp^2 quaternary carbons (δ_C 132.1, 151.3, and 143.0). Detailed comparisons of NMR data (Table 2) of compounds **3**−**5** revealed that these compounds had a carbon skeleton similar to clitocybulols A and C.[11] However, the CHOH group at C-1 and the methyl group at C-14 in compound **3** were replaced by CH_2 at C-1 and a hydroxymethyl at C-14 in compound **4** (Figure 1). In addition, the CHOH group at C-7 in compound **4** was substituted for CH_2 at C-7 in compound **5** (Figure 1).

The stereochemistry of clitocybulols A and C was determined by applying the octant rule[12] and based on the circular dichroic spectra of these compounds.[11] The negative Cotton effects at 212 nm for compound **3**, 216 nm for compound **4**, and 216 nm for compound **5** (see Figure S8 of the Supporting Information) suggest that three compounds have the same configuration as clitocybulols A and C at C-3 and C-6. This configuration was further supported by the same sinistral optical rotations ($[\alpha]_D^{25}$, −50.0 for compound **3**; $[\alpha]_D^{25}$, −45.8 for compound **4**; $[\alpha]_D^{25}$, −51.3 for compound **5**; $[\alpha]_D^{25}$,

DOI: 10.1021/jf504931n
J. Agric. Food Chem. 2015, 63, 545−551

−80.0 for clitocybulol A; and $[\alpha]_D^{25}$, −57.7 for clitocybulol C) and NOESY experiments. NOSEY correlations between H-7 and H_3-13, indicating that they are directed on the same side of compound **3**, and between H-1 and H-8, which are pointed at the other side, were observed and deduced the stereochemistry of compound **3** (Figure 1). The presence of NOESY correlations between H-8 and H_2-15, between H_2-15 and H-10α, and between H-8 and H-1α indicated the α orientation of these protons in compound **4**. Further, the NOESY cross-peak between H-7 and H_3-13 revealed the β orientation of these protons in compound **4** (Figure 1). NOESY correlations between H-8 and H-1α and H-7α and between H_2-15 and H-5α, which showed the α orientation of these protons, and between H-1β and H-7β, between H-10β and H_3-13, and between H-10β and H_3-14, which showed the β orientation, were observed in compound **5** and supported its stereochemistry (Figure 1). Compounds **3**, **4**, and **5** were named clitocybulols D, E, and F, respectively.

Bioactivity Evaluation. The experimental results of the MTT cell viability assay indicated that these new sesquiterpenoids exhibit significant cytotoxicity against two human prostate cancer DU-145 and C42B cells. The median inhibitory concentration (IC_{50}) of compounds **1**−**5** against DU-145 and C42B cells are shown in Table 3. Consistently, the colony formation assay showed that the number of colonies formed in the cells treated with compound **2** significantly decreased in comparison to that of the control group (Figure 2). Furtherly, flow cytometric analysis revealed that the proportion of apoptotic cells after treatment with compound **2** was 13.36%, which was dramatically increased in comparison to 0.29% of the control cells (Figure 3A). Chromatin condensations induced by the treatment with compound **2** for 24 h could be observed by DAPI staining in DU-145 cells (Figure 3B). We observed that the expression levels of pro-apoptotic protein Bak and Bax increased significantly in the treated cells compared to the controls, but the anti-apoptotic protein Bcl-2 level was decreased (Figure 3C). Taken together, these results indicated that compound **2** triggered the apoptosis of the DU-145 cells.

Table 3. Growth Inhibition against DU-145 and C42B Cells of Compounds 1−5

	growth inhibition (IC_{50}, nM)	
compound	DU-145	C42B
1	174	104
2	28	52
3	233	163
4	162	120
5	179	119

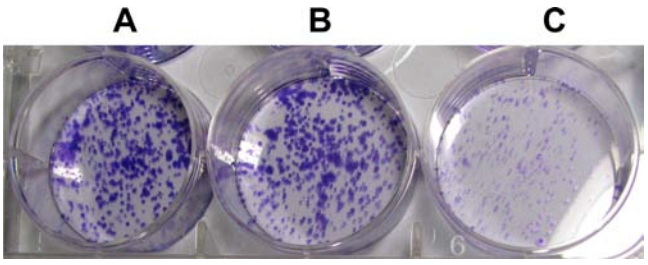

Figure 2. Colony formation assay (A, DU-145 cells were cultured in the medium not containing compound **2**; B, DU-145 cells were cultured in the medium containing compound **2** at 17.5 nM; and C, DU-145 cells were cultured in the medium containing compound **2** at 35 nM).

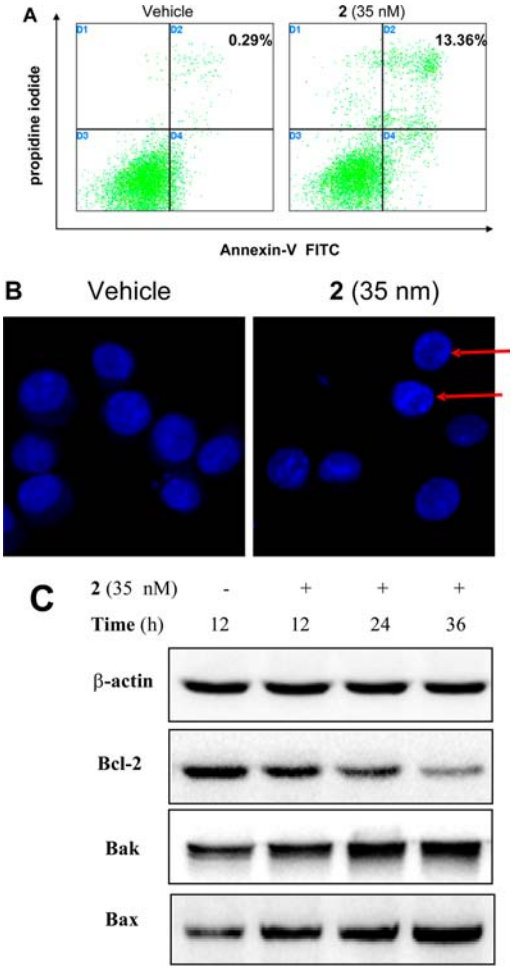

Figure 3. Analysis of apoptosis induced by compound **2**. (A) Detection of apoptosis using annexin V-FITC staining. After treatment with compound **2** at 35 nM for 24 h, DU-145 cells were analyzed by a FACSCalibur flow cytometer. The horizontal axis represents annexin V intensity, and the vertical axis shows PI staining. The lines divide each plot into four quadrants: lower left quadrant, living cells; lower right quadrant, early apoptotic cells; upper left quadrant, necrotic cells; and upper right quadrant, late apoptotic cells. (B) Microscopy of DU-145 cells treated with compound **2**. DU-145 cells were treated with compound **2** at 35 nM for 24 h. The images were captured using fluorescence (at 600×) for nuclear staining with compound **2** at 0 nM (vehicle) or 35 nM. Apoptotic cells with condensed nuclei were observed using nuclear staining, as indicated with red arrows. (C) Western blot analysis for the expression of apoptosis-related proteins in the DU-145 cells. The expression levels of Bcl-2, Bak, and Bax were determined by western blotting in the DU-145 cells after treatment for the indicated time with compound **2** at 35 nM. β-Actin was used for normalization and verification of protein loading.

Sesquiterpenoids **1** and **2** possess a bisabolane-type skeleton, whereas sesquiterpenoids **3**−**5** are clitocybulol derivatives. In the previous reports, cheimonophyllons A−E and cheimonophyllal, analogues of compounds **1** and **2**, exhibited nematicidal, cytotoxic, and antimicrobial activities,[9,10] but no activities were observed about clitocybulols.[11] In the present work, pleuroton B (**2**) exhibited significant cytotoxicity at a higher level than other sesquiterpenoids, pleuroton A (**1**), and clitocybulols D−F (**3**−**5**). In particular, although compound **1** possesses one α,β-

DOI: 10.1021/jf504931n
J. Agric. Food Chem. 2015, 63, 545−551

unsaturated carbonyl moiety and one exomethylene as compound **2**, compound **2** has one additional hydroxyl at C-8 compared to compound **1** and has ca. 2−6 times stronger cytotoxicity against the two prostate cancer cells than compound **1**.

Sesquiterpenoids are the major secondary metabolites of fungi, plant, algae, etc. The diversity of their structures is often beyond people's imagination. In recent years, many new sesquiterpenoids were discovered and possessed a wide variety of bioactivities, such as antidiabetic and anti-inflammatory,[13] anti-aging,[14] antimelanogenesis,[15] antineuroinflammatory,[16] antivirus,[17] antimicrobial,[18] acetylcholinesterase inhibitory activity,[19,20] protein tyrosine phosphatase,[21] antifouling,[22] etc. Moreover, the relationships between the structure and bioactivities of sesquiterpenoids have been summarized in several reviews[23−25] and revealed that the α,β-unsaturated carbonyl structural groups, including α-methylene-γ-lactones, α,β-unsaturated cyclepentanone, etc., are the active functional groups, which could react as Michael acceptors with nucleophiles by Michael addition and display promising cytotoxity, such as bigelovin,[26] ergolide,[26] kaunial,[27] germacranolide,[28] eudesmane derivative,[29] etc. Additionally, several studies in bisabolane-type sesquiterpenoids had revealed more interesting results about structure−activity relationships. The bisabolane-type sesquiterpenoid dihydro-ar-turmerone, which contains an oxidation functional group and the single bond moiety in its skeleton, has a higher acetylcholinesterase inhibitory activity than other analogues.[30] 3,6-Epidioxy-1,10-bisaboladiene (EDBD), the bisabolane sesquiterpenoid endoperoxide, showed stronger antitumor activity than α-curcumene, a bisabolane sesquiterpene that lacks the endoperoxide moiety of EDBD.[31] The additional hydroxyl at C-8 in compound **2** could act as an electron-withdrawing group and polarize the exomethylene, resulting in the susceptibility to nucleophilic attack and forming a bifunctional center, which plays a key role in the cytotoxity against the prostate cancer cells. Structure−activity relationship studies will contribute to the modification of new lead compounds.

■ ASSOCIATED CONTENT

Supporting Information

ITS DNA sequences of *P. cystidiosus* (Figure S1), mycelia of *P. cystidiosus* cultured in a dish (Figure S2), ^{1}H and ^{13}C NMR spectra of compounds **1**−**5** (Figures S3−S7) and circular dichroic spectra of compounds **3**−**5** (Figure S8). This material is available free of charge via the Internet at http://pubs.acs.org.

■ AUTHOR INFORMATION

Corresponding Author

*Telephone/Fax: +86-591-22868193. E-mail: yongbiaozheng@fjnu.edu.cn.

Funding

This work was financially supported by the Natural Science Foundation of Fujian Province of China (2013J01122), the Science Foundation of Fuzhou City (2013G101), and the Science Fund of the National Health and Family Planning Commission of China (WKJ-FJ-20).

Notes

The authors declare no competing financial interest.

■ REFERENCES

(1) Yang, T. K.; Lee, Y. H.; Paudel, U.; Bhattarai, G.; Yun, B. S.; Hwang, P. H.; Yi, H. K. Davallialactone from mushroom reduced premature senescence and inflammation on glucose oxidative stress in human diploid fibroblast cells. *J. Agric. Food Chem.* **2013**, *61*, 7089−7095.

(2) Norikura, T.; Fujiwara, K.; Yanai, T.; Sano, Y.; Sato, T.; Tsunoda, T.; Kushibe, K.; Todate, A.; Morinaga, Y.; Iwai, K.; Matsue, H. *p*-Terphenyl derivatives from the mushroom *Thelephora aurantiotincta* suppress the proliferation of human hepatocellular carcinoma cells via iron chelation. *J. Agric. Food Chem.* **2013**, *61*, 1258−1264.

(3) Wang, S. J.; Bao, L.; Han, J. J.; Wang, Q. X.; Yang, X. L.; Wen, H. A.; Guo, L. D.; Li, S. J.; Zhao, F.; Liu, H. W.; Pleurospiroketals, A.-E. Perhydrobenzannulated 5,5-spiroketal sesquiterpenes from the edible mushroom *Pleurotus cornucopiae*. *J. Nat. Prod.* **2013**, *76*, 45−50.

(4) Wang, S. J.; Bao, L.; Zhao, F.; Wang, Q. X.; Li, S. J.; Ren, J. W.; Li, L.; Wen, H.; Guo, L. D.; Liu, H. W. Isolation, identification, and bioactivity of monoterpenoids and sesquiterpenoids from the mycelia of edible mushroom *Pleurotus cornucopiae*. *J. Agric. Food Chem.* **2013**, *61*, 5122−5129.

(5) Wang, S. J.; Li, Y. X.; Bao, L.; Han, J. J.; Yang, X. J.; Li, H. R.; Wang, Y. Q.; Li, S. J.; Liu, H. W.; Eryngiolide, A. a cytotoxic macrocyclic diterpenoid with an unusual cyclododecane core skeleton produced by the edible mushroom *Pleurotus eryngii*. *Org. Lett.* **2012**, *14*, 3672−3675.

(6) Bae, J. S.; Park, J. W.; Park, S. H.; Park, J. B.; Rho, Y. H.; Ryu, Y. B.; Lee, K. S.; Park, K. H.; Bae, Y. S. Apoptotic cell death of human leukaemia U937 cells by ubiquinone-9 purified from *Pleurotus eryngii*. *Nat. Prod. Res.* **2009**, *23*, 1112−1119.

(7) Liu, L. Y.; Li, Z. H.; Liu, J. K. A new menthane-type monoterpene from *Pleurotus eryngii*. *Chin. J. Nat. Med.* **2013**, *11*, 71−73.

(8) Zervakis, G. I.; Moncalvo, J. M.; Vilgalys, R. Molecular phylogeny, biogeography and speciation of the mushroom species *Pleurotus cystidiosus* and allied taxa. *Microbiology* **2004**, *150*, 715−726.

(9) Stadler, M.; Anke, H. New nematicidal and antimicrobial compounds from the basidiomycete *Cheimonophyllum candidissimum* (Berk & Curt.) sing. I. Producing organism, fermentation, isolation, and biological activities. *J. Antibiot.* **1994**, *47*, 1284−1289.

(10) Stadler, M.; Anke, H.; Stener, O. Six new antimicrobial and nematicidal bisabolanes from the basidiomycete *Cheimonophyllum candidissimum*. *Tetrahedron* **1994**, *50*, 12649−12654.

(11) Ayer, W. A.; Shan, R.; Trifonov, L. S.; Hutchison, L. J. Sesquiterpenes from the nematicidal fungus *Clitocybula oculus* in honour of professor GH Neil Towers 75th birthday. *Phytochemistry* **1998**, *49* (2), 589−592.

(12) Scott, A.; Wrixon, A. A symmetry rule for chiral olefins. *Tetrahedron* **1970**, *26*, 3695−3715.

(13) Chung, Y. M.; Wei, C. K.; Chuang, D. W.; El-Shazly, M.; Hsieh, C. T.; Asai, T.; Oshima, Y.; Hsieh, T. J.; Hwang, T. L.; Wu, Y. C. An epigenetic modifier enhances the production of anti-diabetic and anti-inflammatory sesquiterpenoids from *Aspergillus sydowii*. *Bioorg. Med. Chem.* **2013**, *21*, 3866−3872.

(14) Park, J. H.; Jung, Y. J.; Antar Aziz Mohamed, M.; Hoon Lee, T.; Lee, C. H.; Han, D.; Song, M. C.; Kim, J.; Baek, N. I. New bisabolane sesquiterpenes from the rhizomes of *Curcuma xanthorrhiza* Roxb. and their inhibitory effects on UVB-induced MMP-1 expression in human keratinocytes. *Helv. Chim. Acta* **2014**, *97*, 438−446.

(15) Lee, J. W.; Yun, C. Y.; Roh, E.; Lee, C.; Jin, Q.; Bang, K. K.; Jung, S. H.; Lee, D.; Lee, M. K.; Kim, Y. Melanogenesis inhibitory bisabolane-type sesquiterpenoids from the roots of *Angelica koreana*. *Bioorg. Med. Chem. Lett.* **2012**, *22*, 2927−2931.

(16) Wang, L. J.; Xiong, J.; Liu, S. T.; Liu, X. H.; Hu, J. F. Sesquiterpenoids from *Chloranthus henryi* and their anti-neuroinflammatory activities. *Chem. Biodiversity* **2014**, *11*, 919−928.

(17) Lv, J. J.; Yu, S.; Wang, Y. F.; Wang, D.; Zhu, H. T.; Cheng, R. R.; Yang, C. R.; Xu, M.; Zhang, Y. J. Anti-hepatitis B virus norbisabolane sesquiterpenoids from *Phyllanthus acidus* and the establishment of their absolute configurations using theoretical calculations. *J. Org. Chem.* **2014**, *79*, 5432−5447.

DOI: 10.1021/jf504931n
J. Agric. Food Chem. 2015, 63, 545−551

(18) Ma, K.; Bao, L.; Han, J.; Jin, T.; Yang, X.; Zhao, F.; Li, S.; Song, F.; Liu, M.; Liu, H. New benzoate derivatives and hirsutane type sesquiterpenoids with antimicrobial activity and cytotoxicity from the solid-state fermented rice by the medicinal mushroom *Stereum hirsutum*. *Food Chem.* **2014**, *143*, 239−245.
(19) Chen, P.; Wang, P. P.; Jiao, Z. Z.; Xiang, L. Sesquiterpenoids from the fruits of *Alpinia oxyphylla* and their anti-acetylcholinesterase activity. *Helv. Chim. Acta* **2014**, *97*, 388−397.
(20) Zhang, J.; Fan, P.; Zhu, R.; Li, R.; Lin, Z.; Sun, B.; Zhang, C.; Zhou, J.; Lou, H. Marsupellins A−F *ent*-longipinane-type sesquiterpenoids from the Chinese liverwort *Marsupella alpine* with acetylcholinesterase inhibitory activity. *J. Nat. Prod.* **2014**, *77*, 1031−1036.
(21) Fan, Q. Y.; Dong, Z. J.; Li, Z. H.; Yin, X.; Yang, X. Y.; Feng, T.; Wei, K.; Liu, J. K.; Zhao, B. H. Two new ylangene-type sesquiterpenoids from cultures of the fungus *Postia* sp. *J. Asian Nat. Prod. Res.* **2014**, *16*, 254−258.
(22) Chen, D.; Chen, W.; Liu, D.; van Ofwegen, L.; Proksch, P.; Lin, W. Asteriscane-type sesquiterpenoids from the soft coral *Sinularia capillosa*. *J. Nat. Prod.* **2013**, *76*, 1753−1763.
(23) Wang, G. W.; Qin, J. J.; Cheng, X. R.; Shen, Y. H.; Shan, L.; Jin, H. Z.; Zhang, W. D. Inula sesquiterpenoids: Structural diversity, cytotoxicity and anti-tumor activity. *Expert Opin. Invest. Drugs* **2014**, *23*, 317−345.
(24) Vasas, A.; Hohmann, J. Xanthane sesquiterpenoids: Structure, synthesis and biological activity. *Nat. Prod. Rep.* **2011**, *28*, 824−842.
(25) Ghantous, A.; Gali-Muhtasib, H.; Vuorela, H.; Saliba, N. A.; Darwiche, N. What made sesquiterpene lactones reach cancer clinical trials? *Drug Discovery Today* **2010**, *15*, 668−678.
(26) Wang, Q.; Zhou, B. N.; Zhang, R. W.; Lin, Y. Y.; Lin, L. Z.; Gil, R. R.; Cordell, G. A. Cytotoxicity and NMR spectral assigments of ergolide and bigelovin. *Planta Med.* **1996**, *62*, 166−168.
(27) Maldonado, E. M.; Svensson, D.; Oredsson, S. M.; Sterner, O. A novel cytotoxic terpenoid from the flowers of *Kaunia lasiophthalma* Griseb. *Phytochem. Lett.* **2014**, *8*, 105−108.
(28) Harvala, E.; Aligiannis, N.; Skaltsounis, A. L.; Pratsinis, H.; Lambrinidis, G.; Harvala, C.; Chinou, I. Cytotoxic germacranolides from *Inula verbascifolia* subsp. *methanea*. *J. Nat. Prod.* **2002**, *65*, 1045−1048.
(29) Maldonado, E. M.; Svensson, D.; Oredsson, S. M.; Sterner, O. Cytotoxic sesquiterpene lactones from *Kauna lasiophthalma* Griseb. *Sci. Pharm.* **2014**, *82*, 147−160.
(30) Fujiwara, M.; Yagi, N.; Miyazawa, M. Acetylcholinesterase inhibitory activity of volatile oil from *Peltophorum dasyrachis* Kurz ex Bakar (yellow batai) and bisabolane-type sesquiterpenoids. *J. Agri. Food Chem.* **2010**, *58*, 2824−2829.
(31) Nishikawa, K.; Aburai, N.; Yamada, K.; Koshino, H.; Tsuchiya, E.; Kimura, K. The bisabolane sesquiterpenoid endoperoxide, 3,6-epidioxy-1,10-bisaboladiene, isolated from *Cacalia delphiniifolia* inhibits the growth of human cancer cells and induces apoptosis. *Biosci., Biotechnol., Biochem.* **2008**, *72*, 2463−2466.

DOI: 10.1021/jf504931n
J. Agric. Food Chem. 2015, 63, 545−551

JOURNAL OF AGRICULTURAL AND FOOD CHEMISTRY

Article

pubs.acs.org/JAFC

Purified Anthocyanins from Bilberry and Black Currant Attenuate Hepatic Mitochondrial Dysfunction and Steatohepatitis in Mice with Methionine and Choline Deficiency

Xilan Tang,[†,§] Tianran Shen,[†] Xinwei Jiang,[†] Min Xia,[†,‡] Xujia Sun,[†] Honghui Guo,*[,§] and Wenhua Ling*[,†,‡]

[†]Department of Nutrition, School of Public Health, Sun Yat-Sen University, Guangzhou 510080, P. R. China

[§]Department of Nutrition, Henry Fok School of Food Science and Engineering, Shaoguan University, Shaoguan 512005, P. R. China

[‡]Guangdong Provincial Key Laboratory of Food, Nutrition and Health, Guangzhou 510080, P. R. China

Supporting Information

ABSTRACT: The berries of bilberry and black currant are a rich source of anthocyanins, which are thought to have favorable effects on nonalcoholic steatohepatitis (NASH). This study was designed to examine whether purified anthocyanins from bilberry and black currant are able to limit the disorders related to NASH induced by a methionine-choline-deficient (MCD) diet in mice. The results showed that treatment with anthocyanins not only alleviated inflammation, oxidative stress, steatosis, and even fibrosis but also improved depletion of mitochondrial content and damage of mitochondrial biogenesis and electron transfer chain developed concomitantly in the liver of mice fed the MCD diet. Furthermore, anthocyanins treatment promoted activation of AMP-activated protein kinase (AMPK) and expression of peroxisome proliferator-activated receptor-gamma coactivator-1α (PGC-1α). These data provide evidence that anthocyanins possess significant protective effects against NASH and mitochondrial defects in response to a MCD diet, with a mechanism maybe through affecting the AMPK/PGC-1α signaling pathways.

KEYWORDS: *AMP-activated protein kinase, anthocyanin, mitochondrial dysfunction, nonalcoholic fatty liver disease, oxidative stress*

INTRODUCTION

Nonalcoholic fatty liver disease (NAFLD) is currently the most prevalent chronic liver disease, largely due to the obesity epidemic.[1] It encompasses a spectrum of liver damage ranging from simple steatosis to nonalcoholic steatohepatitis (NASH), an advanced stage of disease comprising progressive steatosis, lobular inflammation, balloon degeneration, and even fibrosis.[2] The pathogenesis responsible for the development and progression of NASH is comprehensive and remains yet to be fully elucidated. Due to this available treatments remain unsatisfactory.

Hepatocytes are commonly enriched in mitochondria (~1000−2000 mitochondria/hepatocyte), signifying their critical roles within hepatocytes, such as the primary site for energy production and β-oxidation of fatty acids. Previous studies have shown that abnormal morphological changes in mitochondria and reduced mitochondrial DNA (mtDNA) copy number are observed in human subjects and animal models with NASH.[3,4] In addition, significantly decreased activity of the hepatic mitochondrial respiratory chain (MRC), particularly complex I and IV, was shown in NASH liver samples compared to controls.[5,6] Moreover, recent evidence has demonstrated impairment of mitochondrial β-oxidation in humans and animals with NASH.[7,8] These studies provide strong evidence to support the possibility that NAFLD might be a mitochondrial disease. They also support seeking therapies that improve mitochondrial function as a useful strategy for preventing NASH and its complications.

Interestingly, several polyphenolic compounds, such as curcumin,[9] quercetin,[10] anthocyanins (ACNs)[11] and green tea catechins,[12] have been demonstrated to have beneficial effects in NAFLD. Among them, ACNs are of great interest due to their abundance in a wide variety of plant foods and the fact that considerable amounts could be ingested from our plant-based daily diets. Existing in vitro data suggest that ACNs exert antisteatosis effects in hepatocytes by inhibiting lipogenesis and/or promoting fatty acid oxidation.[13−15] Mirroring the results obtained in vitro, ample evidence from animal models of NAFLD demonstrates that ACNs diminish hepatic lipid accumulation and inflammation.[16] Furthermore, ACNs are thought to promote antioxidant activity and eventually contribute to an overall positive gain in liver function.[17,18] Despite realizing these benefits, an understanding of the protective role of ACNs and the underlying mechanism of action in the progression of NASH remains unknown and requires further investigation in vivo.

Considering the potential capability of ACNs in NASH and the vital role of mitochondrial dysfunction in the progression of NASH, we set out to determine the influence of purified ACNs from bilberry and black currant on hepatic steatohepatitis and fibrosis as well as mitochondrial content and function in a methionine-choline-deficient (MCD) diet murine model of

Received: October 14, 2014
Revised: December 8, 2014
Accepted: December 23, 2014
Published: December 23, 2014

ACS Publications © 2014 American Chemical Society

DOI: 10.1021/jf504926n
J. Agric. Food Chem. 2015, 63, 552−561

NASH. The influence of ACNs on related signaling pathways was also investigated.

MATERIALS AND METHODS

Purified Anthocyanins. Purified ACNs were kindly provided by Polyphenol AS (Sandnes, Norway). As mentioned in our previous study,[19] the purified ACNs product consisted of 17 different natural ACNs from bilberry (*Vaccinium myrtillus*) and black currant (*Ribes nigrum*). Cyanidin 3-*O*-β-glucoside and delphinidin 3-*O*-β-glucoside are major components of the ACNs supplement. Detailed components and contents are listed in Supporting Information Table 1.

Reagents and Antibodies. Reagents for immunohistochemistry and immunofluorescence, such as serum blocking solution, hydrogen peroxide, and diaminobenzidine (DAB), were obtained from Zhongshan Jinqiao Biotechnology Co. (Beijing, China). Anti-AMP-activated protein kinase (AMPK) and antiphosphorylated AMP-activated protein kinase (p-AMPK) antibodies were purchased from Cell Signaling Technology Inc. (Danvers, MA, USA). Antibodies for cabamoyl phosphate synthase 1 (CPS-1), alpha smooth muscle actin (α-SMA), peroxisome proliferator-activated receptor-gamma coactivator-1β (PGC-1β), nicotinamide adenine dinucleotide dehydrogenase (Complex I), and cytochrome *c* oxidase (Complex IV) were purchased from Abcam (Cambridge, UK). Antibodies for peroxisome proliferator-activated receptor-gamma coactivator-1α (PPAR-α), peroxisome proliferator-activated receptor-1α (PGC-1α), glyceraldehyde 3-phosphate dehydrogenase (GAPDH), and all secondary antibodies were obtained from Santa Cruz Biotechnology (Santa Cruz, CA, USA). Fluorescent probe dihydroethidium (DHE) was purchased from Calbiochem (San Diego, CA, USA). All other reagents and kits were obtained from Sigma-Aldrich (St. Louis, MO, USA) and Invitrogen (Carlsbad, CA, USA) unless otherwise noted.

Animals and Diets. All animal procedures were approved by the Animal Care and Protection Committee of Sun Yat-Sen University (2013-10). Six-week-old male C57BL/6J mice purchased from the Experimental Animal Center of Sun Yat-Sen University (Guangzhou, China) were housed in standard cages within a room with a constant temperature and humidity, under a 12-h light/dark cycle, with free access to food and water. After 2-week adaptation, all mice were body-weight matched and randomly divided into three groups (n = 8 per group): (1) control group, mice were fed a control chow diet; (2) MCD group, mice were fed with a diet deficient in methionine and choline; (3) MCD + ACNs group, mice were fed with the MCD diet with addition of 1 g of purified ACNs per kilogram food. Both the control chow diet and MCD diet were purchased from Research Diets Inc. (New Brunswick, NJ, USA). The control diet was identical to the MCD diet but supplemented with D,L-methionine (3 g/kg) and choline chloride (2 g/kg). Food intake was measured every other day, and body weight was measured weekly.

Biochemical Analyses. At the end of the experiment, all mice were euthanized with sodium pentobarbital (50 mg/kg body weight) and sacrificed after overnight starvation. The serum and liver samples of each mouse were collected and stored at −80 °C for further analysis.

Serum alanine aminotransferase (ALT) and aspartate aminotransferase (AST) were detected using commercial kits from Jiancheng Bioengineering Institute (Nanjing, China) according to the manufacturer's instructions. Serum triglyceride (TG), total cholesterol (TC), and hepatic TG/TC contents were determined using commercial detection kits (Applygen Technologies Inc., Beijing, China) according to manufacturer's protocols.

Histological Assessment. The liver samples were fixed in 10% phosphate-buffered formalin, embedded in paraffin, cut in 5 μm thickness, and applied to slides. The sections were stained with hematoxylin and eosin (H&E) and Sirius Red for histological analysis (NAFLD activity scoring (NAS) and collagen) under light microscopy (Leica, Bensheim, Germany). The Pathology Committee of the NASH Clinical Research Network[20] provided guidance and recommendations for the NAS study by semiquantitatively evaluating the following histological features: steatosis (<5% = 0; 5−33% = 1; 33−66% = 2; >66% = 3); lobular inflammation (none = 0; <2 foci = 1; 2−4 foci = 2; >4 foci = 3); and hepatocellular ballooning (none = 0; few = 1; prominent = 2). All features were scored blindly based on at least 5 samples per group and 10 fields of vision in each sample. Fresh liver tissue was embedded in Tissue Tek OCT, rapidly frozen in liquid nitrogen, and then stored at −80 °C for preparation of frozen sections (5 μm), which were used for staining with Oil Red O and immunofluorescence staining.

Immunohistochemistry and Immunofluorescence. The procedures for immunohistochemistry and immunofluorescence assays were performed as previously described.[21] Briefly, slides were incubated in serum blocking solution for 30 min and incubated overnight with either α-SMA or CPS-1 primary antibody. Then HRP-labeled or fluorescent secondary antibodies were used for immunohistochemistry (α-SMA) and immunofluorescence (CPS-1) analysis, respectively. DAB was applied for immunohistochemistry, and the samples were observed under light microscopy (Leica, Bensheim, Germany). DAPI (Roche, Germany) was utilized for immunofluorescence nuclear staining, and the samples were observed under an Inverted Fluorescence Microscopy (Nikon Eclipse Ti-E, Tokyo, Japan). The fluorescent intensity was analyzed using ImageJ software (Research Services Branch of the NIH, Bethesda, MD).

Western Blot. Liver tissues were homogenized, and 30 μg of total protein lysate were loaded onto 8−15% SDS polyacrylamide gels. After 90 min of electrophoresis, the proteins were transferred onto a polyvinylidene difluoride membrane in ice for 1−2 h. The membrane was blocked with 5% (w/v) bovine serum albumin dissolved in trihydroxymethyl aminomethane buffer salt containing 0.05% (v/v) Tween-20 (TBST). The membrane was then incubated at 4 °C overnight with primary antibodies for AMPK, p-AMPK, CPS-1, PGC-1α, PGC-1β, PPAR-α, Complex I, or Complex IV, followed by incubation with secondary antibodies conjugated with horseradish peroxidase for 2 h at room temperature. Signals were detected by enhanced chemiluminescence reagent (Thermo Fisher Scientific, Waltham, MA, USA). GAPDH was used for normalization. The density of the specific bands was quantified using ImageJ software.

Mitochondrial DNA Quantification. Total DNA was extracted from livers using a DNeasy Blood & Tissue Kit (Qiagen, Dusseldorf, Germany), and real-time PCR was performed using gene-specific primers amplifying mitochondrial DNA (mtDNA) and nuclear DNA (nDNA). The relative values of mtDNA content and nDNA content were used to assess mitochondrial copy numbers. The primer sequences are listed in Supporting Information Table 2.

RNA Extraction and Quantitative RT-PCR. Total RNA (1 μg) was extracted from liver tissues using Trizol reagent and transcribed into cDNA using the PrimeScript RT reagent kit (TaKaRa, Tokyo, Japan) according to the manufacturer's recommendations. Quantitative PCR was performed using a real-time PCR system (Applied Biosystems, Foster City, CA, USA), and reactions were performed using SYBR Green Master Mix (TaKaRa, Tokyo, Japan) with gene-specific primers. Each sample was normalized to β-actin, and the fold change in expression of each target gene relative to β-actin was assessed via the comparative CT ($2^{-\Delta\Delta CT}$) method. Primer sequences are listed in Supporting Information Table 3.

Detection of Hepatic Oxidative Stress. The total reactive oxygen species (ROS) levels in the liver tissues were detected using the fluorescent probe DHE. Briefly, frozen liver sections were incubated in DHE (10 μM) for 30 min in a dark and humidified chamber at 37 °C. DHE is oxidized by superoxide to ethidium bromide, bands to the DNA, and emits red fluorescence,[22] which was detected using inverted fluorescence microscopy. In addition, liver tissue homogenates were prepared to measure hepatic malondialdehyde (MDA) by following the commercial kit's instructions (Beyotime, Shanghai, China). The MDA concentrations were normalized by protein contents.

Statistical Analysis. All results were expressed as mean ± standard deviation (SD) and statistically analyzed with SPSS 16.0 for Windows (SPSS Inc., Chicago, IL, USA). Comparisons between all groups were evaluated using one-way analysis of variance (ANOVA). Differences were considered significant at $P < 0.05$.

DOI: 10.1021/jf504926n
J. Agric. Food Chem. 2015, 63, 552−561

RESULTS

Effects of ACNs on Animal Characteristics. As shown in Table 1, the initial body weight among the 3 groups showed little deviation ($P > 0.05$). After 4 weeks, the MCD mice with or without ACNs treatment displayed a significant reduction in body weight (~50%). Moreover, 1-fold increase in serum AST and more than 10-fold increase in serum ALT were observed in mice fed the MCD diet. Though ACNs did not attenuate the reduction of body weight induced by the MCD diet, their addition effectively decreased serum ALT and AST levels ($P < 0.05$). No significant changes in daily food intake among the 3 groups during the experimental period were observed (data not shown).

Table 1. Animal Characteristics and Serum Liver Enzymes of Mice in Different Study Groups[a]

	control	MCD	MCD + ACNs
initial body weight (g)	25.12 ± 1.30	25.09 ± 1.26	25.35 ± 1.20
final body weight (g)	27.39 ± 2.74	16.93 ± 0.73*	17.19 ± 0.42*
liver weight (g)	0.89 ± 0.13	0.54 ± 0.06*	0.56 ± 0.10*
liver to body weight ratio (%)	3.53 ± 0.62	3.20 ± 0.20	3.40 ± 0.34
serum ALT level (U/L)	6.03 ± 1.68	79.08 ± 36.54*	58.65 ± 25.03*/#
serum AST level (U/L)	23.43 ± 1.66	49.48 ± 3.17*	40.26 ± 2.07*/#

[a]All values are mean ± SD, $n = 8$. Statistical analysis of the data for multiple comparisons was performed by ANOVA. *$P < 0.05$ versus the control group; #$P < 0.05$ versus the MCD group.

Effects of ACNs on Lipid Accumulation. The histological features of Oil Red O staining illustrated a massive accumulation of neutral lipid droplets within the hepatocytes of MCD group, whereas only small lipid droplets were observed in mice treated with ACNs (Figure 1A). Quantitative determination of hepatic TG content further confirmed that a large quantity of TG accumulated in the livers of mice fed the MCD diet, which was significantly decreased by ACNs supplementation ($P < 0.05$) (Figure 1B). Conversely, the serum TG levels in both MCD diet group and MCD + ACNs group declined sharply compared with the control group, while were slightly up-regulated by ACNs though without significance compared with the MCD group ($P > 0.05$) (Figure 1C). This interesting phenomenon probably was

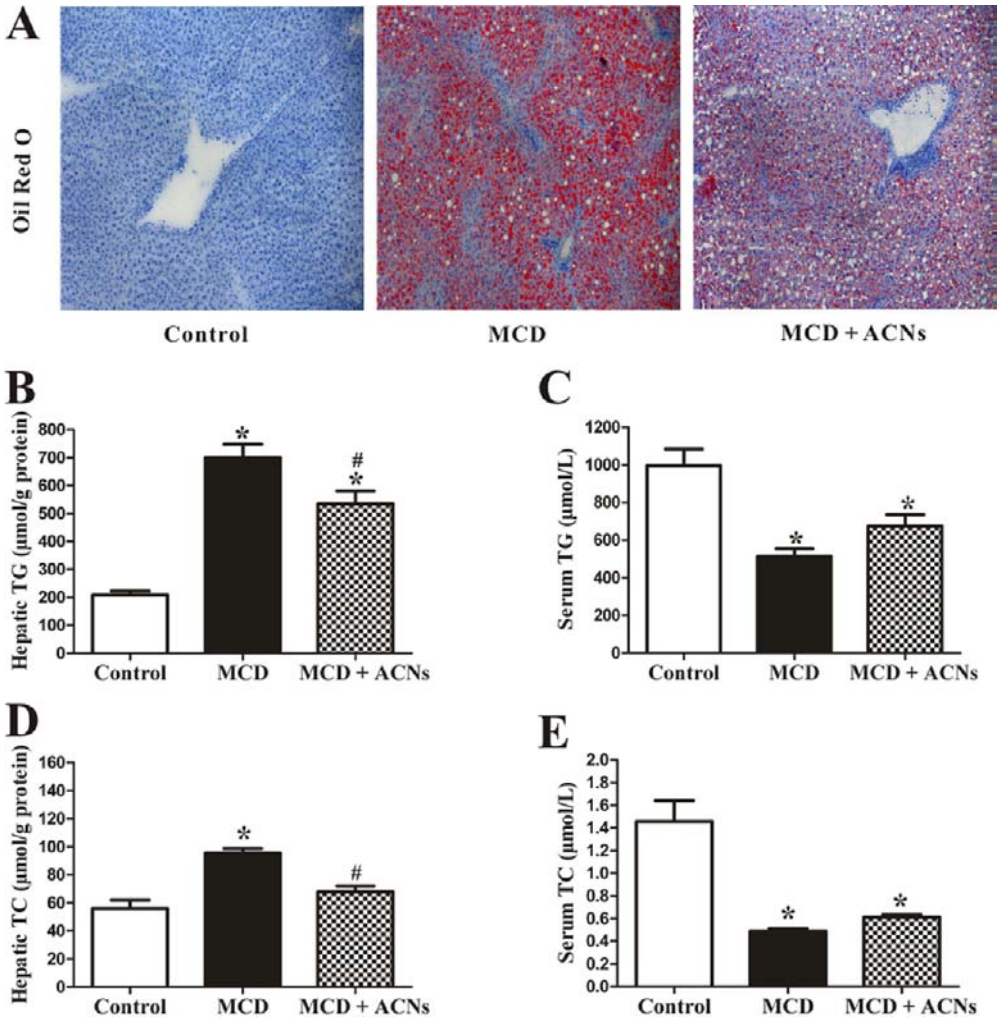

Figure 1. ACNs decreased lipid accumulation in mice fed the MCD diet. (A) Frozen sections (5 μm thick) were stained with Oil Red O, which marked neutral lipid. Representative micrographs (200× magnification) are shown. (B–E) TG and TC levels were measured from all frozen liver specimens and serum. Values are expressed as mean ± SD, $n = 8$. *$P < 0.05$ versus the control group; #$P < 0.05$ versus the MCD group.

DOI: 10.1021/jf504926n
J. Agric. Food Chem. 2015, 63, 552–561

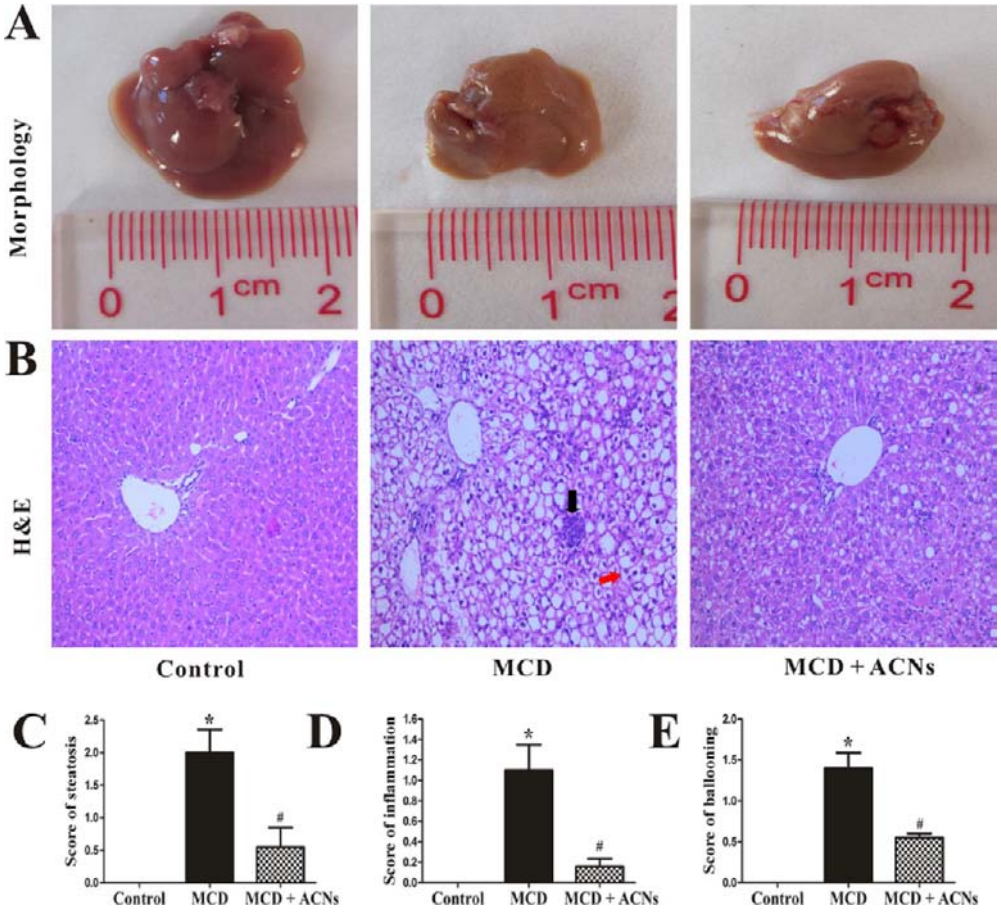

Figure 2. ACNs ameliorated steatohepatitis induced by the MCD diet. (A) Representative gross morphology images are shown. (B) Hepatic histological analysis of H&E staining (200× magnification). Inflammatory infiltration (black arrow) and hepatocyte ballooning (red arrow) were observed in liver sections from the MCD group which were improved in the ACNs-treated group. (C–E) Histological NAS scores of liver tissues. Values are expressed as mean ± SD, $n = 8$. *$P < 0.05$ versus the control group; $^{\#}P < 0.05$ versus the MCD group.

caused by hepatic TG potentially releasing into serum. Similarly, accumulation of hepatic TC was effectively alleviated by ACNs ($P < 0.05$) (Figure 1D). The serum TC levels in the MCD + ACNs group showed an increasing trend but no significant differences compared to the MCD diet only group (Figure 1E).

Amelioration of Steatohepatitis by ACNs. The gross morphology of the livers in the control group displayed red and smooth tissue surface. After 4 weeks feeding with MCD diet, the gross morphology of livers had an obvious increase in tawny and brittle appearance, which was improved greatly by ACNs treatment (Figure 2A). The NAS calculation system was applied to semiquantitatively evaluate the steatosis, inflammation, and ballooning. Indeed, the histological analysis of H&E staining indicated significant microvesicular steatosis, inflammatory cell infiltration, and hepatocyte ballooning in the MCD diet group. However, livers of the ACNs-treated group exhibited only mild hepatic steatosis and effectively ameliorated inflammatory infiltration with reduction by 50% in hepatocyte ballooning compared to the MCD diet only group (Figure 2B–E).

Inhibition of Liver Fibrosis by ACNs. To assess the effect of ACNs on hepatic fibrosis, we carried out a Sirius Red staining of collagen in liver sections. A substantial increase in collagen deposition was observed in the MCD group compared with the control group. However, an obvious decrease in the stained area percentage was observed in the MCD + ACNs group (Figure 3A). Activation of hepatic stellate cells (HSCs), the major effectors in collagen production during hepatic fibrogenesis, is another indicator of fibrogenesis. To further evaluate HSCs activation, immunohistochemical staining of α-SMA was performed. As displayed in Figure 3B, the data indicated that ACNs treatment reduced the expression of α-SMA, suggestive of inhibition of HSCs activation. Besides, both relative mRNA expression of collagen I and α-SMA confirmed that ACNs played a suppressive effect on fibrosis in NASH (Figure 3C and 3D).

Decrease of Oxidative Damage by ACNs. Mitochondria are the major sites for ROS production. Quantitative evaluation of hepatic ROS is also an indicator of mitochondrial impairment. In our present study, the 4-week MCD diet up-regulated ROS levels of liver tissues by approximately 6-fold compared with the control diet, and we unearthed that ACNs were able to significantly subdue ROS production induced by the MCD diet (Figure 4A and 4B). In addition, hepatic malondialdehyde (MDA) content, a widely used marker of oxidative stress, was increased by nearly 4-fold in the MCD group but only slightly increased in ACNs-treated mice (Figure 4C). The results of hepatic ROS and MDA levels clarified that ACNs played a suppressive effect on oxidative damage in NASH.

Attenuation of Reduced Mitochondrial Content and Function by ACNs. One of the common mitochondrial defects observed in NASH is depletion of mitochondrial DNA (mtDNA).[4] In our study, we first investigated the protective effect of ACNs on mtDNA. As shown in Figure 5A, mtDNA indeed displayed an apparent decrease in the MCD group, which was slightly improved through administration of ACNs ($P <$

DOI: 10.1021/jf504926n
J. Agric. Food Chem. 2015, 63, 552–561

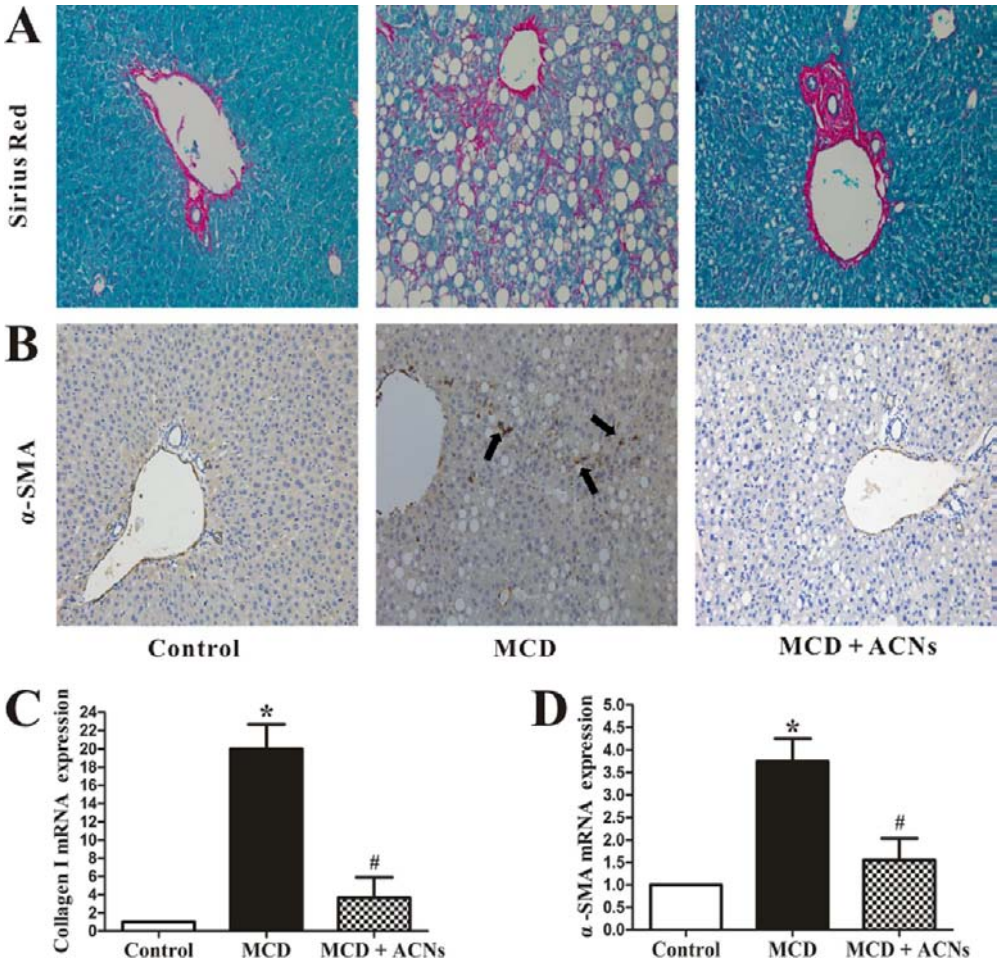

Figure 3. ACNs played an inhibitory role in progression of fibrosis in mice fed an MCD diet. (A) Paraffin-embedded liver specimens were stained with Sirius Red and observed by light microscopy. (B) Paraffin sections were immunoassayed for fibrosis markers, α-SMA (black arrows), to assess hepatic stellate cells activation. Representative photographs (200× magnification) are shown. (C and D) Total RNA was isolated from the livers, and genes expression of collagen I and α-SMA were subjected to RT-PCR analysis; the control group was set to be 1. Values are expressed as mean ± SD, $n = 8$. $^{*}P < 0.05$ versus the control group; $^{\#}P < 0.05$ versus the MCD group.

0.05), though it was still lower than the number observed in the control group. Moreover, CPS-1, a hepatic mitochondrial membrane specific marker and reflection of mitochondrial number and function in liver, declined in NASH but was significantly up-regulated by treatment of ACNs (Figure 5B−5D).

Enhancement of Mitochondrial Biogenesis by ACNs. To investigate whether ACNs are capable of increasing mitochondrial biogenesis, we determined the relative mRNA expression of peroxisome proliferator-activated receptor-gamma coactivator-1α (PGC-1α) and β (PGC-1β), nuclear respiratory factor-1 (NRF-1) and 2 (NRF-2), and mitochondrial transcription factor A (Tfam) (pivotal regulators of mitochondrial biogenesis). As displayed in Figure 6A and B, PGC-1α dropped in NASH ($P < 0.05$) but exhibited sharply increased expression after ACNs intervention, whereas PGC-1β was unaffected by either MCD diet or ACNs treatment. In addition, there was almost 50% reduction in PGC-1α-target genes NRF-1, NRF-2, and TFAM following a MCD diet, while the reduction was effectively suppressed with treatment of ACNs. Likewise, immunoblotting analysis revealed that ACNs reversed the reduction of protein abundance of PGC-1α induced by the MCD diet, while no significant difference in PGC-1β expression was observed among the three groups (Figure 6C). Together, these results indicate that ACNs may induce mitochondrial biogenesis through PGC-1α pathway.

Our previous research has demonstrated activation of AMPK by ACNs in hepatocytes,[14] which could result in phosphorylation of the transcriptional coactivator PGC-1α, thus leading to increased mitochondrial biogenesis.[23,24] Then, we determined the protein levels of p-AMPK and total AMPK and discovered an over 50% decrease in p-AMPK in the liver of NASH mice, which was rescued by ACNs with no change of total AMPK (Figure 6C).

Amelioration of Mitochondrial Electron Transfer Chain (ETC) Defects by ACNs. Mitochondrial ETC is constituted of four respiratory complexes (complexes I−IV).[25] To confirm the alteration of mitochondrial ETC and effects of ACNs on it at a functional level, the protein expression of two major sites of electron input into the electron transport system (complex I and IV) in total liver lysates was examined (Figure 6D). The mice fed the MCD diet had mitochondrial ETC defects, as shown by conspicuously diminished protein expression of mitochondrial complexes I and V, especially complex IV (approximately 4-fold). As expected, dietary ACNs intervention successfully intensified protein expression of mitochondrial complexes I and V, reflecting improvement of mitochondrial oxidative phosphorylation and enhancement of mitochondrial biogenesis and function.

DOI: 10.1021/jf504926n
J. Agric. Food Chem. 2015, 63, 552−561

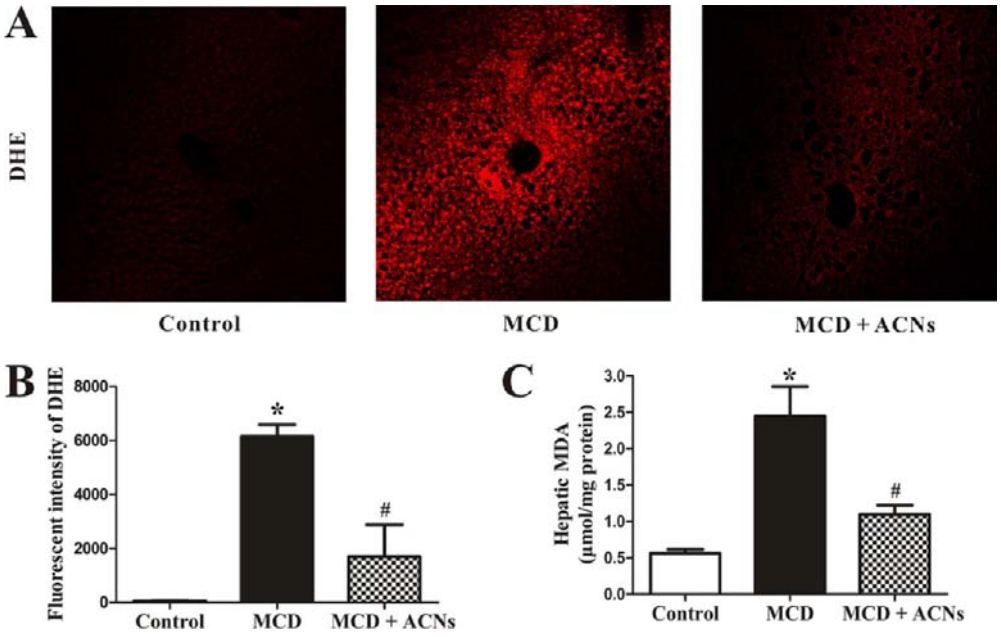

Figure 4. ACNs decreased oxidative damage in NASH. (A) Frozen sections of livers were stained with fluorescent probe DHE, showing red fluorescence in regions of ROS production. Representative fluorescence micrographs (200× magnification) are shown. (B) Fluorescent densitometry of DHE staining was quantified by ImageJ software. (C) MDA content in livers. Values are expressed as mean ± SD, $n = 8$. $^{*}P < 0.05$ versus the control group; $^{\#}P < 0.05$ versus the MCD group.

Improvement of Mitochondrial β-Oxidation by ACNs. Impairment of mitochondrial oxidative phosphorylation is often followed by inhibition of mitochondrial fatty acid β-oxidation. In the present study, we indeed discovered that both protein and mRNA expression of peroxisome proliferator-activated receptor-α (PPAR-α) were nearly halved in NASH but successfully restored by ACNs intervention (Figure 6C and E). PPAR-α is one of a superfamily of nuclear hormone receptors and able to transcriptionally up-regulate nuclear genes encoding mitochondrial fatty acid oxidation enzymes.[26] We then determined gene expression levels of carnitine palmitoyltransferase 1 (CPT-1) and medium chain acyl CoA dehydrogenase (MCAD), two rate-limiting enzymes of fatty acids β-oxidation. As illustrated in Figure 6E, relative mRNA expression of CPT-1 and MCAD dropped significantly in NASH ($P < 0.05$); however, both were augmented with administration of ACNs. These were accompanied by no distinction of fatty acid synthesis (FAS) between the groups. Thus, ACNs seemed to be able to stimulate hepatic lipid oxidation, leading to reduction of TG accumulation within hepatocytes.

DISCUSSION

Previously, we and others have shown that ACNs have hepatoprotective activities in obese and diabetic rodents.[16,27] In the present study, we demonstrated that purified ACNs from bilberry and black currant were capable of ameliorating hepatic steatosis, inflammation, oxidative stress, as well as signs of fibrosis and improving depletion of mitochondrial content and damage of mitochondrial biogenesis, ETC, as well as β-oxidation. To our knowledge, this work provides the first evidence that ACNs, the soluble flavonoids, alleviate complications of NASH and improve degeneration of mitochondrial function in mice fed a MCD diet.

Much research verifies that abnormalities in the number and quality of mitochondria are frequently observed in NASH and involved in its pathogenesis. These mitochondrial abnormalities include ultrastructural lesions, depletion of mtDNA, reduction of respiratory chain activity, impairment of mitochondrial β-oxidation, and induction of uncoupling and apoptosis.[28] As expected, our MCD diet-induced NASH model displayed a reduction in mitochondrial content as well as impairment of mitochondrial biogenesis, ETC activity, and β-oxidation function.

In our study, we discovered that dietary supplement of ACNs could ameliorate the depletion of mtDNA and decrease expression of CPS-1 (Figure 5). Mitochondrial DNA represents mitochondrial self-replication and is involved in mitochondrial biogenesis.[24] It is also crucial for mitochondrial oxidative phosphorylation, encoding 13 MRC polypeptides that embed within complexes I, III, IV, and V, and further for β-oxidation.[29] CPS-1, a hepatic mitochondrial membrane-specific marker, qualitatively reflects hepatic mitochondrial content and function in the liver and is a comprehensive marker of mitochondrial damage.[30] It could be concluded from our work that dietary ACNs mitigate the depletion of mitochondrial content and dysfunction in NASH.

Mitochondrial biogenesis plays a critical role in maintaining the dynamic equilibrium of proliferation and degradation of mitochondria in hepatocytes.[31] Activation of mitochondrial biogenesis is mainly reflected by the activation of NRF-1 and NRF-2, which conversely regulates the expression of Tfam, a protein essential for transcription, replication, and maintenance of the mtDNA. In our study, the mRNA expression of NRF-1, NRF-2, and Tfam was significantly decreased in mice fed the MCD diet, indicating damage to mitochondrial biogenesis. This effect was evidently ameliorated by administration of ACNs, especially with respect to NRF-2 and Tfam (Figure 6B). These data suggest that ACNs stimulate mitochondrial biogenesis in NASH.

As major sites for cellular respiration, mitochondria play a vital role in maintaining energy metabolism and function of hepatocytes, which includes the citric acid cycle and oxidative phosphorylation process. The oxidative phosphorylation process

DOI: 10.1021/jf504926n
J. Agric. Food Chem. 2015, 63, 552−561

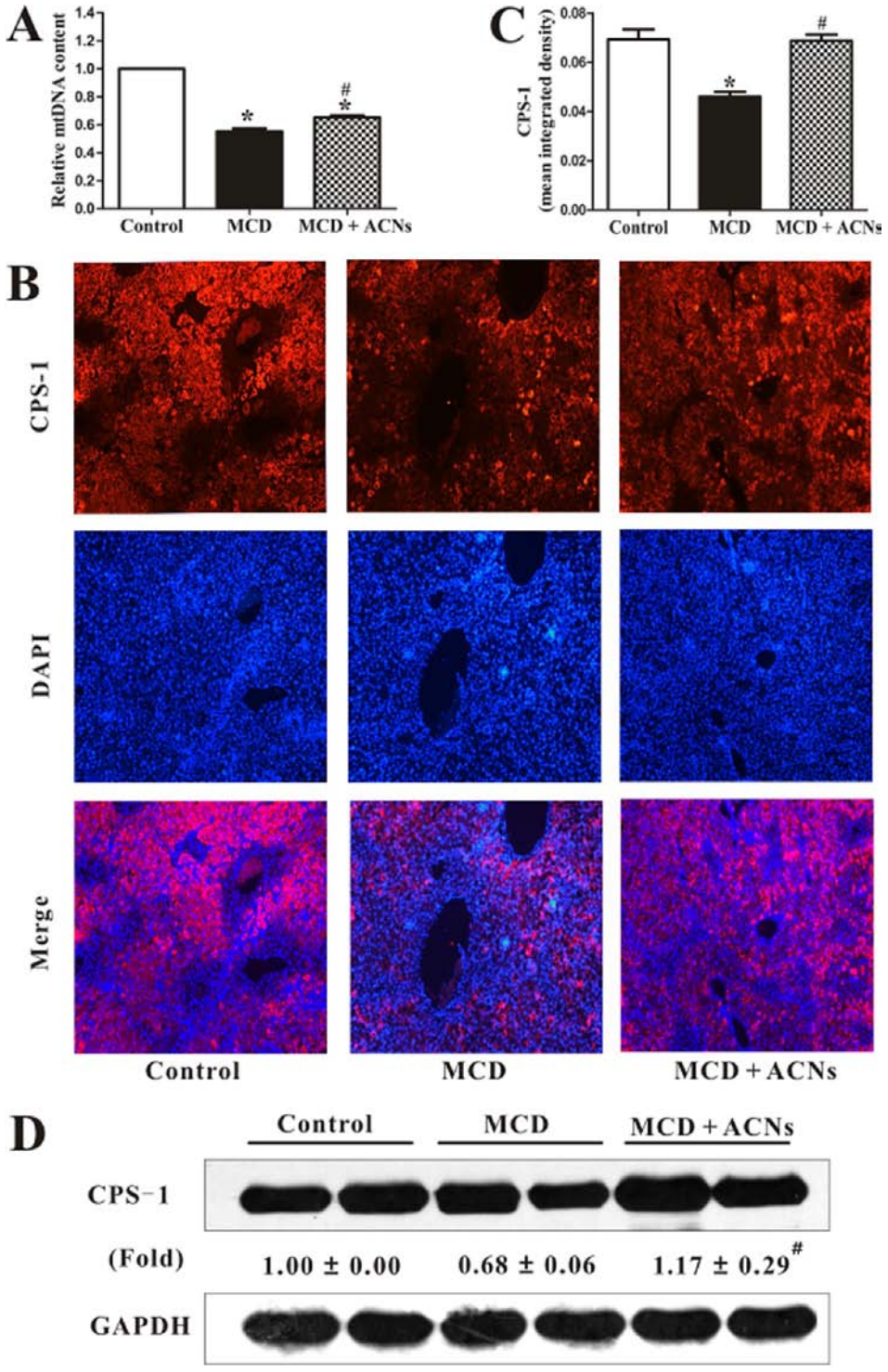

Figure 5. ACNs attenuated reduction of mitochondrial content and function in NASH. (A) Mitochondrial genome copy number was shown as the ratio of mtDNA to nDNA from purified liver DNA, which was determined by quantitative real-time PCR. The control group was set to be 1. (B) Representative immunofluorescent photomicrographs (200× magnification) for mitochondrial marker CPS-1 (red fluorescence) showed granular staining patterns in liver frozen sections. (C) Fluorescent staining of CPS-1 per field was quantified by ImageJ software and reported as mean integrated density. (D) Western blot analysis was performed to semiquantitatively assess expression levels of CPS-1 from liver homogenates. The control group was set to be 1. Values are expressed as mean ± SD, $n = 8$. $^{*}P < 0.05$ versus the control group; $^{\#}P < 0.05$ versus the MCD group.

of ETC is located on the inner membrane of mitochondrion and consisted of four large transmembrane protein complexes (mitochondrial respiratory complexes I–IV).[25] Complexes I and IV are two important and major protein complexes of the electron transfer chain among the four. Via determination of the two representative protein complexes, we ascertained that ETC defects happened in mice fed the MCD diet which, however, were visibly alleviated by ACNs administration (Figure 6D).

One of the most common hepatic cell injuries is the result of accumulation of various lipids, which further contributes to

DOI: 10.1021/jf504926n
J. Agric. Food Chem. 2015, 63, 552–561

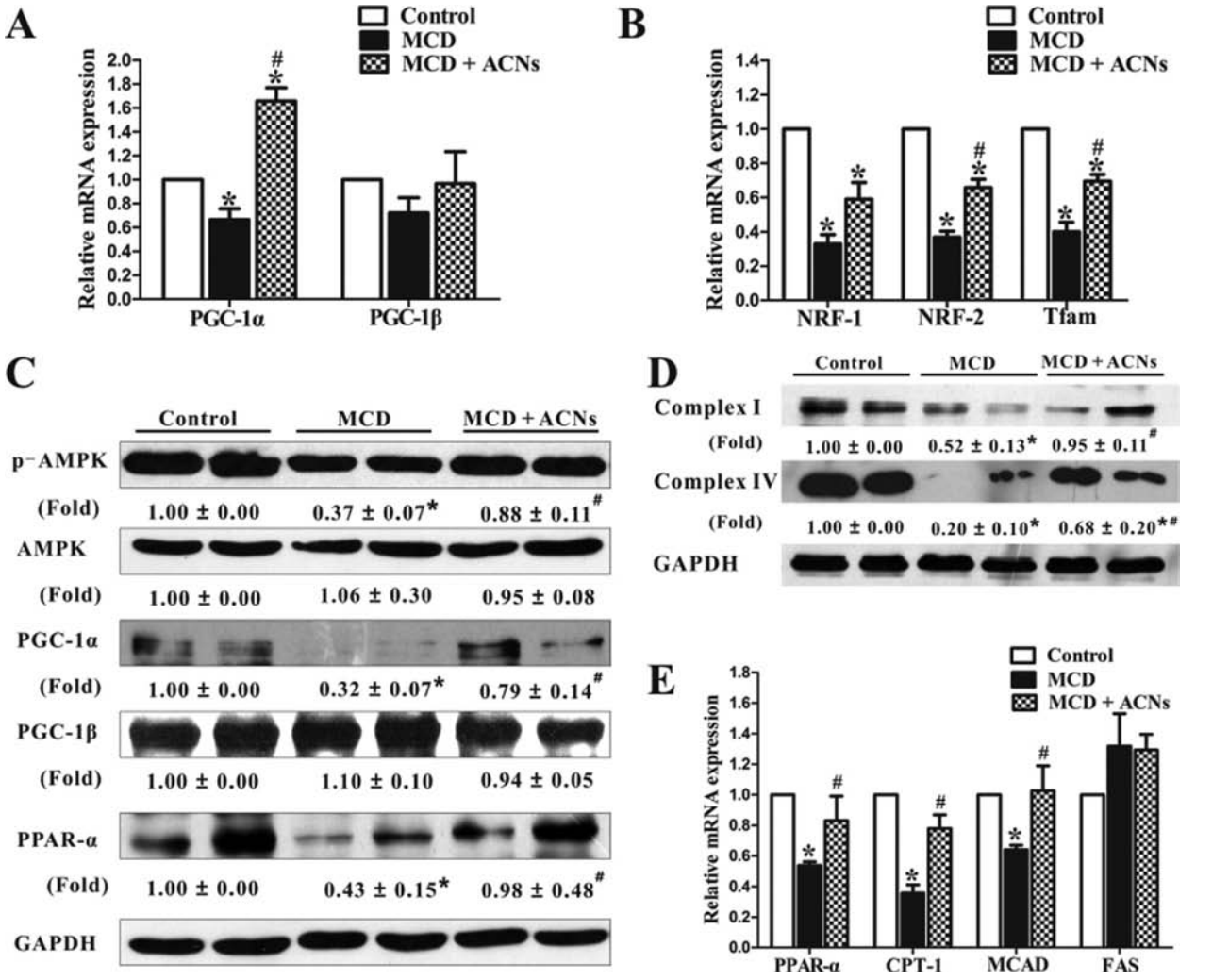

Figure 6. ACNs stimulated mitochondrial biogenesis and improved mitochondrial ETC defects as well as enhanced mitochondrial β-oxidation in NASH. (A and B) Real-time PCR was applied to measure mRNA expression of PGC-1α and PGC-1β (A) and genes related to mitochondrial biogenesis (NRF-1, NRF-2 and Tfam) (B). (C) Protein expression of p-AMPK, total AMPK, PGC-1α, PGC-1β, and PPAR-α in livers was measured by Western blot, quantified using densitometry, and normalized by GAPDH content. (D) Protein levels of complexes I and IV were examined by Western blot. (E) Genes related to fatty acid oxidation (CPT-1, MCAD, and PPAR-α) and lipogenesis (FAS) were subjected to RT-PCR analysis. The control group was set to be 1. Results are expressed as mean ± SD, $n = 6-8$. *$P < 0.05$ versus the control group; #$P < 0.05$ versus the MCD group.

development and progression of fatty liver. The main mechanisms are as follows: increased fatty acid uptake and de novo hepatic lipogenesis, decreased fatty acid β-oxidation and hepatic very low density lipoprotein-triglyceride (VLDL) secretion. One of the mechanisms of NASH induced by the MCD diet is decreased VLDL assembly and secretion, contributing to disturbance in phosphatidylcholine synthesis that is caused by deficiencies in methionine and choline.[32] In our study, we also observed that this model was accompanied by impairment of mitochondrial β-oxidation, manifested by a decrease in gene or protein expression of PPAR-α, CPT-1, and MCAD (Figure 6C and 6E), which consequently cooperated with decreased VLDL to result in the reduction of lipid clearance. Our data show that ACNs treatment significantly up-regulated protein expression of PPAR-α and gene expression of PPAR-α, CPT-1, and MCAD (Figure 6E). PPAR-α is predominantly expressed in the liver where it transcriptionally up-regulates nuclear genes encoding mitochondrial fatty acid oxidation enzymes CPT-1 and MCAD.[26] CPT-1 locates on the outer mitochondrial membrane and is a key rate-limiting enzyme of long-chain fatty acid β-oxidation, while MCAD is a key enzyme in the first step of medium-chain fatty acid β-oxidation. We conclude that ACNs can improve impairment of mitochondrial β-oxidation in NASH induced by the MCD diet, which further counteracts hepatocyte injury resulting from lipid accumulation by promoting TG clearance.

In line with existing research illustrating that ACNs are able to activate protein expression of AMPK in vitro[14] and in vivo,[16] we also found that ACNs could attenuate the reduction of p-AMPK expression induced by the MCD diet (but not total AMPK; Figure 6C). Moreover, emerging evidence showed that the activation of AMPK leads to increased expression of the downstream molecule PGC-1α,[33] which was demonstrated to be a potent stimulator of mitochondrial biogenesis in liver, heart, and skeletal muscle by contributing to activation of NRF-1, NRF-2, and Tfam.[34] In the present study, we showed that protein and gene expression of PGC-1α and its target genes were up-regulated by ACNs, which subsequently potentiated mitochondrial biogenesis. These data suggest that the improvement of mitochondrial dysfunction induced by ACNs treatment is

DOI: 10.1021/jf504926n
J. Agric. Food Chem. 2015, 63, 552−561

attributed to increased phosphorylation of AMPK, which subsequently increased expression of PGC-1α, rather than PGC-1β (Figure 6A and 6C).

In summary, our study shows that ACNs ameliorate liver disease in steatohepatitis progression and improve mitochondrial defects. Our previous study also showed that anthocyanin cyanidin 3-*O*-β-glucoside could notably improve mitochondrial function in high glucose-stressed hepatocytes.[35] Considering previous studies reporting that mitochondrial dysfunction takes precedence over insulin resistance and hepatic steatosis and leads to the natural history of NAFLD[30,36] and combining with our own results, we venture to conclude that administration of ACNs attenuated NASH due to the improvement of mitochondrial dysfunction in mice fed a MCD diet. The possible mechanism may involve activation of AMPK/PGC-1α signaling axis by ACNs, which subsequently contributes to improvement of depletion of mitochondrial mtDNA and mitochondrial biogenesis function, improves ETC activity and β-oxidation, and eventually attenuates lipid accumulation-induced hepatocyte injury by enhancing TG clearance. Due to limitations such as the animal model of NASH and lack of inhibitors or blockers in our current study, further research is needed to investigate the detailed molecular mechanisms and potential clinical applications of ACNs in NAFLD.

■ ASSOCIATED CONTENT

Supporting Information

Composition of the purified anthocyanins and primer sequences used for RT-PCR. This material is available free of charge via the Internet at http://pubs.acs.org.

■ AUTHOR INFORMATION

Corresponding Authors

*Phone:86-751-8120167. Fax: 86-751-8121429. E-mail: guohh1999@hotmail.com.

*Phone: 86-20-87331597. Fax: 86-20-87330446. E-mail: lingwh@mail.sysu.edu.cn.

Funding

This work was funded by grants from the National Basic Research Program (973 Program, 2012CB517506), National Nature Science Foundation (81172655, 81372994), and China Scholarship Council (201308440005).

Notes

The authors declare no competing financial interest.

■ ABBREVIATIONS USED

α-SMA, alpha smooth muscle actin; ACNs, anthocyanins; ALT, alanine aminotransferase; AMPK, AMP-activated protein kinase; AST, aspartate aminotransferase; complex I, nicotinamide adenine dinucleotide dehydrogenase; complex IV, cytochrome *c* oxidase; CPS-1, cabamoyl phosphate synthase 1; CPT-1, carnitine palmitoyltransferase 1; DHE, dihydroethidium; ETC, electron transfer chain; FAS, fatty acid synthesis; H&E, hematoxylin and eosin; HSC, hepatic stellate cell; MCAD, medium chain acyl CoA dehydrogenase; MCD, methionine-choline-deficient diet; MDA, malondialdehyde; MRC, mitochondrial respiratory chain; mtDNA, mitochondrial DNA; NAFLD, nonalcoholic fatty liver disease; NAS, nonalcoholic fatty liver disease activity scoring; NASH, nonalcoholic steatohepatitis; NRF-1/2, nuclear respiratory factor-1/2; p-AMPK, phosphorylated AMP-activated protein kinase; PGC-1α/β, peroxisome proliferator-activated receptor-gamma coactivator-1α/β; PPAR-α, peroxisome proliferator-activated receptor-α; ROS, reactive oxygen species; TC, total cholesterol; Tfam, transcription factor A; TG, triglyceride; VLDL, very low density lipoprotein-triglyceride

■ REFERENCES

(1) Shen, H. C.; Zhao, Z. H.; Hu, Y. C.; Chen, Y. F.; Tung, T. H. Relationship between obesity, metabolic syndrome, and nonalcoholic fatty liver disease in the elderly agricultural and fishing population of Taiwan. *Clin. Interventions Aging* **2014**, *9*, 501−508.

(2) Tiniakos, D. G.; Vos, M. B.; Brunt, E. M. Nonalcoholic fatty liver disease: pathology and pathogenesis. *Annu. Rev. Pathol.* **2010**, *5*, 145−171.

(3) Caldwell, S. H.; Chang, C. Y.; Nakamoto, R. K.; Krugner-Higby, L. Mitochondria in nonalcoholic fatty liver disease. *Clin. Liver Dis.* **2004**, *8*, 595−617 x..

(4) Sobaniec-Lotowska, M. E.; Lebensztejn, D. M. Ultrastructure of hepatocyte mitochondria in nonalcoholic steatohepatitis in pediatric patients: usefulness of electron microscopy in the diagnosis of the disease. *Am. J. Gastroenterol.* **2003**, *98*, 1664−1665.

(5) Perez-Carreras, M.; Del Hoyo, P.; Martin, M. A.; Rubio, J. C.; Martin, A.; Castellano, G.; Colina, F.; Arenas, J.; Solis-Herruzo, J. A. Defective hepatic mitochondrial respiratory chain in patients with nonalcoholic steatohepatitis. *Hepatology* **2003**, *38*, 999−1007.

(6) Finocchietto, P. V.; Holod, S.; Barreyro, F.; Peralta, J. G.; Alippe, Y.; Giovambattista, A.; Carreras, M. C.; Poderoso, J. J. Defective leptin-AMP-dependent kinase pathway induces nitric oxide release and contributes to mitochondrial dysfunction and obesity in ob/ob mice. *Antioxid. Redox Signaling* **2011**, *15*, 2395−2406.

(7) Roglans, N.; Vila, L.; Farre, M.; Alegret, M.; Sanchez, R. M.; Vazquez-Carrera, M.; Laguna, J. C. Impairment of hepatic Stat-3 activation and reduction of PPARalpha activity in fructose-fed rats. *Hepatology* **2007**, *45*, 778−788.

(8) Serviddio, G.; Giudetti, A. M.; Bellanti, F.; Priore, P.; Rollo, T.; Tamborra, R.; Siculella, L.; Vendemiale, G.; Altomare, E.; Gnoni, G. V. Oxidation of hepatic carnitine palmitoyl transferase-I (CPT-I) impairs fatty acid beta-oxidation in rats fed a methionine-choline deficient diet. *PLoS One* **2011**, *6*, e24084.

(9) Kuo, J. J.; Chang, H. H.; Tsai, T. H.; Lee, T. Y. Positive effect of curcumin on inflammation and mitochondrial dysfunction in obese mice with liver steatosis. *Int. J. Mol. Med.* **2012**, *30*, 673−679.

(10) Marcolin, E.; San-Miguel, B.; Vallejo, D.; Tieppo, J.; Marroni, N.; Gonzalez-Gallego, J.; Tunon, M. J. Quercetin treatment ameliorates inflammation and fibrosis in mice with nonalcoholic steatohepatitis. *J. Nutr.* **2012**, *142*, 1821−1828.

(11) Shih, P. H.; Hwang, S. L.; Yeh, C. T.; Yen, G. C. Synergistic effect of cyanidin and PPAR agonist against nonalcoholic steatohepatitis-mediated oxidative stress-induced cytotoxicity through MAPK and Nrf2 transduction pathways. *J. Agric. Food Chem.* **2012**, *60*, 2924−2933.

(12) Masterjohn, C.; Bruno, R. S. Therapeutic potential of green tea in nonalcoholic fatty liver disease. *Nutr. Rev.* **2012**, *70*, 41−56.

(13) Liu, Y.; Wang, D.; Zhang, D.; Lv, Y.; Wei, Y.; Wu, W.; Zhou, F.; Tang, M.; Mao, T.; Li, M.; Ji, B. Inhibitory effect of blueberry polyphenolic compounds on oleic acid-induced hepatic steatosis in vitro. *J. Agric. Food Chem.* **2011**, *59*, 12254−12263.

(14) Guo, H.; Liu, G.; Zhong, R.; Wang, Y.; Wang, D.; Xia, M. Cyanidin-3-O-beta-glucoside regulates fatty acid metabolism via an AMP-activated protein kinase-dependent signaling pathway in human HepG2 cells. *Lipids Health Dis.* **2012**, *11*, 10.

(15) Chang, J. J.; Hsu, M. J.; Huang, H. P.; Chung, D. J.; Chang, Y. C.; Wang, C. J. Mulberry anthocyanins inhibit oleic acid induced lipid accumulation by reduction of lipogenesis and promotion of hepatic lipid clearance. *J. Agric. Food Chem.* **2013**, *61*, 6069−6076.

(16) Hwang, Y. P.; Choi, J. H.; Han, E. H.; Kim, H. G.; Wee, J. H.; Jung, K. O.; Jung, K. H.; Kwon, K. I.; Jeong, T. C.; Chung, Y. C.; Jeong, H. G. Purple sweet potato anthocyanins attenuate hepatic lipid accumulation through activating adenosine monophosphate-activated protein kinase

DOI: 10.1021/jf504926n
J. Agric. Food Chem. 2015, 63, 552−561

in human HepG2 cells and obese mice. *Nutr. Res. (N.Y.)* **2011**, *31*, 896−906.
(17) Cho, B. O.; Ryu, H. W.; Jin, C. H.; Choi, D. S.; Kang, S. Y.; Kim, D. S.; Byun, M. W.; Jeong, I. Y. Blackberry extract attenuates oxidative stress through up-regulation of Nrf2-dependent antioxidant enzymes in carbon tetrachloride-treated rats. *J. Agric. Food Chem.* **2011**, *59*, 11442−11448.
(18) Zhang, Z. F.; Lu, J.; Zheng, Y. L.; Wu, D. M.; Hu, B.; Shan, Q.; Cheng, W.; Li, M. Q.; Sun, Y. Y. Purple sweet potato color attenuates hepatic insulin resistance via blocking oxidative stress and endoplasmic reticulum stress in high-fat-diet-treated mice. *J. Nutr. Biochem.* **2013**, *24*, 1008−1018.
(19) Qin, Y.; Xia, M.; Ma, J.; Hao, Y.; Liu, J.; Mou, H.; Cao, L.; Ling, W. Anthocyanin supplementation improves serum LDL- and HDL-cholesterol concentrations associated with the inhibition of cholesteryl ester transfer protein in dyslipidemic subjects. *Am. J. Clin. Nutr.* **2009**, *90*, 485−492.
(20) Kleiner, D. E.; Brunt, E. M.; Van Natta, M.; Behling, C.; Contos, M. J.; Cummings, O. W.; Ferrell, L. D.; Liu, Y. C.; Torbenson, M. S.; Unalp-Arida, A.; Yeh, M.; McCullough, A. J.; Sanyal, A. J. Design and validation of a histological scoring system for nonalcoholic fatty liver disease. *Hepatology* **2005**, *41*, 1313−1321.
(21) Luo, X.; Xiao, Y.; Song, F.; Yang, Y.; Xia, M.; Ling, W. Increased plasma S-adenosyl-homocysteine levels induce the proliferation and migration of VSMCs through an oxidative stress-ERK1/2 pathway in apoE(−/−) mice. *Cardiovasc. Res.* **2012**, *95*, 241−250.
(22) Aoyama, T.; Hida, K.; Kuroda, S.; Seki, T.; Yano, S.; Shichinohe, H.; Iwasaki, Y. Edaravone (MCI-186) scavenges reactive oxygen species and ameliorates tissue damage in the murine spinal cord injury model. *Neurol. Med. Chir. (Tokyo)* **2008**, *48*, 539−545.
(23) Steinberg, G. R.; Kemp, B. E. AMPK in Health and Disease. *Physiol. Rev.* **2009**, *89*, 1025−1078.
(24) Hock, M. B.; Kralli, A. Transcriptional control of mitochondrial biogenesis and function. *Annu. Rev. Physiol.* **2009**, *71*, 177−203.
(25) Ruiz, L. M.; Jensen, E. L.; Bustos, R. I.; Arguelloa, G.; Gutierrez-Garcia, R.; Gonzalez, M.; Hernandez, C.; Paredes, R.; Simon, F.; Riedel, C.; Ferrick, D.; Elorza, A. A. Adaptive responses of mitochondria to mild copper deprivation involve changes in morphology, OXPHOS remodeling and bioenergetics. *J. Cell. Physiol.* **2014**, *229*, 607−619.
(26) Mandard, S.; Muller, M.; Kersten, S. Peroxisome proliferator-activated receptor alpha target genes. *Cell. Mol. Life Sci.* **2004**, *61*, 393−416.
(27) Guo, H.; Xia, M.; Zou, T.; Ling, W.; Zhong, R.; Zhang, W. Cyanidin 3-glucoside attenuates obesity-associated insulin resistance and hepatic steatosis in high-fat diet-fed and *db/db* mice via the transcription factor FoxO1. *J. Nutr. Biochem.* **2012**, *23*, 349−360.
(28) Begriche, K.; Massart, J.; Robin, M. A.; Bonnet, F.; Fromenty, B. Mitochondrial adaptations and dysfunctions in nonalcoholic fatty liver disease. *Hepatology* **2013**, *58*, 1497−1507.
(29) Begriche, K.; Massart, J.; Robin, M. A.; Borgne-Sanchez, A.; Fromenty, B. Drug-induced toxicity on mitochondria and lipid metabolism: mechanistic diversity and deleterious consequences for the liver. *J. Hepatol.* **2011**, *54*, 773−794.
(30) Rector, R. S.; Thyfault, J. P.; Uptergrove, G. M.; Morris, E. M.; Naples, S. P.; Borengasser, S. J.; Mikus, C. R.; Laye, M. J.; Laughlin, M. H.; Booth, F. W.; Ibdah, J. A. Mitochondrial dysfunction precedes insulin resistance and hepatic steatosis and contributes to the natural history of non-alcoholic fatty liver disease in an obese rodent model. *J. Hepatol.* **2010**, *52*, 727−736.
(31) Kubli, D. A.; Gustafsson, A. B. Mitochondria and mitophagy: the yin and yang of cell death control. *Circ. Res.* **2012**, *111*, 1208−1221.
(32) Anstee, Q. M.; Goldin, R. D. Mouse models in non-alcoholic fatty liver disease and steatohepatitis research. *Int. J. Exp. Pathol.* **2006**, *87*, 1−16.
(33) Lee, W. J.; Kim, M.; Park, H. S.; Kim, H. S.; Jeon, M. J.; Oh, K. S.; Koh, E. H.; Won, J. C.; Kim, M. S.; Oh, G. T.; Yoon, M.; Lee, K. U.; Park, J. Y. AMPK activation increases fatty acid oxidation in skeletal muscle by activating PPARalpha and PGC-1. *Biochem. Biophys. Res. Commun.* **2006**, *340*, 291−295.
(34) Scarpulla, R. C.; Vega, R. B.; Kelly, D. P. Transcriptional integration of mitochondrial biogenesis. *Trends. Endocrinol. Metab.* **2012**, *23*, 459−466.
(35) Jiang, X.; Tang, X.; Zhang, P.; Liu, G.; Guo, H. Cyanidin-3-O-beta-glucoside protects primary mouse hepatocytes against high glucose-induced apoptosis by modulating mitochondrial dysfunction and the PI3K/Akt pathway. *Biochem. Pharmacol.* **2014**, *90*, 135−144.
(36) Lee, S. J.; Zhang, J.; Choi, A. M.; Kim, H. P. Mitochondrial dysfunction induces formation of lipid droplets as a generalized response to stress. *Oxid. Med. Cell. Longevity* **2013**, *2013*, 327167.

DOI: 10.1021/jf504926n
J. Agric. Food Chem. 2015, 63, 552−561

JOURNAL OF AGRICULTURAL AND FOOD CHEMISTRY

Article

pubs.acs.org/JAFC

Characterization of Selenium-Enriched Mycelia of *Catathelasma ventricosum* and Their Antihyperglycemic and Antioxidant Properties

Yuntao Liu,*[,†,‡] Caiming Li,[§] Xiaohu Luo,[§] Guoquan Han,[†] Shude Xu,[∥] Fuge Niu,[§] Xinjie Hu,[†,§] Hejun Wu,[†] and Huimin Zhang[⊥]

[†]College of Food Science, Sichuan Agricultural University, Yaan 625014, China

[‡]Animal Nutrition Institute, Sichuan Agricultural University, Chengdu 611130, China

[§]State Key Laboratory of Food Science and Technology, Jiangnan University, Wuxi 214122, China

[∥]Guangdong VTR Bio-tech Co., Ltd, Zhuhai 519060, China

[⊥]College of Animal Science and Technology, Yangzhou University, Yangzhou 225009, China

ABSTRACT: This is the first report concerning the selenium enrichment of *Catathelasma ventricosum* mycelia. The selenium-containing proteins present in selenium-enriched mycelia (Se-MC) were identified using size-exclusion chromatography−inductively coupled plasma−mass spectrometry (SEC-ICP-MS). The selenium-containing amino acids liberated by hydrolysis of these proteins were identified using anion exchange-ICP-MS. Se-MC was found to contain selenoproteins with molecular weights ranging from 1.7 to 60.5 kDa. The main selenium-containing amino acids within them were selenomethionine and selenocysteine. Furthermore, Se-MC possessed excellent antihyperglycemic and antioxidant properties. Se-MC normalized biochemical parameters like insulin level, blood glucose level, body weight, and antioxidant enzyme activity in streptozocin-induced diabetic mice. It also inhibited the α-amylase and α-glucosidase activities present in in vitro gastric and intestinal models. In conclusion, Se-MC has the potential to serve as a dietary supplement of selenium, an antioxidant, or an ingredient for the formulation of nutraceuticals.

KEYWORDS: *mushroom, antihyperglycemic activity, antioxidant activity, chemical composition, selenium speciation*

INTRODUCTION

Diabetes mellitus, a chronic metabolic disease caused by insulin deficiency or dysfunction, is characterized by high blood glucose levels.[1] Hyperglycemia has been shown to increase oxidative stress through the overproduction of reactive oxygen species.[2] These oxygen radicals cause lipid oxidation and play a role in the development of diabetic complications. Oxidative stress is thought to link diverse mechanisms for the pathogenesis of diabetic complications.[3] Although several hypoglycemic drugs are available to treat diabetes mellitus, many of them have serious side effects.[4] Relatively low cost management of hyperglycemia with minimal clinical side effects remains a challenge for the medical system.[5] Phytochemicals from relatively low cost bioresources have relatively few side effects. Exploiting this resource offers a new approach for the treatment of various diseases, including diabetes.[6]

Catathelasma ventricosum, an edible fungus, is a delicious source of valuable nutrition. Its fruiting body provides an excellent source of nutrients because of its high protein, polysaccharide, and mineral content, as well as its low content of toxic metals, fat, and energy. A previous report has demonstrated that the fruiting body of wild *C. ventricosum* has antihyperglycemic and antioxidative effects.[7] Selenium (Se), a trace element important for human health, is a component of several selenoproteins that perform essential biological functions, including glutathione peroxidase (GSH-Px) and selenoprotein P. The Se-dependent enzyme GSH-Px reduces oxidized glutathione and minimizes lipid peroxidation by catalyzing the reduction of both lipid peroxides and hydrogen peroxide. Selenoprotein P, an extracellular antioxidant present in the vascular endothelium, lowers the level of peroxinitrile ($ONOO^-$), a reactive nitrogen species.[8] Se deficiency has been associated with several diseases, including hepatocyte damage, cardiovascular disease, and cancers.[9−11] Se supplementation using microorganisms may be an excellent solution to the problem of Se deficiency because organic Se compounds are generally believed to be better and safer dietary supplements than inorganic Se compounds. A variety of Se-enriched food supplements have been commercialized, including garlic, yeast, and lactic acid bacteria.[12]

Submerged basidiomycete culture is currently the preferred technique for producing stable, safe mycelia and mushroom biometabolites. Importantly, submerged culture is less time-consuming than mushroom cultivation and leads to the production of products with mushroom metabolite contents that are more consistent than those of products consisting of fruiting bodies.[1] Furthermore, based on our preliminary experiment, the capacity of *C. ventricosum* for selenium enrichment is greater than that of some famous mushrooms, like *Lentinula edodes, Pleurotus ostreatus, Ganoderma lucidum, Coriolus versicolor, Tremella fuciformis,* etc. (data not shown). In order to assess the suitability of Se-enriched mycelia from *C. ventricosum* (Se-MC) as a candidate for diabetes treatment, the

Received: October 17, 2014
Revised: December 22, 2014
Accepted: December 22, 2014
Published: December 22, 2014

ACS Publications © 2014 American Chemical Society

DOI: 10.1021/jf5050316
J. Agric. Food Chem. 2015, 63, 562−568

chemical composition and Se speciation in Se-MC was determined. The antihyperglycemic and antioxidant properties of Se-MC were also investigated.

MATERIALS AND METHODS

Chemicals. Sodium selenite and sodium selenate were obtained from Alfa Aesar (Ward Hill, MA, USA). Working solutions for the determination of total selenium were prepared daily by appropriate dilution of a 1 mg/mL Se (IV) standard solution (Merck, Darmstadt, Germany). Glibenclamide, streptozocin (STZ), 4-nitrophenyl-α-D-glucopyranoside (PNPG), selenocysteine (SeCys), selenomethionine (SeMet), and amino acid standards were purchased from Sigma-Aldrich Co. LLC (St. Louis, MO, USA). Reagent kits for the determination of catalase (CAT), maleic dialdehyde (MDA), superoxide dismutase (SOD), glutathione peroxidase (GSH-Px), and insulin were obtained from the Jianchen Bioengineering Institute (Nanjing, Jiangsu, China). The SXT Blood Glucose Monitoring System and Test Strip were from Sinocare Co., Ltd. (Changsha, Hunan, China). All other materials were of the highest grade commercially available and obtained from Sinopharm Chemical Reagent Co. Ltd. (Shanghai, China).

Se-Enriched Fermentation *C. ventricosum* Mycelia. The seed of *C. ventricosum* was purchased from Mianyang Edible Fungi Research Institute (Mianyang, Sichuan, China) and maintained on synthetic potato dextrose agar (PDA).

C. ventricosum was initially grown on PDA at 22 °C for 4 days. Aliquots (2.5 mL) of this 4-day-old liquid culture were then transferred to two hundred 250 mL flasks. Each flask contained 47.5 mL of Se-enriched fermentation culture medium (medium components were based on our previous reports[13]) and incubated at 22 °C on a shake platform at 100 rpm for 15 days. The harvest mycelia are referred to as Se-MC. *C. ventricosum* was also incubated in an otherwise identical fermentation culture medium without Na_2SeO_3 as a control. This control material is referred to as MC.

In Vitro Simulation of Gastrointestinal Digestion. Gastrointestinal digestion was simulated using a method based upon a published procedure that mimicks the physiological events taking place in the upper gastrointestinal tract (stomach and small intestine).[14] Three-gram samples of powdered *C. ventricosum* mycelia (Se-MC and MC were freeze-dried and ground to a fine powder (40 mesh)) were mixed with 18 mL of saline (140 mM NaCl, 5 mM KCl and 150 μM butylated hydroxytoluene (BHT)), acidified to pH 2 with 0.1 M HCl, and then mixed with 500 μL of pepsin solution. After incubation at 37 °C for 1 h in a shaking water bath, 0.1 M $NaHCO_3$ was added to increase the pH to 6.9. At this point, 2.5 mL of pancreatin-bile solution was added. After incubation at 37 °C for 2 h in a shaking water bath, the simulated gastrointestinal digestion (GI) extract was centrifuged, and then the supernatant was dried under nitrogen gas. The dried powder was used for the in vitro assay. The samples of Se-MC and MC were treated in triplicate.

Chemical Composition. *Proximate Analysis.* The crude protein, crude fat, moisture, ash, and total phenolic contents of Se-MC and MC were determined in triplicate using the Association of Official Analytical Chemists (AOAC) procedures (1995).[15] The determination of carbohydrate content (g) and energy content (KJ) were performed based on the methods of Liu et al. (2012).[7]

Amino Acid Analysis. Extracts were prepared according to the method of Ribeiro et al. (2008).[16] Amino acid analysis was performed using our previously published methods,[7] with slight modifications. Briefly, the amino acid composition was determined using a reversed-phase high-performance liquid chromatography (HPLC, Agilent 1100) system equipped with a 250 × 4.6 mm, 5 μm ODS HYPERSIL column (Agilent) (Santa Clara, CA, USA). The analysis was conducted using gradient elution at 40 °C and a flow rate of 1 mL/min. The mobile phase gradient was formed from buffer A (8 g of sodium acetate dissolved in 1000 mL of deionized water plus 225 μL of triethylamine and 5 mL of tetrahydrofuran; pH adjusted to 7.2 ± 0.05 with acetic acid) and buffer B (8 g of sodium acetate dissolved in 400 mL of deionized water plus 800 mL of acetonitrile and 800 mL of methanol; pH adjusted to 7.2 ± 0.05 with acetic acid). A/B ratios were 92:8, 40:60, 0:100, 0:100, 0:100, and 92:8, at run times of 0, 27.5, 31.5, 32, 34, and 35.5 min, respectively. Samples were derivatized with *o*-phthaldialdehyde (OPA, Sigma) (St. Louis, MO, USA) prior to HPLC; the detection wavelength was set to 338 nm, or 262 nm for proline. Stock solutions of individual amino acids, except for tryptophan, were prepared in 0.1 M HCl. Tryptophan solutions were prepared in water. The concentrations of the individual amino acids were approximately 1 mM. The samples of Se-MC and MC were analyzed in triplicate.

The Content of Se and Its Speciation. *Determination of Total Se.* Dried samples (approximately 0.1 g) were digested with a mixture containing 0.5 mL of H_2O_2 (30%) and 2 mL of HNO_3 (65%). After 24 h, the solutions were digested using a microwave system. A mineralization program was performed based on the method of Wrobel et al. (2004).[17] After digestion, the final solutions were diluted to a total volume of 25 mL with distilled water. The standard solutions and reagent blanks were digested using the same procedure. The samples of Se-MC and MC were treated in triplicate.

The total selenium concentration was determined using inductively coupled plasma mass spectrometetry (ICP-MS, Agilent 7500ce) (Tokyo, Japan). Isotopes ^{77}Se, ^{78}Se, ^{80}Se, and ^{82}Se were monitored. The instrument settings were as follows: forward power, 1590 W; carrier gas flow rate, 1.2 L/min; plasma gas flow rate, 15 L/min; and dwell time, 0.3 s per isotope. All samples were analyzed in triplicate.[18]

Investigation of Selenoproteins in Mycelia. Mycelia samples (1 g) were added to 100 mL of buffer containing 20 mM Tris-HCl (pH 7.5) and 150 mM NaCl. The mixtures were extracted with magnetic stirring at 37 °C for 24 h. After centrifugation (8000 rpm for 10 min), 1 mL of supernatant was transferred to 5 mL of acetone. This mixture was extracted with magnetic stirring at 4 °C for 24 h, and then placed at 5 °C for 24 h. After centrifugation (8000 rpm for 10 min), the supernatant was discarded and the protein precipitate was dried under nitrogen gas. The samples of Se-MC and MC were treated in triplicate.

The dry precipitate was resolubilized with 1 mL of mobile phase buffer for analysis by size exclusion chromatography (SEC)-ICP-MS. Chromatographic separations were performed using an Agilent 1100 liquid chromatograph (Palo Alto, CA, USA) equipped with a Superdex peptide 10-300 GL (300 mm × 10 mm × 15 μm) column. The mobile phase was composed of 20 mM Tris-HCl and 150 mM NaCl (pH 7.5), the injection volume was 50 μL, and the flow rate was 0.5 mL/min.[18] The SEC column was calibrated using a standard mixture of albumin (66 kDa), myoglobin (16 kDa), cytochrome *c* (12.5 kDa), methylcobalamin (1.34 kDa), and $(Gly)_6$ (0.36 kDa). All samples were analyzed in triplicate.

Se Speciation in the Mycelia. Enzymatic hydrolysis was performed to identify the species that possess covalent bonds between Se and proteins or peptides.[19] In this method, the precipitated selenoproteins were resolubilized with 1 mL of a solution containing 20 mM Tris-HCl (pH 7.5), 150 mM NaCl, and 0.03 g of trypsin. After incubation at 50 °C for 24 h in a shaking water bath, 0.03 g of proteinase K was added to the mixture described above, and the resulting solution was kept in a shaking water bath at 50 °C for an additional 24 h. After centrifugation (8000 rpm for 10 min) and filtration (0.45 μm polyvinylidene fluoride filter), the supernatant was passed through 5 kDa molecular weight cutoff filters (Ultrafree-0.5, Millipore) to remove high molecular weight proteins from the extracts before the analysis of the Se-containing species. The samples were treated in triplicate.

Se species were analyzed by anion exchange-HPLC-ICP-MS and identified by comparing their retention times with those of available standards (sodium selenite, sodium selenite, SeCys, and SeMet).[20] Chromatographic separations were performed using an Agilent 1100 liquid chromatograph (Palo Alto, CA, USA) equipped with a Hamilton PRP-X100 (250 mm × 4.1 mm × 10 μm) column. The mobile phase consisted of 5 mM ammonium citrate in 2% methanol (pH 5.2), the flow rate was 1 mL/min, and the injection volume was 50 μL. All samples were analyzed in triplicate.[18]

Antihyperglycemic Assays in Vitro. *α-Glucosidase Inhibitory Activity.* Inhibition of α-glucosidase activity was assayed using the

DOI: 10.1021/jf5050316
J. Agric. Food Chem. 2015, 63, 562−568

Table 1. Moisture (g/100 g of Fresh Weight), Macronutrients (g/100 g of Dry Weight), and Total Energy (kJ/100 g of Dry Weight) of *C. ventricosum*

	components						
C. ventricosum	moisture	ash	crude protein	crude fat	total carbohydrates	total energy	total phenols
selenium-enriched mycelia	93.03 ± 3.67[a]	10.64 ± 1.48	31.22 ± 2.59	2.17 ± 0.34	55.97 ± 4.94	1562.52 ± 87.42	0.44 ± 0.04
mycelia	93.55 ± 2.07	9.29 ± 1.17	21.42 ± 5.03	6.19 ± 0.29	63.10 ± 7.39	1665.87 ± 102.53	0.83 ± 0.08

[a]Each value is expressed as the mean ± SD (n = 3).

method of Palanisamy et al. (2011), with minor modifications.[3] Various dilutions of the GI extracts described above were mixed with α-glucosidase (0.4 IU) dissolved in 2 mL of phosphate buffer (0.1 M, pH 6.8) containing 50 μL of glutathione (1 mg/mL) and 50 μL of PNPG (0.1 M). These reaction mixtures were incubated at 37 °C for 15 min. The reactions were stopped with 10 mL of 0.1 M sodium carbonate, and the extent of reaction was determined by measuring the absorbance at 400 nm using a UV−visible spectrophotometer. Acarbose was used as the positive control, while the absence of sample was used as a negative control. The percentage inhibition was calculated as % inhibition = {1 − [(absorbance of sample)/(absorbance of negative control)]} × 100. The α-glucosidase inhibitory activity was expressed as an EC_{50} value (amount of sample causing 50% inhibition). All samples were analyzed in triplicate.

α-Amylase Inhibitory Activity. Porcine pancreatic α-amylase (1 IU) was dissolved in 0.5 mL of buffer (20 mM phosphate, pH 6.9) containing various dilutions of the GI extracts described above. These mixtures were incubated at 37 °C for 15 min. Each reaction mixture was subsequently added to 0.5 mL of soluble starch solution (1.5%) and incubated at 37 °C for 5 min. Each reaction was stopped at this point using 1.0 mL of 3,5-dinitrosalicylic acid reagent. The samples were then incubated in a boiling water bath for 10 min, cooled to room temperature, and diluted with distilled water. The absorbance was measured at 520 nm. Acarbose was used as the positive control, and reactions lacking sample were used as a negative control. The percentage inhibition was calculated as % inhibition = {1 − [(absorbance of sample)/(absorbance of negative control)]} × 100. The α-amylase inhibitory activity was expressed as an EC_{50} value (amount of sample causing 50% inhibition). All samples were analyzed in triplicate.

Animals. The male ICR mice (body weight 18 ± 2 g) used in this study were purchased from SLAC Laboratory Animal Company (Shanghai, China). The mice were acclimatized for at least 1 week before the experiment was started. Before and during the experiment, the mice were housed in a segregated air-conditioned room at 25 °C with a 12 h light and dark cycle. Mice were provided a basal diet (Shanghai Laboratory Animal Company) and free access to drinking water. This experiment was approved by the Institutional Animal Ethics Committee of Jiangnan University (Wuxi, China). All experimental animals were overseen and approved by the Animal Care and Use Committee of our Institute before and during experiments.

Establishment of a Diabetic Mouse Model. Diabetes was induced in mice by the intraperitoneal (ip) injection of a freshly prepared solution of STZ at a dose of 150 mg/kg body weight.[21] Mice displaying polydipsia and polyuria after 72 h were chosen for measurement of their fasting glucose levels using blood glucose test strips. Hyperglycemic mice (blood glucose level >16.8 mmol/L) were used as the diabetic mice for further studies.

Experimental Design. Based on a preliminary experiment (data not shown), the STZ-induced diabetic mice were randomly divided into five groups (6 mice per group). Group I: normal mice treated with saline solution as control. Group II: STZ-induced diabetic mice treated with saline solution as diabetic control. Group III: STZ-induced diabetic mice receiving oral glibenclamide (20 mg/kg/d) as a positive control. Group IV: STZ-induced diabetic mice receiving oral MC at a dose of 500 mg/kg/d. Group V: STZ-induced diabetic mice receiving oral Se-MC at a dose of 500 mg/kg/d. After 30 days of treatment, the animals were fasted overnight and sacrificed by cervical dislocation. Their blood glucose levels and body weight were measured. Blood collected from their eyes was immediately centrifuged for 5 min to obtain serum (stored at −70 °C). Kidney and liver tissues were excised from the animals, washed with saline solution, and stored at −70 °C.

Biochemical Analysis. Blood glucose levels were determined with blood glucose test strips using blood samples taken from the tail veins of overnight fasted mice. The serum insulin concentration was determined using commercially available kits according to the manufacturer's instructions. Liver and kidney homogenates were immediately assayed for SOD, CAT, GSH-Px, and MDA activities using the procedures described in the instructions contained in their corresponding assay kits.

Statistical Analyses. All of the assays described above were carried out in triplicate. The results are expressed as the mean ± SD. Data were analyzed using one-way analysis of variance (ANOVA) followed by Tukey's test. Statistical analyses were performed using SPSS software, version 16.0. Differences leading to values of $p < 0.05$ were considered statistically significant.

RESULTS

Chemical Composition. The proximate compositions of the investigated mushrooms are shown in Table 1. The order of the contents (g/100 g dry weight) was total carbohydrate > crude protein > ash > crude fat > total phenols. These data demonstrate that Se-MC contained slightly more protein and ash than the control MC, and slightly less total carbohydrate. The crude fat and total phenol contents of Se-MC were about half or less of those of the MC control. The total energy content of the Se-MC was slightly lower than that of the MC control.

The percentage composition of 17 amino acids was investigated in the mycelia of *C. ventricosum*; the results are presented in Table 2. Se-MC and MC were found to contain 13 and 12 amino acids, respectively. Se-MC contained seven of the essential amino acids, lacking only isoleucine. The ratios of the essential amino acids to nonessential amino acids were 0.87 and 0.80 in Se-MC and MC respectively.

The Content of Se and Its Speciation. The total Se contents of Se-MC and the MC control were determined by digesting samples and quantifying the Se by ICP-MS. The total Se content of Se-MC was 867.11 μg/g of dry mycelia. The mycelial yield was about 12.64 g of dry mycelia per L of culture. The conversion of organic Se was approximate 11%. No Se was detected in the MC control.

The SEC-ICP-MS chromatograms of the Se-MC extracts are presented in Figure 1a. The molecular weights (MW) of the three main Se-containing fractions were about 60.5, 11.2, and 1.7 kDa. Based on the description of Kapolna et al. (2007),[18] the fractions with high molecular weights (HMW; 60.5 and 11.2 kDa) represent Se-containing proteins, and those with the low molecular weight (LMW) of 1.7 kDa correspond to Se-containing peptides, while the molecular weights of selenoamino acids and inorganic selenium are less than 1.7 kDa.

A chromatogram of the Se species standards, obtained using anion exchange-HPLC-ICP-MS, is displayed in Figure 1b. The

DOI: 10.1021/jf5050316
J. Agric. Food Chem. 2015, 63, 562−568

Table 2. Free Amino Acid Composition (Wt %) of *C. ventricosum*

amino acids[a]	*C. ventricosum*	
	Se-enriched mycelia (Se-CM)	mycelia (CM)
Val[b]	13.59 ± 0.63[c]	12.14 ± 0.53
Thr[b]	1.45 ± 0.49	7.92 ± 0.82
Met[b]	16.37 ± 0.51	4.06 ± 0.31
Leu[b]	1.07 ± 0.05	ND[d]
Ile[b]	ND	ND
Trp[b]	4.19 ± 0.63	8.63 ± 0.77
Phe[b]	2.73 ± 0.34	5.19 ± 0.49
Lys[b]	7.11 ± 0.39	6.48 ± 0.67
Gly	1.06 ± 0.08	1.53 ± 0.08
His	10.52 ± 0.96	12.15 ± 0.75
Tyr	ND	ND
Asp	ND	ND
Ser	8.74 ± 1.02	17.53 ± 1.24
Cys	9.74 ± 0.18	1.46 ± 0.16
Arg	ND	ND
Ala	18.62 ± 2.74	12.18 ± 0.21
Glu	4.81 ± 0.43	10.73 ± 1.11

[a]Valine (Val); threonine (Thr); methionine (Met); leucine (Leu); isoleucine (Ile); tryptophan (Trp); phenylalanine (Phe); lysine (Lys); glycine (Gly); histidine (His); tyrosine (Tyr); aspartic acid (Asp); serine (Ser); cysteine (Cys); arginine (Arg); alanine (Ala); glutamic acid (Glu). [b]Essential amino acids. [c]Each value is expressed as mean ± SD (n = 3). [d]ND: not detected.

species were identified by comparing their retention times to those of available standards. The selenium species profile of the Se-MC extracts is shown in Figure 1c. Selenomethionine (SeMet) was the predominant selenium species in the Se-MC extracts, comprising approximately 68% of the total selenium content. Other selenium species identified in Se-MC samples included selenocysteine (SeCys, 6%), selenite (Se−IV, 2%), and selenate (Se−VI, 5%).

Antihyperglycemic Activity in Vitro. The antihyperglycemic properties of Se-MC and MC were evaluated using two assays that measured the inhibition of α-glucosidase and α-amylase activities, respectively. Based on the results, the highest α-glucosidase inhibitory activity (EC_{50} = 8.3 μg/mL) was found in Se-MC, and the highest α-amylase inhibitory activity (EC_{50} = 19.4 μg/mL) was found in MC, while the α-glucosidase and α-amylase inhibitory activities of acarbose (positive control) were 15.9 and 26.7 μg/mL, respectively.

Effects of Se-MC and MC on Blood Glucose, Body Weight, and Insulin in STZ-Induced Diabetic Mice. Mice in the diabetic control group (group II) exhibited a severe decrease in insulin level and body weight and a significant increase in blood glucose level, compared with mice in the normal group (group I; $p < 0.05$) (Table 3). After administration of Se-MC, MC, or glibenclamide (positive control) for 30 days, the levels of blood glucose in groups III, IV, and V were much lower than that in group II. On the other hand, the insulin levels and body weights of the mice in groups III, IV, and V showed a significant increase compared with those of the mice in group II.

Effects of Se-MC and MC on MDA and Antioxidant Enzymes in Kidney and Liver of STZ-Induced Diabetic Mice. The MDA levels in the kidney and liver of untreated STZ-induced diabetic mice were significantly increased ($p < 0.05$), whereas the activities of antioxidant enzymes in the kidney and liver of untreated STZ-induced diabetic mice were significantly decreased ($p < 0.05$) compared with those of the mice in group I (Table 4). After administration of Se-MC or MC for 30 days, the MDA levels present in the mice in groups IV and V were significantly decreased ($p < 0.05$), while SOD, GSH-Px, and CAT activity were significantly increased ($p < 0.05$) in the kidney and liver, compared with those of the mice in groups II and III.

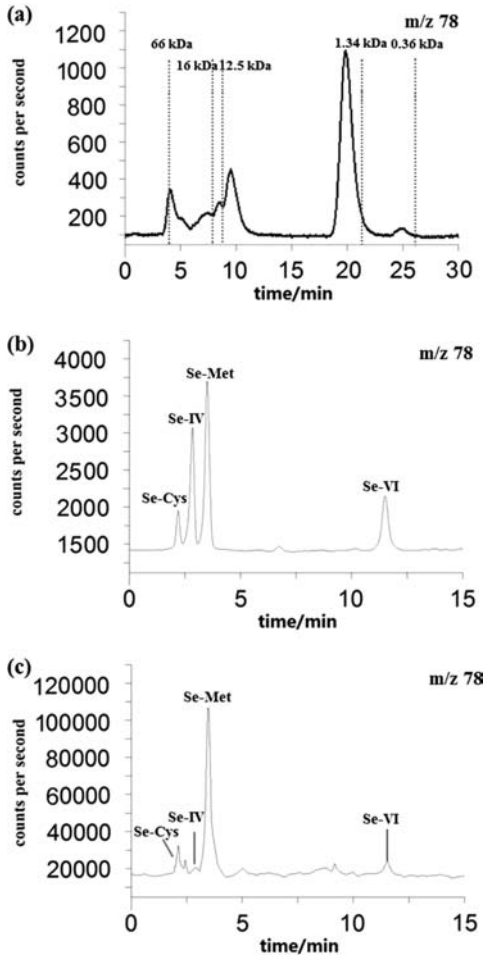

Figure 1. HPLC-ICP-MS chromatograms of the mycelia of Se-enriched *C. ventricosum*. (a) Protein fractions of Se-MC were analyzed by SEC-ICP-MS. (b) Chromatogram of Se species standard obtained by anion-exchange ICP-MS. (c) Chromatogram of Se species profile in Se-MC obtained by anion-exchange ICP-MS.

DISCUSSION

The moisture content of mushrooms ranges from 86−94 g/100g fresh weight. The moisture contents of Se-MC and MC were 93.03 and 93.55 g/100 g fresh weight, respectively, which is higher than that of the fruiting body of *C. ventricosum*.[7] It seems that liquid culture conditions can increase the moisture content of *C. ventricosum*. Kalač (2009) indicated that low dry matter and lipid contents result in mushrooms with low energy values.[22]

The concentration order of the components in the proximate analyses of Se-MC and MC is consistent with that revealed in our previous report.[7] This indicates that the physical state of the culture medium (liquid state or solid state) may have a limited effect on the chemical composition of *C. ventricosum*.

DOI: 10.1021/jf5050316
J. Agric. Food Chem. 2015, 63, 562−568

Table 3. Effects of Selenium-Enriched Mycelia and Mycelia on Body Weight, Blood Glucose, and Insulin in Diabetic Mice[a]

	group I (control)	group II (diabetic mice)	group III (positive control)	group IV (diabetic mice + MC)	group V (diabetic mice + Se-MC)
insulin level (μIU/mL)	28.7 ± 1.7[c]	8.3 ± 0.8 a	19.1 ± 2.0 b	11.2 ± 0.7 a	18.3 ± 1.2 b
blood glucose (mmol/L)	5.8 ± 0.6 a	26.3 ± 3.1 d	11.5 ± 1.1 b	17.7 ± 1.4 c	13.1 ± 0.9 b
body weight (g)	35.3 ± 1.5 d	25.8 ± 3.2 a	32.5 ± 2.4 c	28.7 ± 1.4 b	28.2 ± 1.7 b

[a]Each value is expressed as the mean ± SD (n = 6). Means with different letters within a row are significantly different (p < 0.05).

Table 4. Effect of Selenium-Enriched Mycelia and Mycelia on Antioxidants in Liver and Kidney of Diabetic Mice[a]

	group I (control)	group II (diabetic mice)	group III (positive control)	group IV (diabetic mice + CM)	group V (diabetic mice + Se-CM)
			Liver		
GSH-Px (U/mg protein)	877.1 ± 74.1 d	413.5 ± 32.3 a	442.0 ± 29.7 a	593.6 ± 30.1 b	797.4 ± 59.6 c
SOD (U/mg protein)	478.1 ± 39.5 c	277.3 ± 14.6 a	234.9 ± 10.7 a	299.7 ± 19.4 b	424.5 ± 21.7 c
CAT (U/mg protein)	194.4 ± 20.1 c	41.7 ± 2.6 a	49.9 ± 2.8 a	92.7 ± 10.7 b	167.4 ± 17.3 c
MDA (nmol/mg protein)	4.2 ± 0.8 a	9.0 ± 0.7 c	8.5 ± 0.8 c	6.2 ± 1.1 b	4.7 ± 0.7 a
			Kidney		
GSH-Px (U/mg protein)	564.2 ± 34.9 c	277.4 ± 17.7 a	263.7 ± 20.4 a	400.3 ± 35.2 b	584.5 ± 67.6 c
SOD (U/mg protein)	277.3 ± 14.9 c	104.4 ± 8.5 a	115.8 ± 11.0 a	197.6 ± 20.4 b	283.7 ± 17.7 c
CAT (U/mg protein)	83.8 ± 7.5 c	37.5 ± 3.7 a	42.1 ± 3.5 a	66.3 ± 4.7 b	89.1 ± 9.5 c
MDA (nmol/mg protein)	3.1 ± 0.5 a	7.3 ± 0.4 d	7.3 ± 0.6 d	4.9 ± 0.2 c	3.8 ± 0.7 b

[a]Each value is expressed as the mean ± SD (n = 6). Means with different letters within a row are significantly different (p < 0.05); glutathione peroxidase (GSH-Px); superoxide dismutase (SOD); catalase (CAT); maleic dialdehyde (MDA).

The concentration of protein in Se-MC (31.22% of dry matter) is very high compared with those of most plants and mushrooms. The results are consistent with the conclusions of Belitz and Grosch (1999):[23] Se concentrations are positively correlated with protein content in food. Moreover, Pappa et al. (2006)[24] indicated that the Se concentration is negatively correlated with food fat content. The concentration of crude fat in Se-MC (2.17% of dry matter) is very low compared with those of most plants and mushrooms.[22] In a word, *C. ventricosum* is an ideal candidate for Se enrichment.

The content of crude protein in Se-MC, on the other hand, was 30% higher than that in MC. It seems that the presence of Se in the culture medium can affect protein metabolism in *C. ventricosum*. One possibility is that Se can replace sulfur in amino acids like selenomethionine (SeMet) and selenocysteine (SeCys), due to their physicochemical similarity, which may stimulate the synthesis of protein (especially Met and Cys). The results of the amino acid analysis also support this assumption. The concentration of methionine (Met) and cysteine (Cys) in Se-MC was much higher than that in MC. Moreover, Dumont et al. (2006)[25] indicated that most plants lack the ability to accumulate large amounts of Se (they rarely exceed 100 μg/g dry weight). However, some mushrooms have been recognized as Se accumulators. These mushrooms can take up a large amount of Se (>1000 μg/g dry weight) without exhibiting any negative effects because they increase their intracellular concentrations of SeCys and SeMet, which are normally incorporated into proteins.[8,25]

Although selenium is beneficial to normal biological function when supplied in appropriate quantities, excessive selenium intake can cause toxicosis.[26] The essential and toxic levels of Se are similar. The tolerable upper Se intake level for adults is set at 400 μg/day, while the recommended dietary allowance for Se is 55 μg/day for both men and women.[27] Therefore, determination of the total Se content of Se-MC is of great significance. The total Se content of Se-MC (867.11 μg/g of dry mycelia) is higher than that of some other Se-enriched plants and mushrooms, like *Allium schoenoprasum* (1.07 μg/g), *Lentinula edodes* (770.7 μg/g), and *Cordyceps militaris* (42 μg/g).[18,19,28]

The bioavailability of Se depends strongly on the chemical form of the Se that is ingested. Organic Se compounds are generally more bioavailable than inorganic Se compounds.[8] Ferri et al. (2007)[29] indicated there is a lack of information about the chemical forms of selenium in foods. This lack is mainly the result of the difficulties inherent in their identification. The application of different hyphenated techniques (HPLC-MS, HPLC-ICP-MS, etc.) has begun to change this situation. In this study, we employed HPLC-ICP-MS to analyze the Se species. Previous reports have identified selenate, selenite, SeMet, and SeCys as the primary selenocompounds in mushrooms.[19,28] These reports agree well with the results of this study. In addition, the ratio of organic Se to inorganic Se in Se-MC is 74:7, which is higher than the ratio seen in some Se-enriched foods.[20,28]

Two in vitro assays were carried out to evaluate the antihyperglycemic activity of a simulated gastrointestinal digestion extract of Se-MC and MC: an α-glucosidase inhibition assay and an α-amylase inhibition assay. α-Glucosidase, located in the brush-border surface membrane of intestinal cells, is a key enzyme of carbohydrate digestion. α-Amylase catalyzes the hydrolysis of the α-1,4-glucosidic linkages in glycogen, starch, and other oligosaccharides. Inhibition of the α-glucosidase and α-amylase activities in the human digestive tract can effectively control diabetes by diminishing the absorption of glucose derived from the degradation of starch by these enzymes.[30] There are two main concepts to explain the interaction mechanism between α-glucosidase/α-amylase and their inhibitor: (1) The inhibitor inhibits α-glucosidase/α-amylase activity by hydrolyzing them.[31] (2) α-Glucosidase/α-amylase and their inhibitor combine to form a soluble complex, which inactivates the enzymes.[32] Yasuda (2003)[33] indicated

DOI: 10.1021/jf5050316
J. Agric. Food Chem. 2015, 63, 562−568

that α-glucosidase/α-amylase inhibitor is not a competitive inhibitor that competes with α-glucosidase/α-amylase for starch, disaccharides, or various oligosaccharides. However, the inhibitor will combine with α-glucosidase/α-amylase directly and change their conformations, inactivating them. Acarbose, an inhibitor of a-glucosidase and α-amylase used in the treatment of diabetes mellitus, was chosen as the positive control.[3] The inhibitory activities of Se-MC and MC were significantly greater than those of acarbose ($p < 0.05$), which indicates that Se-MC and MC possess excellent antihyperglycemic activity. Inhibition of intestinal α-glucosidase and α-amylase activities is an important antihyperglycemic mechanism of Se-MC and MC. However, the antihyperglycemic activities of Se-MC and MC are very similar. It seems that adding Se into the culture medium does not have has much of an influence on the α-glucosidase and α-amylase inhibitory activities of *C. ventricosum* mycelium.

Animal models in which diabetes mellitus is induced by the administration of STZ or other chemicals have been reported.[21] The advantages of STZ are its greater stability and relative lack of extrapancreatic toxicity. In the present study, the diabetic mouse model was established by intraperitoneal injection of STZ, and all of the STZ-induced diabetic mice displayed polydipsia and polyuria.

Stapleton (2000)[34] reported that selenium has been found to have insulin-mimetic activities in vitro and in vivo. Based on the results presented here, Se-MC possesses better antihyperglycemic properties than MC. The levels of blood glucose and insulin in the mice in groups III and V were very close ($p > 0.05$), although they did not recover completely (compared with the normal group, $p < 0.05$). However, the body weight of the mice in groups IV and V was significantly lower than that of the mice in the positive control (group III) and normal mice (group I). It seems that both Se-MC and MC lack a strong ability to increase body weight in STZ-induced diabetic mice. Chen and Ianuzzo (1982)[35] suggested that the decrease in body weight observed in diabetic mice might be the result of protein wasting caused by the inability to use carbohydrates as an energy source. Zhao et al. (2011)[36] reported that administration of *Opuntia dillenii* polysaccharides significantly increased the body weight of STZ-induced diabetic mice.

Diabetes mellitus is associated with the generation of reactive oxygen species that cause oxidative damage to the liver and kidney.[37,38] Major antioxidant enzymes, including GSH-Px and SOD, are the first line of defense against the reactive oxygen species generated during oxidative stress in vivo.[39,40] In the present study, a significant increase in MDA levels and a significant decrease in GSH-Px, SOD, and CAT activity were found in kidney and liver of mice with STZ-induced diabetes (group II; compared with mice in group I), which suggests that severe oxidative stress occurred in liver and kidney tissues. However, after treatment with Se-MC (mice in group IV) or MC (mice in group V), MDA levels were significantly decreased ($p < 0.05$) and GSH-Px, SOD, and CAT activity were significantly increased ($p < 0.05$) in liver and kidney, compared with those of mice in group II. In particular, except MDA levels in kidney, activities of GSH-Px, SOD, CAT, and MDA in group V almost returned to their normal level, which indicated that Se-MC possesses a strong effect on increasing the synthesis of these antioxidant enzymes. MDA, the end product of lipid peroxidation, is used as an index of cellular damage and cytotoxicity. The MDA generated by high levels of free radicals can damage proteins and inactivate membrane-bound enzymes.[41] Chen et al. (2013)[39] indicated that decreasing MDA levels in diabetic rats may be associated with a drug's potential organ protective effect through improved glycometabolism and lipid metabolism. Therefore, it can be inferred that Se-MC probably exhibits its antihyperglycemic property by increasing these antioxidant enzymes in diabetic mice. These enzymes protect tissues from peroxidative damage and maintain their function, improving the sensitivity and response of target cells to insulin. Simultaneously, after the administration of glibenclamide, there was no difference among these biochemical parameters in group III compared with group II, which reveals that glibenclamide does not have an obvious ability to stimulate the synthesis of these antioxidant enzymes. This observation is consistent with those of a previous study, which found that glibenclamide is not capable of modulating antioxidant enzymes and diminishing STZ-induced damage to the liver, which is the main organ to synthesize antioxidant enzymes.[13]

In conclusion, the selenoproteins in Se-MC possess a wide range of molecular weights and SeMet and SeCys were identified as the main selenium compounds bound to these proteins. Moreover, Se-MC was found to be an effective antihyperglycemic and antioxidant. These results demonstrate that the mycelia of Se-enriched *C. ventricosum* can be used as a source of nutrients because of their high protein and carbohydrate content and their low fat and energy content. Mushrooms can also be uesd as a natural source of Se supplements for both animals and humans, especially in Se-deficient areas. Future studies may show that the Se-enriched mycelium of *C. ventricosum* is a source of new antidiabetic drugs, chemopreventive preparations, or food supplements.

AUTHOR INFORMATION

Corresponding Author

*College of Food Science, Sichuan Agricultural University, 46 Xinkang Road, Yaan, Sichuan 625014, China. Tel: 86-835-2882212. Fax: 86-835-2882311. E-mail: lyt_taotao@163.com.

Funding

This work was supported by Scientific Research Foundation of Sichuan Agricultural University (No. 06021400).

Notes

The authors declare no competing financial interest.

ABBREVIATIONS USED

CAT, catalase; GSH-Px, glutathione peroxidase; HPLC, high performance liquid chromatography; MDA, maleic dialdehyde; Se-MC, selenium-enriched mycelia; SOD, superoxide dismutase; SEC-ICP-MS, size-exclusion chromatography−inductively coupled plasma−mass spectrometry

REFERENCES

(1) De Silva, D. D.; Rapior, S.; Hyde, K. D.; Bahkali, A. H. Medicinal mushrooms in prevention and control of diabetes mellitus. *Fungal Diversity* **2012**, *56*, 1−29.

(2) Nogueira, F. N.; Carvalho, A. M.; Yamaguti, P. M.; Nicolau, J. Antioxidants parameters and lipid peroxidation in salivary glands of streptozotocin-induced diabetic rats. *Clin. Chim. Acta* **2005**, *353*, 133−139.

(3) Palanisamy, U. D.; Ling, L. T.; Manaharan, T.; Appleton, D. Rapid isolation of geraniin from Nephelium lappaceum rind waste and its anti-hyperglycemic activity. *Food Chem.* **2011**, *127*, 21−27.

DOI: 10.1021/jf5050316
J. Agric. Food Chem. 2015, 63, 562−568

(4) May, L. D.; Lefkowitch, J. H.; Kram, M. T.; Rubin, D. E. Mixed hepatocellular-cholestatic liver injury after pioglitazone therapy. *Ann. Intern. Med.* **2002**, *136*, 449−452.
(5) Sun, J. E.; Ao, Z. H.; Lu, Z. M.; Xu, H. Y.; Zhang, X. M.; Dou, W. F.; Xu, Z. H. Antihyperglycemic and antilipidperoxidative effects of dry matter of culture broth of Inonotus obliquus in submerged culture on normal and alloxan-diabetes mice. *J. Ethnopharmacol.* **2008**, *118*, 7−13.
(6) Li, Y. G.; Ji, D. F.; Zhong, S.; Lv, Z. Q.; Lin, T. B.; Chen, S.; Hu, G. Y. Hybrid of 1-deoxynojirimycin and polysaccharide from mulberry leaves treat diabetes mellitus by activating PDX-1/insulin-1 signaling pathway and regulating the expression of glucokinase, phosphoenol-pyruvate carboxykinase and glucose-6-phosphatase in alloxan-induced diabetic mice. *J. Ethnopharmacol.* **2011**, *134*, 961−970.
(7) Liu, Y. T.; Sun, J.; Luo, Z. Y.; Rao, S. Q.; Su, Y. J.; Xu, R. R.; Yang, Y. J. Chemical composition of five wild edible mushrooms collected from Southwest China and their antihyperglycemic and antioxi-dant activity. *Food Chem. Toxicol.* **2012**, *50*, 1238−1244.
(8) Navarro-Alarcon, M.; Cabrera-Vique, C. Selenium in food and the human body: A review. *Sci. Total Environ.* **2008**, *400*, 115−141.
(9) El-Bayoumy, K. The protective role of selenium on genetic damage and on cancer. *Mutat. Res.* **2001**, *475*, 123−139.
(10) Lubos, E.; Sinning, C. R.; Schnabel, R. B.; Wild, P. S.; Zeller, T.; Rupprecht, H. J.; Bickel, C.; Lackner, K. J.; Peetz, D.; Loscalzo, J.; Münzel, T.; Blankenberg, S. Serum selenium and prognosis in cardiovascular disease: results from the Athero*Gene* study. *Atherosclerosis* **2010**, *209*, 271−277.
(11) Navarro-Alarcon, M.; de la Serrana, H. L-G.; Perez-Valero, V.; Lopez-Martinez, M. C. Selenium concentrations in serum of individuals with liver diseases (cirrhosis or hepatitis): relationship with some nutritional and biochemical markers. *Sci. Total Environ.* **2002**, *291*, 135−141.
(12) Chasteen, T. G.; Bentley, R. Biomethylation of selenium and tellurium: Microorganisms and plants. *Chem. Rev.* **2003**, *103*, 1−26.
(13) Liu, Y. T.; Sun, J.; Rao, S. Q.; Su, Y. J.; Li, J. H.; Li, C. M.; Xu, S. D.; Yang, Y. J. Antidiabetic activity of mycelia selenium-polysaccharide from *Catathelasma ventricosum* in STZ-induced diabetic mice. *Food Chem. Toxicol.* **2013**, *62*, 285−291.
(14) Liang, L. H.; Wu, X. Y.; Zhao, T.; Zhao, J. L.; Li, F.; Zou, Ye.; Mao, G. H.; Yang, L. Q. In vitro bioaccessibility and antioxidant activity of anthocyanins from mulberry (*Morus atropurpurea* Roxb.) following simulated gastro-intestinal digestion. *Food Res. Int.* **2012**, *46*, 76−82.
(15) AOAC. *Official methods of analysis*, 16th ed.; Association of Official Analytical Chemists: Arlington, VA, 1995.
(16) Ribeiro, B.; Andrade, P. B.; Solva, B. M.; Baptista, P.; Seabra, R. M.; Valentao, P. Comparative study on free amino acid composition of wild edible mushroom species. *J. Agric. Food Chem.* **2008**, *56*, 10973−10979.
(17) Wrobel, K.; Wrobel, K.; Kannamkumarath, S. S.; Caruso, J. A.; Wysocka, I. A.; Bulska, E.; Swiatek, J.; Wierzbicka, M. HPLC−ICP-MS speciation of selenium in enriched onion leaves -a potential dietary source of Se-methylselenocysteine. *Food Chem.* **2004**, *86*, 617−623.
(18) Kapolna, E.; Shah, M.; Caruso, J. A.; Fodor, P. Selenium speciation studies in Se-enriched chives (*Allium schoenoprasum*) by HPLC-ICP−MS. *Food Chem.* **2007**, *101*, 1398−1406.
(19) Gergely, V.; Kubachka, K. M.; Mounicou, S.; Fodor, P.; Caruso, J. A. Selenium speciation in *Agaricus bisporus* and *Lentinula edodes* mushroom proteins using multi-dimensional chromatography coupled to inductively coupled plasma mass spectrometry. *J. Chromatogr. A* **2006**, *1101*, 94−102.
(20) Hart, D. J.; Fairweather-Tait, S. J.; Broadley, M. R.; Dickinson, S. J.; Foot, I.; Knott, P.; McGrath, S. P.; Mowat, H.; Norman, K.; Scott, P. R.; Stroud, J. L.; Tucker, M.; White, P. J.; Zhao, F. J.; Hurst, R. Selenium concentration and speciation in biofortified flour and bread: Retention of selenium during grain biofortification, processing and production of Se-enriched food. *Food Chem.* **2011**, *126*, 1771−1778.
(21) Muralidhara, S. B. Early oxidative stress in testis and epididymal sperm in streptozotocin-induced diabetic mice: Its progression and genotoxic consequences. *Reprod. Toxicol.* **2007**, *23*, 578−587.
(22) Kalač, P. Chemical composition and nutritional value of European species of wild growing mushrooms: A review. *Food Chem.* **2009**, *113*, 9−16.
(23) Belitz, H. D.; Grosch, W. *Food chemistry*. Springer: Berlin, Germany, 1999.
(24) Pappa, E. C.; Pappas, A. C.; Surai, P. F. Selenium content in selected foods from the Greek marked and estimation of the daily intake. *Sci. Total Environ.* **2006**, *372*, 100−108.
(25) Dumont, E.; Vanhaecke, F.; Cornelis, R. Selenium speciation from food source to metabolites: a critical review. *Anal. Bioanal. Chem.* **2006**, *385*, 1304−1323.
(26) Rayman, M. P.; Infante, H. G.; Sargent, M. Food-chain selenium and human health: spot-light on speciation. *Br. J. Nutr.* **2008**, *100*, 238−253.
(27) Food and Nutrition Board-USA Institute of Medicine. *Dietary References Intakes for Vitamin C, Vitamin E, Selenium and Carotenoids*; National Academy Press: WA, 2000.
(28) Dong, J. Z.; Ding, J.; Yu, P. Z.; Lei, C.; Zheng, X. J.; Wang, Y. Composition and distribution of the main active components in selenium-enriched fruit bodies of *Cordyceps militaris* link. *Food Chem.* **2013**, *137*, 164−167.
(29) Ferri, T.; Favero, G.; Frasconi, M. Selenium speciation in foods: Preliminary results on potatoes. *Microchem. J.* **2007**, *85*, 222−227.
(30) Heo, S. J.; Hwang, J. Y.; Choi, J. I.; Han, J. S.; Kim, H. J.; Jeon, Y. J. Diphlorethohydroxycarmalol isolated from Ishige okamurae, a brown algae, a potent α-glucosidase and α-amylase inhibitor, alleviates postprandial hyperglycemia in diabetic mice. *Eur. J. Pharmacol.* **2009**, *615*, 252−256.
(31) Layer, P.; Rizza, R. A.; Zinsmeister, A. R.; Carlson, G. L.; DiMagno, E. P. Effect of a purified amylase inhibitor on carbohydrate tolerance in normal subjects and patients with diabetes mellitus. *Mayo Clin. Proc.* **1986**, *61*, 442−447.
(32) Doi, T.; Yoshimatsu, H.; Katsuragi, I.; Kurokawa, M.; Takahashi, H.; Motoshio, A.; Sakata, T. alpha-amylase inhibitor increases plasma 3-hydroxybutyric acid in food-restricted rats. *Experientia* **1995**, *51*, 585−588.
(33) Yasuda, K.; Shimowada, K.; Uno, M.; Odaka, H.; Adachi, T.; Shihara, N.; Suzuki, N.; Tamon, A.; Nagashima, K.; Hosokawa, M.; Tsuda, K.; Seino, Y. Long-term therapeutic effects of voglibose, a potent intestinal alpha-glucosidase inhibitor, in spontaneous diabetic GK rats. *Diabetes Res. Clin. Pract.* **2003**, *59*, 113−22.
(34) Stapleton, S. R. Selenium: An insulin mimetic. *Cell. Mol. Life Sci.* **2000**, *57*, 1874−1879.
(35) Chen, V.; Ianuzzo, C. D. Dosage effect of streptozotocin on rat tissue enzyme activities and glycogen concentration. *Can. J. Physiol. Pharmacol.* **1982**, *60*, 1251−1256.
(36) Zhao, L. Y.; Lan, Q. J.; Huang, Z. C.; Ouyang, L. J.; Zeng, F. H. Antidiabetic effect of a newly identified component of *Opuntia dillenii* polysaccharides. *Phytomedicine* **2011**, *18*, 661−668.
(37) Kakkar, R.; Mantha, S. V.; Radhi, J.; Prasad, K.; Kalra, J. Increased oxidative stress in rat liver and pancreas during progression of streptozotocin induced diabetes. *Clin. Sci.* **1998**, *94*, 623−632.
(38) Mohamed, A. K.; Bierhaus, A.; Schiekofer, S. The role of oxidative stress and NF-kappaB activation in late diabetic complications. *Biofactors* **1999**, *10*, 175−179.
(39) Chen, X. M.; Tang, J.; Xie, W. Y.; Wang, J. J.; Jin, J.; Ren, J.; Jin, L. Q.; Lu, J. X. Protective effect of the polysaccharide from *Ophiopogon japonicus* on streptozotocin-induced diabetic rats. *Carbohydr. Polym.* **2013**, *94*, 378−385.
(40) Irshad, M.; Chaudhuri, P. S. Oxidant-antioxidant system: Role and significance in human body. *Indian J. Exp. Biol.* **2002**, *40*, 1233−1239.
(41) Bagchi, D.; Bagchi, M.; Hassoun, E. A.; Stohs, S. J. In vitro and in vivo generation of reactive oxygen species, DNA damage and lactate dehydrogenase leakage by selected pesticides. *Toxicology* **1995**, *104*, 129−140.

DOI: 10.1021/jf5050316
J. Agric. Food Chem. 2015, 63, 562−568

JOURNAL OF AGRICULTURAL AND FOOD CHEMISTRY

Article

pubs.acs.org/JAFC

A Novel Alkali Extractable Polysaccharide from *Plantago asiatic* L. Seeds and Its Radical-Scavenging and Bile Acid-Binding Activities

Lu Gong,[∥,†] Hua Zhang,[∥,§] Yuge Niu,[*,†] Lei Chen,[†] Jie Liu,[†] Sierkemideke Alaxi,[†] Pingping Shang,[†] Wenjuan Yu,[#] and Liangli (Lucy) Yu[*,†,⊥]

[†]Institute of Food and Nutraceutical Science, School of Agriculture and Biology, Shanghai Jiao Tong University, Shanghai 200240, China

[§]School of Chemical and Environmental Engineering, Shanghai Institute of Technology, Shanghai 201418, China

[#]Instrumental Analysis Center, Shanghai Jiao Tong University, Shanghai 200240, China

[⊥]Department of Nutrition and Food Science, University of Maryland, College Park, Maryland 20742, United States

Supporting Information

ABSTRACT: A new acidic polysaccharide (PLP) was isolated and characterized from *Plantago asiatic* L. seeds by hot alkali extraction and chromatographic purification using DEAE cellulose and Sephacryl S-400 columns. PLP has a molecular weight of 1.15×10^6 Da, and a monosaccharide composition of xylose (Xyl), arabinose (Ara), glucuronic acid (GlcA), and galactose (Gal) in a molar ratio of 18.8:7.2:6.1:1. The results of methylation analysis, FT-IR, and 1D and 2D NMR indicated that PLP was a highly branched heteroxylan of β-1,4-linked Xyl*p* backbone with three α-GlcA*p*-(1→3)-Ara*f* attached to the *O*-3 position and one α-T-linked-GlcA*p* and one α-Ara*f*-(1→5)-Ara*f* attached to the *O*-2 position every eight monosaccharide residues. PLP exhibited scavenging abilities against hydroxyl, peroxyl anion, and DPPH radicals in vitro and showed significant binding capacities against cholic and chenodeoxycholic acids, suggesting its possible cholesterol-lowering activity. The results demonstrated the potential use of PLP in functional foods and nutraceuticals.

KEYWORDS: *Plantago asiatic L. polysaccharides, monosaccharide composition, structure analysis, bile acid-binding capacity, antioxidant*

INTRODUCTION

Plantago L. (Plantaginaceae) is a perennial herb that has more than 270 species all over the world. Polysaccharides from *Plantago* L., such as psyllium, are important health components.[1−4] Psyllium is an arabinoxylan derived from the seed husk of *Plantago ovata* and is a commercial dietary fiber with a bile-acid binding activity, which might be important for its cholesterol-lowering activity.[5]

Psyllium is mostly produced in India. In China, *Plantago major*, *Plantago asiatic*, and *Plantago depressa* have been used in functional foods, and *P. asiatic* is most widely distributed.[6] The hot water extractable polysaccharides from *P.asiatica* L. seeds exhibited antioxidant activity in vitro[7] and were shown to promote defecation.[8] Polysaccharides may bind bile acids and enhance their intestinal elimination and consequently stimulate the conversion of cholesterol to bile acids in liver.[9] As a result, the levels of total plasma and low-density lipoprotein (LDL) cholesterol may be reduced, which may reduce the risk of cardiovascular diseases. Additionally, polysaccharides with antioxidant capacities could suppress LDL oxidation and consequently reduce the risk of cardiovascular disease.

Our previous studies showed that the physicochemical properties and bile acid-binding capacities of psyllium were closely related to its chemical and molecular structures.[9] Alkali-extractable polysaccharides may have bioactivities different from the water-extractable ones because the alkali-sensitive chemical bonds between polysaccharides and cell wall of plants could be broken during extraction, leading to the release of polysaccharide(s) with different chemical and molecular structures.[10,11] To date, little is known about the alkali-extractable polysaccharides of *P. asiatic* L. seeds.

The present study aimed to investigate the alkali-extractable *P. asiatic* L. seed polysaccharides. The ground seeds of *P. asiatic* L. were extracted with alkali and purified by column chromtographies. The chemical structures of individual polysaccharides were characterized by methylation, GC, HPLC, GC-MS, and 1D and 2D NMR spectroscopy analyses. In addition, their hydroxyl, peroxyl, and DPPH radical-scavenging capacities and bile acid-binding activity were examined. The results may serve as a scientific foundation for developing their possible application in functional foods and nutraceuticals.

MATERIALS AND METHODS

Materials. The seeds of *P. asiatic* L. were collected and identified by Dr. Haibo Yin (Liaoning University of Traditional Chinese Medicine) in 2012. Diethylaminoethyl (DEAE) cellulose was purchased from Whatman International Ltd. (Kent, UK). Sephacryl S-400 was purchased from GE Healthcare (Uppsala, Sweden). Dextrans with different molecular weights and standard monosaccharaides including arabinose, glucose, mannose, glucuronic acid, galactose, rhamnose, fucose, and xylose were purchased from the National Institute for Food and Drug Control (Beijing, China). Deuterated

Received: October 28, 2014
Accepted: December 23, 2014
Published: December 23, 2014

ACS Publications © 2014 American Chemical Society

DOI: 10.1021/jf505909k
J. Agric. Food Chem. 2015, 63, 569−577

water (D_2O) was purchased from Cambridge Isotope Laboratories, Inc. (Andover, MA, USA). Fluorescein (FL), iron(III) chloride, 6-hydroxyl-2,5,7,8-tetramethylchroman-2-carboxylic acid (Trolox), dimethyl sulfoxide (DMSO), 2,2-diphenyl-1-picrylhydrazyl radical (DPPH•), cholic and chenodexycholic acids, diphorase, β-nicotinamide adenine dinucleotide, and 3-α-hydroxysterol dehydrogenase were purchased from Sigma-Aldrich (St. Louis, MO, USA). *myo*-Inositol, 2,2′-azobis(2-amidinopropane) dihydrochloride (AAPH), nitro blue tetrazolium (NBT), and 3-methyl-1-phenyl-2-pyrazolin-5-one (PMP) were purchased from J&K Scientific (Beijing, China). Acetic anhydride, pyridine, and sodium borohydride were purchased from Sinopharm (Beijing, China). Other reagents for isolation were of analytical grade without further purification.

Extraction, Isolation, and Purification of Polysaccharide (PLP). The dried seeds of *P. asiatica* L. (100 g) were ground into powder and then defatted by ethanol (95%, v/v) extraction for 9 h. The residues were extracted by hot water (1:30, m/v) three times at 80 °C for 2 h each time. After filtering, the residues were extracted by 0.5 M NaOH (1:25, m/v) twice at 80 °C for 2 h each time. The combined supernatants were neutralized by 37.5% hydrochloric acid and dialyzed with 3500 Da molecular weight cutoff membrane against distilled water for 72 h. The solution was deproteinized according to a Sevag method.[12] Fifteen milliliters of 30% hydrogen peroxide was added to 100 mL of solution to remove the pigment at 60 °C for 6 h. The resulting aqueous solution was collected after centrifugation at 4500 rpm for 10 min and then precipitated using 4-fold volumes of ethanol (95%, v/v). The precipitates were collected by centrifugation (4500 rpm × 10 min), rinsed with anhydrous ethanol, acetone, and ether, and dried with nitrogen (2 L/min, room temperature) to yield crude polysaccharides.

Three milliliters of crude polysaccharide solution (100 mg/mL) was applied to a DEAE column (2.5 cm × 30 cm, Whatman International Ltd.) and eluted first with distilled water at a rate of 0.2 mL/min for 24 h, followed by 0.62 M NaCl solution at the same rate. Fractions were combined according to the result of phenol−sulfuric acid determination. The eluent was concentrated, centrifuged, and loaded onto a Sephacryl S-400 column (1.6 cm × 100 cm, GE Healthcare). The column was washed with distilled water at a rate of 0.2 mL/min. Each eluting peak was collected, concentrated, and lyophilized to give the pure polysaccharide named PLP.

Purity and Molecular Weight Determination. The purity and molecular weight of PLP were determined using a high-performance size exclusion chromatograph (Agilent, Santa Clara, CA, USA) equipped with a gel filtration column (Shodex SUGAR KS-805, 8 mm i.d. × 300 mm, Showa Denko, Japan) and a refractive index detector. Deionized water as the mobile phase eluted at a flow rate of 1.0 mL/min. The molecular weight of PLP was calculated by the standard curve prepared with a series of dextran standards with different molecular weights (180, 2700, 5250, 9750, 13050, 36800, 64650, 135,350, 300,600, and 2,000,000 Da, respectively).

Monosaccharide Composition Analysis. PLP (5 mg) was dissolved in 1 mL of 2 M trifluoroacetic acid (TFA) and kept at 100 °C for 8 h. After being completely hydrolyzed, the excess TFA was removed by codistillation with the added 0.1% HCl−methanol. The residual was dissolved in 1 mL of distilled water for further derivatization.[13]

The hydrolysate was applied to monosaccharide composition analysis using a GC method.[14] Briefly, monosaccharide standards including arabinose, glucose, mannose, glucuronic acid, galactose, rhamnose, fucose, and xylose and the hydrolyzed polysaccharide samples were reduced by $NaBH_4$ at 65 °C for 30 min, followed by incubation with acetic anhydride and pyridine at 100 °C for 2 h. The resulting alditol acetates were applied to a GC (Agilent) equipped with a flame ionization detector and a HP-5 capillary column (30 m × 0.32 mm, 0.25 μm). The oven temperature was raised from 110 to 220 °C at 5 °C/min, held for 2 min, increased to 240 °C at 2 °C/min, held for 2 min, and finally increased to 280 °C at 10 °C/min.

Precolumn derivatization with PMP was used for the identification and quantification of the monosaccharides including uronic acid.[15] After mixing with 50 μL of 0.6 M sodium hydroxide, 50 μL of monosaccharide standard or the hydrolyzed polysaccharide sample solution was mixed with 50 μL of 0.5 M PMP in methanol. The reaction was carried out at 70 °C for 30 min and neutralized with 100 μL of 0.3 M hydrochloric acid, followed by extraction with chloroform (1.0 mL) three times. The aqueous layer was filtered through a 0.45 μm pore membrane filter for HPLC analysis (Agilent Technologies Co. Ltd., Santa Clara, CA, USA) at 250 nm with a Zorbax Eclipse XDB-C18 column (4.6 mm × 250 mm, 5 μm, Agilent, Palo Alto, CA, USA). The mobile phase was composed of ammonium acetate solution (pH 5.5) and acetonitrile at a ratio of 78:22 (v/v).

Infrared Spectral Analysis. The Fourier transform infrared (FT-IR) spectrum was determined on a FT-IR spectrophotometer with an ATR accessory (Nicolet 6700, Thermo Fisher, Waltham, MA, USA) in the range of 4000−400 cm^{-1}.

Methylation and GC-MS Analysis. Methylation analysis of polysaccharide was performed according to the method of Needs and Selvendran with minor modifications.[16] The dried PLP (10 mg) was dissolved in 5 mL of anhydrous DMSO with added NaOH powder (100 mg). CH_3I (2 mL) was added slowly into the solution. The methylated polysaccharide was extracted with chloroform. The methylation was repeated until the polysaccharide was methylated completely. The completion of methylation of PLP was confirmed by the disappearance of the OH band (3200−3700 cm^{-1}) in the IR spectrum.

The methylated polysaccharide was hydrolyzed in 3 mL of formic acid (88%, v/v) at 100 °C for 6 h and further hydrolyzed in 3 mL of 2 M trichloroacetic acid at 100 °C for 3 h. After being reduced with $NaBH_4$ at 60 °C for 1 h, monosaccharides were converted into the alditol acetates by reacting with pyridine and acetic anhydride at 100 °C for 1 h and subjected to linkage analysis using an Agilent 7890A-5975C GC-MS system (Agilent Technologies Co. Ltd., Santa Clara, CA, USA) equipped with a DB-5MS column (30 m × 0.25 mm, 0.25 μm, Agilent, Palo Alto, CA, USA). The oven temperature was from 100 to 190 °C at 20 °C/min, increased to 260 °C at 3 °C/min, and increased to 300 °C at 10 °C/min. The resulting peaks of alditol acetates were identified by their MS fragmentation patterns and the relative retention time in GC spectrum. Their relative amount was estimated as ratios of peak areas.

Nuclear Magnetic Resonance (NMR) Spectroscopy. PLP (50 mg) was dissolved in 0.5 mL of D_2O. The 1D and 2D NMR spectra, including ^1H NMR, ^{13}C NMR, HH COSY, HSQC, and HMBC, were recorded on a Bruker AV-500 MHz NMR spectrometer (Bruker, Rheinstetten, Germany) at 30 °C.

Relative DPPH•-Scavenging Capacity (RDSC). DPPH•-scavenging capacity was determined following a previously reported laboratory protocol[17] using a Synergy 2 Multi-Mode Microplate Reader (BioTek, Winooski, VT, USA). Trolox was employed as an antioxidant standard. Briefly, 100 μL of PLP, Trolox standard solution, or blank was added into each well, then 100 μL of 0.092 mM DPPH• solution was added to initiate the antioxidant radical reaction. The absorbance of the reaction mixture at 515 nm was recorded every minute for 1.5 h, and each sample was tested three times in parallel. The relative scavenging capacity (RDSC) was calculated as micromoles of Trolox equivalents (TE) per gram of PLP using the area under the curve (AUC) calculation.

Hydroxyl Radical-Scavenging Capacity (HOSC). A previously reported laboratory protocol[18] was applied to evaluate the HOSC value of PLP using a Synergy 2 Multi-Mode Microplate Reader (BioTek). Fluorescein (FL) prepared in 75 mM sodium phosphate buffer (pH 7.4) was used as the molecular probe and Trolox as the antioxidant standard. One hundred and seventy microliters of FL solution (9.28×10^{-8} M), 30 μL of PLP, standard, or blank, 40 μL of 0.199 M hydrogen peroxide, and 60 μL of 3.43 M $FeCl_3$ were added into each well successively to initiate the reaction. The fluorescence was recorded every minute for 6 h. The excitation wavelength was 485 nm, and emission wavelength was 528 nm. The experiment was conducted three times in parallel for each sample. The HOSC value was expressed as micromoles of TE per gram of PLP based on the AUC.

DOI: 10.1021/jf505909k
J. Agric. Food Chem. 2015, 63, 569−577

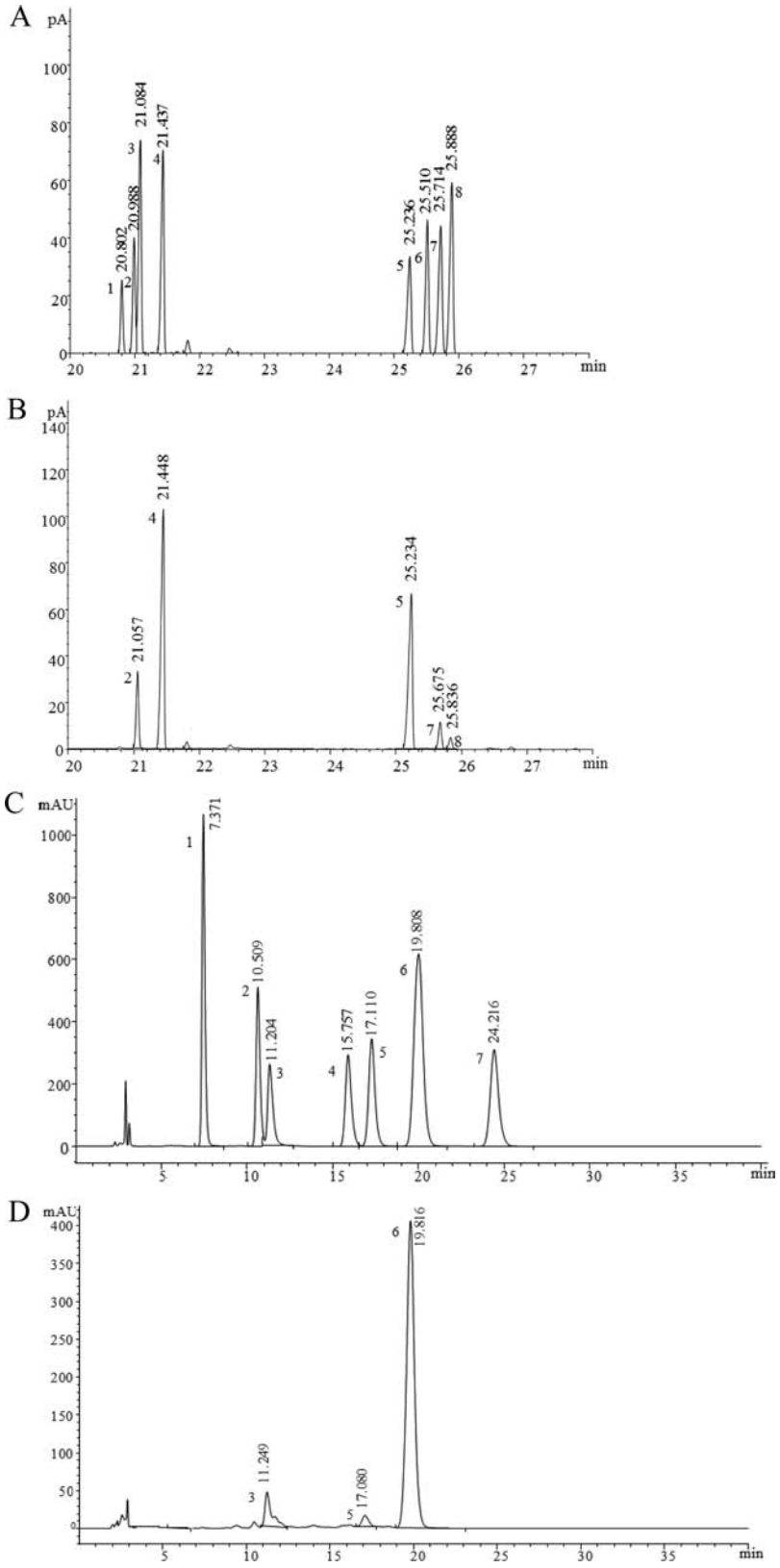

Figure 1. GC chromatograms: standard monosaccharides (A) and monosaccharide composition of PLP (B). Peaks: 1, rhamnose; 2, arabinose; 3, fucose; 4, xylose; 5, inositol; 6, mannose; 7, glucose; 8, galactose. HPLC chromatograms of PMP derivatives: standard monosaccharaides (C) and monosaccharide composition of PLP (D). Peaks: 1, mannose; 2, rhamnose; 3, glucuronic acid; 4, glucose; 5, galactose; 6, xylose and arabinose; 7, fucose.

Oxygen Radical Absorbance Capacity (ORAC). The ORAC assay was conducted according to a previously described laboratory protocol.[19] Fluorescein (FL) was used as the fluorescent probe with Trolox as the antioxidant standard. In brief, 30 μL of PLP, standard, or

DOI: 10.1021/jf505909k
J. Agric. Food Chem. 2015, 63, 569−577

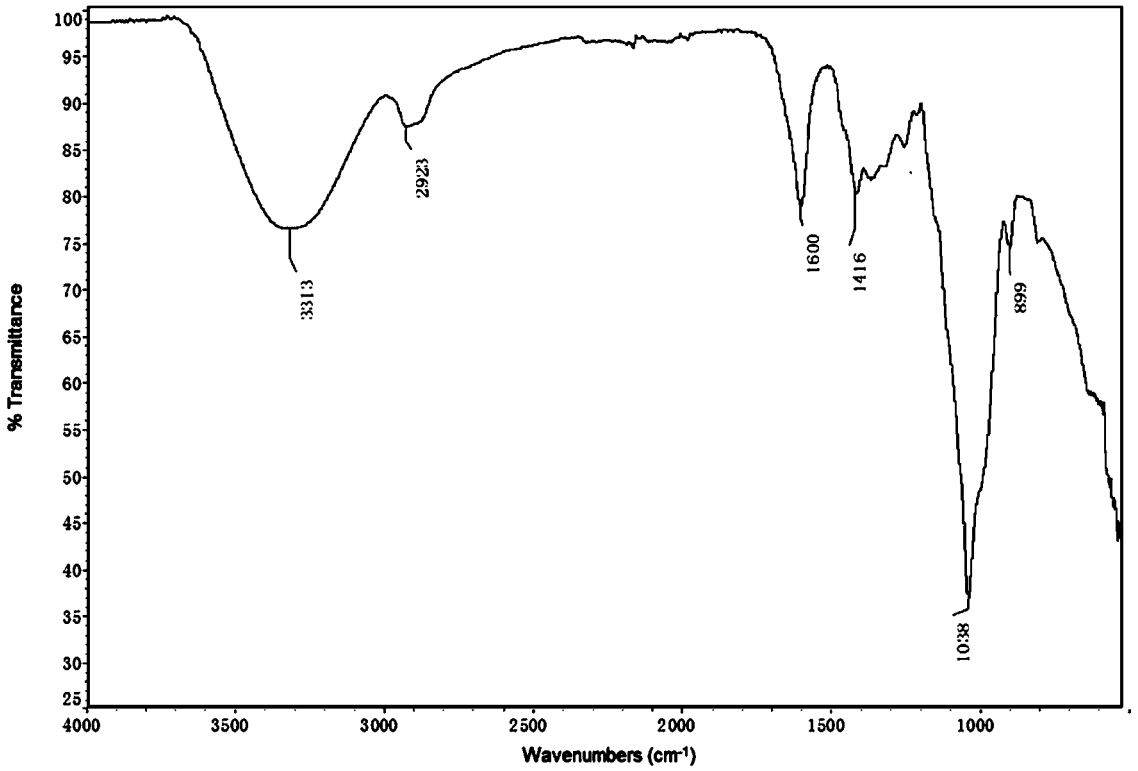

Figure 2. FT-IR spectrum of PLP.

Table 1. Methylation Analysis of PLP

retention time (min)	methylated sugar	mass fragments(m/z)	molar ratio	linkage type
11.827	2,5-Me_2-Ara*f*	43, 58, 87, 99, 113, 117, 129, 159, 233	0.62	1,3-linked Ara*f*
12.203	2,3 -Me_2-Ara*f*	43, 87, 101, 117, 129, 189	0.25	1,5-linked Ara*f*
12.291	2,3,5-Me_3-Ara*f*	43, 45, 71, 87, 101, 117, 129, 145, 161	0.22	1-linked Ara*f*
13.181	3-Me-Xyl*p*	43, 87, 99, 126, 129, 189	0.44	1,2,4-linked Xyl*p*
13.306	2,3-Me_2-Xyl*p*	43, 87, 101, 117, 129, 161, 189, 233	1.85	1,4-linked Xyl*p*
13.344	2-Me-Xyl*p*	43, 85, 101, 117, 127, 159, 201, 233	0.66	1,3,4-linked Xyl*p*
24.027	2,3,4,6-Me_4-GluA*p*	43, 71, 101, 117, 129, 161, 203	1	1-linked GluA*p*

blank was added into 225 μL of 81.63 nM FL solution. After 20 min of preheating at 37 °C in a Synergy 2 Multi-Mode Microplate Reader (BioTek), 25 μL of 0.36 M AAPH was successively added into each well to initiate the reaction. The fluorescence was measured every minute for 2 h at 37 °C. The excitation wavelength was 485 nm, and emission wavelength was 535 nm. The ORAC value was calculated on the basis of AUC and reported as micromoles of TE per gram of PLP.

Bile Acid-Binding Capacity Assay. According to a previous laboratory protocol,[20] 25 mg of each sample was dissolved in 0.25 mL of 0.01 mol/L HCl to simulate gastric condition and then incubated at 37 °C for 60 min with continuous shaking. The solution was adjusted to pH 7.0 by adding 25 μL of 0.1 mol/L NaOH and mixed with 1.25 mL of bile acid stock solution (400 μM in 0.01 M phosphates buffer, pH 7.0) to simulate the intestinal condition. The mixture was incubated for another 60 min at 37 °C, followed by centrifugation at 4500 rpm for 15 min. The supernatant was collected to quantify the unbound bile acid. One hundred microliters of each sample or bile acid standard was mixed with 125 μL of 1.22 mmol/L nicotinamide adenine dinucleotide, 5 mmol/L NBT, 100 μL of diphorase (625 units/L), and 100 μL of 3-α-hydroxysterol dehydrogenase solution (625 units/L). After incubation at ambient temperature for 1 h, 100 μL of 1.33 mmol/L phosphoric acid was added to stop the reaction. The absorbance of each mixture was determined at 530 nm with cholestyramine resin as a positive control and the phosphate buffer without bile acid as the reagent blank. The bile acid-binding capacity (mg/g sample) was calculated according to the standard curves of cholic and chenodeoxycholic acids, respectively. Triplicate tests were conducted.

Statistical Analysis. Data were expressed as the mean ± standard deviation (SD) for each assay. Differences between means were determined by the analysis of one-way ANOVA and Tukey's test, using SPSS (SPSS for Windows, version rel. 16.0, SPSS Inc., Chicago, IL, USA). Statistical significance was declared at $P < 0.05$.

RESULTS AND DISCUSSION

Isolation, Purification, and Molecular Weight of PLP. The crude polysaccharides were obtained from the dry seeds of *P. asiatic* L. by hot alkaline extraction and ethanol precipitation with a yield of approximately 5.45% (w/w). After purification with an ion exchange column (DEAE-32), the alkali-extractable polysaccharide PLP was further purified using a Sephacryl S-400 column chromatograph. No significant absorption band was observed at 260 or 280 nm in the UV spectrum, indicating that PLP contained no protein or nucleic acid (data not shown). PLP showed a single, sharp, and symmetric peak by HPLC analysis, and its purity was calculated as 99.2% (data not shown). The molecular weight of PLP was calculated 1.15×10^6 Da using a dextran standard curve.

Monosaccharide Composition. The result of GC analysis showed that the monosaccharide composition of PLP was

DOI: 10.1021/jf505909k
J. Agric. Food Chem. 2015, 63, 569−577

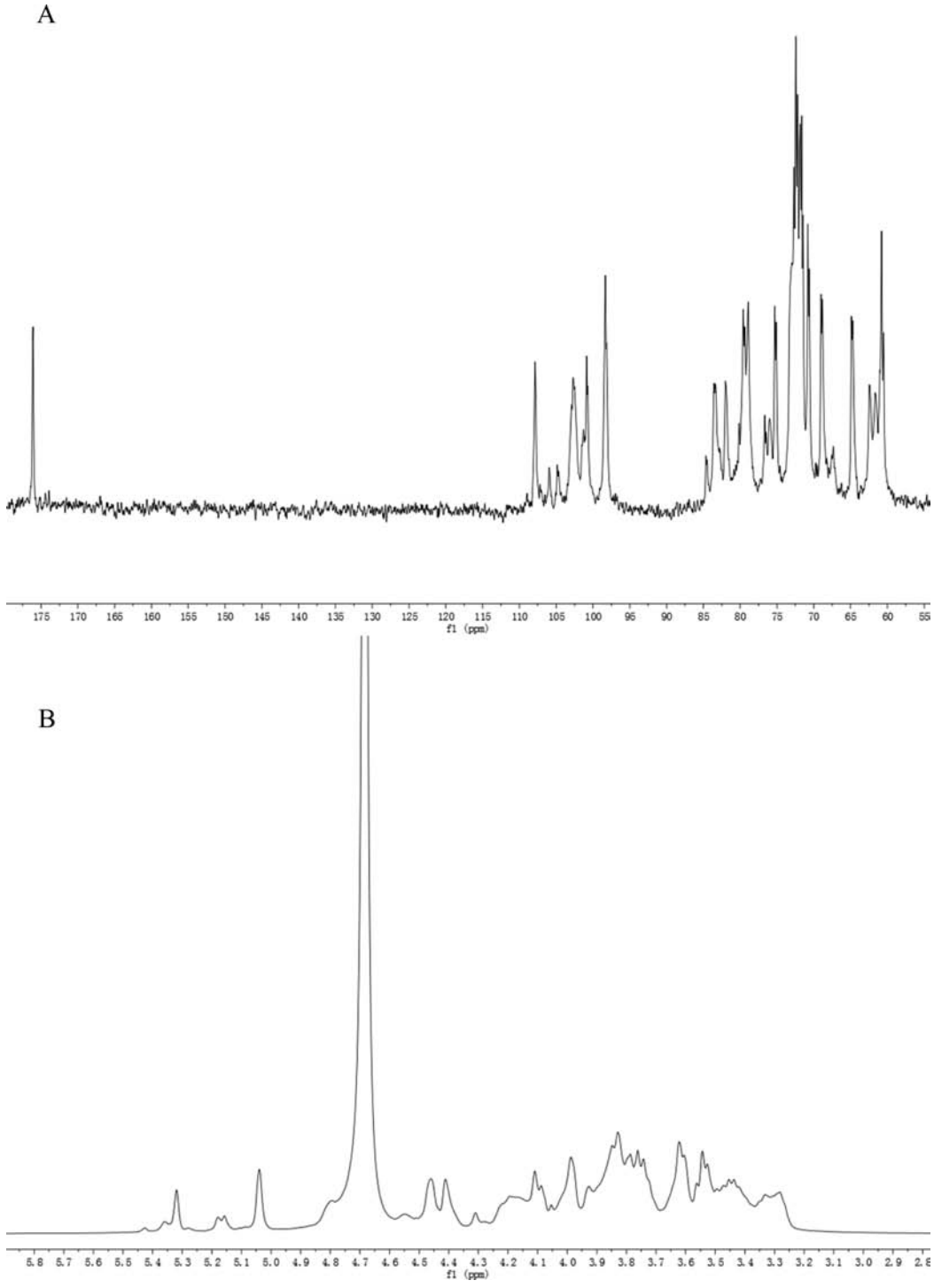

Figure 3. continued

DOI: 10.1021/jf505909k
J. Agric. Food Chem. 2015, 63, 569−577

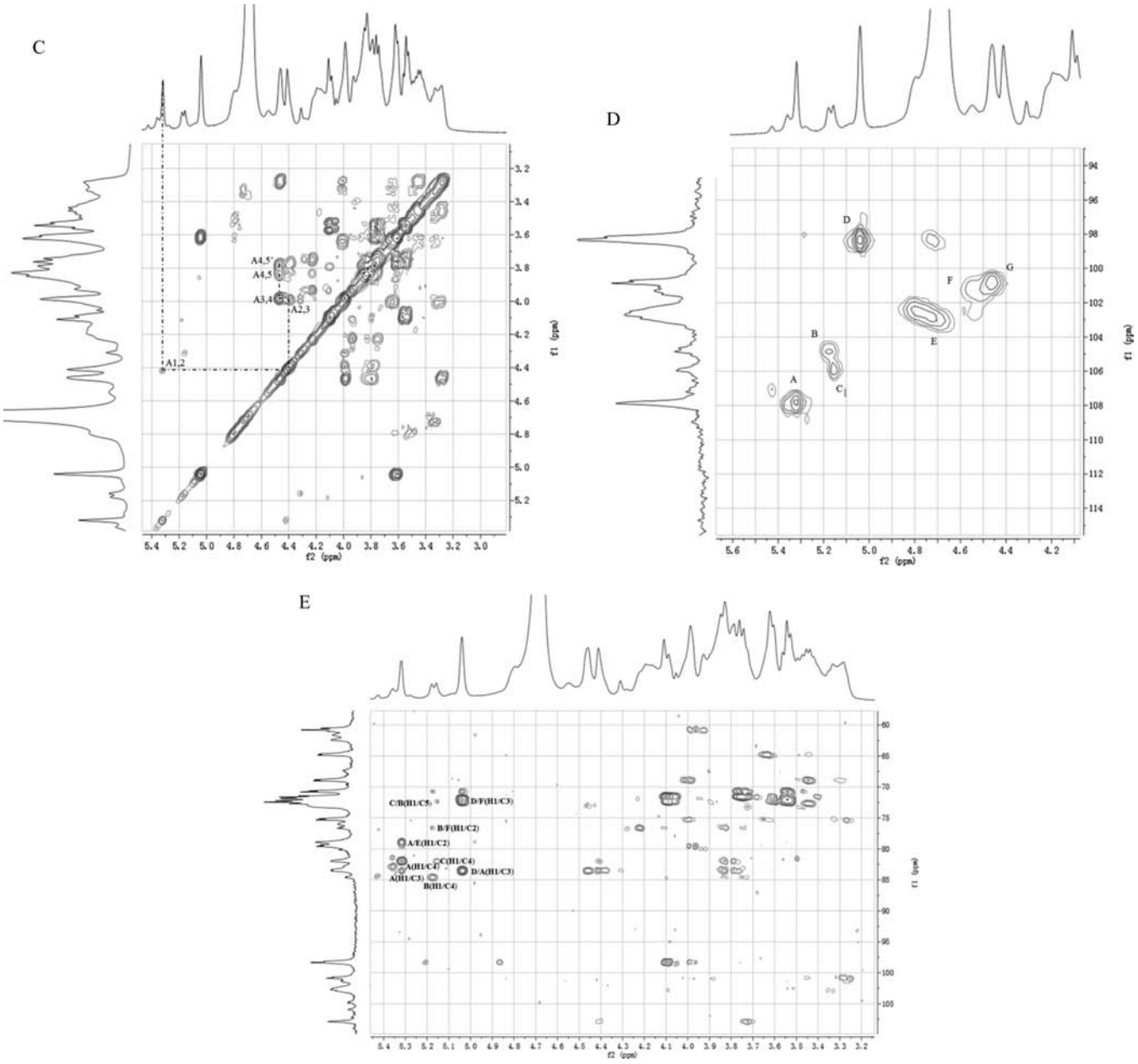

Figure 3. ^{13}C (A) and ^{1}H (B) NMR spectra of PLP; (C) $^{1}H/^{1}H$ COSY spectrum; (D) HSQC spectrum (anomeric region); (E) HMBC spectrum (anomeric region).

Table 2. ^{13}C and ^{1}H Chemical Shifts of PLP

	chemical shifts, δ						
sugar residue	C1/H1	C2/H2	C3/H3	C4/H4	C5/H5	H5′	C6
(A) α-1,3-linked Ara*f*	107.90/5.32	79.41/4.41	83.44/3.99	81.88/4.46	60.80/3.83	3.79	
(B) α-1,5-linked Ara*f*	104.75/5.18	80.12/4.11	76.66/3.92	84.54/3.64	64.63/4.00	3.31	
(C) α-T-linked Ara*f*	105.87/5.16	79.41/4.31	83.51/3.98	81.95/4.39	60.94/3.76		
(D) α-T-linked GlcA*p*	98.47/5.04	70.82/3.62	72.22/3.74	84.57/4.22	76.63/3.93		176
(E) β-1,3,4-linked Xyl*p*	102.50/4.79	75.26/3.46	72.22/3.79	72.43/3.62	68.90/3.44	3.28	
(F) β-1,2,4-linked Xyl*p*	101.41/4.55	78.91/3.56	78.92/3.73	80.12/4.22	61.04/3.83	3.77	
(G) β-1,4-linked Xyl*p*	100.85/4.46	72.56/3.28	75.26/3.44	70.42/3.62	64.74/3.99	3.33	

xylose, arabinose, glucose, and galactose at a molar ratio of 18.8:7.2:6.1:1 according to peak areas and response factors (Figure 1A,B). Considering that glucuronic acid could be reduced to glucose by $NaBH_4$ during acetylation and measured as glucose, a PMP derivatization analysis was further used to measure the possible uronic acid and glucose contents of PLP. The peaks of PMP-labeled monosaccharides in Figure 1D showed the presence of xylose, arabinose, glucuronic acid, and galactose without glucose. Taken together, these data indicated no presence of glucose in the alkali extractable polysaccharide

DOI: 10.1021/jf505909k
J. Agric. Food Chem. 2015, 63, 569−577

Table 3. Significant Connectivities Observed in the HMBC Spectrum for the Anomeric Protons/Carbons of the Sugar Residues of PLP

			observed connectivities		
residue	sugar linkage	H 1/C 1 δ_H/δ_C	δ_H/δ_C	residue	atom
A	1,3-linked Ara*f*	5.32	72.22	E	C 3
			83.44	A	C 3
		107.90	81.88	A	C 4
B	1,5-linked Ara*f*	5.18	78.91	F	C 2
		104.75	84.54	B	C 4
C	T-linked Ara*f*	5.16	60.94	B	C 5
		105.87	81.95	C	C 4
D	T-linked GlcA*p*	5.04	78.91	F	C 2
		98.47	83.44	A	C 3
E	1,3,4-linked Xyl*p*	4.79	3.62	E	H 4
		102.50			
F	1,2,4-linked Xyl*p*	4.55	4.22	F	H 4
		101.41			
G	1,4-linked Xyl*p*	4.46	72.43	E	C 4
			80.12	F	C 4
		100.85	72.56	G	C 2

from *P. asiatic* L. seeds. The monosaccharide composition of PLP was xylose, arabinose, glucuronic acid, and galactose at a molar ratio of 18.8:7.2:6.1:1. It contained no protein or nucleic acid. The content of uronic acid was about 18.4%.

Structural Characterization of PLP. The FT-IR spectrum of PLP is shown in Figure 2. The assignments of functional groups were conducted according to previous literature.[14,21,22] The band centered at 3312 cm^{-1} arose from OH stretching vibrations of hydroxyl groups. The strong band at 2923 cm^{-1} was characteristic of C−H stretching vibrations of a CH_2 group. Moderate IR bands at 1600 and 1416 cm^{-1} arose from asymmetric and symmetric stretching vibrations of carboxylate generated by the reaction of KBr and carboxylic acid. They implied the presence of carboxylic acid, supporting the presence of glucuronic acid suggested by the result of PMP derivatization analysis. Strong overlapped IR bands at 900−1200 cm^{-1} corresponded to coupled C−O, C−C stretching, and C−OH bending vibrations. An IR band at 899 cm^{-1} was characteristic of β-anomeric configuration.

Methylation followed by GC-MS analysis was employed to obtain more structural information on PLP. Demonstrated by the FT-IR spectrum, PLP was methylated completely and then hydrolyzed under an acidic condition to form partially methylated alditol acetates followed by GC-MS analysis.

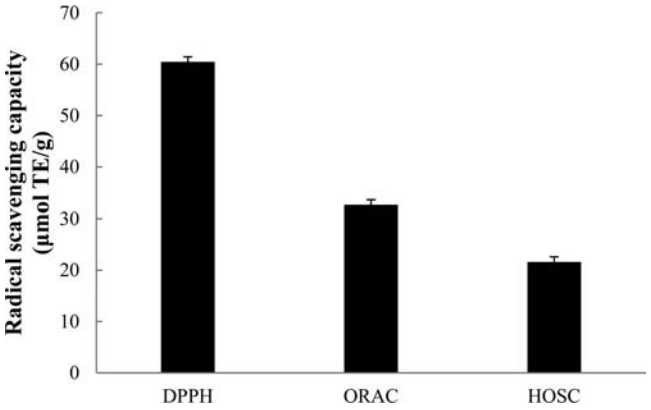

Figure 5. Free radical-scavenging activities of PLP. Data were expressed as Trolox equivalent (TE) in μmol TE/g. Free radical-scavenging activities were calculated using the area under the curve (AUC) against the Trolox standard. Vertical bars represent SD.

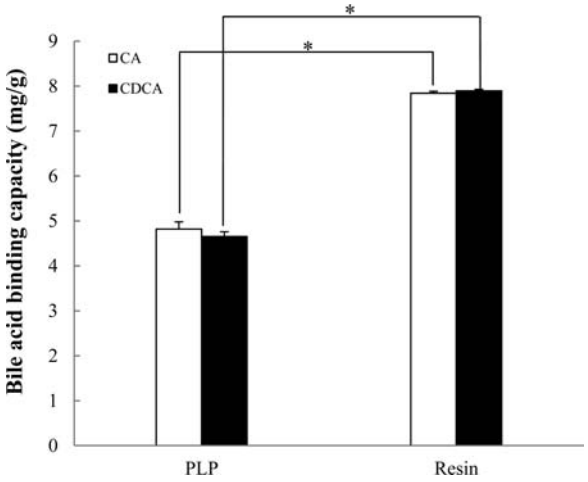

Figure 6. Bile acid-binding capacity of PLP. CA and CDCA represent cholic and chenodeoxycholic acids, respectively. Resin means cholestyramine resin, which is the positive control. Vertical bars represent the SD. * represents significant differences ($P < 0.05$).

According to the results in Table 1, seven homogeneous peaks were observed by GC analysis. According to their retention time, the peaks were identified as 2,5-di-Me-arabitol, 2,3-di-Me-arabitol, 2,3,5-tri-Me-arabitol, 3-Me-xylitol, 2,3-di-Me-xylitol, 2-Me-xylitol, and 2,3,4,6-tetra-Me-gluctiol with a molar ratio of 0.62:0.25:0.22:0.44:1.85:0.66:1, which was in good agreement with the monosaccharide composition. Due to its low content (3%) and possible structural damage during the methylation reaction, the galactose residues were not detected in the GC-MS analysis. The results implied that the possible structure of PLP was a highly branched araboxylan mainly composed of 1,4-linked Xyl*p* as the backbone with side chains

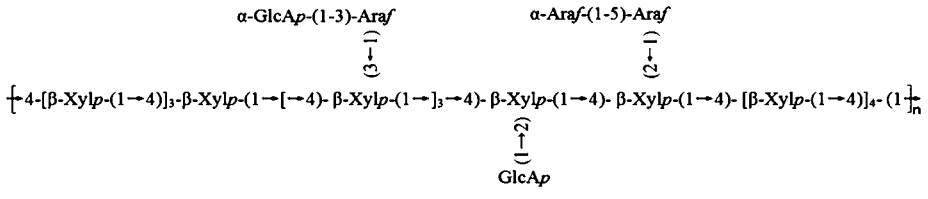

Figure 4. Proposed repeating unit of PLP.

DOI: 10.1021/jf505909k
J. Agric. Food Chem. 2015, 63, 569−577

attached to the *O*-2 or *O*-3 position.[23,24] The side chains consisted of 1,3-linked Ara*f*, 1, 5-linked Ara*f*, T-linked Ara*f*, and T-linked GlcA.

According to the ^{1}H NMR of PLP (Figure 3A), seven signals were displayed in the anomeric region between δ 4.4 and 5.5. Generally, the chemical shifts of α-linked Ara*f* and β-linked Xyl*p* were between δ 5.1 and 5.4 and between δ 4.4−4.8, respectively.[25−27] By comparison with the results of methylation analysis, the anomeric proton signals at δ 4.79, 4.55, and 4.46 and the anomeric carbon signals at δ 102.50, 101.41, and 100.85 corresponded with H-1 and C-1 of β-1,3,4-linked Xyl*p* (residue E), β-1,2,4-linked Xyl*p* (residue F), and β-1,4-linked Xyl*p* (residue G), respectively. The β-anomeric configuration was in a good agreement with the appearance of an FT-IR band at 899 cm^{-1} (Figure 2). The anomeric proton signals at δ 5.32, 5.18, and 5.16 and the anomeric carbon signals at δ 107.9, 104.75, and 105.87 (Figure 3B) could be attributed to H-1 and C-1 of α-1,3-linked Ara*f* (residue A), α-1,5-linked Ara*f* (residue B), and α-T-linked Ara*f* (residue C). The typical signal at δ 176 was ascribed to C-6 of the α-T-linked GlcA*p* (residue D).[28]

From the H−H−COSY spectrum (Figure 3C), the H-1 signal for α-1,3-linked Ara*f* at δ 5.32 might correlate with H-2 at δ 4.41. Similarly, H-3 (δ 3.99), H-4 (δ 4.46), H-5 (δ 3.83), and H-5′ (δ 3.79) were assigned successively. According to these results and the HSQC spectrum (Figure 3D), C-2, C-3, C-4, and C-5 of α-1,3-linked Ara*f* were assigned to δ 79.41, 83.44, 81.88, and 60.80, respectively. Signals of other residues were assigned by the same procedure. All carbon and proton signals are summarized in Table 2.[29] The signals of some terminal residues such as T-linked Xyl and T-linked Gal were not detected by NMR spectroscopy, possibly due to their low molecular ratio in PLP.

For polysaccharides, the HMBC spectra are considered an important tool to give information about the sequence of glycoside residues.[30] From the HMBC spectrum of PLP (Figure 3E), a cross peak was observed between H-1 (δ 5.32) of residue A and C-3 (δ 72.22) of residue E, which implied residue A was linked to *O*-3 of residue E. The cross peak D/F (H1/C2) was also found, indicating residue D was linked to *O*-2 of residue F. Other cross peaks were assigned by a similar procedure, and they are summarized in Table 3.

Taking all information together, PLP was a highly branched heteroxylan of β-1,4-linked Xyl*p* backbone possibly with three α-GlcA*p*-(1→3)-Ara*f* attached to the *O*-3 position and one α-T-linked-GlcA*p* and one α-Ara*f*-(1→5)-Ara*f* attached to the *O*-2 position every eight monosaccharide residues (Figure 4). Furthermore, the glucuronic acid content was greater in PLP compared to the hot water extractable *P. asiatic* L. polysaccharide.[31] The side chains of PLP were also different from that of water-extractable *P. asiatic* L. polysaccharides.

Antioxidant Activity of PLP in Vitro. The DPPH$^\bullet$-scavenging capacity was a widely accepted assay for evaluating the radical-scavenging capacity of natural compounds based on a single electron transfer (SET) mechanism.[14] PLP exhibited a strong scavenging capacity against DPPH$^\bullet$ with a relative DPPH$^\bullet$-scavenging capacity (RDSC) value of 60.5 μmol TE/g (Figure 5). It was much stronger than that of the tobacco seed flour and wheat grains at 2.65−4.37 μmol TE/g[32] and 0.91−1.53 μmol TE/g,[33] respectively. PLP had ORAC and HOSC values of 32.65 and 21.6 μmol TE/g, respectively. The ORAC value of PLP was comparable to that of the tobacco seed flour (25−53 μmol TE/g)[32] and wheat grains (15.7−35.8 μmol TE/g).[33] The HOSC value of PLP was comparable to that of wheat grains (18.6−24.5 μmol TE/g)[33] but lower than those of tobacco seed flour (44−74 μmol TE/g).[32]

Previous studies[19,34] have shown that polysaccharides possess a radical-scavenging effect due to their specific structure features. Their antioxidant effects are related to the number of available active hydroxyl groups in the polysaccharide structure. The results from this study suggested that PLP could effectively scavenge the three free radicals in vitro by either a hydrogen atom or an electron transfer mechanism. It was possibly dependent on the available active hydroxyl groups in its structure.

Bile Acid-Binding Capacity of PLP. Cholic acid (CA) and chenodeoxycholic acid (CDCA) are two primary bile acids synthesized in the liver from cholesterol. Binding bile acids to polymers may enhance their elimination through the gastrointestinal tract, which may promote the metabolism of cholesterol in liver and consequently lower the total plasma and LDL cholesterol levels.[9] As shown in Figure 6, the CA binding capacity for PLP was 65% of that for cholestyramine resin, whereas its CDCA binding capacity was 60% of that for cholestyramine resin on a per same weight basis. These data suggested the potential of PLP in reducing total plasma and LDL cholesterol levels because cholestyramine resin was a commercially used cholesterol-lowering agent. The mechanism of PLP binding bile acid might be similar to that for other psyllium-related and derived polysaccharides and might be related to its highly branched structure.[5] These results warrant additional research in investigating the cholesterol-lowering capacity of PLP from *P. asiatic* L. for its potential application in cholesterol-lowering functional foods.

■ ASSOCIATED CONTENT

Ⓢ Supporting Information

Additional figures. This material is available free of charge via the Internet at http://pubs.acs.org.

■ AUTHOR INFORMATION

Corresponding Authors

*(Y.N.) Phone: (86)-21-34204538. Fax: (86)-21-34204107. E-mail: yugeniu@sjtu.edu.cn.

*(L.Y.) Phone: (301) 405-0761. Fax: (301) 314-3313. E-mail: lyu5@umd.edu.

Author Contributions

‖L.G. and H.Z. contributed equally to this work.

Funding

This work was partly supported by a grant from the National Natural Science Funds of China (Grant 31401490), grants from the National High Technology Research and Development Program of China (Grants 2013AA102202 and 2013AA102207), a special fund for Agro-scientific Research in the Public Interest (Grant 201203069), and a grant from Wilmar (Shanghai) Biotechnology Research & Development Center Co., Ltd.

Notes

The authors declare no competing financial interest.

■ REFERENCES

(1) Cummings, J. H. The effect of dietary fiber on fecal weight and composition. *CRC Handb. Dietary Fiber Hum. Nutr.* **2001**, 3, 183−252.

(2) Beara, I. N.; Orčić, D. Z.; Lesjak, M. M.; Mimica-Dukić, N. M.; Peković, B. A.; Popović, M. R. Liquid chromatography/tandem mass

DOI: 10.1021/jf505909k
J. Agric. Food Chem. 2015, 63, 569−577

spectrometry study of anti-inflammatory activity of plantain (*Plantago* L.) species. *J. Pharm. Biomed. Anal.* **2010**, *52*, 701−706.
(3) Beara, I. N.; Lesjak, M. M.; Orčić, D. Z.; Simin, N. Đ.; Četojević-Simin, D. D.; Božin, B. N.; Mimica-Dukić, N. M. Comparative analysis of phenolic profile, antioxidant, anti-inflammatory and cytotoxic activity of two closely-related Plantain species: *Plantago altissima* L. and *Plantago lanceolata* L. *LWT−Food Sci. Technol.* **2012**, *47*, 64−70.
(4) Rodríguez-Morán, M.; Guerrero-Romero, F.; Lazcano-Burciaga, G. Lipid- and glucose-lowering efficacy of *Plantago* psyllium in type II diabetes. *J. Diabetes Complications* **1998**, *12*, 273−278.
(5) Zhou, K.; Xia, W.; Zhang, C.; Yu, L. *In vitro* binding of bile acids and triglycerides by selected chitosan preparations and their physico-chemical properties. *LWT−Food Sci. Technol.* **2006**, *39*, 1087−1092.
(6) Hu, J. Q.; Cui, H. B.; Li, Z. Y. Plantaginaceae. In *Flora of China*, 1st ed.; Ed.ial Committee of Flora of China in Chinese Academy of Sciences; Science Press: Beijing, China, 2002; Vol. 70, pp 322−343.
(7) Yin, J. Y.; Nie, S. P.; Zhou, C.; Wan, Y.; Xie, M. Y. Chemical characteristics and antioxidant activities of polysaccharide purified from the seeds of *Plantago asiatica* L. *J. Sci. Food Agric.* **2010**, *90*, 210−217.
(8) Hu, J.; Nie, S.; Min, F.; Xie, M. Polysaccharide from seeds of *Plantago asiatica* L. increases short-chain fatty acid production and fecal moisture along with lowering pH in mouse colon. *J. Agric. Food Chem.* **2012**, *60*, 11525−11532.
(9) Niu, Y.; Xie, Z.; Zhang, H.; Sheng, Y.; Yu, L. Effects of structural modifications on physicochemical and bile acid-binding properties of psyllium. *J. Agric. Food Chem.* **2013**, *61*, 596−601.
(10) Prieto, A.; Bernabé, M.; Leal, J. A. Isolation, purification and chemical characterization of alkali-extractable polysaccharides from the cell walls of *Talaromyces* species. *Mycol. Res.* **1995**, *99*, 69−75.
(11) Kim, G.; Choi, G.; Lee, S.; Park, Y. Acidic polysaccharide isolated from *Phellinus linteus* enhances through the up-regulation of nitric oxide and tumor necrosis factor-α from peritoneal macrophages. *J. Ethnopharmacol.* **2004**, *95*, 69−76.
(12) Staub, A. M. Removal of protein-Sevag method. *Methods Carbohydr. Chem.* **1965**, *5*, 5−6.
(13) Yang, X. B.; Gao, X. D.; Han, F.; Xu, B. S.; Song, Y. C.; Tan, R. X. Purification, characterization and enzymatic degradation of YCP, a polysaccharide from marine filamentous fungus *Phoma herbarum* YS4108. *Biochimie* **2005**, *87*, 747−754.
(14) Niu, Y.; Yan, W.; Lv, J.; Yao, W.; Yu, L. L. Characterization of a novel polysaccharide from tetraploid *Gynostemma pentaphyllum Makino*. *J. Agric. Food Chem.* **2013**, *61*, 4882−4889.
(15) Yan, W.; Niu, Y.; Lv, J.; Xie, Z.; Jin, L.; Yao, W.; Gao, X.; Yu, L. L. Characterization of a heteropolysaccharide isolated from diploid *Gynostemma pentaphyllum* Makino. *Carbohydr. Polym.* **2013**, *92*, 2111−2117.
(16) Needs, P. W.; Selvendran, R. R. Avoiding oxidative degradation during sodium hydroxide/methyl iodide-mediated carbohydrate methylation in dimethyl sulfoxide. *Carbohydr. Res.* **1993**, *245*, 1−10.
(17) Cheng, Z.; Moore, J.; Yu, L. High-throughput relative DPPH radical scavenging capacity assay. *J. Agric. Food Chem.* **2006**, *54*, 7429−7436.
(18) Moore, J.; Yin, J. J.; Yu, L. L. Novel fluorometric assay for hydroxyl radical scavenging capacity (HOSC) estimation. *J. Agric. Food Chem.* **2006**, *54*, 617−626.
(19) Moore, J.; Hao, Z. G.; Zhou, K. Q.; Luther, M.; Costa, J.; Yu, L. L. Carotenoid, tocopherol, phenolic acid, and antioxidant properties of Maryland-grown soft wheat. *J. Agric. Food Chem.* **2005**, *53*, 6649−6657.
(20) Niu, Y.; Xie, Z.; Hao, J.; Yao, W.; Yue, J.; Yu, L. L. Preparation of succinylated derivatives of psyllium and their physicochemical and bile acid-binding properties. *Food Chem.* **2012**, *132*, 1025−1032.
(21) Zheng, R.; Jie, S.; Hanchuan, D.; Moucheng, W. Characterization and immunomodulating activities of polysaccharide from *Lentinus edodes*. *Int. Immunopharmacol.* **2005**, *5*, 811−20.
(22) Na, Y. S.; Kim, W. J.; Kim, S. M.; Park, J. K.; Lee, S. M.; Kim, S. O.; Synytsya, A.; Park, Y. I. Purification, characterization and immunostimulating activity of water-soluble polysaccharide isolated from *Capsosiphon fulvescens*. *Int. Immunopharmacol.* **2010**, *10*, 364−370.
(23) Fischer, M. H.; Yu, N.; Gray, G. R.; Ralph, J.; Anderson, L.; Marlett, J. A. The gel-forming polysaccharide of psyllium husk (*Plantago ovata* Forsk). *Carbohydr. Res.* **2004**, *339*, 2009−2017.
(24) Samuelsen, A. B.; Hanne Cohen, E.; Smestad Paulsen, B.; Brüll, L. P.; Thomas-Oates, J. E. Structural studies of a heteroxylan from *Plantago major* L. seeds by partial hydrolysis, HPAEC-PAD, methylation and GC−MS, ESMS and ESMS/MS. *Carbohydr. Res.* **1999**, *315*, 312−318.
(25) Apirattananusorn, S.; Tongta, S.; Cui, S. W.; Wang, Q. Chemical, molecular, and structural characterization of alkali extractable nonstarch polysaccharides from Job's tears. *J. Agric. Food Chem.* **2008**, *56*, 8549−8557.
(26) Ebringerová, A.; Hromádková, Z.; Berth, G. Structural and molecular properties of a water-soluble arabinoxylan-protein complex isolated from rye bran. *Carbohydr. Res.* **1994**, *264*, 97−109.
(27) Hoffman, R. A.; Kamerling, J. P.; Vliegenthart, J. F. Structural features of a water-soluble arabinoxylan from the endosperm of wheat. *Carbohydr. Res.* **1992**, *226*, 303−311.
(28) Saghir, S.; Iqbal, M. S.; Hussain, M. A.; Koschella, A.; Heinze, T. Structure characterization and carboxymethylation of arabinoxylan isolated from Ispaghula (*Plantago ovata*) seed husk. *Carbohydr. Polym.* **2008**, *74*, 309−317.
(29) Cui, S. W. *Food Carbohydrates: Chemistry, Physical Properties, and Applications*; Taylor & Francis Group, CRC Press: Boca Raton, FL, USA, 2005.
(30) Duus, J. Ø.; Gotfredsen, C. H.; Bock, K. Carbohydrate structural determination by NMR spectroscopy: modern methods and limitations. *Chem. Rev.* **2000**, *100*, 4589−4614.
(31) Yin, J. Y.; Lin, H. X.; Li, J.; Wang, Y. X.; Cui, S. W.; Nie, S. P.; Xie, M. Y. Structural characterization of a highly branched polysaccharide from the seeds of *Plantago asiatica* L. *Carbohydr. Polym.* **2012**, *87*, 2416−2424.
(32) Xie, Z.; Whent, M.; Lutterodt, H.; Niu, Y.; Slavin, M.; Kratochvil, R.; Yu, L. L. Phytochemical, antioxidant, and antiproliferative properties of seed oil and flour extracts of Maryland-grown tobacco cultivars. *J. Agric. Food Chem.* **2011**, *59*, 9877−9884.
(33) Zhou, K.; Hao, J.; Griffey, C.; Chung, H.; O'Keefe, S. F.; Chen, J.; Hogan, S. Antioxidant properties of *Fusarium* head blight-resistant and -susceptible soft red winter wheat grains grown in Virginia. *J. Agric. Food Chem.* **2007**, *55*, 3729−3736.
(34) Guo, Z.; Xing, R.; Liu, S.; Yu, H.; Wang, P.; Li, C.; Li, P. The synthesis and antioxidant activity of the Schiff bases of chitosan and carboxymethyl chitosan. *Bioorg. Med. Chem. Lett.* **2005**, *15*, 4600−46033.

DOI: 10.1021/jf505909k
J. Agric. Food Chem. 2015, 63, 569−577

JOURNAL OF AGRICULTURAL AND FOOD CHEMISTRY

Article

Pubs.Acs.Org/Jafc

In Vitro Bioaccessibility of Carotenoids, Flavonoids, and Vitamin C from Differently Processed Oranges and Orange Juices [*Citrus sinensis* (L.) Osbeck]

Julian K. Aschoff,[†] Sabrina Kaufmann,[†] Onur Kalkan,[†] Sybille Neidhart,[†] Reinhold Carle,[†,‡] and Ralf M. Schweiggert*[,†]

[†]Institute of Food Science and Biotechnology, Chair of Plant Foodstuff Technology and Analysis, Hohenheim University, Garbenstraße 25, 70599 Stuttgart, Germany

[‡]King Abdulaziz University, Faculty of Science, Biological Science Department, P.O. Box 80257, Jeddah 21589, Saudi Arabia

Supporting Information

ABSTRACT: Carotenoid, flavonoid, and vitamin C concentrations were determined in fresh orange segments and a puree-like homogenate derived thereof, as well as freshly squeezed, flash-pasteurized, and pasteurized juices. Lutein and β-cryptoxanthin were slightly degraded during dejuicing, whereas β-carotene levels were retained. Vitamin C levels remained unaffected, whereas flavonoid levels decreased 8-fold upon juice extraction, most likely due to the removal of flavonoid-rich albedo and juice vesicles. Likewise, the presence of such fibrous matrix compounds during in vitro digestion was assumed to significantly lower the total bioaccessibility (BA) of all carotenoids from fresh fruit segments (12%) as compared to juices (29−30%). Mechanical disruption of orange segments prior to digestion did not alter carotenoid BA, whereas pasteurization of the freshly squeezed juice slightly increased BA by 9−11%. In addition to carotenoid BA, the stabilities of hesperidin, narirutin, and vitamin C including dehydroascorbic acid during in vitro digestion were monitored, and applied analytical methods were briefly validated.

KEYWORDS: *fruit matrix, bioavailability, dietary fiber, bioactive compounds, health and nutrition*

INTRODUCTION

Orange juice is the most popular fruit juice in the European Union and the United States.[1] Consumers perceive orange juice as a healthy and natural source of vitamins and other health-promoting nutrients, resulting in an increasing worldwide demand and production.[2] Additionally, the convenient packaging and long shelf life of juices are advantageous compared to fresh fruit. Recent intervention studies demonstrated the health benefits of long-term orange juice consumption, such as an increased total antioxidant status, lower total cholesterol levels, and the prevention of endotoxin increases after meals high in fat and carbohydrate.[3−6] However, greater consumption of orange juice has also been criticized because of its high intrinsic sugar level, being associated with a higher risk of type 2 diabetes and cardiovascular diseases.[7]

Oranges [*C. sinensis* (L.) Osbeck] and products thereof are rich sources of carotenoids, flavonoids, and vitamin C.[8−11] The carotenoid profile of oranges has been reported to be one of the most complex in fruits,[12] making its determination a popular research objective over the past few decades.[9] In addition to the provitamin A carotenoids β-cryptoxanthin, α-carotene, and β-carotene, oranges contain a large diversity of free and esterified xanthophylls, among them lutein and zeaxanthin. The latter compounds are believed to play an important role in preventing age-related macular degeneration and, possibly, cognitive impairment in elderly people.[13] Sufficient bioavailability is a prerequisite for their bioactivity in humans, that is, their liberation from the food matrix, incorporation into mixed micelles, and subsequent absorption by the enterocyte.[14] The term "bioaccessibility" refers to "the fraction of a compound that is released from its matrix in the gastrointestinal tract and thus becomes available for intestinal absorption". Because only micellarized carotenoids are potentially bioavailable, common in vitro digestion assays include analyses of the intestinal micellar fraction.[15] In vitro digestion models measuring the bioaccessibility of micro- and macronutrients in food by mimicking the physiological conditions in the intestinal tract have become a popular low-cost−high-throughput research tool.[15,16] Although presenting major drawbacks compared to in vivo studies, in vitro models allow the fast and inexpensive screening of a larger sample set, serving as a scientific basis for further in vivo studies.

Numerous reports have described the bioavailability and bioaccessibility of carotenoids from different food matrices.[14,17−19] Simultaneous intake of fat[20,21] as well as thermal and mechanical processing[22,23] were shown to favor carotenoid liberation and micellarization from tomatoes, carrots, and spinach, thus resulting in higher carotenoid bioavailability. Although some studies evaluated the effects of different orange juice production on carotenoid bioaccessibility,[24−26] comparative data regarding the bioaccessibility of unprocessed orange fruits and products derived thereof are lacking.

In addition to carotenoids, the flavanone glycosides hesperidin and narirutin represent potentially bioactive phytochemicals in oranges. In numerous epidemiological

Received: November 4, 2014
Revised: December 19, 2014
Accepted: December 23, 2014
Published: December 23, 2014

ACS Publications © 2014 American Chemical Society

DOI: 10.1021/jf505297t
J. Agric. Food Chem. 2015, 63, 578−587

studies, an inverse relationship between dietary flavonoid intake and cardiovascular diseases has been demonstrated, mainly due to the antioxidant properties of the flavanones.[11] Various other health-beneficial mechanisms have been reported, such as anti-inflammatory and chemopreventive activities.[11] The metabolism of hesperidin and narirutin involves the deglycosylation of the rhamnose moiety by the colon microbiota, their absorption by colonocytes, and their subsequent conjugation with hydrophilic compounds such as glucuronic acid.[10] The solubilization of flavonoids during processing and digestion is a key factor in this metabolism, thus strongly affecting their bioavailability.[27] In vitro models commonly used for the evaluation of carotenoid bioaccessibility include ultracentrifugation and microfiltration of the digesta,[18] thus also allowing the measurement of soluble flavonoids in the intestinal fluid.

Orange fruits and products thereof contain high amounts of vitamin C, with concentrations averaging 500 mg/L.[8,28] Although the bioavailability of vitamin C (comprising ascorbic acid and dehydroascorbic acid) ranges between 80% and 100% at doses normally ingested,[8] its oxidation and further degradation during processing, storage, and digestion might limit the nutritional value of a dietary source.

The first aim of this work was to evaluate the impacts of different steps of orange fruit processing on levels of carotenoids, flavonoids, and vitamin C. All test foods were produced from the same batch of navel oranges to ensure uniformity of analyte levels. The main objective was then to evaluate the in vitro bioaccessibility of nutritionally relevant carotenoids and flavonoids in these test foods. In addition, levels of vitamin C were monitored before and after in vitro digestion.

MATERIALS AND METHODS

Materials and Reagents. Fresh, untreated oranges [*Citrus sinensis* (L.) Osbeck cv. "Navel Lane Late"] were obtained from a wholesale market (Stuttgart, Germany). Ammonium oxalate (≥99.5%), calcium carbonate (98.5−100.5%), calcium chloride dihydrate (p.a.), dipotassium hydrogen phosphate (≥99%), ethanol (≥99.9%), aqueous hydrochloric acid (37%), potassium dihydrogen phosphate (p.a.), potassium chloride (p.a.), *N*,*N*-dimethylformamide (DMFA, ≥99.8%), sodium hydrogen carbonate (p.a.), sodium hydroxide (1 mol/L, Titrisol), 2-propanol (≥99.8%), methyl *tert*-butyl ether [MTBE, high-performance liquid chromatography (HPLC) gradient grade], and BIOQUANT total dietary fiber kits (1.12979.0001) were purchased from Merck (Darmstadt, Germany). Butylated hydroxytoluene (BHT) was from Merck Schuchhardt (Hohenbrunn, Germany). Ascorbic acid (Ph. Eur.), acetic acid (100%), sodium chloride (100%), potassium hydroxide (85.9%), magnesium chloride hexahydrate (Ph. Eur.), methanol (HPLC grade), metaphosphoric acid (GPR), and petroleum benzine (bp 40−60 °C, GPR rectapur) were purchased from VWR International (Leuven, Belgium). Porcine pancreatic α-amylase (46.4 U/mg), porcine bile extract, cholesterol esterase from porcine pancreas (42.9 U/mg), dehydroascorbic acid, disodium hydrogen phosphate, pancreatin from porcine pancreas, and pepsin from porcine gastric mucosa were obtained from Sigma-Aldrich Chemie (Steinheim, Germany). β-Carotene (≥97%), β-cryptoxanthin (≥97%), 3-*tert*-butylhydroxyanisol (BHA), and hesperidin (~90%) were from Fluka Chemie (Buchs, Switzerland), whereas antheraxanthin (95.0%), zeinoxanthin (97.7%), α-carotene (98.9%), lutein (99.9%), mutatoxanthin (95.5%), violaxanthin (99.3%), and zeaxanthin (99.8%) were purchased from CaroteNature (Ostermundingen, Switzerland). Narirutin (96%) was obtained from ChromaDex (Irvine, CA), and tris(2-carboxyethyl)phosphine hydrochloride (TCEP) was from Alfa Aesat (Karlsruhe, Germany). Ultrapure water (Milli-Q system, Millipore, Bedford, MA) was used for all analyses.

Production of Orange Test Foods. Figure 1 illustrates the processing steps used to obtain five different test products (fresh unprocessed orange segments, homogenized segments, freshly squeezed juice, pasteurized juice, flash-pasteurized juice). A minimum of 8 kg of oranges was used for the production of each test food to minimize the influence of raw-material heterogeneity. Unprocessed orange segments were manually peeled, and the adhering albedo and the columella were almost completely removed. A portion of the obtained segments was immediately frozen in liquid nitrogen, vacuum-sealed in plastic bags, and stored at −80 °C until further analyses. Residual segments were homogenized with a PUC colloid mill (Probst and Class, Rastatt, Germany) at 5050 rpm and a gap width of 1 mm. Subsequently, homogenization was repeated thrice with decreasing gap widths (350, 50, and 50 μm, respectively). The homogenized segments were filled into 20 mL plastic flasks, and the headspace was flushed with nitrogen prior to sealing. The plastic flasks were then immediately frozen in liquid nitrogen and stored at −80 °C until further analyses.

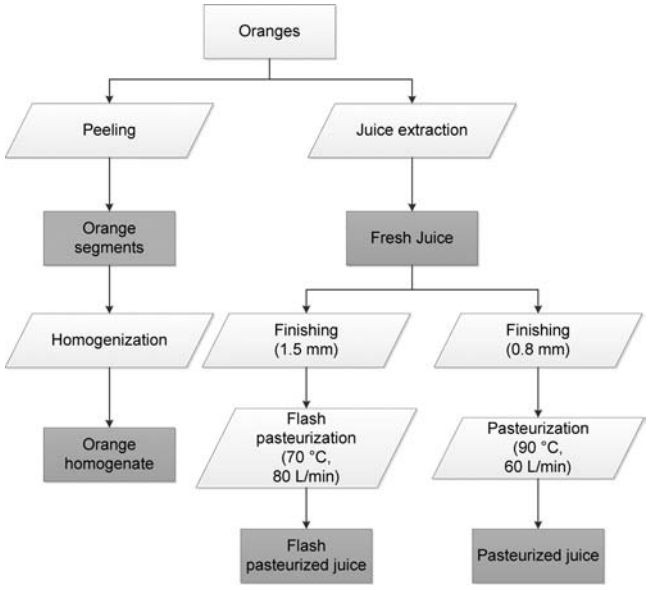

Figure 1. Production of the test foods (gray boxes) for in vitro digestion from the same batch of fresh "Navel Lane Late" orange fruits.

For orange juice production, oranges were washed with cold water and dejuiced using a semiautomatic Orange X-Press extractor (Brimato, Hilter, Germany). An aliquot of the freshly squeezed juice was filled into plastic flasks, frozen with liquid nitrogen, and stored at −80 °C until further use. The remaining freshly squeezed juice was finished using a commercial paddle pulper (PAP 0533, Bertuzzi, Brugherio, Italy) with mesh sizes of 1.5 and 0.8 mm for the production of the flash-pasteurized and pasteurized orange juice, respectively. As shown in Figure 1, the flash-pasteurized juice was continuously heated to 70 °C at a flow rate of 80 L/h using a tubular heater (Ruland Engineering & Consulting, Neustadt/Weinstraße, Germany), whereas the pasteurized juice was heated to 90 °C at 60 L/h. Subsequently, the juices were hot-filled into 500 mL glass bottles and cooled to room temperature in a water bath. The juices were filled into plastic flasks, and the headspace was flushed with nitrogen before sealing and freezing with liquid nitrogen. All samples were stored at −80 °C until further analyses. Product temperature was recorded throughout the process, and pasteurization values were calculated using *Bacillus coagulans* as the reference germ (T_{ref} = 93.3 °C, z = 8.9 K) according to the method of Hirsch et al.[29] Pasteurization values were 0.002 and 0.504 min for the flash- and conventionally pasteurized juices, respectively.

In Vitro Digestion Model. After being thawed at ambient temperature for less than 1 h, unprocessed orange segments were cut into cubic pieces of 5-mm length to mimic coarse comminution obtained by chewing. All other test foods were thawed and subjected

DOI: 10.1021/jf505297t
J. Agric. Food Chem. 2015, 63, 578−587

to the digestion model without further pretreatment. The in vitro digestion protocol was based on the method reported by Schweiggert et al.,[18] with the following modifications. During the oral phase, 10 mL (instead of 5 mL) of artificial saliva solution was used, and 7 mL (instead of 9 mL) of porcine bile extract/pancreatin solution was added at the beginning of the intestinal phase. After completion of the intestinal phase, 35 mL of the artificial intestinal fluid was centrifuged at 75000*g* for 60 min at 10 °C in a JA-25.50 rotor (Avanti J-26 XP/XPI, Beckman Coulter, Krefeld, Germany) to separate solids from the aqueous phase. The thus-obtained supernatant (~35 mL) was considered to contain the nutrients *liberated* from the solid food matrix. A volume of 5 mL of the supernatant was then filtered through a cellulose acetate-based 0.2-μm syringe filter (Klaus Ziemer, Mannheim, Germany) to yield the micellar fraction. Only micellarized lipophilic nutrients such as carotenoids are considered to be potentially available for absorption, thus representing the *bioaccessible* fraction. In vitro liberation and bioaccessibility were calculated as the percentages of the respective nutrient transferred from the test food to the supernatant obtained after centrifugation and to the micellar phase obtained by microfiltration of the supernatant, respectively, as described by Schweiggert et al.[18] The in vitro digestion was performed in triplicate.

Carotenoid, Flavonoid, and Vitamin C Analyses. *Sample Preparation.* Frozen orange segments and homogenized segments were milled under liquid nitrogen using a model 38BL41 blender (Waring, Torrington, CT) prior to analyses, whereas juices and digesta were analyzed without further pretreatment.

Carotenoids. An aliquot of 2.0 ± 0.1 g and 2.0 mL of test food and digesta, respectively, were combined with 50 mg of $CaCO_3$ and 3 mL of petroleum benzine/2-propanol (1:1, v/v), containing 50 mg of BHA and 50 mg of BHT/100 mL solvent mixture. Extraction was supported by a probe sonicator (Sonoplus HD 3080 with MS 72 sonotrode, Bandelin, Berlin, Germany) at 70% amplitude for 30 s. After centrifugation (3000 rpm, 3 min, Labofuge 200, Heraeus, Hanau, Germany), the upper organic layer was collected, and the sample was re-extracted twice with 2 mL of the above-mentioned extraction solvent. The combined organic phases were washed with 2 mL of aqueous NaCl (0.1 M) and dried under a stream of nitrogen at ≤25 °C. Subsequently, the dried extracts were redissolved in 3 mL of petroleum benzine, and saponification was started by adding 3 mL of ethanolic KOH (10%, w/v). After incubation for 3 h under continuous shaking using an orbital shaker at 130 rpm (Type A2, Edmund Bühler, Tübingen, Germany), the samples were washed with 2 mL of aqueous NaCl (0.1 M), centrifuged, and the upper organic layer was separated. The lower ethanolic phase was re-extracted with 1 mL of MTBE, and the combined organic phases were evaporated to dryness under a stream of nitrogen at ≤25 °C. Samples were redissolved in 400 μL of 2-propanol and filtered (0.45 μm) into amber vials prior to HPLC analysis. The extraction procedure was conducted in duplicate under subdued light.

Carotenoid identification and quantification were performed on a series 1100 HPLC instrument (Agilent, Waldbronn, Germany) equipped with a G1379A degasser, a G1312A binary gradient pump, a G1313A autosampler, a G1316A column oven, and a G1315B diode array detector (DAD) coupled to a Bruker 3000+ ion-trap mass spectrometer (Bruker Daltonics, Bremen, Germany). Carotenoids were separated on a YMC C30 reverse-phase column (150 × 3.0 mm i.d., 3-μm particle size, YMC Europe GmbH, Dinslaken, Germany) protected by a YMC C30 guard column (10 × 3.0 mm i.d., 3-μm particle size) and operated at 40 °C. The mobile phase consisted of methanol/water (90:10 v/v, eluent A) and MTBE/methanol/water (78:20:2 v/v/v, eluent B), both containing 1.5 g/L ammonium acetate. The following gradient was used (min/percentage of A): 0/98, 24/83, 28/54, 35/22.5, 35.1/0, 38/0, 41/98, 43/98. The total run time was 43 min at a flow rate of 1 mL/min. The injection volume was 20 and 80 μL for the analyses of test foods and digested samples, respectively. Carotenoids were monitored at 450 nm, and additional UV−vis spectra were recorded between 200 and 700 nm. Carotenoid identification was carried out by comparing the retention times, UV−vis spectra, and mass spectra of detected compounds with those of external standards and literature references.[30] To support the identification of carotenoid (*Z*) isomers, D_B/D_{II} ratios were determined according to the method of Britton.[30] Carotenoids were quantified by HPLC-DAD using linear calibration curves of external standards.

Vitamin C Analyses. Vitamin C analyses were conducted by HPLC-DAD based on the findings of Wechtersbach and Cigić.[31] A sample aliquot of 2.0 ± 0.1 g was transferred to a 20 mL volumetric flask containing 15 mL of metaphosphoric acid (1% w/v) adjusted to pH 3.8 with dipotassium hydrogen phosphate. A second aliquot of 2.0 ± 0.1 g was transferred to an identical buffer additionally containing 10 mM TCEP. The samples were made up to 20 mL with the respective buffer, vortexed, and allowed to stand for 30 min for the reduction of dehydroascorbic acid (DHAA) to ascorbic acid (AA) in the TCEP experiment. Subsequently, samples were membrane-filtered (0.45 μm) and analyzed by HPLC. For quantification of ascorbic acid by HPLC-DAD, the above-described HPLC system (series 1100 HPLC) was equipped with a reverse-phase C18 Sunfire column (250 mm × 4.6 mm i.d., 5-μm particle size, Waters, Eschborn, Germany) operated at 25 °C. The mobile phase consisted of aqueous metaphosphoric acid (1% w/v) adjusted to pH 2.6 with dipotassium hydrogen phosphate (eluent A) and methanol (eluent B). The following gradient was used (min/percentage of A): 0/100, 17/100, 20/0, 30/0, 33/100, 43/100. The total run time was 43 min at a flow rate of 0.8 mL/min. The injection volume was 20 μL. AA was monitored at 254 nm and quantitated by external linear calibration. DHAA concentrations were determined by subtracting the initial AA concentration from that obtained by the above-described TCEP experiment. The reported vitamin C levels represent the sum of AA and DHAA.

Flavonoids. Flavonoid extraction was performed according to method no. 58 of the International Federation of Fruit Juice Producers[32] with some modifications. Exactly weighed samples (2.0 ± 0.1 g of test foods and supernatant, 1.0 ± 0.1 g of micellar phase) were transferred into 50, 10, and 5 mL volumetric flasks for test foods, supernatant, and micellar phase, respectively. The following description refers to the experiment using the 50 mL volumetric flask. Experiments using 10 and 5 mL flasks were carried out identically using proportional amounts of reagents. After addition of 10 mL of ammonium oxalate solution (0.025 M) and 10 mL of DMFA, the samples were made up to 50 mL with deionized water and incubated in a type 461 water bath (Büchi Labortechnik, Flawil, Switzerland) at 90 °C for 10 min. Subsequently, samples were membrane-filtered (0.45 μm, Chromafil RC-45/15MS, Macherey-Nagel, Düren, Germany) into amber HPLC vials. Flavonoid separation was performed on the above-described series 1100 HPLC system, using a reverse-phase C18 Sunfire column (250 × 4.6 mm i.d., 5-μm particle size, Waters, Eschborn, Germany) at 25 °C. The mobile phase consisted of acetic acid (2%, eluent A) and methanol (eluent B) using the following gradient (min/percentage of A): 0/100, 10/100, 20/55, 30/55, 33/0, 40/0, 43/100, 50/100. The total run time was 50 min at a flow rate of 0.8 mL/min. The injection volume was 10 μL, except for supernatant and micellar phases of all juices (20 μL). Flavonoids were monitored at 287 nm and quantitated by external linear calibration curves.

Method Validation of Carotenoid, Flavonoid, and Vitamin C Determinations. *Repeatability.* The intra-assay precision and the time-dependent intermediate precision[33] of the methods described for analysis of the bioactive compounds were determined by analyzing a commercial orange juice in quadruplicate by the same person and with the same equipment on three different days within 1 month.[34] The orange juice was aliquoted and stored at −20 °C prior to the performance of the above-described determinations. Relative standard deviations (RSDs) for quantification of flavonoids and vitamin C were <0.7%. RSDs for quantification of carotenoids were <4.4%, except for the interday RSD of lutein (6.1%). The results illustrate the high precision of the methods applied. Further details are provided in Table S1 (Supporting Information).

Recovery. The accuracy of the methods described for analysis of bioactive compounds was determined by spiking different levels of the

DOI: 10.1021/jf505297t
J. Agric. Food Chem. 2015, 63, 578−587

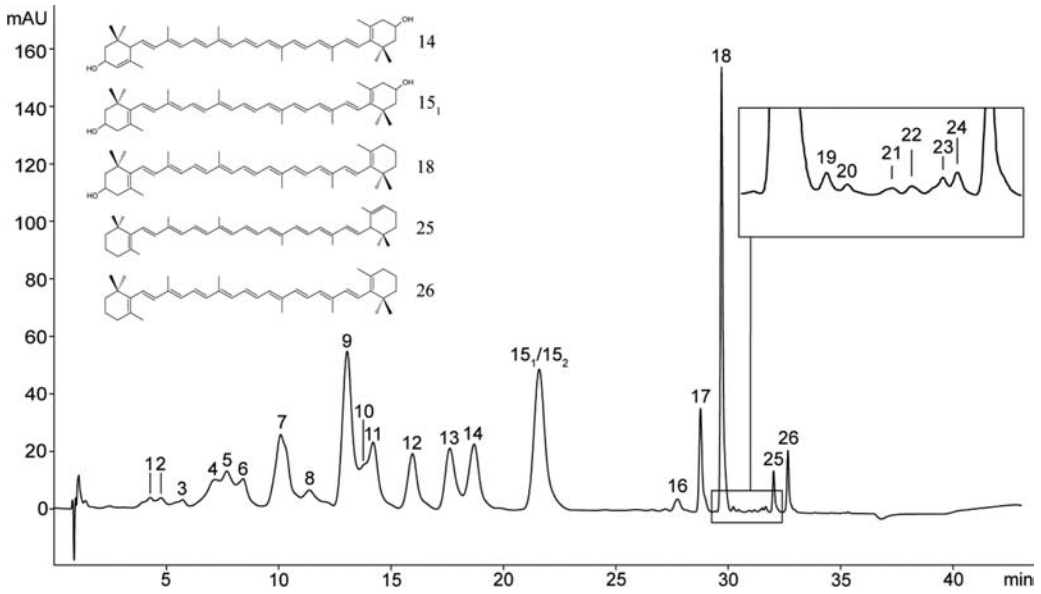

Figure 2. Chromatogram at 450 nm showing carotenoids in the pasteurized orange juice sample. Peak assignments in Table 1.

Table 1. Identification of Carotenoids Found in Orange Fruit and Derived Products

compound no.	retention time (min)	identity	UV−vis absorption maxima (nm)	$[M + H]^+$ m/z
1	4.2	NI[a]	416/440/468	583
2	4.7	NI	418/442/468	601
3	5.7	NI	400/422/448	601
4	7.1	NI	408/432/458	601
5	7.6	NI	418/442/468	601
6	8.3	violaxanthin[b]	418/440/468	601
7	10.0	NI	400/422/448	601
8	11.3	NI	404/426/446	601
9	13.0	(9*Z*)-violaxanthin[c]	328/416/438/464	601
10	13.7	NI	420/444/470	601
11	14.1	NI	396/418/444	601
12	15.9	mutatoxanthin (8*R*/8*S*)[b]	406/428/452	585
13	17.5	mutatoxanthin (8*R*/8*S*)[b]	406/428/452	585
14	18.6	lutein[b]	422/446/472	551[d]
15_1	21.5	zeaxanthin[b]	428/450/476	551[d]
15_2	21.5	(9*Z*)-antheraxanthin[c]	332/420/442/468	585
16	27.7	(13*Z*)-*β*-cryptoxanthin[c]	340/420/444/468	553
17	28.7	zeinoxanthin[b]	422/446/474	553
18	29.6	*β*-cryptoxanthin[b]	430/452/478	553
19	30.2	NI	ND[e]	ND
20	30.4	NI	332/348/368	ND
21	30.9	NI	ND	ND
22	31.1	NI	334/348/368	ND
23	31.4	NI	378/400/424	ND
24	31.6	NI	378/398/422	ND
25	31.9	*α*-carotene[b]	422/446/474	537
26	32.6	*β*-carotene[b]	428/452/478	537

[a]NI = not identified [b]Identified using authentic standards. [c]Tentative identification by UV−vis absorption spectrum and $[M + H]^+$. D_B/D_{II} (compound): 0.078 (9), 0.075 (15_2), 0.459 (16). [d]$[M + H - H_2O]^+$. [e]ND = not detectable (trace amounts).

analytes into orange juice.[33] Relative recovery was calculated based on the predicted and measured concentrations. Recovery rates were generally 98−100%, except for the addition of intermediate levels of *β*-carotene (95.3%) and high levels of *β*-cryptoxanthin (94.8%). Further details are provided in Table S2 (Supporting Information).

Limit of Detection (LOD) and Limit of Quantification (LOQ). LOD and LOQ were determined according to DIN 32645 from the respective calibration curves.[35] All measured concentrations of secondary plant metabolites were above the LOQ. Detailed information can be found in the Supporting Information (Table S2).

Quantitation of Pectin and Total Dietary Fiber. Pectin levels were quantitated spectrophotometrically according to IFU methods.[36] Pectin levels are expressed as milligrams of galacturonic acid (GA) per 100 g of test product. Dietary fiber levels were determined gravimetrically using a BIOQUANT total dietary fiber kit according to the supplier's instructions. Samples were analyzed in quadruplicate.

DOI: 10.1021/jf505297t
J. Agric. Food Chem. 2015, 63, 578−587

Table 2. Carotenoid Levels[a] in Test Foods, Supernatants, and Micelles (Based on Fresh Weight of Test Foods)

	orange segments	orange homogenate	$juice_{fresh}$	$juice_{flash\text{-}pasteurized}$	$juice_{pasteurized}$
			In Test Foods		
sum (C_P)[b]	224.3 ± 5.0 b	271.5 ± 9.5 a	204.5 ± 8.5 bc	178.3 ± 3.5 c	183.5 ± 9.5 c
lutein	96.2 ± 3.7 a	89.2 ± 6.6 a	82.3 ± 0.3 ab	66.3 ± 2.0 c	68.3 ± 3.0 bc
β-cryptoxanthin	104.9 ± 0.9 b	151.4 ± 2.7 a	101.5 ± 6.9 b	91.8 ± 1.3 b	94.8 ± 5.5 b
α-carotene	10.0 ± 0.1 a	9.0 ± 0.2 a	7.8 ± 0.3 b	7.1 ± 0.2 b	7.7 ± 0.4 b
β-carotene	13.2 ± 0.3 b	21.9 ± 0.0 a	12.9 ± 1.0 b	13.1 ± 0.1 b	12.8 ± 0.6 b
ZEA + (9Z)-ANT[c]	61.7 ± 1.6 bc	82.0 ± 2.1 b	51.1 ± 1.5 c	115.1 ± 12.2 a	116.7 ± 4.4 a
			In Supernatant[d]		
sum (C_L)	51.8 ± 2.8 b	61.2 ± 5.5 b	91.9 ± 9.9 a	90.1 ± 3.5 a	99.0 ± 3.7 a
lutein	12.1 ± 0.3 c	14.5 ± 0.9 c	23.9 ± 2.7 b	23.9 ± 1.6 ab	27.3 ± 1.4 a
β-cryptoxanthin	34.5 ± 2.8 b	37.3 ± 3.8 b	55.9 ± 6.0 a	54.2 ± 2.2 a	58.9 ± 2.4 a
α-carotene	1.5 ± 0.1 c	2.9 ± 0.3 b	4.4 ± 0.5 a	4.3 ± 0.1 a	4.9 ± 0.2 a
β-carotene	3.6 ± 0.4 c	6.6 ± 0.6 b	7.7 ± 0.7 a	7.6 ± 0.2 a	7.9 ± 0.2 a
ZEA + (9Z)-ANT[c]	22.7 ± 1.1 c	25.0 ± 1.8 cb	30.0 ± 4.2 a	30.5 ± 2.1 a	27.6 ± 0.6 ab
			In Micelles[e]		
sum (C_M)	24.2 ± 0.4 d	32.4 ± 1.1 c	57.9 ± 5.1 b	67.1 ± 1.1 a	72.7 ± 2.4 a
lutein	6.4 ± 0.3 c	8.2 ± 0.6 c	15.8 ± 0.9 b	17.2 ± 0.3 b	19.4 ± 1.1 a
β-cryptoxanthin	15.2 ± 0.5 c	19.0 ± 0.5 c	34.2 ± 4.1 b	40.6 ± 1.0 a	43.4 ± 1.3 a
α-carotene	0.8 ± 0.1 d	1.4 ± 0.1 c	2.8 ± 0.3 b	3.4 ± 0.2 a	3.7 ± 0.1 a
β-carotene	1.9 ± 0.1 d	3.7 ± 0.2 c	5.0 ± 0.6 b	5.9 ± 0.2 a	6.1 ± 0.1 a
ZEA + (9Z)-ANT[c]	9.7 ± 0.6 b	10.6 ± 0.4 b	17.7 ± 2.5 a	19.0 ± 0.5 a	18.4 ± 1.4 a

[a]Mean ± standard deviation, $n = 2$ for quantification of carotenoids in the test foods, $n = 3$ for in vitro digestion. Units of μg/100 g of FW. Different letters within rows indicate significant differences ($P \leq 0.05$). [b]Sum (C_P) = sum of lutein, β-cryptoxanthin, α- and β-carotene levels. [c]ZEA, zeaxanthin; (9Z)-ANT, (9Z)-antheraxanthin. [d]Obtained after centrifugation of the digesta. [e]Obtained after centrifugation and microfiltration (0.2 μm).

Statistics. Statistically significant differences of means were identified by Tukey's and Duncan's test, using SAS 9.1.3 (SAS Institute, Cary, NC). Differences were considered significant at $p < 0.05$. Normal distribution of the results was verified by the Shapiro–Wilk test. All reported data represent mean ± standard deviation. The standard deviation of the bioaccessibility was calculated by the Gaussian law of error propagation from the standard deviations of the levels in the test foods and of the total bioaccessible amounts of the respective analyte.

RESULTS AND DISCUSSION

Carotenoid Identification in the Test Foods. Figure 2 presents a chromatogram of a carotenoid extract from pasteurized orange juice, showing 26 detected carotenoids. Unambiguous identification of 9 carotenoids (peaks 6, 12–15_1, 17, 18, 25, 26) was achieved by comparing their retention times, UV–vis spectra, and molecular masses with those of authentic standards. Among them, lutein (14), zeaxanthin (15_1), zeinoxanthin (17), and β-cryptoxanthin (18) were the major ones, in accordance with previous studies.[9,28,37−39] The two enantiomeric forms (8*R*)- and (8*S*)-mutatoxanthin were also identified using authentic standards, although the assignment of the enantiomers to the respective peaks (12 and 13) was impossible. Using authentic standards (compounds 6, 25, and 26, respectively), violaxanthin and α- and β-carotene were unambiguously assigned.

Compound 9 was tentatively identified as (9Z)-violaxanthin. Its UV–vis spectrum was highly similar to that of all-*E*-violaxanthin (6), except for a characteristic hypsochromic shift of 2–4 nm (Table 1). In addition, the UV spectrum exhibited a cis peak at 328 nm with a D_B/D_{II} ratio of 0.078, and the compound eluted after its all-trans isomer, both being typical of (9Z)-carotenoid isomers. In agreement with the previous report of Dugo et al.,[40] a predominant quasimolecular ion was detected at m/z 601, thus supporting the identity of compound 9 as (9Z)-violaxanthin.

By analogy, compound 15_2 was tentatively assigned to (9Z)-antheraxanthin. It is noteworthy that this compound coeluted with zeaxanthin (15_1) and was detectable only in the flash-pasteurized and pasteurized orange juices, thus indicating its thermally induced formation. Meléndez-Martínez et al.[41] reported the presence of high amounts of *cis*-antheraxanthin in orange juice. Therefore, the zeaxanthin contents determined for pasteurized juices can be partly attributed to (9Z)- or (9′Z)-antheraxanthin. Because of the observed coelution, the fate of zeaxanthin during processing and digestion remains unclear.

Compound 16 revealed a slightly hypsochromic shift of the UV–vis spectrum similar to β-cryptoxanthin. In contrast to compounds 9 and 15_2, compound 16 eluted before its all-*E* isomer and had a D_B/D_{II} ratio of 0.459, which is characteristic of (13Z) isomers.[39] Therefore, compound 16 was tentatively assigned to (13Z)-β-cryptoxanthin.

Absolute Carotenoid Levels in Test Foods. Table 2 summarizes the carotenoid levels in the test foods, as well as the liberated and micellarized carotenoid fractions after in vitro digestion. Carotenoid epoxides such as violaxanthin and mutatoxanthin are not found in human plasma and thus are considered not to be bioavailable in humans.[42] Accordingly, we limited our bioaccessibility study to bioavailable carotenoids, because only such carotenoids would be relevant for the evaluation of assumed health-beneficial effects. Because of the coelution of the tentative (9Z)-antheraxanthin and zeaxanthin in both flash- and conventionally pasteurized juices, their carotenoid concentrations were apparently higher than those in the freshly squeezed juice. We therefore did not include these carotenoids in the sum of total (bioaccessible) carotenoids reported in Table 2 and Figure 3.

DOI: 10.1021/jf505297t
J. Agric. Food Chem. 2015, 63, 578–587

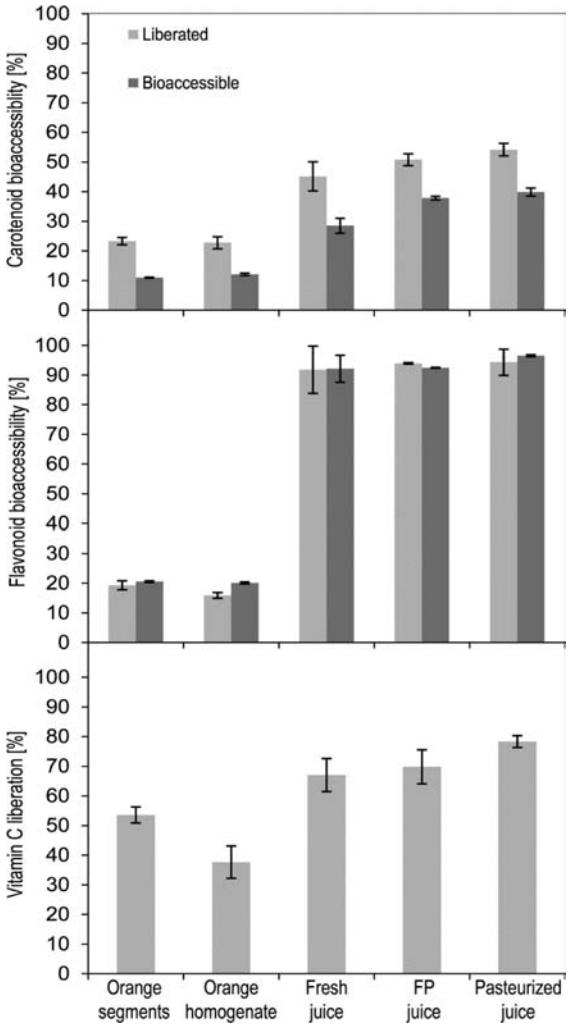

Figure 3. Bioaccessibility of potentially bioavailable carotenoids (lutein, β-cryptoxanthin, α- and β-carotene), flavonoids, and vitamin C from differently processed oranges (FP = flash-pasteurized). Liberated and bioaccessible fractions were calculated as the percentages of the respective nutrients transferred from the test food to the supernatant obtained after centrifugation and to the micellar phase obtained by microfiltration of the supernatant, respectively.

A decrease in total carotenoid levels (C_p) was noted during the processing of fresh oranges (224 μg/100 g of FW) into pasteurized orange juices (178−184 μg/100 g of FW, Table 2). However, the homogenized orange segments showed higher carotenoid levels (272 μg/100 g of FW), possibly due to the inevitable heterogeneity of the fruit or a slightly better carotenoid extractability during analyses. Among the nutritionally relevant carotenoids (Table 2), β-cryptoxanthin was predominant in fresh orange segments, homogenate, and freshly squeezed juice (102−151 μg/100 g of FW), being slightly lowered by 7−10% after pasteurization (92−95 μg/100 g of FW). According to the classification of Britton and Khachik,[43] β-cryptoxanthin levels of orange can be considered as being low (<100 μg/100 g of FW) to moderate (100−500 μg/100 g of FW), whereas papaya fruits (up to ca. 2500 μg/100 g of FW[44]) and red chili peppers (1834 μg/100 g of FW[45]) are among fruits and vegetables rich in β-cryptoxanthin. Lutein had the second highest concentrations in segments, homogenate, and freshly squeezed juice, reaching 82−96 μg/100 g of FW. Its contents were reduced by 17−19% after pasteurization (66−68 μg/100 g of FW, Table 2). Regarding the above-mentioned classification, lutein levels were considered as being low, particularly when compared to those of green leafy vegetables (>2000 mg/100 g of FW[43]). As mentioned above, the exact quantitation of zeaxanthin was hampered by the presence of (9*Z*)-antheraxanthin. Nevertheless, the sum of the aforementioned carotenoids more than doubled after processing of the freshly squeezed juice (51 μg/100 g of FW) to the pasteurized juices (115−117 μg/100 g of FW). This increase was ascribed to the heat-induced formation of the tentative (9*Z*)-antheraxanthin from yet-unknown precursors, because the practical absence of all-*E*-antheraxanthin in the fresh juice was verified using an authentic standard. For α- and β-carotene, degradation and isomerization were insignificant (Table 2), confirming their high stability at temperatures below 120 °C.[46]

Absolute Carotenoid Levels in Micellar Fractions and Bioaccessibility. After in vitro digestion, the so-called bioaccessible carotenoids are contained in the micellarized fraction resulting from microfiltration of the supernatant.[47] The lowest levels of bioaccessible carotenoids were found for orange segments (24.2 ± 0.4 μg of micellarized total carotenoids/100 g of test food). Hence, only 10.8% of the carotenoids contained in fresh orange segments was micellarized and thus bioaccessible (Figure 3). Although the micellarized carotenoid concentration after digestion of homogenized segments was higher (32.4 ± 1.1 μg/100 g), the bioaccessibility was similar (11.9%) to that of intact segments (Figure 3), thus indicating only a minor contribution of mechanical cell disruption to carotenoid BA in oranges. The previously reported supportive effect of comminution on carotenoid bioavailability from tomatoes by disrupting the cell matrix[22] might be less decisive for oranges, because of either the absence of large carotenoid crystals as reported for tomatoes[18] or the high intrinsic fiber levels of oranges (13.9 g/100 g, Table 3) as compared to tomatoes (1.2 g/100 g[48]). The amount of soluble fiber such as pectin can strongly affect micellarization of carotenoids in the duodenum, because previous studies demonstrated hindering of

Table 3. Pectin and Dietary Fiber Contents in the Test Foods

	orange segments	orange homogenate	$juice_{fresh}$	$juice_{flash\text{-}pasteurized}$	$juice_{pasteurized}$
pectin[a]	287.8 ± 7.2 b	425.5 ± 1.9 a	44.2 ± 1.2 c	30.8 ± 0.7 c	27.5 ± 0.4 c
dietary fiber[c]					
soluble	5.7 ± 0.2 a	5.4 ± 0.4 a	0.7 ± 0.0 b	0.6 ± 0.1 b	0.5 ± 0.0 b
insoluble	8.2 ± 0.3 a	8.2 ± 0.3 a	0.7 ± 0.0 b	0.6 ± 0.1 b	0.2 ± 0.0 b
total	13.9 ± 0.5 a	13.6 ± 0.7 a	1.4 ± 0.0 b	1.2 ± 0.1 b	0.7 ± 0.0 b

[a]Mean ± standard deviation, n = 2. Units of mg of GA/100 g of FW, where GA = galacturonic acid. Different letters within rows indicate significant difference ($P \leq 0.05$). [c]Mean ± standard deviation, n = 4. Units of g/100 g of FW. Different letters within rows indicate significant difference ($P \leq 0.05$).

DOI: 10.1021/jf505297t
J. Agric. Food Chem. 2015, 63, 578−587

Table 4. Flavonoid, Ascorbic Acid (AA), and Vitamin C[a] Levels in Test Foods, Supernatants, and Micelles (Based on Fresh Weight of Test Product)

	orange segments	orange homogenate	$juice_{fresh}$	$juice_{flash\text{-}pasteurized}$	$juice_{pasteurized}$
			Flavonoid Levels[a] (mg/100 g of FW)		
			In Test Foods		
hesperidin	241.7 ± 7.9 a	238.8 ± 3.3 a	29.3 ± 0.5 b	28.9 ± 0.0 b	29.7 ± 0.0 b
narirutin	46.6 ± 0.4 a	46.1 ± 1.0 a	5.3 ± 0.0 b	5.5 ± 0.0 b	5.1 ± 0.0 b
			In the Supernatant		
hesperidin	32.1 ± 3.9 a	25.6 ± 1.6 a	26.8 ± 2.3 a	27.3 ± 0.0 a	28.2 ± 1.4 a
narirutin	23.6 ± 0.8 a	19.7 ± 1.1 b	5.0 ± 0.5 c	5.1 ± 0.0 c	4.7 ± 0.2 c
			In Micelles		
hesperidin	33.9 ± 1.4 a	32.3 ± 0.1 a	26.7 ± 1.3 b	26.8 ± 0.0 b	28.8 ± 0.0 b
narirutin	25.4 ± 1.9 a	24.9 ± 0.1 a	5.1 ± 0.2 b	5.0 ± 0.0 b	4.7 ± 0.0 b
			Levels of Ascorbic Acid (AA) and Vitamin C[b] (mg/100 g of FW)		
			In Test Foods		
AA	43.1 ± 0.6 c	32.6 ± 0.2 d	48.6 ± 0.5 a	45.5 ± 0.0 b	44.6 ± 0.1 bc
vitamin C	51.1 ± 0.6 a	47.9 ± 0.2 c	49.4 ± 0.1 b	47.1 ± 0.1 d	46.5 ± 0.1 d
			In the Supernatant		
AA	22.9 ± 0.4 b	12.4 ± 2.5 c	26.1 ± 2.0 b	26.1 ± 2.0 b	33.6 ± 1.1 a
vitamin C	27.4 ± 1.4 b	18.0 ± 2.6 c	33.1 ± 2.8 ab	32.9 ± 2.7 ab	36.5 ± 0.9 a

[a]Calculated as the sum of ascorbic acid and dehydroascorbic acid. [a]Mean ± standard deviation, $n = 3$. Different letters within rows indicate significant differences ($P \leq 0.05$). [b]Mean ± standard deviation, $n = 2$ for quantification of AA and vitamin C in the test foods, $n = 3$ for quantification of AA and vitamin C in the supernatant. Different letters within rows indicate significant differences ($P \leq 0.05$).

β-carotene bioavailability in humans by dietary fibers and, particularly, citrus pectin.[49] In our study, pectin and soluble-fiber levels confirmed their inverse correlation with carotenoid BA. Whereas dietary fiber and bioaccessibility in fresh and homogenated oranges were 13.6−13.9 g/100 g and 10.8−11.9%, respectively, juices containing only 0.7−1.4 g of dietary fiber/100 g had a far higher BA of 28.3−39.5% (Tables 2 and 3).

Because of the diminished content of dietary fiber, micellar carotenoid levels increased to 57.9 ± 5.1 μg/100 g after the digestion of freshly squeezed orange juice, resulting in a 2.6-fold higher bioaccessibility (28.3%) when compared to carotenoids from orange segments. Highest concentrations of bioaccessible carotenoids were observed in the flash-pasteurized (67.1 ± 1.1 μg/100 g) and pasteurized (72.7 ± 2.4 μg/100 g) juices. The bioaccessibility of total carotenoids was significantly higher in the pasteurized juices (37.6−39.5%) than in the freshly squeezed juice (28.3%). Thermal processing and finishing of the fresh juice increased the BA of lutein, β-cryptoxanthin, α-carotene, and β-carotene, whereas the (9Z)-antheraxanthin/zeaxanthin BA decreased from 35% to 17% and 16% in flash-pasteurized and pasteurized juices, respectively. Note that this decrease might be attributable to the instability of epoxy carotenoids such as antheraxanthin during digestion. Higher pasteurization temperatures and intensified finishing with smaller mesh size did not result in significant changes of the carotenoid BA. Consequently, a moderate thermal treatment and finishing appear to be key factors in increasing carotenoid BA. The insignificant change in carotenoid BA from the flash-pasteurized to the pasteurized juice indicates a "saturation" of these processing effects, meaning that further heating or finishing beyond such an "optimum processing" does not further improve carotenoid BA. If this hypothesis is valid, the heat exposure during the production of the flash- and conventionally pasteurized juices (P values of 0.002 and 0.504 min, respectively) exceeded this optimum heating threshold. However, the definition of an "optimum thermal treatment" regarding carotenoid bioaccessibility is expected to be highly intricate because of the numerous interactions with other dietary factors, such as the amount of ingested dietary lipids. Unfortunately, we cannot differentiate whether the thermal treatment or the finishing step had the greater impact on carotenoid BA. Both treatments are assumed to contribute to the enhanced carotenoid bioaccessibility.

In comparison to this study, Stinco et al.[24] reported higher relative carotenoid absorption from simulated digesta, ranging from 34% in fresh hand-squeezed juice to 40% in industrially pasteurized juice and up to 52% in industrially squeezed and finished juice. According to their work, finishing resulted in a particle size reduction, thus improving carotenoid liberation, whereas thermal pasteurization apparently diminished carotenoid liberation during digestion. Note that Stinco et al.[24] did not separate the micellar fraction by microfiltration of the supernatant, which is rather more comparable to the liberated carotenoids displayed in Figure 3 than to the bioaccessible fraction. In agreement with our study, carotenoid liberation was 44.9−53.9% in freshly squeezed and pasteurized juices, thus being significantly higher than the respective bioaccessibility (28.3−39.5%). The observation of higher liberation as compared to bioaccessibility is in accordance with previous studies, which reported significantly lowered carotenoid levels after microfiltration of the aqueous supernatant.[18,47,50]

Flavonoid Levels in Test Foods and Digesta. Flavonoid contents in the orange juices were 8-fold lower than those of orange segments and homogenated segments (Table 4). According to previous studies, hesperidin levels in membranes and albedo of *Citrus sinensis* are between 8.5- and 16.0-fold higher than those in juice vesicles.[51] These findings correlate well with the hesperidin and narirutin levels determined in our test foods, because juice extraction resulted in the extensive separation of membranes and albedo. For instance, the hesperidin content decreased from approximately 240 mg/100 g in fresh orange segments to 30 mg/100 g of juice (Table 4). Despite the large differences in the test foods, the absolute hesperidin and narirutin levels in the supernatant and micellar fractions were similar after their in vitro digestion. Apparently,

DOI: 10.1021/jf505297t
J. Agric. Food Chem. 2015, 63, 578−587

their solubilization was dose-independent in our experiments, indicating a saturation of the intestinal fluid with soluble hesperidin and narirutin at 26−34 mg/100 g and 20−25 mg/100 g, respectively. Consequently, the bioaccessibility of hesperidin and narirutin increased significantly upon juice extraction (Figure 3). Whereas only 20.5% of the flavonoids were bioaccessible from orange segments, a total of 92.1−96.5% of the flavonoids occurring in the juices was bioaccessible, equaling a gain of almost 500% as compared to the orange segments. Comparing the digestion of intact and homogenized segments, differences in flavonoid BA were insignificant. Thus, homogenization of the orange segments turned out to be ineffective regarding flavonoid BA (Figure 3).

Our findings are in good agreement with those of a previous study by Vallejo et al., who found only the soluble fraction of flavonoids in orange juice to be bioavailable.[27] Supported by these findings, it is assumed that the higher hesperidin level in orange fruits compared to orange juice offers only a limited nutritional benefit, because differences in the hesperidin contents in the supernatant and micellar phase from the digested test foods were found to be insignificant. However, it is worth mentioning that our in vitro model did not include the simulation of colonic digestion, where hesperidin is deglycosylated by the microbiota to hesperetin 7-*O*-glucosid and hesperetin.[10] Insoluble hesperidin can thus be further solubilized, metabolized, and absorbed in the colon. Nevertheless, in an in vivo study, Brett et al.[52] found differences in flavonoid bioavailability to be insignificant based on total urinary hesperetin excretion of human subjects after consumption of orange fruit and juice.

Ascorbic Acid and Vitamin C in Test Foods and Digesta (Supernatant). When exposed to oxygen, ascorbic acid (AA) is reversibly oxidized to dehydroascorbic acid (DHAA), which also exerts vitamin efficacy. According to most reports, vitamin C efficacy is lost upon the irreversible degradation of DHAA to 2,3-diketogulonic acid.[31] Consequently, both AA and DHAA levels were monitored in our study (Table 4). AA levels in the fresh and flash-pasteurized juices (48.6 ± 0.5 and 45.5 ± 0.0 mg/100 g, respectively) were slightly higher compared to those in the orange segments (43.1 ± 0.6 mg/100 g) and the pasteurized juice (44.6 ± 0.1 mg/100 g). Although these slight differences might be due to unavoidable heterogeneities within the used batch of oranges, homogenization of the orange segments led to a significant loss of AA from 43.1 to 32.6 mg/100 g and, at the same time, to an increase in DHAA from 8.0 to 15.3 mg/100 g, possibly due to oxygen exposure during homogenization. However, the vitamin C values of all test foods ranged between 46.5 and 51.1 mg/100 g, confirming the stability of AA and DHAA at low pH.

The bioavailability of vitamin C ranges from 80% to 100% at doses normally ingested (≤180 mg).[8] Thus, the concentration in the intestinal digesta is rather a demonstration of vitamin C stability during digestion than of bioaccessibility. Whereas digestion of the orange segments resulted in residual vitamin C levels of 54% as compared to the test food, a level of only 38% was found after digestion of homogenized orange segments. The high input of air during homogenization probably favored further degradation of vitamin C during in vitro digestion. In contrast, the production of the pasteurized orange juice significantly improved vitamin C stability during digestion, resulting in a residual level of 78% as compared to the test food. Vitamin C levels in the digesta of the different juices did not differ significantly (Figure 3).

In conclusion, processing of the oranges into fresh and pasteurized juices slightly diminished carotenoid and vitamin C levels by 3−18%. However, flavonoid and dietary fiber levels were decreased to approximately one-tenth upon dejuicing. At the same time, carotenoid BA from orange segments was enhanced from 10.8% to 28.3% for freshly squeezed orange juice, whereas flavonoid BA was boosted by almost 5-fold to 96.5%. However, the total hesperidin levels in the digesta of all test foods were quite similar. The lower flavonoid levels in orange juices as compared to orange segments might be less relevant regarding their intestinal absorption, because low flavonoid solubility in the digestive fluids is considered to be the limiting factor. In contrast to dejuicing, homogenization of orange segments to a puree did not enhance carotenoid BA, thus indicating a minor role of cell disruption and comminution compared to the removal of fibers in orange products. To substantiate our findings, performing an in vivo bioavailability study is the next aim of our ongoing investigations.

■ ASSOCIATED CONTENT

Ⓢ Supporting Information

Data on reproducibility, recovery, and limit of detection/limit of quantification for carotenoid, flavonoid, and vitamin C quantification. This material is available free of charge via the Internet at http://pubs.acs.org.

■ AUTHOR INFORMATION

Corresponding Author

*Tel.: +49 711 459 22995. Fax: +49 711 459 24110. E-mail: ralf.schweiggert@uni-hohenheim.de.

Notes

The authors declare no competing financial interest.

■ ACKNOWLEDGMENTS

We thank Klaus Mix and Martin Leitenberger for their valuable technical assistance during the production of the test foods and the development of the analytical method, respectively.

■ ABBREVIATIONS USED

AA, ascorbic acid; BA, bioaccessibility; BHA, 3-*tert*-butylhydroxyanisol; BHT, butylated hydroxytoluene; DHAA, dehydroascorbic acid; DMFA, *N*,*N*-dimethylformamide; FP, flash-pasteurized; MTBE, methyl *tert*-butyl ether; TCEP, tris(2-carboxyethyl)phosphine hydrochloride

■ REFERENCES

(1) *AIJN European Fruit Juice Association 2012 Liquid Fruit Market Report*; AIJN: Brussels, Belgium, 2012; available at http://www.aijn.org/pages/main/file.handler?f=AIJNMarketReport2012.pdf (accessed October 2012).

(2) *Citrus Fruit: Fresh and Processed. Annual Statistics 2012*; Report CCP:CI/ST/2012; Food and Agriculture Organization: Rome, Italy, 2012; available at http://www.fao.org/fileadmin/templates/est/COMM_MARKETS_MONITORING/Citrus/Documents/CITRUS_BULLETIN_2012.pdf (accessed September 2014).

(3) Aptekmann, N. P.; Cesar, T. B. Long-term orange juice consumption is associated with low LDL-cholesterol and apolipoprotein B in normal and moderately hypercholesterolemic subjects. *Lipids Health Dis.* **2013**, *12*, 119.

(4) Foroudi, S.; Potter, A. S.; Stamatikos, A.; Patil, B. S.; Deyhim, F. Drinking orange juice increases total antioxidant status and decreases lipid peroxidation in adults. *J. Med. Food* **2014**, *17*, 612−617.

(5) Ghanim, H.; Sia, C. L.; Upadhyay, M.; Korzeniewski, K.; Viswanathan, P.; Abuaysheh, S.; Mohanty, P.; Dandona, P. Orange

DOI: 10.1021/jf505297t
J. Agric. Food Chem. 2015, 63, 578−587

juice neutralizes the proinflammatory effect of a high-fat, high-carbohydrate meal and prevents endotoxin increase and Toll-like receptor expression. *Am. J. Clin. Nutr.* **2010**, *91*, 940−949.
(6) Sánchez-Moreno, C.; Cano, M. P.; Ancos, B.; de Plaza, L.; Olmedilla, B.; Granado, F.; Martín, A. Effect of orange juice intake on vitamin C concentrations and biomarkers of antioxidant status in humans. *Am. J. Clin. Nutr.* **2003**, *78*, 454−460.
(7) Muraki, I.; Imamura, F.; Manson, J. E.; Hu, F. B.; Willett, W. C.; van Dam, R. M.; Sun, Q. Fruit consumption and risk of type 2 diabetes: Results from three prospective longitudinal cohort studies. *BMJ* **2013**, *347*, 1−15.
(8) Davey, M. W.; van Montagu, M.; Inze, D.; Sanmartin, M.; Kanellis, A.; Smirnoff, N.; Benzie, I.; Strain, J. J.; Favel, D.; Fletcher, J. Plant L-ascorbic acid: Chemistry, function, metabolism, bioavailability and effects of processing. *J. Sci. Food Agric.* **2000**, 825−860.
(9) Meléndez-Martínez, A. J.; Vicario, I. M.; Heredia, F. J. Review: Analysis of carotenoids in orange juice. *J. Food Comp. Anal.* **2007**, *20*, 638−649.
(10) Nielsen, I. L. F.; Chee, W. S. S.; Poulsen, L.; Offord-Cavin, E.; Rasmussen, S. E.; Frederiksen, H.; Enslen, M.; Barron, D.; Horcajada, M.; Williamson, G. Bioavailability is improved by enzymatic modification of the citrus flavonoid hesperidin in humans: A randomized, double-blind, crossover trial. *J. Nutr.* **2006**, *136*, 404−408.
(11) Tripoli, E.; La Guardia, M.; Giammanco, S.; Di Majo, D.; Giammanco, M. Citrus flavonoids: Molecular structure, biological activity and nutritional properties: A review. *Food Chem.* **2007**, *104*, 466−479.
(12) Meléndez-Martínez, A. J.; Britton, G.; Vicario, I. M.; Heredia, F. J. The complex carotenoid pattern of orange juices from concentrate. *Food Chem.* **2008**, *109*, 546−553.
(13) Johnson, E. J. A possible role for lutein and zeaxanthin in cognitive function in the elderly. *Am. J. Clin. Nutr.* **2012**, *96*, 1161S−5S.
(14) Canene-Adams, K.; Erdman, J. W., Jr. Absorption, transport, distribution in tissues and bioavailability. In *Carotenoids. Vol. 5: Nutrition and Health*; Britton, G., Liaaen-Jensen, S., Pfander, H., Eds.; Birkhäuser: Basel, Switzerland, 1995; Chapter 7, pp 115−144.
(15) Fernández-García, E.; Carvajal-Lérida, I.; Pérez-Gálvez, A. In vitro bioaccessibility assessment as a prediction tool of nutritional efficiency. *Nutr. Res. (N.Y.)* **2009**, *29*, 751−760.
(16) Minekus, M.; Alminger, M.; Alvito, P.; Ballance, S.; Bohn, T.; Bourlieu, C.; Carrière, F.; Boutrou, R.; Corredig, M.; Dupont, D.; Dufour, C.; Egger, L.; Golding, M.; Karakaya, S.; Kirkhus, B.; Le Feunteun, S.; Lesmes, U.; Macierzanka, A.; Mackie, A.; Marze, S.; McClements, D. J.; Ménard, O.; Recio, I.; Santos, C. N.; Singh, R. P.; Vegarud, G. E.; Wickham, M. S. J.; Weitschies, W.; Brodkorb, A. A standardised static in vitro digestion method suitable for food—An international consensus. *Food Funct.* **2014**, *5*, 1113−1124.
(17) Gupta, R.; Kopec, R. E.; Schwartz, S. J.; Balasubramaniam, V. M. Combined pressure−temperature effects on carotenoid retention and bioaccessibility in tomato juice. *J. Agric. Food Chem.* **2011**, *59*, 7808−7817.
(18) Schweiggert, R. M.; Mezger, D.; Schimpf, F.; Steingass, C. B.; Carle, R. Influence of chromoplast morphology on carotenoid bioaccessibility of carrot, mango, papaya, and tomato. *Food Chem.* **2012**, *135*, 2736−2742.
(19) Schweiggert, R. M.; Kopec, R. E.; Villalobos-Gutierrez, M. G.; Högel, J.; Quesada, S.; Esquivel, P.; Schwartz, S. J.; Carle, R. Carotenoids are more bioavailable from papaya than from tomato and carrot in humans: A randomised cross-over study. *Br. J. Nutr.* **2014**, *111*, 490−498.
(20) Brown, M. J.; Ferruzzi, M. G.; Nguyen, M. L.; Cooper, D. A.; Eldridge, A. L.; Schwartz, S. J.; White, W. S. Carotenoid bioavailability is higher from salads ingested with full-fat than with fat-reduced salad dressings as measured with electrochemical detection. *Am. J. Clin. Nutr.* **2004**, *80*, 396−403.
(21) Unlu, N. Z.; Bohn, T.; Clinton, S. K.; Schwartz, S. J. Carotenoid absorption from salad and salsa by humans is enhanced by the addition of avocado or avocado oil. *J. Nutr.* **2005**, *135*, 431−436.
(22) Gärtner, C.; Stahl, W.; Sies, H. Lycopene is more bioavailable from tomato paste than from fresh tomatoes. *Am. J. Clin. Nutr.* **1997**, *66*, 116−122.
(23) Rock, C. L.; Lovalvo, J. L.; Emenhiser, C.; Ruffin, M. T.; Flatt, S. W.; Schwartz, S. J. Bioavailability of beta-carotene is lower in raw than in processed carrots and spinach in women. *J. Nutr.* **1998**, *128*, 913−916.
(24) Stinco, C. M.; Fernández-Vázquez, R.; Escudero-Gilete, M. L.; Heredia, F. J.; Meléndez-Martínez, A. J.; Vicario, I. M. Effect of orange juice's processing on the color, particle size, and bioaccessibility of carotenoids. *J. Agric. Food Chem.* **2012**, *60*, 1447−1455.
(25) Stinco, C. M.; Fernández-Vázquez, R.; Heredia, F. J.; Meléndez-Martínez, A. J.; Vicario, I. M. Bioaccessibility, antioxidant activity and colour of carotenoids in ultrafrozen orange juices: Influence of thawing conditions. *LWT—Food Sci. Technol.* **2013**, *53*, 458−463.
(26) Dhuique-Mayer, C.; Borel, P.; Reboul, E.; Caporiccio, B.; Besancon, P.; Amiot, M.-J. *β*-Cryptoxanthin from *Citrus* juices: Assessment of bioaccessibility using an *in vitro* digestion/Caco-2 cell culture model. *Br. J. Nutr.* **2007**, *97*, 883.
(27) Vallejo, F.; Larrosa, M.; Escudero, E.; Zafrilla, M. P.; Cerdá, B.; Boza, J.; García-Conesa, M. T.; Espín, J. C.; Tomás-Barberán, F. A. Concentration and solubility of flavanones in orange beverages affect their bioavailability in humans. *J. Agric. Food Chem.* **2010**, *58*, 6516−6524.
(28) Sánchez-Moreno, C.; Plaza, L.; Ancos, B. d.; Cano, M. P. Quantitative bioactive compounds assessment and their relative contribution to the antioxidant capacity of commercial orange juices. *J. Sci. Food Agric.* **2003**, *83*, 430−439.
(29) Hirsch, A. R.; Förch, K.; Neidhart, S.; Wolf, G.; Carle, R. Effects of thermal treatments and storage on pectin methylesterase and peroxidase activity in freshly squeezed orange juice. *J. Agric. Food Chem.* **2008**, *56*, 5691−5699.
(30) Britton, G. UV/visible spectroscopy. In *Carotenoids. Vol. 1B: Spectroscopy*; Britton, G., Liaaen-Jensen, S., Pfander, H., Eds.; Birkhäuser: Basel, Switzerland, 1995; Chapter 1, pp 13−62.
(31) Wechtersbach, L.; Cigić, B. Reduction of dehydroascorbic acid at low pH. *J. Biochem. Biophys. Methods* **2007**, *70*, 767−772.
(32) Determination of Hesperidin and Naringin, HPLC. IFU Method no. 58. In *IFU Methods of Analysis*; International Federation of Fruit Juice Producers (IFU): Paris, France, 1991.
(33) Green, J. M. Peer reviewed: A practical guide to analytical method validation. *Anal. Chem.* **1996**, *68*, 305A−309A.
(34) Hirsch, A. R.; Carle, R.; Neidhart, S. Validation and applicability of a standardized procedure for evaluating freshness of *Citrus* juices based on pectin methylesterase activity quantitation. *J. Appl. Bot. Food Qual.* **2012**, 6−16.
(35) *Chemische Analytik; Nachweis-, Erfassungs- und Bestimmungsgrenze; Ermittlung unter Wiederholbedingungen; Begriffe, Verfahren, Auswertung*; DIN 32645; Beuth Verlag: Berlin, Germany, 1994.
(36) Determination of Pectin. IFU Method no. 26. In *IFU Methods of Analysis*; International Federation of Fruit Juice Producers (IFU): Paris, France, 1995.
(37) Cortés, C.; Torregrosa, F.; Esteve, M. J.; Frígola, A. Carotenoid profile modification during refrigerated storage in untreated and pasteurized orange juice and orange juice treated with high-intensity pulsed electric fields. *J. Agric. Food Chem.* **2006**, *54*, 6247−6254.
(38) Cortés, C.; Esteve, M. J.; Frígola, A.; Torregrosa, F. Identification and quantification of carotenoids including geometrical isomers in fruit and vegetable juices by liquid chromatography with ultraviolet−diode array detection. *J. Agric. Food Chem.* **2004**, *52*, 2203−2212.
(39) Meléndez-Martínez, A. J.; Britton, G.; Vicario, I. M.; Heredia, F. J. Identification of zeinoxanthin in orange juices. *J. Agric. Food Chem.* **2005**, *53*, 6362−6367.
(40) Dugo, P.; Herrero, M.; Giuffrida, D.; Ragonese, C.; Dugo, G.; Mondello, L. Analysis of native carotenoid composition in orange juice using C30 columns in tandem. *J. Sep. Sci.* **2008**, *31*, 2151−2160.

DOI: 10.1021/jf505297t
J. Agric. Food Chem. 2015, 63, 578−587

(41) Meléndez-Martínez, A. J.; Britton, G.; Vicario, I. M.; Heredia, F. J. Identification of isolutein (lutein epoxide) as *cis*-antheraxanthin in orange juice. *J. Agric. Food Chem.* **2005**, *53*, 9369−9373.
(42) Khachik, F. Distribution and metabolism of dietary carotenoids in humans as a criterion for development of nutritional supplements. *Pure Appl. Chem.* **2006**, 78.
(43) Britton, G.; Khachik, F. Carotenoids in food. In *Carotenoids. Vol. 5: Nutrition and Health*; Britton, G., Liaaen-Jensen, S., Pfander, H., Eds.; Birkhäuser: Basel, Switzerland, 2009; Chapter 3, pp 45−66.
(44) Schweiggert, R. M.; Steingass, C. B.; Esquivel, P.; Carle, R. Chemical and morphological characterization of Costa Rican papaya (*Carica papaya* L.) hybrids and lines with particular focus on their genuine carotenoid profiles. *J. Agric. Food Chem.* **2012**, *60*, 2577−2585.
(45) Breithaupt, D. E.; Bamedi, A. Carotenoid esters in vegetables and fruits: A screening with emphasis on β-cryptoxanthin esters. *J. Agric. Food Chem.* **2001**, *49*, 2064−2070.
(46) Marx, M.; Stuparic, M.; Schieber, A.; Carle, R. Effects of thermal processing on trans−cis-isomerization of β-carotene in carrot juices and carotene-containing preparations. *Food Chem.* **2003**, *83*, 609−617.
(47) Garrett, D. A.; Failla, M. L.; Sarama, R. J. Development of an in vitro digestion method to assess carotenoid bioavailability from meals. *J. Agric. Food Chem.* **1999**, *47*, 4301−4309.
(48) *USDA National Nutrient Database for Standard Reference*, release 27; U.S. Department of Agriculture: Washington, DC, 2011; available at http://ndb.nal.usda.gov/ (accessed Oct 2014).
(49) Rock, C. L.; Swendseid, M. E. Plasma beta-carotene response in humans after meals supplemented with dietary pectin. *Am. J. Clin. Nutr.* **1992**, *55*, 96−99.
(50) Bengtsson, A.; Larsson Alminger, M.; Svanberg, U. In vitro bioaccessibility of β-carotene from heat-processed orange-fleshed sweet potato. *J. Agric. Food Chem.* **2009**, *57*, 9693−9698.
(51) Barthe, G. A.; Jourdan, P. S.; McIntosh, C. A.; Mansell, R. L. Radioimmunoassay for the quantitative determination of hesperidin and analysis of its distribution in *Citrus sinensis*. *Phytochemistry* **1988**, *27*, 249−254.
(52) Brett, G. M.; Hollands, W.; Needs, P. W.; Teucher, B.; R. Dainty, J.; Davis, B. D.; Brodbelt, J. S.; Kroon, P. A. Absorption, metabolism and excretion of flavanones from single portions of orange fruit and juice and effects of anthropometric variables and contraceptive pill use on flavanone excretion. *Br. J. Nutr.* **2009**, *101*, 664.

DOI: 10.1021/jf505297t
J. Agric. Food Chem. 2015, 63, 578−587

JOURNAL OF AGRICULTURAL AND FOOD CHEMISTRY

Article

pubs.acs.org/JAFC

Loss of miRNAs during Processing and Storage of Cow's (*Bos taurus*) Milk

Katherine M. Howard,[†] Rio Jati Kusuma,[†] Scott R. Baier,[†] Taylor Friemel,[†] Laura Markham,[‡] Jairam Vanamala,*[,‡,§] and Janos Zempleni*[,†]

[†]Department of Nutrition and Health Sciences, University of Nebraska, 316C Leverton Hall, Lincoln, Nebraska 68583, United States

[‡]Department of Food Science, Pennsylvania State University, University Park, Pennsylvania 16802, United States

[§]Penn State Hershey Cancer Institute, Penn State Milton S. Hershey Medical Center, Hershey, Pennsylvania 17033, United States

ABSTRACT: MicroRNAs (miRs, miRNAs) play central roles in gene regulation. Previously, we reported that miRNAs from pasteurized, store-bought bovine milk have biological activity in humans. Here, we assessed the effects of milk processing, storage, somatic cell content, and handling by consumers on the degradation of miRNAs in milk; we also quantified miRNAs in dairy products. Pasteurization and homogenization caused a 63% loss of miR-200c, whereas a 67% loss observed for miR-29b was statistically significant only in skim milk. Effects of cold storage and somatic cell content were quantitatively minor (<2% loss). Heating in the microwave caused a 40% loss of miR-29b but no loss of miR-200c. The milk fat content had no effect on miRNA stability during storage and microwave heating. The concentrations of miRNAs in dairy products were considerably lower than in store-bought milk. We conclude that processing of milk by dairies and handling by consumers causes a significant loss of miRNAs.

KEYWORDS: *heating, miRNAs, milk, processing, storage*

INTRODUCTION

MicroRNAs (miRs, miRNAs) are small non-coding RNAs that play essential roles in the regulation of genes at the posttranscriptional level in plants and animals.[1] Mature miRNAs are about 22 nucleotides long and bind to complementary sequences in the 3′-untranslated region of mRNAs. Perfect or near perfect base pairing of the miRNAs and its target mRNAs typically results in mRNA degradation, whereas less perfect base pairing typically results in inhibition of mRNA translation.[2,3] Traditionally, miRNAs have been considered endogenous regulators of genes; i.e., miRNAs synthesized by a given host regulate the expression of genes in that host. Recently, our laboratory refuted this paradigm. We provided strong evidence that (1) humans absorb biologically meaningful amounts of miRNAs from nutritionally relevant doses of cow's milk, (2) physiological concentrations of milk miRNAs affect human gene expression *in vivo* and in cell cultures, and (3) endogenous synthesis of miRNAs does not compensate for dietary miRNA deficiency in mice.[4] Our discoveries were largely modeled on miR-29b and miR-200c but likely hold true for all miRNAs encapsulated in milk exosomes.[5,6] To the best of our knowledge, our previous paper is the first to provide unambiguous evidence that miRNAs can be transferred between distinct species through dietary means. In contrast, previous claims that miRNAs from plants affect human gene expression[7,8] are highly controversial and were met with skepticism by the scientific community.[4,9−12] On the basis of the above observations, milk miRNAs are a novel class of bioactive food compounds as defined by the National Cancer Institute in the United States.[13] The discovery that milk miRNAs are bioactive food compounds has broader implications because miRNAs play essential roles in gene regulation,[2,3] cell communication,[14,15] and human health.[16−23]

This study focused on determining the effect of milk processing, storage, somatic cell content, and handling by consumers on two miRNA, miR-29b and miR-200c, levels based on the following rationale. In bovine milk, miR-29b and miR-200c are among the most abundant miRNAs.[20] miR-29b is an important regulator of bone mineralization in humans, because it increases osteoblast differentiation[16] and decreases osteoclast differentiation and function.[17] miR-200c decreases cancer risk by targeting the transcription factor ZEB1, which induces E-cadherin expression, thereby limiting epithelial-to-mesenchymal transition, a key event in metastasis.[24,25] Also, the nucleotide sequences of miR-29b and miR-200c in bovine milk are identical to those of their human orthologues.[26] Our rationale for including the somatic cell count in our analysis was to assess whether an increase in milk cells, as seen in mastitis, might be a confounder in the analysis of milk miRNAs.

In Western societies, the majority of milk is processed prior to consumption. In fact, the production and sale of raw milk dairy products is illegal in many states in the United States, and pasteurization is required.[27] Moreover, while the per capita consumption of milk has declined from 236 pounds in 1982 to 195 pounds in 2012, total dairy consumption increased by 11% during the same time period.[28] Therefore, we considered it worthwhile to assess the effects of processing on the miRNA content in both milk and dairy products.

Received: November 18, 2014
Revised: December 21, 2014
Accepted: December 25, 2014
Published: December 25, 2014

ACS Publications © 2014 American Chemical Society

DOI: 10.1021/jf505526w
J. Agric. Food Chem. 2015, 63, 588−592

Little is known about the effects of processing and storage on milk miRNA levels. In two studies, synthetic miRNAs were added to bovine milk, and their stability after exposure to harsh treatments, such as acid and RNase, was assessed and compared to the stability of endogenous miRNAs in milk.[6,20] Synthetic miRNAs were rapidly degraded, whereas endogenous miRNAs were resistant to treatment. However, the harsh treatments applied in these studies are not representative of the treatments applied in commercial dairy production. In this study, we assessed the effects of pasteurization, fat content, cold storage, heating, and processing into dairy products on the content of milk miRNAs.

MATERIALS AND METHODS

Chemicals. Guanidinium thiocyanate and ethanol were purchased for use in the NucleoSpin miRNA plasma RNA extraction kit (Macherey-Nagel, Inc., Bethlehem, PA). TRIzol was purchased from Life Technologies (Grand Island, NY).

Milk and Dairy Products. Raw, whole, 2%, and skim cow's (*Bos taurus*) milk was obtained from the Pennsylvania State University Creamery (University Park, PA) from separate collections in three consecutive weeks in May 2014. A diagram illustrating the preparation of whole cow's milk is presented in Figure 1. Briefly, the milk was procured from the Penn State Animal Science Department's Holsteins breed herd, using raw milk and cream routinely supplied to the Penn State Berkey Creamery, University Park, PA. The milk was stored under intermittent agitation in a 22 712.5 L raw milk silo at 2.2 °C (Feldmeier Equipment, E-015-05, Little Falls, NY). The milk contained 3.25% fat and 12.15% non-fat solids (near-infrared method, CEM, Turbo Smart5, model 907990, Matthews, NC) and was pasteurized at 75.55 °C with a 28 s holding time (APV Paraflow, serial number 20053003000302, Goldsboro, NC). The milk was homogenized at 145 bar and 60 °C (APV Gaulin homogenizer, serial number 20052410702, Lake Mills, WI) and standardized using a Westfalia separator (MSE 55-01-177, Oelde, Germany), thereby producing whole milk (3.25% fat and skim milk). The 2% fat milk was prepared by mixing 3.25% milk and skim milk. After cooling, the product was transferred to a 7200 L refrigerated storage tank at 2.2 °C (Feldmeier Equipment, E-015-05, Little Falls, NY). The product was bottled on a filling machine (Federal Manufacturing, serial number 1/12.4GL843, Milwaukee, WI) and stored in a conventional cold-milk warehouse at 3.0 °C. On our initial collection dates, milk of all fat levels were stored at 4 °C for up to 15 days, and aliquots were taken and frozen at −80 °C every other day. In a separate experiment, bovine cells were removed from raw milk by centrifugation (500*g* for 10 min at 4 °C) to determine whether somatic cells are a meaningful confounder when analyzing the concentrations of miRNAs in milk from healthy cows. Samples were frozen at −80 °C and shipped on dry ice to Lincoln, NE, for miRNA analysis. Samples from all fat levels of milk on day 15 were heated in the microwave for 15 s and analyzed after cooling off to room temperature. Dairy products other than milk were purchased from grocery stores in Lincoln, NE. All samples were produced and analyzed as biological repeats in triplicate.

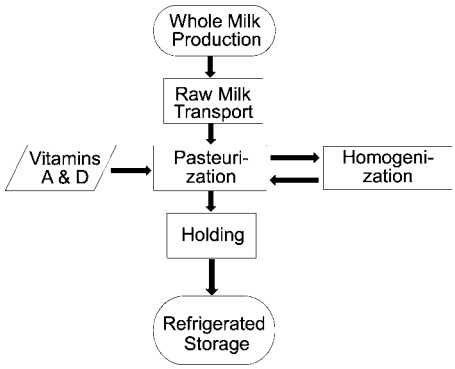

Figure 1. Schematic presentation of milk processing.

miRNA Analysis. Milk samples were spiked with a synthetic internal standard (25 attomoles) prior to extraction of miRNAs using miSPIKE synthetic RNA (IDT Technologies).[4] Dairy products (100 mg) other than milk were extracted using TRIzol prior to the addition of the synthetic internal standard. miR-29b and miR-200c were quantified using quantitative real-time polymerase chain reaction (PCR) as described previously.[4]

Statistics. Analysis by Bartlett's test homogeneity suggested that variances were homogeneous.[29] The paired *t* test was used for pairwise comparisons. One-way analysis of variance (ANOVA) and Fisher's protected least significant differences were used when comparing more than two groups. Repeated measures ANOVA was used for assessing the effects of storage time on the miRNA concentration. StatView 5.0.1 (SAS Institute, Cary, NC) was used for conducting statistical analyses. Means ± standard deviation (SD) are reported. Differences were considered statistically significant if $p \leq 0.05$.

RESULTS

Pasteurization and homogenization of raw milk resulted in a 63 ± 28% decrease of miR-200c in whole milk; effects were similar for 2% fat milk and skim milk (Figure 2A). The effect was less pronounced for miR-29b, for which a significant decrease (67 ± 18%) was observed only in skim milk (Figure 2B). Cold storage of milk did not affect the concentration of mir-29b and miR-200c in whole milk, 2% milk, and skim milk up to 15 days; 2% fat milk is shown as a representative example in Figure 3. Somatic cells are not meaningful confounds regarding the analysis of miRNAs in milk from healthy cows. When somatic cells were removed from raw milk by centrifugation and

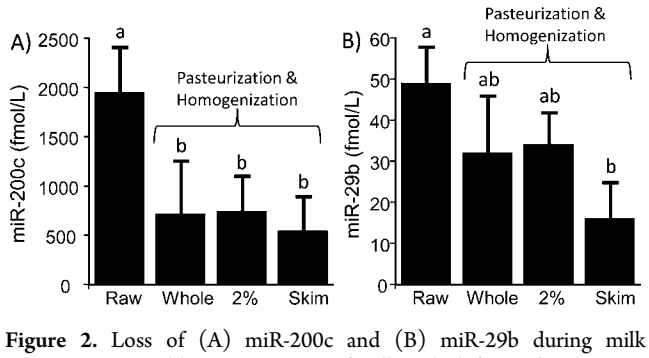

Figure 2. Loss of (A) miR-200c and (B) miR-29b during milk pasteurization and homogenization of milk with different fat contents. (a and b) Significantly different ($n = 3$ biological replicates; $p < 0.05$).

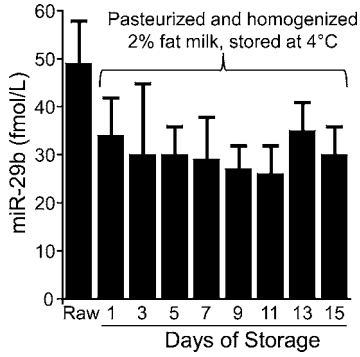

Figure 3. Storage at 4 °C did not affect the concentrations of miR-29b in pasteurized and homogenized 2% fat milk ($n = 3$ biological replicates; $p > 0.05$).

DOI: 10.1021/jf505526w
J. Agric. Food Chem. 2015, 63, 588−592

analyzed for miRNA content, the cellular miRNAs were found to contribute less than 2% of the total miRNAs present in raw milk before centrifugation: 1.1 ± 0.9% for miR-29b and 0.14 ± 0.08% for miR-200c.

Processing in the household has the potential to cause a considerable loss of some miRNAs in milk. For example, the concentration of miR-29b decreased by 40 ± 28% when processed milk was heated in the microwave and cooled to room temperature compared to milk before heating (Figure 4).

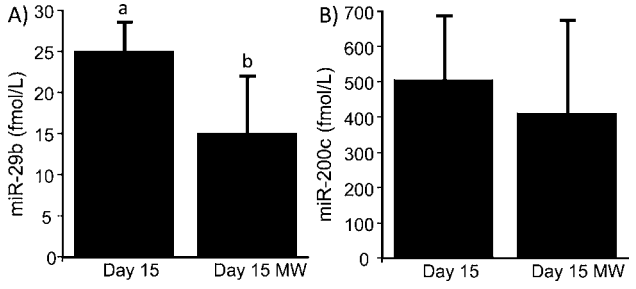

Figure 4. Loss of (A) miR-29b and (B) miR-200c during heating of whole milk in the microwave after 15 days of storage at 4 °C. Abbreviation: MW, microwaved. (a and b) Significantly different (n = 3 biological replicates; $p < 0.05$).

In contrast, when milk was heated in the microwave, the concentration of miR-200c was not statistically different compared to unheated controls. The concentrations of miRNAs varied considerably among the dairy products tested (Table 1) but were generally lower than the concentrations in pasteurized whole milk (compare to Figure 2). Fresco queso dip was a notable exception and contained higher concentrations of miRNAs than those observed in milk.

Table 1. Concentration of miRNAs, miR-29b and miR-200c, in Dairy Products[a]

	miRNA	
product	miR-29b (fmol/kg)	miR-200c (fmol/kg)
Best Choice yogurt	0.9 ± 0.10	37.6 ± 2.8
Fresco queso dip	36.1 ± 5.5	1029.8 ± 478.6
Greek yogurt	14.2 ± 3.9	462.3 ± 126.9
half and half	3.0 ± 0.17	513.3 ± 159.2
heavy whip cream	2.6 ± 1.3	342.0 ± 132.9
parmesan cheese	4.9 ± 1.9	232.0 ± 64.5
Upstate Farm yogurt	2.4 ± 1.0	216.9 ± 93.8

[a]Data are means ± SD; n = 3.

DISCUSSION

In a recent paper, we reported the importance of milk miRNAs for gene regulation in humans.[4] That report has major implications for the roles of milk and possibly other dairy products in human health. Cow's milk contains meaningful quantities of 245 miRNAs,[20,30] and 71.4% of these miRNAs are predicted to target about 11 000 human transcripts (unpublished observations). In addition to the roles of miR-29b and miR-200c in bone health and cancer prevention,[16,17,24,25] respectively, miRNAs have been implicated in various aspects of human health and disease, including hypertension, insulin resistance and diabetes, hyperlipidemia and atherosclerosis, reproduction, immune function, and Crohn's disease.[18,20,21,31−33]

We propose that milk has a meaningful effect on human health, mediated by miRNA-dependent gene regulation. The potential importance of dietary milk miRNA intake is supported by data suggesting that (1) Americans consume large quantities of milk and dairy products,[28] (2) a large proportion of milk miRNAs is encapsulated in extracellular vesicles, thereby providing protection against degradation[5,6] and a pathway for cellular uptake by endocytosis,[34,35] and (3) milk miRNAs are resistant against degradation during storage (this study).

Our previous studies of milk miRNAs in humans and mice were conducted using 1% fat milk from the grocery store.[4] On the basis of this study, the content of miRNAs is about 2 times higher in unprocessed milk compared to pasteurized, store-bought milk. Note that we have no intent recommending the consumption of raw cow's milk by humans, because of food safety concerns associated with raw milk. We observed that a loss of milk miRNAs occurred only during pasteurization, homogenization, and processing to dairy products other than milk. This observation is consistent with previous studies of milk miRNAs. For example, endogenous miRNAs were not degraded when milk was exposed to harsh treatments, such as low pH or treatment with RNase.[6,20] It is reasonable to propose that encapsulation of miRNAs in extracellular vesicles[5] prevents miRNA degradation based on the following lines of evidence: (1) When synthetic miRNAs are added to milk and subjected to low pH or RNase treatment, the miRNAs are rapidly degraded.[6,20] (2) When exosome membranes in milk were disrupted by sonication for preparing miRNA-depleted mouse diets in previous studies, miR-29b was rapidly degraded to concentrations below the detection limit.[4] Presumably, degradation was due to milk RNases gaining access to miRNAs released from exosomes. (3) When milk was fermented to produce yogurt, miRNA concentrations decreased to levels much lower than in milk (this study). We speculate that the decrease was due to the lysis of exosomes during fermentation and the large amounts of RNases produced by microbes. (4) When milk was homogenized, miRNA concentrations decreased by on average 50% (this study). We speculate that the decrease was caused by a disruption of exosome mebranes by shear forces applied during homogenization. Collectively, our studies suggest that milk and perhaps dairy products have the potential to contribute to the miRNA body pool in humans.

Some uncertainties remain to be addressed in future studies. For example, this study was modeled on the basis of miR-29b and miR-200c; however, there is a possibility that distinct miRNAs may be differentially metabolized.[8,36] Another layer of uncertainty is the possible effects of feeding regimens, season, and breed on the miRNA content in milk. Moreover, while this study suggests that somatic cells in milk from healthy cows do not contribute meaningful amounts to the total miRNA content in milk, it is possible that the increased somatic cell count in milk from cows suffering from mastitis[37] may cause an artificial increase in milk miRNA concentrations. Our previous studies suggest that plasma miRNA concentrations decrease by 61% in mice fed a milk miRNA-depleted diet for 4 weeks. This observation is consistent with milk miRNAs contributing meaningful quantities to the miRNA body pool but does not necessarily establish the essentiality of dietary miRNA intake. Clearly, this is an uncertainty that will need to be addressed in future studies. Finally, it is conceivable that miRNAs from foods

DOI: 10.1021/jf505526w
J. Agric. Food Chem. 2015, 63, 588−592

other than milk also contribute toward the total body pool of miRNAs.

There is precedent for degradation of milk compounds during processing. Examples include the thermal and non-thermal degradation of modified peptides[38] and DNA encapsulated in silica.[39] The immediate relevance of these previous publications for the stability of miRNAs in milk is uncertain.

AUTHOR INFORMATION

Corresponding Authors

*Telephone: 814-865-6842. Fax: 814-863-6132. E-mail: juv4@psu.edu.

*Telephone: 402-472-3270. Fax: 402-472-1587. E-mail: jzempleni2@unl.edu.

Funding

Support was provided by National Institutes of Health (NIH) Grant P20GM104320, National Research Initiative Grant 2014-06605, the Gerber Foundation (to Janos Zempleni), the National Research Initiative Grant 2009-55200-05197 from the United States Department of Agriculture (USDA) National Institute for Food and Agriculture, and startup funds from the College of Agricultural Sciences, Penn State University (to Jairam Vanamala).

Notes

The authors declare no competing financial interest.

ACKNOWLEDGMENTS

The authors thank Deanna Jane Bartos and Abigail Sido for help with milk sample collection and processing.

ABBREVIATIONS USED

miR, microRNA; miRNA, microRNA

REFERENCES

(1) Ameres, S. L.; Zamore, P. D. Diversifying microRNA sequence and function. *Nat. Rev. Mol. Cell Biol.* **2013**, *14*, 475−488.

(2) Jing, Q.; Huang, S.; Guth, S.; Zarubin, T.; Motoyama, A.; Chen, J.; Di Padova, F.; Lin, S. C.; Gram, H.; Han, J. Involvement of microRNA in AU-rich element-mediated mRNA instability. *Cell* **2005**, *120*, 623−634.

(3) Djuranovic, S.; Nahvi, A.; Green, R. miRNA-mediated gene silencing by translational repression followed by mRNA deadenylation and decay. *Science* **2012**, *336*, 237−240.

(4) Baier, S. R.; Nguyen, C.; Xie, F.; Wood, J. R.; Zempleni, J. MicroRNAs are absorbed in biologically meaningful amounts from nutritionally relevant doses of cow's milk and affect gene expression in peripheral blood mononuclear cells, HEK-293 kidney cell cultures, and mouse livers. *J. Nutr.* **2014**, *144*, 1495−1500.

(5) Zhou, Q.; Li, M.; Wang, X.; Li, Q.; Wang, T.; Zhu, Q.; Zhou, X.; Wang, X.; Gao, X.; Li, X. Immune-related microRNAs are abundant in breast milk exosomes. *Int. J. Biol. Sci.* **2012**, *8*, 118−123.

(6) Kosaka, N.; Izumi, H.; Sekine, K.; Ochiya, T. microRNA as a new immune-regulatory agent in breast milk. *Silence* **2010**, *1*, 7.

(7) Zhang, L.; Hou, D.; Chen, X.; Li, D.; Zhu, L.; Zhang, Y.; Li, J.; Bian, Z.; Liang, X.; Cai, X.; Yin, Y.; Wang, C.; Zhang, T.; Zhu, D.; Zhang, D.; Xu, J.; Chen, Q.; Ba, Y.; Liu, J.; Wang, Q.; Chen, J.; Wang, J.; Wang, M.; Zhang, Q.; Zhang, J.; Zen, K.; Zhang, C. Y. Exogenous plant MIR168a specifically targets mammalian LDLRAP1: Evidence of cross-kingdom regulation by microRNA. *Cell Res.* **2012**, *22*, 107−126.

(8) Zhou, Z.; Li, X.; Liu, J.; Dong, L.; Chen, Q.; Liu, J.; Kong, H.; Zhang, Q.; Qi, X.; Hou, D.; Zhang, L.; Zhang, G.; Liu, Y.; Zhang, Y.; Li, J.; Wang, J.; Chen, X.; Wang, H.; Zhang, J.; Chen, H.; Zen, K.; Zhang, C. Y. Honeysuckle-encoded atypical microRNA2911 directly targets influenza A viruses. *Cell Res.* **2015**, *25*, 39−49.

(9) Snow, J. W.; Hale, A. E.; Isaacs, S. K.; Baggish, A. L.; Chan, S. Y. Ineffective delivery of diet-derived microRNAs to recipient animal organisms. *RNA Biol.* **2013**, *10*, 1107−1116.

(10) Dickinson, B.; Zhang, Y.; Petrick, J. S.; Heck, G.; Ivashuta, S.; Marshall, W. S. Lack of detectable oral bioavailability of plant microRNAs after feeding in mice. *Nat. Biotechnol.* **2013**, *31*, 965−967.

(11) Chen, X.; Zen, K.; Zhang, C. Y. Reply to lack of detectable oral bioavailability of plant microRNAs after feeding in mice. *Nat. Biotechnol.* **2013**, *31*, 967−969.

(12) Wang, K.; Li, H.; Yuan, Y.; Etheridge, A.; Zhou, Y.; Huang, D.; Wilmes, P.; Galas, D. The complex exogenous RNA spectra in human plasma: An interface with human gut biota? *PLoS One* **2012**, *7*, No. e51009.

(13) National Cancer Institute (NCI). *NCI Dictionary of Cancer Terms*; http://www.cancer.gov/dictionary?cdrid=703278 (accessed July 6, 2014).

(14) Turchinovich, A.; Samatov, T. R.; Tonevitsky, A. G.; Burwinkel, B. Circulating miRNAs: Cell−cell communication function? *Front. Genet.* **2013**, *4*, 119.

(15) Xu, L.; Yang, B. F.; Ai, J. MicroRNA transport: A new way in cell communication. *J. Cell. Physiol.* **2013**, *228*, 1713−1719.

(16) Li, Z.; Hassan, M. Q.; Jafferji, M.; Aqeilan, R. I.; Garzon, R.; Croce, C. M.; van Wijnen, A. J.; Stein, J. L.; Stein, G. S.; Lian, J. B. Biological functions of miR-29b contribute to positive regulation of osteoblast differentiation. *J. Biol. Chem.* **2009**, *284*, 15676−15684.

(17) Rossi, M.; Pitari, M. R.; Amodio, N.; Di Martino, M. T.; Conforti, F.; Leone, E.; Botta, C.; Paolino, F. M.; Del Giudice, T.; Iuliano, E.; Caraglia, M.; Ferrarini, M.; Giordano, A.; Tagliaferri, P.; Tassone, P. miR-29b negatively regulates human osteoclastic cell differentiation and function: Implications for the treatment of multiple myeloma-related bone disease. *J. Cell. Physiol.* **2013**, *228*, 1506−1515.

(18) Nothnick, W. B. The role of micro-RNAs in the female reproductive tract. *Reproduction* **2012**, *143*, 559−576.

(19) Abu-Halima, M.; Hammadeh, M.; Schmitt, J.; Leidinger, P.; Keller, A.; Meese, E.; Backes, C. Altered microRNA expression profiles of human spermatozoa in patients with different spermatogenic impairments. *Fertil. Steril.* **2013**, *99*, 1249−1255.

(20) Izumi, H.; Kosaka, N.; Shimizu, T.; Sekine, K.; Ochiya, T.; Takase, M. Bovine milk contains microRNA and messenger RNA that are stable under degradative conditions. *J. Dairy Sci.* **2012**, *95*, 4831−4841.

(21) Arnold, C. N.; Pirie, E.; Dosenovic, P.; McInerney, G. M.; Xia, Y.; Wang, N.; Li, X.; Siggs, O. M.; Karlsson Hedestam, G. B.; Beutler, B. A forward genetic screen reveals roles for Nfkbid, Zeb1, and Ruvbl2 in humoral immunity. *Proc. Natl. Acad. Sci. U. S. A.* **2012**, *109*, 12286−12293.

(22) Nijhuis, A.; Biancheri, P.; Lewis, A.; Bishop, C. L.; Giuffrida, P.; Chan, C.; Feakins, R.; Poulsom, R.; Di Sabatino, A.; Corazza, G. R.; MacDonald, T. T.; Lindsay, J. O.; Silver, A. R. In Crohn's disease fibrosis-reduced expression of the miR-29 family enhances collagen expression in intestinal fibroblasts. *Clin. Sci.* **2014**, *127*, 341−350.

(23) Amodio, N.; Di Martino, M. T.; Foresta, U.; Leone, E.; Lionetti, M.; Leotta, M.; Gulla, A. M.; Pitari, M. R.; Conforti, F.; Rossi, M.; Agosti, V.; Fulciniti, M.; Misso, G.; Morabito, F.; Ferrarini, M.; Neri, A.; Caraglia, M.; Munshi, N. C.; Anderson, K. C.; Tagliaferri, P.; Tassone, P. miR-29b sensitizes multiple myeloma cells to bortezomib-induced apoptosis through the activation of a feedback loop with the transcription factor Sp1. *Cell Death Dis.* **2012**, *3*, No. e436.

(24) Korpal, M.; Lee, E. S.; Hu, G.; Kang, Y. The miR-200 family inhibits epithelial-mesenchymal transition and cancer cell migration by direct targeting of E-cadherin transcriptional repressors ZEB1 and ZEB2. *J. Biol. Chem.* **2008**, *283*, 14910−14914.

(25) Burk, U.; Schubert, J.; Wellner, U.; Schmalhofer, O.; Vincan, E.; Spaderna, S.; Brabletz, T. A reciprocal repression between ZEB1 and members of the miR-200 family promotes EMT and invasion in cancer cells. *EMBO Rep.* **2008**, *9* (6), 582−589.

(26) Griffiths-Jones, S.; Saini, H. K.; van Dongen, S.; Enright, A. J. miRBase: Tools for microRNA genomics. *Nucleic Acids Res.* **2008**, *36*, D154−D158.

DOI: 10.1021/jf505526w
J. Agric. Food Chem. 2015, 63, 588−592

(27) Langer, A. J.; Ayers, T.; Grass, J.; Lynch, M.; Angulo, F. J.; Mahon, B. E. Nonpasteurized dairy products, disease outbreaks, and state laws—United States, 1993−2006. *Emerging Infect. Dis.* **2012**, *18*, 385−391.
(28) United States Department of Agriculture Economic Research Service. *Dairy Data*; http://www.ers.usda.gov/data-products/dairy-data.aspx (accessed Sept 25, 2013).
(29) Abacus Concepts, Inc. *StatView*; Abacus Concepts, Inc.: Berkeley, CA, 1996.
(30) Chen, X.; Gao, C.; Li, H.; Huang, L.; Sun, Q.; Dong, Y.; Tian, C.; Gao, S.; Dong, H.; Guan, D.; Hu, X.; Zhao, S.; Li, L.; Zhu, L.; Yan, Q.; Zhang, J.; Zen, K.; Zhang, C. Y. Identification and characterization of microRNAs in raw milk during different periods of lactation, commercial fluid, and powdered milk products. *Cell Res.* **2010**, *20*, 1128−1137.
(31) Li, S.; Zhu, J.; Zhang, W.; Chen, Y.; Zhang, K.; Popescu, L. M.; Ma, X.; Lau, W. B.; Rong, R.; Yu, X.; Wang, B.; Li, Y.; Xiao, C.; Zhang, M.; Wang, S.; Yu, L.; Chen, A. F.; Yang, X.; Cai, J. Signature microRNA expression profile of essential hypertension and its novel link to human cytomegalovirus infection. *Circulation* **2011**, *124*, 175−184.
(32) Fernandez-Valverde, S. L.; Taft, R. J.; Mattick, J. S. MicroRNAs in β-cell biology, insulin resistance, diabetes and its complications. *Diabetes* **2011**, *60* (7), 1825−1831.
(33) Soh, J.; Iqbal, J.; Queiroz, J.; Fernandez-Hernando, C.; Hussain, M. M. MicroRNA-30c reduces hyperlipidemia and atherosclerosis in mice by decreasing lipid synthesis and lipoprotein secretion. *Nat. Med.* **2013**, *19*, 892−900.
(34) Feng, D.; Zhao, W. L.; Ye, Y. Y.; Bai, X. C.; Liu, R. Q.; Chang, L. F.; Zhou, Q.; Sui, S. F. Cellular internalization of exosomes occurs through phagocytosis. *Traffic* **2010**, *11*, 675−687.
(35) Escrevente, C.; Keller, S.; Altevogt, P.; Costa, J. Interaction and uptake of exosomes by ovarian cancer cells. *BMC Cancer* **2011**, *11*, 108.
(36) Squadrito, M. L.; Baer, C.; Burdet, F.; Maderna, C.; Gilfillan, G. D.; Lyle, R.; Ibberson, M.; De Palma, M. Endogenous RNAs modulate microRNA sorting to exosomes and transfer to acceptor cells. *Cell Rep.* **2014**, *8*, 1432−1446.
(37) Dohoo, I. R.; Meek, A. H. Somatic cell counts in bovine milk. *Can. Vet. J.* **1982**, *23*, 119−125.
(38) Meltretter, J.; Wust, J.; Pischetsrieder, M. Modified peptides as indicators for thermal and nonthermal reactions in processed milk. *J. Agric. Food Chem.* **2014**, *62*, 10903−10915.
(39) Bloch, M. S.; Paunescu, D.; Stoessel, P. R.; Mora, C. A.; Stark, W. J.; Grass, R. N. Labeling milk along its production chain with DNA encapsulated in silica. *J. Agric. Food Chem.* **2014**, *62*, 10615−10620.

DOI: 10.1021/jf505526w
J. Agric. Food Chem. 2015, 63, 588−592

JOURNAL OF AGRICULTURAL AND FOOD CHEMISTRY

Article

pubs.acs.org/JAFC

Genetic and Biochemical Evaluation of Natural Rubber from Eastern Washington Prickly Lettuce (*Lactuca serriola* L.)

Jared L. Bell,[†] Ian C. Burke,*[,§] and Michael M. Neff[§]

[†]Discovery Research, Dow Agrosciences, Indianapolis, Indiana, United States

[§]Crop and Soil Science Department, Washington State University, Pullman, Washington, United States

Supporting Information

ABSTRACT: Alternative sources of natural rubber are of importance due to economic, biological, and political threats that could diminish supplies of this resource. Prickly lettuce (*Lactuca serriola* L.) synthesizes long-chain natural rubber and was studied to determine underlying genetic and phenotypic characteristics of rubber biosynthesis. Genotypic and phenotypic analysis of an F2 segregating population using EST-SSR markers led to the discovery of genetic regions linked to natural rubber production. Interval mapping (IM) and multiple QTL mapping (MQM) identified several QTL in the mapping population that had significance based on LOD score thresholds. The discovered QTL and the corresponding local markers are genetic resources for understanding rubber biosynthesis in prickly lettuce and could be used in marker-assisted selection (MAS) breeding. Prickly lettuce is an excellent candidate for elucidating the rubber synthesis mechanism and has potential as a crop plant for rubber production.

KEYWORDS: *EST-SSR, Lactuca serriola L., polyisoprene, prickly lettuce, QTL, rubber*

INTRODUCTION

Natural rubber (*cis*-1,4-polyisoprene) is a plant-derived bioproduct that has strategic importance due the number of products that utilize the polymer. Commercial quantities of natural rubber are supplied by the Brazilian rubber tree [*Hevea brasiliensis* (Willd. ex A. Juss.) Müll. Arg.], a native of the Amazon basin. Yearly rubber harvest has steadily increased since rubber was first commercialized. In 2011, worldwide natural rubber production reached 11,031,000 tonnes with consumption closely following at 10,981,000 tonnes.[1] Alternative sources of natural rubber are being investigated for their utilization in rubber production to alleviate the threat of supply shortages.[2,3] Prickly lettuce (*Lactuca serriola* L.) is one of the few rubber-bearing plant species able to produce high M_w rubber,[4] yet, to date, no research has been conducted to identify genetic influences of rubber biosynthesis or molecular markers linked to rubber trait development.

Prickly lettuce is closely related to, and most likely the progenitor of, cultivated lettuce (*Lactuca sativa* L.). It is believed the two species are conspecific[5] and are easily crossed to produce viable offspring. Cultivated lettuce is grown throughout the world and consumed for its nutritious foliage.[6,7] Cultivated lettuce has nine chromosomes and a genome size of approximately 2600 Mb. Prickly lettuce also has nine chromosomes and presumably a similar genome size. The Compositae Genome Project Database (CGPDB[8]) is the most comprehensive genetic resource for study of the Compositae family including cultivated and four closely related lettuce species, *L. serriola* L., *L. saligna* L., *L. virosa* L., and *L. perennis* L., ordered in proposed phylogenetic relatedness to cultivated lettuce. The genetic and genomic architecture of cultivated lettuce and its relatives has been well documented and includes a large inventory of molecular markers. Variable marker types include RFLPs,[9,10] RAPDs,[11] ISSRs,[12] genomic/EST-SSRs,[13−15] AFLPs,[5,16,17] TRAPs,[18] SNPs,[19] and SFPs.[20] The developed molecular markers have been effectively utilized for linkage mapping,[21] gene-tagging, QTL mapping,[16] and genetic diversity studies.[13,22] Although cultivated lettuce is the main research focus, many of the molecular markers are transferable and have been used between lettuce species. Most recently, the lettuce genome has been released[23] and will become a valuable asset in lettuce research as well as close lettuce relatives through sytenic genetic comparisons.

Prickly lettuce is important in lettuce breeding as donors of disease resistance genes[24−29] insect resistance,[30−32] and trait development such as carotenoid content,[33] bolting time,[34] and water use efficiency.[35] On the basis of the gene-pool concept,[36] *Lactuca* species were categorized into three gene pools based on their relationship to cultivated lettuce.[37] The primary gene pool is represented by numerous cultivars of cultivated lettuce, primitive landraces, and wild species where crossing barriers do not exist. Prickly lettuce is the primary representative as the progenitor species of this gene pool[38] and will be the greatest beneficiary of cultivated lettuce genetic advancements.

Prickly lettuce is a potential new crop plant for rubber production. Development of this species will require molecular tools that assist in breeding efforts for desired traits. Of equal scientific importance are the general mechanisms controlling rubber biosynthesis in all rubber-bearing plants. There are few studies that attempt to find genetic associations to rubber traits and no studies in prickly lettuce. The purposes of these studies were (1) to understand the genetic control of rubber traits in prickly lettuce and (2) to identify molecular markers or QTL

Received: August 14, 2014
Revised: December 8, 2014
Accepted: December 16, 2014
Published: December 16, 2014

ACS Publications © 2014 American Chemical Society

DOI: 10.1021/jf503934v
J. Agric. Food Chem. 2015, 63, 593−602

that would lead to a better understanding of the genes involved in rubber biosynthesis and allow for selection of prickly lettuce biotypes that have increased rubber-making potential.

MATERIALS AND METHODS

Plant Material and Population Development. In 2006, 20 eastern Washington prickly lettuce biotypes were collected and later screened for rubber content and quality. Preliminary screening of the collected biotypes for herbicide resistance and latex rubber revealed two with distinct rubber content and quality traits as well as contrasting visual phenotypes (Figure 1). Parent 6-9/13 (P1) had lobed leaves, was resistant to acetolactate synthase (ALS) targeting herbicides, was early to bolt, had average rubber M_w of 2.5×10^6 g mol^{-1}, and contained 4.9% rubber in the latex on average. Parent 4-10/6 (P2) had nonlobed oblanceolate leaves, no herbicide resistance, was late to bolt, an average rubber M_w of 1.1×10^6 g mol^{-1}, and contained an average of 2.2% rubber in the latex. Parental plants were grown in a greenhouse from seed in 16 cm round plastic pots into potting media (LC1Mix. Sun Gro Horticulture Distribution Inc., Bellevue, WA, USA) with temperatures kept at 26 °C daytime and 22 °C nighttime (±3 °C). Natural light was supplemented with sodium vapor lighting to give a 14 h photoperiod that coincided with the daytime portion of the temperature profile. Plants were subirrigated as needed. At anthesis, flowers were crossed using the clip-and-wash method.[39] Reciprocal crosses were made and F1 seeds collected. F1 seeds were planted and evaluated for potential self-pollination using the differential parental phenotypic traits of bolting time and leaf lobing, semidominant and dominant traits, respectively. Successfully crossed F1 plants had an intermediate bolting time between parental phenotypes and inherited leaf lobing traits (lobed in 4-10/6 × 6/9-13 crosses) that allowed for selection of nonselfed individuals. Cross efficiency was 81% with 13 of 16 successful crosses. One F1 plant with cross 6-9/13 female × 4-10/6 male was selected for creation of an F2 segregating population by collecting seed from the selfed F1 plant.

Figure 1. Leaf morphologies of the parents selected for generation of F2 segregating population.

Phenotypic Evaluation. In total, 250 F2 individuals were grown in a greenhouse from seed for 4 weeks prior to planting at Washington State University's Cook Agronomy Farm near Pullman, WA (GPS coordinates 46° 47′ 1.0854″, −117° 5′ 28.755″). Plants were started May 7, 2010, in a greenhouse under the same conditions as the parental and F1 plants but were planted in smaller 100 cm^2 square plastic pots. Plants were transplanted to the field June 7, 2010, at 2 m row spacing with 1 m distance between each plant. Two plants died, leaving a total of 248 individuals in the population. Throughout the growing season phenotypic data were collected from four main categories including latex extract components, rubber qualities, leaf measurements, and growth patterns. Flowering time phenotype was confounded by deer herbivory; however, deer appeared to graze preferentially on certain individuals within the population. Plants were scored with either herbivory or no herbivory. Lobing was scored as either lobed or not lobed. Leaf area and leaf perimeter values were calculated by scanning four fully expanded leaves on a flatbed scanner and using the ImageJ[40] convert to mask and wand tool functions to outline each leaf. Stem number was determined by counting the number of stems on each plant at 90 days after planting. Growth habit was scored on a scale of 1−5, where 1 represented the 6-9/13 parental phenotype, which consists of early bolting and multiple lateral shoots, and 5 represented the 4-10/6 parental phenotype that had a late bolt timing and few lateral shoots.

Latex from each individual was collected from the bolting stem for latex component and biochemical analysis. The percent of water, resin, rubber, and insoluble material from each plant was determined gravimetrically (% wt/wt). Latex was collected by making multiple diagonal incisions with a razor and catching the drips of latex into a tared microcentrifuge tube. Tubes were capped and reweighed to obtain weight of initial latex collection. Latex was then dried for 48 h under vacuum at 35 °C to remove all water. Tubes were reweighed to acquire total contained water. Dried samples were extracted three times with acetone by addition of 1 mL of acetone, vortexing, centrifugation for 5 min at 6822*g*, and collection of supernatant into a clean, tared vial. Acetone was dried under a stream of air, and vials were reweighed to determine resin content. Following acetone extraction, samples were extracted with hexane to dissolve rubber. One milliliter of hexane was added to each tube followed by vortexing and hand stirring with a spatula to dislodge the rubber pellet as needed. Samples were centrifuged, and supernatant was collected into a clean, tared vial. Latex was extracted three times with hexane, the third hexane addition being allowed to sit for 8−10 h before supernatant collection. Hexane was dried under air, and vials were weighed for total contained rubber. Original collection tubes

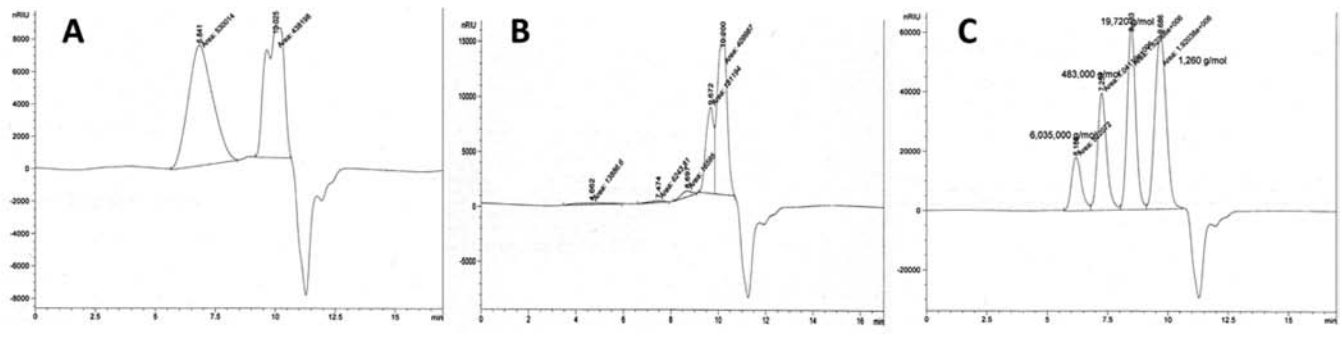

Figure 2. Representative HPLC GPC/SEC chromatograms from individuals of the F2 population with high (A) and low (B) molecular weight rubber as well as the polystyrene standards used to make a calibration curve (C).

DOI: 10.1021/jf503934v
J. Agric. Food Chem. 2015, 63, 593−602

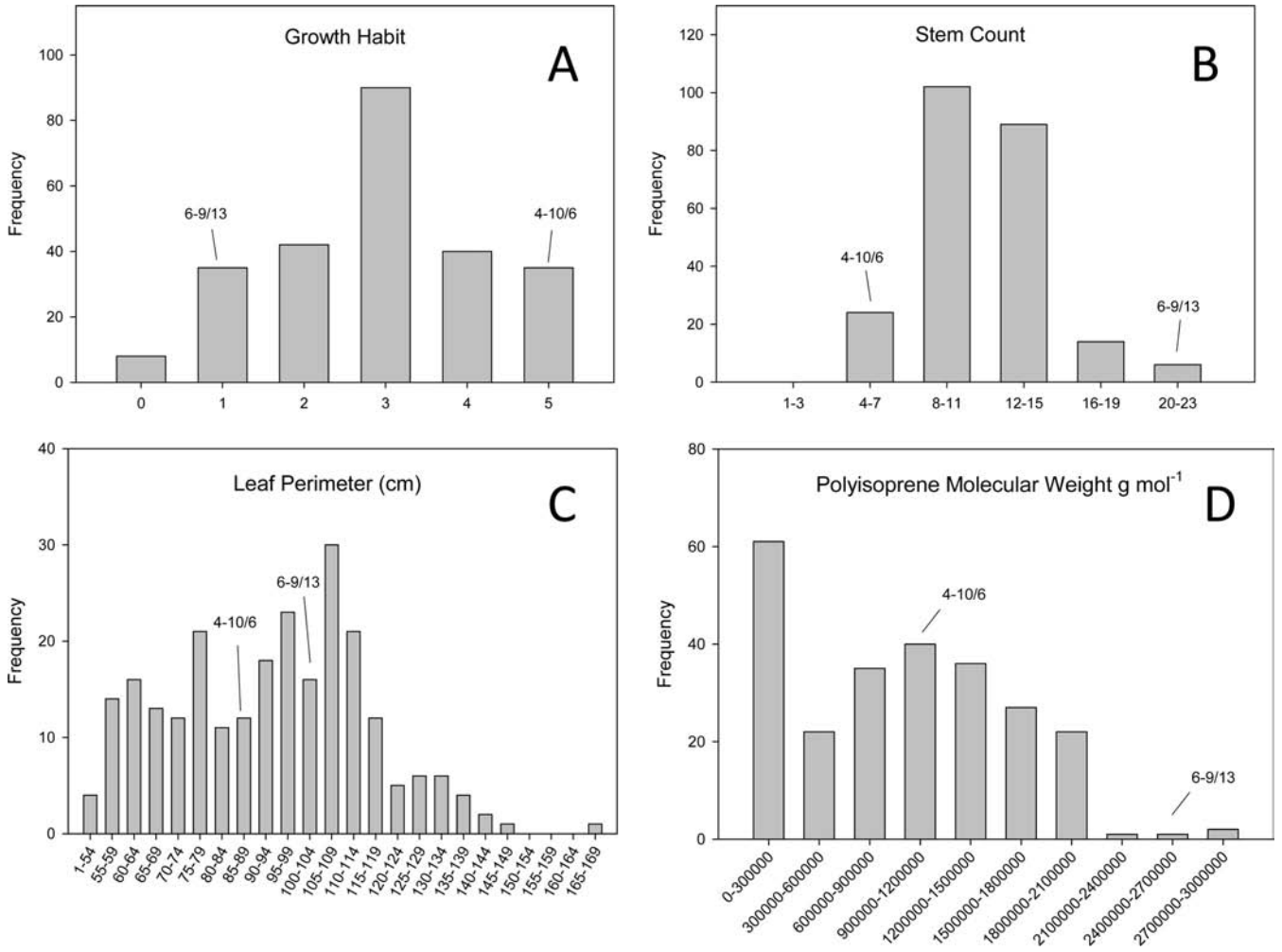

Figure 3. Distribution of selected traits growth habit (A), stem count (B), leaf perimeter (C), and polyisoprene weight (D) showing QTL on groups 4 and 8 from an F2 population derived from a cross of eastern Washington prickly lettuce biotypes 6-9/13 × 4-10/6.

containing insoluble latex material were dried and weighed to find the percentage of insoluble material.

The rubber fraction was further analyzed by high-performance liquid chromatography gel permeation/size exclusion chromatography (HPLC GPC/SEC), with refractive index (RI) detection to evaluate rubber (polyisoprene) polymer chain length (Figure 2). Dried rubber fractions were re-eluted in tetrahydrofuran (THF) to a concentration of approximately 5 mg mL^{-1}. Rubber was allowed to dissolve at room temperature overnight. A 100 μL portion of the dissolved rubber solution was removed from the top, without disturbing any nondissolved material at the bottom of the vial, and transferred to an HPLC vial with a 250 μL glass insert. An autosampler injected 40 μL of the dissolved rubber solution. Samples were analyzed with an Agilent 1100 series HPLC equipped with an Agilent G1362A refractive index detector. Polyisoprene polymers were separated with a Phenogel linear/mixed guard column (10 μM 7.5 × 50 mm), and a PLgel Mixed-B size exclusion column (10 μM 7.5 × 300 mm) using THF as mobile phase. Run time was 17 min with a flow rate of 1 mL min^{-1}. Column and detector were maintained at 40 °C. Molecular weights were extrapolated using polystyrene standards from Varian (EasiVial) to create a semilogarithmic standard curve (Figure 2C). A single standard of 1,4-polyisoprene (M_w 999,000 g mol^{-1}) (Polymer Standards Service) was added to the standard curve as a check against the polystyrene polymers. Agilent GPC software was used together with standards to generate a standard curve and estimate average molecular weight (M_n), weight-average molecular weight (M_w), and polymer dispersity ($Đ$). The values for polyisoprene characterization were determined by selecting the earliest eluting peak (longest polymer). Low $Đ$, a beneficial trait, is independent of polymer M_w but rather reflects the $Đ$ of the selected peak. In this study, the earliest eluting peak may have low M_w and low $Đ$.

Phenotypic values for the entire population were plotted versus frequency to generate histograms (Figures 3 and 4). Analysis of phenotypic frequencies over the population determined if traits were single-gene controlled having expected ratios of 3:1, 1:2:1, or multigenic (quantitative) with a normal distribution. Suspect single-gene traits were examined by chi-square analysis (X^2) and quantitative traits analyzed for QTL (Tables 1 and 2).

Prickly Lettuce Genetic Map. DNA from each individual in the F2 population and parents was extracted from young leaves that were frozen (−80 °C) and freeze-dried. Extraction was performed on approximately 30 mg of dried tissue using a Biosprint 96 DNA Extractor following manufacturer protocols. DNA concentrations were measured with a Nanodrop 2000 spectrophotometer and normalized to 50 ng μL^{-1}. A total of 400 EST-SSR derived primers that were previously mined from the CGPDB to analyze prickly lettuce genetic diversity were used for polymorphic screening.[13] An additional 61 EST-SSR primers developed by Simko[14] were added, giving a total of 461 EST-SSRs available to screen against the crossed parents. Polymorphism of the mined EST-SSRs was carried out using two genotyping platforms. The first employed 10% polyacrylamide gel electrophoresis (PAGE) denaturing gels with silver stain to visualize amplified fragments. Polymerase chain reactions (PCR) were carried out in 20 μL total volume mixtures each containing 100 ng of template DNA, 0.5 μM SSR primers, 250 μM dNTPs, 1.5 mM $MgCl_2$, 0.5× PCR buffer, and 1.0 U *Taq* DNA polymerase (MangoTaq, Bioline

DOI: 10.1021/jf503934v
J. Agric. Food Chem. 2015, 63, 593−602

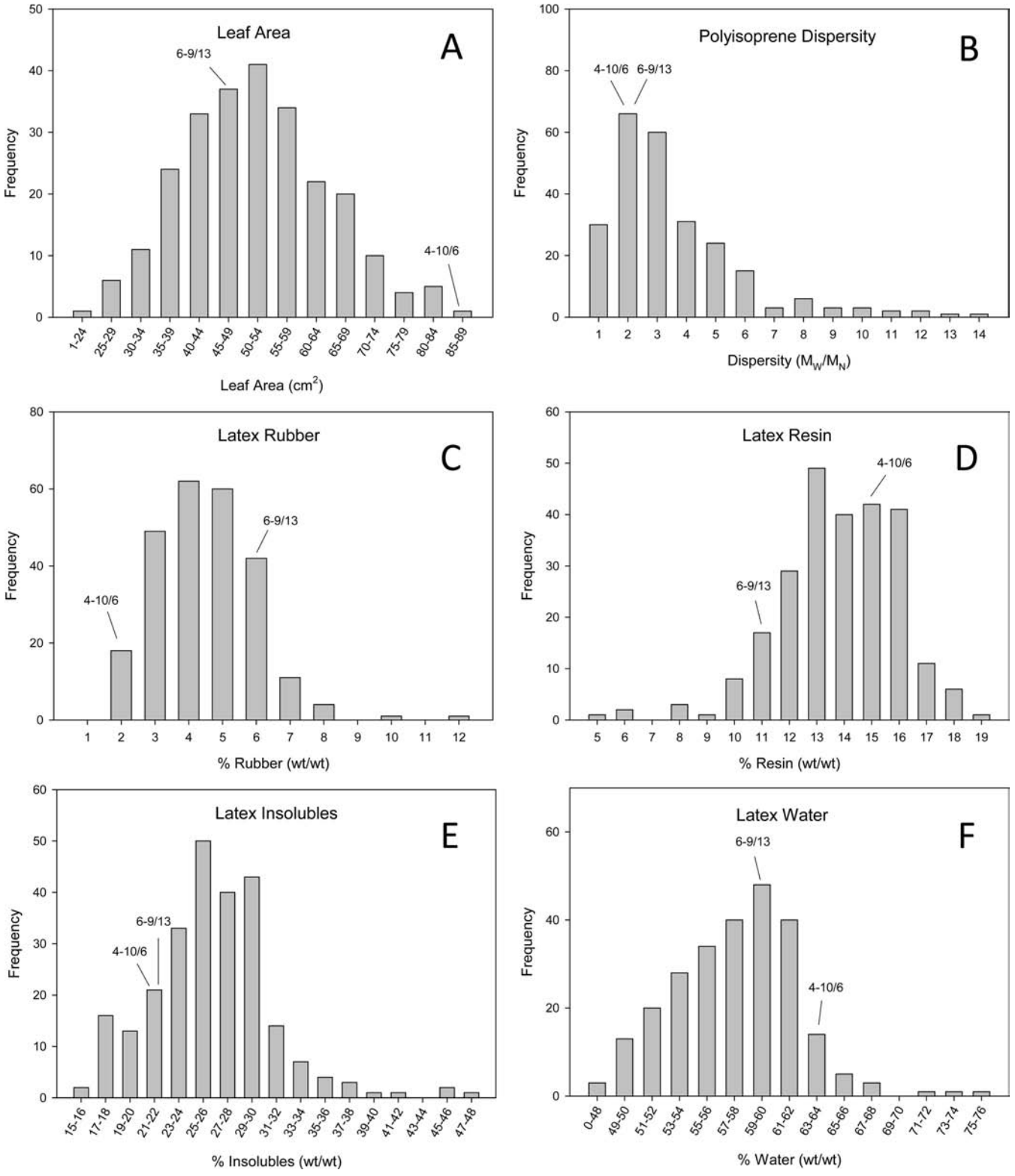

Figure 4. Distribution of phenotypic traits leaf area (A), polyisoprene dispersity (B), latex rubber (C), latex resin (D), latex insolubles (E), and latex water (F) from an F2 population derived from a cross of eastern Washington prickly lettuce biotypes 6-9/13 × 4-10/6.

USA Inc.). Reactions were carried out on a Techne TC-4000 thermocycler with the following PCR profile: initial denaturation at 95 °C for 3 min followed by 40 cycles at 95 °C for 30 s, 57 °C for 30 s, 72 °C for 25 s, and a final extension at 72 °C for 10 min.

Of the 461 primers 380 were further analyzed by a second genotyping platform utilizing an ABI 3730XL DNA analyzer (Applied Biosystems, Foster City, CA, USA). PCR amplifications were carried out in 12 μL reaction mixtures each containing 15 ng of template DNA, and three PCR primers [M13F primer (5′-CACGACGTT-GTAAAACGAC-3′) labeled with one of four fluorescent dyes (6-FAM, PET, VIC, or NED; Applied Biosystems), long forward primer with M13F-tail at its 5′ end and a reverse primer]. Primer concentrations were 0.25 μM reverse primer, 0.20 μM M13F, and 0.05 μM of the long, M13 tagged, forward primer. Other components

DOI: 10.1021/jf503934v
J. Agric. Food Chem. 2015, 63, 593−602

Table 1. Chi-Square Analysis of Potential Prickly Lettuce Single Gene Traits Derived from F2 Population of Cross between Eastern Washington Biotypes 6-9/13 × 4-10/6

	lobing		herbivory		low M_w		
	lobe	no lobe	herb	no herb	M_w > 100000	M_w < 100000	total
observed	186	62	201	47	197	51	248
expected (3:1)	186	62	186	62	186	62	
diff	0	0	15	−15	11	−11	
diff^2	0	0	225	225	121	121	
diff^2/expected	0	0	1.2	3.6	0.7	2.0	
X^2		0		4.8		2.6	

included 200 μM dNTPs, 1.0 mM $MgCl_2$, 1.0× PCR buffer, and 1.0 U of *Taq* DNA polymerase. PCR amplifications were done on a Bio-Rad C1000 or S1000 thermocycler using the following conditions: initial denaturation at 95 °C for 3 min followed by 42 cycles at 95 °C for 40 s, 57 °C for 60 s, 72 °C for 60 s, and a final extension at 72 °C for 10 min.

Segregation Analysis/Linkage Maps. Initially, 89 polymorphic EST-SSR markers were selected and used to create a genetic linkage map (Supporting Information, Supplementary Table 1). Of the 248 individuals in the F2 population, 186 were analyzed to facilitate 96 and 384 well formats. Fragment analysis of markers in the F2 population was carried out using an Applied Biosystems 3730XL DNA analyzer and GENE MARKER software version 1.5.[41] PCR conditions were the same as described for the parental screen in the second genotyping platform. Fragments were scored as either parent 1 (a), parent 2 (b), or heterozygous (h). Scored data were analyzed by JoinMap 4.0[42] using maximum likelihood algorithm with all other parameters set to default. The Haldane mapping function was used to calculate genetic distances. Maps were verified using Mapmaker 3.0b[43] at a LOD score of 3.0. The traits of leaf lobing and herbivory were scored bimodally as presence or absence phenotypes and analyzed by chi square (Table 1).

Polymorphism. Marker polymorphism was determined as the difference in nucleotide base pairs between parents as established by the ABI 3730XL DNA analyzer (Supporting Information, Supplementary Table 1). Fragment sizes were estimated by comparison to a size standard added to each well and tagged with fluorescent dye LIZ.

Trait Genetic Markers/QTL Analysis. F2 genotypic and phenotypic data were analyzed using MapQTL 6.0[44] to assist in identifying marker−trait correlations. Analysis was done using both interval mapping (IM) to allow for possible correlations with the unmapped markers and multiple-QTL model (MQM). Default parameters for IM were used and included algorithm, regression; test statistic, LOD; fit dominance for F2, yes; mapping step size, 1.0; neighboring markers, 5; number of iterations, 200; functional tolerance, 1.0×10^{-8}; and permutation, 1000. MQM model had the same default parameters. Chromosomes with associated QTL were made using MapChart 2.2[45] (Figure 5).

To determine the LOD score significance thresholds, a permutation test of 10000 iterations (p = 0.05) was performed over each chromosome.[46] QTL were considered significant if the output over the chromosome for the trait of interest exceeded the minimum threshold.

RESULTS AND DISCUSSION

Phenotypic Assessment. Phenotypes in the F2 population were quantitative in that they did not follow Mendelian segregation ratios with the exceptions of leaf lobing and low M_w. These traits segregated at a ratio of 3:1 (X^2 = 0 df 1) and (X^2 = 2.6 df 1), respectively (Table 1). Leaf lobing observed in this experiment is consistent with previous reports for inheritance of the trait, where lobing was reported as dominant to nonlobed leaves and controlled by a single gene.[47,48] The plant growth phenotypes growth habit and stem count had normal distributions with the majority of phenotypes intermediate between parents (Figure 3A,B). Leaf perimeter also had a less defined normal distribution pattern (Figure 3C). Leaf area in the F2 population had a normal distribution with the median closer to that of parent 6-9/13 and very few individuals sharing a large leaf area phenotype similar to that of 4-10/6 (Figure 4A). Rubber Đ values over the population were normally distributed (Figure 4B) and appear skewed to higher Đ; however, values cannot fall below the optimal Đ of one.

Normal distributions were observed for all latex components including the amount of rubber, resin, insoluble material, and water contained in the latex (Figure 4C−F). The M_w of the rubber from the F2 population was normally distributed; however, there was an enrichment of individuals with low M_w

Table 2. QTL and Associated Markers Found in an F2 Population Derived from a Cross of the Eastern Washington Prickly Lettuce Biotypes 6-9/13 × 4-10/6

trait	QTL location	phenotypic variation (%)	peak value	threshhold 0.05	additive	dominance	parental allele
rubber M_w	8, WSULs-21	6.9	2.87	2.2	215898	118670	6-9/13
	8, WSULs-374.2	7.7	3.24	2.2	223844	145724	6-9/13
dispersity[a]	WSULs-374.1	11.2	4.79	NA	0.94	−0.27	6-9/13
leaf perimeter	8, WSULs-102	40.3	20.87	2.2	19.15	4.97	6-9/13
	8, WSULs-212	49.2	27.32	2.2	21.09	9.12	6-9/13
lobing	8, WSULs-102	52.0	29.68	2.2	0.37	0.32	6-9/13
	8, WSULs-212	67.5	45.39	2.2	0.42	0.41	6-9/13
herbivory	8, WSULs-374.2	7.7	3.25	2.2	−0.07	−0.17	6-9/13
growth habit	4, WSULs-304	25.6	11.94	2.5	−0.92	0.04	6-9/13
	4, WSULs-383	7.1	2.98	2.5	−0.36	0.41	6-9/13
stem count	4, WSULs-304	29	13.84	2.6	3.55	1.07	6-9/13
	4, WSULs-383	8.1	3.43	2.6	1.62	0.92	6-9/13

[a]Unmapped marker, non-QTL, single-marker association as determined by IM.

DOI: 10.1021/jf503934v
J. Agric. Food Chem. 2015, 63, 593−602

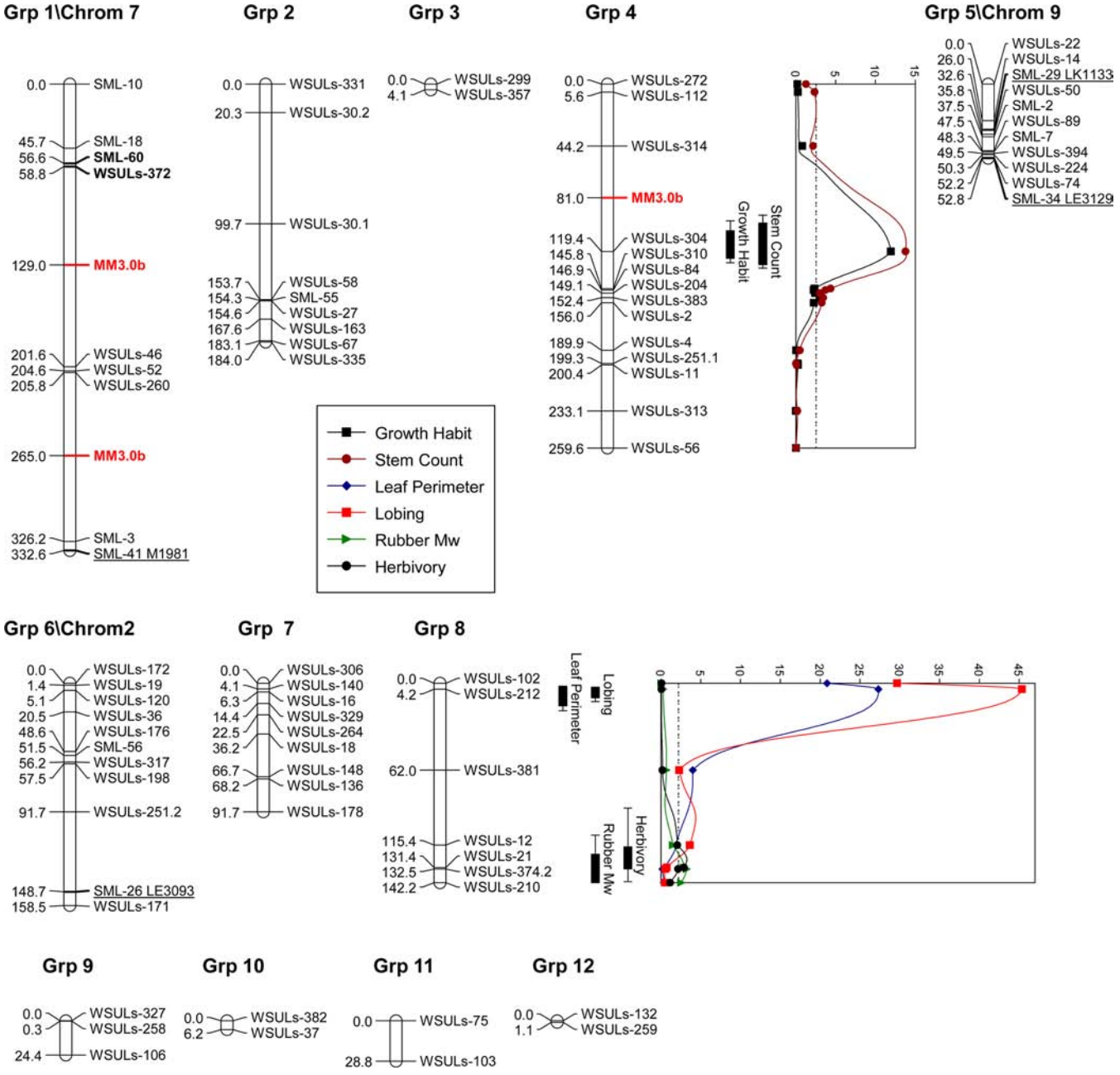

Figure 5. Linkage groups and QTL from eastern Washington prickly lettuce biotype cross (6-9/13 × 4-10/6). Group designations were derived from JoinMap 4.0 software. Bold, red markers with designation MM3.0b are further separation of linkage groups determined by MapMaker 3.0b. Chromosome designations were assigned on the basis of mapped EST markers found in CGPDB and are underlined. The bold markers SML-60 and WSULs-372 were derived from the same EST contig but found in independent SSR mining experiments. Significant QTLs are shown next to linkage groups as black bars with 1 and 2 LOD QTL intervals and corresponding QTL LOD graph.

rubber (Figures 2B and 3D). The reason for the elevated number of extremely low M_w phenotypes is unclear. Rubber from these individuals may have degraded at some point during collection, storage, or extraction. Alternatively, the individuals with low M_w rubber may have underlying genetic influences affecting polymer stability or determinant polymer length. Just under 25% of the F2 population had inferior, low M_w rubber (<100000 g mol^{-1}), suggesting the low M_w phenotype may be a single-gene trait (Table 1). Repeated studies from a recombinant inbred line (RIL) derived from the cross made for this study will assist in determining whether the low M_w phenotype is an artifact of sampling or a defined genetic trait.

Linkage Maps. Of the original 89 markers, 3 were not linked to any linkage group and 5 dominant markers did not map, leaving 81 mapped markers in 12 linkage groups (Figure 5). The chromosome number for lettuce and prickly lettuce is 9.[49] Discrepancies in chromosome number are most likely due to the low number of markers used in this study. A few of the markers previously mapped in the CGPDB and were used as anchors for assigning chromosome names for the associated linkage group. On the basis of maps generated in the CGPDB, some of the linkage groups made by JoinMap 4.0 in this study had distances longer or shorter than would be expected (Figure 5). For example, group 1 is anchored by SML-41 and corresponds to chromosome 7 in CGPDB, MAP 2 JMR2.

DOI: 10.1021/jf503934v
J. Agric. Food Chem. 2015, 63, 593−602

Chromosome 7 is 126.8 cM in length compared to 332.6 cM in this study. Group 5 is anchored by markers SML-29 and SML-34, both on chromosome 9 of MAP 2 JMR2. Chromosome 9 is 102.9 cM compared to our 52.8 cM distance. Group 6 is anchored by SML-26 to chromosome 2, which is 162.1 cM in MAP 2 JMR2, a much closer distance to 158.5 cM of this study; however, SML-26 is placed near the middle of MAP 2 JMR2 at 72.0 cM, whereas in our map SML-26 is nearer the end at 148.7 cM.

MapMaker 3.0b was used to verify grouping made by JoinMap. Mapmaker was more stringent in grouping of markers and further divided some of the linkage groups generated in JoinMap. The distinction is noted by bold, red markers designated as MM3.0b placed half the distance between the flanking mapped markers in the chromosome groupings. In general, JoinMap 4.0 and MapMaker 3.0b grouped markers similarly, lending confidence to the map structure.

Rubber Trait QTL. Of particular interest in this study are the markers and QTL linked to rubber traits. One QTL and one unmapped marker had significant correlations to rubber traits M_w and polymer Đ. Rubber M_w had a QTL associated with group 8 near markers WSULs-374.2 and WSULs-21. The rubber M_w QTL peaks near marker WSULs-374.2, at LOD 3.24, and accounted for 7.7% of the phenotypic variation in the population (Figure 5; Table 2).

Dispersity is a measure of polymer homogeny as measured by weight-average molecular weight divided by the number-average molecular weight (M_w/M_n) (Stepto 2009). An optimal ratio of 1.0 signifies uniform polymers. Dispersity is a beneficial trait if the rubber also has high M_w. The marker WSULs-374.1 had significant linkage to Đ with a peak LOD value of 4.79 and explained 11.2% of the phenotypic variation (Table 2) as determined by IM. It is important to note that the Đ and M_w values were based on the earliest eluting peak by HPLC-SEC/GPC and are therefore not necessarily correlated to one another. Low Đ does not mean high M_w. Review of the Đ and M_w values reveals that the majority of individuals with low Đ were more closely related to the low M_w individuals in the population. Interpretation of the marker is counterintuitive and suggests that the higher Đ values are representative of a beneficial trait. Although high Đ is less desirable, nearly all of the Đ values in the population from the earliest eluting peak would be considered acceptable for production purposes.[50]

The WSULs-374 markers are derived from the same primer yet generated distinct PCR products that segregated sufficiently to separate the two at a LOD threshold of 3.0. At LOD 2.0 WSULs-374.1 and WSULs-374.2 are grouped together; however, at this threshold they are separated by 122.1 cM. Both the rubber M_w QTL and Đ marker are derived from 6-9/13 alleles. This single marker could be used for selection and integration of prickly lettuce with acceptable Đ and high M_w rubber, the two most important traits in determining rubber end-use potential.[51]

Other Beneficial Traits. Cultivated lettuce cultivars have been developed to meet consumer and producer needs. Most have a delayed bolt time and, if allowed to bolt, have only a single stem. Cultivated lettuce produces copious leaf tissue and little latex during vegetative growth.[52] Many of these traits are in stark contrast to those desired in a rubber-producing cultivar. Anecdotal evidence suggests latex production increases with bolt initiation.[4] In this regard, early bolting with multiple stems would both be beneficial traits for rubber lettuce production. A strong growth habit and stem count QTL was identified in our study on group 4 that is highly correlated to marker WSULs-304 (Figure 5). The QTL significance continues at a lower level over a group of adjacent markers WSULs-310, WSULs-84, WSULs-204, WSULs-383, and WSULs-2 with the highest significance at marker WSULs-383 in this group. The growth habit phenotype was characterized by early bolt time with multiple lateral shoots. The growth habit QTL peaked at LOD 11.94 near marker WSULs-304 and LOD 2.98 near WSULs-383 and respectively explained 25.6 and 7.1% of the population phenotypic variation (Figure 5; Table 2).

As expected, stem count is strongly related to growth habit as a numerical reflection of the growth habit phenotype. The stem count QTL also peaked at markers near WSULs-304 and WSULs-383 with respective LOD values 13.84 and 3.43 and phenotypic variances 29.0 and 8.1% (Figure 5; Table 2). Growth habit associated markers will assist in selection of rubber lettuce cultivars that bolt early and have many stems. These traits may also facilitate multiple harvests over the season, increasing rubber yields. Alternative to harvesting fast-bolting multistem plants, crisphead lettuce cultivars possessing high latex and rubber content yet remain as compact heads would be ideal for current lettuce cultivation and harvest practices. Many of the head lettuce cultivars have high biomass (700−1000 g head^{-1}), disease resistance, and reduced chlorophyll content.[52] The crisphead lettuce cv. 'Salinas', released in 1975, is the most widely grown lettuce cultivar in the history of lettuce production.[52] Introgression of alleles that confer high rubber content and M_w in nonbolting head lettuce such as 'Salinas' lettuce leaf tissue would be well suited for current cultivation practices. The identified markers and QTL are useful tools for MAS and introgression of those traits into new rubber lettuce varieties. Further selection of prickly lettuce weedy traits, such as water use efficiency, would allow rubber lettuce to be grown on marginal lands, decreasing competition with existing lettuce production areas and other food crops.

In this study additional interesting marker−phenotype associations, not necessarily related to rubber lettuce development, have been identified. Leaf perimeter, a numerical expression of leaf lobing, and herbivory both had significant QTL on group 8 (Figure 5). As previously noted, lettuce leaf lobing has been identified as a dominant, single-gene trait.[47,48] Leaf perimeter QTL is associated with markers WSULs-102 and WSULs-212, which had respective peak LOD values of 20.87 and 27.32 and explained 40.3 and 49.2% of the phenotypic variation for the population (Figure 5; Table 2). The histogram for leaf perimeter is not normal and may be more indicative of epistatic interactions. The QTL for the lobing phenotype was stronger than the perimeter trait with peak LOD values of 29.7 and 45.4 at respective markers WSULs-102 and WSULs-212. Population phenotypic variance for the lobing trait was 52.0% near marker WSULs-102 and 67.5% at WSULs-212. Leaf lobing is an important horticultural trait in cultivated lettuce.[53] On an evolutionary level, lobed leaves may impart greater hydraulic efficiency and heat dissipative properties.[54,55] There are no reports of a leaf lobing gene in lettuce; however, a single large effect QTL has been identified on chromosome 3 through analysis of the core F7:8 RIL mapping population derived from a cross between *L. sativa* cv. 'Salinas' and *L. serriola* accession UC96US23.[53] The QTL found in this study is most likely the same found by Michelmore placing group 8 markers on chromosome 3 of the lettuce map.

DOI: 10.1021/jf503934v
J. Agric. Food Chem. 2015, 63, 593−602

On the basis of sequence similarity, the EST related to marker WSULs-102 resembles the *Arabidopsis thaliana* cyclin family protein AT5G67260 (CYCD3;2) (Supporting Information, Supplementary Table 1). In general, cyclin proteins act as transcription factors activating cyclin-dependent kinases during the cell cycle, in turn regulating key transitions during mitosis.[56] In *Arabidopsis*, CYCD3;2 is expressed in the shoot apical meristem and persists in young leaves. CYCD3;2 functions by determining cell number in developing lateral organs and mediating the effects of cytokinin on apical growth and development.[57] Leaf morphogenesis in tomato was dependent on cytokinin levels, and overexpression of a cytokinin biosynthesis gene IPK7 caused increased expression of CYCD3.[58]

The EST for WSULs-212 has similarity to AT4G14960 tubulin α-6 chain (TUA6) (Supporting Information, Supplementary Table 1). TUA6 encodes an isoform of tubulin necessary for right-handed helical growth.[59] It is interesting to find that both EST-SSRs markers associated with the leaf perimeter and lobing QTLs are involved in plant organ morphogenesis. Further study of these genes in lettuce would determine if either of the genes is the causal agent for leaf lobing in lettuce. Overexpression of the genes in a nonlobed lettuce background could help identify these candidate genes as the leaf lobing gene in lettuce.

A prickly lettuce herbivory QTL was found on group 8 and peaked at LOD 3.25 near marker WSULs-374.2. The population phenotypic variance for the QTL was 7.7% (Figure 5; Table 2). The phenotype was observed as preferential feeding of bolted stems in the F2 population by white tail deer (*Odocoileus virginianus* Zimmermann.). Evidence suggests latex is a beneficial adaptation to deter herbivory.[60,61] One example in lettuce was found where latex from an insect-resistant cultivar, 'Valmaine', prevented *Diabrotica balteata* (LeConte.) beetles from feeding on latex-painted lima bean leaves; however, feeding was not inhibited when latex from the susceptible cultivar 'Tall Guzmaine' was applied.[62] A follow-up study showed that differential compounds in the semipolar latex extract contained the inhibitory element(s).[63] Prickly lettuce contains an abundance of the sesquiterpine lactones lactucin and lactucopicrin.[64] Increase in the levels of these compounds was correlated to perceived bitterness by sensory analysis.[65] The compounds also have sedative and analgesic affects.[66] Chemical analysis of the resin extracts containing the sesquiterpines compared with plant feeding patterns will help determine if these compounds act as a deer herbivory deterrents or stimulants.

In summary, a set of polymorphic EST-SSRs have been used to generate a linkage map from a cross between two distinct eastern Washington prickly lettuce biotypes. Analysis of the map with phenotypic data has led to the discovery of QTL and markers useful in the development of rubber lettuce cultivars. The identified QTL and corresponding local markers could be used in a MAS breeding scheme to find individuals with high M_w rubber and multibolting traits or introgression of rubber-producing traits into current lettuce cultivars. Importantly, the QTL will allow further investigation of the genes that control these traits now that linked chromosomal regions have been identified. Additional QTL and markers related to lettuce leaf morphology and herbivory could be used in lettuce breeding for horticultural traits and understanding leaf ontogeny or lend evidence to latex herbivory relationships.

■ ASSOCIATED CONTENT

Ⓢ Supporting Information

Supplementary Table 1 referencing markers used to generate the map and subsequent analysis; information includes marker names, contig from which EST-SSR was mined, SSR motif, primer sequences, product size, polymorphism, GCPBD annotation, and putative gene function. This material is available free of charge via the Internet at http://pubs.acs.org.

■ AUTHOR INFORMATION

Corresponding Author

*(I.C.B.) Mail: Department of Crop and Soil Sciences, Johnson Hall 163, Washington State University, Pullman, WA 99164-6420, USA. E-mail: cburke@wsu.edu. Phone: (509) 335-2858. Fax: (509) 335-8674.

Funding

We acknowledge funding for this project through the *Aegilops cylindrica* – Biomass for Biofuels and Bioproducts from Weedy Plants (NIFA/USDA special grant) and Hatch Project WNP00753.

Notes

The authors declare no competing financial interest.

■ ACKNOWLEDGMENTS

Special thanks go to Lydia Baxter, Nicholas Boydston, Madeline Jacobson, Misha Manuchehri, Dennis Pittman, Alan Raeder, Dilpreet Riar, Sachin Rustgi, Sherri Rynearson, Deven See, Jamin Smitchger, and Randall Stevens from the Department of Crop and Soil Sciences, Washington State University, for their technical assistance in laboratory and field studies.

■ REFERENCES

(1) International Rubber Study Group, http://www.rubberstudy.com/ (accessed Sept 17, 2012).

(2) Mooibroek, H.; Cornish, K. Alternative sources of natural rubber. *Appl. Microbiol. Biotechnol.* **2000**, *53*, 355–365.

(3) Van Beilen, J. B.; Poirier, Y. Guayule and Russian dandelion as alternative sources of natural rubber. *Crit. Rev. Biotechnol.* **2007**, *27*, 217–231.

(4) Bushman, B. S.; Scholte, A. A.; Cornish, K.; Scott, D. J.; Brichta, J. L.; Vederas, J. C.; Ochoa, O.; Michelmore, R. W.; Shintani, D. K.; Knapp, S. J. Identification and comparison of natural rubber from two *Lactuca* species. *Phytochemistry* **2006**, *67*, 2590–2596.

(5) Koopman, W. J. M.; Zevenbergen, M. J.; den Berg, R. G. V. Species relationships in *Lactuca s.l.* (Lactuceae, Asteraceae) inferred from AFLP fingerprints. *Am. J. Bot.* **2001**, *88*, 1881–1887.

(6) Mou, B. Nutritional quality of lettuce. *Curr. Nutr. Sci.* **2012**, *8*, 177–187.

(7) Nicolle, C.; Cardinault, N.; Gueux, E.; Jaffrelo, L.; Rock, E.; Mazur, A.; Amouroux, P.; Rémésy, C. Health effect of vegetable-based diet: lettuce consumption improves cholesterol metabolism and antioxidant status in the rat. *Clin. Nutr.* **2004**, *23*, 605–614.

(8) Michelmore, R. *Compositae Genome Project*, http://compgenomics.ucdavis.edu/ (accessed Nov 24, 2012).

(9) Kesseli, R.; Ochoa, O.; Michelmore, R. Variation at RFLP loci in *Lactuca* spp. and origin of cultivated lettuce (*L. sativa*). *Genome* **1991**, *34*, 430–436.

(10) Kesseli, R. V.; Paran, I.; Michelmore, R. W. Analysis of a detailed genetic linkage map of *Lactuca sativa* (lettuce) constructed from RFLP and RAPD markers. *Genetics* **1994**, *136*, 1435–1446.

(11) Waycott, W.; Fort, S. B. Differentiation of nearly identical germplasm accessions by a combination of molecular and morphologic analyses. *Genome Natl. Res. Counc. Can. Genome Cons. Natl. Rech. Can.* **1994**, *37*, 577–583.

DOI: 10.1021/jf503934v
J. Agric. Food Chem. 2015, 63, 593–602

(12) Vicente, M. J.; Conesa, E.; Franco, J. A.; Esteva, J.; Martinez-Sanchez, J. J. Genetic variability in lettuce (*Lactuca sativa*) germplasm using morphologic and molecular analyses. *Acta Hortic.* **2008**, *782*, 59−66.
(13) Riar, D. S.; Rustgi, S.; Burke, I. C.; Gill, K. S.; Yenish, J. P. EST-SSR development from 5 *Lactuca* species and their use in studying genetic diversity among *L. serriola* biotypes. *J. Hered.* **2011**, *102*, 17−28.
(14) Simko, I. Development of EST-SSR markers for the study of population structure in lettuce (*Lactuca sativa* L.). *J. Hered.* **2009**, *100*, 256−262.
(15) Van de Wiel, C.; Arens, P.; Vosman, B. Microsatellite retrieval in lettuce (*Lactuca sativa* L.). *Genome Natl. Res. Counc. Can. Genome Cons. Natl. Rech. Can.* **1999**, *42*, 139−149.
(16) Jeuken, M.; van Wijk, R.; Peleman, J.; Lindhout, P. An integrated interspecific AFLP map of lettuce (*Lactuca*) based on two *L. sativa* × *L. saligna* F2 populations. *Theor. Appl. Genet.* **2001**, *103*, 638−647.
(17) Jansen, J.; Verbakel, H.; Peleman, J.; Hintum, T. J. L. A note on the measurement of genetic diversity within genebank accessions of lettuce (*Lactuca sativa* L.) using AFLP markers. *Theor. Appl. Genet.* **2005**, *112*, 554−561.
(18) Hu, J.; Ochoa, O.; Truco, M.; Vick, B. Application of the TRAP technique to lettuce (*Lactuca sativa*) genotyping. *Euphytica* **2005**, *144*, 225−235.
(19) Moreno-Vázquez, S.; Ochoa, O. E.; Faber, N.; Chao, S.; Jacobs, J. M. E.; Maisonneuve, B.; Kesseli, R. V.; Michelmore, R. W. SNP-based codominant markers for a recessive gene conferring resistance to corky root rot (*Rhizomonas suberifaciens*) in lettuce (*Lactuca sativa*). *Genome* **2003**, *46*, 1059−1069.
(20) Van Leeuwen, H.; Stoffel, K.; Kozik, A.; Cui, X.; Ashrafi, H.; McHale, L.; Lavelle, D.; Wong, G.; Chen, F.; Truco, M.; Van Deynze, A.; Michelmore, R. W. High-density mapping of the lettuce genome with SFP markers in over 15,000 unigenes. *Proceedings of the Plant and Animal Genomes XVII Conference*, San Diego, CA, January 2009.
(21) Truco, M. J.; Antonise, R.; Lavelle, D.; Ochoa, O.; Kozik, A.; Witsenboer, H.; Fort, S. B.; Jeuken, M. J. W.; Kesseli, R. V.; Lindhout, P.; Michelmore, R. W.; Peleman, J. A high-density, integrated genetic linkage map of lettuce (*Lactuca* spp.). *Theor. Appl. Genet.* **2007**, *115*, 735−746.
(22) Kuang, H.; van Eck, H. J.; Sicard, D.; Michelmore, R.; Nevo, E. Evolution and genetic population structure of prickly lettuce (*Lactuca serriola*) and its RGC2 resistance gene cluster. *Genetics* **2008**, *178*, 1547−1558.
(23) Reyes-Chin-Wo, S. *Lettuce Genome Resource*, https://lgr.genomecenter.ucdavis.edu/ (accessed Sept 17, 2012).
(24) Lebeda, A. *Biodiversity of the Interactions between Germplasms of Wild Lactuca spp. and Related Genera and Lettuce Downy Mildew (Bremia lactucae)*; report on research programme OECD Biological Resource Management for Sustainable Agricultural Systems; HRI Wellesbourne: UK, 1998; Vol. 70.
(25) Lebeda, A.; Pink, D. A. C.; Astley, D. Aspects of the interactions between wild *Lactuca* spp. and related genera and lettuce downy mildew (*Bremia lactucae*). In *Advances in Downy Mildew Research*; Spencer-Phillips, P. T. N., Gisi, U., Lebeda, A., Eds.; Springer: Dordrecht, The Netherlands, 2002; pp 85−117.
(26) Reinink, K. Lettuce resistance breeding. Proceedings of the Eucarpia meeting on leafy vegetables genetics and breeding, Olomouc, Czech Republic, Jun 8−11, 1999. Palacky University, 1999.
(27) Ryder, E. J. *Lettuce, Endive, and Chicory*; CABI Publishing: Wallingford, UK, 1999.
(28) Sicard, D.; Woo, S. S.; Arroyo-Garcia, R.; Ochoa, O.; Nguyen, D.; Korol, A.; Nevo, E.; Michelmore, R. W. Molecular diversity at the major cluster of disease resistance genes in cultivated and wild *Lactuca* spp. *Theor. Appl. Genet.* **1999**, *99*, 405−418.
(29) Zohary, D. The wild genetic resources of cultivated lettuce (*Lactuca sativa* L.). *Euphytica* **1991**, *53*, 31−35.
(30) Ellis, P. R.; McClement, S. J.; Saw, P. L.; Phelps, K.; Vice, W. E.; Kift, N. B.; Astley, D.; Pink, D. A. C. Identification of sources of resistance in lettuce to the lettuce root aphid (*Pemphigus bursarius*). *Euphytica* **2002**, *125*, 305−315.
(31) Kishaba, A. N.; McCreight, J. D.; Coudriet, D. L.; Whitaker, T. W.; Pesho, G. R. Studies of ovipositional preference of cabbage looper on progenies from a cross between cultivated lettuce and prickly lettuce. *J. Am. Soc. Hortic. Sci.* **1980**, *105*, 890−892.
(32) Mou, B.; Liu, Y. B. Host plant resistance to leafminers in lettuce. *J. Am. Soc. Hortic. Sci.* **2004**, *129*, 383−388.
(33) Mou, B. Genetic variation of β-carotene and lutein contents in lettuce. *J. Am. Soc. Hortic. Sci.* **2005**, *130*, 870−876.
(34) Ryder, E. J.; Milligan, D. C. Additional genes controlling flowering time in *Lactuca sativa* and *L. serriola*. *J. Am. Soc. Hortic. Sci.* **2005**, *130*, 448−453.
(35) Johnson, W. C.; et al. Lettuce, a shallow-rooted crop, and *Lactuca serriola*, its wild progenitor, differ at QTL determining root architecture and deep soil water exploitation. *Theor. Appl. Genet.* **2000**, *101*, 1066−1073.
(36) Harlan, J. R.; Wet, J. M. J. de Toward a rational classification of cultivated plants. *Taxon* **1971**, *20*, 509−517.
(37) McGuire, P. E.; Ryder, E. J.; Michelmore, R. W.; Clark, R. L.; Antle, R.; Emery, E.; Hannan, R. M.; Kesseli, R. V.; Kurtz, E. A.; Ochoa, O.; Rubatzky, E.; William, W. *Genetic Resources of Lettuce and Lactuca Species in California: An Assessment of the USDA and UC Collections and Recommendations for Long-Term Security*, report 12; University of California Genetic Resources Conservation Program: Los Angeles, CA, USA, 1993.
(38) De Vries, I. M. Origin and domestication of *Lactuca sativa* L. *Genet. Resour. Crop Evol.* **1997**, *44*, 165−174.
(39) Nagata, R. T. Clip-and-wash method of emasculation for lettuce. *HortScience* **1992**, *27*, 907−908.
(40) Rasband, W. S. *Image Processing with ImageJ*; National Institutes of Health, 1997, http://imagej.nih.gov/ij/ (accessed Sept 10, 2010).
(41) SoftGenetics LLC. *GeneMarker*; 2006.
(42) Van Ooijen, J. W. *JoinMap ® 4, Software for the Calculation of Genetic Linkage Maps in Experimental Populations*. Kyazama B.V., 2006.
(43) Lander, E. S.; Green, P.; Abrahamson, J.; Barlow, A.; Daly, M. J.; Lincoln, S. E.; Newburg, L. MAPMAKER: an interactive computer package for constructing primary genetic linkage maps of experimental and natural populations. *Genomics* **1987**, *1*, 174−181.
(44) Van Ooijen, J. W. *MapQTL ® 6, Software for the Mapping of Quantitative Trait Loci in Experimental Populations of Diploid Species*, Kyazama B.V., 2009.
(45) Voorrips, R. E. MapChart: software for the graphical presentation of linkage maps and QTLs. *J. Hered.* **2002**, *93*, 77−78.
(46) Churchill, G. A.; Doerge, R. W. Empirical threshold values for quantitative trait mapping. *Genetics* **1994**, *138*, 963−971.
(47) Durst, C. E. Inheritance in lettuce. *Bull. Ill. Agric. Exp. Stn.* **1930**, *No. 356*, 239−341.
(48) Whitaker, T. W. The genetics of leaf form in cultivated lettuce. I. The inheritance of lobing. *Proc. Am. Soc. Hortic. Sci.* **1950**, *56*, 389−94.
(49) Babcock, E. B.; Stebbins, G. L. J.; Jenkins, J. A. Chromosomes and phylogeny in some genera of the Crepidineae. *Cytol. Fujii Jubil.* **1937**, 188−210.
(50) Kovuttikulrangsie, S.; Sakdapipanich, J. T. The molecular weight (MW) and molecular weight distribution (MWD) of NR from different age and clone *Hevea* trees. *Songklanakarin J. Sci. Technol.* **2004**, *27*, 337−342.
(51) Swanson, C. L.; Buchanan, R. A.; Otey, F. H. Molecular weights of natural rubbers from selected temperate zone plants. *J. Appl. Polym. Sci.* **1979**, *23*, 743−748.
(52) Mou, B. In *Handbook of Plant Breeding, Vol. Veg. Asteraceae, Brassicaceae, Chenopodicaceae, Cucurbitaceae*; Prohens, J., Nuez, F., Eds.; Springer: New York, 2008; Vol. 1.
(53) Michelmore, R. W. *California Leafy Greens Research Program: Genetic Variation in Lettuce*l University of California, Davis, CA, USA, 2009; available at http://calgreens.org/control/uploads/Genetic_Variation_in_Lettuce_-_Michelmore.pdf (accessed Nov 26, 2012).

DOI: 10.1021/jf503934v
J. Agric. Food Chem. 2015, 63, 593−602

(54) Nicotra, A. B.; Leigh, A.; Boyce, C. K.; Jones, C. S.; Niklas, K. J.; Royer, D. L.; Tsukaya, H. The evolution and functional significance of leaf shape in the angiosperms. *Funct. Plant Biol.* **2011**, *38*, 535−552.
(55) Sack, L.; Tyree, M. T. Leaf hydraulics and its implications in plant structure and function. In *Vascular Transport in Plants*; Holbrook, N. M., Zwieniecki, M. A., Eds.; Elsevier Academic Press: Burlington, MA, USA, 2005; pp 93−114.
(56) Jackson, P. K. The hunt for cyclin. *Cell* **2008**, *134*, 199−202.
(57) Dewitte, W.; Scofield, S.; Alcasabas, A. A.; Maughan, S. C.; Menges, M.; Braun, N.; Collins, C.; Nieuwland, J.; Prinsen, E.; Sundaresan, V.; Murray, J. A. H. Arabidopsis CYCD3 D-type cyclins link cell proliferation and endocycles and are rate-limiting for cytokinin responses. *Proc. Natl. Acad. Sci. U.S.A.* **2007**, *104*, 14537−14542.
(58) Shani, E.; Ben-Gera, H.; Shleizer-Burko, S.; Burko, Y.; Weiss, D.; Ori, N. Cytokinin regulates compound leaf development in tomato. *Plant Cell Online* **2010**, *22*, 3206−3217.
(59) Abe, T.; Hashimoto, T. Altered microtubule dynamics by expression of modified α-tubulin protein causes right-handed helical growth in transgenic *Arabidopsis* plants. *Plant J.* **2005**, *43*, 191−204.
(60) Agrawal, A. A.; Konno, K. Latex: a model for understanding mechanisms, ecology, and evolution of plant defense against herbivory. *Annu. Rev. Ecol. Evol. Syst.* **2009**, *40*, 311−331.
(61) Konno, K. Plant latex and other exudates as plant defense systems: roles of various defense chemicals and proteins contained therein. *Phytochemistry* **2011**, *72*, 1510−1530.
(62) Huang, J.; McAuslane, H. J.; Nuessly, G. S. Resistance in lettuce to *Diabrotica balteata* (Coleoptera: Chrysomelidae): the roles of latex and inducible defense. *Environ. Entomol.* **2003**, *32*, 9−16.
(63) Sethi, A.; McAuslane, H. J.; Alborn, H. T.; Nagata, R. T.; Nuessly, G. S. Romaine lettuce latex deters feeding of banded cucumber beetle: a vehicle for deployment of biochemical defenses. *Entomol. Exp. Appl.* **2008**, *128*, 410−420.
(64) Sessa, R. A.; Bennett, M. H.; Lewis, M. J.; Mansfield, J. W.; Beale, M. H. Metabolite profiling of sesquiterpene lactones from *Lactuca* species. *J. Biol. Chem.* **2000**, *275*, 26877−26884.
(65) Price, K. R.; Dupont, M. S.; Shepherd, R.; Chan, H. W.-S.; Fenwick, G. R. Relationship between the chemical and sensory properties of exotic salad crops − coloured lettuce (*Lactuca sativa*) and chicory (*Cichorium intybus*). *J. Sci. Food Agric.* **1990**, *53*, 185−192.
(66) Wesołowska, A.; Nikiforuk, A.; Michalska, K.; Kisiel, W.; Chojnacka-Wójcik, E. Analgesic and sedative activities of lactucin and some lactucin-like guaianolides in mice. *J. Ethnopharmacol.* **2006**, *107*, 254−258.

DOI: 10.1021/jf503934v
J. Agric. Food Chem. 2015, 63, 593−602

JOURNAL OF AGRICULTURAL AND FOOD CHEMISTRY

Article

pubs.acs.org/JAFC

Isolation and Structural Characterization of the Milled Wood Lignin, Dioxane Lignin, and Cellulolytic Lignin Preparations from Brewer's Spent Grain

Jorge Rencoret,[†] Pepijn Prinsen,[†] Ana Gutiérrez,[†] Ángel T. Martínez,[‡] and José C. del Río*[,†]

[†]Instituto de Recursos Naturales y Agrobiología de Sevilla (IRNAS), CSIC, P.O. Box 1052, E-41080 Seville, Spain

[‡]Centro de Investigaciones Biológicas (CIB), CSIC, Ramiro de Maeztu 9, E-28040 Madrid, Spain

ABSTRACT: The structure of the lignin from brewer's spent grain (BSG) has been studied in detail. Three different lignin preparations, the so-called "milled-wood" lignin (MWL), dioxane lignin (DL), and cellulolytic lignin (CEL), were isolated from BSG and then thoroughly characterized by pyrolysis GC/MS, 2D-NMR, and derivatization followed by reductive cleavage (DFRC). The data indicated that BSG lignin presents a predominance of guaiacyl units (syringyl/guaiacyl ratio of 0.4−0.5) with significant amounts of associated *p*-coumarates and ferulates. The flavone tricin was also present in the lignin from BSG, as also occurred in other grasses. 2D-NMR (HSQC) revealed that the main substructures present are *β*-*O*-4′ alkyl-aryl ethers (77−79%) followed by *β*-5′ phenylcoumarans (11−13%) and lower amounts of *β*-*β*′ resinols (5−6%) and 5-5′ dibenzodioxocins (3−5%). The results from 2D-NMR (HMBC) and DFRC indicated that *p*-coumarates are acylating the *γ*-carbon of lignin side chains and are mostly involved in condensed structures. DFRC analyses also indicated a minor degree of *γ*-acylation with acetate groups, which takes place preferentially on S lignin (6% of S units are acetylated) over G lignin (only 1% of G units are acetylated).

KEYWORDS: *brewer's spent grain, lignin, Py-GC/MS, TMAH, HSQC, DFRC*

INTRODUCTION

Brewer's spent grain (BSG) is the solid waste generated during the brewing process and comprises the husk−pericarp−seed coat layers that covered the starting barley (*Hordeum vulgare* L.) grain.[1−4] BSG accounts for around 30% (w/w) of the barley grain, making it a readily available high-volume and low-cost byproduct within the brewing industry that can be regarded as a potentially valuable resource for the production of new added-value products.[1,2] Although BSG is produced in important amounts from brewing companies worldwide, with an estimated production of around 30 million tons per year,[5] the major part of these residues remains mostly underexploited.

BSG is a lignocellulosic material that is primarily composed of cellulose (17−25%), hemicelluloses (25−35%), protein (15−24%), lignin (8−28%), and lower amounts of lipids (10%).[1−6] Due to the high amounts of proteins and fibers, BSG has been predominantly used as animal feed. However, there is a trend nowadays for the more efficient utilization of the lignocellulosic residues generated from agro-forest and alimentary industries as feedstocks to produce new value-added products in the context of the so-called lignocellulosic biorefinery. In this context, the development of new techniques and procedures for a more appropriate valorization and industrial exploitation of this agro-industrial waste is of major importance because BSG is widely available at low cost and in large amounts.

Recent studies regarding the valorization and potential uses of BSG indicate that it could be considered as an important feedstock for the production of new products such as xylitol, lactic acid, and hydroxycinnamic acids or used as a growth medium for microorganisms and enzyme production, for paper manufacturing, or even for energy production, including the production of second-generation bioethanol, among others.[1,2,7,8] However, for an appropriate valorization of BSG as a source of added-value products and to explore newer applications and maximizing the use of existing technologies, a comprehensive characterization of the different components of BSG is of high interest. Previous studies have reported the composition of carbohydrates, proteins, lipids, and *p*-hydroxycinnamic acids in BSG.[4−6,9−11] However, studies regarding the composition of the lignin polymer in BSG have been insufficient and mostly restricted to its interactions with gastrointestinal microbiota[12,13] or to its recovery from the black liquors after alkaline pulping.[7] It is known that the content and composition of the lignin polymer play a decisive role in digestibility and delignification reactions and, therefore, the structural characterization of the lignin from BSG is an important step in the development of suitable methods for lignin depolymerization approaches. Moreover, detailed knowledge of the lignin polymer in BSG will help in the development of lignin-based high-added-value products from this waste material.

The lignin polymer is a complex macromolecule synthesized mainly from three *p*-hydroxycinnamyl alcohols, namely, *p*-coumaryl, coniferyl, and sinapyl alcohols, differing in their degree of methoxylation. These monolignols give rise to the *p*-hydroxyphenyl (H), guaiacyl (G), and syringyl (S) units, respectively, producing a variety of structures and linkages within the lignin polymer.[14,15] Moreover, *p*-hydroxycinnamates

Received: October 23, 2014
Revised: December 16, 2014
Accepted: December 18, 2014
Published: December 18, 2014

ACS Publications © 2014 American Chemical Society

DOI: 10.1021/jf505808c
J. Agric. Food Chem. 2015, 63, 603−613

(*p*-coumarates and ferulates) also occur in the lignins from grasses, such as barley, with *p*-coumarates acylating the γ-OH of the lignin side chain and ferulates and diferulates acylating cell wall polysaccharides and participating in both polysaccharide−polysaccharide and lignin−polysaccharide cross-coupling reactions, in the latter case mainly forming ether linkages similar to those existing between lignin units.[16]

In this study, an in-depth and comprehensive characterization of the lignin polymer in BSG has been performed. Because there is no universal method for the isolation of native lignin and due to the difficulties of isolating a representative lignin preparation from a material such as BSG, different lignin isolation methods were used. For this purpose, different lignin preparations that can be seen as representative of the native lignin due to their relatively low structural modification, namely, "milled-wood" lignin (MWL), dioxane lignin (DL), and cellulolytic lignin (CEL), were isolated according to traditional lignin isolation procedures.[17−19] The isolated lignin preparations were subsequently analyzed by using different analytical techniques, such as pyrolysis GC/MS (Py-GC/MS), in the absence and in the presence of tetramethylammonium hydroxide (TMAH) as methylating agent; 2D-NMR; and derivatization followed by reductive cleavage (DFRC). As far as we know, this is the first time that the detailed study of the structure of BSG lignin has been reported. Knowledge of the composition and structure of BSG lignin will help in maximizing the industrial utilization of this important agro-industrial waste.

MATERIALS AND METHODS

Samples. The BSG sample used in this study was taken from Adnams brewery (Southwold, UK) and was kindly provided by Prof. Craig B. Faulds (INRA, Marseille, France). The sample was the residue resulting from wort prepared from malted barley for ale brewing. Further information about the composition of this particular sample has been previously published.[20] The BSG sample was lyophilized and milled using an IKA knife mill (Janke & Kunkel, Staufen, Germany). Fifty grams of sample was successively extracted with acetone in a Soxhlet apparatus for 16 h and with hot water (100 mL, 3 h at 100 °C). The Klason lignin content was determined as the residue after sulfuric acid hydrolysis of the pre-extracted material according to TAPPI method T222 om-8.[21] The Klason lignin content was then corrected for proteins, determined from the N content obtained by CHN elemental analysis in a CHNS-932 Elemental Analyzer (LECO Corp., St. Joseph, MI, USA) and using a 6.25 factor,[22] and ashes. The acid-soluble lignin content was estimated, after the insoluble lignin was filtered off, by UV spectroscopy at 205 nm wavelength using an extinction coefficient of 110 L/cm/g. Holocellulose was isolated from pre-extracted BSG by delignification during 4 h using the acid chlorite method.[23] The content of α-cellulose was determined by removing the hemicelluloses from the holocellulose by alkali extraction.[23] Finally, the ash content was determined gravimetrically after 6 h of heating at 575 °C. Three replicates were used for each sample.

Isolation of "Milled-Wood Lignin". The MWL was isolated from the BSG sample according to the classical protocol.[17] Around 40 g of extractives-free sample was ball-milled in a PM100 planetary ball mill (Restch, Haan, Germany) at 400 rpm for 36 h in an agate jar and using agate balls (20 × 20 mm). The total ball-milling time was 5 h, with 5 min breaks after every 5 min of milling. The ball-milled powder was subsequently extracted with dioxane/water, 9:1 (v/v), using 20 mL of solvent/g of milled sample for 12 h under agitation, the solution was centrifuged, and the supernatant was evaporated to dryness in a rotary evaporator at 40 °C. The residue obtained (raw MWL) was then redissolved into a solution of acetic acid/water, 9:1 (v/v) (25 mL of solvent/g of raw MWL). The lignin was then precipitated into cold water and separated by centrifugation, milled in an agate mortar, and subsequently dissolved in 1,2-dichloroethane/ethanol, 2:1 (v/v). The mixture was centrifuged to eliminate any insoluble material. The lignin in the supernatant was precipitated in diethyl ether and recovered by centrifugation. This residue was then suspended in diethyl ether overnight, centrifuged, and finally suspended in petroleum ether. The final purified MWL sample was washed with *n*-hexane, recovered by centrifugation, and dried under nitrogen. The final yield was around 10% of the original Klason lignin content.

Isolation of Dioxane Lignin. The isolation of the DL was performed by acidolysis by the dioxane method according to a previously published procedure,[18] with some minor modifications. Fourteen grams of dry extractives-free (by Soxhlet extraction during 16 h with acetone and subsequent extraction with water at 100 °C) ball-milled BSG sample was refluxed for 40 min (3 times) with 150 mL of 0.05 M HCl in dioxane/water, 82:18 (v/v), under nitrogen. The lignin was then filtered and washed with dioxane/water, 82:18 (v/v). The filtrate was evaporated in a rotary evaporator at 40 °C, and then the lignin was precipitated in water. The precipitated lignin was then centrifuged and freeze-dried. After freeze-drying, the lignins were Soxhlet extracted with hexane for 8 h to remove lipid contaminants. The yield of DL was around 50% (based on the Klason lignin content).

Isolation of Cellulolytic Lignin. CEL preparations were isolated by enzymatically hydrolyzing the polysaccharides according to the protocol previously described.[19] For this purpose, we used Cellulysin (Calbiochem-Behring Corp., La Jolla, CA, USA), a crude cellulase preparation from *Trichoderma viride* that also contains hemicellulase activities. Its activity was ≥10000 units/g, estimated as reducing sugars (glucose equivalents) released from a paper filter at 40 °C, pH 4. The extractives-free ball-milled material (200 mg) was suspended in 20 mM NaOAc buffer (30 mL, pH 5.0) in a 50 mL centrifuge tube, 8 mg of Cellulysin was added, and the reaction slurry was incubated at 30 °C for 48 h. The solids were recovered by centrifugation (8000 rpm, 4 °C, 20 min), and the process was repeated twice with fresh buffer and enzyme. The lignin was finally recovered by filtration, washed with water, and then lyophilized. The yield of CEL was around 105% of the Klason lignin, indicating the presence of some contaminants in this lignin preparation.

Analytical Pyrolysis. The pyrolysis of the different lignin preparations (ca. 0.1 mg) was carried out in a 3030 microfurnace pyrolyzer (Frontier Laboratories Ltd., Fukushima, Japan) connected to a GC 7820A (Agilent Technologies, Inc., Santa Clara, CA, USA) and an Agilent 5975 mass selective detector (EI at 70 eV). The column used was a 60 m × 0.25 mm i.d., 0.25 μm film thickness, DB-1701 (J&W Scientific, Folsom, CA, USA). The pyrolysis was performed at 500 °C. The oven temperature was programmed from 45 °C (4 min) to 280 °C at a heating rate of 4 °C/min and held for 10 min. The carrier gas was helium at 2 mL/min. For Py/TMAH, around 0.1 mg of sample was mixed with 0.5 μL of TMAH (25%, w/w, in methanol), and the pyrolysis was performed as described above. The released phenolic compounds were identified by comparison of their mass spectra with those present in the Wiley and NIST libraries and those reported in the literature[24,25] and, when possible, by comparison with retention time and mass spectra of authentic standards. Peak molar areas for each lignin-derived phenolic compound were calculated, the summed areas were normalized, and the data for two repetitive analyses were averaged and expressed as percentages. The relative standard deviation was <5%. The response factors for most of the lignin-derived phenols released were practically identical, except for vanillin,[26] which is a minor peak here. Therefore, no attempt was made to calculate the response factor for every compound released.

NMR Spectroscopy. 2D-NMR spectra of the isolated lignin preparations were recorded at 25 °C on an AVANCE III 500 MHz instrument (Bruker, Karlsruhe, Germany) equipped with a cryogenically cooled 5 mm TCI gradient probe with inverse geometry. The lignin preparations (40 mg) were dissolved in 0.75 mL of dimethyl sulfoxide (DMSO)-d_6. The central solvent peak was used as the internal reference (DMSO, δ_C/δ_H 39.5/2.49). The heteronuclear single-quantum coherence (HSQC) experiment used Bruker's

DOI: 10.1021/jf505808c
J. Agric. Food Chem. 2015, 63, 603−613

"hsqcetgpsisp2.2" adiabatic pulse program with spectral widths from 0 to 10 ppm (5000 Hz) and from 0 to 165 ppm (20625 Hz) for the ^{1}H and ^{13}C dimensions. The number of transients was 64, and 256 time increments were always recorded in the ^{13}C dimension. The $^{1}J_{CH}$ used was 145 Hz. Processing used typical matched Gaussian apodization in the ^{1}H dimension and squared cosine-bell apodization in the ^{13}C dimension. Prior to Fourier transformation, the data matrices were zero-filled to 1024 points in the ^{13}C dimension. For heteronuclear multiple bond correlation (HMBC) acquisition experiments, the long-range *J*-coupling evolution time used was 80 ms.

2D-NMR correlation signals were assigned by literature comparison.[27−30] A semiquantitative analysis of the HSQC signals was performed using Bruker's Topspin 3.1 processing software. Integration of signals was performed separately for the different regions of the spectra corresponding to chemically analogous C−H pairs with similar $^{1}J_{CH}$ coupling values. The relative abundances of side chains involved in the different interunit linkages were estimated in the aliphatic oxygenated region from the C_α−H_α correlations, except for α-oxidized β-*O*-4 substructures (A_{ox}), for which C_β−H_β correlations had to be used. In the aromatic/unsaturated region, C_2−H_2 correlations from H, G, and S lignin units and from *p*-coumarates and ferulates were used to estimate their relative abundances.

DFRC (Derivatization followed by Reductive Cleavage). The DFRC degradation was performed according to the protocol previously developed.[31−33] Lignins (10 mg) were mixed with acetyl bromide in acetic acid, 8:92 (v/v), and stirred at 50 °C for 2 h. The solvents and excess of acetyl bromide were removed by rotary evaporation at reduced pressure. The products were then dissolved in dioxane/acetic acid/water, 5:4:1 (v/v/v), 50 mg of powdered Zn was added, and the mixture was stirred at room temperature for 40 min. After completion, the reaction mixture was transferred into a separation funnel with dichloromethane and saturated ammonium chloride. The aqueous phase was adjusted to pH <3 by adding 3% HCl, the mixture vigorously mixed, and the organic layer separated. The water phase was extracted twice more with dichloromethane. The combined dichloromethane fractions were dried over anhydrous Na_2SO_4, and the filtrate was evaporated on a rotary evaporator. The residue was then acetylated in 1.1 mL of dichloromethane containing 0.2 mL of acetic anhydride and 0.2 mL of pyridine for 1 h. The acetylated lignin degradation products were collected after rotary evaporation of the solvents and analyzed by GC/MS using mass spectra and relative retention times to authenticate the DFRC monomers and their *p*-coumarate conjugates as described in previous papers.[31−33] To investigate the occurrence of native acetylated lignin units, a modification of the standard DFRC method using propionylating instead of acetylating reagents (DFRC′) was used in the present study.[34−36]

The GC/MS analyses were performed with a GCMS-QP2010 Ultra instrument (Shimadzu Co., Kyoto, Japan). The column used was a 30 m × 0.25 mm i.d., 0.10 μm film thickness, DB-5HT (J&W Scientific). The oven was heated from 140 °C (1 min) to 250 °C at 3 °C/min, then ramped at 10 °C/min to 300 °C, and held for 10 min at the final temperature. The injector was set at 250 °C, and the transfer line was kept at 300 °C. Helium was used as the carrier gas at a rate of 1 mL/min. The DFRC compounds were identified on the basis of the mass spectra and relative retention times of authentic standards published previously.[31,32] Quantitation of the released individual (acetylated and propionylated) monomers was performed using tetracosane as external standard and by assuming response factors similar to those of the acetylated monomers reported previously.[30]

RESULTS AND DISCUSSION

The abundance of the main constituents (namely, water-soluble material, lipids, Klason lignin, acid-soluble lignin, polysaccharides, proteins, and ash) of the BSG sample analyzed in this work is indicated in Table 1. Previously published data of this sample are also shown for comparison. The Klason lignin content estimated in this work was relatively low (8.8%) compared to previous published data for the same sample (16−20.1%). One of the main reasons for this discrepancy is that previous works did not consider the high amounts of proteins and ashes when the Klason lignin content was quantitated gravimetically and presented an uncorrected value. In our case, the uncorrected Klason lignin content amounted to ca. 13%,

Table 1. Abundance of the Main Constituents (Percent Dry Weight) of the Brewer's Spent Grain Sample[a]

constituent	content[b]	Robertson et al. (2010)[4]	Faulds et al. (2008)[20]
water-soluble material	8.3 ± 1.0	nd	nd
lipids	9.2 ± 0.2	nd	5.4
Klason lignin	8.8 ± 0.9[c]	16.0	20.1
acid-soluble lignin	4.9 ± 0.3	nd	nd
polysaccharides	49.4 ± 2.0	43.3	51.0
proteins	14.5 ± 1.0	18.8	17.6
ash	4.9 ± 0.1	nd	nd

[a]Data from other papers regarding the same sample are shown for comparison.[4,20] [b]Average of three replicates. [c]Corrected for proteins and ash.

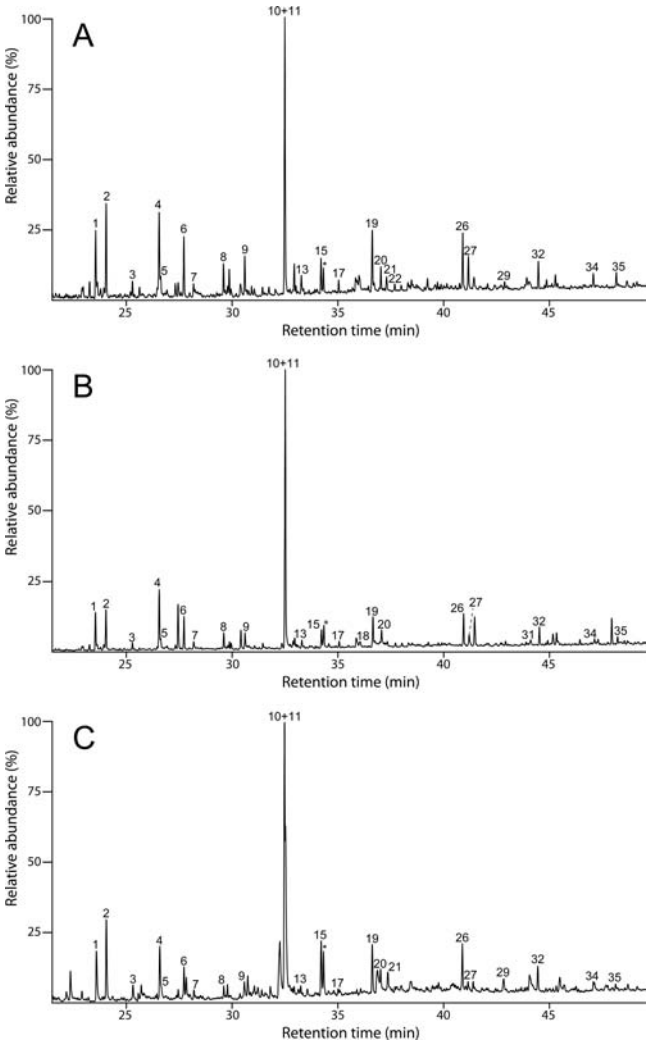

Figure 1. Py-GC/MS chromatograms of the different lignin preparations isolated from BSG: (A) MWL; (B) DL; (C) CEL. The identities and relative abundances of the lignin-derived phenolic compounds released are listed in Table 2. (∗) 1*H*-Indole from proteins.

DOI: 10.1021/jf505808c
J. Agric. Food Chem. 2015, 63, 603−613

Table 2. Identities and Relative Molar Abundances of the Lignin-Derived Compounds Released after Py-GC/MS of MWL, DL, and CEL Preparations Isolated from the BSG Sample

no.	compound	M_w	origin[a]	MWL	DL	CEL
1	phenol	94	H/Pr	9.1	7.9	8.2
2	guaiacol	124	G	8.7	5.6	8.1
3	2-methylphenol (*o*-cresol)	108	H/Pr	1.7	1.2	1.6
4	4-methylphenol (*p*-cresol)	108	H/Pr	11.3	10.6	6.4
5	3-methylphenol (*m*-cresol)	108	H/Pr	2.3	1.8	1.4
6	4-methylguaiacol	138	G	5.3	4.2	2.7
7	2,4-dimethylphenol	122	H/Pr	1.1	1.1	0.8
8	4-ethylphenol	122	H/Pr	3.0	2.3	1.1
9	4-ethylguaiacol	152	G	3.1	2.0	1.2
10	4-vinylphenol	120	H/Pr/PCA	10.4	21.8	23.0
11	4-vinylguaiacol	150	G/FA	15.5	20.5	21.6
12	4-allylphenol	134	H	0.2	0.2	0.2
13	eugenol	164	G	1.6	1.0	0.7
14	4-propylguaiacol	166	G	0.5	0.2	0.2
15	syringol	154	S	2.7	2.3	4.8
16	*cis*-4-propenylphenol	134	H	0.1	0.1	0.1
17	*cis*-isoeugenol	164	G	0.9	0.5	0.4
18	*trans*-4-propenylphenol	134	H	0.6	0.6	0.4
19	*trans*-isoeugenol	164	G	5.0	2.7	4.2
20	4-methylsyringol	168	S	1.5	1.7	1.6
21	vanillin	152	G	1.3	0.6	1.6
22	4-propinylguaiacol	162	G	0.6	0.5	0.3
23	4-propinylguaiacol	162	G	0.5	0.4	0.3
24	4-ethylsyringol	182	S	0.9	0.4	0.3
25	acetovanillone	166	G	0.5	0.3	0.4
26	4-vinylsyringol	180	S	3.7	3.3	3.2
27	guaiacylacetone	180	G	2.5	1.4	0.6
28	4-allylsyringol	194	S	0.4	0.8	0.4
29	*cis*-4-propenylsyringol	194	S	0.5	0.4	0.3
30	4-propinylsyringol	192	S	0.3	0.2	0.1
31	4-propinylsyringol	192	S	0.2	0.2	0.1
32	*trans*-4-propenylsyringol	194	S	1.7	1.6	1.7
33	syringaldehyde	182	S	0.3	0.1	0.4
34	acetosyringone	196	S	1.1	0.4	0.5
35	syringylacetone	210	S	0.7	0.7	0.4
36	propiosyringone	210	S	0.2	0.2	0.1
37	syringyl vinyl ketone	208	S	0.2	0.2	0.3
			S/G ratio =	04	0.5	0.5

[a]H, lignin *p*-hydroxyphenyl-type; G, lignin guaiacyl-type; S, lignin syringyl-type; PCA, *p*-coumarate; FA, ferulate; Pr, proteins. All G- and S-derived peaks were used for the estimation of the S/G ratio, except 4-vinylguaiacol (which also arises from ferulates), and the analogous 4-vinylsyringol.

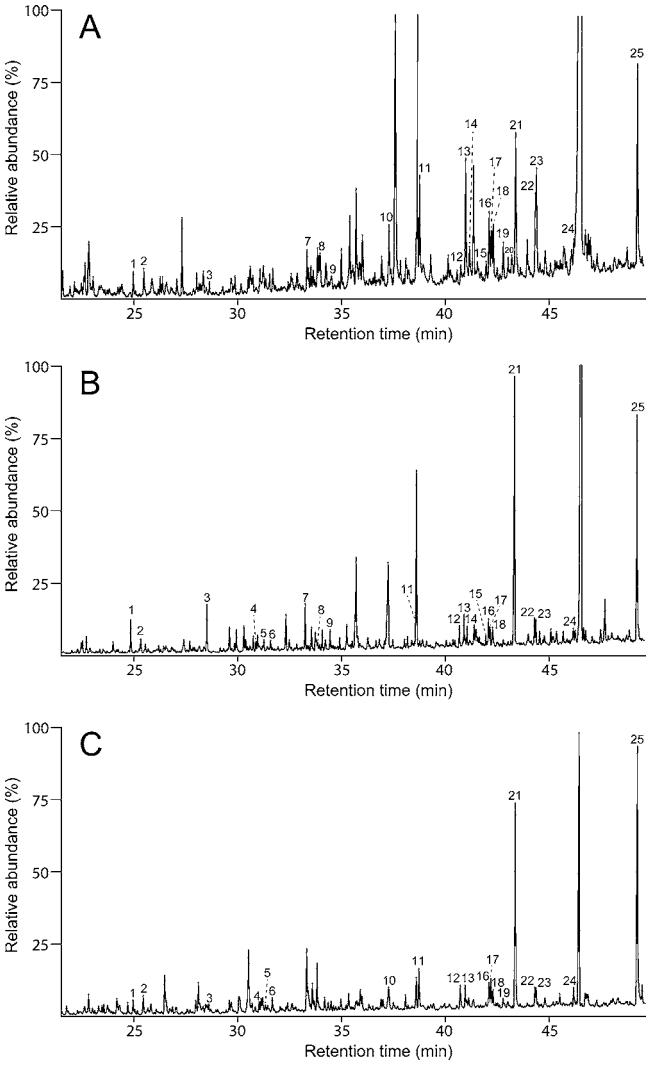

Figure 2. Py-TMAH-GC/MS chromatograms of the different lignin preparations isolated from BSG: (A) MWL; (B) DL; (C) CEL. The identities and relative abundances of the released lignin-derived compounds are listed in Table 3.

but contained appreciable amounts of ashes (ca. 10%) and proteins (ca. 20%) that needed to be corrected. Therefore, it is important to stress the importance of correcting the Klason lignin content in BSG (and related samples) for proteins and ashes to avoid presenting overestimated values.

In this work, we have thoroughly studied the composition and structure of the lignin polymer of BSG. For this purpose, different lignin preparations, MWL, DL, and CEL, were isolated from the BSG sample selected for this study according to traditional lignin isolation procedures.[17−19] However, it is well recognized that these lignin preparations, in particular MWL due to its low yield, represent only a part of the native lignin and may not be representative of the whole lignin present in the plant material.[19,37,38] Indeed, these lignin preparations can also undergo some structural modifications during isolation, especially during extended milling.[38,39] The yields of the lignin preparations isolated from the BSG sample varied from 10% (MWL) to 50% (DL) to 105% (CEL) of the Klason lignin content. However, and although these lignin preparations were purified as described, they still contained appreciable amounts of proteins (calculated from the N content), which accounted for 20% (MWL), 30% (DL), and 21% (CEL), that were difficult to remove and lipids, as shown in the NMR spectra. In any case, and despite the presence of impurities, it was still possible to get information about the structure of the lignin polymer. To obtain a detailed description of the structure of the BSG lignin, these lignin preparations were subsequently

DOI: 10.1021/jf505808c
J. Agric. Food Chem. 2015, 63, 603−613

Table 3. Identities and Relative Molar Abundances of the Compounds Released after Pyrolysis in the Presence of TMAH of MWL, DL, and CEL Preparations Isolated from the BSG Sample

no.	compound	M_w	origin[a]	MWL	DL	CEL
1	4-methoxystyrene	134	H/Pr	2.3	4.2	2.3
2	1,2-dimethoxybenzene	138	G	2.5	1.4	3.2
3	3,4-dimethoxytoluene	152	G	1.2	5.0	0.9
4	4-methoxybenzaldehyde	136	H/Pr	2.7	1.3	1.6
5	4-ethyl-1,2-dimethoxybenzene	166	G	0.9	1.2	0.7
6	1,2,3-trimethoxybenzene	168	S	1.5	0.9	2.2
7	3,4-dimethoxybenzeneethylene	164	G	2.7	4.7	1.8
8	4-methoxybenzoic acid methyl ester	166	H/Pr	2.6	0.7	0.3
9	3,4,5-trimethoxytoluene	185	S	0.7	1.9	1.2
10	1,2-dimethoxy-4-propenylbenzene	178	G	1.5	2.3	1.0
11	3,4-dimethoxybenzaldehyde	166	G	8.5	8.5	5.7
12	*cis*-3-(4-methoxyphenyl)-3-propenoic acid methyl ester	192	PCA	0.7	1.9	3.0
13	3,4-dimethoxybenzoic acid methyl ester	196	G	9.2	2.5	2.4
14	3,4-dimethoxyacetophenone	180	G	2.9	1.8	1.0
15	1-(3,4,5-trimethoxyphenyl)-1-propene	208	S	1.4	0.7	0.4
16	*cis*-1-(3,4-dimethoxyphenyl)-2-methoxyethylene	194	G	5.1	1.7	1.7
17	3,4,5-trimethoxybenzaldehyde	196	S	3.1	1.3	3.0
18	*trans*-1-(3,4-dimethoxyphenyl)-2-methoxyethylene	194	G	3.5	1.5	1.5
19	*cis*-1-(3,4-dimethoxyphenyl)-1-methoxyprop-1-ene	208	G	1.9	0.5	0.9
20	*trans*-1-(3,4-dimethoxyphenyl)-1-methoxyprop-1-ene	208	G	1.0	0.4	0.6
21	*trans*-3-(4-methoxyphenyl)-3-propenoic acid methyl ester	192	PCA	13.6	27.2	26.8
22	3,4,5-trimethoxyacetophenone	210	S	5.4	1.9	1.9
23	3,4,5-trimethoxybenzoic acid methyl ester	226	S	6.8	1.6	1.5
24	*cis*-3-(3,4-dimethoxyphenyl)-3-propenoic acid methyl ester	222	FA	1.3	1.0	1.8
25	*trans*-3-(3,4-dimethoxyphenyl)-3-propenoic acid methyl ester	222	FA	16.9	23.8	32.3
			S/G ratio =	0.5	0.4	0.5
			PCA/FA ratio =	0.8	1.1	0.8

[a]H, lignin *p*-hydroxyphenyl type; G, lignin guaiacyl type; S, lignin syringyl type; PCA, *p*-coumarate; FA, ferulate; Pr, proteins.

analyzed by different analytical methodologies, including Py-GC/MS, 2D-NMR, and DFRC.

Lignin Composition As Observed by Py-GC/MS. The different lignin preparations (MWL, DL, CEL) isolated from the BSG sample selected for this study were first analyzed by Py-GC/MS. The pyrograms are shown in Figure 1, and the identification and relative molar abundances of the released phenolic compounds are listed in Table 2. The pyrograms of the three lignin preparations were rather similar and released phenolic compounds that are derived from *p*-hydroxyphenyl (H), guaiacyl (G), and syringyl (S) lignin units as well as from *p*-hydroxycinnamates (*p*-coumarates and ferulates). The most predominant phenolic compounds released were 4-vinylphenol (**10**) and 4-vinylguaiacol (**11**), with important amounts of other compounds such as phenol (**1**), guaiacol (**2**), 4-methylphenol (**4**), 4-methylguaiacol (**6**), syringol (**15**), *trans*-isoeugenol (**19**), 4-methylsyringol (**20**), 4-vinylsyringol (**26**), guaiacylacetone (**27**), and *trans*-4-propenylsyringol (**32**). Compounds **10** and **11** coelute together in the same chromatographic peak, and their relative abundances in this peak were estimated on the basis of the relative abundance of their respective characteristic fragments ions (*m*/*z* 91 and 120 for 4-vinylphenol; *m*/*z* 107, 135, and 150 for 4-vinylguaiacol).

The high levels of phenol (**1**), 4-methylphenol (**4**), and 4-vinylphenol (**10**), together with the important amounts of 1*H*-indole released from the different lignin preparations, seem to indicate that the major part of these phenolic compounds does not arise from H-lignin structural units but from proteins, in agreement with the high content of protein impurities present in these lignin preparations as shown above. In addition, the high amounts of 4-vinylphenol (**10**) released upon pyrolysis from these lignin preparations, as also occurs in the lignins from other grasses, may also arise from *p*-coumarate esters that are acylating the lignin side chains and which decarboxylate efficiently under pyrolytic conditions.[28,29,40,41] Similarly, 4-vinylguaiacol (**11**), which is also present in high abundance among the pyrolysis products of the different BSG lignin preparations, might also arise from ferulates after decarboxylation upon pyrolysis.[28,29,40,41] Therefore, 4-vinylphenol and 4-vinylguaiacol cannot be used to determine the lignin H:G:S composition upon Py-GC/MS in the BSG lignin preparations because part of them does not arise from lignin structural units but from *p*-hydroxycinnamates or also from proteins in the case of 4-vinylphenol. An estimation of the S/G ratio was, however, obtained by using the molar areas of all the G- and S-derived compounds listed in Table 2, except for 4-vinylguaiacol, which also arises from ferulates, and its respective 4-vinylsyringol. The S/G ratios thus calculated for the different BSG lignin preparations indicated a predominance of G- over S-lignin units, with a S/G ratio in the range of 0.4−0.5.

As stated above, the high amounts of 4-vinylphenol and 4-vinylguaiacol released in the pyrograms point to the occurrence of important amounts of *p*-hydroxycinnamates (*p*-coumarates and ferulates) in the BSG lignin preparations, as usually occurs in all grasses. The occurrence of *p*-hydroxycinnamates in the BSG lignin preparations was therefore assessed by pyrolysis in the presence of TMAH as methylating reagent.[28,29,40,41] Py/TMAH induces transesterification of the *p*-hydroxycinnamate

DOI: 10.1021/jf505808c
J. Agric. Food Chem. 2015, 63, 603−613

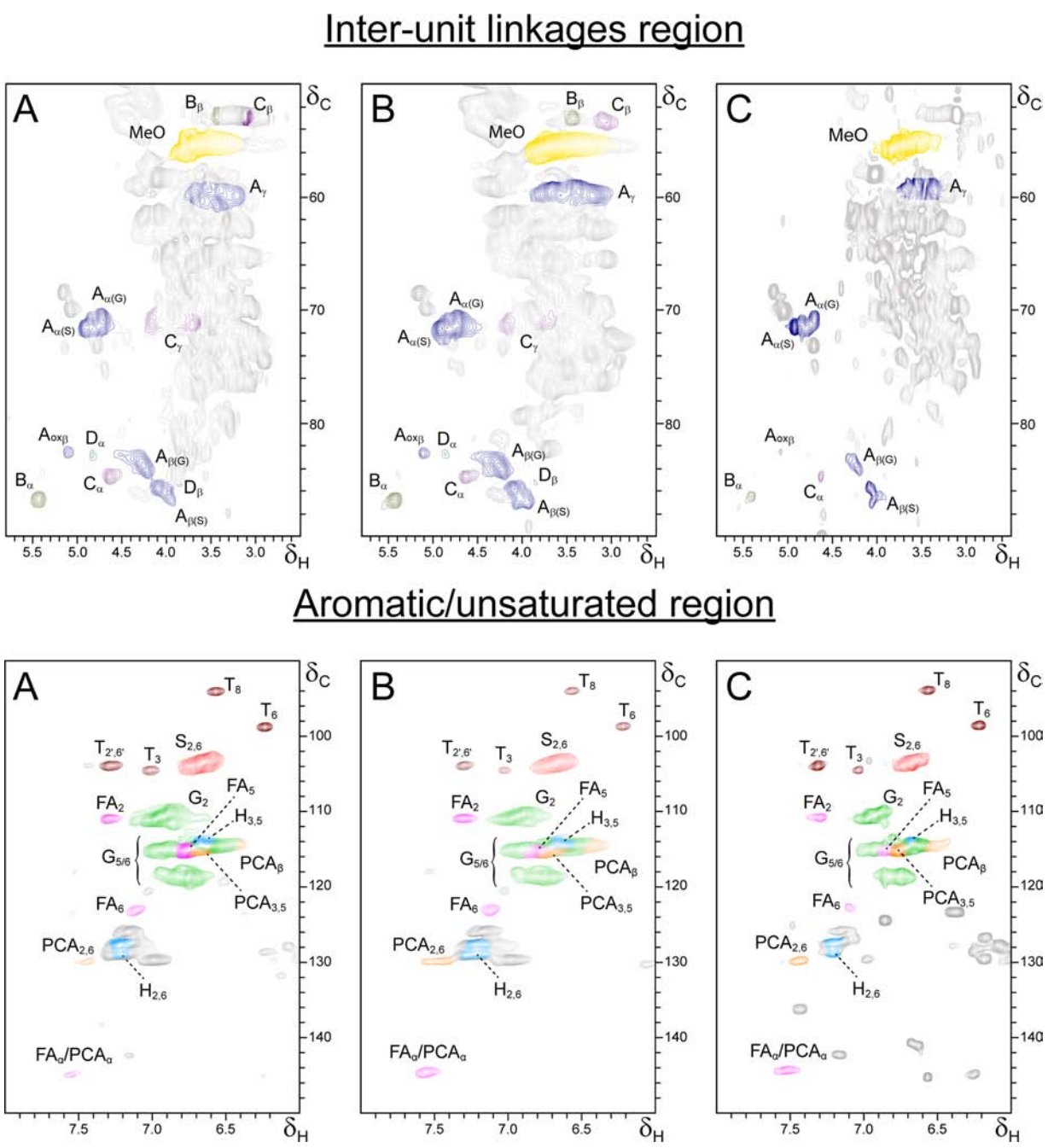

Figure 3. Side-chain (δ_C/δ_H 50–90/2.5–5.8) and aromatic/unsaturated (δ_C/δ_H 90–160/6.0–8.0) regions in the 2D (HSQC) NMR spectra: (A) MWL; (B) DL; (C) CEL. See Table 4 for signal assignments and Figure 4 for the main lignin structures identified.

esters and cleavage of ether linkages at C_4, with subsequent methylation of the formed phenolic groups. The Py/TMAH chromatograms of the BSG lignin preparations are shown in Figure 2. The identities of the compounds released and their relative abundances are listed in Table 3. It is clearly apparent that Py/TMAH of the different BSG lignin preparations released important amounts of the dimethyl derivatives of *p*-coumaric (**21**) and ferulic (**25**) acids, confirming the relatively high amounts of *p*-coumarates and ferulates present in the BSG lignin preparations, as also occurred in the lignin from other grasses. Previous studies have indicated that *p*-coumarates in grasses are acylating the *γ*-OH of the lignin side chains.[16,29,42] Ferulates, on the other hand, are an intrinsic part of the lignin structure in grasses, participating in coupling and cross-coupling reactions with other monolignols.[16,43,44] In all BSG lignin preparations, *p*-coumarates and ferulates were released in nearly similar abundances, with a *p*-coumarates/ferulates ratio around 0.8–1.0. An estimation of the lignin S/G ratio can now be performed upon Py/TMAH with more accuracy because *p*-hydroxycinnamates and lignin release clearly differentiated compounds (Table 3) and revealed a S/G value in the range 0.4–0.5, similar to that estimated upon Py-GC/MS, by ignoring 4-vinylguaiacol and its respective 4-vinylsyringol and confirming that BSG lignin is enriched in G-lignin units.

Lignin Structural Units and Interunit Linkages As Seen by 2D-NMR. To obtain additional information on the structure of BSG lignin, the different lignin preparations (MWL, DL, and CEL) were analyzed by 2D-NMR, which

DOI: 10.1021/jf505808c
J. Agric. Food Chem. 2015, 63, 603–613

Table 4. Assignments of the $^{13}C-^{1}H$ Correlation Signals for the Lignin Structures Shown in Figure 4 and Observed in the 2D HSQC Spectra (Figure 3) of the MWL, DL, and CEL Preparations Isolated from the BSG Sample

label	δ_C/δ_H	assignment
B_β	53.1/3.43	$C_\beta-H_\beta$ in phenylcoumaran substructures (B)
C_β	53.5/3.05	$C_\beta-H_\beta$ in β-β' resinol substructures (C)
$-OCH_3$	55.6/3.73	C−H in methoxyls
A_γ	59.4/3.40 and 3.72	$C_\gamma-H_\gamma$ in β-O-4′ substructures (A)
C_γ	71.0/3.83 and 4.19	$C_\gamma-H_\gamma$ in β-β' resinol substructures (C)
$A_{\alpha(G)}$	71.1/4.71	$C_\alpha-H_\alpha$ in β-O-4′ substructures (A) linked to a G unit
$A_{\alpha(S)}$	71.6/4.84	$C_\alpha-H_\alpha$ in β-O-4′ substructures (A) linked to an S unit
$A_{ox\beta}$	82.6/5.11	$C_\beta-H_\beta$ in α-oxidized β-O-4′ substructures (A_{ox})
D_α	83.0/4.82	$C_\alpha-H_\alpha$ in 5-5′ (dibenzodioxocin) substructures (D)
$A_{\beta(G)}$	83.7/4.26	$C_\beta-H_\beta$ in β-O-4′ substructures (A) linked to a G unit
C_α	84.7/4.64	$C_\alpha-H_\alpha$ in β-β' resinol substructures (C)
D_β	85.2/3.85	$C_\beta-H_\beta$ in 5-5′ (dibenzodioxocin) substructures (D)
$A_{\beta(S)}$	85.8/4.09	$C_\beta-H_\beta$ in β-O-4′ substructures linked (A) to an S unit
B_α	86.8/5.43	$C_\alpha-H_\alpha$ in phenylcoumaran substructures (B)
T_8	94.0/6.56	C_8-H_8 in tricin (T)
T_6	98.7/6.22	C_6-H_6 in tricin (T)
$S_{2,6}$	103.7/6.68	C_2-H_2 and C_6-H_6 in etherified syringyl units (S)
$T_{2',6'}$	103.9/7.30	$C_{2',6'}-H_{2',6'}$ in tricin (T)
T_3	104.5/7.03	C_3-H_3 in tricin (T)
G_2	110.8/6.96	C_2-H_2 in guaiacyl units (G)
F_2	110.9/7.30	C_2-H_2 in ferulate (FA)
PCA_β/FA_β	114.5/6.48	$C_\beta-H_\beta$ in p-coumarates (PCA) and ferulates (FA)
$H_{3,5}$	114.5/6.62	$C_{3,5}-H_{3,5}$ in p-hydroxyphenyl units (H) and proteins
FA_5	115.1/6.76	C_5-H_5 in ferulate (FA)
G_5/G_6	115.0/6.74 and 6.94	C_5-H_5 and C_6-H_6 in guaiacyl units (G)
	118.8/6.79	
FA_6	123.2/7.12	C_6-H_6 in ferulates (FA)
$H_{2,6}$	128.3/7.22	$C_{2,6}-H_{2,6}$ in p-hydroxyphenyl units (H) and proteins
$PCA_{2,6}$	129.9/7.44	$C_{2,6}-H_{2,6}$ in p-coumarates (PCA)
PCA_α/FA_α	144.6/7.56	$C_\alpha-H_\alpha$ in p-coumarates (PCA) and ferulates (FA)

provides information on the interunit linkages as well as the composition of the lignin units. The side-chain (δ_C/δ_H 50−90/2.5−5.8) and the aromatic/unsaturated (δ_C/δ_H 90−160/6.0−8.0) regions of the HSQC NMR spectra of the different lignin preparations are shown in Figure 3. The main lignin cross-signals assigned in the HSQC spectra are listed in Table 4, and the main lignin substructures present are shown in Figure 4.

The side-chain region of the spectra gives important information about the different interunit linkages occurring in the structure of the lignin polymer. The spectra of the different BSG lignin preparations show strong signals from lipids (including linoleic acid), proteins, and carbohydrates; however, they also show intense and characteristic signals for the lignin polymer. Thus, the spectra show prominent signals corresponding to β-O-4′ aryl-ether linkages (substructure A). The $C_\alpha-H_\alpha$ correlations in β-O-4′ substructures were observed at δ_C/δ_H 71.1/4.71 and 71.6/4.84 for structures linked to G or S lignin units, respectively. Likewise, the $C_\beta-H_\beta$ correlations were observed at δ_C/δ_H 83.7/4.26 for β-O-4′ structures linked to G units and at δ_C/δ_H 85.8/4.09 for β-O-4′ structures linked to S units. The $C_\gamma-H_\gamma$ correlations of β-O-4′ substructures were observed at δ_C/δ_H 59.4/3.40 and 3.72, superimposed to other signals. In addition, signals for phenylcoumaran substructures (B) were also found in the spectra of the BSG lignin preparations, the signals for their $C_\alpha-H_\alpha$ and $C_\beta-H_\beta$ correlations being observed at δ_C/δ_H 86.8/5.43 and 53.1/3.43, whereas the $C_\gamma-H_\gamma$ correlation overlaps with other $C_\gamma-H_\gamma$ signals around δ_C/δ_H 62/3.8. Resinol substructures (C) were also clearly observed in the spectra, with their $C_\alpha-H_\alpha$, $C_\beta-H_\beta$, and the double $C_\gamma-H_\gamma$ correlations observed at δ_C/δ_H 84.7/4.64, 53.5/3.05 and 71.0/3.83 and 4.19. Finally, small signals corresponding to dibenzodioxocin (5′-5″/α-O-4′/β-O-4″ linkages) substructures (D) could also be observed in the spectra, with the characteristic $C_\alpha-H_\alpha$ and $C_\beta-H_\beta$ correlations at δ_C/δ_H 83.0/4.82 and 85.2/3.85, as well as signals for the $C_\beta-H_\beta$ correlations of α-keto-β-O-4′-substructures (A_{ox}) at δ_C/δ_H 82.6/5.11.

The main cross-signals in the aromatic/unsaturated region of the HSQC spectra corresponded to the aromatic rings and unsaturated side chains of the different H, G, and S lignin units and to p-coumarates (PCA) and ferulates (FA) that are associated with the lignin. The S lignin units presented a strong signal for the $C_{2,6}-H_{2,6}$ correlation at δ_C/δ_H 103.7/6.68, whereas the G lignin units showed different correlation signals for C_2-H_2 (δ_C/δ_H 110.8/6.96) and C_5-H_5/C_6-H_6 (δ_C/δ_H 115.0/6.74 and 6.94 and δ_C/δ_H 118.8/6.79). Cross-signals corresponding to $C_{3,5}-H_{3,5}$ correlations of H lignin units were observed at δ_C/δ_H 114.5/6.62 overlapping with other lignin signals, whereas the $C_{2,6}-H_{2,6}$ correlations at δ_C/δ_H 128.3/7.22 overlapped with strong signals from proteins. Signals corresponding to p-coumarate structures (PCA) were clearly observed in the spectra of the isolated lignins. Cross-signals corresponding to the $C_{2,6}-H_{2,6}$ at δ_C/δ_H 130.0/7.46 and $C_{3,5}-H_{3,5}$ at δ_C/δ_H 115.5/6.77 correlations of the aromatic ring and signals for the correlations of the unsaturated $C_\alpha-H_\alpha$ at δ_C/δ_H 144.4/7.41 and $C_\beta-H_\beta$ at 113.5/6.27 of the p-coumarate units were observed in this region of the HSQC spectra. Signals corresponding to the C_2-H_2 and C_6-H_6 correlations of ferulate moieties (FA) were also observed at δ_C/δ_H 111.0/7.32 and 123.3/7.10 in the spectra. The signals corresponding to the unsaturated $C_\alpha-H_\alpha$ and $C_\beta-H_\beta$ correlations overlapped with those of the p-coumarate units. Moreover, the signals for the $C_\beta-H_\beta$ correlations of p-coumarates and ferulates indicated that the carboxylic groups were not in free but in ester form. Interestingly, in this region of the HSQC spectra, it was also possible to detect the two distinctive and typical signals at δ_C/δ_H 94.1/6.56 and 98.7/6.22 corresponding to the C_8-H_8 and C_6-H_6 correlations of tricin (T),[28] a flavone that is widely found and is apparently incorporated into the lignin structure in some grasses,[28,45,46] and that also occur in the lignin of other monocotyledons, such as coconut coir.[30] The HSQC spectra also show the C_3-H_3 correlation of tricin at δ_C/δ_H 104.5/7.03, whereas the correlations for $C_{2'}-H_{2'}$ and $C_{6'}-H_{6'}$ are observed at δ_C/δ_H 103.9/7.30. Tricin arises from a different pathway than the usual monolignols, but seems to act as a lignin monomer in grasses. Tricin cannot couple with other tricins, so it can only undergo cross-coupling with monolignols and must be present

DOI: 10.1021/jf505808c
J. Agric. Food Chem. 2015, 63, 603−613

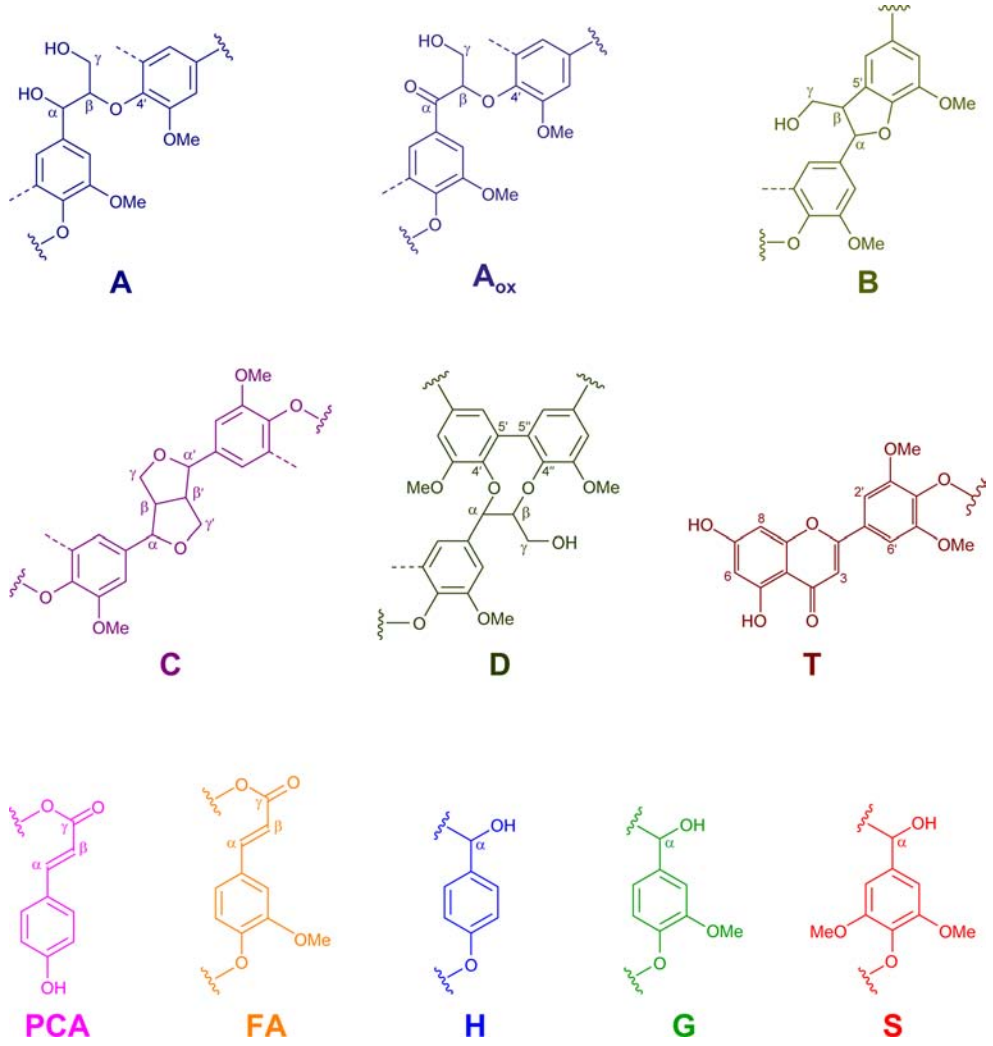

Figure 4. Main structures present in the lignin preparations from brewer's spent grain: (A) *β-O*-4′ alkyl-aryl ethers; (A_{ox}) C_α-oxidized *β-O*-4′ structures; (B) phenylcoumarans; (C) resinols; (D) dibenzodioxocins; (PCA) *p*-coumarates; (FA) ferulates; (H) *p*-hydroxyphenyl units; (G) guaiacyl units; (S) syringyl units; (T) tricin.

at the start of lignification acting as the initiation site. The incorporation of tricin into the lignin polymer through 4-*O*-*β* ether linkages has already been reported.[29]

The relative abundances of the main lignin interunit linkages and the molar abundances of the different lignin units (H, G, and S), *p*-hydroxycinnamates (*p*-coumarates and ferulates), and tricin, all estimated from volume integration of the corresponding cross-signals in the HSQC spectra, are shown in Table 5. The three lignin preparations gave similar results, indicating that they might be considered as representative of the native lignin in BSG. The main substructure present in the lignin of BSG was the *β-O*-4′ alkyl-aryl ether (A and A_{ox}), which accounts for 77−79% of all interunit linkages, followed by *β*-5′ phenylcoumaran substructures (B) that involved 11−13% of all linkages and lower amounts of *β-β*′ resinol substructures (C) with 5−6%, and dibenzodioxocins with 3−5%, depending on the lignin preparation. The exact determination of the H:G:S composition of the BSG lignin preparations was not possible due to the high amounts of proteins present in the lignin preparations, which impairs obtaining an accurate volume integral of the $C_{2,6}$−$H_{2,6}$ correlation of the H units. Therefore, the abundance of H lignin units is overestimated. However, and despite this limitation, the calculation of the S/G ratio can be performed with more accuracy because the characteristic signals are well resolved. The lignin S/G ratio determined upon 2D-NMR gave a value of 0.4, similar to that obtained upon Py-GC/MS and Py/TMAH, and confirmed that the BSG lignin is enriched in G units. With regard to the content of *p*-hydroxycinnamates, a higher abundance of ferulates than *p*-coumarates was observed in all lignin preparations, with *p*-coumarates accounting for 5−6% and ferulates accounting for 7−10% of the total lignin units. Finally, tricin units account for 5−8% of total lignin units, with the highest abundance in the CEL preparation.

Lignin Acylation with *p*-Coumarates and Acetates As Seen by 2D-NMR and DFRC. Whereas ferulates are an intrinsic part of the lignin structure in grasses, participating in coupling and cross-coupling reactions with other monolignols and producing a diversity of linkages, *p*-coumarates are always present acylating the *γ*-carbon of the lignin side chain.[16,28,42] However, the characteristic C_γ−H_γ correlations of *γ*-acylated lignin units at δ_C/δ_H 62.7/3.83−4.30 could not be clearly observed in the HSQC spectra of the different BSG lignin preparations due to overlapping with other signals. In this sense, and to prove that the *p*-coumarates present in BSG lignin are also acylating the *γ*-carbon of the lignin side chain, we

DOI: 10.1021/jf505808c
J. Agric. Food Chem. 2015, 63, 603−613

Table 5. Structural Characteristics (Lignin Interunit Linkages, Aromatic Units, *p*-Coumarates and Ferulates, and Tricin Content) from Integration of $^{13}C-^{1}H$ Correlation Signals in the HSQC Spectra of the MWL, DL, and CEL Lignin Preparations Isolated from the BSG Sample

	MWL	DL	CEL
lignin interunit linkages (%)[a]			
β-*O*-4′ aryl ethers (A)	72	75	75
C*α*-oxidized *β*-*O*-4′ aryl ethers (A_{ox})	5	4	3
phenylcoumarans (B)	12	11	13
resinols (C)	6	5	6
dibenzodioxocins (D)	5	5	3
lignin aromatic units[b]			
H (%)[c]	24	32	20
G (%)	56	50	59
S (%)	20	18	21
S/G ratio	0.4	0.4	0.4
p-hydroxycinnamates[d]			
p-coumarates (%)	5	5	6
ferulates (%)	7	9	10
p-coumarates/ferulates ratio	0.7	0.6	0.6
tricin[d]	5	5	8

[a]Expressed as a fraction of the total lignin interunit linkage types A–D. [b]Molar percentages (H + G + S = 100). [c]Overestimated due to the presence of proteins. [d]Molar content as percentage of lignin content (H + G + S = 100).

performed HMBC experiments that correlate protons with carbons separated by two or three bonds. Figure 5 shows the section of the HMBC of the MWL preparation isolated from BSG with the correlations of the carbonyl carbons of the groups acylating the lignin *γ*-OH. The correlations of the carbonyl carbon at 166.0 ppm with the *α*-protons of *p*-coumarate esters (at 7.56 ppm) indicate that they belong to *p*-coumarate esters, but more important, the correlations of this carbonyl carbon with the protons at 4.08 ppm[28,42] definitively confirm that *p*-coumarates in BSG lignin are acylating the *γ*-position of the lignin side chains, as usually occurs in all grasses. However, the HBMC spectrum did not present any correlation for acetate groups (at 169.8 ppm) acylating the lignin side chain, despite the acetates having been widely found acylating the *γ*-OH in the lignins of many plants, including grasses.[28,29,34−36,47] This result seems to indicate that the extent of lignin *γ*-acetylation, if any, should be very low.

Further information about the acylation of the *γ*-OH of the lignin side chain was obtained from DFRC, a chemical degradative method that cleaves *α*- and *β*-ether bonds but leaves *γ*-esters intact.[31−33] The chromatogram of the DFRC degradation products of the MWL preparation is shown in Figure 6. The MWL from BSG released the *cis*- and *trans*-isomers of guaiacyl (*c*G and *t*G) and syringyl (*c*S and *t*S) lignin monomers (as their acetylated derivatives), arising from normal, non-*γ*-*p*-coumaroylated *β*-ethers in lignin. Only minor amounts of *γ*-*p*-coumaroylated syringyl (tS_{pc}) monomers could be detected in the chromatogram (<0.7% of the peak molar area of all lignin units) despite the significant amounts of *p*-coumarates present in this lignin (5% with respect to the total lignin aromatic units, as estimated by 2D-NMR in Table 5) and the fact that *p*-coumarates are acylating the *γ*-carbon, as observed by HMBC. No traces of *γ*-*p*-coumaroylated guaiacyl (cG_{pc} and tG_{pc}) lignin units could be found in the chromatogram despite this lignin being enriched in G lignin units, confirming that *p*-coumarates preferentially acylate S lignin units, as usually occurs in grasses.[16,29,42] Similar results were recently observed in the lignin from wheat straw, where neither traces of *γ*-*p*-coumaroylated syringyl nor guaiacyl conjugates were released, despite *p*-coumarates being attached to the *γ*-carbon, as clearly revealed by NMR.[28] This finding seems to indicate that, as also occurred in the lignin of wheat straw, *p*-coumarate groups are mostly attached to the lignin *γ*-OH in condensed lignin substructures that are not amenable to DFRC analysis.

The DFRC degradation method originally developed does not allow the analysis of natively acetylated lignin units because the degradation products are acetylated during the procedure. However, with appropriate modification of the original protocol by replacing acetylating reagents with propionylating ones, it is possible to obtain information about the presence of acetate groups originally acylating the *γ*-OH in lignin.[34−36] The results from this analysis indicated only a very minor extent of *γ*-acetylation of this lignin (undetectable by HMBC), which takes place predominantly on syringyl units (6% of S lignin units are acetylated), whereas only traces of acetylated guaiacyl units were detected (1% of G lignin units are acetylated).

In conclusion, the content and structure of the lignin from BSG have been thoroughly studied for the first time in the present work. Three different lignin preparations (MWL, DL, and CEL) were isolated and characterized in detail by different analytical methodologies (Py-GC/MS, 2D-NMR, DFRC). The

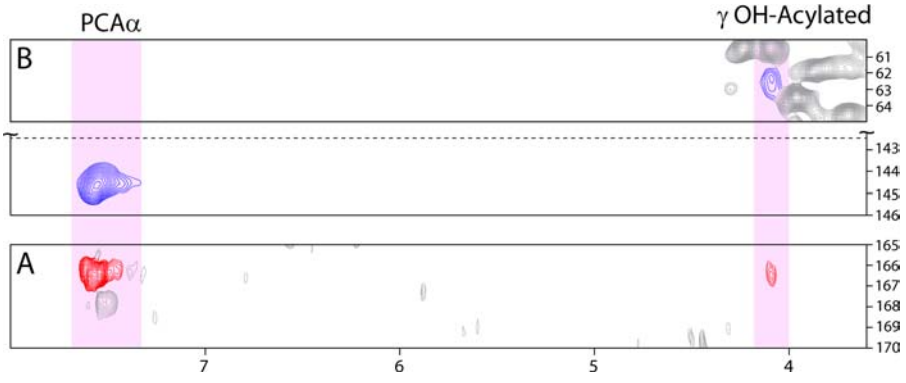

Figure 5. Section of the HMBC spectrum (δ_C/δ_H 165–170/3.5–8.0) of the MWL preparation isolated from BSG showing the main correlations for the carbonyl carbon of *p*-coumarates acylating the *γ*-position of the lignin side chain (A). Appropriate sections of the HSQC spectrum showing the $C_\gamma-H_\gamma$ correlations of the acylated lignin *γ*-carbon (δ_C 60–65) and the $C_\alpha-H_\alpha$ correlations of *p*-coumarates (δ_C 142–146) are also shown (B).

DOI: 10.1021/jf505808c
J. Agric. Food Chem. 2015, 63, 603–613

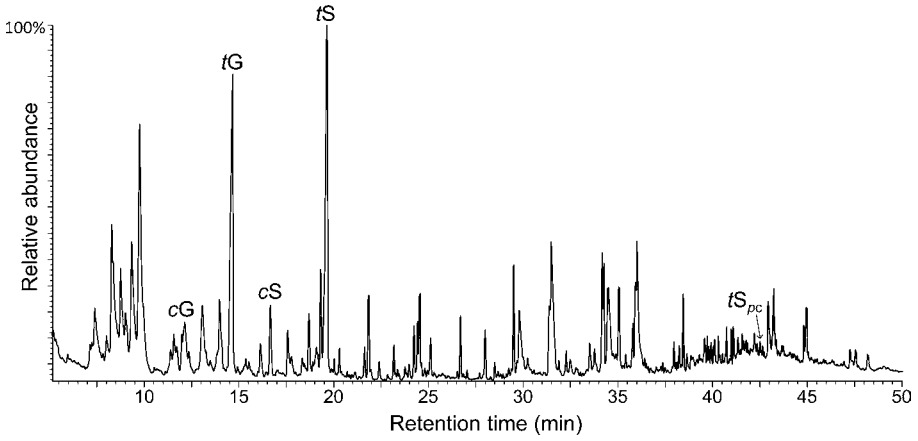

Figure 6. Chromatogram (GC-TIC) of the DFRC degradation products from the MWL preparation isolated from the BSG. *c*G, *t*G, *c*S, and *t*S are the normal *cis*- and *trans*-coniferyl and -sinapyl alcohol (guaiacyl and syringyl) monomers (as their acetate derivatives). tS_{pc} is the *trans*-sinapyl *p*-coumarate (as its acetate derivative).

analyses of these lignin preparations gave similar results and indicated that this lignin presents a strong predominance of G lignin units (S/G ratio of 0.4−0.5) with some amounts of associated *p*-coumarates and ferulates. The main lignin substructures present in BSG include *β*-*O*-4′ alkyl-aryl ethers (77−79% of all interunit linkages), followed by *β*-5′ phenylcoumarans (11−13%) and minor amounts of *β*-*β*′ resinols (5−6%) and 5-5′ dibenzodioxocins (3−5%). Finally, we also found that the flavone tricin is incorporated into the BSG lignin, as seems to occur in all grasses. The comprehensive understanding of the composition and structure of BSG lignin accomplished here will help development of lignin-based high-added-value products from this agro-industrial waste material and design of effective deconstruction strategies for biorefinery purposes.

AUTHOR INFORMATION

Corresponding Author

*(J.C.d.R.) Phone: +34-95-4624711. Fax: +34-95-4624002. E-mail: delrio@irnase.csic.es.

Funding

This study has been funded by the Spanish Project AGL2011-25379 (cofinanced by FEDER funds) and the EU Project LIGNODECO (KBBE-244362). J.R. thanks the CSIC for a JAE-DOC contract of the program "Junta para la Ampliación de Estudios" cofinanced by Fondo Social Europeo (FSE). P.P. thanks the Spanish Ministry of Science and Innovation for an FPI fellowship.

Notes

The authors declare no competing financial interest.

ACKNOWLEDGMENTS

We thank Prof. Craig B. Faulds (INRA, Marseille, France) for providing the BSG sample analyzed in this study. We also thank Dr. Manuel Angulo (CITIUS, University of Seville) for performing the NMR analyses.

REFERENCES

(1) Mussatto, S. I.; Dragone, G.; Roberto, I. C. Brewers' spent grain: generation, characteristics and potential applications. *J. Cereal Sci.* **2006**, *43*, 1−14.

(2) Aliyu, S.; Bala, M. Brewer's spent grain: a review of its potentials and applications. *Afr. J. Biotechnol.* **2011**, *10*, 324−331.

(3) Santos, M.; Jiménez, J. J.; Bartolomé, B.; Gómez-Cordovés, C.; del Nozal, M. J. Variability of brewer's spent grain within a brewery. *Food Chem.* **2003**, *80*, 17−21.

(4) Robertson, J. A.; I'Anson, K. J. A.; Treimo, J.; Faulds, C. B.; Brocklehurst, T. F.; Eijsink, V. G. H.; Waldron, K. W. Profiling brewers' spent grain for composition and microbial ecology at the site of production. *LWT−Food Sci. Technol.* **2010**, *43*, 890−896.

(5) Niemi, P.; Tamminen, T.; Smeds, A.; Viljanen, K.; Ohra-aho, T.; Holopainen-Mantila, U.; Faulds, C. B.; Poutanen, K.; Buchert, J. Characterization of lipids and lignans in brewer's spent grain and its enzymatically extracted fraction. *J. Agric. Food Chem.* **2012**, *60*, 9910−9917.

(6) del Río, J. C.; Prinsen, P.; Gutiérrez, A. Chemical composition of lipids in brewer's spent grain: a promising source of valuable phytochemicals. *J. Cereal Sci.* **2013**, *58*, 248−254.

(7) Mussatto, S. I.; Fernandes, M.; Roberto, I. C. Lignin recovery from brewer's spent grain black liquor. *Carbohydr. Polym.* **2007**, *70*, 218−223.

(8) Wilkinson, S.; Smart, K. A.; Cook, D. J. Optimisation of alkaline reagent based chemical pre-treatment of Brewers spent grains for bioethanol production. *Ind. Crops Prod.* **2014**, *62*, 219−227.

(9) Faulds, C. B.; Mandalari, G.; LoCurto, R.; Bisignano, G.; Waldron, K. W. Arabinoxylan and mono- and dimeric ferulic acid release from brewer's grain and wheat bran by feruloyl esterases and glycosyl hydrolases from *Humicola insolens*. *Appl. Microbiol. Biotechnol.* **2004**, *64*, 644−650.

(10) Hernanz, D.; Nuñez, V.; Sancho, A. I.; Faulds, C. B.; Williamson, G.; Bartolomé, B.; Gómez-Cordovés, C. Hydroxycinnamic acids and ferulic acid dehydrodimers in barley and processed barley. *J. Agric. Food Chem.* **2001**, *49*, 4884−4888.

(11) Mussatto, S. I.; Dragone, G.; Roberto, I. C. Ferulic and *p*-coumaric acids extraction by alkaline hydrolysis of brewer's spent grain. *Ind. Crops Prod.* **2007**, *25*, 231−237.

(12) Aura, A.-M.; Niemi, P.; Mattila, I.; Niemelä, K.; Smeds, A.; Tamminen, T.; Faulds, C. B.; Buchert, J.; Poutanen, K. Release of small phenolic compounds from brewer's spent grain and its lignin fractions by human intestinal microbiota in vitro. *J. Agric. Food Chem.* **2013**, *61*, 9744−9753.

(13) Niemi, P.; Aura, A.-M.; Maukonen, J.; Smeds, A. I.; Mattila, I.; Niemelä, K.; Tamminen, T.; Faulds, C. B.; Buchert, J.; Poutanen, K. Interactions of a lignin-rich fraction from brewer's spent grain with gut microbiota in vitro. *J. Agric. Food Chem.* **2013**, *61*, 6754−6762.

(14) Boerjan, W.; Ralph, J.; Baucher, M. Lignin biosynthesis. *Annu. Rev. Plant Biol.* **2003**, *54*, 519−549.

(15) Ralph, J.; Lundquist, K.; Brunow, G.; Lu, F.; Kim, H.; Schatz, P. F.; Marita, J. M.; Hatfield, R. D.; Ralph, S. A.; Christensen, J. H.; Boerjan, W. Lignins: natural polymers from oxidative coupling of 4-hydroxyphenylpropanoids. *Phytochem. Rev.* **2004**, *3*, 29−60.

DOI: 10.1021/jf505808c
J. Agric. Food Chem. 2015, 63, 603−613

(16) Ralph, J. Hydroxycinnamates in lignification. *Phytochem. Rev.* **2010**, *9*, 65−83.
(17) Björkman, A. Studies on finely divided wood. Part I. Extraction of lignin with neutral solvents. *Sven. Papperstidn.* **1956**, *59*, 477−485.
(18) Evtuguin, D. V.; Neto, C. P.; Silva, A. M. S.; Domingues, P. M.; Amado, F. M. L.; Robert, D.; Faix, O. Comprehensive study on the chemical structure of dioxane lignin from plantation *Eucalyptus globulus* wood. *J. Agric. Food Chem.* **2001**, *49*, 4252−4261.
(19) Chang, H.-M.; Cowling, E. B.; Brown, W.; Adler, E.; Miksche, G. Comparative studies on cellulolytic enzyme lignin and milled wood lignin of sweetgum and spruce. *Holzforschung* **1975**, *29*, 153−159.
(20) Faulds, C. B.; Robertson, J. A.; Waldron, K. W. Effect of pH on the solubilization of brewers' spent grain by microbial carbohydrases and proteases. *J. Agric. Food Chem.* **2008**, *56*, 7038−7043.
(21) Tappi. *Tappi Test Methods 2004−2005*; Tappi Press: Norcoss, GA, USA, 2004.
(22) Darvill, A. G.; McNeil, M.; Albersheim, P.; Delmer, D. The primary cell-walls of flowering plants. In *The Biochemistry of Plants*; Tolbert, N., Ed.; Academic Press: New York, 1980; pp 91−162.
(23) Browning, B. L. *Methods of Wood Chemistry*; Wiley-Interscience: New York, 1967.
(24) Faix, O.; Meier, D.; Fortmann, I. Thermal degradation products of wood. Gas chromatographic separation and mass spectrometric characterization of monomeric lignin-derived products. *Holz Roh-Werkst.* **1990**, *48*, 351−354.
(25) Ralph, J.; Hatfield, R. D. Pyrolysis-GC-MS characterization of forage materials. *J. Agric. Food Chem.* **1991**, *39*, 1426−1437.
(26) Bocchini, P.; Galletti, G. C.; Camarero, S.; Martínez, A. T. Absolute quantitation of lignin pyrolysis products using an internal standard. *J. Chromatogr., A* **1997**, *773*, 227−232.
(27) Ralph, S. A.; Ralph, J.; Landucci, L. *NMR Database of Lignin and Cell Wall Model Compounds*; U.S. Forest Products Laboratory: Madison, WI, USA; http://ars.usda.gov/Services/docs.htm?docid=10491) (accessed January 2009).
(28) del Río, J. C.; Rencoret, J.; Prinsen, P.; Martínez, Á. T.; Ralph, J.; Gutiérrez, A. Structural characterization of wheat straw lignin as revealed by analytical pyrolysis, 2D-NMR, and reductive cleavage methods. *J. Agric. Food Chem.* **2012**, *60*, 5922−5935.
(29) del Río, J. C.; Prinsen, P.; Rencoret, J.; Nieto, L.; Jiménez-Barbero, J.; Ralph, J.; Martínez, Á. T.; Gutiérrez, A. Structural characterization of the lignin in the cortex and pith of elephant grass (*Pennisetum purpureum*) stems. *J. Agric. Food Chem.* **2012**, *60*, 3619−3634.
(30) Rencoret, J.; Ralph, J.; Marques, G.; Gutiérrez, A.; Martínez, Á. T.; del Río, J. C. Structural characterization of lignin isolated from coconut (*Cocos nucifera*) coir fibers. *J. Agric. Food Chem.* **2013**, *61*, 2434−2445.
(31) Lu, F.; Ralph, J. The DFRC method for lignin analysis. 1. A new method for β-aryl ether cleavage: lignin model studies. *J. Agric. Food Chem.* **1997**, *45*, 4655−4660.
(32) Lu, F.; Ralph, J. The DFRC method for lignin analysis. 2. Monomers from isolated lignin. *J. Agric. Food Chem.* **1998**, *46*, 547−552.
(33) Lu, F.; Ralph, J. Detection and determination of *p*-coumaroylated units in lignins. *J. Agric. Food Chem.* **1999**, *47*, 1988−1992.
(34) Ralph, J.; Lu, F. The DFRC method for lignin analysis. 6. A simple modification for identifying natural acetates in lignin. *J. Agric. Food Chem.* **1998**, *46*, 4616−4619.
(35) del Río, J. C.; Marques, G.; Rencoret, J.; Martínez, A. T.; Gutiérrez, A. Occurrence of naturally acetylated lignin units. *J. Agric. Food Chem.* **2007**, *55*, 5461−5468.
(36) del Río, J. C.; Rencoret, J.; Marques, G.; Gutiérrez, A.; Ibarra, D.; Santos, J. I.; Jiménez-Barbero, J.; Zhang, L.; Martínez, A. T. Highly acylated (acetylated and/or *p*-coumaroylated) native lignins from diverse herbaceous plants. *J. Agric. Food Chem.* **2008**, *56*, 9525−9534.
(37) Crestini, C.; Melone, F.; Sette, M.; Saladino, R. Milled wood lignin: a linear oligomer. *Biomacromolecules* **2011**, *12*, 3928−3935.
(38) Capanema, E.; Ballakshin, M.; Katahira, R.; Chang, H.-M.; Jameel, H. How well do MWL and CEL preparations represent the whole hardwood lignin? *J. Wood Chem. Technol.* **2015**, *35*, 17−26.
(39) Fujimoto, A.; Matsumoto, Y.; Chang, H.-M.; Meshitsuka, G. Quantitative evaluation of milling effects on lignin structure during the isolation process of milled wood lignin. *J. Wood Sci.* **2005**, *51*, 89−91.
(40) del Río, J. C.; Gutiérrez, A.; Rodríguez, I. M.; Ibarra, D.; Martínez, Á. T. Composition of non-woody plant lignins and cinnamic acids by Py-GC/MS, Py/TMAH and FT-IR. *J. Anal. Appl. Pyrol.* **2007**, *79*, 39−46.
(41) del Rio, J. C.; Martin, F.; Gonzalez-Vila, F. J. Thermally assisted hydrolysis and alkylation as a novel pyrolytic approach for the structural characterization of natural biopolymers and geomacromolecules. *Trends Anal. Chem.* **1996**, *15*, 70−79.
(42) Ralph, J.; Hatfield, R. D.; Quideau, S.; Helm, R. F.; Grabber, J. H.; Jung, H.-J. G. Pathway of *p*-coumaric acid incorporation into maize lignin as revealed by NMR. *J. Am. Chem. Soc.* **1994**, *116*, 9448−9456.
(43) Grabber, J. H.; Hatfield, R. D.; Ralph, J.; Zon, J.; Amrhein, N. Ferulate cross-linking in cell walls isolated from maize cell suspensions. *Phytochemistry* **1995**, *40*, 1077−1082.
(44) Ralph, J.; Grabber, J. H.; Hatfield, R. D. Lignin-ferulate crosslinks in grasses: active incorporation of ferulate polysaccharide esters into ryegrass lignins. *Carbohydr. Res.* **1995**, *275*, 167−178.
(45) Wen, J.-L.; Sun, S.-L.; Xue, B.-L.; Sun, R.-C. Quantitative structural characterization of the lignins from the stem and pith of bamboo (*Phyllostachys pubescens*). *Holzforschung* **2013**, *67*, 613−627.
(46) You, T.-T.; Mao, J.-Z.; Yuan, T.-Q.; Wen, J.-L.; Xu, F. Structural elucidation of the lignins from stems and foliage of *Arundo donax* Linn. *J. Agric. Food Chem.* **2013**, *61*, 5361−5370.
(47) Ralph, J. An unusual lignin from kenaf. *J. Nat. Prod.* **1996**, *59*, 341−342.

DOI: 10.1021/jf505808c
J. Agric. Food Chem. 2015, 63, 603−613

JOURNAL OF AGRICULTURAL AND FOOD CHEMISTRY

Article

pubs.acs.org/JAFC

Nonenzymatic Modification of Ubiquitin under High-Pressure and -Temperature Treatment: Mass Spectrometric Studies

Monika Kijewska, Karolina Radziszewska, Martyna Kielmas, Piotr Stefanowicz,* and Zbigniew Szewczuk

Faculty of Chemistry, University of Wrocław, Wrocław, Poland

ABSTRACT: The effect of high-pressure and/or high-temperature on the glycation of a model protein (ubiquitin) was investigated by mass spectrometry. This paper reports the impact of high pressure (up to 1200 MPa) on the modification of a ubiquitin using ESI-MS measurements. The application of glucose labeled with stable isotope allows a quantitative assessment of modification under the conditions of high-pressure (HPG) and high-temperature (HTG) glycation. A higher degree of modification was observed for the sample heated at 80 °C for 25 min under atmospheric pressure than for sample treated under high pressure. In samples treated at pressure below 400 MPa an insignificant increase of glycation level was observed, whereas high pressure (>600 MPa) has only a minor effect on the number of hexose moieties (Fru) attached to the lysine residue side chain.

KEYWORDS: *glycation, high-pressure glycation, Amadori products*

INTRODUCTION

High-pressure processing (HPP) preserves nutrients, natural flavor, and other sensory properties of food while extending the shelf life by preventing the growth of microorganisms by inducing structural changes to the cell membrane and inactivating important enzyme systems that disrupt metabolism of microorganisms.[1,2] Some bacteria show resistance[3] to pressures up to 800 MPa and or even higher. However, the application of high-pressure processing combined with increased temperature could be useful for sterilization of many products sensitive to high temperatures, such as food, cosmetics, and pharmaceuticals.[4]

HPP is a nonthermal preservation and pasteurization technique, which causes little or no changes in the sensory and nutritional attributes of the product being processed, unlike most conventional heat treatments.[5] HPP accomplishes this by application of high hydrostatic pressures (between 100 and 1000 MPa) to food products. High pressure to about 3000 MPa does not affect covalent bonds in the molecules; therefore, many vitamins and provitamins as well as dyes, drugs; or other pharmacologically active molecules retain their unique characteristics.[5,6]

Bristow et al.[7] and Moreno et al.[8,9] reported the impact of high-pressure and alkaline conditions on the formation of Maillard products. The condensation of glyceraldehyde with di- and tripeptides was hardly affected by a pressure increase (up to 500 MPa), and the reaction of glyceraldehyde, glycolaldehyde, or xylose with amino acids was slightly suppressed. For a glucose−lysine system, some stages of the Maillard reaction were affected differently.[10]

Staniszewska et al.[11] proved that advanced glycation end products (AGEs) formed under high pressure (850 MPa) differ from those obtained thermally. In general, after high-pressure glycation (HPG), the products have a lower molecular mass than after high-temperature glycation (HTG). Immunoblotting experiments showed that the epitopes of the cross-linked glycation products formed in solution under high pressure are not the same as those originating in dry conditions at high temperature. The antibodies against HTG products recognized HTG but not HPG products. This finding reveals that the biological properties of AGEs obtained by thermal treatment and high-pressure treatment may be different.[11]

The first investigations on the impact of pressure on modifications of proteinaceous amino acid residue side chains using glucose or more reactive dicarbonyl[12] compounds revealed an increased level of pentosidine,[13] whereas the observed formation of carboxyethylarginine from arginine did not occur at atmospheric pressure.[14] In contrast, the generation of other Maillard reaction products, such as pyrraline, is hindered with the application of pressure.[15]

The effect of combined heat and pressure on the Maillard reaction between bovine serum albumin (BSA) and glucose was investigated by Buckow et al.[16] The kinetic results showed that the protein−sugar conjugation rate increased with increasing temperature, but decreased with increasing pressure. However, five modified lysine residues were identified after 30 min of treatment at 200 MPa and 110 °C, that is, lysine residues K75, K204, K297/299, K548, and K557. Glycation of K548 was previously observed by Frolov et al.[17] The effects of pressure and temperature on the reaction kinetics are antagonistic as an increase in pressure at constant temperature leads to a decrease in the entropy of the system.[18] Considine et al.[19] reported that BSA is relatively resistant to pressure denaturation, whereas it is easily denatured by heat and combined heat and high-pressure treatment.

A similar investigation was performed on milk proteins in the absence and presence of different saccharides or dicarbonyl compounds.[20] Without carbohydrates, protein cross-linking of casein is enhanced by pressure through the formation of dehydroalanine-derived lysinoalanine. In contrast, saccharide or

Received: June 11, 2014
Accepted: December 18, 2014
Published: December 18, 2014

ACS Publications © 2014 American Chemical Society

DOI: 10.1021/jf505628e
J. Agric. Food Chem. 2015, 63, 614−619

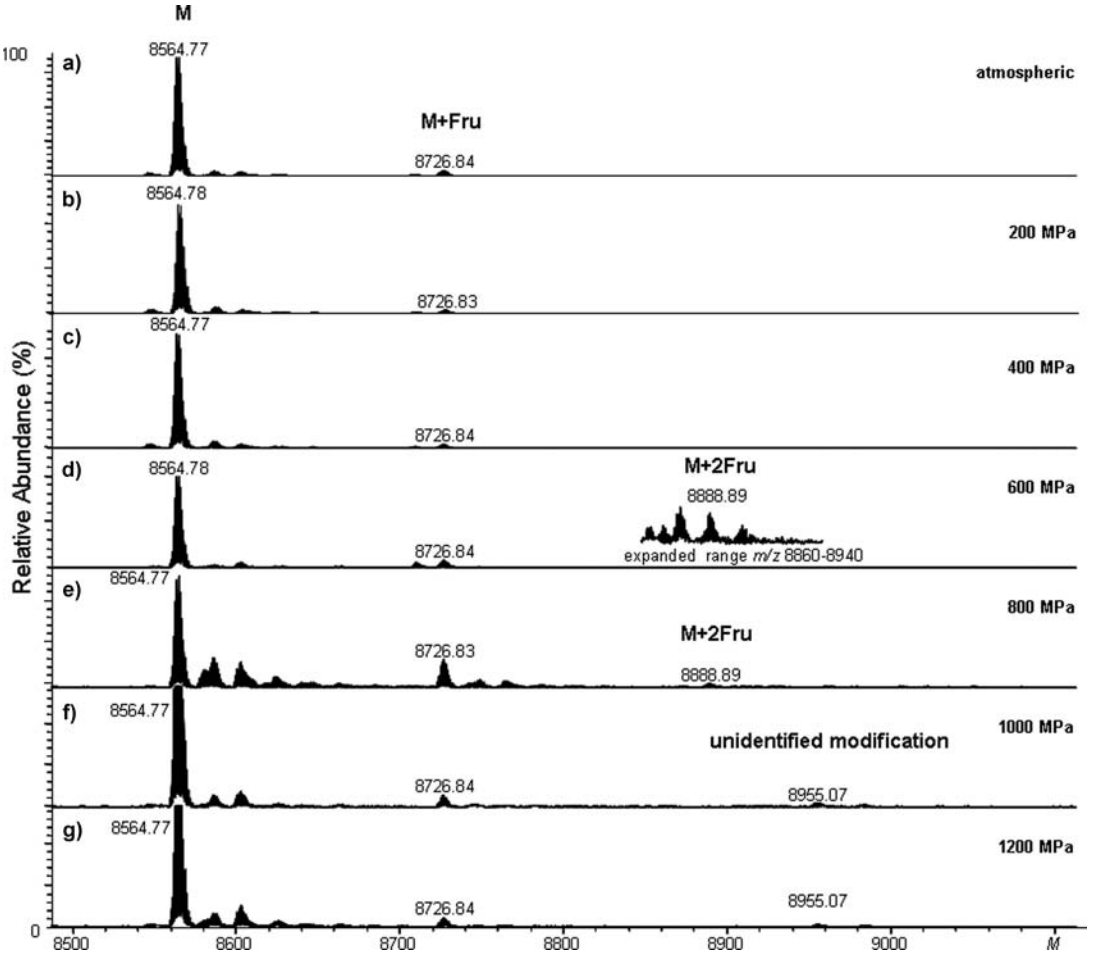

Figure 1. Deconvoluted ESI-MS spectra for ubiquitin glycated under high pressure in the range of 0.1−1200 MPa.

dicarbonyl compound-induced cross-linking is reduced at high pressures. The authors hypothesized that protein cross-linking is decelerated due to either degradation of sugars or carbonyl compounds or formation of early Maillard products.[20]

Our recent work has been focused on the reaction of the lysine moiety with reducing sugars. The Amadori products, including glycoconjugates, are potentially useful markers of some diseases: diabetes, Alzheimer's disease, or the aging process. We have reported an efficient method of synthesis,[21] as well as selective mass spectrometric (ESI-MS) detection based on the neutral losses, borate complex formation,[22,23] and isotopic (^{13}C, ^{18}O) labeling combined with enzymatic hydrolysis[24−26] and sequencing of glycoconjugates using various methods of fragmentation (ECD, CID).[27]

The utilization of high pressure, an emerging technology in the area of food processing, has been increasing over the past two decades. Herein we report the impact of high pressure (up to 1200 MPa) on the level of glycation of a ubiquitin using ESI-MS measurement. The quantification of the glycation level of ubiquitin was based on application of isotopic labeling [$^{13}C_6$].[23]

MATERIALS AND METHODS

Reagents. Reagents (including isotopically labeled [$^{13}C_6$]glucose; 99% ^{13}C and pepsin) and solvents (including formic acid (HPLC grade), acetonitrile (LC-MS grade), and ammonium formate (LC-MS grade)) were purchased from Sigma. Ubiquitin was purchased from Aldrich and D-glucose from Eurochem. The reagents were used without further purification.

High-Pressure Equipment. The high-pressure glycation experiments were carried out using a custom-made cylinder-piston type apparatus.[28,29] The stoppered polypropylene syringe, containing the protein sample, was placed in a high-pressure vessel filled with hexane as a transmission medium and compressed (0.1−1200 MPa).

High-Pressure Glycation. Ubiquitin (0.5 mg) and glucose (0.1 mg) were dissolved in 10 mmol/L aqueous ammonium formate (150 μL) at a 1:10 molar ratio and incubated at a given pressure (0.1−1200 MPa) for 24 h at room temperature (22 °C). After decompression, samples were diluted with 150 μL of a MeCN/H_2O/HCOOH mixture (50:50:0.1 v/v/v). The samples were directly analyzed by ESI-MS. Additionally, the modified ubiquitin treated under a pressure of 800 MPa was hydrolyzed according to the procedure described below.

High-Temperature Glycation. The high-temperature glycation of ubiquitin was performed according to Boratyński's method.[30,31] Briefly, ubiquitin and glucose or [$^{13}C_6$]glucose were dissolved in water at a 1:10 molar ratio and lyophilized. The dry lyophilisate was placed in an air oven at 80 °C for 25 min.[27] The resulting preparation was lyophilized and directly used for MS experiments.

Enzymatic Hydrolysis. Modified ubiquitin (1 mg) was dissolved in 5% aqueous formic acid (100 μL). Pepsin (10 μL of stock solution 1 mg/mL in water) was added, giving a 1:10 enzyme/substrate mass ratio. The reaction mixture was incubated for 5 h at 22 °C. The resulting digest was lyophilized and used for MS experiments.

ESI-MS Measurement. ESI-MS experiments were performed using an Apex-Qe Ultra 7T instrument (Bruker Daltonic, Germany) equipped with an ESI source. The obtained fragments were subsequently analyzed by the ICR mass analyzer. The instrument was operated in the positive-ion mode and calibrated with the Tunemix mixture (Bruker Daltonic). The mass accuracy was better than 5 ppm. Spectra were recorded for 5 μmol/L protein in a MeCN/

DOI: 10.1021/jf505628e
J. Agric. Food Chem. 2015, 63, 614−619

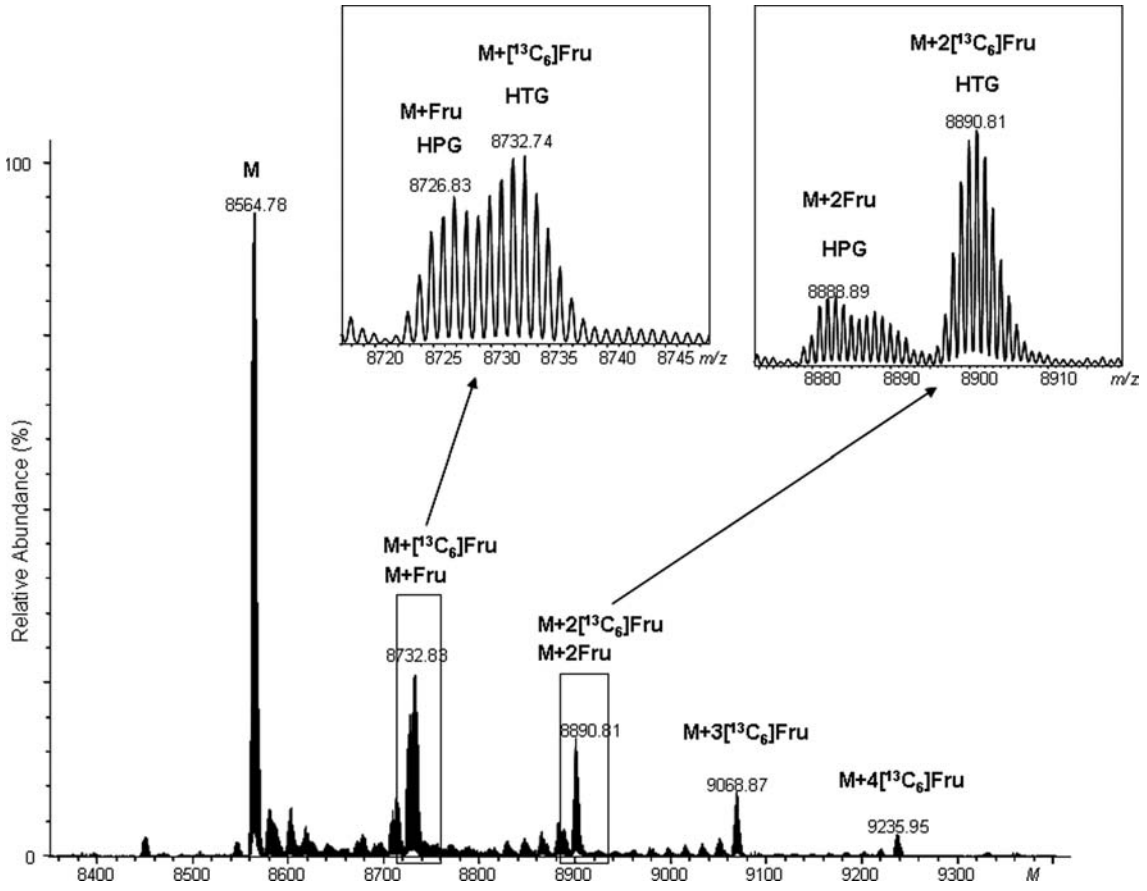

Figure 2. Deconvoluted ESI-MS spectrum of the mixture of ubiquitin modified thermally using [$^{13}C_6$]glucose and under high pressure (800 MPa) using standard glucose.

H_2O/HCOOH mixture (50:50:0.1 v/v/v). The sample was infused at a flow rate of 3 μL/min. The instrumental parameters were as follows: scan range, m/z 300−2500; drying gas, nitrogen; temperature of drying gas, 200 °C; potential between the spray needle and the orifice, 4.5 kV; source accumulation, 0.5 s; ion accumulation time, 0.5 s. The obtained mass spectra were analyzed using Bruker Data Analysis (Bruker Daltonic) software.

RESULTS AND DISCUSSION

High-Pressure Glycation. The effect of pressure on the Millard reaction between the model protein (ubiquitin) and a carbohydrate (glucose) was investigated. The series of experiments, including incubation of ubiquitin and glucose under high pressure in the range of 0.1−1200 MPa, were performed at isothermal conditions. The level of glycation was analyzed by ESI-MS.

The deconvoluted mass spectra (Figure 1) reveal the signals corresponding to mono- and diglycated ubiquitin, although the spectra are dominated by the nonmodified protein. A control sample was prepared using the same molar ratio of reagents and incubated under atmospheric pressure. The peak corresponding to monoglycated ubiquitin was observed for pressures of 0.1 MPa (atmospheric) and 200 and 400 MPa (Figure 1a−c). The average level of glycation calculated according to eq 1 equals 0.08. The approximate level of glycation of a particular Lys residue was calculated by comparing intensities of ions of protein differing by the number of hexose moieties.

$$\bar{n} = \frac{\sum n^* I_n}{\sum I_n} \quad (1)$$

n is the number of Fru and I_n is the intensity of the ion.

For protein samples incubated under pressure >600 MPa (Figure 1c−g), the signals corresponding to diglycated ubiquitin derivatives were observed. According to the literature, the critical pressure for denaturation of ubiquitin is approximately 600 MPa.[32−34] This may explain the appearance of the doubly modified protein under higher pressure (600−1200 MPa). The average level of modification was also calculated for 600 and 800 MPa pressures as 0.083 and 0.25, respectively. A further increase in pressure did not result in incorporation of another hexose moiety. The incubation of ubiquitin and glucose at 1000 MPa led to an additional modification, resulting in a 390.32 Da mass increase, which we were not able to identify accurately.

In Figure 2, the ESI-MS spectrum of the mixture of ubiquitin modified thermally using [$^{13}C_6$]glucose and by a high-pressure (800 MPa) using standard glucose is presented. The signals corresponding to mono- and diglycated ubiquitin confirm the presence of protein modification resulting from the reaction with both labeled and unlabeled glucose. The same experiments were conducted to compare the level of glycation under atmospheric and high pressure (800 MPa), using regular and [$^{13}C_6$]glucose, respectively.

In contrast to the results obtained for a high-temperature glycation using the same molar ratio of reagents as described previously,[27] the application of a high pressure has minor influence on the degree of glycation. However, after the high-pressure treatment, we observed additional signals in the MS spectra that were not observed after thermal treatment. We

DOI: 10.1021/jf505628e
J. Agric. Food Chem. 2015, 63, 614−619

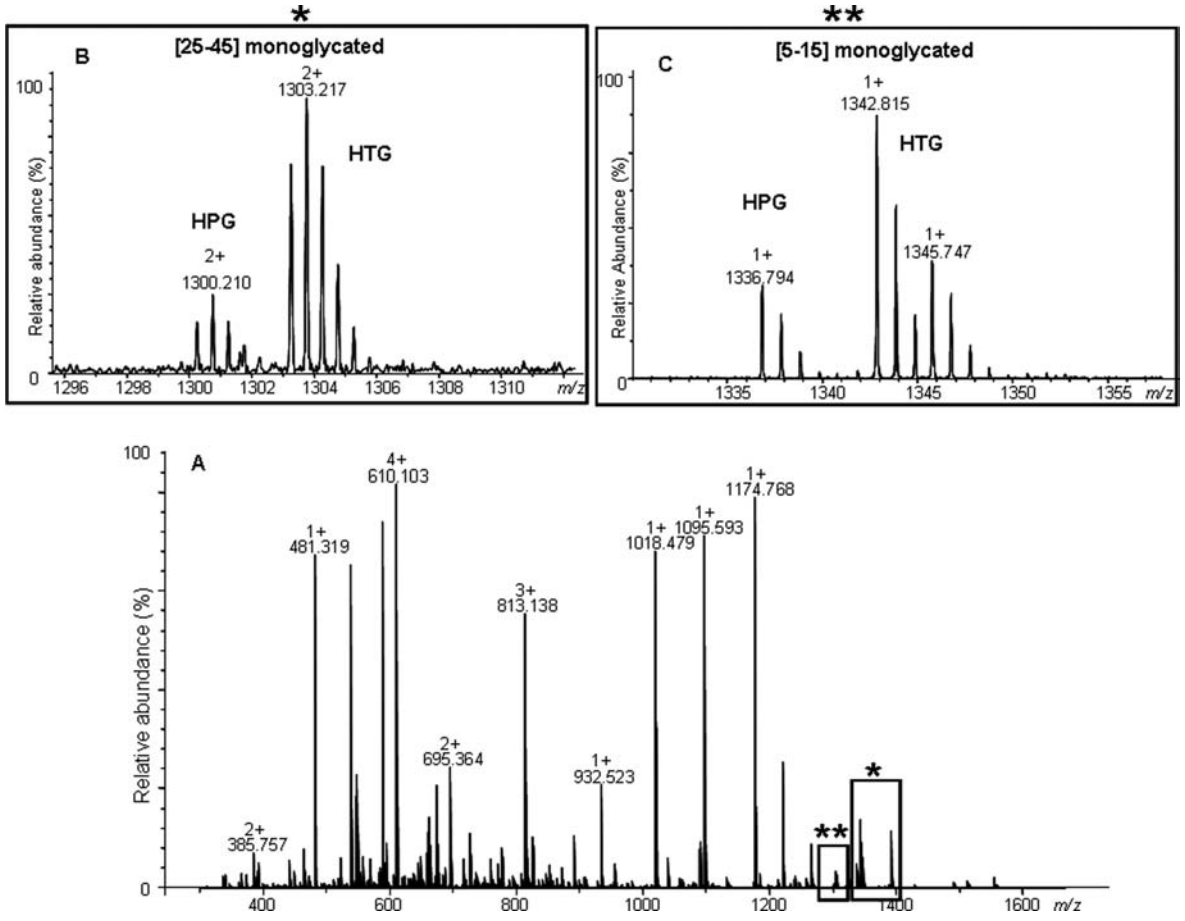

Figure 3. ESI-MS spectrum of the mixture of hydrolysates of ubiquitin glycated thermally (HTG) and under pressure (HPG, 800 MPa).

were not able to identify these byproducts. Further experiments are still needed to characterize these compounds and their mechanism of formation.

The regioselectivity of glycation of lysine moieties in ubiquitin was evaluated by enzymatic hydrolysis of the modified protein (incubated under pressure of 800 MPa) by pepsin followed by a direct ESI-MS measurement. Pepsin is a nonspecific protease, with the preference for peptide bonds at the C-terminus from Phe and Leu.[35] The crude hydrolysate was diluted with MeCN and then analyzed by ESI-MS. The glycation under high temperature and/or high pressure is relatively nonspecific. In the sequence of ubiquitin, there are seven lysine residues and the N-terminal amino group could be also glycated. Even though there are differences in the reactivity of the particular lysine moieties, every amino group may be glycated to some extent. Therefore, the sample of a glycated protein is an extremely complex mixture. In the analyzed hydrolysate, four peptides containing Amadori products, including residues 59−67, 5−15, 4−15, and 25−45, were found. The ECD fragmentation of modified peptide confirmed their sequence and the modification sites.[27] The analysis of the spectra allowed for identification of the glycated lysine residues as Lys6, Lys11, Lys27, Lys29, Lys33, and Lys63 within the sequences of ubiquitin fragments. The modifications of Lys48 and the α-amino groups, which according to the literature[27] are characterized by the lowest reactivity of all the potential glycation sites in ubiquitin, were not observed. In these studies, we received four identical peptide-derived Amadori products as in the case of thermally glycated ubiquitin.[23,27] Due to a much lower degree of modification under high pressure in comparison to the thermal modification of ubiquitin at the same protein/sugar molar ratio, the number of detected modified peptides was lower because of reduced concentration of glycated ubiquitin.

We tested the levels of glycation after the pressure and thermal treatment using isotopic labeling. High-temperature glycation was performed according to Boratyński's method using [$^{13}C_6$]glucose, whereas ubiquitin glycated under a high pressure was prepared using a standard glucose. The obtained modified proteins were mixed at a 1:1 weight ratio and then hydrolyzed in the presence of pepsin. The mixture of peptic fragments was analyzed directly, without a chromatographic separation, on an Apex-Ultra ESI-MS spectrometer. The same procedure was used to compare the efficiency of the glycation under atmospheric (APG) and high pressure (800 MPa) (HPG) using ubiquitin and glucose and [$^{13}C_6$]glucose, respectively.

The Amadori products obtained by the different treatments can be identified on the basis of mass difference caused by the use of [$^{13}C_6$] glucose. The search for glycated peptides can be performed automatically (in-house-designed spreadsheet) or by a visual inspection, recognizing the pairs of peaks with a defined m/z difference (m/z 6 for +1 ion, 3 Th for +2 ion, etc.). In the spectrum, signals corresponding to mixtures of hydrolysates of thermally and high-pressure glycated ubiquitin are presented. In the expanded range of this spectrum (Figure 3), a pair of signals corresponding to Amadori products 5−15 and 25−45 is shown. A significant difference in the signal intensity corresponding to

DOI: 10.1021/jf505628e
J. Agric. Food Chem. 2015, 63, 614−619

Table 1. Identified Glycoconjugates in a Mixture of Hydrolysates of Ubiquitin Glycated Thermally Using Labeled Glucose ([$^{13}C_6$]Glucose) (HTG) and under High Pressure (800 MPa) Using Unlabeled Glucose (HPG) by MS

			m/z				
glycated peptide	charge state	glycation method[a]	found	calcd	intensity	modified Lys residue	intensity ratio I_{HTG}/I_{HPG}
4−15	1+	HPG glucose	1483.864	1483.862	1.6×10^6	K6 or K11	3.88
		HTG [$^{13}C_6$]glucose	1489.882	1489.882	6.2×10^6		
5−15	1+	HPG glucose	1336.794	1336.793	2.2×10^7	K6 or K11	3.18
		HTG [$^{13}C_6$]glucose	1342.815	1342.814	7.0×10^7		
25−45	2+	HPG glucose	1300.210	1300.208	4.8×10^6	K27 or K29 or K33	3.75
		HTG [$^{13}C_6$]glucose	1303.217	1303.218	1.8×10^7		
59−67	1+	HPG glucose	1257.623	1257.621	9.8×10^6	K63	4.08
		HTG [$^{13}C_6$]glucose	1263.640	1263.641	4.0×10^7		

[a]HPG, glycation under high pressure; HTG, high-temperature glycation.

Table 2. Identified Glycoconjugates in a Mixture of Hydrolysates of Ubiquitin Incubated under Atmospheric Pressure Using Unlabeled Glucose (APG) and under High Pressure (800 MPa) Using Labeled Glucose ([$^{13}C_6$]Glucose) (HPG) by MS

			m/z				
glycated peptide	charge state	glycation method[a]	found	calcd	intensity	modified Lys residue	intensity ratio I_{HPG}/I_{APG}
4−15	1+	APG glucose	1483.863	1483.862	2.8×10^6	K6 or K11	2.45
		HPG [$^{13}C_6$]glucose	1489.883	1489.882	6.9×10^6		
5−15	1+	APG glucose	1336.795	1336.793	3.7×10^7	K6 or K11	2.03
		HPG [$^{13}C_6$]glucose	1342.814	1342.814	7.5×10^7		
25−45	2+	APG glucose	1300.210	1300.208	1.0×10^7	K27 or K29 or K33	2.2
		HPG [$^{13}C_6$]glucose	1303.219	1303.218	2.2×10^7		
59−67	1+	APG glucose	1257.622	1257.621	2×10^7	K63	1.9
		HPG [$^{13}C_6$]glucose	1263.642	1263.641	3.8×10^7		

[a]APG, glycation under atmospheric pressure HPG, glycation under high pressure.

the modified peptides was observed. The intensities of signals corresponding to the peptide-derived Amadori products obtained by thermal methods are higher than for the same products obtained under a pressure of 800 MPa. The relative intensity of peaks corresponding to the same fragments containing [$^{13}C_6$]glucose and unlabeled glucose allows for the analysis of the degree of modification of the Amadori products obtained under a high pressure (800 MPa), atmospheric pressure, and thermal glycation. It also makes possible the determination of the distribution of sugar residues in the protein sequence and thus the comparison of the reactivity of individual lysine residues. The results, including only the pairs of modified peptides present after thermal and pressure treatment, are presented in Tables 1 and 2. For ubiquitin glycated according to Boratyński's method, more fragments were found.[23]

On the basis of relative intensities of the peaks we can conclude that the thermal glycation is 4 times as efficient as the glycation under 800 MPa pressure, whereas the glycation under 800 MPa pressure is twice as efficient as incubation at atmospheric pressure (Table 1). The analysis of hydrolysates shows that both thermal and pressure glycation are relatively nonselective.

To summarize, glycation under 800 MPa pressure caused a slight increase in the level of ubiquitin glycation as compared to the atmospheric pressure incubation. Using the same molar ratio in the experiments performed on ubiquitin glycated by Boratyński's thermal method, up to four molecules of sugar moieties can be introduced, in contrast to ubiquitin glycated under pressure, where only a disubstituted protein was obtained. The results of our studies indicate high-pressure processing is a potential method for the preservation of foods, because the analyzed sample treated with a high pressure (<800 MPa) compared with the pressure up to 600 MPa did not cause the formation of unidentified byproducts forming at higher pressure. Moreover, we also noted that the level of glycation of the model protein under high pressure may be compared with the degree of modification under atmospheric pressure for the same time of incubation. In both cases a slight increase of glycation was observed in contrast to thermal glycation. On the basis of the presented results we can conclude that high-pressure treatment, a new method of food preservation enjoying increasing popularity among customers, can reduce the degree of glycation of proteins in comparison to pasteurization. On the other hand, high-pressure processing cannot eliminate a commonly used method of food pasteurization because many advantages of AGEs formed at a high temperature are known, and this area of research is still a matter of dispute.

AUTHOR INFORMATION

Corresponding Author

*(P.S.) Mail: Faculty of Chemistry, University of Wrocław, F. Joliot-Curie 14, 50-383 Wrocław, Poland. Fax: +48-71-

DOI: 10.1021/jf505628e
J. Agric. Food Chem. 2015, 63, 614−619

3282348. Phone: +48-71-3757213. E-mail: piotr.stefanowicz@chem.uni.wroc.pl.

Funding

This work was supported by Grant N N204 180340 from the Ministry of Science and Higher Education of Poland.

Notes

The authors declare no competing financial interest.

REFERENCES

(1) Heinz, V.; Buckow, R. Food preservation by high pressure. *J. Verbr. Lebensm* **2010**, *5*, 73−81.
(2) Fan, D. High pressure technology in the food industry. *Trends Food Sci. Technol.* **1990**, *1*, 14−16.
(3) Garcia-Graells, C.; Hauben, K.-J. A.; Michiels, C.-W. High pressure inactivation and sublethal injury of pressure-resistant *Escherichia coli* mutants in fruit juices. *Appl. Environ. Microbiol.* **1998**, *64*, 1566−1568.
(4) Hendrickx, M.; Ludikhuyze, L.; Van den Broeck, I.; Weemaes, C. Effects of high pressure enzymes related to food quality. *Trends Food Sci.* **1998**, *9*, 197−203.
(5) Barba, F. J.; Esteve, M. J.; Frıgola, A. High pressure treatment effect on physicochemical and nutritional properties of fluid foods during storage: a review. *Compr. Rev. Food Sci. Food Saf.* **2012**, *11*, 307−322.
(6) Boonyaratanakornkit, B.-B.; Park, Ch.-B.; Clark, D.-S. Pressure effects on intra and intermolecular interactions within proteins. *Biochim. Biophys. Acta* **2002**, *1595*, 235−249.
(7) Bristow, M.; Isaacs, N.-S. The effect of high pressure on the formation of volatile products in a model Maillard reaction. *J. Chem. Soc., Perkin Trans.* **1999**, *2*, 2213−2218.
(8) Moreno, F.-J.; Molina, E.; Olano, A.; Lopez-Fandino, R. High pressure effects on Maillard reaction between glucose and lysine. *J. Agric. Food Chem.* **2003**, *5*, 394−400.
(9) Moreno, F.-J.; Villamiel, M.; Olano, A. Effect of high pressure on isomerization and degradation of lactose in alkaline media. *J. Agric. Food Chem.* **2003**, *51*, 1894−1896.
(10) Nursten, H. *The Maillard Reaction: Chemistry, Biochemistry and Implications*; The Royal Society of Chemistry: Cambridge, UK, 2005; 33 pp.
(11) Staniszewska, M.; Jarosz, S.; Jon, M.; Gamian, A. Advanced glycation end-products prepared in solution under high pressure contain epitopes distinct from those formed in the dry reaction at high temperature. *Arch. Immunol. Ther. Exp.* **2005**, *53*, 71−78.
(12) Kocadagli, T.; Gökmen, V. Investigation of α-dicarbonyl compounds in baby foods by high-performance liquid chromatography coupled with electrospray ionization mass spectrometry. *J. Agric. Food Chem.* **2014**, *62*, 7714−7720.
(13) Schwarzenbolz, U.; Klostermeyer, H.; Henle, T. Maillard-type reactions under pressure: formation of pentosidine. *Eur. Food Res. Technol.* **2000**, *211*, 208−210.
(14) Alt, N.; Schieberle, P. Model studies on the influence of high hydrostatic pressure on the formation of glycated arginine modifications at elevated temperatures. *J. Agric. Food Chem.* **2005**, *54*, 5789−5797.
(15) Schwarzenbolz, U.; Klostermeyer, H.; Henle, T. Maillard reaction under high hydrostatic pressure: studies on the formation of protein-bound amino acid derivatives. In *The Maillard Reaction in Food Chemistry and Medical Science: Update for the Postgenomic Era*, 7th International Symposium on the Maillard Reaction, Kumamoto, Japan; Horiuchi, S., Taniguchi, N., Hayase, F., Kurata, T., Osawa, T., Eds.; Elsevier Science: Amsterdam, The Netherlands, 2001; pp 223−227.
(16) Buckow, R.; Wendorff, J.; Hemar, Y. Conjugation of bovine serum albumin and glucose under combined high pressure and heat. *J. Agric. Food Chem.* **2011**, *59*, 3915−3923.
(17) Frolov, A.; Hoffmann, R. Identification and relative quantification of specific glycation sites in human serum albumin. *Anal. Bioanal. Chem.* **2010**, *397*, 2349−2356.
(18) Mozhaev, V.-V.; Heremans, K.; Frank, J.; Masson, P.; Balny, C. High pressure effects on protein structure and function. *Proteins* **1996**, *24*, 81−91.
(19) Considine, T.; Patel, H. A.; Anema, S. G.; Singh, H.; Creamer, L.-K. Interactions of milk proteins during heat and high hydrostatic pressure treatments − a review. *Innovative Food Sci. Emerging Technol.* **2007**, *8*, 1−23.
(20) Schwarzenbolz, U.; Henle, T. Non-enzymatic modifications of proteins under high-pressure treatment. *High Pressure Res.* **2010**, *30*, 458−465.
(21) Stefanowicz, P.; Kijewska, M.; Kapczyńska, K.; Szewczuk, Z. Methods of the site-selective synthesis of peptide-derived Amadori products. *Amino Acids* **2010**, *38*, 881−889.
(22) Kijewska, M.; Kluczyk, A.; Stefanowicz, P.; Szewczuk, Z. ESI-MS investigation of interaction of peptide-derived Amadori products with borate ions. *Rapid Commun. Mass Spectrom.* **2009**, *23*, 4038−4046.
(23) Kijewska, M.; Kuc, A.; Kluczyk, A.; Waliczek, M.; Man-Kupisinska, A.; Łukasiewicz, J.; Stefanowicz, P.; Szewczuk, Z. Selective detection of carbohydrates and their peptide conjugates by ESI-MS using synthetic quaternary ammonium salt derivatives of phenylboronic acids. *J. Am. Soc. Mass Spectrom.* **2014**, *25*, 966−976.
(24) Stefanowicz, P.; Kijewska, M.; Kluczyk, A.; Szewczuk, Z. Detection of glycation sites in proteins by high-resolution mass spectrometry combined with isotopic labeling. *Anal. Biochem.* **2010**, *400*, 237−243.
(25) Kijewska, M.; Stefanowicz, P.; Kluczyk, A.; Szewczuk, Z. The isotopic exchange of oxygen in peptide-derived Amadori products as a tool for selective detection the glycation sites in proteins. *Anal. Biochem.* **2011**, *419*, 81−87.
(26) Kielmas, M.; Stefanowicz, P.; Szewczuk, Z. A study on human serum albumin influence on glycation of fibrynogen. *Biochem. Biophys. Res. Commun.* **2013**, *439*, 78−83.
(27) Stefanowicz, P.; Kijewska, M.; Szewczuk, Z. Sequencing of peptide-derived Amadori products by the electron capture dissociation method. *J. Mass Spectrom.* **2009**, *44*, 1047−1052.
(28) Stefanowicz, P.; Petry-Podgorska, I.; Kowalewska, K.; Jaremko, L.; Jaremko, M.; Szewczuk, Z. Electrospray ionization mass spectrometry as a method for studying the high-pressure denaturation of proteins. *Biosci. Rep.* **2010**, *30*, 91−99.
(29) Jankowska, E.; Stefanowicz, P.; Sosnowska, M.; Karpowicz, P.; Radziszewska, K.; Szewczuk, Z.; Szymańska, A. Pressure as a denaturing agent in studies of single-point mutants of an amyloidogenic protein human cystatin C. *Proteins* **2012**, *80*, 2417−2425.
(30) Stefanowicz, P.; Boratyński, J.; Kańska, U.; Petry, I.; Szewczuk, Z. Evaluation of high temperature glycation of proteins and peptides by electrospray ionization mass spectrometry. *Acta Biochim. Polym.* **2001**, *48*, 1137−1141.
(31) Boratyński, J.; Roy, R. High temperature conjugation of proteins with carbohydrates. *Glycoconjugate J.* **1998**, *15*, 131−138.
(32) Herberhold, H.; Winter, R. Temperature- and pressure-induced unfolding and refolding of ubiquitin: a static and kinetic Fourier transform infrared spectroscopy study. *Biochemistry* **2002**, *41*, 2396−2401.
(33) Jonas, J.; Ballard, L.; Nash, D. High-resolution, high-pressure NMR studies of proteins. *Biophys. J.* **1998**, *75*, 445−452.
(34) Stefanowicz, P.; Petry-Podgórska, I.; Kowalewska, K.; Jaremko, Ł.; Jaremko, M.; Szewczuk, Z. Electrospray ionization mass spectrometry as a method for studying the high-pressure denaturation of proteins. *Biosci. Rep.* **2010**, *29*, 91−99.
(35) Engen, J. R.; Wales, T. E. Hydrogen exchange mass spectrometry for the analysis of protein dynamics. *Mass Spectrom. Rev.* **2006**, *25*, 158−170.

DOI: 10.1021/jf505628e
J. Agric. Food Chem. 2015, 63, 614−619

JOURNAL OF AGRICULTURAL AND FOOD CHEMISTRY

Article

pubs.acs.org/JAFC

Remarkable Proanthocyanidin Adsorption Properties of Monastrell Pomace Cell Wall Material Highlight Its Potential Use as an Alternative Fining Agent in Red Wine Production

Ana Belén Bautista-Ortín, Yolanda Ruiz-García, Fátima Marín, Noelia Molero, Rafael Apolinar-Valiente, and Encarna Gómez-Plaza*

Departamento de Tecnología de Alimentos, Nutrición y Bromatología, Facultad de Veterinaria, Universidad de Murcia, Campus de Espinardo, 30071 Murcia, Spain

Supporting Information

ABSTRACT: The existence of interactions between the polysaccharides of vegetal cell walls and proanthocyanins makes this cell wall material an interesting option for its use as a fining agent to reduce the level of proanthocyanins in wines. Pomace wastes from the winery are widely available and a source of cell wall material, and the identification of varieties whose pomace cell walls present high proanthocyanin binding capacity and of processing methods that could enhance their adsorption properties could be of great interest. This study compared the proanthocyanin adsorption properties of pomace cell wall material from three different grape varieties (Monastrell, Cabernet Sauvignon, and Syrah), and the results were compared with those obtained using fresh grape cell walls. Also, the effect of the vinification method has been studied. Analysis of the proanthocyanidins in the solution after reaction with the cell wall material, using phloroglucinolysis and size exclusion chromatography, provided quantitative and qualitative information on the adsorbed and nonadsorbed compounds. A highlight of this study was the observation that Monastrell pomace cell wall material showed a strong affinity for proanthocyanidins, with values similar to that obtained for fresh grapes cell walls, and a preferential binding of high molecular mass proanthocyanidins, so these pomace cell walls could be used in wines to reduce astringency. The use of maceration enzymes during vinification had little effect on the retention capacity of the pomace cell walls obtained from this vinification, although an increase in the retention of low molecular mass proanthocyanidins was observed, and this might have implications for wine sensory properties.

KEYWORDS: *proanthocyanidins, tannins, cell wall material, grapes, pomace, phloroglucinolysis, size exclusion chromatography*

INTRODUCTION

The properties and characteristics of grape skin and flesh cell wall material (CWM) are closely related to some enological events and some observations concerning phenolic compounds in grapes and wines. In this way, previous studies have demonstrated that the composition and quantity of skin cell walls may determine the mechanical resistance, texture, and ease with which berries are processed, as well as anthocyanin extractability during fermentative maceration.[1,2]

Cell walls (CWs) are composed of polysaccharides, phenolic compounds, and proteins and are stabilized by ionic and covalent linkages. Among the polysaccharides, the presence of hemicellulose, cellulose, and pectins is important, and the last two account for 30−40% of the polysaccharide components of the cell wall.[3]

Cell wall polysaccharides contain hydroxyl groups as well as aromatic and glycosidic oxygen atoms that have the ability to form hydrogen bonds and hydrophobic interactions with some molecules,[4,5] including proanthocyanidins.[6] The existence of CWM−proanthocyanidin interactions may explain some experimental observations such as the decrease in grape proanthocyanidin (PA) extractability as ripening progresses,[7,8] which can be explained as a retention of PAs in the cell wall material,[9−11] and the reduced extractability of PAs during fermentative maceration,[12] which may be related not only to these PAs being retained in the solid parts but also to a substantial proportion of them being adsorbed by the CWM in suspension in the must and finally precipitated during settling. Moreover, some authors have stated that there are differences in the affinity of PAs for the different polysaccharides present in CWs, their affinity for covalently linked pectin being higher than that for xyloglucan and cellulose.[5] This observation may indicate that differences in the CW and PA composition among varieties may be the cause of the varietal differences in PA extractability observed in other experiments.[12]

Another enological practice that may be affected by these interactions is the use of enological tannins. The addition of exogenous commercial tannins to increase their levels in wine is a common practice for several reasons: they may help stabilize color, increase body, mask green characters, etc.[13] Depending on the final objective, they are used in the fermentative or postfermentative phase of winemaking. Their addition during fermentation may result in a large part of these exogenous tannins being eliminated by their interaction with the skin and pulp cell walls present in the must after crushing of the grapes, as reported by Bautista-Ortín et al.[14]

Another point of interest of the capacity of CWs to interact with PAs is their possible use as fining agents. Some red wines

Received: July 30, 2014
Revised: December 14, 2014
Accepted: December 20, 2014
Published: December 20, 2014

ACS Publications © 2014 American Chemical Society

DOI: 10.1021/jf503659y
J. Agric. Food Chem. 2015, 63, 620−633

present high levels of astringency and bitterness, due to an excessive extraction of tannins from grapes or an excessive addition of commercial enological tannins,[15] and may need a fining agent to reduce the concentrations of tannins in wines. Traditionally, proteins have been used for fining purposes, due to their high affinity for PAs. Most of the proteins commonly used are of animal origin, such casein, albumin, and gelatin.[16] Lately, those of vegetal origin (Arabic gum, pea protein) are becoming more popular, mainly due to the allergenic properties of some of the animal-derived proteins and the legal obligation to indicate their presence on the label (EU Directive 2007/68/EC November 27, 2007), a fact that may reduce their attraction for consumers. The ability of CWM to bind PAs makes them an interesting object of study for their possible use as new fining agents. Such studies were initiated by Bindon and Smith[17] and Guerrero et al.,[18] who studied the fining action of insoluble fibers prepared from fresh apple and different grape sources and compared them with commercial proteins, reporting that grape fibers may be considered as alternative fining agents for red wines. It is clear that fiber or purified CWM derived from fresh grapes would not be of commercial interest because grapes are a valuable product, but products derived from the pomace obtained after fermentation and devatting might be an interesting way of adding value to this byproduct, as also stated by Bindon and Smith.[17] However, compositional differences among different varieties, the possible compositional changes that flesh, but especially skin CWM may suffer during the fermentation process, and how these changes affect their binding capacity need to be considered. In fact, previous studies have shown that the fermentation process may alter the polysaccharide composition of the CWM, as may do the different treatments used during fermentative maceration as it is the use of maceration enzymes.[19,20] The use of maceration enzymes decreased the uronic acids and total sugar content of the cell wall due to their action on the pectin matrix[20] and that may change the level of CW−PA interactions.

In this study, the ability of purified CWM derived from pomace (from three different varieties and from two different vinification methods) to bind different types of PAs was studied, searching for a source of pomace material with a high adsorption capacity and clear selectivity for high molecular mass proanthocyanidins that could be used to reduce wine astringency.

MATERIALS AND METHODS

Chemicals. Chromatographic solvents were of high-performance liquid chromatography (HPLC) grade, and chemicals were of analytical reagent grade. Acetonitrile, acetone, methanol, ethanol, formic acid, and trifluoroacetic acid were from Merck (Darmstadt, Germany). The phloroglucinol reagent was sourced from Sigma-Aldrich (St. Louis, MO, USA). Sodium acetate was sourced from J. T. Baker (Deventer, The Netherlands). The standards (+)-catechin, (−)-epicatechin, (−)-epicatechin gallate, and (−)-epigallocatechin were obtained from Extrasynthese (Genay, France).

Instrumentation. The HPLC apparatus was a Waters 2695 (Waters, Milford, MA, USA) equipped with a Syrahstem autosampler and a Waters 2996 photodiode array detector.

Grapes and Pomace. *Vitis vinifera* L. cv. Monastrell, Cabernet Sauvignon, and Syrah grapes, cultivated in Murcia (Spain), were sampled at 23.8, 24.8, and 25.6 °Brix, respectively, and with a titratable acidity ranging from 2.9 to 3.3 g/L, expressed as tartaric acid.

Grapes from each of the three cultivars (90 kg) were destemmed and crushed. The crushed grapes were macerated in 100 L stainless steel tanks. Potassium bisulfite (8 g/100 kg grapes) was added. Fermentation was carried out with temperature control (25 °C); fermentations were initiated with Levuline Gala (commercial dry *Saccharomyces cerevisiae* yeast, OenoFrance, Bordeaux, France) inoculated at 10 g/hL. After 10 days of maceration, the wine was pressed at 150 kPa in a 75 L tank membrane press (Hidro 80L, Ausavil, Spain), and the pomace was recovered. The skins from pomace were separated from seeds and other solid parts, and they represented the pomace from the control vinification. Other vinification was carried out with the addition of a commercial enzyme preparation (3 g/100 kg, Enozym Vintage, Agrovin, Spain) just after crushing. The fermentation, pressing conditions, and pomace recovery were as described for the control vinification.

Cell Wall Material. Purified CWM was extracted from *V. vinifera* L. cv. Monastrell, Cabernet Sauvignon, and Syrah fresh skins and from the pomace obtained after 10 days of fermentative maceration. Cell walls were isolated according to the method of De Vries et al.,[21] as adapted by Apolinar-Valiente et al.[22] Briefly, the grape skin tissue or the pomace skin tissue (10 g) was suspended in 15 mL of boiling water for 5 min and then homogenized. One part of the homogenized material was mixed with two parts of 96% ethanol and extracted for 30 min at 40 °C. The raw alcohol-insoluble solids were separated by filtration on paper and extracted again with fresh 70% ethanol for 30 min at 40 °C. The washing treatment with fresh 70% ethanol was repeated several times until no sugars remained in the 70% ethanol phase. Then, the alcohol-insoluble solids (AIS) were washed twice with 96% ethanol and once with acetone and finally dried overnight under an air stream at 20 °C. The composition of the cell walls can be found in the Supporting Information (Figures S1−S4).

Proanthocyanidins Used in the Interaction Studies. Two purified PA fractions from ripened grape skin (sPA) and seed (sdPA) were selected for the experiment as well as two commercial samples, a skin-derived (T1) and a seed-derived (T2) enological tannin. The purity of the commercial tannins was estimated spectrophotometrically following the method of Riberau-Gayon et al.[23] after acid hydrolysis of the samples.

For the purified fractions, *V. vinifera* L. cv. Monastrell grape berries were used as the source material for grape skin and seed proanthocyanidins. A random sample (1 kg) was collected at technological maturity. Grape berries were kept at −20 °C until processed. For the proanthocyanidin isolation and purification, the skins and seeds were separated from the berry mesocarp and rinsed with distilled−deionized water, and the intact tissues were extracted in covered Erlenmeyer flasks with 2:1 acetone/water at room temperature for 24 h. To minimize proanthocyanidin oxidation, solutions were sparged with nitrogen and the extraction was carried out in the dark. Following extraction, the extract was concentrated under reduced pressure at 35 °C to remove acetone and then lyophilized to a dry powder.

The crude proanthocyanidins were purified using Toyopearl TSK HW 40-F size exclusion media (Sigma-Aldrich). The column (400 × 26 mm) was equilibrated with 1:1 MeOH/water containing 0.1% (v/v) trifluoroacetic acid. The proanthocyanidin powder was dissolved in a minimum amount of this mobile phase and then applied to the column. The column was then rinsed with 5 column volumes of the mobile phase to remove carbohydrate and low-molecular-weight flavan-3-ol monomer material. The proanthocyanidins were then eluted with 3 column volumes of 2:1 acetone/water containing 0.1% (v/v) trifluoroacetic acid. The eluent was concentrated under reduced pressure at 35 °C to remove acetone and then lyophilized to a dry powder.

For fractionation, the method proposed by Kennedy and Taylor[24] was used. Grape skin proanthocyanidin samples (2 g each) were dissolved in 50 mL of MeOH/water/formic acid (49.8:49.8:2.4) and quantitatively applied to a Sephadex LH-20 column (400 × 26 mm, Sigma-Aldrich) equilibrated with MeOH/water/formic acid (49.8:49.8:2.4). The column was then washed sequentially using different solvent systems and volumes. Eluted proanthocyanidin fractions were collected into test tubes. The fractions were rotary evaporated, lyophilized to dryness, and stored at −80 °C. One purified fraction from seed and another from skin were chosen for the experiments, on the basis of their quantitative availability and a mean degree of polymerization closer to that of red Monastrell wines.

Binding Reactions between Tannins and Cell Wall Material. Skin or pomace CWM was weighed into 3 mL tubes. CWM samples

DOI: 10.1021/jf503659y
J. Agric. Food Chem. 2015, 63, 620−633

were then combined with the four different proanthocyanidins: those contained in two different commercial enological tannins (a seed-derived and a skin-derived grape tannin) and the two purified skin- and seed-derived proanthocyanidins. They were dissolved in a model solution (12% ethanol at pH 3.6 adjusted with trifluoroacetic acid) to a concentration of 2 g/L. The reaction volume was 2.5 mL, and the CWM was 13 mg/mL. The different samples were shaken at 300 rpm in an orbital shaker at room temperature for 90 min. Each experiment (each tannin solution with each of the three different CWM, isolated from fresh grape skins and from the pomace of the two different vinifications) was made in duplicate and for each variety.

For each reaction, a blank without CWM and a blank without tannin were also included, the latter to monitor any possible desorption of CWM-bound tannin. After the binding reaction, samples were centrifuged at 13000 rpm, and the supernatant was transferred to a new tube. Samples were then dried under vacuum at 35 °C. Recovered tannin was reconstituted in 250 μL of methanol and then analyzed by phloroglucinolysis and size exclusion chromatography (SEC).

Analysis of Proanthocyanidins Using the Phloroglucinolysis Reagent. The proanthocyanidin content of the control sample (2 g/L) or those remaining in solution after the interaction with the CWs was analyzed using the phloroglucinol reagent, according to the method described by Kennedy and Jones[25] with some modifications described below. A solution of 0.2 M HCl in methanol, containing 100 g/L phloroglucinol and 20 g/L ascorbic acid, was prepared (phloroglucinolysis reagent). The methanolic extract was left to react with the phloroglucinolysis reagent (1:1) in a water bath for 20 min at 50 °C and then combined with 2 volumes of 200 mM aqueous sodium acetate to stop the reaction.

HPLC analysis followed the conditions described by Busse-Valverde et al.[26] Samples (10 μL injection volume) were injected on an Atlantis dC18 column (250 × 4.6 mm, 5 μm packing) protected with a guard column of the same material (20 mm × 4.6 mm, 5 μm packing) (Waters). The elution conditions were as follows: 0.8 mL/min flow rate; oven temperature, 30 °C; solvent A, water/formic acid (98:2, v/v); and solvent B, acetonitrile/solvent A (80:20 v/v). Elution began with 0% B for 5 min, linear gradient from 0 to 10% B in 30 min, and gradient from 10 to 20% in 30 min, followed by washing and re-equilibration of the column.

Proanthocyanidin cleavage products were estimated using their response factors at 280 nm relative to (+)-catechin, which was used as the quantitative standard. These analyses allowed determination of the recovery by mass of the total proanthocyanidin content, the apparent mean degree of polymerization (mDP), and the percentage of each constitutive unit. The mDP was calculated as the sum of all subunits (flavan-3-ol monomer and phloroglucinol adducts, in moles) divided by the sum of all flavan-3-ol monomers (in moles).

The percentage of conversion was calculated gravimetrically from the percentage of conversion of tannins to known proanthocyanin subunits.

To determine the naturally occurring proanthocyanidin monomers (catechin and epicatechin), the methanolic extract was analyzed without reaction with the phloroglucinolysis reagent.

Analysis of Proanthocyanidins by Size Exclusion Chromatography. An adaptation of the method described by Kennedy and Taylor[24] was used for SEC. The method used two PLgel (300 × 7.5 mm, 5 μm, 500 (effective molecular mass range of up to 4000 using polystyrene standards) by 100 Å (effective molecular mass range of 500−30000 using polystyrene standards) columns connected in series and protected by a guard column containing the same material (50 × 7.5 mm, 5 μm), all purchased from Polymer Laboratories (Amherst, MA, USA). The amount of sample injected was 40 μg. The isocratic method used a mobile phase consisting of *N*,*N*-dimethylformamide containing 1% glacial acetic acid, 5% water, and 0.15 M lithium chloride. The flow rate was maintained at 1 mL/min with a column temperature of 60 °C, and elution was monitored at 280 nm.

The SEC peak area results were calibrated to the gravimetric value (A_{280}/mg gravimetric) for each tannin type.

Statistical Analysis. All of the statistical analyses were made using Statgraphics Centurion XVI (Statpoint Technologies Inc., Warranton, VA, USA).

RESULTS AND DISCUSSION

Proanthocyanidins Used in the Experiment. Because it has been suggested that the composition, molecular size, conformational mobility, and shape influence the interactions between tannins and CWM,[4,5] PA samples with different characteristics were used for this study. We have worked with two commercial samples, a skin-derived (T1) and a seed-derived (T2) commercial tannin, and the results were compared with a purified PA fraction from ripened grape skin (sPA) or seed (sdPA). The phloroglucinolysis assay showed that the lowest conversion was observed in T1 and the highest in seed PA, with a conversion of 72% (Table 1). These results were expected because higher conversions are always found when working with seed tannins compared with skin.[7]

It is well-known that grape PAs slightly differ in their composition according to their origin in the berry. Seed proanthocyanidins contain greater levels of flavan-3-ols esterified to gallic acid, they generally have a lower degree of polymerization (mDP) than those from skins, and no trihydroxylation of the B ring has been observed.[25,27] However, and contrary to expectations, the mDP of the skin-derived commercial enological tannin was very low considering its origin (skin tannin sample), with values very similar to those obtained for seed-derived commercial sample. Higher mDPs were observed for the purified samples, the highest being found in sPA.

The maximum galloylation percentage was observed in the seed-derived tannins, especially in the purified samples, and lower values were found in the skin-derived samples, the lowest values in T1.

With regard to the subunit composition, commercial samples differed from purified samples mainly in the lower quantities of terminal units and higher percentage of extension epicatechin. Comparison of both purified samples showed the main differences were in the percentages of epicatechin gallate, both terminal and extension subunits (as was expected, given the higher percentage of galloylation) and the absence of epigallocatechin subunits in the seed samples. The composition of T1, labeled as skin tannin, showing a low mDP, relatively high galloylation percentage, and low percentage of epigallocatechin, may indicate that this sample is really a mix of skin and seed tannins.

The tannin samples and purified fractions were also analyzed using SEC. Given the relatively low conversion percentage of the phloroglucinolysis study, the use of SEC also allows the fraction that was not depolymerized by the phloroglucinolysis assay to be studied. This technique provides complementary information concerning the adsorption rate and molecular mass distribution of the tannins.

The profiles are shown in Figure 1, and differences were observed among the different samples. For the study of the molecular mass distribution, and unlike other studies that reported mass distribution information as a cumulative (% volume elution) molecular mass, in the current study the mass distribution is reported as elution time and the SEC chromatograms were divided in three areas representing the high (those eluting from minute 10 to 11.8, F1 (see Table 2)), medium (from 11.8 to 13.6 min, F2), and low molecular mass PAs (from 13.6 to 15.0 min, F3). The distribution of the eluted area showed that sPA and sdPA had the largest percentages of areas eluting at the first elution time range (67.8 and 66.9%, respectively), indicating a higher percentage of high molecular mass PAs, whereas in T1 and T2 the area in this fraction of elution time was lower

DOI: 10.1021/jf503659y
J. Agric. Food Chem. 2015, 63, 620−633

Table 1. Composition of the Enological Tannins Used in the Experiment[a]

sample	total tannins (mg/L)	% conversion	mDP	%G	tC	tEC	tECG	extC	extEC	extEGC	extECG
T1	771.91 ± 5.24	38.60 ± 0.26	2.67 ± 0.02	3.86 ± 0.00	17.42 ± 0.13	19.33 ± 0.08	0.74 ± 0.00	5.16 ± 0.04	47.89 ± 0.18	6.33 ± 0.01	3.12 ± 0.00
T2	1227.48 ± 5.03	61.37 ± 0.25	2.57 ± 0.01	7.33 ± 0.03	20.27 ± 0.14	16.18 ± 0.04	2.47 ± 0.00	9.66 ± 0.02	46.57 ± 0.12	0.00	4.86 ± 0.03
sPA	1143.72 ± 110.57	57.19 ± 5.53	8.50 ± 0.26	2.78 ± 0.02	6.23 ± 0.03	5.54 ± 0.33	0.00	1.47 ± 0.01	67.53 ± 0.31	16.46 ± 0.02	2.78 ± 0.02
sdPA	1454.78 ± 19.07	72.74 ± 0.95	5.69 ± 0.1	17.01 ± 0.07	6.28 ± 0.11	6.56 ± 0.08	4.74 ± 0.03	7.36 ± 0.01	62.79 ± 0.04	0.00	12.27 ± 0.04

[a]Abbreviations: T1, commercial enological tannin from grape skins; T2, commercial enological tannin from grape seeds; sPA, purified grape skin proanthocyanidin; sdPA, purified grape seed proanthocyanidin; mDP, mean degree of polymerization; %G, percentage of galloylation; extC, percentage of extension (+)-catechin; extEC, percentage of extension (−)-epicatechin; extECG, percentage of extension (−)-epicatechin gallate; tC, percentage of terminal (+)-catechin; tEC, percentage of terminal (−)-epicatechin; tECG, percentage of terminal (−)-epicatechin gallate.

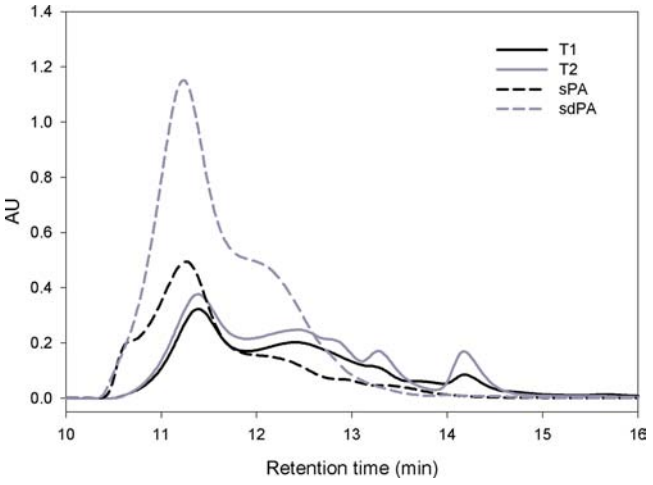

Figure 1. Size exclusion chromatogram of the different tannins used in the experiment.

Table 2. Total Area Observed in the SEC Analysis for Each Tannin and Percentage Eluted from 10 to 11.8 min (F1, Corresponding to High Molecular Mass Proanthocyanidins), from 11.8 to 13.6 min (F2, Corresponding to Medium Molecular Mass Proanthocyanidins), and from 13.6 min to 15.00 min (F3, Corresponding to Low Molecular Mass Proanthocyanidins)[a]

tannin	concentration (mg/L)	F1	F2	F3
T1	1208[b]	37.5	48.2	12.5
T2	1594[c]	36.2	49.3	13.0
sPA	2000	67.8	28.8	1.7
sdPA	2000	66.9	31.5	0.7

[a]Abbreviations: T1, commercial enological tannin from grape skins; T2, commercial enological tannin from grape seeds; sPA, purified grape skin proanthocyanidin; sdPA, purified grape seed proanthocyanidin. [b]This concentration corresponds to the real tannin content of a 2 g of the commercial sample T1, determined by acid hydrolysis. [c]This concentration corresponds to the real tannin content of a 2 g of the commercial sample T2, determined by acid hydrolysis.

(37.5 and 36.2%), which is in agreement with the differences in mDP. At the range of time between 11.8 and 13.6 min, corresponding to medium molecular mass PAs, the values were, this time, higher for T1 and T2 (48.2 and 49.3%) than for sPA (28.8%). Again, a substantial variation was observed at elution time from 13.6 to 15 min (low molecular mass PAs), the relative area being very low for sPA and sdPAs (1.7 and 0.7%) and higher for T1 and T2 (12.5 and 13.0%).

Effect of the Addition of the Different Cell Wall Materials to Model Solutions Containing the Different Proanthocyanidin Samples. The proanthocyanidin samples (commercial tannins and purified fractions) were combined with the purified skin CWM (gCW) from Monastrell, Cabernet Sauvignon, and Syrah grapes and their corresponding CWM from the pomace obtained after a control vinification (cmCW) or a vinification where a maceration enzyme was used (emCW). The different CWs were suspended in model solutions to determine the effect of the interaction in terms of PA concentration, composition, and molecular mass distribution. The effect of CWM additions on PAs was determined by observing the changes in the PAs that remained in solution compared with a control (Tables 3− 5 and Figures 2−5).

DOI: 10.1021/jf503659y
J. Agric. Food Chem. 2015, 63, 620−633

Table 3. Effect of the Addition of the Different Monastrell CWMs on the Reduction in Tannin Concentration and on the Composition of the PAs Remaining in Solution[a]

sample	tannins (mg/L)	% reaction	mDP	%G	tC	tEC	tECG	extC	extEC	extEGC	extECG
T1	771.91 ± 5.24		2.67 ± 0.02	3.86 ± 0.00	17.42 ± 0.13	19.33 ± 0.08	0.74 ± 0.00	5.16 ± 0.04	47.89 ± 0.18	6.33 ± 0.01	3.12 ± 0.00
T1 + gCWM	487.01 ± 20.46	36.9 ± 2.3	2.51 ± 0.00	3.56 ± 0.03	18.46 ± 0.11	20.87 ± 0.19	0.58 ± 0.02	4.95 ± 0.02	45.99 ± 0.00	6.17 ± 0.07	2.98 ± 0.01
T1 + cmCWM	476.60 ± 35.04	38.2 ± 1.8	2.51 ± 0.03	3.43 ± 0.03	18.45 ± 0.45	20.89 ± 0.02	0.58 ± 0.01	5.17 ± 0.03	46.28 ± 0.42	5.79 ± 0.02	2.85 ± 0.04
T1 + emCWM	495.43 ± 12.75	35.8 ± 0.7	2.51 ± 0.00	3.36 ± 0.01	18.58 ± 0.03	20.85 ± 0.10	0.46 ± 0.01	5.16 ± 0.01	45.91 ± 0.03	6.14 ± 0.03	2.90 ± 0.02
T2	1227.48 ± 5.03		2.57 ± 0.01	7.33 ± 0.03	20.27 ± 0.14	16.18 ± 0.04	2.47 ± 0.00	9.66 ± 0.02	46.57 ± 0.12	0.00	4.86 ± 0.03
T2 + gCWM	765.41 ± 11.72	37.6 ± 0.8	2.30 ± 0.02	5.84 ± 0.14	22.67 ± 0.02	18.59 ± 0.33	2.16 ± 0.02	9.49 ± 0.12	43.41 ± 0.36	0.00	3.68 ± 0.11
T2 + cmCWM	802.07 ± 58.76	34.6 ± 1.0	2.36 ± 0.00	7.62 ± 0.02	22.60 ± 0.07	17.57 ± 0.04	2.12 ± 0.00	9.38 ± 0.00	42.83 ± 0.00	0.00	5.50 ± 0.02
T2 + emCWM	838.85 ± 7.51	31.6 ± 0.4	2.40 ± 0.02	7.68 ± 0.09	22.33 ± 0.11	17.25 ± 0.15	2.06 ± 0.01	9.41 ± 0.00	43.34 ± 0.16	0.00	5.63 ± 0.10
sPA	1143.72 ± 110.57		8.50 ± 0.26	2.78 ± 0.02	6.23 ± 0.03	5.54 ± 0.33	0.00	1.47 ± 0.01	67.53 ± 0.31	16.46 ± 0.02	2.78 ± 0.02
sPA + gCWM	500.94 ± 39.30	56.2 ± 2.0	9.01 ± 0.10	2.77 ± 0.03	7.61 ± 0.03	3.49 ± 0.16	0.00	1.64 ± 0.02	68.62 ± 0.16	15.86 ± 0.33	2.77 ± 0.03
sPA + cmCWM	448.28 ± 41.89	60.8 ± 2.1	8.91 ± 0.19	2.70 ± 0.07	7.91 ± 0.06	3.31 ± 0.18	0.00	1.74 ± 0.03	68.16 ± 0.50	16.19 ± 0.35	2.70 ± 0.07
sPA + emCWM	544.37 ± 12.39	52.4 ± 1.5	9.20 ± 0.20	2.72 ± 0.00	7.41 ± 0.17	3.47 ± 0.07	0.00	1.72 ± 0.01	68.08 ± 0.04	16.61 ± 0.20	2.72 ± 0.00
sdPA	1454.78 ± 19.07		5.69 ± 0.1	17.01 ± 0.07	6.28 ± 0.11	6.56 ± 0.08	4.74 ± 0.03	7.36 ± 0.01	62.79 ± 0.04	0.00	12.27 ± 0.04
sdPA + gCWM	834.06 ± 110.23	42.6 ± 1.1	5.80 ± 0.08	16.47 ± 0.03	7.00 ± 0.06	5.09 ± 0.25	5.17 ± 0.05	7.80 ± 0.05	63.63 ± 0.17	0.00	11.31 ± 0.01
sdPA + cmCWM	1049.19 ± 108.70	27.9 ± 4.1	5.72 ± 0.03	16.58 ± 0.03	6.98 ± 0.23	5.56 ± 0.17	4.94 ± 0.03	7.66 ± 0.04	63.21 ± 0.1	0.00	11.65 ± 0.06
sdPA + emCWM	958.05 ± 7.90	34.1 ± 0.3	5.91 ± 0.04	16.56 ± 0.01	6.77 ± 0.05	5.26 ± 0.03	4.87 ± 0.02	7.70 ± 0.01	63.70 ± 0.12	0.00	11.68 ± 0.01

[a]Abbreviations: T1, commercial enological tannin from grape skins; T2, commercial enological tannin from grape seeds; sPA, purified grape skin proanthocyanidin; sdPA, purified grape seed proanthocyanidin; gCWM, CWM from the skin of fresh grapes; cmCWM, cell wall material from the pomace obtained after a control vinification; emCWM, cell wall material from the pomace obtained after a vinification where a maceration enzyme was used; mDP, medium degree of polymerization; %G, percentage of galloylation; extC, percentage of extension (+)-catechin; extEC, percentage of extension (−)-epicatechin; extECG, percentage of extension (−)-epicatechin gallate; tC, percentage of terminal (+)-catechin; tEC, percentage of terminal (−)-epicatechin; tECG, percentage of terminal (−)-epicatechin gallate.

J. Agric. Food Chem. 2015, 63, 620−633
DOI: 10.1021/jf503659y

Table 4. Effect of the Addition of the Different Cabernet Sauvignon CWMs on the Reduction in Tannin Concentration and on the Composition of the PAs Remaining in Solution[a]

sample	tannins (mg/L)	% reaction	mDP	%G	tC	tEC	tECG	extC	extEC	extEGC	extECG
T1	771.91 ± 5.24		2.67 ± 0.02	3.86 ± 0.00	17.42 ± 0.13	19.33 ± 0.08	0.74 ± 0.00	5.16 ± 0.04	47.89 ± 0.18	6.33 ± 0.01	3.12 ± 0.00
T1 + gCWM	367.97 ± 4.21	52.3 ± 0.9	2.62 ± 0.04	4.00 ± 0.01	17.59 ± 0.27	19.99 ± 0.26	0.59 ± 0.02	4.95 ± 0.06	46.29 ± 0.55	7.17 ± 0.09	3.41 ± 0.01
T1 + cmCWM	559.47 ± 10.94	27.5 ± 0.8	2.58 ± 0.02	3.58 ± 0.02	18.14 ± 0.32	20.13 ± 0.09	0.49 ± 0.00	5.25 ± 0.02	46.72 ± 0.27	6.18 ± 0.04	3.09 ± 0.02
T1 + emCWM	508.37 ± 8.30	34.1 ± 1.0	2.56 ± 0.01	3.68 ± 0.03	18.02 ± 0.00	20.54 ± 0.08	0.47 ± 0.00	5.27 ± 0.02	46.25 ± 0.11	6.24 ± 0.02	3.21 ± 0.02
T2	1227.48 ± 5.03		2.57 ± 0.01	7.33 ± 0.03	20.27 ± 0.14	16.18 ± 0.04	2.47 ± 0.00	9.66 ± 0.01	46.57 ± 0.12	0.00	4.86 ± 0.01
T2 + gCWM	668.21 ± 100.11	45.5 ± 2.6	2.41 ± 0.00	6.44 ± 0.02	21.58 ± 0.08	17.75 ± 0.08	2.17 ± 0.02	9.58 ± 0.01	44.65 ± 0.02	0.00	4.27 ± 0.01
T2 + cmCWM	875.46 ± 53.86	28.7 ± 2.0	2.43 ± 0.01	8.22 ± 0.00	21.96 ± 0.18	17.11 ± 0.02	2.15 ± 0.00	9.11 ± 0.03	43.59 ± 0.14	0.00	6.07 ± 0.01
T2 + emCWM	793.85 ± 90.17	35.3 ± 2.3	2.44 ± 0.01	8.19 ± 0.05	21.86 ± 0.10	16.98 ± 0.02	2.13 ± 0.01	9.16 ± 0.02	43.80 ± 0.15	0.00	6.06 ± 0.04
sPA	1143.72 ± 110.57		8.50 ± 0.26	2.78 ± 0.02	6.23 ± 0.03	5.54 ± 0.33	0.00	1.47 ± 0.01	67.53 ± 0.31	16.46 ± 0.02	2.78 ± 0.02
sPA + gCWM	540.17 ± 3.08	52.7 ± 0.7	11.46 ± 0.44	3.00 ± 0.03	7.10 ± 0.30	1.63 ± 0.03	0.00	1.60 ± 0.04	67.27 ± 0.99	19.40 ± 1.39	3.00 ± 0.03
sPA + cmCWM	601.88 ± 2.40	47.4 ± 0.7	11.80 ± 0.06	3.13 ± 0.27	6.90 ± 0.10	1.57 ± 0.06	0.00	1.69 ± 0.08	69.87 ± 0.63	16.84 ± 0.48	3.13 ± 0.27
sPA + emCWM	600.07 ± 2.00	47.5 ± 0.5	11.57 ± 0.16	3.30 ± 0.11	6.99 ± 0.08	1.65 ± 0.04	0.00	1.64 ± 0.03	69.51 ± 0.15	16.91 ± 0.17	3.30 ± 0.11
sdPA	1454.78 ± 19.07		5.69 ± 0.1	17.01 ± 0.07	6.28 ± 0.11	6.56 ± 0.08	4.74 ± 0.03	7.36 ± 0.01	62.79 ± 0.04	0.00	12.27 ± 0.04
sdPA + gCWM	904.68 ± 106.25	37.8 ± 3.5	5.84 ± 0.04	15.65 ± 0.06	6.96 ± 0.18	5.38 ± 0.27	4.78 ± 0.04	7.78 ± 0.01	64.23 ± 0.15	0.00	10.87 ± 0.02
sdPA + cmCWM	1060.66 ± 60.45	27.1 ± 1.8	5.86 ± 0.12	15.64 ± 0.20	6.75 ± 0.10	5.68 ± 0.24	4.64 ± 0.01	7.74 ± 0.02	64.19 ± 0.13	0.00	10.99 ± 0.21
sdPA + emCWM	1027.36 ± 20.15	29.4 ± 1.4	5.87 ± 0.04	15.55 ± 0.02	6.84 ± 0.14	5.57 ± 0.20	4.61 ± 0.02	7.75 ± 0.02	64.29 ± 0.15	0.00	10.93 ± 0.03

[a]Abbreviations: T1, commercial enological tannin from grape skins; T2, commercial enological tannin from grape seeds; sPA, purified grape skin proanthocyanidin; sdPA, purified grape seed proanthocyanidin; gCWM, CWM from the skin of fresh grapes; cmCWM, cell wall material from the pomace obtained after a control vinification; emCWM, cell wall material from the pomace obtained after a vinification where a maceration enzyme was used; mDP, medium degree of polymerization; %G, percentage of galloylation; extC, percentage of extension (+)-catechin; extEC, percentage of extension (−)-epicatechin; extECG, percentage of extension (−)-epicatechin gallate; tC, percentage of terminal (+)-catechin; tEC, percentage of terminal (−)-epicatechin; tECG, percentage of terminal (−)-epicatechin gallate.

DOI: 10.1021/jf503659y
J. Agric. Food Chem. 2015, 63, 620−633

Table 5. Effect of the Addition of the Different Syrah CWMs on the Reduction in Tannin Concentration and on the Composition of the PAs Remaining in Solution[a]

sample	tannins (mg/L)	% reaction	mDP	%G	tC	tEC	tECG	extC	extEC	extEGC	extECG
T1	771.91 ± 5.24		2.67 ± 0.02	3.86 ± 0.00	17.42 ± 0.13	19.33 ± 0.08	0.74 ± 0.00	5.16 ± 0.04	47.89 ± 0.18	6.33 ± 0.01	3.12 ± 0.00
T1 + gCWM	459.25 ± 25.38	35.84 ± 0.9	2.60 ± 0.00	3.92 ± 0.35	18.06 ± 0.18	19.87 ± 0.11	0.56 ± 0.00	5.16 ± 0.04	46.36 ± 0.21	6.63 ± 0.04	3.36 ± 0.35
T1 + cmCWM	536.51 ± 16.16	30.5 ± 0.4	2.56 ± 0.02	3.51 ± 0.07	18.33 ± 0.03	20.19 ± 0.19	0.47 ± 0.01	5.17 ± 0.06	46.69 ± 0.30	6.11 ± 0.09	3.04 ± 0.06
T1 + emCWM	497.29 ± 19.40	35.6 ± 1.1	2.53 ± 0.00	3.49 ± 0.00	18.50 ± 0.10	20.59 ± 0.15	0.47 ± 0.01	5.19 ± 0.04	46.20 ± 0.00	6.03 ± 0.01	3.02 ± 0.01
T2	1227.48 ± 5.03		2.57 ± 0.01	7.33 ± 0.03	20.27 ± 0.14	16.18 ± 0.04	2.47 ± 0.001	9.66 ± 0.02	46.57 ± 0.12	0.00	4.86 ± 0.03
T2 + gCWM	890.28 ± 17.84	27.5 ± 1.2	2.39 ± 0.00	6.58 ± 0.02	22.05 ± 0.04	17.54 ± 0.07	2.21 ± 0.04	9.54 ± 0.07	44.28 ± 0.06	0.00	4.37 ± 0.07
T2 + cmCWM	900.28 ± 57.65	26.6 ± 1.9	2.45 ± 0.00	8.14 ± 0.01	21.77 ± 0.02	16.93 ± 0.03	2.11 ± 0.01	9.33 ± 0.05	43.83 ± 0.10	0.00	6.03 ± 0.05
T2 + emCWM	834.90 ± 17.37	32.0 ± 1.0	2.43 ± 0.01	7.82 ± 0.02	21.96 ± 0.09	17.08 ± 0.01	2.10 ± 0.01	9.40 ± 0.06	43.73 ± 0.12	0.00	5.72 ± 0.03
sPA	1143.72 ± 110.57		8.50 ± 0.26	2.78 ± 0.02	6.23 ± 0.03	5.54 ± 0.33	0.00	1.47 ± 0.01	67.53 ± 0.31	16.46 ± 0.02	2.78 ± 0.02
sPA + gCWM	619.17 ± 62.29	45.9 ± 2.2	8.79 ± 0.46	3.14 ± 0.16	7.35 ± 0.16	4.04 ± 0.43	0.00	1.71 ± 0.05	68.15 ± 0.44	15.61 ± 0.06	3.14 ± 0.16
sPA + cmCWM	593.21 ± 1.85	48.1 ± 0.5	11.36 ± 0.03	2.84 ± 0.04	7.22 ± 0.03	1.58 ± 0.01	0.00	1.76 ± 0.01	70.28 ± 0.04	16.32 ± 0.02	2.84 ± 0.04
sPA + emCWM	572.83 ± 16.47	49.9 ± 1.1	10.96 ± 0.00	2.87 ± 0.01	7.54 ± 0.04	1.58 ± 0.04	0.00	1.75 ± 0.02	69.91 ± 0.02	16.34 ± 0.05	2.87 ± 0.01
sdPA	1454.78 ± 19.07		5.69 ± 0.1	17.01 ± 0.07	6.28 ± 0.11	6.56 ± 0.08	4.74 ± 0.03	7.36 ± 0.01	62.79 ± 0.04	0.00	12.27 ± 0.04
sdPA + gCWM	1023.09 ± 1.24	29.7 ± 0.4	5.85 ± 0.02	15.47 ± 0.22	6.83 ± 0.15	5.58 ± 0.06	4.69 ± 0.04	7.78 ± 0.02	64.35 ± 0.12	0.00	10.78 ± 0.18
sdPA + cmCWM	1047.50 ± 14.10	28.0 ± 1.2	5.68 ± 0.01	15.63 ± 0.07	6.86 ± 0.14	6.04 ± 0.16	4.70 ± 0.02	7.70 ± 0.00	63.77 ± 0.50	0.00	10.93 ± 0.04
sdPA + emCWM	1010.84 ± 24.46	30.5 ± 1.9	5.76 ± 0.01	15.73 ± 0.04	6.88 ± 0.08	5.79 ± 0.07	4.68 ± 0.01	7.70 ± 0.02	63.91 ± 0.51	0.00	11.04 ± 0.05

[a]Abbreviations: T1, commercial enological tannin from grape skins; T2, commercial enological tannin from grape seeds; sPA, purified grape skin proanthocyanidin; sdPA, purified grape seed proanthocyanidin; gCWM, CWM from the skin of fresh grapes; cmCWM, cell wall material from the pomace obtained after a control vinification; emCWM, cell wall material from the pomace obtained after a vinification where a maceration enzyme was used; mDP, medium degree of polymerization; %G, percentage of galloylation; extC, percentage of extension (+)-catechin; extEC, percentage of extension (−)-epicatechin; extECG, percentage of extension (−)-epicatechin gallate; tC, percentage of terminal (+)-catechin; tEC, percentage of terminal (−)-epicatechin; tECG, percentage of terminal (−)-epicatechin gallate.

J. Agric. Food Chem. 2015, 63, 620−633
DOI: 10.1021/jf503659y

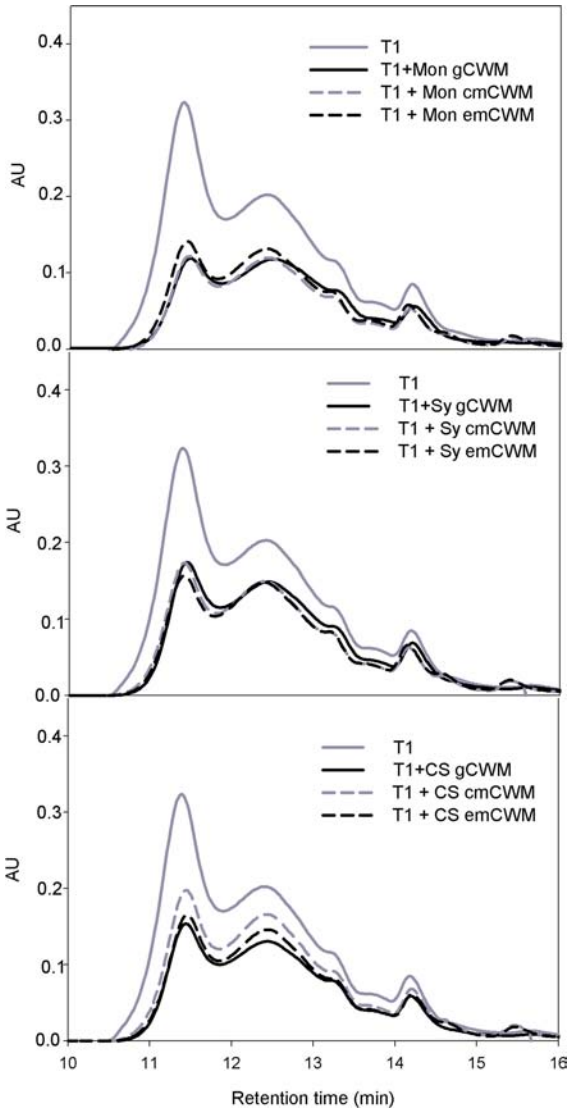

Figure 2. Comparison of the size exclusion chromatography of the commercial enological tannin T1 in solution and that for this remaining after the addition of different CWMs (gCWM, CWM from the skin of fresh grapes; cmCWM, cell wall material from the pomace obtained after a control vinification; emCWM, cell wall material from the pomace obtained after a vinification where a maceration enzyme was used).

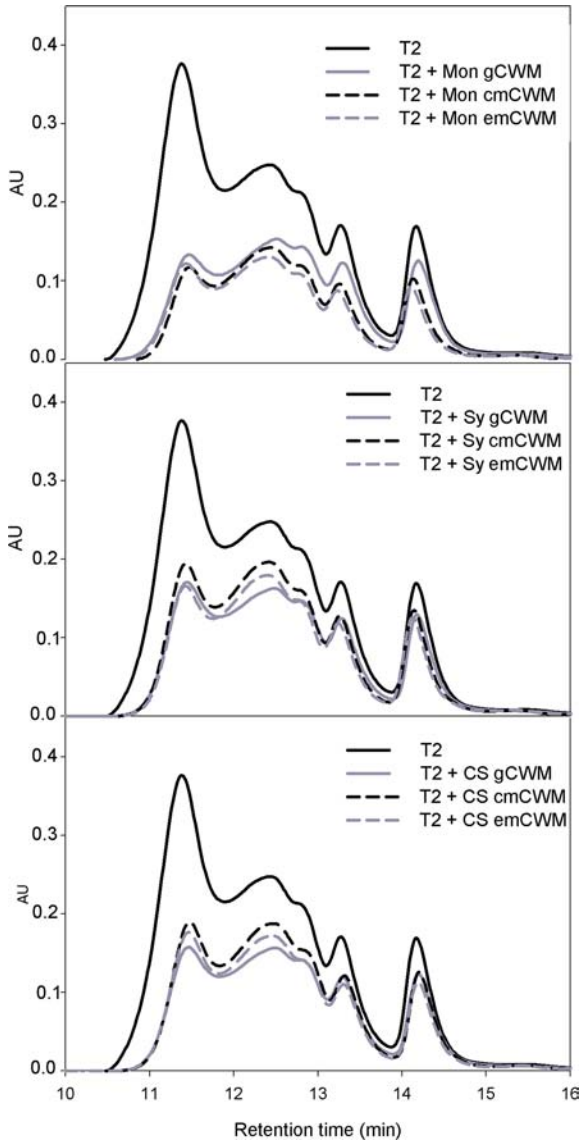

Figure 3. Comparison of the size exclusion chromatography of the T2 in solution and that for this remaining after the addition of different CWMs (gCWM, CWM from the skin of fresh grapes; cmCWM, cell wall material from the pomace obtained after a control vinification; emCWM, cell wall material from the pomace obtained after a vinification where a maceration enzyme was used).

The results of the phloroglucinolysis analysis showed that the addition of the different CWMs to the suspension containing the tannins produced, in all cases, a decrease in the quantity of tannins in the solution; that is, all of them could act as fining agents, reducing tannins in the wine. For Monastrell samples, this decrease ranged from 27.9% for the solution containing sdPA and cmCWM to 60.8% for sPA and cmCWM. The differences in the adsorption capacity of Monastrell fresh skin CWs compared with those of the pomace were not very large, being only slightly lower for cmCW with T1, T2, and sdPA. The data shown in the Supporting Information indicate that the percentual carbohydrate composition did not significantly change between fresh skin CWs and pomace CWs. In Monastrell CW samples, only the use of a maceration enzyme promoted a small decrease in the uronic acid proportion of the pomace CWs, the other sugars barely changing. Guerrero et al.[18] also reported that pomace CWs presented a chemical and polysaccharide composition quite similar to that of fresh grapes, although they seemed to present larger dry volume per unit mass and an increased expansion in hydroalcoholic solution. The potential contribution of an expanded surface area of the hydrated fiber, and therefore greater surface interaction, might well contribute to the high affinity of pomace CWs for PAs.

The adsorption capacity of Monastrell emCWs was always similar to that of fresh skin CWs, even when pectins (measured as uronic acids) were present at lower proportion. Le Bourvellec et al.[28] stated that the elimination of pectins decreased the apparent affinity values of cell walls and PA. However, the increase in cell wall porosity after pectin elimination may enhance the encapsulation of PA within a more open network and explain the very similar behaviors of gCW and emCWs.

Maximum adsorption was observed for purified skin PA samples, with lower values being observed for purified seed PA, the adsorption values of which were similar to those of the commercial samples, which, in turn, showed very similar behavior. Bindon et al.,[29] working with solutions containing different

DOI: 10.1021/jf503659y
J. Agric. Food Chem. 2015, 63, 620−633

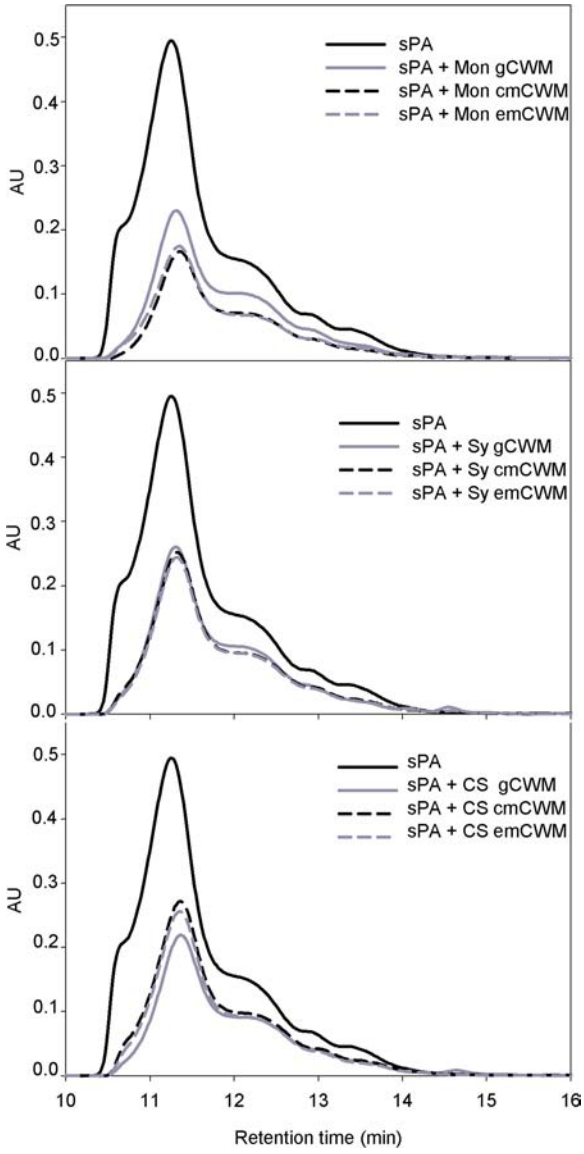

Figure 4. Comparison of the size exclusion chromatography of the purified skin tannin (sPA) in solution and that for this remaining after the addition of different CWMs (gCWM, CWM from the skin of fresh grapes; cmCWM, cell wall material from the pomace obtained after a control vinification; emCWM, cell wall material from the pomace obtained after a vinification where a maceration enzyme was used).

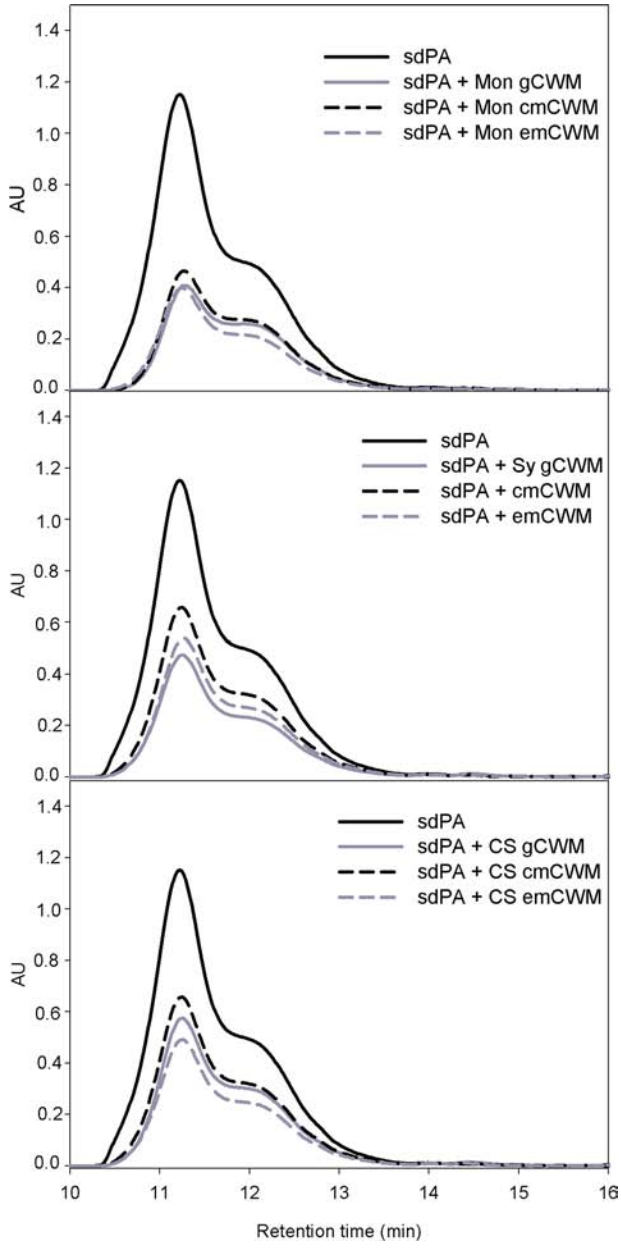

Figure 5. Comparison of the size exclusion chromatography of the purified seed tannin (sdPA) in solution and that for this remaining after the addition of different CWMs (gCWM, CWM from the skin of fresh grapes; cmCWM, cell wall material from the pomace obtained after a control vinification; emCWM, cell wall material from the pomace obtained after a vinification where a maceration enzyme was used).

percentages of skin and seed PAs, found that the total PA amount bound to flesh CWM gradually declined as the proportion of seed PA in the solution increased (from 57% removed for a solution containing 100% skin PA to 47% removed for a solution containing 100% seed PA), although, contrary to our results, they did not find any pattern of PA mass decrease when using skin CWs. The differences in adsorption between skin and seed PA are probably related to their different compositions. Haslam[6] reported that interactions between PAs and CWM increase as mDP increases (because each additional monomer increases the number of reactive sites, allowing the tannin molecule to bind simultaneously to more than one site in the cell wall), whereas the presence of epigallocatechin subunits in the skin tannin composition may also contribute to the differences because epigallocatechin has an additional hydroxyl group on ring B that provides another site for hydrogen bonding to occur.[5]

The percentage of galloylation (%G) slightly decreased in all of the nonadsorbed tannins (except in the case of the interaction of the pomace CWM with T2, where a small increase was observed). The mDP also tended to decrease in the fraction of nonadsorbed tannins, except for the samples where purified seed PA was used, when almost no changes were observed, and in the samples where skin PA was used, when the mDP of the remaining tannins slightly increased. In the case of purified samples, where large quantities of high molecular mass tannins are present, saturation of the available binding sites on the CWM surface might occur, whereas smaller PA molecules might still penetrate the interior of the CWM structure, therefore increasing the mDP of the remaining tannins, as also stated by Bindon et al.[11]

DOI: 10.1021/jf503659y
J. Agric. Food Chem. 2015, 63, 620−633

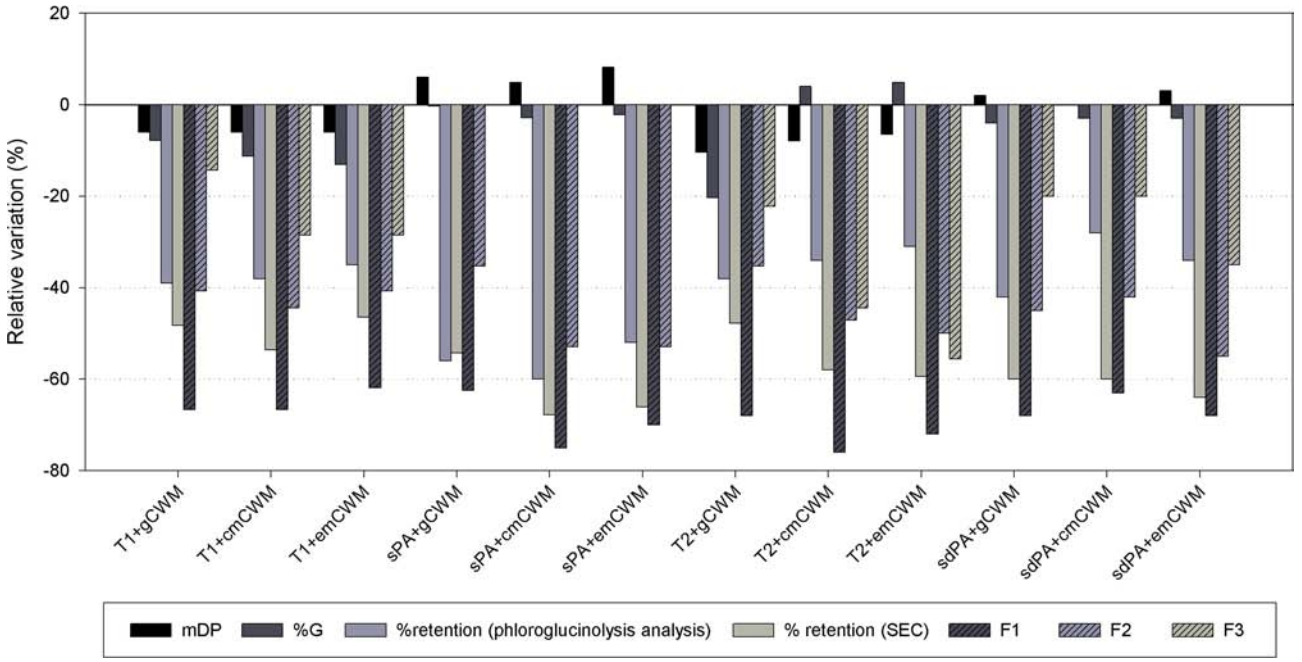

Figure 6. Percent changes in the main parameters when Monastrell CWs are used (T1, commercial enological tannin from grape skins; T2, commercial enological tannin from grape seeds; sPA, purified grape skin proanthocyanidin; sdPA, purified grape seed proanthocyanidin; gCWM, CWM from the skin of fresh grapes; cmCWM, cell wall material from the pomace obtained after a control vinification; emCWM, cell wall material from the pomace obtained after a vinification where a maceration enzyme was used; mDP, medium degree of polymerization; %G, percentage of galloylation; F1, F2, and F3, percentage of area of the size exclusion chromatogram corresponding to high (from 10 to 11.8 min), medium (from 11.8 to 13.6 min), and low (from 13.6 to 15 min) molecular mass PAs).

The terminal and extension subunits changed very little; a decrease in terminal epicatechin was always observed in sPA, concomitant with the increase in mDP.

When Cabernet Sauvignon CWM (Table 4) was used, the results showed that gCWM, in general, retained similar or larger quantities of tannins than Monastrell gCWM, which can be attributed to this variety presenting the highest content in pectins in their CWs, but this retention significantly decreased when the pomace CWM of this variety was used. The losses in sugars and pectins observed when the fresh skin CWs and the pomace CWs of this variety are compared might explain these differences. Also, another key structural difference that could reduce PA adsorption to Cabernet Sauvignon pomace cell walls could be, as suggested by Bindon et al.,[10] the endogenously higher concentrations of insoluble PA and lignin and lower cell wall-bound protein than in fresh skin cell walls. These differences may confer reduced flexibility and porosity to the pomace cell walls. In the case of T1, the retained quantities decreased by almost 50% compared with those retained in gCWM. The decrease was less pronounced when sPA was used, observing, in general, a higher adsorption of tannins when skin PAs (both commercial and purified) were used, similarly to that described for Monastrell. The behaviors of mDP and galloylation were exactly the same as those observed in Monastrell CWM, the observed increases in mDP in the nonadsorbed sPA being even higher.

In the case of Syrah, the retention of PAs on gCWM was the lowest of the three varieties studied, perhaps because the CW pectin content was the lowest and the cellulose content the highest (see Supporting Information, Figure S3). However, the adsorption capacities of gCWM and pomace CWM were almost the same, as in Monastrell, only a small decrease being observed (although much lower than that observed in Cabernet Sauvignon pomace CWM). The effect on mDP and the percentage of galloylation of the remaining PAs in solution was similar to that previously described for the other varieties, as was the higher affinity for skin PA samples.

These results suggest that, regarding binding capacity, important varietal differences exist and Monastrell pomace CWs could be the more interesting for reducing tannins and astringency in wines than pomace from other varieties.

The results of SEC analysis, comparing the PA profiles before and after the addition of CWM, are shown in Figures 2−5, whereas a comparison of the percentages of retention measured in the phloroglucinolysis analysis and SEC, including the retention of high, medium, and low molecular mass PAs, is shown in Figures 6−8.

As can be seen, the results were quite coincident with the phloroglucinolysis analysis, although the retention measured by SEC was greater than that observed by phloroglucinolysis for all of the varieties and all of the different PAs. This was probably due to the presence in the samples of some type of structures, such as oxidized tannins, that are not depolymerized by the phloroglucinol reagent but are measured by the SEC analysis.[30] This chromatographic analysis also showed that the intermediate (those eluting in SEC between 11.8 and 13.6 min) and especially the high molecular mass tannin fractions (those eluting from 10 to 11.8 min) were preferentially removed in all cases.

From a study of each individual tannin, the results for T1 (Figures 2 and 6) indicate that the highest retention was reported for Monastrell CWs. For Syrah (Figures 2 and 7) and Cabernet Sauvignon (Figures 2 and 8) CWs, the quantities of adsorbed tannin were lower when the pomace CWs were in the solution than with that of fresh grapes CWs and lower than that reported for Monastrell.

With regard to T2 (Figure 3), the behavior of Monastrell CWs was very similar to that reported for T1, the CWM of this variety

DOI: 10.1021/jf503659y
J. Agric. Food Chem. 2015, 63, 620−633

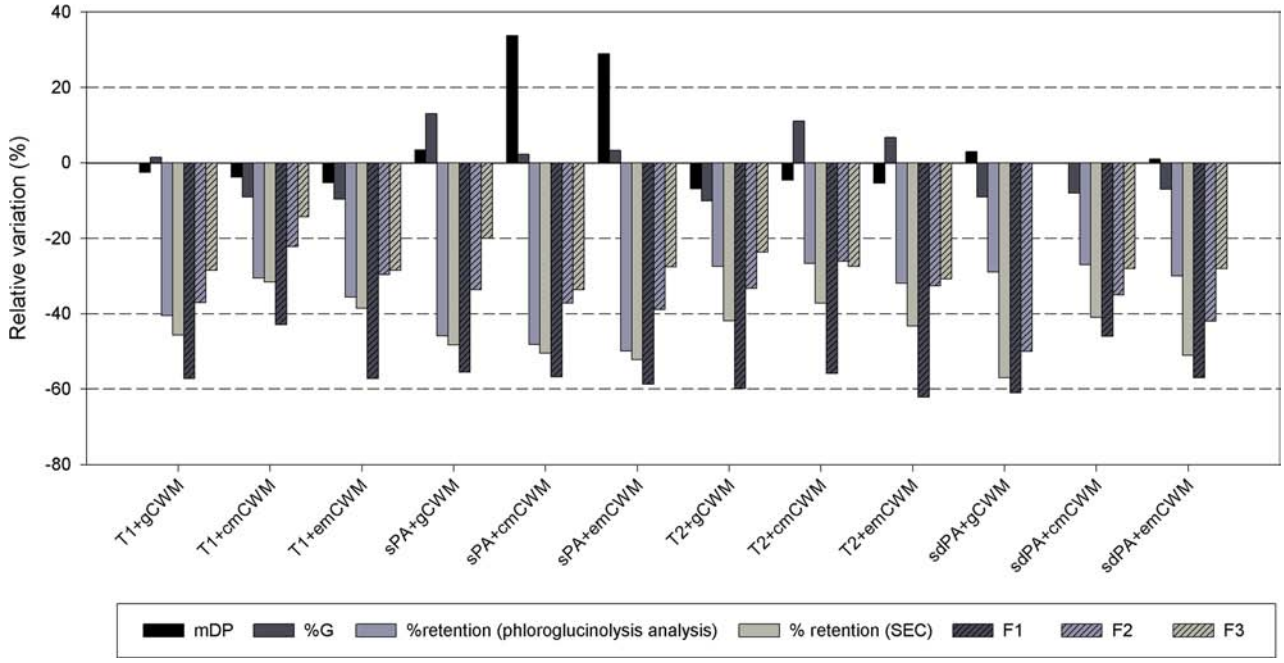

Figure 7. Percent changes in the main parameters when Syrah CWs are used (T1, commercial enological tannin from grape skins; T2, commercial enological tannin from grape seeds; sPA, purified grape skin proanthocyanidin; sdPA, purified grape seed proanthocyanidin; gCWM, CWM from the skin of fresh grapes; cmCWM, cell wall material from the pomace obtained after a control vinification; emCWM, cell wall material from the pomace obtained after a vinification where a maceration enzyme was used; mDP, medium degree of polymerization; %G, percentage of galloylation; F1, F2, and F3, percentage of area of the size exclusion chromatogram corresponding to high (from 10 to 11.8 min), medium (from 11.8 to 13.6 min), and low (from 13.6 to 15 min) molecular mass PAs).

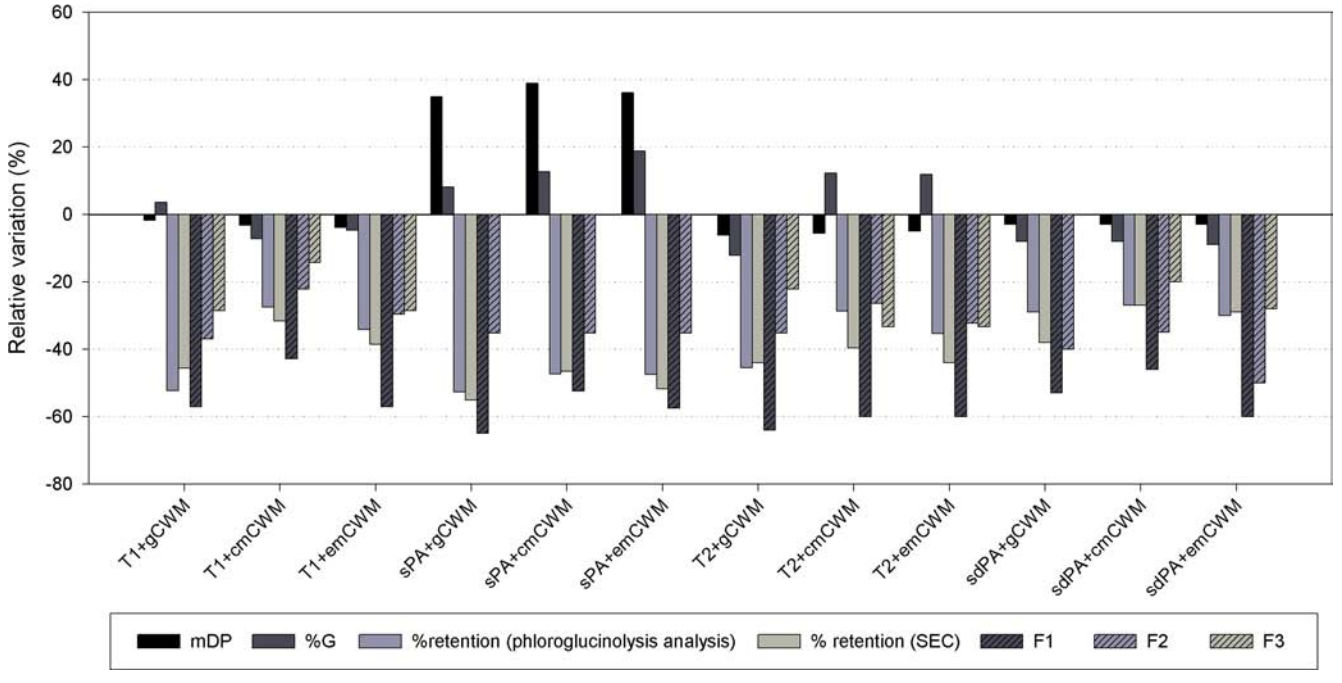

Figure 8. Percent changes in the main parameters when Cabernet Sauvignon CWs are used (T1, commercial enological tannin from grape skins; T2, commercial enological tannin from grape seeds; sPA, purified grape skin proanthocyanidin; sdPA, purified grape seed proanthocyanidin; gCWM, CWM from the skin of fresh grapes; cmCWM, cell wall material from the pomace obtained after a control vinification; emCWM, cell wall material from the pomace obtained after a vinification where a maceration enzyme was used; mDP, medium degree of polymerization; %G, percentage of galloylation; F1, F2, and F3, percentage of area of the size exclusion chromatogram corresponding to high (from 10 to 11.8 min), medium (from 11.8 to 13.6 min), and low (from 13.6 to 15 min) molecular mass PAs).

showing the highest adsorption compared with the results obtained in Cabernet Sauvignon and Syrah, the pomace CWs retaining even more tannins than fresh skin CW. For Syrah and Cabernet Sauvignon, the differences between gCWs and emCWs were almost nonexistent, whereas adsorption was lower in cmCWs.

DOI: 10.1021/jf503659y
J. Agric. Food Chem. 2015, 63, 620−633

In the purified samples, sPA (Figure 4) was highly retained by Monastrell CWs, reaching 67 and 65% in cmCW and emCWs. Also, high values of total adsorption were observed for Syrah and Cabernet Sauvignon CWs, the values being higher than that obtained with commercial tannins and, now, differences in the adsorption capacity between gCW and pomace CW were very small, especially in Syrah.

In the SEC profiles for sdPA (Figure 5), and contrary to the results observed in the phloroglucinolysis analysis, large differences were observed between varieties. The retention in Monastrell reached 64% for emCW, whereas for Cabernet Sauvignon the maximum value was only 38%, the use of pomace CWs leading to a retention of only 27 and 29%. Syrah showed intermediate values. It is clear that the SEC profiles of T1 and T2 and their behaviors were quite similar with regard to the retention properties (similar characteristics, especially the mDP, were observed in both commercial tannins, despite their different origins), whereas for purified samples, sPA and sdPA, behaved clearly differently, the higher adsorption being observed for sPA, as also found by Bindon et al.[29] for flesh CWs.

The results obtained by SEC are quite similar to the results observed with the phloroglucinolysis analysis and confirm that CWs from Monastrell pomace could be a really interesting material for wine tannin fining, being very effective in binding both nonpurified commercial tannins and native skin and seed tannins.

With regard to the molecular mass distribution of the retained tannins, the highest retention was always observed in the high molecular mass PAs, especially with Monastrell CWs, for which values of >70% were obtained for sPA + cmCW and T2 + cmCW. Bindon et al.[29] also found that for a 100% skin PA, the greatest PA-CW adsorption occurred in the higher molecular mass range, with less material removed by CWM in the lower molecular mass range. In general, emCW retained, percentually, lower quantities of high molecular mass PAs than gCW, perhaps due to a more linear structure, with slightly more affinity for low molecular mass tannins. Bindon and Smith[17] also observed that lower molecular PAs were preferentially bound when the Cabernet Sauvignon fibers were used.

These observations and differences can be much more clearly observed using a multivariate analysis of variance, which allows the different affinity properties of CWs (measured as the percentage of retained PAs calculated by phloroglucinolysis or SEC analysis) to be observed separately, taking into account their varietal or technological (fresh or processed skins) origin (Supporting Information, Figures S5 and S6). Monastrell CWs generally retained the highest quantities of PAs, especially when observed by SEC. It could be hypothesized that Monastrell CWs, due to their composition, have a higher capacity to bind oxidized tannins, which would explain the differences in percentage of retention observed between the phloroglucinolysis analysis and SEC. This would also explain why differences between varieties are much higher when the binding capacity is measured by SEC.

The same argument regarding varieties could be applied to the type of CW. Considering all of the data and for all of the varieties, gCWM showed a high PA affinity, in both phloroglucinolysis and SEC analyses. On the other hand, a large difference was observed in the binding capacity of emCWs, depending on the type of analysis. They were seen to retain a high quantity of PAs when the nonadsorbed PAs in solution were analyzed by SEC and much lower quantities when they were determined by the phloroglucinolysis analysis, which suggests that emCWs present a high affinity for oxidized and other nondepolymerized proanthocyanidins, which cannot be measured by the phloroglucinolysis analysis.

Finally, a discriminant algorithm was used to identify the specific variables potentially useful as predictors of discrimination between the three varieties and between the origins of the CWs. The discriminant analysis was based on a backward step algorithm (Table 6 and Figure 9). For the discrimination of varieties, the analysis was conducted with an *F*-to-enter = 2. This strategy resulted in a considerable reduction in the dimensionality of the information, because it led to the selection of very few variables that can be considered as the most important for the differentiation of the samples and which could indicate whether the various types of CWs could really be classified as different. When the variables were used to classify the CWs according to their varietal origin, a 72% correct classification was obtained. CWs from the Monastrell variety were well classified, only one sample being misclassified. CWs from Cabernet Sauvignon and Syrah showed slightly poorer separation, which is coincident with the experimental results, Monastrell CWs showing higher affinity for PAs than the CWs from Cabernet Sauvignon or those from Syrah grapes. The backward discriminant analysis allowed this separation to be reached with only two variables, the percentage of PA adsorbed to the CWs, measured as the percentage of decrease in the SEC area, and the mDP of the nonadsorbed tannins.

Table 6. Discriminant Functions Used To Predict to Which Group the Observations Belong

standardized coefficient	function 1	function 2
Variety		
SEC area	1.24	−0.22
mDP	0.94	0.84
CW Origin		
mDP	1.03	0.30
phloroglucinolysis area	0.75	1.02
% of retention at 90% elution time	−0.84	0.79

The classification obtained according to the technological origin of CW (from fresh skins or pomace from control or enzyme vinifications) was not very good (as low as 63%), indicating that the differences in their adsorption properties were not very different. The mDP of the nonadsorbed tannins, the percentage of adsorbed tannins measured by the area of phloroglucinolysis analysis, and the retention of the low molecular mass tannins were the variables used to discriminate the samples.

In conclusion, this study has confirmed that pomace CWs, a byproduct of the enology industry, present a high affinity for PAs and has demonstrated that this was especially remarkable in those of Monastrell grapes, for which pomace CWs present a very high adsorption capacity of all types of PA structures but especially for those of high molecular mass, and so their use in wines could reduce astringency. However, pomace cell walls present a slightly higher affinity for low molecular mass PAs than CWs from fresh skin grapes, and this might have implications for wine sensory properties such as astringency and bitterness and must be studied in greater depth. Moreover, and given that Guerrero et al.[18] observed that, in general, grape fibers not only reduced PAs but also reduced anthocyanins, total phenolics, and wine color density, to confirm the potential use of Monastrell pomace cell walls as an alternative fining agent to proteins, their role in the retention of other phenolic and volatile compounds in

DOI: 10.1021/jf503659y
J. Agric. Food Chem. 2015, 63, 620−633

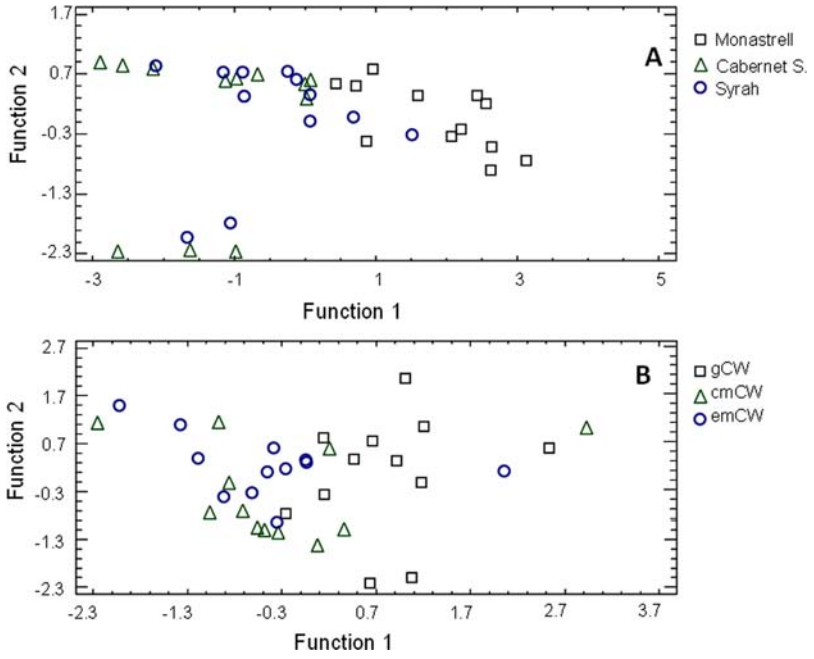

Figure 9. Plot of discriminant functions for (A) variety and (B) type of cell wall.

wine, the effect on wine chromatic characteristics, and some technological aspects, such as the amount of lees formed during their used, need to be study.

■ ASSOCIATED CONTENT

Supporting Information

Figures S1−S5. This material is available free of charge via the Internet at http://pubs.acs.org.

■ AUTHOR INFORMATION

Corresponding Author

*(E.G.-P.) E-mail: encarnag@um.es. Phone: 34 868887323. Fax: 34 868884147.

Funding

This work was made possible by financial assistance of the Ministerio de Economía y Competitividad and FEDER funds, Project AGL2012-39845-C02-01.

Notes

The authors declare no competing financial interest.

■ REFERENCES

(1) Ortega-Regules, A.; Romero-Cascales, I.; Ros-García, J. M.; López-Roca, J. M.; Gómez-Plaza, E. A first approach towars the relationship between grape skin cell-wall composition and anthocyanin extractability. *Anal. Chim. Acta* **2006**, *563*, 26−32.

(2) Rolle, L.; Torchio, F.; Ferrandino, A.; Guidoni, S. Influence of wine-grape skin hardness on the kinetics of anthocyanin extraction. *Int. J. Food Prop.* **2012**, *15*, 249−261.

(3) Nunan, K. J.; Sims, C. A.; Bacic, A.; Robinson, S. P.; Fincher, G. B. Isolation and characterization of cell walls from the mesocarp of mature grape berries (*Vitis vinifera*). *Planta* **1997**, *203*, 93−100.

(4) McManus, J.; Davis, K.; Beart, J.; Gaffney, S.; Lilley, T.; Haslam, E. Polyphenols interactions. I. Introduction, some observations on the reversible complexation of polyphenols with proteins and polysaccharides. *J. Chem. Soc., Perkin Trans. 2* **1985**, 1429−1438.

(5) Le Bourvellec, C.; Guyot, S.; Renard, C. M. Noncovalent interaction between procyanidins and apple cell wall material. Part 1. Effect of some environmental parameters. *Biochim. Biophys. Acta* **2004**, *1672*, 192−202.

(6) Haslam, E. Molecular recognition. Phenols and polyphenols. In *Practical Polyphenolics. From Structure to Molecular Recognition and Physiological Action*; Cambridge University Press: Cambridge, UK, 1998.

(7) Kennedy, J. A.; Matthews, M. A.; Waterhouse, A. L. Changes in grape seed polyphenols during fruit ripening. *Phytochemistry* **2000**, *55*, 77−85.

(8) Bautista-Ortin, A. B.; Rodríguez-Rodríguez, P.; Gil-Muñoz, R.; Jímenez-Pascual, E.; Busse-Valverde, N.; Martínez-Cutillas, A.; López-Roca, J. M.; Gómez-Plaza, E. Influence of berry ripeness on concentration, qualitative composition and extractability of grape seed tannins. *Aust. J. Grape Wine Res.* **2012**, *18*, 123−130.

(9) Bindon, K.; Kennedy, J. Ripening-induced changes in grape skin proanthocyanidins modify their interaction with cell walls. *J. Agric. Food Chem.* **2011**, *59*, 2696−2707.

(10) Bindon, K.; Bacic, A.; Kennedy, J. Tissue-specific and developmental modifications of grape cell walls influence the adsorption of proanthocyanidins. *J. Agric. Food Chem.* **2012**, *60*, 9249−9260.

(11) Bindon, K.; Madani, S.; Pendleton, P.; Smith, P.; Kennedy, J. Factors affecting skin tannin extractability in ripening grapes. *J. Agric. Food Chem.* **2014**, *62*, 1130−1141.

(12) Busse-Valverde, N.; Bautista-Ortín, A. B.; Gómez-Plaza, E.; Fernández-Fernández, J. I.; Gil-Muñoz, R. Influence of skin maceration time on the proanthocyanidin content of red wines. *Eur. Food Res. Technol.* **2012**, *235*, 1117−1123.

(13) Hill, M.; Kaine, G. *The Market Potential of Tannin Related Innovations in the Wine Industry*; Victorian Department of Primary Industries: Australia, 2007; Tatura pp. 41.

(14) Bautista-Ortin, A. B.; Cano-Lechuga, M.; Ruiz-García, Y.; Gómez-Plaza, E. Interactions between grape skin cell wall material and commercial enological tannins. Practical implications. *Food Chem.* **2014**, *152*, 558−565.

(15) Bautista-Ortín, A. B.; Martínez-Cutillas, A.; Ros-García, J. M.; López-Roca, J. M.; Gómez-Plaza, E. Improving colour extraction and stability in red wines: the use of maceration enzymes and enological tannins. *Int. J. Food Sci. Technol.* **2005**, *40*, 1−12.

(16) Boulton, R.; Singleton, V.; Bisson, L.; Kunkee, R. *Principles and Practices of Winemaking*; Chapman & Hall: New York, 1996.

(17) Bindon, K.; Smith, P. Comparison of the affinity and selectivity of insoluble fibres and commercial proteins for wine proanthocyanidins. *Food Chem.* **2013**, *136*, 917−928.

DOI: 10.1021/jf503659y
J. Agric. Food Chem. 2015, 63, 620−633

(18) Guerrero, R.; Smith, P.; Bindon, K. Application of insoluble fibers in the fining of wine phenolics. *J. Agric. Food Chem.* **2013**, *61*, 4424−4432.
(19) Apolinar-Valiente, R. *Pared celular de uva y polisacáridos de vinos de distinta procedencia, elaborados mediante tecnologías enzimáticas y de frio*. Ph.D. thesis, University of Murcia, 2012.
(20) Romero-Cascales, I.; Ros-García, J. M.; López-Roca, J. M.; Gómez-Plaza, E. The effect of a commercial pectolytic enzyme on grape skin cell wall degradation and colour evolution during the maceration process. *Food Chem.* **2012**, *130*, 626−631.
(21) de Vries, J. A.; Voragen, A. G. J.; Rombouts, F. M.; Pilnik, W. Estraction and purification of pectins from alcohol insoluble solids from ripe and unripe apples. *Carbohydr. Polym.* **1981**, *1*, 117−127.
(22) Apolinar-Valiente, R.; Romero-Cascales, I.; López-Roca, J. M.; Gómez-Plaza, E.; Ros-García, J. M. Application and comparation of four selected procedures for the isolation of cell wall material from the skin of grapes cv. Monastrell. *Anal. Chim. Acta* **2010**, *660*, 206−210.
(23) Ribéreau-Gayon, P.; Glories, Y.; Maujean, A.; Dubourdieu, D. *Traité d'Oenologie. 2. Chimie du Vin. Stabilisation et Traitements*; Dunod: Paris, France, 1998.
(24) Kennedy, J. A.; Taylor, A. W. Analysis of proanthocyanidins by high-performance gel permeation chromatography. *J. Chromatogr.* **2003**, *995*, 99−107.
(25) Kennedy, J. A.; Jones, G. P. Analysis of proanthocyanidin cleavage products following acid-catalysis in the presence of excess phloroglucinol. *J. Agric. Food Chem.* **2001**, *49*, 1740−1746.
(26) Busse-Valverde, N.; Gómez-Plaza, E.; López-Roca, J. M.; Gil-Muñoz, R.; Fernández-Fernández, J. I.; Bautista-Ortín, A. B. Effect of different enological practices on skin and seed proanthocyanidins in three varietal wines. *J. Agric. Food Chem.* **2010**, *58*, 11333−11339.
(27) Moutounet, M.; Rigaud, J.; Souquet, J. M.; Cheynier, V. Caracterisation structurale des tanins de las baie de raisin. Quelques exemples de l'incidence du cepage, du terroir et du monde de conduite de la vigne (1). *Bull. O.I.V.* **1996**, 433−443.
(28) Le Bourvellec, C.; Watrelot, A.; Ginies, C.; Imberty, A.; Renard, C. M. Impact of processing on the noncovalent interactions between procyanidin and apple cell wall. *J. Agric. Food Chem.* **2012**, *60*, 9484−9494.
(29) Bindon, K.; Smith, P.; Kennedy, J. Interaction between grape-derived proanthocyanidins and cell wall material. 1. Effect on proanthocyanidin composition and molecular mass. *J. Agric. Food Chem.* **2010**, *58*, 2520−2528.
(30) Poncet-Legrand, C.; Cabane, B.; Bautista-Ortin, A. B.; Carrillo, S.; Fulcrand, H.; Pérez, J.; Vernhet, A. Tannin oxidation: intra- versus intermolecular reactions. *Biomacromolecules* **2010**, *11*, 2376−2386.

DOI: 10.1021/jf503659y
J. Agric. Food Chem. 2015, 63, 620−633

JOURNAL OF AGRICULTURAL AND FOOD CHEMISTRY

Article

pubs.acs.org/JAFC

Preparation and Characterization of Debranched-Starch/Phosphatidylcholine Inclusion Complexes

Weiwei Cheng, Zhigang Luo,* Lin Li, and Xiong Fu*

Carbohydrate Lab, College of Light Industry & Food Sciences, South China University of Technology, Guangzhou 510640, China

ABSTRACT: In this study, debranched-starch/phosphatidylcholine inclusion complexes were prepared. The effect of reaction parameters such as reaction temperature, reaction time, and addition amount of phosphatidylcholine on the phosphatidylcholine payload and inclusion rate was investigated. The phosphatidylcholine payload and inclusion rate prepared under the optimal conditions were 106 mg/g and 84.8%, respectively. The formation of debranched-starch/phosphatidylcholine inclusion complexes was confirmed by the results of XRD and FT-IR. Furthermore, the molecular, cluster, and fractal structures of the complexes were investigated using ^{13}C CP/MAS NMR and SAXS. The results indicated that the inclusion complexes were formed by hydrophobic interactions between alkyl chain of phosphatidylcholine and debranched-starch helix cavity. The complexes possessed a mass fractal structure, and a semicrystalline structure with a Bragg distance of 19.04 nm formed. After complexation, the stability of phosphatidylcholine was significantly improved, and phosphatidylcholine of the complexes can be gradually released with pancreatin treatment. This study revealed that debranched-starch can be used as an effective carrier of phosphatidylcholine for the purpose of improving its stability.

KEYWORDS: *debranched-starch, phosphatidylcholine, complexes, preparation*

INTRODUCTION

Phosphatidylcholine is a naturally occurring mixture with diverse fatty acid side chains such as stearic, oleic, and palmitic acids.[1,2] It is the best known kind of phospholipids.[2] Because of its outstanding physiological functionalities, such as slowing aging, enhancing memory, reducing blood fat, and preventing diabetes, and its surface activity, phosphatidylcholine has been widely used in food, pharmaceutical, and cosmetic industries.[3−5] However, due to its rich content of unsaturated fatty acids, phosphatidylcholine is sensitive to heat and light, and very easy to oxidize during manufacture, storage, and consumption, which restricts its applications in industries. Up to now, there are few reports on improving the stability of phosphatidylcholine.

Amylose, one of the two main fractions of starch, is a predominantly linear polymer, which is composed of α-D-glucose mainly linked by α-1,4 linkages. In the presence of ligands such as alcohols,[6] aroma compounds,[7] and lipids,[8] amylose can undergo a conformation change resulting in a single, left-handed helix that has a hydrophilic surface and hydrophobic inside helical channel. Hence, amylose can be used as a wall material to encapsulate hydrophobic guest molecules to form inclusion complexes, and meanwhile amylose single helices were arranged to form a V-type crystalline structure known as V-amylose.[9] Although the ability of amylose to form inclusion complexes with a wide variety of molecules has been known for several decades, only recently has amylose been systematically studied as a possible vehicle for bioactive compounds.[10−12] In view of the degradability and availability of amylose, the application of amylose as a food-grade delivery material has become a research hotspot in recent years.[13] Conventionally, amylose is obtained by separation of the two components of starch, mainly by methods of aqueous dispersion, aqueous leaching, selective retrogradation, or alcohol precipitation.[14] However, amylose obtained by these methods is often costly because of the complicated production process and the consumption of organic compounds such as alcohol, *n*-butyl, and pentanol.

In this study, to reduce the cost and achieve industrialization, amylose was obtained by hydrolysis of native potato starch with pullulanase, and the obtained debranched-starch (amylose) was used for the first time as wall material to encapsulate phosphatidylcholine by its single helical to improve the stability of phosphatidylcholine. The effect of reaction temperature, reaction time, and addition amount of phosphatidylcholine on the phosphatidylcholine payload and inclusion rate was investigated. In addition, the obtained debranched-starch/phosphatidylcholine complexes were characterized by X-ray diffraction (XRD), Fourier transform infrared spectroscopy (FT-IR), ^{13}C cross-polarization/magic angle spinning nuclear magnetic resonance (^{13}C CP/MAS NMR), small-angle X-ray scattering (SAXS), and scanning electron microscopy (SEM), and the stability and digestibility properties of the complexes were also studied.

MATERIALS AND METHODS

Materials. Commercial food grade potato starch (amylose content 19.42%) was obtained from Qinghai Weston Co. Ltd. (Qinghai, China). Pullulanase (E.C. 3.2.1.41., activity 1000 ASPU/g) was supplied by Genencor (China) Bio-Products Co. Ltd. (Wuxi, China). One unit of pullulanase activity was defined as the amount of enzyme that liberates one glucose reducing equivalent from pullulan per minute at pH 4.5 at 60 °C. Phosphatidylcholine (phosphatidylcholine >95%, Epikuron 200) was obtained from Lucas Meyer (Hamburg,

Received: August 28, 2014
Revised: January 3, 2015
Accepted: January 4, 2015
Published: January 4, 2015

ACS Publications © 2015 American Chemical Society

DOI: 10.1021/jf504133c
J. Agric. Food Chem. 2015, 63, 634−641

Germany) and used without further purification. Pancreatin (8 × USP, from porcine pancreas) was purchased from Sigma-Aldrich (St. Louis, MO). All other chemicals used were of analytical grade.

Preparation of Debranched-Starch. Starch (50 g, dry basis) was mixed with 450 g of water in a 500 mL three necked flask. The slurry was adjusted to pH 4.5 with 0.5 mol/L HCl and gelatinized in a thermostatic water bath at 98 °C with stirring for 1 h. After gelatinization, the mixture was cooled to 60 °C and the debranching reaction was started by adding pullulanase (10 ASPU/g). To completely debranch starch, the solution was incubated at 60 °C, pH 4.5 for 4 h. The thoroughness of the debranched reaction was confirmed by ^{1}H NMR, which can distinguish α-1,6 from α-1,4 linkages of starch according to chemical shifts of 4.7−5.0 ppm for α-1,6 linkages and 5.1−5.4 ppm for α-1,4 linkages.[15,16] According to previous literature,[15,16] when the α-1,6 peak located at 4.7−5.0 ppm disappears altogether, all of the α-1,6 branch linkages are suggested to be completely hydrolyzed. In this study, when potato starch was hydrolyzed by pullulanase at the above reaction conditions, the α-1,6 peak located at 4.7−5.0 ppm disappears altogether, indicating that potato starch has been completely debranched. The hydrolysis percent and blue value of the debranched-starch were determined using the methods of Bruner[17] and Gilbert and Spragg,[18] respectively. Hydrolysis rate and blue value of the debranched-starch made under the above conditions were 15.11% and 1.12, respectively. The debranched-starch solution obtained was stored at 60 °C for further use.

Preparation of Debranched-Starch/Phosphatidylcholine Inclusion Complexes. Different amounts of tetrahydrofuran (10, 15, 20, 25, 30 g) containing 20 wt % phosphatidylcholine were added to the debranched-starch solutions, and after reacting in a thermostatic water bath at a certain temperature (40, 50, 60, 70, 80 °C) for 0.5, 1, 2, 3, and 4 h, respectively, the mixture was slowly cooled to ambient temperature and then stored at 4 °C for 18 h. Samples were centrifuged, washed to remove all tetrahydrofuran with deionized water, and dried in an oven at 40 °C overnight. The recovery of debranched-starch/phosphatidylcholine inclusion complexes is in the range of 35−40 g. The products prepared under the optimal conditions were used for further analysis. As control, a debranched-starch solution sample without phosphatidylcholine was slowly cooled to ambient temperature and then stored at 4 °C for 18 h. The mixture was centrifuged, washed with deionized water, and dried in an oven at 40 °C overnight. The obtained uncomplexed retrograded debranched-starch (URDS) product was used for further analysis.

Determination of the Phosphatidylcholine Payload and Inclusion Rate. The determination of the phosphatidylcholine payload and inclusion rate was done by phosphous molybdenum blue spectrophotometric method.[19] Debranched-starch/phosphatidylcholine complexes (0.5 g) and URDS (0.5 g) were accurately weighed and mineralized by HNO_3 and $HClO_4$, respectively. The mineralized liquid was transferred to a 50 mL flask and diluted with distilled water to volume. After being diluted to an appropriate concentration, the phosphous content of the complexes was determined by the phosphous molybdenum blue spectrophotometric method with URDS as blank, and the phosphatidylcholine payload was obtained by multiplying the phosphous content by a specific conversion coefficient. The phosphatidylcholine payload (X, mg/g) was calculated by the following equation:

$$X = (C \times N \times V_1 \times 25)/m_0 \quad (1)$$

where C (mg/mL) is the phosphous content of the mineralized liquid (after being diluted) determined from the phosphous standard curve, N is the dilution ratio of the mineralized liquid, V_1 (mL) is the total volume of the mineralized liquid, 25 is the conversion coefficient from phosphous to phosphatidylcholine, and m_0 (g) is the amount of the sample weighed.

The inclusion rate (Y) was calculated by the following equation:

$$Y = (m_1 \times X \times 100\%)/(m_2 \times 1000) \quad (2)$$

where m_1 (g) is the weight of the debranched-starch/phosphatidylcholine complexes obtained, X (mg/g) is the phosphatidylcholine payload of the sample, and m_2 (g) is the weight of phosphatidylcholine added.

Characterization of Debranched-Starch/Phosphatidylcholine Complexes. XRD analysis was performed on a D8 ADVANCE X-ray diffractometer (Bruker, Karlsruhe, Germany) operating at 40 mA and 40 kV by using Cu Kα radiation (λ = 0.1542 nm). The scattering angle (2θ) was varied from 5° to 60° with a scanning step of 0.04°.

FT-IR spectra of samples were acquired on a VECTOR 33 FT-IR spectrophotometer (Bruker, Frankfurt, Germany) using KBr disk technique. The samples were mixed with anhydrous KBr and then compressed into thin disk-shaped pellets. The spectra were obtained with a resolution of 2 cm^{-1} in a wavenumber range of 400−4000 cm^{-1}.

^{13}C CP/MAS NMR experiments were performed on a Bruker AVANCE AV 400 spectrometer (Bruker, Rheinstetten, Germany) equipped with a 4 mm MAS probe. Samples (ca. 100 mg) were packed in 4 mm zirconia rotor and spun at 6000 r/min. The spectra were obtained at ambient temperature with a sampling time of 17 ms and a relaxation delay time of 2 s. All chemical shifts were reported in parts per million (ppm).

SAXS measurements were performed using a SAXSess small-angle X-ray scattering system (Anton Paar, Graz, Austria), operated at an acceleration voltage of 40 kV and current of 50 mA. A Cu Kα radiation with a wavelength of 0.1542 nm was used as X-ray source. Prior to analysis, all samples used for the experiments were prepared by mixing the starch with distilled water and equilibrated at ambient temperature for 24 h; the total moisture content of each sample was 60%. Each sample then was filled into a capillary of 0.01 mm wall thickness, the sample-to-detecter distance was 261.2 mm, and the temperature was kept at 26 °C during the measurement. The data were collected by the IP reader softwware and read out by a Perkin-Elmer storage phosphor system. The background and smeared intensity were removed by applying the data to the SAXSquant 3.0 software. The average repeat distance (i.e., thickness of semicrystalline lamellae) of the amorphous and crystalline lamellar of each sample can be calculated as

$$d = 2\pi/q \quad (3)$$

where d (nm) is the lamellar repeat distance and q (nm^{-1}) is the scattering vector;[20] the relationship between q and θ can be calculated as

$$q = (4\pi \sin\theta)/\lambda \quad (4)$$

where λ (nm) is the wavelength of the X-ray source and 2θ is the scattering angle.

SEM observations were performed using a model 1530VP scanning electron microscope (LEO, Oberkochen, Germany). The accelerating voltage was 20 kV. The samples were mounted on an aluminum stub with a double sticky tape, and coated with gold in a vacuum before examination.

Stability of the debranched-starch/phosphatidylcholine inclusion complexes and URDS/phosphatidylcholine physical mixture (phosphatidylcholine payload106 mg/g) was evaluated by measuring peroxide value (POV) after the samples had been stored at 50 °C for 0, 3, 7, 13, and 20 days. The measurement of POV was according to ISO 3960:2001.

Digestion tests in simulated stomach condition and by enzymatic hydrolysis were performed according to previous literature[12] with little modification. The release of phosphatidylcholine from the complexes in simulated stomach conditions was tested by incubating the debranched-starch/phosphatidylcholine complexes (30 mg) with 2 mL of HCl (pH = 2) for 2 h at 37 °C under continuous stirring. The release of phosphatidylcholine from the complexes in simulated small intestine conditions was tested by incubating the debranched-starch/phosphatidylcholine complexes (30 mg) with 2 mL of pancreatin solutions for 24 h at 37 °C. The amount of phosphatidylcholine released following the simulated stomach and simulated small intestine conditions was measured by extracting the reaction substrate (after freeze-drying) with n-hexane, and the phosphatidylcholine payload was

DOI: 10.1021/jf504133c
J. Agric. Food Chem. 2015, 63, 634−641

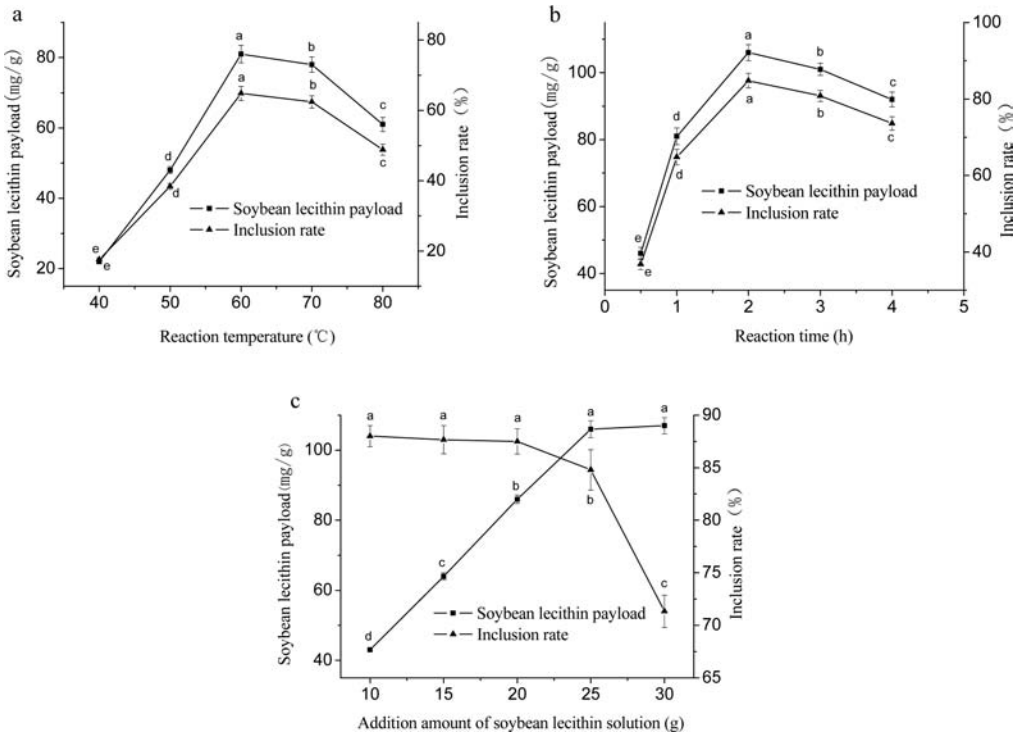

Figure 1. Effect of reaction parameters on soybean lecithin payload and inclusion rate. (a) Effect of reaction temperature (reaction time, 1 h; addition amount of soybean lecithin solution, 25 g). (b) Effect of reaction time (reaction temperature, 60 °C; addition amount of soybean lecithin solution, 25 g). (c) Effect of addition amount of soybean lecithin solution (reaction temperature, 60 °C; reaction time, 2 h). Values in the same curve with different superscript letters are significantly different ($P < 0.05$).

measured by ultraviolet spectrophotometry according to our previous method.[4] The release rate (R) of phosphatidylcholine was calculated as

$$R = (m_1/m_0) \times 100\% \quad (5)$$

where m_1 (g) is the quantity of phosphatidylcholine released calculated according to the ultraviolet spectrophotometric method, and m_0 (g) is the phosphatidylcholine payload of the complexes calculated according to the phosphous molybdenum blue spectrophotometric method.

Statistical Analysis. All determinations were replicated three times, and mean values and standard deviations were reported. Analyses of variance (anova) were performed, and the mean separations were performed by Tukey's HSD test ($P < 0.05$) using SigmaStat version 2.0 (Jandel Scientific/SPSS Science, Chicago, IL).

RESULTS AND DISCUSSION

The complexation of phosphatidylcholine with debranched-starch is influenced by many factors. The effect of reaction parameters (reaction temperature, reaction time, and addition amount of phosphatidylcholine) on the phosphatidylcholine payload and inclusion rate was studied, and the results are shown in Figure 1.

Effect of Reaction Temperature. Reaction temperature had a great influence on the phosphatidylcholine payload and inclusion rate. As shown in Figure 1a, as the reaction temperature increased from 40 to 60 °C, the phosphatidylcholine payload and inclusion rate increased rapidly from 22 to 81 mg/g and 17.6% to 64.8%, respectively. However, when the reaction temperature was higher than 60 °C, a decrease in phosphatidylcholine payload and inclusion rate was observed. The reason for this phenomenon is probably that phosphatidylcholine is prone to deterioration when the reaction temperature is too high.[4] Thus, the optimal reaction temperature of 60 °C was selected for the following runs.

Effect of Reaction Time. As presented in Figure 1b, at the starting hours, the phosphatidylcholine payload and inclusion rate increased steadily with time increasing. However, when the reaction lasted for more than 2 h, an apparent reduction of phosphatidylcholine and inclusion rate was observed ($P < 0.05$). One reason for this phenomenon is probably the oxidative degradation of phosphatidylcholine after reacting at 60 °C for more than 2 h. Another reason might be that, similar to the complexation of cyclodextrin with guest molecules, the complexation of debranched-starch with phosphatidylcholine is also a dynamic process.[21] At the starting hours, phosphatidylcholine entered the hydrophobic cavity of debranched-starch by hydrophobic interactions. However, when the reaction time was too long, part of the phosphatidylcholine was released from the cavity.

Effect of Addition Amount of Phosphatidylcholine. The influence of addition amount of phosphatidylcholine on the phosphatidylcholine payload and inclusion rate was investigated, and the result is shown in Figure 1c. The phosphatidylcholine payload and inclusion rate increased with the increase in the addition amount of phosphatidylcholine at the first stage. As the addition amount of phosphatidylcholine solution increased from 10 to 20 g, the phosphatidylcholine payload increased rapidly from 43 to 86 mg/g, and the inclusion rate almost kept constant ($P < 0.05$). When the addition amount of phosphatidylcholine solution was further increased to 25 g, the phosphatidylcholine payload reached its maximum of 106 mg/g, while the inclusion rate slightly reduced. Therefore, the optimal addition amount of phosphatidylcholine solution was 25 g; that is, the mass ratio of phosphatidylcholine to native starch was 1:10.

DOI: 10.1021/jf504133c
J. Agric. Food Chem. 2015, 63, 634−641

XRD Analysis. X-ray diffraction was used to verify the formation of debranched-starch/phosphatidylcholine inclusion complexes. As shown in Figure 2a, the diffraction pattern of

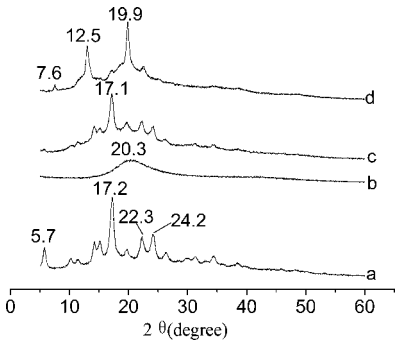

Figure 2. X-ray diffraction spectra. (a) URDS, (b) soybean lecithin, (c) URDS/soybean lecithin physical mixture, and (d) debranched-starch/soybean lecithin inclusion complexes.

URDS was a typical B-type crystalline structure with main diffraction peaks at 5.7°, 17.2°, 22.3°, and 24.2°.[22] The diffractogram of phosphatidylcholine (Figure 2b) exhibited a big and broad peak at around 20.3°, which indicated the amorphous characteristics of phosphatidylcholine.[23] As presented in Figure 2c, the diffractogram of URDS/phosphatidylcholine physical mixture (phosphatidylcholine payload 106 mg/g) was a simple superimposition of URDS and phosphatidylcholine, which remained the main diffraction peaks of URDS and showed the characterictics of phosphatidylcholine. As compared to URDS/phosphatidylcholine physical mixture, the diffractogram of debranched-starch/phosphatidylcholine inclusion complexes (Figure 2d) confirmed the formation of inclusion complexes, as inferred from the diffraction peaks at 7.6°, 12.5°, and 19.9°, which was a typical diffraction pattern of V-type amylose inclusion complexes.[10,24]

FT-IR Analysis. As a common analysis tool, FT-IR spectrum has been widely applied to confirm the formation of inclusion complexes.[25,26] Figure 3 illustrates the FT-IR spectra of URDS (Figure 3a), phosphatidylcholine (Figure 3b), URDS/phosphatidylcholine physical mixture (Figure 3c, phosphatidylcholine payload 106 mg/g), and debranched-starch/phosphatidylcholine inclusion complexes (Figure 3d). In the spectrum of URDS, the extremely broad band at 3384 cm^{-1} and the peak at 2930 cm^{-1} corresponded to the O−H and C−H stretching

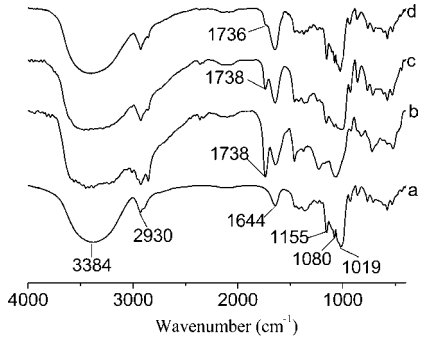

Figure 3. FT-IR spectra. (a) URDS, (b) soybean lecithin, (c) URDS/soybean lecithin physical mixture, and (d) debranched-starch/soybean lecithin inclusion complexes.

vibration, respectively. Three characteristic peaks at 1155, 1080, and 1019 cm^{-1} were assigned to the C−O stretching vibrations. The peak at 1644 cm^{-1} was attributed to the δ(OH) bending vibration.[27] As shown in Figure 3b, the spectrum of phosphatidylcholine was characterized by the absorption at 1738 cm^{-1}, which was attributed to the C═O stretching vibration.[4] The FT-IR spectrum of the URDS/phosphatidylcholine physical mixture showed approximate superimposition of the individual spectrum of URDS and phosphatidylcholine. Most of the absorption bands of phosphatidylcholine were covered by that of URDS, except the C═O stretching vibration located at 1738 cm^{-1}. The FT-IR spectrum of the debranched-starch/phosphatidylcholine complexes was almost the same as that of URDS except the shoulder peak (1736 cm^{-1}) corresponding to the C═O stretching vibration. However, as compared to the physical mixture, the C═O stretching vibration peak of phosphatidylcholine was apparently weakened; the reason is probably that part of the C═O bonds were covered by debranched-starch after the complexation of debranched-starch with phosphatidylcholine. Similar results were found by Yang et al.[25] who investigated the formation of inclusion complexes of amylose and conjugated linoleic acid. From the FT-IR spectra, the authors suggested that the driving force for self-assembly between amylose and conjugated linoleic acid is the hydrophobic interaction.

^{13}C CP/MAS NMR Analysis. The ^{13}C NMR spectrum and the peak data of (a) URDS, (b) URDS/phosphatidylcholine physical mixture (phosphatidylcholine payload 106 mg/g), and (c) debranched-starch/phosphatidylcholine inclusion complexes are presented in Figure 4 and Table 1. The serial

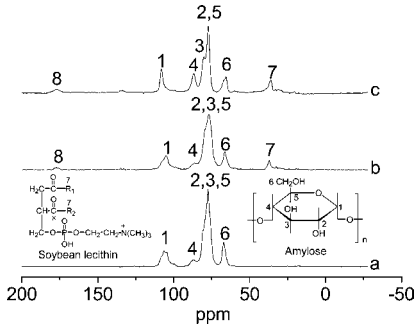

Figure 4. ^{13}C CP/MAS NMR spectra. (a) URDS, (b) URDS/soybean lecithin physical mixture, and (c) debranched-starch/soybean lecithin inclusion complexes.

number of the peaks in Figure 4 and Table 1 corresponds to the carbon atoms of the molecular formula presented in Figure 4. In the spectrum of URDS, the peaks were assigned as follows: 66.59 ppm, C6; 77.44 ppm, C2, C3, C5; 86.53 ppm, C4; and 106.46 ppm, C1.[28] The ^{13}C NMR spectrum of URDS/phosphatidylcholine physical mixture was almost the same as URDS, except two new peaks located at 37.09 and 176.89 ppm, which were attributed to the alkyl carbon and carbonyl carbon atoms, respectively.[29,30] In comparison with URDS and URDS/phosphatidylcholine physical mixture, the spectrum of debranched-starch/phosphatidylcholine inclusion complexes displayed typical characteristics of inclusion complexes, of which the C-4 peak at 86.46 ppm was better resolved from the combined C-2, C-3, C-5 peak and moved downfield, the C-3 peak was partially resolved from the C-2, C-5 peak, and the peak of C-1 was sharper and moved downfield.[31,32] The

DOI: 10.1021/jf504133c
J. Agric. Food Chem. 2015, 63, 634−641

Table 1. Characteristics of ^{13}C CP/MAS NMR Spectra

	ppm						
samples	C-7	C-6	C-3,5	C-2	C-4	C-1	C-8
URDS		66.59	77.44		86.53	106.46	
physical mixture	37.09	66.44	76.85		86.46	106.42	176.89
inclusion complexes	35.92	66.61	77.29	80.19	87.42	108.13	176.95

chemical shifts of C-1 and C-4 were more remarkable because α-1,4 linkages are more sensitive to conformational changes.[33] Morever, the peaks attributed to the alkyl carbon (35.92 ppm) and carbonyl carbon (176.95 ppm) atoms were also observed in the spectrum of the complexes. However, as compared to that of the physical mixture, the peak (35.92 ppm) corresponding to the alkyl carbon atoms of the complexes shifted upfield by 1.17 ppm. The chemical shift was caused by the combined trans and gauche conformation of the fatty acid chain of the lipids upon complexation with debranched-starch. Similar results were found by Lebail et al.[34] who investigated the complexation of amylose with fatty acids. Furthermore, according to Snape et al.[31] who demonstrated that all polar groups larger than carboxyl must lie outside the helix cavity of amylose, we can conclude that the debranched-starch/phosphatidylcholine inclusion complexes were formed by the hydrophobic interactions between the alkyl chain of phosphatidylcholine and the helix cavity of debranched-starch, with the rest of the parts of phosphatidylcholine lying outside the helix cavity.

SAXS Analysis. Characterization of the cluster and fractal structure of (a) native potato starch, (b) URDS, and (c) debranched-starch/phosphatidylcholine inclusion complexes was performed using SAXS, and the scattering patterns are presented in Figure 5. As shown in Figure 5a, native starch

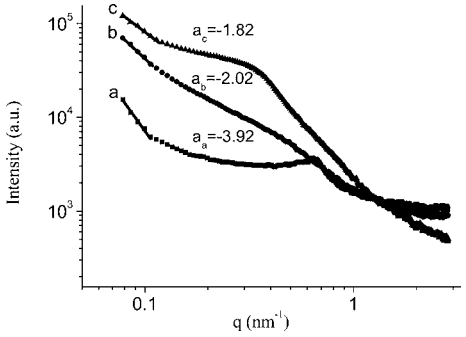

Figure 5. SAXS curves. (a) Native potato starch, (b) URDS, and (c) debranched-starch/soybean lecithin inclusion complexes.

showed one characteristic peak at about q = 0.66 nm^{-1}, which corresponds to a Bragg distance (d) of about 9.52 nm. This peak is thought to arise from the long periodicity occurring from the semicrystalline structure (i.e., alternating crystalline and amorphous lamellae structure) of the starch granules.[35,36] As can be seen from Figure 5b and c, after the gelatinization, enzymatic hydrolysis, and retrogradation process, the crystalline structure of native starch was completely destroyed, and the peak located at about 0.66 nm^{-1} disappeared. The SAXS pattern of URDS was smooth, and no distinct characteristic peak was observed within the testing range. However, after complexation with phosphatidylcholine, a new shoulder peak was observed in the SAXS curve of the complexes at about q = 0.33 nm^{-1}. This shoulder indicated that a semicrystalline structure with a Bragg distance (d) of about 19.04 nm existed in the complexes. In previous literature, similar results were found by Zabar et al.[37] who investigated the nano characteristics of the amylose/fatty acid complexes. In this study, the researchers suggested that interactions between fatty acid and amylose tend to form lamella of distinct nanometric dimensions. The structure of the debranched-starch/phosphatidylcholine complexes may be described as the crystalline regions of folded debranched-starch chains were separated alternately by regions of imperfections, chain ends, and probably residues of phosphatidylcholine, which lay outside the helix cavity of debranched-starch. It was worth noting that the semicrystalline structure in the complexes that was formed by crystallization of linear polymers from solution was different from that of native starch, of which the concentric regions of alternating amorphous and crystalline structures known as growth rings are formed by the radial orientation of the amylopectin molecules.[29]

In previous literature, SAXS data have also been used to analyze the fractal structure of native and modified starch.[19,36] The fractal structures can be characterized by the fractal dimension D, which can be obtained from the scattering power law equation:

$$I \propto q^{\alpha} \tag{6}$$

where I is the scattering intensity, and α is an exponent that can take the range from -1 to -4 and can be obtained from the slope between log I and log q.[20]

In case of $-4 < \alpha < -3$, the scattering can be judged as reflection from the surface, and the objects can be seen as possessing a surface fractal structure with the fractal dimension $D_s = \alpha + 6$, which indicates the irregularity of the surface. When the scattering surface is smooth, D_s becomes 2.[20] In case of $-3 < \alpha < -1$, the scattering objects can be seen as possessing a mass fractal structure (which means that the density profile of the scattering object has a self-similar nature) with the fractal dimension $D_m = -\alpha$, which indicates the degree of compactness of the physical arrangement of the mass.[20]

As can be seen from Figure 5a, native starch had an obvious surface fractal structure with $\alpha = -3.92$ and $D_s = 2.08$, indicating that native starch had a surface fractal structure and the surface of the granules was smooth. However, the slope of the scattering patterns of URDS and debranched-starch/phosphatidylcholine complexes was -2.02 and -1.82, respectively, indicating that both URDS and debranched-starch/phosphatidylcholine complexes possessed a mass fractal structure with D_m = 2.02 and 1.82, respectively. The D_m value of URDS was slightly higher than that of the complexes, which suggested that the molecules of URDS were arranged more tightly than that of the complexes.

SEM Analysis. Scanning electron microscopy was used to investigate the morphology of URDS and debranched-starch/phosphatidylcholine complexes at different magnification. The surface of URDS appeared to be smooth with no distinct features (Figure 6a,b). However, as shown in Figure 6c,d, after complexation with phosphatidylcholine, the complexes dis-

DOI: 10.1021/jf504133c
J. Agric. Food Chem. 2015, 63, 634−641

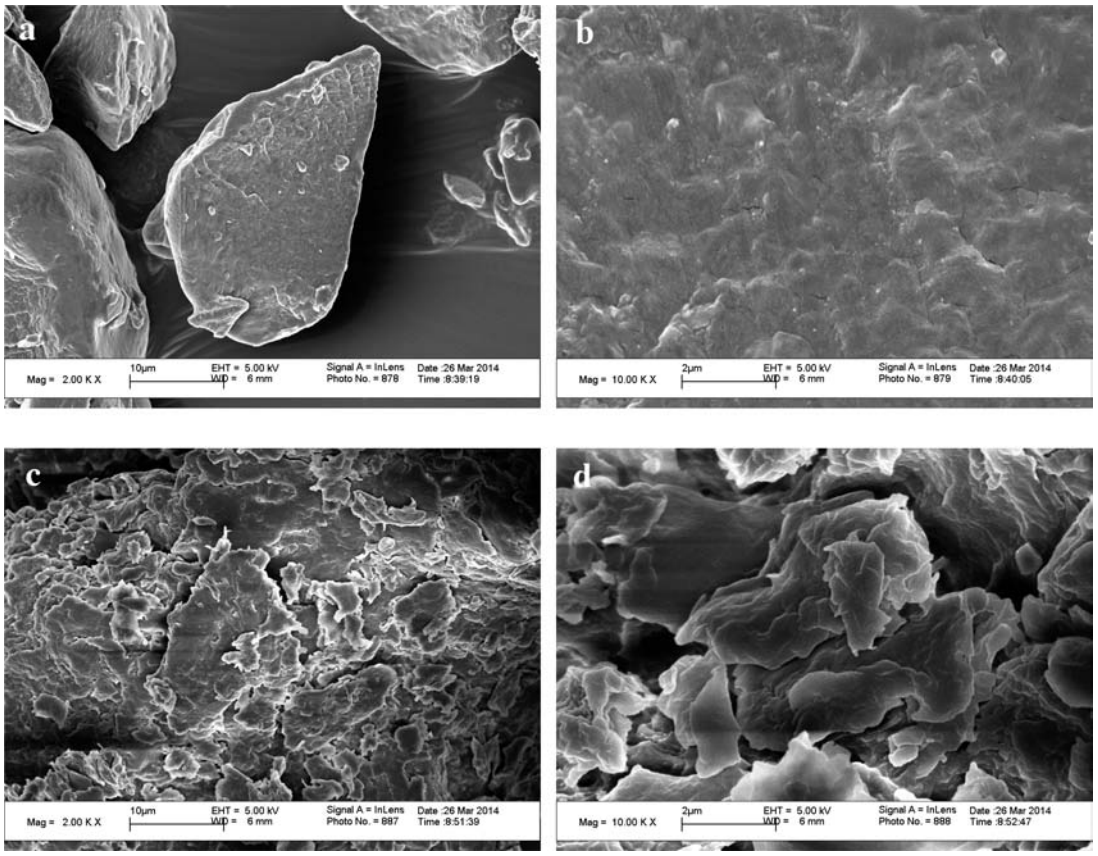

Figure 6. SEM images. (a) URDS ×2000, (b) URDS ×10 000, (c) inclusion complexes ×2000, and (d) inclusion complexes ×10 000.

played a rough appearance with thin lamellar structures embedded in the matrix. This phenomenon is probably due to the fact that the regular arrangement of debranched-starch was disrupted by the phosphatidylcholine molecules with alkyl chain encapsulated in the helix cavity of debranched-starch and the rest of the molecule parts of phosphatidylcholine lying outside the helix cavity. In previous literature, similar results were found in the amylose/fatty acid inclusion complexes.[29,37]

Stability Analysis. The determination of POV is a method that is widely used to evaluate the deterioration of lipids.[13] The higher is the value of POV, the severer is the deterioration of lipids. As can be seen from Figure 7, the POV of both the debranched-starch/phosphatidylcholine inclusion complexes and the URDS/phosphatidylcholine physical mixture increased with storage time increasing. However, the POV of the complexes was significantly lower than that of the physical mixture at any storage time. This result indicated that after complexation with debranched-starch, the stability of phosphatidylcholine was significantly improved. This result was in good agreement with other studies using amylose as embedding material of lipids.[12,13] Therefore, not only amylose extracted from native starch, but also debranched-starch can be used as wall material to improve the stability of lipids.

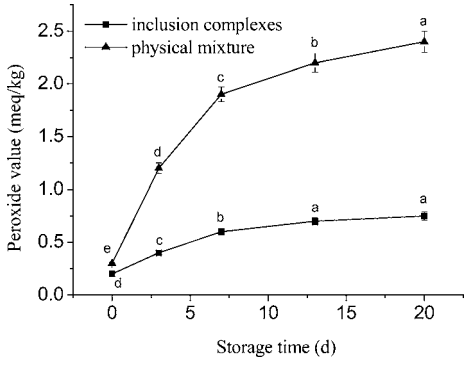

Figure 7. Stability of debranched-starch/soybean lecithin inclusion complexes and URDS/soybean lecithin physical mixture stored at 50 °C for 0, 3, 7, 13, and 20 days. Values in the same curve with different superscript letters are significantly different ($p < 0.05$).

Digestibility Analysis. The percentage of phosphatidylcholine released after the complexes were incubated under the simulated stomach condition and hydrolyzed by pancreatin is shown in Figure 8. As can be seen from Figure 8a, the complexes were relatively stable under stomach conditions, and only 5% of phosphatidylcholine was released after incubating for 2 h at the simulated stomach conditions. However, after being hydrolyzed by pancreatin for 24 h (Figure 8b), nearly all of the phosphatidylcholine was gradually released, which indicated that the debranched-starch/phosphatidylcholine inclusion complexes could be effectively hydrolyzed by pancreatin. Similar results were found by Lalush et al.[12] who studied the enzymatic digestion behaviors of amylose-conjugated linoleic acid complexes.

In conclusion, this Article described an exploratory study on the synthesis of debranched-starch/phosphatidylcholine inclusion complexes, which is a facile method to improve the stability of phosphatidylcholine. The optimum conditions for preparing the debranched-starch/phosphatidylcholine complexes were concluded as follows: reaction temperature, 60 °C; reaction time, 2 h; and the mass ratio of phosphatidylcho-

DOI: 10.1021/jf504133c
J. Agric. Food Chem. 2015, 63, 634−641

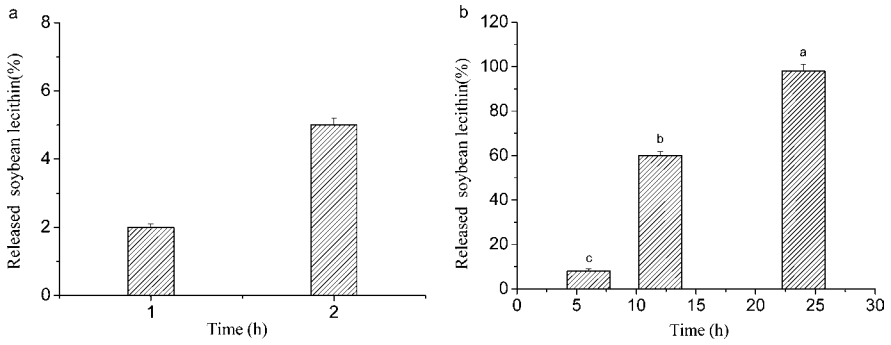

Figure 8. Percentage of soybean lecithin released (a) in simulated stomach condition and (b) after enzymatic treatment with pancreatin. Values in the same curve with different superscript letters are significantly different ($P < 0.05$).

line to native starch (dry basis), 1:10. The phosphatidylcholine payload and inclusion rate measured under optimum conditions were 106 mg/g and 84.8%, respectively. The formation of debranched-starch/phosphatidylcholine inclusion complexes was confirmed by XRD and FT-IR. The debranched-starch/phosphatidylcholine inclusion complexes were formed mainly by the hydrophobic interactions between the alkyl chain of phosphatidylcholine and the helix cavity of debranched-starch, with the rest of the molecule parts of phosphatidylcholine lying outside the helix cavity. Moreover, a new semicrystalline structure with a Bragg distance of about 19.04 nm was formed in the complexes. The complexes possessed a mass fractal structure and displayed a rough appearance with thin lamellar structures embedded in the matrix. After complexation with debranched-starch, the stability of phosphatidylcholine was significantly improved, and the phosphatidylcholine encapsulated can be gradually released upon pancreatin treatment.

AUTHOR INFORMATION

Corresponding Authors

*Tel.: +86-20-87113845. Fax: +86-20-87113848. E-mail: zhgluo@scut.edu.cn.

*Tel.: +86-20-87113845. Fax: +86-20-87113848. E-mail: lfxfu@scut.edu.cn.

Funding

This research was supported by the National Natural Science Foundation of China (31130042, 21376097), the program for New Century Excellent Talents in University (NCET-13-0212), the Guangdong Natural Science Foundation (S2013010012318), the Key Project of Science and Technology of Guangdong Province (2012B091100443, 2012B091100047), and the Fundamental Research Funds for the Central Universities, SCUT (2013ZZ0070).

Notes

The authors declare no competing financial interest.

ABBREVIATIONS USED

URDS, uncomplexed retrograded debranched-starch; XRD, X-ray diffraction; FT-IR, Fourier transform infrared spectroscopy; ^{13}C CP/MAS NMR, ^{13}C cross-polarization/magic angle spinning nuclear magnetic resonance; SAXS, small-angle X-ray scattering; SEM, scanning electron microscopy

REFERENCES

(1) Oke, M.; Jacob, J. K.; Paliyath, G. Effect of soy lecithin in enhancing fruit juice/sauce quality. *Food Res. Int.* **2010**, *43*, 232−240.

(2) Scholfield, C. R. Composition of soybean lecithin. *J. Am. Oil Chem. Soc.* **1981**, *58*, 889−892.

(3) Duric, M.; Sivanesan, S.; Bakovic, M. Phosphatidylcholine functional foods and nutraceuticals: A potential approach to prevent non-alcoholic fatty liver disease. *Eur. J. Lipid Sci. Technol.* **2012**, *114*, 389−398.

(4) Wang, X. G.; Luo, Z. G.; Xiao, Z. G. Preparation, characterization, and thermal stability of β-cyclodextrin/soybean lecithin inclusion complex. *Carbohydr. Polym.* **2014**, *101*, 1027−1032.

(5) Zakharova, T. S.; Fortinskaya, E. S.; Kochetova, M. M.; Babakhanov, I. S.; Torkhovskaya, T. I.; Khalilov, E. M. Surface activity of phosphatidylcholines as the basis for surfactant replacement therapy. *Bull. Exp. Biol. Med.* **2000**, *129*, 144−145.

(6) Kim, J. Y.; Lim, S. T. Preparation of nano-sized starch particles by complex formation with n-butanol. *Carbohydr. Polym.* **2009**, *76*, 110−116.

(7) Arvisenet, G.; Le Bail, P.; Voilley, A.; Cayot, N. Influence of physicochemical interactions between amylose and aroma compounds on the retention of aroma in food-like matrices. *J. Agric. Food Chem.* **2002**, *50*, 7088−7093.

(8) Bhatnagar, S.; Hanna, M. A. Amylose-lipid complex formation during single-screw extrusion of various corn starches. *Cereal Chem.* **1994**, *71*, 582−587.

(9) Biais, B.; Le Bail, P.; Robert, P.; Pontoire, B.; Buléon, A. Structural and stoichiometric studies of complexes between aroma compounds and amylose. *Carbohydr. Polym.* **2006**, *66*, 306−315.

(10) Lesmes, U.; Cohen, S. H.; Shener, Y.; Shimoni, E. Effects of long chain fatty acid unsaturation on the structure and controlled release properties of amylose complexes. *Food Hydrocolloids* **2009**, *23*, 667−675.

(11) Lesmes, U.; Barchechath, J.; Shimoni, E. Continuous dual feed homogenization for the production of starch inclusion complexes for controlled release of nutrients. *Innovative Food Sci. Emerging Technol.* **2008**, *9*, 507−515.

(12) Lalush, I.; Bar, H.; Zakaria, I.; Eichler, S.; Shimoni, E. Utilization of amylose-lipid complexes as molecular nanocapsules for conjugated linoleic acid. *Biomacromolecules* **2005**, *6*, 121−130.

(13) Xu, J.; Zhao, W. X.; Ning, Y. W.; Bashari, M.; Wu, F. F.; Chen, H. Y.; Yang, N.; Jin, Z. Y.; Xu, B. C.; Zhang, L. X.; Xu, X. M. Improved stability and controlled release of $\omega 3/\omega 6$ polyunsaturated fatty acids by spring dextrin encapsulation. *Carbohydr. Polym.* **2013**, *92*, 1633−1640.

(14) Kim, S.; Willett, J. L. Isolation of amylose from starch solutions by phase separation. *Starch/Staerke* **2004**, *56*, 29−36.

(15) Sweedman, M. C.; Hasjim, J.; Tizzotti, M. J.; Schaefer, C.; Gilbert, R. G. Effect of octenylsuccinic anhydride modification on β-amylolysis of starch. *Carbohydr. Polym.* **2013**, *97*, 9−17.

(16) Ward, R. M.; Gao, Q. Y.; de Bruyn, H.; Gilbert, R. G.; Fitzgerald, M. A. Improved methods for the structural analysis of the amylose-rich fraction from rice flour. *Biomacromolecules* **2006**, *7*, 866−876.

DOI: 10.1021/jf504133c
J. Agric. Food Chem. 2015, 63, 634−641

(17) Bruner, R. L. Determination of reducing value: 3,5-Dinitrosalicylic acid method. In *Methods in Carbohydrate Chemistry IV: Starch*, 1st ed.; Whistler, R. L., Smith, R. J., Bemiller, J. N., Wolfrom, M. L., Eds.; Academic Press: New York, 1964; pp 67−71.
(18) Gilbert, G. A.; Spragg, S. P. Iodimetric determination of amylose. In *Methods in Carbohydrate Chemistry IV: Starch*, 1st ed.; Whistler, R. L., Smith, R. J., Bemiller, J. N., Wolfrom, M. L., Eds.; Academic Press: New York, 1964; pp 168−169.
(19) Quinlan, K. P.; DeSesa, M. A. Spectrophotometric determination of phosphorus as molybdovanadophosphoric acid. *Anal. Chem.* **1955**, *27*, 1626−1629.
(20) Suzuki, T.; Chiba, A.; Yarno, T. Interpretation of small angle x-ray scattering from starch on the basis of fractals. *Carbohydr. Polym.* **1997**, *34*, 357−363.
(21) Biliaderis, C. G.; Galloway, G. Crystallization behavior of amylose-V complexes: structure-property relationships. *Carbohydr. Res.* **1989**, *189*, 31−48.
(22) Lu, X. X.; Luo, Z. G.; Yu, S. J.; Fu, X. Lipase-catalyzed synthesis of starch palmitate in mixed ionic liquids. *J. Agric. Food Chem.* **2012**, *60*, 9273−9279.
(23) Formariz, T. P.; Chiavacci, L. A.; Sarmento, V. H. V.; Franzini, C. M.; Silva- Jr, A. A.; Scarpa, M. V.; Santilli, C. V.; Egito, E. S. T.; Oliveira, A. G. Structural changes of biocompatible neutral microemulsions stabilized by mixed surfactant containing soya phosphatidylcholine and their relationship with doxorubicin release. *Colloids Surf., B* **2008**, *63*, 287−295.
(24) Jouquand, C.; Ducruet, V.; Le Bail, P. Formation of amylose complexes with C6-aroma compounds in starch dispersions and its impact on retention. *Food Chem.* **2006**, *96*, 461−470.
(25) Yang, Y.; Gu, Z.; Zhang, G. Delivery of bioactive conjugated linoleic acid with self-assembled amylose-CLA complex. *J. Agric. Food Chem.* **2009**, *57*, 7125−7130.
(26) Lay Ma, U. V.; Floros, J. D.; Ziegler, G. R. Formation of inclusion complexes of starch with fatty acid esters of bioactive compounds. *Carbohydr. Polym.* **2011**, *83*, 1869−1878.
(27) Luo, Z. G.; Cheng, W. W.; Chen, H. M.; Fu, X.; Peng, X. C.; Luo, F. X.; Nie, L. H. Preparation and properties of enzyme-modified cassava starch-zinc complexes. *J. Agric. Food Chem.* **2013**, *61*, 4631−4638.
(28) Cheetham, N. W. H.; Tao, L. Solid state NMR studies on the structural and conformational properties of natural maize starches. *Carbohydr. Polym.* **1998**, *36*, 285−292.
(29) Zabar, S.; Lesmes, U.; Katz, I.; Shimoni, E.; Bianco-Peled, H. Studying different dimensions of amylose-long chain fatty acid complexes: molecular, nano and micro level characteristics. *Food Hydrocolloids* **2009**, *23*, 1918−1925.
(30) Morrison, W. R.; Law, R. V.; Snape, C. E. Evidence for inclusion complexes of lipids with V-amylose in maize, rice and oat starches. *J. Cereal Sci.* **1993**, *18*, 107−109.
(31) Snape, C. E.; Morrison, W. R.; Maroto-Valer, M. M.; Karkalas, J.; Pethrick, R. A. Solid state ^{13}C NMR investigation of lipid ligands in V-amylose inclusion complexes. *Carbohydr. Polym.* **1998**, *36*, 225−237.
(32) Gidley, M. J.; Bociek, S. M. Carbon-13 CP/MAS NMR studies of amylose inclusion complexes, cyclodextrins, and the amorphous phase of starch granules: relationships between glycosidic linkage conformation and solid-state carbon-13 chemical shifts. *J. Am. Chem. Soc.* **1988**, *110*, 3820−3829.
(33) Le Bail, P.; Rondeau, C.; Buléon, A. Structural investigation of amylose complexes with small ligands: helical conformation, crystalline structure and thermostability. *Int. J. Biol. Macromol.* **2005**, *35*, 1−7.
(34) Le Bail, P.; Buleon, A.; Shiftan, D.; Marchessault, R. H. Mobility of lipid in complexes of amylose-fatty acids by deuterium and ^{13}C solid state NMR. *Carbohydr. Polym.* **2000**, *43*, 317−326.
(35) Zhu, J.; Li, L.; Chen, L.; Li, X. X. Study on supramolecular structural changes of ultrasonic treated potato starch granules. *Food Hydrocolloids* **2012**, *29*, 116−122.
(36) Zhang, B. J.; Li, X. X.; Liu, J.; Xie, F. W.; Chen, L. Supramolecular structure of A-and B-type granules of wheat starch. *Food Hydrocolloids* **2013**, *31*, 68−73.
(37) Zabar, S.; Lesmes, U.; Katz, I.; Shimoni, E.; Bianco-Peled, H. Structural characterization of amylose-long chain fatty acid complexes produced via the acidification method. *Food Hydrocolloids* **2010**, *24*, 347−357.

DOI: 10.1021/jf504133c
J. Agric. Food Chem. 2015, 63, 634−641

JOURNAL OF AGRICULTURAL AND FOOD CHEMISTRY

Article

pubs.acs.org/JAFC

Deacidification of Cranberry Juice by Electrodialysis with Bipolar Membranes

Elodie Rozoy,[†] Leslie Boudesocque,[§] and Laurent Bazinet*[,†]

[†]Institute of Nutrition and Functional Foods (INAF) and Department of Food Sciences, Pavillon Paul Comtois, Université Laval, Quebec, QC, Canada G1V 0A6

[§]UMR INRA 1282 Infectiology and Public Health, Faculty of Pharmacy Philippe Maupas, University François Rabelais, 31 avenue Monge, 37200 Tours, France

ABSTRACT: Cranberry is recognized for its many benefits on human health; however, its high acidity may be a limiting factor for its consumption. This study aimed to investigate the deacidification of cranberry juice using a two simultaneous step electrodialysis with bipolar membranes (EDBM) process. In step 1 (deacidification), during the 6 h treatment, the pH of the juice increased from 2.47 to 2.71 and a deacidification rate of 22.84% was obtained, whereas in step 2 (pH lowering) the pH of juice 2 was almost stable. Citric, quinic, and malic acid were extracted with a maximum of 25% and were mainly transferred to the KCl 2 fraction. A significant loss of anthocyanins in juice 2 (step 2) was observed, due to their oxidation by oxygen incorporated by the centrifugal pump. This also affected its coloration. The first step of the EDBM process was successful for cranberry juice deacidification and could be improved by increasing the number of membranes stacked.

KEYWORDS: *cranberry juice, deacidification, electrodialysis, bipolar membranes*

INTRODUCTION

Cranberry juice has a long history of scientific interest regarding its many positive benefits on human health. Particularly, it has a strong activity against *Helicobacter pylori*,[1] reduces urinary tract infection,[2] and can prevent gastrointestinal disorders.[3] All of these health benefits should attract consumers, but the high content of organic acids and low pH of cranberry juice are inconveniences that limit its consumption. The main acids present in cranberry juice are citric, malic, and quinic acids, and there is also the presence of benzoic and glucuronic acids, in lower quantities.[4] Those acids are responsible for the high titratable acidity of the juice and its astringency.

Different acidic juices such as mandarin orange juice,[5] pineapple juice,[6] passion fruit juice,[7] and tropical fruit juice[8] have already been deacidified by electrodialysis. Electrodialysis is an electrochemical process based on the migration of electrically charged species through selective membranes, under the influence of an electrical field. This electrical field is created by the application of a potential difference between the two electrodes present in the cell. This process is affordable, environmentally friendly as it does not use solvents, and easy to use. More recently, bipolar membranes (BM), which are membranes dissociating water molecules in protons (on the cationic side of the BM) and hydroxyls (on the anionic side) under the effect of electric field, were stacked in electrodialysis cells. Hence, electrodialysis with bipolar membranes (EDBM) has found applications in food systems regarding production or separation of organic acids,[9−14] production of hydroxide and hydrochloric acids,[15,16] inhibition of juice enzymatic browning,[17] and deacidification of fruit juices.[5,18]

A configuration already published for the deacidification of red wine[19] was preliminarily tested in the present study on cranberry juice (results not shown), but the results were not satisfying due to the difference in initial pH between cranberry juice and wine, influencing the migration of the acids according to their pK_a. A system more complex and more eco-efficient was then proposed here for cranberry juice deacidification.

The objectives of this work were (1) to use a two-step deacidification process to deacidify and then decrease the pH of the juice to its initial pH, which has never been performed to our knowledge; (2) to study the composition evolution of a cranberry juice deacidified during EDBM treatments; and (3) to study the EDBM parameters evolution and the potential fouling of the membranes during repetitive uses.

MATERIALS AND METHODS

Materials. Food grade Neosepta AMX-SB anion-exchange membrane, CMX-SB cation-exchange membrane, and BP-1 bipolar membrane from Tokuyama Soda Ltd. (Tokyo, Japan) were used. Solutions of 20 g/L NaCl and 2 g/L KCl (Mat Laboratory, Québec, QC, Canada) were prepared.

Treatments were carried out on a pasteurized and clarified cranberry juice produced by Fruit d'Or (Notre-Dame-de-Lourdes, QC, Canada). The juice was stored at −28 °C and thawed at 4 °C before each experiment.

Electrodialysis Cell. The electrodialysis cell was an MP type cell with 100 cm^2 of effective electrode surface (ElectroCell AB, Täby, Sweden) with two AMX-SB anionic membranes, two bipolar membranes, and two CMX-SB cationic membranes (Figure 1). Each membrane was placed behind two rubber gaskets, and there was one polypropylene spacer behind each membrane, representing the cell compartment. Food grade stainless steel cathode and a dimensionally stable anode (DSA-O_2) were used. The KCl and NaCl solutions were connected to their own external tanks and circulated in the compartments using two centrifugal pumps (Iwaki Magnet Pump,

Received: September 3, 2014
Revised: December 16, 2014
Accepted: December 22, 2014
Published: December 22, 2014

ACS Publications © 2014 American Chemical Society

DOI: 10.1021/jf502824f
J. Agric. Food Chem. 2015, 63, 642−651

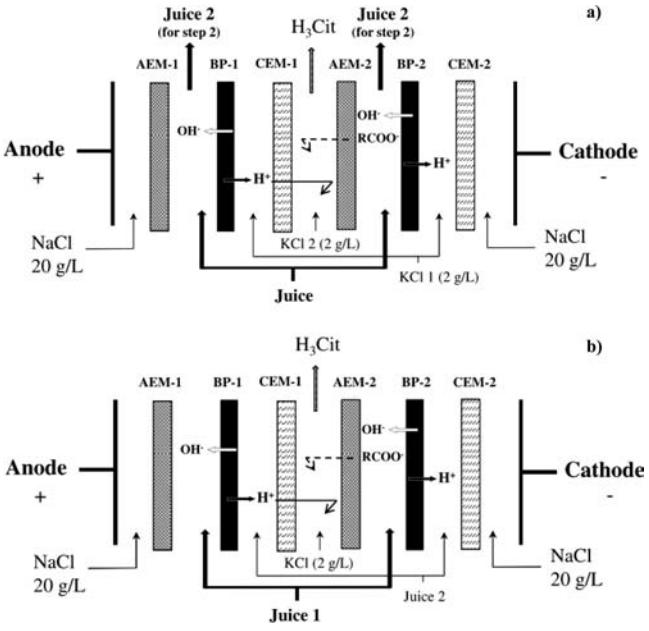

Figure 1. Configuration used for (a) the first and (b) second electrodialysis steps. AEM was an anion-exchange membrane, BP was a bipolar membrane, and CEM was a cation-exchange membrane.

Iwaki Co. Ltd., Tokyo, Japan). The flow rates were controlled using flowmeters (Aalborg Instrument and Controls, Inc., Orangeburg, NY, USA), whereas cranberry juice was circulated using a peristaltic pump (Kate, Barnant Co., Barrington, IL, USA) to avoid oxygen incorporation.

Protocol of Deacidification by ED. The deacidification was performed in two steps; the first was carried out to decrease the quantity of acids in the juice, as well as increase the pH of the juice. The second step was to reduce the pH of the juice previously deacidified to its initial value, in order to not affect its color, and to deacidify in the same time a new batch of juice to optimize the efficiency of the whole process.

Step 1 (Figure 1a). The volume of cranberry juice used in the first step was 750 mL. In the electrode compartment, 900 mL of 20 g/L NaCl was used, and 650 mL of 2 g/L KCl was put in KCl 1 and KCl 2 compartments. The flow rates were 1000 mL/min for the electrolyte (NaCl), 600 mL/min for the juice and KCl 1 (the flow is divided in two circuits in the cell, and consequently the flow rate is equal to 300 mL/min), and 300 mL/min for KCl 2. This study was carried out at room temperature. The first step was performed during 6 h.

During the electrodialysis treatment, the pH of the juice, KCl 1, and KCl 2 was recorded, as well as the conductivity of all those compartments. The current intensity, as well as the temperature of the compartment containing the juice, was also recorded. Samples (15 mL) were taken every hour to perform further analyses concerning the titratable acidity, total polyphenols, anthocyanins, organic acids, and degrees Brix.

After the experiment, the juice that was deacidified and KCl 1 were stored at 4 °C. KCl 2 and NaCl solutions were discarded as they were only necessary for beginning the first step of the process. Then the electrodialysis system was cleaned as follows: 10 min of circulation of hot water, then 30 min of alkaline solution, rinsing with water at 55 °C and circulation for 10 min, then circulation of acidic solution for 20 min. Finally, every compartment was rinsed with water at 55 °C for 4–5 min and then rinsed with distilled water.

Step 2 (Figure 1b). The objective of the second step was to deacidify the cranberry juice (juice 1) as in the first step, as well as to decrease the pH of the juice deacidified in the first step under the action of the bipolar membranes, to restore the initial pH of this juice, with a diminished level of organic acids.

Juice from the first step was reused as juice 2 in the second step. The KCl 1 in the first step was also reused as KCl in the second step, but 250 mL of new solution (2 g/L KCl) was added to the previous one to reach a volume of 550 mL. A new juice called juice 1 was used (Figure 1b). The volumes for juice 1, juice 2, and KCl were 550 mL, and the volume of NaCl remained identical to that in the first step. All flow rates were identical to those of the first step, and the experiments were also performed at room temperature. Every electrodialytic parameter was recorded according to the first step, and samples were also taken to proceed to further analyses.

At the end of the treatment, the electrodialysis system was cleaned as previously.

Analyses. *Conductivity.* A YSI conductivity meter, model 3100, was used with a YSI immersion probe (model 3252, cell constant K = 1 cm^{-1}; Yellow Springs Instrument, Yellow Springs, OH, USA) to measure the conductivity of all solutions.

Global System Resistance. The global resistance of the system was calculated using Ohm's law (U = RI). The values of voltage were read directly from the power supply indicators and the current passing through the electrodes from a multimeter (model 52-0060-2, Mastercraft, Toronto, Canada).

Membrane Electrical Conductivity. The electrical conductivity of the membrane was measured with a specially designed cell (conductivity clip) from the Laboratoire des Matériaux Echangeurs d'Ions (Créteil, France). The membrane's electrical conductivity κ (mS/cm) was calculated as

$$\kappa = \frac{l}{R_m A}$$

where l is the membrane thickness (cm), R_m the transversal electric resistance of the membrane (Ω), and A the electrode area (1 cm^2).

Membrane Thickness. The membrane thickness was measured using a Mitutoyo Corp. IDC type digimatic indicator with absolute encoder (model ID-C112EB, Kanagawa-Ken, Japan) with a resolution of 1 μm and a range of 12.7–0.001 mm. The membrane thickness value was averaged from four measurements at different locations on the membrane.

pH. The pH was measured using a VWR Symphony electrode equipped with an automatic temperature compensation device and connected to a VWR Symphony SP20 portable pH meter (Thermo Orion, West Chester, PA, USA).

Titratable Acidity. The titratable acidity was evaluated according to AOAC method 942.15. Forty milliliters of degassed distilled water was added to 4 mL of juice, and then 0.1 M NaOH was added drop by drop until pH 8.2 was reached. The pH was measured with the same electrode and pH meter as for the pH measurements. The titratable acidity was expressed as milliliters of NaOH (0.1 M) added.

Degrees Brix. The degrees Brix of cranberry juices was measured using a Digital Pocket Refractometer (model PAL-1, 0–53%, Atago, Tokyo, Japan).

Total Polyphenol Content. Total polyphenol content measurements in raw juice, juice step 1 (S1), juice 1–step 2 (S2), and juice 2–step 2 (S2) were performed using the microscale protocol for Folin–Ciocalteu colorimetry of Waterhouse.[20] The samples and the standards of gallic acid absorbances were measured at 765 nm using a UV–visible Agilent 8453 spectrophotometer (Agilent Technologies, Palo Alto, CA, USA). Concentration in total polyphenol was expressed as gallic acid equivalent per liter of juice (mg/L).

Anthocyanin Content. Total anthocyanin concentration was quantified by UV–visible spectroscopy following the method described by Giusti and Wrolstad.[21] Each sample of cranberry juice was diluted 10 times in two distinct aqueous buffers: 0.025 M potassium chloride buffer, pH 1.0; and 0.4 M sodium acetate buffer, pH 4.5. Diluted solutions were equilibrated for 15 min at room temperature before analysis. The absorbance of each diluted sample was measured at 520 and 700 nm using a UV–visible Agilent 8453 spectrophotometer (Agilent technologies, Palo Alto, CA, USA). Absorbance (A) due to the contribution of total anthocyanins was calculated as follows:

DOI: 10.1021/jf502824f
J. Agric. Food Chem. 2015, 63, 642–651

$$A = (A_{510nm} - A_{700nm})_{pH1.0} - (A_{510nm} - A_{700nm})_{pH4.5} \quad (1)$$

Concentration in total anthocyanins was expressed as milligrams of cyanidin-3-glucoside equivalent per liter of juice (mg/L) by applying the equation

$$\text{monomeric cyanidin-3-glucoside pigment (mg/L)} = (A \times MW_{Cyd\text{-}3\text{-}glu} \times \text{dilution factor} \times 1000)/(\varepsilon_{Cyd\text{-}3\text{-}glu} \times L) \quad (2)$$

with $MW_{Cyd\text{-}3\text{-}glu}$ = 449.2 g mol^{-1}, ε = 26900 L mol^{-1} cm^{-1}, and L = 1 cm.

Proanthocyanidins (PACs), Catechin, PAC-A_2, and PAC-B_1 Contents. The content of global PACs content of juices was determined by the BL-DMAC (4-dimethylaminocinamaldehyde) method, adapted from the method described from Prior et al.[22] The quantitative analysis of the global content of PACS of cranberry juices was carried out in triplicate for all three repetitions in 96-well plates. Prior to analysis, juices were freeze-dried to obtain dry residues. Standard calibration of PAC-A_2 controls was performed in methanol from 0.05 to 0.5 mg/mL. Seven microliters of control solution was added to 63 μL of methanol in each well. Dry residues obtained previously were solubilized in distilled water at a concentration of 15 mg/mL, then 20 μL of sample solution was added to 50 μL of methanol in each well. DMAC reagent was solubilized in acidified ethanol at 0.1%, and 210 μL of DMAC solution was added to each well before the reading. Plate readings were performed at 630 nm every 2 min for 20 min, on a Biohit Bp 800 microplate reader, and the DO values used were the ones obtained after stabilization around 16–18 min. A standard curve of PAC-A_2 was then drawn, and a polynomial regression was applied to provide an equation allowing the calculation of the PACs content of samples.

The contents of catechin, PAC-A_2, and PAC-B_1 of juices have been analyzed by densitometric HPTLC using a plate scanner at a wavelength of 225 nm according to the method developed by Boudesocque et al.[23] Dry residues of juices obtained prior to the PACs content analysis were solubilized in distilled water at 75 mg/mL. Stock solution of controls was prepared by solubilization of an appropriate amount of catechin, PAC-A_2, and PAC-B_1 to obtain the initial concentration of 1 mg/mL. Diluted solutions at 0.02, 0.035, 0.05, and 0.07 mg/mL were obtained from the stock solution. Ten microliters of each control and sample solution in triplicate was sprayed by a Linomat 5 Automatic TLC Sampler (CAMAG, Switzerland), at 30 nL/s under nitrogen flow. Plate migration was performed in an automatic ADC 2 tank (CAMAG), with dichloromethane/ethyl acetate/formic acid (6:10:1, v/v) eluent. Plates are then analyzed by a TLC Plate Scanner (CAMAG) at 200, 225, and 279 nm, and quantification was performed at 225 nm through the calibration curve for each standard.

Organic Acid Contents. Prior to analysis, organic acids were extracted from 1/5 diluted cranberry juices with a C18-SPE cartridge (6 mL, 500 mg, Silicycle, Québec, QC, Canada). The cartridges were previously conditioned with elution of 5 mL of methanol, then 5 mL of distilled water, and then 10 mL of acetonitrile/water (50:50 v/v) solution. After drying of the cartridges, 10 mL of sample was dropped off and the last 5 mL was kept for analysis. The individual organic acid contents of cranberry juices and KCl fractions were determined by HPLC based on AOAC method 986.13. The system used was a Waters 600 HPLC system (Milford, MA, USA) equipped with a UV detector (Waters, model 966). Organic acids were analyzed with an Allure Organic Acids column (300 × 4.6 mm, Restek, USA). Standards for all organic acids tested were used with external calibration. A solution of 0.2 M (v/v) KH_2PO_4 (pH 2.4) was used as solvent for elution at a 0.5 mL/min flow rate. The detection wavelength was 226 nm.

Cranberry Juice Color. The color parameters of the cranberry juice were determined with a chromameter (model Minolta meter CR-200, Konica Minolta Inc., Mississauga, ON, Canada). Results were reported as L^* (luminescence or lightness), a^* (intensity of color varying from red to green)m and b^* (intensity of color varying from yellow to blue).[24]

Statistical Analyses. Data obtained during treatments for pH, conductivity, titratable acidity, and organic acids content were subjected to a repeated-measures analysis of variance using SigmaPlot software (version 11.0) or for anthocyanin and total polyphenol content to an analysis of variance. Tukey tests were also performed on data using SigmaPlot software (version 11.0) to allow the determination of treatments that were statistically different from the other at a probability level of $P < 0.05$.

RESULTS AND DISCUSSION

Evolution of the Electrodialytic Parameters. *Global System Resistance.* According to the repeated measures analysis of variance, during the first step of electrodialysis the global system resistance remained almost constant ($P = 0.412$) around 44 Ω (Figure 2). During the second electrodialysis step,

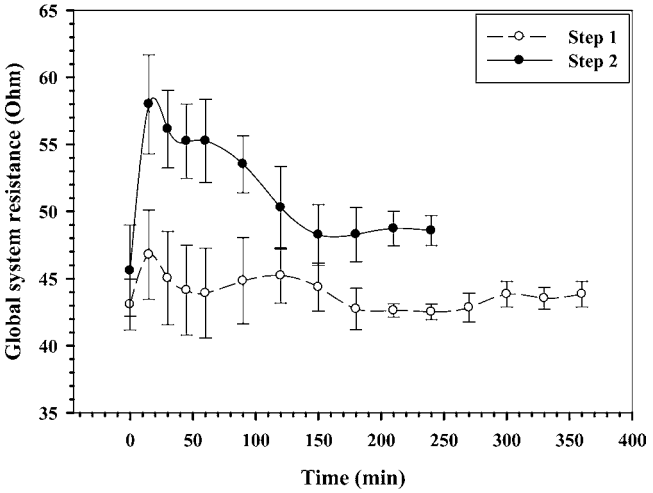

Figure 2. Results of the global system resistance (ohms) of the first and second electrodialysis steps.

the global system resistance increased from 45.60 to 58.00 Ω during the first 15 min and then decreased to 48.26 Ω after 150 min of treatment and reached a plateau until the end of the experiment ($P < 0.001$). The decrease could be due to water dissociation after 15 min of treatment at the surface of the monopolar ion-exchange membranes. Indeed, during water dissociation, the high conductivity of the H^+ ions produced facilitates the transport of the current, decreasing then the resistance.[25]

Membrane Parameters. Table 1 shows the thickness and electrical conductivity values of each membrane used for the EDBM treatments of the cranberry juices. The thickness was not significantly different after ED treatment for CMX-SB-1 membrane ($P = 0.184$) and for the two bipolar membranes ($P = 0.259$ and $P = 0.791$). For the other membranes, the thickness after the treatment was significantly higher ($P < 0.05$). However, the electrical conductivity of every CMX-SB membrane was not significantly different ($P > 0.05$) after use, meaning that their integrities were preserved, although they were in contact with the juice during the second step of the treatment. The electrical conductivity of AMX-SB membranes significantly decreased after the treatment ($P < 0.001$), as well as the conductivity of bipolar membranes ($P < 0.001$). During the two-step process, AEMs were in contact with raw juice in step 1 (see Figure 1a) and juice 1 in step 2 (see Figure 1b):

DOI: 10.1021/jf502824f
J. Agric. Food Chem. 2015, 63, 642–651

Table 1. Thickness and Conductivity of Each Membrane Used before and after Electrodialysis Treatment[a]

	thickness (cm)		conductivity (mS/cm)	
membrane	before treatment	after treatment	before treatment	after treatment
CMX-SB-1	0.170 ± 0.002a	0.173 ± 0.003a	10.31 ± 0.28a	8.67 ± 1.50a
CMX-SB-2	0.172 ± 0.001a	0.175 ± 0.001b	10.67 ± 0.12a	9.24 ± 1.71a
AMX-SB-1	0.136 ± 0.002a	0.146 ± 0.004b	7.62 ± 0.17b	5.50 ± 0.59a
AMX-SB-2	0.140 ± 0.000a	0.146 ± 0.002b	7.46 ± 0.51b	6.02 ± 0.08a
BP-1E-1	0.237 ± 0.001a	0.236 ± 0.004a	6.31 ± 0.09b	5.68 ± 0.31a
BP-1E-2	0.240 ± 0.001a	0.244 ± 0.006a	6.27 ± 0.26b	5.45 ± 0.06a

[a]Data in the same row with different letters for the same parameter are significantly different at a probability level of 0.05.

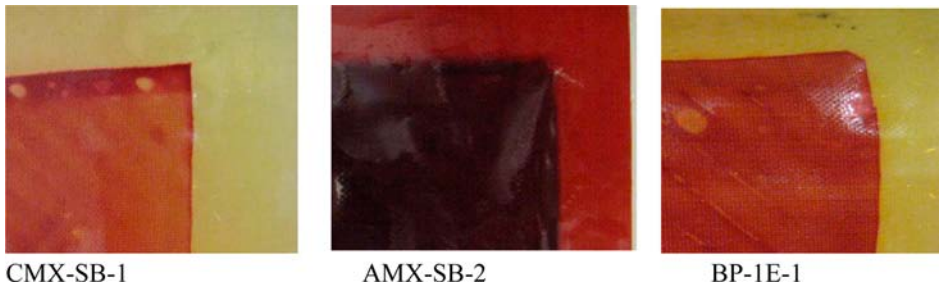

Figure 3. Photographs of anionic (AMX-SB), cationic (CMX-SB), and bipolar (BP-1) membranes.

organic acids and negative ions passed through this membrane during all of the process, but other negative molecules could have built up a deposit on the surface during the treatment, decreasing the conductivity of these membranes. As can be seen in Figure 3, the color of the CEM, AEM, and bipolar membranes changed (active and nonactive surface). These membranes may have interacted with a positively charged compound such as proanthocyanidin, anthocyanin, or other polyphenolic products, as well as negatively charged molecules such as organic acids and other molecules with high molecular weight such as pectin. All of these interactions could explain the difference of color of the membranes and their possible responsibity in fouling. This result is consistent with the literature. Indeed, a study demonstrated that the fouling appears in the AEM when this membrane transports the organic anion and that this fouling could appear when the current density is close to the limiting current.[8] It has been demonstrated in a previous study[26] that organic fouling can decrease the electrical conductivity of the ion-exchange membrane surface. Vera et al.[18] also observed a fouling on the anion-exchange membranes they used that were in contact with the treated passion fruit juice and attributed it to the colored compounds present in the passion fruit juice. Bipolar membranes were in contact with juice in step 1 and both juices in step 2, so that increased the risk of fouling at the surface of this membrane. Indeed, the fouling of membranes by charged compounds present in the juice is dependent on the position of the membranes in the configuration cell as well as the solution they are in contact with, as demonstrated before.[27]

Juice Parameter Evolution. *pH.* On the basis of the results obtained from the repeated measures analysis of variance, the first-step treatment had a significant effect on the pH ($P < 0.001$) of juice and both KCl fractions (Figure 4a). The pH of raw juice increased from 2.47 ± 0.02 to 2.71 ± 0.02 during the 6 h treatment ($P < 0.001$). The pH increase was higher in the first 75 min of treatment. At the initial pH of the juice, >60% of all acids were in the molecular and monoionized form, because the pH of the juice was below their first pK_a.[8]

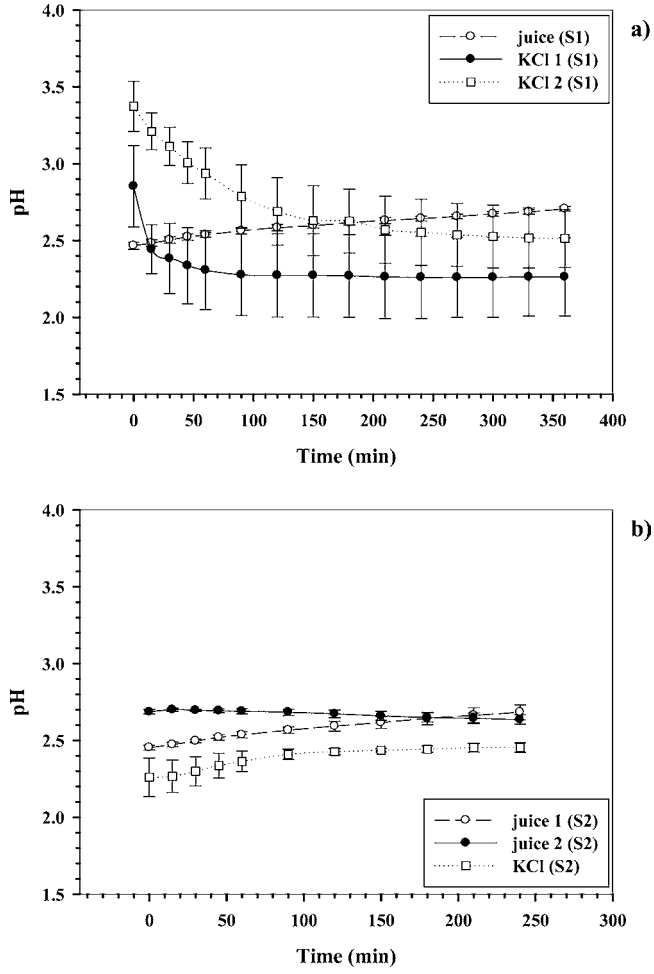

Figure 4. Evolution of the pH as a function of time for (a) the first electrodialysis step of juice 1, KCl 1, and KCl 2 and (b) the second electrodialysis step of juice 1, juice 2, and KCl.

DOI: 10.1021/jf502824f
J. Agric. Food Chem. 2015, 63, 642−651

The fact that a minority of the acids were charged did not help their migration through the anionic membranes. Concerning KCl 1, its pH decreased quickly from 2.85 ± 0.27 to reach a plateau around 2.26 ± 0.25 ($P < 0.001$) after only 55 min. The pH of KCl 2 decreased quickly in the first 75 min from 3.37 ± 0.16 to 2.51 ± 1.89 ($P < 0.001$), its final value. The pH decrease in the KCl 2 compartment followed closely the pH increase observed for juice (S1); the organic acids that left the juice were concentrated in the KCl 2 compartment, as expected with the cell configuration.

In step 2 (Figure 4b), the pH of juice 1 followed the same behavior as juice in step 1, with an increase from pH 2.46 ± 0.02 to 2.68 ± 0.05 ($P < 0.001$); meanwhile, the pH of juice 2 was almost stable during the first 75 min of the treatment and then decreased slightly ($P = 0.019$). Surprisingly, the pH of KCl in step 2 increased quickly from its initial value of 2.26 ± 0.13 to 2.45 ± 0.03 in the first 75 min and then continued to increase, but more slowly ($P = 0.033$).

With regard to the previously reported results obtained with passion fruit juices,[18,28] the pH variation obtained in our study was lower (0.3 pH unit versus >1.0 pH unit), which was explained by a lower initial pH in our study, far below the pK_a of the acids, corresponding to less charged species able to be extracted from the juice, so higher time or energy was required to achieve the transfer.

Conductivity. According to the repeated-measures analysis of variance, the electrodialysis treatment in step 1 had a significant effect on the conductivity values of juice and KCl fractions ($P < 0.001$). During the first step (Figure 5a), the conductivity of juice remained almost constant around 3152 ± 65 μS/cm for the first 75 min and then decreased quickly to 2856 ± 21 μS/cm at the end of the treatment ($P < 0.001$). This is explained by a demineralization of the juice, as well as a neutralization of the protons and the loss of organic acids and other charged molecules, phenomena already reported in the deacidification of passion fruit juices.[8] At the same time, the conductivity of KCl 1 followed a neperian logarithm increase: KCl 1 conductivity increased quickly from 3605 ± 73 μS/cm to reach a plateau at 4996 ± 219 μS/cm after 120 min of treatment ($P < 0.001$). The conductivity of KCl 2 fraction increased also from 3364 ± 22 to 4454 ± 110 μS/cm ($P < 0.001$), but the slope of the curve was slightly higher in the first 100 min compared to the last 300 min of the treatment. As expected, the conductivity of both KCl fractions increased due to the migration of organic acids as well as other charged molecules and ions from the juice into these compartments. To our knowledge, the conductivity of other KCl fractions during deacidification by electrodialysis has never been reported in the literature.

During the second step of electrodialysis (Figure 5b), the conductivity of juice 1 remained almost constant around 3046 ± 51 μS/cm during the first 60 min ($P > 0.05$) and then slightly decreased to reach 2801 ± 106 μS/cm at the end of the 240 min treatment. This behavior was similar to that of juice in step 1, due to the same movement of molecules. The conductivity of juice 2 (the juice obtained in the first step of the treatment) was not significantly different ($P > 0.05$) for the first 30 min and then decreased to reach a plateau at around 2264 ± 66 μS/cm. The conductivity of KCl in step 2 slightly decreased from 3711 ± 240 to 3476 ± 296 μS/cm during the first 90 min and then increased to reach 3929 ± 166 μS/cm at the end of the treatment ($P < 0.001$). In the second step, the KCl fraction seems to compensate for the decrease in conductivity of juice 1 according to step 1; moreover, juice 2 seems to be subjected to a demineralization because its conductivity decreased.

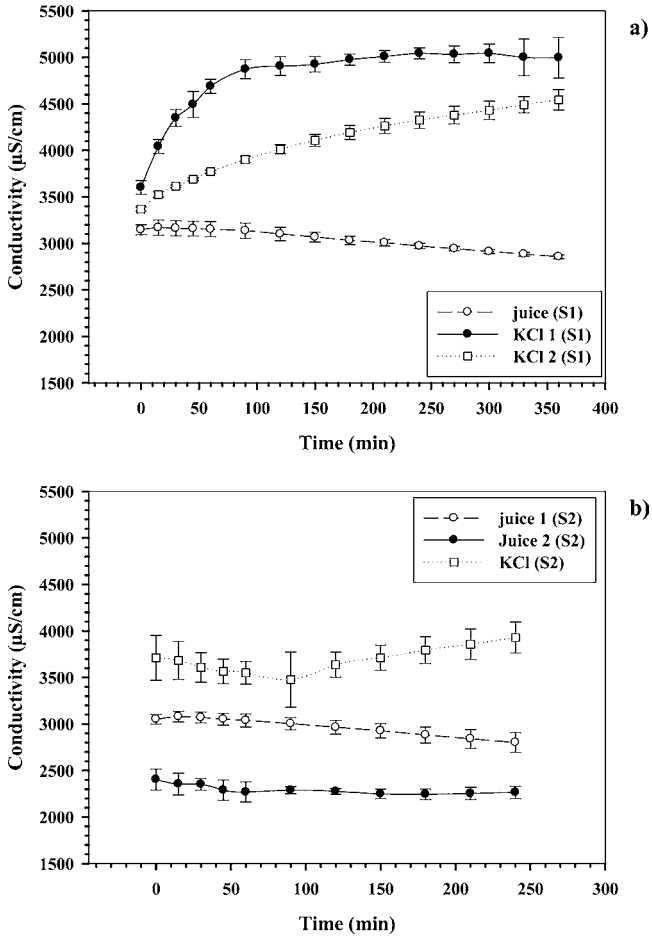

Figure 5. Evolution of the conductivity as a function of time for (a) the first electrodialysis step of juice 1, KCl 1, and KCl 2 and (b) the second electrodialysis step of juice 1, juice 2, and KCl.

Titratable Acidity. The titratable acidity of the juice in step 1 decreased during the 6 h of treatment from 15.90 ± 0.87 mL of 0.1 N NaOH to reach pH 8.2, to 12.27 ± 0.64 mL (Figure 6a), which corresponds to a 22.84 ± 0.22% deacidification. At the same time, the titratable acidity of KCl 1 fraction increased from 0.10 ± 0.00 mL to reach an almost stable value of 0.30 ± 0.00 mL of 0.1 N NaOH at 240 min. The titratable acidity of KCl 2 in the first step increased from 0.10 ± 0.00 mL to 2.85 ± 0.39 mL of 0.1 N NaOH: the KCl 2 compartment seemed to recover the acidity loss from the juice during the treatment. Vera et al.[28] have reported a deacidification of 70% of different clarified tropical fruit juices including passion fruit juices when they reached pH 4, using two electrodialysis cells with bipolar membranes of 20 and 200 cm^2 membrane areas, with various applied current densities between 50 and 400 A/m^2, but the duration of the ED treatment was not known. All of the juices used in this previous study had initial pH values higher than those of the cranberry juices (near pH 3.0), so citric and malic acids, both major acids in those juices, were mainly in their molecular form,[8,29] but at lower percentages than in cranberry juice, allowing a higher migration rate of these charged species.

In the second step (Figure 6b), the titratable acidity of juice 1 decreased from 15.97 ± 1.42 mL to 12.33 ± 1.46 mL of 0.1 N NaOH, corresponding to a deacidification of 22.78 ± 5.89%, comparable to the first step, with 2 h less treatment. During the

DOI: 10.1021/jf502824f
J. Agric. Food Chem. 2015, 63, 642−651

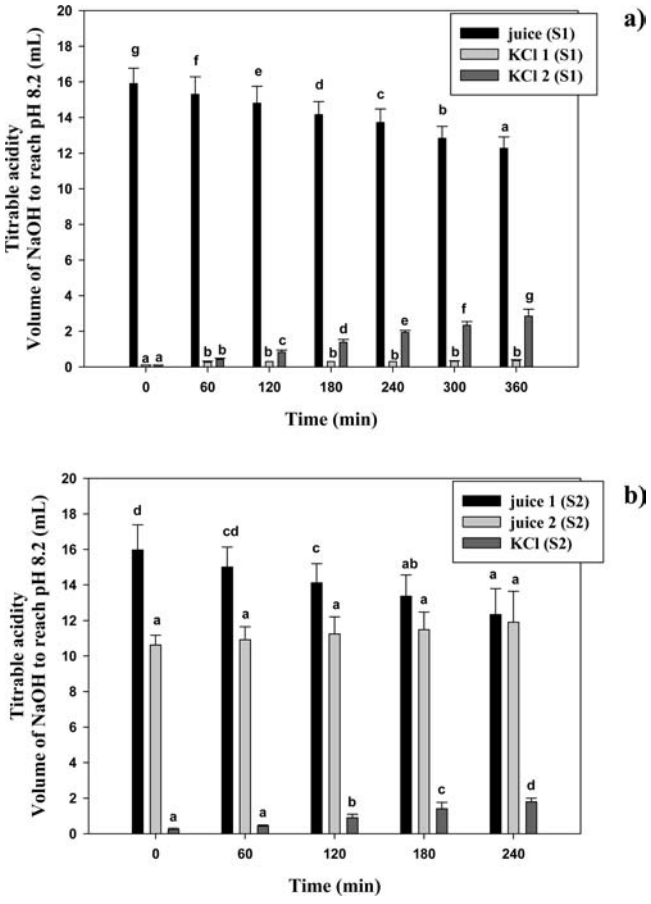

Figure 6. Evolution of the titratable acidity as a function of time for (a) the first electrodialysis step of juice 1, KCl 1, and KCl 2 and (b) the second electrodialysis step of juice 1, juice 2, and KCl.

same time the titratable acidity of juice 2 remained stable ($P > 0.5$) at a lower acidity than juice 1, whereas KCl increased from 0.23 ± 0.08 to 1.80 ± 0.20 mL, possibly compensating for the juice 1 acidity decrease.

Degrees Brix. The degrees Brix of juice in the first step (Figure 7) significantly decreased from 7.37 ± 0.06 to 6.87 ± 0.12 during the 6 h treatment ($P < 0.001$). During the 4 h treatment, the degrees Brix of juice 1−step 2 also decreased significantly ($P < 0.001$) following the same behavior as juice in step 1 ($P > 0.05$). Because the degrees Brix refers to the total soluble solids (primarily sugars and acids) and the titratable acidity decreased for the juice in step 1 and juice 1 in step 2, it was expected that the degrees Brix would decrease in these juices, as seen for the deacidification of tropical fruit juices.[28] However, juice 2 had a constant degrees Brix around 6.23 ± 0.15 during the 4 h treatment of step 2, lower than that of juice in step 1 and juice 1 in step 2 ($P < 0.001$), which is consistent with the titratable acidity results, because it was stable during the treatment for this juice.

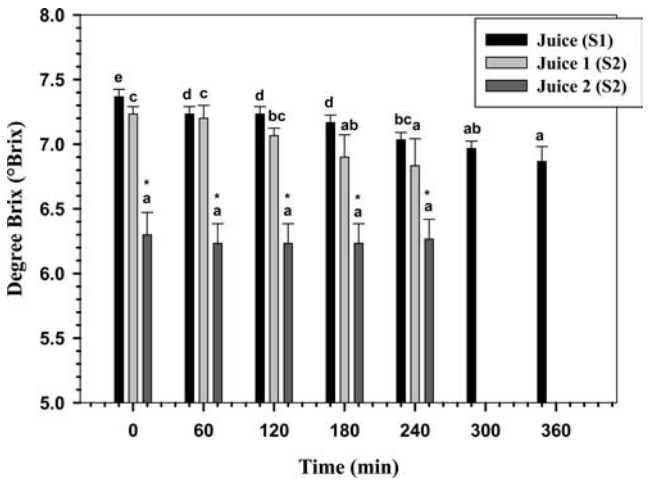

Figure 7. Evolution of the degrees Brix as a function of time for the first electrodialysis step of juice 1 and the second electrodialysis step of juices 1 and 2.

Total Polyphenol Content. On the basis of the results obtained from the analysis of variance, every electrodialysis-treated juice had a significantly lower total polyphenol content than the cranberry control juice ($P < 0.001$, Figure 8). Indeed,

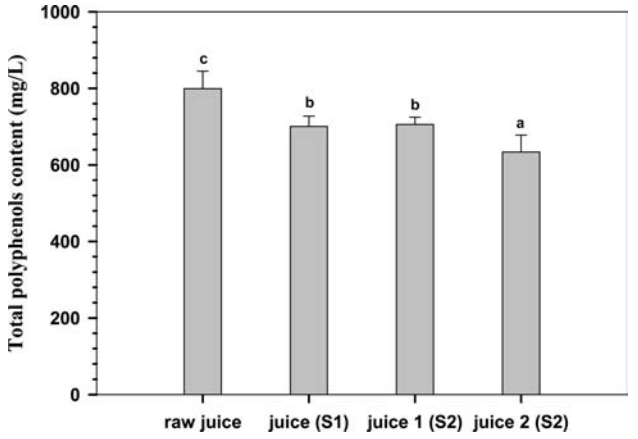

Figure 8. Results of total polyphenols content of the raw juice and the juices at the end of each treatment.

control juice had total polyphenol content of 799.15 ± 46.13 mg/L gallic acid equivalent, compared to around 703.10 ± 23.04 mg/L for juice−step 1 and juice 1−step 2 and 633.80 ± 44.01 mg/L for juice 2−step 2. Those results can be correlated to the fouling of membranes, because the coloration of the different membranes suggested a polyphenol/membrane interaction and a possible anthocyanins/membrane interaction.

Anthocyanin Content. Because the content of total polyphenol decreased for each juice treatment, the anthocyanin content was investigated. It appeared that this content was not significantly different ($P > 0.05$) for juice−step 1 and juice 1−step 2 at around 84.40 ± 1.14 mg/L cyanidin-3-glucoside equivalent before or after electrodialysis treatment, so those molecules did not migrate during the ED treatment. Otherwise, juice 2−step 2 had significantly lower anthocyanin content that other juices at the beginning of the experiment ($P < 0.001$) and even lower content at the end of the treatment ($P < 0.001$) (Figure 9). These results may suggest that there was a loss in anthocyanin between each step, due to storage (even for <3 days) at 4 °C. Indeed, this loss can be due to the oxygen present in the storage beaker used to keep the juice between the first and second steps[30] that may affect the anthocyanins during the storage. Furthermore, the significant loss during the second electrodialysis step could be due to the passage of juice 1 into a centrifugal pump, incorporating oxygen, whereas the peristaltic pump did not for juice−step 1 and juice 1−step 2.

DOI: 10.1021/jf502824f
J. Agric. Food Chem. 2015, 63, 642−651

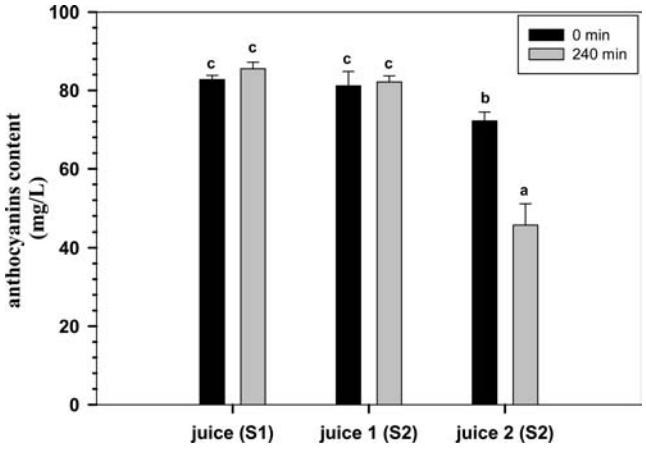

Figure 9. Results of total anthocyanins content at the end of each electrodialysis treatment.

Indeed, the decrease in total polyphenols for juice−step 1 and juice 1−step 2 was not due to anthocyanin degradation or fouling on membranes, contrary to what was suggested.

PACs, Catechin, PAC-A_2, and PAC-B_1 Contents. According to the analysis of variance, raw juice, juice−step 1, juice 1−step 2, and juice 2−step 2 were not significantly different ($P > 0.05$) with regard to their global PACs content, with values between 26.53 ± 3.11 and 28.60 ± 0.70 μg/mL, so these flavonoids were not degraded by the treatment (Table 2). However, this level of PACs was 16 times lower than what was already reported in the literature.[22,31] No catechin and PAC-B_1 have been observed by HTPLC. PAC-A_2 has been detected, but with values below the lower point of the standard curve applied, so its quantity in the different juices was below 0.02 mg/mL of PAC-A_2 standard. Those compounds were also not detected in cranberry juices by HPLC in another study.[32]

Organic Acid Contents. The major organic acids found in cranberry juices determined by HPLC analysis were citric acid (molecular weight (MW) = 192.12 g/mol), malic acid (MW = 134.09 g/mol), and quinic acid (MW = 192.17 g/mol).

The analysis of variance showed that the citric acid content of juice−step 1 (Figure 10a) was not significantly different ($P > 0.05$) throughout the treatment, but there was a tendency to decrease. Indeed, its concentration decreased from 3501.47 ± 215.75 mg/100 mL at 30 min to 2989.38 ± 355.41 mg/100 mL at the end of the treatment. On the other hand, the KCl 2 fraction had a content of citric acid that increased during the 6 h electrodialysis ($P < 0.001$) to reach 401.15 ± 36.58 mg/100 mL, compensating for the slight loss of citric acid in the juice, as expected with the cell configuration. Citric acid was produced in the KCl 2 fraction from citrate ion extracted from the juice and protons provided by BP-1 that went through CEM-1, as demonstrated in another study.[8] It is not visible in Figure 10a, but the content of citric acid in KCl 1 fraction increased slightly during the treatment to reach a 1.24 ± 0.30 mg/100 mL after 360 min. Juice 1 in the second step showed a behavior similar to that of the juice in the first step; indeed, even if there was no significant difference ($P > 0.05$) in the citric acid content as a function of time, there was a tendency to decrease, due to the migration of citrate ions through the AEMs membranes to produce citric acid in the KCl compartment. Indeed, as expected because of the cell configuration, the content of citric acid increased in the KCl compartment to reach 301.84 ± 39.55 mg/100 mL. Juice 2−step 2 remained stable for its content in citric acid during the 240 min of treatment ($P > 0.05$). Furthermore, the citric acid content of juice 2−step 2 was significantly lower than that of juice−step 1 and juice 1−step 2 from the beginning of the treatment until 120 min of electrodialysis, because of the migration of citrate ions during the first step of treatment.

These trends were similar for quinic acid (Figure 10b), except that juice 1−step 2 had a higher content of quinic acid at the beginning of the electrodialysis than at the end at 240 min ($P = 0.022$) and that the content of quinic acid of juice 2 in the second step was lower than for juice−step 1 and juice 1−step 2 during the 240 min of treatment. In that case, the quinic acid also concentrated in KCl 2−step 1 and the KCl−step 2, due to their same position in the cell. It has to be noted that the concentrations of quinic acid at times 0, 60, and 240 min were higher for KCl−step 2 compared to KCl 2−step 1. This can be due to the accumulation of quinic acid during the first passage in the electrodialysis, where the final concentration of KCl 1 was 17.43 ± 1.48 mg/100 mL.

The content of malic acid (Figure 10c) significantly decreased from 846.52 ± 54.13 to 635.13 ± 30.97 mg/100 mL during the treatment of juice−step 1 ($P < 0.001$), which corresponds to an extraction of 211.38 ± 54.65 mg/100 mL or 25% of this acid, whereas the KCl 2 fraction was enriched in this acid to reach a final content of 127.45 ± 22.98 mg/100 mL. A very little content of malic acid passed in the KCl 1 fraction to reach a final value of 1.24 ± 0.30 mg/100 mL. In the second step of the electrodialysis treatment, juice 1 and the KCl fractions had the same behavior as in the first step ($P < 0.001$), whereas juice 2 was not affected by the second electrodialysis treatment ($P > 0.05$), as for the other acids.

In their study, Bazinet et al.[27] also found a migration of citric and malic acid through an ultrafiltration membrane, when enriching a cranberry juice in antioxidants, confirming the migration ability of those acids during electrodialysis treatment. The most abundant organic acid found in the KCl 2−step 1 and KCl−step 2 recovery compartment was the citric acid. Among the acids present in the juice, citric acid was the most available to migrate at the pH of the juice, due to its high concentration (in comparison with other acids), its low molecular weight (192.12 Da), and its first pK_a (3.14), which was the lowest of all the acids.[8]

Table 2. Global Proanthocyanidins (PACs), Catechin, PAC-A_2, and PAC-B_1 Contents (μg/mL) in Cranberry Juices[a]

	raw juice	juice (S1)	juice 1 (S2)	juice 2 (S2)
PACs	26.77 ± 3.57a	26.53 ± 3.11a	28.60 ± 0.70a	28.00 ± 1.11a
catechin	nd[b]	nd	nd	nd
PAC-A2	bdl[c]	bdl	bdl	bdl
PAC-B1	nd	nd	nd	nd

[a]Data in the same row with different letters for the same parameter are significantly different at a probability level of 0.05. [b]nd, not determined (no peak corresponded to the peaks of the standards tested). [c]bdl, below detection level (below the lower point of the standard curve).

DOI: 10.1021/jf502824f
J. Agric. Food Chem. 2015, 63, 642−651

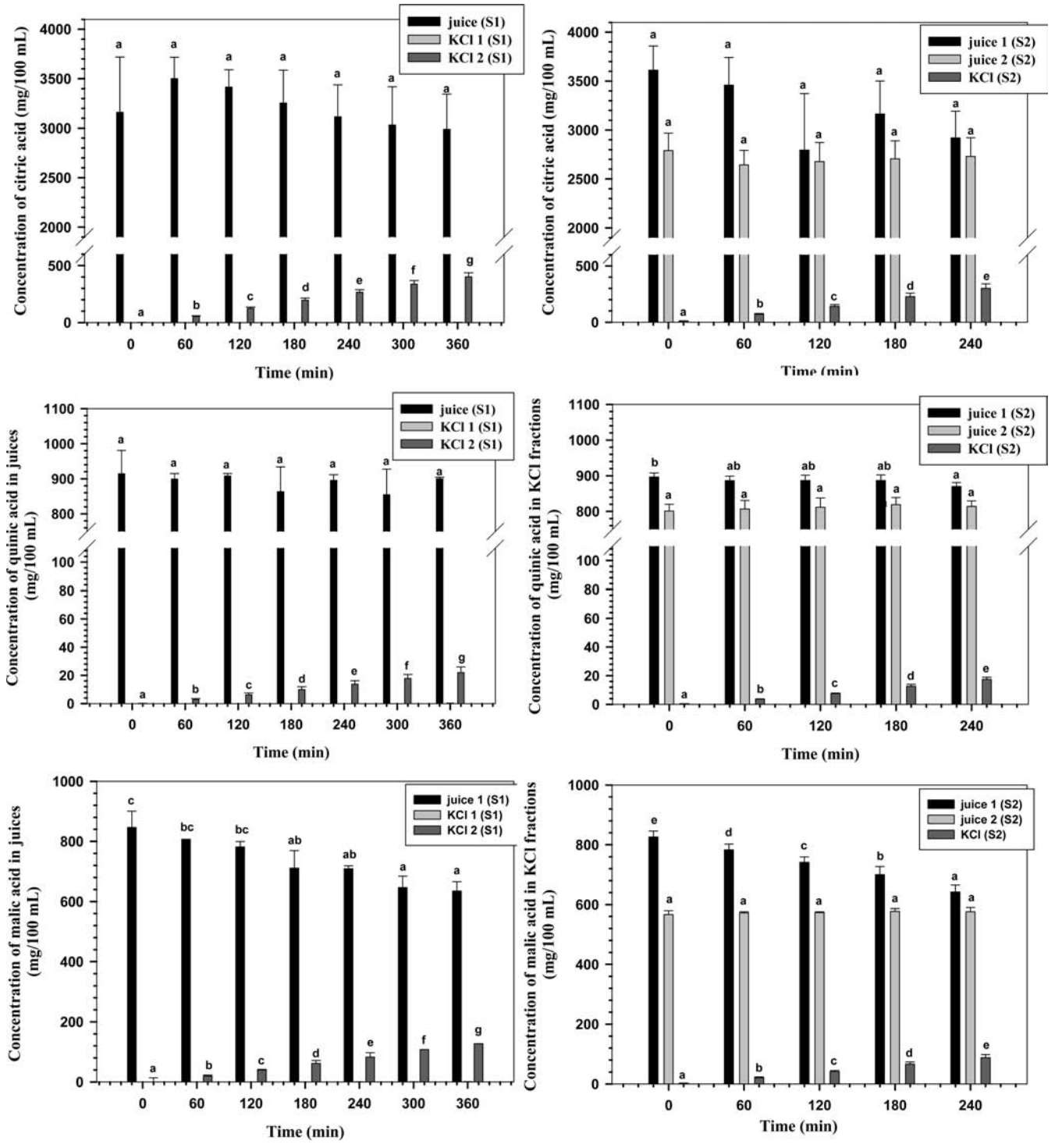

Figure 10. Evolution of (a, top) citric acid, (b, middle) quinic acid, and (c, bottom) malic acid contents of juice 1, KCl 1, and KCl 2 in the first electrodialysis step (6 h), as well as of juice 1, juice 2, and KCl in the second step (4 h). Data with different letters for the same parameter are significantly different at a probability level of 0.05.

Cranberry Juice Color. The cranberry juice color was studied on raw juice, final juice 1−step 2, and juice 2−step 2 because the volume required (30 mL) to do the analysis was not available for juice−step 1, because it was always used for the second step of electrodialysis (Figure 11). Considering that there were no significant differences ($P > 0.05$) for each L^*a^*b parameters between the control juice and juice 1−step 2, there should not be significant differences for juice−step 1. However, juice 2−step 2 was significantly different from other juices regarding component a^*. Indeed, this juice had a lower intensity of red and was visibly affected by the second electrodialysis treatment. Due to the presence of anthocyanins in cranberry juices, particularly cyanidin galactoside, peonidin galactoside, cyanidin arabinoside, and peonidin arabinoside, responsible for the red color of the juice,[33,34] and the variation of the intensity of ,a* parameter, already demonstrated to be correlated with anthocyanin content variation,[25] we can conclude that the significant degradation of anthocyanin in

DOI: 10.1021/jf502824f
J. Agric. Food Chem. 2015, 63, 642−651

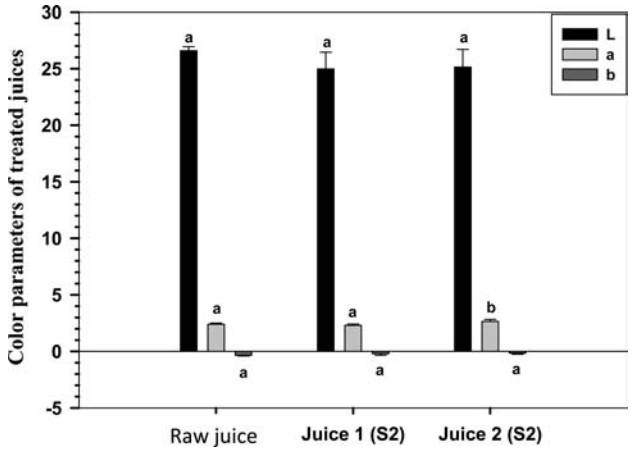

Figure 11. Results for the $L^*a^*b^*$ color parameters of the raw juice, juice 1, and juice 2 in the second electrodialysis step. Data with different letters for the same parameter are significantly different at a probability level of 0.05.

juice 2−step 2 during the electrodialysis treatment influenced its color and confirmed the decrease observed previously for the anthocyanins content.

This study demonstrated that it is possible to increase significantly the pH of a cranberry juice, as well as decrease its titratable acidity and organic acids contents by electrodialysis with bipolar membranes (EDBM). The first step of the treatment allowed better results than the second step concerning the polyphenols and anthocyanins content, as well as the color characteristics. The second step did not allow a pH decrease of juice 2 to recover its original characteristics; on the contrary, it seemed to deteriorate the cranberry juice. With regard to the electrodialytic parameters, the global system resistance decreased after each repetition, supported by the coloration of the different membranes and the diminution of the conductivity of the anionic and bipolar membranes due to the negatively charged molecules that passed through membranes or made a fouling at their surface.

To improve the results obtained in this study, the use of a configuration considering only the first step but with a higher surface of membrane obtained by increasing the number of membranes stacked would increase the rate of juice deacidification. Finally, this study proves that it is possible to remove organic acids with electrodialysis, a green technique using no solvent, even when the pH of the juice is far lower than the pK_a of the acids targeted.

AUTHOR INFORMATION

Corresponding Author

*(L.B.) Phone: (418) 656-2131, ext. 7445. Fax: (418) 656-3353. E-mail: Laurent.Bazinet@fsaa.ulaval.ca.

Funding

We thank the Natural Sciences and Engineering Research Council of Canada (NSERC) and the Ministère de l'agriculture, Pêcheries et Alimentation du Québec (MAPAQ) for their financial support.

Notes

The authors declare no competing financial interest.

ACKNOWLEDGMENTS

We thank Pascal Dubé and Alain Brousseau for their analytical help.

ABBREVIATIONS USED

EDBM, electrodialysis with bipolar membrane; S1, step 1; S2, step 2; PACs, proanthocyanidins; DMAC, dimethylaminocinamaldehyde; CEM, cation-exchange membrane; AEM, anion-exchange membrane; HPLC, high-performance liquid chromatography; MW, molecular weight

REFERENCES

(1) Burger, O.; Weiss, E.; Sharon, N.; Tabak, M.; Neeman, I.; Ofek, I. Inhibition of *Helicobacter pylori* adhesion to human gastric mucus by a high-molecular-weight constituent of cranberry juice. *Crit. Rev. Food Sci. Nutr.* **2002**, *42*, 279−284.

(2) Blatherwick, N. R.; Long, M. L. Studies of urinary acidity. II. The increased acidity produces by eating prunes and cranberries. *J. Biol. Chem.* **1923**, *57*, 815−818.

(3) Vattem, D. A.; Ghaedian, R.; Shetty, K. Enhancing health benefits of berries through phenolic antioxidant enrichment: focus on cranberry. *Asia Pac. J. Clin. Nutr.* **2005**, *14*, 120−130.

(4) Raz, R.; Chazan, B.; Dan, M. Cranberry juice and urinary tract infection. *Clin. Infect. Dis.* **2004**, *38*, 1413−1419.

(5) Kang, J. J.; Rhee, K. C. Deacidification of mandarin orange juice by electrodialysis combined with ultrafiltration. *Nutraceuticals Food* **2002**, *4*, 411−416.

(6) Sairi, M.; Jeng Yih, L.; Roji Sarmidi, M. Chemical composition and sensory analysis of fresh pineapple and deacidified pineapple juice using electrodialysis. In *Regional Symposium on Membrane Science and Technology*; uteri Pan Pacific Hotel, Johor Bahru, Johor, Malaysia, 2004; pp 1−9.

(7) Vera Calle, E.; Ruales, J.; Dornier, M.; Sandeaux, J.; Sandeaux, R.; Pourcelly, G. Deacidification of the clarified passion fruit juice (*P. edulis* f. *flavicarpa*). *Desalination* **2002**, *149*, 357−361.

(8) Vera, E.; Sandeaux, J.; Persin, F.; Pourcelly, G.; Dornier, M.; Ruales, J. Deacidification of clarified tropical fruit juices by electrodialysis. Part I. Influence of operating conditions on the process performances. *J. Food Eng.* **2007**, *78*, 1427−1438.

(9) Boyaval, P.; Seta, J.; Gavach, C. Concentrated propionic acid production by electrodialysis. *Enzyme Microb. Technol.* **1993**, *15*, 683−686.

(10) Tongwen, X.; Weihua, Y. Citric acid production by electrodialysis with bipolar membranes. *Chem. Eng. Process.: Process Intensification* **2002**, *41*, 519−524.

(11) Siebold, M.; Frieling, P. V.; Joppien, R.; Rindfleisch, D.; Schügerl, K.; Röper, H. Comparison of the production of lactic acid by three different Lactobacilli and its recovery by extraction and electrodialysis. *Process Biochem.* **1995**, *30*, 81−95.

(12) Trivedi, G. S.; Shah, B. G.; Adhikary, S. K.; Indusekhar, V. K.; Rangarajan, R. Studies on bipolar membranes. Part II — Conversion of sodium acetate to acetic acid and sodium hydroxide. *React. Funct. Polym.* **1997**, *32*, 209−215.

(13) Wang, Y.; Zhang, X.; Xu, T. Integration of conventional electrodialysis and electrodialysis with bipolar membranes for production of organic acids. *J. Membr. Sci.* **2010**, *365*, 294−301.

(14) Voss, H. Deacidification of citric acid solutions by electrodialysis. *J. Membr. Sci.* **1986**, *27*, 165−171.

(15) Mazrou, S.; Kerdjoudj, H.; Che'Rif, A. T.; Mole'Nat, J. Sodium hydroxide and hydrochloric acid generation from sodium chloride and rock salt by electro-electrodialysis. *J. Appl. Electrochem.* **1997**, *27*, 558−567.

(16) Gineste, J. L.; Pourcelly, G.; Lorrain, Y.; Persin, F.; Gavach, C. Analysis of factors limiting the use of bipolar membranes: a simplified model to determine trends. *J. Membr. Sci.* **1996**, *112*, 199−208.

(17) Quoc, A. L.; Mondor, M.; Lamarche, F.; Ippersiel, D.; Bazinet, L.; Makhlouf, J. Effect of a combination of electrodialysis with bipolar membranes and mild heat treatment on the browning and opalescence stability of cloudy apple juice. *Food Res. Int.* **2006**, *39*, 755−760.

(18) Vera, E.; Sandeaux, J.; Persin, F.; Pourcelly, G.; Dornier, M.; Ruales, J. Deacidification of passion fruit juice by electrodialysis with

DOI: 10.1021/jf502824f
J. Agric. Food Chem. 2015, 63, 642−651

bipolar membrane after different pretreatments. *J. Food Eng.* **2009**, *90*, 67−73.
(19) Rozoy, E.; Bazinet, L.; Gagné, F.; Bouissou, D.; Escudier, J.-L.; le Gratiet, Y.; Lutin, F.; d'Hauteville, J.; Bes, M. Développement d'un procédé de désacidification des vins par électrodialyse à membrane bipolaire: étude de faisabilité à l'échelle laboratoire. *OIV* **2013**, *86*, 187−208.
(20) Waterhouse, A. L. Determination of total phenolics. In *Current Protocols in Food Analytical Chemistry*; Wiley: Hoboken, NJ, USA, 2002; pp I1.1.1−I1.1.8.
(21) Giusti, M. M.; Wrolstad, R. E. Characterization and measurement of anthocyanins by UV-visible spectroscopy. In *Current Protocols in Food Analytical Chemistry*; Wiley: Hoboken, NJ, USA, 2001; pp F1.2.1−F1.2.13.
(22) Prior, R. L.; Fan, E.; Ji, H.; Howell, A.; Nio, C.; Payne, M. J.; Reed, J. Multi-laboratory validation of a standard method for quantifying proanthocyanidins in cranberry powders. *J. Sci. Food Agric.* **2010**, *90*, 1473−1478.
(23) Boudesocque, L.; Dorat, J.; Pothier, J.; Gueiffier, A.; Enguehard-Gueiffier, C. High performance thin layer chromatography−densitometry: a step further for quality control of cranberry extracts. *Food Chem.* **2013**, *139*, 866−871.
(24) CIE. *Recommendations on Uniform Color Spaces, Color-difference Equations, Psychometric Color Terms*; CIE Publication 15 (E-1.3.1) 1971, Suppl. 2. Bureau Central de la CIE: Vienna, Austria, 1978.
(25) Bazinet, L.; Cossec, C.; Gaudreau, H.; Desjardins, Y. Production of a phenolic antioxidant enriched cranberry juice by electrodialysis with filtration membrane. *J. Agric. Food Chem.* **2009**, *57*, 10245−10251.
(26) Grebenyuk, V. D.; Chebotareva, R. D.; Peters, S.; Linkov, V. Surface modification of anion-exchange electrodialysis membranes to enhance anti-fouling characteristics. *Desalination* **1998**, *115*, 313−329.
(27) Bazinet, L.; Brianceau, S.; Dubé, P.; Desjardins, Y. Evolution of cranberry juice physico-chemical parameters during phenolic anti-oxidant enrichment by electrodialysis with filtration membrane. *Sep. Purif. Technol.* **2012**, *87*, 31−39.
(28) Vera, E.; Sandeaux, J.; Persin, F.; Pourcelly, G.; Dornier, M.; Piombo, G.; Ruales, J. Deacidification of clarified tropical fruit juices by electrodialysis. Part II. Characteristics of the deacidified juices. *J. Food Eng.* **2007**, *78*, 1439−1445.
(29) Novalic, S.; Jagschits, F.; Okwor, J.; Kulbe, K. D. Behaviour of citric acid during electrodialysis. *J. Membr. Sci.* **1995**, *108*, 201−205.
(30) Markakis, P.; Jurd, L. Anthocyanins and their stability in foods. *CRC Crit. Rev. Food Technol.* **1974**, *4*, 437−456.
(31) Cunningham, D. G.; Vannozzi, S.; O'Shea, E.; Turk, R. Analysis and standardization of cranberry products. In *Quality Management of Nutraceuticals*; American Chemical Society: Washington, DC, USA, 2001; Vol. 803, pp 151−166.
(32) Biswas, N.; Balac, P.; Narlakanti, S. K.; Enamul Haque, M. D.; Mehedi Hassan, M. D. Identification of phenolic compounds in processed cranberries by HPLC method. *J. Nutr. Food Sci.* **2013**, *3*, 1−5.
(33) Neto, C. C.; Vinson, J. A. 6. Cranberry. In *Herbal Medicine: Biomolecular and Clinical Aspects*, 2nd ed.; Wachtel-Galor, S., Ed.; CRC Press: Boca Raton, FL, USA, 2011; pp 107−130.
(34) Gu, L.; Kelm, M. A.; Hammerstone, J. F.; Beecher, G.; Holden, J.; Haytowitz, D.; Gebhardt, S.; Prior, R. L. Concentrations of proanthocyanidins in common foods and estimations of normal consumption. *J. Nutr.* **2004**, *134*, 613−617.

DOI: 10.1021/jf502824f
J. Agric. Food Chem. 2015, 63, 642−651

JOURNAL OF AGRICULTURAL AND FOOD CHEMISTRY

Article

pubs.acs.org/JAFC

Influence of Processing Parameters on Morphology of Polymethoxyflavone in Emulsions

Yuwen Ting, Colin C. Li, Yin Wang, Chi-Tang Ho, and Qingrong Huang*

Department of Food Science, Rutgers, The State University of New Jersey, 65 Dudley Road, New Brunswick, New Jersey 08901, United States

ABSTRACT: Polymethoxyflavones (PMFs) are groups of compounds isolated from citrus peels that have been documented with wide arrays of health-promoting bioactivities. Because of their hydrophobic structure and high melting point, crystallized PMFs usually have poor systemic bioavailability when consumed orally. To improve the oral efficiency of PMFs, a viscoelastic emulsion system was formulated. Because of the crystalline nature, the inclusion of PMFs into the emulsion system faces great challenges in having sufficient loading capacity and stabilities. In this study, the process of optimizing the quality of emulsion-based formulation intended for PMF oral delivery was systematically studied. With alteration of the PMF loading concentration, processing temperature, and pressure, the emulsion with the desired droplet and crystal size can be effectively fabricated. Moreover, storage temperatures significantly influenced the stability of the crystal-containing emulsion system. The results from this study are a good illustration of system optimization and serve as a great reference for future formulation design of other hydrophobic crystalline compounds.

KEYWORDS: *polymethoxyflavone, morphology, emulsions, crystal size*

INTRODUCTION

With the advances in medical sciences and informational technologies, people are more educated on disease pathologies. Instead of receiving therapeutic treatments after a disease has been diagnosed, engaging in preventive behavior has gained popularity among health-conscious individuals. The discoveries of many bioactive compounds from dietary sources have become the popular trend in research of disease prevention. The term nutraceutical is being used to identify these types of bioactive ingredients. Well-known examples of such bioactive compounds, including curcumin, quercetin, resveratrol, lutein, β-carotene, epigallocatechin gallate (EGCG), lycopene, etc., are widely investigated and documented on their ability to provide health-promoting benefits to living organisms. For chronic consumption, oral ingestion is the user-friendliest method for consumers to use the biofunctionalities provided by bioactive ingredients. However, many of those nutraceuticals are poorly absorbed when consumed orally because of their unfavorable chemical characteristics, which leads to fast degradation, low solubility, poor intestinal uptake and transport, extensive metabolism, and rapid excretion rate. For these reasons, various delivery systems have been developed to enhance their oral bioavailability.[1−4]

When consumed with lipids, the oral bioavailabilities of highly hydrophobic compounds were shown to be significantly improved.[1−3] Thus, many lipid-based delivery formulations have been developed for the oral consumption of nutraceuticals with poor aqueous solubility.[4] Emulsion, in this sense, has a long history of being applied as a convenient method to contain, protect, and facilitate uptake and transport of hydrophobic dietary ingredients. Because of this adaptable nature, many derivatives, supplemented with additional functional mechanisms, have been produced to broaden the applications of emulsion-based delivery systems for food and pharmaceutical uses. Moreover, because many studies have suggested an inverse relationship between the particle size and oral absorption of bioactive ingredients, the applications of technologies to physically reduce the emulsion particle to micro- or nanoscale have become a popular trend. However, with the reduction of the particle size, emulsion-based delivery systems face the challenge of low compound loading capacity and higher sedimentation rate because of the presence of highly crystalline hydrophobic ingredients.[5]

Polymethoxyflavones (PMFs), such as nobeletin, tangeretin, sinensetin, 3,5,6,7,8,3′,4′-heptamethoxyflavone (HMF), and others, contain multiple methoxy ($-OCH_3$) groups on their characteristic 15-carbon benzo-γ-pyrone structures and are categorized as a subgroup of flavonoids. PMFs and their hydroxylated derivatives have been proven to be potent therapeutic agents in preventing diseases, such as chronic inflammation, tumor development, atherosclerosis, thrombosis, and oxidation damage.[6−11] Multiple methoxyl groups on the structure of PMFs contribute to their highly hydrophobic nature, which results in a low aqueous solubility and poor oral bioavailability. The application of an emulsion-based delivery technology has been investigated for PMF oral ingestion with the interest of improving its bioavailability.[5,12,13] However, the high melting point and fast crystallization behavior of PMFs pose great challenges in designing, processing, storing, and applying emulsion formulations.[5,12−14] Because of their poor solubility in both oil and water at ambient temperatures, the loading capacity of PMF emulsion systems is generally unsatisfactorily low and the formula is subject to precipitation

Received: September 16, 2014
Revised: December 18, 2014
Accepted: December 22, 2014
Published: December 23, 2014

ACS Publications © 2014 American Chemical Society

DOI: 10.1021/jf504465a
J. Agric. Food Chem. 2015, 63, 652−659

during storage. In our previous studies, a viscoelastic emulsion was designed to maximize the PMF loading capacity while maintaining a stable system, even if crystallization did occur.[13] During the process of optimizing the formulation, interestingly, the crystallization kinetics and the resulting crystal morphology were affected by the processing parameters. In the present study, we aim to systematically examine the effect of different processing conditions on the crystalline compound in an emulsion system. Moreover, the effect of various storage environments on the crystalline emulsion system was also included as a part of our discussion. Here, for the convenience of the study design, only tangeretin was selected as the model PMF compound in the emulsion system (Figure 1). The knowledge obtained from this study will serve as a useful reference for the future development of oral formulations targeting highly crystalline compounds.

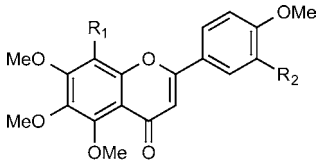

Tangeretin R_1 = OMe R_2 = H

Figure 1. Structure of PMF with a detailed functional group of tangeretin.

MATERIALS AND METHODS

Materials. Tangeretin of 98% purity was purchased from Quality Phytochemicals, LLC (Edison, NJ). Rapeseed PC75 lecithin containing 75% phosphatidylcholine was a gift from American Lecithin Company (Oxford, CT). Neobee 1053 medium-chain triacylglycerol (MCT) was a sample requested from Stepan Company (Northfield, IL). Milli-Q water was used throughout the experiment.

Preparation and Processing of PMF Emulsion Samples. PMF emulsions were prepared according to a previously published method, with necessary modifications.[13] The distribution of each emulsion phase of the studied samples was kept constant at 46% aqueous phase, 1.5% emulsifier, and 52.5% oil phase. To evaluate the effect of the PMF loading concentration on the resulting crystal in the emulsion, various concentrations (0.3−2.0%) of the PMF compound were added to the carrier oil, composed of 100% medium-chain triacylglycerol (MCT), at 130 °C with continuous stirring until they were completely dissolved (Table 1). After PMF was dissolved in MCT, 0.45 g of lecithin was then added to the 130 °C PMF oil solution as the emulsifier and then stirred until fully solubilized. The aqueous phase [100% double deionized (DI) water] was preheated to 70 °C to prevent rapid PMF crystallization induced by impulsive temperature drops. To avoid excessive water loss, the disperse phase solution (MCT with solubilized PMF compound and lecithin) was adjusted to 70 °C immediately before mixing with the preheated aqueous phase. Once the aqueous phase had been added to the oil phase, the solution was maintained at 70 °C and continuously stirred until one phase of crude emulsion was formed. Because the crude emulsion formed was very viscous and could cause processing difficulty during high-pressure homogenization (EmulsiFlex-C6, AVESTIN, Inc., Ottawa, Ontario, Canada), the crude emulsion was then subjected to high-speed homogenization (ULTRA-TURRAX T-25 basic, IKA Works, Inc., Wilmington, NC) at 24 000 rpm. During high-pressure homogenization, all samples used for compound loading and storage studies were processed under 500 bar at 55 °C. However, samples used for comparing the effect of different processing parameters on the emulsion sample quality were produced at various combinations of temperatures (55, 65, and 75 °C) and pressures (500, 1000, and 1500 bar). Finally, approximately 25−30 g of emulsion sample was collected from each processing batch.

Table 1. Formulations for Emulsion Samples of Various Tangeretin (PMF) Loading

emulsion formulation compostion				
	oil phase (52.5%)		emulsifier (1.5%)	aqueous phase (46%)
PMF loading concentration (%)	PMF (g)	MCT (g)	lecithin (g)	DI water (g)
0.30	0.09	15.66	0.45	13.80
0.50	0.15	15.60	0.45	13.80
0.60	0.18	15.57	0.45	13.80
0.70	0.21	15.54	0.45	13.80
0.80	0.24	15.51	0.45	13.80
0.90	0.27	15.48	0.45	13.80
1.10	0.33	15.42	0.45	13.80
1.30	0.39	15.36	0.45	13.80
1.50	0.45	15.30	0.45	13.80
2.00	0.60	15.15	0.45	13.80

Particle Size Measurement. Because the particle size is an important quality parameter for an emulsion system, the average particle size was determined. A BIC 90 Plus particle size analyzer equipped with a Brookhaven BI-9000AT digital correlator (Brookhaven Instrument Corporation, New York, NY) was used for determining the average particle sizes from all emulsion samples produced. Emulsion samples were diluted in DI water by a dilution factor of 5000 to avoid multiple scattering effects. The light source was a solid-state laser operating at the wavelength of 658 nm with 30 mW of power, and a high-sensitivity avalanche photodiode detector was used for signal detection. Measurements were conducted at a fixed scattering angle of 90° at 25 ± 1 °C. Results were reported in triplicate (n = 3) as the mean particle size and size distribution.

Moisture Content Analysis. The moisture contents of emulsion samples were calculated as the percent sample weight loss when dried by an IR-200 moisture analyzer (Denver Instrument Co., Arvada, CO). To determine the moisture content, emulsion samples (≤0.2 g) were placed on a balanced aluminum weight pan (diameter = 100 mm) located on the scale section of the instrument. The samples were continuously heated by four parallel quartz infrared heaters at 200 °C until completely dried. The moisture content was then calculated using the following equation:

$$\text{moisture } (\%) = \frac{W_i - W_f}{W_i} \times 100 \quad (1)$$

where W_i is the initial sample weight being placed on the scale and W_f is the final sample weight after drying.

Crystal Size and Morphology Evaluation. To obtain higher loading concentrations of hydrophobic crystalline compounds, the resulting emulsion formulations are sometimes a system containing heterogeneous particles. In a mixed emulsion system, compounds are either solubilized within the emulsion droplet or present as entrapped small solid crystals. Variation of the processing parameters and storage conditions may result in different droplet and crystal characteristics. In this part of the study, crystal size and morphology were monitored using a direct microscopic observation. Undiluted emulsion samples were placed on a microscope slide and then mounted using a cover glass. An inverted optical microscope (Nikon TE 2000, Nikon Corporation, Japan) equipped with a charge-coupled device (CCD) camera (Retiga EXi, QImaging) was used for crystal morphology observation. All images were processed by C-Imaging software (SimplePCI, Compix, Inc.). The average sizes of the crystal (n = 100) were measured using Java-based image processing software (ImageJ) with corrected reference scaling.

X-ray Diffraction (XRD). The information on the crystal characteristics from emulsion samples containing various concentrations of PMF was studied using an XRD method. Powder X-ray

DOI: 10.1021/jf504465a
J. Agric. Food Chem. 2015, 63, 652−659

diffraction (PXRD) experiments were conducted using a D/M-2200T automated system (Ultima+, Rigaku) with Cu Kα radiation (λ = 1.5406 Å). The PXRD patterns were collected at 2θ angles from 3° to 40° at a scan rate of 2°/min. A graphite monochromator was used, and the generator power settings were 40 kV and 40 mA.

Study of Rheological Characteristics. The rheological properties of the emulsion samples were performed using an ARES rheometer (Rheometric Scientific, Piscataway, NJ) with parallel plate geometry (diameter of 25 mm) at room temperature (20.0 ± 0.2 °C). About 1 mL of the emulsion sample was deposited onto the plate geometry. Prior to each dynamic frequency sweep test, a dynamic strain sweep test ranging from 0 to 100% was performed at 2 rad/s angular frequency and the strain value of 5% in the linear viscoelastic region was adopted. The angular frequency ω ranged from 1 to 100 rad/s with 20 data points per decade. The gap between the two parallel plates was properly selected to prevent sample slip. A small amount of mineral oil was used to seal the sample edge to prevent solvent evaporation.

Storage Stability Evaluation. It is desirable to have a stable emulsion system for long-term storage. In this part of the study, the stability and quality changes under different storage conditions were evaluated. The emulsion sample quality was examined by monitoring the changes of the emulsion droplet size and crystal length over 30 days of storage at 4, 25, and 60 °C. All emulsion samples used in this study were processed in one single batch with a composition of 2.0% PMF, 50.5% MCT, 1.5% lecithin, and 46% DI water.

Statistical Analysis. A single-tailed student's *t* test was performed using Sigmaplot 10.0 software.

RESULTS AND DISCUSSION

Effect of the Tangeretin Loading Concentration on the Emulsion Property. For oral formulation, it is equally desirable to have adequate stability as well as sufficient loading of the active ingredient, so that a therapeutically meaningful dosage can be reached in a practical serving portion. Dependent upon the purpose and form of consumption, the requirements for a qualified oral formulation can vary significantly. For example, it is essential for an oral formulation to avoid creaming and precipitation when incorporated into a beverage product. On the other hand, when consumed as a soft gel or tablet, it is desirable for the oral system to have a higher concentration and sophisticated storage stability of the active ingredient. Therefore, it is necessary for investigators to explore the highest possible loading concentrations of the target compound in the designated oral applications. In our previously published paper, we had successfully developed a viscoelastic emulsion system to contain PMF with sufficient loading capacity and storage stability. Here, in this part of the experiment, we aim to systematically examine the effect of incorporating various tangeretin concentrations (0.3, 0.5, 0.6, 0.7, 0.8, 0.9, 1.1, 1.3, 1.5, and 2.0%) on the physical characteristics and related application potentials of the emulsion system. As suggested by previous studies, the particle size of oral formulation was a critical factor in determining the digestion, absorption, and bioavailability of hydrophobic active ingredients.[12,15−20] That is, smaller emulsion droplets often resulted in higher bioavailability because of faster digestion kinetics and potential direct uptake by gut wall and lymphatic systems. When the amount of emulsifier was held constant, the emulsion droplet size increased progressively (from 378.4 ± 5.3 to 565.2 ± 3.3 nm) as the percentage (from 0.3 to 2.0%) of tangeretin increased in the system, while no significant change in the moisture content was observed (Table 2). In general, the concentration of the emulsifier in the system was inversely related to the particle size. As the loading of PMF increased, the

Table 2. Physical Characteristic Information for the Emulsion of Different Tangeretin (PMF) Loadings

loading concentration (%)	0.3	0.5	0.6	0.7	0.8	0.9	1.1	1.3	1.5	2
particle size (nm)	378.4 ± 5.3	388.7 ± 4.4	385.8 ± 4.2	410.1 ± 6.1	463.0 ± 8.6	499.3 ± 5.9	507.6 ± 7.7	513.5 ± 7.0	550.8 ± 5.4	565.2 ± 3.3
moisture content (%)	46.08 ± 0.09	46.14 ± 0.10	46.81 ± 10.06	46.93 ± 0.11	45.81 ± 0.04	46.17 ± 0.09	45.65 ± 0.4	46.18 ± 0.08	48.12 ± 0.13	46.07 ± 0.07
crystal length (μm)				196.17 ± 42.44	109.69 ± 24.60	55.89 ± 12.68	23.52 ± 5.88	18.13 ± 4.13	13.38 ± 3.95	10.11 ± 13.16

DOI: 10.1021/jf504465a
J. Agric. Food Chem. 2015, 63, 652−659

larger particle size may have been the result of the various degrees of emulsifier consumed to support the PMF solubility of the system.

Moreover, the inclusion of crystalline hydrophobic compounds into emulsion formulations could sometimes result in a mixed system containing bioactives solubilized as dispersed droplets or present as entrapped crystalline particles. To maximize the loading of hydrophobic crystalline components in an emulsion system, the carrier oil was usually supersaturated using high processing temperatures. As a result, the reduction in temperature caused the compound to be expelled from the supersaturated oil phase and crystallized in the continuous phase. When the compound concentration (<0.6%) in the system was below the saturation concentration, no crystal formation was observed in the emulsion systems (panels a and b of Figure 2A). As the loading concentration increased to the

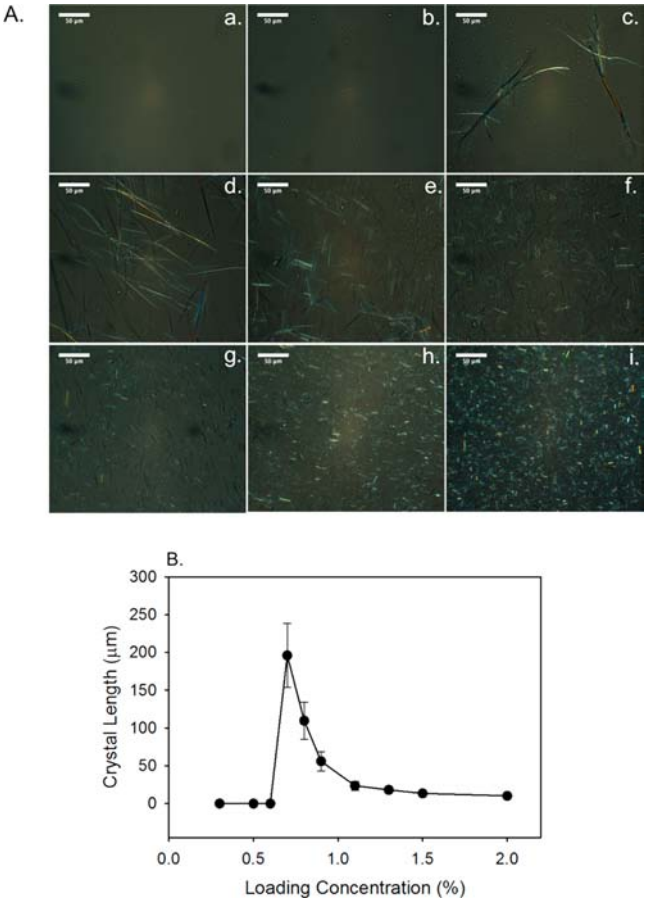

Figure 2. (A) Microscopic picture of emulsion samples with different tangeretin (PMF) loadings: (a) 0.5%, (b) 0.6%, (c) 0.7%, (d) 0.8%, (e) 0.9%, (f) 1.1%, (g) 1.3%, (h) 1.5%, and (i) 2.0%. (B) Quantitative plots of crystal lengths as a function of PMF loading concentrations.

critical concentration (0.7%), where it was only supersaturated, low amounts of tangeretin crystals appeared in bundles, with a maximum crystal size of 196.17 ± 42.44 μm scattered among the emulsion droplets. With the continuous increase in supersaturation, the number of tangeretin crystals increased (panels c–i of Figure 2A) as the size decreased (Figure 2B). As established by others, the size of a crystal produced is inversely proportional to the number of nuclei formed.[21−23] The number of nucleation sites considerably increased with a higher degree of supersaturation, because the number of molecules required for the formation of nucleating clusters decreased.[21] Therefore, smaller crystals were produced as the number of nuclei expanded more rapidly than the crystal growth. To be absorbed in the gastrointestinal (GI) tract, a hydrophobic crystalline compound has to be either solubilized or dispersed in the aqueous GI environment. Upon oral ingestion, large clusters of crystalline hydrophobic components are prone to gravitational precipitation, which causes them to be excluded from the body. On the other hand, the bioavailability of crystalline hydrophobic compounds may benefit from the smaller size. Small crystals are more advantageous for GI absorption because they are more easily incorporated into mixed micelles or directly absorbed by the gut wall.

Because of the crystalline structure, the variation in the PMF loading concentrations changed the physical characteristics of the viscoelastic emulsion systems, affecting the potential consumer applications. Specifically, the rheological properties of the viscoelastic emulsion are the most important factor in sustaining and stabilizing the PMF-incorporated system. Here, we explore the effects of different PMF loads on the rheological properties in relation to its crystalline characteristic. All of the samples containing different degrees of PMF loading had a higher storage modulus value ($G2$) than lost modulus value ($G2$), indicating a gel-like elastic behavior. Figure 3A shows G'

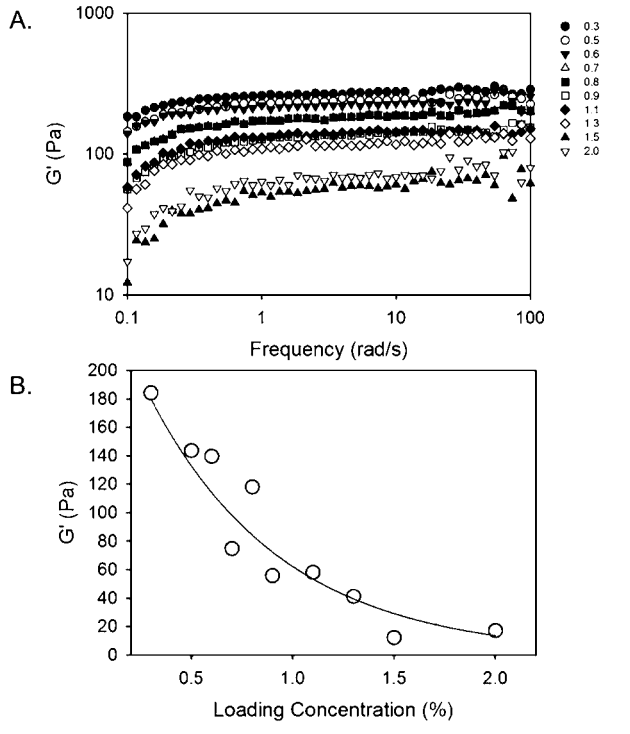

Figure 3. (A) Storage modulus ($G2$) versus frequency curve of emulsion containing various tangeretin (PMF) concentrations from 0.3 to 2.0%. (B) Plot of the $G2$ value at 0.1 rad/s frequency as a function of PMF concentrations.

as a function of the frequency for viscoelastic emulsion samples with PMF loading of 0.3, 0.5, 0.6, 0.7, 0.8, 0.9, 1.1, 1.3, 1.5, and 2.0%. To elucidate the effect of PMF loading on the $G2$ value, Figure 3B presents the changes to the $G2$ value at 0.1 rad/s frequency as a function of PMF concentrations. The increase in the PMF concentration from 0.3 to 2.0% in emulsion formulation is matched with a decreasing trend in $G2$ values. Because the $G2$ value is usually used as an indicator of the

DOI: 10.1021/jf504465a
J. Agric. Food Chem. 2015, 63, 652−659

network interaction, the lowering $G2$ values suggested the weakening of the gel-like structure in the emulsion. As reported in our previous investigation, the interactions between emulsion droplets contribute to the viscoelastic property of emulsion systems.[13] The weakening of the network interactions can be mainly attributed to the increasing number of crystals entrapped within the system. The increases of the emulsion crystalline structure were further confirmed by XRD analysis. In Figure 4, there was no characteristic peak observed in the

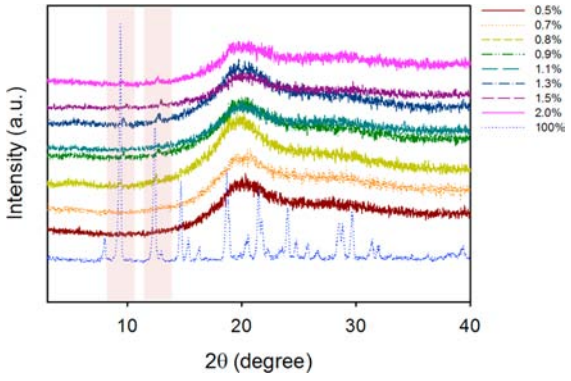

Figure 4. XRD pattern for emulsion samples with tangeretin (PMF) loading concentrations ranging from 0.5 to 2.0%. The pattern from 100% tangeretin crystal (blue dotted line) was also included as a characteristic peak reference.

emulsion sample with lower PMF concentrations (0.5 and 0.7%). However, the characteristic peak for PMF was detected in emulsion samples with higher PMF concentrations.

Effects of Processing Parameters on the Emulsion Property. Because smaller particles may have higher oral bioavailability, it is desirable to reduce the particle size in oral formulations containing hydrophobic components. High-pressure homogenization (HPH) is a common technique for reducing the droplet size in an emulsion-based system. As previously reported, smaller droplet sizes were obtained when higher processing pressure and temperature were applied.[24] To investigate the influence of HPH on the particle sizes of the crystalline emulsion system, different combinations of temperatures and pressures were used for producing PMF viscoelastic emulsions. Because PMF crystallization is sensitive to temperature variation, it is critical to maintain an elevated processing temperature during emulsion production. During HPH, temperatures lower than 50 °C promoted massive PMF crystallization and caused blockage of the HPH instrument. To prevent rapid crystallization, three temperatures (55, 65, and 75 °C) were selected for emulsion optimization trials. The three processing temperatures were applied in combination with three different pressure levels of 500, 1000, or 1500 bar, giving a total of nine production combinations. However, samples processed at 75 °C were excluded from the discussion, because it had excessive moisture loss and did not form a stable one-phase emulsion system (data not shown). Under all processing conditions, emulsion samples had an average droplet size of around ∼500 nm with no significant intersample deviation. However, the size of crystalline structures in the emulsion system was greatly influenced by different processing parameters. Under the same processing pressures, samples processed at 65 °C produced a larger crystal size than samples processed at 55 °C (Figure 5A). The results indicated that the rate of PMF crystallization in the viscoelastic emulsion was

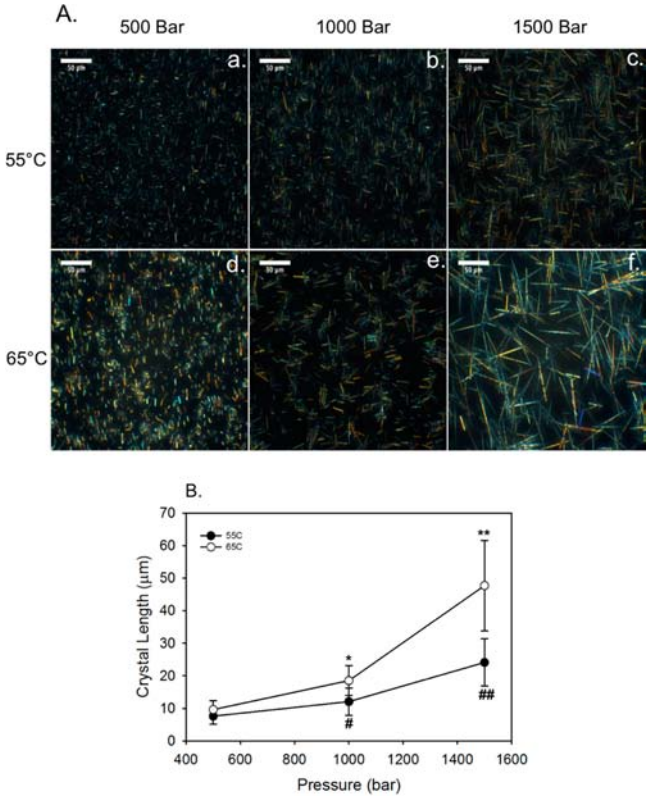

Figure 5. (A) Microscopic pictures of emulsion samples processed at different combinations of temperature/pressure level: (a) 55 °C/500 bar, (b) 55 °C/1000 bar, (c) 55 °C/1500 bar, (d) 65 °C/500 bar, (e) 65 °C/1000 bar, and (f) 65 °C/1500 bar. (B) Plot of the crystal length at 55 °C (○) and 65 °C (●) as a function of the processing pressure. (∗) $p < 0.05$: the crystal size of 55 °C/1000 bar is significantly different from the crystal size of 55 °C/500 bar and 65 °C/1000 bar. (∗∗) $p < 0.05$: the crystal size of 55 °C/1500 bar is significantly different from the crystal size of 55 °C/500 bar, 55 °C/1000 bar, and 65 °C/1500 bar. (#) $p < 0.05$: the crystal size of 65 °C/1000 bar is significantly different from the crystal size of 65 °C/500 bar. (##) $p < 0.05$: the crystal size of 65 °C/1500 bar is significantly different from the crystal size of 65 °C/500 bar and 65 °C/1000 bar.

positively associated with the temperature ($\nu \propto T$). The production of larger crystals at higher processing temperatures is likely due to the higher temperature providing the system with more free energy (ΔG), which is required for nucleation as well as for fostering frequent collisions of crystalline molecules.[25,26] Besides processing temperature, the pressure under which the sample is produced also plays a critical role in determining the PMF crystal size. Under similar processing temperatures, crystal sizes became larger when the applied pressure increased (Figure 5B). The phenomenon of pressure application on the elevation of crystallization kinetics has been well-studied by previous investigations. Under high pressure, the melting temperature shifted toward a higher temperature, which increased the degree of undercooling and resulted in higher nucleation rates.[26−28] Moreover, the crystal growth was promoted because the physical distance of crystalline components was decreased under high-pressure conditions.[28,29] From our study, the crystal was smallest with a temperature/pressure combination of 55 °C/500 bar and largest at 65 °C/1500 bar with sizes of 7.58 ± 2.48 and 47.72 ± 13.94 μm, respectively.

DOI: 10.1021/jf504465a
J. Agric. Food Chem. 2015, 63, 652−659

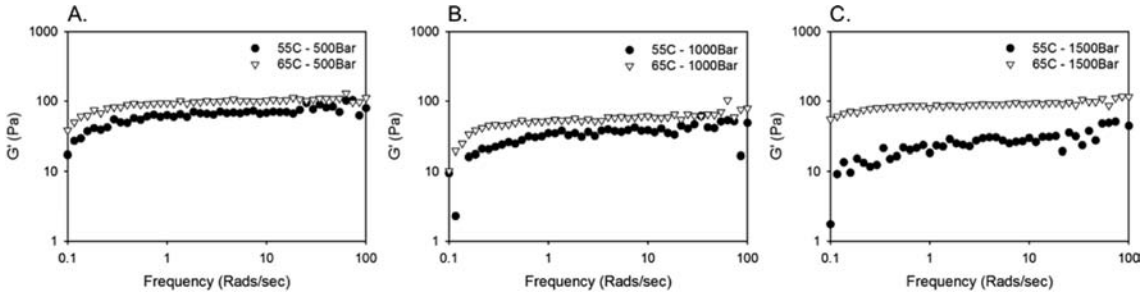

Figure 6. Storage modulus ($G2$) versus angular frequency curves for emulsion samples processed at different combinations of the temperature/pressure level: (A) 55 and 65 °C at 500 bar pressure, (B) 55 and 65 °C at 1000 bar pressure, and (C) 55 and 65 °C at 1500 bar pressure.

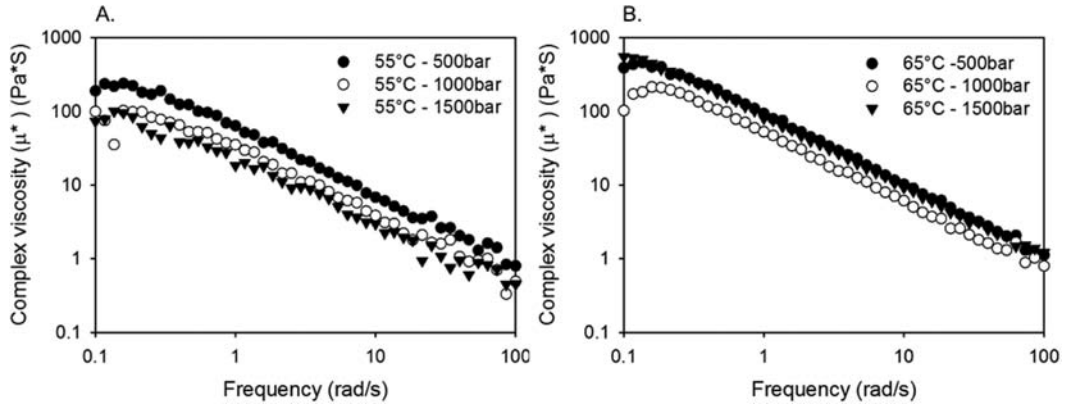

Figure 7. Complex viscosity η^* of emulsion samples processed at different combinations of the temperature/pressure level: (A) 55 °C at 500, 1000, and 1500 bar pressure and (B) 65 °C at 500, 1000, and 1500 bar pressure.

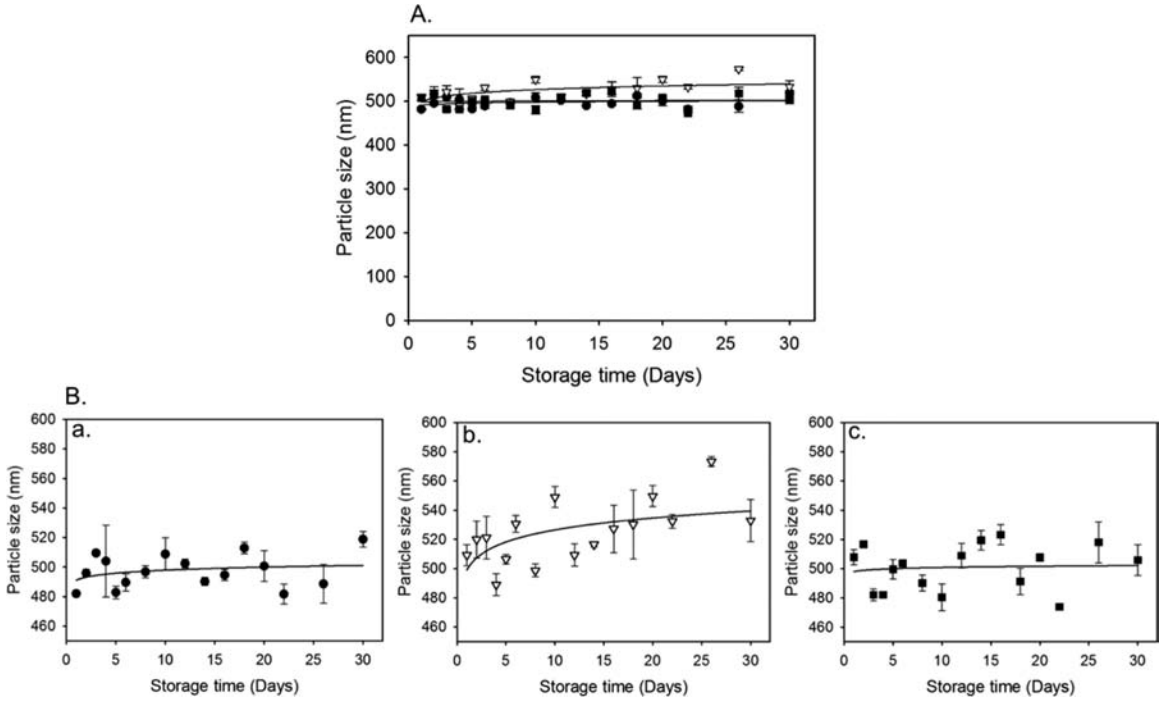

Figure 8. (A) Particle sizes of emulsion samples stored under 4, 25, and 60 °C. (B) Enlarged plots for particle size analysis at each storage temperature: (a) 4 °C, (b) 25 °C, and (c) 60 °C. All emulsion samples used in the storage study contain 2.0% tangeretin (PMF).

The influence on the gel-like structure of the PMF viscoelastic emulsion by the pressure and temperature is given in panels A−C of Figure 6. For all pressure conditions, higher processing temperatures reduced the network interaction more than lower temperatures. While the network interaction of samples processed under 500 and 1000 bar was not significantly affected by temperature variation, the gel structure was greatly weakened when the temperature was raised at 1500 bar. The results from this study suggested that larger crystals in the emulsion system disrupt the gel-like

DOI: 10.1021/jf504465a
J. Agric. Food Chem. 2015, 63, 652−659

structure more by interfering with the emulsion droplet interaction. In Figure 7, the viscoelastic characteristics of emulsion samples under different pressure treatments are compared. Interestingly, the viscoelastic property of the emulsion system was not significantly changed by the pressure variation when the temperature was kept constant (55 or 65 °C). The results from the rheological study indicated that all emulsion samples sustained a viscoelastic structure, even though the network strength was variable.

PMF Emulsion Stability under Different Storage Temperatures. For the general population to benefit from oral formulations, it is important for products to have an adequate shelf life. In this part of the experiment, the storage stability of crystalline PMF viscoelastic emulsion was studied under three storage temperatures (4, 25, and 60 °C) over a 1 month period. Because the emulsion system was a mixed system, any change in the particle size of both emulsion droplets and crystalline components was monitored as indicators of potential instability. To minimize the variability, all emulsion samples were produced in one single batch, distributed between three bottles, and stored in the selected temperature environments. During the 1 month study, the emulsion droplets of all three samples remained stable one-phase systems and did not have noteworthy changes in particle size (Figure 8A). Upon closer examination of the droplet particle size, the droplet particles of the 25 °C sample were slightly larger than those of the other two storage conditions (panels a and c of Figure 8B). The results from this observation indicated that the stability of viscoelastic emulsion might not only benefit from storage in lower temperatures, where the molecular diffusion rate was limited, but also in higher temperatures, where the gel-like surface interaction was stronger. In Figure 9A, the observed microscopic crystal morphology under three storage conditions is presented in chronological order over a 1 month period. To clarify the effect of the storage temperature on the crystal growth, the crystal length from all temperature environments as a function of days elapsed is plotted in Figure 9B. According to our analysis, the crystal growth rate at 4 and 25 °C was minimal and showed no significant variability. However, at 60 °C storage temperature, the crystal growth rate was significantly accelerated. The growth rate of the crystalline structure is highly dependent upon the molecular diffusion rate and activation energy for the crystalline component to fit into the crystal lattice.[26] In this sense, higher storage temperatures provided all factors required for rapid crystal growth and, in our case, caused higher instability for the crystalline emulsion system.

In summary, we systematically optimized an oral formulation that included crystalline components. Formulations with PMF loading no more than 0.6% did not show the existence of crystal structures in the emulsion system. However, to achieve a higher PMF loading and smaller crystal sizes, PMF loadings higher than 1.5% should be selected. Processing parameters also play a critical role in determining the sample quality when a smaller particle size is desired. Because lower temperatures and pressures may create samples with a smaller crystalline structure, the processing temperature and pressure should be set at the optimum processing conditions. During storage, higher temperatures promoted faster growth in the size of both emulsion droplets and crystals. Therefore, to better preserve the quality, a sample containing a crystalline component should preferably be stored in cooler conditions. The results clearly illustrate that the loading concentration, processing parameters, and storage conditions are critical factors to produce crystals with desired sizes and specifications. The methods from this study can be used for future reference when designing oral delivery formulations for crystalline hydrophobic ingredients.

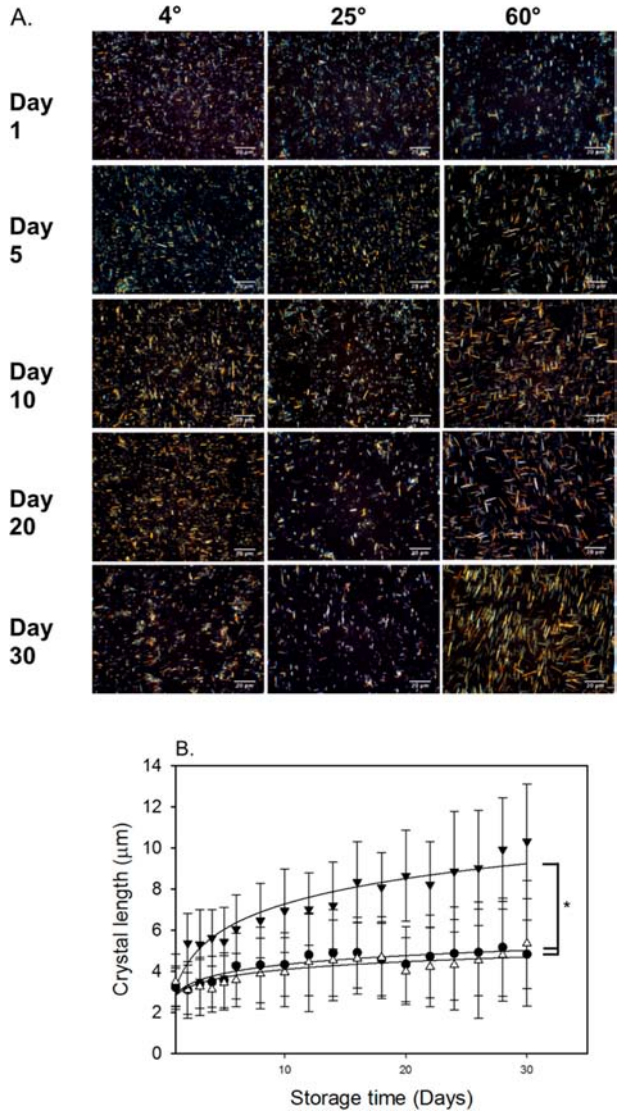

Figure 9. (A) Microscopic pictures of emulsion samples stored at 4, 25, and 60 °C over 1 month. (B) Crystal length of PMF in emulsion samples stored at 4 °C (△), 25 °C (●), and 60 °C (▼) as a function of storage days. (*) $p < 0.05$: the crystal length of the sample stored under 60 °C is significantly different from the sample stored under 4 and 25 °C.

AUTHOR INFORMATION

Corresponding Author

*Telephone: 848-932-5514. Fax: 732-732-6776. E-mail: qhuang@aesop.rutgers.edu.

Notes

The authors declare no competing financial interest.

REFERENCES

(1) Chakraborty, S.; Shukla, D.; Mishra, B.; Singh, S. Lipid—An emerging platform for oral delivery of drugs with poor bioavailability. *Eur. J. Pharm. Biopharm.* **2009**, *73*, 1−15.

DOI: 10.1021/jf504465a
J. Agric. Food Chem. 2015, 63, 652−659

(2) Humberstone, A. J.; Charman, W. N. Lipid-based vehicles for the oral delivery of poorly water soluble drugs. *Adv. Drug Delivery Rev.* **1997**, *25*, 103−128.
(3) Fricker, G.; Kromp, T.; Wendel, A.; Blume, A.; Zirkel, J.; Rebmann, H.; Setzer, C.; Quinkert, R.-O.; Martin, F.; Müller-Goymann, C. Phospholipids and lipid-based formulations in oral drug delivery. *Pharm. Res.* **2010**, *27*, 1469−1486.
(4) Ting, Y.; Jiang, Y.; Ho, C.-T.; Huang, Q. Common delivery systems for enhancing in vivo bioavailability and biological efficacy of nutraceuticals. *J. Funct. Foods* **2014**, *7*, 112−128.
(5) Li, Y.; Zheng, J.; Xiao, H.; McClements, D. J. Nanoemulsion-based delivery systems for poorly water-soluble bioactive compounds: Influence of formulation parameters on polymethoxyflavone crystallization. *Food Hydrocolloids* **2012**, *27*, 517−528.
(6) Li, S. M.; Pan, M. H.; Lo, C. Y.; Tan, D.; Wang, Y.; Shahidi, F.; Ho, C. T. Chemistry and health effects of polymethoxyflavones and hydroxylated polymethoxyflavones. *J. Funct. Foods* **2009**, *1*, 2−12.
(7) Reddel, R. R.; Ke, Y.; Gerwin, B. I.; Mcmenamin, M. G.; Lechner, J. F.; Su, R. T.; Brash, D. E.; Park, J. B.; Rhim, J. S.; Harris, C. C. Transformation of human bronchial epithelial-cells by infection with SV40 or adenovirus-12 SV40 hybrid virus, or transfection via strontium phosphate coprecipitation with a plasmid containing SV40 early region genes. *Cancer Res.* **1988**, *48*, 1904−1909.
(8) Stoner, G. D.; Kaighn, M. E.; Reddel, R. R.; Resau, J. H.; Bowman, D.; Naito, Z.; Matsukura, N.; You, M.; Galati, A. J.; Harris, C. C. Establishment and characterization of SV40 T-antigen immortalized human esophageal epithelial cells. *Cancer Res.* **1991**, *51*, 365−71.
(9) Janakiram, N. B.; Rao, C. V. Molecular markers and targets for colorectal cancer prevention. *Acta Pharmacol. Sin.* **2008**, *29*, 1−20.
(10) Pan, M. H.; Ho, C. T. Chemopreventive effects of natural dietary compounds on cancer development. *Chem. Soc. Rev.* **2008**, *37*, 2558−2574.
(11) Pan, M. H.; Lai, C. S.; Wu, J. C.; Ho, C. T. Molecular mechanisms for chemoprevention of colorectal cancer by natural dietary compounds. *Mol. Nutr. Food Res.* **2011**, *55*, 32−45.
(12) Ting, Y.; Li, C. C.; Pan, M.-H.; Ho, C.-T.; Huang, Q. Effect of labile methyl donor on the transformation of 5-demethyl tangeretin and related implication on bioactivity. *J. Agric. Food Chem.* **2013**, *61*, 8090−8097.
(13) Ting, Y.; Xia, Q.; Li, S.; Ho, C.-T.; Huang, Q. Design of high-loading and high-stability viscoelastic emulsions for polymethoxyflavones. *Food Res. Int.* **2013**, *54*, 633−640.
(14) McClements, D. J. Crystals and crystallization in oil-in-water emulsions: Implications for emulsion-based delivery systems. *Adv. Colloid Interface Sci.* **2012**, *174*, 1−30.
(15) Acosta, E. Bioavailability of nanoparticles in nutrient and nutraceutical delivery. *Curr. Opin. Colloid Interface Sci.* **2009**, *14*, 3−15.
(16) Huang, Q. R.; Yu, H. L.; Ru, Q. M. Bioavailability and delivery of nutraceuticals using nanotechnology. *J. Food Sci.* **2010**, *75*, R50−R57.
(17) McClements, D. J.; Rao, J. Food-grade nanoemulsions: Formulation, fabrication, properties, performance, biological fate, and potential toxicity. *Crit. Rev. Food Sci. Nutr.* **2011**, *51*, 285−330.
(18) McClements, D. J.; Xiao, H. Potential biological fate of ingested nanoemulsions: Influence of particle characteristics. *Food Funct.* **2012**, *3*, 202−220.
(19) Moraru, C.; Huang, Q. R.; Takhistov, P.; Dogan, H.; Kokini, J. Food nanotechnology: Current developments and future prospects. In *Global Issues in Food Science and Technology*; Barbosa-Cánovas, G. V., Mortimer, A., Colonna, P., Lineback, D., Spiess, W., Buckle, K., Eds.; Academic Press: New York, 2009; pp 369−399.
(20) Yu, H.; Huang, Q. Improving the oral bioavailability of curcumin using novel organogel-based nanoemulsions. *J. Agric. Food Chem.* **2012**, *60*, 5373−5379.
(21) Bancroft, W. D. Supersaturation and crystal size. *J. Phys. Chem.* **1920**, *24*, 100−107.
(22) Davey, R.; Garside, J.; Hilton, A.; McEwan, D.; Morrison, J. Purification of molecular mixtures below the eutectic by emulsion crystallization. *Nature* **1995**, *375*, 664−666.
(23) Rodríguez-hornedo, N.; Murphy, D. Significance of controlling crystallization mechanisms and kinetics in pharmaceutical systems. *J. Pharm. Sci.* **1999**, *88*, 651−660.
(24) Donsì, F.; Wang, Y.; Li, J.; Huang, Q. Preparation of curcumin sub-micrometer dispersions by high-pressure homogenization. *J. Agric. Food Chem.* **2010**, *58*, 2848−2853.
(25) Málek, J. Kinetic analysis of crystallization processes in amorphous materials. *Thermochim. Acta* **2000**, *355*, 239−253.
(26) Marangoni, A. G. *Fat Crystal Networks*; CRC Press: Boca Raton, FL, 2010; Vol. *140*.
(27) Ito, H.; Tsutsumi, Y.; Minagawa, K.; Takimoto, J.-i.; Koyama, K. Simulations of polymer crystallization under high pressure. *Colloid Polym. Sci.* **1995**, *273*, 811−815.
(28) Kyotani, M.; Kanetsuna, H. Crystallization kinetics of polyethylene under high pressure. *J. Polym. Sci., Polym. Phys. Ed.* **1974**, *12*, 2331−2345.
(29) Prewitt, C. T.; Downs, R. T. High-pressure crystal chemistry. *Rev. Mineral.* **1998**, *37*, 284−318.

DOI: 10.1021/jf504465a
J. Agric. Food Chem. 2015, 63, 652−659

JOURNAL OF AGRICULTURAL AND FOOD CHEMISTRY

Article

pubs.acs.org/JAFC

Sorption of Grape Proanthocyanidins and Wine Polyphenols by Yeasts, Inactivated Yeasts, and Yeast Cell Walls

J. Mekoue Nguela,[†,‡,§,∥] N. Sieczkowski,[∥] S. Roi,[†,‡,§] and A. Vernhet*[,†,‡,§]

[†]INRA, UMR 1083 SPO, F-34060 Montpellier, France

[‡]Montpellier SupAgro, UMR 1083 SPO, F-34060 Montpellier, France

[§]Université Montpellier 1, UMR 1083 SPO, F-34060 Montpellier, France

[∥]Lallemand SAS, 19 rue des Briquetiers, BP 59, 31 702 Blagnac, France

ABSTRACT: Inactivated yeast fractions (IYFs) can be used in enology to improve the stability and mouthfeel of red wines. However, information concerning the mechanisms involved and the impact of the IYF characteristics is scarce. Adsorption isotherms were used to investigate interactions between grape proanthocyanidin fractions (PAs) or wine polyphenols (WP) and a commercial yeast strain (Y), the inactivated yeast (IY), the yeast submitted to autolyzis and inactivation (A-IY), and the cell walls obtained by mechanical disruption (CW). High affinity isotherms and high adsorption capacities were observed for grape PAs and whole cells (Y, IY, and A-IY). Affinity and adsorbed amount were lower with wine PAs, due to chemical changes occurring during winemaking. By contrast to whole cells, grape PAs and WP adsorption on CW remained very low. This raises the issue of the part played by cell walls in the interactions between yeast and proanthocyanidins and suggests the passage of the latter through the wall pores and their interaction with the plasma membrane.

KEYWORDS: *inactivated yeast fractions, physicochemical properties, polyphenols, sorption isotherms*

INTRODUCTION

Inactivated yeast fractions (IYFs) are yeast derivatives produced from enological yeasts (*Saccharomyces cerevisiae*) previously inactivated to suppress their fermentative capacity. Depending on the treatment applied, inactivated whole yeasts, yeast autolysates, yeast extracts, cell walls, or mannoproteins can be obtained. IYFs are used in enology to improve fermentation steps,[1,2] to adsorb pigments,[3−6] or to enhance the safety,[7] the sensory characteristics,[8−11] the color and the colloidal stability of wines.[7,11−13] Regarding sensory properties and stability, the aim is to obtain characteristics similar to those of wines aged on lees.[3,14]

Despite their increasing use, there is limited information concerning the exact composition of IYFs and the mechanisms involved in their potential effect on the organoleptic properties and stability of wines. In fact, IYFs are usually complex products. Their impact can be related to the release of compounds that modify wine taste as well as to the removal of some wine components by parietal adsorption (insoluble fractions) or precipitation (soluble fractions). When dealing with red wines, this impact is mainly attributed to physicochemical interactions involving wine polyphenols and soluble or insoluble IYF components, especially mannoproteins[15,16] and cell walls.[17−19] However, the respective impact of IYF soluble and insoluble components and the exact mechanisms involved are not clearly established yet, and some contradictory results may be found in the literature[20,8] as well as in winemaking practice. This can be related either to the use of very different yeast derived products, obtained from different strains submitted to diverse treatments (thermal inactivation, autolysis, drying, etc.) and presenting different composition and structure, or to the variability of wine composition and initial characteristics.

The aim of the present work was to study interactions between polyphenols and yeast cells (parietal adsorption) and to compare the effect of different treatments (drying, autolysis, and mechanical disruption) on them. Interactions were studied by means of adsorption kinetics and isotherms established in a model winelike solution using grape seed and skin proanthocyanidins (PAs) with different average molecular weight and a pool of polyphenols purified from a red wine. This allowed evidencing (i) the impact of PA molecular weight on their adsorption and (ii) the impact of chemical changes that occur during winemaking. Indeed polyphenols, due to their high reactivity, undergo chemical changes once extracted from grapes. This leads to the formation of derived tannins and pigments, the properties of which are likely to be different from those of their precursors.[21−23] In addition, these derived products are poorly characterized using current analytical techniques.

MATERIALS AND METHODS

Yeasts, Inactivated Yeast Fractions, and Yeast Cell Walls. The yeast strain used in the present work is a commercial *Saccharomyces cerevisiae* strain (Lallemand, Montreal, Canada) commonly used in enology. Yeast was propagated aerobically at 32 °C in a fed-batch manner, with a growth rate of 0.18 h^{-1}, for a total of 17 h. Feed substrate was beet molasses diluted to allow suitable delivery of the molasses to the propagation, and ammonia hydroxide

Received: September 19, 2014
Revised: November 28, 2014
Accepted: December 19, 2014
Published: December 19, 2014

ACS Publications © 2014 American Chemical Society

DOI: 10.1021/jf504494m
J. Agric. Food Chem. 2015, 63, 660−670

(5%) was used as the nitrogen source. The yeast biomass (Y) was either frozen at −20 °C and conserved as such or submitted to further postharvesting treatments to obtain inactivated yeast fractions. The viability of frozen cells (Y) was determined prior interaction assays through flow cytometry associated with staining techniques and growth on Petri plates. Results (1 and 2.4% respectively) indicated that most cells were dead. A part of the biomass was inactivated by thermal treatment, achieved by holding the yeast cream at 70 °C for 15 min in a temperature controlled vessel. The inactivated yeast biomass was spray-dried in a Büchi B290 spray dryer (Büchi, New Castle, DE, USA). This enabled the inactivated yeast fraction (IY) to be obtained. Another part was submitted to autolysis. Autolysis was carried out by incubating the yeast biomass at a pH of 5.5 at 55 °C for 20 h. After autolysis the yeast was centrifuged at 15000*g* for 15 min in order to separate the soluble fraction from the insoluble fraction. The insoluble part (A-IY) was spray-dried.

A cell wall fraction (CW) was purified from the biomass Y at the laboratory scale by mechanical disruption, according to the protocol described by Dallies et al. (1998).[24] Before disruption, the yeast biomass was washed three times in a 5 mM phosphate buffer (pH 7.5) by successive resuspension and centrifugation steps (1000*g*, 5 min, 5 °C). Cells were then dispersed in the phosphate buffer at a concentration of 10^9 cells·mL^{-1} and 2 mL aliquots distributed in suitable glass tubes containing 5.3 g of 0.5 mm diameter yttria-stabilized zirconium oxide beads. Complete cell disruption was achieved with a tissue homogenizer (Precellys 24, Bertin Technologies, France) by the application of 13 periods of shaking of 20 s each at 5500 rpm, with 1 min intervals on ice between each period. Cell disruption was followed by optical microscopy. The cell suspension was then collected, and beads were extensively washed with the phosphate buffer. The supernatant and washing solution were pooled and centrifuged at 3800*g* for 5 min.[24] The pellet, containing the cell walls, was washed four times with phosphate buffer and twice with deionized water. The cell wall suspension was heated at 72 °C for 15 min to remove residual enzymatic activities, and sodium azide (0.02% w/v) was added to prevent any microbiological development. The suspension was then stored at 4 °C until use. The dry weight per milliliter of suspension, 4.4 mg·mL^{-1}, was determined by freeze-drying of aliquots. In accordance with literature data,[25,26] it was calculated that cell walls accounted for about 20% of the whole cell dry weight. Neutral sugars[24] and Kjeldhal analyses performed on CW indicated a neutral sugar content of 80% (w/w) and a nitrogen content of about 2% (w/w).

Physicochemical Characterization of Yeast and Inactivated Yeast Fractions. *Transmission Electron Microscopy (TEM).* TEM observations were performed to assess the impact of the process on yeast structure and integrity. Yeast and inactivated yeast fractions were washed three times in Milli-Q water before being dispersed in a 2.5% glutaraldehyde solution in Sorensen's buffer (0.1 M, pH 7.4) overnight at 4 °C. They were then washed twice in Sorensen's buffer and postfixed in a 0.5% osmic acid solution for 2 h in darkness and at room temperature. After two further washes in Sorensen's buffer, cells and cell walls were dehydrated in a graded series of ethanol solutions (30−100%). Samples were embedded in EmBed 812 using an automated microwave tissue processor for electronic microscopy (Leica EM AMW). Thin sections (70 nm; Leica-Reichert Ultracut E) were collected at different levels of each block. These sections were counterstained with uranyl acetate and observed using a Hitachi 7100 transmission electron microscope (Centre de Ressources en Imagerie Cellulaire de Montpellier, IURC, Montpellier, France).

Surface Hydrophobicity and Lewis Acid/Base Properties. Hydrophobicity and Lewis acid (electron acceptor)/base (electron donor) properties of the yeast and of the IYFs were determined by the microbial adhesion to solvents (MATS) method.[27] In aqueous media, polar acid/base forces usually occur under the form of hydrogen donor/hydrogen acceptor (Brønsted acid/base) interactions. However, the use of the Lewis model, more general, is preferable. The affinity of cells (Y, IY, A-IY) for two pairs of solvents of similar Lifshitz−van der Waals surface tension components was compared: (i) the apolar solvent hexadecane and its paired acidic monopolar solvent, chloroform, and (ii) the apolar solvent decane and its paired strongly basic, monopolar solvent, ethyl acetate. Because of the surface tension properties of these solvents, differences between the affinity for chloroform and hexadecane and the affinity for ethyl acetate and decane indicate electron-donor or electron-acceptor properties of the yeast surface, respectively. The hydrophobic/hydrophilic character is revealed by their affinity for apolar solvents.

Yeast biomass and yeast fractions were washed twice and suspended in 9 g·L^{-1} (155 mM) NaCl solution at pH 3.5 (adjusted with HCl) to get an optical density of about 0.7 at 620 nm. In a test tube, 0.4 mL of solvent was added to 2.4 mL of cell suspension. The mixture was vortex-mixed for 60 s and allowed to stand for 15 min to achieve the complete separation of the two phases. The aqueous phase was recovered, and the optical density at 620 nm measured. The percentage of cells bound to a given solvent (or the affinity) is expressed as

$$\%\ \text{affinity} = [1 - ((A - A_T)/A_0)] \times 100$$

A_0 and A being the optical density at 620 nm of the yeast suspension before and after contact with the solvent, respectively, and A_T the optical density at 620 nm of the control. Each assay was performed in triplicate.

Surface Charge. Yeast cells (Y, IY, A-IY) were rehydrated (IY and A-IY only), washed twice, and suspended in a 1 mM NaCl solution. Their electrophoretic mobility was measured at different pH, adjusted between 3 and 7 with HCl and NaOH, using a laser zetasizer (Zetasizer HS 3000, Malvern Instruments, Orsay, France). Each result represents a mean of at least 6 separate experiments.

Purification and Analysis of Polyphenols from a Red Wine. *Purification.* A wine polyphenol pool (WP) was purified from 9 L of a Merlot wine, produced in 2012 at the INRA Experimental Unit of Pech Rouge (Gruissan, France). Separation was achieved by applying the wine to a 7 L bed volume column filled with a styrene/divinylbenzene Diaion resin. The wine flow rate was of 4.2 L·h^{-1}. The resin was rinsed with two bed volumes of distilled water (flow rate 4.2 L·h^{-1}) to remove water-soluble compounds. The elution was followed by refractometry. The phenolic pool was finally eluted with 5 L of methanol and 12 L of 96/4 v/v ethanol/water, both solvents being acidified with TFA (0.05%). The ethanolic and methanolic extracts were pooled and the solvents removed by vacuum evaporation at 40 °C. The polyphenol pool was then freeze-dried and stored at −80 °C under argon atmosphere before further use. The total yield was 5 g of freeze-dried powder per 1 L of treated wine.

Polyphenol Analysis. The wine polyphenol pool WP was dissolved in a winelike medium at a concentration of 5 g·L^{-1}, giving an absorbance at 280 nm of 55.0 (total polyphenols index, TPI). The reconstituted wine had a color intensity ($A_{420nm} + A_{520nm} + A_{620nm}$, optical path 1 cm) of 16.1 and a color tint (A_{420nm}/A_{520nm}, optical path 1 cm) of 0.6. Spectrophotometric measurements were made with a SAFAS UV-MC^2 spectrophotometer (Monaco).

High performance liquid chromatography analyses on the reconstituted wine before and after phloroglucinolysis[28,29] were performed to obtain the composition of the pool. Before phloroglucinolysis, the wine was applied on a C-18 solid-phase extraction cartridge (Waters, Vac tC18 3 cm^3) to remove tartaric acid and salts.[30] The polyphenol composition of the fraction was (on a dry weight basis): 29.3 mg·g^{-1} anthocyanins, 7.7 mg·g^{-1} flavan-3-ol monomers, 32.7 mg·g^{-1} phenolic acids, 24.2 mg·g^{-1} stilbenes, 5.9 mg·g^{-1} flavonols, and 95.0 mg·g^{-1} tannins. The mean degree of polymerization of the tannins was 7.3 ± 1.1, with a % of epigallocatechin and of epicatechin-gallate units of 24.2 ± 2.3 and 3.3 ± 0.3, respectively. This low yield is related to the fact that most polyphenols in the wine pool consisted of derived pigments and tannins, formed by chemical reactions during winemaking and aging and resistant to the usual depolymerization methods.[22,23,31] The possible presence of residual nitrogenous compounds or polysaccharides in the wine pool was also assessed by the Kjeldhal method and the analysis of neutral sugars. Neutral glycosyl-residue composition of polysaccharides in the fraction was determined after hydrolysis with 2 M trifluoroacetic acid (120 °C, 75 min)[32] by converting the

DOI: 10.1021/jf504494m
J. Agric. Food Chem. 2015, 63, 660−670

monosaccharides into their alditol acetate derivatives.[33] Hydrolysis was performed on the reconstituted wine according to the procedure described previously.[34] Analyses indicated the presence of residual pectic polysaccharides, accounting for 2% of the dry mass, and of nitrogen (0.02 $g \cdot g^{-1}$). Assuming that nitrogen is related to peptides or proteins, this content would indicate the presence of about 12.5% peptides/proteins in the dried powder. Considering these results, it was considered that a TPI of 55.0 (obtained by dissolving WP in a winelike medium at a concentration of 5 $g \cdot L^{-1}$) corresponded to a whole polyphenol concentration of 4.275 $g \cdot L^{-1}$. This value was used to convert the TPI into adsorbed polyphenol amount.

Grape Seed and Skin Proanthocyanidin Fractions. Two proanthocyanidin (PA) fractions from *Vitis vinifera* grape seeds (variety Carignan) and a PA fraction from grape skin (variety Muscat), previously purified at the laboratory and stored at −80 °C under argon in sealed vials, were also used for sorption experiments. Grape seed PAs were purified as described by Ducasse (2010).[30] The first fraction, named thereafter Seed3, had a mean degree of polymerization of 3.0 ± 0.1 and a percentage of galloylation of 14.9 ± 0.2%, whereas the second one, named Seed12, had a mean degree of polymerization of 11.8 ± 0.5 and a percentage of galloylation of 26.0 ± 0.5%. The yields of the depolymerization reaction were 64.3 and 41.6% for Seed3 and Seed12, respectively. The grape skin PA fraction was purified from the skin of 1.25 kg of Muscat berries. PAs were extracted with 2.5 L of acetone/H_2O/methanol (51/34/15), under stirring and during 2 h.[35] The mixture was centrifuged for 20 min at 2000*g* and 20 °C. The solid phase was extracted again with the same solvent during one night at 4 °C, and the mixture was centrifuged. The supernatants were pooled, filtrated, concentrated under vacuum at 30 °C (final volume 200 mL), and stored at −80 °C before the following steps. Chlorophyll was removed by three extractions with hexane and the PA extract applied on a styrene/divinylbenzene Diaion resin in batch conditions. The resin was washed several times with H_2O acidified with trifluoroacetic acid (TFA, 0.05% v/v) to remove sugars and proteins (followed by refractometry), and PAs were recovered with MeOH acidified with TFA (0.05% v/v). Methanol was evaporated, and the samples were dispersed in distilled water and freeze-dried. This PA extract was dissolved in H_2O acidified with TFA (0.05% v/v) (5 mL, 47 $mg \cdot mL^{-1}$) and further applied on a Toyopearl TSK HW-50 (F) gel (Tosoh Corp., Tokyo, Japan) (diameter, 2.7 cm; 18 cm height) equilibrated with the same solvent. The column was then extensively washed with H_2O:TFA (0.05% v/v, 300 mL). Elution by 55:45:0.05 v:v:v EtOH:H_2O:TFA (450 at 10 $mL \cdot min^{-1}$) was performed first to remove low molecular weight polyphenols. High molecular weight proanthocyanidins were eluted with a 60:40:0.05 acetone:H_2O:TFA v:v:v mixture (450 mL). After concentration under vacuum (rotary evaporator at 30 °C), the high molecular weight PA fraction was freeze-dried and stored at −80 °C. This fraction, named Skin21, had a mean degree of polymerization of 20.1 ± 0.7, and its percentage of epigallocatechin units was 16.8 ± 1.2%. The yield of the depolymerization reaction was 73.9%.

Adsorption Experiments. Adsorption experiments were performed in a 12% v/v ethanol model winelike solution with 2 $g \cdot L^{-1}$ tartaric acid, the pH of which was adjusted to 3.5 with KOH 1 M. The ionic strength was set at 50 mM by NaCl (2.16 $g \cdot L^{-1}$). SO_2 (25 $mg \cdot L^{-1}$) was added to prevent polyphenol oxidation. Before experiments, the yeast biomass Y and the cell walls CW were washed twice in the winelike solution and resuspended at the final desired concentration in the same medium. Inactivated yeast IY and autolyzed−inactivated yeast A-IY, under the form of dried powders, were first rehydrated in water for 30 min at 37 °C, under stirring. Supernatant was removed by centrifugation (1500*g*, 5 min, 5 °C), and the pellets were washed twice and resuspended in the winelike solution, as described for Y and CW. All suspensions were dispersed properly in model wine using ultrasound (Branson Sonifier 250, 150 W, 40 s).

Adsorption Kinetics. In order to determine the contact time required to reach the adsorption equilibrium, experiments were performed first at different concentrations of the wine polyphenol pool using the yeast biomass at a concentration of 10^8 $cells \cdot mL^{-1}$. Samples were stirred continuously for 3 days, and an aliquot was taken at several time intervals. Yeast cells were removed by centrifugation (1000*g* for YC, 5 min, 5 °C) and the supernatants recovered for spectrophotometric measurements. The total polyphenol concentrations in the bulk were determined by absorbency measurements at 280 nm after adequate dilution. Total adsorbed polyphenols (TAP) were calculated from the difference in absorbance between the samples and the corresponding controls using

$$\mathrm{TAP} = \mathrm{TPI}^{\mathrm{PPcontrol}} - (\mathrm{TPI}^{\mathrm{sample}} - A_{280}^{\mathrm{Ycontrol}})$$

$\mathrm{TPI}^{\mathrm{PPcontrol}}$ being the total polyphenols index (A_{280} × dilution factor) of the polyphenol solution without yeast cells, $\mathrm{TPI}^{\mathrm{PPsample}}$ the total polyphenols index of the supernatant recovered after contact with yeasts, and A^{Ycontrol} the absorbance related to a possible release of compounds by yeasts. Indeed, Y, IY or A-IY may release compounds that absorb at 280 nm. Though very low, this absorbance affects the measurements at the lowest polyphenol concentrations. Therefore, yeast controls, i.e., 10^8 $cells \cdot mL^{-1}$ suspensions in the model wine without polyphenols, were also performed. With the wine polyphenol pool, absorbency measurements at 420, 520, and 620 nm were also performed to determine the impact of yeast and yeast fractions on color intensity and tint.[36]

Kinetics were repeated with the yeast biomass and the three tannin fractions, and then with the inactivated yeasts, the cell walls, and the WP and Skin21 tannins to confirm the contact time needed in sorption isotherm studies to reach equilibrium. Centrifugation conditions adopted to remove cells and cell walls for spectrophotometric measurements were 1500*g*, 5 min, 5 °C and 10000*g*, 5 min, 5 °C, respectively.

Adsorption Isotherms. From kinetic studies, a contact time of 24 h was chosen for adsorption experiments. Polyphenol stock solutions were prepared by dissolving the polyphenol fractions in the model wine at a concentration of 10 $g \cdot L^{-1}$. Dilution of these stock solutions was performed to get a final concentration range between 0.01 and 5 $g \cdot L^{-1}$. All sorption experiments were carried out by mixing equal volumes of a $2x$ $g \cdot L^{-1}$ polyphenol solution (x being the final desired polyphenol concentration) and of a 2×10^8 $cells \cdot mL^{-1}$ suspension (final concentration 10^8 $cells \cdot mL^{-1}$). For cell walls and considering that yeast walls account for 20% of the cell weight, the final concentration of the suspension was set at 0.44 $mg \cdot mL^{-1}$. Samples (2 mL) were placed in 2 mL tightly closed eppendorfs in order to minimize headspace and were stirred continuously (Stuart rotator SB3, 40 rpm) in darkness and at room temperature. After 24 h, samples were clarified by centrifugation (as above mentioned), and supernatants were recovered for spectrophotometric measurements and HPLC analyses (wine polyphenol pool only). Data represent a mean of at least two separate experiments.

Reversibility upon Dilution. The Y and IYF pellets obtained by centrifugation after adsorption were resuspended in 2 mL of model wine without polyphenols. Samples were stirred for 24 h and the supernatants recovered. The adsorption reversibility was evaluated through the quantity of polyphenols recovered in supernatants.

RESULTS AND DISCUSSION

Characterization of the Yeast Biomass and the Inactivated Yeast Fractions. TEM observations of Y, IY, A-IY, and CW are presented Figure 1. In the conditions adopted in the present work, neither the drying process nor the autolysis induced any detectable changes of the yeast ultrastructure (cell wall damage, release of the intracellular material, membrane collapse). All cells presented dimensions between 1.5 and 3 μm, and the measured thickness of the cell wall lay between 100 and 200 nm. The mechanical disruption procedure allowed close to complete removal of the intracellular material and the recovery of cell walls.

Though not visible by TEM, postharvesting processes significantly modified the surface physicochemical properties of cells, which reflects changes in their surface composition

DOI: 10.1021/jf504494m
J. Agric. Food Chem. 2015, 63, 660−670

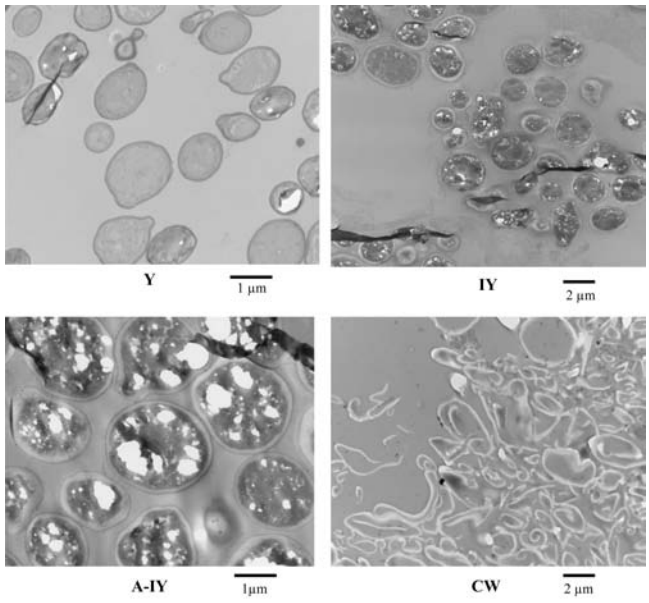

Figure 1. TEM views of the yeast biomass Y, the inactivated yeast IY, the yeast following to autolysis and inactivation A-IY and cell walls CW.

and/or structure (Figure 2). Indeed, IY and A-IY exhibited higher hydrophobicity than the untreated biomass Y, evidenced by their much higher affinity for apolar solvents hexadecane and decane (Figure 2B). All cells also exhibited a higher affinity for chloroform than for hexadecane, and a lower affinity for ethyl acetate than for decane. This allows their classification as basic (i.e., as electron donor), without any apparent electron-acceptor component. This electron-donor character was more pronounced for IY and A-IY than for Y, as shown by the greater differences in affinity observed with solvent pairs. Modification in surface polarity was coupled with a decrease of cell electrophoretic mobility and thus surface charge (Figure 2A). These results are in accordance with previous reports[37,38] and can be attributed to the drying process. Drying has been shown to modify the yeast cell wall structure, inducing changes that are not fully reversible upon rehydration and that are dependent on both the drying (heat-treatment, freeze-drying) and the rehydration procedure.[37,39] Electrophoretic mobility measurements and MATS experiments were not performed on cell walls because these latter present two very different surfaces in terms of composition (outer and inner surface). In addition, they are under the form of fragments of different size and shape. Thus, they cannot be easily compared to whole yeast cells.

Adsorption Kinetics. Kinetic studies were performed first with the wine polyphenol pool (WP) and the yeast biomass Y using different initial polyphenol concentrations. Polyphenol adsorption was followed during 64 h by the measurement of the total polyphenol index (TPI) and of the color parameters (Figure 3). After a rapid decrease of the TPI during the first hour, a plateau value was obtained for the two lowest polyphenol concentrations (0.5 and 1 $g{\cdot}L^{-1}$). This plateau value, indicating that the equilibrium was reached, was observed after 16 and 24 h at concentrations of 2.5 and 5 $g{\cdot}L^{-1}$, respectively. Maximum decrease in color intensity was obtained after 1 h of contact whatever the initial polyphenol concentration, and the color tint was not modified. The percentage of polyphenols fixed by yeast cells decreased from 30 to 16% when the polyphenol concentration in the model wine was increased from 0.5 to 5.0 $g{\cdot}L^{-1}$. In parallel, the decrease in color intensity varied from 33 to 17%. These results are comparable to those obtained by previous work,[17] where the interaction kinetic between yeast lees (1.35×10^8 $cells{\cdot}mL^{-1}$) and a pool of red wine polyphenols was studied in a model winelike solution. For a TPI of 23, close to the one measured in the present study at a WP concentration of 2.5 $g{\cdot}L^{-1}$, the loss in TPI at equilibrium was similar, on the order of 22% for a yeast population of 10^8 $cells{\cdot}mL^{-1}$ (instead of 23% here). In the above-mentioned study,[17] where samples were stirred once a day, much slower adsorption kinetics were obtained than those observed in the present work. This is likely related to the continuous agitation mode chosen in the present work, which favors contact between polyphenols and yeast cells. From these first results, the contact time for sorption isotherm experiments was set at 24 h. Kinetics were repeated with the yeast biomass and the tannin fractions, as well as with the inactivated yeasts and the cell walls, to check that equilibrium was reached (results not shown).

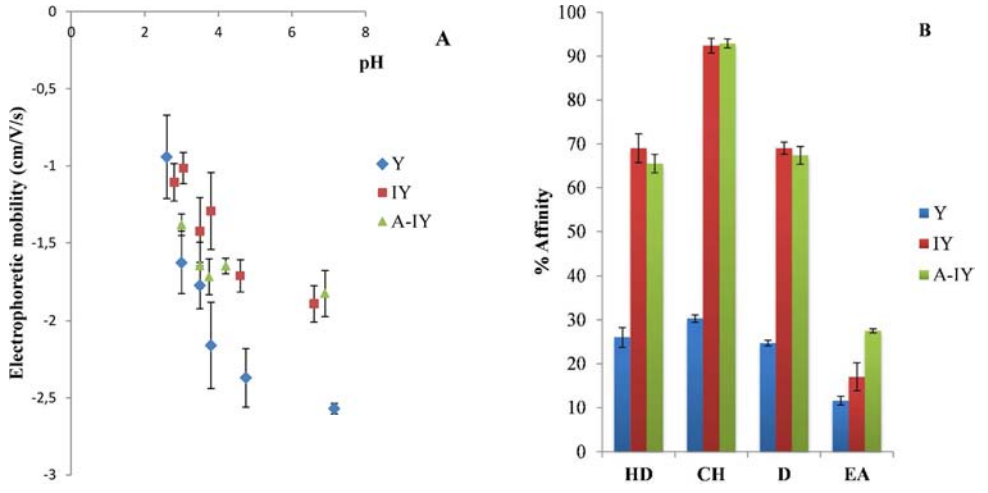

Figure 2. (A) Electrophoretic mobility of Y, IY and A-IY in 1 mM NaCl solutions, at various pH. (B) Adhesion of Y, IY and A-IY suspended in 9 $g.L^{-1}$ NaCl solution, pH 3.5, to various solvent-water interfaces. HD: hexadecane; CH: chloroform; D: decane; EA: ethyl acetate.

DOI: 10.1021/jf504494m
J. Agric. Food Chem. 2015, 63, 660−670

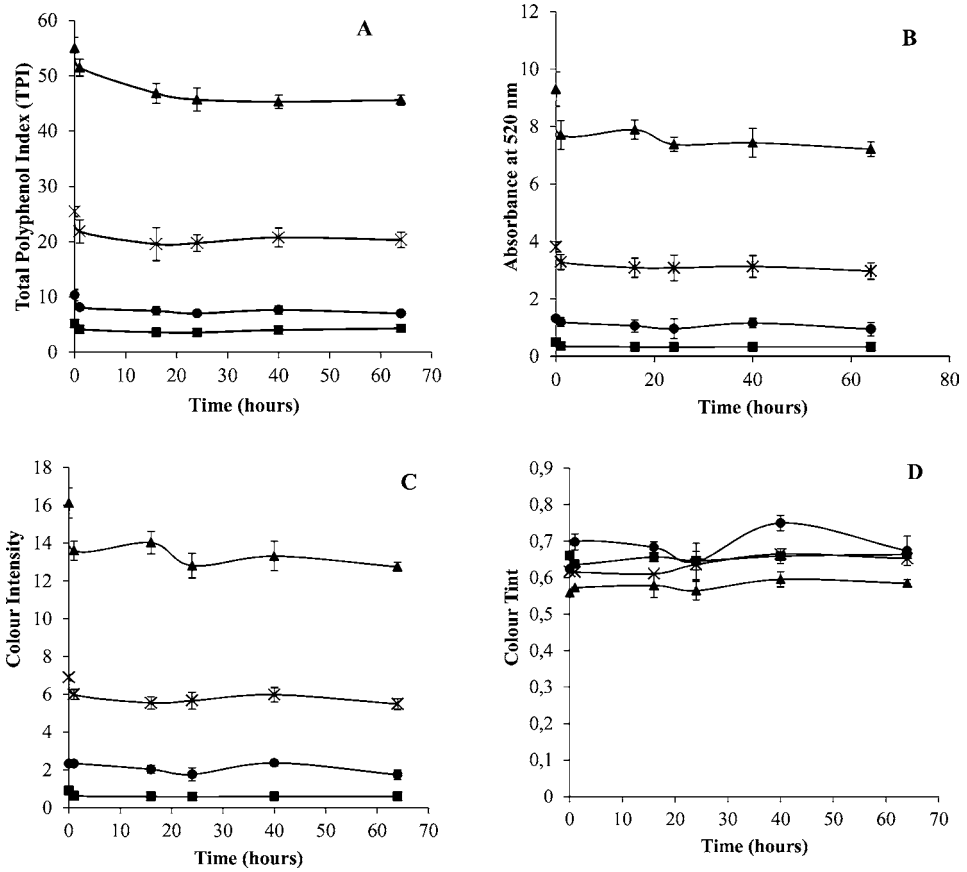

Figure 3. Adsorption kinetics of wine polyphenols on yeast biomass (Y, 10^8 cells·mL^{-1}) in model wine. The concentrations of the wine polyphenol pool were 5 g·L^{-1} (filled triangle), 2.5 g·L^{-1} (filled star), 1 g·L^{-1} (filled circle), and 0.5 g·L^{-1} (filled square). Polyphenol adsorption was monitored by the measurement of the total polyphenol index (TPI, A_{280nm} × dilution factor)) (A); the A_{520nm} (B); the color intensity (C); the color tint (D).

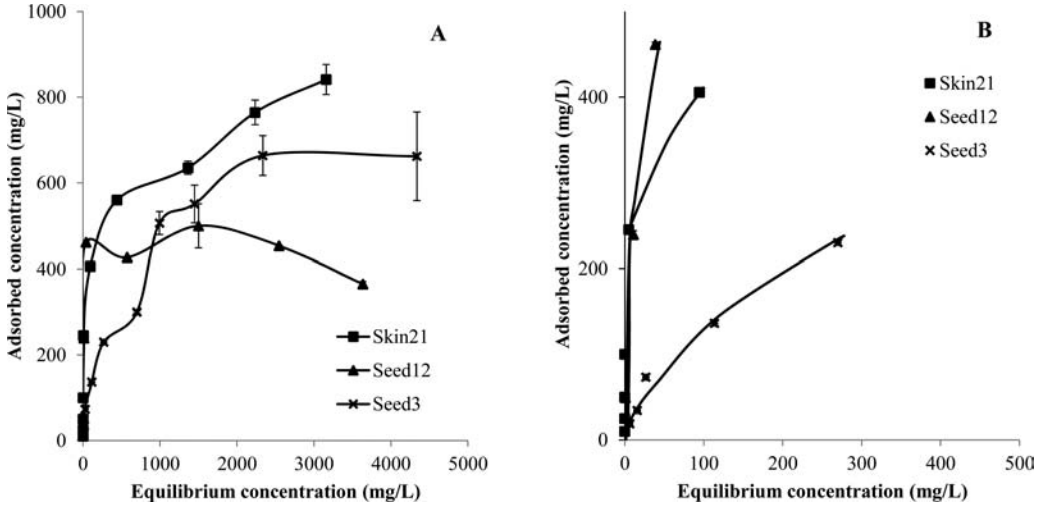

Figure 4. (A) Adsorption isotherms of grape skin (Skin 21) and grape seed (Seed 3 and Seed12) PA by the yeast biomass Y. (B) Enlarged view of the initial adsorption.

Adsorption of Grape Proanthocyanidins by the Yeast Biomass. Adsorption from solution is driven by a complex interplay between solute/solvent, solute/surface, surface/solvent physicochemical interactions, and solvent cohesion. The affinity for the surface (initial adsorption) as well as the maximum adsorbed amount will be dependent not only on the number of binding sites and accessibility to these binding sites but also on possible conformational rearrangements of the solute when dealing with polymers and on possible lateral interactions between adsorbed species. Adsorption isotherms (adsorbed concentration C_{sorbed} versus bulk equilibrium concentration C_{eq}) obtained on the yeast biomass with the grape seed (Seed3 and Seed12) and skin (Skin21) proanthocyanidin fractions are reported in Figure 4A. Skin21 and Seed12 exhibited very high affinity adsorption isotherms, with a complete adsorption at low concentrations, up to 0.5 g·

DOI: 10.1021/jf504494m
J. Agric. Food Chem. 2015, 63, 660−670

L^{-1} (Figure 4B and Table 1). This was followed by a continuous and very progressive increase of the adsorbed amount for Skin21, and no plateau value could be observed within the tested concentration range. With Seed12, a maximum plateau value was obtained from 0.5 $g \cdot L^{-1}$. A lower sorption was found for the lower aDP seed PA (Seed3) with an initial slope, calculated from the initial part of the curve of 2.62 and a progressive increase up to a plateau reached for an initial concentration of 3 $g \cdot L^{-1}$. There was no relationship between PA aDP and the maximum adsorbed amount. The lower affinity of Seed3 compared with Seed12 and Seed21 and the complete sorption of the latter at low concentrations suggest the involvement of multiple binding in their interactions with yeast cells.

Table 1. Initial Slopes C_{ads}/C_{eq} Deduced from the Initial Part of the Sorption Isotherms and Maximum Adsorbed Values (Q_{max}) Obtained with the Grape Seed and Skin Proanthocyanidin Fractions[a]

	C_{ads}/C_{eq}	C_{max} ($mg \cdot L^{-1}$)	Q_{max} ($mg \cdot g^{-1}$)	Q_{max}[b] ($mg \cdot m^{-2}$)
Seed3	2.62	664	352	221
Seed12	∞	500	265	167
Skin21	∞	840	445	280

[a] C_{ads}: sorbed concentration. C_{eq}: equilibrium concentration. Results are expressed in $mg \cdot L^{-1}$ and in $mg \cdot g^{-1}$ of dried yeast cells. [b] Yeast cells are considered as spheres with a mean diameter of 3 μm, so that 1 g (5.3×10^{10} cells) represents surface area of 1.47 m^2.

It is usually considered that polyphenol adsorption by yeast is related to their interactions with the cell wall components, and more especially mannoproteins. Yeast cell walls are composed of a network of β-1,3- and β-1,6-linked glucans, mannoproteins, and chitin.[25,26] Schematically, they can be described as two layered structures: an inner microfibrillar layer mainly composed of β-glucans cross-linked or not to chitin and an outer brushlike layer that mostly consists of mannoproteins. Mannoproteins present on the outer layer may be linked either to β-1,6-glucans by a remnant of their glycosyl phosphatidyl inositol (GPI) anchor or to β-1,3-glucans by an alkali-labile linkage.[40] Various proteins/mannoproteins are also attached to the cell wall outer network via disulfide bridges. Considering yeast cells as spheres with a radius of 1.5 μm, 1 g (5.3×10^{10} cells) represents a surface area of 1.47 m^2 (Table 1). This gives for whole cells adsorbed PA amount ranging from 167 to 280 $mg \cdot m^{-2}$, which is several tens to hundred times more than usually found on dense surfaces (in the order of few $mg \cdot m^{-2}$).[41] This result is consistent with PA location on several sites within the wall thickness. These sites can be mannoproteins, but also β-glucans and chitins. Unfortunately, information concerning PA interactions with mannoproteins remains scarce and is missing for β-glucans and chitins.

If polyphenol adsorption by yeasts is often attributed to cell walls,[7] it has also been suggested that small polyphenols may pass through the cell wall and interact with the plasma membrane lipids.[42] This hypothesis has been done to explain the protective effect of yeast lees toward polyphenol oxidation in white wines. In vitro experiments have evidenced that interactions between membrane sterols (ergosterol) and catechin or small (mainly dimers) oxidation reaction products are possible. We are working here with quite different polyphenolic structures (proanthocyanidins), with molecular weight ranging from 950 (Seed3) to 5840 Da (Skin21). The comparison of the adsorption isotherms does not evidence any impact of PA molecular weight on adsorbed amount. The question of the passage of these proanthocyanidins though the cell wall and interaction with the membrane will be further discussed later.

Impact of Postharvesting Treatments and Cell Disruption on Skin21 PA Adsorption by Yeast. The adsorption of polyphenols by the two inactivated yeasts (IY and A-IY) and the cell walls (CW) was compared to that of the yeast biomass (Y) using the Skin21 PA fraction (Figure 5A). Results evidenced very different adsorption behaviors between the whole cells on one hand and the purified cell walls on the other hand. On the whole, purified cell walls exhibited much lower adsorption capacity than the three others. At concentrations below 3 $g \cdot L^{-1}$, the adsorption of skin PA on CW was between 10 and 20 times less than that obtained with the whole cells. An unexpected and significant increase of the adsorbed amount was observed at the highest initial PA concentration, but it remains much lower than that observed with cells. These results are consistent with those of previous studies,[6] that showed a lower adsorption of oxidized phenolic compounds by cell walls than by whole yeast cells in white

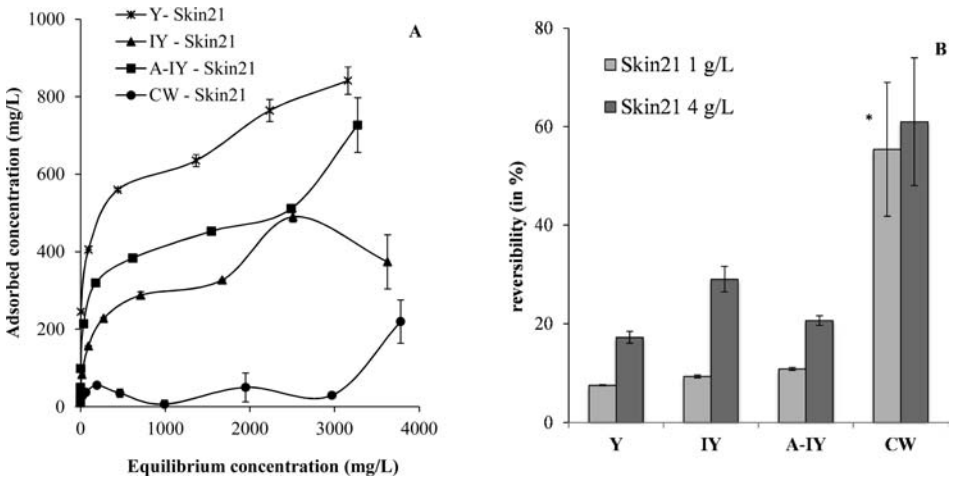

Figure 5. (A) Impact of postharvesting processes and cell disruption on the adsorption of grape skin PA (Skin 21): Y, yeast biomass; IY, inactivated yeast; A-IY, yeast submitted to autolysis and inactivation; CW, cell walls recovered from mechanical disruption. (B) Reversibility.

DOI: 10.1021/jf504494m
J. Agric. Food Chem. 2015, 63, 660−670

Table 2. Maximum Sorbed Values (Q_{max}) and Initial Slopes C_{ads}/C_{eq} Deduced from the Initial Part of the Sorption Isotherms for Yeast Biomass (Y), Inactived Yeast (IY), Autolyzed Inactived Yeast (A-IY), and Cell Walls (CW)

		C_{ads}/C_{eq}	Q_{max} (mg·L^{-1})	Q_{max} (mg.g^{-1})	Q_{max} (mg·m^{-2})[a]
Skin21 TPI	Y	∞	841 ± 35	440 ± 18	279 ± 11
	IY	∞	373 ± 69	197 ± 36	124 ± 23
	A-IY	∞	726 ± 70	382 ± 37	241 ± 23
	CW	*b*	219 ± 56	115 ± 29	72 ± 18
wine pool TPI	Y	0.27	350 ± 29	185 ± 15	116 ± 9
	IY	0.57	350 ± 25	185 ± 13	116 ± 8
	A-IY	0.39	350 ± 40	185 ± 21	116 ± 13
	CW	0.17	10 ± 55	5.29 ± 28	3.32 ± 18
wine pool anthocyanins	Y	0.09	8.8 ± 3	4.6 ± 1.0	2.9 ±
	IY	*b*	5.5 ± 1	2.9 ± 0.7	1.8 ± 0.4
	A-IY	*b*	1.8 ± 1	0.9 ± 0.7	0.6 ± 0.4
	CW	*b*	0.0	0.0	0.0
wine pool phenol acids	Y	*b*	5.6 ±	2.9 ± 0.4	1.9 ± 0,2
	IY	*b*	14.1 ± 2	7.4 ± 0.8	4.7 ± 1
	A-IY	0.1256	12.2 ± 2	6.4 ± 0.9	4.1 ± 1
	CW	*b*	1.6 ± 1	0.8 ± 0.3	0.5 ± 0.1

[a]For cell walls, we assumed that yeast walls account for 20% of the whole cell weight and that the outer surface developed by cell walls is about twice that developed by whole cells. [b]This value could not be calculated due to the very low adsorption.

wine. As for the untreated biomass, a complete adsorption of Skin21 PA was noticed at low polyphenol concentrations with IY and A-IY, followed by a progressive increase of the adsorbed amount, with fluctuations at the highest tested concentrations. However, some differences were observed between the untreated biomass and the others, and cells could be classified by decreasing order of maximum PA adsorption as follows: Y > A-IY > IY (Figure 5A and Table 2). Though much less than cell disruption, heat treatment and yeast autolysis thus affected the adsorption of polyphenols by yeasts. The reversibility of PA adsorption was evaluated at different initial PA concentrations. Results are summarized in Figure 5B for concentrations of 1 and 4 g·L^{-1}. As can be seen, much higher reversibility was found with the cell walls than with the whole cells. This suggests higher interaction strength between PA and whole yeast than PA and cell wall, and indicates different interaction mechanisms.

Part Played by Cell Wall in PA Adsorption? The much smaller adsorption observed with CW by comparison to whole cells is quite unexpected if PA adsorption occurs only within the wall network thickness. Considering that the outer surface developed by cell walls is about twice that developed by whole cells (Table 2), PA amount adsorbed at initial concentrations below 3 g·L^{-1} fell to values on the order of 2 to 3 mg·m^{-2}. This much smaller adsorption by comparison to whole cells could first be due to a loss of some cell wall constituents involved in interactions with polyphenols during mechanical disruption and/or to an important alteration of their three-dimensional structure, affecting the accessibility to interaction sites and proanthocyanidin accumulation within the wall network thickness. However, these results also raise the question of PA passage through the CW to the periplasmic space and of their interaction with the plasma membrane. As stated before, such transfer and interaction have been hypothesized in the case of small polyphenols.[42]

The question here is the pore size of yeast cell wall and the possible transfer within the network of PA with aDP as large as 21. The pore sizes of yeast cell wall and their permeability to solutes can vary significantly with the strain as well as with growth and environmental conditions. Reports underline a large variability in the data, which can be attributed to cell wall and membrane dynamic behavior, to the very different structures and conformations of the molecules used to study this permeability and to the different treatments applied on cells.[43−45] Thus, if Scherrer and collaborators[43] stated that only molecules smaller than 700 Da and with a maximum Stokes radius of 0.85 nm could diffuse freely through the cell wall, it is known that high molecular weight secreted proteins such as invertase (53 kDa) are able to pass through the cell wall barrier. According to Gerhardt and Judge,[46] the maximum "pore" size of yeast cell walls is around 36 Å and polyethylene glycol or dextran polymers of 4.5 kDa and above are excluded. The average molecular weights of the studied PAs are 5.84, 3.98, and 0.95 kDa for Skin21, Seed12, and Seed3, respectively. Grape or apple tannins are wormlike chain polymers with gyration radius ranging from 2 nm for an aDP 9 grape seed tannin fraction to 5.6 nm for an aDP 40 apple tannin fraction,[22] the radius of the cross section being within the range 0.3 to 0.45 nm. In addition, dynamic light scattering experiments indicated a hydrodynamic diameter on the order of 3 nm for an aDP 28 apple proanthocyanidin.[47] Thus, the passage of the studied grape tannins through the cell wall pores is possible.

In that case, polyphenols may interact not only with cell wall constituents but also with the plasma membrane and/or accumulate in the periplasmic space. The hypothesis of tannin passage through the cell wall and interactions with the plasma membrane would account for the very different reversibility found between cell walls and whole cells. Indeed, if only a passive diffusion mechanism with PA accumulation in the periplasmic space was involved, the reversibility would be higher. Further specific studies will be needed to validate these hypotheses. It is also important to note that most of the data on cell wall permeability/porosity concerns living cells. We are dealing here with the biomass (Y) that presents a very low viability (2.4%) and with inactivated cells. This lack of viability, which is consistent with the context of wine aging and of the use of inactivated yeast, may induce differences in cell wall permeability.

Impact of Autolysis, Inactivation, and Drying on PA Adsorption by Whole Cells. Adsorption isotherm evidenced

DOI: 10.1021/jf504494m
J. Agric. Food Chem. 2015, 63, 660−670

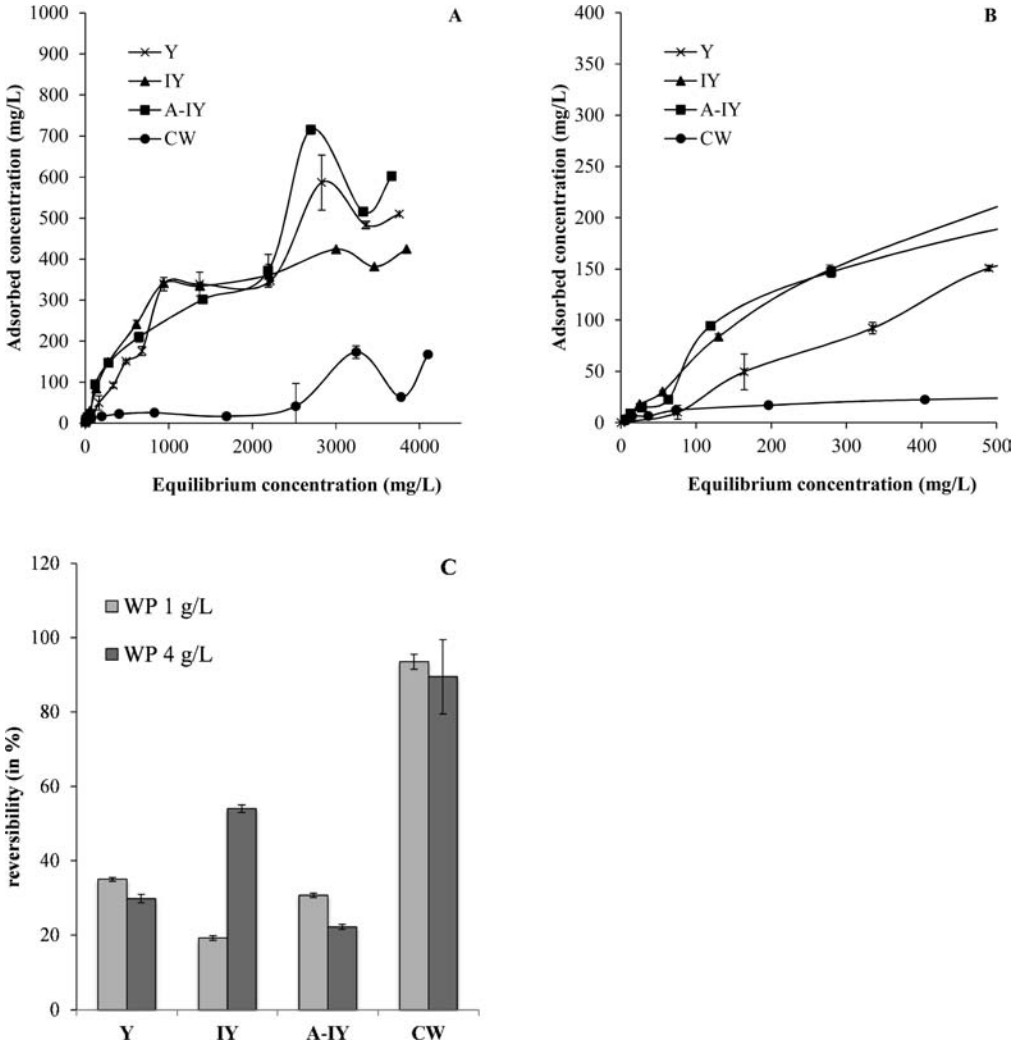

Figure 6. (A) Impact of postharvesting processes and cell disruption on the adsorption of wine polyphenols (WP): Y, yeast biomass; IY, inactivated yeast; A-IY, yeast submitted to autolysis and inactivation; CW, cell walls recovered from mechanical disruption. (B) Enlarged view of the initial adsorption. (C) Reversibility.

that autolysis, inactivation, and drying treatments decrease the maximum adsorbed amount of Skin21 PAs (Figure 5A). As stated before, maximum adsorbed amount on Y, IY, and A-IY indicates that PA adsorption is not limited to the outer cell surface but occurs within the cell wall thickness and may also involve the passage of PAs through the wall and accumulation in the periplasmic space. Thus, the composition and the three-dimensional structure of the cell wall will determine proanthocyanidin adsorption (affinity, adsorbed amount, and strength of the interactions) and wall permeability. Inactivation, autolysis, or spray-drying likely affect yeast cell wall characteristics,[37,38] and the MATS method, along with electrokinetic measurements, indicated an impact of these processes on the surface physicochemical properties of cells. The decrease in polarity observed for IY and A-IY by comparison to Y, which indicates a global decrease of sites for H-bond formation, could explain part of the observed differences between the untreated biomass and the two others. Indeed, proanthocyanidin adsorption on surfaces or complexation with other biopolymers (proteins, polysaccharides) in aqueous media have been shown to be mostly driven by hydrophobic attraction and H-bond formation, and thus by polar acid−base forces.[41,48−50] However, MATS and electrokinetic measurements provide information that only concerns the surface (outer mannoprotein layer). They provide neither any information concerning the three-dimensional organization of the cell wall network nor information about possible physicochemical changes inside this network. Thus, the greater adsorption capacity of Y by comparison to YI and AIY can also be related to a higher accessibility of PA to interaction sites. Especially, drying processes are known to affect the three-dimensional structure of biopolymer networks, inducing a collapse of their structure and a decrease of their porosity that are not fully reversible upon rehydration.[51]

Wine Polyphenols: Impact of Structural Changes on Tannin Sorption by Yeast Cells. Polyphenols from the wine pool WP exhibited much lower affinity than grape PA for the untreated and inactivated yeast cells, and maximum adsorbed amounts were also significantly lower (Figure 6 and Table 2). In agreement with that observed for PA, WP sorption on CW was about 15 times lower than on whole cells at concentrations below 3 $g{\cdot}L^{-1}$. With Y and A-IY, sorption curves presented a first plateau value for initial WP concentrations between 1.5 and 3 $g{\cdot}L^{-1}$, followed by a significant increase in adsorbed amount associated with strong fluctuations at higher concentrations. This increase at high WP concentrations was also

DOI: 10.1021/jf504494m
J. Agric. Food Chem. 2015, 63, 660−670

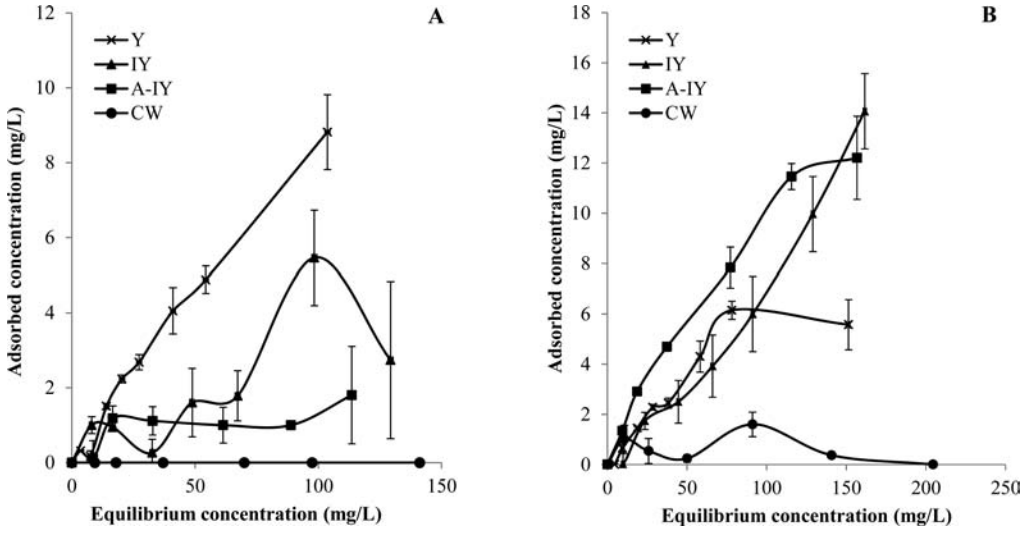

Figure 7. Adsorption of anthocyanins (A) and cinnamic acids (B) on the yeast biomass Y, the inactivated yeast IY, the yeast submitted to autolysis and inactivation A-IY; and the cell walls recovered from mechanical disruption CW.

noticed with cell walls, in accordance with that found with PA with this fraction, and was also associated with strong fluctuations. The exact origin of these fluctuations could not be identified in the present work.

The involvement of tannins and anthocyanins in oxidation reactions during winemaking and aging leads to the formation of a huge diversity of derived tannins and pigments, including polymeric pigments.[52] These structural changes result in the formation of modified units/subunits that cannot be easily analyzed, in a decrease of the yield of the acid-catalyzed cleavage reaction used for the analysis of oligomers and polymers, and induce bias in the determination of the average degree of polymerization of the latter.[53,22] This is the reason why adsorption was studied for WP using spectrophotometric measurements. HPLC analyses were however performed to distinguish between the adsorption of monomers (free anthocyanins and their derivatives, cinnamic acids, flavonols, flavanol monomers) and that of wine PAs and polymeric pigments. Among monomers, only anthocyanins and phenolic acids were adsorbed by yeast cells (Figure 7). This adsorption remained very low and nonspecific. Thus, adsorption of red wine polyphenols by yeast cells or yeast cell walls mainly concerns oligomeric and polymeric structures, and the lowest sorption of wine PAs by comparison to skin and seed PAs is not related to a competition with more simple phenols or to a different aDP but to structural changes. In addition, the higher reversibility found with WP by comparison to PAs indicates weaker interactions.

Structural changes related to oxidation reactions (intermolecular and intramolecular reactions) have been shown to induce an increase of the molecular weight of PAs, along with changes in their conformation.[22,31] This can first induce a lower accessibility of wine PAs to CW interaction sites and/or interfere with their diffusion through the cell walls. Moreover, changes in PA structure associated with winemaking and aging have been shown to modify their interactions with poly(L-proline). Isothermal titration calorimetry experiments indicated a decrease in hydrophobic attraction and hydrogen bond formation between PAs and poly(L-proline) for wine PAs by comparison to grape ones, a decrease that was enhanced with wine age.[31] This was attributed to fewer accessible PA interaction sites due to conformational modifications. However, it can also be due to chemical changes at the molecular level that modify their hydrophobic character and H-donor character. This is consistent with the higher affinity found at low concentrations for IY and A-IY by comparison to Y: postharvesting treatments increased the hydrophobicity and basic character of yeast surface by comparison to the untreated biomass.

This work allowed thus to evidence a very strong affinity of grape seed and skin proanthocyanidins for yeast cells, associated with high adsorption levels. Yeast cells in the context of this work were an untreated biomass with viability close to zero and inactivated yeast fractions. Wine polyphenols exhibited lower affinity for cells than grape PAs, attributed to structural changes that occur during winemaking and aging. A preferential adsorption of wine oligomeric and polymeric PAs and pigments was observed, while the adsorption of monomers remained very small. An important result here was the different adsorption behavior between whole cells and cell walls. Results raise the question of the exact part played by cell walls in the adsorption of wine polyphenols and suggest a quite easy diffusion of proanthocyanidins (up to an average DP of 21) and of wine PAs through this cell wall, accumulation in the periplasmic space, and interactions with the yeast cell membrane. This hypothesis needs to be confirmed, and future works will be devoted to the identification of polyphenol location in whole cells.

AUTHOR INFORMATION

Corresponding Author

*Montpellier SupAgro, UMR 1083 Sciences pour l'œnologie (SPO), bât. 28, 2 place Viala, F-34060 Montpellier, France. Phone: 33 (0)4 99 61 27 58. Fax: 33 (0)4 99 61 28 57. E-mail: vernhet@supagro.inra.fr.

Notes

The authors declare no competing financial interest.

ACKNOWLEDGMENTS

The authors thank Jean-Paul Mazauric, Jean-Marc Souquet, and Stéphanie Carrillo for their precious help in the experiments and during polyphenol purification and analysis; Chantal

DOI: 10.1021/jf504494m
J. Agric. Food Chem. 2015, 63, 660−670

Cazevieille and Cécile Sanchez for microscopy analysis; Céline Poncet-Legrand, Virginie Hugouvieux, and Jean-Marc Brillouet for very profitable discussions.

■ ABBREVIATIONS USED

aDP, average degree of polymerization; A-IY, autolyzed and inactivated yeast; CW, cell wall; IY, inactivated yeast; IYFs, inactivated yeast fractions; MATS, microbial adhesion to solvents; PAs, proanthocyanidins; Seed12, grape seed proanthocyanidins with an average degree of polymerization 12; Seed3, grape seed proanthocyanidins with an average degree of polymerization 3; Skin 21, grape skin proanthocyanidins with an average degree of polymerization 21; TEM, transmission electron microscopy; WP, wine polyphenols; Y, yeast biomass

■ REFERENCES

(1) Guilloux-Benatier, M.; Chassagne, D. Comparison of components released by fermented or active dried yeasts after aging on lees in a model wine. *J. Agric. Food Chem.* **2003**, *51*, 746−751.

(2) Soubeyrand, V.; Luparia, V.; Williams, P.; Doco, T.; Vernhet, A.; Ortiz-Julien, A.; Salmon, J.-M. Formation of micella containing solubilized sterols during rehydration of active dry yeasts improves their fermenting capacity. *J. Agric. Food Chem.* **2005**, *53*, 8025−8032.

(3) Loira, I.; Vejarano, R.; Morata, A.; Ricardo-da-Silva, J. M.; Laureano, O.; González, M. C.; Suárez-Lepe, J. A. Effect of *Saccharomyces* strains on the quality of red wines aged on lees. *Food Chem.* **2013**, *139*, 1044−1051.

(4) Merida, J.; Lopez-Toledano, A.; Marquez, T.; Millan, C.; Ortega, J. M.; Medina, M. Retention of browning compounds by yeasts involved in the winemaking of sherry type wines. *Biotechnol. Lett.* **2005**, *27*, 1565−1570.

(5) Morata, A.; Gómez-Cordovés, M. C.; Suberviola, J.; Bartolomé, B.; Colomo, B.; Suárez, J. A. Adsorption of anthocyanins by yeast cell walls during the fermentation of red wines. *J. Agric. Food Chem.* **2003**, *51*, 4084−4088.

(6) Razmkhab, S.; Lopez-Toledano, A.; Ortega, J. M.; Mayen, M.; Merida, J.; Medina, M. Adsorption of phenolic compounds and browning products in white wines by yeasts and their cell walls. *J. Agric. Food Chem.* **2002**, *50*, 7432−7437.

(7) Caridi, A. New perspectives in safety and quality enhancement of wine through selection of yeasts based on the parietal adsorption activity. *Int. J. Food Microbiol.* **2007**, *120*, 167−172.

(8) Del Barrio-Galan, R.; Perez-Magarino, S.; Ortega-Heras, M.; Guadalupe, Z.; Ayestaran, B. Polysaccharide characterization of commercial dry yeast preparations and their effect on white and red wine composition. *LWT—Food Sci. Technol.* **2012**, *48*, 215−223.

(9) Comuzzo, P.; Tat, L.; Tonizzo, A.; Battistutta, F. Yeast derivatives (extracts and autolysates) in winemaking: Release of volatile compounds and effects on wine aroma volatility. *Food Chem.* **2006**, *99*, 217−230.

(10) Comuzzo, P.; Tat, L.; Fenzi, D.; Brotto, L.; Battistutta, F.; Zironi, R. Interactions between yeast autolysates and volatile compounds in wine and model solution. *Food Chem.* **2011**, *127*, 473−480.

(11) Del Barrio-Galán, R.; Perez-Magarino, S.; Ortega-Heras, M.; Williams, P.; Doco, T. Effect of aging on lees and of three different dry yeast derivatives products on verdejo white wine composition and sensorial characteristics. *J. Agric. Food Chem.* **2011**, *59*, 12433−12442.

(12) Moine-ledoux, V.; Dubourdieu, D. Role of yeast mannoproteins with regard to tartaric stabilization of wines. *Bull. O.I.V.* **2002**, *75*, 857−858.

(13) Waters, E. J.; Pellerin, P.; Brillouet, J.-M. A *Saccharomyces* mannoprotein that protects wine from protein haze. *Carbohydr. Polym.* **1994**, *23*, 185−191.

(14) Pérez-Serradilla, J. A.; Luque de Castro, M. D. Role of lees in wine production: A review. *Food Chem.* **2008**, *111*, 447−456.

(15) Escot, S.; Feuillat, M.; Dulau, L.; Charpentier, C. Release of polysaccharides by yeasts and the influence of released polysaccharides on colour stability and wine astringency. *Aust. J. Grape Wine Res.* **2001**, *7*, 153−159.

(16) Rodrigues, A.; Ricardo-da-silva, J. M.; Lucas, C.; Laureano, O. Effect of commercial mannoproteins on wine colour and tannins stability. *Food Chem.* **2012**, *131*, 907−914.

(17) Mazauric, J.-P.; Salmon, J.-M. Interactions between yeast lees and wine polyphenols during simulation of wine aging: I. Analysis of remnant polyphenolic compounds in the resulting wines. *J. Agric. Food Chem.* **2005**, *53*, 5647−5653.

(18) Mazauric, J.-P.; Salmon, J.-M. Interactions between Yeast Lees and Wine Polyphenols during Simulation of Wine Aging: II. Analysis of Desorbed Polyphenol Compounds from Yeast Lees. *J. Agric. Food Chem.* **2006**, *54*, 3876−3881.

(19) Vasserot, Y.; Caillet, S.; Maujean, A. Study of anthocyanin adsorption by yeast lees. Effect of some physicochemical parameters. *Am. J. Enol. Vitic.* **1997**, *48*, 433−437.

(20) Guadalupe, Z.; Ayestaran, B. Effect of commercial mannoprotein addition on polysaccharide, polyphenolic, and color composition in red wines. *J. Agric. Food Chem.* **2008**, *55*, 10720−10728.

(21) Fulcrand, H.; Duenas, M.; Salas, E.; Cheynier, V. Phenolic reactions during winemaking and aging. *Am. J. Enol. Vitic.* **2006**, *57:3*, 289−297.

(22) Poncet-Legrand, C.; Cabane, B.; Bautista-Ortin, A. B.; Carrillo, S.; Fulcrand, H.; Perez, J.; Vernhet, A. Tannin oxidation: intra- versus intermolecular reactions. *Biomacromolecules* **2010**, *11*, 2376−2386.

(23) Vernhet, A.; Dubascoux, S.; Cabane, B.; Fulcrand, H.; Dubreucq, E.; Poncet-Legrand, C. Characterization of oxidized tannins: comparison of depolymerization methods, asymmetric flow field-flow fractionation and small-angle X-ray scattering. *Anal. Bioanal. Chem.* **2011**, *401*, 1559−1569.

(24) Dallies, N.; François, J.-M.; Paquet, V. A new method for quantitative determination of polysaccharides in the yeast cell wall. Application to the cell wall defective mutants of *Saccharomyces cerevisiae*. *Yeast* **1998**, *14*, 1297−1306.

(25) Klis, F. M.; Boorsma, A.; De Groot, P. W. J. Cell wall construction in Saccharomyces cerevisiae. *Yeast* **2006**, *23*, 185−202.

(26) Orlean, P. Architecture and biosynthesis of the *Saccharomyces cerevisiae* cell wall. *Genetics* **2012**, *192*, 775−818.

(27) Bellon-Fontaine, M.-N.; Rault, J.; van Oss, C. J. Microbial adhesion to solvents: a novel method to determine the electron-donor/electron-acceptor or Lewis acid-base properties of microbial cells. *Colloids Surf., B* **1996**, *7*, 47−53.

(28) Fournand, D.; Vicens, A.; Sidhoum, L.; Souquet, J.-M. M.; Moutounet, M.; Cheynier, V. Accumulation and extractability of grape skin tannins and anthocyanins at different advanced physiological stages. *J. Agric. Food Chem.* **2006**, *54*, 7331−7338.

(29) Kennedy, J. A.; Matthews, M. A.; Waterhouse, A. L. Changes in grape seed polyphenols during fruit ripening. *Phytochemistry* **2000**, *55*, 77−85.

(30) Ducasse, M.-A. *Impact des enzymes de macération sur la composition en polysaccharides et en polyphénols des vins rouges-Etude de l'évolution de ces composés en solution modèle vin*. PhD thesis; University of Montpellier II: 2009; pp 71.

(31) McRae, J. M.; Falconer, R. J.; Kennedy, J. A. Thermodynamics of grape and wine tannin interaction with polyproline: implications for red wine astringency. *J. Agric. Food Chem.* **2010**, *58*, 12510−12518.

(32) Albersheim, P.; Nevins, D. J.; English, P. D.; Karr, A. A method for the analysis of sugars in plant cell wall polysaccharides by gas−liquid chromatography. *Carbohydr. Res.* **1967**, *5*, 240−245.

(33) Harris, P. J.; Henri, R. J.; Blakeney, A. B.; Stone, B. A. An improved method for the methylation analysis of oligosaccharides and polysaccharides. *Carbohydr. Res.* **1984**, *55*, 205−208.

(34) Doco, T.; Williams, P.; Cheynier, V. Effect of flash release and pectinolytic enzyme treatments on wine polysaccharide composition. *J. Agric. Food Chem.* **2007**, *55*, 6643−6649.

(35) Mane, C. *Phénomènes oxydants et composés phénoliques dans les vins blancs de Champagne: developpements methodologiques pour*

DOI: 10.1021/jf504494m
J. Agric. Food Chem. 2015, 63, 660−670

l'analyse des polymères. PhD thesis; Montpellier SupAgro: 2007; pp 56−58.
(36) Ayala, F.; Echavarri, J. F.; Negueruela, A. I. A new simplified method for measuring the color of wines. I. Red and Rosé wines. *Am. J. Enol. Vitic.* **1997**, *48*, 357−363.
(37) Pradelles, R.; Vichi, S.; Alexandre, H.; Chassagne, D. Influence of the drying processes of yeasts on their volatile phenol sorption capacity in model wine. *Int. J. Food Microbiol.* **2009**, *135*, 152−157.
(38) Vergnault, H.; Willemot, R.-M.; Mercier Bonin, M. Non-electrostatic interactions between cultured *Saccharomyces cerevisiae* yeast cells and adsorbent beads in expanded bed adsorption: Influence of cell wall properties. *Process Biochem.* **2007**, *42*, 244−251.
(39) Scherrer, R.; Berlin, E.; Gerhardt, P. Density, Porosity, and Structure of dried cell walls isolated from *Bacillus megaterium* and *Saccharomyces cerevisiae*. *J. Bacteriol.* **1977**, *129*, 1162−1164.
(40) Klis, F. M.; Brul, S.; De Groot, P. W. J. Covalently linked wall proteins in ascomycetous fungi. *Yeast* **2010**, *27*, 489−493.
(41) Cartalade, D.; Vernhet, A. Polar interactions in flavan-3-ol adsorption on solid surfaces. *J. Agric. Food Chem.* **2006**, *54*, 3086−3094.
(42) Marquez, T.; Millan, C.; Salmon, J.-M. Plasma membrane sterols are involved in yeast's ability ao adsorb polyphenolic compounds resulting from wine model solution browning. *J. Agric. Food Chem.* **2009**, *57*, 8026−8032.
(43) Scherrer, R.; Louden, L.; Gerhardt, P. Porosity of the yeast cell wall and membrane. *J. Bacteriol.* **1974**, *118*, 534−540.
(44) De Nobel, J. G. Increased Cell Wall Porosity in *Saccharomyces cerevisiae* after treatment with dithiothreitol or EDTA. *J. Gen. Microbiol.* **1989**, *135*, 2077−2084.
(45) Normand, V.; Dardelle, G.; Bouquerand, P.-E.; Nicolas, L.; Johnston, D. Flavor encapsulation in yeasts: limonene used as a model system for characterization of the release mechanism. *J. Agric. Food Chem.* **2005**, *53*, 7532−7543.
(46) Gerhardt, P.; Judge, J. A. Porosity of isolated cell walls of *Saccharomyces cerevisiae* and *Bacillus megaterium*. *J. Bacteriol.* **1964**, *87*, 945−951.
(47) Zanchi, D.; Konarev, P. V.; Tribet, C.; Baron, A.; Svergun, D. I.; Guyot, S. Rigidity, conformation, and solvation of native and oxidized tannin macromolecules in water-ethanol solution. *J. Chem. Phys.* **2009**, *130*, 245103.
(48) Le Bourvellec, C.; Guyot, S.; Renard, C. Non-covalent interaction between procyanidins and apple cell wall material: Part I. Effect of some environmental parameters. *Biochim. Biophys. Acta, Gen. Subj.* **2004**, *1672*, 192−202.
(49) Oh, H. I.; Hoff, J. E.; Armstrong, G. S.; Haff, L. A. Hydrophobic interaction in tannin-protein complexes. *J. Agric. Food Chem.* **1980**, *28*, 394−398.
(50) McManus, J. P.; Davis, K. G.; Beart, J. E.; Gaffney, S. H.; Lilley, T. H.; Haslam, E. Polyphenol interactions. Part I. Introduction; some observations on the reversible complexation of polyphenols with proteins and polysaccharides. *J. Chem. Soc., Perkin Trans.* **1985**, *II*, 1429−1438.
(51) Hromadkova, Z.; Ebringerova, A.; Sasinkova, V.; Sandula, J.; Hribalova, V.; Omelkova, J. Influence of the drying method on the physical properties and immunomodulatory activity of the particulate (1−3)-beta-D-glucan from *Saccharomyces cerevisiae*. *Carbohydr. Polym.* **2003**, *51*, 9−15.
(52) Mouls, L.; Fulcrand, H. UPLC-ESI-MS study of the oxidation markers released from tannin depolymerization: toward a better characterization of the tannin evolution over food and beverage processing. *J. Mass Spectrom.* **2012**, *47*, 1450−1457.
(53) Aron, P. M.; Kennedy, J. A. Compositional investigation of phenolic polymers isolated from Vitis vinifera L. Cv. Pinot Noir during fermentation. *J. Agric. Food Chem.* **2007**, *55*, 5670−5680.

DOI: 10.1021/jf504494m
J. Agric. Food Chem. 2015, 63, 660−670

JOURNAL OF AGRICULTURAL AND FOOD CHEMISTRY

Article

pubs.acs.org/JAFC

Complex Carbohydrates of Red Wine: Characterization of the Extreme Diversity of Neutral Oligosaccharides by ESI-MS

Thierry Doco,*[,†] Pascale Williams,[†] Emmanuelle Meudec,[‡] Véronique Cheynier,[†,‡] and Nicolas Sommerer[‡]

[†]Team BCP2, and [‡]Polyphenols Platform, UMR1083 Sciences pour l'Œnologie, INRA, 2 Place Viala, F-34060 Montpellier, France

ABSTRACT: The major neutral oligosaccharides of a Carignan red wine have been characterized for the first time. The oligosaccharides were prepared after removal of phenolic compounds by polyamide chromatography and of polysaccharides by alcohol precipitation and then were fractionated by anion exchange and size-exclusion chromatography. In a second step, the glycosyl composition and linkages of wine oligosaccharides were determined. Oligosaccharide fractions were analyzed by mass spectrometry (MS) with an electrospray ionization (ESI) source and an ion trap mass analyzer after separation by hydrophilic interaction liquid chromatography on a Nucleodur HILIC column (zwitterionic sulfoalkyl betaine stationary phase). Glycosyl residue composition analysis showed the predominant presence of arabinose, with galactose, rhamnose, and mannose in lower proportion. Neutral oligosaccharides were present at a concentration of 185 mg/L in this wine. The MS spectra in the negative ion mode of the oligosaccharide fractions showed a series of oligosaccharidic structures corresponding to oligo-arabinans often linked to the basic unit α-L-Rha*p*-(1 → 4)-α-D-Gal*p*A. The wine oligosaccharides identified correspond to arabino-oligosaccharides, rhamno-arabino-oligosaccharides, and different rhamnogalacturonan-arabino-oligosaccharides with DP ranging from 5 to 49, resulting from the degradation of grape cell wall pectins. Oligosaccharides have an extreme diversity, with more than 100 peaks detected in HPLC-ESI-MS spectra corresponding each to at least one oligosaccharidic structure.

KEYWORDS: *wines, oligosaccharides, HILIC, HPLC-ESI-MS/MS*

INTRODUCTION

Wine polysaccharides have been thoroughly studied because of their technological and sensory properties in wines. They have been shown to interact with tannins,[1,2] to decrease astringency,[3] to inhibit hydrogen tartrate crystallization,[4] to interact with wine aroma compounds,[5] to prevent or limit aggregation and flocculation and the formation of protein haze in white wine,[6−10] and to form specific coordination complexes with Pb^{2+} ions.[11,12] For sparkling wines, foam properties have been correlated with the type, the molecular weight, and the composition of polysaccharides.[13−16]

Although their presence in wine is known,[17−22] information on oligosaccharide composition is still limited, because of the difficulty in separating and characterizing them. Sucrose and other diholosides have been identified in wines,[22] and a global fraction of oligomers of homo- and rhamno-galacturonan was described and shown to decrease during wine aging.[23] The structure and amounts of polysaccharides and oligosaccharides released into the wines also depend on the grape varieties and the wine-making process and can be modified by enzyme treatment.[18,20,24−27]

Oligosaccharides can be found in various areas, in food, and in nonfood applications.[28] Their main applications include elicitation of plant defenses[29] and a role in prebiotics,[30] but they are also significant for their physicochemical properties such as chelations of cations[31] which can be important for wines. It is important to determine the exact composition of oligosaccharides in wines and to analyze their molecular structures in order to better understand the technological and organoleptic properties associated with them. Characterization of oligosaccharide structure has been classically performed by glycosyl and linkage analyses, by NMR, or by mass spectrometry techniques.[32] The direct analysis of oligosaccharide mixtures by MS has been made possible by the development of soft ionization techniques such as ESI (electrospray ionization).[33−35] The ion fragmentation patterns obtain by MS/MS or MS^n spectra provided information for structural characterization of oligosaccharides.[36] Acidic oligosaccharides have been identified previously,[17,18] and some neutral oligosaccharides have been characterized by high resolution and high mass accuracy matrix-assisted laser desorption/ionization Fourier transform ion cyclotron resonance mass spectrometry (MALDI-FTICR MS) in Grignolino and Chardonnay wines.[19]

We describe herein the purification of neutral and acidic oligosaccharides from a red wine of Carignan and the characterization of the main neutral oligosaccharides after chromatographic separation using a HILIC column by mass spectrometry coupled to an electrospray ionization source and an ion trap mass analyzer. The MS technique proved to be particularly efficient for the analysis of mixtures of wine oligosaccharides without prior derivatization.

EXPERIMENTAL SECTION

Wine Samples. Carignan red wine was made from the grapes of *Vitis vinifera* cv. Carignan grown at the INRA Experimental Unit Station (Gruissan, Southern France) and harvested in 2004 at

Received: October 8, 2014
Revised: December 9, 2014
Accepted: December 20, 2014
Published: December 20, 2014

ACS Publications © 2014 American Chemical Society

DOI: 10.1021/jf504795g
J. Agric. Food Chem. 2015, 63, 671−682

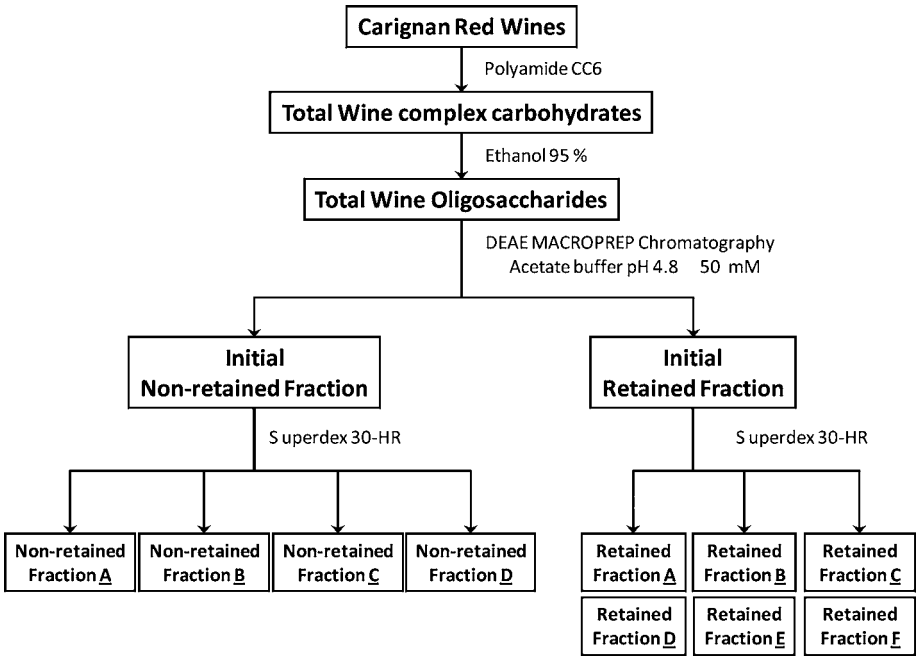

Figure 1. Scheme of fractionation of wine oligosaccharides by decolorization, alcohol precipitation, and anion-exchange and size-exclusion chromatography.

commercial maturity (21.8°Brix). A 100 kg amount of grapes was crushed and destemmed using a destemmer−crusher and put in 100-L stainless steel tanks. Alcoholic fermentation was carried out in tanks equipped with temperature control (28 °C), enabling regulation of fermentation kinetics. At the end of alcoholic fermentation, the must was pressed, the wine was stored in 50-L tanks, and lactic bacteria was subsequently added to induce malolactic fermentation. At the end of malolactic fermentation, the wine was racked in a 30-L inox tank and stored at low temperature (−4 °C) to induce tartaric stability. The wine was then bottled and stored in a cellar at 18 °C until analysis.[18,26]

Isolation of Oligosaccharide Fractions. As described in Figure 1, wines (500 mL) added to 1 M NaCl were partially decolorized on a column of MN Polyamide CC6 (28 × 2.8 cm) previously equilibrated with 1 M NaCl. Wine polysaccharides and oligosaccharides not retained on the polyamide column were eluted by two bed volumes of 1 M NaCl.[37] The wine complex carbohydrates were precipitated by ethanolic dehydration. This was performed by adding ethanol 95% acidified by 0.5% HCl to obtain a final concentration of 80% ethanol.[23,24] After one night at 4 °C, the supernatant, which contained the total oligosaccharide fraction, was recovered by centrifugation (30 min, 6288*g*, 4 °C) and dialyzed extensively against distilled water (MWCO 1 kDa), concentrated, and freeze-dried. Then a step of anion-exchange chromatography was performed. The solution containing oligosaccharides was loaded on a DEAE-MACROPREP column (17 × 5 cm; Bio-Rad, Hercules, CA) equilibrated with 50 mM sodium acetate buffer pH 4.8. An unbound fraction (nonretained fraction) was recovered, and a bound fraction (retained fraction) of oligosaccharides was eluted by 1 M NaCl in the same buffer. The unbound fraction and the bound fraction from DEAE-Macroprep were extensively dialyzed against distilled water (MWCO 1 kDa), concentrated, and freeze-dried.

The oligosaccharides of unbound (initial nonretained fraction) and bound (initial retained fraction) fractions were finally purified by size exclusion chromatography. The chromatography was performed by loading 2 mL of initial nonretained or initial retained fractions containing 30 mg of the freeze-dried fraction on a Superdex 30-HR column (60 × 1.6 cm, GE Healthcare, Uppsala, Sweden) with a precolumn (0.6 × 4 cm), equilibrated at 1 mL/min in 30 mM ammonium formate pH 5.6. The elution of oligosaccharides was monitored with an Erma-ERC 7512 (Erma, Tokyo, Japan) refractive index detector combined with Chromeleon software (Dionex, Sunnyvale, CA). Four and six fractions, according to elution time, were collected for the unbound DEAE fraction (initial nonretained fraction) and bound DEAE fraction (initial retained fraction), respectively. The isolated fractions, called nonretained fractions A, B, C, and D and retained fractions A, B, C, D, E, and F were freeze-dried, redissolved in water, and freeze-dried again four times to remove completely the ammonium salt (Figure 1). The molecular weight distribution of oligosaccharides present in the nonretained fractions A, B, C, D and retained fractions A, B, C, D, E, and F was determined by high-performance size-exclusion chromatography (HPSEC) using a LC-10 AS Shimadzu pump (Kyoto, Japan). HPSEC elution was performed on two serial Shodex Ohpak KB-803 and KB-805 columns (0.8 × 30 cm; Showa Denkko, Japan) connected to a ERC-7512 refractometer (Erma, Japan), at 1 mL/min flow rate in 0.1 M $LiNO_3$. The apparent molecular weights were deduced from the calibration curve established with a pullulan calibration kit (P-400, MW = 380 000 P-200, MW = 186 000; P-100, MW = 100 000; P-50, MW = 48 000; P-20, MW = 23 700; P-10, MW = 12 200; P-5, MW = 5800; Showa Denko K.K., Japan). The calibration equation was log MW = 27.746 − 1.03 × t_R (t_R = column retention-time at peak maximum, and r^2 = 0.997).

Neutral Sugar Composition as Alditol Acetates. Neutral sugars were determined as alditol acetates by GLC after TFA hydrolysis.[38] Separation was carried out on a DB225 column (30 m × 0.25 mm i.d.; 0.25 μm film; J&W Scientific, Agilent Technologies, Santa Clara, CA) with hydrogen as carrier gas (0.6 bar inlet pressure) on a Shimadzu GC-2010*plus* gas chromatograph. The alditol acetates were identified from their retention times by comparison with those of standard monosaccharides. Neutral sugars amounts were calculated relative to the internal standards. Allose and myo-inositol were used as internal standards.[39]

Neutral and Acidic Sugar Composition as Trimethylsilyl Derivatives. The neutral and acidic sugar composition was determined after solvolysis with anhydrous MeOH containing 0.5 M HCL (80 °C, 16 h), by GC of their per-O-trimethylsilylated (TMS) methyl glycoside derivatives.[40] The TMS derivatives were separated on two DB-1 capillary columns (30 m × 0.25 mm i.d., 0.25 μm film) (temperature programming 120−145 °C at 1.5 °C/min, then 145−180 °C at 0.9 °C/min, and finally−180−230 °C at 50 °C/min), coupled to a single injector inlet through a two-holed ferrule, with H_2 as the carrier gas on a Shimadzu GCMS-QP2010SE gas chromato-

DOI: 10.1021/jf504795g
J. Agric. Food Chem. 2015, 63, 671−682

Table 1. Composition Analysis of Nonretained and Retained Oligosaccharide Fractions on a DEAE-Macroprep Column (mol %)

	Rha	Ara	Xyl	Gal	Glc	Man	GalA	GlcA	ratio Ara/Gal	MW[a]	conc[b]
initial nonretained fraction	3.0	75.6	-	6.3	3.0	8.4	2.7	1.1	12.00	-	184.8
nonretained fraction A	1.0	70.9	-	4.0	4.8	19.4	-	-	17.72	8187	4.0
nonretained fraction B	1.4	89.1	-	5.2	1.2	2.3	0.8	-	17.13	3828	44.4
nonretained fraction C	1.7	82.1	-	7.0	1.9	5.0	1.1	1.1	11.72	2250	85.0
nonretained fraction D	8.9	29.3	6.0	6.1	10.9	30.4	6.2	2.4	4.80	929	36.2
initial retained fraction	27.5	29.9	-	8.8	2.5	0.8	29.2	1.2	3.39	-	261.6
retained fraction A	17.6	48.5	-	12.1	3.7	3.4	13.6	1.2	4.00	7641	25.6
retained fraction B	27.2	39.2	-	9.1	2.4	Tr[c]	20.5	1.3	4.30	2591	110.0
retained fraction C	35.0	24.0	-	7.4	2.0	Tr[c]	29.7	1.3	3.24	1790	16.8
retained fraction D	39.6	15.1	-	7.1	2.2	Tr[c]	34.1	1.5	2.12	1516	34.8
retained fraction E	49.9	3.4	-	2.4	2.2	Tr[c]	40.9	0.8	1.41	1255	30.0
retained fraction F	38.0	-	-	-	9.0	0.7	52.3	-	-	966	11.6

[a]Molecular weight. [b]Concentration mg/L. [c]Tr = trace, less than 0.5%.

graph. The outlet of one column was directly connected to a FID at 250 °C, and the second column via a deactived fused-silica column (0.25 m × 0.11 μm i.d.) was connected to a mass detector. Samples were injected in the pulsed split mode with a split ratio of 20:1. The transfer line to the mass was set at 280 °C. EI mass spectra were obtained from m/z 50 to 400 every 0.2 s in the total ion-monitoring mode using an ion source temperature of 200 °C, a filament emission current of 60 μA, and an ionization voltage of 70 eV.

Glycosyl-Linkage Determination. The glycosyl-linkage compositions were determined by GC-MS of the partially methylated alditol acetates. Two milligrams of polysaccharides in 0.5 mL of dimethyl sulfoxide were methylated using methyl sulfinyl carbanion and methyl iodide.[41] Only for the retained fractions A, B, C, D, E, and F, half of the methylated sample was then carboxyl-reduced with lithium triethylborodeuteride (Superdeuteride, Aldrich, Milwaukee, WI).[42] Both methylated and methylated-carboxyl-reduced samples were hydrolyzed with 2 M trifluoroacetic acid (75 min at 120 °C). The released methylated or carboxyl-reduced monosaccharides were converted to their corresponding alditols by treatment with $NaBD_4$ and then acetylated.[38] Partially methylated alditol acetates were analyzed by GC GC-EI-MS using a DB-1 capillary column (30 m × 0.32 mm i.d., 0.25 μm film); temperature programming 135 °C for 10 min and then 1.2 °C/min to 180 °C, with H_2 as the carrier gas on a Shimadzu GCMS-QP2010SE gas chromatograph.[43] Identity of each methyl ether was confirmed by EIMS, and their areas were corrected by response factors.

UPLC-ESI-MS^n. Separations of oligosaccharide fractions were performed using a Waters Acquity UPLC-DAD system (Milford, MA), on a (100 × 1 mm i.d.) Nucleodur HILIC column, 1.8 μm (zwitterionic sulfoalkyl betaine stationary phase, Macherey-Nagel, Düren, Germany), operated at 35 °C. The mobile phase consisted of acetonitrile/formic acid (99.5/0.5, v/v) (eluent A) and water/formic acid (99.5/0.5,v/v) (eluent B). Flow rate was 0.3 mL/min. The elution program was as follows: 1−40% B (0−20 min), 40−90% B (20−21 min), isocratic with 90% B (21−25 min), 90−1% B (25−26 min), isocratic with 1% B (26−33 min).

ESI-MS^n analyses were performed with a Bruker Daltonics Amazon (Bremen, Germany) mass spectrometer equipped with an electrospray source and an ion trap mass analyzer. The spectrometer was operated in the negative ion mode (capillary voltage, 4 kV; end plate off set: −300 V; temperature, 200 °C; nebulizer gas: 36 psi and dry gas, 7 L/min). Collision energy for fragmentation used for MS^2 and MS^3 experiments was set at 1. The mass spectra were acquired over a mass range of 300−2500 Da with target mass at 1200 Da, and 500−3000 Da with target mass at 2000 Da.

RESULTS AND DISCUSSION

Purification and Characterization of Oligosaccharide Fractions. Wine carbohydrates from Carignan were decolorized on Polyamide CC6 and then were precipitated by acidified alcohol in order to separate polysaccharides (mannoproteins, polysaccharides rich in arabinose and galactose (PRAGs), RGII, and glucans) from oligosaccharides (Figure 1). The passage of the supernatant through a column of anion exchange allowed us to separate wine oligosaccharides into two fractions, a first fraction not retained on the column and a second charged and retained on the column and then eluted by 1 M of NaCl. The glycosyl residue composition determined by GC after methanolysis and trimethysylilation,[40] is summarized in Table 1. The nonretained fraction contained low amounts of uronic acids, 2.7 mol % for galacturonic acid, and 1.1 mol % for glucuronic acid and is predominantly composed of arabinose (75.6%). In the retained fraction, galacturonic acid, rhamnose, and arabinose presented the highest molar percentages (29.2, 27.5, and 29.9, respectively). The total amount of oligosaccharides before the anion exchange represented a concentration of 446 mg per liter (184 mg for initial nonretained fraction and 261 mg for the initial retained fraction, Table 1). These results are slightly higher than those previously reported for Merlot and Carignan,[17,18] or Grignolino and Chardonnay wines,[19] but they were similar to those reported for Monastrell wine oligosaccharide fractions.[20]

The initial nonretained fraction and the initial retained fraction were finally separated by SEC on superdex HR30. The MW determined for the oligosaccharide fractions obtained by SEC are given in Table 1. The nonretained fraction and retained fractions yielded four and six subfractions, respectively, with molecular weight (MW) ranging from 8000 Da (fraction A) to 1000 Da (fractions D and F, respectively). Table 1 also shows the glycosyl residue composition of the oligosaccharide fractions obtain after solvolysis by GC of their per-O-trimethylsilylated (TMS) methyl glycoside derivatives. They contained most of the sugars known to take part in the composition of wine carbohydrates. Oligosaccharides of nonretained fractions A, B, C, and D and retained fractions A, B, C, D, E, and F included sugars such as rhamnose, arabinose, galactose, and galacturonic acid derived from the pecto-cellulosic cell walls of grape berries but also mannose and glucose released from yeast and/or bacteria polysaccharides.[17−21] The nonretained fractions A, B, and C were rich in arabinose (70.9%, 89.1%, and 82.1%, respectively), whereas nonretained fraction D contained similar proportions of arabinose and mannose (30%), and larger proportions of

DOI: 10.1021/jf504795g
J. Agric. Food Chem. 2015, 63, 671−682

Table 2. Glycosyl Linkage Composition (mole percentage) of Oligosaccharides Fractions Isolated from Carignan Red Wine

		nonretained fractions				retained fractions					
methyl ether	linkage	A	B	C	D	A	B	C	D	E	F
2,3,4-Rha[a]	terminal	-	-	-	1.5	0.9	1.4	2.4	3.4	11.3	13.8
3,4-Rha	2-linked	0.8	0.9	1.7	5.9	5.4	14.1	29.1	36.5	42.9	34.7
3-Rha	2,4-linked	-	-	-	-	13.8	12.3	6.0	3.6	1.3	Tr[c]
total rhamnose[b]		0.8	0.9	1.7	7.4	20.1	27.9	37.4	43.2	55.4	48.8
2,3,5-Ara	terminal	4.3	7.9	8.2	6.9	16.7	14.6	11.4	9.0	1.9	0.5
2,5-Ara	3-linked	5.8	4.7	2.6	1.0	1.7	1.0	Tr	-	-	-
2,3-Ara	5-linked	29.3	46.6	44.9	15.8	18.7	15.4	10.2	4.6	-	-
2-Ara	3,5-linked	22.5	25.1	19.6	4.9	7.8	5.6	1.2	Tr	-	-
Ara	2,3,5-linked	-	2.2	1.3	-	-	-	-	-	-	-
total arabinose		61.9	86.5	76.6	28.6	44.9	36.6	23.1	13.9	1.9	0.5
3-Xyl	2,4-linked	-	-	-	5.1	-	-	-	-	-	-
total xylose					5.1						
2,3,4,6-Gal	terminal	Tr	-	Tr	0.9	1.8	1.1	0.7	Tr	Tr	-
2,3,4-Gal	6-linked	-	-	1.1	2.0	1.1	0.6	0.4	-	-	-
2,4,6-Gal	3-linked	1.6	-	1.0	2.4	1.6	1.8	2.3	1.6	Tr	-
2,3,6-Gal	4-linked	-	-	1.4	5.0	3.3	3.6	3.3	4.0	1.9	1.4
2,4-Gal	3,6-linked	2.6	1.0	1.6	2.5	2.0	0.6	-	-	-	-
2,6-Gal	3,4-linked	-	-	-	-	6.6	7.3	6.3	6.1	1.6	Tr
2 -Gal	3,4,6-linked	-	-	-	-	1.1	Tr	Tr	-	-	-
total galactose		4.6	1.0	5.3	12.8	17.5	15.5	13.2	12.2	4.5	1.8
2,3,4,6-Glc	terminal	0.7	Tr	Tr	2.0	0.8	Tr	Tr	Tr	Tr	1.4
2,3,4-Glc	6-linked	3.3	-	-	4.0	1.3	0.8	0.7	0.9	1.5	1.0
3,4,6-Glc	2-linked	3.5	-	-	-	-	-	-	-	-	-
2,4-Glc	3,6-linked	-	-	-	2.4	-	-	-	-	-	-
2,3-Glc	4,6-linked	-	2.7	3.4	-	-	-	-	-	-	-
3,4-Glc	2,6-linked	4.5	-	-	-	-	-	-	-	-	-
2-Glc	3,4,6 linked	1.7	5.2	5.2	3.2	-	-	-	-	-	-
total glucose		13.7	8.3	9.1	11.6	2.1	1.1	1.0	1.2	1.8	2.4
2,3,4,6-Man	terminal	5.1	Tr	1.2	8.4	0.8	-	-	-	-	-
3,4,6-Man	2-linked	-	Tr	1.7	9.4	-	-	-	-	-	-
2,4,6-Man	3-linked	5.1	-	-	5.1	0.6	-	-	-	-	-
2,3,6-Man	4-linked	-	-	1.1	-	-	-	-	-	-	-
2,3,4-Man	6-linked	-	-	-	1.8	-	-	-	-	-	-
2,4-Man	3,6-linked	-	-	-	2.4	-	-	-	-	-	-
mannose	2,3,4,6-linked	8.0	0.9	1.0	1.3	-	-	-	-	-	-
total mannose		18.2	1.8	5.0	28.4	1.4					
2,3,4-GlcA[d]	terminal	-	-	-	-		-	0.9	1.6	1.5	-
total glucuronic acid								0.9	1.6	1.5	
2,3,4-GalA[d]	terminal	-	-	-	-	-	0.5	1.0	1.4	2.6	11.6
2,3-GalA[d]	4-linked	-	-	-	-	12.6	16.5	21.5	25.9	33.5	34.9
2 -GalA[d]	3,4-linked	-	-	-		1.2		1.1	1.0	0.7	Tr
-											
total galacturonic acid						13.8	18.1	23.5	28.0	36.6	46.5
ratio terminal/branched		0.21	0.20	0.05	0.84	0.63	0.67	1.17	1.50	4.88	39.0
ratio linear/terminal		4.70	6.06	29.21	2.93	2.20	2.86	3.90	4.57	4.84	2.64

[a]2,3,4-Rha: 1,5-di-*O*-acetyl-2,3,4-tri-*O*-methyl rhamnitol, etc. [b]Relative mole percent of each parent sugar family (sum of ethers from one sugar type) within total sugars. [c]Tr = trace, less than 0.5%. [d]6,6′-dideuterated ether only for the retained fractions.

rhamnose and glucose than the other three fraction, as well as xylose and galacturonic acid (6% each). In the retained fractions, the proportions of rhamnose and galacturonic acid increased from 15% to 50% in fractions A through F while that of arabinose decreased (48% in retained fraction A to 0% in the retained fraction F, Table 1). This composition indicated that the retained fractions with lower MW correspond to structures of the rhamnogalacturonan of type-I (RGI). The glycosyl-linkage compositions for nonretained and retained fractions are given in Table 2. Nonretained fractions A, B, C, and D are mainly constituted by arabinose linked at position 5 or arabinose linked at 3,5 (Table 2). Presence, after the methylation analysis, of these methyl ethers indicates the presence of a branched (1 → 5)-oligo-arabinan composed of the following repeating unit [→ 5)-Ara*f*-(1 → 5)[Ara*f*-(1 → 3)]-Ara*f*-(1 → 5)-Ara*f*-(1→], with more arabinosyl residues involved in the linear (1 → 5)-arabinan chain, and terminal arabinose linked in 3 on the (1 → 5)-arabinan chain. Analysis of glycosidic linkages (Table 2) indicates the presence of other oligosaccharides, in particular originating from mannoproteins, but at low levels in the nonretained fractions. Oligosaccharides from retained fractions are mainly constituted by rhamnose

DOI: 10.1021/jf504795g
J. Agric. Food Chem. 2015, 63, 671−682

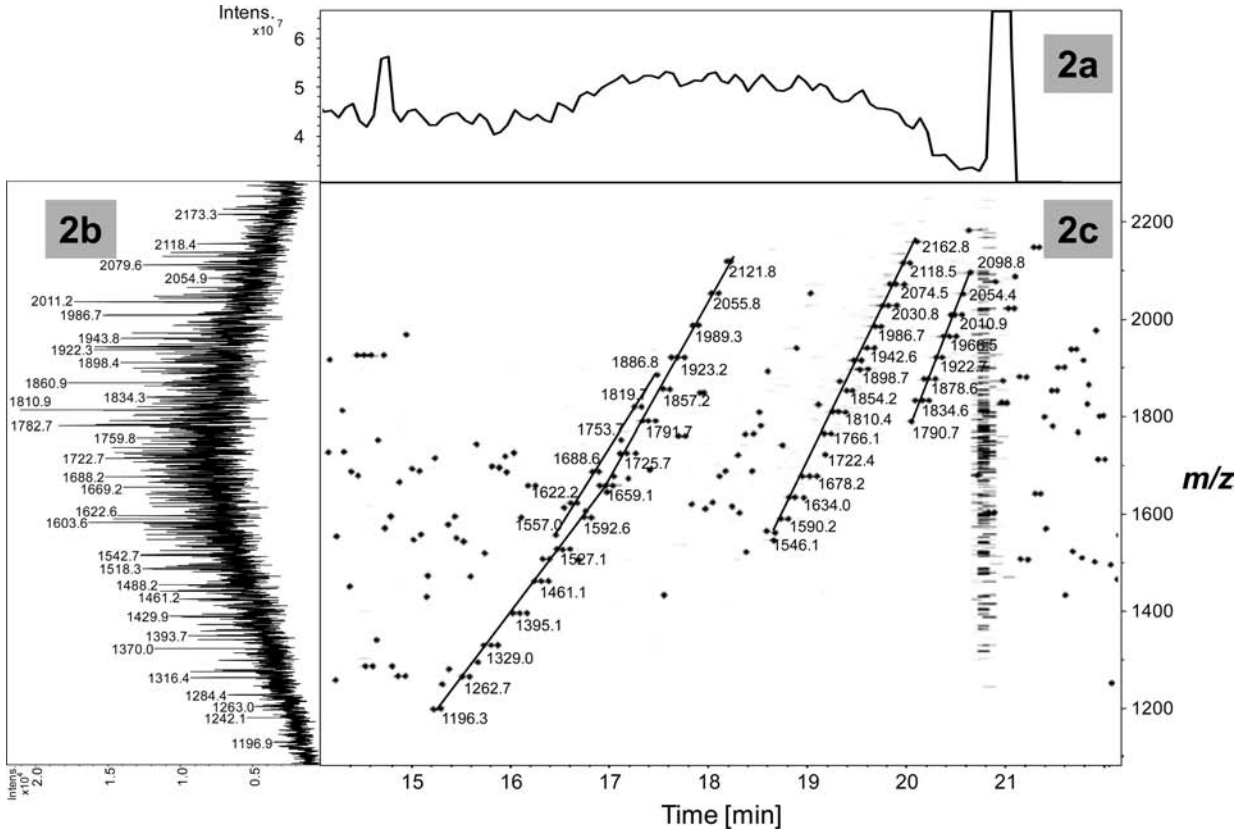

Figure 2. UPLC-MS analysis of nonretained fraction B: (a) total ion chromatogram; (b) full-scan mass spectrum of nonretained fraction B; (c) 2D projection of the full-scan mass spectra as a function of oligosaccharide retention times on the HILIC column.

linked at position 2 and 2,4, and by galacturonic acid linked at 4 (Table 2, per-O-methylated-6,6′-dideuterated ethers for uronic acids), indicating that fractions were oligo-rhamnogalacturonans organized with a repeat unit of [(→2)-α-L-Rha*p*-(1 → 4)-α-D-Gal*p*A-(1 →]$_n$.[44,45] The presence of 2,4-linked rhamnose along with methyl ethers from arabinose and galactose, obtained after methylation analysis (Table 2), indicated that side chains were attached to the oligorhamnogalacturonan backbone through the rhamnose moieties.[45] These oligosaccharides arise from the rhamnogalacturonan regions of pectins as a result of degradation of the grape berry cell wall by pectinases during grape maturation and/or wine making[46] and have been isolated for oligosaccharides of Carignan or Merlot wines.[17] Analysis of the glycosidic linkages enabled determination of the structure of oligosaccharides that were released into the wines but not their structural organizations, for example the degree of polymerization (DP) of the oligosaccharides.

UPLC-ESI-MS^n of the Nonretained Oligosaccharide Fractions. Figures 2a, 4a, and 5a show the total ion chromatogram of nonretained fractions B, C, and D on the HILIC column. HPLC coupled with mass spectrometry is a very powerful technique for oligosaccharide analysis and characterization, and ESI has been a good technique for the introduction of sugar components into an MS.[35,36] Recently, hydrophilic interaction liquid chromatography (HILIC), an alternative method for separation of highly polar compounds such as carbohydrates, and negative-ion ESI-MS^n were applied for structural analysis of oligosaccharides.[47−49]

The nonretained fraction A was also injected on the column but did not give a total ion chromatogram by MS. The masses of the oligosaccharides are too large (up to 8 kDa) to be analyzed in our ESI-MS spectrometer. Analysis of the full-scan mass spectra of nonretained fractions B, C, and D (Figures 2b, 4b, and 5b) show a multitude of mass signals between m/z 800 and m/z 2500 Da. The 2D projection of the full-scan mass spectra as a function of oligosaccharide retention times on the HILIC column (Figures 2c, 4c, and 5c) shows the separation as a function of the masses. Due to the low background noise in negative-ion mode, this 2D representation makes it possible to highlight oligosaccharides with different degrees of polymerization (DP). The negative ionization consists of a selective deprotonation of the anomeric hydroxyl at the reducing end of the oligosaccharide chain. Once the negative charge is localized at the reducing end, the ion fragmentation of the ring occurs rapidly and the mass losses observed are found to be diagnostic of the glycoside type. The signals obtained correspond to negatively charged oligosaccharides as deprotonated $[M - H]^-$, $[M - 2H]^{2-}$, and $[M - 3H]^{3-}$ ions determined by the isotopic distribution (1 for single deprotonated, 0.5 for doubly deprotonated, and 0.33 for triply deprotonated ions). In Figure 2c, a series of ions was observed at m/z 1557.0, 1622.2, 1688.6, 1753.7, 1819.7, and 1886.8, which correspond to a difference of 66 Da between the different ions (M = 3116 Da to M = 3776 Da). A second series of ions was observed at m/z 1196.3, 1263.0, 1329.0, 1395.1, 1461.1, 1527.1, 1592.6, 1659.1, 1725.7, 1791.7, 1857.2, 1923.2, 1989.3, 2055.8, and 2121.8 which also correspond to a difference of 66 Da. The ions of the two series correspond to oligosaccharide molecules detected as doubly deprotonated $[M - 2H]^{2-}$ ions. The difference of 66 Da (m/z 132 with z=2) between the first two series of ions corresponds to the presence of a pentose, likely an arabinose residue (Table

DOI: 10.1021/jf504795g
J. Agric. Food Chem. 2015, 63, 671−682

Table 3. Degrees of Polymerization (DP) of the Different Series of Oligosaccharides from Nonretained Fractions B, C, and D[a]

	fraction nonretained B			fraction nonretained C				fraction nonretained D		
DP	$(Ara)_n$-Rha-GalA	$(Ara)_n$	$(Ara)_n$-Rha-GalA-Rha	$(Ara)_n$-Rha-GalA	$(Ara)_n$	$(Ara)_n$-Rha	$(Ara)_n$-Rha-GalA-Rha	$(Ara)_n$-Rha	$(Ara)_n$	$(Ara)_n$
5	-	-	-	-	-	-	-	823.3	-	-
6	-	-	-	-	-	-	-	955.5	-	-
7	-	-	-	-	-	-	-	1087.5	943.4	-
8	-	-	-	-	-	-	-	1219.5	1076.0	-
9	-	-	-	-	-	-	-	1352.2	1208.1	-
10	-	-	-	-	-	-	-	1484.2	1340.3	818.7 $^{(2-)}$
11	-	-	-	-	-	-	-	741.2$^{(2-)}$	1472.2	899.3 $^{(2-)}$
12	-	-	-	-	-	-	-	807.3 $^{(2-)}$	-	980.7 $^{(2-)}$
13	-	-	-	-	-	-	-	873.3 $^{(2-)}$	867.4 $^{(2-)}$	1061.4 $^{(2-)}$
14	-	-	-	-	-	-	-	939.3 $^{(2-)}$	933.4 $^{(2-)}$	1142.9 $^{(2-)}$
15	-	-	-	1027.4 $^{(2-)}$	998.9 $^{(2-)}$	1005.3 $^{(2-)}$	-	1005.4 $^{(2-)}$	999.8 $^{(2-)}$	1223.9 $^{(2-)}$
16	-	-	-	1093.9 $^{(2-)}$	1064.9 $^{(2-)}$	1071.9 $^{(2-)}$	-	1071.9 $^{(2-)}$	1065.9 $^{(2-)}$	-
17	-	-	-	1159.4 $^{(2-)}$	1131.0 $^{(2-)}$	1137.9 $^{(2-)}$	-	1137.4 $^{(2-)}$	1131.4 $^{(2-)}$	-
18	-	1196.5 $^{(2-)}$	-	1225.9 $^{(2-)}$	1196.9 $^{(2-)}$	1203.4 $^{(2-)}$	-		1197.4 $^{(2-)}$	-
19	-	1263.0 $^{(2-)}$	-	1291.9 $^{(2-)}$	1263.0 $^{(2-)}$	1269.5 $^{(2-)}$	1299.4 $^{(2-)}$	-		-
20	-	1329.0 $^{(2-)}$	-	1357.5 $^{(2-)}$	1328.5 $^{(2-)}$	1336.0 $^{(2-)}$	1365.0 $^{(2-)}$	-	-	-
21	-	1395.1 $^{(2-)}$	-	1424.0 $^{(2-)}$	1395.1 $^{(2-)}$	1401.9 $^{(2-)}$	1431.0 $^{(2-)}$	-	-	-
22	-	1461.1 $^{(2-)}$	-	-	1461.1 $^{(2-)}$	-	1497.0 $^{(2-)}$	-	-	-
23	1557.0 $^{(2-)}$	1527.1 $^{(2-)}$	-	-	1527.6 $^{(2-)}$	-	1563.1 $^{(2-)}$	-	-	-
24	1622.2 $^{(2-)}$	1595.6 $^{(2-)}$	-	-	1595.0 $^{(2-)}$	-	1629.1 $^{(2-)(2-)}$	-	-	-
25	1688.6 $^{(2-)}$	1659.1 $^{(2-)}$	-	-	-	-	1695.6 $^{(2-)}$	-	-	-
26	1753.7 $^{(2-)}$	1725.7 $^{(2-)}$	-	-	-	-	1173.7 $^{(3-)}$	-	-	-
27	1819.7 $^{(2-)}$	1791.7 $^{(2-)}$	-	-	-	-	1217.5 $^{(3-)}$	-	-	-
28	1886.8 $^{(2-)}$	1857.2 $^{(2-)}$	-	-	-	-	1261.8 $^{(3-)}$	-	-	-
29	-	1923.2 $^{(2-)}$	-	-	-	-	1305.7 $^{(3-)}$	-	-	-
30	-	1989.3 $^{(2-)}$	-	-	-	-	1349.9 $^{(3-)}$	-	-	-
31	-	2055.8 $^{(2-)}$	-	-	-	-	1393.8 $^{(3-)}$	-	-	-
32	-	2121.8 $^{(2-)}$	-	-	-	-	1437.8 $^{(3-)}$	-	-	-
33	-	-	-	-	-	-	1482.1 $^{(3-)}$	-	-	-
34	-	-	-	-	-	-	-	-	-	-
35	-	1546.1 $^{(3-)}$	-	-	-	-	-	-	-	-
36	-	1590.2 $^{(3-)}$	-	-	-	-	-	-	-	-
37	-	1634.0 $^{(3-)}$	-	-	-	-	-	-	-	-
38	-	1678.2 $^{(3-)}$	-	-	-	-	-	-	-	-
39	-	1722.4 $^{(3-)}$	-	-	-	-	-	-	-	-
40	-	1766.1 $^{(3-)}$	1790.7 $^{(3-)}$	-	-	-	-	-	-	-
41	-	1810.4 $^{(3-)}$	1834.6 $^{(3-)}$	-	-	-	-	-	-	-
42	-	1854.2 $^{(3-)}$	1878.6 $^{(3-)}$	-	-	-	-	-	-	-
43	-	1898.7 $^{(3-)}$	1922.7 $^{(3-)}$	-	-	-	-	-	-	-
44	-	1942.6 $^{(3-)}$	1966.5 $^{(3-)}$							
45	-	1986.7 $^{(3-)}$	2010.0 $^{(3-)}$							
46	-	2030.8 $^{(3-)}$	2054.4 $^{(3-)}$							
47	-	2074.5 $^{(3-)}$	2098.8 $^{(3-)}$							
48	-	2118.5 $^{(3-)}$	-							
49	-	2162.8 $^{(3-)}$	-							

[a]The ions of the series correspond to negatively charged oligosaccharides detected as deprotonated $[M - H]^-$, $[M - 2H]^{2-}$, and $[M - 3H]^{3-}$ ions. The charge is indicated in parentheses.

1). The first series starting at m/z 1557.0 corresponds to the deprotonated oligosaccharides with the following structures: $[Ara]_n$-(1 → 4)-α-L-Rha*p*-(1 → 4)-α-D-Gal*p*A, where the number n of arabinose residue is between 21 to 26, and the first arabinose residue is linked at (1 → 4) on the rhamnose residue (Table 2). The second series starting at m/z 1196.3, 1263.0,.... corresponds to doubly deprotonated $[M - 2H]^{2-}$ oligo-arabinans with DP ranging from 18 (m/z 1196.3, M = 2396) to 32 (m/z 2121.8, M = 4246). A third series of ions at m/z 1546.1, 1590.2, 1634.0, 1722.4, 1766.1, 1810.4, 1854.2, 1898.7, 1942.7, 1986.8, 2074.5, 2118.5, and 2162.8 presented a difference of 44 Da between all the ions of the series. The difference of 44 corresponds of a triply charged arabinose residue (m/z 44 where m = 132 and z = 3), and this series of ions correspond to $[M - 3H]^{3-}$ ions of oligo-arabinans with a DP between 35 (m/z 1546.1, M = 4641) and 49 (m/z 2162.8, M = 6492). The separation on the HILIC column depends on the number of hydroxyl groups that each oligosaccharide has and the number of hydrogen bonds established with the stationary phase. Within a homologous series, e.g. oligo-

DOI: 10.1021/jf504795g
J. Agric. Food Chem. 2015, 63, 671−682

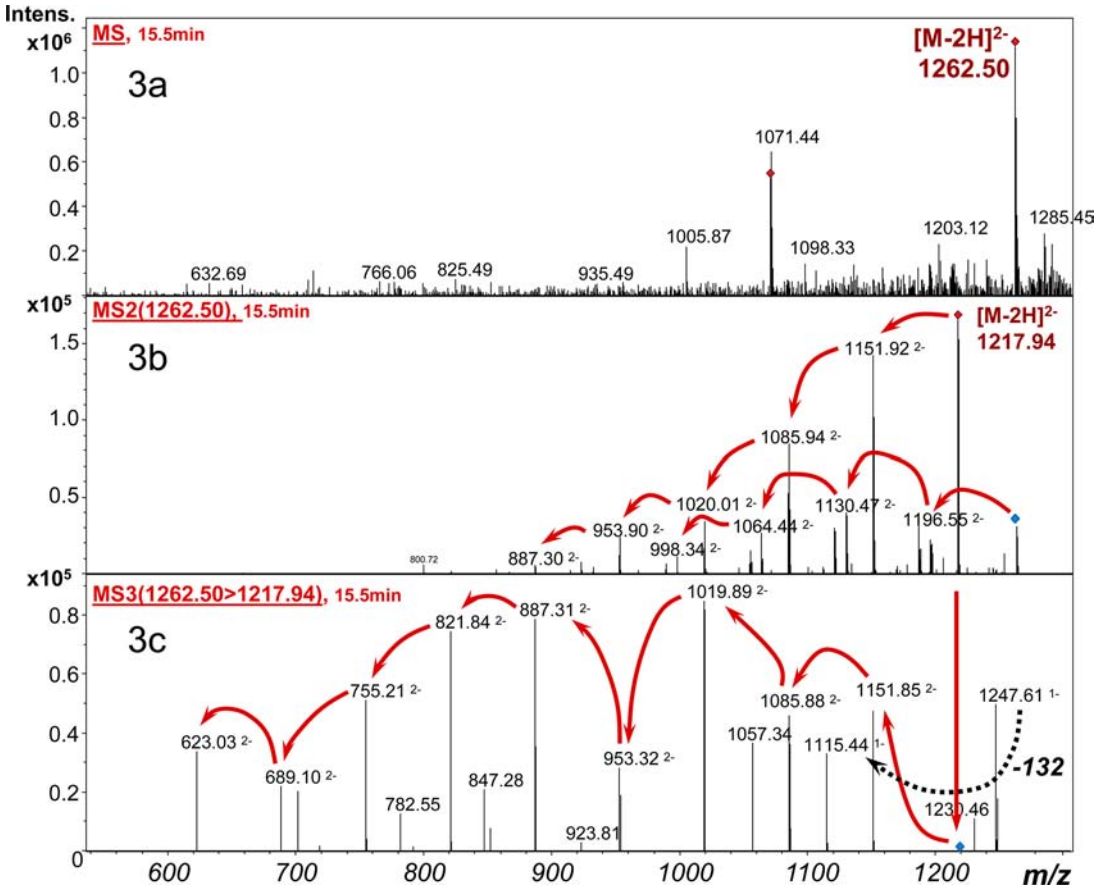

Figure 3. Spectra of MS^3 fragmentation by ESI-TI in negative mode of ion parent at m/z 1262.5 (a). MS spectrum of ion at m/z at 1262 $[M - 2H)^{2-}$. (b). MS^2 spectrum of the ion at m/z 1262.5 $[M - 2H)^{2-}$. (c). MS^3 spectrum of the ion at m/z at1217.94 $[M - 2H)^{2-}$ from the m/z 1262.5 ion $[M - 2H)^{2-}$. (red →) Loss of a fragment of m/z 66.

arabinans, this allows the prediction of elution positions as a function of DP. The oligo-arabinan of DP 18 (m/z 1196.3, M = 2396) has a retention time of 15.2 min, while the oligo-arabinan with a DP 49 (m/z 2162.8, M = 6492) has a retention time of 20.1 min. In this series, other oligo-arabinans with DP between 18 and 49 are eluted between 15 and 20 min on the column. The results of nonretained fractions B are summarized in Table 3.

The MS^n fragmentations of each oligosaccharide from nonretained fractions B, C and D, were performed by ESI-IT-MS^n in the negative ion mode. Figure 3 shows, as an example, the MS^n spectra of the $[M - 2H]^{2-}$ ion at m/z 1262.5 obtained from the nonretained fraction B. Under negative-ionization ESI-MS^n conditions, the fragmentation process of oligosaccharides involves the glycosidic cleavage between two sugar residues and cross-ring opening of sugar (cleavage of two bonds within the sugar ring). MS^n spectra of deprotonated oligosaccharides can be read "from right to left". The fragment ions observed in the MS^n spectra are usually named according to the nomenclature of Domon and Costello (1988).[50]

The MS^2 fragmentation (Figure 3b) of the parent ion at m/z 1262.5 showed the presence of a fragment ion at m/z 1196.5, due to the loss of an arabinose residue (m/z 66 where m = 132 and z = 2). This fragment ion at m/z 1196.5 loses a first arabinose residue to give the fragment ion at m/z 1130.5 and after successive losses of arabinose residues yields fragment ions at m/z 1064.4, 998.3,... Another point of the MS^2 spectra was the presence of a fragment ion due to the loss of 90 mass units (45 amu from the doubly charged parent ion), i.e. ion at m/z 1217.9 for parent ion at m/z 1262.5 (Figure 3b, MS^2 spectrum). The loss of this fragment corresponds to a fragmentation $^{0,2}X_n$ of a residue of arabinose in a nonreducing terminal position of the oligosaccharide studied.[50] Then from this ion, we observe a series of fragment ions produced by loss of arabinose residues: the fragment ion at m/z gives an ion at m/z 1151.9 and m/z 1085.9 and so on until a fragment ion at m/z 887.3 corresponding to the loss of five residues of arabinose from the ion at m/z 1217.9. All fragment ions obtained are doubly charged ions. In the same manner, the MS^3 fragmentation (Figure 3c) of the fragment ion at m/z 1217.9 showed the presence of fragment ions arising from successive losses of arabinose residues. The last fragment ion at m/z 623.1 corresponds to the loss of nine residues of arabinose from the fragment ion at m/z 1217.9. The fragment ion at m/z 623.1 corresponds to a doubly charged fragment, but it is also present as a singly charged fragment ion $[M - H]^-$ at m/z 1247.6. This fragment ion at m/z 1247.6 then loses an arabinose residue to give an ion $[M - H]^-$ at 1115.4 amu. All the ions present in the spectrum of the nonretained fraction B (Figure 2) were fragmented in MS^2 and MS^3 (data not shown). All ions identified on Figure 2C provide a MS/MS fragmentation spectrum similar to that of the ion at m/z 1262.5.

Figures 4c and 5c show mass spectra of wine oligosaccharides from the nonretained fractions C and D. We observe several series of oligosaccharides with different structures and degrees of polymerization. The results are summarized in Table 3. A

DOI: 10.1021/jf504795g
J. Agric. Food Chem. 2015, 63, 671−682

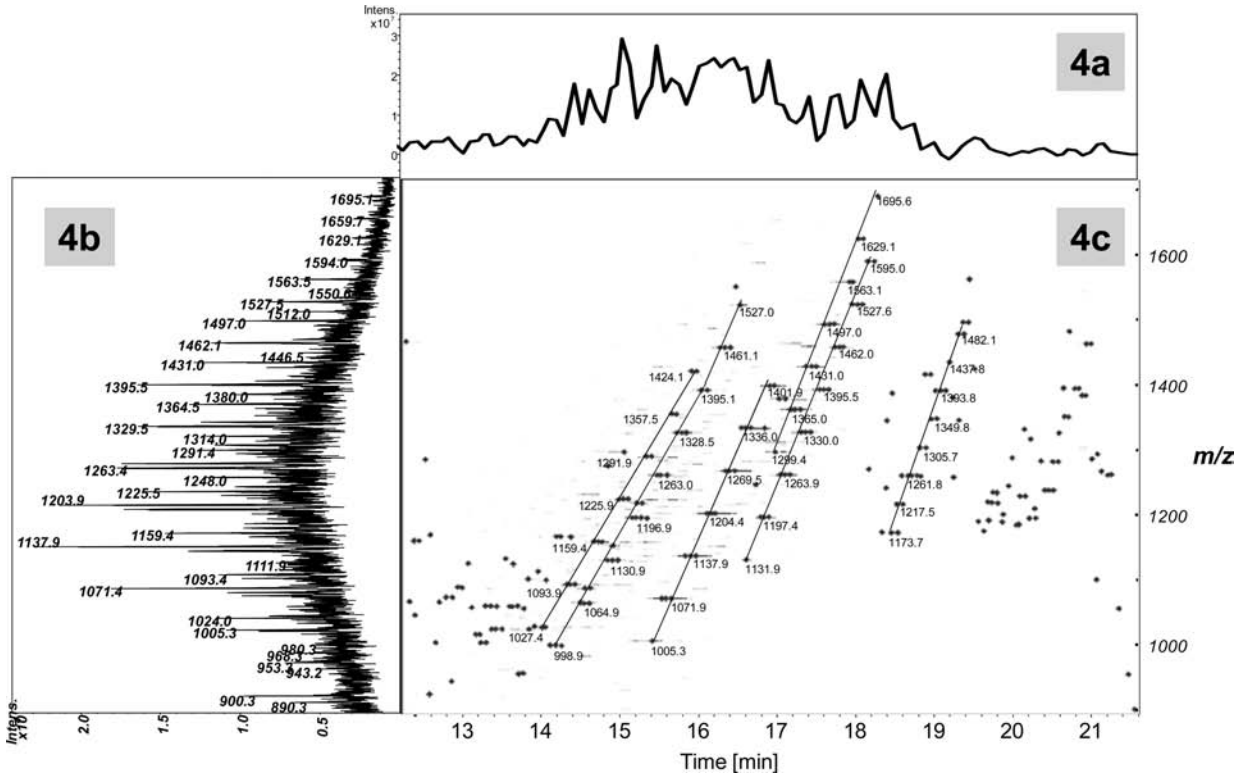

Figure 4. UPLC-MS analysis of nonretained fraction C: (a) total ion chromatogram; (b) full-scan mass spectrum; (c) 2D projection of the full-scan mass spectra as a function of oligosaccharide retention times on the HILIC column.

series starting from the $[M - 2H]^{2-}$ ion at m/z 1027.4 corresponds to the deprotonated oligosaccharides with the following structures: disaccharide α-L-Rha*p*-(1→4)-α-D-Gal*p*A substituted on the Rha by a lateral chain of arabinans. The first and last oligosaccharides of the series correspond to a DP of 15 and a DP of 21, respectively. The following two series, identified as $[M - 2H]^{2-}$ ions, correspond to the structure of oligo-arabinans with a DP ranging from 15 to 24, and rhamno-oligo-arabinans consisting of one residue of Rha substituted at the 4 position by arabinans of DP 15 to DP 21 (Table 3). The last series identified in the nonretained fraction C (Table 3) correspond to oligosaccharide molecules with the following structures: α-L-Rha*p*-(1→4)-α-D-Gal*p*A-(1→2)-α-L-Rha*p*, where one residue of rhamnose was substituted at (1→4) by *n* residues of arabinose with *n* between 16 to 30 (see Table 3). Our results indicated that these oligosaccharides are constituted by a core structure of degraded RGI, in which the oligo-rhamnogalacturonan backbone was substituted through the rhamnose moieties by (1→5)-arabinan branched at the 3-position by terminal nonreducing arabinose. These types of arabinan chains have been found in red wine as the side chains of RGI[51] while arabinans were rarely found.[22,52] RGI originates from grape cell walls. It is present in low amounts in wine,[22] presumably because it is hydrolyzed by glycoside hydrolases and/or "polysaccharidases" from grapes or from yeast used during the fermentation step. The detection of these oligosaccharides suggests that they have been released from grape cell wall polysaccharides under the action of rhamnogalacturonase, arabinanase, and α-arabinofuranosidase activities at least.

The oligosaccharide series identified in the nonretained Fraction D (Table 3) correspond to oligosaccharide with the following structures: One residue of rhamnose substituted by arabinan with a DP between 7 and 18, and oligo-hexose, where hexoses are galactose, glucose, or mannose (see Table 1) with a DP between 10 to 15.

UPLC-ESI-MS^n of the Retained Oligosaccharide Fractions. The retained fractions A, B, C, D, E, and F, corresponding to acidic oligosaccharides (Table 1), were also analyzed by LC-ESI-MS with the HILIC column. No mass signal was detected in retained fraction A, while retained fractions B and C provided mass signals of low intensity (Figure 6a–d) and the retained fractions E and F gave mass spectra corresponding to the oligosaccharides already identified.[17,18,20] The majority of masses could be assigned to an oligosaccharide structure. All oligosaccharide molecules were detected as the deprotonated $[M - H]^-$ and doubly deprotonated $[M - 2H]^{2-}$ ions. The predominant ions (the most intense) observed in the mass spectra were ions at m/z 485, 545, 661, 807, 837, 983, 1130, 1160, 1306, and 1452 for oligosaccharides from retained fractions E and F. The ion observed at m/z 661 corresponds to the deprotonated tetrasaccharide: [(→2)-α-L-Rha*p*-(1→4)-α-D-Gal*p*A(1→]$_2$, the ion at m/z 837 corresponds to the deprotonated pentasaccharide: α-D-Gal*p*A(1→[(→2)-α-L-Rha*p*-(1→4)-α-D-Gal*p*A(1→]$_2$, the ion at m/z 983 to the hexasaccharide: [(→2)-α-L-Rha*p*-(1→4)-α-D-Gal*p*A(1→]$_3$, the ion at m/z 1160 to the heptasaccharide and the ion at m/z 1306 to the octasaccharide: [(→2)-α-L-Rha*p*-(1→4)-α-D-Gal*p*A(1→]$_4$. The ions observed at m/z 485, 661, 807, 983, 1130, 1306, and 1452 correspond to the deprotonated rhamnogalacturonan oligosaccharides where the first oligosaccharide (m/z 485) has the following structure [α-L-Rha*p*-(1→4)-α-D-Gal*p*A(1→2)-α-L-Rha*p*]. The last ion of the series at m/z 1452 is an oligosaccharide of DP 9 with the following structure: [α-L-Rha*p*-(1→4)-α-D-Gal*p*A(1→2)-]$_4$α-L-Rha*p*. The ion at m/z 545 present in the MS spectrum of the

DOI: 10.1021/jf504795g
J. Agric. Food Chem. 2015, 63, 671–682

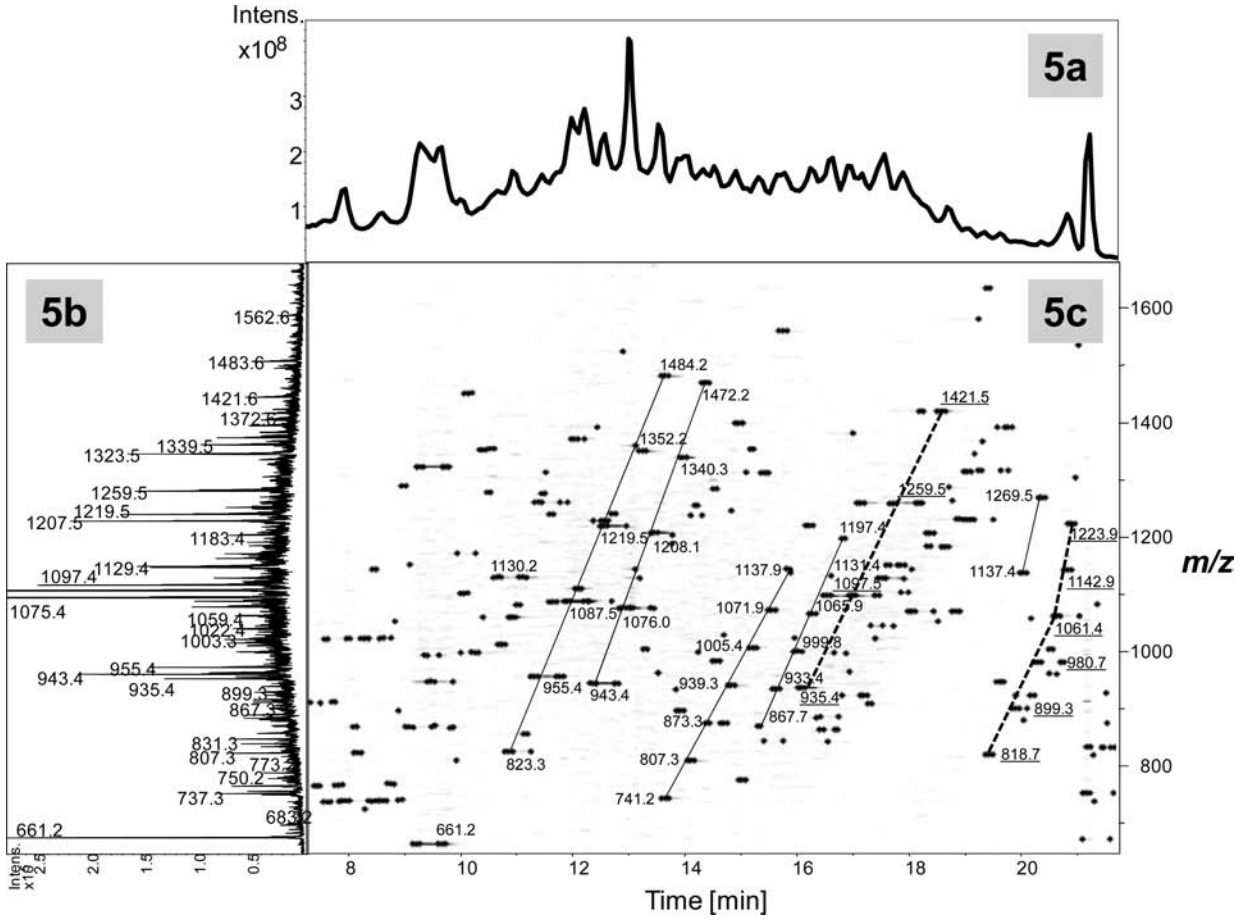

Figure 5. UPLC-MS analysis of nonretained fraction D: (a) total ion chromatogram; (b) full-scan mass spectrum; (c) 2D projection of the full-scan mass spectra as a function of oligosaccharide retention times on the HILIC column.

retained fraction F corresponds to the trigalacturonic acid coming from the homogalacturonan backbones of the pectins. These acidic oligosaccharides arise from the rhamnogalacturonan or homogalacturonan regions of pectins as a result of degradation of grape cell wall berries by pectinases during grape maturation and/or wine making.

In conclusion, we have isolated and characterized the neutral and acidic oligosaccharide fractions of Carignan red wines by complementary methods: glycosyl composition analysis, glycosidic-linkage analysis, and mass spectrometry. Mass spectrometry is a powerful tool used to identify and determine the structure of the oligosaccharides and in particular those coming from pectins.[36] Its use has enabled us to identify the various structures of oligosaccharides present in the fractions isolated from wines. We particularly focused on neutral wine oligosaccharide fractions (nonretained fractions A, B, C, and D), and for the first time, we have characterized by ESI-TOF MS a large number of neutral oligosaccharides rich in arabinose. We also found acid oligosaccharide structures previously characterized in our laboratory.[17,18,20] These molecules, neutral and acidic oligosaccharides identified in our previous works, and other oligosaccharides identified in Grignolino and Chardonnay wines by Bordiga et al.[19] (hexose-oligosaccharides, xyloglucans, and arabinogalactans), represent the degraded structures of polysaccharides originating from the grape berry cell wall, as a result of endogenous (present in grapes) or exogenous (added by the winemakers) enzyme activities present during the various stages of the wine making. The mass spectra of fractions of neutral sugars eluted from a HILIC column, used for the first time for separating wine oligosaccharides, showed a high variety of oligosaccharides (detected as $[M - H]^-$, $[M - 2H]^{2-}$, and $[M - 3H]^{3-}$ ions) corresponding to arabino-oligosaccharides composed of 8 to 49 arabinose residues, rhamnose substituted with arabino-oligosaccharides with a DP between 5 to 21, and different rhamnogalacturonan arabino-oligosaccharides composed of one or two residues of rhamnose, one residue of galacturonic acid, and side chains of 13 to 30 residues of arabinose. The oligosaccharides rich in arabinose are present in significant amounts (185 mg/L) in red wine, and are degradation products originating from the pectic polysaccharides of grape cell walls. Arabinans are known to participate in haze formation by self-aggregation when they have a low degree of branching. However, oligosaccharides rich in arabinan side chains isolated and identified in this study are highly branched with low molecular masses. It would be interesting to determine the impact of these structures on wines, especially their implications in haze development. Arabinans are known to be involved in clarification and stabilization problems of apple juices and concentrates.[53] No information is available on the properties of oligosaccharides rich in arabinose. However, our preliminary results show that in a wine model solution, oligosaccharides rich in arabinose can interact with purified tannins and form haze, but these results need to be confirmed. Knowledge of these oligosaccharides should allow us to study their physicochemical properties, their interactions with other

DOI: 10.1021/jf504795g
J. Agric. Food Chem. 2015, 63, 671−682

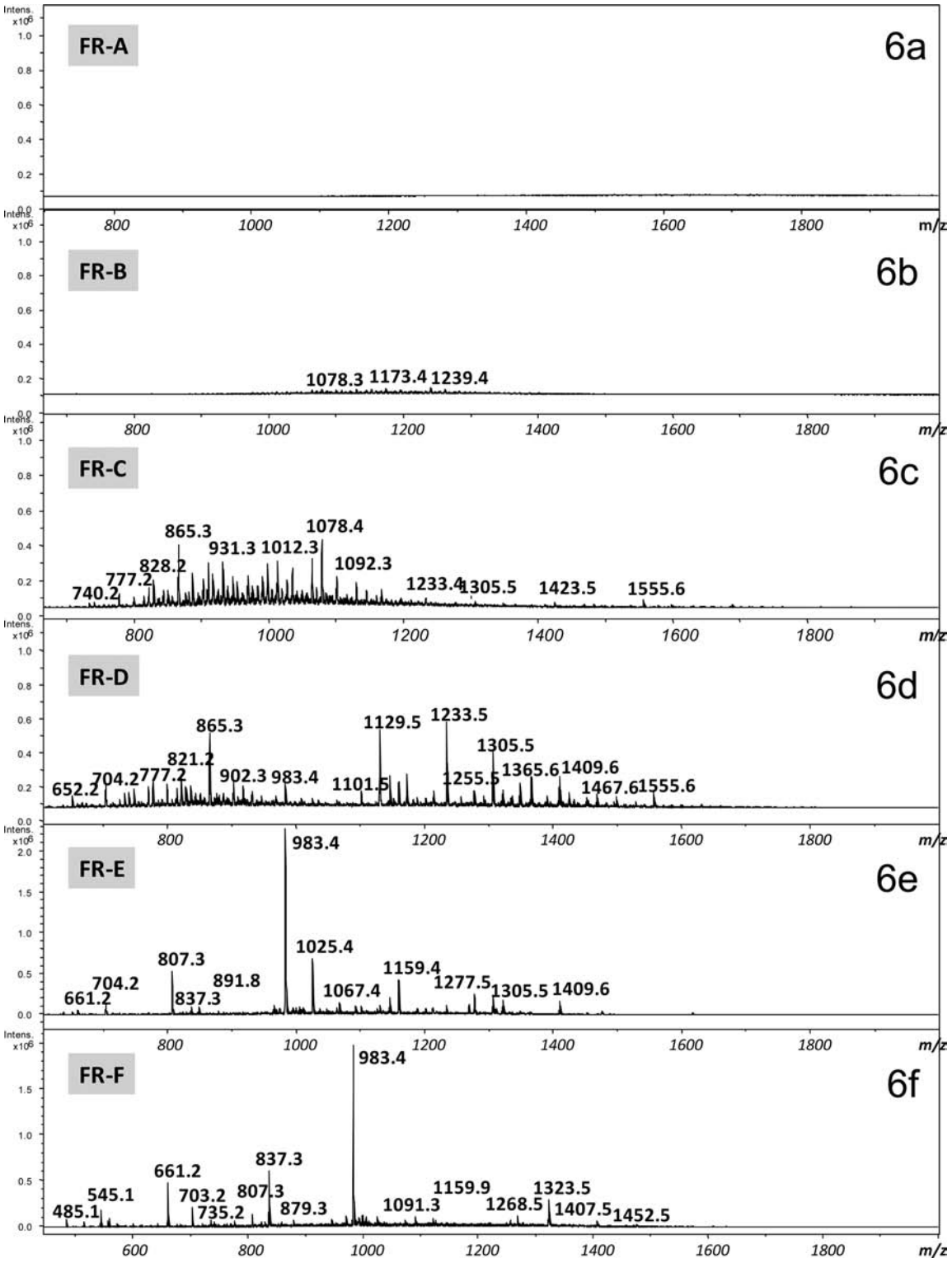

Figure 6. Negative ESI-TOF spectrum of oligosaccharide from retained fractions A, B, C, D, E, and F.

components present in wine (polyphenols, proteins, and aroma compounds), and possibly their beneficial health effects as prebiotics.

AUTHOR INFORMATION

Corresponding Author

*Tel: +33 499612585; fax: +33 499612857; e-mail: thierry.doco@supagro.inra.fr.

Notes

The authors declare no competing financial interest.

REFERENCES

(1) Riou, V.; Vernhet, A.; Doco, T.; Moutounet, M. Aggregation of grape seed tannins in model wine - effect of wine polysaccharides. *Food Hydrocolloids* **2002**, *16*, 17−23.

(2) Poncet-Legrand, C.; Doco, T.; Williams, P.; Vernhet, A. Inhibition of grape seed tannin aggregation by wine mannoproteins:

DOI: 10.1021/jf504795g
J. Agric. Food Chem. 2015, 63, 671−682

Effect of polysaccharide molecular weight. *Am. J. Enol. Vitic.* **2007**, *58*, 87−91.
(3) Vidal, S.; Courcoux, P.; Francis, L.; Kwiatkowski, M.; Gawel, R.; Williams, P.; Waters, E.; Cheynier, V. Use of an experimental design approach for evaluation of key wine components on mouth-feel perception. *Food Quality Preference* **2004**, *15*, 209−217.
(4) Gerbaud, V.; Gabas, N.; Laguerie, C.; Blouin, J.; Vidal, S.; Moutounet, M.; Pellerin, P. Effect of wine polysaccharides on the nucleation of potassium hydrogen tartrate in model solutions. *Trans. Inst. Chem. Eng.* **1996**, *74*, 782−790.
(5) Chalier, P.; Angot, B.; Delteil, D.; Doco, T.; Gunata, Z. Interactions between aroma compounds and whole mannoprotein extract or fractions of mannoproteins isolated from *saccharomyces cerevisiae* strains. *Food Chem.* **2007**, *100*, 22−30.
(6) Waters, E. J.; Pellerin, P.; Brillouet, J.-M. *Saccharomyces* mannoprotein that protects wine from protein haze. *Carbohydr. Polym.* **1994**, *23*, 185−191.
(7) Moine-Ledoux, V.; Dubourdieu, D. An invertase fragment responsible for improving the protein stability of dry white wines. *J. Sci. Food Agric.* **1999**, *79*, 537−543.
(8) Dupin, I.; Mc Kinnon, B. M.; Boulay, M.; Markides, A. J.; Jones, G. P.; Williams, J. P.; Waters, E. J. *Saccharomyces cerevisiae* mannoproteins that protect wine from protein haze: Their release during fermentation and lees contact and a proposal for their mechanism of action. *J. Agric. Food Chem.* **2000**, *48*, 3098−3105.
(9) Lomolino, G.; Curioni, A. Protein haze formation in white wines: Effect of *Saccharomyces cerevisiae* cell wall components prepared with different procedures. *J. Agric. Food Chem.* **2007**, *55*, 8737−8744.
(10) Schmidt, S. A.; Tan, E. L.; Brown, S.; Nasution, U. L.; Pettonilo, F.; MacInttyre, O. J.; Lopes, M. D.; Waters, E. J.; Anderson, P. A. Hpf2 glycan structure is critical for protection against protein haze formation in white wine. *J. Agric. Food Chem.* **2009**, *57*, 3308−3315.
(11) O'Neill, M. A.; Warrenfeltz, D.; Kates, K.; Pellerin, P.; Doco, T.; Darvill, A. G.; Albersheim, P. Rhamnogalacturonan II, a pectic polysaccharide in the walls of growing plant cells, forms a dimer that is covalently cross-linked by a borate ester. *J. Biol. Chem.* **1996**, *271*, 22923−22930.
(12) Pellerin, P.; O'Neill, M. A.; Pierre, C.; Cabanis, M. T.; Darvill, A.; Albersheim, P.; Moutounet, M. Le plomb est complexé dans les vins par les dimères de rhamnogalacturonane II, un polysaccharide pectique du raisin. *J. Int. Sci. Vigne Vin* **1997**, 33−41.
(13) Andrés-Lacueva, C.; Lamuela-Raventós, R. M.; Buxaderas, S.; de la Torre-Boronat, M. C. Influence of variety and aging on foaming properties of cava (sparkling wine). *J. Agric. Food Chem.* **1997**, *45*, 2520−2525.
(14) López-Barajas, M.; López-Tamames, E.; Buxaderas, S.; Torre-Boronat, M. C. Effect of vinification and variety on foam capacity of wine. *Am. J. Enol. Vitic.* **1998**, *49*, 397−402.
(15) Abdallah, Z.; Aguié-Béghin, V.; Abou-Saleh, K.; Douillard, R.; Bliard, C. Isolation and analysis of macromolecular fractions responsible for the surface properties in native Champagne wines. *Food Res. Int.* **2010**, *43*, 982−987.
(16) Martínez-Lapuente, L.; Guadalupe, Z.; Ayestarán, B.; Ortega-Heras, M.; Pérez-Magariño, S. Changes in polysaccharide composition during sparkling wine making and aging. *J. Agric. Food Chem.* **2013**, *61*, 12362−12373.
(17) Ducasse, M.-A.; Williams, P.; Meudec, E.; Cheynier, V.; Doco, T. Isolation of Carignan and Merlot red wine oligosaccharides and their characterization by ESI-MS. *Carbohydr. Polym.* **2010**, *79*, 747−754.
(18) Ducasse, M.-A.; Williams, P.; Canal-Llauberes, R.-M.; Mazerolles, G.; Cheynier, V.; Doco, T. Effect of macerating enzymes on the oligosaccharide profiles of merlot red wines. *J. Agric. Food Chem.* **2011**, *59*, 6558−6567.
(19) Bordiga, M.; Travaglia, F.; Meyrand, M.; German, J. B.; Lebrilla, C. B.; Coisson, J. D.; Arlorio, M.; Barile, D. Identification and characterization of complex bioactive oligosaccharides in white and red wine by a combination of mass spectrometry and gas chromatography. *J. Agric. Food Chem.* **2012**, *60* (14), 3700−3707.
(20) Apolinar-Valiente, R.; Williams, P.; Mazerolles, G.; Romero-Cascales, I.; Gómez-Plaza, E.; López-Roca, J. M.; Ros-García, J. M.; Doco, T. Effect of enzyme additions on the oligosaccharide composition of Monastrell red wines from four different wine-growing origins in Spain. *Food Chem.* **2014**, *156*, 151−159.
(21) Quijada-Morín, N.; Williams, P.; Rivas-Gonzalo, J. C.; Doco, T.; Escribano-Bailón, M. T. Polyphenolic, polysaccharide and oligosaccharide composition of Tempranillo red wines and their relationship with the perceived astringency. *Food Chem.* **2014**, *154*, 44−51.
(22) Pellerin, P.; Cabanis, J. C. Les Glucides. In *Elements d'œnologie. Fondements scientifiques et techniques*; Technique et Documentation; Flanzy, C., Ed.; Lavoisier: Paris, 1998; pp 40−93.
(23) Doco, T.; Quellec, N.; Moutounet, M.; Pellerin, P. Polysaccharide patterns during the aging of Carignan noir red wines. *Am. J. Enol. Vitic.* **1999**, *50* (1), 25−32.
(24) Ayestaran, B.; Guadalupe, Z.; Leon, D. Quantification of major grape polysaccharides (Tempranillo v.) released by maceration enzymes during the fermentation process. *Anal. Chim. Acta* **2004**, *513* (1), 29−39.
(25) Guadalupe, Z.; Palacios, A.; Ayestaran, B. Maceration enzymes and mannoproteins: A possible strategy to increase colloidal stability and color extraction in red wines. *J. Agric. Food Chem.* **2007**, *55* (12), 4854−4862.
(26) Doco, T.; Williams, P.; Cheynier, V. Effect of flash release and pectinolytic enzyme treatments on wine polysaccharide composition. *J. Agric. Food Chem.* **2007**, *55*, 6643−6649.
(27) Ducasse, M.-A.; Canal-Llauberes, R.-M.; Lumley, M. D.; Williams, P.; Souquet, J.-M.; Fulcrand, H.; Doco, T.; Cheynier, V. Effect of macerating enzyme treatment on the polyphenol and polysaccharide composition of red wines. *Food Chem.* **2010**, *118*, 369−376.
(28) Qiang, X.; YongLie, C.; QianBing, W. Health benefit application of functional oligosaccharides. *Carbohydr. Polym.* **2009**, *77*, 435−441.
(29) Darvill, A. G.; Albersheim, P. Phytoalexins and their elicitors-A defense against microbial infection in plants. *Annu. Rev. Plant Physiol.* **1984**, *155*, 507−516.
(30) Broekaert, W. F.; Courtin, C. M.; Verbeke, K.; Van de Wiele, T.; Verstraete, W.; Delcour, J. A. Prebiotic and other health-related effects of cereal-derived arabinoxylans, arabinoxylan-oligosaccharides, and xylooligosaccharides. *Crit. Rev. Food Sci. Nutr.* **2011**, *51*, 178−194.
(31) Cescutti, P.; Rizzo, R. Divalent cation interactions with oligogalacturonides. *J. Agric. Food Chem.* **2001**, *49*, 3262−3267.
(32) Duarte, F. I.; Godejohann, M.; Braumann, U.; Spraul, M.; Gil, A. M. Application of NMR spectroscopy and LC-NMR/MS to the identification of carbohydrates in beer. *J. Agric. Food Chem.* **2003**, *51* (17), 4847−4852.
(33) Reis, A.; Coimbra, M. A.; Domingues, P.; Ferrer-Correia, A. J.; Domingues, M. R. M. Fragmentation pattern of underivatised xylo-oligosaccharides and their alditol derivatives by electrospray tandem mass spectrometry. *Carbohydr. Polym.* **2004**, *55*, 401−409.
(34) Quemener, B.; Ordaz-Ortiz, J. J.; Saulnier, L. Structural characterization of underivatized arabino-xylo-oligosaccharides by negative-ion electrospray mass spectrometry. *Carbohyd. Res.* **2006**, *341*, 1834−1847.
(35) Fernández, L. E. M. Introduction to ion trap mass spectrometry: Application to the structural characterization of plant oligosaccharides. *Carbohyd. Polymers* **2007**, *68*, 797−807.
(36) Ralet, M.-C.; Lerouge, P.; Quéméner, B. Mass spectrometry for pectin structure analysis. *Carbohyd. Res.* **2009**, *334*, 1798−1807.
(37) Brillouet, J.-M.; Moutounet, M.; Escudier, J.-L. Fate of yeast and grape pectic polysaccharides of a young red wine in the cross-flow microfiltration process. *Vitis* **1989**, *28*, 49−63.
(38) Harris, P. J.; Henri, R. J.; Blakeney, A. B.; Stone, B. A. An improved method for the methylation analysis of oligosaccharides and polysaccharides. *Carbohyd. Res.* **1984**, *127* (1), 59−73.
(39) Hilz, H.; Williams, P.; Doco, T.; Schols, H. A.; Voragen, A. G. J. The pectic polysaccharide rhamnogalacturonan II is present as a dimer in pectic populations of bilberries and black currants in muro and in juice. *Carbohyd. Polym.* **2006**, *65* (4), 521−528.

DOI: 10.1021/jf504795g
J. Agric. Food Chem. 2015, 63, 671−682

(40) Doco, T.; O'Neill, M. A.; Pellerin, P. Determination of the neutral and acidic glycosyl residue compositions of plant cell polysaccharides by GC-EI-MS analysis of the trimethylsilyl methyl glucoside derivatives. *Carbohydr. Polym.* **2001**, *46*, 249−259.
(41) Hakomori, S. I. A rapid permethylation of glycolipid, and polysaccharide catalyzed by methylsulfinyl carbanion in dimethyl sulfoxide. *J. Biochem. (Tokyo)* **1964**, *55*, 205−208.
(42) Pellerin, P.; Vidal, S.; Williams, P.; Brillouet, J.-M. Characterization of five type II arabinogalactan-protein complexes from red wine with increasing uronic acid content. *Carbohyd. Res.* **1995**, *190*, 183−197.
(43) Vidal, S.; Williams, P.; Doco, T.; Moutounet, M.; Pellerin, P. The polysaccharides of red wine: Total fractionation and characterisation. *Carbohydr. Polym.* **2003**, *54*, 439−447.
(44) Schols, H. A.; Voragen, A. G. J.; Colquhoun, I. J. Hairy (ramified) regions of pectins. Isolation and characterization of rhamnogalacturonan oligomers, liberated during degradation of pectic hairy regions by rhamnogalacturonase. *Carbohydr. Res.* **1994**, *256*, 97−111.
(45) Mohnen, D. Pectin structure and biosynthesis. *Curr. Opin. Plant Biol.* **2008**, *11* (3), 266−277.
(46) Arnous, A.; Meyer, A. S. Quantitative prediction of cell wall polysaccharide composition in grape (*Vitis vinifera* L.) and apple (*Malus domestica*) skins from acid hydrolysis monosaccharide profiles. *J. Agric. Food Chem.* **2009**, *57* (9), 3611−3619.
(47) Liu, Y.; Urgaonkar, S.; Verkade, J. G.; Armstrong, D. W. Separation and characterization of underivatized oligosaccharides using liquid chromatography and liquid chromatography−electrospray ionization mass spectrometry. *J. Chromatogr. A* **2005**, *1079*, 146−152.
(48) Leijdekkers, A. G. M.; Sanders, M. G.; Schols, H. A.; Gruppen, H. Characterizing plant cell wall derived oligosaccharides using hydrophilic interaction chromatography with mass spectrometry detection. *J. Chromatogr.* **2011**, *1218* (51), 9227−9235.
(49) Fu, Q.; Liang, T.; Li, Z.; Xu, X.; Ke, Y.; Jin, Y.; Liang, X. Separation of carbohydrates using hydrophilic interaction liquid chromatography. *Carbohyd. Res.* **2013**, *379*, 13−17.
(50) Domon, B.; Costello, C. E. Asystematic nomenclature for carbohydrate fragmentation in FAB-MS/MS spectra of glycoconjugates. *Glycoconjugate J.* **1988**, *5*, 397−409.
(51) Vidal, S.; Williams, P.; O'Neill, M. A.; Pellerin, P. Polysaccharides from grape berry cell walls. Part I: Tissue distribution and structural characterization of the pectic polysaccharides. *Carbohydr. Polym.* **2001**, *45*, 315−323.
(52) Belleville, M. P.; Williams, P.; Brillouet, J.-M. A linear arabinan from a red wine. *Phytochemistry* **1993**, *33*, 227−229.
(53) Mehrlander, K.; Dietrich, H.; Sembries, S.; Dongowski, G.; Will, F. Structural characterization of oligosaccharides and polysaccharides from apple juices produced by enzymatic pomace liquefaction. *J. Agric. Food Chem.* **2002**, *50*, 1230−1236.

DOI: 10.1021/jf504795g
J. Agric. Food Chem. 2015, 63, 671−682

JOURNAL OF AGRICULTURAL AND FOOD CHEMISTRY

Article

pubs.acs.org/JAFC

Comprehensive NMR Analysis of Compositional Changes of Black Garlic during Thermal Processing

Tingfu Liang,[†] Feifei Wei,[†] Yi Lu,[†] Yoshinori Kodani,[†] Mitsuhiko Nakada,[‡] Takuya Miyakawa,[†] and Masaru Tanokura*,[†]

[†]Department of Applied Biological Chemistry, Graduate School of Agricultural and Life Sciences, The University of Tokyo, 1-1-1 Yayoi, Bunkyo-ku, Tokyo 113-8657, Japan

[‡]Salad Cosmo Company, Ltd., 1-15 Sendanbayashi, Nakatsugawa, Gifu 509-9131, Japan

Supporting Information

ABSTRACT: Black garlic is a processed food product obtained by subjecting whole raw garlic to thermal processing that causes chemical reactions, such as the Maillard reaction, which change the composition of the garlic. In this paper, we report a nuclear magnetic resonance (NMR)-based comprehensive analysis of raw garlic and black garlic extracts to determine the compositional changes resulting from thermal processing. ^{1}H NMR spectra with a detailed signal assignment showed that 38 components were altered by thermal processing of raw garlic. For example, the contents of 11 L-amino acids increased during the first step of thermal processing over 5 days and then decreased. Multivariate data analysis revealed changes in the contents of fructose, glucose, acetic acid, formic acid, pyroglutamic acid, cycloalliin, and 5-(hydroxymethyl)furfural (5-HMF). Our results provide comprehensive information on changes in NMR-detectable components during thermal processing of whole garlic.

KEYWORDS: *black garlic, thermal process, Maillard reaction, NMR, multivariate statistical analysis*

INTRODUCTION

Garlic (*Allium sativum* L.) is widely used as a spice in many parts of the world, such as Asia, Europe, and the United States, because of its unique flavor and taste. Garlic has been reported to exert many health benefits, including antimicrobial,[1] anticancer,[2] and antioxidant[3] activities, and to improve the effects of hypoglycemic activity.[4] Among the chemical compounds of garlic, organosulfur compounds such as allicin are primarily responsible for its flavor,[5] and the derivatives of these compounds are responsible for its health benefits.[3,6]

Black garlic is a newly processed food that is made by subjecting whole raw garlic to thermal processing at approximately 70−80 °C under controlled humidity conditions for 1−3 months without any additives.[3] This processed food has a fruity taste and is edible without any cooking processes. The thermal processing induces many chemical reactions, such as the enzymatic browning reaction and Maillard reaction, which causes the color to change from white and yellow to dark brown. Compared with raw garlic, black garlic has a less pungent odor because of a decrease in allicin content,[7] whereas *S*-allylcysteine (SAC) contents have been reported to be increased.[7,8] SAC is a water-soluble sulfur compound with high antioxidant activity and shows at least a 5-fold increase in black garlic compared with raw garlic.[8] In addition, increments in the content of polyphenols and flavonoids[9] along with increments in antitumor effects in vitro[2] and immunostimulatory activity[10] are observed in black garlic after thermal processing. There are other reports that showed the potential health benefits of black garlic by chemical analysis,[11,12] cell culture experiments,[13,14] and animal experiments.[15,16]

Nuclear magnetic resonance (NMR) is a useful tool for studying the physicochemical state of foods and does not require the separation of their constituents, which may change the condition of the food samples; therefore, this technique has been applied in food science because of its simplicity and because it is a direct method to obtain comprehensive information about food products.[17−19] In addition, nondestructive NMR is commonly used to study the metabolome of many types of food, such as potato,[17] coffee,[20] mango juice,[21] and milk.[22,23] Although NMR is less sensitive than other analytical techniques, such as absorption spectroscopy and mass spectrometry combined with liquid or gas chromatography, it remains an indispensable and useful technique when combined with multivariate data analysis to provide a comprehensive observation of complex mixtures. Furthermore, the application of quantitative NMR (qNMR) was also reported on food due to the enormous potential in metabolomics profiling,[24] resulting from a feature of NMR techniques, that is, precise compound identification and quantification. NMR techniques are useful for monitoring composition changes during food processing such as fermentation, thermal processing, and ripening.[21,23−25] With untargeted multivariate statistical methods, such as principal component analysis (PCA), different origins,[25] cultivars,[21] processes,[23] or fermentations[24] in foods are clearly distinguished by the ^{1}H NMR spectra.

To date, metabolite changes in black garlic during thermal processing have not been reported. These changes could be detected by the one-dimensional (1D) and two-dimensional (2D) NMR spectra of black garlic with different degrees of thermal processing. Multivariate analyses are also used to obtain

Received: October 8, 2014
Revised: December 18, 2014
Accepted: December 30, 2014
Published: December 30, 2014

ACS Publications © 2014 American Chemical Society

DOI: 10.1021/jf504836d
J. Agric. Food Chem. 2015, 63, 683−691

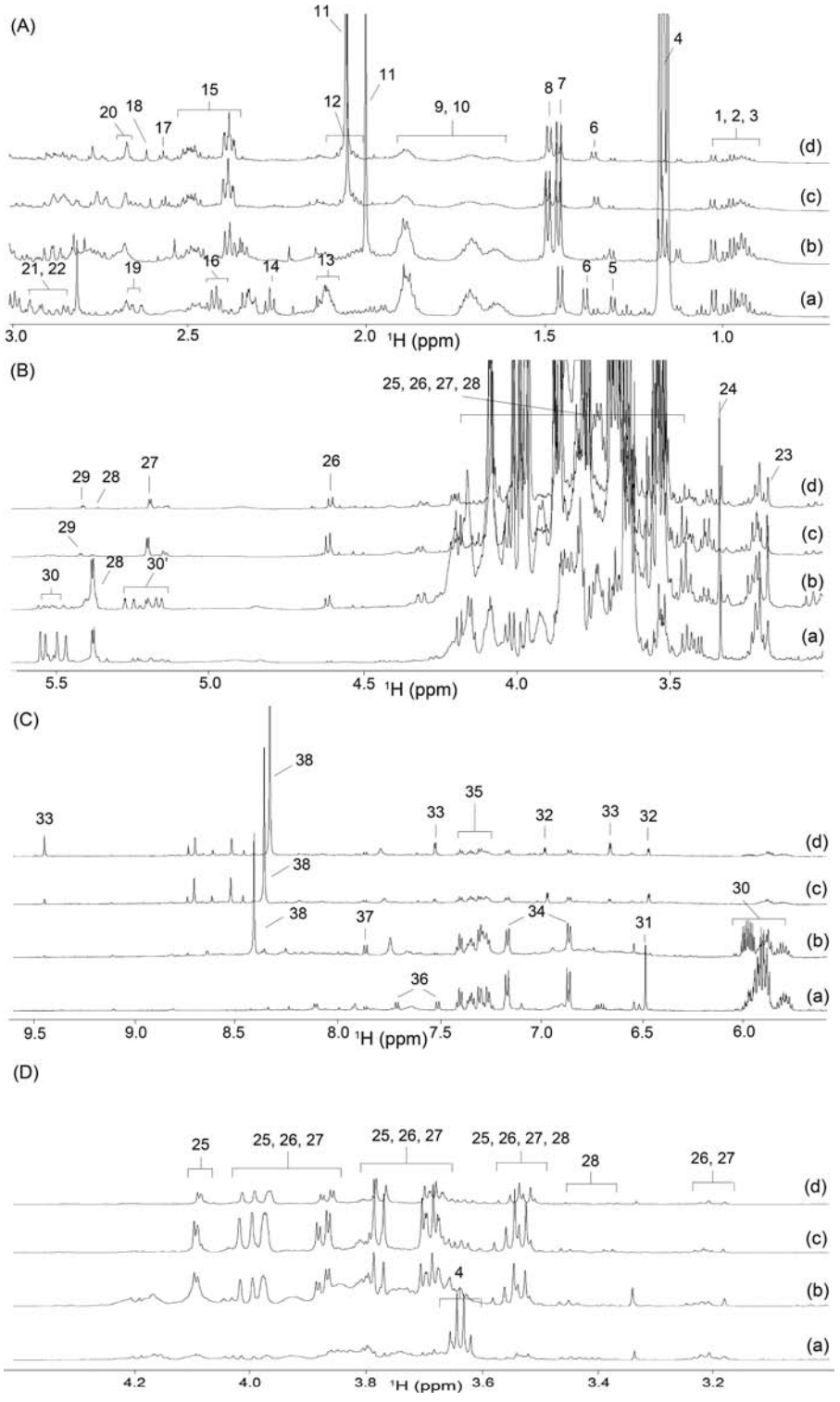

Figure 1. (A, B) High-field, (C) low-field, and (D) sugar regions of the ^{1}H NMR spectra of the (a) raw garlic extract and (b) 5 day, (c) 25 day, and (d) over 90 day black garlic extracts with the following signal assignments: 1, valine; 2, leucine; 3, isoleucine; 4, ethanol; 5, threonine; 6, lactic acid; 7, alanine; 8, cycloalliin; 9, lysine; 10, arginine; 11, acetic acid; 12, proline; 13, glutamine; 14, γ-aminobutyric acid (GABA); 15, pyroglutamic acid; 16, glutamic acid; 17, 3-hydroxypropionic acid; 18, succinic acid; 19, malic acid; 20, citric acid; 21, asparagine; 22, aspartic acid; 23, choline; 24, methanol; 25, fructose; 26, β-glucose; 27,α-glucose; 28, sucrose; 29, glucosamine; 30, 30′, allicin and other allyl organosulfur compounds; 31, fumaric acid; 32, 5-(hydroxymethyl)-2-furoic acid; 33, 5-(hydroxymethyl)furfural; 34, tyrosine; 35, phenylalanine; 36, tryptophan; 37, uridine; 38, formic acid.

comprehensive information regarding the compositional changes of black garlic from the NMR spectra. In this study, we report a ^{1}H NMR-based comprehensive analysis of raw garlic and black garlic extracts. The chemical compositional changes resulting from thermal processing are characterized using 1D ^{1}H NMR spectra, the signal assignment information is provided by analyses of 2D NMR spectra, and the resulting PCA is provided as score and loading plots.

DOI: 10.1021/jf504836d
J. Agric. Food Chem. 2015, 63, 683−691

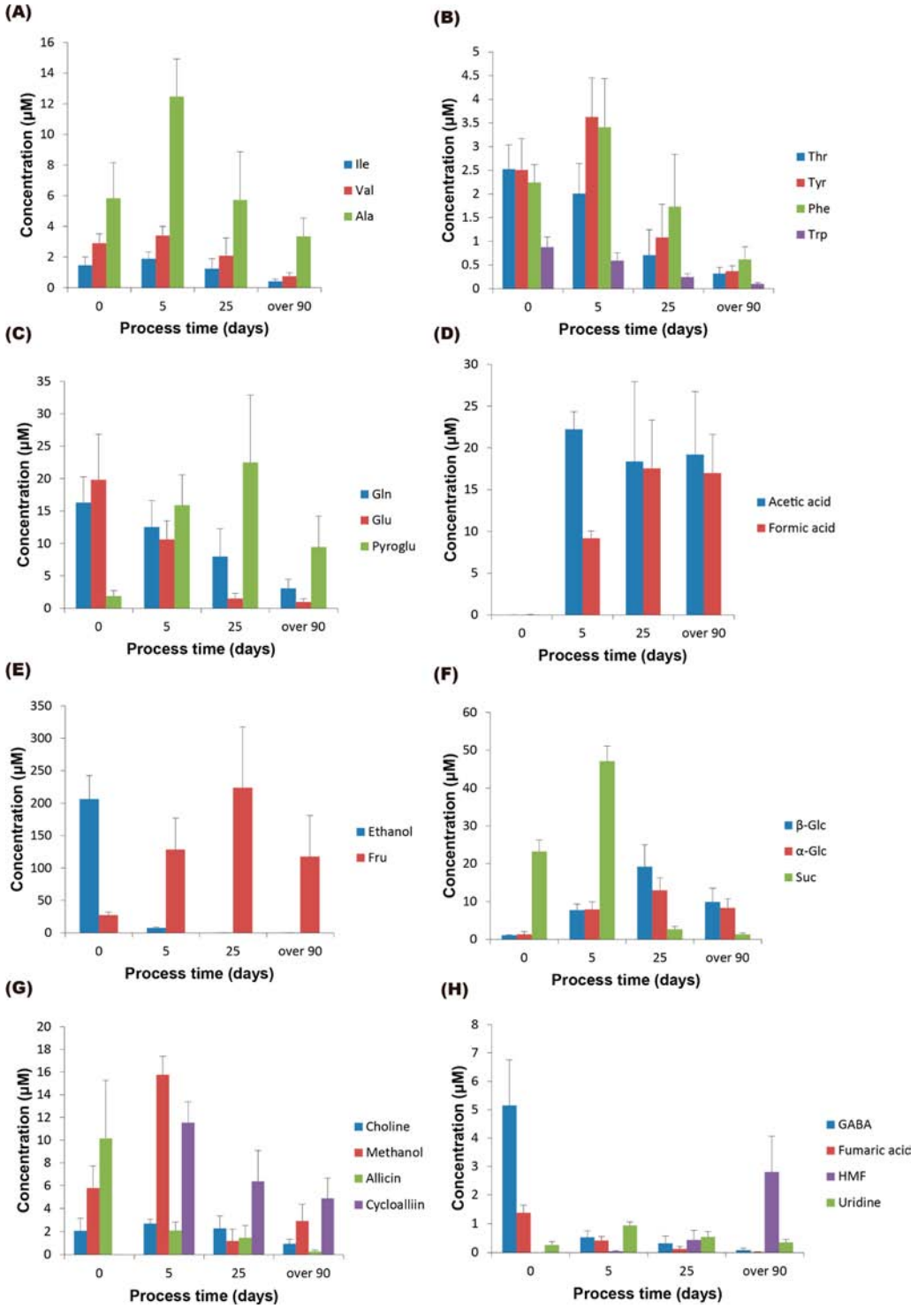

Figure 2. Changes in black garlic extract content during thermal processing: (A–C) amino acids, (D) organic acids, (E, F) ethanol and sugars, (G, H) other compounds. Abbreviations: Pyroglu, pyroglutamic acid; Fru, fructose; α-Glc, α-glucose; β-Glc, β-glucose; Suc, sucrose; GABA, γ-aminobutyric acid; HMF, 5-(hydroxymethyl)furfural. The L-amino acids are represented by the universal three-letter codes. The integral value of the DSS signal (trimethylsilyl protons) was set to unity. The integral values of the signals from the individual constituents were normalized to the value of a proton and then used to calculate the concentration. The data are the mean ± standard deviation (SD; n = 3).

MATERIALS AND METHODS

Materials. The raw garlic and black garlic samples were prepared by Salad Cosmo, Co., Ltd. (Japan) and stored at −30 °C until use. The garlic samples were divided into four groups including raw garlic and black garlic with three different degrees of thermal processing as follows: 5 day black garlic, which represents the early step of thermal processing, i.e., thermal processing of raw garlic at 75 °C for 5 days; 25 day black garlic, which represents the late step of thermal processing, consisting of subsequent thermal processing of the 5 day black garlic at 67 °C for 20 days; over 90 day black garlic, which represents the state offered for sale and is stored at room temperature for approximately 2 months after thermal processing of 25 day black garlic at 35 °C for 14 days.

DOI: 10.1021/jf504836d
J. Agric. Food Chem. 2015, 63, 683–691

NMR Samples. Samples of raw garlic and three types of black garlic (seven samples for each group) were peeled and sliced. The garlic samples (1 g) were soaked in 1 mL of 10% dimethyl sulfoxide-d_6 (DMSO-d_6; Cambridge Isotope Laboratories, Inc.)/90% D_2O (99.7%; Shoko Co., Ltd., Tokyo, Japan) for 1 h at room temperature. The extracts were centrifuged at 10000*g* at 4 °C for 10 min. The supernatants were removed and centrifuged again under the same conditions. Then 5 μL of 178 μM 4,4-dimethyl-4-silapentane-1-sulfonic acid, sodium salt (DSS; Wako Pure Chemical Industries, Ltd., Osaka, Japan) was added to the supernatants (600 μL) as an internal reference (final concentration of 1.47 μM),[21] with a chemical shift that was set to 0 ppm, and the solution was transferred into 5 mm NMR tubes.

NMR Spectroscopy. Quantitative ^{1}H NMR spectra were measured at 20 °C with a 600 MHz Agilent Unity INOVA-600 spectrometer equipped with a cryogenic probe. The signal of water was suppressed by the presaturation method, and the parameters of the measurements were as follows: number of data points, 64K; spectral width, 7764 Hz; acquisition time, 4.22 s; delay time, 30.0 s; number of scans, 32. The delay time was determined by the spin−lattice relaxation time (T_1) measurement, as used in a previous study.[20]

The ^{13}C NMR spectra were measured at 20 °C and 125.65 MHz on an Agilent Unity INOVA-500 spectrometer equipped with a 5 mm broad-band probe, and the parameters for ^{13}C NMR spectra were as follows: number of data points, 64K; spectral width, 31446 Hz; acquisition time, 1.04 s; delay time, 2.0 s; number of scans, 28128.

All of the 2D NMR spectra were measured at 20 °C on an Agilent Unity INOVA-500 spectrometer equipped with a 5 mm triple-resonance probe. For ^{1}H−^{1}H double-quantum-filtered correlation spectroscopy (DQF-COSY), the signal of water was suppressed by the presaturation method, and the acquisition parameters were as follows: number of data points, 2048 in F_2 (^{1}H) and 1024 in F_1 (^{1}H); spectral width, 5195 Hz in F_2 and F_1; acquisition time, 0.197 s; number of scans, 72. ^{1}H−^{13}C heteronuclear single-quantum coherence (HSQC) in the phase-sensitive mode was measured with the following parameters: number of data points, 2048 for ^{1}H and 512 for ^{13}C; spectral width, 5195 Hz for ^{1}H and 25141 Hz for ^{13}C; acquisition time, 0.160 s; delay time, 1.5 s; number of scans, 64. ^{1}H−^{13}C constant-time heteronuclear multiple-bond correlation (CT-HMBC) was obtained in the absolute mode with the following parameters: number of data points, 2048 for ^{1}H and 512 for ^{13}C; spectral width, 5751 Hz for ^{1}H and 30166 Hz for ^{13}C; acquisition time, 0.259 s; delay time, 2.0 s; number of scans, 512.

NMR Signal Assignments and Data Processing. The free-induction decay (FID) data were processed using ACD/NMR Workbook Suite V2012 (Advanced Chemistry Development, Inc., Canada). The signal assignments were performed as follows: (1) Certain signals in the 1D NMR spectra of the raw garlic extracts were assigned by comparison with the published data.[5,26] (2) For the assignments of the unreported signals in the 1D NMR spectra, we predicted candidate compounds using the Biological Magnetic Resonance Bank (BMRB)[27] and previous reports for the compounds of black garlic.[6,9] (3) We confirmed that the signals were correctly assigned to the candidate compounds using the 2D NMR spectra. The correlations between the carbons and their attached protons were confirmed by the ^{1}H−^{13}C HSQC spectra, and the ^{1}H−^{13}C CT-HMBC spectra were used to identify two- or three-bond coupling between the carbons and protons to detect linkages to the quaternary carbons. Couplings between two protons up to three bonds away were confirmed by the ^{1}H−^{1}H DQF-COSY spectrum. When the signals in the 1D NMR spectra were not distinguished or were undetectable in the 2D NMR spectra because of heavy overlaps or low sensitivity, respectively, spiking experiments[20] were performed in which analytical-grade chemicals were added to the NMR samples of the raw garlic or black garlic extracts to confirm the existence of the components. To observe the changes in metabolites in the garlic resulting from thermal processing, the integral values of the signals were calculated by the ACD/NMR Workbook Suite V2012. The integral value of the DSS signal at 0 ppm (the trimethylsilyl protons) was set to unity as an internal standard.

Multivariate Statistical Analysis. The ^{1}H NMR spectra were reduced into 0.04 ppm spectral buckets, the region of D_2O (4.8−5.1 ppm) was removed, and the ^{1}H NMR spectra from 0.8 to 9.5 ppm were then normalized. For the multivariate statistical analysis, the resulting data sets were imported into SIMCA-P, version 13 (Umetrics, Umeå, Sweden). PCA was performed to examine the variation in the data sets as an unsupervised classification method. The modeled variation in the score plot was defined with a 95% confidence interval, and the spectral data were Pareto scaled (Par). The goodness of fit (R^2x) and the predictability (Q^2) were described for the quality of the model.

RESULTS

^{1}H and ^{13}C NMR Spectra of Raw Garlic and Black Garlic Extracts. Figure 1 shows a representative 1D ^{1}H NMR spectrum of the raw garlic extract, 5 day, 25 day, and over 90 day black garlic extracts. On the basis of the 2D NMR analysis and the spiking experiments, 38 components were identified in the raw garlic and black garlic extracts (Table S1 in the Supporting Information). Among these components, 27 constituents of the raw garlic extracts, i.e., sucrose, α-glucose, β-glucose, fructose, L-alanine, L-valine, L-leucine, L-isoleucine, L-threonine, L-lysine, L-arginine, L-glutamine, L-glutamic acid, L-proline, L-asparagine, L-aspartic acid, L-tyrosine, L-phenylalanine, L-tryptophan, γ-aminobutyric acid (GABA), methanol, ethanol, citric acid, malic acid, fumaric acid, choline, and allyl organosulfur compounds such as allicin, have also been reported in previous studies on Italian raw garlic,[5] and all of these components were observed in the ^{1}H NMR spectrum of the raw garlic extract. In addition, uridine and lactic acid were detected in the raw garlic extract for the first time in this study. The following nine components were produced after thermal processing and were identified only in the black garlic extracts: pyroglutamic acid, cycloalliin, formic acid, acetic acid, succinic acid, 3-hydroxypropionic acid, glucosamine, 5-(hydroxymethyl)furfural (5-HMF), and 5-(hydroxymethyl)-2-furoic acid (5-HMFA). Four of the components observed in the raw garlic, i.e., GABA, L-tryptophan, ethanol, and fumaric acid, disappeared in the spectra of the black garlic extracts.

Changes in Garlic Components Resulting from Thermal Processing. To investigate the changes in the garlic components resulting from thermal processing, the contents of the garlic components were determined from the integral values of the ^{1}H signals corresponding to the individual components. Among the detectable components, 25 were quantitatively analyzed because their signals were separately observed (Figure 2).

Among the 17 detected amino acids, the contents of L-alanine, L-valine, L-leucine, L-isoleucine, L-lysine, L-arginine, L-proline, L-asparagine, L-aspartic acid, L-tyrosine, and L-phenylalanine increased in the 5 day black garlic extracts after the early step of the thermal processing and then decreased in the 25 and over 90 day black garlic extracts (Figure 2). Among the other detected amino acids, the contents of L-threonine, L-glutamine, and L-glutamic acid decreased with the progression of thermal processing. The pyroglutamic acid content increased in the 5 and 25 day black garlic extracts but decreased in the over 90 day black garlic extracts. The signals of GABA and L-tryptophan in the 1D ^{1}H NMR spectra nearly disappeared in the 5 day black garlic extract and showed a trace amount in the 25 and over 90 day black garlic extracts (Figure 1).

Among the four detected sugars, α-glucose, β-glucose, and fructose showed changes similar to those of pyroglutamic acid with the progression of thermal processing (Figure 2). The content of these sugars increased in the 5 and 25 day black garlic extracts and then decreased in the over 90 day black garlic extract. However, the sucrose content showed a 2.0-fold increase in the 5

DOI: 10.1021/jf504836d
J. Agric. Food Chem. 2015, 63, 683−691

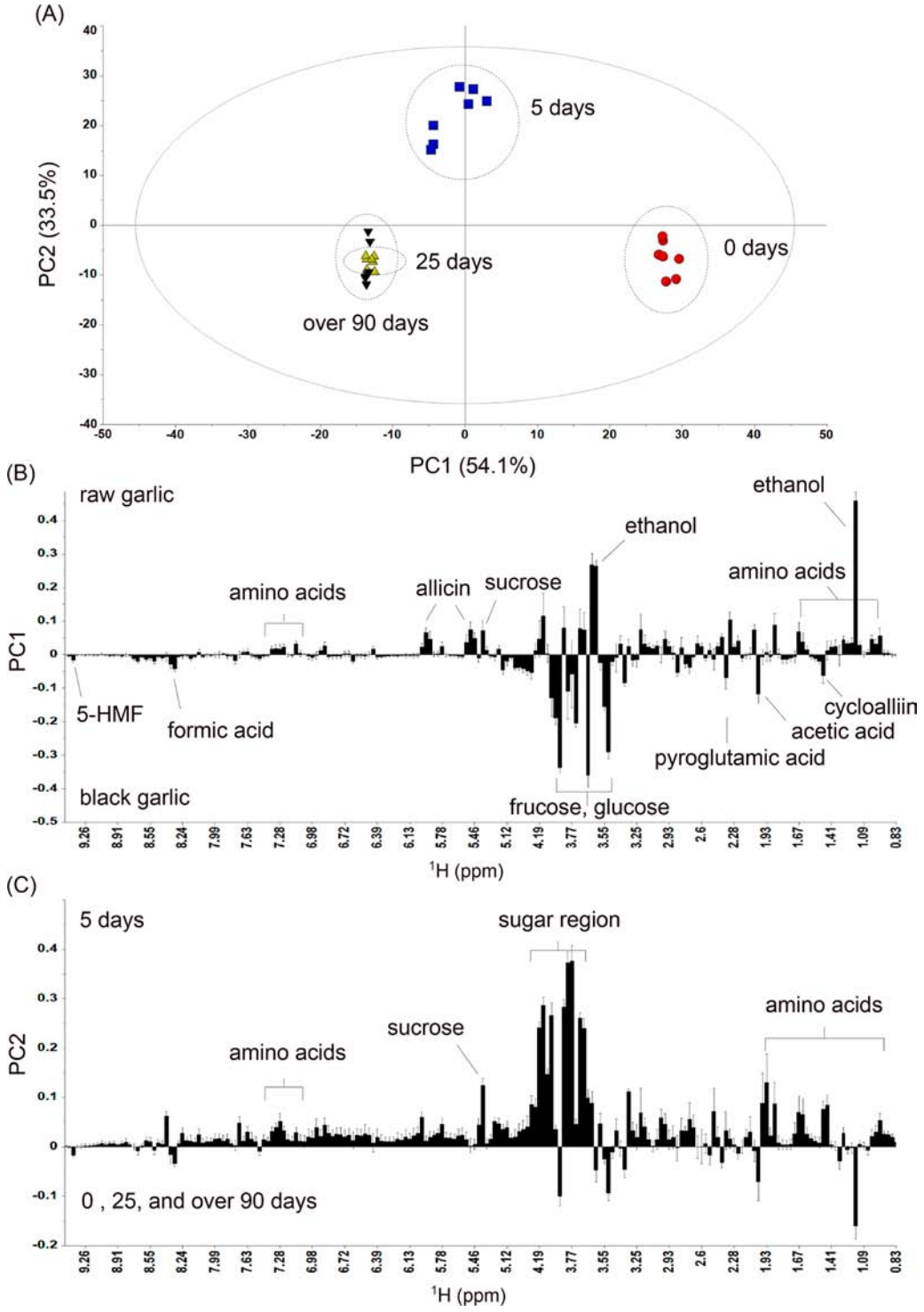

Figure 3. (A) PCA score plot, (B) loading plot for PC1, and (C) loading plot for PC2 for the extracts of raw garlic (0 days) and black garlic with different degrees of thermal processing (5, 25, and over 90 days). The PCA model with seven components was computed, and the goodness of fit (R^2x) was 54.1% and 33.5% for PC1 and PC2, respectively. The goodness of predictability was indicated by a Q^2 value of 0.95.

day black garlic extract compared with the raw garlic extract and significantly decreased in the 25 day black garlic extracts.

Among the observed organic acids, the ^{1}H signal of acetic acid was not observed in the raw garlic extract (Figure 1a), but it appeared in the 5 day black garlic extracts, and the content did not significantly change in the 25 and over 90 day black garlic extracts (Figure 2). The ^{1}H signal of formic acid also appeared in the 5 day black garlic extract and showed a small increase in the 25 and over 90 day black garlic extracts. The chemical shifts of acetic acid and formic acid changed in the ^{1}H NMR spectra during thermal processing (Figure 1), possibly as a result of changes in pH. However, the fumaric acid content decreased with the progression of thermal processing, and fumaric acid was not detected in the over 90 day black garlic extract. Succinic acid and 3-hydroxypropionic acid were detected only in the black garlic extracts (Figure 1). The contents of both of these

DOI: 10.1021/jf504836d
J. Agric. Food Chem. 2015, 63, 683−691

components increased in the 5 and 25 day black garlic extracts and then decreased in the over 90 day black garlic extracts.

Ethanol showed strong signals in the ^{1}H NMR spectra in the raw garlic extract but disappeared after thermal processing (Figures 1 and 2). Methanol showed a 2.7-fold increase in the 5 day black garlic extract compared with the raw garlic extract, and its content was significantly decreased in the 25 day black garlic extracts (Figure 2). However, a slight increase of methanol content was observed in the over 90 day black garlic extracts.

Among the other five detected components, the content of choline increased in the 5 day black garlic extracts and then decreased in the 25 and over 90 day black garlic extracts. The multiple signals at approximately 5.5 ppm in the ^{1}H NMR spectra of the raw garlic extracts were assigned to the allyl protons of allicin (Figure 1), and the content of allicin decreased during the thermal process (Figure 2). The multiplet signals at approximately 5.2 ppm were assigned to the allyl protons of organosulfur compounds. These signals increased in the 5 day black garlic extract and then decreased in the 25 day black garlic extract (Figure 1). Other compounds in the black garlic, such as cycloalliin, 5-HMF, and 5-HMFA, were detected in the 5 day black garlic extract (Figure 1). The content of cycloalliin decreased in the 25 and over 90 day black garlic extracts, whereas that of 5-HMF and 5-HMFA increased in the 25 day black garlic extracts. At the later thermal processing step of the over 90 day black garlic extracts, the content of 5-HMF was increased by more than 6-fold compared with that in the 25 day black garlic extracts.

Variations in Black Garlic Constituents Resulting from Thermal Processing. To determine the overall compositional changes in black garlic during thermal processing, PCA was performed on the quantitative ^{1}H NMR spectral data for all of the garlic extracts. As shown in Figure 3A, the raw garlic and 5 and 25 day black garlic extracts were clearly distinguished from one another on the PCA score plot with high statistical values of R^2x (54.1% for PC1 and 33.5% for PC2) and Q^2 (0.95). However, the over 90 day black garlic extracts were not distinguished from the 25 day black garlic extracts, indicating that the overall composition of the 25 day black garlic extracts was similar to that of the over 90 day extracts. The PCA loading plots demonstrated that the components in the raw garlic extracts and the black garlic extracts were different (Figure 3B). The PC1 negative loading indicated that the black garlic extracts contained higher amounts of fructose, glucose, acetic acid, formic acid, cycloalliin, pyroglutamic acid, and 5-HMF than the raw garlic extracts. On the basis of the PC1 positive loading, the raw garlic extract contained higher amounts of ethanol, amino acids, sucrose, and allicin than the black garlic extracts. However, the PC2 loading plot showed that the 5 day black garlic extract was chemically different from the raw garlic, 25 day black garlic, and over 90 day black garlic extracts. The differences were primarily observed in the amino acid and sugar contents.

DISCUSSION

Amino Acids. The ^{1}H NMR spectra showed that most of the amino acid content of garlic, except for that of GABA, L-tryptophan, L-threonine, L-glutamic acid, L-glutamine, and pyroglutamic acid, changed in a similar manner during thermal processing as follows: the content increased at the early step of thermal processing up to 5 days and decreased during the later thermal processing. The increased content of the amino acids, including L-alanine, L-valine, L-leucine, L-isoleucine, L-lysine, L-arginine, L-proline, L-asparagine, L-aspartic acid, L-tyrosine, and L-phenylalanine, in the 5 day black garlic most likely resulted from the degradation of proteins or peptides, which may result from enzymatic hydrolysis or nonenzymatic hydrolysis, such as pyrolysis. In addition, the pH value decreased from 7.1 for the raw garlic extract to 5.3 for the 5 day black garlic extract as thermal processing progressed, which may have led to further enzymatic hydrolysis of proteins under acidic conditions. However, additional data are required to verify that the increase in the amino acid content of garlic after 5 days of thermal processing is derived from proteins. In the 25 day black garlic extracts, the decrease in amino acids may have been caused by reactions with reducing sugars, such as the Maillard reaction. The amounts of glucose and fructose increased in the 25 day black garlic extracts, providing good conditions for the Maillard reaction, which frequently occurs during thermal treatment of foods such as coffee and chocolate.[28]

The decreased level of L-tryptophan in the black garlic extracts likely resulted from consumption of L-tryptophan in the chemical reaction to produce carboline, which has been reported in aged garlic extracts.[29] During this reaction, L-tryptophan reacts with an aldehyde or an α-oxo acid, such as pyruvic acid, which is produced from the Maillard reaction or from alliin metabolism, via Pictet−Spengler condensation to form tetrahydro-β-carboline derivatives (THβCs).[29,30] The THβCs exert high antioxidant activity in short-term-fermented black garlic and aged garlic extracts but were not detected in the ^{1}H NMR spectra in our study, likely because of the extraction method used. The THβCs in the aged garlic were extracted by ethanol or a relatively high ratio of an organic solvent in water solution.[29,30]

Levels of pyroglutamic acid increased in the 5 and 25 day black garlic extracts, most likely through conversion from glutamic acid or glutamine by enzymatic or nonenzymatic reactions.[31] The decrease in the contents of glutamic acid and glutamine supports their conversion to pyroglutamic acid during thermal processing. Pyroglutamic acid is a cyclic lactam of glutamic acid that is an agonist of glutamic acid and is beneficial for the prevention of amnesia or memory loss in rats.[32]

Sugars and Organic Acids. In the 5 day black garlic extracts, the sugars content, especially that of sucrose, glucose, and fructose, increased, possibly through the degradation of polysaccharides. The polysaccharides in garlic have been reported to include fructan and galactan.[33,34] The remarkable increase in fructose levels in the 5 and 25 day black garlic extracts may also have resulted from degradation of the abundant fructan in the garlic.[35] Degradation of the polysaccharides could occur under acidic and high-temperature conditions,[36] which have been well studied in food products such as coffee beans after thermal processing.[37,38] In plants, degradation of cell wall polysaccharides causes tissue softening; therefore, the texture of black garlic is more gumlike than that of raw garlic. The decrease in pH and the heat treatment during thermal processing could promote further hydrolysis of sucrose to glucose and fructose, which may also be supported by the increase in glucose and fructose contents accompanying the reduced sucrose levels in the 25 day black garlic extracts.

Signals of organic acids, such as acetic acid, formic acid, succinic acid, and 3-hydroxypropionic acid, were identified in the 1D ^{1}H NMR spectra and the 2D NMR spectra of the black garlic extracts. The contents of acetic acid were significantly increased in the 5 day black garlic extracts, as demonstrated by the differences between the raw garlic extract and the black garlic extracts in the PC1 loading plot. This change in acetic acid content may result from sugar fragmentation.[39,40] During

DOI: 10.1021/jf504836d
J. Agric. Food Chem. 2015, 63, 683−691

thermal processing, the production of short-chain carboxylic acid results from α-dicarbonyl and β-dicarbonyl cleavage of hexose or pentose.[39−41] These reactions may also produce formic acid, succinic acid, and 3-hydroxypropionic acid.[42] Fumaric acid was detected in the raw garlic extracts, but its content decreased after thermal processing, most likely because it was converted to other metabolites. Malic acid and citric acid were detectable in the 1D and 2D NMR spectra, but their signals in the ^{1}H NMR spectra were highly overlapped with other signals, which made it difficult to determine the integral values. The increased organic acid content reduced the pH of the solution, which thus affected the degradation of the proteins, peptides, and polysaccharides. In black garlic, the increased organic acid and sugar (fructose and glucose) contents most likely contribute to sourness and sweetness, respectively, which result in the fruity taste. The over 90 day black garlic may show better taste than 25 day black garlic due to the texture change after further thermal processing.

Other Compounds. Ethanol showed extremely strong signals in the 1D and 2D NMR spectra of the raw garlic extracts and was dominant in the PC1 positive loading. However, the ethanol contents were significantly decreased in the 5 day black garlic extracts and not detected in the 25 and over 90 day black garlic extracts. Because ethanol is a volatile compound, it may have been vaporized during the thermal treatment. Moreover, ethanol may be converted to acetaldehyde, which then reacts with L-tryptophan via Pictet−Spengler condensation to form THβCs.[29] The methanol signal in the ^{1}H NMR spectra increased in the 5 day black garlic extracts and then decreased during additional thermal processing. The changes in methanol content were unclear because similar changes have been reported only in plant growth.[43,44] In addition, the decrease in methanol content in the 25 day black garlic extracts may have occurred through evaporation, similar to the results observed for ethanol, because methanol is also volatile.

The content of allicin, a metabolite largely responsible for the strong odor of garlic, decreased with the progression of thermal processing in black garlic, as detected in the ^{1}H NMR spectra. Allicin could be converted from alliin by the enzymatic reaction of alliinase in raw garlic under conditions above pH 3.6.[7] In our experimental conditions, the pH values of raw garlic and 5 day black garlic extracts were around 7.1 and 5.3, respectively, and the pH value of over 90 day black garlic extracts was around 4.1. Therefore, allicin could be generated under these conditions. Although allicin is an unstable sulfur compound and it could be changed to other sulfur compounds by any processing, it was still detected in ^{1}H NMR spectra of raw and black garlic extracts with our extraction conditions and those described in the previous report.[5] The decrease in the allicin content results in a "smoother" taste of black garlic. However, the increased signal at approximately 5.2 ppm in the 5 day black garlic extracts suggests that other allyl organosulfur compounds may be produced from allicin at this stage. The 1D ^{13}C NMR and 2D NMR spectra showed that the signals were not from allicin but may represent other allyl organosulfur compounds described in previous studies, such as diallyl disulfide or other allicin derivatives.[1,5,7] As an important organosulfur compound in garlic, allicin has been studied for its health potential, including its antibacterial, antifungal, and antiviral activities.[45] However, allicin and other organosulfur compounds in garlic are eliminated by processing, such as long-time extraction and thermal processing.[7] Thus, allicin could not be the primary functional factor underlying the health benefits of black garlic. Processed garlic products, including aged garlic extract and black garlic, also showed higher antioxidant activity along with other potential health benefits compared with raw garlic.[46] These effects resulted from the formation of other functional compounds, such as SAC and THβCs. We have tried to assign the signals of major organosulfur compounds γ-glutamyl-*S*-alk(en)ylcysteines and *S*-alk(en)ylcysteine sulfoxides in garlic, but the existence of a cysteine structure, which is a methylene group linked to a sulfur atom ($-S-CH_2-$), was not detected in our NMR data. Signals of cycloalliin, a sulfur imino acid, appeared in the ^{1}H NMR spectra of the 5 day black garlic extracts. Although this organosulfur compound has been reported to exist in *Allium* species, such as onions and garlic,[47] it was not detected in the raw garlic extracts in our study or in a previous study[5] by NMR. Cycloalliin has been reported to have many biological effects, such as serum triacylglycerol-lowering effects[47] in rats and cancer risk reduction.[48] A previous report also indicated that cycloalliin could be generated from isoalliin by storage of raw garlic.[49] Because isoalliin is produced by γ-glutamyl transpeptidase and oxidase, the increased cycloalliin contents in black garlic extracts may result from thermal processing that enhances the enzymatic activity. Therefore, the increased amount of cycloalliin in the black garlic extracts may contribute to their higher functionality after thermal processing when compared with that of raw garlic.

In the thermal processing of foods, the Maillard reaction and caramelization products including 5-HMF and 5-HMFA[13,50] were also detected in the ^{1}H NMR spectra of the black garlic extracts. The increased contents of 5-HMF and 5-HMFA in the 25 and over 90 day black garlic extracts indicated that further thermal processing may have a positive correlation with the amount of 5-HMF in black garlic. 5-HMF and 5-HMFA were generated from fructose and glucose, which in turn were produced by sugar decomposition in the black garlic during the thermal treatments.

In summary, we characterized the compositional changes of black garlic through thermal processing using ^{1}H NMR spectra combined with multivariate statistical analysis. The PCA score plot indicated differences between the raw garlic extracts and black garlic extracts, although the 25 day black garlic extract was not clearly distinguished from the over 90 day black garlic extract. However, the amount of 5-HMF was different in the 25 day extract compared with the over 90 day black garlic extract as determined by detailed signal assignments. In total, 38 NMR-visible components in the raw garlic and black garlic extracts were identified by the present nondestructive NMR method, and the changes in the content of these compounds, including amino acids, sugars, organic acids, and other metabolites, were successfully monitored throughout the thermal processing. Thermal processing of garlic is important not only for generating a functional food but also for improving the taste of garlic as a processed food product. The insights into the changes in metabolite levels during thermal processing in the present study shed light on the changes in color, flavor, and taste of food products resulting from the Maillard reaction, browning reaction, and other reactions caused by thermal treatments.

■ ASSOCIATED CONTENT

Supporting Information

Detailed signal assignment data for the NMR experiments of the raw and black garlic extracts. This material is available free of charge via the Internet at http://pubs.acs.org.

DOI: 10.1021/jf504836d
J. Agric. Food Chem. 2015, 63, 683−691

AUTHOR INFORMATION

Corresponding Author

*Phone: +81-3-5841-5165. E-mail: amtanok@mail.ecc.u-tokyo.ac.jp.

Funding

This study was supported by a Japan Society for the Promotion of Science (JSPS) Grant-in-Aid for Scientific Research (S) (Grant 23228003).

Notes

The authors declare no competing financial interest.

REFERENCES

(1) Casella, S.; Leonardi, M.; Melai, B.; Fratini, F.; Pistelli, L. The role of diallyl sulfides and dipropyl sulfides in the *in vitro* antimicrobial activity of the essential oil of garlic, *Allium sativum* L., and leek, *Allium porrum* L. *Phytother. Res.* **2013**, *27*, 380−383.

(2) Wang, X.; Jiao, F.; Wang, Q.; Wang, J.; Yang, K.; Hu, R.; Liu, H.; Wang, H.; Wang, Y. Aged black garlic extract induces inhibition of gastric cancer cell growth *in vitro* and *in vivo*. *Mol. Med. Rep.* **2012**, *5*, 66−72.

(3) Kim, J.; Nam, S.; Rico, C.; Kang, M. A comparative study on the antioxidative and anti-allergic activities of fresh and aged black garlic extracts. *Int. J. Food Sci. Technol.* **2012**, *47*, 1176−1182.

(4) Sher, A.; Fakhar-ul-mahmood, M.; Shah, S.; Bukhsh, S.; Murtaza, G. Effect of garlic extract on blood glucose level and lipid profile in normal and alloxan diabetic rabbits. *Adv. Clin. Exp. Med.* **2012**, *21* (6), 705−711.

(5) Ritota, M.; Casciani, L.; Han, B.; Cozzolino, S.; Leita, L.; Sequi, P.; Valentini, M. Traceability of Italian garlic (*Allium sativum* L.) by means of HRMAS-NMR spectroscopy and multivariate data analysis. *Food Chem.* **2012**, *135*, 684−693.

(6) Kharazi, P. GC and mass-spectrometric comparison of organo sulfur compounds in two varieties of Iranian garlic. *Phosphorus, Sulfur Silicon Relat Elem.* **2005**, *180*, 1399−1403.

(7) Amagase, H. Clarifying the real bioactive constituents of garlic. *J. Nutr.* **2006**, *136*, 716S−725S.

(8) Bae, S.; Cho, S.; Won, Y.; Lee, S.; Park, H. Changes in S-allyl cysteine contents and physicochemical properties of black garlic during heat treatment. *Lebensm.-Wiss. Technol.* **2014**, *55*, 397−402.

(9) Kim, J.; Kang, O.; Gweon, O. Comparison of phenolic acids and flavonoids in black garlic at different thermal processing steps. *J. Funct. Foods* **2013**, *5*, 80−86.

(10) Purev, U.; Chung, M.; Oh, D. Individual differences on immunostimulatory activity of raw and black garlic extract in human primary immune cells. *Immunopharmacol. Immunotoxicol.* **2012**, *34*, 651−660.

(11) Kim, S.; Jung, E.; Kang, D.; Chang, U.; Hon, Y.; Suh, H. Physical stability, antioxidative properties, and photoprotective effects of a functionalized formulation containing black garlic extract. *J. Photochem. Photobiol., B* **2012**, *117*, 104−110.

(12) Sato, E.; Kohno, M.; Hamano, H.; Niwano, Y. Increased antioxidative potency of garlic by spontaneous short-term fermentation. *Plant Food Hum. Nutr.* **2006**, *61*, 157−160.

(13) Kim, H.; Choi, Y.; Lee, E.; Park, J.; Kim, S.; Park, D.; Kim, B.; Lim, Y.; Yoon, S. 5-Hydroxymethylfurfural from black garlic extract prevents TNFα-induced monocytic cell adhesion to HUVECs by suppression of vascular cell adhesion molecule-1 expression, reactive oxygen species generation and NF-κB activation. *Phytother. Res.* **2011**, *25*, 965−974.

(14) Wang, D.; Feng, Y.; Liu, J.; Yan, J.; Wang, M.; Sasaki, J.; Lu, C. Black garlic (*Allium sativum*) extracts enhance the immune system. *Med. Aromat. Plant Sci. Biotechnol.* **2010**, *4*, 37−40.

(15) Lee, Y.; Gweon, O.; Seo, Y.; Im, J.; Kang, M.; Kim, M.; Kim, J. Antioxidant effect of garlic and aged black garlic in animal model of type 2 diabetes mellitus. *Nutr. Res. Pract.* **2009**, *3*, 156−161.

(16) Kim, I.; Kim, J.; Hwang, Y.; Hwang, K.; Om, A.; Kim, J.; Cho, K. The beneficial effects of aged black garlic extract on obesity and hyperlipidemia in rats fed a high-fat diet. *J. Med. Plants Res.* **2011**, *5*, 3159−3168.

(17) Daniela, P.; Lorena, C.; Mena, R.; Giuseppem, M.; Chiara, O.; Anna, M.; Bruno, P.; Caterina, C.; Massimiliano, V. NMR-based metabolomics for organic farming traceability of early potatoes. *J. Agric. Food Chem.* **2013**, *61*, 11201−11211.

(18) Clausen, M.; Edelenbos, M.; Bertram, H. Mapping the variation of the carrot metabolome using ^{1}H NMR spectroscopy and consensus PCA. *J. Agric. Food Chem.* **2014**, *62*, 4392−4398.

(19) Monakhova, Y.; Kuballa, T.; Lachenmeier, D. Chemometric methods in NMR spectroscopic analysis of food products. *J. Anal. Chem.* **2013**, *68*, 755−766.

(20) Wei, F.; Furihata, K.; Koda, M.; Hu, F.; Miyakawa, T.; Tanokura, M. Roasting process of coffee beans as studied by nuclear magnetic resonance: time course of changes in composition. *J. Agric. Food Chem.* **2012**, *60*, 1005−1012.

(21) Koda, M.; Furihata, K.; Wei, F.; Miyakawa, T.; Tanokura, M. Metabolic discrimination of mango juice from various cultivars by band-selective NMR spectroscopy. *J. Agric. Food Chem.* **2012**, *60*, 1158−1166.

(22) Sundekilde, U.; Frederiksen, P.; Clausen, M.; Larsen, L.; Bertram, H. Relationship between the metabolite profile and technological properties of bovine milk from two dairy breeds elucidated by NMR-based metabolomics. *J. Agric. Food Chem.* **2011**, *59*, 7360−7367.

(23) Hu, F.; Furihata, K.; Kato, Y.; Tanokura, M. Nondestructive quantification of organic compounds in whole milk without pretreatment by two-dimensional NMR spectroscopy. *J. Agric. Food Chem.* **2007**, *55*, 4307−4311.

(24) López-rituerto, E.; Cabredo, S.; López, M.; Avenoza, A.; Busto, J.; Peregrina, J. A thorough study on the use of quantitative ^{1}H NMR in Rioja red wine fermentation processes. *J. Agric. Food Chem.* **2009**, *57*, 2112−2118.

(25) Schievano, E.; Peggion, E.; Mammi, S. ^{1}H nuclear magnetic resonance spectra of chloroform extracts of honey for chemometric determination of its botanical origin. *J. Agric. Food Chem.* **2010**, *58*, 57−65.

(26) Kimura, Y.; Tani, S.; Hayashi, A.; Ohtani, K.; Fujioka, S.; Kawano, T.; Shimada, A. Nematicidal activity of 5-hydroxymethyl-2-furoic acid against plant-parasitic nematodes. *Z. Naturforsch.* **2007**, *62c*, 234−238.

(27) Ulrich, E. L.; Akutsu, H.; Doreleijers, J. F.; Harano, Y.; Ioannidis, Y. E.; Lin, J.; Livny, M.; Mading, S.; Maziuk, D.; Miller, Z.; Nakatani, E.; Schulte, C. F.; Tolmie, D. E.; Kent Wenger, R.; Yao, H.; Markley, J. L. BioMagResBank. *Nucleic Acids Res.* **2008**, *36*, D402−D408.

(28) Kim, S.; Hyun, S.; Yang, S.; Choi, H.; Lee, B. ^{1}H NMR-based discrimination of thermal and vinegar treated ginseng roots. *J. Food Sci.* **2010**, *75*, C577−581.

(29) Ichikawa, M.; Yoshida, J.; Ide, N.; Sasaoka, T.; Yamaguchi, H.; Ono, K. Tetrahydro-β-carboline derivatives in aged garlic extract show antioxidant properties. *J. Nutr.* **2006**, *136*, 726S−731S.

(30) Sato, E.; Kohno, M.; Hamano, H.; Niwano, Y. Increased level of tetrahydro-β-carboline derivatives in short-term fermented garlic. *Plant Foods Hum. Nutr.* **2006**, *61*, 175−178.

(31) Kumar, A.; Bachhawat, A. Pyroglutamic acid: throwing light on a lightly studied metabolite. *Curr. Sci.* **2012**, *102*, 288−297.

(32) Drago, F.; Valerio, C.; D'Agata, V.; Astuto, C.; Spadaro, F.; Continella, G.; Scapagnini, U. Pyroglutamic acid improves learning and memory capacities in old rats. *Funct. Neurol.* **1988**, *3*, 137−143.

(33) Das, N.; Das, A. Structure of the D-fructan isolated from garlic (*Allium sativum*) bulbs. *Carbohydr. Res.* **1978**, *64*, 155−167.

(34) Das, N.; Das, A. Structure of the D-galactan isolated from garlic (*Allium sativum*) bulbs. *Carbohydr. Res.* **1977**, *56*, 337−349.

(35) Baumgartner, S.; Dax, G.; Praznik, W.; Falk, H. Characterisation of the high-molecular weight fructan isolated from garlic (*Allium sativum* L.). *Carbohydr. Res.* **2000**, *328*, 177−183.

(36) Mankarios, A.; Jones, C.; Jarvis, M.; Therelfall, D.; Friend, J. Hydrolysis of plant polysaccharides and glc analysis of their consitituent neutral sugars. *Phytochemistry* **1979**, *18*, 419−422.

(37) Oosterveld, A.; Voragen, A.; Schols, H. Effect of roasting on the carbohydrate composition of *Coffea arabica* beans. *Carbohydr. Polym.* **2003**, *54*, 183−192.

DOI: 10.1021/jf504836d
J. Agric. Food Chem. 2015, 63, 683−691

(38) Redgwell, R.; Trovato, V.; Curti, D.; Fischer, M. Effect of roasting on degradation and structural features of polysaccharides in Arabica coffee beans. *Carbohydr. Res.* **2002**, *337*, 421−431.
(39) Davidek, T.; Robert, F.; Devaud, S.; Vera, F.; Blank, I. Sugar fragmentation in the Maillard reaction cascade: formation of short-chain carboxylic acids by a new oxidative α-dicarbonyl cleavage pathway. *J. Agric. Food Chem.* **2006**, *54*, 6677−6684.
(40) Davidek, T.; Devaud, S.; Robert, F.; Blank, I. Sugar fragmentation in the Maillard reaction cascade: isotope labeling studies on the formation of acetic acid by a hydrolytic β-dicarbonyl cleavage mechanism. *J. Agric. Food Chem.* **2006**, *54*, 6667−6676.
(41) Davidek, T.; Goúezec, E.; Devaud, S.; Blank, I. Origin and yields of acetic acid in pentose-based Maillard reaction systems. *Ann. N.Y. Acad. Sci.* **2008**, *1126*, 241−243.
(42) Fagerson, I. Thermal degradation of carbohydrates. A review. *J. Agric. Food Chem.* **1969**, *17*, 747−750.
(43) Sharkey, T. Emission of low molecular mass hydrocarbons from plants. *Trends Plant Sci.* **1996**, *1*, 78−82.
(44) Fall, R.; Benson, A. Leaf methanol—the simplest natural product from plants. *Trends Plant Sci.* **1996**, *1*, 296−301.
(45) Ankri, S.; Mirelman, D. Antimicrobial properties of allicin from garlic. *Microbes Infect.* **1999**, *2*, 125−129.
(46) Matsutomo, T.; Stark, T.; Hofmann, T. In vitro activity-guided identification of antioxidants in aged garlic extract. *J. Agric. Food Chem.* **2013**, *61*, 3059−3067.
(47) Yanagita, T.; Han, S.; Wang, Y.; Tsuruta, Y.; Anno, T. Cycloalliin, a cyclic sulfur imino acid, reduces serum triacylglycerol in rats. *Nutrition* **2003**, *19*, 140−143.
(48) Ichikawa, M.; Mizuno, I.; Yoshida, J.; Ide, N.; Ushijima, M.; Kodera, Y.; Hayama, M.; Ono, K. Pharmacokinetics of cycloalliin, an organosulfur compound found in garlic and onion, in rats. *J. Agric. Food Chem.* **2006**, *54*, 9811−9819.
(49) Ichikawa, M.; Ide, N.; Ono, K. Changes in organosulfur compounds in garlic cloves during storage. *J. Agric. Food Chem.* **2006**, *54*, 4849−4854.
(50) Murkovic, M.; Bornik, M. Formation of 5-hydroxymethyl-2-furfural (HMF) and 5-hydroxymethyl-2-furoic acid during roasting of coffee. *Mol. Nutr. Food Res.* **2007**, *51*, 390−394.

DOI: 10.1021/jf504836d
J. Agric. Food Chem. 2015, 63, 683−691

JOURNAL OF AGRICULTURAL AND FOOD CHEMISTRY

Article

pubs.acs.org/JAFC

Determination of Fatty Acids and Stable Carbon Isotopic Ratio in Subcutaneous Fat to Identify the Feeding Regime of Iberian Pigs

María Asunción López-Bascón,[†,‡] Feliciano Priego-Capote,*[,†,‡,§] Mónica Calderón-Santiago,[†,‡,§] Verónica Sánchez de Medina,[†,‡,§] José Manuel Moreno-Rojas,[∥] Juan María García-Casco,[⊥] and María Dolores Luque de Castro*[,†,‡,§]

[†]Department of Analytical Chemistry, University of Córdoba, Annex C-3, Campus of Rabanales, Córdoba, Spain

[‡]University of Córdoba Agroalimentary Excellence Campus, ceiA3, Córdoba, Spain

[§]Institute of Biomedical Research Maimónides (IMIBIC), Reina Sofía Hospital, University of Córdoba, Córdoba, Spain

[∥]Postharvest Technology and Agrifood Industry, IFAPA Center, Alameda del Obispo, Córdoba, Spain

[⊥]INIA - Center I+D of Cerdo Ibérico, Ctra Ex-101 km 4.7, Zafra, Badajoz, Spain

Supporting Information

ABSTRACT: Discrimination among the types of feeding regimes for Iberian pigs is currently a highly demanded challenge by the Iberian pig sector. In the present research, discrimination among feeding regimes has been achieved by the combination of two analytical methods (based on FAMEs analysis by GC−FID and determination of $\delta^{13}C$ by IRMS) previously used independently without success. In the present study, 80 samples of adipose tissue from Iberian pigs subjected to four different feedings were analyzed. The study of the variables more influenced by the feeding regime has allowed us to configure panels of markers with predictive power for the studied feedings by multivariate ROC analysis. The results provided values of specificity and sensitivity higher than 85% in most cases. The statistical combination of results from different analytical methods could be the key to develop models for the correct discrimination of Iberian pigs according to the feeding regime.

KEYWORDS: *Iberian pig, subcutaneous fat, IRMS, GC−FID, feeding regimes, ROC analysis, fatty acid methyl esters, stable carbon isotopes*

INTRODUCTION

The Iberian pig is well adapted to the environmental and ecological conditions of the dehesa, where it eats basically acorns, the fruit of the genus *Quercus*. Studies have shown that this feeding habit yields Iberian pigs with large amounts of monounsaturated fatty acids (MFAs), triglycerides, and phospholipids;[1,2] therefore, the fat composition in these animals is characterized by a content of polyunsaturated fatty acids (PUFAs) lower than that in those fed with prepared feeds.[3]

In the last 30 years, the increased demand for Iberian pork products has led to a rise in production, which has not been in-parallel with the available natural resources. The dehesa forest cannot support the density of animals demanded by consumers; therefore, Iberian pigs are most times fed with grains and prepared feeds,[4] and the obtained products are endowed with nutritional and organoleptical properties different from those of pigs subjected to the *montanera* feeding (traditional name for the feeding regime exclusively based on the natural resources of the dehesa). Differences in the feeding regime have a direct impact on the economic value of cured products obtained from slaughtered pigs. The high economic value of cured products from animals fed under the *montanera* regime has made mandatory regulation and identification of Iberian products. Therefore, legislation (a Royal Decree, RD) to regulate their quality according to animal feeding was promoted and approved in 2001.[5] Designation of the different types of feeding has undergone changes with time, which are defined according to the Spanish RD[6] as follows:

1. *Bellota* (*montanera*): feeding based on acorns, grass and other natural resources present in the dehesa without any contribution of prepared feeds (mainly composed by cereals and legumes).
2. *Recebo*: feeding up to a minimum weight in *montanera* conditions, then supplemented with prepared feeds.
3. *Cebo de Campo*: feeding based on prepared feeds but with a final stay in the dehesa for at least 60 days combined with prepared feeds.
4. *Cebo*: feeding based exclusively on prepared feeds.

Currently, some modifications in the new RD of 2014[7] have included the *Recebo* class into the *Cebo de Campo* class. Thus, the new *Cebo de Campo* class is a type of feeding based on prepared feeds but also, in some cases, on acorns and grasses of the dehesa.

Among the methods used for classification of products according to the feeding regime of Iberian pigs, the most common approach has been analysis of the relative proportions of fatty acids (FAs) in adipose tissues by gas chromatography (GC) separation and flame ionization detection (FID).[3,4] Analysis of FAs is of great interest in the meat industry because

Received: October 28, 2014
Revised: December 23, 2014
Accepted: December 26, 2014
Published: December 26, 2014

ACS Publications © 2014 American Chemical Society

DOI: 10.1021/jf505189x
J. Agric. Food Chem. 2015, 63, 692−699

of the technological, nutritional, and sensory aspects resulting from their composition. Nevertheless, the determination of FAs in the subcutaneous tissue related with the feeding regime of pigs has given rise to an increase of prepared feeds defined by a composition of FAs similar to that in acorns.[8] Therefore, the composition of the most important fatty acids in animals fed with prepared feeds is very similar to that in those fed by *montanera* regime, and the power of the analytical method to distinguish among the categories decreases as a result.[4]

The feasibility of using near-infrared spectroscopy (NIRS) for discrimination among subcutaneous fat from Iberian pigs reared on different fattening diets has also been evaluated in diverse studies.[9,10] This technology is based on the analysis of the spectra in the near-infrared region provided by direct determination of cured products or fresh meat. Nevertheless, the models developed so far do not allow successful discrimination of all types of diets.

It is clear that new and more specific analytical methods are needed at present to discriminate among feeding regimes. The application of isotope ratio mass spectrometry (IRMS) has become an interesting tool to analyze the quality and authenticity of food.[8] Some of the methods based on this technique have been adopted as official in the EU, for example, for the characterization of wine[11] and fruit juices.[12] Isotopic analysis of carbon and sulfur in adipose tissue has also led to an alternative method to discriminate between *Bellota* and *Cebo* regimes.[13,14] Pioneers in the study of the influence of diet on stable carbon isotope ratio in animals were De Niro et al.[15] Their results showed the possibility of performing dietary analysis based on the determination of the $^{13}C/^{12}C$ ratio. In the field of this research, González-Martin et al.[13] were pioneers in the determination of the isotopic $^{13}C/^{12}C$ ratio in subcutaneous fat of Iberian pigs to differentiate feeding regimes. Subsequently, other authors have studied the applicability of this technique in other fresh pig tissues, mainly muscle,[13] liver,[4,13−16] adipose tissue,[4,11,15] and intramuscular fat,[3,14,17−19] for the prediction of feeding regimes in Iberian pigs.[4] In general, the different techniques presented difficulty in discerning between other feedings and *Recebo*. The authors emphasized that application of only one method is not enough for the discrimination of four feeding categories; therefore, they combined several methods. Nevertheless, they did not combine their data to develop a unique discrimination model.

The aim of the research presented here was to combine the classical method for the determination of FAs based GC−FID and that for monitoring carbon isotopic abundances by IRMS to develop discrimination models and search for panels of markers with capability to classify slaughtered animals by their feeding regime.

MATERIALS AND METHODS

Samples. Eighty Iberian pigs were selected in different farms located North of the province of Sevilla (Spain) within an area delimited by 25 km from South to North and 50 km from East to West. Collection of samples was carried out in 2012 by personnel belonging to the National Institute of Agriculture and Food Research and Technology (INIA, Extremadura, Spain). The animals were classified into four groups according to the feeding regime as set by the official legislation[6]. Each group was composed of 20 samples. Subcutaneous fat samples from slaughtered pigs were collected following the established Spanish official method.[20] The fat tissues were cut and put into individual microwave-resistant glass containers, then heated in a domestic microwave oven (700 W power and 2450 MHz microwave frequency) for 5 min at the maximum power, after which the melted samples were homogenized prior to sampling 5 mL of the liquid fat.[21] The treated samples were then stored at −20 °C until analysis.

Reagents and Standards. *n*-Hexane from Scharlau (Barcelona, Spain) was used for fat solubilization. Commercial standards of FA methyl esters (FAMEs) were acquired from Fluka Analytical (Buches, Switzerland) and corresponded to the following acids: lauric (C12:0), myristic (C14:0), palmitic (C16:0), palmitoleic (C16:1n9), hepatadecanoic (C17:0), stearic (C18:0), oleic (C18:1n9), eicosanoic (C20:0), eicosenoic (C20:1), eicosadienoic (C20:2n6), eicosatrienoic (C20:3n6), eicosatetraenoic (C20:4n3), arachidonic (C20:4n6), eicosapentaenoic (20:5n3), behenic (C22:0), tetracosenoic (C24:0), docosatetraenoic (C22:4n6), docosapentanoic (C22:5n3), docosahexaenoic (C22:6n3), hexacosanoic (C26:0), and octacosanoic (C28:0). A mixture of cis/trans isomers of linoleic (C18:2) and linolenic (C18:3) FAMEs was from Supelco Analytical Sigma-Aldrich (St. Louis, MO, USA). Tridecanoic acid methyl ester (C13:0) was used as external standard (ES) in the determination step. The C13:0 methyl ester was selected as this FA is not present in the samples, and its physicochemical properties are similar to those of the target FAs. Individual stock standard solutions and multistandard solutions at different concentrations were prepared by dilution in *n*-hexane. The concentrations were selected according to those of the FAs in subcutaneous fat in pork, and the solutions were stored at −20 °C. The international isotopic standards (IIS) used for the determination of $\delta^{13}C$ values by IRMS were mineral oil (IAEA NBS22) and sacarose (IAEA CH_6), provided by the International Atomic Energy Agency (IAEA, Vienna, Austria).

Instruments. An Agilent 7820A GC System equipped with an FID was used to separate and determine the esterified FAs in each extract. The GC was furnished with an autosampler and a split/splitless injector. An SP-2380 fused silica capillary column (60 m × 0.25 mm I.D., 0.2 μm film thickness) provided by Supelco (Bellefonte, PA, USA) was used as the analytical column. EZ Chrom Elite Compact software (version 3.3.2 from Agilent Technologies, Santa Clara, CA, USA) was used for acquisition and processing of data in the GC−FID system.

A Delta V Advantage Isotope Ratio Mass Spectrometer from Thermo Fisher Scientific (Bremen, Germany) was also used. This system was equipped with a ConFlo IV Universal Interface for continuous flow analysis and a Flash 2000 HT elemental analyzer. A molecular sieve packed column (5 Å, 1 m × 1/8″ × 2 mm) from Thermo Scientific (Bremen, Germany) was used for sample cleanup. Isodat Gas Isotope Ratio MS Software (version 3.0 from Thermo Scientific, Bremen, Germany) was used to acquire and process the signal obtained by IRMS analysis.

Statgraphics Centurion XV, version 15.1.02 for Windows, and the Mass Profiler Professional (MPP) software package (version 2.0 from Agilent Technologies, Santa Clara, CA, USA) were used for statistical analysis of the generated data. Roccet software (version online, http://www.roccet.ca/) was used for data pretreatment and analysis of receiver operating characteristic (ROC) curves.

Preparation of FAMEs. Conversion of FAs into their more volatile FAMEs is mandatory prior to individual GC separation. Subcutaneous fat (0.1 g) was shaken with 2 mL of hexane and vortexed for 1 min to complete solubilization. Then, 0.2 mL of 2 M methanolic potassium hydroxide solution was added, and the byphasic system was vortexed for 1 min. The two phases were easily separated, and 1.5 mL of the upper phase, containing the esterified FAs, was pipetted in a glass vial. This solution was 1:100 (v/v) diluted in hexane, and the resulting analytical sample was spiked with the ES (40 μg/mL) prior to injection into the GC.

Determination of FAMEs by GC−FID. Two microliters of each analytical sample was injected into the GC−FID equipment for analysis of FAMEs. The injector and detector were maintained at 250 and 295 °C, respectively. All samples were prepared and analyzed in triplicate. The injection was 1:10 split, and the program of the temperature gradient was as follows: the initial oven temperature was kept at 50 °C for 2 min, then raised at 15 °C/min to a final temperature of 250 °C, which was held for 15 min. The equilibration time was 3 min. The mobile phase was helium at a flow rate of 1 mL/min. The corresponding standard was used to confirm identification of each FAME in the fat samples. Quantitative analysis was carried out by preparation of a

DOI: 10.1021/jf505189x
J. Agric. Food Chem. 2015, 63, 692−699

Table 1. Maximum, Minimum, and Mean Concentration Values Expressed as Percentages of FAs and $\delta^{13}C$ as per Thousand as a Function of the Feeding Regime

type of sample		C14:0	C16:0	C16:1n9	C17:0	C18:0	C18:1 n9	*c,c*, C18:2	*c, c, c* C18:3	C20:0	C20:2	$\delta^{13}C$
Bellota	maximum	1.38	21.42	2.48	0.40	9.76	60.73	10.05	1.03	1.42	0.59	−28.01
	minimum	1.03	17.07	1.44	0.27	7.22	51.29	8.10	0.40	0.71	0.40	−24.77
	mean	1.18	19.62	1.84	0.33	8.35	55.44	9.00	0.65	0.93	0.49	−27.05
	N	20.00	20.00	20.00	20.00	20.00	20.00	20.00	20.00	20.00	20.00	20.00
	RSD (%)[a]	9.78	5.31	13.60	10.81	9.72	4.86	8.65	27.84	20.24	13.45	2.59
Recebo	maximum	1.54	22.22	2.51	0.45	10.79	59.92	10.07	0.83	1.49	0.63	−27.83
	minimum	1.00	17.75	1.69	0.29	7.40	49.07	7.12	0.34	0.68	0.04	−25.48
	mean	1.25	20.12	1.94	0.34	8.82	56.03	8.59	0.54	1.01	0.41	−26.26
	N	20.00	20.00	20.00	20	20	20.00	20.00	20.00	20.00	20.00	20.00
	RSD (%)[a]	10.51	6.10	9.98	12.40	11.96	5.82	10.00	24.57	23.37	36.70	3.02
Cebo de Campo	maximum	1.77	27.24	3.49	0.54	13.60	53.80	11.11	0.80	1.53	0.75	−25.38
	minimum	1.13	17.68	1.67	0.27	7.15	37.85	7.15	0.41	0.95	0.31	−24.54
	mean	1.43	23.57	2.50	0.36	11.16	44.73	8.98	0.52	1.27	0.59	−24.93
	N	20.00	20.00	20.00	20.00	20.00	20.00	20.00	20.00	20.00	20.00	20.00
	RSD (%)[a]	9.67	9.59	19.18	17.06	15.15	8.85	13.02	17.08	11.65	18.26	1.08
Cebo	maximum	1.74	26.80	3.06	0.89	14.45	52.90	9.71	0.54	1.01	0.55	−27.80
	minimum	1.12	21.32	1.66	0.18	9.08	41.50	6.17	0.29	0.53	0.22	−25.55
	mean	1.39	23.99	2.17	0.39	11.28	46.92	8.35	0.42	0.72	0.39	−26.40
	N	20.00	20.00	20.00	20.00	20.00	20.00	20.00	20.00	20.00	20.00	20.00
	RSD (%)[a]	13.91	9.40	18.48	56.45	15.03	7.98	14.69	16.86	20.02	24.92	2.33

[a]RSD: relative standard deviation.

calibration model for each FA by using the multistandard solution at different concentrations spiked with the ES at 40 μg/mL. The concentrations of the target FAs were expressed as a percentage in relative terms.

Determination of $^{13}C/^{12}C$ Isotopic Ratio by IRMS. Sacarose ($\delta^{13}C$ −10.45 ‰) and NBS22-Oil ($\delta^{13}C$ −30.03 ‰) were used as IIS within the ranges 350−450 and 550−750 μg, respectively, to achieve a signal intensity of 7600 mV. Samples (within the range 320−420 μg) were weighed into a tin capsule (3.3 × 5 mm, IVA Analysentechnik e. K., Düsseldorf, Germany). The analyses were carried out in batches of 10 samples, sandwiched by standards as the internal control. The carrier and reference gases (He in both cases) were circulated at 80 and 200 mL/min, respectively. The temperatures of the elemental analyzer were set at 65 and 1020 °C for the oven temperature and combustion reactor, respectively. The results of the carbon isotope ratio ($\delta^{13}C$) analyses were reported as the per mil (‰) enrichment relative to the international standard, V-PDB (Vienna Pee Dee Belemnite) for carbon isotope ratio, according to the following equation:

$$X(‰) = [(R_{sample}/R_{reference}) - 1] \times 1000$$

where X is the ratio of the heavy to the light stable isotope (e.g., $^{13}C/^{12}C$) in the sample (R_{Sample}) and in the standard ($R_{Reference}$).[22] The fat samples were analyzed in duplicate with a variability less than 0.20‰ for $\delta^{13}C$ measurements.

Statistical Analysis. Raw data files were used to create a data set formed by samples (columns) and the quantitative variables (concentrations of FAs and $\delta^{13}C$ values). The data set, formed by 11 variables × 80 samples, was exported as comma separated value files (.csv) into the Roccet and MPP softwares for processing.

Normalization by logarithmic transformation was used as a preprocessing step since the data obtained from the two different analyses were combined. An ANOVA test was executed with the normalized data to evaluate the significance of each variable (p-value lower than 0.05). Statistical analysis was carried out by principal component analysis (PCA) and partial least squares discriminant analysis (PLS-DA). In the latter case, an N-fold cross-validation model was used. With this model, the classes of the input data are randomly divided into N equal parts; $N - 1$ parts are used for model training, and the remaining part is used for testing. The process is iteratively repeated N times using each time a different subset for testing. Thus, each row is used at least once in training and once in testing, and a confusion matrix is generated. This whole process can then be repeated as many times as specified by the number of repetitions. Ten repetitions and a fold number of three were selected in all PLS-DA models.

The ROC curves were individually obtained for different panels of variables in order to find discrimination trends between pairs of feedings.

RESULTS AND DISCUSSION

Development of Calibration Models for the Analysis of FAMEs. The calibration models were prepared from 25 FAMEs prior to analysis of the samples by using multistandard solutions at different concentrations as a function of the abundance of each compound in subcutaneous pork fat.[1,3,23] The most concentrated FAs, C16:0, C18:0, and, particularly, C18:1n9, ranged from 1.8 to 187.5 μg/mL; a second set (C14:0, C:16:1n9, and the C18:2 isomers) ranged from 0.90 to 93.75 μg/mL, and a third calibration range (from 0.48 to 48.75 μg/mL) was applied to C12:0, C17:0, C18:3 isomers, C20:1n9, C20:2, C20:3, and C20:4. Finally, the resting FAs were modeled from 0.125 to 12.5 μg/mL. Six dilutions (1:2, 1:5, 1:10, 1:25, 1:50, 1:100, and 1:250) of the multistandard stock solution, each injected in triplicate, were used to run the calibration curves. All the solutions at the different concentrations were spiked with the ES at 40 μg/mL. The calibration curves were obtained by plotting the ratio between the peak area for each FA and the peak area of the ES. The calibration equations and regression coefficients are listed in Supporting Information, Table 1. As can be seen, the regression coefficients were above 0.99 for all the compounds. It is also worth mentioning that the eight C18:3 isomers could not be independently quantified, except for the *t,t,t* and *c,c,c* isomers. A similar situation was found for C20:3 and C20:4 owing to the overlapping of their chromatographic peaks.

Analysis of FAs in the Target Samples by GC−FID and IRMS Characterization. Taking into account the variable concentration of the FAs in subcutaneous pig fat, different dilution factors were tested for analysis of the derivatized samples to obtain quantitative information on the maximum number of FAs. Thus, an 1/100 (v/v) dilution factor was adopted for

DOI: 10.1021/jf505189x
J. Agric. Food Chem. 2015, 63, 692−699

analysis of the 10 most concentrated FAs (C14:0, C16:0, C16:1n9, C17:0, C18:0, C18:1n9, *c,c* C18:2, *c,c,c* C18:3, C20:0, and C20:2); while the rest of FAs were detected at lower dilution factors at which quantitative analysis of the most concentrated FAs was compromised; therefore, they were discarded from the results obtained at dilutions lower than 1/100. Supporting Information, Figure 1 shows a GC−FID chromatogram obtained by analysis of subcutaneous fat from a *Bellota* sample.

After analysis, the data were processed to obtain the FA concentration profile from each sample. Table 1 summarizes the results provided by the 80 samples with information on the maximum and minimum concentrations found for each FA and the mean concentration and standard deviation for each target feeding. The $\delta^{13}C$ value is also included to show the variability of this parameter. As Table 1 shows, four FAs (C18:1n9, C16:1n9, C18:0, and *c,c* C18:2) clearly dominated the concentration profile of subcutaneous fat, which is in agreement with characterization studies previously reported.[1,3] The rest of the FAs were present at relative concentrations below 5%.

The comparison of the FA profile among the four types of samples grouped by feeding revealed that the content of major FAs was similar for *Cebo* and *Cebo de Campo* feedings (*p*-value above 0.0713), while samples from *Recebo* and *Bellota* also provided a similar profile (*p*-value above 0.1239); this is quite foreseeable behavior taking into account that these two feedings are the most similar among the four classes under study. It is also worth emphasizing that C18:1n9 was the most concentrated FA in the four groups of samples (about 50% of relative concentration), but mean values were higher for *Recebo* and *Bellota* (56.03 and 55.44%, respectively), which could be ascribed to similarity between these two feeding regimes. Animals subjected to the *Recebo* regime are fattened in *montanera* conditions up till they reach a cutoff weight, while *Bellota* animals are fed under *montanera* conditions up till they are slaughtered.

The only official method for discrimination of feeding regimes of Iberian pigs was based on GC−FID analysis of FA composition in subcutaneous adipose tissue.[6,18] This method was discarded as the official method in 2007 as it was not able to detect fraud imvolving Iberigan pigs fed with prepared feeds.[18] B.O.E. 2004[20] includes a summary of the criteria used for classification of the three defined feedings: *Cebo*, *Recebo*, and *Bellota*. The relative standard deviation (RSD %) was quite similar among the four groups under study (Table 1): below 10% for all FAs, except for the two most relevant, C16:0 and C18:1.

The $\delta^{13}C$ values (see Supporting Information, Figure 1, which shows an IRMS spectrum provided by analysis of a subcutaneous adipose *Bellota* sample) ranged from −28.01 to −24.54‰, with RSD below 3‰. Attending to this variability, the inclusion of $\delta^{13}C$ in classical discrimination models based on FAME analysis could aid in feeding classification. In this research, only carbon isotopic ratios were studied. The isotopic analysis of hydrogen and oxygen has been applied mainly for geographical discrimination of different types of food such as durum wheat semolina and potatoes.[4,16,24−30] Geographical discrimination is out of the scope of the present research as all samples were collected in a delimited area, as specified under Materials and Methods.

Influence of Feeding on the FA Profile and $\delta^{13}C$ Value. The data set was normalized by logarithmic transformation because of the two analytical methods used. The effect of this preprocessing step was proved by application of the Kurtosis and Skewness tests. Then, the normalized data set was analyzed by ANOVA to evaluate the influence of the feeding type on both the concentration of FAs and the value of the $^{13}C/^{12}C$ isotopic ratio (dependent variables). Table 2 summarizes the results provided by ANOVA of the 11 dependent variables as a function of the predictive factor, the feeding type. The variance is decomposed into two components: between-groups variability (intergroups) and within-group variability (intragroup). As can be seen, most of the variables reported a very high significance with *p*-values below 0.001, except for C17:0 and *c,c* C18:2 which did not show any level of significance. Therefore, the feeding factor exerted a noticeable influence on the FA profile and $^{13}C/^{12}C$ ratio. In fact, feeding was identified as the main variability source to explain the levels of the most concentrated FAs (C16:0, C18:0, C18:1n9, and C20:0) as well as the $^{13}C/^{12}C$ ratio, which was deduced by comparing the sum of squares between and within the target

Table 2. Sum of Squares between and within Groups, Mean Square, and Significance (*p*-Values) Obtained after Application of the ANOVA Test

compound	variability	sum of squares	D.f.	mean square	significance
C14:0	between-groups	0.95	3	0.32	0.0000
	within-group	1.93	76	0.03	
	total	2.88	79		
C16:0	between-groups	1.32	3	0.44	0.0000
	within-groups	1.03	76	0.01	
	total	2.35	79		
C16:1n9	between-groups	2.15	3	0.72	0.0000
	within-groups	3.66	76	0.05	
	total	5.82	79		
C17:0	between-groups	0.13	3	0.04	0.8263
	within-groups	10.71	76	0.14	
	total	10.83	79		
C18:0	between-groups	2.92	3	0.97	0.0000
	within-groups	2.83	76	0.04	
	total	5.75	79		
C18:1n9	between-groups	1.68	3	0.56	0.0000
	within-groups	0.78	76	0.01	
	total	2.46	79		
c,c C18:2	between-groups	0.18	3	0.06	0.1210
	within-groups	2.31	76	0.03	
	total	2.50	79		
c,c,c C18:3	between-groups	3.52	3	1.17	0.0000
	within-groups	7.19	76	0.09	
	total	10.71	79		
C20:0	between-groups	6.96	3	2.32	0.0000
	within-groups	5.35	76	0.07	
	total	12.32	79		
C20:2	between-groups	5.06	3	1.69	0.0000
	within-groups	14.19	76	0.19	
	total	19.25	79		
$\delta^{13}C$	between-groups	0.15	3	0.05	0.0000
	within-groups	0.09	76	0.00	
	total	0.24	79		

DOI: 10.1021/jf505189x
J. Agric. Food Chem. 2015, 63, 692−699

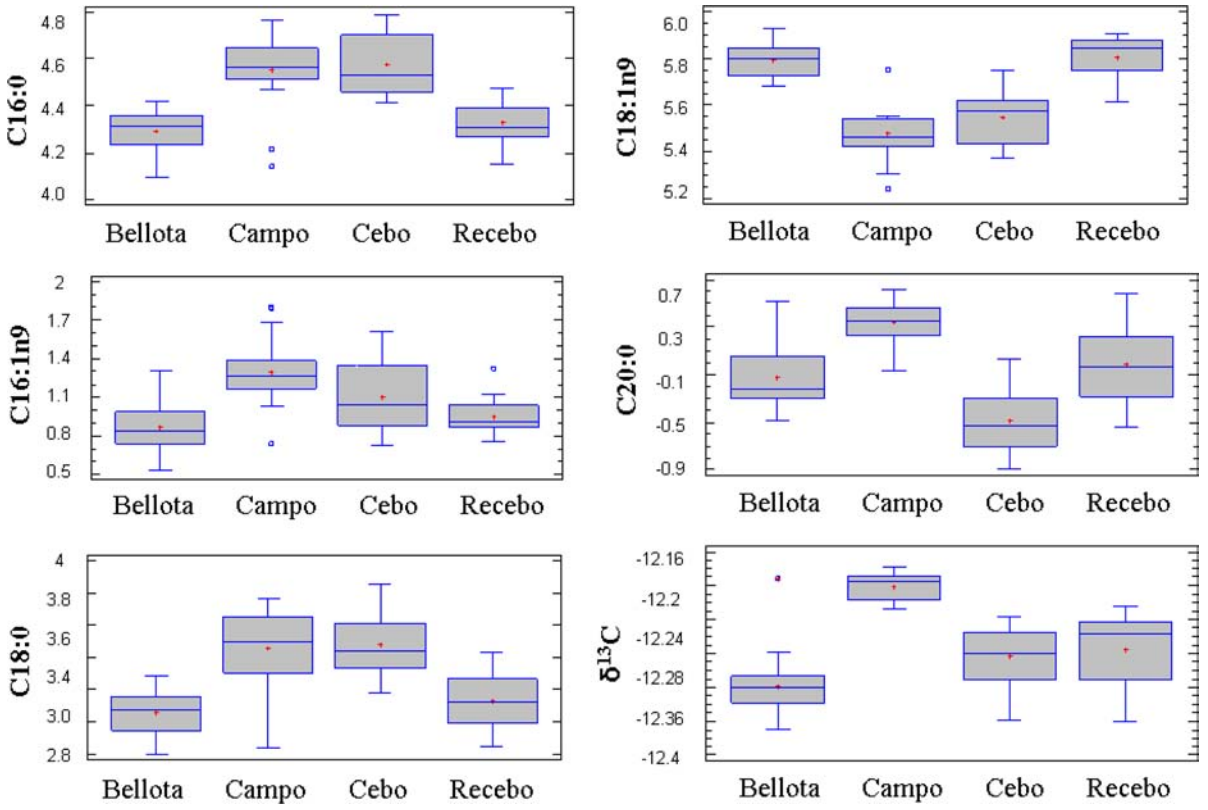

Figure 1. Box-and-whisker plots provided by comparison of normalized concentrations of significant FAs (%) and $\delta^{13}C$ (‰) according to the feeding regime.

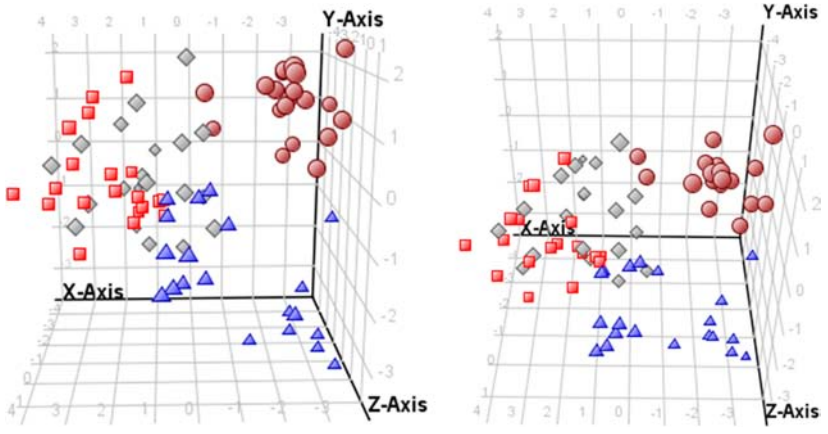

Figure 2. PLS-DA scores plot (different views) of samples from slaughtered pigs subjected to different feeding regimes. *X*-axis, t_0; *Y*-axis, t_1; *Z*-axis, t_2. Explained variability: *X*-axis, 40.95%; *Y*-axis, 19.56%; *Z*-axis, 9.65%. Square, *Bellota*; circle, *Cebo de Campo*; triangle, *Cebo*; rhombus, *Recebo*.

groups. Figure 1 shows the box-and-whisker plots obtained by normalized concentrations of the significant variables, which allowed us to detect some differences among the four groups. Thus, the $\delta^{13}C$ values revealed differences between *Cebo de Campo* samples and the other three feedings. However, C16:0, C16:1n9, and C18:0 were characterized by a similar trend since they were clearly more concentrated in *Cebo de Campo* and *Cebo* samples than in those from *Bellota* and *Recebo*. The opposite situation was observed with C18:1n9, which was more concentrated in animals subjected to the *montanera* regime during a given period. A different trend was observed for C20:0, which provided discrimination in concentration between *Cebo de Campo* and *Cebo* samples, while *Bellota* and *Recebo* samples gave levels between the two previous groups.

The influence of feeding on the FA profile and $\delta^{13}C$ values led us to apply multivariate analysis to find discrimination trends among groups. Thus, PCA was first applied to check the incidence of the breeding type on the FA profile and the $^{13}C/^{12}C$ ratio. The three-dimensional PCA scores plot with samples identified by symbols as a function of the type of feeding is shown in Supporting Information, Figure 2. The 3D-plot allowed us to explain 70.6% of the total variability. One cluster formed by *Cebo de Campo* samples can be clearly differentiated from the other three groups. Thus, the *Cebo de Campo* class was the feeding type providing the most discriminating pattern in the FA profile and the $^{13}C/^{12}C$ ratio. However, a partial separation can be observed for the other three feeding classes (*Cebo*, *Recebo*, and *Bellota*), which allows us to set differences. A particular behavior was

DOI: 10.1021/jf505189x
J. Agric. Food Chem. 2015, 63, 692−699

Table 3. *p*-Values Obtained by Application of the ANOVA Test between Pairs of Regimes

p-value	*Cebo de Campo* vs *Recebo*	*Cebo de Campo* vs *Bellota*	*Cebo de Campo* vs *Cebo*	*Bellota* vs *Cebo*	*Recebo* vs *Bellota*	*Recebo* vs *Cebo*
0.05−0.01			C16:1n9	C18:2	C18:3, C20:2	C14:0, C16:1n9
0.01−0.001	C20:2	C18:3, C20:2		δ^{13}C, C16:1n9	δ^{13}C	C18:3
<0.001	δ^{13}C, C16:0	δ^{13}C, C16:0	δ^{13}C, C18:3	C18:0, C18:1n9		C18:0, C18:1n9
	C18:0, C18:1n9, C14:0	C18:0, C18:1n9, C14:0	C20:0,, C20:2	C16:0, C18:3		C16:0, C20:0
	C20:0, C16:1n9	C20:0, C16:1n9		C20:0, C14:0, C20:2		

visualized for *Cebo* samples as two subclusters were found, one of them completely separated and a second subcluster that overlapped with *Recebo* and *Bellota* samples. No details were provided by farmers about this result, but it could be associated with differences in the provided feeding. The results obtained with PCA seem to be quite logical since the maximum overlap was detected between *Recebo* and *Bellota* samples that constitute the most similar classes since animals subjected to *Recebo* feeding must reach a minimum weight in the dehesa (*montanera* regime).

The next step was application of supervised statistical analysis by PLS-DA to evaluate the capability of the data set for development of predictive/discrimination models. Figure 2 shows the PLS scores plot that allows discrimination between *Cebo de Campo* and *Cebo* samples, while *Bellota* and *Recebo* samples overlapped. This behavior was checked in the confusion matrix provided by this PLS-DA model both in the training and validation steps, which were carried out by cross-validation. Thus, *Bellota*, *Cebo de Campo*, and *Cebo* were classified with accuracy above 90%, while the model failed in the classification of *Recebo* samples with a 45% of accuracy. In fact, the model confused 35% of the *Recebo* samples, which were erroneously classified as *Bellota* samples.

Multivariate Analysis between Pairs of Feedings. Since the variability in the concentrations of FAs and δ^{13}C values does not allow complete discrimination of the four groups of feedings, multivariate analysis was applied to pairs of feedings to precisely identify the patterns that differentiate them. For this purpose, one PLS-DA model was created for each pair of feedings, and then, ANOVA analysis revealed the main statistical differences in subcutaneous fat of animals subjected to each feeding (Supporting Information, Figure 3). Supporting Information, Table 2 shows the discrimination capability for training and cross-validation obtained from the six cases. As expected, high-discriminating models were found in all pairs of feedings, except for that involving *Bellota* and *Recebo* samples, which provided discrimination capabilities above 75% in the training step and 65% in the validation step. Supporting Information, Figure 3 shows the 3D-plots obtained by PLS-DA with clear separation between each pair of feedings. Therefore, if the variability study is focused on two types of feedings then the discrimination models gain in prediction capability, even for *Bellota* and *Recebo* samples, which seems to be the two most similar feedings.

After supervised analysis, an ANOVA test was independently applied to each pair of feedings to evaluate its influence on the concentration of FAs and δ^{13}C. Table 3 lists the variables that are significantly different by comparison of two feedings and the *p*-values obtained for them. As can be seen, the δ^{13}C value was significantly altered by the feeding in all cases, with a *p*-value below 0.001, except for the pair *Recebo* vs *Cebo*. The most concentrated FAs in subcutaneous fat, C16:0, C18:0, and C18:1n9, were significant in most of the evaluated pairs, except for *Cebo de Campo* vs *Cebo* and *Recebo* vs *Bellota*. It is worth mentioning that the significance level was quite high in all cases with *p*-values below 0.001. Only two FAs, C17:0 and *c,c* C18:2, were not significantly affected by the type of feeding.

Prediction Analysis by Multivariate ROC Analysis. The influence of feeding on the variability of FA concentration and δ^{13}C values in subcutaneous fat from Iberian pigs supports the assessment of predictive models based on panels formed by a combination of significant variables according to the ANOVA test. ROC curves are generally considered the method of choice for evaluating the performance of potential biomarkers associated with biological processes. In this research, panels were prepared by multivariate ROC analysis, which involves a preliminary study of the individual predictive capability of all the variables and, then, the combination of variables in panels to maximize the predictive capability. Taking into account that *Bellota* is the most appreciated class, prediction models were created for the classification of *Bellota* vs *Cebo de Campo*, *Bellota* vs *Cebo*, and *Bellota* vs *Recebo*. Other panels with commercial interest were also configured for discrimination between *Cebo* vs *Cebo de Campo* and *Cebo* vs *Recebo*. Predictive models were developed by dividing the set of samples into training and validation sets, which included 75% and 25% of the samples of each condition, respectively. The samples used for validation were not included in the training step, which means that this was carried out with an external set. The algorithm used for classification and selection of variables in the panels was PLS-DA with three latent variables. All of the panels were formed by three variables, except for *Bellota* vs *Recebo*, in which the best predictive behavior was provided by δ^{13}C, and no improvement provided the inclusion of additional variables. In the studies involving other combinations of feeding regimes, the sensitivity and/or specificity was not improved by inclusion of more variables either. It is also worth mentioning that all panels constituted by three variables were formed by δ^{13}C and the most concentrated FA, oleic acid. Additionally, stearic acid contributed to the prediction of *Bellota* vs *Cebo de Campo* and *Bellota* vs *Cebo*, while palmitic acid and eicosanoic acid improved the models for the discrimination of *Cebo* vs *Recebo* and *Cebo* vs *Cebo de Campo*, respectively. The models involving *Bellota* vs *Cebo de Campo* and *Cebo* reported high sensitivity and specificity, always above 90%, which led to quite good predictive models. The most complicated case was the model involving *Bellota* vs *Recebo*, based on a unique variable, δ^{13}C, which reported a specificity of 80%, while sensitivity decreased to 63%. This result agrees with that provided by the PLS-DA study for the same two feeding regimes. The efficiency of this model can be compared with that provided by previous studies based on IRMS analysis, such as that carried out by García Casco et al.,[4] who provided a model based on the analysis of stable isotopes of carbon (δ^{13}C) and sulfur (δ^{34}S) with lower discrimination capability than the model obtained in this research. The sensitivity and specificity of the models for the discrimination of *Cebo* vs *Recebo* and *Cebo* vs *Cebo de Campo* were 93% and 85%, respectively. The most compromised case was the model involving *Recebo* vs *Bellota* that reported a specificity of 80% and sensitivity of 63%. Thus,

DOI: 10.1021/jf505189x
J. Agric. Food Chem. 2015, 63, 692−699

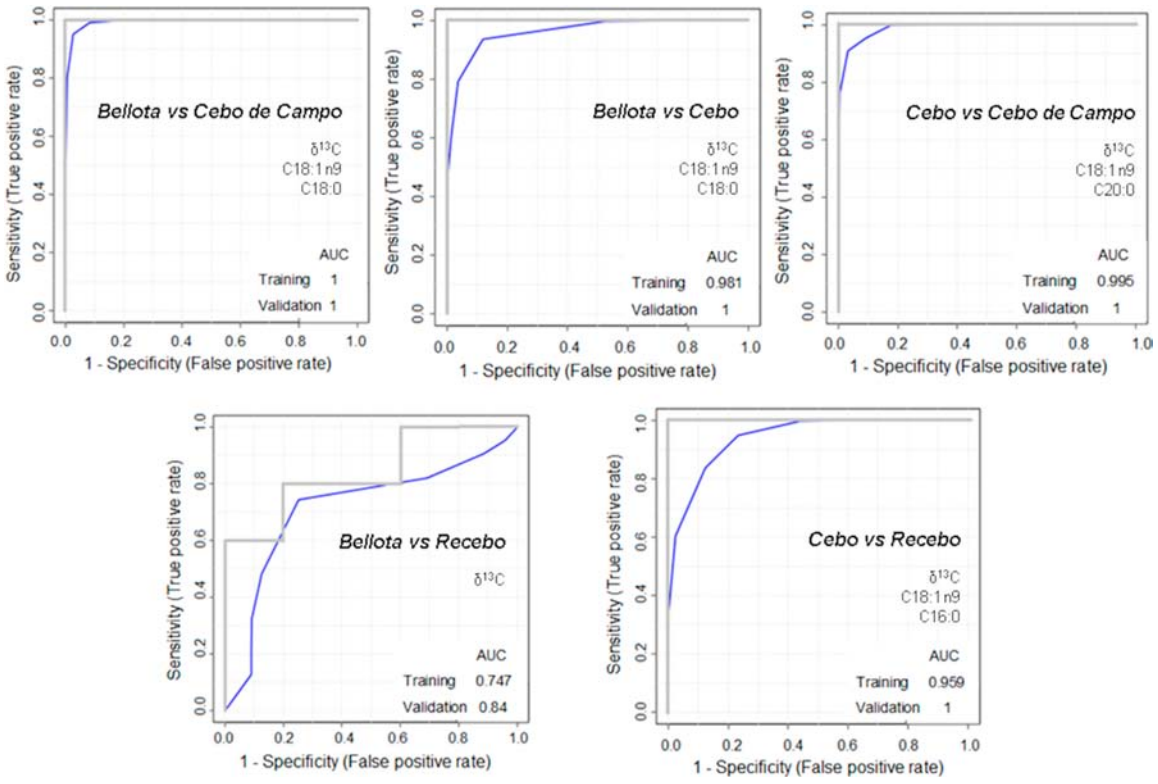

Figure 3. Individual ROC curves obtained from panels of biomarkers for discrimination between pairs of diets. The thick line corresponds to validation (external), and the fine line corresponds to training. *Bellota* vs *Cebo de Campo*: variables, δ^{13}C, C18:1n9, C18:0. *Bellota* vs *Cebo*: variables, δ^{13}C, C18:1n9, C18:0. *Cebo* vs *Cebo de Campo*: variables, δ^{13}C, C18:1n9, C20:0. *Bellota* vs *Recebo*: variables, δ^{13}C. *Cebo* vs *Recebo*: variables, δ^{13}C, C18:1n9, C16:0.

these models enabled us to classify samples according to their feeding regimes. These good prediction parameters can be explained by the ROC curves illustrated in Figure 3.

The results of sensitivity and specificity for each panel can be combined with the estimations of prediction capability for each class and the false positive rates listed in Supporting Information, Table 3. Thus, these values associated with the validation set were quite consistent with the results provided by the training set. As the validation set was formed by samples not included in the training set, the quality and statistical support are considerably enhanced.

At present, there are no discrimination methods able to identify the feeding regime used with capability to detect fraud. Different techniques have been independently assayed. However, no methods based on the application of different analytical techniques had been combined so far. In view of these results, the statistical combination of the results obtained by different analytical methods could be the key for the correct discrimination of feeding regimes in the sector of Iberian pigs. Taking into account the demand for methods to discriminate feeding regimes, this approach could be implemented in routine laboratories since the analysis of fatty acids is already carried out at this level, while IRMS analysis is frequently used in reference food laboratories.

■ ASSOCIATED CONTENT

Supporting Information

Calibration models for quantitative analyses of FAMEs by GC−FID; accuracy values (expressed as %) for the training and validation sets obtained by PLS-DA as a function of feeding regime; prediction capability values and false positive rates (expressed as %) obtained for the training and validation models created for different pairs of feedings; GC−FID chromatogram and IRMS spectrum obtained by analysis of subcutaneous adipose tissue from a *Bellota* sample; PCA score plots (different views) associated with FAs and δ^{13}C as a function of the feeding regime; and 3D-plots obtained by PLS-DA analysis of FAs and δ^{13}C to discriminate between pair of diets. This material is available free of charge via the Internet at http://pubs.acs.org.

■ AUTHOR INFORMATION

Corresponding Authors

*(F.P.-C.) Phone: +34957218615. Fax: +34957218615. E-mail: q72prcaf@uco.es.

*(M.L.C) Phone: +34957218615. Fax: +34957218615. E-mail: qa1lucam@uco.es.

Funding

The Spanish Ministerio de Economía y Competitividad (MINECO) and European FEDER program are thanked for financial support through project CTQ2012-37428. F.P.C. is also grateful to Ministerio de Ciencia e Innovación (MICINN) for a Ramón y Cajal contract (RYC-2009-03921).

Notes

The authors declare no competing financial interest.

■ ABBREVIATIONS USED

EFA, esterified fatty acid; ES, external standard; EU, Europe Union; FA, fatty acid; FAME, fatty acid methyl ester; FID, flame ionization detector; GC, gas chromatography; IAEA, International Energy Agency; IIS, international isotopic standard; INIA, National Institute of Agriculture and Food Research and Technology; IRMS, isotope-ratio mass spectrometry; MAGRAMA, Ministerio de Agricultura, Alimentación y Medio Ambiente;

DOI: 10.1021/jf505189x
J. Agric. Food Chem. 2015, 63, 692−699

MFA, monounsatured fatty acid; MHz, megahertz; MPP, Mass Profiler Professional; NIRS, near-infrared spectroscopy; PCA, principal component analysis; PLS-DA, partial least-squares discriminant analysis; RD, royal decree; V-PDB, Vienna Pee Dee Belemnite; W, watt

REFERENCES

(1) Rey, A. I.; Isabel, B.; Cava, R.; Lopez-Bote, C. J. Dietary acorns provide a source of gamma-tocopherol to pigs raised extensively. *Can. J. Anim. Sci.* **1998**, *78*, 441−443.

(2) Tejerina, D.; García-Torres, S.; Cabeza de Vaca, M.; Vázquez, F. M.; Cava, R. Acorns (*Quercus rotundifolia Lam.*) and grass as natural sources of antioxidants and fatty acids in the "montanera" feeding of Iberian pig: Intra- and inter-annual variations. *Food Chem.* **2011**, *124*, 997−1004.

(3) Cava, R.; Ruiz, J.; López-Bote, C.; Martín, L.; García, C.; Ventanas, J.; Antequera, T. Influence of finishing diet on fatty acid profiles of intramuscular lipids, triglycerides and phospholipids in muscles of the Iberian pig. *Meat Sci.* **1997**, *45*, 263−270.

(4) García Casco, J. M.; Muñoz, M.; González, E. Predictive ability of the feeding system in Iberian pig by means of several analytical methods. *Grasas Aceites* **2013**, *64*, 191−200.

(5) Royal Decree, 1083/2001, 5 October. Quality Standard for Iberian Products Made in Spain. B.O.E. 2001; Vol. *247*, pp 37830−37833.

(6) Royal Decree, 1469/2007, 2 November. Quality Standard for Iberian Products Made in Spain. B.O.E. 2007; Vol. *264*, pp 45087−45104.

(7) Royal Decree, 4/2014, 10 January. New Quality Standard for Iberian Products Made in Spain. B.O.E. 2014; Vol. *10*, pp 1569−1585.

(8) Vinci, G.; Preti, R.; Tieri, A.; Vieri, S. Authenticity and quality of animal origin food investigated by stable-isotope ratio analysis. *J. Sci. Food Agric.* **2012**, *93*, 439−448.

(9) Arce, L.; Domínguez-Vidal, A.; Rodríguez-Estévez, V.; López-Vidal, S.; Ayora-Canada, M. J.; Valcárcel, M. Feasibility study on the use of infrared spectroscopy for the direct authentication of Iberian pig fattening diet. *Anal. Chim. Acta* **2009**, *636*, 183−189.

(10) Fernández-Cabanás, V. M.; Garrido-Varo, A.; García Olmo, J.; De Pedro, E.; Dardenne, P. Optimisation of the spectral pre-treatments used for Iberian pig fat NIR calibrations. *Chemom. Intell. Lab. Syst.* **2007**, *87*, 104−112.

(11) European Commission No. 2676/90. Community Methods of Analysis Applicable in the Wine Sector, 1990; pp 1−192.

(12) Jamin, E.; Martin, F.; Martin, G. G. Determination of the 13C/12C ratio of ethanol derived from fruit juices and maple syrup by isotope ratio mass spectrometry: collaborative study. *J. AOAC Int.* **2004**, *87*, 621−31.

(13) González-Martín, I.; González-Pérez, C.; Hernández Menéndez, J.; Marqués-Macías, E.; Sanz Poveda, F. Use of isotope analysis to characterize meat from Iberian breed swine. *Meat Sci.* **1999**, *52*, 437−441.

(14) González-Martín, I.; González-Pérez, C.; Hernández-Menéndez, J.; Sánchez-González, C. Differentiation of dietary regimen of Iberian swine by means of isotopic analysis of carbon and sulphur in hepatic tissue. *Meat Sci.* **2001**, *58*, 25−30.

(15) Deniro, M. J.; Samuel Epstein, S. Influence of diet on the distribution of carbon isotopes in animals. *Geochim. Cosmochim. Acta* **1978**, *42*, 495−506.

(16) Sanabria, C.; Martín-Mateos, M. J.; González-Cantillo, N.; Moreno-Indias, I.; García-Casco, J. M. Fatty acid analysis of subcutaneous fat from animals with a reliable and safe feeding. *Grasas Aceites* **2013**, *64*, 148−156.

(17) Nürnberg, K.; Wegner, J.; Ender, K. Factors influencing fat composition in muscle and adipose tissue of farm animals. *Livest. Prod. Sci.* **1998**, *56*, 145−156.

(18) Pascual, J. V.; Rafecas, M.; Canela, M. A.; Boatella, J. R.; Barroeta, A. C.; Codony, R. Effect of increasing amounts of a linoleic-rich dietary fat on the fat composition of four pig breeds. Part II: Fatty acid composition in muscle and fat tissues. *Food Chem.* **2007**, *100*, 1639−1648.

(19) Narváez-Rivas, M.; Vicario, I. M.; Alcalde, M. J.; Camacho, M. L. Volatile hydrocarbon profile of Iberian dry-cured hams. A possible tool for authentication of hams according to the fattening diet. *Talanta* **2010**, *81*, 1224−1228.

(20) Orden PRE/3844/2004, 18 November. Official Methods of Sampling Channels Iberian Pigs and the Method of Analysis for Determining the Fatty Acid Composition of Total Lipids from Subcutaneous Fat of Iberian Pigs. B.O.E. 2004; Vol. *283*, pp 38770−38779.

(21) De Pedro, E.; Casillas, M.; Miranda, C. M. Microwave oven application in the extraction of fat from the subcutaneous tissue of Iberian pig ham. *Meat Sci.* **1997**, *45*, 45−51.

(22) Moreno-Rojas, J. M.; Vasta, V.; Lanza, A.; Luciano, G.; Ladroue1, V.; Claude Guillou, C.; Priolo, A. Stable isotopes to discriminate lambs fed herbage or concentrate both obtained from C3 plants. *Rapid Commun. Mass Spectrom.* **2008**, *22*, 3701−3705.

(23) García-Olmo, J.; De Pedro, E.; Garrido, A.; Paredes, A.; Sanabria, C.; Santolallad, M.; Salas, J.; García-Hierro, J. R.; Gonzalez, I.; García-Cachan, M. D.; Guirao, J. Determination of the precision of the fatty acid analysis of Iberian pig fat by gas chromatography. Results of a mini collaborative study. *Meat Sci.* **2002**, *60*, 103−109.

(24) Sacco, D.; Brescia, M. A.; Buccolieri, A.; Caputi Jambrenghi, A. Geographical origin and breed discrimination of Apulian lamb meat samples by means of analytical and spectroscopic determinations. *Meat Sci.* **2005**, *71*, 542−548.

(25) Camin, F.; Bontempo, L.; Heinrich, K.; Horacek, M.; Kelly, S. D.; Schlicht, C.; Thomas, F.; Monahan, F. J.; Hoogewerff, J.; Rossmann, A. Multi-element (H,C,N,S) stable isotope characteristics of lamb meat from different European regions. *Anal. Bioanal. Chem.* **2007**, *389*, 309−320.

(26) Schmidt, O.; Quilter, J. M.; Bahar, B.; Moloney, A. P.; Scrimgeour, C. M.; Begley, I. S.; Monahan, F. J. Inferring the origin and dietary history of beef from C, N and S stable isotope ratio analysis. *Food Chem.* **2005**, *91*, 545−549.

(27) Osorio, M. T.; Moloney, A. P.; Schmidt, O.; Monahan, F. J. Multielement isotope analysis of bovine muscle for determination of international geographical origin of meat. *J. Agric. Food Chem.* **2011**, *59*, 3285−3294.

(28) Horacek, M.; Min, J. S. Discrimination of Korean beef from beef of other origin by stable isotope measurements. *Food Chem.* **2010**, *121*, 517−520.

(29) Horacek, M.; Min, J. S.; Heo, S. C.; Soja, G. Discrimination between ginseng from Korea and China by light stable isotope analysis. *Anal. Chim. Acta* **2010**, *682*, 77−81.

(30) Longobardi, F.; Casiello, G.; Sacco, D.; Tedone, L.; Sacco, A. Characterisation of the geographical origin of Italian potatoes, based on stable isotope and volatile compound analyses. *Food Chem.* **2010**, *124*, 1708−1713.

DOI: 10.1021/jf505189x
J. Agric. Food Chem. 2015, 63, 692−699

JOURNAL OF AGRICULTURAL AND FOOD CHEMISTRY

Article

pubs.acs.org/JAFC

Changes in the Levels of Off-Flavor Generation in Soybean through Biotic Elicitor Treatments

Sweta Kumari,*[,†] Anil Dahuja,[†] T. Vinutha,[†] Sanjay Kumar Lal,[‡] Abhijit Kar,[§] and Raj D. Rai[†]

[†]Division of Biochemistry, [‡]Division of Genetics, and [§]Division of Food Science & Post harvest Technology, Indian Agricultural Research Institute, New Delhi-110012, India

ABSTRACT: The nutritional benefits of soybean remain underutilized as the off-flavor present in it limits the consumption and acceptability among people. The aim of the present study was to unveil the effect of the phytohormones methyl jasmonate (MJ: 0, 50 μM, 1 mM, and 15 mM) and salicylic acid (SA: 0, 50 μM, 0.1 mM, and 10 mM) as elicitors on two contrasting off-flavor soybean varieties at different growth stages (1, bloom; 2, pod development; 3, seed development). The effects of two elicitors varied widely and were found to be dose dependent and growth stage independent. SA reduces the lipoxygenase (LOX) and hydroperoxide lyase (HPL) activity, which in turn resulted in reduction in the TBA number and carbonyl value in contrast to MJ. SA 0.1 mM is the most effective dose in reduction of off-flavor determining parameters and protein oxidation, and it reduces the LOX and HPL activity by 2.3- and 2.4-fold, respectively in "high off-flavor" cultivar 'Bragg' compared to "low off-flavor" cultivar 'DS 2706' which showed 1.4- and 2.1-fold, respectively. This reduction in protein oxidation is also supported by enhanced content of antioxidant enzymes. Thus, phytohormone SA can be used in reduction of off-flavor generation, more effectively than MJ treatments, in soybean.

KEYWORDS: *soybean, off-flavor, elicitation, protein oxidation, antioxidant enzymes*

INTRODUCTION

Soybean is fast emerging as one of the most important food crops in the developing countries, especially India, to cater to the needs for protein as well as oil. It has also been described as the "functional food of the century" for a plethora of nutraceuticals it possesses: anthocyanins, isoflavones, tocopherols, etc.[1] Indians are predominantly vegetarian, and the vegetable proteins have special significance. India has been struggling hard and importing oils and pulses to bridge the gap; the importance of production and consumption of soybean has, of late, gained the attention of the researchers and policy-planners. The consumption of soy protein as human food is being encouraged due to its economical source of high quality protein. Though soybean contains about 40% protein and 20% oil, it is classified as an oil crop. Although consumption of food products made from soybeans has registered steady increase during the past 30 years, the acceptance, popularity, and market of these products has, however, been limited due to "off-flavor"—beany, grassy—associated with soybean and its products.[2]

The off-flavor development in soybean seeds and its products is a serious problem. Soybean oil, in general, contains about 55% linoleic and 10% linolenic acid. Lipoxygenase (LOX), present in a relatively large amount (about 2%), is implicated as a major culprit in the peroxidation of lipids especially polyunsaturated fatty acids (PUFAs), containing *cis*,*cis*-1,4-pentadienes.[3] The products of this enzyme are subsequently acted upon by other enzymes like hydroperoxide lyase leading to the production of the off-flavor causing compounds such as pentanal, hexanal, heptanal, and even nonanal along with their unsaturated forms. These volatile and offensive smelling aldehydes are very reactive, bind covalently with proteins, and thus cause flavor problems both in protein and in oil products.[4] Out of three lipoxygenase enzymes (LOX1, LOX2, and LOX3) found in soybean seeds, LOX2 has been pinpointed to be largely responsible for generation of hexanal.[5]

Heat treatment is given to seeds before processing, to reduce LOX activity and production of volatiles, but the treatment may have undesirable effects on the texture. While processing methods for soymilk have considerably improved, processed soybean products often have undesirable chalky texture caused by processing. Breeders have, however, tried to reduce the off-flavor problem by developing varieties with low PUFA content/ratio[6] or by silencing/removing seed lipoxygenases.[5] This approach however is not without disadvantages as Lox is essential for formation of several important secondary products, including jasmonic acid, which plays a desirable role in various important physiological processes. Lox in soybean has also been reported to maintain the appropriate level of protease inhibitors which are vital for the protection of plants against insects and pests.[7] Hence, complete elimination of the lox isozymes from soybean may adversely affect plant defense mechanism. It has though been demonstrated that stacking mutations in all three LOX genes can reduce undesirable flavors, but these mutants still have been shown to contain considerable levels of off-flavor.[8] Furthermore, these mutations have not been incorporated into the elite breeding lines because of the technical difficulties in selecting for three recessive mutations that segregate independently.[9]

Inherent antioxidant potential in soybean seeds has been shown to reduce the off-flavor, and the effect is partially

Received: October 29, 2014
Revised: December 9, 2014
Accepted: December 22, 2014
Published: December 22, 2014

ACS Publications © 2014 American Chemical Society

DOI: 10.1021/jf505199a
J. Agric. Food Chem. 2015, 63, 700−706

mediated through secondary metabolites, especially tocopherol, anthocyanins, phenolics, etc.[3] Enhancement of desirable secondary metabolites by elicitation is an area of active investigation, and few strategies have found commercial application. It can, therefore, be explored to obtain soybean and its products with reduced off-flavor and enhanced consumer acceptability. Elicitors are chemical molecules which, when added in small amount to a living cell system, advance the biosynthesis of specific compounds and induce physiological changes in the plant.[10] Elicitors may be of biological or nonbiological origin, which upon contact with the higher plant cells trigger the increased production of the secondary metabolites like pigments, flavones, antioxidants, phytoalexins, and other related compounds. Biotic elicitors have biological origin and are commonly applied to enhance the phytochemical composition of plants.

Biotic elicitors (having biological origin) such as methyl jasmonate (MJ), salicylic acid (SA), etc. have been reported to increase production of secondary metabolites, isoflavonoid,[11] betalain,[12] saponin,[13] and glucosinolates,[14] through various mechanisms. They are natural plant growth regulator phytohormones playing key roles in the signal interplay during biotic and abiotic stresses.[15] In view of the above, it is quite apperent that biotic elicitors have a great potential to enhance the qualities, especially production of nutraceuticals, but this strategy has not been tried for the reduction of off-flavor in soybean. The main aim of this study is, therefore, to investigate the effect of the two most potent elicitors, namely, SA and MJ on the reduction levels of off-flavor generation in soybean. The approach was to determine the effect of concentration and stage of application of these elicitors on soybean genotype differing widely in their off-flavor generation potential.

MATERIALS AND METHODS

Chemicals. Salicylic acid and methyl jasmonate were purchased from Sigma-Aldrich Co. (Germany). Linoleic acid, 2,4-dinitrophenylhydrazine, and 5,5′-dithiobis(2-nitrobenzoate) [DTNB reagent] were obtained from Sigma-Aldrich Co. (USA). Ascorbic acid and glutathione were purchased from Sigma-Aldrich Co. (Bangalore, India). Lipoxygenase, Tween-20, tetraethoxypropane (TEP), riboflavin, methionine, nitro-blue tetrazolium chloride (NBT), and NADPH were purchased from Sisco Research Laboratory (Mumbai, India). Other chemicals and solvents used for estimation of various parameters were also of analytical grade.

Plant Materials and Elicitor Treatment. Two contrasting (high and low) off-flavor soybean varieties, viz., Bragg (high off-flavor) and DS 2706 (low off-flavor), were selected.[3] The field experiments were conducted in plots (size 1 m^2) in the research farm, IARI, New Delhi, following standard cultural practices. Treatments (sprays) were imposed at various growth stages of the crops, and three replications were maintained for each treatment. The total volume applied to one plot was 500 mL for high vegetative growth cultivar 'DS 2706' and 300 mL for low vegetative growth cultivar 'Bragg'. Different concentrations of the elicitors tried were as follows: MJ (0, 50 μM, 1 mM, and 15 mM) and SA (0, 50 μM, 0.1 mM, and 10 mM). Solutions of the elicitors were prepared by dissolving MJ in 0.01% (v/v) Triton X-100 and SA in distilled water. Elicitors were sprayed at three growth stages: GS-1 (beginning to full bloom), GS-2 (beginning to full pod), and GS-3 (beginning to full seed) with a hand sprayer. Spray was given to cover uniformly the whole plant. Seeds from the treated plants were harvested at full maturity in mid-November and were stored at room temperature for three months for off-flavor generation, after which seeds were processed for estimation of different parameters. Seeds from plants sprayed with only Triton X-100 or water were used as control. Soybean seeds were milled with a laboratory electric mill to make a fine particle size of 0.5 mm.

Assay of Lipoxygenase (LOX) Activity. The LOX activity in soybean extracts was assayed by a modified method of Axelrod et al.,[16] and the time course of the peroxide formation was measured by the increase in absorbance at 234 nm using a spectrophotometer. Overnight soaked soybean seeds (1 g) in distilled water were homogenized in 6 mL of ice-cooled extraction buffer (0.1 M phosphate buffer, pH 6.8) using a mortar and pestle. The homogenate was allowed to stand for 10 min at 4 °C and centrifuged at 15000*g* for 30 min at 4 °C. The resultant supernatant was kept at 4 °C for further estimations. To 2.99 mL of substrate was added 10 μL of enzyme extract, and the increase in OD was measured at 234 nm for 6 min at room temperature. A unit of enzyme was defined as the amount which produced a change in OD of 0.001 per min at 234 nm in 3 mL of reaction mixture. The peroxide identification in all solvents and extracts was done using the potassium iodide test and was found to be negative.

Assay of Hydroperoxide Lyase (HPL) Activity. In the present study HPL activity has been estimated by a coupled enzyme assay, which is conducted spectrophotometrically at 340 nm and measures the oxidation of nicotinamide adenenine dinucleotide, reduced form (NADH). It is based on the ability of hydroperoxide lyase products, aldehydes and ω-oxoacids, to serve as substrates for yeast alcohol dehydrogenase.[17] For the preparation of substrate for HPL, 3 mL of lipoxygenase (60 mg of lipoxygenase in 6 mL of 10 mM borate buffer, pH 8.9) solution was added to 35.5 mL of double distilled water and 7.5 mL of 8 mM linoleic acid. This solution was stirred on a magnetic stirrer for 20 min, to provide oxygen continuously to obtain fatty acid hydroperoxide. HPL was extracted from 1 g of soy flour by homogenizing in 6 mL of extraction buffer (50 mM potassium phosphate buffer, pH 7.0) through continuous stirring for 2−3 h on a magnetic stirrer. Supernatant was collected after centrifugation. In a 3 mL cuvette were taken 2600 μL of assay mixture (50 mL of 100 mM phosphate buffer, pH 6.0, 3.5 mg of NADH, and 6.6 mg of yeast alcohol dehydrogenase) and 200 μL of substrate (fatty acid hydroperoxide). To this was added 200 μL of enzyme extract, and the absorbance was measured at 340 nm at every 30 s interval for 6 min. A unit of enzyme was defined as the amount which produced a change in OD of 0.001 per min at 340 nm in 3 mL of reaction mixture. Total protein content of this extract was determined by Bradford method using bovine serum albumin as a standard.

Estimation of Thiobarbituric Acid (TBA) Number. TBA number is a measure of amount of malondialdehyde produced by the decomposition of various primary and secondary lipid peroxidation products. Its estimation was based on the reaction of TBA with malondialdehyde (MDA) to form a pink colored MDA−TBA adduct.[18] Overnight soaked soybean seeds (0.2 g), in distilled water, were homogenized with 2.0 mL of distilled water, and the homogenate was centrifuged at 15000*g* for 30 min. Thus, the extract obtained was filtered to obtain the clear extract through filter paper. Then, 0.2 mL of this extract was taken in a test tube, and 0.2 mL of 8.1% SDS, 1.5 mL of 20% acetic acid (pH 3.5), and 1.5 mL of 0.8% TBA were added. The final volume was made to 4.0 mL with distilled water and heated in a boiling water bath for 60 min. After cooling, 1.0 mL of distilled water and 5.0 mL of *n*-butanol−pyridine (15:1) was added and the tubes were shaken vigorously and centrifuged at 4000 rpm for 10 min. The pink color organic layer formed at the top was separated from the aqueous phase, and absorbance was taken at 532 nm. The standard curve was prepared using TEP ranging from 10 to 70 nmol and the level of lipid peroxides expressed as nmol of MDA/g fresh weight.

Estimation of Carbonyl Value. The carbonyls were estimated by the method described by Henick et al.[19] 2,4-Dinitrophenylhydrazine reacts with the lipids to form 2,4-dinitrophenylhydrazone derivatives that converted to wine red colored complex under alkaline conditions provided by KOH. The sample extraction for estimation of carbonyls was done in the same way as that for TBA number. For estimation, to a 2.5 mL centrifuge tube were added 0.5 mL of sample extract and 0.5 mL of 2,4-dinitrophenylhydrazine, and the mixture was heated in a water bath at 60 °C for 30 min. After cooling, 1.0 mL of KOH was added and a characteristic wine red color was appeared. Ten minutes

DOI: 10.1021/jf505199a
J. Agric. Food Chem. 2015, 63, 700−706

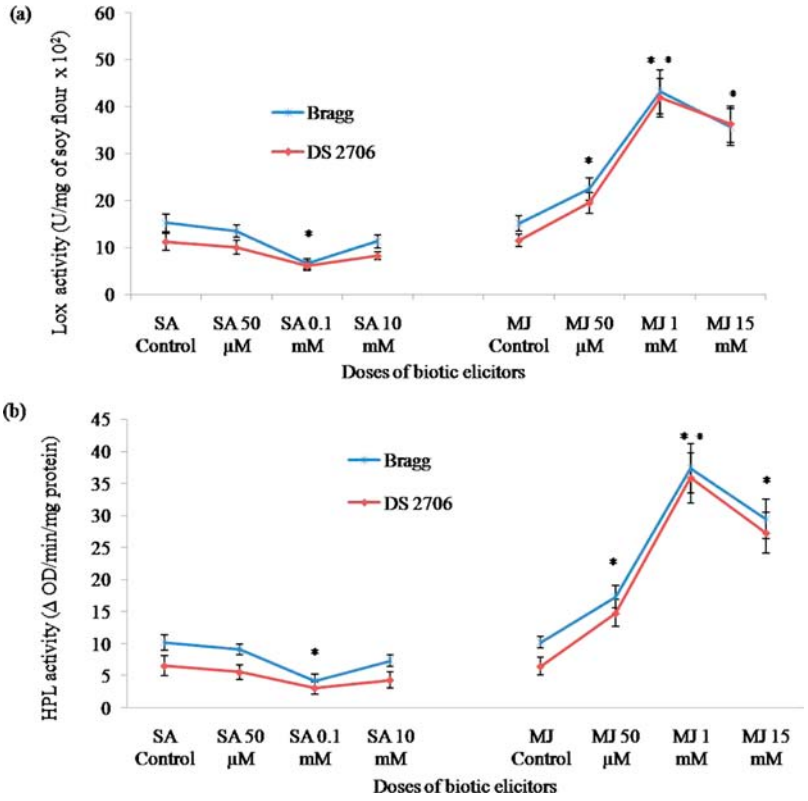

Figure 1. Effect of elicitors (SA and MJ) application at different doses in two soybean cultivars on (a) LOX activity and (b) HPL activity. Values are means ± SD of three determinations. *P* values as compared to control (* indicates that values are significant at $P < 0.05$, ** $P < 0.01$).

after the appearance of wine red color, absorbance was read at 480 nm. Amount of carbonyls was estimated by using the formula

$$A = \varepsilon CL$$

where A = absorbance; $\varepsilon = 2.72 \times 10^4$; C = concentration, and L = path length.

Estimation of Sulfhydryl Content of Protein. The sulfhydryl group of proteins were determined by titration with 5,5′-dithiobis(2-nitrobenzoate) (DNTB), using the general procedure of Ellman (1959).[20] Samples (75 mg) were suspended in 10 mL of 0.1 M phosphate buffer (pH 8.0), 1 mM EDTA, and 1% sodium dodecyl sulfate by stirring with a 1.25 cm stir bar in a 20 mL beaker on medium speed for 30 min at 20 °C. For SH determinations, to 3 mL of protein solution were added 3 mL of 0.l M phosphate buffer with EDTA and SDS and 0.1 mL of DTNB reagent, and the mixture was vortexed and incubated at 25 °C for 1.0 h. This mixture was centrifuged at 10000*g* for 30 min. Absorbance was measured at 412 nm vs reagent blanks. Calculations were based on extinction coefficient of 13,600 M^{-1} cm^{-1} for the thiolate chromogen according to the equation

$$\mu M\ SH/g = 73.53 A_{412} D/C$$

where A_{412} = the absorbance at 412 nm; C = the sample concentration in mg solids/mL; D = the dilution factor, 2.03 for SH; and 73.53 is derived from $10^6/(1.36 \times 10^4)$; 1.36×10^4 is the molar absorptivity (Ellman, 1959), and 10^6 is for conversions from the molar basis to the μM/mL basis and from mg solids to g solids.

Estimation of Antioxidant Enzyme Activity. Enzyme extract for superoxide dismutase (SOD), ascorbate peroxidase (APx), and glutathione reductase (GR) was prepared by homogenizing 1 g of overnight soaked soybean seed in 6.0 mL of extraction buffer (0.1 M phosphate buffer, pH 7.0, containing 0.5 mM EDTA). The homogenate was passed through four layers of muslin cloth, the filtrate was centrifuged at 16000 rpm for 30 min, and the supernatant obtained was used as the enzyme extract. Total protein content of this extract was determined by Bradford method using bovine serum albumin as a standard.

Superoxide Dismutase (SOD) Activity. SOD activity was assayed on the basis of its ability to inhibit photochemical reduction of nitro-blue tetrazolium (NBT) resulting in the decrease in optical density at wavelength 560 nm due to formazone formed by superoxide radical and NBT dye in the presence of the enzyme.[21] One unit of SOD activity was defined as the amount of enzyme that causes 50% inhibition of the initial rate of the reaction in the absence of enzyme, i.e., absorbance control.

Ascorbate Peroxidase (APx) Activity Assay. Ascorbate peroxidase (APx) reduces hydrogen peroxide to water with the help of ascorbic acid, which is oxidized to mono-dehydro ascorbic acid, which is spontaneously metabolized to dehydroascorbate. Hence, the assay is based on decrease in absorbance of ascorbic acid to mono-dehydroascorbic acid and dehydroascorbic acid.[22] The 3 mL reaction mixture contained 50 mM potassium phosphate buffer (pH 7.0), 0.5 mM ascorbic acid, 0.1 mM EDTA, 0.1 mM H_2O_2, and 0.1 mL of enzyme. The reaction was started with the addition of 0.1 mM hydrogen peroxide. Decrease in absorbance for a period of 30 s was measured at 290 nm in a UV−vis spectrophotometer. A unit of enzyme was defined as the amonnt which produced a change in OD of 0.01 per min at 290 nm in 3 mL of reaction mixture.

Glutathione Reductase (GR) Activity Assay. Glutathione reductase activity was assayed by recording the increase in absorbance in the presence of oxidized glutathione and DTNB (5,5-dithiobis-2-nitrobenzoic acid).[23] The reaction mixture contained 6.67 mM potassium phosphate buffer (pH 7.5) containing 33.33 mM EDTA, 0.5 mM DTNB in 0.01 M potassium phosphate buffer (pH 7.5), 66.67 mM NADPH, 0.1 mL of enzyme extract, and distilled water to make up a final volume of 2.9 mL. Reaction was initiated by adding 66.67 mM GSSG (oxidized glutathione). The increase in absorbance at 412 nm was recorded at 25 °C over a period of 5 min on a spectrophotometer. One enzyme unit is equivalent to 0.01 OD change per minute.

Statistical Analysis. All extractions and quantifications were carried out in triplicate ($n = 3$), and data are expressed as mean ± SD. The data were subjected to analysis of variance (ANOVA) Tukey test

DOI: 10.1021/jf505199a
J. Agric. Food Chem. 2015, 63, 700−706

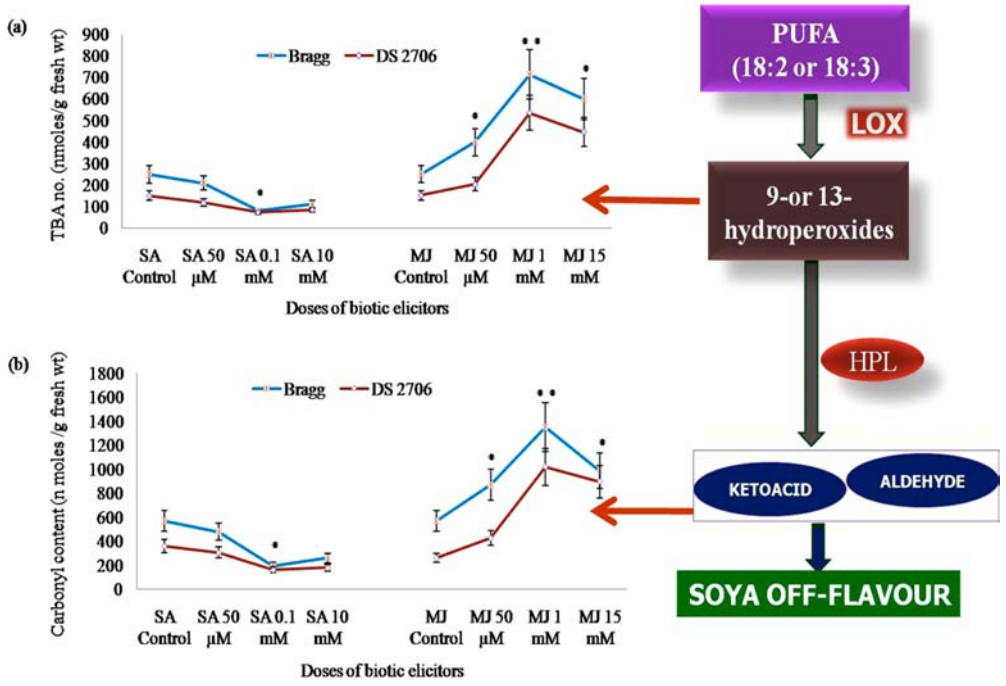

Figure 2. Effect of application of elicitors (SA and MJ) at different doses on off-flavor parameters (a) TBA number and (b) carbonyl value in two soybean cultivars. Values are means ± SD of three determinations. *P* values as compared to control (* indicates that values are significant at $P < 0.05$, ** $P < 0.01$).

to compare mean values, and the level of significance was set at 5% ($\alpha = 0.05$).

RESULTS AND DISCUSSION

Effect of Elicitor Application on Lipoxygenase (LOX) and Hydroperoxide Lyase (HPL) Activities. LOX and HPL are the two important enzymes of oxylipin pathway, which is responsible for the production of off-flavor causing volatile aldehydes and ketones. In the present study two elicitors, MJ (0, 50 μM, 1 mM, and 15 mM) and SA (0, 50 μM, 0.1 mM, and 10 mM), were used. With regard to MJ application, with increasing concentration an increase in the LOX and HPL activities was observed up to 1 mM application followed by a decline. The maximum increase (2.8-fold in Bragg and 3.6-fold in DS 2706 for LOX and 3.6-fold in Bragg and 5.5-fold in DS 2706 for HPL) was observed at 1 mM MJ application (Figure 1). However, the increase observed at 1.5 mM MJ was less compared to 1 mM MJ application. In SA application, with increasing concentration a decrease in the LOX and HPL was observed, further, the maximum decrease (2.3-fold in Bragg and 1.4-fold in DS 2706 for LOX and 2.4-fold in Bragg and 2.1-fold in DS 2706 for HPL) was observed at 0.1 mM SA application. However, the decrease observed at 10 mM SA was less compared to 0.1 mM SA application. A maximum decrease observed due to SA application at a dose of 0.1 mM and a maximum increase observed due to MJ application at a dose of 1 mM for LOX and HPL in both cultivars was significant at $P < 0.05$ compared to control. MJ has been found to effectively upregulate the LOX and HPL activity while SA has been found to effectively downregulate the LOX and HPL activity. SA and MJ appear to be important signaling molecules in plants, and they have been shown to be able to alter activity of plant proteins when applied exogenously. Hence, in the present study, it seems that a product of the oxylipin pathway, MJ derived from the linolenic acid, may have a positive feedback effect on one of the enzymes involved in its own production, LOX. Previously, a similar result has been obtained by Grimes et al.[24] wherein MJ has been shown to be regulatory for some enzymes directly involved in the oxylipin pathway, since it induces the accumulation of LOX in soybean. We also provide here evidence that MJ significantly increased levels of LOX and HPL associated with the oxylipin pathway. Similarly, Avdiushko et al.[5] also reported that the exogenous application of gaseous MJ effectively increased both LOX and HPL activity which was persistent and did not significantly change for at least 7 d after termination of MJ exposure.

In the present study, it seems that SA is acting antagonistically to MJ and decreases the activities of the off-flavor causing LOX and HPL that may be leading to reduced MJ biosynthesis and reduction of off-flavor generating volatile aldehydes and ketones as well. Previously, Leon-Reyes et al.[26] concluded that the antagonistic effect of SA on MJ signaling could be due to its action at a site that functions downstream of MJ biosynthesis. They also analyzed the MJ-responsive MJ biosynthesis genes LOX2, AOS, AOC2, and OPR3, and their results revealed that all were downregulated by exogenous application of SA, confirming their hypothesis that the MJ biosynthesis pathway could be a potential target of the antagonistic effect of SA on MJ signaling in *Arabidopsis*.

Effect of Elicitor Application on Thiobarbituric Acid (TBA) Number and Carbonyl Value. Estimation of the products of LOX and HPL action, i.e., peroxides, volatile aldehydes and ketones, and carbonylated proteins, were carried out in terms of TBA number and carbonyl value, respectively (Figure 2). In the present study, for change in the TBA number and carbonyl value, a pattern similar to the one obtained for LOX and HPL activity was obtained. With regard to MJ application, with increasing concentration an increase in the TBA number and carbonyl value was observed; further, the maximum increase (2.8-fold in Bragg and 4.4-fold in DS 2706

DOI: 10.1021/jf505199a
J. Agric. Food Chem. 2015, 63, 700−706

for TBA number and 2.4-fold in Bragg and 3.9-fold in DS 2706 for carbonyl value) was observed at 1 mM MJ application. However, the increase observed at 1.5 mM MJ was less compared to 1 mM MJ application. In SA application, with increasing concentration a decrease in the TBA number and carbonyl value was observed; further, the maximum decrease (3.1-fold in Bragg and 2.8-fold in DS 2706 for TBA number and 2.9-fold in Bragg and 2.2-fold in DS 2706 for carbonyl value) was observed at 0.1 mM SA application. However, the decrease observed at 10 mM SA was less compared to 0.1 mM SA application. The data presented here provide evidence that MJ directly or indirectly enhances certain enzymes of the oxylipin pathway (LOX and HPL) and SA inhibits the MJ responsive factors and thereby affects the direction the pathway takes and ultimately the type of fatty acid per oxidation products formed that leads to off-flavor generation in soybean. Hence, we may conclude that the MJ application mediated enhancement in LOX activity could lead to accumulation of the fatty acid oxidation product, i.e., hydroperoxides as indicated by high TBA number, which in turn may further stimulate the HPL activity thereby triggering the pathway toward the production of more volatile aldehydes and ketones. From this result one would expect to see a shift in the balance of oxylipin pathway products after MJ and SA application to increased production of fatty acid peroxidation products by MJ and decrease in fatty acid peroxidation products by SA from the HPL branch. Avdiushko et al.[25] compared the ability of MJ-treated tissues to evolve C_6 volatiles with that of control tissue in cucumber, tobacco, and *Arabidopsis* and found that all three plant species showed greater potential to form a variety of C_6 volatiles than controls. Hexanal, derived from linoleic acid, increased 2.5-fold in cucumber, 3-fold in tobacco, and 5-fold in *Arabidopsis*. Similarly, (*E*)-2-hexenal, derived from linolenic acid, increased above control plants by 80% in tobacco, 60% in cucumber, and 460% in *Arabidopsis*. Hence, if the levels of linoleic and linolenic acids available to LOX-catalyzed peroxidation are limiting in the pathway, the increase in HPL could shift the oxylipin pathway away from production of JA by allene oxide synthase. Hence, we can conclude that methyl jasmonate and salicylic acid selectively altered the activity of certain enzymes of the oxylipin pathway (lipoxygenase and hydroperoxide lyase) and increased and decreased the potential for greatly enhanced six-carbon-volatile production, respectively.

Effect of Elicitor Application on Antioxidant Enzyme Activity. Plants have developed enzymatic and nonenzymatic mechanisms to scavenge ROS. Among the active oxygen species, superoxide is converted by the SOD enzyme into H_2O_2, which is further scavenged by ascorbate glutathione cycle enzymes such as APx and GR.[27] The study on application of biotic elicitors on antioxidant enzyme activities showed that SA and MJ effectively influence the activity of SOD, APx, and GR in dose dependent manners in both of the cultivars 'Bragg' and 'DS 2706' (Figures 3 and 4). In the present study, both biotic elicitors SA and MJ increased the antioxidant enzyme activities maximal at 0.1 mM and 1 mM dose, respectively. However, declines in the antioxidant enzyme activities were observed in both of the cultivars at higher dose 10 mM and 15 mM, respectively. We also observed that high off-flavor cultivar 'Bragg' showed higher fold enhancement due to SA and MJ application (9.2- and 8.5-fold, respectively) in total antioxidant enzyme activity compared to low off-flavor cultivar 'DS 2706' (8.5- and 6-fold, respectively). Previously, Agarwal et al.[28]

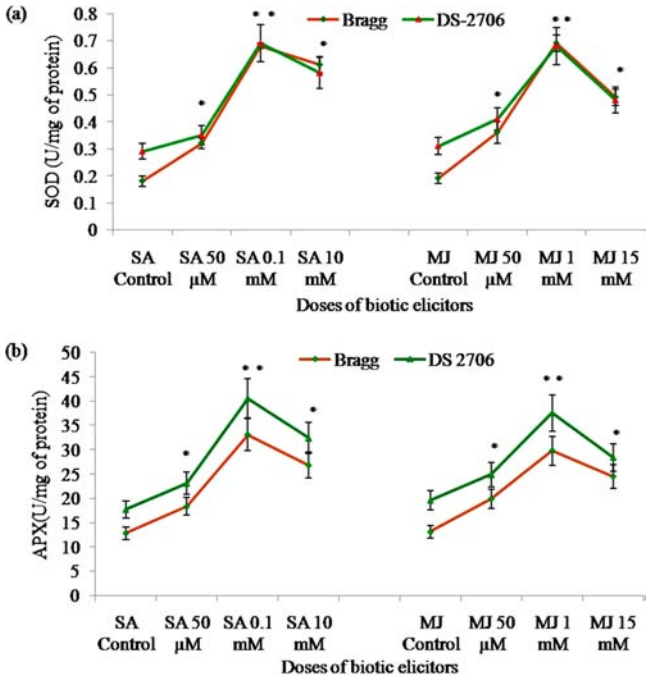

Figure 3. Effect of application of elicitors (SA and MJ) at different doses on activity of antioxidant enzyme (a) SOD and (b) APx in two soybean cultivars. Values are means ± SD of three determinations. *P* values as compared to control (* indicates that values are significant at $P < 0.05$, ** $P < 0.01$).

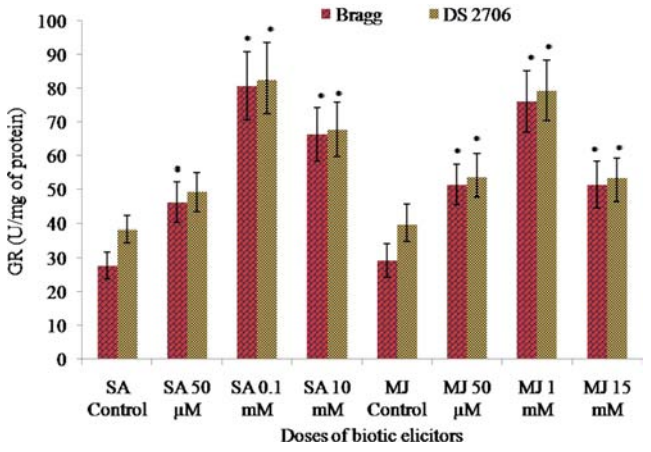

Figure 4. Effect of application of elicitors (SA and MJ) at different doses on activity of antioxidant enzyme glutathione reductase (GR) in two soybean cultivars. Values are means ± SD of three determinations. *P* values as compared to control (* indicates that values are significant at $P < 0.05$).

showed that application of 1 mM SA on wheat seedlings resulted in significant increase in SOD, APx over control. Similarly, Manar et al.[29] reported increase in SOD and APx by 210% and 344%, respectively in egg plant embryos after MJ application. Ali et al.[30] also reported that methyl jasmonate and salicylic acid elicitation induces enzymatic and nonenzymatic antioxidant in suspension culture *Panax ginseng* roots in bioreactors and significantly induced the activity of the APx and GR and SOD.

Hence, application of biotic elicitors MJ and SA causes the generation of excessive reactive oxygen species (ROS) by

DOI: 10.1021/jf505199a
J. Agric. Food Chem. 2015, 63, 700−706

NADPH oxidase present in the membrane, which leads to oxidative burst in the cell.[31]

Effect of Elicitor Application on the Level of Protein Oxidation. The measurement of protein oxidation on the basis of sulfhydryl (−SH) group content revealed that protein oxidation is low in cultivar 'Bragg' compared to 'DS 2706' (Figure 5). SA 0.1 mM is the most effective dose in reduction

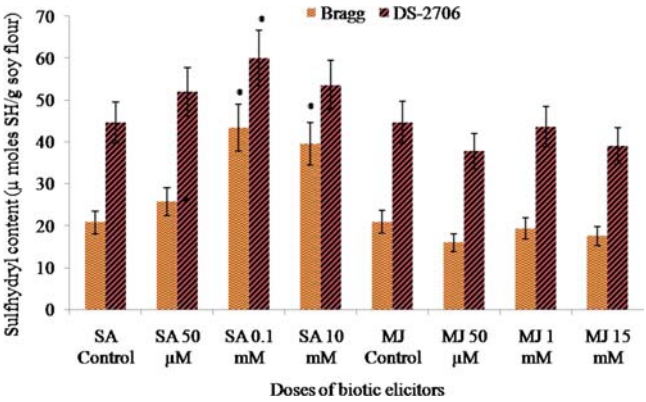

Figure 5. Effect of application of elicitors (SA and MJ) at different doses on levels of protein oxidation (measured in terms of −SH group) in two soybean cultivars. Values are means ± SD of three determinations. *P* values as compared to control (* indicates that values are significant at $P < 0.05$).

of protein oxidation in both of the cultivars while reduction is high in cultivar 'Bragg' (100%) compared to 'DS 2706' (36%). However, in the protein oxidation, application of MJ on the enhancement observed was not found to be proportionate. It could be due to increase in antioxidant enzyme system due to MJ application thereby providing protection to the proteins against oxidation. As Huang[32] showed, soybean protein oxidation and aggregation induced by lipoxygenase catalyzed linoleic acid oxidation. They suggested that linoleic acid oxidation products induced by LOX were very reactive substances that could react with soybean proteins, lead to its oxidation, and change the structural characteristics of soybean proteins. It seems that increase in antioxidant enzymes like superoxide dismutase, glutathione reductase, and ascorbate peroxidase by SA and MJ helps in reduction of protein oxidation and protection from oxidative stress. Previously, Dahuja and Madaan[3] also reported that presence of high levels of antioxidant enzymes and molecules in the soybean seeds leads to reduction in the lipid oxidation thereby resulting in low off-flavor generation in soybean.

Effects of Elicitors on the Growth Stage of Application. Considering the all important role of LOX in off-flavor generation, the effect of growth stage of the plant on its response to elicitors' application with regard to LOX2 activity was evaulated. Lipoxygenase from soybean seeds was extracted and its activity assayed from elicitor-treated and untreated plants of two varieties, viz., Bragg and DS 2706. The results of effect of growth stage of the plants on its response to both of the elicitors are depicted in Figure 6. The values of LOX2 concentrations from all treatments were compared with the untreated control. No significant variations were observed with respect to growth stages for both of the elicitors at all of the concentrations used in this study. Both of the genotypes of soybean exhibited a similar response to elicitors at all of the growth stages. Hence, our study suggested that, for a given

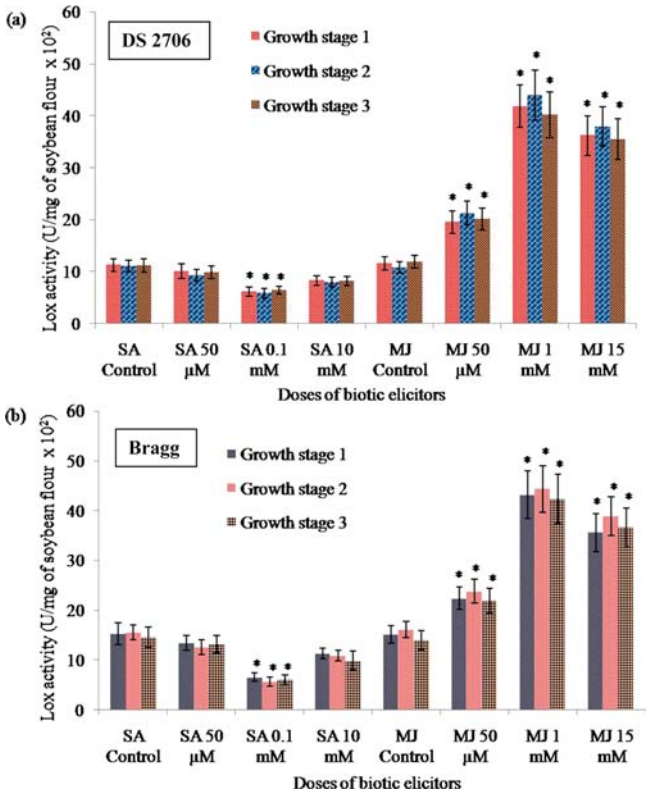

Figure 6. Effect of application of elicitors (SA and MJ) at different growth stages on LOX activity in soybean cultivars (a) DS 2706 and (b) Bragg. Values are means ± SD of three determinations. *P* values as compared to control (* indicates that values are significant at $P < 0.05$).

variety and elicitor, the concentration is an important factor for reduction of LOX2. Zhang et al.[11] while studying the effect of elicitor treatment on isoflavones also reported that, with all of the elicitors tested, concentration was a more important factor than growth stage Similarly, Eswaranandam et al.[13] reported that the overall effect of elicitor on total soy saponin content was not dependent on growth stage, however, elicitors sprayed at different growth stages showed differences among elicitors applied on soybeans.

Hence, biotic elicitors SA have the potential for reducing off-flavor content in soybean seeds when applied to plants in the field. The mechanism for off-flavor reduction as indicated by the results of the present study could be through reduction in LOX and HPL activity or due to enhancement in the levels of the antioxidant enzymes in response to oxidative burst caused by elicitors' treatments. We hereby propose a schematic model for representing the plausible sequence of events leading to off-flavor reduction in soybean after biotic elicitor treatments in abstract graphics. The effect of JA treatment on flavor quality of soybean seems to be contrasting to SA application. However, the dosage and duration of the elicitors' treatment need to be standardized further to get the optimal reduction in the level of off-flavor generation in soybean.

AUTHOR INFORMATION

Corresponding Author

*Tel: + 91 11 25834374. Fax: +91 11 25846420. E-mail: swetaarunbiochem@gmail.com.

DOI: 10.1021/jf505199a
J. Agric. Food Chem. 2015, 63, 700−706

Funding

The authors sincerely thank Indian Agricultural Research Institute (IARI) and Indian Council of Agricultural Research (ICAR) for providing financial support under institutional project.

Notes

The authors declare no competing financial interest.

■ ACKNOWLEDGMENTS

The authors duly acknowledge Upendra Pradhan, Scientist, Indian Agricultural Statistics Research Institute (IASRI), New Delhi, for data analysis.

■ REFERENCES

(1) Yu, L. L.; Tsao, R.; Shahidi, F. *Cereals and Pulses: Nutraceutical Properties and Health Benefits*; John Wiley & Sons: 2012; 328 pp.

(2) Kumar, V.; Rani, A.; Tindwani, C.; Jain, M. Lipoxygenase isozymes and trypsin inhibitor activities in soybean as influenced by growing location. *Food Chem.* **2003**, *83*, 79−83.

(3) Dahuja, A.; Madaan, T. R. Estimation of parameters responsible for the generation of off-flavour in some Indian varieties of soybeans. *Plant Food Hum. Nutr.* **2003**, *58*, 1−8.

(4) Dahuja, A.; Madaan, T. R. Off-flavour development in soybeans: comparative role of some antioxidants and related enzymes. *J. Sci. Food Agri.* **2004**, *84*, 547−550.

(5) Reinprecht, Y.; Luk-Labey, S. Y.; Yu, K.; Poysa, V. W.; Rajcan, I.; Ablett, G. R.; et al. Molecular basis of seed lipoxygenase null traits in soybean line OX948. *Theor. Appl. Genet.* **2011**, *122*, 1247−1264.

(6) Mandal, S.; Dahuja, A.; Kar, A.; Santha, I. M. In vitro kinetics of soybean lipoxygenase with combinatorial fatty substrates and its functional significance in off flavour development. *Food Chem.* **2014**, *146*, 394−403.

(7) Carvalho, W. L.; Oliveira, M. G. A.; Barros, E. G.; Moreira, M.; Carvolho, W. L.; Barros, E. G. Lipoxygenase affects protease inhibitor levels in soybean seeds. *Plant Physiol. Biotechnol.* **1999**, *37*, 497−501.

(8) Iassonova, D. R.; Johnson, L. A.; Hammond, E. G.; Beattie, S. E. Evidence of an enzymatic source of off flavors in "lipoxygenase-null" soybeans. *J. Am. Oil Chem. Soc.* **2009**, *86*, 59−64.

(9) Reinprecht, Y.; Luk-Labey, S.-Y.; Yu, K.; Poysa, V. W.; Rajcan, I.; Ablett, G. R.; Pauls, K. P. Molecular basis of seed lipoxygenase null traits in soybean line OX948. *Theor. Appl. Genet.* **2011**, *122*, 1247−1264.

(10) Angelova, Z.; Georgiev, S.; Roos, W. Elicitation of plants. *Biotechnol. Equip.* **2006**, *20*.

(11) Zhang, B.; Hettiarachchy, N.; Chen, P.; Horax, R.; Cornelious, B.; Zhu, D. Influence of the application of three different elicitors on soybean plants on the concentrations of several isoflavones in soybean seeds. *J. Agric. Food Chem.* **2006**, *54*, 5548−5554.

(12) Savitha, B. C.; Thimmaraju, R.; Bhagyalakshmi, N.; Ravishankar, G. A. Different biotic and abiotic elicitors influence betalain production in hairy root cultures of *Beta vulgaris* in shake-flask and bioreactor. *Proc. Biochem.* **2006**, *41*, 50−60.

(13) Eswaranandam, S.; Salyer, J.; Chen, P.; Lee, S. O. Effect of elicitor spray at different reproductive stages on saponin content of soybean. *J. Food Sci.* **2012**, *77* (2), H81−H86.

(14) Baenas, N.; García-Viguera, C.; Moreno, D. A. Biotic elicitors effectively increase the glucosinolates content in brassicaceae sprouts. *J. Agric. Food Chem.* **2014**, *62*, 1881−1889.

(15) Poulev, A.; O'Neal, J. M.; Logendra, S.; Pouleva, R. B.; Timeva, V.; Garvey, A. S.; Gleba, D.; Jenkins, I. S.; Halpern, B. T.; Kneer, R.; Cragg, G. M.; Raskin, I. Elicitation, a new window into plant chemodiversity and phytochemical drug discovery. *J. Med. Chem.* **2003**, *6*, 2542−2547.

(16) Axelrod, B.; Cheesebrough, T. M.; Laakso, S. Lipoxygenases in soybeans. *Methods Enzymol.* **1981**, *71*, 441−451.

(17) Vick, B. A. A spectrophotometric assay for hydroperoxide lyase. *Lipid* **1991**, *26*, 315−320.

(18) Ohkawa, H.; Ohishin, N.; Vagi, K. Assay for lipid peroxide in animal tissues by Thiobarbiyuric acid reaction. *Anal. Biochem.* **1979**, *95*, 351−358.

(19) Henick, A. S.; Benca, M. F.; Mitchell, J. H. Estimating carbonyl compounds in rancid fats and foods. *J. Am. Oil Chem. Soc.* **1954**, *31*, 88−91.

(20) Ellman, G. L. Tissue sulfhydryl groups. *Arch. Biochem. Biophys.* **1959**, *82*, 70−77.

(21) Beauchamp, C.; Fridovich, I. Superoxide dismutase: improved assays and an assay applicable to acrylamide gels. *Anal. Biochem.* **1971**, *44*, 276−287.

(22) Nakano, Y.; Asada, K. Hydrogen peroxide is scavenged by ascorbate specific peroxides in spinach chloroplasts. *Plant Cell Physiol.* **1981**, *22*, 867−880.

(23) Smith, I. K.; Vierheller, T. L.; Thorne, C. A. Assay of glutathione reductase in crude tissue homogenates using 5,5′-dithiobis(2-nitobenzoic acid). *Anal. Biochem.* **1988**, *175*, 408−413.

(24) Grimes, H. D.; Koetje, D. S.; Francheschi, V. R. Expression, .activity, and cellular accumulation of methyl jasmonate-induced lipoxygenase in soybean seedlings. *Plant Physiol.* **1992**, *100*, 433−443.

(25) Avdiushko, S.; Crof, K. P.; Brown, G. C.; Jackson, D. M.; Hamilton-Kemp, T. R.; Hildebrand, D. Effect of volatile methyl jasmonate on the oxylipin pathway in tobacco, cucumber, and *Arabidopsis*. *Plant Physiol.* **1 995**, *109*, 1227−1230.

(26) Leon-Reyes, A.; Van der Does, D.; De Lange, E. S.; Delker, C.; Casternack, C.; Van Wees, S. C. M.; Ritsema, T.; Pieterse, C. M. J. Salicylate-mediated suppression of jasmonate-responsive gene expression in *Arabidopsis* is targeted downstream of the jasmonate biosynthesis pathway. *Planta* **2010**, *232*, 1423−1432.

(27) Sevengor, S.; Yasar, F.; Kusvuran, S.; Ellialtıoglu, S. The effect of salt stress on growth, chlorophyll content, lipid peroxidation and antioxidative enzymes of pumpkin seedling. *Afr. J. Agric. Res.* **2011**, *6* (21), 4920−4924.

(28) Agarwal, S.; Sairam, R. K.; Srivastava, G. C.; Tyagi, A.; Meena, R. C. Role of ABA, salicylic acid, calcium and hydrogen peroxide on antioxidant enzymes induction in wheat seedlings. *Plant Sci.* **2005**, *169*, 559−570.

(29) Manar, M.; Banu1, G.; Fikret, Y.; Şebnem, K.; Özlem, U.; Şebnem, E. The effects of JA treatment on the growth and some enzyme activities of eggplant embryos grown *in vitro* under salt stress conditions. *Res. J. Biotechnol.* **2013**, *8* (12), 101−106.

(30) Ali, M. B.; Yu, K.-W.; Hahn, E.-J.; Paek, K.-Y. Methyl jasmonate and salicylic acid elicitation induces ginsenosides accumulation, enzymatic and non-enzymatic antioxidant in suspension culture *Panax ginseng* roots in bioreactors. *Plant Cell Rep.* **2006**, *25*, 613−620.

(31) Vellosillo, T.; Vicente, J.; Kulasekaran, S.; Hamberg, M.; Castresana, C. Emerging complexity in reactive oxygen species production and signaling during the response of plants to pathogens. *Plant Physiol.* **2010**, *154* (2), 444−448.

(32) Huang, Y.; Hua, Y.; Qiu, A. Soybean protein aggregation induced by lipoxygenase catalyzed linoleic acid oxidation. *Food Res. Int.* **2006**, *39*, 240−249.

DOI: 10.1021/jf505199a
J. Agric. Food Chem. 2015, 63, 700−706

JOURNAL OF AGRICULTURAL AND FOOD CHEMISTRY

Article

pubs.acs.org/JAFC

Neutral Pectin Side Chains of Amaranth (*Amaranthus hypochondriacus*) Contain Long, Partially Branched Arabinans and Short Galactans, Both with Terminal Arabinopyranoses

Daniel Wefers,[†] Catrin E. Tyl,[§] and Mirko Bunzel*[,†]

[†]Department of Food Chemistry and Phytochemistry, Institute of Applied Biosciences, Karlsruhe Institute of Technology (KIT), Adenauerring 20a, 76131 Karlsruhe, Germany

[§]Department of Food Science and Nutrition, University of Minnesota, 1334 Eckles Avenue, St. Paul, Minnesota 55108, United States

Supporting Information

ABSTRACT: Amaranth is a pseudocereal of high nutritional value, including a high dietary fiber content. Amaranth dietary fiber was suggested to contain large amounts of neutral rhamnogalacturonan I side chains. In this study, *endo*-arabinanase and *endo*-galactanase were used to liberate arabinan and galactan oligosaccharides from amaranth fiber. The liberated oligosaccharides were identified by high-performance anion exchange chromatography with pulsed amperometric detection (HPAEC-PAD) and HPLC-MS^n using standard compounds, which were isolated from amaranth, sugar beet, potato, and red clover sprouts and characterized by one- and two-dimensional NMR spectroscopy. It was demonstrated that insoluble amaranth arabinans have linear and branched areas, with the *O*-3 position being the dominant branching point. Minor amounts of branches at position *O*-2 and double substitution were also found. Amaranth arabinans were also demonstrated to contain terminal α-(1→5)-linked L-arabinopyranose units. In addition, it was evidenced that galactans from amaranth seeds are composed of β-(1→4)-linked D-galactopyranose units, which can also be terminated with L-arabinopyranose units. In direct comparison to structural elucidation of amaranth fiber by using methylation analysis, the advantage of the enzymatic approach over methylation analysis was demonstrated.

KEYWORDS: *Amaranthus hypochrondriacus, dietary fiber, cell wall, arabinans, galactans, oligosaccharides, NMR, arabinopyranose, methylation analysis*

INTRODUCTION

Amaranth is a pseudocereal, which gained increasing interest by the food industry and consumers over the past decade. Due to their high starch content and their beneficial nutritional profile, amaranth seeds are used in many applications to replace common cereal grains. Amaranth seeds are reported to have a higher protein content than common cereal grains and a high protein quality because they are rich in lysine.[1] In addition, they are gluten-free, which makes them suitable for people suffering from celiac disease.[2] The seeds are usually used as whole grains, for example, in granola and cereal-based snacks. Thus, they also contribute to the intake of dietary fiber, which is mainly composed of cell wall polysaccharides and associated substances.[3] The seeds of *Amaranthus caudatus* are reported to have a total dietary fiber content ranging from 7.6 to 16.4%, depending on the variety.[4] Most recently, Lamothe et al.[5] analyzed monosaccharide units and glycosidic linkages of *A. caudatus* dietary fiber polysaccharides. They demonstrated that amaranth fiber contained high amounts of pectic substances such as homogalacturonan, arabinans, and galactans. In another study, ferulic acid esterified arabinan and galactan oligosaccharides were isolated from *A. caudatus*.[6] Arabinans and galactans are side chains of rhamnogalacturonan I, which is part of the pectic polysaccharides. Rhamnogalacturonan I consists of a backbone of repeating α-D-galacturonic acid and α-L-rhamnose units with neutral side chains being linked to the *O*-4-position of the rhamnose residues. Arabinans are composed of a backbone made up of α-(1→5)-L-arabinofuranose units, with potential branches at positions *O*-2 and/or *O*-3. Galactans have a backbone of β-(1→4)-D-galactopyranoses to which galactopyranoses and arabinofuranoses can be attached.[7] The structures of arabinans and galactans are important factors in plant physiology.[8] Also, depending on the structural elements present, different enzymes may be necessary for their degradation by human microbiota. Thus, the physiological properties of dietary fibers are greatly affected by their structural features.[9,10]

Because previous studies investigated only the main structural features of *A. caudatus* seeds by using methylation analysis,[5] the aim of this study was to obtain more detailed information on fiber polysaccharides of *Amaranthus hypochondriacus* seeds by using an enzymatic approach in addition to methylation analysis. Besides the isolation and characterization of novel arabinan and galactan structural elements, the focus of this study was to determine branched units as structural elements with potential impact on fiber fermentation.

Received: November 2, 2014
Revised: December 18, 2014
Accepted: December 20, 2014
Published: December 22, 2014

ACS Publications © 2014 American Chemical Society

DOI: 10.1021/jf505283x
J. Agric. Food Chem. 2015, 63, 707−715

MATERIALS AND METHODS

General. Thermostable α-amylase (EC 3.2.1.1, from *B. licheniformis*, 20000−60000 U/mL) (Sigma-Aldrich, Schnelldorf, Germany), protease (EC 3.4.21.14, subtilisin A from *B. licheniformis*, 300 U/mL) (Megazyme, Bray, Ireland), and amyloglucosidase (EC 3.2.1.3, from *A. niger*, 200 U/mL) (Megazyme) were used to analyze dietary fiber contents. The enzymes for preparative fiber isolation, Termamyl 120 L (EC 3.2.1.1, from *B. licheniformis*, 120 KNU/g), Alcalase 1.5 MG type FG (EC 3.4.21.62, from *B. licheniformis*, 1.5 AU/g), and AMG 300L (EC 3.2.1.3, from *A. niger*, 300 AGU/g) were kindly donated by Novozymes (Bagsvaerd, Denmark). *endo*-Arabinanase (EC 3.2.1.99, from *A. niger*, 9 U/mg) and *endo*-galactanase (EC 3.2.1.89, from *A. niger*, 408 U/mg) were purchased from Megazyme. Bio-Gel P-2 was from Bio-Rad Laboratories (Hercules, CA, USA). Amberlite FPA53 (OH^-) and Ambersep 200 (H^+) were purchased from Megazyme.

Materials. Amaranth seeds from *A. hypochondriacus* were grown and harvested in 2012 in Moersingen (Germany). The seeds were milled to a size <0.5 mm using an IKA MF10 basic mill and defatted with acetone. Arabinan from sugar beet and pectic galactan from potato were purchased from Megazyme. Red clover sprouts (*Trifolium pratense* L. cv. Rozeta) were grown and harvested in 2013.

Determination of Dietary Fiber Content. The defatted amaranth flour was analyzed for its dietary fiber content according to the method of Prosky et al.[11] using 1 g of flour, 100 μL of thermostable α-amylase, 100 μL of protease, and 200 μL of amyloglucosidase. The analysis was performed in duplicate, and fiber contents were corrected for ash (incineration for 5 h at 525 °C) and protein (determined as NH_4^+ according to the method of Willis et al.[12] after Kjeldahl digestion, nitrogen conversion factor = 6.25).

Dietary Fiber Preparation. Dietary fiber for preparative purposes was isolated by incubating 20 g of defatted amaranth flour or lyophilized red clover sprouts, suspended in 200 mL of 0.08 M phosphate buffer (pH 6.2), with 1.5 mL of thermostable α-amylase (Termamyl 120 L) at 92 °C for 20 min. After adjustment of the pH to 7.5 with sodium hydroxide, 1.12 g of protease (Alcalase 1.5 MG type FG) was added. The mixture was incubated for 30 min at 60 °C. The pH was adjusted to 4.5 with hydrochloric acid, 700 μL of amyloglucosidase (AMG 300L) was added, and the suspension was incubated for 30 min at 60 °C. The undigested residue was obtained through filtration, washed with water, ethanol (96%, v/v), and acetone and used as amaranth insoluble fiber. The soluble fiber was precipitated from the supernatant by adding 4 volumes of ethanol (96%, v/v), isolated by filtration, and washed with ethanol (96%, v/v)/water (4:1, v/v), ethanol (96%, v/v), and acetone. The soluble fiber was redissolved in water and dialyzed against water for 24 h (molecular weight cutoff = 3500 Da) to eliminate coprecipitated salts. The water was changed at least three times to ensure maximum dialysis.

Monosaccharide Analysis. The polymeric sugar composition of amaranth insoluble dietary fiber was analyzed after sulfuric acid hydrolysis according to the method of Saeman et al.[13] The fiber (100 mg) was swollen in 1.5 mL of 12 M sulfuric acid for 2.5 h, diluted with 9.75 mL of water, and hydrolyzed for 3 h at 100 °C. After filtration and dilution, the hydrolysate was analyzed by HPAEC-PAD as described below. Methanolysis was performed as described by De Ruiter et al.[14] with minor modifications. Hydrogen chloride in methanol (1.25 M, 2 mL) was added to 10−25 mg of sample, and hydrolysis was performed for 16 h at 80 °C. An aliquot (40 μL) was evaporated, and the 1-methylglycosides and 1-methylglycoside-6-methylesters were hydrolyzed with 500 μL of 2 M trifluoroacetic acid (TFA) at 121 °C for 1 h. After evaporation and coevaporation with ethanol, samples were dissolved in water. Samples were analyzed by HPAEC-PAD on an ICS-5000 System (Thermo Scientific Dionex, Sunnyvale, CA, USA) equipped with a CarboPac PA20 column (150 mm × 3 mm i.d., 6.5 μm particle size, Thermo Scientific Dionex) at 25 °C using a flow rate of 0.4 mL/min. The eluents used were (A) bidistilled water, (B) 0.1 M NaOH, and (C) 0.1 M NaOH + 0.2 M sodium acetate (NaOAc). Before every run, the column was rinsed with 100% B for 10 min and equilibrated for 20 min with 90% A and 10% B. After injection, the following gradient was applied: 0−1.5 min, from 90% A and 10% B to 96% A and 4% B; 1.5−22 min, isocratic, 96% A and 4% B; 22−32 min from 96% A and 4% B to 100% B; 32−42 min, isocratic, 100% C.

For monosaccharide analysis of oligosaccharides, an aliquot of the sample was hydrolyzed with 2 M TFA for 60 min at 121 °C and analyzed by HPAEC as described above. Determination of the D/L-configuration of the monosaccharides was performed by heating the evaporated TFA hydrolysate overnight at 130 °C with 150 μL of (*R*)-2-octanol and 5 μL of TFA.[15] Solvent was removed, and samples were silylated with 80 μL of *N*,*O*-bis(trimethylsilyl)trifluoroacetamide and 20 μL of pyridine. Analysis was performed on a GC-MS system (GC-2010 Plus and GCMS-QP2010 Ultra, Shimadzu, Kyoto, Japan) equipped with an Rxi-5Sil MS column (30 m × 0.25 mm i.d., 0.25 μm film thickness, Restek, Bad Homburg, Germany). The following conditions were used: initial column temperature, 150 °C; ramped at 1 °C/min to 200 °C; ramped at 15 °C/min to 300 °C. Injection temperature was 275 °C, and split injection was used at a split ratio of 10:1. Helium was used as carrier gas at 40 cm/s, and the transfer line was held at 275 °C.

Isolation of Standard Oligosaccharides. Red clover sprouts insoluble fiber (15 g) was extracted with 0.6 g of $Ca(OH)_2$ in 150 mL of water for 30 min at 95 °C. Polysaccharides were precipitated from the supernatant with 4 volumes of ethanol (96%, v/v), separated, redissolved in water, and dialyzed for 24 h (molecular weight cutoff = 3500 Da). For the isolation of oligosaccharide standards, 1−10 g of red clover sprout polysaccharides, arabinans from sugar beet, pectic galactans from potato, or amaranth insoluble fiber was dissolved or suspended in water (10 mg/mL) and incubated with *endo*-arabinanase or *endo*-galactanase (at least 1 U/100 mg sample) for 24 or 48 h. The hydrolysate was centrifuged, and the supernatant was freeze-dried and redissolved in water. The solution was fractionated by gel filtration using Bio-Gel P-2 as stationary phase (gel bed: 85 cm × 2.6 cm). Bidistilled water was used as eluent (1 mL/min), and the temperature was held at 45 °C. The oligosaccharides were detected using a Smartline RI detector 2300 (Knauer, Berlin, Germany). Fractions were collected every 2.5 min, combined according to the chromatograms, and freeze-dried. Fractions containing multiple compounds (as determined by HPAEC analysis) were further fractionated by HPLC (L-7100 pump, L-7490 RI detector, Merck/Hitachi, Darmstadt, Germany) using a semipreparative C18 column (250 mm × 8 mm i.d., 5 μm particle size, Eurosphere 100, Knauer). Water was used as eluent (1−1.5 mL/min) at various temperatures (5−35 °C). The fractions were collected according to the chromatograms and freeze-dried.

NMR Spectroscopic Characterization. After hydrogen−deuterium exchange, the samples were dissolved in D_2O, and spectra were collected on a Bruker Ultrashield 700 MHz NMR spectrometer (Bruker, Rheinstetten, Germany). Acetone was used as an internal reference (δ_H 2.22 ppm, δ_C 30.89 ppm).[16] The structures of the isolated oligosaccharides were identified by using ^{1}H, H,H-correlated spectroscopy (COSY), heteronuclear single-quantum coherence/heteronuclear multiple-quantum correlation (HSQC/HMQC), and heteronuclear multiple-bond correlation (HMBC) experiments. Standard Bruker pulse sequences were used (^{1}H, zg30; COSY, cosygpqf; HSQC, hsqcetgpsi2; HMQC, hmqcgpqf; HMBC, hmbcgplpndqf); spectra were acquired at 298 K.

Liberation of Oligosaccharides from Amaranth Fiber. Amaranth insoluble and dialyzed soluble fibers (10 mg/mL each) were incubated by using *endo*-arabinanase (2 U/100 mg fiber) for 24 h at 40 °C. Before *endo*-galactanase incubation, the insoluble fiber (400 mg) was suspended in 20 mL of water and heated to 90 °C. $Ca(OH)_2$ (28 mg) was added, and the mixture was heated for 90 min at 90 °C. After neutralization with hydrochloric acid, the supernatant was precipitated with 4 volumes of ethanol (96%, v/v). The precipitate was redissolved and desalted by passing over a column filled with 4 g of Amberlite FPA53 and 4 g of Ambersep 200. An aliquot (1 mL) of the eluate (20 mL) was incubated with *endo*-galactanase (4 U) for 24 h at 40 °C.

HPAEC-PAD Analysis of the Oligosaccharides. HPAEC-PAD oligosaccharide analysis was performed on an ICS-5000 system (Thermo Scientific Dionex) using a Carbopac PA100 column (250

DOI: 10.1021/jf505283x
J. Agric. Food Chem. 2015, 63, 707−715

mm × 4 mm i.d., 8.5 μm particle size, Thermo Scientific Dionex). The temperature was held at 25 °C, and a flow rate of 1 mL/min was applied using the following eluents: (A) bidistilled water, (B) 0.1 M NaOH, (C) 0.1 M NaOH + 0.5 M NaOAc. Before every run, the column was washed with 100% C for 10 min and equilibrated with 90% A and 10% B for 20 min. After injection, the following gradient was applied: 0−10 min, isocratic 90% A and 10% B; 10−20 min, from 90% A and 10% B to 100% B; 20−65 min, from 100% B to 50% B and 50% C; 65−68 min, isocratic 50% B and 50% C; 68−85 min, 100% C.

LC-MS Analysis of the Liberated Amaranth Fiber Oligosaccharides. The galacto-oligosaccharides were reduced according to the method of Pitson et al.[17] with minor modifications. In brief, after reduction with aqueous $NaBH_4$ (2 mL of 250 mM $NaBH_4$ per 5 mg of sample, 2 h at room temperature), the reaction was terminated by adding hydrochloric acid, and the samples were desalted using an ion-exchange column packed with 4 g of Amberlite FPA53 and 4 g of Ambersep 200. LC-MS analysis was performed on a Surveyor HPLC System, coupled to an LXQ linear ion trap MS^n system (Thermo Fisher Scientific, Waltham, MA, USA). Chromatographic separation was performed on a porous graphitized carbon (PGC) column (Hypercarb, 100 mm × 2.1 mm i.d., 3 μm particle size, Thermo Fisher Scientific) at 60 °C using a flow rate of 0.4 mL/min. The following gradient composed of 25 μM aqueous LiCl (A) and acetonitrile (ACN) (B) was used: 0−1 min, 100% A; 1−20 min, from 100% A to 90% A; 20−28 min, from 90% A to 30% A; 28−31 min, from 30% A to 20% A; 31−35 min, isocratic 20% A; 35−36 min, from 20% A to 100% A; 36−41 min, equilibration with 100% A.

Methylation Analysis. Methylation analysis was performed as described by Nunes and Coimbra[18] with minor modifications. Briefly, the sample was dissolved in 2 mL of dimethyl sulfoxide, and freshly ground sodium hydroxide (ca. 100 mg) was added. The solution was sonicated for 90 min and incubated at room temperature for 90 min. Methyl iodide (1 mL) was added, followed by 30 min of sonication and 30 min of incubation at room temperature. The solution was extracted with dichloromethane, and the organic phase was washed with 3 mL of 0.1 M sodium thiosulfate and twice with 3 mL of water. After evaporation and drying, the methylated polysaccharides were hydrolyzed by adding 2 mL of 2 M TFA and incubation at 121 °C for 90 min. After evaporation, 20 mg of $NaBD_4$ in 300 μL of an aqueous NH_3 solution (2 M) was added. After 1 h at room temperature, the reaction was terminated by adding glacial acetic acid. During cooling with ice, 450 μL of 1-methylimidazole and 3 mL of acetic anhydride were added, and the solution was incubated for 30 min at room temperature. After the addition of 3 mL of water, the partially methylated alditol acetates (PMAA) were extracted by using 5 mL of dichloromethane. The organic layer was washed three times with water, and residual water was removed by freezing overnight at −18 °C. The PMAAs in dichloromethane were analyzed by GC-MS (GC-2010 Plus and GCMS-QP2010 SE, Shimadzu) on a DB-225MS column (30 m × 0.25 mm i.d., 0.25 μm film thickness, Agilent Technologies, Santa Clara, CA, USA) using the following conditions: initial column temperature, 140 °C, held for 1 min; ramped at 20 °C/min to 220 °C, held for 25 min. Helium was used as carrier gas at 40 cm/s. Split injection with a split ratio of 30:1 was used. The injection temperature was 220 °C. The transfer line was held at 220 °C, and electron impact mass spectra were recorded at 70 eV. The relative quantification of the partially methylated alditol acetates was carried out on a GC-FID system (GC-2010 Plus, Shimadzu) using a DB-225 column (30 m × 0.25 mm i.d., 0.25 μm film thickness, Agilent Technologies) and the same GC conditions as described for the GC-MS experiments, with the exception of a reduced split ratio of 10:1. FID temperature was 240 °C, and nitrogen was used as makeup gas. Molar response factors according to Sweet et al.[19] were used for semiquantitative calculations.

RESULTS AND DISCUSSION

Amaranth Dietary Fiber Content and Fiber Monosaccharide Composition. The insoluble and soluble dietary fiber contents of *A. hypochondriacus* seeds were 6.0 and 2.4%. These values are comparable with fiber contents of *A. caudatus* reported previously.[4,5] The monosaccharide compositions of the preparatively isolated insoluble and soluble fiber polysaccharides were analyzed after H_2SO_4 hydrolysis according to the method of Saeman et al.[13] and after methanolysis according to the method of De Ruiter et al.[14] (Table 1). Whereas sulfuric acid hydrolysis of the insoluble fiber underestimates uronic acids, methanolysis of amaranth insoluble fiber does not hydrolyze crystalline cellulose. The high contents of arabinose and galactose (sulfuric acid hydrolysis: 24.3% and 5.6% of the liberated monosaccharides) indicate high amounts of arabinans and galactans in the amaranth insoluble fiber. The low amount of rhamnose (2.0%) suggests long arabinan chains and rather short galactan chains. Comparable results were obtained from methanolysis. Methanolysis of the insoluble fiber demonstrated the galacturonic acid/rhamnose ratio to be 3.8:1 (H_2SO_4 hydrolysis: 1.7:1). Thus, amaranth fiber also contains significant amounts of homogalacturonan. Studies on the monosaccharide composition of *A. caudatus* insoluble fiber also reported high contents of pectic polysaccharides, however, with galacturonic acid as dominating monosaccharide.[4,5] The polymeric glucose and xylose units can be assigned to cellulose, xyloglucans, and xylans. Analysis of the soluble fiber yielded comparable proportions of the rhamnogalacturonan I sugars. The relatively high amount of mannose may indicate the presence of galactomannans in amaranth soluble fiber.

Table 1. Monosaccharide Composition (Percent) of Amaranth Insoluble Fiber after Sulfuric Acid Hydrolysis and Methanolysis and of Soluble Fiber after Methanolysis

monosaccharide	insoluble fiber (H_2SO_4)	insoluble fiber (methanolysis)	soluble fiber (methanolysis)
fucose	tr[a]	0.9	tr
rhamnose	2.0	5.9	4.5
arabinose	24.3	30.3	30.8
galactose	5.6	6.7	13.2
glucose	48.6	20.1	9.5
xylose	12.7	10.4	15.5
mannose	3.4	1.9	16.8
galacturonic acid	3.4	22.2	7.9
glucuronic acid	tr	1.7	1.7

[a]tr, traces.

Isolation and Characterization of Standard Compounds of Arabino- and Galacto-oligosaccharides. Preliminary studies showed that the hydrolysis of amaranth fiber with *endo* enzymes is not very effective, yielding only small amounts of some diagnostic oligosaccharides. The isolation of quantities sufficient for 2D NMR characterization of these diagnostic oligosaccharides would be an extremely time-consuming task. Thus, some standard compounds were isolated from sugar beet arabinans, potato galactans, and red clover sprout polysaccharides. These materials are more susceptible to arabinan and galactan hydrolysis by *endo* enzymes, yielding satisfactory amounts of the required diagnostic oligosaccharides. The purity of these oligosaccharides allowed for a detailed structural characterization by 1D and 2D NMR (structures shown in Figure 1). The oligosaccharides were hydrolyzed under acidic conditions, derivatized with (*R*)-2-octanol, silylated, and analyzed by GC-MS. This analysis showed that

DOI: 10.1021/jf505283x
J. Agric. Food Chem. 2015, 63, 707−715

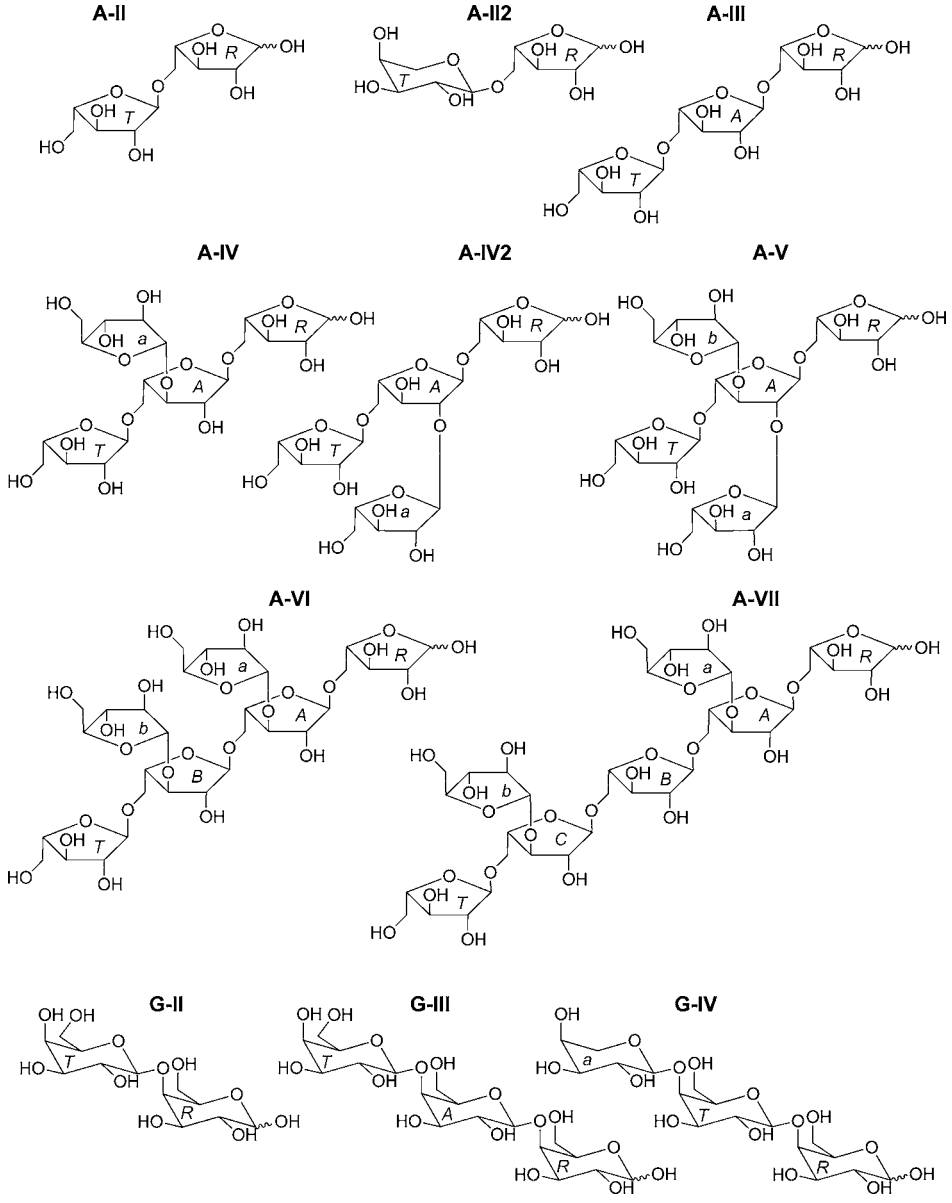

Figure 1. Structures of arabino-oligosaccharides isolated from sugar beet arabinan (**A-II**–**A-VII**), amaranth (**A-II2**), and red clover sprouts (**A-IV2**) and structures of galacto-oligosaccharides isolated from potato galactan (**G-II**–**G-IV**). Letters R, A, B, C, T, a, and b are used to describe the sugar units for the NMR spectroscopic assignment (Table 2 and Supporting Information).

arabinose was present in its L-form and galactose in its D-form in all oligosaccharides.

The isolated arabino-oligosaccharides represent many different substitution patterns of the arabinan backbone. These linear and branched arabino-oligosaccharides (Figure 1) with the exceptions of **A-II2** and **A-IV2** were previously isolated and characterized by Westphal et al.[20] The NMR spectroscopic data of the isolated oligosaccharides (Supporting Information) were in good agreement with data published by Westphal et al.[20]

The novel arabinan tetramer branched at position *O*-2 (**A-IV2**) was liberated in very low quantities from sugar beet arabinans and was also difficult to separate from the *O*-3 branched tetramer by RP18-HPLC. Thus, this tetramer was isolated from red clover sprout polysaccharides, where compound **A-IV2** was dominant over **A-IV**. It was possible to distinguish the *O*-2-branched tetramer from the *O*-3-branched tetramer by NMR spectroscopy analysis because their anomeric protons showed different ^{1}H chemical shifts. The other protons and carbons showed similar δ_C and δ_H values except H/C2 and H/C3 of the central arabinose unit A. The δ_C values were diagnostic because the C3 signal shifted downfield (83.10 ppm, Supporting Information) in the spectrum of compound **A-IV**, whereas the C2 signal shifted downfield (87.86 ppm, Table 2) in the spectrum of compound **A-IV2**. These values are in good agreement with literature data for *O*-3 and *O*-2 substituted arabinans.[20−23] The substitution at position *O*-2 was confirmed by an HMBC cross peak between H1 of the terminal arabinofuranose *a* and C2 of the central (1→5)-linked arabinose *A*.

Compound **A-II2**, which was isolated from an *endo*-arabinanase hydrolysate of amaranth insoluble fiber, contains an *α*-L-arabinopyranose attached to *O*-5 of an arabinofuranose. The ring form was unambiguously demonstrated by the ^{13}C chemical shifts (Table 2) and by an HMBC cross peak between C1 and H5. The (1→5)-linkage was evidenced by a long-range correlation between H1 of the arabinopyranose and C5 of the

DOI: 10.1021/jf505283x
J. Agric. Food Chem. 2015, 63, 707−715

Table 2. ^{1}H and ^{13}C Chemical Shifts and Anomeric Proton Coupling Constants of Structures A-II2, A-IV2, and G-IV[a]

	H1 (^{3}J)	H2	H3	H4	H5	H6	C1	C2	C3	C4	C5	C6
						A-II2						
R-α	5.26 (nd)	4.03	4.03	4.22	3.86/3.98		101.72	81.96	76.43	82.22	69.72	
R-β	5.29 (3.7)	4.09	4.09	3.94	3.84/3.97		95.85	76.52	74.87	80.02	71.13	
T	4.44/4.45* (7.8)	3.29	3.44	3.62	3.32/3.96		103.87	73.59	76.19	69.84	65.82	
						A-IV2						
R-α	5.26 (nd)	4.03	4.05	4.24	3.78/3.88		101.96	82.07	76.88	82.09	67.25	
R-β	5.29 (3.7)	4.09	4.09	3.95	3.78/3.88		96.12	76.57	75.24	81.90	67.25	
A	5.19/5.20* (nd)	4.16	4.16	4.19	3.83/3.90		107.39	87.86	76.01	82.32	67.07	
T	5.08 (nd)	4.13	3.95	4.08	3.71/3.83		108.21	81.80	77.26	84.41	61.85	
a	5.19 (nd)	4.13	3.95	4.04	3.71/3.83		107.90	81.80	77.26	84.71	61.85	
						G-IV						
R-α	5.27 (3.7)	3.86	3.96	4.23	4.13	3.70/3.79	93.06	69.89	70.09	79.38	70.34	61.55
R-β	4.61 (8.0)	3.57	3.75	4.16	3.75	3.70/3.79	97.15	72.74	74.19	78.43	74.19	61.55
T	4.63* (7.7)	3.67	3.75	4.13	3.72	3.79	105.13	73.34	74.19	77.86	75.33	61.51
a	4.56 (7.4)	3.63	3.67	3.92	3.63/3.92		105.30	72.27	73.34	69.04	67.14	

[a]The corresponding structures including R, T, A, and descriptors are shown in Figure 1. Chemical shifts are given in ppm, coupling constants in Hz. nd, not determined. *, signal splitting due to the long-range effect of the anomeric protons of the reducing monosaccharide unit.

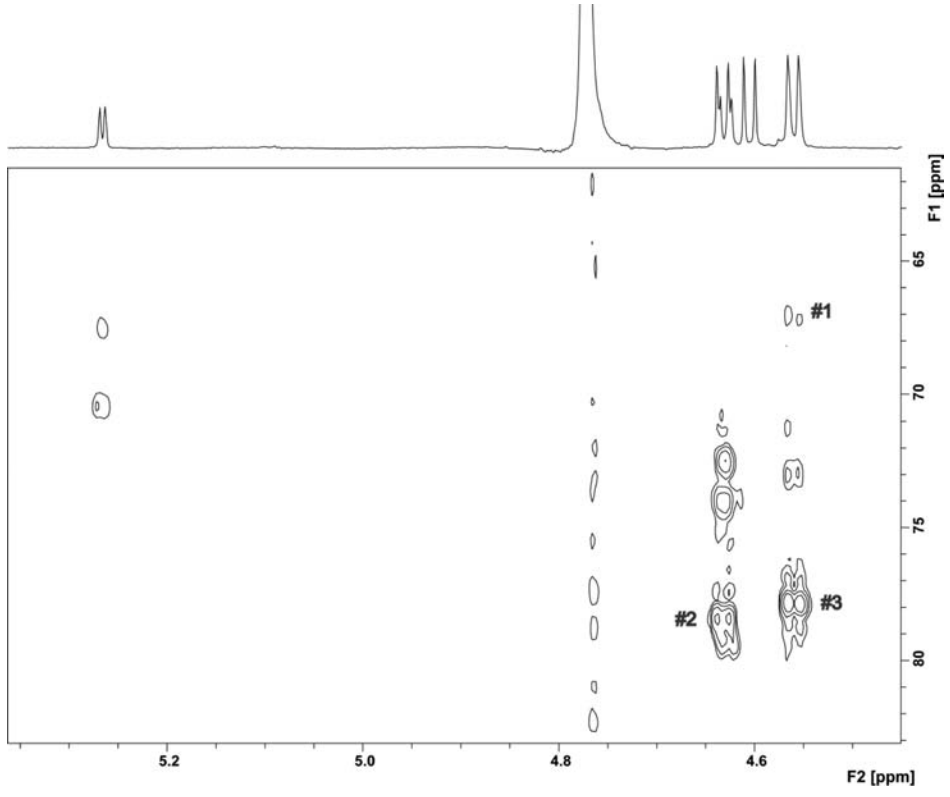

Figure 2. HMBC spectrum of compound **G-IV**. The marked cross-peaks show coupling of C5 and H1 of the arabinose (signal 1), coupling of C4 of the reducing galactose and H1 of the nonreducing galactose (signal 2), and coupling of C4 of the nonreducing galactose and H1 of the arabinose (signal 3).

arabinofuranose. Arabinopyranoses are rarely described as structural elements of arabinans. Ishii et al.[24] described the enzymatic transfer of a β-arabinopyranose to the *O*-3-position of an arabinan backbone. Swamy and Salimath[23] suggested the presence of terminal arabinopyranoses in an arabinan from *Cajanus cajan* cotyledons based on methylation analysis and ^{13}C NMR; however, the exact position in the arabinan backbone was not determined. The reported ^{13}C chemical shifts are comparable to those of **A-II2**, suggesting that a similar structural element was present in Swamy and Salimath's study. Besides demonstrating the occurrence of arabinopyranoses as structural elements of amaranth arabinans, the isolation of compound **A-II2** unambiguously demonstrates that arabinan chains can be terminated by arabinopyranoses.

Hydrolysis of the potato galactan yielded a heterogeneous mixture of oligosaccharides. Only structures relevant for this study are described here. As shown in Figure 1, linear β-(1→4)-linked galactopyranose dimers and trimers were isolated and characterized. The NMR data were in good agreement with previously published data (Supporting Information).[25,26] These structures are well-known as constituents of the galactan backbone.

DOI: 10.1021/jf505283x
J. Agric. Food Chem. 2015, 63, 707−715

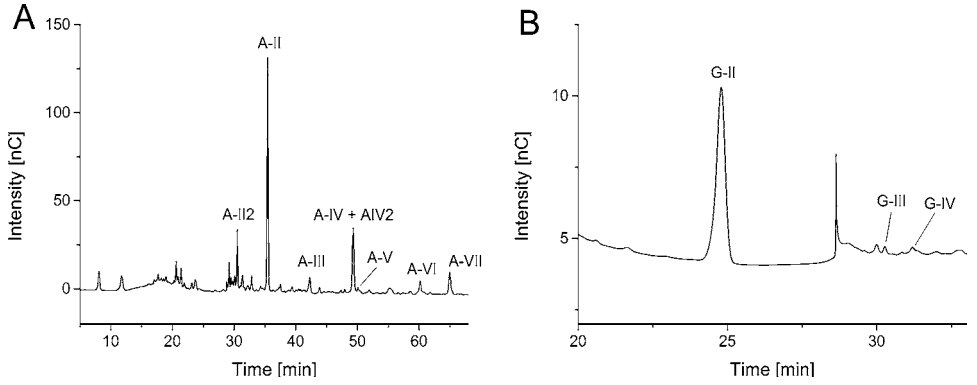

Figure 3. HPAEC chromatograms of the *endo*-arabinanase hydrolysate of amaranth insoluble fiber (A) and the *endo*-galactanase hydrolysate of the $Ca(OH)_2$ extract from amaranth insoluble fiber (B). A-II–A-VII and G-II–G-IV assign the signals to the structures shown in Figure 1 as evidenced by comparison of HPAEC and LC-PGC-MS retention times and MS^2 fragmentation patterns. The peaks around compound **A-II2** in the *endo*-arabinanase incubation were also present in an incubation mixture without enzyme.

The monosaccharide analysis of **G-IV**, however, revealed the occurrence of galactose and arabinose in a 2:1 ratio. Besides three anomeric proton signals for a reducing and a β-linked galactose, the ^{1}H NMR spectrum contained a signal at 4.56 ppm with a 7.4 Hz coupling constant (Table 2), suggesting the presence of an α-arabinopyranose. This hypothesis was confirmed by the ^{13}C chemical shifts, which were in good agreement with literature data for a terminal α-arabinopyranose,[27] and by an HMBC cross peak between H1 and C5 (signal 1 in Figure 2). A cross peak between C4 of the reducing galactose and H1 of the nonreducing galactose demonstrated the (1→4)-linkage between these residues (signal 2 in Figure 2). The long-range correlation between H1 of the arabinopyranose and C4 of the nonreducing galactose showed that the arabinopyranose is attached to *O*-4 of the nonreducing galactopyranose (signal 3 in Figure 2). Thus, **G-IV** contains a terminal arabinopyranose linked to the *O*-4-position of a β-(1→4)-linked galactan dimer. There have been few reports on such a structural element. Huisman et al.[28] demonstrated the presence of terminal arabinopyranoses in hydrolysates of soybean pectins by methylation analysis. Also, Ishii et al.[27] synthesized β-(1→4)-linked galacto-oligosaccharides containing terminal arabinopyranoses by using microsomal membranes from mung beans. However, NMR spectroscopic characterization of such an oligosaccharide isolated from plants has not been achieved yet. Because *endo*-galactanases should not be able to cleave glycosidic linkages between arabinose and galactose units, the liberation of this oligosaccharide strongly supports the hypothesis that arabinopyranose units terminate galactan chains, as previously suggested by Huisman et al.[28] and Ishii et al.[27]

Characterization of Amaranth Fiber Galactans and Arabinans via Liberated Galacto- and Arabino-oligosaccharides. To characterize structural elements of amaranth arabinans and galactans, the insoluble and soluble fibers were incubated with *endo*-arabinanase and *endo*-galactanase. No significant amounts of oligosaccharides were liberated from insoluble fiber by using *endo*-galactanase. This was probably due to an incorporation of the galactans into the complex cell wall matrix. Different pretreatments (extraction with hydrochloric acid, sodium hydroxide, $Ca(OH)_2$, or 1,2-diaminocyclohexane tetraacetic acid; enzymatic pretreatment with *endo*-polygalacturonase or cellulase) were tested to improve the enzymatic degradation. $Ca(OH)_2$ extraction of galactans was proven to be most efficient. As shown in Figure 3, several arabino-oligosaccharides and galacto-oligosaccharides were liberated by enzymatic hydrolysis of the insoluble fiber and the $Ca(OH)_2$ extract. Incubation of the soluble fiber liberated the same arabino-oligosaccharides (data not shown), but galacto-oligosaccharides were not detected. Thus, the polymeric galactose that was detected in amaranth soluble fiber after methanolysis is incorporated in linkages other than β-(1→4)-linkages or is part of galactomannans.

Identification of the liberated oligosaccharides was performed by HPAEC analysis (Figure 3) and comparison with the isolated standard compounds. However, because some of the oligosaccharides were present in very low amounts only, the LC-PGC-MS retention time and the fragmentation pattern of the lithium adducts were additionally used to confirm the presence of the oligosaccharides. Extensive peak broadening was obtained for the galacto-oligosaccharides on the PGC column. Thus, they were reduced with sodium borohydride to obtain sharp peaks and a good separation. Westphal et al.[29] described a coelution of the linear arabinotetraose with branched arabinotetraoses such as structure **A-IV** if analyzed by HPAEC. As also described by this group, the different tetramers can be separated on a PGC column. The mass trace of the lithium adduct of arabinotetraose (m/z 553) is shown in Figure 4 for the analysis of the hydrolyzed amaranth insoluble fiber, demonstrating the occurrence of both branched arabinotetraoses. The MS^2 fragmentation pattern yielded m/z

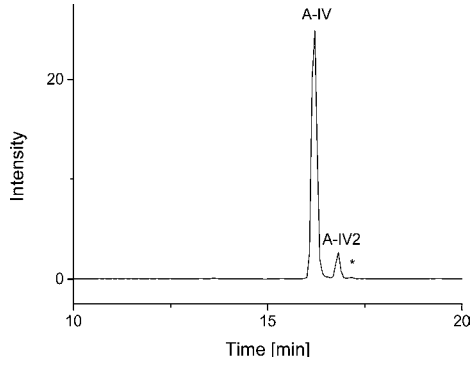

Figure 4. LC-PGC-MS mass trace of the lithium adduct of arabinotetraose (m/z 553) for the hydrolysate of amaranth insoluble fiber. The structures for **A-IV** and **A-IV2** are shown in Figure 1. The peak representing linear arabinotetraose is marked with an asterisk.

DOI: 10.1021/jf505283x
J. Agric. Food Chem. 2015, 63, 707–715

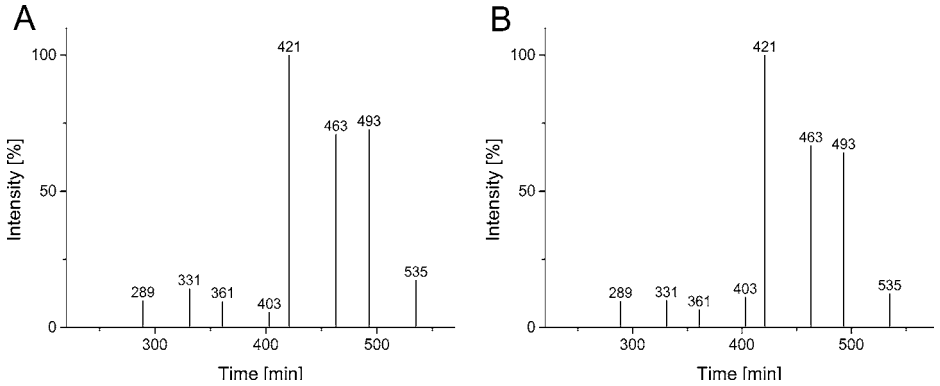

Figure 5. Fragmentation patterns of the lithium adducts of standard compounds **A-IV** (A) and **A-IV2** (B) (*m*/*z* 553).

421 as the main fragment ion in both peaks, which is typical for a branched arabinotetraose.[29] Compounds **A-IV** and **A-IV2** also showed *m*/*z* 421 as their dominating fragment. Due to their very similar structures, the fragmentation patterns of these branched arabinotetraoses showed only minor differences (Figure 5). Linear arabinotetraose was only found in traces, eluting after the branched arabinotetraoses (Figure 4). Because *endo*-arabinanase incubations were performed for 24 h, higher linear oligomers including linear arabinotetraose, which were initially liberated, were further degraded to yield mostly linear arabinobiose. Arabinotriose can also be cleaved by *endo*-arabinanase, but the conditions used here allow for their detection by HPAEC (Figure 3) and LC-PGC-MS. The amount of the trimer decreased with increasing incubation times. On the other hand, reduced incubation times favored the detection of the linear trimer (data not shown). This is in good agreement with previous findings by Dunkel and Amado.[30] A similar result was found for the galacto-oligosaccharides, with galactobiose and galactotriose being the only unsubstituted galacto-oligosaccharides detected. These are described as incubation end products.[31−33] Detection of these galacto-oligosaccharides confirms the occurrence of β-(1→4)-linked galactans in amaranth. The finding of the terminal arabinopyranoses (**G-IV**, Figure 1) suggests that this structural element may be a conserved one, because it was now demonstrated to exist in soybean, potato, and amaranth. The identification of compound **A-II2** demonstrates that arabinan chains in amaranth can also be terminated by arabinopyranoses. Because this structural element was only found to terminate the chains, there could be a special plant physiological function of this substituent. Also, degradation of these arabinans by human microbiota may be influenced in the absence of an arabinopyranosidase. The high abundance of arabinobiose suggests a high percentage of linear arabinans. However, the detection of the branched oligosaccharides shows some ramification with side chains mostly attached to the *O*-3 positions of the arabinan backbone. Double-substituted arabinan oligosaccharides (**A-V**) and areas with higher degree of branching at position *O*-3 (**A-VI** and **A-VII**) were found in small amounts only.

Methylation Analysis of Amaranth Dietary Fibers. The analysis of the PMAA obtained from methylation analysis (Table 3) confirmed these hypothesized structures. In insoluble fiber, there was a high amount of PMAA representing (1→5)-linked arabinose, whereas PMAA representing branched arabinoses were of lower abundance. The ratio of 1,3,5- and 1,2,5-substituted arabinofuranoses as determined by methyl-

Table 3. Percentages of the Partially Methylated Alditol Acetates in Amaranth Insoluble Fiber[a]

glycosidic linkage	insoluble fiber	soluble fiber
t-Ara*f*	6.9	9.4
1,5-Ara*f*	15.1	30.4
1,3,5-Ara*f*	6.2	1.7
1,2,5-Ara*f*	1.6	14.9
1,2,3,5-Ara*f*	0.8	
t-Gal*p*	1.3	1.0
1,4-Gal*p*	1.1	
1,3,6-Gal*p*		10.0
1,2-Rha*p*	1,5	1.3
1,2,4-Rha*p*	0.5	
t-Glc*p*	3.4	3.2
1,4-Glc*p*	47.0	2.7
1,4,6-Glc*p*	5.1	
t-Xyl*p*	5.9	16.6
1,4-Xyl*p*	2.5	0.6
1,2,4-Xyl*p*	0.2	
t-Man*p*		8.1
1,4-Man*p*	0.9	

[a]Ara, arabinose; Gal, galactose; Rha, rhamnose; Glc, glucose; Xyl, xylose; Man, mannose; *f*, furanose; *p*, pyranose.

ation analysis seemed to be comparable to that of the two branched arabinotetraoses as analyzed by LC-PGC-MS[2]. (1→4)-Linked galactose and terminal galactose were found in comparably low amounts. This supports the hypothesis of short galactan chains. Different from our enzymatic studies, terminal arabinopyranose units were not detected by methylation analysis, demonstrating the advantage of the enzymatic approach over methylation analysis. PMAA formed from (1→4)-linked glucose and terminal xylose represent cellulose and xyloglucans. However, a small part of the xylose may also be part of xylogalacturonan. The detection of (1→4)-linked xylose units suggests the presence of low amounts of xylans in the cell wall of the dicotyledonous amaranth seeds. Lamothe et al.[5] also detected a higher amount of linear arabinans in insoluble fiber of *A. caudatus*, but *O*-3 was the only branching position found. Also, the amount of PMAA representing galactans was significantly higher, and 1,4-substitued xylopyranoses were not detected. This may be due to species differences between *A.*

DOI: 10.1021/jf505283x
J. Agric. Food Chem. 2015, 63, 707−715

caudatus and *A. hypochondriacus*. The PMAA of amaranth soluble fiber (Table 3) suggest a high amount of arabinans, which are mostly composed of linear and, different from the insoluble fiber, *O*-2 substituted sections. However, **A-IV** was liberated in higher amounts than **A-IV2** from amaranth soluble fiber. Thus, the 1,2,5-substituted arabinofuranoses are probably involved in structural elements that are not cleaved by *endo*-arabinanase or liberated as oligosaccharides with a high degree of polymerization. For example, Eriksson et al.[34] already demonstrated that 1,2,5-substituted arabinofuranose can be part of complex arabinan side chains. The 1,3,6-substituted galactopyranoses demonstrate that (1→4)-linked galactans are not present, which is in good agreement with the results of the enzymatic digestion. These results are again different from the data for *A. caudatus* soluble fiber, where (1→4)-linked galactans and other arabinan structural elements were present.[5] Mannose is probably derived from structural elements other than mannans and galactomannans because it appears only in its terminal form.

By combining the results, it can be concluded that large amounts of neutral rhamnogalacturonan I side chains occur in amaranth seeds. As evident by our enzymatic approach and methylation analysis, they contain mostly linear arabinans, which are partially branched in position *O*-3 and/or *O*-2. The galactans, which are strongly incorporated in the cell wall matrix, are probably short and (1→4)-linked. We were also able to demonstrate that arabinan and galactan chains contain terminal arabinopyranoses. Our investigations showed that amaranth fiber is composed of arabinans and galactans with novel and unique structural features. The plant physiological functions of these structural elements as well as the consequences for human physiology and processing are difficult to deduce from our structural studies and may be part of future investigations.

■ ASSOCIATED CONTENT

Supporting Information

NMR data for the compounds already characterized by Westphal et al.[20] and Fransen et al.[25] This material is available free of charge via the Internet at http://pubs.acs.org.

■ AUTHOR INFORMATION

Corresponding Author

*(M.B.) E-mail: mirko.bunzel@kit.edu. Phone: +49 721 608 42936. Fax: +49 721 608 47255.

Funding

Funding for NMR instrumentation was provided by the Office of the Vice President for Research, the Medical School, the College of Biological Science, NIH, NSF, and the Minnesota Medical Foundation.

Notes

The authors declare no competing financial interest.

■ ACKNOWLEDGMENTS

We are grateful to Lillie Nguyen and David Schmitt for experimental support and to Ewelina Brzozowska for providing the red clover sprouts.

■ ABBREVIATIONS USED

HPAEC-PAD, high-performance anion exchange chromatography with pulsed amperometric detection; TFA, trifluoroacetic acid; NaOAc, sodium acetate; COSY, correlated spectroscopy; HSQC, heteronuclear single-quantum coherence; HMQC, heteronuclear multiple-quantum correlation; HMBC, heteronuclear multiple-bond correlation; PGC, porous graphitized carbon; ACN, acetonitrile; PMAA, partially methylated alditol acetates

■ REFERENCES

(1) Bressani, R.; Gonzales, J. M.; Zuniga, J.; Breuner, M.; Elias, L. G. Yield, selected chemical composition and nutritive value of 14 selections of amaranth grain representing four species. *J. Sci. Food Agric.* **1987**, *38*, 347−356.

(2) Alvarez-Jubete, L.; Arendt, E. K.; Gallagher, E. Nutritive value and chemical composition of pseudocereals as gluten-free ingredients. *Int. J. Food Sci. Nutr.* **2009**, *60*, 240−257.

(3) AACC. The definition of dietary fiber. *Cereal Foods World* **2001**, *46*, 112−126.

(4) Pedersen, B.; Knudsen, K. E. B.; Eggum, B. O. The nutritive value of amaranth grain (*Amaranthus caudatus*) 3. Energy and fibre of raw and processed grain. *Plant Foods Hum. Nutr.* **1990**, *40*, 61−71.

(5) Lamothe, L. M.; Srichuwong, S.; Reuhs, B. L.; Hamaker, B. R. Quinoa (*Chenopodium quinoa* W.) and amaranth (*Amaranthus caudatus* L.) provide dietary fibres high in pectic substances and xyloglucans. *Food Chem.* **2015**, *167*, 490−496.

(6) Bunzel, M.; Ralph, J.; Steinhart, H. Association of non-starch polysaccharides and ferulic acid in grain amaranth (*Amaranthus caudatus* L.) dietary fiber. *Mol. Nutr. Food Res.* **2005**, *49*, 551−559.

(7) Voragen, A. G. J.; Coenen, G. J.; Verhoef, R. P.; Schols, H. A. Pectin, a versatile polysaccharide present in plant cell walls. *Struct. Chem.* **2009**, *20*, 263−275.

(8) Pena, M. J.; Carpita, N. C. Loss of highly branched arabinans and debranching of rhamnogalacturonan I accompany loss of firm texture and cell separation during prolonged storage of apple. *Plant Physiol.* **2004**, *135*, 1305−1313.

(9) Kabel, M. A.; Kortenoeven, L.; Schols, H. A.; Voragen, A. G. J. In vitro fermentability of differently substituted xylo-oligosaccharides. *J. Agric. Food Chem.* **2002**, *50*, 6205−6210.

(10) Gniechwitz, D.; Reichardt, N.; Blaut, M.; Steinhart, H.; Bunzel, M. Dietary fiber from coffee beverage: degradation by human fecal microbiota. *J. Agric. Food Chem.* **2007**, *55*, 6989−6996.

(11) Prosky, L.; Asp, N. G.; Schweizer, T. F.; Devries, J. W.; Furda, I. Determination of insoluble, soluble, and total dietary fiber in foods and food products: Interlaboratory study. *J. Assoc. Off. Anal. Chem.* **1988**, *71*, 1017−1023.

(12) Willis, R. B.; Montgomery, M. E.; Allen, P. R. Improved method for manual, colorimetry determination of total Kjeldahl nitrogen using salicylate. *J. Agric. Food Chem.* **1996**, *44*, 1804−1807.

(13) Saeman, J. F.; Bubl, J. L.; Harris, E. E. Quantitative saccharification of wood and cellulose. *Ind. Eng. Chem., Anal. Ed.* **1945**, *17*, 35−37.

(14) De Ruiter, G. A.; Schols, H. A.; Voragen, A. G. J.; Rombouts, F. M. Carbohydrate analysis of water-soluble uronic acid-containing polysaccharides with high-performance anion-exchange chromatography using methanolysis combined with TFA hydrolysis is superior to four other methods. *Anal. Biochem.* **1992**, *207*, 176−185.

(15) Leontein, K.; Lindberg, B.; Lonngren, J. Assignment of absolute configuration of sugars by GLC of their acetylated glycosides formed from chiral alcohols. *Carbohydr. Res.* **1978**, *62*, 359−362.

(16) Gottlieb, H. E.; Kotlyar, V.; Nudelman, A. NMR chemical shifts of common laboratory solvents as trace impurities. *J. Org. Chem.* **1997**, *62*, 7512−7515.

(17) Pitson, S. M.; Voragen, A. G. J.; Vincken, J. P.; Beldman, G. Action patterns and mapping of the substrate-binding regions of *endo*-(1→5)-α-L-arabinanases from *Aspergillus niger* and *Aspergillus aculeatus*. *Carbohydr. Res.* **1997**, *303*, 207−218.

(18) Nunes, F. M.; Coimbra, M. A. Chemical characterization of the high molecular weight material extracted with hot water from green and roasted arabica coffee. *J. Agric. Food Chem.* **2001**, *49*, 1773−1782.

DOI: 10.1021/jf505283x
J. Agric. Food Chem. 2015, 63, 707−715

(19) Sweet, D. P.; Shapiro, R. H.; Albersheim, P. Quantitative-analysis by various GLC response-factor theories for partially methylated and partially ethylated alditol acetates. *Carbohydr. Res.* **1975**, *40*, 217−225.
(20) Westphal, Y.; Kühnel, S.; de Waard, P.; Hinz, S. W. A.; Schols, H. A.; Voragen, A. G. J.; Gruppen, H. Branched arabino-oligosaccharides isolated from sugar beet arabinan. *Carbohydr. Res.* **2010**, *345*, 1180−1189.
(21) Navarro, D. A.; Cerezo, A. S.; Stortz, C. A. NMR spectroscopy and chemical studies of an arabinan-rich system from the endosperm of the seed of *Gleditsia triacanthos*. *Carbohydr. Res.* **2002**, *337*, 255−263.
(22) Capek, P.; Toman, R.; Kardosova, A.; Rosik, J. Polysaccharides from the roots of the marsh mallow (*Althaea officinalis* L., var. Rhobusta): structure of an arabinan. *Carbohydr. Res.* **1983**, *117*, 133−140.
(23) Swamy, N. R.; Salimath, P. V. Arabinans from *Cajanus cajan* cotyledon. *Phytochemistry* **1991**, *30*, 263−265.
(24) Ishii, T.; Konishi, T.; Ito, Y.; Ono, H.; Ohnishi-Kameyama, M.; Maeda, I. A β-(1→3)-arabinopyranosyltransferase that transfers a single arabinopyranose onto arabino-oligosaccharides in mung bean (*Vigna radiate*) hypocotyls. *Phytochemistry* **2005**, *66*, 2418−2425.
(25) Fransen, C. T. M.; Van Laere, K. M. J.; van Wijk, A. A. C.; Brull, L. P.; Dignum, M.; Thomas-Oates, J. E.; Haverkamp, J.; Schols, H. A.; Voragen, A. G. J.; Kamerling, J. P.; Vliegenthart, J. F. G. α-D-Glc*p*-(1↔1)-β-D-Gal*p*-containing oligosaccharides, novel products from lactose by the action of β-galactosidase. *Carbohydr. Res.* **1998**, *314*, 101−114.
(26) Lichtenthaler, F. W.; Oberthur, M.; Peters, S. Directed and efficient syntheses of β(1→4)-linked galacto-oligosaccharides. *Eur. J. Org. Chem.* **2001**, *2001*, 3849−3869.
(27) Ishii, T.; Ono, H.; Ohnishi-Kameyama, M.; Maeda, I. Enzymic transfer of α-L-arabinopyranosyl residues to exogenous 1,4-linked β-D-galacto-oligosaccharides using solubilized mung bean (*Vigna radiata*) hypocotyl microsomes and UDP-β-L-arabinopyranose. *Planta* **2005**, *221*, 953−963.
(28) Huisman, M. M. H.; Brull, L. P.; Thomas-Oates, J. E.; Haverkamp, J.; Schols, H. A.; Voragen, A. G. J. The occurrence of internal (1→5)-linked arabinofuranose and arabinopyranose residues in arabinogalactan side chains from soybean pectic substances. *Carbohydr. Res.* **2001**, *330*, 103−114.
(29) Westphal, Y.; Kühnel, S.; Schols, H. A.; Voragen, A. G. J.; Gruppen, H. LC/CE-MS tools for the analysis of complex arabino-oligosaccharides. *Carbohydr. Res.* **2010**, *345*, 2239−2251.
(30) Dunkel, M. P. H.; Amado, R. Analysis of *endo*-(1→5)-α-L-arabinanase degradation patterns of linear (1→5)-α-L-arabino-oligosaccharides by high-performance anion-exchange chromatography with pulsed amperometric detection. *Carbohydr. Res.* **1995**, *268*, 151−158.
(31) Yamaguchi, F.; Inoue, S.; Hatanaka, C. Purification and properties of endo-β-1,4-galactanase from *Aspergillus niger*. *Biosci., Biotechnol., Biochem.* **1995**, *59*, 1742−1744.
(32) Luonteri, E.; Laine, C.; Uusitalo, S.; Teleman, A.; Siika-aho, M.; Tenkanen, M. Purification and characterization of *Aspergillus* β-D-galactanases acting on β-1,4- and β-1,3/6-linked arabinogalactans. *Carbohydr. Polym.* **2003**, *53*, 155−168.
(33) Van de Vis, J. W.; Searle-van Leeuwen, M. J. F.; Siliha, H. A.; Kormelink, F. J. M.; Voragen, A. G. J. Purification and characterization of *endo*-1,4-β-D-galactanases from *Aspergillus niger* and *Aspergillus aculeatus*: Use in combination with arabinanases from *Aspergillus niger* in enzymatic conversion of potato arabinogalactan. *Carbohydr. Polym.* **1991**, *16*, 167−187.
(34) Eriksson, I.; Andersson, R.; Westerlund, E.; Andersson, R.; Aman, P. Structural features of an arabinan fragment isolated from the water-soluble fraction of dehulled rapeseed. *Carbohydr. Res.* **1996**, *281*, 161−172.

DOI: 10.1021/jf505283x
J. Agric. Food Chem. 2015, 63, 707−715

JOURNAL OF AGRICULTURAL AND FOOD CHEMISTRY

Article

pubs.acs.org/JAFC

Alpha-Substituted Derivatives of Cinnamaldehyde as Tyrosinase Inhibitors: Inhibitory Mechanism and Molecular Analysis

Yi Cui, Ge Liang, Yong-Hua Hu, Yan Shi, Yi-Xiang Cai, Huan-Juan Gao, Qing-Xi Chen, and Qin Wang*

State Key Laboratory of Cellular Stress Biology and Key Laboratory of the Ministry of Education for Coastal and Wetland Ecosystems, Xiamen University, Xiamen 361102, China

ABSTRACT: Alpha-substituted derivatives of cinnamaldehyde (alpha-bromocinnamaldehyde, alpha-chlorocinnamaldehyde, and alpha-methylcinnamaldehyde) were used as inhibitors on mushroom tyrosinase. The result showed that three compounds can reduce both monophenolase and diphenolase activity on tyrosinase, and the inhibition was reversible. The IC_{50} values of alpha-bromocinnamaldehyde, alpha-chlorocinnamaldehyde, and alpha-methylcinnamaldehyde were 0.075, 0.140, and 0.440 mM on monophenolase and 0.049, 0.110, and 0.450 mM on diphenolase, respectively. The inhibition types and constants on diphenolase for these inhibitors were further studied. The molecular inhibition mechanisms of tyrosinase by the derivatives were investigated by UV-scanning study, fluorescence quenching, and molecular docking. These assays demonstrated that the derivatives could decrease the formation of *o*-quinones, and all derivatives were static quenchers of mushroom tyrosinase. Docking results implied that they could not form metal interactions with the copper ions of the enzyme, whereas they could interact with the amino acid residues of active site center. This research on alpha-substituted derivatives of cinnamaldehyde as tyrosinase inhibitors would lead to advances in the field of antityrosinase.

KEYWORDS: *tyrosinase, derivatives of cinnamaldehyde, fluorescence quenching, molecular docking*

INTRODUCTION

Tyrosinase (EC 1.14.18.1) is a copper-containing, mixed function oxidase widely distributed in animals, plants, and microorganisms.[1] It catalyzes two distinct reactions of melanin biosynthesis by hydroxylation of monophenols to *o*-diphenols and oxidation of *o*-diphenols to the corresponding *o*-quinones, which are the initial steps whereafter a series of highly reactive quinones are produced to initiate the pigmentation and excessive activation of tyrosinase can cause various dermatological disorders.[2]

Tyrosinase inhibitors are widely used in dermatological treatments and in cosmetics. Plenty of tyrosinase inhibitors are obtained from natural or synthetic sources, which have been further investigated.[3] Cinnamaldehyde, a low molecular weight cinnamic acid analogue with relatively broad distribution in plants, has shown various activities such as antitumor, cytotoxic, and mutagenic.[4,5] It has also been proven to have strong activity against a wide variety of wood decay fungi.[6,7] Cinnamaldehyde is considered to be a safe fragrant constituent without acute and chronic toxicity, and no case of mutagenecity or genotoxicity and carcinogenicity due to cinnamaldehyde has ever been reported in mammalian.[8]

In the previous study, Ikuyo et al.[9] reported that cinnamaldehyde inhibited the oxidation of L-DOPA by mushroom tyrosinase with an IC_{50} of 129 μg/mL (0.98 mM). Several kinds of derivatives of cinnamaldehyde have been reported. 2′-Hydroxycinnamaldehyde derivative isolated from *C. cassia* has been reported to have an inhibitory effect on farnesyl protein transferase activity and inhibited proliferation of several human cancer cell lines including breast, leukemia, ovarian, lung, and colon tumor.[10,11] Dimeric cinnamaldehydes strongly inhibited the growth of human tumor cells through the inducing of apoptosis in tumor cells and in vivo growth of human colon tumor xenograft in nude mice.[12] Yoshio et al.[13] reported that alpha-bromocinnamaldehyde has been used widely as an antifungal agent for optical, electric, and musical instruments, and they also proposed the metabolic pathway of alpha-bromocinnamaldehyde in rats.

Based on the above, we paid attention to the relationship between derivatives of cinnamaldehyde on alpha-substituted and mushroom tyrosinase. This research aims to understand the mechanism of the alpha-substituted derivatives on tyrosinase and to clarify molecular interaction between derivatives and enzyme structure.

MATERIALS AND METHODS

Materials. Mushroom tyrosinase (EC 1.14.18.1) from mushroom (*Agaricus bisporus*) was the product of Sigma-Aldrich (St. Louis, MO). The specific activity of the enzyme was 6680 U/mg. L-3,4-Dihydroxyphenylalanine (L-DOPA), L-tyrosine (L-Tyr), alpha-bromocinnamaldehyde (aBCA), alpha-chlorocinnamaldehyde (aCCA), alpha-methylcinnamaldehyde (aMCA), dimethylsulfoxide (DMSO), and $NaIO_4$ were also obtained from Sigma-Aldrich. Other reagents with standard analytical purity were acquired from Sinopharm (Shanghai, China). The water used was redistilled and ion-free.

Enzyme Activity Assay. Monophenolase and diphenolase activity assay were performed as previously reported.[14] In this reaction, L-Tyr and L-DOPA were used as the substrate for monophenolase and diphenolase activity assay, respectively. The reaction media (3 mL) for enzyme activity assay contained 1 mM L-Tyr or 0.5 mM L-DOPA in 50 mM Na_2HPO_4–NaH_2PO_4 buffer (PH 6.8) and 100 mL of different concentrations of inhibitor. The final concentrations of mushroom tyrosinase were 33.33 and 3.33 μg/mL for monophenolase and

Received: November 12, 2014
Revised: December 29, 2014
Accepted: December 29, 2014
Published: December 29, 2014

ACS Publications © 2014 American Chemical Society

DOI: 10.1021/jf505469k
J. Agric. Food Chem. 2015, 63, 716−722

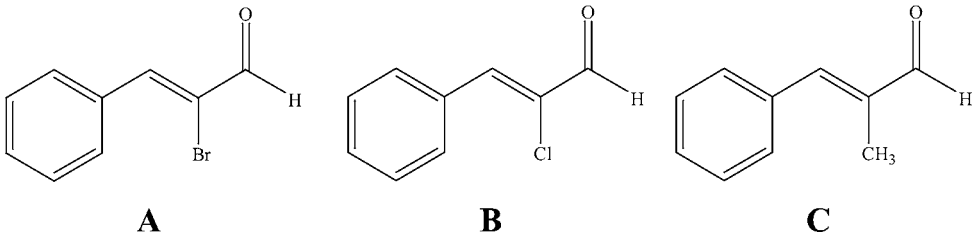

Figure 1. Chemical structures of the derivatives of cinnamaldehyde. (A), (B), and (C) represent aBCA, aCCA, and aMCA, respectively.

diphenolase activity, respectively.[15,16] Enzyme assay was performed by following the increase of optical density at 475 nm (ε = 3700 M^{-1} cm^{-1}) accompanying the oxidation of substrates. The reaction was carried out at 30 °C. A Beckman DU800 spectophotometer was used for absorbance and kinetic measure.[17]

The inhibitor was dissolved in 3.3% DMSO and diluted to appropriate concentration. The controls without inhibitor but containing 3.3% DMSO in the reaction media were routinely carried out. The inhibitory effects of inhibitors on the enzyme were expressed as the concentrations that inhibited 50% of the enzyme activity (IC_{50}). The inhibition types were obtained by the Line-weaver Burk plot, and the inhibition constants were determined by the secondary plots of the apparent K_m/V_m or $1/V_m$ versus the concentrations of the inhibitors.[18]

UV Scanning Study. The experiment was carried out according to the method of Jiménez-Atiénzar et al.[19] with slight modifications. The oxidation of L-DOPA was carried out with and without the presence of inhibitor. The reaction media (3 mL) contained 0.5 mM L-DOPA in 50 mM Na_2HPO_4–NaH_2PO_4 buffer (pH 6.8) and 0.1 mL of inhibitor (dissolved in DMSO). The final concentration of the mushroom tyrosinase was 16.67 μg/mL. The UV spectra were recorded using a Beckman DU-800 spectrophotometer.

Nonenzymatic Generation of the Quinones. The experiment was carried out by methods of Espin and Wichers.[20] L-DOPA (100 μM) was oxidized by $NaIO_4$ (100 μM). The spectra in the absence and presence of the inhibitor (9, 18, 27, and 36 μM) were recorded with the DU800 spectrophotometer.

Fluorescence Spectrum Quenching. The experiment was performed with reference to Kim et al.[21] Fluorescence spectra were recorded using an Cary Eclipse fluorescence spectrophotometer. Fluorescence emission spectra were recorded at wavelengths of 300–420 nm upon excitation at 280 nm. The excitation and emission bandwidths were both 5 nm.[22,23] For each data point, 10 μL of inhibitor solution was added to 2 mL of tyrosinase solution to make sure each inhibitor was at the appropriate range of concentration. Each measurement was done thrice, and the means were calculated. The fluorescence quenching data were plotted as the fluorescence intensity against the inhibitor concentration. Fluorescence quenching was described by the Stern–Volmer equation[24]

$$F_0/F = 1 + K_q\tau_0[Q] = 1 + K_{SV}[Q]$$

where F_0 and F are the fluorescence intensities before and after the addition of the quencher, respectively, K_q is the bimolecular quenching constant, τ_0 (10^{-8} s) is the lifetime of the fluorophore in the absence of the quencher, [Q] is the concentration of the quencher, and K_{SV} is the Stern–Volmer quenching constant. Hence, the above equation was applied to determine the K_{SV} using linear regression of a plot of F_0/F against [Q]. For the calculation of bimolecular quenching constants, the data were plotted as F_0/F against [Q], with the bimolecular quenching constants calculated by linear regression.

There were two types of fluorescence-quenching mechanisms: static (by complex formation) and dynamic (by collisional processes).[25] When the type was static, the apparent binding constant (K_A) and the binding affinity (n) were estimated by plotting $\log[(F_0 - F)/F]$ against $\log[Q]$ with the following equation[26]

$$\log[(F_0 - F)/F] = \log K_A + n\log[Q]$$

where [Q] is the quencher concentration

Molecular Docking with Ligand. In this research, molecular operation environment 2010 software (MOE) was used for protein–ligand docking. The method was consulted with reference to Chen.[27] Before docking, the 3D structures of the inhibitors and tyrosinase were energy minimized. Hydrogens were added using the energy minimization module of the MOE. The parameters for molecular docking were as follows: the receptor and site were set to receptor atoms and dummy atoms, respectively; the refinement was set to force field; the retain of both the first and second scoring were set to 10; both the first and second rescoring were set to London dG; the MM/GBVI binding free energy scoring was used to rank the docking poses. A more negative value reflects a stronger interaction. Other parameters used were the default settings of the software. The docked conformation, which had the highest score, was selected to analyze the mode of binding.

RESULTS

Effects of Derivatives of Cinnamaldehyde on the Monophenolase Activity of Mushroom Tyrosinase. Taking aBCA, aCCA, and aMCA (see Figure 1 for structures) as the effectors, we probed the effects of these compounds on the activity of mushroom tyrosinase for the oxidation of L-Tyr. The lag time and characteristic of monophenolase activity were observed. The reaction system reached a steady state after the lag time. After the steady state, the curve of product increased linearly with increasing reaction time. The results are shown in Figure 2. Increasing concentrations of these effectors not only changed the lag time of the enzyme (Figure 2A-II, Figure 2B-II, and Figure 2C-II), but also the steady-state rates decreased obviously (Figure 2A-III, Figure 2B-III, and Figure 2C-III). When the concentrations of effectors were increased to 0.2 mM, the lag time was extended by aBCA, aCCA, and aMCA up to 115%, 75%, and 9%, respectively. As shown in Table 1, the concentrations for aBCA, aCCA, and aMCA leading to 50% enzyme activity (IC_{50}) were 0.075, 0.140, and 0.440 mM, respectively.

Effects of Derivatives of Cinnamaldehyde on the Diphenolase Activity. Effects of the derivatives on the oxidation of L-DOPA catalyzed by mushroom tyrosinase were investigated. The results showed that the inhibition was dose-dependent, while the relative activity of the enzyme reaction was reduced with increasing concentration of the inhibitors (Figure 3). The concentrations of aBCA, aCCA, and aMCA for leading to 50% enzyme activity loss (IC_{50}) were 0.049, 0.110, and 0.450 mM, respectively. The values are given in Table 1 as well.

Inhibition Mechanism of Derivatives of Cinnamaldehyde on the Diphenolase Activity. To ascertain the inhibition mechanism of derivatives of cinnamaldehyde, the oxidation of L-DOPA by derivatives was studied. Figure 4 shows that the plots of the remaining enzyme activity versus the concentrations of enzyme at different concentrations of aBCA gave a family of straight lines, which all passed through the origin. The slopes of the lines descended with an increase of the

DOI: 10.1021/jf505469k
J. Agric. Food Chem. 2015, 63, 716–722

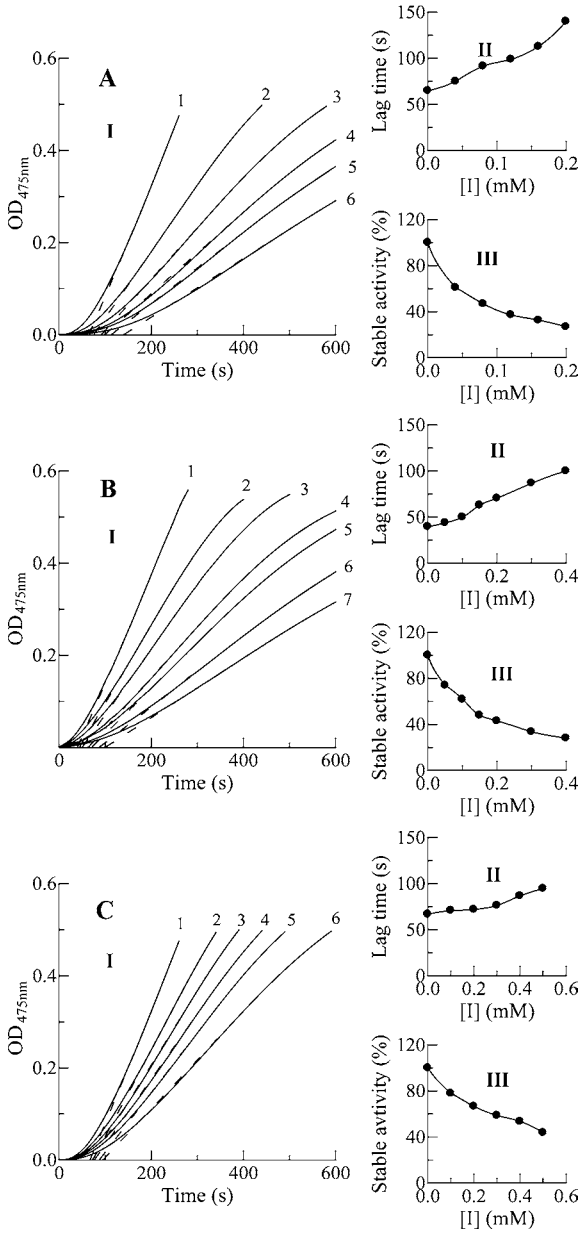

Figure 2. Inhibitory activity of the derivatives of cinnamaldehyde on monophenolase activity of mushroom tyrosinase. (I) Progress curves for the oxidation of L-Tyr by the enzyme. (II) Effects on the lag time of monophenolase. (III) Effects on the stable activity of L-Tyr by the enzyme. (A), (B), and (C) represent aBCA, aCCA, and aMCA, respectively. The concentrations of aBCA for curves 1−6 were 0, 0.04, 0.08, 0.12, 0.16, and 0.20 mM. The concentrations of aCCA for curves 1−7 were 0, 0.05, 0.1, 0.15, 0.2, 0.3, and 0.4 mM. The concentrations of aMCA for curves 1−6 were 0, 0.1, 0.2, 0.3, 0.4, and 0.5 mM.

concentrations of inhibitor, indicating that the presence of aBCA did not bring down the amount of active enzyme but just led to a decrease in the enzyme activity. Therefore, the inhibition of tyrosinase by aBCA was reversible. We also studied the inhibition mechanisms of aCCA and aMCA, as above. Results indicated that both aCCA and aMCA were reversible inhibitors of mushroom tyrosinase.

Inhibition Types and Constants on the Diphenolase Activity by Derivatives of Cinnamaldehyde. The plots of $1/v$ versus $1/[S]$ gave a family of straight lines indicating that aBCA was mixed type inhibitor (Figure 5A-I). Figure 5B-I indicated that aCCA was a noncompetitive inhibitor of the enzyme. As shown in Figure 5C-I, the result domenstrated that aMCA was an uncompetitive inhibitor of mushroom tyrosinase.

The inhibition constants (K_I) were obtained from the plots of the slopes versus the concentrations of the inhibitors (Figure 5A-II and Figure 5B-II), and the enzyme−substrate complexes (K_{IS}) were obtained from the vertical intercepts versus the concentrations of these compounds (Figure 5A-III and Figure 5C-II). The values obtained are summarized in Table 1 for comparison.

Oxidation of L-DOPA in the Presence and Absence of Derivatives of Cinnamaldehyde. The spectra obtained during the oxidation of L-DOPA in the absence (Figure 6A) and presence (Figure 6B, Figure 6C, and Figure 6D) of aBCA, aCCA, and aMCA by mushroom tyrosinase are given. In the absence of these compounds, the absorbance of the typical peak at 475 nm was 0.75. With the existence of aBCA, aCCA, and aMCA, at 10 min after the addition of the enzyme the peak intensity was reduced by 67%, 48%, and 24%, respectively. The results were consistent with the enzyme activity assay.

Interaction of Derivatives of Cinnamaldehyde with *o*-Quinones. Ultraviolet−visible scan was used to research the inhibitory mechanism of the compounds on mushroom tyrosinase. The *o*-diphenol (L-DOPA) was oxidized by sodium-periodate ($NaIO_4$) in the absence and presence of the inhibitors. Figure 7A, curve 1 shows spectrum of L-DOPA without any characteristic peaks. Curves 2−5 show the oxidation of L-DOPA by $NaIO_4$ for 1−4 min with a characteristic peak at 475 nm. Because the absorption did not increase as time goes by, L-DOPA (100 μM) was considered to be totally oxidized by $NaIO_4$ (100 μM).

Curves 1 in Figure 7B, 7C, and 7D are spectra of aBCA, aCCA, and aMCA, respectively. None of them showed characteristic peak at 475 nm. However, when the compounds were added to the mixture of L-DOPA and $NaIO_4$, a decrease of absorbance at the peak occurred (Figure 7B, Figure 7C, and Figure 7D curves 2−5).

Oxidation of L-DOPA by tyrosinase and $NaIO_4$ had the same typical peak at 475 nm indicating that they produced the same products. After addition of effectors, both the enzymatic and nonenzymatic reactions, the product peak became lower. The results indicated that effectors could bring down the oxidative product of L-DOPA, meaning that they prevented the formation of *o*-quinones, so the generation of melanin had

Table 1. Inhibition Constants of Cinnamaldehyde Derivatives

	IC_{50} (mM)		inhibition (mM)		inhibition constants (mM)	
compd	monophenolase	diphenolase	mechanism	type	K_I	K_{IS}
aBCA	0.075	0.049	reversible	mixed	0.044	0.063
aCCA	0.140	0.110	reversible	noncompetitive	0.116	0.116
aMCA	0.440	0.450	reversible	uncompetitive		0.194

DOI: 10.1021/jf505469k
J. Agric. Food Chem. 2015, 63, 716−722

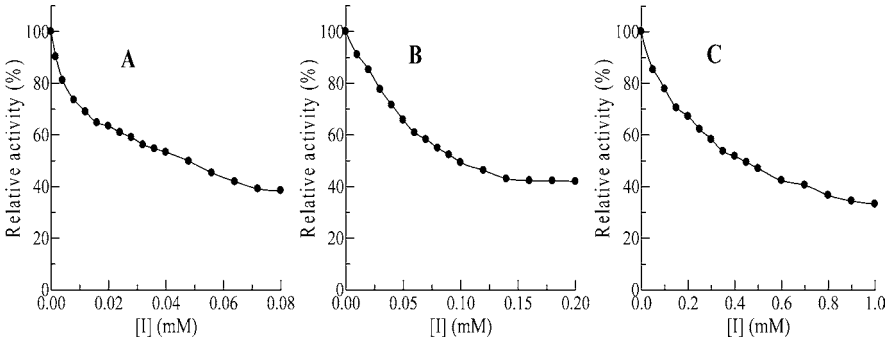

Figure 3. Inhibitory activity of the derivatives of cinnamaldehyde on diphenolase activity of tyrosinase. (A), (B), and (C) represent aBCA, aCCA and aMCA, respectively.

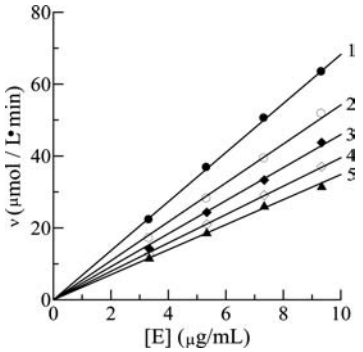

Figure 4. Effect of concentrations of mushroom tyrosinase on its activity for the oxidation of L-DOPA at different concentrations of aBCA. The concentrations of aBCA for curves 1−5 were 0, 0.0125, 0.025, 0.0375, and 0.05 mM.

been reduced. This was the other process to restrain the activity of tyrosinase.

Analysis of Fluorescence Quenching of Tyrosinase with Derivatives of Cinnamaldehyde. Fluorescence quenching was applied to investigate the interactions of ligands and proteins.[28] The fluorescence emission spectra of tyrosinase in the absence and presence of aBCA are shown in Figure 8A. The fluorescence intensities of the emission peaks at 338 nm were inversely decreased with increasing concentration of aBCA (Figure 8B). Figure 8C is the Stern−Volmer plot which measured the Stern−Volmer quenching constants of aBCA. The results, shown in Table 2, suggested a good linear Stern−Volmer plot with K_q and K_{SV} values of 3.77×10^{12} M^{-1} s^{-1} and 3.77×10^4 M^{-1}, respectively. Due to the fact that the K_{SV} for dynamic cannot be larger than 100 L/M,[26] the K_{SV} we got demonstrated that the type of fluorescence-quenching mechanism between tyrosinase and aBCA was static.

Figure 8D shows the plot of $\log[(F_0 - F)/F]$ against $\log[Q]$ for tyrosinase with various concentrations of aBCA. From this graph, the values of K_A and n were obtained from the intercept and the slope. We obtain an equation of linear regression:

$$\log[(F_0 - F)/F] = 5.89 + 1.29 \log[Q], \quad R^2 = 0.9965$$

We have studied the fluorescence quenching of tyrosinase with aCCA and aMCA as well. Results were similar to aBCA, which indicated that both aCCA and aMCA were static quenchers of mushroom tyrosinase. All the values of K_{SV}, K_q, K_A, and n are shown in Table 2.

Molecular Docking Analysis. Docking simulations were further performed to understand the mechanism underlying the

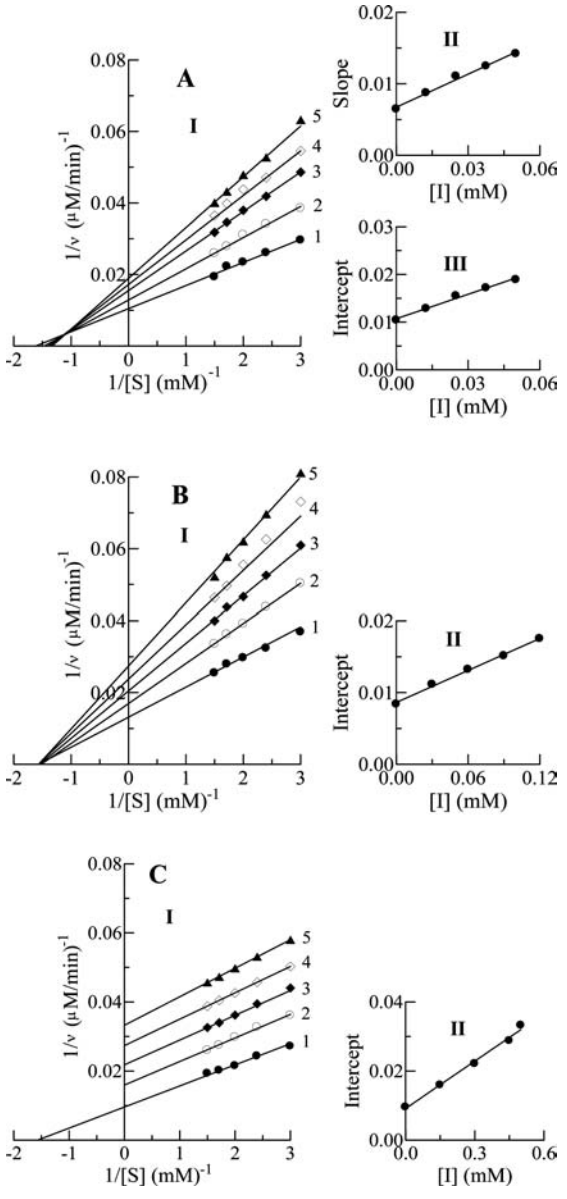

Figure 5. Determination of the inhibition type and constants of the compounds of tyrosinase. (A), (B), and (C) represent aBCA, aCCA and aMCA, respectively. The concentrations of aBCA for curves 1−5 were 0, 0.0125, 0.0250, 0.0375, and 0.0500 mM. The concentrations of aCCA for curves 1−5 were 0, 0.5, 1.0, 1.5, and 2.0 mM. The concentrations of aMCA for curves 1−5 were 0, 0.15, 0.30, 0.45, and 0.60 mM.

DOI: 10.1021/jf505469k
J. Agric. Food Chem. 2015, 63, 716−722

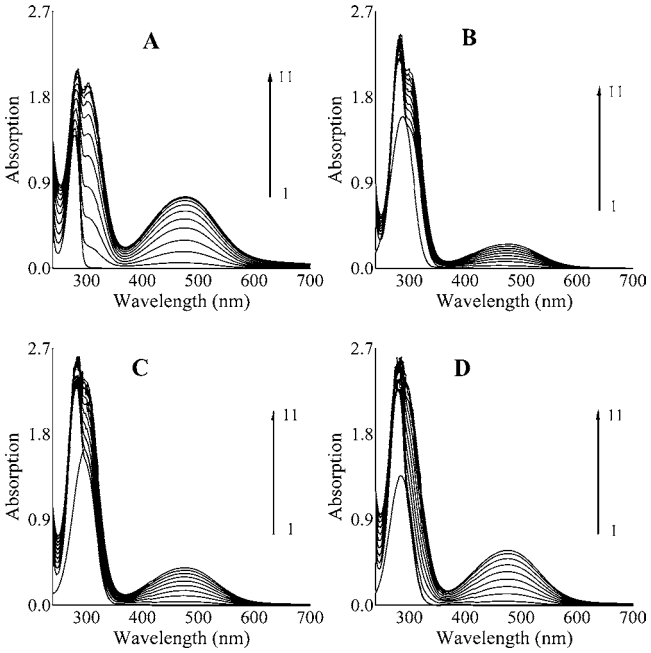

Figure 6. Consecutive spectra obtained during the oxidation of L-DOPA in the absence (A) and presence (B), (C), and (D) of inhibitors (0.2 mM) by mushroom tyrosinase. (B), (C), and (D) represent aBCA, aCCA, and aMCA, respectively. Curves 1−11 represent 0−10 min after the addition of the enzyme.

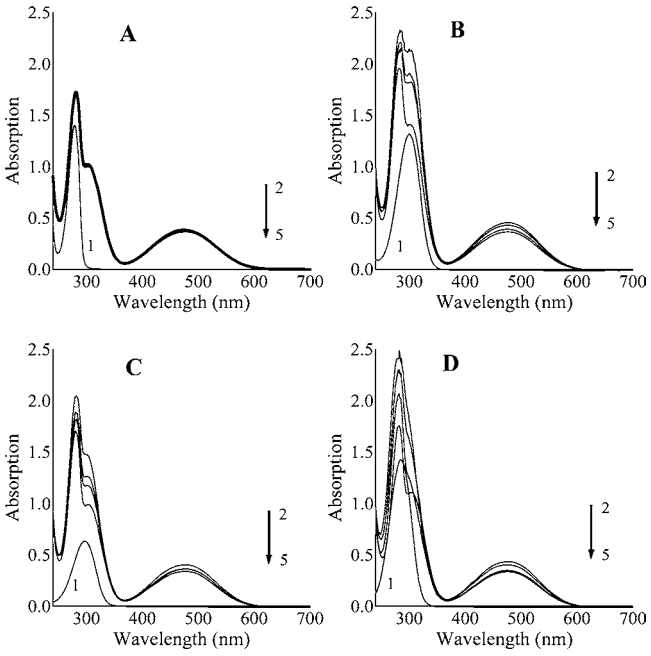

Figure 7. UV−vis spectra for the oxidation of L-DOPA. Line 1 is 100 μM L-DOPA or compounds alone. Curves 2−5 in (A) represent 1−4 min after adding $NaIO_4$; curves 2−5 in (B), (C), and (D) are different concentrations (9, 18, 27, and 36 μM) of aBCA, aCCA, and aMCA, respectively.

antityrosinase activities of the derivatives of cinnamaldehyde. The docking modes of aBCA, aCCA, and aMCA were examined in the enzyme catalytic site. The docked conformations revealed that all compounds have similar mechnism with mushroom tyrosinase (Figure 9). They could not form metal interactions with the copper irons of the

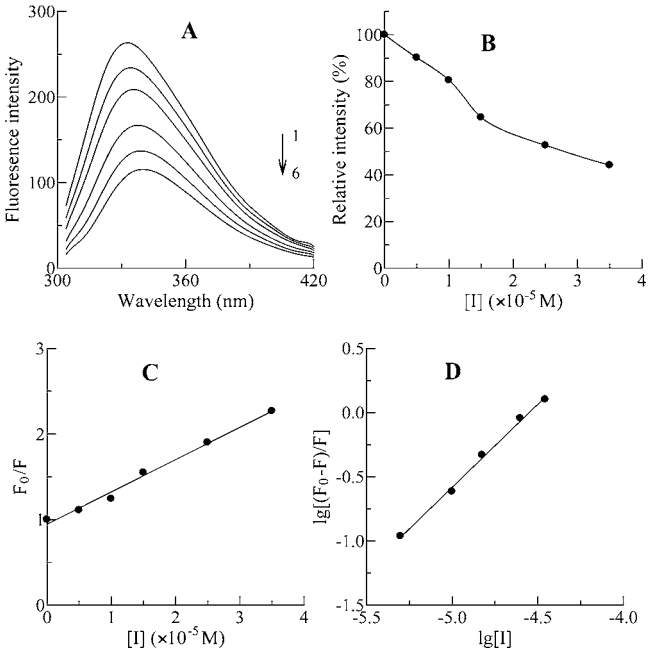

Figure 8. Changes in intrinsic tyrosinase fluorescence at different concentrations of aBCA. (A) Emission spectra 1−6 of tyrosinase in the presence of aBCA for 0, 0.005, 0.010, 0.015, 0.025, and 0.035 μM, respectively; (B) maximum florescence intensity changes; (C) Stern−Volmer plot describing the tyrosinase quenching caused by association with quencher; (D) plot of $\log[(F_0 - F)/F]$ against $\log[Q]$ for tyrosinase and various concentrations of quencher. F_0 and F are the fluorescence intensities before and after the addition of the quencher.

Table 2. Stern−Volmer Equation for the Interaction between Quenchers and Tyrosinase

compd	type of quenching	K_{SV} (M^{-1})	K_q (M^{-1} s^{-1})	K_A (M^{-1})	n
aBCA	static	3.77×10^4	3.77×10^{12}	7.76×10^5	1.29
aCCA	static	3.84×10^4	3.84×10^{12}	5.75×10^5	1.05
aMCA	static	4.86×10^4	4.86×10^{12}	3.47×10	0.97

enzyme. whereas all of them could interact the amino acid residues in the center of active site. The oxygen for aBCA on the aldehyde group could directly act on His_{85} and His_{61}. Besides, aBCA could form intercations with tyrosinase residues, such $asAla_{286}$, His_{244}, Glu_{256}, Phe_{264}, Asn_{260}, Phe_{292}, His_{263},Val_{283}, His_{295}, and Ser_{282}. (Figure 9A).

The same analyses were carried out on aCCA and aMCA, which indicated the oxygen on the aldehyde group for aCCA and aMCA could directly act on His_{94} (Figure 9B) and His_{85} (Figure 9C), respectively. In addition, aCCA and aMCA could also interact with another 10 (Figure 9B) or 9 (Figure 9C) amino acid residues in tyrosinase. These interactions might enhance the inhibitory potency of derivatives on the enzyme.

DISCUSSION

This paper explained the relationship between the cinnamaldehyde derivatives and mushroom tyrosinase. For monophenolase activity, three derivatives could extend the lag time and inhibit the steady-state activity. Comparing the inhibitory effects of three derivatives, we found that aBCA was better than aCCA, and aMCA was weakest.

With respect to diphenolase activity, the IC_{50} showed the same results with the inhibitory effects of monophenolase.

DOI: 10.1021/jf505469k
J. Agric. Food Chem. 2015, 63, 716−722

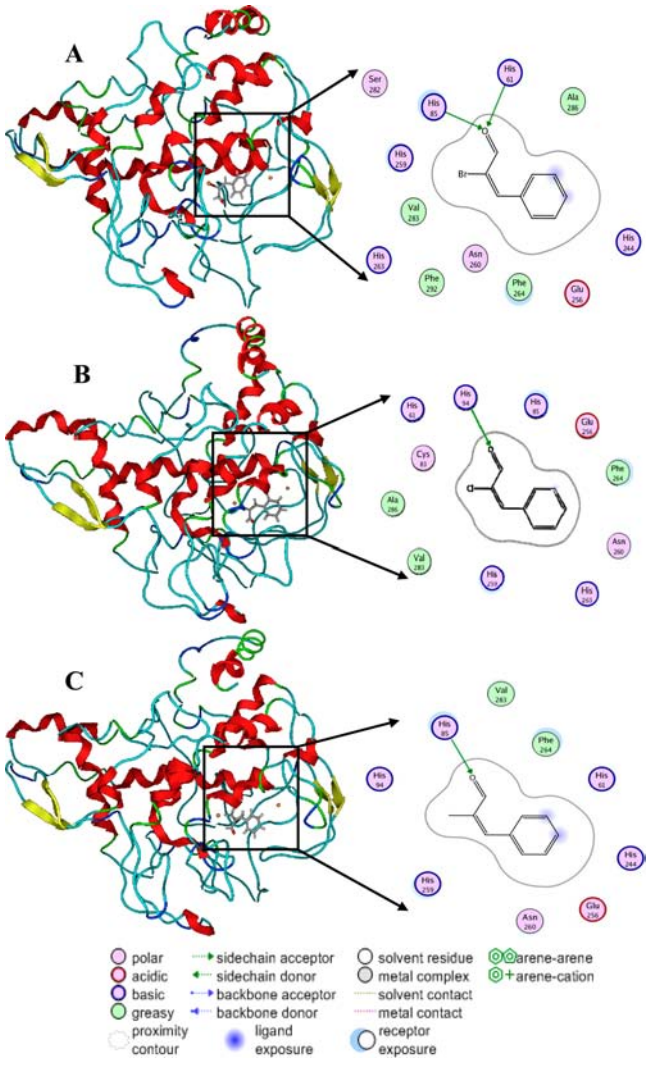

Figure 9. Binding mode of the ligands with tyrosinase residues. The receptor exposure differences were shown by the size and intensity of the turquoise discs surrounding the residues. (A), (B), and (C) represent aBCA, aCCA, and aMCA, respectively.

aBCA was the strongest inhibitor, and aMCA was the weakest. The inhibitions of three derivatives were reversible demonstrating that the effectors did not reduce the amount of the efficient enzyme, but just decreased the activity of tyrosinase.[29] It was interesting that each inhibition type of three compounds was different and this phenomenon may result in the different inhibitory capacities for derivatives. Compared with cinnamaldehyde, whose IC_{50} of diphenolase was 0.98 mM,[9] alpha-substituted derivatives showed better inhibitory effects. Due to the existence of alpha substituents, the terpenes on derivatives became unstable and easier to interfere with tyrosinase. Moreover, Xiao et al.[30] reported that alpha halogeno group can enhance cinnamaldehyde antibacterial ability greatly. Perhaps the substituents hindered the activity of enzyme and thus restrained bacterial growth.

Fluorescence quenching was used to investigate the interactions of ligands and proteins. The presented results showed that the tyrosinase fluorescence intensity decreased in the presence of derivatives; however, there was no apparent λ_{em} shift in the fluorescence emission spectra of tyrosinase with the addition of derivatives. Therefore, the interaction between effectors and tyrosinase only affected the microenvironment in close proximity to the fluorophore of tyrosinase, as no other changes in the immediate surroundings of the quenched residues were observed.[31] This mode was also observed by Mu et al.[32] in fluorescence quenching between 4-methoxycinnamic acid and tyrosinase. Moreover, tricin[30] and thiobarbituric acid[33] showed similar quenching mechanisms. Compared with the values in Table 2, for aBCA, aCCA, and aMCA, the K_{SV} increased in turn; meanwhile, the binding constant (K_A) and the binding affinity (n) decreased in turn. All the trends of the changes declared that tyrosinase and aBCA had the strongest interaction while the interaction between aMCA and enzyme was the weakest. The results were consistent with enzyme assay.

The results of molecular docking by MOE suggested that the inhibition on tyrosinase by three derivatives represented a different strategy for inactivating tyrosinase compared to simple copper chelators. They did not bind directly to the copper ions of the active site. An example of such inhibitor was 4-methoxycinnamic acid, which can occupy the position of CuA to suppress the monophenolase activity.[32]

The scores for aBCA, aCCA, and aMCA docking with tyrosinase were −9.59, −9.35,l and −8.84 kcal/mol, respectively. The score meant that the docking between tyrosinase and all compounds was successful. The molecular docking showed that aMCA could bind residues within free enzyme whereas the inhibition type demonstrated that aMCA could not interact with enzyme directly. L-DOPA may reduce the affinity of aMCA and enzyme, and aMCA prefers to combine with the complex rather than free enzyme.

Taken together, three derivatives of cinnamaldehyde could inhibit the acitvity of tyrosinase in two ways. First, the effectors combined with enzyme to affect the microenvironment in close proximity to the active site of tyrosinase. At the same time, alpha-substituent group enhanced the reciprocity between effectors and the residues within active site, which caused activity of tyrosinase to be restricted. The second way was enzyme, inhibitor, and the substrate to form ternary compound, and effectors could prevent the oxidative process of substrate, which brings down the formation of melanin. This was the other approach was to restrict the activity of tyrosinase. Among three derivatives, aBCA had the best inhibitory effect on tyrosinase. In addition, Lu et al.[34] reported that aBCA was a low toxical compound, with slight nonspecific inflammatory irritation effects on the skin and eye. The minimun effective dose of subacute toxicity experiment (oral) was 369 mg/kg body weight. In conclusion, aBCA was a good tyrosinase inhibitor and could be widely used as insecticide, bactericide, and so on.

AUTHOR INFORMATION

Corresponding Author

*Phone/fax: +86-592-2184648. E-mail: qwang@xmu.edu.cn.

Funding

The present investigation was supported by the Natural Science Foundation of China (Grant No. 31271952 and 31371857), the Fundamental Research Funds for the Central Universities (Grant No. 20720140541), and the National Science Foundation for Fostering Talents in Basic Research of the National Natural Science Foundation of China (Grant No. J1310027).

DOI: 10.1021/jf505469k
J. Agric. Food Chem. 2015, 63, 716−722

Notes

The authors declare no competing financial interest.

■ ABBREVIATIONS USED

aBCA, alpha-bromocinnamaldehyde; aCCA, alpha-chlorocinnamaldehyde; aMCA, alpha-methylcinnamaldehyde; L-DOPA, L-3, 4-dihydroxyphenylalanine; L-Tyr, L-tyrosine; DMSO, dimethylsulfoxide; K_m, Michaelis−Menten constant; K_I, equilibrium constant of the inhibitor combining with the free enzyme; K_{IS}, equilibrium constant of the inhibitor combining with the enzyme−substrate complex

■ REFERENCES

(1) Chen, Q. X.; Song, K. K.; Wang, Q.; Huang, H. Inhibitory effects of mushroom tyrosinase by some alkylbenzaldehydes. *J. Enzyme Inhib. Med. Chem.* **2003**, *18*, 491−496.

(2) Valko, M.; Leibfritz, D.; Moncol, J.; Cronin, M. T. D.; Mazur, M.; Telser, J. Free radicals and antioxidants in normal physiological functions and human disease. *Int. J. Biochem. Cell Biol.* **2007**, *39*, 44−84.

(3) Chang, T. M. Tyrosinase and tyrosinase inhibitors. *J. Biocatal. Biotransform.* **2012**, *1*, 1−2.

(4) Kwon, B. M.; Lee, S. H.; Choi, S. U.; Park, S. H.; Lee, C. O.; Cho, Y. K. Synthesis and in vitro cytotoxicity of cinnamaldehydes to human solid tumor cells. *Arch. Pharmacal Res.* **1998**, *21*, 147−152.

(5) Shaughnessy, D. T.; Setzer, R. W.; DeMarini, D. M. The antimutagenic effect of vanillin and cinnamaldehyde on spontaneous mutation in *Salmonella* TA104 is due to a reduction in mutations at GC but not AT sites. *Mutat. Res.* **2001**, *480*, 55−69.

(6) Wang, S. Y.; Chen, P. F.; Chang, S. T. Antifungal activities of essential oils and their constituents from indigenous cinnamon (*Cinnamomum osmophloeum*) leaves against wood decay fungi. *Bioresour. Technol.* **2005**, *96*, 813−818.

(7) Cheng, S. S.; Liu, J. Y.; Hsui, Y. R.; Chang, S. T. Chemical polymorphism and antifungal activity of essential oils from leaves of different provenances of indigenous cinnamon (*Cinnamomum osmophloeum*). *Bioresour. Technol.* **2006**, *97*, 306−312.

(8) Bickers, D.; Calow, P.; Greim, H.; Hanifin, J. M.; Rogers, A. E.; Saurat, J. H.; Sipes, I. G.; Smith, R. L.; Tagami, H. A toxicologic and dermatologic assessment of cinnamyl alcohol, cinnamaldehyde, and cinnamic acid when used as fragrance ingredients. *Food Chem. Toxicol.* **2005**, *43*, 799−836.

(9) Isao, K.; Ikuyo, K.-H. Tyrosinase inhibitory activity of the olive oil flavor compounds. *J. Agric. Food Chem.* **1999**, *47*, 4574−4578.

(10) Kwon, B. M.; Cho, Y. K.; Lee, S. H.; Nam, J. Y.; Bok, S. H.; Chun, S. K.; Kim, J. A.; Lee, I. R. 2′-Hydroxycinnamaldehyde from stem bark of *Cinnamomum cassia*. *Planta Med.* **1996**, *62*, 183−184.

(11) Lee, C. W.; Hong, D. H.; Han, S. B.; Park, S. H.; Kim, H. K.; Kwon, B. M.; Kim, H. M. Inhibition of human tumor growth by 2′-hydroxy- and 2′-benzoyloxycinnamaldehydes. *Planta Med.* **1999**, *65*, 263−266.

(12) Shin, D. S.; Kim, J. H.; Lee, S. K.; Han, D. C.; Son, K. H. Synthesis and biological evaluation of dimeric cinnamaldehydes as potent antitumor agents. *Bioorg. Med. Chem.* **2006**, *14*, 2498−2506.

(13) Akimoto, Y.; Nito, S.; Urakubo, G. Studies on the metabolic fate of a-bromocinnamaldehyde (an anti-fungal agent) in rat. *Pharm. Soc. Jpn.* **1988**, *34* (4), 303−312.

(14) Chen, L. H.; Hu, Y. H.; Wei, S.; Song, K. K.; Liu, X.; Jia, Y. L.; Zhuang, J. X.; Chen, Q. X. Synthesis and antityrosinase mechanism of benzaldehyde thiosemicarbazones: Novel tyrosinase inhibitors. *J. Agric. Food Chem.* **2012**, *60*, 1542−1547.

(15) Huang, X. H.; Chen, Q. X.; Wang, Q.; Song, K. K.; Wang, J.; Li, S.; Guan, X. Inhibition of the activity of mushroom tyrosinase by alkylbenzoic acids. *Food Chem.* **2006**, *94*, 1−6.

(16) Chai, W. M.; Shi, Y.; Feng, H. L.; Qiu, L.; Zhou, H. C.; Deng, Z. W.; Yan, C. L.; Chen, Q. X. NMR, HPLC-ESI-MS, and MALDI-TOF MS analysis of condensed tannins from *Delonix regia* (Bojer ex Hook.) Rat and their bioactivities. *J. Agric. Food Chem.* **2012**, *60*, 5013−5022.

(17) Li, Z. C.; Chen, L. H.; Yu, X. J.; Hu, Y. H.; Song, K. K.; Zhou, X. W.; Chen, Q. X. Inhibition kinetics of chlorobenzaldehyde thiosemicarbazones on mushroom tyrosinase. *J. Agric. Food Chem.* **2010**, *58*, 12537−12540.

(18) Lin, M.; Ke, L. N.; Han, P.; Qiu, L.; Chen, Q. X.; Lin, H. T.; Wang, Q. Inhibitory effects of *p*-alkylbenzoic acids on the activity of polyphenol oxidase from potato (*Solanum tuberosum*). *Food Chem.* **2010**, *119*, 660−663.

(19) Jiménez-Atiénzar, M.; Cabanes, J.; Gandıa-Herrero, F. Kinetic analysis of catechin oxidation by polyphenol oxidase at neutral pH. *Biochem. Biophys. Res. Commun.* **2004**, *319*, 902−910.

(20) Espin, J. C.; Wichers, H. J. Effect of captopril on mushroom tyrosinase activity in vitro. *Biochim. Biophys. Acta* **2001**, *1544*, 289−300.

(21) Kim, D.; Park, J.; Kim, J.; Han, C.; Yoon, J.; Kim, N.; Seo, J.; Lee, C. Flavonoids as mushroom tyrosinase inhibitors: A fluorescence quenching study. *J. Agric. Food Chem.* **2006**, *54*, 935−941.

(22) Tian, J.; Liu, J.; Xie, J.; Yao, X.; Hu, Z.; Chen, X. Binding of wogonin to human serum albumin: A common binding site of wogonin in subdomain IIA. *J. Photochem. Photobiol., B* **2004**, *74*, 39−45.

(23) Wang, H. R.; Zhu, W. J.; Wang, X. Y. Mechanism of inhibition of arginine kinase by flavonoids consistent with thermodynamics of docking simulation. *Int. J. Biol. Macromol.* **2011**, *49*, 985−991.

(24) Eftinka, M. R.; Ghirona, C. A. Fluorescence quenching studies with proteins. *Anal. Biochem.* **1981**, *114*, 199−227.

(25) Li, Y.; He, W.; Liu, J.; Sheng, F.; Hu, Z.; Chen, X. Binding of the bioactive component Jatrorrhizine to human serum albumin. *Biochim. Biophys. Acta* **2005**, *1722*, 15−21.

(26) Zhao, Y.; Cao, Y.; Han, F. M.; Chen, Y. Study on the interaction between cinnamic acid and human serum albumin by fluorescence quenching method. *Spectrosc. Spectral Anal.* **2008**, *44*, 904−907.

(27) Chen, X. X.; Zhang, J.; Chai, W. M.; Feng, H. L.; Xiang, Z. H.; Shen, D. Y.; Chen, Q. X. Reversible and competitive inhibitory kinetics of amoxicillin on mushroom tyrosinase. *Int. J. Biol. Macromol.* **2013**, *62*, 726−733.

(28) Anand, U.; Jash, C.; Boddepalli, R. K.; Shrivastava, A.; Mukherjee, S. Exploring the mechanism of fluorescence quenching in proteins induced by tetracycline. *J. Phys. Chem. B* **2011**, *115*, 6312−6320.

(29) Chai, W. M.; Shi, Y.; Feng, H. L.; Qiu, L.; Zhou, H. C.; Deng, Z. W.; Yan, C. L.; Chen, Q. X. Structure characterization and anti-tyrosinase mechanism of polymeric proanthocyanidins fractionated from kiwifruit pericarp. *J. Agric. Food Chem.* **2012**, *60*, 5013−5022.

(30) Xiao, K. J.; Ning, Z. X. Preparation antimicrobial activity of α-bromo-cinnamaldehyde and its application. *Food Mach.* **1995**, *5*, 26−28.

(31) Mu, Y.; Li, L.; Hu, S. Q. Molecular inhibitory mechanism of tricin on tyrosinase. *Spectrochim. Acta, Part A* **2013**, *107*, 235−240.

(32) Mu, Y.; Li, L.; Dong, F. Y.; Hu, S. Q. Inhibition mechanism of 4-methoxycinnamic acid to tyrosinase. *J. South China Univ. Technol., Nat. Sci.* **2012**, *40*, 134−138.

(33) Yin, S. J.; Si, Y. X.; Wang, Z. J.; Wang, S. F.; Oh, S.; Lee, S.; Sim, S. M.; Yang, J. M.; Qian, G. Y.; Lee, J.; Park, Y. D. The effect of thiobarbituric acid on tyrosinase: Inhibition kinetic and computational simulation. *J. Biomol. Struct. Dyn.* **2011**, *29* (3), 463−370.

(34) Lu, D.; Bi, J.; He, Q. Y.; Wang, J.; Chen, Y. F.; Yin, M. Q. Study on the toxicities of alpha-bromocinnamaldehyde and structure−effect relationship. *Carcinog., Teratog. Mutagen.* **1992**, *4* (5), 22−25.

DOI: 10.1021/jf505469k
J. Agric. Food Chem. 2015, 63, 716−722

JOURNAL OF AGRICULTURAL AND FOOD CHEMISTRY

Article

pubs.acs.org/JAFC

Transfer Rates of 19 Typical Pesticides and the Relationship with Their Physicochemical Property

Hongping Chen,[†,‡,§] Meiling Pan,[‡] Rong Pan,[†] Minglu Zhang,[†] Xin Liu,*[,†,‡,§] and Chengyin Lu*[,†,‡,§]

[†]Tea Research Institute, Chinese Academy of Agricultural Sciences, Hangzhou 310008, China

[‡]Ministry of Agriculture, Tea Quality and Supervision Testing Center, Hangzhou 310008, China

[§]CAAS Key Laboratory of Tea Quality and Safety & Risk Assessment, Hangzhou 310008, China

Supporting Information

ABSTRACT: Determining the transfer rate of pesticides during tea brewing is important to identify the potential exposure risks from pesticide residues in tea. In this study, the transfer rates of 19 typical pesticides from tea to brewing were investigated using gas chromatography tandem mass and ultraperformance liquid chromatography tandem mass. The leaching rates of five pesticides (isocarbophos, triazophos, fenvalerate, buprofezin, and pyridaben) during tea brewing were first reported. The pesticides exhibited different transfer rates; however, this result was not related to residual concentrations and tea types. Pesticides with low octanol−water partition coefficients (Logkow) and high water solubility demonstrated high transfer rates. The transfer rates of pesticides with water solubility > 29 mg L^{-1} (or <15 mg L^{-1}) were >25% (or <10%), and those of pesticides with LogKow < 1.52 (or >2.48) were >65% (or <35%). This result indicates that water solubility at approximately 20 mg L^{-1} and LogKow at approximately 2.0 could be the demarcation lines of transfer rate. The results of this study can be used as a guide in the application of pesticides to tea trees and establishment of maximum residue limits of pesticides in tea to reduce pesticide exposure in humans.

KEYWORDS: *tea brewing, pesticides,transfer rate, water solubility, octanol−water partition coefficient*

INTRODUCTION

Tea made from dried leaves of *Camellia sinensis* is the second most widely consumed beverage worldwide after water.[1] Tea polyphenols and polysaccharides exhibit anticancer, anti-HIV, hypoglycemic, and immunological activities.[2,3] These active substances, along with harmful substances such as pesticides and heavy metals, are leached during tea brewing. Tea plants are treated with pesticides to prevent pests and diseases as well as achieve high yields. However, pesticide residues in fresh leaves are transferred from made tea to infusion during tea brewing. At present, the maximum residue limits (MRLs) of several hundred types of pesticides in tea have been regulated by China,[4] Japan,[5] the European Union,[6] and Codex Alimentarius Commission.[7] However, the pesticide MRLs have great differences in the formulation of the same pesticide. The absence of global unified pesticide MRLs makes pesticide management difficult. Thus, the establishment of unified and reasonable MRLs of typical pesticide residues in tea is urgently needed. The exposure level of toxic substances is crucial for risk assessment and establishment of MRLs. Therefore, the transfer rate of pesticides during tea brewing should be investigated because tea infusion is the most important pathway of pesticide exposure to humans during tea drinking.

Several studies have investigated the transfer rates of pesticides during tea brewing.[8−12] Neonicotinoid pesticides were easily leached into tea brewing. The transfer rates of acetamiprid, imidacloprid, and thiamethoxam are 78.3−80.6%, 62.2−63.1%, and 80.5−81.6%, respectively.[8] Wang et al.[9] determined 12 pesticide residue transfer rates during tea brewing using high-performance liquid chromatography tandem mass spectrometry (HPLC-MS/MS). High transfer rates were found for quizalofop (44.5%), thiacloprid (49.7%), thiabendazole (61.3%), methidathion (65.4%), carbary (78.9%), carbendazim (83.4%), imidacloprid (84.9%), monocrotophos (87.4%), methomyl (92.4%), thiamethoram (92.6%), 3-hydroxucarbofuran (99.4%), and clothianidin (99.8%). Pyrethroid pesticides, such as cypermethrin, bifenthrin, deltamethrin, permethrin, and cyhalothrin, are prone to be retained in tea spent because their transfer rates are lower than 10% or even equal to 0.[10,11] Benzoylurea pesticides have low transfer rates of less than 10%, except for iflubenzuron (45.6%) and triflumuron (13.1%).[12] However, several pesticides, such as triazophos,[13,14] buprofezin,[15] fenvalerate,[16,17] and isocarbophos,[18,19] have been detected in tea samples. To the best of the authors' knowledge, the transfer rates of these pesticides have not been reported. The present study investigated the transfer rates of 19 typical pesticide residues from tea into brewing and analyzed the relationship between the transfer rate and the property of these pesticides. The results would provide important information for the establishment of pesticide MRLs in tea and help farmers select suitable pesticides with low transfer rates to reduce pesticide exposure to humans.

Received: September 19, 2014
Accepted: December 23, 2014
Published: December 23, 2014

ACS Publications © 2014 American Chemical Society

DOI: 10.1021/jf506103d
J. Agric. Food Chem. 2015, 63, 723−730

Figure 1. Tea brewing and sample preparation for GC-MS/MS and UPLC-MS/MS analysis of pesticide residues in made tea, infusion, and tea spent. Notes: (a) SPE column was conditioned with 5 mL of MeCN/tubene 3:1 (v/v) prior to sample. (b) Tea spent was directly extracted with 15 mL of MeCN but not addition of 5 mL of boiled water; the next steps of sample preparation were the same as "made tea".

MATERIALS AND METHODS

Selection of Pesticides. In this study, the selected pesticides have the following characteristics: (1) widely applied pesticides in tea plantations, such as bifenthrin, cypermethrin, cyhalothrin, fenpropathrin, carbendazim, difenoconazole, and propargite; (2) banned but detectable pesticides, such as dicofol, fenvelerate, and methomyl;[20,21] (3) ability to be substituted and highly detectable pesticides, such as imidacloprid, acetamiprid, buprofezin, and thiamethoxam; (4) non-authorized but detectable pesticides, such as isocarbophos, triazophos, chlorpyrifos, and pyridaben;[22] (5) newly applied pesticides in tea plantations, such as indoxacarb. The maximum residual levels (MRLs) of 11 of the 19 pesticides have been established by the Chinese government,[23] whereas those of the other 8 pesticides have yet to be established. Although the MRLs of 8 pesticides have been established by the European Union or Japan, these MRLs cannot be used because MRLs vary with different countries or organizations.[4−6] For example, the MRLs of imidacloprid established by China, Japan, and EU are 0.5, 10, and 0.05 mg kg^{-1}, respectively. The MRLs of 19 pesticides formulated by China, Japan, and the European Union are shown in Table S-1, Supporting Information. Determining the transfer rates and then accessing the exposure level of pesticides through tea brewing are beneficial for establishment of standard MRLs of pesticides in tea.

Materials. HPLC-grade acetonitrile (MeCN), acetone, methanol, dichloromethane (DCM), and toluene were purchased from Sigma−Aldrich (Merck, Germany). Primary secondary amine-bond graphite carbon black SPE columns (PSA/GCB, 500 mg/6 mL) were purchased from Varian (USA). A Milli-Q plus ultrapure water system from Millipore (Miford, USA) was used throughout the study to obtain HPLC-grade water. Analytical-grade NaCl, anhydrous Na_2SO_4, and anhydrous $MgSO_4$ (Zhejiang Medicine, China) were baked for 3 h at 650 °C prior to use. Certified pesticide standards and triphenyl phosphate (TPP) were purchased from Sigma−Aldrich (Steinheim, Germany).

Positive samples (including 22 green tea and 18 oolong tea) were selected from over 2000 samples that were collected from 2012 to 2014 from supermarkets, monopoly stores, wholesale markets, or field experiments for pesticide dissipation. Collected samples were stored in the dark at 1−4 °C and returned to room temperature before testing. Organic tea samples containing no pesticides were used as controls to prepare matrix-matched standard solutions.

Tea Brewing. Tea brewing was prepared with boiled water for certain times in duplicate or triplicate. To simulate the traditional green tea and oolong tea brewing, 3.0 g of tea samples was transferred into a sensory evaluation cup and added with 150 mL of boiled water. The cup was sealed with a cap and allowed to stand for 5 min. Tea soup was transferred into a baker and cooled to room temperature, which was the first soup. The boiled water (150 mL) was reinfused with tea spent and then collected as the second infusion.

Sample Preparations. The overall sample preparation is presented in Figure 1.

Made Tea. Approximately 250 g of each tea sample was ground into powder and then sieved through a membrane with a pore size of 200 μm. Tea power (4.0 g) was placed in a 50 mL centrifuge tube and then mixed with 10 mL of boiled water for 15 min. A 50 μL amount of 20 μg mL^{-1} internal standard triphenyl phosphate (IS TPP) surrogate standard solution in acetonitrile was added into the mixtures prior to extraction. Target pesticides were extracted with 20 mLof MeCN by homogenization at 12 000 rpm for 2 min. Approximately 5 g of NaCl and 2 g of $MgSO_4$ were added into a centrifuge tube, vigorously shaken for 1 min by hand, and then centrifuged at 10 000 rpm for 2

DOI: 10.1021/jf506103d
J. Agric. Food Chem. 2015, 63, 723−730

Table 1. GC-MS/MS and UPLC Parameters of Retention Time (RT), Ion Transitions, Collision Energy (CE), and Declustering Pressure (DP)

GC-MS/MS						
no.	pesticides	RT (min)	ion transitions (m/z)	CE (eV)	ion transitions (m/z)	CE (eV)
1	chlorpyrifos	14.575	314 > 258	15	314 > 286	10
2	dichlorobenzophenone*	15.143	139 > 111	10	250 > 139	20
3	isocarbophos	20.187	289 > 136	10	230 > 212	5
4	triazophos	20.187	257 > 162	14	161 > 134	10
5	bifenthrin	22.658	181 > 141	20	181 > 153	20
6	fenpropathrin	23.033	181 > 152	25	209 > 181	10
7	cyhalothrin	24.272	181 > 152	25	181 > 127	25
		24.613				
8	cypermethrin	27.839	163 > 127	5	181 > 152	25
		28.056				
		28.149				
		28.243				
9	fenvalerate	29.534	167 > 125	10	125 > 89	20
		29.954				
	tpp		326 > 228	8	26 > 233	10

UPLC-MS/MS								
no.	pesticides	RT (min)	ion transitions (m/z)	DP (V)	CE (V)	ion transitions (m/z)	DP (V)	CE (V)
1	carbendazim	4.4	192.1 > 160.1	36	23	192.1 > 132.1	36	42
2	methomyl	4.6	163.1 > 88.1	11	14	163.1 > 88.1	18	12
3	thiamethoxam	4.7	292.1 > 211.2	31	18	292.1 > 181.2	32	29
4	imidacloprid	5.4	256.1 > 209.1	34	22	256.1 > 175.1	36	22
5	acetamiprid	5.9	223.1 > 56.1	41	25	223.1 > 126.1	42	27
6	indoxacarb	10.0	528.0 > 150.0	41	29	528.0 > 218.0	41	31
7	difenoconazole	10.1	406.1 > 251.1	61	34	406.1 > 337.2	58	24
8	buprofezin	10.3	306.2 > 201.0	25	20	306.2 > 116.1	25	20
9	propargite	10.8	368.1 > 231.0	35	20	368.1 > 175.1	35	20
10	pyridaben	11.1	365.2 > 147.2	62	34	365.2 > 309.2	59	17
	tpp	9.78	326.9 > 152.1	52	48	326.9 > 168.1	52	52

min. The supernatant (5 mL) was added in the GCB/PSA SPE column (SPE column was conditioned with 5 mL of MeCN/toluene 3:1 (v/v) prior to sample). Target pesticides were eluted from the SPE column with 25 mL of MeCN/toluene 3:1 (v/v). The elutes were evaporated into dryness and dissolved in 5 mL of acetone. Approximately 2 mL was filtered through a 0.22 μm membrane into an autosampler vial for GC-MS/MS analysis. Exactly 2 mL of the rest was solvent changed with 2 mL of methanol for UPLC-MS/MS analysis.

Tea Infusion. NaCl (10 g) was added into 100 mL of infusion and then transferred into a 250 mL separating funnel. IS TPP (50 μL) was added to achieve a concentration of 10 μg L^{-1} prior to extraction. DCM (100 mL) was used to extract the target pesticides from infusion by liquid−liquid extraction. The lower liquid (DCM phase) was filtered into a 150 mL heart-shaped bottle through a filter paper, which was filled with 15−20 g of Na_2SO_4. The infusion was re-extracted with 100 mL of DCM by LLE. Approximately 50 mL of DCM was used to wash Na_2SO_4 and then collected. The combined extractions (DCM phase from two LLE extraction) were evaporated into dryness at 40 °C and then dissolved with 5 mL of acetone. Approximately 2 mL of acetone solution was filtered through a 0.22 μm membrane into an autosampler vial for GC-MS/MS analysis. Exactly 2 mL of the rest was solvent changed with 2 mL of methanol for UPLC-MS/MS analysis.

Tea Spent. The tea spent (means all the solid residues of made tea after brewing twice) was cut into small pieces and then transferred into a 50 mL centrifuge tube. IS TPP (50 μL) was added to achieve a concentration of 25 μg kg^{-1} prior to extraction. Then, 15 mL of MeCN was added into the samples and then homogenized at 12 000 rpm for 2 min. The following steps were the same as the made tea in Made Tea section.

Preparation of Standard Solutions. Individual pesticide stock solutions at 1000 mg L^{-1} (200 mg L^{-1} for carbendazim) were prepared with acetone for 9 pesticides analyzed by GC-MS/MS and methanol for 10 pesticides analyzed by UPLC-MS/MS. IS TPP at 1000 mg L^{-1} was prepared with acetone. Intermediate mixed standard solutions at 40 mg L^{-1} and IS TPP solution at 20 mg L^{-1} were prepared by dilution of stock standard solutions with acetone (for GC-MS/MS) and methanol (for UPLC-MS/MS). All stock solutions and intermediate solutions were stored in the dark at −18 °C.

Matrix-matched standard solutions were prepared for quantification of 19 pesticides. A 5 mL amount of liquids obtained from blank sample (made tea, tea infusion, and spent tea) with the proposed treatment was evaporated to dryness. Afterward, 5 mL of solvent standard solutions (containing IS TPP at 50 μg L^{-1}) with concentrations ranging from 1 to 1000 μg L^{-1} for the pesticides analyzed by UPLC-MS/MS and 2 to 2000 μg L^{-1} for the pesticides analyzed by GC-MS/MS were added to produce solutions with final concentrations corresponding to the levels of matrix-matched calibration standards.

GC-MS/MS Analysis. Volatile and thermally stable pesticides, such as bifenthrin, chlorpyrifos, cyhalothrin, cypermethrin, dicofol (expressed as dichlorobenzophenone), fenpropathin, fenvalerate, isocarbophos, and triazophos, were analyzed by GC-MS/MS using a Bruker 450 GC coupled with a 300 MS. Separation was performed on a VF-5 MS column (30 m × 0.25 mm × 0.25 μm; Agilent, USA). The column temperature was maintained at 80 °C for 1.0 min and then ramped at 15 °C min^{-1} up to 180 °C, held for 2 min, and then at 5 °C min^{-1} up to 280 °C, held for 10 min. The injection volume was 1.0 μL, and splitless mode was adopted. Helium (99.99%) at a flow rate of 1.0 mL min^{-1} was used as the carrier gas and argon (99.99%) as the collision gas. The MSD transfer line, ion source, and manifold temperatures were 280, 230, and 40 °C, respectively. The triple-quadrupole mass spectrometer was operated in electron impact ionization mode. Two mass transitions were acquired for each

DOI: 10.1021/jf506103d
J. Agric. Food Chem. 2015, 63, 723−730

Table 2. Transfer Rates of 19 Pesticides from Made Tea into Infusion during Tea Brewing

pesticides by UPLC-MS/MS analysis	tea sample (numbers)	concentration in made tea (μg kg^{-1})	mean residual rate in tea spent ± SD (%)	mean transfer rate ± SD (%)		
				first soup	second soup	total soup
methomyl	green tea (3)	68−453	7.6 ± 5.7	75.1 ± 7.9	13.5 ± 4.6	91.3 ± 14.2
	oolong tea (4)	54−310	6.4 ± 5.3	73.7 ± 5.9	13.1 ± 6.2	89.5 ± 15.1
imidacloprid	green tea (8)	12−1030	11.2 ± 3.2	62.6 ± 8.2	12.6 ± 5.4	76.5 ± 8.5
	oolong tea (10)	30−1330	10.1 ± 4.7	64.5 ± 9.9	12.9 ± 6.7	77.3 ± 10.6
carbendazim	green tea (7)	49−1470	8.9 ± 4.0	63.2 ± 10.2	17.6 ± 7.4	79.6 ± 11.4
	oolong tea (7)	39−1211	11.6 ± 5.2	64.5 ± 13.7	16.1 ± 6.9	81.2 ± 13.3
acetamiprid	green tea (10)	43−1520	22.5 ± 8.4	53.8 ± 11.5	14.5 ± 7.2	68.3 ± 9.7
	oolong tea (10)	20−2780	24.0 ± 9.3	50.9 ± 9.7	16.7 ± 7.7	67.8 ± 11.5
difenoconazole	green tea (3)	29−371	92.7 ± 6.7	4.1 ± 2.6	4.7 ± 3.1	8.4 ± 3.3
	oolong tea (3)	22−288	90.4 ± 7.6	5.2 ± 3.4	3.4 ± 2.1	8.2 ± 2.5
propargite	green tea (3)	27−795	91.7 ± 9.3	0	0	0
	oolong tea (4)	25−638	93.3 ± 11.2	0	0	0
pyridaben	green tea (4)	219−1974	95.9 ± 8.1	0.8 ± 0.7	0.8 ± 0.6	1.1 ± 0.7
	oolong tea (3)	337−1550	96.3 ± 5.6	0.8 ± 0.6	0.8 ± 0.8	0.9 ± 0.8
buprofezin	green tea (6)	227−2550	85.2 ± 4.4	2.4 ± 0.9	2.3 ± 1.1	4.5 ± 1.3
	oolong tea (8)	316−6017	83.5 ± 6.1	2.3 ± 1.2	2.4 ± 0.7	4.2 ± 0.9
thiamethoxam	green tea (4)	47−675	4.1 ± 2.1	72.1 ± 10.4	14.5 ± 6.5	90.6 ± 10.2
	oolong tea (5)	39−515	3.5 ± 1.0	70.6 ± 14.4	17.8 ± 4.4	90.4 ± 11.7
indoxacarb	green tea (1)	28	7.1 ± 2.6	0	0	0
	oolong tea (0)					

pesticides by GC-MS/MS analysis	tea sample (numbers)	concentration in made tea, (mg kg^{-1})	tea spent	mean transfer rate ± SD (%)		
			mean residual rate ± SD (%)	first soup	second soup	total soup
chlorpyrifos	green tea (7)	218−1935	89.1 ± 11.5	0.4 ± 0.3	0.5 ± 0.3	0.8 ± 0.5
	oolong tea (6)	37−849	93.6 ± 11.5	0.3 ± 0.2	0.5 ± 0.4	0.7 ± 0.6
isocarbophos	green tea (3)	17−886	49.7 ± 22.8	26.1 ± 9.5	4.7 ± 2.9	31.4 ± 8.5
	oolong tea (4)	36−1705	54.0 ± 29.3	26.9 ± 8.2	5.4 ± 3.2	32.2 ± 9.2
triazophos	green tea (3)	19−906	49.8 ± 28.4	23.1 ± 4.6	6.7 ± 3.1	29.6 ± 8.9
	oolong tea (3)	15−838	56.0 ± 29.7	21.9 ± 5.2	5.7 ± 6.9	27.1 ± 10.2
dicofol	green tea (6)	11−2117	91.4 ± 8.4	2.2 ± 1.7	3.4 ± 0.7	5.4 ± 1.3
	oolong tea (8)	11−4139	93.4 ± 9.5	2.9 ± 1.4	4.0 ± 2.1	5.6 ± 1.7
bifenthrin	green tea (12)	334−3515	94.9 ± 7.6	0	0	0
	oolong tea (12)	437−7495	92.4 ± 8.5	0.5 ± 0.5	0.5 ± 0.5	0.9 ± 0.8
fenpropathrin	green tea (8)	15−1527	98.3 ± 1.3	0	0	0
	oolong tea (6)	34−995	97.1 ± 1.9	0	0	0
cyhalothrin	green tea (5)	27−525	98.3 ± 1.2	0	0	0
	oolong tea (5)	32−2165	97.6 ± 1.7	0	0	0
cypermethrin	green tea (4)	309−1094	93.8 ± 5.5	0	0	0
	oolong tea (6)	211−3465	89.4 ± 10.1	0	0	0
fenvalerate	green tea (2)	11−72	90.2 ± 9.3	0	0	0
	oolong tea (2)	46−1020	88.5 ± 9.9	0	0	0

compound, the higher sensitivity of which was used for quantification. The GC-MS/MS parameters for nine pesticides are shown in Table 1.

UPLC-MS/MS Analysis. UPLC-MS/MS was used to analyze 10 pesticides (acetamiprid, buprofezin, carbendazim, difenoconazole, imidacloprid, indoxacarb, methomyl, propargite, pyridaben, and thiamethoxam). A Waters Acquity UPLC system equipped with an applied Biosystems 3200 QTRAP system (ABI, USA) and controlled Analyst 1.5 software was used. Chromatography was performed on an Acquity UPLC HSS T3 column (100 mm × 2.1 mm i.d., 1.8 μm particle size, Waters, USA). The mobile phase consisted of water (A) and methanol (B) containing 0.1% formic acid (v/v). Gradient elution was performed as follows: 90% A initially, 5% A for 1−10 min (held for 2 min), and then 90% A for 12−13 min (held for 1 min). The flow rate, autosampler temperature, and injection volume were 0.25 mL min^{-1}, 4 °C, and 3 μL, respectively. Analysis was performed in electron spray ionization mode, and analytes were detected by selective reaction monitoring. The UPLC-MS/MS parameters of the 10 pesticides are shown in Table 1.

Calculating the Transfer Rate of Pesticides. The transfer rate was calculated by two models. In one model, the rates of the first and second brewing are added (eq 1), whereas the other model involves indirect calculation of the residual rate of pesticides in tea spent (eq 2)

$$R_{in} = C_{in} \times V_{in}/C \times M \times 100\% \quad (1)$$

$$Re_{spent} = C_{spent}/C \times 100\% \quad (2)$$

where R_{in} is the transfer rate (%), C_{in} is the concentration of pesticides in tea infusion (ng mL^{-1}), V_{in} is the volume of tea infusion (mL), C is the concentration of pesticides in made tea (μg kg^{-1}), M is the mass of made tea (g), Re_{spent}(%) is the residual rate calculated by spent tea, and C_{spent} is the concentration of pesticides in tea spent (μg kg^{-1}).

RESULTS AND DISCUSSION

Method Validation. Method validation was evaluated with selectivity, linearity, accuracy, precision, and limits of

DOI: 10.1021/jf506103d
J. Agric. Food Chem. 2015, 63, 723−730

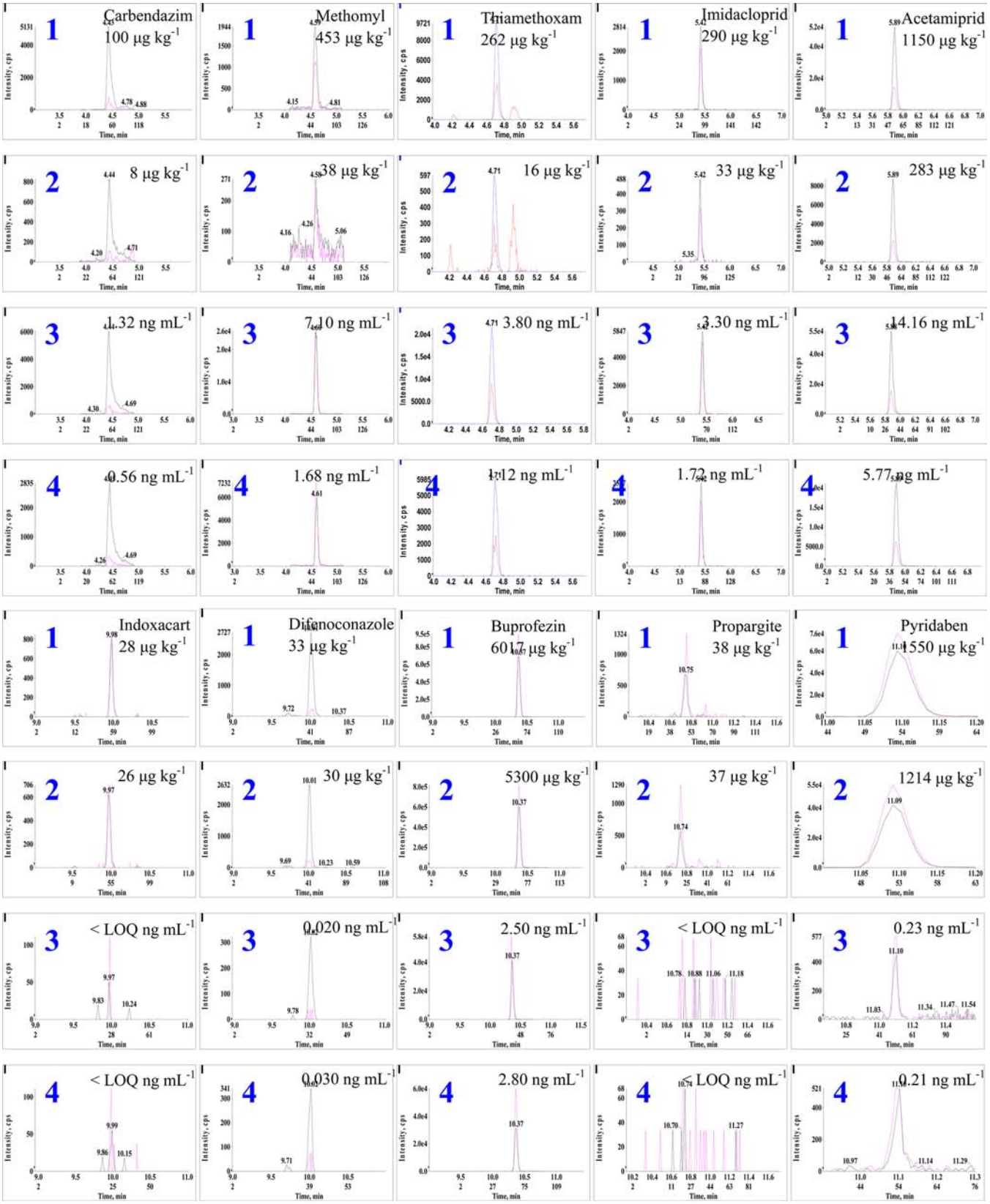

Figure 2. Typical UPLC-MS/MS chromatograms of 9 pesticides in made tea (1), tea spent (2), first soup (3), and second soup (4).

quantification (LOQs) (Table S-2, Supporting Information). Matrix-matched calibration solutions were used for quantification. No interfering peaks were observed for UPLC-MS/MS and GC-MS/MS because of the high selectivity of tandem mass (Figures 1 and 2, Supporting Information). The linearity obtained with $r^2 > 0.995$ for 10 pesticides analyzed by UPLC-MS/MS ranged from 1 to 1000 μg L^{-1} (except for methomyl, 8−2000 ug L^{-1}), whereas that obtained with $r^2 > 0.991$ for 9

DOI: 10.1021/jf506103d
J. Agric. Food Chem. 2015, 63, 723−730

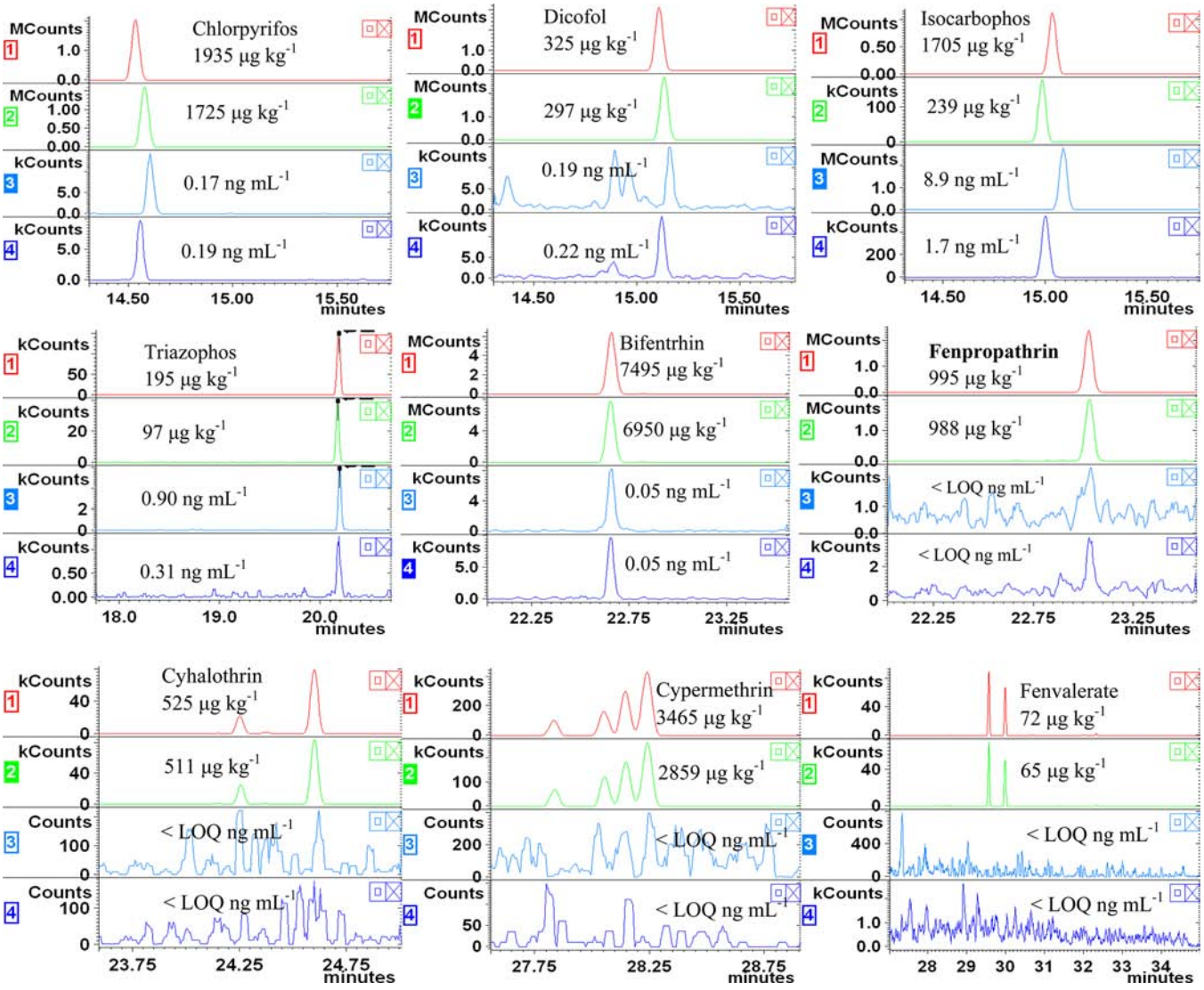

Figure 3. Typical GC-MS/MS chromatograms of 9 pesticides in made tea (1), tea spent (2), first soup (3), and second soup (4).

pesticides analyzed by GC-MS/MS was 2−2000 μg L^{-1} (except for cypermethrin, 4−2000 ug L^{-1}). The accuracy of the method was verified by measuring the recovery from blank samples of made tea, tea spent, and infusion spiked with the analytes at two concentrations of 80 and 400 μg kg^{-1} for both made tea and tea spent but 8 and 40 μg L^{-1} for tea infusion. For all matrices, satisfactory accuracy was achieved with a recovery of 80.4−119.3% for 10 pesticides analyzed by UPLC-MS/MS and 83.4−113.4% for 9 pesticides analyzed by GC-MS/MS. Method precision was determined five times (n = 5) at the two spiked levels. Good precision was obtained with relative standard deviations (RSDs) < 10% for all pesticides with two spiked levels. LOQs were defined when the signal-to-noise ratio was 10 times above the blank signal. The LOQs of 19 pesticides were 1−20 μg kg^{-1} in made tea and tea spent and 0.005−0.150 ng L^{-1} in tea soup.

Transfer Rate of Pesticides during Tea Brewing. The transfer rates of 19 pesticides are summarized in Table 2. The typical UPLC-MS/MS or GC-MS/MS chromatograms for 19 pesticides in made tea, spent, and infusion are shown in Figures 2 and 3, respectively. Compared with the pesticides analyzed by GC-MS/MS, those analyzed by UPLC-MS/MS were easier to leach into the infusion during tea brewing. The transfer rates of thiamethoxam, methomyl, carbendazim, imidacloprid, and acetamiprid were 90.4−90.6%, 89.5−91.3%, 79.6−81.2%, 76.5−77.3%, and 67.8−68.3%, respectively, which were much higher than those of the other 14 pesticides. These results were in accordance with previous studies by Hou et al.[8] and Wang et al.[9] but higher than the results from Gupta et al., where the transfer rates of acetamiprid and imidacloprid were lower than 50%.[24−26] This study is the first to report the transfer rates of pyridaben and buprofezin, which were all lower than 15%. Similar with the results from Cho et al.[27] the transfer rate of difenoconazole was found with nearly 8%. The lowest transfer rate of pesticides analyzed by UPLC-MS/MS was nearly 0% for propargite and indoxacart. Nearly no residues in tea infusion were observed for the pesticides (chlorpyrifos, dicofol, bifenthrin, fenpropathrin, cyhalothrin, cypermethrin, and fenvelerate) analyzed by GC-MS/MS. The results were in accordance with previous studies by Manikandan et al.,[10] Jaggi et al.,[11] and Tewary et al.[28] The transfer rates of isocarbophos (31.4−32.2%) and triazophos (27.1−29.6%) were also first reported in this study.

DOI: 10.1021/jf506103d
J. Agric. Food Chem. 2015, 63, 723−730

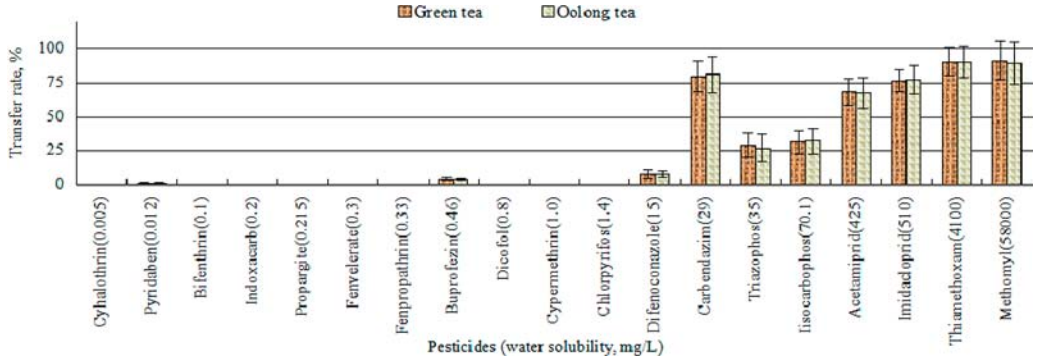

Figure 4. Relationship between water solubility and transfer rates of pesticides during tea brewing.

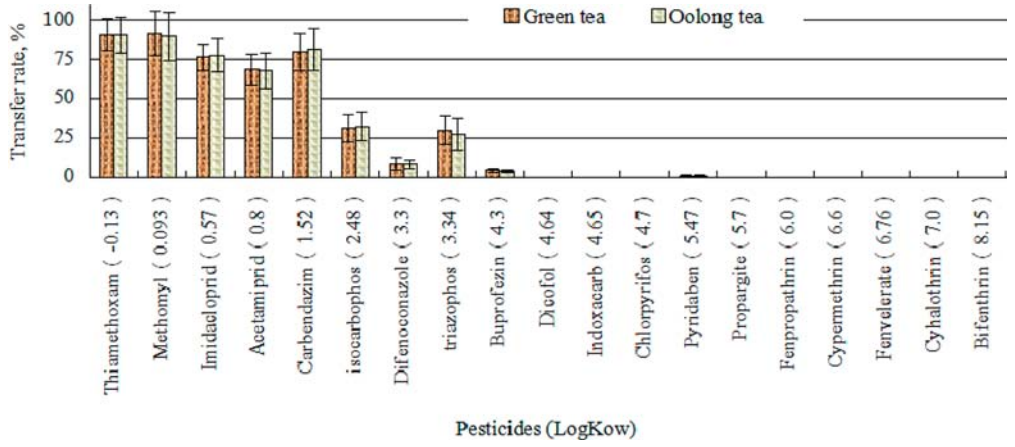

Figure 5. Relationship between octanol–water partition coefficient (Logkow) and transfer rates of pesticides during tea brewing.

In general, the transfer rates of 19 pesticides have no significant relation with their concentrations in made tea. For example, three tea samples containing acetamiprid at 43, 571, and 1150 μg kg^{-1} had transfer rates of 69.5%, 76.2%, and 72.1%, respectively. Similar to previous studies,[8] the present study found no significant difference between green and oolong teas. The deviations in the transfer rates from the same tea type were much higher than those between green tea and oolong tea samples.

Tea is usually brewed twice because its taste and aroma in the first and second infusions are favorable, but both taste and aroma rapidly decrease in the third or subsequent infusions. Thus, this study investigated the transfer rates of 19 pesticides during the first and second brewing. For pesticides with transfer rates higher than 20%, the ratios between the first and the second soups were 2:1–5:1. For the pesticides with transfer rates lower than 10%, transfer rates were similar during the first and second brewing. The transfer rates determined by indirect calculation of the residual rate in tea spent ($R_{in} = 1 - Re_{spent}$) were higher than the total transfer rates of the first and second infusions. This result indicated that suspended particles were leached into tea infusion and the mass of tea spent was lower than the original amount of made tea (3.0 g). The amounts of pesticides exposed to human during tea brewing should be indirectly calculated by the residual rate of tea spent since the suspended particles containing pesticides could also be adsorbed by humans during tea drinking.

Relationship between Transfer Rates and Physicochemical Properties of Pesticides. Water solubility is one of the crucial physical and chemical parameters that influences the transfer rates of pesticides from made tea to infusion because water is the most important carryover of pesticides during tea brewing. The relationship between transfer rate and water solubility of 19 pesticides is shown in Figure 4. The transfer rates increased as the water solubility of the pesticides increased. Low transfer rates of <15% were observed when the water solubility of pesticides was lower than 20 mg L^{-1}, but the rates increased from 22.6% (triazophos, 35 mg L^{-1}) to 90.6% (thiamethoxam, 4100 mg L^{-1}). This result indicated that the water solubility of certain pesticides at 20 mg L^{-1} could be a demarcation line of the transfer rate. However, carbendazim, methomyl, and buprofezin showed a different relationship between transfer rate and water solubility. Carbendazim with a low solubility of 29 mg L^{-1} exhibited a high transfer rate of 79.6–81.2%, whereas methomyl with an extrahigh solubility of 58 000 mg L^{-1} demonstrated a similar transfer rate of 89.5–91.3% to thiamethoxam at 4100 mg L^{-1} (90.4–90.6%). This result indicated that the transfer rate depended on other physicochemical properties of pesticides, such as Logkow.[29−32]

The relationship between the octanol–water partition coefficient (Logkow) and the transfer rate of 19 pesticides is shown in Figure 5. Obviously, the transfer rates of pesticides decreased with increasing LogKow. Five pesticides (thiamethoxam, methomyl, imidacloprid, acetamiprid, and carbendazim) with low LogKow values were mostly leached from made tea into infusion, whereas the pesticides (pyrethoid pesticides, dicofol, propargite, and indoxacarb) with high LogKow values were mostly retained in tea spent. The transfer rates dropped from approximately 80% to 30% when the LogKow value increased from 1.52 (carbendazim) to 2.48 (isocarbophos).

DOI: 10.1021/jf506103d
J. Agric. Food Chem. 2015, 63, 723–730

This result indicated that LogKow at approximately 2.0 can be a demarcation line of transfer rate.

Therefore, pesticides with low octanol−water partition coefficients (Logkow) or high water solubility were easily leached into tea infusion. The pesticides with LogKow at less than 2.0 and water solubility at higher than 20 mg L^{-1} are more exposed for human being by drinking tea because of their high transfer rates. The results from this study can be used as a guide in the application of pesticides to tea trees and establishment of MRLs of pesticides in tea to reduce pesticide exposure in humans.

■ ASSOCIATED CONTENT

Supporting Information

Maximum residue limits of 19 pesticides. Data of method validation. UPLC-MS/MS and GC-MS/MS chromatograms of analytes from matrix matched standard solutions, blank samples, and spiked samples. This material is available free of charge via the Internet at http://pubs.acs.org.

■ AUTHOR INFORMATION

Corresponding Authors

*E-mail: LiuXin@mail.tricaas.com.

*E-mail: Lchy@mail.tricaas.com.

Funding

This work was supported by the earmarked fund for Modern Agro-Industry Technology Research System (NYCYTX-26) and Innovative Research Term in Chinese Academy of Agricultural Sciences.

Notes

The authors declare no competing financial interest.

■ REFERENCES

(1) Harbowy, M. E.; Balentine, D. A. Tea chemistry. *Crit. Rev. Plant Sci.* **1997**, *16* (5), 415−480.

(2) Nie, S. P.; Xie, M. Y. A review on the isolation and structure of tea polysaccharides and their bioactivities. *Food Hydrocolloids* **2011**, *25*, 144−149.

(3) Hodgson, J. M.; Croft, K. D. Tea flavonoids and cardiovascular health. *Mol. Aspects Med.* **2010**, *31*, 495−502.

(4) GB 2763-2014. *National food safety standard-Maximum residue limits for pesticide in food*. 2014.

(5) The Japan Food Chemical Research Foundation. Table of MRLs in Foods (Tea); http://www.m5.ws001.squarestart.ne.jp/foundation/foodtl.php?f_inq=13200, accessed by Nov 26, 2014.

(6) EU Pesticides Database. Pesticide EU-MRLs. http://ec.europa.eu/sanco_pesticides/public/?event=homepage; accessed by Nov 26, 2014.

(7) CODEX alimentarius. Pesticide Residues in Food and Feed. http://www.codexalimentarius.net/pestres/data/pesticides/results.html?pesticideText=&pestClassId=-1&commodityText=tea&commodityCode=&searchBy=com; accessed by Nov 26, 2014.

(8) Hou, R. Y.; Hu, J. F.; Qian, X. S.; Su, T.; Wang, X. H.; Zhao, X. X.; Wan, X. C. Comparison of the dissipation behaviour of three neonicothinoids insecticides in tea. *Food Addit. Contam., Part A.* **2013**, *30* (10), 1761−1769.

(9) Wang, J.; Cheung, W.; Leung, D. Determination of pesticide residue transfer rates (percent) from dried tea leaves to brewed tea. *J. Agric. Food Chem.* **2014**, *62*, 966−983.

(10) Manikandan, N.; Seenivasan, S.; Ganapathy, M. N. K.; Muraleedharan, N. N.; Selvasundaram, R. Leaching of residues of certain pesticides from black tea to brew. *Food Chem.* **2009**, 522−525.

(11) Jaggi, S.; Sood, C.; Kummar, V.; Ravindranath, S. D.; Shanker, A. Leaching of pesticides in tea brew. *J. Agric. Food Chem.* **2001**, *49*, 5479−5483.

(12) Chen, L.; Chen, J. F.; Guo, Y.; Li, J. R.; Yang, Y. Q.; Xu, L. J.; Fu, F. Study on the simultaneous determination of seven benzoylurea pesticides in Oolong tea and their leaching characteristics during infusing process by HPLC-MS/MS. *Food Chem.* **2014**, *143*, 405−410.

(13) Huang, Z.; Zhang, Y.; Wang, L.; Ding, L.; Wang, M.; Yan, H.; Li, Y.; Zhu, S. Simulanteous determination of 103 pesticide residues in tea samples by LC-MS/MS. *J. Sep. Sci.* **2009**, *32*, 1294−1301.

(14) Chen, G.; Cao, P.; Liu, R. A multi-residue method for fast determination of pesticides in tea by ultra performance liquid chromatography-electrospray tandem mass spectrometry combined with modified QuEChERS sample preparation procedure. *Food Chem.* **2011**, *125*, 1406−1411.

(15) Huang, Z.; Li, Y.; Chen, B.; Yao, S. Simultaneous determination of 102 pesticide residues in Chinese tea by gas chromatography-mass spectrometry. *J. Chromatogr, B* **2007**, *853*, 154−162.

(16) Zhu, P.; Miao, H.; Du, J.; Zou, J.; Zhang, G.; Zhao, Y.; Wu, Y. Organochlorine pesticides and pyrethroids in Chinese tea by screening and confirmatory detection using GC-NCI-MS and GC-MS/MS. *J. Agric. Food Chem.* **2014**, *62*, 7092−7100.

(17) Feng, J.; Tang, H.; Chen, D.; Li, L. Monitoring and risk assessment of pesticide residues in tea samples from China. *Hum. Ecol. Risk Assess.* **2015**, *00*, 1−15.

(18) Wang, X.; Cheng, J.; Zhou, H.; Wang, X.; Cheng, M. Development of a simple combining apparatus to perform a magnetic stirring-assisted diepersive liquid-liquid microextraction and its application for the analysis of carbamate and organophosphorus pesticides in tea drinks. *Anal. Chim. Acta* **2013**, *787*, 71−77.

(19) Xu, X.; Yu, C.; Han, J.; Li, J.; El-sepai, F.; Zhu, Y.; Huang, B.; Cai, Z.; Wu, H.; Ren, Y. Multi-residue analysis of pesticides in tea by online SEG-GC/MS. *J. Sep. Sci.* **2011**, *34*, 210−216.

(20) Bulletin No. 199th, The People's Republic of China Ministry of Agriculture, June 5, 2002.

(21) Bulletin No. 1586th, The People's Republic of China Ministry of Agriculture, Oct 31, 2011.

(22) China Pesticide information network; http://www.chinapesticide.gov.cn/service/aspx/B4.aspx; accessed by Nov 26, 2014.

(23) National Standard of the People's Republic of China. GB 2763-2014. National food safety standard-Maximum residue limits for pesticide in food. 2014.

(24) Gupta, M.; Sharma, A.; Shanker, A. Dissipation of imidaclorprid in Orthodox tea and its transfer from made tea to infusion. *Food Chem.* **2008**, *106*, 158−164.

(25) Gupta, M.; Shanker, A. Fate of imidacloprid and acetamiprid residues during black tea manufacture and transfer into tea infusion. *Food Addit. Contam., Part A.* **2009**, *26* (2), 157−163.

(26) Gupta, M.; Shanker, A. Persistence of acetamiprid in tea and its transfer from made tea to infusion. *Food Chem.* **2008**, 805−810.

(27) Cho, S. K.; El-Aty, A. M. A.; Rahman, M. M.; Choi, J. H.; Shim, J. H. Simultaneous multi-determination and transfer of eight pesticide residues from green tea leaves to infusion using gas chromatography. *Food Chem.* **2014**, *165*, 532−539.

(28) Tewary, D. K.; Kumar, V.; Ravindranath, S. D.; Shanker, A. Dissipation behaviour of bifenthrin residues in tea and its brew. *Food Control.* **2005**, *16*, 231−237.

(29) Ozbey, A.; Uygun, U. Behaviour of some organophosphorus pesticide residues in peppermint tea during the infusion process. *Food Chem.* **2007**, *104*, 237−241.

(30) Satheshkumar, A.; Senthurpandian, V. K.; Shanmugaselvan, V. A. Dissipation kinetics of bifenazate in tea under tropical conditions. *Food Chem.* **2014**, *145*, 1092−1096.

(31) Pérez-parada, A.; González, J.; Pareja, L.; Geis-Asteggiante, L.; Colazzo, M.; Niell, S.; Besil, N.; González, G.; Cesio, V.; Heinzen, H. Transfer of pesticides to the brew during mate drinking process and their relationship with physicochemical properties. *J. Environ. Sci. Health B* **2010**, *45* (8), 796−803.

(32) Xue, J.; Li, H.; Liu, F.; Xue, J.; Chen, X.; Zhan, J. Transfer of difenocozole and azoxustrobin residues from chrysanthemum flower tea to its infusion. *Food Addit. Contam., Part A.* **2014**, *31* (4), 666−675.

DOI: 10.1021/jf506103d
J. Agric. Food Chem. 2015, 63, 723−730

JOURNAL OF AGRICULTURAL AND FOOD CHEMISTRY

Article

pubs.acs.org/JAFC

Anomericity of T-2 Toxin-glucoside: Masked Mycotoxin in Cereal Crops

Susan P. McCormick,*[,†] Takayuki Kato,[‡] Chris M. Maragos,[†] Mark Busman,[†] Veronica M. T. Lattanzio,[§] Gianni Galaverna,[#] Chiara Dall-Asta,[#] David Crich,[‡] Neil P. J. Price,[⊥] and Cletus P. Kurtzman[†]

[†]Bacterial Foodborne Pathogens and Mycology Research Unit, National Center for Agricultural Utilization Research, U.S. Department of Agriculture, Peoria, Illinois 61604, United States

[‡]Department of Chemistry, Wayne State University, Detroit, Michigan 48202, United States

[§]Institute of Sciences of Food Production, National Research Council of Italy, Bari 70126, Italy

[#]Department of Food Science, University of Parma, Parma 43124, Italy

[⊥]Renewable Product Technology Research Unit, National Center for Agricultural Utilization Research, U.S. Department of Agriculture, Peoria, Illinois 61604, United States

Supporting Information

ABSTRACT: T-2 toxin is a trichothecene mycotoxin produced when *Fusarium* fungi infect grains, especially oats and wheat. Ingestion of T-2 toxin contaminated grain can cause diarrhea, hemorrhaging, and feed refusal in livestock. Cereal crops infected with mycotoxin-producing fungi form toxin glycosides, sometimes called masked mycotoxins, which are a potential food safety concern because they are not detectable by standard approaches and may be converted back to the parent toxin during digestion or food processing. The work reported here addresses four aspects of T-2 toxin-glucosides: phytotoxicity, stability after ingestion, antibody detection, and the anomericity of the naturally occurring T-2 toxin-glucoside found in cereal plants. T-2 toxin-β-glucoside was chemically synthesized and compared to T-2 toxin-α-glucoside prepared with *Blastobotrys muscicola* cultures and the T-2 toxin-glucoside found in naturally contaminated oats and wheat. The anomeric forms were separated chromatographically and differ in both NMR and mass spectrometry. Both anomers were significantly degraded to T-2 toxin and HT-2 toxin under conditions that mimic human digestion, but with different kinetics and metabolic end products. The naturally occurring T-2 toxin-glucoside from plants was found to be identical to T-2 toxin-α-glucoside prepared with *B. muscicola*. An antibody test for the detection of T-2 toxin was not effective for the detection of T-2 toxin-α-glucoside. This anomer was produced in sufficient quantity to assess its animal toxicity.

KEYWORDS: *mycotoxins, trichothecene, masked mycotoxins, ELISA, T-2 toxin, T-2 toxin-glucoside*

INTRODUCTION

Species of the genus *Fusarium* are among the most destructive fungal plant pathogens known and are responsible for major yield losses during cultivation of wheat, maize, barley, and soybeans.[1−4] Many species of *Fusarium* produce mycotoxins as they grow parasitically within the plant, and ingestion of contaminated grain and food products processed from this grain causes acute and chronic health problems for both humans and animals.[5,6] Some species of *Fusarium* produce trichothecenes, sesquiterpenoid mycotoxins that inhibit eukaryotic protein synthesis and other cellular functions in animals that ingest contaminated feed.[7] Type A trichothecenes (e.g., T-2 toxin, HT-2 toxin, diacetoxyscirpenol) are of particular concern because they are considerably more toxic than the type B group (e.g., deoxynivalenol and nivalenol). As part of their defense response to xenobiotics, plants can modify the structure of several mycotoxins, including trichothecenes, by conjugation to sugars, organic acids, or sulfates, which reduce their phytotoxicity and may facilitate their sequestration.[8−12] Whereas conjugation to sugars may protect plants from the ill effects of the toxins,[13] these so-called "masked mycotoxins" present a potential food safety concern because, although toxicological data are scarce, several studies highlight the potential threat to consumer safety from these substances.[9,14−17] In particular, the possible hydrolysis of masked mycotoxins back to their toxic parents during mammalian digestion is of considerable concern.

Structurally T-2 toxin, **1**, R = Ac (Figure 1) is (2α,3α,4β,8α)-4,15-bis(acetyloxy)-3-hydroxy-12,13-epoxytrichothec-9-en-8-yl 3-methylbutanoate, which in animals is known to be predominantly metabolized to the 4-*O*-deacetylated form known as HT-2 toxin, **1**, R = H (Figure 1).[10,11] Glucoside conjugates of T-2 toxin have been reported in *Fusarium*-infected grain and *Fusarium* culture material,[10,11] although to date the anomericity of the 3-*O*-linked glucosyl group is unknown. T-2 toxin-α-glucoside, **2**, and T-2 toxin-β-glucoside, **3** (Figure 1), are anticipated to have very different physical properties. More importantly, the relative toxicities of the two anomers are as yet unknown, and the ability to test the naturally occurring form needs to be addressed.

One of the most studied masked trichothecenes is deoxynivalenol-3-glucoside, which has been reported from

Received: September 30, 2014
Revised: December 15, 2014
Accepted: December 18, 2014
Published: December 18, 2014

ACS Publications © 2014 American Chemical Society

DOI: 10.1021/jf504737f
J. Agric. Food Chem. 2015, 63, 731−738

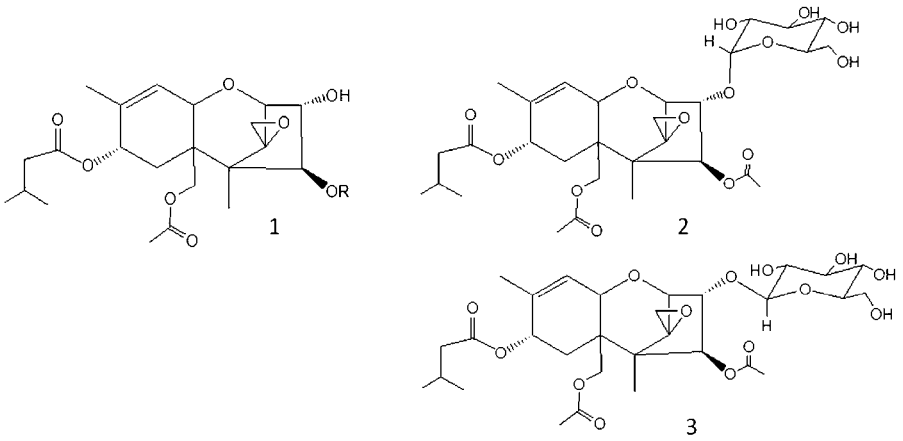

Figure 1. Structures of T-2 toxin, **1** (R = Ac), HT-2 toxin, **1** (R = H), T-2 toxin-α-glucoside, **2**, and T-2 toxin-β-glucoside, **3**.

contaminated cereal crops[18] and in food products derived from these crops.[19] Nuclear magnetic resonance (NMR) studies have shown that the naturally occurring glucoside is deoxynivalenol-3-β-glucoside.[8,20] Plant glucosyltransferase genes that control the conversion of deoxynivalenol to deoxynivalenol-3-β-glucoside have been identified,[21−23] and a barley glucosyltransferase gene has been engineered into wheat to improve resistance to *Fusarium* head scab. In addition, a deoxynivalenol glucosyltransferase gene has been cloned and expressed in yeast.[21] As a result, deoxynivalenol-3-β-glucoside has been prepared using yeast expression and has been available for studies on its stability during food processing and the digestive fate of this masked mycotoxin.[17,24]

Although initial studies reported that deoxynivalenol-3-β-glucoside is relatively stable to gastric conditions,[17,24,25] it was recently reported that masked mycotoxins can be deconjugated by human colon microbiota, thus releasing their parent forms.[14,26] Because parent toxins may be absorbed in the intestine, this cleavage should be considered of toxicological relevance depending on the colonic absorption of the target compound.[14]

We have recently shown that three species of *Blastobotrys* are able to biotransform T-2 toxin to T-2 toxin-α-glucoside, **2** (Figure 1),[27] and these yeast species appeared to provide an efficient way to produce the material necessary to study the digestive fate or animal toxicity of T-2 toxin-glucoside and related compounds,[27] as well as develop methods for their detection.[28] It was first important to determine which anomeric form of T-2 toxin-glucoside was produced in *Fusarium*-contaminated cereals before proceeding with larger scale studies using the yeast biotransformation product. For this reason, T-2 toxin-β-glucoside, **3** (Figure 1), was chemically synthesized, and along with T-2 toxin-α-glucoside, **2** (Figure 1), the yeast biotransformation product, compared to the T-2 toxin-glucoside found in contaminated grain. We present here a comparison of the chromatographic and spectroscopic properties of the two anomeric forms, their relative reactivities to antibodies prepared with T-2 toxin-α-glucoside[28] or T-2 toxin, their relative phytotoxicities, the stabilities and bioavailabilities of these masked mycotoxins after ingestion, and the anomeric form of the naturally occurring T-2 toxin-glucoside. These results become particularly relevant if international standards are developed for the detection and quantitation of T-2 toxin and T-2 toxin-glucoside in cereal grains and products made from them.

MATERIALS AND METHODS

NMR Spectroscopy. NMR experiments were performed with acetone-d_6 as the solvent on a Bruker Avance AMX 500 spectrometer (Bruker BioSpin Corp., Billerica, MA, USA) operating at 500.11 MHz using a standard 5 mm *z*-gradient BBI probe at 27 °C. Chemical shifts are reported as parts per million from tetramethylsilane calculated from the lock solvent. The deuterated solvents used were obtained from Cambridge Isotope Laboratories (Andover, MA, USA). The pulse sequences used were those supplied by Bruker, and processing was done with the Bruker TOPSPIN software package (v. 1.3). Additional NMR experiments with tetra-*O*-TIPS-β-glucosyl T-2 toxin, **6**, and T-2 toxin-β-glucoside, **3**, were performed on an Agilent 600 MHz NMR spectrometer (Agilent, Santa Clara, CA, USA).

Naturally Contaminated Cereal Samples. One wheat and one oat sample were extracted for comparison with T-2 toxin-glucoside standards. Samples were finely ground with a Tecator Cyclotec 1093 (International PBI, Milan, Italy) laboratory mill equipped with a 500 mm sieve. Ten grams of each ground sample was extracted with 30 mL of acetonitrile/water (84:16 v/v) by orbital shaking for 2 h. After filtration through filter paper, 10 mL of extract was cleaned with a Mycosep 227 column (Romer Laboratories, Union, MO, USA). Purified extract (6 mL, equivalent to 2 g of sample) was dried under an air stream at 50 °C.

Liquid Chromatography−Mass Spectrometry (LC-MS) Analysis. Extracts of naturally contaminated cereals or T-2 toxin-glucoside standards were analyzed by LC coupled to tandem mass spectrometry (MS/MS) as previously described.[10,11] LC-MS/MS analyses were performed by a QTrap MS/MS system, from Applied Biosystems (Foster City, CA, USA) equipped with an electrospray ionization (ESI) interface and an 1100 series micro-LC system comprising a binary pump and a microautosampler from Agilent Technologies (Waldbronn, Germany). The column used was a 150 × 3 mm i.d., 4 μm, Synergi Hydro, with a 4 mm × 2 mm i.d., 10 μm, Aqua C18 guard column (Phenomenex, Torrance, CA, USA). The flow rate of the mobile phase was 200 μL/min, whereas the injection volume was 20 μL. Eluent A was water and eluent B was methanol, both containing 5 mM ammonium acetate. The elution was performed by changing the mobile phase composition as follows. Eluent B was increased from 20 to 40% in 3 min, then increased to 63% in 35 min, and kept constant for 9 min. For column re-equilibration, eluent B was decreased to 20% in 1 min and kept constant for 9 min. For MS analyses, the ESI interface was used with the following settings: temperature, 350 °C; curtain gas, nitrogen, 30 psi; nebulizer gas, air, 10 psi; auxiliary gas, air, 30 psi; ion spray voltage, +4500 V, positive ion mode.

The MS was operated in enhanced product ion (EPI) mode, applying a collision energy (CE) for stimulation of ion fragmentation of 10, or multiple reaction monitoring (MRM) mode to observe several distinctive ions produced upon fragmentation of the toxin with ammonium adduct $[M + NH_4]^+$ ion. For T-2 toxin-glucoside, the parent ion (m/z 646) and fragment ions were monitored to observe

DOI: 10.1021/jf504737f
J. Agric. Food Chem. 2015, 63, 731−738

elution of the separated T-2 toxin conjugates. Operation of the LC-MS/MS instrument and interpretation of the acquired data were done utilizing the Analyst (ABSCIEX) software provided by the MS instrument manufacturer.

Preparation of T-2 Toxin-glucosides. T-2 toxin-glucosides were prepared using T-2 toxin that had been isolated and purified from liquid cultures of *Fusarium sporotrichioides* strain 5493cos9-1#11 as described previously.[27] T-2 toxin-α-glucoside, **2** (optical rotation, $[\alpha]_D^{20}$ = +79.74, *c* 0.153, CH_3OH), was prepared by feeding T-2 toxin to *Blastobotrys muscicola* cultures as described previously.[27] T-2 toxin-β-glucoside, **3**, was synthesized as described below (Figure 2).

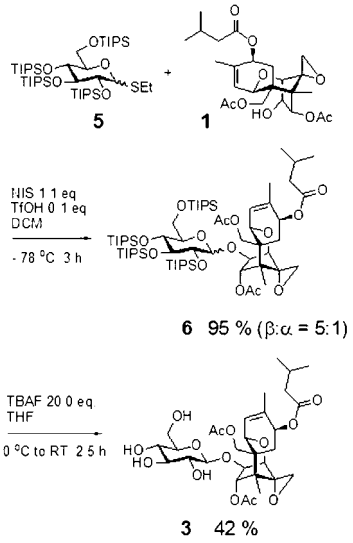

Figure 2. Synthesis of T-2 toxin-β-glucoside, **3**.

Ethyl 2,3,4,6-Tetra-*O*-acetyl-1-thio-D-glucopyranoside, 4.[29] Pentaacetyl-β-glucopyranose (1.0 g, 2.56 mmol) was dissolved in dichloromethane (20 mL), and ethanethiol (220 μL, 3.07 mmol) was added followed by BF_3OEt (1.6 mL, 12.8 mmol) at ambient temperature under an argon atmosphere. After 2 h, the reaction mixture was diluted with dichloromethane and washed with saturated sodium bicarbonate. The aqueous phase was extracted with dichloromethane, and the combined organic phase was washed with brine and dried over sodium sulfate. The filtrate was concentrated, and the residue was purified by column chromatography over silica gel (hexane/ethyl acetate, 1:1), giving 660 mg (67%) of a colorless oil in the form of a 1:1 α,β-mixture.

Ethyl 2,3,4,6-Tetra-*O*-triisopropylsilyl-1-thio-D-glucopyranoside, 5.[30] To a solution of **4** (660 mg, 1.68 mmol) in methanol (16.5 mL) was added sodium methoxide (10 mg, 0.17 mmol) at ambient temperature. After 1 h, the reaction mixture was neutralized with Amberlite 120. The resin was filtered off, and the filtrate was concentrated to give a colorless oil (340 mg),[31] which was dissolved in 2,6-lutidine (15 mL) (Sigma-Aldrich, St. Louis, MO, USA) and treated with triisopropylsilyl trifluoromethanesulfonate (2 mL, 4.9 mmol) (Sigma-Aldrich). The reaction mixture was heated to 130 °C, and after 1.5 h, further triisopropylsilyl trifluoromethanesulfonate (2 mL, 4.9 mmol) was added. The reaction mixture was maintained at 130 °C for 2 h, then further triisopropylsilyl trifluoromethanesulfonate (2 mL, 4.9 mmol) was added. After 2 h, the reaction mixture was cooled to room temperature, diluted with hexane, and washed with 0.1 M HCl until the water phase remained acidic. The organic layer was washed with brine and dried over sodium sulfate. The filtrate was concentrated and purified by column chromatography over silica gel eluting with hexane, a colorless oil (680 mg, 53%) as a 1:1 mixture of α,β-isomers.

Tetra-*O*-TIPS-β-glucosyl T-2 Toxin, 6. A solution of **5** (110 mg, 0.13 mmol) and T-2 toxin (40 mg, 0.086 mmol) was dissolved in dry dichloromethane (0.4 mL) with 3 Å acid-washed molecular sieves (Alfa Aesar, Ward Hill, MA, USA). The reaction mixture was cooled to −78 °C under an argon atmosphere, and then *N*-iodosuccinimide (26 mg, 0.15 mmol) (Chem-Impex Int. Inc., Wood Dale, IL, USA) was added. After 0.5 h, trifluoromethanesulfonic acid (2.3 μL, 0.04 mmol) (Sigma-Aldrich) was added to the cold solution. After 3 h, the reaction mixture was quenched with triethylamine (EMD, Philadelphia, PA, USA), and the molecular sieves were filtered off. The filtrate was concentrated and purified by column chromatography over silica gel (eluent, hexane/ethyl acetate 4:1) to give a colorless oil (100 mg, 95%) as a 1:5 mixture of α,β-isomers.

^{1}H NMR (600 MHz in $CDCl_3$) for β-isomer: δ 5.66 (d, *J* = 3.3 Hz, 1H, H-4), 5.63 (d, *J* = 5.9 Hz, 1H, H-10), 5.27 (d, *J* = 5.5 Hz, 1H, H-8), 4.91 (d, *J* = 5.9 Hz, 1H, H-26), 4.31 (d, *J* = 12.1 Hz, 1H, H-15a), 4.27 (dd, *J* = 4.8, 3.67 Hz, 1H, H-3), 4.10 (d, *J* = 5.5 Hz, 1H, H-11), 4.08 (overlapped with H-15b, 1H, H-28), 4.07 (d, *J* = 12.5 Hz, 1H, H-15b), 3.95 (d, *J* = 2.9 Hz, 1H, H-29), 3.90 (d, *J* = 5.9 Hz, 1H, H-27), 3.89 (d, *J* = 5.8 Hz, 1H, H-30), 3.84 (d, *J* = 5.1 Hz, 2H, H-31a,b), 3.73 (d, *J* = 4.8 Hz, 1H, H-2), 2.92 (d, *J* = 4.0 Hz, 1H, H-13a), 2.75 (d, *J* = 4.0 Hz, 1H, H-13b), 2.29 (dd, *J* = 15.0, 5.9 Hz, 1H, H-7a), 2.09 (m, 1H, H-18), 2.07 (s, 1H, H-23), 2.05 (m, 1H, H-19), 2.00 (s, H-25), 1.99 (overlapped with H-25, 1H, H-7b), 1.72 (s, H-16), 0.95 (d, *J* = 6.2 or 5.1 Hz, 1H, H-20), 0.94 (d, *J* = 6.2 or 5.1 Hz, 1H, H-21), 0.67 (s, H-14); ^{13}C NMR (150 MHz in CD_2Cl_3) δ 172.4 (C-17), 170.2 (C-22), 169.8 (C-24), 135.1 (C-9), 124.1 (C-10), 103.4 (C-26), 83.5 (C-30), 82.8 (C-3), 80.6 (C-4), 79.5 (C-2), 78.0 (C-28), 77.3 (C-27), 71.1 (C-29), 68.0 (C-8), 66.8 (C-11), 65.7 (C-31), 64.3 (C-15), 64.1 (C-12), 48.5 (C-5), 46.7 (C-13), 43.4 (C-18), 43.0 (C-6), 26.9 (C-7), 25.7 (C-19), 22.1 (C-20), 22.1 (C-21), 20.9 (C-25), 20.6 (C-23), 20.1 (C-16), 6.2 (C-14); HRMS-ESI (*m*/*z*) $[M + Na]^+$ calcd for $C_{66}H_{124}O_{14}Si_4Na$ 1275.7966, found 1275.7947.

T-2 Toxin-β-glucoside, 3. The above α,β-mixture of **6** (100 mg, 0.08 mmol) was dissolved in THF (1.0 mL) and treated at 0 °C with tetrabutylammonium fluoride (1.6 mL, 1.6 mmol) (Acros-Thermo Fisher Scientific Inc., Waltham, MA, USA). The reaction mixture was allowed to warm to room temperature and stirred for 2.5 h, after which it was concentrated and purified by column chromatography over silica gel (eluent, chloroform/methanol, 8:1) to give a colorless oil (42 mg, 84%) of a 1:5 α,β-mixture. Further purification of this mixture by C18 HPLC (water−acetonitrile 25−40%) and freeze-drying gave 21 mg (42%) of the pure β-isomer, **3**, as a white amorphous powder.

^{1}H NMR (600 MHz in CD_3OD) δ 5.96 (d, *J* = 3.0 Hz, 1H, H-4), 5.77 (d, *J* = 6.00 Hz, 1H, H-10), 5.31 (d, *J* = 5.6 Hz, 1H, H-8), 4.46 (dd, *J* = 4.9, 3.2 Hz, 1H, H-3), 4.43 (d, *J* = 7.7 Hz, 1H, H-26), 4.37 (d, *J* = 6.2 Hz, 1H, H-11), 4.36 (d, *J* = 12.7 Hz, 1H, H-15a), 4.08 (d, *J* = 12.5 Hz, 1H, H-15b), 3.81 (dd, *J* = 12.0, 2.2 Hz, 1H, H-31a), 3.70 (d, *J* = 5.0 Hz, 1H, H-2), 3.63 (dd, *J* = 12.0, 5.8 Hz, 1H, H-31b), 3.34 (t, *J* = 9.0, 8.9 Hz, 1H, H-28), 3.28 (t, *J* = 9.0, 9.0 Hz, 1H, H-29), 3.24 (dd, *J* = 9.0, 7.8 Hz, 1H, H-27), 3.19 (ddd, *J* = 9.6, 5.8, 2.2 Hz, 1H, H-30), 3.03 (d, *J* = 3.8 Hz, 1H, H-13a), 2.85 (d, *J* = 3.9 Hz, 1H, H-13b), 2.36 (dd, *J* = 15.2, 6.0 Hz, 1H, H-7a), 2.14 (dd, *J* = 7.6, 2.4 Hz, 1H, H-18), 2.07 (s, H-23), 2.05 (s, 1H, H-25), 2.05 (m, H-19), 1.92 (d, *J* = 15.2 Hz, 1H, H-7b), 1.73 (s, H-16), 0.95 (d, *J* = 6.6 Hz, 1H, H-20), 0.94 (d, *J* = 6.6 Hz, 1H, H-21), 0.72 (s, 1H, H-14); ^{13}C NMR (150 MHz in CD_2Cl_3) δ 174.1 (C-17), 170.8 (C-24), 170.7 (C-22), 137.2 (C-9), 125.2 (C-10), 103.8 (C-26), 83.9 (C-3), 81.3 (C-4), 80.6 (C-2), 78.4 (C-30), 78.2 (C-28), 74.9 (C-27), 71.6 (C-29), 69.4 (C-8), 68.6 (C-11), 65.9 (C-15), 65.4 (C-12), 62.8 (C-31), 50.2 (C-5), 48.0 (C-13), 44.6 (C-18), 44.5 (C-6), 28.9 (C-7), 27.0 (C-19), 22.9 (C-20), 22.8 (C-21), 21.3 (C-25), 20.9 (C-23), 20.6 (C-16), 7.2 (C-14); HRMS-ESI (*m*/*z*) $[M + Na]^+$ calcd for $C_{30}H_{44}O_{14}Na$ 651.2629, found 651.2618; optical rotation $[\alpha]_D^{20}$ = +7.51 (*c* 0.080, CH_3OH).

ELISA Tests. The responses of the T-2 glucoside anomers were evaluated in two immunoassay formats. The first of these was a competitive indirect enzyme-linked immunosorbent assay (CI-ELISA) based upon an antibody (Mab 2-13) developed against T-2 toxin-3-α-glucoside, conjugated to ovalbumin (e.g., T-2G−OVA), as described previously.[28] The second immunoassay format was a commercial test kit previously validated to detect T-2 toxin and HT-2 toxin (Veratox for T-2/HT-2) (Neogen Corp., Lansing, MI, USA). Assays were performed as described in the test kit instructions. For consistency with the methanol content indicated in the test kit instructions, the

DOI: 10.1021/jf504737f
J. Agric. Food Chem. 2015, 63, 731−738

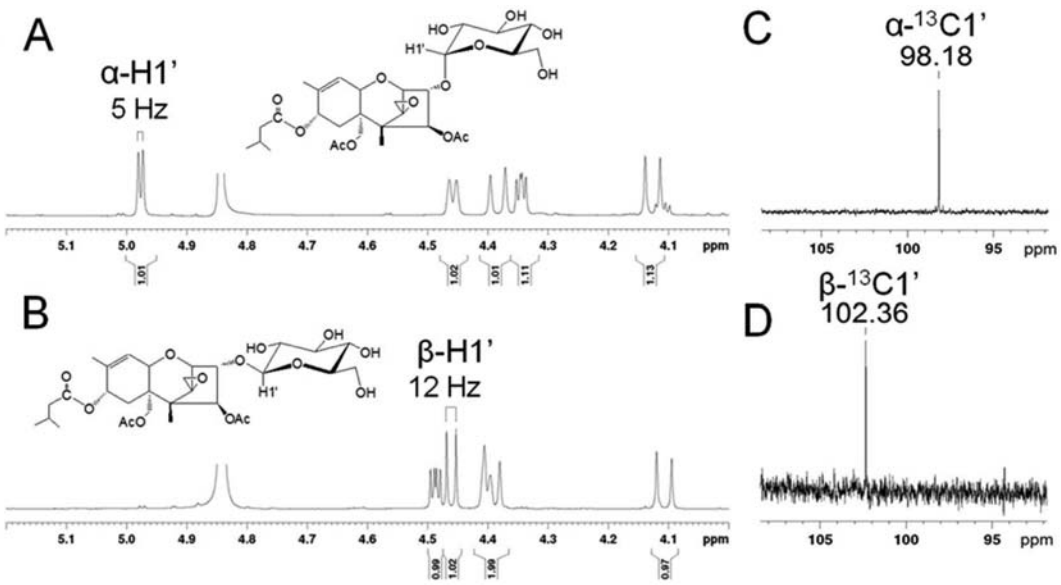

Figure 3. Proton NMR spectra of (A) T-2 toxin-α-glucoside, (B) T-2 toxin-β-glucoside with signals for the H1 anomeric proton indicated and ^{13}C NMR anomeric carbon signals of (C) T-2 toxin-α-glucoside (98.18 ppm) and (D) T-2 toxin-β-glucoside (102.36 ppm).

T-2 toxin-glucoside standards were prepared in 35% (v/v) methanol/water.

Phytotoxicity. The single-celled alga *Chlamydomonas reinhardtii* was used to assess the relative phytotoxicity of T-2 toxin, T-2 toxin-α-glucoside, and T-2 toxin-β-glucoside, as described previously.[27,32] Triplicate cultures (10 mL) were initiated with 10^5 cells/mL containing a 100 μM concentration of an individual trichothecene and grown for 6 days under fluorescent lights, with agitation of 200 rpm. Culture doublings were calculated as follows: (log of the final density − log of the initial cell density)/log 2.

Artificial Saliva Digestion Assay. The in vitro digestion experiment was performed as described previously.[16] Briefly, the main digestive juices were prepared by mixing salts and enzymes[33] and were preheated at 37 °C before use. A volume of 200 μL of a water/methanol (25:75, v/v) solution containing the target compounds was transferred in a 4 mL septum vial, and the solvent was evaporated under nitrogen. The in vitro digestion was started by adding 75 μL of artificial saliva to 200 μL of the water/methanol (25:75 v/v) solution containing the target analyte (500 μg/L). After 5 min of incubation at 37 °C, 150 μL of artificial gastric juice was added and the mixture was incubated again for 2 h. At the end of the gastric step, 25 μL of 1 M bicarbonate solution with 150 μL of artificial duodenal juice and 75 μL of artificial bile juice were added, and then a final incubation step of 2 h was performed. Finally, 25 μL of acetonitrile was added to stop the reactions, and the sample was centrifuged for 10 min at 10000 rpm, prior to direct LC-MS/MS analysis.

In Vitro Human Colonic Fermentation Assay. Human colonic fermentation of T-2 toxin-α-glucoside, T-2 toxin-β-glucoside, and T-2 toxin was carried out as described previously.[14] Fresh feces were collected from three different healthy and nonsmoker donors. These samples were immediately placed in an anaerobic environment and then mixed and weighed to obtain a 10% fecal solution in a phosphate saline buffer (PBS). For each sample 1.8 mL of growth medium, prepared as described previously,[14] and 1.8 mL of fecal solution were mixed and added to 0.4 mL of a toxin solution, at a final concentration of 500 μg/L. Each vial was then treated with a slight nitrogen flow to eliminate oxygen and perform fermentations under anaerobic condition. Samples were incubated in a water bath at 37 °C and shaken at a rate of 200 strokes/min. Fermentations were stopped immediately to have controls and then after 30 min and 24 h, by cooling samples to room temperature and adding 0.4 mL of acetonitrile. Samples were immediately centrifuged at 14000 rpm for 10 min and stored at −20 °C. At the same time, samples without added mycotoxin were prepared. All of the fermentations were performed in triplicate. Samples were diluted adding acetonitrile (1:2 v/v) and directly analyzed for T-2 toxin-glucoside, T-2 toxin, and HT-2 toxin by LC-MS/MS using MRM as described above.

RESULTS AND DISCUSSION

NMR Analysis of T-2 Toxin-α-glucoside, 2, and T-2 Toxin-β-glucoside, 3. NMR spectra were recorded for T-2 toxin-α-glucoside, obtained by yeast biotransformation (Figure 3A,C) and for chemically synthesized T-2 toxin-β-glucoside (Figure 3B,D). Both compounds are characterized by two spin systems due to a single glucopyranosyl ring and the trichothecene aglycone. The anomeric linkages are characterized by proton signals in the 4.5−5.5 ppm range and the ^{13}C signals by proton signals between 95 and 105 ppm. Consistent with expectations, T-2 toxin-α-glucoside gave a doublet at 4.98 ppm that integrates to a single proton (Figure 3A) and correlates to an adjacent ^{13}C signal at 98.18 ppm (Figure 3C). The observed $J_{1,2}$ coupling constant of 5 Hz is consistent with a small H1eq−H2ax dihedral angle that is characteristic for α anomers. The chemically synthesized T-2 toxin-β-glucoside is similarly characterized by a larger H1ax−H2ax bond angle, resulting in a definitive $J_{1,2}$ coupling constant of 12 Hz for the β-anomeric proton at 4.46 ppm (Figure 3B). This H-1 proton correlates to the β-C1 ^{13}C NMR anomeric signal at 102.36 ppm (Figure 3D). Hence, the T-2 toxin-glucoside anomers are defined by the observed ^1H and ^{13}C chemical shifts and by the characteristic $J_{1,2}$ coupling constants. These assignments were confirmed by HSQC and, together with HMBC, DEPT, COSY, and NOESY experiments, enable the complete NMR assignment of both epimers.

LC-MS Analysis of T-2 Toxin-α-glucoside and T-2 Toxin-β-glucoside Standards. The two epimeric standards, T-2 toxin-α-glucoside prepared with yeast and the synthetic T-2 toxin-β-glucoside, could be separated with LC (Figure 4). In EPI mode, T-2 toxin-α-glucoside and T-2 toxin-β-glucoside $[M + NH_4]^+$ ions were subjected to collision-induced dissociation. Under these conditions, T-2 toxin-α-glucoside more readily ionized to yield an $[M + H]^+$ ion than the T-2 toxin β-glucoside, as shown by the relative intensities of the

DOI: 10.1021/jf504737f
J. Agric. Food Chem. 2015, 63, 731−738

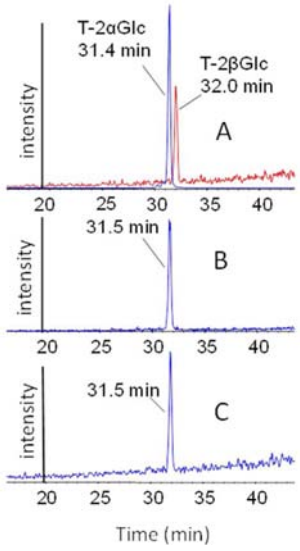

Figure 4. LC-MS/MS chromatograms of (A) T-2 toxin-α-glucoside (T-2αGlc) and T-2 toxin-β-glucoside (T-2βGlc) standards, (B) T-2 toxin-glucoside extracted from wheat, and (C) T-2 toxin-glucoside extracted from oats.

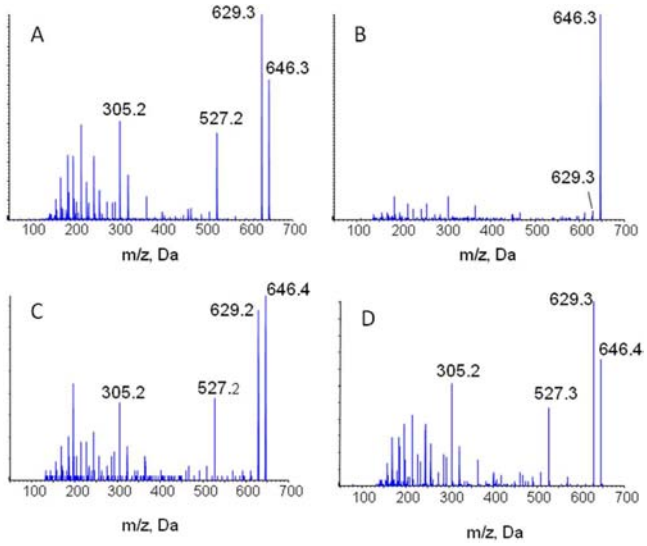

Figure 5. Tandem mass spectrum of the $[M + NH_4]^+$ ion of (A) T-2 toxin-α-glucoside, (B) T-2 toxin-β-glucoside, (C) T-2 toxin-glucoside from oats, and (D) T-2 toxin-glucoside from wheat.

residual $[M + NH_4]^+$ and $[M + H]^+$ ions (Figure 5). Other fragment ions were similar to those previously observed from *Fusarium*-infected grain.[10,11]

LC-MS Analysis of Naturally Contaminated Cereals. To determine the form of T-2 toxin-glucoside present in contaminated oats and wheat, extracts were analyzed with LC-MS/MS and compared to the standard T-2 toxin-α-glucoside and T-2 toxin-β-glucoside (Figure 4). Under the conditions used, T-2 toxin-α-glucoside eluted at 31.4 min and T-2 toxin-β-glucoside at 32.0 min. T-2 toxin-glucoside was detected at 31.5 min in oat and wheat samples, consistent with T-2 toxin-α-glucoside (Figure 4). In addition, there were differences in the mass spectra of the two isomers, showing the same fragment ions but with different relative intensities. Similar to T-2 toxin-α-glucoside, the yeast biotransformation product, the T-2 toxin-glucoside from oats and wheat, had the prominent $[M + H]^+$ product ion from the $[M + NH_4]^+$ ion (Figure 5).

Digestive Study on Anomeric Forms of T-2 Toxin-glucoside. In this study, the stability under in vitro gastrointestinal conditions and the catabolic fate of both T-2 toxin-α-glucoside and T-2 toxin-β-glucoside were tested in a human gut microbioma assay and compared to T-2 toxin. The simulated digestion assay used was developed to mimic the human gastrointestinal process.[14,16]

We found that the T-2 toxin-glucosides were unchanged after incubation with human artificial saliva. These results are similar to those reported for deoxynivalenol glucoside and zearalenone glucoside[14] and further demonstrate the stability of some α- and β-glucosidic bonds upon digestion.

In contrast to zearalenone glucoside, which was hydrolyzed in the first 30 min of colonic fermentation,[9] T-2 toxin and the T-2 toxin-glucosides were relatively stable for the first 30 min (Figure 6). There was significant degradation after 24 h (Figure 6). T-2 toxin was mainly transformed into its derivative HT-2 toxin (83% at t = 24 h). T-2 toxin-α-glucoside and T-2 toxin-β-glucoside were both strongly degraded after 24 h, with <30% of the starting material remaining. The degradation pathway is different between α- and β-forms. The latter was mainly cleaved to release its precursor T-2 toxin (58%) with a smaller percentage of HT-2 toxin (12%), whereas the former is converted into T-2 toxin (13%), HT-2 toxin (30%), and other metabolites of unknown structure and toxicity (33%).

Because smaller amounts of T-2 toxin remained following colonic fermentation with T-2 toxin-α-glucoside, it may pose less of a risk than T-2 toxin-β-glucoside, which is not known to occur in crops. However, T-2 toxin-α-glucoside was also converted into other, as yet uncharacterized, compounds (Figure 6). In addition to T-2 toxin and HT-2 toxin, other possible products of T-2 toxin-glucoside include HT-2 toxin-glucoside, T-2 triol, and T-2 tetraol. It is important to consider the toxicity of all of the products when the risk posed by T-2 toxin-α-glucoside in grain is assessed.

Phytotoxicity. The relative toxicity of T-2 toxin and the T-2 toxin-glucosides was tested with *C. reinhardtii* cultures. Previous studies have shown that T-2 toxin is quite phytotoxic[32] and T-2 toxin-α-glucoside is nontoxic.[27] In this study, cultures grown in 100 μM T-2 had only a slight increase in the number of cells, with 0.6 doubling after 4 days. In contrast, neither T-2 toxin-α-glucoside nor T-2 toxin-β-glucoside was phytotoxic, with 5.4 and

Table 1. Cross-Reactivity of ELISA toward T-2 Toxin-α-glucoside and T-2 Toxin-β-glucoside

analogue	av IC_{50} ± 1 SD (ng/mL)	cross-reactivity (relative to T-2 toxin, %)
Mab 2-13 ELISA		
T-2 toxin[a]	3.3 ± 0.1	100
T-2 toxin-α-glucoside	3.04 ± 0.16	108 ± 5.7
T-2 toxin-β-glucoside	5.80 ± 0.16	56.9 ± 1.6
Commercial T-2 Toxin/HT-2 Toxin Kit		
T-2 toxin	3.03 ± 0.13	100
T-2 toxin-α-glucoside	18.9 ± 2.4	16.0 ± 2.0
T-2 toxin-β-glucoside	6.65 ± 0.58	45.5 ± 4.0

[a]Data for T-2 toxin with this immunoassay are from Maragos et al.[28]

DOI: 10.1021/jf504737f
J. Agric. Food Chem. 2015, 63, 731−738

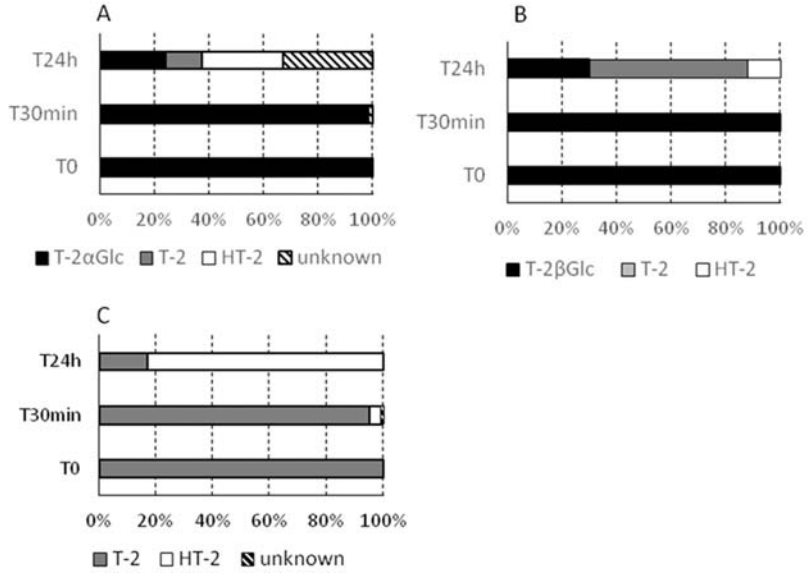

Figure 6. Degradation upon human colonic microbiota fermentation of (A) T-2 toxin-α-glucoside (T-2αGlc), (B) T-2 toxin-β-glucoside (T-2βGlc), and (C) T-2 toxin (T-2). HT-2 toxin (HT-2).

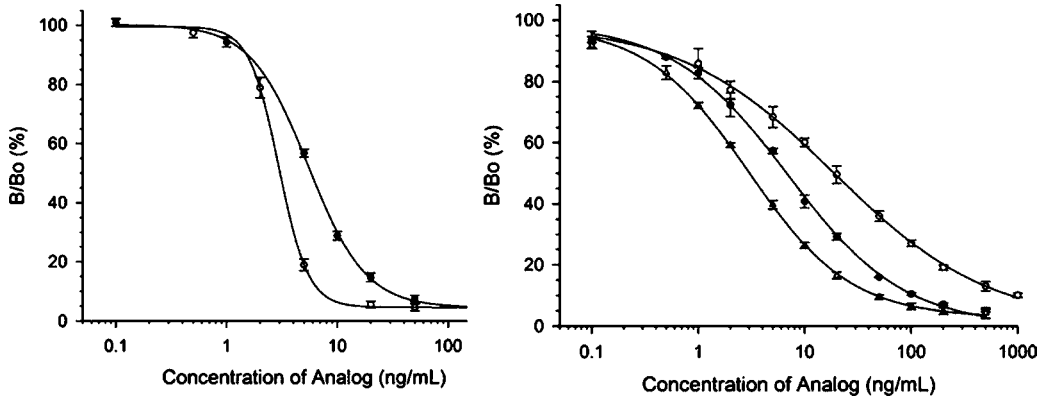

Figure 7. ELISA responses. (A) CI-ELISA responses of T-2 toxin-α-glucoside (open circles) and T-2 toxin-β-glucoside (solid circles) with Mab 2-13. Data shown are the averages from four plates, with six replicates per toxin concentration per plate (n = 24), ± 1 standard deviation. Curves represent the fit of a logistic dose−response equation over the indicated concentration range (0.1−200 ng/mL). (B) ELISA responses of T-2 toxin (open triangles), T-2 toxin-α-glucoside (open circles), and T-2 toxin-β-glucoside (solid circles) to Neogen Veratox T-2/HT-2 antibody. Data shown are the averages from three plates per toxin, with four replicates per toxin concentration per plate (n = 12), ± 1 standard deviation. Curves represent the fit of a logistic dose−response equation over the indicated concentration range (0.1−1000 ng/mL).

5.5 doublings, respectively, which are similar to the 5.3 doublings observed for cultures treated with acetone alone.

Antibody Detection of T-2 Toxin and T-2 Toxin-glucosides with Two Immunoassays. T-2 toxin-glucoside standards were each tested in two immunoassays. The first immunoassay was a competitive indirect ELISA format using Mab 2-13, an antibody developed with T-2 toxin-α-glucoside.[28] Mab 2-13 recognized T-2 toxin α-glucoside slightly better than T-2 toxin (cross reaction 108%), whereas T-2 toxin-β-glucoside was recognized more poorly, at about 57% relative to T-2 toxin (Table 1; Figure 7A). This makes this antibody-based test suitable for the detection of both T-2 toxin and the naturally occurring T-2 toxin-α-glucoside.

The second immunoassay was a commercially available T-2/HT-2 kit. This kit was used to determine if an ELISA, developed before the glucosides of T-2 and HT-2 toxins were even discovered, could detect these "masked" mycotoxins. The commercial ELISA test kit for T-2 toxin and HT-2 toxin detection performed very well for detecting T-2 toxin with good sensitivity and good reproducibility. In addition, the kit cross-reacted fairly well with the T-2 toxin-β-glucoside, but poorly with the T-2 toxin-α-glucoside (Table 1; Figure 7B). However, given that T-2 toxin-α-glucoside is the form found in naturally contaminated samples and that the cross-reaction with this anomer was only about 16%, this test kit would not be recommended for the simultaneous screening of T-2 toxin and T-2 toxin-α-glucoside.

The ability of plants to form trichothecene glucosides can be seen as a detoxification mechanism that plants use when infected with trichothecene-producing fungi. Because trichothecenes can be virulence factors in plant disease,[34] expression of trichothecene UGT genes in plants is a potential way to increase disease resistance to trichothecene-producing fungi. This approach may reduce disease and thereby decrease the amount of trichothecenes. However, both the trichothecenes and their masked forms need to be considered to accurately

DOI: 10.1021/jf504737f
J. Agric. Food Chem. 2015, 63, 731−738

assess the risk to human and animal health posed by plant material contaminated with trichothecenes.

Sufficient amounts of T-2 toxin-glucoside are needed to determine the risk posed by the masked form of T-2 toxin in cereals, to develop reliable methods for their detection, and to study the stability, digestive fate, and toxicity of T-2 toxin-glucoside formed in plant materials. Whereas the synthesis of deoxynivalenol-glucoside is relatively straightforward,[35] this method was not amenable to the preparation of T-2 toxin-glucosides because the isovaleryl and acetyl groups are labile during the synthesis. A synthesis employing a superarmed tetra-*O*-triisopropylsilyl protected donor[36] offered a way to selectively remove the protecting groups from the sugar portion of the glucoside without disturbing the isovaleryl and acetyl groups of T-2 toxin, thus providing a means to synthesize T-2 toxin-β-glucoside. Microbial T-2 toxin-α-glucoside was prepared as a single anomer with *B. muscicola* yeast cultures,[27] On the basis of LC and LC-MS chromatographic comparisons and MS/MS analyses, the T-2 toxin-glucoside occurring in contaminated wheat and oats was found to be identical to the yeast biotransformation product, T-2 toxin-α-glucoside.

It is notable that naturally occurring T-2 glucoside has an α-linked sugar, whereas naturally occurring deoxynivalenol glucoside has a β-linked sugar. Although β-linked sugars are more commonly found with xenobiotics and natural products including flavonoids,[37] there is a report of *Fusarium* cultures producing an α-linked glycoside, 15-monoacetoxyscirpenol-4-α-glucoside.[38] The *Blastobotrys* glucosyltransferase that converts T-2 toxin to T-2 toxin-α-glucoside has not been identified, but there may be substrate preferences between the UGT that lead to trichothecene α- or β-glucosides.

Although the focus of this study was the T-2 toxin-glucosides, HT-2 toxin-glucosides have also been reported in contaminated grain[11] and in culture material.[10] They may be formed either by hydrolysis of T-2 toxin-α-glucoside or by conversion of T-2 toxin to HT-2 toxin followed by glycosylation at C-3 or C-4. It is possible that the latter route may utilize different glucosyltransferases that result in a β orientation. To date, no plant UGT that converts T-2 toxin to T-2 toxin-α-glucoside has been identified. Numerous glucosyltransferases were screened to identify one that had good substrate specificity for deoxynivalenol.[23] Although the T-2 toxin-glucoside found in naturally contaminated oats and wheat was identical to the T-2 toxin-α-glucoside prepared with yeast cultures,[27] the anomericity of HT-2 toxin-glucosides has not been determined.

The present study has demonstrated that naturally occurring T-2 toxin-glucoside has an α-linked sugar and that T-2 toxin-α-glucoside can be prepared with *B. muscicola* in sufficient quantity to study its animal toxicity. The U.S. FDA has not provided guidance levels to the agricultural industry for T-2 toxin or related trichothecenes. The European Food Safety Authority (EFSA) established a group tolerable daily intake of 100 ng/kg body weight for T-2 and HT-2 toxins.[39] However, at present it is not possible to perform a proper risk assessment for masked mycotoxins in food, due to the lack of data on exposure and toxic properties. Masked mycotoxins may elude analysis because of altered physical properties or because of modification of an epitope recognized by antibodies used for the detection, leading to an underestimation of the total mycotoxin load. Possible release during food processing is also a concern, and EFSA currently has a working group on the public health risk of masked mycotoxins in food and animal feed. Research on masked mycotoxins is hampered by the nonavailability of analytical standards or calibrants, and only one compound, deoxynivalenol-3-β-glucoside, is commercially available.

The occurrence of T-2 toxin-α-glucoside in wheat and oat samples, and its metabolism by microbes during digestion, suggests that there is a risk in underestimation of the total T-2 toxin load and a need to monitor both mycotoxins and their conjugated forms in cereals and food products. To promote research efforts in the area of masked mycotoxins, T-2 toxin-α-glucoside has now been made available to the scientific community by the authors.

■ ASSOCIATED CONTENT

Ⓢ Supporting Information

Figures S1−S11. This material is available free of charge via the Internet at http://pubs.acs.org.

■ AUTHOR INFORMATION

Corresponding Author

*(S.P.M.) Phone:(309) 681-6381. Fax: (309) 681-6627. E-mail: Susan.McCormick@ars.usda.gov.

Funding

D.C. thanks the NIH (GM62160) for support of the synthetic work.

Notes

The authors declare no competing financial interest.

■ ACKNOWLEDGMENTS

We thank Karl Vermillion for NMR analyses and Jennifer Teresi for technical assistance with *Chlamydomonas* assays. D.C. thanks the NSF (MRI-084043) for funds to purchase the 600 MHz NMR spectrometer in the Lumigen Instrument Center at WSU.

■ REFERENCES

(1) Aoki, T.; O'Donnell, K.; Homma, Y.; Lattanzi, A. R. Sudden-death syndrome of soybean is caused by two morphologically and phylogenetically distinct speces with the *Fusarium solani* species complex, *F. virguliforme* in North America and *F. tucumaniae* in South America. *Mycologia* **2003**, *95*, 660−684.

(2) McMullen, M.; Bergstrom, G.; De Wolf, E.; Dill-Macky, R.; Hershman, D.; Shaner, G.; Van Sanford, D. A unified effort to flight an enemy of wheat and barley: *Fusarium* head blight. *Plant Dis.* **2012**, *96*, 1712−1728.

(3) McMullen, M.; Jones, R.; Gallenberg, D. Scab of wheat and barley: a re-emerging disease of devastating impact. *Plant Dis.* **1997**, *81*, 1340−1348.

(4) Mesterhazy, A.; Lemmens, M.; Reid, L. M. Breeding for resistance to ear rots caused by *Fusarium* spp. in maize − a review. *Plant Breed.* **2012**, *131*, 1−19.

(5) Wu, F.; Groopman, J. D.; Pestka, J. J. Public health impacts of foodborne mycotoxins. *Annu. Rev. Food Sci. Technol.* **2014**, *5*, 351−372.

(6) Richard, J. L. Some major mycotoxins and their mycotoxicoses − an overview. *Int. J. Food Microbiol.* **2007**, *119*, 3−10.

(7) Rocha, O.; Ansari, K.; Doohan, F. M. Effects of trichothecene mycotoxins on eukaryotic cells: a review. *Food Addit.Contam.* **2005**, *22*, 369−378.

(8) Sewald, N.; Lepschy von Gleissenthall, J.; Schuster, M.; Müller, G.; Alpin, R. T. Structure elucidation of a plant metabolite of 4-desoxynivalenol. *Tetrahedron: Asymmetry* **1992**, *3*, 953−960.

(9) Paris, M. P. K.; Schweiger, W.; Hametner, C.; Stückler, R.; Muehlbauer, G. J.; Varga, E.; Krska, R.; Berthiller, F.; Adam, G.

DOI: 10.1021/jf504737f
J. Agric. Food Chem. 2015, 63, 731−738

Zearalenone-16-*O*-glucoside: a new masked mycotoxin. *J. Agric. Food Chem.* **2014**, *62*, 1181−1189.
(10) Busman, M.; Poling, S. M.; Maragos, C. M. Observation of T-2 toxin and HT-2 toxin glucosides from *Fusarium sporotrichioides* by liquid chromatography coupled to tandem mass spectrometry (LC-MS/MS). *Toxins* **2011**, *3*, 1554−1568.
(11) Lattanzio, V. M. T.; Visconti, A.; Haidukowski, M.; Pascale, M. Identification and characterization of new *Fusarium* masked mycotoxins, T2 and HT2 glycosyl derivatives, in naturally contaminated wheat and oats by liquid chromatography-high resolution mass spectrometry. *J. Mass Spectrom.* **2011**, *47*, 466−475.
(12) Berthiller, F.; Crews, C.; Dall-Asta, C.; De Saeger, S.; Haesaert, G.; Karlovsky, P.; Oswald, I. P.; Seefelder, W.; Speijers, G.; Stroka, J. Masked mycotoxins: a review. *Mol. Nutr. Food Res.* **2013**, *57*, 165−186.
(13) Shin, S.; Torres-Acosta, J. A.; Heinen, S. J.; McCormick, S.; Lemmens, M.; Kovalsky Paris, M. P.; Berthiller, F.; Adam, G.; Muehlbauer, G. J. Transgenic *Arabidopsis thaliana* expressing a barley UDP-glucosyltransferase exhibit resistance to the mycotoxin deoxynivalenol. *J. Exp. Bot.* **2012**, *63*, 4731−4740.
(14) Dall-Erta, A.; Cirlini, M.; Dall-Aasta, M.; Del Rio, D.; Galaverna, G.; Dall'Asta, C. Masked mycotoxins are efficiently hydrolyzed by human colonic microbiota releasing their aglycones. *Chem. Res. Toxicol.* **2013**, *25*, 305−312.
(15) De Angelis, E.; Monaci, L.; Pascale, M.; Visconti, A. Fate of deoxynivalenol, T-2 and HT-2 toxins and their glucoside conjugates from flour to bread: an investigation by high-performance liquid chromatography high-resolution mass spectrometry. *Food Addit. Contam., Part A* **2013**, *30*, 345−355.
(16) Dall'Asta, C.; Falavigna, C.; Galaverna, G.; Dossena, A.; Marchelli, R. In vitro digestion assay for determination of hidden fumonisins in maize. *J. Agric. Food Chem.* **2010**, *58*, 12042−12047.
(17) Nagl, V.; Schwarz, H.; Krska, R.; Moll, W. D.; Knasmüller, S.; Ritzmann, M.; G, A.; Berthiller, F. Metabolism of the masked mycotoxin deoxynivalenol-3-glucoside in rats. *Toxicol. Lett.* **2012**, *213*, 367−373.
(18) Berthiller, F.; Dall'Asta, C.; Corrodini, R.; Marchelli, R.; Sulyok, M.; Krska, R.; Adam, G.; Schuhmacher, R. Occurrence of deoxynivalenol and its 3-*β*-D-glucoside in wheat and maize. *Food Addit. Contam.* **2009**, *26*, 507−511.
(19) Kostelanska, M.; Hajslova, J.; Zachariasova, M.; Malachova, A.; Kalachova, K.; Postka, J.; Fiala, J.; Scott, P. M.; Berthiller, F.; Krska, R. Occurrence of deoxynivalenol and its major conjugate, deoxynivalenol-3-glucoside, in beer and some brewing intermediates. *J. Agric. Food Chem.* **2009**, *57*, 3187−3194.
(20) Berthiller, F.; Dall'Asta, C.; Schuhmacher, R.; Lemmens, M.; Adam, G.; Krska, R. Masked mycotoxins: determination of a deoxynivalenol glucoside in artificially and naturally contaminated wheat by liquid chromatography-tandem mass spectrometry. *J. Agric. Food Chem.* **2005**, 3421−3425.
(21) Schweiger, W.; Boddu, J.; Shin, S.; Poppenberger, B.; Berthiller, F.; Lemmens, M.; Muehlbauer, G. J.; Adam, G. Validation of a candidate deoxynivalenol-inactivating UDP-glucosyltransferase from barley by heterologous expression in yeast. *Mol. Plant−Microbe Interact.* **2010**, *23*, 977−986.
(22) Schweiger, W.; Pasquel, J.-C.; Nussbaumer, T.; Kovalsky Paris, M. P.; Wiesenberger, G.; Macadré, C.; Ametz, C.; Berthiller, F.; Lemmens, M.; Saindrenan, P.; Mewes, H.-W.; Mayer, K. F. X.; Dufresne, M.; Adam, G. Functional characterization of two clusters of *Brachypodium distachyon* UDP-glycosyltransferases encoding putative deoxynivalenol detoxification genes. *Mol. Plant−Microbe Interact.* **2013**, *26*, 781−792.
(23) Schweiger, W.; Steiner, B.; Limmongkon, A.; Brunner, K. Cloning and heterologous expression of candidate DON-inactivating UDP-glucosyltransferases from rice and wheat in yeast. *Plant Breed. Seed Sci.* **2011**, *64*, 105−111.
(24) Berthiller, F.; Krska, R.; Domig, K. J.; Kneifel, W.; Juge, N.; Schuhmacher, R.; Adam, G. Hydrolytic fate of deoxynivalenol-3-glucoside during digestion. *Toxicol. Lett.* **2011**, *206*, 264−267.
(25) De Nijs, M.; Van den Top, H. J.; Portier, L.; Oegema, G.; Kramer, E.; Can Egmond, H. P.; Hoogenboom, L. A. P. Digestibility and absorption of deoxynivalenol 3-*β*-glucoside in in vitro models. *World Mycotox. J.* **2012**, *5*, 325−334.
(26) Gratz, S. W.; Duncan, G.; Richardson, A. J. The human fecal microbiotia metabolizes deoxynivalenol and deoxynivalenol-3-glucoside and may be responsible for urinary deepoxy-deoxynivalenol. *Appl. Environ. Microbiol.* **2013**, *79*, 1821−1825.
(27) McCormick, S. P.; Price, N. P. J.; Kurtzman, C. P. Glucosylation and other biotransformations of T-2 toxin by yeasts of the *Trichomonascus* clade. *Appl. Environ. Microbiol.* **2012**, *78*, 8694−8702.
(28) Maragos, C. M.; Kurtzman, C.; Busman, M.; Price, N.; McCormick, S. Development and evaluation of monoclonal antibodies for the glucoside of T-2 toxin (T2-Glc). *Toxins* **2013**, *5*, 1299−1313.
(29) Samhueza, C. A.; Dorta, R. L.; Vázquez, J. T. Involvement of the S-aglycon in the conformational preferences of thioglucosides. *Tetrahedron: Asymmetry* **2008**, *19*, 258−264.
(30) Okada, Y.; Mukae, T.; Okajima, K.; Taira, M.; Fujita, M.; Yamada, H. Highly *β*-selective O-glucosidation due to the restricted twist-boat conformation. *Org. Lett.* **2007**, *9*, 1573−1576.
(31) Vic, G.; Hasting, J. J.; Howarth, O. W.; Crout, D. H. G. Chemoenzymatic synthesis of ethyl 1-thio-(*β*-D-galactopyranosyl)-*O*-[*O*-*β*-D-glycopyranosyl disaccharides using the *β*-galactosidase from *Bacillus circulans*. *Tetrahedron: Asymmetry* **1996**, *7*, 709−720.
(32) Alexander, N. J.; McCormick, S. P.; Ziegenhorn, S. L. Phytotoxicity of selected trichothecenes using *Chlamydomonas reinhardtii* as a model system. *Nat. Toxins* **1999**, *7*, 265−269.
(33) Versantvoort, C. H. M.; Oomen, A. G.; Van de Kamp, E.; Rompelberg, C. J. M.; Sips, A. J. Applicability of an *in vitro* digestion model in assessing the bioaccessibility of mycotoxins from food. *Food Chem. Toxicol.* **2005**, *43*, 31−40.
(34) Desjardins, A. E.; Proctor, R. H.; Bai, G.; McCormick, S. P.; Shaner, G.; Beuchley, G.; Hohn, T. M. Reduced virulence of trichothecene-non-producing mutants of *Gibberella zeae* in wheat field tests. *Mol. Plant−Microbe Interact.* **1996**, *9*, 775−781.
(35) Savard, M. E. Deoxynivalenol fatty acid and glucoside conjugates. *J. Agric. Food Chem.* **1991**, *39*, 570−574.
(36) Pedersen, C. M.; Marinescu, L. G.; Bols, M. Glycosyl donors in "unusual" conformations − influence on reactivity and selectivity. *C. R. Chim.* **2011**, *14*, 17−43.
(37) Bowles, D.; Isayenkova, J.; Lim, E.-K.; Poppenberger, B. Glycosyltransferases: managers of small molecules. *Curr. Opin. Plant Biol.* **2005**, *8*, 254−263.
(38) Gorst-Allman, C. P.; Steyn, P. S.; Vleggaar, R. Structure elucidation of a novel trichothecene glucoside using ^{1}H and ^{13}C nuclear magnetic resonance spectroscopy. *J. Chem. Soc., Perkin Trans. 1* **1985**, *1985*, 1553−1555.
(39) European Food Safety Authority. Commision recommendation of 27 March 2013 on the presence of T-2 and HT-2 toxin in cereals and cereal products. *Off. J. Eur. Union* **2013**, *L91*, 12−14.

DOI: 10.1021/jf504737f
J. Agric. Food Chem. 2015, 63, 731−738

JOURNAL OF AGRICULTURAL AND FOOD CHEMISTRY

Article

pubs.acs.org/JAFC

Fruit of *Ziziphus jujuba* (Jujube) at Two Stages of Maturity: Distinction by Metabolic Profiling and Biological Assessment

Jianping Chen,[†,§,#] Pui H. Chan,[‡,§,#] Candy T. W. Lam,[§] Zhonggui Li,[†] Kelly Y. C. Lam,[§] Ping Yao,[§] Tina T. X. Dong,[§] Huangquan Lin,[§] Henry Lam,[‡] and Karl W. K. Tsim*[,§]

[†]Pharmaceutical Department, Shenzhen Traditional Chinese Medicine Hospital, Guangzhou University of Chinese Medicine, Shenzhen, China

[‡]Department of Chemical and Biomolecular Engineering, and Division of Biomedical Engineering, The Hong Kong University of Science and Technology, Hong Kong, China

[§]Division of Life Science and Center for Chinese Medicine, The Hong Kong University of Science and Technology, Hong Kong, China

ABSTRACT: The fruit of *Ziziphus jujuba*, named as jujube or Chinese date, is used as a health supplement worldwide. Two kinds of jujubes are commonly found in the market: immature jujubes eaten as fruits, and mature jujubes employed as medicinal herbs. To study the variation of jujubes at two developmental stages, we investigated their chemical and biological properties by metabolic profiling and cellular assays. In NMR profiling, the levels of 11 metabolites were measured. Statistically differences in the levels of threonine, alanine, acetate, creatine, glucose, sucrose, and formate were found between mature and immature jujubes. In parallel, their neuro-protecting and erythropoietic activities were compared. The water extract of mature jujube possessed better effect in inducing neurofilament expression than that of the immature one, while immature jujube extract performed better in activating HRE-mediated transcriptional activity. These findings suggest the maturity of jujube has to be considered when it is being used for health food products.

KEYWORDS: *Rhamnaceae, Ziziphus jujuba, maturity, NMR, metabolic profiling, neurofilament expression, hypoxia response element*

INTRODUCTION

Jujube is the fruit of *Ziziphus jujuba* Mill. from the Rhamnaceae family, commonly named Chinese date or red date. According to ancient Chinese medical theory in *Shennong Bencao Jing* (300 BC−200 AD), one of the usages of jujube was to play a trophic role in our brain by calming down the mind and improving quality of sleep, as such, which prolonged one's life-span. In addition, the daily consumption of jujube-containing herbal decoction is also considered to enhance the "Qi" (the vital energy) and to nourish the "Blood" (body circulation) of individuals.

Current nutritional findings have reported that carbohydrates, minerals, vitamins, and amino acids are major ingredients in jujube.[1,2] Moreover, pharmacological data have shown that the fruit has abilities to perform antioxidant actions,[3,4] immunological activity,[5] a potential sedative effect,[6] treatment of jaundice,[7] and anti-inflammatory effects.[8] Previously, we have demonstrated the neuronal activity of jujube in defending cultured PC12 cells against oxidative stress,[9] and its beneficial roles in neuronal differentiation.[10] Jujube could stimulate the expression of neurotrophic factor in cultured astrocytes.[11] Besides, jujube water extract has abilities to stimulate the expression of erythropoietin (EPO) in cultured Hep3B cells[12] and to regulate cytokine expression in cultured RAW 264.7 cells.[13]

Two forms of jujubes are usually found in the marketplace: unripe jujubes eaten as fruits and ripe jujubes considered as medicinal herbs. However, it is unclear whether the unripe jujube is exactly the same as the ripe one in terms of chemical composition and pharmacological activity. Currently, metabolic profiling methods are employed increasingly to seek quality control of medicinal herbs.[14] Here, we aim to employ ^{1}H NMR (nuclear magnetic resonance) metabolic profiling to identify jujube water extracts at two stages of maturity. In addition, the pharmacological properties of two developmental stages of jujube were compared, which included: (i) the neuro-protecting activity by using the induction of neurofilament in cultured PC12 cells, and (ii) the erythropoietic activity by revealing the activation of the hypoxia response element (HRE) in cultured Hep3B cells.

MATERIALS AND METHODS

Preparation of Herbal Extract. The fruits of *Z. jujuba* cultivated in Hebei Cangzhou at two stages of maturity were collected in 2012. Classification of jujube: unripe jujube was collected in September 2012 with a yellow-green background having mahogany-colored spots. Ripe jujube was harvested in October 2012 when its appearance turned entirely red, and the fruit began to soften and wrinkle. The raw materials were authenticated by Dr. Tina Dong according to their morphological properties, having the voucher numbers voucher #12-09-A for immature jujube and voucher #12-10-A for mature jujube. The voucher specimens are kept at the Center for Chinese Medicine, The Hong Kong University of Science and Technology. After removing the kernel and chopping into slices, the fruits were dried by using a freeze-dryer. The dried fruits were powdered to

Received: August 29, 2014
Revised: December 8, 2014
Accepted: December 28, 2014
Published: December 29, 2014

ACS Publications © 2014 American Chemical Society

DOI: 10.1021/jf5041564
J. Agric. Food Chem. 2015, 63, 739−744

homogeneous size (40 mesh). Fifty grams of the dried powder was weighed accurately and extracted in 1 L of boiling water twice for 1 h. The extract was lyophilized to dryness and stored at −80 °C. The powder was redissolved with water, or other solvents, and vortexed at room temperature before use.[9]

NMR Metabolic Analysis. Sample preparation for NMR spectroscopy was performed as in previous studies.[14] Briefly, dried jujube extract (50 mg) was redissolved in 1000 μL of aquae, from which 550 μL was mixed with 50 μL of a D_2O solution with 0.2% TSP-d_4 and 3 mM sodium azide. All particulates were discarded by centrifugation at 13,000*g* for 1 min, and the supernatant was transferred to a standard 5 mm NMR tube. NMR spectra were acquired using a Bruker AV 400 MHz NMR spectrometer. Gradient shimming was employed to improve the magnetic field homogeneity prior to all acquisition. The ^{1}H NMR spectra of the samples were acquired on a ^{1}D NOESY pulse sequence to generate a spectrum with a reduced residual solvent peak. Each sample was performed around 5 min (64 scans). All spectral data were integrated using the rNMR program.[15] The data were then formatted in XML for importing into MATLAB version 2009b and SIMCA-P version 12.0. Each ^{1}H NMR spectrum was Pareto scaled and divided into 1300 bins. The summed intensity in each bin was used as a data point for Principle Component Analysis (PCA). Metabolites were identified and assigned using a Chenomx Profiler with input from online databases hmdb.ca,[16] bmrb.wisc.edu,[17] and literature data.[18] The statistical significance of the changes in the integrated area of these assigned peaks was evaluated using a two-tailed Student's *t* test.

Cell Cultures. PC12 cells were purchased from American Type Culture Collection (ATCC, Manassas, VA). The PC12 cells were cultured in Dulbecco's modified Eagles medium (DMEM) added with 6% fetal bovine serum (FBS), 6% horse serum (HS), 100 U/mL penicillin, and 100 μg/mL streptomycin. Cultures were placed in a water-saturated 7.5% CO_2 incubator at 37 °C. Medium was renewed every 2−3 days. Human hepatocellular carcinoma Hep3B from ATCC was maintained in DMEM added with 100 IU/mL penicillin, 100 μg/mL streptomycin, and FBS to a final concentration of 10%. For subculturing, cultures were rinsed with 5 mL of 1X PBS (phosphate buffered saline) having 1 mM EDTA twice, followed by adding 1 mL of tripsin/EDTA solution to detach the cells. Reagents for cell cultures were obtained from Invitrogen Technologies (Carlsbad, CA). Cobalt chloride ($CoCl_2$, ≥97%; an inhibitor of HIF-α degradation) was obtained from Sigma (St. Louis, MO). Nerve growth factor (NGF; PC12 cells differentiation inducer) was from Alomone Laboratories (Jerusalem, Israel).

Expression of Neurofilament 68. The determination of neurofilament expression in cultures was performed according to a previous method.[10] Briefly, cultured PC12 cells were plated into 12-well plates for 24 h and then transferred to low serum for 3 h prior to treatment with jujube extract. After 3 days of treatment, the cells were harvested. The concentration of total proteins was determined by Bradford assay. Equal amounts of total protein were separated on SDS-PAGE, transferred to a nitrocellulose membrane, and incubated with an antibody specific to neurofilament 68 (NF68; Sigma) using GAPDH (Abcam Ltd., Cambridge, U.K.) as loading control. The nitrocellulose was conjugated with horseradish peroxidase antimouse secondary antibody. The intensity of the protein bands was quantified using an image analyzer.

Determination of pHRE-Luc Activity. The DNA construct of HRE and the vector were generated as described previously.[12] Briefly, cultured Hep3B cells were seeded into 24-well plates and transfected with pHRE-Luc using Lipofectamine reagent (Invitrogen), according to the manufacturer's protocol. The luciferase activity in the cell lysates was evaluated in a Tropix TR717TM Microplate Luminometer (Bedford, MA), and the activity was expressed as absorbance (up to 560 nm) per mg of protein.

Statistical and Other Analyses. The amount of total protein was measured by Bradford's assay (Hercules, CA). Data were presented as Mean ± Standard Error of Mean (SEM). Statistical analyses were evaluated using *t* test (version 13.0, SPSS, IBM Corporation, Armonk, NY). $p < 0.05$ was considered as significant (*), $p < 0.01$ as more significant (**), and $p < 0.001$ as highly significant (***).

RESULTS

Metabolic Profiles of Jujubes at Two Stages of Maturity. Before NMR analysis and cell treatment, the water extracts of jujube were chemically standardized as reported previously.[9,10] The below chemical parameters were applied to the water extracts from both mature and immature jujubes. The contents of nucleobases, including uracil, xanthine, hypoxanthine, guanine, and/or adenine in water extract should be more than 45 and 80 μg/g of dried extract of jujube. The contents of nucleosides, including cytidine, uridine, and/or guanosine in jujube extract, should be more than 80 and 150 μg/g. The contents of cyclic nucleotides, including cGMP and cAMP, in the extract should be more than 85 and 100 μg/g. The amounts of flavonoids, including quercetin 3-O-rutinoside, quercetin 3-O-galactoside, quercetin 3-O-β-D-glucoside, and kaempferol 3-O-rutinoside, in jujube extract should be more than 50 and 35 μg/g. Thus, the jujubes extracts were chemically standardized, and only samples that met the standardization criteria would be selected for all below analyses.

Jujube samples at two stages of maturity were collected from Cangzhou of China (Figure 1). Morphologically, there was a considerable difference between mature and immature jujubes, i.e. color and texture. In order to investigate the metabolic profiling of jujube extracts, ^{1}H NMR was employed to measure their primary metabolites. The average spectra of the jujube extracts were obtained, as indicated in Figure 2. Visual observation demonstrated that the spectrum of mature jujube showed similarity with that of the immature one. The top intense peaks were found at between 3.3 and 4 ppm, which belonged to the sugar compounds. Among these peaks, the two highest concentrations were sucrose and glucose. In addition, we identified other primary metabolites (Table 1), such as amino acid and organic acid. PCA, the most basic and efficient approach for evaluating complex data in metabolic profiling, was applied for data analysis.[19] Here, PCA was performed to analyze the integrated peak areas of identified metabolites. Clear separation of immature jujube and mature jujube was successfully observed (Figure 3A). The corresponding loading plot indicated that jujube at the immature stage showed a greater concentration of sucrose, alanine, and formate, while the others were found to be higher in mature jujube (Figure 3B). All identified and integrated peaks were further analyzed (Figure 4). Sucrose was shown to be the highest intensity in jujube, and then glucose and creatine. The metabolites of mature and immature jujubes were compared. The levels of

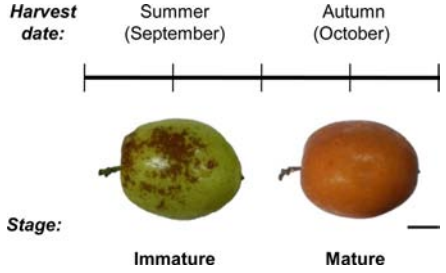

Figure 1. Morphology of mature and immature jujubes. Immature fruit was collected in summer with a yellow-green background having mahogany-colored spots (left panel). The mature fruit was collected in autumn when its appearance became entirely red and the fruit began to soften and wrinkle (right panel). Jujube samples were obtained from Cangzhou, Hebei. Bar: 1 cm.

DOI: 10.1021/jf5041564
J. Agric. Food Chem. 2015, 63, 739−744

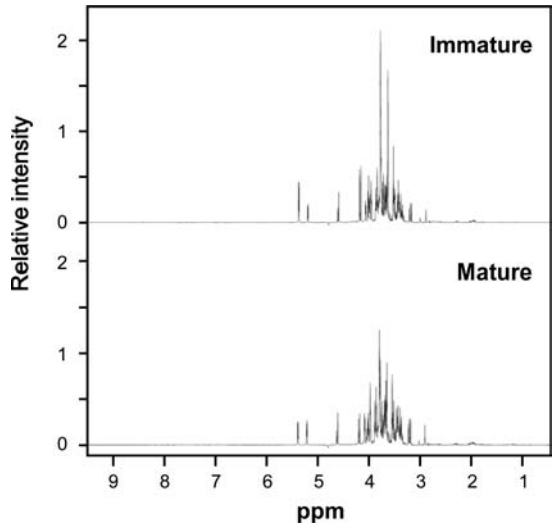

Figure 2. Average ^{1}H NMR spectra of mature and immature jujube water extracts. Each representative ^{1}H NMR spectrum of mature and immature jujube water extracts was the mean of five replicates (n = 5). The overall features for both spectra are indeed very similar. The NMR condition was described in the Materials and Methods. The experimental time for each sample was around 5 min (64 scans).

Table 1. Chemical Shifts of Metabolites Identified in ^{1}H-NMR Spectra of Jujube Extracts Used for Quantification

Metabolite	Chemical shift (ppm)[a]
Acetate	1.9 (s)[b]
Alanine	1.5 (d)
Asparagine	2.93 (m)
Choline	3.2 (s)
Creatine	3.9 (d)
Formate	8.4 (s)
Glucose	5.2 (d)
Isoleucine	1.2 (d)
Sucrose	5.4 (d)
Threonine	1.3 (d)
Valine	1.1 (d)

[a]Chemical shifts are determined by references, databases, and software described in the Materials and Methods section. [b]s: singlet; d: doublet; m: multiplet.

alanine, sucrose, and formate were higher in immature jujube than that of the mature one, while the levels of isoleucine, threonine, acetate, creatine, and glucose were higher in mature jujube than that of the immature one. The levels of valine, asparagine, and choline did not show a significant difference between mature and immature jujubes (Figure 4).

Pharmacological Properties of Jujubes at Two Stages of Maturity. PC12 cells are a commonly used model for the evaluation of neuronal differentiation.[20] The differentiation could be analyzed by a biochemical analysis in determining the expressions of neurofilaments that are the neuronal cell-specific cytoskeleton proteins, including NF68, NF160, and NF200. Our previous studies reported that jujube water extract stimulated the expressions of neurofilaments, especially NF68 in a concentration-dependent manner, and the submaximal concentration of jujube extract was revealed at ~2 mg/mL.[10] To compare the difference between mature and immature jujubes on NF68 expression, different jujube extracts at 2 mg/mL were applied onto cultured PC12 cells for 72 h. The results

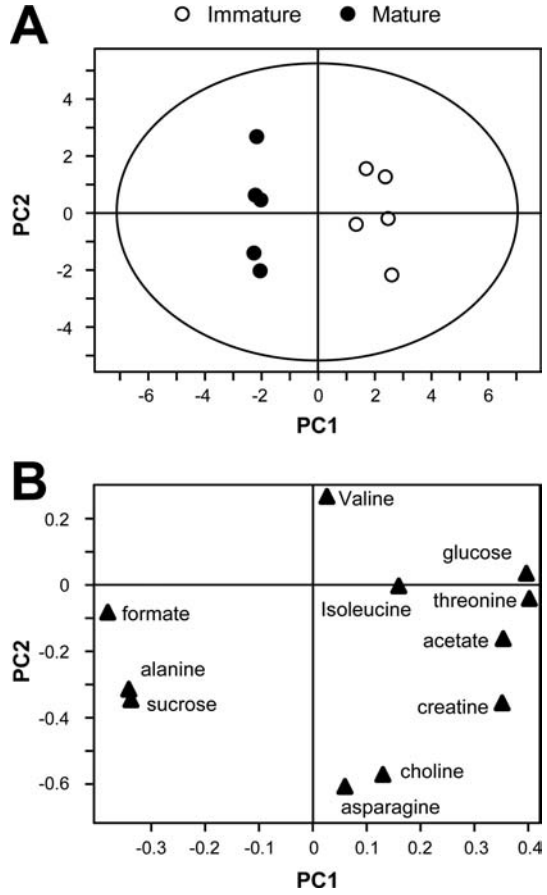

Figure 3. Chemometric analysis by PCA. (A) Scores from pattern recognition (PCA) of a selection of targeted molecules. (B) Loading plots from pattern recognition (PCA) of a selection of targeted molecules. Data are unit-variance scaled. The score plot can successfully discriminate mature and immature jujube. Loading plat shows which molecules contributed most to the discrimination. Immature jujube has a higher concentration in formate, sucrose, and alanine.

showed that both immature jujube and mature jujube possessed the ability to stimulate neurofilament expression (Figure 5A, upper panel). Moreover, the effect of mature jujube was ~60% higher than that of the immature one (Figure 5B, lower panel).

Jujube was reported to induce the expression of EPO, a specific hematopoietic growth factor, by activation of the transcriptional activity of HRE in cultured Hep3B cells, and the submaximal concentration of jujube was revealed at about 2 mg/mL.[12] To investigate the transcriptional activity of HRE, a luciferase-reporter construct (pHRE-Luc), having six HREs derived from the enhancer of EPO gene and tagged upstream of a luciferase gene, was transfected into cultured Hep3B cells (Figure 6, upper panel). Here, the HRE-mediated transcriptional activity of jujube at two stages of maturity was investigated. Different jujube extracts at 2 mg/mL were added onto HRE-expressed Hep3B cells. The data demonstrated that both immature jujube and mature jujube activated HRE-mediated transcriptional activity. And immature jujube possessed better effect, ~30% higher than that of mature jujube (Figure 6, lower panel).

DOI: 10.1021/jf5041564
J. Agric. Food Chem. 2015, 63, 739−744

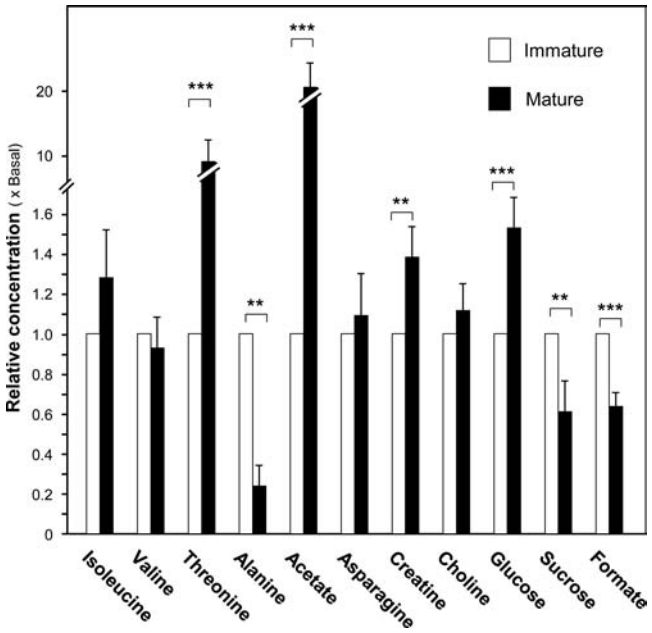

Figure 4. Quantification of identified metabolites between mature and immature jujube extract. Peaks associated with identified metabolites in all of the ^{1}H NMR spectra were integrated to yield the concentrations in the extracts relative to the mean value for immature jujube (basal level set at 1.0). The most noticeable feature was the concentration of sucrose and glucose; that of sucrose is higher in immature jujube, but mature jujube has a higher concentration in glucose. Values are expressed as mean ± SEM (n = 5). Statistical comparison was made between mature and immature jujubes; * p < 0.05; ** p < 0.01; *** p < 0.001, by student's t test.

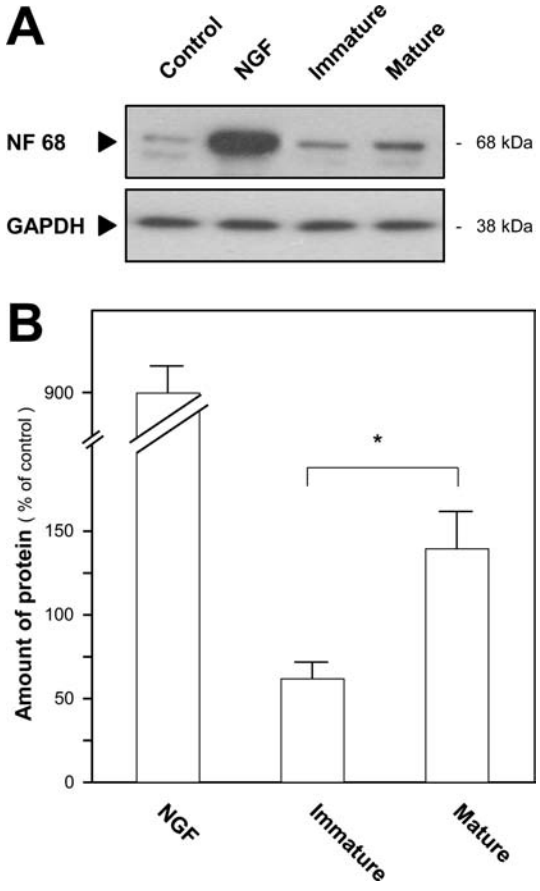

Figure 5. The inductive role of jujubes at two stages of maturity in neurofilament expression. (A) Cultured PC12 cells were treated with mature and immature jujube water extracts (2 mg/mL) for 72 h. The cell lysates were collected to determine the expressions of NF68 at ~68 kDa. NGF (50 ng/mL) served as a positive control. GAPDH at ~38 kDa served as loading control. (B) Quantification plot was shown in histograms. Data are expressed as the percentage of increase to basal reading (untreated culture), mean ± SEM, n = 4. Statistical comparison was made between mature and immature jujubes; *p < 0.05.

DISCUSSION

Jujube can be found all around the world today due to its health benefits both as food and herbal medicine. China has over 1.5 million hectares of total farm area and is the sole country known to be outputting jujube. The output of fresh jujube is about 400,000 tons, while 4,700 tons of jujubes are dried annually.[21] In China, jujube has been consumed into numerous products, i.e. juice, vinegar, and wine. In Korea, jujube is featured in the popular ginseng chicken dish. A candy called "jujube", being made from jujube paste, is available in America.[22] Among folk, dried jujubes have been commonly consumed as a snack or with tea. It can be further smoked to boost their taste.

Recently, the variation of chemical contents at different stages of the fruits was reported, indicating the specific usages of different stages of jujubes. In chemical analysis, the total phenolic content and total flavonoidic content rapidly decreased during maturity.[23−25] In good agreement with this notion, our studies revealed that the content of flavonoids fell sharply during maturity.[9] As for nucleotide and its derivatives, the contents of 7 compounds were higher in mature jujubes than that of immature ones, including xanthine, hypoxanthine, adenine, uridine, guanosine, cGMP, and cAMP.[9] The content of polysaccharide in jujube has not been significantly changed by the developmental stage.[9] In line with this, our current studies revealed that the total amount of sugars, including glucose and sucrose, did not show a significant difference between mature and immature jujubes. However, a report showed that the pectin contents increased during ripening.[26] Indeed, our data demonstrated that the content of glucose was higher in mature jujube than that of immature jujube, yet the sucrose amount was higher in immature jujube than that of the mature one. Choi et al. (2012) revealed that mature jujube had a lower level of protein than that of the immature one, while mature jujube contained higher amounts of free amino acids than that of the immature one.[23] Our NMR results showed that the total amount of tested amino acids was higher in mature jujube than that of the immure one, which was in line with the studies by Choi et al. (2012).[23] Fatty acid profiles of fruits were also reported to be affected by maturity.[27] Besides, we revealed that the total amount of organic acids including acetate and formate was higher in mature jujube than that of the immature one.

In biological analysis, the variation between mature and immature jujubes in antioxidative effect has been reported. Flavonoids were considered as one of the ingredients in jujube contributing to this effect, yet whether the levels of flavonoids were correlated with the activity is still debatable. Zhang et al. (2010) reported that the ferric reducing activity power (FRAP) effect was great related with the content of total flavonoids.[28] Immature jujube containing significantly higher amount of flavonoidic compounds showed better antioxidative activity

DOI: 10.1021/jf5041564
J. Agric. Food Chem. 2015, 63, 739−744

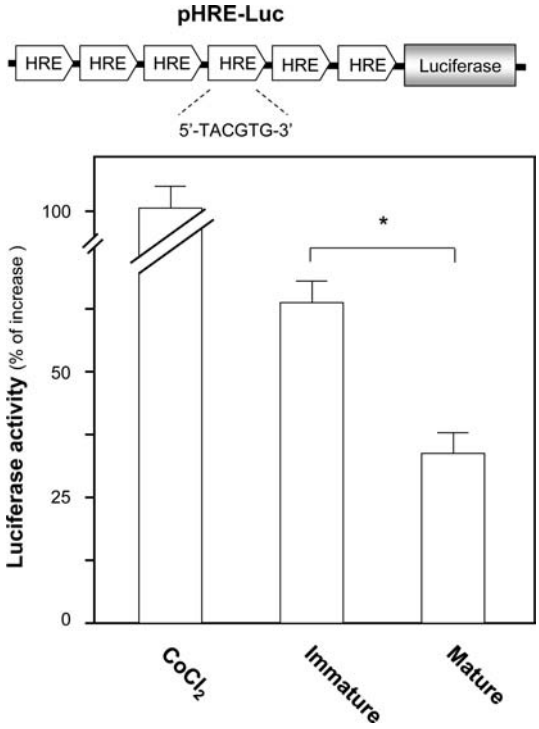

Figure 6. Comparison of HRE-mediated transcriptional activity on jujubes at two stages of maturity. A luciferase-reporter containing six HREs and a downstream luciferase-reporter gene, namely as pHRE-Luc, was used as a study tool (upper panel). Cultured Hep3B cells, transfected with pHRE-Luc, were treated with mature and immature jujube water extracts (2 mg/mL) for 24 h. The cell lysates were subjected to luciferase assay. $CoCl_2$ at 100 μM served as a positive control. Values are expressed as the percentage of increase to basal reading (untreated culture), and they are in mean ± SEM, where n = 4, each with triplicate samples. Statistical comparison was made between mature and immature jujubes; * $p < 0.05$.

than that of the mature one.[23] Zozio et al. (2014) proposed that, during ripening, the antioxidant activity may be more impacted by the flavonols and condensed tannins.[25] In contrast, other studies demonstrated that the antioxidative activity did not show significant correlation with the amount of flavonoids.[4,9] Here, immature jujube was shown to have higher levels of flavonoids, which performed better with regard to pHRE-Luc activity than that of mature jujube. However, our previous studies have shown that cAMP and polysaccharide, rather than flavonoid, in jujube could also achieve this activity.[12] This suggests that the pHRE-Luc activity of jujube does not relate to the content of flavonoids. In parallel to this notion, flavonoids derived from herbal medicines have been reported to be able to induce the expression of EPO,[29] suggesting that flavonoids may be one of the active ingredients for this action. In addition, we also revealed that mature jujube had a better effect in inducing neurofilament expression than that of the immature one: this higher induction could be an outcome of the higher amount of cAMP in mature jujube.[10] Besides, a report demonstrated that as the fruit matured, the activity of jujube in inhibiting Hel299 normal lung and A549 lung cancer cells declined.[23]

AUTHOR INFORMATION

Corresponding Author

*Phone: +852- 2358 7332; fax: +852- 2358 1559; e-mail: botsim@ust.hk.

Funding

This research was supported by Hong Kong Research Grants Council Theme-based Research Scheme (T13-607/12R), GRF (661110, 662911, 660411, 663012, 662713), TUYF12SC03, TUYF15SC01, The Hong Kong Jockey Club Charities Trust, and Foundation of The Awareness of Nature (TAON12SC01) to K.T. J.C. received a scholarship from the Hong Kong Chiu Chow Chamber of Commerce.

Notes

The authors declare no competing financial interest.

#J.C. and P.H.C. contributed equally.

ABBREVIATIONS USED

HRE, hypoxia response element; NMR, nuclear magnetic resonance; PCA, principal component analysis; EPO, erythropoietin; NGF, nerve growth factor; cGMP, guanosine 3′,5′-cyclic monophosphate; cAMP, adenosine 3′,5′-cyclic monophosphate

REFERENCES

(1) Li, J. W.; Fan, L. P.; Ding, S. D.; Ding, X. L. Nutritional composition of five cultivars of Chinese jujube. *Food Chem.* **2007**, *103*, 454−460.

(2) U.S. Department of Agriculture. ARS. USDA National Nutrient Database for Standard Reference, release 25, 2012.

(3) Xue, Z. P.; Feng, W. H.; Cao, J. K.; Cao, D. D.; Jiang, W. B. Antioxidant activity and total phenolic contents in peel and pulp of Chinese jujube (*Ziziphus jujuba* Mill.) fruit. *J. Food Biochem.* **2009**, *33*, 613−629.

(4) Choi, S. H.; Ahn, J. B.; Kozukue, N.; Levin, C. E.; Friedman, M. Distribution of free amino acids, flavonoids, total phenolics, and antioxidative activities of jujube (*Ziziphus jujuba*) fruits and seeds harvested from plants grown in Korea. *J. Agric. Food Chem.* **2011**, *59*, 6594−6604.

(5) Zhao, Z. H.; Li, J.; Wu, X. M.; Dai, H.; Gao, X. M.; Liu, M. J.; Tu, P. F. Structures and immunological activities of two pectic polysaccharides from the fruits of *Ziziphus jujuba* Mill. cv. *jinsixiaozao* Hort. *Food Res. Int.* **2006**, *39*, 917−923.

(6) Jiang, J. G.; Huang, X. J.; Chen, J.; Lin, Q. S. Comparison of the sedative and hypnotic effects of flavonoids, saponins, and polysaccharides extracted from Semen Ziziphus Jujube. *Nat. Prod. Res.* **2007**, *21*, 310−320.

(7) Ebrahimi, S.; Ashkani-Esfahani, S.; Poormahmudi, A. Investigating the efficacy of *Zizyphus jujuba* on neonatal jaundice. *Iran. J. Pediatr.* **2011**, *21*, 320−324.

(8) Goyal, R.; Sharma, P. L.; Singh, M. Possible attenuation of nitric oxide expression in anti-inflammatory effect of *Ziziphus jujuba* in rat. *J. Nat. Med.* **2011**, *65*, 514−518.

(9) Chen, J. P.; Li, Z. G.; Maiwulanjiang, M.; Zhang, W. L.; Zhan, J. Y. X.; Lam, C. T. W.; Zhu, K. Y.; Yao, P.; Choi, R. C. Y.; Lau, D. T. W.; Dong, T. T. X.; Tsim, K. W. K. Chemical and biological assessment of *Ziziphus jujuba* fruits from China: different geographical sources and developmental stages. *J. Agric. Food Chem.* **2013**, *61*, 7315−7324.

(10) Chen, J. P.; Maiwulanjiang, M.; Lam, K. Y.; Zhang, W. L.; Zhan, J. Y. X.; Lam, C. T. W.; Xu, S. L.; Zhu, K. Y.; Yao, P.; Lau, D. T. W.; Dong, T. T. X.; Tsim, K. W. K. A standardized extract of the fruit of *Ziziphus jujuba* (jujube) induces neuronal differentiation of cultured PC12 Cells: a signaling mediated by protein kinase A. *J. Agric. Food Chem.* **2014**, *62*, 1890−1897.

(11) Chen, J. P.; Yan, A. L.; Lam, K. Y. C.; Lam, C. T. W.; Zhang, W. L.; Xu, S. L.; Zhu, K. Y.; Yao, P.; Dong, T. T. X.; Tsim, K. W. K. A chemically standardized extract of *Ziziphus jujuba* fruit (jujube)

DOI: 10.1021/jf5041564
J. Agric. Food Chem. 2015, 63, 739−744

stimulates expressions of neurotrophic factors and anti-oxidant enzymes in cultured astrocytes. *Phytother. Res.* **2014**, DOI: 10.1002/ptr.5202.
(12) Chen, J. P.; Lam, C. T. W.; Guo, A. Y. Y.; Zhang, W. L.; Zhan, J. Y. X.; Bi, C. W. C.; Chan, G. K. L.; Lam, K. Y. C.; Yao, P.; Dong, T. T. X.; Tsim, K. W. K. The extract of *Ziziphus jujuba* fruit (jujube) induces expression of erythropoietin via hypoxia-inducible factor-1 α in cultured Hep3B cells. *Planta Med.* **2014**, *80*, 1622−1627.
(13) Chen, J. P.; Du, C. Y. Q.; Lam, K. Y. C.; Zhang, W. L.; Lam, C. T. W.; Yan, A. L.; Yao, P.; Lau, D. T. W.; Dong, T. T. X.; Tsim, K. W. K. The standardized extract of *Ziziphus jujuba* fruit (jujube) regulates pro-inflammatory cytokine expression in cultured murine macrophages: suppression of lipopolysaccharide-stimulated NF-κB Activity. *Phytother. Res.* **2014**, DOI: 10.1002/ptr.5160.
(14) Chan, P. H.; Zhang, W. L.; Lau, C. H.; Cheung, C. Y.; Keun, H. C.; Tsim, K. W. K.; Lam, H. Metabonomic analysis of water extracts from different *Angelica* roots by ^{1}H-nuclear magnetic resonance spectroscopy. *Molecules* **2014**, *19*, 3460−3470.
(15) Lewis, I. A.; Schommer, S. C.; Markley, J. L. rNMR: open source software for identifying and quantifying metabolites in NMR spectra. *Magn. Reson. Chem.* **2009**, *47* (Suppl 1), S123−126.
(16) Wishart, D. S.; Tzur, D.; Knox, C.; et al. HMDB: the human metabolome database. *Nucleic Acids Res.* **2007**, *35* (Database issue), D521−526.
(17) Ulrich, E. L.; Akutsu, H.; Doreleijers, J. F. BioMagResBank. *Nucleic Acids Res.* **2008**, *36*, (Database issue), D402−408.
(18) Fan, W. M. T. Metabolite profiling by one and two-dimensional NMR analysis of complex mixtures. *Prog. Nucl. Magn. Reson. Spectrosc.* **1996**, *28*, 161−219.
(19) Trygg, J.; Holmes, E.; Lundstedt, T. Chemometrics in metabonomics. *J. Proteome Res.* **2007**, *6*, 469−479.
(20) Greene, L. A.; Aletta, J. M.; Rukenstein, A.; Green, S. H. PC12 pheochromocytoma cells—Culture, nerve growth factor treatment, and experimental explitation. *Methods Enzymol.* **1987**, *147*, 207−216.
(21) Gao, Q. H.; Wu, C. S.; Wang, M. The jujube (*Ziziphus jujuba* Mill.) fruit: a review of current knowledge of fruit composition and health benefits. *J. Agric. Food Chem.* **2013**, *61*, 3351−3363.
(22) Lim, T. K. *Ziziphus jujuba*. In *Edible Medicinal And Non-Medicinal Plants*; Springer Science+Business Media: Dordrecht, Netherlands, 2013; Vol. *5*., pp 578−604.
(23) Choi, S. H.; Ahn, J. B.; Kim, H. J.; Im, N. K.; Kozukue, N.; Levin, C. E.; Friedman, M. Changes in free amino acid, protein, and flavonoid content in jujube (*Ziziphus jujube*) fruit during eight stages of growth and antioxidative and cancer cell inhibitory effects by extracts. *J. Agric. Food Chem.* **2012**, *60*, 10245−10255.
(24) Wang, C. T.; Cheng, D.; Cao, J. K.; Jiang, W. B. Antioxidant capacity and chemical constituents of Chinese jujube (*Ziziphus jujuba* Mill.) at different ripening stages. *Food Sci. Biotechnol.* **2013**, *22*, 639−644.
(25) Zozio, S.; Servent, A.; Cazal, G.; Mbeguie-A-Mbeguie, D.; Ravion, S.; Pallet, D.; Abel, H. Changes in antioxidant activity during the ripening of jujube (*Ziziphus mauritiana* Lamk.). *Food Chem.* **2014**, *150*, 448−456.
(26) Wang, H. J.; Chen, F. S.; Yang, H. S.; Chen, Y. M.; Zhang, L. F.; An, H. J. Effects of ripening stage and cultivar on physicochemical properties and pectin nanostructures of jujubes. *Carbohydr. Polym.* **2012**, *89*, 1180−1188.
(27) Guil-Guerrero, J. L.; Delgado, A. D.; Gonzalez, M. C. M.; Isasa, M. E. T. Fatty acids and carotenes in some ber (*Ziziphus jujuba* Mill.) varieties. *Plant Foods Hum. Nutr.* **2004**, *59*, 23−27.
(28) Zhang, H.; Jiang, L.; Ye, S.; Ye, Y. B.; Ren, F. Z. Systematic evaluation of antioxidant capacities of the ethanolic extract of different tissues of jujube (*Ziziphus jujuba* Mill.) from China. *Food Chem. Toxicol.* **2010**, *48*, 1461−1465.
(29) Zheng, K. Y. Z.; Choi, R. C. Y.; Cheung, A. W. H.; Guo, A. J. Y.; Bi, C. W. C.; Zhu, K. Y.; Fu, Q. A.; Du, Y. Q.; Zhang, W. L.; Zhan, J. Y. X.; Duan, R.; Lau, D. T. W.; Dong, T. T. X.; Tsim, K. W. K. Flavonoids from Radix Astragali induce the expression of erythropoietin in cultured cells: a signaling mediated via the accumulation of hypoxia-inducible factor-1 alpha. *J. Agric. Food Chem.* **2011**, *59*, 1697−1704.

DOI: 10.1021/jf5041564
J. Agric. Food Chem. 2015, 63, 739−744

JOURNAL OF AGRICULTURAL AND FOOD CHEMISTRY

Review

pubs.acs.org/JAFC

Novel Strategies To Enhance Lateral Flow Immunoassay Sensitivity for Detecting Foodborne Pathogens

Shan Shan, Weihua Lai,* Yonghua Xiong, Hua Wei, and Hengyi Xu

State Key Laboratory of Food Science and Technology, Nanchang University, Nanchang 330047, China

ABSTRACT: Food contaminated by foodborne pathogens causes diseases, affects individuals, and even kills those affected individuals. As such, rapid and sensitive detection methods should be developed to screen pathogens in food. One current detection method is lateral flow immunoassay, an efficient technique because of several advantages, including rapidity, simplicity, stability, portability, and sensitivity. This review presents the format and principle of lateral flow immunoassay strip and the development of conventional lateral flow immunoassay for detecting foodborne pathogens. Furthermore, novel strategies that can be applied to enhance the sensitivity of lateral flow immunoassay to detect foodborne pathogens are presented; these strategies include innovating new label application, designing new formats of lateral flow immunoassay, combining with other methods, and developing signal amplification systems. With these advancements, detection sensitivity and detection time can be greatly improved.

KEYWORDS: *lateral flow immunoassay, foodborne pathogens, sensitivity enhancement*

INTRODUCTION

Food safety is an important public health priority. Foodborne diseases are serious global problems and impose a significant burden not only on infected individuals but also on the economy. Although a majority of cases are mild, occasional cases can lead to serious or long-term conditions or even death. The Centers for Disease Control and Prevention estimated that each year roughly one in six Americans (or 48 million people) becomes adversely affected by foodborne diseases.[1] The World Health Organization estimated that approximately a million people suffered from foodborne diseases each year in the United Kingdom.[2] Foodborne pathogens contaminate food at some parts of the food chain from farm to fork. *Salmonella*, enterohemorrhagic *Escherichia coli* (EHEC), *Listeria monocytogenes*, *Staphylococcus aureus*, *Campylobacter*, *Cronobacter*, *Vibrio*, and *Shigella* are reported frequently. For instance, *Salmonella* is one of the most common causes of food poisoning in the world and can cause more serious illnesses in older adults, infants, and persons with chronic diseases. Every year, *Salmonella* is estimated to cause approximately 1.2 million illnesses in the United States.[3] Another case involves EHEC; this pathogen is often reported as one of the most common causes of foodborne outbreaks. For example, approximately 265,000 EHEC infections occur each year in the United States. EHEC O157 also causes approximately 36% of these infections, and non-O157 EHEC accounts for the remaining cases.[4] In other instances, *L. monocytogenes* primarily affects older adults, pregnant women, newborns, and adults with weakened immune systems. In the United States, *L. monocytogenes* causes nearly 2500 cases of listeriosis per year.[5] Foods that are most frequently associated with foodborne illnesses include meat, fish, poultry, vegetables, and fruits. These foods may cause illnesses when they are eaten.

In traditional methods, analytes are initially cultured in enrichment media for 18−24 h and then cultured in selective media for 18−24 h; biochemical and serological tests are subsequently performed to confirm suspected colonies for another 3−5 days. Conventional detection methods require 5−7 days to identify target bacteria. The methods of conventional isolation and culture are time-consuming and laborious. Therefore, a simple, specific, and sensitive method that can be used to detect pathogens should be developed. Several methods based on nucleic detection, such as real-time polymerase chain reaction (PCR),[6−8] multiplex PCR,[9−11] and loop-mediated isothermal amplification (LAMP) methods,[12−14] have been developed rapidly. Enzyme-linked immunosorbent assay (ELISA),[15−17] biosensing,[18−21] and electrochemical strategies[22,23] have also been extensively investigated. On the one hand, these methods are sensitive and specific; on the other hand, these methods require technical expertise, laborious procedures, and expensive instrumentation. In addition, these technologies are inappropriate for on-site tests. With these drawbacks, detection techniques have been developed and improved. For instance, lateral flow immunoassay (LFI) has been considered as a promising diagnostic tool extensively applied to detect drugs,[24−27] toxins,[28,29] hormones,[30,31] heavy metals,[32,33] pesticides,[34,35] and pathogens.[36,37] LFI provides several advantages, including rapid procedure, convenient operational requirements, sensitivity, and cost-effective equipment. Review papers have described the strengths, weaknesses, opportunities, and threats of LFI,[38] as well as its advanced ability to detect mycotoxins, phycotoxins, and pesticides.[39,40] In this paper, recent advances on LFI applied to detect foodborne pathogens are described. Furthermore, sensitivity enhancement methods are presented and discussed.

FORMAT AND PRINCIPLE OF TRADITIONAL LFI

Components of the LFI Format. Immunochromatography test paper technology, which was developed in the early 1980s,

Received: October 1, 2014
Revised: December 23, 2014
Accepted: December 24, 2014
Published: December 24, 2014

ACS Publications © 2014 American Chemical Society

DOI: 10.1021/jf5046415
J. Agric. Food Chem. 2015, 63, 745−753

involves rapid detection based on immunological techniques. A LFI device consists of a sample pad, a conjugate pad, a nitrocellulose membrane, and an absorbent pad. A test zone and a control zone are found on the nitrocellulose membrane (Figure 1A).

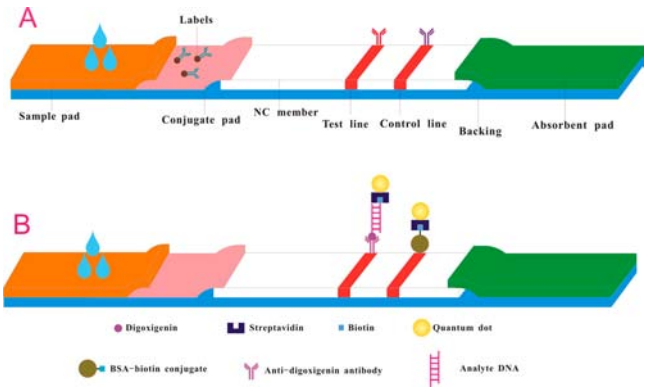

Figure 1. (A) Components of LFI strip format. (B) Schematic of detecting *S. aureus* principles of nucleic acid LFI. (Adapted from Chen et al.[87])

Sample pads are used to filter specific sample components; these pads can also change the pH of a sample and release analytes with high efficiency.

Conjugate pads are used to accept recognition labels and keep these labels stable during their entire shelf life period. Recognition labels are added to a treated conjugate pad by impregnating them in a conjugate suspension or dispensing them with quantitative noncontact dispensers.

After a sample is added to a strip, this sample migrates through a sample pad to a conjugate pad, where recognition labels are immobilized. Analytes in a given sample then interact with recognition labels when they migrate to an analytical region. Specific biological components are then bound at a test line and a control line via quantitative dispensers.

The absorbent pad resembles the engine of a LFI device; the absorbent pad pulls fluid and retains this fluid during the whole assay.

LFI Principle To Detect Foodborne Pathogens. Competitive assay and sandwich assay are the two kinds of formats commonly used in LFI. Competitive assay is preferred when target analytes exhibit low molecular weight or present a single specific antigen. Sandwich assay is performed when target analytes present several epitopes, such as pathogens. In a sandwich assay, the first analyte ligand (monoclonal antibodies are commonly used) is used to label markers. The second ligand (polyclonal antibodies are widely used) is placed on the test zone of a nitrocellulose membrane and assigned as the test line. The specific antibodies coating the control line capture excess labeled antibodies and conjugates. As sample extract is applied to the LFI device, the labeled first ligand initially binds to the target analyte to form an analyte−ligand complex; this complex then migrates forward by capillary force to the test zone. The second ligand in the test zone subsequently binds to the target analyte. Detectable signal enhancement in the test zone directly corresponds to the amount of a target analyte in a sample. In sandwich assay, detectable signal enhancement is observed as target analyte concentration increases.

CONVENTIONAL LFI TO DETECT FOODBORNE PATHOGENS

Colloidal gold lateral flow strip is considered as one of the most widely used tools to detect foodborne pathogens. Colloidal gold is essentially inert and forms spherical particles. Antibodies bind to the surfaces of these gold particles with enormous strength when correctly coupled, thus providing a high degree of long-term stability.[41,42] Hence, ligands exhibit good compatibility with biomolecules and can retain biochemical activities of tagged biomolecules. Colloidal gold-based LFI has been applied to detect foodborne pathogens.[43−50] Furthermore, a LFI device has been used to determine the analytical sensitivity of *E. coli* O157 of approximately 10^5 CFU/mL.[51,52] Preechakasedkit et al.[53] also used colloidal gold-based LFI strip to detect *S. typhimurium*, and the limit of detection was 1.14×10^5 CFU/mL. Ueda et al.[54] applied the colloidal gold LFI strip to detect *L. monocytogenes*, and the detection limit of this assay was 10^6 CFU/mL. The detection limit of *Vibrio harveyi* was 10^6 CFU/mL when a colloidal gold LFI was used.[55] Wiriyachaiporn et al.[56] further developed a LFI device to detect *Staphylococcus aureus*, and the result showed a detection limit of 10^6 CFU/mL. Colloidal gold-based LFI has also been widely applied in commercial detection. Table 1 summarizes the information regarding conventional colloidal gold LFI applied to detect foodborne pathogens in industries from some manufacturers. Although this summary includes only several commercial products, the main trends of colloidal gold LFI in the detection of foodborne pathogens are shown.

Table 1. Commercial Colloidal Gold LFI Applied To Detect Foodborne Pathogens

company	Web site	analytes
Beijing Kwinbon Biotechnology	www.kwinbon.com	*E. coli* O157:H7, *Listeria monocytogens*
Biocontrol	www.biocontrolsys.com	EHEC, *Salmonella*, *Listeria monocytogens*
DuPont	www.dupont.com	*E. coli* O157:H7, *Salmonella*, *Listeria monocytogens*
Invisible Sentinel	invisiblesentinel.com	*E. coli* O157:H7, STEC, *Salmonella*, *Listeria* spp., *Campylobacter*
Merck KGaA/EMD Chemicals	www.merck.com	*E. coli* O157:H7, *Salmonella*, *Campylobacter*
Neogen	www.neogen.com	*E. coli* O157:H7, *Salmonella*, *Listeria monocytogens*
New Horizons Diagnostic	www.nhdiag.com	*E. coli* O157:H7, *Salmonella*.spp.
Nippon Meat Packers	www.nipponham.co.jp	*E. coli* O157, O26, O111, *Salmonella enteritidis*, *Listeria* spp., *Campylobacter jejuni*
Quicking Biotech	www.quicking.cn	*E. coli* O157:H7, *Salmonella*, *Listeria monocytogens*
Romer Laboratories	www.romerlabs.com	*E. coli* O157:H7, *Salmonella*, *Listeria monocytogens*
Ubio Biotechnology System	www.ubio.in	*E. coli* O157:H7, *Salmonella*, *Listeria*, *Shigella*, *Vibrio cholera*, *V. parahemolyticus*

RECENT ADVANCEMENTS IN LFI TO DETECT FOODBORNE PATHOGENS

Researchers have devoted efforts to develop a rapid and sensitive lateral flow assay platform to screen foodborne pathogens (Table 2). New advancements in lateral flow assay have also been developed to detect foodborne pathogens; these advancements include innovating novel labels, designing new formats of LFI, combining with other methods, and developing signal amplification systems.

Innovation of Novel Label Application. An ideal label should be stable, have low nonspecific binding, be cost-effective,

DOI: 10.1021/jf5046415
J. Agric. Food Chem. 2015, 63, 745−753

Table 2. Novel Strategies Applied in LFI for Detecting Foodborne Pathogens

methods to enhance detection sensitivity		target	limit of detection	ref
new label application	colored labels	Shiga toxin-producing *E. coli*	$10^4/10^5$ CFU/mL	58
		Cronobacter spp.	8 ng	59
	luminescent NPs	*E. coli* O157:H7	10^4 CFU/mL	64
		E. coli O157:H7	6×10^2 CFU/mL	68
		V. anguillarum	10^2 CFU/mL	62
	other labels	*B. anthracis*	200 spores/mg	75
		E. coli O157:H7	10^3 CFU/mL	78
		S. typhimurium	10^2 CFU/mL	81
new formats of LFI	nucleic acid LFI	*S. aureus*	3 CFU/mL	87
	AMPs LFI and simultaneous detection	Shiga toxin-producing *E. coli*	10^4 CFU/mL	95
combined with other methods	combined with IMS	*E. coli* O157:H7	7.6×10^3 CFU/mL	105
signal amplification system	biotin−streptavidin system	*E. coli* O157:H7	2.3×10^3 CFU/mL	111
	enzyme amplification	*L. monocytogenes*	95 CFU/mL	112
	silver enhancement	*Salmonella*	10^4 CFU/mL	118

and be easily conjugated; an ideal label could also be used for multianalyte detection. Many efforts have also been devoted to discover novel labels to enhance detection sensitivity. In this paper, the types of the new labels successfully applied to enhance the sensitivity of LFI to detect foodborne pathogens are described; these new labels include colored labels, luminescent nanoparticles (NPs), and labels based on other properties.

Colored Labels. Colored labels are visible to the naked eye. They have been widely used in many fields owing to their convenience; colloidal gold and colored latexes are the most common labels in LFI. Carbon nanoparticles have also been applied as labels owing to their low price, nontoxicity, and high signal intensity; they can easily bind ligands to their large surface area, and they are suitable for LFI detection because of their "black-on-white" test results.[57,58]

Blažková[59] used carbon as a label to develop a nucleic acid test strip to detect *Cronobacter* spp. The PCR products of the analytes were conjugated with biotin on one side and digoxigenin on the other side. Carbon NPs were labeled with neutravidin as capture conjugate. Anti-digoxigenin antibodies and biotin−protein conjugates were sprayed on NC membrane as test line and control line, respectively. The detection limit of PCR product was 8 ng.

Luminescent NPs. Luminescent NPs have been extensively investigated because these NPs exhibit high sensitivity and spectral characteristics. Fluorescent dyes,[60] quantum dots,[61] and up-converting emitters[62] have been applied as labels to detect *Campylobacter jejuni*, *E. coli* O157:H7, and *Vibrio* in a LFI system.

Fluorescent dyes display low photostability and are highly quenched by the environment and concentration.[63] To overcome these drawbacks, researchers should couple multiple fluorescent dyes to a carrier or produce particles loaded with fluorescent dyes. Xie et al.[64] applied LFI based on fluorescent microspheres as labels to detect *E. coli* O157:H7 with the reader, which was from Shanghai Huguo Science Instrument Co. Ltd. (excitation wavelength = 470 nm; emission wavelength = 520 nm). The results showed that the sensitivity of this LFI system was 10^4 CFU/mL, whereas the sensitivity of LFI based on colloidal gold was 10^5 CFU/mL.

Quantum dots have been applied to bioassays and biosensors due to excellent signal brightness, size-tunable light emission, broad excitation spectrum, narrow emission spectrum, and excellent stability resisting photobleaching.[65−67] Bruno[68] compared colloidal gold with quantum dot versions in lateral flow test strips to detect *E. coli* O157:H7. A hand-held long-wave UV light (365 nm) and an orange Schott glass filter were used for illumination and enhancing visual detection of quantum dot particles. The limits of detection of *E. coli* O157:H7 were 6000 and 600 cells per test in a buffer by using colloidal gold lateral flow assay system and quantum dot lateral flow assay system, respectively.

Up-converting emitters are reportedly more sensitive than conventional labels such as colloidal gold or colored latex beads.[69] Up-converting emitters exhibit several advantages, including long lifetime and sequential two-photon absorption possible in a microsecond time scale. With these emitters, background absorption can be minimized because of anti-Stokes luminescence, and biomolecular photodegradation does not occur because of excitation occurring in the infrared area and the ease of production.[70] An ultrasensitive up-conversion fluorescent lateral flow strip based on NaYF4:Yb,Er NPs was applied to detect *Vibrio anguillarum*.[62] Carboxyl-modified β-NaYF4:Yb,Er NPs were synthesized by a facile one-pot solvothermal approach and then coupled with mAb as a conjugate probe in lateral flow assay. Continuous wave near-infrared spectrum laser at λ = 980 nm was used to excite the up-conversion nanoparticles on the strip by the up-converting nanoparticles−LFI biosensor. The sensitivity of the up-converting fluorescent strip was 10^2 CFU/mL and 100 times higher than that in enzyme-linked immunosorbent assays and exhibited good specificity attributed to no cross reaction with eight other pathogens.

Other Labels. In addition to colored and luminescent particles, new labels, including magnetic beads, enzymes, and liposomes, are also applied in LFI.

Magnetic beads have been widely used to separate target analytes; these magnetic beads have also been used as carriers and labels to detect pathogens.[71−74] Wang et al.[75] developed a superparamagnetic lateral flow assay to detect *Bacillus anthracis* spores. Anti-*B. anthracis* mAbs were conjugated to 300 nm superparamagnetic beads to capture bacterial spores. Different anti-*B. anthracis* mAbs were sprayed onto a nitrocellulose membrane as a test line, and goat anti-mouse IgG was used as a control line. The detection system yielded a linear range from 4×10^3 CFU/mL to 4×10^6 CFU/mL, and reproducible

DOI: 10.1021/jf5046415
J. Agric. Food Chem. 2015, 63, 745−753

detection limits were 200 spores mg^{-1} in milk powder. These superparamagnetic beads were larger and reaction time was longer than other types of strip tests because spores were larger (approximately 1 μm in diameter) than other analytes (such as proteins). The conjugates that run through a membrane required a long reaction time when the conjugates of magnetic beads and antibodies captured the spores. Small-diameter particles were also used as labels. With these particles, the flow rate was higher and reaction time was shorter; however, the use of these materials reduced detection sensitivity. Yan et al.[76] discussed the effect of the characteristics of Fe_3O_4 NPs (including particle size, size distribution, surface biomodification, magnetic property, and colloidal stability) on LFI when these Fe_3O_4 NPs were used as labels to detect *V. parahemolyticus*. To increase sensitivity and decrease false-positive reaction, they chose Fe_3O_4 NPs, which had small size and good colloidal stability as the labels. The 200 nm Fe_3O_4 nanoparticles were selected for the detection system.

In another approach, enzymes as labels were introduced to lateral flow assay to decrease the limit of detection. Enzymes can be linked to biomolecules to form complexes and exhibit enzymatic and immunological activities. The reaction between enzymes and substrates amplifies optical signals. Enzyme-linked immunosorbent assay (ELISA) based on the reaction between enzymes and substrates is considered to be one of the most outstanding assays. Hence, ELISA combined with lateral flow assay to detect analytes could be an excellent strategy to amplify signals.[77] Park et al.[78] fabricated a LFI based on sandwich ELISA to detect *E. coli* O157:H7. Optical signals were generated by the reaction between horseradish peroxidase (HRP) and its substrate, which could be read directly by the naked eye. The lower limit of detection was 10^3 CFU/mL.[78] A similar method was applied to detect *S. typhimurium*. An immunostrip was used to quantitatively determine *S. typhimurium* in the range from 9.2×10^3 CFU/mL to 9.2×10^6 CFU/mL based on chemiluminescent signals.[79]

Liposomes are formed from amphiphilic molecules and can encapsulate and immobilize molecular markers, such as dyes, via covalent or hydrophobic interactions. Khreich et al.[80] encapsulated sulfordamine B in liposomes as labels to detect fluorescent signals and obtained a 15-fold increase in sensitivity compared with the optical detection sensitivity of colored labels. Immunoliposome-encapsulated sulforhodamine B has also been applied as a capture label to detect *S. typhimurium* and compared with traditional colloidal gold lateral flow strip.[81−83] The result showed that the sensitivity of the immunoliposome immunoassay strip was higher than that of the traditional colloidal gold immunoassay strip; this high sensitivity was appropriate to detect food matrix.

New Formats of LFI. The application of antibodies in a LFI system exhibits several weaknesses, including difficult preparation and poor stability. A new ligand should be discovered to replace antibody. With advances in nucleic acid- and genomic sequence-based techniques, various detection methods have been developed using nucleic acid rather than antibodies. A rapid and sensitive detection system, which is called nucleic acid LFI,[84−86] has been developed. In the detection of *S. aureus* by nucleic acid LFI, quantum dot−streptavidin conjugate was used as a capture probe. Anti-digoxigenin antibody and BSA−biotin conjugate were sprayed on a membrane as a control line and a test line, respectively.[87] This detection system was based on two reaction systems, including digoxigenin and anti-digoxigenin, streptavidin, and biotin. DNA extracted from the analytes in a sample was labeled with digoxigenin on one side and with biotin on the other side. The schematic of detection principles is shown in Figure 1B. The limits of detection of *S. aureus* were 3 CFU/mL and 30 CFU/g in spiked milk powder and meat samples, respectively. Extracted DNA from analytes in a sample is usually amplified by PCR. LAMP was applied to perform rapid and sensitive nucleic acid amplification combined with lateral flow assay.[88−90] A shorter time is needed to amplify target DNA by LAMP than by PCR because a set of four primers that recognize a total of six distinct sequences on the target DNA is used in LAMP; LAMP also relies on the autocycling strand displacement of DNA synthesis performed by the large DNA polymerase under isothermal conditions.

Aptamers are another choice to replace antibodies as recognition molecules used for bacterial detection methods to bind specific analytes.[91−94] Yonekita et al.[95] used antimicrobial peptides (AMPs) as recognition probes for bacteria in a LFI. Streptavidin−colloidal gold was conjugated with biotinylated AMP, which was used as a capture probe. Anti-analyte antibodies were then sprayed on a test line, whereas anti-streptavidin antibodies were sprayed on a control line. Moreover, LFI was applied to simultaneously detect and identify Shiga toxin-producing *E. coli* O157, O26, and O111 (Figure 2). Studies have focused on the simultaneous detection

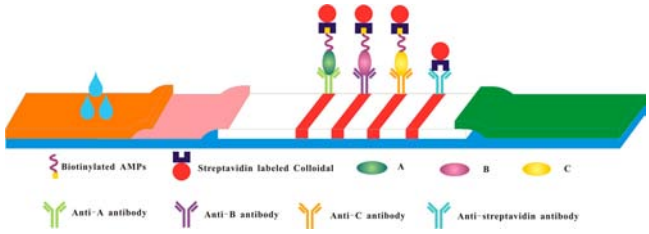

Figure 2. Schematic of the multiplex LFI strip. Antianalyte antibodies were sprayed on test lines to capture *E. coli* O157 (A), *E. coli* O26 (B), and *E. coli* O111 (C). Analytes were mixed with streptavidin-colloidal gold conjugate solution, and the mixtures were added to the sample pad of the LFI strip. After 15 min, positive or negative results could be determined. (Adapted from Yonekita et al.[95])

by LFI.[96,97] A simultaneous detection system exhibits several advantages, such as simplicity, rapidity, and sample-saving, compared with single detection. Yu et al.[98] developed a colloidal gold LFI to simultaneously detect *V. cholerae* serogroups O1 and O139, which could cause epidemic and pandemic cholera. The result showed that 100% sensitivity and 100% specificity were obtained for O1 and O139 in all of the tested strains. The loss of intensity in the test line after 21 weeks was not significant compared with that after 4 weeks; LFI remained stable for at least 3 months when stored dry at room temperature.

Combination with Other Methods. The sensitivity and specificity of methods used to detect foodborne pathogens should be improved. Immunomagnetic separation (IMS) performs an increasingly important function in the isolation and concentration of foodborne pathogens in food samples.[99−101] A detection method of combined IMS and LFI can significantly improve sensitivity, decrease detection time, and eliminate interference from food matrices.[102−104] Cui et al.[105] used IMS and traditional colloidal gold LFI to detect *E. coli* O157:H7. The results showed that the detection limit was 7.6×10^3 CFU/mL; thus, the result was 10 times higher than that of colloidal gold lateral flow assay. The schematic is shown in Figure 3. Chen et al.[106] developed a LFI test to detect *Cronobacter* and used silica-coated magnetic NPs to separate nucleic acid from

DOI: 10.1021/jf5046415
J. Agric. Food Chem. 2015, 63, 745−753

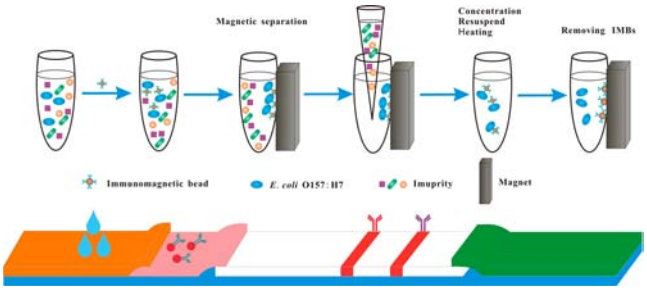

Figure 3. Schematic of immunomagnetic separation combined with colloidal gold LFI. (Adapted from Cui et al.[105])

Cronobacter lysate. The detection limit of this technique was 10^7 CFU/mL in pure culture, and 1 mL of 10^5 CFU *Cronobacter* was detected as positive in pure culture after silica-coated magnetic NP treatment was administered.

In a food matrix, some nontarget analytes may cause false-positive results. In the primary enrichment phase, the growth of closely related nontarget bacteria should be suppressed to improve detection sensitivity. Muldoon and co-workers[107] applied specific bacteriophages, which could suppress non-*Salmonella* bacterial growth for the control of cross-reactive non-*Salmonella* bacteria during primary sample enrichment. The bacteriophage cocktail that was added into primary enrichment significantly reduced the false positives of the immunochromatographic test strip. False positives were reduced from 32 of 115 samples tested to 0 in naturally contaminated beef samples.

Development of the Signal Amplification System. *Application of a Biotin−Streptavidin System.* Several approaches have been used to amplify signals of traditional gold colloidal LFI. These approaches aim to improve LFI sensitivity. To increase sensitivity effectively, a biotin−streptavidin system has been applied in lateral flow assay. The biotin−streptavidin system exhibits good reaction specificity and high affinity; hence, this system has been widely applied in many field detections.[108,109] Furthermore, this system can greatly contribute to signal amplification and background activity reduction.[110] Zhao et al.[111] prepared colloidal gold immunochromatographic strip based on a biotin−streptavidin system to detect *E. coli* O157:H7. Colloidal gold labeled anti-*E. coli* O157 monoclonal antibodies and biotinylated anti-*E. coli* O157 polyclonal antibodies were impregnated in a conjugated pad and a sample pad, respectively. Streptavidin and goat anti-mouse antibodies were immobilized in a test line and a control line of nitrocellulose membrane, respectively. *E. coli* O157 bound to biotinylated antibody and colloidal gold-labeled antibody to form a biotinylated antibody−analyte−colloidal gold-labeled antibody complex. This complex migrated to the detection zone by capillary action. The test line became red when the complex was captured by streptavidin via high-affinity biotin−streptavidin interaction (Figure 4). Streptavidin coated in the test line could reduce the background signal and amplify the detection signal owing to the high affinity between biotin and streptavidin. This method could detect *E. coli* O157 at a minimum of 2.3×10^3 CFU/mL without enrichment. Sensitivity was nearly 100 times higher than that of traditional lateral flow assay.[52]

Enzyme Amplification. In another approach involving signal amplification, enzymes are introduced to a lateral flow assay. Cho et al.[112] prepared an antibody−enzyme−magnetic NP complex as a label to detect *L. monocytogenes* by employing a lateral flow assay. In this strategy, magnetic properties and enzyme catalytic

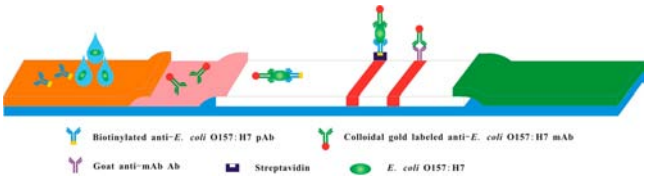

Figure 4. Schematic of the colloidal gold LFI based on biotin−streptavidin system to detect *E. coli* O157:H7.

amplifications were combined, thereby generating a darker signal on magnetic beads because of enzyme−substrate reaction (Figure 5). The study included three steps as follows: (1)

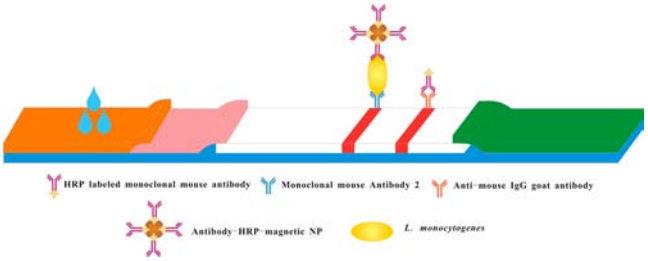

Figure 5. Schematic of LFI based on enzyme combined with magnetic separation step to detect *L. monocytogenes*. (Adapted from Cho et al.[112])

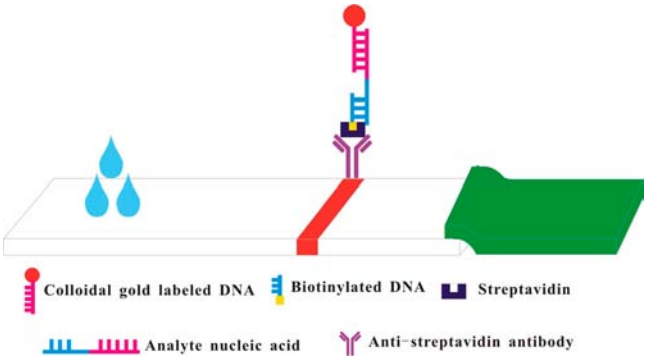

Figure 6. Schematic of LFI. As immunoreaction was completed, test strip was soaked in silver enhancer reagent to intensify the signal of gold nanoparticles. (Adapted from Liu et al.[118])

magnetic separation and concentration; (2) lateral flow immunochromatography; and (3) signal generation by placing HRP substrates on the absorption pad on the lateral side of a nitrocellulose membrane pad (Figure 5). Signals were captured as images using a scanner. The optical densities of the images were digitized by using image analysis program (Multianalyst version 1.1, Bio-Rad Laboratories, Hercules, CA, USA) to obtain the signal value. After the signal was amplified, the limit of detection of 95 CFU/mL was obtained in buffer solution.

Silver Enhancement. Silver nucleation on gold has been applied to perform sensitive biosensing and achieve signal amplification.[113−116] Silver precipitates on gold and can enhance electrochemical and colorimetric signals; silver can also vary the resistance or conductance of a substrate.[117] Color is greatly enhanced on the basis of the reaction between silver salt and reducing agent when silver is deposited on gold. Liu et al.[118] utilized a 16S rDNA/rRNA probe-conjugated AuNPs and silver enhancement method based on sandwich LFI to detect *Salmonella*. In this assay, anti-avidin antibody was sprayed onto a nitrocellulose membrane to capture avidin. A biotinylated

DOI: 10.1021/jf5046415
J. Agric. Food Chem. 2015, 63, 745−753

capture probe was conjugated with avidin and 16S rDNA/rRNA probe-conjugated AuNPs as a capture probe to capture *Salmonella*-targeted nucleic acid. Both biotinylated probe and probe-conjugated AuNPs could capture *Salmonella*-targeted nucleic acid; these probes then constituted sandwich LFI. To improve detection sensitivity and intensify AuNP signal, researchers soaked test strips in silver enhancer reagents. Nucleic acids were detected from 10^7 bacterial cells. The detection limit was as low as 10^4 cells after silver enhancement was performed (Figure 6).

CONCLUSIONS

Traditional lateral flow assay has been widely applied to detect foodborne pathogens. However, detection sensitivity is limited. As such, future studies should focus on enhancing detection sensitivity and decreasing detection time of LFI to detect foodborne pathogens. Scientists have devoted efforts to attain these goals. This review described recent LFI advancements, including using new labels, applying new formats, combining other methods, and utilizing signal amplification systems, in foodborne pathogen detection. With these advancements, detection sensitivity and detection time can be greatly improved. In the future, hard work should be done to further improve the stability and convenience of these sensitive lateral flow immunoassays.

AUTHOR INFORMATION

Corresponding Author

*(W.L.) Mail: State Key Laboratory of Food Science and Technology, Nanchang University, 235 Nanjing East Road, Nanchang 330047, China. Phone: 0086-13879178802. Fax: 0086-791-88157619. E-mail: talktolaiwh@163.com.

Funding

We are grateful to the Research Program of the State Key Laboratory of Food Science and Technology, Nanchang University (Project SKLF-ZZB-201307), earmarked fund for Jiangxi Agriculture Research System (JXARS-03), and the Nanchang Technological Program (2012-CYH-DW-SP-001) for financial support.

Notes

The authors declare no competing financial interest.

REFERENCES

(1) The Centers for Disease Control and Prevention (CDC). 2011 Estimates of Foodborne Illness in the United States; http://www.cdc.gov/Features/dsFoodborneEstimates (updated April 15, 2011).

(2) World Health Organization. Foodborne Disease Strategy: 2010 update. United Kingdom; http://multimedia.food.gov.uk/multimedia/pdfs/fds2015.pdf (published May 2011).

(3) The Centers for Disease Control and Prevention (CDC). *Salmonella*.; http://www.cdc.gov/salmonella/ (updated June 13, 2014).

(4) The Centers for Disease Control and Prevention (CDC). General Information, *Escherichia coli (E. coli)*; http://www.cdc.gov/ecoli/general/index.html (updated Aug 3, 2012).

(5) The Centers for Disease Control and Prevention (CDC). *Listeria monocytogenes*, Pathogens & Protocols; http://www.cdc.gov/pulsenet/pathogens/listeria.html (updated Aug 5, 2013).

(6) Wang, L. J.; Li, P.; Zhang, Z. L.; Chen, Q.; Aguilar, P. Z.; Xu, H.; Yang, L.; Xu, F.; Lai, W. H.; Xiong, Y. H.; Wei, H. Rapid and accurate detection of viable *Escherichia coli* O157:H7 in milk using a combined IMS, sodium deoxycholate, PMA and real-time quantitative PCR process. *Food Control* **2014**, *36* (1), 119−125.

(7) Haldar, M.; Butler, M.; Quinn, D. C.; Stratton, W. C.; Tang, Y. W.; Burnham, C. A. D. Evaluation of a real-time PCR assay for simultaneous detection of *Kingella kingae* and *Staphylococcus aureus* from synovial fluid in suspected septic arthritis. *Ann. Lab. Med.* **2014**, *34* (4), 313−316.

(8) Liu, Y. R.; Mustapha, A. Detection of viable *Escherichia coli* O157:H7 in ground beef by propidium monoazide real-time PCR. *Int. J. Food Microbiol.* **2014**, *170*, 48−54.

(9) Chandra, M.; Cheng, P.; Rondeau, G.; Porwollik, S.; McClelland, M. A single step multiplex PCR for identification of six diarrheagenic *E. coli* pathotypes and *Salmonella*. *Int. J. Med. Microbiol.* **2013**, *303* (4), 210−216.

(10) Yang, Y. J.; Xu, F.; Xu, H. Y.; Aguilar, Z. P.; Niu, R. J.; Yuan, Y.; Sun, J. C.; Lai, W. H.; You, X. H.; Wan, C. X.; Wei, H. Magnetic nanobeads based separation combined with propidium monoazide treatment and multiplex PCR assay for simultaneous detection of viable *Salmonella typhimurium*, *Escherichia coli* O157:H7 and *Listeria monocytogenes* in food products. *Food Microbiol.* **2013**, *34* (2), 418−424.

(11) Binet, R.; Deer, M. D.; Uhlfelder, J. S. Rapid detection of *Shigella* and enteroinvasive *Escherichia coli* in produce enrichments by a conventional multiplex PCR assay. *Food Microbiol.* **2014**, *40*, 48−54.

(12) Soli, K. W.; Kas, M.; Maure, T.; Umezaki, M.; Morita, A.; Siba, P. M.; Greenhill, A. R.; Horwood, P. F. Evaluation of colorimetric detection methods for *Shigella*, *Salmonella*, and *Vibrio cholerae* by loop-mediated isothermal amplification. *Diagn. Microbiol. Infect. Dis.* **2013**, *77* (4), 321−323.

(13) Wang, L.; Shi, L.; Su, J. Y.; Ye, Y. X.; Zhong, Q. Q. Detection of *Vibrio parahaemolyticus* in food samples using in situ loop-mediated isothermal amplification method. *Gene* **2013**, *515* (2), 421−425.

(14) Niessen, L.; Luo, J.; Denschlag, C.; Vogel, R. F. The application of loop-mediated isothermal amplification (LAMP) in food testing for bacterial pathogens and fungal contaminants. *Food Microbiol.* **2013**, *36* (2), 191−206.

(15) Jain, S.; Chattopadhyay, S.; Jackeray, R.; Abid, C. K. V.; Kohli, G. S.; Singh, H. Highly sensitive detection of *Salmonella typhi* using surface aminated polycarbonate membrane enhanced-ELISA. *Biosens. Bioelectron.* **2012**, *31* (1), 37−43.

(16) Cho, I. H.; Irudayaraj, J. In-situ immuno-gold nanoparticle network ELISA biosensors for pathogen detection. *Int. J. Food Microbiol.* **2013**, *164* (1), 70−75.

(17) Nyman, A. K. J.; Ågren, E. C. C.; Bergström, K.; Wahlström, H. Evaluation of the specificity of three enzyme-linked immunosorbent assays for detection of antibodies against *Salmonella* in bovine bulk milk. *Acta Vet. Scand.* **2013**, *55* (1), 5.

(18) Liu, T.; Zhao, Y.; Zhang, Z. H.; Zhang, P. P.; Li, J.; Yang, R. F.; Yang, C. X.; Zhou, L. A fiber optic biosensor for specific identification of dead *Escherichia coli* O157:H7. *Sens. Actuators, B* **2014**, *196*, 161−167.

(19) Ma, X. Y.; Jiang, Y. H.; Jia, F.; Yu, Y.; Chen, J.; Wang, Z. P. An aptamer-based electrochemical biosensor for the detection of *Salmonella*. *J. Microbiol. Methods* **2014**, *98*, 94−98.

(20) Li, Y. X.; Afrasiabi, R.; Fathi, F.; Wang, N.; Xiang, C. L.; Love, R.; She, Z.; Kraatz, H. B. Impedance based detection of pathogenic *E. coli* O157:H7 using a ferrocene-antimicrobial peptide modified biosensor. *Biosens. Bioelectron.* **2014**, *58*, 193−199.

(21) Song, Y.; Li, W.; Duan, Y. F.; Li, Z. J.; Deng, L. Nicking enzyme-assisted biosensor for *Salmonella enteritidis* detection based on fluorescence resonance energy transfer. *Biosens. Bioelectron.* **2014**, *55*, 400−404.

(22) Cheng, C. N.; Peng, Y.; Bai, J. L.; Zhang, X. Y.; Liu, Y. Y.; Fan, X. J.; Ningb, B.; Gao, Z. X. Rapid detection of *Listeria monocytogenes* in milk by self-assembled electrochemical immunosensor. *Sens. Actuators, B* **2014**, *190*, 900−906.

(23) Zhou, J.; Du, L. P.; Zou, L.; Zou, Y. C.; Hu, N.; Wang, P. An ultrasensitive electrochemical immunosensor for carcinoembryonic antigen detection based on staphylococcal protein A-Au nanoparticle modified gold electrode. *Sens. Actuators, B* **2014**, *197*, 220−227.

(24) Hayden, J. A.; Schmeling, M.; Hoofnagle, A. N. Lot-to-lot variations in a qualitative lateral-flow immunoassay for chronic pain drug monitoring. *Clin. Chem.* **2014**, *60* (6), 896−897.

(25) Taranova, N. A.; Byzova, N. A.; Zaiko, V. V.; Starovoitova, T. A.; Yu, Y.; Vengerov, Z. A. V.; Dzantiev, B. B. Integration of lateral flow and microarray technologies for multiplex immunoassay: application to the

DOI: 10.1021/jf5046415
J. Agric. Food Chem. 2015, 63, 745−753

determination of drugs of abuse. *Microchim. Acta* **2013**, *180* (11−12), 1165−1172.
(26) Lai, W. H.; Fung, D. Y. C.; Xu, Y.; Xiong, Y. H. Screening procedures for clenbuterol residue determination in raw swine livers using lateral-flow assay and enzyme-linked immunosorbent assay. *J. Food Prot.* **2008**, *71* (4), 865−869.
(27) Lai, W. H.; Xu, Y.; Fung, D. Y. C.; Xiong, Y. H. Development of a lateral-flow assay for rapid screening of the performance-enhancing sympathomimetic drug clenbuterol used in animal production; food safety assessments. *Asia Pac. J. Clin. Nutr.* **2007**, *16* (1), 106−110.
(28) Lai, W. H.; Fung, D. Y. C.; Xu, Y.; Liu, R. R.; Xiong, Y. H. Development of a colloidal gold strip for rapid detection of ochratoxin A with mimotope peptide. *Food Control* **2009**, *20* (9), 791−795.
(29) Wang, Z. H.; Li, H.; Li, C. L.; Yu, Q.; Shen, J. Z.; De Saeger, S. Development and application of a quantitative fluorescence-based immunochromatographic assay for fumonisin B1 in maize. *J. Agric. Food Chem.* **2014**, *62* (27), 6294−6298.
(30) Chang, H. F.; Wang, J. Q.; Wang, B.; Deng, A. An immunochromatographic assay for rapid and simultaneous detection of levonorgestrel and methylprednisolone in water samples. *Chin. Chem. Lett.* **2013**, *24* (10), 937−940.
(31) Xu, C. L.; Wang, H. T.; Peng, C. F.; Jin, Z. Y.; Liu, L. Q. Colloidal gold-based immumochromatographic assay for detection of diethylstilbestrol residues. *Biomed. Chromatogr.* **2006**, *20* (12), 1390−1394.
(32) Zhu, M. Y.; Wang, Y.; Deng, Y.; Yao, L.; Adeloju, S. B.; Pan, D. D.; Xue, F.; Wu, Y. C.; Zheng, L.; Chen, W. Ultrasensitive detection of mercury with a novel one-step signal amplified lateral flow strip based on gold nanoparticle-labeled ssDNA recognition and enhancement probes. *Biosens. Bioelectron.* **2014**, *61*, 14−20.
(33) Fu, Q. Q.; Tang, Y.; Shi, C. Y.; Zhang, X. L.; Xiang, J. J.; Liu, X. A novel fluorescence-quenching immunochromatographic sensor for detection of the heavy metal chromium. *Biosens. Bioelectron.* **2013**, *49*, 399−402.
(34) Lee, E. H.; Kim, Y. A.; Lee, Y. T.; Hammock, B. D.; Lee, H. S. Competitive immunochromatographic assay for the detection of the organophosphorus pesticide EPN. *Food Agric. Immunol.* **2013**, *24* (2), 129−138.
(35) Wang, L. M.; Cai, J.; Wang, Y. L.; Fang, Q. K.; Wang, S. Y.; Cheng, Q.; Du, D.; Lin, Y. H.; Liu, F. Q. A bare-eye-based lateral flow immunoassay based on the use of gold nanoparticles for simultaneous detection of three pesticides. *Microchim. Acta* **2014**, 1−8.
(36) Chaivisuthangkura, P.; Pengsuk, C.; Longyant, S.; Sithigorngul, P. Evaluation of monoclonal antibody based immunochromatographic strip test for direct detection of *Vibrio cholerae* O1 contamination in seafood samples. *J. Microbiol. Methods* **2013**, *95* (2), 304−311.
(37) Chen, W. X.; Zhang, J.; Lu, G.; Yuan, Z. W.; Wu, Q.; Li, J. J.; Xu, G. P.; He, A.; Zheng, J.; Zhang, J. Development of an immunochromatographic lateral flow device for rapid diagnosis of *Vibrio cholerae* O1 serotype Ogawa. *Clin. Biochem.* **2014**, *47* (6), 448−454.
(38) Posthuma, T. G. A.; Korf, J.; Van Amerongen, A. Lateral flow (immuno)assay: its strengths, weaknesses, opportunities and threats. A literature survey. *Anal. Bioanal. Chem.* **2009**, *393* (2), 569−582.
(39) Anfossi, L.; Baggiani, C.; Giovannoli, C.; D'Arco, G.; Giraudi, G. Lateral-flow immunoassays for mycotoxins and phycotoxins: a review. *Anal. Bioanal. Chem.* **2013**, *405* (2−3), 467−480.
(40) Dzantiev, B. B.; Byzova, A. N.; Urusov, E. A.; Zherdev, V. A. Immunochromatographic methods in food analysis. *Trends Anal. Chem.* **2014**, *55*, 81−93.
(41) Zhang, Z.; Lin, M.; Zhang, S.; Vardhanabhuti, B. Detection of aflatoxin M1 in milk by dynamic light scattering coupled with superparamagnetic beads and gold nanoprobes. *J. Agric. Food Chem.* **2013**, *61* (19), 4520−4525.
(42) Sperling, R. A.; Parak, W. J. Surface modification, functionalization and bioconjugation of colloidal inorganic nanoparticles. *Philos. Trans. R. Soc. London, A* **2010**, *368* (1915), 1333−1383.
(43) Gryko, R.; Sobieszczanska, B. M.; Stopa, P. J.; Bartoszcze, A. M. Comparison of multiplex PCR, and an immunochromatographic method sensitivity for the detection of *Escherichia coli* O157:H7 in minced beef. *Acta Microbiol. Pol.* **2002**, *51* (2), 121−129.
(44) Nakasone, N.; Toma, C.; Lu, Y.; Iwanaga, M. Development of a rapid immunochromatographic test to identify enteropathogenic and enterohemorrhagic *Escherichia coli* by detecting EspB. *Diagn. Microbiol. Infect. Dis.* **2007**, *57* (1), 21−25.
(45) Brinkman, E.; Van Beurden, R.; Mackintosh, R.; Beumer, R. Evaluation of a new dip-stick test for the rapid detection of *Salmonella* in food. *J. Food Prot.* **1995**, *58* (9), 1023−1027.
(46) Bautista, D. A.; Elankumaran, S.; Arking, J. A.; Heckert, R. A. Evaluation of an immunochromatography strip assay for the detection of *Salmonella* sp. from poultry. *J. Vet. Diagn. Invest.* **2002**, *14* (5), 427−430.
(47) Seo, K. H.; Holt, P. S.; Stone, H. D.; Gast, R. K. Simple and rapid methods for detecting *Salmonella enteritidis* in raw eggs. *Int. J. Food Microbiol.* **2003**, *87* (1), 139−144.
(48) Muller, J. D.; Wilks, C. R.; O'Riley, K. J.; Condron, R. J.; Bull, R.; Mateczun, A. Specificity of an immunochromato-graphic test for anthrax. *Aust. Vet. J.* **2004**, *82* (4), 220−222.
(49) Huang, S. H.; Wei, H.; Lee, Y. C. One-step immunochromatographic assay for the detection of *Staphylococcus aureus*. *Food Control* **2007**, *18* (8), 893−897.
(50) Shim, W. B.; Choi, J. G.; Kim, J. Y.; Yang, Z. Y.; Lee, K. H.; Kim, M. G.; Ha, S. D.; Kim, K. S.; Kim, K. Y.; Kim, C. H.; Ha, K. S.; Eremin, S. A.; Chung, D. H. Production of monoclonal antibody against *Listeria monocytogenes* and its application to immunochromatography strip test. *J. Microbiol. Biotechnol.* **2007**, *17* (7), 1152−1161.
(51) Takeda, T.; Yamagata, K.; Yoshida, Y.; Yoshino, K.; Nomura, T.; Kansenshogaku, Z. Evaluation of immunochromatography-based rapid detection kit for fecal *Escherichia coli* O157. *J. Jpn. Assoc. Infect. Dis.* **1998**, *72* (8), 834−839.
(52) Byeong, Y. J.; Suk, C. J.; Chang, H. K. Development of a rapid immunochromatographic strip for detection of *Escherichia coli* O157. *J. Food Prot.* **2005**, *68* (10), 2140−2143.
(53) Preechakasedkit, P.; Pinwattana, K.; Dungchaic, W.; Siangproh, W.; Chaicumpa, W.; Tongtawe, P.; Chailapakul, O. Development of a one-step immunochromatographic strip test using gold nanoparticles for the rapid detection of *Salmonella typhi* in human serum. *Biosens. Bioelectron.* **2012**, *31* (1), 562−566.
(54) Ueda, S.; Iwase, M.; Kuwabara, Y. Evaluation of immunochromatography for the rapid and specific identification of *Listeria monocytogenes* from food. *Biocontrol Sci.* **2013**, *18* (3), 157−161.
(55) Sithigorngul, P.; Rukpratanporn, S.; Pecharaburanin, N.; Suksawat, P.; Longyant, S.; Chaivisuthangkura, P.; Sithigorngul, W. A simple and rapid immunochromatographic test strip for detection of pathogenic isolates of *Vibrio harveyi*. *J. Microbiol. Methods* **2007**, *71* (3), 256−264.
(56) Wiriyachaiporn, S.; Howarth, P. H.; Bruce, K. D.; Dailey, L. A. Evaluation of a rapid lateralflow immunoassay for *Staphylococcus aureus* detection in respiratory samples. *Diagn. Microbiol. Infect. Dis.* **2013**, *75* (1), 28−36.
(57) Lönnberg, M.; Carlsson, J. Quantitative detection in the attomole range for immunochromatographic tests by means of a flatbed scanner. *Anal. Biochem.* **2001**, *293* (2), 224−231.
(58) Noguera, P.; Posthuma-Trumpie, G. A.; Van Tuil, M.; Van der Wal, F. J.; De Boer, A.; Moers, A. P. H. A.; Van Amerongen, A. Carbon nanoparticles in lateral flow methods to detect genes encoding virulence factors of Shiga toxin-producing *Escherichia coli*. *Anal. Bioanal. Chem.* **2011**, *399* (2), 831−838.
(59) Blažková, M.; Javůrková, B.; Fukal, L.; Rauch, P. Immunochromatographic strip test for detection of genus *Cronobacter*. *Biosens. Bioelectron.* **2011**, *26* (6), 2828−2834.
(60) Xu, D.; Wu, X. L.; Li, B.; Li, P.; Ming, X.; Wei, H.; Xu, F. Rapid detection of *Campylobacter jejuni* using fluorescent microspheres as label for immunochromatographic strip test. *Food Sci. Biotechnol.* **2013**, *22* (2), 585−591.
(61) Xu, F.; Xu, D.; Ming, X.; Xu, H. Y.; Li, B.; Li, P.; Aguilar, Z. P.; Cheng, T. T.; Wu, X. L.; Wei, H. Quantum dot-based immunochromatography test strip for rapid detection of *Campylobacter jejuni*. *J. Nanosci. Nanotechnol.* **2013**, *13* (7), 4552−4559.

DOI: 10.1021/jf5046415
J. Agric. Food Chem. 2015, 63, 745−753

(62) Zhao, P.; Wu, Y.; Zhu, Y.; Yang, X.; Jiang, X.; Xiao, J.; Zhang, Y.; Li, C. Upconversion fluorescent strip sensor for rapid determination of *Vibrio anguillarum*. *Nanoscale* **2014**, *6* (7), 3804−3809.
(63) Wang, F.; Tan, W. B.; Zhang, Y.; Fan, X. P.; Wang, M. Q. Luminescent nanomaterials for biological labeling. *Nanotechnology* **2006**, *17* (1), R1−R13.
(64) Xie, Q. Y.; Wu, Y. H.; Xiong, Q. R.; Xu, H. Y.; Xiong, Y. H.; Liu, K.; Jin, Y.; Lai, W. H. Advantages of fluorescent microspheres compared with colloidal gold as a label in immunochromatographic lateral flow assays. *Biosens. Bioelectron.* **2014**, *54*, 262−265.
(65) Li, Z.; Wang, Y.; Wang, J.; Tang, Z.; Pounds, J. G.; Lin, Y. Rapid and sensitive detection of protein biomarker using a portable fluorescence biosensor based on quantum dots and a lateral flow test strip. *Anal. Chem.* **2010**, *82* (16), 7008−7014.
(66) Yang, H.; Li, D.; He, R.; Guo, Q.; Wang, K.; Zhang, X.; Huang, P.; Cui, D. A novel quantum dots-based point of care test for syphilis. *Nanoscale Res. Lett.* **2010**, *5* (5), 875−881.
(67) Zou, Z.; Du, D.; Wang, J.; Smith, J. N.; Timchalk, C.; Li, Y.; Lin, Y. Quantum dot-based immunochromatographic fluorescent biosensor for biomonitoring trichloropyridinol, a biomarker of exposure to chlorpyrifos. *Anal. Chem.* **2010**, *82* (12), 5125−5133.
(68) Bruno, G. J. Application of DNA aptamers and quantum dots to lateral flow test strips for detection of foodborne pathogens with improved sensitivity versus colloidal gold. *Pathogens* **2014**, *3* (2), 341−355.
(69) Hampl, J.; Hall, M.; Mufti, N. A.; Yao, Y. M. M.; MacQueen, D. B.; Wright, W. H.; Cooper, D. E. Upconverting phosphor reporters in immunochromatographic assays. *Anal. Biochem.* **2001**, *288* (2), 176−187.
(70) Goryacheva, Y. I.; Lenain, P.; De Saeger, S. Nanosized labels for rapid immunotests. *Trends Anal. Chem.* **2013**, *46*, 30−43.
(71) Mohamad, N. N.; Abdul, R. K.; Tan, S. C.; Noordin, R. Properties of surface functionalized iron oxide nanoparticles (ferrofluid) conjugated antibody for lateral flow immunoassay application. *J. Alloys Compd.* **2012**, *538*, 100−106.
(72) Tang, Y. J.; Li, Z. Y.; He, N. Y.; Zhang, L. M.; Ma, C.; Li, X. L.; Li, C. Y.; Wang, Z. F.; Deng, Y.; He, L. Preparation of functional magnetic nanoparticles mediated with PEG-4000 and application in *Pseudomonas aeruginosa* rapid detection. *J. Biomed. Nanotechnol.* **2013**, *9* (2), 312−317.
(73) He, N.; Wang, F.; Ma, C.; L, C. Y.; Zeng, X.; Deng, Y.; Zhang, L. M.; Li, Z. Y. Chemiluminescence analysis for HBV-DNA hybridization detection with magnetic nanoparticles based DNA extraction from positive whole blood samples. *J. Biomed. Nanotechnol.* **2013**, *9* (2), 267−273.
(74) Wang, D. B.; Tian, B.; Zhang, Z. P.; Wang, X. Y.; Fleming, J.; Bi, L. J.; Yang, R. F.; Zhang, X. E. Detection of *Bacillus anthracis* spores by super-paramagnetic lateral-flow immunoassays based on "road closure". *Biosens. Bioelectron.* **2014**, DOI: 10.1016/j.bios.2014.09.067.
(75) Wang, D. B.; Tian, B.; Zhang, Z. P.; Deng, J. Y.; Cui, Z. Q.; Yang, F. R.; Wang, X. Y.; Wei, H. P.; Zhang, X. Rapid detection of *Bacillus anthracis* spores using a super-paramagnetic lateral-flow immunological detection system. *Biosens. Bioelectron.* **2013**, *42*, 661−667.
(76) Yan, J.; Liu, Y. Y.; Wang, Y. L.; Xu, X. W.; Lu, Y.; Pan, Y. J.; Guo, F. F.; Shi, D. L. Effect of physiochemical property of Fe_3O_4 particle on magnetic lateral flow immunochromatographic assay. *Sens. Actuators, B* **2014**, *197*, 129−136.
(77) Joung, H. A.; Oh, Y. K.; Kim, M. G. An automatic enzyme immunoassay based on a chemiluminescent lateral flow immunosensor. *Biosens. Bioelectron.* **2014**, *53*, 330−335.
(78) Park, S.; Kim, H.; Paek, S. H.; Hong, W. J.; Kim, Y. K. Enzyme-linked immuno-strip biosensor to detect *Escherichia coli* O157:H7. *Ultramicroscopy* **2008**, *108* (10), 1348−1351.
(79) Park, S.; Kim, Y. T.; Kim, Y. K. Optical enzyme-linked immunosorbent assay on a strip for detection of *Salmonella typhimurium*. *BioChip J.* **2010**, *4* (2), 110−116.
(80) Khreich, N.; Lamourette, P.; Boutal, H.; Devilliers, K.; Créminon, C.; Volland, H. Detection of *Staphylococcus* enterotoxin B using fluorescent immunoliposomes as label for immunochromatographic testing. *Anal. Biochem.* **2008**, *377* (2), 182−188.
(81) Shukla, S.; Leem, H.; Kim, M. Development of a liposome-based immunochromatographic strip assay for the detection of *Salmonella*. *Anal. Bioanal. Chem.* **2011**, *401* (8), 2581−2590.
(82) Leem, H.; Shukla, S.; Song, X. J.; Heu, S.; Kim, M. An efficient liposome-based immunochromatographic strip assay for the sensitive detection of *Salmonella* Typhimurium in pure culture. *J. Food Saf.* **2014**, DOI: 10.1111/jfs.12119
(83) Shukla, S.; Leem, H.; Lee, J. S.; Kim, M. Immunochromatographic strip assay for the rapid and sensitive detection of *Salmonella* Typhimurium in artificially contaminated tomato samples. *Can. J. Microbiol.* **2014**, *60* (6), 399−406.
(84) Blažková, M.; Koets, M.; Rauch, P.; Van Amerongen, A. Development of a nucleic acid lateral flow immunoassay for simultaneous detection of *Listeria* spp. and *Listeria monocytogenes* in food. *Eur. Food Res. Technol.* **2009**, *229* (6), 867−874.
(85) Yeung, C. Y.; Liu, C. C.; Tseng, Y. T.; Tsai, K. C.; Hsieh, M. A.; Chan, W. T.; Liu, H. L.; Lee, H. C.; Hou, S. Y. Rapid identification of *Salmonella* using Hektoen enteric agar and 16S ribosomal DNA probe-gold nanoparticle immunochromatography assay in clinical faecal specimens. *Lett. Appl. Microbiol.* **2014**, *58* (4), 311−317.
(86) Fang, Z. Y.; Wu, W.; Lu, X. W.; Zeng, L. W. Lateral flow biosensor for DNA extraction-free detection of salmonella based on aptamer mediated strand displacement amplification. *Biosens. Bioelectron.* **2014**, *56* (15), 192−197.
(87) Chen, X. X.; Gan, M.; Xu, H.; Chen, F.; Ming, X.; Xu, H. Y.; Wei, H.; Xu, F.; Liu, C. W. Development of a rapid and sensitive quantum dot-based immunochromatographic strip by double labeling PCR products for detection of *Staphylococcus aureus* in food. *Food Control* **2014**, *46*, 225−232.
(88) Surasilp, T.; Longyant, S.; Rukpratanporn, S.; Sridulyakul, P.; Sithigorngul, P.; Chaivisuthangkura, P. Rapid and sensitive detection of *Vibrio vulnificus* by loop-mediated isothermal amplification combined with lateral flow dipstick targeted to *rpoS* gene. *Mol. Cell Probe* **2011**, *25* (4), 158−163.
(89) Prompamorn, P.; Sithigorngul, P.; Rukpratanporn, S.; Longyant, S.; Sridulyakul, P.; Chaivisuthangkura, P. The development of loop-mediated isothermal amplification combined with lateral flow dipstick for detection of *Vibrio parahaemolyticus*. *Lett. Appl. Microbiol.* **2011**, *52* (4), 344−351.
(90) Thongkao, K.; Longyant, S.; Silprasit, K.; Sithigorngul, P.; Chaivisuthangkura, P. Rapid and sensitive detection of *Vibrio harveyi* by loop-mediated isothermal amplification combined with lateral flow dipstick targeted to vhhP2 gene. *Aquacult. Res.* **2013**, 1−10.
(91) Arcidiacono, S.; Pivarnik, P.; Mello, C. M.; Senecal, A. Cy5 labeled antimicrobial peptides for enhanced detection of *Escherichia coli* O157:H7. *Biosens. Bioelectron.* **2008**, *23* (11), 1721−1727.
(92) Kulagina, N. V.; Lassman, M. E.; Ligler, F. S.; Taitt, C. R. Antimicrobial peptides for detection of bacteria in biosensor assays. *Anal. Chem.* **2005**, *77* (19), 6504−6508.
(93) Kulagina, N. V.; Shaffer, K. M.; Anderson, G. P.; Ligler, F. S.; Taitt, C. R. Antimicrobial peptide-based array for *Escherichia coli* and *Salmonella* screening. *Anal. Chim. Acta* **2006**, *575* (1), 9−15.
(94) Mannoor, M. S.; Zhang, S. Y.; Link, A. J.; McAlpine, C. M. Electrical detection of pathogenic bacteria via immobilized antimicrobial peptides. *Proc. Natl. Acad. Sci. U.S.A.* **2010**, *107* (45), 19207−19212.
(95) Yonekita, T.; Ohtsuki, R.; Hojo, E.; Morishita, N.; Matsumoto, T.; Aizawa, T.; Morimatsu, F. Development of a novel multiplex lateral flow assay using an antimicrobial peptide for the detection of Shiga toxin-producing *Escherichia coli*. *J. Microbiol. Methods* **2013**, *93* (3), 251−256.
(96) Le, T.; Yan, P. F.; Xu, J.; Hao, Y. J. A novel colloidal gold-based lateral flow immunoassay for rapid simultaneous detection of cyromazine and melamine in foods of animal origin. *Food Chem.* **2013**, *138* (2), 1610−1615.
(97) Wang, Y. K.; Yan, Y. X.; Ji, W. H.; Wang, H. G.; Li, S. Q.; Zou, Q.; Sun, J. H. Rapid simultaneous quantification of zearalenone and fumonisin B1 in corn and wheat by lateral flow dual immunoassay. *J. Agric. Food Chem.* **2013**, *61* (21), 5031−5036.

DOI: 10.1021/jf5046415
J. Agric. Food Chem. 2015, 63, 745−753

(98) Yu, C. Y.; Ang, G. Y.; Chua, A. L.; Tan, E. H.; Lee, S. Y.; Falero, D. G.; Otero, O.; Rodríguez, I.; Reyes, F.; Acosta, A.; Sarmiento, M. E.; Ghosh, S.; Ramamurthy, T.; Yean, C. Y.; Lalitha, P.; Ravichandran, M. Dry-reagent gold nanoparticle-based lateral flow biosensor for the simultaneous detection of *Vibrio cholerae* serogroups O1 and O139. *J. Microbiol. Methods* **2011**, *86* (3), 277−282.
(99) Varshney, M.; Yang, L. J.; Su, X. L.; Li, Y. B. Magnetic nanoparticle-antibody conjugates for the separation of *Escherichia coli* O157:H7 in ground beef. *J. Food Prot.* **2005**, *68* (9), 1804−1811.
(100) Xiong, Q. R.; Cui, X.; Saini, J. K.; Liu, D. F.; Shan, S.; Jin, Y.; Lai, W. H. Development of an immunomagnetic separation method for efficient enrichment of *Escherichia coli* O157:H7. *Food Control* **2014**, *37*, 41−45.
(101) Shan, S.; Zhong, Z. Q.; Lai, W. H.; Xiong, Y. H.; Cui, X.; Liu, D. F. Immunomagnetic nanobeads based on a streptavidin-biotin system for the highly efficient and specific separation of *Listeria monocytogenes*. *Food Control* **2014**, *45*, 138−142.
(102) Shim, W. B.; Choi, J. G.; Kim, J. Y.; Yang, Z. Y.; Lee, K. H.; Kim, M. G.; Ha, S. D.; Kim, K. S.; Kim, K. Y.; Kim, C. H.; Eremin, S. A.; Chung, D. H. Enhanced rapidity for qualitative detection of *Listeria monocytogenes* using an enzyme-linked immunosorbent assay and immunochromatography strip test combined with immunomagnetic bead separation. *J. Food Prot.* **2008**, *71* (4), 781−789.
(103) Fisher, M.; Atiya, N. Y.; Simon, I.; Gordin, M.; Mechaly, A.; Yitzhakiet, S. A combined immunomagnetic separation and lateral flow method for a sensitive on-site detection of *Bacillus anthracis* spores − assessment in water and dairy products. *Lett. Appl. Microbiol.* **2009**, *48* (4), 413−418.
(104) Qi, H.; Zhong, Z.; Zhou, H. X.; Deng, C. Y.; Zhu, H.; Li, J. F.; Wang, X. L.; Li, F. R. A rapid and highly sensitive protocol for the detection of *Escherichia coli* O157:H7 based on immunochromatography assay combined with the enrichment technique of immunomagnetic nanoparticles. *Int. J. Nanomed.* **2011**, *6*, 3033−3039.
(105) Cui, X.; Xiong, Q. R.; Xiong, Y. H.; Shan, S.; Lai, W. H. Establishing of a method combined immunomagnetic separation with colloidal gold lateral flow assay and its application in rapid detection of *Escherichia coli* O157:H7. *Chin. J. Anal Chem.* **2013**, *41* (12), 1812−1816.
(106) Chen, F.; Ming, X.; Chen, X. X.; Gan, M.; Wang, B. G.; Xu, F.; Wei, H. Immunochromatographic strip for rapid detection of *Cronobacter* in powdered infant formula in combination with silica-coated magnetic nanoparticles separation and 16S rRNA probe. *Biosens. Bioelectron.* **2014**, *61* (15), 306−313.
(107) Muldoon, M. T.; Teaney, G.; Li, J. K.; Onisk Dale, V.; Stave, J. W. Bacteriophage-based enrichment coupled to immunochromatographic strip−based detection for the determination of *Salmonella* in meat and poultry. *J. Food Prot.* **2007**, *70* (10), 2235−2242.
(108) Ahmed, R.; Spikings, E.; Zhou, S.; Thompsett, A.; Zhang, T. Pre-hybridisation: an efficient way of suppressing endogenous biotin-binding activity inherent to biotin-streptavidin detection system. *J. Immunol. Methods* **2014**, *406*, 143−147.
(109) Hu, C. M.; Dou, W. C.; Zhao, G. Y. Enzyme immunosensor based on gold nanoparticles electroposition and Streptavidin-biotin system for detection of *S. pullorum* and *S. gallinarum*. *Electrochim. Acta* **2014**, *117*, 239−245.
(110) Rosebrough, S. F.; Hartley, D. F. Biochemical modification of streptavidin and avidin: in vitro and in vivo analysis. *J. Nucl. Med.* **1996**, 1380−1384.
(111) Zhao, X. H.; He, X. W.; Li, W. M.; Liu, Y.; Yang, L. S.; Wang, J. H. Development and evaluation of colloidal gold immunochromatographic strip for detection of *Escherichia coli* O157. *Afr. J. Microbiol. Res.* **2010**, *4* (9), 663−670.
(112) Cho, I. H.; Irudayaraj, J. Lateral-flow enzyme immunoconcentration for rapid detection of *Listeria monocytogenes*. *Anal. Bioanal. Chem.* **2013**, *405*, 3313−3319.
(113) Liu, R.; Zhang, Y.; Zhang, S. Y.; Qiu, W.; Gao, Y. Silver enhancement of gold nanoparticles for biosensing: from qualitative to quantitative. *Appl. Spectrosc. Rev.* **2014**, *49* (2), 121−138.
(114) Anfossi, L.; Di, N. F.; Giovannoli, C.; Passini, C.; Baggiani, C. Increased sensitivity of lateral flow immunoassay for ochratoxin A through silver enhancement. *Anal. Bioanal. Chem.* **2013**, *405* (30), 9859−9867.
(115) Yang, W.; Li, X. B.; Liu, G. W.; Zhang, B. B.; Zhang, Y.; Kong, T.; Tang, J. J.; Li, D. N.; Wang, Z. A colloidal gold probe-based silver enhancement immunochromatographic assay for the rapid detection of abrin-a. *Biosens. Bioelectron.* **2011**, *26* (8), 3710−3713.
(116) Wen, J. L.; Zhou, S. G.; Yuan, Y. Graphene oxide as nanogold carrier for ultrasensitive electrochemical immunoassay of *Shewanella oneidensis* with silver enhancement strategy. *Biosens. Bioelectron.* **2014**, *52*, 44−49.
(117) Cao, X. D.; Ye, Y. K.; Liu, S. Q. Gold nanoparticle-based signal amplification for biosensing. *Anal. Biochem.* **2011**, *417* (1), 1−16.
(118) Liu, C. C.; Yeung, C. Y.; Chen, P. H.; Yeh, M. K.; Hou, S. Y. *Salmonella* detection using 16S ribosomal DNA/RNA probe-gold nanoparticles and lateral flow immunoassay. *Food Chem.* **2013**, *141* (3), 2526−2532.

DOI: 10.1021/jf5046415
J. Agric. Food Chem. 2015, 63, 745−753

JOURNAL OF AGRICULTURAL AND FOOD CHEMISTRY

Article

pubs.acs.org/JAFC

Rapid Metabolite Discovery, Identification, and Accurate Comparison of the Stereoselective Metabolism of Metalaxyl in Rat Hepatic Microsomes

Xinru Wang,[†] Jing Qiu,[‡] Peng Xu,[§] Ping Zhang,[†] Yao Wang,[†] Zhiqiang Zhou,[†] and Wentao Zhu*,[†]

[†]Department of Applied Chemistry, China Agricultural University, Beijing 100193, China

[‡]Institute of Quality Standards & Testing Technology for Agro-Products, Key Laboratory of Agro-product Quality and Safety, Chinese Academy of Agricultural Sciences, Beijing, China

[§]Research Center for Eco-Environmental Sciences, Chinese Academy of Sciences, Beijing, China

ABSTRACT: Metabolite identification and quantitation impose great challenges on risk assessment of agrochemicals, as many metabolite standards are generally unavailable. In this study, metalaxyl metabolites were identified by time-of-flight mass spectrometry and semiquantified by triple quadrupole tandem mass spectrometry with self-prepared ^{13}C-labeled metalaxyl metabolites as internal standards. Such methodology was employed to characterize the stereoselective metabolism of metalaxyl in rat hepatic microsomes successfully. Metabolites derived from hydroxylation, demethylation, and didemethylation were identified and semiquantified. The results indicated that (+)-*S*-metalaxyl eliminated preferentially as the enantiomer fraction was 0.32 after 60 min incubation. The amounts of hydroxymetalaxyl and demethylmetalaxyl derived from (−)-*R*-metalaxyl were 1.76 and 1.82 times higher than that of (+)-*S*-metalaxyl, whereas didemethylmetalaxyl derived from (+)-*S*-metalaxyl was 1.44 times larger than that from (−)-*R*-metalaxyl. This study highlights a new quantitation approach for stereoselective metabolism of chiral agrochemicals and provides more knowledge on metalaxyl risk assessment.

KEYWORDS: *metabolic profile, LC-MS, rat hepatic microsome, stereoselective metabolism, metabolite identification*

INTRODUCTION

To facilitate the elimination and/or utilization of exogenous chemicals, all living creatures perform a certain level of metabolism, which might result in the activation of drugs or even the production of new toxic species.[1,2] In some cases, metabolites show better bioactivities than the parent compound, such as acetaminophen from acetanilide.[3] In some other cases, metabolites exhibit more toxicities than the parent compound.[4−6] For example, Mitchell proposed that a toxic metabolite of acetaminophen is the main cause of acetaminophen-induced hepatic necrosis.[7] Also, metabolites are always important indicators of biological processes. Therefore, identification and quantitation of metabolites are very important in metabolism research as well as risk assessments of xenobiotics.[8] As for chiral drugs, it is well-known that stereochemistry has a marked impact on biological activity as well as biological processes such as absorption, degradation, metabolism, and excretion behavior in organisms. Enantiomers of a chiral compound can interact with biomacromolecules stereoselectively, leading to entirely different and even contradictory biological effects.[9] Consequently, stereoselective metabolic investigation is important for ecotoxicological and environmental risk assessment of current chiral pesticides. The main purpose of this study is to introduce a new way to facilitate the accurate comparison of the stereoselective metabolism of a chiral xenobiotic.

Nowadays, regarding the analytical tools used for qualitative and quantitative analysis of metabolites, mass spectrometry (MS) coupled with liquid chromatography (LC) is considered to be the most preeminent and widely used tool,[10−12] due primarily to its superior sensitivity, selectivity, speed of analysis, cost effectiveness, and ability to separate, detect, and identify metabolites even in the presence of many endogenous interferences.[13] Since molecular weight determination is always the first and basic step for qualitative analysis of metabolites, MS instruments with high-resolution mass measurement, such as time-of-flight (TOF) or Fourier transform (FT) mass spectrometers, are always preferred in this step. Then, for further structural confirmation, tandem mass spectrometry (MS/MS) is often used mainly because it covers a variety of scanning techniques including product ion, precursor ion, and neutral loss scanning. The results provide information on a series of characteristic fragment ion masses, all of which correspond to part of the unknown molecule. For metabolite quantitation, triple quadrupole MS coupled with LC operated in the multiple reaction monitoring (MRM) mode is considered as the gold standard.[14]

Traditionally, discovery of new metabolites from a single parent molecule is performed by tracking radioactive tracers that are catabolized from a radioactive parent compound.[15,16] Another widely used approach is stable isotope labeling.[17] For instance, Chowdhury et al. utilized stable isotope-labeled drugs to aid the detection and identification of ribavirin metabolites in rats.[18] The advantage of stable isotope labeling is that the metabolites are labeled in complex biological matrixes, which

Received: May 27, 2014
Revised: January 6, 2015
Accepted: January 12, 2015
Published: January 12, 2015

ACS Publications © 2015 American Chemical Society

DOI: 10.1021/jf5025104
J. Agric. Food Chem. 2015, 63, 754−760

can be distinguished from various interferences and possible laboratory contaminants.[19]

For the quantitative analysis of metabolites, the lack of metabolite standards always imposes a significant limitation. This is also the bottleneck for comprehensive metabolism research for chiral pesticides. Although synthesis of some potential metabolites can be achieved in theory, it would be a quite expensive and complex endeavor. Another possible approach to get metabolites might be incubation of substrates with in vivo methods[20] or some in vitro systems.[21,22] For example, in vivo methods often include administering fluorescent, isotopic, or radioactive labeled substrates to the living biological model, while potential in vitro systems often include cell cultures, enzyme mixtures, and liver microsomes. Simplicity and availability are the most obvious advantages of in vitro technologies. The relatively high concentration of substrate as well as metabolites in an in vitro system makes the metabolic study much easier than that with in vivo systems.[23] Microsomal incubation is a valuable and the most widely used tool for metabolism research on xenobiotics,[24] as it contains a significant amount of metabolic enzymes. Clements et al. developed a strategy of using liver microsomal incubation with drug candidates for the preparation of phase I drug metabolites, which could then be used as standards for in vivo experiments.[25] This approach inspired us that the microsomal incubation could be a possible and convenient way to produce metabolite "standards" of a pesticide.

Metalaxyl [*N*-(2,6-dimethylphenyl)-*N*-(methoxyacetyl)-D,L-alanine methyl ester, MX, Figure 1] is a systemic fungicide

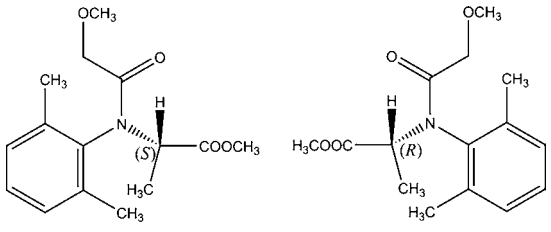

Figure 1. Chemical structure of metalaxyl enantiomers.

with protective and curative actions against oomycetes. Since introduction in 1977, it has been widely used in agriculture and horticulture.[26] It has also been reported that metalaxyl has many hazardous effects on humans and other nontarget organisms.[27,28] Recently, metalaxyl and its metabolites were detected in groundwater.[29,30] For a comprehensive risk assessment of metalaxyl, data on the stereoselective metabolism are indispensable. Therefore, the present work involved the following four aspects: (1) TOF-MS was employed to acquire the accurate molecular mass information and preliminary structural presumption of MX metabolites; (2) ^{13}C-labeled MX incubation and MS/MS detection were carried out for further structure identification; (3) ^{13}C-labeled metabolites were prepared and used as internal standards for quantitation; (4) stereoselective metabolism of MX enantiomers were quantitively investigated in rat hepatic microsomes.

MATERIALS AND METHODS

Chemicals. Racemic MX (*rac*-MX) standard (>99% purity) was provided by Institute for Control of Agrochemicals, China Ministry of Agriculture. (+)-*S*-MX and (−)-*R*-MX were prepared on an Agilent high-performance liquid chromatography (HPLC) with a preparative chiral column containing cellulose-tris(3,5-methylphenylcarbamate)-based chiral stationary phase (CDMPC−CSP, provided by the Department of Applied Chemistry, China Agricultural University, Beijing). $^{13}C_6$-MX and β-nicotinamide adenine dinucleotide phosphate (NADPH) were purchased from Sigma-Aldrich (St Louis, MO). $^{13}C_6$-MX acid [*N*-(2, 6-dimethylphenyl)-*N*-(methoxyacetyl)-alanine] was synthesized in our own laboratory. HPLC grade solvents were purchased from Beijing Chemicals (Beijing, China). All other chemicals and solvents were analytical grade and purchased from standard commercial sources. Water was purified with a Milli-Q system.

Stock solutions of *rac*-, (+)-*S*-, and (−)-*R*-MX were prepared in 2-propanol and were stored at −20 °C. Working standard solutions were obtained by dilutions of the stock solution in 2-propanol.

Animals. Adult male Sprague−Dawley rats (200−250 g, 5−6 weeks old) were purchased from the Vital River Laboratory Animal Company (Beijing, China) and were fed with a standard diet before use. All rats were handled in accordance with the standard guidelines for care and use of laboratory animals as laid down in the EU directive 2010/63/EU. Rat hepatic microsomes were prepared with a procedure as described by Zhu[31] and were stored at −80 °C.

Incubation of MX with Microsomes for Metabolite Identification. For the detection and identification of MX metabolites, rat hepatic microsomal incubations with MX of various time periods were carried out with a series of samples and controls in parallel. In particular, *rac*-MX (100 μM) was prepared in ethanol and added into the microsomal incubation system, which was made up of 1 mg of microsomal protein and 50 mM Tris-HCl buffer (pH7.4) with 5.0 mM $MgCl_2$. The ethanol added to each incubate was less than 1.0% v/v. After preincubation in a water bath at 37 °C for 5 min, NADPH at a final reaction concentration of 1.0 mM was added to the mixtures to initiate the reaction, resulting in a final total reaction volume of 1.0 mL. By adding 1 mL of acetonitrile containing 0.1% formic acid(v/v), the reactions were terminated after incubation in the water bath (37 °C) for 5, 10, 20, 30, and 60 min. The samples were vortexed for 3 min. To obtain a clear extract for analysis, samples were frozen at −20 °C for 1 h for protein precipitation and then centrifuged at 12 000*g* at 4 °C for 4 min, and the supernatant was transferred to a new tube for one more centrifugation. Eventually the clear extract was collected for analysis.

Qualitative Analysis of MX and Its Metabolites in Microsomes. Samples were first analyzed by Agilent 1290 UPLC/microTOF Q II system (Bruker Co., DE); thus, the accurate molecular weights of the metabolites were acquired. A reversed-phase Agilent UPLC C18 analytical column (50 × 2.1 mm i.d., 1.8 μm) was used. The electrospray ionization (ESI) source was operated at 4 kV and a desolvation temperature of 200 °C. The mobile phase was water/acetonitrile (90/10), and the flow rate was 0.1 mL/min. All MS spectra were obtained in the positive mode, and argon was used as collision gas for the MS/MS measurements. The instrument was calibrated in the *m*/*z* range 50−600. MS data were processed via Bruker Data Analysis software 4.1.

The metabolites were further identified by an API 2000 LC-MS/MS System (AB Sciex Instruments) equipped with a turbo electrospray ionization probe in the MRM scan mode. Liquid chromatography was carried out using an Agilent 1200 (Santa Clara, CA) series HPLC equipped with a G1322 degasser, G1311A quatpump, G1316B column compartment, and G1329A autosampler (Wilmington, DE). A Waters Atlantis T3 column (150 × 2.1 mm i.d., 3 μm) (Eschborn, Germany) was used. The mobile phase system was 0.1% formic acid in water (v/v):0.1% formic acid in acetonitrile (v/v) 50:50. A flow rate of 0.3 mL/min and an injection volume of 40 μL were adopted in all steps. Positive ionization mode was used for detection of all analytes. The ion spray voltage was 4000 V, and the ion source temperature was 450 °C. The curtain gas was set at 10 psig, while ion source gas 1 and 2 were set at 45 and 50 psig, respectively. For data acquisition and analysis, Analyst v.1.4.2 (Applied Biosystems/MDS SCIEX) was used.

Finally, rat hepatic microsomal incubation with ^{13}C-labeled MX was performed to reconfirm metabolites as well as to produce the ^{13}C-

DOI: 10.1021/jf5025104
J. Agric. Food Chem. 2015, 63, 754−760

labeled metabolites, which along with the synthesized ^{13}C-labeled MX acid were used as internal standard in the subsequent stereoselective metabolism research of MX enantiomers.

Quantitative Analysis for Stereoselective Metabolism of MX Enantiomers. (+)-*S*- and (−)-*R*-MX were incubated in the microsomal system described above, respectively. After 0, 5, 10, 20, 30, and 60 min, 10 μL of internal standard and 140 μL of acetonitrile containing 0.1% formic acid (v/v) were added to 50 μL of the incubation mixture to terminate the reaction. Then the samples were vortexed and centrifuged, and the supernatant was collected and stored at −20 °C until analysis. Triple quadrupole MS coupled with LC was used for quantitation. The LC solvents, column, and MS parameters used for the sample analysis were identical to those of the qualitative analysis described above.

RESULTS AND DISCUSSION

Identification of the Possible MX Metabolites by Rat Hepatic Microsomes. Data from LC-TOF-MS indicated that possible metabolites of hydroxylation, probably at two sites (M1 and M2), demethylation (M3), and didemethylation (M4) were detected after the microsomal incubation with 100 μM MX. Figure 2 shows the full-scan chromatogram and the extracted mass chromatograms of the metabolites formed by 60 min incubation. Table 1 lists the exact masses and fragmentation of MX and the detected metabolites. The fragment ions of these potential metabolites corresponded to the proposed structures.

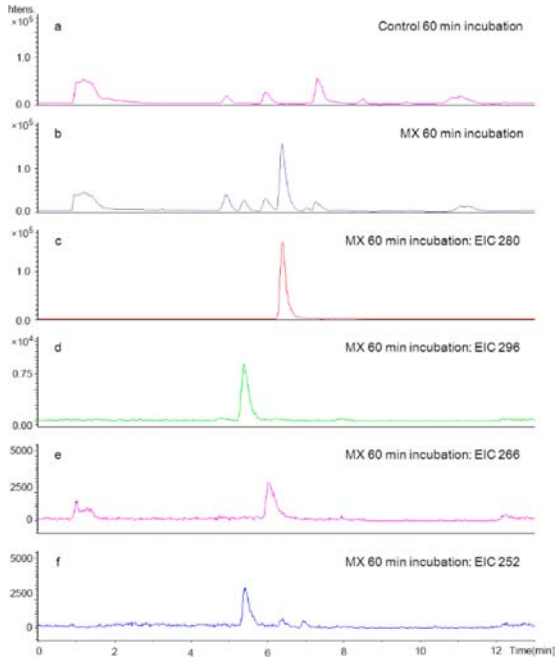

Figure 2. Total ion current chromatograms of UPLC-TOF-MS from the 60 min microsome incubations of (a) the control and (b) metalaxyl. Extracted ion chromatograms of (c) *m*/*z* 280, (d) *m*/*z* 296, (e) *m*/*z* 266, and (f) *m*/*z* 252.

In the present study, the structure of the potential metabolites was presumed based on the LC-TOF-MS data and previously reported in vivo metabolic data.[32] In general, the demethylation metabolite (*m*/*z* 266) should be *N*-(2,6-dimethylphenyl)-*N*-(methoxyacetyl)alanine (M3), the MX acid. The didemethylation metabolite (*m*/*z* 252) should be *N*-(2,6-dimethylphenyl)-*N*-(hydroxyacetyl)alanine (M4). For the hydroxylation metabolite (*m*/*z* 296), the two possible positions of hydroxylation resulted in two possible structures: *N*-(2,6-dimethyl-5-hydroxyphenyl)-*N*-(methoxyacetyl)alanine methyl ester (M1) and *N*-(2-hydroxymethyl-6-methylphenyl)-*N*-(methoxyacetyl)alanine methyl ester (M2). M1 and M2 are two isomers of hydroxymetalaxyl. Figure 3 summarizes the proposed biotransformation pathways of MX in rat hepatic microsomes.

Much research has focused on the metabolism of MX in matrixes such as soil,[33,34] plants,[26] fungus[35] and microsomes.[36,37] In general, MX acid was the main metabolite in most soil matrixes.[38,39] In human liver microsomes, as reported by Abass, hydroxylation, didemethylation, and lactone formation were the main biotransformation reactions.[37] Since the metabolic profile of a compound always varies with the species used, the difference in metabolic behavior between human and rat liver microsomes may be partly attributed to different CYPs participating in MX metabolism.

Quantitation Method for Metabolite Analysis. After preliminary confirmation of MX metabolites, ^{13}C-labeled MX was incubated with rat hepatic microsomes (1) for further confirmation of the formation of the metabolites and (2) to obtain ^{13}C-labeled metabolites, which were then used as the "internal standards" for identification and quantitative analysis of metabolites in the subsequent stereoselective metabolism study of MX. As a result, hydroxymetalaxyl (*m*/*z* 296), demethylmetalaxyl (*m*/*z* 266), and didemethylmetalaxyl (*m*/*z* 252) were all reconfirmed in this step. A 60 min incubation time was considered as optimal, giving the highest yield of ^{13}C-labeled metabolites. Thus, besides a minor level of $^{13}C_6$-MX acid, the demethylation metabolite (*m*/*z* 266), which was synthesized through a hydrolysis method, other labeled metabolites were successfully achieved with the incubation of $^{13}C_6$-MX for 60 min.

Quantitative analysis of MX metabolites was carried out by LC-MS/MS. All analytes showed a strong signal of the quasimolecular ion $[M + H]^+$ under positive electrospray ionization mode. The parameters of MRM mode for all analytes were optimized by selecting the most abundant product ion. Table 2 listed the MRM parameters for all analytes. Figure 4 illustrated a set of MRM chromatograms for the 60 min

Table 1. Tentative Identification of Metalaxyl Metabolites Formed in Vitro by Rat Liver Microsomes, on the Basis of Exact Mass Determination by TOF-MS

metabolite	biotransformation	accurate mass	fragments	molecular formula
M1[a]	hydroxylation	296.1984	278.1853, 252.1662, 198.2208, 149.0540, 122.1127	$C_{15}H_{21}NO_5$
M2[b]	hydroxylation	296.1984		
M3	demethylation	266.1879	234.1559, 198.2236, 149.0550, 122.1135	$C_{14}H_{19}NO_4$
M4	didemethylation	252.1666	198.2208, 149.0537, 122.1118	$C_{13}H_{17}NO_4$
metalaxyl	–	280.1973	248.1665, 220.1681, 192.1692, 122.1108	$C_{15}H_{21}NO_4$

[a]Hydroxylation of the phenyl ring. [b]Hydroxylation of the aromatic methyl group.

DOI: 10.1021/jf5025104
J. Agric. Food Chem. 2015, 63, 754−760

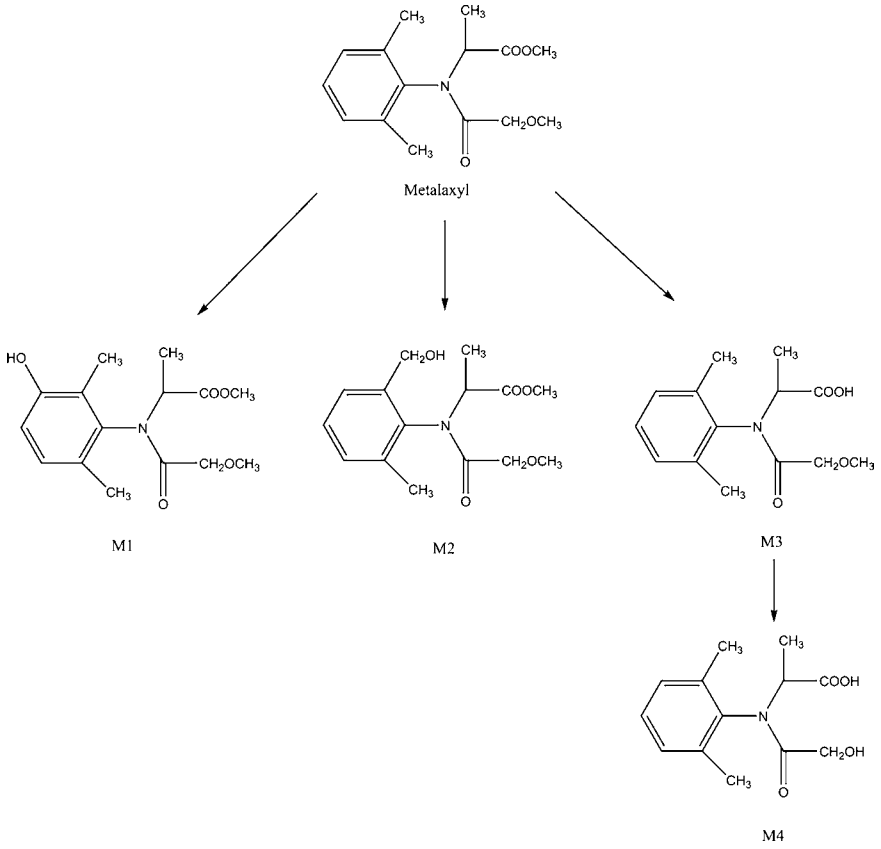

Figure 3. Proposed metabolic pathways of metalaxyl by rat hepatic microsomes. (M1 and M2) Hydroxymetalaxyl metabolite (m/z 296), (M3) demethylmetalaxyl metabolite (m/z 266), (M4) didemethylmetalaxyl metabolite (m/z 252).

Table 2. Mass Spectrometry Parameters for Determination of Metalaxyl and Its Metabolites by LC-MS/MS

compound	retention time (min)	Q1 mass (amu)	Q3 mass (amu)	DP[a](V)	CE[b](V)	CXP[c](V)
metalaxyl	5.83	280.2	220.0	61	15	8
hydroxymetalaxyl metabolites (m/z 296)	2.43	296.1	146.4	46	29	6
demethylmetalaxyl metabolite (m/z 266)	2.96	266.2	220.0	71	17	4
didemethylmetalaxyl metabolite (m/z 252)	2.32	252.0	206.0	10	15	4

[a]DP, declustering potential. [b]CE, collision energy. [c]CXP, cell exit potential.

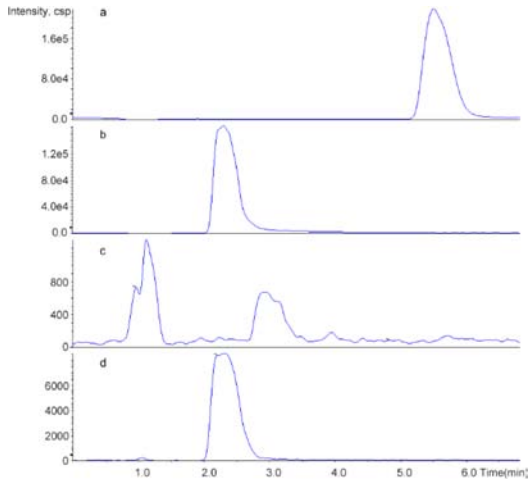

Figure 4. MRM chromatograms of LC-MS/MS from the 60 min microsome incubations of (a) m/z 280, (b) m/z 296, (c) m/z 266, and (d) m/z 252.

microsomal incubation of MX. Hydroxymetalaxyl (m/z 296), didemethylmetalaxyl (m/z 252), and demethylmetalaxyl (m/z 266) were detected. None of them were detected in the absence of rat hepatic microsomes.

Stereoselective Metabolism of (+)-*S*- and (−)-*R*-MX. (+)-*S*- and (−)-*R*-MX at a concentration of 100 μM were incubated with rat hepatic microsomes, respectively. The degradation curves for MX enantiomers are shown in Figure 5a. (+)-*S*-MX degraded faster than its antipode through the incubation period with a $t_{1/2}$ of 21.00 and 36.47 min for (+)-*S*- and (−)-*R*-MX, respectively. In addition, the enantiomer fraction (EF) was used to measure the stereoselective metabolism of MX (Figure 6). EF was calculated from the peak areas of (+)-*S*- and (−)-*R*-MX following the equation:

$$\text{EF} = (+)\text{-}S\text{-MX}/[(+)\text{-}S\text{-MX} + (-)\text{-}R\text{-MX}] \quad (1)$$

The EF was 0.32 after 60 min incubation, also indicating that degradation of MX in rat hepatic microsomes was stereoselective. This was consistent with the degradation aspect of *rac*-MX in rat hepatic microsomes in a previous study.[36]

In the present study, the peak area ratio of each metabolite and its corresponding ^{13}C-labeled internal standard was used to

DOI: 10.1021/jf5025104
J. Agric. Food Chem. 2015, 63, 754−760

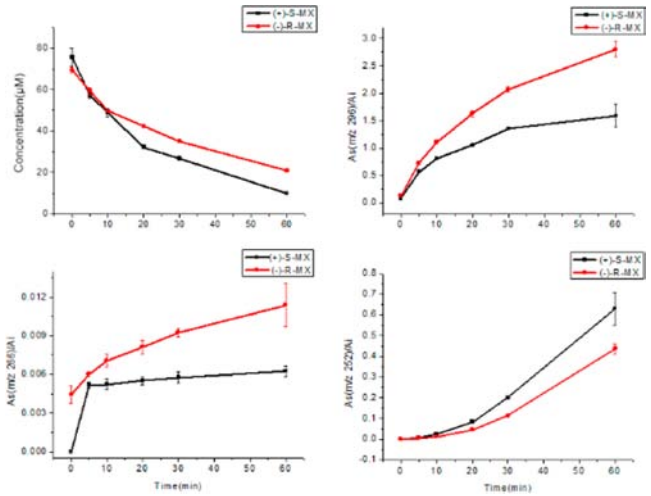

Figure 5. Concentration−time curves of (a) metalaxyl, (b) the hydroxymetalaxyl metabolites (m/z 296), (c) the demethylmetalaxyl metabolite (m/z 266), and (d) the didemethylmetalaxyl metabolite (m/z 252) after incubation of 100 μM (+)-*S*- and (−)-*R*-metalaxyl with rat hepatic microsomes, respectively.

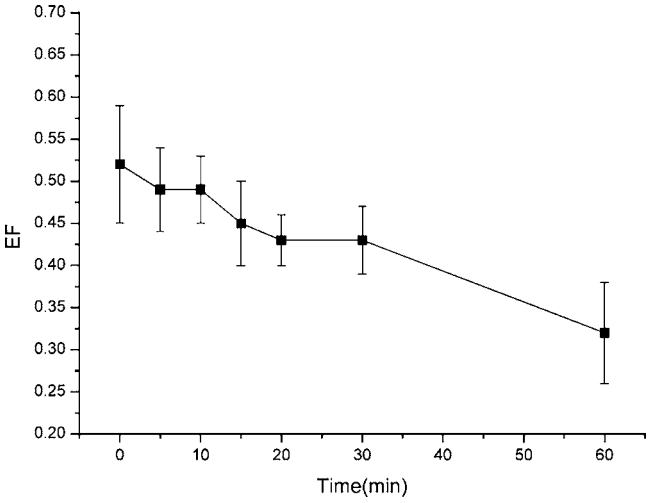

Figure 6. Temporal variations of EFs of metalaxyl in the rat hepatic microsome in the 60 min time course after exposure to 100 μM metalaxyl enantiomers.

compare the differences of metabolic profile between the two enantiomers of MX. Therefore, with the ratio values at different incubation times figured out, metabolite formation from (+)-*S*- and (−)-*R*-MX by rat hepatic microsomes during the incubation is shown in Figure 5b−d.

The amount of all metabolites increased over incubation time. For both enantiomers of MX, the hydroxymetalaxyl metabolites (m/z 296) were the major metabolites. The didemethylmetalaxyl metabolite (m/z 252) was at a moderate level, and demethylmetalaxyl metabolite (m/z 266) was found as the minor metabolite, probably because it could undergo further demethylation. A previous in vivo study indicated that metabolites resulted from didemethylation, hydroxylation of the aromatic methyl group, and demethylation of the ester group were major metabolites, while phenyl ring hydroxyl, ether group demethylated, and lactone metabolites were minor metabolites.[40] Compared with in vitro systems, more complex metabolic pathways exist in vivo, and conditions such as cofactors and concentration of NADPH are also different. These might explain the difference in metabolite formation between the in vitro and in vivo systems.

Except for a small quantity of demethylmetalaxyl metabolite (m/z 266), other metabolites were not detected in the control group. It seemed that MX underwent a slight hydrolysis in the absence of NADPH system.

It is obvious that rat hepatic microsome exhibited significant stereoselectivity in the formation of all detected metabolites. (+)-*S*- and (−)-*R*-MX demonstrated quantitatively different metabolite patterns. Transformation of (−)-*R*-MX to its hydroxymetalaxyl (m/z 296) and demethylmetalaxyl metabolite (m/z 266) was markedly preponderant over its (+)-*S*-isomer, while the case of didemethylmetalaxyl metabolite (m/z 252), a secondary dimethyl metabolite of demethylmetalaxyl metabolite (m/z 266), was just the opposite. Specifically, after 60 min incubation, the amounts of hydroxymetalaxyl and demethylmetalaxyl derived from (−)-*R*-MX were 1.76 and 1.82 times higher than that of (+)-*S*-MX, whereas the production of didemethylmetalaxyl from (+)-*S*-MX was 1.44 times more than that from (−)-*R*-MX. Therefore, the minor amount of demethylmetalaxyl metabolite (m/z 266) from (+)-*S*-MX might well be attributed to the preferential transformation to its secondary dimethyl metabolite (m/z 252). As the fungicidal activity of metalaxyl was mainly attributed to the (−)-*R*-MX, it is interesting that the more active isomer (for target organism) also showed a higher metabolic activity in the in vitro system of the nontarget organism.

Abundant reports suggested that two enantiomers of a chiral compound could always show differences in pharmacokinetic processes (absorption, distribution, metabolism, protein binding, and excretion).[41] Optically active biological macromolecules might behave stereoselectivity when interacting with a chiral drug. In the present study, our results demonstrated that degradation of the parent MX as well as formation of the metabolites in rat hepatic microsomes were observably stereoselective, which should be highly attributed to the existence of several microsomal mono-oxygenases differing in their stereoselectivities and inducibilities for the enantiomers.

In summary, we proposed a new approach using the peak area ratio of each metabolite and its corresponding stable isotope-labeled internal standard to quantitatively compare the stereoselective metabolic behavior of two enantiomers of a chiral compound. According to P. Schieberle,[42] the quantitation method proposed in the present study should be categorized into the "Stable Isotope Dilution Assays (SIDA)". As commercially unavailability of many labeled analytes was claimed as the main drawback of SIDA, our present study proposed a method using real biological samples to obtain the labeled standards. But the absolute quantities of the labeled metabolites were unclear, and it is difficult to establish the MRM method for some minor metabolites at very low concentrations. This should be regarded as the main limitation of our microsomal incubation method. With most of the main metabolites having been quantified, this approach could be of great value for its extensive application in the field of stereoselective metabolism research of a chiral compound, which is important for its comprehensive ecotoxicological and environmental risk assessment.

DOI: 10.1021/jf5025104
J. Agric. Food Chem. 2015, 63, 754−760

AUTHOR INFORMATION

Corresponding Author

*E-mail: wentaozhu@cau.edu.cn. Fax: +861062733547. Tel:+861062733547.

Funding

We gratefully acknowledge financial support from the National Natural Science Foundation of China (contract grant numbers: 21207158 and 21021058) and Chinese Universities Scientific Fund (2012RC026).

Notes

The authors declare no competing financial interest.

REFERENCES

(1) Chen, C.; Gonzalez, F. J.; Idle, J. R. LC-MS-based metabolomics in drug metabolism. *Drug Metab Rev.* **2007**, *39*, 581−97.

(2) Clarke, N. J.; Rindgen, D.; Korfmacher, W. A.; Cox, K. A. Peer Reviewed: Systematic LC/MS Metabolite Identification in Drug Discovery. *Anal. Chem.* **2001**, *73*, 430 A−439 A.

(3) Brodie, B. B.; Axelrod, J. The estimation of acetanilide and its metabolic products, aniline, N-acetyl p-aminophenol and p-aminophenol, free and total conjugated, in biological fluids and tissues. *J. Pharmacol Exp Ther* **1948**, *94*, 22−8.

(4) Gillette, J. R.; Mitchell, J. R.; Brodie, B. B. Biochemical Mechanisms of Drug Toxicity. *Annu. Rev. Pharmacol. Toxicol.* **1974**, *14*, 271−288.

(5) Knowles, S. R.; Uetrecht, J.; Shear, N. H. Idiosyncratic drug reactions: the reactive metabolite syndromes. *Lancet* **2000**, *356*, 1587−91.

(6) Liebler, D. C.; Guengerich, F. P. Elucidating mechanisms of drug-induced toxicity. *Nat. Rev. Drug Discovery* **2005**, *4*, 410−20.

(7) Mitchell, J. R.; Jollow, D. J.; Potter, W. Z.; Davis, D. C.; Gillette, J. R.; Brodie, B. B. Acetaminophen-induced hepatic necrosis. I. Role of drug metabolism. *J. Pharmacol. Exp. Ther.* **1973**, *187*, 185−94.

(8) Yang, W. C.; Regnier, F. E.; Jiang, Q.; Adamec, J. In vitro stable isotope labeling for discovery of novel metabolites by liquid chromatography-mass spectrometry: Confirmation of gamma-tocopherol metabolism in human A549 cell. *J. Chromatogr. A* **2010**, *1217*, 667−75.

(9) Kurihara, N.; Miyamoto, J.; Paulson, G. D.; Zeeh, B.; Skidmore, M. W.; Hollingworth, R. M.; Kuiper, H. A. Chirality in synthetic agrochemicals: bioactivity and safety considerations. *Pestic. Sci.* **1999**, *55*, 219−219.

(10) Lu, X.; Zhao, X.; Bai, C.; Zhao, C.; Lu, G.; Xu, G. LC-MS-based metabonomics analysis. *J. Chromatogr. B: Anal. Technol. Biomed. Life Sci.* **2008**, *866*, 64−76.

(11) Lu, W.; Bennett, B. D.; Rabinowitz, J. D. Analytical strategies for LC-MS-based targeted metabolomics. *J. Chromatogr. B: Anal. Technol. Biomed. Life Sci.* **2008**, *871*, 236−42.

(12) Ji, C.; Walton, J.; Su, Y.; Tella, M. Simultaneous determination of plasma epinephrine and norepinephrine using an integrated strategy of a fully automated protein precipitation technique, reductive ethylation labeling and UPLC-MS/MS. *Anal. Chim. Acta* **2010**, *670*, 84−91.

(13) Lee, M. S.; Kerns, E. H. LC/MS applications in drug development. *Mass Spectrom. Rev.* **1999**, *18*, 187−279.

(14) Chen, S.; Kong, H.; Lu, X.; Li, Y.; Yin, P.; Zeng, Z.; Xu, G. Pseudotargeted metabolomics method and its application in serum biomarker discovery for hepatocellular carcinoma based on ultra high-performance liquid chromatography/triple quadrupole mass spectrometry. *Anal. Chem.* **2013**, *85*, 8326−8333.

(15) Chiku, S.; Hamamura, K.; Nakamura, T. Novel urinary metabolite of d-delta-tocopherol in rats. *J. Lipid Res.* **1984**, *25*, 40−8.

(16) Simon, E. J.; Gross, C. S.; Milhorat, A. T. The Metabolism of Vitamin E: I. The Absorption and Excretion of D-α-Tocopheryl-5-methyl-C14-succinate. *J. Biol. Chem.* **1956**, *221*, 797−805.

(17) Parks, E. J.; Hellerstein, M. K. Thematic review series: Patient-oriented research. Recent advances in liver triacylglycerol and fatty acid metabolism using stable isotope labeling techniques. *J. Lipid Res.* **2006**, *47*, 1651−60.

(18) Chowdhury, S. K.; Gopaul, V. S.; Blumenkrantz, N.; Zhong, R.; Kulmatycki, K. M.; Alton, K. B. Detection and characterization of highly polar metabolites by LC-MS: Proper selection of LC column and use of stable isotope-labeled drug to study metabolism of ribavirin in rats. *Prog. Pharm. Biomed. Anal.* **2005**, *6*, 277−293.

(19) Birkemeyer, C.; Luedemann, A.; Wagner, C.; Erban, A.; Kopka, J. Metabolome analysis: the potential of in vivo labeling with stable isotopes for metabolite profiling. *Trends Biotechnol.* **2005**, *23*, 28−33.

(20) Zhang, N. Y.; Fountain, S. T.; Bi, H. G.; Rossi, D. T. Quantification and rapid metabolite identification in drug discovery using API time-of-flight LC/MS. *Anal. Chem.* **2000**, *72*, 800−806.

(21) Baranczewski, P.; Stanczak, A.; Kautiainen, A.; Sandin, P.; Edlund, P. O. Introduction to early in vitro identification of metabolites of new chemical entities in drug discovery and development. *Pharmacol. Rep.* **2006**, *58*, 341−52.

(22) Holcapek, M.; Kolarova, L.; Nobilis, M. High-performance liquid chromatography-tandem mass spectrometry in the identification and determination of phase I and phase II drug metabolites. *Anal. Bioanal. Chem.* **2008**, *391*, 59−78.

(23) Venkatakrishnan, K.; von Moltke, L. L.; Obach, R.; Greenblatt, D. J. Drug metabolism and drug interactions: application and clinical value of in vitro models. *Curr. Drug Metab.* **2003**, *4*, 423−459.

(24) Tolleson, W. H.; Doerge, D. R.; Churchwell, M. I.; Marques, M. M.; Roberts, D. W. Metabolism of biochanin A and formononetin by human liver microsomes in vitro. *J. Agric. Food Chem.* **2002**, *50*, 4783−90.

(25) Clements, M.; Li, L. Strategy of using microsome-based metabolite production to facilitate the identification of endogenous metabolites by liquid chromatography mass spectrometry. *Anal. Chim. Acta* **2011**, *685*, 36−44.

(26) Zadra, C.; Marucchini, C.; Zazzerini, A. Behavior of metalaxyl and its pure *R*-enantiomer in sunflower plants (*Helianthus annus*). *J. Agric. Food Chem.* **2002**, *50*, 5373−7.

(27) Demsia, G.; Vlastos, D.; Goumenou, M.; Matthopoulos, D. P. Assessment of the genotoxicity of imidacloprid and metalaxyl in cultured human lymphocytes and rat bone-marrow. *Mutat. Res., Genet. Toxicol. Environ. Mutagen.* **2007**, *634*, 32−39.

(28) Al-Amoudi, W. M. Haematological and biochemical effects of metalaxyl fungicide on albino mice. *Am. J. Biochem.* **2012**, *2*, 62−66.

(29) Hildebrandt, A.; Guillamón, M.; Lacorte, S.; Tauler, R.; Barceló, D. Impact of pesticides used in agriculture and vineyards to surface and groundwater quality (North Spain). *Water Res.* **2008**, *42*, 3315−3326.

(30) Reemtsma, T.; Alder, L.; Banasiak, U. A multimethod for the determination of 150 pesticide metabolites in surface water and groundwater using direct injection liquid chromatography−mass spectrometry. *J. Chromatogr. A* **2013**, *1271*, 95−104.

(31) Zhu, W.; Dang, Z.; Qiu, J.; Liu, Y.; Lv, C.; Diao, J.; Zhou, Z. Species differences for stereoselective metabolism of ethofumesate and its enantiomers in vitro. *Xenobiotica* **2009**, *39*, 649−655.

(32) Vleminckx, C. *Pesticide residues in food-2002*; Joint FAO/WHO Meeting on Pesticide Residues; Rome, Italy, September 16−25, 2002.

(33) Droby, S.; Coffey, M. D. Biodegradation Process and the Nature of Metabolism of Metalaxyl in Soil. *Ann. Appl. Biol.* **1991**, *118*, 543−553.

(34) Sukul, P.; Spiteller, M. Persistence, fate, and metabolism of [^{14}C]metalaxyl in typical Indian soils. *J. Agric. Food Chem.* **2001**, *49*, 2352−2358.

(35) Zheng, Z.; Liu, S. Y.; Freyer, A. J.; Bollag, J. M. Transformation of Metalaxyl by the Fungus Syncephalastrum racemosum. *Appl. Environ. Microbiol.* **1989**, *55*, 66−71.

(36) Zhang, P.; Shen, Z.; Xu, X.; Zhu, W.; Dang, Z.; Wang, X.; Liu, D.; Zhou, Z. Stereoselective degradation of metalaxyl and its enantiomers in rat and rabbit hepatic microsomes in vitro. *Xenobiotica* **2012**, *42*, 580−586.

DOI: 10.1021/jf5025104
J. Agric. Food Chem. 2015, 63, 754−760

(37) Abass, K.; Reponen, P.; Jalonen, J.; Pelkonen, O. In vitro metabolism and interactions of the fungicide metalaxyl in human liver preparations. *Environ. Toxicol. Pharmacol.* **2007**, *23*, 39−47.
(38) Buser, H.-R.; Müller, M. D.; Poiger, T.; Balmer, M. E. Environmental Behavior of the Chiral Acetamide Pesticide Metalaxyl: Enantioselective Degradation and Chiral Stability in Soil. *Environ. Sci. Technol.* **2002**, *36*, 221−226.
(39) Saha, T.; Sukul, P. Metalaxyl—its persistence and metabolism in soil. *Toxicol. Environ. Chem.* **2008**, *58*, 251−258.
(40) Hambock, H. Metabolic pathways of CGA 48988 in the rat. Project unpublished report 31/81 from Ciba-Geigy Ltd., Basle, Switzerland, submitted to the World Health Organization by Ciba-Geigy, Ltd., 1981.
(41) Brocks, D. R. Drug disposition in three dimensions: An update on stereoselectivity in pharmacokinetics. *Biopharm. Drug Dispos.* **2006**, *27*, 387−406.
(42) Schieberle, P.; Molyneux, R. J. Quantitation of sensory-active and bioactive constituents of food: a journal of agricultural and food chemistry perspective. *J. Agric. Food Chem.* **2012**, *60*, 2404−2408.

DOI: 10.1021/jf5025104
J. Agric. Food Chem. 2015, 63, 754−760

JOURNAL OF AGRICULTURAL AND FOOD CHEMISTRY

Article

pubs.acs.org/JAFC

Effects of High CO_2 Levels on Fermentation, Peroxidation, and Cellular Water Stress in *Fragaria vesca* Stored at Low Temperature in Conditions of Unlimited O_2

Maria Blanch,[†] Raquel Rosales,[†] Raquel Mateos,[‡] María B. Perez-Gago,[§] Maria T. Sanchez-Ballesta,[†] María I. Escribano,[†] and Carmen Merodio*[,†]

[†]Department of Characterization, Quality and Security and [‡]Department of Metabolism and Nutrition, Institute of Food Science Technology and Nutrition (ICTAN-CSIC), Madrid, Spain

[§]Postharvest Technology Center, Valencian Institute of Agricultural Research (IVIA), Valencia, Spain

ABSTRACT: To better understand the tolerance of strawberries (*Fragaria vesca* L.) to high CO_2 in storage atmospheres, fermentation and cellular damage were investigated. Fruits were stored for 3 and 6 days at 0 °C in the presence of different CO_2 levels (0, 20, or 40%) with 20% O_2. Changes in pyruvate decarboxylase (PDC) and alcohol dehydrogenase (ADH) gene expression and in fermentative metabolites, as well as in bound water and malondialdehyde (MDA) concentrations, were analyzed. In strawberries stored without added CO_2, up-regulation of *PDC* and *ADH* was not associated with an increase in fermentative metabolites. By contrast, moderate ethanol fermentation in fruits exposed to 20% CO_2 seems to be essential to maintain fruit metabolism, reducing both lipid peroxidation and cellular water stress. However, if the CO_2 concentration increases (40%), the excess acetaldehyde and ethanol produced were closely correlated with a decrease in bound water and production of MDA.

KEYWORDS: *high CO_2 levels, fermentative genes, acetaldehyde, ethanol, MDA, bound water*

INTRODUCTION

Low temperature is used to prolong the storage life of strawberries and to slow fungal decay, mainly caused by gray mold (*Botrytis cinerea*) that grows at temperatures as low as 0 °C. Thus, relying on low-temperature storage to efficiently control gray mold must involve coadjuvant treatment to preserve the quality of the fruit while enhancing disease resistance. High CO_2 levels (15−20%) are used commercially as an effective means of limiting fungal decay.[1] Strawberries are tolerant to elevated high CO_2 concentrations, although distinct cultivars exhibit different degrees of high CO_2 tolerance, and they accumulated different levels of fermentative metabolites, such as acetaldehyde and ethanol.[2] These fermentative products influence fruit quality and may also act as natural fungicides or insecticides.[3]

Strawberries are highly appreciated for their tasty flavor and nutritional value, and in particular they are a particularly good source of polyphenols, of which proanthocyanidins, produced from the condensation of flavan-3-ol units, are the main phenolics.[4] Genetic and growth conditions affect the content and composition of proanthocyanidins,[5] although quantitative differences are often driven by environmental storage conditions. Flavan-3-ols have positive effects on human health,[6] as well as contributing to defense and stress resistance toward different fungi.[7] Interestingly, short-term high-CO_2 treatment (20% CO_2 for 3 days) is an effective treatment for the accumulation of (+)-catechin and procyanidins B1 and B3.[8] In some astringent-type fruits such as persimmon, the effectiveness of high-CO_2 treatment (95−100% CO_2) to promote deastringency is based on the decrease of soluble tannins concentrations through their polymerization by acetaldehyde.[9,10] This role of acetaldehyde as the main polymerizing agent was demonstrated in model solution systems with (+)-catechin or (−)-epicatechin.[11]

In addition to the above, high CO_2 levels also modified the water status of several high-CO_2-tolerant fruits, such as table grapes and strawberries, affecting the unfreezable (bound) water fraction as detected by differential scanning calorimetry (DSC).[12,13] Although ethanol is a small, polar molecule able to enter the hydration layer of membranes and weaken interlipid hydrogen bonding,[14,15] its influence on fruit cellular water has scarcely been investigated. Water molecules have a primary structural role in the maintenance of cell membrane, participating in the hydrogen-bonded network or hydration layer. In yeast, ethanol concentrations as low as 5% (w/v) reduce water availability sufficiently to have metabolic consequences.[16] Thus, we hypothesize that perturbations in bound water, which are essential to maintain cell membrane structure, may be associated with changes in the accumulation of fermentative metabolites. Moreover, and consistent with the above, it is likely that some of the reported effects of high CO_2 treatment occur through the accumulation of fermentative metabolites.

Nevertheless, excessively high-CO_2 treatments may also have an adverse effect on strawberry quality associated with oxidative stress. Enhanced rate of active oxygen species (ROS), often leading to oxidative damage, is an integral part of many stressful

Received: July 18, 2014
Revised: January 7, 2015
Accepted: January 8, 2015
Published: January 8, 2015

ACS Publications © 2015 American Chemical Society

DOI: 10.1021/jf505715s
J. Agric. Food Chem. 2015, 63, 761−768

environmental conditions.[17] ROS have been recognized as contributing to injury via direct lipid peroxidation that may disrupt membrane integrity.[18,19] Peroxidation of lipids may lead to a radical chain reaction that is usually accompanied by the formation of a wide variety of products, including alkanes and carbonyl compounds. The most widely used index of lipid peroxidation is malondialdehyde (MDA) formation, often assayed through thiobarbituric acid (TBA). However, several other compounds are also reactive toward TBA, leading to an overestimation of MDA content. The quantitative determination of MDA by HPLC with UV detection after its derivatization with dinitrophenylhydrazone (DNPH) greatly improves the selectivity and the analytical detection limit of the MDA assay.[20] Thus, using this technique, in the present work we have tried to see if the damage produced by excessively high-CO_2 treatment (40%) or severely low-temperature (0 °C) storage could be also attributed to oxidative stress.

Fermentative metabolism is closely linked to the availability of respiratory substrates, including malic acid, the oxidative decarboxylation of which results in the formation of pyruvic acid that may eventually be converted to fermentative compounds. The activation of ethanolic fermentative metabolism should allow NAD^+ regeneration so that a net ATP production can be generated. In the first step of the ethanol fermentation pathway, pyruvate is the substrate of pyruvate decarboxylase (PDC), yielding CO_2 and acetaldehyde. Subsequently, acetaldehyde is reduced to ethanol with the concomitant oxidation of NADH to NAD^+ by alcohol dehydrogenase (ADH). Changes in the activities and gene expression of *PDC* and *ADH* under high-CO_2/low-O_2 conditions have been reported in *Fragaria* × *ananassa*,[21−23] yet there is little information about the specific effect of high-CO_2 levels under unlimited O_2 conditions in *Fragaria vesca*.

The aim of this study was to first determine the effect of low-temperature and high-CO_2 levels on *ADH* and *PDC* expression as well as on levels of fermentative metabolites, ethanol and acetaldehyde. Accordingly, the transcript abundance of these genes and fermentative metabolites were analyzed in Mara des Bois strawberries exposed for 3 and 6 days to different CO_2 concentrations (0, 20, and 40%) during storage at 0 °C. In addition, we set out to stablish the CO_2 doses and exposure times capable of activating fermentative metabolism. To achieve this, the availability of respiratory substrates was determined, as was the potential damage of the accumulated ethanol and acetaldehyde on lipid peroxidation and cellular water stress. This was done by analyzing bound water content and MDA.

MATERIALS AND METHODS

Plant Material. The organic strawberries used in this study (*F. vesca* L. Mara des Bois) were grown in an orchard in San Sebastian de los Reyes (Madrid, Spain). Strawberries belonging to the first and second inflorescences were harvested, immediately transported to the Institute of Food Science Technology and Nutrition, and selected for uniform size and color. The strawberries with 1 mg flavonoids/g FW and a harvest maturity index of 12 (total soluble solids/titratable acidity ratio) were stored at 0 °C (±0.5) and >95% relative humidity in three sealed containers with a capacity of 1 m^3. Fifteen plastic boxes, each containing approximately 0.5 kg of fruit, were stored in each container and exposed to different CO_2 concentrations (0, 20, or 40%) with 20% O_2 under a continuous flow. Strawberries were analyzed after 3 and 6 days of treatment using fruit analyzed at harvest as a control. The CO_2 and O_2 concentrations were measured using a gas analyzer (PBI Dansensor mod, Checkmate 9900). At harvest and from each treatment group (0, 20, and 40% CO_2-treated fruit), 45 strawberries were selected for quality analysis (pH, soluble solids content, titratable acidity) and fermentative metabolites quantification. Another 45 fruits were removed at random from each of group, divided into three batches of 15 strawberries, frozen in liquid nitrogen, and stored at −80 °C for further analysis. The 15 strawberries from each batch served as a biological replicate, and two different measurements were taken from each of the three biological replicates.

Relative Gene Expression Assessed by Quantitative RT-PCR. RNA extraction was conducted according to the protocol of Yu et al.,[24] with modifications from samples of strawberry treated with 0, 20, and 40% CO_2 stored for 0 or 3 days. Total RNA was extracted three times from 0.4 g of each sample with CTBA-based extraction buffer. The quality and purity of the total RNA were evaluated by agarose gel electrophoresis and spectrometry (NanoDrop 2000, Thermo Scientific), and it was then treated with DNase (DNase I, RNase-free, Thermo) to remove any genomic DNA before synthesizing cDNAs from 1 μg of each sample using the iScript TM Reverse Transcription Supermix for RT-qPCR (Bio-Rad). RT-PCR amplification was carried out in a 96-well plate iCycler iQ thermal cycler (Bio-Rad) and quantified using iCycler iQTM-associated software (Real Time Detection System Software, version 2.0), evaluating each gene in at least two independent runs. Sequences from the NCBI database and from the available literature (in particular, refs 21 and 25) were used to design the following gene specific primers using Primer3 software. The primer pairs used in the RT-qPCR for pyruvate decarboxylase (XM_004302484) were FvPDC_F, GTTGCTTGAGTGGGGGTC-TA, and FvPDC_R, ATCTGTGAATGCGAATGAAGG; and those for alcohol dehydrogenase (XM_004290520) were FvADH_QFw2, GCCCTTCTATACTGTGTCCTC, and FvADH_QRv2, ACTGTT-CTGGCTGACTGGTT.

The relative expression of all the genes studied was assayed using quantitative RT-PCR (RT-qPCR). To calculate the efficiency of the reaction (optimal range 90−110%) and to establish the most suitable template concentration, the cDNAs synthesized from serial dilutions of total RNA were amplified (between 40 and 2.5 ng). Standard curves and linear equations were determined by plotting cycle threshold (Ct) values (*y*-axis) against the logs of the total RNA (*x*-axis). The efficiency of each individual run was calculated on the basis of the raw fluorescence data (ΔRn) exported as output file and subsequently imported into the LinReg PCR program. The specificity of the products was validated by analyzing the dissociation curves, evaluating in agarose gels, and sequencing (Genomic Department of the CIB-CSIC). The *actin-97-like* housekeeping gene from *F. vesca* (XM_004307470) was not regulated by low-temperature or high-CO_2 levels (data not shown) and, thus, it was used as the internal reference gene to normalize the transcript profiles according to the $2^{-\Delta\Delta Ct}$ method and relative to the calibrator sample (fruit at harvest). The *actin-97-like* was amplified with the primers FvActin_Fw, GGGTTTGCTGGAGATGATG, and FvActin_Rv, CACGATTGG-CCTTGGGATTC. Similarly, the specificity of the products was validated by analyzing the dissociation curve in agarose gels and by sequencing. Three biological replicates were assessed for each treatment and sample, each with three technical replicates.

Ethanol and Acetaldehyde Content. Ethanol and acetaldehyde were analyzed from the headspace of juice of three replicates of 15 strawberries without calyx, immediately after harvest and for each storage period. An aliquot (5 mL) of juice was transferred to 10 mL vials, closed tightly with crimp-top caps and TFE/silicone septum seals, and frozen at −80 °C. Gas chromatography (Thermo Trace, Thermo Fisher Scientific) was used to measure the ethanol and acetaldehyde according to the procedure of Valencia-Chamorro et al.[26] The setup included an autosampler (model HS 2000), a flame ionization detector (FID), and a 1.2 m × 0.32 cm (i.d.) Poropack QS 80/100 column, with the injector set at 175 °C, the column at 150 °C, the detector at 200 °C, and the carrier gas at 28 mL/min. A 1 mL sample of the headspace was withdrawn from vials previously equilibrated in a water bath at 20 °C for 1 h and for 15 min at 40 °C, and it was then injected onto the GC. Ethanol and acetaldehyde were identified by comparison of the retention times with standards, and the results were expressed as milligrams per 100 mL of juice.

DOI: 10.1021/jf505715s
J. Agric. Food Chem. 2015, 63, 761−768

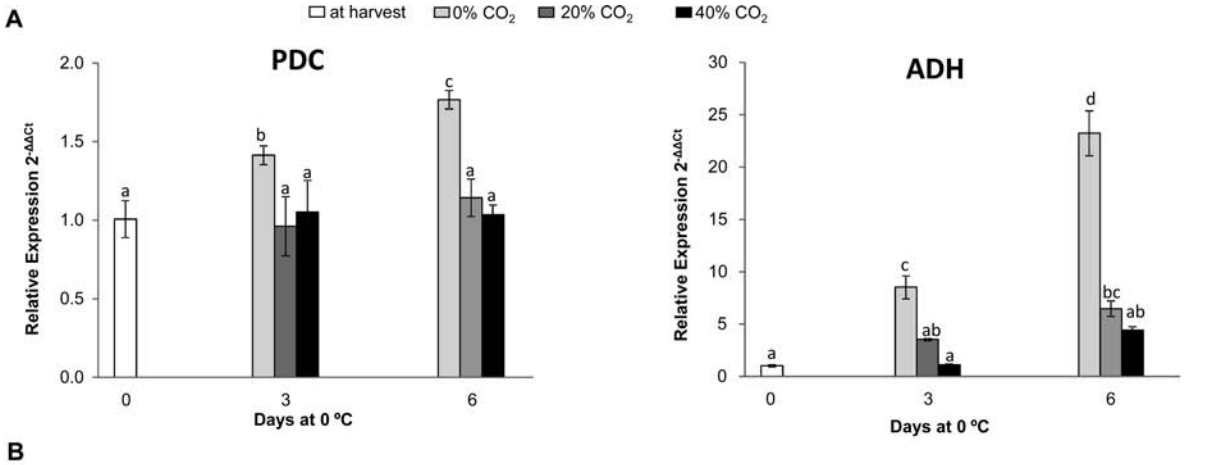

B

Acetaldehyde (mg /100 mL)

	3 days			6 days		
at harvest	0% CO_2	20% CO_2	40% CO_2	0% CO_2	20% CO_2	40% CO_2
0.12±0.0a	0.23±0.0a	0.92±0.8ab	10.56±1.4d	0.09±0.0a	1.70±0.2b	5.45±0.2c

Ethanol (mg /100 mL)

	3 days			6 days		
at harvest	0% CO_2	20% CO_2	40% CO_2	0% CO_2	20% CO_2	40% CO_2
1.05±0.1a	0.20±0.2a	5.32±0.6b	43.07±1.7d	0.00a	13.19±1.5c	67.72±2.8d

Figure 1. Two histograms (A) represent the relative expression of fermentative genes and the two tables (B) show the levels of fermentative metabolites. The histograms reflect the relative expressions of the *PDC* gene XM_004302484 and the *ADH* gene M_004290520 in Mara des Bois strawberries *Fragaria vesca*, immediately after harvesting (day 0) and after 3 and 6 days of storage at 0 °C in different concentrations of CO_2 (0, 20, or 40%), maintaining a constant concentration of O_2 (20%). Transcripts were measured by quantitative RT-PCR and normalized against those *actin-97-like* used as a reference gene. The results were calculated relative to a calibrator sample (day 0) using the formula $2^{-\Delta\Delta Ct}$ and the values representing the means ± SE of three replicates (n = 6). The tables show changes in acetaldehyde and ethanol (mg/100 mL) under the same conditions described above. Each letter indicates significant differences between the means determined by Tukey's test (P < 0.05).

Determination of Water Fractions Content. The water fractions content were determined on a differential scanning calorimeter (DSC822e, Mettler-Toledo Inc., Columbus, OH, USA) equipped with a liquid nitrogen cooling accessory, according to the procedure of Goñi et al.[27] The method based on the heat of fusion was used to calculate the unfreezable water (bound) content, whereas the total water content was determined after a stable weight had been obtained following drying at 105 °C.

Chromatographic Determination of MDA. MDA was determined as its hydrazone by high-performance liquid chromatography using 2,4-dinitrophenylhydrazine (DNPH) for derivatization and following the method previously described by Mateos et al.,[28] with slight modifications in the chromatographic conditions. Frozen fruit samples of approximately 1 g were homogenized in 10 mL of ultrapure water and centrifuged at 30000*g* for 20 min; after filtering through a 0.45 μm pore size membrane, the supernatants were collected to quantify MDA.

An aliquot (250 μL) of the sample was placed in a 1.5 mL Eppendorf, and 50 μL of 6 M NaOH was added to achieve alkaline to hydrolyze protein-bound MDA by incubating this mixture in a 60 °C water bath for 30 min. The protein was then precipitated with 125 μL of 35% (v/v) perchloric acid, and the mixture was centrifuged at 2800*g* for 10 min. A 250 μL aliquot of the supernatant was transferred to another Eppendorf vial and mixed with 25 μL of DNPH prepared as a 5 mM solution in 2 M hydrochloric acid. Finally, this reaction mixture was incubated for 20 min at room temperature, protected from light. An aliquot of 50 μL of this reaction mixture was injected onto an Agilent 1100 HPLC-DAD with a Nucleosil 100 RP-18 column (4.0 mm × 125 mm, 5 μm particle size, Agilent) preceded by a Lichrospher guard column (4.0 mm × 4.0 mm). Samples were isocratically eluted with a mixture of 0.2% (v/v) acetic acid in deionized water and acetonitrile (75:25 v/v), applied at a flow rate of 0.7 mL/min at room temperature for 40 min. Chromatograms were acquired at 310 nm. Standard MDA was prepared by acidic hydrolysis of 1,1,3,3-tetraethoxypropane in 1% sulfuric acid. Like the experimental samples, the standards were treated with 6 M NaOH for 30 min at 60 °C, followed by protein precipitation with 35% perchloric acid and derivatization with DNPH. Concentrations were expressed as nanomoles of MDA per gram of FW.

Determination of Sucrose and Malic Acid Contents. Sucrose and malic acid were measured according to the method of Blanch et al.[15] using a Metrohm Advanced compac ion chromatography apparatus (867 IC Metrohm). Sucrose was determined by HPAEC-PAD with a Metrosep Carb 1-250 IC column (4.6 mm × 250 mm) and malic acid by HPAEC with an IC-819 conductivity detector equipped with a Metrosep Organic Acids column (7.8 mm × 100 mm). Sucrose and malic acid were identified by their retention times and quantified on the basis of calibration curves derived from standards; their contents were expressed as milligrams per gram of FW of the sample. The data represent the means of the three replicates on which two different measurements were taken.

Determination of Total Soluble Solids and Titratable Acidity. The total soluble solids were determined using a digital refractometer (Atago PR-101, Atago, Japan), expressed as a percentage. The titratable acidity was analyzed by titration with 0.1 N NaOH to pH 8.1 (Mettler DL-70, Mettler-Toledo, Spain).

Statistical Analysis. The analysis of variance (ANOVA) was performed using SPSS v. 19.0. Multicomparison of the means was performed using Tukey's test, with the level of significance set at P < 0.05. The main effects of CO_2 treatment and storage time and the treatment × time interaction were analyzed.

RESULTS AND DISCUSSION

Effect of CO_2 on *PDC* and *ADH* transcripts and on fermentative metabolites. To better understand the effect of low-temperature and high-CO_2 levels on fermentative metabolism, we analyzed the expression of genes encoding for PDC and ADH by RT-qPCR in strawberries stored for 3 and 6 days with 0, 20, or 40% CO_2 in 20% O_2 (Figure 1). We analyzed the expression of the gene codifying for the Fvpdc isoform 2-like (XP_004302532), which is the PDC isoform in *F. vesca* with the highest homology to the Fapdc1 (AF333772) from *Fragaria* × *ananassa* that has been shown to be induced by

DOI: 10.1021/jf505715s
J. Agric. Food Chem. 2015, 63, 761−768

stress conditions.[23] Likewise, we studied the expression of genes codifying for the predicted *F. vesca* ADH isoform XP_004290568, which was the sequence with the highest homology to the ADH from *Fragaria* × *ananassa* (P17648) involved in cold tolerance.[25] The expression of *PDC* was already high at harvest, but storage at 0 °C without added CO_2 induced a progressive accumulation of its transcripts. After 3 days, *PDC* expression had increased 40%, and this increase reached 77% after 6 days. However, in fruit exposed to 20 and 40% CO_2 *PDC* expression was similar to that found in fruit at harvest, suggesting that application of high-CO_2 levels prevented the increase in *PDC* transcription induced by low temperature. These results agree with those of Ponze-Valadez et al.,[21] who found that CO_2 inhibited *PDC* expression in Jewel strawberries during the first days of storage at 2 °C. Even with an atmosphere of 60% CO_2 for 7 days,[23] no effect in PDC mRNA levels in Chandler strawberries was detected. Low temperature induced its transcription even more drastically. After 3 and 6 days without added CO_2, *ADH* expression was 8.5- and 23-fold higher than that of fruit at harvest, respectively. This increase was more moderate in the fruit exposed to 20% CO_2, and it was even less pronounced when fruits were exposed to 40% CO_2. *ADH* mRNA accumulation by low temperature has been reported in several plant species.[29,30] Also in Jewel strawberries, the *ADH* expression, which was low at harvest, increased after the second day of storage at low temperature,[21] although accumulation of ethanol was not shown. Considering that in the present work all samples exhibited the same O_2 (20%), our results indicate that factors other than O_2 are influencing the expression of *PDC* and *ADH* genes. The observed marked accumulation of *PDC* and *ADH* transcripts in strawberries stored without added CO_2 seems to indicate that low temperature is involved in the induction of both genes.

The lowest ethanol values were found in strawberries stored without added CO_2 (Figure 1B), and ethanol was not even detected after 6 days. By contrast, a marked increase in ethanol content was detected following exposure to CO_2, and whereas a 4-fold increase was measured after 3 days in 20% CO_2, the increase was 41-fold in 40% CO_2. When fruits were exposed to CO_2 for 6 days, the increase in ethanol was more pronounced, whereas no such increase was found in fruit that was not exposed to CO_2. In the case of acetaldehyde, again the highest levels were found in fruit treated with 40% CO_2. Furthermore, after a 3 day exposure to 40% CO_2, the increase in acetaldehyde in fruit was higher than that observed for ethanol. Also in Chandler strawberries treated with 50% CO_2 and with oxygen kept at 21%, acetaldehyde markedly increased with respect to untreated fruit, and its levels were higher compared with those under hypoxia conditions.[31] A progressive increase in acetaldehyde and ethanol concentrations has also been reported in other fruits during ripening at 20 °C and under elevated CO_2 and normal atmospheric oxygen concentration.[32] Moreover, Zhang and Watkins[22] showed that accumulation of fermentative metabolites and *ADH* transcripts in CO_2-treated strawberries was temperature dependent, being higher at 20 °C than at 2 °C. Our results indicate that the highest ethanol values were obtained in fruit exposed to 40% CO_2 for 6 days (67.7 ± 2.8 mg/100 mL). Despite its accumulation, there was significantly less ethanol than in the juice of other fruits such as oranges[26,33] and less than the level indicated by Ben-Aire et al.[34] as an off-flavor developed in persimmons (75 mg/100 mL). Also in 40% CO_2-treated fruit the highest levels of acetaldehyde were quantified, reaching values of 10 mg/100 mL. In 20% CO_2-treated fruit the maximum ethanol and acetaldehyde levels were 4- and 10-fold lower than those found in 40% CO_2-treated ones. Furthermore, the accumulation of such fermentative metabolites was not correlated with the strongest expression of *PDC* and *ADH*. Our results show that *PDC* and *ADH* expression was up-regulated by low temperature and it was unmodified (*PDC*) or weakly induced (*ADH*) by high levels of CO_2. The sharp induction of *PDC* and *ADH* driven by low temperature was not accompanied by a shift toward ethanolic fermentation, such that the levels of acetaldehyde and ethanol did not increase concomitantly. Although high CO_2 appears to exert a clear influence in avoiding the specific induction of *PDC* and *ADH* genes analyzed in this work, fruit is able to maintain an active fermentative metabolism based on the accumulation of ethanol and acetaldehyde. In light of the discrepancies between *ADH* transcripts and ethanol content described elsewhere[21,22] and the data shown here, the correlation between fermentative metabolites and *PDC* and *ADH* gene expression still requires further study. Accordingly, other experiments should be performed to determine if there is a *PDC* or *ADH* isoform specifically induced by high concentrations of CO_2.

Cellular Water Stress in Response to Various CO_2 Levels. The determination of bound water content by DSC showed a clear difference between CO_2 doses and duration of exposure (Figure 2). In freshly harvested strawberries, the bound water (2.5 g/g DW) was slightly lower than in fruit exposed to 20% CO_2, which exhibited the highest values. By contrast, the bound water content decreased in fruit stored at low temperature in air, although less so than in fruit maintained in 40% CO_2 in which a marked depletion was quantified after 3 days. The low bound water content then remained constant for a further 3 days, reaching values of 0.71 g/g DW. Modifications

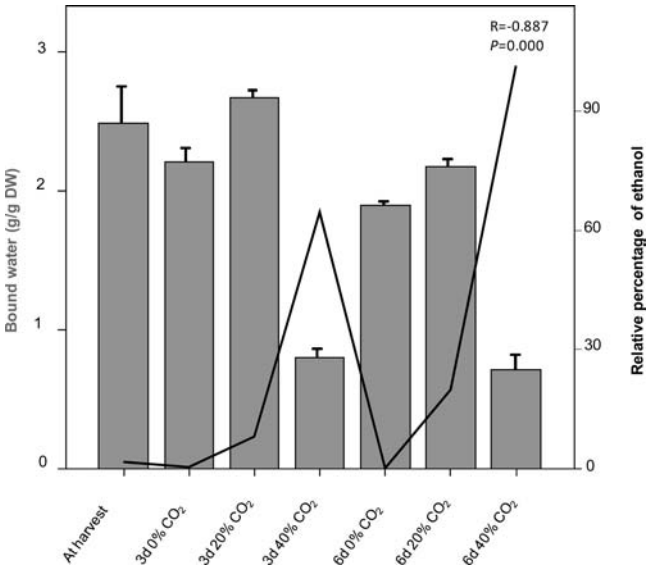

Figure 2. Correlation between ethanol and bound water in Mara des Bois strawberries *Fragaria vesca* immediately after harvesting (day 0) and after 3 days of storage at 0 °C in different CO_2 concentrations (0, 20, or 40%), maintaining a constant concentration of O_2 (20%). The bound water content is represented by the shaded bars, whereas the line shows the relative percent of ethanol over maximum level. The *R* value and significance level are indicated in the top right-hand corner of the figure. An inverse correlation was also found between bound water and acetaldehyde ($R = -0.836$; $P = 0.000$) (data not shown).

DOI: 10.1021/jf505715s
J. Agric. Food Chem. 2015, 63, 761−768

of water fractions have already been detected in several fruits during ripening and storage.[12,27] Our present results indicate that excessively high CO_2 leads to a significant conversion of bound water to free water content, with the consequent implications on the availability of water in the cell. Interestingly, the decrease in the content of bound water was inversely correlated with the increase in the levels of ethanol (R = −0.887) (Figure 2) and acetaldehyde (R = −0.836, data not shown). Strawberries treated with 40% CO_2 showed the highest fermentative volatile values and the lowest values for bound water. This good correlation seems to indicate that there is competition between acetaldehyde and/or ethanol and bound water, and excessive fermentative metabolites can disrupt membrane structures. Klemm[35] reported that alcohol and water compete with each other on target membrane molecules, specifically, lipids and proteins near the membrane surface. Ethanol could bind certain targets preferentially and displace water, leading to conformational consequences. Using model membrane systems, FTIR spectroscopic evidence revealed that alcohol has a nonstereospecific binding capacity for membrane surface molecules and that such binding occurs at sites that would otherwise be occupied by hydrogen-bonded water.[36] Our results suggest that fermentative metabolites can modulate the displacement of water from the hydrogen-bonded network in the hydration layer, resulting in a reduction of bound water. Ethanol also perturbed cell membranes by weakening interlipid hydrogen bonding, involving water.[14] Furthermore, as we previously reported that 40% CO_2 treatment affected cellular structure and water potential in strawberries,[13] our results suggest that excess alcohol might trigger cellular water stress. Alternatively, the lack of ethanol in fruit stored without added CO_2 may restrain the flexibility of the membrane, in part, through the changes in membrane rigidity associated with storage at low temperature.[37] Consequently, the beneficial effect of 20% CO_2 treatment may be attributed to the stabilization of membrane component interactions, involving water. Indeed, keeping the water fractions within normal parameters seems to be important to maintain a relatively constant distance between membrane components and to stabilize lipid−lipid interactions that strongly influence the structure of biological membranes.

Oxidative Damage in Response to Various CO_2 Levels. Oxidative damage was quantified by measuring MDA using HPLC-UV detection as the DNPH derivative. Figure 3 shows the HPLC chromatogram at 310 nm of strawberry homogenates after treatment for MDA determination, indicating the hydrazone derivative of MDA, which was confirmed by spiking samples with standard MDA before the treatment. A good chromatographic peak resolution was obtained, with no interfering peaks, which allowed a straightforward determination of the MDA derivative. Using this precise and sensitive method, the effect of low temperature and high CO_2 concentrations on lipid peroxidation was evident (Figure 3). After 3 days, MDA levels increased in fruit stored without added CO_2 with respect to freshly harvested fruit and then declined, indicating that radical-induced damage is involved in the initial stage of storage at low temperature. When strawberries were treated with 20% CO_2 for 3 days, the MDA levels increased, but to lower levels than for strawberries stored without added CO_2, and then remained constant for a further 3 days. In fruits treated with 40% CO_2, higher levels of MDA were detected than for strawberries stored without added CO_2, mainly after 6 days of treatment.

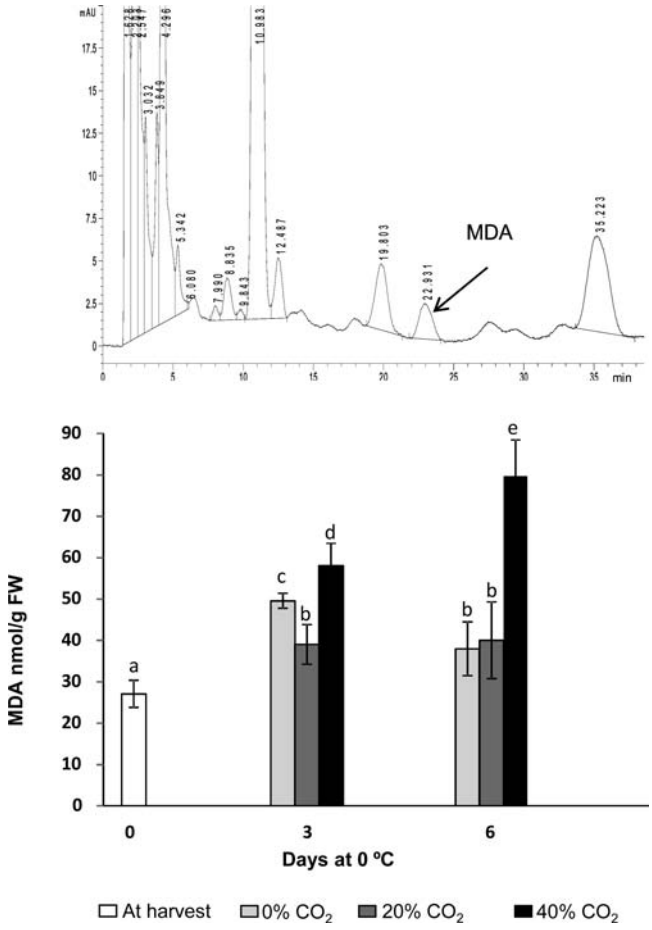

Figure 3. Chromatogram showing the MDA peak and a graph indicating the changes in the levels of MDA in Mara des Bois strawberries *Fragaria vesca* immediately after harvesting (day 0) and after 3 days of storage at 0 °C in different CO_2 concentrations (0, 20, or 40%), maintaining a constant concentration of O_2 (20%). Each letter indicates significant differences between the means determined by Tukey's test (P < 0.05).

Membrane phospholipids, and especially the group of polyunsaturated fatty acids, are susceptible to reactions with free radicals. The significant increase in MDA in fruit tissues indicates enhanced lipid peroxidation. Lipid peroxidation may be the result of more than one environmental factor, including chilling temperature.[38] Our data indicate that 20% CO_2 reduces the oxidative stress caused by severely low temperature, supporting the significant increase previously observed in several tissues of table grape bunches as a response to low-temperature storage.[39,40] Given the high MDA levels in 40% CO_2-treated fruit, we suggest that the decomposition of lipid hydroperoxide is possibly enhanced by the accumulation of potentially toxic levels of acetaldehyde and/or ethanol that disproportionally affect the displacement of water molecules in this hydrogen-bonded water network, thereby disrupting membrane structure. The above changes in membrane stability associated with excessive fermentative metabolites might also accelerate the oxidative damage determined by an increase in MDA levels.

Changes in Sucrose, Malic Acid, Total Soluble Solids, pH, and Titratable Acidity in Response to Various CO_2 Levels. At harvest, a steady-state level of sucrose was maintained in CO_2-treated fruit, this being the main constituent

DOI: 10.1021/jf505715s
J. Agric. Food Chem. 2015, 63, 761−768

Table 1. Changes in the Content of Sucrose and Malic Acid Determined by HPAEC and in the Quality Parameters (Total Soluble Solids (°Brix), pH, and Titratable Acidity (TA)) in *Fragaria vesca* Mara des Bois Strawberries Immediately after Harvesting and after 3 and 6 Days of Storage at 0 °C in Different CO_2 Concentrations (0, 20, or 40% CO_2), Maintaining a Constant Concentration of O_2 (20%)[a]

		3 days			6 days		
	at harvest	0% CO_2	20% CO_2	40% CO_2	0% CO_2	20% CO_2	40% CO_2
sucrose (mg/g fw)	17.92 ± 1.2bc	12.36 ± 0.9a	17.83 ± 0.2bc	16.98 ± 1.1bc	13.25 ± 0.5a	19.13 ± 1.6c	17.63 ± 1.8bc
°Brix (%)	9.80 ± 0.2cd	9.80 ± 0.2cd	9.27 ± 0.2ab	9.47 ± 0.1bc	9.03 ± 0.1a	10.10 ± 0.0d	9.93 ± 0.1d
malic acid(mg/g fw)	3.48 ± 0.2d	2.91 ± 0.1c	2.09 ± 0.2a	2.93 ± 0.2c	2.36 ± 0.1ab	2.49 ± 0.1b	2.74 ± 0.0bc
pH	3.57 ± 0.0a	3.71 ± 0.0d	3.64 ± 0.0c	3.72 ± 0.0d	3.60 ± 0.0b	3.64 ± 0.0c	3.69 ± 0.0d
TA (% citric acid)	0.80 ± 0.0c	0.85 ± 0.0d	0.78 ± 0.0b	0.73 ± 0.0a	0.78 ± 0.0b	0.81 ± 0.0c	0.73 ± 0.0a

[a]Data are presented as the means ± SE of three replicates (n = 6); different letters (a–d) within rows indicate significant differences at $P < 0.05$.

of carbohydrate reserve (Table 1). By contrast, a decrease in sucrose was observed in fruit stored without additional CO_2 (0%) after both 3 and 6 days in storage at 0 °C. These results reveal that without added CO_2, fruits deplete their energy reserves, leading to a decrease in sucrose and lower levels of total soluble solids after 6 days in storage. Conversely, fruits saved energy reserves when exposed to CO_2 and had more abundant sucrose than fruits stored at low temperature without added CO_2. Ethanol synthesis has generally been regarded as the means to regenerate NAD^+ required to sustain glycolytic energy production. Furthermore, and consistent with the pH-stat mechanism for H^+ consumption, the activation of ethanol synthesis in CO_2-treated fruit could be an important role given that ethanol synthesis is not accompanied by H^+ production and, so, it could be a way to limit cytoplasmic acidification. Although cytoplasmic pH determination has not been performed in this study, the fruit extract pH indicated that fruit with excessive CO_2 levels (40%) exhibited the highest pH levels and the lowest titratable acidity (Table 1). Increasing pH and decreasing titratable acidity in strawberry tissues was more marked in fruit stored in high CO_2 atmospheres.[41] Malic acid content is involved in regulating cytoplasmic pH, and changes in endogenous malate levels in response to experimental treatment are expected to cause cytoplasmic pH shifts.[42] The lowest values of malic acid were found in fruit exposed to 20% CO_2 for 3 days (Table 1). The decrease in malic acid in fruit treated with 20% CO_2 for 3 days might prevent a drop in the cytoplasmic pH and, consequently, a high degree of fermentation might not be required in accordance with the aforementioned hypothesis. A significant role for malate in the regulation of cytoplasmic pH in hypoxic plant tissue has been proposed.[43] However, when the exposure to CO_2 treatment was stronger and persisted longer, this pattern changed. In the case of fruit stored at 0 °C without added CO_2, the up-regulation of fermentative genes while ethanol formation was restricted implies that the potential capacity for ethanolic fermentation was insufficient. Ethanolic fermentation not only is considered to be the main factor in providing energy under low oxygen concentrations but also has additional important functions in the presence of atmospheric oxygen.[44]

Our results show that following exposure to high CO_2 under unlimited oxygen conditions, the activation of fermentative metabolism in fruit with the associated production of ethanol and acetaldehyde may represent an essential supplementary metabolic pathway for energy production. Favorable fermentative metabolism in strawberries exposed to 20% CO_2, with a marked increase in the levels of fermentative metabolites, should promote the consumption of reducing power and H^+. Moreover, the reoxidation of NADH in 20% CO_2-treated fruit seems to be potentiated by the activation of malic acid decarboxylation in accordance with the decrease in malic acid quantified in these treated fruit. Stimulation of NADP-ME activity in 20% CO_2-treated fruit has already been reported.[45] Thus, the activation of fermentative metabolism has been described as an adaptive response of fruit to stressful conditions.[21] Therefore, the controlled modulation of ethanol and acetaldehyde levels that are allowed to accumulate in strawberry tissues in fruit seems to be an extremely important protective mechanism for conferring tolerance to high-CO_2 levels, thus reducing damage to severely low temperature.

Our data indicate that the expression of *PDC* and *ADH* genes in *Fragaria vesca* Mara des Bois strawberries stored at low temperature without added CO_2 is greatly in excess of the rate of fermentation metabolites. Moreover, the progressive decrease in the transcript levels of *PDC* and *ADH* as CO_2 increases suggests that the induction of fermentative genes is correlated with low-temperature storage. Our results demonstrate that treating strawberries with 20% CO_2 activates fermentative metabolism by means of a marked increase in the levels of fermentative metabolites. Moreover, favorable fermentative metabolism combined with the activation of malic acid decarboxylation may represent a protective mechanism. On exposure to 40% CO_2, the exclusive disposition of fermentative metabolism caused damage due to the excessive accumulation of fermentative metabolites in the fruit, leading to elevated oxidative stress as witnessed by acute MDA production. Moreover, excess ethanol and acetaldehyde accumulation could potentially accelerate the loss of membrane integrity, provoking the loss of bound water fraction that resembles cellular water stress. Therefore, the controlled modulation of ethanol and acetaldehyde levels in fruit concomitant with an activation of malic decarboxylation may in part explain complex processes such as cross tolerance between low temperature and beneficial high-CO_2 concentrations.

This study demonstrates the up-regulation of ADC and PDC in strawberries at 0 °C in conditions of unlimited O_2 while nonaccumulation of fermentative products occurred. Moreover, storage at low temperature was coupled to oxidative stress, exacerbated by excessive high CO_2 (40%) and controlled by beneficially high-CO_2 (20%) levels. Furthermore, the accumulation of fermentative products was correlated with marked changes in fruit water status, without the influence of extra surrounding water.

DOI: 10.1021/jf505715s
J. Agric. Food Chem. 2015, 63, 761–768

AUTHOR INFORMATION

Corresponding Author

*(C.M.) Phone: 34-91-5492300. Fax: 34-91-5493627. E-mail: merodio@ictan.csic.es.

Funding

This work was financed by CICYT Projects AGL2008-02949 and AGL2011-26742 from MICINN of the Spanish government. R.R. was supported by a postdoctoral JAE contract from the CSIC.

Notes

The authors declare no competing financial interest.

REFERENCES

(1) Wszelaki, A. L.; Mitcham, E. J. Effect of combination of hot water dips, biological control and controlled atmospheres for control of gray mold on harvested strawberries. *Postharvest Biol. Technol.* **2003**, *27*, 255−264.

(2) Fernandez-Trujillo, J. P.; Nock, J. F.; Watkins, C. B. Fermentative metabolism and organic acid concentrations in fruit of selected strawberry cultivars with different tolerances to carbon dioxide. *J. Am. Soc. Hortic. Sci.* **1999**, *124*, 696−701.

(3) Pesis, E. The role of the anaerobic metabolites, acetaldehyde and ethanol, in fruit ripening, enhancement of fruit quality and fruit deterioration. *Postharvest Biol. Technol.* **2005**, *37*, 1−19.

(4) Buendia, B.; Gil, M. I.; Tudela, J. A.; Gady, A. L.; Medina, J. J.; Soria, C.; López, J. M.; Tomás-Barberán, F. A. HPLC-MS analysis of proanthocyanidin oligomers and other phenolics in 15 strawberry cultivars. *J. Agric. Food Chem.* **2010**, *58*, 3916−3926.

(5) Akhatou, I.; Fernández-Recamales, A. Nutritional and nutraceutical quality of strawberries in relation to harvest time and crop conditions. *J. Agric. Food Chem.* **2014**, *62*, 5749−5760.

(6) Aron, P. M.; Kennedy, J. A. Flavan-3-ols: nature, occurrence and biological activity. *Mol. Nutr. Food Res.* **2008**, *52*, 79−104.

(7) Panjehkeh, N.; Backhouse, D.; Taji, A. Role of proanthocyanidins in resistance of the legume Swainsona formosa to *Phytophthora cinnammi*. *J. Phytopathol.* **2010**, *158*, 365−371.

(8) Blanch, M.; Alvarez, I.; Sanchez-Ballesta, M. T.; Escribano, M. I.; Merodio, C. Increasing catechin and procyanidin accumulation in high CO_2-treated *Fragaria vesca* strawberries. *J. Agric. Food Chem.* **2012**, *60*, 7489−7496.

(9) Arnal, L.; Del Río, M. A. Removing astringency by carbon dioxide and nitrogen-enriched atmospheres in persimmon fruit cv. 'Rojo brillante'. *J. Food Sci.* **2003**, *68*, 1516−1518.

(10) Min, T.; Yin, X.; Shi, Y.; Luo, Z.; Yao, Y.; Grierson, D.; Ferguson, I. B.; Chen, K. Ethylene-responsive transcription factors interact with promoters of ADH and PDC involved in persimmon (*Diospyros kaki*) fruit de-astringency. *J. Exp. Bot.* **2012**, *63*, 6393−6405.

(11) Es-Safi, N.; Fulcrand, H.; Cheynier, V.; Moutounet, M. Competition between (+)-catechin and (−)-epicatechin in acetaldehyde induced polymerization of flavanols. *J. Agric. Food Chem.* **1999**, *47*, 2088−2095.

(12) Goñi, O.; Fernandez-Caballero, C.; Sanchez-Ballesta, M. T.; Escribano, M. I.; Merodio, C. Water status and quality improvement in high-CO_2 treated table grapes. *Food Chem.* **2011**, *128*, 34−39.

(13) Blanch, M.; Goñi, O.; Sanchez-Ballesta, M. T.; Escribano, M. I.; Merodio, C. Characterisation and functionality of fructo-oligosaccharides affecting water status of strawberry fruit (*Fragaria vesca* L. cv. Mara des Bois) during postharvest storage. *Food Chem.* **2012**, *134*, 912−919.

(14) Slater, S. J.; Frank, C. H.; Taddeo, F. J.; Kelly, M. B.; Stubbs, C. D. Contribution of hydrogen bonding to lipid-lipid interactions in membranes and the role of lipid order: effects of cholesterol, increased phospholipid unsaturation, and ethanol. *Biochemistry* **1993**, *32*, 3714−3721.

(15) Fujita, Y.; Yoshikawa, M. Vapor permeation of aqueous ethanol mixtures through agarose membranes. *J. Membr. Sci.* **2014**, *459*, 114−121.

(16) Hallsworth, J. E. Ethanol-induced water stress in yeast. *J. Ferment. Bioeng.* **1998**, *85*, 125−137.

(17) Mitller, R. Oxidative stress, antioxidant and stress tolerance. *Trends Plant Sci.* **2002**, *7*, 405−410.

(18) de Lima, V. R. D.; Morfim, M. P.; Teixeira, A.; Creczynski-Pasa, T. B. Relationship between the action of reactive oxygen and nitrogen species on bilayer membranes and antioxidants. *Chem. Phys. Lipids* **2004**, *132*, 197−208.

(19) Xu, M.; Dong, J.; Zhang, M.; Xu, X.; Sun, L. Cold-induced endogenous nitric oxide generation plays a role in chilling tolerance of loquat fruit during postharvest storage. *Postharvest Biol. Technol.* **2012**, *65*, 5−12.

(20) De Zwart, L. L.; Meerman, J. H. N.; Commandeur, J. N. M.; Vermeulen, N. P. E. Biomarkers of free radical damage applications in experimental animals and in humans. *Free Radical Biol. Med.* **1999**, *26*, 202−226.

(21) Ponce-Valadez, M.; Watkins, C. B. Fermentation and malate metabolism in response to elevated CO_2 concentrations in two strawberry cultivars. *Physiol. Plant.* **2008**, *134*, 121−33.

(22) Zhang, J. J.; Watkins, C. B. Fruit quality, fermentation products, and activities of associated enzymes during elevated CO_2 treatment of strawberry fruit at high and low temperatures. *J. Am. Soc. Hortic. Sci.* **2005**, *130*, 124−130.

(23) Moyano, E.; Encinas-Villarejo, S.; López-Ráez, J.; Redondo-Nevado, J.; Blanco-Portales, R.; Bellido, M. L.; Sanz, C.; Caballero, J. L.; Muñoz-Blanco, J. Comparative study between two strawberry pyruvate decarboxylase genes along fruit development and ripening, post-harvest and stress conditions. *Plant Sci.* **2004**, *166*, 835−845.

(24) Yu, D.; Tang, H.; Zhang, Y.; Du, Z.; Yu, H.; Chen, Q. Comparison and improvement of different methods of RNA isolation from strawberry (*Fragraria* × *ananassa*). *J. Agric. Sci.* **2012**, *4*, 51−56.

(25) Koehler, G.; Wilson, R. C.; Goodpaster, J. V.; Sønsteby, A.; Lai, X.; Witzmann, F. A.; You, J. S.; Rohloff, J.; Randall, S. K.; Alsheikh, M. Proteomic study of low-temperature responses in strawberry cultivars (*Fragaria* × *ananassa*) that differ in cold tolerance. *Plant Physiol.* **2012**, *159*, 1787−1805.

(26) Valencia-Chamorro, S. A.; Pérez-Gago, M. B.; del Río, M. A.; Palou, L. Effect of antifungal hydroxypropyl methylcellulose (HPMC)-lipid edible composite coatings on postharvest decay development and quality attributes of cold-stored 'Valencia' oranges. *Postharvest Biol. Technol.* **2009**, *54*, 72−79.

(27) Goñi, O.; Muñoz, M.; Ruiz-Cabello, J.; Escribano, M. I.; Merodio, C. Changes in water status of cherimoya fruit during ripening. *Postharvest Biol. Technol.* **2007**, *45*, 147−150.

(28) Mateos, M.; Lecumberri, E.; Ramos, S.; Goya, L.; Bravo, L. Determination of malondialdehyde (MDA) by high-performance liquid chromatography in serum and liver as a biomarker for oxidative stress. Application to a rat model for hypercholesterolemia and evaluation of the effect of diets rich in phenolic antioxidants from fruits. *J. Chromatogr., B* **2005**, *827*, 76−82.

(29) Christie, P. J.; Hahn, M.; Walbot, V. Low-temperature of *alcohol dehydrogenase-1* mRNA and protein activity in maize and rice seedlings. *Plant Physiol.* **1991**, *95*, 699−706.

(30) Jarillo, J. A.; Leyva, A.; Salinas, J.; Martínez-Zapater, J. M. Low temperature induces the accumulation of alcohol dehydrogenase mRNA in *Arabidopsis thaliana*, a chilling-tolerant plant. *Plant Physiol.* **1993**, *101*, 833−837.

(31) Ke, D.; Zhou, L.; Kader, A. A. Mode of oxygen and carbon dioxide action on strawberry ester biosynthesis. *J. Am. Soc. Hortic. Sci.* **1994**, *119*, 971−975.

(32) Muñoz, M. T.; Escribano, M. I.; Merodio, C. Ethanolic metabolism in cherimoya fruit during storage at ambiente and under high CO_2 atmosphere. *J. Hortic. Sci. Biotechnol.* **1997**, *72*, 976−982.

(33) Pérez-Gago, M. B.; Rojas, C.; del Río, M. A. Effect of lipid type and amount of edible hydroxypropyl methylcellulose−lipid composite coatings used to protect postharvest quality of mandarins cv. Fortune. *J. Food Sci.* **2002**, *67*, 2903−2910.

DOI: 10.1021/jf505715s
J. Agric. Food Chem. 2015, 63, 761−768

(34) Ben-Aire, R.; Zutkhi, Y.; Sonego, L.; Klein, J. Modified atmosphere packaging for long-term storage of astringent persimmons. *Postharvest Biol. Technol.* **1991**, *1*, 169−179.
(35) Klemm, W. R. Biological water and its role in the effects of alcohol. *Alcohol* **1998**, *15*, 249−267.
(36) Chiou, J. S.; Kuo, C. C.; Lin, S. H.; Kamaya, H.; Ueda, I. Interfacial dehydration by alcohols: hydrogen bonding of alcohols to phospholipids. *Alcohol* **1991**, *8*, 143−150.
(37) Gualanduzzi, S.; Baraldi, E.; Braschi, I.; Carnevali, F.; Gessa, C. E.; De Santis, A. Respiration, hydrogen peroxide levels and antioxidant enzyme activities during cold storage of zucchini squash fruit. *Postharvest Biol. Technol.* **2009**, *52*, 16−23.
(38) Hodges, D. M.; Lester, G. E.; Munro, K. D.; Toivonen, P. M. A. Oxidative stress: importance for postharvest quality. *HortScience* **2004**, *39*, 924−929.
(39) Rosales, R.; Fernandez-Caballero, C.; Romero, I.; Escribano, M. I.; Merodio, C.; Sanchez-Ballesta, M. T. Molecular analysis of the improvement in rachis quality by high CO_2 levels in table grapes stored at low temperature. *Postharvest Biol. Technol.* **2013**, *77*, 50−58.
(40) Romero, I.; Sanchez-Ballesta, M. T.; Maldonado, R.; Escribano, M. I.; Merodio, C. Anthocyanin, antioxidant activity and stress-induced gene expression in high CO_2-treated table grapes stored at low temperature. *J. Plant Physiol.* **2008**, *165*, 522−530.
(41) Holcroft, D. M.; Kader, A. A. Controlled atmosphere-induced changes in pH and organic acid metabolism may affect color and stored strawberry fruit. *Postharvest Biol. Technol.* **1999**, *17*, 19−32.
(42) Sakano, K. Metabolic regulation of pH in plant cells: role of cytoplasmic pH in defense reaction and secondary metabolism. *Int. Rev.Cytol.* **2001**, *206*, 1−44.
(43) Roberts, J. K. M.; Hooks, M. A.; Miaullis, A. P.; Edwards, S.; Webster, C. Contribution of malate and amino acid metabolism to cytoplasmic pH regulation in hypoxic maize root tips studied using nuclear magnetic resonance spectroscopy. *Plant Physiol.* **1992**, *98*, 480−487.
(44) Tadege, M.; Dupuis, I.; Kuhlemeier, C. Ethanolic fermentation: new functions for an old pathway. *Trends Plant Sci.* **1999**, *8*, 320−325.
(45) Blanch, M.; Rosales, R.; Goya, L.; Sanchez-Ballesta, M. T.; Escribano, M. I.; Merodio, C. NADP-malic enzyme and glutathione reductase contribute to glutathione regeneration in *Fragaria vesca* fruit treated with protective high CO_2 concentrations. *Postharvest Biol. Technol.* **2013**, *86*, 431−436.

DOI: 10.1021/jf505715s
J. Agric. Food Chem. 2015, 63, 761−768

JOURNAL OF AGRICULTURAL AND FOOD CHEMISTRY

Article

pubs.acs.org/JAFC

Characterization of Typical Potent Odorants in Cola-Flavored Carbonated Beverages by Aroma Extract Dilution Analysis

Yaowapa Lorjaroenphon[†] and Keith R. Cadwallader*[,‡]

[†]Department of Food Science and Technology, Faculty of Agro-Industry, Kasetsart University, 50 Ngamwongwan Road, Bangkok 10900, Thailand

[‡]Department of Food Science and Human Nutrition, University of Illinois at Urbana-Champaign, 1302 West Pennsylvania Avenue, Urbana, Illinois 61801, United States

ABSTRACT: The aroma-active compounds in typical cola-flavored carbonated beverages were characterized using gas chromatography−olfactometry and gas chromatography−mass spectrometry. The potent odorants in the top three U.S. brands of regular colas were identified by aroma extract dilution analysis (AEDA). Among the numerous odorants identified, eugenol (spicy, clovelike, sweet) and coumarin (sweet, herbaceous) were predominant in all colas. Other predominant odorants in at least one brand included guaiacol (smoky) and linalool (floral, sweet), while 1,8-cineole (minty, eucalyptus-like) was a moderately potent odorant in all colas. Determination of the enantiomeric compositions indicated that (*R*)-(−)-linalool (34.5%) was a more potent odorant than the (*S*)-(+)-enantiomer (65.6%) due to its much lower odor detection threshold. In addition, lemon-lime and cooling attributes determined by sensory descriptive analysis had the highest odor intensities among the eight sensory descriptors. The aroma profiles of the three colas were in good agreement with the potent odorants identified by AEDA.

KEYWORDS: *cola-flavored carbonated beverage, potent odorant, aroma extract dilution analysis, enantiomer, sensory descriptive analysis*

INTRODUCTION

Carbonated beverages are the largest segment of the soft drink industry, and cola is the predominant flavor accounting for 54.0% of the global revenues generated by the soft drink and bottled water industry.[1] The sales of cola-flavored carbonated beverages in 2010 were about $14 billion of the soft drink market in the United States.[2,3] According to product labels and published literature, the uniqueness and complexity of cola is a result of the mixture of natural flavors derived from vanilla extract and essential oils of citrus, cassia or cinnamon, coriander, nutmeg, and neroli.[4,5]

Despite its popularity, there are only a few studies on the flavor chemistry of cola. Cola aroma has been studied by both sensory[6] and instrumental[7−9] techniques. Headspace volatiles of decarbonated colas were evaluated by solid-phase microextraction (SPME) and dynamic headspace analysis.[8] These researchers reported that terpenes and aldehydes were the major volatiles, and those in highest abundance were limonene and a mixture of α- and γ-terpineol. Limonene along with γ-terpinene and *p*-cymene were identified as the three most abundant headspace volatiles in off-flavored cola.[7] Another study asserted that (*Z*)-terpin hydrate could be used as a volatile marker to differentiate cola stains from the dark color stains caused by other beverages, including beer, coffee, black tea, Oolong tea, and green tea.[9]

However, the potent odorants of cola have not been reported. Gas chromatography−olfactometry (GCO), which uses the human nose as a detector of GC, was developed and applied to indicate the odorants from the complex mixture of both aroma volatiles and odorless volatiles. Aroma extract dilution analysis (AEDA), which is frequently used, is a screening method used to rank the relative potency of aroma-active compounds found in foods.[10,11] It has been used to identify the potent odorants in foods, beverages, and nonfoods, including pomegranate juice[12] and scented candles.[13]

In the present study we aimed to determine the potent odorants in the top three U.S. brands of regular cola-flavored carbonated beverages on the basis of AEDA. The aroma-active compounds in typical cola were characterized using GCO and GC−mass spectrometry (GC−MS). The aroma-active compounds with the most impact were then identified by AEDA. The results of this study can provide a foundation for further studies leading to the identification of key aroma components and improvements in the flavor and shelf life stability of cola-flavored carbonated beverages.

MATERIALS AND METHODS

Materials. The top three U.S. brands of regular cola-flavored carbonated beverages (Coca-Cola, Pepsi, and RC, designated as cola A, cola B, and cola C, respectively) and the references used in sensory evaluation (Table 1) were purchased from local markets (Urbana, IL) during 2010−2011. Odor-free water used in this experiment was prepared by boiling deionized−distilled water to two-thirds of its initial volume.

Chemicals. General-reagent- or HPLC-grade chemicals, such as anhydrous diethyl ether, anhydrous sodium sulfate, dichloromethane, hydrochloric acid, sodium bicarbonate, and sodium chloride, were obtained from Fisher Scientific (Fair Lawn, NJ). Ultra-high-purity (UHP) nitrogen and UHP helium were purchased from S.J. Smith (Davenport, IA).

Received: October 13, 2014
Revised: December 20, 2014
Accepted: December 21, 2014
Published: December 21, 2014

ACS Publications © 2014 American Chemical Society

DOI: 10.1021/jf504953s
J. Agric. Food Chem. 2015, 63, 769−775

Table 1. Attributes, Definitions, and References Used for Sensory Descriptive Analysis of Cola-Flavored Carbonated Beverages

attribute	definition	reference		
		product (manufacturer)	preparation[a]	intensity[b]
lemon-lime	aromatic reminiscent of lemon or lime	Sprite (lemon-lime soda) (Coca-Cola Co., Atlanta, GA)	50 mL	7
orange	aromatic reminiscent of orange	Sunkist (orange soda) (Sunkist Growers, Inc., Sherman Oaks, CA)	50 mL	9
brown spice	aromatic associated with allspice, cinnamon, clove, mace, nutmeg (spicy)	whole cloves (McCormick & Co., Inc., Hunt Valley, MD)	0.2 g	10
herbal	aromatic associated with dried herbs, hay, or grass	dried long grass (cut into 2 cm pieces)	3 g	9
vanilla	vanilla-like aroma	vanillin (compound **58**; Fluka, Buchs, Switzerland)	10 mL (50 ppm in water)	8
caramel	sweet aromatic	Werther's Original (chewy caramels) (made in Germany for Storck USA L.P., Chicago, IL)	one piece (~6 g)	6
cooling	cooling aroma, but not identical to mint	Halls (Mentho-Lyptus) (made in Canada, distributed by Cadbury Adams USA LLC, Parsippany, NJ)	10 mL (3.5 mg/mL of water)	7
pine	aromatic reminiscent of pine needles	Pine-Sol (original) (Fabricado Para the Clorox Co., Oakland, CA)	10 mL (100 ppm in water)	7

[a]Prepared in a 125 mL Teflon sniff bottle. [b]Relative intensity on a 15 cm line with two anchor scales from none to strong.

Reference Standard Compounds. The standard compounds used to confirm the structures of the aroma compounds listed in Table 2 were supplied by the companies given in parentheses: compounds **1**−**6**, **8b**, **9**−**11**, **13**, **14**, **16**, **19**−**22** (**22a** and **22b**), **24**, **25** (**25a** and **25b**), **26**−**29**, mixture of **30** and **34**, **31** (**31a** and **31b**), **32**, **37**, **38**, **41**, **43**, **45**−**49**, **51**, **52**, **56**, and **57** (Sigma-Aldrich, St. Louis, MO); **12** (TCI, Portland, OR); **33**, **36**, and **39** (Bedoukian, Danbury, CT); **40** (Firmenich, Princeton, NJ); mixture of **53** and **54** (Alfa Aesar, Lancashire, U.K.); **8a**, **22a**, **58** (Fluka, Buchs, Switzerland). 2,3-Dehydro-1,8-cineole (compound **7**) was synthesized according to the published literature.[14]

Isolation of Volatile Compounds. Odor-free deionized−distilled water (200 mL) and diethyl ether (150 mL) were added to the extraction chamber of a continuous liquid−liquid extraction (CLLE) apparatus (part no. Z562440, Sigma-Aldrich) equipped with a 5 °C condenser, 48 °C water bath (250 mL distillation flask), and magnetic stirrer. One can of cola sample (355 mL) was poured through the cooled condenser to avoid loss of aroma compounds and rinsed with 50 mL of water. After extraction for 18 h at a condensation rate of 2 drops/s, the solvent layer was concentrated to 50 mL by Vigreux column distillation at 43 °C. The volatile compounds were isolated from any nonvolatile compounds by solvent-assisted flavor evaporation (SAFE) according to the litelature.[13,15] The aroma extract was fractionated with aqueous 0.5 M $NaHCO_3$ (3 × 20 mL) into acidic (aqueous phase) and neutral-basic (organic phase) fractions. The aqueous layer was acidified to pH 2 with aqueous 4 N HCl and extracted with diethyl ether (3 × 20 mL). Each fraction was washed with saturated aqueous NaCl (2 × 15 mL), concentrated to 10 mL by Vigreux column distillation, and dried over 2 g of anhydrous Na_2SO_4. The ether extract was further concentrated by Vigreux column distillation to 350 μL and kept at −70 °C until analysis.

Identification of Aroma-Active Compounds. The aroma extracts were analyzed by GCO and GC−MS.

GCO. GCO was conducted using a 6890 gas chromatograph (Agilent Technologies, Inc., Santa Clara, CA) equipped with a flame ionization detector (FID) and olfactory detection port (DATU Technology Transfer, Geneva, NY). The aroma extract (2 μL) was injected in the cool on-column mode (+3 °C oven tracking mode) to avoid injection bias and reduce the chance for thermal degradation of any labile compounds. Separations were performed on RTX-Wax and RTX-5 SILMS capillary columns (both 15 m × 0.32 mm i.d. × 0.5 μm df; Restek, Bellefonte, PA). The column effluent was split 1:5 between the FID (250 °C) and olfactory detection port, respectively. The oven temperature was programed from 40 to 225 °C at a ramp rate of 10 °C/min for the RTX-Wax column or a ramp rate of 6 °C/min for the RTX-5 SILMS column, with initial and final hold times of 5 and 20 min, respectively. The flow rate of the helium carrier gas was 2 mL/min.

GC−MS. The GC−MS system consisted of a 6890 GC/5973 mass selective detector (Agilent Technologies, Inc.). A 1 μL volume of extract was injected into either the Stabilwax (30 m × 0.25 mm i.d. × 0.25 μm df; Restek) or SAC-5 (30 m × 0.25 mm i.d. × 0.25 μm df; Supelco, Bellefonte, PA) capillary columns in the cool on-column mode (+3 °C oven tracking mode). The initial oven temperature was 35 °C. After 5 min, the oven temperature was increased at 4 °C/min to the final temperature (225 °C for Stabilwax or 240 °C for SAC-5) and held for 20 min. The flow rate of helium carrier gas was 1 mL/min. The mass spectra were recorded in full scan mode (35−300 amu, scan rate 5.27 scans/s, interface temperature 280 °C, and ionization energy 70 eV).

The retention index (RI) of each compound was calculated using the retention time (RT) of that compound compared against the RTs of a series of standard *n*-alkanes.[16] The aroma-active compounds were positively identified on the basis of comparison of their RI values (on two different polarity stationary phases), odor properties, and mass spectra against those of authentic standard compounds to avoid erroneous identifications. A compound was considered to be tentatively identified if no authentic standard was available for comparison. In this case mass spectra were compared against those in the NIST2008 mass spectral database, and retention indices were compared to literature values.

Aroma Extract Dilution Analysis. The aroma extract was diluted stepwise (1:3, v/v) using diethyl ether as described previously.[13,17] Each dilution was performed by GCO on an RTX-Wax column. The sniffing time for each panelist was about 30 min per run. The flavor dilution (FD) factor for a specific odorant, which is the highest dilution at which panelists can smell that compound, was reported on the basis of averaging the $\log_3$ FD factors of three panelists (one female and two males, 20−47 years old) after rounding off to the nearest whole number.

Determination of Enantiomer Composition. The enantiomeric compositions of selected aroma-active compounds were investigated by GC-FID using an InertCap CHIRAMIX column (30 m × 0.32 mm i.d. × 0.25 μm df; GL Sciences Inc., Tokyo, Japan). A 2 μL volume of the aroma extract or standard solution (~1 ppm in dichloromethane) was injected in the hot split (5:1) mode at 250 °C. The oven temperature program started from 100 °C for 1 min, then was ramped at 1 °C/min to 180 °C, and was held for 10 min. Helium was used as a carrier gas at a flow rate of 2.5 mL/min. The configuration of each chiral compound was determined on the basis of comparison of its retention time against that of an authentic standard compound. The relative composition of each enantiomer pair in cola A was based on the average from four aroma extracts.

Sensory Descriptive Analysis. The human subject protocol number 11249 was approved by The University of Illinois at Urbana-Champaign Institutional Review Board (IRB). Ten panelists (students

DOI: 10.1021/jf504953s
J. Agric. Food Chem. 2015, 63, 769−775

Table 2. Aroma-Active Compounds in Three Commercial Brands of Regular Cola-Flavored Carbonated Beverages Determined by Aroma Extract Dilution Analysis

compd no.[a]	RI[b] RTX-Wax	RI[b] RTX-5	F[c]	compd name	odor[d]	FD factor[e] A	FD factor[e] B	FD factor[e] C	identification[f]
1	1019	939	NB	α-pinene	camphorous, cool	27	<3	3	RI, O, MS, S
2	1073	941[g]	NB	camphene	camphorous	3		3	RI, O, MS, S
3	1108		NB	β-pinene	fresh	9	9	9	O, S
4	1154	1013	NB	δ-3-carene	citrus, minty	9	27	3	RI, O, MS, S
5	1175	993	NB	β-myrcene	rubbery, terpene	3	3	3	RI, O, MS, S
6	1186	1025	NB	α-terpinene	rubbery, pine	3	9	9	RI, O, MS, S
7	1208	986[g]	NB	2,3-dehydro-1,8-cineole	minty	<3		<3	RI, O, MS, S
8	1221	1048	NB	limonene	orange, terpene	<3		3	RI, O, MS, S
9	1225	1044	NB	1,8-cineole	minty, eucalyptus	81	81	81	RI, O, MS, S
10	1252	1072	NB	γ-terpinene	terpene	<3		<3	RI, O, MS, S
11	1271	1024[g]	NB	p-cymene	herbal, pine	<3	9	3	RI, O, MS, S
12	1297	1089	NB	α-terpinolene	pine, plastic		3	9	RI, O, MS, S
13	1307	1005	NB	octanal	orange, citrus	9	9	9	RI, O, MS, S
14	1340		NB	6-methyl-5-hepten-2-one	mushroom	3		<3	O, MS, S
15	1380		NB	unknown	fruity	27	9	9	O
16	1416	1111	NB	nonanal	orange, green, sweet, fresh	9	3	9	RI, O, MS, S
17	1434		NB	α-p-dimethylstyrene	orange, fresh	3	3	3	O, MS
18	1445	1070[g]	NB	linalool oxide	floral	3	3		RI, O, MS
19	1463	<700[g]	A	acetic acid	vinegar	<3	<3	<3	RI, O, MS, S
20	1475	829[g]	NB	furfural	sweet	9			RI, O, MS, S
21	1517	1205[g]	NB	decanal	orange, fresh, green	<3	9	3	RI, O, MS, S
22	1555	1102	NB	linalool	floral, sweet	243	9	729	RI, O, MS, S
23	1592	1130	NB	1-terpineol	soapy			<3	RI, O, MS
24	1602	1415[g]	NB	β-caryophyllene	earthy, woody	27	3	9	RI, O, MS, S
25	1623	1191	NB	4-terpineol	earthy, soapy, woody	81	3	9	RI, O, MS, S
26	1637	807[g]	A	butanoic acid	cheesy, buttery	<3	<3	<3	RI, O, MS, S
27	1669	860[g]	A	2-furanmethanol	popcorn, sweet	<3			RI, O, MS, S
28	1681	888	A	3-methylbutanoic acid	cheesy, stinky feet	<3	<3	<3	RI, O, S
29	1688	1175	NB	isoborneol	earthy, camphorous	27	9	9	RI, O, MS, S
30	1699		NB	neral	soapy, lemon	9	9	3	O, MS, S
31	1713	1206	NB	α-terpineol	phenolic, pine	3	<3	9	RI, O, MS, S
32	1723	1184	NB	borneol	earthy, camphorous, phenolic	3	<3	<3	RI, O, MS, S
33	1735	1531	NB	(+)-valencene	camphorous, earthy	27	3		RI, O, MS, S
34	1755		NB	geranial	sweet, terpene	<3			O, MS, S
35	1759		NB	(*E*)-piperitol	saffron, straw, haylike, stale	9	<3		O, MS
36	1799	1238	NB	nerol	floral, sweet	27	3	3	RI, O, MS, S
37	1841		NB	2-phenethyl acetate	floral	<3		<3	O, MS, S
38	1843	1325[g]	NB	(*E*,*E*)-2,4-decadienal	fatty, fried, oily	3	9	3	RI, O, MS, S
39	1854	1259	NB	geraniol	cleaner, lemon Pledge			<3	RI, O, MS, S
40	1857		NB	β-damascenone	apple sauce, sweet	27	<3	81	O, S
41	1878		NB	guaiacol	smoky	729	243	27	O, MS, S
42	1893	1284[g]	NB	safrol	burnt sugar, spice	3	3	<3	RI, O, MS
43	1935	1120	NB	2-phenylethanol	rose, sweet	27	27	3	RI, O, MS, S
44	1970	1238[g]	NB	2-methoxybenzaldehyde	herbaceous, lactone, sweet, vanilla, grape	27		9	RI, O, MS
45	1981	1114	A	maltol	sweet	<3		<3	RI, O, MS, S
46	2004	1403[g]	NB	methyleugenol	haylike, dried grass	243	27	3	RI, O, MS, S
47	2053	1064	NB	4-hydroxy-2,5-dimethyl-3(2*H*)-furanone	burnt sugar, sweet	9	9	<3	RI, O, S
48	2091	1283	NB	(*E*)-cinnamaldehyde	cinnamon, sweet	81	3	3	RI, O, MS, S
49	2100	1093[g]	NB	p-cresol	dung, animal stable	9	27	27	RI, O, MS, S
50	2147	1442[g]	NB	cinnamyl acetate	cloves, cinnamon, sweet	9	3	3	RI, O, MS
51	2195	1361	NB	eugenol	spicy, cloves, sweet	729	243	729	RI, O, MS, S
52	2220	1130	A	3-hydroxy-4,5-dimethyl-2(5*H*)-furanone (sotolon)	burnt sugar, curry, spicy	9	3	9	RI, O, S
53	2299	1411	NB	(*Z*)-isoeugenol	cloves, sweet	81	27	9	RI, O, S
54	2373	1456	NB	(*E*)-isoeugenol	sweet, cloves	81	<3	3	RI, O, S
55	2399		NB	unknown	cloves, sweet	81	<3	3	O
56	2507	1451	NB	coumarin	sweet, herbaceous	729	243	729	RI, O, MS, S

DOI: 10.1021/jf504953s
J. Agric. Food Chem. 2015, 63, 769−775

Table 2. continued

compd no.[a]	RI[b] RTX-Wax	RTX-5	F[c]	compd name	odor[d]	FD factor[e] A	B	C	identification[f]
57	2583	1263[g]	A	phenylacetic acid	rosy, sweet, plastic	9	3	<3	RI, O, MS, S
58	2596	1404	A	vanillin	vanilla	27	9		RI, O, MS, S

[a]Numbers correspond to those in Table 3. [b]Retention indices determined by GCO on two different stationary phases (RTX-Wax and RTX-5 SILMS). [c]Fraction: acidic (A); neutral-basic (NB). [d]Odor quality determined by GCO. [e]Flavor dilution factors were determined on an RTX-Wax column and were derived from average $\log_3$ FD factors [n = 3 (1 female and 2 males, 20−47 years old)] after rounding off to the nearest whole number. [f]Identification criteria: retention index (RI); odor quality (O); mass spectra (MS); reference standard compound (S). [g]RI determined by GC−MS.

and staff, seven females and three males, 22−38 years old) were selected on the basis of the participants' abilities to detect and describe differences in aroma characteristics. They were trained for approximately 15 h to evaluate the aroma (by nose) of authentic cola samples consisting of different brands, lots, packages, and colas stored under various conditions. Terminologies with definitions and commercially available references were developed and are listed in Table 1. Cola-flavored carbonated beverage (50 mL) was prepared in a 125 mL Teflon sniff bottle (Nalgene PTFE wash bottle without a siphon tube; Nalge Nunc International, Rochester, NY). The bottles were covered with aluminum foil and labeled with randomly generated three-digit codes. To minimize nasal irritation caused by high levels of carbon dioxide, the sample bottles were kept open at room temperature for 30 min before evaluation, which allowed most the of carbon dioxide to passively escape. The serving orders of test samples were randomized, and the colas were presented one at a time to the panelist. In individual booths, the panelists evaluated the samples by gently squeezing the bottle and sniffing the expressed air. They were asked to rate the intensity of each attribute on a 15 cm line scale with two end anchors from none to strong.

Statistical analysis. The mean score of each attribute/term was calculated and then plotted to establish the aroma profile as spider web plots. Analysis of variance (ANOVA) was performed with the SAS program (SAS Institute Inc., Cary, NC) to detect significant differences among cola samples. If there was a significant difference (p-value < 0.05), the least significant difference (LSD) was used to check which samples differed.

RESULTS AND DISCUSSION

The top three U.S. brands of regular cola-flavored carbonated beverages were chosen for comprehensive aroma analysis. The CLLE method was used to isolate the aroma compounds from colas because decarbonation and extraction could be performed at the same time. The odor representativeness of the extract was checked by using strip paper, and the aroma extract obtained from each cola by CLLE had a characteristic colalike odor. This confirmed that the extract contained the typical aroma-active compounds of the colas.

Volatile Components. Total ion chromatograms were similar for all three cola-flavored carbonated beverages. Monoterpenes and sesquiterpenes were the major compounds in all colas. Among these, the most abundant were limonene (**8**), α-terpineol (**31**), and γ-terpinene (**10**). However, not all volatile compounds found in foods significantly contribute to food aroma. In the past, flavor scientists have not been successful in creating aroma models from the most abundant volatiles. For this reason, GCO has been applied to help identify trace-level potent odorants and to distinguish aroma-active compounds (odorants) from volatiles that contribute essentially no odor.

Aroma-Active Components. A combined total of 58 odorants were detected in the colas (Table 2), of which 2 were unidentified. Most of the odorants found in colas originate from the flavoring ingredients, including vanilla extract and essential oils of citrus, cassia or cinnamon, coriander, nutmeg, and neroli.[4,5] However, some may have been derived from nonvolatile components, for example, furfural (**20**), which was reported as an acid hydrolysis product of *d*-fructose.[18] Moreover, some of these compounds can be derived from other odorants, such as formation of α-terpineol (**31**) from limonene (**8**) due to acid-catalyzed reaction.[19]

It should also be noted that the highly volatile aroma compounds with RI values on a polar column (RTX-Wax) of less than 1000 were not identified in the present study. They might be lost during extraction and concentration of the extract or might not be present in the colas considering the list of ingredients used in cola flavorings. Essential oils are generally obtained by distillation methods which cause loss of highly volatile compounds.

The odor activity value (OAV) concept has been used to estimate the degree to which a particular volatile contributes to the overall aroma of food. It is defined as the ratio of the concentration of an aroma compound in the food to its odor detection threshold in the food matrix. The accuracy of an OAV depends on accurate quantification and determination of the odor threshold. However, the odor detection thresholds of some compounds, especially unknowns, cannot be measured. For this reason, AEDA was used to indicate the impact of an aroma compound in colas in the present study. This technique can rank the odorants by their relative potency on the basis of OAVs in air.

Potent Odorants. The FD factors of all odorants found in the colas are shown in Table 2. Eugenol (**51**) (spicy, clovelike, sweet) and coumarin (**56**) (sweet, herbaceous) were predominant odorants in all colas. These odorants have been reported in cinnamon and cassia (Chinese cinnamon) oils.[20,21] Eugenol is also a common volatile compound of nutmeg oil.[22]

Guaiacol (**41**) (smoky note) was a potent odorant in colas A and B, while linalool (**22**) (floral, sweet) had high odor potency in cola C. Linalool also had relatively high potency in cola A. This odorant is reported as one of the most aroma-active compounds contributing to the overall flavor of lemon oil[23] and orange peel oil.[24] It is also a major component of the essential oils of coriander[25] and neroli.[26] In addition, linalool is reported as a dominant alcohol in orange oil,[27] and it was perceived in highest aroma intensity after octanal and wine lactone.[28]

The compound 1,8-cineole (**9**) (minty, eucalyptus-like) was a moderately potent odorant in all colas. It was reported as one of the aroma compounds with the most impact in orange peel oil.[24] This compound was also the second most abundant volatile found in cinnamon oil distillated from root bark.[20] 1,8-Cineole not only is present naturally in essential oils, but also is reported as a secondary degradation product of limonene and α-terpineol by acid-catalyzed reactions.[19]

DOI: 10.1021/jf504953s
J. Agric. Food Chem. 2015, 63, 769−775

However, the most abundant volatiles, including limonene, α-terpineol, and γ-terpinene, had low odor potencies in the colas. The FD factors of highly potent odorants found in citrus oil, such as neral (**30**) and geranial (**34**), were also low in all colas because of their possible degradation by acid-catalyzed reactions. It is well-known that citral (a mixture of neral and geranial) is extremely unstable under acidic conditions, resulting in the formation of various products.[29] The half-life of citral in carbonated soft drinks is about 6 days.[30] Oxidation of citral can occur under certain conditions,[31] but this is unlikely to occur in carbonated beverages due to the very low level of oxygen. The degradation mechanism for citral has already been proposed.[30−33] Neral (*cis*-isomer) and geranial (*trans*-isomer) can rearrange by isomerization reactions. Then, *p*-menthadien-8-ols can be converted directly from neral by the series of acid-catalyzed reactions starting from cyclization. These intermediates are further degraded by disproportionation, redox, and dehydration reactions to form α,*p*-dimethylstyrene (**17**) and *p*-cymene (**11**), which are more stable. The compound 2,3-dehydro-1,8-cineole (**7**) is also formed as a result of the deterioration of citral by acid-catalyzed reactions. It is very unstable in acid conditions, but it is found at low levels in colas due to the steady state reached among various precursor compounds via reversible acid-catalyzed reactions.[33] It should also be noted that this compound was a predominant odorant in lemon-lime carbonated beverages.[14]

Among the three brands, the aroma profile of cola A was the most complex. Additional moderately potent odorants in cola A included methyleugenol (**46**) (haylike, dried grass), 4-terpineol (**25**) (earthy, soapy, woody), (*E*)-cinnamaldehyde (**48**) (cinnamon-like, sweet), (*Z*)- and (*E*)-isoeugenols (**53** and **54**) (clovelike, sweet), and an unknown with an RI of 2399 on the RTX-Wax column (**55**) (clovelike, sweet). It is interesting to note that 4-terpineol, which is a major volatile in nutmeg oil,[34] may be a degradation product of some terpenes via acid-catalyzed reactions.[19] It was also reported to be a potent odorant in a stored emulsion of lemon oil in an aqueous citric acid solution.[23]

β-Damascenone (**40**) (apple sauce, sweet) was another moderately potent odorant in cola C. Vanillin (**58**), however, was not detected by GCO in this beverage. This finding suggests that vanilla extract may be used at only a low concentration in cola C. The low level of vanillin is also supported by low potency of guaiacol (**41**) in the cola since both compounds are important aroma components of vanilla extract.[35] Furthermore, it was indicated that the main component influencing the sweet note of cola C was coumarin, not vanillin. Coumarin mixed with vanillin is reportedly used in cream soda because it is not highly volatile and its aroma intensity is 3 times higher than that of vanillin.[36] Tonga bean extract which contains coumarin has also been used as a vanilla substitute.[36] However, coumarin, tonga bean, and tonga extract are not permitted for use in human foods in the United States[37] because of toxicity concerns.[38] Although coumarin is prohibited for use as a flavoring compound, it occurs naturally in cinnamon oil[20] and vanilla extract,[39] which are natural flavors used in cola-flavored carbonated beverages.

While AEDA is the useful screening technique to rank the aroma compounds in order of potency, the method is, however, based on the odor activity of the aroma compound in air. The effect of the food matrix on cola odor was not taken into account in the present study. The potent odorants identified in colas should be further analyzed by OAVs to correct for the limitations of AEDA. Additional sensory studies on aroma reconstitution and omission models should also be conducted to verify the OAV calculation.

Enantiomeric Composition. Cola A was chosen to investigate the enantiomeric composition of selected aroma-active compounds since some of them had high FD factors. Furthermore, different enantiomers may have different odor detection thresholds and odor characteristics. The chemical structures and enantiomeric distributions of chiral compounds identified in cola A are shown in Table 3. *d*-Limonene or the (*R*)-(+)-isomer (**8b**) was present in greatest abundance (97.2%). This is to be expected because it is well-known that *d*-limonene is commonly present in citrus oils. The majority of *d*-limonene results in more fresh citruslike odor characteristics in the essential oils, while *l*-limonene has a harsh, turpentine note.[40]

Table 3. Enantiomeric Distribution of Aroma Compounds Identified in Cola A

compd no.[a]	compd name	distribution ratio[b]
8a:8b	(*S*)-(−)-limonene:(*R*)-(+)-limonene	2.8:97.2
22a:22b	(*R*)-(−)-linalool:(*S*)-(+)-linalool	34.5:65.5
25a:25b	(*S*)-(+)-4-terpineol:(*R*)-(−)-4-terpineol	51.0:49.0
31a:31b	(*S*)-(−)-α-terpineol:(*R*)-(+)-α-terpineol	55.1:44.9

[a]Numbers correspond to those in Table 2, and the letters following the numbers indicate the elution order of enantiomers from an InertCap CHIRAMIX column. [b]Enantiomeric excess expressed as a percentage (n = 4).

Linalool found in natural flavor is usually present as a mixture of the (*R*)-(−)-isomer (**22a**) and (*S*)-(+)-isomer (**22b**) at different ratios. The odor description of **22a** is floral, with a woody lavender note, while **22b** is perceived as sweet and floral.[40] The enantiomeric composition of linalool in cola A was 34.5% (*R*)-(−)-enantiomer and 65.5% (*S*)-(+)-enantiomer. (*R*)-(−)-Linalool is predominant in neroli oil, while (*S*)-(+)-linalool comprises 60−70% of coriander oil.[41] Although the amount of (*S*)-(+)-linalool in cola was almost 2-fold higher than that of (*R*)-(−)-linalool, the odor threshold in water of the latter enantiomer is about 9 times lower than that of the former stereoisomer (0.8 and 7.4 ppb, respectively[42]). Thus, at similar concentrations (*R*)-(−)-linalool should make a greater aroma contribution than (*S*)-(+)-linalool in cola-flavored carbonated beverage.

In addition, the enantiomeric compositions of the 4-terpineols (51.0% (*S*)-(+)-enantiomer (**25a**) and 49.0% (*R*)-(−)-enantiomer (**25b**)) and α-terpineols (55.1% (*S*)-(−)-enantiomer (**31a**) and 44.9% (*R*)-(+)-enantiomer (**31b**)) in cola occurred as approximately racemic mixtures. The enantiomeric pairs of 2,3-dehydro-1,8-cineole (**7**), isoborneol (**29**), and borneol (**32**) were, however, not determined on the chiral GC capillary column because of their low concentrations in cola extracts.

Sensory Analysis. Aroma (by nose) of decarbonated colas was described by eight attributes, including lemon-lime, orange, brown spice, herbal, vanilla, caramel, cooling, and pine (Table 1). Citrus, caramel, and vanilla have been reported as aromas and aromatics (aroma-by-mouth) of regular and diet colas by descriptive analysis.[6] In the present study, all colas (A, B, and C) had similar aroma profiles, except the lemon-lime intensity in cola B was significantly lower than in colas A and C (*p*-value

DOI: 10.1021/jf504953s
J. Agric. Food Chem. 2015, 63, 769−775

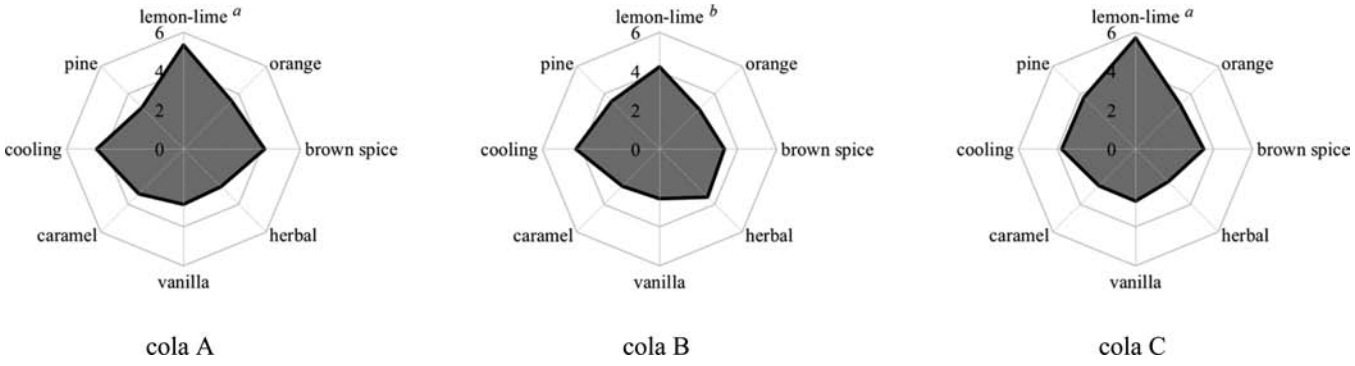

Figure 1. Aroma (by nose) profiles of cola-flavored carbonated beverages from sensory descriptive analysis. Attributes followed by different italic superscript letters are significantly different (p-value < 0.05) [n = 10 (7 females and 3 males, 22−38 years old)]. Odor intensity was rated on a 15 cm line scale.

< 0.05) (Figure 1). Lemon-lime and cooling attributes were dominant attributes in all colas. Brown spice, herbal, and pine attributes were moderate intensities in all colas. The results of sensory analysis agreed well with potent odorants identified by AEDA (Table 2) when the odor characteristic of high FD factor compounds was considered. The low intensity of the lemon-lime note in cola B was probably due to the low potency of linalool (**22**) in that product. This finding was supported by the previous research which revealed that linalool has the highest FD factor in lemon-lime carbonated beverages.[14] Furthermore, the cooling note of cola could be associated with a higher level of 1,8-cineole (**9**). The high-potency aroma compounds were also responsible for the other aroma attributes, such as brown spice aroma from eugenol (**51**) or vanilla note from coumarin (**56**). Additionally, the moderately spicy note of cola A compared to the other colas was possibly the result of the impact of methyleugenol (**46**) and the isoeugenols (**53** and **54**).

AUTHOR INFORMATION

Corresponding Author

*Phone: 217-333-5803. Fax: 217-333-1875. E-mail: cadwlldr@illinois.edu.

Funding

Partial support for this project was provided by the National Institute of Food and Agriculture, U.S. Department of Agriculture, under Project ILLU-698-366.

Notes

The authors declare no competing financial interest.

ABBREVIATIONS USED

AEDA, aroma extract dilution analysis; ANOVA, analysis of variance; CLLE, continuous liquid−liquid extraction; FD, flavor dilution; FID, flame ionization detector; GC−MS, gas chromatography−mass spectrometry; GCO, gas chromatography−olfactometry; LSD, least significant difference; OAV, odor activity value; RI, retention index; RT, retention time; SAFE, solvent-assisted flavor evaporation; SPME, solid-phase microextraction; UHP, ultra-high-purity

REFERENCES

(1) IBISWorld. *Global Soft Drink & Bottled Water Manufacturing* [Online]; Global Industry Report C1124-GL; IBISWorld: Melbourne, Australia, Nov 9, 2011; p 14. http://clients.ibisworld.com/globalindustry/default.aspx?indid=420 (accessed Jan 12, 2012).

(2) Kaczanowska, A. *Soft Drink Production in the US* [Online]; IBISWorld Industry Report 31211; IBISWorld: Melbourne, Australia, August 2010, pp 13−14. http://www.ibisworld.com/industryus/default.aspx?indid=284 (accessed Dec 9, 2010).

(3) Kaczanowska, A. *Carbonated Soft Drink Production in the US* [Online]; IBISWorld Industry Report 31211a; IBISWorld: Melbourne, Australia, December 2010, p 12. http://www.ibisworld.com/industryus/default.aspx?indid=285 (accessed Dec 9, 2010).

(4) Tchudi, S. N. *Soda Poppery*; Charles Scribner's Sons: New York, 1986; pp 32−34.

(5) Pendergrast, M. *For God, Country and Coca-Cola*; Basic Books: New York, 2000; pp 456−460.

(6) Kappes, S. M.; Schmidt, S. J.; Lee, S.-Y. Descriptive analysis of cola and lemon/lime carbonated beverages. *J. Food Sci.* **2006**, *71*, S583−S589.

(7) Wiley, R. C.; Louie, M. K.; Sheu, M.-J. Studies on turpentine-like off-odor in cola. *J. Food Sci.* **1984**, *49*, 485−488.

(8) Elmore, J. S.; Erbahadir, M. A.; Mottram, D. S. Comparison of dynamic headspace concentration on Tenax with solid phase microextraction for the analysis of aroma volatiles. *J. Agric. Food Chem.* **1997**, *45*, 2638−2641.

(9) Hida, Y.; Matsumoto, M.; Kudo, K.; Imamura, T.; Ikeda, N. Identification of beverages and beverage stains by GC/MS using aroma components as indicators. *Int. J. Leg. Med.* **1998**, *111*, 13−16.

(10) Grosch, W. Detection of potent odorants in foods by aroma extract dilution analysis. *Trends Food Sci. Tecnol.* **1993**, *4*, 68−73.

(11) Grosch, W. Determination of potent odourants in foods by aroma extract dilution analysis (AEDA) and calculation of odour activity values (OAVs). *Flavour Fragrance J.* **1994**, *9*, 147−158.

(12) Cadwallader, K. R.; Tamamoto, L. C.; Sajuti, S. C. Aroma components of fresh and stored pomegranate (*Punica granatum* L.). In *Flavors in Noncarbonated Beverages*; Da Costa, N. C., Cannon, R. J., Eds.; ACS Symposium Series 1036; American Chemical Society: Washington, DC, 2010; pp 93−101.

(13) Watcharananun, W.; Cadwallader, K. R.; Huangrak, K.; Kim, H.; Lorjaroenphon, Y. Identification of predominant odorants in Thai desserts flavored by smoking with "Tian Op", a traditional Thai scented candle. *J. Agric. Food Chem.* **2009**, *57*, 996−1005.

(14) Hausch, B.j.; Lorjaroenphon, Y.; Cadwallader, K. R. Flavor chemistry of lemon-lime carbonated beverages. *J. Agric. Food Chem.* [Online early access]. DOI: 10.1021/jf504852z. Published Online: Dec 12, 2014. http://pubs.acs.org/doi/abs/10.1021/jf504852z.

(15) Engel, W.; Bahr, W.; Schieberle, P. Solvent assisted flavour evaporation—a new and versatile technique for the careful and direct isolation of aroma compounds from complex food matrices. *Eur. Food Res. Technol.* **1999**, *209*, 237−241.

(16) van den Dool, H.; Kratz, P. D. A generalization of the retention index system including linear temperature programmed gas-liquid partition chromatography. *J. Chromatogr.* **1963**, *11*, 463−471.

DOI: 10.1021/jf504953s
J. Agric. Food Chem. 2015, 63, 769−775

(17) Ullrich, F.; Grosch, W. Identification of the most intense volatile flavour compounds formed during autoxidation of linoleic acid. *Z. Lebensm.-Unters. -Forsch.* **1987**, *184*, 277−282.
(18) Shaw, P. E.; Tatum, J. H.; Berry, R. E. Acid-catalyzed degradation of *d*-fructose. *Carbohydr. Res.* **1967**, *5*, 266−273.
(19) Clark, B. C., Jr.; Chamblee, T. S. Acid-catalyzed reactions of citrus oils and other terpene-containing flavors. In *Off-Flavors in Foods and Beverages*; Charalambous, G., Ed.; Elsevier: Amsterdam, 1992; pp 229−285.
(20) Senanayake, U. M.; Lee, T. H.; Wills, R. B. H. Volatile constituents of cinnamon (*Cinnamomum zeylanicum*) oils. *J. Agric. Food Chem.* **1978**, *26*, 822−824.
(21) He, Z.-D.; Qiao, C.-F.; Han, Q.-B.; Cheng, C.-L.; Xu, H.-X.; Jiang, R.-W.; But, P.P-H.; Shaw, P.-C. Authentication and quantitative analysis on the chemical profile of cassia bark (cortex cinnamomi) by high-pressure liquid chromatography. *J. Agric. Food Chem.* **2005**, *53*, 2424−2428.
(22) Jukié, M.; Politeo, O.; Miloš, M. Chemical composition and antioxidant effect of free volatile aglycones from nutmeg (*Myristica fragrans* Houtt.) compared to its essential oil. *Croat. Chem. Acta* **2006**, *79*, 209−214.
(23) Schieberle, P.; Grosch, W. Identification of potent flavor compounds formed in an aqueous lemon oil/citric acid emulsion. *J. Agric. Food Chem.* **1988**, *36*, 797−800.
(24) Fischer, A.; Grab, W.; Schieberle, P. Characterisation of the most odour-active compounds in a peel oil extract from Pontianak oranges (*Citrus nobilis* var. Lour. *microcarpa* Hassk.). *Eur. Food Res. Technol.* **2008**, *227*, 735−744.
(25) Ravi, R.; Prakash, M.; Bhat, K. K. Aroma characterization of coriander (*Coriandrum sativum* L.) oil samples. *Eur. Food Res. Technol.* **2007**, *225*, 367−374.
(26) Toyoda, T.; Nohara, I.; Sato, T. Headspace analysis of volatile compounds emitted from various citrus blossoms. In *Bioactive Volatile Compounds from Plants*; Teranishi, R., Buttery, R. G., Sugisawa, H., Eds.; ACS Symposium Series 525; American Chemical Society: Washington, DC, 1993; pp 205−219.
(27) Sawamur, M.; Tu, N. T. M.; Yu, X.; Xu, B. Volatile constituents of the peel oils of several sweet oranges in China. *J. Essent. Oil Res.* **2005**, *17*, 2−6.
(28) Högnadóttir, Á.; Rouseff, R. L. Identification of aroma active compounds in orange essence oil using gas chromatography-olfactometry and gas chromatography-mass spectrometry. *J. Chromatogr. A* **2003**, *998*, 201−211.
(29) Clark, B. C., Jr.; Powell, C. C.; Radford, T. The acid catalyzed cyclization of citral. *Tetrahedron* **1977**, *33*, 2187−2191.
(30) Peacock, V. E.; Kuneman, D. W. Inhibition of the formation of α-*p*-dimethylstyrene and *p*-cymen-8-ol in a carbonated citral-containing beverage system. *J. Agric. Food Chem.* **1985**, *33*, 330−335.
(31) Kimura, K.; Nishimura, H.; Iwata, I.; Mizutani, J. Deterioration mechanism of lemon flavor. 2. Formation mechanism of off-odor substances arising from citral. *J. Agric. Food Chem.* **1983**, *31*, 801−804.
(32) Kimura, K.; Iwata, I.; Nishimura, H. Relationship between acid-catalyzed cyclization of citral and deterioration of lemon flavor. *Agric. Biol. Chem.* **1982**, *46*, 1387−1389.
(33) Lorjaroenphon, Y.; Hausch, B. J.; Cadwallader, K. R. Formation and stability of 2,3-dehydro-1,8-cineol in a model carbonated beverage system. In *Flavour Science: Proceedings from XIII Weurman Flavour Research Symposium*; Ferreira, V., Lopez, R., Eds.; Elsevier Inc.: San Diego, CA, 2014; pp 231−235.
(34) Choo, L.-C.; Wong, S.-M.; Liew, K.-Y. Essential oil of nutmeg pericarp. *J. Sci. Food Agric.* **1999**, *79*, 1954−1957.
(35) Pérez-Silva, A.; Odoux, E.; Brat, P.; Ribeyre, F.; Rodriguez-Jimenes, G.; Robles-Olvera, V.; García-Alvarado, M. A.; Günata, Z. GC-MS and GC-olfactometry analysis of aroma compounds in a representative organic aroma extract from cured vanilla (*Vanilla planifolia* G. Jackson) beans. *Food Chem.* **2006**, *99*, 728−735.
(36) Abernethy, J. L. The historical and current interest in coumarin. *J. Chem. Educ.* **1969**, *46*, 561−568.
(37) U.S. Food and Drug Administration. Code of Federal Regulations Title 21, Section 189.130 Coumarin. http://www.accessdata.fda.gov/scripts/cdrh/cfdocs/cfcfr/CFRSearch.cfm?fr=189.130&SearchTerm=coumarin (accessed Nov 29, 2014).
(38) Lake, B. G. Coumarin metabolism, toxicity and carcinogenicity: relevance for human risk assessment. *Food Chem. Toxicol.* **1999**, *37*, 423−453.
(39) Boyce, M. C.; Haddad, P. R.; Sostaric, T. Determination of flavour components in natural vanilla extracts and synthetic flavouring by mixed micellar electrokinetic capillary chromatography. *Anal. Chim. Acta* **2003**, *485*, 179−186.
(40) Leffingwell, J. C. Chirality & Odour Perception. http://www.leffingwell.com/chirality/chirality.htm (accessed Nov 29, 2014).
(41) Opdyke, D. L. J.; Linalool. *Food Cosmet. Toxicol.* **1975**, *13*, 827−832.
(42) Padrayuttawat, A.; Yoshizawa, T.; Tamura, H.; Tokunaga, T. Optical isomers and odor thresholds of volatile constituents in *Citrus sudachi*. *Food Sci. Technol. Int., Tokyo* **1997**, *3*, 402−408.

DOI: 10.1021/jf504953s
J. Agric. Food Chem. 2015, 63, 769−775

JOURNAL OF AGRICULTURAL AND FOOD CHEMISTRY

Article

pubs.acs.org/JAFC

Identification of Character-Impact Odorants in a Cola-Flavored Carbonated Beverage by Quantitative Analysis and Omission Studies of Aroma Reconstitution Models

Yaowapa Lorjaroenphon[†] and Keith R. Cadwallader*[,‡]

[†]Department of Food Science and Technology, Faculty of Agro-Industry, Kasetsart University, 50 Ngamwongwan Road, Bangkok 10900, Thailand

[‡]Department of Food Science and Human Nutrition, University of Illinois at Urbana-Champaign, 1302 West Pennsylvania Avenue, Urbana, Illinois 61801, United States

Supporting Information

ABSTRACT: Thirty aroma-active components of a cola-flavored carbonated beverage were quantitated by stable isotope dilution assays, and their odor activity values (OAVs) were calculated. The OAV results revealed that 1,8-cineole, (*R*)-(−)-linalool, and octanal made the greatest contribution to the overall aroma of the cola. A cola aroma reconstitution model was constructed by adding 20 high-purity standards to an aqueous sucrose−phosphoric acid solution. The results of headspace solid-phase microextraction and sensory analyses were used to adjust the model to better match authentic cola. The rebalanced model was used as a complete model for the omission study. Sensory results indicated that omission of a group consisting of methyleugenol, (*E*)-cinnamaldehyde, eugenol, and (*Z*)- and (*E*)-isoeugenols differed from the complete model, while omission of the individual components of this group did not differ from the complete model. These results indicate that a balance of numerous odorants is responsible for the characteristic aroma of cola-flavored carbonated beverages.

KEYWORDS: *cola-flavored carbonated beverage, odor activity value, stable isotope dilution assay, aroma reconstitution model, omission study*

INTRODUCTION

Cola is the predominant flavor among the various types of carbonated beverages. The uniqueness and complexity of cola flavor is due to a mixture of various natural flavor ingredients, including vanilla extract and essential oils of citrus, cassia or cinnamon, coriander, nutmeg, and neroli.[1,2] Despite its popularity, there is limited information about the flavor chemistry of cola. In our previous study, 58 odorants from the top three U.S. brands of regular cola were identified by gas chromatography−olfactometry (GCO) and aroma extract dilution analysis (AEDA).[3] On the basis of those findings, the most potent odorants in all colas were eugenol and coumarin. Guaiacol and linalool were predominant odorants in at least one brand, while 1,8-cineole was a moderately potent odorant in all colas. Among enantiomeric aroma compounds, (*R*)-(−)-linalool, despite being the less abundant enantiomer in cola, was regarded as a more potent odorant than the (*S*)-(+)-enantiomer because of its much lower odor detection threshold. GCO and AEDA were also found to be in good agreement with aroma profiles generated by sensory descriptive analysis.

The application of AEDA is a useful method for ranking the relative potency of odorants, but the interactions between the odorants and food matrix is not taken into account. Calculation of odor activity values (OAVs) is the next step of flavor analysis, and it is necessary to verify the analytical data by aroma recombination studies.[4] Omission tests which compare the complete model with models in which one or more odorants have been omitted may also be conducted to identify the character-impact odorants.[5] Furthermore, suppression and synergistic effects of aroma compounds can be identified by omission studies as well.[6]

The objectives of the present study were to (1) quantitate the potent odorants by stable isotope dilution assays (SIDAs), (2) identify key potent odorants by calculation of OAVs, and (3) investigate character-impact odorants by sensory evaluation of aroma reconstitution and omission models. Knowledge of key odorants which contribute to the typical flavor of cola could be used as quality indicator compounds to develop products with superior flavors and to investigate the flavor changes which occur during storage.

MATERIALS AND METHODS

Materials. Regular Coca-Cola and the references for sensory descriptive analysis were purchased from local markets (Urbana, IL) in 2011−2012.

Chemicals. General-reagent- or HPLC-grade chemicals were purchased from Fisher Scientific (Fair Lawn, NJ). Sucrose was supplied by Sigma-Aldrich (St. Louis, MO).

Standard Compounds. The standard compounds listed in Tables 1−4 were supplied by the companies given in parentheses: **8b**, **9**, **13**, **16**, **19**, **21**, **22** (**22a** and **22b**), **25** (**25a** and **25b**), **26**, **28**, **29** (**29a** and **29b**), mixture of **30** and **34**, **31** (**31a** and **31b**), **32a**, **32b**, **37**, **41**, **43**, **46**, **48**, **49**, **51**, **56**, and **57** (Sigma-Aldrich); **36** and **39** (Bedoukian, Danbury, CT);

Received: October 13, 2014
Revised: December 20, 2014
Accepted: December 21, 2014
Published: December 21, 2014

ACS Publications © 2014 American Chemical Society

DOI: 10.1021/jf504954p
J. Agric. Food Chem. 2015, 63, 776−786

Table 1. Concentrations, Odor Detection Thresholds, and Odor Activity Values of Selected Odorants Identified in Coca-Cola

		selected ion (m/z)					threshold[d] (ng/g)		
compd no.[a]	compd name	labeled	unlabeled	R_f[b]	concn[c] (ng/g)			ref	OAV[e]
8	limonene	138	136	0.98 (0.99+)	10000	(±17%)	10	44	1000
9	1,8-cineole	157	154	0.97 (0.99+)	104	(±29%)	1.3	44	80
13	octanal	114	110	0.49 (0.99+)	34.5	(±3%)	0.7	45	49
16	nonanal	116	114	0.44 (0.99)	12.8	(±6%)	1	45	13
19	acetic acid	63	60	0.95 (0.94)	3390	(±15%)	22000	46	<1
21	decanal	130	128	1.92 (0.99+)	17.5	(±7%)	2	45	9
22	linalool	123	121	1.01 (0.99+)	140	(±3%)	6	47	23
25	4-terpineol	75	71	0.68 (0.99+)	708	(±3%)	340	44	2
26	butanoic acid	63	60	1.65 (0.91)	11.5	(±6%)	240	46	<1
28	3-methylbutanoic acid	89	87	0.86 (0.99+)	2.8	(±14%)	250	48	<1
29	isoborneol	113	110	1.07 (0.99+)	15.1	(±17%)	16.4[f]	8	<1
30	neral	75	69	0.68 (0.99+)	<10[g]		30	49	
31	α-terpineol	62	59	0.91 (0.99+)	4200	(±9%)	350	44	12
32	borneol	113	110	0.83 (0.99+)	191	(±5%)	180[h]/80[i]	35	1[h]/2[i]
34	geranial	75	69	0.69 (0.99+)	<20[g]		32	48	
36	nerol	75	69	0.68 (0.99+)	16.9	(±3%)	300	50	<1
37	2-phenethyl acetate	106	104	1.00 (0.90)	4.8	(±3%)	20	51	<1
39	geraniol	75	69	0.96 (0.99+)	23.9	(±4%)	40	31	<1
40	β-damascenone	73	69	1.04 (0.99)	<10[g]		0.002	49	
41	guaiacol	127	124	1.49 (0.99+)	1.5	(±10%)	3	31	<1
43	2-phenylethanol	124	122	0.27 (0.98)	3.7	(±3%)	1100	31	<1
46	methyleugenol	184	178	1.04 (0.99+)	8.6	(±3%)	68	44	<1
48	(*E*)-cinnamaldehyde	137	131	0.57 (0.99+)	808	(±2%)	1180	*j*	<1
49	*p*-cresol	111	108	1.27 (0.99+)	0.9	(±33%)	55	45	<1
51	eugenol	167	164	1.06 (0.99)	6.6	(±3%)	6	31	1
53	(*Z*)-isoeugenol	167	164	0.67 (0.99+)	0.3	(±5%)			
54	(*E*)-isoeugenol	167	164	2.22 (0.99+)	2.6	(±4%)			
56	coumarin	124	118	0.85 (0.99+)	46.5	(±4%)	25	52	2
57	phenylacetic acid	138	136	1.45 (0.99+)	0.8	(±33%)	1000	53	<1
58	vanillin	155	152	1.25 (0.99+)	95.1	(±4%)	25	54	4

[a]Numbers correspond to those in Tables 2−4, 6, and 7 and Figure 2. [b]Response factor with the R^2 of the calibration plot given in parentheses. [c]Mean concentration (with the coefficient of variation in parentheses) calculated from the peak area on a Stabilwax column, except for borneol (quantitated on an SAC-5 column) (n = 4). [d]Odor detection thresholds in water obtained from the published literature[6,29,33,42−52] or determined in our laboratory. [e]Odor activity value. [f]Racemic mixture of *d*- and *l*-isomers. [g]Not detected (reported as the concentrations of spiked isotope standards). [h](+)-Borneol. [i](−)-Borneol. [j]Determined in our laboratory.

Table 2. Concentrations, Odor Detection Thresholds, and Odor Activity Values of Enantiomers Identified in Coca-Cola

compd no.[a]	compd name	enantiomeric excess[b]	concn[c] (ng/g)	threshold[d] (ng/g)	OAV[e]
8a	(*S*)-(−)-limonene	2.8	279	1040	<1
8b	(*R*)-(+)-limonene	97.2	9740	1200	8
22a	(*R*)-(−)-linalool	34.5	48.1	0.8	60
22b	(*S*)-(+)-linalool	65.5	91.4	7.4	12
25a	(*S*)-(+)-4-terpinenol	51.0	361	1290	<1
25b	(*R*)-(−)-4-terpinenol	49.0	347	1190	<1
31a	(*S*)-(−)-α-terpineol	55.1	2320	9180	<1
31b	(*R*)-(+)-α-terpineol	44.9	1890	6800	<1

[a]Numbers correspond to those in Tables 1, 4, and 6 and Figure 2, and the letters after the numbers indicate the elution order of enantiomers from the InertCap CHIRAMIX column. [b]Expressed as a percentage from the previous study.[3] [c]Calculated from concentrations in Table 1 according to the enantiomeric excess. [d]Odor detection thresholds in water obtained from the literature.[35] [e]Odor activity value.

40 (Firmenich, Princeton, NJ); mixture of **53** and **54** (Alfa Aesar, Lancashire, U.K.); **58** (Fluka, Buchs, Switzerland).

All aroma compounds used for odor threshold determination and reconstitution study were purified by vacuum distillation and/or flash chromatography before use. Chemical purities were determined by neat injection (hot split) GC-FID analysis. Each compound was determined to be free of any odor impurities by analysis of a 100 mg/L solution by the GCO technique previously described.[3]

All the enantiomeric distributions were determined using the method previously described.[3]

Isotope Standard Compounds. The following isotopically labeled standards were obtained from the commercial sources listed in parentheses: [$^2H_3$]acetic acid (**I-19**), [$^2H_7$]butanoic acid (**I-26**), 2-methoxy-[$^2H_3$]phenol ([$^2H_3$]guaiacol) (**I-41**), and [$^2H_3$]-*p*-cresol (**I-49**) (CDN, Quebec, Canada); [$^{13}C_2$]phenylacetic acid (**I-57**) (Isotec, Miamisburg, OH).

DOI: 10.1021/jf504954p
J. Agric. Food Chem. 2015, 63, 776−786

Table 3. Relative Odor Detection Thresholds in Air of Isoeugenols Determined by GCO

compd no.[a]	compd name	relative odor detection threshold in air[b] (ng/L of air)
53	(*Z*)-isoeugenol	0.4−0.6
54	(*E*)-isoeugenol	0.1−0.2

[a]Numbers correspond to those in Tables 1, 4, 6, and 7 and Figure 2. [b]Using eugenol (**51**) as the internal standard.

Syntheses. The following compounds were synthesized according to the procedures reported in the literature: [$^2H_2$]limonene (**I-8**);[7] [$^2H_3$]-1,8-cineole (**I-9**), [$^2H_4$]octanal (**I-13**), [$^2H_4$]nonanal (**I-16**), [$^2H_4$]decanal (**I-21**), [$^2H_7$]-4-terpineol (**I-25**), [$^2H_3$]isoborneol (**I-29**), [$^2H_6$]neral (**I-30**), [$^2H_3$]-*α*-terpineol (**I-31**), [$^2H_3$]borneol (**I-32**), [$^2H_6$]geranial (**I-34**), [$^2H_6$]nerol (**I-36**), and [$^2H_6$]geraniol (**I-39**);[8] [$^2H_2$]linalool (**I-22**);[9] [$^2H_2$]-3-methylbutanoic acid (**I-28**);[10] [$^2H_4$]-*β*-damascenone (**I-40**);[11] [$^{13}C_2$]-2-phenylethanol (**I-43**);[12] [$^2H_3$]vanillin (**I-58**).[13] The synthetic procedures used to prepare the following compounds are provided in the Supporting Information: [$^{13}C_2$]-2-phenethyl acetate (**I-37**), [$^2H_3$]eugenol (**I-51**), [$^2H_6$]methyleugenol (**I-46**), [$^2H_3$]-(*Z*)- and [$^2H_3$]-(*E*)-isoeugenols (**I-53** and **I-54**), (*Z*)- and (*E*)-isoeugenols (**53** and **54**), [$^2H_5$]cinnamaldehyde (**I-48**), and [$^2H_6$]coumarin (**I-56**).

Stable Isotope Dilution Assay. The isotopically labeled standards of selected aroma-active compounds were prepared individually in dichloromethane (∼1 mg/mL) instead of methanol to avoid decomposition. The chemical and isotopic stabilities were confirmed using an aqueous citrate buffer (pH 2.3, 0.12% (w/v) citric acid) for 18 h. The appropriate amounts of all isotope standards, determined by preliminary experiments, were added into cola as internal standards before extraction.

Isolation of Limonene and α-Terpineol. About 5 mL of cola from the original can were poured into a 20 mL scintillation vial containing 5 mL of diethyl ether to prevent loss of volatiles. The exact weight of cola was recorded as the weight difference. The isotope standards were added into the cola layer before extraction. The sample was decarbonated by sonication (model 2200; Branson Ultrasonics, Co., Danbury, CT) using an ice−water bath at 10 °C for 5 min and then shaken (DS-500 orbital shaker; VWR Scientific, Batavia, IL) at 200 rpm for 10 min. The separated aroma extract was dried over 1 g of anhydrous Na_2SO_4 and concentrated to 0.5 mL by Vigreux column distillation at 43 °C before analysis by gas chromatography−mass spectrometry (GC−MS).

Isolation of Other Aroma Compounds. The volatile compounds were extracted from one can of cola (335 mL) in the same manner as previously described.[3] The aroma components were isolated by continuous liquid−liquid extraction (CLLE), and any nonvolatiles were removed by solvent-assisted flavor evaporation (SAFE) before fractionation into acidic and neutral-basic fractions as previously described.[3]

A 1 μL volume of the aroma extract was injected into a GC−MS system in the cold splitless mode (−50 °C held for 0.1 min and then raised at 12 °C/s to 250 °C). Volatile compounds were separated on either a Stabilwax (polar phase) or an SAC-5 (nonpolar phase) capillary column. For quantitation, the mass ions for isotopes and unlabeled target compounds were chosen on the basis of uniqueness and relative intensity. The peak areas for selected ions were integrated using MSD ChemStation software (Agilent Technologies, Inc.). The concentration of each target compound was calculated from the area ratio and GC−MS response factor (R_f) using eq 1. R_f was calculated as the inverse of the slope of the calibration plot of the area ratio versus mass ratio (eq 2), determined by analysis of five levels of a standard compound (unlabeled) against the isotope (labeled) compound. The reported average concentration value was determined from four cans of cola from the same code date.

$$\text{concentration}_t = (\text{concentration}_i)R_f\left[\frac{\text{area of ion}_t}{\text{area of ion}_i}\right] \quad (1)$$

$$R_f = \frac{\Delta[\text{mass}_t/\text{mass}_i]}{\Delta[\text{area of ion}_t/\text{area of ion}_i]} \quad (2)$$

Here i = labeled internal standard and t = target compound.

Table 4. Concentration of High-Purity Standard Compounds Used in Cola Models

compd no.[a]	compd name	purity[b] (%)	enantiomeric excess[c]	concn (ng/g) original	concn (ng/g) rebalanced
8b	(*R*)-(+)-limonene	99.5		10100	5050[d]
9	1,8-cineole	99.3		101	101
13	octanal	99.5		35.2	35.2
16	nonanal	99.9		13.2	26.4[e]
21	decanal	99.8		17.6	17.6
22	linalool	99.7	49.7:50.3	148	74.1[e]
25	4-terpineol	99.9+	78.5:21.5	702	702
29	isoborneol	98.7[f]	49.1:50.9	15.8	15.8
31	*α*-terpineol	99.9	61.1:38.9	4180	4180
32a	(−)-borneol	99.3		99.3	99.3
32b	(+)-borneol	96.5[g]		107	107
36	nerol	99.4		17.2	11.5[e]
39	geraniol	99.8		23.3	23.3
41	guaiacol	99.8		1.5	1.5
46	methyleugenol	99.9+		8.7	8.7
48	(*E*)-cinnamaldehyde	99.9+		800	1600[d]
51	eugenol	99.9+		6.3	6.3
53	(*Z*)-isoeugenol	8.0[h]		0.2	0.2
54	(*E*)-isoeugenol	92.0[h]		2.7	2.7
56	coumarin	99.1		46.0	46.0
58	vanillin	99.9+		88.0	176[d]

[a]Numbers correspond to those in Tables 1, 2, 3, 6, and 7 and Figure 2. [b]Determined by neat injection (hot split) GC-FID analysis. [c]Expressed as a percentage, and orders of enantiomers correspond to those in Table 1. [d]Adjusted by sensory data. [e]Adjusted by SPME data. [f]Contained additional 1.3% borneol (**32**). [g]Contained additional 3.5% isoborneol (**29**). [h]Mixture of two isomers.

DOI: 10.1021/jf504954p
J. Agric. Food Chem. 2015, 63, 776−786

Odor Activity Values. The OAV of a compound was calculated as the ratio of its concentration in cola to its odor threshold in water. The odor detection thresholds in water of the aroma-active compounds were obtained from the literature or determined in our laboratory.

Determination of Odor Thresholds in Water. The odor detection threshold of high-purity (*E*)-cinnamaldehyde (**48**) (99.9+%) was determined orthonasally following a published procedure[6] by 11 panelists (7 females and 4 males, 22−47 years old).

Determination of Odor Thresholds in Air. The relative odor thresholds of (*Z*)- and (*E*)-isoeugenols (**53** and **54**) in air were evaluated by GCO according to a method reported in the literature[14] using eugenol (**51**) as the internal standard. The high-purity standards of isoeugenols and eugenol were prepared in CH_2Cl_2 and diluted stepwise (1:3, v/v). The panelists evaluated each dilution by GCO (following the same procedure in the previous study[3]) until they were not able to smell any odor. The highest dilution of each aroma compound was recorded, and the relative odor thresholds of (*Z*)- and (*E*)-isoeugenols were calculated on the basis of that of eugenol (0.2−0.3 ng/L of air[15]). The group threshold was calculated as the geometric mean of individual thresholds of seven panelists (three females and four males, 21−38 years old).

Aroma Reconstitution Model. The cola composition, including pH, soluble solids, and titratable acidity, was determined for a decarbonated (by sonication) cola on the basis of three samples with different code dates. The model matrix was prepared on the basis of the information in Table 5 using a sucrose−phosphoric acid solution. The cola base was adjusted to pH 2.31 using aqueous 1 M NaOH or HCl.

Table 5. pH and Chemical Composition of Decarbonated Cola

	mean ± SD[a]
pH (at 25 °C)	2.31 ± 0.03
soluble solids (°Brix, corrected to 20 °C)	10.73 ± 0.06
titratable acidity (g of citric acid/100 mL)	0.1226 ± 0.0011
titratable acidity (g of phosphoric acid/100 mL)	0.0625 ± 0.0006

[a]Mean and standard deviation of products having three different code dates.

The model was constructed on the basis of quantitation data from SIDA. The high-purity standards (Table 4) were prepared individually in methanol, except octanal, nonanal, and decanal (**13**, **16**, **21**). High-purity standards of these aldehydes were dissolved in pentane to avoid degradation reactions and diluted in methanol just before preparation of the model. The solutions of aroma compounds were spiked into the cola matrix. To determine if the model was similar to the actual product, the model was compared to decarbonated cola (authentic cola) by sensory descriptive aroma profiling following the procedure from our previous study.[3] The approval protocol number from the University of Illinois at Urbana-Champaign Institutional Review Board (IRB) for conducting all sensory analyses in this experiment was 11249. The aroma profile provided information about the major aroma attributes (terms) of cola and the cola model and how they were similar or how they differed, thus allowing for the possibility of adjusting the model to better match the authentic cola. The model was deemed appropriate for omission studies on the basis of the similarity (or "matching") of its aroma profile to that of the authentic cola. Ten trained panelists (seven females and three males, 23−45 years old) participated in this descriptive analysis in individual sensory booths.

Solid-Phase Microextraction. Headspace solid-phase microextraction (HS-SPME) was also used to compare the HS volatiles of authentic cola and those of cola models for the purpose of adjusting the model to better match the authentic cola. Commercial cola or cola models (5 mL) and 1 g of NaCl were prepared in 20 mL screw top headspace vials equipped with a Teflon-coated stir bar and a Teflon-lined silicon closure. The sample vial was incubated at 40 °C for 10 min at an agitator speed of 250 rpm. The SPME fiber (50/30 μm DVB/Carboxen/PDMS StableFlex; Supelco, Bellefonte, PA) was exposed into the HS of the sample vial, and the HS volatiles were extracted for 20 min at the same temperature. Then the aroma volatiles in SPME fiber were desorbed in the hot splitless injection port of the GC−MS or GCO system at 260 °C for 14 min with a 4 min GC valve delay. The volatiles were separated on a polar capillary column (RTX-Wax or Stabilwax), and the GC parameters were the same as previously described.[3] The semi-quantitation of HS volatiles was determined by use of 2-methyl-3-heptanone as the internal standard.

Omission Studies of Aroma Reconstitution Models. Omission studies were performed by comparing the complete model against the omission models using the *R*-index ranking test following the procedure in the literature.[6] Potent odorants were grouped on the basis of their similar odor characteristics, properties, or origins of the compounds (Table 6). The complete model of cola was constructed as described above, and the omission models were prepared by omitting a group of odorants (methanol was spiked instead). All samples (50 mL) were prepared in sniff bottles (Nalgene PTFE wash bottle without a siphon tube; Nalge Nunc International, Rochester, NY) covered with aluminum foil. The complete model was labeled as the control, and the omission models and another set of complete model were labeled with random three-digit codes.

Table 6. *R*-Index Values for the Omission Test of Groups of Compounds

group[a]	odorants omitted[b]	*R*-index, JB[c]
1, citrus/floral	(*R*)-(+)-limonene (**8b**), linalool (**22**), nerol (**36**), geraniol (**39**)	53.57
2, herbal/cooling	1,8-cineole (**9**), 4-terpineol (**25**), isoborneol (**29**), α-terpineol (**31**), borneol (**32a** and **32b**)	32.14
3, aldehyde	octanal (**13**), nonanal (**16**), decanal (**21**)	53.57
4, vanilla	guaiacol (**41**), coumarin (**56**), vanillin (**58**)	53.57
5, brown spice	methyleugenol (**46**), (*E*)-cinnamaldehyde (**48**), eugenol (**51**), (*Z*)-isoeugenol (**53**), (*E*)-isoeugenol (**54**)	67.86*

[a]Description of each group. [b]Compound numbers correspond to those in Tables 1−4 and 7 and Figure 2. [c]Calculated by using John Brown computation against the complete model and expressed as a percentage. *Significantly different from the complete model at α = 0.05 (the critical value for the two-tailed test, α = 0.05 and n = 28 (19 females and 9 males, 20−48 years old), is 17.65).

The test samples (omission models and complete model) were presented to the panelists [n = 28 (19 females and 9 males, 20−48 years old)] using randomized and balance serving orders. After the panelists evaluated the samples, they were asked to rank the test samples on how similar they were to the control (complete model). The *R*-index values were calculated as the percentage of times the sample was ranked less similar to the complete model using the John Brown computation.[16] These values were compared to the critical value of *R*-index 50% for the two-tailed test at α = 0.05. For example, the sample is significantly different from the control if its *R*-index is more than 67.65 (50 + 7.65, which is the critical value for n = 28).

Additional omission studies were conducted for individual components of a group whenever a group omission model was determined to be significantly different from the complete model. Twenty-six panelists (eighteen females and eight males, 20−48 years old) evaluated the test samples against the control sample in the same manner as recently described. In addition, the omission model which significantly differed from the complete model was subjected to sensory descriptive (aroma profile) analysis by an eight-member trained panel (five females and three males; 26−45 years old). A paired t test performed with the SAS program (SAS Institute Inc., Cary, NC) was used to compare the attribute means of the complete model and those of the omission model.

DOI: 10.1021/jf504954p
J. Agric. Food Chem. 2015, 63, 776−786

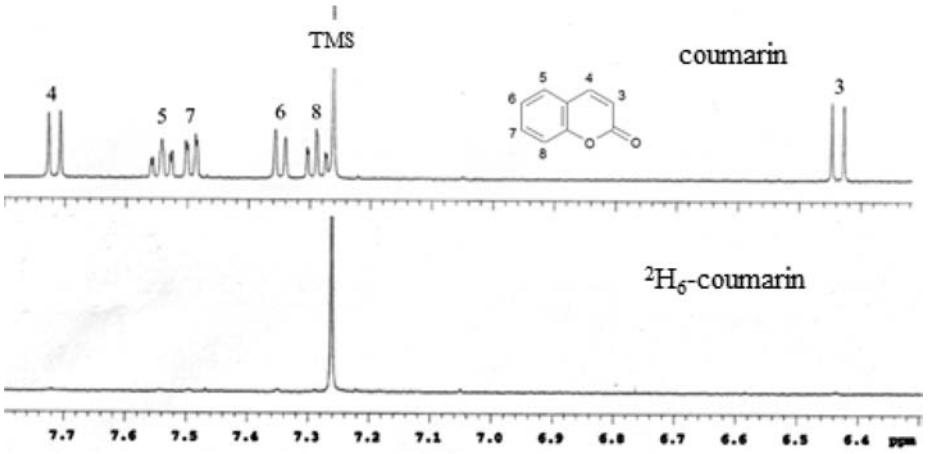

Figure 1. ^{1}H NMR spectra of coumarin and [$^2H_6$]coumarin in $CDCl_3$ (contains TMS as the internal standard).

RESULTS AND DISCUSSION

On the basis of results from our previous study,[3] Coca-Cola, which contained most of the potent odorants found in other cola-flavored carbonated beverages, was chosen as the representative sample for the present study. The odor-active compounds from AEDA were selected for calculation of OAVs based on their high potency (high flavor dilution (FD) factor). Some less potent odorants were also quantitated. In particular, limonene (**8**) and α-terpineol (**31**), which had low FD factors, were included in this experiment since these two odorants were present at the highest abundance in all colas,[3] so they might exert some influence on the perception of cola aroma.

Quantitation by Stable Isotope Dilution Assay. In the present study, SIDA was used for accurate quantitation. The SIDA method is highly accurate since isotopically labeled compounds are used as internal standards. However, the perfect integration of isotope standard solution into the original food matrix has to be taken into account. If the isotope is prepared in an organic solvent, the recovery experiment should be conducted. In addition, it is preferable that the isotope standard should be more than 3 mass units higher than the analyte to ensure a linear calibration curve.[17]

All isotopes used in this study (Figure 2) were labeled with deuterium, except for phenylacetic acid (**I-57**) and its derivatives (**I-37** and **I-43**), which were labeled with ^{13}C. Among synthesized isotopes, [$^2H_6$]coumarin (**I-56**) was prepared by exchanging the hydrogen atoms with deuterium atoms. The electron-impact (EI) mass spectrum of **I-56** indicated that six atoms of hydrogen were substituted, but it was important to confirm the chemical structure of this isotope by nuclear magnetic resonance (NMR). The ^{1}H NMR spectra of **I-56** showed no signal (Figure 1), except for internal standard (TMS) and solvent ($CDCl_3$) peaks. This confirmed that all hydrogen atoms were nearly completely replaced by deuterium atoms.

The concentrations of selected odorants identified in the cola are shown in Table 1. Among 30 aroma compounds, limonene (**8**) was in highest abundance, followed by α-terpineol (**31**) and acetic acid (**19**). Neral (**30**), geranial (**34**), and β-damascenone (**40**) were present at levels below their limits of detection by either full scan or SIM modes of GC−(EI)MS.

Odor Detection Thresholds. The odor thresholds determined in different matrixes will not be the same because of interaction with other components.[18] Odor thresholds in water were used to calculate OAVs of potent odorants in cola since the solubilities, which affect the volatilities, in cola should be very close to those in water. A previous study of flavor release from sucrose solution indicated that flavor release of the 13 aroma compounds studied, including compounds such as linalool and β-damascenone in water and those in aqueous 20% (w/v) sucrose solution, were not significantly different.[19]

Most odor thresholds in water of potent odorants were obtained from the literature (Tables 1 and 2). It is also important to note that the odor threshold of isoborneol (**29**) is for a racemic mixture (49.1:50.9) of the two enantiomers. Enantiomers can have different odor thresholds; therefore, the configuration of chiral compounds should be considered. Among chiral aroma compounds in cola, linalool (**22**) showed the greatest difference (more than 9-fold) with respect to the odor detection thresholds of the two enantiomers.

The aroma compound used to determine the odor threshold must be highly pure before testing. Sometimes this is difficult or nearly impossible, such as in the case of the two isomers of isoeugenol, which could not be separated by using flash chromatography or high-pressure flash chromatography, so determination of their odor thresholds in water was not possible. Their odor thresholds in air should, however, give some indication of how much they influence cola aroma. Unfortunately, these values are not available in the literature. For this reason, the relative odor thresholds in air of the (*Z*)- and (*E*)-isoeugenols (**53** and **54**) were determined by GCO in the present study.

Eugenol (**51**), which has an odor threshold in air of 0.2−0.3 ng/L of air,[15] was used as the internal standard. The relative odor threshold in air of (*Z*)-isoeugenol (0.4−0.6 ng/L of air) was about 2-fold higher than that of eugenol, while the value of (*E*)-isoeugenol (0.1−0.2 ng/L of air) was slightly lower (Table 3).

Odor Activity Values. OAVs of specific aroma-active compounds in cola were calculated as the ratio of the concentrations of the aroma compounds in cola to their odor detection thresholds in water (Tables 1 and 2). In cola-flavored carbonated beverages, limonene (**8**) had the highest OAV followed by 1,8-cineole (**9**), octanal (**13**), and linalool (**22**). OAVs for some potent odorants from our previous study[3] could not be calculated due to a lack of concentration data (e.g., neral (**30**), geranial (**34**), and β-damascenone (**40**)), or their odor detection thresholds in water were unavailable (e.g., (*Z*)-isoeugenol (**53**) and (*E*)-isoeugenol (**54**)). Additionally, the OAVs of borneol (**32**) were reported as the values of the (+)- and

DOI: 10.1021/jf504954p
J. Agric. Food Chem. 2015, 63, 776−786

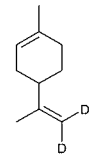

I-8[a] [$^2H_2$]-limonene

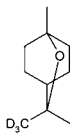

I-9 [$^2H_3$]-1,8-cineole

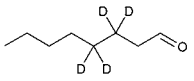

I-13 [$^2H_4$]-octanal

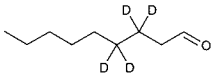

I-16 [$^2H_4$]-nonanal

I-19 [$^2H_3$]-acetic acid

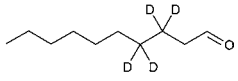

I-21 [$^2H_4$]-decanal

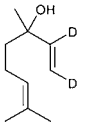

I-22 [$^2H_2$]-linalool

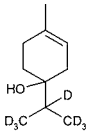

I-25 [$^2H_7$]-4-terpineol

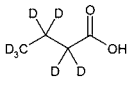

I-26 [$^2H_7$]-butanoic acid

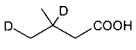

I-28 [$^2H_2$]-3-methylbutanoic acid

I-29 [$^2H_3$]-isoborneol

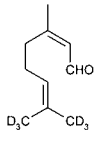

I-30 [$^2H_6$]-neral

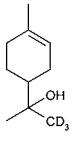

I-31 [$^2H_3$]-α-terpineol

I-32 [$^2H_3$]-borneol

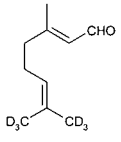

I-34 [$^2H_6$]-geranial

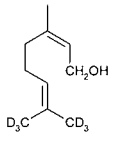

I-36 [$^2H_6$]-nerol

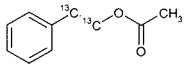

I-37 [$^{13}C_2$]-2-phenethyl acetate

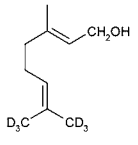

I-39 [$^2H_6$]-geraniol

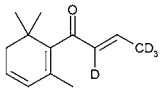

I-40 [$^2H_4$]-β-damascenone

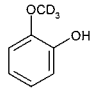

I-41 [$^2H_3$]-guaiacol

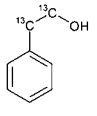

I-43 [$^{13}C_2$]-2-phenylethanol

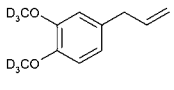

I-46 [$^2H_6$]-methyleugenol

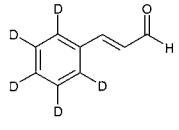

I-48 [$^2H_5$]-cinnamaldehyde

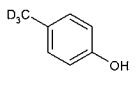

I-49 [$^2H_3$]-p-cresol

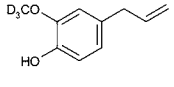

I-51 [$^2H_3$]-eugenol

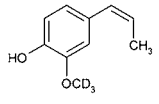

I-53 [$^2H_3$]-(Z)-isoeugenol

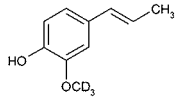

I-54 [$^2H_3$]-(E)-isoeugenol

Figure 2. continued

DOI: 10.1021/jf504954p
J. Agric. Food Chem. 2015, 63, 776−786

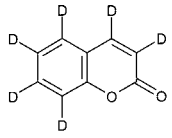

I-56 [$^2H_6$]-coumarin

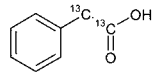

I-57 [$^{13}C_2$]-phenylacetic acid

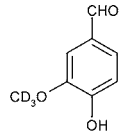

I-58 [$^2H_3$]-vanillin

Figure 2. Chemical structures of isotope standards. Note a: The letter "I" means isotopically labeled compound followed by the numbers which correspond to those in Tables 1 and 2.

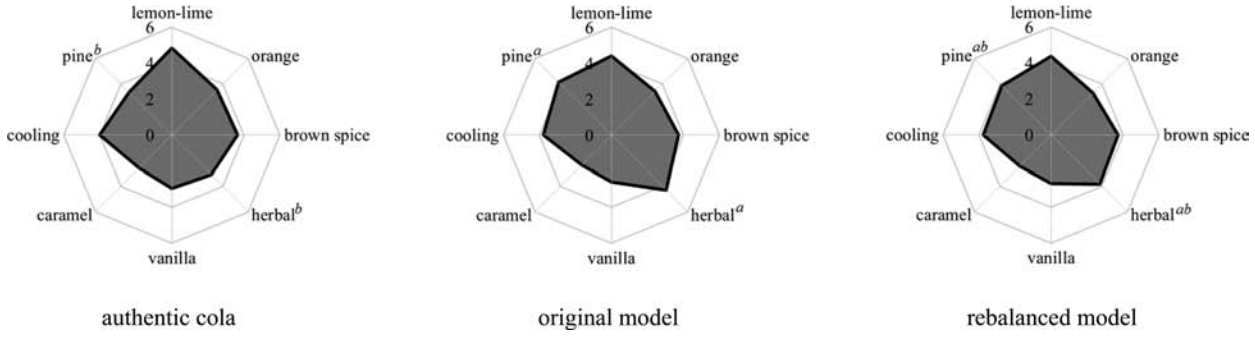

Figure 3. Aroma (by nose) profiles by means of sensory descriptive analysis of cola models compared to authentic cola. Attributes followed by different italic superscript letters are significantly different (p-value < 0.05) [n = 10 (7 females and 3 males, 23−45 years old)]. Odor intensity was rated on a 15 cm line scale.

(−)-isomers because the enantiomeric excess of borneol in cola could not be determined.[3]

When the enantiomeric composition was taken into account, the OAVs of (*S*)-(−)-limonene (**8a**; *l*-isomer) and (*R*)-(+)-limonene (**8b**; *d*-isomer) decreased to 0.3 and 8, respectively, while the OAV of (*R*)-(−)-linalool (**22a**) increased to 60. The other enantiomer pairs ((*S*)-(+)- and (*R*)-(−)-4-terpineols (**25a** and **25b**); (*S*)-(−)- and (*R*)-(+)-α-terpineols (**31a** and **31b**)) showed lower OAVs than the racemic mixtures (**25** and **31**). Furthermore, their values decreased to below 1 (were not considered as aroma-active compounds).

By means of OAV calculations, 1,8-cineole (**9**), (*R*)-(−)-linalool (**22a**), and octanal (**13**) were the most potent odorants which contribute to the overall aroma of cola. Compounds of moderate potency included nonanal (**16**), (*S*)-(+)-linalool (**22b**), decanal (**21**), and (*R*)-(+)-limonene (**8b**).

1,8-Cineole (**9**) is one of the most odor-active compounds in orange peel oil,[18] and it is reported as a secondary degradation product of limonene and α-terpineol by acid-catalyzed reactions.[20] Additionally, it is the second most abundant volatile compound found in cinnamon oil distilled from root bark.[21]

The higher potency of octanal (**13**) by means of OAV calculation compared to AEDA results[3] was due to its low odor detection threshold in water. AEDA is proportional to OAV in air. The nonpolar aroma is volatilized easier from the aqueous phase, resulting in a higher OAV when compared to a polar compound with a similar FD. Octanal is the highest intensity aroma compound in orange oil,[22] and this aldehyde was reported as a moderately potent odorant in orange oil[23] and fresh lemon oil.[24]

As mentioned in our previous study,[3] linalool (**22**) is an important potent odorant of lemon oil[24] and orange peel oil.[23] This compound is highly abundant in coriander oil,[25] neroli oil,[26] and orange oil.[27] (*S*)-(+)-Linalool (**22b**) comprises 60−70% of coriander oil, while the (*R*)-(−)-enantiomer (**22a**) is predominant in neroli oil.[28] The higher potency on the basis of the OAV of (*R*)-(−)-linalool over (*S*)-(+)-linalool in cola flavor was due to the lower odor detection threshold of the (*R*)-(−)-enantiomer.

Limonene (**8**) is the major volatile component of lemon oil,[29] lime peel oil,[30] and orange oil.[22] It was also present at the highest concentration in cola. The major enantiomer of limonene in cola was the (*R*)-(+)-isomer (**8b**), accounting for 97%.[3] Its odor threshold is very high compared to those of the other aroma-active compounds found in cola, so it is important to note that the high potency of this enantiomer was due to its high concentration, not its low odor detection threshold.

The other important potent odorants were vanillin (**58**), borneol (**32**), coumarin (**56**), and eugenol (**51**). The lower potencies, by means of OAV calculation, of coumarin and eugenol as compared to their high FD factors from AEDA[3] are due to the low volatilities of these compounds. For example, the odor threshold in air of eugenol is 0.2−0.3 ng/L of air,[15] while its threshold in water is considerably higher at 6 ng/g.[31] Since the concentrations and in-air thresholds (Table 3) of the (*Z*)- and (*E*)-isoeugenols (**53** and **54**) are similar to those of eugenol, their odor potencies in cola may be equally low. In addition, the OAV of coumarin was less than that of vanillin, but the intensity of coumarin is considered to be about 3 times higher than that of vanillin.[32]

Aroma Reconstitution Models. All aroma compounds which had OAVs higher than 1 in Table 1 (**8**, **9**, **13**, **16**, **21**, **22**, **25**, **31**, **32**, **51**, **56**, and **58**) were used to construct the cola aroma reconstitution model. Some odorants which had OAVs lower than 1 were included in the model reconstitution since they could impact the cola flavor or flavor release/partitioning. In this case, isoborneol (**29**), nerol (**36**), geraniol (**39**), guaiacol (**41**), methyleugenol (**46**), (*E*)-cinnamaldehyde (**48**), (*Z*)-isoeugenol (**53**), and (*E*)-isoeugenol (**54**), which had medium or high FD factors in colas,[3] were used to prepare the cola aroma model.

The high-purity aroma compounds listed in Table 4 were used to prepare the model. The purities of the aroma compounds were more than 99%, except for isoborneol (**29**; 98.7%; plus 1.3% borneol) and (+)-borneol (**32b**, 96.5%; plus 3.5% isoborneol).

DOI: 10.1021/jf504954p
J. Agric. Food Chem. 2015, 63, 776−786

Isoeugenol was present as a mixture of (*Z*)- and (*E*)-isomers (**53** and **54**). (*R*)-(+)-Limonene (**8b**) was used to prepare the cola model because it is present at 97% enantiomer excess in cola,[3] while isoborneol (**29**) and borneol (**32**) were added as racemic mixtures since their enantiomeric distributions could not be evaluated in commercial cola.[3] It is, however, important to note that linalool (**22**), 4-terpineol (**25**), and α-terpineol (**31**) used in this experiment had enantiomeric ratios different from those reported in our previous study.[3] These standard compounds were used to construct the cola model on the basis of quantitation data determined by SIDA.

The chemical composition and pH of commercial cola were examined after decarbonation by sonication. The mean values were a pH of 2.31, soluble solids content of 10.73 °Brix, and titratable acid content of 0.1226 g of citric acid/100 mL or 0.0625 g of phosphoric acid/100 mL (Table 5). The variation was slight among three different code dates of cola, and the above values are close to the values published by Coca-Cola's scientists for acidity of 0.1246% (w/v) and a pH value of 2.4.[33] Soluble solids contents were 11.1 °Brix for original Coca-Cola and 11.5 °Brix for Pepsi.[34] The composition in this table was used to make the matrix of cola model (sucrose−phosphoric acid solution). This cola base was odorless, and it did not differ from odor-free water.

The actual concentration of each aroma compound used to construct the cola aroma reconstitution model is shown in Table 4. The "original" model prepared from a cola matrix and high-purity standards on the basis of quantitation data had a characteristic cola aroma, but could be distinguished from the authentic sample in terms of the intensity of some aroma descriptors. In particular, the herbal and pine attributes of the original cola model were significantly higher than those of commercial cola (Figure 3). The differences between the two aroma profiles may be caused by (1) the matrix or (2) aroma volatiles and/or the balance of odorants above the headspace. To confirm that the synthetic cola base was comparable to the odorless authentic cola base, an odorless matrix was prepared from commercial cola. The aroma volatiles of decarbonated authentic cola were removed by diethyl ether extraction (three times, 1 h each) followed by SAFE for 8 h. The nonvolatile residue was then reconstituted with odor-free water to its original composition. The procedure was repeated to obtain the odorless authentic matrix. By comparison of the overall aroma, the odor characteristic of the cola model obtained from this matrix was similar to that of the cola model prepared from a synthetic base. It was thus concluded that the synthetic matrix was identical to the commercial cola base.

Another possible reason was verified by using SPME. The HS aromas of authentic cola and the model determined by GCO had similar profiles, except for β-damascenone (**40**), which was not detected in the model. The results from GC−MS also indicated that the relative HS concentrations of some aroma-active compounds in the model were different from those in commercial cola (data not shown). For example, the HS concentration of linalool (**22**) in the model was higher than that in authentic cola. Moreover, the high-purity standard of linalool contained a higher percentage of the (*R*)-(−)-enantiomer (**22a**), which has a lower odor threshold than the (*S*)-(+)-enantiomer (**22b**),[35] than the original cola reported in the previous study.[3] Thus, the concentrations of nonanal (**16**), linalool (**22**), and nerol (**36**) above the HS were adjusted one by one to better match (within 0.5-fold of the HS concentration of commercial cola), and this model was designated as "rebalanced". On the basis of HS data, (*R*)-(+)-limonene (**8b**) and (*E*)-cinnamaldehyde (**48**) had to be increased by about 3- and 5-fold, respectively. Unfortunately, the adjusted models seemed obviously different from the authentic cola and were noticeably higher in piney or cinnamon odors. The appropriate amounts of these two aroma components were further adjusted by sensory analysis. Furthermore, the concentration of vanillin, which could not be detected by SPME on GC−MS, was increased. Compounds not quantitated but which had high FD factors[3] included β-damascenone (**40**), 4-hydroxy-2,5-dimethyl-3(2*H*)-furanone (**47**), and sotolon (**52**). These were also evaluated by addition to the model in an attempt to improve the overall aroma. Each of them was added at the odor threshold level or increased by up to 10 times their threshold, but they were not included in the rebalanced model since they caused no improvement or had a negative effect. The actual concentration of each aroma compound in the rebalanced model is reported in Table 4. On the basis of sensory descriptive analysis, the aroma profile of the model did not differ from that of the authentic cola (Figure 3). Therefore, this model was used as the complete model for the omission study.

Omission Studies. Omission studies of the cola aroma reconstitution models involved the omission of various groups of compounds instead of single odorants. The 20 high-purity standard compounds used to construct the cola aroma reconstitution model were categorized into five groups (Table 6). (*R*)-(+)-Limonene (**8b**), linalool (**22**), nerol (**36**), and geraniol (**39**), which had odor characteristic of citrus/floral perceived by GCO,[1] comprised group 1. The aroma compounds in group 2, including 1,8-cineole (**9**), 4-terpineol (**25**), isoborneol (**29**), α-terpineol (**31**), and borneol (**32a** and **32b**), had similar herbal/cooling notes as determined by GCO.[1] Meanwhile, group 5 consisted of methyleugenol (**46**), (*E*)-cinnamaldehyde (**48**), eugenol (**51**), and (*Z*)- and (*E*)-isoeugenols (**53** and **54**) and was designated as the brown spice group according to the aroma characters identified during descriptive analysis in the previous study.[3] Furthermore, not only is eugenol present in nutmeg oil, but it is also a major volatile in cinnamon oil distillated from leaf.[21,36] Guaiacol (**41**) was classified in group 4 along with coumarin (**56**) and vanillin (**58**) because of the origin of these compounds in vanilla bean.[37] Octanal (**13**), nonanal (**16**), and decanal (**21**) were categorized in group 3 as the aldehyde group due to their similar properties. These three aliphatic straight-chain aldehydes are known to cross-adapt because of their similar odor qualities,[38] and they also share the same I7 mammalian odorant receptors.[39]

Omission models were compared against the complete model by sensory evaluation. There are several sensory techniques used to discriminate the omission models from the complete model. The *R*-index ranking test is superior to different general tests because this method can provide the degree of difference among samples in a single experiment.[16] In addition, the *R*-index ranking test can reduce the error of numerical estimates of rating scale testing, and John Brown's *R*-index computation is not difficult to perform.[16] The ranking test is also appropriate for untrained panelists.[40]

The *R*-index results revealed that only the group 5 omission model was statistically different from the complete model (Table 6). Nineteen of the total twenty-eight panelists (67.86%) ranked this omission model as less similar to the complete model. This indicated that methyleugenol (**46**), (*E*)-cinnamaldehyde (**48**), eugenol (**51**), and (*Z*)- and (*E*)-isoeugenols (**53** and **54**) were the most important aroma compounds which contribute to the cola flavor. However, the impact of the "brown spice" group on

DOI: 10.1021/jf504954p
J. Agric. Food Chem. 2015, 63, 776−786

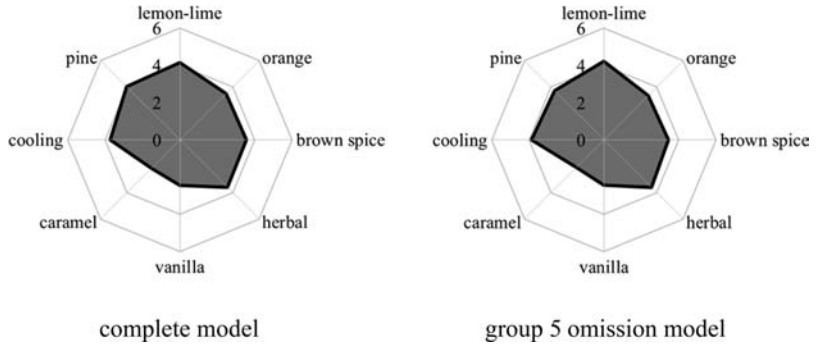

Figure 4. Aroma (by nose) profiles of the group 5 omission model compared to the complete model [n = 8 (5 females and 3 males, 26−45 years old)]. Odor intensity was rated on a 15 cm line scale.

the overall aroma was not in agreement with the main contributors as indicated by the OAVs. This may be because odor thresholds in the cola matrix may differ from those in water. Odor thresholds of some odorants are also affected by the pH of the matrix, for example, 4-hydroxy-2,5-dimethyl-3(2*H*)-furanone.[41] In addition, the mixture suppression or synergy of aroma compounds was not taken into account for OAV calculations.

The descriptive analysis of aroma (by nose) was also performed to compare between the group 5 omission model (brown spice) and the complete model. The two models could not be differentiated by the sensory descriptive analysis results (Figure 4). The complexity of the cola flavor and cross-adaptation might be the reasons to explain this result. The omission model contained guaiacol (**41**) and coumarin (**56**), which were described as having a spicy note. Not only similar odor quality,[42] but also similar chemical structure[43] can result in cross-adaptation. The chemical structure of guaiacol consists of −OH and $-OCH_3$ functional groups on the six-membered ring, which is similar to the structure of eugenol (**51**). Additionally, it could be concluded that the *R*-index ranking test is more powerful than descriptive analysis to discriminate the omission models from the complete model.

The additional omission test was conducted on the basis of omission of each of the aroma compounds in group 5 singularly. However, all omission models did not differ from the complete model (Table 7). This means that the omission of the individual odorants could not be recognized. Food flavor is a result of several odorants, and a change in odor quality or intensity caused by omission of a single or sometimes even several odorants is usually hard to detect.[4]

Table 7. *R*-Index Values for Omission Studies of Single Compounds

odorants omitted[a]	*R*-index, JB[b]
methyleugenol (**46**)	34.62
(*E*)-cinnamaldehyde (**48**)	53.85
eugenol (**51**)	50.00
(*Z*)- and (*E*)-isoeugenols (**53** and **54**)	42.31

[a]Compound numbers correspond to those in Tables 1−4 and 6 and Figure 2. [b]Calculated by using John Brown computation against the complete model and expressed as a percentage (the critical value for the two-tailed test, α = 0.05 and n = 26 (18 females and 8 males, 20−48 years), is 18.25).

■ ASSOCIATED CONTENT

Supporting Information

Synthetic procedures for compounds **I-37**, **I-51**, **I-46**, **I-53**, **I-54**, **53**, **54**, **I-48**, and **I-56**. This material is available free of charge via the Internet at http://pubs.acs.org.

■ AUTHOR INFORMATION

Corresponding Author

*Phone: 217-333-5803. Fax: 217-333-1875. E-mail: cadwlldr@illinois.edu.

Funding

Partial support for this project was provided by the National Institute of Food and Agriculture, U.S. Department of Agriculture, under Project ILLU-698-366.

Notes

The authors declare no competing financial interest.

■ ABBREVIATIONS USED

AEDA, aroma extract dilution analysis; CLLE, continuous liquid−liquid extraction; EI, electron impact; FD, flavor dilution; FID, flame ionization detector; GC−MS, gas chromatography−mass spectrometry; GCO, gas chromatography−olfactometry; HS, headspace; NMR, nuclear magnetic resonance; OAV, odor activity value; R_f, response factor; SAFE, solvent-assisted flavor evaporation; SIDA, stable isotope dilution assay; SPME, solid-phase microextraction

■ REFERENCES

(1) Tchudi, S. N. *Soda Poppery*; Charles Scribner's Sons: New York, 1986; pp 32−34.

(2) Pendergrast, M. *For God, Country and Coca-Cola*; Basic Books: New York, 2000; pp 456−460.

(3) Lorjaroenphon, Y.; Cadwallader, K. R. Characterization of typical potent odorants in cola-flavored carbonated beverages by aroma extract dilution analysis. *J. Agric. Food Chem.* **2015**, *63*, DOI: 10.1021/jf504953s (previous paper in this issue).

(4) Grosch, W. Evaluation of the key odorants of foods by dilution experiments, aroma models and omission. *Chem. Senses* **2001**, *26*, 533−545.

(5) Czerny, M.; Mayer, F.; Grosch, W. Sensory study on the character impact odorants of roasted Arabica coffee. *J. Agric. Food Chem.* **1999**, *47*, 695−699.

(6) Lorjaroenphon, Y.; Cadwallader, K. R.; Kim, H.; Lee, S.-Y. Evaluation of key odorants in chipotle pepper by quantitative analysis, calculation of odor activity values and omission studies. In *Recent Highlights in Flavor Chemistry and Biology*, Proceedings of the 8th Wartburg Symposium on Flavor Chemistry & Biology, Eisenach, Germany, Feb 28 to March 2, 2007; Hofmann, T., Meyerhof, W.,

DOI: 10.1021/jf504954p
J. Agric. Food Chem. 2015, 63, 776−786

Schieberle, P., Eds.; Deutsche Forschungsanstalt für Lebensmittelchemie: Garching, Germany, 2008; pp 191−200.
(7) Chen, H.; Chan, K. K.; Budd, T. Pharmacokinetics of *d*-limonene in the rat by GC-MS assay. *J. Pharm. Biomed. Anal.* **1998**, *17*, 631−640.
(8) Hausch, B. J.; Lorjaroenphon, Y.; Cadwallader, K. R. Flavor chemistry of lemon-lime carbonated beverages. *J. Agric. Food Chem.* [Online early access]. DOI: 10.1021/jf504852z. Published Online: Dec 12, 2014. http://pubs.acs.org/doi/abs/10.1021/jf504852z.
(9) Steinhaus, M.; Fritsch, H.; Schieberle, P. Quantitation of (*R*)- and (*S*)-linalool in beer using solid phase microextraction (SPME) in combination with a stable isotope dilution assay (SIDA). *J. Agric. Food Chem.* **2003**, *51*, 7100−7105.
(10) Steinhaus, M.; Schieberle, P. Characterization of odorants causing an atypical aroma in white pepper powder (*Piper nigrum* L.) based on quantitative measurements and orthonasal breakthrough thresholds. *J. Agric. Food Chem.* **2005**, *53*, 6049−6055.
(11) Kotseridis, Y.; Baumes, R.; Skouroumounis, G. K. Synthesis of labeled [$^2H_4$]β-damascenone, [$^2H_2$]2-methoxy-3-isobutylpyrazine, [$^2H_3$]α-ionone, and [$^2H_3$]β-ionone, for quantification in grapes, juices and wines. *J. Chromatogr. A* **1998**, *824*, 71−78.
(12) Schuh, C.; Schieberle, P. Characterization of the key aroma compounds in the beverages prepared from Darjeeling black tea: quantitative differences between tea leaves and infusion. *J. Agric. Food Chem.* **2006**, *54*, 916−924.
(13) Schneider, S.; Rolando, C. One step synthesis of vanillin d_3 (4-hydroxy-3-(methoxy d_3)-benzaldehyde. *J. Labelled Compd. Radiopharm.* **1992**, *31*, 489−492.
(14) Ullrich, F.; Grosch, W. Identification of the most intense volatile flavour compounds formed during autoxidation of linoleic acid. *Z. Lebensm.-Unters. -Forsch.* **1987**, *184*, 277−282.
(15) Blank, I.; Fischer, K.-H.; Grosch, W. Intensive neutral odourants of linden honey. *Z. Lebensm.-Unters. -Forsch.* **1989**, *189*, 426−433.
(16) O'Mahony, M. Understanding discrimination tests: a user-friendly treatment of response bias, rating and ranking R-index tests and their relationship to signal detection. *J. Sens. Stud.* **1992**, *7*, 1−47.
(17) Fay, L. B.; Metairon, S.; Lin, J.; Blank, I. Stable isotope dilution assay mass spectrometry in flavour research: Internal standard and calibration issues. In *Frontiers of Flavour Science*, Proceeding of the 9th Weurman Flavour Research Symposium, Freising, Germany, June 22−25, 1999; Schieberle, P., Engel, K. H., Eds.; Deutsche Forschungsanstalt für Lebensmittlechemie: Garching, Germany, 2000; pp 125−131.
(18) Mistry, B. S.; Reineccius, T.; Olson, L. K. Gas chromatography-olfactometry for the determination of key odorants in foods. In *Techniques for Analyzing Food Aroma*; Marsili, R., Ed.; Marcel Dekker: New York, 1997; pp 265−292.
(19) Rabe, S.; Krings, U.; Berger, R. G. Dynamic flavor release from sucrose solutions. *J. Agric. Food Chem.* **2003**, *51*, 5058−5066.
(20) Clark, B. C., Jr.; Chamblee, T. S. Acid-catalyzed reactions of citrus oils and other terpene-containing flavors. In *Off-Flavors in Foods and Beverages*; Charalambous, G., Ed.; Elsevier: Amsterdam, 1992; pp 229−285.
(21) Senanayake, U. M.; Lee, T. H.; Wills, R. B. H. Volatile constituents of cinnamon (*Cinnamomum zeylanicum*) oils. *J. Agric. Food Chem.* **1978**, *26*, 822−824.
(22) Högnadóttir, Á.; Rouseff, R. L. Identification of aroma active compounds in orange essence oil using gas chromatography-olfactometry and gas chromatography-mass spectrometry. *J. Chromatogr. A* **2003**, *998*, 201−211.
(23) Fischer, A.; Grab, W.; Schieberle, P. Characterisation of the most odour-active compounds in a peel oil extract from Pontianak oranges (*Citrus nobilis* var. Lour. *microcarpa* Hassk.). *Eur. Food Res. Technol.* **2008**, *227*, 735−744.
(24) Schieberle, P.; Grosch, W. Identification of potent flavor compounds formed in an aqueous lemon oil/citric acid emulsion. *J. Agric. Food Chem.* **1988**, *36*, 797−800.
(25) Gil, A.; de la Fuente, E. B.; Lenardis, A. E.; Pereira, M. L.; Suarez, S. A.; Bandoni, A.; van Baren, C.; Lira, P. D. L.; Ghersa, C. M. Coriander essential oil composition from two genotypes grown in different environmental conditions. *J. Agric. Food Chem.* **2002**, *50*, 2870−2877.
(26) Toyoda, T.; Nohara, I.; Sato, T. Headspace analysis of volatile compounds emitted from various citrus blossoms. In *Bioactive Volatile Compounds from Plants*; Teranishi, R., Buttery, R. G., Sugisawa, H., Eds.; ACS Symposium Series 525; American Chemical Society: Washington, DC, 1993; pp 205−219.
(27) Sawamur, M.; Tu, N. T. M.; Yu, X.; Xu, B. Volatile constituents of the peel oils of several sweet oranges in China. *J. Essent. Oil Res.* **2005**, *17*, 2−6.
(28) Opdyke, D. L. J. Linalool. *Food Cosmet. Toxicol.* **1975**, *13*, 827−832.
(29) Njoroge, S. M.; Ukeda, H.; Kusunose, H.; Sawamura, M. Volatile components of Japanese Yuzu and lemon oils. *Flavour Fragrance. J.* **1994**, *9*, 159−166.
(30) Minh Tu, N. T.; Thanh, L. X.; Une, A.; Ukeda, H.; Sawamura, M. Volatile constituents of Vietnamese pummel, orange, tangerine and lime peel oils. *Flavour Fragrance J.* **2002**, *17*, 169−174.
(31) Buttery, R. G.; Ling, L. C.; Light, D. M. Tomato leaf volatile aroma components. *J. Agric. Food Chem.* **1987**, *35*, 1039−1042.
(32) Abernethy, J. L. The historical and current interest in coumarin. *J. Chem. Educ.* **1969**, *46*, 561−568.
(33) Clos, J. F.; DuBois, G. E.; Prakash, I. Photostability of rebaudioside A and stevioside in beverages. *J. Agric. Food Chem.* **2008**, *56*, 8507−8513.
(34) Liu, F.; He, Y. Use of visible and near infrared spectroscopy and least squares-support vector machine to determine soluble solids content and pH of cola beverage. *J. Agric. Food Chem.* **2007**, *55*, 8883−8888.
(35) Padrayuttawat, A.; Yoshizawa, T.; Tamura, H.; Tokunaga, T. Optical isomers and odor thresholds of volatile constituents in *Citrus sudachi*. *Food Sci. Technol. Int. Tokyo* **1997**, *3*, 402−408.
(36) Huang, T.-C.; Ho, C.-T.; Fu, H.-Y.; Pan, M.-H. Cytotoxin properties of leaf essential oil and components from indigenous cinnamon (*Cinnamomum osmophloeum* Kaneh). In *Herbs: Challenges in Chemistry and Biology*; Wang, M., Sang, S., Hwang, L. S., Ho, C.-T., Eds.; ACS Symposium Series 925; American Chemical Society: Washington, DC, 2006; pp 299−313.
(37) Pérez-Silva, A.; Odoux, E.; Brat, P.; Ribeyre, F.; Rodriguez-Jimenes, G.; Robles-Olvera, V.; García-Alvarado, M. A.; Günata, Z. GC-MS and GC-olfactometry analysis of aroma compounds in a representative organic aroma extract from cured vanilla (*Vanilla planifolia* G. Jackson) beans. *Food Chem.* **2006**, *99*, 728−735.
(38) Kurtz, A. J.; Lawless, H. T.; Acree, T. E. The cross-adaptation of green and citrus odorants. *Chemosens. Percept.* **2010**, *3*, 149−155.
(39) Zhao, H.; Ivic, L.; Otaki, J. M.; Hashimoto, M.; Mikoshiba, K.; Firestein, S. Functional expression of a mammalian odorant receptor. *Science* **1998**, *279*, 237−242.
(40) O'Mahony, M. Additional nonparametric tests. *Sensory Evaluation of Food: Statistical Methods and Procedures*; Marcel Dakker, Inc.: New York, 1986; pp 303−370.
(41) Buttery, R. G.; Takeoka, R.; Ling, L. C. Furaneol: odor threshold and importance to tomato aroma. *J. Agric. Food Chem.* **1995**, *43*, 1638−1640.
(42) Gottfried, J. A.; Winston, J. S.; Dolan, R. J. Dissociable codes of odor quality and odorant structure in human piriform cortex. *Neuron* **2006**, *49*, 467−479.
(43) Pierce, J. D.; Wysocki, C. J., Jr.; Aronov, E. V.; Webb, J. B.; Boden, R. M. The role of perceptual and structural similarity in cross-adaptation. *Chem. Senses* **1996**, *21*, 223−237.
(44) Buttery, R. G.; Black, D. R.; Guadagni, D. G.; Ling, L. C.; Connolly, G.; Teranishi, R. California bay oil: I. Constituents, odor properties. *J. Agric. Food Chem.* **1974**, *22*, 773−777.
(45) Buttery, R. G.; Turnbaugh, J. G.; Ling, L. C. Contribution of volatiles to rice aroma. *J. Agric. Food Chem.* **1988**, *36*, 1006−1009.
(46) Buttery, R. G.; Ling, L. C. Additional studies on flavor components of corn tortilla chips. *J. Agric. Food Chem.* **1998**, *46*, 2764−2769.
(47) Guadagni, D. G.; Buttery, R. G.; Harris, J. Odour intensities of hop oil components. *J. Sci. Food Agric.* **1966**, *17*, 142−144.

DOI: 10.1021/jf504954p
J. Agric. Food Chem. 2015, 63, 776−786

(48) Buttery, R. G.; Teranishi, R.; Ling, L. C.; Turnbaugh, J. G. Quantitative and sensory studies on tomato paste volatiles. *J. Agric. Food Chem.* **1990**, *38*, 336−340.
(49) Buttery, R. G.; Teranishi, R.; Flath, R. A.; Ling, L. C. Fresh tomato volatiles, composition and sensory studies. In *Flavor Chemistry: Trends and Developments*; Teranishi, R., Buttery, R. G., Shahidi, F., Eds.; ACS Symposium Series 388; American Chemical Society: Washington, DC, 1989; pp 213−222.
(50) Ohloff, G. Importance of minor components in flavors and fragrances. *Perfum. Flavor.* **1978**, *3*, 11−22.
(51) Liu, S.-Q.; Holland, R.; Crow, V. L. Ester and their biosynthesis in fermented dairy products: a review. *Int. Dairy J.* **2004**, *14*, 923−945.
(52) Masanetz, C.; Grosch, W. Hay-like off-flavour of dry parsley. *Z. Lebensm.-Unters. -Forsch. A* **1998**, *206*, 114−120.
(53) Rychlik, M.; Schieberle, P.; Grosch, W. *Compilation of Odor Thresholds, Odor Qualities and Retention Indices of Key Food Odorants*; Deutsche Forschungsanstalt für Lebensmittelchemie and Institut für Lebensmittelchemie der Technischen Universitä München: Garching, Germany, 1998; p 47.
(54) Semmelroch, P.; Laskawy, G.; Blank, I.; Grosch, W. Determination of potent odourants in roasted coffee by stable isotope dilution assays. *Flavour Fragrance. J.* **1995**, *10*, 1−7.

DOI: 10.1021/jf504954p
J. Agric. Food Chem. 2015, 63, 776−786

JOURNAL OF AGRICULTURAL AND FOOD CHEMISTRY

Article

pubs.acs.org/JAFC

Characterization of Phenolic Constituents Inhibiting the Formation of Sulfur-Containing Volatiles Produced during Garlic Processing

Wen-Qing Li,[†] Hua Zhou,*[,†] Mei-Yun Zhou,[‡] Xing-Peng Hu,[†] Shi-Yi Ou,[†] Ri-An Yan,[†] Xiao-Jian Liao,[‡] Xue-Song Huang,[†] and Liang Fu[†]

[†]Department of Food Science and Engineering, and [‡]Department of Chemistry, Jinan University, Guangzhou 510632, Guangdong China

Supporting Information

ABSTRACT: Garlic (*Allium sativum* L.), which is a widely distributed plant, is globally used as both spice and food. This study identified five novel phenolic compounds, namely, 8-(3-methyl-(*E*)-1-butenyl)diosmetin, 8-(3-methyl-(*E*)-1-butenyl)chrysin, 6-(3-methyl-(*E*)-1-butenyl)chrysin, and Alliumones A and B, along with nine known compounds **6**−**14** from the ethanol extract of garlic. The structures of these five novel phenolic compounds were established via extensive 1D- and 2D-nuclear magnetic resonance spectroscopy experiments. The effects of the phenolic compounds isolated from garlic on the enzymatical or nonenzymatical formation of sulfur-containing compounds produced during garlic processing were examined. Compound **12** significantly reduced the thermal decomposition of alliin, whereas compound **4** exhibited the highest percentage of alliinase inhibition activity (36.6%).

KEYWORDS: *Allium sativum, phenolic compounds, alliin, alliinase*

INTRODUCTION

Garlic (*Allium sativum* L.), which is a widely distributed plant, has been used as spice, food, and folk medicine worldwide for hundreds of years.[1,2] Garlic is a leading herbal remedy used by alternative medical practitioners. Garlic exhibits a wide range of therapeutic effects, such as hypolipidaemic,[3] antiatherosclerotic,[4] antidiabetic,[5] antimicrobial,[6] anticarcinogen,[7] and immunomodulatory[8] activities.

The characteristic smell and health activities of garlic result from sulfur-containing volatiles;[9] these substances are formed when fresh, raw garlic is chopped or crushed, thereby rupturing the intracellular compartments that contain the nonprotein amino acid alliin (*S*-allyl-L-cysteine sulfoxide), pyridoxal-5-phosphate-dependent enzyme alliinase (L-(+)-*S*-alk(en)-ylcysteine sulfoxide lyase, EC 4.4.1.4), and α, β-eliminating endogenous lyase from *Allium* spp.[10,11] or from alliin, which is also a product nonenzymatically formed when garlic or alliin is thermally processed at temperatures >100 °C.[9,12−14]

Aside from S-containing volatiles, garlic also contains phenolic compounds, including the flavonoids[15−17] myricetin, quercetin, and apigenin, as well as phenolic acids,[18] such as gallic, chlorogenic, ferulic, *o*-coumaric, and cinnamic acids, the contents of which were affected by the genotype and location of garlic and the processing condition of "seed" cloves. For instance, the white and Chinese garlic cultivars contained higher contents of total phenolics and ferulic acid than those of the purple garlic cultivars;[18] phenolic compounds were more abundant in the leaves than in the bulbs;[19] and low-temperature conditioning of garlic seed cloves increased the synthesis of phenolic compounds, resulting in a threefold content increase compared with those conditioned at room temperature.[20] Most phenolic compounds exhibit interesting biochemical properties, such as anti-HIV property,[21] capability to protect low-density lipoprotein cholesterol from oxidation,[22] antioxidative characteristics,[23−26] inhibition of ACE activity.[27] and binding affinity toward P-glycoprotein.[28]

Besides having various biological activities, phenolic compounds usually play important roles in food processing.[29] They easily form complexes with other food component such as protein and lipid via hydrogen bonding interactions, leading to changes in physicochemical properties of the latter such as solubility, thermal stability, and digestibility.[30−34] Therefore, phenolic compounds, as the major metabolites of garlic, could interact with alliin or alliinase during garlic processing. These phenolic compounds affect the formation of S-containing compounds, thereby altering the flavor and health benefits of garlic. However, little information is available on the systematic isolation of the phenolic compounds from garlic and the effect of such compounds on alliin or alliinase.

This research aimed to characterize phenolic compounds from garlic and study the effects of them on the enzymatical or nonenzymatical formation of S-containing compounds. Fourteen phenolic compounds that were isolated from garlic, including five novel flavones, were investigated to determine the inhibitory activities of the compounds on the enzymatical or nonenzymatical formation of S-containing compounds. To our knowledge, this study provided the first evidence of the functions of phenolic compounds in garlic during alliinase catalyst reaction and thermal decomposition of alliin.

MATERIALS AND METHODS

General Experimental Procedures. All chemicals, including alliin (98.5%) and alliinase (EC 4.4.1.4, 1000 U/mg), were purchased

Received: September 28, 2014
Revised: January 6, 2015
Accepted: January 11, 2015
Published: January 11, 2015

ACS Publications © 2015 American Chemical Society

DOI: 10.1021/jf505982f
J. Agric. Food Chem. 2015, 63, 787−794

from Aladdin Industrial Corporation (China). Distilled water was used throughout the experiments. All the experiments were performed at room temperature unless stated otherwise. UV/vis spectra were obtained using a Spectrumlab 53 UV−visible spectrophotometer (Shanghai Lengguang Technology Co., Ltd., Shanghai, China). Nuclear magnetic resonance (NMR) spectra were acquired using a 400 MHz NMR machine (Bruker), and IR spectra were obtained using a Fourier transform-infrared spectrophotometer (Nicolet Avatar). All the experiments were performed in triplicate.

Plant Material. In January 2014, garlic (*Allium sativum* L.) was collected from Guangzhou, which is located in the Guangdong province of China. Voucher specimens (Accession No. 201410005) were deposited at the herbarium of the Jinan University.

Extraction and Isolation. Around 25 kg of air-dried garlic was peeled and extracted thrice with 95% ethanol (3 × 30 L) at 80 °C. The extract was evaporated to dryness in a vacuum at 60 °C, and 1500.5 g of the crude extract was obtained. The crude extract was purified using an Amberlite A21 column (dimension of column: 10 cm, flow rate: 20 mL/min, eluted with 0%, 25%, 50%, 75%, 90%, and 100% ethanol, volume of solvent: 6 × 40 L) to afford six fractions, namely, fractions 1−6. Fraction 1 contained high amounts of sugar and amino acids, which were not further separated. Fraction 2 (10.1 g, 25% ethanol fraction) was further separated by passing the compounds to a Sephadex LH-20 column (dimension of column: 4 cm, flow rate: 2 mL/min, solvent: MeOH, volume of solvent: 2000 mL) to afford two fractions, namely, fractions 2A and 2B. After evaporation of the solvent at a reduced pressure, fraction 2A (4.2 g) was passed through a 100 g silica gel column by using MeOH/CH_2Cl_2 (2:10) as the eluting solvent to afford compound **12** (300 mg). Fraction 2B (2.4 g) was also passed through a 50 g silica gel column, developed with PE/EtOAc (5:0.5, 5:1, and 5:2), and monitored via thin-layer chromatography by using PE/EtOAc (5:1) to afford compounds **8** (20 mg, R_f = 0.35) and **9** (10 mg, R_f = 0.40). Fraction 3 (14.0 g, 50% ethanol fraction) was separated using a silica gel column (200 g) and eluted by PE/EtOAc (5:1). Subsequently, the fraction was separated by a Sephadex LH-20 column (dimension of columns: 1 cm, flow rate: 0.2 mL/min, solvent: MeOH, volume of solvent: 200 mL) to afford compound **10** (8.8 mg) and another fraction (subfraction A). Subfraction A was further purified by HPLC [250 mm × 10 mm YMC-Pack-C_{18} column, mobile phase: MeOH/H_2O (30:70), detection wavelength: 254 nm, flow rate: 1.0 mL/min] to obtain compound **7** (8.3 mg, Rt = 10.5 min). Fraction 4 (12.1 g, 75% ethanol fraction) was subjected to RP_{18} gel (200 g) column by using MeOH−H_2O (from 8:2 to 9:1) as the eluting solvent to obtain two fractions, namely, 4A and 4B. Fraction 4A was separated using a silica gel column and EtOAc/PE (1:5) as the eluting solvent. Fraction 4A was then purified via preparative TLC CH_2Cl_2/PE(1:1) to afford compound **1** (11 mg, R_f = 0.5). Fraction 4B was subjected to a Sephadex LH-20 column (dimension of column: 1 cm, flow rate: 0.1 mL/min, solvent: MeOH, volume of solvent: 180 mL) and then purified via preparative HPLC [250 mm × 10 mm YMC-Pack-C_{18} column, mobile phase: MeOH/H_2O (20:80), detection wavelength: 254 nm, flow rate: 1.0 mL/min] to obtain compounds **4** (10 mg, Rt = 13.5 min) and **5** (11 mg, Rt = 14.8 min). Fraction 5 (25.8 g, 90% ethanol fraction) was separated using a silica gel column and EtOAc/PE (1:5) to afford three fractions, including 5A−5C. Fraction 5A was separated by a Sephadex LH-20 column (dimension of column: 1 cm, flow rate: 0.2 mL/min, solvent: CH_3COCH_3, volume of solvent: 170 mL) to obtain compound **14** (14.6 mg), and fraction 5B was chromatographed using a silica gel column (400 g) with CH_2Cl_2/MeOH mixtures of increasing polarity to afford compound **11** (10.4 mg). Fraction 5C was separated using a Sephadex LH-20 column (dimension of column: 1 cm, flow rate: 0.2 mL/min, solvent: MeOH/H_2O (1:1), volume of solvent: 240 mL) to yield compound **6** (18.8 mg). Meanwhile, fraction 6 (10.2 g, 100% ethanol fraction) was separated by silica and developed with CH_2Cl_2/MeOH (100:1, 100:5, 10:1) to obtain two fractions, namely, fractions 6A and 6B. Fraction 6A was purified using a silica gel column [30g, CH_2Cl_2/CH_3COCH_3 (100:1)] and further prepared via preparative TLC (EtOAc/PE (5:1) to obtain compounds **2** (8.1 mg, R_f = 0.4) and **3** (8.4 mg, R_f = 0.34). Fraction 6B was separated using a silica gel column (30 g, CH_2Cl_2/MeOH [50:1]) to obtain compound **13** (10.9 mg).

*8-(3-Methyl-(E)-1-butenyl)diosmetin (**1**).* Yellow powder; $C_{21}H_{20}O_6$; m.p.194−196 °C; UV (MeOH) λ_{max} (log ϵ) 220 (2.24), 267 (4.12) nm; IR (KBr) υ_{max}: 3377, 2949, 1643, 1580, 1399, and 851 cm^{-1}; ^1H NMR (CD_3OD, 400 MHz) δ 6.58 (1H, s, H-3), 6.24 (1H, s, H-6), 7.39 (1H, d, J = 2.0 Hz, H-2′), 7.04 (1H, d, J = 8.4 Hz, H-5′), 7.48 (1H, dd, J = 8.4 and 2.0 Hz, H-6′), 3.94 (3H, s, OCH_3), 6.54 (1H, d, J = 16.4 Hz, H-1″), 6.48 (1H, dd, J = 16.4 and 6.8 Hz, H-2″), 2.53 (1H, m, H-3″), and 1.18 (6H, d, J = 6.8 Hz, H-4″ and H-5″); HR−ESI−MS, m/z 369.1331 $[M + H]^+$ (calcd for $C_{21}H_{21}O_6$, 369.1333).

*8-(3-Methyl-(E)-1-butenyl)chrysin (**2**).* Yellow powder; $C_{20}H_{18}O_4$; m.p.184−186 °C; UV (MeOH) λ_{max} (log ϵ) 223 (2.38), 276 (4.49) nm; IR (KBr) υ_{max}: 3401, 2926, 1607, 1578, 1422, and 872 cm^{-1}; ^1H NMR (CD_3OD, 400 MHz) δ 6.61 (1H, s, H-3), 6.17 (1H, s, H-6), 7.88 (2H, d, J = 7.6 Hz, H-2′ and H-6′), 7.52 (3H, m, H-3′, H-4′, and H-5′), 6.46 (1H, d, J = 16.4 Hz, H-1″), 6.43 (1H, dd, J = 16.4 and 6.4 Hz, H-2″), 2.46 (1H, m, H-3″), and 0.89 (6H, d, J = 6.8 Hz, H-4″ and H-5″); HR−ESI−MS, m/z 323.1279 $[M + H]^+$ (calcd for $C_{20}H_{19}O_4$, 323.1278).

*6-(3-Methyl-(E)-1-butenyl)chrysin (**3**).* Yellow powder; $C_{20}H_{18}O_4$; m.p.188−189 °C; UV (MeOH) λ_{max} (log ϵ) 218 (2.36), 275 (3.11) nm; IR (KBr) υ_{max}: 3363, 2924, 1644, 1580, 1379, and 850 cm^{-1}; ^1H NMR (CD_3OD, 400 MHz) δ 6.67 (1H, s, H-3), 6.43 (1H, s, H-8), 7.54 (2H, d, J = 6.8 Hz, H-2′ and H-6′), 7.95 (2H, dd, J = 6.8 and 2.0 Hz, H-3′ and H-5′), 7.56 (1H, d, J = 6.8 Hz, H-4′), 6.63 (1H, d, J = 16.4 Hz, H-1″), 6.68 (1H, dd, J = 16.4 and 6.4 Hz, H-2″), 2.44 (1H, m, H-3″), 1.07 (6H, d, J = 6.8 Hz, H-4″ and H-5″); HR−ESI−MS, m/z 323.1271 $[M + H]^+$ (calcd for $C_{20}H_{19}O_4$, 323.1278).

*Alliumone A (**4**).* Yellow powder; $C_{35}H_{28}O_8$; m.p.312−314 °C; UV (MeOH) λ_{max} (log ϵ) 216 (2.44), 277 (5.19), nm; IR (KBr) υ_{max}: 3469, 2924, 1647, 1580, 1397, and 845 cm^{-1}; ^1H NMR (CD_3OD, 400 MHz) δ 6.61 (2H, s, H-3), 6.16 (2H, s, H-6), 7.14 (4H, dd, J = 8.0 and 7.8 Hz, H-2′ and H-6′), 7.62 (4H, d, J = 7.8 Hz, H-3′ and H-5′), 7.22 (2H, dd, J = 8.0 and 7.8 Hz, H-4′), 5.54 (1H, t, J = 8.0 Hz, H-1″), 2.12 (2H, t, J = 8.0 Hz, H-2″), 1.44 (1H, m, H-3″), 0.84 (6H, d, J = 6.4 Hz, H-4″ and H-5″); HR−ESI−MS, m/z 577.1840 $[M + H]^+$ (calcd for $C_{35}H_{29}O_8$, 577.1857).

*Alliumone B (**5**).* Yellow powder; $C_{35}H_{28}O_8$; m.p.331−333 °C; $[\alpha]_{20}^{D}$ +10.04 (c 0.001, methanol); UV (MeOH) λ_{max} (log ϵ) 216 (2.78), 277 (5.79), and 345 (2.45) nm; IR (KBr) υ_{max}: 3433, 2953, 1656, 1590, 1416, and 878 cm^{-1}; ^1H NMR (CD_3OD, 400 MHz) unit I: δ 6.72 (1H, s, H-3), 6.34 (1H, s, H-8), 7.59 (2H, m, H-2′ and H-6′), 8.34 (2H, dd, J = 7.8 and 1.2 Hz, H-3′ and H-5′), 7.51 (1H, m, H-4′), 5.74 (1H, t, J = 8.4 Hz, H-1″), 2.28 (1H, m, H-2″α), 2.21 (1H, m, H-2″β), 1.44 (1H, m, H-3″), 0.92 (3H, m, H-4″), 0.93 (3H, m, H-5″); unit II: δ 6.60 (1H, s, H-3), 6.12 (1H, s, H-6), 7.50 (2H, m, H-2′ and H-6′), 7.94 (2H, d, J = 7.0 Hz, H-3′ and H-5′), 7.57 (1H, m, H-4′); HR−ESI−MS, m/z 577.1857 $[M + H]^+$ (calcd for $C_{35}H_{29}O_8$, 577.1857).

Alliin and Allicin Analysis. Quantitative analyses of alliin and allicin were performed using an Agilent 1260 infinity quaternary liquid chromatography (Hewlett-Packard, Wilmington, NC) equipped with a 250 cm × 4.6 mm ODS-A-C_{18} (5 nm particle size) column. The HPLC conditions were as follows: alliin and allicin, as mobile phase of MeOH/H_2O (20:80) and (15:85), detection wavelength of 220 and 254 nm, and flow rate of 0.8 and 1.0 mL/min, respectively.

Allicin Synthesis. Alliin was synthesized as previously described with slight modifications.[35] Diallyl disulfide was placed under vacuum at 0 °C to remove traces of allyl disulfide. A solution of diallyl disulfide (1.00 g, 7.0 mmol) in chloroform (30 mL) and *m*-chloroperbenzoic acid (77%, 1.79 g, 8.0 mmol) in chloroform (5 mL) was added dropwise at 0 °C. The reaction mixture was stirred at 0 °C for 1 h. Anhydrous sodium carbonate (8 g) was added in small portions with vigorous stirring. The reaction mixture was stirred for an additional 0.5 h at 0 °C and then filtered through a pad of Celite and magnesium sulfate. The filtrate was concentrated under reduced pressure to yield 0.90 g (85% yields) of crude allicin, which was purified by column chromatography (PE: EtOAc, 80:20). ^{1}HNMR (400 MHz,

DOI: 10.1021/jf505982f
J. Agric. Food Chem. 2015, 63, 787−794

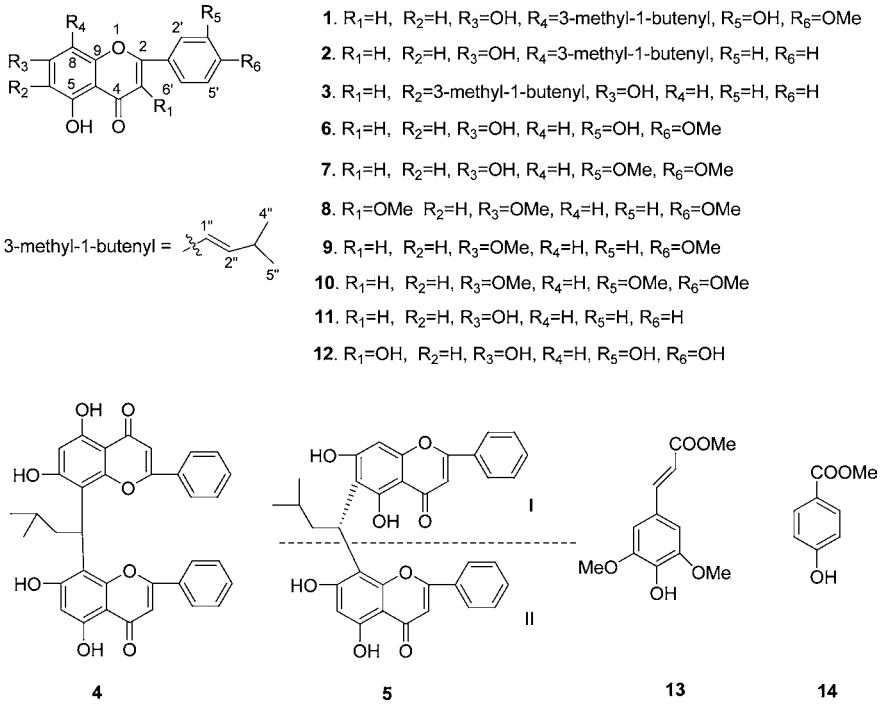

Figure 1. Structures of compounds **1**−**14**.

CD_3CO_2D): δ 3.72−3.92 (m, 4H), 5.20−5.56 (m, 4H), 5.88−5.99 (m, 2H); ^{13}CNMR (100 MHz, CD_3CO_2D): δ 35.0, 59.9, 119.1, 124.0, 125.8, 132.9 ppm.

Thermal Decomposition of Alliin. The thermal decomposition of alliin was estimated by determining its content in the samples according to a previously described method.[12,36] Exactly 5 mg of alliin, 1.0 mg of phenolic compounds isolated from garlic (control: no phenolic compound added), and water were placed in a 5 mL glass tube. The tube was then sealed and equilibrated for 24 h. After equilibration, the tube was heated in an oven at 120 °C for 2 h, cooled in a freezer to −18 °C, and crushed into water to a total volume of 5 mL. The resulting solution was immediately analyzed for alliin content.[10,21] The inhibition percentage was calculated as follows: inhibition percent = [(content of alliin − content of control)/content of control] × 100%. Triplicate measurements were performed.

Assay of Alliinase Activity. Alliinase activity was assayed by determining the production of pyruvate from alliin according to a previously described method with slight modifications.[10] Briefly, the alliinase activity was assayed by determining the production of allicin from alliin. Around 0.5 mL of a 890 U mL^{-1} alliinase sample was added to 1 mL of the standard reaction mixture containing 60 mmol L^{-1} sodium phosphate buffer (pH = 6.5), 25 μmol L^{-1} pyridoxal phosphate, 1 mmol L^{-1} phenolic compounds isolated from garlic (control: no addition of phenolic compound), and 20 mmol L^{-1} pure alliin as substrate. The enzymatic reaction was incubated at 25 °C for 5 min, and the reaction was terminated by adding 2 mL of 0.1 g L^{-1} trichloroacetic acid. The solution was centrifuged to remove the precipitated protein, and the supernatant was assayed for pyruvate concentration via colorimetric analysis. Around 0.5 mL of 1.0 g kg^{-1} 2,4-dinitrophenylhydrazine was added to the supernatant and incubated at 25 °C for 5 min. Exactly 5 mL of 0.5 mol L^{-1} NaOH was then added to the solution and incubated at 25 °C for 10 min. The absorbance at 520 nm was determined using a Spectrumlab 53 UV−visible spectrophotometer (Shanghai Lengguang Technology Co., Ltd., Shanghai, China). The pyruvate concentration was calculated according to the pyruvate standard curve, and the inhibition percentage was calculated as follows: alliinase inhibition (%) = [(content of control − content of pyruvate)/content of control] × 100%. Triplicate measurements were performed.

Procedure for Allicin Decomposition. Allicin decomposition was estimated by determining the content of allicin in the samples according to a previously described method.[35] Exactly 0.5 mg of phenolic compound (control: no phenolic compound added) was added into 0.5 mL of 10 mmol L^{-1} allicin aqueous solution at room temperature. The aliquots were withdrawn from the reaction mixture at a regular time interval (24 h). The resulting solution was immediately analyzed for allicin content, after which the decomposition percentage of allicin was calculated. Each value is the average obtained from three runs of chromatography performed on the sample. Allicin decomposition (%) = [(initial content of allicin − content of allicin)/initial content of allicin] × 100%.

RESULTS AND DISCUSSION

Identification of Compounds 1−14. Exactly 95% aqueous ethanol extract of garlic was separated successively by partitioning the extract using Amberlite A21 column (eluted with 0%, 25%, 50%, 75%, 90%, and 100% ethanol) and repeated Sephadex LH-20 columns. Gel column chromatography afforded five new phenolic compounds **1**−**5** (Figure 1). Nine known compounds, namely, diosmetin (**6**),[37] 2-(3,4-dimethoxyphenyl)-5,7-dihydroxy-4*H*-chromen-4-one (**7**),[38] 5-hydroxy-3,7-dimethoxy-2-(4-methoxyphenyl)-4*H*-chromen-4-one (**8**),[39] 5-hydroxy-7-methoxy-2-(4-methoxyphenyl)-4*H*-chromen-4-one (**9**),[40] 2-(3,4-dimethoxyphenyl)-5-hydroxy-7-methoxy-4*H*-chromen-4-one (**10**),[41] chrysin (**11**),[42] quercetin (**12**),[4,43] (*E*)-methyl 3-(4-hydroxy-3,5-dimethoxyphenyl)-acrylate (**13**),[44] and methyl-4-hydroxybenzoate (**14**),[45] were also obtained and identified based on their spectral data and comparison with literature reports.

Compound **1** exhibited the molecular structure $C_{21}H_{20}O_6$. This result was inferred from the HR-EIMS, ^{13}C NMR, and DEPT data, which indicated 12 degrees of unsaturation. The IR spectrum indicated the presence of hydroxyl groups (3377 cm^{-1}) and a carbonyl group (1643 cm^{-1}), which was conjugated with an aromatic ring. The ^{1}H NMR spectrum provided signals of most functional groups, including five

DOI: 10.1021/jf505982f
J. Agric. Food Chem. 2015, 63, 787−794

aromatic protons [δH 6.58 (1H, s), 6.24 (1H, s), 7.39 (1H, d, *J* = 2.0) 7.04 (1H, d, *J* = 8.4 Hz), and 7.48 (1H, dd, *J* = 8.4 and 2.0 Hz)] and a 3-methyl-1-butenyl group [6.54 (1H, d, *J* = 16.4 Hz, H-1″), 6.48 (1H, dd, *J* = 16.4 and 6.8 Hz, H-2″), 2.53 (1H, m, H-3″), and 1.18 (6H, d, *J* = 6.8 Hz, H-4″ and H-5″)]. The ^{13}C NMR spectrum (Table 1) also exhibited signals for one carbonyl group, seven aromatic methane groups, and seven aromatic quaternary C, including at least four oxygenated C signals at δC 155.9, 161.1, 164.1, and 166.1. This result revealed that compound **1** contained a flavone skeleton. Compound **1** was deduced as 3-methyl-1-butenyl group-substituted diosmetin[22] based on 2D NMR spectrum. In the HMBC spectrum, the following long-range cross peaks (^2J and ^3J) were observed in a ring: singlet at δH 6.24 (H-6) with C-5 (δC 161.1), C-7 (δC 164.1), C-8 (δC 106.6), and C-10 (δC 105.3); as well as methane doublet at δH 6.54 (H-1″) correlated with C-7 (δC 164.1), C-8 (δC 106.6), and C-9 (δC 155.9), which indicated that the 3-methyl-1-butenyl group was attached at C-8. An aromatic methoxy group at δH 3.94 correlated with C-4′ (δC 152.6), and another proton at δH 6.48 (H-2′) showed cross peaks with C-6′ (δC 120.1), C-3′ (δC 148.3), and C-4′ (δC 152.6). These results indicated the presence of a 3′-hydroxyl-4′-methoxybenzoyl moiety. The stereochemistry at C-2″ was *E* because the coupling constant between H-1″ and H-2″ was 16.4 Hz.[46] Thus, the structure of compound **1** was (*E*)-5,7-dihydroxy-2-(3-hydroxy-4-methoxyphenyl)-8-(3-methylbut-1-enyl)-4*H*-chromen-4-one, which was named as 8-(3-methyl-(*E*)-1-butenyl) diosmetin.

Table 1. ^{13}C NMR Chemical Shift Assignments (δ) of 1−5 (in CD_3OD, 100 MHz)

				4	5	
positions	1	2	3	unit I, II	unit I	unit II
2	166.1	165.3	164.7	165.5	165.3	164.5
3	104.3	105.7	105.6	106.2	105.3	105.0
4	184.2	184.0	183.4	183.6	183.1	184.0
5	161.1	161.1	160.3	161.2	161.0	160.8
6	100.0	100.5	111.5	103.5	116.7	103.3
7	164.1	165.5	168.6	172.1	171.4	172.8
8	106.6	106.8	95.7	110.4	97.7	112.0
9	155.9	155.9	157.7	157.3	158.3	157.2
10	105.3	105.1	104.3	104.0	104.1	103.4
1′	125.3	132.7	132.6	132.2	133.1	132.9
2′	114.2	130.1	130.2	129.8	130.1	129.9
3′	148.3	127.5	127.3	127.3	128.0	127.2
4′	152.6	132.9	132.6	132.2	132.7	132.6
5′	112.4	127.5	127.3	127.3	128.0	127.2
6′	120.1	130.1	130.2	129.8	130.1	129.9
1″	116.9	117.3	118.2	30.1	28.0	
2″	142.7	142.3	141.9	42.0	41.0	
3″	34.2	34.1	34.5	26.9	27.7	
4″	23.2	23.0	23.3	23.0	23.1	
5″	23.2	23.0	23.3	23.0	23.3	
MeO	56.4					

Compound **2** was obtained as a yellow amorphous powder. The EIMS exhibited a molecular ion peak at *m*/*z* 323 [M + 1]. The elemental formula of the compound was $C_{20}H_{18}O_4$, as confirmed by the results of HR−ESI−MS ([M + H] 323.1279; calcd for $C_{20}H_{19}O_4$, 323.1278). The IR and UV data of compound **2** were compared with those of compound **1**, and the same basic skeleton as compound **1** was observed in compound **2**. The ^{13}C NMR spectra of **2** displayed signals for one carbonyl group, seven aromatic methane groups, including two symmetrical aromatic methane groups, as well as seven aromatic quaternary C, including three oxygenated C signals at δC 165.3, 161.1, and 165.5. Analysis of the ^{13}C NMR of compound **2** showed that an aromatic methoxy and two oxygenated aromatic quaternary C signals were eliminated, and two aromatic methane signals were added compared with those of compound **1**, which indicated that the C-3′ and C-4′ positions cannot be substituted by the methoxy and hydroxyl groups. The results revealed that compound **2** contained a chrysin skeleton.[42] Compound **2** was deduced as an isomer of 8-prenychrysin.[47] By contrast, the ^{13}C NMR and DEPT data of **2** are similar to those of 8-prenylchrysin, except that a downfield quaternary carbon signal and a methylene signal in 8-prenylchrysin were replaced by two methane signals in **2**, which indicated that **2** contained 3-methyl-1-butenyl group instead of prenyl group in 8-prenylchrysin.[44] In the HMBC NMR experiments, proton δH 6.46 (H-1″) showed correlations with C-7 (δC 165.5), C-8 (δC 106.8), and C-9 (δC 155.9), thereby confirming that the 3-methyl-1-butenyl group was attached at C-8. Accordingly, compound **2** was identified as (*E*)-5,7-dihydroxy-8-(3-methylbut-1-enyl)-2-phenyl-4*H*-chromen-4-one, which was named as 8-(3-methyl-(*E*)-1-butenyl)-chrysin.

Compound **3** exhibited the same molecular formula ($C_{20}H_{18}O_4$) according to the HR−ESI−MS ([M + H] 323.1271; calcd for $C_{20}H_{19}O_4$, 323.1278). The IR bands showed the presence of OH groups (3363 cm^{-1}). A comparison of the NMR spectra of compounds **2** and **3** (Table 1) showed the similarity of the two compounds. The major difference indicated that one aromatic methane signal at δC 100.5 and an aromatic quaternary C signal at δC 106.8 in compound **2** were replaced by that at δC 95.7 and δC 111.5 in compound **3**. This finding implied that the 3-methyl-1-butenyl group, which substituted the position in compound **3**, was different from that in compound **2**. The correlations between a methane doublet at δH 6.63 (H-1″) and C-7 (δC 168.6), C-8 (δC 95.7), and C-9 (δC 157.7) in the HMBC spectrum suggested that the 3-methyl-1-butenyl group was linked to a C-6 carbon. Thus, the structure was characterized as (*E*)-5,7-dihydroxy-6-(3-methylbut-1-enyl)-2-phenyl-4*H*-chromen-4-one, which was named as 6-(3-methyl-(*E*)-1-butenyl)chrysin.

Compound **4** was isolated as a yellow powder. The molecular formula of compound **4** was $C_{35}H_{28}O_8$ according to the results of ^{13}C (DEPT), NMR spectra, and HR−ESI−MS ([M + H] 577.1840; calcd for $C_{35}H_{29}O_8$, 577.1857). The ^{1}H and ^{13}C NMR spectral data of compound **4** were analogous to those of compound **2**. The ^{13}C NMR spectrum showed that two signals, which were ascribed to methane C atoms (δC = 30.1 ppm) at C-1″ and C-2″ (δC = 42.0 ppm) in compound **4**, were observed in place of the two olefinic C atoms (δC = 117.3 and 142.3 ppm, respectively) in compound **2**. The characteristic proton signal at δH = 5.54 ppm, which was attributed to C-1″ (δC = 30.1 ppm), suggested that C-1″ was linked with two symmetric flavone moieties that combined the molecular formula with ^{13}C NMR spectral data and was confirmed by the significant HMBC cross peaks from the methane proton at δH 5.54 to C-8 (δC = 110.4 ppm) and C-7 (δC = 172.1 ppm). Thus, compound **4** was determined as 8,8′-(3-methylbutane-1,1-diyl)bis(5,7-dihydroxy-2-phenyl-4*H*-chromen-4-one), which is a novel natural compound named *Alliumone A*.

DOI: 10.1021/jf505982f
J. Agric. Food Chem. 2015, 63, 787−794

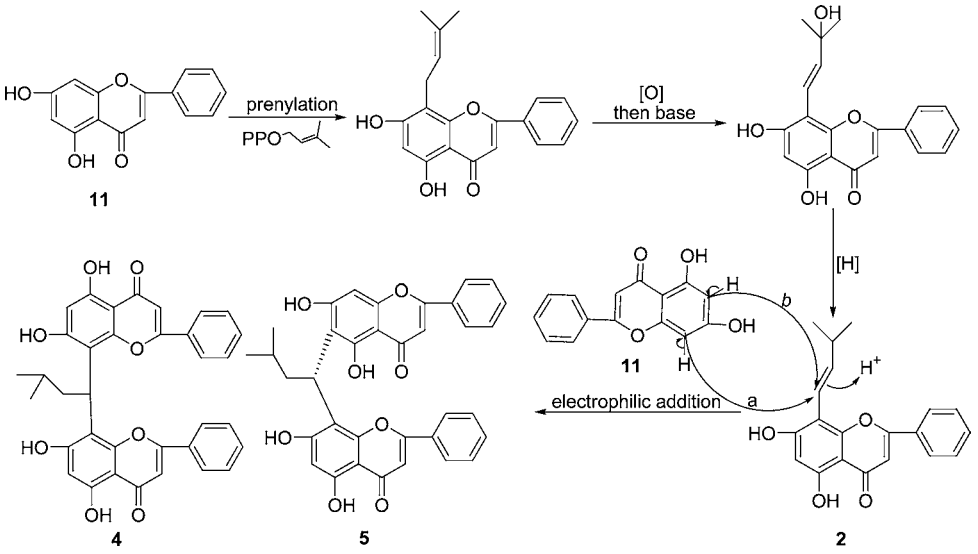

Figure 2. Proposed biosynthesis of **4** and **5**.

Compound **5** was obtained as a yellow amorphous powder. The molecular formula of compound **5** was $C_{35}H_{28}O_8$ according to the ^{13}C (DEPT), NMR spectra, and HR−ESI−MS ([M + H] 577.1857; calcd for $C_{35}H_{28}O_8$, 577.1857). These results were the same as those for compound **4**. The NMR signals of compound **5** appeared in pairs at the same region as those of compound **4**, which suggested that compound **5** was the nonsymmetrical isomer of compound **4**. The presence of a correlation peak from the characteristic proton signal at δH = 5.74 ppm, which was ascribed to C-1″, C-8, and C-6, in the HMBC experiment (δC = 28.0 ppm), demonstrated that C-1″ was attached to the C-8 of unit I and C-6 of unit II. A detailed analysis of the HMBC, H-2″(I) to C-4″(I) and C-1″(I), H-8(I) to C-10(I) and C-7(I), H-6(II) to C-10(II) and C-8(II), H-3(I II) to C-4(I II), C-10(I II), and C-1′(I II), as well as H-4′(I II) to C-3′/5′(I II) and C-2′/6′(I II), facilitated the assignment of all the protons and Cs. An *S* configuration of a chiral center was tentatively assigned according to the optical rotation [$(\alpha)_{20}^{D}$ +10.04 (c 0.001, methanol)] of compound **5** with that of (*S*)-1-ferrocenyl-4-(1-cyclopentylethyl)benzene.[48] In conclusion, the structure of compound **5** was determined as (*S*)-8-(1-(5,7-dihydroxy-4-oxo-2-phenyl-4*H*- chromen-6-yl)-3-methylbutyl)-5,7-dihydroxy-2-phenyl-4*H*-chromen-4-one, which is a novel natural compound named *Alliumone B*.

A plausible biogenetic pathway to **4** and **5** was proposed (Figure 2). Compound **11** generated 8-prenylchrysin though prenylation reaction. The prenyl group of the latter was oxidized and then basified, leading to form 8-(3-hydroxy-3-methyl-but-1-enyl)chrysin, which was similar to the last step of the formation of hyperualones B.[49] The resulting compound was reduced to generate **2**, which further produced the electrophilic addition reaction at the C(1″)= C(2″) bond with C-8 of **11** via a or C-6 of **11** via b (Figure 2), thereby forming **4** and **5**, respectively.

Effect of Phenolic Compounds on Thermal Degradation of Alliin. Previous research reported that alliin is self-degraded or thermally decomposed to generate volatile S-containing compounds.[12−14] These compounds are generated from alliin via hydrolysis or free-radical rearrangement.[14] Most phenolic compounds are strong radical scavengers; thus, we investigated the effects of phenolic compounds isolated from garlic on the thermal decomposition of alliin (Figure 3). The phenolic

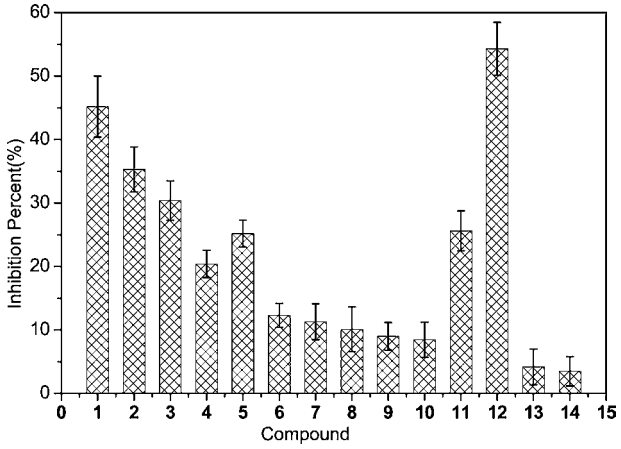

Figure 3. Effect of phenolic compounds from garlic on thermal degradation of alliin.

compounds positively affected the inhibition of the thermal degradation of alliin, in which addition of flavones, such as compounds **11** and **12,** led to stronger inhibition than that of other phenolic compounds, including **13** and **14**. Compound **12** exhibited a maximum inhibition of about 51% compared with compound **14,** which exhibited 5.2% inhibition.

The hydroxyl group in the flavones affected the inhibition ability of the compounds. Compound **11** exhibited more potential inhibition ability than those of compounds **9** and **10** because the latter compounds lacked a hydroxyl substituent at the 7-position of the A ring. This result suggested that the hydroxyl group substituent at the 7-position of the A ring can increase the inhibition ability of the compound. The 3-methyl-1-butenyl group substituent on the flavone skeleton also increased the inhibition capability of the flavone, particularly when the substituent was located at the 8-position of the A ring. This result was exhibited by compounds **2**, **3**, and **11**. Compounds **2** and **3** exhibited one 3-methyl-1-butenyl group substituent at the 8- and 6-positions, respectively, whereas compound **11** lacked a 3-methyl-1-butenyl group substituent in the skeleton. Thermal degradation assay results showed that compounds **2** and **3** exhibited stronger inhibition ability than that of compound **11**. Compound **2** also exhibited better

DOI: 10.1021/jf505982f
J. Agric. Food Chem. 2015, 63, 787−794

inhibition activity than compound **3**, which suggested that the presence of a 3-methyl-1-butenyl group at the 8-position in the skeleton caused stronger inhibition ability relative to that with a 3-methyl-1-butenyl group at the 6-position.

The above results indicated that most flavones clearly exhibited strong inhibition during the alliin degradation. This finding was expected because the flavones behaved as strong radical scavengers, which prevented free radical reaction during the thermal process. The 3-methyl-1-butenyl group substituent, which behaved as an electron-donating substituent at the ring, also decreased the vertical ionization potentials, thereby resulting in better antioxidant activity.[50] This behavior can strongly inhibit the thermal degradation of alliin.

Effect of Phenolic Compounds on Alliinase Activity. The alliinase catalyst reaction was affected by the temperature, pH, concentration, solvent, and presence of additives.[8,9,51,52] However, the functions of the phenolic compounds, which are major secondary metabolites of garlic in the alliinase activity, remain unknown. Figure 4 shows the effects of 14

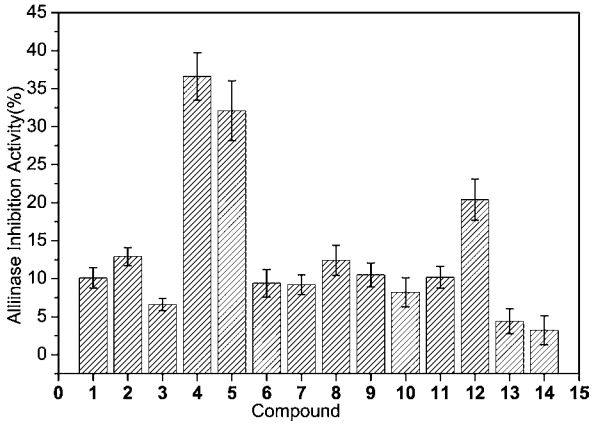

Figure 4. Alliinase inhibition activity of phenolic compounds isolated from garlic.

phenolic compounds isolated from garlic on the alliinase activity. The results indicated that flavones with more hydroxyls (e.g., compound **12**) exhibited higher inhibitory activity than that with more methoxyls (e.g., compounds **8** and **9**). Biflavone **4** also showed the highest percentage of alliinase inhibition activity at 36.6%. Moreover, compound **5** exhibited 32.7% alliinase inhibition activity. The alliinase inhibition activities of compounds **4** and **5** were correspondingly 3.6 and 3.2 times more potent than that of compound **11**. These results implied that the efficiency of flavones as inhibitors of alliinase depended largely on their chemical structures, relative orientation, and number of hydroxyl groups attached to the aromatic ring.

In addition to interactions with alliinase and alliin, phenolics may also interact with allicin as the reactive species formed upon the alliinase cleavage of alliin. Allicin is very unstable and thus easily decomposes into S-containing volatiles. Phenolics could affect allicin stability. Therefore, two phenolics **4** and **12**, which respectively showed strong interaction with alliinase and alliin, were selected to evaluate their effects on allicin stability (Figure 5). After 144 h of the test, the addition of phenolics **4** and **12** caused the decomposition percentage of allicin to reach 47% and 48%, respectively, compared with the control at 52%. This finding is consistent with that obtained by Fujisawa.[53] This result implies that the addition of phenolics slightly promoted allicin stability at room temperature.

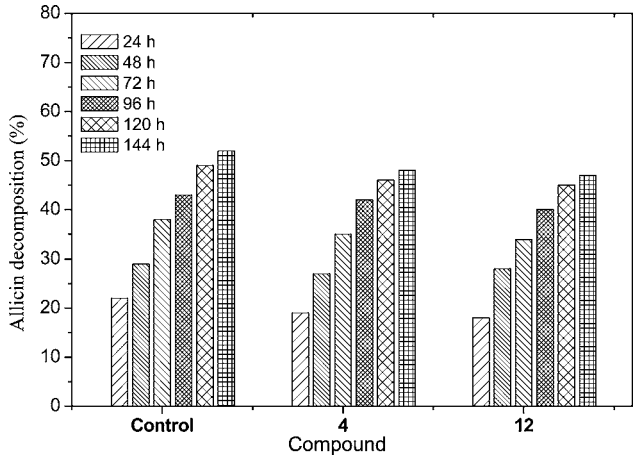

Figure 5. Decomposition percentage of allicin with phenolic compounds **4** and **12**. Each value is the average obtained from three runs of chromatography performed on the sample.

In the present study, five novel flavones, namely, 8-(3-methyl-(*E*)-1-butenyl)diosmetin, 8-(3-methyl-(*E*)-1-butenyl)-chrysin, 6-(3-methyl-(*E*)-1-butenyl)chrysin, and Alliumones A and B, together with nine known compounds **6**−**14**, were identified from the ethanol extract of garlic. To our knowledge, this research is the first systematic report on phenolic compounds from garlic and thus provides the first evidence of the effects of phenolic compounds in garlic on the enzymatical or nonenzymatical formation of S-containing compounds. This study demonstrated that compounds **12** exhibited the strongest inhibition ability for the thermal degradation of alliin (51%), and biflavone **4** showed the highest percentage of alliinase inhibition activity (36.6%). The results may serve as important references for garlic processing.

■ ASSOCIATED CONTENT

Ⓢ Supporting Information

^{1}H NMR, ^{13}C (DEPT) NMR, HSQC, HMBC, and ^{1}H−^{1}H COSY spectra and HR−ESI−MS data of compounds **1**−**5** and ^{1}H and ^{13}C NMR data of compounds **6**−**14**. This material is available free of charge via the Internet at http://pubs.acs.org.

■ AUTHOR INFORMATION

Corresponding Author

*Phone: +8620-85226630. Fax: +8620-85226630. E-mail: zhouhua5460@jnu.edu.cn.

Funding

This work was financially supported by the NSFC of China (Nos. 31101323 and 31000816) and the high-performance computing platform of Jinan University.

Notes

The authors declare no competing financial interest.

■ ABBREVIATIONS USED

PE, petroleum ether; EtOAc, ethyl acetate; R_f, retention factor; Rt, retention time; HIV, human immunodeficiency virus; ACE, angiotensin 1 converting enzyme; TLC, thin-layer chromatography

■ REFERENCES

(1) Eric, B. *Garlic and Other Alliums: The Lore and the Science*; Royal Society of Chemistry: Cambridge, U.K., 2010.

DOI: 10.1021/jf505982f
J. Agric. Food Chem. 2015, 63, 787−794

(2) Koch, H. P.; Lawson, L. D. *Garlic. The Science and Therapeutic Application of Allium sativum L. and Related Species*, 2nd ed.; Williams & Wilkens: Baltimore, MD, 1996.
(3) Sher, A.; Fakhar-ul-Mahmood, M.; Shah Syed Nisar, H.; Bukhsh, S.; Murtaza, G. Effect of garlic extract on blood glucose level and lipid profile in normal and alloxan diabetic rabbits. *Adv. Clin. Exp. Med.* **2013**, *21*, 705−711.
(4) Ide, N.; Lau, B. H. S. Garlic compounds minimize intracellular oxidative stress and inhibit nuclear factor-κB activation. *J. Nutr.* **2001**, *131*, 1020S−1026S.
(5) Padiya, R.; Banerjee, S. K. Garlic as an anti-diabetic agent: Recent progress and patent reviews. *Recent Pat. Food, Nutr. Agric.* **2013**, *5*, 105−127.
(6) Marques, A.; Encarnacao, S.; Pedro, S.; Nunes, M. L. In vitro antimicrobial activity of garlic, oregano and chitosan against Salmonella enterica. *World J. Microbiol. Biotechnol.* **2008**, *24*, 2357−2360.
(7) Modem, S.; Di Carlo, S. E.; Reddy, T. R. Fresh garlic extract induces growth arrest and morphological differentiation of MCF7 breast cancer cells. *Genes Cancer* **2014**, *3*, 177−186.
(8) Schafer, G.; Kaschula, C. H. The immunomodulation and anti-inflammatory effects of garlic organosulfur compounds in cancer chemoprevention. *Anti-Cancer Agents Med. Chem.* **2014**, *14*, 233−240.
(9) Zhang, M.; Lei, N.; Zhu, T.; Zhang, Z. Thermal processing effects on the chemical constituent and antioxidant activity of S-alk(en)-ylcysteine S-oxides (alliin) extract. *LWT—Food Sci. Technol.* **2012**, *51*, 309−313.
(10) Wang, J.; Cao, Y.; Wang, C.; Sun, B. Low-frequency and low-intensity ultrasound accelerates alliinase-catalyzed synthesis of allicin in freshly crushed garlic. *J. Sci. Food Agric.* **2011**, *91*, 1766−1772.
(11) Wang, J.; Cao, Y.; Sun, B.; Wang, C.; Mo, Y. Effect of ultrasound on the activity of alliinase from fresh garlic. *Ultrason. Sonochem.* **2010**, *18*, 534−540.
(12) Kubec, R.; Velisek, J.; Dolezal, M.; Kubelka, V. Sulfur-containing volatiles arising by thermal degradation of alliin and deoxyalliin. *J. Agric. Food Chem.* **1997**, *45*, 3580−3585.
(13) Yu, T. H.; Wu, C. M.; Ho, C. T. Meat-like flavor generated from thermal interactions of glucose and alliin or deoxyalliin. *J. Agric. Food Chem.* **1994**, *42*, 1005−1009.
(14) Yu, T. H.; Wu, C. M.; Rosen, R. T.; Hartman, T. G.; Ho, C. T. Volatile compounds generated from thermal degradation of alliin and deoxyalliin in an aqueous solution. *J. Agric. Food Chem.* **1994**, *42*, 146−153.
(15) Lanzotti, V. The analysis of onion and garlic. *J. Chromatogr., A* **2006**, *1112*, 3−22.
(16) Kim, J. S.; Kang, O. J.; Gweon, O. C. Comparison of phenolic acids and flavonoids in black garlic at different thermal processing steps. *J. Funct. Foods* **2012**, *5*, 80−86.
(17) Isabel Alarcon-Flores, M.; Romero-Gonzalez, R.; Martinez Vidal, J. L.; Garrido Frenich, A. Determination of phenolic compounds in artichoke, garlic and spinach by ultra-high- performance liquid chromatography coupled to tandem mass spectrometry. *Food Anal. Method* **2014**, *7*, 2095−2106.
(18) Manuel Beato, V.; Orgaz, F.; Mansilla, F.; Montano, A. Changes in phenolic compounds in garlic (*Allium sativum l.*) owing to the cultivar and location of growth. *Plant Foods Hum. Nutr.* **2011**, *66*, 218−223.
(19) Tuan, P. A.; Li, X.; Park, N. I.; Lee, S. Y.; Kim, H. H.; Park, S. U. Molecular cloning of 4-coumarate: CoA ligase and total phenolic content in garlic (*Allium sativum*). *Plant Omics* **2011**, *4*, 25−28.
(20) Dufoo-Hurtado, M. D.; Zavala-Gutierrez, K. G.; Cao, C. M.; Cisneros-Zevallos, L.; Guevara-Gonzalez, R. G.; Torres-Pacheco, I.; Vazquez-Barrios, M. E.; Rivera-Pastrana, D. M.; Mercado-Silva, E. M. Low-temperature conditioning of "seed" cloves enhances the expression of phenolic metabolism related genes and anthocyanin content in "coreano" garlic (*Allium sativum*) during plant development. *J. Agric. Food Chem.* **2013**, *61*, 10439−10446.
(21) Murata, R. M.; Pasetto, S.; Pardi, V. The anti-HIV activity of flavonoids: Quercetin and Pinocembrin. *Planta Med.* **2014**, *80*, 811−811.
(22) Gong, M. K.; Garige, M.; Varatharajalu, R.; Marmillot, P.; Gottipatti, C.; Leckey, L. C.; Lakshman, R. M. Quercetin up-regulates paraoxonase 1 gene expression with concomitant protection against LDL oxidation. *Biochem. Biophys. Res. Commum.* **2009**, *379*, 1001−1004.
(23) Lu, X.; Ross, C. F.; Powers, J. R.; Aston, D. E.; Rasco, B. A. Determination of total phenolic content and antioxidant activity of garlic (*Allium sativum*) and elephant garlic by attenuated total reflectance-fourier transformed infrared spectroscopy. *J. Agric. Food Chem.* **2012**, *59*, 5215−5221.
(24) Chen, S. X.; Shen, X. Q.; Cheng, S. Q.; Li, P. P.; Du, J. N.; Chang, Y. X.; Meng, H. W. Evaluation of garlic cultivars for polyphenolic content and antioxidant properties. *PLoS One* **2013**, *8*, 1−12.
(25) Bozin, B.; Mimica-Dukic, N.; Samojlik, I.; Goran, A.; Igic, R. Phenolics as antioxidants in garlic (*Allium sativum L.*, Alliaceae). *Food Chem.* **2008**, *111*, 925−929.
(26) Du, J.; Chen, S.; Cheng, Z.; Chang, Y.; Zhou, J. Response surface methodology for optimization of extraction conditions of total phenolic compounds from garlic and determination of antioxidant activity. *Food Sci.* **2012**, *33*, 72−77.
(27) Oboh, G.; Akinyemi, A. J.; Ademiluyi, A. O. Inhibitory effect of phenolic extract from garlic on angiotensin-1 converting enzyme and cisplatin induced lipid peroxidation-in vitro. *Int. J. Biomed. Sci.* **2013**, *9*, 98−106.
(28) Comte, G.; Daskiewicz, J. B.; Bayet, C.; Conseil, G.; Viornery-Vanier, A.; Dumontet, C.; Di Pietro, A.; Barron, D. C-isoprenylation of flavonoids enhances binding affinity toward P-glycoprotein and modulation of cancer cell chemoresistance. *J. Med. Chem.* **2001**, *44*, 763−768.
(29) Ozdal, T.; Esra, C.; Altay, F. A review on protein−phenolic interactions and associated changes. *Food Res. Int.* **2013**, *51*, 954−970.
(30) Jung, D. M.; Ropp, J. S. D.; Ebeler, S. E. Study of interactions between food phenolics and aromatic flavors using one- and two-dimensional ^{1}H NMR spectroscopy. *J. Agric. Food Chem.* **2000**, *48*, 407−412.
(31) Viljanen, K.; Kivikari, R.; Heinonen, M. Lipid interactions during liposome oxidation with added anthocyanin and other phenolic compound. *J. Agric. Food Chem.* **2004**, *52*, 1104−1111.
(32) Tramer, Z.; Shugar, D. Studies on phenolic hydroxyl binding in proteins. *Acta Biochim. Polym.* **1959**, *6*, 235−251.
(33) Hassan, Z. M. R.; Fakhr El Din, H. M.; Ali, A. A.; Mehanna, N. S.; El-Messery, T. M. Interaction of some low molecular weight phenolics with milk proteins. *World Appl. Sci. J.* **2013**, *23*, 182−187.
(34) Alu'datt, M. H.; Rababah, T.; Ereifej, K.; Brewer, S.; Alli, I. Phenolic−protein interactions in oilseed protein isolates. *Food Res. Int.* **2013**, *52*, 178−184.
(35) Vaidya, V.; Ungold, K. U.; Pratt, D. A. Garlic: Source of the ultimate antioxidants−sulfenic acids. *Angew. Chem., Int. Ed.* **2009**, *48*, 157−160.
(36) Yu, T. H.; Shu, C. K.; Ho, C. T. Thermal decomposition of alliin, the major flavor component of garlic, in an aqueous solution. *ACS Symp. Ser.* **1994**, *546*, 144−152.
(37) Park, Y.; Moon, B. H.; Yang, H.; Lee, Y.; Lee, E.; Lim, Y. Spectral assignments and reference data complete assignments of NMR data of 13 hydroxymethoxy-flavones. *Magn. Reson. Chem.* **2007**, *45*, 1072−1075.
(38) Seijas, J. A.; Vazquez-Tato, M. P.; Carballido-Reboredo, R. Solvent-free synthesis of functionalized flavones under microwave irradiation. *J. Org. Chem.* **2005**, *70*, 2855−2858.
(39) Lu, K.; Chu, J.; Wang, H.; Fu, X.; Quan, D.; Ding, H.; Yao, Q.; Yu, P. Regioselective iodination of flavonoids by N-iodosuccinimide under neutral conditions. *Tetrahedron Lett.* **2013**, *54*, 6345−6348.
(40) Kim, J.; Park, K.-S.; Lee, C.; Chong, Y. Synthesis of a complete series of O-methyl analogues of naringenin and apigenin. *Bull. Korean Chem. Soc.* **2007**, *28*, 2527−2530.

DOI: 10.1021/jf505982f
J. Agric. Food Chem. 2015, 63, 787−794

(41) Nguyen, T. K. P.; Nguyen, K. P. P.; Kamounah, F. S.; Zhang, W.; Hansen, P. E. NMR of a series of novel hydroxyflavothiones. *Magn. Reson. Chem.* **2009**, *47*, 1043−1054.
(42) Pandurangan, N. A new synthesis for acacetin, chrysoeriol, diosmetin, tricin and other hydroxylated flavones by modified baker-venkataraman transformation. *Lett. Org. Chem.* **2014**, *11*, 225−229.
(43) Lopes, R. M.; Agostini-Costa, T. d. S.; Gimenes, M. A.; Silveira, D. Chemical composition and biological activities of *Arachis species*. *J. Agric. Food Chem.* **2011**, *59*, 4321−4330.
(44) Kim, H. J.; Chen, F.; Choi, J. H.; Wang, X.; Jiang, Y. Identification and evaluation of antioxidant phenolic compounds in parsley (*Petroselinum crispum neapolitanum*) and radish (*Raphanus sativus* L.) sprout. *ACS Symp. Ser.* **2008**, *993*, 165−180.
(45) Deleon, S.; Hope, P. H.; Macias, C. Synthesis of *p*-hydroxybenzoic acid and its ester. *Rev. Soc. Quim. Mex.* **1964**, *8*, 13−18.
(46) Zheng, Z. P.; Xu, Y.; Qin, Q.; Zhang, S.; Gu, X. H.; Lin, Y. Y.; Xie, G..B.; Wang, M. F.; Chen, J. Characterization of antiproliferative activity constituents from *Artocarpus heterophyllus*. *J. Agric. Food Chem.* **2014**, *62*, 5519−5527.
(47) Daskiewicz, J. B.; Bayet, C.; Barron, D. Regioselective syntheses of 6-(1,1-dimethylallyl)chrysin and 8-(3,3-dimethylallyl)chrysin. *Tetrahedron* **2002**, *58*, 3589−3595.
(48) Binder, J. T.; Cordier, C. J.; Fu, G. C. Catalytic enantioselective cross-couplings of secondary alkyl electrophiles with secondary alkylmetal nucleophiles: Negishi reactions of racemic benzylic bromides with achiral alkylzinc reagents. *J. Am. Chem. Soc.* **2012**, *134*, 17003−17006.
(49) Zhang, J. J.; Yang, J.; Liao, Y.; Yang, X. W.; Ma, J. Z.; Xiao, Q. L.; Yang, L. X.; Xu, G. Hyperuralones A and B, new acylphloroglucinol derivatives with intricately caged cores from *Hypericum uralum*. *Org. Lett.* **2014**, *16*, 4912−4915.
(50) Reis, M.; Lobato, B.; Lameira, J.; Santos, A. S.; Alves, C. N. A theoretical study of phenolic compounds with antioxidant properties. *Eur. J. Med. Chem.* **2007**, *42*, 440−446.
(51) Kim, K. W.; Kim, Y. T.; Kim, M.; Noh, B. S.; Choi, W. S. Effect of high hydrostatic pressure (HHP) treatment on flavor, physicochemical properties, and biological functionalities of garlic. *LWT—Food Sci. Technol.* **2013**, *55*, 347−354.
(52) Anifantaki, E.; Touloupakis, E.; Ghanotakis, D. F. Alliinase immobilization in calcium alginate beads and layered double hydroxides matrices. *J. Food Biochem.* **2012**, *36*, 12−20.
(53) Fujisawa, H.; Suma, K.; Origuchi, K.; Kumagai, H.; Seki, T.; Ariga, T. Biological and chemical stability of garlic-derived allicin. *J. Agric. Food Chem.* **2008**, *56*, 4229−4235.

DOI: 10.1021/jf505982f
J. Agric. Food Chem. 2015, 63, 787−794

JOURNAL OF AGRICULTURAL AND FOOD CHEMISTRY

Article

pubs.acs.org/JAFC

Analysis and Evaluation of Tasty Components in the Pileus and Stipe of *Lentinula edodes* at Different Growth Stages

Wanchao Chen,[†,‡,§,⊥] Wen Li,[†,‡,⊥] Yan Yang,*[,†,‡] Hailong Yu,[†,‡] Shuai Zhou,[†,‡] Jie Feng,[†,‡] Xiaobei Li,[†,‡] and Yanfang Liu[†,‡]

[†]Institute of Edible Fungi, Shanghai Academy of Agricultural Sciences, Key Laboratory of Edible Fungi Resources and Utilization (South), Ministry of Agriculture, Shanghai 201403, P.R. China

[‡]National Engineering Research Center of Edible Fungi, No. 1000 Jinqi Road, Shanghai 201403, P.R. China

[§]College of Food Science and Technology, Shanghai Ocean University, Shanghai 201306, P.R. China

ABSTRACT: Tasty components in *Lentinula edodes* pileus and stipe at different growth stages were studied. Mannitol, trehalose, arabitol, and glucose were the main soluble polyols and sugars, whereas succinic acid, malic acid, and citric acid were the main organic acids. Mannitol contents were the highest in the pileus and increased at mature growth stages, although arabitol contents were the highest in the stipe and peaked at stage 5. Succinic acid contents peaked at stage 5 in the pileus and stipe during mature growth stages. Threonine (sweet taste) values were the highest among all the detected amino acids, followed by glutamic acid (MSG-like taste). MSG-like 5′-nucleotide contents could account for nearly 50% of the total 5′-nucleotides. Equivalent umami concentration (EUC) values of stage 5 exhibited higher levels during mature growth stages. Tasty components in the stipe were rich and EUC values were high, which might be useful for further processing and byproduct development of *L. edodes*.

KEYWORDS: *Lentinula edodes, tasty components, equivalent umami concentration, growth stages*

INTRODUCTION

Lentinula edodes (Berk.), usually called Xianggu in China, shiitake in Japan, is one of the most important traditional edible and medicinal fungus in China and other East Asian countries for its desirable tasty flavor and great medicinal properties.[1−6] The tasty components in edible mushrooms are primarily several water-soluble substances, including soluble sugars, free amino acids, 5′-nucleotides, and organic acids, which present a variety of taste, such as sweet, umami, sour, and so on. Soluble sugars and polyols, contained in mushrooms, contribute to a sweet taste but not to the typical mushroom taste.[7] Organic acids, related to the metabolic processes of synthetic phenols, amino acids, esters, and aromatic substances,[8] contribute an important part of edible mushroom flavor. Umami taste is recognized as a basic taste, typified by glutamic acid and its salt monosodium glutamate (MSG), which give a savory meat soup or rich meaty taste sensation.[9] Aspartic acid, glutamic acid, and some 5′-nucleotides were also considered as MSG-like components, and values of equivalent umami concentration (EUC) were used to evaluate umami of mushrooms.[10]

Currently, both the pileus and stipe of *L. edodes* were available for food flavor components in China. Recent literatures were just aimed at the tasty components in fruiting bodies of *L. edodes*.[11−13] However, there were few reports about the profiles of tasty components of *L. edodes* in different parts (pileus and stipe) or at different growth stages. Therefore, the aims of our study were to systematically evaluate the main tasty components in *L. edodes* pileus and stipe at different growth stages, in order to further elucidate the synergistic effect of umami tasty components and mechanism of flavor producing in the pileus and stipe during growth stages. The results would be beneficial for further processing in the flavors and fragrances industry.

MATERIALS AND METHODS

Mushroom Materials. *L. edodes* used in this study were cultivated in Xiufeng Edible Fungi Cooperative, Jinshan district, Shanghai, China. The strain, Shenxiang 16 ((2009) No. 002, was recognized by Edible Fungus of Shanghai Agricultural Commodities) and bred by the Improved and Standardized Spawn Breeding Center (ISSBC), Shanghai Academy of Agricultural Sciences, China. Fresh *L. edodes* were harvested at six different stages (Figure 1) according to their growth characteristics (Table 1). The stipe of *L. edodes* formed at stage 1 and was fully extended at stage 6. After stage 4, its inner membrane would crack naturally. Samples were dried by hot air (DHG-9145A, Hengke Technology Ltd., Shanghai, China) at 50 ± 2 °C with maximum air speed, and samples were ground using an ultracentrifugal mill and sieving machine to obtain powder (80 mesh).

Analysis of Soluble Sugars by HPAEC-PAD. Soluble sugars and polyols were extracted and analyzed according to Ajlouni et al.[14] Suspensions of powdered mushroom (0.5 g) in 50 mL of 80% ethanol were shaken at 150 rpm for 45 min at room temperature (26 °C). After filtration through Whatman No. 3 filter paper, the residue was washed five times with additional 25 mL volumes of 80% ethanol. The combined filtrate and rinsed water were evaporated to dryness at 50 °C on

Received: November 14, 2014
Revised: January 5, 2015
Accepted: January 6, 2015
Published: January 6, 2015

ACS Publications © 2015 American Chemical Society

DOI: 10.1021/jf505410a
J. Agric. Food Chem. 2015, 63, 795−801

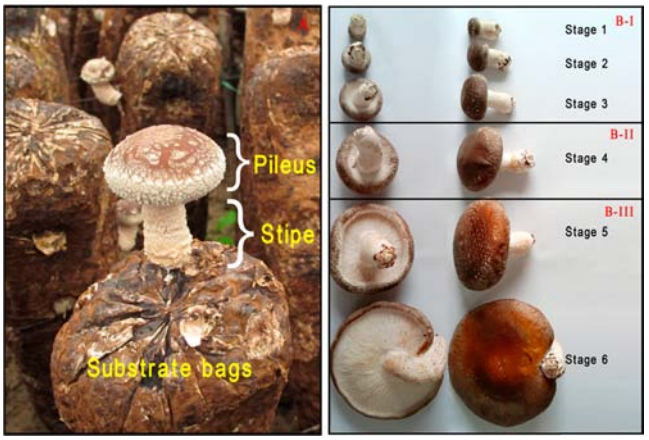

Figure 1. Photograph of *L. edodes* at different growth stages. **A** The fruit body consists of pileus (cap) and stipe (stalk) growing on substrate bags. Developmental processes were divided into three phases: **B−I**, primary developing stages; **B−II**, middle stage; and **B−III**, mature stages.

a rotary evaporator. Extracted solids were redissolved in deionized water to a final volume of 10 mL, and the solution was filtered (0.22 μm cellulose filter, Millipore) prior to analysis. Components were identified by high performance anion exchange chromatography with pulsed amperometric detection (HPAEC-PAD) using the Dionex ICS2500 HPAEC-PAD system (Thermo Fisher China Ltd., Shanghai). Corresponding condition of test method referenced the report by Li et al.[15] Each sugar or polyol was identified and quantified using authentic sugar or polyol standards (Sigma-Aldrich, St. Louis, United States).

Analysis of Organic Acids by HPLC. The extraction of organic acids was modified from a method described by Li et al.[16] Mushroom powder (1.0 g) diluted with 50 mL of 0.1 N HCl (analytical reagent, Sinopharm) was shaken for 60 min at 60 °C for analysis of organic acids. The suspension was centrifuged at 10 000 rpm (15 000*g*) for 20 min after cooling. Then the extraction was filtered through 0.22 μm mixed cellulose esters filter (Welch) to inject into HPLC. The HPLC conditions were carried by Li et al.[16] Each organic acid was identified and quantified using authentic standards (Sinopharm Chemical Reagent Co. Ltd., Shanghai, China) based on their retention time; samples were further quantified by comparing their peak area with the relevant calibration curves of the standard compounds.

Analysis of Free Amino Acids by Amino Acid Analyzer. Free amino acids were extracted and analyzed according to Li et al.[16] Dried *L. edodes* powder sample (0.5 g) was mixed with 30 mL of 0.1 mol/L HCl (GR) solution and then placed into an ultrasonic bath for 30 min at 40 °C. The sample was left to stand for 30 min and then centrifuged at 6000 rpm (4000*g*) for 3 min. The supernatant and 10% sulfosalicylic acid solution were mixed according to the proportion of 1:1 (v/v). The mixture was left at 4 °C for 1 h and then centrifuged at 12 000 rpm (18 000*g*) for 30 min at 4 °C, immediately transferred the supernatant to the tube, and adjusted pH value to 2.0 with 10 mol/L NaOH/HCl. The final supernatant liquid was filtered with Millipore 0.45 μm PES filters (Milford, U.S.A.). The filtrate was loaded onto L-8800 high-speed amino acid analyzer (Hitachi, Japan). The standard amino acid solutions, type ANII and type B, were obtained from Wako (Wako-shi, Japan).

Analysis of 5′-Nucleotides by HPLC. 5′-Nucleotides were extracted and analyzed as described by Taylor et al.[17] A suspension of *L. edodes* powder (1.0 g) in 25 mL of deionized water was boiled for 1 min, cooled, and then centrifuged at 12 000 rpm (18 000*g*) for 15 min. The sediment was repeated with 20 mL of deionized water, and the combined extraction was filtered through a 0.22 μm cellulose membrane (Millipore) prior to analysis by high-performance liquid chromatography (HPLC). The HPLC conditions were carried by Li et al.[15] Each 5′-nucleotide was identified and quantified using 5′-nucleotide standards (Sigma-Aldrich, St. Louis, United States).

Formula of Equivalent Umami Concentration (EUC). The equivalent umami concentration [EUC, g monosodium glutamate (MSG) per 100 g dry raw material weight] is the concentration of MSG equivalent to the umami intensity of that given by the mixture of MSG and a 5′-nucleotide and is represented by the following addition equation:[18]

$$Y = \sum a_i b_i + 1218\left(\sum a_i b_i\right)\left(\sum a_j b_j\right)$$

where Y is the EUC of the mixture in terms of g MSG per 100 g dry raw material weight; a_i is the concentration (g per 100 g dry raw material weight) of each umami amino acid [aspartic acid (Asp) or glutamic acid (Glu)]; a_j is the concentration (g per 100 g dry raw material weight) of each umami 5′-nucleotide [5′-inosine monophosphate (5′-IMP), 5′-guanosine monophosphate (5′-GMP), 5′-xanthosine monophosphate (5′-XMP) or 5′-adenosine monophosphate (5′-AMP)]; b_i is the relative umami concentration (RUC) for each umami amino acid to MSG (Glu, 1 and Asp, 0.077); b_j is the RUC for each umami 5′-nucleotide to 5′-IMP (5′-IMP, 1; 5′-GMP, 2.3; 5′-XMP, 0.61 and 5′-AMP, 0.18); and 1218 is a synergistic constant based on the concentration of g per 100 g dry raw material weight used.

Statistical Analysis. All experiments were performed three times. Tukey's Honestly Significant Difference (Tukey HSD) test was conducted when the samples exhibited a significance

Table 1. Growth Characteristics of *L.edodes* Fruiting Body at Different Stages of Maturity

	stipe		pileus		
stage	diameter (cm)	thickness (cm)	diameter (cm)	length (cm)	mass (g)
1	1.93 ± 0.23f	1.22 ± 0.20e	1.48 ± 0.26c	2.13 ± 0.32d	3.73 ± 1.04e
2	2.56 ± 0.16e	1.62 ± 0.11d	1.59 ± 0.23c	2.50 ± 0.40d	7.17 ± 1.52e
3	4.03 ± 0.22d	2.16 ± 0.14c	1.56 ± 0.32c	3.27 ± 0.49c	15.06 ± 1.96d
4	5.13 ± 0.45c	2.42 ± 0.37b	1.90 ± 0.21b	3.74 ± 0.48b	28.86 ± 5.24c
5	7.73 ± 0.57b	2.82 ± 0.16a	2.48 ± 0.46a	4.70 ± 0.43a	69.95 ± 11.45b
6	11.70 ± 0.57a	2.83 ± 0.21a	2.71 ± 0.22a	5.26 ± 0.65a	99.26 ± 13.31a

Each value is expressed as mean ± standard deviation (n = 3). Means with different letters within a column are significantly different (P < 0.05).

DOI: 10.1021/jf505410a
J. Agric. Food Chem. 2015, 63, 795−801

Table 2. Contents of Soluble Sugars and Polyols in the Pileus and Stipe of *L. edodes* at Different Stages of Maturity

	content (mg/g dry weight)								
	arabitol	mannitol	trehalose	arabinose	fructose	fucose	glucose	rhamnose	total
in the pileus									
stage 1	27.10 ± 0.15e[a]	37.65 ± 0.41f	10.85 ± 0.16b	nd[b]	nd	0.88 ± 0.02d	2.10 ± 0.03d	nd	78.65 ± 0.06a
stage 2	24.15 ± 0.23d	44.49 ± 0.54h	22.19 ± 0.23d	nd	0.52 ± 0.04 cd	0.81 ± 0.01d	2.99 ± 0.01e	nd	95.24 ± 0.58bc
stage 3	17.06 ± 0.06b	54.79 ± 0.60i	32.37 ± 0.12i	0.08 ± 0.03b	0.35 ± 0.03bc	0.86 ± 0.02d	3.30 ± 0.03f	nd	108.9 ± 0.57f
stage 4	19.21 ± 0.29c	34.22 ± 0.32e	35.35 ± 0.43j	0.00 ± 0.00a	0.82 ± 0.08d	0.97 ± 0.01e	5.60 ± 0.04i	nd	96.35 ± 0.29c
stage 5	18.58 ± 0.18c	41.88 ± 0.47g	27.63 ± 0.17g	0.00 ± 0.00a	0.48 ± 0.04de	0.84 ± 0.03d	5.03 ± 0.02h	nd	94.58 ± 0.22bc
stage 6	12.34 ± 0.09a	56.65 ± 0.31j	36.58 ± 0.28j	0.03 ± 0.00b	0.67 ± 0.05e	0.85 ± 0.02d	4.34 ± 0.03j	nd	111.6 ± 0.08g
in the stipe									
stage 1	60.75 ± 0.25i	22.86 ± 0.32a	7.32 ± 0.14a	0.50 ± 0.03d	0.21 ± 0.03a	0.14 ± 0.03bc	1.11 ± 0.04b	0.05 ± 0.01a	92.98 ± 0.32b
stage 2	64.46 ± 0.67j	25.44 ± 0.22b	13.11 ± 0.22c	0.36 ± 0.07c	0.33 ± 0.05b	0.16 ± 0.03c	0.65 ± 0.08a	0.11 ± 0.03b	104.7 ± 0.25d
stage 3	54.11 ± 0.25h	27.09 ± 0.20c	25.33 ± 0.09f	0.41 ± 0.01 cd	0.38 ± 0.01bc	0.02 ± 0.01a	0.82 ± 0.05a	0.11 ± 0.02b	108.9 ± 0.22ef
stage 4	51.60 ± 0.25g	23.07 ± 0.18a	30.85 ± 0.13h	0.50 ± 0.05d	0.27 ± 0.02ab	0.06 ± 0.01ab	0.59 ± 0.02a	0.02 ± 0.00a	107.0 ± 0.19e
stage 5	71.70 ± 0.54k	29.36 ± 0.34d	23.14 ± 0.13e	0.47 ± 0.04d	0.31 ± 0.03ab	0.08 ± 0.01b	0.99 ± 0.12b	nd	126.1 ± 1.06i
stage 6	47.83 ± 0.42f	34.40 ± 0.26e	40.10 ± 0.15k	0.39 ± 0.08c	0.43 ± 0.06c	0.09 ± 0.02bc	1.57 ± 0.08c	nd	125.0 ± 1.01h

[a]Each value is expressed as mean ± standard deviation (n = 3). Means with different letters within a row are significantly different (P < 0.05). [b]Not detected.

Table 3. Contents of Organic Acids in the Pileus and Stipe of *L. edodes* at Different Stages of Maturity

	content (mg/g dry weight)							
	acetic acid	ascorbic acid	citric acid	fumaric acid	malic acid	succinic acid	tartaric acid	total
in the pileus								
stage 1	6.39 ± 0.63d	nd[b]	67.64 ± 3.21e	3.36 ± 0.06c	21.60 ± 0.94c	122.9 ± 4.76c	4.33 ± 0.22b[a]	226.1 ± 3.91e
stage 2	10.54 ± 0.85e	nd	77.60 ± 2.76f	4.41 ± 0.04d	79.93 ± 1.24e	197.1 ± 5.32h	5.21 ± 0.38c	374.7 ± 4.88h
stage 3	3.82 ± 0.45b	nd	53.22 ± 1.88d	3.10 ± 0.05bc	52.65 ± 0.75d	155.8 ± 3.55d	4.39 ± 0.26b	272.9 ± 3.27f
stage 4	5.60 ± 0.68c	nd	65.54 ± 2.07e	3.03 ± 0.03bc	57.52 ± 1.33d	184.3 ± 5.89g	4.43 ± 0.27b	320.3 ± 4.84g
stage 5	5.29 ± 0.87bc	nd	59.20 ± 2.14d	2.40 ± 0.04b	53.60 ± 1.28d	196.9 ± 5.12h	4.22 ± 0.29b	321.5 ± 4.68g
stage 6	4.81 ± 0.96bc	nd	59.11 ± 2.41d	3.19 ± 0.03bc	26.57 ± 1.17c	174.1 ± 7.83e	1.76 ± 0.11a	269.5 ± 5.93f
in the stipe								
stage 1	5.03 ± 0.13	0.50 ± 0.06c	40.6 ± 1.21c	2.36 ± 0.04b	16.8 ± 0.97b	60.0 ± 2.65ab	7.91 ± 0.53e	133.2 ± 1.87d
stage 2	2.16 ± 0.21a	0.34 ± 0.07b	22.5 ± 0.67ab	1.30 ± 0.01a	16.1 ± 0.81b	47.2 ± 3.11a	6.30 ± 0.29d	95.84 ± 2.34b
stage 3	2.62 ± 0.28a	0.42 ± 0.01bc	29.8 ± 0.74b	2.02 ± 0.03b	16.1 ± 0.87b	69.5 ± 3.43b	6.23 ± 0.42d	126.7 ± 1.98d
stage 4	nd	0.18 ± 0.03a	19.8 ± 0.97a	1.00 ± 0.05a	16.5 ± 0.77b	43.5 ± 2.96a	5.24 ± 0.27c	85.40 ± 2.04a
stage 5	2.56 ± 0.34a	0.35 ± 0.04b	27.1 ± 1.03b	0.94 ± 0.05a	10.1 ± 0.92ab	70.5 ± 3.04b	5.00 ± 0.45c	116.5 ± 2.65 cd
stage 6	nd	0.35 ± 0.05b	27.6 ± 1.11b	1.54 ± 0.03ab	7.71 ± 0.79a	68.4 ± 2.11b	5.01 ± 0.37c	109.8 ± 1.72c

[a]Each value is expressed as mean ± standard deviation (n = 3). Means with different letters within a row are significantly different (P < 0.05). [b]Not detected.

difference between samples, with the level of significance set at P < 0.05. Both ANOVA and Tukey HSD were performed with IBM SPSS Statistics 20.

RESULTS AND DISCUSSION

Analysis of Tasty Components in *Lentinula edodes* at Different Stages and Parts. The tasty components of fruit body (pileus and stipe) and different developmental stages of *L. edodes* were investigated. Results were compared with other findings in the literature.

Soluble Sugars and Polyols. Mannitol, trehalose, arabitol, and glucose, considered as the main mushroom polyols or soluble sugars in former reports,[11,12,15,19] were found in the pileus and stipe of *L. edodes* at different growth stages in this research (Table 2). The contents of mannitol were the highest in the pileus, whereas arabitol values were highest in the stipe. In the pileus, the contents of mannitol appeared as an "N" shape developing curve during all the growth stages. It had increased profiles at primary developing stages (stages 1−3) and stages 4−6, whereas it decreased from stage 3 to stage 4. Both mannitol and trehalose increased profiles in the pileus and stipe during mature growth stages. Arabitol showed a high peak at stage 5 in the stipe and had different profiles compared with the results reported by Yang et al.[11] Fucose, arabinose, and frutocose were detected both in the pileus and stipe, but rhamnose was just detected in the stipes. Kim et al.[12] found that freeze-dried *L. edodes* (Strain No. KKU-05, Hwago) fruiting body contained ribose, xylcose, manose, and sucrose (2.40, 7.98, 23.12, and 2.33 mg/g, respectively). Yang et al.[11] found that *L. edodes* (271) and *L. edodes* (Tainung 1) contained manninol, glucose, and trehalose (83.8 and 134 mg/g, 28.6 and 14.2 mg/g, 29.2 and 3.74 mg/g, respectively). The discrepancy in varieties and contents of main soluble sugars and polyols might be due to the difference in strains and cultivation media of fungus, and fucose, rhamnose, and fructose in *L. edodes* have not been reported or detected in the previous studies.

Organic Acids. As main organic acids, succinic acid, citric acid, and malic acid were detected both in the pileus and stipes of *L. edodes*, with descending order of succinic acid > citric acid > malic acid at each growth stage (Table 3). Hiroshi[20] reported that malic acid, fumaric acid, and citric acid were the main organic acids in shiitake (*L. edodes*), whereas in this research,

DOI: 10.1021/jf505410a
J. Agric. Food Chem. 2015, 63, 795−801

Table 4. Contents of Free Amino Acids, 5′-Nucleotides and Equivalent Umami Concentration (EUC) in the Pileus of *L. edodes* at Different Stages of Maturity

	content (mg/g dry weight)					
	stage 1	stage 2	stage 3	stage 4	stage 5	stage 6
amino acids						
alanine	0.91 ± 0.04b	0.94 ± 0.06b	1.40 ± 0.05c	0.64 ± 0.02a	1.54 ± 0.09c	1.01 ± 0.11b
arginine	2.75 ± 0.05h	2.01 ± 0.04g	1.46 ± 0.04e	1.33 ± 0.08d	1.48 ± 0.11e	1.39 ± 0.12d
aspartic acid	0.63 ± 0.04c[a]	0.47 ± 0.03b	0.25 ± 0.01a	0.74 ± 0.03d	0.26 ± 0.03a	0.24 ± 0.02a
cysteine	0.21 ± 0.03c	0.10 ± 0.02b	0.45 ± 0.03d	0.23 ± 0.03c	0.09 ± 0.01b	0.40 ± 0.04d
GABA	0.31 ± 0.02bc	0.35 ± 0.02c	0.27 ± 0.04b	0.27 ± 0.03b	0.35 ± 0.03c	0.17 ± 0.02a
glutamic acid	4.02 ± 0.03f	3.49 ± 0.08e	2.66 ± 0.06 cd	2.28 ± 0.05c	2.96 ± 0.14d	2.10 ± 0.08c
glycine	0.66 ± 0.01d	0.34 ± 0.03b	0.76 ± 0.04e	0.24 ± 0.02ab	0.26 ± 0.01ab	0.65 ± 0.03d
histidine	0.68 ± 0.04f	0.51 ± 0.02e	0.37 ± 0.05c	0.40 ± 0.02 cd	0.33 ± 0.03c	0.45 ± 0.01d
hydroxyproline	0.08 ± 0.01b	0.07 ± 0.02ab	0.11 ± 0.02c	0.12 ± 0.02c	0.07 ± 0.01ab	0.13 ± 0.02c
isoleucine	0.28 ± 0.03c	0.20 ± 0.01c	0.29 ± 0.04c	0.09 ± 0.02b	0.10 ± 0.01b	0.24 ± 0.01c
leucine	0.47 ± 0.05d	0.32 ± 0.04c	0.41 ± 0.06d	0.14 ± 0.08b	0.16 ± 0.02b	0.35 ± 0.03c
lysine	1.44 ± 0.07e	1.36 ± 0.04d	1.08 ± 0.08c	0.92 ± 0.03c	0.92 ± 0.07c	1.02 ± 0.03c
methionine	0.08 ± 0.02e	0.06 ± 0.02d	0.06 ± 0.08d	0.06 ± 0.02d	0.04 ± 0.01b	0.06 ± 0.01d
ornithine	0.69 ± 0.06a	1.82 ± 0.06e	1.86 ± 0.06e	1.86 ± 0.09e	2.79 ± 0.09g	2.40 ± 0.04f
phenylalanine	0.90 ± 0.05e	0.89 ± 0.05c	0.89 ± 0.08c	0.73 ± 0.05c	0.70 ± 0.05c	0.90 ± 0.03e
proline	0.00 ± 0.00a	0.00 ± 0.00a	0.11 ± 0.04e	0.00 ± 0.00a	0.00 ± 0.00a	0.08 ± 0.03d
serine	1.36 ± 0.02g	0.97 ± 0.05f	0.74 ± 0.05e	0.43 ± 0.04c	0.71 ± 0.03d	0.73 ± 0.04d
tyrosine	0.33 ± 0.03ab	0.45 ± 0.07b	0.64 ± 0.05c	0.40 ± 0.06b	0.48 ± 0.01b	0.68 ± 0.05c
tryptophan	0.00 ± 0.00a	0.11 ± 0.03c	0.13 ± 0.01c	0.05 ± 0.02b	0.02 ± 0.01ab	0.26 ± 0.03d
threonine	8.04 ± 0.03c	11.9 ± 0.07g	9.61 ± 0.10ef	10.1 ± 0.14f	8.67 ± 0.07 cd	9.20 ± 0.05d
valine	1.81 ± 0.05h	1.37 ± 0.05g	1.22 ± 0.05g	0.99 ± 0.08e	0.99 ± 0.04e	1.12 ± 0.08f
taste characteristics[b]						
bitter	6.97 ± 0.08h	5.47 ± 0.03g	4.83 ± 0.07f	3.79 ± 0.11e	3.82 ± 0.10e	4.77 ± 0.04f
MSG-like	4.65 ± 0.05g	3.96 ± 0.06f	2.91 ± 0.02d	3.02 ± 0.05d	3.22 ± 0.07de	2.34 ± 0.13bc
sweet	11.0 ± 0.07f	14.1 ± 0.09h	12.6 ± 0.03g	11.4 ± 0.09f	11.2 ± 0.13f	11.7 ± 0.08f
tasteless	1.98 ± 0.03d	1.91 ± 0.04d	2.17 ± 0.05e	1.55 ± 0.08c	1.49 ± 0.05c	2.10 ± 0.11e
total	25.7 ± 0.11g	27.7 ± 0.09h	24.8 ± 0.15f	22.0 ± 0.22d	22.9 ± 0.17d	23.6 ± 0.27e
5′-nucleotides[c]						
5′-AMP	2.47 ± 0.13e	1.11 ± 0.11b	1.77 ± 0.14d	1.34 ± 0.12b	1.53 ± 0.09c	1.88 ± 0.11d
5′-CMP	3.34 ± 0.14e	1.51 ± 0.10a	2.59 ± 0.15	2.29 ± 0.12c	2.24 ± 0.11c	2.46 ± 0.12d
5′-GMP	2.81 ± 0.12g	1.34 ± 0.11c	2.12 ± 0.15f	1.53 ± 0.12d	1.67 ± 0.09e	2.16 ± 0.11f
5′-UMP	2.81 ± 0.13f	1.05 ± 0.09c	1.70 ± 0.13e	1.51 ± 0.13d	1.56 ± 0.10d	1.61 ± 0.10d
MSG-like 5′-nucleotides[d]	5.28 ± 0.12h	2.45 ± 0.09c	3.89 ± 0.13f	2.87 ± 0.11d	3.21 ± 0.10e	4.04 ± 0.11g
flavor 5′-nucleotides[e]	2.81 ± 0.12g	1.34 ± 0.11c	2.12 ± 0.15f	1.53 ± 0.12d	1.67 ± 0.09e	2.16 ± 0.11f

[a]Each value is expressed as mean ± standard deviation ($n = 3$). Means with different letters within a row are significantly different ($P < 0.05$). [b]MSG-like (monosodium glutamate-like): Asp + Glu; Sweet: Ala + Gly + Ser + Thr; Bitter: Arg + His + Ile + Leu + Met + Phe + Try + Val; Tasteless: Lys + Tyr + GABA. [c]5′-CMP: 5′-sytosine monophosphate; 5′-UMP: 5′-uridine monophosphate; 5;-GMP: 5′-guanosine monophosphate; 5′-AMP: 5′-adenosine monophosphate. [d]MSG-like 5′-nucleotides: 5′-AMP + 5′-GMP + 5′-IMP + 5′-XMP, while 5′-IMP and 5′-XMP was not detected in this study. [e]Flavor 5′-nucleotides defined by Chen (1986): 5′-GMP + 5′-IMP + 5′-XMP, while only 5′-GMP was detected in this study.

the contents of succinic acid were significantly higher than those of other detected organic acids, peaked at stage 2 in the pileus and stage 3 in the stipe, respectively, during primary developing stages, and came to a relatively stable levels at mature growth stages. Succinic acid and its sodium salt were the characteristic umami components, rich in marine shellfishes, such as scallop (370 mg/g) and oyster (50 mg/g).[21] Those results would be benefit to a further research of the umami formation mechanism in *L. edodes*. The contents of succinic acid were from 122.9 mg/g to 197.1 mg/g in the pileus and 43.5 mg/g to70.5 mg/g in the stipe during the growth of *L. edodes* fruiting body, higher than the contents of succinic acid in several cultivated mushrooms reported by Li et al.[15] Citric acid, had a mild and refreshing acidity,[22] as the second highest organic acid in pileus and stipe ranged from 53.22 mg/g to 77.60 mg/g and 19.8 mg/g to 40.6 mg/g, respectively, and reached certain steady values at mature growth stages. It also got a top value at stage 2 in the pileus and stage 1 in the stipe, respectively. Malic acid, with a refreshing acidity and a slightly bitter taste,[23] ranked at the third level at mature growth stages in pileus and stipe. At mature stages, the contents of succinic acid in pelius were approximately 3-fold higher than those in stipe, whereas values of citric acid in pelius were 2-fold compared with those in stipe.

Free Amino Acids and 5′-Nucleotides. In this study, 21 amino acids were identified in the pileus and stipe of the growth stages of *L. edodes* (Table 4 and Table 5). The results showed that the contents of threonine were the highest among all amino acids, accounting for 90% of sweet amino acids, with higher values in pileus compared with those of stipe, and achieved relatively steady level at mature growth stages. Glutamic acid as the second highest free amino acid, also accounting for 90% of MSG-like amino acids, were higher in pileus than those of stipe and peaked at stage 5 during the

DOI: 10.1021/jf505410a
J. Agric. Food Chem. 2015, 63, 795−801

Table 5. Contents of Free Amino Acids, 5′-Nucleotides and Equivalent Umami Concentration (EUC) in the Stipe of *L. edodes* at Different Stages of Maturity[a]

	content (mg/g dry weight)					
	stage 1	stage 2	stage 3	stage 4	stage 5	stage 6
amino acids						
alanine	0.59 ± 0.01a	1.09 ± 0.01b	0.70 ± 0.01a	0.69 ± 0.04a	1.42 ± 0.02c	0.66 ± 0.03a
arginine	1.56 ± 0.01f	1.22 ± 0.02c	1.15 ± 0.01bc	0.80 ± 0.03a	1.01 ± 0.03b	0.89 ± 0.01a
aspartic acid	1.04 ± 0.01f	0.42 ± 0.01b	0.23 ± 0.02a	0.87 ± 0.01e	0.25 ± 0.01a	0.22 ± 0.02a
cysteine	0.25 ± 0.02c	0.26 ± 0.01c	0.24 ± 0.01c	0.19 ± 0.01c	0.00 ± 0.00a	0.22 ± 0.01c
GABA	0.16 ± 0.01a	0.35 ± 0.02c	0.17 ± 0.01a	0.25 ± 0.01b	0.32 ± 0.01c	0.17 ± 0.01a
glutamic acid	2.52 ± 0.01 cd	2.19 ± 0.04c	1.33 ± 0.02a	1.29 ± 0.01a	1.86 ± 0.02b	1.36 ± 0.02a
glycine	0.45 ± 0.01c	0.31 ± 0.03b	0.40 ± 0.01c	0.19 ± 0.01a	0.15 ± 0.01a	0.31 ± 0.02b
histidine	0.32 ± 0.01c	0.21 ± 0.01b	0.13 ± 0.01a	0.15 ± 0.01a	0.13 ± 0.02a	0.12 ± 0.03a
hydroxyproline	0.04 ± 0.01a	0.04 ± 0.01a	0.04 ± 0.01a	0.09 ± 0.01b	0.05 ± 0.01a	0.04 ± 0.02a
isoleucine	0.10 ± 0.01b	0.07 ± 0.02ab	0.10 ± 0.01b	0.02 ± 0.01a	0.03 ± 0.01a	0.08 ± 0.02b
leucine	0.16 ± 0.01b	0.11 ± 0.01b	0.13 ± 0.01b	0.04 ± 0.00a	0.05 ± 0.01a	0.11 ± 0.02b
lysine	0.66 ± 0.02b	0.96 ± 0.00c	0.56 ± 0.03ab	0.60 ± 0.02b	0.63 ± 0.01b	0.42 ± 0.01a
methionine	0.05 ± 0.01c	0.03 ± 0.01a	0.04 ± 0.01b	0.03 ± 0.01a	0.03 ± 0.01a	0.04 ± 0.01b
ornithine	0.67 ± 0.01a	0.97 ± 0.01c	0.79 ± 0.02b	0.83 ± 0.01b	1.13 ± 0.03d	1.12 ± 0.02d
phenylalanine	0.45 ± 0.01b	0.39 ± 0.01b	0.40 ± 0.02b	0.27 ± 0.02a	0.30 ± 0.01a	0.35 ± 0.03ab
proline	0.00 ± 0.00a	0.00 ± 0.00a	0.06 ± 0.01c	0.00 ± 0.00a	0.00 ± 0.00a	0.04 ± 0.01b
serine	0.65 ± 0.02d	0.48 ± 0.02c	0.33 ± 0.01b	0.19 ± 0.02a	0.20 ± 0.01a	0.24 ± 0.01a
tyrosine	0.22 ± 0.01a	0.20 ± 0.02a	0.20 ± 0.02a	0.35 ± 0.01ab	0.16 ± 0.02a	0.19 ± 0.01a
tryptophan	0.00 ± 0.00a	0.00 ± 0.00a	0.05 ± 0.01b	0.00 ± 0.00a	0.01 ± 0.00ab	0.01 ± 0.00ab
threonine	9.05 ± 0.03d	5.82 ± 0.02b	5.06 ± 0.02ab	4.52 ± 0.03a	4.36 ± 0.03a	5.05 ± 0.03ab
valine	0.87 ± 0.01d	0.68 ± 0.03c	0.53 ± 0.01b	0.40 ± 0.02a	0.35 ± 0.01a	0.42 ± 0.01a
taste characteristics[b]						
bitter	3.51 ± 0.01d	2.71 ± 0.04c	2.53 ± 0.02bc	1.71 ± 0.01a	1.91 ± 0.02ab	2.02 ± 0.01b
MSG-like	3.56 ± 0.02e	2.61 ± 0.04c	1.56 ± 0.00a	2.16 ± 0.03b	2.11 ± 0.01b	1.58 ± 0.02a
sweet	10.7 ± 0.06e	7.70 ± 0.03d	6.55 ± 0.01c	5.59 ± 0.04a	6.13 ± 0.01b	6.30 ± 0.02bc
tasteless	1.13 ± 0.03bc	1.42 ± 0.01c	1.00 ± 0.01b	1.14 ± 0.02bc	0.79 ± 0.01a	0.83 ± 0.04a
total	19.8 ± 0.12c	15.8 ± 0.03b	12.6 ± 0.04a	11.8 ± 0.03a	12.4 ± 0.03a	12.1 ± 0.05a
5′-nucleotides[c]						
5′-AMP	0.88 ± 0.09a	1.49 ± 0.10c	0.92 ± 0.07a	1.11 ± 0.07b	1.28 ± 0.09b	0.87 ± 0.07a
5′-CMP	1.48 ± 0.09a	2.49 ± 0.08d	1.54 ± 0.11a	1.82 ± 0.07b	1.96 ± 0.12b	1.44 ± 0.08a
5′-GMP	0.95 ± 0.09ab	1.41 ± 0.09c	0.92 ± 0.11a	1.03 ± 0.08b	1.14 ± 0.08bc	0.86 ± 0.12a
5′-UMP	0.92 ± 0.11bc	1.45 ± 0.09d	0.81 ± 0.10b	1.00 ± 0.07c	1.07 ± 0.12c	0.61 ± 0.06a
MSG-like 5′-nucleotides[d]	1.83 ± 0.10a	2.90 ± 0.09d	1.84 ± 0.10a	2.14 ± 0.08b	2.42 ± 0.11c	1.73 ± 0.08a
flavor 5′-nucleotides[e]	0.95 ± 0.09ab	1.41 ± 0.09c	0.92 ± 0.11a	1.03 ± 0.08b	1.14 ± 0.08bc	0.86 ± 0.12a

[a]Each value is expressed as mean ± standard deviation ($n = 3$). Means with different letters within a row are significantly different ($P < 0.05$). [b]MSG-like (monosodium glutamate-like): Asp + Glu; Sweet: Ala + Gly + Ser + Thr; Bitter: Arg + His + Ile + Leu + Met + Phe + Try + Val; Tasteless: Lys + Tyr + GABA. [c]5′-CMP: 5′-sytosine monophosphate; 5′-UMP: 5′-uridine monophosphate; 5;-GMP: 5′-guanosine monophosphate; 5′-AMP: 5′-adenosine monophosphate. [d]MSG-like 5′-nucleotides: 5′-AMP + 5′-GMP + 5′-IMP + 5′-XMP, while 5′-IMP and 5′-XMP was not detected in this study. [e]Flavor 5′-nucleotides defined by Chen (1986): 5′-GMP + 5′-IMP + 5′-XMP, while only 5′-GMP was detected in this study.

mature growth stages. The contents of total free amino acids were in the range of 22.0−27.7 mg/g in the pileus and 11.8−19.8 mg/g in the stipe, which peaked at stage 2 in the former and stage 1 in the latter during the primary developing stages, and both reached steady levels at mature stages. Komata grouped the free amino acids into several classes on the basis of their taste characteristics (Table 4).[24] Asp and Glu acids were MSG-like components, which gave the most mushroom taste (the umami taste or palatable taste).[25] The contents of MSG-like amino acids were in the range of 2.34−4.65 mg/g in the pileus and 1.56−3.56 mg/g in the stipe. The values of sweet amino acids in the pileus (11.0−14.1 mg/g) were higher than those in the stipe (5.59−10.7 mg/g). The MSG-like amino acids and sweet amino acids were considered as the main amino acids in *L. edodes* fruiting body. γ−Aminobutyric acid (GABA) is a biologically active compound, and the presence of GABA in *L. edodes* would be beneficial to humans in addition to their palatable taste and other therapeutic effects.[26,27]

Yang et al. reported that contents of MSG-like taste active amino acids could be divided into three ranges: low (<5 mg/g), middle (5−20 mg/g), and high ranges (>20 mg/g).[11] Our study found that the contents of MSG-like taste active amino acids in the growth of *L. edodes* (1.56−4.65 mg/g) were in the low range, but they were higher than some medicinal mushrooms (0.17−0.50 mg/g) reported by Mau et al.[28] and most commercial mushrooms reported by Yang et al.[11]

Yamaguchi et al. reported that 5′-nucleotides, detected in mushrooms, could contribute to MSG-like taste.[10] Our study identified four 5′-nucleotides (5′-CMP, 5′-AMP, 5′-GMP and 5′-UMP) in the pileus and stipe of *L. edodes* fruiting body (Table 4 and Table 5). As for the MSG-like taste active 5′-nucleotides, their contents were 2.45−5.28 mg/g in the pileus and 1.73−2.90 mg/g in the stipe, and they accounted for nearly

DOI: 10.1021/jf505410a
J. Agric. Food Chem. 2015, 63, 795−801

50% of total 5′-nucleotides contents at each growth stage of pileus and stipe. The contents of 5′-AMP (0.87−2.47 mg/g) and 5′-GMP (0.86−2.81 mg/g) were similar during the whole stages in the pileus and stipe, and their contents were mostly higher in the pileus than those of stipe.

5′-GMP gave the meaty favor, and is also a flavor enhancer, which could induce much umami taste production, and these umami tastes were stronger than MSG.[7] The contents of flavor 5′-nucleotides were 1.34−2.81 mg/g in the pileus and 0.86−1.41 mg/g in the stipe during the growth of *L. edodes* fruiting body in this research (Table 4 and Table 5). It demonstrated a peak at stage 1 in the pileus and stage 2 in the stipe during the primary developing stages, with slightly increasing profiles in the pileus and stable levels in the stipe, respectively, at mature growth stages. Yang[11] reported that contents of flavor 5′-nucleotides could be divided into three ranges: low (<1 mg/g), middle (1−5 mg/g), and high (>5 mg/g), and found the contents of flavor 5′-nucleotides in *L. edodes* (271) and *L. edodes* (Tainung 1) were, respectively, in high range and middle range, whereas the contents of flavor 5′-nucleotides in the pileus of *L. edodes* during whole growth stages in this research were all in the middle range.

Evaluation of *Lentinula edodes* at Different Stages and Parts Using Equivalent Umami Concentration (EUC). Yamaguchi et al. reported that the combination of umami amino acids and umami 5′-nucleotides would synergistically increase the umami taste of mushrooms. Using the equation derived from sensory evaluation,[18] the EUC value of stage 1 in the pileus was the highest among all the *L. edodes* growth stages (Figure 2). However, *L. edodes* fruit bodies were

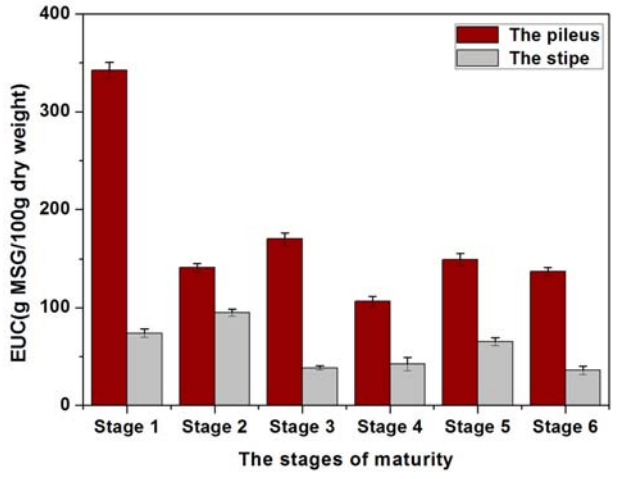

Figure 2. Changes in the equivalent uamami concentration (EUC) of *L. edodes* at different stages of maturity in the pileus and stipe. Each value was expressed as mean ± standard deviation (n = 3).

usually picked at stage 5, which exhibited higher EUC values at mature stage. At stage 6, when *L. edodes* fruit bodies pileus are exposed completely, the fruit bodies became overmatured, and their EUC values decreased. These results were different from those reported by Tsai et al.[29]

Mau reported that the EUC values of flavor components in mushroom were usually classified into four levels: first level of >1000 g MSG/100 g dry weight, second level of 100−1000 g MSG/100 g dry weight, third level of 10−100 g MSG/100 g dry weight, and fourth level of <10 g MSG/100 g dry weight.[30] EUC values of several cultivated mushrooms were at third level (11.19−88.37 g MSG/100g dry weight),[19] and those of several medicinal mushrooms were at the fourth level (0.66−7.92 g MSG/100g dry weight).[30] In this study, EUC values of the pileus (106.8−342.7 g MSG/100 g dry weight) were at the second level, and those of the stipe (35.93−95.11 g MSG/100g dry weight) were at the third level. The EUC values of the pileus were mostly higher than those of *L. edodes* (271), and significantly higher than those of *L. edodes* (Tainung 1).[11] Furthermore, tasty components in the stipe of *L. edodes* were rich and EUC values were higher than other several cultivated mushrooms[15] and medical mushrooms,[30] which might be useful for further processing and byproduct development of *L. edodes*.

AUTHOR INFORMATION

Corresponding Author

*E-mail: yangyan@saas.sh.cn. Phone/Fax: +86 21 62209765.

Author Contributions

⊥W.C. and W.L. contributed equally to this work.

Funding

This work was supported financially by Shanghai Municipal Agricultural Commission of China (No. Hu 2013610) and Shanghai Academy of Agricultural Sciences Fund for Distinguished Young Scientists (2013(28)).

Notes

The authors declare no competing financial interest.

REFERENCES

(1) Huang, N. L.; Lin, Z. B.; Chen, G. L. *Medicinal and Edible Fungi*; Shanghai Science and Technology References Press: China, 2010; pp 1244−1247.

(2) Jin, M.; Jeon, H.; Jung, H. J.; Kim, B.; Shin, S. S.; Choi, J. J.; Lee, J. K.; Kang, C. Y.; Kim, S. Enhancement of repopulation and hematopoiesis of bone marrow cells in irradiated mice by oral administration of PG101, a water-soluble extract from Lentinus lepideus. *Exp. Biol. Med.* **2003**, *228* (6), 759−766.

(3) Kupfahl, C.; Geginat, G.; Hof, H. Lentinan has a stimulatory effect on innate and adaptive immunity against murine Listeria monocytogenes infection. *Int. Immunopharmacol.* **2006**, *6* (4), 686−696.

(4) Caglarirmak, N. The nutrients of exotic mushrooms (*Lentinula edodes* and *Pleurotus* species) and an estimated approach to the volatile compounds. *Food Chem.* **2007**, *105* (3), 1188−1194.

(5) Hamuro, J. Anticancer immunotherapy with perorally effective lentinan. *Gan to Kagaku Ryoho* **2005**, *32* (8), 1209−1215.

(6) Shi, X.; Ding, Q.; Yang, Q. Lentinan combined with chemotherapy in the treatment of advanced non-small cell lung cancer. *Bull. Chinese Cancer* **2007**, *11*, 946−948.

(7) Litchfield, J. H. Morel mushroom mycelium as a food flavoring material. *Biotechnol. Bioeng.* **1967**, *9*, 289−304.

(8) Chen, F. X.; Liu, X. H.; Chen, L. S. Advances in research on organic acid metabolism in fruits. *J. Fruit Sci.* **2005**, *22* (5), 526−531.

(9) Yamaguchi, S. Fundamental properties of umami taste. *J. Agric. Chem. Soc. of Japan* **1991**, *65* (5), 903−906.

(10) Yamaguchi, S.; Yoshikawa, T.; Ikeda, S.; Ninomiya, T. Measurement of the relative taste intensity of some a amino acid and 50-nucleotides. *J. Food Sci.* **1971**, *36*, 846−849.

(11) Yang, J.-H.; Lin, H.-C.; Mau, J.-L. Non-volatile taste components of several commercial mushrooms. *Food Chem.* **2001**, *72*, 465−471.

(12) Kim, M.-Y.; Chung, L.-M.; Lee, S.-J.; Ahn, J.-K.; Kim, E.-H.; Kim, M.-J.; Kim, S.-L.; Moon, H.-I.; Ro, H.-M.; Kang, E.-Y.; Seo, S.-H.; Song, H.-K. Comparison of free amino acid, carbohydrates concentrations in Korean edible and medicinal mushrooms. *Food Chem.* **2009**, *113* (2), 386−393.

(13) Dermiki, M.; Phanphensophon, N.; Mottram, D. S.; Methven, L. Contributions of non-volatile and volatile compounds to the umami

DOI: 10.1021/jf505410a
J. Agric. Food Chem. 2015, 63, 795−801

taste and overall flavour of shiitake mushroom extracts and their application as flavour enhancers in cooked minced meat. *Food Chem.* **2013**, *141* (1), 77−83.
(14) Ajlouni, S. O.; Beelman, R. B.; Thompson, D. B.; Mau, J. L. Changes in soluble sugars in various tissues of cultivated mushrooms, *Agaricus bisporus*, during postharvest storage. In *Food Flavors*. Charalambous, G., Ed.; Elsevier Science Publisher.: Amsterdam, The Netherlands, 1995; pp 1865−1880.
(15) Li, W.; Gu, Z.; Yang, Y.; Zhou, S.; Liu, Y. F.; Zhang, J. S. Non-volatile taste components of several cultivated mushrooms. *Food Chem.* **2014**, *143*, 427−431.
(16) Li, X. B.; Feng, T.; Zhou, S.; Liu, Y.-F.; Li, W.; Ye, R.; Yang, Y. Effects of drying methods on the tasty compounds of *Pleurotus eryngii*. *Food Chem.* **2015**, *166*, 358−364.
(17) Taylor, M. W.; Hershey, R. A.; Levine, R. A.; Coy, K.; Olivelle, S. Improved method of resolving nucleotides by reverse-phase high performance liquid chromatography. *J. Chromatogr.* **1981**, *219*, 133−139.
(18) Yamaguchi, S.; Yoshikawa, T.; Ikeda, S.; Ninomiya, T. Measurement of the relative taste intensity of some a amino acid and 50-nucleotides. *J. Food Sci.* **1971**, *36*, 846−849.
(19) Mau, J. L.; Chyau, C. C.; Li, J. Y.; Tseng, Y. H. Flavor compounds in straw mushrooms *Volvariella volvacea* harvested at different stages of maturity. *J. Agric. Food Chem.* **1997**, *45*, 4726−4729.
(20) Hiroshi, Y.; et al. The content of free sugars, free polyols and organic acids in shiitake. *J. Jpn. Soc. Food Sci. Technol.* **1979**, *28* (8), 356−359.
(21) Motono, M. *Chemistry of foods and beverages: recent developments*; Academic press: New York, 1982; pp 181−183.
(22) Jiming, Li; Hui, D.; Rong-hua, Z.; Yan, X.; Dong, W. Study on Main Components of Apple Wine. *Food Sci.* **2007**, *28* (12), 362−365.
(23) Da-yun, Z.; Xiao-lin, D. Detection and analysis of amino acids and organic acids in pickled Brassica juncea, Coss. *Chinese Condiment* **2000**, *12*, 13−16.
(24) Komata, Y. The taste and constituents of foods. *J. Jpn. Soc. Food Sci. Technol.* **1969**, *3*, 26.
(25) Yamaguchi, S.. The umami taste. In *Food taste chemistry*. Boudreau, J. C., Ed.; ACS symposium series; American Chemical Society: Washington, DC, 1979; Vol. *115*, pp 33−51.
(26) Kohama, Y.; Matsumoto, S.; Mimura, T.; Tanabe, N.; Inada, a.; Nakanishi, T. Isolation and identification of hypotenxive principles in red-mold rice. *Chem. Pharm. Bull.* **1987**, *35*, 2484−2489.
(27) Tsai, S.-Y.; Huang, S.-J.; Lo, S.-H.; Wu, T.-P.; Lian, P.-Y.; Mau, J.-L. Flavour components and antioxidant properties of several cultivated mushrooms. *Food Chem.* **2009**, *113*, 578−584.
(28) Mau, J.-L.; Lin, H.-C.; Chen, C.-C. Non-volatile components of several medicinal mushrooms. *Food Res. Int.* **2001**, *34* (6), 521−526.
(29) Tsai, S.-Y.; Wu, T.-P.; Huang, S.-J.; Mau, J.-L. Nonvolatile taste components of *Agaricus bisporus* harvested at different stages of maturity. *Food Chem.* **2007**, *103*, 1457−1464.
(30) Mau, J. The umami taste of edible and medicinal mushrooms. *Int. J. Med. Mushrooms* **2005**, *7* (1/2), 119.

DOI: 10.1021/jf505410a
J. Agric. Food Chem. 2015, 63, 795−801

JOURNAL OF AGRICULTURAL AND FOOD CHEMISTRY

Article

pubs.acs.org/JAFC

Applying Population Genetics for Authentication of Marine Fish: The Case of Saithe (*Pollachius virens*)

Konstanze Behrmann,[†,‡] Hartmut Rehbein,[‡] Annika von Appen,[§] and Markus Fischer*[,†]

[†]Hamburg School of Food Science, University of Hamburg, Grindelallee 117, 20146 Hamburg, Germany

[‡]Federal Research Institute for Nutrition and Food, Department of Safety and Quality of Milk and Fish products, Max-Rubner-Institut, Palmaille 9, 22767 Hamburg, Germany

[§]Life Science, Hamburg University of Applied Sciences, Ulmenliet 20, 21033 Hamburg, Germany

ABSTRACT: The number of fishery products with a quite detailed description of the origin is increasing. This trend is driven by the interest of consumers and the fight against illegal unregulated and unreported fisheries. Unfortunately, there is a lack of methods to prove this information experimentally besides the document-based traceability assessments. For marine fish population genetics is a promising strategy, but research is concentrated only on a few species. Saithe is a commercially important fish species, despite the fact that genetic knowledge is scarce regarding the specification of populations. For a comparative study cost- and time-effective strategies were tested: We found RAPD-PCR to be a useful method for low-budget research or prestudies. Adoption of microsatellites from closely related species turned out to be possible with limited success quota. Our results suggest a clustered structure of populations within the Northeast Atlantic, probably overlapping in the northern North Sea.

KEYWORDS: *RAPD, microsatellites, saithe, populations*

INTRODUCTION

On the fish and seafood market an increasing number of products are labeled regarding to the origin in much detail. Market analyses throughout the EU showed that consumers are highly interested in the origin of their seafood.[1] Labeling ranges from local-marketing strategies ("Fish from our own coast") or ways of direct marketing from fisheries[2] to the labeling of origin because of environmental concerns of consumers. From December 2014 EU regulation No. 1379/2013 will apply for all fishery products.[3] Article 38 of this regulation prescribes obligatory information about the subcatch area or subdivision for all unprocessed and smoked fishery products being sold to the consumer. Notably, this rule is valid only when the fish originates from the oceans surrounding the EU: Northeast Atlantic (FAO 27) or Mediterranean and Black Sea (FAO 37).

If scientific data should be used to uncover fraud regarding the origin and fight against illegal, unreported, and unregulated (IUU) fishing activities, it is inevitable to connect the area of origin to specific data, which are also available in a fillet.[4]

The actual tracing system for fishery products is very detailed and employs high bureaucratic effort.[3,5] It sets high standards for fresh and frozen unprocessed fishery products. Processed products are covered by the general traceability requirement of food law.[6] During processing the composition may change, due to heading, gutting, adding of ingredients, or water loss by salting or smoking. This makes tracing along the food chain very complex in real life, especially because production chains are often split into single operations taking place in several different countries or even continents.

Most of the fishery products are placed on the market as a fillet or as part of a processed food. DNA is still available in highly processed products even when damaged due to low pH values or enzymatic ripening processes, but population genetic-based methods are still on the level of scientific investigation and not suitable for routine analysis. Mass spectrometry-based strategies have been shown to work well for coastal organisms[7] but are not suitable for pelagic fish because these methods are based on the climate and composition of plankton in the area of production which is much more leveled in the open water.

While identification of species is already common practice in food control laboratories,[8,9] validation of the authentication of origin is possible only in a few cases, like, for example, herring, Atlantic cod, and Pacific salmon species.[10]

Currently, data derived from population genetic investigations of marine fishes had mostly been used to answer biological questions or optimize management areas.[11,12] Furthermore, to date population genetic research of North Atlantic fish species used for human consumption has been performed only for a limited number of species. Reiss et al.[12] and Olsson (p 121f)[13] provided an overview on the number and quality of genetic population studies of managed species in the Northeast Atlantic. It can be seen that herring (*Clupea harengus*), cod (*Gadus morhua*), and salmon (*Salmo salar*) have been studied in detail. On the other hand, there is almost no population genetic knowledge of commercially important species like sprat (*Sprattus sprattus*), Norway pout (*Trisopterus esmarkii*), and saithe (*Pollachius virens*), all of these species providing a TAC quota (total annual catch) of more than 100 kt each.[14]

Before population genetics can be applied for authentication purposes, the population genetic structure of the respective

Received: August 31, 2014
Revised: January 2, 2015
Accepted: January 3, 2015
Published: January 3, 2015

ACS Publications © 2015 American Chemical Society

DOI: 10.1021/jf506201m
J. Agric. Food Chem. 2015, 63, 802−809

species and migratory processes have to be understood. Furthermore, a lot of data and samples have to be collected, but the question is how to design a study for a species where genetic knowledge is very low. For the development of specific markers and their validation a large number of sequences and samples are required. Each project has to be planed as detailed as possible, which appears to be difficult if there is no knowledge available regarding the number of populations present. We have chosen RAPD-PCR as examples for easy-access methods. An attempt to employ Exon primed Intron crossing PCR had to be abandoned because the number of variable markers was too small.[15] Our other approach was the adoption of microsatellite primers from closely related species, in our case from the family of *Gadidae*.

Biology of Saithe. The literature about saithe populations is dominated by data from tagging studies. The deficiency is that tagging can only be carried out on juvenile fish, not on larvae. This does not take into account the larval drift by the subtropical gyre, and most of the large-scale tagging studies were carried out before the 1990s.[16,17]

There are historical reports about unusual larval drifts of saithe into the Spitzbergen fjords (1967), the southern North Sea (1967), or the Limfjord (1932/33).[18] Furthermore, there are indications that migration routes of saithe are being affected in recent years by salmon farming.[17]

It is known that juvenile saithe remain in the area they have been drifted to for some years. For fisheries the year classes 4 and 5 are most important, because they migrate out of the fjords and live in the open water forming schools. The assumption that saithe return to their spawning grounds has never been convincingly proved, but there are indications that larger fully mature saithe (older than 6 years or larger than 60 cm) enter the spawning areas at spawning times.[19,20] Larger saithe, which are more than 60 cm long, seem to wander through the whole Northeast Atlantic.[16]

Actually the ICES expect four independent stocks of saithe within the Northeast Atlantic (FAO 27): (i) Northeast Arctic (Norwegian) saithe, (ii) saithe from North Sea/Western Scotland, (iii) Icelandic saithe, and (iv) Faroese saithe.[14]

To date, papers dealing with population genetics of saithe are rare.[12,22] After early publications of Child[21] and Denovan and Wright,[22] saithe was no longer the focus of population genetic researchers. In recent years, Eiriksson and Arnason sequenced fragments of the mitochondrial cytochrome oxidase 1 (MT-CO1) gene of 1160 individuals from Canada, Norway, Iceland, and Faroer.[23] This fragment of mitochondrial DNA did not show a significant differentiation between sampling areas but found connections between sex and migratory behavior. In another project 270 fish were genotyped from Canada, Norway, Faroer, and Barents Sea using a set of 115 SNPs, but detailed data have not been published, yet.[24]

Population Genetic. Population genetic tools can be divided into two main groups: easy-access methods and species-specific methods.

Easy-access methods are transferable between species, require relatively low cost and development times, and are useful tools in small-scale research and prestudies. Examples are fingerprinting methods, like RAPD (random amplified polymorphic DNA) and AFLP (amplified fragment-length polymorphism). Also easy access are methods using defined loci being still interspecific like EPIC-PCR (exon primed intron crossing) and assays based on mitochondrial DNA.

Species-specific methods like MSats (Microsatellites) and SNPs (single-nucleotide polymorphism) are generally suitable for automation, making them candidate systems for routine analysis, but their development is time consuming and normally requires more or less high-throughput sequencing.[4,25]

Random Amplified Polymorphic DNA (RAPD)-PCR. The idea of RAPD-PCR is that only one single short primer (10−15 bp long) is used for PCR. Because these primers are that short, they statistically will find some sites to anneal on opposite strands of a given template DNA.[26] The resulting band pattern (fingerprint) is individual and will therefore contain DNA bands which are characteristic for individuals.

RAPD-PCR is a DNA fingerprinting technique that has often been used in species identification and population genetic research for species, whose genome has not been sequenced very extensive as being the case for most of the fish used for human consumption. RAPD-PCR was widely applied in the past for population genetics.[27,28] On the other hand, it was not used very often in recent years due to development of next-generation sequencing (NGS) technologies and more sophisticated methods with higher resolution and reproducibility.

The problem is that very short primers require a relatively low annealing temperature (often 36 °C is used) giving rise to unspecific bands which are not reproducible.[29] Despite these drawbacks RAPD-PCR became a popular tool in population genetics because of its simplicity, low cost, and low requirements regarding laboratory equipment.

Microsatellite (MSat)-PCR. Microsatellites do frequently occur in the noncoding region of the genome. They consist of repeats of 2−5 base pairs. Copy mistakes are likely to occur in these regions, adding or removing one repeat motive. This leads to length polymorphisms providing a lot of markers because after many generations each population develops its characteristic profile of MSat frequencies. If enough data (from many individuals and more than 5 loci) are available it is possible to make meta-analysis giving information about timelines when populations did depart. Furthermore, the method can be automated easily, if fully developed.

This makes microsatellites one of the working horses, being widely used in population genetics.[11,12] Their potential for use even in processed fishery products is high, because the respective amplicons are quite short (100−300 bp). The major drawback is that markers have to be developed for every species anew, requiring a lot of time and resources.[30]

O'Reilly showed that many primers he developed for Alaska Pollack (*Theragra chalcogramma*) could be used for other gadoid species, too.[31] Charrier found 7 MSat primers for whiting (*Merlangius merlangus*) by testing 37 primers developed for other fish of the same family (*Gadidae*).[32]

The current study is aimed to give insights into the toolbox of population genetics. We developed a modus operandi how to design a pilot study providing a first glimpse of the population structure enabling the scientist to plan a detailed study on the species of interest. As a model we used saithe.

MATERIALS AND METHODS

Samples. The origin of samples is shown in Figure 1. Most samples were taken by the German research vessel Walther Herwig III. The commercial sample "CS" was bought from German North Sea Saithe trawl fisheries, catch position defined by tracking code (vessel Susanne, NC 120). Fish were kept under melting ice until filleted. A piece of the fillet was frozen and used for later DNA extraction. Samples "IS" were taken by Icelandic scientists (vessel Ottó N. Porláksson, ID 1578) and

DOI: 10.1021/jf506201m
J. Agric. Food Chem. 2015, 63, 802−809

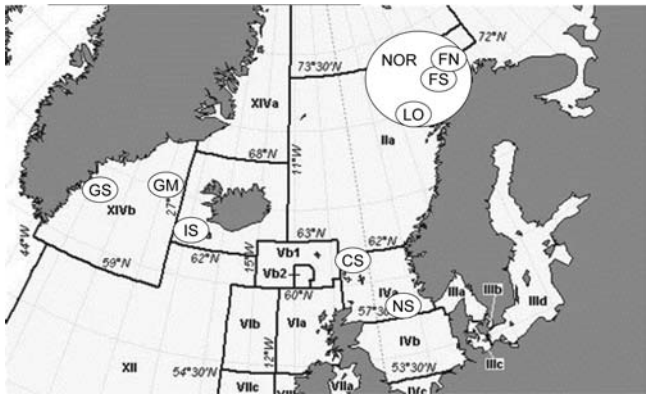

Figure 1. Sampling areas of *P. virens*. Year of sampling 2009 (NS), 2010 (GM, GS), 2011 (IS), and 2012 (NOR, CS).

reached our lab preserved in ethanol. A geographic overview is given in Figure 1. More details are given in Table 3.

The three Norwegian samples (LO, FS, FN) only consisted of 10 individuals, each of which is a very small number for population genetic analyses. Because they came from a similar sampling area and had been collected within 2 days they were combined to one "Norway" sample (NOR, 30 individuals).

DNA Extraction and General PCR Conditions. DNA was extracted using the CTAB (cetyltrimethylammonium bromide) DNA extraction protocol.[33] The DNA concentration was adjusted to 10 ng/μL after fluorimetric quantification using Hoechst 33258.[34]

HOT FIREPol DNA Polymerase kits from Solis Biodyne (Cat. Nos. 01-02 and 02-31, Tartu, Estonia) and HotStarTaq Master Mix from QIAGEN (Cat. No. 203443, Hilden, Germany) were used for PCR. The reaction mixtures both contained Tris-HCl, $(NH_4)_2SO_4$ and detergents, 2.5 mM $MgCl_2$, 0.1 μM of primers (each), 200 μM dNTP mix, and 2 ng DNA/μL PCR assay; assay volume was 12 or 16 μL (depending on cycler requirements).

In RAPD-PCR, 0.16 μM primer (just one per reaction) was used. Reproducibility of DNA patterns was tested by repeating the PCR assays for three times with a set of 15 samples.

Gel Electrophoresis. Electrophoresis was carried out under different conditions: agarose gels and large homemade polyacrylamide gels.

Agarose gel electrophoresis was done using gels containing 2% (w/v) agarose; PCR products were visualized by staining with ethidium bromide (0.1 μg/mL final concentration).

Native PAGE for Msat Analysis. Large polyacrylamide gels (16 × 18 cm) were prepared according to Wang et al.[35] Total acrylamide concentration and duration of an electrophoretic run varied depending on allele sizes from 2.5 h, 8% to 4 h, 6.6%.

Gels were stained with silver and afterward scanned using a desktop scanner.[36] The sizes of the alleles were calculated semiautomatically by the software package QUANTITY ONE (version 4.6.8, BioRad laboratories, Inc.).

RAPD-PCR Analysis. The Random Primer Kit A (Art. No. HP22.1; Roth, Karlsruhe, Germany) was chosen for RAPD-PCR. The kit contains 20 different primers having a length of 10 nucleotides. All of the 20 primers of the Roth Random Primer Kit A were used for screening.

The PCR conditions were optimized according to Welsh and McClelland for better reproducibility:[37] preheating 95 °C/15 min, then 10 cycles of 95 °C/20 s, annealing temperature 1 (AT1)/40 s, 72 °C/90 s, followed by 30 cycles of 95 °C/20 s, AT2/40 s, 72 °C/90 s, and a final heating at 72 °C for 10 min; then the temperature was held at 10 °C. AT1 was 2−4 °C lower than AT2 (compare Table 1).

Reproducibility was checked by repeated analyses of a set of 14 samples for three times.

MSat-Analysis. All microsatellite markers, chosen from the literature, contained repeats of 4 base pairs. Furthermore, they were described to work with more than one gadoid species or successfully used in a study on Pollock (*Pollachius pollachius*).[38] Accordingly, 10 primers were selected originally described for *Gadus morhua* and 8 primers developed for *Theragra chalcogramma*.[31,39−41] The scientific name of Alaska Pollock recently changed from *Theragra chalcogramma* to *Gadus chalcogrammus* by taxonomical considerations.[42] Furthermore, two *Merlangius merlangus* primers were tested as well as single primers for *Macruronus magellanicus* and *Micromesistius poutassou*.[32,43,44]

PCR conditions were standardized using the following protocol: Initial denaturation (15 min 95 °C), followed by 35 cycles (20 s 95 °C, 40 s AT, 90 s 70 °C), and a final annealing (10 min 72 °C). Annealing temperature was taken from literature and varied within the test for every primer set.

Amplification was possible with 10 primer pairs (Tch18-F/R,[31] Tch20-F/R,[31] Gmo1-F/R,[39] Gmo24-F/R,[40] Gmo37-F/R,[48] Gmo46-F/R,[40] Gmo132-F/R,[39] Pop14c-F/R,[32] Pop18a-F/R,[32] Tch12-F/R[31]). Only Gmo24-F/R (AT = 52 °C), Gmo46-F/R (AT = 55 °C), and Pop18a-F/R (AT = 56 °C) showed variability typical for microsatellites.

These three primers were used for further analyses using large polyacrylamide gels as described above.

Data Processing: Statistical Analyses. For binary markers (RAPD, RFLP, SNP) the presence or absence of the chosen bands was determined by visual inspection and brought into a matrix. Thus, a binary pattern was evaluated for every individual. This matrix was used for analysis using GenAlEx.[45,46]

Expected and observed heterozygosity (H_e) was calculated per sample, per loci, and for all loci and all samples.

The population genetic structure between the samples was analyzed using two independent methods. Nei's genetic distance and F, R, and Φ statistics were computed using GenAlEx. The larger the value of Nei's D is, the larger is the difference between two samples. The resulting values are not to be seen on an absolute scale but should rather be compared within one study. Genetic differentiation analysis

Table 1. *P. virens*, Primers from the Roth RAPD Kit A, Annealing Temperature (AT) for Touch-up PCR, Allele Size and Name, Heterozygosity (He), Molecular Variance among Samples[a]

primer	sequence 5′ → 3′	AT1 (°C)	AT2 (°C)	allele size (bp)	name of locus	He	Φ_{PT}
A 5	AGG GGT CTT G	36	40	800	A5A	0.479	0.030
A 7	GAA ACG GGT G	36	40	390	A7B	0.187	0.083**
				410	A7C	0.459	−0.029
				980	A7D	0.134	0.105**
A 8	GTG ACG TAG G	40	42	380	A8E	0.330	0.252**
				1400	A8F	0.253	0.556**
A 9	GGG TAA CGC C	38	42	680	A9G	0.325	0.147**
A 14	TCT GTG CTG G	40	42	450	A14H	0.333	0.006
				1200	A14J	0.141	0.137**

[a]F_{st}, probability for Φ statistics by locus based on standard permutation is shown by asterisks. **$p < 0.01$; *$p < 0.05$.

DOI: 10.1021/jf506201m
J. Agric. Food Chem. 2015, 63, 802−809

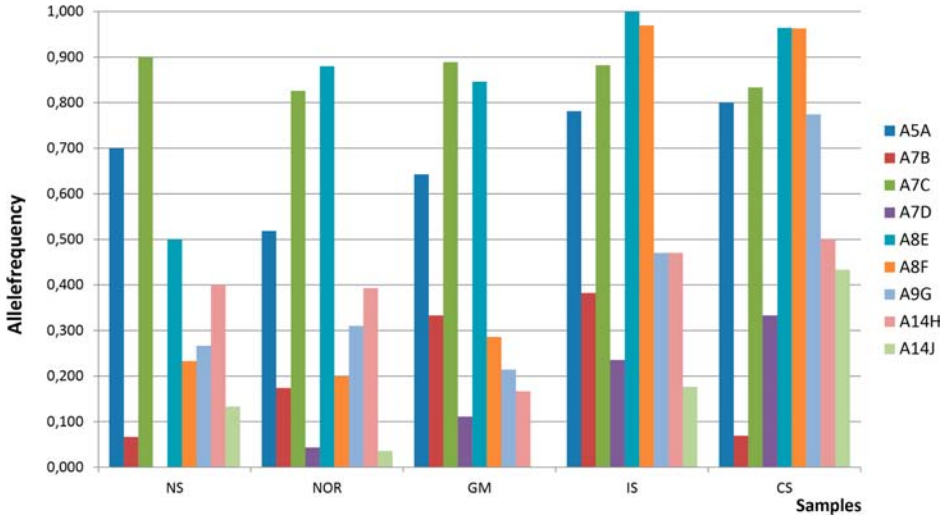

Figure 2. Differences in allele frequency among samples from different origin using RAPD-PCR. Detailed description of markers is shown in Table 1.

using Nei's D is based on similarities but does not differentiate between similarity by chance and statistically significant similarities. Values range from zero to infinity.

AMOVA is a distance-based analysis that allows the hierarchical partitioning of genetic variation among populations.[47]

Calculation of Φ_{PT} is similar to F statistics but a special adoption for binary and diploid data, while R statistics take into account the stepwise mutation model, which can be assumed for microsatellites.[45,46] Populations were tested for significant differentiation based on 999 permutations. Similar to Nei's D statistics a high similarity between samples leads to small values, while the p value gives the probability that two samples do not differ. Accordingly, $p < 0.05$ indicates significant differentiation and $p < 0.01$ can be interpreted as highly significant.

The matrices of Nei's D were used for construction of an UPGMA (unweighted pair-group method with arithmetic mean) dendrogram using the online tool of Edwards.[48]

RESULTS

RAPDs. Five primers were elected, providing nine variable alleles that matched our requirement regarding reproducibility (Table 1). The sample from location GS did not amplify with all primers and was withdrawn from analysis. The loci-specific data are shown in Table 1, pointing out that six out of nine alleles showed significant variation among samples, marked by an asterisk in column Φ_{PT}.

The differences in allele frequency among samples is outlined in Figure 2. The illustration was chosen to point out the fingerprinting character of this approach. A similar pattern also led to similarity detected by Nei's D (see Figure 4A) and Φ_{PT} statistics (see Table 4). The molecular variance among samples was 16% (Φ_{PT} = 0.159, p = 0.001).

MSats. Analyses of MSats were performed using large self-made polyacrylamide gels being suitable for MSat analyses.[35] Exemplary, a gel can be seen in Figure 3. A 25 bp ladder was used as a ruler for the sizing of the alleles. According to our experience a resolution of less than ±1% is not achievable using large self-cast gels. Therefore, it was necessary to choose 4 bp repeats in the project. The general problem was that locus Gmo24 provided alleles from 300 bp to 400 bp, so an error of 1% is the same size as one repeat. Furthermore, the long run times of 4 h, necessary to separate these larger alleles sufficiently, led to increased influence of laminary effects on the gel.

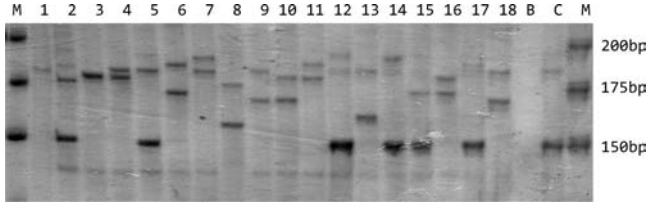

Figure 3. *P. virens* from the North Sea. Primer: Pop18a on a large self-cast polyacrylamide gel. M: DNA ladder 25bp, 1−18. Samples: B blind and C control sample.

The statistical data from the MSat analyses are shown in Table 2. Microsatellite analyses provide much higher statistical power than binary dominant markers.[27] Data analyses can treat every allele independently (F statistics) or take into account the stepwise mutation model (R statistics).[46]

The F_{st} values indicate very low but highly significant molecular variation among samples (2% among samples, 10% among individuals, and 88% within population), while the R_{st} values show higher differentiation (24% among samples, 7% among individuals, and 69% within samples). However, this differentiation is mostly caused by the primer Gmo24-F/R. Taking into account that the sizing at this locus provided the lowest reliability and R_{st} statistics are even more vulnerable to sizing errors than others, we concentrate on the F statistics for further interpretation.

Comparison of Population Genetic Data. Statistical data of all samples are shown in Table 3.

We are aware of the logical gap for applying the H_e value to dominant markers like RAPDs and RFLP patterns,[28] because differentiation between homozygotes and heterozygotes is not possible. Homozygous organisms carrying two identical copies of the same (dominant) allele provide the same pattern as if only one haplotype contains the dominant allele. Despite the fact that we show this value for comparison of our results with other publications, but we do not make any conclusions from this value.

The genetic distance was analyzed using Nei's D statistics. The results were transferred into an UPGMA dendrogram for visualization purposes and can be seen in Figure 4.

DOI: 10.1021/jf506201m
J. Agric. Food Chem. 2015, 63, 802−809

Table 2. *P. virens*, Microsatellite Primers Adopted from Charrier[47] and Westgaard,[49] Allele Sizes, Observed and Expected Heterozygosity (Ho, He), Comparison of F and R Statstics Showing Molecular Variance within (F_{is}, R_{is}) and among Samples (F_{st}, R_{st}), Probability for F and R Statistics by Locus Based on Standard Permutation Shown by Asterisks[a]

primer	allele size (bp)	number of allele	H_o	H_e	F_{st}	F_{it}	R_{st}	R_{it}
Gmo46-F/R	132−188	12	0.827	0.814	0.008*	0.024	0.014	0.177*
Gmo24-F/R	308−400	24	0.704	0.866	0.020**	0.185**	0.339**	0.303**
Pop18a F/R	148−204	15	0.771	0.853	0.016**	0.130**	0.060**	0.260**
all MSats			0.768	0.844	0.014**	0.115**	0.203**	0.273**

[a]**$p < 0.01$; *$p < 0.05$.

Table 3. *P. virens* from Northeast Atlantic, Data and Characteristics Per Sample[a]

						RAPD	MSat	
origin of samples	code	ICES area	no. of indiv.	mean length/cm	year of samp-ling	H_e	H_o	H_e
North Sea	NS	IV a	30	44	2009	0.314	0.757	0.852
Greenland Middle	GM	XIV	14	73	2010	0.270	0.701	0.802
Greenland South	GS	XIV	15	96	2010		0.711	0.819
Norway	NOR	II a	30	49	2012	0.269	0.722	0.869
Iceland	IS	Va	32−35	58	2011	0.306	0.765	0.859
commercial sample	CS	IV a	31	51	2012	0.361	0.956	0.865
all samples H_e						0.304	0.769	0.844
molecular variance between samples						Φ_{PT} 15%	F_{st} 2%	

[a]Sample sizes, mean length, and year of sampling. Comparison of H_e values from RAPD and MSat study.

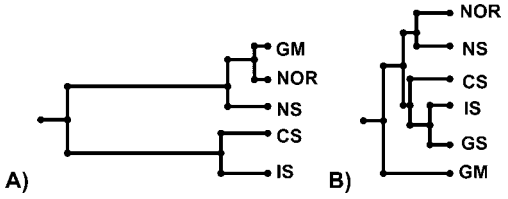

Figure 4. *P. virens* from Northeast Atlantic. UPGMA dendrogram showing relationships among samples based on values of Nei's genetic distances (Nei's D) from (A) RAPD-PCR using 9 loci and (B) Microsatellites using 3 loci.

Results of AMOVA-based analyses of RAPD (pairwise Φ statistics) and MSat (pairwise Fst statistics) are shown in Table 4.

DISCUSSION

Data Assessment from a Population Genetic View. Because of the small number of samples the final number of populations stays unclear, but we observed two main clusters that were detected independently by RAPD and by MSat analyses: (i) One continental cluster containing samples NS and NOR and (ii) a second cluster containing samples IS and CS. However, Φ_{PT} and F_{st} statistics also detected significant differentiation within these clusters.

Despite samples NS and CS being both caught in waters belonging to the northern North Sea area (ICES Region IVa), both statistics indicate a definite differentiation between these samples. This is an indication that in the northern part of the North Sea probably more than one population is present.

The small numbers of individuals in the samples from Greenland does not allow an interpretation of this data.

Tagging studies revealed a close relationship between Norwegian and North Sea Saithe on one hand and between Faroese and Icelandic Saithe on the other.[16,17]

Eiriksson and Arnasson found only limited transatlantic genetic structure by sequencing a 460 bp fragment of the mitochondrial cytochrome *c* oxidase subunit I (MT-CO1) gene of 1162 individuals.[23] No differentiation between Canadian, Icelandic, Faroese, and Norwegian samples was found (F_{CT} = −0.0037, p = 0.93). A small but significant differentiation was found if female and male individuals were separated. Ogden described mitochondrial markers to be suitable for differentiation of species with a very limited gene flow for many generations, and the MT-CO1 gene especially is used as a barcoding gene due to its very low intraspecific variation.[11] Neutral nuclear loci like microsatellites provide higher potential of detecting regional genetic differentiation, which could explain the differences between these results.

Table 4. *P. virens*: Population Structure of North East Atlantic, Differentiation between Samples[a]

	NS	GM	NOR	IS	CS	GS
NS		0.023**	0.007	0.016**	0.022**	0.024**
GM	0.040		0.027**	0.033**	0.031**	0.040**
NOR	0.038*	0.000		0.004	0.027**	0.019*
IS	0.247**	0.164**	0.204**		0.013*	0.000
CS	0.292**	0.278**	0.276**	0.062**		0.018*

[a]Pairwise F_{st} values of MSat analyses using 3 loci above diagonal. Pairwise Φ_{PT} values of RAPD analyses using 9 loci below diagonal. Significance is shown by asterisks. **$p < 0.01$; *$p < 0.05$.

DOI: 10.1021/jf506201m
J. Agric. Food Chem. 2015, 63, 802−809

A recent change in the migratory behavior of saithe as a consequence of large-scale salmon farming is indicated by a comparison of migratory behavior before 1990, when salmon farming started its exponential growth, and recent studies. There are indications that outward migration of young saithe from the Norwegian fjords is delayed or that the fish do not migrate offshore at all.[17]

Population Genetics as a Tool for Authentication Purposes. Population genetic research is always based on statistical analysis. It has to be kept in mind that genetic variation within a population is subject to constant change by genetic drift, despite this influence being very small in large populations.[49]

The application of population genetic methods for authentication purposes is actually only possible for a very limited number of species which have been studied in recent years as case studies like herring (*Clupea harengus*) and cod (*Gadus morhua*).[25] However, for many other species population genetic knowledge is very low.[12] Undoubtedly the goal is to develop methods suitable for routine analysis and validation between laboratories, because they are intended to be a tool for forensic argumentation. To gain this sufficient biological data are required regarding stock structure, habitats, and migration routes before development of markers suitable for routine analysis will start.

Thus, normally a biological study is the starting point, based on scientific samples with known origin, size, weight, and sex. Depending on the knowledge of a species, the first problem often is the tailoring of the study. We chose saithe as an example of a well-known fish, whose population structure is still not fully understood, despite a lot of tagging studies being made in recent decades.[16,17]

The methods available in population genetics can be divided into two groups: easy-access markers, which do not need species-specific development, and markers suitable for robotic testing.

Examples for easy-access markers are fingerprinting methods, like RAPD or AFLP, or locus-specific but not species-specific markers (like EPIC). Such markers are not suitable for routine analysis but can shed a first light on a genetic structure within a species, and they may provide a starting point for further marker development. Methods based on mitochondrial genes like MT-CO1 or cytochrome *b* are easy to access as well, but long evolutionary time is necessary before populations do differ.[4,11]

RAPD-PCR is still a powerful tool for low-cost population genetic studies.[27,28] Primer sets are commercially available, 10 bp long primers are cheap, and only simple agarose gels are necessary for detection. The major drawback is that this method is known for its reproducibility problems,[29] but these problems should be solvable within a single laboratory. PCR conditions, reagents (kits), and thermocyclers have to be kept constant for the whole study. We strongly recommend choosing the allele carefully and confirming their reproducibility. In conclusion, RAPD-PCR gives a chance for laboratories to provide a fast and cost-efficient impression of an underexplored species within a few months without employing large-scale sequencing technology. Thus, RAPD-PCR is a useful tool for prestudies that can help to plan a detailed working program. Detected variable loci can be sequenced and might provide an alternative source for development of species-specific markers.

We expected EPIC-PCR to be a very easy to access method as well. However, a large number of loci have to be checked to find suitable markers. The occurrence of pseudo genes bears problems. Cloning is an option for few samples but not for a large numbers of samples as required in population genetics. The resulting laborious optimization of markers stays in contrast to our idea of easy-access markers. If a group is working on many species in parallel EPIC might be a useful start. In our opinion EPIC is a powerful tool for development of species-specific markers, because SNPs and MSats are very likely to occur at introns, but they are not as easy to access as RAPD markers and being binary dominant markers too do not provide a higher statistical power.

For authentication purposes "markers suitable for robotic testing" are required, providing the chance for validated methods answering the question of origin within a few days.[4] Their development is very laborious and costly and requires a large number of sequences to be analyzed.[25,30] For a sufficient database a set of at least 5 microsatellites is required,[12] which we did not achieve in our study. For studies based on SNPs a much higher number of loci is necessary; because they provide only binary data, studies are often based on more than 50 single-nucleotide polymorphisms.[4]

The adoption of MSat loci from closely related species might provide a shortcut, but a lot of loci have to be checked. We tried 25 MSats loci described for fishes of the same family (*Gadidae*) finding that only three of them flanked a region containing Msats. Charrier made similar experience in a study regarding Pollock (*Pollachius pollachius*) detecting 6 MSat loci from testing 37 primers.[32]

Prestudies using easy-access markers are a tool on the way of marker development. They give an imprint of the genetic diversity of a species. This can help to tailor large-scale studies regarding the amount of markers and samples needed. Easy-access markers are also a suitable starting point for further marker development. If population genetics should be applied for authentication purposes development of species-specific markers is inevitable as well as validation of data in large-scale studies that also take into account long-term stability of markers and migration routes.

AUTHOR INFORMATION

Corresponding Author

*Tel: +49-40-428384357. Fax: +49-40-428384342. E-mail: markus.fischer@chemie.uni-hamburg.de.

Funding

This research was financially supported by the Bundesverband der deutschen Fischindustrie und des Fischgroßhandels e.V., Hamburg, Germany.

Notes

The authors declare no competing financial interest.

ACKNOWLEDGMENTS

We thank Heiða Pálmadóttir (MATIS, Reykjavík, Iceland) for organizing samples of Icelandic saithe for our study and Malte Damerau (Thünen Institut, Hamburg, Germany) for his guidance to population genetics.

ABBREVIATIONS USED

Sample Abbreviations

CS, commercial sample (Northern North Sea)
IS, Icelandic
NOR, Norwegian (LO, Lofoten; FS, Fugloybanken South, FN, Fugloybanken North)

DOI: 10.1021/jf506201m
J. Agric. Food Chem. 2015, 63, 802−809

NS, North Sea
GM, Greenland (middle)
GS, Greenland (south)

Other Abbreviations

AFLP, amplified fragment-length polymorphism
AT, annealing temperature
EPIC, exon primed intron crossing
MSat, microsatellites
MT-CO1, mitochondrial cytochrome oxidase 1
PAGE, polyacryl gel electrophoresis
RAPD, random amplified polymorphic DNA
SNP, single nucleotide polymorphism
FAO, Food and Agriculture Organization of the United Nations
ICES, International Council for the Exploration of the Sea
TAC, total annual catch

REFERENCES

(1) Calvo, D. Quality of fish products, traceability and labelling: Discovering new challenges and opportunities. Presented at the ISLAS Conference, Vigo, Spain, November 2014.

(2) ThisFish | Seafood Traceability http://thisfish.info/ (accessed Nov 28, 2014).

(3) Regulation (EU) No 1379/2013 of the European Parliament and of the Council of 11 December 2013 on the common organisation of the markets in fishery and aquaculture products, amending Council Regulations (EC) No 1184/2006 and (EC) No 1224/2009 and repealing Council Regulation (EC) No 104/2000; *OJEU*, 28.12.2013, *L 354*, 1.

(4) Martinsohn, J. T. *Detering illegal activities in the fisheries sector: genetics, genomics, chemistry and forensics to fight IUU fishing and in support of fish product traceability*. European Union; European Commission; Joint Research Centre. Luxembourg, 2011.

(5) Council Regulation (EC) No 1224/2009 of 20 November 2009 establishing a Community control system for ensuring compliance with the rules of the common fisheries policy, amending Regulations (EC) No 847/96, (EC) No 2371/2002, (EC) No 811/2004, (EC) No 768/2005, (EC) No 2115/2005, (EC) No 2166/2005, (EC) No 388/2006, (EC) No 509/2007, (EC) No 676/2007, (EC) No 1098/2007, (EC) No 1300/2008, (EC) No 1342/2008 and repealing Regulations (EEC) No 2847/93, (EC) No 1627/94 and (EC) No 1966/2006; *OJEU*, 22.11.2019, *L 343*, 1.

(6) Regulation (EC) No 178/2002 of the European Parliament and of the Council of 28 January 2002 laying down the general principles and requirements of food law, establishing the European Food Safety Authority and laying down procedures in matters of food safety; *OJEU*, 01.02.2002, *L 031*, 1.

(7) Ratel, J.; Berge, P.; Berdague, J.-L.; Cardinal, M.; Engel, E. Mass Spectrometry Based Sensor Strategies for the Authentication of Oysters According to Geographical Origin. *J. Agric. Food Chem.* **2008**, *56*, 321−327.

(8) Herrero, B.; Madriñán, M.; Vieites, J. M.; Espiñeira, M. Authentication of Atlantic Cod (*Gadus morhua*) Using Real Time PCR. *J. Agric. Food Chem.* **2010**, *58*, 4794−4799.

(9) Griffiths, A. M.; Sotelo, C. G.; Mendes, R.; Pérez-Martín, R. I.; Schröder, U.; Shorten, M.; Silva, H. A.; Verrez-Bagnis, V.; Mariani, S. Current methods for seafood authenticity testing in Europe: Is there a need for harmonisation? *Food Control* **2014**, *45*, 95−100.

(10) Nielsen, E. E.; Cariani, A.; Aoidh, E. M.; Maes, G. E.; Milano, I.; Ogden, R.; Taylor, M.; Hemmer-Hansen, J.; Babbucci, M.; Bargelloni, L.; et al. Gene-associated markers provide tools for tackling illegal fishing and false eco-certification. *Nat. Commun.* **2012**, *3*, 851.

(11) Ogden, R. Fisheries forensics: the use of DNA tools for improving compliance, traceability and enforcement in the fishing industry. *Fish and Fisheries* **2008**, *9*, 462−472.

(12) Reiss, H.; Hoarau, G.; Dickey-Collas, M.; Wolff, W. J. Genetic population structure of marine fish: mismatch between biological and fisheries management units. *Fish and Fisheries* **2009**, *10*, 361−395.

(13) Olsson, J. *Genetic research on commercially exploited fish species in Nordic countries*; Nordic Council of Ministers: Copenhagen, 2007.

(14) Barz, K. Zimmermann, C. (Ed.): Fischbestände online. Thünen-Institut für Ostseefischerei. http://www.fischbestaende-online.de (accessed Feb 05, 2014).

(15) Fritsch, A. *Differenzierung von Seelachsbeständen mit Hilfe der EPIC-PCR*. Master-Thesis, Hamburg University of Applied Science, Germany, Nov. 2012.

(16) Homrum, E. í; Hansen, B.; Jónsson, S. P.; Michalsen, K.; Burgos, J.; Righton, D.; Steingrund, P.; Jakobsen, T.; Mouritsen, R.; Hátún, H.; et al. Migration of saithe (*Pollachius virens*) in the Northeast Atlantic. *ICES J. Mar. Sci.* **2013**, *70*, 782−792.

(17) Ottera, H.; Skilbrei, O. T. Possible influence of salmon farming on long-term resident behaviour of wild saithe (*Pollachius virens* L.). *ICES J. Mar. Sci.* **2014**, *71*, 2484−2493.

(18) Reinsch, H.-H. *Köhler und Steinköhler*; Die Neue Brehm-Bücherei; A. Ziemsen Verlag, DDR: Wittenberge, 1976; Vol. *496*, pp 24−27, 81.

(19) Homrum, E. Í.; Hansen, B.; Steingrund, P.; Hátún, H. Growth, maturation, diet and distribution of saithe (*Pollachius virens*) in Faroese waters (NE Atlantic). *Mar. Biol. Res.* **2012**, *8*, 246−254.

(20) Reinsch, H. H. Zur Verbreitung der einzelnen Altersklassen des Köhlers, Pollachius virens (L.), in der nördlichen Nordsee (lCES-Div. IV a). *Infn. Fischw.* **1994**, *41*, 124−135.

(21) Child, A. R. Population Genetics of Cod (*Gadus morhua* (L.)), Haddock (*Melanogrammus aeglefinus* (L.)), Whiting (*Merlangius merlangus* (L.)) and Saithe (*Pollachius virens* (L.)). Technical Report No. 87, Ministry of Agriculture, Fisheries and Food, Directorate of Fisheries Research, Lowestoft, UK, 1988.

(22) Denovan, E. M.; Wright, J. M. A satellite DNA family from pollock (*Pollachius virens*). *Gene* **1990**, *87*, 279−283.

(23) Eiríksson, G.; Árnason, E. Gene flow across the N-Atlantic and sex-biased dispersal inferred from mtDNA sequence variation in saithe, Pollachius virens. *Environ. Biol. Fish.* **2015**, *98*, 67−79.

(24) Saha, A.; Kirubakaran, T. G.; Kent, M.; Lien, S.; Westgaard, J.-I.; Fevolden, S. E.; Hauser, L.; Knutsen, H.; Cadrin, S.; Johansen, T. *Consistency between management units and genetic structure in saithe (Pollachius virens)? Application of modern genetic tools to an exploited species in the North Atlantic*. Presented at the ICES Annual Science Conference Bergen, Norway, 17−21 Sep. 2012.

(25) Nielsen, E. E.; Cariani, A.; Aoidh, E. M.; Maes, G. E.; Milano, I.; Ogden, R.; Taylor, M.; Hemmer-Hansen, J.; Babbucci, M.; Bargelloni, L.; et al. Gene-associated markers provide tools for tackling illegal fishing and false eco-certification. *Nat. Commun.* **2012**, *3*, 851.

(26) Williams, J. G.; Kubelik, A. R.; Livak, K. J.; Rafalski, J. A.; Tingey, S. V. DNA polymorphisms amplified by arbitrary primers are useful as genetic markers. *Nucleic Acids Res.* **1990**, *18*, 6531−6535.

(27) Bardakci, F. Random Amplified Polymorphic DNA (RAPD) Markers. *Turk. J. Biol.* **2001**, *25*, 185−196.

(28) Smith, P. Ramdom Amplified Polymorphic DNA (RAPD). In *Stock identification methods applications in fishery science*; Cadrin, S. X.; Friedland, K. D.; Waldman, J. R., Eds.; Elsevier Academic Press: Burlington, MA, 2005; pp 371−387.

(29) Bagley, M.; Anderson, S.; May, B. Choice of Methodology for Assessing Genetic Impacts of Environmental Stressors: Polymorphism and Reproducibility of RAPD and AFLP Fingerprints. *Ecotoxicology* **2001**, *10*, 239−244.

(30) Zane, L.; Bargelloni, L.; Patarnello, T. Strategies for microsatellite isolation: a review. *Mol. Ecol.* **2002**, *11*, 1−16.

(31) O'Reilly, P. Isolation of twenty low stutter di- and tetranucleotide microsatellites for population analyses of walleye pollock and other gadoids. *J. Fish Biol.* **2000**, *56*, 1074−1086.

(32) Charrier, G.; Coombs, S.; McQuinn, I.; Laroche, J. Genetic structure of whiting *Merlangius merlangus* in the northeast Atlantic and adjacent waters. *Mar. Ecol.: Prog. Ser.* **2007**, *330*, 201−211.

DOI: 10.1021/jf506201m
J. Agric. Food Chem. 2015, 63, 802−809

(33) Rehbein, H.; Kress, G. Detection of short mRNA sequences in fishery products. *Dtsch. Lebensm.-Rundsch.* **2005**, *101*, 333−337.
(34) Downs, T. R.; Wilfinger, W. W. Fluorometric quantification of DNA in cells and tissue. *Anal. Biochem.* **1983**, *131*, 538−547.
(35) Wang, D.; Shi, J.; Carlson, S. R.; Cregan, P. B.; Ward, R. W.; Diers, B. W. A Low-Cost, High-Throughput Polyacrylamide Gel Electrophoresis System for Genotyping with Microsatellite DNA Markers. *Crop Sci.* **2003**, *43*, 1828.
(36) Rehbein, H. Identification of the fish species of raw or cold-smoked salmon and salmon caviar by single-strand conformation polymorphism (SSCP) analysis. *Eur. Food Res. Technol.* **2005**, *220*, 625−632.
(37) Welsh, J.; McClelland, M. Fingerprinting genomes using PCR with arbitrary primers. *Nucleic Acids Res.* **1990**, *18*, 7213−7218.
(38) Charrier, G.; Durand, J.; Quiniou, L.; Laroche, J. An investigation of the population genetic structure of pollack (*Pollachius pollachius*) based on microsatellite markers. *ICES J. Mar. Sci.* **2006**, *63*, 1705−1709.
(39) Brooker, A. L.; Cook, D.; Bentzen, P.; Wright, J. M.; Doyle, R. W. Organization of Microsatellites Differs between Mammals and Cold-water Teleost Fishes. *Can. J. Fish. Aquat. Sci.* **1994**, *51*, 1959−1966.
(40) Westgaard, J.-I.; Tafese, T.; Wesmajervi, M. S.; Nilsen, F.; Fjalestad, K. T.; Damsgård, B.; Delghandi, M. Development of ten new EST-derived microsatellites in Atlantic cod (*Gadus morhua* L.). *Conserv. Genet.* **2007**, *8*, 1503−1506.
(41) Miller, K. M.; Le, K. D.; beacham, T. D. Development of tri- and tetranucleotide repeat microsatellite loci in Atlantic cod (*Gadus morhua*). *Mol. Ecol.* **2000**, *9*, 238−239.
(42) Page, L. M.; H. Espinosa-Pérez; Findley, L. D.; ; Gilbert, C. R.; ; Lea, R. N.; ; Mandrak, N. E.; ; Mayden, R. L.; ; J. S. Nelson *Common and scientific names of fishes from the United States, Canada, and Mexico*; 7th ed.; American Fisheries Society, 2013; Vol. Special Publication 34. I, XII, 1−384.
(43) D'Amato, M. E.; Lunt, D. H.; Garry, R. Carvalho. Microsatellite markers for the hake *Macruronus magellanicus* amplify other gadoid fish. *Mol. Ecol.* **1999**, *8*, 1086−1088.
(44) Moran, P.; Rico, C.; Hewitt, G. M. Four microsatellite loci in the gadoid fish, blue whiting *Micromesistius poutassou* (Riso 1826). *Anim. Genet.* **1999**, *30*, 463−464.
(45) Peakall, R.; Smouse, P. E. GenAlEx 6.5: genetic analysis in Excel. Population genetic software for teaching and research—an update. *Bioinformatics* **2012**, *28*, 2537−2539.
(46) Peakall, R.; Smouse, P. E. GenAlEx 6: genetic analysis in Excel. Population genetic software for teaching and research. *Mol. Ecol. Notes* **2006**, *6*, 288−295.
(47) Excoffier, L.; Smouse, P. E.; Quattro, J. M. Analysis of molecular variance inferred from metric distances among DNA haplotypes: application to human mitochondrial DNA restriction data. *Genetics* **1992**, *131*, 479−491.
(48) Edwards, R. UPGMA Node Clustering UPGMA. http://bioware.soton.ac.uk/upgma.html (accessed Mar 20, 2014).
(49) Flint-Garcia, S. A. Genetics and Consequences of Crop Domestication. *J. Agric. Food Chem.* **2013**, *61*, 8267−8276.

DOI: 10.1021/jf506201m
J. Agric. Food Chem. 2015, 63, 802−809

JOURNAL OF AGRICULTURAL AND FOOD CHEMISTRY

Article

pubs.acs.org/JAFC

Rapid Discrimination and Feature Extraction of Three *Chamaecyparis* Species by Static-HS/GC−MS

Ying-Ju Chen,[†,‡] Chun-Ya Lin,[†] Sen-Sung Cheng,[§] and Shang-Tzen Chang*[,†]

[†]School of Forest and Resource Conservation, National Taiwan University, Taipei 10617, Taiwan

[‡]Division of Forest Chemistry, Taiwan Forestry Research Institute, Taipei 10070, Taiwan

[§]Experimental Forest, National Taiwan University, Nan-Tou 55750, Taiwan

ABSTRACT: This study aimed to develop a rapid and accurate analytical method for discriminating three *Chamaecyparis* species (*C. formosensis*, *C. obtusa*, and *C. obtusa* var. *formosana*) that could not be easily distinguished by volatile compounds. A total of 23 leaf samples from three species were analyzed by static-headspace (static-HS) coupled with gas chromatography−mass spectrometry (GC−MS). The static-HS procedure, whose experimental parameters were properly optimized, yielded a high Pearson correlation-based similarity between essential oil and VOC composition (r = 0.555−0.999). Thirty-six major constituents were identified; along with the results of cluster analysis (CA), a large variation in contents among the three different species was observed. Principal component analysis (PCA) methods illustrated graphically the relationships between characteristic components and tree species. It was clearly demonstrated that the static-HS-based procedure enhanced greatly the speed of precise analysis of chemical fingerprint in small sample amounts, thus providing a fast and reliable tool for the prediction of constituent characteristics in essential oil, and also offering good opportunities for studying the role of these feature compounds in chemotaxonomy or ecophysiology.

KEYWORDS: *VOCs, Chamaecyparis species, cluster analysis, principal component analysis, static-HS/GC−MS*

INTRODUCTION

The wood of *Chamaecyparis* is strong and fragrant, even-grained, and highly valued, with high-quality termite and decay resistance.[1,2] *Chamaecyparis formosensis* (Cf) and *Chamaecyparis obtusa* var. *formosana* (Cof) are two species belonging to the *Chamaecyparis* genus in Taiwan. They are the premier coniferous timber trees of the island. However, a critical habitat designation (along with cool temperatures and high moisture content) and shade intolerance led to minimal regeneration in established stand and decline of both species.[1] On a restricted habitat, these two species usually grow together, but with distinct overlapping elevation bands, Cf at lower elevations (850−2600 m) and Cof above it (1200−2800 m). *Chamaecyparis obtusa* (Co), another species belonging to *Chamaecyparis*, is also found in Taiwan. It has been highly valued and heavily exploited in Japan for centuries.[2−4] It is a tough task to differentiate the subtle characteristics among these three species, in contrast to strong chemical differentiation which was consistent also in specimens collected from sympatric populations.[5] Terpene composition of conifers is usually strongly inherited and has been widely used as a biochemical marker in chemotaxonomic studies to characterize plant species and their geographical or botanical origins.[6−8] In a previous study, the phylogenetic relationships of the *Chamaecyparis* were established, according to their chemical compositions of leaf essential oils, to account for the characteristic compounds of Cf, Cof, and Co, respectively.[7] Lin et al. (2011) subsequently demonstrated that solid-phase microextraction (SPME) could be a rapid technique for differentiating these three species.[9] However, the major feature compounds were not in good agreement with those of essential oils.

Static headspace (static-HS) is an ideal technique that has been proven to be an efficient and convenient sampling method.[10,11] It was in particular advantageous for the analysis of volatile compounds in intricate and heterogeneous matrices.[12] In the past decade, this technique has been employed to investigate various differences in aromatic profile, and to characterize components within different provenances, structures, or vegetative stages.[10,13−15]

The purpose of this study was to develop an accurate and stalwart technique, static-HS coupled with gas chromatography−mass spectrometry (GC−MS), and chemometrics to discriminate three *Chamaecyparis* species according to their feature volatile compounds. The experimental conditions are optimized, and comparative studies are conducted on the typical static-HS and conventional hydrodistillation profiles of leaf samples collected from different regions in the hope of confirming the applicability of the method developed for the chemical characterization of their volatile compounds and for the prediction of main compositions of essential oils in plants.

MATERIALS AND METHODS

Plant Materials. In the present study, fresh mature leaves of three species of *Chamaecyparis* (*C. formosensis* (Cf), *C. obtusa* var. *formosana* (Cof), and *C. obtusa* (Co)) were obtained from different locations in Taiwan. Depending on the availability and accessibility of trees, leaves of Cf were collected from trees growing in Huisun Experimental Forestry (2 trees), Dueigaoyue Tract (2 trees), Chiayi (2 trees),

Received: September 14, 2014
Revised: December 29, 2014
Accepted: January 2, 2015
Published: January 15, 2015

ACS Publications © 2015 American Chemical Society

DOI: 10.1021/jf505587w
J. Agric. Food Chem. 2015, 63, 810−820

Table 1. *Chamaecyparis* Leaf Samples Used in This Study

species	tree no.	sample ID	locality	latitude and longitude	altitude (m)	temp, °C	collecting season
Cf	CF 006−007	Cf1	Huisun Experimental Forestry	121.03438°E 24.08738°N	799	23.5	June
	CF 008−009	Cf2	Dueigaoyue Tract	120.84744°E 23.47429°N	2280	19.8	July
	CF 14 and 16	Cf3	Chiayi	120.80579°E 23.50386°N	2305	6	January
	CF 18−19	Cf4	Taichung	120.99206°E 24.26913°N	2222	6.5	January
	CF 20	Cf5	Chutung	121.11481°E 24.50364°N	2037	8	January
Cof	COF CL	Cof1	Chilan Mt.	121.41666°E 24.58333°N	1650	20.5	August
	COF 06	Cof2	Neimaopu Tract	120.79536°E 23.64950°N	2032	15.5	January
	COF 10−11	Cof3	Taichung	120.99296°E 24.26755°N	2205	6.5	January
	COF 13−15	Cof4	Chutung	121.11481°E 24.50364°N	2037	8	January
Co	CO 04−07	Co1	Sitou	120.79762°E 23.67249°N	1181	14.7	March
	CO 005−006	Co2	Huisun Experimental Forestry	121.03114°E 24.08272°N	1068	23.5	June
	CO 007	Co3	Hoshe	120.87513°E 23.55742°N	1130	22.7	July
total	23	12	9				

Taichung (2 trees), and Chutung (single tree); Cof leaves were collected from trees growing in Mt. Chilan (single tree), Neimaopu Tract (single tree), Taichung (2 trees), and Chutung (3 trees); and Co leaves were collected from trees growing in Sitou (4 trees), Huisun Experimental Forestry (2 trees), and Hoshe (single tree). Samples were obtained by clipping the foliage from healthy noninfected trees of each species. Table 1 lists the coniferous leaf specimens studied. There are 23 trees sampled in current study, and each tree sample was extracted in triplicate. The composition data of all tree samples from the same location were averaged and given a sample ID, and therefore, a total of 12 samples are presented in the following results. Voucher specimens were deposited with the Laboratory of Wood Chemistry (School of Forestry and Resource Conservation, National Taiwan University), and the leaves studied were kept frozen at −80 °C until analysis.

Headspace Analysis Conditions. A PerkinElmer Headspace Turbomatrix 40 (PerkinElmer, USA) was used for headspace analysis. Fresh leaves were clipped into small pieces, and 20 mg samples were placed in 22 mL vials sealed with headspace PTFE-coated silicone rubber septa and caps (PerkinElmer, USA). To develop an optimal headspace procedure for the determination of volatile organic compounds (VOCs) from three *Chamaecyparis* species, key parameters such as equilibration time and temperature were adjusted. The headspace parameters are listed in Table 2.

Volatile Compound Analyses. Volatile compounds were analyzed using a Turbomatrix 40 headspace autosampler, connected to a Clarus 600 gas chromatograph mass spectrometer (PerkinElmer Inc.), equipped with a DB-5ms column (J&W Scientific, Folsom, CA). A chromatographic temperature program was run as follows: from 50 to 200 °C at 3 °C/min, then heating at 5 °C/min to 250 °C, and held for 5 min. Helium was used as the carrier gas at a flow rate of 1 mL/min. The temperatures of the injection port and transfer line were both 250 °C. The MS parameters were ionization voltage (EI), 70 eV; mass range, 45−400 amu; and ion source temperature, 230 °C. The Kovats indices (KI)[16] were calculated for all compounds using a homologous series of *n*-alkanes (C_9−C_{22}) on the DB-5ms column. Identification of individual components was performed using the Wiley/NBS Registry of Mass Spectral Database (version 7) and NIST MS Search (version 2), published literature, and several authentic reference compounds. Quantitative analysis was carried out using a Trace GC Ultra (Thermo Scientific, Waltham, MA) with an FID (Thermo Scientific). The temperatures of the injection port and the detector were 250 and 270 °C, respectively. The parameters of the column, split ratio, oven temperature program, carrier gas, and flow rate of GC-FID were identical to those of GC/MS. The quantity of compounds was obtained by integrating the peak area of the chromatograms, and quantification was performed using percentage peak area calculations using the GC-FID.

Table 2. Headspace Parameter Studied

thermostating temp	50 °C, 100 °C, 150 °C
thermostating time	30 min, 50 min
needle temp	more than 10 deg above thermo temp
transfer line temp	more than 10 deg above needle temp
pressurization time	0.3 min
injection time	0.02 min
carrier gas pressure	103.4 kPa

Statistical Analyses. Statistical analyses were performed using the SPSS program package (SPSS 17.0). Pearson correlation was performed to evaluate the significance and direction of an obtainable correlation between equilibrium time, temperature, and measurable variables (VOCs), and to determine the headspace parameters that achieve maximum correlation with compounds of essential oils. Data collected were subjected to analysis of variance (ANOVA), and the means were separated by the Scheffé test at $P \leq 0.05$. In addition, the method of Chen et al. was employed to evaluate the similarity of volatile compounds extracted from fresh leaves.[7]

The results were further processed with a discriminative study by cluster analysis (CA) and principal component analysis (PCA) to detect clustering formation and to establish the relationships between species and their volatile components. PCA biplot was utilized to highlight the interaction between samples and variables.[17] CA and PCA were performed using the MVSP software (Multivariate

DOI: 10.1021/jf505587w
J. Agric. Food Chem. 2015, 63, 810−820

Table 3. Pearson Correlation Coefficients between Essential Oil and VOC Composition on Different Static-HS Experimental Parameters[a]

		30 min			50 min		
species	location	50 °C	100 °C	150 °C	50 °C	100 °C	150 °C
Cf	Huisun	1.000	0.992	0.980	1.000	0.993	0.985
	DueiGaoYue	0.997	0.988	0.958	0.997	0.985	0.960
	Chiayi	0.999	0.990	0.925	0.999	0.992	0.939
	Taichung	0.961	0.956	0.950	0.961	0.958	0.956
	Chutung	0.999	0.990	0.960	0.999	0.986	0.955
Cof	Chilan Mt	0.275*	0.551	0.759**	0.181	0.574	0.752
	Neimaopu		0.836	0.831		0.849	0.840
	Taichung		0.373**	0.796		0.370**	0.782
	Chutung		0.295**	0.846		0.266*	0.863
Co	Sitou		0.842	0.885		0.877	0.906
	Huisun		0.839	0.731		0.866	0.768
	Hoshe		0.733	0.584		0.817	0.555

[a]*Significant at $P < 0.05$. **Significant at $P < 0.01$; the rest were significant at the $P < 0.001$ level. (Two-tailed.)

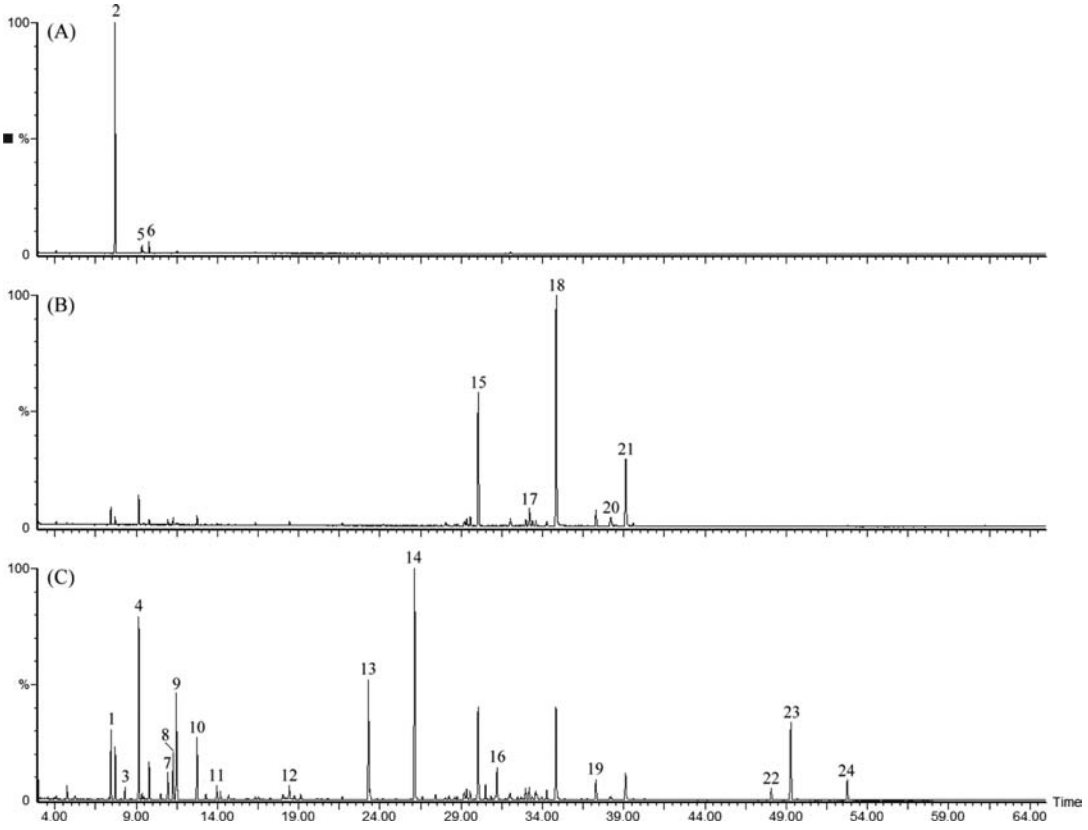

Figure 1. HS-GC/MS chromatogram of volatile compounds of leaves from *Chamaecyparis* species: (A) Cf; (B) Cof; (C) Co. Key: 1, α-thujene; 2, α-pinene; 3, camphene; 4, sabinene; 5, β-pinene; 6, β-myrcene; 7, α-terpinene; 8, *p*-cymene; 9, limonene; 10, γ-terpinene; 11, terpinolene; 12, terpinen-4-ol; 13, L-bornyl acetate; 14, α-terpinyl acetate; 15, thujopsene; 16, bicyclosesquiphellandrene; 17, (+)-cuparene; 18, β-elemol; 19, humulene epoxide III; 20, γ-eudesmol; 21, α+β-eudesmol; 22, rimuene; 23, beyerene; 24, *ent*-16-kaurene.

Statistical Package for Windows, version 3.1, Kovach Computing Services, Anglesey, U.K.).

RESULTS AND DISCUSSION

Optimization of HS Parameters. Series of preliminary tests had been made for optimizing the experimental conditions of sample preparation and instrumental analysis. To elaborate on mutual relationships between the quantities of compounds or classes of components in the essential oils and VOCs extracted by HS technique, the static-HS analysis was optimized by studying the effects of the relevant experimental parameters (equilibration time and temperature) on the volatile composition profile. Furthermore, to screen for optimal parameters under which the volatile composition profiles correspond well with essential oils, the two databases were integrated and correlation analysis between the essential oils and the volatile composition database was performed. As shown in Table 3, at HS equilibrium time of both 30 min and 50 min and oven temperature of 50 °C, a highly significant positive correlation (Pearson's $r = 0.961-1.000$, $P < 0.001$) occurred

DOI: 10.1021/jf505587w
J. Agric. Food Chem. 2015, 63, 810−820

between the leaf volatile composition and essential oil component of Cf. As for Cof, leaves from Chutung showed good statistical significance (Pearson's $r = 0.863$, $P < 0.001$) between volatile components and essential oil composition at HS equilibrium time of 50 min and oven temperature of 150 °C, while volatiles extracted from leaves collected at the other three locations also showed a statistically significant positive correlation (Pearson's $r = 0.759-0.849$, $P < 0.001$) with their essential oils. Regarding Co, leaves from Sitou equilibrated at oven temperature of 150 °C for 50 min showed a highly significant positive correlation (Pearson's $r = 0.906$, $P < 0.001$) between the volatiles and essential oils, while volatiles extracted from leaves collected at Huisun and Hoshe exhibited significant correlations (Pearson's $r = 0.817-0.866$, $P < 0.001$) with essential oil on HS at oven temperature of 100 °C for equilibrium time of 50 min.

According to previous research, the leaf essential oils of Cf contained a predominance of monoterpene hydrocarbons. As for the essential oils of Cof, sesquiterpene hydrocarbons and oxygenated sesquiterpenes constituted the major fractions; while monoterpene hydrocarbons and oxygenated monoterpenes accounted for the largest fractions in the oils of Co.[7] Taken as a whole, the essential oil components found in Cof and Co had higher proportion of polar compounds, and their molecular weights were higher than those of compounds found in Cf. The reason that Cof and Co have higher boiling points than Cf might be the additional energy required to break the hydrogen bonds for vaporization of the molecules. Alternatively, the association of molecules through hydrogen bonding increases the molecular weight, thereby reducing volatility.[18]

In addition, as seen in Table 3, the equilibrium temperature seems to be a much more important factor than equilibrium time on volatile composition profiles. All samples treated at equilibrium time of 50 min and oven temperature of 150 °C showed good correlation (Pearson's $r > 0.555$) between VOCs and essential oils. Terpenes are the main volatile components of plant essential oils. Several studies have been conducted on the bioactivities of essential oils and some of their major constituents.[19,20] The bioactivities of essential oils are attributable to monoterpenes, sesquiterpenes, and other hydrocarbons.[21] For "biomining", the experimental parameters obtained in this study could be employed to screen for unraveled species, which might have economic or potential bioactive compounds. According to an overview published by Goren et al.,[22] the higher the equilibrium temperature, the greater the number of compounds were detected in the chromatogram. The optimum sample temperature (200 °C) for analyzing *Satureja trhymbra* was determined by the maximum number of compounds detected.[22] However, the correlations between essential oils and volatile profiles were not examined by statistical tests.

Volatile Organic Compound Analyses. To investigate the VOCs extracted from three *Chamaecyparis* species (Cf, Cof, and Co), a static-HS was employed to extract the volatile compounds from fresh leaves and the composition of VOCs was then analyzed using GC-FID and GC/MS. From the static-HS/GC–MS chromatogram (Figure 1), 24 apparent peaks were detected and there were significant differences among the volatile components patterns of these three *Chamaecyparis*. The volatile components identified were separated into five categories, i.e., monoterpene hydrocarbons, oxygenated monoterpenes, sesquiterpene hydrocarbons, oxygenated sesquiterpenes, and others. Integrating the GC-FID peak areas of individual constituents showed that the leaf VOCs of Cf contained a predominance of monoterpene hydrocarbons (98.23–99.82%), among which α-pinene (89.30–96.90%) was the main constituent, followed by β-myrcene (0.82–4.70%) and β-pinene (1.94–3.44%) (Table 4). For Cof, sesquiterpene hydrocarbons (52.29%, 44.46%) and oxygenated sesquiterpenes (30.95%, 42.20%) constituted the two major fractions in the VOCs of leaves collected from Taichung and Chutung, respectively. These were in agreement with the constituents in leaf essential oils.[7] As for the VOCs of leaves collected from Mt. Chilan, sesquiterpene hydrocarbons (74.96%) constituted the major fraction, while sesquiterpene hydrocarbons (57.03%) and monoterpenoids hydrocarbons (32.04%) accounted for the largest fraction in the VOCs of leaves collected from Neimaopu. Variations in VOC composition of Cof leaves collected from four locations were observed; since leaves were collected from Taichung and Chutung in the same season and with similar environmental factors—high altitude (2037–2205 m) and low temperature (6.5–8 °C)—they had relatively higher contents of sesquiterpenes compared to the other two locations. A similar variation in VOC composition was also observed for Co leaves collected from different locations. Even though three Co samples have similar altitude distribution, leaves collected from Huisun and Hoseh, with higher temperature (22.7–23.5 °C), were characterized by higher contents of monoterpenes. Chemical compositions of secondary metabolites typically affected by different factors, such as temperature, precipitation, light, and growing site, might alter the qualitative/quantitative amount of the volatile composition. Season is related to a combination of these environmentally regulated factors.[23] In the present study, most of the samples were collected in winter and summer, and such environmental information (Table 1) is insufficient to provide an adequate basis for analyzing the environmental influence on the chemical variations. A further investigation concerning correlation between chemical composition and seasonal variation is warranted.

The VOCs extracted from Cof leaves contained primarily thujopsene (30.35–49.77%), β-elemol (0.87–28.60%), sabinene (1.03–14.97%), *cis*-thujopsenal (0.00–14.72%), and β-himachalene (0.61–9.43%). In addition, *cis*-thujopsenal was found mainly in VOCs extracted from leaves collected at Mt. Chilan, β-elemol was found primarily in VOCs extracted from leaves collected at Taichung and Chutung, and thujopsene was the dominant compound in VOCs from leaves collected at all locations. These results are similar to previous findings, in which the major/characteristic compounds of leaf essential oils from Cof are thujopsene (Taichung), β-elemol (Chutung), and *cis*-thujopsenal (Mt. Chilan). As for Co, the leaf VOCs comprise mainly sabinene (8.55–24.58%), α-terpinyl acetate (16.98–23.50%), L-bornyl acetate (6.48–11.38%), β-elemol (0.51–11.95%), and thujopsene (2.81–9.78%). These data are also in agreement with previous findings;[7] the leaf essential oil of Co was characterized by α-terpinyl acetate and L-bornyl acetate. To sum up, the leaf compositions of these three *Chamaecyparis* species extracted using the static-HS technique correspond well to those from hydrodistillation (i.e., essential oils).[7]

Multivariate Data Analyses. To investigate the variation in compositions of VOCs among three *Chamaecyparis* species, the data in Table 4 were examined using CA. The resulting dendrogram shows the existence of three major clusters (Figure

DOI: 10.1021/jf505587w
J. Agric. Food Chem. 2015, 63, 810–820

Table 4. Constituents and Relative Contents of VOCs of Leaves from Three *Chamaecyparis* Species

	C. formosensis					*C. obtusa* var. *formosana*				*C. obtusa*				significance[e]		
compds	Cf1[a]	Cf2	Cf3	Cf4	Cf5	Cof1	Cof2	Cof3	Cof4	Co1	Co2	Co3	identification[d]	Cf	Cof	Co
monoterpene hydrocarbon	98.80[b]	98.62	99.82	98.23	98.42	6.45	32.04	2.18	6.20	21.63	49.05	52.93				
α-thujene						0.23	2.91	0.18	0.82	1.07	0.92	0.69	MS, KI, STD	A	A	A
						(0.11)	(0.02)	(0.07)	(0.76)	(1.51)	(0.01)	(0.03)				
α-pinene	89.30	90.50	96.90	94.20	93.13	0.17	6.12	0.12	0.77	1.21	2.27	1.86	MS, KI, STD	A	B	B
	(1.15)[c]	(1.64)	(0.34)	(1.97)	(0.35)	(0.05)	(0.15)	(0.03)	(0.58)	(0.38)	(0.15)	(0.19)				
sabinene						1.27	14.97	1.03	2.07	8.55	23.23	24.58	MS, KI, STD	B	B	A
						(1.51)	(0.72)	(0.05)	(0.46)	(0.66)	(1.5)	(1.63)				
β-pinene	3.44	2.67	1.94	2.06	2.65					0.24	0.72	0.23	MS, KI, STD	A	B	B
	(0.03)	(0.19)	(0.17)	(0.02)	(0.08)					(0.04)	(0.28)	(0.03)				
β-myrcene	4.70	4.12	0.82	1.34	2.07	1.33	1.05	0.23	0.66	2.44	6.11	11.28	MS, KI, STD	AB	B	A
	(0.69)	(0.11)	(0.07)	(0.4)	(0.09)	(0.42)	(0.3)	(0.22)	(0.63)	(1.2)	(0.78)	(1.96)				
α-terpinene						1.13	0.11	0.08	0.44	0.60	0.36	0.47	MS, KI, STD	A	A	A
						(1)	(0.01)	(0.02)	(0.48)	(0.34)	(0.1)	(0.16)				
p-cymene							4.73	0.24	0.42	0.72	0.79	0.24	MS, KI, STD	A	A	A
							(0.05)	(0.1)	(0.26)	(0.77)	(0.26)	(0.04)				
limonene	0.42	0.30	0.07	0.35	0.28	0.25	0.22	0.10	0.07	4.10	10.39	9.01	MS, KI, STD	B	B	A
	(0.17)	(0.43)	(0.1)	(0.16)	(0.19)	(0.25)	(0.02)	(0.06)	(0.06)	(0.13)	(1.58)	(0.74)				
β-phellandrene	0.94	1.04	0.09	0.28	0.30	0.29	0.04	0.05	0.14	0.11			MS, KI	A	A	A
	(0.23)	(0.31)	(0.13)	(0.39)	(0.26)	(0.21)	(0.07)	(0.04)	(0.17)	(0)						
γ-terpinene						1.41	2.40	0.11	0.67	2.09	3.25	3.57	MS, KI, STD	B	B	A
						(1.22)	(0.02)	(0.03)	(0.73)	(0.35)	(0.35)	(0.07)				
terpinolene						0.37	0.16	0.05	0.13	0.50	1.01	1.00	MS, KI, STD	B	B	A
						(0.32)	(0.02)	(0.07)	(0.14)	(0.01)	(0.03)	(0.06)				
oxygenated monoterpenes						2.80	4.91	0.44	1.84	24.35	33.56	36.20				
L-borneol									0.02	0.20	0.08	0.11	MS, KI	B	B	A
									(0.04)	(0.28)	(0.11)	(0.03)				
terpinen-4-ol						2.80	4.40	0.18	0.49	0.29	0.24	0.42	MS, KI, STD	A	A	A
						(2.01)	(1.46)	(0.06)	(0.33)	(0.16)	(0.34)	(0.08)				
α-terpineol							0.12		0.02	0.27	0.15	0.25	MS, KI, STD	B	B	A
							(0.06)		(0.03)	(0.02)	(0.21)	(0.04)				
linalyl acetate							0.22	0.06	1.03	0.13	0.73	0.54	MS, KI, STD	A	A	A
							(0.07)	(0.02)	(0.91)	(0.08)	(0.35)	(0.33)				
L-bornyl acetate							0.03	0.03	0.11	6.48	9.94	11.38	MS, KI, STD	B	B	A
							(0.07)	(0.05)	(0.04)	(2.24)	(1.93)	(1.31)				
α-terpinyl acetate							0.14	0.16	0.17	16.98	22.43	23.50	MS, KI, STD	B	B	A
							(0.06)	(0.15)	(0.14)	(5.61)	(0.63)	(3.32)				
sesquiterpene hydrocarbons	0.49	0.09	0.09	0.67	0.66	74.96	57.03	52.29	44.46	22.36	10.99	5.76				
(−)-*α*-cedrene						5.28	0.58	1.00	1.03	0.53	0.46	0.08	MS, KI, STD	A	A	A
						(4.09)	(0.05)	(0.00)	(0.50)	(0.06)	(0.28)	(0.03)				
trans-*β*-caryophyllene		0.09		0.21	0.20	0.37	0.14	1.01	1.27	0.94	1.00	0.28	MS, KI	A	A	A

J. Agric. Food Chem. 2015, 63, 810−820
DOI: 10.1021/jf505587w

Table 4. continued

compds	*C. formosensis*					*C. obtusa* var. *formosana*				*C. obtusa*			identification[d]	significance[e]		
	Cf1[a]	Cf2	Cf3	Cf4	Cf5	Cof1	Cof2	Cof3	Cof4	Co1	Co2	Co3		Cf	Cof	Co
		(0.03)		(0.05)	(0.07)	(0.37)	(0.02)	(0.47)	(0.49)	(0.13)	(0.62)	(0.05)				
(+)-β-cedrene						2.39	1.88	1.48	1.53	0.63	0.57	0.12	MS, KI, STD	B	A	B
						(0.82)	(0.03)	(0.26)	(0.58)	(0.05)	(0.32)	(0.06)				
thujopsene						30.35	49.77	33.90	30.51	9.78	6.51	2.81	MS, KI, STD	B	A	B
						(12.93)	(0.59)	(11.03)	(8.99)	(2.29)	(2.09)	(0.74)				
bicyclosesquiphellandrene									0.03	5.14	0.77	0.76	MS, KI	A	A	A
									(0.03)	(0.95)	(0.07)	(0.26)				
τ-cadinene	0.49		0.03	0.47	0.46	2.61	0.02	0.33	0.37	0.16		0.02	MS, KI	A	A	A
	(0.27)		(0.02)	(0.26)	(0.07)	(2.73)	(0.07)	(0.09)	(0.1)	(0.13)		(0.02)				
(−)-β-chamigrene						4.12	3.47	4.38	3.58	1.21	0.81	0.96	MS, KI, STD	C	A	B
						(0.99)	(1.48)	(1.13)	(1.94)	(0.48)	(0.63)	(0.36)				
epizonarene			0.02			2.29		0.07	0.13	0.43		0.06	MS, KI	A	A	A
			(0.01)			(2.64)		(0.1)	(0.02)	(0.09)		(0.06)				
β-himachalene						9.43	0.61	1.60	1.61	1.24	0.66	0.20	MS, KI	A	A	A
						(5.88)	(0.04)	(0.24)	(0.70)	(0.65)	(0.46)	(0.07)				
(+)-cuparene						1.00	1.66	2.81	2.07	0.49	0.21	0.03	MS, KI, STD	B	A	B
						(0.59)	(0.06)	(0.65)	(1.11)	(0.35)	(0.08)	(0.03)				
γ-cadinene						1.01	0.01	0.45	0.85	0.47		0.12	MS, KI	A	A	A
						(0.44)	(0.03)	(0.12)	(0.27)	(0.38)		(0.07)				
δ-cadinene			0.03			1.39	0.01	0.48	1.02	1.25	0.01	0.33	MS, KI	A	A	A
			(0.02)			(0.94)	(0.04)	(0.06)	(0.15)	(0.74)	(0.02)	(0.18)				
cis-thujopsenal						14.72		4.78	0.48	0.09			MS	A	A	A
						(1.05)		(3.10)	(0.82)	(0.03)						
oxygenated sesquiterpenes						10.44	3.21	30.95	42.20	16.51	1.08	1.70				
β-elemol						3.81	0.87	15.43	28.60	11.95	0.51	1.31	MS, KI, STD	A	A	AB
						(2.17)	(0.04)	(6.58)	(7.40)	(1.07)	(0.01)	(0.05)				
humulene epoxide III						2.20	1.01	5.94	3.46	2.25	0.45	0.13	MS, KI	C	A	AB
						(2.57)	(0.03)	(0.52)	(0.71)	(0.92)	(0.35)	(0.05)				
γ-eudesmol						0.70	0.06	1.42	1.75	0.33	0.06	0.03	MS, KI, STD	C	A	AB
						(0.51)	(0.1)	(1.2)	(1.37)	(0.02)	(0.08)	(0.04)				
α+β-eudesmol						3.72	0.01	8.16	8.39	1.98	0.06	0.23	MS, KI	A	B	AB
						(3.11)	(0.02)	(6.24)	(4.39)	(0.63)	(0.08)	(0.05)				
diterpene hydrocarbons						0.10	0.01	8.83	0.39	4.37	1.35	0.22				
beyerene						0.06	0.01		0.11	4.15	1.35	0.22	MS, KI	A	A	A
						(0.05)	(0.04)		(0.15)	(2.75)	(0.01)	(0.01)				
ent-16-kaurene						0.04		8.83	0.27	0.22			MS, KI, STD	A	A	A
						(0.05)		(12.1)	(0.09)	(0.31)						
unknown						1.61	0.23	1.35	1.45	1.50	0.48	0.18				
unknown-19										2.26	0.36	0.27		A	A	A

J. Agric. Food Chem. 2015, 63, 810−820 DOI: 10.1021/jf505587w

Table 4. continued

compds	*C. formosensis*					*C. obtusa* var. *formosana*				*C. obtusa*			identification[d]	significance[e]		
	Cf1[a]	Cf2	Cf3	Cf4	Cf5	Cof1	Cof2	Cof3	Cof4	Co1	Co2	Co3		Cf	Cof	Co
										(0.62)	(0.07)	(0.07)				
unknown-29						1.61		0.15	0.09	0.35		0.03		A	A	A
						(1.86)		(0.21)	(0.03)	(0.07)		(0.04)				
unknown-35							0.23	1.20	1.35	1.16	0.48	0.15		A	A	A
							(0.01)	(0.54)	(0.63)	(0.46)	(0.39)	(0.07)				

[a]Cf1: Huisun. Cf2: Dueigaoyue. Cf3: Chiayi. Cf4: Taichung. Cf5: Chutung. Cof1: Chilan. Cof2: Neimaopu. Cof3: Taichung. Cof4: Chutung. Co1: Sitou. Co2: Huisun. Co3: Hoshe. [b]Relative content, percent of normalized peak areas. [c]Standard deviation given in parentheses. [d]Identification according to comparison of mass spectrum (MS), Kovats index (KI), and coinjection with standard compounds (STD). [e]Species sharing the same letter are not significantly different in relative content (Scheffé, $P = 0.05$).

2). The first group, Cof, comprised Neimaopu, Chutung, Taichung, and Chilan areas, and the similarity between these samples was 48.17%. The second group (Co) was composed of Hoshe, Huisun, and Sitou areas, and the similarity within this group was 59.01%. The third group (Cf) included Chutung, Taichung, Chiayi, Dueigaoyue, and Huisun areas, and the similarity within this group was 94.97%. There was only a 25.12% similarity between Co and Cof, revealing that these two species were considerably different. Furthermore, the similarity between Cf and these two species was significantly low, only 4.01%. These results are not only in good agreement with our previous findings but also in accordance with morphological and genetic classifications.[24,25] In addition, PCA was also performed to differentiate the data listed in Table 4. The results of the PCA score plot (Figure 3) indicated that PC1 and PC2 explained 84.77% and 10.52%, respectively, of the total variance. PCA can be quite useful in visualizing the relationships between responses of characteristic components in different species. As reported in the "Biplot Analysis" (Figure 3), the distribution of the groups indicated significant statistical differences among the different species. The PCA mapping clearly distinguished the samples according to their dominant volatile compounds, and they were clustered into three groups. The species Cf belongs to the group with a high content of α-pinene, while the other two species Cof and Co cluster in the opposite part of the graph since they contain only small amounts of this component. By contrast, the second group, Cof, contains high levels of thujopsene and β-elemol. The last group includes the species Co that contains higher contents of α-terpinyl acetate, L-bornyl acetate, sabinene, and limonene. These results showed that the above-mentioned compounds could be useful indicators for distinguishing Cf, Cof, and Co. Although it has been demonstrated that essential oil or SPME technique could be employed to discriminate these species, static-HS, compared with a conventional technique, hydrodistillation, involves shorter extraction time (50 min against 6 h for hydrodistillation) and lower energy cost. Furthermore, static-HS can accurately perform the essential oil/VOC compositions for different species, while the SPME technique shows highly selective adsorption toward chemicals, with the results slightly different from the real chemical profiles, even though it is a feasible and rapid technique for differentiating *Chamaecyparis* species.

It is notable that the major limitation of static-HS is that the concentrations of volatiles in the vapor phase were dependent on the partition coefficients. The sensitivity of headspace analysis is directly affected by the vapor pressure and boiling point of analyzed compounds. High and medium volatile compounds, such as monoterpene and sesquiterpene, usually have a reliable reproducibility; high-molecular-weight compounds, as well as tightly bound and encapsulated volatiles, are usually not suitably analyzed by headspace system.[26,27] The utility of headspace technique depends on whether the target analytes have enough concentration in a small amount of gas sample to be detected reliably by GC, due to limited capacity of gas chromatograph injection port (0.1−2.0 mL). One part per million (ppm) may be assayed in a reproducible way in general analytes (in some practical terms will reach ppb level) using this technique, but the technique is still less sensitive when compared to the purge and trap method (ppt level).[28] Equilibrium of volatile compounds in the headspace is highly temperature dependent. Elevating the temperature of the sample can assist in achieving equilibrium more quickly by

DOI: 10.1021/jf505587w
J. Agric. Food Chem. 2015, 63, 810−820

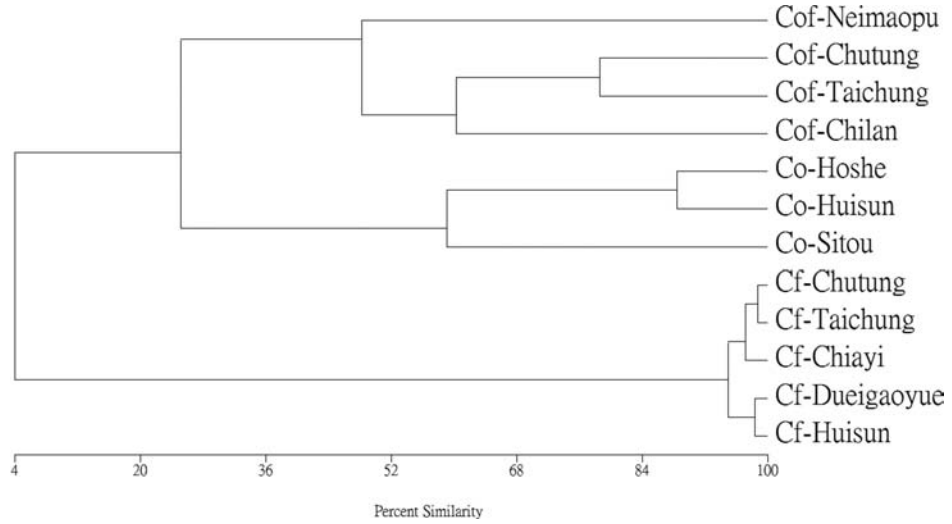

Figure 2. Similarity analysis of the volatile compositions from the three *Chamaecyparis* species.

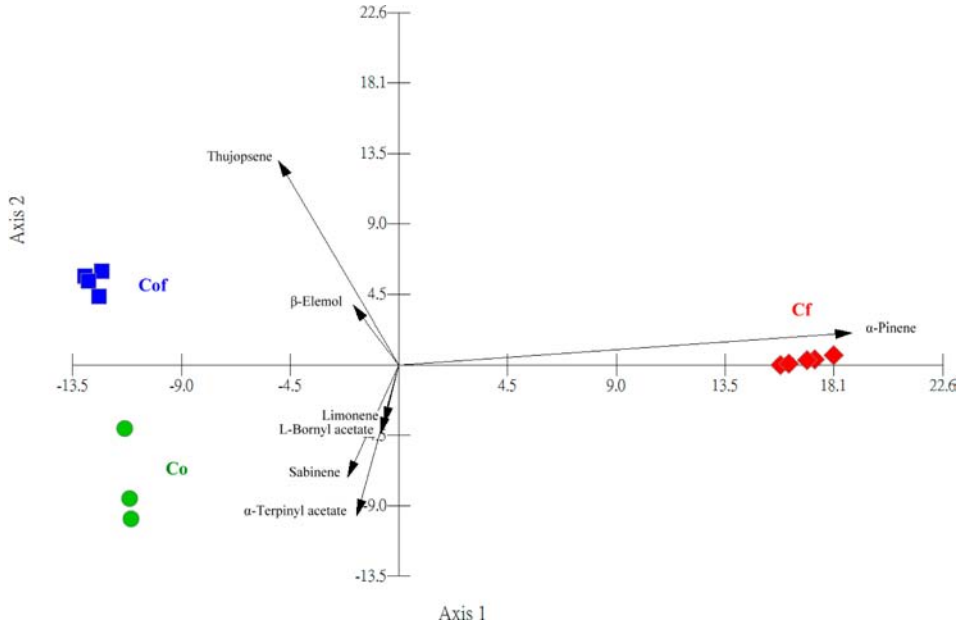

Figure 3. Biplot for PCA (principal component analysis) carried out on volatile compound contents of three *Chamaecyparis* species.

increasing the volatility of the analytes. Some sample matrices, such as oil samples, require higher temperature (160−200 °C) and longer equilibration times due to the slower diffusion rate in viscous or fusible crystalline systems.[26] However, in this experiment, 100−150 °C equilibrium temperature has shown a good correlation and identical chromatogram between VOCs and essential oils for most samples. It demonstrated that selectivity and loss of heavy compounds were not diminished with static-HS sampling in this study. In particular, static-HS has also been shown to be a good technique for agricultural quality management, such as bioactive components of medical plants and aroma quality control of grapes, by discriminating the characteristic compounds being used as indicators of different harvesting times/maturation stages.[11,29] These applications demonstrated that static-HS is a reproducible and reliable technique used in biochemical research and quality management.

Secondary metabolites (e.g., terpenoids and alkaloids) play important ecological roles in the relation of plants to their environment adaptation. Some kinds of phytochemical data are likely to be meaningful in determining phylogeny.[30] Terpenoids constitute an important class of secondary plant compounds that are further classified into various groups such as monoterpenoids (C_{10}), sesquiterpenoids (C_{15}), diterpenoids (C_{20}), triterpenoids (C_{30}), tetraterpenoids (C_{40}) and poly-C polyterpenoids. These compounds have been used in plant taxonomic studies, such as specific and subspecific distinction, geographic races, and hybrid detection.[31,32] Volatile monoterpenoids and sesquiterpenoids, the major components of essential oils, are the compounds most commonly used in taxonomy. For *Juniperus* (Cupressaceae), many studies have been conducted to determine the intraindividual, ontogenetic, seasonal, and population variations in these compounds.[32] Therefore, biochemical characteristics of plants have been employed taxonomically for a long time, and chemical compounds can be analyzed quantitatively using gas chromatography by integrating areas under the peaks for each compound, and qualitatively, which has been used extensively

DOI: 10.1021/jf505587w
J. Agric. Food Chem. 2015, 63, 810−820

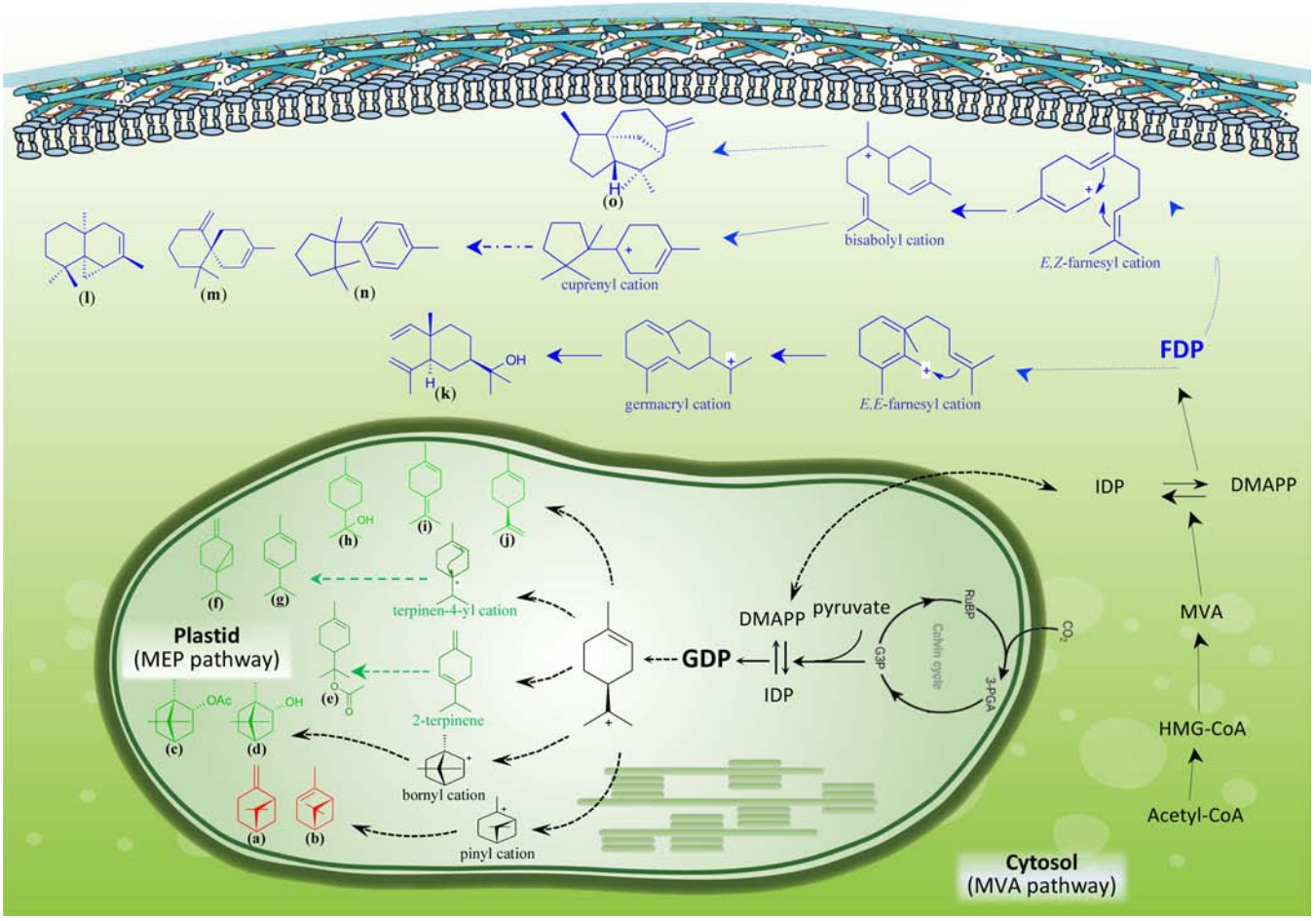

Figure 4. Biosynthetic pathway of the minor characteristic compounds from three *Chamaecyparis* species: (a) β-pinene; (b) α-pinene; (c) bornyl acetate; (d) L-borneol; (e) α-terpinyl acetate; (f) sabinene; (g) γ-terpinene; (h) α-terpineol; (i) terpinolene; (j) limonene; (k) β-elemol; (l) thujopsene; (m) (−)-β-chamigrene; (n) (+)-cuparene; (o) (+)-β-cedrene.

in plant systematics, using analyses of infraspecific variations to determine phylogenetic relationship of families and other high-level taxonomic groups.[31−33]

Characteristic Compounds. In addition to the aforementioned results, α-pinene, (−)-thujopsene, and α-terpinyl acetate play important roles as leading discriminators for distinguishing Cf, Cof, and Co. A few minor compounds also showed significant differences ($p < 0.05$) of relative abundance between these species. As can be seen from Table 4, sabinene, β-pinene, limonene, γ-terpinene, terpinolene, L-borneol, α-terpineol, L-bornyl acetate, α-terpinyl acetate, (+)-β-cedrene, thujopsene, (−)-β-chamigrene, and (+)-cuparene showed statistically significant difference between the three species, among which, for β-pinene, Cf had the highest content (1.94−3.44%), while the other two species had only rare contents. As for sabinene (8.55−24.58%), limonene (4.10−10.39%), γ-terpinene (2.09−3.57%), terpinolene (0.50−1.01%), L-borneol (0.08−0.20%), α-terpineol (0.15−0.27%), and L-bornyl acetate (6.48−11.38%), the species with a relatively high content of these compounds is Co. In the same way, for (+)-β-cedrene, (−)-β-chamigrene, and (+)-cuparene, Cof had the highest content among these three species. All characteristic compounds are widely occurring in coniferous trees as a constituent of essential oils. Various bioactivities have been demonstrated, such as inhibiting root growth of weed species,[34] antimicrobial and antioxidant properties,[35] and usage as an anticancer agent.[36] Some trends in distribution of terpenoids in distinct conifer families may already be observed and can be taken as valuable chemical characteristics, i.e., cedrene, chamigrene, and cuparene were usually associated with Cupressaceae.[37] Furthermore, β-pinene and γ-terpinene were assumed to be responsible for water stress in various studies.[20,38−40]

Interestingly, in terms of the biosynthesis pathway, these characteristic compounds associated with Cof were essentially derived from the mevalonate (MVA) pathway, while the compounds belonging to both Cf and Co were derived from the methylerythritol phosphate (MEP) pathway (Figure 4). MVA and MEP were two independent pathways for the biosynthesis of isoprenoid (also referred to as terpenoids) precursors coexisting within the plant cells.[41] The MVA pathway supplies acetyl CoA-derived precursors for the production of sesquiterpenes and triterpenes in cytosol, whereas the MEP pathway provides pyruvate-derived IPP and DMAPP for the biosynthesis of monoterpenes, diterpenes, and tetraterpenes in plastid.[42] Terpenoids characterize the greatest variety of metabolites with great diversities in structures and functions.[43] Monoterpenes and sesquiterpenes act as natural defense agents and are involved in communications between plants and their environments.[44] In many plant species, diterpenes and sesquiterpenes also act as phytoalexins.[45] They fulfill the same role but have some functional differences.[46] Terpenoids have a myriad of functions in ecological

DOI: 10.1021/jf505587w
J. Agric. Food Chem. 2015, 63, 810−820

interactions of living organisms. It is generally recognized that the most abundant compounds associate with activity toward pollinators, herbivores, or herbivore enemies. According to recent research perspectives, compounds present in minor amounts rather than major members of volatile blends are responsible for their biological activity.[47]

Furthermore, some terpenoids and primary metabolites function as antioxidants and play important roles in photosynthesis, with regulation of growth and development[48] attributed to the MEP pathway.[44,49] Many studies have confirmed that photosynthesis is the major source for the synthesis of IPP for MEP-derived terpenoids. Compared with the MVA pathway, the MEP pathway was closely connected with sugar metabolism.[50] On the other hand, plants treated with MEP or MVA pathway-specific inhibitors confirmed that the MVA pathway functions for plant development, and the MEP pathway functions for pigment formation in young tissues.[50] It was suggested that allocation of resources varies by species, and depends especially on the specific chemical defensive compounds produced.[51] Depending on species, phenological stages, ages, and genetics, plants might increase growth, secondary metabolite production, or combination of both in response to varied nutrients.[52] Terpenoids constitute the most diverse group of natural products, and have been used as models for the study of the evolution of chemical functions and of the ecological impacts of evolutionary change.[53] According to the distribution of habitat type and our preliminary experiment, Cof and Cf exhibit different characteristics of water use. It is worth further investigation to examine whether the characteristic compounds' coming from the MEP or MVA pathway would influence the plants' habitat adaptation.

In spite of inconsistent findings on a possible relationship between abiotic stress and essential oil quality,[40] the significant changes in relative contents could be a defense mechanism and a biochemical adaptation to environment constraints.[20] The potential relationship between these characteristic compounds and the regional distribution or evolution in these three *Chamaecyparis* species warrants more in-depth study.

In conclusion, the present study provides a novel strategy for objective discrimination of three *Chamaecyparis* species, according to the potential volatile compounds analyzed by static-HS/GC−MS. The parameters affecting the extraction efficiency were optimized. Besides being useful in chemotaxomical studies, this method opens new opportunities for estimating or determining the leaf essential oils of uninvestigated species. Additionally, chemometric methods, like one-way ANOVA, CA, and PCA, can highlight significant differences between the indiscernible species. For complete functional characteristics of feature compounds, further research is required to ascertain the possible correlation between chemical markers, environmental factors, and the evolution of the genus *Chamaecyparis*.

AUTHOR INFORMATION

Corresponding Author

*Phone: +886-2-33664626. Fax: +886-2-23654520. E-mail: peter@ntu.edu.tw.

Funding

This study was supported by a grant (103-2313-B-002-005-MY3) from the MOST (Ministry of Science and Technology, Taiwan).

Notes

The authors declare no competing financial interest.

ACKNOWLEDGMENTS

We thank Prof. B. T. Guan, Prof. S. T. Lin, Prof. I. L. Shiau, Prof. S. Y. Wang, Prof. Y. H. Tseng, and Y. R. Hsui for providing samples, and all members of the CHEMTREE laboratory for technical assistance. We also thank Prof. S. R. Kuo, Dr. T. F. Yeh, and Dr. K. F. Chung for their constructive and valuable comments. Special thanks to Chih-Kai Yang for contributing his photos.

REFERENCES

(1) Eckenwalder, J. E. *Conifers of the world: the complete reference*; Timber Press: Portland, 2009.

(2) Farjon, A. *A natural history of conifers*; Timber Press: Portland, OR, 2008.

(3) Matsui, N.; Ohira, T.; Hiramatsu, Y.; Imai, Y.; Miyazaki, Y. The composition of volatiles from tatami mats containing hinoki (*Chamaecyparis obtusa*) wood-wool and its decline over the long term. *J. Wood Sci.* **2007**, *53*, 529−532.

(4) Miyamoto, K.; Okuda, S.; Inagaki, Y.; Noguchi, M.; Itou, T. Within- and between-site variations in leaf longevity in hinoki cypress (*Chamaecyparis obtusa*) plantations in southwestern Japan. *J. For. Res.* **2013**, *18*, 256−269.

(5) Gerber, S.; Baradat, P.; Marpeau, A.; Arbez, M. Geographic variation in terpene composition of *Pinus nigra* Arn. *For. Genet.* **1995**, *2*, 1−10.

(6) Beltran Sanahuja, A.; Ramos Santonja, M.; Grane Teruel, N.; Martin Carratala, M. L.; Garrigos Selva, M. C. Classification of almond cultivars using oil volatile compound determination by HS-SPME-GC-MS. *J. Am. Oil Chem. Soc.* **2011**, *88*, 329−336.

(7) Chen, Y. J.; Lin, C. Y.; Cheng, S. S.; Chang, S. T. Phylogenetic relationships of the genus *Chamaecyparis* inferred from leaf essential oil. *Chem. Biodiversity* **2011**, *8*, 1083−1097.

(8) Lin, J.; Zhang, P.; Pan, Z.; Xu, H.; Luo, Y.; Wang, X. Discrimination of oolong tea (*Camellia sinensis*) varieties based on feature extraction and selection from aromatic profiles analysed by HS-SPME/GC−MS. *Food Chem.* **2013**, *141*, 259−265.

(9) Lin, C. Y.; Chen, Y. J.; Cheng, S. S.; Chang, S. T. Rapid differentiation of three *Chamaecyparis* species (Cupressaceae) grown in Taiwan using solid-phase microextraction-gas chromatography/mass spectrometry, cluster analysis, and principal component analysis. *J. Agric. Food Chem.* **2011**, *59*, 10854−10859.

(10) Escriche, I.; Kadar, M.; Juan-Borras, M.; Domenech, E. Using flavonoids, phenolic compounds and headspace volatile profile for botanical authentication of lemon and orange honeys. *Food Res. Int.* **2011**, *44*, 1504−1513.

(11) Gonzalez-Mas, M. C.; Garcia-Riano, L. M.; Alfaro, C.; Rambla, J. L.; Padilla, A. I.; Gutierrez, A. Headspace-based techniques to identify the principal volatile compounds in red grape cultivars. *Int. J. Food Sci. Technol.* **2009**, *44*, 510−518.

(12) Marton, D.; Tapparo, A.; Di Marco, V. B.; Repice, C.; Giorio, C.; Bogialli, S. Ultratrace determination of total and available cyanides in industrial wastewaters through a rapid headspace-based sample preparation and gas chromatography with nitrogen phosphorous detection analysis. *J. Chromatogr. A* **2013**, *1300*, 209−216.

(13) Chatzopoulou, P. S.; Katsiotis, S. T. Headspace analysis of the volatile constituents from *Juniperus communis* L 'berries' (cones) grown wild in Greece. *Flavour Fragrance J.* **2006**, *21*, 492−496.

(14) Kruma, Z.; Karklina, D.; Zalane, I.; Sabovics, M. Total phenol content and aromatic compounds variation among *Latvian medical* plants depending on vegetative stage. *Planta Med.* **2009**, *75*, 1065−1065.

(15) Silvestrini, E.; Michelozzi, M.; Skroppa, T.; Brancaleoni, E.; Ciccioli, P. Characterisation of different clones of *Picea abies* (L.) Karst using head-space sampling of cortical tissues combined with enantioselective capillary gas chromatography for the separation of

DOI: 10.1021/jf505587w
J. Agric. Food Chem. 2015, 63, 810−820

chiral and non-chiral monoterpenes. *J. Chromatogr. A* **2004**, *1034*, 183−189.
(16) Adams, R. P. *Identification of essential oil components by gas chromatography/mass spectorscopy*; Allured Pub. Corp.: Carol Stream, IL, 2007.
(17) Gabriel, K. R. The biplot graphic display of matrices with application to principal component analysis. *Biometrika* **1971**, *58*, 453−467.
(18) Anslyn, E. V.; Dougherty, D. A. *Modern physical organic chemistry*; University Science: Sausalito, CA, 2006.
(19) Cheng, S. S.; Lin, C. Y.; Gu, H. J.; Chang, S. T. Antifungal activities and chemical composition of wood and leaf essential oils from *Cunninghamia konishii*. *J. Wood Chem. Technol.* **2011**, *31*, 204−217.
(20) Rebey, I. B.; Jabri-Karoui, I.; Hamrouni-Sellami, I.; Bourgou, S.; Limam, F.; Marzouk, B. Effect of drought on the biochemical composition and antioxidant activities of cumin (*Cuminum cyminum* L.) seeds. *Ind. Crop. Prod.* **2012**, *36*, 238−245.
(21) Raveane, L.; Tisato, F.; Isak, I.; Traldi, P. Analyses of BioVOCs variation related to vegetation predominance in the natural park of ampezzo dolomites, UNESCO world heritage area of dolomites. *J. For. Res.* **2013**, *24*, 439−448.
(22) Goren, A. C.; Topcu, G.; Bilsel, G.; Bilsel, M.; Wilkinson, J. M.; Cavanagh, H. M. A. Analysis of essential oil of *Satureja thymbra* by hydrodistillation, thermal desorber, and headspace GC/MS techniques and its antimicrobial activity. *Nat. Prod. Res.* **2004**, *18*, 189−195.
(23) Barra, A. Factors affecting chemical variability of essential oils: a review of recent developments. *Nat. Prod. Commun.* **2009**, *4*, 1147−1154.
(24) Liao, P. C.; Lin, T. P.; Hwang, S. Y. Reexamination of the pattern of geographical disjunction of *Chamaecyparis* (Cupressaceae) in North America and East Asia. *Bot. Stud.* **2010**, *51*, 511−520.
(25) Lin, T. P.; Lee, T. Y.; Yang, L. F.; Chung, Y. L.; Yang, J. C. Comparison of the allozyme diversity in several populations of *Chamaecyparis formosensis* and *Chamaecyparis taiwanensis*. *Can. J. For. Res.* **1994**, *24*, 2128−2134.
(26) Hui, Y. H. *Handbook of fruit and vegetable flavors*; Wiley: Hoboken, NJ, 2010.
(27) Warner, K.; Eskin, N. A. M. *Methods to assess quality and stability of oils and fat-containing foods*; AOCS Press: Champaign, IL, 1995.
(28) Marsili, R. *Flavor, fragrance, and odor analysis*; Marcel Dekker: New York, 2002.
(29) Fang, F.; Cheng, Z. H.; Guo, Y. L.; Cai, Y. B. Comparative analysis of the volatile components in the fresh roots and rhizomes of *Curcuma wenyujin* by static headspace gas chromatography mass spectrometry. *Chin. J. Chem.* **2006**, *24*, 1346−1351.
(30) Stuessy, T. F. *Plant Taxonomy: The Systematic Evaluation of Comparative Data*, 2nd ed.; Columbia University Press: 2009.
(31) Neilson, E. H.; Goodger, J. Q. D.; Woodrow, I. E.; Moller, B. L. Plant chemical defense: at what cost? *Trends Plant Sci.* **2013**, *18*, 250−258.
(32) Menze, B. H.; Kelm, B. M.; Masuch, R.; Himmelreich, U.; Bachert, P.; Petrich, W.; Hamprecht, F. A. A comparison of random forest and its Gini importance with standard chemometric methods for the feature selection and classification of spectral data. *BMC Bioinf.* **2009**, *10*, 213.
(33) Lienert, D.; Anklam, E.; Panne, U. Gas chromatography mass spectral analysis of roots of *Echinacea* species and classification by multivariate data analysis. *Phytochem. Anal.* **1998**, *9*, 88−98.
(34) Chowhan, N.; Singh, H.; Batish, D.; Kaur, S.; Ahuja, N.; Kohli, R. β-Pinene inhibited germination and early growth involves membrane peroxidation. *Protoplasma* **2013**, *250*, 691−700.
(35) Jordán, M. J.; Lax, V.; Rota, M. C.; Lorán, S.; Sotomayor, J. A. Effect of the phenological stage on the chemical composition, and antimicrobial and antioxidant properties of *Rosmarinus officinalis* L essential oil and its polyphenolic extract. *Ind. Crop. Prod.* **2013**, *48*, 144−152.
(36) Aydin, E.; Turkez, H.; Geyikoglu, F. Antioxidative, anticancer and genotoxic properties of α-pinene on N2a neuroblastoma cells. *Biologia* **2013**, *68*, 1004−1009.
(37) Otto, A.; Wilde, V. Sesqui-, di-, and triterpenoids as chemosystematic markers in extant conifers—A review. *Bot. Rev.* **2001**, *67*, 141−238.
(38) Bettaieb, I.; Knioua, S.; Hamrouni, I.; Limam, F.; Marzouk, B. Water-deficit impact on fatty acid and essential oil composition and antioxidant activities of Cumin (*Cuminum cyminum* L.) Aerial Parts. *J. Agric. Food Chem.* **2011**, *59*, 328−334.
(39) Khorasaninejad, S.; Mousavi, A.; Soltanloo, H.; Hemmati, K.; Khalighi, A. The effect of drought stress on growth parameters, essential oil yield and constituent of Peppermint (*Mentha piperita* L.). *J. Med. Plants Res.* **2011**, *5*, 5360−5365.
(40) Leicach, S. R.; Garau, A. M.; Guarnaschelli, A. B.; Grass, M. A. Y.; Sztarker, N. D.; Dato, A. Changes in *Eucalyptus camaldulensis* essential oil composition as response to drought preconditioning. *J. Plant Interact.* **2010**, *5*, 205−210.
(41) Saiman, M. Z.; Mustafa, N. R.; Pomahocova, B.; Verberne, M.; Verpoorte, R.; Choi, Y. H.; Schulte, A. E. Analysis of metabolites in the terpenoid pathway of *Catharanthus roseus* cell suspensions. *Plant Cell, Tissue Organ Cult.* **2014**, *117*, 225−239.
(42) Besser, K.; Harper, A.; Welsby, N.; Schauvinhold, I.; Slocombe, S.; Li, Y.; Dixon, R. A.; Broun, P. Divergent regulation of terpenoid metabolism in the trichomes of wild and cultivated tomato species. *Plant Physiol.* **2009**, *149*, 499−514.
(43) Hemmerlin, A. Post-translational events and modifications regulating plant enzymes involved in isoprenoid precursor biosynthesis. *Plant Sci.* **2013**, *203*, 41−54.
(44) Kumari, S.; Priya, P.; Misra, G.; Yadav, G. Structural and biochemical perspectives in plant isoprenoid biosynthesis. *Phytochem. Rev.* **2013**, *12*, 255−291.
(45) Cheng, A. X.; Lou, Y. G.; Mao, Y. B.; Lu, S.; Wang, L. J.; Chen, X. Y. Plant terpenoids: biosynthesis and ecological functions. *J. Integr. Plant Biol.* **2007**, *49*, 179−186.
(46) Chadwick, M.; Trewin, H.; Gawthrop, F.; Wagstaff, C. Sesquiterpenoids lactones: benefits to plants and people. *Int. J. Mol. Sci.* **2013**, *14*, 12780−12805.
(47) Clavijo McCormick, A.; Gershenzon, J.; Unsicker, S. B. Little peaks with big effects: establishing the role of minor plant volatiles in plant-insect interactions. *Plant Cell Environ.* **2014**, *37*, 1836−44.
(48) Rodriguez-Concepcion, M.; Fores, O.; Martinez-Garcia, J. F.; Gonzalez, V.; Phillips, M. A.; Ferrer, A.; Boronat, A. Distinct light-mediated pathways regulate the biosynthesis and exchange of isoprenoid precursors during *Arabidopsis* seedling development. *Plant Cell* **2004**, *16*, 144−156.
(49) Bouvier, F.; Rahier, A.; Camara, B. Biogenesis, molecular regulation and function of plant isoprenoids. *Prog. Lipid Res.* **2005**, *44*, 357−429.
(50) Hemmerlin, A.; Harwood, J. L.; Bach, T. J. A raison d'être for two distinct pathways in the early steps of plant isoprenoid biosynthesis? *Prog. Lipid Res.* **2012**, *51*, 95−148.
(51) Burney, O. T.; Jacobs, D. F. Ungulate herbivory of regenerating conifers in relation to foliar nutrition and terpenoid production. *For. Ecol. Manage.* **2011**, *262*, 1834−1845.
(52) Burney, O. T.; Jacobs, D. F. Ungulate herbivory of boreal and temperate forest regeneration in relation to seedling mineral nutrition and secondary metabolites. *New For.* **2013**, *44*, 753−768.
(53) Theis, N.; Lerdau, M. The evolution of function in plant secondary metabolites. *Int. J. Plant Sci.* **2003**, *164*, S93.

DOI: 10.1021/jf505587w
J. Agric. Food Chem. 2015, 63, 810−820

JOURNAL OF AGRICULTURAL AND FOOD CHEMISTRY

Article

pubs.acs.org/JAFC

Development of an Isoform-Specific Tandem Mass Spectrometry Assay for Absolute Quantitation of Maize Lipid Transfer Proteins

Severin E. Stevenson,[†] Scott McClain,[‡] and Jay J. Thelen*[,†]

[†]University of Missouri, Department of Biochemistry, Christopher Bond Life Sciences Center, 1201 Rollins Avenue, Columbia, Missouri 65211, United States

[‡]Syngenta Crop Protection, LLC, 3054 East Cornwallis Road, Research Triangle Park, North Carolina 27709, United States

Supporting Information

ABSTRACT: Precise and accurate quantitation of maize grain allergens is important for seed and food industries. The major allergen in maize grain is Zea m 14, a lipid transfer protein (LTP). The B73 maize genome encodes for at least six LTPs sharing 15%−87% sequence identity to Zea m 14. Phylogenetic analysis of the maize LTP family revealed one gene that corresponds to Zea m 14 (denoted as LTPa) and two other genes sharing 43% (LTPc) and 74% (LTPb) identity with Zea m 14 that are putative homologues. Using stable isotope peptide mimics as internal standards for LTPs, we present a multiple reaction monitoring mass spectrometry approach for multiplexed, absolute quantitation of all three LTP proteins and alternative transcript models therein. To validate quantitative accuracy, a redundant peptide, simultaneously representing the two most abundant LTPs, was included. Analysis of 21 maize varieties revealed LTPa was most prominently expressed in maize grain, ranging from 9 to 32 μg LTP/mg protein. Proteins belonging to the LTPb and LTPc gene models were also expressed but at approximately 10- and 100-fold lower levels than LTPa, respectively. The quantitative results provided by the redundant peptide show around 95% agreement with the sum of the two unique peptides, thus providing support for the LTP gene models and validating the accuracy of this method. Though not all Zea m 14-related LTPs are abundant in grain, their high sequence homology and detectable expression in maize grain signify that LTPb and LTPc are putative allergens and should be accounted for in any quantitation strategy for maize LTP allergens.

KEYWORDS: *LC-MS/MS, MRM, LTP, lipid transfer protein, allergen, maize, Zea mays, AQUA-MRM, quantitation*

INTRODUCTION

Reports on the food allergenicity of maize grain are few despite significant maize consumption on a global basis.[1,2] Some cases of allergenicity to maize have been reported;[3−8] though not all cases can be confirmed as representing true food allergenicity. For example, research by Jones et al.[7] and, separately, Pasini et al.[9] have found that less than half of subjects with positive skin prick tests (SPT) or CAP-FEIA (fluorescence enzyme immunoassay) to maize reacted clinically to an oral challenge. In 2000, Pastorello et al. discovered a salt-soluble IgE-binding component of maize flour, a 9 kDa protein, Zea m 14, and suggested it represents the major allergen of maize responsible for food induced allergic reactions.[3] Zea m 14 was identified as lipid transfer protein (LTP), a ubiquitous protein belonging to the pathogen resistant group of plant proteins. Sera from 86% of patients with systemic symptoms after maize grain ingestion and positive SPT exhibited immunoreactivity to this 9 kDa protein.[3,10] LTP is now acknowledged to be the major allergen in maize grain.

At the cellular level, LTPs are generally located in the apoplast, and most of these proteins contain eight conserved cysteines forming four disulfide bridges, which make them highly resistant to loss of transfer function at high temperature or pH changes.[11] As a group, plant LTPs display a high degree of structural homology, as revealed by sequence alignment and hydrophobic cluster analysis.[12,13] In 1994, a unifying nomenclature for pathogenesis-related proteins (PRs) was proposed on the basis of their sequence, enzymatic, or biological activity.[14] Recently this list has been extended to contain 14 families, including the PR-14-type proteins referred to as LTPs.

Expression analysis by immunoblotting of Zea m 14, based on IgG polyclonal antibody detection specific for an LTP peptide, indicated that its abundance varies in mature grain from various maize hybrids grown under different conditions. Significant differences in relative LTP abundance (up to 10-fold differences) between maize hybrids were demonstrated and occurred across a greater range (up to 20-fold) in nonirrigated plots, indicating differences in allergenic potential.[15,16] The natural variation in protein allergen expression in food crops is in part due to differences in the genetic backgrounds of commercial nongenetically modified (GM) varieties, and interactions with the environment such as nutrient and water availability, differences in moisture, temperature, plant pathogens, harvest timing, and storage conditions.[17] Recent work in soybean shows that both genetics and environmental differences contribute to allergen expression levels, with environment playing the larger role among related breeding lines.[18] Although LTPs from botanically related plants share IgE-binding epitopes,[19] it has been shown that patients allergic to LTPs show a high variability in the IgE reactivity to vegetable

Received: September 29, 2014
Revised: December 19, 2014
Accepted: December 24, 2014
Published: December 24, 2014

ACS Publications © 2014 American Chemical Society

DOI: 10.1021/jf504708u
J. Agric. Food Chem. 2015, 63, 821−828

foods, including maize.[15] However, at present it remains unclear how patient allergy to maize LTP may vary in response to the actual exposure levels in various maize-derived foods.

The technical objectives for developing a LTP detection method were focused on verifying the number of related LTP isoforms and whether these can be quantified individually with precision, reliability, and accuracy. Currently there is no rapid quantitative method for analyzing multiple isoforms of LTP in a multiplexed manner. Western blot analysis represents a well-established, robust, and reliable method to accurately detect specific proteins within a multitude of matrix compounds, such as those found in seeds, including endogenous allergens in their host plant matrices.[20,21] LTP was first characterized by IgE-binding studies using the Western blot format.[22] Typically, LTP has been studied with human serum and detecting IgE antibody binding, as is the case with most allergens for the purpose of characterizing patient responses, as well as identifying newly discovered protein allergens. However, for the purpose of characterizing LTP content (and isoforms therein) in maize, a more selective and accurate analytical approach is desirable and may be preferred for supporting further study of all related LTP isoforms and their content in foods, allergen preparations (used for clinical allergy studies), and GMO plants (as a means to identify allergen risk).

MATERIALS AND METHODS

Reagents. All reagents were purchased from Research Products International Corp. (Mount Prospect, IL, USA) unless stated otherwise. Organic solvents were purchased from Sigma-Aldrich (St. Louis, MO, USA) unless stated otherwise. AQUA peptide standards, containing either a C-terminal heavy lysine or arginine, were custom synthesized by Sigma Life Science Custom Products (The Woodlands, TX, USA).

LTP Homology Assessment. Phylogenetic analysis was performed using the "One-click" Phylogeny.fr.[23] Pairwise alignments were performed using ClustalO on UniProtKB (http://www.uniprot.org/uniprot/), and percent identity values were recorded.

Maize Grain Samples. The goal was to develop LTP analytical capability using a broad sampling of maize across various breeding backgrounds and production locations under varying environmental conditions. Samples of grain (approximately 50 g of whole grain) were taken as subsamples from bags of mature and harvested maize. The maize varietal characteristics and breeding histories were not taken into account in the LTP analysis in this work in terms of data interpretation. Supporting Information (SI) Table 1 is provided to show the variety of production years, hybrid varieties, and production locations.

Protein Extraction. Total protein was extracted from a sample subset of five maize kernels from each maize variety. Five replicates were prepared for each variety. Each sample was homogenized and total protein was extracted using a phenol partition protocol[24] modified for smaller volumes. Briefly, five maize kernels from each replicate in each variety were weighed and pulverized for 30 s using a 50 mL Waring blender. One hundred milligrams (±5 mg) were portioned for each sample, which represents a single biological replicate. Extraction buffer (1:1 mix of sucrose buffer (0.9 M sucrose, 100 mM Tris-HCl pH 8.0, 10 mM EDTA, 0.4% ß-mercaptoethanol) and Tris buffered phenol (pH 8.0) were added to each sample in a 1:60 ratio (mL buffer: mg sample). Samples were shaken for 1 h at 4 °C using a Bead Ruptor 24 (Omni International, Kennesaw, GA, USA) on speed 1. Sample tubes were centrifuged at 17000*g* at 4 °C for 5 min in a benchtop centrifuge. The upper phenol phase was transferred to a new tube and was back extracted with 1 volume of fresh sucrose buffer by vortexing lightly at room temperature for 5 min and repeating the centrifugation step above. The phenol phase was removed and protein precipitated with five volumes of ice-cold precipitation solution (0.1 M ammonium acetate in 100% methanol). The samples were vortexed and incubated for 16 h at −20 °C to precipitate the protein. Protein was pelleted by centrifugation at 4000*g* for 10 min at 4 °C and then washed twice with 1 mL of 0.1 M ammonium acetate in methanol, twice with 1 mL of ice-cold 80% (v/v) acetone in water, and once in 1 mL of 70% (v/v) ethanol in water. Protein pellets were stored in 0.5 mL of 70% (v/v) ethanol at −20 °C. Each of the five replicates was analyzed separately using mass spectrometry.

Preparation of Samples for AQUA-MRM. Protein was dissolved in a chaotrope-containing buffer (8 M urea, 50 mM Tris-HCl, pH 8.0) followed by quantification using the Bradford assay (Bio-Rad Laboratories Inc., Hercules, CA, USA) with bovine gamma globulin standard (2 mg/mL, Bio-Rad). Maize protein was portioned (20 μg/sample) and spiked with AQUA peptides (dissolved in 50% (v/v) acetonitrile (ACN), 1% (v/v) formic acid) at 50 fmol/μg, prior to chemical treatment. Protein was reduced by adding dithiothreitol (DTT) to 10 mM and incubated for 1 h at RT. Alkylation was performed by adding iodoacetamide (IAA) to 50 mM and incubated at RT in the dark for 1 h. Urea was diluted and IAA neutralized by adding 3 volumes of a solution containing 10 mM ammonium bicarbonate and 10 mM DTT. Trypsin (Promega, Madison, WI, USA) was added to sample protein at a 1:49 ratio and digestion proceeded for 18 h at 37 °C. After digestion, samples were frozen at −80 °C and evaporated to dryness using a Centrivap (ThermoFisher Scientific, Waltham, MA, USA). Dried protein digests were dissolved immediately prior to mass spectrometry analysis to a concentration of 0.40 μg/μL with 5% (v/v) ACN, 0.1% formic acid (v/v) in water.

Verification of Complete Protein Digestion. Trypsin digests of proteins were qualitatively assessed by SDS-PAGE and staining with colloidal Coomassie Brilliant Blue dye (CBB). Briefly, digested protein remaining from the samples used for the AQUA-MRM analysis was combined from the five sample replicates and lyophilized to dryness. Remaining undigested protein from samples prepared for AQUA-MRM analysis was also pooled from the five sample replicates. Both undigested and digested samples were diluted or dissolved, respectively, with SDS-PAGE sample buffer to 1 μg/μL, based upon calculations prior to digestion. Twenty-five microliters (25 μg) was loaded into wells of Any kD Mini-PROTEAN TGX PAGE gels (Bio-Rad Laboratories Inc., Hercules, CA, USA). PageRuler Plus (Thermo Scientific, Carlesbad, CA, USA) was used as protein standard. Gels were resolved as recommended by the manufacturer, until the dye front was ∼1.0 cm from the bottom of the gel. Gels were stained overnight with CBB and destained in water for 6 h before imaging.

Sample Preparation for Discovery Analysis. To assess the LTP component in maize kernels, four representative kernel varieties were assayed using two complementary untargeted "discovery" proteomics workflows: GeLC and in-solution digestion. Protein for these experiments was extracted, dissolved, and assayed for concentration as described in *Protein extraction* and *Verification of complete protein digestion*. Fifty micrograms of protein from each variety was either digested in-solution (without AQUA addition) or resolved by SDS-PAGE. SDS-PAGE and in-solution digestion were performed as described in *Verification of complete protein digestion* and *Preparation of samples for AQUA-MRM*, but using Precision Plus protein standard for SDS-PAGE (Bio-Rad Laboratories Inc., Hercules, CA, USA). For in-gel digestion, the stained region between 20 kDa and 10 kDa was excised and processed as in ref 24.

Discovery Mass Spectrometry. Discovery LC-MS/MS was performed with an Orbitrap mass spectrometer (Thermo Fisher Scientific, Bremen, DE). Resolution settings were 30,000 for MS1 (m/z range of 300−2000) and unit resolution for MS2 acquisitions. Data-dependent acquisition was employed using one MS scan followed by nine MS2 scans for the nine most abundant ions, with dynamic exclusion enabled. Peptides were concentrated and desalted in-line using a C_8 CapTrap, peptide trapping cartridge (Michrom Bioresources, Auburn, CA USA) prior to MS analysis. HPLC separations were performed using in-house fused silica nanospray needles, 10.5 cm length, (360 μm outer diameter, 150 μm inner diameter; Polymicro Technologies, Phoenix, AZ USA), that were packed with "Magic C18AQ" (200 Å, 5 μm particles; Michrom

DOI: 10.1021/jf504708u
J. Agric. Food Chem. 2015, 63, 821−828

Table 1. LTPs Identified during the Discovery Proteomics Experiment[a]

Accession	Description	Organism	MM (kDa)
GRMZM2G071575_T01	LTP	maize	18.89
GRMZM5G898755_T01	nonspecificLTP4pre	maize	12.29
GRMZM5G898755_T02	nonspecificLTP4pre	maize	13.32
GRMZM2G101958_T01	phosphoLTP1	maize	11.74
GRMZM2G010868_T01	LTP	maize	11.72
GRMZM2G010868_T02	LTP	maize	11.51
P19656	NLTP_MAIZE|phosphoLTP1	maize	11.70
GRMZM2G137329_T01	nonspecific_LTPpre	maize	9.86
GRMZM2G081464_T01	nonspecific_LTP2	maize	10.30
P83506	NLTP2	maize	7.31
Q2QYL2	NLT2B_ORYSJ|nLTP2b1pre	rice	11.44
Q7XJ39	NLT2A_ORYSJ|nLTP2a	rice	11.49
Q43194	NLTP2_SORBI|nLTP2	sorghum	11.95

[a]All proteins that shared homology with Zea m 14 based on local BLAST analysis against the list of all identified proteins, and less than 20 kDa, are listed here. Descriptions were provided by maizesequence.org or UniProt.org websites. Molecular mass (MM) for each entry is noted.

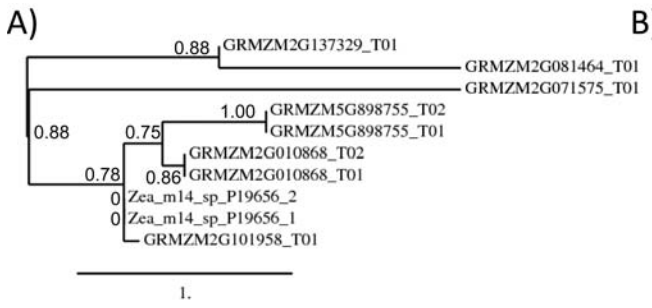

B)

Abbv	Accession	% Identity
Zea m 14	Zea m 14 (sp|P19656-2)	100.0%
	Zea m 14 (sp|P19656-1)	92.2%
LTPa	GRMZM2G101958_T01	86.8%
LTPb	GRMZM2G010868_T01	74.4%
	GRMZM2G010868_T02	74.4%
LTPc	GRMZM5G898755_T01	43.1%
	GRMZM5G898755_T02	42.9%
	GRMZM2G137329_T01	28.9%
	GRMZM2G081464_T01	20.9%
	GRMZM2G071575_T01	15.1%

Figure 1. Sequence homology of LTPs found by LC-MS/MS showing relatedness to Zea m 14 (sp|P19656). (A) Phylogram of the top maize proteins (translated gene sequences) identified during the discovery experiment. Zea_m14_sp_P19656_1 and 2 represent the two isoforms of UniProt entry P19656, both of which are recognized as LTP allergen Zea m 14. Other entries containing T01 and T02 indicate putative, annotated splice variants. Numbers at branch points are branch support values. (B) Pairwise Clustal Omega percent identity scores from alignments performed between Zea m 14 isovariant 2 and the other listed accessions. LTPs in gray have greater than 42% sequence identity with Zea m 14−2 and were given an abbreviation (Abbv column) to simplify nomenclature. These same LTPs were also clustered together phylogenetically (shown in A).

Bioresources) with an ACN gradient from 2 to 45% ACN over 80 min, followed by 17 min for column washing and equilibration. RAW files were searched using SEQUEST (v 1.20) via Proteome Discoverer (v 1.3.0.339) with three databases: UniProt/SwissProt (November, 2012), B73 genome (5b.60, maizesequence.org), and Zea maize UniGene translated transcriptome (Zm166, via NCBI) with carbamidomethylation as a fixed modification for cysteines, methionine oxidation as a variable modification, a parent ion mass tolerance of 20 ppm, and a fragment ion mass tolerance of 0.80 Da. Results were filtered using mass accuracy and confidence filters of 10 ppm and high, respectively.

Targeted AQUA-MRM Mass Spectrometry. Targeted mass spectrometric analysis was performed on a column with 2 μg of protein digestion and a 5 μL loading volume. The linear range of the endogenous analyte was assessed from the maximum possible loading amount, 2.4 μg/injection to 0.0038 μg/injection by 5-fold serial dilutions (SI Figure 1). Autosampling, chromatography, and mass spectrometry were performed as described in ref 18 while using the application-specific transition ions for the LTP AQUA-MRM (SI Table 2). Analysis was conducted within the predetermined linear range of quantification for the AQUA peptides, which was determined for individual transition ions (four most intense). Each LTP AQUA peptide was used as an internal control at 200 fmol/injection, which is within the linear quantitative range.

Determination of LTP Concentration in Biological Samples. The concentration of each native LTP isoform and variants therein was calculated using the response ratio (native/AQUA peptide) for a single transition ion, multiplied by the concentration of the AQUA internal standard. The concentration was expressed as μg LTP/mg of total protein extracted from maize kernel for each LTP in each maize extract and was calculated as follows:

Calculation 1: [Response ratio from mass spectrometer × fmol of AQUA peptide/1 μg of protein sample = fmol of native peptide/μg of protein sample]; Calculation 2: [moles of native LTP × FW (g/mol) of LTP = g LTP/μg of protein sample]; Calculation 3: [g LTP × (1 × 10^6 μg LTP/g LTP) × (1000 μg protein sample/1 mg protein sample) = μg LTP/mg protein sample].

RESULTS

LTP Discovery Proteomics. Although the Zea m 14 allergen has been described as the major maize grain allergen, the recognition that LTP proteins would likely be expressed as a family of isoforms provided the impetus to survey and characterize the "total LTP load" that a maize variety may express. An initial discovery experiment was conducted to assess the diversity of LTPs in representative samples. Orbitrap mass spectrometry was used to accurately identify measurable peptides for the targeted and expressed LTPs in four representative varieties of maize. Two complementary peptide preparation methodologies were used: one method utilized fractionation by SDS-PAGE while the other used unfractionated "total" protein. Both peptide preparations were subjected to LC-MS/MS and protein identification workflows searching three databases: UniProt/Swiss-Prot, *Zea mays* B73 inbred translated genome, and the *Zea mays* UniGene transcriptome. Putative LTPs were extracted from the list of discovered

DOI: 10.1021/jf504708u
J. Agric. Food Chem. 2015, 63, 821−828

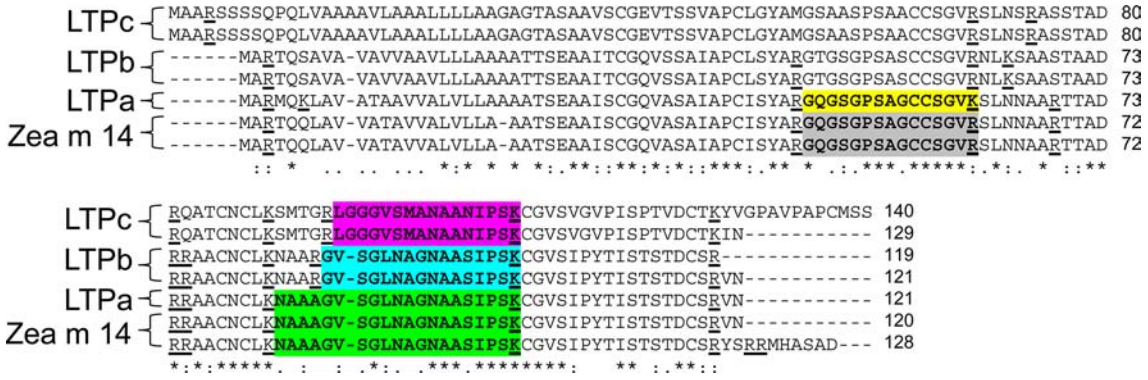

Figure 2. LTP protein alignment showing peptides for AQUA analysis. Ideal, quantitative tryptic peptides are highlighted. Specificity is indicated by color. Putative splice variants are paired by brackets. Each LTP has at least one peptide that distinguishes it, and two of them share one peptide (green). Trypsin cleavage sites are heavy underscored. Amino acid positions are indicated at the ends of each line.

proteins using molecular weight filters (20 kDa) and local BLAST analysis via BioEdit software using Zea m 14 as a query sequence; 20 kDa was the upper limit as a rational filter considering the LTP proteins are not likely to exceed ~13−15 kDa. In total, 13 LTP sequence listings (accessions) were identified from the four biological samples with high confidence, including Zea m 14 (P19656 in UniProt, Table 1). Two of the 13 accessions, GRMZM2G010868 and GRMZM5G898755, each had two splice variants annotated in the maize genome database (www.maizesequence.org). One of them, P19656, had an isoform annotated in UniProt, P19656-2 (http://www.uniprot.org/uniprot/). Three others, Q2QYL2, Q7XJ39, and Q43194, were from nonmaize sources, and were excluded.

LTP Homology Assessment. To create an AQUA-MRM assay that quantified all selected LTP paralogs to allergen Zea m 14, the ten maize LTPs discovered during our proteomic screen of various maize proteomes were grouped by their phylogenetic relationships (Figure 1A). A clear relationship was apparent between Zea m 14 and maize gene loci GRMZM2G10 1958, GRMZM2G010868, and GRMZM5G898755, including both presumptive splice variants for the two latter loci. In addition, sequence identity was assessed by pairwise sequence alignments between each LTP and Zea m 14 (Figure 1B). The percent identity scores for the seven proteins that grouped closest to Zea m 14 in the phylogram also shared the highest sequence identity with greater than 42% identity. It should be noted that none of the maize B73 loci were 100% identical to Zea m 14, although GRMZM2G101958 was closest at 87%. Taken together, these results show that, of the maize LTP candidate proteins, GRMZM2G101958, GRMZM2G010868, and GRMZM5G898755 are most similar to Zea m 14 and reasonably could contribute to food allergenicity based on a level of shared identity and function homology that may lead to cross-reactivity/cross-sensitization; for well described allergens such as those from pollen, this would generally be 50% shared identify or more.[25] To simplify nomenclature, the isoforms and splice variants for LTPs with greater than 42% identity to Zea m 14 were grouped and named LTPa, b and c (Figure 1B).

Sequence Assessment of LTPs. The feasibility of using AQUA-MRM as a quantitation method for these small and highly similar proteins was assessed using sequence alignment and manual sequence inspection. All isoforms and splice variants of Zea m 14, LTPa, LTPb, and LTPc were aligned using Clustal Omega (Figure 2). Possible tryptic peptides were critiqued for their selectivity and appropriateness for use as AQUA-MRM standards (i.e., labeled peptides to be included in each sample analysis[26]). The N-terminus of all LTPs had very few tryptic cleavage sites. LTPa has a peptide that starts at residue 48, and an analogous peptide in Zea m 14 starts at residue 47. These peptides differ in the C-terminal cleavage site, with LTPa having a Lys and Zea m 14 having an Arg (GQGSGPSAGCCSGVK and GQGSGPSAGCCSGVR). Neither peptide has neighboring downstream cleavage sites or double cleavage sites that could lead to "ragged ends", as was the case for the analogous peptide in LTPb, which has a C-terminal arginine with a lysine two residues away (GTGSGP SASCCSGV**R**NL**K**). LTPb also has only one available peptide at residue 87 (GVSGLNAGNAASIPSK). LTPc has only one available peptide which starts at residue 88 (LGGGVSMANAA NIPSK). LTPa and Zea m 14 both have a second available peptide which is shared between them, which starts at residue 84 in LTPb and 83 in Zea m 14 (NAAAGVSGLNAGNA ASIPSK). This second peptide is an improvement on the first peptide, as it is free from modifiable amino acids which negatively affect protein quantitation by AQUA-MRM. In addition, this second peptide can be used in parallel to measure both of these proteins (Zea m 14s and LTPa) together, while their first peptide can provide the quantities of each separately. Because AQUA-MRM quantitation yields molar quantities for target analytes, the quantities of Zea m 14 and LTPa as measured by their independent peptides can be directly compared to the signal of the second, conserved peptide (NAAAGVSGLNAGNAASIPSK; Figure 2, green). Theoretically, the quantity of the second peptide, which is shared between them, should equal the sum of the concentration of the two isoform-specific peptides (Figure 2, gray and yellow peptides). This assay design was pursued to reveal whether Zea m 14 (P19656-1) and its isovariant (P19656-2) were *bona fide* proteins, as neither is a perfect match to B73 gene locus GRMZ M2G101958 (LTPa). A matrix presentation of the LTP sequences and their representative peptides is shown in Table 2. To ensure that each of these peptides is protein specific, BLAST analysis of the translated B73 genome and the *Zea mays* (Zm166) UniGene transcriptome was performed. None of the peptides had an exact match to any protein other than the expected LTPs. Finally, none of these peptides discriminate between the putative splice variants observed for each of the three gene loci, which differ at the C-terminus (Figure 2). However, resolving these variants was not necessary to devise a comprehensive, absolute quantitative assay for each of the classes of endogenous LTP allergens in maize.

DOI: 10.1021/jf504708u
J. Agric. Food Chem. 2015, 63, 821−828

Table 2. LTP Protein/Peptide Matrix[a]

	Tryptic peptides				
LTP protein accessions	GQGSGPSAGCCSGVK	GQGSGPSAGCCSGVR	NAAAGVSGLNAGNAASIPSK	GVSGLNAGNAASIPSK	LGGGVSMANAANIPSK
GRMZM2G101958 (LTPa)	*		*		
GRMZM2G010868 (LTPb)				*	
GRMZM5G898755 (LTPc)					*
Zea m 14		*	*		

[a]Tryptic peptides are in columns, and the LTP accessions in rows. Asterisks are placed at the intersections of peptides and LTP accessions to which they belong. The peptide highlighted in gray is shared by two LTPs (the same as the green peptide in Figure 2). All other peptides are unique to the respective LTP isoform.

Bioanalytical Method Validation for Native and AQUA Peptides. Bioanalytical method validation requires the determination of many parameters, including specificity, precision, linear quantitative range, and carryover. Carryover between analytical runs was assessed during the AQUA peptide dilution series experiments, which used a fixed amount of maize grain protein as matrix and the cognate endogenous peptide therein as the control to calculate a response ratio. A blank run between each dilution in the series was assessed for residual native peptide signal and compared to that of the previous analytical runs. Each analytical run contained 2 μg of native peptides. Background was subtracted for both analytical runs and blank runs. The resulting signals for the blank runs were divided by the sum of the blank signal and the average area from the analytical runs, and multiplied by 100 to find the percent of total signal present in the blank run. Each peptide was assessed individually. On average, all were below 0.9% except the LTPc peptide, which was at 1.30%.

The linear range of native (endogenous) peptides used in these assays was determined by a six point, 5-fold dilution series from 2.4 μg to 0.0038 μg/injection (including a zero control), with duplicate injections. AQUA peptides were spiked at 40 fmol/μL. When the log5 values of the response ratios (RRs, endogenous/AQUA) were plotted against the log5 values of the matrix amounts, R^2 values for all transition ions were between 0.9842 and 1.000, and slope values were between 1.05 and 0.885 when the zero control was excluded. The experimentally verified linear dynamic range was nearly 4 orders of magnitude for each peptide, although the current instrument and column capabilities likely offer a broader range. Duplicate injections provided percent relative standard deviation (%RSD) values that averaged less than 11% across all dilutions and all peptides except LTPc, which was 36% (SI Figure 1).

The linear range of AQUA peptides was assessed by a seven-point, 5-fold dilution series from 0.5 pmol to 0.16 fmol/injection including a zero control with duplicate injections (SI Figure 2). For all peptides and transition ions therein, except LTPc, this six point dilution series was linear with R^2 values ranging from 0.996 to 0.9999, when excluding the zero control. For most of these assays, the LLOD and ULOQ exceeded the six point dilution series. However, for the LTPc peptide the LLOD was 0.16 fmol and the ULOQ was 100 fmol. The LLOQ of 0.8 fmol and linear range from 0.8 to 100 fmol offered R^2 values ranging between 0.991 and 0.9996 when excluding the zero control. Considering the linear range for all AQUA peptide dilution series, the slopes ranged from 0.8873 to 1.0038, with the majority being less than 5% under 1.00 (without zero control). Duplicate injections yielded response ratio %RSDs that averaged less than 8% across all dilutions. AQUA-MRM assay parameters for all peptides are listed in SI Table 2. The lower and upper limits of quantification (LLOQ/ULOQ) were assessed in terms of their surrogate proteins, by converting the molar quantity for each peptide into the gram quantity for the respective protein (Table 3). For LTPa, the LLOQ was 9.39 pg/injection (0.8 fmol). For LTPb, the LLOQ was 1.88 pg/injection (0.16 fmol). The LLOQ for LTPc was 10.66 pg/injection (0.8 fmol). For Zea m 14 and LTPa/Zea m 14, the LLOQ was 2.03 pg/injection (0.16 fmol) for both.

LTP AQUA-MRM Analysis. Absolute measures of the concentration in maize grain extracts for all LTPs in each variety are graphed in Figure 3. Figure 3 (top panel) shows the higher abundance LTPa and Zea m 14, while Figure 3 (bottom) contains the quantities of the lower abundance LTPb and LTPc isoforms. In most samples, both LTPa and Zea m 14 were present at similar concentrations. However, in four of the samples (variety 1, 2, 14, and 15), one of those LTPs is below either detection or quantification limits. The third series in Figure 3 (top), labeled "LTPa/Zea m 14", shows the result which simultaneously quantifies both LTPa and Zea m 14 together via a shared peptide. In all cases where either LTPa or Zea m 14 proteins are low or undetected, the quantity of the single, representative LTP is similar to the concentration of the peptide that is common to both LTPa and Zea m 14 (i.e., LTPa/Zea m 14). In addition, for the samples where both Zea m 14 and LTPa are present in similar concentrations, the additive value of the two independent assays (each protein represented by its unique peptide) is similar to the LTPa/Zea m 14 value. When the sums of the independent LTPa and Zea

Table 3. Summary Table for Proteins and Peptides[a]

Prot Abbv	IUIS allergen nomenclature	MM (g/mol)	AQUA peptide sequence	AQUA assay LLOQ (pg/injection)	AQUA assay ULOQ (ng/injection)
LTPa	none	11742.84	GQGSGPSAGCCSGVK	9.39	5.87
LTPb	none	11718.82	GVSGLNAGNAASIPSK	1.88	5.86
LTPc	none	13319.46	LGGGVSMANAANIPSK	10.66	6.66
Zea m 14	Zea m 14	12659.23	GQGSGPSAGCCSGVR	2.03	6.33
LTPa/Zea m 14	Zea m 14	12659.23	NAAAGVSGLNAGNAASIPSK	2.03	6.33

[a]LLOQ is the lower limit of quantitation and represents the lowest point at which we demonstrated quantitative accuracy during our assay development. ULOQ is the highest amount tested with AQUA peptides, though assays with native peptides showed linearity of response beyond this value.

DOI: 10.1021/jf504708u
J. Agric. Food Chem. 2015, 63, 821−828

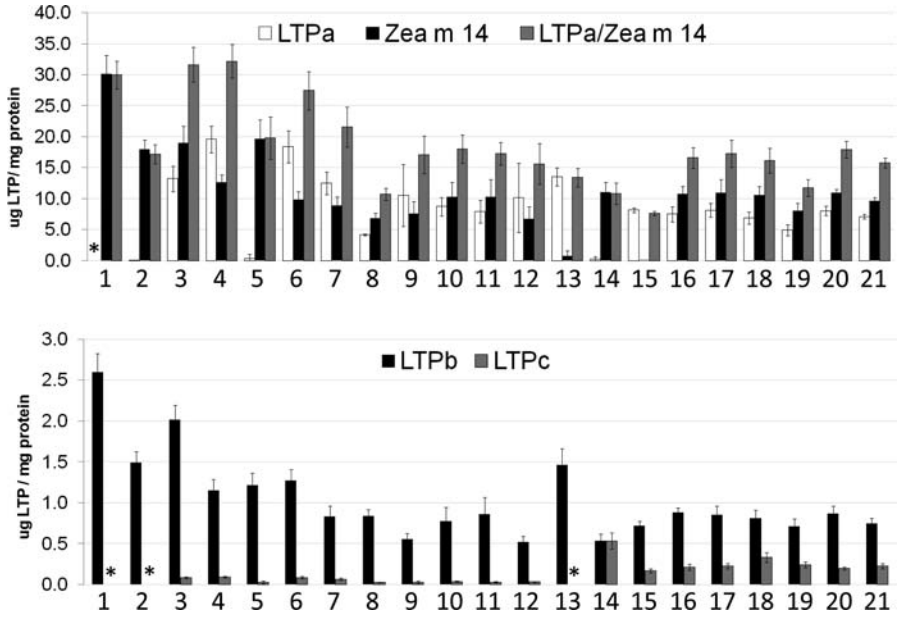

Figure 3. Absolute quantities of LTPs in each variety. LTPa/Zea m 14 represents the quantity provided by the peptide assay which monitors both LTPa and Zea m 14 simultaneously using a peptide that is shared by both proteins. Error bars represent standard deviation for five biological replicates. Numbers below the *x*-axis are variety identifiers. Asterisks indicate samples below detection limits.

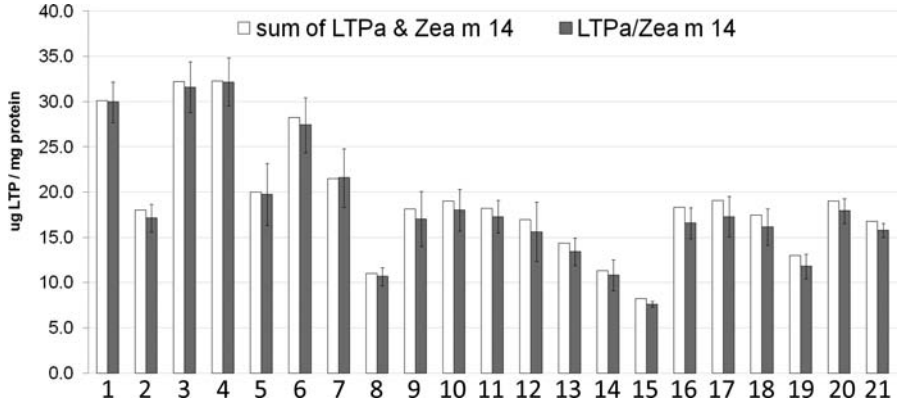

Figure 4. Stoichiometric agreement between three separate LTP AQUA-MRM assays. Error bars represent standard deviation for five biological replicates. Numbers below the *x*-axis are variety identifiers.

m 14 are plotted with the shared peptide LTPa/Zea m 14 values, it is evident that the shared peptide represents the sum of the individual peptides (Figure 4). The average percent error for the sum of LTPa and Zea m 14 versus the value measured by the LTPa/Zea m 14 is only 5.3%. LTPb and LTPc isoforms are less abundant, with LTPb being the more abundant species (Figure 3, bottom panel). LTPc was below detection or quantification limits in five varieties, numbers 1, 2, 5, 11, and 13.

DISCUSSION

The premise behind developing analytical approaches for measuring food allergens is to gain a better understanding of their precise expression levels (referred to as absolute) in various plant organs and to extend this technology toward their identification in processed foods and the environment. Traditionally, allergen detection and quantification methods have relied primarily on antibody-based approaches, employing either IgE antibodies derived from allergic patient sera or IgG antibodies raised in animals against individual allergens. However, it is generally understood that most antibody-based methods provide semiquantitative, relative estimates of content and that specificity and reproducibility can be affected by matrix components in the grain and foods in which allergens are usually monitored. Using a comparative approach to determine feasible assays for soybean allergens, Pedersen et al.[27] found that matrix component interference could be minimized. By using a general ranking of abundance of the targeted soy within a given food type, calculated soy levels were consistent across assays (higher abundance equaled a higher level of measured soy); however, "...the measured soy levels given by each of these assays were not in correlation with each other, allowing only semi-quantitative estimations of the soy content". In contrast, absolute measures of protein allergens, such as has been developed for LTP by mass spectrometry, when paired with an understanding of genetic/bioinformatic background, can provide reliable concentration values for the total abundance of related isoforms *in planta*.

The sequence of the B73 maize genome, coupled with in-depth transcriptomics, provided predictive gene models for the

DOI: 10.1021/jf504708u
J. Agric. Food Chem. 2015, 63, 821−828

LTP family of proteins. Amino acid sequence alignment revealed three genes sharing between 43% and 87% amino acid identity with Zea m 14. Three additional genes shared between 15% and 29% sequence identity and clustered phylogenetically apart from the others, and were therefore not considered close homologues to Zea m 14. The most closely related gene to Zea m 14 was GRMZM2G101958 (LTPa), which due to a presumptive alternative translation termination site shared 87% identity. Therefore, it is likely that the Zea m 14 allergen arose from this gene. This is supported by the observation that one of the two reported Zea m 14 transcript variants is identical to the LTPa gene at the variable C-terminus. Three of the peptides for this multiplexed maize LTP assay were developed to verify the existence of both the reported sequence for Zea m 14 as well as the LTPa transcript. The two discriminating peptides GQGSGPSAGCCSGV(R/K) differed only in the terminating residue. A third peptide was developed to a conserved sequence for LTPa and the two variants for Zea m 14 (NAAAGVSGLNAGNAASIPSK). Quantitative analysis of 21 maize varieties revealed the existence of both the LTPa and Zea m 14 proteins, albeit with varying abundance among them (Figure 3). The levels of LTPa varied from undetectable to almost 20 μg LTPa/mg maize grain protein among the 21 varieties studied. Zea m 14 ranged from undetectable to 30 μg LTP/mg maize grain protein. To confirm the accuracy of these results, the third peptide was designed against a domain conserved in all three transcripts and was included in the multiplexed assay performed for each sample. This peptide overlapped with the multiple gene variants documented for LTPa and was included in each analysis. The results confirmed the values for the two independent peptides, with an average percent error of 5.3%. The results from this peptide demonstrate signals from the two specific peptides were authentic and accurate, as the sum was equivalent to the conserved peptide representing all three gene products in all varieties (Figure 4). These proteins are considered to represent the bulk of LTP expression in maize grain.

LTP homologues encoded by genes GRMZM2G010868 (LTPb) and GRMZM5G898755 (LTPc) were 74% and 43% identical to Zea m 14, respectively, at the amino acid level. Each of these two gene assemblies were represented by two transcript variants exclusively variable at the C-terminus (Figure 2). Two peptides were designed to discern these two genes but not the transcript variants that arose from them (Figure 2). Analysis of the 21 maize varieties revealed both proteins are present within maize grain at variable levels. Expression of LTPb ranged from 0.5 to 2.5 μg LTPb/mg maize grain protein. LTPc exhibited a low level of expression, varying from undetectable to 0.5 μg LTPc/mg maize grain protein. Although the levels of LTPb and LTPc gene products were lower than LTPa, this is dependent upon the specific maize variety being analyzed (Figure 3). Therefore, to accurately assess the total LTP allergen "load" in maize grain, it is essential to monitor all three LTP isoforms related to Zea m 14.

To our knowledge, only one other nonantibody-based method for quantifying maize LTPs has been described, which uses LC-UV/MS.[28] In this method, LTPs were selectively extracted and analyzed intact utilizing liquid chromatography coupled to UV absorbance for quantitation. Quantitation was performed using external calibration curves with a prepared mix of LTPs standardized by amino acid analysis. Analysis of maize grain revealed an LTP concentration ranging from 58 to 678 μg/g grain fresh weight from 14 maize varieties. Using the AQUA-MRM approach, we determined total LTPa (Zea m 14) concentration to be 9 to 32 μg LTP/mg protein among 21 maize varieties. Assuming maize grain is 10% protein by weight, the values from Kuppannan et al.[28] convert to 0.58−6.78 μg LTP/mg protein. Two LTP variants were observed in 2010 by Kuppannan et al.,[28] and it is likely variant A is the Lys-containing version of Zea m 14 (GQGSGPSAGCC SGVK/R) denoted as LTPa in Figure 2, as determined by MS analysis of this tryptic peptide. Thus, for direct comparison to the values reported here for Zea m 14 (LTPa), it is necessary to sum the values for "LTP" and "LTP variant A" in ref 28. This produced a range of 2.23−8.14 μg LTP/mg protein, which is close to values reported here using AQUA-MRM. The slightly lower estimate of maize grain LTP concentration by Kuppannan et al. could be due to varietal or methodological differences between these two approaches. Variant B observed by Kuppannan et al.[28] was up to 20-fold less abundant than the other LTP variants; therefore, it would be reasonable to conclude this represented one of the related LTP genes (i.e., LTPb or LTPc in our study) based upon values reported here.The method presented here has the advantage of added selectivity by utilizing signal derived from individual peptide ions present in each chromatographic peak, so that even coeluting species are distinguished during quantitative analysis. In addition, each assay utilizes internal reference standards that are isotope-labeled and analyzed simultaneously, which increases quantitative accuracy and reproducibility.

In summary, the maize allergen Zea m 14 is part of a family of LTPs with related gene isoforms and putative splice or translation variants. Additionally, LTPs are small, 7−10 kDa proteins and therefore contain few proteotypic peptides for quantitation in a typical bottom-up AQUA-MRM workflow. Despite these limitations, we demonstrated a robust, multiplexed assay for three LTP genes and the 2−3 variants of each of these genes, which varied by as little as a single amino acid. We rigorously validated this multiplexed assay for absolute quantitation from extracts of maize grain in order to provide reliable and repeatable concentration measurements in a complex seed matrix. As a control, a redundant peptide that represents the theoretical sum of two specific peptides was employed as part of the methodology. The quantitative results from this redundant peptide support the theoretical sum and thus verify the accuracy of these predictive gene models as well as the AQUA-MRM method (Figure 4). In total, this quantitative study design accounted for all LTPs related to Zea m 14. It provided the specificity, accuracy, reproducibility, sensitivity, and linear quantitative range to be employed for comprehensive Zea m 14 allergen assessment in maize with the possibility of validation with other food matrices. In the future, experimental field designs that help elucidate the natural variability in LTP expression may be useful in providing a baseline. It is becoming well established that environmental factors and the genetic background of various crop varieties are the basis for largest percentage of variability. This variability will need to be better studied in order to work toward an understanding of exposure risk for the LTP allergen.

■ ASSOCIATED CONTENT

Supporting Information

Table listing maize production year, maize varietal name, and production (growing) location for the maize varieties analyzed in this study; table summary of MRM acquisition parameters

DOI: 10.1021/jf504708u
J. Agric. Food Chem. 2015, 63, 821−828

for analysis of maize LTP peptides; figure showing the endogenous (native) peptide dilution series, and figure showing the AQUA peptide dilution series. This material is available free of charge via the Internet at http://pubs.acs.org.

AUTHOR INFORMATION

Corresponding Author

*Phone: 573.884.1325. E-mail: thelenj@missouri.edu.

Funding

This research was funded by a grant from Syngenta Crop Sciences.

Notes

The authors declare the following competing financial interest(s): The research described here was conducted through financial support to J.J.T. from Syngenta Crop Sciences.

ACKNOWLEDGMENTS

The authors wish to acknowledge Trent Stevens for reference management.

ABBREVIATIONS USED

LC-MS/MS, liquid chromatography tandem mass spectrometry; LTP, lipid transfer protein; MRM, multiple reaction monitoring; SDS-PAGE, sodium dodecyl sulfate polyacrylamide gel electrophoresis; kDa, kilodalton; DTT, dithiothreitol; IAA, iodoacetamide; RT, room temperature; ACN, acetonitrile; CBB, Coomassie Brilliant Blue

REFERENCES

(1) Frisner, H.; Rosendal, A.; Barkholt, V. Identification of immunogenic maize proteins in a casein hydrolysate formula. *Pediatr. Allergy Immunol.* **2000**, *11*, 106−110.

(2) Metcalfe, D.; Sampson, H.; Simon, R. *Food allergy: adverse reactions to foods and food additives*, 3rd ed.; Blackwell Publishing: Malden, MA, 2003.

(3) Pastorello, E. A.; Farioli, L.; Pravettoni, V.; Ispano, M.; Scibola, E.; Trambaioli, C.; Giuffrida, M. G.; Ansaloni, R.; Godovac-Zimmermann, J.; Conti, A.; Fortunato, D.; Ortolani, C. The maize major allergen, which is responsible for food-induced allergic reactions, is a lipid transfer protein. *J. Allergy Clin. Immunol.* **2000**, *106*, 744−751.

(4) Tanaka, L. G.; El-Dahr, J. M.; Lehrer, S. B. Double-blind, placebo-controlled corn challenge resulting in anaphylaxis. *J. Allergy Clin. Immunol.* **2001**, *107*, 744.

(5) Pauls, J. D.; Cross, D. Food-dependent exercise-induced anaphylaxis to corn. *J. Allergy Clin. Immunol.* **1998**, *101*, 853−854.

(6) Ispano, M.; Colafrancesco, M.; Ansaloni, R.; Vighi, G.; Ortolani, C. Comparison of the results of skin prick tests, CAP system and ENEA system in the diagnosis of food allergy. *Monogr. Allergy* **1996**, *32*, 181−186.

(7) Jones, S. M.; Magnolfi, C. F.; Cooke, S. K.; Sampson, H. A. Immunologic cross-reactivity among cereal grains and grasses in children with food hypersensitivity. *J. Allergy Clin. Immunol.* **1995**, *96*, 341−351.

(8) Venter, C.; Skypala, I.; Dean, T. Maize allergy: what we have learned so far. *Clin. Exp. Allergy* **2008**, *38*, 1844−1846.

(9) Pasini, G.; Simonato, B.; Curioni, A.; Vincenzi, S.; Cristaudo, A.; Santucci, B.; Peruffo, A. D.; Giannattasio, M. IgE-mediated allergy to corn: a 50 kDa protein, belonging to the Reduced Soluble Proteins, is a major allergen. *Allergy* **2002**, *57*, 98−106.

(10) Pastorello, E. A.; Robino, A. M. Clinical role of lipid transfer proteins in food allergy. *Mol. Nutr. Food Res.* **2004**, *48*, 356−362.

(11) Kader, J. C. LIPID-TRANSFER PROTEINS IN PLANTS. *Annu. Rev. Plant Physiol. Plant Mol. Biol.* **1996**, *47*, 627−654.

(12) Henrissat, B.; Popineau, Y.; Kader, J. C. Hydrophobic-cluster analysis of plant protein sequences. A domain homology between storage and lipid-transfer proteins. *Biochem. J.* **1988**, *255*, 901−905.

(13) Tchang, F.; This, P.; Stiefel, V.; Arondel, V.; Morch, M. D.; Pages, M.; Puigdomenech, P.; Grellet, F.; Delseny, M.; Bouillon, P.; et al. Phospholipid transfer protein: full-length cDNA and amino acid sequence in maize. Amino acid sequence homologies between plant phospholipid transfer proteins. *J. Biol. Chem.* **1988**, *263*, 16849−16855.

(14) Van Loon, L.; Pierpoint, W.; Boller, T.; Conejero, V. Recommendations for naming plant pathogenesis-related proteins. *Plant Mol. Biol. Rep.* **1994**, *12*, 245−264.

(15) Ariyarathna, H.; Pramod, S.; Goodman, R. The abundance of lipid transfer protein(LTP), the major food allergen of corn, varies between hybrids and growth conditions. *J. Allergy Clin. Immunol.* **2009**, *123*, S28.

(16) Goodman, R. E.; Panda, R.; Ariyarathna, H. Evaluation of endogenous allergens for the safety evaluation of genetically engineered food crops: review of potential risks, test methods, examples and relevance. *J. Agric. Food Chem.* **2013**, *61*, 8317−8332.

(17) Goodman, R. E.; Vieths, S.; Sampson, H. A.; Hill, D.; Ebisawa, M.; Taylor, S. L.; van Ree, R. Allergenicity assessment of genetically modified crops—what makes sense? *Nat. Biotechnol.* **2008**, *26*, 73−81.

(18) Stevenson, S. E.; Woods, C. A.; Hong, B.; Kong, X.; Thelen, J. J.; Ladics, G. S. Environmental effects on allergen levels in commercially grown non-genetically modified soybeans: assessing variation across north america. *Front. Plant Sci.* **2012**, *3* (196), 1−13.

(19) Borges, J. P.; Barre, A.; Culerrier, R.; Granier, C.; Didier, A.; Rougé, P. Lipid transfer proteins from Rosaceae fruits share consensus epitopes responsible for their IgE-binding cross-reactivity. *Biochem. Biophys. Res. Commun.* **2008**, *365*, 685−690.

(20) Su, M.; Venkatachalam, M.; Teuber, S. S.; Roux, K. H.; Sathe, S. K. Impact of γ-irradiation and thermal processing on the antigenicity of almond, cashew nut and walnut proteins. *J. Sci. Food Agric.* **2004**, *84*, 1119−1125.

(21) Roux, K. H.; Teuber, S. S.; Robotham, J. M.; Sathe, S. K. Detection and stability of the major almond allergen in foods. *J. Agric. Food Chem.* **2001**, *49*, 2131−2136.

(22) Pastorello, E. A.; Pompei, C.; Pravettoni, V.; Farioli, L.; Calamari, A. M.; Scibilia, J.; Robino, A. M.; Conti, A.; Iametti, S.; Fortunato, D.; Bonomi, S.; Ortolani, C. Lipid-transfer protein is the major maize allergen maintaining IgE-binding activity after cooking at 100 degrees C, as demonstrated in anaphylactic patients and patients with positive double-blind, placebo-controlled food challenge results. *J. Allergy Clin. Immunol.* **2003**, *112*, 775−783.

(23) Dereeper, A.; Guignon, V.; Blanc, G.; Audic, S.; Buffet, S.; Chevenet, F.; Dufayard, J. F.; Guindon, S.; Lefort, V.; Lescot, M.; Claverie, J. M.; Gascuel, O. Phylogeny.fr: robust phylogenetic analysis for the non-specialist. *Nucleic Acids Res.* **2008**, *36*, W465−469.

(24) Hajduch, M.; Ganapathy, A.; Stein, J. W.; Thelen, J. J. A systematic proteomic study of seed filling in soybean. Establishment of high-resolution two-dimensional reference maps, expression profiles, and an interactive proteome database. *Plant Physiol.* **2005**, *137*, 1397−1419.

(25) Radauer, C.; Breiteneder, H. Pollen allergens are restricted to few protein families and show distinct patterns of species distribution. *J. Allergy Clin. Immunol.* **2006**, *117*, 141−147.

(26) Houston, N. L.; Lee, D. G.; Stevenson, S. E.; Ladics, G. S.; Bannon, G. A.; McClain, S.; Privalle, L.; Stagg, N.; Hérouet-Guicheney, C.; MacIntosh, S. C.; Thelen, J. J. Quantitation of soybean allergens using tandem mass spectrometry. *J. Proteome Res.* **2011**, *10*, 763−773.

(27) Pedersen, M. H.; Holzhauser, T.; Bisson, C.; Conti, A.; Jensen, L. B.; Skov, P. S.; Bindslev-Jensen, C.; Brinch, D. S.; Poulsen, L. K. Soybean allergen detection methods—a comparison study. *Mol. Nutr. Food Res.* **2008**, *52*, 1486−1496.

(28) Kuppannan, K.; Albers, D. R.; Schafer, B. W.; Dielman, D.; Young, S. A. Quantification and characterization of maize lipid transfer protein, a food allergen, by liquid chromatography with ultraviolet and mass spectrometric detection. *Anal. Chem.* **2011**, *83*, 516−524.

DOI: 10.1021/jf504708u
J. Agric. Food Chem. 2015, 63, 821−828

JOURNAL OF AGRICULTURAL AND FOOD CHEMISTRY

Article

pubs.acs.org/JAFC

Selected Ion Flow Tube−Mass Spectrometry for Online Monitoring of Submerged Fermentations: A Case Study of Sourdough Fermentation

Simon Van Kerrebroeck,[†] Joeri Vercammen,[‡] Roel Wuyts,[‡] and Luc De Vuyst*[,†]

[†]Research Group of Industrial Microbiology and Food Biotechnology, Vrije Universiteit Brussel, Pleinlaan 2, B-1050 Brussels, Belgium

[‡]Interscience bvba, Avenue Jean-Etienne Lenoir 2, B-1348 Louvain-la-Neuve, Belgium

Supporting Information

ABSTRACT: Selected ion flow tube−mass spectrometry (SIFT-MS) has recently gained interest as an alternative method to traditional GC-MS for the detection of targeted volatile sample compounds, due to its ease of use, its speed and sensitivity, and its potential for real-time quantification. The feasibility of this technique was demonstrated using the case of the production of ethanol during sourdough fermentation. The potential of SIFT-MS as an online monitoring device for food fermentations was further demonstrated by the detection of acetoin in certain sourdough fermentations. This allowed discrimination between sourdough fermentation processes and illustrated the importance of real-time monitoring of food fermentations.

KEYWORDS: *SIFT-MS, GC-MS, fermentation, online monitoring, sourdough, Lactobacillus, volatile organic compounds*

INTRODUCTION

Food fermentation processes have been performed since ancient times, in the first place as a way to preserve food products and in the second place to increase their nutritional value and organoleptic properties.[1] In contrast to the action of desirable microorganisms (bacteria, yeasts, and to a lesser extent, filamentous fungi), the outgrowth or action of undesirable microorganisms can lead to spoilage of the end-products. Therefore, considerable research efforts have been made to the control and monitoring of food fermentation processes. One such way is the application of (functional) starter cultures, i.e., the inoculation of a large number of cultivated dedicated microbial cells.[2] An example of a fermented food that has benefited from this development is sourdough. Sourdough is a fermented cereal-based product initially made through spontaneous fermentation of a cereal flour−water mixture or continuous reinoculation of fresh flour by the addition of a part of a previous fermentation batch.[3] A more industrial approach to the production of sourdough involves the addition of selected starter cultures, which can be lactic acid bacteria (LAB) and/or yeasts.[2,3] However, even modern sourdough production is subjected to considerable batch-to-batch variations. One way to minimize end-product variations is to improve the control of the fermentation processes, preferably through online monitoring of microbial growth, substrate consumption, and/or metabolite production.[4] However, online monitoring through chromatography and/or mass spectrometry of food fermentation processes, whether spontaneous or starter culture-initiated, is challenging, in particular with respect to the analysis of volatile organic compounds in real-time. To the authors' knowledge, only online gas chromatography for the quantitative analysis of off-gases has been implemented.[5] Semiquantitative analysis of volatile organic compounds has been made possible by means of membrane inlet mass spectrometry and direct-injection mass spectrometric techniques.[6,7]

Selected ion flow tube−mass spectrometry (SIFT-MS) is a relatively new mass spectrometric technique that finds its origin in the study of gas-phase ion−molecule reactions.[8,9] It applies soft chemical ionization of volatile compounds with selected reagent ions, i.e., H_3O^+, NO^+, and O_2^+, which are generated in situ. As a result of the reaction of these reagent ions with the volatile organic compounds produced from the fermentation process, product ions of the volatile organic compounds are formed. Because of the soft ionization employed, little fragmentation of these product ions occurs. A quantitative measurement of the volatile compounds at ultratrace levels can be achieved without external calibration providing the fundamental kinetic parameters for the reagent ion-volatile organic compound reactions are known. The signal amplitudes of the selected product ions are used to calculate the concentrations of the targeted volatile compounds present in the sample. The use of three selected reagent ions and the ability to directly analyze the headspace above samples increase the identification power of the technique, rendering a priori separation and tedious or discriminating sample preparation obsolete, hence allowing real-time measurements.

Since it was first described by Španěl and Smith in 1996, the SIFT-MS technique has advanced tremendously.[10] Its selectivity, sensitivity, and ease and speed of measurement have boosted its applications. So far, SIFT-MS has gained attention in the areas of environmental monitoring,[11,12] (petro)chemical applications,[13,14] and clinical analysis.[15−17]

Received: October 24, 2014
Revised: December 15, 2014
Accepted: December 29, 2014
Published: December 29, 2014

ACS Publications © 2014 American Chemical Society

DOI: 10.1021/jf505111m
J. Agric. Food Chem. 2015, 63, 829−835

Because of the complexity of targeted chemicals and their concomitant matrices, applications of SIFT-MS in the field of food and flavor analysis present promising results.[18−21] Indeed, the use of SIFT-MS for the identification and quantification of volatile organic compounds, suitable as biomarkers and often emitted by microbial cultures or related to (fermented) foods, has been described.[22−24] However, the potential of SIFT-MS for the analysis of volatile organic compounds, indicating spoilage or contributing to the aroma of (fermented) foods, has not yet been realized fully.[25−34] Moreover, no reports exist on the use of SIFT-MS as an online measurement technique for the monitoring of (food) fermentation processes.

The aim of the present study was to develop and validate a SIFT-MS setup that is useful for the online monitoring of volatile metabolites during sourdough fermentations in parallel with quantitative online gas analysis.

MATERIALS AND METHODS

Design of an Online Monitoring SIFT-MS Setup. A unique SIFT-MS setup for the online monitoring of the headspace of fermentation vessels was designed (Figure 1). Sourdough fermentations involving heterofermentative LAB and generating typical volatile compounds, such as ethanol and acetic acid, were performed as a case study. To sweep volatiles toward the SIFT instrument (Syft Voice 200; Syft Technologies Ltd., Christchurch, New Zealand), nitrogen gas was added to the fermentation vessels (Biostat B-DCU fermentors; Sartorius AG, Melsungen, Germany) at 0.35 bar. In addition, this created a small overpressure (0.2 bar) area at the inlet of the autosampler (CGM2000; Umwelttechnik MCZ, Bad Nauheim, Germany), needed for its proper operation. Condensation pots (100 mL glass bottles) were connected directly with the headspace of the fermentors, bypassing the condensors and filters present at their standard gas outlets and operating as a physical water trap for water condensation at room temperature. Heated (105 °C) 1/4′′ polytetrafluoroethylene (PTFE) transfer lines connected these glass bottles with the entrance of the autosampler to avoid condensation of water and volatile compounds. The autosampler was equipped with four digital mass flow controllers and a mixing chamber. Three mass flow controllers were connected to the fermentation vessels and one to the dilution gas. The mass flow controllers were operated by the autosampler software, allowing the selection of gas inflow from a fermentation vessel and an appropriate amount of dilution gas (high-grade nitrogen gas), hence enabling the autosampler to act both as a selection and a dilution device. Dilution and sample gases were mixed in the mixing chamber and an amount of 25 mL min^{-1} of the gas blend was transferred to the SIFT-MS by means of the MS vacuum. This way, the evolution of volatile compound signals were followed as a function of time for multiple fermentation vessels and the SIFT-MS, controlled by LabSyft software (Syft Technologies Ltd.), could be operated under the analytical conditions required. Additionally, the autosampler device was equipped with a permeation oven, through which internal standards were added to the gas blend. Two internal standards were applied by means of permeation tubes, i.e., toluene (Metronics Inc. Poulsbo, WA, USA) with a diffusion rate of 75 ng min^{-1} at 50 °C and fluorobenzene (KIN-TEK Laboratories, La Marque, TX, USA) with a diffusion rate of 8.511 ng min^{-1} at 60 °C. This adaptation allowed the continuous monitoring of the performance of the SIFT-MS, correcting for incidental instrumental variations. The standards were applied separately. The permeation oven was set at 50 or 60 °C, depending on the permeation tubes used. A constant flow of permeation gas (nitrogen gas) at 200 mL min^{-1} was applied, which was mixed with the gas blend in the mixing chamber. To evaluate this setup, the breakthrough time, which was defined as the time needed to get 10% of the equilibrium response, and the mixing time, which was defined as the time needed to obtain a response in the SIFT-MS corresponding to 95% of the final equilibrium response, were determined by the addition of ethanol as a tracer compound, in a concentration of 34 mM, to a 2-L Biostat B-DCU fermentor (Sartorius AG, Melsungen, Germany) filled with 1.5 L of ultrapure water. Three aeration methods were compared, namely, headspace aeration and aeration through a ring sparger or a microsparger (Figure 2).

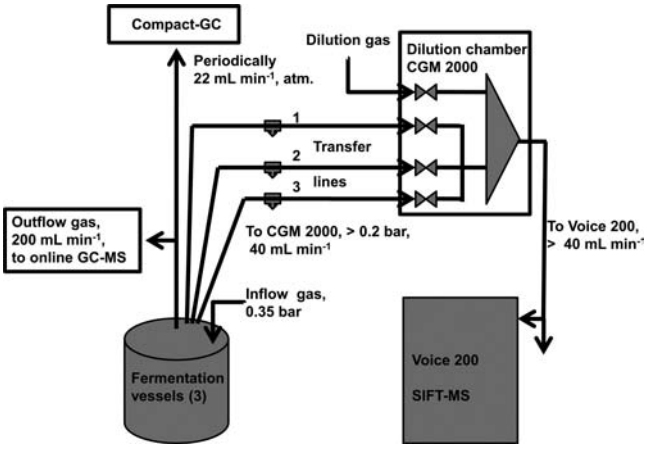

Figure 1. Scheme of the SIFT-MS setup to measure volatile sample compounds from multiple fermentation vessels in parallel with off-gases through SIFT-MS/GC-MS and Compact-GC, respectively.

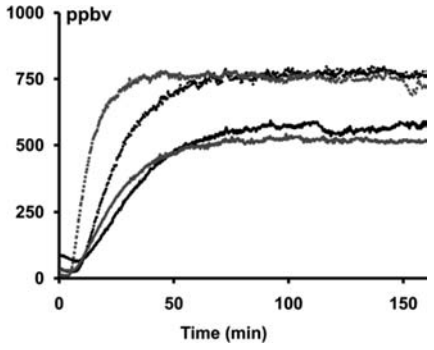

Figure 2. Influence of the aeration device and sample gas flow rate (in mL min^{-1}) on the online monitoring of ethanol through SIFT-MS, when ethanol is injected into the fermentor at $t = 0$. Ring sparger, 40 mL min^{-1}, upper gray line; ring sparger, 10 mL min^{-1}, upper black line; microsparger, 10 mL min^{-1}, lower black line; headspace aeration, 10 mL min^{-1}, lower gray line.

Applications. *Strains and Media.* *Lactobacillus fermentum* IMDO 130101, a strain previously isolated from a spontaneous laboratory rye sourdough, was used for the fermentations in wheat sourdough simulation medium (W-SSM).[35,36] *Lactobacillus sanfranciscensis* IMDO 150101, a strain isolated from a spontaneous laboratory teff sourdough (unpublished results), was used for the starter culture-initiated sourdough fermentations based on teff flour. The strains were stored at −80 °C in modified de Man-Rogosa-Sharpe-5 (mMRS-5) medium,[37] supplemented with 25% (vol vol^{-1}) glycerol as cryoprotectant. Solid media of W-SSM and mMRS-5 were prepared by adding 1.5% (wt vol^{-1}) agar (Oxoid Ltd., Basingstoke, Hampshire, UK) to the broth.

Fermentations in Wheat Sourdough Simulation Medium. W-SSM was composed of (per liter) wheat peptone, 12.0 g; granulated yeast extract, 12.0 g; $MgSO_4 \cdot 7H_2O$, 0.2 g; $MnSO_4 \cdot H_2O$, 0.05 g; KH_2PO_4, 4.0 g; K_2HPO_4, 4.0 g; Tween 80, 1.0 mL; and vitamin solution, 1.0 mL. The latter had the following composition (per liter): cobalamine, 0.2 g; folic acid, 0.2 g; nicotinamide, 0.2 g; pantothenic acid, 0.2 g; pyridoxal-phosphate, 0.2 g; and thiamine, 0.2 g.[36] All chemicals were obtained from VWR International (Darmstadt, Germany). Three W-SSM fermentations were carried out in parallel in 2-L Biostat B-DCU fermentors (Sartorius AG, Melsungen,

DOI: 10.1021/jf505111m
J. Agric. Food Chem. 2015, 63, 829−835

Germany). To estimate the variability of the methodology developed, each of these three parallel fermentations were carried out in triplicate. All medium components, except for carbohydrates and the vitamin solution, were dissolved in 1.25 L of distilled water, and the pH of the medium was adjusted to 5.5 by adding HCl and/or NaOH, prior to sterilization (121 °C, 2.1 bar, 20 min) of the fermentors. The carbohydrate mixture (250 mL), consisting of maltose, sucrose, glucose, and fructose in a final concentration of 10 g L^{-1}, 2 g L^{-1}, 0.5 g L^{-1}, and 0.5 g L^{-1}, respectively, was sterilized (121 °C, 2.1 bar, 20 min) separately, and the vitamin solution was filter-sterilized (0.2-μm Minisart PES filters; Sartorius AG, Goettingen, Germany); both were added aseptically to the sterile fermentors, prior to inoculation. The fermentation temperature was kept at 30 °C. The pH of the medium was kept constant at 5.5 through automatic addition of a 1.5 M NaOH solution to the fermentation broth. The stirring speed was fixed at 300 rpm. Temperature, pH, and agitation were controlled online (MicroMFCS for Windows NT software, Sartorius AG, Melsungen, Germany). Sterile nitrogen gas was continuously blown through the fermentation medium at a rate of 200 mL min^{-1}. The inoculum was prepared through three subcultures of 12 h in W-SSM. The first two subcultures were carried out in 10 mL of medium; the third subculture in 100 mL. The transfer volume was always 1.0% (vol vol^{-1}).

Starter Culture-Initiated Teff Sourdough Fermentations. Starter culture-initiated sourdough fermentations (8 kg) were carried out in duplicate in 15-L Biostat C fermentors (Sartorius AG, Melsungen, Germany) filled with 6 L of sterile water and 2 kg of teff flour.[38] An inoculum of 1.0% (vol vol^{-1}) of the starter culture, subcultured twice in mMRS-5 overnight, was used. This dough was incubated at 30 °C for 72 h, while the mixture was kept homogeneous through stirring (300 rpm). The headspace of the fermentors was flushed with sterile air at a flow rate of 1 L min^{-1}.

Off-Line Sample Analyses. During fermentation, samples were regularly withdrawn from the fermentors for the determination of bacterial counts, residual carbohydrates, and metabolites produced, as described previously.[36] Briefly, bacterial counts were determined by plating 10-fold dilutions of W-SSM fermentation samples or samples of fresh mixtures of 10 g of teff sourdough sample with 90 mL of sterile saline (0.85%, wt vol^{-1}, NaCl) on W-SSM agar (W-SSM fermentations) or mMRS-5 agar (starter culture-initiated teff sourdough fermentations), followed by incubation at 30 °C for 48 h.

For metabolite target analysis, a given amount of W-SSM (50 mL) or sourdough sample (approximately 100 g) was centrifuged (8,041*g* for 20 min at 4 °C) to remove solids, and the supernatant was stored at −20 °C until further analysis. Concentrations of residual carbohydrates (maltose, sucrose, fructose, and glucose) and mannitol produced were determined through high-performance anion exchange chromatography with pulsed amperometric detection, applying a standard addition protocol.[39] Concentrations of lactic acid were determined using high-performance liquid chromatography with refractive index detection (HPLC-RI), through external standards.[39] Concentrations of acetic acid, ethanol, and acetoin were determined through HPLC-RI and gas chromatography (GC) with flame ionization detection, using external standards.[40] Concentrations of volatile compounds were determined through static headspace-GC-MS (SH-GC-MS).[41] Peak identification was achieved by comparison with pure standard compounds and library confirmation (NIST 08, National Institute of Standards and Technology, Gaithersburg, MD, USA).

Online Analysis of Gases and Volatile Compounds. The headspace of the fermentation vessels was analyzed for carbon dioxide and targeted volatile compounds during the sourdough fermentation processes for either 48 or 72 h. Carbon dioxide was quantified through online gas chromatography by means of a Compact-GC (Interscience, Louvain-la-Neuve, Belgium).[5] Briefly, a headspace sample was pumped through an analytical cell, containing a PoraBOND Q column (Varian, Palo Alto, CA, USA) coupled to a thermal conductivity detector. Helium was used as carrier gas. The following conditions were applied: valve temperature, 60 °C; injection volume, 20 μL; carrier gas module mode, constant pressure (70 kPa); split flow, 5 mL min^{-1}; reference flow, 1 mL min^{-1}; column temperature, 60 °C; and detector temperature, 110 °C. A four-position selection valve allowed automated sequential sampling of the three fermentation vessels and injection of calibration gas mixtures (Saphir calibration gases; Air Liquide, Paris, France). Each fermentor was sampled twice every hour. The carbon dioxide concentration was summarized over the entire fermentation period and expressed in millimolars.

Volatile sample compounds were monitored through SIFT-MS. All fermentors were sampled consecutively during 20 min so that each fermentor was sampled once per hour. During the sampling time, a full scan (m/z^{-1} 10 to 250 for H_3O^+, 15−250 for NO^+, and 15−250 for O_2^+) and a selected ion mode (SIM) scan (settle time, 80 s; measurement time, 100 s) were run.[42] A list of the ions measured is presented in Supporting Information, Table S1.

To verify the results obtained by SIFT-MS, an online dynamic headspace-GC-MS analysis (Agilent 6890 gas chromatograph coupled to an Agilent 5973N mass spectrometer; Agilent Technologies, Santa Clara, CA, USA), was performed. Every hour, a gas sample of 1 mL was withdrawn from a Pall flow cell (CTC Analytics AG, Zwingen, Switzerland), which was connected to the gas outflow of one fermentation vessel by means of a 1/4″ PTFE transfer line, and injected into a capillary column (DB-WAXetr, Agilent Technologies) at a rate of 500 μL s^{-1}.

The carbon recovery was calculated by dividing the total amount of carbon present in the metabolites by the total amount of carbon added as carbohydrates.

RESULTS AND DISCUSSION

Optimization of the Online Monitoring SIFT-MS Setup. The Syft Voice200 instrument is a very sensitive device since its linear range is a magnitude lower than the anticipated concentrations of volatile compounds emitted by a microbial culture.[42,43] Consequently, it was necessary to dilute the headspace samples with dilution gas (nitrogen gas) prior to introduction into the instrument in a dilution chamber (part of the autosampler) to obtain more appropriate concentrations (Figure 1).

The mass flow controllers of the autosampler required an input pressure of 0.2 bar, hence making it necessary to put the fermentation vessels under overpressure. It was found that the required pressure of the inflowing gas had to be 0.35 bar to compensate for the pressure drop between the gas inlet of the fermentors and the mass flow controllers of the autosampler. However, this altered the measurement of the carbon dioxide concentration with the Compact-GC. Indeed, when the gas outflow was restricted, the concentration of carbon dioxide quickly increased to values out of the linear range of the apparatus. Therefore, a sufficiently high gas flow rate of 200 mL min^{-1} was applied. A valve, regulating the outflow of gas and a union tee were installed, making continuous gas flow and decompression to atmospheric pressure possible. This way, the disturbance of the system, for instance by pressure swings influencing biological and physicochemical parameters of the fermentation processes, was minimized, and simultaneous measurements by Compact-GC and SIFT-MS were feasible.

Addition of the condensation pots substantially increased the system's mixing time to around 60 min, as measured with a sample gas flow rate of 10 mL min^{-1}. This made it the limiting step of the measurements and hence determined the overall reaction time of the setup (Figure 2). To compensate for this, the sample gas flow rate was increased to 40 mL min^{-1}. This in turn lowered the breakthrough time from around 9−11 to 6 min. With respect to the time frame of sourdough fermentation (48 h), both the mixing time and breakthrough time were considered acceptable. Unfortunately, an increase of the sample gas flow rate required a proportional increase of the dilution gas

DOI: 10.1021/jf505111m
J. Agric. Food Chem. 2015, 63, 829−835

flow rate, to maintain a linear system response. To limit dilution gas usage, however, this load was allowed to be below 10 ppmv. Also, it is noteworthy that the aeration method did not determine the breakthrough time due to the installment of a condensation pot.

A method for the determination of the concentrations of metabolites of heterofermentative LAB metabolism was developed. Additionally, common organic contaminants were included in the method to control the risk of misinterpretation due to pollution by laboratory air. The internal standards were added and measured to monitor the system performance of the SIFT-MS setup. Toluene exhibited interference with one or more volatile sample compounds, while the measured signal of fluorobenzene did not alter during the course of a W-SSM fermentation. Therefore, fluorobenzene was preferred as the internal standard and was used during subsequent experiments. Product ions that, according to the LabSyft software library, could cause interference were removed from the method in several optimization rounds. An initial screening, using online GC-MS and SH-GC-MS, showed that ethanol was the main volatile present. It was preferably detected by SIFT-MS. As a result, ethanol impeded the determination of other volatile sample compounds. No additional compounds were found upon dilution of the sample gas. The response of these compounds could have disappeared in the elevated noise due to their low expected level.

Application of SIFT-MS during W-SSM Fermentation. The unique technical setup for the online monitoring of carbon dioxide and microbial volatiles and the method developed for the quantitative determination of these microbial volatiles were applied to follow up a fermentation with *Lb. fermentum* IMDO 130101 in W-SSM. Online SIFT-MS measurements of volatile compounds present in the headspace of the fermentors were compared with HPLC-RI measurements of the concentrations of these volatiles in the fermentation broth. A typical fermentation pattern, represented in Figure 3, shows the simultaneous production of lactic acid, ethanol, acetic acid, and carbon dioxide, along with the consumption of the carbohydrates. As described previously, maltose and glucose were the preferred energy sources, while sucrose was consumed once these carbohydrates were exhausted.[36] Fructose was used mainly as an alternative external electron acceptor and converted into mannitol, allowing concomitant production of acetate instead of ethanol.[36] However, the limited concentration of fructose (5 mM) present in W-SSM limited acetate formation to 5 mM.

Only 80−85% of the carbon supplied under the form of carbohydrates could be accounted for in the metabolites measured. Following the heterofermentative metabolism of *Lb. fermentum*, 65 mM of carbon dioxide was produced, as measured by online gas chromatography. This was stoichiometrically correct, indicating a successful coupling of the Compact-GC with the fermentors as part of the whole configuration for online measurements of fermentation gases and microbial volatiles. Although lactic acid (60 mM) was produced equimolar to the sum of the ethanol and acetic acid concentrations, its concentration in the headspace of the fermentors was too low for detection by SIFT-MS. This might be due to several factors. First, the Henry coefficient, describing the division of volatile organic compounds between the gaseous and liquid phases, is much higher for ethanol than that for lactic acid.[44,45] Second, as for all organic acids, the pH of the medium, which was automatically adjusted to 5.5, influenced the equilibrium.[46] The latter effect also influenced the concentration of acetic acid in the headspace of the fermentors. Third, charged compounds could have been adsorbed on parts of the setup, removing them from the headspace.[47] Therefore, neither lactic acid nor acetic acid could be found in the headspace of the fermentors by means of the current online SIFT-MS setup. In addition, ethanol evaporation, due to the high gas flow rates through the system, was not taken into account.[48] Finally, a comparison of the current setup with a closed model system showed a pressure loss of around 10%.

Nevertheless, a comparison between the concentrations of ethanol in the medium, as measured by off-line SH-GC-MS, and the concentrations of ethanol in the dynamic headspace, as measured by online SIFT-MS, showed their parallel evolution (Figure 4). Additionally, the online GC-MS measurements showed the same parallel evolution as the online SIFT-MS measurements. This indicates that online measurement of ethanol concentrations in the dynamic headspace of a fermentor by SIFT-MS can be used as a tool to monitor the production of ethanol in the fermentation broth. As ethanol is a key metabolite of the heterofermentative metabolism of LAB, it

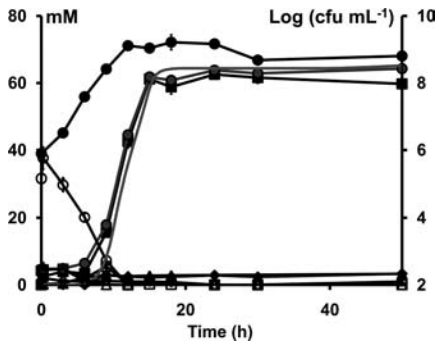

Figure 3. Bacterial growth of and carbohydrate consumption and metabolite production by *Lactobacillus fermentum* IMDO 130101 during fermentation in wheat sourdough simulation medium at a constant pH of 5.5. Growth is represented as counts of colony forming units per mL (cfu mL^{-1}, black circle); maltose (○), glucose (□), fructose (Δ), sucrose (◇), lactic acid (gray circle), ethanol (■), acetic acid (◆), mannitol (▲), carbon dioxide (−).

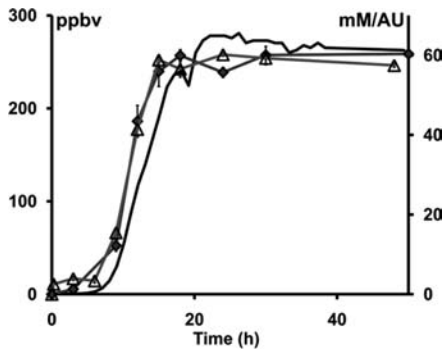

Figure 4. Comparison between the concentrations of ethanol in the fermentation broth as measured off-line by HPLC-RI (mM, Δ) and SH-GC-MS (AU, ♦) and in the dynamic headspace of the fermentation vessels as measured by online SIFT-MS (ppbv, —), during fermentation with *Lactobacillus fermentum* IMDO 130101 in a wheat sourdough simulation medium.

DOI: 10.1021/jf505111m
J. Agric. Food Chem. 2015, 63, 829−835

can be used as biomarker for the online monitoring of food fermentations involving heterofermentative LAB.

To correct for biological variation, the ratio between the ethanol concentrations in the headspace, as measured by online SIFT-MS, and the ethanol concentrations in the fermentation broths, as measured by HPLC-RI, was calculated and averaged, based on three series of fermentations carried out in triplicate, and was $(1.1 \pm 0.1)\ 10^{-4}$ (mol per liter in the gas phase) (mol per liter in the liquid phase)$^{-1}$. Hence, analysis of the dynamic headspace by online SIFT-MS according to the setup of the present study could be used as a tool to monitor fermentations with a variability of only 13%. However, this variability may still be lowered, as the present study included changes in methodology or setup, for example, by the introduction of a SIM method. The advantage of a SIM method over a full mass scan is that only those volatile organic compounds of interest are monitored, and in the SIM mode of operation, ion products from these volatile organic compounds are averaged over longer periods, thus improving the accuracy of the measurements.[42,49]

Application of Online SIFT-MS during Starter Culture-Initiated Teff Sourdough Fermentation. Heterofermentative metabolism of *Lb. sanfranciscensis* IMDO 150101 resulted in the production of lactic acid, ethanol, acetic acid, and mannitol out of maltose, glucose, fructose, and sucrose during teff sourdough fermentation (data not shown). Besides ethanol and acetic acid, the application of online SIFT-MS during a *Lb. sanfranciscensis*-initiated teff sourdough fermentation showed the production of another volatile sample compound, namely, acetoin (Figure 5), known to be produced by cocultures of *Lb.*

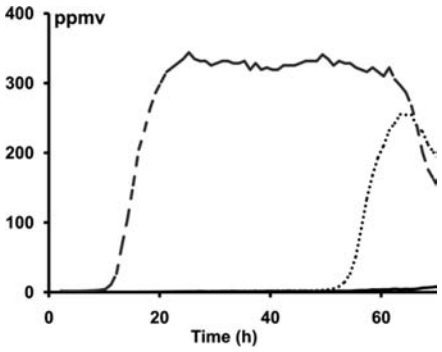

Figure 5. Profile of targeted sample compounds measured by online SIFT-MS, namely, ethanol (– – –), acetoin (···), and acetic acid (–).

sanfranciscensis and *Saccharomyces cerevisiae* under (acid) stress conditions.[50] The low concentrations present in this sourdough (5 mM) corresponded with a large response (255 ppmv) in the SIFT-MS, which was in contrast with the low response for acetic acid (12 ppmv), despite the high concentrations of the latter in this sourdough (70 mM). Several factors could be accountable for the discrepancy. However, all this seems to limit the use of SIFT-MS to the monitoring of noncharged, volatile compounds, unless precautions are taken to trap these compounds. Nevertheless, the detection of acetoin and ethanol demonstrated the feasibility of SIFT-MS as a real-time monitoring unit for sourdough fermentation processes. Interestingly, extensive microbiological analysis of these fermentation processes showed that the *Lb. sanfranciscensis* IMDO 150101 starter culture added did not dominate all of the fermentations performed (data not shown), allowing other microbiota to grow out, which was confirmed by differences in the volatile sample compounds found through SIFT-MS, i.e., a lowered production of ethanol and acetoin.

In conclusion, the feasibility of SIFT-MS to monitor fermentations through gas sampling in the headspace of fermentation vessels was illustrated, using the case of the production of ethanol during sourdough fermentation. The setup and methodology presented could be used not only to monitor a fermentation process online but also to (semi)-quantify volatiles in real-time without the need for additional samplings. The potential of SIFT-MS as an online monitoring device for food fermentations was further demonstrated by the detection of acetoin in certain sourdough fermentations. This allowed discrimination between sourdough fermentation processes and illustrated the importance of real-time monitoring of food fermentations. However, the performance of the SIFT-MS technique in complex matrices needs further examination, as the current device is restricted to the monitoring of sufficiently volatile compounds.

■ ASSOCIATED CONTENT

Supporting Information

Ions measured during SIM scans. This material is available free of charge via the Internet at http://pubs.acs.org.

■ AUTHOR INFORMATION

Corresponding Author

*Phone: +32 2 6293245. Fax: +32 2 6292720. E-mail: ldvuyst@vub.ac.be.

Funding

We acknowledge the financial support from Research Council of the Vrije Universiteit Brussel (SRP, IRP, and IOF projects), the Hercules Foundation, and Flanders' FOOD. S.V.K. is the recipient of a Ph.D. fellowship from the Vrije Universiteit Brussel.

Notes

The authors declare the following competing financial interest(s): Joeri Vercammen and Roel Wuyts belong to Interscience bvba, the official distributor of the SIFT instrument in the Benelux. They intensively contributed to the engineering of the unique SIFT-MS set-up (interface, transfer lines, etc.).

■ ACKNOWLEDGMENTS

We thank the technical support of Interscience bvba, in particular by Michel Verhaegen and Nico van der Groef. Also, Gunter Eerdekens (Interscience bvba) and Tom Balzarini (Vrije Universiteit Brussel) are gratefully acknowledged for their technical advice.

■ REFERENCES

(1) Caplice, E.; Fitzgerald, G. F. Food fermentations: role of microorganisms in food production and preservation. *Int. J. Food Microbiol.* **1999**, *50*, 131–149.

(2) Leroy, F.; De Vuyst, L. Lactic acid bacteria as functional starter cultures for the food fermentation industry. *Trends Food Sci. Technol.* **2004**, *15*, 67–78.

(3) De Vuyst, L.; Van Kerrebroeck, S.; Harth, H.; Huys, G.; Daniel, H.-M.; Weckx, S. Microbial ecology of sourdough fermentations: diverse or uniform? *Food Microbiol.* **2014**, *37*, 11–29.

(4) Maiti, S. K.; Srivastava, R. K.; Bhushan, M.; Wangikar, P. P. Real time phase detection based online monitoring of batch fermentation processes. *Process Biochem.* **2009**, *44*, 799–811.

DOI: 10.1021/jf505111m
J. Agric. Food Chem. 2015, 63, 829–835

(5) Falony, G.; Verschaeren, A.; De Bruycker, F.; De Preter, V.; Verbeke, K.; Leroy, F.; De Vuyst, L. In vitro kinetics of prebiotic inulin-type fructan fermentation by butyrate-producing colon bacteria: implementation of online gas chromatography for quantitative analysis of carbon dioxide and hydrogen gas production. *Appl. Environ. Microbiol.* **2009**, *75*, 5884−5892.
(6) Bastidas-Oyanedel, J.-R.; Mohd-Zaki, Z.; Pratt, S.; Steyer, J.-P.; Batstone, D. J. Development of membrane inlet mass spectrometry for examination of fermentation processes. *Talanta* **2010**, *83*, 482−492.
(7) Biasioli, F.; Yeretzian, C.; Märk, T. D.; Dewulf, J.; Van Langenhove, H. Direct-injection mass spectrometry adds the time dimension to (B)VOC analysis. *Trends Anal. Chem.* **2011**, *30*, 1003−1017.
(8) Adams, N. G.; Smith, D. The selected ion flow tube (SIFT); a technique for studying ion-neutral reactions. *Int. J. Mass Spectrom Ion Phys.* **1976**, *21*, 349−359.
(9) Španěl, P.; Smith, D. Advances in on-line absolute trace gas analysis by SIFT-MS. *Curr. Anal. Chem.* **2013**, *9*, 525−539.
(10) Španěl, P.; Smith, D. Selected ion flow tube: a technique for quantitative trace gas analysis of air and breath. *Med. Biol. Eng. Comput.* **1996**, *34*, 409−419.
(11) Smith, D.; Španěl, P. Direct, rapid quantitative analyses of BVOCs using SIFT-MS and PTR-MS obviating sample collection. *Trends Anal. Chem.* **2011**, *30*, 945−959.
(12) Heynderickx, P. M.; Van Huffel, K.; Dewulf, J.; Van Langenhove, H. Application of similarity coefficients to SIFT-MS data for livestock emission characterization. *Biosyst. Eng.* **2013**, *114*, 44−54.
(13) Langford, V. S.; Gray, J. D. C.; McEwan, M. J. Selected ion flow tube studies of several siloxanes. *Rapid Commun. Mass Spectrom.* **2013**, *27*, 700−706.
(14) Heynderickx, P. M.; De Clercq, S.; Saveyn, P.; Dewulf, J.; Van Langenhove, H. Determination of the sorption and desorption kinetics of perfume raw materials in the liquid phase with vesicular dispersion: Application of SIFT-MS. *Chem. Eng. J.* **2013**, *217*, 281−288.
(15) Havlíček, V.; Lemr, K.; Schug, K. A. Current trends in microbial diagnostics based on mass spectrometry. *Anal. Chem.* **2013**, *85*, 790−797.
(16) Storer, M. K.; Hibbard-Melles, K.; Davis, B.; Scotter, J. Detection of volatile compounds produced by microbial growth in urine by selected ion flow tube mass spectrometry (SIFT-MS). *J. Microbiol. Methods* **2011**, *87*, 111−113.
(17) Dummer, J.; Storer, M.; Swanney, M.; McEwan, M.; Scott-Thomas, A.; Bhandari, S.; Chambers, S.; Dweik, R.; Epton, M. Analysis of biogenic volatile organic compounds in human health and disease. *Trends Anal. Chem.* **2011**, *30*, 960−967.
(18) West, R.; Seetharaman, K.; Duizer, L. M. Whole grain macaroni: Flavour interactions with sodium-reduced cheese sauce. *Food Res. Int.* **2013**, *53*, 149−155.
(19) Langford, V. S.; Reed, C. J.; Milligan, D. B.; McEwan, M. J.; Barringer, S. A.; Harper, W. J. Headspace analysis of Italian and New Zealand parmesan cheeses. *J. Food Sci.* **2012**, *77*, C719−C726.
(20) De Clippeleer, J.; Van Opstaele, F.; Vercammen, J.; Francis, G. J.; De Cooman, L.; Aerts, G. Real-time profiling of volatile malt aldehydes using selected ion flow tube mass spectrometry. *LCGC North Am.* **2010**, *28*, 386.
(21) Huang, X. S.; Duan, H. Y.; Barringer, S. A. Effects of buffer and temperature on formation of furan, acetic acid and formic acid from carbohydrate model systems. *Food Sci. Technol.* **2011**, *44*, 1761−1765.
(22) Thorn, R. M. S.; Reynolds, D. M.; Greenman, J. Multivariate analysis of bacterial volatile compound profiles for discrimination between selected species and strains *in vitro*. *J. Microbiol. Methods* **2011**, *84*, 258−264.
(23) Shestivska, V.; Španěl, P.; Dryahina, K.; Sovova, K.; Smith, D.; Musilek, M.; Nemec, A. Variability in the concentrations of volatile metabolites emitted by genotypically different strains of *Pseudomonas aeruginosa*. *J. Appl. Microbiol.* **2012**, *113*, 701−713.
(24) Scotter, J. M.; Langford, V. S.; Wilson, P. F.; McEwan, M. J.; Chambers, S. T. Real-time detection of common microbial volatile organic compounds from medically important fungi by selected ion flow tube-mass spectrometry (SIFT-MS). *J. Microbiol. Methods* **2005**, *63*, 127−134.
(25) Langford, V.; Gray, J.; Foulkes, B.; Bray, P.; McEwan, M. J. Application of selected ion flow tube-mass spectrometry to the characterization of monofloral New Zealand honeys. *J. Agric. Food Chem.* **2012**, *60*, 6806−6815.
(26) Olivares, A.; Dryahina, K.; Navarro, J. L.; Smith, D.; Španěl, P.; Flores, M. SPME-GC-MS versus selected ion flow tube mass spectrometry (SIFT-MS) analyses for the study of volatile compound generation and oxidation status during dry fermented sausage processing. *J. Agric. Food Chem.* **2011**, *59*, 1931−1938.
(27) Noseda, B.; Islam, M. T.; Eriksson, M.; Heyndrickx, M.; De Reu, K.; Van Langenhove, H.; Devlieghere, F. Microbiological spoilage of vacuum and modified atmosphere packaged Vietnamese *Pangasius hypophthalmus* fillets. *Food Microbiol.* **2012**, *30*, 408−419.
(28) Amadei, G.; Ross, B. M. Quantification of character-impacting compounds in *Ocimum basilicum* and 'Pesto alla Genovese' with selected ion flow tube mass spectrometry. *Rapid Commun. Mass Spectrom.* **2012**, *26*, 219−225.
(29) Sharp, M. D.; Kocaoglu-Vurma, N. A.; Langford, V.; Rodriguez-Saona, L. E.; Harper, W. J. Rapid discrimination and characterization of vanilla bean extracts by attenuated total reflection infrared spectroscopy and selected ion flow tube mass spectrometry. *J. Food Sci.* **2012**, *77*, C284−C292.
(30) Bowman, T.; Barringer, S. Analysis of factors affecting volatile compound formation in roasted pumpkin seeds with selected ion flow tube-mass spectrometry (SIFT-MS) and sensory analysis. *J. Food Sci.* **2012**, *77*, C51−C60.
(31) Huang, Y.; Barringer, S. A. Alkylpyrazines and other volatiles in cocoa liquors at pH 5 to 8, by selected ion flow tube-mass spectrometry (SIFT-MS). *J. Food Sci.* **2010**, *75*, C121−C127.
(32) Davis, B. M.; Senthilmohan, S. T.; McEwan, M. J. Direct determination of antioxidants in whole olive oil using the SIFT-MS-TOSC assay. *J. Am. Oil Chem. Soc.* **2011**, *88*, 785−792.
(33) Sumonsiri, N.; Barringer, S. A. Application of SIFT-MS in monitoring volatile compounds in fruits and vegetables. *Curr. Anal. Chem.* **2013**, *9*, 631−641.
(34) Huang, Y.; Barringer, S. A. Monitoring of cocoa volatiles produced during roasting by selected ion flow tube-mass spectrometry (SIFT-MS). *J. Food Sci.* **2011**, *76*, C279−C286.
(35) Van der Meulen, R.; Scheirlinck, I.; Van Schoor, A.; Huys, G.; Vancanneyt, M.; Vandamme, P.; De Vuyst, L. Population dynamics and metabolite target analysis of lactic acid bacteria during laboratory fermentations of wheat and spelt sourdoughs. *Appl. Environ. Microbiol.* **2007**, *73*, 4741−4750.
(36) Vrancken, G.; Rimaux, T.; De Vuyst, L.; Leroy, F. Kinetic analysis of growth and sugar consumption by *Lactobacillus fermentum* IMDO 130101 reveals adaptation to the acidic sourdough ecosystem. *Int. J. Food Microbiol.* **2008**, *128*, 58−66.
(37) Meroth, C. B.; Walter, J.; Hertel, C.; Brandt, M. J.; Hammes, W. P. Monitoring the bacterial population dynamics in sourdough fermentation processes by using PCR-denaturing gradient gel electrophoresis. *Appl. Environ. Microbiol.* **2003**, *69*, 475−482.
(38) Ravyts, F.; De Vuyst, L. Prevalence and impact of single-strain starter cultures of lactic acid bacteria on metabolite formation in sourdough. *Food Microbiol.* **2011**, *28*, 1129−1139.
(39) Vrancken, G.; Rimaux, T.; Weckx, S.; Leroy, F.; De Vuyst, L. Influence of temperature and backslopping time on the microbiota of a type I propagated laboratory wheat sourdough fermentation. *Appl. Environ. Microbiol.* **2011**, *77*, 2716−2726.
(40) Lefeber, T.; Gobert, W.; Vrancken, G.; Camu, N.; De Vuyst, L. Dynamics and species diversity of communities of lactic acid bacteria and acetic acid bacteria during spontaneous cocoa bean fermentation in vessels. *Food Microbiol.* **2011**, *28*, 457−464.
(41) Ravyts, F.; Vrancken, G.; D'Hondt, K.; Vasilopoulos, C.; De Vuyst, L.; Leroy, F. Kinetics of growth and 3-methyl-1-butanol production by meat-borne, coagulase-negative staphylococci in view of sausage fermentation. *Int. J. Food Microbiol.* **2009**, *134*, 89−95.

DOI: 10.1021/jf505111m
J. Agric. Food Chem. 2015, 63, 829−835

(42) Syft Technologies Ltd. Development of SIFT-MS Methods. In *SIFT-MS Primer: An Introduction to the Chemistry and Methodology of SIFT-MS*; Syft Technologies Ltd.: Christchurch, New Zealand, 2009; pp 59−72.
(43) Prince, B. J.; Milligan, D. B.; McEwan, M. J. Application of selected ion flow tube mass spectrometry to real-time atmospheric monitoring. *Rapid Commun. Mass Spectrom.* **2010**, *24*, 1763−1769.
(44) Saxena, P.; Hildemann, L. M. Water-soluble organics in atmospheric particles: A critical review of the literature and application of thermodynamics to identify candidate compounds. *J. Atmos. Chem.* **1996**, *24*, 57−109.
(45) Yaws, C. L.; Yang, H.-C. Henry's Law Constant for Compound in Water. In *Thermodynamic and Physical Property Data*; Yaws, C. L., Ed.; Gulf Publishing Company: Houston, TX, 1992; pp 181−206.
(46) Smith, F. L.; Harvey, A. H. Avoid common pitfalls when using Henry's law. *Chem. Eng. Prog.* **2007**, *103*, 33−39.
(47) Yokelson, R. J.; Christian, T. J.; Bertschi, I. T.; Hao, W. M. Evaluation of adsorption effects on measurements of ammonia, acetic acid, and methanol. *J. Geophys. Res.* **2003**, *108*, 4649.
(48) Moens, F.; Lefeber, T.; De Vuyst, L. Oxidation of metabolites highlights the microbial interactions and role of *Acetobacter pasteurianus* during cocoa bean fermentation. *Appl. Environ. Microbiol.* **2014**, *80*, 1848−1857.
(49) Masucci, J. A.; Caldwell, G. W. Techniques for Gas Chromatography/Mass Spectrometry. In *Modern Practice of Gas Chromatography*, 4th ed.; Grob, R. L., Barry, E. F., Eds.; Wiley-Interscience: New York, 2004; pp 354−355.
(50) Guerzoni, M. E.; Vernocchi, P.; Ndagijimana, M.; Gianotti, A.; Lanciotti, R. Generation of aroma compounds in sourdough: Effects of stress exposure and lactobacilli-yeasts interactions. *Food Microbiol.* **2007**, *24*, 139−148.

DOI: 10.1021/jf505111m
J. Agric. Food Chem. 2015, 63, 829−835

JOURNAL OF AGRICULTURAL AND FOOD CHEMISTRY

Article

pubs.acs.org/JAFC

Naturally Occurring Hydroxytyrosol Derivatives: Hydroxytyrosyl Acetate and 3,4-Dihydroxyphenylglycol Modulate Inflammatory Response in Murine Peritoneal Macrophages. Potential Utility as New Dietary Supplements

Marina Aparicio-Soto,[†] Susana Sánchez-Fidalgo,[†] Alejandro González-Benjumea,[‡] Inés Maya,[‡] José G. Fernández-Bolaños,[‡] and Catalina Alarcón-de-la-Lastra*[,†]

[†]Department of Pharmacology, Faculty of Pharmacy, University of Seville, Profesor García González Street 2, 41012 Seville, Spain

[‡]Department of Organic Chemistry, Faculty of Chemistry, University of Seville, Profesor García González Street 1, 41012 Seville, Spain

ABSTRACT: This work evaluated the effects of extra virgin olive oil (EVOO) phenols, hydroxytyrosyl acetate (**2**) and 3,4-dihydroxyphenylglycol (**3**), as well as two new acyl derivatives of **3**, 4-(1,2-di(butanoyloxy)ethyl)benzene-1,2-diol (**7**) and 4-(1,2-di(lauroyloxy)ethyl)benzene-1,2-diol (**8**), on LPS-stimulated murine peritoneal macrophages in comparison with hydroxytyrosol (HTy, **1**). Compounds **2**, **3**, **7**, and **8** showed a strong reactive oxygen species (ROS)-scavenging activity, reducing significantly nitrite levels with a significant decrease on iNOS expression [**2** (50 μM, 0.44 ± 0.03; 100 μM, 0.44 ± 0.01; $p < 0.01$); **3** (50 μM, 0.37 ± 0.03; 100 μM, 0.37 ± 0.01; $p < 0.001$); **7** (50 μM, 0.45 ± 0.06; $p < 0.01$)] . However, only **2** and **3** down-regulated COX-2 expression [**2** (50 μM, 0.72 ± 0.04, $p < 0.05$; 100 μM, 0.54 ± 0.06, $p < 0.01$); **3** (50 μM, 0.56 ± 0.05, $p < 0.05$; 100 μM, 0.37 ± 0.04; $p < 0.001$)] and prevented IKBα degradation [**2** (100 μM, 1.63 ± 0.14, $p < 0.01$); **3** (100 μM, 1.82 ± 0.09; $p < 0.01$)] ; the diacylated compounds **7** and **8** showed worse anti-inflammatory activity than the parent **3**. In conclusion, **2** and **3** phenolic derivatives could play an important role in the anti-inflammatory effect of EVOO. The implication of this study for the nutrition and general health of the population rests in the possible use of natural HTy derivatives with better hydrophilic/lipophilic balance, thus improving its pharmacodynamic and pharmacokinetic profiles, as new dietary supplements in foods.

KEYWORDS: *EVOO, phenols, inflammation, macrophages, NF-κB*

INTRODUCTION

Macrophages are major components of the innate immune system and play a critical role in the inflammation process. Resident macrophages produce pro-inflammatory cytokines and chemokines that attract other cells, including neutrophils and additional macrophages. These cells are activated by exposure to bacterial lipopolysaccharide (LPS) among others. LPS-stimulated macrophages disrupt the balance of the intracellular reduction−oxidation state, which leads to oxidative stress characterized by a major shift in the cellular redox balance and usually accompanied by reactive oxygen species (ROS)-mediated damage.[1] Macrophages express enzymes such as inducible nitric oxide synthase (iNOS) and cylcooxygenase-2 (COX-2) that regulate inflammatory processes.[2] Actually, both proteins are responsible for the overproduction of NO and prostaglandin E_2 (PGE_2), respectively, in inflammation. The process of gene expression of these pro-inflammatory mediators involves multiple signal transduction pathways such as mitogen-activated protein kinases (MAPKs) and nuclear transcription factor κB (NF-κB) pathways. These pro-inflammatory mediators and pathways are regarded as essential anti-inflammatory targets.[3] For this reason, the stimulation of macrophages with LPS constitutes an excellent model for the screening and subsequent evaluation of the effects of candidate drugs on the inflammatory pathway.[4]

Extra virgin olive oil (EVOO), the characteristic fatty component of the Mediterranean diet, is rich in a variety of phenolic compounds, mainly constituted by secoiridoid derivatives of 2-(3,4-dihydroxyphenyl)ethanol (hydroxytyrosol, HTy) (**1**) and 2-(4-hydroxyphenyl)ethanol (tyrosol) along with minor amounts of free HTy and hydroxytyrosyl acetate (HTy-Ac) (**2**).[5]

Evidence has accumulated on the favorable properties of these EVOO phenolic compounds, which have shown a broad spectrum of beneficial activities such as antioxidant, free radical scavenging, anti-inflammatory, or anticancer,[6−8] as well as very good available safety/toxicity.[9] HTy is one of the most studied phenols, which has demonstrated important biological properties acting as a powerful antioxidant scavenger of free radicals[10−13] and modulating signaling pathways involved in antioxidant/detoxifying enzyme regulation, contributing to prevent oxidative stress associated cell damage.[14] In addition, HTy reduces DNA, lipid, and protein damages and strengthens the intracellular antioxidant enzyme mechanisms, protecting the peripheral blood mononuclear cells against oxidative stress.[15] Moreover, antiplatelet aggregation, antiatherogenic,

Received: July 15, 2014
Revised: December 18, 2014
Accepted: December 19, 2014
Published: December 19, 2014

ACS Publications © 2014 American Chemical Society

DOI: 10.1021/jf503357s
J. Agric. Food Chem. 2015, 63, 836−846

cardioprotective, antimicrobial, antiviral, anticancer, and anti-inflammatory activities have been reported.[11] Recently, we have demonstrated that supplementation of the diet with HTy may improve chronic colitis through inducible nitric oxide synthase (iNOS) down-regulation plus its antioxidant capacity.[16] Nevertheless, the low lipophilicity of this compound has encouraged us to study two HTy derivatives also present in EVOO: one more lipophilic, hydroxytyrosyl acetate (**2**), and another more hydrophilic, 3,4-dihydroxyphenylglycol (**3**), than HTy (**1**)[17,18] to improve the pharmacokinetic profile and increase bioavailability. The concentration of **2** is approximately equal to that of HTy in some olive oil varieties such as Arbequina, but is twice as high as that of HTy in the Picual variety and 3−4 times as high in the Manzanilla and Hojiblanca varieties.[5] Previous studies have shown that **2** exerts an in vitro neuroprotective effect and an antiplatelet effect in vivo[19] acting as a potential alternative to HTy (**1**) as platelet antiaggregant in prophylaxis for vascular disease. Moreover, another study has demonstrated its ability to increase glucose consumption in 3T3-L1 adipocytes and C2C12 myotubes through the down-regulation of PPARγ, C/EBPα, and SREBP-1c and their downstream target genes (GLUT4, CD36, and FAS).[20] On the other hand, dihydroxyphenylglycol (**3**) is an important phenolic compound that appears in higher concentration than HTy in certain table olive preparations (naturally processed olives)[21] and also importantly presents in the solid olive waste of olive oil extraction.[22] This phenol has shown higher antioxidant and antiradical capacities than HTy and a lipid peroxidation prevention comparable with that of vitamin E.[23] In addition, its bioavailability and antioxidant properties have been demonstrated in vitamin E-deficient rats,[24] and it may also protect against platelet activation and adhesion.[25] However, the anti-inflammatory properties of **2** and **3** and the molecular mechanisms involved remain unexplored.

Furthermore, different studies on phenolic compounds have shown the importance of acyl derivatives of natural phenols because their lipophilic nature allows them to cross the cytoplasmic cell membranes and their uptake by cells, providing a potential protection of membrane constituents.[26,27] Besides, the native phenols that contain several hydroxyl groups often undergo conjugation reactions such as the formation of β-glucuronides catalyzed by a family of enzymes known as the uridine diphosphoglucuronosyl transferases (UGTs). Conjugation with a sulfate moiety or with glutathione also occurs, catalyzed by various sulfotransferases and glutathione-*S*-transferases, respectively. These conjugated products are ideal substrates for various excretory transmembrane transport processes in the liver and kidneys.[26] A deacylation step by lipases of the human digestive system prior to glucuronidation or sulfation may delay the excretion process. In this context, two new derivatives from 3,4-dihydroxyphenylglycol (**3**), 4-(1,2-bis(butanoyloxy)ethyl)benzene-1,2-diol (**7**), and 4-(1,2-bis(lauroyloxy)ethyl)benzene-1,2-diol (**8**) have been synthesized and tested in peritonea macrophages.

Taking this background into account, the aim of the present work was to investigate the potential effects of compounds **2**, **3**, **7**, and **8** in murine macrophage inflammatory response induced by LPS in comparison with hydroxytyrosol (**1**). In this sense, antioxidant activity and protein expression of pro-inflammatory (iNOS and COX-2) enzymes as well as the role of mitogen-activated protein kinases (MAPKs) and nuclear transcription factor-kappa B (NF-κB) signaling pathways involved in the anti-inflammatory effects were determined.

MATERIALS AND METHODS

Chemicals. *General Chemical Procedures.* ^{1}H (300.1 MHz) and ^{13}C (75.5 MHz) NMR spectra were recorded on a Bruker Avance-300 spectrometer. Mass spectra (LSI-MS) were recorded on a Micromass AutoSpec-Q mass spectrometer. IR spectra were recorded on a Jasco FT-IR 4100 spectrophotometer. TLC was performed on silica-coated aluminum sheets from Merck (silica gel 60 F_{254}); spots were visualized by UV light and by staining with vanillin/H_2SO_4 in EtOH (1.5 g of vanillin in 100 mL of 95% EtOH/concentrated H_2SO_4 100:1). Column chromatography was performed using silica gel 60 (particle size 63−200 μm, Merck). All reactions were carried out under a nitrogen or argon atmosphere with dry solvents. Hydroxytyrosol (**1**), obtained from olive mill wastewaters,[28] was used after purification by column chromatography (EtOAc/hexane 1:5 → 1:2).

*3,4-Bis(benzyloxy)phenylglycol (**4**).* To a solution of **3** (200 mg, 0.57 mmol) in dry acetone (20 mL) were added K_2CO_3 (640 mg, 4.63 mmol) and BrBn (320 μL, 2.72 mmol). The mixture was refluxed in the dark for 12 h, filtered, and concentrated to dryness. Column chromatography (EtOAc/hexane 1:5 → 1:1) gave **4** as a white solid (162 mg, 81%): ^{1}H NMR (300 MHz, CD_3OD) δ 7.50−7.29 (m, 10H, Ph), 7.11 (d, 1H, $J_{2,6}$ = 1.9 Hz, Ar-2), 7.02 (d, 1H, $J_{5,6}$ = 8.3 Hz, Ar-5), 6.93 (dd, 1H, $J_{6,5}$ = 8.3 Hz, $J_{6,2}$= 1.9 Hz, Ar-6), 5.15 and 5.13 (2 s, 2H each, 2 OCH_2Ph), 4.62 (t, 1H, J = 6.0 Hz, CH), 3.58 (d, 2H, J = 6.0 Hz, CH_2); ^{13}C NMR (75.5 MHz, CD_3OD) δ 151.1, 150.5 (Ar-3, Ar-4), 139.7, 139.7 (2 Ph-*ipso*), 137.9 (Ar-1), 130.3 (4 Ph-*m*), 129.7 (2 Ph-*p*), 129.6, 129.5 (4 Ph-*o*), 121.6 (Ar-6), 117.2 (Ar-5), 115.6 (Ar-2), 76.4 (CH), 73.4 and 73.3 (2 OCH_2Ph), 69.5 (CH_2); IR (cm^{-1}) 3382, 1515, 1258, 1226, 1135, 1012, 737, 694; HR-LSI-MS m/z calcd for $C_{22}H_{22}NaO_4$ ([M + Na]$^+$) 373.1410, found 373.1429.

*1,2-Bis(benzyloxy)-4-(1,2-bis(butanoyloxy)ethyl)benzene (**5**).* To a solution of **4** (553 mg, 1.58 mmol) in pyridine (3 mL) at 0 °C was added butanoyl chloride (500 μL, 4.81 mmol), and the mixture was stirred for 15 min. The solution was kept at 0 °C overnight. Some drops of water were added, and the solution was diluted with CH_2Cl_2 (90 mL). The solution was washed with 1 M HCl (30 mL) until the pH value reached 1; then it was washed with 1 M $NaHCO_3$ (30 mL) and finally with water. The organic phase was dried ($MgSO_4$), filtered, and concentrated to dryness. The residue was purified by column chromatography (EtOAc/hexane 1:5 → 1:1) to give the product as a colorless syrup (775 mg, quant): ^{1}H NMR (300 MHz, CD_3OD) δ 7.48−7.29 (m, 10H, Ph), 7.06 (d, 1H, $J_{3,5}$ = 1.9 Hz, Ar-3), 7.04 (d, 1H, $J_{6,5}$ = 8.3 Hz, Ar-6), 6.94 (dd, 1H, $J_{5,6}$ = 8.3 Hz, $J_{5,3}$ = 1.9 Hz, Ar-5), 5.95 (dd, 1H, J = 7.0 Hz, J = 5.0 Hz, CH), 5.16 and 5.15 (2s, 2H each, 2 OCH_2Ph), 4.33−4.24 (m, 2H, CH_2O), 2.33 (m, 2H, αCH_2), 2.27 (t, 2H, J = 7.3 Hz, $\alpha'CH_2$), 1.65 and 1.62 (2 sext, 2H each, J = 7.4 Hz, 2 βCH_2), 0.95 and 0.94 (2 t, 3H each, J = 7.4 Hz, 2 CH_3); ^{13}C NMR (75.5 MHz, CD_3OD) δ 175.6, 175.1 (2 CO), 151.4, 151.1 (Ar-1, Ar-2), 139.5 (2 Ph-*ipso*), 132.3 (Ar-4), 130.3 (4 Ph-*m*), 129.8 (2 Ph-*p*), 129.6, 129.5 (4 Ph-*o*), 122.2 (Ar-5), 117.1 (Ar-6), 116.1 (Ar-3), 75.1 (CH), 73.4 and 73.3 (2 OCH_2Ph), 67.8 (CH_2), 37.9, 37.7 (αCH_2), 20.3, 20.2 (βCH_2), 14.7 (2 CH_3); IR (cm^{-1}) 2967, 1736, 1514, 1248, 1166, 1137, 1007, 735, 696; HR-LSI-MS m/z calcd for $C_{30}H_{34}O_6$ ([M]$^+$) 490.2355, found 490.2341.

*1,2-Bis(benzyloxy)-4-(1,2-bis(lauroyloxy)ethyl)benzene (**6**).* To a solution of **4** (400 mg, 1.12 mmol) in pyridine (2.5 mL) at 0 °C was added lauroyl chloride (780 μL, 3.37 mmol), and the mixture was stirred for 15 min. The solution was kept at room temperature for 72 h. Some drops of water were added, and the solution was diluted with CH_2Cl_2 (150 mL). The solution was washed with 1 M HCl (30 mL) until the pH value reached 1; then it was washed with 1 M $NaHCO_3$ (30 mL) and finally with water. The organic phase was dried ($MgSO_4$), filtered, and concentrated to dryness. The residue was purified by column chromatography (EtOAc/hexane 1:5 → 1:1) to give the product as a colorless syrup (0.76 g, 95%): ^{1}H NMR (300 MHz, $(CD_3)_2CO$) δ 7.57−7.32 (m, 10H, Ph), 6.93 (d, 1H, $J_{3,5}$ = 1.9 Hz, Ar-3), 6.86 (d, 1H, $J_{6,5}$ = 8.1 Hz, Ar-6), 6.79 (dd, 1H, $J_{5,6}$ = 8.1 Hz, $J_{5,3}$ = 1.9 Hz, Ar-5), 5.94 (dd, 1H, J = 7.5 Hz, J = 4.8 Hz, CH), 5.23 and 5.20 (2s, 2H each, 2 OCH_2Ph), 4.33−4.24 (m, 2H, CH_2O), 2.38 (m, 2H, αCH_2), 2.32 (m, 2H, $\alpha'CH_2$), 1.67−1.58 (m, 4H, βCH_2

DOI: 10.1021/jf503357s
J. Agric. Food Chem. 2015, 63, 836−846

ester), 1.33 (m, 32H, 16 CH_2 ester), 0.94−0.90 (m, 6H, 2 CH_3 ester); ^{13}C NMR (75.5 MHz, $(CD_3)_2CO$) δ 172.6 (2 CO), 149.8, 149.7 (Ar-1, Ar-2), 138.3 (2 Ph-*ipso*), 130.9 (Ar-4), 128.9 (4 Ph-*m*), 128.3 (2 Ph-*p*), 128.2, 128.0 (4 Ph-*o*), 120.5 (Ar-5), 115.2 (Ar-6), 114.1 (Ar-3), 73.1 (CH), 71.4, 71.3 (2 OCH_2Ph), 66.1 (CH_2O), 34.5, 34.3, 33.9, 32.4, 25.5, 25.4, 23.1 (20 CH_2 ester), 14.1 (2 CH_3 ester); IR (cm^{-1}) 2922, 2852, 1739, 1263, 1155, 733, 659; HR-LSI-MS *m*/*z* calcd for $C_{46}H_{67}O_6$ ($[M + H]^+$) 715.4932, found 715.4925.

*4-(1,2-Bis(butanoyloxy)ethyl)benzene-1,2-diol (**7**).* A solution of **5** (240 mg, 0.49 mmol) in absolute EtOH (4 mL) was reduced in the dark with 10% Pd/C (115 mg) under atmospheric pressure at room temperature for 24 h. The mixture was filtered through a Celite pad and concentrated to dryness. The residue was purified by column chromatography (EtOAc/hexane 1:1) to give a product as a colorless syrup (137 mg, 90%): ^{1}H NMR (300 MHz, $CDCl_3$) δ 6.87−6.86 (m, 1H, Ar-3), 6.82 (d, 1H, $J_{6,5}$ = 8.1 Hz, Ar-6), 6.76 (dd, 1H, $J_{5,6}$ = 8.1 Hz, $J_{5,3}$ = 1.5 Hz, Ar-5), 5.89 (t, 1H, *J* = 6.0 Hz, CH), 4.27 (d, 2H, *J* = 6 Hz, CH_2O), 2.35 (t, 2H, *J* = 7.4 Hz, αCH_2), 2.29 (t, 2H, *J* = 7.4 Hz, $\alpha' CH_2$), 1.64 (sext, 2H, *J* = 7.4 Hz, βCH_2), 1.63 (sext, 2H, *J* = 7.4 Hz, $\beta' CH_2$), 0.92 (t, 6H, *J* = 7.4 Hz, 2 CH_3); ^{13}C NMR (75.5 MHz, $CDCl_3$) δ 174.1, 173.7 (2 CO), 144.7, 144.3 (Ar-1, Ar-2), 129.3 (Ar-4), 119.6 (Ar-5), 115.7 (Ar-6), 114.3 (Ar-3), 73.4 (CH), 66.3 (CH_2), 36.5, 36.4 (2 αCH_2), 18.7, 18.6 (2 βCH_2), 13.9 (2 CH_3); IR (cm^{-1}) 3400, 2967, 1720, 1170; HR-LSI-MS *m*/*z* calcd for $C_{16}H_{22}NaO_6$ ($[M + Na]^+$) 333.1309, found 333.1315.

*4-(1,2-Bis(lauroyloxy)ethyl)benzene-1,2-diol (**8**).* A solution of **6** (350 mg, 0.47 mmol) in THF (5 mL) was reduced in the dark with 10% Pd/C (160 mg) under atmospheric pressure at room temperature for 24 h. The mixture was filtered through a Celite pad and concentrated to dryness. The residue was purified by column chromatography (EtOAc/hexane 1:3) to give a product as a white solid (199 mg, 79%): ^{1}H NMR (300 MHz, $(CD_3)_2CO$) δ 6.93 (d, 1H, $J_{3,5}$ = 1.9 Hz, Ar-3), 6.86 (d, 1H, *J* = 8.1 Hz, Ar-6), 6.79 (dd, 1H, *J* = 1.9 Hz, *J* = 8.1 Hz, Ar-5), 5.94 (dd, 1H, *J* = 7.5 Hz, *J* = 4.8 Hz, CH), 4.33−4.24 (m, 2H, CH_2O), 2.34−2.29 (m, 4H, 2 αCH_2 ester), 1.67−1.58 (m, 4H, 2 βCH_2 ester), 1.33 (m, 32H, 16 CH_2 ester), 0.94−0.90 (m, 6H, 2 CH_3); ^{13}C NMR (75.5 MHz, $(CD_3)_2CO$) δ 173.1, 172.6 (2 CO), 145.8, 145.6 (Ar-1, Ar-2), 129.3 (Ar-4), 119.0 (Ar-5), 115.7 (Ar-6), 114.5 (Ar-3), 73.2 (CH), 66.2 (CH_2), 34.5, 34.3, 33.9, 32.4, 29.3, 25.3, 25.2, 22.9 (CH_2 ester), 14.4 (2 CH_3); IR (cm^{-1}) 2917, 2849, 1734, 1699, 1169; HR-LSI-MS *m*/*z* calcd for $C_{32}H_{54}NaO_6$ ($[M + Na]^+$) 557.3813, found 557.3797.

DPPH Radical Scavenging Activity. The free radical scavenging activities of **1**−**3**, **7**, and **8** were measured by decrease in the absorbance of methanolic solution of 1,1-diphenyl-2-picrylhydrazyl radical (DPPH) and was used for the determination of the antioxidant capacity of the compounds in the study.[28,29] Increasing concentrations of each product (1.56−100 μM, in methanol) were added at an equal volume (10 mL) to methanol solution of DPPH (400 μg mL^{-1}). Different concentrations of L-ascorbic acid (1.25−100 mg mL^{-1}) were used as the standard antioxidant. This acid has been widely used as a reference standard in the DPPH assay of polyphenols.[30−32] After 30 min at room temperature, the absorbance values were measured at 517 nm on a spectrophotometer and converted into the percentage antioxidant activity using the following equation: DPPH antiradical scavenging capacity (%) = (absorbance of sample − absorbance of blank) × 100/absorbance of blank. Methanol plus different concentrations of product solution was used as a blank, whereas DPPH solution plus methanol was used as a control. Dose−response curves (1.25−100 μg mL^{-1}) were performed for each product to obtain the respective half-maximum inhibitory concentration (IC_{50}), a value that denotes the concentration of sample required to scavenge 50% of DPPH radicals.

Animals. Fifteen 8−10-week-old male Swiss mice provided by Harlan Interfauna Ibérica (Barcelona, Spain), weighing 20−30 g, were randomly placed in cages (5 mice/cage) and maintained under constant conditions of temperature (20−25 °C) and humidity (40−60%) with a 12 h light/dark cycle and fed standard rodent chow (Panlab A04, Seville, Spain) and water ad libitum throughout the experiment in our Animal Laboratory Center (Faculty of Pharmacy, University of Seville, Spain). All animal care and experimental procedures complied with the Guidelines of the European Union regarding animal experimentation (Directive of the European Counsel 2010/63/EU) and followed a protocol observed by the Animal Ethics Committee of the University of Seville. All studies involving animals are reported in accordance with the ARRIVE guidelines for reporting experiments involving animals.

Isolation and Culture of Murine Peritoneal Macrophages. After 1 week of acclimation, peritoneal macrophages from five mice were elicited by intraperitoneal injection of 1 mL of sterile thioglycollate medium (10% w/v) (Scharlau, Barcelona, Spain), and behavioral observation, water and food consumptions, loss of body weight, and survival were daily monitored until sacrifice. After 3 days, mice were euthanized in the laboratory surgical area by CO_2 exposure and peritoneal exudate cells were obtained by lavage with ice-cold PBS. After centrifugation, cells were suspended in RPMI 1640 medium (PAA, Pasching, Austria) supplemented with 10% heat-inactivated fetal calf serum (FCS) (PAA), L-glutamine (2 mM), glucose (4.5 g l^{-1}), and HEPES buffer (10 mM), in the presence of 100 mg mL^{-1} streptomycin and 100 U mL^{-1} penicillin (PAA) and then seeded in culture plates (1 × 10^6 cells mL^{-1}) for 2 h at 37 °C in a 5% CO_2 humidified atmosphere. After 2 h, nonadherent cells were removed by washing with PBS and fresh RPMI 1640 medium supplemented with 5% FCS containing **1**−**3**, **7**, and **8**, respectively, was added. After 30 min, murine peritoneal macrophages (1 × 10^6 cells mL^{-1}) were treated with 5 μg mL^{-1} of LPS from *Escherichia coli* (Sigma-Aldrich, St. Louis, MO, USA) in the absence or presence of each compound in the study for 18 h. In each experiment, viability was always ≥95%. Stock solutions of **1**−**3**, **7**, and **8** at a concentration of 100 mg mL^{-1} were always freshly prepared in dimethyl sulfoxide (DMSO) (Panreac, Barcelona, Spain) and diluted to the desired concentration in the culture medium. The final concentration of DMSO in the culture medium was ≤1% in all experiments, and it had no significant influence on cell response.

Cell Viability Assay. Cells seeded in 96-well plates (1 × 10^5 cells $well^{-1}$) were incubated in the presence or absence of **1**−**3**, **7**, and **8** for 18 h. At the end of the exposure time, the effect of these compounds on cell growth/viability was analyzed by sulforhodamine B (SRB) assay.[33] After incubation time, adherent cell cultures were fixed in situ by adding 50 μL of 50% (w/v) cold of trichloroacetic acid (Sigma-Aldrich) and incubated for 60 min at 4 °C. The supernatant was discarded, and plates were washed five times with deionized water and dried. Fifty microliters of SRB (Sigma-Aldrich) solution (0.4% w/v) in 1% acetic acid (Panreac) was added to each well and incubated for 30 min at room temperature. Plates containing SRB solution were washed five times with 1% acetic acid. Then, plates were air-dried, and 100 μL per well of 10 mmol L^{-1} Tris base, pH 10.5 (Sigma-Aldrich), was added, and the absorbance of each well was read on an enzyme-linked immunosorbent assay reader at 510 nm (BioTek, Bad Friedrichshall, Germany). Finally, cell survival was measured as the percentage of absorbance compared with that obtained in control cells (nontreated cells).

Measurement of Nitrite Production. Cells in a 24-well plate were untreated or treated with different concentrations of **1**−**3**, **7**, and **8** and 30 min later stimulated with LPS for 18 h. The culture supernatants (100 μL) were transferred to a 96-well assay plate mixed with Griess reagent (Sigma, St. Louis, MO, USA) and incubated for 15 min at room temperature. The amount of nitrite, as an index of NO generation, was determined by a spectrophotometric method using the Griess reaction[34] and obtained by extrapolation from a standard curve with sodium nitrite. The absorbance at 540 nm was measured by an enzyme-linked immunosorbent assay reader (BioTek). Results were expressed as the nitrite production percentage compared with LPS control cells (stimulated untreated cells). One micromolar dexamethasone (Sigma) was used as positive control (data not shown).

Immunoblotting Detection. Cells (1 × 10^6 cells mL^{-1}) were untreated or treated with **1**−**3**, **7**, and **8** and stimulated with LPS for 18 h. After incubation, cells were rinsed, scraped off, and collected in ice-cold PBS containing a cocktail of protease and phosphatase inhibitors and processed as described by Sánchez-Hidalgo et al.[35] to isolate

DOI: 10.1021/jf503357s
J. Agric. Food Chem. 2015, 63, 836−846

proteins. Protein concentration was measured for each sample using a protein assay reagent (Bio-Rad, Hercules, CA, USA) according to the Bradford method and using γ-globulin as a standard.[36] Aliquots of supernatant containing equal amounts of protein (20 μg) were separated on 10% acrylamide gel by sodium dodecyl sulfate–polyacryamide gel electrophoresis. In the next step, the proteins were electrophoretically transferred into a nitrocellulose membrane and incubated with specific primary antibodies: rabbit anti-COX-2 and rabbit anti-iNOS (Cayman Chemical, Ann Arbor, MI, USA) (1:2500 and 1:1000, respectively); rabbit anti-IκBα, (Cell Signaling, Danvers, MA, USA) (1:1000); mouse anti-pJNK, rabbit anti-JNK, mouse anti-pp38, and rabbit anti-p38 (Santa Cruz Biotechnology, Santa Cruz, CA, USA) (1:1000) overnight at 4 °C. After rinsing, the membranes were incubated with a horseradish peroxidase-labeled (HRP) secondary antibody antirabbit (Cayman Chemical) (1:50000) or anti-mouse (Dako, Atlanta, GA, USA) (1:2000) containing blocking solution for 1–2 h at room temperature. To prove equal loading, the blots were analyzed for β-actin expression using an anti-β-actin antibody (Sigma-Aldrich). Immunodetection was performed using enhanced chemiluminescence light-detecting kit (Pierce, Rockford, IL, USA). The immunosignals were captured using an LAS-3000 Imaging System from Fujifilm Image Reader (Stamford, CT, USA), and densitometric data were studied following normalization to the housekeeping loading control. The signals were analyzed and quantified by an Image Processing and Analysis in Java (ImageJ, Softonic) and expressed in relation to the DMSO–LPS-treated cells.

Statistical Evaluation. All values in the figures and text are expressed as arithmetic means ± standard error (SEM). Experiments were carried out in triplicate. Data were evaluated with Graph Pad Prism version 5.01 software (San Diego, CA, USA). The statistical significance of any difference in each parameter among the groups was evaluated by one-way analysis of variance (ANOVA), using Tukey's multiple-comparisons test as post hoc test. P values of <0.05 were considered statistically significant. In the experiments involving densitometry, the figures shown are representative of at least three different experiments performed on different days.

RESULTS

Chemistry. The synthesis of HTy-Ac (**2**) was carried out from hydroxytyrosol (**1**) by a chemoselective acid-catalyzed transacetylation reaction (74%) by refluxing in EtOAc in the presence of a strong acidic resin (Scheme 1), following a proprietary procedure.[37] The naturally occurring 3,4-dihydroxyphenylglycol (**3**) was prepared from 3,4-dihydroxyphenacyl chloride following a procedure reported elsewhere (Sánchez-Fidalgo et al. 2014, submitted for publication).

Scheme 1. Synthesis of Hydroxytyrosyl Acetate (2) by Chemoselective Transesterification Reaction of 1

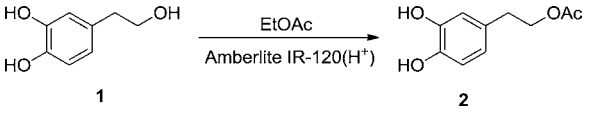

Although hydroxytyrosol and its lipophilic derivatives have been widely studied, there are many fewer reports on the biological properties and the chemical transformations of compound **3**. Herein we describe for the first time the synthesis of diacyl derivatives of **3** in order of increasing its reduced lipophilia.

Chemoselective protection of catechol fragment of **3** was performed in good yield (81%) by treatment with benzyl bromide in acetone under reflux the presence of potassium carbonate (Scheme 2). The higher acidity of the phenolic hydroxyl groups compared to the aliphatic alcohol explains the observed selectivity. The exhaustive acylation of the glycol moiety with butanoyl and lauroyl chlorides (3 equiv) in pyridine gave **5** and **6** in excellent yield (quant and 95%, respectively). Finally, deprotection of the catechol moiety of **5** and **6** by hydrogenolysis afforded **7** and **8** in a good yield (90 and 79%, respectively).

Scheme 2. Synthesis of Diacylated 3,4-Dihydroxyphenylglycols, 7 and 8, from 3[a]

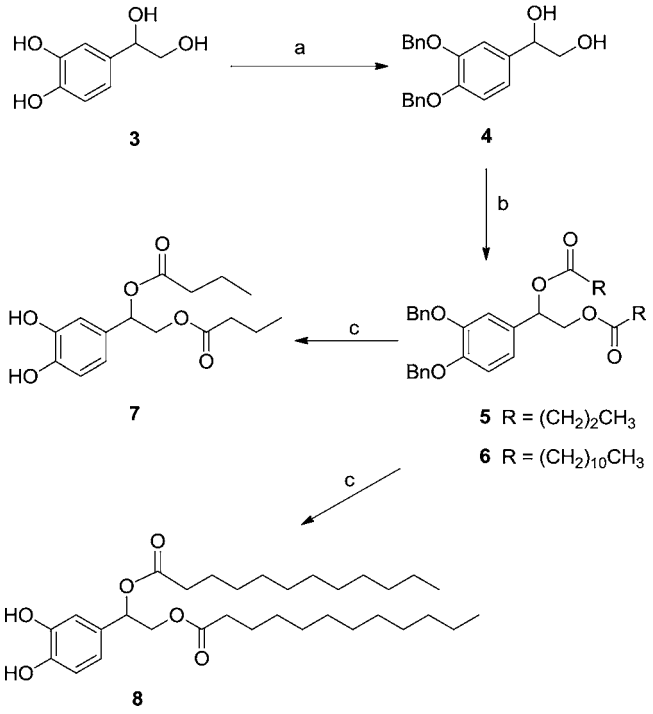

[a]Conditions: (a) BnBr, K_2CO_3, acetone, reflux, 12 h; (b) acyl chloride, pyridine, room temperature, 72 h; (c) H_2, 10% Pd/C, EtOH, or THF, room temperature, 24 h.

DPPH Radical Scavenging Activity of 1–3, 7, and 8. DPPH scavenging activity assay is a useful method for determination free radical scavenging activities of antioxidant compounds. As shown in Figure 1, the DPPH radical scavenging rates of the compounds were found to be higher than those of the standard ascorbic acid. However, compounds **1–3** have shown the best antioxidant activities. The IC_{50} values, defined as the effective concentration at which the antioxidant activity was 50% of **1–3**, **7**, and **8** and ascorbic acid, were 1.60 ± 0.21, 1.73 ± 0.26, 1.55 ± 0.11, 7.49 ± 0.26, 5.04 ± 0.215, and 14.30 ± 0.60 μM, respectively.

Effects of 1–3, 7, and 8 on Cell Viability. To evaluate the anti-inflammatory effect of these compounds, we determinate their effect on the viability of mouse peritoneal macrophages by SRB assay. After 18 h, our data demonstrated that the viability of cells treated with **1**, **2** and **3** separately was not significantly reduced at concentrations of 25–100 μM (data not shown). However, **7** and **8** at 100 μM had cell viability <90%; therefore, these compounds were assayed at 25 and 50 μM in the next studies.

Effects of 1–3, 7, and 8 on Nitrite Production. LPS induces the synthesis and release of NO into murine macrophage cell medium by iNOS protein expression.[38] As shown in Figure 2, co-incubation with **2**, **3**, and **7**, separately, significantly reduced nitrite production at similar levels of **1** (***, p < 0.001 vs DMSO–LPS control).

DOI: 10.1021/jf503357s
J. Agric. Food Chem. 2015, 63, 836–846

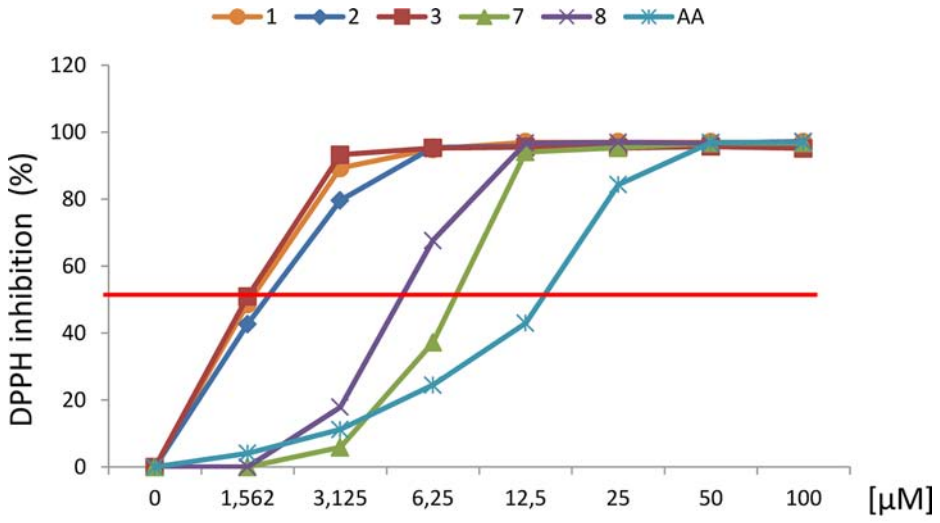

Substance (μM)	DPPH radical scavenging activity (IC_{50})
1	1.60 ± 0.21
2	1.73 ± 0.26
3	1.55 ± 0.11
7	7.49 ± 0.26
8	5.04 ± 0.22
AA	14.3 ± 0.60

Figure 1. DPPH scavenging effect of hydroxytyrosol (**1**), hydroxytyrosyl acetate (**2**), 3,4-dihydroxyphenylglycol (**3**), 4-(1,2-bis(butanoyloxy)-ethyl)benzene-1,2-diol (**7**), and 4-(1,2-bis(lauroyloxy)ethyl)benzene-1,2-diol (**8**). Values are expressed as the mean ± SEM. Values are the mean of three experiments. IC_{50} values represent the means ± SEM of three measurements.

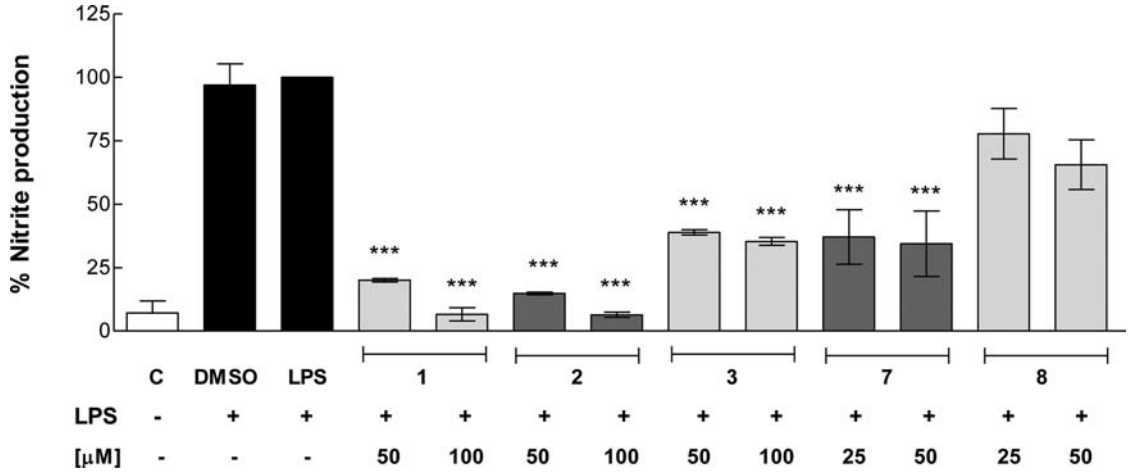

Figure 2. Effect of hydroxytyrosol (**1**), hydroxytyrosyl acetate (**2**), 3,4-dihydroxyphenylglycol (**3**), 4-(1,2-bis(butanoyloxy)ethyl)benzene-1,2-diol (**7**), and 4-(1,2-bis(lauroyloxy)ethyl)benzene-1,2-diol (**8**) on LPS-induced NO production. Each value represents the mean ± SEM for three independent experiments. (***) $p < 0.001$ versus DMSO-treated control cells.

Effects 1−3, 7, and 8 on iNOS Expression. The above data suggest that these compounds could down-regulate iNOS enzyme activity. This hypothesis was assessed by measuring of iNOS protein levels by Western blotting. Immunoblotting analysis demonstrated that **1**−**3** caused a significant inhibition of LPS-induced iNOS expression at 50 and 100 μM (** $p <$ 0.01, and ***, $p < 0.001$ vs DMSO−LPS control, respectively) (Figure 3). However, a significant iNOS reduction was observed only with the highest concentration (50 μM) of **7**

DOI: 10.1021/jf503357s
J. Agric. Food Chem. 2015, 63, 836−846

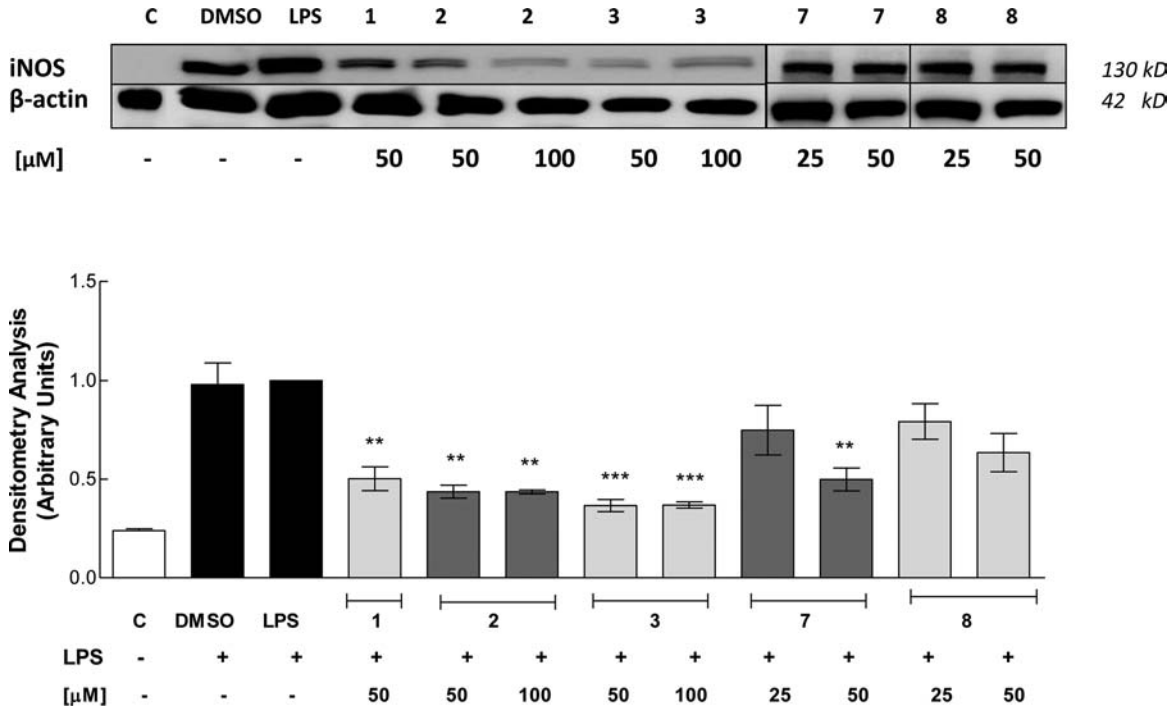

Figure 3. Effect of hydroxytyrosol (**1**), hydroxytyrosyl acetate (**2**), 3,4-dihydroxyphenylglycol (**3**), 4-(1,2-bis(butanoyloxy)ethyl)benzene-1,2-diol (**7**), and 4-(1,2-bis(lauroyloxy)ethyl)benzene-1,2-diol (**8**) on iNOS protein expression in mouse peritoneal macrophages. Cells were incubated with the compounds separately, and after 30 min, macrophages were treated with LPS for 18 h. As controls, cells were also treated with DMSO (solvent control) and LPS or untreated in the absence of LPS. Densitometry was performed following normalization to the control (*β*-actin housekeeping gene). Each value represents the mean ± SEM of three independent experiments. (**) $p < 0.01$ and (***) $p < 0.001$ versus DMSO-treated control cells.

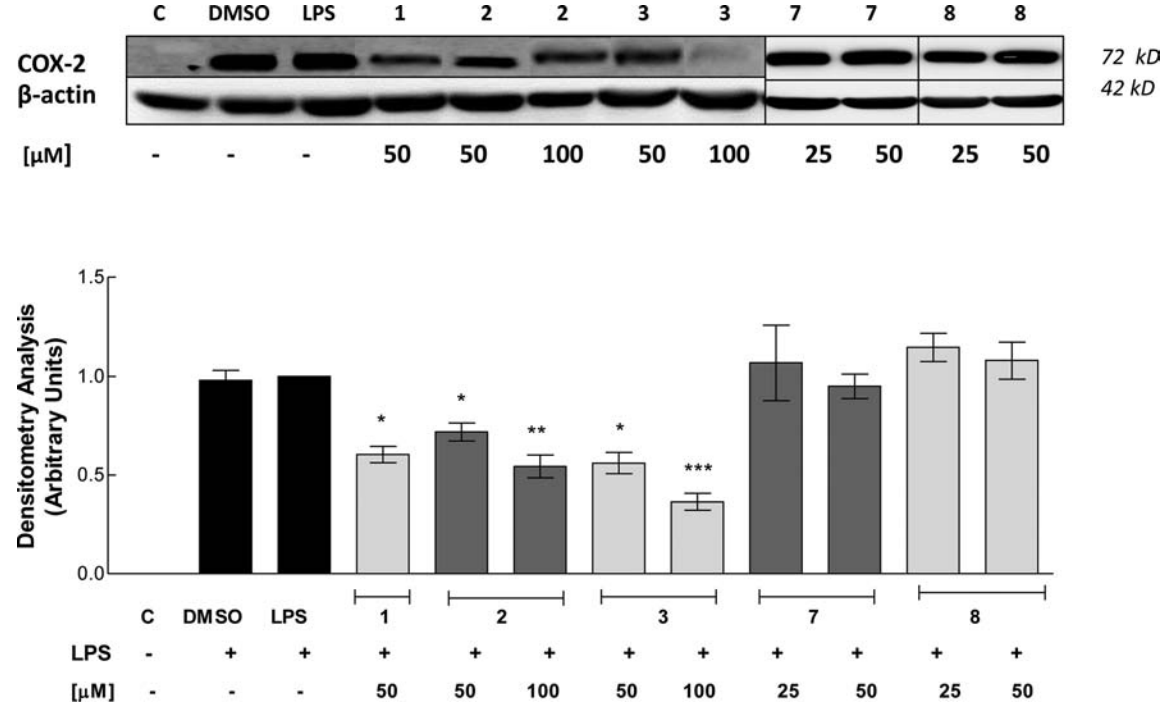

Figure 4. Effect of hydroxytyrosol (**1**), hydroxytyrosyl acetate (**2**), 3,4-dihydroxyphenylglycol (**3**), 4-(1,2-bis(butanoyloxy)ethyl)benzene-1,2-diol (**7**), and 4-(1,2-bis(lauroyloxy)ethyl)benzene-1,2-diol (**8**) on COX-2 protein expression in murine peritoneal macrophages. Cells were untreated or treated with **1**−**3**, **7**, and **8** for 18 h in the presence of LPS. As controls, cells were also treated with DMSO (solvent control) and LPS or untreated in the absence of LPS. Densitometry was performed following normalization to the control (*β*-actin housekeeping gene). Data are represented as the mean ± SEM. (*) $p < 0.05$, (**) $p < 0.01$, and (***) $p < 0.001$ versus DMSO-treated control cells.

(**, $p < 0.01$ vs DMSO−LPS control). No effects were observed on iNOS expression after incubation with **8**.

Effects of 1−3, 7, and 8 on COX-2 Overexpression Induced by LPS. Subsequently, we investigated the possible

DOI: 10.1021/jf503357s
J. Agric. Food Chem. 2015, 63, 836−846

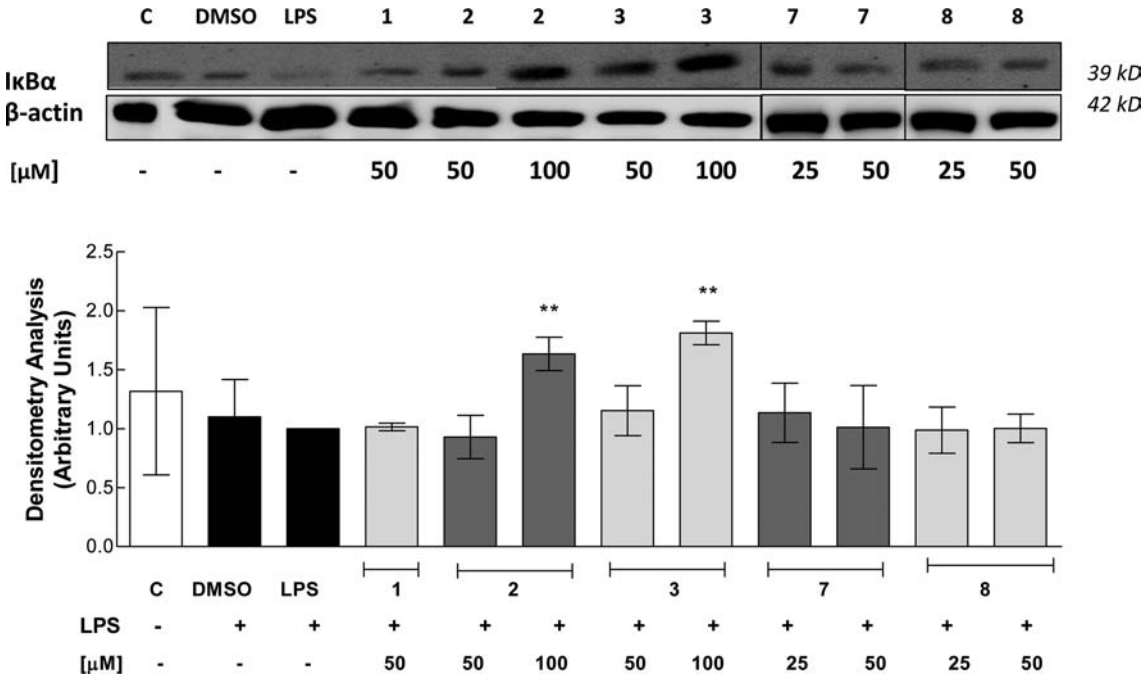

Figure 5. Effect of hydroxytyrosol (**1**), hydroxytyrosyl acetate (**2**), 3,4-dihydroxyphenylglycol (**3**), 4-(1,2-bis(butanoyloxy)ethyl)benzene-1,2-diol (**7**), and 4-(1,2-bis(lauroyloxy)ethyl)benzene-1,2-diol (**8**) on IKBα degradation in murine peritoneal isolated macrophages. Cells were untreated or treated with **1**−**3**, **7**, and **8** for 18 h in the presence of LPS. As controls, cells were also treated with DMSO (solvent control) and LPS or untreated in the absence of LPS. The results are representative of three independent experiments. Densitometry was performed following normalization to the control (β-actin housekeeping gene). Data are expressed as the mean ± SEM. (**) $p < 0.01$ versus DMSO-treated control cells.

effects of **1**−**3**, **7**, and **8** on COX-2 inflammation-related enzyme. COX-2 protein expression was remarkably increased after LPS stimulation, whereas a significant down-regulation on this pro-inflammatory protein expression was seen in macrophages treated with 50 μM **1** and 50 and 100 μM **2** and **3**: (**1**) *, $p < 0.05$; (**2**) *, $p < 0.05$, and **, $p < 0.01$, respectively; and (**3**) *, $p < 0.05$, and ***, $p < 0.001$, respectively, vs DMSO−LPS control) (Figure 4). However, no COX-2 expression changes were observed after treatment with **7** and **8**.

Effects of 1−3, 7, and 8 on LPS-Induced IKBα Degradation in LPS-Murine Peritoneal Macrophages. NF-κB is a pleiotropic mediator in the control of several inducible and tissue-specific genes and is one of the key regulators of the cellular responses to oxidative stress in mammalian cells.[39] NF-κB activation is initiated by the LPS-activated IκBα kinase signal followed by phosphorylation and degradation of IκBα. After IκBα is degraded, NF-κB in the NF-κB−IκBα complex is free to be translocated into the nucleus, where it can induce the expression of pro-inflammatory genes contributing to the damage. To determine whether pro-inflammatory protein down-regulation is regulated by the IκBα pathway, we measured the expression levels of IκBα in cytosolic fractions of mouse peritoneal macrophages treated with 5 μg mL^{-1} LPS and incubated in the presence or absence of the compounds individually for 18 h. As shown in Figure 5, pretreatment with **2** and **3** at 100 μM significantly prevented IκBα translocation (**, $p < 0.01$ vs DMSO control). Nevertheless, no changes were observed after **1**, **7**, and **8** treatments.

Effects of 2 and 3 on LPS-Induced MAPKs Activation in Murine Peritoneal Macrophages. To explore the possible molecular mechanisms of compounds **2** and **3** underlying the anti-inflammatory effects, we determined their potential effects on the MAPKs signaling pathway. We evaluated whether both concentrations (50 and 100 μM) were able to modulate JNK and p38 MAPKs activation after 18 h of LPS stimulation by Western blotting. Our findings demonstrated no significant changes in p38 and JNK protein phosphorylation after both treatments, suggesting that the MAPKs signaling pathway does not make a consistent contribution in the anti-inflammatory activities of **2** and **3** HTy derivatives on mouse peritoneal macrophages (Figure 6).

DISCUSSION

Our findings have shown for the first time that these phenol compounds, mainly compounds **2** and **3**, showed significant antiradical and antioxidant activities and thus prevented the progression of cellular damage induced by LPS acting as effective antioxidants. Balance disruption of the intracellular reduction−oxidation state has been observed in activated macrophages, which leads to oxidative stress characterized by a major shift in the cellular redox balance and usually accompanied by ROS-mediated damage.[1] Therefore, modulators of ROS production and ROS-induced signaling pathways, especially in macrophages, could represent potential targets for anti-inflammatory intervention.[40] Our findings are in agreement with other in vitro studies in which EVOO-isolated phenols, that is, **1** or oleuropein showed strong antioxidant effects acting as powerful scavenger of free radicals in a similar range and higher than those tested in our study (50−100 μM).[41,42] In addition, **2** has shown protective effects against oxidative DNA damage in blood cells[43] and against iron-induced oxidative stress in human cervical cells (HeLa)[44] as well as a neuroprotective effect in a model of hypoxia−reoxygenation in rat brain slices, both in vitro and after oral administration.[12] On the other hand, **3** presented higher antioxidant and antiradical capacities and reducing power than **1** and prevented lipid peroxidation to a degree that was comparable with that of

DOI: 10.1021/jf503357s
J. Agric. Food Chem. 2015, 63, 836−846

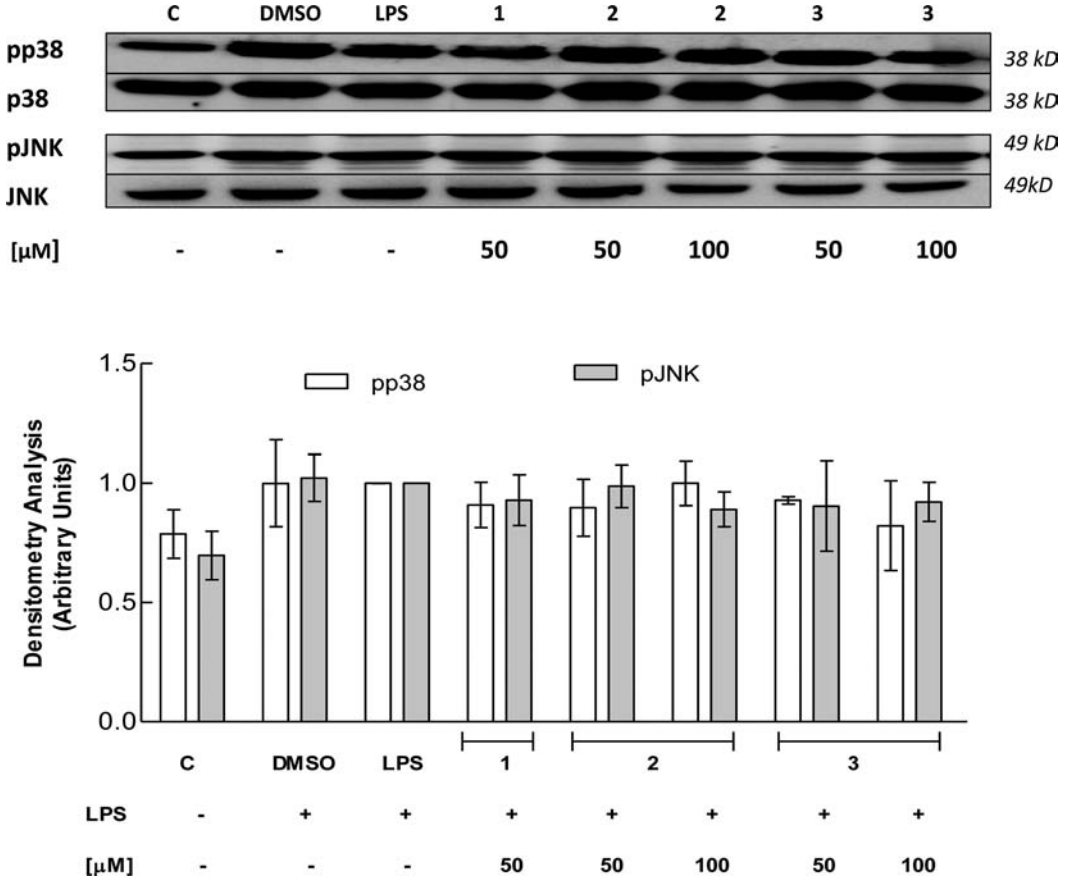

Figure 6. Effect of hydroxytyrosol (**1**), hydroxytyrosyl acetate (**2**), and 3,4-dihydroxyphenylglycol (**3**) on p38 and JNK MAPKs activation in murine peritoneal macrophages. Cells were untreated or treated with **1**−**3** (50 and 100 μM) for 18 h in the presence of LPS. As controls, cells were also treated with DMSO (solvent control) and LPS or left untreated in the absence of LPS. The results are representative of three independent experiments. Densitometry was performed following normalization to the control (JNK and p38 housekeeping genes, respectively).

vitamin E.[21] Furthermore, **1** and **3** have shown free radical scavenging properties after measuring plasma levels of thiobarbituric acid reactive substances by HPLC in a vitamin E-deficient rats in vivo model, which may represent relevant antioxidant activities by which these olive phenolics could have beneficial impact on health.[24]

Stimulation of macrophages by LPS induces transcription of the iNOS gene and generation of large amounts of NO. NO acts as an intracellular messenger, which modulates the formation of endogenous ROS including hydrogen peroxide, peroxynitrite, and other potential oxidants that orchestrate the inflammatory response.[40] In the present study we found that exposure of peritoneal macrophages to LPS resulted in a significant increase of nitrite/nitrate levels as a NO production indicator and an up-regulation of iNOS protein expression. However, **1**−**3** and **7** reduced significantly both nitrite production and iNOS expression, in contrast to **8**, which showed a lower reduction of NO production at 50 μM but no changes in LPS-induced iNOS expression.

COX-2, the inducible isoform of COX, is the key enzyme that catalyzes the two sequential steps in the biosynthesis of prostaglandins (PGs) from arachidonic acid and plays a critical role in inflammatory response. Our data showed that COX-2 protein expression was significantly induced by LPS stimulation, but treatments of LPS-stimulated murine macrophages with **1**−**3** produced a remarkable down-regulation of COX-2 expression. Nevertheless, no changes were observed after treatment with **7** and **8**. These results are in accordance with a previous study by Richard et al. in which **1** prevented the up-regulation of iNOS and COX-2 and inhibited the production of PGE_2 in RAW murine macrophages.[45] Similar data were obtained in THP-1 cells and in cultured endothelial cells.[46,47]

Toll-like receptors (TLRs) are located as well as macrophages on other immune cells such as dendritic cells and T and B cells, where they play an important role in the detection of pathogens and enable their elimination from the body.[48,49] LPS can trigger groups of different TLR especially TLR4, starting downstream signaling cascades, including mitogen-activated protein kinases (MAPKs) and the nuclear transcription factor kappa-B (NF-κB) pathways. NF-κB, as a dimeric transcription factor, exists in the cytoplasm as an inactive complex with the inhibitory protein IκBα. When cells are challenged with pro-inflammatory stimuli, for example, LPS, IκBα undergoes phosphorylation and subsequently ubiquitination, allowing NF-κB to translocate to the nucleus. As a result, NF-κB binds to κB enhancer elements present in the promoter region of many pro-inflammatory genes, for instance, iNOS and COX-2.[50] Our results show that pretreatment with **2** and **3** significantly prevented IκBα degradation after LPS stimulus. However, no significant changes were observed in IκBα expression after **1**, **7**, and **8** treatments. Other researchers have shown that anti-inflammatory activity by EVOO isolated phenols is mediated, at least in part, by NF-κB signaling. For instance, **1** at 25−100 μM has been demonstrated to block NF-κB intracellular oxidative stress attenuating iNOS and COX-2 expressions in human monocytes.[46] This capacity to regulate

DOI: 10.1021/jf503357s
J. Agric. Food Chem. 2015, 63, 836−846

NF-κB genes was also described in J774 murine macrophages and in N2a cells against amyloid-β-induced toxicity.[51,52] Nevertheless, our data are in agreement with another previous paper in which no significant changes after co-incubation with **1** in HT-29 human cells were observed.[53] Moreover, a recent paper has showed that HTy suppressed NO production by decreasing iNOS gene expression through a mechanism independent of the NF-κB signaling pathway.[54] Maybe these discrepancies could be explained in terms of different phenol concentrations and changes on cell experimental conditions.

As above-mentioned, LPS can induce MAPK activation. MAPKs are a family of serine−threonine kinase enzymes that orchestrate the recruitment of gene transcription, protein biosynthesis, cell cycle control, apoptosis, and differentiation and allow cells to respond to oxidative stress and inflammatory stimuli from their extracellular environment.[55] MAPKs include extracellular signal-regulated kinases (ERKs-1 and -2), c-Jun N-terminal kinases (JNKs), and p38 MAPKs. In fact, MAPKs have been shown to play important roles in iNOS and COX-2 up-regulation induced by various stimuli in mammalian cells. Nevertheless, our findings demonstrated no significant changes in p38 and JNK protein phosphorylation after treatments, suggesting that MAPKs signaling pathway does not make a consistent contribution in the anti-inflammatory effects of **2** and **3** in mouse peritoneal macrophages. In conclusion, this study establishes for the first time that the natural HTy derivatives **2** and **3** present in EVOO inhibit LPS-induced oxidative stress and inflammatory response via direct down-regulation of NO generation. These protective effects seem to be due to a down-regulation of iNOS and COX-2 protein expression via inhibition of the NF-κB signaling pathway. Acylation of the side chain of 3,4-hydroxyphenylglycol **3** by catechol protection, acylation of aliphatic hydroxyl groups, and deprotection afforded diacylated **7** and **8**. which show worse anti-inflammatory activity than the parent **3**. Furthermore, **8**, with the longer acyl chains, showed the worst behavior on the stimulated macrophages. The implication of this study for nutrition and general health of the population rests in the possible use of natural HTy derivatives with better hydrophilic/lipophilic balance, thus improving their pharmacodynamic and pharmacokinetic profiles, as new dietary supplements in foods; however, further in vivo studies are in progress to fully understand the role of EVOO phenols in the management of inflammation-related diseases.

AUTHOR INFORMATION

Corresponding Author

*(C.A.-L.) Phone: +34 954559877. Fax: +34 954556774. E-mail: calarcon@us.es.

Funding

This work was supported by funds from the Spanish Ministerio de Economía y Competitividad (AGL 2011-26949) and Junta de Andalucía (CTS-259, FQM134, P-10-AGR-6609 and P-08-AGR-03751 cofinanced with FEDER funds). M.A.-S. gratefully acknowledges support from a Postgraduate National Program of FPU fellowship and financial sponsorship from the Spanish Ministerio de Educación, Cultura y Deporte.

Notes

The authors declare no competing financial interest.

ACKNOWLEDGMENTS

We gratefully acknowledge the assistance of the Center for Technology and Innovation Research, University of Seville (CITIUS).

ABBREVIATIONS USED

COX-2, cyclooxygenase-2; DMSO, dimethyl sulfoxide; DPPH, 1,1-diphenyl-2-picrylhydrazyl radical; ERK, extracellular signal-regulated kinase; FCS, fetal calf serum; iNOS, inducible nitric oxide synthase; IκBα, inhibitory NF-κB protein alpha; HTy, hydroxytyrosol; JNK, c-Jun N-terminal kinase; LPS, lipopolysaccharide; MAPKs, mitogen-activated protein kinases; NF-κB, nuclear transcription factor-kappa B; NO, nitric oxide; PGE_2, prostaglandin E_2; ROS, reactive oxygen species; SRB, sulforhodamine B; UGT, uridine diphosphoglucuronosyl transferases

REFERENCES

(1) Brüne, B.; Dehne, N.; Grossmann, N.; Jung, M.; Namgaladze, D.; Schmid, T.; von Knethen, A.; Weigert, A. Redox control of inflammation in macrophages. *Antioxid. Redox Signal.* **2013**, *19*, 595−637.

(2) Chang, W. T.; Huang, W. C.; Liou, C. J. Evaluation of the anti-inflammatory effects of phloretin and phlorizin in lipopolysaccharide-stimulated mouse macrophages. *Food Chem.* **2012**, *134*, 972−979.

(3) Lawrence, T.; Willoughby, D. A.; Gilroy, D. W. Anti-inflammatory lipid mediators and insights into the resolution of inflammation. *Nat. Rev. Immunol.* **2002**, *2*, 787−795.

(4) Sánchez-Miranda, E.; Lemus-Bautista, J.; Pérez, S.; Pérez-Ramos, J. Effect of kramecyne on the inflammatory response in lipopolysaccharide-stimulated peritoneal macrophages. *Evidence-Based Complement. Altern. Med.* **2013**, *2013*, No. 762020.

(5) Mateos, R.; Trujillo, M.; Pereira-Caro, G.; Madrona, A.; Cert, A.; Espartero, J. L. New lipophilic tyrosyl esters. Comparative antioxidant evaluation with hydroxytyrosyl esters. *J. Agric. Food Chem.* **2008**, *56*, 10960−10966.

(6) Cárdeno, A.; Sánchez-Hidalgo, M.; Alarcón-de-la-Lastra, C. An up-date of olive oil phenols in inflammation and cancer: molecular mechanisms and clinical implications. *Curr. Med. Chem.* **2013**, *20*, 4758−4776.

(7) Grossi, C.; Rigacci, S.; Ambrosini, S.; Dami, T. E.; Luccarini, I.; Traini, C.; Failli, P.; Berti, A.; Casamenti, F.; Stefani, M. The polyphenol oleuropein aglycone protects TgCRND8 mice against Aβ plaque pathology. *PLoS One* **2013**, *8*, No. e71702.

(8) Parkinson, L.; Keast, R. Oleocanthal, a phenolic derived from virgin olive oil: a review of the beneficial effects on inflammatory disease. *Int. J. Mol. Sci.* **2014**, *15*, 12323−12334.

(9) Soni, M. G.; Burdock, G. A.; Christian, M. S.; Bitler, C. M.; Crea, R. Safety assessment of aqueous olive pulp extract as an antioxidant or antimicrobial agent in foods. *Food Chem. Toxicol.* **2006**, *44*, 903−915.

(10) Rubio-Senent, F.; Rodríguez-Gutíerrez, G.; Lama-Muñoz, A.; Fernández-Bolaños, J. New phenolic compounds hydrothermally extracted from the olive oil byproduct alperujo and their antioxidative activities. *J. Agric. Food Chem.* **2012**, *60*, 1175−1186.

(11) Granados-Principal, S.; Quiles, J. L.; Ramirez-Tortosa, C. L.; Sanchez-Rovira, P.; Ramirez-Tortosa, M. C. Hydroxytyrosol: from laboratory investigations to future clinical trials. *Nutr. Rev.* **2010**, *68*, 191−206.

(12) González-Correa, J. A.; Navas, M. D.; Lopez-Villodres, J. A.; Trujillo, M.; Espartero, J. L.; De La Cruz, J. P. Neuroprotective effect of hydroxytyrosol and hydroxytyrosol acetate in rat brain slices subjected to hypoxia-reoxygenation. *Neurosci. Lett.* **2008**, *446*, 143−146.

(13) Angelino, D.; Gennari, L.; Blasa, M.; Selvaggini, R.; Urbani, S.; Esposto, S.; Servili, M.; Ninfali, P. Chemical and cellular antioxidant activity of phytochemicals purified from olive mill waste waters. *J. Agric. Food Chem.* **2011**, *59*, 2011−2018.

DOI: 10.1021/jf503357s
J. Agric. Food Chem. 2015, 63, 836−846

(14) Martín, M. A.; Ramos, S.; Granado-Serrano, A. B.; Rodríguez-Ramiro, I.; Trujillo, M.; Bravo, L.; Goya, L. Hydroxytyrosol induces antioxidant/detoxificant enzymes and Nrf2 translocation via extracellular regulated kinases and phosphatidylinositol-3-kinase/protein kinase B pathways in HepG2 cells. *Mol. Nutr. Food Res.* **2010**, *54*, 956−966.
(15) Ilavarasi, K.; Kiruthiga, P. V.; Pandian, S. K.; Devi, K. P. Hydroxytyrosol, the phenolic compound of olive oil protects human PBMC against oxidative stress and DNA damage mediated by 2,3,7,8-TCDD. *Chemosphere* **2011**, *84*, 888−893.
(16) Sánchez-Fidalgo, S.; Sánchez de Ibargüen, L.; Cárdeno, A.; Alarcón de la Lastra, C. Influence of extra virgin olive oil diet enriched with hydroxytyrosol in a chronic DSS colitis model. *Eur. J. Nutr* **2012**, *51*, 497−506.
(17) Medina, E.; de Castro, A.; Romero, C.; Brenes, M. Comparison of the concentrations of phenolic compounds in olive oils and other plant oils: correlation with antimicrobial activity. *J. Agric. Food Chem.* **2006**, *54*, 4954−4961.
(18) Neveu, V.; Perez-Jiménez, J.; Vos, F.; Crespy, V.; du Chaffaut, L.; Mennen, L.; Knox, C.; Eisner, R.; Cruz, J.; Wishart, D.; Scalbert, A. Phenol-Explorer: an online comprehensive database on polyphenol contents in foods. *Database (Oxford)* **2010**, *2010*, No. bap024.
(19) González-Correa, J. A.; Navas, M. D.; Muñoz-Marín, J.; Trujillo, M.; Fernández-Bolaños, J.; de la Cruz, J. P. Effects of hydroxytyrosol and hydroxytyrosol acetate administration to rats on platelet function compared to acetylsalicylic acid. *J. Agric. Food Chem.* **2008**, *56*, 7872−7876.
(20) Drira, R.; Sakamoto, K. Modulation of adipogenesis, lipolysis and glucose consumption in 3T3-L1 adipocytes and C2C12 myotubes by hydroxytyrosol acetate: a comparative study. *Biochem. Biophys. Res. Commun.* **2013**, *440*, 576−581.
(21) Guillermo, R.; Rocío, R.; Juan, F.-B.; Rafael, G.; Ana, J. Antioxidant activity of effluents during the purification of hydroxytyrosol and 3,4-dihydroxyphenyl glycol from olive oil waste. *Eur. Food Res. Technol.* **2007**, *224*, 733−741.
(22) Lama-Muñoz, A.; Rodríguez-Gutiérrez, G.; Rubio-Senent, F.; Palacios-Díaz, R.; Fernández-Bolaños, J. A study of the precursors of the natural antioxidant phenol 3,4-dihydroxyphenylglycol in olive oil waste. *Food Chem.* **2013**, *140*, 154−160.
(23) Rodríguez, G.; Lama, A.; Jaramillo, S.; Fuentes-Alventosa, J. M.; Guillén, R.; Jiménez-Araujo, A.; Rodríguez-Arcos, R.; Fernández-Bolaños, J. 3,4-Dihydroxyphenylglycol (DHPG): an important phenolic compound present in natural table olives. *J. Agric. Food Chem.* **2009**, *57*, 6298−6304.
(24) Rodríguez-Gutiérrez, G.; Duthie, G. G.; Wood, S.; Morrice, P.; Nicol, F.; Reid, M.; Cantlay, L. L.; Kelder, T.; Horgan, G. W.; Fernández-Bolaños Guzmán, J.; de Roos, B. Alperujo extract, hydroxytyrosol, and 3,4-dihydroxyphenylglycol are bioavailable and have antioxidant properties in vitamin E-deficient rats − a proteomics and network analysis approach. *Mol. Nutr. Food Res.* **2012**, *56*, 1137−1147.
(25) de Roos, B.; Zhang, X.; Rodriguez Gutierrez, G.; Wood, S.; Rucklidge, G. J.; Reid, M. D.; Duncan, G. J.; Cantlay, L. L.; Duthie, G. G.; O'Kennedy, N. Anti-platelet effects of olive oil extract: in vitro functional and proteomic studies. *Eur. J. Nutr.* **2011**, *50*, 553−562.
(26) Scheepens, A.; Tan, K.; Paxton, J. W. Improving the oral bioavailability of beneficial polyphenols through designed synergies. *Genes Nutr.* **2010**, *5*, 75−87.
(27) Fragopoulou, E.; Nomikos, T.; Karantonis, H. C.; Apostolakis, C.; Pliakis, E.; Samiotaki, M.; Panayotou, G.; Antonopoulou, S. Biological activity of acetylated phenolic compounds. *J. Agric. Food Chem.* **2007**, *55*, 80−89.
(28) Fernández-Bolaños, J.; Rodríguez, G.; Rodríguez, R.; Heredia, A.; Guillén, R.; Jiménez, A. Production in large quantities of highly purified hydroxytyrosol from liquid-solid waste of two-phase olive oil processing or 'Alperujo'. *J. Agric. Food Chem.* **2002**, *50*, 6804−6811.
(29) Ablat, A.; Mohamad, J.; Awang, K.; Shilpi, J. A.; Arya, A. Evaluation of antidiabetic and antioxidant properties of *Brucea javanica* seed. *Sci. World J.* **2014**, *2014*, No. 786130.
(30) Barua, R.; Sultana, S.; Uddin Talukder, M. E.; Chakma, K.; Hasan, C. M. M.; Islam, M. S. Antioxidant and cytotoxic activity of crude flavonoid fraction from the fruits of hybrid variety of *Momordica charantia* (bitter gourd). *Br. J. Pharm. Res.* **2014**, *4* (7), 778−786.
(31) Hajihashemi, S.; Geuns, J. M. C. Free radical scavenging activity of steviol glycosides, steviol glucuronide, hydroxytyrosol, metformin, aspirin and leaf extract of *Stevia rebaudiana*. *Free Radical Antioxid.* **2013**, *3* (2s), s34−s41.
(32) Sun, B.; Spranger, I.; Yang, J.; Leandro, C.; Guo, L.; Canário, S.; Zhao, Y.; Wu, C. Red wine phenolic complexes and their in vitro antioxidant activity. *J. Agric. Food Chem.* **2009**, *57*, 8623−8627.
(33) Skehan, P.; Storeng, R.; Scudiero, D.; Monks, A.; McMahon, J.; Vistica, D.; Warren, J. T.; Bokesch, H.; Kenney, S.; Boyd, M. R. New colorimetric cytotoxicity assay for anticancer-drug screening. *J. Natl. Cancer Inst.* **1990**, *82*, 1107−1112.
(34) Moorcroft, M. J.; Davis, J.; Compton, R. G. Detection and determination of nitrate and nitrite: a review. *Talanta* **2001**, *54*, 785−803.
(35) Sánchez-Hidalgo, M.; Martín, A. R.; Villegas, I.; Alarcón De La Lastra, C. Rosiglitazone, an agonist of peroxisome proliferator-activated receptor gamma, reduces chronic colonic inflammation in rats. *Biochem. Pharmacol.* **2005**, *69*, 1733−1744.
(36) Bradford, M. M. A rapid and sensitive method for the quantitation of microgram quantities of protein utilizing the principle of protein-dye binding. *Anal. Biochem.* **1976**, *72*, 248−254.
(37) Fernandez-Bolaños, J.; Rodriguez, G.; Lama-Muñoz, A.; Senent-Rubio. F.; Fernandez-Bolaños, J. G.; Maya, I.; Lopez-Lopez, O.; Marset-Castro, A. Method for obtaining hydroxytyrosol extract, mixture of hydroxytyrosol and 3,4-dihydroxyphenylglycol extract, and hydroxytyrosyl acetate extract, from by-products of the olive tree, and the purification thereof. PCT/ES2012/070491, 2013.
(38) Xie, Q. W.; Cho, H. J.; Calaycay, J.; Mumford, R. A.; Swiderek, K. M.; Lee, T. D.; Ding, A.; Troso, T.; Nathan, C. Cloning and characterization of inducible nitric oxide synthase from mouse macrophages. *Science* **1992**, *256*, 225−228.
(39) Helenius, M.; Kyrylenko, S.; Vehviläinen, P.; Salminen, A. Characterization of aging-associated up-regulation of constitutive nuclear factor-κB binding activity. *Antioxid. Redox Signal.* **2001**, *3*, 147−156.
(40) Li, D. Y.; Xue, M. Y.; Geng, Z. R.; Chen, P. Y. The suppressive effects of Bursopentine (BP5) on oxidative stress and NF-κB activation in lipopolysaccharide-activated murine peritoneal macrophages. *Cell Physiol. Biochem.* **2012**, *29*, 9−20.
(41) Raederstorff, D. Antioxidant activity of olive polyphenols in humans: a review. *Int. J. Vitam. Nutr. Res.* **2009**, *79*, 152−165.
(42) Granados-Principal, S.; Quiles, J. L.; Ramirez-Tortosa, C.; Camacho-Corencia, P.; Sanchez-Rovira, P.; Vera-Ramirez, L.; Ramirez-Tortosa, M. C. Hydroxytyrosol inhibits growth and cell proliferation and promotes high expression of sfrp4 in rat mammary tumours. *Mol. Nutr. Food Res.* **2011**, *55* (Suppl.1), S117−S126.
(43) Grasso, S.; Siracusa, L.; Spatafora, C.; Renis, M.; Tringali, C. Hydroxytyrosol lipophilic analogues: enzymatic synthesis, radical scavenging activity and DNA oxidative damage protection. *Bioorg. Chem.* **2007**, *35*, 137−152.
(44) Bouallagui, Z.; Bouaziz, M.; Lassoued, S.; Engasser, J. M.; Ghoul, M.; Sayadi, S. Hydroxytyrosol acyl esters: biosynthesis and activities. *Appl. Biochem. Biotechnol.* **2011**, *163*, 592−599.
(45) Richard, N.; Arnold, S.; Hoeller, U.; Kilpert, C.; Wertz, K.; Schwager, J. Hydroxytyrosol is the major anti-inflammatory compound in aqueous olive extracts and impairs cytokine and chemokine production in macrophages. *Planta Med.* **2011**, *77*, 1890−1897.
(46) Zhang, X.; Cao, J.; Jiang, L.; Zhong, L. Suppressive effects of hydroxytyrosol on oxidative stress and nuclear factor-κB activation in THP-1 cells. *Biol. Pharm. Bull.* **2009**, *32*, 578−582.
(47) Scoditti, E.; Calabriso, N.; Massaro, M.; Pellegrino, M.; Storelli, C.; Martines, G.; De Caterina, R.; Carluccio, M. A. Mediterranean diet polyphenols reduce inflammatory angiogenesis through MMP-9 and COX-2 inhibition in human vascular endothelial cells: a potentially

DOI: 10.1021/jf503357s
J. Agric. Food Chem. 2015, 63, 836−846

protective mechanism in atherosclerotic vascular disease and cancer. *Arch. Biochem. Biophys.* **2012**, *527*, 81−89.
(48) Rakoff-Nahoum, S.; Medzhitov, R. Role of Toll-like receptors in tissue repair and tumorigenesis. *Biochemistry (Moscow)* **2008**, *73*, 555−561.
(49) Charles, P. E.; Barbar, S. D. Toll-like receptors: a link between mechanical ventilation, innate immunity and lung injury? *Intensive Care Med.* **2010**, *36*, 909−911.
(50) Lee, H. N.; Surh, Y. J. Therapeutic potential of resolvins in the prevention and treatment of inflammatory disorders. *Biochem. Pharmacol.* **2012**, *84*, 1340−1350.
(51) Maiuri, M. C.; De Stefano, D.; Di Meglio, P.; Irace, C.; Savarese, M.; Sacchi, R.; Cinelli, M. P.; Carnuccio, R. Hydroxytyrosol, a phenolic compound from virgin olive oil, prevents macrophage activation. *Naunyn Schmiedebergs Arch. Pharmacol.* **2005**, *371*, 457−465.
(52) St-Laurent-Thibault, C.; Arseneault, M.; Longpré, F.; Ramassamy, C. Tyrosol and hydroxytyrosol, two main components of olive oil, protect N2a cells against amyloid-β-induced toxicity. Involvement of the NF-κB signaling. *Curr. Alzheimer Res.* **2011**, *8*, 543−551.
(53) Cárdeno, A.; Sánchez-Hidalgo, M.; Cortes-Delgado, A.; Alarcón de la Lastra, C. Mechanisms involved in the antiproliferative and proapoptotic effects of unsaponifiable fraction of extra virgin olive oil on HT-29 cancer cells. *Nutr. Cancer* **2013**, *65*, 908−918.
(54) Takeda, Y.; Bui, V. N.; Iwasaki, K.; Kobayashi, T.; Ogawa, H.; Imai, K. Influence of olive-derived hydroxytyrosol on the Toll-like receptor 4-dependent inflammatory response of mouse peritoneal macrophages. *Biochem. Biophys. Res. Commun.* **2014**, *446*, 1225−1230.
(55) Munoz, L.; Ammit, A. J. Targeting p38 MAPK pathway for the treatment of Alzheimer's disease. *Neuropharmacology* **2010**, *58*, 561−568.

DOI: 10.1021/jf503357s
J. Agric. Food Chem. 2015, 63, 836−846

JOURNAL OF AGRICULTURAL AND FOOD CHEMISTRY

Article

pubs.acs.org/JAFC

Demethoxycurcumin Modulates Human P-Glycoprotein Function via Uncompetitive Inhibition of ATPase Hydrolysis Activity

Yu-Ning Teng,[†] Yow-Wen Hsieh,[†,‡] Chin-Chuan Hung,*[,†,‡,∥] and Hui-Yi Lin*[,†,‡,∥]

[†]Department of Pharmacy, College of Pharmacy, China Medical University, Taichung, Taiwan

[‡]Department of Pharmacy, China Medical University Hospital, Taichung, Taiwan

ABSTRACT: Curcuminoids are major components of *Curcuma longa* L., which is widely used as spice in food. This study aimed at identifying whether curcumin, demethoxycurcumin, and bisdemethoxycurcumin could modulate efflux function of human P-glycoprotein and be used as chemosensitizers in cancer treatments. Without altering P-glycoprotein expression levels and conformation, the purified curcuminoids significantly inhibited P-glycoprotein efflux function. In rhodamine 123 efflux and calcein-AM accumulation assays, demethoxycurcumin demonstrated the highest inhibition potency (inhibitory IC_{50} = 1.56 ± 0.13 μM) among the purified curcuminoids, as well as in the fold of reversal assays. Demethoxycurcumin inhibited P-glycoprotein-mediated ATP hydrolysis under concentrations of <1 μM and efficiently inhibited 200 μM verapamil-stimulated ATPase activity, indicating a high affinity of demethoxycurcumin for P-glycoprotein. These results suggested that demethoxycurcumin may be a potential additive natural product in combination with chemotherapeutic agents in drug-resistant cancers.

KEYWORDS: *curcuminoids, demethoxycurcumin, P-glycoprotein, multidrug resistance, kinetic mechanism*

INTRODUCTION

Human P-glycoprotein (P-gp), encoded by the *ABCB1* gene, is an efflux transporter that belongs to the ATP-binding cassette (ABC) transporter superfamily.[1] It is a 170 kDa transmembrane protein and expresses abundantly in the apical membranes of major excretory organs, such as the kidney, liver, and intestines, as well as the luminal surface of blood−tissue interfaces, such as the blood−brain, blood−testis, and blood−ovarian barriers.[2] A wide range of therapeutics drugs are substrates of P-gp, including anticancer agents (e.g., vinca alkaloids, anthracyclines, and taxanes), HIV protease inhibitors, immunosuppressive drugs, antidepressants, and steroids.[3] It affects the absorption, distribution, and elimination of these substrates and contributes a major role in multidrug resistance (MDR) in cancer treatment.[4] The overexpressed P-gp has been found in several human tumors and confers resistance to chemotherapeutic agents.[5] Therefore, identifying molecules that interfere with human P-gp function or expression may be a potential target for reversing MDR in cancers.

To date, three generations of P-gp inhibitors have been developed.[6] However, none of these compounds could achieve beneficial clinical outcomes.[7] The most considerable reasons for the failure of these synthetic compounds were the toxicities and pharmacokinetic interactions.[4] These clinical reports led to the search for P-gp inhibitors from natural products, which are generally considered to be safer and nontoxic at usual doses. Curcuminoids are natural phenolic compounds extracted from the rhizome of *Curcuma longa* Linn. and are commonly used as spices in food and health products. The three major isolated curcuminoids are curcumin, demethoxycurcumin, and bisdemethoxycurcumin.[8] Previous studies have shown that natural curcuminoids possess many pharmacological activities, such as anti-inflammation, antioxidant, and anticancer effects.[9−13] Besides these effects, several studies have shown that the commercial grade mixture of curcuminoids, composed of approximately 77% curcumin, 17% demethoxycurcumin, and 3% bisdemethoxycurcumin, were able to modulate P-gp expression and function in hepatocytes and cancer cells.[14,15] Most of the previous studies utilized the commercial grade curcuminoids and were unable to identify the individual effect of the three major curcuminoids on P-gp. Recently, limited studies reported that the isolated curcumin, demethoxycurcumin, and bisdemethoxycurcumin may diversely contribute to the influence of P-gp expression and function.[16,17] However, inconsistent results have been obtained among different studies, and kinetic mechanisms of interactions between P-gp and the three major curcuminoids were not investigated.

The present study aimed to evaluate the effect of individual curcuminoids, including curcumin, demethoxycurcumin, and bisdemethoxycurcumin, on human P-gp expression and function. Further in-depth biochemical and kinetic mechanism investigation was performed to elucidate the differential P-gp inhibition potency of these major curcuminoids. The effect of the most potent curcuminoid on the sensitivity of the chemotherapeutic agent in the P-gp overexpression cells was also examined to evaluate the potential of curcuminoids to overcome P-gp-mediated MDR in cancer chemotherapy.

MATERIALS AND METHODS

Chemicals. *R*-(+)-Verapamil, doxorubicin, MTT reagent, DMSO, rhodamine 123, and calcein-AM were purchased from Sigma Chemical Co (St. Louis, MO, USA). The Flp-In system and all cell culture medium were obtained from Invitrogen (Carlsbad, CA, USA). The full-length human *ABCB1* cDNA in pMDRA1 was supplied by the Riken BRC DNA bank (RDB No. 1372) (Ibaraki, Japan). Curcumin (C), demethoxycurcumin (DMC), and bisdemethoxycurcumin

Received: September 2, 2014
Revised: December 11, 2014
Accepted: January 2, 2015
Published: January 16, 2015

ACS Publications © 2015 American Chemical Society

DOI: 10.1021/jf5042307
J. Agric. Food Chem. 2015, 63, 847−855

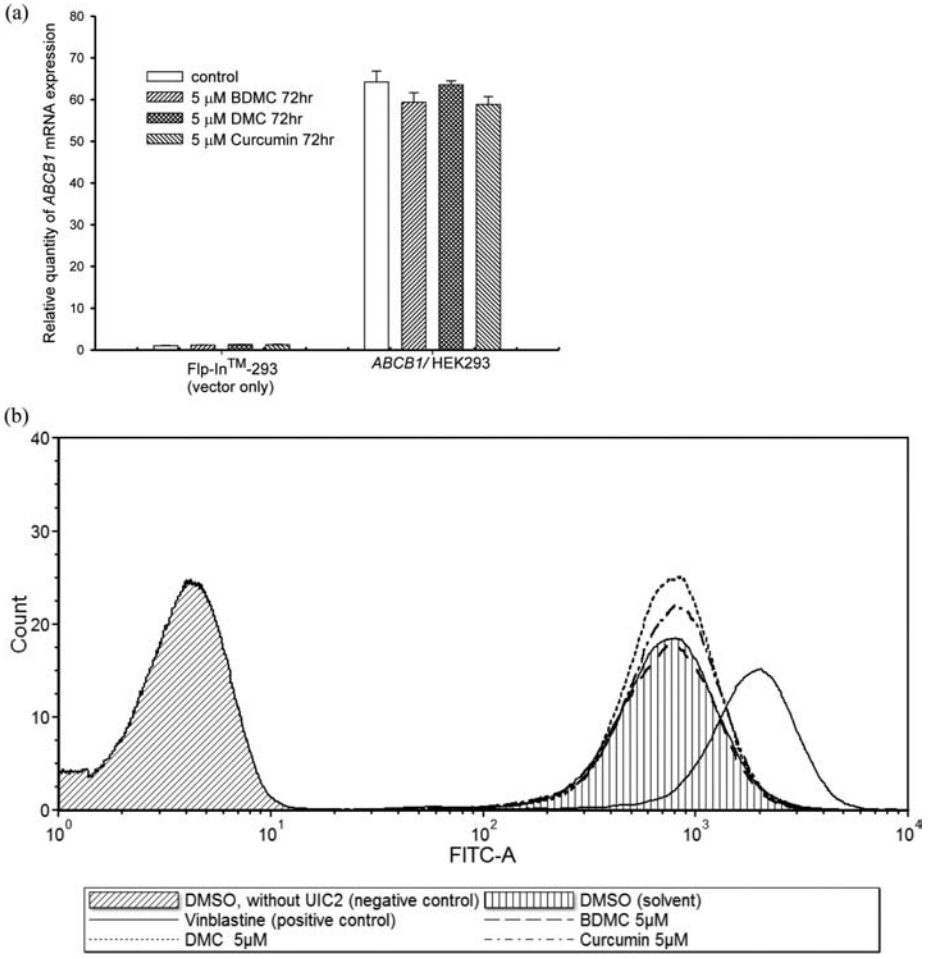

Figure 1. Effect of purified curcuminoids on P-gp mRNA expression and conformational changes. (a) Human P-gp mRNA levels were detected by real-time quantitative RT-PCR. There were no significant differences between no treatment and 72 h of treatment of 5 μM purified curcuminoids. Data are presented as the mean ± SE of at least three experiments, each in triplicate. (b) MDR1 shift assay was applied to examine the effect of 5 μM purified curcuminoids on P-gp conformational changes. Vinblastine, a P-gp substrate, was used as a positive control. The peaks of purified curcuminoids did not shift, as compared to the solvent, indicating that the purified curcuminoids did not change the conformation of P-gp to the open form.

(BDMC) were extracted and isolated from roots of *Curcuma longa* as in our previous study;[18] the isolated three pigments were identified to be >98% pure.

Cell Culture. The human P-gp overexpression cells were established and verified in our previous studies.[19,20] To be brief, the host Flp-In-293 cells were cultured in DMEM containing 10% fetal bovine serum and 100 μg/mL zeocin at 37 °C, 95% humidity, and 5% CO_2. The constructed pcDNA5/*ABCB1* plasmid and pOG44 plasmid were cotransfected into the Flp-In-293 cells. The human P-gp stable transfected cells (*ABCB1*/HEK293) were selected on the basis of hygromycin B resistance.

Cytotoxicity Assay. Cytotoxicities of curcuminoids toward Flp-In-293 and *ABCB1*/HEK293 cells were determined by MTT assay. The cells were seeded into 24-well plates overnight, and series concentrations of curcuminoids (from 1 to 500 μM) were added. After 72 h of incubation, the medium was removed, and 200 μL of fresh culture medium containing 0.5 mg/mL MTT was added. The medium was removed after incubation at 37 °C for 4 h, and 200 μL of DMSO was added. After incubation at room temperature for 30 min, 100 μL of solution was transferred to a 96-well plate, and absorbance was measured using an ELISA plate reader (Molecular Devices, Sunnyvale, CA, USA) at 570 nm with a reference wavelength of 650 nm. The sensitivities of Flp-In-293 and *ABCB1*/HEK293 cells to doxorubicin were also evaluated by the MTT assay. The concentration reaching 50% cell growth inhibition (IC_{50}) was calculated, and the fold reversal factor was further determined according to the previous study.[21]

Real-Time Quantitative RT-PCR and MDR1 Shift Assay. *ABCB1* mRNA expression levels were evaluated by real-time quantitative RT-PCR. The Qiagen RNeasy kit (Valencia, CA, USA) was used to extract total RNA from the transfected cells. The primers and probes for human *ABCB1* and *GAPDH* genes were Taqman Assay on Demand reagents (Applied Biosystem, Foster City, CA, USA). The relative expression of *ABCB1* mRNA was analyzed using an ABI Prism 7900 Sequence Detection System and normalized to the amount of *GAPDH* in the same cDNA by using the standard curve method described by the manufacturer.

The conformation change of P-gp after the addition of test compound was examined by using a MDR1 Shift Assay kit (EMD Millipore Corp., Billerica, MA, USA) according to the manufacturer's protocol. UIC2 shift was shown in the presence of a P-gp substrate such as vinblastine. A total of 5×10^5–1×10^6 cells were prepared per reaction and resuspended with warm UIC2 binding buffer. Cells were incubated at 37 °C for 10 min and then treated with DMSO or vinblastine or test compounds. Cells were incubated at 37 °C for 30 min and then treated with IgG2a (negative control antibody) or UIC2 working solution (P-gp conformational sensitive antibody). Cells were incubated at 37 °C for 15 min and then washed with iced UIC2 binding buffer twice. A secondary antibody, goat anti-mouse IgG ALEXA 488, was added at 4 °C for 15 min, and then iced UIC2 binding buffer was added. The fluorescence was measured by FACS analysis (BD FACSCanto System).

DOI: 10.1021/jf5042307
J. Agric. Food Chem. 2015, 63, 847–855

P-gp ATPase Activity Assays. The Pgp-GIO assay system (Promega, Madison, WI, USA) was used to evaluate the effect of curcuminoids on P-gp ATPase activity according to the manufacturer's protocol. In a 96-well untreated white plate, curcuminoids (from 1 to 100 μM) were incubated with 25 μg of recombinant human Pgp membrane. The P-gp-GIO assay buffer was used as the untreated control, 200 μM verapamil was used as the positive control of drug-induced P-gp ATPase activity, and 100 μM sodium orthovanadate was used as the selective inhibitor of P-gp ATPase activity. The ATPase activity was initiated by the addition of 5 mM MgATP and incubated at 37 °C for 60 min. Further luminescence was initiated by adding 50 μL of ATP detection reagent; after 20 min of incubation at room temperature, the plate was read on the SpectraMax Gemini XS microplate spectrofluorometer (Molecular Devices Co.).

Rhodamine 123 Efflux Assay. For the rhodamine 123 efflux assays, 1×10^5 cells/well were seeded on 96-well plates and cultured for 24 h. The cells were washed and preincubated with Hanks' balanced salt solution (HBSS) for 30 min, and subsequently incubated in 1 μM rhodamine 123 for 30 min with or without curcuminoids in triplicate. After a washing with warm PBS, cells were allowed to efflux rhodamine 123 for 10 min at 37 °C in the incubator. Samples (100 μL) were collected and transferred to 96-well black plates. The fluorescence was measured by the SpectraMax Gemini XS microplate spectrofluorometer (Molecular Devices Co.) with the excitation set at 485 nm and the emission set at 535 nm. The rhodamine 123 concentration was obtained by comparison to the standard curve. Each experiment was performed at least three times, each in triplicate on different days.

Calcein-AM Uptake Assay. For the calcein-AM uptake study, 1×10^5 cells/well were placed on 96-well black plates and cultured overnight. Before the uptake assay, cells were washed and preincubated with HBSS for 30 min and subsequently with curcuminoids for 30 min. After preincubation, calcein-AM was added and incubated at 37 °C in the incubator for 30 min. After a washing with ice-cold HBSS, cells were lysed with 1% Triton X-100, and intracellular calcein fluorescence was analyzed by the SpectraMax Gemini XS microplate spectrofluorometer (Molecular Devices Co.) with the excitation at 485 nm and the emission at 535 nm. Each experiment was performed at least three times, each in triplicate on different days.

Fluorescent Doxorubicin Efflux Assay. For doxorubicin efflux assays, 1×10^5 cells/well were seeded on 96-well plates. After overnight incubation, cells were washed and incubated with HBSS for 30 min. Then, the cells were subsequently incubated in 10, 20, or 30 μM fluorescent doxorubicin for 3 h with or without curcuminoids in triplicate. After being washed with warm PBS, cells were allowed to efflux fluorescent doxorubicin for 2 h at 37 °C in the incubator. Samples (100 μL) were collected and transferred to 96-well black plates. The fluorescence of doxorubicin was measured by the SpectraMax Gemini XS microplate spectrofluorometer (Molecular Devices Co.) with the excitation set at 485 nm and the emission set at 590 nm. The doxorubicin concentration was obtained by comparison to the standard curve. Each experiment was performed at least three times, each in triplicate on different days.

Data and Statistical Analysis. For evaluation of inhibitor potency, IC_{50} values were calculated by using the equation

$$E = E_0\left(\frac{IC_{50}^s}{IC_{50}^s + I^s}\right)$$

where E is the observed efflux in the presence of inhibitor; E_0, the efflux in the absence of inhibitor; I, the inhibitor concentration; IC_{50}, the concentration that caused 50% inhibition of the maximal drug effect; and s, the slope factor.

For kinetic studies, kinetic parameters were estimated by nonlinear regression using Scientist v2.01 (MicroMath Scientific Software, Salt Lake City, UT, USA) according to the equation

$$V = \frac{V_{max} \times C}{K_m + C}$$

where V denotes the efflux rate; V_{max}, the maximal efflux rate; K_m, the Michaelis–Menten constant; and C, the substrate concentration.

Statistical differences were evaluated by ANOVA followed by post hoc analysis (Tukey's test) or Student's t test. The statistical significance was set at p value <0.05.

RESULTS

Expression and Basic Function Evaluation of Human P-gp in Established Cell Line. The *ABCB1* mRNA expression was significantly higher in stable transfected HEK293 cells (*ABCB1*/HEK293) than in the Flp-In-293 cells (vector only; host cells) ($p < 0.001$; Figure 1a). After 72 h of treatment with 5 μM curcumin (C), demethoxycurcumin (DMC), or bisdemethoxycurcumin (BDMC), the *ABCB1* mRNA expression remained unchanged (Figure 1a). The cytotoxicity assays indicated that curcuminoids at concentrations ranging from 1 to 5 μM did not affect *ABCB1*/HEK293 cell viability. The cytotoxicities IC_{50} of curcumin, demethoxycurcumin, and bisdemethoxycurcumin for *ABCB1*/HEK293 cells were 7.29 ± 0.51, 8.31 ± 0.71, and 10.72 ± 1.42 μM, respectively.

The basic P-gp function of *ABCB1*/HEK293 cells was confirmed by MDR1-shift assay utilizing UIC2 antibody. The conformation-specific antibody, UIC2, recognizes the extracellular epitopes of P-gp after conformation change induced by substrates or inhibitors.[22,23] The addition of the positive control drug vinblastine to *ABCB1*/HEK293 cells resulted in increased UIC2 binding to P-gp, whereas none of the curcuminoids induced P-gp conformation change (Figure 1b).

Effects of Curcuminoids on P-gp Efflux Function. The P-gp fluorescence substrate, rhodamine123, was used as a model compound to investigate the effects of curcuminoids on P-gp function. The efflux of rhodamine 123 was significantly inhibited by curcuminoids in *ABCB1*/HEK293 cells (Figure 2a). As compared to the no-treatment control, the addition of C, DMC, or BDMC, as well as the well-known P-gp inhibitor verapamil, to *ABCB1*/HEK293 cells reduced rhodamine 123 efflux significantly ($p < 0.01$; Figure 2a).

The effects of curcuminoids on P-gp efflux function were further confirmed by the calcein-AM uptake assay. Calcein-AM is a nonfluorescent lipophilic P-gp substrate. After entering living cells, it would be hydrolyzed by esterase and become fluorescent calcein. Therefore, the intracellular calcein fluorescence was inversely correlated to P-gp function. The addition of C, DMC, or BDMC significantly increased the intracellular accumulation of calcein as compared to the no-treatment control ($p < 0.01$; Figure 2c).

Molecular and Kinetic Mechanisms of Interactions between Curcuminoids and P-gp. To detect the influence of curcuminoids on the P-gp ATPase activity, series concentrations of curcuminoids (from 1 to 10 μM) were incubated with recombinant human P-gp membranes. DMC and BDMC were demonstrated to inhibit both P-gp basal ATPase activity and 200 μM verapamil-stimulated P-gp ATPase activity, whereas C was demonstrated to inhibit P-gp basal ATPase activity but was unable to inhibit 200 μM verapamil-stimulated P-gp ATPase activity (Figure 3).

The rhodamine 123 efflux inhibition kinetics of curcuminoids was further investigated by Lineweaver–Burk plot (Figure 4). In *ABCB1*/HEK293 cells, when the concentration of C, DMC, or BDMC increased, both the maximum rate (V_{max}) and the affinity (K_m) of rhodamine 123 efflux decreased (Figure 4; Table 1). These results suggested that curcuminoids may inhibit human P-gp via uncompetitive inhibition. The P-gp inhibition

DOI: 10.1021/jf5042307
J. Agric. Food Chem. 2015, 63, 847–855

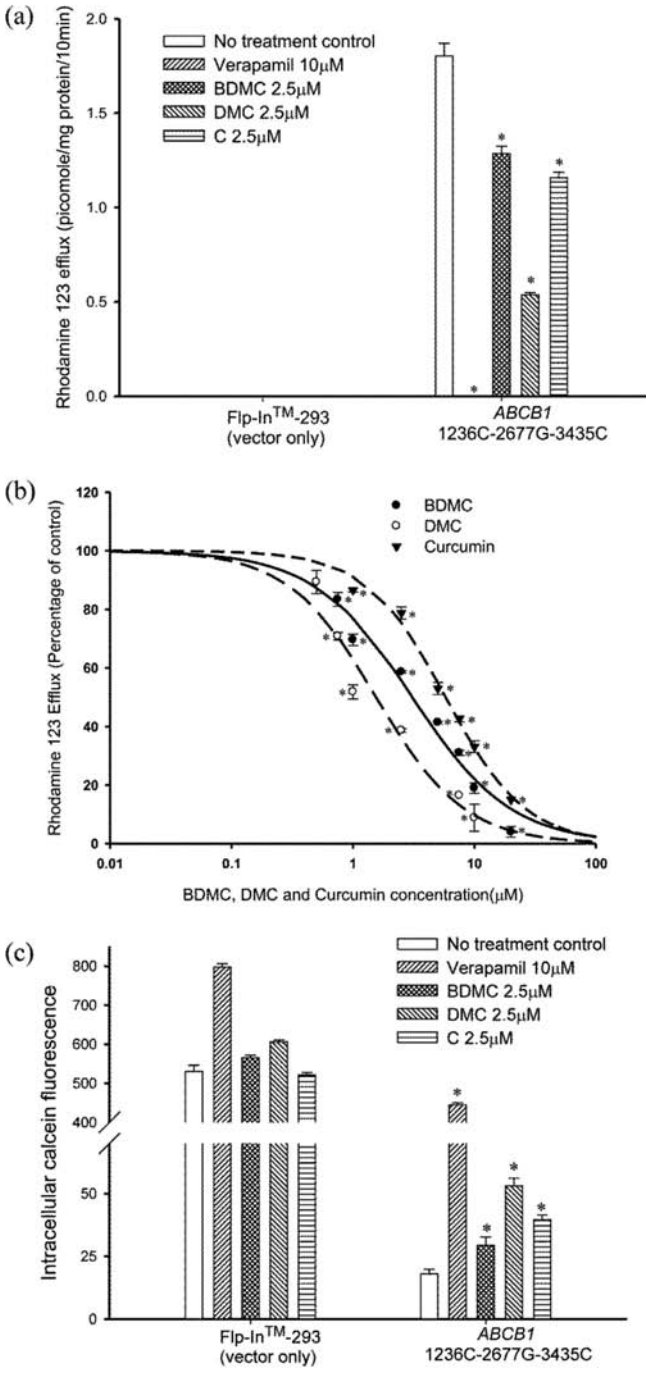

Figure 2. Evaluation of influences of purified curcuminoids on P-glycoprotein efflux function. (a) In the rhodamine 123 efflux assay, purified curcuminoids significantly inhibited P-gp mediated efflux of rhodamine 123 under nontoxic concentrations. Verapamil 10 μM was used as a positive control. (*) $p < 0.05$ as compared to rhodamine 123 efflux without purified curcuminoids (no treatment control). (b) The IC_{50} values of the inhibitory effect of C, DMC, and BDMC on rhodamine 123 efflux by P-gp were 5.8 ± 0.32, 1.56 ± 0.13, and 3.08 ± 0.19 μM, respectively, indicating that DMC possessed the most potent effect on rhodamine 123 efflux by P-gp. (c) In the calcein-AM uptake assay, purified curcuminoids increased intracellular accumulation of calcein under nontoxic concentrations in P-gp. Verapamil 10 μM was used as a positive control. (*) $p < 0.05$ as compared to calcein-AM uptake without purified curcuminoids (no treatment control). The above data are presented as the mean ± SE of at least three experiments, each in triplicate.

potency of curcuminoids was demonstrated by dose response study, and DMC was the most potent P-gp inhibitor among the curcuminoids (Figure 2b; Table 1).

Effects of Curcuminoids on the Sensitivity of Doxorubicin in P-gp Overexpressed ABCB1/HEK293 Cells. The multidrug resistant reversal abilities of curcuminoids were evaluated by co-administered P-gp overexpressed cells with curcuminoids and doxorubicin. The IC_{50} of doxorubicin with or without curcumunoids was calculated, and the fold of reversal was further determined (Table 2). The combinations of purified curcuminoids significantly lower the IC_{50} of doxorubicin in human P-glycoprotein expressed cells. The fold of reversal of DMC was the highest among the tested curcuminoids.

The effect of DMC on P-gp-mediated doxorubicin efflux and the kinetic mechanism were further investigated. DMC significantly inhibited doxorubicin efflux in a dose-dependent manner (Figure 5a,b). As for the kinetic mechanism of P-gp-mediated doxorubicin efflux, when the concentration of DMC increased, the V_{max} decreased with the K_m of doxorubicin remaining unchanged (Figure 5c; Table 3). These results suggested that DMC may inhibit doxorubicin efflux by P-gp via noncompetitive inhibition.

DISCUSSION

Multidrug resistance remains one of the major problems to be resolved in cancer chemotherapy. Although quantities of human P-gp inhibitors have been developed, none of them can provide clinical benefits without toxic side effects. Therefore, efforts have turned to identifying natural products with P-gp inhibitory effects and without systemic toxicities. In the present study, curcuminoids were demonstrated to possess P-gp inhibitory effects under nontoxic concentrations. Among the major curcuminoids, DMC exhibited the strongest P-gp inhibition potency with the highest multidrug resistance reversal ability. The kinetic studies revealed that DMC may interact with P-gp transport of rhodamine 123 via uncompetitive inhibition and doxorubicin through noncompetitive inhibition. Furthermore, ATPase assay demonstrated that DMC was capable of inhibition of both P-gp basal ATPase activity and verapamil-stimulated P-gp ATPase activity. These results indicated that DMC was a potential candidate to be developed as a multidrug resistance reversal agent.

Previous studies have reported the anticancer effects of curcuminoids.[24] It has been suggested that the cancer preventive activities of commercial curcuminoids may be related to the suppression of NF-κB, the regulation of Wnt signaling pathway, and also the inhibition of mTOR signaling.[25−29] In terms of the reversal of multidrug resistance, commercial curcuminoids were reported to be able to increase the accumulation of daunorubicin in P-gp overexpressing human carcinoma KB-C2 cells in a concentration-dependent manner.[30] The efflux of the P-gp fluorescence substrate, rhodamine 123, by KB-C2 cells was also reduced by commercial curcuminoids.[30] Furthermore, the expression of P-gp in multidrug-resistant human cervical carcinoma cells was reported to be down-regulated by commercial curcuminoids in another study.[14] The individual effects of C, DMC, and BDMC on P-gp expression and function were tested in limited studies.[16,17] One study focused on the characterization of C, DMC, and BDMC effects on P-gp function using KB-V1 and KB-3-1 cells, which were multidrug resistance and drug sensitive cervical carcinoma cells, respectively.[17] Their results demonstrated that

DOI: 10.1021/jf5042307
J. Agric. Food Chem. 2015, 63, 847−855

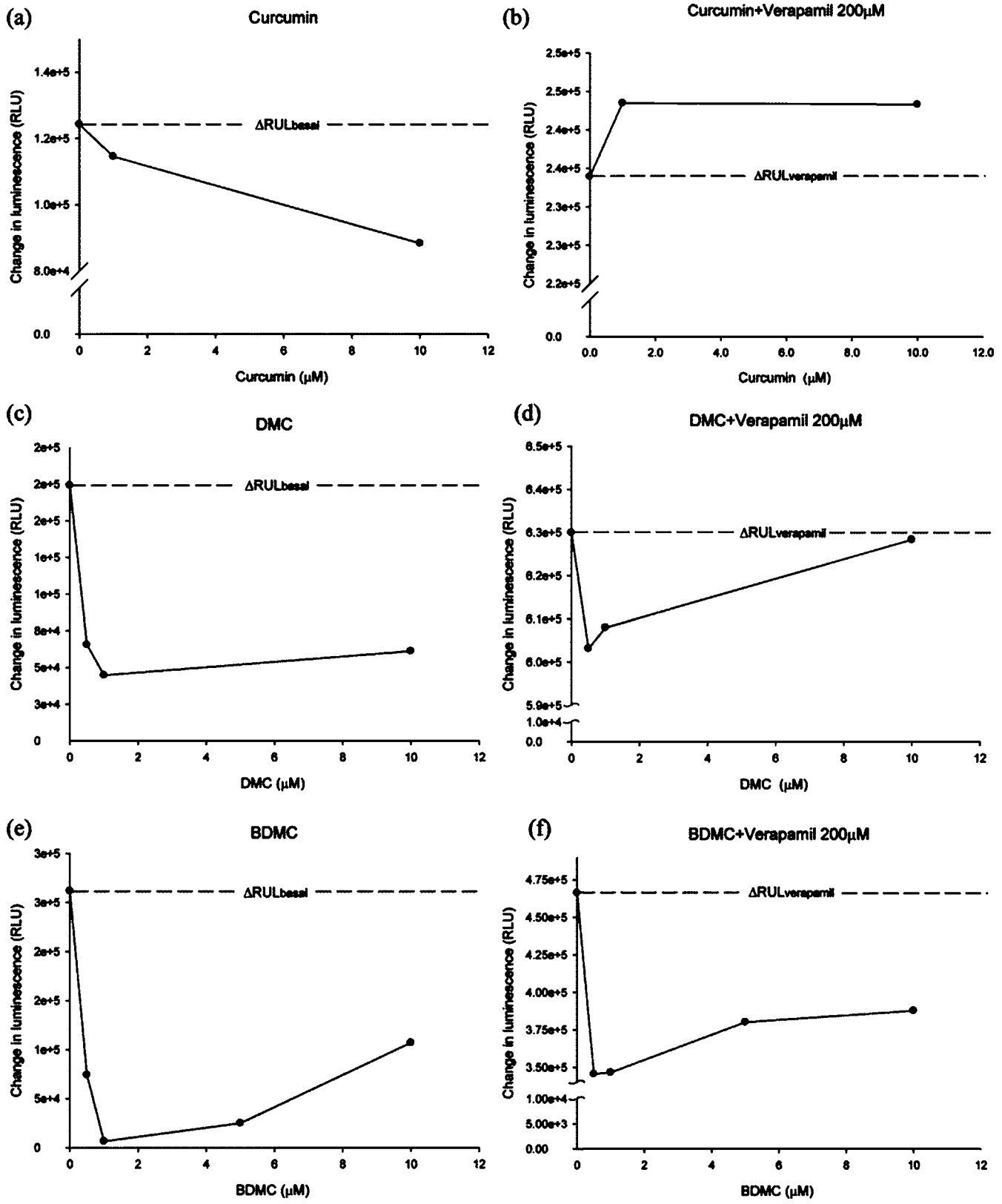

Figure 3. Effect of purified curcuminoids on P-glycoprotein ATPase activity. Data were analyzed in terms of RLUs. (a, c, e) Incubation with C, DMC, or BDMC (0.5−10 μM) inhibited the P-gp ATPase activity. (b, d, f) C, DMC, or BDMC (0.5−10 μM) was tested for its capacity to inhibit 200 μM verapamil-stimulated P-gp ATPase activity. C showed stimulatory effect on 200 μM verapamil-stimulated P-gp ATPase activity at a concentration of 5 μM, whereas DMC or BDMC inhibited 200 μM verapamil-stimulated P-gp ATPase activity at a concentration of 5 μM.

C, DMC, and BDMC all can inhibit P-gp function, and C was shown to be the most active form among the major curcuminoids.[17] In another study, the effects of C, DMC, and BDMC on P-gp transport function were examined by using

DOI: 10.1021/jf5042307
J. Agric. Food Chem. 2015, 63, 847−855

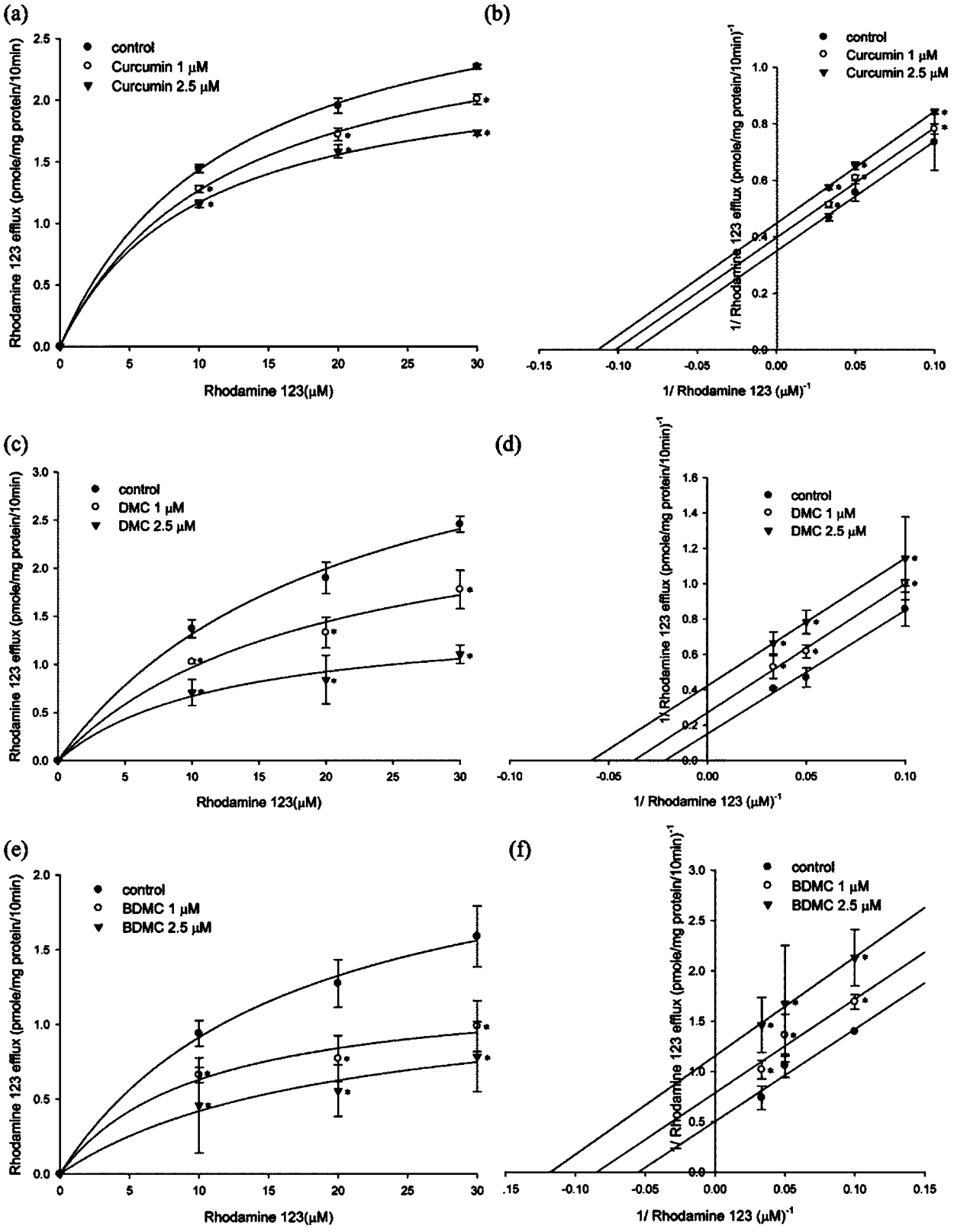

Figure 4. Concentration-dependent rhodamine 123 efflux (10−30 μM) in the presence or absence of purified curcuminoids: (a, b) curcumin; (c, d) DMC; (e, f) BDMC. The left panels show the nonlinear regression analysis of rhodamine 123 efflux, and the right panels demonstrate the Lineweaver−Burk plot analysis of rhodamine 123 efflux. Data are presented as the mean ± SE of at least three experiments, each in triplicate. (∗) $p < 0.05$ as compared to rhodamine 123 efflux without purified curcuminoids (control).

Caco-2 and vinblastine-selected Caco-2 cells.[16] It showed that C and DMC could inhibit P-gp function; however, BDMC showed no effect on P-gp function.[16] These discrepancies may result from the use of different cell lines and drugs to induce resistance. To clarify whether curcuminoids have the potential to be used as multidrug resistance reversal agents, we performed

DOI: 10.1021/jf5042307
J. Agric. Food Chem. 2015, 63, 847−855

Table 1. Effect of the Purified Curcuminoids on Rhodamine 123 Transport by Human P-Glycoprotein

	Nonlinear Kinetic Parameters		
	V_m (pmol/mg protein/10 min)	K_m (μM)	
Bisdemethoxycurcumin (BDMC)			
nonlinear regression			
Rhodamine 123 only	3.84 ± 0.21	20.43 ± 0.98	
+ BDMC, 1 μM	1.62 ± 0.23*[a]	14.31 ± 1.99*	
+ BDMC, 2.5 μM	1.03 ± 0.31*	9.16 ± 2.58*	
K_i from Lineweaver–Burk (μM)			1.23 ± 0.07
efflux IC_{50} (μM)			3.08 ± 0.19
Demethoxycurcumin (DMC)			
nonlinear regression			
Rhodamine 123 only	3.84 ± 0.21	20.43 ± 0.98	
+ DMC, 1 μM	2 ± 0.15*	8.86 ± 1.89*	
+ DMC,2.5 μM	1.48 ± 0.09*	4.93 ± 2.44*	
K_i from Lineweaver–Burk (μM)			0.96 ± 0.09
efflux IC_{50} (μM)			1.56 ± 0.13
Curcumin (C)			
nonlinear regression			
Rhodamine 123 only	3.84 ± 0.21	20.43 ± 0.98	
+ C, 1 μM	2.68 ± 0.05*	11.46 ± 0.43*	
+ C, 2.5 μM	2.34 ± 0.02*	10.00 ± 0.47*	
K_i from Lineweaver–Burk (μM)			2.57 ± 0.71
efflux IC_{50} (μM)			5.8 ± 0.32

[a]* denotes $p < 0.05$ as compared to rhodamine 123 transport without purified curcuminoids.

Table 2. Effects of Purified Curcuminoids on Doxorubicin Cytotoxicity

	IC_{50} (mean ± SD, nM) (fold reversal factor)	
compound	Flp-In 293 cells	*ABCB1*/HEK293 cells
doxorubicin (Dox) only	6.15 ± 1.78	196.34 ± 5.01 (1.00)
Dox + 1 μM BDMC	5.36 ± 0.95	13.89 ± 1.51 (14.14)*[a]
Dox + 2.5 μM BDMC	6.30 ± 1.14	10.41 ± 1.76 (18.86)*
Dox + 1 μM DMC	7.75 ± 1.43	11.61 ± 1.94 (16.91)*
Dox + 2.5 μM DMC	5.47 ± 0.17	8.76 ± 1.31 (22.41)*
Dox + 1 μM C	7.78 ± 0.24	13.21 ± 2.53 (14.86)*
Dox + 2.5 μM C	6.58 ± 0.74	10.90 ± 1.55 (18.01)*

[a]* denotes $p < 0.05$ as compared to doxorubicin treatment.

the analyses in HEK293 cells, which were stably transfected with human P-gp to avoid the disturbance of baseline expression of transporters and the different drug-induced transporter expression levels.

In the present study, DMC was demonstrated to be the most potent P-gp inhibitor among the major curcuminoids. Several studies also showed that DMC possessed the most efficient cytotoxic effects toward breast cancer and prostate cancer cells.[18,31,32] It was reported that DMC may activate AMPK and thus inhibit energy metabolic and oncogenic signaling pathways in triple-negative breast cancer cells.[31] It was also shown in another study that DMC may down-regulate HSP70 and EGFR and further influence the proliferation of prostate cancer cells.[18] DMC was also shown to induce human glioma cells arrested at G2/M phase and apoptosis.[33] Although C is the most abundant form of natural curcuminoids, it can be degraded easily both in vivo and in vitro.[34] The instability of C limited its biological activity, and thus the efficacy of anticancer and P-gp inhibition was reduced; on the other hand, compared to C, DMC lacks the methoxy group, which links directly to the benzene ring, and this slight difference led to the more stable chemical character of DMC.[35] In the present study, DMC was demonstrated to be a 3.5-fold more potent P-gp inhibitor than C. The kinetic mechanisms of C, DMC, and BDMC were similar. These curcuminoids acted as uncompetitive inhibitors of human P-gp and inhibited ATPase activity of P-gp. These results indicated that the structural stability plays a critical role for the potency of curcuminoids. The difference among C, DMC, and BDMC was the ability to inhibit verapamil-induced ATPase activity. Only C was unable to inhibit verapamil-induced ATPase activity; both DMC and BDMC inhibited verapamil-induced ATPase activity under low concentration. These results suggested that DMC and BDMC may compete for the ATPase binding sites of verapamil, whereas C might act on the other binding pockets.

Table 3. Effect of Demethoxycurcumin on Doxorubicin Transport by Human P-Glycoprotein

	Nonlinear Kinetic Parameters		
	V_m (pmol/mg protein/120 min)	K_m (μM)	
nonlinear regression			
doxorubicin only	144.63 ± 4.78	36.87 ± 3.27	
+ DMC, 1 μM	92.42 ± 4.41*[a]	32.67 ± 3.59	
+ DMC, 2.5 μM	85.24 ± 1.43*	30.49 ± 4.69	
K_i from Lineweaver–Burk (μM)			0.44 ± 0.07

[a]* denotes $p < 0.05$ as compared to doxorubicin transport without DMC.

DOI: 10.1021/jf5042307
J. Agric. Food Chem. 2015, 63, 847–855

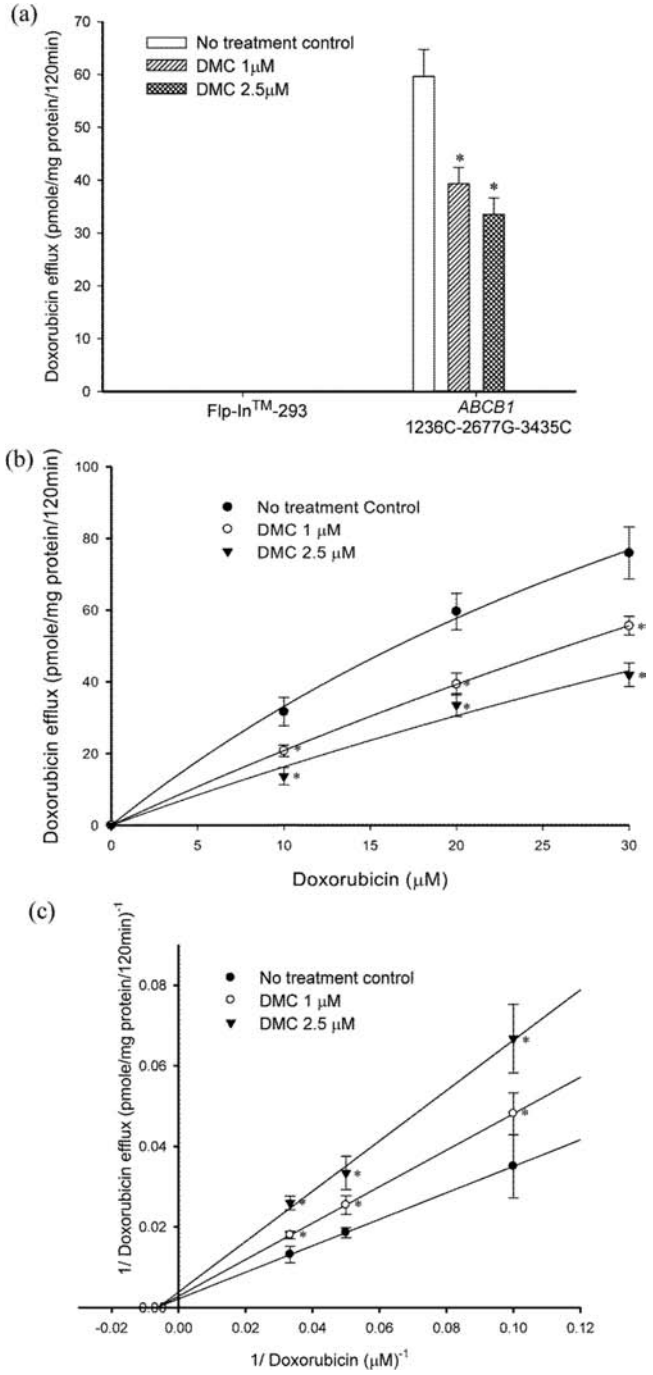

Figure 5. Concentration-dependent doxorubicin efflux (10−30 μM) in the presence or absence of DMC: (a) dose-dependent effect of DMC on doxorubicin efflux by P-gp; (b) nonlinear regression analysis of the inhibition effect of DMC on doxorubicin efflux; (c) Lineweaver−Burk plot analysis of the inhibition effect of DMC on doxorubicin efflux. Data are presented as the mean ± SE of at least three experiments, each in triplicate. (*) $p < 0.05$ as compared to doxorubicin efflux without DMC (control).

The strength of this study was the use of stable cloned human P-gp expression cells. With the stable and identical P-gp expression level, the kinetic mechanisms and potency of C, DMC, and BDMC were clarified. The fold of reversal factor of doxorubicin further demonstrated the reversal of drug sensitivity by treatment of individual major curcuminoids. However, there were still weakness in this study. The effects of multidrug-resistant reversal curcuminoids still need to be verified in animal models. The other important issue is the low bioavailability of curcuminoids irrespective of the route of administration. There are several strategies to improve the bioavailability of curcuminoids, including utilization of nanoparticle preparations, concomitant administration with metabolic pathway blocking agents, or modification of the structures of curcuminoids.

In conclusion, the results of this study demonstrated that DMC treatment inhibited human P-gp function through ATPase inhibition via uncompetitive inhibition. It also reversed the doxorubicin-resistant cells to doxorubicin-sensitive cells. Further in vivo studies about the P-gp inhibition effect of DMC may provide evidence to support DMC used as an add-on natural product in chemotherapy patients.

AUTHOR INFORMATION

Corresponding Authors

*(H.-Y.L.) E-mail: hylin@mail.cmu.edu.tw. Phone: +886-4-22053366, ext. 5112. Fax: +886-4-22078083.

*(C.-C.H.) E-mail: cc0206hung@gmail.com. Phone: +886-4-22053366, ext. 5155. Fax: +886-4-22078083.

Author Contributions

‖C.-C.H. and H.-Y.L. contributed equally.

Funding

This work was supported by grants from the Ministry of Science and Technology in Taiwan (MOST 103-2320-B-039-014), the Taiwan Department of Health Clinical Trial and Research Center of Excellence (DOH102-TD-B-111-004), and the National Health Research Institutes in Taiwan (NHRI-102A1-PDCO-1312141). The funders had no role in study design, data collection and analysis, decision to publish, or preparation of the manuscript.

Notes

The authors declare no competing financial interest.

ACKNOWLEDGMENTS

We acknowledge Dr. Kazumitsu Ueda (Kyoto University) for providing the human MDR1 cDNA.

REFERENCES

(1) Ueda, K. ABC proteins protect the human body and maintain optimal health. *Biosci., Biotechnol., Biochem.* **2011**, *75*, 401−409.

(2) Fromm, M. F. Importance of P-glycoprotein at blood-tissue barriers. *Trends Pharmacol. Sci.* **2004**, *25*, 423−429.

(3) Sarkadi, B.; Homolya, L.; Szakacs, G.; Varadi, A. Human multidrug resistance ABCB and ABCG transporters: participation in a chemoimmunity defense system. *Physiol. Rev.* **2006**, *86*, 1179−1236.

(4) Callaghan, R.; Luk, F.; Bebawy, M. Inhibition of the multidrug resistance P-glycoprotein: time for a change of strategy? *Drug Metab. Disposition: Biol. Fate Chem.* **2014**, *42*, 623−631.

(5) Yu, M.; Ocana, A.; Tannock, I. F. Reversal of ATP-binding cassette drug transporter activity to modulate chemoresistance: why has it failed to provide clinical benefit? *Cancer Metastasis Rev.* **2013**, *32*, 211−227.

(6) Saneja, A.; Khare, V.; Alam, N.; Dubey, R. D.; Gupta, P. N. Advances in P-glycoprotein-based approaches for delivering anticancer drugs: pharmacokinetic perspective and clinical relevance. *Expert Opin. Drug Delivery* **2014**, *11*, 121−138.

(7) Lopez, D.; Martinez-Luis, S. Marine natural products with P-glycoprotein inhibitor properties. *Mar. Drugs* **2014**, *12*, 525−546.

(8) Ammon, H. P.; Wahl, M. A. Pharmacology of *Curcuma longa*. *Planta Med.* **1991**, *57*, 1−7.

DOI: 10.1021/jf5042307
J. Agric. Food Chem. 2015, 63, 847−855

(9) Gota, V. S.; Maru, G. B.; Soni, T. G.; Gandhi, T. R.; Kochar, N.; Agarwal, M. G. Safety and pharmacokinetics of a solid lipid curcumin particle formulation in osteosarcoma patients and healthy volunteers. *J. Agric. Food Chem.* **2010**, *58*, 2095−2099.
(10) Huang, T. Y.; Tsai, T. H.; Hsu, C. W.; Hsu, Y. C. Curcuminoids suppress the growth and induce apoptosis through caspase-3-dependent pathways in glioblastoma multiforme (GBM) 8401 cells. *J. Agric. Food Chem.* **2010**, *58*, 10639−10645.
(11) Lin, Y. T.; Wang, L. F.; Hsu, Y. C. Curcuminoids suppress the growth of pharynx and nasopharyngeal carcinoma cells through induced apoptosis. *J. Agric. Food Chem.* **2009**, *57*, 3765−3770.
(12) Liao, K. K.; Wu, M. J.; Chen, P. Y.; Huang, S. W.; Chiu, S. J.; Ho, C. T.; Yen, J. H. Curcuminoids promote neurite outgrowth in PC12 cells through MAPK/ERK- and PKC-dependent pathways. *J. Agric. Food Chem.* **2012**, *60*, 433−443.
(13) Shishu; Gupta, N.; Aggarwal, N. Bioavailability enhancement and targeting of stomach tumors using gastro-retentive floating drug delivery system of curcumin − "a technical note". *AAPS PharmSciTech* **2008**, *9*, 810−813.
(14) Anuchapreeda, S.; Leechanachai, P.; Smith, M. M.; Ambudkar, S. V.; Limtrakul, P. N. Modulation of P-glycoprotein expression and function by curcumin in multidrug-resistant human KB cells. *Biochem. Pharmacol.* **2002**, *64*, 573−582.
(15) Romiti, N.; Tongiani, R.; Cervelli, F.; Chieli, E. Effects of curcumin on P-glycoprotein in primary cultures of rat hepatocytes. *Life Sci.* **1998**, *62*, 2349−2358.
(16) Ampasavate, C.; Sotanaphun, U.; Phattanawasin, P.; Piyapolrungroj, N. Effects of *Curcuma* spp. on P-glycoprotein function. *Phytomedicine: Int. J. Phytother. Phytopharmacol.* **2010**, *17*, 506−512.
(17) Chearwae, W.; Anuchapreeda, S.; Nandigama, K.; Ambudkar, S. V.; Limtrakul, P. Biochemical mechanism of modulation of human P-glycoprotein (ABCB1) by curcumin I, II, and III purified from turmeric powder. *Biochem. Pharmacol.* **2004**, *68*, 2043−2052.
(18) Hung, C. M.; Su, Y. H.; Lin, H. Y.; Lin, J. N.; Liu, L. C.; Ho, C. T.; Way, T. D. Demethoxycurcumin modulates prostate cancer cell proliferation via AMPK-induced down-regulation of HSP70 and EGFR. *J. Agric. Food Chem.* **2012**, *60*, 8427−8434.
(19) Hung, C. C.; Chiou, M. H.; Teng, Y. N.; Hsieh, Y. W.; Huang, C. L.; Lane, H. Y. Functional impact of ABCB1 variants on interactions between P-glycoprotein and methadone. *PLoS One* **2013**, *8*, No. e59419.
(20) Sheu, M. J.; Teng, Y. N.; Chen, Y. Y.; Hung, C. C. The functional influences of common ABCB1 genetic variants on the inhibition of P-glycoprotein by *Antrodia cinnamomea* extracts. *PLoS One* **2014**, *9*, No. e89622.
(21) Liu, K. J.; He, J. H.; Su, X. D.; Sim, H. M.; Xie, J. D.; Chen, X. G.; Wang, F.; Liang, Y. J.; Singh, S.; Sodani, K.; Talele, T. T.; Ambudkar, S. V.; Chen, Z. S.; Wu, H. Y.; Fu, L. W. Saracatinib (AZD0530) is a potent modulator of ABCB1-mediated multidrug resistance in vitro and in vivo. *Int. J. Cancer* **2013**, *132*, 224−235.
(22) Krasznai, Z. T.; Toth, A.; Mikecz, P.; Fodor, Z.; Szabo, G.; Galuska, L.; Hernadi, Z.; Goda, K. Pgp inhibition by UIC2 antibody can be followed in vitro by using tumor-diagnostic radiotracers, 99mTc-MIBI and 18FDG. *Eur. J. Pharm. Sci.* **2010**, *41*, 665−669.
(23) Ritchie, T. K.; Kwon, H.; Atkins, W. M. Conformational analysis of human ATP-binding cassette transporter ABCB1 in lipid nanodiscs and inhibition by the antibodies MRK16 and UIC2. *J. Biol. Chem.* **2011**, *286*, 39489−39496.
(24) Nabekura, T. Overcoming multidrug resistance in human cancer cells by natural compounds. *Toxins* **2010**, *2*, 1207−1224.
(25) Singh, S.; Aggarwal, B. B. Activation of transcription factor NF-κB is suppressed by curcumin (diferuloylmethane) [corrected]. *J. Biol. Chem.* **1995**, *270*, 24995−25000.
(26) Jaiswal, A. S.; Marlow, B. P.; Gupta, N.; Narayan, S. β-Catenin-mediated transactivation and cell-cell adhesion pathways are important in curcumin (diferuylmethane)-induced growth arrest and apoptosis in colon cancer cells. *Oncogene* **2002**, *21*, 8414−8427.
(27) Park, C. H.; Hahm, E. R.; Park, S.; Kim, H. K.; Yang, C. H. The inhibitory mechanism of curcumin and its derivative against β-catenin/Tcf signaling. *FEBS Lett.* **2005**, *579*, 2965−2971.
(28) Beevers, C. S.; Li, F.; Liu, L.; Huang, S. Curcumin inhibits the mammalian target of rapamycin-mediated signaling pathways in cancer cells. *Int. J. Cancer* **2006**, *119*, 757−764.
(29) Yu, S.; Shen, G.; Khor, T. O.; Kim, J. H.; Kong, A. N. Curcumin inhibits Akt/mammalian target of rapamycin signaling through protein phosphatase-dependent mechanism. *Mol. Cancer Ther.* **2008**, *7*, 2609−2620.
(30) Nabekura, T.; Kamiyama, S.; Kitagawa, S. Effects of dietary chemopreventive phytochemicals on P-glycoprotein function. *Biochem. Biophys. Res. Commun.* **2005**, *327*, 866−870.
(31) Shieh, J. M.; Chen, Y. C.; Lin, Y. C.; Lin, J. N.; Chen, W. C.; Chen, Y. Y.; Ho, C. T.; Way, T. D. Demethoxycurcumin inhibits energy metabolic and oncogenic signaling pathways through AMPK activation in triple-negative breast cancer cells. *J. Agric. Food Chem.* **2013**, *61*, 6366−6375.
(32) Simon, A.; Allais, D. P.; Duroux, J. L.; Basly, J. P.; Durand-Fontanier, S.; Delage, C. Inhibitory effect of curcuminoids on MCF-7 cell proliferation and structure-activity relationships. *Cancer Lett.* **1998**, *129*, 111−116.
(33) Luthra, P. M.; Kumar, R.; Prakash, A. Demethoxycurcumin induces Bcl-2 mediated G2/M arrest and apoptosis in human glioma U87 cells. *Biochem. Biophys. Res. Commun.* **2009**, *384*, 420−425.
(34) Ireson, C.; Orr, S.; Jones, D. J.; Verschoyle, R.; Lim, C. K.; Luo, J. L.; Howells, L.; Plummer, S.; Jukes, R.; Williams, M.; Steward, W. P.; Gescher, A. Characterization of metabolites of the chemopreventive agent curcumin in human and rat hepatocytes and in the rat in vivo, and evaluation of their ability to inhibit phorbol ester-induced prostaglandin E2 production. *Cancer Res.* **2001**, *61*, 1058−1064.
(35) Han, G.; Bi, R.; Le, Q.; Zhao, L. L.; Dong, Y.; Lin, Q. H. [Study on effect of demethoxycurcumin in *Curcuma longa* on stability of curcumin]. *J. Chin. Med. Mater.* **2008**, *31*, 592−594.

DOI: 10.1021/jf5042307
J. Agric. Food Chem. 2015, 63, 847−855

JOURNAL OF AGRICULTURAL AND FOOD CHEMISTRY

Article

pubs.acs.org/JAFC

Metagenomic Insights into the Effects of Fructo-oligosaccharides (FOS) on the Composition of Fecal Microbiota in Mice

Bingyong Mao,[†,∥] Dongyao Li,[†,∥] Jianxin Zhao,[†] Xiaoming Liu,[†] Zhennan Gu,[†,‡] Yong Q. Chen,[†,‡] Hao Zhang,*[,†,‡] and Wei Chen*[,†,‡]

[†]State Key Laboratory of Food Science and Technology, School of Food Science and Technology, Jiangnan University, Wuxi 214122, People's Republic of China

[‡]Synergistic Innovation Center for Food Safety and Nutrition, Wuxi 214122, People's Republic of China

Supporting Information

ABSTRACT: Fructo-oligosaccharides (FOS) are usually regarded as a type of prebiotic, favorably stimulating the growth of bifidobacteria and lactobacilli. However, they are not the specific substrates for these target species, and other bacteria, such as *Streptococcus*, *Escherichia*, and *Clostridium*, have been shown to be able to utilize FOS. Previous studies have mainly investigated only a few bacteria groups, and few reports analyzed the global effects of FOS on intestinal microbial communities. In this study the effects of FOS on gut bacteria in mice were investigated through a 16S rRNA metagenomic analysis. In the FOS-low group, the abundance of *Actinobacteria* significantly increased and that of *Bacteroidetes* decreased after FOS diet (5%) for 3 weeks. In the FOS-high group, *Enterococcus* was promoted and levels of *Bifidobacterium* and *Olsenella* both notably increased after FOS diet (25%) and the microbiota tended to revert to initial structure 2 weeks after FOS treatment ceased. The most striking observation was that *Olsenella* became a dominant genus comparable with *Bifidobacterium* after FOS treatment, and one strain of *Olsenella*, isolated from mice feces, was confirmed, for the first time, to be capable of using FOS. The results indicated that metagenomic analysis was helpful to reveal the FOS effects on the global composition of gut communities and new target for future studies.

KEYWORDS: *fructo-oligosaccharides, prebiotic, intestinal microbiota, 16S rRNA metagenomic, Olsenella*

INTRODUCTION

The human gastrointestinal tract is home to >10^{12} organisms.[1] Maintaining the balance of the microbial communities is crucial for host health, and perturbation of their composition may induce a range of diseases including obesity, diabetes, and inflammatory bowel disease.[2−4] It is well recognized that the composition of gut microbiota is dependent on individual genotype[5] and environmental factors,[6−8] among which diet is of particular importance.

Nondigestible oligosaccharides are able to reach the large intestine and modify the microbial community. Fructo-oligosaccharides (FOS) are regarded as a prebiotic and have well documented beneficial health effects,[9,10] which are achieved by restructuring of the gut microbiota. Although FOS are usually considered to favorably stimulate the growth of bifidobacteria and lactobacilli, there is increasing evidence that FOS are not entirely specific for these bacteria and can also be used by non-bifidobacteria, such as *Streptococcus*,[11] *Escherichia*,[12] and *Clostridium*.[13] Valcheva et al. found that FOS treatment increased the abundance of *Clostridium leptum* in rats[14] and stimulated the growth of *Faecalibacterium prausnitzii* in humans.[15] Shen et al. assessed the effects of FOS on *Bifidobacterium*, the *Clostridium leptum* subgroup, and *Bacteriodes* in human flora-associated piglets and found that the effects varied at different developmental stages.[16] In contrast to most expectations, Licht et al. and Bovee-Oudehoven et al. found that dietary FOS increased colonic permeability in rats[17,18] and dose-dependently increased the translocation of *Salmonella* in mice and rats,[19−21] indicating the adverse effects of FOS consumption. Moreover, an overdose of prebiotics can lead to the development of intestinal discomfort,[9,22−24] including borborygmi and tympanites, which might be caused by the increase in gas production and osmotic pressure.[22−24] Thus, the effects of FOS on gut bacteria are far more complex than the bifidogenic effects. Being limited to the analytical technologies, previous studies mainly focused on the changes of given groups of bacteria during FOS consumption, and there were few reports on the global effects of FOS use on the gut communities.[25] Therefore, more detailed and extensive studies are required to investigate the effects of FOS on the composition of gut microbiota using the available advanced analytical technologies.

In this study, mice were fed FOS at low and high doses, and the composition of the fecal microbiota was determined using a high-throughput MiSeq sequencing technique to assess the effects of the FOS treatment. 16S rRNA metagenomic analysis was performed on both bifidobacteria and non-bifidobacteria to reveal the relationship between FOS and gut bacteria.

MATERIALS AND METHODS

Chemicals and Reagents. Fructo-oligosaccharides (Meioligo P, Meiji Seika Kaisha, Ltd., Japan) comprised 6.5% fructosylfructosyl nystose (GF5), 43.4% 1F-β-fructofuranosyl nystose (GF4), 40.9% nystose (GF3), 7.1% 1-kestose (GF2), and 2.1% glucose and fructose.

Received: October 24, 2014
Revised: January 6, 2015
Accepted: January 8, 2015
Published: January 8, 2015

ACS Publications © 2015 American Chemical Society

DOI: 10.1021/jf505156h
J. Agric. Food Chem. 2015, 63, 856−863

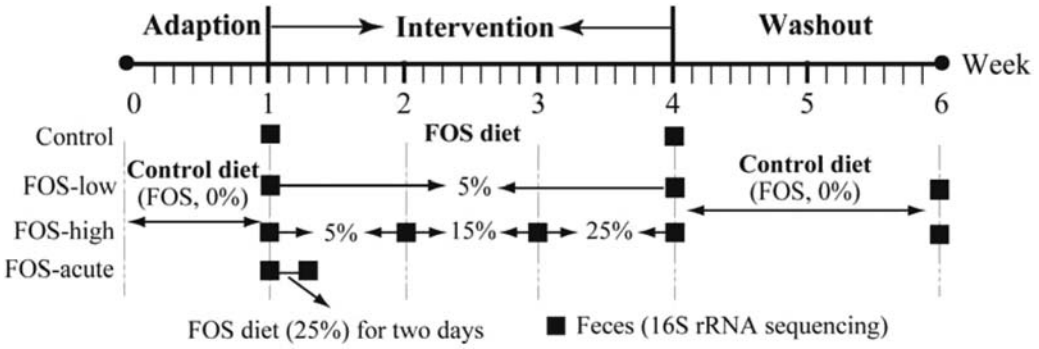

Figure 1. Experimental design. Thirty-two mice were randomly and equally divided into four groups (control, FOS-low, FOS-high, and FOS-acute). In the control group, mice were fed the control diet (FOS, 0%), and feces were collected at the 1st and 4th weeks. In the FOS-low group, mice were fed diet supplemented with FOS (5%) for 3 weeks, and feces were collected at the 1st, 4th, and 6th weeks. In the FOS-high group, mice were fed diet with FOS at increasing proportions, 5% for the 2nd week, 15% for the 3rd week, and 25% for the 4th week. Feces were collected at the 1st, 2nd, 3rd, 4th, and 6th weeks. In the FOS-acute group, mice were fed diet with FOS (25%) for 2 days and feces were collected before and after the FOS treatment.

Animals and Sample Collection. Six-week-old male C57BL/6J mice were obtained from the Shanghai Laboratory Animal Center (Shanghai, China) and maintained in an IVC rodent caging system. The mice were housed in a temperature- and humidity-controlled room under a strict 12 h light cycle and fed a commercial mouse diet; water was given ad libitum. All of the protocols used in this study were approved by the Ethics Committee of Jiangnan University, China (JN No. 20140306-0910-7), and the procedures were carried out in accordance with the European Community guidelines (Directive 2010/63/EU) for the care and use of experimental animals.

The mice were randomly divided into four groups (n = 8 for each group), as shown in Figure 1. The average body weight was 19.6 ± 0.8 g. The mice were adapted to the new environment for 1 week, followed by a 3 week intervention period and a 2 week washout period. The commercial diet was smashed and amended with FOS at different proportions, and pellets were formed. In this study, the dose of FOS was determined according to a pre-experiment. Twenty-four 6-week old male C57BL/6J mice were randomly and equally divided into six groups, which were given diets supplemented with FOS at proportions of 2, 5, 10, 20, 25, and 30%. The diet was weighed daily to calculate the FOS intake, and the FOS proportions corresponded to doses of 0.1, 0.2, 0.4, 0.6, 0.8, and 1.0 g of FOS per mouse per day (PMPD), respectively. Feces were daily collected for observation. Diarrhea was diagnosed as poorly formed, looser, and more watery feces than normal. Slight diarrhea was found in the 25 and 30% groups after 1 week. Therefore, the FOS proportion was set at 5% for the FOS-low group and 25% for the FOS-high group. The dose was based on a body weight of 20 g. As shown in Figure 1, the control group was fed the control diet (FOS, 0%) throughout the experiment, and the other three groups were fed the diets supplemented with FOS at different proportions (5, 15, and 25%) during the intervention period. Diet was weighed daily and recorded for calculating the actual FOS intake (Supporting Information, Figure S1), and body weight was recorded every week. At the times indicated in Figure 1, mice were transferred to separate sterilized cages, and feces were collected in individual sterile EP tubes on ice, which were taken to the laboratory within 2 h of collection for further study. After the experiment, the mice were euthanized by intraperitoneal injection of 200 mg/kg sodium pentobarbital euthanasia solution.

DNA Extraction, PCR Amplification, Quantification, and Sequencing. Microbial genome DNA was extracted from fecal samples using FastDNA Spin Kit for Soil (MP Biomedicals, catalog no. 6560-200) following the manufacturer's instructions. The V4 region of the 16S rRNA was PCR amplified from microbial genome DNA using the primers (forward primer, 5′-AYTGGGYDTAAAGNG-3′; reverse primer, 5′-TACNVGGGTATCTAATCC-3′) as described previously.[26] The PCR procedures were 95 °C for 5 min; 95 °C for 30 s, 50 °C for 30 s, and 72 °C for 30 s, repeat for 30 cycles; and 72 °C for 10 min. The PCR products were excised from a 1.5% agarose gel, purified by GeneClean Turbo (MP Biomedicals, catalog no. 111102400) and quantified by Quant-iT PicoGreen dsDNA Assay Kit (Life Technologies, catalog no. P7589) according to the instructions. Libraries were prepared using TruSeq DNA LT Sample Preparation Kit (Illumina, catalog no. FC-121-2001) and sequenced for 500+7 cycles on Illumina Miseq using the MiSeq Reagent Kit (500 cycles-PE, catalog no. MS-102-2003).

Bioinformatic Analysis. Sequences with an average quality score <30, containing ambiguous bases, homopolymer run exceeds 6, having mismatches in primers, or sequence length <200 bp were removed. Pair-end reads that overlapped longer than 10 bp and without any mismatch were assembled according to their overlap sequence. Reads that could not be assembled were discarded. Barcode and sequencing primers were trimmed from the sequences.

Sets of trimmed sequences with >97% identity were defined as an operational taxonomic unit (OTU). The OTUs were assigned to a taxonomy using the Ribosomal Database Project (RDP) Naive Bayes classifier.[27] Representative sequences from each cluster were aligned with the PyNAST aligner[28] to the greengenes core set in QIIME.[29] A phylogeny was constructed within QIIME using FastTree.[30] Rarefaction curves, alpha diversity, and beta diversity calculations were also performed using QIIME. The Chao1 estimator and Shannon diversity index were estimated to evaluate the ecological diversity of the microbiota in each sample. The similarity among the microbial communities was determined using UniFrac analysis[31] with weighted and unweighted principal coordinate analysis (PCoA).

Statistical Analysis. The differences among groups were analyzed using ANOVA with Tukey's honestly significant difference post hoc test, and Student's t test was used to identify the differences between two groups. The analyses were performed using SPSS software (version 16.0; SPSS Inc., Chicago, IL, USA). Significance was accepted at $P < 0.05$.

Nucleotide Sequence Accession Numbers. The sequences reported in this paper have been deposited in the Rapid Annotation using Subsystems Technology for Metagenomes database (MG-RAST) under the accession no. 4578758.3−4578850.3.

Isolation and Identification of *Olsenella* from Mice Feces. To isolate *Olsenella* from mice feces, three mice were fed a diet supplemented with FOS at a dose of 0.8 g PMPD for 1 week. On day 7, the mice were transferred to sterilized individual cages. Fresh feces were collected in 5 mL sterile EP tubes and immediately dispersed in 0.9% salt solution. Fecal samples were diluted 10^{-5}, 10^{-6}, and 10^{-7}, plated on brain−heart infusion (BHI, Oxoid) agar, and incubated anaerobically at 37 °C for 48 h. Colonies were selected, Gram-strained, and identified using 16S rRNA gene sequencing.

Growth of *Olsenella* on FOS. Strains of *Olsenella* were cultured anaerobically in BHI media with and without FOS (8 g/L) at 37 °C for 24 h. The absorbance at 600 nm (OD_{600}) was recorded every 2 h, and the amount of FOS in the culture supernatant was determined on a Waters 600 high-performance liquid chromatography system (Waters Corp., Milford, MA, USA), equipped with a 600 pump, an autosampler, and a refractive index detector. Separations were carried out using a

DOI: 10.1021/jf505156h
J. Agric. Food Chem. 2015, 63, 856−863

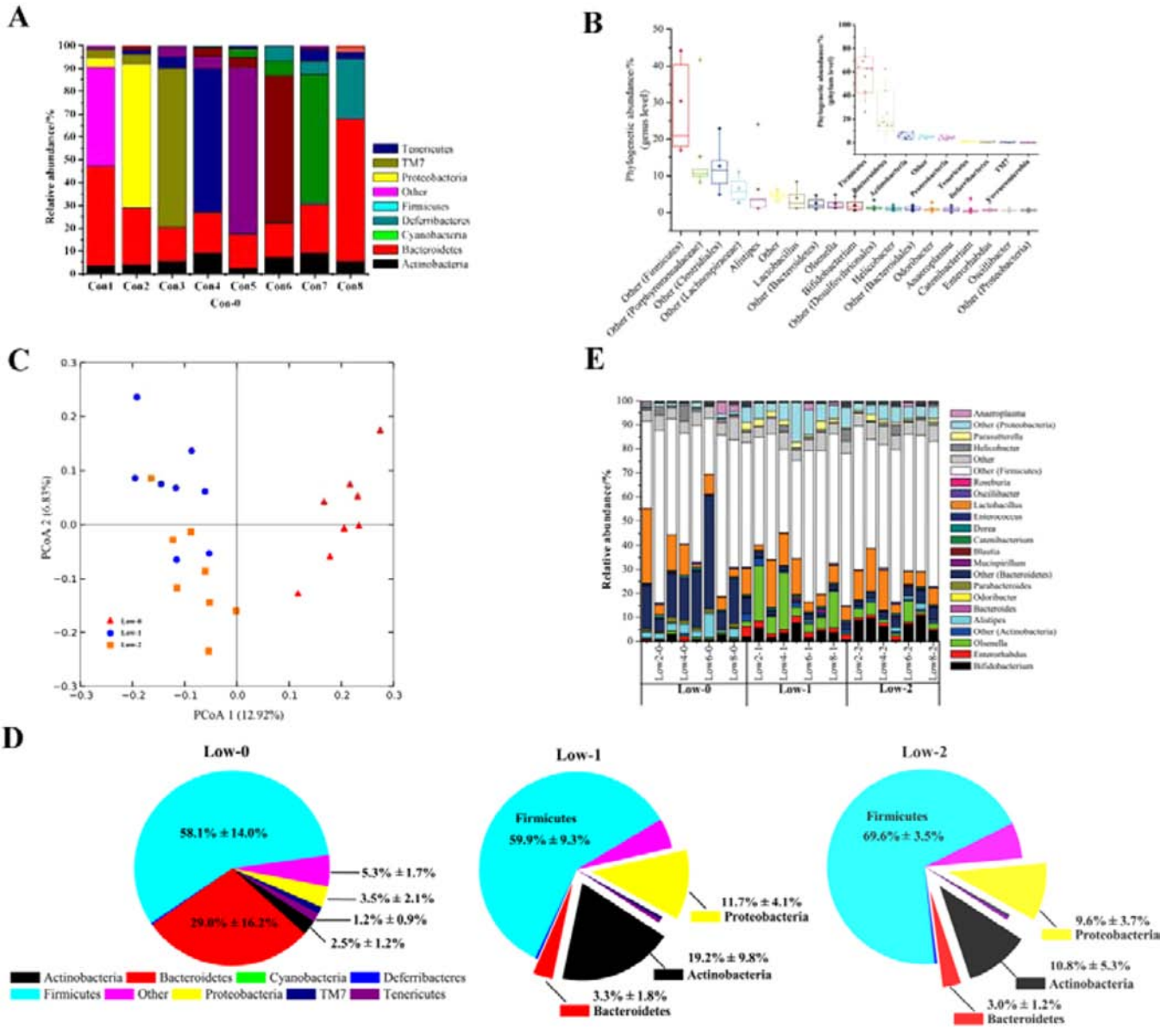

Figure 2. Effect of FOS at a low dose on the fecal microbiota: (A) interindividual variation in the proportion of major phyla for the control group; (B) bacterial diversity at the phylum and genus levels (>0.5%) for the control group; (C) principal coordinate (PCoA) score plots based on unweighted UniFrac metrics at the different periods (each point represents the composition of fecal microbiota of one mouse); relative abundance of main phyla (D) and genera >0.1% (E) at different periods. Sequences that could not be classified into any known group were assigned as "other". Con, control group; Low, FOS-low group. The number following the abbreviations stands for the mouse number. For example, Con1 and Con2 stand for the first and second mice in the control group. Con-0 stands for the 1st week. The number following "Low-" stands for the period: "0", before FOS treatment; "1", intervention period; "2", washout period. The abundance of main phyla is expressed as the mean ± SEM.

Waters SugarPak1 column (6.5 × 300 mm, i.d. = 3.5 μm), and the column temperature was set at 85 °C. The mobile phase was water with the flow rate of 0.4 mL/min, and the injection volume was 10 μL.

RESULTS

A data set consisting of 1,265,448 high-quality, classifiable 16S rRNA gene sequences was generated from 93 fecal samples through MiSeq sequencing analysis. The average sequence read was 13607 per sample (Supporting Information, Table S1). All of the sequences were clustered with representative sequences, and a 97% sequence identity cutoff was used. The number of OTUs per sample ranged between 334 and 2936 (Table S1).

Effect of FOS at Low Dose on the Composition of Fecal Microbiota. At the phylum level (Figure 2A,B), the gut bacteria community was mostly dominated by *Firmicutes* and *Bacteroidetes*, and the average ratio between *Firmicutes* and *Bacteroidetes* was 3.04 (ranging from 0.42 to 5.04). At the genus level (Figure 2B), unknown genera belonging to *Firmicutes*, *Porphyromonadaceae*, *Clostridiales*, *Lachnospiraceae*, *Bacteroidetes*, *Desulfovibrionales*, *Bacteroidales*, and *Proteobacteria* and *Alistipes*, *Lactobacillus*, *Olsenella*, *Bifidobacterium*, *Helicobacter*, *Odoribacter*, *Anaeroplasma*, *Catenibacterium*, *Enterorhabdus*, and *Oscillibacter* all comprised >0.5% of the microbiota.

The fecal microbiota was profoundly affected after FOS treatment (0.2 g PMPD) for 3 weeks (Figure 2C). The abundance of *Firmicutes* was maintained at about 60%, whereas that of *Bacteroidetes* dropped markedly from 29.0 to 3.3% (Figure 2D). Accordingly, the average ratio of *Firmicutes* and *Bacteroidetes*

DOI: 10.1021/jf505156h
J. Agric. Food Chem. 2015, 63, 856−863

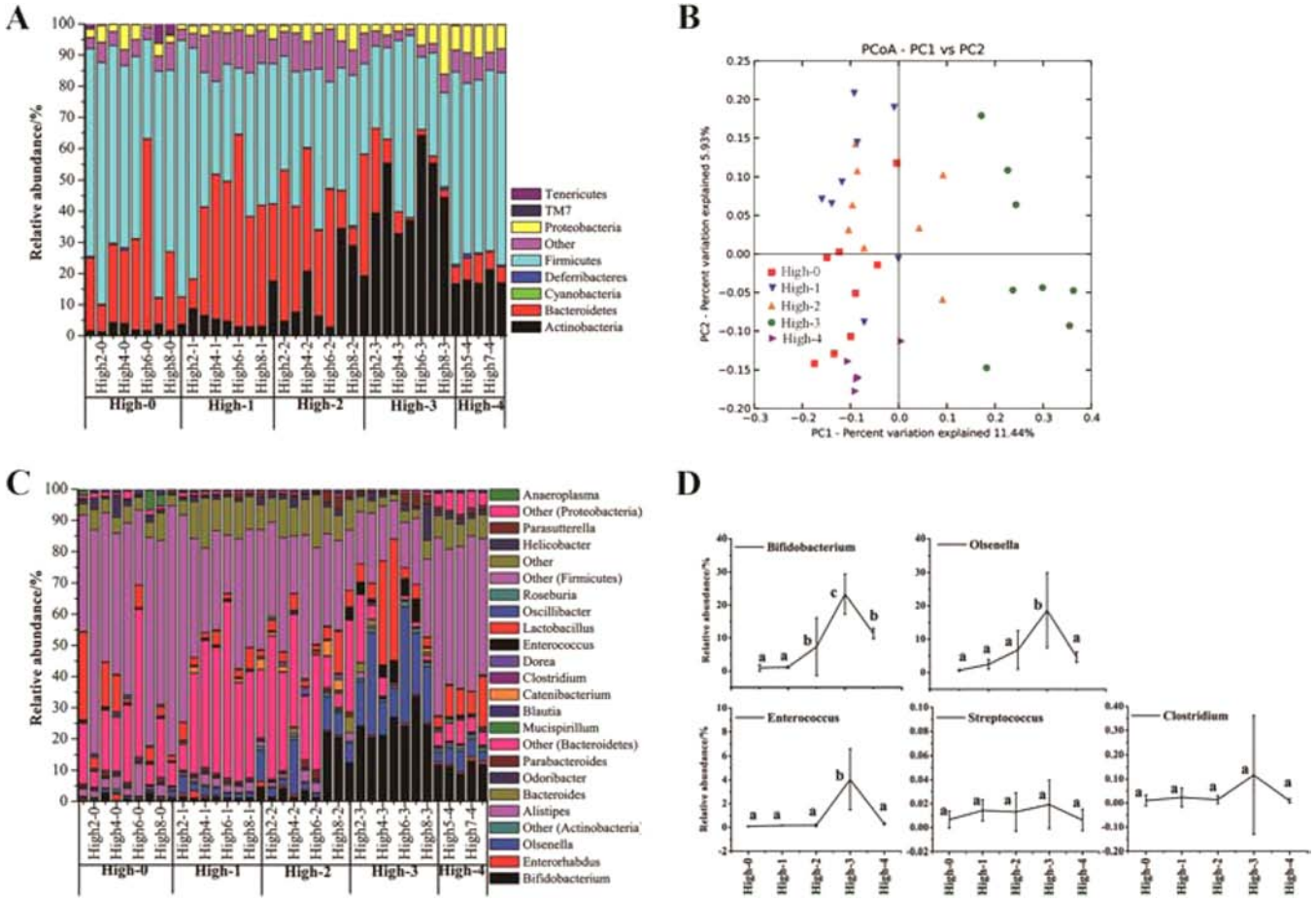

Figure 3. Effect of FOS with increasing doses on the fecal microbiota. (A) Relative abundance of main phyla at different periods. Sequences that could not be classified into any known group were assigned as "other". High, FOS-high group. High1, High2, High3, High4, High5, High6, High7, and High8 stand for the first, second, third, fourth, fifth, sixth, seventh, and eighth mice in the FOS-high group. The number following "High-" stands for the period. "0", before FOS treatment; "1", intervention period (FOS, 5%); "2", intervention period (FOS, 15%); "3", intervention period (FOS, 25%); "4", washout period. (B) Principal coordinate (PCoA) score plots were based on unweighted UniFrac metrics at the different periods. Each point represents the composition of fecal microbiota of one mouse. (C) Relative abundance of main genera >0.1% at different periods. (D) Changes of the abundance of selected genera at different periods. Mean values ± SEM are plotted. Significant differences ($P < 0.05$) are indicated with different letters (a, b, c).

increased to 34.97 (ranging from 9.97 to 79.89). Moreover, significant increases in *Actinobacteria* ($P < 0.01$, Student's *t* test) were observed.

As expected, the abundance of *Bifidobacterium* was significantly increased (Figure 2E, $P < 0.05$), confirming the bifidogenic property of FOS. However, the level of *Lactobacillus* remained stable during the FOS treatment. In addition, the levels of many non-bifidobacteria increased after the FOS treatment. Interestingly, the level of *Olsenella* belonging to *Actinobacteria* increased significantly from 0.7 to 10.7% ($P < 0.01$, Student's *t* test), which was even higher than that of *Bifidobacterium*.

During the washout period, the diet was reverted to the control diet. Slight decreases in *Actinobacteria* and *Proteobacteria* were observed (Figure 2D). The abundance of *Olsenella* was also reduced (Figure 2E). It seems that the effect of FOS on the fecal microbiota did not last long, although the original composition had not fully recovered after 2 weeks.

Effects of FOS at High Dose on the Composition of Fecal Microbiota. During the intervention period, the proportion of *Actinobacteria* continued to increase and reached 44.8% ($P < 0.01$, Student's *t* test), whereas that of *Firmicutes* declined from 57.1 to 34.2% (Figure 3A, $P < 0.01$, Student's *t* test). As shown in Figure 3A, a significant increase in *Actinobacteria* ($P < 0.01$, Student's *t* test) and a decrease in *Bacteroidetes* were observed at the fourth week (High-3). The data points shift from the left of the score plot (High-2) to the right side of the graph (High-3) at the fourth week, indicating significant changes in the fecal microbiota (Figure 3B).

Among the *Actinobacteria*, *Bifidobacterium* and *Olsenella* were the two most abundant genera. During the first 3 weeks, the levels of these genera remained lower. However, they both increased significantly (Figure 3C, $P < 0.05$, Student's *t* test) at the fourth week when the dose reached 0.8 g PMPD. For *Lactobacillus*, no significant changes were observed during the FOS treatment except for significant increases in two mice at the fourth week. Two weeks after the FOS treatment stopped, the fecal microbiota changed and tended to revert to the original levels before the FOS treatment as indicated by the cluster results between the data points of High-4 and High-0 (Figure 3B).

During the first 3 weeks, the level of *Enterococcus* remained low at 0.1%. However, it significantly increased to 4.0% at the fourth week (Figure 3D). The levels of *Streptococcus* and *Clostridium* were also increased at the fourth week, although the increases were not significant and their abundance remained low (Figure 3D). Similarly to *Bifidobacterium*, the abundance of *Olsenella* significantly increased, and it was even higher than that of

DOI: 10.1021/jf505156h
J. Agric. Food Chem. 2015, 63, 856−863

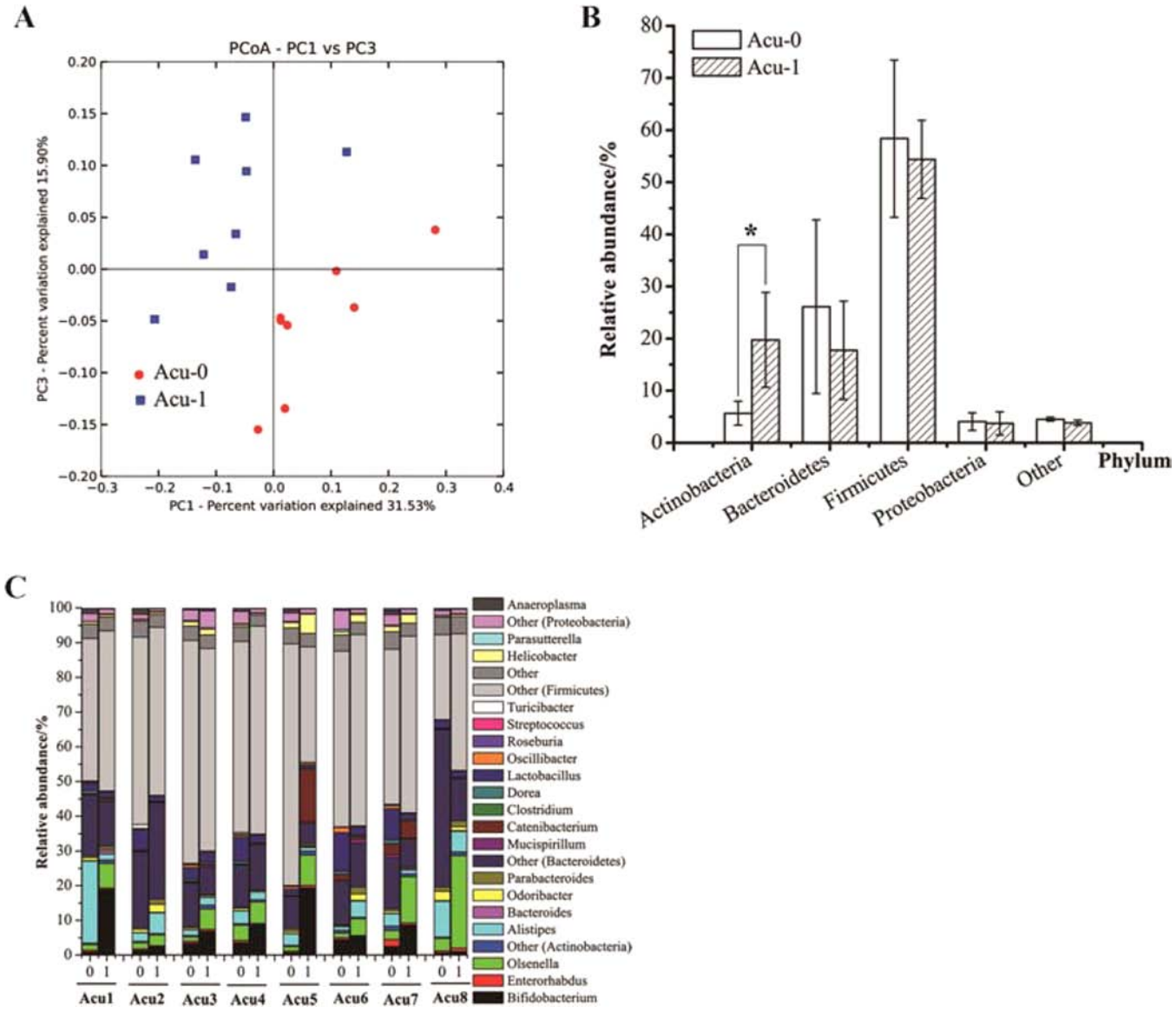

Figure 4. Effect of one-time consumption of FOS on the fecal microbiota. (A) Principal coordinate (PCoA) score plots based on weighted UniFrac metrics. Each point represents the composition of fecal microbiota of one mouse. Relative abundance of five phyla >1% (B) and main genera of different mice before and after FOS treatment (C). Sequences that could not be classified into any known group were assigned as "other". Acu, FOS-acute group; Acu-0, before FOS treatment; Acu-1, after FOS treatment. Acu1, Acu2, Acu3, Acu4, Acu5, Acu6, Acu7, and Acu8 stand for the first, second, third, fourth, fifth, sixth, seventh, and eighth mice in the FOS-acute group. The abundance of main phyla is expressed as the mean ± SEM (∗, $P < 0.05$, Student's t test).

Table 1. Ratio of *Bifidobacterium* and *Olsenella* before and after FOS Treatment

mice		Acu1	Acu2	Acu3	Acu4	Acu5	Acu6	Acu7	Acu8
Bifidobacterium/ *Olsenella* (B/O)	Acu-0	0.53	0.77	2.61	0.79	0.53	3.30	0.92	0.16
	Acu-1	2.65	0.76	1.15	1.42	2.21	1.09	0.64	0.04

Bifidobacterium in several mice at the fourth week. Therefore, more attention needs to be paid to the non-bifidobacteria, especially *Olsenella* and *Enterococcus*, during FOS treatment at high doses.

Effects of FOS on the Fecal Microbiota in an Acute Model. An acute model was established to study the effect of one-time consumption of FOS on fecal microbiota. After 2 days of FOS treatment (FOS, 25%), feces were collected and sequenced. A PCoA based on unweighted Unifrac distances was performed using the obtained sequence data (Figure 4A). Points representing the fecal microbiota of mice before (Acu-0) and after treatment (Acu-1) clustered at the bottom right and top left, respectively. There were significant increases in *Actinobacteria* ($P < 0.001$, Student's t test) and slight decreases in *Bacteroidetes* and *Firmicutes* (Figure 4B). The dramatic increase of *Actinobacteria* was mainly attributable to the significant increases in *Bifidobacterium* and *Olsenella* (Figure 4C, $P < 0.05$, Student's t test). However, the level of *Bifidobacterium* was not significantly different from that of *Olsenella*. Therefore, the FOS were able to selectively stimulate the rapid growth of both *Bifidobacterium* and *Olsenella* in the gut. To make clear the effects of initial abundance of bacteria on the final abundance,

DOI: 10.1021/jf505156h
J. Agric. Food Chem. 2015, 63, 856−863

correlation between the initial and final ratios of *Bifidobacterium* and *Olsenella* (B/O) was investigated (Table 1). The Pearson correlation coefficient was −0.07, which suggests that the final B/O was not correlated with the initial B/O.

Isolation and Identification of *Olsenella* from Mouse Feces and Characterization of Its Growth on FOS. After 7 days of enrichment, seven purified isolates from fecal samples were identified by 16S rRNA sequencing, one of which was confirmed as the genus *Olsenella* (Table 2). The most positive match was *Olsenella* sp. F0004 (accession no. EU592964.1). However, the "Ident" was only 93%, indicating that this strain may belong to unknown species of the genus *Olsenella*. In addition, the sequence of the V4 region of 16S rRNA for *Olsenella* (206 bp) was obtained from the established MiSeq library, which could be found in the sequences of 16S rRNA for mou02 (1373 bp).

Table 2. Identified Strains Isolated from Mouse Feces

no.	strain	most positive match	Ident (%)	GenBank
1	Mou01	*Lactobacillus animalis* JCM 8697 (AB911535.1)	99	KM405313
2	Mou02	*Olsenella* sp. F0004 (EU592964.1)	93	KM405314
3	Mou03	*Lactobacillus animalis* JCM 8697 (AB911535.1)	99	KM405315
4	Mou04	*Lactobacillus* sp. sy4 (KJ801851.1)	99	KM405316
5	Mou09	*Lactobacillus johnsonii* strain LB-19 (HM772969.1)	99	KM405318
6	Mou12	*Lactobacillus taiwanensis* JCM 8687 (AB911525.1)	99	KM405319
7	Mou19	*Lactobacillus taiwanensis* JCM 8687 (AB911525.1)	99	KM405320

The strain mou02 grew faster in BHI medium with the addition of FOS (Figure 5A), indicating that FOS could be used by the *Olsenella* strain mou02, which was confirmed by HPLC analysis (Figure 5B).

DISCUSSION

FOS have long been known to act as a prebiotic that can improve human health by selectively stimulating the growth of beneficial bacteria and reducing the levels of putrefactive bacteria. However, previous studies have mainly focused on specific organisms, such as bifidobacteria, lactobacilli, clostridia, and bacteriodes.[16,32−34] In this study, the effects of FOS on intestinal bacterial populations were investigated using 16S rRNA metagenomic analysis, which can cover the genera existing in the gut.

The FOS were found to alter the intestinal microbiota. Significant increases in the abundance of *Actinobacteria* and decreases in *Bacteroidetes* were observed after FOS treatment (Figures 2D and 3A, High-3), consistent with the results of Rycroft et al.,[33] who evaluated the in vitro fermentation properties of prebiotics on fecal slurry. However, no effect or higher *Bacteroidetes* were observed in mice fed FOS,[34,35] which was consistent with the results at lower doses (Figure 3A, High-1, High-2), indicating that the effect of FOS on *Bacteroidetes* was dependent on dose and time. After 3 weeks, the abundance of *Firmicutes* remained at 60% for the FOS-low group (Figure 2D), but dropped to 35% for the FOS-high group (Figure 3A), indicating that the effect of FOS on the composition of the intestinal microbiota was dependent on the dose. Moreover, the microbial diversity within each group was quantified at given time points (α diversity) (Figure 6). The Shannon index (SI) was estimated to evaluate the ecological diversity of the microbiota in each fecal sample, with a higher SI indicating greater diversity. Significant decreases in α diversity were detected for High-3 and Acu-1 ($P < 0.05$). The decrease for Acu-0 occurred after only 2 days on the FOS diet (FOS, 25%), demonstrating that diet rapidly altered the gut bacteria.[36] Therefore, FOS treatment at a dose of 0.8 g PMPD had a profound effect on the composition and diversity of the intestinal microbiota. Furthermore, the microbiota reverted to their original structure during the washout period (Figure 6), suggesting that the bacterial populations gradually reverted to their prefeeding structures once the FOS treatment ceased.[34,37]

During the FOS treatment, the most striking change in the fecal microbiota was the increase in *Actinobacteria*, of which *Bifidobacterium* and *Olsenella* were the two most dominant genera. It is not surprising that the FOS stimulated the growth of *Bifidobacterium*. However, the abundance of *Olsenella* was also significantly increased and was even higher than *Bifidobacterium* in certain mice (Figures 3B and 4C). *Olsenella* has been described as a member of the oral microbiota[38,39] and is considered an

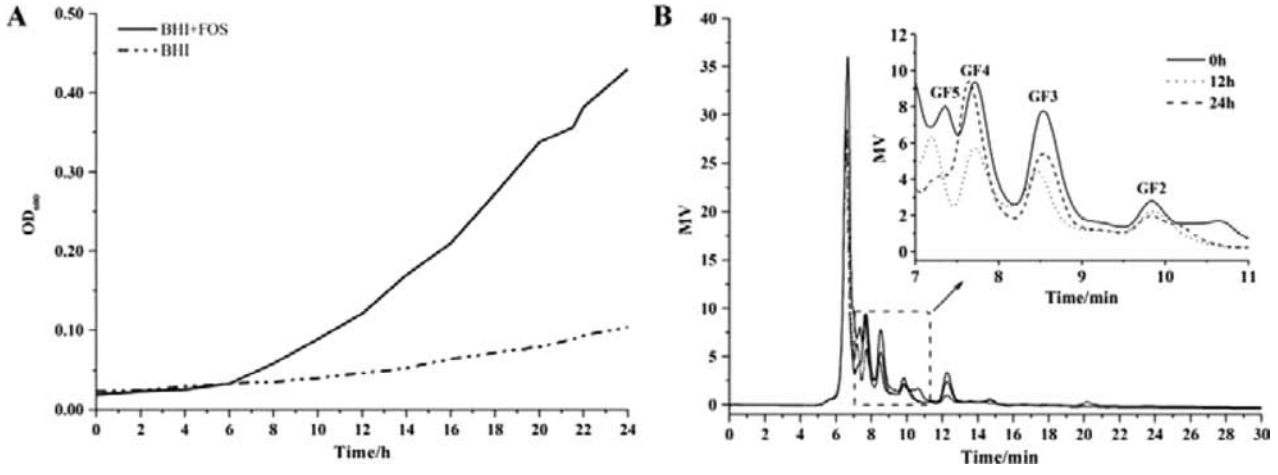

Figure 5. (A) Growth of the *Olsenella* strain mou02 in BHI and BHI-FOS media. The concentration of FOS was 8 g/L. (B) HPLC analysis of the supernatant for the *Olsenella* strain mou02 in BHI-FOS medium at different times: ——, 0 h; ···, 12 h; - - -, 24 h. Peaks at 7.3, 7.7, 8.5, and 9.9 min were assigned as GF5, GF4, GF3, and GF2, respectively.

DOI: 10.1021/jf505156h
J. Agric. Food Chem. 2015, 63, 856−863

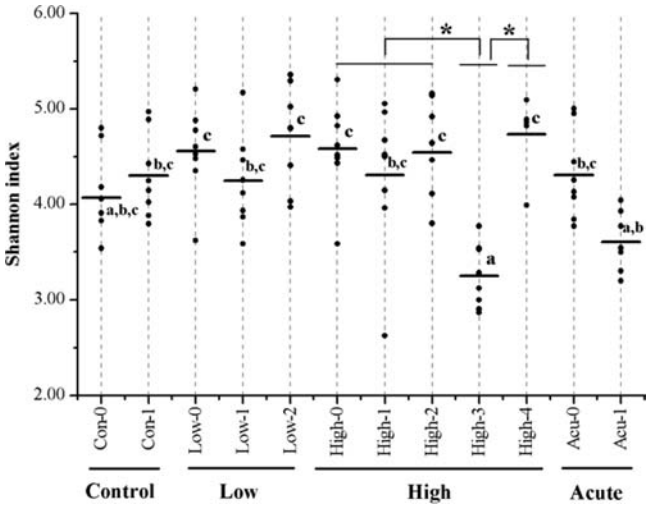

Figure 6. Shannon index of fecal samples at different periods (α diversity.). Con, control group; Low, FOS-low group; High, FOS-high group; Acu, FOS-acute group. Low-0, before FOS treatment; Low-1, intervention period; Low-2, washout period; High-0, before FOS treatment; High-1, intervention period (FOS, 5%); High-2, intervention period (FOS, 15%); High-3, intervention period (FOS, 25%); High-4, washout period; Acu-0, before FOS treatment; Acu-1, after FOS treatment. Significant differences ($P < 0.05$) are indicated with different letters (a, b, c). *, $P < 0.05$.

opportunistic pathogen according to Technische Regeln für Biologische Arbeitstoffe (TRBA 466) and the Human Opportunistic Pathogen (HOP) Library (Gifu University, Genetic information Genetic Resource Center of Human Pathogens) that is closely related to endodontic disease.[38,39] *Olsenella* is also part of the normal bacterial flora in the human gut (http://www.hmpdacc.org/resources/data_browser.php).[40] However, little is known about the role that *Olsenella* plays in the gut, and the genus is seldom mentioned in previous studies on the effects of FOS on intestinal microbiota. Owing to the high-throughput MiSeq sequencing technique used in this study, *Olsenella* was found to be greatly stimulated by FOS and became the dominant genus comparable with *Bifidobacterium* after the FOS treatment. Moreover, we extensively explored the changes of all genera in the gut, rather than focusing on only limited and specific bacteria. Therefore, we suspect that the FOS preferentially stimulated the growth of beneficial bacteria such as *Bifidobacterium* at a low dose but that they also promoted the non-bifidobacteria such as *Olsenella* and *Enterococcus* when the dose was sufficiently high.

One strain of *Olsenella* was isolated from the mouse feces and was confirmed to be capable of utilizing FOS (Table 2; Figure 5). This may be the first reported finding on the utilization of FOS by *Olsenella*. Although not examined in this study, some bacteria in the *Enterococcus*, *Streptococcus*, and *Clostridium* genera may also have the ability to use FOS.

In conclusion, 16S rRNA metagenomic analysis was helpful in investigating the global effects of FOS on the composition of intestinal microbiota. The FOS were found to alter the microbiota, stimulating the growth of *Bifidobacterium* and *Olsenella* at low doses and promoting the growth of non-bifidobacteria such as *Enterococcus* at high doses. However, the FOS effects were not permanent and the microbiota gradually reverted to their initial structure after the FOS treatment ceased. Owing to the high-throughput MiSeq sequencing technique, we found that *Olsenella* became a dominant genus comparable with *Bifidobacterium* after FOS treatment, especially at high doses, and we proved for the first time that one strain of *Olsenella* was able to grow on FOS. More attention should be paid to the non-bifidobacteria, such as *Olsenella* and *Enterococcus*, in future studies to reveal the interactions between FOS and human gut bacteria.

■ ASSOCIATED CONTENT

Supporting Information

Table S1 and Figure S1. This material is available free of charge via the Internet at http://pubs.acs.org.

■ AUTHOR INFORMATION

Corresponding Authors

*(H.Z.) Phone: 86-510-85912155. Fax: 86-510-85912155. E-mail: zhanghao@jiangnan.edu.cn.

*(W.C.) Phone: 86-510-85912155. Fax: 86-510-85912155. E-mail: chenwei66@jiangnan.edu.cn

Author Contributions

‖B.M. and D.L. contributed equally to this work.

Funding

This work was supported by the key projects in the national science and technology pillar program during the 12th five-year plan period (No. 2012BAD28B07, 2012BAD28B08, 2013BAD18B01, and 2013BAD18B02), the 111 project B07029, the Program for Changjiang Scholars and Innovative Research Team in University (IRT1249), and the Priority Academic Program Development of Jiangsu Higher Education Institutions.

Notes

The authors declare no competing financial interest.

■ ACKNOWLEDGMENTS

We thank Shunhe Wang for technical assistance with mouse care and treatment.

■ ABBREVIATIONS USED

FOS, fructo-oligosaccharides; OTU, operational taxonomic unit; PMPD, per mouse per day; PCoA, principal coordinate analysis; BHI, brain−heart infusion; Acu, acute

■ REFERENCES

(1) Backhed, F.; Ley, R. E.; Sonnenburg, J. L.; Peterson, D. A.; Gordon, J. I. Host-bacterial mutualism in the human intestine. *Science* **2005**, *307*, 1915−1920.

(2) Wang, J.; Tang, H.; Zhang, C.; Zhao, Y.; Derrien, M.; Rocher, E.; van-Hylckama Vlieg, J. E.; Strissel, K.; Zhao, L.; Obin, M.; Shen, J. Modulation of gut microbiota during probiotic-mediated attenuation of metabolic syndrome in high fat diet-fed mice. *ISME J.* **2014**, 1−15.

(3) Cani, P. D.; Bibiloni, R.; Knauf, C.; Waget, A.; Neyrinck, A. M.; Delzenne, N. M.; Burcelin, R. Changes in gut microbiota control metabolic endotoxemia-induced inflammation in high-fat diet-induced obesity and diabetes in mice. *Diabetes* **2008**, *57*, 1470−1481.

(4) Frank, D. N.; Robertson, C. E.; Hamm, C. M.; Kpadeh, Z.; Zhang, T.; Chen, H.; Zhu, W.; Sartor, R. B.; Boedeker, E. C.; Harpaz, N.; Pace, N. R.; Li, E. Disease phenotype and genotype are associated with shifts in intestinal-associated microbiota in inflammatory bowel diseases. *Inflamm. Bowel Dis.* **2011**, *17*, 179−184.

(5) Kovacs, A.; Ben-Jacob, N.; Tayem, H.; Halperin, E.; Iraqi, F. A.; Gophna, U. Genotype is a stronger determinant than sex of the mouse gut microbiota. *Microb. Ecol.* **2011**, *61*, 423−428.

(6) Muegge, B. D.; Kuczynski, J.; Knights, D.; Clemente, J. C.; Gonzalez, A.; Fontana, L.; Henrissat, B.; Knight, R.; Gordon, J. I. Diet

DOI: 10.1021/jf505156h
J. Agric. Food Chem. 2015, 63, 856−863

drives convergence in gut microbiome functions across mammalian phylogeny and within humans. *Science* **2011**, *332*, 970−974.
(7) De Filippo, C.; Cavalieri, D.; Di Paola, M.; Ramazzotti, M.; Poullet, J. B.; Massart, S.; Collini, S.; Pieraccini, G.; Lionetti, P. Impact of diet in shaping gut microbiota revealed by a comparative study in children from Europe and rural Africa. *Proc. Natl. Acad. Sci. U.S.A.* **2010**, *107*, 14691−14696.
(8) Bolnick, D. I.; Snowberg, L. K.; Hirsch, P. E.; Lauber, C. L.; Org, E.; Parks, B.; Lusis, A. J.; Knight, R.; Caporaso, J. G.; Svanbäck, R. Individual diet has sex-dependent effects on vertebrate gut microbiota. *Nat. Commun.* **2014**, *5*, 4500.
(9) Lee, Y. K.; Salminen, S. *Handbook of Probiotics and Prebiotics*, 2nd ed.; Wiley: Hoboken, NJ, USA, 2008.
(10) Sabater-Molina, M.; Larqué, E.; Torrella, F.; Zamora, S. Dietary fructooligosaccharides and potential benefits on health. *J. Physiol. Biochem.* **2009**, *65*, 315−328.
(11) Hartemink, R.; Quataert, M. C.; van Laere, K. M.; Nout, M. J.; Rombouts, F. M. Degradation and fermentation of fructo-oligosaccharides by oral streptococci. *J. Appl. Bacteriol.* **1995**, *79*, 551−557.
(12) Hartemink, R.; Van Laere, K. M. J.; Rombouts, F. M. Growth of enterobacteria on fructo-oligosaccharides. *J. Appl. Bacteriol.* **1997**, *83*, 367−374.
(13) Van Laere, K. M.; Hartemink, R.; Bosveld, M.; Schols, H. A.; Voragen, A. G. Fermentation of plant cell wall derived polysaccharides and their corresponding oligosaccharides by intestinal bacteria. *J. Agric. Food Chem.* **2000**, *48*, 1644−1652.
(14) Valcheva, R.; Slingerland, B.; Farrant, A.; Gaenzle, M.; Dieleman, L. Prebiotics prevent loss of intestinal biodiversity and reduce colitis in HLA-B27 transgenic rats. Canadian Digestive Diseases Week. *Can. J. Gastroenterol.* **2009**, poster session 2-168.
(15) Ramirez-Farias, C.; Slezak, K.; Fuller, Z.; Duncan, A.; Holtrop, G.; Louis, P. Effect of inulin on the human gut microbiota: stimulation of *Bifidobacterium adolescentis* and *Faecalibacterium prausnitzii*. *Br. J. Nutr.* **2009**, *101*, 541−550.
(16) Shen, J.; Zhang, B.; Wei, H.; Che, C.; Ding, D.; Hua, X.; Bucheli, P.; Wang, L.; Li, Y.; Pang, X.; Zhao, L. Assessment of the modulating effects of fructo-oligosaccharides on fecal microbiota using human flora-associated piglets. *Arch. Microbiol.* **2010**, *192*, 959−968.
(17) Ten Bruggencate, S. J. M.; Bovee-Oudenhoven, I. M. J.; Lettink-Wissink, M. L. G.; Van der Meer, R. Dietary fructooligosaccharides increase intestinal permeability in rats. *J. Nutr.* **2005**, *135*, 837−842.
(18) Schepens, M. A.; Rijnierse, A.; Schonewille, A. J.; Vink, C.; Brummer, R. J.; Willemsen, L. E.; van der Meer, R.; Bovee-Oudenhoven, I. M. Dietary calcium decreases but short-chain fructo-oligosaccharides increase colonic permeability in rats. *Br. J. Nutr.* **2010**, *104*, 1780−1786.
(19) Bovee-Oudenhoven, I. M.; ten Bruggencate, S. J.; Lettink-Wissink, M. L.; van der Meer, R. Dietary fructo-oligosaccharides and lactulose inhibit intestinal colonisation but stimulate translocation of *Salmonella* in rats. *Gut* **2003**, *52*, 1572−1578.
(20) Ten Bruggencate, S. J.; Bovee-Oudenhoven, I. M.; Lettink-Wissink, M. L.; Van der Meer, R. Dietary fructo-oligosaccharides dose-dependently increase translocation of *Salmonella* in rats. *J. Nutr.* **2003**, *133*, 2313−2318.
(21) Petersen, A.; Heegaard, P. M.; Pedersen, A. L.; Andersen, J. B.; Sorensen, R. B.; Frokiaer, H.; Lahtinen, S. J.; Ouwehand, A. C.; Poulsen, M.; Licht, T. R. Some putative prebiotics increase the severity of *Salmonella enterica* serovar *Typhimurium* infection in mice. *BMC Microbiol.* **2009**, *9*, 245.
(22) Kawaguchi, M.; Tashiro, Y.; Adachi, T.; Tamura, Z. Changes in intestinal condition, fecal microflora and composition of rectal gas after administration of fructooligosaccharide and lactulose at different doses. *Bifidobacteria Microflora* **1993**, *12*, 57−67.
(23) Coussement, P. A. Inulin and oligofructose: safe intakes and legal status. *J. Nutr.* **1999**, *129*, 1412S−1417S.
(24) Gibson, G. R.; Rastall, R. A. When we eat, which bacteria should we be feeding? *ASM News* **2004**, *70*, 224−231.
(25) Macfarlane, G. T.; Steed, H.; Macfarlane, S. Bacterial metabolism and health-related effects of galacto-oligosaccharides and other prebiotics. *J. Appl. Microbiol.* **2008**, *104*, 305−344.
(26) Zhao, L.; Wang, G.; Siegel, P.; He, C.; Wang, H.; Zhao, W.; Zhai, Z.; Tian, F.; Zhao, J.; Zhang, H.; Sun, Z.; Chen, W.; Zhang, Y.; Meng, H. Quantitative genetic background of the host influences gut microbiomes in chickens. *Sci. Rep.* **2013**, *3*, 1163.
(27) Wang, Q.; Garrity, G. M.; Tiedje, J. M.; Cole, J. R. Naive Bayesian classifier for rapid assignment of rRNA sequences into the new bacterial taxonomy. *Appl. Environ. Microbiol.* **2007**, *73*, 5261−5267.
(28) Caporaso, J. G.; Bittinger, K.; Bushman, F. D.; DeSantis, T. Z.; Andersen, G. L.; Knight, R. PyNAST: a flexible tool for aligning sequences to a template alignment. *Bioinformatics* **2010**, *26*, 266−267.
(29) Caporaso, J. G.; Kuczynski, J.; Stombaugh, J.; Bittinger, K.; Bushman, F. D.; Costello, E. K.; Fierer, N.; Pena, A. G.; Goodrich, J. K.; Gordon, J. I.; Huttley, G. A.; Kelley, S. T.; Knights, D.; Koenig, J. E.; Ley, R. E.; Lozupone, C. A.; McDonald, D.; Muegge, B. D.; Pirrung, M.; Reeder, J.; Sevinsky, J. R.; Turnbaugh, P. J.; Walters, W. A.; Widmann, J.; Yatsunenko, T.; Zaneveld, J.; Knight, R. QIIME allows analysis of high-throughput community sequencing data. *Nat. Methods* **2010**, *7*, 335−336.
(30) Price, M. N.; Dehal, P. S.; Arkin, A. P. FastTree: computing large minimum evolution trees with profiles instead of a distance matrix. *Mol. Biol. Evol.* **2009**, *26*, 1641−1650.
(31) Lozupone, C.; Knight, R. UniFrac: a new phylogenetic method for comparing microbial communities. *Appl. Environ. Microbiol.* **2005**, *71*, 8228−8235.
(32) Roberfroid, M. Prebiotics: the concept revisited. *J. Nutr.* **2007**, *137*, 830S−837S.
(33) Rycroft, C. E.; Jones, M. R.; Gibson, G. R.; Rastall, R. A. A comparative in vitro evaluation of the fermentation properties of prebiotic oligosaccharides. *J. Appl. Microbiol.* **2001**, *91*, 878−887.
(34) Santos, A.; San Mauro, M.; Díaz, D. M. Prebiotics and their long-term influence on the microbial populations of the mouse bowel. *Food Microbiol.* **2006**, *23*, 498−503.
(35) Petersen, A.; Bergström, A.; Andersen, J. B.; Hansen, M.; Lahtinen, S. J.; Wilcks, A.; Licht, T. R. Analysis of the intestinal microbiota of oligosaccharide fed mice exhibiting reduced resistance to *Salmonella* infection. *Benef. Microbes* **2010**, *1*, 271−281.
(36) David, L. A.; Maurice, C. F.; Carmody, R. N.; Gootenberg, D. B.; Button, J. E.; Wolfe, B. E.; Ling, A. V.; Devlin, A. S.; Varma, Y.; Fischbach, M. A.; Biddinger, S. B.; Dutton, R. J.; Turnbaugh, P. J. Diet rapidly and reproducibly alters the human gut microbiome. *Nature* **2014**, *505*, 559−563.
(37) Bouhnik, Y.; Raskine, L.; Simoneau, G.; Paineau, D.; Bornet, F. The capacity of short-chain fructo-oligosaccharides to stimulate faecal bifidobacteria: a dose-response relationship study in healthy humans. *Nutr. J.* **2006**, *5*, 8.
(38) Rôças, I. N.; Siqueira, J. F., Jr. Species-directed 16S rRNA gene nested PCR detection of *Olsenella* species in association with endodontic diseases. *Lett. Appl. Microbiol.* **2005**, *41*, 12−16.
(39) Jiang, W.; Ling, Z.; Lin, X.; Chen, Y.; Zhang, J.; Yu, J.; Xiang, C.; Chen, H. Pyrosequencing analysis of oral microbiota shifting in various caries states in childhood. *Microb. Ecol.* **2014**, *67*, 962−969.
(40) Zhang, J.; Guo, Z.; Lim, A. A. Q.; Zheng, Y.; Koh, E. Y.; Ho, D.; Qiao, J.; Huo, D.; Hou, Q.; Huang, W.; Wang, L.; Javzandulam, C.; Narangerel, C.; Jirimutu; Menghebilige; Lee, Y. K.; Zhang, H. Mongolians core gut microbiota and its correlation with seasonal dietary changes. *Sci. Rep.* **2014**, *4*, 5001.

DOI: 10.1021/jf505156h
J. Agric. Food Chem. 2015, 63, 856−863

JOURNAL OF AGRICULTURAL AND FOOD CHEMISTRY

Article

pubs.acs.org/JAFC

Antioxidant Potential of Date (*Phoenix dactylifera* L.) Seed Protein Hydrolysates and Carnosine in Food and Biological Systems

Priyatharini Ambigaipalan and Fereidoon Shahidi*

Department of Biochemistry, Memorial University of Newfoundland, St. John's, Newfoundland, Canada A1B 3X9

ABSTRACT: Date seed protein hydrolysates were evaluated for antioxidant activity as well as solubility and water-holding capacity in food and biological model systems. Date seed protein hydrolysates as well as carnosine exhibited >80% of solubility over a pH range of 2−12. The hydrolysates and carnosine at 0.5% (w/w) were also found to be effective in enhancing water-holding capacity and cooking yield in a fish model system, which was nearly similar to sodium tripolyphosphate (STPP; 0.3%, w/w). Incorporation of hydrolysates (200 ppm) in fish model systems resulted in the highest inhibition (30%) of oxidation in comparison to butylated hydroxytoluene (BHT; 9%). In addition, hydrolysates and carnosine inhibited β-carotene oxidation by 75%. The hydrolysates (0.1 mg/mL) inhibited LDL cholesterol oxidation by 60%, whereas carnosine inhibited oxidation by 80% after 12 h of incubation. Additionally, hydrolysates and carnosine effectively inhibited hydroxyl (6 mg/mL) and peroxyl (0.1 mg/mL) radical-induced DNA scission. Therefore, date seed protein hydrolysates could be used as a potential functional food ingredient for health promotion.

KEYWORDS: *date seed, protein hydrolysate, solubility, water-holding capacity, carnosine, LDL cholesterol, DNA scission*

INTRODUCTION

Hydrolysates are defined as proteins that are chemically or biologically broken down to peptides of various sizes. Enzymatic hydrolysis of food proteins is an efficient way to recover potent bioactive peptides.[1] Hydrolysis of proteins using various enzymes could improve the functional properties by influencing the molecular size, hydrophobicity, and polar groups of peptides.[2] Functional properties of protein hydrolysates such as solubility, water-holding capacity, and emulsifying and foaming properties are substantially useful characteristics for many food applications.[1] Apart from functionalities, several studies have shown the potential application of protein hydrolysates for the nutritional or pharmaceutical industry due to their antioxidant activity.[3−6]

Bioactive peptides generally contain 3−20 amino acid units,[7] but in some cases this range may be extended. Lunasin, for example, is a food-derived peptide with anticancer activity, composed of 43 amino acids with a molecular weight of 5400 Da.[8] Depending on the amino acid sequence, these peptides may be involved in various biological functions such as antihypertension, opioid agonists or antagonists, immunomodulatory, antithrombotic, antioxidant, anticancer, and antimicrobial activities, in addition to nutrient utilization.[9,10]

The reactivity of free radicals on biological molecules (lipids, proteins, and DNA) may be considered as the initiating stage for several chronic diseases. For example, oxidation of low-density lipoprotein (LDL) cholesterol by free radicals or metal ions is an important cause for developing atherosclerotic lesions that lead to coronary heart disease.[11] Furthermore, Wettasinghe and Shahidi[12] reported that oxidation of DNA and strand scission play an important role in carcinogenesis. Thus, researchers have a greater interest in developing novel antioxidative compounds from various plant and animal sources. Carnosine is a β-alanylhistidine dipeptide, present at millimolar concentrations in skeletal muscle and absorbed into plasma, that has been shown to have antioxidative property.[13−15] Thus, a well-known bioactive peptide, carnosine, was used in this study to compare the functional and antioxidative properties of date seed protein hydrolysates. In this study, date seed protein hydrolysates hydrolyzed using various enzymes (Alcalase, Flavourzyme, and Thermolysin) were compared to carnosine, an antioxidative peptide, with respect to functional (solubility and water-holding capacity) and antioxidative properties in various food (cooked comminuted fish model and β-carotene−linoleate model) and biological (human LDL and DNA) model systems.

MATERIALS AND METHODS

Materials. Ground date (*Phoenix dactylifera* L.) seed sample was provided by Dr. A. S. Al-Khalifa of King Saud University, Riyadh, Saudi Arabia. Alcalase (2.4 AU/g) and Flavourzyme (1000 LAPU/g) were procured from Novozymes, Bagsvaerd, Denmark. Thermolysin (50−100 units/mg protein) was purchased from Sigma-Aldrich Canada Ltd. (Oakville, ON, Canada). All chemicals used were obtained from Fisher Scientific Ltd. (Ottawa, ON, Canada) or Sigma-Aldrich Canada Ltd. The solvents used were of ACS grade, pesticide grade, or HPLC grade and were used without any further purification.

Preparation of Protein Hydrolysate. Ground date seed sample was defatted with hexane (1:5, w/v) for 5 min. The crude protein content was determined by using micro-Kjeldhal analysis.[16] The date seed protein hydrolysates were prepared using Alcalase (AL), Flavourzyme (FL), and Thermolysin (TH) by individual or sequential treatment as described in Table 1. Twenty grams of defatted date seed sample was suspended in 100 mL of water and hydrolyzed batchwise in a reaction vessel, equipped with a stirrer, thermometer, and pH electrode according to the conditions presented in Table 1. The pH (changes as a result of hydrolysis) was kept constant by the addition of

Received: November 4, 2014
Revised: December 31, 2014
Accepted: January 1, 2015
Published: January 1, 2015

ACS Publications © 2015 American Chemical Society

DOI: 10.1021/jf505327b
J. Agric. Food Chem. 2015, 63, 864−871

Table 1. Hydrolysis Conditions Used for Preparation of Date Seed Protein Hydrolysates

sample	enzyme	enzyme/protein	temperature (°C)	pH	time (h)
AL	Alcalase	0.3 AU/g	50	8	1
FL	Flavourzyme	50 LAPU/g	50	7	2
TH	Thermolysin	50 U/mg	50	8	3
AL + FL	Alcalase + Flavourzyme	0.3 AU/g 50 LAPU/g	50	8 7	1 2
AL + TH	Alcalase + Thermolysin	0.3 AU/g 50 U/mg	50	8 8	1 3
FL + TH	Flavourzyme + Thermolysin	50 LAPU/g 50 U/mg	50	7 8	2 3
AL + FL + TH	Alcalase + Flavourzyme + Thermolysin	0.3 AU/g 50 LAPU/g 50 U/mg	50	8 7 8	1 2 3

a known amount of 4 M NaOH. The degree of hydrolysis (%) was then determined by the trinitrobenzenesulfonic acid (TNBS) method described by Alder-Nissen (1979). The date seed protein hydrolysates obtained were freeze-dried and stored at −20 °C for subsequent analyses.

Solubility of Protein Hydrolysates. The solubility of date seed protein hydrolysate was determined according to the method described by Shahidi, Han, and Synoweicki[17] with modifications. Freeze-dried date seed protein hydrolysate (10 mg/mL, w/v) was dispersed in distilled water, and its pH was adjusted to 2, 5, 8, and 12 by the addition of a 1 N or 6 N HCl or 1 N or 6 N NaOH solution. The contents were mixed, and the mixture was centrifuged at 7500*g* for 15 min. The protein contents in the supernatant were determined using the Biuret method, and the total protein content in the sample was determined by solubilizing the sample in 0.5 N NaoH. The solubility of date seed protein hydrolysates was determined using the following equation:

$$\text{solubility (\%)} = \frac{\text{protein content in supernatant}}{\text{total protein content in sample}} \times 100$$

Determination of Water-Holding Capacity. The water-holding capacity of date seed protein hydrolysates was determined according to the method described by Shahidi and Synowiecki.[18] A fish model system was prepared using 8.5 g of ground salmon and 1.5 g of distilled water in a preweighed 50 mL centrifuge tube. Date seed protein hydrolysates (0.5%, w/w) were added and mixed thoroughly. A control without any protein hydrolysate and positive controls sodium tripolyphosphate (0.3%, w/w) and carnosine were also prepared. The mixture was allowed to stand in a cold room for 1 h and subsequently cooked at 95 °C in a water bath for 1 h. The cooked samples were cooled under a stream of cold tap water, and the drip water was determined using a filter paper. The final weight of the cooked fish was recorded. The drip volume was calculated as the difference between the initial weight and final weight. The water-holding capacity for different date seed protein hydrolysates was expressed as decrease of drip volume against the control.

Antioxidant Activity in Cooked Comminuted Fish Model System. The antioxidant activity of date seed protein hydrolysates in the cooked comminuted fish model system was determined as described by Wettasinghe and Shahidi.[19] Ground salmon (40 g) was mixed with 10 g of deionized water in Mason jars. Date seed protein hydrolysate (200 ppm) was added directly to the mixture. A control without protein hydrolysate and a positive control using butylated hydroxytoluene (BHT; 200 ppm) were also prepared. Samples were cooked in a thermostated water bath at 80 °C for 40 min while stirring every 5 min with a glass rod. After cooling to room temperature, the fish samples were transferred into plastic bags and stored in a refrigerator at 4 °C for 14 days. Thiobarbituric acid reactive substances (TBARS) were analyzed on days 0, 7, and 14 using a modified version of the method described by Wijeratne, Abou-Zaid, and Shahidi.[20] Fish samples (1 g) in centrifuge tubes were mixed with trichloroacetic acid (10%, 2.5 mL) and vortexed for 2 min at high speed. TBA reagent (0.02 M, 2.5 mL) was then added to the tube, followed by further vortexing for 30 s. Samples were centrifuged at 3000*g* for 10 min and the supernatants filtered through Whatman no. 3 filter paper. The tubes were covered with aluminum foil, placed in a boiling water bath for 45 min, and subsequently cooled to room temperature under running cold tap water. The absorbance of the resultant pink TBA−MDA (malondialdehyde) adduct was read at 532 nm. A standard curve was prepared using 1,1,3,3-tetramethoxypropane, a precursor of MDA (0−6 ppm). TBARS values, calculated using the standard curve, were expressed as milligrams of MDA equivalent per kilogram of sample.

Antioxidant Activity in Oil-in-Water Emulsions. A β-carotene−linoleate model system was used to evaluate the antioxidant activity of date seed protein hydrolysates in an oil-in-water emulsion.[1] β-Carotene (10 mg) was dissolved in chloroform (10 mL), and an aliquot (1.2 mL) of it was transferred into a flask containing linoleic acid (40 mg) and Tween 40 (400 mg). A blank without β-carotene was also prepared (40 mg of linoleic acid + 400 mg of Tween 40). Chloroform was removed under a nitrogen stream; 100 mL of oxygenated distilled water was added to the flask, and the mixture was stirred vigorously for 30 min. Date seed protein hydrolysates (0.5 mg/mL; 0.5 mL) dissolved in deionized water were mixed with 4.5 mL of the above emulsion. A control without protein hydrolysate and a mixture of blank (without β-carotene) was prepared for each sample. The absorbance at 470 nm was read immediately after the addition of the emulsion. The tubes were incubated in a shaking water bath at 50 °C, and the absorbance was read over a 105 min period at 15 min intervals. A kinetic curve was plotted against blank-corrected absorbance and time. One hundred parts per million of Trolox and carnosine were used as a positive control. Antioxidant activity of date seed protein hydrolysates in protecting β-carotene/linoleic acid oxidation was calculated using the equation

$$\text{antioxidant activity (\%)} = [(A_0 - A_t)/(A^\circ_0 - A^\circ_t)] \times 100$$

where A_0 and A_t are corrected absorbance values for test samples measured at zero time and after incubation, respectively, whereas A°_0 and A°_t are corrected absorbance values for control at time zero and at time t after incubation, respectively.

Cupric Ion-Induced Human Low-Density Lipoprotein (LDL) Peroxidation. The inhibitiory effect of cupric ion-induced human LDL peroxidation was determined according to the method described by Liyana-Pathirana and Shahidi.[21] LDL (5 mg/mL) was dialyzed against 100 volumes of 10 mM phosphate buffer (pH 7.4, 0.15 M NaCl) using a dialysis tube with a molecular weight cutoff of 12−14 kDa (Fisher Scientific, Nepean, ON, Canada) at 4 °C under a nitrogen blanket in the dark for 12 h. Diluted LDL cholesterol (0.04 mg LDL/mL) was mixed with the date seed protein hydrolysate solutions (0.1 mg/mL). Carnosine was used as a positive control. The samples were preincubated at 37 °C for 15 min. The reaction was initiated by adding a solution of cupric sulfate (50 μM), and the samples were then incubated at 37 °C for 22 h. The formation of conjugated dienes (CD) was recorded at 234 nm using a diode array spectrophotometer (Agilent, Palo Alto, CA, USA). The appropriate blanks were run for each sample by replacing LDL cholesterol and $CuSO_4$ with distilled water for background correction. The inhibitory effect of tested samples on the formation of conjugated dienes (% inhibition CD) was then calculated using the equation

$$\text{\% inhibition CD} = [(\text{Abs}_{\text{control}} - \text{Abs}_{\text{sample}})/(\text{Abs}_{\text{control}} - \text{Abs}_{\text{native}})] \times 100$$

$$\text{Abs}_{\text{control}} = (A^\circ_0 - A^\circ_t)$$

$$\text{Abs}_{\text{sample}} = (A_0 - A_t)$$

DOI: 10.1021/jf505327b
J. Agric. Food Chem. 2015, 63, 864−871

where $Abs_{control}$ is the absorbance of LDL + $CuSO_4$ + PBS, Abs_{sample} is the absorbance of LDL + $CuSO_4$ + sample/standard, and Abs_{native} is the absorbance of LDL + PBS. A_0 and A_t are absorbance values for test samples measured at zero time and at time t after incubation, respectively, whereas $A°_0$ and $A°_t$ are corrected absorbance values for control at time zero and at time t after incubation, respectively.

Inhibition of Peroxyl and Hydroxyl Radical-Induced Supercoiled DNA Strand Scission. Peroxyl and hydroxyl radical-induced supercoiled plasmid DNA strand scission inhibitory activity of date seed protein hydrolysate was determined according to the method described by Chandrasekara and Shahidi.[22] Supercoiled plasmid DNA (pBR 322) (50 μg/mL) was dissolved in 10 mM phosphate buffer (PBS, pH 7.4), and date seed protein hydrolysates were dissolved in distilled water. In a 0.5 mL eppendorf tube date seed protein hydrolysate (0.1 mg/mL, 2 μL), PBS (2 μL), pBR 322 (50 μg/mL, 2 μL), and 4 μL of 7 mM 2,2′-azobis(2-methylpropanimidamide dihydrochloride (AAPH) were added to generate peroxyl radicals, whereas date seed protein hydrolysate (6 mg/mL, 2 μL), PBS (2 μL), pBR 322 (50 μg/mL, 2 μL), $FeSO_4$ (0.5 mM, 2 μL), and H_2O_2 (0.5 mM, 2 μL) were added to produce hydroxyl radicals. The mixture was incubated at 37 °C for 1 h in the dark. A control with DNA alone, a positive control with carnosine (0.1 mg/mL), and a blank devoid of protein hydrolysates were also prepared. After incubation, 1 μL of the loading dye (0.25% bromophenol blue, 0.25% xylene cyanol, and 50% glycerol) were added to the reaction mixture. The mixture (10 μL) was loaded onto 0.7% agarose gel prepared in Tris−acetic acid−EDTA (TAE) buffer (40 mM Tri−-acetate containing 1 mM EDTA, pH 8.5). SYBR safe (5 μL) was added into agarose gel solution (50 mL) as a gel stain. Electrophoresis was conducted at 80 V for 90 min using a model B1A horizontal mini gel electrophoresis system (Owl Separation Systems Inc., Portsmonth, NH, USA) and a model 300 V power supply (VWR International Inc., West Chester, PA, USA) in TAE buffer. The DNA bands were visualized under trans-illumination of UV light using the Alpha-Imager gel documentation system (Cell Biosciences, Santa Clara, CA, USA). The intensity (area %) of bands was quantified with the Chemi-Imager 4400 software (Cell Biosciences). The retention of supercoiled DNA strand (%) was calculated using the following equation:

$$\text{DNA retention (\%)} = (\text{area of supercoiled DNA with oxidative radical and protein hydrolysate/area of supercoiled DNA in control})$$

Statistical Analysis. All determinations were replicated three times and mean values and standard deviations reported. One-way ANOVA was performed, and the mean separations were performed by Tukey's HSD test ($p < 0.05$) using SPSS 16.0 for Windows (SPSS Inc., Chicago, IL, USA).

RESULTS AND DISCUSSION

Solubility of Protein Hydrolysates. The protein content of defatted date seed sample was 6.7%, on a dry weight basis, and the degree of hydrolysis ranged between 11 and 13%. Molecular weights of peptides, determined using a quadrupole orthogonal time-of-flight hybrid tandem mass spectrometer, ranged from 2062.9 ± 0.0 to 116803.8 ± 0.4 Da (unpublished data). Solubility is one of the most important properties of protein hydrolysates, which is required in many functional applications such as emulsions, foams, and gels.[2,3] The solubility of date seed protein hydrolysate in the pH range of 2−12 is shown in Figure 1. All date seed protein hydrolysates as well as carnosine exhibited >80% of solubility at range of pH 2−12. Solubility of date seed hydrolysates increased to 97% with increasing pH. Hydrolysis of proteins by enzymes potentially affects the molecular size and hydrophobicity, as well as polar and ionizable groups of protein hydrolysates.[23] Dong, Zeng, Wang, Liu, Zhao, and Yang[4] showed that the solubility of silver carp hydrolysates increases with lower molecular mass protein fraction at high degrees of hydrolysis. Gbogouri, Linder, Fanni, and Parmentier[24] suggested that the smaller peptides from proteins have proportionally more polar residues, which could form hydrogen bonds with water and thus increase solubility. The high solubility of date seed protein hydrolysate reveals its potential applications in formulated food systems.

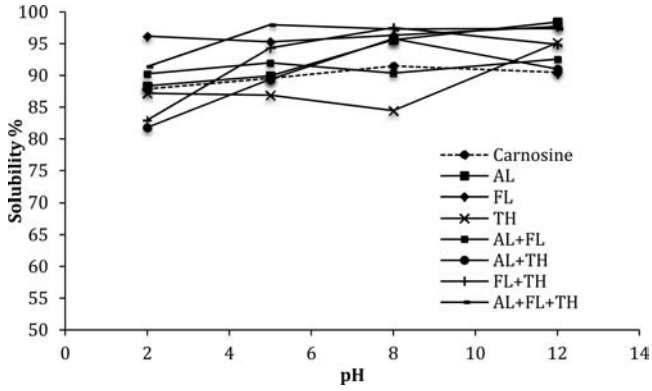

Figure 1. Solubility of date seed protein hydrolysates and carnosine at various pH values.

Water-Holding Capacity. All date seed protein hydrolysates enhanced the water-holding capacity of salmon fish and thus improved cooking yield (Figure 2). There was no siginificant difference among protein hydrolysates (0.5%) and sodium tripolyphosphate (STTP; 0.3%) with respect to decrease in drip volume. However, date seed flour exhibited a low water-holding capacity (1.8%) in comparison to protein hydrolysates. Cumby, Zhong, Naczk, and Shahidi[25] observed an increase water-holding capacity of ground pork meat model system for rapeseed proteins hydrolyzed using Alcalase and Flavourzyme. The authors suggested that that lower molecular weight peptides could be more effective in holding water than are larger-sized peptides due to its greater hydrophilicity. However, the type of amino acid present in the peptides could also play an important role. Decrease in drip volume percentage of carnosine (4.3%) was also lower than date seed protein hydrolysates. Das, Anjaneyulu, and Biswas[26] showed that ground buffalo meat containing 1.0 and 1.5% carnosine significantly improved water-holding capacity and lowered cooking loss. Thomsen and Zeuthen[27] showed that the water-holding capacity increases with increasing meat pH. Thus, the

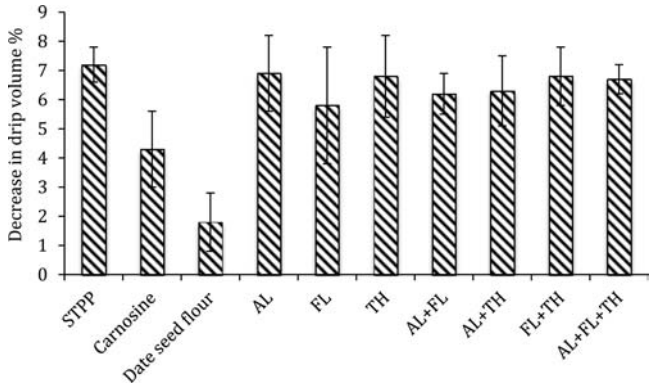

Figure 2. Decrease in drip volume (%) of date seed protein hydrolysates, date seed flour, carnosine, and STPP.

DOI: 10.1021/jf505327b
J. Agric. Food Chem. 2015, 63, 864−871

authors[26] concluded that the increase in meat pH by carnosine probably accounts for the decrease in cooking loss. Our study shows that 0.5% of date seed protein hydrolysates could be used as an alternative to STPP to increase cooking yield of fish meat.

Antioxidant Activity of Date Seed Protein Hydrolysates in Cooked Comminuted Fish Meat Model System. The antioxidant activity of date seed protein hydrolysates in cooked salmon was measured by the thiobarbituric acid (TBA) assay. TBA assay is a spectrophotometric detection of TBARS, namely, MDA, one of the secondary lipid peroxidation products used to measure the extent of lipid degradation. Ground salmon was treated with BHT (200 ppm) or carnosine (200 ppm) or date seed protein hydrolysates (200 ppm) before cooking. Table 2 shows the

Table 2. TBARS Values of Fish Model System Containing Date Seed Protein Hydrolysates, BHT, and Carnosine Stored for 14 Days

	TBARS[a] (mg/kg)		
	0 days	7 days	14 days
control	4.6 ± 0.1e	5.6 ± 0.2e	5.9 ± 0.0
BHT	3.8 ± 0.0cd	5.2 ± 0.0de	5.6 ± 0.1
carnosine	4.0 ± 0.0d	4.9 ± 0.0cd	5.0 ± 0.1
AL	4.1 ± 0.2d	5.4 ± 0.1e	5.7 ± 0.0
FL	4.7 ± 0.1e	5.5 ± 0.1e	5.9 ± 0.0
TH	3.4 ± 0.2bc	5.0 ± 0.1cd	5.5 ± 0.0
AL + FL	3.6 ± 0.0c	3.8 ± 0.0a	5.5 ± 0.1
AL + TH	3.0 ± 0.1b	4.6 ± 0.0b	5.0 ± 0.0
FL + TH	2.5 ± 0.2a	3.9 ± 0.1a	4.8 ± 0.3
AL + FL + TH	4.6 ± 0.1e	4.8 ± 0.0bc	5.5 ± 0.0

[a]All data represent the mean of triplicates. Values followed by the same letter are not significantly different ($P > 0.05$) by Tukey's HSD test.

TBARS values of samples throughout the storage period. The initial TBARS value of salmon (4.6 mg MDA equiv/kg) were found to be higher than that of pork model system (~1.0 mg MDA equiv/kg) studied elsewhere.[6] This could be due to the presence of polyunsaturated fatty acids in fish that could increase TBARS during cooking. The fish system containing FL + TH hydrolysate displayed significantly ($p < 0.05$) lower TBARS value compared to BHT upon cooking. Generally, the TBARS of cooked salmon increased as the storage time increased up to 14 days of storage ($p < 0.05$). Inhibition percentage of TBARS production in fish model system containing date seed protein hydrolysates or carnosine or BHT is shown in Figure 3. After 7 days of storage, fish systems with AL + FL (32%) and FL + TH (30%) hydrolysate showed the highest percentages of TBARS inhibition in comparison to BHT (7%). Carnosine exhibited a higher percentage of inhibition (12%) compared to BHT (6.6%) after 7 days of storage. Decker and Crum[28] showed that the antioxidant activity of carnosine (0.5−1.5%) in cooked salted and unsalted ground pork is greater than those of the lipid-soluble free radical scavengers BHT and α-tocopherol but less than that of STPP. In another study on ground buffalo meat, carnosine at 1.0 and 1.5% significantly lowered the TBARS values as compared to control sample. The inhibition of TBARS production in the fish system containing date seed protein hydrolysate could be most likely due to its radical-scavenging activity as well as chelating activity toward Fe^{2+}. In comparison

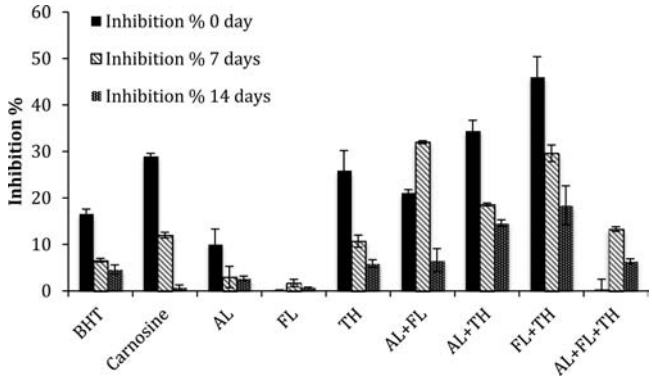

Figure 3. Inhibition of TBARS production in fish model system containing date seed protein hydrolysates, carnosine, and BHT.

to fish system containing AL + FL, AL + TH, and FL + TH hydrolysates (200 ppm), BHT (200 ppm) showed a lower inhibition after 7 days of storage. Thus, date seed protein hydrolysates prepared using combinations of AL + FL, AL + TH, and FL + TH could be used to control oxidation in a fish model system.

Antioxidant Activity of Date Seed Protein Hydrolysates in Oil-in-Water Emulsion. A β-carotene−linoleate model system was used to evaluate the antioxidant activity of date seed protein hydrolysates in an oil-in-water emulsion. Oxidation of linoleic acid in the emulsion system gives rise to the formation of free radicals and hydroperoxides. The free radicals so formed attack the β-carotene molecule, causing it to lose its conjugation and eventually decolorize. This loss of color could be monitored spectrophotometrically at 470 nm. The presence of antioxidants can counteract the bleaching of β-carotene during the coupled oxidation of linoleic acid and β-carotene in the emulsified aqueous system. Figure 4 shows the effect of date seed protein hydrolysates, at a concentration of 0.1 mg/mL, on β-carotene bleaching in the aforementioned system. β-Carotene content in the control samples decreased to a greater extent compared to those containing date seed protein hydrolysates or trolox or carnosine, which retained high amounts of β-carotene after 105 min. Positive controls trolox (~54−63%) and carnosine (~58−75%) showed significantly ($p < 0.05$) higher inhibitory effect against β-carotene bleaching than date seed protein hydrolysates up to 60 min. The percent inhibition of β-carotene oxidation inhibition by date seed protein hydrolysates ranged between 66.9 and 73.7%. Hydrolysates prepared using a combination of FL and TH showed the highest inhibition (73.7%) followed by AL + TH ~ FL ~ AL > AL + FL+TH ~ TH ~ AL + FL. Several studies have shown that amino acids possess strong antioxidant activity in linoleic acid and methyl linoleate model systems,[29] for example, tryptophan and lysine in butter fat,[30] proline in sardine oil,[31] methionine in vegetable oils,[32] and histidine, threonine, lysine, and methionine in a sunflower oil emulsion.[33] Furthermore, Aruoma, Laughton, and Halliwell[34] showed the antioxidative effect for taurine, hypotaurine, carnosine, and anserine using in vivo models. However, Pratt and Hudson[35] reported that some amino acids such as cysteine, histidine, and tryptophan at higher concentration may act as prooxidants. Copper bound to amino acids or peptides has been shown to have a strong catalyzing effect on the oxidation of linoleic acid.[1] Amarowicz and Shahidi[1] suggested that differences in the antioxidant properties of peptides might originate from their synergistic

DOI: 10.1021/jf505327b
J. Agric. Food Chem. 2015, 63, 864−871

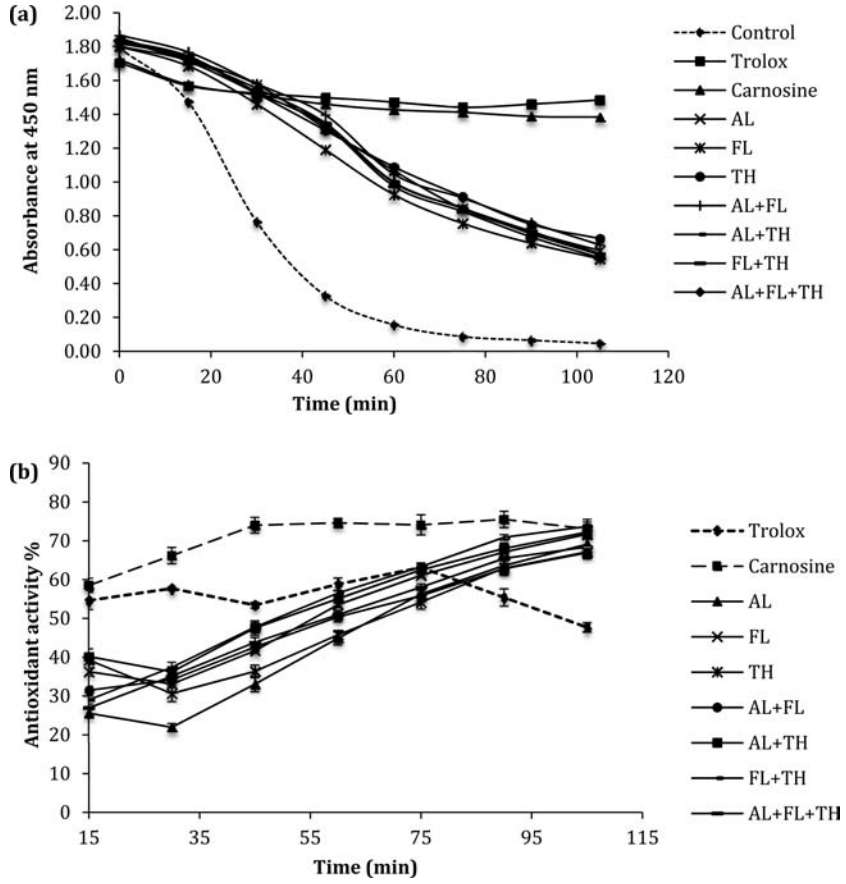

Figure 4. (a) β-Carotene bleaching as affected by date seed protein hydrolysates, trolox, and carnosine as measured by changes in absorbance value at 450 nm; (b) antioxidant activity of date seed protein hydrolysates, trolox, and carnosine against β-carotene bleaching.

action with the emulsifier (Tween 40) used in the analysis. Furthermore, Wijeratne, Abou-Zaid, and Shahidi[20] reported that hydrophobic antioxidants have higher efficiency than hydrophilic ones in preventing oxidation in oil-in-water emulsion systems by preferentially orienting themselves at the oil−water interface. Emulsifiers decrease the particle size of peptides and increase the contact surface of the phases.[29] This lends support to findings of this study that could be attributable to the presence of hydrophobic amino acids in date seed protein hydrolysates.

Cupric Ion-Induced Human Low-Density Lipoprotein Peroxidation. Cupric ion has been shown to be effective in initiating the oxidation of EDTA-free human LDL, as measured by the formation of conjugated dienes. The presence of both cholesteryl linoleate and cholesteryl arachidonate within the LDL core provides a rich source of lipid peroxidation substrate.[36] Therefore, the greater the lipophilic property of the antioxidant, the more effective it will be to extend the LDL oxidation lag phase once induced by[37] Cu^{2+}. LDL oxidation plays a major role in atherogenesis and coronary heart disease. Date seed protein hydrolysates and carnosine at a concentration of 0.1 mg/mL rendered a protective effect against human LDL oxidation (Figure 5), and this was higher. Date seed protein hydrolysates and carnosine exhibited higher after 12 h of incubation, being 50−60 and 80.9%, respectively. There was no significant difference ($p > 0.05$) among date seed protein hydrolysates after 12 h of incubation. Hydrolyates prepared using AL and TH showed the highest percentage of inhibition among all enzymatic treatments. Hydrolysate

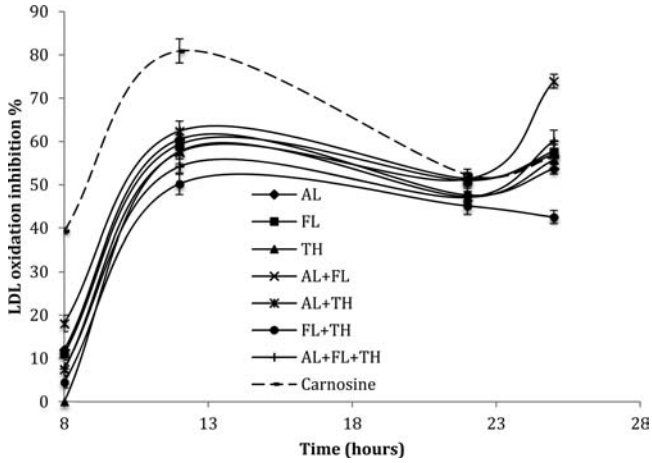

Figure 5. Inhibition against human LDL cholesterol oxidation by date seed protein hydrolysates and carnosine incubated at 37 °C for 25 h.

prepared using only TH had no inhibition at 8 h, but it increased to ∼57% after 12 h. However, percent inhibition decreased after 22 h of incubation in all date seed hydrolydates as well as in carnosine. Decker, Ivanov, Zhu, and Frei[16] investigated the ability of carnosine to inhibit the oxidation of LDL in comparison to its constituent amino acid, histidine. They showed that carnosine is capable of inhibiting copper-promoted oxidation reactions by chelating copper ions. However, carnosine's inhibitory activity against copper is shown to be less than that of histidine in LDL model, due to

DOI: 10.1021/jf505327b
J. Agric. Food Chem. 2015, 63, 864−871

its lower ability to remove copper from the surface of the macromolecules.[16] Alvarez-Parrilla, de la Rosa, Amarowicz, and Shahidi[5] reported that the inhibition of LDL oxidation by polyphenols could be attributed to different mechanisms, including hydrogen donation, lipid radical scavenging, metal chelation,[38] and protein binding.[21] Chen and Frei[39] reported that direct binding of cupric ions to LDL is important for copper reactivity because modification of histidine decreased the binding of copper to LDL and decreased copper-promoted oxidation rates. In this study, the inhibitiory effect of date seed protein hydrolysates on human LDL cholesterol oxidation could be attributed to the chelating power of protein hydrolysates for copper ions as well as scavenging of free radicals in LDL. In a previous study, Kittiphattanabawon, Benjakul, Visessanguan, and Shahidi[6] showed that gelatin hydrolysate from blacktip shark at various degrees of hydrolysis showed promising inhibitiory effect on LDL cholesterol oxidation. Several studies have shown that the presence of certain amino acids in protein hydrolysates, such as histidine, tryptophan, tyrosine, phenylalanine, methionine, leucine, glycine, or proline enhances the scavenging and chelating activities of peptides.[40−42] Thus, date seed protein hydrolyzed using Alcalase, Flavourzyme, and Thermolysin alone or in combination could protect human LDL cholesterol from oxidation and reduce oxidative stress in the body.

Inhibition of Peroxyl and Hydroxyl Radical-Induced Supercoiled DNA Strand Scission. Free radicals generated in living cells have been shown to induce base modification and DNA strand breakage, which may subsequently lead to mutation and carcinogenesis.[43] The most common radical in biological systems is the superoxide radical anion, which is produced mostly within the mitochondria of a cell.[44] Superoxide alone or combination with other free radicals could damage the DNA at both the phosphate backbone and the nucleotide bases. Davies[45] reported that this could lead to strand scission, sister chromatid exchange, and DNA−DNA and DNA−protein cross-links. Supercoiled DNA (form I) may be converted to a nicked open circular form (form II) and a linear form (form III) when its single strands are cleaved by free radicals.[43] To assess the protective effect of date seed protein hydrolysates on hydroxyl and peroxyl radical-induced DNA scission, agarose gel electrophoresis was used, which could be used to detect the forms of DNA separately. Percentage inhibition of DNA strand scission induced by peroxyl and hydroxyl radicals is presented in Table 3. Date seed protein hydrolysates exhibited inhibitory effects against peroxyl and hydroxyl radical-induced DNA scission in a concentration-dependent manner (Figure 6). Although date seed protein hydrolysates exhibited a protective effect against peroxyl radical-induced DNA scission at a concentration of 0.1 mg/mL, they were effective only at 6 mg/mL against hydroxyl radical-induced DNA scission, ranging from 13.8 to 33.0%. The positive control, carnosine, exhibited an inhibition of 30.6%. AL hydrolysate exhibited the highest inhibition of 33.0% against hydroxyl radical, which is slightly higher than that rendered by carnosine, whereas the mixture of three enzymes (AL + FL + TH) showed the lowest inhibition of 13.8%. All other enzymatic treatments exhibited no significant difference ($p > 0.05$) in inhibition of hydroxyl radicals (19.5−24.2%). For peroxyl radical-induced DNA scission, inhibition by the date seed protein hydrolysates ranged from 22.1 to 83.2% at a concentration of 0.1 mg/mL. All enzymatic treatments of date seed proteins exhibited significantly ($p < 0.05$) higher percentage of inhibition against peroxyl radical compared to that of carnosine (22.1%). Decker, Livisay, and Zhou[46] observed the changes in carnosine concentrations in oxidizing skeletal muscle and suggested that carnosine may not be as effective a free radical scavenger in vivo as other antioxidants such as α-tocopherol. This seems plausible, because carnosine exhibited a lower percentage of inhibition against peroxyl radical-induced DNA scission compared to date seed protein hydrolysates. AL hydrolysate showed significantly ($p < 0.05$) higher inhibition percentage of both peroxyl and hydroxyl radical-induced DNA scission, whereas the mixture of three enzymes (AL + FL + TH) showed the lowest percentage of inhibition. The inhibitory effect of date seed protein hydrolysates may be due to their ability to scavenge hydroxyl and peroxyl radicals and via their chelating activity. In this experiment, it was evident that the level of inhibition against hydroxyl radical was substantially lower compared to that against peroxyl radical even at a higher concentration. A similar observation was reported by Madhujith and Shahidi[47] for barley extracts. Hydroxyl radicals are short-lived and extremely reactive among all reactive oxygen species.[22] In contrast, peroxyl radicals exhibit a long half-life and have a greater affinity to diffuse into cells.[6] Thus, Hunag, Ou, and Prior[48] suggested that the direct scavenging of the hydroxyl radical by dietary antioxidants in a biological system is unrealistic as the cellular concentration of dietary antioxidants is negligible compared with DNA and other biological molecules. Therefore, the protective effect of date seed protein hydrolysates toward hydroxyl radical could be mainly due to the chetaltion of Fe(II), whereas that of peroxyl radicals may be due to a scavenging effect. This may explain the large variations observed in inhibition efficacies observed for hydroxyl and peroxyl radical-induced DNA scission. Regardless, this study demonstrated that date seed protein hydrolysates could serve as potential antimutagenic agents in food and biological systems.

Table 3. Inhibition of Peroxyl Radical-Induced DNA Scission by Date Seed Protein Hydrolystes and Carnosine[a]

	DNA scission inhibition (%)	
protein hydrolysate	hydroxyl radical	peroxyl radical
carnosine	30.6 ± 2.1c	22.1 ± 0.4a
AL	33.0 ± 1.4c	83.2 ± 1.5e
FL	20.5 ± 1.6b	47.8 ± 1.0b
TH	24.2 ± 1.6b	78.5 ± 2.4de
AL + FL	23.9 ± 1.4b	76.8 ± 1.3d
AL + TH	19.5 ± 1.9ab	75.2 ± 2.2d
FL + TH	21.4 ± 1.3b	77.4 ± 1.0d
AL + FL + TH	13.8 ± 2.2a	55.2 ± 0.4c

[a]All data represent the mean of triplicates. Values followed by the same letter are not significantly different ($P > 0.05$) by Tukey's HSD test.

This study revealed that date seed protein hydrolysates have a good solubility over a wide range of pH (pH 2−12) and improved water-holding capacity of fish products. In addition, date seed protein hydrolysates exhibited different antioxidant activities depending on the test model systems. Thus, date seed protein hydrolysates could be used as a natural additive possessing functionalities and antioxidative properties in food systems. Furthermore, date seed protein hydrolysates inhibited human LDL cholesterol oxidation and peroxyl and hydroxyl radical-induced supercoiled plasmid DNA strand scission.

DOI: 10.1021/jf505327b
J. Agric. Food Chem. 2015, 63, 864−871

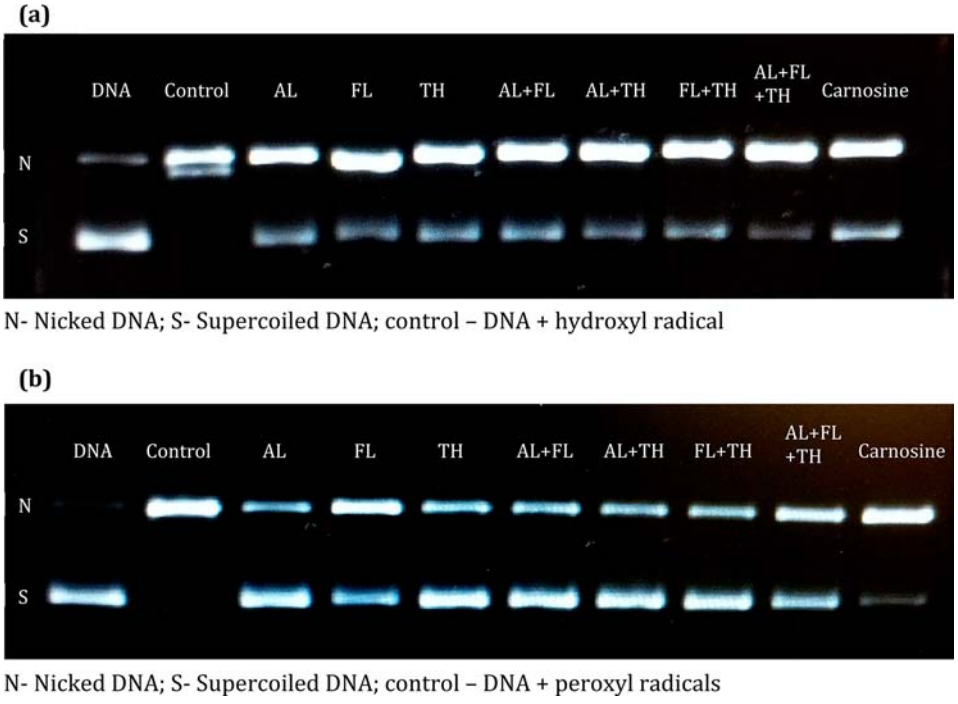

Figure 6. (a) Agarose gel electrophoresis of inhibition of hydroxyl radical-induced DNA scission by date seed protein hydrolystes and carnosine (6 mg/mL); (b) peroxyl radical-induced DNA scission by date seed protein hydrolystes and carnosine (0.1 mg/mL).

Therefore, it could be a potential functional food ingredient for health promotion. However, the antioxidant effect of date seed protein hydrolysate could also be influenced by the presence of other biomolecules, including minute amounts of water-soluble phenolics in the crude material, but this effect is considered to be minimal. Therefore, purification of date seed proteins, fractionation of the resultant peptides, and their sequencing may provide further clarity.

AUTHOR INFORMATION

Corresponding Author

*(F.S.) Phone: (709) 864-8552. Fax: (709) 864-4000. E-mail: fshahidi@mun.ca.

Funding

We are grateful to the Natural Science and Engineering Council (NSERC) of Canada for financial support in the form of a discovery grant to F.S.

Notes

The authors declare no competing financial interest.

ABBREVIATIONS USED

AL, Alcalase; FL, Flavourzyme; TH, Thermolysin

REFERENCES

(1) Amarowicz, R.; Shahidi, F. Antioxidant activity of peptide fractions of capelin protein hydrolysates. *Food Chem.* **1997**, *58*, 355–359.

(2) Kristinsson, H. G.; Rasco, B. A. Fish protein hydrolysates: production, biochemical, and functional properties. *Crit. Rev. Food Sci. Nutr.* **2000**, *40*, 43–81.

(3) Thiansilakul, Y.; Benjakul, S.; Shahidi, F. Compositions, functional properties and antioxidative activity of protein hydrolysates prepared from round scad (*Decapterus maruadsi*). *Food Chem.* **2007**, *103*, 1385–1394.

(4) Dong, S.; Zeng, M.; Wang, D.; Liu, Z.; Zhao, Y.; Yang, H. Antioxidant and biochemical properties of protein hydrolysates prepared from silver carp (*Hypophthalmichthys molitrix*). *Food Chem.* **2008**, *107*, 1485–1493.

(5) Alvarez-Parrilla, E.; de la Rosa, L. A.; Amarowicz, R.; Shahidi, F. Protective effect of fresh and processed Jalapeño and Serrano peppers against food lipid and human LDL cholesterol oxidation. *Food Chem.* **2012**, *133*, 827–834.

(6) Kittiphattanabawon, P.; Benjakul, S.; Visessanguan, W.; Shahidi, F. Inhibition of angiotensin converting enzyme, human LDL cholesterol and DNA oxidation by hydrolysates from blacktip shark gelatin. *LWT–Food Sci. Technol.* **2013**, *51*, 177–182.

(7) Pihlanto-Leppala, A. Bioactive peptides derived from bovine proteins: opioid and ACE-inhibitory peptides. *Trends Food Sci. Technol.* **2001**, *11*, 347–356.

(8) Jeong, H. J.; Lam, Y.; de Lumen, B. O. Barley lunasin suppresses *ras*-induced colony formation and inhibits core histone acetylation in mammalian cells. *J. Agric. Food Chem.* **2002**, *50*, 5903–5908.

(9) Clare, D. A.; Swaisgood, H. E. Bioactive milk peptides: a prospectus. *J. Dairy Sci.* **2000**, *83*, 1187–1195.

(10) Elias, R. J.; Kellerby, S. S.; Decker, E. A. Antioxidant activity of proteins and peptides. *Crit. Rev. Food Sci. Nutr.* **2008**, *48*, 430–441.

(11) Halliwell, B.; Zentella, A.; Gomez, E. O.; Kershenobich, D. Antioxidants and human disease: a general introduction. *Nutr. Rev.* **1997**, *55*, S44–S52.

(12) Wettasinghe, M.; Shahidi, F. Scavenging of reactive-oxygen species and DPPH free radicals by extracts of borage and evening primrose meals. *Food Chem.* **2000**, *70*, 17–26.

(13) Boldyrev, A. A.; Dupin, A. M.; Bunin, A. Y.; Babizhaev, M. A.; Severin, S. E. The antioxidative properties of carnosine, a histidine containing dipeptide. *Biochem. Int.* **1987**, *15*, 1105–1113.

(14) Kohen, R.; Yamamoto, Y.; Cundy, K. C.; Ames, B. Antioxidant activity of carnosine, homocarnosine, and anserine present in muscle and brain. *Proc. Natl. Acad. Sci. U.S.A.* **1998**, *85*, 3175–3179.

(15) Decker, E. A.; Ivanov, V.; Zhu, B. Z.; Frei, B. Inhibition of low-density lipoprotein oxidation by carnosine and histidine. *J. Agric. Food Chem.* **2001**, *49*, 511–516.

(16) AOAC. Protein (crude) determination in animal feed: copper catalyst Kjeldahl method (984.13). *Official Methods of Analysis*, 15th ed.; Association of Official Analytical Chemists: Rockville, MD, USA, 1990.

DOI: 10.1021/jf505327b
J. Agric. Food Chem. 2015, 63, 864–871

(17) Shahidi, F.; Han, X.-Q.; Synowiecki, J. Production and characteristics of protein hydrolysates from capelin (*Mallotus villosus*). *Food Chem.* **1995**, *53*, 285−293.
(18) Shahidi, F.; Synowiecki, J. Protein hydrolyzates from seal meat as phosphate alternatives in food processing applications. *Food Chem.* **1997**, *60*, 29−32.
(19) Wettasinghe, M.; Shahidi, F. Antioxidant and free radical-scavenging properties of ethanolic extracts of defatted borage (*Borago officinalis* L.) seeds. *Food Chem.* **1999**, *67*, 399−414.
(20) Wijeratne, S. S.; Abou-Zaid, M. M.; Shahidi, F. Antioxidant polyphenols in almond and its coproducts. *J. Agric. Food Chem.* **2006**, *54*, 312−318.
(21) Liyana-Pathirana, C. M.; Shahidi, F. Antioxidant properties of commercial soft and hard winter wheat (*Triticum aestivum* L.) and their milling fractions. *J. Sci. Food Agric.* **2006**, *83*, 477−485.
(22) Chandrasekara, A.; Shahidi, F. Inhibitory activities of soluble and bound millet seed phenolics on free radicals and reactive oxygen species. *J. Agric. Food Chem.* **2011**, *59*, 428−436.
(23) Mutilangi, W. A. M.; Panyam, D.; Kilara, A. Functional properties of hydrolysates from proteolysis of heat-denatured whey protein isolate. *J. Food Sci.* **1996**, *61*, 270−303.
(24) Gbogouri, G. A.; Linder, M.; Fanni, J.; Parmentier, M. Influence of hydrolysis degree on the functional properties of salmon byproduct hydrolysates. *J. Food Sci.* **2004**, *69*, 615−622.
(25) Cumby, N.; Zhong, Y.; Naczk, M.; Shahidi, F. Antioxidant activity and water-holding capacity of canola protein hydrolysates. *Food Chem.* **2008**, *109*, 144−148.
(26) Das, A. K.; Anjaneyulu, A. S. R; Biswas, S. Effect of carnosine preblending on the quality of ground buffalo meat. *Food Chem.* **2006**, *97*, 531−538.
(27) Thomsen, H. H.; Zeuthen, P. The influence of mechanically deboned meat and pH on the water-holding capacity and texture of emulsion type meat products. *Meat Sci.* **1988**, *22*, 189−201.
(28) Decker, E.; Crum, A. D. Antioxidant activity of carnosine in cooked ground pork. *Meat Sci.* **1993**, *34*, 245−253.
(29) Marcuse, R. The effect of some amino acids on oxidation of linoleic acid and its methyl esters. *J. Am. Oil Chem. Soc.* **1962**, *39*, 97−103.
(30) Merzametov, M. M.; Gadzhieva, L. I. Certain amino acids as antioxidants in butterfat. *Zzv. Ucheb. Zaved. Pischew. Technol.* **1976**, *115*, 21−27.
(31) Revankar, G. D. Proline as an antioxidant in fish oil. *J. Food Sci. Technol. Mysore* **1974**, *11*, 1−11.
(32) Sims, R. J.; Fioriti, J. A. Methional as an antioxidant for vegetable oils. *J. Am. Oil Chem. Soc.* **1977**, *54*, 4−7.
(33) Riison, T.; Sims, R. J.; Fioriti, J. A. Effect of amino acids on the autoxidaton of safflower oil in emulsions. *J. Am. Oil Chem. Soc.* **1980**, *57*, 354−359.
(34) Aruoma, 0. I.; Laughton, M. I.; Halliwell, B. Camosine, homocamosine and serine, could they act as antioxidants in vivo? *Biochem. J.* **1989**, *264*, 863−869.
(35) Pratt, D. E.; Hudson, B. J. F. Natural antioxidants not exploited commercially. In *Food Antioxidants*; Hudson. B. J. F., Ed.; Elsevier Applied Science: London, UK, 1990; pp 171−191.
(36) Thomas, S. R.; Stocker, R. Molecular action of vitamin E in lipoprotein oxidation: implications for atherosclerosis. *Free Radical Biol. Med.* **2000**, *28*, 1795−1805.
(37) Hu, C.; Kitts, D. D. Evaluation of antioxidant activity of epigallocatechin gallate in biphasic model systems in vitro. *Mol. Cell. Biochem.* **2001**, *218*, 147−155.
(38) Brand-Williams, W.; Cuvelier, M. E.; Berset, C. Use of a free radical method to evaluate antioxidant activity. *LWT−Food Sci. Technol.* **1995**, *28*, 25−30.
(39) Chen, K.; Frei, B. The effect of histidine modification on copper-dependent lipid peroxidation in human low-density lipoprotein. *Redox Rep.* **1997**, *3*, 175−181.
(40) Chen, H. M.; Muramoto, K.; Yamauchi, F.; Nokihara, K. Antioxidant activity of designed peptides based on the antioxidative peptide isolated from digests of a soybean protein. *J. Agric. Food Chem.* **1996**, *44*, 2619−2623.
(41) Park, P. J.; Jung, W. K.; Nam, K. S.; Shahidi, F.; Kim, S. K. Purification and characterization of antioxidative peptides from protein hydrolysate of lecithin-free egg yolk. *J. Am. Oil Chem. Soc.* **2001**, *78*, 651−656.
(42) Li, B.; Chen, F.; Wang, X.; Ji, B.; Wu, Y. Isolation and identification of antioxidative peptides from porcine collagen hydrolysate by consecutive chromatography and electrospray ionization-mass spectrometry. *Food Chem.* **2007**, *102*, 1135−1143.
(43) Hiramoto, K.; Ojima, N.; Sako, K. I.; Kikugawa, K. Effect of plant phenolics on the formation of the spin-adduct of hydroxyl radical and the DNA strand breaking by hydroxyl radical. *Biol. Pharm. Bull.* **1996**, *19*, 558−563.
(44) Valko, M.; Izakovic, M.; Mazur, M.; Rhodes, C. J.; Telser, J. Role of oxygen radicals in DNA damage and cancer incidence. *Mol. Cell. Biochem.* **2004**, *266*, 37−56.
(45) Davies, K. J. A. Oxidative stress: the paradox of aerobic life. In *Free Radical and Oxidative Stress: Environments, Drugs and Food Additives*; Rice-Evans, C., Halliwell, B., Lunt, G. G., Eds.; Portland Press: London, UK, 1995; pp 1−31.
(46) Decker, E. A.; Zhou, S.; Livisay, S. A. A re-evaluation of the antioxidant activity of purified carnosine. *Biochemistry (Moscow)* **2000**, *65*, 766−770.
(47) Madhujith, T.; Shahidi, F. Optimization of the extraction of antioxidative constituents of six barley cultivars and their antioxidant properties. *J. Agric. Food Chem.* **2006**, *54*, 8048−8057.
(48) Hunag, D.; Ou, B.; Prior, R. The chemistry behind the antioxidant capacity assays. *J. Agric. Food Chem.* **2005**, *53*, 1841−1856.

DOI: 10.1021/jf505327b
J. Agric. Food Chem. 2015, 63, 864−871

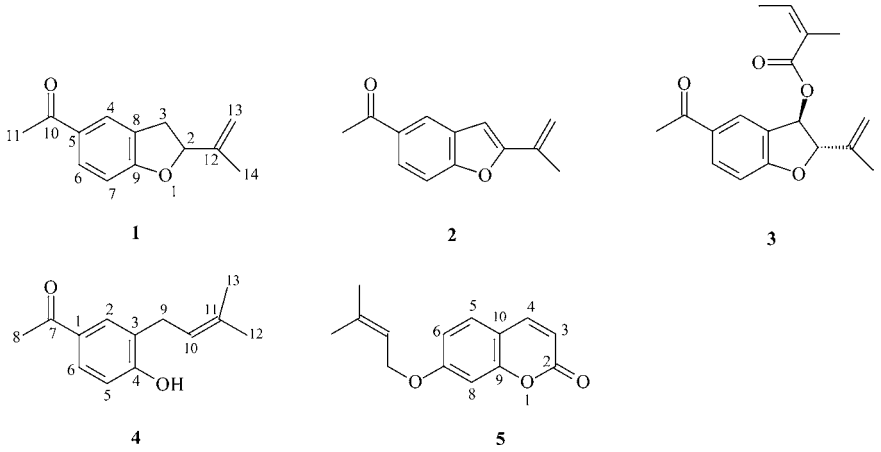

Figure 2. Chemical structures of tremetone, **1**, dehydrotremetone, **2**, 3-oxyangeloyltremetone, **3**, 4-hydroxy-3-(3-methyl-2-butenyl)acetophenone, **4**, and 7-isopentenyloxycoumarin, **5**.

Table 1. *Isocoma* spp. Collection Sites, Dates, and Herbarium Accession Numbers

Isocoma spp.	site	state	county	GPS coordinates	collection date month/day/year	accession no.
I. pluriflora	Pecos	TX	Reeves	31°23.969′ N/103°29.969′ W	08/25/2014	4606
I. pluriflora	Carlsbad	NM	Eddy	32°14.073′ N/104°06.006′ W	08/21/2014	4605
I. tenuisecta	Tucson	AZ	Pima	32°17.687′ N/111°02.127′ W	08/26/2014	4595
I. tenuisecta	Red Rock	AZ	Pinal	32°33.115′ N/111°18.212′ W	08/26/2014	4594
I. azteca	Newcomb	NM	San Juan	36°20.636′ N/108°42.843′ W	08/25/2014	4600
I. azteca	Tsaya	NM	San Juan	36°13.031′ N/108°15.978′ W	08/25/2014	4598
I. acradenia	Mesa	AZ	Pinal	33°18.325′ N/111°35.301′ W	08/26/2014	4549
I. acradenia	Kingman	AZ	Mohave	35°23.090′ N/114°02.202′ W	08/27/2014	4593
I. acradenia	Wickenburg	AZ	Yavapai	34°07.080′ N/112°56.553′ W	09/03/2014	4607
I. rusbyi	Marble Canyon	AZ	Coconino	36°46.835′ N/111°41.444′ W	08/25/2014	4603
I. rusbyi	Tuba City	AZ	Coconino	36°05.254′ N/111°23.569′ W	08/25/2014	4601
I. rusbyi	Holbrook	AZ	Navajo	35°03.681′ N/110°05.829′ W	08/26/2014	4597

putative toxins (i.e., tremetone, **1**, dehydrotremetone, **2**, etc.) in any of the other *Isocoma* spp. Review literature[4,21] has suggested that *Isocoma hartwegii*, *I. coronopifolia*, and *I. tenuisecta* may be toxic and cause the same disease syndrome as *I. pluriflora*. In the past year we investigated a case of poisoning in cattle near Mesa, AZ, where *Isocoma acradenia* was the suspected causative agent. Using previously described analytical methods for *I. pluriflora*,[19] relatively high concentrations of tremetone, **1**, dehydrotremetone, **2**, and 3-oxyangeloyltremetone, **3**, were detected in the *I. acradenia* as well as two unidentified compounds not detected in *I. pluriflora*.

The discovery of tremetone, **1**, dehydrotremetone, **2**, and 3-oxyangeloyltremetone, **3**, in *I. acradenia*, in addition to the overall absence of reported livestock poisonings and lack of chemical analyses of the *Isocoma* spp. native to the southwestern United States, prompted us to undertake a systematic study to analyze the different *Isocoma* spp. for the suspected *I. pluriflora* toxins, tremetone, **1**, dehydrotremetone, **2**, and other structurally related compounds using both field collections and herbarium specimens.

MATERIALS AND METHODS

Plant Material. Five different *Isocoma* spp. were collected from 12 different locations (Table 1) and dried at ambient temperature. Composite collections of the above ground parts (the top 15 cm of green stems with leaves) of at least nine plants were collected randomly at each site. The plants collected were in early to full flower. *Isocoma* plants were identified by Robert Johnson, Plant Collection Manager, Stanley L. Welsh Herbarium at Brigham Young University, Provo, UT. Voucher specimens for the different *Isocoma* spp. collections were deposited at the Poisonous Plant Research Laboratory Herbarium, Logan, UT, and accession numbers are listed in Table 1. Leaf tissue from the *Isocoma* spp. specimens at the Poisonous Plant Research Laboratory, Intermountain Herbarium at Utah State University, S. L. Welsh Herbarium at Brigham Young University, University of Texas Herbarium, S. M. Tracy Herbarium at Texas A & M University, Arizona State University Herbarium, University of New Mexico Herbarium, University of Arizona Herbarium, and the University of California at Riverside Herbarium was sampled for analysis of tremetone, **1**, dehydrotremetone, **2**, 3-oxyangeloyltremetone, **3**, and other structurally related compounds. All plant specimens were ground to pass through a 1 mm screen.

Extraction and Isolation of Compounds. Dry, ground plant material (150 g) was Soxhlet-extracted for 72 h with hexane (700 mL). The hexane extract was rotary-evaporated to 200 mL and extracted with an equal volume of MeOH:H_2O (90:10) three times. MeOH:H_2O (90:10) was rotary-evaporated to a viscous dark green residue. Residue was dissolved in MeOH:H_2O (90:10) to result in a concentration of 50 mg/mL, filtered through a 30 mm Nylon 0.45 μm syringe filter (National Scientific Co., Rockwood, TN) and a 1.5 mL sample injected onto a Waters Prep LC2000 preparative chromatography system equipped with a UV/vis detector (Millipore Co., Millford, MA) monitoring at λ 280 nm. The HPLC column (150 mm × 21.20 mm i.d., 10 μm, Luna C18(2) with a 50 mm × 21.20 mm guard column of the same material (Phenomenex Inc., Torrance, CA). The mobile phase flow rate was 25 mL/min. The mobile phase program was water−acetonitrile, (65:35, v:v) for 5 min followed by a linear gradient to a composition of 65% acetonitrile at 20 min; the mobile phase composition was then held at 65% acetonitrile for an additional 5 min for total run time of 25 min. The major peaks were

DOI: 10.1021/jf505423h
J. Agric. Food Chem. 2015, 63, 872−879

Table 2. Concentrations of Tremetone, 1, Dehydrotremetone, 2, 3-Oxyangeloyltremetone, 3, 4-Hydroxy-3-(3-methyl-2-butenyl)acetophenone,4, and 7-Isopentenyloxycoumarin, 5, in *Isocoma* spp. Field Collections[a]

	av compd concn ± SD (n = 10), μg/mg dry weight				
site	1	2	3	4	5
			I. pluriflora		
Pecos	0.4 ± 0.3	2.6 ± 0.7	4 ± 1		
Carlsbad	0.16 ± 0.08	0.8 ± 0.2	1.9 ± 0.7		
			I. tenuisecta		
Tucson	0.2 ± 0.1	1.7 ± 0.5	2 ± 1	*0.4 ± 0.4*[b]	*1.1 ± 0.4*
Red Rock	0.11 ± 0.08	0.7 ± 0.5	1.3 ± 0.9	*0.09 ± 1.0*	*0.1 ± 0.5*
			I. azteca		
Newcomb	6 ± 2	0.8 ± 1	2 ± 3	*0.7 ± 0.4*	
Tsaya	8 ± 2	0.0004 ± 0.001	0.5 ± 0.3	*0.8 ± 0.4*	
			I. acradenia		
Mesa	1.0 ± 0.2	1.0 ± 0.4	1.1 ± 0.9	*0.4 ± 0.4*	*0.10 ± 0.04*
Kingman	0.3 ± 0.3	4 ± 2	4 ± 2	*1 ± 1*	*0.10 ± 0.02*
Wickenburg	1.1 ± 0.4	1.1 ± 0.5	1.2 ± 0.4	*0.6 ± 0.4*	*0.09 ± 0.03*
			I. rusbyi		
Marble Canyon	0.7 ± 0.6	0.6 ± 0.6	4 ± 1	*0.07 ± 0.03*	*0.4 ± 0.3*
Tuba City	2 ± 1		0.4 ± 0.2	*0.02 ± 0.02*	*0.07 ± 0.1*
Holbrook	2 ± 1	2 ± 2	7 ± 3	*0.13 ± 0.07*	

[a] n = 10 for all sites except Pecos, Carlsbad, and Marble Canyon where n = 9. [b] The concentrations in italics are expressed in tremetone equivalents.

collected separately from multiple injections. The combined fractions, corresponding to each of the major peaks, were each evaporated to <30% of the original volume and extracted three times with equal volumes of $CHCl_3$. These three $CHCl_3$ extracts were combined, dried over anhydrous Na_2SO_4, filtered, and rotary-evaporated to dryness. Using this method, 4-hydroxy-3-(3-methyl-2-butenyl)acetophenone, **4**, and 7-isopentenyloxycoumarin, **5**, were isolated from *I. acradenia* collected at the Mesa, AZ, site.

NMR Analysis. NMR spectra of compounds in $CDCl_3$ were recorded using a JEOL ECX-300 300 MHz NMR spectrometer (JEOL Ltd., Peabody, MA). ^{1}H NMR and ^{13}C NMR assignments were determined using HSQC and HMBC experiments.

Gas Chromatography–Mass Spectrometry. GC/MS data were acquired using a Trace GC Ultra and Polaris Q mass spectrometer (Thermo Fisher Scientific, Waltham, MA) equipped with a split/splitless injector and a 30 m × 0.25 mm, 0.25 μm film thickness DB-5MS (Agilent Technologies Inc., Santa Clara, CA) column. The injection volume was 1.5 μL, the injection port temperature was 250 °C, and the injector was operated in the splitless mode. Split vent flow rate was 50 mL/min and purged after 0.80 min. Oven temperature was 80 °C for 1 min, increased 80–300 °C at 30 °C/min, and held at 300 °C for 3.0 min. Electron impact ionization (EI) at 70 eV was used with an ion source temperature of 200 °C. The detector scanned the mass range from m/z 50 to m/z 650.

*4-Hydroxy-3-(3-methyl-2-butenyl)acetophenone, **4**.* ^{1}H NMR, ^{13}C NMR, EIMS, and UV were in agreement with previously reported literature.[22,23]

*7-Isopentenyloxycoumarin, **5**.* ^{1}H NMR, ^{13}C NMR, EIMS, and UV were in agreement with previously reported literature.[24−26]

Analytical Scale Extraction and HPLC Analysis. Using a HPLC method developed for the quantitation of tremetone, **1**, dehydrotremetone, **2**, and 3-oxyangeloyltremetone, **3**, in white snakeroot and rayless goldenrod,[19] the concentrations of **1**−**5** were determined in the different *Isocoma* spp. collections. Dry, ground aerial plant material was weighed (100 mg) into a screw top glass test tube (16 mL). The plant material was extracted (16 h) by mechanical rotation with hexane:ethyl acetate (70:30, v:v) (8 mL) at ambient temperature. HPLC was performed using an LC-20AT (Shimadzu Co., Kyoto, Japan) equipped with an autosampler and PDA detector from the same vendor and a 100 mm × 2.1 mm i.d., 5 μm, Betasil C_{18}, with a 10 mm × 2.1 mm i.d. guard column of the same material (Thermo Hypersil-Keystone, Bellefonte, PA). Samples (10 μL) in hexane:ethyl acetate (70:30, v:v) were injected on to the column and eluted with a 20 mM ammonium acetate–acetonitrile mobile phase at a flow rate of 0.4 mL/min. The mobile phase program was 20 mM ammonium acetate–acetonitrile (65:35, v:v) for 4 min followed by a linear gradient to a composition of 65% acetonitrile at 20 min. At 21 min the composition was increased to 100% acetonitrile for 5 min. The eluant was monitored at 280 nm. Under these conditions tremetone, **1**, dehydrotremetone, **2**, 3-oxyangeloyltremetone, **3**, 4-hydroxy-3-(3-methyl-2-butenyl)-acetophenone, **4**, and 7-isopentenyloxycoumarin, **5**, eluted at 10, 14.4, 17.8, 7.7, and 12.7 min, respectively. The concentrations of tremetone, **1**, dehydrotremetone, **2**, and 3-oxyangeloyltremetone, **3**, in plant field collections were quantitated against seven point tremetone, **1**, dehydrotremetone, **2**, and 3-oxyangeloyltremetone, **3**, calibration curves using previously isolated tremetone, **1**, dehydrotremetone, **2**, and 3-oxyangeloyltremetone, **3**.[19] 4-Hydroxy-3-(3-methyl-2-butenyl)-acetophenone, **4**, and 7-isopentenyloxycoumarin, **5**, were quantitated against the tremetone, **1**, standard curve and are thus expressed in tremetone equivalents. The standard solutions were prepared by serial dilution with hexane:ethyl acetate (70:30, v:v) over the range of 0.78 μg/mL to 200.0 μg/mL. The calibration curve had R^2 of 0.9999. Plant material (25 mg) from herbarium specimens was extracted in 2 mL of hexane/ethyl acetate (70:30, v:v). Qualitative analysis for the compounds of interest was performed as described above.

Maps. Distribution maps of *Isocoma* spp. were created using ArcGIS software by ESRI. State boundary data was downloaded from the U.S. Census Bureau TIGER/Line shapefiles.[27]

RESULTS AND DISCUSSION

Isolation and Identification of Compounds. Tremetone, **1**, dehydrotremetone, **2**, and 3-oxyangeloyltremetone, **3**, were previously isolated from *I. pluriflora*.[19] In this study, 4-hydroxy-3-(3-methyl-2-butenyl)acetophenone, **4**, and 7-isopentenyloxycoumarin, **5**, were isolated from *I. acradenia* plant material collected from the Mesa, AZ (Figure 1), site by Soxhlet extraction with hexane and reversed phase HPLC. The identification of 4-hydroxy-3-(3-methyl-2-butenyl)-acetophenone, **4**, and 7-isopentenyloxycoumarin, **5**, was confirmed based on comparison of spectroscopic data with those previously reported.

Isocoma pluriflora. *I. pluriflora* is native to Arizona, New Mexico, West Texas, and Northern Mexico (Figure 1).[1] Tremetone, **1**, dehydrotremetone, **2**, and 3-oxyangeloyltreme-

DOI: 10.1021/jf505423h
J. Agric. Food Chem. 2015, 63, 872−879

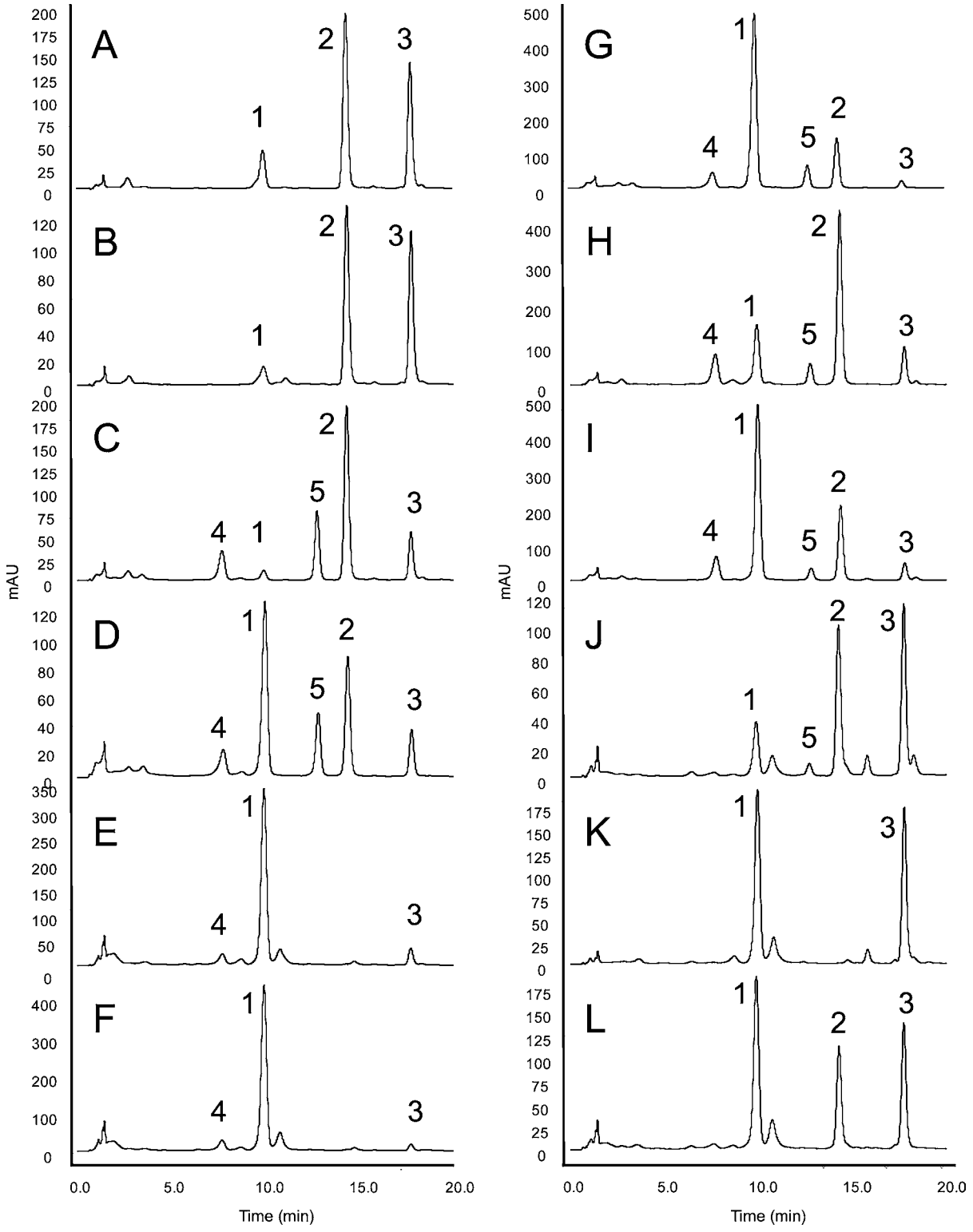

Figure 3. HPLC chromatograms of extracts from *Isocoma* spp. collected from (A) *I. pluriflora*, Pecos; (B) *I. pluriflora*, Carlsbad; (C) *I. tenuisecta*, Tucson; (D) *I. tenuisecta*, Red Rock; (E) *I. azteca*, Newcomb; (F) *I. azteca*, Tsaya; (G) *I. acradenia*, Mesa; (H) *I. acradenia*, Kingman; (I) *I. acradenia*, Wickenburg; (J) *I. rusbyi*, Marble Canyon; (K) *I. rusbyi*, Tuba City; (L) *I. rusbyi*, Holbrook. Peak numbers refer to compound structures in Figure 2.

tone, **3**, were present in all the field collected plants at Pecos, TX, and Carlsbad, NM (Table 2, Figure 3). Compounds **4** and **5** were not present in any of the field collected plants (Table 2, Figure 3). The presence of these three benzofurans and the concentrations of these compounds are consistent with previously analyzed plant material from the same Pecos site collected in 2008 and 2009 and from a site in Palo Duro Canyon also in Reeves County, TX, collected in 2009.[19,28] The mean concentrations of the three benzofuran ketones in the *I. pluriflora* plants from the Pecos site were approximately double the concentration from the Carlsbad site. *I. pluriflora* collected at the Pecos site in 2008 was poisonous and produced trembles

DOI: 10.1021/jf505423h
J. Agric. Food Chem. 2015, 63, 872−879

in both goats and horses under controlled dosing conditions.[5−8] Tremetone, **1**, dehydrotremetone, **2**, 3-oxyangeloyltremetone, **3**, and 7-isopentenyloxycoumarin, **5**, were present in *I. pluriflora* sampled from herbarium specimens (n = 33) representing locations from 21 different counties in Texas and New Mexico as well as Mexico at a frequency of 82, 12, 45, and 36%, respectively (Table 3). The herbarium data and field collection data differed in the frequency of detection of dehydrotremetone and 3-oxyangeloyltremetone. Additionally, 7-isopentenyloxycoumarin, **5**, was detected in herbarium specimens but not field collections. This is the first report of this compound in *I. pluriflora*. Consistent between the field collections and herbarium collection was the high frequency of tremetone and the absence of 4-hydroxy-3-(3-methyl-2-butenyl)acetophenone, **4**.

Table 3. Frequency of Tremetone, 1, Dehydrotremetone, 2, 3-Oxyangeloyltremetone, 3, 4-Hydroxy-3-(3-methyl-2-butenyl)acetophenone, 4, and 7-Isopentenyloxycoumarin, 5, Observed in *Isocoma* spp. Herbarium Survey

		freq of compds obsd (%)				
Isocoma spp.	*n*	**1**	**2**	**3**	**4**	**5**
I. pluriflora	33	82	12	45	0	36
I. tenuisecta	22	50	27	82	23	100
I. azteca	18	100	56	61	0	0
I. acradenia	46	89	26	67	48	90
I. rusbyi	25	88	0	88	0	40
I. menziesii	36	33	8	81	22	69
I. coronopifolia	17	6	0	76	0	0
I. drummondi	16	0	0	81	0	0
I. veneta	10	20	0	70	0	10
I. hartwegii	4	25	0	75	0	0
I. gypsophila	2	0	0	50	0	0
I. tomentosa	1	0	0	100	100	0
I. arguta	1	0	0	100	0	0

Isocoma tenuisecta. *I. tenuisecta* is native to southern Arizona and southwestern New Mexico (Figure 1).[1] Tremetone, **1**, dehydrotremetone, **2**, 3-oxyangeloyltremetone, **3**, 4-hydroxy-3-(3-methyl-2-butenyl)acetophenone, **4**, and 7-isopentenyloxycoumarin, **5**, were present in 95% or greater of all the field collected plants at Tucson, AZ, and Red Rock, AZ (Table 2, Figure 3). This is the first report of these compounds in *I. tenuisecta*. The mean concentrations of these compounds at the Tucson site were approximately double the mean concentration from the Red Rock site. Tremetone, **1**, dehydrotremetone, **2**, 3-oxyangeloyltremetone, **3**, 4-hydroxy-3-(3-methyl-2-butenyl)-acetophenone, **4**, and 7-isopentenyloxycoumarin, **5**, were present in *I. tenuisecta* sampled from herbarium specimens (n = 22) representing locations from 8 counties in Arizona and New Mexico at a frequency of 50, 27, 82, 23 and 100%, respectively (Table 3). The herbarium data and field collection data differed in the frequency of detection of tremetone, **1**, dehydrotremetone, **2**, and 4-hydroxy-3-(3-methyl-2-butenyl)-acetophenone, **4**. Consistent between the field collections and herbarium collection was the high frequency of 3-oxyangeloyltremetone, **3**, and 7-isopentenyloxycoumarin, **5**.

Isocoma azteca. *I. azteca* is native primarily to northwest New Mexico and northeast Arizona (Figure 1).[1] Tremetone, **1**, dehydrotremetone, **2**, 3-oxyangeloyltremetone, **3**, and 4-hydroxy-3-(3-methyl-2-butenyl)acetophenone, **4**, were present in 90% or greater of all the field collected plants at Newcomb, NM, and Tsaya, NM, with the exception of dehydrotremetone, **2**, which was detected in only 20% of the plants collected at Tsaya, NM (Table 2, Figure 3). This is the first report of these compounds in *I. azteca*. The mean concentrations of tremetone, **1**, 4-hydroxy-3-(3-methyl-2-butenyl)acetophenone, **4**, and 3-oxyangeloyltremetone, **3**, were similar between the two collections, however, the mean concentration of dehydrotremetone, **2**, was very low at the Tsaya site as only two of the plants contained dehydrotremetone, **2**, and they both had relatively low concentrations (<0.005 μg/mg). Plants from the *I. azteca* collection sites had the highest concentration of tremetone, **1**, of any of the other major compounds observed in any of the field collections of *Isocoma* spp. with the average concentration of tremetone, **1**, in plants at the Tsaya site approaching 1% of the dry plant material. *I. azteca* samples from herbarium specimens (n = 18) representing locations from 3 counties in Arizona and New Mexico were qualitatively analyzed (Table 3). Tremetone, **1**, dehydrotremetone, **2**, and 3-oxyangeloyltremetone, **3**, were present in sampled herbarium specimens (n = 18) representing locations from 3 counties in Arizona and New Mexico at a frequency of 100, 56 and 61%, respectively. Consistent between the field and herbarium collections was the high frequency of tremetone, **1** (100%), and the absence of 7-isopentenyloxycoumarin, **5**. Somewhat similar between the field and herbarium collections was the frequency of occurrence of dehydrotremetone, **2**, and 3-oxyangeloyltremetone, **3**. Most inconsistent between the field and herbarium collections was the absence of 4-hydroxy-3-(3-methyl-2-butenyl)acetophenone, **4**, in the herbarium specimens.

Isocoma acradenia. *I. acradenia* is native to southern California, southern Nevada, the western half of Arizona, and northwest Mexico (Figure 1).[1] Tremetone, **1**, dehydrotremetone, **2**, 3-oxyangeloyltremetone, **3**, 4-hydroxy-3-(3-methyl-2-butenyl)acetophenone, **4**, and 7-isopentenyloxycoumarin, **5**, were present in all the field collected plants at Mesa, AZ, Kingman, AZ, and Wickenburg, AZ (Table 2, Figure 3). This is the first report of these compounds in *I. acradenia*. The mean concentrations of the 5 major compounds in plants from the Mesa site and Wickenburg site were similar but differed from the Kingman site. Plants collected from the Kingman site had approximately double the concentration of 4-hydroxy-3-(3-methyl-2-butenyl)acetophenone, **4**, and 4 times the concentrations of dehydrotremetone, **2**, and 3-oxyangeloyltremetone, **3**, but half the mean concentration of tremetone, **1**, compared to the Mesa and Wickenburg sites. Tremetone, **1**, dehydrotremetone **2**, 3-oxyangeloyltremetone, **3**, 4-hydroxy-3-(3-methyl-2-butenyl)acetophenone, **4**, and 7-isopentenyloxycoumarin, **5**, were present in *I. acradenia* sampled herbarium specimens (n = 46) representing 23 different counties in California, Arizona, and Nevada as well as Mexico at a frequency of 89, 26, 67, 48, and 90%, respectively. Consistent between the field and herbarium collections was the frequency of occurrence of tremetone, **1**, and 7-isopentenyloxycoumarin, **5**, while 3-oxyangeloyltremetone, **3**, was somewhat similar between the two different collections. Dehydrotremetone, **2**, and 4-hydroxy-3-(3-methyl-2-butenyl)acetophenone, **4**, occurred at a lower frequency in herbarium specimens compared to the field samples.

Isocoma rusbyi. *I. rusbyi* is primarily native to central southeastern Utah, and central northeastern Arizona (Figure 1).[1] Tremetone, **1**, dehydrotremetone, **2**, 3-oxyangeloyltremetone, **3**, 4-hydroxy-3-(3-methyl-2-butenyl)acetophenone, **4**, and

DOI: 10.1021/jf505423h
J. Agric. Food Chem. 2015, 63, 872−879

7-isopentenyloxycoumarin, **5**, were present in all the field collected plants from Marble Canyon, AZ. Plants collected from Holbrook, AZ, and Tuba City, AZ were qualitatively similar to those from Marble Canyon, AZ, other than that 7-isopentenyloxycoumarin, **5**, was not detected in the plants from Holbrook and dehydrotremetone, **2**, was not present in the plants from Tuba City. Quantitatively, plants from Holbrook, AZ, had approximately double the mean concentration or more of dehydrotremetone, **2**, 3-oxyangeloyl-tremetone, **3**, and 4-hydroxy-3-(3-methyl-2-butenyl)acetophenone, **4**, compared to the other two sites. This is the first report of these compounds in *I. rusbyi*. Tremetone, **1**, 3-oxyangeloyltremetone, **3**, and 7-isopentenyloxycoumarin, **5**, were present in *I. rusbyi* sampled herbarium specimens (n = 25) representing 9 different counties in Arizona, Colorado, New Mexico, and Utah at a frequency of 88, 88, and 40%, respectively. Consistent between field and herbarium collections was the occurrence of tremetone, **1**, 3-oxyangeloyltremetone, **3**, and 7-isopentenyloxycoumarin, **5**. Inconsistent between field and herbarium collections was the presence of 4-hydroxy-3-(3-methyl-2-butenyl)acetophenone, **4**, and dehydrotremetone, **2**, although compound **4** was detected at low concentrations in field collections, which may partially explain it being not present in the herbarium specimens.

Other *Isocoma* Species. In addition to the five species above for which field and herbarium collections were analyzed, we also analyzed herbarium specimens from 8 other species, *I. menziesii*, *I. coronopilofolia*, *I. drummondi*, *I. veneta*, *I. hartwegii*, *I. gypsophila*, *I. tomentosa*, and *I. arguta*. The distribution of these species is shown in Figure 4.[1] The number of herbarium

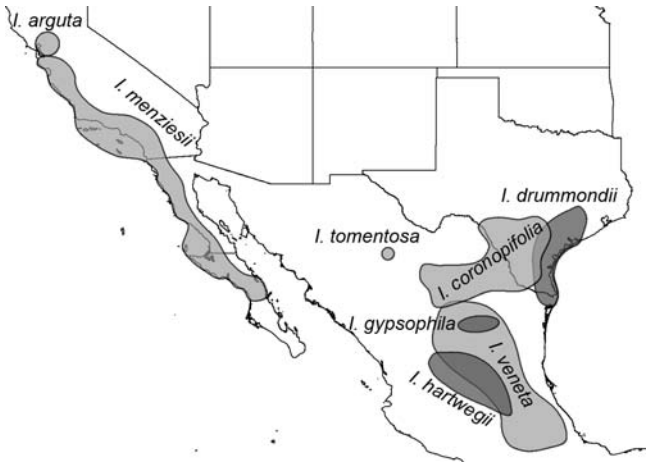

Figure 4. Map of the distribution of *Isocoma menziesii*, *I. coronopilofolia*, *I. drummondi*, *I. veneta*, *I. hartwegii*, *I. gypsophila*, *I. tomentosa*, and *I. arguta*.

specimens analyzed for each of these species ranged from 1 to 36 (Table 3). The number analyzed was limited by the available specimens from cooperating herbaria. 3-Oxyangeloyltremetone, **3**, was present in each of these species generally at frequencies ranging from 70 to 100% (Table 3). Other benzofuran ketones including tremetone, **1**, and structurally similar compounds (**4** and **5**) were also detected in select species. This is the first report of these compounds in *Isocoma menziesii*, *I. coronopilofolia*, *I. drummondi*, *I. veneta*, *I. hartwegii*, *I. gypsophila*, *I. tomentosa*, and *I. arguta*. In conclusion, one or more of the benzofuran ketones and similar compounds were found in all the *Isocoma* species analyzed to date.

In this study we analyzed both field collections and herbarium samples for tremetone, **1**, dehydrotremetone, **2**, 3-oxyangeloyltremetone, **3**, and structurally related compounds from the 5 major *Isocoma* spp. native to the southwestern United States. Both collections demonstrated that all three of the benzofuran ketones and at least one of the structurally related compounds were present in all 5 of the major *Isocoma* spp. native to the southwestern United States. This is the first report of these compounds in *I. tenuisecta*, *I. azteca*, *I. acradenia*, and *I. rusbyi*. The herbarium samples were of interest because we could sample a large number of plants from a large geographical area in a relatively short amount of time, however, since we were sampling limited leaf material from the specimens, the specimens were collected at different times of the year, and the specimens were collected over many different years, these samples were analyzed qualitatively but not quantitatively. In contrast, with the field collections we were able to sample representative samples from each species, collect replicate samples, and make collections at the same time of the year and during the same phenological stage. We were able to perform both qualitative and quantitative analysis with the field samples, however, we were limited to two or three locations for each of the 5 *Isocoma* spp. Due to the differences in the field and herbarium collections we were only able to make some broad qualitative comparisons between the two types of collections. Overall, the most consistent observations between the two types of collections were that tremetone, **1**, and 3-oxyangeloylytremetone, **3**, were the most observed benzofuran ketones. Inconsistent between the two types of collections was that dehydrotremetone, **2**, was present in the majority of the field collections, but was conspicuously absent in many of the herbarium specimens. To investigate the low frequency of dehydrotremetone, **2**, in the herbarium specimens, we sampled a herbarium specimen of *I. pluriflora* from the Pecos site held at the Intermountain Herbarium at Utah State University that we collected on May 8, 2008, and analyzed this herbarium specimen by HPLC.[19] We initially analyzed plant material collected at the Pecos site collected on May 8, 2008, by HPLC on February 18, 2009. The concentrations of tremetone, **1**, dehydrotremetone, **2**, and 3-oxyangeloyltremetone, **3**, were all lower in the herbarium specimen than in plant material from the same collection analyzed over 5 years earlier (Figure 5). All three benzofuran ketones appeared to decrease at herbarium storage conditions over the 5+ year time period; however, dehydrotremetone, **2**, appeared to decrease the most under these conditions. Although this data is limited, this comparison offers a possible explanation to the low frequency of dehydrotremetone, **2**, observed in the herbarium samples compared to the recently collected field samples. This comparison is also a caution that herbarium specimens may not accurately reflect the composition of secondary compounds in the field and should be evaluated in conjunction with samples analyzed shortly after collection. This comparison with *I. pluriflora* also suggests that tremetone, **1**, and dehydrotremetone, **2**, may be present in the *Isocoma* spp. *I. menziesii*, *I. coronopilofolia*, *I. drummondi*, *I. veneta*, *I. hartwegii*, *I. gypsophila*, *I. tomentosa*, and *I. arguta*, but no conclusions can be made as we only sampled herbarium specimens. As tremetone, **1**, and dehydrotremetone, **2**, have been suggested as the toxins in *I. pluriflora*,[13−15] and in light of the apparent loss of these compounds in *Isocoma* spp. over time at room temperature, a study documenting this phenomenon is warranted.

DOI: 10.1021/jf505423h
J. Agric. Food Chem. 2015, 63, 872−879

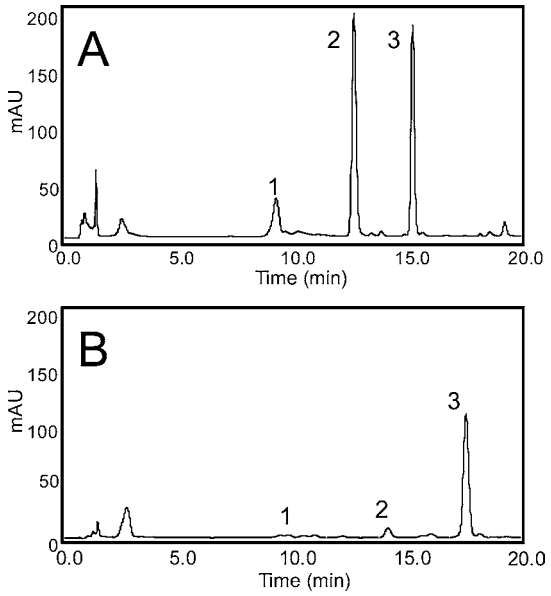

Figure 5. HPLC chromatograms of extracts from *I. pluriflora*, Pecos, collected on May 8, 2008: (A) analyzed February 18, 2009, (B) leaf tissue from voucher specimen #250012 held at the Intermountain Herbarium at Utah State University and analyzed November 4, 2014. Peak retention times are different due to a different Betasil C_{18} column used in the analysis. Peak numbers refer to compound structures in Figure 2.

It has been well established that *I. pluriflora* is poisonous, causing a disease called trembles and milksickness in livestock.[2−4] Tremetone, **1**, and dehydrotremetone, **2**, have been suggested as the toxins in *I. pluriflora* responsible for the disease[13−15] and have also been suggested as the toxins responsible for the same disease caused by white snakeroot, native to the eastern and midwestern United States.[4,14,15] Four other *Isocoma* spp., *I. tenuisecta*, *I. azteca*, *I. acradenia*, and *I. rusbyi*, are native to southwestern United States on land used extensively for livestock production. These plants were analyzed and found to contain tremetone, **1**, dehydrotremetone, **2**, and other compounds of similar structure at concentrations comparable to *I. pluriflora*.[5−8] These results raise the question: Why is there an absence of reports in the literature of livestock poisoning due to *I. tenuisecta*, *I. azteca*, *I. acradenia*, and *I. rusbyi*? One answer may be that tremetone, **1**, dehydrotremetone, **2**, and other compounds of similar structure are not the compounds responsible for toxicity in *I. pluriflora* or in white snakeroot even though they are common to both plants. Tremetone, **1**, and dehydrotremetone, **2**, as isolated compounds have not been documented to cause toxicity in a mammalian or livestock model. This may suggest that *I. pluriflora* and/or white snakeroot may share another unique compound(s) responsible for causing the same disease. However, in order to determine if *I. tenuisecta*, *I. azteca*, *I. acradenia*, and *I. rusbyi* are or are not toxic, well designed, controlled dosing studies in livestock using the toxic *I. plurifora* as a control must be conducted. Dosing studies in livestock using these different *Isocoma* spp. can result in valuable information into the toxic compound. For example if *I. azteca* from the Tsaya site, which contains approximately 1% of tremetone, **1**, and relatively low concentrations of dehydrotremetone, **2**, and other compounds, is dosed to livestock under the same regimen as toxic *I. pluriflora* and is found not to be toxic, serious doubt must be given into the role of tremetone, **1**, as the singular toxin.

In conclusion, this is the first report of tremetone, **1**, dehydrotremetone, **2**, 3-oxyangeloyltremetone, **3**, and similar compounds in *I. tenuisecta*, *I. azteca*, *I. acradenia*, and *I. rusbyi*. Tremetone, **1**, and dehydrotremetone, **2**, have been suggested as the toxins in *I. pluriflora*. The concentrations of tremetone, **1**, dehydrotremetone, **2**, and 3-oxyangeloyltremetone, **3**, in *I. tenuisecta*, *I. azteca*, *I. acradenia*, and *I. rusbyi* are similar to those in toxic *I. pluriflora*. In addition, tremetone, **1**, 3-oxyangeloyltremetone, **3**, and stucturally related compounds were reported for the first time in 8 other species, *Isocoma menziesii*, *I. coronoplofolia*, *I. drummondi*, *I. veneta*, *I. hartwegii*, *I. gypsophila*, *I. tometosa*, and *I. arguta*.

■ ASSOCIATED CONTENT

Ⓢ Supporting Information

List of *Isocoma* species, their voucher numbers, and their locations. This material is available free of charge via the Internet at http://pubs.acs.org.

■ AUTHOR INFORMATION

Corresponding Author

*Tel: (435) 752-2941. Fax: (435) 753-5681. E-mail: stephen.lee@ars.usda.gov.

Notes

The authors declare no competing financial interest.

■ ACKNOWLEDGMENTS

We thank Charles Hailes and Katie Lott for technical assistance as well as Edward Knoppel and Dr. Anthony Knight for assistance in plant collection. We appreciate the assistance of M. B. Piep, Assistant Curator, of the Intermountain Herbarium at Utah State University.

■ REFERENCES

(1) Neesom, G. L. Taxonomy of Isocoma (Asteraceae: Astereae). *Phytologia* **1991**, *70*, 69−114.

(2) Marsh, C. D.; Roe, G. C. The "Alkali Disease" of livestock in the Pecos Valley. *U.S., Dep. Agric., Circ.* **1921**, *180*, 3−8.

(3) Kingsbury, J. M. *Poionous plants of the United States and Canada*; Prentice Hall: Upper Saddle River, NJ, 1964.

(4) Burrows, G. E.; Tyrl, R. J. In *Toxic Plants of North America*, 2nd ed.; John Wiley and Sons: Ames, IA, 2013; p 190.

(5) Stegelmeier, B. L.; Davis, T. Z.; Green, B. T.; Lee, S. T.; Hall, J. O. Experimental rayless goldenrod (*Isocoma pluriflora*) toxicosis in goats. *J. Vet. Diagn. Invest.* **2010**, *22*, 570−577.

(6) Stegelmeier, B. L.; Davis, T. Z.; Green, B. T.; Lee, S. T.; Hall, J. O. The resolution of rayless goldenrod (*Isocoma pluriflora*) poisoning in goats. *Int. J. Poisonous Plant Res.* **2012**, *2*, 27−33.

(7) Davis, T. Z.; Green, B. T.; Stegelmeier, B. L.; Lee, S. T.; Welch, K. D.; Pfister, J. A. Physiological and serum biochemical changes associated with rayless goldenrod (*Isocoma pluriflora*) poisoning in goats. *Toxicon* **2013**, *76*, 247−254.

(8) Davis, T. Z.; Stegelmeier, B. L.; Lee, S. T.; Green, B. T.; Hall, J. O. Experimental rayless goldenrod (*Isocoma pluriflora*) toxicosis in horses. *Toxicon* **2013**, *73*, 88−95.

(9) Couch, J. F. Tremetol, the compound that produces "trembles" (milksickness). *J. Am. Chem. Soc.* **1929**, *51*, 3617−3619.

(10) Couch, J. F. The toxic constituent of rayless goldenrod. *J. Agric. Res.* **1930**, *40*, 649−658.

(11) Zalkow, L. H.; Burke, N.; Cabat, G.; Grula, E. A. Toxic constituents of rayless goldenrod. *J. Med. Chem.* **1962**, *5*, 1342−1351.

(12) Zalkow, L. H.; Ekpo, B. A.; Gelbaum, L. T.; Harris, R. N., III; Keinan, E.; Novak, J. R., Jr.; Ramming, C. T.; Van Derveer, D. The

DOI: 10.1021/jf505423h
J. Agric. Food Chem. 2015, 63, 872−879

benzofurans of *Isocoma wrightii*, structure and stereochemistry. *J. Nat. Prod.* **1979**, *42*, 203−219.
(13) Bowen, D. M.; DeGraw, J. I., Jr.; Shah, V. R.; Bonner, W. A. The synthesis and pharmacological action of tremetone. *J. Med. Chem.* **1963**, *6*, 315−319.
(14) Beier, R. C.; Norman, J. O.; Irvin, R. T.; Witzel, D. A. Microsomal activation of constituents of white snakeroot (*Eupatorium rugosum* Houtt) to form toxic products. *Am. J. Vet. Res.* **1987**, *48*, 583−585.
(15) Beier, R. C.; Norman, J. O.; Reagor, M. C.; Rees, M. S.; Mundy, B. P. Isolation of the major component in white snakeroot that is toxic after microsomal activation: possible explanation of sporadic toxicity of white snakeroot plants and extracts. *Nat. Toxins* **1993**, *1*, 286−293.
(16) Moseley, E. L. *Milk sickness caused by white snakeroot*; The Ohio Academy of Science, Edwards Brothers, Inc.: Ann Arbor, MI, 1917; p 171.
(17) Couch, J. F. The toxic constituent of richweed or white snakeroot (*Eupatorium urticaefolium*). *J. Agric. Res.* **1927**, *35*, 547−576.
(18) Bonner, W. A.; DeGraw, J. I., Jr. Ketones from "white snakeroot" *Eupatorium urticaefolium*. *Tetrahedron* **1962**, *18*, 1295−1309.
(19) Lee, S. T.; Davis, T. Z.; Gardner, D. R.; Stegelmeier, B. L.; Evans, T. J. A quantitiative method for the measurement of three benzofuran ketones in rayless goldenrod (*Isocoma pluriflora*) and white snakeroot (*Ageratina altissima*) by HPLC. *J. Agric. Food Chem.* **2009**, *57*, 5639−5643.
(20) Lee, S. T.; Davis, T. Z.; Gardner, D. R.; Colegate, S. M.; Cook, D.; Green, B. T.; Meyerholtz, K. A.; Wilson, C. R.; Stegelmeier, B. L.; Evans, T. J. Tremetone and structurally related compounds in white snakeroot (*Ageratina altissima*): A plant associated with trembles and milk sickness. *J. Agric. Food Chem.* **2010**, *58*, 8560−8565.
(21) Buehrer, T. F.; Mason, C. M.; Crowder, J. A. The chemical composition of rayless goldenrod (*Aplopappus hartwegi*). *Am. J. Pharm.* **1939**, *111*, 105−112.
(22) Tomas-Barberan, F.; Iniesta-Sanmartin, E.; Tomas-Lorente, F.; Rumero, A. Antimicrobial phenolic compounds from three Spanish *Helichrysum* species. *Phytochemistry* **1990**, *29*, 1093−1095.
(23) Piro, O. E.; Echeverria, G. A.; Lizarraga, E.; Romano, E.; Catalan, C. A. N.; Brandan, S. A. Molecular structure of 4-hidroxy-3-(3-methyl-2-butenyl)acetophenone, a plant antifungal, by X-ray diffraction, DFT calculation, and NMR and FTIT spectroscopy. *Spectrochim. Acta, Part A* **2013**, *101*, 196−203.
(24) Lassak, E. V.; Southwell, I. A. The coumarins from the resin of *Euodia vitiflora*. *Aust. J. Chem.* **1972**, *25*, 2491−2496.
(25) Latip, J.; Hartley, T. G.; Waterman, P. G. Lignans and coumarin metabolites from *Meticope hayseii*. *Phytochemistry* **1999**, *51*, 107−110.
(26) Askari, M.; Sahebkar, A.; Iranshahi, M. Synthesis and purification of 7-prenyloxycoumarins and herniarian as bioactive natural coumarins. *Iran J. Basic Med. Sci.* **2009**, *12*, 63−69.
(27) TIGER/line shapefiles prepared by the U.S. Census Bureau, 2013. https://www.census.gov/geo/maps-data/data/tiger-line.html. (Accessed: 03/22/2013.)
(28) Lee, S. T.; Davis, T. Z.; Cook, D.; Stegelemeier, B. L. Evaluation of drying methods and toxicity of rayless goldenrod (*Isocoma pluriflora*) and white snakeroot (*Ageratina altissima*) in goats. *J. Agric. Food Chem.* **2012**, *60*, 4849−4853.

DOI: 10.1021/jf505423h
J. Agric. Food Chem. 2015, 63, 872−879

Jackson (Muskegon, MI). HPLC-grade chloroform, methyl pentadecanoate, and methanolic hydrochloride were purchased from Sigma-Aldrich (St. Louis, MO).

Strains and Culture Conditions. The *D. tertiolecta* strain UTEX LB999 (henceforth referred to simply as "LB999") acclimated to an optimal temperature of 21 °C was obtained from the culture collection of algae at the University of Texas at Austin, and another strain, SCCAP K-0591 (henceforth referred to simply as "K-0591"), acclimated to an optimal temperature of 15 °C was obtained from the Scandinavian Culture Collection in Copenhagen, Denmark. To enable direct comparison, both strains were grown photoautotrophically under the same conditions—except for temperature—under illumination from fluorescent lamps at 50 μE/(m^2 s) in 3-fold f/2 medium[19] without vitamins. The culture medium consisted of 225 mg/L $NaNO_3$, 15 mg/L $NaH_2PO_4{\cdot}7H_2O$, and 1 mL of trace-elements stock solution (4.16 g/L Na_2EDTA, 3.15 g/L $FeCl_3{\cdot}6H_2O$, 0.01 g/L $CuSO_4{\cdot}5H_2O$, 0.022 g/L $ZnSO_4{\cdot}7H_2O$, 0.01 g/L $CoCl_2{\cdot}6H_2O$, 0.18 g/L $MnCl_2{\cdot}4H_2O$, and 0.006 g/L $Na_2MoO_4{\cdot}2H_2O$) in artificial seawater (24.7 g/L NaCl, 0.66 g/L KCl, 8.48/L $MgCl_2{\cdot}6H_2O$, 1.9 g/L $CaCl_2{\cdot}2H_2O$, 3.07 g/L $MgSO_4{\cdot}7H_2O$, and 0.18 g/L $NaHCO_3$). The concentration of nitrate was kept at 2.68 mM throughout the culture period by measuring it every 24 h and adding nitrate stock solution as required.

Algal cultures were set up in 400 mL bubble-column photobioreactors at a fresh cell weight (FCW) inoculation concentration of 0.1 g/L and with 0.1 vvm aeration using 2% CO_2-enriched air to provide a carbon source for the culture. The microalgal concentration (cells/mL) and FCW (g/L) were determined daily using a Multisizer 3 Coulter counter (Beckman Coulter, Miami, FL).

Culture shifting was performed when the FCWs (cell concentrations) of LB999 and K-0591 were 1.76 g/L (7.7×10^6 cells/L) and 1.12 g/L (4.3×10^6 cells/L), respectively (Figure S1 in the Supporting Information). The time point at which ND was triggered—when the FCW reached half that measured at the beginning of the stationary phase for each strain—was determined on the basis of a preliminary study that the most-significant changes in FA profiles were observed in that time point.[20] The cells were harvested at that point and washed three times with centrifugation at 1500 rpm for 5 min (UNION 32R PLUS, Hanil Science Industrial, Incheon, Korea) to remove the nutrients. The cells were then transferred to either nitrate-sufficient (NS) or ND medium and cultured for 12 h. The algal cells were harvested by transferring 400 mL of the cell suspensions to 50 mL tubes, and then they were precipitated by centrifugation at 1500 rpm for 5 min. The transparent supernatant was discarded, and the cell pellets were completely washed four times with distilled water by centrifugation and resuspension. The collected algal cells were freeze-dried and kept in labeled tubes at −80 °C before extraction.

Extraction of Total Lipids. Glycerolipids and glycerophospholipids were extracted from 1 mg of dried biomass from each sample extracted using a modified Folch procedure, as described previously.[9] The extracts were dried with nitrogen gas, capped, and stored at −20 °C for chip-based nanoelectrospray ionization (nano-ESI) direct infusion.

Methylation of FAs. FAs were extracted by adding 200 μL of chloroform/methanol (2:1, v/v) to 5 mg of dried cells. The FAs were then converted into fatty acid methyl esters (FAMEs) by incubating the samples in 300 μL of 1.25 M methanolic hydrochloride for 1 h at 85 °C[21] and then adding 1 mL of hexane and incubating for 1 h at room temperature. A 90 μL aliquot of the upper layer was transferred to a vial, 10 μL of methyl pentadecanoate was added, and the mixture was vortexed.

Analysis of Glycerolipids and Glycerophospholipids. Glycerolipids and glycerophospholipids were analyzed in positive and negative ion modes on a linear ion-trap mass spectrometer (LTQ-XL, ThermoFisher Scientific, San Jose, CA) equipped with an automated nanoinfusion/nanospray source (Triversa NanoMate System, Advion Biosciences, Ithaca, NY). The ionization voltage and gas pressure were set to 1.4 kV and 0.4 psi, respectively, and the ion source was controlled using Chipsoft 8.3.1 software (Advion Biosciences). All lipid samples were dissolved in 500 μL of methanol/chloroform (9:1, v/v) containing 7.5 mM ammonium acetate; 15 μL of each sample was loaded into a 96-well plate (Eppendorf, Hamburg, Germany), which was then sealed with aluminum film (ThermoFisher Scientific) using a heat sealer. The 96-well plate was placed onto a NanoMate cooling plate set at a temperature of 5 °C. A 5 μL volume of each of the samples was aspirated and infused into a mass spectrometer via an Advion ESI chip with 5.5 μm [inner diameter (i.d.)] emitter nozzles. Biological triplicates of the LB999 samples were each analyzed in triplicate by nano-ESI mass spectrometry (MS), while biological duplicates of the K-5091 samples were each analyzed in triplicate.

Full-scan spectra were collected in mass-to-charge ratio (m/z) ranges of 400−1200 and 500−1300 in positive and negative ion modes, respectively. The mass spectra of each sample were acquired in profile mode over a 2 min period. The capillary temperature was set to 200 °C; the capillary voltage and tube lens were set to 47 and 145 V, respectively, in positive mode, and to −44 and −132 V in negative mode. The target automatic gain control values for full MS and multistage MS were 30000 and 10000, respectively. MS/MS was applied to pooled samples for identification of lipid species. The normalized collision energy was set to 35% with an isolated width of 3 m/z units and a charge state of 1. The dynamic exclusion parameters were a repeat duration of 60 s, an exclusion duration of 60 s, and an exclusion list size of 50.

Analysis of FAMEs. The samples were analyzed using a gas chromatograph (model 7890A, Agilent Technologies, Santa Clara, CA) equipped with a mass-selective detector (model 5975C, Agilent Technologies), an autosampler (7683B series, Agilent Technologies), a split/splitless injector, an injection module, and ChemStation software. The GC inlet temperature was set to 250 °C, and 1.0 μL of sample was injected in duplicate. Helium was used as the carrier gas in constant-flow mode at 1.0 mL/min. A fused silica capillary column of 5% phenyl methylpolysiloxane phase (DB-5, Agilent Technologies) with film dimensions of 30 m × 0.25 mm (i.d.) × 0.25 μm was used for analysis. The detector voltage was set to 1812 V, and the auxiliary, MS source, and MS quadrupole temperatures were set to 280, 230, and 150 °C, respectively.

The split ratio and mass range for the FAME analysis were 5:1 and 40−400 Da, respectively, and data were obtained in full-scan mode. The initial oven temperature of 70 °C was held for 3 min before being ramped first to 130 °C at a rate of 20 °C/min, to 178 °C at 4 °C/min, to 200 °C at 1 °C/min, and finally to 290 °C at 10 °C/min. The total run time was 40 min.

Data Acquisition and Processing. The full-scan data were acquired using a nano-ESI-MS system and processed with Expressionist MSX v2013.0.39 software (Genedata, Basel, Switzerland). The spectral scans obtained between 0.5 and 1.5 min were averaged, then spectrum smoothing, m/z alignment, and baseline subtraction were performed, and the obtained data were prepared for multivariate analysis. One-way analysis of variance was performed using Expressionist MSX software. The data matrices exported from Expressionist MSX were imported to SIMCA-P software (version 13.0, Umetrics, Umeå, Sweden) for principal component analysis (PCA), for which Pareto scaling and mean centering were applied.

For the GC−MS-based FAME analysis, mass spectral data were processed using the AMDIS (Automated Mass Spectral Deconvolution and Identification System) and SpectConnect (http://spectconnect.mit.edu/). The AMDIS was initially used for mass spectrum deconvolution, which isolates the target peaks from the noise and overlapping peaks.[22] The following settings were used: a component width of 12, adjacent peaks subtraction of 1, medium resolution, low sensitivity, and medium shape requirement. The resulting *.elu files were subsequently analyzed using an online peak-filtering algorithm. The FAs were identified using the National Institute of Standards and Technology mass spectral search program, with a match quality greater than 70% set as the criterion for peak assignment. Normalization was then performed by dividing the base peak intensity of each compound by that of methyl pentadecanoate (the internal standard) to obtain the relative intensities of the FAs in each sample. The composition of each FA in *D. tertiolecta* samples is presented as a percentage, which was

DOI: 10.1021/jf502967k
J. Agric. Food Chem. 2015, 63, 880−887

Table 1. Fatty Acid (FA) Composition (%) of Algal Lipids Extracted from Two *D. tertiolecta* Strains Cultivated in Nitrate-Sufficient (NS) and Nitrate-Deficient (ND) Conditions[a−c]

			K-0591		LB999	
FA[d]	RT (min)	MS fragment ion (m/z)	NS	ND	NS	ND
C12:0	13.6	43, 55, 69, 74, 87	0.01 ± 0.01	0.01 ± 0.01 (ns)	0.04 ± 0.02	0.04 ± 0.01 (ns)
C14:0	18.3	74, 87, 143, 199, 211	0.16 ± 0.02	0.19 ± 0.02 (ns)	0.23 ± 0.02	0.24 ± 0.00 (ns)
C16:0	23.9	74, 87, 143, 227, 270	23.64 ± 0.51	24.06 ± 0.70 (ns)	24.73 ± 0.39	26.67 ± 0.11 (↑)
C16:1	23.0	55, 67, 74, 84, 96	1.69 ± 0.04	2.31 ± 0.12 (↑)	1.92 ± 0.20	2.23 ± 0.22 (↑)
	23.7	55, 67, 74, 83, 96				
C16:2	22.8	67, 81, 95, 109, 135	1.00 ± 0.03	1.17 ± 0.01 (↑)	2.23 ± 0.28	2.09 ± 0.10 (ns)
C16:3	22.3	79, 105, 119, 133, 147	0.62 ± 0.03	0.59 ± 0.03 (ns)	1.86 ± 0.12	1.67 ± 0.10 (↓)
C18:0	30.8	74, 87, 143, 255, 298	0.58 ± 0.04	0.55 ± 0.04 (ns)	1.14 ± 0.44	1.15 ± 0.21 (ns)
C18:1	30.0	55, 69, 83, 97, 110	0.76 ± 0.04	0.78 ± 0.11 (ns)	1.24 ± 0.16	0.94 ± 0.06 (↓)
C18:2	29.2	67, 81, 95, 109, 121	8.18 ± 0.46	8.49 ± 0.04 (ns)	11.31 ± 0.56	11.10 ± 0.15 (ns)
	29.5	67, 81, 95, 109, 123				
C18:3	22.9	79, 93, 108, 121, 135	63.13 ± 1.01	61.60 ± 0.92 (↓)	54.93 ± 0.73	53.47 ± 0.38 (↓)
	28.9	79, 93, 107, 121, 150				
	29.8	79, 95, 108, 121, 135				
	30.2	79, 87, 95, 135, 149				
	30.3	79, 87, 121, 149, 163				
C20:0	38.4	74, 87, 143, 283, 326	0.04 ± 0.01	0.05 ± 0.00 (↑)	0.08 ± 0.01	0.13 ± 0.01 (↑)
C20:1	17.6	55, 67, 74, 81, 96	0.09 ± 0.01	0.10 ± 0.01 (↑)	0.12 ± 0.01	0.12 ± 0.00 (ns)
C20:2	37.6	81, 95, 109, 120, 322	0.07 ± 0.02	0.07 ± 0.00 (ns)	0.12 ± 0.02	0.09 ± 0.02 (↓)
C22:0	41.7	74, 87, 143, 207, 354	0.02 ± 0.01	0.03 ± 0.00 (↑)	0.07 ± 0.01	0.07 ± 0.01 (ns)
∑SFAs			24.46 ± 0.52	24.89 ± 0.77	26.28 ± 0.86	28.29 ± 0.18
∑MUFAs			2.54 ± 0.08	3.19 ± 0.22	3.27 ± 0.15	3.29 ± 0.19
∑PUFAs			73.01 ± 0.59	71.91 ± 0.99	70.44 ± 0.89	68.43 ± 0.14

[a]Abbreviations: RT, retention time; SFA, saturated FA; MUFA, monounsaturated FA; PUFA, polyunsaturated FA; MS, mass spectrometry; m/z, mass-to-charge ratio. [b]Data are the mean ± SD values for biological and experimental repetitions at $n = 6$ for LB999 and $n = 4$ for K-0591. [c]A t test was conducted for the NS and ND conditions. Key: ns, no significant difference ($p < 0.05$); ↑, significantly high percentage composition compared with that of the NS condition; ↓, significantly low percentage composition compared with that of the NS condition. [d]Cx:y, FA annotation, where x is the number of carbon atoms and y is the number of double bonds.

obtained by dividing the relative intensity of the FA by the sum of the total FA relative intensity. Significant differences were detected by a t test using the PASW Statistics 19 software (IBM, Somers, NY). The cutoff for statistical significance was set at $p < 0.05$.

RESULTS AND DISCUSSION

FA Profiles. Table 1 presents the FA composition of algal oil extracted from the two *D. tertiolecta* strains (K-0591 and LB999) with different optimal growth temperatures (15 and 21 °C, respectively). The dominant FAs were C18:3, C16:0, and C18:2, results which are similar to those of previous studies finding the main components of *D. tertiolecta* to be C18:3 and C16:0.[16,23] Linolenic acid (C18:3) was the most abundant FA in both strains, but was the predominant FA in K-0591. It is known that microalgae change their FA composition at low temperature as a method of maintaining their membrane fluidity.[24] It has been reported that the level of unsaturated lipids in *Dunaliella salina* increases when the temperature is reduced from 30 to 12 °C.[25] In this context, the main alteration implemented to prevent membrane rigidification is an increase in polyunsaturated FAs (PUFAs), including C18:3. Preserving the fluidity of the chloroplast membrane is essential for effective photosynthetic function at low temperature. For example, membrane fluidity is crucial for electron transport among the photosynthetic complexes, as well as for gas exchange.[26] In addition, PUFAs have a protective effect against the damage caused by high light intensity and UV radiation.[27]

When nitrate was deficient, the percentage compositions of C16:1 and C20:0 were significantly increased in both strains, whereas that of C18:3 was decreased in both. Nitrogen deficiency generally takes place toward the end of cell growth, when cell division is attenuated following an energy-storing process. Palmitoleic acid (C16:1) is associated with energy storage.[28] Conversely, the biosynthesis of PUFAs usually occurs during the growth phase.[29] Therefore, ND conditions seem to transfer the cell status from a growth stage to an energy-storage stage in both the low- and higher-temperature-acclimated *D. tertiolecta* strains.

Meanwhile, the FAs extracted from K-0591 and LB999 that had changed most significantly (in terms of the percentage composition) were linolenic acid (C18:3) and palmitic acid (C16:0), respectively. Interestingly, it appears that the reduction in C18:3 in K-0591 might have been affected by the decline of two lipid species: digalactosyldiacylglycerol (DGDG) 18:3/16:4 and *lyso*-diacylglyceryl-*N*,*N*,*N*-trimethylhomoserine (DGTS; *lyso*-DGTS) 18:3 (Table 2). In addition, the increase in C16:0 in LB999 under ND conditions was consistent with the elevation of lipid species containing C16:0 (Table 2). Together these results show that the characteristic changes in FA profiles in both strains were caused by changes in their lipid profiles.

PCA Using the Nano-ESI-MS Data Set. *D. tertiolecta* samples were characterized according to their lipid profiles, which were detected by nano-ESI-MS in both the positive and negative ion modes. The processed mass spectral data were then subjected to PCA. The PCA score plot revealed a clear separation between LB999 and K-0591 when using the detected ions in the two ion modes (Figure 1). The algal

DOI: 10.1021/jf502967k
J. Agric. Food Chem. 2015, 63, 880−887

Table 2. Identification of Lipid Species from Two *D. tertiolecta* Strains Cultivated in Nitrate-Sufficient (NS) and Nitrate-Deficient (ND) Conditions by Nanoelectrospray Ionization MS Along with *p* Values from *t* Tests and the Relative Changes in Identified Peak Intensities[a]

				K-0591 (NS) / LB999 (NS)		LB999 (ND)/LB999 (NS)		K-0591 (ND)/ K-0591 (NS)	
ion mode	ion species	*m/z*	proposed composition	*p*	fold change[b]	*p*	fold change[b]	*p*	fold change[b]
				DGTS					
(+)	$[M + H]^+$	680.2	C16:0/C14:2	0.01	1.37 (↑)	0.50	1.06 (ns)	0.60	1.07 (ns)
(+)	$[M + H]^+$	704.7	C16:0/C16:4	0.00	7.59 (↑)	0.03	1.52 (↑)	0.53	1.13 (ns)
(+)	$[M + H]^+$	706.8	C16:0/C16:3	0.00	5.66 (↑)	0.02	1.46 (↑)	0.66	1.09 (ns)
(+)	$[M + H]^+$	708.8	C16:0/C16:2	0.00	3.16 (↑)	0.00	1.65 (↑)	0.93	1.02 (ns)
(+)	$[M + H]^+$	732.7	C18:4/C16:0	0.00	3.58 (↑)	0.26	0.85 (ns)	0.86	0.97 (ns)
(+)	$[M + H]^+$	734.7	C18:3/C16:0	0.00	1.91 (↑)	0.04	1.36 (↑)	0.71	0.93 (ns)
(+)	$[M + H]^+$	736.8	C18:2/C16:0	0.00	1.89 (↑)	0.00	2.15 (↑)	0.92	1.02 (ns)
(+)	$[M + H]^+$	738.8	C18:1/C16:0	0.00	1.82 (↑)	0.00	2.25 (↑)	0.06	1.46 (ns)
(+)	$[M + H]^+$	748.7	C18:3/C17:0	0.16	1.16 (ns)	0.00	1.40 (↑)	0.73	0.95 (ns)
			C19:3/C16:0						
(+)	$[M + H]^+$	756.7	C18:3/C18:3	0.00	2.76 (↑)	0.55	0.93 (ns)	0.85	1.04 (ns)
(+)	$[M + H]^+$	758.7	C18:2/C18:3	0.00	2.30 (↑)	0.70	1.05 (ns)	0.77	1.06 (ns)
(+)	$[M + H]^+$	760.8	C18:2/C18:2	0.00	1.89 (↑)	0.24	1.20 (ns)	0.36	1.22 (ns)
			C18:1/C18:3						
(+)	$[M + H]^+$	762.4	C18:1/C18:2	0.00	1.87 (↑)	0.43	0.93 (ns)	0.74	0.94 (ns)
			C18:0/C18:3						
(+)	$[M + H]^+$	764.5	C18:1/C18:1	0.56	1.07 (ns)	0.04	0.84 (↓)	1.00	1.00 (ns)
			C18:2/C18:0						
(+)	$[M + H]^+$	776.6	C19:0/C18:3	0.00	2.84 (↑)	0.46	1.12 (ns)	0.71	0.95 (ns)
			C19:1/C18:2						
			C21:3/C16:0						
(+)	$[M + H]^+$	778.6	C 21:2/C16:0	0.00	1.97 (↑)	0.00	0.74 (↓)	0.59	0.96 (ns)
			C19:0/C18:2						
				DGDG					
(+)	$[M + Na]^+$	928.3	C18:3/C16:4	0.06	0.84 (ns)	0.18	0.88 (ns)	0.01	0.61 (↓)
(+)	$[M + Na]^+$	932.4	C18:3/C16:3	0.85	0.98 (ns)	0.11	1.18 (ns)	0.43	0.84 (ns)
(+)	$[M + Na]^+$	934.4	C18:3/C16:2	0.03	0.80 (↓)	0.00	1.41 (↑)	0.53	0.91 (ns)
(+)	$[M + Na]^+$	935.5	C18:3/C16:1	0.04	0.50 (↓)	0.05	1.41 (ns)	0.10	2.46 (ns)
			C18:2/C16:2						
			C18:1/C16:3						
(+)	$[M + Na]^+$	937.4	C 18:3/16:0	0.02	1.39 (↑)	0.06	1.15 (ns)	0.07	1.40 (ns)
(+)	$[M + Na]^+$	939.4	C 18:2/16:0	0.11	1.22 (ns)	0.76	0.98 (ns)	0.29	1.13 (ns)
(+)	$[M + Na]^+$	941.5	C 18:1/16:0	0.16	1.19 (ns)	0.40	1.07 (ns)	0.29	1.13 (ns)
				lyso-DGTS					
(+)	$[M + H]^+$	474.5	C16:0	0.95	1.02 (ns)	0.95	1.01 (ns)	0.78	0.93 (ns)
(+)	$[M + H]^+$	496.5	C18:3	0.04	1.66 (↑)	0.00	0.41 (↓)	0.01	0.56 (↓)
(+)	$[M + H]^+$	498.6	C18:2	0.72	1.08 (ns)	0.01	0.59 (↓)	0.26	0.79 (ns)
				MGDG					
(+)	$[M + Na]^+$	767.6	C18:3/C16:4	0.00	1.72 (↑)	0.86	1.03 (ns)	0.92	1.02 (ns)
(+)	$[M + Na]^+$	769.6	C18:2/C16:4	0.39	1.16 (ns)	0.64	0.92 (ns)	0.35	0.83 (ns)
			C18:3/C16:3						
(−)	$[M + OAc]^-$	803.9	C18:3/C16:4	0.05	0.83 (ns)	0.31	1.18 (ns)	0.98	1.00 (ns)
				SQDG					
(−)	$[M - H]^-$	794.2	C16:0/C16:0	0.89	1.01 (ns)	0.08	1.24 (ns)	0.41	0.89 (ns)
(−)	$[M - H]^-$	816.1	C18:3/C16:0	0.33	1.10 (ns)	0.94	0.99 (ns)	0.16	0.82 (ns)
(−)	$[M - H]^-$	819.2	C18:1/C16:0	0.83	1.02 (ns)	0.52	0.92 (ns)	0.36	0.88 (ns)
				PG					
(−)	$[M - H]^-$	744.1	C18:3/C16:0	0.75	1.04 (ns)	0.29	0.89 (ns)	0.33	0.82 (ns)
(−)	$[M - H]^-$	746.2	C18:1/C16:1	0.18	1.16 (ns)	0.40	0.90 (ns)	0.11	0.76 (ns)
(−)	$[M - H]^-$	748.2	C18:1/C16:0	0.40	0.90 (ns)	0.00	2.30 (↑)	0.84	1.03 (ns)
				PI					
(−)	$[M - H]^-$	836.1	C18:1/C16:0	0.38	0.92 (ns)	0.00	1.82 (↑)	0.79	0.96 (ns)

[a]Abbreviations: DGTS, diacylglyceryl-*N,N,N*-trimethylhomoserine; DGDG, digalactosyldiacylglycerol; MGDG, monogalactosyldiacylglycerol; SQDG, sulfoquinovosyldiacylglycerol; PG, phosphatidylglycerol; PI, phosphatidylinositol. [b]Key: ns, no significant difference ($p < 0.05$); ↑, significant difference ($p < 0.05$) and relative change >1; ↓, significant difference ($p < 0.05$) and relative change <1.

DOI: 10.1021/jf502967k
J. Agric. Food Chem. 2015, 63, 880−887

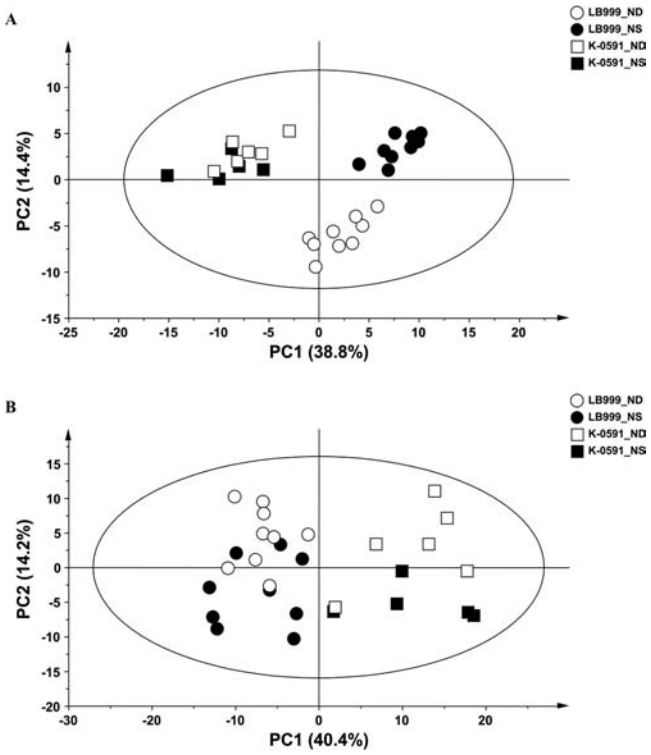

Figure 1. Principal component analysis score plot derived from the nanoelectrospray ionization mass spectrometry (nano-ESI-MS) data of two *D. tertiolecta* samples, a 21 °C-optimized strain (LB999; circles) and a 15 °C-optimized strain (K-0591; squares), under nitrate-sufficient (NS; filled symbols) and nitrate-deficient (ND; open symbols) conditions in (A) positive ion mode and (B) negative ion mode. Abbreviations: PC1, principal component 1; PC2, principal component 2.

strains exhibited different trends according to their response to the nitrate condition. Interestingly, the lipid profile of LB999 exhibited a clearer separation between the NS and ND conditions than did K-0591 in the positive ion mode. This implies that nitrate deficiency markedly alters the lipid profile in LB999 but not in K-0591.

Lipid Profile. Figure 2 shows representative spectra of lipids from a pooled lipid extract sample of the two *D. tertiolecta* strains in positive and negative ion modes. In total, 16 DGTS species, 7 DGDG species, 3 *lyso*-DGTS species, and 2 monogalactosyldiacylglycerol (MGDG) species were detected in positive ion mode, and 3 sulfoquinovosyldiacylglycerol (SQDG) species, 3 phosphatidylglycerol (PG) species, and 1 phosphatidylinositol (PI) species were detected in negative ion mode. MGDG 34:7 was detected in both ion modes (Table 2).

Comparison of K-0591 and LB999 under the normal, NS conditions revealed significantly higher levels of DGTS in K-0591. DGTS is known to be a substrate for the further desaturation of FAs. For example, DGTS appears to act as a major substrate for the sequential desaturation of C18:1 to C18:3. Moreover, DGTS is regarded as a donor of eicosapentaenoic acid (C20:5) for chloroplast lipids.[30] Therefore, it can be hypothesized that the high levels of DGTS species with unsaturated fatty acyl chains in K-0591 could aid the maintenance of a highly unsaturated, adequately fluid chloroplast membrane at low temperatures.

To investigate the association of DGTS with low-temperature adaptation, lipid profiles were compared using the LB999 cultures cultivated at different temperatures (15 and 21 °C). Each cell was harvested at mid exponential phase on the basis of the growth curve under each temperature condition. The growth of LB999 cells was significantly retarded in the 15 °C culture, and they entered the stationary phase earlier than those cultivated at 21 °C (data not shown). These results imply that cultivation at a temperature (15 °C) that is lower than the normal cultivation temperature (21 °C) caused cold stress and physiological changes in LB999 cells.

Interestingly, the levels of DGTS species were lower in LB999 cells cultivated at 15 °C than those cultivated at 21 °C (Table S1 in the Supporting Information). DGTS was previously shown to be involved in desaturation of FAs, and the biosynthesis of PUFA was found to be generally enhanced during the dramatic exponential growth of microalgae.[28,31] The higher levels of DGTS species in the K-0591 strain seemed to be positively associated with robust growth even at low temperature, which is a consequence of long-term cold adaptation of that strain over many years. However, the lower levels of DGTS species in LB999 cells cultivated at 15 °C might be caused by short-term exposure stress to a low-temperature condition rather than to long-term cold adaptation. It is assumed that the contribution of DGTS species to low- temperature conditions is feasible only in long-term adaptation and evolution, as in the case of the K-0591 strain.

DGTS species with odd-numbered fatty acyl chains, such as C17 and C19, were also detected. The role of odd-numbered FAs in algae remains unclear; however, it has been reported that odd-numbered, branched-chain FAs such as C15:0 and C17:0 have a relatively low melting point and thus contribute to cold adaptation in the bacterium *Listeria monocytogenes*.[32]

The levels of DGDG 18:3/16:0 and MGDG 18:3/16:4 were higher in K-0591 than in LB999, while those of two DGDG species (DGDG 18:3/16:2 and DGDG 18:3/16:1) were lower. Johnson et al revealed that MGDG 16:0/18:1 is the preferred precursor moiety of DGDG biosynthesis.[33] Moreover, it was observed that DGDG 16:0/18:2 (rather than DGDG 16:0/18:1) was found in *Brassica napus* leaves grown at low temperature.[32] It can therefore be assumed that the higher level of DGDG 18:3/16:0 may be the result of sequential desaturation of MGDG 16:0/18:1 as a base form under low-temperature conditions. In addition, it was reported that rapid desaturation of the MGDG fatty acyl groups occurred in both the C16 and C18 species at low temperature, resulting in highly desaturated fatty acyl chains in MGDG from *B. napus* leaves.[34] This is supported by the present finding that the level of the highly unsaturated formed MGDG 18:3/16:4 was higher in the low-temperature K-0591 strain than in LB999. Therefore, these unique DGDG and MGDG patterns of fatty acyl chains were presumably caused by cold adaptation of *D. tertiolecta*.

The lipid compositions of organisms grown with and without nitrate (i.e., NS and ND conditions) were compared to determine which lipid species affect the metabolism of *D. tertiolecta* under ND conditions. Most of the DGTS species were increased in LB999 after 12 h of ND conditions. It is known that oil globules accumulate under nutrient-limited conditions. DGTS appears to play a role as a polar lipid monolayer that aids the formation of oil globules in green algae.[35] However, the levels of most lipids, including the DGTS species, were not changed in K-0591 under the same conditions. K-0591 was initially collected from the North Sea close to Denmark, where concentrations of dissolved nitrogen

DOI: 10.1021/jf502967k
J. Agric. Food Chem. 2015, 63, 880−887

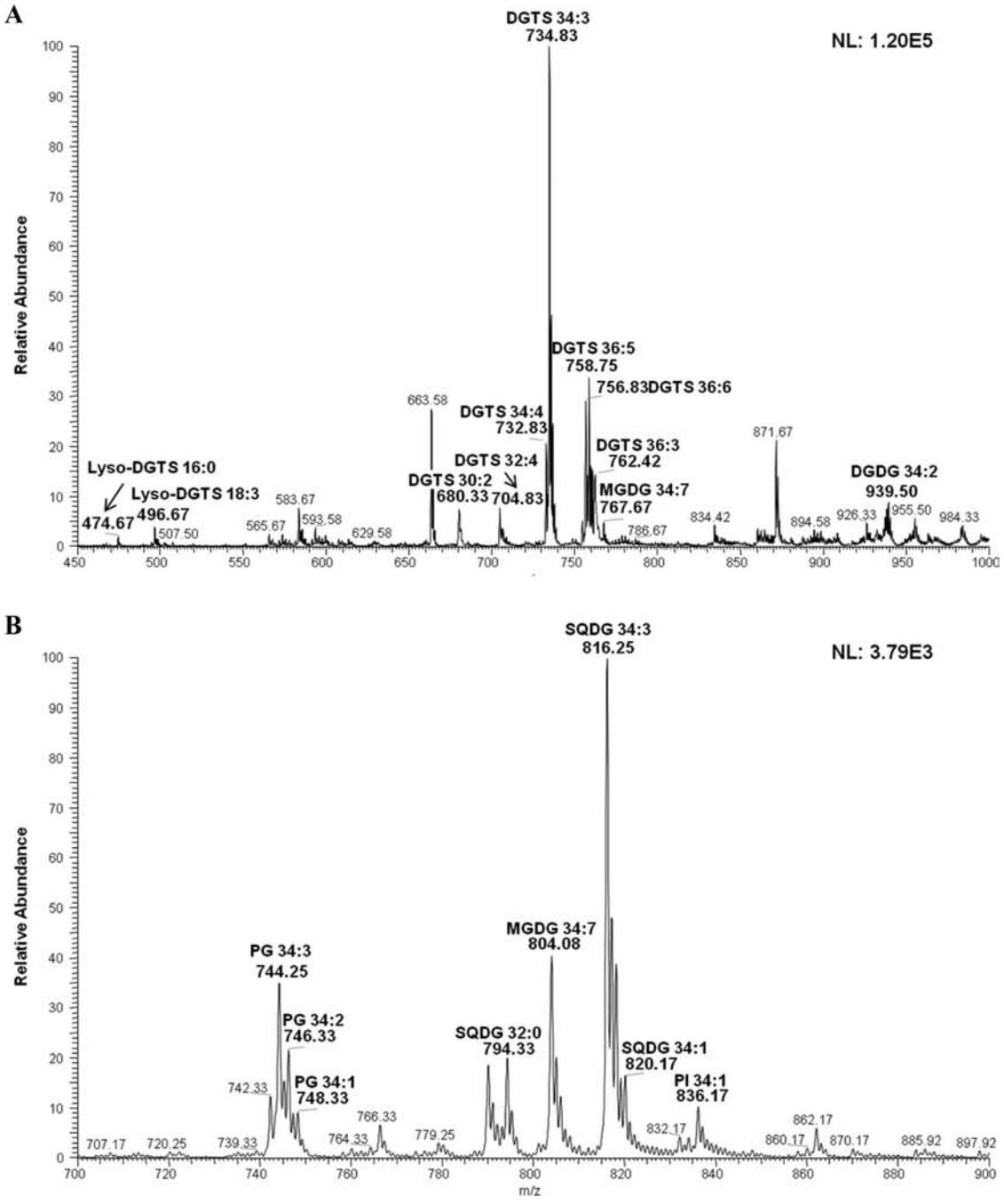

Figure 2. Representative spectra of lipid profiles from *D. tertiolecta* derived from nano-ESI-MS in (A) positive ion mode and (B) negative ion mode. Abbreviations: DGTS, diacylglyceryl-*N*,*N*,*N*-trimethylhomoserine; MGDG, monogalactosyldiacylglycerol; DGDG, digalactosyldiacylglycerol; SQDG, sulfoquinovosyldiacylglycerol; PG, phosphatidylglycerol; PI, phosphatidylinositol; *m*/*z*, mass-to-charge ratio; NL, normalized intensity level.

are very low.[36] It was therefore speculated that K-0591 has already acclimated to extreme conditions in which nitrogen is deficient. Meanwhile, the level of lyso-DGTS 18:3 was decreased in both strains.

There were no changes in the levels of MGDG and SQDG species in LB999, but there were significant increases in those of DGDG 18:3/16:2, PI 18:1/16:0, and PG 18:1/16:0. Mock and Kroon[37] demonstrated that the levels of DGDG, PG, and PI increase under nitrogen-deficient conditions in Antarctic sea-ice diatoms. They showed that photosynthesis was reduced under these conditions, resulting in the loss of proteins that regulate photosynthesis in the thylakoid membrane. Consequently, the level of DGDG and phospholipids—which are bilayer-forming lipids—seemed to be increased to stabilize the membrane structures.[37] Meanwhile, exposing K-0591 to nitrate deficiency produced no significant changes in lipid species except for reductions in the levels of *lyso*-DGTS 18:3 and DGDG 18:3/16:4.

In this study we conducted a comprehensive lipid analysis based on GC−MS and nano-ESI-MS of *D. tertiolecta*. The lipid profiles of two *D. tertiolecta* strains with different optimal growth temperatures were compared to determine the lipid species affecting the acclimation to low-temperature and ND conditions. The significant feature of the low-temperature (15

DOI: 10.1021/jf502967k
J. Agric. Food Chem. 2015, 63, 880−887

°C) strain K-0591 was that its levels of C18:3, DGTS species, MGDG 18:3/16:4, and DGDG 18:3/16:0 were higher than those of the LB999 strain grown at 21 °C. It appears that these lipid species contribute to desaturation of the cell membrane to maintain its fluidity under low-temperature conditions. K-0591 changed little under ND conditions, whereas large amounts of DGTS, DGDG, PI, and PG species had accumulated in LB999. These changes in the lipid profiles of LB999 could be the result of an increased number of oil globules and a compensation response to the reduced level of photosynthetic proteins observed under ND conditions. Notably, the levels of DGTS species in *D. tertiolecta* were higher under low-temperature and ND conditions. This implies that DGTS species could be candidate compounds related to acclimation to low temperature and nitrate deficiency. However, further experiments should be conducted to observe the changes in DGTS species at various time points and temperatures in each of these strains to verify this hypothesis.

The development of microalgal strains with tolerance of low temperature appears to be important from an economic viewpoint, because this would make the large-scale, open-pond cultivation of these microalgae possible even at relatively low temperatures. Such development could improve one of the current drawbacks of open-pond systems: diurnal and seasonal temperature fluctuations. In addition, prolonged cultivation while retaining a consistent FA composition under ND conditions would be feasible if microalgal strains with tolerance of such conditions can be developed. Although different nitrogen levels could induce changes in lipid and FA profiles in microalge,[38,39] it is not easy to control the nitrogen concentration in an open-pond system in a natural environment subject to events such as rain or evaporative water loss. Therefore, maintaining a constant lipid profile is necessary for the quality-controlled production of microalgal biofuel.

The findings of this study provide a deeper understanding of the differential lipid metabolism in two *D. tertiolecta* strains with different optimized growth temperatures when they are subjected to nitrate deficiency. This lipidomics tool could be a useful technique for elucidating certain lipid species potentially related to adaptation under various environmental conditions. Furthermore, this study provides new insight into the development of new strains that can survive under low-temperature and low-nutrient conditions using metabolic engineering targeting certain lipid species such as DGTS.

■ ASSOCIATED CONTENT

Ⓢ Supporting Information

Growth of *D. tertiolecta* strains LB999 and K-0591 and description of the lipid profiles of LB999 cells cultivated at different temperatures. This material is available free of charge via the Internet at http://pubs.acs.org.

■ AUTHOR INFORMATION

Corresponding Author

*Phone: +82-2-8205605. Fax: 82-2-8123921. E-mail: hykychoi@cau.ac.kr.

Funding

This research was supported by the Chung-Ang University Excellent Student Scholarship program and by a grant from the National Research Foundation of Korea funded by the Korean government (MIST) (NRF-2011-0021055).

Notes

The authors declare no competing financial interest.

■ ABBREVIATIONS USED

D. tertiolecta, *Dunaliella tertiolecta*; DGTS, diacylglyceryl-*N*,*N*,*N*-trimethylhomoserine; MGDG, monogalactosyldiacylglycerol; DGDG, digalactosyldiacylglycerol; SQDG, sulfoquinovosyldiacylglycerol; PG, phosphatidylglycerol; PI, phosphatidylinositol; FAME, fatty acid methyl ester; GC, gas chromatography; FCW, fresh cell weight; nano-ESI, nanoelectrospray ionization; MS, mass spectrometry; PCA, principal component analysis; PUFA, polyunsaturated fatty acid; NS, nitrate-sufficient; ND, nitrate-deficient; AMDIS, Automated Mass Spectral Deconvolution and Identification System

■ REFERENCES

(1) Hong, J. W.; Choi, H.; Kang, S.; Yoon, H. Axenic purification and cultivation of an Arctic cyanobacterium, *Nodularia spumigena* KNUA005, with cold tolerance potential for sustainable production of algae-based biofuel. *Algae* **2010**, *25*, 99−104.

(2) Knothe, G. A technical evaluation of biodiesel from vegetable oils vs. algae. Will algae-derived biodiesel perform? *Green Chem.* **2011**, *13*, 3048−3065.

(3) Radakovits, R.; Jinkerson, R. E.; Darzins, A.; Posewitz, M. C. Genetic engineering of algae for enhanced biofuel production. *Eukaryotic Cell.* **2010**, *9*, 486−501.

(4) Radakovits, R.; Eduafo, P. M.; Posewitz, M. C. Genetic engineering of fatty acid chain length in *Phaeodactylum tricornutum*. *Metab. Eng.* **2011**, *13*, 89−95.

(5) Yu, W.; Ansari, W.; Schoepp, N. G.; Hannon, M. J.; Mayfield, S. P.; Burkart, M. D. Modifications of the metabolic pathways of lipid and triacylglycerol production in microalgae. *Microb. Cell Fact.* **2011**, *10*, 91−101.

(6) Ndimba, B. K.; Ndimba, R. J.; Johnson, T. S.; Waditee-Sirisattha, R.; Baba, M.; Sirisattha, S.; Shiraiwa, Y.; Agrawal, G. K.; Rakwal, R. Biofuels as a sustainable energy source: an update of the applications of proteomics in bioenergy crops and algae. *J. Proteomics* **2013**, *93*, 234−244.

(7) Lu, N.; Wei, D.; Chen, F.; Yang, S. Lipidomic profiling and discovery of lipid biomarkers in snow alga *Chlamydomonas nivalis* under salt stress. *Eur. J. Lipid Sci. Technol.* **2012**, *114*, 253−265.

(8) MacDougall, K. M.; McNichol, J.; McGinn, P. J.; O'Leary, S. J.; Melanson, J. E. Triacylglycerol profiling of microalgae strains for biofuel feedstock by liquid chromatography−high-resolution mass spectrometry. *Anal. Bioanal. Chem.* **2011**, *401*, 2609−2616.

(9) Kim, S. H.; Liu, K. H.; Lee, S. Y.; Hong, S. J.; Cho, B. K.; Lee, H.; Lee, C. G.; Choi, H. K. Effects of light intensity and nitrogen starvation on glycerolipid, glycerophospholipid, and carotenoid composition in *Dunaliella tertiolecta* culture. *PLoS One* **2013**, *8*, e72415.

(10) Kind, T.; Meissen, J. K.; Yang, D.; Nocito, F.; Vaniya, A.; Cheng, Y.; VanderGheynst, J. S.; Fiehn, O. Qualitative analysis of algal secretions with multiple mass spectrometric platforms. *J. Chromatogr. A* **2012**, *1244*, 139−147.

(11) Holguin, F. O.; Schaub, T. Characterization of microalgal lipid feedstock by direct-infusion FT-ICR mass spectrometry. *Algal Res.* **2013**, *2*, 43−50.

(12) Bartley, M. L.; Boeing, W. J.; Corcoran, A. A.; Holguin, F. O.; Schaub, T. Effects of salinity on growth and lipid accumulation of biofuel microalga *Nannochloropsis salina* and invading organisms. *Biomass Bioenergy* **2013**, *54*, 83−88.

(13) Barzegari, A.; Hejazi, M. A.; Hosseinzadeh, N.; Eslami, S.; Aghdam, E. M.; Hejazi, M. S. Dunaliella as an attractive candidate for molecular farming. *Mol. Biol. Rep.* **2010**, *37*, 3427−3430.

(14) Hosseini Tafreshi, A.; Shariati, M. Dunaliella biotechnology: methods and applications. *J. Appl. Microbiol.* **2009**, *107*, 14−35.

(15) Rismani-Yazdi, H.; Haznedaroglu, B. Z.; Bibby, K.; Peccia, J. Transcriptome sequencing and annotation of the microalgae *Dunaliella*

DOI: 10.1021/jf502967k
J. Agric. Food Chem. 2015, 63, 880−887

tertiolecta: pathway description and gene discovery for production of next-generation biofuels. *BMC Genomics* **2011**, *12*, 148−164.
(16) Chen, M.; Tang, H.; Ma, H.; Holland, T. C.; Ng, K.; Salley, S. O. Effect of nutrients on growth and lipid accumulation in the green algae *Dunaliella tertiolecta*. *Bioresour. Technol.* **2011**, *102*, 1649−1655.
(17) Mujtaba, G.; Choi, W.; Lee, C.; Lee, K. Lipid production by *Chlorella vulgaris* after a shift from nutrient-rich to nitrogen starvation conditions. *Bioresour. Technol.* **2012**, *123*, 279−283.
(18) Yeh, K.; Chang, J. Nitrogen starvation strategies and photobioreactor design for enhancing lipid content and lipid production of a newly isolated microalga *Chlorella vulgaris* ESP-31: implications for biofuels. *Biotechnol. J.* **2011**, *6*, 1358−1366.
(19) Guillard, R.R. L. Culture of phytoplankton for feeding marine invertebrates. In *Culture of Marine Invertebrate Animals*; Smith, W. L., Chanley, M. H., Eds.; Plenum Press: New York, 1975; pp 29−60.
(20) Lee, S. Y.; Kim, S. H.; Hyun, S. H.; Suh, H. W.; Hong, S. J.; Cho, B. K.; Lee, C. G.; Lee, H.; Choi, H. K. Fatty acids and global metabolites profiling of *Dunaliella tertiolecta* by shifting culture conditions to nitrate deficiency and high light at different growth phases. *Process Biochem.* **2014**, *49*, 996−1004.
(21) Laurens, L. M.; Quinn, M.; Van Wychen, S.; Templeton, D. W.; Wolfrum, E. J. Accurate and reliable quantification of total microalgal fuel potential as fatty acid methyl esters by in situ transesterification. *Anal. Bioanal. Chem.* **2012**, *403*, 167−178.
(22) Styczynski, M. P.; Moxley, J. F.; Tong, L. V.; Walther, J. L.; Jensen, K. L.; Stephanopoulos, G. N. Systematic identification of conserved metabolites in GC/MS data for metabolomics and biomarker discovery. *Anal. Chem.* **2007**, *79*, 966−973.
(23) Lang, I.; Hodac, L.; Friedl, T.; Feussner, I. Fatty acid profiles and their distribution patterns in microalgae: a comprehensive analysis of more than 2000 strains from the SAG culture collection. *BMC Plant Biol.* **2011**, *11*, 124−139.
(24) Sharma, K. K.; Schuhmann, H.; Schenk, P. M. High lipid induction in microalgae for biodiesel production. *Energies* **2012**, *5*, 1532−1553.
(25) Thompson, G. A. Lipids and membrane function in green algae. *Biochim. Biophys. Acta, Lipids Lipid Metab.* **1996**, *1302*, 17−25.
(26) Morgan-Kiss, R. M.; Priscu, J. C.; Pocock, T.; Gudynaite-Savitch, L.; Huner, N. P. Adaptation and acclimation of photosynthetic microorganisms to permanently cold environments. *Microbiol. Mol. Biol. Rev.* **2006**, *70*, 222−252.
(27) Whitelam, G.; Codd, G. Damaging effects of light on microorganisms. In *Microbes in Extreme Environments*; Herbert, R. A., Codd, G. A., Eds.; Academic: San Diego, CA, 1986; pp 129−169.
(28) Siron, R.; Giusti, G.; Berland, B. Changes in the fatty acid composition of *Phaeodactylum tricornutum* and *Dunaliella tertiolecta* during growth and under phosphorus deficiency. *Mar. Ecol.: Prog. Ser.* **1989**, *55*, 95−100.
(29) Solovchenko, A.; Khozin-Goldberg, I.; Didi-Cohen, S.; Cohen, Z.; Merzlyak, M. Effects of light intensity and nitrogen starvation on growth, total fatty acids and arachidonic acid in the green microalga *Parietochloris incisa*. *J. Appl. Phycol.* **2008**, *20*, 245−251.
(30) Guschina, I. A.; Harwood, J. L. Lipids and lipid metabolism in eukaryotic algae. *Prog. Lipid Res.* **2006**, *45*, 160−186.
(31) Vidoudez, C.; Pohnert, G. Comparative metabolomics of the diatom *Skeletonema marinoi* in different growth phases. *Metabolomics* **2012**, *8*, 654−669.
(32) Chattopadhyay, M.; Jagannadham, M. A branched chain fatty acid promotes cold adaptation in bacteria. *J. Biosci.* **2003**, *28*, 363−364.
(33) Williams, J. P.; Khan, M. U.; Mitchell, K. The molecular species of diacylglycerol precursors used in monogalactosyldiacylglycerol biosynthesis in the leaves of a number of higher plant species. *Plant Cell Physiol.* **1988**, *29*, 849−854.
(34) Johnson, G.; Williams, J. P. Effect of Growth Temperature on the Biosynthesis of Chloroplastic Galactosyldiacylglycerol Molecular Species in *Brassica napus* leaves. *Plant Physiol.* **1989**, *91*, 924−929.
(35) Peled, E.; Leu, S.; Zarka, A.; Weiss, M.; Pick, U.; Khozin-Goldberg, I.; Boussiba, S. Isolation of a novel oil globule protein from the green alga *Haematococcus pluvialis* (Chlorophyceae). *Lipids* **2011**, *46*, 851−861.
(36) Brandsma, J.; Hopmans, E. C.; Brussaard, C. P.; Witte, H. J.; Schouten, S.; Sinninghe Damsté, J. S. Spatial distribution of intact polar lipids in North Sea surface waters: relationship with environmental conditions and microbial community composition. *Limnol. Oceanogr.* **2012**, *57*, 959−973.
(37) Mock, T.; Kroon, B. Photosynthetic energy conversion under extreme conditions—I: important role of lipids as structural modulators and energy sink under *N*-limited growth in Antarctic sea ice diatoms. *Phytochemistry* **2002**, *61*, 41−51.
(38) Xiao, Y.; Zhang, J.; Cui, J.; Feng, Y.; Cui, Q. Metabolic profiles of *Nannochloropsis oceanica* IMET1 under nitrogen-deficiency stress. *Bioresour. Technol.* **2013**, *130*, 731−738.
(39) Piorreck, M.; Pohl, P. Formation of biomass, total protein, chlorophylls, lipids and fatty acids in green and blue-green algae during one growth phase. *Phytochemistry* **1984**, *23*, 217−223.

DOI: 10.1021/jf502967k
J. Agric. Food Chem. 2015, 63, 880−887

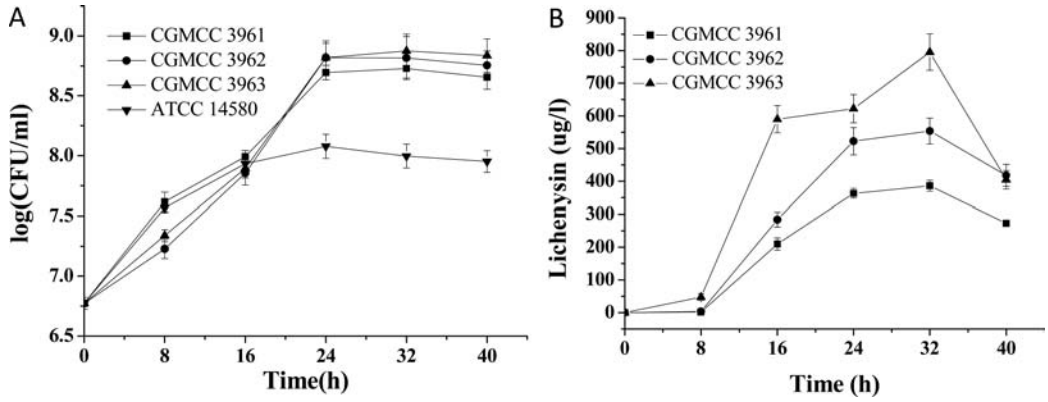

Figure 1. Time profile of lichenysin produced by different strains of *B. licheniformis* cultured in sorghum extract. (A) Biomass; (B) lichenysin concentration.

liquor is a symbolic drink of China, just as whisky is for Scotland and brandy for France. It is produced by a unique spontaneous and solid-state fermentation process with sorghum as the main material.[19] This process is rich in nutrition and accumulates a complex microbial community, including bacteria, yeast, and fungi. In this process, fungi produce amylase and glucoamylase to hydrolyze starch in cereal to oligosaccharide and also produce protease and peptidase to hydrolyze protein to oligopeptides and amino acids. These small molecular compounds are then consumed and transformed to ethanol and flavor compounds by yeast and bacteria.[20] *B. licheniformis* is a dominant species in this process. Its biosynthetic activity of lichenysin might be important for its survival and predominance in this community, because the produced lichenysin might show inhibition of other strains. Since there are rich nutritional and complex microbial communities in the liquor-making process, it is important to reveal the mechanism of lichenysin biosynthesis by producers in the Maotai-flavor liquor-making process. Therefore, the comparative transcriptome of these producers and a non-producer, *B. licheniformis*strain ATCC 14580, was carried out in a simulated liquor-making process. It is important to reveal the mechanism of the lichenysin biosynthetic process, including the substance supply and transformation by these strains in this complex process. This work would supplement the knowledge of lichensysin biosynthesis and promote the lichenysin production industry.

MATERIALS AND METHODS

Strains. Lichenysin producers were isolated from Chinese Maotai-flavor liquor-making process, on the basis of hemolysis zone on blood agar.[21] Then the obtained strains were cultured in sorghum extract, and their lichenysin productivity was determined by ultra-performance liquid chromatography (UPLC). Strains *B. licheniformis* CGMCC 3961, 3962,[22] and 3963[23] showed the highest lichenysin productivity. *B. licheniformis* ATCC 14580, obtaining from Shanghai Institute of Industrial Microbiology, did not originate from Maotai-liquor fermentation process.

Culture Conditions. In order to simulate the fermentation process of liquor making, the fermentation medium was prepared with sorghum. Sorghum extract was prepared as previously reported.[19] Strains were inoculated in 50 mL of sorghum extract medium and incubated at 37 °C for 40 h with an agitation speed of 150 rpm. To investigate the effect of different substrates on lichenysin production, strains were inoculated in synthetic medium with different substrates: 20 g/L glucose, amino acids, casein hydrolysate, respectively. The amino acids contained 5 g/L each L-leucine, L-aspartate, L-isoleucine, L-valine, and L-glutamine (the component unit of lichenysin). The synthetic medium was prepared according to a previous report[24] with minor modifications. It included 20 g/L glucose, 24 g/L $(NH_4)_2HPO_4$, 14.2 g/L $Na_2HPO_4{\cdot}12H_2O$, 3.0 g/L KH_2PO_4, 0.5 g/L NaCl, 0.24 g/L $MgSO_4{\cdot}7H_2O$, and 0.014 g/L $CaCl_2$, with the addition of 10 mL of metal ions mixture. Metal ions mixture contained 1.6 g/L $FeSO_4{\cdot}7H_2O$, 0.1 g/L $MnCl_2{\cdot}H_2O$, 0.17 g/L $ZnCl_2$, 0.043 g/L $CuCl_2{\cdot}H_2O$, 0.06 g/L $CoCl_2{\cdot}H_2O$, and 0.06 g/L $Na_2MoO_4{\cdot}2H_2O$. Strains were inoculated in 50 mL of the synthetic medium and incubated at 37 °C with an agitation speed of 150 rpm. The strain was incubated for 32 h to determine lichenysin yield and incubated for 24 h to determine the gene expression levels by quantitative real-time polymerase chain reaction (qRT-PCR).

RNA Extraction and cDNA Preparation. Total RNA was extracted from *B. licheniformis* CGMCC 3961, 3962, and 3963 and *B. licheniformis* ATCC 14580 cells cultured in sorghum extract and synthetic medium by use of RNeasy micro kits (Qiagen). DNase I was used to remove DNA contamination. The obtained RNA was determined by a nanobiosizing assay (Agilent) and then amplified and labeled by use of a one-color DNA labeling kit (NimbleGen) to obtain the cDNA sample.

Gene Expression Arrays. The obtained cDNA samples from strains cultured in sorghum extract were used for gene expression array processing. The expression array chip used contained 385 000 probes representing 4196 genes (NimbleGen). Target cDNA was hybridized to microarrays, and the processed slides after hybridization were scanned as reported.[22] The raw data of fluorescent intensity were extracted, normalized, background-corrected, and statistically analyzed as reported.[22] Genes with an absolute change >2.0-fold were identified as significantly differentially expressed genes.

Quantitative Real-Time Polymerase Chain Reaction. To verify the microarray results, two differentially expressed genes (*dppA* and *dppC*) were further analyzed by qRT-PCR. To investigate the effect of substrate on lichenysin production, strains were inoculated in synthetic medium with different substrates for 24 h. The obtained cDNA samples were also used for qRT-PCR. Relative transcript abundance was detected by SYBRGreen (Invitrogen) on the ABI 7900HT thermal cycler by use of gene-specific primers. The primer pairs were as follows: *dppA* (BLi01392), 5′-GGCTTATTTCGGGAGATGT-3′ (forward) and 5′-TTTCTTTGACGGCTGCTG-3′ (reverse); *dppB* (BLi01393), 5′-CACGACATTGACCTTTGTGA-3′ (forward) and 5′-ACGAAACGGGAAATCCTC-3′ (reverse); *dppC* (BLi01394), 5′-ATCGTCCAGATGACCTTG-3′ (forward) and 5′-CAGTCCGTCTCCAACAAC-3′ (reverse); *dppD* (BLi01395), 5′-TTGAGGCAGTATCCGCAC-3′ (forward) and 5′-TCACGGCGATTCTGTCTG-3′ (reverse); *dppE* (BLi01396), 5′-CGAAAGAAACGGCTGGAG-3′ (forward) and 5′-CATTTGGCATCATCACGG-3′ (reverse); 16S rDNA (reference gene), 5′-GTAACCTGCCTGTAAGACTG-3′ (forward) and 5′-TGTCTCAGTCCCAGTGTG-3′ (reverse); *ypqE* (BLi02359), 5′-TGATGGGTGACGGAATG-3′ (forward) and 5′-

DOI: 10.1021/jf5036806
J. Agric. Food Chem. 2015, 63, 888−893

Table 1. Different Metabolic Pathways Derived from Different Responsive Genes

entry	term	differential gene count	upregulated gene count	*P*-value
bld02010	ABC transporters	81	29	5.28×10^{-8}
bld00562	inositol phosphate metabolism	11	9	0.000128
bld00680	methane metabolism	18	8	0.012394
bld00281	geraniol degradation	8	8	0.016741
bld00362	benzoate degradation	10	8	0.017837
bld02060	phosphotransferase system (PTS)	22	16	0.019500
bld00280	valine, leucine, and isoleucine degradation	15	10	0.023497
bld00380	tryptophan metabolism	10	9	0.032104
bld00626	naphthalene degradation	7	5	0.034043
bld00051	fructose and mannose metabolism	15	9	0.035269
bld02040	flagellar assembly	17	10	0.042324

TGTGAAACCTTCGCCTT-3′ (reverse); *ptsG* (BLi01598), 5′-CGACATTGGCAACGGGA-3′ (forward) and 5′-CGACCGCTT-CATTGGCT-3′ (reverse).

Quantification of Lichenysin in Fermentation Broth. *B. licheniformis* was inoculated into 50 mL of sorghum extract and then shaken at 150 rpm for 24 h. Lichenysin was extracted with methanol as reported.[25] The methanol-soluble fraction was concentrated to 1 mL by rotary evaporation. To determine lichenysin concentration, UPLC was performed with a Waters Acquity UPLC system equipped with a UV detector (Milford, MA). The chromatographic separation was performed on a Waters Acquity C18 column (2.1 × 50 mm). The injection volume was 10 μL. The mobile phase was a gradient prepared from methanol (component A) and water containing 0.1% formic acid (component B). Elution started with 15% B for 0.1 min, and the proportion of B was decreased linearly to 0% in 10 min and then returned to 15% in 1 min. The flow rate was 300 μL/min. The experiments were carried out in triplicate.

RESULTS AND DISCUSSION

***B. licheniformis* CGMCC 3961, 3962, and 3963 Produce Lichenysin Efficiently in Simulated Liquor Fermentation Process.** *B. licheniformis* CGMCC 3961, 3962, and 3963 were isolated in Chinese Maotai-flavor liquor-making process.[22,23] They showed the highest lichenysin productivity among the isolated strains by the hemolysis reaction method[21] and UPLC determination. There are seven different fractions, which we reported previously.[4] The concentration of lichenysin is the total amount of these different fractions. Time profiles of lichenysin production by these strains and the type strain ATCC 14580 in sorghum extract medium were determined and are shown in Figure 1. *B. licheniformis* CGMCC 3961, 3962, and 3963 grew much better than ATCC 14580 in this medium. This indicated the three producers had adapted to this medium after long-time survival in the environment for liquor fermentation. In addition, all three strains produced lichenysin efficiently, and *B. licheniformis* CGMCC 3963 had stronger producing activity than the other two, while the type strain *B. licheniformis* ATCC 14580, of non-liquor-making origin, did not produce lichenysin. Lichenysin increased quickly after 8 h, reached a maximum value at 32 h (386.3, 553.5, and 795.2 μg/L, respectively), and then decreased until the end of fermentation by *B. licheniformis* CGMCC 3961, 3962, and 3963. The decrease of lichenysin might be due to further degradation by the strains. In addition, lichenysin was produced 8 h after initiation of cell growth, since it was produced as a secondary metabolite.[15]

Lichenysin is an amphiphile and shows strong antibacterial activity. It could inhibit the growth of many strains, including *Pseudomonas*, *Staphylococcus*, *Escherichis coli*, *Acinetobacter*, *Alcaligenes*, *Micrococcus*, etc.[11,22,26] Among them, *Pseudomonas* and *Staphylococcus* have been discovered in Chinese liquor.[27] The antibacterial activity of lichenysin would not only be beneficial for the dominance of *B. licheniformis* in Maotai-flavor liquor making but could also prevent liquor fermentation from contamination by those harmful microbes, achieving a successful product.

Transcriptome Analysis between Three Producers and Nonproducer. To gain further insight into the metabolic mechanism of overproduction of lichenysin by *B. licheniformis* CGMCC 3961, 3962 and 3963, the mean global differences of gene expression levels of these three producers were compared with those of nonproducer ATCC 14580. Of the 4196 genes on the microarray, a total of 1574 genes (37.5%), with a change of at least 2.0-fold, were identified as differentially expressed genes: 803 genes were upregulated and 771 genes were downregulated. Metabolic pathways obtained from the KEGG databases were characterized from the 1574 genes. As shown in Table 1 and Table S1 (Supporting Information), 11 metabolic pathways had *P*-value <0.05. Among them, ABC transporters (bld02010) constituted the most significantly different pathway. This might be related to membrane transport of substance absorption and lichenysin secretion, as well as the phosphotransferase system (PTS) (bld02060). Inositol phosphate metabolism (bld00562) and methane metabolism (bld00680) were related to energy metabolism, which might supply energy for vigorous cell growth and lichenysin biosynthesis and secretion processes. Benzoate degradation (bld00362), naphthalene degradation (bld00626), and geraniol degradation (bld00281) might be responsive to the fermentation environment, since there were terpenes and aromatic compounds in liquor fermentation materials. Fructose and mannose metabolism (bld00051) might be responsive to the high oligosaccharide content in sorghum, since these sugars were the nutrient for cell growth. Certain amino acids in cells were not only nutrients for cell growth but also direct substrates for lichenysin synthesis. The responsive metabolic pathways of valine, leucine, and isoleucine degradation (bld00280) and tryptophan metabolism (bld00380) might be related to substance degradation for cell growth and providing substance for lichenysin synthesis.

Increased Expression Pattern of Lichenysin Synthetases and Certain Regulators. Compared with the type strain ATCC 14580, *B. licheniformis* CGMCC 3961, 3962, and 3963 showed strong lichenysin-producing activities, which was essentially due to the difference in expression pattern of lichenysin synthetases. Lichenysin was reported to be produced by a multienzyme peptide synthetase complex expressed by the *lchA* operon, consisting of *lchAA*−*AD*.[15,16] To gain further

DOI: 10.1021/jf5036806
J. Agric. Food Chem. 2015, 63, 888−893

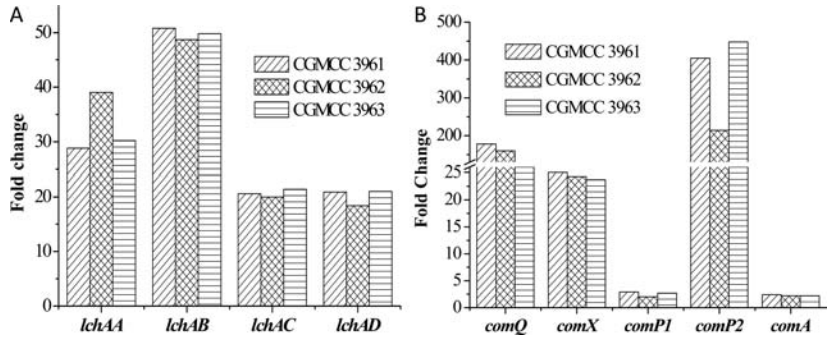

Figure 2. Expression pattern of lichenysin synthetases and regulators in *B. licheniformis* GMCC 3961, 3962, and 3963 compared with ATCC 14580. (A) *lchAA*−*AD*; (B) different regulators.

insight into the expression pattern of *lchA* operon in these three producers, the expression patterns of *lchAA*−*AD* were analyzed and are shown in Figure 2A. The average expression values of *lchAA*−*AD* in the three producers were 32.7-, 49.8-, 20.7-, and 20.1-fold greater than those of the type strain, respectively. The high expression level of lichenysin synthetase genes confirmed the overproduction of lichenysin.

LchAA is a three-module enzyme. The first module activated the acylation of the first amino acid, the second and third module assembled the following two amino acid residues, and the third module also converted L-amino acid into the D-isomer. LchAB and LchAC incorporated the following three and the last amino acids, respectively. LchAD is a repair enzyme.[28] The gene allele distribution of *lch* operon in the genome was analyzed in the genome of *B. licheniformis* CGMCC 3963.[23] It was found that *lchAA*−*AD* were in one gene cluster all with one copy in the genome level, which was the same as in ATCC 14580.[29] Therefore, the higher expression level in the producers might be due to the difference in transcription levels. However, the expression levels of *lchAA* and *lchAB* were higher than those of *lchAC* and *lchAD*. The sequence lengths of *lchAA* and *lchAB* were 10 757 and 10 766 bp, while the lengths of *lchAC* and *lchAD* were only 3848 and 740 bp in CGMCC 3963.[23] The long gene sequence of *lchAA* and *lchAB* might lead to weak transcription levels of the following genes, *lchAC* and *lchAD*. Since the reactions catalyzed by LchAA and LchAB were more complex, the higher expression levels of *lchAA* and *lchAB* would consequently increase the synthesis reaction and lichenysin yield. This represents the cell's economy of costs and benefits, which result from the adaptation evolution of this strain, due to long-term habitation in the liquor fermentation environment.

The expression levels of lichenysin synthetases were regulated by additional regulators. Therefore, it was necessary to find the expression pattern of the involved regulators. ComX was the initial regulator of surfactin (the homologue of lichenysin) biosynthesis in *B. subtilis*. It became active after being modified by ComQ and then controlled *srfA* expression when it interacted with ComP and ComA.[1,18] Therefore, in order to investigate whether the lichenysin synthesis regulatory pathway was the same in the producers, these related regulators were all analyzed, as shown in Figure 2B. Expression levels of *comQ* in these strains were more than 94.4-fold greater than that in the type strain, and the expression levels of *comX* were more than 23.7-fold. There were two histidine protein kinases ComP, but the expression pattern was significantly different: *comP2* expression in *B. licheniformis* CGMCC 3961, 3962, and 3963 was 404.9-, 214.3-, and 447.7-fold greater than that in the type strain, indicating ComP2 might be important for lichenysin synthesis. Although *comP1* and *comA* directly activate transcription of *lchAA*−*AD*,[17,18] the expression increase was only around 2.0−2.9-fold. This indicated that a small amount of *comP1* and *comA* would lead to the overproduction of *lchAA*−*AD*. The high expression of these regulators indicated that regulation of lichenysin biosynthesis might be also related to these regulators in the three lichenysin producers.

Increased Expression Pattern of Peptide Transport-Related Genes. ABC transporters (bld02010) constituted the most significant responsive metabolic pathway. Of the 29 upregulated genes, 14 of them were related to dipeptide and peptide transport, including *dppABCDE*, *appCDF*, *oppA*-like, *appBCDF*-like, and *ykfD* genes (Tables S1 and S2, Supporting Information). As shown in Figure 3, the expression level of

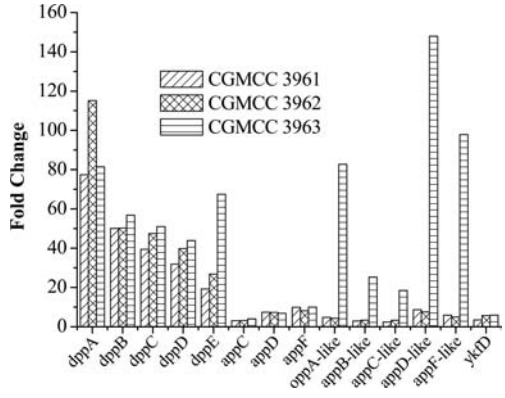

Figure 3. Expression pattern of genes related to peptide transport in the pathway of ABC transporters (bld02010) in *B. licheniformis* GMCC 3961, 3962, and 3963 compared with ATCC 14580.

dppABCDE increased more than 19.2-fold in CGMCC 3961, 3962, and 3963. In addition, the average upregulated expression level of *dppABCDE* in the three strains gradually decreased from 91.3- to 37.8-fold, although the expression level of *dppE* was higher than that of *dppBCD* in CGMCC 3963. Since the five genes were in the same operon, the subsequent gene expression gradually became weaker during the transcription process, due to premature termination of transcription of the subsequent genes by several attenuators.[30]

In addition, we found that the expression of *dppE*, *oppA*-like, and *appBCDF*-like genes was significantly higher in the highest lichenysin producer CGMCC 3963: about 67.5-, 82.7-, 25.3-, 18.4-, 147.9-, and 97.9-fold greater than in ATCC14580, respectively. These more highly expressed genes might be related to the higher productivity of lichenysin.

DOI: 10.1021/jf5036806
J. Agric. Food Chem. 2015, 63, 888−893

Table 2. Lichenysin Production in Synthetic Medium with Addition of Different Substrates[a]

	control	glucose	amino acids	casein hydrolysate
biomass, log(CFU/mL)	8.65 ± 0.03	8.75 ± 0.06	7.84 ± 0.08	8.51 ± 0.01
lichenysin yield (μg/L)	28.2 ± 2.6	42.7 ± 3.9	12.8 ± 2.1	47.5 ± 4.4

[a]*B. licheniformis* CGMCC 3963 was cultured in synthetic medium for 32 h. Control represents the culture in synthetic medium without additional substrates. The added concentrations of glucose, amino acids, and casein hydrolysate were all 20 g/L.

To confirm the microarray data, we analyzed the relative mRNA levels of two genes (*dppA* and *dppC*) in the three producers by qRT-PCR, and the results suggested that the expression levels of *dppA* in CGMCC 3961, 3962, and 3963 were 58.4-, 89.3-, and 66.2-fold greater than that in ATCC14580, respectively, while the expression levels of *dppC* in these three strains were 24.2-, 31.3-, and 30.5-fold greater, respectively (data not shown), which showed good agreement between the microarray and qRT-PCR analysis.

Relationship of Peptide Transport Genes to Lichenysin Production. It was reported that *Bacillus* will use glucose as the main substance to produce lichenysin.[15] However, we found that the average expression levels of the glucose transport-related genes *ptsG* (BLi01598) and *ypqE* (BLi02359) were both 0.4-fold in the three producers. Since lichenysin was mainly composed of amino acids, which would be hydrolyzed from peptides, the high peptide transporter expression value indicated peptide would also be a good candidate for the substrate of lichenysin synthesis. In order to investigate the relationship between lichenysin production and the substrates (glucose and peptide), we cultured *B. licheniformis* CGMCC 3963 (the most efficient among the three producers) in synthetic medium with different substrates, including glucose, five types of amino acids (the component unit of lichenysin), and casein hydrolysate (containing various types of peptides), respectively. As shown in Table 2, with the addition of amino acids, cell growth decreased slightly and lichenysin production also decreased. This implied that amino acids could not stimulate cell growth and lichenysin production. *Bacillus* species could utilize amino acids as the substrate to grow, however, some strains evolved to preferentially take up dipeptide or oligopeptide rather than amino acids. Although *B. licheniformis* CGMCC 3963 could grow with amino acids as the only nitrogen in our previous work (data not shown), it still preferred to utilize peptide in the environment full of peptides. With the addition of glucose and casein hydrolysate, lichenysin production increased significantly, from 28.2 to 42.7 and 47.5 μg/L, respectively. Since cell growth remained nearly the same between the control and the sample cultured with glucose or casein hydrolysate, it indicated that glucose and peptide would both improve the metabolic activity of lichenysin biosynthesis. It might be due to the increase of substrate supplements, such as glucose and peptide. In addition, glucose might also provide energy for lichenysin biosynthesis. Since the nonribosomal peptide synthetase and ABC transporter systems for lichenysin synthesis would both expend a lot of energy, glucose may benefit as a respiratory substrate to create energy.

In addition, we determined the expression levels of transport-related genes in the synthetic medium with the addition of these substrates. As shown in Table 3, the expression levels of *dppABCDE* remained nearly stable when glucose or amino acids were added in synthetic medium, but the expression of all these genes increased about 2-fold when casein hydrolysate was added. This indicated that peptide transport might be strengthened with the addition of casein hydrolysate, which was full of peptides. In addition, the expression levels of glucose-related genes, *ypqE* and *ptsG*, both increased about 2-fold with the addition of glucose, indicating glucose might induce higher expression of these two genes. However, the expression levels of these two genes both decreased to less than 0.21-fold with the addition of amino acids and casein hydrolysate. It was consistent with the transcriptome analysis result that the expression of the two genes decreased in sorghum extract. When it came to Chinese liquor fermentation, the fermentation environment was rich in peptide, and the concentration of glucose was at a relatively low level, because it is a simultaneous saccharification and fermentation process. This explained the high expression levels of peptide transporter genes (*dppABCDE*) and the low expression levels of glucose transporter genes (*ptsG* and *ypqE*) in the simulated liquor fermentation process. Since these producers were long-term inhabitants in an environment full of various types of peptides, then the strains might have evolved to preferentially take up peptides to synthesize lichenysin, rather than the in vivo pathway. This was also the energy and nutrition−cost principle, which was also the result of adaptation of long-term evolution. This would be a supplement for the previously reported substrate glucose.[15] On the other hand, the competition for nutrients and space was another way of exploitative competition by producers. The high efficiency of peptide transport by the producers competitively absorbed these available substances in this microbial community. It had stronger transport ability for substances for both cell growth and lichenysin biosynthesis. Then the high efficiency of peptide transport would be beneficial for both cell survival and lichenysin production, which turns out to be beneficial for cell competition.

Table 3. Expression of Substrate Transport-Related Genes in *B. licheniformis* CGMCC 3963 Cultures in Synthetic Medium with Different Additions[a]

gene	glucose	amino acids	casein hydrolysate
dppA	0.79	0.67	2.06
dppB	1.05	0.95	2.74
dppC	1.16	0.99	2.69
dppD	0.86	0.73	1.93
dppE	1.44	1.25	4.01
ypqE	2.87	0.08	0.21
ptsG	2.10	0.05	0.18

[a]*B. licheniformis* CGMCC 3963 was cultured in synthetic medium for 24 h. The concentrations of glucose, amino acids and casein hydrolysate were all 20 g/L. Strain cultured in the synthetic medium served as the control for qRT-PCR.

This work not only deepened insight into the mechanism for lichenysin biosynthesis but also found a new explanation of the biological mechanism of lichenysin produced by *B. licheniformis*. It should ultimately promote the production efficiency of lichenysin.

DOI: 10.1021/jf5036806
J. Agric. Food Chem. 2015, 63, 888−893

■ ASSOCIATED CONTENT

Supporting Information

Two tables, listing global expression patterns in *B. licheniformis* GMCC 3961, 3962, and 3963 compared with *B. licheniformis* ATCC 14580 and significant metabolic pathways obtained from the KEGG databases, characterized from the 1574 differentially expressed genes. This material is available free of charge via the Internet at http://pubs.acs.org.

■ AUTHOR INFORMATION

Corresponding Author

*Phone 86 510-85864112; fax +86 510-85864112; e-mail yxu@jiangnan.edu.cn.

Funding

This work was supported by the National High Technology Research and Development Program of China (2013AA102108, 2012AA021301), National Natural Science Foundation of China (31371822, 31271921), China Postdoctoral Science Foundation (2014M550265), Priority Academic Program Development of Jiangsu Higher Education Institutions, 111 Project (111-2-06), and Jiangsu province "Collaborative Innovation Center for Advanced Industrial Fermentation" industry development program.

Notes

The authors declare no competing financial interest.

■ REFERENCES

(1) Stein, T. *Bacillus subtilis* antibiotics: Structures, syntheses and specific functions. *Mol. Microbiol.* **2005**, *56*, 845−857.

(2) Joshi, S.; Yadav, S.; Desai, A. J. Application of response-surface methodology to evaluate the optimum medium components for the enhanced production of lichenysin by *Bacillus licheniformis* R2. *Biochem. Eng. J.* **2008**, *41*, 122−127.

(3) Li, Y. M.; Haddad, N. I. A.; Yang, S.; Mu, B. Variants of lipopeptides produced by *Bacillus licheniformis* HSN221 in different medium components evaluated by a rapid method ESI-MS. *Int. J. Pept. Res. Ther.* **2008**, *14*, 229−235.

(4) Zhang, R.; Wu, Q.; Xu, Y.; Qian, M. C. Isolation, identification and quantification of lichenysin, a novel nonvolatile compound in Chinese distilled spirits. *J. Food Sci.* **2014**, *79*, C1907−C1915.

(5) Zhang, R.; Wu, Q.; Xu, Y. Lichenysin, a cyclooctapeptide occurring in Chinese liquor Jiannanchun, reduced the headspace concentration of phenolic off-flavors via hydrogen-bond interactions. *J. Agric. Food. Chem.* **2014**, *62*, 8302−8307.

(6) Compaoré, C. S.; Nielsen, D. S.; Sawadogo-Lingani, H.; Berner, T. S.; Nielsen, K. F.; Adimpong, D. B.; Diawara1, B.; Ouédraogo, G. A.; Jakobsen, M.; Thorsen, L. *Bacillus amyloliquefaciens* ssp. *plantarum* strains as potential protective starter cultures for the production of Bikalga, an alkaline fermented food. *J. Appl. Microbiol.* **2013**, *115*, 133−146.

(7) Grangemard, I.; Wallach, J.; Maget-Dana, R.; Peypoux, F. Lichenysin, a more efficient cation chelator than surfactin. *Appl. Biochem. Biotechnol.* **2001**, *90*, 199−210.

(8) Lin, S. C.; Minton, M. A.; Sharma, M. M.; Georgiou, G. Structural and immunological characterization of a biosurfactant produced by *Bacillus licheniformis* JF-2. *Appl. Environ. Microbiol.* **1994**, *60*, 31−38.

(9) Horowitz, S.; Griftin, W. M. Structural analysis of *Bacillus licheniformis* 86 surfactant. *J. Ind. Microbiol.* **1991**, *7*, 45−52.

(10) Yakimov, M. M.; Abraham, W. R.; Meyer, H.; Giuliano, L.; Golyshin, P. N. Structural characterization of lichenysin A components by fast atom bombardment tandem mass spectrometry. *Biochim. Biophys. Acta* **1999**, *1438*, 273−280.

(11) Yakimov, M. M.; Timmis, K. N.; Wray, V. Characterization of new lipopeptide surfactant produced by thermotolerant and halotolerant subsurface *Bacillus licheniformis* BAS50. *Appl. Environ. Microbiol.* **1995**, *61*, 1706−1713.

(12) Grangemard, I.; Bonmatin, J. M.; Bernillon, J.; Das, B. C.; Peypoux, F.; Lichemysin, G. A novel family of lipopeptide biosurfactants from *Bacillus licheniformis* IM1307: Production, isolation and structural evaluation by NMR and mass spectrometry. *J. Antibiot.* **1999**, *52*, 363−373.

(13) Konz, D.; Doekel, S.; Marahiel, M. A. Molecular and biochemical characterization of the protein template controlling biosynthesis of the lipopeptide lichenysin. *J. Bacteriol.* **1999**, *181*, 133−140.

(14) Makkar, R.; Cameotra, S. An update on the use of unconventional substrates for biosurfactant production and their new applications. *Appl. Microbiol. Biotechnol.* **2002**, *58*, 428−434.

(15) Nerurkar, A. S. Structural and molecular characteristics of lichenysin and its relationship with surface activity. In *Biosurfactants*; Sen, R., Ed.; Springer Science+Business Media LLC: New York, 2010; pp 301−315.

(16) Das, P.; Mukherjee, S.; Sen, R. Genetic regulations of the biosynthesis of microbial surfactants: an overview. *Biotechnol. Genet. Eng. Rev.* **2008**, *25*, 165−186.

(17) Yakimov, M. M.; Golyshin, P. N. ComA-dependent transcriptional activation of lichenysin A synthetase promoter in *Bacillus subtilis* cells. *Biotechnol. Prog.* **1997**, *13*, 757−761.

(18) Hamoen, L. W.; Venema, G.; Kuipers, O. P. Controlling competence in *Bacillus subtilis*: Shared use of regulators. *Microbiol.* **2003**, *149*, 9−17.

(19) Wu, Q.; Xu, Y.; Chen, L. Diversity of yeast species during fermentative process contributing to Chinese Maotai-flavour liquor making. *Lett. Appl. Microbiol.* **2012**, *55*, 301−307.

(20) Wu, Q.; Chen, L.; Xu, Y. Yeast community associated with the solid state fermentation of traditional Chinese Maotai-flavor liquor. *Int. J. Food. Microbiol.* **2013**, *166*, 323−330.

(21) Carrillo, P. G.; Mardaraz, C.; Pitta-Alvarez, S. I.; Giulietti, A. M. Isolation and selection of biosurfactant-producing bacteria. *World J. Microbiol. Biotechnol.* **1996**, *12*, 82−84.

(22) Wu, Q.; Xu, Y. Transcriptome profiling of heat-resistant strain *Bacillus licheniformis* CGMCC3962 producing Maotai-flavor. *J. Agric. Food. Chem.* **2012**, *60*, 2033−2038.

(23) Wu, Q.; Peng, S.; Yu, Y.; Li, Y.; Xu, Y. Genome sequence of *Bacillus licheniformis* CGMCC3963, a stress-resistant strain isolated from Chinese traditional solid-state liquor making process. *Genome Announc.* **2013**, *1* (1), No. e00060.

(24) Tännler, S.; Decasper, S.; Sauer, U. Maintenance metabolism and carbon fluxes in *Bacillus* species. *Microb. Cell Factories* **2008**, *7*, 19.

(25) Das, P.; Mukherjee, S.; Sen, R. Antimicrobial potential of a lipopeptide biosurfactant derived from a marine *Bacillus circulans*. *J. Appl. Microbiol.* **2008**, *104*, 1675−1684.

(26) Zhang, W.; Li, Z.; Miao, X.; Zhang, F. The screening of antimicrobial bacteria with diverse novel nonribosomal peptide synthetase (NRPS) genes from south China sea sponges. *Mar. Biotechnol.* **2009**, *11*, 346−355.

(27) Wang, H.; Gao, Y.; Fan, Q.; Xu, Y. Characterization and comparison of microbial community of different typical Chinese liquor Daqus by PCR−DGGE. *Lett. Appl. Microbiol.* **2011**, *53*, 134−140.

(28) Kraas, F. I.; Helmetag, V.; Wittmann, M.; Strieker, M.; Marahiel, M. A. Functional dissection of surfactin synthetase initiation module reveals insights into the mechanism of lipoinitiation. *Chem. Biol.* **2010**, *17*, 872−880.

(29) Rey, M. W.; Ramaiya, P.; Nelson, B. A.; Brody-Karpin, S. D.; Zaretsky, E. J.; Tang, M.; de Leon, A. L.; Xiang, H.; Gusti, V.; Clausen, I. G.; Olsen, P. B.; Rasmussen, M. D.; Andersen, J. T.; Jørgensen, P. L.; Larsen, T. S.; Sorokin, A.; Bolotin, A.; Lapidus, A.; Galleron, N.; Ehrlich, S. D.; Berka, R. M. Complete genome sequence of the industrial bacterium *Bacillus licheniformis* and comparisons with closely related *Bacillus* species. *Genome Biol.* **2004**, *5*, R77.

(30) Merino, E.; Yanofsky, C. Transcription attenuation: A highly conserved regulatory strategy used by bacteria. *Trends Genet.* **2005**, *21*, 260−264.

DOI: 10.1021/jf5036806
J. Agric. Food Chem. 2015, 63, 888−893

hydrolytic activity and transglycosylation toward lactose. Interestingly, a much higher synthetic ability of Bgal1-3 was observed in an organic−aqueous biphasic system than in aqueous system. To evaluate the effect of the immobilization as CLEAs on the GOS synthetic ability of the enzyme, its CLEAs were prepared. The enzymatic properties of Bgal1-3-CLEAs were investigated and compared with that of the free enzyme, including optimal pH, optimal temperature, pH stability, thermostability, storage stability, and kinetic parameters. The GOS synthesis of Bgal1-3-CLEAs was also conducted in the organic−aqueous biphasic system, and their reusability was evaluated by repeated consecutive batches. The aim of this study was to provide more information about the CLEAs of β-galactosidase and their potential application in the GOS synthesis.

MATERIALS AND METHODS

Strains, Vectors, and Chemicals. *E. coli* DH5α (Invitrogen, Carlsbad, CA, USA) was used as the host for gene cloning. A modified plasmid pUC19Δ*LacZ* was used to construct metagenomic libraries. The plasmid pUC19Δ*LacZ* was obtained by eliminating the *LacZ* fragment of plasmid pUC19 and replacing the ampicillin resistance gene with kanamycin resistance gene. *E. coli* BL21 (DE3) and pET-32a (+) (Novagen, Madison, WI, USA) were used for protein expression. Restriction endonucleases, DNA polymerase, and T4 DNA ligase were purchased from Thermo Fisher Scientific (Hudson, NH, USA). Lactose, glucose, and galactose were purchased from Sigma-Aldrich (St. Louis, MO, USA). All other chemicals and reagents were of analytical grade and purchased from commercial sources, unless indicated otherwise.

Construction and Screening of Metagenomic Library. Marine sediment samples were collected from Qiongdongnan basin of South China Sea (17°33′17″ N, 110°30′26″ E; water depth of 716.8 m) and stored at −80 °C until the DNA extraction was performed. The total genomic DNA from the marine sediment sample was extracted by using QIAamp DNA stool Mini kit according to the product manual (QIAGEN, Hilden, Germany). The genomic DNA was then partially digested with *Bam*HI and DNA fragments of 2.5−7.5 kb were purified using a QIAquick Gel Extraction Kit (QIAGEN) and inserted into the pUC19Δ*LacZ* vector, which had been previously digested with *Bam*HI and dephosphorylated with calf intestine alkaline phosphatase (CIAP). Next, the recombinant plasmid was transformed into *E. coli* DH5α and the transformants were cultured on LB agar plates containing 24 μg/mL isopropyl-β-D-1-thiogalactopyranoside (IPTG), 40 μg/mL 5-bromo-4-chloro-3-indolyl-β-D-galactopyranoside (X-Gal), and 50 μg/mL kanamycin at 37 °C overnight. The positive colonies were visibly selected based on their blue color, which was caused by the hydrolysis of X-Gal.

Overexpression and Purification of the Target Protein. The overexpression and purification of the target protein in pET32a (+) and *E. coli* BL21 (DE3) were performed as previously described elsewhere.[8] After purification using a His Bind Purification Kit (Novagen) according to the product manual, the purified enzyme in the elution buffer (1 M imidazole, 0.5 M NaCl, 20 mM Tris-HCl, pH 7.9) was further dialyzed three times in phosphate buffer (50 mM, pH 7.0), and then stored at 4 °C for further study. Sodium dodecyl sulfate−polyacrylamide gel electrophoresis (SDS−PAGE) was used to determine the molecular mass of the denatured recombinant protein with suitable size of protein markers (Thermo Fisher Scientific, Waltham, MA, USA) as standards. The concentration of the recombinant protein was determined by using CoomassiePlus (Bradford) Assay Kit (Thermo Fisher Scientific, Waltham, MA, USA) according to the product manual.

Enzyme Activity Assay. The enzyme activity was determined using lactose as substrate. Appropriately diluted enzyme solution (50 μL) was added into 450 μL of lactose solution (50 g/L in 50 mM phosphate buffer, pH 7.0). After being incubated for 15 min at 50 °C, the reaction mixture was boiled for 10 min to terminate the reaction. The concentration of glucose released from lactose was determined using a glucose oxidase-peroxidase assay kit (Sigma-Aldrich). One unit of enzyme activity was defined as the amount of enzyme required to release 1 μmol of glucose per min.

Preparation and Structure Analysis of Bgal1-3-CLEAs. The CLEAs of Bgal1-3 were prepared in a 25-mL flask with a magnetic stirrer bar. Initially, 9 mL of different protein precipitating agents including saturated ammonium sulfate, acetone, isopropanol, acetonitrile, and dimethyl sulfoxide (DMSO) was added into 1 mL of β-galactosidase solution, respectively. After keeping the mixture with stirring for 30 min at 4 °C for precipitation, glutaraldehyde was added to different final concentrations (10, 25, 50, 75, 100, and 125 mM) and stirred for 3 h at 25 °C. The pellets were collected by centrifugation at 12 000*g* for 10 min, washed twice with 10 mL of phosphate buffer (50 mM, pH 7.0), and stored in the same buffer at 4 °C.

The scanning electron micrographs (SEM) of CLEAs were recorded on a JSM-6330F field emission scanning electron microscope (Japan Electron Optics Laboratory Co., Ltd., Japan). The sample preparation consisted of freeze-drying by lyophilizer (Alpha 2-4/LSC, Christ, Germany) and coating with gold using an Emitech K550 sputter coater (Ashford, UK).

Effect of pH and Temperature on the Activity of the Free and Immobilized Bgal1-3. The optimal pH of the free and immobilized Bgal1-3 was determined using lactose as substrate in the pH range of 4.5−8.5 at 50 °C, respectively. The pH buffers were 50 mM citric acid−sodium citrate buffer (pH 3.0−6.0), 50 mM phosphate buffer (pH 6.0−8.0), and 50 mM Tris-HCl buffer (pH 8.0−9.0). The optimal temperature of the free and immobilized Bgal1-3 was determined by measuring the initial reaction rate in the temperature range of 35−65 °C in phosphate buffer (50 mM, pH 7.0). Moreover, the pH stability of the free and immobilized enzyme was investigated by measuring the residual activity after incubating the free and immobilized enzyme at 4 °C for 24 h in the above buffer systems, and the thermostability of the enzyme was measured by residual activity analysis after incubating the free and immobilized enzyme for various times intervals at 40 °C in 50 mM phosphate buffer (pH 7.0). All these reactions were performed according to the method in the Enzyme Activity Assay section.

The storage stability of the free and immobilized β-galactosidase was determined at 25 °C in 50 mM phosphate buffer (pH 7.0). After different storage times (0−90 days), the residual activities were tested. The activity of the free and immobilized enzyme after fresh preparation was defined as 100%, respectively.

Determination of Kinetic Parameters of the Free and Immobilized Bgal1-3. The kinetic parameters (K_{cat} and K_m) of the free and immobilized β-galactosidase were determined by assaying the enzymatic activity in 50 mM phosphate buffer (pH 7.0) at 50 °C with seven different concentrations (5, 10, 15, 20, 30, 50, and 100 mM) of lactose as substrate. The Michaelis−Menten equation was used to make all kinetic data fit to Lineweaver−Burk, and SigmaPlot software (Systat Software, Chicago, IL, USA) was applied to calculate the kinetic parameters.

Effect of Galactose and Glucose on the Activity of the Free and Immobilized Bgal1-3. The effect of galactose and glucose on the activity of the free and immobilized Bgal1-3 was determined according to the method reported by Husain et al.[28] In brief, the activity of the free and immobilized β-galactosidase was determined in the presence of increasing concentrations of galactose or glucose (100−500 mM) in 50 mM phosphate buffer (pH 7.0) at 50 °C using 5 mM *o*-nitrophenyl-β-D-galactopyranoside (oNPG) as substrate. Ten μL of enzyme solution was added into 490 μL of oNPG solution. After the reaction mixture was incubated for 10 min at 50 °C, 500 μL of 10% (w/v) sodium carbonate was added to terminate the reaction. The enzyme activity was quantified by following the *o*-nitrophenyl (oNP) release at 405 nm. The activity of enzyme without galactose or glucose was considered as 100%, respectively.

GOS Synthesis in Organic−Aqueous Biphasic System Using the Free and Immobilized Bgal1-3. The synthesis of GOS using lactose as substrate via the free and immobilized Bgal1-3 was performed in an organic−aqueous biphasic system. Ethyl acetate

DOI: 10.1021/jf504473k
J. Agric. Food Chem. 2015, 63, 894−901

(2.5 mL) was added into 22.5 mL of aqueous phase, which was prepared by adding 9 g of lactose and 450 U enzyme into phosphate buffer (50 mM, pH 7.0). The reaction mixture was added into a 100-mL flask and the reaction was carried out at 40 °C for 10 h in a shaking oscillator (250 rpm). The reaction was then terminated by boiling the mixture for 10 min. After centrifugation at 12 000*g* for 10 min, the supernatant of aqueous phase was collected for sugar analysis.

Sugar Analysis. Qualitative analysis of the GOS syrup was performed by thin-layer chromatography (TLC). Butanol−ethanol−water (5:3:2, v/v/v) was used as the mobile phase, and visualization was achieved by spraying a solution containing 20% (v/v) sulfuric acid and 0.5% (w/v) 3,5-dihydroxytoluene onto a plate (TLC Silica gel 60 F254, Merck, Germany) and heating it at 85 °C for 15 min. Further analysis of the individual oligosaccharide in the GOS syrup was investigated by high-resolution electrospray ionization mass spectrometry (HR-ESI-MS) via hybrid mass spectrometer LTQ Orbitrap Velos (Thermo Scientific, FL, USA). The detection was performed in the positive mode under the working conditions as follows: spray voltage of 3.5 kV, heated capillary temperature of 300 °C, and heated capillary voltage of 20 V with nitrogen used as sheath and auxiliary gas. Quantitative analysis of the GOS syrup was carried out by high-performance liquid chromatography (HPLC) with a refractive index detector via a system equipped with a degassing system (LC-20A SHIMADZU, Japan) and a pump (SHIMADZU). A Shodex SUGAR SP0810 column (8.0 × 300 mm, 7 μm, Shodex, Japan) was used for the HPLC analysis. HPLC-grade water was used as the mobile phase at a flow rate of 0.25 mL/min at 80 °C. The injection volume was 10 μL. Individual sugars in the mixtures were identified by comparison of their retention times with those of the standards (1% glucose, 1% galactose, 1% lactose; their response factors were 2.953×10^{-7}, 3.422×10^{-7}, and 3.376×10^{-7}, respectively) and quantified from the peak area calibrated against sugar standards.[29] The GOS yield was calculated according to the following formula:

$$\text{GOS yield (\%)} = \frac{\text{GOS formed}}{\text{total saccharides}} \times 100$$

Total saccharides is the sum of all sugars (glucose, galactose, residual lactose, and GOS), and it is approximately equal to the initial lactose content.

Reusability Assay of Bgal1-3-CLEAs. The reusability of Bgal1-3-CLEAs was assessed by carrying out the GOS synthesis for ten consecutive batches under the same synthetic condition described above. After each cycle of operation, the pellets were recovered by centrifugation at 12 000*g* for 10 min and washed twice with phosphate buffer (50 mM, pH 7.0). The recovered CLEAs and 2.5 mL of ethyl acetate were then added into 22.5 mL of phosphate buffer (50 mM, pH 7.0) which contained 9 g of lactose to initiate the next batch reaction. The residual enzymatic activity after each operation was compared with that of fresh CLEAs, which was defined as 100%. The GOS yield of each batch was determined according to the method in the Sugar Analysis section.

Statistical Analysis. All data were treated by analysis of variance (ANOVA) using IBM SPSS (Statistical Package for the Social Sciences, IBM SPSS. Inc., Chicago, IL, US). Significant differences were defined as $P < 0.05$.

Nucleotide Sequence Accession Number. The nucleotide sequence of *bgal1-3* has been submitted to GenBank, and its accession number is KC521353.

RESULTS AND DISCUSSION

***β*-Galactosidase Screening from Metagenomic Library and Sequence Analysis.** A plasmid metagenomic library containing nearly 3150 Mb of metagenomic DNA was successfully constructed using the DNA extracted from marine sediment samples of South China Sea for screening novel *β*-galactosidase. Twenty-eight positive clones were identified from the metagenomic library by functional screening, and one of the positive clones was finally selected for further study due to its high activity toward natural substrate lactose. Sequence analysis of the positive clone revealed an open reading frame (named *bgal1-3*) of 2202 bp which encoded a 733-amino-acid protein (Bgal1-3). A protein blast (Blastp) result showed that all its closest homologues were *β*-D-galactosidase. A search of Conserved Domains Database (CDD) revealed contained conserved regions of the glycosyl hydrolases family 2 sugar binding domain (1−140 aa, pfam02836) and glycosyl hydrolases family 2 triosephosphate isomerase barrel domain (249−547 aa, pfam02837), which indicated that this protein was a member of the glycosyl hydrolases family 2 (GH2).

Overexpression and Purification of the Recombinant Bgal1-3. The *bgal1-3* gene was inserted into the expression vector pET-32a (+) and overexpressed in a soluble protein fraction in *E. coli* BL21 (DE3). The recombinant Bgal1-3 was purified by affinity chromatography, and the activity of the pure protein toward lactose was 67.18 ± 1.22 U/mg. SDS−PAGE analysis revealed that the molecular mass of the recombinant Bgal1-3 was about 100 kDa (Supporting Information (SI) Figure S1), which agreed with the predicted size of Bgal1-3 (82.26 kDa) plus the N-terminal fusion protein of the expression vector (18 kDa).

Preparation and Structural Characterization of Bgal1-3-CLEAs. The preparation of CLEAs usually includes two procedures: precipitation of the enzyme from aqueous buffer as physical aggregates and cross-linking of the aggregates by bifunctional agent.[21] In this study, five kinds of protein precipitating agents were used for the precipitation of Bgal1-3 (Figure 1A). Activity assay demonstrated that ammonium sulfate (90% saturation) worked best among them. The activity recovery of the precipitated protein was 92.3 ± 3.7%. The optimum quantity of glutaraldehyde required for activity recovery was then investigated by adding glutaraldehyde to different final concentrations (10−125 mM), and the results showed that the CLEAs retained 96.2 ± 1.6% activity after cross-linking with 25 mM glutaraldehyde at 25 °C for 3 h (Figure 1B).

The scanning electron micrographs of Bgal1-3-CLEAs revealed a spherical structure of the aggregates. The enzyme molecules were packed together into "balls" with diameter of about 0.2 μm (Figure 2B), and then the "balls" were cross-linked to be aggregate clusters with the diameter of about 5 μm (Figure 2A). The structure of Bgal1-3-CLEAs was similar to that of the type 1 aggregates described by Schoevaart et al.[30]

Effect of pH and Temperature on the Enzymatic Activity and Stability of the Free and Immobilized Bgal1-3. The free and immobilized Bgal1-3 both showed an optimal pH of 7.0 (Figure 3A). However, the immobilized Bgal1-3 maintained higher pH stability than the free enzyme (Figure 3B), which was similar to the reports previously published.[18,25] The optimal temperature of the immobilized Bgal1-3 was 50 °C, the same as that of the free enzyme (Figure 3C). The thermostability of the immobilized enzyme was distinctly improved than that of the free enzyme, and its enzymatic activity stayed almost constant after incubation at 40 °C for 120 h, whereas the residual activity of the free enzyme was only about 60% under the same processing conditions (Figure 3D). This phenomenon has been observed in some previous studies. For example, the CLEAs of aminoacylase from *Aspergillus melleus* conserved about 52% activity after incubation at 47 °C for 24 h, while the free aminoacylase lost almost all activity;[31] the CLEAs of phenylalanine ammonia lyase from *Rhodotorula glutinis* maintained approximately 75% activity

DOI: 10.1021/jf504473k
J. Agric. Food Chem. 2015, 63, 894−901

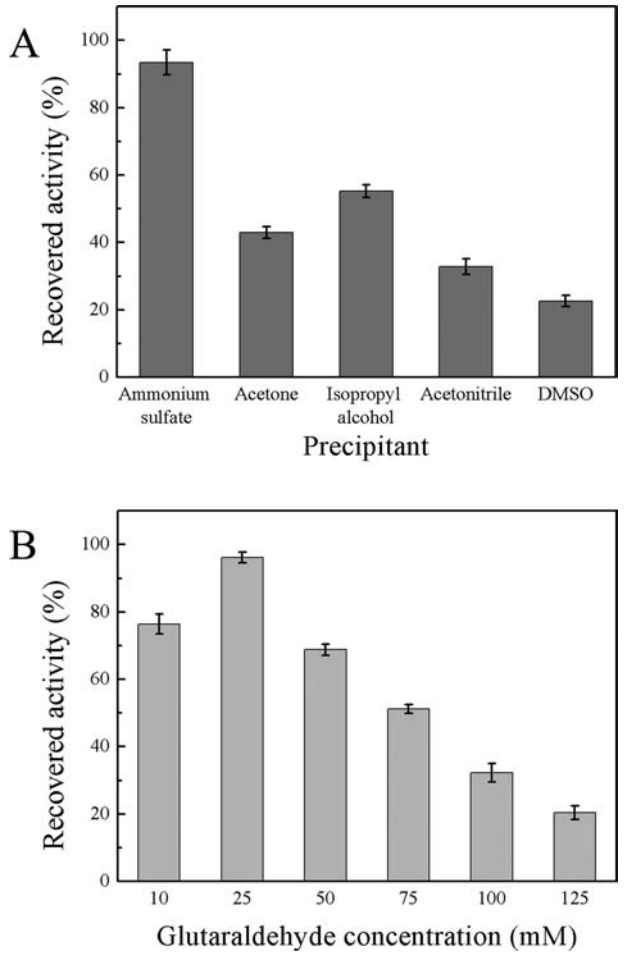

Figure 1. (A) Precipitation of Bgal1-3 with different precipitants. (B) Effect of glutaraldehyde concentration on the activity recovery of the protein precipitated with ammonium sulfate. Data represent the means of three experiments and error bars represent standard deviation.

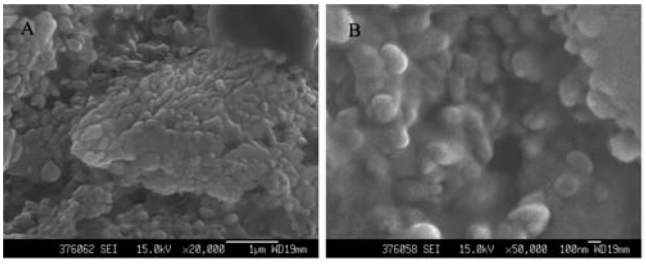

Figure 2. Scanning electron microscope images of Bgal1-3-CLEAs: (A) magnification ×20 000; (B) magnification ×50 000.

when stored at 60 °C for 10 h, whereas its soluble counterpart maintained only 20% activity at the same temperature for 1 h;[25] the CLEAs of alpha amylase (CLARASE L-40,000), glucoamylase (OPTIDEX L-300) and pullulanase (OPTIMAX L-300) retained 85%, 70%, and 38% activity after the incubation at 65 °C for 3 h, while their free counterparts retained only 46%, 35%, and 15% activity, respectively.[32] The enhanced thermostability of the CLEAs indicated that cross-linking as aggregates provided more molecular conformation stability of these enzymes.[25,31,32]

The storage stability of Bgal1-3-CLEAs was also determined. After storage at 25 °C for 90 days, the residual activity of the immobilized enzyme was 79.5 ± 3.1%, whereas the free enzyme was only 16.2 ± 2.3% (Table 1). Therefore, the immobilization of Bgal1-3 as CLEAs conferred extended storage life of the enzyme.

Kinetic Parameters of the Free and Immobilized Bgal1-3. The kinetic parameters of the free and immobilized Bgal1-3 are listed in Table 2. The catalytic efficiency (K_{cat}/K_m) of Bgal1-3 decreased after the immobilization, which was mainly due to the increase of the K_m value (from 17.98 ± 0.35 mM to 19.39 ± 0.21 mM). Similar change of the kinetics parameters has also been reported in the cases of other enzymes. The K_m value of the immobilized aminoacylase was 1.497 mM, higher than that of free enzyme (0.964 mM);[31] the immobilized β-galactosidase from *Aspergillus oryzae* displayed higher K_m value (60.30 mM) than its soluble counterpart (52.13 mM).[33] The increase of K_m value of immobilized enzyme may be partially attributed to the occurrence of mass transfer resistance between the substrate and the immobilized enzyme.[34]

GOS Synthesis in Organic−Aqueous Biphasic System Using the Free and Immobilized Bgal1-3. To assess the GOS synthetic ability of the free enzyme in the organic−aqueous biphasic system, the reaction condition was optimized by a single factorial experiment (method and data are provided in detail in the SI). Ethyl acetate was chosen as the organic phase because its existence (10−90%, v/v) did not affect the thermostability of either the free Bgal1-3 or Bgal1-3-CLEAs (data not shown). The GOS synthesis of Bgal1-3-CLEAs was then conducted under the same condition in order to investigate the effect of the immobilization on the GOS synthetic ability of Bgal1-3. After the reaction, TLC was used for the preliminary analysis of the GOS syrups synthesized by the free enzyme and Bgal1-3-CLEAs. As shown in Figure 4A, the GOS content and composition of the two kinds of syrups were similar. The bands of the sugar distribution in Figure 4A also suggested the rich diversity of the oligosaccharide. Each individual oligosaccharide was then further distinguished by mass spectrometry. HR-ESI-MS analysis revealed that both of the GOS syrups synthesized by the free enzyme and Bgal1-3-CLEAs contained at least seven different oligosaccharides, with the degree of polymerization (DP) ranging between 3 and 9 (SI Figure S3 and SI Table S1). At last, the GOS yields were quantified according to the method in the Sugar Analysis section. (Figure 4B). Results showed that the GOS yield of Bgal1-3-CLEAs (59.4 ± 1.5%) was slightly higher than that of the free enzyme (57.1 ± 1.7%) ($n = 6$, $P < 0.05$, SI Figure S4, and SI Table S2). High GOS yield is an attractive property of the β-galactosidases that is of interest for the potential application. According to the reported literature, GOS yields were commonly achieved between 17.1% and 45%, only a few exceeded 50%.[35] Therefore, the high GOS yields of the free enzyme and CLEAs in this work would be very useful in the GOS production.

Although the CLEAs of a variety of enzymes have been applied to many different biochemical reactions, there is only one report on the GOS synthesis by using β-galactosidase CLEAs up to now. Gaur et al.[27] reported that the transglycosylation activity of the β-galactosidase from *Aspergillus oryzae* drastically dropped after it was immobilized as CLEAs, with the decrease of the GOS yield from 24.1% to 1.4%. In contrast, the GOS yield of Bgal1-3 increased after the immobilization. The possible reasons behind this were mainly ascribed to the following points: First, the conformational change of Bgal1-3 after immobilization may affect its trans-

DOI: 10.1021/jf504473k
J. Agric. Food Chem. 2015, 63, 894−901

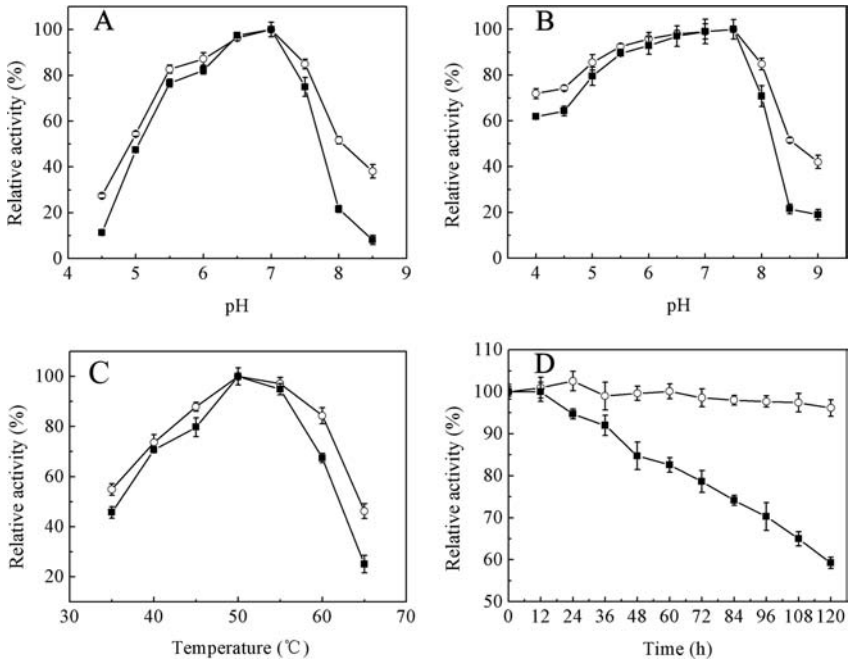

Figure 3. Effect of pH and temperature on the initial reaction rate and stability of the free and immobilized Bgal1-3. (A) Effect of pH on the initial reaction rate of the free (■) and immobilized (○) Bgal1-3 when the reactions were performed at 50 °C. (B) Effect of pH on the stability of the free (■) and immobilized (○) Bgal1-3 when the reactions were performed at 50 °C after the enzymes were incubated at 4 °C for 24 h. (C) Effect of temperature on the initial reaction rate of the free (■) and immobilized (○) Bgal1-3 when the reactions were performed at pH 7.0. (D) Effect of temperature on the stability of the free (■) and immobilized (○) Bgal1-3 when the enzymes were incubated at pH 7.0 and the reactions were performed at pH 7.0. Data points are the average of triplicate measurements, and error bars represent standard deviation.

Table 1. Storage Stability of the Free and Immobilized Bgal1-3 at 25 °C

	residual activity (%)	
storage time (days)	free Bgal1-3	immobilized Bgal1-3
0	100.0 ± 0.8	100.0 ± 0.6
5	98.5 ± 1.4	100.0 ± 0.3
10	97.6 ± 0.5	99.8 ± 1.1
20	92.5 ± 1.8	99.2 ± 1.8
30	86.2 ± 2.4	98.8 ± 2.5
60	43.6 ± 3.1	86.5 ± 2.7
90	16.2 ± 2.3	79.5 ± 3.1

Table 2. Kinetic Parameters of the Free and Immobilized Bgal1-3

enzyme	substrate	K_m (mM)	K_{cat} (s^{-1})	K_{cat}/K_m (s^{-1} mM^{-1})
free Bgal1-3	lactose	17.98 ± 0.35	131.16 ± 2.38	7.29
immobilized Bgal1-3	lactose	19.39 ± 0.21	128.46 ± 1.54	6.63

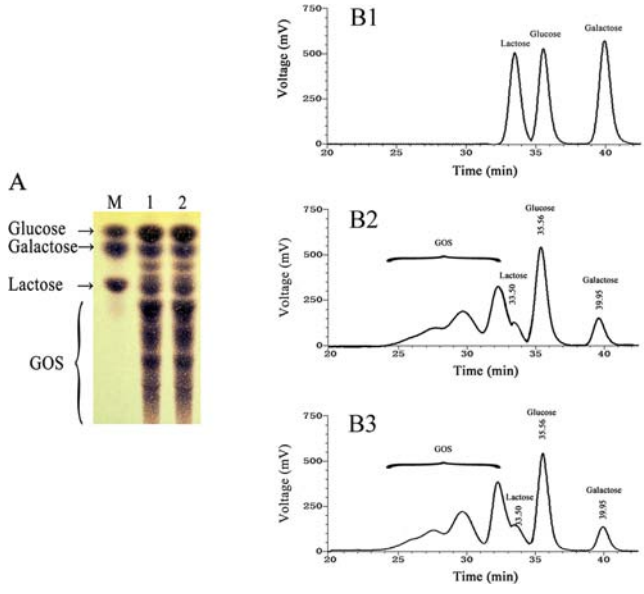

Figure 4. Sugar analysis of the GOS syrups synthesized by the free Bgal1-3 and Bgal1-3-CLEAs in organic−aqueous biphasic system. (A) TLC analysis. Lane M: standard sugar marker. Lane 1: GOS syrup synthesized by the free Bgal1-3. Lane 2: GOS syrup synthesized by Bgal1-3-CLEAs. (B) HPLC analysis. B1. The standard sugar samples (lactose, glucose, and galactose). B2. GOS syrup synthesized by the free Bgal1-3. B3. GOS syrup synthesized by Bgal1-3-CLEAs. The peaks were lactose, 33.50 min; glucose, 35.56 min; and galactose, 39.95 min; several other peaks were synthetic GOS.

glycosylation ability. The conformation of the enzyme molecular could be significantly changed in the process of precipitation and then the changed conformation was "locked" by the cross-linking, which would greatly affect the selectivity of the enzymes.[36] In line with this, the conformation "locked" by the CLEAs of Bgal1-3 may be more conducive to trans-glycosylation. Previous studies on the lipase CLEAs also showed that increased specific activity and/or enantioselectivity can be achieved by changing the conformation of the enzymes to more favorable forms.[36] Second, the enhanced galactose-tolerance of Bgal1-3-CLEAs might be another reason for the increased GOS yield. As shown in Figure 5, Bgal1-3-CLEAs showed glucose tolerance similar to that of the free enzyme; they both retained more than 90% activity in the presence of 500 mM glucose. Whereas, when the same concentration of

DOI: 10.1021/jf504473k
J. Agric. Food Chem. 2015, 63, 894−901

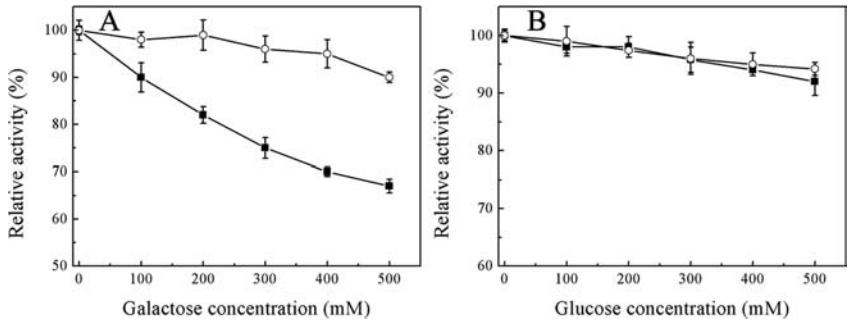

Figure 5. Effect of D-galactose (A) and D-glucose (B) on the activity of Bgal1-3 (■) and Bgal1-3-CLEAs (○). Data represent the means of three experiments and error bars represent standard deviation.

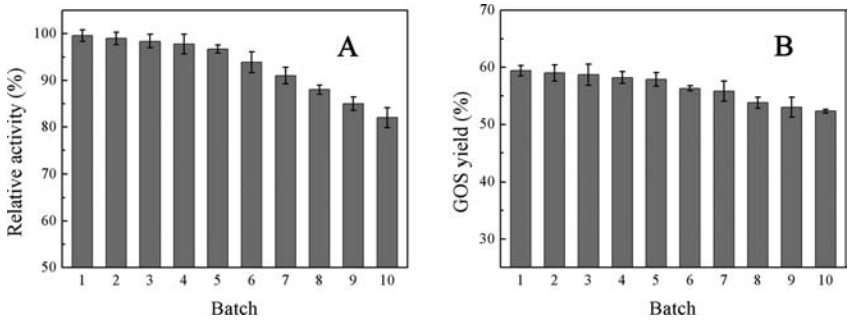

Figure 6. Reusability of Bgal1-3-CLEAs for GOS synthesis in organic−aqueous biphasic system. (A) Residual activity of Bgal1-3-CLEAs after each batch. (B) GOS yields of each batch. Data represent the means of three experiments and error bars represent standard deviation.

galactose existed, the residual activity of Bgal1-3-CLEAs was much higher than that of the free enzyme (92.3 ± 1.3% vs 68.1 ± 1.5%). The enhanced galactose-tolerance of Bgal1-3-CLEAs could relieve the inhibitory effect during the reaction and thus benefit the GOS synthesis.[37] Similar phenomena of other β-galactosidases have been reported before.[33,38] Last, it is worth noting that the organic−aqueous biphasic system used in this work may also contribute to the higher GOS yield of Bgal1-3-CLEAs. As mentioned above, Bgal1-3-CLEAs showed lower hydrolytic efficiency toward lactose than the free enzyme in aqueous phase, which may be partially attributed to the occurrence of diffusional limitations. However, when the Bgal1-3-CLEAs and the free enzyme were used for the GOS synthesis in the organic−aqueous biphasic system, higher GOS yield was achieved by Bgal1-3-CLEAs, which indicated undiminished catalytic efficiency and negligible diffusional limitations in the process of GOS synthesis. Similar phenomenon has been reported by Sheldon[21] when using CLEAs in colorimetric assays (aqueous system, diffusional limitations observed) and organic synthesis (nonaqueous system, no diffusional limitations observed). These results suggested that the catalytic property of CLEAs in aqueous and nonaqueous system was not fully corresponding. The activity of CLEAs based on colorimetric assays in aqueous system may lead one to underrate its real catalytic capability in nonaqueous system. Hence, more caution and attempts are needed when one tries to evaluate the suitability of CLEAs for the reactions in nonaqueous system.

Reusability of Bgal1-3-CLEAs. Reusability of the immobilized enzymes is a key factor in industrial applications, because it results in simplification of downstream processing and reduction in enzyme costs.[21] In this study, the reusability of Bgal1-3-CLEAs was evaluated through GOS synthesis for successive batches. As shown in Figure 6, Bgal1-3-CLEAs retained 82 ± 2.1% of their initial activity after ten batches; the GOS yield of the tenth batch was 52.3 ± 0.3%, which was still higher than that of the most former reports.[35] Considering the fact that the activity of Bgal1-3-CLEAs was almost constant after incubation for 120 h at 40 °C (Figure 3D) and the existence of ethyl acetate also did not affect their thermostability (data not shown), the decline of catalytic activity of CLEAs during repeated use might be mainly attributed to the washing and centrifugation.[39] This phenomenon was also supported by the determination of enzyme activity left in the supernatant (data not shown). These results demonstrated that CLEAs of Bgal1-3 had a robust reusability and good application potential in the GOS production.

In conclusion, a novel β-galactosidase Bgal1-3 was isolated from a marine metagenomic library, and its CLEAs were then successfully prepared. Furthermore, the enzymatic properties and GOS yields of the free and immobilized enzyme were also investigated. In comparison with the free enzyme, the immobilized enzyme displayed slightly higher GOS yield, much higher thermostability, and robust reusability, as well as good storage stability. These results open an attractive way toward the feasibility and high-efficiency synthesis of GOS by β-galactosidases-CLEAs.

■ ASSOCIATED CONTENT

Supporting Information

SDS−PAGE figure, single factorial experiments of the GOS synthesis using free Bgal1-3 in organic−aqueous biphasic system, and HR-ESI-MS spectrum analysis of the oligosaccharides. This material is available free of charge via the Internet at http://pubs.acs.org.

DOI: 10.1021/jf504473k
J. Agric. Food Chem. 2015, 63, 894−901

AUTHOR INFORMATION

Corresponding Author

*E-mail: lsslyh@mail.sysu.edu.cn. Tel: 86-20-84113712. Fax: 86-20-84036215.

Author Contributions

†Authors L.L. and G.L. contributed equally to this work.

Notes

The authors declare no competing financial interest.

ACKNOWLEDGMENTS

This research was supported by National Natural Science Foundation of China (31170117, 31270156), Science & Technology Projects of Guangdong Provincial Oceanic and Fishery Bureau (A201301C04), National Marine Research Special Funds for Public Welfare Projects of China (201205020), Major Science and Technology Projects of Guangdong Province, China (2011A080403006), Natural Science Foundation of Guangdong Province, China (S2012010010464), the Research (Innovative) Fund of Laboratory Sun Yat-sen University (YJ201027), and the Fundamental Research Fund for the Central Universities of Sun Yat-sen University (11lgpy23).

ABBREVIATIONS USED

CLEAs, cross-linked enzyme aggregates; GOS, galacto-oligosaccharides; *E. coli*, *Escherichia coli*; CIAP, calf intestine alkaline phosphatase; IPTG, isopropyl-β-D-1-thiogalactopyranoside; X-Gal, 5-bromo-4-chloro-3-indolyl-β-D-galactopyranoside; SDS−PAGE, sodium dodecyl sulfate−polyacrylamide gel electrophoresis; oNPG, *o*-nitrophenyl-β-D-galactopyranoside; TLC, thin-layer chromatography; HR-ESI-MS, high-resolution electrospray ionization mass spectrometry; HPLC, high-performance liquid chromatography

REFERENCES

(1) Kunz, C.; Rudloff, S. Biological functions of oligosaccharides in human milk. *Acta. Paediatr.* **2008**, *82*, 903−912.

(2) Weaver, C. M.; Martin, B. R.; Nakatsu, C. H.; Armstrong, A. P.; Clavijo, A.; McCabe, L. D.; McCabe, G. P.; Duignan, S.; Schoterman, M. H. C.; van den Heuvel, E. G. H. M. Galactooligosaccharides improve mineral absorption and bone properties in growing rats through gut fermentation. *J. Agric. Food Chem.* **2011**, *59*, 6501−6510.

(3) Hughes, C.; Davoodi-Semiromi, Y.; Colee, J. C.; Culpepper, T.; Dahl, W. J.; Mai, V.; Christman, M. C.; Langkamp-Henken, B. Galactooligosaccharide supplementation reduces stress-induced gastrointestinal dysfunction and days of cold or flu: a randomized, double-blind, controlled trial in healthy university students. *Am. J. Clin. Nutr.* **2011**, *93*, 1305−1311.

(4) Mussatto, S. I.; Mancilha, I. M. Non-digestible oligosaccharides: A review. *Carbohydr. Polym.* **2007**, *68*, 587−597.

(5) Sears, P.; Wong, C. H. Toward automated synthesis of oligosaccharides and glycoproteins. *Science* **2001**, *291*, 2344−2350.

(6) Gosling, A.; Stevens, G. W.; Barber, A. R.; Kentish, S. E.; Gras, S. L. Effect of the substrate concentration and water activity on the yield and rate of the transfer reaction of β-galactosidase from *Bacillus circulans*. *J. Agric. Food Chem.* **2011**, *59*, 3366−3372.

(7) Torres, D. P. M.; Goncalves, M. P.; Teixeira, J. A.; Rodrigues, L. R. Galacto-oligosaccharides: production, properties, applications, and significance as prebiotics. *Compr. Rev. Food Sci. Food Saf.* **2010**, *9*, 438−454.

(8) Wang, K.; Li, G.; Yu, S. Q.; Zhang, C. T.; Liu, Y. H. A novel metagenome-derived β-galactosidase: gene cloning, overexpression, purification and characterization. *Appl. Microbiol. Biotechnol.* **2010**, *88*, 155−165.

(9) Otieno, D. O. Synthesis of β-galactooligosaccharides from lactose using microbial β-galactosidases. *Compr. Rev. Food Sci. Food Saf.* **2010**, *9*, 471−482.

(10) Gosling, A.; Stevens, G. W.; Barber, A. R.; Kentish, S. E.; Gras, S. L. Recent advances refining galactooligosaccharide production from lactose. *Food Chem.* **2010**, *121*, 307−318.

(11) Lu, L.; Xu, S.; Zhao, R.; Zhang, D.; Li, Z.; Li, Y.; Xiao, M. Synthesis of galactooligosaccharides by CBD fusion β-galactosidase immobilized on cellulose. *Bioresour. Technol.* **2012**, *116*, 327−333.

(12) Vera, C.; Guerrero, C.; Conejeros, R.; Illanes, A. Synthesis of galacto-oligosaccharides by galactosidase from *Aspergillus oryzae* using partially dissolved and supersaturated solution of lactose. *Enzyme Microb. Technol.* **2012**, *50*, 188−194.

(13) Husain, Q. β-Galactosidases and their potential applications: a review. *Crit. Rev. Biotechnol.* **2010**, *30*, 41−62.

(14) Urrutia, P.; Bernal, C.; Wilson, L.; Illanes, A. Improvement of chitosan derivatization for the immobilization of *Bacillus circulans* β-galactosidase and its further application in galacto-oligosaccharides synthesis. *J. Agric. Food Chem.* **2014**, *62*, 10126−10135.

(15) Zheng, P.; Yu, H.; Sun, Z.; Ni, Y.; Zhang, W.; Fan, Y.; Xu, Y. Production of galacto-oligosaccharides by immobilized recombinant beta-galactosidase from *Aspergillus candidus*. *Biotechnol. J.* **2006**, *1*, 1464−1470.

(16) Cao, L.; Langen, L. v.; Sheldon, R. A. Immobilised enzymes: carrier-bound or carrier-free? *Curr. Opin. Biotechnol.* **2003**, *14*, 387−394.

(17) Gupta, P.; Dutt, K.; Misra, S.; Raghuwanshi, S.; Saxena, R. Characterization of cross-linked immobilized lipase from thermophilic mould *Thermomyces lanuginosa* using glutaraldehyde. *Bioresour. Technol.* **2009**, *100*, 4074−4076.

(18) Hormigo, D.; Garcia-Hidalgo, J.; Acebal, C.; de la Mata, I.; Arroyo, M. Preparation and characterization of cross-linked enzyme aggregates (CLEAs) of recombinant poly-3-hydroxybutyrate depolymerase from *Streptomyces exfoliatus*. *Bioresour. Technol.* **2012**, *115*, 177−182.

(19) Vaidya, B. K.; Kuwar, S. S.; Golegaonkar, S. B.; Nene, S. N. Preparation of cross-linked enzyme aggregates of L-aminoacylase via co-aggregation with polyethyleneimine. *J. Mol. Catal. B: Enzym.* **2012**, *74*, 184−191.

(20) Cao, L.; van Langen, L. M.; van Rantwijk, F.; Sheldon, R. A. Cross-linked aggregates of penicillin acylase: robust catalysts for the synthesis of beta-lactam antibiotics. *J. Mol. Catal. B: Enzym.* **2001**, *11*, 665−670.

(21) Sheldon, R. A. Characteristic features and biotechnological applications of cross-linked enzyme aggregates (CLEAs). *Appl. Microbiol. Biotechnol.* **2011**, *92*, 467−477.

(22) Illanes, A.; Wilson, L.; Caballero, E.; Fernández-Lafuente, R.; Guisán, J. M. Crosslinked penicillin acylase aggregates for synthesis of β-lactam antibiotics in organic medium. *Appl. Biochem. Biotechnol.* **2006**, *133*, 189−202.

(23) Fazary, A. E.; Ismadji, S.; Ju, Y. H. Biochemical studies on native and cross-linked aggregates of *Aspergillus awamori* feruloyl esterase. *Int. J. Biol. Macromol.* **2009**, *44*, 240−248.

(24) Talekar, S.; Ghodake, V.; Ghotage, T.; Rathod, P.; Deshmukh, P.; Nadar, S.; Mulla, M.; Ladole, M. Novel magnetic cross-linked enzyme aggregates (magnetic CLEAs) of alpha amylase. *Bioresour. Technol.* **2012**, *123*, 542−547.

(25) Cui, J.-D.; Zhang, S.; Sun, L.-M. Cross-linked enzyme aggregates of phenylalanine ammonia lyase: novel biocatalysts for synthesis of L-phenylalanine. *Appl. Biochem. Biotechnol.* **2012**, *167*, 835−844.

(26) Hassani, T.; Ba, S.; Cabana, H. Formation of enzyme polymer engineered structure for laccase and cross-linked laccase aggregates stabilization. *Bioresour. Technol.* **2013**, *128*, 640−645.

(27) Gaur, R.; Pant, H.; Jain, R.; Khare, S. Galacto-oligosaccharide synthesis by immobilized *Aspergillus oryzae* β-galactosidase. *Food Chem.* **2006**, *97*, 426−430.

(28) Husain, Q.; Ansari, S. A.; Alam, F.; Azam, A. Immobilization of *Aspergillus oryzae* -galactosidase on zinc oxide nanoparticles via simple adsorption mechanism. *Int. J. Biol. Macromol.* **2011**, *49*, 37−43.

DOI: 10.1021/jf504473k
J. Agric. Food Chem. 2015, 63, 894−901

(29) Placier, G.; Watzlawick, H.; Rabiller, C.; Mattes, R. Evolved β-galactosidases from *Geobacillus stearothermophilus* with improved transgalactosylation yield for galacto-oligosaccharide production. *Appl. Environ. Microbiol.* **2009**, *75*, 6312−6321.
(30) Schoevaart, R.; Wolbers, M.; Golubovic, M.; Ottens, M.; Kieboom, A.; Van Rantwijk, F.; Van der Wielen, L.; Sheldon, R. Preparation, optimization, and structures of cross-linked enzyme aggregates (CLEAs). *Biotechnol. Bioeng.* **2004**, *87*, 754−762.
(31) Dong, T.; Zhao, L.; Huang, Y.; Tan, X. Preparation of cross-linked aggregates of aminoacylase from *Aspergillus melleus* by using bovine serum albumin as an inert additive. *Bioresour. Technol.* **2010**, *101*, 6569−6571.
(32) Talekar, S.; Pandharbale, A.; Ladole, M.; Nadar, S.; Mulla, M.; Japhalekar, K.; Pattankude, K.; Arage, D. Carrier free co-immobilization of alpha amylase, glucoamylase and pullulanase as combined cross-linked enzyme aggregates (combi-CLEAs): A tri-enzyme biocatalyst with one pot starch hydrolytic activity. *Bioresour. Technol.* **2013**, *147*, 269−275.
(33) Freitas, F. F.; Marquez, L. D.; Ribeiro, G. P.; Brandão, G. C.; Cardoso, V. L.; Ribeiro, E. J. A comparison of the kinetic properties of free and immobilized *Aspergillus oryzae* β-galactosidase. *Biochem. Eng. J.* **2011**, *58*, 33−38.
(34) Ortiz-Soto, M. E.; Rudiño-Piñera, E.; Rodriguez-Alegria, M. E.; Munguia, A. L. Evaluation of cross-linked aggregates from purified *Bacillus subtilis* levansucrase mutants for transfructosylation reactions. *BMC Biotechnol.* **2009**, *9*, 68.
(35) Park, A.-R.; Oh, D.-K. Galacto-oligosaccharide production using microbial β-galactosidase: current state and perspectives. *Appl. Microbiol. Biotechnol.* **2010**, *85*, 1279−1286.
(36) Cao, L. Immobilised enzymes: science or art? *Curr. Opin. Chem. Biol.* **2005**, *9*, 217−226.
(37) Neri, D. F.; Balcão, V. M.; Costa, R. S.; Rocha, I. C.; Ferreira, E. M.; Torres, D. P.; Rodrigues, L. R.; Carvalho, L. B.; Teixeira, J. A. Galacto-oligosaccharides production during lactose hydrolysis by free *Aspergillus oryzae* β-galactosidase and immobilized on magnetic polysiloxane-polyvinyl alcohol. *Food Chem.* **2009**, *115*, 92−99.
(38) Pessela, B. C. C.; Mateo, C.; Fuentes, M.; Vian, A.; García, J. L.; Carrascosa, A. V.; Guisán, J. M.; Fernández-Lafuente, R. The immobilization of a thermophilic β-galactosidase on Sepabeads supports decreases product inhibition: complete hydrolysis of lactose in dairy products. *Enzyme Microb. Technol.* **2003**, *33*, 199−05.
(39) Alvarenga, A. E.; Amoroso, M. J.; Illanes, A.; Castro, G. R. Cross-linked α-L-rhamnosidase aggregates with potential application in food industry. *Eur. Food Res. Technol.* **2014**, *238*, 797−801.

DOI: 10.1021/jf504473k
J. Agric. Food Chem. 2015, 63, 894−901

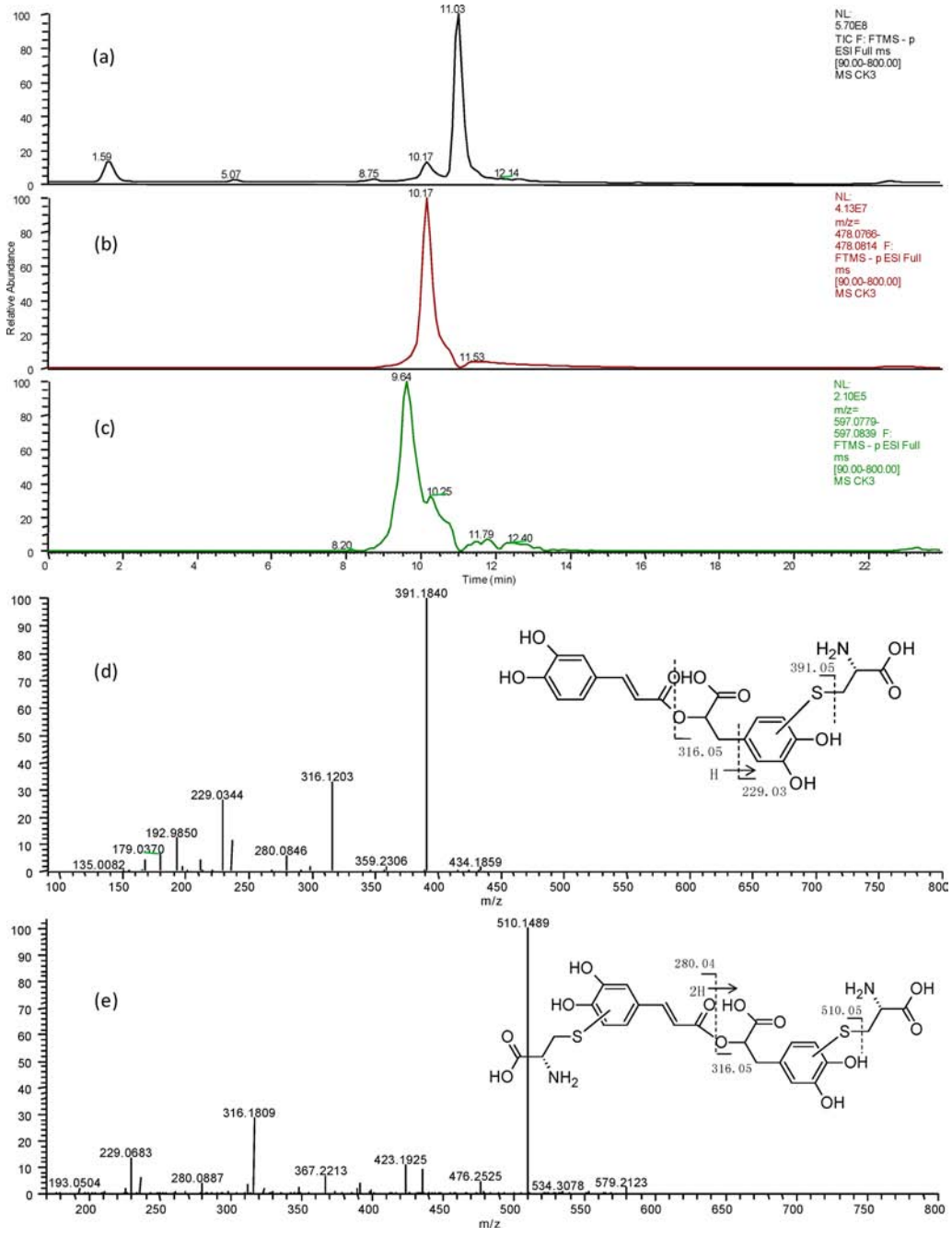

Figure 1. Cys (1.0 mM) and RosA (0.5 mM) incubated in maleic acid buffer (0.1 M) at pH 5.8, with $FeSO_4$ (0.1 mM) and H_2O_2 (30 mM) at 30 °C: (a) TIC of the incubation solution; extracted chromatograms of (b) M1 and (c) M2 from TIC; MS^2 fragmentation patterns of (d) M1 and (e) M2 show the structures of the products with fragmentation pathways noted.

distributed in Lamiaceae herbs.[22] The Lamiaceae herbs, including rosemary, sage, and melissa, are rich in RosA; these herbs are used as food additives in many food products.[23−26] Although Fujimoto[33] has demonstrated the addition reaction between RosA and 1-dodecanethiol, there are still questions about whether RosA can react with myofibrillar proteins, which is closely related to the quality of resulting meat products. As of this writing, little information is available to elucidate the effects of processing conditions, including stirring time, temperature, and oxidative stress, on the formation of adducts. Thus, the objective of this study was to identify the structures of adducts by the reaction of RosA and thiol compounds including cysteine (Cys), glutathione (GSH), and peptides digested from myosin; determine the occurrence of the adduction reaction between RosA and myosin, which is the main protein of myofibrillar proteins in meat; and investigate the influence of processing conditions on the formation of adducts.

MATERIALS AND METHODS

Materials. RosA (96%, MW 360.33), maleic acid, formic acid, Cys (96%, MW 121.15), and GSH (reduced Biotech grade, MW 307.32) were obtained from Sigma-Aldrich Inc. (St. Louis, MO, USA). Hydrochloric acid, sodium hydroxide, acetonitrile, sodium dihydrogen phosphate, sodium chloride, magnesium chloride, ethylenebis-(oxyethylenenitrilo)tetraacetic acid, and hydrogen peroxide (30%) were obtained from Sino Pharm Chemical Reagent Co., Ltd. (Shanghai, China). Water was purified by a Milli-Q system (Millipore,

DOI: 10.1021/jf5044713
J. Agric. Food Chem. 2015, 63, 902−911

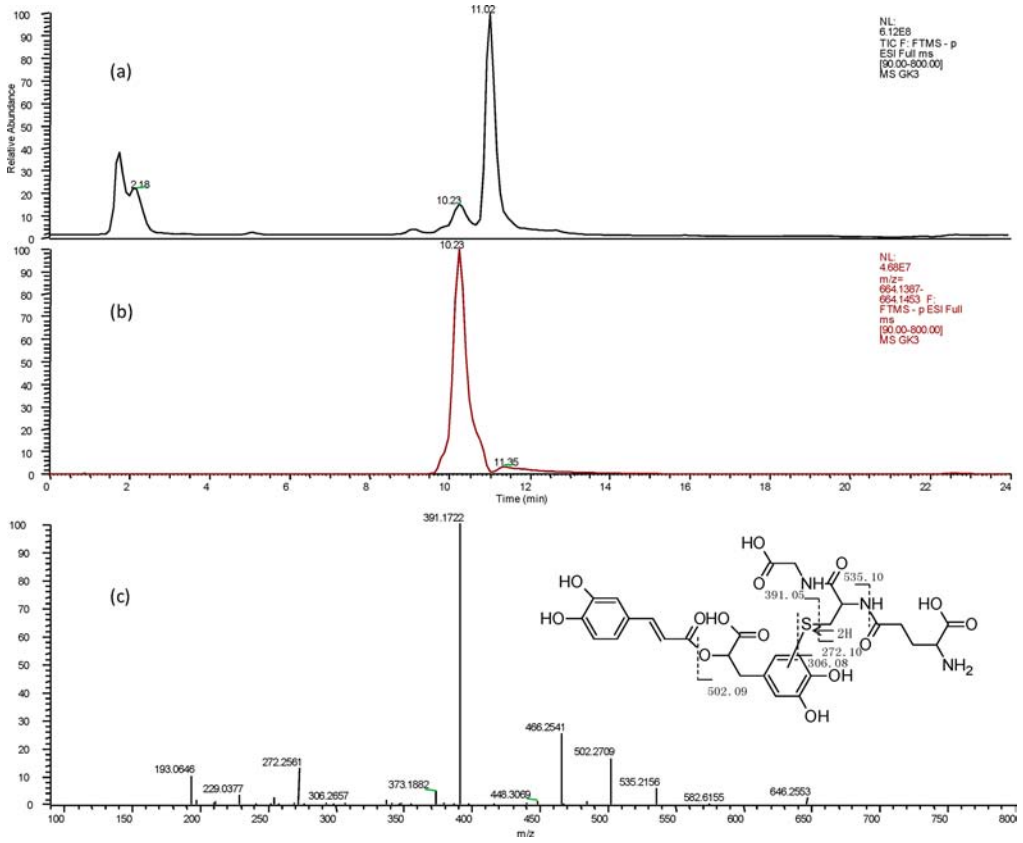

Figure 2. GSH (1.0 mM) and RosA (0.5 mM) incubated in maleic acid buffer (0.1 M) at pH 5.8, with $FeSO_4$ (0.1 mM) and H_2O_2 (30 mM) at 30 °C: (a) TIC of the incubated solution; (b) extracted chromatogram of M3 from TIC; (c) MS^2 fragmentation patterns of M3 show the structures of the products with fragmentation pathways noted.

Scheme 1. Proposed Oxidation Mechanism of Rosmarinic Acid in Meat Model Systems: (I) Oxidation of Compounds Containing Thiol Groups (R−SH) Resulting in Dipolymer by Disulfides to Form Cross-Linked Proteins; (II) Quinone of Rosmarinic Acid Reacted with Compounds Containing Thiol Groups (R−SH), Forming a Thiol−Quinone Adduct

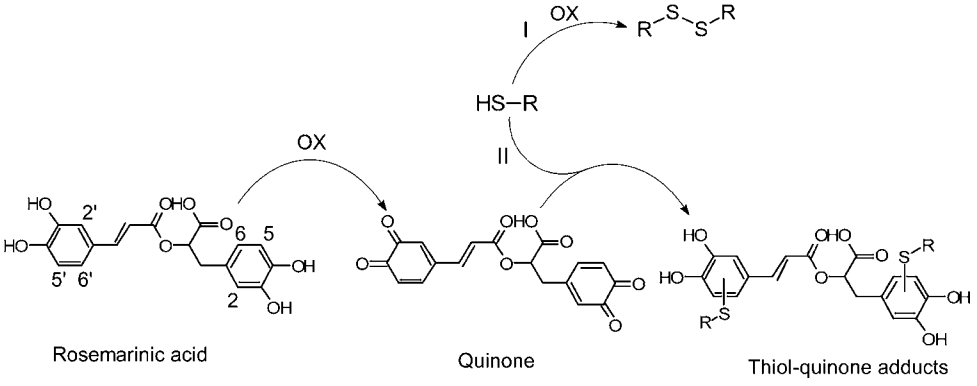

Thermo, Bedford, MA, USA). The following three synthetic peptides (96% enrichment) were obtained from China Peptides Co., Ltd. (Shanghai, China): hexapeptide-1, Cys-Ala-Ser-Leu-Glu-Lys (MW 649.76); heptapeptide-2, His-Asp-Cys-Asp-Leu-Leu-Arg (MW 870.98); and nonapeptide-3, Leu-Glu-Asp-Glu-Cys-Ser-Glu-Leu-Lys (MW 1065.16).

Preparation of Model Solution Sample. The method used for generating adducts was based on the method formerly described;[10,27] thiol compounds including Cys, GSH, and peptides from myosin were diluted in 0.1 M maleic acid buffer adjusted to pH 5.8 with NaOH. The solutions were then separately incubated with RosA, $FeSO_4$, and H_2O_2 at 30 °C and stirred in the dark for 5 h. The concentrations of samples are presented in Table 1.

Preparation of Meat Samples. Freshly ground pork was purchased from Walmart supermarket, Nanjing, China. The meat was chopped and divided in two parts (100 g): to one part was added 50 mg of RosA, and the other part without RosA was used as the control. Aliquots of 5.0 g samples were transferred to plastic bags, which were filled with pure oxygen and sealed. The meat samples in triplicate were kept in storage in the dark at 4 °C for 6 days.

Extraction of MPI. MPI was extracted from the meat samples after 6 days of storage according to the method of Park et al.[28] with slight modifications. An aliquot of 4.0 g of meat was homogenized in 20 mL of isolation buffer (100 mM NaCl, 10 mM NaH_2PO_4, 2 mM $MgCl_2$, 1 mM EGTA, pH 7.0) in 50 mL centrifuge tubes. The homogenate was centrifuged at 2600*g* at 4 °C for 12 min, and the pellet was

DOI: 10.1021/jf5044713
J. Agric. Food Chem. 2015, 63, 902−911

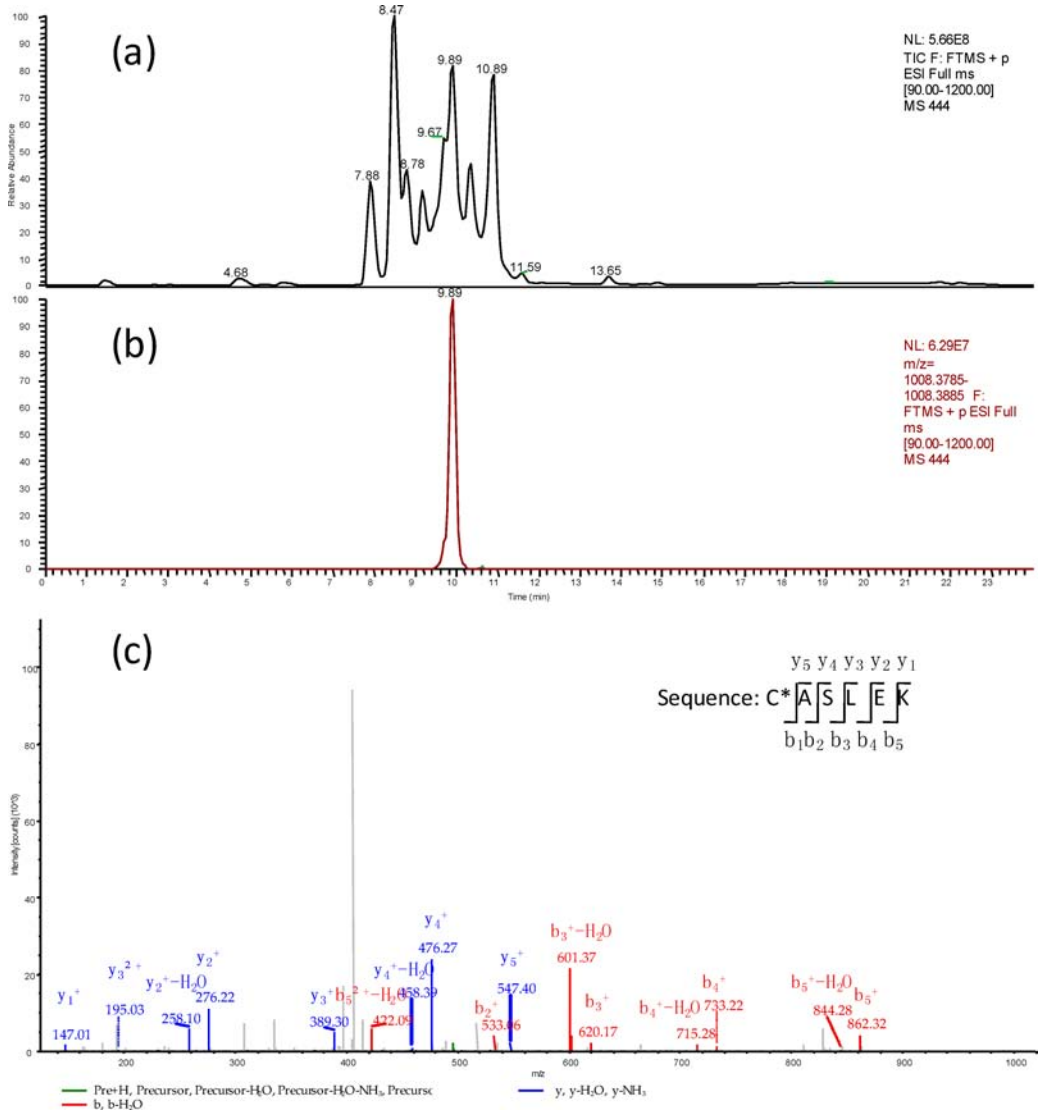

Figure 3. Hexapeptide (0.5 mM) and RosA (0.5 mM) incubated in maleic acid buffer (0.1 M) at pH 5.8, with $FeSO_4$ (0.1 mM) and H_2O_2 (30 mM) at 30 °C: (a) TIC of the incubated solution; (b) extracted chromatogram of M4 from TIC; (c) MS^2 fragmentation patterns of M4 show the structures of the products with fragmentation pathways noted.

resuspended in 10 mL of isolation buffer by homogenization and centrifugation, which was repeated three times. Before the last centrifugation, the suspension was filtered through cheesecloth, and the protein pellet was stored in ice for use.

Influence of Processing Condition on Adducts. To evaluate the effects of stirring time, temperature, and oxidizing intensity on adduct production, the above reaction mixtures were incubated at 30, 40, and 50 °C and stirred for either 1, 3, 5, or 7 h in the presence of 10, 30, 50, or 70 mM H_2O_2. Aliquots (10 mL) of each reaction were prepared in amber vials. Reactions were stopped by the addition of 50 mM potassium bisulfate solution. All reactions were performed in triplicate. The residue was filtered through a 0.45 μm membrane filter for mass spectrometer analysis.

UHPLC-LTQ-Orbitrap MS Analysis. The thiol sources, including Cys, GSH, and peptides of myosin, and their adducts with quinones oxidized from RosA were monitored by the UHPLC-LTQ-Orbitrap system, which consisted of UHPLC (Dionex, ThermoFisher Scientific, New York, USA) coupled with LTQ Orbitrap XL MS (Thermo Fisher Scientific). Instruments were charged by Tune 2.6.0 and Cheomeleon programs. The chromatographic column used was Hypersil GOLD C18 (100 mm × 2.10 mm, 3 μm particle size, Thermo Fisher Scientific). UHPLC mobile phase A was water with 0.1% formic acid, and UHPLC mobile phase D was 100% acetonitrile. Separations were performed in 20 min with a flow rate of 0.2 mL/min under the following programs: 0−4 min, 5% D; 4−12 min, 5−95% D; 12−15 min, 95% D; 15−15.5 min, 95−5% D; and 15.5−20 min, 5% D. The oven temperature of the column was set at 35 °C, and the injection volume was 5 μL.

MS was operated in negative mode to analyze adducts formed by Cys and GSH and monitor the calculated ions of $[M - H]^-$ = 478.0813 (Cys−RosA, M1), $[M - H]^-$ = 597.0854 (Cys−RosA−Cys, M2), and $[M - H]^-$ = 664.1454 (GSH−RosA, M3). The positive mode was used to analyze the adducts formed by peptides and monitor the calculated ions of $[M^+H]^+$ = 1008.3866 (hexapeptide−RosA, M4), $[M + 2H]^{2+}$ = 615.2428 (heptapeptide−RosA, M5), and $[M + 2H]^{2+}$ = 712.2767 (nonapeptide−RosA, M6).

MALDI-TOF/TOF MS Analysis. MALDI-TOF/TOF-MS equipped with a 355 nm laser was applied to examine the precise sites of adduct between RosA and myosin in MPI. The protein samples were reduced and alkylated by the routine method of Biotech Proteome kit (Shimadzu, Osaka, Japan). Finally, the sample (2 μg) was digested in 5 μL of 100 mM NH_4CO_3 (pH 8.0) containing 10 μg/mL trypsin for 10 h at 37 °C. After desalting by C18 Tip, 1 μL of sample solution was spotted on the MALDI plate (Shimadzu GLC, Osaka, Japan) with DHB as the matrix. The digests were analyzed on a MALDI-TOF/TOF

DOI: 10.1021/jf5044713
J. Agric. Food Chem. 2015, 63, 902−911

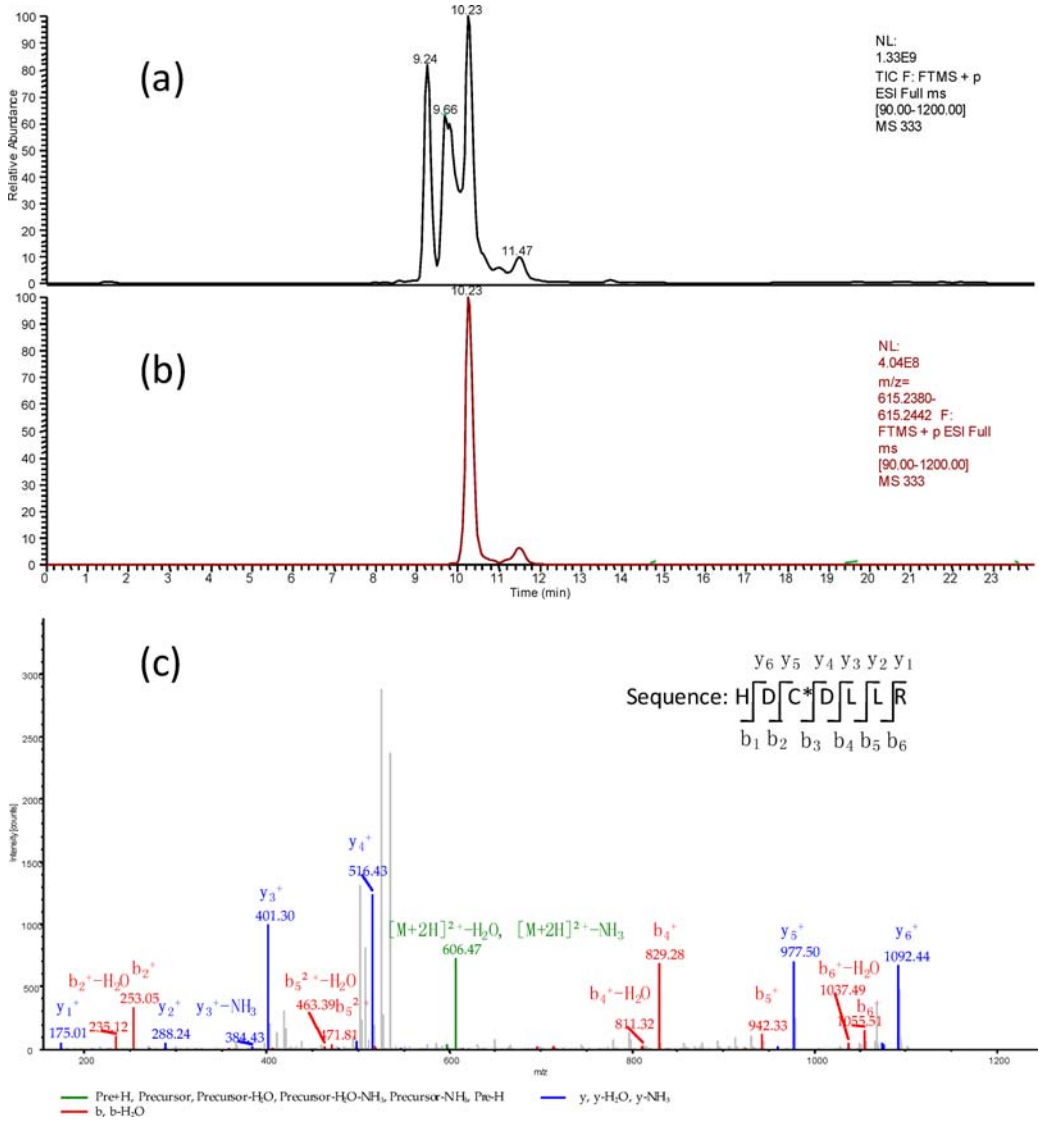

Figure 4. Heptapeptide (0.5 mM) and RosA (0.5 mM) incubated in maleic acid buffer (0.1 M) at pH 5.8, with $FeSO_4$ (0.1 mM) and H_2O_2 (30 mM) at 30 °C: (a) TIC of the incubated solution; (b) extracted chromatogram of M5 from TIC; (c) MS^2 fragmentation patterns of M5 show the structures of the products with fragmentation pathways noted.

instrument (AXIMA Performance; Shimadzu, Manchester, UK) with Kompact version 2.8.

Protein identification was operated by using the MS ion and MS/MS ion search of Mascot. The following parameters were set for searching peptides containing cysteine modified by rosmarinic acid: database, SwissProt; allowing one missed cleavage; enzyme, trypsin; peptide mass tolerance, 100 ppm; fragment mass tolerance, ±1.5 Da; fixed modification, carbamidomethyl (C); and variable modification, oxidation (M). A Mascot threshold of 63 was used to achieve a false identification rate of 5%.

RESULTS AND DISCUSSION

Identification of Adducts Formed between Cys and Quinone Derived from RosA. Two adducts formed between Cys and quinone derived from RosA were named quinone−RosA/Cys adduct (M1) and quinone−RosA/2Cys adduct (M2), respectively. A typical total ion chromatogram (TIC) for adducts in the solutions is presented in Figure 1a. Extracted chromatograms from the TIC with different accurate mass settings are shown in Figure 1b,c. M1 and M2 were identified using the exact mass of two peaks at retention times of 2.81 and 2.96 min, displaying the accurate mass of 478.0813 (Figure 1b) and *m/z* 664.1454 (Figure 1c) for each peak, respectively.

The structure of M1 was identified by the data-dependent MS/MS spectra and fragments for further examination (Figure 1d). The ratio of *m/z* 391.05 suggested the base peak of the RosA moiety with sulfur residue. Given the ester bond cleavage, *m/z* 316.05 was attributed to the 2-oxyphenylpropanoyl moiety with the conjunction Cys, which implied that the Cys residue occurred on the right benzene moiety of RosA. In M2 (Figure 1e), which consisted of RosA with two Cys residues caused by ester bond cleavage, *m/z* 316.05 was attributed to the 2-oxyphenylpropanoyl moiety with the conjunction Cys, and *m/z* 280.04 suggested the loss of the caffeoyl moiety with the conjunction Cys. The ion fragmentation patterns of the adducts were similar to those of RosA, which confirmed our results.[29−31]

According to the 1,4-Michael addition reaction, Cys could add to the 2- and 2′-positions (Scheme 1) of quinone derived from RosA. Cys reacts with 4-MC on the 2-position.[10] Caftaric acid, which is similar to the left benzene moiety of the RosA ring, also reacts with 3SH on the 2′-position.[32] However, RosA

DOI: 10.1021/jf5044713
J. Agric. Food Chem. 2015, 63, 902−911

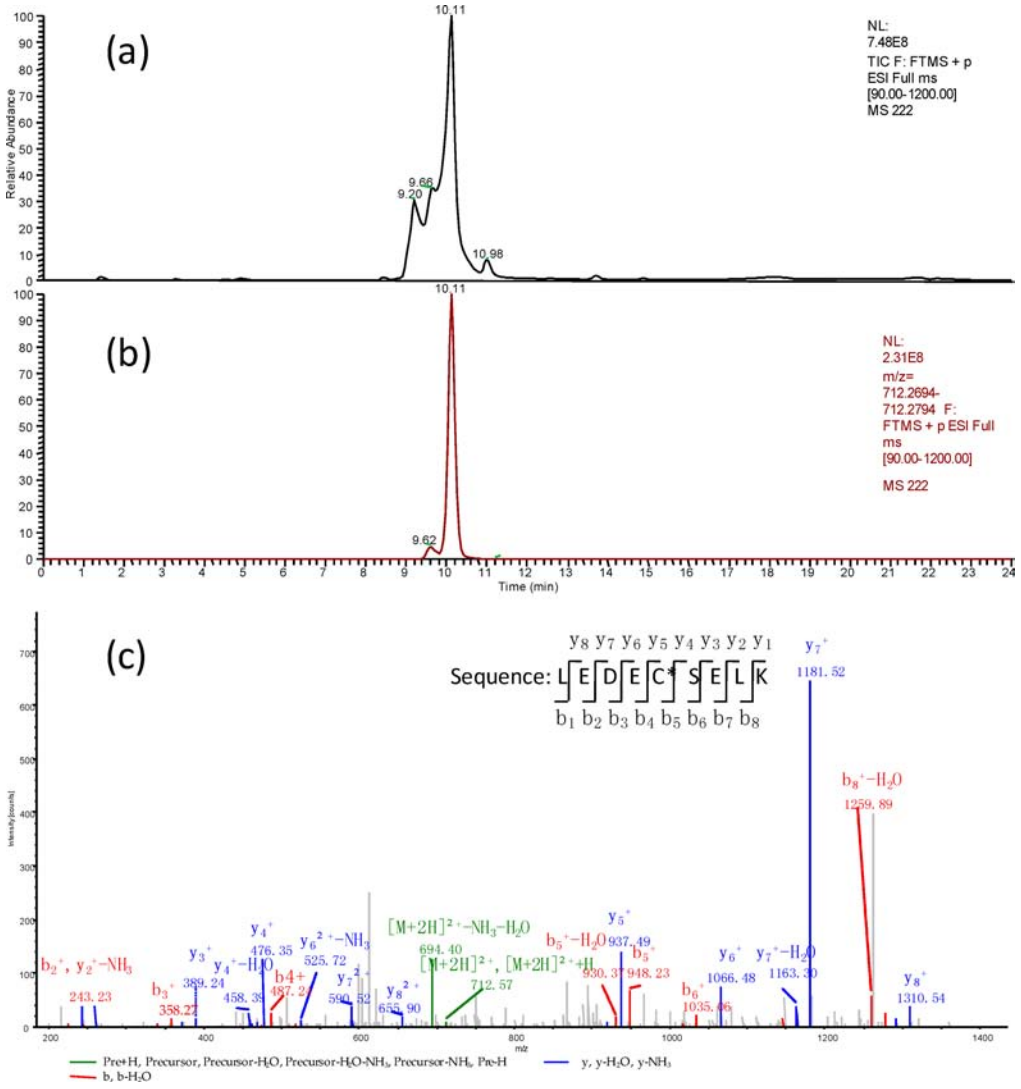

Figure 5. Nonapeptide (0.5 mM) and RosA (0.5 mM) incubated in maleic acid buffer (0.1 M) at pH 5.8, with $FeSO_4$ (0.1 mM) and H_2O_2 (30 mM) at 30 °C: (a) TIC of the incubated solution; (b) extracted chromatogram of M6 from TIC; (c) MS^2 fragmentation patterns of M6 show the structures of the products with fragmentation pathways noted.

reacted with 1-dodecanethiol to form three thiol adducts, in which the binding sites were on the 5-, 6-, and 2′-positions of the benzene rings.[33] Further research should be conducted to confirm the reaction position on the benzene moiety of the RosA ring.

Identification of Adducts Formed between GSH and Quinones Derived from RosA. M3, which was formed between GSH and quinones derived from RosA, was identified using the exact mass of the peak at a retention time of 10.23 min, and an accurate mass of 664.1413 was obtained (Figure 2b). Fragments were performed to identify the structure of M3 (Figure 2c). The ratio of m/z 502.09 suggested the 2-oxyphenylpropanoyl moiety with the conjunction of GSH. This finding indicates that the GSH residue occurred on the right benzene moiety of RosA. Given the fracture of the GSH thiol, m/z 391.05 was attributed to the base peak of RosA, and m/z 272.10 indicated the GSH residue with the removal of 2H. The ratio of m/z 353.10 suggested the loss of the glutamyl residue, and m/z 306.08 suggested the GSH residue.

Other quinones from 4-methylcatechol,[10] tocopherol,[34] and epigallocatechin gallate (EGCG)[35] were confirmed to undergo an adduct reaction with GSH. The structure of those adducts could not be understood because MS/MS ion fragmentation analysis was not accomplished in the current study. However, we can confirm that only one GSH reacted with the corresponding phenolics.

Identification of Adducts Formed between Peptides of Myosin and Quinones Derived from RosA. A series of trypsin-digested peptides of myosin with Cys residue were selected to evaluate the formation of adducts between quinones derived from RosA and myosin, and the positive mode was used for analyzing adducts. The results of peptides were CASLEK, HDCDLLR, and LEDECSELK, and RosA acted as a modification group on the Cys residues for analysis. Adducts were named M4, M5, and M6.

UHPLC-MS TICs for adducts in the solution are presented in Figures 3a, 4a, and 5a. As shown in Figures 3b, 4b, and 5b, the ions from the molecular masses of adducts (M4, M5, and M6) were determined to be $[M + H]^+$ = 1008.3835 m/z (retention time = 9.89 min), $[M + 2H]^{2+}$ = 615.2412 m/z (retention time = 10.23 min), and $[M + 2H]^{2+}$ = 712.2744 m/z (retention time = 10.11 min), respectively. The MS/MS spectra

DOI: 10.1021/jf5044713
J. Agric. Food Chem. 2015, 63, 902−911

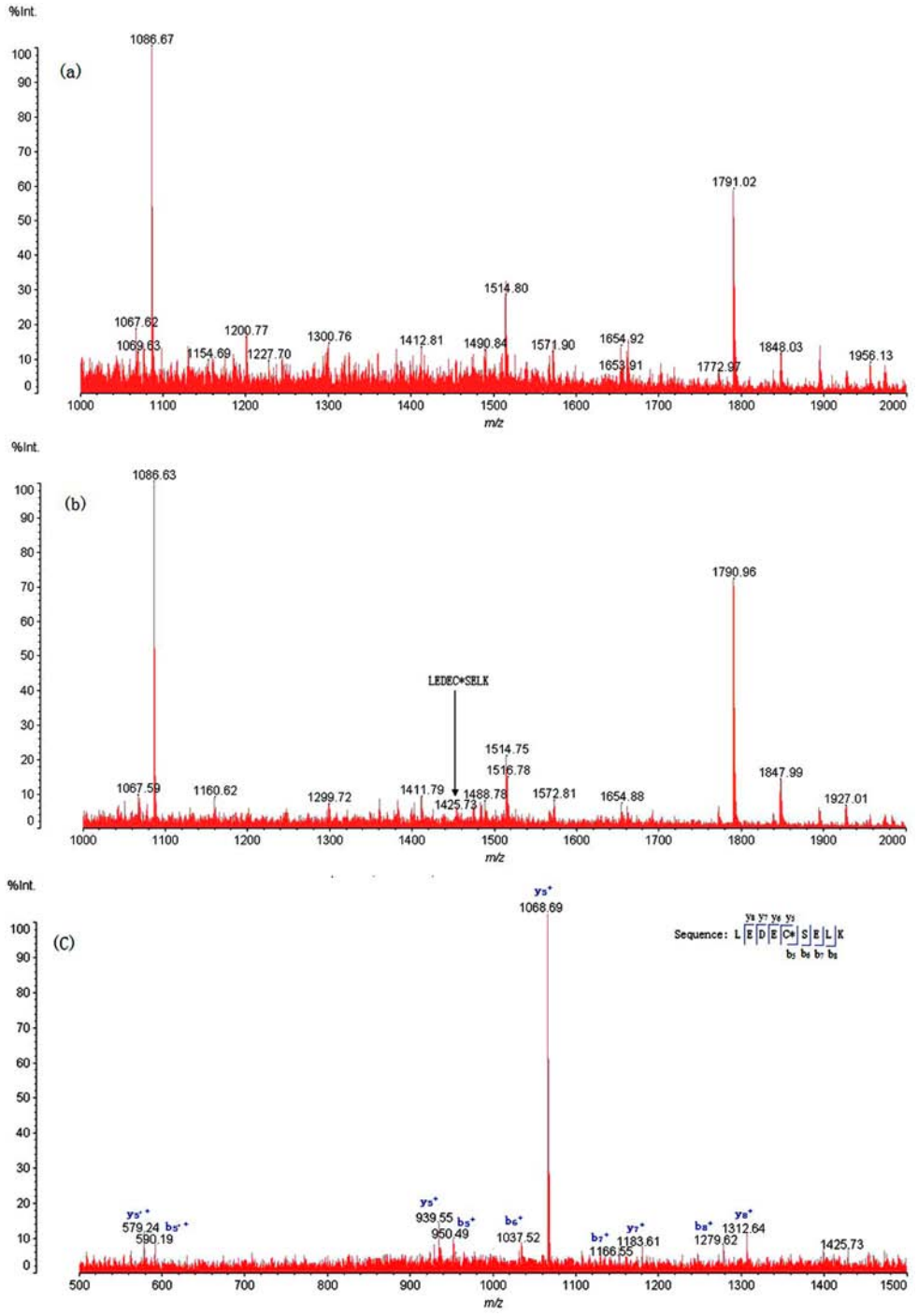

Figure 6. MALDI-TOF/MS spectrum of the tryptic digest of (a) myosin in MPI extracted from sample as control, (b) myosin in MPI extracted from sample with RosA (500 ppm), (c) MS/MS spectrum of m/z 1425.73 peptide (LEDEC*SELK) acquired with MALDI-TOF/TOF MS (C*, cysteines adducted with RosA).

and fragments were studied to identify the structures of M4, M5, and M6 (Figures 3c, 4c, and 5c), and Xcalibur 2.1.0 was used for analysis. Peptides were identified by peptide mass mapping using the Mascot database search program. We found the corresponding ions, from which we confirmed that RosA could react with peptides on the Cys residues.

The Cys−quinone adduct was determined to investigate the adduction reaction between MPI and 4-MC.[10] Rawel[38] found that whey proteins are modified by reactions with selected phenolic compounds using MALDI-MS. However, no study has identified and further analyzed the structures of adducts formed between RosA and peptides digested from myosin. To analyze the mechanism of adduction between phenolic compounds and proteins, structural identification of adducts is necessary.

However, quinones may also react with delta-amino groups located in the side chains of alkaline amino acids (e.g., lysine, proline, and arginine) to form the corresponding semialdehydes.[39,40] The outcome of this reaction is the carbonylation of that side chain, which may also influence the quality of muscle foods.[41,42]

DOI: 10.1021/jf5044713
J. Agric. Food Chem. 2015, 63, 902−911

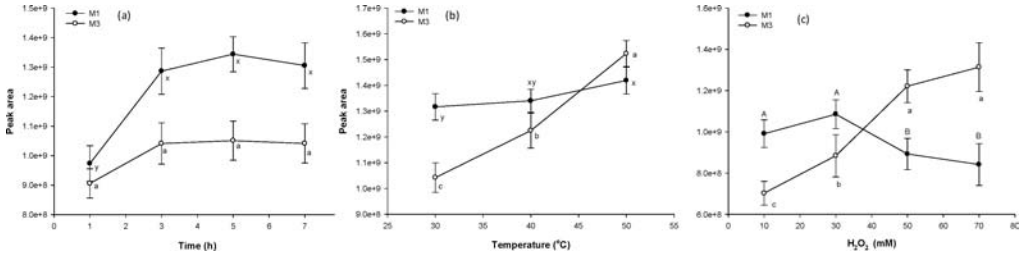

Figure 7. Stirring time effects of (a) oxidation reaction, (b) temperature, and (c) oxidation stress on the concentrations of M1 and M3. Data are expressed as the mean ± standard deviation (SD) (n = 3).

Identification of Adduction Reaction Sites between RosA and Myosin in MPI. To identify adduction sites between myosin and RosA, we performed MALDI-TOF/TOF analysis with PTM Finder. Figure 6a shows the spectrum of peptides digested from MPI sample as control. A Swissprot database search of the MS data yielded 11% sequence coverage with "MYH4-PIG". Figure 6b shows the spectrum of peptides digested from MPI sample with RosA, identifying the adduction peptide m/z 1425.73 LEDEC*SELK (C*, cysteines adducted with RosA). With the MS/MS spectrum of "LEDEC*SELK" in Figure 6c, we confirmed the peptide sequence of the observed fragment ions and demonstrated Cys949 was the adduction site. We herein, for the first time, managed to determine the accurate adduction site between RosA and myosin and to demonstrate the adduction between polyphenols and proteins during meat storage and processing.

Influence of Processing Condition on the Reactivity of RosA and Thiol Compounds. To understand the influence of processing conditions (stirring time, temperature, and oxidation stress) on the reactivity of RosA and thiol compounds, 1 mM Cys or 1 mM GSH was reacted with 1 mM RosA and incubated by chemical oxidation (30 mM H_2O_2). Adduct formation was determined by UHPLC-LTQ-Orbitrap with a proton detector for ion peak area. M2 was ignored because its contents were significantly lower than those of M1 and M3.

Different incubation times (1, 3, 5, and 7 h) were used. The effect of stirring time was examined, as shown in Figure 7a. The formation of M1 and M3 initially increased followed by a lag phase, and the maximum yield was observed at 3 h. In the study of adducts between oxidized grape phenolic compounds and odoriferous volatile thiol in grape wine, seven adducts showed similar increasing trends.[36] The chemical oxidation of RosA to yield peroxyl radicals results in the formation of quinones (Scheme 1).[37] Quinones, which are reactive electrophilic intermediates, are inclined to react easily with thiol compounds, including Cys and GSH, to form thiol−quinone adducts by 1,4-Michael addition reactions. However, the yield rate of M1 was faster than that of M3 from 1 to 3 h. Some similar findings were reported with EGCG[35] or quercetin,[43] in which Cys was more reactive than GSH. Nikolantonaki[44] explained that Cys, a primary thiol, is expected to have less sterically hindered sulfhydryl groups than GSH thiols; thus, Cys has greater reactivity with the quinones.

The effect of different temperatures on the formation of M1 and M3 was investigated. As shown in Figure 7b, two adducts presented an increasing trend as the temperature increased from 30 to 50 °C. The generation of M1 significantly increased with temperature (ion intensity of M1 increased by 46.15%), whereas that of M3 changed more gradually from 30 to 50 °C (M3 increased by only 7.58%). Besides accelerating RosA to quinone, an increase in temperature converted the autoxidation of thiol compounds to polymerization (Scheme 1, reaction I), which could hinder 1,4-Michael addition reactions to form the thiol−quinone adduct. Given its nucleophilic properties,[44] Cys autoxidation reacts faster than GSH, which hinders the formation of adduct 1. Thus, the addition reaction also increased with rising temperature. The order of the reactivity of the addition reaction was GSH > CYS.

The effect of different types of oxidation stress on the formation of M1 and M3 is investigated in Figure 7c. With increasing oxidation stress, M3 demonstrated an increasing trend. Growing oxidation stress can increase the oxidation of RosA to quinone and improve the addition reaction.[45] M1 showed a decreasing trend with higher oxidation stress (50−70 mM). Besides accelerated oxidation of RosA, high H_2O_2 concentration also induced the polymerization reaction of Cys to form the Cys−Cys dimer (Scheme 1, reaction I), which could inhibit M1 formation. Considering the less sterically hindered sulfhydryl group, M1 itself could further oxidize or polymerize, thereby causing the decreasing trend of M1. These findings indicate that oxidation potentials played an important role in adduct formation, and sulfhydryls of different molecular weights exhibited different reaction capacities to form adducts.

Overall, we successfully identified the structures of adducts between RosA and thiols under chemical oxidation conditions. The amount of adducts was regulated by chemical reaction conditions including stirring time, temperature, and oxidation stress. We further determined the accurate adduction site between RosA and myosin in meat samples. In addition, polyphenols and proteins were subjected to adduction reaction during meat storage and processing. Further studies are necessary to investigate how these adducts regulate the quality and nutritional value of food products in processing.

AUTHOR INFORMATION

Corresponding Author

*(G.Z.) Phone/fax: +86 025 84395341. E-mail: ghzhou@njau.edu.cn.

Funding

The research was funded by the Twelfth Five Issues of Rural Areas of People's Republic of China (2012BAD28B03).

Notes

The authors declare no competing financial interest.

REFERENCES

(1) Salminen, H.; Estévez, M.; Kivikari, R.; Heinonen, M. Inhibition of protein and lipid oxidation by rapeseed, camelina and soy meal in cooked pork meat patties. *Eur. Food Res. Technol.* **2006**, *223*, 461−468.

(2) Estévez, M.; Ventanas, S.; Cava, R. Protein oxidation in frankfurters with increasing levels of added rosemary essential oil: effect on color and texture deterioration. *J. Food Sci.* **2005**, *70*, 427−432.

DOI: 10.1021/jf5044713
J. Agric. Food Chem. 2015, 63, 902−911

(3) Lund, M. N.; Hviid, M. S.; Skibsted, L. H. The combined effect of antioxidants and modified atmosphere packaging on protein and lipid oxidation in beef patties during chill storage. *Meat Sci.* **2007**, *76*, 226−233.
(4) Ganhão, R.; Morcuende, D.; Estévez, M. Protein oxidation in emulsified cooked burger patties with added fruit extracts: influence on colour and texture deterioration during chill storage. *Meat Sci.* **2010**, *85*, 402−409.
(5) Jongberg, S.; Lund, M. N.; Waterhouse, A. L.; Skibsted, L. H. 4-Methylcatechol inhibits protein oxidation in meat but not disulfide formation. *J. Agric. Food. Chem.* **2011**, *59*, 10329−10335.
(6) Kim, Y. H. B.; Bødker, S.; Rosenvold, K. Influence of lamb age and high-oxygen modified atmosphere packaging on protein polymerization of long-term aged lamb loins. *Food Chem.* **2012**, *135*, 122−126.
(7) Lund, M. N.; Hviid, M. S.; Skibsted, L. H. The combined effect of antioxidants and modified atmosphere packaging on protein and lipid oxidation in beef patties during chill storage. *Meat Sci.* **2007**, *76*, 226−233.
(8) Lund, M. N.; Lametsch, R.; Hviid, M. S.; Jensen, O. N.; Skibsted, L. H. High-oxygen packaging atmosphere influences protein oxidation and tenderness of porcine longissimusdorsi during chill storage. *Meat Sci.* **2007**, *77*, 295−303.
(9) Zakrys-Waliwander, P. I.; O'Sullivan, M. G.; O'Neill, E. E.; Kerry, J. P. The effects of high oxygen modified atmosphere packaging on protein oxidation of bovine M. longissimusdorsi muscle during chilled storage. *Food Chem.* **2012**, *131*, 527−532.
(10) Jongberg, S.; Lund, M. N.; Gislason, N.; Skibsted, L. H.; Waterhouse, A. L. Thiol-quinone adduct formation in myofibrillar proteins detected by LC-MS. *J. Agric. Food Chem.* **2011**, *59*, 6900−6905.
(11) Prigent, S. V. E.; Voragen, A. G. J.; Visser, A. J. W. G.; van Koningsveld, G. A.; Gruppen, H. Covalent interactions between proteins and oxidation products of caffeoylquinic acid (chlorogenic acid). *J. Sci. Food Agric.* **2007**, *87*, 2502−2510.
(12) Rawel, H. M.; Rohn, S.; Kruse, H. P.; Kroll, J. Structural changes induced in bovine serum albumin by covalent attachment of chlorogenic acid. *Food Chem.* **2002**, *78*, 443−455.
(13) Rawel, H. M.; Kroll, J.; Hohl, U. C. Model studies on reactions of plant phenols with whey proteins. *Nahrung Food* **2001**, *45*, 72−81.
(14) Kroll, J.; Rawel, H. M. Reactions of plant phenols with myoglobin: influence of chemical structure of the phenolic compounds. *J. Food Sci.* **2001**, *66*, 48−58.
(15) Makarov, A.; Scigelova, M. Coupling liquid chromatography to Orbitrap mass spectrometry. *J. Chromatogr., A* **2010**, *25*, 3938−3945.
(16) Hogenboom, A. C.; van Leerdam, J. A.; de Voogt, P. Accurate mass screening and identification of emerging contaminants in environmental samples by liquid chromatography−hybrid linear ion trap Orbitrap mass spectrometry. *J. Chromatogr., A* **2009**, *1216*, 510−519.
(17) Kečkeš, S.; Gašić, U.; Veličković, T. Ć.; Milojković-Opsenica, D.; Natić, M.; Tešić, Ž. The determination of phenolic profiles of Serbian unifloral honeys using ultra-high-performance liquid chromatography/high resolution accurate mass spectrometry. *Food Chem.* **2013**, *138*, 32−40.
(18) Wong, C. C. L.; Cociorva, D.; Venable, J. D.; Xu, T.; Yates, J. R. Comparison of different signal thresholds ondata dependent sampling in Orbitrap and LTQ mass spectrometry for the identification of peptides and proteins in complex mixtures. *J. Am. Soc. Mass Spectrom.* **2009**, *20*, 1405−1414.
(19) Jang, K. S.; Baik, J. E.; Kang, S. S.; Jeon, J. H.; Choi, S.; Yang, Y. H.; Kim, B. G.; Yun, C. H.; Han, S. H. Identification of staphylococcal lipoteichoic acid-binding proteins in humanserum by high-resolution LTQ-Orbitrap mass spectrometry. *Mol. Immunol.* **2012**, *50*, 177−183.
(20) Bakry, R.; Rainer, M.; Huck, C. W.; Bonn, G. K. Protein profiling for cancer biomarker discovery using matrix-assisted laser desorption/ionization time-of-flight mass spectrometry and infrared imaging: a review. *Anal. Chim. Acta* **2011**, *690*, 26−34.
(21) Jurinke, C.; Oeth, P.; van den Boom, D. MALDI-TOF mass spectrometry: a versatiletool for high-performance DNA analysis. *Mol. Biotechnol.* **2004**, *26*, 147−164.
(22) Petersen, M.; Simmonds, M. S. Rosmarinic acid. *Phytochemistry* **2003**, *62*, 121−125.
(23) Lara, M. S.; Gutierrez, J. I.; Timón, M.; Andrés, A. I. Evaluation of two natural extracts (*Rosmarinus officinalis* L. and *Melissa officinalis* L.) as antioxidants in cooked pork patties packed in MAP. *Meat Sci.* **2011**, *88*, 481−488.
(24) Zhang, L.; Lin, Y. H.; Leng, X. J.; Huang, M.; Zhou, G. H. Effect of sage (*Salvia officinalis*) on the oxidative stability of Chinese-style sausage during refrigerated storage. *Meat Sci.* **2013**, *95*, 145−150.
(25) Kim, H.; Cadwallader, K. R.; Kido, H.; Watanabe, Y. Effect of addition of commercial rosemary extracts on potent odorants in cooked beef. *Meat Sci.* **2013**, *94*, 170−176.
(26) Zhang, W.; Xiao, S.; Samaraweera, H.; Lee, E. J.; Ahn, D. U. Improving functional value of meat products. *Meat Sci.* **2010**, *86*, 15−31.
(27) Gallo, M.; Vinci, G.; Graziani, G.; Simone, C. D.; Ferranti, P. The interaction of cocoa polyphenols with milk proteins studied by proteomic techniques. *Food Res. Int.* **2013**, *54*, 406−415.
(28) Park, D.; Xiong, Y. L. L.; Alderton, A. L. Concentration effects of hydroxyl radical oxidizing systems on biochemical properties of porcine muscle myofibrillar protein. *Food Chem.* **2007**, *101*, 1239−1246.
(29) Hong, E. Y.; Park, K. H.; Kim, G. H. Phenolic-reriched fractions from *Perilla frutescens* var. *acuta*: determination rosmarinic acid and antioxidant activity. *J. Food Biochem.* **2011**, *35*, 1637−1645.
(30) Kang, N. S.; Lee, J. H. Characterisation of phenolic phytochemicals andquality changes related to the harvest times from the leaves of Korean purple (*Perilla frutescens*). *Food Chem.* **2011**, *124*, 556−562.
(31) Lee, J. H.; Park, K. H.; Lee, M. H.; Kim, H. T.; Seo, W. D.; Kim, J. Y.; Baek, I. Y.; Jang, D. S.; Ha, T. J. Identification, characterization, and quantification of phenolic compounds in the antioxidant activity-containing fraction from the seeds of Korean perilla (*Perilla fertescens*) cultivars. *Food Chem.* **2013**, *136*, 843−852.
(32) Nikolantonaki, M.; Chichuc, I.; Teissedre, P. L.; Darriet, P. Reactivity of volatile thiols with polyphenols in a wine-model medium: impact of oxygen, iron, and sulfur dioxide. *Anal. Chim. Acta* **2010**, *660*, 102−109.
(33) Fujimoto, A.; Masuda, T. Antioxidation mechanism of rosmarinic acid, identification of an unstable quinone derivative by the addition of odourless thiol. *Food Chem.* **2012**, *132*, 901−906.
(34) Cornwell, D. G.; Kim, S.; Mazzer, P. A.; Jones, K. H.; Hatcher, P. G. Electrophile tocopheryl quinones in apoptosis and mutagenesis: thermochemolysis of thiol adducts with proteins and in cells. *Lipids* **2003**, *38*, 973−979.
(35) Sang, S.; Lambert, J. D.; Hong, J.; Tian, S.; Lee, M. J.; Stark, R. E.; Ho, C. T.; Yang, C. S. Synthesis and structure identification of thiol conjugates of (−)-epigallocatechin gallate and their urinary levels in mice. *Chem. Res. Toxicol.* **2005**, *18*, 1762−1769.
(36) Nikolantonaki, M.; Jourdes, M.; Shinoda, K.; Teissedre, P. L.; Quideau, S.; Darriet, P. Identification of adducts between an odoriferous volatile thiol and oxidized grape phenolic compounds: kinetic study of adduct formation under chemical and enzymatic oxidation conditions. *J. Agric. Food Chem.* **2012**, *60*, 2647−2656.
(37) Kroll, N. G.; Rawel, H. M.; Rohn, S. Reactions of plantphenolics with food proteins and enzymes under special considerationof covalent bonds. *Food Sci. Technol. Int.* **2003**, *9*, 205−218.
(38) Nausheel, R.; Unnadkat; Elias, R. J. Oxidative stability of (−)-epigallocatechin gallate in the presence of thiols. *J. Agric. Food Chem.* **2012**, *60*, 10815−10821.
(39) Akagawa, M.; Sasaki, T.; Suyama, K. Oxidative deamination of lysine residue in plasma protein of diabetic rats. *Eur. J. Biochem.* **2002**, *269*, 5451−5458.
(40) Estévez, M.; Heinonen, M. Effect of phenolic compounds on the formation of α-aminoadipic and γ-glutamic semialdehydes from

DOI: 10.1021/jf5044713
J. Agric. Food Chem. 2015, 63, 902−911

myofibrillar proteins oxidized by copper, iron, and myoglobin. *J. Agric. Food Chem.* **2010**, *58*, 4448−4455.
(41) Utrera, M.; Estévez, M. Oxidation of myofibrillar proteins and impaired functionality: underlying mechanisms of the carbonylation pathway. *J. Agric. Food Chem.* **2012**, *60*, 8002−8011.
(42) Estévez, M. Protein carbonyls in meat systems: a review. *Meat Sci.* **2011**, *89*, 259−279.
(43) Awad, H. M.; Boersma, M. G.; Boeren, S.; van Bladeren, P. J.; Vervoort, J.; Rietjens, I. Quenching of quercetin quinone/quinine methides by different thiolate scavengers: stability and reversibility of conjugate formation. *Chem. Res. Toxicol.* **2003**, *16*, 822−831.
(44) Nikolantonaki, M.; Chichuc, I.; Teissedre, P. L.; Darriet, P. Reactivity of volatile thiols with polyphenols in a wine-model medium: Impact of oxygen, iron, and sulfur dioxide. *Anal. Chim. Acta* **2010**, *660*, 102−109.
(45) Danilewicz, J. C.; Seccombe, J. T.; Whelan, J. Mechanism of interaction of polyphenols, oxygen, and sulfur dioxide in model wine and wine. *Am. J. Enol. Vitic.* **2008**, *59*, 128−136.

DOI: 10.1021/jf5044713
J. Agric. Food Chem. 2015, 63, 902−911

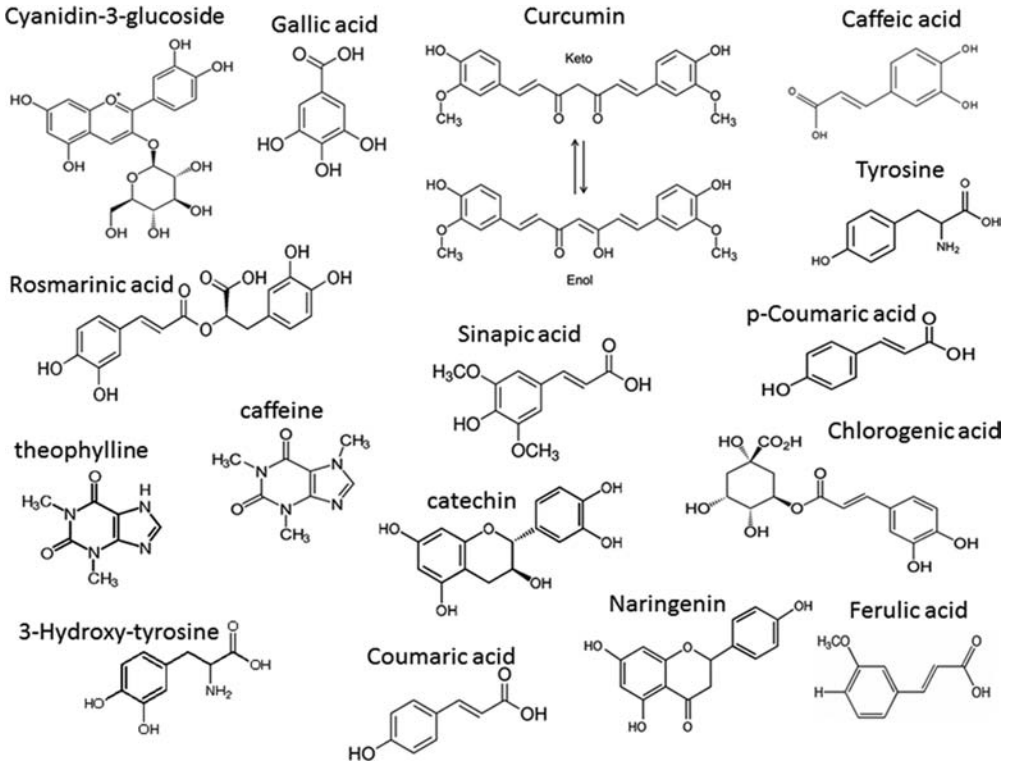

Figure 1. Molecular structures of phenolic compounds tested in the present experimental work.

bind weakly to nanoparticle surfaces and eventually desorb or exchange with bulk solution, affecting the stability of colloidal suspensions. In addition, processes to coat nanoparticles are often cumbersome, time-consuming, expensive, and characterized by low yield, limiting massive productions. Finally, nanoparticle coating reduces the average magnetic moment of the material by introducing a nonmagnetic component in the final nanoparticle.[4,10] Therefore, magnetic nanoparticles, to be a real competitor for standard technologies, need to respond to specific requirements, that is, colloidal stability, proper surface reactivity, and superparamagnetism.

Recently, we developed a novel synthetic procedure for nanostructured superparamagnetic material in the size range around 10 nm, constituted of stoichiometric maghemite (γ-Fe_2O_3) and showing peculiar surface chemical behavior, called surface active maghemite nanoparticles (SAMNs).[11,12] SAMNs present a high average magnetic moment and high water stability as colloidal suspensions without any superficial modification or coating derivatization. Because of their unique physical and chemical properties, these naked iron oxide nanoparticles are currently used to immobilize various biomolecules.[13−16] Biomolecule immobilization is carried out in water, without any chemical reactant, and the total derivatization process is mild, minimizing alteration/oxidation of ligands, low cost, ecologically green, and reversible. These peculiarities make SAMNs an elective competitor to standard methods for biomolecule purification.

In the present work, the binding properties of SAMNs were tested with different ligands of high interest in the pharmaceutical and food industries. Interestingly, among tested molecules, SAMNs displayed high specificity for curcumin binding.

Curcumin (IUPAC name, (1*E*,6*E*)-1,7-bis(4-hydroxy-3-methoxyphenyl)-1,6-heptadiene-3,5-dione; CAS Registry No. 458-37-7) is a homodimer of feruloyl-methane, containing a methoxy group and a hydroxyl group, a heptadiene with two Michael acceptors, and an α,β-diketone (see Figure 1).

Curcumin has shown significant efficacy as a chemopreventive in cell culture studies, as it elicits efficacy in various clinical studies.[17,18] Numerous experimental studies on in vitro and in vivo activities of this compound have been reported.[19] A special attribute of curcumin resides in its antioxidant potency,[20] namely, the ability to scavenge free radicals in blood and body tissues, helping the prevention of various cardiovascular, viral, and other chronic diseases.[21] In particular, curcumin's ability to affect gene transcription and induce apoptosis in preclinical models advocates its potential utility in cancer chemoprevention and chemotherapy.[22]

In *Curcuma longa* rhizome, a combination of substances called curcuminoids, namely, curcumin, demethoxycurcumin, and bis-demethoxycurcumin, can be found, curcumin being the major compound.

In the present work naked SAMNs were successfully applied for the purification of curcuminoids, and curcumin, from extracts of *C. longa* rhizome.

MATERIALS AND METHODS

Materials. Chemicals were purchased at the highest commercially available purity, and they were used without further treatment. Iron(III) chloride hexahydrate (97%), sodium borohydride ($NaBH_4$), and tetramethylammonium hydroxide ($N(CH_3)_4OH$) were obtained from Aldrich (Sigma-Aldrich, Italy), as well as catechin, tyrosine, hydroxytyrosine, ferulic acid, coumaric acid, rosmarinic acid, naringenin, curcumin, and cyanidin-3-glucoside.

A mixture of curcuminoids (curcumin, demethoxycurcumin, and bis-demethoxycurcumin) (purity ≥ 94.0%), being curcumin ≥80.0% (by TLC), was obtained from Aldrich (cod. C7727, Sigma-Aldrich, Italy).

DOI: 10.1021/jf504624u
J. Agric. Food Chem. 2015, 63, 912−920

The cultivations of *Eryngium fetidum* and *Curcuma longa* were carried out in a greenhouse in the experimental farm of the State University of São Paulo 'Júlio de Mesquita Filho' in Botucatu, São Paulo, Brazil (22°53′09″ S latitude, 48°26′42″ W longitude, and at 804 m altitude), with harvest at the optimal period. The soil used in the experiment showed the following characteristics: pH 6.3; M.O = 23 g dm^{-3}; P = 60 mg dm^{-3}; H + Al = 19 mmol dm^{-3}; K = 7 mmol dm^{-3}; Ca = 44 mmol dm^{-3}; Mg = 25 mmol dm^{-3}; SB = 77 mmol dm^{-3}; CTC = 95, V% = 80; B = 0.31 mg dm^{-3}; Cu = 2.2 mg dm^{-3}; Fe = 26 mg dm^{-3}; Mn = 2.4 mg dm^{-3}; Zn = 5.3 mg dm^{-3}.

Instrumentation. Optical spectroscopy measurements were performed in 1 cm quartz cuvettes using a Cary 50 spectrophotometer (Varian Inc., Palo Alto, CA, USA). Transmission electron microscope (TEM) micrographs were taken on a JEOL 2010 operating at 160 kV with a point-to-point resolution of 1.9 Å. A series of Nd−Fe−B magnets (N35, 263−287 kJ/m3 BH, 1170−1210 mT flux density by Powermagnet, Germany) was used for the magnetic driving of nanoparticles.

Synthesis of Surface Active Magnetic Nanoparticles. A typical synthesis of nanoparticles was already described[11,12] and can be summarized as follows: $FeCl_3{\cdot}6H_2O$ (10.0 g, 37 mmol) was dissolved in Milli-Q grade water (800 mL) under vigorous stirring at room temperature. $NaBH_4$ solution (2 g, 53 mmol) in ammonia (3.5%, 100 mL, 4.86 mol mol^{-1} Fe) was quickly added to the mixture. Soon after the reduction reaction occurrence, the temperature of the system was increased to 100 °C and kept constant for 2 h. Then, the material was cooled at room temperature and aged in water, as prepared, for another 24 h. This product was separated by imposition of an external magnet and washed several times with water. This material can be transformed into a red-brown powder (final synthesis product) by drying and curing at 400 °C for 2 h. The resulting nanopowder showed a magnetic response upon exposure to a magnetic field. The final mass of product was 2.0 g (12.5 mmol) of Fe_2O_3, and a yield of 68% was calculated.

The nanoparticulated resulting material was characterized by Mössbauer spectroscopy, FT-IR spectroscopy, high-resolution transmission electron microscopy, XRD, and magnetization measurements[12] and was constituted of stoichiometric maghemite (γ-Fe_2O_3) with a mean diameter (d_{av}) of 11 ± 2 nm, which can lead to the formation, upon ultrasound application in water (Bransonic, model 221, 48 kHz, 50 W), of a stable colloidal suspension, without any organic or inorganic coating or derivatization. The surface of these bare maghemite nanoparticles shows peculiar binding properties and can be reversibly derivatized with selected organic molecules. We called these bare nanoparticles surface active maghemite nanoparticles (SAMNs).

Quantitative Determination of Free Phenolic Acids and Curcuminoids by HPLC. Curcuminoids, chlorogenic acid, ferulic acid, *p*-coumaric acid, caffeic acid, gallic acid, cyanidin-3-glucoside, and synaptic acid were separated and quantified using an HPLC (model X-LC, Jasco, Japan). The liquid chromatography apparatus consisted of a PU-2080 pump, an MD-2015 diode array detector, an AS-2055 autosampler, and a CO-2060 column oven. ChromNAV chromatography software was used for chromatographic data analysis. The separation of phenolic acids was obtained on a Tracer Extrasil ODS2 (5 mm, 250 mm, Teknokroma, Spain) operating at room temperature. The mobile phase consisted of formic acid, pH 2.8 (A), and acetonitrile (B). Elution gradient was carried out in 50 min, and the flow rate was 0.8 mL min^{-1} (10−80% B). All standards were dissolved in 50% ethanol, and the calibration curves were built with standard concentrations ranging from 0.06 to 60 mg L^{-1}. Two wavelengths (325 and 310 nm) were used to detect phenolic acids. Measurements at 325 nm were used for the identification of chlorogenic acid, caffeic acid, and ferulic acid. The identification of *p*-coumaric acid was performed at 310 nm.

HPLC determination of curcuminoids (bis-demethoxy-curcumin, demethoxy-curcumin, and curcumin) was carried out according to a procedure derived from that of He with some modification.[23] A UHPLC system (Ultimate 3000 BioRS, Dionex-Thermo Fisher Scientific Inc., USA) equipped with a diode array detector was used. An Ace 5 C18 (Advanced Chromatography Technologies, UK) column (5 μm, 25 cm × 4.6 mm) was used for curcuminoid analysis, at 48 °C. The gradient profile of the mobile phase, (A) water (0.25% acetic acid, Mallinckrodt) and (B) acetonitrile (HPLC grade, Mallinckrodt), was as follows: 0−17 min, 40−60% B; 17−32 min, 60−85% B; 32−38 min, 85% B; 38−40 min, 85−40% B; 40−45 min, 40% B; the flow rate was 0.5 mL min^{-1}. The injection volume was 20 μL (full loop). All samples were filtered through 0.22 μm membrane filters before the injections. Curcuminoid peaks were identified by retention times and injections tests with standards (curcumin, demethoxy-curcumin, and bisdemethoxy-curcumin).

RESULTS

A list of biomolecules of interest for the pharmaceutical and food industries, namely, catechin, tyrosine, hydroxytyrosine, ferulic acid, coumaric acid, rosmarinic acid, naringenin, curcumin, and cyanidin-3-glucoside, was screened to test the recognition properties of SAMN surface toward different compounds. Thus, the binding efficiency and reversibility on SAMNs were evaluated by UV−vis spectroscopy. Moreover, with the aim of broadening the applicability spectrum of SAMNs in the field of biomolecule purification, a general approach for predicting SAMN suitability for selective magnetic separation of compounds of interest from complex matrices was studied. Selected molecules present chemical features potentially able to anchor, by metal chelation, on iron(III) available sites on the SAMN surface, the presence of which was recently demonstrated.[16] The comparison of the interactions of different molecular functionalities with SAMNs, from binding to desorption, allowed the individuation of chemical features required for stable and, at the same time, reversible binding on the SAMN surface.

Structural and magnetic properties of as-prepared iron oxide nanoparticles were investigated by zero-field and in-field Mössbauer spectroscopy and SQUID magnetization measurements.[12] In-field Mössbauer spectroscopy was used due to its unique ability to distinguish between structurally isomorphous maghemite and magnetite and also to quantify the distribution of cations in tetrahedral (T) an octahedral (O) sites of these spinel structures. The in-field Mössbauer spectrum, collected at 5 K in an external magnetic field of 5 T, corresponded with that reported for maghemite. Taking into account the maghemite stoichiometric formula, given by $(Fe^{3+})^{T}(Fe^{3+}_{5/3}\ o_{1/3})^{O}O_4$, where "o" stands for vacancies, the prepared maghemite was perfectly stoichiometric.

To monitor the magnetic response of SAMNs, hysteresis loops were measured at 2 and 300 K. At 2 K, the isothermal magnetization curve showed hysteresis with the values of coercivity and remanent magnetization comparable with those reported for bulk maghemite. As prepared SAMNs showed a maximum magnetization of 71.4 Am^2 kg^{-1}, which was similar to that of bulk maghemite[12] and higher than values reported for other magnetic nanoparticles in the literature.[24] The value of the maximum magnetization at 7 T was slightly lower than that reported for bulk maghemite, which was caused by a nanometer size of the particles. The hysteresis loop at 2 K was symmetric (i.e., equal values of positive and negative coercivity and positive and negative remanent magnetization), and no exchange bias phenomenon was present. Thus, the degree of magnetic disorder occurring at the surface layers of nanoparticles was not significant. Some misalignment of the surface atomic magnetic moments of each particle is present, in accordance with in-field Mössbauer data; however, it does not crucially govern the overall magnetic response of the system.

DOI: 10.1021/jf504624u
J. Agric. Food Chem. 2015, 63, 912−920

From the application point of view, it is important that a very high magnetization is achievable already at very low applied fields at room temperature. Thus, we can conclude that the prepared magnetic particles would act as an excellent magnetic carrier due to their well-defined stoichiometric structure, single-phase character, suitable magnetic properties, and uniform size distribution. Moreover, as a unique aspect of the preparation procedure, the particles exhibit colloidal behavior with no indications of the sedimentation and/or aggregation process even within several months.

Tentatively, phenolic compounds were incubated with aqueous suspensions of SAMNs, and the resulting nanoconjugates were extensively washed with water, by alternating magnetic separations, to eliminate loosely bound molecules. Finally, the release of the phenolic compounds from the nanoconjugate was tested under different conditions. All tested compounds present at least one phenol ring in their molecular structure (see Figure 1); thus, the whole process was easily followed by UV−vis spectroscopy. The characteristic wavelength of maximum absorbance and the molar extinction coefficients of tested compounds are reported in Table S1 in the Supporting Information. Because the focus of the present paper is providing a purification strategy for real applications, we aimed at obtaining the best compromise between yield and purity of phenolic compounds, minimizing the operations during the purification steps. For this last reason we avoided any other modification of the extracting and binding solutions, such as pH or ionic strength modifications.

First, because the tested substances could possibly be easily oxidized at room temperature, their stability was, as well, assessed by UV−vis spectroscopy. Optical spectra were acquired within 24 h, and the residual concentration of phenolics, with respect to freshly prepared solutions, is reported in Table S1 (in the Supporting Information, last column). Experimental data indicated that the stability of tested substances was acceptable, and, anyway, the magnetic purification tests carried out with SAMNs was performed within 2 h.

The tested phenolic compounds (10.0 μM) were incubated in the presence of SAMNs (0.5 g L^{-1}), and experimental results evidenced different behaviors in terms of efficiency and reversibility of the binding. In all of the explored cases, phenolic−SAMN nanoconjugates showed remarkable stability and no oxidation of bound phenolics was observed.

It is known that catechols and ene-diols, bearing multiple hydroxyl groups, as well as carboxylic groups, are able to form complexes with transition metals and metal oxide-based nanomaterials.[25,26] Recently, we demonstrated the presence of available under-coordinated iron(III) atoms on the surface of SAMNs,[27] and these phenolic ligands can lead to the formation of very stable complexes, as they convert under-coordinated iron atoms on the nanoparticle surface to a bulk-like lattice structure.[28]

Interestingly, most of the tested phenolic substances led to the formation of irreversible complexes with SAMNs, in agreement with Rajh, who reported, with bidentate ene-diol ligands, the formation of very stable complexes with metal oxide nanoparticles.[29] In fact, the protocol used for releasing ligands from the nanoparticle surface, consisting of an incubation of the complex in 0.5 M NH_4OH,[27] was inefficient with the tested group of molecules (see Table 1).

As an example, a remarkable binding efficiency on the SAMN surface was shown by catechin, and the subsequent incubation

Table 1. Binding and Release Efficiencies of Tested Compounds on the Surface of SAMNs[a]

polyphenol	binding (%)	release (%)
catechin	61.7 ± 5.0	4.7 ± 1.1
tyrosin	0.23 ± 0.1	nd
3-hydroxytyrosine	37.5 ± 6.3	4.2 ± 0.6
ferulic acid	17.2 ± 0.7	1.7 ± 0.2
coumaric acid	26.6 ± 0.7	nd
rosmarinic acid	57.7 ± 3.4	1.0 ± 0.8
naringenin	45.3 ± 3.7	7.7 ± 0.4
curcumin	94.3 ± 1.4	97.2 ± 2.4
cyanidin-3-glucoside	94.1 ± 0.8	3.0 ± 0.2

[a]Incubations were performed with 50.0 μM of the tested compound in the presence of 1.0 g L^{-1} SAMNs. The releasing process from the nanoparticles was performed with 99.6% ethanol. Values are the mean of three experiments.

of the complex of SAMNs with catechin (SAMN@catechin) in 99.6% ethanol led to the release of only 4.7 ± 1.1% of the bound molecule, indicating that catechin formed stable complexes on the iron oxide surface, as it completed the dangling boundaries of truncated crystalline structure of the nanoparticle.[30] Moreover, the comparison between the behavior of tyrosine and 3-hydroxytyrosine highlighted the role of the catechol structure, with respect to simple phenolic groups. The catechol structure was responsible for a 160-fold increase of substance binding with respect to simple phenolic rings. As in the case of catechin, the catechol structure of 3-hydroxytyrosine generated an irreversible binding, and the incubation of its SAMN complex in 99.6% ethanol led to a releasing yield of 4.2 ± 0.6% (n = 5).

The strong intimate interaction between phenolics and the surface iron oxide nanoparticles was evidenced by UV−vis spectroscopy. The electronic absorption spectrum of bare SAMNs, acquired in water, showed a wide band with a maximum at about 400 nm (Figure 2, black line) characterized by an extinction coefficient of 1520 $M^{-1}cm^{-1}$, expressed as Fe_2O_3 molar concentration. Differently, the SAMN@catechin spectrum was characterized by a peak at 440 and a shoulder at 520 nm (see Figure 2, red line). The observed red shift and

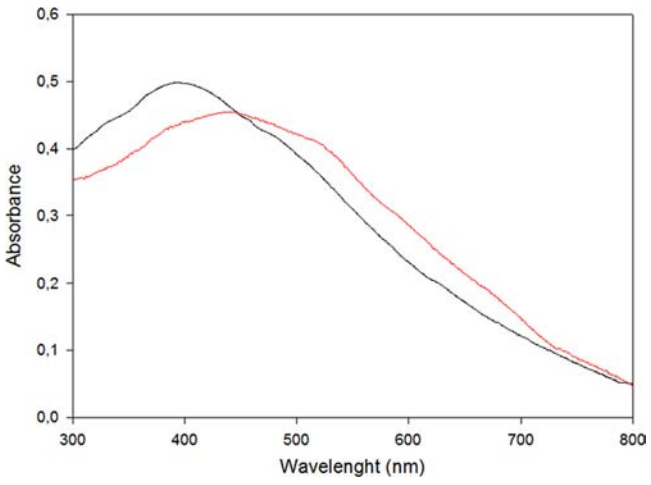

Figure 2. UV−vis spectra of naked and catechin-coated SAMNs (SAMN@catechin): (black line) SAMN; (red line) SAMN@catechin. Spectra were acquired in water. The concentrations in suspension were 40 and 200 μg mL^{-1} for SAMN and SAMN@catechin, respectively.

DOI: 10.1021/jf504624u
J. Agric. Food Chem. 2015, 63, 912−920

change in the absorption envelope (shape) of the SAMN spectrum upon catechin binding was not surprising. A similar phenomenon was observed with other biomolecules following their interaction with the nanoparticle surface.[14] We suggest that the recorded red shift in the absorption spectrum of modified nanoparticles was due to the excitation of localized electrons from the surface modifier to the conduction band of iron oxide nanoparticles.[29] In the present case, it was due to the presence of catechin on the SAMN surface.

Moreover, the SAMN@catechin complex was studied by electron transmission microscopy (see Figure 3). TEM

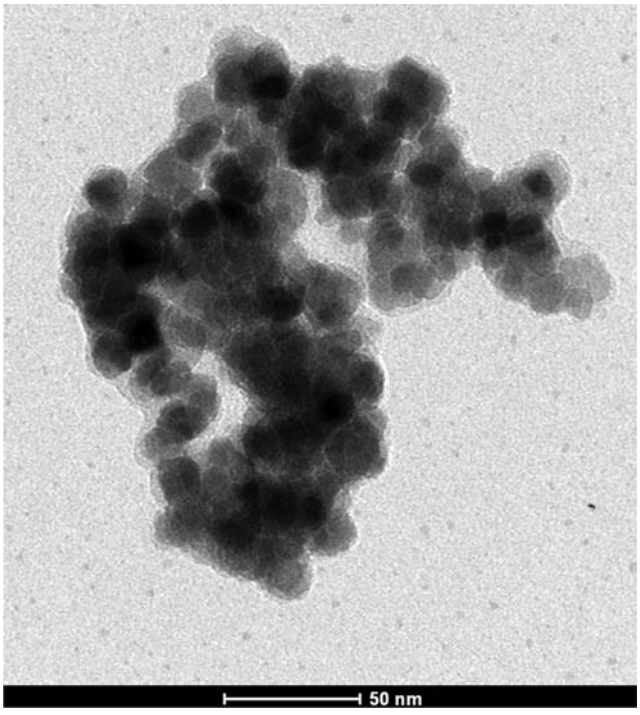

Figure 3. TEM micrograph of SAMN@catechin complex.

microscopy images of the SAMN@catechin complex indicated the presence of an organic matrix, forming a shell of about 2.0 nm around iron oxide nanoparticles, characterized by a lower electron density, attributable to catechin molecules layering on the SAMN surface. The resulting SAMN@catechin complex was extremely stable and, if stored at 4 °C, catechin remained firmly bound to the iron oxide nanoparticle surface for at least 12 months.

Considering the binding behavior of similar molecules (ferulic, coumaric, and rosmarinic acid), we observed the best binding efficiency on SAMN surface by rosmarinic acid, which presents two catechol moieties, with free hydroxyl groups, at the extremities of the organic chain (see Figure 1), therefore confirming that catechol-containing ligands showed a more efficient anchoring function on the SAMN surface with respect to simple phenol moieties and single-carboxylate ligands. Furthermore, the presence of a methoxy substituent ($-OCH_3$) in the aromatic ring, such as in the molecule of ferulic acid, led to a considerably less efficient ligand binding.

Narigenin and curcumin, presenting a keto−enol functionality, showed very good binding proclivity toward the SAMN surface. In particular, curcumin appeared as one of the best ligands for the SAMN surface (Table 1), confirming the literature reporting that curcumin has a remarkable ability to create stable complexes with iron(III).[31] In addition, its complex with SAMN (SAMN@curcumin) was completely reversible, and the molecule was completely released from the nanoparticle surface by incubation in 99.6% ethanol (see Table 1).

It should be mentioned that different solvent mixtures, based on ethanol, acetic acid, and ammonia, were tested for phenolic release from the SAMN surface (data not shown). Some of them were already used for controlling SAMN complex formation.[13] Ethanol was chosen for subsequent experiments aimed at the release of phenolic compounds from the SAMN surface. The use of ethanol for releasing oleic acid from iron oxide nanoparticles was already reported in the literature.[32]

Comparable binding efficiency on SAMNs with respect to curcumin was observed for cyanidin-3-glucoside, which presents a sugar ring as a distinctive chemical feature, a resorcinol, and a catechol moiety.

As a general result, substances characterized by catechol and/or keto−enol functionalities were able to efficiently bind on the SAMN surface, even if, at the same time, no easy general strategy for compound release from the nanoparticle surface was individuated. For comparison, as negative controls, two alkaloid molecules were tested, namely, caffeine and theophylline (Figure 1), both presenting no chemical features particularly prone to iron(III) chelation. Even at high concentration (1 mM), the incubation of these two substances with SAMNs did not lead to significant complex formation. In both cases, a negligible binding efficiency, with respect to previously tested phenolics, was observed (see Table 1).

As a first test on a real sample, SAMNs were subsequently used for the magnetic separation of biomolecules in water−ethanol extracts of *Eryingium fetidum* L. (Apiaceae family). *E. fetidum* is an aromatic plant, used as a spice and medicinal plant in tropical regions. The leaves are used to treat several diseases, such as fever, pains, and hypertension.[33−35] This species is also an important item in the perfumery and cosmetic industries due to the properties of its essential oil.[36,37] Several studies have reported the presence of phenolic compounds in leaves of *E. fetidum*.[38,39] However, researchers mainly focused their attention on the essential oil, and scarce information is available on other phytochemicals,[40] such as phenolic compounds.

The HPLC profiles of phenolic acids extracted from *E. fetidum* in 50% ethanol showed peaks attributable to chlorogenic, ferulic, *p*-coumaric, caffeic, gallic, and sinapic acid. All of these compounds may form complexes with undercoordinated iron(III) on the SAMN surface (see Figure 1). Ethanolic extracts of *E. fetidum* leaves (20 mg mL^{-1}) were incubated in the presence of 0.5 g L^{-1} SAMNs to test binding specificities. After magnetic separation, SAMN-bound molecules were removed by incubation in 99.6% ethanol, and supernatants were analyzed by HPLC for the determination of phenolic acids. No enrichment of a specific phenolic acid was evidenced, and the chromatographic profile was unaltered with respect to that of the untreated sample, demonstrating that phenolic acids were purified by magnetic purification with SAMNs, but without any specificity (see Figure S1 in the Supporting Information). This behavior can be attributed to the concomitant presence of the catechol function on most of the phenolic acids in the extract. Molecules bearing chemical features with similar affinity toward iron(III) chelation compete for complex formation with the SAMN surface, without showing particular selectivity.

DOI: 10.1021/jf504624u
J. Agric. Food Chem. 2015, 63, 912−920

Curcumin Purification from *Curcuma longa* Rhizome. Experimental results showed that curcumin stands out, among all tested molecules, in terms of both binding efficiency on SAMNs and complex reversibility. Therefore, the magnetic separation of this molecule by SAMNs was tested on real samples of *C. longa* rhizome.

HPLC analyses were performed to evaluate the efficiency of the magnetic purification and isolation yield of curcumin and curcuminoids as a function of experimental conditions and nanoparticle concentrations. As a control, commercial curcuminoid mixture, purified from *C. longa* rhizome at the highest commercial purity available, namely, a combination of curcumin, demethoxy-curcumin, and bis-demethoxy-curcumin, was subjected to chromatographic analysis.

Rhizomes of *C. longa* collected after 65 days of cultivation were manually finely ground and then dried at 45 °C in a ventilated oven. Dried and powdered *C. longa* rhizome was extracted (20 mg mL^{-1}) with different water−ethanol mixtures, where ethanol concentration was in the 0−100% range.

Then, the extracts were incubated with SAMNs, in the 1.25−10.0 g L^{-1} concentration range. After 1 h of incubation, SAMNs and the corresponding bound material were magnetically recovered. Then, SAMNs were resuspended in 99.6% ethanol for the release of bound curcuminoids. After 1 h of incubation and a further magnetic separation, SAMNs were finally removed, and the resulting supernatants were collected and characterized by HPLC.

As reported in the literature,[41] we found that curcumin represented the main curcuminoid compound in the *C. longa* rhizome (87.02% curcumin, 2.08% demethoxy-curcumin, and 10.90% bis-demethoxy-curcumin). As shown in Figure 4, the isolation yield of curcuminoids increased with ethanol concentration used during the extraction and depended, as well, on SAMN concentration. The best results were observed by extraction in 99.6% ethanol and using 10 g L^{-1} SAMNs for the magnetic purification. Under these conditions it was possible to isolate >80% of curcuminoids from *C. longa* rhizome extracts, namely, 155.37 mg L^{-1}. Notwithstanding the highest ethanol concentration (99.6%) represented the worst binding condition on nanoparticles, as it is used for the release of curcuminoids from SAMNs, it represented the best extraction condition in terms of yield. According to the le Chatellier principle, the high concentration of curcuminoids in the extract strongly favored the binding to the formation of the complex with nanoparticles; thus, under these conditions, curcuminoids successfully competed for SAMNs in the presence of extraction contaminants. Conversely, when curcuminoid-loaded nanoparticles were incubated in 99.6% pure ethanol, the equilibrium leads to the dissociation of the complexes.

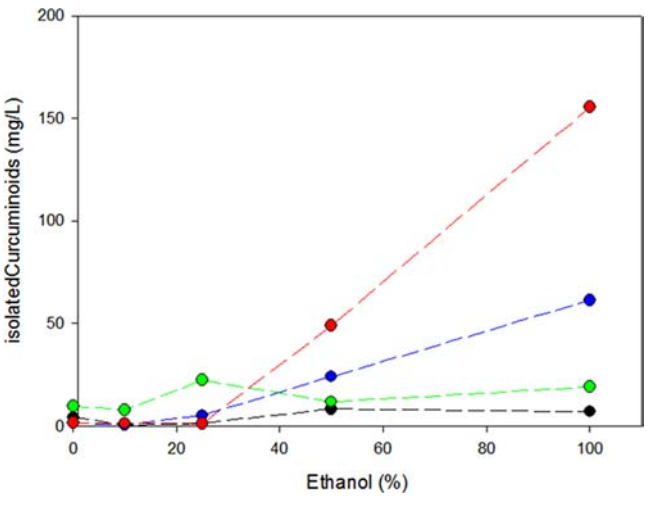

Figure 4. Isolation yield of curcuminoids as a function of ethanol and SAMN concentrations. Powdered *C. longa* rhizome was extracted (20 mg mL^{-1}) with different water−ethanol mixtures, and the resulting solutions were incubated with SAMNs. Recovered SAMNs and the corresponding bound material were resuspended in 99.6% ethanol for the release of bound molecules. SAMN concentrations used for the magnetic purification of curcuminoids were (black symbols) 1.25 g L^{-1}, (green symbols) 2.5 g L^{-1}, (blue symbols) 5.0 g L^{-1}, and (red symbols) 10.0 g L^{-1}.

Moreover, the curcumin purification yield, with respect to the total amount of curcuminoids, obtained from the magnetic purification, was assessed by comparison of chromatographic peak areas by HPLC. In Figure S2 in the Supporting Information the fractions of purified curcumin are reported as a function of ethanol concentration, for all of the tested concentrations of SAMNs. The highest yield of curcumin, with respect to total curcuminoids, was observed using 25% ethanol for extraction. Interestingly, the combination of 25% ethanol for *C. longa* rhizome extraction and 1.25 g L^{-1} SAMNs for magnetic purification, which is the lowest nanoparticle concentration tested, led to the highest curcumin/curcuminoid ratio (>80.0%). For other tested ethanol and SAMN concentrations, the curcumin/curcuminoid ratio was about 65%.

The proposed procedure for curcumin purification can be summarized as follows: dried powder of *C. longa* rhizome (10 g) was extracted with 99.6% ethanol (600 mL) with the aid of 5 min of sonication (Bransonic, model 221, 48 kHz, 50 W).

Control experiments showed that the extraction of the same amount of powdered *C. longa* rhizome with ethanol led to the isolation, after drying in a rotary evaporator, of 50.7 mg g^{-1} of a residual oil. As reported in the literature, *C. longa* rhizome contains a considerable amount of essential oil; thus, the separation of curcuminoids from this hydrophobic matrix represents a problematic task.[42]

After decantation (10 min), the supernatant was incubated with SAMNs (10 g L^{-1}) for 1 h, under stirring, at room temperature. The nanoparticle-containing suspension was subjected to magnetic separation, and the resulting supernatant was eliminated. The release of curcuminoids bound to nanoparticles was accomplished by subsequent incubation of SAMN@curcumin in 99.6% ethanol (600 mL) for 1 h, at room temperature. Released curcumin in ethanol was dried under low vacuum (100 torr) in a rotary evaporator at 40 °C, leading to 3.95 mg g^{-1} of a yellow powder, consisting of 64.0% curcumin, 17.0% demethoxy-curcumin, and 19.0% bis-demethoxy-curcumin (by HPLC), with a purity >98% with respect to the total dry mass of the extract. The total process can be accomplished within 80 min. The HPLC profile of curcuminoids after magnetic separation by SAMNs is shown in Figure 5. The amount of purified curcuminoids from *C. longa* extracts well agreed with literature values,[43] and a yield of 45% with respect to its total content in the first ethanol extract was calculated. It should be mentioned that the total amount of curcuminoids, as well as the curcumin/curcuminoids ratio, will depend on the original composition of the *C. longa* rhizome sample.

DOI: 10.1021/jf504624u
J. Agric. Food Chem. 2015, 63, 912−920

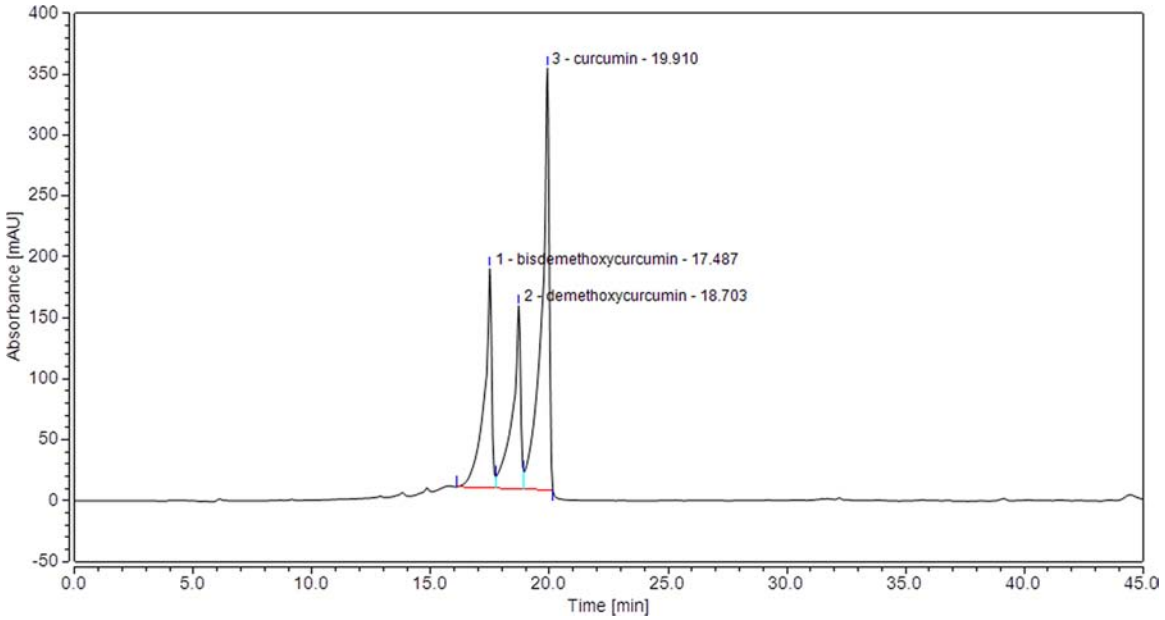

Figure 5. HPLC profile of curcuminoids after magnetic purification by SAMN on *Curcuma longa* extracts. The separation of curcuminoids in the supernatant obtained from magnetic purification was carried out as described under Materials and Methods.

DISCUSSION

Novel maghemite nanoparticles (SAMNs) were studied for phenolic binding and were applied for the purification of curcumin from *C. longa* rhizome extracts. The peculiar properties of the SAMN surface, due to the presence of under-coordinated iron(III) sites, confer high specificity to select iron chelating molecules from complex matrices. These nanoparticles easily match with interests in biotechnology, revealing different surface characteristics from other reported magnetic nanoparticles, justifying the peculiar behavior of SAMN suspensions, their high colloidal stability in aqueous solutions, and their ability to reversibly adsorb biomolecules. These features led us to apply SAMNs as a novel tool to isolate and purify substances from natural matrices, which could be attractive for the pharmaceutical and food industries. SAMNs showed high specificity to reversibly bind curcumin and were used for isolating this biomolecule from *C. longa* rhizome extracts.

The present paper envisages new possibilities offered by SAMNs for the isolation of curcumin and, moreover, proposes an easy procedure based on magnetic purification of curcuminoids, which could be easily modified for scaling-up, moving from a laboratory scale to an industrial level. The complete purification process, from SAMN synthesis to application, is fast and ecologically green, avoiding the use of large volumes of solvents, as typically required by elution in standard chromatographic methods, and the ethanol employed for extraction is easily recyclable. As well, SAMNs can be easily regenerated after the purification process by sonication in water and reutilized for further purification cycles. Therefore, the proposed process is cost-effective and does not involve production of wastes, being based on green chemistry processes, suitable for scaling-up. In the present case an estimated yield of 45% of pure curcuminoids, characterized by a purity >98%, was obtained from *C. longa* rhizomes.

ASSOCIATED CONTENT

Supporting Information

HPLC profiles of *E. fetidum* extracts in 50% ethanol, before and after incubation with SAMNs (Figure S1), curcumin purification yield with respect to total curcuminoids after magnetic purification of Curcuma longa rhizome extracts as a function of ethanol concentration and SAMN concentration (Figure S2), and optical characteristics of catechin, tyrosine, 3-hydroxytyrosine, ferulic acid, coumaric acid, rosmarinic acid, naringenin, curcumin and cyanidin-3-glucoside (Table S1). This material is available free of charge via the Internet at http://pubs.acs.org.

AUTHOR INFORMATION

Corresponding Author

*(F.V.) Mail: Department of Comparative Biomedicine and Food Safety, University of Padua, Agripolis, Viale dell'Università 16, Legnaro, 35020 (PD), Italy. Phone: +39-049-8276863. Fax: +39-049-8073310. E-mail: fabio.vianello@unipd.it.

Funding

The present experimental work was partially funded by "Fondazione CARIPARO" and by Italian Institutional Ministry Grants cod. 60A06-7411 and 60A06-8055.

Notes

The authors declare no competing financial interest.

ACKNOWLEDGMENTS

We gratefully acknowledge the support by the São Paulo Research Foundation, Process 2013/05644-3, and Brazilian National Counsel of Technological and Scientific Development, Process 478372/2013-2.

ABBREVIATIONS USED

SAMNs, surface active maghemite nanoparticles; TEM, transmission electron microscope; FT-IR, Fourier transform infrared

DOI: 10.1021/jf504624u
J. Agric. Food Chem. 2015, 63, 912−920

spectroscopy; XRD, X-ray powder diffraction; SQUID, superconducting quantum interference device

REFERENCES

(1) Kitts, D. D.; Weiler, K. Bioactive proteins and peptides from food sources. Applications of bioprocesses used in isolation and recovery. *Curr. Pharm. Des.* **2003**, *9*, 1309−1323.

(2) Hage, D. S.; Cazes, J. *Handbook of Affinity Chromatography*, 2nd ed.; Taylor and Francis, CRC Press: Boca Raton, FL, USA, 2005.

(3) Turkova, J. *Affinity Chromatography*, 1st ed.; Elsevier Scientific Publishing: Amsterdam, The Netherlands, 1978.

(4) Horak, D.; Babic, M.; Mackova, H.; Benes, M. J. Preparation and properties of magnetic nano- and microsized particles for biological and environmental separations. *J. Sep. Sci.* **2007**, *30*, 1751−1772.

(5) Safarik, I.; Safarikova, M. Magnetic techniques for the isolation and purification of proteins and peptides. *Biomagn. Res. Technol.* **2004**, *2*, 7−24.

(6) Lyon, J. L.; Fleming, D. A.; Stone, M. B.; Schiffer, P.; Williams, M. E. Synthesis of Fe oxide core/Au shell nanoparticles by iterative hydroxylamine seeding. *Nano Lett.* **2004**, *4*, 719−723.

(7) Zhang, Y.; Kohler, N.; Zhang, M. Surface modification of superparamagnetic magnetite nanoparticles and their intracellular uptake. *Biomaterials* **2002**, *23*, 1553−1561.

(8) Lu, Y.; Yin, Y. D.; Mayers, B. T.; Xia, Y. N. Modifying the surface properties of superparamagnetic iron oxide nanoparticles through a sol−gel approach. *Nano Lett.* **2002**, *2*, 183−186.

(9) Urbanova, V.; Magro, M.; Gedanken, A.; Baratella, D.; Vianello, F.; Zboril, R. Nanocrystalline iron oxides, composites and related materials as a platform for electrochemical, magnetic, and chemical biosensors. *Chem. Mater.* **2104**, *26*, 6653−6673.

(10) Mackay, M. E.; Tuteja, A.; Duxbury, P. M.; Hawker, C. J.; Van Horn, B.; Guan, Z.; Chen, G.; Krishnan, R. S. General strategies for nanoparticle dispersion. *Science* **2006**, *311*, 1740−1743.

(11) Magro, M.; Valle, G.; Russo, U.; Nodari, L.; Vianello, F. Maghemite nanoparticles and method for preparing thereof. World Patent WO/2012/010200, 2012.

(12) Magro, M.; Sinigaglia, G.; Nodari, L.; Tucek, J.; Polakova, K.; Marusak, Z.; Cardillo, S.; Salviulo, G.; Russo, U.; Stevanato, R.; Zboril, R.; Vianello, F. Charge binding of rhodamine derivative to OH-stabilized nanomaghemite: universal nanocarrier for construction of magnetofluorescent biosensors. *Acta Biomater.* **2012**, *8*, 2068−2076.

(13) Sinigaglia, G.; Magro, M.; Miotto, G.; Cardillo, S.; Agostinelli, E.; Zboril, R.; Bidollari, E.; Vianello, F. Catalytically active bovine serum amine oxidase bound to fluorescent and magnetically drivable nanoparticles. *Int. J. Nanomed.* **2012**, *7*, 2249−2259.

(14) Magro, M.; Faralli, A.; Baratella, D.; Bertipaglia, I.; Giannetti, S.; Salviulo, G.; Zboril, R.; Vianello, F. Avidin functionalized maghemite nanoparticles and their application for recombinant human biotinyl-SERCA purification. *Langmuir* **2012**, *28*, 15392−15401.

(15) Venerando, R.; Miotto, G.; Magro, M.; Dallan, M.; Baratella, D.; Bonaiuto, E.; Zboril, R.; Vianello, F. Magnetic nanoparticles with covalently bound self-assembled protein corona for advanced biomedical applications. *J. Phys. Chem. C* **2013**, *117*, 20320−20331.

(16) Magro, M.; Campos, R.; Baratella, D.; Lima, G.; Holà, K.; Divoky, C.; Stollberger, R.; Malina, O.; Aparicio, C.; Zoppellaro, G.; Zboril, R.; Vianello, F. A magnetically drivable nanovehicle for curcumin with antioxidant capacity and MRI relaxation properties. *Chem.−Eur. J.* **2014**, *20*, 11913−11920.

(17) Nagpal, M.; Sood, S. Role of curcumin in systemic and oral health: an overview. *J. Nat. Sci. Biol. Med.* **2013**, *4*, 3−7.

(18) Liu, D.; Chen, Z. The effect of curcumin on breast cancer cells. *J. Breast Cancer* **2013**, *16*, 133−137.

(19) Yallapu, M. M.; Jaggi, M.; Chauhan, S. C. Cyclodextrin-curcumin self-assembly enhances curcumin delivery in prostate cancer cells. *Colloids Surf. B: Biointerfaces* **2010**, *79*, 113−125.

(20) Anand, P.; Thomas, S. G.; Kunnumakkara, A. B.; Sundaram, C.; Harikumar, K. B.; Sung, B.; Tharakan, S. T.; Misr, K.; Priyadarsini, I. K.; Rajasekharan, K. N.; Aggarwal, B. B. Biological activities of curcumin and its analogues (congeners) made by man and mother nature. *Biochem. Pharmacol.* **2008**, *76*, 1590−1611.

(21) Maheshwari, R. K.; Singh, A. K.; Gaddipati, J.; Srimal, R. C. Multiple biological activities of curcumin: a short review. *Life Sci.* **2006**, *78*, 2081−2087.

(22) Grynkiewicz, G.; Ślifirski, P. Curcumin and curcuminoids in quest for medicinal status. *Acta Biochim. Polym.* **2012**, *59*, 201−212.

(23) He, X.-G.; Lin, L.-Z.; Lian, L.-Z.; Lindenmaier, M. Liquid chromatography−electrospray mass spectrometric analysis of curcuminoids and sesquiterpenoids in turmeric (*Curcuma longa*). *J. Chromatogr., A* **1998**, *818*, 127−132.

(24) Gupta, A. K.; Gupta, M. Synthesis and surface engineering of iron oxide nanoparticles for biomedical applications. *Biomaterials* **2005**, *26*, 3995−4021.

(25) Thanh, N. T. K.; Green, L. A. W. Functionalization of nanoparticles for biomedical applications. *Nano Today* **2010**, *5*, 213−230.

(26) Laurent, S.; Forge, D.; Port, M.; Roch, A.; Robic, C.; Vander Elst, L.; Muller, R. N. Magnetic iron oxide nanoparticles: synthesis, stabilization, vectorization, physicochemical characterizations, and biological applications. *Chem. Rev.* **2008**, *108*, 2064−2110.

(27) Magro, M.; Baratella, D.; Salviulo, G.; Polakova, K.; Zoppellaro, G.; Tucek, J.; Kaslik, J.; Zboril, R.; Vianello, F. Core−shell hybrid nanomaterial based on prussian blue and surface active maghemite nanoparticles as stable electrocatalyst. *Biosens. Bioelectron.* **2014**, *52*, 159−165.

(28) Chen, L. X.; Liu, T.; Thurnauer, M. C.; Csencsits, R.; Rajh, T. Fe_2O_3 nanoparticle structures investigated by X-ray absorption near-edge structure, surface modifications, and model calculations. *J. Phys. Chem. B* **2002**, *106*, 8539−8546.

(29) Rajh, T.; Chen, L. X.; Lukas, K.; Liu, T.; Thurnauer, M. C.; Tiede, D. M. Surface restructuring of nanoparticles: an efficient route for ligand−metal oxide crosstalk. *J. Phys. Chem. B* **2002**, *106*, 10543−10552.

(30) Rodriguez, J. A.; Fernández-García, M. *Synthesis, Properties, and Applications of Oxide Nanomaterials*; Wiley: Hoboken, NJ, USA, 2007.

(31) Borsari, M.; Ferrari, E.; Grandi, R.; Saladini, M. Curcuminoids as potential new iron-chelating agents: spectroscopic, polarographic and potentiometric study on their Fe(III) complexing ability. *Inorg. Chim. Acta* **2002**, *328*, 61−68.

(32) White, M. A.; Johnson, J. A.; Koberstein, J. T.; Turro, N. J. Toward the syntheses of universal ligands for metal oxide surfaces: controlling surface functionality through click chemistry. *J. Am. Chem. Soc.* **2006**, *128*, 11356−11357.

(33) Singh, S.; Singh, D. R.; Banu, S.; Salim, K. M. Determination of bioactives and antioxidant activity in *Eryngium foetidum* L.: a traditional culinary and medicinal herb. *Proc. Natl. Acad. Sci. India Sect. B: Biol. Sci.* **2013**, *83*, 453−460.

(34) Singh, B. K.; Ramakrishna, Y.; Ngachan, S. V. Spiny coriander (*Eryngium foetidum* L.): a commonly used, neglected spicing-culinary herb of Mizoram, India. *Genet. Resour. Crop Evol.* **2014**, *61*, 1085−1090.

(35) Duke, J. *Duke's Handbook of Medicinal Plants of Latin America*; Taylor and Francis, CRC Press: Boca Raton, FL, USA, 2009.

(36) Essia Ngang, J. J.; Nyegue, M. A.; Ndoye, F. C.; Tchuenchieu Kamgain, A. D.; Sado Kamdem, S. L.; Lanciotti, R.; Gardini, F.; Etoa, F.-X. Characterization of Mexican coriander (*Eryngium foetidum*) essential oil and its inactivation of *Listeria monocytogenes* in vitro and during mild thermal pasteurization of pineapple juice. *J. Food Prot.* **2014**, *77*, 435−443.

(37) Garcia, M.; Sáenz, M.; Gómes, M.; Fernándes, M. Topical anti-inflammatory activity of phytosterols isolated from Eryngium foetidum on chronic and acute inflammation models. *Phytother. Res.* **1999**, *13*, 78−80.

(38) Craig, W. Health-promoting properties of common herbs. *Am. J. Clin. Nutr.* **1999**, *70*, 491s−499s.

(39) Wong, S.; Leong, L.; Koh, J. Antioxidant activities of aqueous extract of selected plants. *Food Chem.* **2006**, *99*, 775−783.

DOI: 10.1021/jf504624u
J. Agric. Food Chem. 2015, 63, 912−920

(40) Dawilai, S.; Muangnoi, C.; Praengamthanachoti, P.; Tuntipopipat, S. Anti-inflammatory activity of bioaccessible fraction from *Eryngium foetidum* leaves. *BioMed. Res. Int.* **2013**, *2013*, No. 958567.
(41) Wichitnithad, W.; Jongaroonngamsang, N.; Pummangura, S.; Rojsitthisak, P. A simple isocratic HPLC method for the simultaneous determination of curcuminoids in commercial turmeric extracts. *Phytochem. Anal.* **2009**, *20*, 314−319.
(42) Funk, J. L.; Frye, J. B.; Oyarzo, J. N.; Zhang, H.; Timmermann, B. N. Anti-arthritic effects and toxicity of the essential oils of turmeric. *J. Agric. Food Chem.* **2010**, *58*, 842−849.
(43) Tayyem, R. F.; Heath, D. D.; Al-Delaimy, W. K.; Rock, C. L. Content of turmeric and curry powders. *Nutr. Cancer* **2006**, *55*, 126−131.

DOI: 10.1021/jf504624u
J. Agric. Food Chem. 2015, 63, 912−920

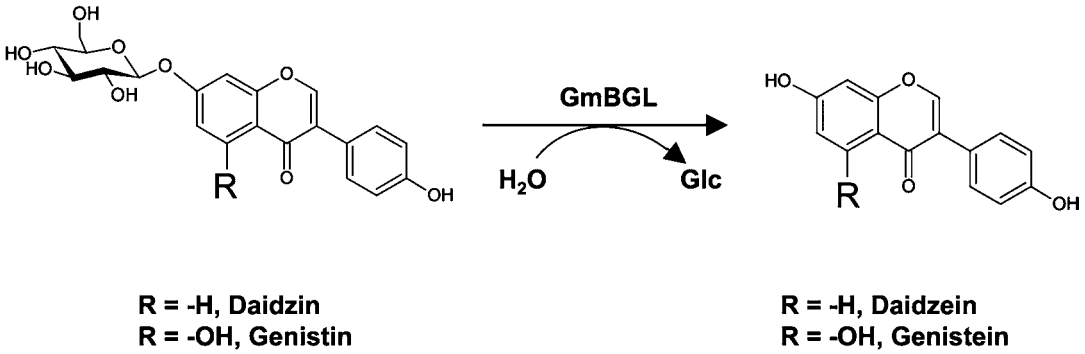

Figure 1. *Glycine max* β-glucosidase (GmBGL)-catalyzed hydrolysis of glycosyl isoflavones. Isoflavone 7-*O*-glucosides including daidzin and genistin are hydrolyzed by GmBGL into the corresponding aglycones. Glc, glucose.

been characterized. β-Glucosidase has been purified from soy cotyledons that hydrolyze isoflavone glucosides to release aglycones.[22,23] Suzuki et al.[24] reported cloning a gene encoding isoflavone conjugate-hydrolyzing β-glucosidase (GmICHG). GmICHG is a member of the glycoside hydrolase 1 (GH1) family, which can hydrolyze both malonylated and non-malonylated forms of isoflavone-7-*O*-β-D-glucosides.

In soybean, although β-glucosidase is believed to play an important role in the transformation and regulation of isoflavones, most of the biochemical and molecular properties remain unclear. In our previous study, we purified a novel β-glucosidase with high specificity toward glucosidic isoflavones (Figure 1), but not malonylglucosidic isoflavone from soybean okara, the byproduct of soy milk and tofu-making, and we determined the N-terminal amino acid sequence of the enzyme.[25] Here, we obtained and characterized the full-length *GmBGL* cDNA. Moreover, transgenic rice harboring *GmBGL* was created, and β-glucosidase activities toward isoflavone conjugate were determined. *GmBGL* may be a functional β-glucosidase for use in producing isoflavone aglycone-rich soybean by genetic engineering.

MATERIALS AND METHODS

Plant Materials and Chemicals. Soybean (*Glycine max* L.) Kaohsiung No. 12 was obtained from the agricultural research and extension station in Kaohsiung district, Taiwan. Soybean seeds were washed with running water, soaked in tap water overnight, and then ground in liquid nitrogen for RNA extraction. *Japonica*-type rice (*Oryza sativa* L.) Tainung 67 (TNG 67) was used for heterologous expression. *p*-Nitrophenol (*p*NP), dithiothreitol, and electrophoresis reagents were from Sigma-Aldrich Co. (St. Louis, MO, USA). CM-Sepharose CL-6B cation exchanger, Hiload 16/60 Superdex 75 columns, and protein standards were from GE Healthcare Bio-Sciences Co. (Piscataway, NJ, USA). Isoflavone standards were purchased from Sigma-Aldrich Co. Liquid chromatography grade acetonitrile, methanol, and *n*-hexane were from Merck (Darmstadt, Germany). DIAION HP-20 was from Mitsubishi Chemical Co. (Tokyo, Japan). All chemicals used were of analytical grade.

Rapid Amplification of cDNA ends (RACE). Total RNA was extracted from soybean seeds as described.[26] Purified RNA was used to construct the RACE library by use of the SMART RACE cDNA Amplification kit (Clontech, Palo Alto, CA, USA). Our previous paper[25] gave the partial N-terminal amino acid sequence for soybean β-glucosidase. To obtain the full-length cDNA encoding soybean β-glucosidase, pairs of degenerate primers were designed on the basis of this partial protein sequence and the conserved sequences of β-glucosidase from other plants in Genbank. After obtaining the gene's partial sequence, gene-specific primers (GmBGL-F1, 5′-GCTGCGACCTGGCAGCAAATGGTGAATC-3′; GmBGL-R1, 5′-CCGCAATGCATGGAGCAAAGACATACGG-3′) were designed by use of the PrimerSelect program of Lasergene 6 (DNASTAR, Inc., Madison, WI, USA) for 5′ and 3′ RACE. PCR involved a Mastercycler gradient thermal cycler (Eppendorf, Hamburg, Germany). The high-fidelity Platinum Taq DNA polymerase (Invitrogen, Carlsbad, CA, USA) was used for the amplification of the *GmBGL* cDNA. PCR products were cloned with use of the pGEM-T Easy Vector System II (Promega, Madison, WI, USA). An ABI Prism 3730XL DNA Sequencer (Applied Biosystems, Foster City, CA, USA) was used to determine the nucleotide sequences of positive clones. After sequencing, we obtained a full-length cDNA of the soybean β-glucosidase gene (*GmBGL*, GenBank accession no. KF740479).

Sequence and Phylogenetic Analysis. DNA sequences were analyzed by use of BLAST (http://www.ncbi.nlm.nih.gov/blast/) and InterProScan (http://www.ebi.ac.uk/Tools/pfa/iprscan/). The amino acid sequences of β-glucosidase from soybean and other plants including *Medicago truncatula*, *Zea mays*, *Arabidopsis thaliana*, *Hordeum vulgare*, *Nicotiana tabacum*, *Triticum aestivum*, *Tropaeolum majus*, and *Oryza sativa* deposited in GenBank were used for phylogenetic analysis. The alignment of the deduced protein sequences and phylogenetic tree were computed by use of Megalign in Lasergene 6 (DNASTAR, Inc., Madison, WI, USA) and MEGA5,[27] respectively, with standard parameters.

Rice Transformation and Growth Conditions. The maize ubiquitin 1 promoter together with its first intron was used to drive the overexpression of *GmBGL* in rice. The hygromycin phosphotransferase gene was chosen as a selectable marker. The cassette was cloned into the binary vector pCambia1302 and then transferred into *Agrobacterium tumefaciens* strain EHA101 by electroporation. Embryogenic calli from immature seeds of TNG67 were transfected as described.[28] Three independent T2 homozygous lines (oxBGL1, oxBGL2, and oxBGL3) were used for molecular and biochemical analysis. Seeds of wild-type and transgenic rice were hydroponically cultivated at 30/25 °C (day/night) in a phytotron (Agricultural Experimental Station, National Taiwan University, Taipei) with natural sunlight and 90% relative humidity.

Semiquantitative RT-PCR. Total RNA was isolated from 2-week-old rice leaves and soybean tissues by use of Trizol reagent (Invitrogen). RNA samples were treated with TURBO DNase (Ambion, Grand Island, NY, USA) at 37 °C for 30 min to avoid DNA contamination. First-strand cDNA was synthesized by use of MMLV high-performance reverse transcriptase (EPICENTRE Biotechnologies, Madison, WI, USA) according to the manufacturer's instructions. For amplifying the full-length cDNA of *GmBGL*, we designed a gene-specific primer pair (GmBGL-F2, 5′-ACTAGTAGTCCACTCAATTTTAGATTTTTAAGTGTCTGGT-3′; GmBGL-R2, 5′-ACTAGTAACAATAGTAATCAAAATGAAAAGTCTGCCCTAG-3′; *Spe*I underlined for subcloning). To quantify the relative amount of *GmBGL* transcripts in transgenic rice and soybean, we designed two pairs of gene-specific primers (OsActin-F, 5′-ATGCTCTCCCCCATGCTATC-3′; OsActin-R, 5′-TCTCCTTGCTCATCCTGTC-3′; GmEF-1-F, 5′-ACATCCCAAGCTGACTGTGC-3′; GmEF-1-R, 5′-TACCTGGCCTTGGAATACTTGG-3′) for rice

DOI: 10.1021/jf504778x
J. Agric. Food Chem. 2015, 63, 921−928

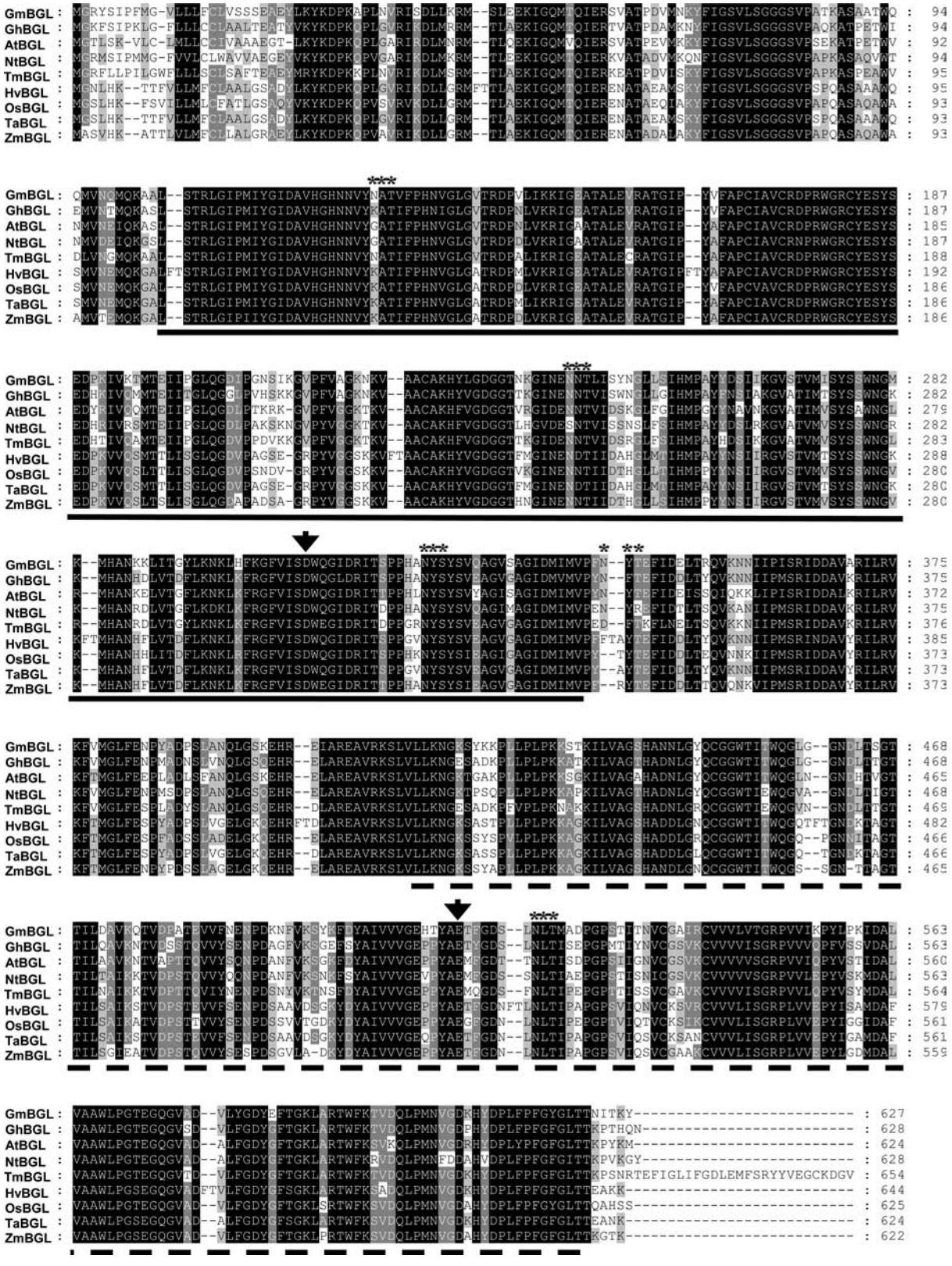

Figure 2. Multiple sequence alignment of deduced amino acid sequences of *β*-glucosidase genes from *Glycine max* (GmBGL, KF740479), *Arabidopsis thaliana* (AtBGL, NM_122104), *Gossypium hirsutum* (GhBGL, AAQ17461), *Hordeum vulgare* (HvBGL, U46003), *Nicotiana tabacum* (NtBGL, AB017502), *Oryza sativa* (OsBGL, NM_001057810), *Triticum aestivum* (TaBGL, AY091513), *Tropaeolum majus* (TmBGL, AJ006501), and *Zea mays* (ZmBGL, NM_001136824). Conserved stretches and residues are indicated in bold and shading, respectively. N-terminal and C-terminal domains of glycosyl hydrolase 3 (GH3) family members are underlined with continuous and dashed lines, respectively. The positions of potential N-glycosylation sites are denoted by asterisks. Arrows indicate the catalytic nucleophile (Asp) and the catalytic acid/base (Glu) responsible for GH3 activities.

DOI: 10.1021/jf504778x
J. Agric. Food Chem. 2015, 63, 921−928

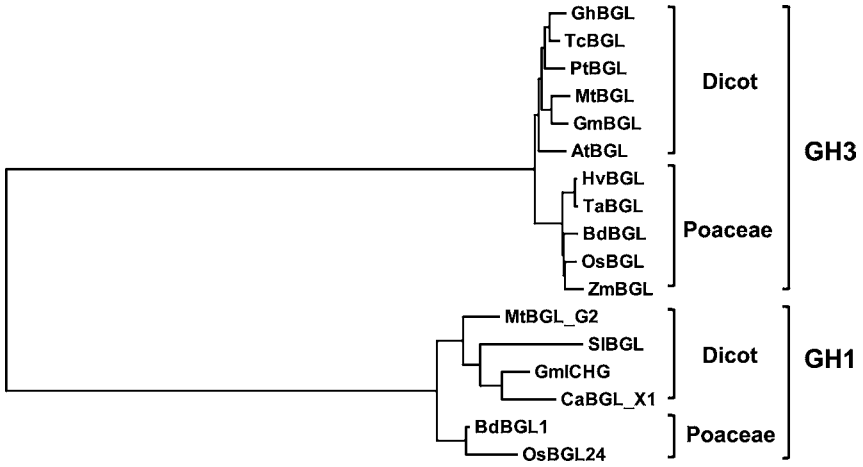

Figure 3. Phylogenetic tree of plant β-glucosidases. The tree was generated with the full-length BGL protein sequences by use of Clustal W and the neighbor-joining method (MEGA 5.0). The bar beneath the dendrogram represents a distance of 0.05 change per amino acid. Branches are labeled with species names as follows: *G. max* (GmBGL, KF740479; GmICHG, NP_001237501), *A. thaliana* (AtBGL, NP 197595), *Brachypodium distachyon* (BdBGL, XP 00355; BdBGL1, Bradi1g42690), *Cicer arietinum* (CaBGL_X1, XP_004507133), *G. hirsutum* (GhBGL, AAQ17461), *H. vulgare* (HvBGL, AAC49170), *Medicago truncatula* (MtBGL, XP 003601350; MtBGL_G2, ABW76287), *O. sativa* (OsBGL, Os03g0749300; OsBGL24, LOC_Os06g21570), *Populus trichocarpa* (PtBGL, XP 00231363), *Solanum lycopersicum* (SlBGL, Solyc08g044510), *Theobroma cacao* (TcBGL, EOY33198), *T. aestivum* (TaBGL, AAM13694), and *Z. mays* (ZmBGL, NP 001130296).

Actin1 and soybean *elongation factor-1α*, respectively, as normalization controls.

Enzyme Extraction and Activity Assay. Shoots from 2-week-old rice plants were ground to powder in liquid nitrogen, and 2 mM EDTA aqueous solution was added to a volume of approximately 10 mL g^{-1} fresh weight. After centrifuging at 13000*g* for 15 min, the supernatant was discarded to remove water-soluble parts. The residue was then extracted twice with 10 mL of 3% NaCl aqueous solution for 30 min at room temperature. The homogenates were centrifuged at 13000*g* for 15 min at 4 °C. The supernatant as crude β-glucosidase was assayed for GmBGL activity and protein content. β-Glucosidase activity was assessed by measuring *p*NP release from *p*-nitrophenyl-β-D-glucopyranoside (*p*NPG) at pH 9.5 by absorption spectrophotometry at 405 nm absorbance.[25] The enzyme reaction was initiated by mixing 20 μL of crude β-glucosidase with 25 μL of 10 mM *p*NPG and 55 μL of 50 mM acetate buffer, pH 4.5. After incubation at 45 °C for 15 min, 100 μL of 1 M sodium carbonate solution was added to stop the reaction, and the released *p*NP was measured. A quantitative curve was prepared for authentic *p*NP at 0−0.5 mM. β-Glucosidase activity was calculated from the angular coefficient of the linear slope and normalized to protein content by using the Bradford method.

Antiserum Preparation. The full-length coding region of *GmBGL* was cloned into the *pET32a* vector at the *Nco*I and *Xho*I sites for protein expression in the *Escherichia coli* BL21 (DE3) strain by induction with isopropyl-D-thiogalactopyranoside. For purification of recombinant protein, bacterial extracts were initially passed through an Ni^{2+} column (GE Healthcare Life Sciences) according to the manufacturer's protocol, and then purified recombinant GmBGL was used as the rabbit antigen for antibody production (LTK BioLaboratories, Taoyuan, Taiwan).

Western Blot Analysis. In total, 2 μg of crude extract from shoots was separated by 10% SDS-PAGE, and proteins were transferred to an Immobilon-P PVDF transfer membrane (Merck Millipore, Darmstadt, Germany), which was blocked with 5% skim milk for 1 h and incubated with primary antibody at a 1:500 dilution at 4 °C for 12 h and then with horseradish peroxidase-conjugated secondary goat anti-rabbit IgG antibody (GeneTex, Irvine, CA, USA) at 1:50000 dilution for 1 h. Immunoreactivity was detected by enhanced chemiluminescence (Amersham International PLC, Gloucester, UK). The positive control from soybean was purified as described.[25] Briefly, 200 g of okara was homogenized in 1 L of 3% (w/v) NaCl aqueous solution; after filtration, the filtrate was concentrated by ultrafiltration (Hollow Fiber Cartridge, MWCO 5 kDa, GE Healthcare Life Science), treated with dithiothreitol, and then further purified by CM-Sepharose CL-6B cation-exchange chromatography to obtain soybean β-glucosidase.

Hydrolyzing Test of Malonylglucosidic and Glucosidic Forms of Isoflavone. Malonylglucosidic and glucosidic forms of isoflavone were prepared as described.[29] Briefly, isoflavones were extracted from soybean with 60% methanol, and then solvents were removed under reduced pressure to obtain the crude extracts of isoflavone, which were further fractionated by passing through a column prepacked with Diaion HP20 resins. The HP20 adsorbed fraction was eluted sequentially with a bed volume of 40% methanol, 70% methanol, and pure methanol to obtain the corresponding fractions that contained the dominant constituent with malonylglucosidic, glucosidic, and aglycone forms of isoflavone, respectively. The isolated isoflavones in each of the eluents was identified by comparison with authentic isoflavone standards through high-performance liquid chromatography (HPLC). After evaporation to dryness under vacuum, the isolated fraction with dominant glucosyl isoflavone was used as the substrate for analyzing the enzyme activity of recombinant β-glucosidase. For evaluating the substrate affinity of enzyme, both malonylglucosidic and glucosidic forms of isoflavone were used as substrates. The hydrolysis was initiated by adding 100 μL of the substrate isoflavone at 3000 μg/mL into the reaction mixture, which consisted of 10 μg of crude extract protein and 100 μL of 50 mM acetate buffer, pH 4.5, with a final volume of 350 μL. After incubation at 45 °C for 60 min, the reaction was stopped by adding 350 μL of methanol containing 1000 μg/mL benzoic acid. The insoluble substances were removed by centrifugation, and the supernatant was used for analyzing isoflavone content by HPLC. HPLC involved the model 584 Solvent Delivery Module (ESA Biosciences, Chelmsford, MA, USA) equipped with a YMC-Pack ODS-AM C18 column (4.6 × 250 mm, 5 μm) and a Thermo SpectroMonitor 3200 digital UV−vis detector. The linear mobile phase gradient was obtained with 0.1% acetic acid in H_2O (solvent A) and 0.1% acetic acid in acetonitrile (solvent B). After injection of 20 μL of sample, solvent B was increased from 15 to 20% over 20 min, to 24% within the next 10 min, isocratic at 24% over 6 min, increased to 35% within the next 8 min, then isocratic at 35% over 6 min, and finally to decreased to 15% within 5 min and held at that percentage for the next 15 min. The flow rate was set at 1 mL/min. The eluted components were detected at 254 nm.

Statistical Analysis. Data are expressed as mean ± SE (n = 4). Comparisons involved ANOVA, and means were compared by Duncan's multiple-range test (P < 0.05).

DOI: 10.1021/jf504778x
J. Agric. Food Chem. 2015, 63, 921−928

RESULTS

Characterization of GmBGL Gene. After RACE analysis, we obtained a 2190 bp DNA fragment containing a poly-A signal region in the 3′-UTR. Sequence analysis revealed a single open reading frame of 1884 bp encoding a polypeptide of 627 amino acids. The open reading frame was designated the *G. max β-glucosidase* gene (*GmBGL*). The amino acid sequences for GmBGL shared 90% similarity with β-D-glucosidase of *Gossypium hirsutum* (GhBGL, GenBank accession no. AAQ17461). The cDNA and amino acid sequence of *GmBGL* have been deposited at GenBank (accession no. KF740479) (Figure 2).

GmBGL Is a Member of the Glycosyl Hydrolase 3 Family. A BLAST search of the soybean genome database (http://www.phytozome.net/soybean) revealed four highly homologous genes for *GmBGL*. Soybean clones Glyma10g15980.1, Glyma02g33550.1, Glyma02g43990.1, and Glyma14g04940.2 share 99, 96.5, 86.1, and 86.0% identity, respectively, to *GmBGL*, and all genes were annotated as members of the β-glucosidase family. However, N-terminal amino acid sequence analysis demonstrated that only the Glyma10g15980.1 was identical to the N-terminal sequence we identified previously.[25] As compared with Glyma10g15980.1, two single-nucleotide polymorphisms were found in the *GmBGL* cDNA sequence, which may result from different soybean genetic backgrounds.

Multiple sequence alignment of β-glucosidase among *G. max*, *A. thaliana*, *G. hirsutum*, *H. vulgare*, *N tabacum*, *O. sativa*, *T. aestivum*, *T. majus*, and *Z. mays* demonstrated that the GH3 family shared high similarity of the N-terminal domain (^{105}Leu−Val^{340}) and C-terminal domain (^{412}Leu−Thr^{621}) (Figure 2). Aspartic acid, located in the conserved motif ^{303}GFVISDW^{309} of all GH3 family members, was thought to be one of the active sites of amino acid residues. Another putatively catalytic residue of glutamic acid was located in E^{514}. The phylogenetic tree shown in Figure 3 summarizes the β-glucosidases identified in the soybean genome and other species. It revealed a clear divergence between GH1 and GH3 isoforms (Figure 3). Both GH1 and GH3 isoforms could be divided into dicot and Poaceae subgroups. The novel GmBGL belongs to the dicot GH3 subgroup. The sequences in this group are restricted to dicot plants and have been identified in *G. hirsutum*, *Theobroma cacao*, *Populus trichocarpa*, *M. truncatula*, and *A. thaliana*. No isoform from this group was found in the Poaceae genome. In contrast, another soybean β-glucosidase, GmICHG, is included in GH1 (Figure 3).

Expression of GmBGL Gene in Soybean Plants. We analyzed the spatial *GmBGL* gene expression in soybean by semiquantitative RT-PCR. The *GmBGL* transcript was present in both vegetative and reproductive tissues. Roots and leaves accumulated more *GmBGL* transcript than did other tissues (Figure 4).

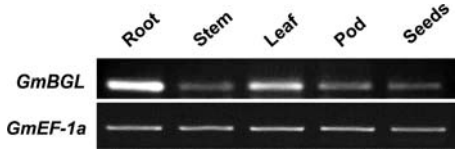

Figure 4. Semiquantitative RT-PCR of *GmBGL* transcript levels in root, stem, leaf, pod, and mature seeds. *G. max elongation factor-1α* (*GmEF-1α*) was used as an internal control.

Analysis of Transgenic Rice Plants Harboring the GmBGL Gene. Figure 5a illustrates the plasmid construct used for heterologous expression of *GmBGL* in rice. After *Agrobacterium*-mediated transformation, 15 independent transgenic lines were obtained. Three randomly selected transgenic lines were analyzed. RT-PCR analysis revealed increased *GmBGL* transcript in oxBGL1- and oxBGL3-overexpressing lines and markedly increased *GmBGL* transcript in the oxBGL2-overexpressing line, with no *GmBGL* transcript detected in nontransformants (WT) and plants transformed with empty vector (Figure 5b). To examine the translation of GmBGL in transgenic rice, we produced a polyclonal antibody to detect GmBGL protein. GmBGL protein highly accumulated in oxBGL1 and oxBGL2 lines and slightly in oxBGL3. Moreover, GmBGL antibody strongly bound to the purified soybean BGL protein, with no signal detected in the WT or rice plants transformed with empty vector (Figure 5c).

β-Glucosidase Activity in Transgenic Rice and Substrate Specificity toward Isoflavones. To examine the β-glucosidase activity of recombinant GmBGL in transgenic rice, we performed a chromogenic assay with *p*NPG as a substrate. As compared with the WT, oxBGL1 and oxBGL2 showed 6- and 31-fold increased activity, respectively (Figure 6). The β-glucosidase activity of oxBGL3 and the WT was similar. The substrate specificities of recombinant GmBGLs toward glucosidic and malonylglucosidic isoflavones are in Figure 7. Figure 7a shows the chromatogram for isoflavone substrate before hydrolysis. After hydrolyzation by crude GmBGLs from oxBGL1 and oxBGL2 at 45 °C and pH 4.5 for 30 min, the contents of daidzin and genistin were decreased to 42 and 46% of the original content with β-glucosidase from oxBGL1 (Figure 7b) and to 97 and 80% with β-glucosidase from oxBGL2 (Figure 7c), but the corresponding contents of daidzein and genistein with both treatments were increased. Daidzin and genistin contents were not reduced in oxBGL3, the WT, or the empty vector control (Figure 7d−f). Thus, both GmBGLs from transgenic rice oxBGL1 and oxBGL2 could effectively hydrolyze glucosyl-conjugated isoflavones into their corresponding aglycones. The content of malonylglucosidic isoflavones in all treatments remained relatively stable. Thus, the β-glucosidase activity of GmBGL from transgenic rice, which possesses high substrate specificity toward glycosyl isoflavones rather than malonylglucosidic isoflavones, could be markedly increased by overexpressing *GmBGL*.

DISCUSSION

We previously purified and characterized a β-glucosidase with isoflavone glucoside-hydrolyzing activity from soybean okara.[25] In this study, we isolated *GmBGL*, a novel gene encoding β-glucosidase, and validated the enzyme activity and substrate specificity in transgenic rice. *GmBGL* encodes for a polypeptide of 627 amino acids with molecular mass of 69 kDa. The deduced amino acid sequence had a high isoelectric point at pH 8.98, which agrees with our previous finding of native GmBGL from soybean okara being capable of separation by adsorption to CM-Sepharose CL-6B cation-exchange resin.[25]

GmBGL was transformed into the rice genome and could be transmitted to progenies. Among three randomly selected transgenic lines overexpressing *GmBGL*, oxBGL2 expressed the highest mRNA levels of β-glucosidase, and oxBGL1 and oxBGL3 expressed lower levels (Figure 5b). As well, oxBGL2 expressed the most abundant GmBGL protein, followed by oxBGL1, with the least by oxBGL3. Both oxBGL1 and oxBGL3

DOI: 10.1021/jf504778x
J. Agric. Food Chem. 2015, 63, 921−928

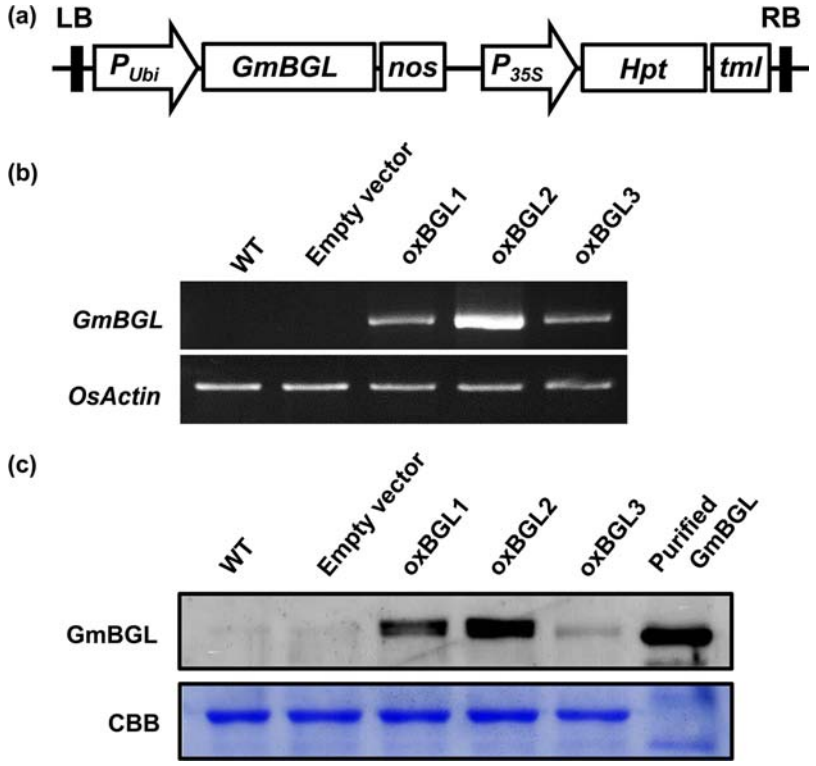

Figure 5. Heterologous expression of *GmBGL* in rice. (a) Schematic representation of the expression cassette used for rice transformation. LB, left border; RB, right border; P_{ubi}, maize ubiquitin 1 promoter together with its first intron; *nos*, terminator of the nopaline synthase gene; P_{35S}, CaMV 35S promoter; *hpt*, coding sequence of hygromycin phosphotransferase; *tml*, terminator of a tumor morphology large gene; oxBGL, overexpressing BGL line. (b) Semiquantitative RT-PCR of expression of *GmBGL* in the wild type (WT) and transformants. Semiquantitative RT-PCR was performed with gene-specific primers of *GmBGL* and the rice *Actin1* as a control. (c) Western blot analysis of GmBGL protein level in the WT and transformants. Equal loading of extracted proteins (2 μg each lane) is shown by Coomassie brilliant blue (CBB) R250 staining. Partially purified GmBGL protein from soybean was used as a positive control to demonstrate antibody specificity.

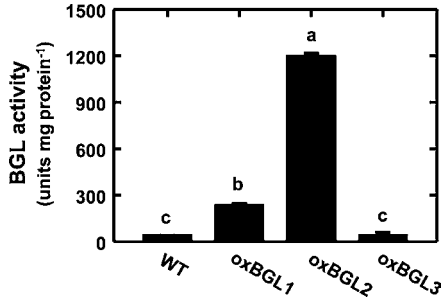

Figure 6. β-Glucosidase activity in transgenic rice plants. Proteins were extracted from shoots of WT and transgenic rice plants. Data are expressed as specific activity. β-Glucosidase activity was assayed with *p*-nitrophenyl-β-D-glucopyranoside (*p*NPG) as the substrate, and activity was calculated from measuring *p*NP release by absorbance at 405 nm. Data are the mean ± SE (n = 4). Bars with the same letter are not significantly different at $P < 0.05$.

expressed similar mRNA levels of *GmBGL*, but a very low protein level in oxBGL3 (Figure 5c). This suggests that mRNA levels of GmBGL in transgenes may, but not necessarily, contribute to corresponding protein levels.

The molecular mass of GmBGL in transgenic rice was slightly higher than that for β-glucosidase purified from soybean okara (Figure 5c). An explanation for the difference in molecular mass could be that recombinant GmBGL underwent post-translational modification such as glycosylation. Many foreign proteins, including soybean proteins, overexpressed in rice are glycosylated.[30,31] We found five potential N-glycosylation sites in the GmBGL amino acid sequence (Figure 2), so the higher molecular mass of GmBGL in transgenic rice than in soybean okara may be due to glycosylation.

The β-glucosidases have been characterized into five families—GH1, GH3, GH5, GH9, and GH30—by amino acid sequence similarity.[32] Most of the identified genes encoding β-glucosidases belong to the GH1 family. The first isoflavone-7-*O*-glucoside-specific β-glucosidase was isolated from chick pea (*Cicer arietinum*). Three isozymes, including R3, H1, and L1, were isolated from roots, hypocotyls, and leaves, respectively.[19] Among the isoflavone-related leguminous β-glucosidases, two members of the GH1 family, dalcochinin-8′-*O*-β-glucoside β-glucosidase (dalcochinase) from *Dalbergia cochinchinensis* and *Dalbergia nigrescens* β-glucosidase, have been cloned and characterized. Dalcochinase, showing high aglycone specificity for isoflavonoids, can hydrolyze both β-glucosides and β-fucosides, and *D. nigrescens* β-glucosidase can efficiently remove disaccharides from dalpatein 7-*O*-β-D-apiofuranosyl-(1→6)-β-D-glucopyranoside and 7-hydroxy-2′,4′,5′,6-tetramethoxy-7-*O*-β-D-apiofuranosyl-(1→6)-β-D-glucopyranoside. They can also remove a single glucose residue from isoflavonoid 7-*O*-glucosides such as daidzin and genistin.[33,34] Our phylogenetic analysis revealed that GmBGL is a novel GH3 protein in soybean (Figure 3). *GmBGL* is preferentially expressed in roots and leaves (Figure 4), which is a similar expression pattern as for the soybean GH1 gene *GmICHG*.[29] However, soybean GH1 and GH3 β-glucosidases show divergence in substrate specificity. The GmICHG (GH1 family) can hydrolyze both malonylated and nonmalonylated

DOI: 10.1021/jf504778x
J. Agric. Food Chem. 2015, 63, 921−928

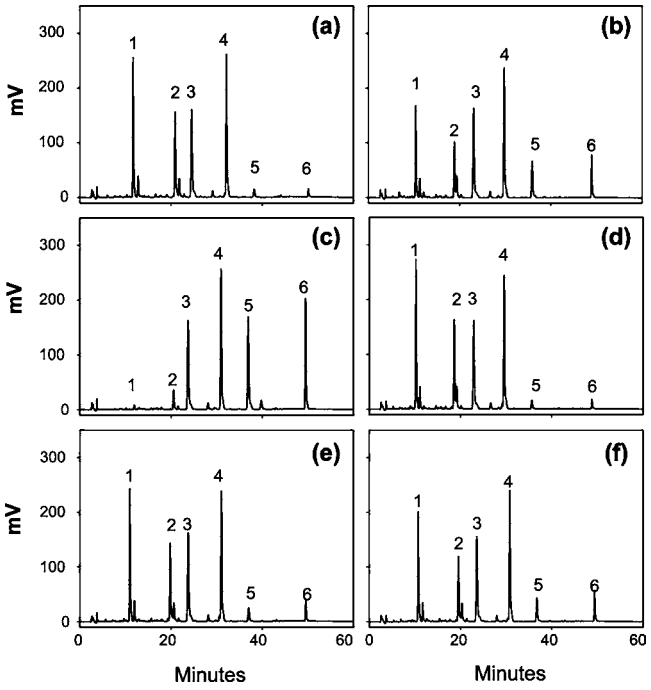

Figure 7. High-performance liquid chromatograms of substrate isoflavones after hydrolysis by crude β-glucosidases from transgenic rice oxBG lines at 45 °C and pH 4.5: (a) original substrate before hydrolysis as a blank control; (b–f) isoflavones were hydrolyzed for 30 min by the crude enzyme from oxBGL1, 2, 3, the WT (TNG 67), and the empty vector control, respectively. Peaks: 1, daidzin; 2, genistin; 3, internal standard (benzoic acid); 4, malonyl-genistin; 5, daidzein; 6, genistein.

forms of isoflavone-7-*O*-β-D-glucosides, the malonylated form being the preferred substrate. In contrast, the GmBGL (GH3 family) has strict substrate specificity toward glucosyl but not malonylglucosidic isoflavones.

GmBGL shares 72% sequence identity with a barley β-D-glucan exohydrolase isoenzyme *Exo*I, which also belongs to the GH3 family. The 3D structure of *Exo*I demonstrated that its first 357 residues represent an $(\alpha/\beta)_8$ barrel domain and the 374–559 residues, an $(\alpha/\beta)_6$ sheet.[35] Protein engineering predicted that GmBGL likely shares similar protein folding. According to Varghese et al.,[35] Asp^{285} and Glu^{491}, representing two conserved residues of the barley β-D-glucan exohydrolase, were suggested to be involved in the nucleophilic catalytic sites within general acid/base catalysis. We found these two conserved amino acids in GmBGL (Asp^{308} and Glu^{514}) and also in other GH3 family members (Figure 2).

Many studies have described the efficient transformation of isoflavone glycosides to aglycones by exogenous enzymatic hydrolysis and microbial fermentation, but only a few have characterized β-glucosidase from soybean. Because aglyconic isoflavones are considered practically to be the bioactive form of soy isoflavones, which could have a role as chemoattractants to attract nodule bacteria occurring in soy plant rhizosphere,[21,36] the amount of aglyconic forms of isoflavone in mature soybean seeds is actually negligible; the predominant forms of isoflavone are malonylglucosides and glucosides.[37] Therefore, most isoflavones in soybean have to undergo a hydrolysis process for their function while soybean seeds are sprouting and growing. We found greater *GmBGL* transcript level in roots and leaves than in other tissues of soybean seedlings (Figure 4), so GmBGL may play an important role in conversion of isoflavone conjugates into bioactive aglycones in soybean.

In conclusion, the cloning and identification of functional β-glucosidase helps us investigate its physiological role and provides the opportunity for genetic engineering of soybean seeds with high levels of aglycone.

AUTHOR INFORMATION

Corresponding Authors

*(N.-W. Su) Phone: +886 2 33664819. E-mail: snw@ntu.edu.tw.

*(C.-Y. Hong) Phone: +886 2 33663839. E-mail: cyhong@ntu.edu.tw.

Author Contributions

‖C.-C. Hsu and T.-M. Wu have equally contributed to this work.

Notes

The authors declare no competing financial interest.

REFERENCES

(1) Setchell, K. D.; Cassidy, A. Dietary isoflavones: biological effects and relevance to human health. *J. Nutr.* **1999**, *129*, 758S–767S.

(2) Messina, M.; Nagata, C.; Wu, A. H. Estimated Asian adult soy protein and isoflavone intakes. *Nutr. Cancer* **2006**, *55*, 1–12.

(3) Albertazzi, P. Purified phytoestrogens in postmenopausal bone health: is there a role for genistein? *Climacteric: J. Int. Menopause Soc.* **2002**, *5*, 190–196.

(4) Khaodhiar, L.; Ricciotti, H. A.; Li, L.; Pan, W.; Schickel, M.; Zhou, J.; Blackburn, G. L. Daidzein-rich isoflavone aglycones are potentially effective in reducing hot flashes in menopausal women. *Menopause* **2008**, *15*, 125–132.

(5) Kurzer, M. S. Hormonal effects of soy isoflavones: studies in premenopausal and postmenopausal women. *J. Nutr.* **2000**, *130*, 660S–661S.

(6) Andres, S.; Abraham, K.; Appel, K. E.; Lampen, A. Risks and benefits of dietary isoflavones for cancer. *Crit. Rev. Toxicol.* **2011**, *41*, 463–506.

(7) Anthony, M. S.; Clarkson, T. B.; Hughes, C. L., Jr.; Morgan, T. M.; Burke, G. L. Soybean isoflavones improve cardiovascular risk factors without affecting the reproductive system of peripubertal rhesus monkeys. *J. Nutr.* **1996**, *126*, 43–50.

(8) Muthyala, R. S.; Ju, Y. H.; Sheng, S. B.; Williams, L. D.; Doerge, D. R.; Katzenellenbogen, B. S.; Helferich, W. G.; Katzenellenbogen, J. A. Equol, a natural estrogenic metabolite from soy isoflavones: convenient preparation and resolution of *R*- and *S*-equols and their differing binding and biological activity through estrogen receptors α and β. *Bioorg. Med. Chem.* **2004**, *12*, 1559–1567.

(9) Setchell, K. D.; Clerici, C.; Lephart, E. D.; Cole, S. J.; Heenan, C.; Castellani, D.; Wolfe, B. E.; Nechemias-Zimmer, L.; Brown, N. M.; Lund, T. D.; Handa, R. J.; Heubi, J. E. *S*-Equol, a potent ligand for estrogen receptor β, is the exclusive enantiomeric form of the soy isoflavone metabolite produced by human intestinal bacterial flora. *Am. J. Clin. Nutr.* **2005**, *81*, 1072–1079.

(10) Izumi, T.; Piskula, M. K.; Osawa, S.; Obata, A.; Tobe, K.; Saito, M.; Kataoka, S.; Kubota, Y.; Kikuchi, M. Soy isoflavone aglycones are absorbed faster and in higher amounts than their glucosides in humans. *J. Nutr.* **2000**, *130*, 1695–1699.

(11) Xu, X.; Harris, K. S.; Wang, H. J.; Murphy, P. A.; Hendrich, S. Bioavailability of soybean isoflavones depends upon gut microflora in women. *J. Nutr.* **1995**, *125*, 2307–2315.

(12) Lin, C. H.; Wei, Y. T.; Chou, C. C. Enhanced antioxidative activity of soybean koji prepared with various filamentous fungi. *Food Microbiol.* **2006**, *23*, 628–633.

(13) Kuo, L. C.; Cheng, W. Y.; Wu, R. Y.; Huang, C. J.; Lee, K. T. Hydrolysis of black soybean isoflavone glycosides by *Bacillus subtilis* natto. *Appl. Microbiol. Biotechnol.* **2006**, *73*, 314–320.

DOI: 10.1021/jf504778x
J. Agric. Food Chem. 2015, 63, 921–928

(14) Ketudat Cairns, J. R.; Esen, A. β-Glucosidases. *Cell. Mol. Life Sci.: CMLS* **2010**, *67*, 3389−3405.
(15) Morant, A. V.; Jorgensen, K.; Jorgensen, C.; Paquette, S. M.; Sanchez-Perez, R.; Moller, B. L.; Bak, S. β-Glucosidases as detonators of plant chemical defense. *Phytochemistry* **2008**, *69*, 1795−1813.
(16) Leah, R.; Kigel, J.; Svendsen, I.; Mundy, J. Biochemical and molecular characterization of a barley seed β-glucosidase. *J. Biol. Chem.* **1995**, *270*, 15789−15797.
(17) Brzobohaty, B.; Moore, I.; Kristoffersen, P.; Bako, L.; Campos, N.; Schell, J.; Palme, K. Release of active cytokinin by a β-glucosidase localized to the maize root meristem. *Science* **1993**, *262*, 1051−1054.
(18) Warzecha, H.; Gerasimenko, I.; Kutchan, T. M.; Stockigt, J. Molecular cloning and functional bacterial expression of a plant glucosidase specifically involved in alkaloid biosynthesis. *Phytochemistry* **2000**, *54*, 657−666.
(19) Hosel, W.; Barz, W. β-Glucosidases from *Cicer arietinum* L. Purification and properties of isoflavone-7-*O*-glucoside-specific β-glucosidases. *Eur. J. Biochem./FEBS* **1975**, *57*, 607−616.
(20) Hinderer, W. Purification and properties of a specific isoflavone 7-*O*-glucoside-6″-malonate malonylesterase from roots of chickpea. *Arch. Biochem. Biophys.* **1986**, *248*, 570−578.
(21) Dakora, F. D.; Phillips, D. A. Diverse functions of isoflavonoids in legumes transcend anti-microbial definitions of phytoalexins. *Physiol. Mol. Plant Pathol.* **1996**, *49*, 1−20.
(22) Matsuura, M.; Sasaki, J.; Murao, S. Studies on β-glucosidases from soybeans that hydrolyze daidzin and genistin − isolation and characterization of an isozyme. *Biosci., Biotechnol., Biochem.* **1995**, *59*, 1623−1627.
(23) Santos, R. F.; Oliveira, C. F.; Varéa, G. S.; Orradi da silva, M. L. C.; Ida, E. I.; Mandarino, J. M. G.; Carrão-Panizzi, M. C.; Ribeiro, M. L. L. Purification and characterization of soy cotyledon β-glucosidase. *J. Food Biochem.* **2012**, *37*, 302−312.
(24) Suzuki, H.; Takahashi, S.; Watanabe, R.; Fukushima, Y.; Fujita, N.; Noguchi, A.; Yokoyama, R.; Nishitani, K.; Nishino, T.; Nakayama, T. An isoflavone conjugate-hydrolyzing β-glucosidase from the roots of soybean (*Glycine max*) seedlings: purification, gene cloning, phylogenetics, and cellular localization. *J. Biol. Chem.* **2006**, *281*, 30251−30259.
(25) Chiou, T. Y.; Lin, Y. H.; Su, N. W.; Lee, M. H. β-Glucosidase isolated from soybean okara shows specificity toward glucosyl isoflavones. *J. Agric. Food Chem.* **2010**, *58*, 8872−8878.
(26) Wang, C. S.; Vodkin, L. O. Extraction of RNA from tissues containing high levels of procyanidins that bind RNA. *Plant Mol. Biol.* **1994**, *12*, 132−145.
(27) Tamura, K.; Peterson, D.; Peterson, N.; Stecher, G.; Nei, M.; Kumar, S. MEGA5: molecular evolutionary genetics analysis using maximum likelihood, evolutionary distance, and maximum parsimony methods. *Mol. Biol. Evol.* **2011**, *28*, 2731−2739.
(28) Hong, C. Y.; Cheng, K. J.; Tseng, T. H.; Wang, C. S.; Liu, L. F.; Yu, S. M. Production of two highly active bacterial phytases with broad pH optima in germinated transgenic rice seeds. *Transgenic Res.* **2004**, *13*, 29−39.
(29) Hsu, C.; Hoa, H. W.; Chang, C. F.; Wang, S. T.; Fang, T. F.; Lee, M. H.; Su, N. W. Soy isoflavone-phosphate conjugates derived by cultivating *Bacillus subtilis* varS. natto BCRC 80517 with isoflavone. *Food Res. Int.* **2013**, *53*, 487−495.
(30) Motoyama, T.; Maruyama, N.; Amari, Y.; Kobayashi, K.; Washida, H.; Higasa, T.; Takaiwa, F.; Utsumi, S. α′ Subunit of soybean β-conglycinin forms complex with rice glutelin via a disulphide bond in transgenic rice seeds. *J. Exp. Bot.* **2009**, *60*, 4015−4027.
(31) Kuo, Y. C.; Tan, C. C.; Ku, J. T.; Hsu, W. C.; Su, S. C.; Lu, C. A.; Huang, L. F. Improving pharmaceutical protein production in *Oryza sativa*. *Int. J. Mol. Sci.* **2013**, *14*, 8719−8739.
(32) Henrissat, B. A classification of glycosyl hydrolases based on amino acid sequence similarities. *Biochem. J.* **1991**, *280* (Part 2), 309−316.
(33) Ketudat Cairns, J. R.; Champattanachai, V.; Srisomsap, C.; Wittman-Liebold, B.; Thiede, B.; Svasti, J. Sequence and expression of Thai Rosewood β-glucosidase/β-fucosidase, a family 1 glycosyl hydrolase glycoprotein. *J. Biochem.* **2000**, *128*, 999−1008.
(34) Chuankhayan, P.; Rimlumduan, T.; Tantanuch, W.; Mothong, N.; Kongsaeree, P. T.; Metheenukul, P.; Svasti, J.; Jensen, O. N.; Cairns, J. R. K. Functional and structural differences between isoflavonoid beta-glycosidases from *Dalbergia* sp. *Arch. Biochem. Biophys.* **2007**, *468*, 205−216.
(35) Varghese, J. N.; Hrmova, M.; Fincher, G. B. Three-dimensional structure of a barley β-D-glucan exohydrolase, a family 3 glycosyl hydrolase. *Structure* **1999**, *7*, 179−190.
(36) Cesco, S.; Neumann, G.; Tomasi, N.; Pinton, R.; Weisskopf, L. Release of plant-borne flavonoids into the rhizosphere and their role in plant nutrition. *Plant Soil* **2010**, *329*, 1−25.
(37) Suzuki, H.; Nishino, T.; Nakayama, T. cDNA cloning of a BAHD acyltransferase from soybean (*Glycine max*): isoflavone 7-*O*-glucoside-6″-*O*-malonyltransferase. *Phytochemistry* **2007**, *68*, 2035−2042.

DOI: 10.1021/jf504778x
J. Agric. Food Chem. 2015, 63, 921−928

been associated with consumer acceptance and can be promoted in the marketplace.[9]

Plant starches are synthesized by several enzymatic reactions.[10−12] ADP-glucose (ADPG) pyrophosphorylase (AGP) (also called glucose-1-phosphate adenyltransferase [EC 2.7.7.27]) activities generate a major source of the glucosyl donor ADPG for starch biosynthesis.[13−15] Starch synthase (SS) including soluble SS (SSS) [EC 2.4.1.21] and granule-bound SS (GBSS) [EC 2.4.1.242] add glucosyl units at the nonreducing end of linear chains through new $\alpha(1\rightarrow4)$ linkages. Starch branching enzyme (SBE) (also called 1,4-α-glucan branching enzyme [EC 2.4.1.18]) introduces branch linkages in the starch by cleaving interior $\alpha(1\rightarrow4)$ bonds and forming a new glycoside bond between the C1 reducing end of the released glucan and a C6 within an adjoining linear chain. Starch debranching enzyme (SDBE) including isoamylase [EC 3.2.1.68] and pullulanase [EC 3.2.1.41] hydrolyzes branch linkages and is needed for creation of normal branching patterns in amylopectin. Multiple isoforms exist for each enzyme, although their specific roles in starch biosynthesis generally are not known.[16] Starch biosynthesis is probably best studied in *Arabidopsis* leaves, potato tubers, and maize endosperm.[12,17,18] Maize (*Zea mays*) contains at least five different genes coding for SS,[19] three genes coding for SBE,[20] and two genes coding for SDBE.[21] In addition, ADPG is transported from the cytosol into amyloplasts by the adenylate transporter/adenylate translocator (ANT) coded for by the *brittle1* gene in maize endosperm.[15,22]

Starch biosynthesis has not been studied in chestnut. One study identified a homologue of *Arabidopsis* DSP4 (SEX4) involved in starch degradation in chestnut that was induced in response to cold and accumulated in stem amyloplasts during winter.[23] New technologies such as transcriptome and microarray have been used to uncover the genes involved in chestnut blight infection. A number of genes have been identified and characterized by comparative transcriptomes of American chestnut (*Castanea dentata*) and Chinese chestnut (*Castanea mollissima*) in response to the chestnut blight infection.[24] This technology has provided insightful information for chestnut resistance to blight disease.[25] cDNA microarray has also been used to monitor transcriptional responses of the chestnut blight fungus *Cryphonectria parasitica* to infection by virulence-attenuating hypoviruses.[26] However, there is no molecular level study of starch biosynthesis and sucrose metabolism in chestnut tree. This study evaluated metabolite profiles and identified genes coding for enzymes in starch and sucrose metabolism by transcriptome and quantitative real-time polymerase chain reaction (qPCR).

MATERIALS AND METHODS

Plant Materials. Chinese chestnut (*Castanea mollissima* Mill.) cultivar 'Yanshanzaofeng' was used in this study. The plants were planted in Qianxi county, Tangshan city, Hebei province, China. Chestnut fruits were collected from three 8-year-old trees at five developmental stages (30, 45, 60, 75, and 90 days after flowering, DAF). To ensure the same developmental stages of the seeds from different trees, we conducted controlled pollination on the three trees. Three chestnut fruits were removed from each of the south, east, west, and north directions of each tree, resulting in a total of 12 fruits per developmental stage per tree. Seeds were taken out of the fruits, and the seed coat and skin were removed. The endosperm was wrapped with silver paper and stored in liquid nitrogen immediately until being used for RNA extraction and metabolite analyses. No specific permit was required for sample collection because the trees were publicly owned, and the field studies did not involve protected species.

Seed Composition Analysis. The seed endosperms were dried in an 80 °C oven. Each dried sample was ground into fine powder with a homogenizer followed by filtration through a 0.5 mm filter before being used for seed composition analyses. Soluble sugar content was determined by the colorimetric Anthrone method.[27,28] Starch (amylose and amylopectin) content was determined by dual-wavelength spectroscopy with wavelength scans of the amylose−iodine and amylopectin−iodine complexes at 450−800 nm in a spectrophotometer (DU 800 Beckman Coulter).[3] Protein content was determined according to the Kjeldahl method based on nitrogen released after strong acid digestion.[29] Oil was extracted from powders by using the Soxhlet extraction method according to the standard protocol of "Determination of crude fat in foods" (State Standard of the People's Republic of China, GB/T 14772-2008).[29]

RNA Isolation. For cDNA library construction and transcriptome sequencing, total RNA was isolated from frozen endosperms of developmental seeds collected at 45 DAF (corresponding to the beginning of starch synthesis peak phase) and 75 DAF (corresponding to the end of starch synthesis peak phase) using a PureLink RNA Mini Kit (Life Technologies, USA). For qPCR analyses, all five stages of seed endosperms were used for RNA extraction using a Microto-Midi Total RNA Purification System according to the manufacturer's protocols (Life Technologies). The quality and quantity of the purified RNA samples were characterized initially by agarose gel electrophoresis and NanoDrop ND1000 spectrophotometer (NanoDrop Technologies, Wilmington, DE, USA) and further assessed by RNA Integrity Number (RIN) and rRNA ratio using an Agilent 2100 Bioanalyzer (Santa Clara, CA, USA) as described.[30] These RNA isolation kits resulted in high-quality RNA preparations with RIN larger than eight (data not shown).

cDNA Library Construction. Poly-A containing mRNA was purified from 2 μg of total RNA using oligo (dT) magnetic beads and fragmented into 200−500 bp pieces with divalent cations at 94 °C for 5 min using a similar procedure for tung tree seed transcriptome cDNA library construction.[31] The mRNA fragments were reverse transcribed into first-strand cDNA using SuperScript II reverse transcriptase and random primers (Life Technologies). After double-stranded cDNA synthesis, fragments were end-repaired and A-tailed. The final cDNA library was created by purifying and enriching the double-stranded cDNA by PCR.

Unigene Assembly and Analysis. The cDNA sequencing was performed using a paired-end flow cell with an Illumina Solexa HiSeq 2000 Sequencing System (Biomarker Technologies Co.). Clean DNA sequencing reads were de novo assembled using Trinity with default *K*-mers = 25.[32] The contigs without ambiguous bases were obtained by conjoining the *K*-mers in an unambiguous path. The clean reads were mapped back to contigs using Trinity to construct unigenes with the paired-end information. This program detected contigs from the same transcript as well as the distances between these contigs. Finally, the contigs were connected with Trinity, and sequences that could not be extended on either end were defined as unigenes for each library. Finally, the two sets of unigenes were integrated into one set of unigenes using the BLAST-Like Alignment Tool (http://genome.ucsc.edu/cgi-bin/hgBlat). The Kyoto Encyclopedia of Genes and Genomes (KEGG) protein databases were used to annotate unigenes using InterProScan software.[33] KEGG annotation was used initially to identify unigenes in starch and sucrose metabolism and glycosyltransferase pathways. Because there is a limitation of using bacterially derived KEGG maps for unigene annotation, a keyword search was performed to identify additional unigenes related to starch and sucrose metabolism.

Digital Analysis of Differentially Expressed Genes in Two Seed Developmental Stages. To compare differences in gene expression, tag frequencies of both libraries were analyzed by IDEG6 software (http://telethon.bio.unipd.it/bioinfo/IDEG6/) according to the method described by Audic and Claverie.[34] The false discovery rate (FDR) was used to determine the threshold *P* value for multiple testing. Calculation of unigene expression used the reads per kilobase

DOI: 10.1021/jf505247d
J. Agric. Food Chem. 2015, 63, 929−942

Table 1. Unigenes and Sequences of 22 Primer Pairs for qPCR Analysis

ID[a]	unigene ID[b]	annotation	reference no.	forward primer (5′−3′)	reverse primer (5′−3′)	amplicon (bp)
A	C1Ug19275	sucrose synthase [EC 2.4.1.13]	AFW99069.1	GACACCCTTGGACAGTATGAGAGT	CACAATGTTGAACCTAGGATCGAA	105
B	C1Ug22044	pectinesterase [EC 3.1.1.11]	XP_007013011.1	GGCGACCCTAATCGTGAAATG	CGGAGCCATCAATGAAGGTAA	151
C	C1Ug31955	sucrose synthase [EC 2.4.1.13]	AGV22113.1	TTCGTCATAGCCAGCACATAC	CGTTGATGCCTGAAACTACTC	118
D	C1Ug36303	trehalose-phosphatase [EC 3.1.3.12]	XP_008238210.1	GAGGAAGAGGTTCAATAGGGTAA	GAATCCGATGAGGTCAGAGTT	133
E	C1Ug38445	ADP-glucose pyrophosphorylase, large subunit [EC 2.7.7.27]	XP_002313036.1	CCTCAATCGCCACATTTCAC	AACCACTTCATTCCTGCTTCC	114
F	C1Ug39763	α,α-trehalose-phosphate synthase [EC 2.4.1.15	EXB54073.1	ATTGGCGTGATAAAGTAGTGTT	TGATGTATGGGAACTGCTGAC	148
G	C1Ug41090	UDP-glucuronate 4-epimerase [EC 5.1.3.6]	XP_004138968.1	ACTGGCTCCGCTGGCTTCA	GGCTTGTCTGGCACGCTTC	126
H	C1Ug41228	soluble starch synthase [EC 2.4.1.21]	XP_008230773.1	CTTGGAGATGTTGCTGGTGCTT	CTTCCGAACTCCTGTATCTTGG	117
I	C1Ug41886	sucrose synthase [EC 2.4.1.13]	AGV22112.1	ACTGGTGGGCAGGTTGTTTAT	AGGAGTCGGGTGACAATGA	122
J	C1Ug42679	β-fructofuranosidase [EC 3.2.1.26]	XP_007024490.1	ATGGTTGCTGGTCAGGTTC	AAGGTATGGGTCAGAGAGATT	131
K	C1Ug43056	β-1,4-D-xylan synthase [EC 2.4.2.24]	XP_007051035.1	GTGGGGAATGTCTACTGTTTGTGAA	TTGGGTTGCGAAGGTTTGGA	143
L	C1Ug44159	α-amylase [EC 3.2.1.1]	AHL44839.1	ACACTCGTTATTGTGATGGC	CCCGATTTCAGTCTTTAGC	137
M	C1Ug46084	α-glucosidase [EC 3.2.1.20]	XP_006468478.1	GGGGTTACAAGAATGTGGCTGAC	GGGAAGTTGATGGGATGAAGG	139
N	C2Ug23382	sucrose synthase [EC 2.4.1.13]	XP_007035651.1	TTGTTGTGGTTGGCGGTTAC	TACGAGCACGGTTCATTTGG	147
O	C2Ug24779	pectinesterase [EC 3.1.1.11]	XP_006828586.1	TGTAATCACAGCCCAAGGTC	TTTGTGGGTAAGGTTGAAGGT	101
P	C2Ug24961	pectinesterase [EC 3.1.1.11]	XP_008235120.1	AGCACATTGTATTATGCCGAGTA	AGCCAGCAAGAAGTTAGCCAC	138
Q	C2Ug26944	soluble starch synthase [EC 2.4.1.21]	XP_008234756.1	GCTCCATTAGTGCTTCCATTG	GCTTGCGTGCCAGTCATT	78
R	C2Ug29276	sucrose synthase [EC 2.4.1.13]	AGV22111.1	ATGAATCGAGCACGTAATGG	CAAGTGGCAAATGTAGGAAGG	140
S	C2Ug29836	ADP-glucose pyrophosphorylase, small subunit [EC 2.7.7.27]	XP_002524583.1	TTACTTGTATGACGGTTACTGGG	GGGTTGGGTGTAGATAGGAGAT	133
T	C2Ug30790	soluble starch synthase [EC 2.4.1.21]	XP_008230284.1	ACAGTGGACATAATGCTTCCTTTC	TGAGATGCCTGAAACTAACCC	144
U	C2Ug31317	α-amylase [EC 3.2.1.1]	P17859.1	CTCCTTCTCAATCTGCTGCTA	CAACGGCTTTAATTCCTTTCT	141
REF	C2Ug31919	elongation factor 1-α2 (EF1-α2)	FK868440	TGACGCCCTTGACCAGAT	GGGACAGTTCCAATACCACCA	102

[a]A−U represent the sample ID of unigene analyzed by qPCR and correspond to those listed in Figure 3 and Table 5. REF represents the reference gene used for qPCR assays. [b]C and U represent the initials of "chestnut" and "unigene" followed by the ID of the unigene identified in the Chinese chestnut transcriptomes.

J. Agric. Food Chem. 2015, 63, 929−942
DOI: 10.1021/jf505247d

per million mapped reads (RPKM) method.[35] FDR <0.001 and absolute value of the log2 RPKM ratio >1 (or RPKM ratio more/less than 2-fold) were used as the threshold to determine significant differences in gene expression.

Quantitative Real-Time PCR Analysis of Gene Expression in Five Seed Developmental Stages. The expression patterns of 21 unigenes mostly in the starch and sucrose metabolism pathway in developing Chinese chestnut seeds were studied by qPCR using the SYBR Green method essentially as described in Cao and Shockey.[36] Elongation factor 1-α2 (*EF1-α2*) (C2Ug31919) was used as the reference gene (primer sequences were identical between Chinese chestnut unigene C2Ug31919 and Portuguese chestnut GenBank accession no. FK868440). PCR primers were designed with "Primer Express" software as used previously.[30] The names and primer sequences of the 22 unigenes are listed in Table 1. The qPCR assay was carried out with three replicates in each reaction using the Bio-Rad CFX system (Bio-Rad). PCR was performed in a 20 μL volume containing 2 μL of diluted cDNA, 250 nM of each primer and 1× SYBR Premix Ex *Taq*II (TaKaRa). The results were analyzed using the comparative Cq method, which uses an arithmetic formula, $2^{-\Delta\Delta Cq}$, to obtain results for relative quantification.[37] The significant difference of $2^{-\Delta\Delta Cq}$ among the different stages of seeds was analyzed using Duncan's multiple-range test with IBM SPSS Statistics 20.0. The correlation between gene expression levels and starch content was analyzed using the method of Pearson correlation coefficient with IBM SPSS Statistics 20.0.

RESULTS

Metabolite Profiles during Fruit Development in Chinese Chestnut Tree. During the developmental stages from 30 to 90 days after flowering, water contents in the fruits collected at 30, 45, 60, 75, and 90 DAF were 82.67 ± 3.23, 75.38 ± 1.12, 66.88 ± 2.30, 60.34 ± 2.21, and 52.89 ± 1.81%, respectively. Whereas water content in the nuts was gradually decreased, the dry mass of the chestnut fruits was rapidly increased from 0.5 to >4 g per fruit, an increase of 7.6-fold (Figure 1A). The increase of dry mass in the fruit was primarily due to starch accumulation in the endosperm (Figure 1B). The amylose portion of starch was increased 32.8-fold by weight (Figure 1B) and 5-fold by ratio (Figure 1C), whereas the amylopectin portion of starch was increased 22.9-fold by weight (Figure 1B) and 3-fold by ratio (Figure 1C). Amylopectin was the major component of starch with approximately 2−3 times the amylose content in the endosperm (Figure 1B). Other metabolites in the endosperm were also increased by weight (6.3-fold for soluble sugars, 4.3-fold for proteins, and 3.6-fold for lipids) (Figure 1B), but their ratios in the endosperm were decreased accordingly until 75 DAF followed by a slight increase at 90 DAF at the expense of amylose in the seeds (Figure 1C).

Identification of Starch and Sucrose Metabolism Genes in Chestnut Seed Transcriptome. RNA was extracted from chestnut seed endosperms collected at 45 and 75 DAF to achieve a broad survey of genes associated with seed development. These RNAs were reverse transcribed into cDNAs and sequenced by an Illumina paired-end sequencing platform. De novo assembly of Chinese chestnut seed transcriptomes generated a total of 56671 nonredundant unigenes (complete transcriptome analysis to be published elsewhere). Pathway-based analysis using KEGG annotation identified 6323 unigenes involved in 302 pathways (data not shown). The default starch and sucrose metabolism pathway contained 141 unigenes including 136 annotated unigenes (Table 2), 2 unannotated unigenes, and 3 unigenes with

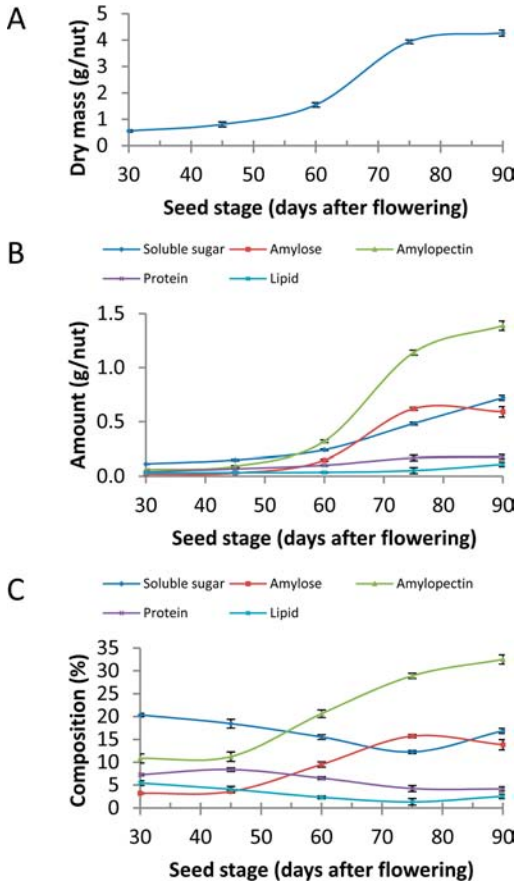

Figure 1. Developmental profiles of dry mass, soluble sugars, amylose, amylopectin, protein, and lipid contents in Chinese chestnut endosperm: (A) dry mass accumulation in developmental nuts; (B) major metabolite accumulation in developmental nuts; (C) composition profiles in developmental nuts (% of dried endosperm).

undetectable RPKM value in the seed transcriptomes (data not shown).

Examination of the unigene list in the KEGG annotated starch and sucrose metabolism pathway revealed that a significant number of known enzymes and transporters were not included in the pathway. Therefore, we manually searched additional unigenes with keywords in the glucosyltransferase family and the whole unigene databases. Glucosyltransferase family contained one unigene (C1Ug17153) coding for glycogenin glucosyltransferase (GLG) [EC.2.4.1.186] and four unigenes (C2Ug23993, C1Ug17740, C1Ug26954 and C1Ug98040) coding for GBSS in the seed transcriptomes (Table 2). Manual search was also used to identify if chestnut transcriptomes contained orthologues of maize Brittle1-type ADPG transporter and Brittle2/Shrunken2-type cytosolic AGP.[15,22,38,39] Keyword search of the annotated chestnut unigene database with "*brittle*" resulted in 4 unigenes related to "*brittle1*" of grape (C1Ug30622, C1Ug33748 and C1Ug29007) and castor bean (C1Ug39668) (Table 2) but none with "*brittle2*." Keyword search with "*shrunken*" did not yield any unigene. Additional keyword search of the annotated unigene database with "isoamylase" and "pullulanase" resulted in the identification of two unigenes for isoamylase-type (C1Ug44378 and C1Ug45762) and three unigenes for pullulanase-type (C1Ug30670, C2Ug20485 and C1Ug22898) of starch debranching enzyme in Chinese chestnuts (Table 2). Manual

DOI: 10.1021/jf505247d
J. Agric. Food Chem. 2015, 63, 929−942

Table 2. Identification and Expression of 152 Starch and Sucrose Metabolism Unigenes in the Chinese Chestnut Endosperm Transcriptomes

unigene ID[a]	C1 (no.)[b]	C1 (RPKM)[c]	C2 (no.)[b]	C2 (RPKM)[c]	C2/C1 (expression)[d]	KEGG annotation [international enzyme name]
C2Ug12839	0	0.00	2	**0.33**		α,α-trehalose-phosphate synthase (UDP-forming) [EC 2.4.1.15]
C2Ug13210	0	0.00	7	**1.39**		pectinesterase [EC 3.1.1.11]
C2Ug13693	0	0.00	18	**3.53**		polygalacturonase [EC 3.2.1.15]
C2Ug16708	0	0.00	15	**2.64**		polygalacturonase [EC 3.2.1.15]
C2Ug17590	0	0.00	2	**0.49**		starch phosphorylase [EC 2.4.1.1]
C2Ug19250	0	0.00	0	**0.00**		hexokinase [EC 2.7.1.1]
C2Ug21630	0	0.00	1	**0.28**		α-1,4-glucan branching enzyme [EC 2.4.1.18]
C2Ug29100	0	0.00	16	**2.59**		polygalacturonase [EC 3.2.1.15]
C2Ug58430	0	0.00	4	**0.79**		trehalose-6-phosphate hydrolase [EC 3.2.1.93]
C2Ug61450	0	0.00	7	**1.38**		UDP-glucose 6-dehydrogenase [EC 1.1.1.22]
C2Ug68900	0	0.00	3	**0.63**		soluble starch synthase [EC 2.4.1.21]
C2Ug80000	0	0.00	3	**0.64**		β-amylase [EC 3.2.1.2]
C2Ug81480	0	0.00	3	**0.61**		PTS, maltose and glucose-specific IIC component
C2Ug82270	0	0.00	4	**0.82**		PTS, trehalose-specific IIC component
C2Ug82280	0	0.00	2	**0.51**		PTS, trehalose-specific IIC component
C2Ug26008	6	0.80	92	11.72	**14.7**	α-amylase/subtilisin inhibitor-like [*Vitis vinifera*]
C2Ug24961	261	8.47	2973	92.20	**10.9**	pectinesterase [EC 3.1.1.11]
C2Ug36490	1	0.15	7	1.00	**6.7**	UDP-glucose 6-dehydrogenase [EC 1.1.1.22]
C2Ug54180	3	0.24	13	1.01	**4.2**	α,α-trehalose-phosphate synthase (UDP-forming) [EC 2.4.1.15]
C2Ug31317	338	13.39	1425	53.93	**4.0**	α-amylase [EC 3.2.1.1]
C2Ug24779	507	29.68	1896	106.05	**3.6**	pectinesterase [EC 3.1.1.11]
C2Ug19146	178	7.05	518	19.59	**2.8**	trehalose-phosphatase [EC 3.1.3.12]
C2Ug23993	40586	994.32	100097	2343.23	**2.4**	granule-bound starch synthase [EC 2.4.1.242]
C1Ug17740	5	0.90	11	1.88	**2.1**	granule-bound starch synthase [EC 2.4.1.242]
C2Ug14771	293	24.53	609	48.72	**2.0**	UDP-glucose 6-dehydrogenase [EC 1.1.1.22]
C1Ug36444	375	12.98	778	25.73	**2.0**	endoglucanase [EC:3.2.1.4]
C2Ug19251	61	4.31	115	7.77	1.8	hexokinase [EC 2.7.1.1]
C1Ug26059	4	0.73	7	1.22	1.7	β-glucosidase [EC 3.2.1.21]
C1Ug44094	2145	46.34	3424	70.68	1.5	starch phosphorylase [EC 2.4.1.1]
C1Ug39221	2820	74.64	4454	112.65	1.5	glucose-1-phosphate adenylyltransferase [EC 2.7.7.27]
C1Ug38157	1721	48.57	2573	69.38	1.4	glucose-6-phosphate isomerase [EC 5.3.1.9]
C1Ug24051	315	22.00	462	30.84	1.4	UDP-glucose 6-dehydrogenase [EC 1.1.1.22]
C2Ug29836	7256	158.82	10398	217.48	1.4	glucose-1-phosphate adenylyltransferase [EC 2.7.7.27]
C2Ug28357	889	17.22	1273	23.56	1.4	trehalose-phosphatase [EC 3.1.3.12]
C1Ug35570	9061	177.54	12900	241.52	1.4	starch phosphorylase [EC 2.4.1.1]
C2Ug19115	776	29.84	1084	39.83	1.3	fructokinase [EC 2.7.1.4]
C2Ug23382	24521	565.36	33715	742.76	1.3	sucrose synthase [EC 2.4.1.13]
C2Ug30240	1494	51.50	1985	65.38	1.3	pectinesterase [EC 3.1.1.11]
C1Ug39534	391	15.24	516	19.22	1.3	hexokinase [EC 2.7.1.1]
C1Ug30240	5456	284.62	7185	358.15	1.3	fructokinase [EC 2.7.1.4]
C1Ug35422	196	7.63	248	9.23	1.2	maltose excess protein 1 [*Malus x domestica*]
C2Ug26944	664	18.29	822	21.64	1.2	soluble starch synthase [EC 2.4.1.21]
C1Ug38445	6201	165.73	7555	192.94	1.2	glucose-1-phosphate adenylyltransferase [EC 2.7.7.27]
C1Ug42386	353	13.03	424	14.96	1.1	α-4-glucanotransferase [EC 2.4.1.25]
C1Ug37665	2416	90.44	2843	101.69	1.1	UDP-glucuronate 4-epimerase [EC 5.1.3.6]
C1Ug42915	2993	71.52	3394	77.50	1.1	phosphoglucomutase [EC 5.4.2.2]
C2Ug19249	45	3.78	51	4.09	1.1	hexokinase [EC 2.7.1.1]
C1Ug37892	428	8.48	465	8.81	1.0	trehalose-phosphatase [EC 3.1.3.12]
C2Ug30776	6064	128.28	6308	127.50	1.0	α-1,4-glucan branching enzyme [EC 2.4.1.18]
C2Ug31571	1844	33.20	1902	32.72	1.0	sucrose-phosphate synthase [EC 2.4.1.14]
C1Ug46204	998	25.19	1019	24.57	1.0	β-glucosidase [EC 3.2.1.21]
C1Ug44205	1459	28.77	1469	27.68	1.0	phosphoglucomutase [EC 5.4.2.2]
C1Ug33458	6077	199.30	6009	188.30	0.9	UTP-glucose-1-phosphate uridylyltransferase [EC 2.7.7.9]
C2Ug32747	473	11.82	461	11.01	0.9	α-4-glucanotransferase [EC 2.4.1.25]
C1Ug41035	412	9.90	393	9.03	0.9	α-1,4-galacturonosyltransferase [EC 2.4.1.43]
C2Ug29276	3727	99.81	3545	90.71	0.9	sucrose synthase [EC 2.4.1.13]
C1Ug44378	1168	25.15	1110	22.84	0.9	isoamylase 1 [EC 3.2.1.68]
C2Ug30790	381	10.68	361	9.67	0.9	soluble starch synthase [EC 2.4.1.21]
C1Ug27848	18	1.60	17	1.45	0.9	UDP-glucuronate 4-epimerase [EC 5.1.3.6]
C1Ug29007	902	33.37	844	29.84	0.9	*brittle1* [*Vitis vinifera*]
C1Ug33748	166	7.89	155	7.04	0.9	*brittle1* [*Vitis vinifera*]
C1Ug40531	1958	53.34	1813	47.20	0.9	hexokinase [EC 2.7.1.1]
C1Ug37149	51	6.00	46	5.17	0.9	α,α-trehalose-phosphate synthase (UDP-forming) [EC 2.4.1.15]
C1Ug35638	833	38.21	741	32.48	0.9	pectinesterase [EC 3.1.1.11]
C1Ug39668	276	8.58	238	7.07	0.8	*brittle1* [*Ricinus communis*]

DOI: 10.1021/jf505247d
J. Agric. Food Chem. 2015, 63, 929−942

Table 2. continued

unigene ID[a]	C1 (no.)[b]	C1 (RPKM)[c]	C2 (no.)[b]	C2 (RPKM)[c]	C2/C1 (expression)[d]	KEGG annotation [international enzyme name]
C1Ug39284	5545	200.21	4753	163.98	0.8	UDP-glucose 6-dehydrogenase [EC 1.1.1.22]
C1Ug30622	119	5.66	102	4.64	0.8	*brittle1* [*Vitis vinifera*]
C1Ug40998	570	10.11	483	8.19	0.8	sucrose-phosphate synthase [EC 2.4.1.14]
C1Ug15639	26	3.84	22	3.10	0.8	β-glucosidase [EC 3.2.1.21]
C1Ug42595	482	15.50	406	12.48	0.8	pectinesterase [EC 3.1.1.11]
C1Ug41899	382	20.69	317	16.41	0.8	fructokinase [EC 2.7.1.4]
C2Ug16554	143	10.13	115	7.78	0.8	UDP-glucuronate 4-epimerase [EC 5.1.3.6]
C1Ug45762	703	15.95	550	11.93	0.7	isoamylase 2 [EC 3.2.1.68]
C1Ug36599	175	13.26	135	9.77	0.7	trehalose-phosphatase [EC 3.1.3.12]
C1Ug38446	182	6.70	140	4.93	0.7	β-glucosidase [EC 3.2.1.21]
C1Ug38663	459	13.27	345	9.53	0.7	α-1,4-Galacturonosyltransferase [EC 2.4.1.43]
C1Ug22898	67	5.53	49	3.86	0.7	pullulanase 1 [EC 3.2.1.41]
C2Ug20485	111	5.94	81	4.14	0.7	pullulanase 1 [EC 3.2.1.41]
C2Ug29274	221	15.13	161	10.53	0.7	sucrose synthase [EC 2.4.1.13]
C1Ug40932	5966	187.57	4332	130.14	0.7	pectinesterase [EC 3.1.1.11]
C1Ug34303	495	17.21	348	11.56	0.7	α-1,4-galacturonosyltransferase [EC 2.4.1.43]
C1Ug38532	277	10.72	184	6.81	0.6	α-1,4-Galacturonosyltransferase [EC 2.4.1.43]
C2Ug29185	823	18.34	513	10.92	0.6	α-4-Glucanotransferase [EC 2.4.1.25]
C1Ug43881	774	23.56	482	14.02	0.6	α-1,4-Galacturonosyltransferase [EC 2.4.1.43]
C2Ug21161	93	9.70	57	5.68	0.6	α,α-Trehalase [EC 3.2.1.28]
C1Ug28970	125	4.40	75	2.52	0.6	ß-Fructofuranosidase [EC 3.2.1.26]
C1Ug44096	3589	102.77	2111	57.76	0.6	α-1,4-Galacturonosyltransferase [EC 2.4.1.43]
C1Ug44159	491	13.07	270	6.87	0.5	α-amylase [EC 3.2.1.1]
C1Ug40350	2360	70.86	1272	36.49	0.5	glucose-6-phosphate isomerase [EC 5.3.1.9]
C1Ug34856	770	27.83	412	14.23	0.5	pectinesterase [EC 3.1.1.11]
C1Ug44802	2227	38.98	1191	19.92	0.5	α-glucosidase [EC 3.2.1.20]
C1Ug30670	139	6.68	71	3.26	0.5	pullulanase 1 [EC 3.2.1.41]
C1Ug44890	5025	51.99	2524	24.95	0.5	α-1,4-galacturonosyltransferase [EC 2.4.1.43]
C1Ug43271	791	20.50	394	9.76	0.5	α-1,4-galacturonosyltransferase [EC 2.4.1.43]
C1Ug31899	124	8.07	61	3.79	0.5	α,α-trehalose-phosphate synthase (UDP-forming) [EC 2.4.1.15]
C1Ug41431	473	13.38	227	6.14	0.5	α-1,4-galacturonosyltransferase [EC 2.4.1.43]
C1Ug41090	3518	137.05	1672	62.24	0.5	UDP-glucuronate 4-epimerase [EC 5.1.3.6]
C2Ug18295	66	8.28	31	3.72	0.4	α,α-trehalase [EC 3.2.1.28]
C1Ug38949	49	7.96	23	3.57	0.4	β-glucosidase [EC 3.2.1.21]
C1Ug26057	15	1.41	7	0.63	0.4	β-glucosidase [EC 3.2.1.21]
C1Ug35697	336	12.53	154	5.49	0.4	α-1,4-galacturonosyltransferase [EC 2.4.1.43]
C1Ug35708	584	19.21	267	8.39	0.4	hexokinase [EC 2.7.1.1]
C1Ug41904	688	14.51	308	6.21	0.4	sucrose-phosphate synthase [EC 2.4.1.14]
C1Ug38374	964	24.10	425	10.15	0.4	α-1,4-galacturonosyltransferase [EC 2.4.1.43]
C2Ug10408	32	6.49	14	2.71	0.4	α,α-trehalase [EC 3.2.1.28]
C1Ug20270	7	1.41	3	0.58	0.4	α,α-trehalase [EC 3.2.1.28]
C1Ug41228	1903	43.98	807	17.82	0.4	soluble starch synthase [EC 2.4.1.21]
C1Ug15756	10	1.39	4	0.53	0.4	β-fructofuranosidase [EC 3.2.1.26]
C1Ug41886	18711	447.14	6903	157.63	0.4	sucrose synthase [EC 2.4.1.13]
C1Ug31046	118	9.65	43	3.36	0.3	UDP-glucuronate 4-epimerase [EC 5.1.3.6]
C1Ug37482	9	1.70	3	0.54	0.3	sucrose synthase [EC 2.4.1.13]
C1Ug44475	581	13.67	192	4.32	0.3	β-fructofuranosidase [EC 3.2.1.26]
C1Ug46084	1931	44.18	602	13.16	0.3	α-glucosidase [EC 3.2.1.20]
C1Ug42679	772	27.90	230	7.94	0.3	β-fructofuranosidase [EC 3.2.1.26]
C1Ug39763	2867	54.83	783	14.31	0.3	α,α-trehalose-phosphate synthase (UDP-forming) [EC 2.4.1.15]
C1Ug37147	130	5.10	34	1.28	0.3	α,α-trehalose-phosphate synthase (UDP-forming) [EC 2.4.1.15]
C1Ug19275	32	3.43	6	0.61	0.2	sucrose synthase [EC 2.4.1.13]
C1Ug25979	110	13.04	19	2.15	0.2	sucrose synthase [EC 2.4.1.13]
C1Ug36303	1693	35.42	287	5.74	0.2	trehalose-phosphatase [EC 3.1.3.12]
C1Ug40923	122	4.57	20	0.72	0.2	β-glucosidase [EC 3.2.1.21]
C1Ug22044	473	26.20	77	4.08	0.2	pectinesterase [EC 3.1.1.11]
C1Ug42785	13	2.14	2	0.31	0.1	hexokinase [EC 2.7.1.1]
C1Ug45378	130	5.58	19	0.78	0.1	sucrose synthase [EC 2.4.1.13]
C1Ug31555	149	4.69	21	0.63	0.1	β-glucosidase [EC 3.2.1.21]
C1Ug44316	169	10.32	22	1.28	0.1	α,α-trehalase [EC 3.2.1.28]
C1Ug10256	16	2.89	2	0.35	0.1	sucrose synthase [EC 2.4.1.13]
C1Ug31955	137	4.46	17	0.53	0.1	sucrose synthase [EC 2.4.1.13]
C1Ug22933	17	1.71	2	0.19	0.1	pectinesterase [EC 3.1.1.11]
C1Ug44317	198	10.70	21	1.08	0.1	α,α-trehalase [EC 3.2.1.28]
C1Ug43056	1683	27.54	137	2.14	0.1	β-1,4-D-xylan synthase [EC 2.4.2.24]
C1Ug29708	38	4.00	3	0.30	0.1	pectinesterase [EC 3.1.1.11]

DOI: 10.1021/jf505247d
J. Agric. Food Chem. 2015, 63, 929−942

Table 2. continued

unigene ID[a]	C1 (no.)[b]	C1 (RPKM)[c]	C2 (no.)[b]	C2 (RPKM)[c]	C2/C1 (expression)[d]	KEGG annotation [international enzyme name]
C1Ug29709	32	4.18	2	0.25	**0.1**	pectinesterase [EC 3.1.1.11]
C1Ug32041	287	9.90	17	0.56	**0.1**	α-1,4-galacturonosyltransferase [EC 2.4.1.43]
C1Ug29710	19	2.36	1	0.12	**0.1**	pectinesterase [EC 3.1.1.11]
C1Ug26954	29	**2.34**	1	0.08	0.0	granule-bound starch synthase [EC 2.4.1.242]
C1Ug98040	33	**3.08**	1	0.09	0.0	granule-bound starch synthase [EC 2.4.1.242]
C1Ug10451	10	**1.40**	0	0.00	0.0	pectinesterase [EC 3.1.1.11]
C1Ug16890	2	**0.43**	0	0.00	0.0	β-amylase [EC 3.2.1.2]
C1Ug17153	25	**2.52**	0	0.00	0.0	glycogenin glucosyltransferase [EC 2.4.1.186]
C1Ug18181	5	**0.96**	0	0.00	0.0	pectinesterase [EC 3.1.1.11]
C1Ug18182	12	**1.22**	0	0.00	0.0	pectinesterase [EC 3.1.1.11]
C1Ug18383	2	**0.57**	0	0.00	0.0	starch phosphorylase [EC 2.4.1.1]
C1Ug19276	2	**0.44**	0	0.00	0.0	sucrose synthase [EC 2.4.1.13]
C1Ug22754	17	**2.24**	0	0.00	0.0	pectinesterase [EC 3.1.1.11]
C1Ug24817	9	**0.95**	0	0.00	0.0	β-glucosidase [EC 3.2.1.21]
C1Ug25204	8	**1.64**	0	0.00	0.0	α-1,4-galacturonosyltransferase [EC 2.4.1.43]
C1Ug25512	25	**2.73**	0	0.00	0.0	β-glucosidase [EC 3.2.1.21]
C1Ug25513	11	**1.77**	0	0.00	0.0	β-glucosidase [EC 3.2.1.21]
C1Ug26058	5	**0.83**	0	0.00	0.0	β-glucosidase [EC 3.2.1.21]
C1Ug31121	19	**1.35**	0	0.00	0.0	gructokinase [EC 2.7.1.4]
C1Ug75300	5	**0.80**	0	0.00	0.0	α-amylase [EC 3.2.1.1]
C1Ug88270	3	**0.86**	0	0.00	0.0	β-fructofuranosidase [EC 3.2.1.26]

[a]Unigene ID highlighted with yellow and green colors represent unigenes identified from "glycosyltransferases" categories according to the KEGG protein database, and manually searched, respectively. [b]The numbers under the "C1 (no.)" and "C2 (no.)" columns represent the number of total reads in each unigene identified in the chestnut transcriptomes. [c]Highlighted RPKM values under the "C1 (RPKM)" and "C2 (RPKM)"columns represent those almost exclusively expressed in the nuts collected 45 and 75 DAF, respectively. [d]Highlighted RPKM values under the "C2/C1 (expression)" column represent those 58 unigenes that showed ≥2-fold of expression difference between the 45 and 75 DAF seed stages.

search using keyword "maltose" identified one unigene (C1Ug35422) in the unigene database putatively coding for maltose exporter (Mex1), a transporter important for starch degradation.[40] Finally, one α-amylase/subtilisin inhibitor-like unigene (C2Ug26008), an orthologue of grape wine, was found in the 75 DAF transcriptome (Table 2). Taken together, 152 annotated unigenes with detectable RPKM values involved in starch and sucrose metabolism were identified from the Chinese chestnut transcriptomes (Table 2).

Digital Analysis of Differentially Expressed Genes in Two Seed Developmental Stages. The RPKM (reads per kb per million mapped reads) method was used to identify unigenes with significant differences in expression levels between the two libraries. A total of 1537 unigenes showed ≥2-fold change (complete transcriptome analysis to be published elsewhere). Among the 152 unigenes coding for starch and sucrose metabolism, 58 unigenes showed ≥2-fold of expression difference between the 45 and 75 DAF seeds including 11 up- and 47 down-regulated unigenes (Table 2). In addition, transcripts for 18 unigenes were almost exclusively detected in 45 DAF seeds whereas 15 unigene transcripts were exclusively detected in 75 DAF seeds as judged by apparent RPKM value in their respective nut stages (Table 2).

Digital Analysis of Major Expressed Genes in Two Seed Developmental Stages. Among the 152 unigenes discovered in starch and sucrose metabolism pathway, 13 unigenes from the 45 DAF cDNA library and 14 unigenes from the 75 DAF cDNA library had RPKM value over 100 (Table 3). Among them, 11 of the unigenes with PRKM values over 100 were presented in both 45 and 75 DAF cDNA libraries (C2Ug23993, C1Ug30240, C1Ug33458, C1Ug35570, C1Ug38445, C1Ug39284, C1Ug40932, C1Ug41886, C2Ug23382, C2Ug29836 and C2Ug30776) (Table 3). C2Ug23993 had the highest RPKM value at 994 and 2343 in the 45 and 75 DFA cDNA libraries, respectively. C2Ug23993 putatively coded for a GBSS, the most abundant transcript identified in the endosperms.

Classification of Starch and Sucrose Metabolism Genes in Chestnut Seed Transcriptome. The 152 starch and sucrose metabolism unigenes identified from the chestnut transcriptomes coded for 37 protein families (Table 4). The gene families coding for pectinesterase, α-1,4-galacturonosyltransferase, β-glucosidase, and SuS had the most unigenes with 17, 13, 12, and 11 unigenes identified from the transcriptomes, respectively (Table 4). These unigenes coded for well-known components in the starch and sucrose metabolism pathway, including 1 unigene for GLG, 1 unigene for Mex1, 4 unigenes for Brittle1-type ANT, 3 unigenes for AGP, 8 unigenes for SS (4 for SSS and 4 for GBSS), 2 unigenes for SBE, 5 unigenes for SDBE (2 for isoamylase and 3 for pullulanase), 11 unigenes for sucrose synthase (SuS), 3 unigenes for sucrose-phosphate synthase (SuPS), 3 unigenes for α-amylase (α-AMY), 2 unigenes for β-AMY, and 4 unigenes for starch phosphorylase (SP) (Table 4). These families of unigenes (red color) were mapped onto the generalized starch and sucrose metabolism pathway generated by KEGG protein database (black color) (Figure 2). Among the identified unigenes, 23 unigenes coding for AGP, ANT, GLG, SSS, GBSS, SBE, and SDBE were involved in starch biosynthesis, whereas 11 unigenes coding for AMY, SP, Mex1, and α-amylase/subtilisin inhibitor were involved in starch degradation (Figure 2). A total of 14 unigenes coding for SuS and SuPS were involved in sucrose metabolism and 9 unigenes coding for enzymes to convert sucrose into β-D-fructose (Figure 2). Ten unigenes converted UDP-glucose into α-D-glucose, whereas 13 unigenes were used to convert cellulose into β-D-glucose (Figure 2). In addition, 40 unigenes starting from UDP-glucose were committed to pectin and pectate biosynthesis (Figure 2). Finally, 11 unigenes starting from UDP-glucose were committed to trehalose biosynthesis and 6 unigenes encoding trehalase for pectate hydrolysis to glucose (Figure 2).

DOI: 10.1021/jf505247d
J. Agric. Food Chem. 2015, 63, 929−942

Table 3. Digital Expression Analysis of Major Starch and Sucrose Metabolism Genes Expressed in Chinese Chestnut Endosperm (RPKM > 50)

unigene ID	C1 (no.)[a]	C1 (RPKM)[b]	C2 (no.)[a]	C2 (RPKM)[b]	KEGG annotation [international enzyme name]
C2Ug23993	40586	994.32	100097	2343.23	granule-bound starch synthase [EC 2.4.1.242]
C2Ug23382	24521	565.36	33715	742.76	sucrose synthase [EC 2.4.1.13]
C1Ug41886	18711	447.14	6903	157.63	sucrose synthase [EC 2.4.1.13]
C1Ug30240	5456	284.62	7185	358.15	fructokinase [EC 2.7.1.4]
C1Ug39284	5545	200.21	4753	163.98	UDP-glucose 6-dehydrogenase [EC 1.1.1.22]
C1Ug33458	6077	199.30	6009	188.30	UTP-glucose-1-phosphate uridylyltransferase [EC 2.7.7.9]
C1Ug40932	5966	187.57	4332	130.14	pectinesterase [EC 3.1.1.11]
C1Ug35570	9061	177.54	12900	241.52	starch phosphorylase [EC 2.4.1.1]
C1Ug38445	6201	165.73	7555	192.94	glucose-1-phosphate adenylyltransferase [EC 2.7.7.27]
C2Ug29836	7256	158.82	10398	217.48	glucose-1-phosphate adenylyltransferase [EC 2.7.7.27]
C2Ug30776	6064	128.28	6308	127.50	α-1,4-glucan branching enzyme [EC 2.4.1.18]
C1Ug41090	3518	137.05	1672	62.24	UDP-glucuronate 4-epimerase [EC 5.1.3.6]
C1Ug44096	3589	102.77	2111	57.76	α-1,4-galacturonosyltransferase [EC 2.4.1.43]
C2Ug29276	3727	99.81	3545	90.71	sucrose synthase [EC 2.4.1.13]
C1Ug37665	2416	90.44	2843	101.69	UDP-glucuronate 4-epimerase [EC 5.1.3.6]
C1Ug39221	2820	74.64	4454	112.65	glucose-1-phosphate adenylyltransferase [EC 2.7.7.27]
C1Ug42915	2993	71.52	3394	77.50	phosphoglucomutase [EC 5.4.2.2]
C1Ug40350	2360	70.86	1272	36.49	glucose-6-phosphate isomerase [EC 5.3.1.9]
C1Ug39763	2867	54.83	783	14.31	α,α-trehalose-phosphate synthase (UDP-forming) [EC 2.4.1.15]
C1Ug40531	1958	53.34	1813	47.20	hexokinase [EC 2.7.1.1]
C1Ug44890	5025	51.99	2524	24.95	α-1,4-galacturonosyltransferase [EC 2.4.1.43]
C2Ug30240	1494	51.50	1985	65.38	pectinesterase [EC 3.1.1.11]
C1Ug38157	1721	48.57	2573	69.38	glucose-6-phosphate isomerase [EC 5.3.1.9]
C1Ug44094	2145	46.34	3424	70.68	starch phosphorylase [EC 2.4.1.1]
C2Ug24779	507	29.68	1896	106.05	pectinesterase [EC 3.1.1.11]
C2Ug31317	338	13.39	1425	53.93	α-amylase [EC 3.2.1.1]
C2Ug24961	261	8.47	2973	92.20	pectinesterase [EC 3.1.1.11]
summary	**173183**	**4514.09**	**238842**	**5946.77**	

[a]The numbers under "C1 (no.)" and "C2 (no.)" columns represent the number of total reads in each unigene identified in the chestnut transcriptomes. [b]The numbers under "C1 (RPKM)" and "C2 (RPKM)"columns represent those most abundantly expressed unigenes with at least 50 RPKM in at least one of the two nut stages collected 45 and 75 DAF.

Digital Expression Analysis of Starch and Sucrose Metabolism Gene Families in Chestnut Seed Transcriptome. RPKM values of individual unigenes were pooled together according to the classified gene families (Table 4). Thirteen families of unigenes had RPKM values >100 in both 45 and 75 DAF seed transcriptomes (Table 4). The most abundantly expressed unigenes represented by total RPKM values were SuS (1159), GBSS (1001), pectinesterase (403), and AGP (399) in 45 DAF seed transcriptome, but the order of the abundance of expression was changed to GBSS (2345), SuS (1007), AGP (523), and pectinesterase (459) in 75 DAF seed transcriptome (Table 4). Soluble SS, isoamylase- and pullulanase-type SDBE, brittle1-type ANT, and Mex1 had <100 RPKM in either transcriptome, but SP had >200 RPKM in both seed stages (Table 4). GLG RPKM was extremely low in 45 DFA and undetectable in 75 DAF transcriptomes (Table 4). In addition, three unigenes were identified in the nut transcriptomes, which coded for phosphotransferase system (PTS), including one unigene for maltose- and glucose-specific IIC component and two unigenes for trehalose-specific IIC component.

Quantitative Analysis of Selected Genes Involved in Starch and Sucrose Pathways. We used qPCR to evaluate the expression profiles of 11 genes involved in starch and sucrose metabolism pathway as well as 10 other genes predicted to be important in chestnut tree carbohydrate metabolism using primers designed according to the sequences of the unigenes (Table 1). The qPCR results showed that five of these genes were significantly up-regulated and peaked at 75 DAF with >2-fold of increases in mRNA levels compared to those at 30 DAF (Figure 3E, C1Ug38445; 3H, C1Ug41228; 3Q, C2Ug26944; 3S, C2Ug29836; and 3T, C2Ug30790). These five genes were important enzymes for starch synthesis because they coded for AGP large subunit (C1Ug38445) and small subunit (C2Ug29836), GBSS2 (C1Ug41228), SSS1 (C2Ug26944), and SSS4 (C2Ug30790) (Table 1). Twelve of the genes were down-regulated during seed development (Figure 3A, C1Ug19275; 3B, C1Ug22044; 3C, C1Ug31955; 3D, C1Ug36303; 3F, C1Ug39763; 3G, C1Ug41090; 3I, C1Ug41886; 3J, C1Ug42679; 3K, C1Ug43056; 3M, C1Ug46084; 3N, C2Ug23382; and 3R, C2Ug29276). Five of the down-regulated genes coded for sucrose synthase (C1Ug41886, C1Ug19275, C2Ug23382, C2Ug29276, and C1Ug31955) (Table 1).

Correlation between Gene Expression Levels and Starch Content in Chestnut Seeds. The correlation between gene expression levels and starch content was performed by SPSS software (Table 5). Expression levels of five genes were highly correlated with the amount of starch including both amylose and amylopectin with correlation

DOI: 10.1021/jf505247d
J. Agric. Food Chem. 2015, 63, 929−942

Table 4. Classification and Digital Expression Analysis of Unigenes Coding for 37 Protein Families in Starch and Sucrose Metabolism in Chinese Chestnut Endosperm Transcriptomes

family	KEGG annotation [international enzyme name][a]	unigene no.[b]	C1 (no.)[c]	C1 (RPKM)[d]	C2 (no.)[c]	C2 (RPKM)[d]
1	1,4-α-glucan branching enzyme [EC 2.4.1.18] (SBE)	2	6064	128.28	6309	127.79
2	1,4-β-D-xylan synthase [EC 2.4.2.24]	1	1683	27.54	137	2.14
3	4-α-glucanotransferase [EC 2.4.1.25]	3	1649	43.20	1398	36.89
4	α,α-trehalase [EC 3.2.1.28]	6	565	46.91	148	15.06
5	α,α-trehalose-phosphate synthase (UDP-forming) [EC 2.4.1.15]	6	3175	74.24	939	25.89
6	α-1,4-galacturonosyltransferase [EC 2.4.1.43]	13	13890	311.48	7604	165.75
7	α-amylase [EC 3.2.1.1]	3	834	27.26	1695	60.80
8	**α-amylase/subtilisin inhibitor [*Vitis vinifera*]**	1	6	0.80	92	11.72
9	**adenylate transporter (brittle1 type)**	4	1463	55.50	1339	48.58
10	α-glucosidase [EC 3.2.1.20]	2	4158	83.16	1793	33.08
11	β-amylase [EC 3.2.1.2]	2	2	0.43	3	0.64
12	β-fructofuranosidase [EC 3.2.1.26]	5	1491	48.22	501	15.31
13	β-glucosidase [EC 3.2.1.21]	12	1595	61.36	1259	39.37
14	endoglucanase [EC 3.2.1.4]	1	375	12.98	778	25.73
15	fructokinase [EC 2.7.1.4]	4	6633	336.52	8586	414.39
16	glucose-1-phosphate adenylyltransferase [EC 2.7.7.27] (AGP)	3	16277	399.20	22407	523.07
17	glucose-6-phosphate isomerase [EC 5.3.1.9]	2	4081	119.43	3845	105.88
18	**glycogenin glucosyltransferase [EC 2.4.1.186] (GLG)**	1	25	2.52	0	0.00
19	**granule-bound starch synthase [EC 2.4.1.242] (GBSS)**	4	40653	1000.64	100110	2345.28
20	hexokinase [EC 2.7.1.1]	7	3052	98.02	2764	86.98
21	**isoamylase [EC 3.2.1.68] (SBDE)**	2	1871	41.10	1660	34.76
22	**naltose excess protein 1 [*Malus* × *domestica*] (Mex1)**	1	196	7.63	248	9.23
23	pectinesterase [EC 3.1.1.11]	17	10936	403.03	12837	459.28
24	phosphoglucomutase [EC 5.4.2.2]	2	4452	100.30	4863	105.18
25	polygalacturonase [EC 3.2.1.15]	3	0	0.00	49	8.77
26	PTS system, maltose- and glucose-specific IIC component	1	0	0.00	3	0.61
27	PTS system, trehalose-specific IIC component	2	0	0.00	6	1.32
28	**pullulanase [EC 3.2.1.41] (SDBE)**	3	317	18.15	201	11.27
29	soluble starch synthase [EC 2.4.1.21] (SSS)	4	2948	72.96	1993	49.76
30	starch phosphorylase [EC 2.4.1.1] (SP)	4	11208	224.44	16326	312.68
31	sucrose synthase [EC 2.4.1.13] (*SuS)	11	47616	1158.98	44390	1006.60
32	sucrose-phosphate synthase [EC 2.4.1.14] (SuPS)	3	3102	57.82	2693	47.12
33	trehalose-6-phosphate hydrolase [EC 3.2.1.93]	1	0	0.00	4	0.79
34	trehalose-phosphatase [EC 3.1.3.12]	5	3363	81.43	2678	67.47
35	UDP-glucose 6-dehydrogenase [EC 1.1.1.22]	5	6154	246.90	5838	245.92
36	UDP-glucuronate 4-epimerase [EC 5.1.3.6]	5	6213	248.87	4690	176.52
37	UTP-glucose-1-phosphate uridylyltransferase [EC 2.7.7.9] (UGP)	1	6077	199.30	6009	188.30
	summary	**152**	**212124**	**5738.60**	**266195**	**6809.95**

[a]Gene families 18 and 19 were identified from "glycosyltransferases" categories according to the KEGG protein database; gene families 8, 9, 21, 22, and 28 were identified by keyword search of unigene database manually. [b]The numbers under "unigene no." column represent the total number of unigenes in each enzyme family identified in the chestnut transcriptomes. [c]The numbers under the "C1 (no.)" and "C2 (no.)" columns represent the total reads in each enzyme family identified in the chestnut transcriptomes. [d]The numbers under "C1 (RPKM)" and "C2 (RPKM)" columns represent the total values of unigene RPKM in each enzyme families identified in the chestnut transcriptomes.

coefficients >0.9 (boldfaced in Table 5). These five genes (C1Ug38445, C1Ug41228, 2Ug26944, C2Ug29836, and C2Ug30790) were identical to those genes for which mRNA levels were up-regulated in later stage of nuts (75 DAF) at least 2-fold relative to those in early stage of nuts (30 DAF) (Figure 3E, C1Ug38445; 3H, C1Ug41228; 3Q, C2Ug26944; 3S, C2Ug29836; and 3T, C2Ug30790). Similarly, all down-regulated genes were negatively correlated with starch content in the nuts (Table 5 vs Figure 3).

DISCUSSION

Chinese chestnuts are a major source of starch, but little has been reported about starch biosynthesis in the seeds. To our knowledge, no prior research has been conducted at the biochemical and molecular levels of starch biosynthesis in chestnuts. Our objectives in this study were to analyze composition profiles and characterize genes involved in starch biosynthesis in developing nuts. As expected, starch constituted approximately half of the dry mass including 33% of amylopectin and 14% of amylose in the seed endosperm collected 90 DAF. In addition, 17% of the dry mass was soluble sugars, but there were only 4% protein and <3% lipid in the nuts. The Chinese chestnut cultivar 'Yanshanzaofeng' used in this study contained less starch than most of the other Chinese chestnut cultivars.[3] The endosperm from this Chinese chestnut contained approximately 15% less starch and 1.5% more lipids than Portuguese chestnuts.[1] The ratio of amylose to amylopectin in Chinese chestnut was similar to that of

DOI: 10.1021/jf505247d
J. Agric. Food Chem. 2015, 63, 929−942

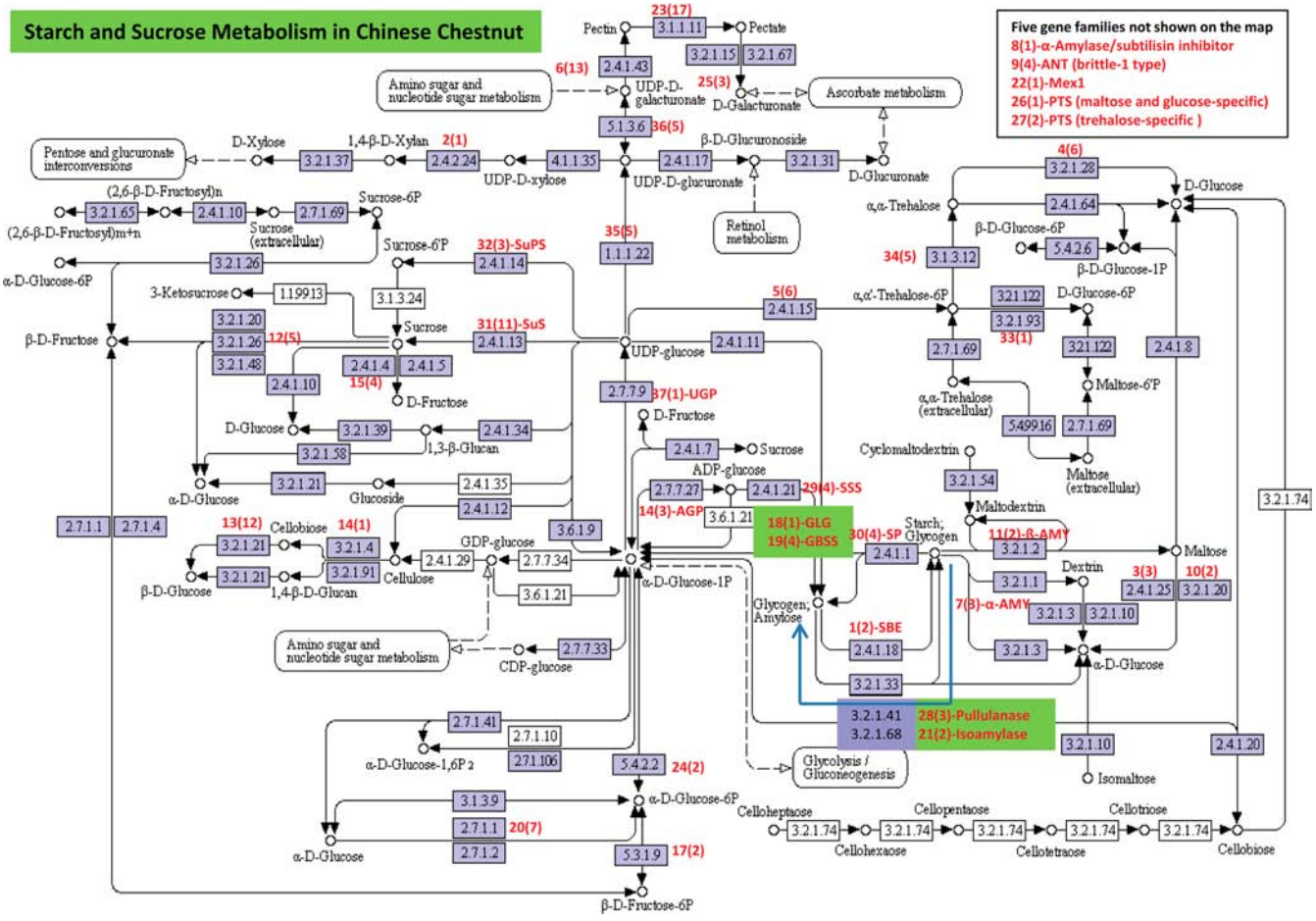

Figure 2. Starch and sucrose metabolism pathway in Chinese chestnut endosperm. The map represents a general starch and sucrose metabolism pathway and was generated from the KEGG pathway, which outlines the steps involved in starch and sucrose metabolism. The numbers in the rectangle represent the standardized international enzyme names in the pathway. The numbers next to the rectangle (in red) represent the family of enzymes corresponding to those in Table 4 followed by the total number of unigenes in that family discovered in the seed transcriptomes (in parentheses).

Portuguese chestnut.[4] The compositions of soluble sugars in Chinese chestnut were not determined as those in Portuguese chestnut.[5]

We coupled transcriptomic analysis with qPCR assays for selected genes to understand the global gene expression involved in starch and sucrose metabolism in Chinese chestnuts. Transcriptomic technology identified 152 unigenes in the starch and sucrose metabolism pathway and classified them into 37 protein families in which pectinesterase, α-1,4-galacturonosyltransferase, β-glucosidase, and SuS families had the most unigenes from the transcriptomes. We used this novel information to construct a general view of starch and sucrose metabolism in Chinese chestnuts (Figure 2). These unigenes coded for well-known components in starch biosynthesis (one unigene for GLG, four unigenes for Brittle1 type ANT, three unigenes for AGP, eight unigenes for SS, two unigenes for SBE, five unigenes for SDBE) and starch degradation (three unigenes for α-AMY, two unigenes for β-AMY, four unigenes for SP, one unigene for Mex1). Sucrose metabolism contained 11 unigenes for SuS, three unigenes for SuPS, four unigenes for fructokinase, and five unigenes for β-fructofuranosidase. In addition, 10 unigenes converted UDP-glucose into α-D-glucose and 13 unigenes converted cellulose into β-D-glucose (Figure 2). Pectin and pectate biosynthesis from UDP-glucose contained 40 unigenes in the transcriptomes. Finally, trehalose contained 11 unigenes for its biosynthesis from UDP-glucose and 6 unigenes for its hydrolysis to glucose (Figure 2). These high numbers of unigenes for glucose and fructose metabolism may represent its property of the nuts having a sweet taste, whereas significant numbers of unigenes for trehalose metabolism may represent the nuts being able to withstand prolonged periods of desiccation. Because there is a limitation of using bacterially derived KEGG maps for unigene annotation, it is possible that more unigenes could be identified in Chinese chestnut transcriptomes using plant-specific software such as MapMan and MetaCyc in the future.

Plant starches are synthesized by a series of enzymatic reactions.[41] Two major starch biosynthesis pathways have been proposed in plants based on the subcellular localization of generating ADPG, the major if not the sole sugar donor for starch biosynthesis. In cereal endosperm such as maize (*Zea mays*),[16] ADPG is mainly synthesized in the cytosol[42] by cytosolic AGP encoded by *brittle2* and *shrunken2* genes.[15,38] ADPG is transported into amyloplasts by brittle1 ADPG transporter.[15,22,39,43] In other plant tissues such as potato tubers, *Arabidopsis* leaves, and pea embryos, ADPG is mainly synthesized in the plastids by plastidic AGP and ANT is mainly used to exchange ATP/ADP across plastid envelopes.[12,44] Adenylate transporters in these tissues are probably divergent from maize brittle1 ADPG transporter because maize brittle1

DOI: 10.1021/jf505247d
J. Agric. Food Chem. 2015, 63, 929−942

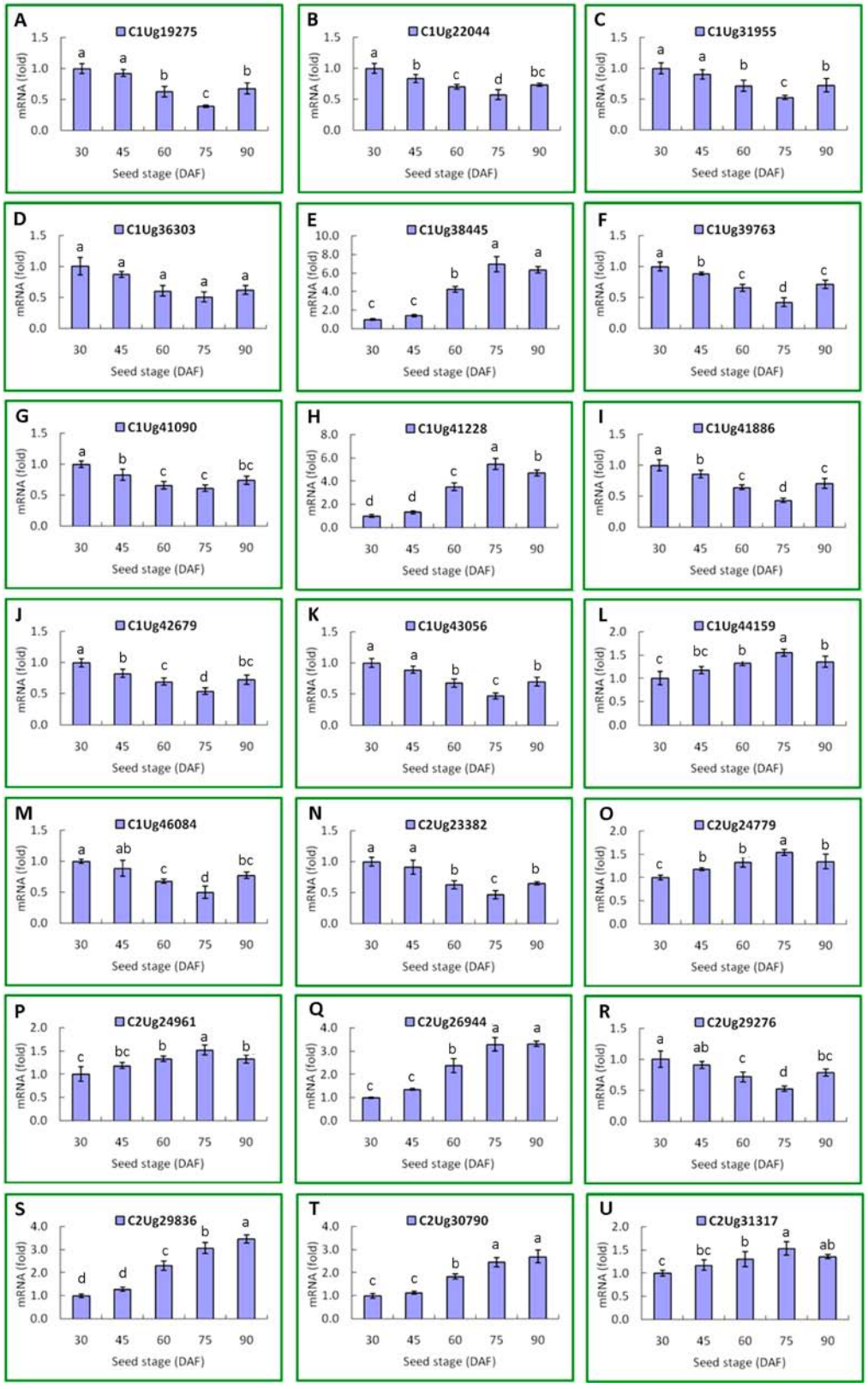

Figure 3. Expression profiles of starch and sucrose metabolism genes in Chinese chestnut endosperm: (A) C1Ug19275 (sucrose synthase [EC 2.4.1.13]); (B) C1Ug22044 (pectinesterase [EC 3.1.1.11]); (C) C1Ug31955 (sucrose synthase [EC 2.4.1.13]); (D) C1Ug36303 (trehalose-phosphatase [EC 3.1.3.12]); (E) C1Ug38445 (ADP-glucose pyrophosphorylase, large subunit [EC 2.7.7.27]); (F) C1Ug39763 (α,α-trehalose-phosphate synthase [EC 2.4.1.15]; (G) C1Ug41090 (UDP-glucuronate 4-epimerase [EC 5.1.3.6]); (H) C1Ug41228 (soluble starch synthase [EC 2.4.1.21]); (I) C1Ug41886 (sucrose synthase [EC 2.4.1.13]); (J) C1Ug42679 (β-fructofuranosidase [EC 3.2.1.26]); (K) C1Ug43056 (β-1,4-D-xylan synthase [EC 2.4.2.24]); (L) C1Ug44159 (α-amylase [EC 3.2.1.1]); (M) C1Ug46084 (α-glucosidase [EC 3.2.1.20]); (N) C2Ug23382 (sucrose synthase [EC 2.4.1.13]); (O) C2Ug24779 (pectinesterase [EC 3.1.1.11]); (P) C2Ug24961 (pectinesterase [EC 3.1.1.11]); (Q) C2Ug26944 (soluble starch synthase [EC 2.4.1.21]); (R) C2Ug29276 (sucrose synthase [EC 2.4.1.13]); (S) C2Ug29836 (ADP-glucose pyrophosphorylase,

DOI: 10.1021/jf505247d
J. Agric. Food Chem. 2015, 63, 929−942

Figure 3. continued

small subunit [EC 2.7.7.27]); (T) C2Ug30790 (soluble starch synthase [EC 2.4.1.21]); (U) C2Ug31317 (α-amylase [EC 3.2.1.1]). The mRNA levels were quantified by qPCR using total RNA from five seed developmental stages. The relative abundance of mRNA levels at 30 DAF was set at 1.0. qPCR was performed in triplicates by SYBR Green qPCR assay using *EF1A* gene as the reference gene. The mean and SD from triplicates are presented. The lower case letters above the columns represent mRNA levels significantly different at $P < 0.05$.

Table 5. Correlation between Gene Expression Levels and Starch Content in Chinese Chestnut Endosperm

ID[a]	unigene	annotation	starch (amylose)[b]	starch (amylopectin)[b]
A	C1Ug19275	sucrose synthase [EC 2.4.1.13]	−0.808	−0.725
B	C1Ug22044	pectinesterase [EC 3.1.1.11]	−0.755	−0.683
C	C1Ug31955	sucrose synthase [EC 2.4.1.13]	−0.832	−0.755
D	C1Ug36303	trehalose-phosphatase [EC 3.1.3.12]	−0.802	−0.758
E	**C1Ug38445**	**ADP-glucose pyrophosphorylase, large subunit [EC 2.7.7.27]**	**0.953***	**0.928***
F	C1Ug39763	α,α-trehalose-phosphate synthase [EC 2.4.1.15	−0.781	−0.690
G	C1Ug41090	UDP-glucuronate 4-epimerase [EC 5.1.3.6]	−0.670	−0.610
H	**C1Ug41228**	**soluble starch synthase [EC 2.4.1.21]**	**0.936***	**0.901***
I	C1Ug41886	sucrose synthase [EC 2.4.1.13]	−0.773	−0.685
J	C1Ug42679	β-fructofuranosidase [EC 3.2.1.26]	−0.762	−0.687
K	C1Ug43056	β-1,4-D-xylan synthase [EC 2.4.2.24]	−0.819	−0.740
L	C1Ug44159	α-amylase [EC 3.2.1.1]	0.845	0.777
M	C1Ug46084	α-glucosidase [EC 3.2.1.20]	−0.729	−0.631
N	C2Ug23382	sucrose synthase [EC 2.4.1.13]	−0.824	−0.762
O	C2Ug24779	pectinesterase [EC 3.1.1.11]	0.823	0.754
P	C2Ug24961	pectinesterase [EC 3.1.1.11]	0.803	0.733
Q	**C2Ug26944**	**soluble starch synthase [EC 2.4.1.21]**	**0.947***	**0.938***
R	C2Ug29276	sucrose synthase [EC 2.4.1.13]	−0.760	−0.663
S	**C2Ug29836**	**ADP-glucose pyrophosphorylase, small subunit [EC 2.7.7.27]**	**0.942***	**0.954***
T	**C2Ug30790**	**soluble starch synthase [EC 2.4.1.21]**	**0.957***	**0.965****
U	C2Ug31317	α-amylase [EC 3.2.1.1]	0.861	0.799

[a]Bolded ID, unigene, and annotations represent those genes showing a positive correlation between their mRNA levels and starch content in the chestnuts. [b]"*" and "**"after the correlation coefficients represent positive correlation between their mRNA levels and starch content in the chestnuts differently at $P < 0.05$ and $P < 0.01$, respectively.

antibodies did not recognize any protein in a number of tissues as well as maize endosperm suspension cultured cells.[45,46] In Chinese chestnut transcriptomes, a keyword search of the annotated unigene database with "*brittle*" resulted in four unigenes related to "*brittle1*" of grape and castor bean but none with "*brittle2*." A keyword search with "*shrunken*" did not yield any unigenes. These results suggest that most if not all AGP resides inside the amyloplasts in Chinese chestnut endosperm cells and that chestnut brittle1 orthologues may function in ATP/ADP transport instead of ADPG transport into amyloplasts. This is the same biochemical mechanism used by *Arabidopsis* leaves and potato tubers.[12,44,47] The fact that high levels of gene expression related to starch degradation (α-AMY, β-AMY, SP, Mex1) were detected in the transcriptomes suggests that starch degradation is probably an active process to ensure sweetness of chestnuts upon harvest.

Digital expression analysis indicated that 13 families of unigenes had RPKM values >100 in both 45 and 75 DAF seed transcriptomes. The most abundantly expressed unigenes represented by total RPKM values were SuS (1159), GBSS (1001), pectinesterase (403), and AGP (399) in 45 DAF seed transcriptome, but the order of the abundance of expression was changed to GBSS (2345), SuS (1007), AGP (523), and pectinesterase (459) in 75 DAF seed transcriptome (Table 4). The altered key gene expression implies that sucrose metabolism is more active in the earlier stages of nut development and that starch accumulation becomes more predominant in the later stages. It is interesting to note that soluble SS, isoamylase- and pullulanase-type SDBE, brittle1 type ANT and GLG had <100 RPKM in either transcriptome but SP had >200 RPKM in both seed stages. These observations suggest that SSS, SBDE, ANT, and GLG are possibly limiting factors for starch biosynthesis, and SP is the major enzyme for starch degradation in the seeds. Future experiments will be needed to characterize the significance of PTS genes discovered from this transcriptome analysis.

Digital expression analysis showed that 58 of 152 unigenes in starch and sucrose metabolism exhibited ≥2-fold of expression difference between the two seed stages. Transcripts for 18 unigenes were almost exclusively detected in 45 DAF seeds, whereas 15 unigene transcripts were exclusively detected in 75 DAF seeds. Additional experiments will be required to understand the physiological significance of these stage-specific unigenes in the chestnuts. The expression profiles of 21 unigenes putatively coding for major enzymes in starch and sucrose metabolism were confirmed by qPCR using RNA from five seed stages. Expression profiles and correlation analyses indicated that the mRNA levels of AGP (large and small subunits), GBSS2, and soluble SS1 and SS4 were well-correlated with starch accumulation in the seeds. Interestingly, two of the most abundant transcripts with RPKM values >1000 in chestnut seed transcriptomes coded for GBSSII-1 (C2Ug23993) and fructose-bisphosphate aldolase (C1Ug33347). GBSS is responsible for amylose synthesis,[48] whereas fructose-bisphosphate aldolase is an important enzyme in the glycolytic pathway regulating carbohydrate metabolism.[49]

DOI: 10.1021/jf505247d
J. Agric. Food Chem. 2015, 63, 929−942

We also noted that gene expression profiles by RPKM and qPCR methods were generally in agreement. Ten of the 11 unigenes (C1Ug22044, C2Ug24779, C2Ug24961, C2Ug31317, C1Ug39763, C1Ug41090, C1Ug41886, C1Ug42679, C1Ug43056, and C1Ug46084) selected for qPCR assays exhibited similar patterns of expression to those estimated by RPKM. The expression of the other unigene (C1Ug36303) showed a similar trend between the two methods, but the expression levels were not significantly different among the seed stages (Figure 3). These results suggest that both methods are reliable and complementary to each other for estimating gene expression.

In conclusion, metabolite analysis showed that starch was the major component and rapidly accumulated during Chinese chestnut seed development. Amylopectin was approximately 3-fold of amylose content in chestnut starch. Transcriptome sequencing identified 152 unigenes involved in starch and sucrose metabolism, which are classified into 37 gene families including glycogenin glucosyltransferase, adenylate transporter, ADP-glucose pyrophosphorylase, starch synthase, starch branching enzyme, starch debranching enzyme, sucrose synthase, and sucrose-phosphate synthase. Among them, 58 unigenes showed a ≥2-fold expression difference between the 45 and 75 DAF seeds including 11 up- and 47 down-regulated unigenes. The expression of 21 unigenes putatively coding for major enzymes in starch and sucrose metabolism was validated by qPCR using RNA from five seed stages. Expression profiles and correlation analysis indicated that the mRNA levels of AGP, granule-bound SS2, and soluble SS1 and SS4 were well-correlated with starch accumulation in the seeds. Our data suggest that the starch biosynthesis pathway in Chinese chestnut endosperm is similar to that of potato tubers and *Arabidopsis* leaves and differs from that of maize endosperm. This study provides valuable metabolic and genetic resources for future research in starch and sucrose metabolism in the Chinese chestnut tree.

AUTHOR INFORMATION

Corresponding Author

*(H.C.) E-mail: Heping.Cao@ars.usda.gov. Phone: (504) 286-4351. Fax: (504) 286-4367.

Present Address

⊥(X.Z.) School of Life Science and Environmental Resources, Yichun University, Yichun, Jiangxi Province 336000, People's Republic of China.

Funding

This work was supported by the Chinese National Science and Technology Pillar Program (2013BAD14B04) and USDA-ARS Quality and Utilization of Agricultural Products Research Program 306 through CRIS 6435-41000-102-00D. Mention of trade names or commercial products in this publication is solely for the purpose of providing specific information and does not imply recommendation or endorsement by the U.S. Department of Agriculture.

Notes

The authors declare no competing financial interest.

ACKNOWLEDGMENTS

We thank Dr. Chris Mattison (USDA-ARS) for helpful comments on the manuscript.

ABBREVIATIONS USED

ADPG, ADP-glucose; AGP, ADP-glucose pyrophosphorylase; AMY, amylase; ANT, adenylate transporter; DAF, days after flowering; FDR, false discovery rate; GBSS, granule-bound starch synthase; GLG, glycogenin glucosyltransferase; KEGG, Kyoto Encyclopedia of Genes and Genomes; Mex, maltose exporter; qPCR, quantitative real-time polymerase chain reaction; PTS, phosphotransferase system; RIN, RNA integrity number; RPKM, reads per kilobase per million mapped reads; SBE, starch branching enzyme; SDBE, starch debranching enzyme; SP, starch phosphorylase; SSS, soluble starch synthase; SuPS, sucrose-phosphate synthase; SuS, sucrose synthase; UGP, UDP-glucose pyrophosphorylase

REFERENCES

(1) De Vasconcelos, M. C. B. M.; Bennett, R. N.; Rosa, E. A.; Ferreira Cardoso, J. V. Primary and secondary metabolite composition of kernels from three cultivars of Portuguese chestnut (*Castanea sativa* Mill.) at different stages of industrial transformation. *J. Agric. Food Chem.* **2007**, *55* (9), 3508−3516.

(2) Borges, O.; Gon+°alves, B.; de Carvalho, J. L. S.; Correia, P.; Silva, A. P. Nutritional quality of chestnut (*Castanea sativa* Mill.) cultivars from Portugal. *Food Chem.* **2008**, *106* (3), 976−984.

(3) Liang, L.; Xu, J.; Wang, G.; Ma, H. Relationship between starch pasting, amylose content and starch granule size in different Chinese chestnut variety groups. *Sci. Agric. Sinica* **2009**, *42*, 251−260.

(4) Cruz, B. R.; Abraao, A. S.; Lemos, A. M.; Nunes, F. M. Chemical composition and functional properties of native chestnut starch (*Castanea sativa* Mill). *Carbohydr. Polym.* **2013**, *94* (1), 594−602.

(5) Barreira, J. C.; Pereira, J. A.; Oliveira, M. B.; Ferreira, I. C. Sugars profiles of different chestnut (*Castanea sativa* Mill.) and almond (*Prunus dulcis*) cultivars by HPLC-RI. *Plant Foods Hum. Nutr.* **2010**, *65* (1), 38−43.

(6) Pizzoferrato, L.; Rotilio, G.; Paci, M. Modification of structure and digestibility of chestnut starch upon cooking: a solid state (13)C CP MAS NMR and enzymatic degradation study. *J. Agric. Food Chem.* **1999**, *47* (10), 4060−4063.

(7) Tsujita, T.; Yamada, M.; Takaku, T.; Shintani, T.; Teramoto, K.; Sato, T. Purification and characterization of polyphenols from chestnut astringent skin. *J. Agric. Food Chem.* **2011**, *59* (16), 8646−8654.

(8) Blaiotta, G.; La Gatta, B.; Di Capua, M.; Di Luccia, A.; Coppola, R.; Aponte, M. Effect of chestnut extract and chestnut fiber on viability of potential probiotic *Lactobacillus* strains under gastrointestinal tract conditions. *Food Microbiol.* **2013**, *36* (2), 161−169.

(9) Warmund, M. R.; Elmore, J. R.; Adhikari, K.; McGraw, S. Descriptive sensory analysis and free sugar contents of chestnut cultivars grown in North America. *J. Sci. Food Agric.* **2011**, *91* (11), 1940−1945.

(10) Emes, M. J.; Bowsher, C. G.; Hedley, C.; Burrell, M. M.; Scrase-Field, E. S.; Tetlow, I. J. Starch synthesis and carbon partitioning in developing endosperm. *J. Exp. Bot.* **2003**, *54* (382), 569−575.

(11) Morell, M. K.; Myers, A. M. Towards the rational design of cereal starches. *Curr. Opin. Plant Biol.* **2005**, *8* (2), 204−210.

(12) Zeeman, S. C.; Kossmann, J.; Smith, A. M. Starch: its metabolism, evolution, and biotechnological modification in plants. *Annu. Rev. Plant Biol.* **2010**, *61*, 209−234.

(13) Baroja-Fernandez, E.; Munoz, F. J.; Akazawa, T.; Pozueta-Romero, J. Reappraisal of the currently prevailing model of starch biosynthesis in photosynthetic tissues: a proposal involving the cytosolic production of ADP-glucose by sucrose synthase and occurrence of cyclic turnover of starch in the chloroplast. *Plant Cell Physiol* **2001**, *42* (12), 1311−1320.

(14) Preiss, J. ADPglucose pyrophosphorylase: basic science and applications in biotechnology. *Biotechnol. Annu. Rev.* **1996**, *2*, 259−279.

(15) Shannon, J. C.; Pien, F. M.; Cao, H.; Liu, K. C. Brittle-1, an adenylate translocator, facilitates transfer of extraplastidial synthesized

DOI: 10.1021/jf505247d
J. Agric. Food Chem. 2015, 63, 929−942

ADP-glucose into amyloplasts of maize endosperms. *Plant Physiol.* **1998**, *117* (4), 1235−1252.
(16) James, M. G.; Denyer, K.; Myers, A. M. Starch synthesis in the cereal endosperm. *Curr. Opin. Plant Biol.* **2003**, *6* (3), 215−222.
(17) Hannah, L. C.; James, M. The complexities of starch biosynthesis in cereal endosperms. *Curr. Opin. Biotechnol.* **2008**, *19* (2), 160−165.
(18) Keeling, P. L.; Myers, A. M. Biochemistry and genetics of starch synthesis. *Annu. Rev. Food Sci. Technol.* **2010**, *1*, 271−303.
(19) Cao, H.; Imparl-Radosevich, J.; Guan, H.; Keeling, P. L.; James, M. G.; Myers, A. M. Identification of the soluble starch synthase activities of maize endosperm. *Plant Physiol.* **1999**, *120* (1), 205−216.
(20) Cao, H.; James, M. G.; Myers, A. M. Purification and characterization of soluble starch synthases from maize endosperm. *Arch. Biochem. Biophys.* **2000**, *373* (1), 135−146.
(21) Beatty, M. K.; Rahman, A.; Cao, H.; Woodman, W.; Lee, M.; Myers, A. M.; James, M. G. Purification and molecular genetic characterization of ZPU1, a pullulanase-type starch-debranching enzyme from maize. *Plant Physiol.* **1999**, *119* (1), 255−266.
(22) Cao, H.; Sullivan, T. D.; Boyer, C. D.; Shannon, J. C. *Bt1*, a structural gene for the major 39−44 kDa amyloplast membrane polypeptides. *Physiol. Plant.* **1995**, *95* (2), 176−186.
(23) Berrocal-Lobo, M.; Ibanez, C.; Acebo, P.; Ramos, A.; Perez-Solis, E.; Collada, C.; Casado, R.; Aragoncillo, C.; Allona, I. Identification of a homolog of *Arabidopsis* DSP4 (SEX4) in chestnut: its induction and accumulation in stem amyloplasts during winter or in response to the cold. *Plant Cell Environ.* **2011**, *34* (10), 1693−1704.
(24) Barakat, A.; DiLoreto, D. S.; Zhang, Y.; Smith, C.; Baier, K.; Powell, W. A.; Wheeler, N.; Sederoff, R.; Carlson, J. E. Comparison of the transcriptomes of American chestnut (*Castanea dentata*) and Chinese chestnut (*Castanea mollissima*) in response to the chestnut blight infection. *BMC Plant Biol.* **2009**, *9*, 51.
(25) Barakat, A.; Staton, M.; Cheng, C. H.; Park, J.; Yassin, N. B.; Ficklin, S.; Yeh, C. C.; Hebard, F.; Baier, K.; Powell, W.; Schuster, S. C.; Wheeler, N.; Abbott, A.; Carlson, J. E.; Sederoff, R. Chestnut resistance to the blight disease: insights from transcriptome analysis. *BMC Plant Biol.* **2012**, *12*, 38.
(26) Allen, T. D.; Dawe, A. L.; Nuss, D. L. Use of cDNA microarrays to monitor transcriptional responses of the chestnut blight fungus *Cryphonectria parasitica* to infection by virulence-attenuating hypoviruses. *Eukaryot. Cell* **2003**, *2* (6), 1253−1265.
(27) Morris, D. L. Quantitative determination of carbohydrates with Dreywood's anthrone reagent. *Science* **1948**, *107* (2775), 254−255.
(28) Liu, T.; Hu, Y.; Li, X. Comparison of dynamic changes in endogenous hormones and sugars between abnormal and normal *Castanea mollissima*. *Prog. Nat. Sci.* **2008**, *18*, 685−690.
(29) Liang, L.; Lin, S.; Zhang, B.; Wang, G. Effect of de-fat and de-protein treatments on swelling power of Chinese chestnut (*C. mollissima* BI.) powder. *Sci. Agric. Sinica* **2012**, *45*, 3820−3831.
(30) Cao, H.; Shockey, J. M. Comparison of TaqMan and SYBR Green qPCR methods for quantitative gene expression in tung tree tissues. *J. Agric. Food Chem.* **2012**, *60* (50), 12296−12303.
(31) Zhang, L.; Jia, B.; Tan, X.; Thammina, C. S.; Long, H.; Liu, M.; Wen, S.; Song, X.; Cao, H. Fatty acid profile and unigene-derived simple sequence repeat markers in tung tree (*Vernicia fordii*). *PLoS One* **2014**, *9* (8), No. e105298.
(32) Grabherr, M. G.; Haas, B. J.; Yassour, M.; Levin, J. Z.; Thompson, D. A.; Amit, I.; Adiconis, X.; Fan, L.; Raychowdhury, R.; Zeng, Q.; Chen, Z.; Mauceli, E.; Hacohen, N.; Gnirke, A.; Rhind, N.; di, P. F.; Birren, B. W.; Nusbaum, C.; Lindblad-Toh, K.; Friedman, N.; Regev, A. Full-length transcriptome assembly from RNA-Seq data without a reference genome. *Nat. Biotechnol.* **2011**, *29* (7), 644−652.
(33) Jones, P.; Binns, D.; Chang, H. Y.; Fraser, M.; Li, W.; McAnulla, C.; McWilliam, H.; Maslen, J.; Mitchell, A.; Nuka, G.; Pesseat, S.; Quinn, A. F.; Sangrador-Vegas, A.; Scheremetjew, M.; Yong, S. Y.; Lopez, R.; Hunter, S. InterProScan 5: genome-scale protein function classification. *Bioinformatics* **2014**, *30* (9), 1236−1240.
(34) Audic, S.; Claverie, J. M. The significance of digital gene expression profiles. *Genome Res.* **1997**, *7* (10), 986−995.
(35) Mortazavi, A.; Williams, B. A.; McCue, K.; Schaeffer, L.; Wold, B. Mapping and quantifying mammalian transcriptomes by RNA-Seq. *Nat. Methods* **2008**, *5* (7), 621−628.
(36) Cao, H.; Shockey, J. M.; Klasson, K. T.; Mason, C. B.; Scheffler, B. E. Developmental regulation of diacylglycerol acyltransferase family gene expression in tung tree tissues. *PLoS One* **2013**, *8* (10), No. e76946.
(37) Livak, K. J.; Schmittgen, T. D. Analysis of relative gene expression data using real-time quantitative PCR and the 2(-ΔΔC(T)) method. *Methods* **2001**, *25* (4), 402−408.
(38) Denyer, K.; Dunlap, F.; Thorbjornsen, T.; Keeling, P.; Smith, A. M. The major form of ADP-glucose pyrophosphorylase in maize endosperm is extra-plastidial. *Plant Physiol.* **1996**, *112* (2), 779−785.
(39) Sullivan, T. D.; Strelow, L. I.; Illingworth, C. A.; Phillips, R. L.; Nelson, O. E., Jr. Analysis of maize brittle-1 alleles and a defective suppressor-mutator-induced mutable allele. *Plant Cell* **1991**, *3* (12), 1337−1348.
(40) Niittyla, T.; Messerli, G.; Trevisan, M.; Chen, J.; Smith, A. M.; Zeeman, S. C. A previously unknown maltose transporter essential for starch degradation in leaves. *Science* **2004**, *303* (5654), 87−89.
(41) Bahaji, A.; Li, J.; Sanchez-Lopez, A. M.; Baroja-Fernandez, E.; Munoz, F. J.; Ovecka, M.; Almagro, G.; Montero, M.; Ezquer, I.; Etxeberria, E.; Pozueta-Romero, J. Starch biosynthesis, its regulation and biotechnological approaches to improve crop yields. *Biotechnol. Adv.* **2014**, *32* (1), 87−106.
(42) Shannon, J. C.; Pien, F. M.; Liu, K. C. Nucleotides and nucleotide sugars in developing maize endosperms (synthesis of ADP-glucose in *brittle-1*). *Plant Physiol.* **1996**, *110* (3), 835−843.
(43) Sullivan, T. D.; Kaneko, Y. The maize brittle 1 gene encodes amyloplast membrane polypeptides. *Planta* **1995**, *196* (3), 477−484.
(44) Smith, A. M. The biosynthesis of starch granules. *Biomacromolecules* **2001**, *2* (2), 335−341.
(45) Cao, H.; Shannon, J. C. BT1, a protein critical for in vivo starch accumulation in maize endosperm, is not detected in maize endosperm suspension cultures. *Physiol. Plant.* **1996**, *97* (4), 665−673.
(46) Cao, H.; Shannon, J. C. BT1, a possible adenylate translocator, is developmentally expressed in maize endosperm but not detected in starchy tissues from several other species. *Physiol. Plant.* **1997**, *100* (2), 400−406.
(47) Martin, C.; Smith, A. M. Starch biosynthesis. *Plant Cell* **1995**, *7* (7), 971−985.
(48) Shure, M.; Wessler, S.; Fedoroff, N. Molecular identification and isolation of the Waxy locus in maize. *Cell* **1983**, *35* (1), 225−233.
(49) Zeng, Y.; Tan, X.; Zhang, L.; Jiang, N.; Cao, H. Identification and expression of fructose-1,6-bisphosphate aldolase genes and their relations to oil content in developing seeds of tea oil tree (*Camellia oleifera*). *PLoS One* **2014**, *9* (9), No. e107422.

DOI: 10.1021/jf505247d
J. Agric. Food Chem. 2015, 63, 929−942

pepsin from porcine gastric mucosa (P7000, 561 U/mg solid), and all other chemicals were purchased from Sigma-Aldrich (Steinheim, Germany).

Citrobacter braakii and *Peniophora lycii* (variant optimized for intestinal and thermal stability[13]) phytases expressed in *Aspergillus oryzae* (trade names Ronozyme HiPhos (L) and Ronozyme NP (L), hereafter abbreviated to H and R, respectively), were kindly provided by DSM (Heerlen, The Netherlands) and Novozymes (Bagsværd, Denmark), respectively. *Escherichia coli* phytase expressed in *Pichia pastoris* (trade name Granular phytase), hereafter abbreviated to G, and *Aspergillus niger* phytase expressed in *A. niger* (trade name SukaPhy phytase), hereafter abbreviated to S, were kindly provided by Challenge Group (Beijing, China) and Sukahan Biotechnology (Weifang, China), respectively. Wheat phytase, hereafter abbreviated to W, was purchased from Sigma-Aldrich. *A. niger* phytase expressed in *P. pastoris*, hereafter abbreviated to N, was produced in house as described below.

Production of *Aspergillus niger* Phytase. *Vector and Strain Construction.* An *A. niger* phytase (GenBank accession no. Z16414.1) without the 21 amino acid long N-terminal signal peptide, but including a C-terminal c-myc epitope and a His_6-tag, was codon-optimized for expression in *P. pastoris* and synthesized by DNA2.0 (Menlo Park, CA, USA) (this codon-optimized nucleotide sequence has been deposited in the GenBank database; NCBI KP001509). The synthesized gene was inserted in the vector pJ912, generating a translational fusion to the α-factor signal sequence. The resulting plasmid, pJ912_AnPhy, was propagated in *E. coli* DH5α grown at 37 °C with shaking in low-salt LB medium (10 g/L tryptone, 5 g/L yeast extract, and 5 g/L NaCl) supplemented with 25 μg/mL Zeocin.

The *P. pastoris* strain X-33 (Life Technologies, Carlsbad, CA, USA) was used as the host strain. X-33 electrocompetent cells were prepared as follows. *P. pastoris* X-33 was grown in nonselective YPD medium to an OD_{600} of 1, centrifuged, and resuspended in PPD buffer (50 mM potassium phosphate, pH 7.5, 25 mM DTT). After 15 min of incubation at 30 °C without shaking, cells were washed three times with STM buffer at 25 °C (10 mM Tris-HCl, pH 7.5, 270 mM sucrose, 1 mM $MgCl_2$) and resuspended in ice-cold STM buffer. Cells were frozen in liquid nitrogen and stored at −80 °C until use. For each transformation, 60 μL of cells were mixed with 0.5−1 μg of *Sac*I-linearized plasmid DNA in a prechilled 2 mm electroporation cuvette. Electroporation was performed using a MicroPulser Electroporator (Bio-Rad, Hercules, CA, USA) with settings according to the manufacturer's instructions. Immediately after the pulse, 1 mL of ice-cold YPD was added to the cuvette, and the cells were incubated at 30 °C for 1 h without shaking. Cells were washed once with 0.68% YNB (without amino acids) supplemented with 20% dextrose and plated on YPDS plates supplemented with 100 μg/mL Zeocin followed by incubation at 30 °C for 2−3 days.

Protein Production and Purification. Of 20 Zeocin-resistant *P. pastoris* X-33 transformants harboring the pJ912_AnPhy, the clone expressing the enzyme of interest in highest amounts, was selected as follows: Transformants were grown for 3 days in 50 mL of BMMY (10 g/L yeast extract, 20 g/L peptone, 100 mM potassium phosphate, pH 6, 13.4 g/L yeast nitrogen base, 0.4 mg/L biotin, and 0.5% (v/v) methanol) during shaking at 28 °C. Protein synthesis was induced every 24 h by addition of methanol to a final concentration of 0.5% (v/v). After 72 h of expression, cells were removed by centrifugation and sterile filtration and the supernatants containing secreted proteins analyzed by SDS-PAGE. To test for N-glycosylation and determine the molecular mass of the nonglycosylated enzyme, the secreted protein fraction was treated with endoglycosidase H for 1 h at 37 °C.

For large-scale phytase expression, the strain identified to produce the highest levels of enzyme in small scale was selected for fermentation in a 5 L Sartorius Biostat Aplus fermentor as described previously.[14] The phytase was purified either (i) from the ultrafiltered cell-free extract from *P. pastoris* by Ni^{2+} affinity column chromatography using a HisTrap HP column (GE Healthcare, Uppsala, Sweden) or (ii) directly from the fermentation broth by Cu^{2+} affinity column chromatography using a Microradial flow column (Proxcys, Nieuw-Amsterdam, The Netherlands), charged with IDA Chelating Cellthru BigBead (Sterogene, Carlsbad, CA, USA). After purification, the enzyme was dialyzed overnight against 20 mM ammonium bicarbonate at room temperature, lyophilized, and frozen at −20 °C.

Determination of Protein Concentration. Protein contents of the phytase formulations were measured with the BCA assay according to the manufacturer's instructions (microplate scale). Bovine serum albumin was used as a standard. For circular dichroism (CD) measurements, protein concentration was determined by absorption at 280 nm (see below).

Phytase Activity Assay. Phytase activity was evaluated at 37 °C in 200 mM acetate buffer at pH 5.5 using 5 mM phytic acid[15] and an enzyme dose corresponding to 0.05% E/S (enzyme/substrate % weight/weight) based on the determined protein content of the enzyme formulations for the R, H, G, and S phytases and 0.3% E/S (w/w) for the N phytase. The higher inclusion level for the N phytase was due to the low specific activity of this enzyme. Three hundred and fifty microliters of substrate solution was preheated to 37 °C, after which 50 μL of phytase solution was added. Reaction was stopped by adding 50 μL of 3.6 M HCl and incubating at 99 °C for 10 min. Samples were diluted with Milli-Q water and analyzed for InsP6 by ion exchange chromatography[15,16] (see below). Activity was evaluated as initial rate of net (compared to control without phytase) inositol hexakisphosphate elimination in micromoles per minute per milligram of enzyme protein during the first minute of reaction.

Quantification of Inositol Phosphates. Inositol phosphates were resolved using an ICS-3000 ion exchange chromatography system from Dionex (Sunnyvale, CA, USA) equipped with a CarboPac PA100 guard column (4 × 50 mm) and a CarboPac PA100 analytical column (4 × 250 mm). Samples (100 μL) were loaded with an autosampler. Bis- to hexakisphosphates were resolved using a gradient from 5 to 95% 1 M HCl, and for analysis of hexakisphosphate only, 80% 1 M HCl was used isocratically.[16] The eluent (0.8 mL/min) was mixed in a postcolumn PTFE knitted open tubular reaction coil (4 m × 0.25 mm i.d.) (Biotech, Onsala, Sweden) with 0.4 mL/min 0.1% (w/v) $Fe(NO_3)_3{\cdot}9H_2O$ in 2% (v/v) $HClO_4$ pumped by an AXP Auxiliary Pump (Dionex). The inositol phosphates were detected with a photodiode array detector at 290 nm.

A reference hydrolysate of phytic acid was prepared by reflux boiling with 0.5 M HCl, evaporation of the acid solution, and reconstitution in Milli-Q water followed by filtration through a 0.22 μm filter. This sample was analyzed according to the bis- to hexakisphosphate method described above, and the chromatogram served as a reference for peak identification by comparison with assigned chromatograms from previous studies.[15,17] Ins(1,2,5,6)P4 and Ins(1,2,4,5,6)P5 standards were run as confirmation for correct assignment of postreaction peaks. InsP3, InsP4, and InsP5 were quantified as InsP6 equiv using the same quantification factor as for InsP6 (slope of standard curve of area under the curve versus molar concentration).

Thermostability of Phytases. The thermostability of the five different phytases (H, R, G, S, N) was tested by incubation (n = 2) of phytases for 2, 10, 20, and 30 min at 37, 45, 50, 60, and 70 °C in 200 mM acetate buffer, pH 5.5, after which the residual activity was assayed as described above.

pH Profiles of Phytases. The pH profiles (n = 3) were determined at 37 °C according to the method described above, except for the solvent of the assays, which was exchanged for a buffer cocktail consisting of 50 mM glycine, 50 mM acetic acid, and 50 mM Bis-Tris.[18] The pH was adjusted to 13 different values between pH 1 and 7. Activities were normalized according to the activity optimum for each phytase to simplify comparison between phytases, as the enzymes were dosed on a protein/substrate (w/w) basis rather than on specific activity.

Stability of Phytases to Pepsin and Low pH. Pepsin stability of the six different phytases (H, R, G, S, W, N) was tested by incubation of phytases (n =2) with 5000 U/mL pepsin (based on gastric conditions as simulated by Haraldsson et al.[19]) in 0.01 M HCl (pH 2) at 37 °C for 10, 20, 30, 60, and 120 min, after which 50 μL of the phytase/pepsin solution was transferred to 350 μL of substrate solution and the activity assayed as described above. Activities were compared with the activity before pepsin addition yielding the residual

DOI: 10.1021/jf5050469
J. Agric. Food Chem. 2015, 63, 943−950

activities. A corresponding assay was conducted to investigate the stability at pH 2 without pepsin (H, R, G, S, and N phytases). Activities were normalized according to the initial activities (for individual replicate series) for each of the phytases.

Degradation of InsP3−6 under Simulated Gastric Conditions. Degradation of inositol hexakis- to triphosphates was investigated at pH 1 (100 mM HCl), pH 2 (10 mM HCl), and pH 5 (200 mM acetate buffer) with and without pepsin (5000 U/mL) with five different phytases (H, R, G, S, N) using 4 mM phytic acid. Each reaction was stopped as described for the phytase assay.

Circular Dichroism. To ensure enzyme purity, commercial phytase formulations were filtered through 0.22 μm syringe filters. Subsequently, they were washed twice with Milli-Q water in Vivaspin 500 sample concentrators (VWR, Radnor, PA, USA) with a molecular weight cutoff of 30 kDa to retain the phytases. Phytases were reconstituted in Milli-Q water. Solutions were diluted with either 10 mM HCl at pH 2 or 10 mM acetate buffer at pH 5 to approximately 2 μM. Concentrations were verified by measuring baseline-corrected absorption using a UV-2401 PC spectrophotometer (Shimadzu, Tokyo, Japan) at 280 nm. Extinction coefficients were calculated from the amino acid sequence using the ProtParam tool.[20]

Baseline-corrected far-UV CD spectra of the five phytases (H, R, G, S, N) were obtained using a Jasco J815 circular dichroism spectropolarimeter (Jasco Inc., Easton, MD, USA) equipped with a temperature control unit. Measurements were performed at 37 °C and a path length of 0.5 mm. Mean residue ellipticities were calculated by normalizing for enzyme concentration and number of amino acids in the respective phytases. Secondary structure contents were estimated from the spectra using the software package CDSSTR[21] through the Dichroweb analysis Web server.[22]

Sequence Alignment and Homology Modeling. Primary sequences for the phytases were found in GenBank with accession numbers AJ310696.1 (*P. lycii*, R), AAS45884.1 (*C. braakii*, H), X05471.1 (*E. coli*, G), Z16414.1 (*A. niger*), and XM_746871.2 (*A. fumigatus*). Sequences were aligned using Clustal Omega.[23,24] The *P. lycii* sequence was submitted to Phyre[25] using the intensive modeling mode for construction of a homology model of the phytase.

Statistical Analyses. For the thermal and low-pH/pepsin data, regression analyses of logarithmically transformed data were done with the aid of Minitab 14 (State College, PA, USA). For significant ($p < 0.05$) regressions, half-lives were determined from the regression parameters. Significance ($p < 0.05$) of differences in decay constants between enzymes were tested in Minitab 14 using a one-way analysis of variance followed by Bonferroni's multiple-comparison test. For the InsP3−6 degradation data, regression analysis was carried out with nontransformed data. For the data from circular dichroism, principal component analysis (PCA) was used to extract a single value expressing the differences in molar ellipticities between the spectra at pH 2 and 5 for each phytase over the entire range of wavelengths.[26] R[27] was used for the PCA.

RESULTS AND DISCUSSION

Thermostability of Phytases. Generally, all tested phytases were stable for 30 min at 50 °C (Figure 1). A direct comparison of half-lives at 60 and 70 °C showed that the R phytase had a significantly longer half-life than the other phytases (Figure 1). Notably, no significant loss of activity could be observed for the R phytase at 60 °C, whereas the half-life of the H phytase was significantly higher than the half-lives of the G, S, and N phytases, and the half-life of the G phytase was significantly higher than that of the N phytase (Figure 1). At 70 °C, no significant differences between half-lives among the S, H, G, and N phytases were observed.

The high thermal stability of the *P. lycii* phytase, R, is supported by previous findings,[28] whereas other studies reported much lower stabilities.[29,30] Some of these discrepancies might be due to different assay conditions in studies or the use of a different, non-optimized variant of the *P. lycii*

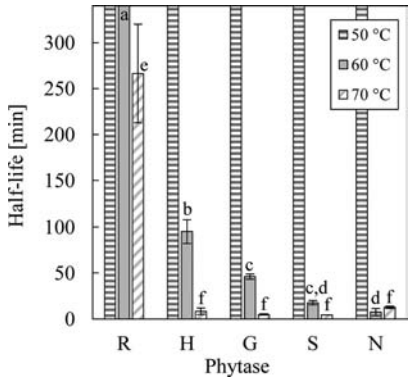

Figure 1. Average (n = 2) half-lives of different phytases (R, Ronozyme NP (L); H, Ronozyme HiPhos (L); G, Granular phytase; S, SukaPhy phytase; N, *A. niger* phytase) at 50, 60, and 70 °C. No decrease in activity of the phytases at 50 °C and, furthermore, the R phytase at 60 °C could be measured, so a half-life is plotted as out of range. Stability was tested in 200 mM acetate buffer, pH 5.5. Error bars correspond to the standard deviation for the duplicate measurements. Different letters correspond to significantly different half-lives ($p < 0.05$).

phytase. For the *A. niger* phytase (the N and S phytases of the present study), results similar to the present study have previously been reported,[29] except for a study that found the *P. lycii* phytase to be less stable than the *A. niger* phytase.[30] The thermal stabilities for the *E. coli* phytase found here are also similar to previously published results.[12,29] For the *C. braakii* phytase (the H phytase of the present study), thermal stability was a little higher than previously reported.[10]

pH Profiles of Phytases. The pH dependence of phytase activities (Figure 2) followed regular symmetrical response

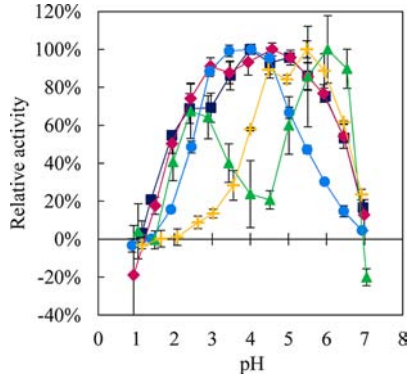

Figure 2. Relative activity of different phytases against pH: (dark blue squares) Granular phytase, G; (red diamonds) SukaPhy phytase, S; (blue circles) Ronozyme HiPhos (L), H; (yellow crosses) Ronozyme NP (L), R; (green triangles) *A. niger* phytase, N. Activity was evaluated as InsP6 elimination rate at 37 °C in a buffer consisting of 50 mM glycine, 50 mM acetic acid and 50 mM Bis-Tris. All activities have been normalized to the activity optimum for the given phytase. Error bars represent the standard deviations (n = 3).

curves for the H, G, and S phytases with pH optima at approximately pH 4, 4, and 4.5, respectively. Compared to the other phytases, the R phytase had a narrower pH profile with the curve slightly skewed toward the higher pH values and an optimum around pH 5.5. For the N phytase, the characteristic double-optimum profile believed to be due to interactions between acidic and alkaline amino acids in the substrate

DOI: 10.1021/jf5050469
J. Agric. Food Chem. 2015, 63, 943−950

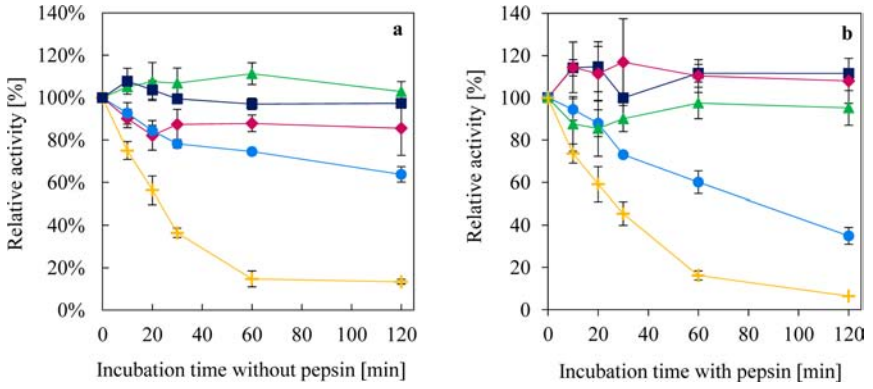

Figure 3. (a) Activity retention against incubation time at pH 2 of different phytases: (dark blue squares) granular phytase, G; (red diamonds) SukaPhy phytase, S; (blue circles) Ronozyme HiPhos (L), H; (yellow crosses) Ronozyme NP (L), R; (green triangles) *A. niger* phytase, N. (b) Activity retention against incubation time with pepsin (5000 U/mL) at pH 2 of different phytases (legend as for panel a). Activity was evaluated as InsP6 elimination rate at pH 5.5 and 37 °C, and all phytases have been normalized to their activity before pepsin incubation (0 min). Error bars represent the standard deviation (n = 2).

specificity site[31] was seen with optima around 3 and 6, respectively. The negative values of relative activities correspond to very small absolute activities with a high relative inaccuracy. As the S phytase was declared to be an *A. niger* phytase, it was surprising that the pH profile did not agree with the expected double optimum reported by previous studies.[32,33] This indicated that the enzyme might not be the wild type *A. niger* phytase, but instead a mutant (or perhaps an enzyme from a different source, e.g., *E. coli*, which has a similar pH profile).

For the R phytase, the pH profile found in these experiments was slightly more skewed toward the alkaline pH range compared with previous studies,[11,34,35] whereas another study using different assay conditions reported a similar pH activity profile.[30] For the *C. braakii* phytase (H phytase), the pH profile determined in the present work was similar to previous findings,[10,34] although the similarity was generally lower at the extreme ends of the pH profile (around pH 2 and 7). The pH activity profile for the G phytase found in the present study was similar, but broader than previously reported.[12]

Stability of Phytases to Pepsin and Low pH. The activities of the G, H, and R phytases decreased significantly when incubated at pH 2 in the absence of pepsin (Figure 3a), whereas the activities of only the H and R phytases decreased significantly in the presence of pepsin (Figure 3b). In agreement with previous findings,[36] the wheat phytase showed no activity after incubation at pH 2 with or without pepsin (data not shown). The wheat phytase was therefore not expected to exert measurable activity in gastric conditions and was not included in further experiments.

Initial rates (linear fit of first 30 min) of activity loss were 27% (R) and 11% (H) higher in the presence of pepsin compared to activity loss at pH 2 without pepsin (Figure 3). The rate of activity loss at pH 2 (no pepsin) was significantly higher ($p < 0.05$) for the R phytase than for the other phytases (half-lives in Table 1). These rates did not differ significantly among the remaining phytases (half-lives in Table 1).

For the S and G phytases, there was a slight tendency toward an increase in activity in the presence of pepsin. The activity increase following pepsin-catalyzed proteolysis was previously reported for the *E. coli* acid phosphatase and was speculated to be due to the presence of pepsin-resistant polypeptides internally in the phosphatase sequence with a higher phytase activity than the original protein.[37] This potential increase in activity might also obscure the activity loss due to low pH, which was observed in the experiment without pepsin (Figure 3a).

Table 1. Half-Lives (min) (± Standard Deviations, n = 2) of Phytases Incubated at pH 2 with or without Pepsin

phytase	without pepsin	with pepsin
G	1200 ± 144	NS[a]
H	205 ± 38	78 ± 7
R	40 ± 3	30 ± 0.3

[a]NS, regression was not significant.

When compared with other studies, it appears that the varying methods of testing pepsin resilience highly influence the conclusions. Other studies[29,38] conducted at pH 2 reported high activity losses of the *P. lycii* phytase, similar to the present study, whereas another study conducted at pH 3−5 reported much lower activity loss.[39] Similarly for the *E. coli* phytase, high pepsin stability was reported at pH 2,[29] similar to the present study, whereas a study using pH 1.2 reported extensive activity loss.[40] With respect to stability to pH 2 (without pepsin), the stability found in the present study agrees with previous results reported for *E. coli*.[12]

Previous studies disagree on pepsin resilience of *A. niger* phytase, with some[29,38] reporting lower pepsin stability than found in this study (Figure 3b) and others reporting similarly high stabilities.[36,37] This might be a result of the use of a different variant of the *A. niger* phytase or an entirely different source organism as mentioned in connection to the pH activity profiles. For the *C. braakii* phytase (the H phytase of the present study), a previous study[10] reported much higher pepsin stability than we found, but because neither pepsin activity nor pH were reported, comparisons are difficult.

Regardless of differences in assay conditions among the various studies, a comparison of different phytases using the same assay conditions is of interest to assess performance of the enzymes in question relative to each other.

Interestingly, in the present study it was observed that the phytases which were least stable at low pH also showed lower resistance toward proteolytic inactivation by pepsin (Figure 3). This could be explained by partial unfolding of the acid labile H and R phytases at low pH, which leads to a better accessibility for the protease pepsin.[35] This hypothesis was corroborated by the observed increase in activity decay rates upon pepsin

DOI: 10.1021/jf5050469
J. Agric. Food Chem. 2015, 63, 943−950

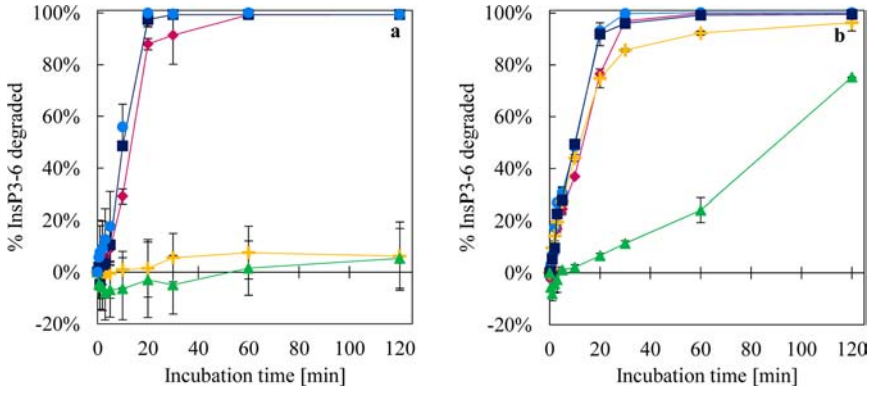

Figure 4. (a) Degradation of InsP3−6 at pH 2 catalyzed by different phytases, (dark blue squares) Granular phytase, G; (red diamonds) SukaPhy phytase, S; (blue circles) Ronozyme HiPhos (L), H; (yellow crosses) Ronozyme NP (L), R; (green triangles) *A. niger* phytase, N, against incubation time with pepsin (5000 U/mL). (b) Degradation of InsP3−6 at pH 5 catalyzed by different phytases (legend as in panel a).

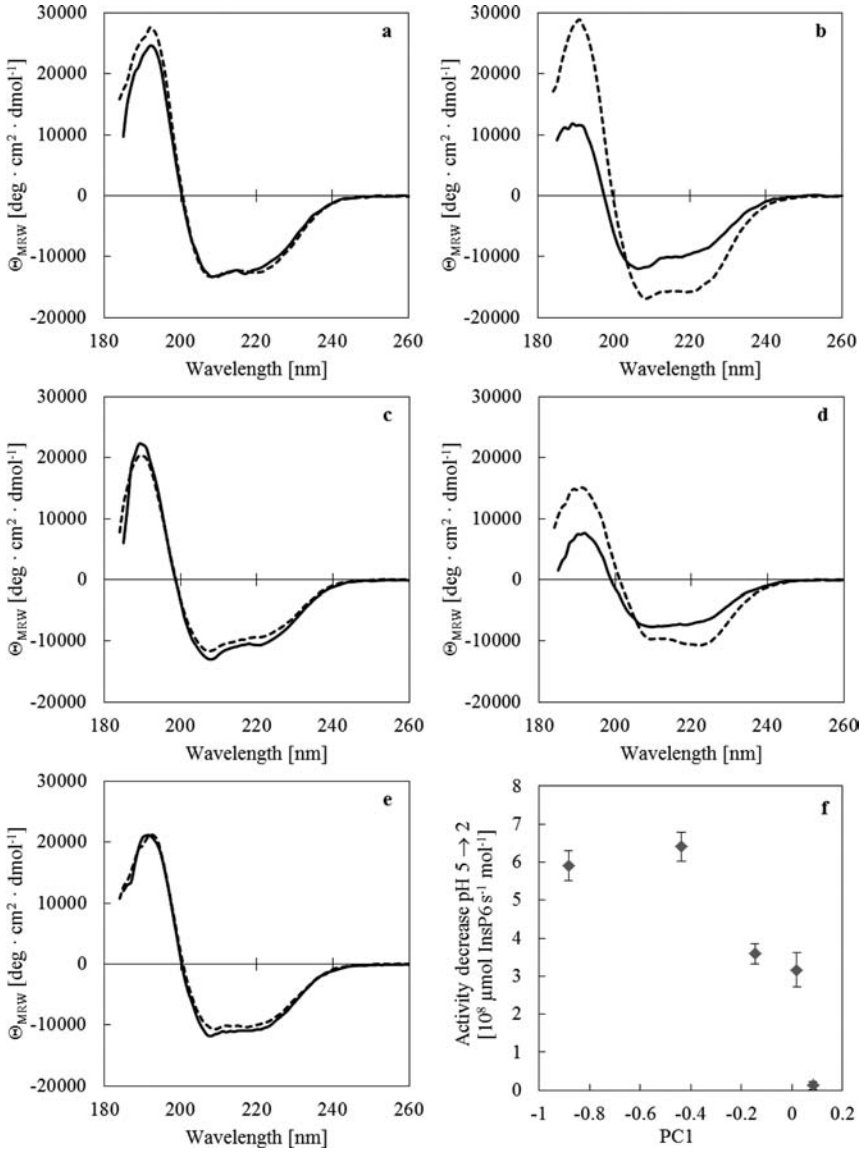

Figure 5. (a−e) CD spectra of the different phytases at pH 2 (solid lines) and pH 5 (dashed lines): (a) G, Granular phytase; (b) H, Ronozyme HiPhos (L); (c) N, *A. niger* phytase; (d) R, Ronozyme NP (L); (e) S, SukaPhy phytase. (f) Difference in molar activity between pH 5 and 2 plotted against the first principal component (PC1) from the principal component analysis.

addition (H and R phytases). An exception was the G phytase as described above.

Finally, it was noted that there appeared to be no connection between pH/pepsin stability and thermostability (Figures 1 and

DOI: 10.1021/jf5050469
J. Agric. Food Chem. 2015, 63, 943−950

3), as the R phytase with the longest half-lives at 60 and 70 °C had the shortest half-lives when incubated at pH 2 with or without pepsin. In a similar fashion, stability toward heat and low pH/pepsin appeared to be inversely correlated for the other phytases.

Degradation of InsP3−6 under Simulated Gastric Conditions. At pH 2, the H, S, and G phytases significantly reduced InsP3−6 content (measured as InsP6 equiv) (Figure 4a) by >90% after 30 min, whereas no significant reduction was seen for the N and R phytases. For the N phytase, even negative average values were observed. The negative values are believed to be a result of minor inaccuracies of chromatography quantifications of small peak values compared to reference values that become magnified when multiplied by a dilution factor for diluted samples. As the R phytase in the pH profiling showed low activity at pH 2 (Figure 2) and in addition showed low activity retention after incubation at pH 2 with or without pepsin (Figure 3), this phytase was not expected to perform well with pepsin at pH 2. The N phytase having significant activity at pH 2 (Figure 2) and good stability toward low pH/pepsin (Figure3) was expected to demonstrate better performance in this assay. However, due to the low specific activity of this enzyme, the amount of enzymatic activity was not sufficient to compare with the other phytases, so a higher dosage would be required for this phytase.

At pH 5 (Figure 4b), all phytases except the N phytase reduced InsP3−6 content by at least 86% after 30 min. The R phytase performed significantly better at this pH compared to pH 2, but the H, G, and S phytases catalyzed a significantly higher degradation of InsP3−6 than the R phytase after 30 and 60 min. At 120 min degradation of InsP3−6 did not differ significantly between the R phytase and H, S, and G phytases (Figure 4b). The N phytase once again suffered from low specific activity, resulting in low InsP3−6 removal in these incubations. Given the high resistance to pepsin and low pH as well as reasonable activity retention at both pH 2 and 5, the N phytase is expected to perform well given a higher dosage. At pH 1, none of the phytases caused a significant reduction in InsP3−6 (data not shown), which was in coherence with the pH profiles showing very low activities for all of the phytases at this pH (Figure 2).

When considering the practical implication of these results, we can take a serving (50 g) of oatmeal as an example. Oatmeal contains ∼1 g phytic acid/100 g,[41] resulting in a total intake of ∼0.5 g of phytic acid. Using the same dosage of enzyme per substrate mass as in the present experiment, ∼0.25 mg of phytase protein would then be required to obtain the same degradation kinetics as seen in the present study (Figure 4). However, different kinetics may occur in the gastric ventricle in vivo due to lower substrate accessibility. Phytate in grains is incorporated in complex globoids,[15] and viscosity effects provided by the food components may lower mass transfer rates. These issues might be overcome by increasing phytase dosage.

As a final note on the practical applications of the results, it should be mentioned that the pH in the fed gastric environment is highly dependent on the nature of the recently consumed meal and is expected to be in a range of pH 3−6. Several studies[42−44] use 0.1 M HCl (corresponding to pH 1) as in vitro gastric medium. Therefore, gastric conditions were initially simulated at pH 1, but because none of the phytases showed activity at this pH value (Figure 2), only results at pH 2 and 5 are reported (Figure 4). Although the average pH value in the fed stomach is in the range of ∼3−6, phytases might experience considerably lower pH values locally due to the secretion of hydrochloric acid. Therefore, a high resistance to acid-induced denaturation is desirable for the optimal phytase. However, to allow for catalysis at the pH in the food chyme, some activity in the pH range of 5−6 and maybe even up to pH 7 is desirable. Finally, high pepsin resistance is desirable to continue catalysis throughout the retention of phytase in the gastric environment. Combining these demands for the optimal phytase, the *E. coli* (G) and SukaPhy (S) phytases appear to have a competitive edge in performance as compared to the other phytases tested. If thermostability is essential for the specific application (including, e.g., preparation of a food or feed product), *P. lycii* (R) and *C. braakii* (H) phytases are good candidates. Native *A. niger* phytase (the N phytase), being the only phytase approved for use in food,[8] appears to be a relatively poor choice due to the low activity between pH 3 and 6. This might be counteracted by increasing dosage as the acid and pepsin stabilities of this phytase are high (Figure 3).

Circular Dichroism. The CD spectra (Figure 5a−e) and estimated contents of secondary structural contents (Table 2) showed that the secondary structures of the H and R phytases changed more between pH 5 and 2 compared with the G, S, and N phytases. The ratio of unassigned (neither α-helix, β-strand, nor turn) secondary structure increased between pH 5 and 2 for the H and R phytases, but decreased or remained constant for the N, G, and S phytases. Using PCA, a principal component able to explain 98.4% of the variation over the entire spectra between pH 2 and 5 was extracted. This principal component appeared to correlate with the difference in activities displayed by the different phytases at pH 5 and 2 (Figure 5f), corroborating that the extent of loss in secondary structure correlates positively with the loss in enzymatic activity.

Table 2. Secondary Structural Contents (Percent) of the Five Phytases at pH 2 and 5[a]

phytase	pH	helix	strand	turn	unassigned
G	5	44	12	16	27
	2	50	20	17	13
H	5	49	12	14	25
	2	31	19	20	30
N	5	33	18	19	30
	2	25	30	15	30
R	5	31	20	19	30
	2	19	28	22	31
S	5	34	18	20	28
	2	37	17	19	27

[a]Numbers are estimated by the CDSSTR software package.

An investigation of potential correlations between secondary structure composition at pH 5 and stability toward heat, low pH, and pepsin indicated that helix content (at pH 5) correlated negatively with half-life at pH 2, whereas strand and turn contents correlated positively (Figure 6a; because no significant loss of activity was observed for S and N phytases, their half-lives have been plotted at 3000 min). On the other hand, higher helix content (at pH 5) and lower contents of

DOI: 10.1021/jf5050469
J. Agric. Food Chem. 2015, 63, 943−950

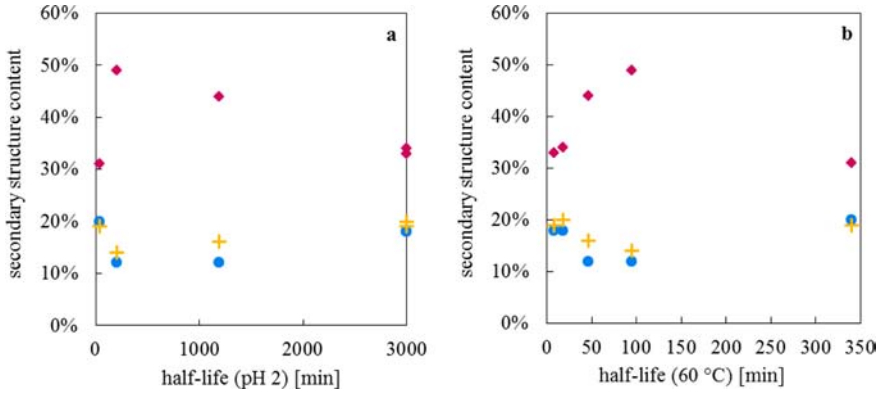

Figure 6. (a) Secondary structure contents against enzymatic activity half-life at pH 2: (red diamonds) helix; (blue circles) strand; (yellow crosses) turns. (b) Secondary structure contents against enzymatic activity half-life at 60 °C (legend as in panel a).

strands and turns appeared to imply a longer half-life at 60 °C (Figure 6b). These tendencies with regard to stability toward heat and low pH were observed for the G, S, N, and H phytases, whereas the R phytase apparently evaded these trends. It is believed that the *P. lycii* phytase (R), which is an optimized version of the native *P. lycii* phytase, differs significantly from the other phytases, for example due to single amino acid changes that may play a crucial role in the structural integrity of the enzyme.

In conclusion, the CD results clearly established a relationship between loss of secondary structure and loss of activity at a low pH. To our knowledge, this relationship has not previously been reported for these phytases.

Sequence Alignment and Homology Modeling. As expected, sequence alignment showed highest sequence identity within the fungal phytases and bacterial phytases, respectively (Table 3). Crystal structures are available for *E. coli* (G), *C. braakii* (H), and *A. niger* (S/N) phytases with PDB entries 1DKL, 3ZHC and 3K4P, respectively. No crystal structure is available for the *P. lycii* (R) phytase. Homology modeling rendered a model using phytases from *A. ficuum* (PDB entry 1IHP) and *A. fumigatus* (PDB entry 1QWO) as templates. Each *Aspergillus* phytase (the two templates, which had 65% sequence identity) had 40% sequence identity with *P. lycii*. The secondary structure contents of the modeled 3D structure for the *P. lycii* phytase were 43% helix, 11% strand, and 16% disordered, which correlates poorly with the secondary structure content determined from the CD spectra (Table 2). This poor agreement with experimental data points toward differences in structure of the homologous enzymes despite their moderate similarity in the amino acid sequence.

Overall, the stability and activity assessments using the soluble phytic acid substrate reported here have provided a decision base for conducting further trials, also including the use of a food model system with digestion.

Table 3. Sequence Identities As Determined from Sequence Alignment Carried out by Clustal Omega

% sequence identity	*C. braakii*	*E. coli*	*A. niger*	*P. lycii*
C. braakii		63.33	19.78	20.64
E. coli	63.33		20.11	21.23
A. niger	19.78	20.11		39.71
P. lycii	20.64	21.23	39.71	

AUTHOR INFORMATION

Corresponding Author

*(A.S.M.) Phone: +45 4525 2800. E-mail: am@kt.dtu.dk.

Funding

This work was partially funded by the FENAMI (Functional Nanomicrostructures for Food and Bioengineering Applications) project, Danish Strategic Research Council.

Notes

The authors declare no competing financial interest.

ACKNOWLEDGMENTS

We thank Peter Waaben Thulstrup (Department of Chemistry, University of Copenhagen) for kindly providing access to the circular dichroism spectropolarimeter.

ABBREVIATIONS USED

H, Ronozyme HiPhos (L); R, Ronozyme NP (L); G, granular phytase; S, SukaPhy phytase; N, in-house-produced *Aspergillus niger* phytase; W, wheat phytase; InsP*X*, inositol phosphate (*X* indicates the number of phosphate groups)

REFERENCES

(1) World Health Organization. *Essential Nutrition Actions*; WHO Press: Geneva, Switzerland, 2013.

(2) Nielsen, A. V. F.; Tetens, I.; Meyer, A. S. Potential of phytase-mediated iron release from cereal-based foods: a quantitative view. *Nutrients* **2013**, *5*, 3074−3098.

(3) Troesch, B.; Jing, H.; Laillou, A.; Fowler, A. Absorption studies show that phytase from *Aspergillus niger* significantly increases iron and zinc bioavailability from phytate-rich foods. *Food Nutr. Bull.* **2013**, *34*, S90−S101.

(4) Bohn, L.; Meyer, A. S.; Rasmussen, S. K. Phytate: impact on environment and human nutrition. A challenge for molecular breeding. *J. Zhejiang Univ. Sci. B* **2008**, *9*, 165−191.

(5) Sandberg, A.-S.; Brune, M.; Carlsson, N.-G.; Hallberg, L.; Skoglund, E.; Rossander-Hulthén, L. Inositol phosphates with different numbers of phosphate groups influence iron absorption in humans. *Am. J. Clin. Nutr.* **1999**, *70*, 240−246.

(6) Pontoppidan, K.; Pettersson, D.; Sandberg, A.-S. Interaction of phytate with protein and minerals in a soybean−maize meal blend depends on pH and calcium addition. *J. Sci. Food Agric.* **2007**, *87*, 1886−1892.

(7) Andrews, N. C. Iron metabolism. In *Principles of Molecular Medicine*; Runge, M. S., Patterson, C., Eds.; Humana Press: Totowa, NJ, USA, 2006; pp 848−853.

DOI: 10.1021/jf5050469
J. Agric. Food Chem. 2015, 63, 943−950

(8) World Health Organization. *Safety Evaluation of Certain Food Additives*; WHO Food Additives Series 67; WHO Press: Geneva, Switzerland, 2012.
(9) Xiang, T.; Liu, Q.; Deacon, A. M.; Koshy, M.; Kriksunov, I. A.; Lei, X. G.; Hao, Q.; Thiel, D. J. Crystal structure of a heat-resilient phytase from *Aspergillus fumigatus*, carrying a phosphorylated histidine. *J. Mol. Biol.* **2004**, *339*, 437−445.
(10) Kim, H.-W.; Kim, Y.-O.; Lee, J.-H.; Kim, K.-K.; Kim, Y.-J. Isolation and characterization of a phytase with improved properties from *Citrobacter braakii*. *Biotechnol. Lett.* **2003**, *25*, 1231−1234.
(11) Lassen, S. F.; Bech, L.; Fuglsang, C. C.; Ohmann, A.; Breinholt, J.; Østergaard, P. R. Peniophora phytase. U.S. Patent 6,054,306, April 25, 2000.
(12) Greiner, R.; Konietzny, U.; Jany, K.-D. Purification and characterization of two phytases from *Escherichia coli*. *Arch. Biochem. Biophys.* **1993**, *303*, 107−113.
(13) Ariza, A.; Moroz, O. V.; Blagova, E. V.; Turkenburg, J. P.; Waterman, J.; Roberts, S. M.; Vind, J.; Sjøholm, C.; Lassen, S. F.; De Maria, L.; Glitsoe, V.; Skov, L. K.; Wilson, K. S. Degradation of phytate by the 6-phytase from *Hafnia alvei*: a combined structural and solution study. *PLoS One* **2013**, *8*, No. e65062.
(14) Michalak, M.; Thomassen, L. V.; Roytio, H.; Ouwehand, A. C.; Meyer, A. S.; Mikkelsen, J. D. Expression and characterization of an endo-1,4-β-galactanase from *Emericella nidulans* in *Pichia pastoris* for enzymatic design of potentially prebiotic oligosaccharides from potato galactans. *Enzyme Microb. Technol.* **2012**, *50*, 121−129.
(15) Bohn, L.; Josefsen, L.; Meyer, A. S.; Rasmussen, S. K. Quantitative analysis of phytate globoids isolated from wheat bran and characterization of their sequential dephosphorylation by wheat phytase. *J. Agric. Food Chem.* **2007**, *55*, 7547−7552.
(16) Carlsson, N.-G.; Bergman, E.-L.; Skoglund, E.; Hasselblad, K.; Sandberg, A.-S. Rapid analysis of inositol phosphates. *J. Agric. Food Chem.* **2001**, *49*, 1695−1701.
(17) Skoglund, E.; Carlsson, N.-G.; Sandberg, A.-S. High-performance chromatographic separation of inositol phosphate isomers on strong anion exchange columns. *J. Agric. Food Chem.* **1998**, *46*, 1877−1882.
(18) Brask-Pedersen, D. N.; Glitsø, L. V.; Skov, L. K.; Lund, P.; Sehested, J. Effect of exogenous phytase on feed inositol phosphate hydrolysis in an *in vitro* rumen fluid buffer system. *J. Dairy Sci.* **2011**, *94*, 951−959.
(19) Haraldsson, A.-K.; Veide, J.; Andlid, T.; Alminger, M. L.; Sandberg, A.-S. Degradation of phytate by high-phytase *Saccharomyces cerevisiae* strains during simulated gastrointestinal digestion. *J. Agric. Food Chem.* **2005**, *53*, 5438−5444.
(20) Gasteiger, E.; Hoogland, C.; Gattiker, A.; Duvaud, S.; Wilkins, M. R.; Appel, R. D.; Bairoch, A. Protein identification and analysis tools on the ExPASy server. In *The Proteomics Protocols Handbook*; Walker, J. M., Ed.; Humana Press: Totowa, NJ, USA, 2005; pp 571−607.
(21) Sreerama, N.; Woody, R. W. Estimation of protein secondary structure from circular dichroism spectra: comparison of CONTIN, SELCON, and CDSSTR methods with an expanded reference set. *Anal. Biochem.* **2000**, *287*, 252−260.
(22) Whitmore, L.; Wallace, B. A. Protein secondary structure analyses from circular dichroism spectroscopy: methods and reference databases. *Biopolymers* **2008**, *89*, 392−400.
(23) Goujon, M.; McWilliam, H.; Li, W.; Valentin, F.; Squizzato, S.; Paern, J.; Lopez, R. A new bioinformatics analysis tools framework at EMBL-EBI. *Nucleic Acids Res.* **2010**, *38*, W695−W699.
(24) Sievers, F.; Wilm, A.; Dineen, D.; Gibson, T. J.; Karplus, K.; Li, W.; Lopez, R.; McWilliam, H.; Remmert, M.; Söding, J.; Thompson, J. D.; Higgins, D. G. Fast, scalable generation of high-quality protein multiple sequence alignments using Clustal Omega. *Mol. Syst. Biol.* **2011**, *7*, 539.
(25) Kelley, L. A.; Sternberg, M. J. E. Protein structure prediction on the Web: a case study using the Phyre server. *Nat. Protoc.* **2009**, *4*, 363−371.
(26) Baum, A.; Agger, J.; Meyer, A. S.; Egebo, M.; Mikkelsen, J. D. Rapid near infrared spectroscopy for prediction of enzymatic hydrolysis of corn bran after various pretreatments. *Nat. Biotechnol.* **2012**, *29*, 293−301.
(27) R Development Core Team. R: A Language and Environment for Statistical Computing, 2008.
(28) Lassen, S. F.; Breinholt, J.; Østergaard, P. R.; Brugger, R.; Bischoff, A.; Wyss, M.; Fuglsang, C. C. Expression, gene cloning, and characterization of five novel phytases from four Basidiomycete fungi: *Peniophora lycii*, *Agrocybe pediades*, a *Ceriporia* sp., and *Trametes pubescens*. *Appl. Environ. Microbiol.* **2001**, *67*, 4701−4707.
(29) Igbasan, F. A.; Männer, K.; Miksch, G.; Borriss, R.; Farouk, A.; Simon, O. Comparative studies on the *in vitro* properties of phytases from various microbial origins. *Arch. Tierernaehrung* **2000**, *53*, 353−373.
(30) Ullah, A. H.; Sethumadhavan, K. PhyA gene product of *Aspergillus ficuum* and *Peniophora lycii* produces dissimilar phytases. *Biochem. Biophys. Res. Commun.* **2003**, *303*, 463−468.
(31) Lei, X.; Mullaney, E. J.; Ullah, A. H. J. Using mutations to improve *Aspergillus niger* phytases. U.S. Patent 7,309,505 B2, Dec 18, 2007.
(32) Sandberg, A.-S.; Hulthén, L. R.; Türk, M. Dietary *Aspergillus niger* phytase increases iron absorption in humans. *J. Nutr.* **1996**, *126*, 476−480.
(33) Kim, T.; Mullaney, E. J.; Porres, J. M.; Roneker, K. R.; Crowe, S.; Rice, S.; Ko, T.; Ullah, A. H. J.; Daly, C. B.; Welch, R.; Lei, X. G. Shifting the pH profile of *Aspergillus niger* PhyA phytase to match the stomach pH enhances its effectiveness as an animal feed additive. *Appl. Environ. Microbiol.* **2006**, *72*, 4397−4403.
(34) Brejnholt, S. M.; Dionisio, G.; Glitsoe, V.; Skov, L. K.; Brinch-Pedersen, H. The degradation of phytate by microbial and wheat phytases is dependent on the phytate matrix and the phytase origin. *J. Sci. Food Agric.* **2011**, *91*, 1398−1405.
(35) Simon, O.; Igbasan, F. *In vitro* properties of phytases from various microbial origins. *Int. J. Food Sci. Technol.* **2002**, *37*, 813−822.
(36) Phillippy, B. Q. Susceptibility of wheat and *Aspergillus niger* phytases to inactivation by gastrointestinal enzymes. *J. Agric. Food Chem.* **1999**, *47*, 1385−1388.
(37) Rodriguez, E.; Porres, J. M.; Han, Y.; Lei, X. G. Different sensitivity of recombinant *Aspergillus niger* phytase (r-PhyA) and *Escherichia coli* pH 2.5 acid phosphatase (r-AppA) to trypsin and pepsin *in vitro*. *Arch. Biochem. Biophys.* **1999**, *365*, 262−267.
(38) Greiner, R.; Farouk, A.-E. Purification and characterization of a bacterial phytase whose properties make it exceptionally useful as a feed supplement. *Protein J.* **2007**, *26*, 467−474.
(39) Pontoppidan, K.; Pettersson, D.; Sandberg, A.-S. *Peniophora lycii* phytase is stabile and degrades phytate and solubilises minerals *in vitro* during simulation of gastrointestinal digestion in the pig. *J. Sci. Food Agric.* **2007**, *87*, 2700−2708.
(40) Garrett, J. B.; Kretz, K. A.; O'Donoghue, E.; Kerovuo, J.; Kim, W.; Barton, N. R.; Hazlewood, G. P.; Short, J. M.; Robertson, D. E.; Gray, K. A. Enhancing the thermal tolerance and gastric performance of a microbial phytase for use as a phosphate-mobilizing monogastric-feed supplement. *Appl. Environ. Microbiol.* **2004**, *70*, 3041−3046.
(41) Reddy, N. R. Occurrence, distribution, content, and dietary intake of phytate. In *Food Phytates*; Reddy, N. R., Sathe, S. K., Eds.; CRC Press: Boca Raton, FL, USA, 2002.
(42) Shockravi, S.; Almgren, A.; Carlsson, N.-G.; Sandberg, A.-S. Dephytinisation of Sangak and Barbari bread made from different extraction rate flours increases iron and zinc bioaccessibility in Caco-2 cells. *Int. J. Food Sci. Technol.* **2012**, *47*, 2252−2258.
(43) Shilpa, K. S.; Lakshmi, A. J. Comparison of enhancement in bioaccessible iron and zinc in native and fortified high-phytate oilseed and cereal composites by activating endogenous phytase. *Int. J. Food Sci. Technol.* **2012**, *47*, 1613−1619.
(44) Glahn, R. P.; Lee, O. A.; Yeung, A.; Goldman, M. I.; Miller, D. D. Caco-2 cell ferritin formation predicts nonradiolabeled food iron availability in an *in vitro* digestion/Caco-2 cell culture model. *J. Nutr.* **1998**, *128*, 1555−1561.

DOI: 10.1021/jf5050469
J. Agric. Food Chem. 2015, 63, 943−950

these compounds. Freezing has been shown as an effective method of minimizing the oxidative degradation of these compounds during storage.[4,10]

MATERIALS AND METHODS

Raw Materials. Vegetable seeds were donated by the Seminis Vegetable Seed Co., Inc., Woodland, CA. Six replicate samples were harvested from different randomly selected points along linear rows for each commodity. Commodities were harvested according to the times and locations listed in Table 1.

Table 1. Harvest Times and Locations for Each Commodity Studied

commodity	month and year	harvest location
spinach	December 2012	Full Belly Farm (Guinda, CA)
carrots	November 2012	UC Davis (Davis, CA)
broccoli	February 2013	UC Davis (Davis, CA)
blueberries	March 2013	California Coastal Blueberry Farms (Oxnard, CA)
peas	April 2013	Iacopi Farm (Half Moon Bay, CA)
green beans	June 2013	UC Davis (Davis, CA)
strawberries	July 2013	Driscoll's (Watsonville, CA)
corn	August 2013	UC Davis (Davis, CA)

All commodities were harvested at uniform maturity as determined by both color and approximate size, as recommended by the grower. All commodities were transported to the UC Davis (University of California, Davis) Food Science and Technology pilot processing plant in refrigerated Styrofoam coolers (Lifoam Industries, Hunt Valley, MD) and processed immediately.

Processing. Throughout the processing and storage chains, each of the six field replicates was maintained as discrete samples. All commodities were given a preliminary rinse with water prior to entering the pilot plant to avoid unnecessary contamination of the facilities. Commodities were then submerged in a flume wash (Food Science and Technology Machine Shop, Davis, CA) filled with water and rinsed thoroughly to remove any surface dirt. Some commodities received additional processing steps prior to blanching: carrots were diced into 1.5 cm cubes using an Urschel G-A dicer (Urschel Laboratories, Inc., Valparaiso, IN), strawberries had their crowns removed by hand, green beans and peas were destemmed by hand, broccoli was cut into 3−5 cm florets by hand, and individual corn kernels were removed from the cob by hand using a Zyliss corn stripper (Zyliss, Irvine, CA).

For each field replicate of each commodity, cleaned, prepared samples were randomized and separated into two parts. Half of each field replicate was then marked for fresh storage, while the other half was blanched and frozen. The samples to be blanched were loaded onto the steam blanching line (Food Science and Technology Machine Shop) in stainless steel baskets for the specified amount of time and temperature (Table 2). Following blanching, the samples were transferred onto wire mesh racks and placed immediately into a −32 °C walk-in freezer (Estes Refrigeration, Inc., Richmond, CA). After 1 h, the frozen commodity was divided into three 300 g storage samples which were packaged in UltraSource 3 mil polyethylene pouches (UltraSource LLC, Kansas City, MO) and stored at −27.5 °C (18 °F) for up to 90 days. Blueberries and strawberries were not blanched prior to freezing, in accordance with industry practices.

Table 2. Blanching Protocols for Each Commodity

commodity	blanch time (min)	blanch temp (°C)	commodity	blanch time (min)	blanch temp (°C)
blueberries	N/A	N/A	corn	3.5	93.3
strawberries	N/A	N/A	green beans	3.5	93.3
broccoli	1.5	90.5	peas	2	93.3
carrots	2	96.1	spinach	3	93.3

Stability Study. The fresh half of each field replicate was divided into three 300 g storage samples which were stored in breathable Tuf-R low-density polyethylene bags (U.S. Plastic Corp., Lima, OH) at 2 °C (35.6 °F) in a walk-in refrigerator (Estes Refrigeration, Inc.) for up to 10 days. The frozen half of each field replicate was divided into three 300 g storage samples which were packaged in UltraSource 3 mil polyethylene pouches (UltraSource LLC) and stored at −27.5 °C (18 °F) for up to 90 days. For each field replicate, one frozen pouch and one fresh pouch were analyzed within 24 h of harvest (day 0) and after each storage time: 3 and 10 days for fresh; 10 and 90 days for frozen. Upon completion of each storage period, samples were removed from storage and transported in refrigerated coolers to the UC Davis Analytical Laboratory facilities for analysis.

Minerals. *Acid Digestion.* A 0.5 g portion of dried, homogenized sample was weighed and transferred to a Teflon PFA double-wall digestion vessel with a 200 psi relief seal (CEM Corp., Matthews, NC). A 1 mL volume of nitric acid and 2 mL of hydrogen peroxide (Fisher Scientific Co., Pittsburgh, PA) were added and gently mixed with the sample. The vessel was capped tightly and allowed to predigest for 10−15 min. Samples were digested for 5 min at 40% power and 8 min at 90% power in a CEM MDS 2000 microwave digestion system (CEM Corp.). After cooling, the digest was transferred to a 15 mL centrifuge tube using deionized water to rinse the vessel. The volume was adjusted to 15 mL with deionized water. The test tube was mixed by being shaken vigorously and allowed to sit overnight to allow particles to settle out. A 1 mL aliquot of the digest was diluted with 3 mL of deionized water and analyzed on a Thermo iCAP 6500 inductively coupled plasma atomic emission spectrometer (Thermo Fisher Scientific, Hudson, NH).

Fiber. *Reagents.* Acid detergent solution was prepared by thoroughly mixing 2 L of Ankom acid detergent liquid (Ankom Technology, Macedon, NY) with 8 L of deionized water. Sulfuric acid solution was prepared by diluting 650 mL of concentrated sulfuric acid (Fisher Scientific Co.) to 2 L with deionized water.

Acid Digestion. Approximately 1 g of dried, ground sample material was weighed into an aluminum weigh dish (Fisher Scientific Co.). The sample was washed into a 600 mL refluxing beaker using acid detergent solution. Additional acid detergent solution was added to fill the beaker to the 100 mL mark. The sample solution was heated under reflux for 60 min and then filtered using a coarse porosity fritted glass crucible (Corning, Tewksbury, MA). The sample was rinsed twice with 90−100 °C water and twice with acetone, then dried for 3 h at 105 °C, cooled, and weighed.

Total Phenols. *Reagents.* Sodium carbonate solution consisted of 75 g of sodium carbonate (Fisher Scientific Co.) diluted in 1 L of deionized water. Gallic acid standards of 40, 100, and 2500 mg/L concentrations were prepared by mixing gallic acid (Arcos Organics, Geel, Belgium) with acetone to the appropriate concentration. Folin and Ciocalteu's phenol reagent (2 N) was obtained from Sigma-Aldrich, Buchs, Switzerland.

Folin−Ciocalteu Treatment. Samples were homogenized with 60% water by weight of sample. A 6.4 g mass of each of the blended samples was weighed into a 50 mL plastic centrifuge tube. Samples were homogenized with 27.6 mL of 76% (v/v) aqueous acetone (Fisher Scientific Co.) for 30 s using an Ultra Turrax T25 basic homogenizer (IKA Works, Inc., Wilmington, NC). After being shaken for 10 min, the samples were centrifuged at 2000 rpm for 10 min. To 1 mL of extract was added 0.36 mL of 2 N Folin reagent. The solution was vortexed and allowed to stand for 5 min, then 6 mL of sodium carbonate was added, and the solution was vortexed again. Deionized water (2.64 mL) was added, and the solution was vortexed and incubated at 50 °C for 5 min. After the solution was cooled to room temperature for 1 h, the absorbance was read at 760 nm and compared to a calibration curve of derivatized gallic acid.

Statistical Analysis. Statistical analysis was performed using JMP statistical software version 9.0.0 (SAS Institute Inc., Cary, NJ). A blocked analysis of variance (ANOVA) was run with storage time point and processing treatment as the treatments. Tukey comparisons

DOI: 10.1021/jf504890k
J. Agric. Food Chem. 2015, 63, 951−956

Table 3. Mineral, Fiber, and Total Phenolic Content of Eight Commodities Stored under Either Refrigeration or Frozen Conditions for Three Storage Times[a]

	storage time (days)	calcium content (%)	magnesium content (%)	zinc content (mg/kg)	copper content (mg/kg)	iron content (mg/kg)	fiber content (%)	phenolics content (mg GAE/g)
				Peas				
fresh	0	0.325 bc (0.018)	0.186 b (0.004)	29.9 bc (0.3)	2.8 bc (0.0)	55.0 c (1.0)	8.3 a (0.5)	3.78 c (0.10)
fresh	3	N/A	N/A	N/A	N/A	N/A	8.4 a (0.3)	3.97 b (0.15)
fresh	10	N/A	N/A	N/A	N/A	N/A	8.4 a (0.4)	4.13 a (0.13)
frozen	0	0.308 c (0.011)	0.173 c (0.004)	28.3 d (0.3)	2.7 bc (0.1)	54.5 c (1.4)	6.0 b (0.0)	3.22 d (0.11)
frozen	10	N/A	N/A	N/A	N/A	N/A	5.9 b (0.0)	3.17 d (0.13)
frozen	90	N/A	N/A	N/A	N/A	N/A	6.3 b (0.3)	2.93 e (0.06)
				Spinach				
fresh	0	0.719 a (0.073)	1.126 a (0.030)	79.8 a (5.2)	11.7 a (0.8)	777.6 a (169.7)	8.9 a (0.5)	7.71 b (0.29)
fresh	3	N/A	N/A	N/A	N/A	768.6 a (154.0)	10.5 a (0.5)	8.90 a (0.39)
fresh	10	N/A	N/A	N/A	N/A	761.7 a (168.4)	10.1 a (0.5)	9.12 a (0.35)
frozen	0	0.705 a (0.066)	0.928 b (0.071)	71.4 a (5.2)	11.7 a (1.5)	448.3 b (61.5)	9.6 a (0.5)	8.00 b (0.53)
frozen	10	N/A	N/A	N/A	N/A	414.8 b (58.6)	8.8 a (0.5)	9.58 a (0.81)
frozen	90	N/A	N/A	N/A	N/A	421.5 b (74.0)	8.6 a (2.2)	9.19 a (0.44)
				Green Beans				
fresh	0	0.542 a (0.0.047)	0.267 ab (0.014)	34.0 a (1.5)	8.1 a (0.5)	72.3 a (4.0)	15.9 ab (0.7)	2.23 ab (0.06)
fresh	3	N/A	N/A	N/A	N/A	N/A	15.9 ab (0.7)	2.09 b (0.09)
fresh	10	N/A	N/A	N/A	N/A	N/A	16.8 a (0.9)	2.19 ab (0.10)
frozen	0	0.532 a (0.056)	0.259 b (0.017)	33.1 ab (3.3)	7.9 a (0.8)	76.6 a (7.0)	15.3 bc (1.0)	2.22 ab (0.20)
frozen	10	N/A	N/A	N/A	N/A	N/A	15.0 bc (1.2)	2.17 ab (0.13)
frozen	90	N/A	N/A	N/A	N/A	N/A	14.6 c (1.3)	2.31 a (0.20)
				Broccoli				
fresh	0	0.292 a (0.049)	0.251 b (0.020)	39.6 a (5.5)	4.7 a (0.5)	91.2 ab (18.3)	11.3 b (0.6)	8.04 c (0.29)
fresh	3	N/A	N/A	N/A	N/A	N/A	11.8 b (0.5)	8.73 c (0.40)
fresh	10	N/A	N/A	N/A	N/A	N/A	13.7 a (0.9)	11.09 a (0.41)
frozen	0	0.302 a (0.038)	0.251 b (0.017)	39.7 a (6.0)	4.4 a (0.4)	70.4 b (9.5)	11.2 b (0.8)	7.99 c (0.36)
frozen	10	N/A	N/A	N/A	N/A	N/A	10.8 b (1.1)	9.57 b (0.43)
frozen	90	N/A	N/A	N/A	N/A	N/A	11.4 b (0.5)	8.29 c (0.36)
				Carrots				
fresh	0	0.32 a (0.015)	0.228 a (0.021)	17.7 ab (0.7)	6.9 a (0.8)	71.1 a (12.3)	12.6 a (1.7)	1.08 ab (0.15)
fresh	3	N/A	N/A	N/A	N/A	N/A	12.0 a (0.6)	1.05 b (0.13)
fresh	10	N/A	N/A	N/A	N/A	N/A	13.5 a (1.5)	1.05 b (0.16)
frozen	0	0.306 a (0.010)	0.223 a (0.016)	18.5 a (0.5)	6.5 a (0.8)	60.5 a (7.4)	12.3 a (0.5)	1.33 a (0.26)
frozen	10	N/A	N/A	N/A	N/A	N/A	12.2 a (0.8)	1.22 ab (0.21)
frozen	90	N/A	N/A	N/A	N/A	N/A	9.2 b (0.3)	1.12 ab (0.26)
				Corn				
fresh	0	N/A	0.119 ab (0.005)	23.6 ab (1.1)	2.1 a (0.4)	16.6 a (1.2)	2.7 c (0.2)	2.42 a (0.07)
fresh	3	N/A	N/A	N/A	N/A	N/A	2.9 bc (0.2)	2.28 a (0.06)
fresh	10	N/A	N/A	N/A	N/A	N/A	2.9 bc (0.0)	1.97 b (0.16)
frozen	0	N/A	0.106 c (0.006)	21.8 b (1.0)	2.0 a (0.2)	14.6 a (1.3)	3.3 a (0.3)	2.45 a (0.12)
frozen	10	N/A	N/A	N/A	N/A	N/A	3.2 ab (0.1)	2.29 a (0.08)
frozen	90	N/A	N/A	N/A	N/A	N/A	3.1 ab (0.3)	1.76 c (0.07)
				Blueberries				
fresh	0	0.102 a (0.008)	0.061 b (0.000)	4.7 b (0.2)	2.8 a (0.3)	26.1 a (2.7)	7.0 a (0.3)	21.31 d (0.69)
fresh	3	N/A	N/A	N/A	N/A	N/A	7.1 a (0.4)	21.48 d (1.14)
fresh	10	N/A	N/A	N/A	N/A	N/A	6.8 ab (0.4)	22.07 cd (1.43)
frozen	0	0.102 a (0.006)	0.060 b (0.001)	4.8 b (0.1)	2.5 a (0.2)	24.7 a (4.1)	6.4 bc (0.3)	23.39 bc (0.74)
frozen	10	N/A	N/A	N/A	N/A	N/A	6.3 c (0.4)	24.57 ab (0.72)
frozen	90	N/A	N/A	N/A	N/A	N/A	6.9 ab (0.0)	26.13 a (0.61)
				Strawberries				
fresh	0	0.306 a (0.011)	0.170 a (0.013)	14.1 ab (0.6)	6.1 ab (0.5)	56.3 a (5.1)	8.8 a (0.5)	22.21 a (1.34)
fresh	3	N/A	N/A	N/A	N/A	N/A	8.8 a (0.5)	23.22 a (1.31)
fresh	10	N/A	N/A	N/A	N/A	N/A	8.7 a (0.7)	22.60 a (0.99)
frozen	0	0.290 a (0.036)	0.153 a (0.007)	14.0 ab (0.7)	5.6 ab (0.5)	46.6 b (2.2)	8.8 a (0.5)	21.91 a (0.40)
frozen	10	N/A	N/A	N/A	N/A	N/A	9.1 a (0.6)	22.43 a (0.78)
frozen	90	N/A	N/A	N/A	N/A	N/A	8.3 a (0.5)	22.03 a (1.49)

[a]Each data point represents the mean of six field replicates and is followed by the standard deviation for those replicates in parentheses. Significantly different values between storage points for a given commodity and nutrient are followed by different letters.

DOI: 10.1021/jf504890k
J. Agric. Food Chem. 2015, 63, 951−956

were used to determine the significance of differences between both fresh and frozen treatments and storage time points for each commodity and nutrient.

RESULTS AND DISCUSSION

The results of this study are presented in Table 3. The content of five minerals as well as fiber and total phenolics was evaluated in eight different commodities stored under either refrigeration (fresh) or frozen conditions over three storage points.

Minerals. Rickman et al.[4] and previous authors have found that minerals are unaffected by the thermal treatments implemented during conventional food processing.[12,13] In fact, leaching of minerals during blanching is the only significant cause of loss of minerals that has been reported that is relevant to the conditions of this study. Water-soluble minerals can be extracted into the water used during the blanching process, causing losses in mineral content of food blanched before further processing.[4,6,14]

While all commodities were washed and scrubbed thoroughly prior to sampling, it is possible that some soil may have remained on the samples, which would have artificially augmented the baseline fresh values and would have caused an apparent decrease in frozen values due to the fact that the mineral-rich soil had been removed during blanching. To evaluate this possibility, an extra set of carrot samples was analyzed. The carrots were peeled after washing and sampled according to the same experimental protocol as the other samples in this study. Half of the peeled carrot samples were stored fresh, and the other half were blanched and frozen. There were no significant differences in mineral content between the fresh and frozen peeled carrots. This suggests that some of the difference in mineral content of samples immediately after blanching is due to removal of residual soil particles.

Calcium. Calcium was one of the best-retained nutrients in the fresh and frozen stored commodities evaluated over the course of this study. In all commodities, there were no significant differences between the frozen samples and those that were stored fresh (Table 3). These results were consistent with the findings of Wills et al.[15] and Maklouf et al.,[16] who found that the calcium content of frozen vegetables was highly conserved, if not higher than in fresh-stored produce.

Magnesium. Magnesium was largely well conserved over both fresh and frozen storage in most commodities. Broccoli, carrots, blueberries, and strawberries showed no significant difference in magnesium content between fresh and frozen samples (Table 3).

Frozen peas, spinach, and corn contained between ~7% and 18% less magnesium when compared to fresh samples (Table 3). These changes were apparent immediately following processing, indicating that minor losses were most likely caused by leaching of magnesium into the blanching water.[16,17]

Zinc. The trends in retention of zinc in frozen fruits and vegetables were similar to those of magnesium. Broccoli, carrots, strawberries, green beans, corn, blueberries, and spinach showed no significant difference between fresh and frozen treatments, while peas showed small losses (~5%) in frozen samples (Table 3).

Copper. Copper, like calcium, was well retained in frozen as compared to fresh produce. In all commodities, there were no significant decreases in the frozen samples (Table 3). This indicates that there were no losses due to leaching of nutrients during blanching, which is the only reason cited in the literature for loss of minerals during the freezing process where no tissue is removed.[4,12,13]

Iron. Two general trends were apparent in the retention of iron in frozen and fresh produce. In green beans, broccoli, carrot variety B, blueberries, strawberries, and peas, there were no significant differences in the iron content between the two treatments. However, in spinach and carrot variety A, the frozen samples had between 10% and 45% less iron than the fresh samples (Table 3). This could be due to leaching of iron during blanching,[14,16,17] since as illustrated with spinach, the loss occurs immediately after blanching and freezing. It may also have been due to small traces of soil left on the surface of products that was washed off during blanching. The amount of surface area exposed to blanching may have also contributed, since the carrots were diced prior to blanching and the spinach had high surface area naturally.

Acid-Digestible Fiber (ADF). Most of the commodities (blueberries, strawberries, green beans, peas, spinach, and corn) showed no significant change in fiber content over the course of fresh or frozen processing and storage (Table 3); however, some commodities showed increases during storage or declines as a result of either blanching or frozen storage. Broccoli showed an increase (21.2%) in fiber content during fresh storage (Figure 1). This could be due to continued respiration

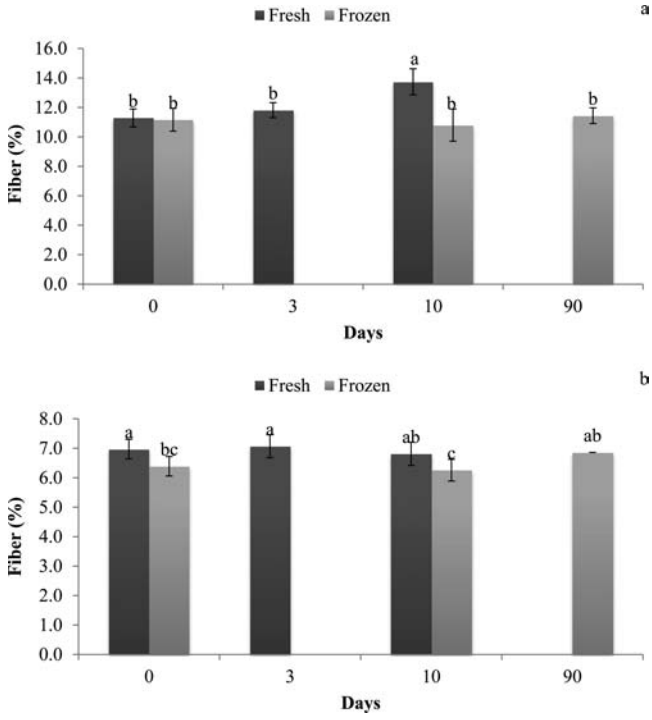

Figure 1. Fiber content of (a) broccoli and (b) blueberries during fresh and frozen storage. Values reported on a dry weight basis. Values that share the same letter (a, b, c) are not significantly different ($p \leq 0.05$).

and thickening of cell walls within broccoli tissue during storage.[18] Some commodities, such as bamboo shoots, have been known to exhibit such behavior during postharvest storage as a stress response.[19] It should be noted that while increases in fiber content were found in vegetables such as onions in previous studies,[20] the increases occurred over much longer periods of fresh storage than in this study. Onions respire

DOI: 10.1021/jf504890k
J. Agric. Food Chem. 2015, 63, 951−956

slower than broccoli, so that may be the reason for the difference. This increase in fiber content during fresh storage caused fresh broccoli to appear to have higher fiber content than frozen broccoli, even though the fiber content of frozen broccoli was unaltered during processing and storage.

Both varieties of carrots lost fiber (~25%) during frozen storage. This could be due to degradation of cell wall components such as cellulose, hemicellulose, pectin, and lignin, which is known to occur during frozen storage of some commodities.[21] Degradation of these polysaccharides in these tissues could have caused the apparent decrease in fiber over storage time.

Fiber losses in peas appear to be due to physical losses during the blanching and freezing process, as the decline occurs immediately after these processes on day 0. According to Kunzek et al.,[22] thermal processing can cause changes in the solubility of plant carbohydrates, which could account for the losses seen in peas, which were among the commodities blanched before freezing. This seems to be corroborated by the fact that two of the commodities with the best retention of fiber were strawberries and blueberries, the two commodities that received no blanching treatment prior to freezing.

Some variability in the method of analysis of fiber, or variability in the raw material, may have had an impact on these results, as frozen blueberries showed slight decreases in fiber levels initially (~8%), but by the end of the 90 day frozen storage period, the frozen product was not significantly different from the fresh product (Figure 1). Previous studies indicated little to no loss of fiber for any commodities during processing apart from methods that involved peeling or otherwise removing plant tissue.[4,14]

Phenolics. Overall, phenolics were well retained in both fresh and frozen produce, and some commodities retained higher concentrations with frozen storage. Spinach, green beans, and carrots showed no significant differences between fresh and frozen produce, while broccoli, corn, and peas had lower levels of phenolic compounds in frozen samples (Figure 2). This could be due to either oxidation of phenolic compounds or leaching of water-soluble phenolic compounds during blanching.[14,23] The decline in phenolic content of peas during frozen storage may be due to oxidation of sensitive phenolic compounds, which can occur nonenzymatically even at temperatures encountered in frozen storage.[4,14] The increases in phenolics in broccoli and peas over the fresh storage period contrast with the findings of Vallejo et al.,[23] who found large losses in phenolic content of fresh broccoli over a period of 10 days, but are supported by Olivera et al.,[24] who proposed that rupture of cellular compartments such as vacuoles during processing could lead to increased availability of phenolic compounds. Blueberries showed higher values of phenolics in frozen compared to fresh samples. This may be due to high oxidative enzymatic activity in fresh blueberries, which would have been minimized by frozen storage.[24,25]

Conclusions. With regard to the nutrients studied, frozen fruits and vegetables represent nutritionally viable alternatives to fresh produce subjected to typical postharvest holding times. Total phenolics, fiber, and minerals were for the most part well conserved in frozen samples as compared to fresh, and when there were decreases in frozen samples, they were usually small and may have been due to some variability in the raw material.

In this study we sought to evaluate the nutritional quality of fruits and vegetables as they arrived to the consumer. A logical progression to future studies would include evaluation of what happens to that nutrient content during preparation for consumption in the home. Knowledge about basic culinary practices involved in preparation of these commodities for consumption in the home would provide useful insight into how they can best be preserved.

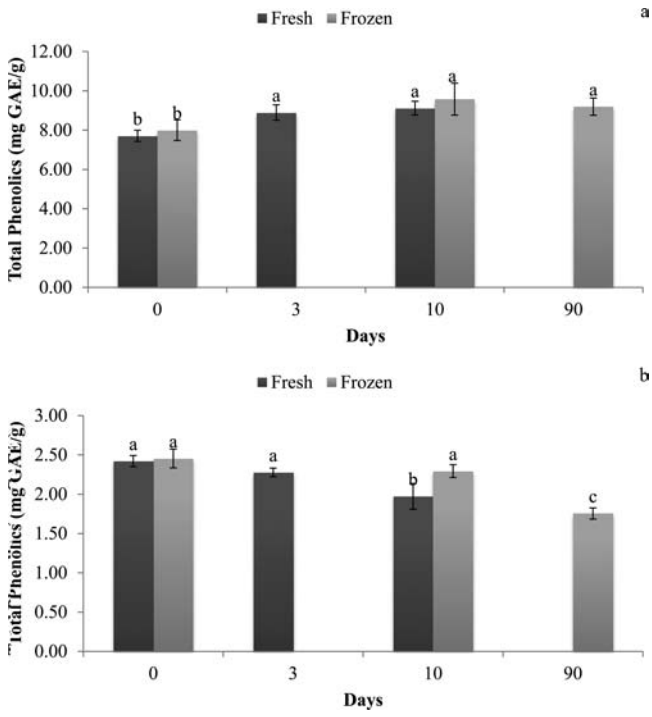

Figure 2. Phenolics content of (a) spinach and (b) corn during fresh and frozen storage. Values reported on a dry weight basis. Values that share the same letter (a, b, c, d, e) are not significantly different ($p \leq 0.05$).

AUTHOR INFORMATION

Notes

The authors declare no competing financial interest.

REFERENCES

(1) World Health Organization (WHO). *Diet, Nutrition, and the Prevention of Chronic Diseases*; Technical Report Series 797; WHO: Geneva, Switzerland, 1990.

(2) Liu, R. H. Health benefits of fruit and vegetables are from additive and synergistic combinations of phytochemicals. *Am. J. Clin. Nutr.* **2003**, *78*, 517S−520S.

(3) Barrett, D. M. Maximizing the nutritional value of fruits & vegetables. *Food Technol.* **2007**, *61*, 40−44.

(4) Rickman, J. C.; Bruhn, C. M.; Barrett, D. M. Nutritional comparison of fresh, frozen, and canned fruits and vegetables—II. Vitamin A and carotenoids, vitamin E, minerals and fiber. *J. Sci. Food Agric.* **2007**, *87*, 1185−1196.

(5) Koh, E.; Wimalasiri, K. M. S.; Chassy, A. W.; Mitchell, A. E. Content of ascorbic acid, quercetin, kaempferol and total phenolics in commercial broccoli. *J. Food Compos. Anal.* **2009**, *22*, 637−643.

(6) Goyal, R. K. Nutritive value of fruits, vegetables, and their products. In *Postharvest Technology of Fruits & Vegetables*; Verma, L. R., Joshi, V. K., Eds.; Indus: New Delhi, 2000; pp 377−389.

(7) Kmiecik, W.; Lisiewska, Z.; Korus, A. Retention of mineral constituents in frozen brassicas depending on the method of preliminary processing of the raw material and preparation of frozen products for consumption. *Eur. Food Res. Technol.* **2007**, *224*, 573−579.

DOI: 10.1021/jf504890k
J. Agric. Food Chem. 2015, 63, 951−956

(8) Barringer, S. Canned tomatoes: production and storage. In *Handbook of Vegetable Preservation and Processing*; Hyu, Y. H., Ghazala, S., Graham, D. M., Murrell, K. D., Nip, W., Eds.; Marcel Dekker: New York, 2004; pp 109−120.
(9) Dreher, M. L. Dietary fiber overview. In *Handbook of Dietary Fiber*; Cho, S. S., Dreher, M. L., Eds.; CRC Press: Boca Raton, FL, 2001; pp 1−15.
(10) Ngo, T.; Wrolstad, R. E.; Zhao, Y. Color quality of Oregon strawberries—impact of genotype, composition, and processing. *J. Food Sci.* **2007**, *72*, C25−C32.
(11) Myojin, C.; Enami, N.; Nagata, A.; Yamaguchi, T.; Takamura, H.; Matoba, T. Changes in the radical-scavenging activity of bitter gourd (*Momordica charantia* L.) during freezing and frozen storage with or without blanching. *J. Food Sci.* **2008**, *73*, C546−C550.
(12) Martin-Belloso, O.; Llanos-Barriobero, E. Proximate composition, minerals and vitamins in selected canned vegetables. *Eur. Food Res. Technol.* **2001**, *212*, 182−187.
(13) Elkins, E. R. Nutrient content of raw and canned grean beans, peaches, and sweet potatoes. *Food Technol.* **1979**, *33*, 66−70.
(14) Puuponen-Pimia, R.; Hakkinen, S. T.; Aarni, M.; Suortti, T.; Lampi, A. M.; Eurola, M.; Piironen, V.; Nuutila, A. M.; Oksman-Caldentey, K. M. Blanching and long-term freezing affect various bioactive compounds of vegetables in different ways. *J. Sci. Food Agric.* **2003**, *83*, 1389−1402.
(15) Wills, R. B. H.; Evans, T. J.; Lim, J. S. K.; Scriven, F. M.; Greenfield, H. Composition of Australian foods. 25. Peas and beans. *Food Technol. Aust.* **1984**, *36*, 512−514.
(16) Makhlouf, J.; Zee, J.; Tremblay, N.; Belanger, A.; Michaud, M. H.; Gosselin, A. Some nutritional characteristics of beans, sweet corn, and peas (raw, canned, and frozen) produced in the province of Quebec. *Food Res. Int.* **1995**, *28*, 253−259.
(17) Severi, S.; Bedogni, G.; Manzieri, A. M.; Poli, M.; Battistini, N. Effects of cooking and storage methods on the micronutrient content of foods. *Eur. J. Cancer Prev.* **1997**, *6*, S21−S24.
(18) Muller, S.; Jardine, W. G.; Evans, B. W.; Vietor, R. J.; Snape, C. E.; Jarvis, M. C. Cell wall composition of vascular and parenchyma tissues in broccoli stems. *J. Sci. Food Agric.* **2003**, *83*, 1289−1292.
(19) Luo, Z. S.; Xu, X. L.; Cai, Z. Z.; Yan, M. Effects of ethylene and 1-methylcyclopropene (1-MCP) on lignification of postharvest bamboo shoot. *Food Chem.* **2007**, *105*, 521−527.
(20) Marlett, J. A. Changes in content and composition of dietary fiber in yellow onions and red delicious apples during commercial storage. *J. AOAC Int.* **2000**, *83*, 992−996.
(21) Khan, A. A.; Vincent, J. F. V. Mechanical damage induced by controlled freezing in apple and potato. *J. Texture Stud.* **1996**, *27*, 143−157.
(22) Kunzek, H.; Kabbert, R.; Gloyna, D. Aspects of material science in food processing: changes in plant cell walls of fruits and vegetables. *Z. Lebensm.-Unters. -Forsch. A* **1999**, *208*, 233−250.
(23) Vallejo, F.; Tomas-Barberan, F.; Garcia-Viguera, C. Health-promoting compounds in broccoli as influenced by refrigerated transport and retail sale period. *J. Agric. Food Chem.* **2003**, *51*, 3029−3034.
(24) Olivera, D. F.; Vina, S. Z.; Marani, C. M.; Ferreyra, R. M.; Mugridge, A.; Chaves, A. R.; Mascheroni, R. H. Effect of blanching on the quality of brussels sprouts (*Brassica oleracea* L. *gemmifera* DC) after frozen storage. *J. Food Eng.* **2008**, *84*, 148−155.
(25) Smith, J. P.; Zagory, D.; Ramaswamy, H. S. Packaging of fruits and vegetables. In *Processing Fruits: Science and Technology*; Barrett, D. M., Somogyi, L., Ramaswamy, H., Eds.; CRC Press: Boca Raton, FL, 2005; pp 355−395.

DOI: 10.1021/jf504890k
J. Agric. Food Chem. 2015, 63, 951−956

While fat-soluble vitamin A is not normally found in fruits and vegetables, it can be indirectly obtained through consumption of the carotenoid compound β-carotene. β-Carotene is a metabolic precursor to vitamin A, and in fact, many dietary descriptions of plant-based foods report a vitamin A correlation that is based on the concentration of β-carotene in the product. β-Carotene does not leach out of produce during washing and blanching but is very sensitive to degradation due to oxidation. This potential for oxidation is dependent on the various processing and storage conditions which include exposure to high temperatures, light, and oxygen.[6,19] Retention of β-carotene in frozen storage seems to vary by commodity, with studies showing decreases to different degrees in β-carotene over a prolonged period of frozen storage.[6,20] This is in contrast to fresh storage, where there is reported to be little degradation.[13]

MATERIALS AND METHODS

Raw Materials. Vegetable seeds were donated by the Seminis Vegetable Seed Co., Inc., Woodland, CA. Six replicate samples were harvested from different randomly selected points along linear rows for each commodity. Commodities were harvested according to the times and locations listed in Table 1.

Table 1. Harvest Times and Locations for Each Commodity Studied

commodity	month and year	harvest location
spinach	December 2012	Full Belly Farm (Guinda, CA)
carrots	November 2012	UC Davis (Davis, CA)
broccoli	February 2013	UC Davis (Davis, CA)
blueberries	March 2013	California Coastal Blueberry Farms (Oxnard, CA)
peas	April 2013	Iacopi Farm (Half Moon Bay, CA)
green beans	June 2013	UC Davis (Davis, CA)
strawberries	July 2013	Driscoll's (Watsonville, CA)
corn	August 2013	UC Davis (Davis, CA)

All commodities were harvested at uniform maturity as determined by both color and approximate size, as recommended by the grower. All commodities were transported to the UC Davis (University of California, Davis) Food Science and Technology pilot processing plant in refrigerated Styrofoam coolers (Lifoam Industries, Hunt Valley, MD) and processed immediately.

Processing. Throughout the processing and storage chains, each of the six field replicates was maintained as discrete samples. All commodities were given a preliminary rinse with water prior to entering the pilot plant to avoid unnecessary contamination of the facilities. Commodities were then submerged in a flume wash (Food Science and Technology Machine Shop, Davis, CA) filled with water and rinsed thoroughly to remove any surface dirt. Some commodities received additional processing steps prior to blanching: carrots were diced into 1.5 cm cubes using an Urschel G-A dicer (Urschel Laboratories, Inc., Valparaiso, IN), strawberries had their crowns removed by hand, green beans and peas were destemmed by hand, broccoli was cut into 3−5 cm florets by hand, and individual corn kernels were removed from the cob by hand using a Zyliss corn stripper (Zyliss, Irvine, CA).

For each field replicate of each commodity, cleaned, prepared samples were randomized and separated into two parts. Half of each field replicate was then marked for fresh storage, while the other was blanched and frozen. The samples to be blanched were loaded onto the steam blanching line (Food Science and Technology Machine Shop) in stainless steel baskets for the specified amount of time and temperature (Table 2). Following blanching, the samples were transferred onto wire mesh racks and placed immediately into a −32 °C walk-in freezer (Estes Refrigeration, Inc., Richmond, CA). After 1 h, the frozen commodity was divided into three 300 g storage samples which were packaged in UltraSource 3 mil polyethylene pouches (UltraSource LLC, Kansas City, MO) and stored at −27.5 °C (18 °F) for up to 90 days. Blueberries and strawberries were not blanched prior to freezing, in accordance with industry practices.

Table 2. Blanching Protocols for Each Commodity

commodity	blanch time (min)	blanch temp (°C)	commodity	blanch time (min)	blanch temp (°C)
blueberries	N/A	N/A	corn	3.5	93.3
strawberries	N/A	N/A	green beans	3.5	93.3
broccoli	1.5	90.5	peas	2	93.3
carrots	2	96.1	spinach	3	93.3

Stability Study. The fresh half of each field replicate was divided into three 300 g storage samples which were stored in breathable Tuf-R low-density polyethylene bags (U.S. Plastic Corp., Lima, OH) and stored at 2 °C (35.6 °F) in a walk-in refrigerator (Estes Refrigeration, Inc.) for up to 10 days. The frozen half of each field replicate was divided into three 300 g storage samples which were packaged in UltraSource 3 mil polyethylene pouches (UltraSource LLC) and stored at −27.5 °C (18 °F) for up to 90 days. For each field replicate, one frozen pouch and one fresh pouch were analyzed within 24 h of harvest (day 0) and after each storage time: 3 and 10 days for fresh; 10 and 90 days for frozen. Upon completion of each storage period, samples were removed from storage and transported in refrigerated coolers to the UC Davis Analytical Laboratory facilities for analysis.

Homogenization and Sample Preparation. Fresh or frozen samples were blended in a blender (Vita-Prep 3, Vitamix, Cleveland, OH) with the addition of 6 g of deionized water for every 10 g sample.

Riboflavin. *Extraction.* Homogenized sample (3.2 g, equivalent to 2 g of sample) was weighed into 50 mL plastic centrifuge tubes. To this was added 20 mL of 0.1 M HCl (Fisher Scientific Co., Pittsburgh, PA), and the tubes were capped, shaken for 5 min, and then incubated at 100 °C for 30 min. Once cool, 2.5 mL of 2.5 M sodium acetate (Fisher Scientific Co.) was added, to an approximate pH of 4.87, and then 100 mg of amyloglucosidase (Sigma-Aldrich, St. Louis, MO) was added to each sample. The samples were shaken and incubated at 37 °C for 15 h. After cooling, 2 mL of trichloroacetic acid (Fisher Scientific Co.) was added to each tube, and the samples were heated to 60 °C for 15 min. After cooling, the samples were diluted with deionized water to a final volume of 40 mL, shaken, and centrifuged for 10 min at 4000 rpm. From the supernatant, 10 mL aliquots were taken, 50 μL of 10 ppm internal standard ($[^{13}C_4,^{15}N_2]$riboflavin, Sigma-Aldrich) was added, and the tubes were vortexed. A 10 mL sample aliquot was loaded onto an Oasis HLB 3 mL[3] (60 mg) extraction cartridge (Waters Corp., Milford, MA) which was prewashed with 1 column volume of methanol followed by 1 column volume of deionized water. The extraction column was washed with 2.5 mL of trichloroacetic acid and dried for 5 min under vacuum. The column was eluted with 1 mL of methanol (Fisher Scientific Co.) into glass test tubes. The extracts were filtered through 0.20 μm IC Millex-LG (EMD Millipore Corp., Billerica, MA) filters into autosampler vials. A 15 μL aliquot of sample was then injected onto the high-performance liquid chromatography (HPLC) column for liquid chromatography/mass spectrometry (LC/MS) determination.

Analysis. The samples were analyzed using HPLC in conjunction with MS. The apparatus consisted of a PerkinElmer LC-200 chromatograph (PerkinElmer, Waltham, MA) with a Sciex API 2000 mass spectrometer (AB SCIEX, Framingham, MA) in the positive ion ESI mode. The transition ions m/z 377 to m/z 243 (riboflavin) and m/z 283 to m/z 249 ($[^{13}C_4,^{15}N_2]$riboflavin, internal standard) were used. An isocratic mobile phase of 90% methanol with 0.2% acetic acid (Fisher Scientific Co.) and 10% water with 0.2% acetic acid (v/v) at 0.4 mL/min was used on a Waters XTerra RP18 column, 3.5 μm pore size, 4.6 × 150 mm (Waters Corp.).

Ascorbic Acid. *Extraction.* Homogenized sample (6.4 g) was mixed with 13.6 mL of 2% oxalic acid (Fisher Scientific Co.) and

DOI: 10.1021/jf5058793
J. Agric. Food Chem. 2015, 63, 957−962

Table 3. Vitamin Content of Eight Commodities Stored under Either Refrigeration or Frozen Conditions for Three Storage Times[a]

	storage time (days)	ascorbic acid content (mg/kg)	riboflavin content (mg/kg)	α-tocopherol content (mg/kg)	β-carotene content(mg/kg)
			Peas		
fresh	0	3786 abc (240)	6.74 a (0.16)	10.95 b (1.73)	65.6 b (2.9)
fresh	3	3595 c (84)	6.73 a (0.37)	9.42 bc (1.18)	65.5 b (4.8)
fresh	10	4056 a (168)	6.91 a (0.52)	7.82 c (1.71)	55.1 c (10.9)
frozen	0	3716 bc (145)	6.57 a (0.34)	29.83 a (1.57)	89.2 a (4.5)
frozen	10	3737 bc (186)	6.61 a (0.48)	30.71 a (1.92)	89.2 a (2.2)
frozen	90	3998 ab (214)	5.19 b (0.32)	31.10 a (1.07)	28.2 d (1.4)
			Spinach		
fresh	0	2969 bc (477)	24.38 a (0.80)	231.30 b (31.37)	1019.1 ab (55.8)
fresh	3	3568 ab (477)	22.98 ab (1.14)	246.85 b (14.99)	990.3 ab (136.5)
fresh	10	2956 bc (482)	22.05 abc (1.08)	246.00 b (14.75)	914.0 b (51.1)
frozen	0	2916 c (395)	20.05 c (1.29)	311.88 a (23.14)	1013.5 ab (50.7)
frozen	10	3864 a (394)	22.97 d (0.82)	304.52 a (11.47)	1113.8 b (76.7)
frozen	90	3475 abc (364)	21.53 bc (1.19)	329.30 a (12.41)	466.0 c (30.8)
			Green Beans		
fresh	0	943 b (55)	6.23 a (1.02)	9.22 b (0.64)	17.7 b (1.7)
fresh	3	805 c (79)	6.09 a (0.26)	8.41 b (0.71)	17.6 b (0.7)
fresh	10	595 d (77)	6.66 a (0.55)	8.56 b (1.80)	21.3 a (1.5)
frozen	0	1056 ab (93)	6.63 a (0.41)	23.39 a (2.18)	22.9 a (0.7)
frozen	10	1085 a (115)	6.44 a (0.34)	23.56 a (1.62)	21.7 a (1.2)
frozen	90	1051 ab (102)	6.24 a (0.22)	24.79 a (2.59)	22.7 a (0.9)
			Broccoli		
fresh	0	6202 b (424)	7.08 d (0.77)	139.32 c (7.63)	32.6 b (4.2)
fresh	3	6481 b (588)	7.97 cd (0.56)	141.11 c (12.24)	33.8 b (2.8)
fresh	10	7045 ab (556)	9.22 c (0.80)	174.32 b (19.60)	41.9 a (6.2)
frozen	0	7001 ab (394)	11.63 b (0.32)	208.42 a (10.28)	42.0 a (5.0)
frozen	10	6852 ab (345)	11.92 b (1.32)	176.7 b (20.62)	47.5 a (4.0)
frozen	90	7422 a (661)	14.0 8 a (0.83)	179.46 b (16.21)	45.1 a (3.9)
			Carrots		
fresh	0	264 a (22)	1.74 a (0.21)	53.15 bc (4.18)	1382.8 a (229.3)
fresh	3	281 a (14)	1.84 a (0.27)	50.36 bc (4.20)	1244.8 ab (58.2)
fresh	10	227 a (22)	1.84 a (0.16)	53.00 bc (5.94)	1110.6 bc (59.4)
frozen	0	252 a (20)	1.93 a (0.22)	56.37 ab (5.70)	959.6 cd (131.7)
frozen	10	249 a (21)	1.64 a (0.31)	64.34 a (6.97)	813.8 d (94.3)
frozen	90	267 a (28)	1.45 a (0.17)	48.00 c (8.51)	398.7 e (68.8)
			Corn		
fresh	0	707 a (21)	2.20 c (0.19)	6.71 a (0.73)	<1.0
fresh	3	587 b (30)	2.27 c (0.12)	4.22 bc (0.97)	<1.0
fresh	10	446 d (52)	2.82 b (0.21)	3.88 c (0.99)	<1.0
frozen	0	484 cd (49)	2.97 ab (0.26)	6.40 a (0.80)	<1.0
frozen	10	489 cd (35)	3.23 a (0.11)	5.90 a (0.71)	<1.0
frozen	90	537 bc (35)	3.09 ab (0.23)	5.40 ab (0.84)	<1.0
			Blueberries		
fresh	0	489 bc (26)	2.42 b (0.12)	75.81 c (4.98)	<1.0
fresh	3	454 c (25)	2.43 b (0.12)	80.12 c (6.98)	<1.0
fresh	10	389 d (15)	2.71 ab (0.28)	93.19 b (6.73)	<1.0
frozen	0	505 b (32)	2.44 b (0.16)	84.63 bc (6.68)	<1.0
frozen	10	509 b (15)	2.74 ab (0.18)	93.14 b (6.24)	<1.0
frozen	90	567 a (16)	3.11 a (0.55)	104.86 a (3.87)	<1.0
			Strawberries		
fresh	0	6193 ab (410)	2.08 a (0.13)	37.23 ab (2.17)	<1.0
fresh	3	5928 b (287)	1.77 ab (0.21)	37.74 a (1.90)	<1.0
fresh	10	6561 a (287)	1.89 ab (0.31)	34.20 ab (1.57)	<1.0
frozen	0	5840 b (476)	1.41 b (0.21)	37.42 ab (1.17)	<1.0
frozen	10	6199 ab (415)	1.82 ab (0.27)	34.94 ab (0.66)	<1.0
frozen	90	6383 ab (689)	1.47 b (0.36)	32.72 b (2.85)	<1.0

[a]Each data point represents the mean of six field replicates and is followed by the standard deviation for those replicates in parentheses. Significantly different values between storage points for a given commodity and nutrient are followed by different online letters.

DOI: 10.1021/jf5058793
J. Agric. Food Chem. 2015, 63, 957−962

homogenized for 30 s. From this mixture, 10 mL was transferred to a 15 mL centrifuge tube and centrifuged at 10 000 rpm for 10 min at 4 °C. A 1.8 mL aliquot was taken, 400 μL of 5% dithiothreitol (Sigma-Aldrich) was added, and the sample was filtered through a 0.2 μm filter. The filtered sample was transferred to an autosampler vial for HPLC analysis.

Analysis. The samples were analyzed using HPLC with UV/vis diode array detection at 261 nm. The apparatus consisted of a PerkinElmer 200 quaternary HPLC system with a PerkinElmer 200 diode array detector (PerkinElmer). A Phenomenex Luna C-18 HPLC column (100 mm × 4.6 mm, 100A) with a C-18 guard column (Phenomenex, Torrance, CA) was used. The mobile phase was 95% water and 5% methanol with 5 mM hexadecyltrimethylammonium bromide and 50 mM potassium dihydrogen phosphate (Sigma-Aldrich) at 1.2 mL/min.

α-Tocopherol and β-Carotene. *Extraction.* Homogenized sample (1.6 g) was weighed into a 50 mL glass centrifuge tube along with 5 mL of ethanol containing 6% (w/v) pyrogallol (Sigma-Aldrich), and the mixture was sonicated for 10 min. A 1 mL volume of 50% KOH (aqueous) (Fisher Scientific Co.) was added, the mixture was mixed by vortexing and heated at 70 °C for 10 min, and mixed and heated for an additional 10 min. The sample was cooled to room temperature, and 5 mL of 5% NaCl was added. The sample was extracted with 30 mL of extraction solvent (85:15 (v/v) hexane/ethyl acetate with 0.05% BHT, Sigma-Aldrich). A 7.5 mL aliquot was evaporated to dryness at 40 °C under nitrogen using a Zymark TurboVap LV. The extract was redissolved in 200 μL of ethyl acetate followed by 1.8 mL of methanol, mixed, and filtered into an autosampler vial for HPLC analysis.

Analysis. The samples were analyzed using HPLC with UV/vis and fluorescence detection. The apparatus consisted of a PerkinElmer 200 quaternary HPLC system with a PerkinElmer 200 UV/vis detector (PerkinElmer) and a Shimadzu 10Axs fluorescence detector (Shimadzu Scientific Instruments, Columbia, MD). Excitation and emission wavelengths of 295 and 340 nm were used to detect α-tocopherol, and an absorbance wavelength of 450 nm was used to detect β-carotene. A Phenomenex Kinetex C-18 HPLC column (100 mm × 4.6 mm, 100A) with a C-18 guard column (Phenomenex) and a mobile phase of 9:1 (v/v) acetonitrile/methanol (Fisher Scientific Co.) at 1 mL/min was used.

Statistical Analysis. Statistical analysis was performed using JMP statistical software version 9.0.0 (SAS Institute Inc., Cary, NJ). A blocked analysis of variance (ANOVA) was run with storage time point and processing treatment as the treatments. Tukey comparisons were used to determine the significance of differences between both fresh and frozen treatments and storage time points for each commodity and nutrient.

RESULTS AND DISCUSSION

The concentrations of four different compounds were evaluated in eight different commodities stored under either refrigeration (fresh) or frozen conditions over three time points (Table 3).

Ascorbic Acid. Ascorbic acid was degraded less in frozen-stored samples than in fresh-stored samples (Figure 1). None of the eight commodities showed losses during frozen storage. In strawberries, carrots, spinach, peas, and broccoli, the ascorbic acid content of fresh-stored products was not significantly different from that of frozen-stored products. In corn, green beans, and blueberries, significantly higher levels of ascorbic acid were found in frozen-stored samples when compared to fresh-stored samples, which could possibly be attributed to arrested enzymatic activity and slowed oxidative degradation of ascorbic acid in the frozen samples.[6] Extensive degradation of ascorbic acid in fresh-stored produce has been previously reported in vegetables, as compared to their frozen counterparts.[21−23]

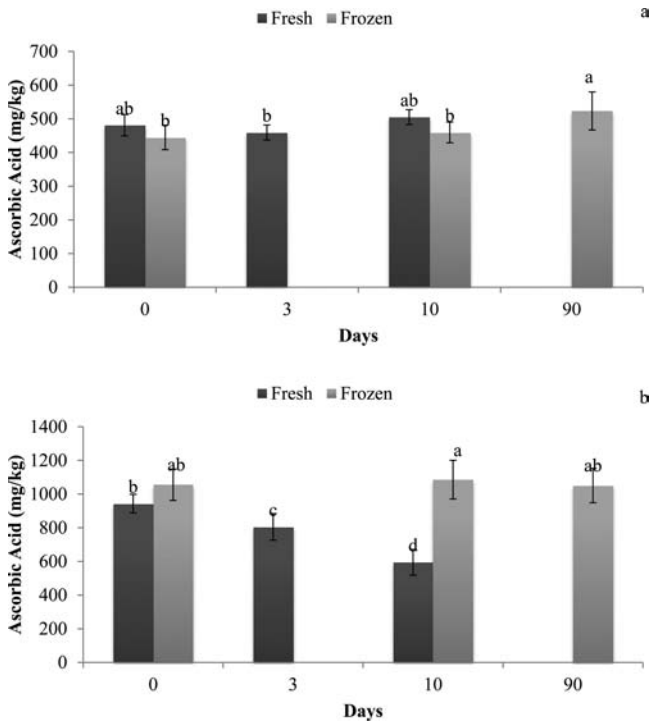

Figure 1. Ascorbic acid content of (a) strawberries and (b) green beans during fresh and frozen storage. Values reported on a dry weight basis. Values that share the same letter (a, b, c, d) are not significantly different ($p \leq 0.05$).

Riboflavin. Riboflavin was well conserved in most frozen samples. Carrots, corn, broccoli, blueberries, and green beans all followed the same trend, with fresh samples containing the same riboflavin content as frozen samples (Figure 2a). Of the eight commodities studied, only peas lost riboflavin during frozen storage (Figure 2b). The loss of riboflavin in peas is most likely due to oxidative degradation of the nutrient. Similar results were found by Gleim et al.,[24] who noted large decreases in riboflavin in asparagus and spinach.

Broccoli (Figure 2c) actually had higher riboflavin content in frozen-stored vs fresh-stored samples. This contrasts with the majority of the literature, such as Makhlouf et al.,[25] who found that, while riboflavin content was higher in frozen vegetables than canned, it was not higher in frozen vegetables than fresh. Similarly, while Van Duyne et al.[26] found riboflavin to be well retained in frozen peas, beans, and spinach, it was not found to be present in any higher amounts in frozen produce as compare to fresh produce.

α-Tocopherol. Of all of the nutrients determined in this study, the α-tocopherol content in fruits and vegetables benefited the most from blanching, freezing, and frozen storage, as compared to fresh storage. When stored fresh, peas, carrots, and corn showed significant decreases in α-tocopherol content (Figure 3). Fresh green beans had much lower levels of α-tocopherol than frozen, but the levels of α-tocopherol did not decrease over the course of fresh storage. In the remaining commodities blueberries, broccoli, green beans, spinach, and strawberries, no significant difference between fresh- and frozen-stored samples was observed (Figure 3). Frozen peas and green beans exhibited more than 2-fold higher levels of α-tocopherol, while blueberries, spinach, and corn also had significantly higher levels (12−39%) in frozen-stored samples, as compared to fresh-stored samples (Figure 3).

DOI: 10.1021/jf5058793
J. Agric. Food Chem. 2015, 63, 957−962

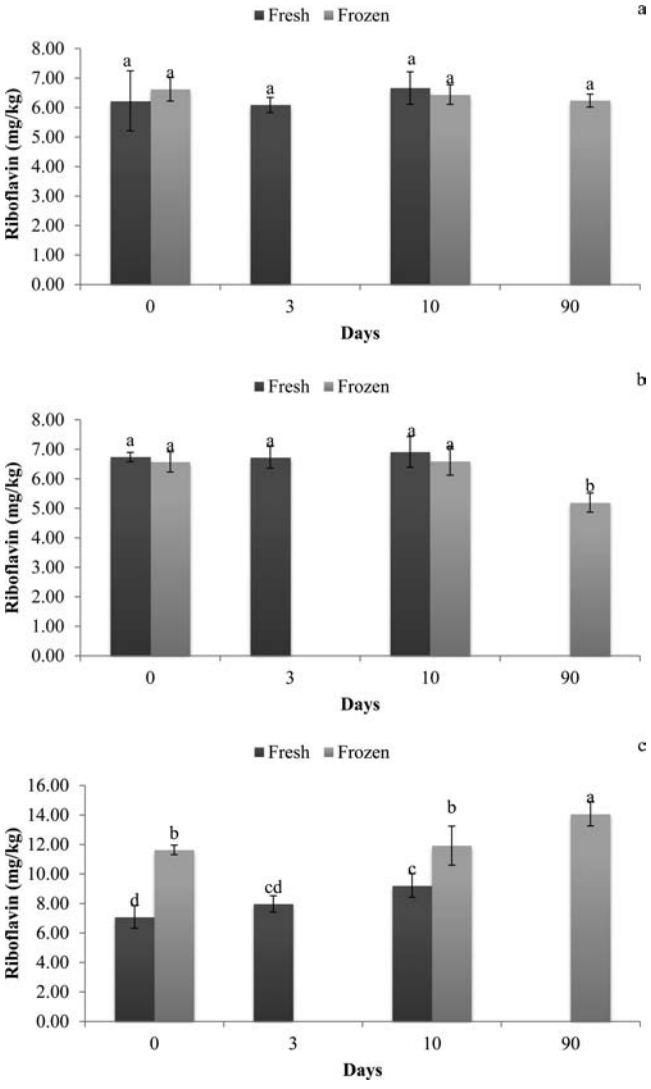

Figure 2. Riboflavin content of (a) green beans, (b) peas, and (c) broccoli during fresh and frozen storage. Values reported on a dry weight basis. Values that share the same letter (a, b, c, d) are not significantly different ($p \leq 0.05$).

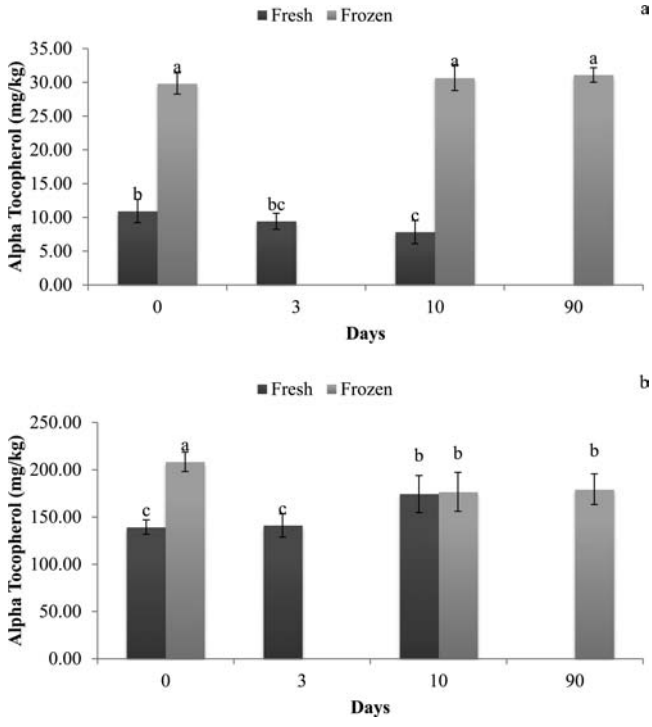

Figure 3. α-Tocopherol content of (a) peas and (b) broccoli during fresh and frozen storage. Values reported on a dry weight basis. Values that share the same letter (a, b, c) are not significantly different ($p \leq 0.05$).

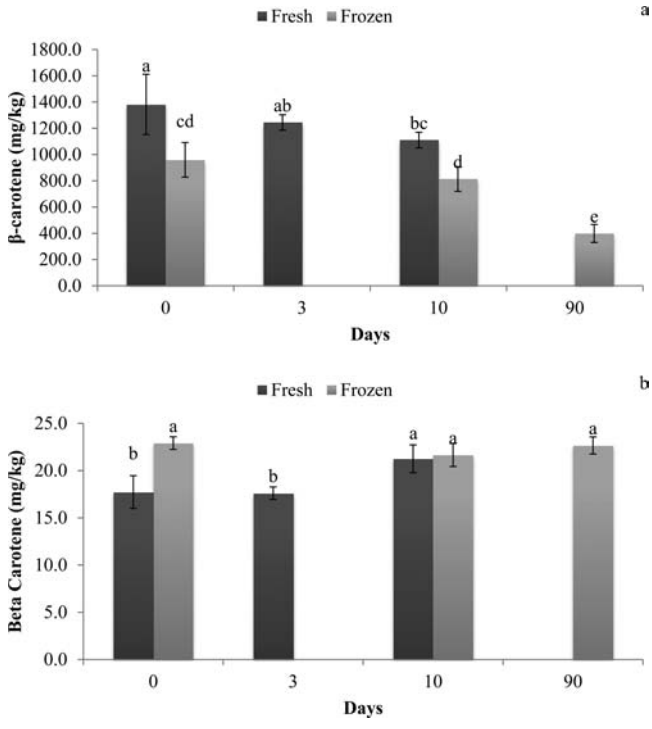

Figure 4. β-Carotene content of (a) carrots and (b) green beans during fresh and frozen storage. Values reported on a dry weight basis. Values that share the same letter (a, b, c, d, e) are not significantly different ($p \leq 0.05$).

The observed higher levels of α-tocopherol in some commodities, which is evident immediately after blanching and freezing on day 0, may be due to its increased availability after steam blanching.[26] α-Tocopherol levels in fresh broccoli were found to be more than 2-fold higher after heat treatments such as steaming or boiling by previous authors.[26] The heat treatment administered during blanching could have a similar effect on the commodities in this study. Previous authors have not studied the effects of freezing on peas in any detail, but lipid oxidation in peas caused by enzymatic or nonenzymatic pathways has been reported to consume α-tocopherol, a potent antioxidant.[27] Both of these oxidative pathways could have been responsible for preferentially lowering the levels of α-tocopherol in fresh samples. It is also unlikely that any leaching of fat-soluble α-tocopherol would occur during blanching in an aqueous environment.

***β*-Carotene.** β-Carotene was not found in any significant amount in blueberries, strawberries, and corn, even in fresh samples (<1.0 mg/kg). Over the course of frozen storage, peas, spinach, and carrots showed losses of more than 50% of the initial β-carotene content (Figure 4). Over the course of fresh storage, peas, green beans, and carrots lost at least 15% of the initial β-carotene content. Losses in β-carotene occurred both immediately after processing and over the course of frozen

DOI: 10.1021/jf5058793
J. Agric. Food Chem. 2015, 63, 957−962

storage. Losses during blanching are most likely not related to leaching because β-carotene is water insoluble,[6] but may be attributed to oxidation of β-carotene.[20] In all of the commodities that showed decreased levels of β-carotene, the 90 day frozen samples were by far the lowest levels detected. These decreases were most likely due to oxidation during frozen storage, which was found to occur in previous studies by Desobry et al.,[29] but these findings are contrary to some other previous findings.[20,26] One possible explanation for such a drastic decrease in β-carotene in carrots is that extensive cell damage and larger surface area after dicing encouraged oxidation of the tissue.[28] Green beans and broccoli showed no significant differences in β-carotene as a result of processing and storage (Figure 4).

Conclusions. For most nutrients in this study, frozen versions of a given commodity present viable substitutes for fresh in terms of nutritional value. While the results were highly dependent on commodity and nutrient, there were certain trends within the specific nutrients. In frozen samples of the commodities analyzed, riboflavin, α-tocopherol, and ascorbic acid were not only preserved in quantities equivalent to those of fresh samples, but in many cases were found in quantities much higher than those of the fresh samples. The most prevalent negative trend in the nutrient content of frozen fruits and vegetables is in β-carotene, which was drastically degraded over frozen storage in many of the commodities studied.

AUTHOR INFORMATION

Notes

The authors declare no competing financial interest.

REFERENCES

(1) Cho, E. Y.; Seddon, J. M.; Rosner, B.; Willett, W. C.; Hankinson, S. E. Prospective study of intake of fruits, vegetables, vitamins, and carotenoids and risk of age-related maculopathy. *Arch. Ophthalmol.* **2004**, *122*, 883−892.

(2) World Cancer Research Fund (WCRF) and American Institute for Cancer Research (AICR). *Food, Nutrition, Physical Activity, and the Prevention of Cancer: A Global Perspective*; AICR: Washington, DC, 2007.

(3) Carter, P.; Gray, L. J.; Troughton, J.; Khunti, K.; Davies, M. J. Fruit and vegetable intake and incidence of type 2 diabetes mellitus: systematic review and meta-analysis. *Br. Med. J.* **2010**, *341*, c4229.

(4) Appel, L. J.; Moore, T. J.; Obarzanek, E.; Vollmer, W. M.; Svetkey, L. P.; Sacks, F. M.; Bray, G. A.; Vogt, T. M.; Cutler, J. A.; Windhauser, M. M.; Lin, P. H.; Karanja, N. (DASH Collaborative Research Group). A clinical trial of the effects of dietary patterns on blood pressure. *N. Engl. J. Med.* **1997**, *336*, 1117−24.

(5) Barrett, D. M. Maximizing the nutritional value of fruits & vegetables. *Food Technol.* **2007**, *61*, 40−44.

(6) Rickman, J. C.; Bruhn, C. M.; Barrett, D. M. Nutritional comparison of fresh, frozen, and canned fruits and vegetables—II. Vitamin A and carotenoids, vitamin E, minerals and fiber. *J. Sci. Food Agric.* **2007**, *87*, 1185−1196.

(7) Koh, E.; Wimalasiri, K. M. S.; Chassy, A. W.; Mitchell, A. E. Content of ascorbic acid, quercetin, kaempferol and total phenolics in commercial broccoli. *J. Food Compos. Anal.* **2009**, *22*, 637−643.

(8) Favell, D. J. A comparison of the vitamin c content of fresh and frozen vegetables. *Food Chem.* **1998**, *62*, 59−64.

(9) Hartmann, A.; Patz, C. D.; Andlauer, W.; Dietrich, H.; Ludwig, M. Influence of processing on quality parameters of strawberries. *J. Agric. Food Chem.* **2008**, *56*, 9484−9489.

(10) Volden, J.; Bengtsson, G. B.; Wicklund, T. Glucosinolates, L-ascorbic acid, total phenols, anthocyanins, antioxidant capacities and colour in cauliflower (*Brassica oleracea* L. ssp. *botrytis*); effects of long-term freezer storage. *Food Chem.* **2009**, *112*, 967−976.

(11) Turkmen, N.; Sari, F.; Velioglu, Y. S. The effect of cooking methods on total phenolics and antioxidant activity of selected green vegetables. *Food Chem.* **2005**, *93*, 713−718.

(12) Melse-Boonstra, A.; Verhoef, P.; Konings, E. J. M.; van Dusseldorp, M.; Matser, A.; Hollman, P. C. H.; Meyboom, S.; Kok, F. J.; West, C. E. Influence of processing on total, monoglutamate and polyglutamate folate contents of leeks, cauliflower, and green beans. *J. Agric. Food Chem.* **2002**, *50*, 3473−3478.

(13) Salunkhe, D. K.; Bolin, H. R.; Reddy, N. R. Freezing. *Storage, Processing, and Nutritional Quality of Fruits and Vegetables*; CRC Press: Boca Raton, FL, 1991; Vol. *2*, pp 41−47.

(14) Klein, B. P. Stability of nutrients in fresh and processed vegetables. Pillsbury product communication, 1997.

(15) Davey, M. W.; Van Montagu, M.; Inze, D.; Sanmartin, M.; Kanellis, A.; Smirnoff, N.; Benzie, I. J. J.; Strain, J. J.; Favell, D.; Fletcher, J. Plant L-ascorbic acid: chemistry, function, metabolism, bioavailability and effects of processing. *J. Sci. Food Agric.* **2000**, *80*, 825−860.

(16) Elkins, E. R. Nutrient content of raw and canned green beans, peaches, and sweet potatoes. *Food Technol.* **1979**, *33*, 66−70.

(17) Chun, J.; Lee, J.; Ye, L.; Exler, J.; Eitenmiller, R. R. Tocopherol and tocotrienol contents of raw and processed fruits and vegetables in the United States diet. *J. Food Compos. Anal.* **2006**, *19*, 196−204.

(18) Psomiadou, E.; Tsimidou, M. Stability of virgin olive oil. 2. Photo-oxidation studies. *J. Agric. Food Chem.* **2002**, *50*, 722−727.

(19) Rupérez, F. J.; Martín, D.; Herrera, E.; Barbas, C. Chromatographic analysis of α-tocopherol and related compounds in various matrices. *J. Chromatogr., A* **2001**, *935*, 45−69.

(20) Scott, C. E.; Eldridge, A. L. Comparison of carotenoid content in fresh, frozen and canned corn. *J. Food Compos. Anal.* **2005**, *18*, 551−559.

(21) Howard, L. A.; Wong, A. D.; Perry, A. K.; Klein, B. P. β-Carotene and ascorbic acid retention in fresh and processed vegetables. *J. Food Sci.* **1999**, *64*, 929−936.

(22) Jenkins, R. R.; Tressler, D. K.; Fitzgerald, G. A. Vitamin c content of vegetables VIII. Frozen peas 1. *J. Food Sci.* **1938**, *3*, 133−140.

(23) Hunter, K. J.; Fletcher, J. M. The antioxidant activity and composition of fresh, frozen, jarred and canned vegetables. *Innovative Food Sci. Emerging Technol.* **2002**, *3*, 399−406.

(24) Gleim, E. G.; Tressler, D. K.; Fenton, F. Ascorbic acid, thiamin, riboflavin, and carotene contents of asparagus and spinach in the fresh, stored, and frozen states, both before and after cooking. *J. Food Sci.* **1944**, *9*, 471−490.

(25) Makhlouf, J.; Zee, J.; Tremblay, N.; Belanger, A.; Michaud, M. H.; Gosselin, A. Some nutritional characteristics of beans, sweet corn, and peas (raw, canned, and frozen) produced in the province of Quebec. *Food Res. Int.* **1995**, *28*, 253−259.

(26) Van Duyne, F. O.; Wolfe, J. C.; Owen, R. F. Retention of riboflavin in vegetables preserved by freezing. 1. *J. Food Sci.* **1950**, *15*, 53−61.

(27) Bernhardt, S.; Schlich, E. Impact of different cooking methods on food quality: retention of lipophilic vitamins in fresh and frozen vegetables. *J. Food Eng.* **2006**, *77*, 327−333.

(28) Dornenburg, H.; Davies, C. The relationship between lipid oxidation and antioxidant content in postharvest vegetables. *Food Rev. Int.* **1999**, *15*, 435−453.

(29) Desobry, S. A.; Netto, F. M.; Labuza, T. P. Preservation of beta-carotene from carrots. *Crit. Rev. Food Sci. Nutr.* **1998**, *38*, 381−396.

DOI: 10.1021/jf5058793
J. Agric. Food Chem. 2015, 63, 957−962

Table 1. Chemical Composition and Fatty Acid Profile of Feeds and of the Rumen-Protected Conjugated Linoleic Acid (rpCLA) Offered to Experimental Lambs[a]

	feeds			
	pasture	meadow hay	concentrate	rpCLA[b]
dry matter	19.9	89.6	88.5	98.4
crude protein	15.9	9.9	19.8	
ether extract	3.0	1.9	4.3	81.3
NDF	41.1	63.0	25.6	
ash	11.2	8.8	8.6	18.1
major fatty acids (g/100 g total FA)				
C16:0	15	25	12	9.7
C18:0	3	5	2	55.2
C18:1*c*9	3	10	26	9.7
C18:2n-6	17	21	57	1.0
C18:3n-3	53	25	1	
CLA*c*9,*t*11				11.3
CLA*t*10,*c*12				10.9

[a]Data expressed as g/100 g of DM, if not otherwise indicated; $n = 3$. [b]rpCLA, commercial product coated with hydrogenated soybean oil (SILA, Noale, Italy).

Table 2. Experimental Conditions and Descriptive Statistics of the Lambs Used in This Study

	feeding system[a]		
	pasture	indoor-control	indoor-CLA
rearing and feeding conditions	pasture	barn (pens)	barn (pens)
lambs (*n*)	12	12	12
males (*n*)	6	6	6
females (*n*)	6	6	6
feedstuffs offered			
pasture	ad libitum		
meadow hay		ad libitum	ad libitum
concentrate (g/day)		267	267
rpCLA supplement[b] (g/day)			9
slaughter			
age (days)	221 ± 26	220 ± 24	216 ± 28
body weight (kg)	33.9 ± 3.6	27.5 ± 6.5	28.6 ± 9.2
body condition score[c]	3.4 ± 0.3	3.2 ± 0.3	3.1 ± 0.3
carcass yield (%)	45.4 ± 2.4	41.1 ± 1.9	40.3 ± 2.5

[a]Pasture, based on pasture feeding; indoor-control, based on hay and concentrates; indoor-CLA, based on hay and concentrates with supplementation of rpCLA. [b]rpCLA, rumen protected conjugated linoleic acid (SILA, Noale, Venice, Italy). [c]Body condition score on a 1−5 point scale, where 1 = emaciated and 5 = obese.

ethyl ether (447534, Carlo Erba) were used as reagents. Mixtures of pure FA (674, Nu-Chek Prep Inc., Elysian, MN, USA), bacterial acid methyl esters (BAMEs) (Sigma-Aldrich) plus CLA*c*9,*t*11 (UC-60M, Nu-Chek Prep Inc.), CLA*t*10,*c*12 (UC-61M, Nu-Chek Prep, Inc.), CLA*c*9,*c*11 (1256, Matreya LLC, Pleasant Gap, PA, USA), CLA*c*11,*t*13 (1259, Matreya LLC), and CLA*t*9,*t*11 (1257, Matreya LLC) were used as reference standards, whereas methyl-12-tridecenoate (U-35 M, Nu-Chek Prep Inc.) was used as internal standard.

Animals and Feeding Systems. The present study followed the "Guidelines for the Care and Use of Agricultural Animals in Agricultural Research and Teaching".[14] Data regarding growth performance and carcass traits of the lambs used in the current experiments are given in Pellattiero et al.[15] Briefly, the lambs were selected from the two largest flocks on an in situ conservation program. Given the need for breed conservation, the number of lambs included in the

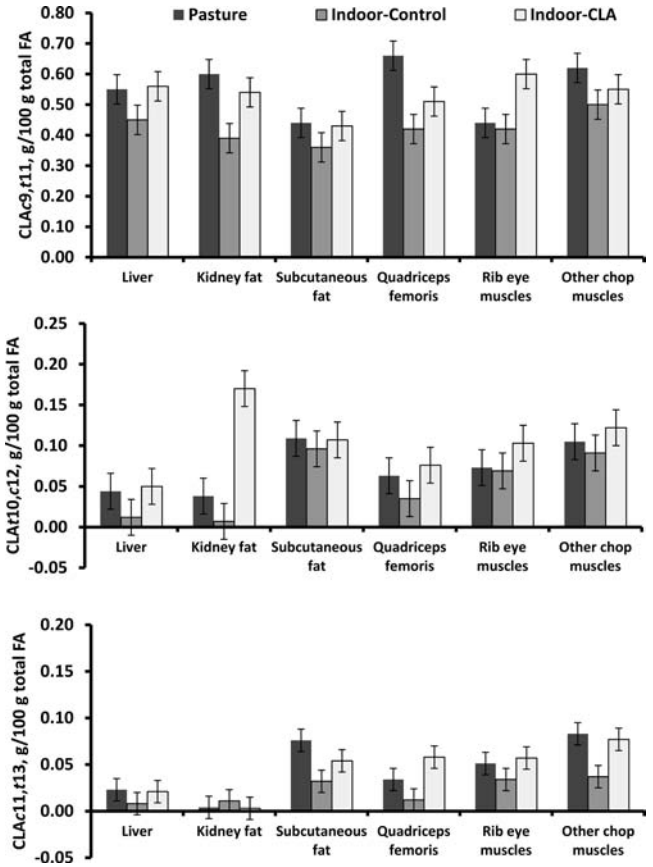

Figure 1. Effect of feeding system (pasture; indoor-control, based on hay and concentrates; indoor-CLA, based on hay and concentrates top dressed with 8 g/day of a commercial rumen-protected CLA mixture) on the content of CLA,*c*9,*t*11, CLA*t*10,*c*12, and CLA*c*11,*t*13 of six lamb tissues. Each bar is the least-squares mean from 12 observations; vertical bars indicate SEM. The level of significance of the feeding system × tissue interaction was $p = 0.07$, $p = 0.10$, and $p = 0.23$ for CLA,*c*9,*t*11, CLA*t*10,*c*12, and CLA*c*11,*t*13, respectively.

experiment was kept to a minimum yet was sufficient to attain adequate statistical power. In total, 36 weaned lambs of three breeds, Foza, Brogna, and Alpagota, were used (12 lambs/breed, 6 males and 6 females). To obtain carcasses with FA profiles varying according to the different feeding systems (FS) used in the Veneto region, lambs were divided into three groups (two males and two females of each breed in each group). All of the lambs in the first group were kept together in a fenced pasture on the experimental farm to ensure the same feeding conditions (pasture). The second group of lambs was kept indoors in an open barn and fed ad libitum hay plus 267 g/day of a commercial concentrate mixture (indoor-control), whereas the third group was also kept indoors on the same diet, but supplemented with 8.0 g/head of a commercial rpCLA product (SILA, Noale, Venice, Italy) providing 0.71 g/day of CLA*c*9,*t*11 and 0.69 g/day of CLA*t*10,*c*12 per lamb (indoor-CLA). The chemical compositions of the pasture, hay, concentrate, and rpCLA product are given in Table 1; further details on rpCLA are given in Schiavon et al.[16]

At the beginning of the trial, lambs were weighed and given a body condition score (BCS) on a scale from 1 (emaciated) to 5 (obese). Mean initial body weight (BW) was 20.1 kg for ewe lambs and 21.8 kg for ram lambs; initial BCS was 3.1 for ewe lambs and 3.0 for ram lambs. The trial lasted 113 days. The final average BW was 28.1 kg for ewe lambs and 31.7 kg for ram lambs. Average age, BW, BCS at slaughter, and carcass yields of the three groups are given in Table 2.

Tissue Sampling. Immediately after slaughter, liver and kidney fat samples were collected from all of the animals and stored at −20 °C. Each carcass was divided into two halves, which were weighed and

DOI: 10.1021/jf504956x
J. Agric. Food Chem. 2015, 63, 963−974

Table 3. Effects of Feeding System (Pasture; Indoor-Control, Based on Hay and Concentrates; Indoor-CLA, Based on Hay and Concentrates plus 8 g/day of a Commercial Rumen-Protected CLA) and Gender on the Proportion of Saturated Fatty Acids of Six Tissues of Lambs (Grams per 100 g of Total FA)[a]

	feeding system				gender		
		indoor					
	pasture[b]	control	CLA[b]	SEM[c]	ram[b]	ewes	SEM[c]
C8:0	0.03	0.03	0.03	0.002	0.03	0.03	0.002
C10:0	0.17	0.20	0.19	0.009	0.18	0.19	0.007
C12:0	0.16	0.19	0.19	0.017	0.18	0.17	0.014
C13:0	0.33	0.30	0.33	0.022	0.32	0.31	0.018
$C14:0_{iso}$	0.10**	0.13	0.14	0.006	0.13	0.11	0.005
C14:0	2.70	3.04	2.95	0.171	2.93	2.87	0.143
$C15:0_{iso}$	0.30**	0.37	0.37	0.013	0.35	0.34	0.011
$C15:0_{anteiso}$	0.33**	0.43	0.44	0.017	0.43*	0.38	0.014
C15:0	0.83**	0.91	0.93	0.026	0.93**	0.85	0.022
$C16:0_{iso}$	0.25**	0.37	0.37	0.013	0.34	0.33	0.011
C16:0	20.7*	22.1	21.6	0.394	21.3	21.6	0.328
$C17:0_{iso}$	0.52**	0.66	0.64	0.017	0.62	0.59	0.014
$C17:0_{anteiso}$	0.68**	0.95	0.93	0.031	0.87	0.84	0.026
C17:0	1.71**	1.96	1.94	0.062	1.88	1.86	0.052
$C18:0_{iso}$	0.18**	0.26	0.25	0.008	0.23	0.23	0.007
C18:0	26.3**	24.1	24.9	0.633	25.2	25.0	0.538
$C19:0_{iso}$	0.03	0.03	0.03	0.003	0.03	0.03	0.003
C19:0	0.22**	0.29	0.27	0.013	0.27	0.25	0.011
C20:0	0.34*	0.41	0.41	0.022	0.41	0.36	0.018
C22:0	0.21	0.17	0.18	0.036	0.21	0.16	0.028
C23:0	0.02	0.02	0.02	0.003	0.02	0.02	0.002

[a]Data are least-squares means (feeding system, $n = 72$; gender $n = 108$). [b]The asterisks (*, $p < 0.05$, or **, $p < 0.01$) on entries in pasture, CLA, or ram columns indicates that pasture differed from the average of the two indoors diets, indoor-CLA differed from indoor-control, or ram differed from ewes, respectively. [c]Standard error of the means.

cold stored at 4 °C. The day after slaughter, all semicarcasses were weighed again, and the right semicarcasses were divided into five cuts (hind leg, foreleg and shoulder, ribs−loin, withers, brisket). Each cut was weighed, and the ribs−loins and hind legs were collected and stored under vacuum for 6 days at 4 °C. These two cuts were then cut up and weighed. Ribs−loin was divided into ribs and loin. Ribs were divided into ribeye muscle, other chop muscles, bones, and subcutaneous fat and weighed. Only the inner part of the hind leg (quadriceps femoris) was separated and weighed. Samples of subcutaneous fat, ribeye muscle, other chop muscles, and leg muscle were collected and stored at −20 °C prior to analysis.

Sample Preparation. All of the tissues collected were ground and mixed for 10 s at 4500*g* (Grindomix GM200, Retsch, Haan, Düsseldorf, Germany). Fresh samples were weighed (liver, 3.26 ± 0.32 g; kidney fat, 2.24 ± 0.21 g; subcutaneous fat, 1.14 ± 0.35 g; leg muscle, 2.60 ± 0.28 g; ribeye muscle, 2.56 ± 0.04 g; other chop muscles, 2.65 ± 0.27 g) and homogenized with Hydromatrix (Phenomenex, Castel Maggiore, Bologna, Italy) and then transferred into 10 mL stainless steel extraction cells for ASE (Dionex ASE 350, Thermo Fisher Scientific Inc., Waltham, MA, USA) with petroleum ether as solvent. Extraction conditions as reported in ASE Application note 334 for meat samples (ASE, Dionex, Sunnyvale, CA, USA) were as follows: temperature, 125 °C; pressure, 10 MPa; static time, 2 min; number of static cycles, 2; rinse, 60%; and purge, 60 s of purge using 20 mL/sample of fresh solvent. Following extraction the solution was heated and maintained at 50 °C under N_2 stream for about 20 min to complete solvent evaporation and then placed in an oven at 60 °C for 15 min and cooled in a dryer; the resulting ether extract was weighed. About 40 mg of ether extract was transferred to test tubes to be methylated using sodium methoxide in methanol (1 M) at room temperature.[17] Briefly, 2 mL of *n*-hexane containing 2 mg/mL of methyl 12-tridecenoate as internal standard and 100 μL of sodium methoxide (1 M) in methanol was collected with a GC microsyringe (1701N, Hamilton, Bonaduz, Switzerland) and added to the ether extract. The solution containing the ether extract was mixed with the solvent for 10 min using a laboratory multimixer (717+, ASAL s.r.l., MI, Italy) at room temperature. After this step, 150 μL of oxalic acid in ethyl ether was added to stop the reaction and obtain the fatty acid methyl ester (FAME) solution. The solution was mixed for 30 s and centrifuged at 8000*g* for 10 min (Sigma Laborzentrifugen 3K15, Osterrode am Harz, Germany). The upper phase was collected (1 mL) and transferred to a vial for the GC×GC analysis. The resulting FAME solution was stored in GC vials at −20 °C prior to analysis.

Gas Chromatographic Analysis. FA profiles of the samples were obtained by GC×GC (Agilent 7890A, Agilent Technologies, Santa Clara, CA, USA) employing two columns in series and fitted with a modulator (G3486A CFT, Agilent Technologies), an automatic sampler (7693, Agilent Technologies), and a flame ionization detector (FID) connected to the chromatography data system software (Agilent Chem Station, Agilent Technologies). This instrument was chosen because the double column enables a much better two-dimensional separation and identification of FAs compared with the traditional one-column GC.[18] Between the two columns the modulator unit collects the analyte bands of the first column in a fixed volume channel, and these are successively launched into the short second column in narrow bands. The operating conditions of the GC apparatus were as follows: first column, 20 m × 100 μm (internal diameter) × 0.1 μm film thickness (J&W 127-0122, Agilent Technologies); H_2 carrier flow, 0.3 mL/min; second column, 5 m × 250 μm (internal diameter) × 0.15 μm film thickness (Agilent 19091N-030, Agilent Technologies); H_2 carrier flow, 24 mL/min. Planned oven temperature variation was an increase from 40 °C (held for 2 min) to 260 °C (held for 5 min) at 5 °C/min. Valves were set for a modulation delay of 0.115 min, a modulation period of 2.0 s, and a sample time of 1.75 s. Detector (FID) conditions were as follows: heater, 250 °C; H_2 carrier flow, 20 mL/min; air flow, 450 mL/min. Splitless inlet temperature was 250 °C and pressure, 37.758 MPa, with a septum purge of 3 mL/min and a split ratio of 15 mL/min.

DOI: 10.1021/jf504956x
J. Agric. Food Chem. 2015, 63, 963−974

Table 4. Effects of Feeding System (Pasture; Indoor-Control, Based on Hay and Concentrates; Indoor-CLA, Based on Hay and Concentrates plus 8 g/day of a Commercial Rumen-Protected CLA) and Gender on the Proportion of Unsaturated Fatty Acids of Six Tissues of Lambs (Grams per 100 g of Total FA)[a]

	feeding system				gender		
		indoor					
	pasture[b]	control	CLA[b]	SEM[c]	ram[b]	ewes	SEM[c]
C14:1*c*9	0.07	0.08	0.08	0.009	0.08	0.07	0.008
ΣC15:1 others	0.06**	0.07	0.08	0.006	0.07	0.07	0.005
C16:1*n*7	0.04*	0.02	0.03	0.005	0.03	0.03	0.004
C16:1*t*7	0.16**	0.09	0.10	0.012	0.11	0.12	0.010
C16:1*c*7	0.53	0.53	0.52	0.018	0.55**	0.50	0.015
C16:1*c*9	1.05	1.18	1.12	0.047	1.12	1.11	0.039
ΣC16:1 others	0.21	0.24	0.25	0.038	0.25	0.22	0.032
C17:1*c*10	0.53*	0.61	0.62	0.027	0.58	0.59	0.021
ΣC17:1 others	0.31	0.38	0.34	0.034	0.37	0.32	0.029
C18:1*c*7[d]	0.52**	0.78	0.78	0.023	0.69	0.69	0.019
C18:1*t*9(+*t*11)[e]	4.23**	3.48	3.72	0.147	3.81	3.81	0.123
C18:1*c*9	26.2	27.3	26.2	0.520	26.2	26.9	0.430
ΣC18:1 others	1.19**	0.82	0.83	0.092	0.95	0.95	0.077
C19:1*n*9*t*	0.01**	0.03	0.03	0.005	0.02	0.03	0.004
C19:1*n*9*c*	0.11	0.12	0.11	0.011	0.12	0.11	0.009
C20:1*n*9*t*	0.02	0.02	0.02	0.006	0.02	0.02	0.004
C20:1*n*9	0.03**	0.06	0.05	0.005	0.05	0.05	0.004
C20:1*n*7	0.03*	0.05	0.05	0.002	0.04	0.04	0.004
C20:1*n*11[d]	0.03**	0.05	0.05	0.006	0.05	0.05	0.005
ΣC16:2 others	0.06**	0.03	0.03	0.033	0.04	0.04	0.043
C18:2n-6	2.94**	3.22	3.49	0.116	3.15	3.29	0.096
ΣC18:2 others	1.27**	0.92	0.91	0.057	1.05	1.02	0.047
CLA*c*9*t*11	0.55*	0.42	0.53**	0.027	0.51	0.49	0.023
CLA*t*9,*t*11[d]	0.19**	0.06	0.08	0.009	0.11	0.12	0.007
CLA*c*11*t*13	0.05	0.02	0.05*	0.009	0.04	0.03	0.006
CLA*t*10*c*12	0.10	0.07	0.12*	0.017	0.10	0.10	0.015
CLA*c*9*c*11	0.03	0.02	0.02	0.005	0.02	0.02	0.004
C18:3n-6	0.06**	0.12	0.11	0.006	0.10	0.10	0.005
C18:3n-3	1.44**	0.72	0.71	0.053	0.98	0.93	0.044
C18:4n-3	0.06	0.06	0.05	0.136	0.07	0.05	0.055
C20:2n-6	0.03	0.03	0.04	0.003	0.03	0.04	0.002
C20:3n-6	0.09**	0.12	0.13	0.008	0.11	0.11	0.006
C20:4n-6	1.12**	1.58	1.71	0.009	1.52	1.42	0.071
C20:5n-3 EPA	0.59**	0.30	0.37	0.004	0.51	0.33	0.003
C20:2n-3[d]	0.15**	0.40	0.35	0.032	0.31	0.29	0.026
C20:3n-3[f]	0.07	0.09	0.08	0.011	0.09	0.07	0.009
C20:4n-3[f]	0.07**	0.03	0.03	0.006	0.05	0.04	0.005
C22:4n-6[f]	0.14**	0.51	0.55	0.049	0.43	0.38	0.041
C22:6n-3 (DHA)[f]	2.03**	1.01	1.23	0.234	1.55	1.31	0.195
C22:5n-6[f]	0.09	0.32	0.34	0.036	0.28	0.23	0.031

[a]Data are least-squares means (feeding system, $n = 72$; gender $n = 108$). [b]The asterisks (*, $p < 0.05$, or **, $p < 0.01$) on entries in pasture, CLA, or ram columns indicate that pasture differed from the average of the two indoors diets, indoor-CLA differed from indoor-control, or ram differed from ewes, respectively. [c]Standard error of the means. [d]Found only in liver and kidney fat. [e]Co-eluted isomers. [f]Found only in liver.

The resulting two-dimensional chromatograms were analyzed with the comprehensive GC×GC software (GC Imagine Software, Zoex Corp., Houston, TX, USA) to ascertain the cone volume of each FA.

Identification and Quantification of FA. Identification was made first by comparing the cone position in the chromatogram with the cone position of the FA contained in reference standards. The second FA identification method was by elution order and position of each FA in the two-dimensional chromatogram produced by the comprehensive GC×GC software. Quantification of each FA was calculated from the cone volume of each FA peak compared to the volume of total FA, and FA content was expressed as grams per 100 g of total FA on the basis of the concentration in weight of the methyl 12-tridecenoate contained in the solution used as internal standard. Some peaks were excluded from the statistical analysis and from the tables (C4:0, C6:0, C7:0, C13:0$_{iso}$, C13:0$_{anteiso}$, C19:0$_{anteiso}$, C23:0, C24:0, C13:1 unknown isomer, ΣC14:1 unknown isomers, ΣC19:1 unknown isomers, ΣC20:1 unknown isomers, C23:1, C24:1) because they were absent from the large majority of samples. Some long-chain PUFAs are presented separately because they were detected in significant amounts in only liver and kidney fat.

Saturated FAs (SFA) were the sum of C8:0, C9:0, C10:0, C11:0, C12:0, C13:0, C13:0$_{iso}$, C13:0$_{anteiso}$, C14:0, C14:0$_{iso}$, C15:0, C15:0$_{iso}$, C15:0$_{anteiso}$, C16:0, C16:0$_{iso}$, C16:0$_{anteiso}$, C17:0, C17:0$_{iso}$, C17:0$_{anteiso}$, C18:0, C18:0$_{iso}$, C19:0, C19:0$_{iso}$, C19:0$_{anteiso}$, C20:0, C21:0, C22:0, C23:0, and C24:0. Monounsaturated FAs (MUFA) were the sum of C13:1 unknown isomer, C14:1*c*9, ΣC14:1 unknown isomer, ΣC15:1

DOI: 10.1021/jf504956x
J. Agric. Food Chem. 2015, 63, 963−974

Table 5. Effects of Feeding System (Pasture; Indoor-Control, Based on Hay and Concentrates; Indoor-CLA, Based on Hay and Concentrates plus 8 g/day of a Commercial Rumen-Protected CLA) and Gender on the Average Fat Content (Grams per 100 g of Tissue), Proportion of Fatty Acid Categories (Grams per 100 g of Total FA), and FA Indices of Six Tissues of Lambs[a]

	feeding system				gender		
		indoor					
	pasture[b]	control	CLA[b]	SEM[c]	ram[b]	ewes	SEM[c]
fat content	28.7**	23.8	22.3	1.699	25.3	24.6	1.410
SFA	56.1	57.0	57.3	0.645	57.0	56.6	0.538
MUFA	34.8	35.1	34.2	0.521	34.4	35.0	0.434
PUFA	8.91*	7.78	8.33	0.307	8.44	8.23	0.255
FA unknown	0.17**	0.08	0.08	0.009	0.12	0.11	0.007
ΣCLA	0.79*	0.55	0.75**	0.048	0.72	0.68	0.041
n-3 PUFA	2.70**	1.46	1.54	0.138	2.00	1.80	0.114
n-6 PUFA	3.76**	4.41	4.75	0.170	4.26	4.36	0.141
n-6/n-3 PUFA	2.10**	4.05	4.19	0.205	3.33	3.56	0.171
<C16	5.07**	5.77	5.84	0.209	5.72	5.40	0.174
C16	22.9**	24.5	24.0	0.427	23.7	23.9	0.712
>C16	71.9**	69.7	70.1	0.594	70.5	70.6	0.495
branched	2.37**	3.26	3.21	0.102	3.04	2.85	0.085
odd chain	5.88**	7.11	7.04	0.102	6.84	6.51	0.085
desaturases:[d]							
C14	0.04	0.02	0.03	0.009	0.03	0.03	0.008
C16	0.05	0.05	0.05	0.002	0.05	0.05	0.002
C18	0.49	0.53	0.51	0.010	0.50	0.52	0.009
CLA*c*9,*t*11	0.12	0.11	0.13*	0.004	0.12	0.12	0.004
IT[e]	1.81	1.83	1.86	0.043	1.85	1.82	0.035
IAT[e]	0.77*	0.85	0.84	0.028	0.83	0.81	0.023

[a]Data are least-squares means (feeding system, $n = 72$; gender $n = 108$). [b]The asterisks (*, $p < 0.05$, or **, $p < 0.01$) on entries in the pasture, CLA, or ram columns indicate that pasture differed the average of the two indoors diets, indoor-CLA differed from indoor-control, or ram differed from ewes, respectively. [c]Standard error of the means. [d]Δ^9-desaturase indices: calculated according to the method of Kelsey et al.[22] [e]Thrombogenic index and atherogenic index were calculated according to the method of Ulbricht and Southgate.[23]

other, C16:1*n*5, C16:1*t*7, C16:1*c*7, C16:1*c*9, ΣC16:1 other, C17:1*c*10, ΣC17:1 other, C18:1*t*7, C18:1*t*9(+*t*11), C18:1*c*9, C18:1*c*7, C18:1n-3, ΣC18:1 other, C19:1*n*9*t*, C19:1*n*9*c*, ΣC19:1 unknown isomer, C20:1*n*7, C20:1*n*9, C20:1*n*11, C20:1*n*9*t*, ΣC20:1 unknown isomer, C23:1, and C24:1. Polyunsaturated FAs (PUFA) were the sum of ΣC16:2 unknown isomers, C18:2n-6, ΣC18:2 unknown isomers, ΣC19:2 unknown isomers, C20:2n-6, C20:2n-3, ΣC20:2 unknown isomers, ΣC16:3 unknown isomers, C18:3*n*-3, C18:3n-6, ΣC18:3 unknown isomers, C20:3n-3, C20:3n-6, ΣC20:3 unknown isomers, C18:4n-3, C20:4n-3, C20:4n-6, ΣC20:4 unknown isomers, C20:5n-3 (EPA), C20:5n-6, ΣC20:5 unknown isomers, C22:2n-6, C22:4n-6, C18:5n-3, C22:5n-6, ΣC22:5 unknown isomers, C22:6n-3 (DHA), CLA*c*9,*t*11, CLA*c*11,*t*13, CLA*t*10,*c*12, CLA*c*9,*c*11, CLA*t*9,*t*11, and ΣCLA unknown isomers. Unknown FAs are the sum of 10 peaks not identified by standard or by position in two-dimensional chromatograms.

Branched FAs, calculated according to Raes et al.,[19] were the sum of $C13:0_{iso}$, $C13:0_{anteiso}$, $C14:0_{iso}$, $C15:0_{iso}$, $C15:0_{anteiso}$, $C16:0_{iso}$, $C16:0_{anteiso}$, $C17:0_{iso}$, $C17:0_{anteiso}$, $C18:0_{iso}$, $C19:0_{iso}$, and $C19:0_{anteiso}$. Odd-chain FAs were calculated according to the method of Or-Rashid et al.[20] The sum of the identified CLA isomers was indicated as ΣCLA and was calculated as the sum of isomers identified by standard and position: CLA*c*9,*t*11, CLA*c*11,*t*13, CLA*t*10,*c*12, CLA*c*9,*c*11, and CLA*t*9,*t*11 plus the ΣCLA of other unknown isomers. The sums of omega-3 PUFAs (n-3 PUFA) and of omega-6 PUFAs (n-6 PUFA) were calculated according to Givens et al.;[21] as an example, n-3 PUFA was computed as the sum of C18:3n-3, C18:4n-3, C18:5n-3, C20:2n-3, C20:3n-3, C20:4n-3, C20:5n-3 (EPA), C22:5n-3, and C22:6n-3 (DHA).

The Δ^9-desaturase indices were calculated according to the method of Kelsey et al.[22] for four pairs of FAs representing products and substrates for Δ^9-desaturase. These FA pairs were 14:1*c*9 and 14:0, 16:1*c*9 and 16:0, 18:1*c*9 and 18:0, and CLA*c*9,*t*11 and C18:1*t*11. The desaturase index was defined as product of Δ^9-desaturase/(product of Δ^9-desaturase + substrate of Δ^9-desaturase). The atherogenic index (AI) and thrombogenic index (TI) were calculated according to the method of Ulbricht and Southgate[23] as AI = (C12:0 + 4 × C14:0 + C16:0)/(n-3 PUFA + n-6 PUFA + MUFA) and TI = (C14:0 + C16:0 + C18:0)/[0.5 × MUFA + 0.5 × n-6 PUFA + 3 × (n-3 PUFA/n-6 PUFA)].

Statistical Analysis. The 216 data obtained for each FA or FA category from the combination of 6 tissues (T) × 3 feeding systems (FS) × 3 breeds ×2 sexes ×2 lambs were analyzed using a linear mixed-effects model (MIXED) procedure in SAS[24] with T, FS, breed, and sex as fixed effects. The random effect of animal was used to test FS, breed, and sex, whereas the effects of T and the FS × T interaction were tested on the residual. Orthogonal contrasts between least-squares means were fitted to test pasture versus indoor diets and indoor-control versus indoor-CLA diets ($p < 0.05$). Further contrasts were fitted to test liver versus other tissues, fatty tissues versus muscles, kidney fat versus subcutaneous fat, leg versus chop muscles, and ribeye versus other chop muscles ($p < 0.05$). As a preliminary analysis revealed the effect of breed to be seldom significant and no interactions of breed with other sources of variation were found, breed was excluded from the model. Because the experimental design was balanced, only one standard error of the least-squares means (SEM) was reported for each source of variation.

RESULTS AND DISCUSSION

Two-Dimensional Gas Chromatography. The GC×GC system revealed the presence of 128 peaks, 56 of which were identified using standard references: 21 SFAs, 16 MUFAs, and 19 PUFAs. Seventy-two other FA peaks were found, but as identification was incomplete, they were placed into 6 family groups (ΣC15:1 other, ΣC16:1 other, ΣC17:1 other, ΣC18:1 other, ΣC16:2 other, and ΣC18:2 other) according to their

DOI: 10.1021/jf504956x
J. Agric. Food Chem. 2015, 63, 963−974

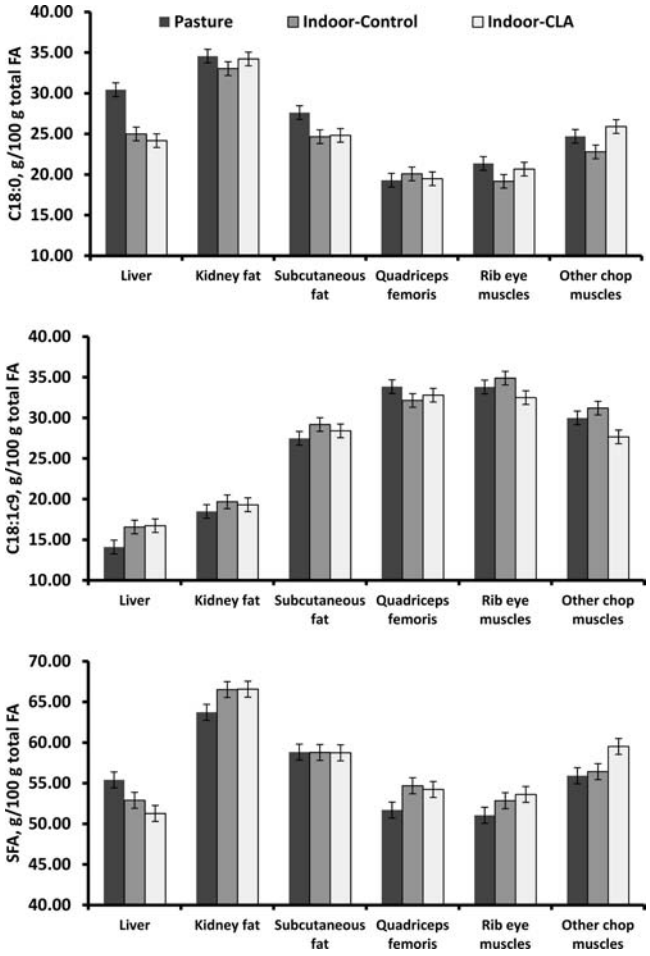

Figure 2. Effect of feeding system (pasture; indoor-control, based on hay and concentrates; indoor-CLA, based on hay and concentrates top dressed with 8 g/day of a commercial rumen-protected CLA mixture) on content of C18:0, C18:1*c*9, and saturated FA in six lamb tissues. Each bar is the least-squares mean from 12 observations; vertical bar indicate SEM. The significance of the feeding system × tissue interaction was $p < 0.01$, < 0.01, and 0.28 for C18:0, C18:1*c*9, and saturated FA, respectively.

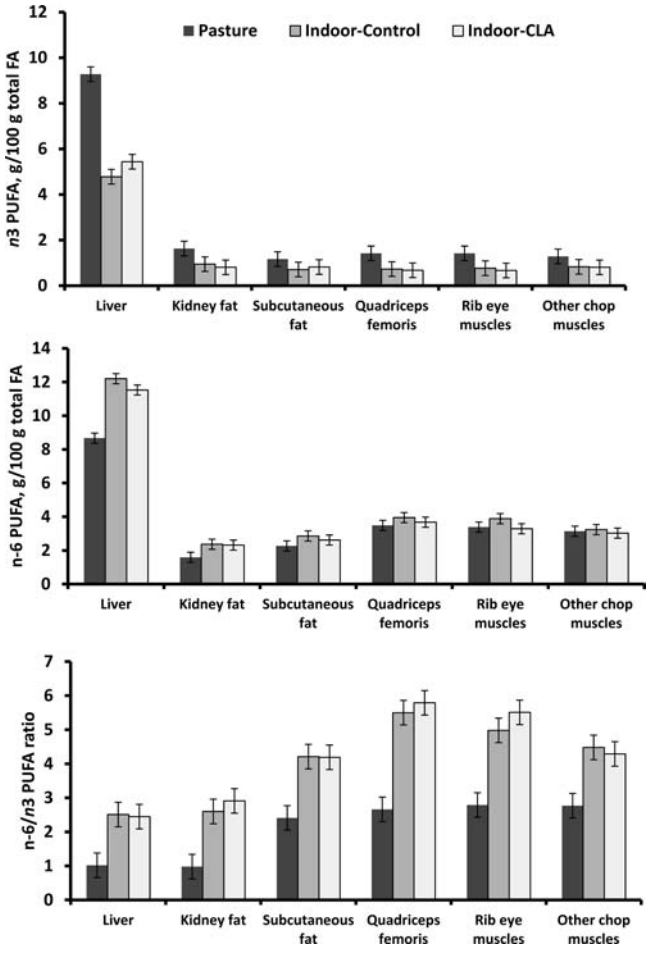

Figure 3. Effect of feeding system (pasture; indoor-control, based on hay and concentrates; indoor-CLA, based on hay and concentrates top dressed with 8 g/day of a commercial rumen-protected CLA mixture) on content of n-3 and n-6 fatty acids and on their ratio in six lamb tissues. Each bar is the least-squares mean from 12 observations; vertical bars indicate SEM. The significance of the feeding system × tissue interaction was $p < 0.01$, < 0.01, and 0.28 for n-3, n-6, and n-3/n-6, respectively.

elution time in the ordered GC×GC chromatograms. Identification of compounds is more reliable with GC×GC than with traditional GC, particularly in combination with columns with different polarities.[4] The various FAs are aligned in the chromatograms in grid form according to their number of carbon atoms and double bounds.[25] The GC×GC system therefore appeared to be well suited to the analysis of matrices containing complex mixtures of FAs, such as meat samples, in which a large number of FAs are present in very different concentrations. Some studies have shown that near-infrared spectroscopy (NIRS) is a useful technique for satisfactorily predicting some FAs in meat, particularly the major SFAs and MUFAs, but is less reliable in predicting PUFAs.[26] This NIRS technique is based on calibrations resulting from FA analysis conducted with a monodimensional GC. A tool such as the GC×GC, which is suitable for accurately detecting numerous FAs in very different concentrations, would be useful in improving NIRS calibration and prediction potential, particularly with regard to the less numerous but most biologically active PUFAs. GC×GC-based calibration of NIRS is desirable as it would allow NIRS to make measures at population levels, which would open up a variety of applications, including genetic selection and online meat quality evaluation at slaughterhouses.

Feeding System. Dietary manipulation is considered to be one of the most effective ways to improve the FA composition of sheep meat.[1,27,28] In the current experiment, the feeding system (FS) affected the average proportions of the large majority of individual FAs in tissues. The FA profile of lambs reared on pasture differed from those fed on the two indoor diets; the only quantitatively notable FAs not influenced by pasture were C14:0 among the SFAs (Table 3) and C16:1*c*9 and C18:1*c*9 among the MUFAs (Table 4). Tissues from lambs kept on pasture were fattier ($p < 0.01$) than those of lambs on indoor diets (Table 5), suggesting that, under the conditions of the current experiment, the lambs' net energy intake was greater from pasture than from the indoor diets. Despite the differences observed in individual FAs and in tissue fat content, FS had little influence on SFAs and MUFAs, although there was a slightly higher proportion of PUFAs in lambs reared on pasture than those on indoor diets ($p < 0.05$), mainly due to increased proportions of C18:3n-3, C20:5n-3 (EPA), and C22:6n-3 (DHA) in pasture-fed lambs ($p < 0.01$). Pasture

DOI: 10.1021/jf504956x
J. Agric. Food Chem. 2015, 63, 963−974

Table 6. Proportion of Saturated Fatty Acids (Grams per 100 g of Total FA) in Six Tissues Collected from Lambs Kept on Three Different Feeding Systems (FS) and *p* Value of the FS × T Interaction[a]

	tissue[b] (T)							T contrasts (*p* value)					
		fats		muscles									
					chop								
	liver	KF	SF	leg	RE	OM	SEM[c]	liver vs others	fats vs muscles	KF vs SF	leg vs chop	RE vs OM	FS × T
C8:0	0.03	0.03	0.03	0.03	0.03	0.03	0.003						
C10:0		0.18	0.19	0.21	0.19	0.18	0.009		*				
C12:0	0.04	0.15	0.17	0.31	0.20	0.21	0.014	**	**				
C13:0	0.91	0.60	0.07	0.06	0.04	0.23	0.046	**		**	*	**	
C14:0$_{iso}$	0.08	0.15	0.15	0.12	0.10	0.12	0.006	**	**		**	**	
C14:0	0.89	2.76	3.13	3.98	3.27	3.36	0.133	**		*			
C15:0$_{iso}$	0.31	0.43	0.44	0.27	0.28	0.35	0.012	**	**		**	**	**
C15:0$_{anteiso}$	0.38	0.47	0.47	0.36	0.33	0.40	0.151		**		**	**	**
C15:0	0.78	0.91	1.02	0.89	0.77	0.97	0.025	**	**	**	**	**	*
C16:0$_{iso}$	0.28	0.38	0.40	0.32	0.30	0.33	0.012	**	**		**	*	**
C16:0	16.4	20.4	22.6	23.7	23.2	22.4	0.330	**		**		*	
C17:0$_{iso}$	0.64	0.61	0.66	0.57	0.58	0.59	0.015	*	**	**	*		**
C17:0$_{anteiso}$	0.79	0.91	1.00	0.77	0.80	0.86	0.026	**	**	**	**	*	**
C17:0	1.77	2.06	2.20	1.62	1.66	1.91	0.053	**	**	*	**	**	**
C18:0$_{iso}$	0.23	0.19	0.27	0.22	0.25	0.23	0.008			**			**
C18:0	26.5	33.9	25.7	19.6	20.4	24.5	0.591	**	**	**	**	**	**
C19:0$_{iso}$	0.04	0.06	0.01	0.02	0.01	0.03	0.004	**	*	**		*	**
C19:0	0.53	0.36	0.17	0.13	0.12	0.25	0.013	**		**	**	**	**
C20:0	1.27	0.35	0.16	0.15	0.13	0.24	0.026	**	**	**	*	**	*
C22:0	0.94	0.08	0.03	0.01	0.02	0.03	0.044	**	**				
C23:0	0.06	0.02	0.01	0.01	0.03	0.01	0.002	**	*	**	*	*	

[a]Data are least-squares means (for tissue, $n = 36$; for FS × T, $n = 12$); a significant difference for a given FA is indicated as * ($p < 0.05$) or ** ($p < 0.01$) for each contrast and FS × T interaction. [b]KF, kidney fat; SF, subcutaneous fat; leg, leg inner muscle (quadriceps femoris); RE, rib ye muscle; OM, other chop muscles. [c]Standard error of the means.

increased the sums of CLA ($p < 0.05$) and n-3 PUFA ($p < 0.01$), reduced n-6 PUFA ($p < 0.01$), and lowered the n-6/n-3 PUFA ratio compared to the indoor diets ($p < 0.01$), the main reason for this being that grass is a rich natural source of C18:3n-3, a precursor of other n-3 PUFAs, whereas concentrates are rich in C18:2n-6, a precursor of other n-6 PUFAs.[27] Pasture feeding also increased long-chain FAs and reduced the proportions of medium- and short-chain FAs as well as the incidences of branched and odd FAs compared to the indoor diets. This would reflect greater rumen activity and lower rumen escape of intermediary products of biohydrogenation with pasture compared to concentrate-based diets.[29] The reduced proportions of odd FAs found in the tissues of lambs kept on pasture might also reflect a lower availability of propionic acid for lipogenesis in fat tissues.[30]

Compared to the indoor-control, the rpCLA diet did not alter the average tissue fat content and influenced only the proportions of individual CLA isomers ($p < 0.05$), the CLA sum ($p < 0.01$), and the desaturation index for CLA*c*9,*t*11 ($p < 0.05$). The CLA*c*9,*t*11 isomer is formed in the rumen or is synthesized in tissues from *trans*-vaccenic acid (C18:1*t*11).[31,32] The C18:1*t*11 is formed in the rumen from C18:1*n*9, C18:2n-6, and C18:3n-3[11] diets that promote the greatest activity of the stearoyl-CoA desaturase (SCD); that is, starchy concentrate diets are also associated with a lower duodenal flow of the C18:1*t*11 precursor, with forage-based diets resulting in the highest flow of this FA from the rumen.[27] This is consistent with the results of the current experiment, which showed that tissues of lambs on indoor diets contained lower proportions of C18:1*t*11 and CLA*c*9,*t*11 than those of lambs on pasture. Unfortunately, in the current experiment we were unable to achieve a good separation of the C18:1*t*11 isomer, as it was coeluted with C18:1*t*9. Separation of the two isomers is desirable, and in light of this a better combination of operative conditions and column characteristics of the GC×GC system needs to be studied.

The CLA*t*10,*c*12 isomer is produced in the rumen from biohydrogenation of linoleic acid (C18:2n-6), especially in cows, sheep, and lambs on starchy and low-fiber diets[33] or on diets supplemented with oils rich in linoleic acid.[34] There are generally low proportions of this CLA isomer in ruminant products,[2] and an rpCLA supplement is considered to be the most effective way of increasing its presence in ruminant tissues.[13] In the current study, the indoor diet with rpCLA increased the average content of CLA*c*9,*t*11 and CLA*t*10,*c*12 in tissues by about 30 and 100%, respectively, compared to the similar diet without rpCLA (Figure 1). The magnitude of response to rpCLA supplementation was broadly similar to that to pasture, except in kidney fat, where a notable increase in CLA*t*10,*c*12 was found when rpCLA was given to the lambs. Previous experiments on lambs found that CLA supplementation effected a dose-dependent increase in the content of these isomers in tissues, but had no influence on the proportions of the other FAs, as also found in the current experiment.[35,36] This suggests that rpCLA supplementation has a much smaller effect on the FA profile of tissue than was previously observed by others in milk.[33]

The relative proportions of CLA*c*11,*t*13 were highest in lambs kept on pasture and lowest in lambs on the indoor-control diet ($p = 0.03$), whereas rpCLA supplementation increased the

DOI: 10.1021/jf504956x
J. Agric. Food Chem. 2015, 63, 963−974

Table 7. Proportion of Unsaturated Fatty Acids (Grams per 100 g of Total FA) in Six Tissues (T) Collected from Lambs Kept under Three Different Feeding Systems (FS) and Significance of Contrasts and of FS × T Interaction[a]

	tissue[b] (T)							T contrasts (p value)					
		fats		muscles	chop								
	liver	KF	SF	leg	RE	OM	SEM[c]	liver vs others	fats vs muscles	KF vs SF	leg vs chop	RE vs OM	FS × T
C14:1*c*9	0.02	0.04	0.07	0.12	0.10	0.09	0.009	**	**	*	**		
ΣC15:1 others	0.06	0.10	0.07	0.05	0.05	0.08	0.007		**	**	**	**	
C16:1n7	0.03	0.03	0.03	0.02	0.04	0.03	0.006						
C16:1*t*7	0.23	0.08	0.09	0.12	0.10	0.07	0.013	**	**				
C16:1*c*7	0.59	0.56	0.53	0.47	0.51	0.48	0.022	**					
C16:1*c*9	0.82	0.65	1.18	1.46	1.37	1.22	0.048	**	**	**	**	*	
ΣC16:1 others	0.48	0.30	0.10	0.17	0.16	0.19	0.045	**		**			
C17:1*c*10	0.11	0.39	0.77	0.74	0.75	0.75	0.035	**		**			
ΣC17:1 others	0.73	0.41	0.17	0.27	0.15	0.32	0.050	**		**		*	**
C18:1*c*7[d]	0.83	0.56					0.185	**					**
C18:1*t*9(+*t*11)[e]	3.32	4.99	4.19	3.38	3.49	3.50	0.103	**	**	**	**		**
C18:1*c*9	15.8	19.2	28.4	32.9	33.7	29.6	0.480	**	**	**	**	**	**
ΣC18:1 others	1.51	1.59	0.63	0.68	0.51	0.77	0.106	**	**	**			**
C19:1n9*t*	0.03	0.02				0.02	0.002	*					*
C19:1n9*c*	0.07	0.02	0.14	0.15	0.14	0.18	0.013	**	**	**		*	
C20:1n9*t*	0.06	0.02	0.01	0.01	0.02	0.01	0.007	**					**
C20:1n9	0.11	0.05	0.02	0.03	0.03	0.04	0.006	**	**	**			**
C20:1n7	0.03	0.06	0.02	0.05	0.04	0.06	0.007	*		**		*	
C20:1n11[d]	0.08	0.02					0.005	**					**
ΣC16:2 others	0.05	0.07	0.03	0.03	0.04	0.03	0.004	**	**	**			**
C18:2n-6	5.39	1.93	2.54	3.33	3.19	2.92	0.109	**	**	**	**	*	
ΣC18:2 others	1.45	1.17	0.98	0.88	1.02	0.72	0.065	**		*	*	**	
CLA*c*9*t*11	0.52	0.51	0.41	0.53	0.49	0.56	0.280	*			**	*	
CLA*t*9*t*11	0.12	0.11					0.006						**
CLA*c*11*t*13	0.02	<0.01	0.05	0.03	0.05	0.07	0.007	**	**		**		
CLA*t*10*c*12	0.05	0.09	0.10	0.08	0.13	0.14	0.022	*	*				
CLA*c*9*c*11	0.04	0.02	0.02	0.03	0.007	0.02	0.014		*				*
C18:3n-6	0.32	0.08	0.04	0.04	0.05	0.05	0.009	**	**	**			**
C18:3n-3	1.34	0.87	0.90	0.83	0.89	0.90	0.056	**	*				**
C18:4n-3	0.16	0.09	0.02	0.02	0.02	0.04	0.018	**		*			
C20:2n-6	0.09	0.01		0.02		0.02	0.003	**	**				**
C20:3n-6	0.37	0.01		0.02		0.01	0.010	**	**				**
C20:4n-6	4.21	0.06				0.14	0.108	**	**				**
C20:5n-3 (EPA)	1.17	0.07				0.01	0.104	**	**				**
C20:2n-3[d]	0.57	0.03					0.026						**
C20:3n-3[f]	0.08						0.040						
C20:4n-3[f]	0.04						0.021						
C22:4n-6[f]	0.41						0.172						
C22:6n-3 (DHA)[f]	1.43						0.827						
C22:5n-6[f]	0.26						0.134						

[a]Data are least-squares means (tissue, n = 36; FS × T interaction, n = 12); a significant difference for a given FA is indicated as * (p < 0.05) or ** (p < 0.01) for each contrast and FS × T interaction. [b]KF, kidney fat; SF, subcutaneous fat; leg, leg inner muscle (quadriceps femoris); RE, ribeye muscle; OM, other chop muscles. [c]Standard error of the means. [d]Found only in liver and kidney fat. [e]Co-eluted isomers. [f]Found only in liver.

amounts of this isomer in all tissues except kidney fat, even though the FS × T interaction was not significant (p = 0.23). This isomer was not present in the rpCLA mixture used in this trial, so the reason for the increase in CLA*c*11,*t*13 when rpCLA is added to the feed is unknown. To our knowledge, this effect has not been observed before, and it may be hypothesized that one or both of the two CLA isomers supplied with rpCLA is directly or indirectly involved in CLA*c*11*t*13 formation.

Depending on the circumstances, gender may be an important factor in FA composition, because of its relationship with carcass fatness.[37] However, in this study no significant or notable effect of gender was observed, likely because the fatness of males and females did not differ as they were slaughtered at the onset of puberty.[15]

Tissue. The FA profile of liver largely differed from that of the other tissues for the majority of single FAs or FA categories (Tables 6−8), as described in the literature.[30,38]

Liver tissue was the richest in PUFAs (21%), mainly due to the contribution of C18:2, C18:3, and FAs with chains longer than 18 C, including 5 FAs present in trace amounts or not detectable in other tissues, among them C20:4n-6, C20:5n-3, and C22:6n-3. Liver also contained high levels of very long

DOI: 10.1021/jf504956x
J. Agric. Food Chem. 2015, 63, 963−974

Table 8. Fat Content (Grams per 100 g of Tissue), Proportion of Fatty Acid Categories (Grams per 100 g of Total FA), FA Indices of Six Tissues (T) Collected from Lambs Kept under Three Different Feeding Systems (FS), and *p* Value of the FS × T Interaction[a]

	tissue[b] (T)							T contrasts (*p* value)					
		fats		muscles	chop								
	liver	KF	SF	leg	RE	OM	SEM[c]	liver vs others	fats vs muscles	KF vs SF	leg vs chop	RE vs OM	FS × T
fat content	5.70	69.2	54.9	3.30	2.80	13.5	1.866	**	**	**	**	**	**
SFA	53.2	65.6	58.8	53.3	52.7	57.3	0.572	**	**	**	**	**	**
MUFA	25.1	28.9	36.1	40.3	41.0	36.9	0.508	**	**	**	**	**	**
PUFA	21.2	5.44	5.15	6.31	6.18	5.79	0.352	**	**				
FA unknown	0.56	0.05	0.02	0.03	0.01	0.01	0.010	**	**	**			**
ΣCLA	0.75	0.74	0.57	0.67	0.67	0.79	0.051	*			*		
n-3 PUFA	6.50	1.13	0.90	0.94	0.96	0.98	0.187	**	**				**
n-6 PUFA	10.8	2.09	2.58	3.71	3.52	3.14	0.176	**	**	*	**		**
n-6/n-3 PUFA	1.99	2.16	3.61	4.65	4.43	3.85	0.210	**	**	**	**	*	
<C16	3.57	6.23	5.73	6.35	5.40	6.08	0.183	**	**	*	**	**	
C16	18.8	22.4	24.9	26.3	25.6	24.7	0.356	**		**	*	*	
>C16	77.1	71.2	69.3	67.4	69.0	69.2	0.479	**		**			
branched	2.91	3.26	3.34	2.64	2.64	2.88	0.089		**		**		**
odd chain	7.76	7.68	6.87	5.59	5.57	6.59	0.091	**	**	**	**	**	**
desaturases:[d]													
C14	0.03	0.02	0.02	0.03	0.03	0.05	0.013						
C16	0.05	0.03	0.05	0.06	0.05	0.05	0.002		**	**			**
C18	0.37	0.36	0.53	0.63	0.62	0.55	0.010	**	**	**	**	**	**
CLA*c*9,*t*11	0.14	0.09	0.09	0.14	0.12	0.14	0.005	**	**			**	
IT[e]	1.15	2.73	2.02	1.61	1.59	1.90	0.042	**	**	**	**	**	
IAT[e]	0.48	0.99	0.90	0.88	0.80	0.88	0.021	**	**	**	**	**	

[a]Data are least-squares means (for tissue, $n = 36$; for FS × T interaction, $n = 12$); a significant difference for a given FA category or index is indicated as * ($p < 0.05$) or ** ($p < 0.01$) for each contrast and FS × T interaction. [b]KF, kidney fat; SF, subcutaneous fat; leg, leg inner muscle (quadriceps femoris); RE, ribeye muscle; OM, other chop muscles. [c]Standard error of the mean. [d]Δ^9-desaturase indices: calculated according to the method of Kelsey et al.[22] [e]Thrombogenic Index and Atherogenic Index were calculated according to the method of Ulbricht and Southgate.[23]

chain SFAs, C20:0, C22:0, and C23:0, and of n-3 and n-6 PUFAs and odd-chain FAs, but had the lowest n-6/n-3 PUFA ratio compared to all other tissues ($p < 0.01$). The Δ^9-desaturation index for C18 was lower in liver than in other tissues, but the opposite was found for the CLA*c*9,*t*11 desaturation index. The FA profile of liver is influenced by dynamic conditions caused by incoming and outgoing FAs. Ruminant liver has less effect on de novo synthesis than adipose tissues or muscles do; nevertheless, a low rate of de novo biosynthesis occurs when acetate is the main carbon source. However, the pool of long-chain FAs in the liver is mainly derived from plasma NEFA.[38,39]

The FA profiles of the two adipose tissues differed from those of muscles with respect to the large majority of single saturated and unsaturated FAs. Fatty depots had higher proportions of SFAs but lower MUFAs and PUFAs, higher proportions of n-3 PUFA, lower proportions of n-6 PUFA, a lower n-6/n-3 PUFA ratio, similar proportions of short-, medium- and long-chain FAs, and higher proportions of branched- and odd-chain FAs compared to muscles. Adipose tissues are considered to be the major sites of de novo FA synthesis, palmitic acid (C16:0) being the main product, which can be further elongated to stearic acid (C18:0) and desaturated to oleic acid by SCD.[27] Ward et al.[40] demonstrated that, in sheep, SCD is produced from a single gene, the expression of which is under hormonal control, independent of total fat synthesis, and the activity of which varies according to fat depot, being higher in subcutaneous fat that in internal depots. In the current experiment, subcutaneous fat and kidney fat differed substantially, the latter being richer in SFAs, particularly C18:0, but poorer in MUFAs, particularly C18:1*c*9.

Differences among the FA profiles of muscles were less pronounced than among those of fat depots; in general the three muscles contained higher proportions of C18:1*c*9 (32%) and C18:2n-6 (3.1%), a similar proportion of C16:0 (23.1%), and a lower proportion of C18:0 (21.5%) compared to subcutaneous fat. The general trend was that the other chop muscles tended to have an FA profile intermediate between that of the leg and ribeye muscles and that of the fatty depots. Differences among muscles are related to differences in the presence of fibers with different oxidative, glycolytic, or oxidoglycolytic properties. These fibers are present in various proportions in muscles depending on animal species, location of the muscle in the body, and other nutritional and physiological characteristics, such as physical movement. Red oxidative fibers have a higher proportion of phospholipids than white and, consequently, a higher percentage of PUFAs.[39]

Feeding System × Tissue Interaction. A significant FS × T interaction was observed for the fat content of tissue. Feeding system had a small or negligible effect on the fat content of liver and muscles, but the proportion of fat in the subcutaneous tissue was higher with pasture than with the two indoor diets (65.0 vs 49.8 g/100 g tissue, respectively). The fat content of kidney exhibited a consistent progressive decrease from 80.0 g/100 g of tissue for pasture to 68.0 g/g for indoor-control to 59.0 g/g for indoor-CLA. This suggests that the

DOI: 10.1021/jf504956x
J. Agric. Food Chem. 2015, 63, 963−974

muscles, the most valuable components of the carcass, have a lower response to changes in dietary energy supply in terms of fat content than other fat tissues, which are less important for human nutrition.

The FS × T interaction was significant for many FAs: a total of 41 single FAs, categories, and indices. The number and the complexity of these interactions made it impossible to go into all of these interactions in depth, so only some examples are presented and discussed.

In all tissues, the most highly represented FAs were C18:0 and C18:1*c*9, both of which exhibited a significant FS × T interaction ($p < 0.01$) (Figure 2). Compared to pasture, the indoor-control diet reduced by an average of 11% the relative proportion of C18:0 in all tissues, except the quadriceps femoris. Indoor-CLA increased the proportion of C18:0 by an average of 11% over indoor-control in ribeye muscle and in other chop muscles, but no differences were found in the other tissues. The trend observed for C18:1*c*9 in tissues, according to FS, mirrored that described for C18:0. Thus, the pattern of the FS × T interaction for SFAs largely reflected the patterns of their major FA constituents, C18:0 and C18:1*c*9. In pasture-fed lambs as opposed to indoor diets the proportions of SFAs decreased in liver (from 55.4 to 51.3 g/100 g total FA), were constant in subcutaneous fat (58.8 g/100 total FA), and increased in muscle (from 52.9 to 55.2 g/100 g total FA). The opposite pattern was observed for MUFAs, whereas PUFAs remained unchanged. These results suggests that different tissues would respond differently to a change in FS in terms of the relative presence of some FAs. However, for the large majority of FAs, the direction of the response to a change in FS was similar in the various tissues, although the relative amounts differed. For example, liver contained higher proportions of both n-3 and n-6 FAs, and in all tissues pasture effected an increase in the proportions of n-3 PUFA, and a decrease in the proportions of n-6 PUFA and in the n-6/n-3 PUFA ratio compared to the other FSs (Figure 3). The n-6/n-3 ratio was smaller with pasture than the other diets in all tissues. Irrespective of the FS, this ratio ranged from 1.0 to 2.5 in liver and from 2.5 to 6.0 in other tissues. Replacing pasture with indoor diets also increases branched and odd FAs in all tissues (Figure 4), but it is more pronounced in liver and kidney fat.

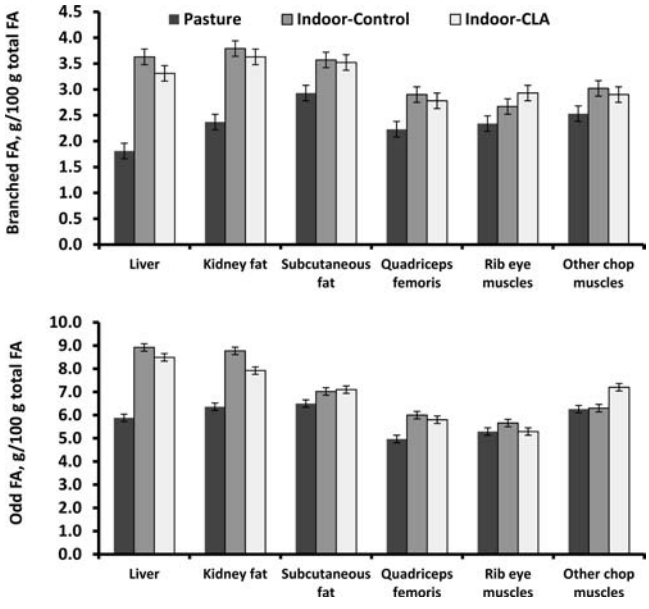

Figure 4. Effect of feeding system (pasture; indoor-control, based on hay and concentrates; indoor-CLA, based on hay and concentrates top dressed with 8 g/day of a commercial rumen-protected CLA mixture) on branched-chain and odd-chain fatty acid contents of six lamb tissues. Each bar is the least-squares mean from 12 observations; vertical bars indicate SEM. The significance of the feeding system × tissue interaction was $p < 0.01$ and < 0.01 for branched and odd FA, respectively.

In conclusion, the use of two-dimensional GC provided a very detailed FA profile of the lipid fraction contained in various tissues of lambs, with 128 single FAs quantified, making available new information on this issue and allowing for a deeper insight of the effect of nutrition on lipid metabolism of ruminants. Despite the relatively low number of observations, this technique allowed us to evaluate the effects of the FS × T interaction even for FAs present in low or very low concentrations, and in general the standard errors of the means were proportional to the value of the corresponding means. It was found that the replacement of pasture with indoor diets altered the FA profile, with an increase in the average n-6/n-3 PUFA ratio toward values that can still be considered acceptable.[38] A commercial CLA mixture containing CLA*c*9,*t*11 and CLA*t*10,*c*12 notably increased the CLA*c*11,*t*13 content in all tissues, except kidney fat, demonstrating the effectiveness of rumen-protected molecules in delivering specific bioactive substances to lamb tissues. The effects of feeding systems with or without rpCLA on the FA profiles were similar, but not identical, in almost all of the tissues analyzed.

■ ASSOCIATED CONTENT

Ⓢ Supporting Information

Ordered structure of GC×GC chromatogram of a liver sample and CLA*c*9,*t*11 levels in tissues. This material is available free of charge via the Internet at http://pubs.acs.org.

■ AUTHOR INFORMATION

Corresponding Author

*(F.T.) Phone: +39 049 8272622. Fax: +39 049 8272633. E-mail: franco.tagliapietra@unipd.it.

Funding

This work was partially supported by MURST ex60% funds.

Notes

The authors declare no competing financial interest.

■ ACKNOWLEDGMENTS

We acknowledge the Veneto Region project Bionet (misura 214—pagamenti agroambientali—sottomisura H — Rete regionale della biodiversità) and the technical assistance of Dr. Alberto Simonetto and Luca Grigoletto. We thank SILA s.r.l. (Noale, VE, Italy) for providing the rumen-protected CLA used in this experiment.

■ ABBREVIATIONS USED

AI, atherogenic index; BCS, body condition score; BW, body weight; DHA, docosahexaenoic acid; EPA, eicosapentaenoic acid; FA, fatty acid; FAME, fatty acid methyl esters; GC×GC, two-dimensional gas chromatography; MUFA, monounsaturated fatty acid; PUFA, polyunsaturated fatty acid; rpCLA, rumen-protected conjugated linoleic acid; SCD, starchy concentrate diets; SFA, saturated fatty acid; TI, thrombogenic index

DOI: 10.1021/jf504956x
J. Agric. Food Chem. 2015, 63, 963−974

REFERENCES

(1) Shingfield, K. J.; Bonnet, M.; Scollan, N. D. Recent developments in altering the fatty acid composition of ruminant-derived foods. *Animal* **2013**, *7*, 132−162.

(2) Dilzer, A.; Park, Y. Implication of conjugated linoleic acid (CLA) in human health. *Crit. Rev. Food Sci. Nutr.* **2012**, *52*, 488−513.

(3) Dannenberger, D.; Nuernberg, K.; Herdmann, A.; Nuernberg, G.; Hagemann, E.; Kienast, W. Dietary PUFA intervention affects fatty acid and micronutrient profiles of beef and related beef products. *Foods* **2013**, *2*, 295−309.

(4) Manzano, P.; Arnáiz, E.; Diego, J. C.; Toribio, L.; García-Viguera, C.; Bernal, J. L.; Bernal, J. Comprehensive two-dimensional gas chromatography with capillary flow modulation to separate FAME isomers. *J. Chromatogr., A* **2011**, *1218*, 4952−4959.

(5) Bittante, G.; Pastore, E. Effect of Finnsheep crossbreeding on Lamon sheep performance − *in vivo* traits. *J. Agric. Sci. Finl.* **1988**, *60*, 511−514.

(6) Ramanzin, M.; Bittante, G.; Bailoni, L. Evaluation of different chromium-mordanted wheat straws for passage rate studies. *J. Dairy Sci.* **1991**, *74*, 2989−2996.

(7) Bittante, G. Italian animal genetic resources in the Domestic Animal Diversity Information System of FAO. *Ital. J. Anim. Sci.* **2011**, *10*, 151−158.

(8) Kouba, M.; Mourot, J. A review of nutritional effects on fat composition of animal products with special emphasis on *n*-3 polyunsaturated fatty acids. *Biochimie* **2011**, *93*, 13−17.

(9) Nuernberg, K.; Nuernberg, G.; Ender, K.; Lorenz, S.; Winkler, K.; Rickert, R.; Steinhart, H. *n*-3 fatty acids and conjugated linoleic acids of *longissimus* muscle in beef cattle. *Eur. J. Lipid Sci. Technol.* **2002**, *104*, 463−471.

(10) Nuernberg, K.; Dannenberger, D.; Nuernberg, G.; Ender, K.; Voigt, J.; Scollan, N. D.; Wood, J. D.; Nute, G. R.; Richardson, R. I. Effect of a grass-based and a concentrate feeding system on meat quality characteristics and fatty acid composition of *longissimus* muscle in different cattle breeds. *Livest. Prod. Sci.* **2005**, *94*, 137−147.

(11) Kim, S. C.; Adesogan, A. T.; Badinga, L.; Staples, C. R. Effects of dietary n-6:n-3 fatty acid ratio on fed intake, digestibility, and fatty acid profiles of the ruminal contents, liver, and muscle of growing lambs. *J. Anim. Sci.* **2007**, *85*, 706−716.

(12) Kitessa, S. M.; Young, P.; Nattrass, G.; Gardner, G.; Pearce, K.; Pethick, D. W. When balanced for precursor fatty acid supply echium oil is not superior to linseed oil in enriching lamb tissues with long-chain n-3 PUFA. *Br. J. Nutr.* **2012**, *108*, 71−79.

(13) Schiavon, S.; De Marchi, M.; Tagliapietra, F.; Bailoni, L.; Cecchinato, A.; Bittante, G. Effect of high or low protein ration combined or not with rumen protected conjugated-linoleic acid (CLA) on meat CLA content and quality traits of double-muscled Piemontese bulls. *Meat Sci.* **2011**, *89*, 133−142.

(14) Consortium. In *Guide for the Care and Use of Agricultural Animals in Research and Teaching*, 3rd ed.; Federation of Animal Science Societies: Champaign, IL, USA, 2010.

(15) Pellattiero, E.; Cecchinato, A.; De Marchi, M.; Penasa, M.; Tormen, N.; Schiavon, S.; Cassandro, M.; Bittante, G. Growth rate, slaughter traits and meat quality of lambs of three Alpine sheep breeds. *Agric. Conspec. Sci.* **2011**, *76*, 1−4.

(16) Schiavon, S.; Tagliapietra, F.; Dal Maso, M.; Bailoni, L.; Bittante, G. Effects of low-protein diets and rumen-protected conjugated linoleic acid on production and carcass traits of growing double-muscled Piemontese bulls. *J. Anim. Sci.* **2010**, *88*, 3372−3383.

(17) Christie, W. W.; Dobson, G.; Adlof, R. O. A practical guide to the isolation, analysis and identification of conjugated linoleic acid. *Lipids* **2007**, *42*, 1073−1084.

(18) Cesaro, G.; Tagliapietra, F.; Grigoletto, L.; Cecchinato, A.; Dannenberger, D.; Bittante, G.; Schiavon, S. Fecal sample preparation methods for gas chromatography analysis of fatty acids of ruminants fed different amounts of rumen protected conjugated linoleic acid (CLA). *Anim. Feed Sci. Technol.* **2013**, *183*, 184−194.

(19) Raes, K.; De Smet, S.; Demeyer, D. Effect of dietary fatty acids on incorporation of long chain polyunsaturated fatty acids and conjugated linoleic acid in lamb, beef and pork meat: a review. *Anim. Feed Sci. Technol.* **2004**, *113*, 199−221.

(20) Or-Rashid, M. M.; Odongo, N. E.; McBride, B. W. Fatty acid composition of ruminal bacteria and protozoa, with emphasis on conjugated linoleic acid, vaccenic acid, and odd-chain and branched-chain fatty acids. *J. Anim. Sci.* **2007**, *85*, 1228−1234.

(21) Givens, D. I.; Kliem, K. E.; Gibb, R. A. The role of meat as a source of n-3 polyunsaturated fatty acids in the human diet. *Meat Sci.* **2006**, *74*, 209−218.

(22) Kelsey, J. A.; Corl, B. A.; Collier, R. J.; Bauman, D. E. The effect of breed, parity, and stage of lactation on conjugated linoleic acid (CLA) in milk fat from dairy cows. *J. Dairy Sci.* **2003**, *86*, 2588−2597.

(23) Ulbricht, T. L. V.; Southgate, D. A. T. Coronary heart disease: seven dietary factors. *Lancet* **1991**, *338*, 985−992.

(24) SAS. In *SAS/STAT User's Guide*, 4th ed.; SAS Institute: Cary, NC, USA, 1996; Vol. 2.

(25) Vlaeminck, B.; Harynuk, J.; Fievez, V.; Marriot, P. Comprehensive two-dimensional gas chromatography for the separation of fatty acids in milk. *Eur. J. Lipid Sci. Technol.* **2007**, *109*, 757−766.

(26) Cecchinato, A.; De Marchi, M.; Penasa, M.; Casellas, J.; Schiavon, S.; Bittante, G. Genetic analysis of beef fatty acids composition predicted by near-infrared spectroscopy. *J. Anim. Sci.* **2011**, *90*, 429−438.

(27) Sinclair, L. A. Nutritional manipulation of the fatty acid composition of sheep meat: a review. *J. Agric. Sci.* **2007**, *145*, 419−434.

(28) Serra, A.; Mele, M.; La Comba, F.; Conte, G.; Buccioni, A.; Secchiari, P. Conjugated linoleic acid (CLA) content of meat from three muscles of Massese suckling lambs slaughtered at different weights. *Meat Sci.* **2009**, *81*, 396−404.

(29) Serra, A.; Macciotta, N. P. P.; Mele, M.; Nudda, A.; Conte, G.; Secchiari, P. Effect of weight of slaughter and feeding regimen on conjugated linoleic acid and trans fatty acid content in lamb meat: a meta-analysis approach. *Ital. J. Anim. Sci.* **2009**, *8*, 540−542.

(30) Demirel, G.; Wachira, A. M.; Sinclair, L. A.; Wilkinson, R. G.; Wood, J. D.; Enser, M. Effects of dietary n-3 polyunsaturated fatty acids, breed and dietary vitamin E on the fatty acids of lamb muscle, liver and adipose tissue. *Br. J. Nutr.* **2004**, *91*, 551−565.

(31) Pariza, M. W.; Park, Y.; Cook, M. E. The biologically active isomers of conjugated linoleic acid. *Prog. Lipid Res.* **2001**, *40*, 283−298.

(32) Cecchinato, A.; Ribeca, C.; Maurmayr, A.; Penasa, M.; De Marchi, M.; Macciotta, N. P. P.; Mele, M.; Secchiari, P.; Pagnacco, G.; Bittante, G. Short communication: effect of β-lactoglobulin, stearoyl-coenzyme A desaturase 1, and sterol regulatory element binding protein gene allelic variants on milk production, composition, acidity, and coagulation properties of Brown Swiss cows. *J. Dairy Sci.* **2012**, *95*, 450−454.

(33) Pulina, G.; Nudda, A.; Bataccone, G.; Cannas, A. Effect of nutrition on the contents of fat, protein, somatic cells, aromatic compounds, and undesirable substances in sheep milk. *Anim. Feed Sci. Technol.* **2006**, *131*, 255−291.

(34) Antongiovanni, M.; Mele, M.; Boccioni, A.; Petacchi, F.; Serra, A.; Melis, M. P.; Cordeddu, L.; Banni, S.; Secchiari, P. Effect of forage/concentrate ratio and oil supplementation on C18:1 and CLA isomers in milk fat from Sarda ewes. *J. Anim. Feed Sci.* **2004**, *13*, 669−672.

(35) Wynn, R. J.; Daniel, Z. C. T. R.; Flux, C. L.; Craigon, J.; Salter, A. M.; Buttery, P. J. Effect of feeding rumen-protected conjugated linoleic acid on carcass characteristics and fatty acid composition of sheep tissues. *J. Anim. Sci.* **2006**, *84*, 3440−3450.

(36) Terré, M.; Nudda, A.; Boe, F.; Gaias, G.; Bach, A. Performance, immune response and fatty acid profile in lambs supplemented with a CLA-mixture. *Anim. Feed Sci. Technol.* **2011**, *165*, 1−7.

(37) Vacca, G. M.; Carcangiu, V.; Dettori, M. L.; Pazzola, M.; Mura, M. C.; Luridiana, S.; Tilloca, G. Productive performance and meat quality of Mouflon × Sarda and Sarda × Sarda suckling lambs. *Meat Sci.* **2008**, *80*, 326−334.

(38) Herdmann, A.; Martin, J.; Nuernberg, G.; Wegner, J.; Dannenberger, D.; Nuerberg, K. How do n-3 fatty acid (short-time restricted *vs* unrestricted) and n-6 fatty acid enriched diets affect the

DOI: 10.1021/jf504956x
J. Agric. Food Chem. 2015, 63, 963−974

fatty acid profile in different tissues on German Simmental bulls? *Meat Sci.* **2010**, *86*, 712−719.
(39) Hocquette, J. F.; Bouchart, D. Intestinal absorption, blood and hepatic and muscle metabolism of fatty acids in preruminant and ruminant animals. *Reprod. Nutr. Dev.* **1999**, *39*, 27−48.
(40) Ward, R. J.; Travers, M. T.; Richards, S. E.; Vernon, R. G.; Salter, A. M.; Buttery, P. J.; Barber, M. C. Stearoyl-CoA desaturase mRNA is transcribed from a single gene in the ovine genome. *Biochim. Biophys. Acta* **1998**, *1391*, 145−156.

DOI: 10.1021/jf504956x
J. Agric. Food Chem. 2015, 63, 963−974

Table 1. Descriptions of the Ciders Analyzed in This Study

sample	brand	location	country code	region[a]	ingredients	declared ABV %	calcd C_4 sugar[b] (%)	sugars identifed
1	Wild	Tipperary, Ireland	IRL	EU	apple/strawberry	4.0	0	
2	Magners	Tipperary, Ireland	IRL	EU	pear	4.5	0	
3	Henry Westons	Herfordshire, UK	GB	EU	apple	8.2	0	
4	Aspall	Suffolk, UK	GB	EU	apple	4.0	0	
5	Loic Raison	Domagné, France	F	EU	apple	4.5	0	
6	Verano	San Sebastain, Spain	E	EU	apple	4.5	68	HFCS
7	Apple Head	Belgium	BY	EU	apple	4.5	0	
8	Stassen	Aubel, Belgium	BY	EU	apple	4.5	0	
9	Rekorderlig	Vimmery, Sweden	S	EU	apple	4.5	0	
10	+46	Herrljunga, Sweden	S	EU	apple	4.5	3	
11	Kopparberg	Kopparberg, Sweden	S	EU	apple	4.5	0	
12	Mercury	TAS, Australia	AU*	ANZ	apple	5.2	85	cane
13	Cheeky Rascal	VIC, Australia	AU	ANZ	apple/pomegranate	8.0	78	HFCS
14	The Barossa Cider Co.	SA, Australia	AU	ANZ	apple	5.0	15	
15	Matsos	WA, Australia	AU	ANZ	apple/lime/ginger	4.0	79	cane/HFCS
16	Bulmers	NSW, Australia	AU	ANZ	pear	4.7	52	cane
17	Miracle	SA, Australia	AU	ANZ	apple	5.0	7	
18	Kirin	NSW, Australia	AU	ANZ	apple	8.0	3	
19	Monteiths	Greymouth, New Zealand	NZ	ANZ	apple/pear	4.5	83	glucose
20	Newton's	New Zealand	NZ	ANZ	apple	4.0	32	cane
21	Old Mout	New Zealand	NZ	ANZ	apple	5.5	56	HFCS

[a]Ciders were categorized as European (EU) or Australia/New Zealand (ANZ). [b]Calculated according to the method of Brooks et al.[21]

cations and anions. The primary aim of this survey was to determine whether the techniques already established for beers[20] could be applied to identify the geographical origin of ciders and/or the addition of C_4 sugars. A further outcome of the study was to provide background data against which suspected substitute or counterfeit products can be compared.

MATERIALS AND METHODS

Sample Collection and Processing. Twenty bottled and one canned cider were purchased from licensed retail outlets in the Brisbane metropolitan area (Queensland, Australia). The packaging of each sample was examined to verify the integrity and authenticity of the product and to confirm the location of manufacture. As with many studies of food authenticity, it was difficult to obtain truly authentic samples. In obtaining the samples for this study our strategy was to seek out reputable vendors.

Prior to analysis, the samples were stored at room temperature. Once opened, samples were filtered through hardened ashless paper to remove the majority of the dissolved carbon dioxide and then through 0.45 μm Durapore filters (Merck Millipore, Billerica, MA, USA) into two 50 mL sterile containers for cation and anion determination. Degassed samples intended for δ^2H and δ^{18}O analysis were dispensed into 2 mL autosampler vials. To obtain a solid residue, approximately 5 mL aliquots of unfiltered ciders were heated in wide beakers at 102 °C until visibly dry.

Stable Isotopic Analysis. All isotopic measurements were performed using a Thermo Scientific (Bremen, Germany) Delta V^{PLUS} isotope ratio mass spectrometer (IRMS) coupled to a ConFlo IV interface for working gas introduction and sample dilution.

The carbon isotopic analysis of solid samples and hydrogen and oxygen isotopic analyses of liquid samples were performed using a Thermo Scientific Flash 2000 HT operated in Elemental Analyzer (EA) or Thermal Conversion EA (TC/EA) mode, respectively, as previously described.[20] The median standard deviations for replicate measurements of samples were 0.03‰ for solid ^{13}C measurements (n = 3) and 0.3 and 0.1‰, respectively, for aqueous ^{2}H and ^{18}O measurements (n = 5).

Solid samples intended for δ^{18}O analysis were measured into 4 × 3.2 mm silver capsules (IVA Analysentechnik, Meerbusch, Germany) and dried under vacuum, over phosphorus pentoxide for a minimum of 5 days. The ^{18}O composition was determined using the TC/EA with the same operating conditions used for liquid samples. Capsules were crimped closed prior to analysis and introduced into the reactor by a Zero-Blank autosampler (Costech Analytical Technologies Inc., Valencia, CA, USA). Each sample was analyzed in triplicate with a median standard deviations of 0.2‰.

Data were normalized to the international isotope scales (VPDB-LSVEC or VSMOW-SLAP) by two-point calibration; a list of the reference materials and quality control (QC) materials used is given in the Supporting Information (cider supp 2). No attempt was made to measure the δ^2H compositions of the solid residues as these samples contained exchangeable hydrogen and were highly deliquescent. In the face of ongoing controversy regarding the measurement of δ^2H values for materials with exchangeable hydrogen,[26] the authors considered that δ^2H_{VSMOW} data for these samples should not be compared to published data.

Cation Analysis. Aliquots of approximately 2 g of sample were accurately weighed into PTFE vessels and digested with 4 mL of high-purity nitric acid (69%, Seastar Chemicals, Sidney, BC, Canada) using a MarXpress microwave digestion system (CEM, Matthews, NC, USA). Digested samples were analyzed using a Vista Pro inductively coupled plasma−optical emission spectrometer (ICP-OES) (Varian Australia Inc., VIC, Australia) and a 7700 ICP-MS (Agilent Technologies Australia Pty Ltd., VIC, Australia) as previously described.[20] Reference materials and recovery spikes were used for quality control and assurance. Recoveries ranged from 77 to 119% and were deemed satisfactory (Supporting Information, cider supp 3).

Anion Analysis. Samples were diluted 500-fold and transferred to autosampler tubes. Anion concentrations were measured using a Compact ion chromatograph (Metrohm, Gladesvile, Australia) as previously described.[20] The recoveries for anions from spiked sample and aqueous solutions were satisfactory and >90% (Supporting Information, cider supp 3).

Sugar Analysis. Degassed, filtered samples were diluted 10-fold and transferred to autosampler vials. Sugars were separated and quantified using a Shimadzu UFLC-20A High-performance liquid

DOI: 10.1021/jf5030054
J. Agric. Food Chem. 2015, 63, 975−982

chromatograph (HPLC) system coupled to an RID-10A refractive index detector. Separation was achieved using a 150 mm × 4.6 mm Alltima NH_2 3 μm column (Grace, Archerfield, QLD, Australia) maintained at 30 °C with an isocratic mobile phase of water/acetonitrile (30:70). Standard solutions were prepared at concentrations of 10, 5.0, and 2.5 g/L from high-purity fructose, glucose, and sucrose (Sigma-Aldrich, Castle Hill, NSW, Australia).

Statistical Analysis. Data were analyzed and plotted using R 3.0.1 software environment for statistical computing and graphics.[27] Least absolute deviation (LAD) regression was applied to plotted data to determine the equation of robust fit and the correlation R^2 (observed vs predicted). Principal component analysis (PCA) was performed on the chemical data to determine which parameters accounted for the largest differences between samples. This was performed using the L_1-norm to increase robustness to outliers compared to traditional PCA.[28] Canonical discriminant analysis (CDA) was applied to both chemical and isotopic data to determine to what extent these parameters distinguish between the different regions of origin. These results represent the recognition ability based on the samples used to generate the model.

RESULTS

Overview of Samples. Although the number of samples in this study was limited, it was considered to be representative of the brands readily available within Australia at the time of the survey (October 2013). The analytical data are presented in the Supporting Information (cider supp 1).

The ciders obtained for this study are detailed in Table 1, categorized by country and region of origin and ingredients. Seven of the samples were produced in Australia, three in New Zealand (NZ), and 12 in European Union (EU) countries (Belgium, France, Ireland, Spain, Sweden, and the United Kingdom). Within Australia and New Zealand the composition of cider is controlled by the Food Standards Australia and New Zealand (FSANZ) code. There is no common EU legislation governing cider, but the majority of cider-producing countries adhere to the AVIC (L'Association des Industries des Cidres et Vins de fruit de l'U.E.) code of practice.

The declared alcoholic content of the ciders (reported in Table 1) ranged from 4.0 to 8.2% alcohol by volume (ABV) with a median value of 4.5% ABV. (For a product to be described as cider, FSANZ and AVIC codes require an alcoholic strength between 1.5 and 8.5% ABV.) Two of the ciders claimed to be manufactured from pears (samples 2 and 16) and one from apples and pears (sample 19). Both FSANZ and AVIC codes allow apple cider to contain up to 25% pear juice and vice versa. Three samples (1, 13, and 15) contained novel ingredients: strawberry, pomegranate, lime, or ginger. The authors assumed that these ingredients would be added in small amounts, principally for flavor, and, consequently, contribute little to the chemical or isotopic composition of the finished product. None of the analytical data acquired suggested differences between beverages produced from apples or pears or due to the inclusion of novel flavoring ingredients. This finding was in agreement with AIJN (The European Fruit Juice Assocaition) reference guides for apples and pears,[29,30] which indicate no significant differences between the juices of the two fruits. The sole sample of canned cider was not distinct from the bottled varieties other than containing the lowest concentration of sulfur. It was assumed that a canned product would be pasteurized, negating the need for added preservative.

Chemical Composition. All measured parameters that were below the limit of detection for the majority of the samples were removed from the overall data. Complete data are reported for nine cations (Na, Ca, K, Mg, Si, V, Mn, Sr, and Ba), four anions (Cl, NO_3, S, and P), the δ^2H and δ^{18}O compositions of the whole ciders (predominantly water), and the δ^{13}C and δ^{18}O compositions of the dry residues (predominantly sugar). A previous study[24] has identified the concentrations of a similar combination of cations (Na, Ca, K, Mg, Si, V, Mn, Sr, Ba, Al, Ti, Zn, As, Rb, and Mo) were sufficient to classify ciders according to country of origin, and the findings of this study were broadly in agreement with that conclusion.

A Pearson correlation matrix was determined for all of the measured parameters (Supporting Information, cider supp 1) and, in contrast to results previously reported for beers,[20] few strong correlations were observed. Correlations observed within the data for beer were attributed to the addition of brewing salts, such as calcium chloride and calcium sulfate, used to control the character of the brewing water and of the finished beer. There is no documented evidence for the addition of brewing salts to ciders, which may account for the general lack of correlations between anion and cation concentrations. In common with the data obtained for beer, significant correlations were observed between the concentrations of potassium, magnesium, and manganese. There was no apparent explanation for these relationships other than all three elements being important nutritional elements for plants.

PCA was applied to the combined anion and cation concentrations to determine which parameters accounted for the largest differences between samples. The loading factors for PC1 were dominated by potassium concentration, as was the case for an earlier study of beer, and the loading factors for PC2 were dominated by sulfur concentration. The latter finding could be explained because all but two of the ciders (samples 1 and 7) declared the preservative sulfur dioxide (or sulfite) as an ingredient. As confirmation, samples 1 and 7 contained the lowest concentrations of sulfur of the samples tested, 30 and 11 mg/kg, respectively, compared to a median concentration of 173 mg/kg. The loading factors for PC3 were predominantly the concentrations of phosphorus, sodium, and calcium. Overall, these finding were in broad agreement with an earlier study of beer,[31] which identified the concentrations of potassium and phosphate as important factors in distinguishing between styles of beers and the region of production.

Isotopic Composition. A Pearson correlation matrix (Supporting Information, cider supp 1) showed that a strong correlation existed between the δ^2H and δ^{18}O compositions of the liquid component of ciders. Both the δ^2H and δ^{18}O compositions of the liquid component correlated with the δ^{18}O composition of the solid residue and with the concentrations of potassium, magnesium, manganese, and silicon. A correlation was also observed between the δ^{13}C and δ^{18}O compositions of the solid residue.

Sugar in Cider. Figure 1 shows the distribution of the δ^{13}C compositions determined for the dry residues of the ciders (predominantly sugar). The majority of samples had $\delta^{13}C_{VPDB}$ values of approximately −26‰, which is typical of C_3 plant material, that is, unadulterated apple or pear sugars, consistent with AIJN guidelines. Other samples were, however, significantly enriched in ^{13}C, suggesting the inclusion of C_4 sugar. An estimate of the proportion of C_4 sugar present in the samples was calculated using the equation adapted from Brooks et al.[28]

$$\%C_4 \text{ carbon} = \frac{(\delta^{13}C_{cider} - \delta^{13}C_3)}{(\delta^{13}C_4 - \delta^{13}C_3)}$$

DOI: 10.1021/jf5030054
J. Agric. Food Chem. 2015, 63, 975−982

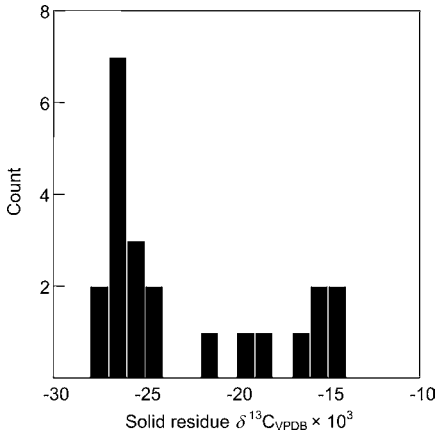

Figure 1. Histogram showing the distribution of $\delta^{13}C$ compositions for the solid residues from ciders.

in which $\delta^{13}C_3$ and $\delta^{13}C_4$ are the typical $\delta^{13}C_{VPDB}$ values for C_3 and C_4 plant material, respectively. (In this study $\delta^{13}C_3$ was taken to be the average value for the ciders that did not appear to contain C_4 sugar (−26.1‰): $\delta^{13}C_4$ was taken as the value reported by Brooks et al. (−12.5‰).) Applying this equation to the $\delta^{13}C$ compositions of the dry residues gave the results presented in Table 1 and revealed that seven of the nine ANZ samples contained C_4 sugar, in contrast to a single EU sample. The EU sample (sample 6) was produced in Spain and claimed to be made from "100% local ingredients". In France, the UNICID (L'Union Natioale Interprofessionnelle Cidricole) code distinguishes between products branded with the English or French spellings, *cider* or *Cidre*, and the addition of water or sugar to the latter is strictly prohibited. Reassuringly, the $\delta^{13}C$ composition of Normandy *Cidre* (sample 5) showed no evidence of adulteration with C_4 sugar.

Ciders that were considered to contain >25% C_4 sugar were analyzed by HPLC to identify the sugars present (Supporting Information, cider supp 1). It was assumed that most of the sugars originally present in the fruit juice would be consumed during primary fermentation and that the profile of the sugars present in the final product would reflect those added after the primary fermentation. The AIJN guidelines suggest that the glucose/fructose ratio of natural apple and pear juice should not exceed approximately 0.5 and, therefore, samples with ratios of approximately unity were deemed to contain HFCS. A single sample (sample 19) was found to have a glucose/fructose ratio >3 and was assumed to contain added glucose syrup. The AIJN guidelines also suggest that the sucrose/fructose ratio of natural apple and pear juice should not exceed approximately 0.4. Ciders with a sucrose concentration exceeding 0.5 (in combination with ^{13}C enrichment) were deemed to contain added cane sugar. On the basis of these guidelines the nature of the added sugar is reported in Table 1.

In this study ANZ and Spanish cider producers were found to use a variety of sugar types (cane sucrose, HFCS, and glucose) or combinations to sweeten their products. In contrast, manufacturers in other EU countries appeared to rely on natural fruit sugars. FSANZ, AVIC, and local Spanish codes (BOE-A-1979-21034) allow for the addition of sugar (and water) to ciders and do not restrict the source of added sugar. This practice makes it difficult to distinguish the origin of ciders based on $\delta^{13}C$ measurements and, although C_4 sweetened products may be indicative of an ANZ origin, it would not be possible to distinguish them from a Spanish cider sweetened with HFCS.

Figure 2a shows a scatter plot of the $\delta^{18}O$ composition of the solid residues against that of the corresponding whole ciders defined by

$$\delta^{18}O_{solid} = \delta^{18}O_{liquid} \times 0.59 + 33 \ (R^2 = 0.87)$$

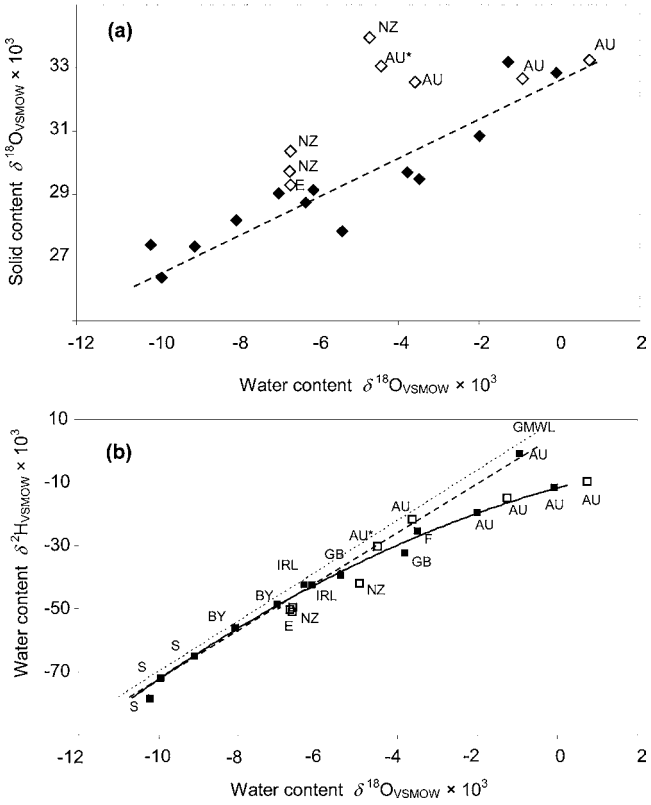

Figure 2. (a) Plot of $\delta^{18}O$ for solid residue against water content; (b) plot of δ^2H against $\delta\ ^{18}O$ for the water content of cider samples (Global Meteoric Water Line shown dotted). Open symbols indicate samples for which $\delta^{13}C$ results suggest the inclusion of C_4 sugars.

The enrichment in ^{18}O of the residues with respect to the whole ciders was consistent with biosynthesis.[32] The robust trend line shown was derived from the samples considered not to contain C_4 sugar (shown as solid symbols, ◆). All of the solid residues that were deemed to contain C_4 sugar (shown as open symbols, ◇) were observed to be enriched in ^{18}O with respect to the robust trend.

Water in Cider. Applying LAD regression to the δ^2H and $\delta^{18}O$ data for the whole ciders produced, the results shown in Figure 3a are defined by the relationship

$$\delta^2H = \delta^{18}O \times 7.6 + 4.3 \ (R^2 = 0.98)$$

with a slope that approximated to that of the Global Meteoric Water Line,[33] which defines all natural waters according to

$$\delta^2H = \delta^{18}O \times 8 + 10$$

The liquid components of all ciders were found to be enriched in ^{18}O with respect to meteoric waters. A recent study has demonstrated that an offset from the GWML develops during the manufacture of beer,[34] which was attributed largely to the boiling of brewery water. Although boiling should not occur during cider making, it is proposed that slower

DOI: 10.1021/jf5030054
J. Agric. Food Chem. 2015, 63, 975−982

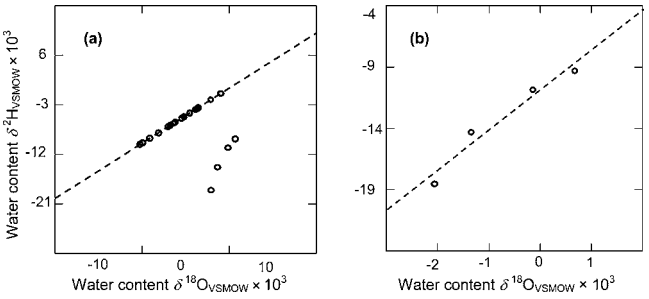

Figure 3. Least absolute deviation (LAD) regression plots of δ^2H against δ^{18}O for the water content of (a) all cider samples and (b) samples identified as outliers. Robust fit lines are shown dashed.

evaporation, from open vats, during initial fermentation may have a similar effect. Another possibility is that the observed offset results from the presence of alcohol and sugar in the analyte, of which cider typically contains more than beer.[35]

Four ciders produced in Australia (samples 13, 14, 17, and 18) deviated significantly from the robust trend line shown in Figure 3a. Applying LAD regression to these data alone produced the result shown in Figure 3b with a relationship defined by

$$\delta^2H = \delta^{18}O \times 3.3 - 11 \ (R^2 = 0.95)$$

This result is consistent with published δ^2H and δ^{18}O compositions of orange and grape juices,[36] which have been reported to have a relationship of approximately 4. This enrichment in ^{18}O with respect to groundwater was reported to result from evapotranspiration and to be more apparent in slow-growing fruits such as apples and pears, which are typically grown in cooler climates than grapes or oranges.

From Figures 2a and 3 it was apparent that the water content of ciders reflected the meteoric water available to the parent fruit tree but, when grown in warmer climates, such as Australia, isotopic enrichment occurred as a result of evaporation. It is also possible that some of the isotopic enrichment observed in the Australian samples resulted from evaporative enrichment of the waters used for irrigation or through water loss during storage or transportation of fruit.

DISCUSSION

Classification. The results of CDA applied to the chemical, isotopic, and combined compositions of the ciders in an attempt to distinguish the country of origin are summarized in Table 2. When considering the chemical data, it was possible to assign the ciders to their country of origin with 100% correct classification. In agreement with PCA, the discriminant functions were dominated by the concentrations of potassium, phosphorus, calcium, and magnesium. Although the concentration of sulfur dominated PC2, it did not feature strongly in the discriminant functions, most likely because the majority of sulfur was derived from an additive rather than from a natural component of the fruit juice. Combining the chemical and isotopic data again provided 100% correct classification.

CDA analysis of the isotopic data in isolation proved somewhat less successful in discriminating the country of origin, and some U.K. samples were variously misclassified as France or New Zealand possibly because these regions share similar geography and/or climate. All of the isotopic parameters contributed approximately equal weighting to the discriminant functions.

Table 2. Percentage Correct Classification by CDA

	country code[a]							
	AU	BY	E	F	GB	IRL	NZ	S
isotopic data	100	100	100	100	50	100	67	100
chemical data	100	100	100	100	100	100	100	100
all data	100	100	100	100	100	100	100	100

	regional code		
	AU	NZ	EU
isotopic data	100	100	91
chemical data	100	100	100
all data	100	100	100

[a]Australia (AU), Belgium (BY), Spain (E), France (F), UK (GB), Ireland (IRL), New Zealand (NZ), Sweden (S).

Applying CDA to data composed of a large number of variables with only a small number of samples assigned to each class might be considered disingenuous. In an initial attempt to address this concern, CDA was applied to two broader groupings, ANZ and EU countries. This approach proved unsuccessful as it transpired the NZ ciders had many characteristics intermediate between those of the Australian and EU samples. CDA was, therefore, recalculated using NZ as a separate grouping, which gave the results shown in Table 2. Figure 4a shows the results of CDA applied to the isotopic data. Although Australian and EU samples formed discrete groupings, the NZ grouping overlapped both and encompassed the sample from Spain, clearly demonstrating why a single ANZ grouping was ineffective. All of the isotopic data contributed similar weighting to the discriminant functions. A similar pattern was observed for the chemical data (Figure 4b), the three classes forming discrete grouping with the Spanish sample correctly classified. In contrast to PCA results, the discriminant functions were dominated by the concentrations of strontium and barium. When the isotopic and chemical data were combined (Figure 4c), there was a clear distinction between Australian and EU samples. From this figure it was also apparent that the NZ samples had more in common with the EU samples than with those from Australia. The discriminant functions were again dominated by the concentrations of strontium and barium with significant contributions from manganese and chloride. In contrast to PCA results, the concentrations of potassium and phosphorus made little contribution; that is, the discriminatory information was not aligned with the direction of maximum variance.

It will be necessary to check the established discrimination functions with a new suite of samples to evaluate fully the real discriminating power.

Geo-location or *CyderSpace*. Figure 2b shows a scatter plot of the δ^2H and δ^{18}O compositions of the whole ciders. As discussed above, these parameters appeared to be controlled by two factors, groundwater and evaporation. To reflect this, two trend lines are shown in Figure 2b; the dashed line shows the robust trend determined by LAD regression (above), and the solid line shows a polynomial fit to all data according to

$$\delta^2H = -0.2 \times \delta^{18}O^2 + 3.7 \times \delta^{18}O - 10 \ (R^2 = 0.99)$$

Of note, the linear part of this equation was similar to the evapotranspiration line determined in Figure 3b ($\delta^2H = \delta^{18}O \times 3.3-11$).

DOI: 10.1021/jf5030054
J. Agric. Food Chem. 2015, 63, 975−982

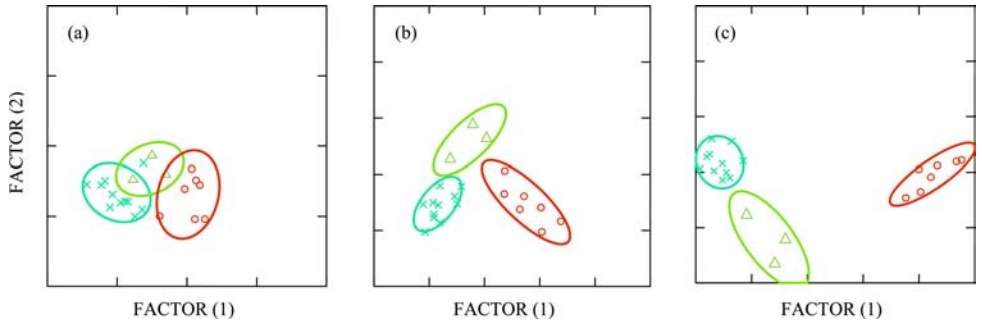

Figure 4. Factor plots derived from canonical discriminant analysis of (a) isotopic data, (b) chemical data, and (c) combined data: Australian (red, ○), EU (blue, ×), and NZ (green, △).

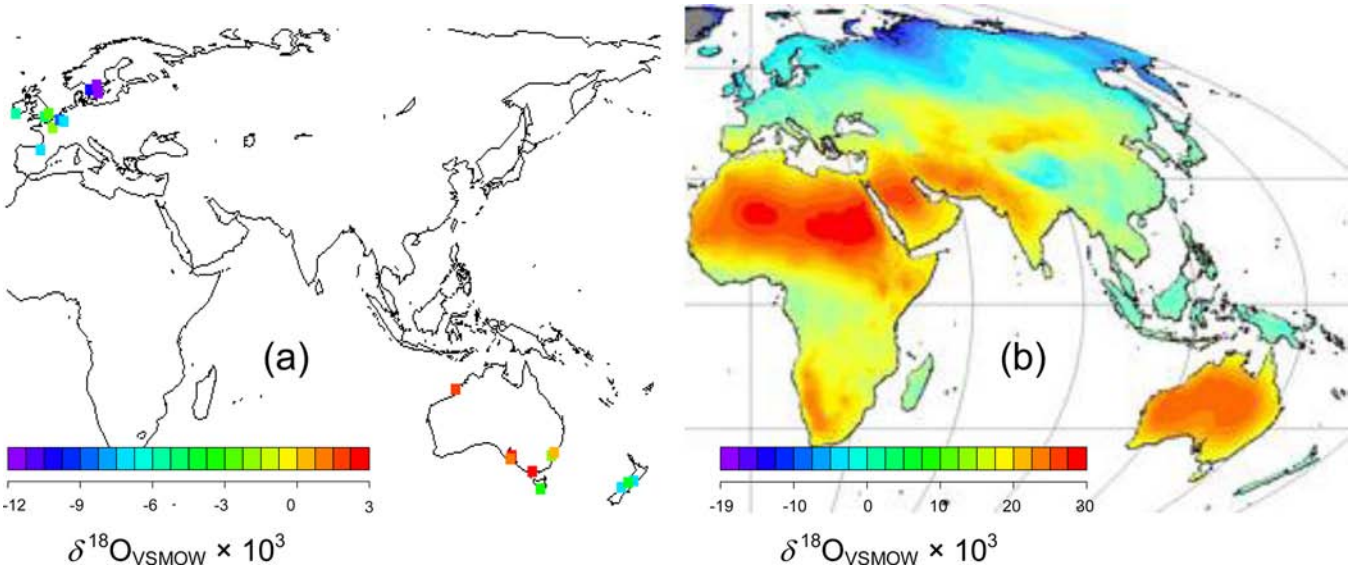

Figure 5. Isoscape of (a) the oxygen isotopic composition of whole ciders compared to (b) the predicted isotopic composition of leaf water. Reprinted with permission from ref 38. Copyright 2008 Public Library of Science.

It was possible to use these data to make inferences about geographical origin. Simplistically, from Figure 2b the most isotopically depleted samples originated from Sweden (S) or Belgium (BY), whereas the most enriched samples originated from Australia (AU). Although AIJN guidelines recommend a minimum $\delta^{18}O_{VSMOW}$ composition for both apple and pear juice of −6.5‰, it was clear that all of the Swedish samples fell below this value, but these guidelines do note that "lower values are possible due to the effects of geographical origins...".

It was difficult to interpret data in the central region of Figure 2b because samples from similar geographical regions such as the United Kingdom (GBR), France (F), or Ireland (IRL) had similar isotopic compositions, as did samples from regions with similar climates, EU, NZ, and Tasmania (AU*), especially Spanish and NZ samples.

Figure 5a shows the $\delta^{18}O$ composition of the whole ciders, color scaled and projected onto a map, often referred to as an *isoscape*[37] or, in this example, *CyderSpace*. This map was compared to a map in which records of the isotopic composition of precipitation were used to predict the $\delta^{18}O$ composition leaf water[38] (Figure 5b). The extent of isotopic enrichment of water within plant tissue is generally assumed to be leaves > fruit > stem > groundwater.[36] Although the water in fruit was expected to be less enriched than in leaves, it was possible to compare fruits and leaves in these maps because both were scaled to encompass the full range of data rather than presented on an absolute scale. Although limited data were available for ciders, the visual similarity between the two maps was apparent. A similar comparison was obtained when the $\delta^{18}O$ data derived from analysis of the dry residues were mapped, which might be expected given the strong correlation observed between the solid and liquid $\delta^{18}O$ data.

The presentation of data in a geo-spatial framework provided a more refined tool to determine country of origin by addressing the following question: Is the isotopic composition of a cider consistent with the claimed country of origin? Such an approach will allow an assessment of the authenticity of ciders for which no reference samples can be obtained. Caution, however, must be applied when the isotopic composition of ciders is compared to isoscapes derived from precipitation. First, ciders have been shown to be enriched in ^{18}O with respect to meteoric waters and, second, plants may be exposed to waters from a combination of precipitation and irrigation, which may vary with time.[39] As a further caveat, it should be noted that once harvested, apples, pears, juice, or sugar may be transported considerable distances, and the composition of a finished cider may not reflect the region of production of any single ingredient.

As with any comparison, it is vital to understand variability to know if differences are significant. The next goal of this study

DOI: 10.1021/jf5030054
J. Agric. Food Chem. 2015, 63, 975−982

will be to examine intraproduct heterogeneity as a function of time because growing conditions will vary from year-to-year and suppliers of fruit and sugar may change.

■ ASSOCIATED CONTENT

Supporting Information

Supplementary data (cider supp 1, cider supp 2, and cider supp 3). This material is available free of charge via the Internet at http://pubs.acs.org.

■ AUTHOR INFORMATION

Corresponding Author

*(J.F.C.) Phone: +61 (07) 3274 9228. Fax: +61 (07) 3274 9229. E-mail: Jim.Carter@health.qld.gov.au.

Notes

The authors declare no competing financial interest.

■ ACKNOWLEDGMENTS

We thank a number of reviewers who have provided insightful feedback and additional references that have greatly improved this paper. We also extend thanks to Stefan Petry and Elizabeth Harrison for their technical assistance with anion analysis, and we thank Jason B. West of Texas A&M University for permission to reproduce part of Figure 1 from ref 36 as Figure 5b.

■ REFERENCES

(1) The Apple Journal; http://www.applejournal.com/fr05.htm (accessed June 12, 2014).

(2) Blenkinsop P. Insight: cider, the golden apple of brewer's eyes. *Rueters* Dec 20, **2012**.

(3) Boffey D. Cider's cool new image to lead the way in British export push. *Observer* Oct 20, **2013**.

(4) Asche, S.; Michaud, A. L.; Brenna, J. T. Sourcing organic compounds based on natural variations measured by high precision isotope ratio mass spectrometry. *Curr. Org. Chem.* **2003**, *7*, 1527−1543.

(5) LeBot, B.; Oulhote, Y.; Deguen, S.; Glorennec, P. Using and interpreting isotope data for source identification. *Trends Anal. Chem.* **2011**, *30* (2), 302−312.

(6) Martin, A. E.; Watling, R. J.; Lee, G. S. The multi-element determination and regional discrimination of Australian wines. *Food Chem.* **2012**, *133* (3), 1081−1089.

(7) Baxter, M. J.; Crews, H. M.; John Dennis, M.; Goodall, I.; Anderson, D. The determination of the authenticity of wine from its trace element composition. *Food Chem.* **1997**, *60* (3), 443−450.

(8) Geana, I.; Iordache, A.; Ionete, R.; Marinescu, A.; Ranca, A.; Culea, M. Geographical origin identification of Romanian wines by ICP-MS elemental analysis. *Food Chem.* **2013**, *138* (2−3), 1125−1134.

(9) Fabani, M. P.; Arrúa, R. C.; Vázquez, F.; Diaz, M. P.; Baroni, M. V.; Wunderlin, D. A. Evaluation of elemental profile coupled to chemometrics to assess the geographical origin of Argentinean wines. *Food Chem.* **2010**, *119* (1), 372−379.

(10) Gonzálvez, A.; Llorens, A.; Cervera, M. L.; Armenta, S.; de la Guardia, M. Elemental fingerprint of wines from the protected designation of origin Valencia. *Food Chem.* **2009**, *112* (1), 26−34.

(11) Ogrinc, N.; Košir, I. J.; Kocjančič, M.; Kidrič, J. Determination of authenticy, regional origin, and vintage of Slovenian wines using a combination of IRMS and SNIF-NMR analyses. *J. Agric. Food Chem.* **2001**, *49* (3), 1432−1440.

(12) Marchionni, S.; Braschi, E.; Tommasini, S.; Bollati, A.; Cifelli, F.; Mulinacci, N.; Mattei, M.; Conticelli, S. High-precision $^{87}Sr/^{86}Sr$ analyses in wines and their use as a geological fingerprint for tracing geographic provenance. *J. Agric. Food Chem.* **2013**, *61* (28), 6822−6831.

(13) Dutra, S. V.; Adami, L.; Marcon, A. R.; Carnieli, G. J.; Roani, C. A.; Spinelli, F. R.; Leonardelli, S.; Vanderlinde, R. Characterization of wines according the geographical origin by analysis of isotopes and minerals and the influence of harvest on the isotope values. *Food Chem.* **2013**, *141* (3), 2148−2153.

(14) Cabañero, A. I.; Recio, J. L.; Rupérez, M. Simultaneous stable carbon isotopic analysis of wine glycerol and ethanol by liquid chromatography coupled to isotope ratio mass spectrometry. *J. Agric. Food Chem.* **2009**, *58* (2), 722−728.

(15) Perini, M.; Camin, F. $\delta^{18}O$ of ethanol in wine and spirits for authentication purposes. *J. Food Sci.* **2013**, *78* (6), C839−C844.

(16) Martinelli, L. A.; Moreira, M. Z.; Ometto, J. P. H. B.; Alcarde, A. R.; Rizzon, L. A.; Stange, E.; Ehleringer, J. R. Stable carbon isotopic composition of the wine and CO_2 bubbles of sparkling wines: detecting C4 sugar additions. *J. Agric. Food Chem.* **2003**, *51* (9), 2625−2631.

(17) Cabañero, A. I.; San-Hipólito, T.; Rupérez, M. GasBench/isotope ratio mass spectrometry: a carbon isotope approach to detect exogenous CO_2 in sparkling drinks. *Rapid Commun. Mass Spectrom.* **2007**, *21* (20), 3323−3328.

(18) Christoph, N.; Rossmann, A.; Schlicht, C.; Voerkelius, S. Wine authentication using stable isotope ratio analysis: significance of geographic origin, climate, and viticultural parameters. In *Authentication of Food and Wine*; American Chemical Society: Washington, DC, USA, 2006; Vol. 952, pp 166−179.

(19) Chesson, L. A.; Valenzuela, L. O.; O'Grady, S. P.; Cerling, T. E.; Ehleringer, J. R. Links between purchase location and stable isotope ratios of bottled water, soda, and beer in the United States. *J. Agric. Food Chem.* **2010**, *58* (12), 7311−7316.

(20) Carter, J. F.; Yates, H. S. A.; Tinggi, U. A global survey of the stable isotope and chemical compositions of bottled and canned beers as a guide to authenticity. *Sci. Justice* **2014**, DOI: /10.1016/j.scijus.2014.05.002.

(21) Brooks, J. R.; Buchmann, N.; Phillips, S.; Ehleringer, B.; Evans, R. D.; Lott, M.; Martinelli, L. A.; Pockman, W. T.; Sandquist, D.; Sparks, J. P.; Sperry, L.; Williams, D.; Ehleringer, J. R. Heavy and light beer: a carbon isotope approach to detect C4 carbon in beers of different origins, styles, and prices. *J. Agric. Food Chem.* **2002**, *50* (22), 6413−6418.

(22) Alonso-Salces, R. M.; Guyot, S.; Herrero, C.; Berrueta, L. A.; Drilleau, J.-F.; Gallo, B.; Vicente, F. Chemometric classification of Basque and French ciders based on their total polyphenol contents and CIELab parameters. *Food Chem.* **2005**, *91* (1), 91−98.

(23) Alonso-Salces, R. M.; Herrero, C.; Barranco, A.; López-Márquez, D. M.; Berrueta, L. A.; Gallo, B.; Vicente, F. Polyphenolic compositions of Basque natural ciders: a chemometric study. *Food Chem.* **2006**, *97* (3), 438−446.

(24) García-Ruiz, S.; Moldovan, M.; Fortunato, G.; Wunderli, S.; García Alonso, J. I. Evaluation of strontium isotope abundance ratios in combination with multi-elemental analysis as a possible tool to study the geographical origin of ciders. *Anal. Chim. Acta* **2007**, *590* (1), 55−66.

(25) Cabañero, A. I.; Rupérez, M. Carbon isotopic characterization of cider CO_2 by isotope ratio mass spectrometry: a tool for quality and authenticity assessment. *Rapid Commun. Mass Spectrom.* **2012**, *26* (16), 1753−1760.

(26) Coplen, T. B.; Qi, H. Recognizing the potential pitfalls of hydrogen isotopic analysis of keratins with steam equilibration to infer origins of wildlife, food, and people. *Rapid Commun. Mass Spectrom.* **2013**, *27* (22), 2569−2569.

(27) R. C. Team. *R: A Language and Nnvironment for Statistical Computing*; R Foundation for Statistical Computing: Vienna, Austria, 2010.

(28) Brooks, J. P.; Dulá, J. H.; Boone, E. L. A pure -norm principal component analysis. *Comput. Stat. Data Anal.* **2013**, *61* (0), 83−98.

(29) Association of the Industry of Juices and Nectars from fruits and vegetables of the EEC. COP 6.3 Reference guideline for apple − revision April 2014; AIJN: Brussels, Belgium, 2004.

DOI: 10.1021/jf5030054
J. Agric. Food Chem. 2015, 63, 975−982

(30) Association of the Industry of Juices and Nectars from fruits and vegetables of the EEC. COP 6.8 Reference guideline for Pear – revision April 2014; AIJN: Brussels, Belgium, 2004.
(31) Alcázar, A.; Jurado, J. M.; Palacios-Morillo, A.; de Pablos, F.; Martin, M. J. Recognition of the geographical origin of beer based on support vector machines applied to chemical descriptors. *Food Control* **2012**, *23* (1), 258–262.
(32) Schmidt, H.-L.; Werner, R. A.; Roßmann, A. ^{18}O pattern and biosynthesis of natural plant products. *Phytochemistry* **2001**, *58* (1), 9–32.
(33) Craig, H. Isotopic variation in meteoric waters. *Science* **1961**, *133*, 1702–1703.
(34) Brettell, R.; Montgomery, J.; Evans, J. Brewing and stewing: the effect of culturally mediated behaviour on the oxygen isotope composition of ingested fluids and the implications for human provenance studies. *J. Anal. At. Spectrom.* **2012**, *27* (5), 778–785.
(35) Kirk, R. S.; Sawyer, R. S. *Pearson's Composition and Chemical Analysis of Foods*, 9th ed.; Longman: Harlow, UK, 1991.
(36) Dunbar, J.; Wilson, A. T. Oxygen and hydrogen isotopes in fruit and vegetable juices. *Plant Physiol.* **1983**, *72*, 725–727.
(37) Bowen, G. J. Isoscapes: Spatial pattern in isotopic biogeochemistry. *Annu. Rev. Earth Planet. Sci.* **2010**, *38*, 161–187.
(38) West, J. B.; Sobek, A.; Ehleringer, J. R. A simplified GIS approach to modelling global leaf water isoscapes. *PLoS One* **2008**, *13* (6), No. e2447.
(39) Kennedy, C. D.; Bowen, G. J.; Ehleringer, J. R. Temporal variation of oxygen isotope ratios ($\delta^{18}O$) in drinking water: implications for specifying location of origin with human scalp hair. *Forensic Sci. Int.* **2011**, *208* (1–3), 156–166.

DOI: 10.1021/jf5030054
J. Agric. Food Chem. 2015, 63, 975–982

(21 °C) and verified to be isotropic using the below method were treated as microemulsions and used to construct a partial ternary phase diagram. Controls containing 1−6% (w/w) lecithin and 1% (w/w) peppermint oil without Tween 20 were also prepared by the same procedures stated above.

Determination of the Phase Inversion Temperature (PIT). *Viscosity Method.* Determination of the PIT based on viscosity data during cooling was adopted from a previous study.[16] Tests were conducted using a model AR2000 rheometer (TA Instruments, New Castle, DE) and a concentric cylinder geometry (bob outer diameter 28 mm, cup inner diameter 30 mm). A 13 mL volume of a mixture with 20% (w/w) Tween 20, 6% (w/w) lecithin, and 20% (w/w) peppermint oil after brief hand-shaking was loaded into the cup, heated to 95 °C, equilibrated for 2 min, and subsequently cooled to 25 °C at 3 °C/min using a fixed shear rate of 100 s^{-1}.

Turbidity Method. The turbidity of emulsions before and after heating at 20−90 °C for 5 min was measured for absorbance at 600 nm using a UV/vis spectrophotometer (model Evolution 201, Thermo Scientific Co., Waltham, MA).

Physicochemical Properties of Microemulsions. Microemulsions with the highest oil loading capability of various lecithin concentrations were used to characterize the following physical and chemical properties. The specific sample numbers and corresponding compositions are listed in Table 1.

Table 1. Sample Numbers and Their Corresponding Compositions Showing the Highest Content of Peppermint Oil Being Dissolved by the Surfactant Combinations as Microemulsions

	composition (%, w/w)		
sample no.	Tween 20	lecithin	peppermint oil
S1	20	1	5
S2	20	2	7
S3	20	3	9
S4	20	4	12
S5	20	5	16
S6	20	6	20

Particle Size Distribution. The particle size distribution of microemulsions was measured using a Delsa Nano C particle size/ζ potential analyzer (Beckman Coulter, Fullerton, CA). To fit the instrument sensitivity requirement, microemulsions were diluted 20−60-fold in diwater. All measurements were performed four times with two from each of two independent repetitions. Both volume fraction-length ($d_{4,3}$) and area-volume ($d_{3,2}$) mean diameters were calculated using eqs 1 and 2, respectively, where n_i is the number of particles with diameter d_i.

$$d_{4,3} = \frac{\sum_{i=1} n_i d_i^4}{\sum_{i=1} n_i d_i^3} \quad (1)$$

$$d_{3,2} = \frac{\sum_{i=1} n_i d_i^3}{\sum_{i=1} n_i d_i^2} \quad (2)$$

Rheological Property. The viscosity of microemulsions was determined using the above rheometer and concentric cylinder geometry. The shear rate ramps were performed from 0.1 to 100 s^{-1} at 25 °C.

Optical Microscopy. To verify the formation of isotropic microemulsions, samples were examined using an Olympus BX51 polarized light microscope and a 40× objective (Olympus Corp. of America, Hauppauge, NY).

Dilution Stability. Microemulsions were diluted 50-, 100-, and 200-fold in diwater. The chemical stability of peppermint oil components and physical stability of the mixtures were monitored at 240 and 600 nm, respectively, using the above UV/vis spectrophotometer during storage at room temperature (21 °C) for 72 h.

Storage Stability. The stability of microemulsions was evaluated after storage for 30 and 70 d at room temperature (21 °C) by measuring particle size changes.

Microemulsions with Dissolved Coenzyme Q_{10}. *Preparation of Microemulsions with CoQ_{10}.* Microemulsions containing CoQ_{10} were prepared using procedures similar to those described above. Briefly, 0.018 mg of CoQ_{10} and 0.54 mg of peppermint oil were mixed on a magnetic stir plate at room temperature (21 °C) until visually completely dissolved. Subsequently, the oil phase was mixed with the 12% (w/w) lecithin stock suspension, diwater, and Tween 20 to a total mass of 18 g containing 0.1% (w/v) CoQ_{10}, 3% (w/w) peppermint oil,

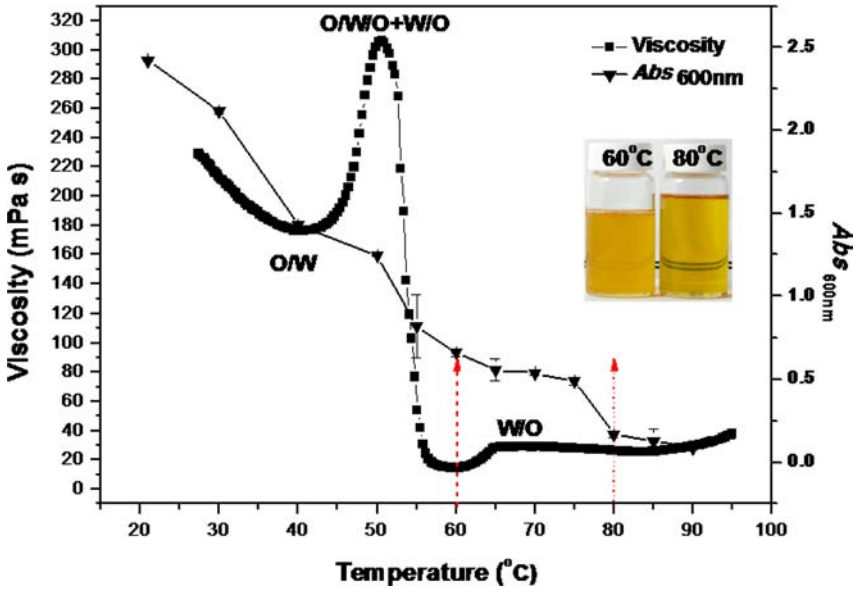

Figure 1. Changes of the viscosity of the coarse emulsion during cooling from 95 to 25 °C at 3 °C/min, in comparison to the absorbance at 600 nm (Abs_{600nm}) after heating of the coarse emulsion at a fixed temperature from 20 to 90 °C for 5 min and cooling in an ice/water bath. The coarse emulsion contained 20% (w/w) Tween 20, 6% (w/w) lecithin, and 20% (w/w) peppermint oil. The inset image compares the visual appearance of two samples heated at 60 and 80 °C for 5 min.

DOI: 10.1021/jf504146t
J. Agric. Food Chem. 2015, 63, 983−989

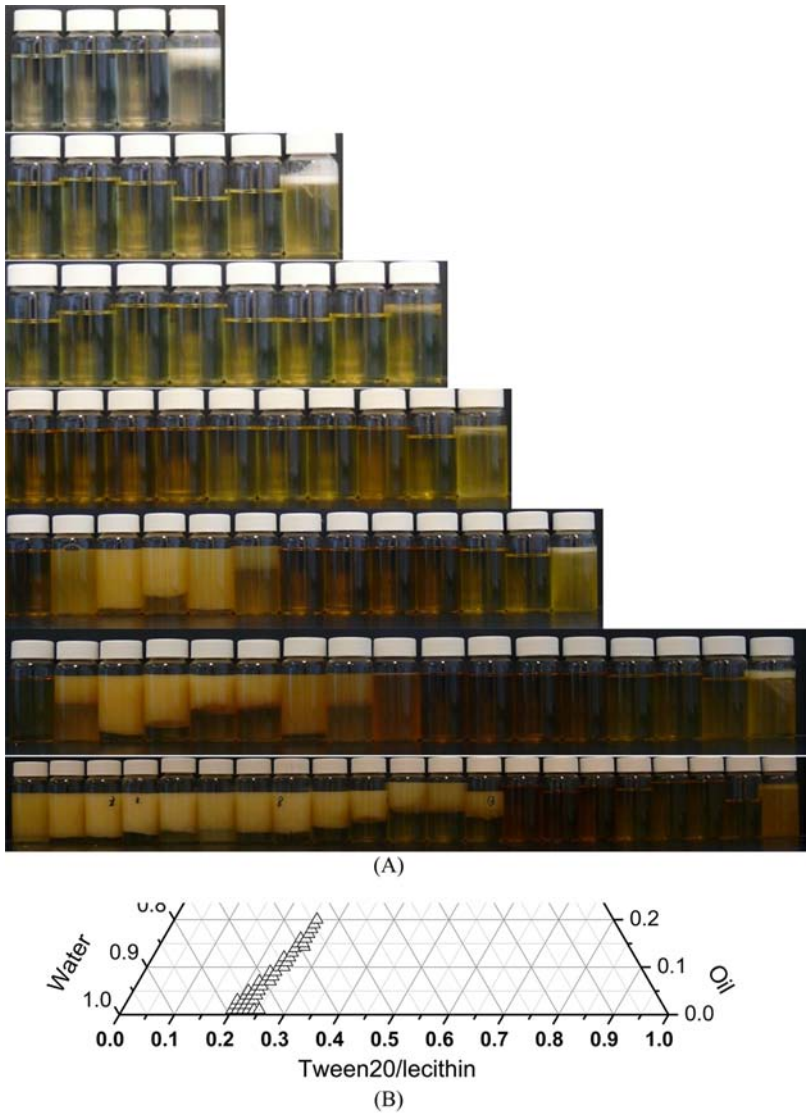

Figure 2. (A) Appearance of oil/water/surfactant mixtures after phase inversion by heating at 80 °C for 5 min. From the top to the bottom, the Tween 20 content was kept at 20% (w/w), while the lecithin content was 0%, 1%, 2%, 3%, 4%, 5%, and 6% (w/w), respectively. In each row, the peppermint oil content from left to right increased by 1% (w/w) successively from 1% (w/w). (B) Partial ternary phase diagram of Tween−lecithin, peppermint oil, and water mixtures confirmed to form transparent microemulsions.

20% (w/w) Tween 20, and 0% or 3% (w/w) lecithin. After brief hand-shaking, the coarse emulsion was heated at 80 °C for 5 min, followed by cooling in an ice/water bath. The CoQ_{10} control solution was prepared by dissolving CoQ_{10} at 0.1% (w/v) in ethyl acetate directly.

Kinetics of CoQ_{10} Degradation under UV Radiation. A 3.5 mL volume of the above microemulsions with CoQ_{10} and control solution in 4 mL clear glass vials were placed at 15 cm under a 15 W UV tube (254 or 302 nm) attached to an XX-15 series UV system from UVP, LLC (Upland, CA). After UV radiation at ambient conditions (21 °C) in the dark for up to 32 h, the samples were diluted 5-fold, and the absorbance at 420 nm was measured using a Biomate 5 UV/vis spectrophotometer (Thermo Scientific). The residual concentration of CoQ_{10} was then determined on the basis of a calibration curve established from standard solutions with 0.03125−1 mg/mL CoQ_{10} dissolved in ethyl acetate. The determined CoQ_{10} concentrations were fit to eq 3, where c_0 and c_t are CoQ_{10} concentrations before and after radiation for a duration of t (h), on the basis of the first-order degradation kinetics.[17,18] The degradation rate constant (k) and half-life ($t_{1/2}$), the duration corresponding to the reduction of the CoQ_{10} concentration to half its initial value (eq 4), were determined.

$$c_t = c_0 e^{-kt} \quad (3)$$

$$t_{1/2} = -(\ln 0.5)k^{-1} \quad (4)$$

Statistical Analysis. The data are reported as the mean ± standard deviation from replicates. Statistical analyses were performed using SAS software (version 9.3, SAS Institute Inc., Cary, NC). One-way ANOVA Tukey's test was used to compare the significant difference of mean values at a P level of 0.05.

RESULTS AND DISCUSSION

Determination of the PIT. The first set of experiments was to identify an appropriate temperature to form microemulsions. The coarse emulsion with 20% (w/w) Tween 20, 6% (w/w) lecithin, and 20% (w/w) peppermint oil was used to determine the PIT. There are several ways to determine the PIT, such as monitoring viscosity changes during cooling,[16,19] electrical conductivity at various temperatures,[20] and turbidity changes during/after heating.[20] In this study, viscosity changes during

DOI: 10.1021/jf504146t
J. Agric. Food Chem. 2015, 63, 983−989

Table 2. Volume Fraction-Length ($d_{4,3}$) and Area-Volume ($d_{3,2}$) Mean Diameters of the Microemulsions in Table 1 before and after 30 and 70 d of Storage at Room Temperature (21 °C)[a]

	$d_{4,3}$ (nm)			$d_{3,2}$ (nm)		
sample	0 d	30 d	70 d	0 d	30 d	70 d
S1	11.1 ± 1.2	7.6 ± 0.9	7.9 ± 1.3	10.5 ± 1.5	6.9 ± 1.0	7.3 ± 1.4
S2	9.2 ± 0.4	9.5 ± 0.8	8.8 ± 0.3	8.5 ± 0.4	8.8 ± 1.0	8.0 ± 0.3
S3	9.4 ± 0.5	8.1 ± 0.6	9.1 ± 0.3	8.7 ± 0.7	7.4 ± 0.6	8.3 ± 0.4
S4	9.2 ± 0.1	7.5 ± 0.3	8.4 ± 0.2	8.3 ± 0.0	6.9 ± 0.4	7.9 ± 0.0
S5	11.0 ± 3.6	7.4 ± 0.9	9.8 ± 0.5	10.3 ± 3.6	6.7 ± 0.9	9.0 ± 0.6
S6	10.1 ± 0.8	9.1 ± 0.5	11.1 ± 0.2	9.1 ± 0.7	8.4 ± 0.6	10.2 ± 0.2

[a]Numbers are the mean ± standard deviation from two measurements of two independent repetitions ($n = 4$). No significance difference ($P > 0.05$) was observed for all treatments.

cooling and turbidity changes after heating were used to determine the PIT.

Figure 1 demonstrates changes of the viscosities of the coarse emulsion during cooling from 95 to 25 °C. During cooling, the coarse emulsion can change from a water (W)/oil (O) emulsion to a W/O/W emulsion, with partial W/O emulsion, and finally to an O/W emulsion.[21] The PIT can be determined as the lowest temperature at which the emulsion converts from a fine W/O emulsion to a W/O/W emulsion.[21] On the basis of the viscosity data, the PIT was determined to be 60.7 °C (Figure 1). When the turbidity data were compared, samples heated at a higher temperature had lower turbidity (Figure 1). The sample heated at 60 °C showed some degree of phase inversion when compared to the coarse emulsion but had a higher absorbance than samples heated at 80 °C or higher, corresponding to turbid and transparent dispersions, respectively. Since the turbidity was similar at 80 °C and above, heating treatment at 80 °C for 5 min was chosen for further study.

Influence of the Lecithin Content on Microemulsion Formation. The impacts of the lecithin content on the phase behavior of oil/water/surfactant mixtures with a base composition of 20% (w/w) Tween 20 were studied after the samples were heated at 80 °C for 5 min. The sample appearance after ambient incubation overnight is shown in Figure 2A. Emulsions prepared with 1−6% (w/w) lecithin alone were turbid even with only 1% (w/w) peppermint oil, and treatments prepared with 1−3% (w/w) lecithin showed some creaming after overnight storage (data not shown). Tween 20 (20%, w/w) alone was able to dissolve 3% (w/w) peppermint oil. The combinations of 20% (w/w) Tween 20 and 1%, 2%, and 3% (w/w) lecithin increased the amount of dissolved peppermint oil to 5%, 7%, and 9% (w/w), respectively. With 4% (w/w) lecithin, the treatments with 1% (w/w) and 7−12% (w/w) peppermint oil were transparent, while the ones with 2−6% (w/w) oil showed phase separation. Similar observations were noted for treatments with 5% (w/w) lecithin, with higher peppermint oil levels in transparent samples (10−16%, w/w). At the highest lecithin content (6%, w/w) studied, 14−20% (w/w) peppermint oil was dissolved as transparent dispersions. For mixtures with 4−6% (w/w) lecithin, samples separated into a clear lower phase (O/W microemulsion) and a turbid upper phase (with excess lecithin) after storage have the characteristics of Winsor-I phase behavior.[22] When transparent samples were examined for sample homogeneity and birefringence using a polarized light microscope, all samples appeared completely dark (data not shown). Therefore, these samples were isotropic, which is a distinct feature of microemulsions.[23] Formulations resulting in isotropic transparent dispersions after confirming Newtonian viscosity and stable and small monodispersed droplets, as presented in the following sections, are treated as microemulsions and summarized in Figure 2B, and those with the highest peppermint oil content at different lecithin concentrations are listed in Table 1.

The hydrophile−lipophile balance (HLB) is commonly used to indicate the properties of surfactants emulsifying oils. Theoretically, surfactants with higher HLB values have better solubility in water,[24] and surfactants with HLB values higher and lower than 7 are usually used to form O/W and W/O emulsions, respectively.[24] The HLB of a surfactant mixture (HLB_{mix}) can be estimated using the summation of the product of HLB and mass percentage of individual surfactants.[25] When the HLB of a surfactant or surfactant mixture is similar to the required HLB of the oil phase, the system provides the minimum energy condition for microemulsion formation.[26] Tween 20 and soybean lecithin have respective HLB values of 16.7 and 8.[27] Assuming similar HLB of sunflower and soybean lecithin, HLB_{mix} decreases from 16.7 (of Tween 20) to 14.69 when the lecithin content increases from 0% to 6% (w/w). Therefore, the addition of lecithin decreased HLB_{mix} to be closer to 12.3, which was found to be the most appropriate HLB value to form O/W emulsions of peppermint oil.[28] Additionally, two long hydrocarbon chains of lecithin facilitate the dissolving of oil in the dispersed phase of O/W microemulsions.[29] These two factors may have resulted in a high loading of peppermint oil in the microemulsions of the present study.

Particle Size and Stability of Selected Microemulsions. Microemulsions are thermodynamically stable systems that typically contain particles with a dimension in the range from 2 to 50 nm.[30] The particle sizes of selected microemulsions containing 1−6% lecithin and 5−20% peppermint oil (Table 1) were tested. No significant differences ($P > 0.05$) were observed from the values of $d_{4,3}$ and $d_{3,2}$ of all samples before and after storage for 30 and 70 d at room temperature (21 °C, Table 2). Particle dimensions ranging from ∼7 to ∼11 nm enabled their transparent appearance. A single narrow peak was observed for all the measured transparent samples (data not shown). The nanoemulsions of peppermint oil typically show the growth of particle dimensions during storage due to Ostwald ripening.[31] Because a stable particle dimension and visible appearance were always observed for all transparent dispersions, it can be concluded that they are microemulsions.

Viscosity of Selected Microemulsions. Shear rate ramps of microemulsions in Table 1 are presented in Figure 3. Linear correlations between shear rate and shear stress, with R^2 values all greater than 0.99 (Table 3), and an intercept of zero indicate

DOI: 10.1021/jf504146t
J. Agric. Food Chem. 2015, 63, 983−989

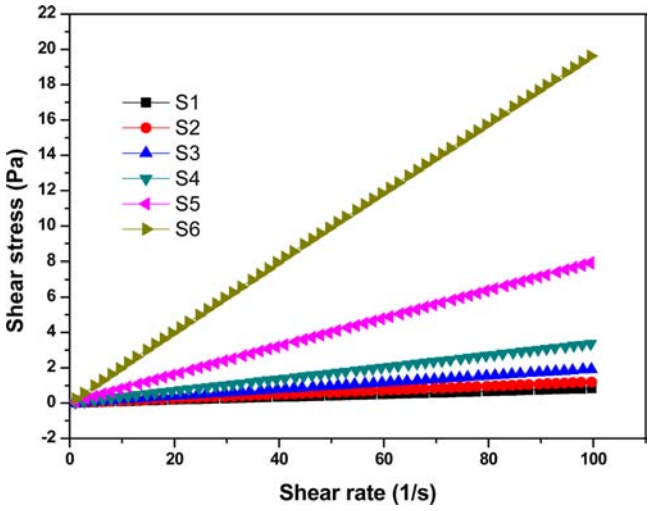

Figure 3. Rheogram of freshly prepared microemulsions S1−S6 with the compositions listed in Table 1 at 25 °C.

Table 3. Summary of Fitting Shear Rate−Shear Stress Data into the Newtonian Model for the Microemulsions in Table 1 at 25 °C[a]

sample	Newtonian viscosity (Pa s)	R^2
S1	0.0085 ± 0.0001 f	0.9978 ± 0.0009
S2	0.0122 ± 0.0003 e	0.9991 ± 0.0002
S3	0.0187 ± 0.0008 d	0.9995 ± 0.0001
S4	0.0334 ± 0.0012 c	0.9999 ± 0.0001
S5	0.0781 ± 0.0025 b	0.9997 ± 0.0003
S6	0.1969 ± 0.0011 a	0.9999 ± 0.0000

[a]Numbers are the mean ± standard deviation from three independent measurements. Different online Roman letters indicate the statistical difference in the mean ($P < 0.05$).

these microemulsions are Newtonian fluids. The Newtonian viscosity ranged from 0.0085 Pa s for the sample with 1% lecithin and 5% peppermint oil to 0.1969 Pa s for that with 6% lecithin and 20% peppermint oil (Table 3). A higher viscosity of microemulsions with higher contents of peppermint oil and lecithin is expected. The trend agreed with the literature microemulsion systems with isopropyl myristate dissolved by a soybean lecithin and Tween 80 mixture and orange oil by a sucrose laurate/soybean lecithin mixture.[29,32]

Stability of Microemulsions after Dilution. The stability of microemulsions diluted 50-, 100-, and 200-fold using diwater was monitored at 240 and 600 nm to indicate the chemical stability of peppermint oil and physical stability (turbidity), respectively, at 21 °C for up to 72 h. The wavelength of 240 nm, corresponding to the maximum absorbance of peppermint oil in the UV/vis regime, was used to monitor the amount of peppermint oil. All diluted samples showed no significant change in the absorbance at 240 nm (presented in Figure 4 for microemulsions after 200-fold dilution), indicating good chemical stability of peppermint oil in microemulsions after dilution. The absorbance at 600 nm of all detected samples after 50-, 100-, and 200-fold dilution using diwater was smaller than 0.1. The excellent dilution stability of microemulsions may be due to the close HLB values of surfactant mixtures and peppermint oil, as discussed above. Because flavor oils such as peppermint oil are used at low concentrations, the excellent

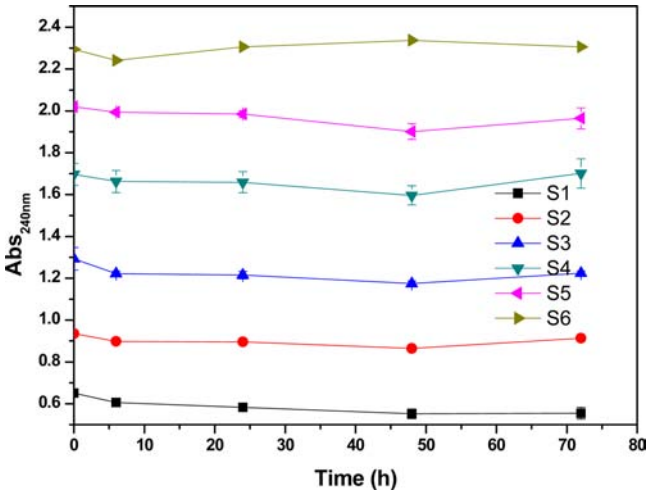

Figure 4. Absorbance of microemulsions S1−S6 at 240 nm (the maximum absorbance of peppermint oil) after 200-fold dilution and incubation at 21 °C for up to 72 h. The sample compositions are listed in Table 1.

dilutability of microemulsions is an important feature for practical applications.

Photostability of CoQ_{10} in Microemulsions. Microemulsions after dissolving CoQ_{10} had a $d_{3,2}$ smaller than 7 nm (Table 4), and there was no significant ($P > 0.05$) difference for

Table 4. Area-Volume Mean Diameters ($d_{3,2}$) of Microemulsions with 20% (w/w) Tween 20, 3% (w/w) Peppermint Oil, 0.1% (w/w) CoQ_{10}, and 0% or 3% (w/w) Lecithin before and after Treatment at 302 nm and Ambient Conditions (21 °C) for up to 32 h[a]

	$d_{3,2}$ (nm)	
UV treatment duration (h)	with 0% lecithin	with 3% lecithin
0	5.98 ± 1.47	5.24 ± 0.87
2	4.78 ± 0.79	6.05 ± 1.30
4	6.09 ± 1.13	4.53 ± 0.25
8	6.85 ± 0.69	4.69 ± 0.55
16	5.57 ± 0.67	4.85 ± 0.80
32	6.45 ± 1.56	4.29 ± 0.68

[a]Numbers are the mean ± standard deviation from two measurements from two independent repetitions. No significance difference ($P > 0.05$) was observed for all treatments.

the treatments with 0% or 3% (w/w) lecithin. These dimensions were similar ($P > 0.05$) to those of microemulsions without CoQ_{10} (Table 2). $d_{3,2}$ did not change significantly ($P > 0.05$) after UV radiation at 302 nm for up to 32 h (Table 4).

The UV stability of CoQ_{10} was studied at 254 and 302 nm. As demonstrated in Figure 5, no significant degradation of CoQ_{10} in the control solution was observed after radiation at 254 nm for 32 h ($P > 0.05$), which was the same as previously reported.[14] However, significant ($P < 0.05$) degradation of CoQ_{10} in the control solution was observed after radiation at 302 nm, decreasing to less than 25% of the initial concentration after 8 h of radiation. The energy of photons is proportional to the frequency of electromagnetic waves, and UV 254 nm, with a higher frequency (shorter wavelength) than UV 302 nm, is expected to cause a greater extent of structural degradation, including the mechanism related to heat after energy conversion.[33,34] Conversely, the electromagnetic energy (P) at

DOI: 10.1021/jf504146t
J. Agric. Food Chem. 2015, 63, 983−989

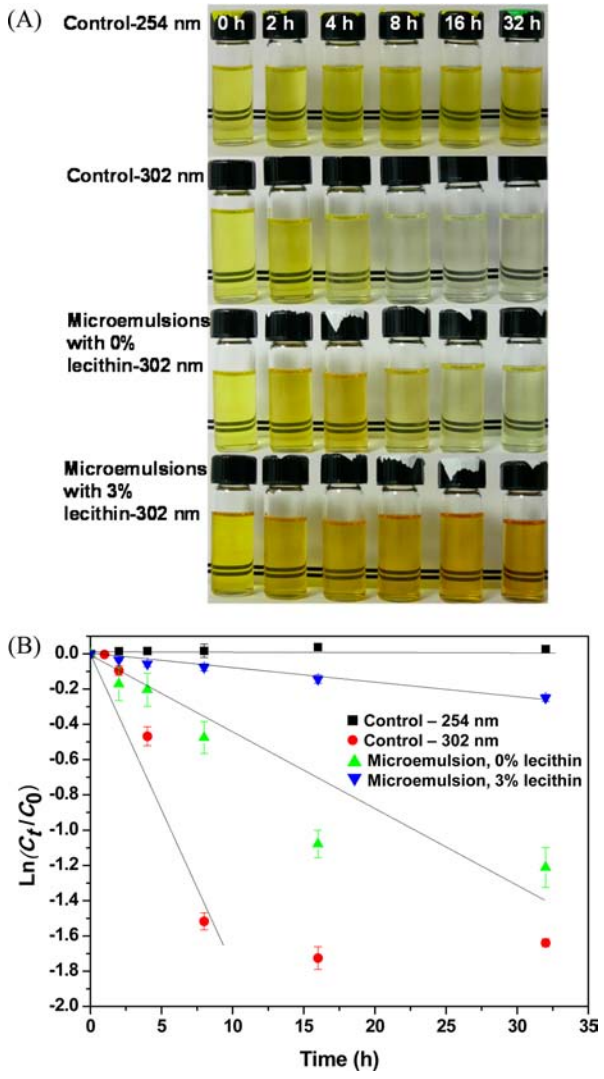

Figure 5. Appearance (A) and normalized residual concentrations (B) of 0.1% (w/w) CoQ_{10} dissolved in microemulsions with 20% (w/w) Tween 20, 3% (w/w) peppermint oil, and 0% or 3% (w/w) lecithin after radiation at UV 302 nm under ambient conditions in the dark for up to 32 h. The control solution contained 0.1% (w/w) CoQ_{10} dissolved in ethyl acetate and was treated at both 254 and 302 nm. Error bars are standard deviations (n = 4).

a depth z decays exponentially from the energy on the surface (P_0), as expressed in the well-known Beer–Lambert law:

$$P = P_0 e^{-\alpha z} \quad (5)$$

where α is a constant and equals $1/d_p$, with d_p being the penetration depth that corresponds to a z value where P becomes 1/e of P_0.[35]

UV 302 nm has a longer penetration depth[36] and therefore has a greater impact on reactions induced by radiation than UV 254 nm, despite the lower photon energy.[37] Therefore, a quicker degradation of CoQ_{10} at 302 nm than at 254 nm was observed in the present study, as well as others.[14,38] The stability of CoQ_{10} in microemulsions was therefore only tested for 302 nm treatments.

The appearance and residual CoQ_{10} concentration after UV 302 nm treatments are shown in Figure 5, and the estimated parameters according to eqs 3 and 4 are compiled in Table 5. The microemulsions improved the photostability of CoQ_{10}, and the improvement was more apparent for the treatment with lecithin. The first-order kinetic model fits the degradation data well, with coefficients of determination above 0.8, which agrees with previous reports.[17,18] The degradation rate constant decreased from 0.167 h^{-1} in the control solution to 0.0448 and 0.00825 h^{-1} in the microemulsion without and with lecithin, respectively. Accordingly, the half-life increased 3.7- and 20.3-fold, respectively, for CoQ_{10} in the microemulsion without and with lecithin.

It is well-established that Tween 20 does not have antioxidant capacity, while lecithin is a good antioxidant.[39] The improved photostability of CoQ_{10} in the microemulsion without lecithin likely resulted from the antioxidant capacity of peppermint oil.[40] The combination of antioxidant properties of lecithin and peppermint oil apparently improved the stability of CoQ_{10} dissolved in the microemulsion with lecithin. On the basis of a previous report,[39] Tween 20 at the O/W interface cannot prevent the diffusion of peroxyl radicals into the oil body, while the opposite is the case for lecithin. Because Tween 20 is present at a higher content than lecithin in the microemulsion (20% vs 3%), the much improved stability of CoQ_{10} in the microemulsion with lecithin further indicates that the two surfactants synergistically dissolved peppermint oil, as discussed previously.

Overall, the combination of sunflower lecithin and Tween 20 enabled the formation of stable microemulsions capable of dissolving high levels of peppermint oil, increasing from 3% to 20% when the lecithin content increased from 0% to 6%. Microemulsions were isotropic and transparent with particle sizes smaller than 12 nm and had relatively low Newtonian viscosity and excellent water-dilution and storage stability at ambient conditions. Additionally, microemulsions had the capability of dissolving CoQ_{10} and reducing its degradation under UV radiation at 302 nm, which likely resulted from the presence of both peppermint oil and lecithin. Our findings indicate that the microemulsions in the present study are promising systems to deliver both flavor oils and lipophilic bioactive compounds in transparent products such as beverages.

Table 5. Degradation Rate Constant (k), Half-Life ($t_{1/2}$), and R^2 When Fitting the Degradation Data at 302 nm (Figure 5) to the First-Order Kinetics Model[a]

sample	k (h^{-1})	R^2	$t_{1/2}$ (h)
control solution	0.167 ± 0.00150 a	0.905 ± 0.0249	4.15 ± 0.0380 c
microemulsion with 0% lecithin	0.0448 ± 0.00293 b	0.828 ± 0.0693	15.5 ± 0.975 b
microemulsion with 3% lecithin	0.00825 ± 0.000785 c	0.953 ± 0.0180	84.6 ± 8.08 a

[a]The control solution had 0.1% (w/w) coenzyme Q_{10} dissolved in ethyl acetate. Microemulsions contained 20% (w/w) Tween 20, 3% (w/w) peppermint oil, 0.1% (w/w) CoQ_{10}, and 0% or 3% (w/w) lecithin. Numbers are the mean ± standard deviation (n = 4). Different online Roman letters indicate the statistical difference (P < 0.05).

DOI: 10.1021/jf504146t
J. Agric. Food Chem. 2015, 63, 983–989

AUTHOR INFORMATION

Corresponding Author

*Phone: 865-974-6196. Fax: 865-974-7332. E-mail: qzhong@utk.edu.

Notes

The authors declare no competing financial interest.

REFERENCES

(1) Ziani, K.; Fang, Y.; McClements, D. J. Fabrication and stability of colloidal delivery systems for flavor oils: effect of composition and storage conditions. *Food Res. Int.* **2012**, *46*, 209−216.

(2) Klossek, M. L.; Marcus, J.; Touraud, D.; Kunz, W. Highly water dilutable green microemulsions. *Colloids Surf., A* **2014**, *442*, 105−110.

(3) Yaghmur, A.; Aserin, A.; Garti, N. Phase behavior of microemulsions based on food-grade nonionic surfactants: effect of polyols and short-chains alcohols. *Colloids Surf., A* **2002**, *209*, 71−81.

(4) Artman, N. R. Safety of emulsifiers in fats and oils. *J. Am. Oil Chem. Soc.* **1975**, *52*, 49−52.

(5) Csaki, K. F. Synthetic surfactant food additives can cause intestinal barrier dysfunction. *Med. Hypotheses* **2011**, *76*, 676−681.

(6) Ema, M.; Hara, H.; Matsumoto, M.; Hirata-Koizumi, M.; Hirose, A.; Kamata, E. Evaluation of developmental neurotoxicity of polysorbate 80 in rats. *Reprod. Toxicol.* **2008**, *25*, 89−99.

(7) Cilek, A.; Celebi, N.; Tirnaksiz, F. Lecithin-based microemulsion of a peptide for oral administration: preparation, characterization, and physical stability of the formulation. *Drug Delivery* **2006**, *13*, 19−24.

(8) Gosenca, M.; Bester-Rogac, M.; Gasperlin, M. Lecithin based lamellar liquid crystals as a physiologically acceptable dermal delivery system for ascorbyl palmitate. *Eur. J. Pharm. Sci.* **2013**, *50*, 114−122.

(9) Arnold, G.; Schuldt, S.; Schneider, Y.; Friedrichs, J.; Babick, F.; Werner, C.; Rohm, H. The impact of lecithin on rheology, sedimentation and particle interactions in oil-based dispersions. *Colloids Surf., A* **2013**, *418*, 147−156.

(10) Hanning, S. M.; Yu, T.; Jones, D. S.; Andrews, G. P.; Kieser, J. A.; Medlicott, N. J. Lecithin-based emulsions for potential use as saliva substitutes in patients with xerostomia-viscoelastic properties. *Int. J. Pharm.* **2013**, *456*, 560−568.

(11) Sheweita, S. A.; Tilmisany, A. M.; Al-Sawaf, H. Mechanisms of male infertility: role of antioxidants. *Curr. Drug Metab.* **2005**, *6*, 495−501.

(12) Flint Beal, M. Coenzyme Q 10 as a possible treatment for neurodegenerative diseases. *Free Radical Res.* **2002**, *36*, 455−460.

(13) Mortensen, S. A.; Kumar, A.; Dolliner, P.; Filipiak, K. J.; Pella, D.; Alehagen, U.; Steurer, G.; Ping, C. S.; Littarru, G. P.; Rosenfeldt, F. ASSA13-13-1 long-term results with coenzyme Q10 as adjunctive therapy in chronic heart failure. *Heart* **2013**, *99*, 55−56.

(14) Fir, M. M.; Smidovnik, A.; Milivojevic, L.; Zmitek, J.; Prosek, M. Studies of CoQ10 and cyclodextrin complexes: solubility, thermo- and photo-stability. *J. Inclusion Phenom. Macrocyclic Chem.* **2009**, *64*, 225−232.

(15) Kommuru, T. R.; Ashraf, M.; Khan, M. A.; Reddy, I. K. Stability and bioequivalence studies of two marketed formulations of coenzyme Q_{10} in beagle dogs. *Chem. Pharm. Bull.* **1999**, *47*, 1024−1048.

(16) Zhang, L.; Hayes, D. G.; Chen, G.; Zhong, Q. Transparent dispersions of milk-fat-based nanostructured lipid carriers for delivery of β-carotene. *J. Agric. Food Chem.* **2013**, *61*, 9435−9443.

(17) Zou, J.; Yu, B.; Song, Y.; Zhang, L.; Wang, F.; Deng, Y. Effects of particle size and concentration on photodegradation kinetics of coenzyme Q_{10} liposomes. *J. Shenyang Pharm. Univ.* **2010**, *5*.

(18) Onoue, S.; Uchida, A.; Kuriyama, K.; Nakamura, T.; Seto, Y.; Kato, M.; Hatanaka, J.; Tanaka, T.; Miyoshi, H.; Yamada, S. Novel solid self-emulsifying drug delivery system of coenzyme Q_{10} with improved photochemical and pharmacokinetic behaviors. *Eur. J. Pharm. Sci.* **2012**, *46*, 492−499.

(19) Souza, V. B.; Spinelli, L. S.; Gonzalez, G.; Mansur, C. R. E. Determination of the phase inversion temperature of orange oil/water emulsions by rheology and microcalorimetry. *Anal. Lett.* **2009**, *42*, 2864−2878.

(20) Rao, J.; McClements, D. J. Stabilization of phase inversion temperature nanoemulsions by surfactant displacement. *J. Agric. Food Chem.* **2010**, *58*, 7059−7066.

(21) Allouche, J.; Tyrode, E.; Sadtler, V.; Choplin, L.; Salager, J. L. Simultaneous conductivity and viscosity measurements as a technique to track emulsion inversion by the phase-inversion-temperature method. *Langmuir* **2004**, *20*, 2134−2140.

(22) Flanagan, J.; Singh, H. Microemulsions: a potential delivery system for bioactives in food. *Crit. Rev. Food Sci.* **2006**, *46* (3), 221−237.

(23) Patel, R. B.; Patel, M. R.; Bhatt, K. K.; Patel, B. G. Formulation consideration and characterization of microemulsion drug delivery system for transnasal administration of carbamazepine. *Bull. Fac. Sci., Cairo Univ.* **2013**, *51*, 243−253.

(24) Walstra, P. Surface phenomena. In *Physical Chemistry of Foods*; CRC Press: New York, Basel, 2002; p 348.

(25) Yu, L.; Li, C.; Xu, J.; Hao, J.; Sun, D. Highly stable concentrated nanoemulsions by the phase inversion composition method at elevated temperature. *Langmuir* **2012**, *28*, 14547−14552.

(26) Pestana, K. C.; Formariz, T. P.; Franzini, C. M.; Sarmento, V. H. V.; Chiavacci, L. A.; Scarpa, M. V.; Egito, E. S. T.; Oliveira, A. G. Oil-in-water lecithin-based microemulsions as a potential delivery system for amphotericin B. *Colloids Surf., B* **2008**, *66*, 253−259.

(27) Rodriguez, M.; Oses, J.; Ziani, K.; Mate, J. I. Combined effect of plasticizers and surfactants on the physical properties of starch based edible films. *Food Res. Int.* **2006**, *39*, 840−846.

(28) Orafidiya, L. O.; Oladimeji, F. A. Determination of the required HLB values of some essential oils. *Int. J. Pharm.* **2002**, *237*, 241−249.

(29) Moreno, M. A.; Ballesteros, M. P.; Frutos, P. Lecithin-based oil-in-water microemulsions for parenteral use: pseudoternary phase diagrams, characterization and toxicity studies. *J. Pharm. Sci.* **2003**, *92*, 1428−1437.

(30) McClements, D. J.; Rao, J. Food-grade nanoemulsions: formulation, fabrication, properties, performance, biological fate, and potential toxicity. *Crit. Rev. Food Sci.* **2011**, *51*, 285−330.

(31) Liang, R.; Xu, S.; Shoemaker, C. F.; Li, Y.; Zhong, F.; Huang, Q. Physical and antimicrobial properties of peppermint oil nanoemulsions. *J. Agric. Food Chem.* **2012**, *60*, 7548−7555.

(32) Tchakalova, V.; Bailly, C.; Fieber, W. Food-grade bicontinuous microemulsions. *Flavour Fragrance J.* **2014**, *29*, 67−74.

(33) Derossi, A.; De Pilli, T.; Fiore, A. G. Vitamin C kinetic degradation of strawberry juice stored under non-isothermal conditions. *LWT—Food Sci. Technol.* **2010**, *43*, 590−595.

(34) Zhao, M.; Li, Y.; Xu, X.; Wu, J.; Liao, X.; Chen, F. Degradation kinetics of malvidin-3-glucoside and malvidin-3,5-diglucoside exposed to microwave treatment. *J. Agric. Food Chem.* **2013**, *61*, 373−8.

(35) Larsen, M. L.; Clark, A. S. On the link between particle size and deviations from the Beer−Lambert−Bouguer law for direct transmission. *J. Quant. Spectrosc. Radiat. Transfer* **2014**, *133*, 646−651.

(36) Vincent, W. F.; Roy, S. Solar ultraviolet-B radiation and aquatic primary production: damage, protection, and recovery. *Environ. Rev.* **1993**, *1*, 1−12.

(37) Rodil, R.; Moeder, M.; Altenburger, R.; Schmitt-Jansen, M. Photostability and phytotoxicity of selected sunscreen agents and their degradation mixtures in water. *Anal. Bioanal. Chem.* **2009**, *395*, 1513−24.

(38) Kwon, S. S.; Nam, Y. S.; Lee, J. S.; Ku, B. S.; Han, S. H.; Lee, J. Y.; Chang, I. S. Preparation and characterization of coenzyme Q_{10}-loaded PMMA nanoparticles by a new emulsification process based on microfluidization. *Colloids Surf., A* **2002**, *210*, 95−104.

(39) Pan, Y.; Tikekar, R. V.; Nitin, N. Effect of antioxidant properties of lecithin emulsifier on oxidative stability of encapsulated bioactive compounds. *Int. J. Pharm.* **2013**, *450*, 129−137.

(40) Fatemi, F.; Dini, S.; Rezaei, M. B.; Dadkhah, A.; Dabbagh, R.; Naij, S. The effect of γ-irradiation on the chemical composition and antioxidant activities of peppermint essential oil and extract. *J. Essent. Oil Res.* **2014**, *26*, 97−104.

DOI: 10.1021/jf504146t
J. Agric. Food Chem. 2015, 63, 983−989

purchased from Fisher Scientific Co. (Fair Lawn, NJ, USA). All other chemicals used were of analytical grade. Double-distilled water was used to prepare all solutions and emulsions.

Nanoemulsion Preparation. We carried out a study using three delivery systems with different compositions and structures.

Delivery System 1: Solubilized β-Carotene (Emulsion). β-Carotene crystals were dissolved in corn oil (digestible oil) and then converted into an oil-in-water nanoemulsion. This group simulates the consumption of functional foods or beverages containing solubilized carotenoids.

Delivery System 2: Crystalline β-Carotene (Emulsion). β-Carotene crystals were mixed with an oil-in-water emulsion immediately before introduction into the GIT model. This group simulates the consumption of crystalline forms of carotenoids (such as those in tablets, powders, cereals, or baked goods) with fatty foods.

Delivery System 3: Crystalline β-Carotene (Buffer). β-Carotene crystals were mixed with a phosphate buffer saline (PBS) solution immediately before introduction into the GIT model. This group simulates the consumption of crystalline forms of carotenoids without co-ingestion of fatty foods (e.g., a crystalline suspension taken with a glass of water).

Initially, an aqueous phase was prepared by mixing 0.5% (w/w) Tween 20 with aqueous buffer solution (10.0 mM PBS, pH 7.0).

β-Carotene-Enriched Nanoemulsion Preparation. An oil phase was prepared by dispersing 0.5% (w/w) of crystalline β-carotene into corn oil followed by mild heating at 50 °C for 5 min followed by stirring at ambient temperature for about 1 h to ensure full dissolution. A coarse emulsion was then formed by mixing the oil phase (4% w/w) with an aqueous phase (96% w/w) and then blending for 2 min at ambient temperature using a high-shear mixer (Tissue-Tearor, Biospec Products, Bartlesville, OK, USA). The coarse emulsion was then passed through a high-pressure microfluidizer (model 101, Microfluidics, Newton, MA, USA) three times at 9000 psi. The freshly prepared β-carotene nanoemulsions were then protected from light in a glass container and stored at 20 °C before digestion.

Nanoemulsion Preparation. Oil-in-water nanoemulsions were prepared by homogenizing 4% (w/w) corn oil with 96% (w/w) aqueous phase using the same method as described above. The freshly made nanoemulsions were then covered by parafilm in a glass container and stored at 20 °C before digestion.

Particle Characterization. The mean particle diameters (*Z*-average) and particle size distribution of the original nanoemulsion and samples at each digestion step were monitored using a dynamic light scattering instrument (Nano-ZS, Malvern Instruments, Worcestershire, UK). Prior to analysis, dilution (1:20) was carried out by adding 0.5 mL of sample to 9.5 mL of buffer solution with the same pH and ionic composition as the sample being analyzed. Dilution was necessary to avoid multiple scattering effects.

The electrical charges (ζ-potential) of the original nanoemulsion and the digesta were monitored using a microelectrophoresis instrument (Nano-ZS, Malvern Instruments). The same diluted samples used above were used for measuring electrical charge. The ζ-potential was determined by measuring the direction and velocity of droplet movement in an oscillating electric field.

Microstructural Analysis. The microstructural changes of the samples within the simulated GIT were observed using confocal scanning fluorescence microscopy. The physical changes of β-carotene crystals were observed using a cross-polarized lens (C1 Digital Eclipse, Nikon, Tokyo, Japan). Samples from each GIT step were dyed with Nile Red (0.1%) to highlight the location of the lipid phases. All images were taken using a 10× eyepiece and a 60× objective lens (oil immersion).

In Vitro Digestion. Three groups of samples were prepared: (1) solubilized β-carotene; (2) crystalline β-carotene (emulsion); (3) crystalline β-carotene (buffer). The β-carotene crystals were introduced into the nanoemulsions and buffer solutions just before the GIT model was started to mimic the way people may ingest nutraceutical tablets with food emulsions or water, respectively. The initial concentration of β-carotene in all three groups was the same. Each sample was passed through a three-step GIT model that consisted of mouth, gastric, and small intestine phases.

Mouth Phase. Simulated saliva fluid (SSF), containing 3% mucin and various salts, was prepared as described previously.[17,18] Ten milliliters of sample was placed in a beaker and mixed with 10 mL of SSF. The mixture was then adjusted to pH 6.8 and placed in a shaker at 100 rpm and 37 °C for 10 min to mimic oral conditions (Innova Incubator Shaker, 132 model 4080, New Brunswick Scientific, NJ, USA).

Gastric Phase. Simulated gastric fluid (SGF) was prepared according to a protocol described before.[19] The "bolus" sample from the mouth phase was mixed with SGF at a 1:1 mass ratio. The mixture was then adjusted to pH 2.5 and placed in a shaker at 100 rpm and 37 °C for 2 h to mimic gastric conditions.

Small Intestine Phase. Gastric digesta (30 mL) was incubated in a water bath (37 °C) for 10 min and then NaOH solution used to adjust the pH to 7.0. Then 1.0 mL of $CaCl_2$ solution, containing 110 mg of $CaCl_2$ (pH 7.0, PBS), was added into the 30 mL digesta. Then 4 mL bile extract, containing 187.5 mg of bile extract (pH 7.0, PBS), was added with stirring, and the resulting system was adjusted to pH 7.0. Finally, 2.5 mL of pancreatic suspension, containing 60 mg of lipase (pH 7.0, PBS), was added to the solution. At this point, titration was started automatically. The pH-stat (Metrohm, USA Inc.) was used to monitor and control the pH (at pH 7.0) of the digestion solution. As the triacylglycerol of fat was digested into free fatty acids (FFAs) by lipolysis, the NaOH solution (0.25 M) was added to neutralize the pH (7.0). The amount of FFAs released in the system was calculated from the volume of NaOH required to maintain neutral pH as described previously.[20] The small intestine digestion phase lasted for 2 h.

Bioaccessibility Determination. After in vitro digestion, digesta of each sample group was collected and centrifuged (14000 rpm, Thermo Scientific, USA) at 25 °C for 40 min. Centrifuged samples separated into three phases: sediment phase at the bottom, a relatively clear watery phase in the middle, and sometimes an undigested oil phase at the top. The middle phase was assumed to contain mixed micelles that entrapped the β-carotene, that is, the bioaccessible fraction. The micelle phase was passed through a syringe filter with the pore size of 0.45 μm. β-Carotene was extracted using organic solvent isopropanol/isooctane solution (1:1 v/v). The micelle phase and total digesta (0.2 mL) from the small intestine were added to 4.8 mL of isopropanol/isooctane solution and centrifuged at 14000 rpm at 25 °C for 10 min. The β-carotene concentrations were then analyzed using a UV−visible spectrophotometer (Ultrospec 3000 pro, GE Health Sciences, USA) at 450 nm. The concentration of β-carotene was calculated from the absorbance using a standard curve. The bioaccessibility was calculated using the following equation:

$$\text{bioaccessibility} = 100 \times \left(\frac{C_{\text{micelle}}}{C_{\text{digesta}}}\right)$$

In this equation, C_{micelle} stands for the concentration of β-carotene in the micelle fraction and C_{digesta} is the concentration of β-carotene in the overall sample (total digesta) after the pH-stat experiment.

Statistical Analysis. All measurements were performed at least three times on freshly prepared samples and were reported as calculated means and standard deviations.

RESULTS AND DISCUSSION

Impact of Physical State of β-Carotene on Gastrointestinal Fate. *Particle Size and Microstructure.* To investigate the influence of the physical state of β-carotene on its bioaccessibility, the three types of delivery system were passed through the GIT model: (1) solubilized β-carotene (emulsion); (2) crystalline β-carotene (emulsion); (3) crystalline β-carotene (buffer). The mean particle sizes (*Z*-average diameters) (Figure 1a), particle size distribution (Figure 1b,c), particle charges (Figure 2), and microstructures (Figures 3 and 4) of the initial nanoemulsions and the samples collected after each GIT stage were measured. Particle size and charge measurements are reported only on the

DOI: 10.1021/jf504673v
J. Agric. Food Chem. 2015, 63, 990−997

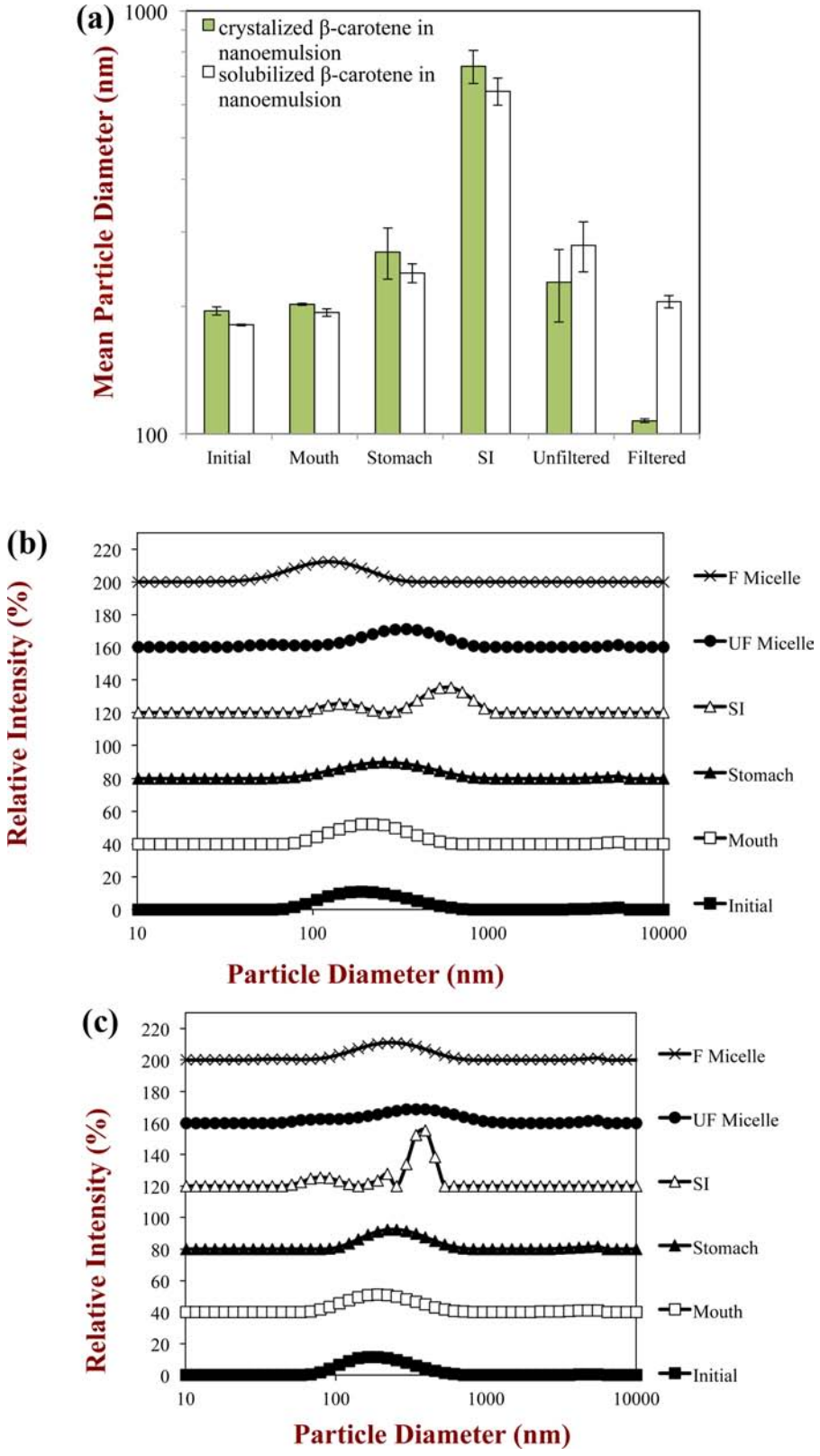

Figure 1. (a) Influence of physical state of β-carotene and in vitro digestion on the mean diameter of the particles in oil-in-water nanoemulsions subjected to a simulated gastrointestinal model. SI, small intestine; unfiltered, unfiltered micelles; filtered, filtered micelles. (b) Influence of in vitro digestion on the particle size distribution of oil-in-water nanoemulsions subjected to a simulated gastrointestinal model with (b) crystallized β-carotene and (c) solubilized β-carotene.

delivery systems initially containing nanoemulsion droplets, because the samples containing crystals in buffer solution could not be reliably analyzed using these analytical techniques.

(a) Initial Samples. The nanoemulsions used to form the solubilized β-carotene (delivery system 1) and the crystalline β-carotene (emulsion) (delivery system 2) had relatively small

DOI: 10.1021/jf504673v
J. Agric. Food Chem. 2015, 63, 990−997

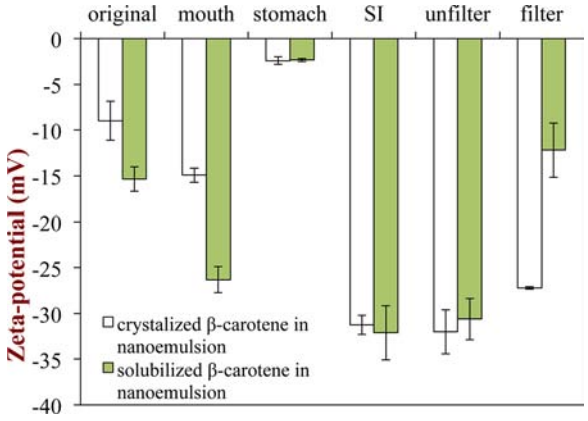

Figure 2. Influence of physical state of β-carotene and in vitro digestion on the charge (ζ-potential) of the particles in oil-in-water nanoemulsions subjected to a simulated gastrointestinal model.

mean particle diameters (d < 200 nm, Figure 1a) and monomodal particle size distributions (Figure 1b,c), which suggested that they were stable under initial solution conditions (pH 7). The confocal microscopy images indicated that the lipid droplets were relatively small and evenly distributed throughout the initial samples (Figure 3).

(b) Mouth Stage. The dynamic light scattering (DLS) measurements suggested that the particles in delivery systems 1 and 2 remained relatively small after passing through the simulated mouth stage, that is, d < 210 nm (Figure 1). However, this may have been an artifact of the DLS method (which is not sensitive to slow-moving large particles), because the confocal microscopy images indicated the presence of some relatively large particles (Figure 3). Droplet aggregation may have occurred as a result of the presence of mucin within the artificial saliva used in the mouth model. Mucin is a complex biopolymer that has previously been shown to be able to promote bridging or depletion flocculation of lipid droplets.[21,22] Nevertheless, the confocal images do suggest that a fraction of the lipid droplets did remain relatively small and evenly distributed (Figure 3). These droplets may have remained stable to aggregation due to the strong steric repulsion generated by the hydrophilic head groups of the nonionic surfactant coating them.[10,23,24] Only a fraction of the lipid droplets may have aggregated because of differences in droplet size (larger droplets are more prone to depletion flocculation than smaller ones) or polymer concentration (there may have been insufficient mucin present to promote bridging or depletion flocculation of all the droplets).

(c) Stomach Stage. After the stomach stage, the DLS measurements indicated that there was a slight increase in particle size, although the mean diameter remained relatively small, that is, d < 270 nm (Figure 1). Again, this appears to be an artifact of the DLS method, because the confocal microscopy images indicated the presence of some large aggregates (Figure 3). Droplet aggregation in the stomach may have been the result of bridging or depletion flocculation caused by the presence of mucin (from the mouth stage) or due to changes in the pH and ionic strength of the intestinal fluids in the stomach phase. The magnitude of the electrical charge on the particles was considerably smaller under stomach conditions than mouth conditions (Figure 3), which would have reduced the electrostatic repulsion between the lipid droplets.

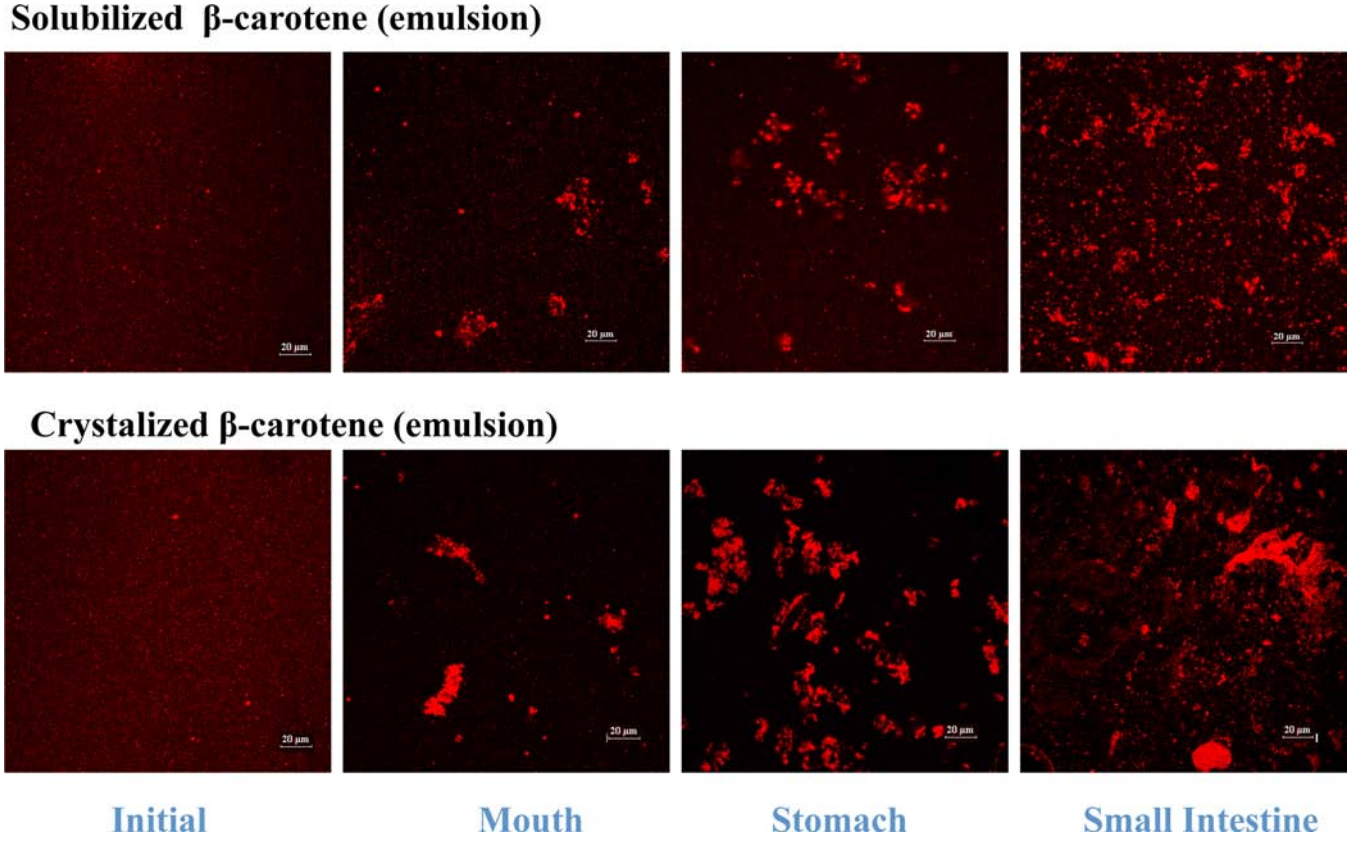

Figure 3. Influence of physical state of β-carotene on the microstructure of lipid measured by confocal microscopy at various stages in an in vitro gastrointestinal tract model. Scale bars = 20 μm.

DOI: 10.1021/jf504673v
J. Agric. Food Chem. 2015, 63, 990−997

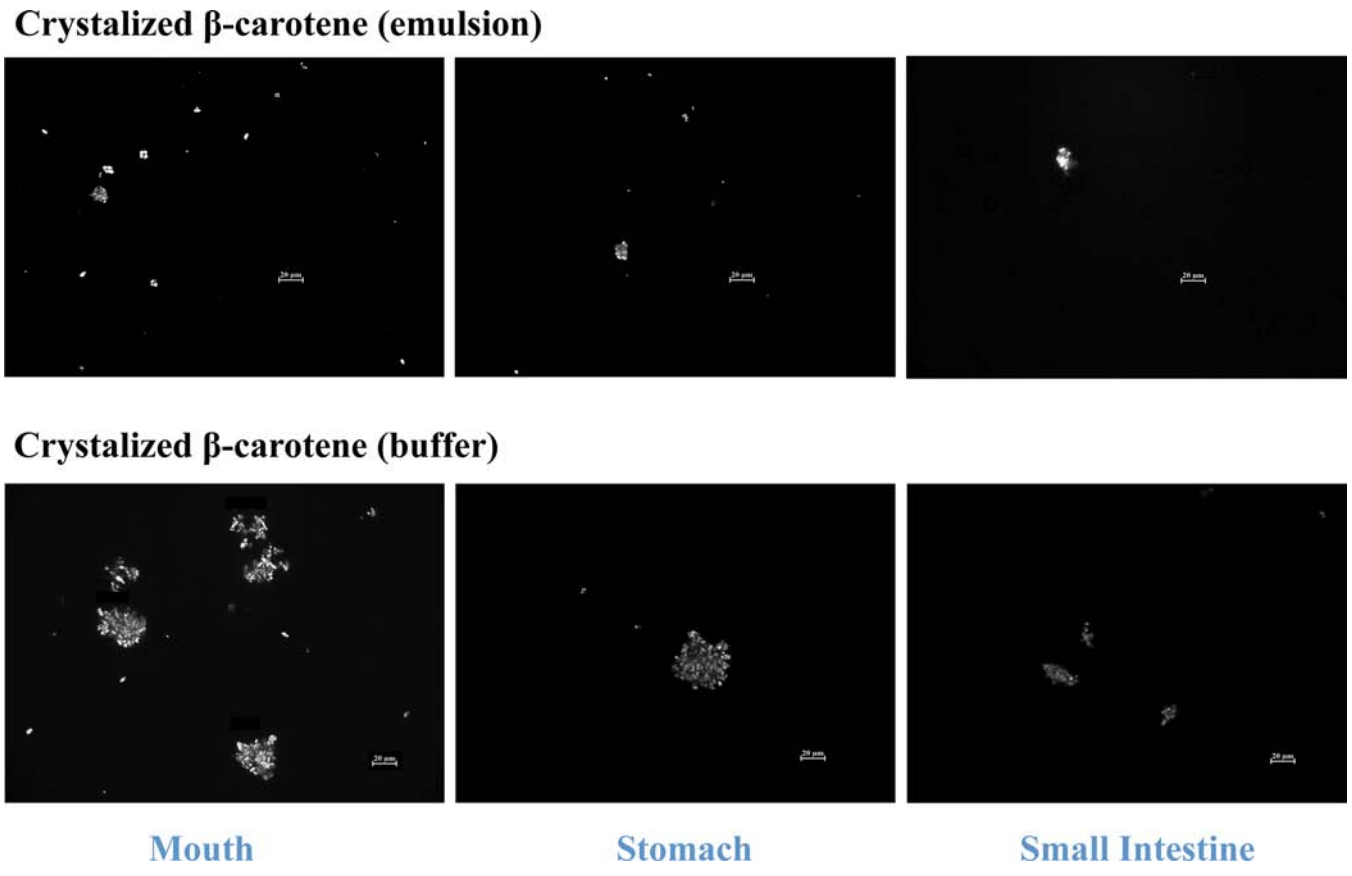

Figure 4. Influence of physical state of β-carotene on the microstructure of β-carotene crystals measured by optical microscopy with a crossed polarizer at various stages in an in vitro gastrointestinal tract model. Scale bars = 20 μm.

(d) Small Intestine Stage. After the small intestine stage, delivery systems 1 and 2 showed a large increase in particle size (Figures 1 and 3), which suggested that extensive droplet aggregation occurred. According to previous studies, several physicochemical mechanisms may have been responsible for this change in aggregation state.[18,23,25] First, the displacement of the original surface active species coating the droplets (i.e., Tween 20) with surface active species from the simulated GIT fluids (i.e., phospholipids, bile salts, FFAs, and monoacyglycerols) may have altered the colloidal interactions between the droplets, thereby promoting aggregation.[26−28] Second, the conversion of emulsified triacylglycerols into FFAs and monoacylglycerols by lipase changes the internal and surface composition of the lipid droplets, which will alter their morphology and aggregation stability.[25]

(e) Micelle Phase. The micelle phase was obtained by centrifuging the digesta from the small intestine phase. The properties of the micelle phase were then analyzed before ("unfiltered") and after ("filtered") they were passed through a 450 nm filter. The mean particle diameters of the unfiltered (228 and 279 nm) and filtered (107 and 205 nm) micelle phases measured by DLS were relatively small for delivery systems 1 and 2, respectively (Figure 1a). The sizes in the unfiltered groups were larger than those in the filtered groups, which indicated that some of the larger particles had been removed by the filter. The micelle phase would be expected to contain β-carotene solubilized within mixed micelles, which are actually a complex mixture of various colloidal structures, including micelles and vesicles.[29] Micelles are expected to be only a few nanometers big (<10 nm), whereas vesicles are much larger (10−1000 nm). Our results therefore suggest that the mixed micelle phase resulting from digestion of the nanoemulsions contained an appreciable amount of vesicles.

Overall, we did not find an appreciable difference between the behavior of the lipid droplets in the two delivery systems containing nanoemulsions (i.e., with either solubilized or crystalline β-carotene). This suggests that the physical state of the carotenoids did not have a major influence on the gastrointestinal fate of the nanoemulsions.

Crystal Structure. Images of the β-carotene crystals within the different delivery systems were captured using a crossed polarizer lens (Figure 4). No crystals were observed in the samples initially containing solubilized β-carotene (delivery system 1), which suggests that the carotenoids did not crystallize during passage through the simulated GIT (data not shown). The number of crystals appearing in the images of the samples initially containing crystalline β-carotene decreased as they were passed through successive stages of the simulated GIT (Figure 4). The most likely reason for this observation is that the samples were progressively diluted at each GIT stage. It is also possible that some of the crystals dissolved during passage through the GIT, but the results of the bioaccessibility study (discussed below) suggest that this was not an appreciable amount.

Particle Charge. We also measured the electrical charge of the particles in the samples after each stage of the GIT model to provide some information about changes in their surface characteristics. Initially, the lipid droplets in the nanoemulsions used to prepare delivery systems 1 and 2 had negative charges (Figure 2). Tween 20 is actually a nonionic surfactant and might therefore be expected to produce neutral lipid droplets. However, it is well established that lipid droplets stabilized by

DOI: 10.1021/jf504673v
J. Agric. Food Chem. 2015, 63, 990−997

this surfactant can have a substantial negative charge, which has been attributed to the presence of anionic impurities in the surfactant or lipids used to prepare them (e.g., phospholipids or FFAs) or due to preferential adsorption of hydroxide ions (OH^-) in water to the droplet surfaces.[10] The electrical charge became more negative when the delivery systems were exposed to the simulated saliva in the mouth (Figure 2), which may have been due to adsorption of anionic mucin molecules to the droplet surfaces. The magnitude of the negative charge on the droplets decreased appreciably after exposure to simulated gastric fluids, which can be attributed to the appreciable decrease in pH in the stomach environment. The particles in the samples had a large negative charge after exposure to the simulated intestinal fluids (Figure 2), which can be attributed to adsorption of anionic species to the droplet surfaces, such as surface active species from the simulated intestinal fluids (e.g., bile salts and phospholipids) or generated during triacylglycerol digestion (e.g., FFAs). The electrical charges on the unfiltered and filtered micelles are also highly negative (Figure 2) because they are primarily composed of anionic species, such as bile salts, phospholipids, and FFAs. The particles in the filtered micelle phase resulting from digestion of the nanoemulsions containing solubilized β-carotene appeared to be less negative than those initially containing crystallized β-carotene. The origin of this effect is unknown, but it suggests that there may have been some differences in the compositions of the mixed micelles in the different systems.

Influence of Physical States of β-Carotene on Lipid Digestion. In this section, the rate and extent of lipid digestion in the small intestine phase was monitored using an automatic titration method (pH-stat). This method measures the amount of alkaline solution required to neutralize the FFAs released from triglycerides during digestion by lipase.[30] As expected, there was little change in the pH of the sample that contained only β-carotene crystals dispersed in buffer solution, because there was no fat in the system and so no FFAs were released during digestion (Figure 5). The slight consumption of NaOH

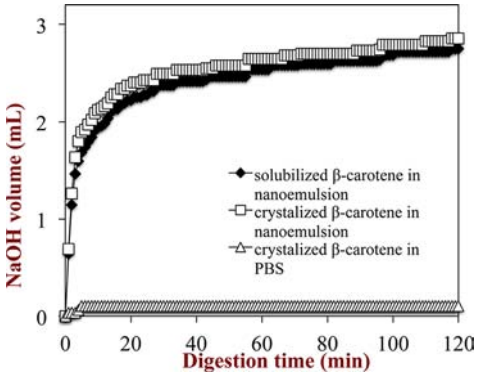

Figure 5. Influence of physical state of β-carotene on the pH-stat titration curves of oil-in-water nanoemulsions. The curves show the volume of 0.25 M NaOH solution that had to be added to the samples to maintain the pH at a constant value of 7.

observed may have been due to some digestible materials in the nonionic surfactant (present in buffer solution) or the chemicals used to prepare the gastrointestinal fluids, for example, phospholipids or proteins. A recent study showed that several nonionic surfactants have ester bonds that are susceptible to lipase digestion, leading to FFA release.[31,32]

In the two delivery systems containing digestible nanoemulsions, there was a steep increase in the volume of NaOH added during the first 20 min of digestion and then it leveled off (Figure 5). The FFA release profiles followed a similar trend as the NaOH consumption (Figure 6). These results suggested that

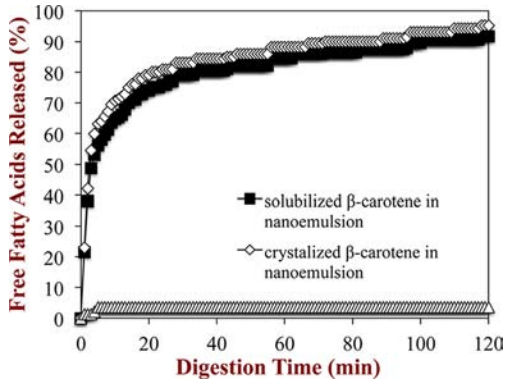

Figure 6. Influence of physical state of β-carotene on the pH-stat titration curves of oil-in-water nanoemulsions. The curves show the calculated percentage of free fatty acids (FFA) released from the nanoemulsions after digestion of the triacylglycerol phase by lipase.

lipase rapidly attached to the surface of the lipid droplets and promoted triacylglycerol digestion. There was no appreciable difference in the FFA release profiles for the solubilized β-carotene samples and for the crystallized β-carotene samples, which suggested that the physical state of β-carotene did not have a major impact on the rate or extent of lipid digestion.

Influence of Physical States of β-Carotene on Its Bioaccessibility. Finally, we measured the influence of the physical state and environment of β-carotene on its bioaccessibility after it passed through the simulated GIT model (Figure 7).

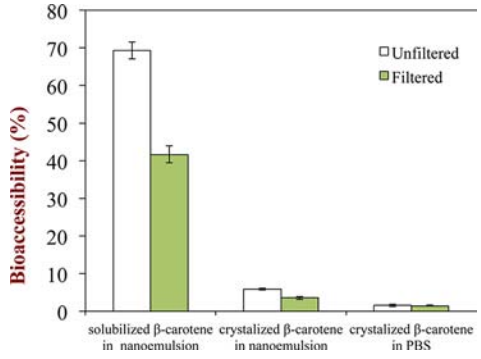

Figure 7. Effect of physical states of β-carotene on bioaccessibility of β- carotene measured after centrifugation of nanoemulsions passed through an in vitro digestion model.

The bioaccessibility was taken to be the amount of β-carotene in the "micelle" phase divided by the portion in the digesta collected after the small intestine phase. The bioaccessibility was measured for both unfiltered and filtered micelle phases. It was assumed that the data for the filtered samples would be more representative of the actual bioaccessibility because particles >~450 nm should not be able to pass through the mucus layer that normally coats the intestinal epithelium cells.[33]

The lowest bioaccessibilities were measured for the unfiltered (1.5%) and filtered (1.4%) samples that initially contained β-carotene crystals dispersed in buffer solution (Figure 7), which

DOI: 10.1021/jf504673v
J. Agric. Food Chem. 2015, 63, 990−997

can be attributed to the fact that there were few mixed micelles available to solubilize the carotenoid crystals. The carotenoid crystals are dense and relatively large (Figure 4) and therefore they sedimented to the bottom of the test tubes after the small intestine stage and did not appear in the micelle phase. The bioaccessibility was also relatively low for the samples that initially contained crystallized β-carotene in nanoemulsions: 5.9 and 3.6% for unfiltered and filtered samples, respectively. In this case, there would be a relatively high concentration of mixed micelles present because the lipid droplets were digested by lipase during the small intestine phase (Figure 5b). This result suggests that there was insufficient time for the β-carotene crystals to dissolve within the mixed micelles in the gastrointestinal fluids, as confirmed by the presence of crystals in the optical microscopy images (Figure 4).

The samples initially containing β-carotene fully dissolved within the nanoemulsions had by far the highest bioaccessibilities: 69 and 42% for unfiltered and filtered samples, respectively. This result suggests that the solubilized β-carotene molecules were able to be transported from the lipid droplets into the mixed micelles during the lipid digestion process, without any crystallization occurring. Overall, our results suggest that the most effective means of delivering β-carotene is by solubilizing it within digestible lipid droplets. Crystalline β-carotene appears to have a relatively low bioaccessibility, whether consumed with water or with an emulsion; however, co-ingestion with an emulsion does lead to an appreciably higher bioaccessibility.

In conclusion, this study showed the bioaccessibility of β-carotene is highly dependent on its physical state, that is, solubilized versus crystalline. Three delivery systems with different properties were tested: (1) solubilized β-carotene in a nanoemulsion; (2) crystallized β-carotene in a nanoemulsion; and (3) crystalline β-carotene in buffer solution. The bioaccessibility of solubilized β-carotene (delivery system 1) was much higher than that of crystallized β-carotene (delivery systems 2 and 3). However, co-ingestion of crystallized β-carotene with a nanoemulsion did lead to an appreciable increase in bioaccessibility. These results have important implications for the development of functional foods or beverages to deliver bioactive lipophilic compounds, such as carotenoids. Our results suggest that the most effective way to obtain a relatively high bioaccessibility is to dissolve the carotenoids in an emulsion. Nevertheless, the bioaccessibility of crystalline carotenoids can also be improved considerably by their consumption with an emulsion.

AUTHOR INFORMATION

Corresponding Author

*(H.X.) Phone: (413) 545-2281. E-mail: hangxiao@foodsci.umass.edu.

Author Contributions

‖D.J.M. and H.X. contributed equally to this paper.

Funding

This material is based upon work supported by the U.S. Department of Agriculture NRI (Grants 2011-67021, 2014-67021, 2011-03539, and 2013-03795), the Massachusetts Agricultural Experiment Station (Projects 995 and 831), and the International Life Science Institute North America.

Notes

The authors declare no competing financial interest.

REFERENCES

(1) Rao, A.; Rao, L. G. Carotenoids and human health. *Pharmacol. Res.* **2007**, *55*, 207−216.

(2) Agarwal, S.; Rao, A. Carotenoids and chronic diseases. *Drug Metab. Drug Interact.* **2000**, *17*, 189−210.

(3) Elliott, R. Mechanisms of genomic and non-genomic actions of carotenoids. *Biochim. Biophys. Acta (BBA)−Mol. Basis Dis.* **2005**, *1740*, 147−154.

(4) Johnson, E. J. The role of carotenoids in human health. *Nutr. Clin. Care* **2002**, *5*, 56−65.

(5) Castenmiller, J. J.; West, C. E. Bioavailability and bioconversion of carotenoids. *Annu. Rev. Nutr.* **1998**, *18*, 19−38.

(6) Thakkar, S. K.; Maziya-Dixon, B.; Dixon, A. G.; Failla, M. L. β-Carotene micellarization during in vitro digestion and uptake by Caco-2 cells is directly proportional to β-carotene content in different genotypes of cassava. *J. Nutr.* **2007**, *137*, 2229−2233.

(7) van het Hof, K. H.; West, C. E.; Weststrate, J. A.; Hautvast, J. G. Dietary factors that affect the bioavailability of carotenoids. *J. Nutr.* **2000**, *130*, 503−506.

(8) Yonekura, L.; Nagao, A. Intestinal absorption of dietary carotenoids. *Mol. Nutr. Food Res.* **2007**, *51*, 107−115.

(9) Hörter, D.; Dressman, J. Influence of physicochemical properties on dissolution of drugs in the gastrointestinal tract. *Adv. Drug Delivery Rev.* **2001**, *46*, 75−87.

(10) Qian, C.; Decker, E. A.; Xiao, H.; McClements, D. J. Nanoemulsion delivery systems: Influence of carrier oil on β-carotene bioaccessibility. *Food Chem.* **2012**, *135*, 1440−1447.

(11) Rao, J.; Decker, E. A.; Xiao, H.; McClements, D. J. Nutraceutical nanoemulsions: influence of carrier oil composition (digestible versus indigestible oil) on β-carotene bioavailability. *J. Sci. Food Agric.* **2013**, *93*, 3175−3183.

(12) Cornacchia, L.; Roos, Y. H. State of dispersed lipid carrier and interface composition as determinants of β-carotene stability in oil-in-water emulsions. *J. Food Sci.* **2011**, *76*, C1211−C1218.

(13) Liu, Y.; Hou, Z.; Lei, F.; Chang, Y.; Gao, Y. Investigation into the bioaccessibility and microstructure changes of β-carotene emulsions during in vitro digestion. *Innovative Food Sci. Emerging Technol.* **2012**, *15*, 86−95.

(14) Silva, H. D.; Cerqueira, M. A.; Souza, B. W.; Ribeiro, C.; Avides, M. C.; Quintas, M. A.; Coimbra, J. S.; Carneiro-da-Cunha, M. G.; Vicente, A. A. Nanoemulsions of β-carotene using a high-energy emulsification−evaporation technique. *J. Food Eng.* **2011**, *102*, 130−135.

(15) Yuan, Y.; Gao, Y.; Zhao, J.; Mao, L. Characterization and stability evaluation of β-carotene nanoemulsions prepared by high pressure homogenization under various emulsifying conditions. *Food Res. Int.* **2008**, *41*, 61−68.

(16) Goltz, S. R.; Campbell, W. W.; Chitchumroonchokchai, C.; Failla, M. L.; Ferruzzi, M. G. Meal triacylglycerol profile modulates postprandial absorption of carotenoids in humans. *Mol. Nutr. Food Res.* **2012**, *56*, 866−877.

(17) Mao, Y.; McClements, D. J. Influence of electrostatic heteroaggregation of lipid droplets on their stability and digestibility under simulated gastrointestinal conditions. *Food Funct.* **2012**, *3*, 1025−1034.

(18) Sarkar, A.; Goh, K. K. T.; Singh, H. Colloidal stability and interactions of milk-protein-stabilized emulsions in an artificial saliva. *Food Hydrocolloids* **2009**, *23*, 1270−1278.

(19) Sarkar, A.; Goh, K. K.; Singh, R. P.; Singh, H. Behaviour of an oil-in-water emulsion stabilized by β-lactoglobulin in an in vitro gastric model. *Food Hydrocolloids* **2009**, *23*, 1563−1569.

(20) Li, Y.; McClements, D. J. New mathematical model for interpreting pH-stat digestion profiles: impact of lipid droplet characteristics on in vitro digestibility. *J. Agric. Food Chem.* **2010**, *58*, 8085−8092.

(21) Silletti, E.; Vingerhoeds, M. H.; Norde, W.; Van Aken, G. A. The role of electrostatics in saliva-induced emulsion flocculation. *Food Hydrocolloids* **2007**, *21*, 596−606.

DOI: 10.1021/jf504673v
J. Agric. Food Chem. 2015, 63, 990−997

(22) Vingerhoeds, M. H.; Blijdenstein, T. B. J.; Zoet, F. D.; van Aken, G. A. Emulsion flocculation induced by saliva and mucin. *Food Hydrocolloids* **2005**, *19*, 915−922.
(23) Golding, M.; Wooster, T. J.; Day, L.; Xu, M.; Lundin, L.; Keogh, J.; Clifton, P. Impact of gastric structuring on the lipolysis of emulsified lipids. *Soft Matter* **2011**, *7*, 3513−3523.
(24) Nik, A. M.; Langmaid, S.; Wright, A. J. Digestibility and β-carotene release from lipid nanodispersions depend on dispersed phase crystallinity and interfacial properties. *Food Funct.* **2012**, *3*, 234−245.
(25) McClements, D. J.; Xiao, H. Potential biological fate of ingested nanoemulsions: influence of particle characteristics. *Food Funct.* **2012**, *3*, 202−220.
(26) Bellesi, F. A.; Ruiz-Henestrosa, V. M. P.; Pilosof, A. M. R. Behavior of protein interfacial films upon bile salts addition. *Food Hydrocolloids* **2014**, *36*, 115−122.
(27) Nik, A. M.; Wright, A. J.; Corredig, M. Impact of interfacial composition on emulsion digestion and rate of lipid hydrolysis using different in vitro digestion models. *Colloids Surf. B−Biointerfaces* **2011**, *83*, 321−330.
(28) Torcello-Gomez, A.; Maldonado-Valderrama, J.; Jodar-Reyes, A. B.; Foster, T. J. Interactions between pluronics (F127 and F68) and bile salts (NaTDC) in the aqueous phase and the interface of oil-in-water emulsions. *Langmuir* **2013**, *29*, 2520−2529.
(29) Yao, M. F.; Xiao, H.; McClements, D. J. Delivery of lipophilic bioactives: assembly, disassembly, and reassembly of lipid nanoparticles. *Annu. Rev. Food Sci. Technol.* **2014**, *5*, 53−81.
(30) McClements, D. J.; Li, Y. Review of in vitro digestion models for rapid screening of emulsion-based systems. *Food Funct.* **2010**, *1*, 32−59.
(31) Li, Y.; McClements, D. J. Inhibition of lipase-catalyzed hydrolysis of emulsified triglyceride oils by low-molecular weight surfactants under simulated gastrointestinal conditions. *Eur. J. Pharm. Biopharm.* **2011**, *79*, 423−431.
(32) Li, Y.; Hu, M.; McClements, D. J. Factors affecting lipase digestibility of emulsified lipids using an in vitro digestion model: proposal for a standardised pH-stat method. *Food Chem.* **2011**, *126*, 498−505.
(33) Ensign, L. M.; Cone, R.; Hanes, J. Oral drug delivery with polymeric nanoparticles: the gastrointestinal mucus barriers. *Adv. Drug Delivery Rev.* **2012**, *64*, 557−570.

DOI: 10.1021/jf504673v
J. Agric. Food Chem. 2015, 63, 990−997

include degumming with different reagents (phosphoric acid, glacial acetic acid, oxalic acid, and citric acid), neutralization with alkali to remove the free fatty acids, bleaching with different individual adsorbents or their combinations (activated charcoal powder, kaolin light, Fuller's earth, cellulose powder, and purified chitin powder), and deodorization by vacuum distillation to remove the low molecular weight volatile compounds. The changes in ^{1}H NMR signal characteristics after degumming and bleaching processes were compared to those of the crude sardine oil. The volatile compounds distilled off during the deodorization process were evaluated by gas chromatography−mass spectroscopic (GC-MS) analysis.

MATERIALS AND METHODS

Preparation of Crude Sardine Oil. Fresh samples of *S. longiceps* (Valenciennes, 1847) (Indian oil sardine) were collected from the fishing harbors in Cochin (9.97° N, 76.28° E; southwestern coast of India) during the monsoon season and were brought to the laboratory in an icebox. After a washing in sterile water, the internal organs were removed and the edible tissues were cut into slices before being minced in a grinder. The minced edible tissue (100 g) was cooked in a pressure cooker for 30 min at 75 °C, and the cooked tissue was pressed in a screw expeller (PIC-106; Four Brothers Ex-Imp Pvt. Ltd., Chennai, India) before being centrifuged (8000*g*, 30 min) to afford the cooked and pressed crude sardine oil (CSO, 8.3 g).

Oil Refinement Methodology. The steps of the crude oil refinement process (degumming, neutralization, bleaching, and deodorization) were carried out by using the operating conditions as described as follows. Each stage of these refining processes was monitored by evaluating the percent recovery and quality parameters such as FFAs, peroxide (PV), *p*-anisidine (pAV), total oxidation (TOTOX), thiobarbituric acid reactive species (TBARS), Lovibond L^*, a^*, b^* color, chroma, hue angle, total color (ΔE) values, and fatty acid composition.

Crude sardine oil (100 g) was stirred in a temperature-controlled water bath (70 °C) for 20 min separately with 85% phosphoric acid (1 mL, DG_1), 99% glacial acetic acid (1 mL, DG_2), 10% oxalic acid (5 mL, DG_3), and 10% citric acid (5 mL, DG_4). The oil was then cooled to room temperature and centrifuged (10000*g*, 10 min) to remove the precipitated gum. The optimum method of degumming was found by studying the percent recovery and common physicochemical characteristics of the oil.

The degummed oil (100 g) obtained by optimum degumming method (i.e., with phosphoric acid DG_1) was further refined by caustic neutralization according to AOCS Official Method Ca 9b-52.[9] This was performed by the addition of NaOH solution (1 N, 30 mL) dropwise to the degummed oil with constant stirring and heating (65 °C) for 20 min until a pH of 7.0 was attained. This oil was then heated at 70 °C for 20 min, cooled to room temperature, and centrifuged (10000*g*, 10 min), and the oil was decanted to remove the precipitated soap. The oil thus obtained was washed three times with 10% deionized water (in relation to the oil mass) by agitation (500 rpm) and heating at 50 °C under vacuum. Water and other impurities were further removed by centrifuging (2500*g*, 10 min) to obtain the neutralized sardine oil (NSO). The quality of the degummed oil was studied by ^{1}H NMR spectroscopy. The proton integral as observed by the ^{1}H NMR analysis of the degummed oil vis-à-vis crude oil were compared to understand the reduction of the hydrocarbon residues from the externalities.

The neutralized sardine oil (NSO) was treated separately with activated charcoal powder (AC), kaolin light (KL), Fuller's earth (FE; fulmont 700C), cellulose powder (CP), and chitin purified powder (CH) to study the individual effect of different adsorbents (at 5%, w/w of oil) on the color and other quality parameters of the oil. The effect of different experimental combinations (at 5% w/w of oil) of the best adsorbents selected, (i.e., AC and FE) on bleaching of the oil was further evaluated. The five experimental combinations of AC and FE were BC_1, AC + FE (90:10); BC_2, AC + FE (75:25); BC_3, AC + FE (50:50); BC_4, AC + FE (25:75); and BC_5, AC + FE (10:90). The best adsorbent combination was optimized by studying their effects on the oil quality parameters such as FFAs, PV, pAV, TOTOX, TBARS, Lovibond L^*, a^*, b^* color, chroma, hue angle, and ΔE values after bleaching. For the above bleaching processes, the neutralized oil was stirred separately with the adsorbents at 300 rpm (using a magnetic stirrer) with heating at 60 °C for 10 min under N_2. The effect of the best adsorbent combination, that is, BC_4 (AC + FE, 25:75), was further studied for optimizing two experimental factors, namely, adsorbent amount and contact time of bleaching as shown in Table 1.

Table 1. Concentration of Different Adsorbents[a] and Contact Time of Bleaching of Crude Sardine Oil

	adsorbents			
treatment	AC (g)	FE (g)	amount of adsorbent (g in 100 g of oil)	contact time[b] (min)
BC_{4A}	1.25	3.75	5	20
BC_{4B}	1.25	3.75	5	40
BC_{4C}	1.25	3.75	5	60
BC_{4D}	0.75	2.25	3	20
BC_{4E}	0.75	2.25	3	40
BC_{4F}	0.75	2.25	3	60
BC_{4G}	0.25	0.75	1	20
BC_{4H}	0.25	0.75	1	40
BC_{4I}	0.25	0.75	1	60

[a]AC, activated charcoal; FE, Fuller's earth. [b]Contact time implies the time used for stirring the oil with the adsorbent combination by heating at 60 °C.

The optimum methodology of the bleaching process of the oil was validated through ^{1}H NMR spectroscopy conjugated with ^{13}C NMR methodology to understand the signals related to the coloring impurities at different regions.

The deodorization of the bleached sardine oil (BSO) was carried out using a modified method of Karahadian and Lindsay[7] with a laboratory distillation unit containing a round-bottom boiling flask (500 mL) having two outlets. One outlet was connected to a condenser, which was connected to a vacuum, and the other was connected to a thermometer. Aqueous acetic acid solution (0.25 N, 5 mL) was added with an aliquot containing the BSO in a round-bottom flask, and the contents were heated to 100 °C under vacuum (5 mmHg) for a period of 1 h. The vacuum line was turned off at different time intervals (5, 15, 30, and 60 min), and the distillates (designated DO_1−DO_4, respectively) were analyzed using GC-MS to estimate the traces of volatile compounds distilled off during the deodorization process. The traces of volatile compounds distilled off during the deodorization process of the degummed oil were analyzed at different intervals (5, 15, 30, and 60 min) using GC-MS analysis.

Analytical Methodologies. FFA (Ca 5a-40), PV (Cd 8−53), and pAV (Cd 18-90) values were determined according to American Oil Chemists' Society (AOCS) methodologies.[10] FFA value was expressed as percent oleic acid = (28.2 × 0.1 × volume of 0.1 N NaOH in mL) × 100/weight of oil in g, and PV was expressed as milliequivalents of O_2 (mequiv O_2)/kg oil. The pAV was calculated as $[25 \times (1.2A_S - A_B)]/W$, where A_S = absorbance of the oil solution after reaction with the *p*-anisidine reagent, A_B = absorbance of the oil solution, W = grams of sample, 25 mL = dilution volume, and 1.2 = correction factor. TOTOX value was calculated as TOTOX = (2 × PV) + pAV.[11] TBARS value was determined by using a spectrophotometric method[12] with a standard curve (with 0−10 ppm concentration) of 1,1,3,3-tetramethoxypropane (malondialdehyde; MDA) with thiobarbituric acid. TBARS values were expressed as milligrams of MDA equivalent compounds (MDAEQ) per kilogram of oil.

The oil color was determined using the Lovibond method (Lovibond Color Staler Tintometer, model F, UK), as described by Sathivel et al.[13] The results were expressed as L^*, a^*, and b^* values. The L^* values indicated lightness (0 = black and 100 = white),

DOI: 10.1021/jf505127e
J. Agric. Food Chem. 2015, 63, 998−1009

whereas a^* values represented redness (+) and greenness (−) and b^* values represented yellowness (+) and blueness (−). From a^* and b^*, the psychometric parameters, namely, hue angle (h_{ab}; actual color) and chroma (C^*_{ab}; intensity of color) were calculated as $h_{ab} = \tan^{-1}(b^*/a^*)$ and $C^*_{ab} = \sqrt{(a^*)^2 + (b^{*2})}$. The total color difference was calculated by $(\Delta E) = \sqrt{(\Delta L^{*2} + \Delta a^{*2} + \Delta b^{*2})}$. The UV−vis spectral scanning of the bleached and nonbleached fish oils in *n*-hexane (0.02% w/v) was performed on a UV−visible spectrophotometer equipped with a 1 cm cell (Varian Cary 50, USA).

Fatty acid profiles were evaluated by converting the triglycerides to their corresponding methyl esters.[14] The lipid (0.2 g) was saponified under reflux (20 min, 70−80 °C) with alkaline reagent (3 mL, 0.5 N KOH/MeOH). The saponifiable materials were reacted with methylating mixture (14% BF_3/CH_3OH, 1 mL) for 5 min, yielding fatty acid methyl esters (FAMEs), which were extracted in *n*-hexane/H_2O (1:2, v/v). The *n*-hexane layer was dried to be reconstituted in petroleum ether (40−60 °C) before being injected on a PerkinElmer (PerkinElmer, Shelton, CT, USA) AutoSystem XL gas chromatograph (HP 5890 series II) connected with an SP 2560 (crossbond 5% diphenyl−95% dimethyl polysiloxane) capillary column (100 m × 0.25 mm i.d., 0.50 μm film thickness, Sigma-Aldrich/Supelco, Bellefonte, PA, USA) using a flame ionization detector (FID) equipped with a split/splitless injector, which was used in the split (1:15) mode. FAMEs were identified by comparing the retention time of the samples with FAME standards (Supelco 37 Component FAME Mix, catalog no. 47885-U, Bellefonte, PA, USA), and the results were expressed as percent of total fatty acids (%). Chromatograms were analyzed using PerkinElmer Chromstation (version 4.02) software. The GC-MS analyses of the *N*-acyl pyrrolidides of fatty acids were performed using the electronic impact (EI) ionization mode in a Varian GC (CP-3800, Palo Alto, CA, USA) interfaced with a Varian instrument 1200L single-quadruple mass spectrometer for confirmation of fatty acid identification as described earlier.[14] Mass spectra were analyzed using Varian Workstation (version 6.2) software.

The ^{1}H NMR spectra of the fish oil were measured using the modified method on a Bruker Avance III, 400 MHz (Bruker Inc., Bremen, Germany) NMR spectrometer using tetramethylsilane (TMS) as an internal standard and $CDCl_3$ as solvent (in δ).[15,16] The acquisition parameters for ^{1}H NMR were as follows: time domain data points (TD) = 65536, number of scans (NS) = 64, number of dummy scans (DS) = 0, sweep width (SWH) = 8223.685 Hz, temporal resolution of the free induction decay (FIDRES) = 0.125483 Hz, acquisition time (AQ) = 3.9846 s, receiver gain (RG) = 16, dwell time (DW) = 60.800 μs, relaxation delay (D1) = 2 s.

The qualitative GC-MS analyses of the volatile components obtained during deodorization were performed using electronic impact (EI) ionization mode in a PerkinElmer Clarus 680 GC-MS instrument. The separation of volatile components was achieved on an Elite 5 MS nonpolar, bonded phase capillary column (50 m × 0.22 mm i.d. × 0.25 μm film thicknesses). Helium (He) was used as the carrier gas, and the flow rate used was 1 mL/min. The temperature was programmed at an initial temperature of 50 °C for 2 min, then raised at 10 °C/min to 180 °C, held for 2 min, and finally raised at 4 °C/min to 280 °C and held for 15 min. About 1 μL of the extract was injected into the column, in the splitless mode. Electron ionization energy was set at 70 eV. The mass range, electron multiplier voltage, and scan rates were set at 35−400 u, 1550 V, and 10 spectra/s, respectively. Ion source temperature was maintained at 200 °C. Mass spectra were analyzed using PerkinElmer Clarus software. The identity of the compounds has been confirmed by fragmentation analyses and by comparison with NIIST database.

Statistical Methodology. The means of all parameters were examined for significance by analysis of variance (ANOVA) and carried out with the Statistical Program for Social Sciences 13.0 (SPSS Inc., Chicago, IL, USA; ver. 13.0). The level of significance for all analyses was $p \leq 0.05$.

RESULTS AND DISCUSSION

Characteristics of Sardine Oil during Different Stages of Refining. *Degumming.* The yield of CSO obtained by cooking followed by pressing was found to be 8.3% (w/w). Degumming with phosphoric acid (DG_1) yielded a dark residue (14%, w/w) with 86% oil recovery (w/w), whereas oxalic acid treatment (DG_3) yielded a dark residue (9.8%, w/w) with 90.2% oil recovery (Table 2). An increase in FFA (5.6−7.8%) was observed for oil after degumming in relation to CSO (4.4%) (Table 2), which was expected due to the trace amount of acids added. PV exhibited maximum reduction for DG_1 followed by DG_3, DG_2, and DG_4. DG_{1-4} observed lesser pAV in relation to CSO with maximum percent reduction observed for DG_1 (16%). TBARS value showed 19.4% reduction for DG_1 in relation to the CSO. Initial L^*, a^*, and b^* values of CSO were recorded to be 50.25, 7.58, and 42.51, respectively, which indicated the brownish orange color of the oil due to the deposition of dietary carotenoids.[17] Increases in L^* and a^* (51.02 and 8.0, respectively) and a reduction in b^* value (42.0) were observed for DG_1, whereas other degumming modes showed no substantial changes in the L^*, a^*, and b^* values (Table 2). This increase in L^* and a^* values could be attributed to the increase in FFA content, resulting in the formation of lipid−protein complexes, thereby consequently increasing color.[18]

Fatty acid compositions of CSO before and after degumming (DG_1, DG_2, DG_3, and DG_4) are shown in Table 3. The saturated fatty acid (SFA) fraction of CSO was 41.0%, which remained unchanged after treatment with different degumming agents. The predominant SFA in CSO was 16:0, accounting for around 53% of total SFA fraction. The monounsaturated fatty acid (MUFA) fraction was 29.2% with predominant fatty acids being 16:1n-7 (13%) followed by 18:1n-9 (12%). The total PUFA of CSO was 26.5% with total n-3 PUFAs (18:3n-3, 20:5n-3, 22:5n-3, and 22:6 n-3) accounting for 83% of the PUFA fractions with a greater share of 20:5n-3 (15.5%) and 22:6n-3 (5%). No significant differences were apparent in MUFA or PUFA compositions after the degumming process ($p > 0.05$). However, a marginal reduction in EPA, ∑PUFA, and ∑n-3PUFA contents might be due to the involvement of heat during the process of degumming. Thus, evaluation of the quality parameters after degumming showed the greater quality of phosphoric acid as degumming agent of the crude sardine oil.

The ^{1}H NMR spectrum of the degummed sardine oil DG_1 was compared with that of CSO (control) for qualitative representation of the various functionalities present in them. The integrated areas of the characteristic regions of the ^{1}H NMR spectra of the oils studied were found to be linearly correlated with the fatty acid data, and ^{1}H NMR was proposed as a new method for determining the degree of degumming. The characteristic fatty acid signals of CSO as identified by ^{1}H NMR were confirmed using literature data[16,19] and by recording spectra of standard compounds. This revealed the presence of n-3 fatty acids as confirmed by a sharp triplet at δ 0.974, a structural feature for methyl proton (-C$\underline{\mathbf{H}}_3$) in n-3 PUFAs (Figure 1). The signals at δ 1.18−1.43 could be explained due to the methylene envelope ($-(C\underline{\mathbf{H}}_2)_n$) in the long alkyl chain. The sandwiched CH_2 bis-allylic protons (−CH═CH—C$\underline{\mathbf{H}}_2$—CH═CH−) were overlapped and displayed at δ 2.74−2.92 (multiplets). These bis-allylic peaks indicate the predominance of PUFA in the sardine oil. The proton integral as observed by the ^{1}H NMR analysis of DG_1 revealed significant reduction of the hydrocarbon residues compared with DG_3 and

DOI: 10.1021/jf505127e
J. Agric. Food Chem. 2015, 63, 998−1009

Table 2. Physicochemical Indices of the Sardine Oil during Different Stages of Refining

physicochemical index[a]	% recovery	FFA	PV	pAV	TOTOX	TBARS	L^*	a^*	b^*	hue angle	chroma	ΔE
CSO	8.3	4.4 ± 0.04a	11.88 ± 0.08a	16.2 ± 0.02a	39.96 ± 0.08a	6.18 ± 0.02a	50.25 ± 0.03a	7.58 ± 0.75a	42.51 ± 1.26ad	79.89 ± 0.8a	43.17 ± 0.45a	
DG_1	86	7.85 ± 0.09b	7.2 ± 0.01bc	13.6 ± 0.06b	28 ± 0.08b	4.98 ± 0.05bc	51.02 ± 1.11a	8 ± 0.8a	42.01 ± 0.2ad	79.21 ± 0.65a	42.76 ± 0.46a	1.03 ± 0.01a
DG_2	93.06	6.98 ± 0.01c	8.01 ± 0.08c	14.1 ± 0.01bc	30.12 ± 0.01b	5.21 ± 0.02c	49.58 ± 2.97a	7.45 ± 0.75a	43.01 ± 2.29ad	80.16 ± 0.81a	43.64 ± 0.47a	0.87 ± 0.01ab
DG_3	90.05	6.01 ± 0.06d	7.56 ± 0.06c	14.68 ± 0.07cd	29.8 ± 0.09b	5.69 ± 0.07ac	50.01 ± 1.01a	7.58 ± 0.76a	42 ± 4.2ad	79.77 ± 0.8a	42.68 ± 0.43a	0.54 ± 0.01b
DG_4	92.56	5.65 ± 0.07d	8.25 ± 0.03c	15.01 ± 0.03d	31.51 ± 0.06c	5.88 ± 0.09ac	50.21 ± 0.02a	7.88 ± 0.79a	42.01 ± 2.2ad	79.37 ± 0.79a	42.73 ± 0.43a	0.58 ± 0.01b
NSO	93.44	3.21 ± 0.02ef	6.09 ± 0.08d	10.01 ± 0.06efg	22.19 ± 0.02d	4.02 ± 0.04d	51.34 ± 5.13a	8.21 ± 0.82a	43.65 ± 4.37ad	79.33 ± 0.79a	44.37 ± 0.35b	1.68 ± 0.02a
AC (5%)	93.84	2.79 ± 0.09e	4.37 ± 0.14e	9.42 ± 0.04fh	18.16 ± 0.02e	3.66 ± 0.07e	75.06 ± 1.51b	3.65 ± 0.37b	38.85 ± 3.89b	84.62 ± 0.83b	38.97 ± 0.39c	25.38 ± 0.25c
KA (5%)	97.74	3.37 ± 0.04f	6.45 ± 0.05bdf	10.45 ± 0.05gh	23.35 ± 0.05d	4.12 ± 0.01e	51.06 ± 0.11a	6.52 ± 0.65c	41.69 ± 4.17ad	81.09 ± 0.81a	42.11 ± 0.42a	1.6 ± 0.02a
FE (5%)	96.63	3.16 ± 0.02ef	5.02 ± 0.05de	9.52 ± 0.05ef	19.56 ± 0.05dg	3.64 ± 0.06e	70.74 ± 1.08b	3.66 ± 0.37b	39.89 ± 1.99ab	84.74 ± 0.85b	39.97 ± 0.4c	21.05 ± 0.21c
CE (5%)	97.08	3.41 ± 0.04eg	6.03 ± 0.06d	9.91 ± 0.09efg	21.97 ± 0.09dg	4.01 ± 0.04e	51.42 ± 1.14a	7.52 ± 0.75a	40.64 ± 0.06ab	79.51 ± 0.78a	41.29 ± 0.56a	2.25 ± 0.02a
CH (5%)	98.32	3.39 ± 0.04h	5.73 ± 0.08d	9.94 ± 0.09efg	21.4 ± 0.05df	4.01 ± 0.04e	51.45 ± 2.15a	4.99 ± 0.5d	40.61 ± 0.06b	82.99 ± 0.83b	40.91 ± 0.41c	3.43 ± 0.03d
BC_1	94.19	3.18 ± 0.01e	4.67 ± 0.07e	9.47 ± 0.05ef	18.81 ± 0.09e	3.67 ± 0.07e	75.28 ± 1.53b	3.67 ± 0.37b	39.96 ± 4b	84.74 ± 0.86b	40.07 ± 0.04c	25.44 ± 0.25c
BC_2	94.43	2.74 ± 0.07ei	4.56 ± 0.07e	9.47 ± 0.05ef	18.59 ± 0.09e	3.68 ± 0.07e	75.23 ± 3.52b	3.65 ± 0.37b	39.78 ± 2.9b	84.75 ± 0.85b	39.87 ± 0.54c	25.46 ± 0.25c
BC_3	94	2.94 ± 0.09e	4.95 ± 0.05e	9.3 ± 0.03ef	19.2 ± 0.03ef	3.5 ± 0.05e	74.16 ± 0.42b	3.61 ± 0.36b	39.86 ± 3.99b	84.81 ± 0.98b	39.96 ± 0.4c	24.38 ± 0.14c
BC_4	92.23	2.79 ± 0.07e	4.3 ± 0.03e	9.42 ± 0.04ef	18.02 ± 0.03e	3.64 ± 0.06e	83.57 ± 2.35b	3.6 ± 0.36b	39.61 ± 1.96b	84.8 ± 0.85b	39.76 ± 0.4c	33.66 ± 0.34e
BC_5	93.5	3.01 ± 0.03e	5.08 ± 0.05e	9.3 ± 0.03ef	19.46 ± 0.03de	3.68 ± 0.07e	81.51 ± 0.15b	3.61 ± 0.36b	39.24 ± 0.93b	84.74 ± 0.85b	39.37 ± 0.09cd	31.72 ± 0.02e
BC_{4A}	93.5	2.79 ± 0.09ej	3.62 ± 0.06e	9.49 ± 0.05ef	16.73 ± 0.07e	3.67 ± 0.37e	83.54 ± 1.35b	3.6 ± 0.36b	37 ± 0.7b	84.44 ± 0.25b	37.17 ± 0.37d	33.99 ± 0.34e
BC_{4B}	92.23	2.78 ± 0.08ej	3.92 ± 0.09e	9.4 ± 0.04ef	17.24 ± 0.02e	3.75 ± 0.38e	83.74 ± 8.37b	3.64 ± 0.36b	37.02 ± 3.7b	84.38 ± 0.84b	37.18 ± 0.54d	34.18 ± 0.34e
BC_{4C}	89.78	2.78 ± 0.08ej	4.15 ± 0.02e	10.34 ± 0.03egi	18.64 ± 0.07ef	4.08 ± 0.41e	81.89 ± 2.19b	3.62 ± 0.36b	37.16 ± 2.71b	84.43 ± 0.84b	37.28 ± 0.37d	32.3 ± 0.32e
BC_{4D}	93.31	2.74 ± 0.07ehj	3.92 ± 0.09e	9.22 ± 0.02ef	17.06 ± 0.07e	3.67 ± 0.37e	81.9 ± 0.19b	3.56 ± 0.36b	38.01 ± 3.8b	84.64 ± 0.05b	38.17 ± 0.32d	32.27 ± 0.32e
BC_{4E}	93.06	2.94 ± 0.03e	3.65 ± 0.08e	9.4 ± 0.04ef	16.7 ± 0.07e	3.62 ± 0.36e	83.74 ± 0.37b	3.61 ± 0.36b	37.99 ± 3.8b	84.56 ± 0.85b	38.07 ± 0.38d	34.05 ± 0.34e
BC_{4F}	91.65	2.76 ± 0.08ej	4.13 ± 0.01e	9.87 ± 0.09efg	18.13 ± 0.01e	4.56 ± 0.46bce	83.73 ± 8.37b	3.54 ± 0.35b	37.56 ± 3.77b	84.6 ± 0.61b	37.67 ± 0.38d	34.11 ± 0.34e
BC_{4G}	90.23	2.96 ± 0.03e	5.09 ± 0.01ef	10.45 ± 0.05egi	20.63 ± 0.07de	3.89 ± 0.39e	81.63 ± 8.16b	5.22 ± 0.52d	39.94 ± 0.98b	82.54 ± 0.83ab	40.24 ± 0.4c	31.6 ± 0.32e
BC_{4H}	88.66	2.97 ± 0.03e	5.15 ± 0.02ef	10.89 ± 0.09egi	21.19 ± 0.03d	4.08 ± 0.41be	81.36 ± 8.14b	5.21 ± 0.52d	39.28 ± 3.93b	82.42 ± 0.82ab	39.54 ± 0.41c	31.36 ± 0.01e
BC_{4I}	87.49	3.14 ± 0.03e	6.29 ± 0.04d	11.25 ± 0.13hi	23.83 ± 0.01d	5.08 ± 0.51bc	81.34 ± 8.13b	5.4 ± 0.54d	39.91 ± 1.99a	82.29 ± 0.54ab	40.26 ± 0.4c	31.28 ± 0.31e
DO_4	97.62	2.34 ± 0.02eh	4.58 ± 0.02e	9.98 ± 0.02efg	19.14 ± 0.02efg	3.69 ± 0.36e	83.46 ± 0.42b	3.64 ± 0.02b	38.66 ± 0.42a	84.47 ± 0.87b	38.2 ± 0.45d	34.12 ± 0.34e

[a]CSO, crude sardine oil; DG_1, DG_2, DG_3, and DG_4 represent the sardine oil degummed using phosphoric acid (85%, 1 mL), glacial acetic acid (99%, 1 mL), oxalic acid (10%, 5 mL), and citric acid (10%, 5 mL), respectively; NSO, neutralized oil; activated charcoal (AC), kaolin (KA), Fuller's earth (FE), cellulose powder (CE), and chitin (CH) were used individually (5% concentration to oil) as adsorbents; BC_1, BC_2, BC_3, BC_4, and BC_5 represent AC + FE used in the ratios 2.5:2.5, 4.5:0.5, 3.75:1.25, 1.25:3.75, and 0.5:4.5, respectively; BC_{4A}, BC_{4B}, BC_{4C}, BC_{4D}, and BC_{4E} represent AC/FE (1.25:3.75) at different contact times and temperatures as detailed in Table 1. Data are expressed as the mean ± standard deviation of three replicates. Means with different letters (a, b, c, etc.) in the same column indicate significant statistical difference ($p < 0.05$). Other notations are as represented under Materials and Methods.

J. Agric. Food Chem. 2015, 63, 998−1009
DOI: 10.1021/jf505127e

Table 3. Fatty Acid Profiles of Sardine Oil after Different Stages of Refining[a]

fatty acid	CSO	DG_1	DG_2	DG_3	DG_4	neutralized oil	bleached oil	deodorized oil
saturated								
14:0	13.02 ± 0.03a	13.01 ± 0.30a	13 ± 0.20a	12.86 ± 0.09b	13.11 ± 0.01c	12.28 ± 0.03d	11.62 ± 0.06e	12.91 ± 1.29c
16:0	21.65 ± 0.08a	20.65 ± 0.07b	21.02 ± 2.10c	21.41 ± 3.14d	20.89 ± 0.08e	20.94 ± 2.08e	20.11 ± 1.02f	21.8 ± 0.26g
18:0	4.23 ± 0.02a	4.34 ± 0.43b	4.36 ± 0.44c	4.37 ± 0.44d	4.32 ± 0.43e	4.81 ± 0.48b	4.29 ± 0.43f	4.31 ± 0.43d
∑SFA	41.03 ± 1.11a	40.15 ± 1.03a	40.56 ± 2.97a	40.79 ± 0.09a	40.41 ± 1.02a	40.18 ± 2.01a	38.21 ± 2.83a	40.86 ± 1.90a
monounsaturated								
16:1n-7 *trans*	0.01 ± 0.00a	0.02 ± 0.00b	0.01 ± 0.00cd	0.01 ± 0.00d	0.01 ± 0.00c	0.03 ± 0.00c	0.01 ± 0.00e	0.04 ± 0.00b
16:1n-7	13.04 ± 1.3a	13.21 ± 1.32a	13.35 ± 1.34a	13.31 ± 1.32a	13.41 ± 1.34a	13.41 ± 1.65a	12.44 ± 1.24a	13.22 ± 1.32a
18:1n-9 *trans*	0.02 ± 0.00a	0.01 ± 0.00a	0.01 ± 0.00a	0.01 ± 0.00a	0.01 ± 0.00a	0.03 ± 0.00a	0.02 ± 0.00a	0.03 ± 0.00a
18:1n-9	12.05 ± 1.20a	12.01 ± 1.20a	12 ± 1.20a	11.89 ± 1.19b	11.21 ± 1.12c	10.49 ± 1.05d	11.54 ± 0.14e	9.53 ± 0.95f
22:1n-9	3.08 ± 0.31a	3.11 ± 0.31ab	3.26 ± 0.33c	3.16 ± 0.31bd	3.24 ± 0.33c	3.1 ± 0.30ad	3.23 ± 0.32cd	2.94 ± 0.29e
∑MUFA	29.19 ± 0.91a	29.5 ± 0.95b	29.7 ± 0.97c	29.52 ± 0.95b	28.92 ± 0.89d	28.98 ± 0.20e	28.49 ± 0.86f	26.79 ± 0.68g
polyunsaturated								
18:2n-6 *trans*	0.01 ± 0.00a	0.01 ± 0.00a	0.01 ± 0.00a	0.01 ± 0.00a	0.01 ± 0.00a	0.03 ± 0.00a	0.02 ± 0.00a	0.03 ± 0.00a
18:2n-6	1.99 ± 0.20a	1.81 ± 0.18b	1.82 ± 0.18bc	1.85 ± 0.19bd	1.86 ± 0.18bd	1.89 ± 0.19cd	1.87 ± 0.19b	1.89 ± 0.19cd
20:2n-6	1.29 ± 0.13a	1.27 ± 0.13a	1.29 ± 0.13a	1.29 ± 0.13a	1.29 ± 0.13a	1.26 ± 0.13a	1.26 ± 0.13a	1.25 ± 0.13a
20:5n-3	15.48 ± 1.56a	15.08 ± 1.51b	15.31 ± 1.52c	15.41 ± 1.54a	15.24 ± 1.52c	15.02 ± 1.5b	15.25 ± 1.24c	14.67 ± 1.47d
22:5n-3	1.37 ± 0.14a	0.88 ± 0.09b	0.9 ± 0.09b	1.26 ± 0.13c	1.27 ± 0.13c	0.7 ± 0.07d	0.75 ± 0.08d	0.53 ± 0.05e
22:6n-3	4.97 ± 0.50a	5.26 ± 0.53b	5.31 ± 0.53b	5.11 ± 0.51c	5.12 ± 0.51c	5.28 ± 0.53b	5.81 ± 0.58d	5.71 ± 0.58e
∑PUFA	26.48 ± 0.67a	26.04 ± 20.6b	26.39 ± 20.64c	26.31 ± 0.63d	26.21 ± 20.62e	25.55 ± 0.55f	26.63 ± 0.69g	25.78 ± 0.58h
20:5n-3 + 22:6n-3	20.45 ± 0.06a	20.34 ± 0.03a	20.62 ± 0.06a	20.52 ± 0.05a	20.36 ± 0.04b	20.3 ± 0.03b	21.06 ± 0.11c	20.38 ± 0.04b
∑n-3 PUFA	22.11 ± 1.23a	21.92 ± 2.19b	22.23 ± 2.22c	22.09 ± 2.21a	21.95 ± 2.2b	21.71 ± 2.17d	22.1 ± 2.11a	21.57 ± 2.16e
∑n-6 PUFA	4.36 ± 0.44a	4.11 ± 0.41b	4.15 ± 0.42bc	4.21 ± 0.42cd	4.25 ± 0.43c	3.81 ± 0.38e	4.51 ± 0.45f	4.17 ± 0.41bd
∑n-3/∑n-6 PUFA	5.07 ± 1.07a	5.33 ± 0.53b	5.36 ± 0.54b	5.25 ± 0.53c	5.16 ± 0.52d	5.7 ± 2.71e	4.9 ± 0.49f	5.17 ± 0.54d
∑*trans* fatty acids	0.04 ± 0.00a	0.04 ± 0.00a	0.03 ± 0.00a	0.03 ± 0.00a	0.03 ± 0.00a	0.09 ± 0.00a	0.05 ± 0.01a	0.1 ± 0.01a

[a]Data are expressed as the mean ± standard deviation of three replicates. ∑SFA, total saturated fatty acids; ∑MUFA, total monounsaturated fatty acids; ∑PUFA, total polyunsaturated fatty acids. Means with different letters (a, b, c, etc.) in the same row indicate significant statistical difference ($p < 0.05$). ND, not detected. Minor fatty acids are not shown in the table.

J. Agric. Food Chem. 2015, 63, 998−1009
DOI: 10.1021/jf505127e

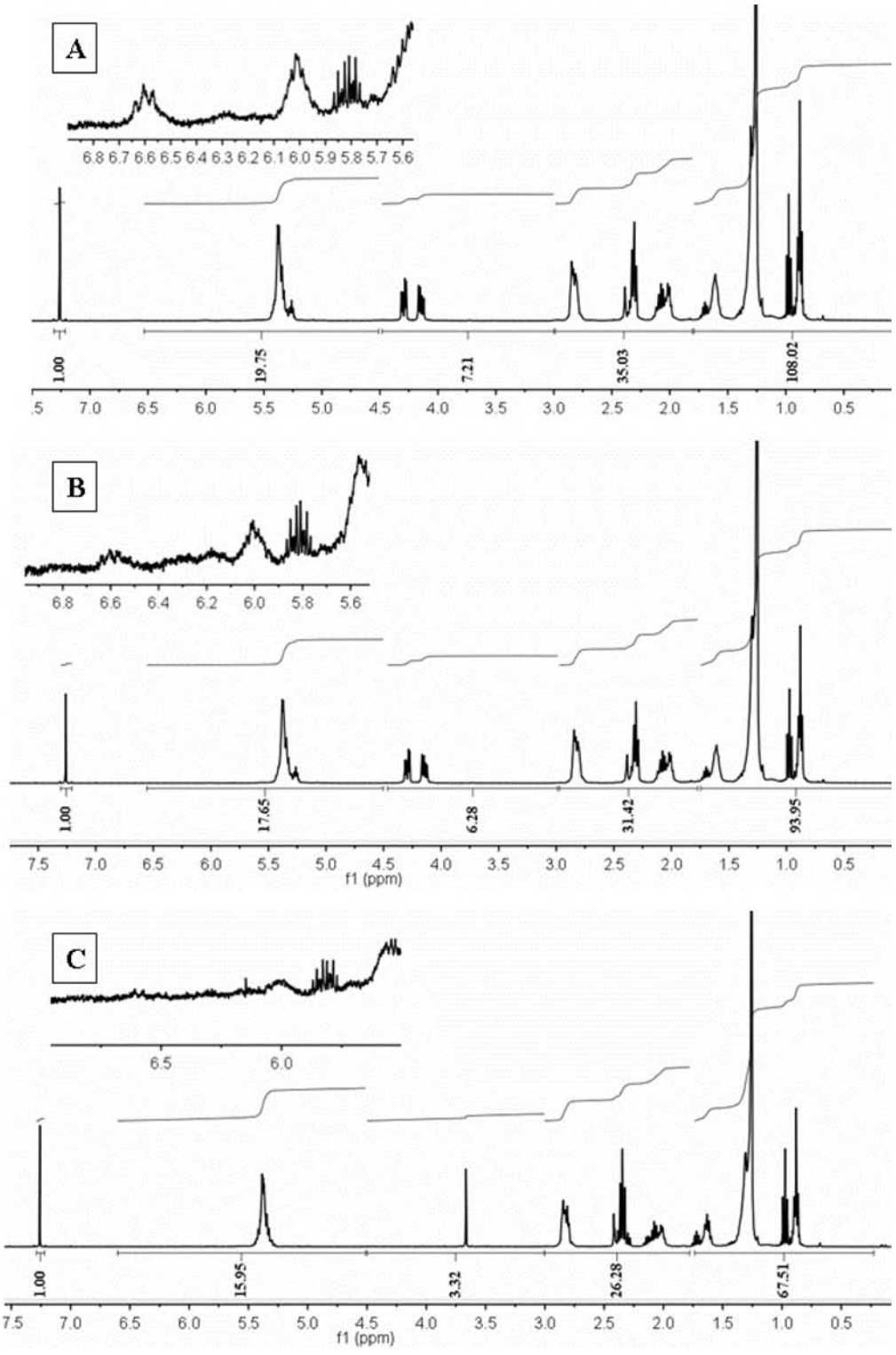

Figure 1. ^{1}H NMR spectra of the (A) crude (CSO), (B) degummed (DG_1), and (C) bleached sardine oils. (Insets) ^{1}H NMR proton signals at δ 5.2−7.0.

CSO (Figure 1). The effect of degumming using the phosphoric acid was determined by the ratio of the proton integrals of the degummed oil (DG_1) to the control oil (CSO) at the region δ 0.2−1.8 (signals exhibited by $-CH_3$ and $-CH_2-$ protons), δ 1.8−3.0 (−CH< and $-C(=O)CH_3$), δ 3.0−4.5 (free $-NH_2$ and −OH), and δ 4.5−6.5 (olefinic protons). A greater reduction in the proton integral was observed for DG_1 at these regions with 13.0 (δ 0.2−1.8), 10.3 (δ 1.8−3.0), 12.9 (δ 3.0−4.5), and 10.6 (δ 4.5−6.5) percent in relation to CSO. Overall, lesser intensity of the peak at δ 6−7 for DG_1 as compared to CSO was observed.

Neutralization of the Degummed Sardine Oil. The neutralization of DG_1 afforded a dark residue (6.6 g) with 80.4% oil yield (w/w) with respect to CSO. The neutralization step effectively reduced the FFA value of DG_1 to 3.21% (Table 2). Similarly, reduction in PV, pAV, and TOTOX values

DOI: 10.1021/jf505127e
J. Agric. Food Chem. 2015, 63, 998−1009

was observed after neutralization ($p > 0.05$) (Table 2). The reduction in the TBARS value of NSO in relation to CSO was approximately 35%. Neutralized oil was lighter ($L^* = 51.34$) and more yellowish ($b^* = 43.65$) in color than CSO. No reduction in redness ($a^* = 8.21$) indicated that the neutralization process might not have significantly removed the carotenoid pigments (Table 2). Neutralization increased the chroma values and decreased the hue angle values of the oil. The ∑SFA, ∑MUFA, and ∑PUFA did not show any significant difference ($p > 0.05$) after neutralization (Table 3).

Bleaching of the Neutralized Sardine Oil. The reduction in FFA content of NSO (13.1 and 1.6% reduction, respectively, with respect to NSO) when AC and FE were added individually indicated the effect of these adsorbents in removing the soap stock residues from NSO (Table 2). The FFA value was further reduced to <2.8% when the combinations of AC:FE at 4.5:0.5 and 1.25:3.75 (BC_2 and BC_4) were used. The FFA value exhibited a marginal increase from 2.8% (BC_4) to 3−3.1% ($BC_{4G\text{-}I}$) when a lower concentration of AC:FE (1%) was used. The reduction of PV, pAV, and TOTOX values after bleaching with individual adsorbents confirmed the capacity of AC and FE to adsorb primary and secondary oxidation products or similar compounds.[20,21] BC_4 showed maximum reduction in the PV and TOTOX values as compared to other combinations (BC_1, BC_2, BC_3, and BC_5). Similarly, maximum reductions in PV and TOTOX values were observed for BC_{4E}. Interestingly, the TOTOX value recorded an increase for $BC_{4G\text{-}I}$ that might be due to the adsorption of impurities together with the natural antioxidants present in the oil, thereby affecting the stability of the fish oil. List et al.[22] reported that the sunflower oil treated with bleaching earth (6%) had unacceptable flavor and oxidative stability relative to the bleached oil with a lower concentration of activated earth (2%). A lower TBARS value was observed when AC and FE were used individually as compared to other adsorbents studied. For the different combinations, TBARS values were in the order $BC_3 < BC_4 < BC_1 < BC_3 \sim BC_5$. Furthermore, the combination of AC and FE used at 3% as in BC_{4E} (with stirring time of 40 min at 40 °C) was found to be optimum for the TBARS reduction to the minimum.

Activated charcoal and Fuller's earth increased the lightness of the oil ($L^* = 75$ and 71, respectively). Besides, the adsorption process using AC and FE effectively reduced the a^* value (3.7), indicating a decrease in red pigment. The b^* value of the bleached oils was observed to be reduced (<40) when AC and FE were used. Among the different combinations, BC_4 exhibited an increment in L^* value and a reduction in a^* value compared to other combinations of AC and FE (Table 2). The highest L^* value (83.74) was achieved for BC_{4B} and BC_{4E}. The combination of chitosan and activated earth was earlier reported to increase the L^* value during the purification process of the salmon oil.[21] The lower a^* value of bleached oil reached ≤3.64 for 3 and 5% concentrations (BC_{4A-F}), which indicated a decrease in the red pigmentation pattern. As a consequence, the oil samples became lighter and more transparent. However, a lesser adsorbent concentration (1%) did not effectively reduce the a^* value (>5), whereas an increase in adsorbent concentration and adsorption time resulted in a more greenish color to sardine oil ($a^* \leq 3.64$). An earlier study in salmon oil revealed the reduction of carotenoid pigments such as astaxanthin and canthaxanthin during adsorption with a decrease in a^* value (redness) and an increase in $-a^*$ value (greenness) while using chitosan and activated earth as adsorbents.[21] Likewise, a greater reduction in b^* value was observed for BC_{4A-F}, which denotes a yellowish color of the bleached sardine oil. The chroma value, which represents the intensity of color, was found to be reduced for BC_{4E} (≤38), whereas the hue angle value increased with the concentration of the adsorbent. Hence, considering the above quality parameters, the combination of activated charcoal and Fuller's earth (1.25:3.75) at 3% concentration with 40 min of stirring time was found to be optimum for obtaining the BSO. The fatty acid profile of the BSO (BC_{4E}) is shown in Table 3. No significant differences were observed in the fatty acid composition of the bleached oil compared to the neutralized oil ($p > 0.05$) (Figure 2).

Spectroscopic Analyses of Sardine Oil after Bleaching. The extent of the bleaching process of the oil was further studied by ^{1}H NMR spectroscopy to understand the signals and proton integrals of the conjugated olefinic double-bond protons as impurities, which resonated at δ 4−4.5 (Figure 1). The region at δ 4−4.5 showing the peaks of conjugated double bonds were reduced for BSO. A greater reduction in the proton integral in the final bleached oil (BSO/BC_{4E}) at the ^{1}H NMR regions with 37.5 (δ 0.2−1.8), 25 (δ 1.8−3.0), 53.9 (δ 3.0−4.5), and 19.2 (δ 4.5−6.5) percent in relation to CSO was recorded. The reductions in proton integral with respect to the degummed oil were 28.1% (δ 0.2−1.8), 16.3% (δ 1.8−3.0), 47.1% (δ 3.0−4.5), and 9.6% (δ 4.5−6.5). These greater reductions in the proton integrals supported the bleaching ability of AC:FE (1.25:3.75) at 3% concentration with a stirring time of 40 min were further confirmed by their L^*, a^*, and b^* values as well as the spectral scanning data (Figure 3). The UV−vis spectra of BSO showed a reduction in their peak intensities in the region between 340 and 370 nm (Figure 3), which apparently signifies the reduction in the unsaturation and auxochromes bearing the electronegative groups. A characteristic absorption of control oil (NSO) in the visible range as shown in Figure 3 might be caused by the chromophores with conjugated π-electron systems resulting in red shifts, thereby giving an undesirable color to the fish oil. The bleaching process led to the removal of the color causing auxochrome and chromophoric systems in the treatment combinations. The absorption of the fish oils in the visible regions was apparently due to the lipid-soluble pigments or pigment-like substances bearing multiple unsaturations in their structures. This indicated that fatty acid glycerides with nonconjugated double bonds did not absorb significantly in the visible region (340−800 nm).

Deodorization of the Bleached Sardine Oil. The BSO on vacuum distillation for 1 h yielded 97.6 g of the deodorized oil with 73% yield (w/w) with respect to CSO. A reduction in FFAs after the deodorization step (DO_4) was observed (4.08%), and this might be due to the vaporization of odoriferous compounds and FFAs during the deodorization process.[8] The deodorization step reduced FFA content by up to 47% to afford an acceptable FFA level (i.e., between 1.8 and 3.5%)[13] for the refined oil. A reduction in PV, pAV, and TOTOX values was observed (Table 2) after the deodorization process. It is significant to note that PV was recorded below the threshold level of acceptance for human consumption (8 mequiv O_2/kg oil),[23] which indicated the oxidative quality index of the refined sardine oil. Thus, it is evident that the conditions used for the deodorization in the present study did not induce oxidative deterioration, which might involve the formation of ring cyclization of fatty acids and the formation of various forms of cyclic fatty acid analogues. An example of the formation of the cyclic fatty acid product 5-(2-((6-(prop-1-enyl)cyclohex-3-enyl)methyl)cyclopent-3-enyl)pentatonic acid

DOI: 10.1021/jf505127e
J. Agric. Food Chem. 2015, 63, 998−1009

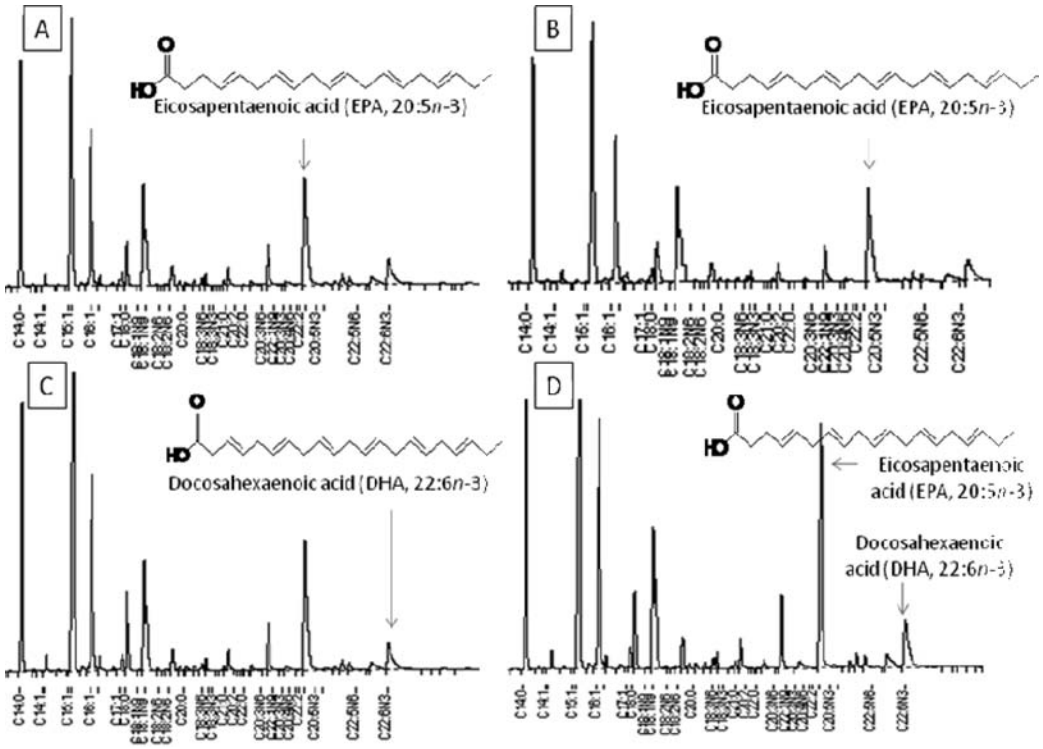

Figure 2. Fatty acid chromatogram of degummed and neutralized sardine oil treated with (A) activated charcoal (AC), (B) Fuller's earth (FE), (C) BC_4 [AC + FE in the ratio (25 g/75 g)], and (D) BC_{4E} [AC + FE in the ratio (25 g/75 g) at 3% concentration].

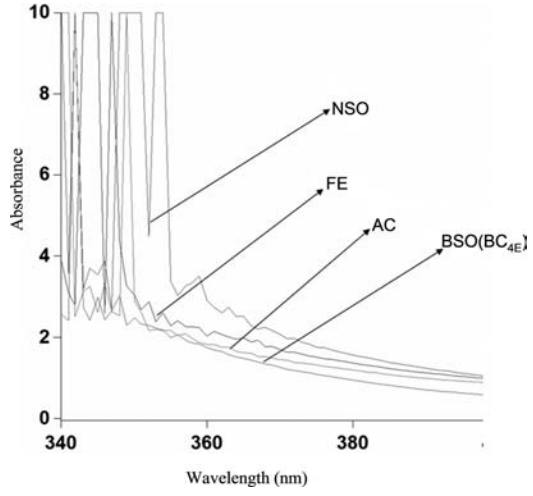

Figure 3. UV spectra of neutralized sardine oil (NSO), oil bleached with activated charcoal (AC), Fuller' earth (FE), and a combination of activated charcoal (0.75 g) plus Fuller's earth (2.25 g) at 3% concentration and 40 min of stirring time (BSO/BC_{4E}).

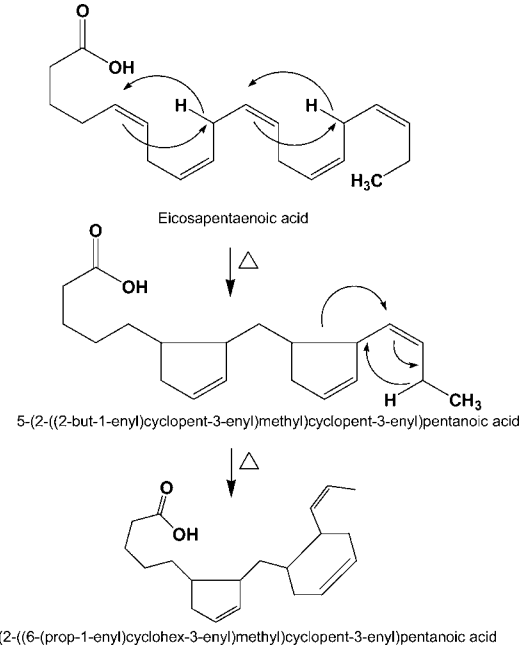

Figure 4. Poposed pathways of the formation of cyclic fatty acid analogue (5-(2-((6-(prop-1-enyl)cyclohex-3-enyl)methyl)cyclopent-3-enyl)pentanoic acid) from EPA.

via the intermediate 5-(2-((2-but-1-enyl)cyclopent-3-enyl)-methyl)cyclopent-3-enyl)pentanoic acid from eicosapentaenoic acid has been proposed under Figure 4. The reduction in the content of TBARS in the deodorized oil in relation to CSO was found to be about 40%. However, a lesser increment in L^*, a^*, and b^* values for the deodorized oil (DO_4) than in BSO confirmed the absence of formation of conjugation in the fatty acid double bonds due to heating.

The contents of ∑SFA, ∑MUFA, and ∑PUFA did not show significant difference ($p > 0.05$) between the CSO and deodorized (refined) sardine oil (Table 3). An insignificant reduction ($p > 0.05$) in n-3 PUFA (decrease of 2.4%) and DHA (decrease of 5.2%) contents was observed in DO_4 as compared with CSO. A study by Sathivel et al.[13] reported an approximate 19% reduction in the n-3 PUFAs of catfish viscera after the oil refining processes including degumming, neutralizing, bleaching, and deodorization. The share of EPA and DHA in the refined fish oil was 20%, which was greater than earlier cited[24] for crude oils of five commercially important species of Brazilian fish, namely, sardine, croaker, tilapia, curimbata, and

DOI: 10.1021/jf505127e
J. Agric. Food Chem. 2015, 63, 998−1009

Table 4. Volatile Compounds Obtained during the Deodorization Process of the Sardine Oil[a]

peak	t_R (min)	compound	base peak[b]	mol wt [M^+]
DO_1				
1	5.880	octamethyl cyclotetrasiloxane[c]	281	284
2	8.201	decamethyl cyclopentasiloxane[c]	73	358
3	10.577	dodecamethyl cyclohexasiloxane[c]	73	432
4	12.723	tetradecamethyl cycloheptasiloxane[c]	73	505
5	14.633	hexadecamethyl cyclooctasiloxane[c]	73	489
DO_2				
1	9.19	dodecane	57	207
2	11.81	tetradecene	55	343
3	11.91	tetradecane	57	281
4	12.667	tetradecamethyl cycloheptasiloxane[c]	73	505
5	13.163	pentadecane	57	212
DO_3				
1	8.015	(*E*,*Z*)-2,6-nonadienal	41	138
2	8.965	(*E*,*E*)-2,4-nonadienal	81	139
3	10.046	(*E*,*E*)-2,4-decadienal	81	341
4	14.748	*E*-2-octadecadecen-1-ol	55	206
DO_4				
1	5.819	(*E*,*E*)-2,4-heptadienal	81	111
2	10.416	(*E*,*E*)-2,4-decadienal	81	153

[a] DO_1, DO_2, DO_3, and DO_4, distillates obtained at 5, 15, 30, and 60 min, respectively, during the deodorization process of the sardine oil. The prefixes (*E*)- (*Z*)- denote *trans*- and *cis*-isomers, respectively. [b] Base peak in GC-MS spectra refers to the *m*/*e* peak with 100% intensity. [c] The siloxane derivatives of fatty acids were formed by reaction between the GLC column stationary phase and the fatty acid reaction products.

shrimps (11.6−13.4%). The increase in the content of *trans* fatty acids was statistically insignificant ($p > 0.05$) after the process of deodorization, which might be due to the exposure of fatty acid at the high temperature used during the deodorization step. The contents of *trans* fatty acids in the refined oil obtained in this study were recorded below the threshold limit (1.0%) as prescribed by EU guidelines.[8] An increase in the human dietary n-3/n-6 fatty acid ratio observed for deodorized oil showed its ability to prevent coronary heart disease by reducing plasma lipids and to reduce cancer risk.[16] In this study, the deodorized oil with superior qualities was obtained with the utilization of a lesser process time as compared to the conditions utilized by Fournier et al.[2]

Gas Chromatographic−Mass Spectroscopic Analysis of the Volatile Components during Deodorization. Table 4 lists the volatile components identified in the fish oil during the deodorization process with acetic acid treatment after 5, 15, 30, and 60 min of distillation. The distillate obtained after 5 min (as in DO_1) showed siloxane derivatives such as octamethyl cyclotetrasiloxane, decamethyl cyclopentasiloxane, dodecamethyl cyclohexasiloxane, tetradecamethyl cycloheptasiloxane, and hexadecamethyl cycloocatasiloxane (Table 4). The appearance of these siloxane derivatives could be attributed to the reaction between the stationary phases of the GC reverse phase column with the eluted components. GC-MS spectra of the distillate obtained after 15 min (DO_2) showed the presence of volatiles, mainly alkanes/alkenes (dodecane t_R 9.19 min, tetradecene t_R 11.81 min, tetradecane t_R 11.91 min, pentadecane t_R 13.16 min). The dodecane was earlier identified in menhaden fish oil, whitefish oil, and tuna oil,[6,25,26] whereas pentadecane was identified in the menhaden fish oil and salmon oil.[6,27] Pentadecane was the

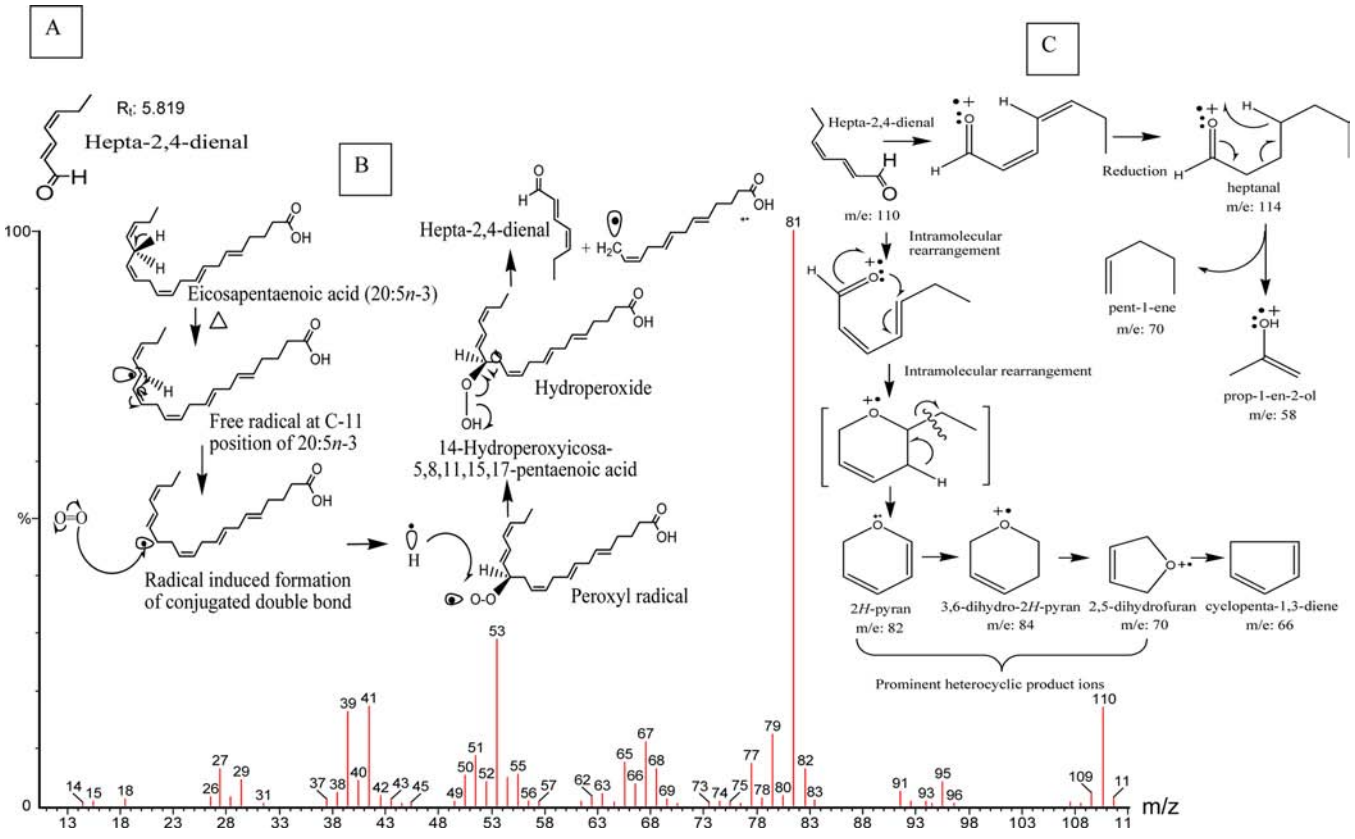

Figure 5. (A) GC-MS spectrum of 2,4-heptadienal; (B) free radical induced formation of 2,4-heptadienal from n-3 polyunsaturated fatty acids (EPA, 20:5n-3); (C) poposed GC-MS fragmentation pathways for generation of fragment ions during EI-MS analysis of 2,4-heptadienal from DO-04.

DOI: 10.1021/jf505127e
J. Agric. Food Chem. 2015, 63, 998−1009

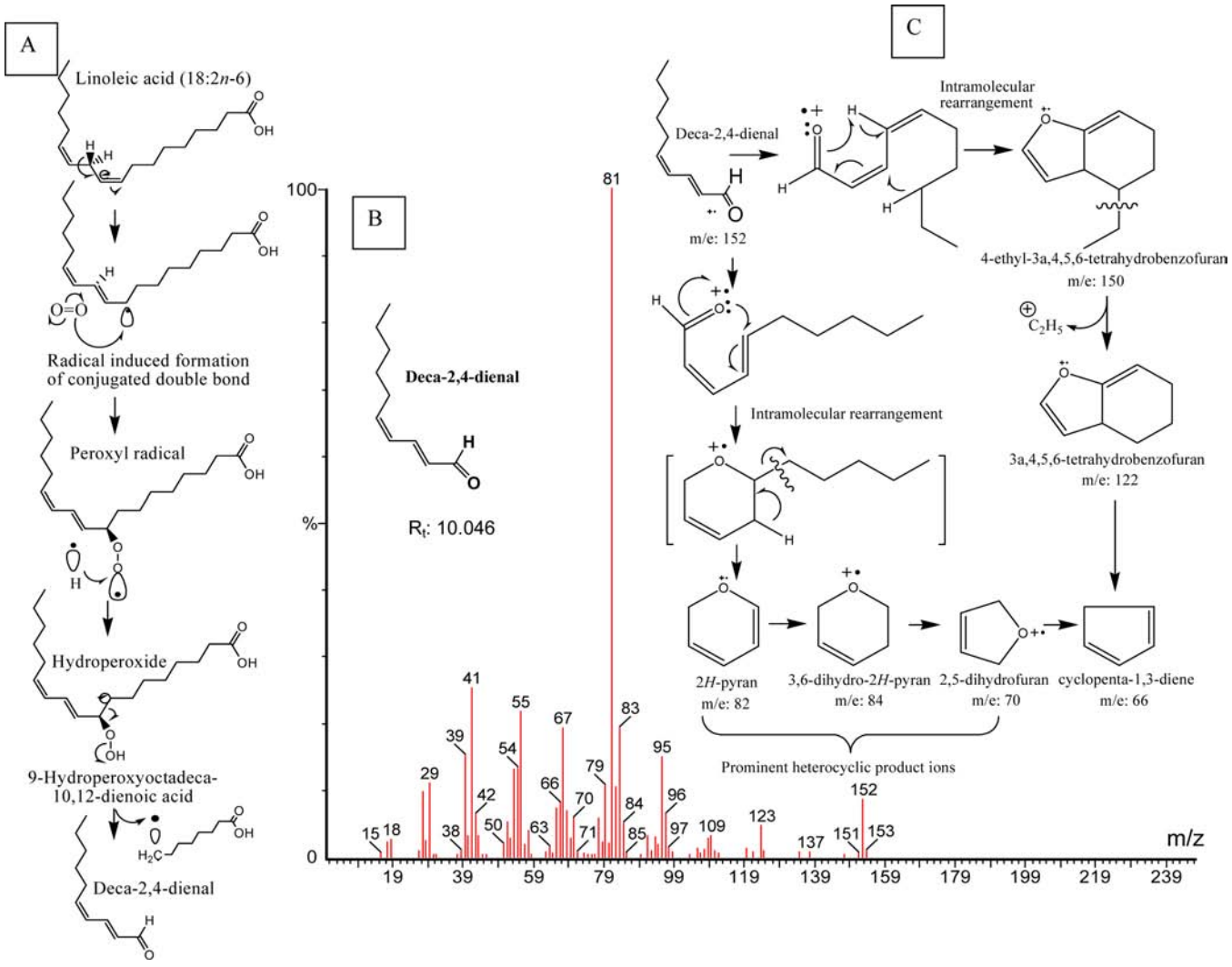

Figure 6. (A) Free radical induced formation of 2,4-decadienal from n-6 polyunsaturated fatty acids (linoleic acid, 18:2n-6); (B) GC-MS spectrum of 2,4-decadienal; (C) proposed GC-MS fragmentation pathways for generation of fragment ions during EI-MS analysis of 2,4-decadienal from DO-04.

major *n*-alkane found in oil sardines and horse mackerel oil.[28] GC-MS spectra of the distillate after 30 min (DO_3) showed four abundant aldehydic volatile compounds, namely, (*E*,*Z*)-2,6-nonadienal, (*E*,*E*)-isomers of 2,4-nonadienal and 2,4-decadienal, and an alcohol, *E*-2-octadecadecen-1-ol (Table 4). Aldehydes play an important role in many food products and are responsible for a wide range of oxidized flavors.[29] Milo and Grosch[30] demonstrated that (*E*,*Z*)-2,6-nonadienal and (*E*,E)-2,4-decadienal were the key aroma compounds of raw and boiled salmon. GC-MS spectra of the distillate obtained after 60 min (DO-04) demonstrated the presence of two prominent aldehydes, namely, (*E*,*E*)-isomers of 2,4-heptadienal and 2,4-decadienal. Rahimabadi[31] recorded (*E*,*Z*)-2,6-nonadienal and (*E*,*E*)-2,4-heptadienal on the distillation of raw narrow-barred Spanish mackerel (*Scomberomorous commerson*). Volatiles such as (*E*,*Z*)-2,6-nonadienal and (*E*,*E*)-2,4-decadienal were separated earlier from cod liver oil by means of deodorization at 200 °C for 2 h.[32] (*E*,*Z*)-2,6-Nonadienal was identified as the compound contributing to the green and melon flavors encountered in fish oils.[7] Furthermore, (*E*,*E*)-2,4-heptadienal was reported as strong fat odor and fish smell inducing compound in the oil.[33] The presence of these unsaturated volatile aldehydes in the fish oil was apparently due to the greater contents of PUFAs. A schematic representation of the peroxidation of polyunsaturated fatty acids (eicosapentaenoic and linoleic acids have been taken as a model systems) leading to the formation of aldehydes is shown in Figures 5 and 6.

It is challenging to characterize the long-chain fatty aldehydes (in free forms) within biological matrices, apparently due to their greater reactive properties. These highly unstable compounds react with nucleophiles in the matrix leading to their rapid metabolism. Of the fatty aldehydes, 2,4-decadienal (particularly from the n-6 fatty acids) and hepta-2,4-dienal (from n-3 fatty acids) are of greater importance due to their contribution to the characteristic unpleasant odor of the oil.

The hydroperoxides formed by free radical induced autoxidation process of n-3 polyunsaturated acids are highly unstable and undergo prompt β-scission to form carbonyl compounds such as hepta-2,4-dienal. For example, 14-hydroperoxyicosa-5,8,11,15,17-pentaenoic acid has been demonstrated to be formed from EPA (20:5n-3) by free radical induced formation of conjugated double bond, which thereafter form hepta-2,4-dienal as the predominant reaction product. EI-induced mass spectrometry of hepta-2,4-dienal with a conjugated diene system yields a characteristic molecular ion at *m*/*e* $[M]^+$ 110 and ragment ions at *m*/*e* 114 (heptanal), *m*/*e* 70 (pent-1-ene),

DOI: 10.1021/jf505127e
J. Agric. Food Chem. 2015, 63, 998−1009

and *m/e* 58 (prop-1-en-2-ol) due to reduction of the molecular ion followed by intramolecular McLafferty type rearrangement. The *β*-cleavage of heptanal (*m/e* 114) with the gain of *γ*-hydrogen atom led to the formation of pent-1-ene and prop-1-en-2-ol. Hepta-2,4-dienal generates prominent heterocyclic product ions with *m/e* 82 (2*H*-pyran), *m/e* 84 (3, 6-dihydro-2*H*-pyran), and *m/e* 70 (2,5-dihydrofuran) (Figure 5) by intramolecular rearrangement of the parent molecular ion.

The diene n-6 polyunsaturated fatty acids have been shown to be good precursors in some defined oxidative conditions to form deca-2,4-dienal along with other reaction products. To rationalize the formation of aldehydic products, as is the case for 2,4-decadienal, linoleic acid (18:2n-6) has been taken as an example. This n-6 dienoic fatty acid may undergo oxidation via 9-hydroperoxyoctadeca-10,12-dienoic acid, forming the fatty acid aldehyde with a conjugated diene system (2,4-decadienal) as the major product. The conjugated unsaturated aldehydes may undergo changes by autoxidation, producing shorter chain aldehydes and other volatile compounds (data not shown). EI-induced mass spectrometry of deca-2,4-dienal yields characteristic molecular ion at *m/e* $[M]^+$ 152 and fragment ions at *m/e* 150 (4-ethyl-3a,4,5,6-tetrahydrobenzofuran) due to intramolecular rearrangement and at *m/e* 122 (3a,4,5,6-tetrahydrobenzofuran) due to the loss of ethyl ion from the former. In particular, deca-2,4-dienal generates prominent heterocyclic product ions with *m/e* 82 (2*H*-pyran), *m/e* 84 (3,6-dihydro-2*H*-pyran), and *m/e* 70 (2,5-dihydrofuran), as demonstrated for hepta-2,4-dienal (Figure 6).

Other volatile decomposition products of hydroperoxides reported in severely oxidized fish oil were alkatrienals, mainly 2,4,7-decatrienal (PV > 70 mequiv/kg).[34] However, in the present study no trace of alkatrienal in the distillate was observed. Thus, a distillation period of 1 h could optimally be able to remove the major volatile components from the sardine oil.

The crude oil obtained from *S. longiceps* was refined by the stepwise process of degumming, bleaching, and deodorization. The effective degumming agent was found to be 1% phosphoric acid, which could keep the PV, pAV, TOTOX, and TBARS values below threshold limits. The utilities of NMR-based proton signal characteristics as new analytical tools to understand the signature peaks and relative abundance of different fatty acids and monitoring the refining process of fish oil have been demonstrated. The region between *δ* 4 and 4.5 in the ^{1}H NMR spectra was taken into account to explain the bleaching process of the oil, and the characteristic signals at *δ* 1.8−3.0, 3.0−4.5, and 4.5−6.5 were considered as indicator regions to explain the variability of the oil qualities under different treatment combinations during the degumming process. A significant reduction in the contents of hydrocarbon functionalities (as shown by the decrease in proton integral in the characteristic ^{1}H NMR region) was demonstrated by using 1% H_3PO_4 during the course of the degumming process. A combination of activated charcoal and Fuller's earth (1.25:3.75, 3% w/w, contact time of 60 min) was found to be efficient in bleaching the sardine oil and to eliminate the colored impurities. This study also demonstrated that unfavorable odor-causing components, particularly low molecular weight carbonyl compounds and alcohols, could successfully be removed by distillation under vacuum with 0.25 N acetic acid (100 °C). A four-stage refinement process of sardine oil resulting in a significant improvement in nutritional values and fish oil characteristics has been demonstrated in the present study. This study is significant in the quest to obtain refined marine fish oil with greater nutritional and oxidative quality for use in the food and pharmaceutical industries.

AUTHOR INFORMATION

Corresponding Author

*(K.C.) Phone: +91-484-2394867. Fax: +91-484-2394909. E-mail: kajal_cmfri@yahoo.com.

Funding

This work is supported by funding under the Department of Science and Technology (SR/S0/HS-0124/2012), New Delhi, India.

Notes

The authors declare no competing financial interest.

ACKNOWLEDGMENTS

We are thankful to the Indian Council of Agricultural Research, New Delhi, for providing facilities to carry out the work. We thank the Director, Central Marine Fisheries Research Institute, for support. We alsao thank the Head, Marine Biotechnology Division, Central Marine Fisheries Research Institute, for facilitating the research activity.

ABBREVIATIONS USED

FFA, free fatty acid; PV, peroxide value; pAV, *para*-anisidine value; TOTOX, total oxidation; TBARS, thiobarbituric acid reactive species; ^{1}H NMR, proton nuclear agnetic resonance; PUFA, polyunsaturated fatty acids; EPA, eicosapentaenoic acid; DHA, docosahexaenoic acid; TAG, triacylglycerides; DEPT, distortionless enhancement by polarization transfer; CSO, crude sardine oil; DG_1, oil degummed with phosphoric acid acid; DG_2, oil degummed with oxalic acid; DG_3, oil degummed with citric acid; DG_4, oil degummed with acetic acid; NSO, neutralized sardine oil; AC, activated charcoal powder; KL, kaolin light; FE, Fuller's earth; CP, cellulose powder; CH, chitin purified powder; BSO, bleached sardine oil; ANOVA, analysis of variance (ANOVA); SPSS, Statistical Program for Social Sciences; FAME, fatty acid methyl esters; FID, flame ionization detector; MDA, malondialdehyde; MDAEQ, malondialdehyde equivalent compounds; AOCS, American Oil Chemists' Society; DO, deodorized oil

REFERENCES

(1) El-Badry, A. M.; Graf, R.; Clavien, P. A. Omega-3-omega 6: what is right for the liver? *J. Hepatol.* **2007**, *47*, 718−725.

(2) Fournier, V.; Destaillats, F.; Hug, B.; Golay, P. A.; Joffre, F.; Juaneda, P.; Semon, E.; Dionisi, F.; Lambelet, P.; Sebedio, J. L.; Berdeaux, O. Quantification of eicosapentaenoic and docosahexaenoic acidgeometrical isomers formed during fish oil deodorization by gas−liquid chromatography. *J. Chromatogr., A* **2007**, *1154*, 353−359.

(3) Morais, M. M.; Pinto, L. A. A.; Ortiz, S. C. A.; Crexi, V. T.; Silva, R. L.; Silva, J. D. Study of fish oil refining process. *Rev. Inst. Adolfo Lutz* **2001**, *60* (1), 23−33.

(4) Menegazzo, M. L.; Petenuci, M. E.; Fonseca, G. G. Production and characterization of crude and refined oils obtained from the co-products of Nile tilapia and hybrid sorubim processing. *Food Chem.* **2014**, *157*, 100−104.

(5) Chang, H. R.; Assenijevic, D.; Pechere, J. C.; Pigaet, P. F.; Mensi, N.; Gisardier, L.; Dalloo, A. G. Dietary supplementation of fish oil enhances *in vivo* synthesis of tumour necrosis factor. *Immunol. Lett.* **1992**, *34* (1), 13−18.

(6) Hsieh, T. C. Y.; Williams, S. S.; Vejaphan, W.; Meyers, S. P. Characterization of volatile components of menhaden fish (*Brevoortia tyrannus*) oil. *J. Am. Oil Chem. Soc.* **1989**, *66*, 114−117.

DOI: 10.1021/jf505127e
J. Agric. Food Chem. 2015, 63, 998−1009

(7) Karahadian, C.; Lindsay, R. C. Evaluation of compounds contributing characterizing fishy flavors in fish oils. *J. Am. Oil Chem. Soc.* **1989**, *66*, 953−960.
(8) Ceriane, R.; Meirelless, J. A. Formation of trans PUFA during deodorization of canola oil: A study through computational simulation. *Chem. Eng. Process.* **2007**, *46*, 375−385.
(9) *Official Methods and Recommended Practices of the American Oil Chemists' Society*; Firestone, D., Ed.; AOCS: Champaign, IL, USA, 1989.
(10) AOCS method Ca 5a-40. *Official Methods and Recommended Practices of the American Oil Chemists' Society*, 5th ed.; AOCS: Champaign, IL, USA, 1998.
(11) Shahidi, F.; Wanasundara, U. Methods for measuring oxidative rancidity in fats and oils. In *Food Lipids: Chemistry, Nutrition and Biotechnology*; Akoh, C. C., Min, D. B, Eds.; Dekker: New York, 2002.
(12) Buege, J. A.; Aust, S. D. Microsomal lipid peroxidation methods. *Enzymology* **1978**, *52*, 302−310.
(13) Sathivel, S.; Prinyawiwatkul, W.; King, J. M.; Grimm, C. C.; Lloyd, S. Oil production from catfish viscera. *J. Am. Oil Chem. Soc.* **2003**, *80* (4), 378−382.
(14) Chakraborty, K.; Paulraj, R. Selective enrichment of *n*-3 polyunsaturated fatty acids with C18-C20 acyl chain length from sardine oil using *Pseudomonas fluorescens* MTCC 2421 lipase. *Food Chem.* **2009**, *114*, 142−150.
(15) Igarashi, T.; Aursand, M.; Sacchi, R.; Paolillo, L.; Nonaka, M.; Wada, S. Determination of docosahexaenoic acid and n-3 fatty acids in refined fish oils by ^{1}H-NMR spectroscopy: IUPAC inter laboratory study. *J. AOAC Int.* **2002**, *85* (6), 1341−1354.
(16) Vidal, N. P.; Manzanos, M. J.; Goicoechea, E.; Guillén, M. D. Quality of farmed and wild sea bass lipids studied by ^{1}H-NMR: usefulness of this technique for differentiation on a qualitative and a quantitative basis. *Food Chem.* **2012**, *135*, 1583−1591.
(17) Luterotti, S.; Franko, M.; Bicanic, D. Ultrasensitive determination of β-carotene in fish oil-based supplementary drugs by HPLC-TLS. *J. Pharm. Biomed. Anal.* **1999**, *21*, 901−909.
(18) Crexi, V. T.; Monte, M. L.; Soares, L. A. S.; Pinto, L. A. A. Production and refinement of oil from carp (*Cyprinus carpio*) viscera. *Food Chem.* **2010**, *119*, 945−950.
(19) Siddiqui, N.; Sim, J.; Silwood, C. J. L.; Toms, H.; Iles, R. A.; Grootweld, M. Multicomponent analysis of encapsulated marine oil supplements using high-resolution ^{1}H and ^{13}C NMR techniques. *J. Lipid Res.* **2003**, *44* (12), 2406−2427.
(20) Rossi, M.; Gianazza, M.; Alamprese, C.; Stanga, F. The role of bleaching clays and synthetic silica in palm oil physical refining. *Food Chem.* **2003**, *82* (2), 291−296.
(21) Huang, J.; Sathivel, S. Purifying salmon oil using adsorption, neutralization, and a combined neutralization and adsorption process. *J. Food Eng.* **2010**, *96* (1), 51−58.
(22) List, G. R.; Evans, C. D.; Moser, H. A. Flavor and oxidative stability of northern-grown sunflower seed oil. *J. Am. Oil Chem. Soc.* **1972**, *49* (5), 287−292.
(23) Boran, G.; Karacam, H.; Boran, M. Changes in the quality of fish oils due to storage temperature and time. *Food Chem.* **2006**, *98*, 693−398.
(24) Luzia, L. A.; Sampaio, G. R.; Castellucci, C. M. N.; Torres, E. A. F. S. The influence of season on the lipid profiles of five commercially important species of Brazilian fish. *Food Chem.* **2003**, *83* (1), 93−97.
(25) Josephson, D. B. Seafood. In *Volatile Compounds in Foods and Beverages*; Maarse, H., Ed.; Dekker: New York, 1991; pp 179−202.
(26) Crawford, L.; Kretsch, M. J. GC-MS identification of the volatile compounds extracted from roasted turkeys fed a basal diet supplemented with tuna oil some comments on fishy flavor. *J. Food Sci.* **1976**, *41* (6), 1470.
(27) Josephson, D. B.; Lindsay, R. C.; Stuiber, D. A. Identification of compounds characterizing the aroma of fresh whitefish (*Coregonus clupeaformis*). *J. Agric. Food Chem.* **1983**, *31*, 326−330.
(28) Moffat, C. F.; McGill, A. S.; Hardy, R.; Anderson, R. S. The production of fish oils enriched in polyunsaturated fatty acids-containing triglycerides. *J. Am. Oil Chem. Soc.* **1995**, *70*, 133−138.
(29) Vejaphan, W.; Hsieh, T. C. Y.; Williams, S. S. Volatile flavor components from boiled crayfish (*Procambarus clarkii*) tail meat. *J. Food Sci.* **1988**, *3* (6), 1666−1670.
(30) Milo, C.; Grosch, W. Changes in the odorants of boiled salmon and cod as affected by the storage of the raw material. *J. Agric. Food Chem.* **1996**, *44*, 2366−2371.
(31) Rahimabadi, Z.; Bakar, J.; Che Man, Y. B.; Hamid, A. N.; Arshadi, A. The impact of lipid content, cooking and reheating on volatile compounds found in narrow-barred Spanish mackerel (*Scomberomorous commerson*). *Iran. J. Fish. Sci.* **2011**, *10* (2), 336.
(32) Karahadian, C.; Lindsay, R. C. Low temperature deodorizations of fish oils with volatile acidic and basic steam sources. *J. Am. Oil Chem. Soc.* **1990**, *67* (2), 85−91.
(33) Roh, H. S.; Park, J. Y.; Park, S. Y.; Chun, B. S. Isolation of off flavours and odours from tuna fish oil using supercritical carbon dioxide. *Biotechnol. Bioprocess Eng.* **2006**, *11*, 496−502.
(34) Ke, P. J.; Ackman, R. G.; Linke, B. A. Autoxidation of polyunsaturated fatty compounds in mackerel oil: formation of 2,4,7-decatrienals. *J. Am. Oil Chem. Soc.* **1975**, *52*, 349−353.

DOI: 10.1021/jf505127e
J. Agric. Food Chem. 2015, 63, 998−1009

difficult to establish scientifically.[15,16,24,27] Moreover, comparative studies on the sensory quality of conventional and organic strawberries are rather scarce, and studies investigating strawberry chemical composition usually concentrate on restricted compound groups such as polyphenols or volatile compounds.

In this study, three strawberry cultivars grown both conventionally and organically were subjected to nontargeted metabolite profiling analysis with liquid chromatography connected with negative electrospray ionization in a quadrupole−time-of-flight−mass spectrometer (LC-qTOF-ESI-MS) and to descriptive sensory evaluation by a trained panel in a sensory laboratory. Metabolite and sensory data were tested statistically to investigate the dependence of strawberry metabolome on cultivar and farming practice and to examine the effects of cultivar, farming practice, and chemical composition on the sensory quality of strawberry.

MATERIALS AND METHODS

Strawberries. Samples from three strawberry (*Fragaria* × *ananassa* Duch.) cultivars, 'Bounty' (B), 'Jonsok' (J), and 'Polka' (P), were collected from both conventional (CON) and organic (OR) fields in northern Savonia, eastern Finland, in June−July 2013. The farming locations were Leppävirta (62.30° N, 27.475° E; J-CON and P-CON), Kaavi (62.586° N, 28.295° E; B-CON), and Lapinlahti (63.216° N, 27.232° E, B-OR, J-OR, and P-OR). Organic cultivation was implemented according to EU Council Regulation (EC 834/2007). The collected berries were in the same, fully mature stage and grown approximately in the same compass direction. Of each cultivar (conventional and organic), ∼7 kg was harvested; ∼2 and ∼5 kg were used for metabolome analysis and sensory evaluation, respectively. After harvesting, pooled whole berry samples were immediately placed on ice and frozen as soon as possible. Berries were stored at −20 °C until further processing.

Nontargeted Metabolite Profiling. *Sample Preparation.* For the metabolite extraction, 10 frozen berries (81.46−149.09 g) for each cultivar × farming practice combination were gently thawed in a microwave oven (defrost setting, 1.5 min; AM Kodinkoneet Inc., Helsinki, Finland) and homogenized with a stick blender. Chemical compounds were extracted from pureed strawberries with 80% methanol; for 10 g of strawberry puree, 30 mL of methanol was used. Suspensions were quickly vortexed and extracted in a horizontal shaker (Unimax 2010, Heidolph Instruments, Schwabach, Germany) at 400 rpm for 15 min at room temperature. Extracts were filtered through a gauze (Mölnlycke Health Care, Gothenburg, Sweden) and centrifuged (Centrifuge 5810R, Eppendorf, Hamburg, Germany) at 3220*g* for 5 min. The clarified supernatants were stored at −75 °C until analysis. Prior to the metabolite analysis, samples were again centrifuged and filtered (Acrodisc 0.22 μm PTFE filter, PALL, Port Washington, NY, USA).

The total phenolic contents of strawberry extracts were measured with the Folin−Ciocalteu method,[28] with some modifications. Briefly, 200 μL of strawberry extract dilution (1:10 or 1:20) was combined with 1000 μL of 10% (v/v) Folin−Ciocalteu reagent (VWR International, Darmstadt, Germany) and 800 μL of 7.5% (w/v) Na_2CO_3 (Sigma-Aldrich, St. Louis, MO, USA) solution; the reagent mixture was incubated at room temperature for 60 min and vortexed every 20 min. The mixture absorbance was measured at 765 nm (Ultrospec 2000, Pharmacia Biotech, Uppsala, Sweden), and the total phenolic content was calculated as gallic acid (GA) (Sigma-Aldrich) equivalent according to a standard curve (0.01, 0.03, 0.05, 0.07, and 0.1 mg GA/mL).

LC-MS Conditions. The samples were analyzed by LC-qTOF-ESI-MS (Agilent Technologies, Waldbronn, Karlsruhe, Germany) that consisted of a 1290 LC system, a Jetstream electrospray ionization (ESI) source, and a 6540 UHD accurate-mass qTOF spectrometer. The samples were analyzed with reversed phase (RP) chromatographic separation, and data were acquired in negative electrospray ionization (ESI−). The sample tray was kept at 4 °C during the analysis.

Two microliters of the sample solution was injected onto a column (Zorbax Eclipse XDB-C18, 2.1 × 100 mm, 1.8 μm) (Agilent Technologies, Palo Alto, CA, USA) kept at 50 °C. Mobile phases, delivered at 0.4 mL/min, consisted of water (eluent A) and methanol (eluent B) (Sigma-Aldrich), both containing 0.1% (v/v) of formic acid (Sigma-Aldrich). The following gradient profile was employed: 0−10 min, 2 → 100% B; 10−14.5 min, 100% B; 14.5−14.51 min, 100 → 2% B; 14.51−16.5 min, 2% B.

A Jetstream ESI source was operated in negative ionization mode. The conditions were as follows: drying gas temperature, 325 °C, and flow, 10 L/min; sheath gas temperature, 350 °C, and flow, 11 L/min; nebulizer pressure, 45 psi; capillary voltage, 3500 V; nozzle voltage, 1000 V; fragmentor voltage, 100 V; and skimmer, 45 V. For data acquisition, 2 GHz extended dynamic range mode was used, and the instrument was set to acquire over m/z 20−1600. For automatic data-dependent MS/MS analyses, precursor isolation width was 1.3 Da, and from every precursor scan cycle, the four most abundant ions were selected for fragmentation. Collision energies were 10, 20, and 40 V in subsequent runs. Continuous mass axis calibration was performed by monitoring two reference ions from an infusion solution throughout the runs. The reference ions were m/z 112.985587 and 966.000725.

Data Processing. Initial data processing was performed using MassHunter Qualitative Analysis B.05.00 (Agilent Technologies, Palo Alto, CA, USA). Ions were extracted to compounds exhibiting isotopic peaks, dimers, and common adducts. Mass Profiler Professional software (version 2.2, Agilent Technologies, Palo Alto, CA, USA) was used for compound alignment. Noise and low-abundance metabolites were removed from the data matrix according to their abundance and appearance frequency in the samples. The final data set contained 3669 molecular features. For the comparison of the sample groups, the data matrix was exported to Excel and filtered according to their maximum peak area value, indicating high relative abundance in one or more sample types focusing on the 131 most intense compound signals. After initial reduction, preliminary partial least-squares regression (PLS) analysis (Unscrambler 9.8, Camo Process AS, Oslo, Norway), using molecular features as *X*-variables, that is, predictors, and sensory properties as *Y*-variables, that is, responses, was performed to perceive the most relevant compounds in terms of sensory characteristics; this resulted in 60 final entities, which were then subjected to spectral inspection and identification.

Principal component analysis (PCA) (Simca 13.0, Umeå, Sweden) was utilized to monitor the relationship between samples and sample replicates in their metabolite profiles. Hierarchical clustering analysis with heat map representation (TM4Microarray Software Suite, available at www.tm4.org/mev.html; algorithm according to Eisen et al.[29]) was applied to analyze and display the similarity of sample replicates and compound accumulation patterns and to visualize the differences in normalized metabolite signal abundances between sample types.

The identification of metabolites was performed on the basis of the fragmentation patterns in the data-dependent MS/MS acquisition. The MS/MS data and the molecular masses were compared against The METLIN Metabolite Database (http://metlin.scripps.edu/), SciFinder (https://scifinder.cas.org), Dictionary of Natural Products (http://dnp.chemnetbase.com/), or earlier published work describing fragmentation patterns.

Sensory Analyses. *Sample Preparation.* For sensory analyses, 200 g of frozen strawberries/cultivar × farming practice combination was gently thawed in a microwave oven (defrost setting, 120 W, 2.5 min; Rosenlew, Stockholm, Sweden). Thawed berries were homogenized with a stick blender, and 30 g of strawberry puree was measured into 50 mL beakers. The beakers were covered with small watch glasses, and the samples were kept at room temperature to stabilize the headspace and to reach the serving temperature (∼20 °C).

Sensory Panel. The descriptive profiling was carried out with 15 voluntary assessors familiar with sensory profiling. Assessors were known to be able to rank taste solutions and recognize flavor differences and odor samples.

DOI: 10.1021/jf505183j
J. Agric. Food Chem. 2015, 63, 1010−1019

Table 1. Attributes, Definitions, and References Used in Sensory Evaluations

attribute	description	reference	intensity
orosensory			
total intensity of flavor	perceived first expression of flavor		
sourness	taste of acids	0.1% citric acid	8
bitterness	bitter taste	0.07% caffeine	8
astringency 1	soft, mouth-drying mouthfeel	0.1% $AlNH_4(SO_4)_2$	8
astringency 2	rough, sharp mouthfeel	0.1% $Al_2(SO_4)_3$	8
sweetness	taste of sugars and other sweeteners	2% sucrose	8
off-flavor	flavors that are not innate for strawberries		
odor			
total intensity of odor	perceived first expression of odor		
fruity	an ester-like odor	5 mL of 10 ppm ethyl butyrate	7
green	freshly cut grass, leaves, or vegetables	1 μL of 200 ppm *cis*-3-hexenol	9
strawberry-like		1 μL of wild strawberry aroma concentrate (Roberts, Turku, Finland)	8
off-odor	odors that are not innate for strawberries		

Panel Training. The panelists were trained according to ISO 8586 standard. Descriptions for strawberry samples were adapted from Hakala et al.[24] and Sandell et al.[30] In four 1 h sessions, assessors were trained to recognize and evaluate the intensity of seven orosensory attributes and five odor attributes in reference samples (Table 1) and in strawberry puree samples.

Intensity Evaluations. The sensory evaluations were performed in December 2013 in a sensory laboratory (ISO 8589). Three parallel evaluation sessions were organized, and each panelist assessed the same six-sample set in each session. The sample set consisted of three cultivars cultivated both conventionally and organically (B-CON, B-OR, J-CON, J-OR, P-CON, and P-OR). Sample cups were coded with three-digit numbers, and the sample order was randomized. The intensities of sensory attributes were rated with a line scale (from 0 = "none" to 10 = "very strong") in nonrandom order, using reference samples (Table 1) in every session. In addition, the possible off-flavors and off-odors were described freely in writing. Data were collected with Compusense *five* software (Compusense Inc., Guelph, Canada).

Statistical Analyses. Differences among the sensory attributes of strawberry samples were analyzed by ANOVA together with Tukey's *t* test and the Tamhane test ($p < 0.05$) (SPSS 16.0, SPSS Inc., H, Chicago, IL, USA). Relationships between sensory and chemical characteristics were tested with the PLS method (Unascrambler 9.8, Camo Process AS, Oslo, Norway). Cross-validation was used to estimate the number of principal components for a statistically reliable model. The reproducibility, agreement, and sensitivity of assessors were also tested (PanelCheck, Nofima, Tromsø, Norway).

RESULTS AND DISCUSSION

Sensory-Active Metabolites in Organic and Conventional Strawberries. From the 3669 molecular features observed in the strawberry metabolite profiling analysis, 60 compounds were selected for further analysis on the basis of preliminary partial least-squares regression (PLS) analysis: the peak areas of 131 molecular features having highest abundance of response in the LC-MS analysis were used as predictors, and the intensities of 7 orosensory attributes and 5 odor attributes (Table 1) evaluated from frozen, pureed strawberry samples were used as responses. The 60 major compounds found to be related to the sensory profile were tentatively identified on the basis of their accurate mass and product ion spectrum. This compound group included mainly flavonoids, hydrolyzable and condensed tannins, organic and phenolic acids, and fatty acids, as well as some terpenoids, furans, and a lactone derivative (Table 2).[6,8,21,31−37] The identified compounds are depicted in the total ion chromatogram of conventional 'Jonsok' sample (Figure 1).

The relatively good stability of 'Bounty" and 'Polka' chemical composition in different horticultural systems was demonstrated by the PCA separating individual sample replicates on the basis of the 60 tentatively identified metabolites: for these two cultivars, conventional and organic samples were closely accumulated (Figure 2). In the hierarchical clustering analysis, conventional 'Polka' (P-CON) and organic 'Polka' (P-OR) further indicated quite similar metabolite profiles regardless of cultivation system (Figure 3). The sample replicates of conventional 'Jonsok' (J-CON) and organic 'Jonsok' (J-OR) were clearly clustered according to farming practice, therefore demonstrating the most conspicuous intracultivar differences between organic and conventional samples (Figures 2 and 3). Especially many organic and cinnamic acids were markedly more abundant in J-CON in comparison to J-OR or to any other sample (Figure 3). When organic 'Bounty' (B-OR) and conventional 'Bounty' (B-CON) were compared, for example, isorhamnetin aglycone, tryptophan, salidroside, an epiafzelechin hexose, a sesquiterpenoid, and a dicaffeoylquinic acid were on average significantly more abundant in B-OR (Figure 3).

In general, the compositional differences between cultivars were much more pronounced than the differences caused by cultivation methods. For example, differing flavonoid glycosylation patterns between cultivars were visualized in the heat map (Figure 3). Both J-CON and J-OR totally lacked a kaempferol pentose. The abundances of some small carboxylic and/or aromatic compounds and salidroside were regulated in a cultivar-dependent manner. A sapogenin compound was found to be more abundant in all organic samples in comparison to conventional analogues, but no other consistent, significant differences were found according to farming practice within the selected compound group.

Earlier studies have shown that flavonoids (e.g., anthocyanins and quercetin glycosides), hydroxycinnamic acids, flavan-3-ols, hydrolyzable and condensed tannins, and triterpene-derived metabolites are important constituents in many strawberry tissues.[7−9,11,14,38,39] Several members of these compound groups were identified as orosensory-active features in this study. In nature, phenolic compounds and terpenoids are often associated with bitter taste perceived by a large family of receptors,[17,40] and the astringent mouthfeel of berries and other polyphenol-rich foods is a consequence of phenolic compounds binding to salivary proteins.[41] Bitterness and astringency, although important quality traits of many beverages (e.g.,

DOI: 10.1021/jf505183j
J. Agric. Food Chem. 2015, 63, 1010−1019

Table 2. Metabolites Tentatively Identified from Strawberry Fruit by LC-qTOF-MS and MS/MS Analysis[a]

peak	t_R (min)	MM	m/z ESI(−)	tentative identification	ref
3	1.09	174.0165	173.0799, 155.0327, 111.0059	dehydroascorbic acid	6, 31
12	1.12	130.02638	129.0199, 116.9357, 85.0290	2-methyl-2-butenedioic acid variant	Dictionary of Natural Products, Metlin
14	1.12	192.02711	191.0186, 173.0080, 111.0086	citric acid	Metlin
62	1.28	104.0475	103.0400, 59.0141	malonic acid	Metlin
78	1.32	134.05775	133.0129, 115.0032, 71.0137	malic acid	Metlin
216	1.68	112.0161	111.0071, 67.0190	furoic acid	Metlin
240	1.73	206.04272	205.0286, 111.0088, 67.0179	furan derivative	Metlin
370	2.08	369.10675	368.1009, 161.0486, 131.0372, 101.0249	methyl cinnamate	Metlin, SciFinder
384	2.12	302.06467	301.0563, 272.4473, 227.0569	quercetin aglycone	SciFinder
466	2.31	316.08017	315.0723, 152.0110, 109.0291	isorhamnetin aglycone	Metlin
498	2.36	296.1112	295.1046, 249.1008, 87.0454, 44.9982	butyric acid conjugate	Metlin
523	2.40	866.20764	865.1974, 575.1197, 287.0560	proanthocyanidin trimer	8
536	2.43	204.08987	203.0797, 186.0565, 142.0644, 116.0497, 74.0248	tryptophan	Metlin
611	2.59	300.08524	299.1139, 137.0618, 89.0232, 59.0137	salidroside	Metlin
618	2.60	332.11142	331.1027, 169.0098, 125.0250	glucogallin	8, 32
655	2.69	144.0242	143.0349, 84.1061, 55.0182	caprylic acid	33, Metlin
661	2.71	346.12735	345.1220, 299.1138, 179.0564, 161.0452, 89.0243, 59.0142	salidroside derivative	Metlin
675	2.72	176.06854	175.0223, 115.0028, 87.0069, 71.1334	L-ascorbic acid	Metlin
844	3.06	418.11182	417.1046, 285.0600, 241.0698, 163.0388, 152.0110	kaempferol pentose	8, 32, SciFinder
887	3.15	326.10114	325.0933, 307.0819, 163.0399, 145.0296	coumaric acid hexose	8
973	3.30	292.0224	291.0156, 247.0288, 163.0413, 147.0457, 117.0344	coumaric acid derivative	Metlin
1083	3.51	466.11182	465.1032, 447.0832, 285.0388, 241.0457, 151.0024	kaempferol hexose	8, 32
1090	3.53	432.10712	431.0996, 269.0462, 253.0528, 225.0552, 147.0082	pelargonidin hexose	6, Metlin
1111	3.56	596.1752	595.1669, 269.0438, 224.6179, 105.5180, 79.2842	unknown	Metlin
1139	3.64	450.1177	449.1094, 431.1024, 287.0583, 269.0448	ferulic acid hexose derivative	21
1185	3.71	578.1647	577.1592, 425.0822, 407.0565, 289.0669, 269.0441, 147.0060	flavan-3-ol derivative	34, Metlin
1211	3.75	480.12738	479.1204, 271.0628, 253.0506, 227.0704, 164.0107, 83.0130	naringenin derivative	32, SciFinder
1244	3.82	356.1118	355.1046, 309.0967, 147.0453, 103.0537	cinnamic acid derivative	Metlin
1253	3.84	332.09055	(751.1387, 561.9384) 331.0821, 289.0719, 271.0554, 125.0237	propelargonidin cleavage product	8
1254	3.84	376.0803	(751.1387, 561.9384) 375.0720, 289.0705, 271.0592, 125.0241	propelargonidin cleavage product	8
1368	4.02	520.1591	519.1185, 271.0613, 253.0503, 227.0734, 164.0103	naringenin derivative	32, SciFinder
1388	4.07	358.12668	357.1193, 195.0649, 151.0765	phenylpropanoid hexose derivative	35, Metlin
1473	4.23	434.12186	433.2065, 271.0583, 253.5903, 227.6108	naringenin hexose	8, SciFinder
1507	4.29	518.1069	517.0959, 473.1056, 269.0456, 225.0560, 163.0040, 147.0404	pelargonidin malonylhexose	6, Metlin
1660	4.54	448.1021	447.0932, 315.0104, 284.0331, 227.0324	kaempferol hexose	Metlin
1763	4.69	434.04922	433.0329, 299.9912, 271.9984, 216.0056, 145.0287	quercetin pentose	8, Metlin
1821	4.77	478.07626	477.0670, 301.0358, 151.0027	quercetin glucuronide	34, Metlin
1823	4.77	956.1505	955.1465, 477.0684, 301.0311, 227.0457	quercetin glucuronide dimer	
1839	4.80	310.1058	309.0983, 147.0426	cinnamic acid hexose	6
1857	4.83	358.12726	357.1203, 195.0662, 151.0761	phenylpropanoid hexose derivative	35, Metlin
1874	4.85	448.06552	447.0584, 300.9994, 257.0115, 229.0145, 200.0048	ellagic acid deoxyhexose	8
1933	4.96	302.00665	300.9998, 284.0042, 257.6011, 229.0150, 200.0099	ellagic acid aglycone	8
1997	5.06	476.1328	475.0.682	unknown	
2089	5.21	462.0812	461.0724, 285.0410, 229.0505, 175.0228, 113.0246	kaempferol glucuronide	8, Metlin
2090	5.21	436.12785	435.1299, 273.0772, 167.0359	epiafzelechin hexose	8, Metlin
2133	5.27	462.08133	461.0738, 285.0408, 175.0246, 113.0247	kaempferol glucuronide	8, Metlin
2272	2.48	436.10193	435.1285, 273.0761, 167.0343	epiafzelechin hexose	8, Metlin
2326	5.57	490.1129	489.1046, 285.0406, 229.0494	kaempferol acetylhexose	8, Metlin
2407	5.74	140.12	139.1123	unknown	
2529	6.09	350.1946	349.1867, 179.0558, 169.1227, 89.0242, 87.0057, 59.0130, 57.0347	lactone hexose	Metlin
2675	6.51	464.26373	463.2546, 417.2496, 255.1918	sesquiterpenoid	8
2744	6.74	464.26276	463.2550, 417.2463, 255.1844, 161.0466	sesquiterpenoid	8
3040	8.64	562.29956	561.2902, 515.2831, 191.0532, 161.0454	dicaffeoylquinic acid	Metlin

DOI: 10.1021/jf505183j
J. Agric. Food Chem. 2015, 63, 1010−1019

Table 2. continued

peak	t_R (min)	MM	m/z ESI(−)	tentative identification	ref
3046	8.71	562.29987	561.2930, 515.2878, 353.6063, 179.4866, 85.0302, 44.9973	dicaffeoylquinic acid	Metlin
3056	8.80	488.35153	487.3432, 469.3330, 407.3308, 135.0753	sapogenin	8, Metlin
3322	10.09	541.33966	540.3286, 480.3092, 255.2323	palmitic acid derivative	6, 36
3358	10.19	567.35455	566.3363, 506.3248, 281.2486, 245.0757	oleic acid derivative	6, 36
3470	10.51	280.24063	279.2334, 153.6057, 75.2451	linoleic acid	6, 36
3533	10.73	282.2561	281.2489, 126.5730	oleic acid	6, 36
3655	11.60	622.446	621.4382, 486.8462, 271.7586, 153.4179	triterpenoid	37, Metlin

[a]Data were acquired in negative electrospray ionization (ESI−). t_R, retention time.

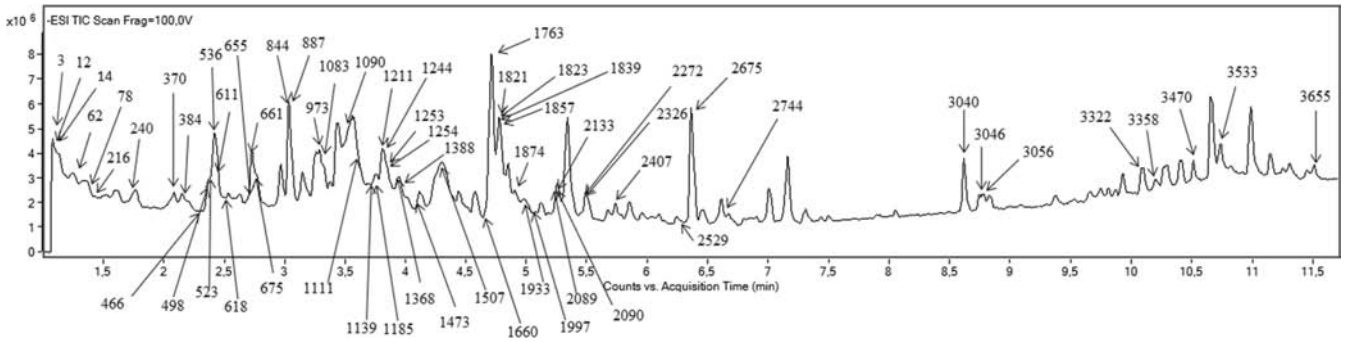

Figure 1. Total ion chromatogram of strawberry obtained in reversed phase liquid chromatography connected with negative electrospray ionization in qTOF-MS analysis. Sixty sensory-active strawberry metabolites are depicted. The peaks are marked by numbers, referring to the tentative identifications in Table 2.

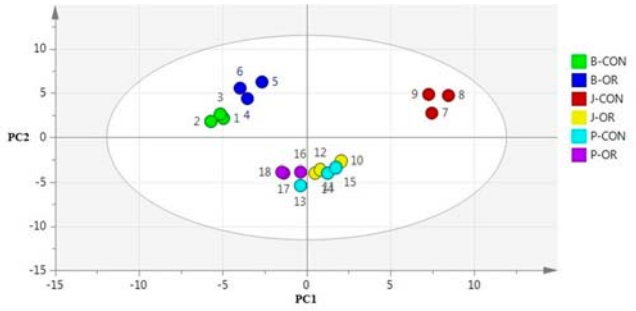

Figure 2. Principal component analysis (PCA) of the metabolite contents of three conventionally and organically grown strawberry cultivars. The PCA plot shows differences between strawberry sample replicates according to their metabolite profiles based on metabolite-specific signal abundances. Each replicate is a pool of 10 strawberry fruits. Numbered circles indicate sample replicates. 1−3, B-CON, conventional 'Bounty'; 4−6, B-OR, organic 'Bounty'; 7−9, J-CON, conventional 'Jonsok'; 10−12, J-OR, organic 'Jonsok'; 13−15, P-CON, conventional 'Polka'; 16−18, P-OR, organic 'Polka'.

wine, tea),[41] are frequently experienced as unpleasant properties of berries.[20]

For instance, citric, malic, and malonic acids were indicated to contribute to strawberry sensory quality in our analyses. Organic acids are an important compound group in strawberry and, indeed, participate and act in synergy with sugars in strawberry flavor formation and perception.[2]

Esters, alcohols, aldehydes, ketones, lactones, furanones, and terpenoids are dominant factors in the strawberry aroma profile.[22,26,42] In addition to furans, terpenoids, and a lactone derivative, many types of fatty acids were among the selected compounds considered in the present study. Several volatile aroma- and/or flavor-active plant secondary metabolites are, in fact, derived from primary metabolites:[17,22,32] for example, lactones are typical products of essential fatty acid degradation[17] and are known to participate in, for instance, the formation of strawberry fruity aroma.[25]

Environment × genotype interactions are important determinants of strawberry phenolic content and metabolite profile. Growth season temperature,[43] fertilization level,[15] harvesting time,[42] and growth location[1] may affect the strawberry metabolome in inter- and intracultivar manners, and some compounds show more plasticity according to environmental conditions.[1] Wounding, microbial attack, and UV radiation, for instance, may induce kaempferol derivative accumulation.[12] As 'Jonsok' samples contained all kaempferol derivatives analyzed in this study except the pentose derivative, it can be proposed that genotype-dependent patterns regulate the glycosylation of flavonols in response to a stress factor. Saponins are synthesized during normal plant development, but biotic threats can also trigger their accumulation.[13]

Total Phenolic Contents of Strawberry Samples. When compared to any other sample, J-CON showed significantly higher total phenolic (TP) values (199 ± 11 mg/100 g fw GAE). J-OR had the second highest TP content (176 ± 11 mg/100 g fw). B-CON had the lowest TP concentration (155 ± 6 mg/100 g fw). The TP contents of J-OR and B-CON differed significantly from each other. The TP contents of P-OR, P-CON, and B-OR were 165 ± 5, 170 ± 4, and 171 ± 2 mg/100 g fw, respectively.

The TP contents of our samples were in line with previous studies.[1,39] No consistent intracultivar alteration of TP content has been observed according to organic versus conventional production.[14,27] Cultivar-dependent, significant differences in the TP values as well as in absolute and relative concentrations of strawberry metabolites have been observed frequently in earlier studies.[1,10,25,27,39]

Strawberry Sensory Properties and Their Relationships with the Identified Metabolites. Some significant

DOI: 10.1021/jf505183j
J. Agric. Food Chem. 2015, 63, 1010−1019

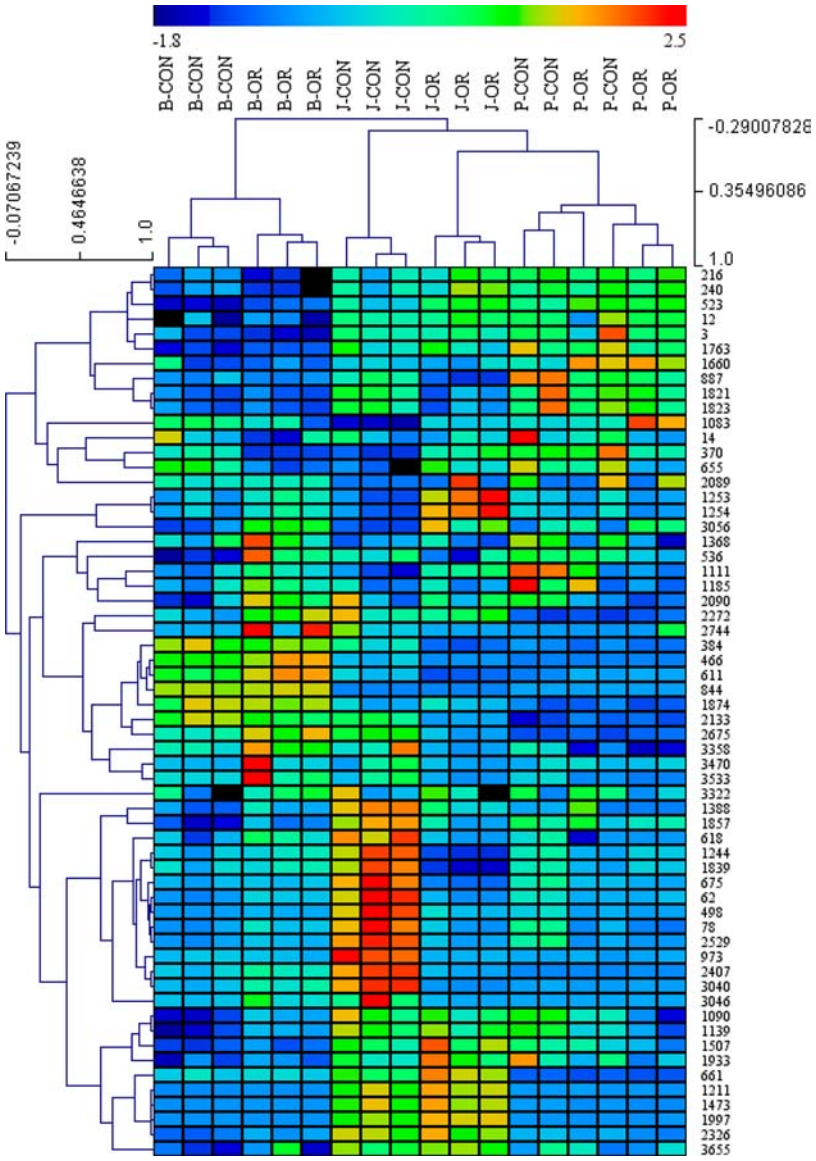

Figure 3. Heat map representation of the hierarchical clustering analysis based on Pearson correlation of the strawberry sample replicates. The analysis is based on the normalized signal abundances of the tentatively identified strawberry metabolites across all analyzed samples. The metabolites are marked by numbers, referring to the tentative identifications in Table 2. The color-coding scale indicates the relative abundance within each metabolite: blue, low abundance; red, high abundance; green/yellow, average abundance. Each replicate is a pool of 10 strawberry fruits. B, 'Bounty'; J, 'Jonsok'; P, 'Polka'; CON, conventional; OR, organic.

differences were detected in all orosensory attribute intensities evaluated from the frozen, pureed strawberry samples (Figure 4A). Nevertheless, there was no consistent correlation between cultivar or farming practice and orosensory property intensities. Sourness and sweetness were the dominating taste properties. J-OR showed both the lowest sweetness intensity and the highest sourness intensity, whereas B-OR was the sweetest and the least sour. B-OR had significantly lower type 1 astringency intensity in comparison to all other samples. Off-flavor was detected in every sample type in at least one evaluation session by at least one assessor.

Green and strawberry odors demonstrated statistically significant differences between samples (Figure 4B). With respect to strawberry odor intensity, J-CON and J-OR represented the extremes and were significantly different from each other; J-CON had considerably higher strawberry odor intensity than J-OR. B-OR had significantly higher green odor intensity than J-OR and P-OR. Off-odors were observed in all sample types with no significant intensity differences.

When the identified chemical compounds were used to explain the sensory attributes of strawberry samples in the PLS model (Figure 5), with three factors, 79% variation in the metabolome data explained 88% variation in the sensory profiles. Bitterness and astringencies were related to the sample-specific combinations of several flavonoid and flavan-3-ol derivatives, a salidroside conjugate, and a triterpenoid. Astringencies and bitterness, in turn, were important contributors in the total intensity of flavor. Two propelargonidin-derived products, citric and caprylic acids and methyl cinnamate, were related to both sourness and rough, sharp type 2 astringency. The aglycones of quercetin and isorhamnetin seemed to be somewhat meaningful in sweet taste intensity, whereas ellagic acid aglycone contributed to bitterness. Green and strawberry odors, as well as sweet taste, were connected

DOI: 10.1021/jf505183j
J. Agric. Food Chem. 2015, 63, 1010−1019

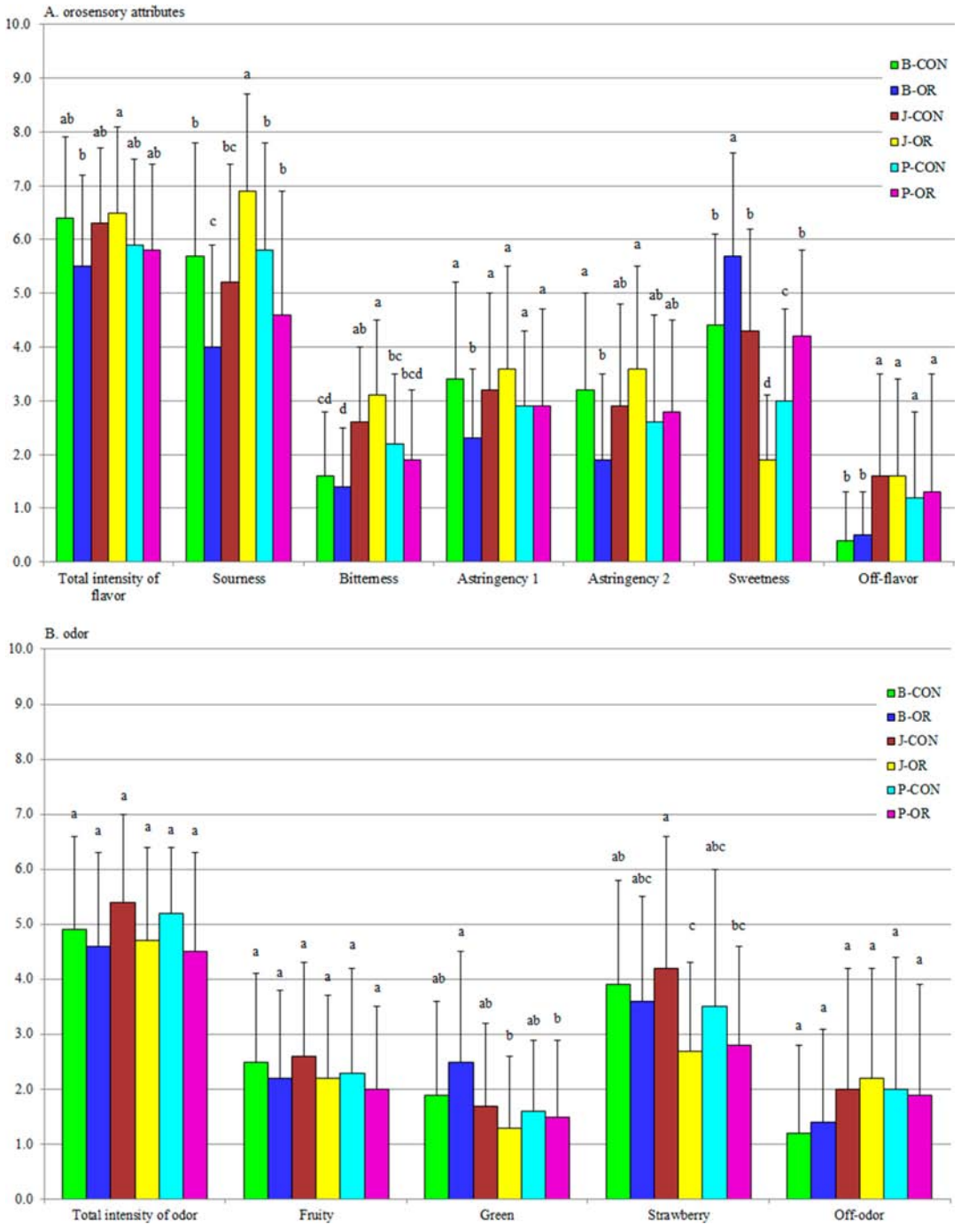

Figure 4. Mean intensities (±SD) of (A) orosensory attributes and (B) odor attributes of three strawberry cultivars (B, 'Bounty'; J, 'Jonsok'; P, 'Polka') cultivated conventionally (CON) and organically (OR). Samples with the same letters for each attribute do not differ significantly.

with fatty acids and fatty acid derivatives. Oleic and linoleic acids were related to green odor formation; an oleic acid derivative was a more determinant factor in strawberry odor. A sesquiterpenoid compound contributed to strawberry odor and salidroside to green odor.

Flavonol glycosides are strongly astringent and contribute especially to velvety, mouth-drying astringency.[20,44−46] Glycosylation patterns of different flavonols are, however, crucial for astringency detection thresholds, depending on the aglycone structure.[44,45] Proanthocyanidins, a compound group including propelargonidins, induce puckering and rough astringency at low concentrations.[45,46] Anthocyanins and proanthocyanidins may also form polymeric pigment compounds having astringent properties in a food matrix.[47] Many compounds having astringent properties may have bitter properties as well, depending on their structure, polymerization level, and concentration.[45,46] Because flavan-3-ols (e.g., (epi)catechin and (epi)afzelechin) tend to polymerize,[8] they possibly contribute to bitterness, along with astringency. Moreover, when chemical mixtures are assessed for their sensory quality, astringency and bitterness are easily linked.[45,46] In a previous study, flavonol aglycones have been observed to correlate with the bitterness of wine,[48] but in our data, flavonol aglycones seemed to be related to the sweetness of B-OR. As for

DOI: 10.1021/jf505183j
J. Agric. Food Chem. 2015, 63, 1010−1019

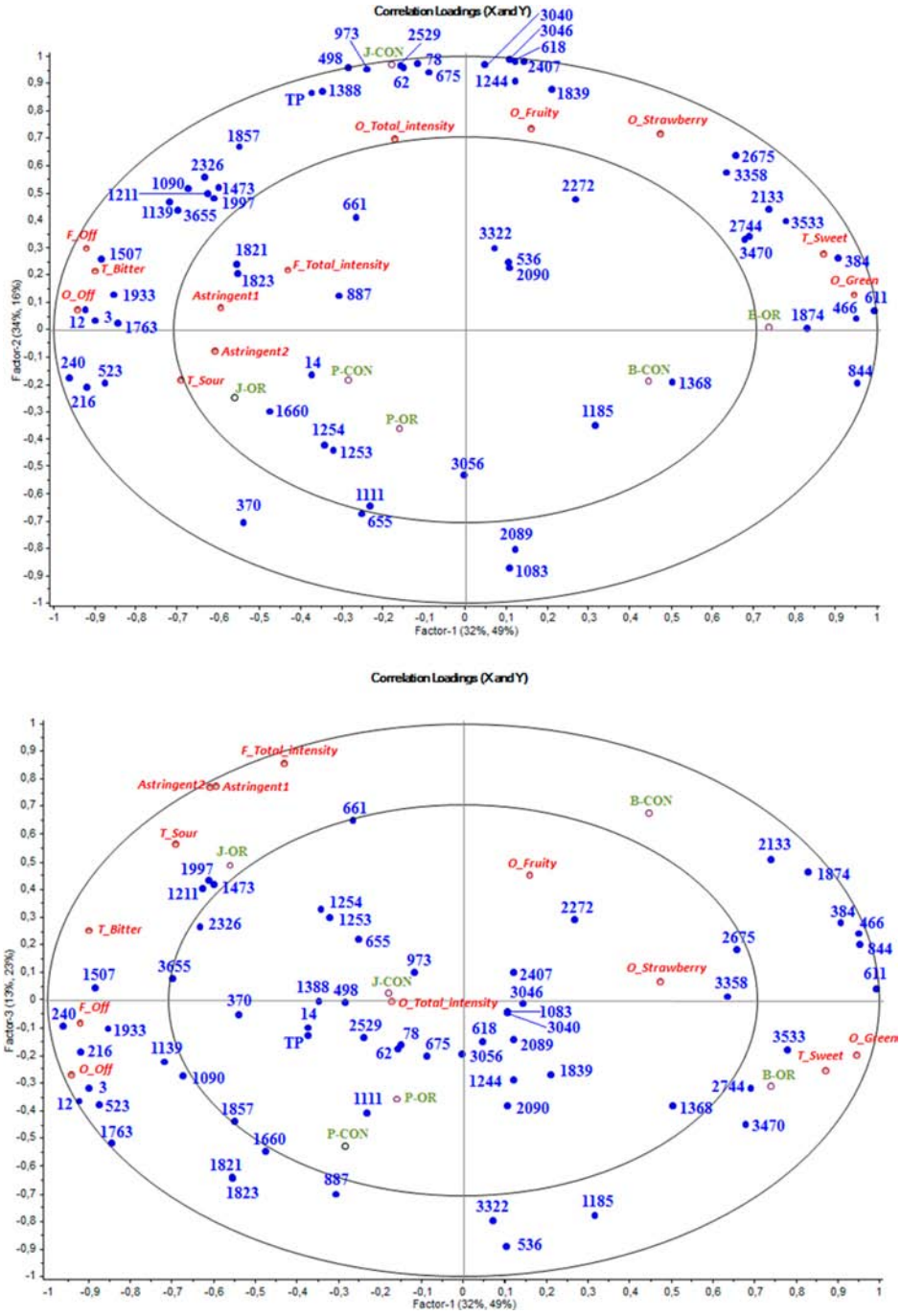

Figure 5. Partial least-squares regression (PLS) plots of the interactions between sensory and tentative metabolite profiles in three strawberry cultivars (B, 'Bounty'; J, 'Jonsok'; P, 'Polka') cultivated conventionally (CON) and organically (OR). Tentatively identified metabolites are used as *X*-variables (predictors) and sensory properties as *Y*-variables (responses). The metabolites are marked by numbers, referring to the tentative identifications in Table 2. Factors 1 and 2 are in the upper plot, and factors 1 and 3 are in the lower plot. Sensory attributes are in italics. O, odor; T, taste; F, flavor; TP, total phenolics.

terpenoids in general, they are well-known bitter, toxicity-implying defense compounds.[17]

Organic acids have been previously found to contribute to both sourness and astringency, two attributes having positive correlation with total acid content and titratable acidity and negative correlation with sugar content.[49] In sensory evaluations, astringency and sourness can be correlated with each other in a berry fruit sample,[49] and this makes distinguishing the effects of individual chemical compounds on fruit sensory properties more difficult.

Oleic and linoleic acids—being long-chained, *cis*-polymerized fatty acids—are distinctive precursors of volatiles involved in plant flavor formation.[17] The catabolism of essential fatty acids is also apt to cause off-flavors.[17] Salidroside is a glucoside of phenylethyl alcohol, and the cleavage of its moieties is likely to profit, for example, rosy odor.[50,51] Yet, the orthonasally perceived aroma of strawberry—derived from the balanced combination of hundreds of plant metabolites, their conjugates. and derivatives—is a complex, polygenic trait fluctuating from

DOI: 10.1021/jf505183j
J. Agric. Food Chem. 2015, 63, 1010−1019

one cultivar to the other and between plants cultivated under different environmental conditions.[22,50]

Sucrose content is a determinant factor in strawberry sweetness and also correlates positively with the total volatile content of strawberry; in addition, some volatile compounds have been observed to enhance sweet taste perception from strawberry samples.[22] The contents and ratios of strawberry sugars (i.e., fructose, glucose, and sucrose) vary according to cultivar, and this may affect the sweet taste perception because sugars differ in their relative sweetness.[2,52] Sweetness may decrease both astringency and bitterness: increased sucrose levels have been found to reduce these properties in polyphenol-rich solutions, and this can be explained both physiologically and cognitively.[53] In addition, sample color can modify flavor perception.[54]

The sugar contents or more accurate volatile profiles of frozen strawberries were not determined in this study, and overall, all samples had moderate sensory attribute intensities. Yet it can be concluded that either high sucrose content, the low concentrations of some flavonoid glycosides, distinct fatty acid metabolism, advantageous volatile profile, or all of these factors may explain the relatively high green odor and sweet taste intensities and relatively low astringency and bitterness intensities evaluated from B-OR (Figures 4 and 5). In this study, we have considered a small but prominent fraction of the strawberry metabolome. Adequate peak area, indicating metabolite abundance in the strawberry sample, was one of the criteria used for compound qualification in our analyses. Among the thousands of chemical compounds detected in our samples, there are yet many minor constituents that undoubtedly contribute to the taste, flavor, and odor of strawberries. Therefore, it is our aim to take a broader perspective in clarifying the relationship between the metabolome and sensory quality of strawberries.

The present results indicate that the stability of strawberry chemical composition and sensory quality in different horticultural systems vary mainly according to cultivar. Organic farming practices may enhance the accumulation of some health-related plant metabolites in specific strawberry genotypes. Hence, careful cultivar selection is a key factor in combining sustainable farming practices and the enhanced nutritional quality of strawberry. Furthermore, appropriate cultivar selection may help to increase the marketing value of organically grown strawberry. This study has further verified that strawberry cultivars differ in their chemical composition and sensory characteristics. Many types of flavonoids, hydrolyzable tannins, and flavan-3-ol derivatives are among the most abundant compounds in strawberries, and these compounds contribute to strawberry sensory attributes, as well.

AUTHOR INFORMATION

Corresponding Author

*(M.S.) Phone: +358 2 333 6835. Fax: +358 2 333 6862. E-mail: mari.sandell@utu.fi.

Funding

This study was financially supported by the Finnish Cultural Foundation, the Maiju and Yrjö Rikala Horticultural Foundation, the Northern Savo ELY-center, and the Academy of Finland (MS252005, 256176, 263747).

Notes

The authors declare no competing financial interest.

ACKNOWLEDGMENTS

We are grateful to Saila Mattila for her technical help and to Gregory Suszko and Billy Braithwaite for English language consultation.

REFERENCES

(1) Josuttis, M.; Verrall, S.; Stewart, D.; Krüger, E.; McDougall, G. J. Genetic and environmental effects on tannin composition in strawberry (*Fragaria* × *ananassa*) cultivars grown in different European locations. *J. Agric. Food Chem.* **2013**, *61*, 790−800.

(2) Akhatou, I.; Fernández Recamales, Á. Influence of cultivar and culture system on nutritional and organoleptic quality of strawberry. *J. Sci. Food Agric.* **2014**, *94*, 866−875.

(3) Basu, A.; Nguyen, A.; Betts, N. M.; Lyons, T. J. Strawberry as a functional food: an evidence-based review. *Crit. Rev. Food Sci. Nutr.* **2014**, *54*, 790−806.

(4) Kårlund, A.; Moor, U.; Sandell, M.; Karjalainen, R. O. The impact of harvesting, storage and processing factors on health-promoting phytochemicals in berries and fruits. *Processes* **2014**, *2*, 596−624.

(5) Hakala, M.; Lapveteläinen, A.; Huopalahti, R.; Kallio, H.; Tahvonen, R. Effect of varieties and cultivation conditions on the composition of strawberries. *J. Food Compos. Anal.* **2003**, *16*, 67−80.

(6) Aharoni, A.; Ric de Vos, C.; Verhoeven, H. A.; Maliepaard, C. A.; Kruppa, G.; Bino, R.; Goodenowe, D. B. Nontargeted metabolome analysis by use of Fourier transform ion cyclotron mass spectrometry. *Omics* **2002**, *6*, 217−234.

(7) Hukkanen, A. T.; Kokko, H. I.; Buchala, A. J.; McDougall, G. J.; Stewart, D.; Kärenlampi, S. O.; Karjalainen, R. O. Benzothiadiazole induces the accumulation of phenolics and improves resistance to powdery mildew in strawberries. *J. Agric. Food Chem.* **2007**, *55*, 1862−1870.

(8) Hanhineva, K.; Rogachev, I.; Kokko, H.; Mintz-Oron, S.; Venger, I.; Kärenlampi, S.; Aharoni, A. Non-targeted analysis of spatial metabolite composition in strawberry (*Fragaria* × *ananassa*) flowers. *Phytochemistry* **2008**, *69*, 2463−2481.

(9) Buendía, B.; Gil, M. I.; Tudela, J. A.; Gady, A. L.; Medina, J. J.; Soria, C.; López, J. M.; Tomás-Barberán, F. A. HPLC-MS analysis of proanthocyanidin oligomers and other phenolics in 15 strawberry cultivars. *J. Agric. Food Chem.* **2010**, *58*, 3916−3926.

(10) Fredericks, C. H.; Fanning, K. J.; Gidley, M. J.; Netzel, G.; Zabaras, D.; Herrington, M.; Netzel, M. High-anthocyanin strawberries through cultivar selection. *J. Sci. Food Agric.* **2013**, *93*, 846−852.

(11) Kårlund, A.; Salminen, J.; Koskinen, P.; Ahern, J. R.; Karonen, M.; Tiilikkala, K.; Karjalainen, R. Polyphenols in strawberry (*Fragaria* × *ananassa*) leaves induced by plant activators. *J. Agric. Food Chem.* **2014**, *62*, 4592−4600.

(12) Dixon, R. A.; Paiva, N. L. Stress-induced phenylpropanoid metabolism. *Plant Cell* **1995**, *7*, 1085−1097.

(13) Augustin, J. M.; Kuzina, V.; Andersen, S. B.; Bak, S. Molecular activities, biosynthesis and evolution of triterpenoid saponins. *Phytochemistry* **2011**, *72*, 435−457.

(14) Crecente-Campo, J.; Nunes-Damaceno, M.; Romero-Rodriguez, M.; Vázquez-Odériz, M. Color, anthocyanin pigment, ascorbic acid and total phenolic compound determination in organic versus conventional strawberries (*Fragaria* × *ananassa* Duch, cv Selva). *J. Food Compos. Anal.* **2012**, *28*, 23−30.

(15) Anttonen, M. J.; Hoppula, K. I.; Nestby, R.; Verheul, M. K.; Karjalainen, R. O. Influence of fertilization, mulch color, early forcing, fruit order, planting date, shading, growing environment, and genotype on the contents of selected phenolics in strawberry (*Fragaria* × *ananassa* Duch.) fruits. *J. Agric. Food Chem.* **2006**, *54*, 2614−2620.

(16) Reganold, J. P.; Andrews, P. K.; Reeve, J. R.; Carpenter-Boggs, L.; Schadt, C. W.; Alldredge, J. R.; Ross, C. F.; Davies, N. M.; Zhou, J. Fruit and soil quality of organic and conventional strawberry agroecosystems. *PLoS One* **2010**, *5*, No. e12346.

(17) Goff, S. A.; Klee, H. J. Plant volatile compounds: sensory cues for health and nutritional value? *Science* **2006**, *311*, 815−819.

DOI: 10.1021/jf505183j
J. Agric. Food Chem. 2015, 63, 1010−1019

(18) Capocasa, F.; Diamanti, J.; Tulipani, S.; Battino, M.; Mezzetti, B. Breeding strawberry (*Fragaria* × *ananassa* Duch) to increase fruit nutritional quality. *BioFactors* **2008**, *34*, 67−72.
(19) Sandell, M.; Tiitinen, K.; Pohjanheimo, T.; Kallio, H.; Breslin, P. A. S. Why naturally healthy berries may be seen as unpleasant and non-appetitive? In *Food Flavor: Chemistry, Sensory Evaluation and Biological Activity*; ACS Symposium Series 988; American Chemical Society, Oxford University Press: Washington, DC, USA, 2007; pp 219−228.
(20) Laaksonen, O.; Ahola, J.; Sandell, M. Explaining and predicting individually experienced liking of berry fractions by the *hTAS2R38* taste receptor genotype. *Appetite* **2013**, *61*, 85−96.
(21) Ornelas-Paz, J. d. J.; Yahia, E. M.; Ramírez-Bustamante, N.; Pérez-Martínez, J. D.; Escalante-Minakata, M. d. P.; Ibarra-Junquera, V.; Acosta-Muñiz, C.; Guerrero-Prieto, V.; Ochoa-Reyes, E. Physical attributes and chemical composition of organic strawberry fruit (*Fragaria* × *ananassa*) Duch, cv. Albion) at six stages of ripening. *Food Chem.* **2013**, *138*, 372−381.
(22) Schwieterman, M. L.; Colquhoun, T. A.; Jaworski, E. A.; Bartoshuk, L. M.; Gilbert, J. L.; Tieman, D. M.; Odabasi, A. Z.; Moskowitz, H. R.; Folta, K. M.; Klee, H. J. Strawberry flavor: diverse chemical compositions, a seasonal influence, and effects on sensory perception. *PLoS One* **2014**, *9*, No. e88446.
(23) Laaksonen, O.; Mäkilä, L.; Tahvonen, R.; Kallio, H.; Yang, B. Sensory quality and compositional characteristics of blackcurrant juices produced by different processes. *Food Chem.* **2013**, *138*, 2421−2429.
(24) Hakala, M. A.; Kallio, H.; Lapveteläinen A. Relationship between the sensory quality and physico-chemical properties of strawberry varieties. In *Factors Affecting the Internal Quality of Strawberry (Fragaria* × *ananassa Duch.) Fruit*, academic dissertation, Original publication V, Department of Biochemistry and Food Chemistry, University of Turku, Finland, 2003; 89 pp.
(25) Du, X.; Plotto, A.; Baldwin, E.; Rouseff, R. Evaluation of volatiles from two subtropical strawberry cultivars using GC−olfactometry, GC-MS odor activity values, and sensory analysis. *J. Agric. Food Chem.* **2011**, *59*, 12569−12577.
(26) Hakala, M.; Lapveteläinen, A.; Kallio, H. Volatile compounds of selected Strawberry varieties analyzed by purge-and-trap headspace GC-MS. *J. Agric. Food Chem.* **2002**, *50*, 1133−1142.
(27) Olsson, M. E.; Andersson, C. S.; Oredsson, S.; Berglund, R. H.; Gustavsson, K. Antioxidant levels and inhibition of cancer cell proliferation in vitro by extracts from organically and conventionally cultivated strawberries. *J. Agric. Food Chem.* **2006**, *54*, 1248−1255.
(28) Everette, J. D.; Bryant, Q. M.; Green, A. M.; Abbey, Y. A.; Wangila, G. W.; Walker, R. B. Thorough study of reactivity of various compound classes toward the Folin−Ciocalteu reagent. *J. Agric. Food Chem.* **2010**, *58*, 8139−8144.
(29) Eisen, M. B.; Spellman, P. T.; Brown, P. O.; Botstein, D. Cluster analysis and display of genome-wide expression patterns. *Proc. Natl. Acad. Sci. U.S.A.* **1998**, *95*, 14863−14868.
(30) Sandell, M.; Laaksonen, O.; Järvinen, R.; Rostiala, N.; Pohjanheimo, T.; Tiitinen, K.; Kallio, H. Orosensory profiles and chemical composition of black currant (*Ribes nigrum*) juice and fractions of press residue. *J. Agric. Food Chem.* **2009**, *57*, 3718−3728.
(31) Frenich, A. G.; Torres, M. H.; Vega, A. B.; Vidal, J. M.; Bolanos, P. P. Determination of ascorbic acid and carotenoids in food commodities by liquid chromatography with mass spectrometry detection. *J. Agric. Food Chem.* **2005**, *53*, 7371−7376.
(32) Calani, L.; Beghè, D.; Mena, P.; Del Rio, D.; Bruni, R.; Fabbri, A.; Dall'Asta, C.; Galaverna, G. Ultra-HPLC−MS^n (poly)phenolic profiling and chemometric analysis of juices from ancient *Punica granatum* L. cultivars: a nontargeted approach. *J. Agric. Food Chem.* **2013**, *61*, 5600−5609.
(33) Zabetakis, I.; Holden, M. A. Strawberry flavour: analysis and biosynthesis. *J. Sci. Food Agric.* **1997**, *74*, 421−434.
(34) Aaby, K.; Mazur, S.; Nes, A.; Skrede, G. Phenolic compounds in strawberry (*Fragaria* × *ananassa* Duch.) fruits: composition in 27 cultivars and changes during ripening. *Food Chem.* **2012**, *132*, 86−97.
(35) Mullen, W.; Borges, G.; Lean, M. E.; Roberts, S. A.; Crozier, A. Identification of metabolites in human plasma and urine after consumption of a polyphenol-rich juice drink. *J. Agric. Food Chem.* **2010**, *58*, 2586−2595.
(36) Kerwin, J. L.; Wiens, A. M.; Ericsson, L. H. Identification of fatty acids by electrospray mass spectrometry and tandem mass spectrometry. *J. Mass Spectrom.* **1996**, *31*, 184−192.
(37) Guo, S.; Duan, J.-A.; Tang, Y.-P.; Yang, N.-Y.; Qian, D.-W.; Su, S.-L.; Shang, E.-X. Characterization of triterpenic acids in fruits of *Ziziphus* species by HPLC-ELSD-MS. *J. Agric. Food Chem.* **2010**, *58*, 6285−6289.
(38) Fernandes, V. C.; Domingues, V. F.; de Freitas, V.; Delerue-Matos, C.; Mateus, N. Strawberries from integrated pest management and organic farming: phenolic composition and antioxidant properties. *Food Chem.* **2012**, *134*, 1926−1931.
(39) Padula, M. C.; Lepore, L.; Milella, L.; Ovesna, J.; Malafronte, N.; Martelli, G.; de Tommasi, N. Cultivar based selection and genetic analysis of strawberry fruits with high levels of health promoting compounds. *Food Chem.* **2013**, *140*, 639−646.
(40) Sandell, M.; Breslin, P. A. S. Variability in a taste-receptor gene determines whether we taste toxins in food. *Curr. Biol.* **2006**, *16*, R792−R794.
(41) Jöbstl, E.; O'Connell, J.; Fairclough, J. P. A.; Williamson, M. P. Molecular model for astringency produced by polyphenol/protein interactions. *Biomacromolecules* **2004**, *5*, 942−949.
(42) Jouquand, C.; Chandler, C.; Plotto, A.; Goodner, K. A sensory and chemical analysis of fresh strawberries over harvest dates and seasons reveals factors that affect eating quality. *J. Am. Soc. Hortic. Sci.* **2008**, *133*, 859−867.
(43) Wang, S. Y.; Zheng, W. Effect of plant growth temperature on antioxidant capacity in strawberry. *J. Agric. Food Chem.* **2001**, *49*, 4977−4982.
(44) Schwarz, B.; Hofmann, T. Sensory-guided decomposition of red currant juice (*Ribes rubrum*) and structure determination of key astringent compounds. *J. Agric. Food Chem.* **2007**, *55*, 1394−1404.
(45) Hufnagel, J. C.; Hofmann, T. Orosensory-directed identification of astringent mouthfeel and bitter-tasting compounds in red wine. *J. Agric. Food Chem.* **2008**, *56*, 1376−1386.
(46) Hufnagel, J. C.; Hofmann, T. Quantitative reconstruction of the nonvolatile sensometabolome of a red wine. *J. Agric. Food Chem.* **2008**, *56*, 9190−9199.
(47) Cascassa, L. F.; Harbertson, J. F. Extraction, evolution, and sensory impact of phenolic compounds during red wine meaceration. *Annu. Rev. Sci. Technol.* **2014**, *5*, 83−109.
(48) Preys, S.; Mazerolles, G.; Courcoux, P.; Samson, A.; Fischer, U.; Hanafi, M.; Bertrand, D.; Cheynier, V. Relationship between polyphenolic composition and some sensory properties in red wines using multiway analyses. *Anal. Chim. Acta* **2006**, *563*, 126−136.
(49) Tiitinen, K. M.; Hakala, M. A.; Kallio, H. P. Quality components of sea buckthorn (*Hippophaë rhamnoides*) varieties. *J. Agric. Food Chem.* **2005**, *53*, 1692−1699.
(50) Ubeda, C.; San-Juan, F.; Concejero, B.; Callejón, R. M.; Troncoso, A. M.; Morales, M. L.; Ferreira, V.; Hernández-Orte, P. Glycosidically bound aroma compounds and impact odorants of four strawberry varieties. *J. Agric. Food Chem.* **2012**, *60*, 6095−6102.
(51) Sáenz-Navajas, M.; Campo, E.; Fernández-Zurbano, P.; Valentin, D.; Ferreira, V. An assessment of the effects of wine volatiles on the perception of taste and astringency in wine. *Food Chem.* **2010**, *121*, 1139−1149.
(52) Kallio, H.; Hakala, M.; Pelkkikangas, A.; Lapveteläinen, A. Sugars and acids of strawberry varieties. *Eur. Food Res. Technol.* **2000**, *212*, 81−85.
(53) Ares, G.; Barreiro, C.; Deliza, R.; Gámbaro, A. Alternatives to reduce the bitterness, astringency and characteristic flavour of antioxidant extracts. *Food Res. Int.* **2009**, *42*, 871−878.
(54) Shankar, M. U.; Levitan, C. A.; Spence, C. Grape expectations: the role of cognitive influences in color-flavor interaction. *Conscious. Cogn.* **2010**, *19*, 380−390.

DOI: 10.1021/jf505183j
J. Agric. Food Chem. 2015, 63, 1010−1019

Table 1. Effect of MAP on Carbon Dioxide (%), Oxygen (%) and Weight Loss (%) in 'Star Ruby' Grapefruit; Fruits Were Stored for 4, 8, 12, and 16 Weeks in Microperforated and Macroperforated Bags at 10 °C, Followed by 1 Week of Storage at Shelf Conditions (20 °C)[a]

	carbon dioxide (%)			oxygen (%)			weight loss (%)		
weeks	control	micro	macro	control	micro	macro	control	micro	macro
4	0.10 ± 0.18 a	2.97 ± 0.18 b	0.40 ± 0.18 a	21.00 ± 0.13 a	18.83 ± 0.13 b	20.60 ± 0.13 a	1.70 ± 0.07 a	1.11 ± 0.07 b	1.18 ± 0.07 b
8	0.20 ± 0.04 a	3.53 ± 0.04 b	0.30 ± 0.04 a	20.70 ± 0.02 a	18.30 ± 0.02 b	20.13 ± 0.02 c	2.04 ± 0.08 a	1.47 ± 0.08 b	1.53 ± 0.08 b
12	0.30 ± 0.13 a	3.10 ± 0.09 b	0.37 ± 0.07 a	20.00 ± 0.09 a	18.20 ± 0.07 b	20.03 ± 0.05 a	3.08 ± 0.16 a	2.12 ± 0.16 b	2.17 ± 0.16 b
16	0.30 ± 0.27 a	3.47 ± 0.16 b	0.50 ± 0.16 a	20.40 ± 0.09 a	18.40 ± 0.08 b	20.10 ± 0.08 a	4.24 ± 0.20 a	3.29 ± 0.20 b	3.74 ± 0.20 b

[a]Data are means ± SE of three replications. For weight loss (%) study, $n = 10$. Different letters denote significant differences ($P < 0.05$) among treatments at each storage period for individual parameters.

MATERIALS AND METHODS

Plant Materials. 'Star Ruby' grapefruits of uniform size were harvested from a commercial grove on the southern coast of Israel (January 26, 2010). Each treatment included four cartons of 10 kg of grapefruits, i.e., 40 kg of fruit per treatment. In the current study, the "bag in box" method of MAP was used. Fruits were stored at 10 °C for 16 weeks, followed by 1 week of storage at shelf conditions (20 °C) with the following treatments: (a) control (untreated); (b) microperforated Xtend bag (MIPB; modified atmosphere and humidity); (c) macroperforated Xtend bag (MAPB; modified humidity). The relative humidity in the 10 °C cold storage room was between 80 and 85%. The optimum humidity for postharvest storage of citrus fruit is ∼90−95%.

The MIPB and MAPB liners used included 20 μm thick Xtend films (StePac LA, Tefen, Israel), which were used in our previously published report,[5] and the total area of pores as a percentage of the film surface area were 0.002% for MIPB and 0.06% for MAPB. The water vapor transmission rate of the film was 18×10^{-10} mol s^{-1} m^{-2} Pa^{-1}, and the oxygen transmission rate was 24×10^{-14} mol s^{-1} m^{-2} at 23 °C. The O_2 and CO_2 concentrations in the atmosphere surrounding the untreated control fruit were similar to those of the regular air (0.1−0.3% CO_2 and 20.5−21.0% O_2) (Table 1). In the MAPB, the atmospheric gas concentrations were also similar to those of regular air. In contrast, the fruit in the MIPB experienced a modified atmosphere with constant levels of 3.5% CO_2 and 18.2% O_2. The relative humidity inside both perforated bags was ∼97−98% as compared with ∼80% for the untreated control fruit. The approximate cost of an Xtend MAP bag for 10 kg of fruits (per carton) is ∼25 cents, and the cost of production will not increase significantly using this material.

Fruit samples were collected at intervals of 4 weeks and were further stored for 1 week at room temperature (20 °C) before analysis, to simulate market conditions. Three juice samples per treatment at each time interval were prepared by blending three peeled fruits from different cartons, i.e., a total of nine fruits for each time point. The juice samples were lyophilized and sent in plastic containers to the Vegetable and Fruit Improvement Center (Texas A&M University, College Station, Texas, USA) for quantification of phytochemicals. Lyophilized juice samples were stored at −20 °C until further phytochemical analysis.

Chemicals. Butylated hydroxytoluene (BHT), lycopene, β-carotene, narirutin, naringin, didymin, poncirin, limonin, and 6′,7′-dihydroxybergamottin (DHB) were procured from Sigma-Aldrich Co. (St. Louis, MO, USA). Analytical-grade solvents used for quantitative analysis were obtained from Fisher Scientific Research (Pittsburgh, PA, USA).

Fruit Quality Analysis. Fruit quality parameters such as total soluble solids (TSS), titratable acidity, ripening ratio (TSS/acidity), weight loss, and disease incidence were measured. TSS was determined using a digital refractometer (model PAL-1, Atago, Tokyo, Japan) and is expressed as °Brix. Titratable acidity was determined by titrating the juice with 0.1 M NaOH to pH 8.3 using a model CH-9101 automatic titrator (Metrohm, Herisau, Switzerland). Each measurement included five replications, and each replication included three fruits. Weight loss was determined by weighing fruits ($n = 10$) at intervals of 4 weeks (plus the subsequent 1 week of storage at 20 °C) and was expressed as percent weight loss compared to the prestorage weight. Decay incidence was determined by monitoring the number of fruits with disease symptoms and was expressed as the percentage of decayed fruit per carton.

Sensory Analysis. Fruit sensory quality was evaluated at 4 weeks intervals (plus the subsequent 1 week of storage at 20 °C). Fruits were peeled, and the separated segments were cut in halves and placed into covered glass cups. Each treatment included a mixture of cut segments from five different fruits. Sensory evaluations were conducted by a trained panel consisting of five males and five females aged between 25 and 62 years, who were well-trained and experienced in tasting citrus fruit. The sensory training included open panel sessions with tasting of reference standards. Each panelist assessed the various attributes of the three samples, according to an unstructured 100 mm scale, with anchor points "very weak" and "very strong" for each attribute, and the sensory data were recorded as distances (mm) from the origin. Overall flavor preference was recorded on a hedonic scale of 1 to 10. The samples were identified by randomly assigned three-digit codes.

Quantification of Ascorbic Acid. Direct titration of juice with 2,6-dichlorophenolindophenol (DCIP) was used to determine ascorbic acid content by measuring the reduction of DCIP with ascorbic acid in an acidic solution.[17] Titration volumes were compared with 0.1% ascorbic acid (Sigma-Aldrich, St. Louis, MO), and the results were expressed as mg of ascorbic acid per 100 mL of juice.

Quantification of Carotenoids. Carotenoids were extracted and analyzed using a previously described method.[18] Freeze-dried samples (1 g + 5 mL of water) were extracted using chloroform (15 mL) containing BHT (0.2%). The reconstituted juice was sequentially extracted three times under yellow light. The organic layer was allowed to separate, and extracts from each sample were pooled, filtered using Whatman grade 1 filter paper, and subjected to high-performance liquid chromatography (HPLC) analysis. Carotenoids were quantified by HPLC using a Gemini C-18, 5 μm column (250 mm × 4.6 mm i.d.) with a guard cartridge (Phenomenex, Torrance, CA, USA) on an Agilent 1200 series HPLC (Foster City, CA, USA). Acetonitrile (A) and isopropyl alcohol (B) were used for the mobile phase at the flow rate of 0.8 mL/min with 10 μL injection volume. External standards were used to quantify β-carotene and lycopene at 450 nm wavelength.

Quantification of Limonoids, Furocoumarins, and Flavonoids. *Sample Preparation.* Extraction of samples was carried out according to our previously published method.[18] Each freeze-dried juice sample was reconstituted (1 g + 5 mL of water) and extracted with 15 mL of ethyl acetate on a shaker for 4 h. The organic layer was separated; the residue was extracted twice and pooled; and the solvent was evaporated to dryness. The dried residue was reconstituted with acetone (4 mL), filtered using a 0.45 μm poly(tetrafluoroethylene) (PTFE) filter, and analyzed by HPLC for limonoids, flavonoids, and furocoumarins. In the current study, a common extraction solvent was used for measuring the levels of limonoids, flavonoids, and furocoumarins, to allow comparison and minimize the extraction errors caused by using different solvents.

Quantification of Limonoids and Flavonoids with HPLC. A Waters HPLC (Milford, MA, USA), spectra model with a photodiode array detector (2996), a binary HPLC pump 1525, and a 717 plus

DOI: 10.1021/jf505278x
J. Agric. Food Chem. 2015, 63, 1020−1028

autosampler, was used for quantification of limonoids and flavonoids. The chromatographic separations were performed according to a previously published method[18] on a Gemini C-18, 5 μm column (250 mm × 4.6 mm i.d.) from Phenomenex (Torrance, CA, USA). The limonoids and flavonoids were detected at 210 and 280 nm, respectively. Data analysis was carried out using the Empower pro software. The chromatographic separation was performed using a gradient mobile phase of 0.03 M phosphoric acid (A) and acetonitrile (B) with 1 mL/min flow rate. Each sample was injected three times, and all measurements were conducted in triplicate.

Confirmation of Limonoids and Flavonoids by Liquid Chromatography–Mass Spectrometry. The structures of limonoids and flavonoids in samples were confirmed by ultrahigh performance liquid chromatography–time-of-flight-mass spectrometry (UPLC-QTOF-MS) (maXis impact, Bruker Daltonics, Billerica, MA, USA). Limonoids and flavonoids were separated on an Eclipse Plus C18 LC-MS column (2.1 × 100 mm), 1.8 μm partical size, connected to an Agilent 1290 UPLC instrument (Agilent, Santa Clara, CA) at 70 °C with a flow rate of 0.2 mL/min using binary gradient elution of 0.1% formic acid and acetonitrile. Compounds were separated by a gradient of 98% A to 10% in 0–9 min followed by equilibration for 2 min before the next injection. The 1290 UPLC is equipped with auto sampler, binary pump, solvent degasser, thermostated column compartment, and diode-array detector (DAD). The LC peaks were monitored at 210 and 280 nm for limonoids and flavonoids, respectively. Mass spectral analyses were performed using the ESI-Q-TOF mass spectrometer equipped with an electrospray ionization. Both positive and negative modes were used for ionization. Mass spectrometer conditions are as follows: MS scan range, 50–1000 m/z; end plate offset, −500 V; capillary voltage, 3000 V; nebulizer gas (N_2), 4 bar; dry gas (N_2) flow rate, 12 L/min; dry gas temperature, 200 °C; ion transfer conditions funnel radio frequency (RF), 200 Vpp; multiple RF, 200 Vpp; quadruple low mass, 55 m/z; collision energy, 5.0 eV; collision RF, 600 Vpp; ion cooler RF, 50–250 Vpp ramping; transfer time, 121 μs; prepulse storage time, 1 μs. Calibration was done before each run through a loop injector of 20 μL of 10 mM sodium formate. The Bruker Compass Data analysis 4.1 software was used for data acquisition.

Quantification of Furocoumarins with HPLC. Furocoumarins were analyzed using our previously described method, with slight modifications.[19] A PerkinElmer HPLC system consisting of a series 200 pump, photodiode array (PDA) detector (235C), and autosampler (Norwalk, CT, USA) was used for analysis. The separations were carried out on a Gemini C-18, 5 μm column (250 mm × 4.6 mm i.d.), with a guard cartridge from Phenomenex (Torrance, CA, USA). The peaks were detected at 320 nm, and the data were integrated using Turbochrom software (PerkinElmer, Norwalk, CT, USA). The gradient mobile phase consisted of 0.03 M phosphoric acid (A) and acetonitrile (B) with 10 μL injection volume at the flow rate of 1 mL/min. Each sample was analyzed three times, and all measurements were conducted in triplicate.

Statistical Analysis. Statistical analysis was performed using one-way analysis of variance (ANOVA) with PASW Statistics 18 software (SPSS Inc., 2009). A general linear model was used to test significant differences, and means were compared using Tukey's HSD test at the 5% probability level. The results were expressed as means ± SE.

RESULTS AND DISCUSSION

Weight Loss. Overall, we observed no significantly detrimental weight loss in any of the three treatments, but in the control fruits, weight loss gradually increased during the postharvest storage from 1.7% after 4 weeks to 4.2% after 16 weeks of storage (Table 1). MIPB and MAPB significantly ($P < 0.05$) reduced weight loss during the 16-week storage period. Humidity, temperature, and storage period strongly affect weight loss in fruits.[20] Moisture loss from the peel, a primary reason for weight loss in citrus fruits, can lead to peel disorders and affect the fruit's appearance.[21,22] In the current experiment, the reduction in weight loss observed in grapefruits stored in MAP can be attributed to reduced transpiration due to the high humidity maintained in the MAP. Similar results were reported in previous experiments where individual film wrapping[22] and use of box liner bags[5] for storage of citrus fruits significantly reduced weight loss.

Visual Appearance and Color. At the time of harvest (January 26, 2010), the fruits were attractive, with an external yellowish color with red cheeks (Figure 1). During the prolonged storage at 10 °C, the control fruits gradually became more reddish as compared to time zero (at harvest). Packing the fruits in perforated bags slightly delayed the development of external color. Low oxygen and high carbon dioxide levels inhibit ethylene production and action,[23,24] which may cause the delay in peel color development in grapefruits stored in MAP.[25] Modified atmosphere storage delays ripening and color development in plums,[26] avocado,[27] and Marsh grapefruit.[22] With respect to internal appearance, the fruit flesh was red at harvest, and no further remarkable changes occurred during storage.

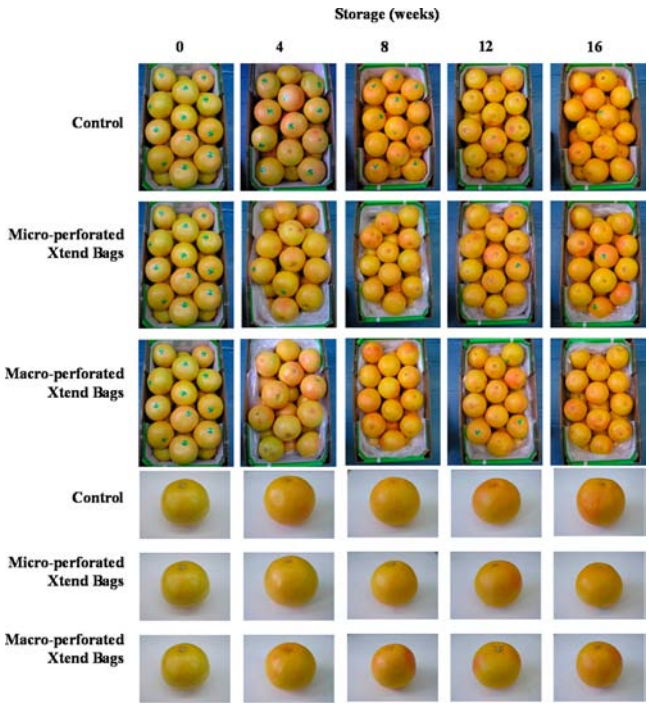

Figure 1. Effect of MAP on the appearance of 'Star Ruby' grapefruit. Fruits were untreated or kept in perforated bags, and pictures were taken after 4, 8, 12, and 16 weeks of storage at 10 °C, followed by 1 week of storage at shelf conditions (20 °C).

Juice TSS and Acid Percentages. Juice TSS was 12.2% at harvest and remained mostly constant during postharvest storage in all treatments (Table 2). By contrast, acidity levels were 1.9% at harvest and slightly decreased to 1.6–1.7% after prolonged storage. Overall, the observed changes in juice TSS and acidity levels resulted in a slight increase in ripening ratio from 6.5 at harvest to 8.0 after 16 weeks of storage. Fruit stored in perforated bags showed only a slight reduction in acidity levels. Similar results were observed in previous studies where MAP had no significant effect on TSS and acidity levels in citrus fruits.[5,28]

Decay Development. The incidence of decay was very low throughout the course of the experiment, and after 16 weeks of

DOI: 10.1021/jf505278x
J. Agric. Food Chem. 2015, 63, 1020–1028

Table 2. Effect of MAP on TSS, Acidity (%), TSS/Acidity Ratio, and Taste Score in 'Star Ruby' Grapefruit; Fruits Were Stored for 4, 8, 12, and 16 Weeks in Microperforated and Macroperforated Bags at 10 °C, Followed by 1 Week of Storage at Shelf Conditions (20 °C)[a]

	storage duration (weeks)				
	0	4	8	12	16
TSS (%)					
control	12.2 ± 0.2 a	12.2 ± 0.4 a	11.6 ± 0.3 a	11.8 ± 0.1 ab	11.6 ± 0.3 a
micro	12.2 ± 0.2 a	10.7 ± 0.4 a	12.3 ± 0.3 a	11.9 ± 0.1 a	12.5 ± 0.3 a
macro	12.2 ± 0.2 a	11.4 ± 0.4 a	10.3 ± 0.3 b	11.3 ± 0.1 b	12.2 ± 0.3 a
acidity (%)					
control	2.0 ± 0.1 a	1.9 ± 0.1 a	2.0 ± 0.1 a	1.8 ± 0.0 a	1.7 ± 0.1 a
micro	2.0 ± 0.1 a	1.6 ± 0.1 a	1.9 ± 0.1 a	1.7 ± 0.0 a	1.6 ± 0.1 a
macro	2.0 ± 0.1 a	1.6 ± 0.1 a	1.7 ± 0.1 b	1.7 ± 0.0 a	1.6 ± 0.1 a
TSS/acidity ratio					
control	6.3 ± 0.2 a	6.5 ± 0.4 a	5.8 ± 0.2 b	6.5 ± 0.2 a	6.8 ± 0.3 a
micro	6.3 ± 0.2 a	6.8 ± 0.4 a	6.6 ± 0.2 a	7.0 ± 0.2 a	8.0 ± 0.3 a
macro	6.3 ± 0.2 a	7.1 ± 0.4 a	6.2 ± 0.2 ab	6.6 ± 0.2 a	7.5 ± 0.3 a
taste score					
control	8.8 ± 0.5 a	8.1 ± 1.1 a	8.1 ± 0.6 b	8.0 ± 0.9 a	7.4 ± 1.2 a
micro	8.8 ± 0.5 a	7.9 ± 0.7 a	8.9 ± 0.7 a	8.1 ± 0.7 a	7.1 ± 1.6 a
macro	8.8 ± 0.5 a	7.7 ± 1.0 a	8.7 ± 1.0 a	7.8 ± 0.9 a	7.6 ± 0.8 a

[a]Data are means ± SE of 3 replications, each from 3 different fruits. Different letters denote significant differences ($P < 0.05$) among treatments at each storage period for individual parameters.

storage only 3−4% decay was observed in all the treatments (data not shown). Thus, the increased humidity in the MAP did not increase the incidence of decay. MAP is recommended as it reduces various rind disorders in citrus fruits including oranges, tangerines, and grapefruit.[5,6]

Fruit Taste. At harvest, fruits achieved a high taste score of 8.8 on a scale of 1 to 10 (Table 2). Although the fruit taste remained good during the entire experiment, the taste score gradually decreased to 7.2−7.5 after 16 weeks of storage. Overall, storing the fruits in MAP had no significant effect on fruit taste or sensory acceptability (Table 2). Taste is an important factor in determining the quality of fruits, especially in fruits stored for prolonged periods. Sugars (TSS) and acids are the primary factors affecting taste, and MAP did not alter these in the current study. Other studies conducted using MAP have reported retention of taste for longer periods than control.[29] However, care must be taken to avoid very high CO_2 (>7−8%) or low O_2 (<14−15%), which can lead to anaerobic conditions and result in off-flavors.[5]

Ascorbic Acid. Ascorbic acid content was 40 mg per 100 mL of juice at harvest and was retained during postharvest storage in all three treatments (Figure 2). MAP had no significant effect on ascorbic acid levels during the storage period. Ascorbic acid levels increased in all three treatments at 8 weeks after storage; nevertheless, at the end of the 16-week storage period, fruits in all three treatments had ascorbic acid levels similar to initial levels. Ascorbic acid is a major antioxidant present in citrus fruits and acts as a first defense response against oxidative stress.[30,31] Increase in ascorbic acid up to 8 weeks can be attributed to de novo biosynthesis and regeneration of ascorbic acid due to increase in stress after harvest and during initial storage weeks of the fruits.[32] In another study in 'Cara Cara' navel orange, an increase in ascorbic acid was observed during prolonged storage of 105 days as a result of ripening of the fruit after harvest and reduced degradation due to lower metabolic rate.[33] Ascorbic acid was higher in broccoli stored in MAP due to its low autoxidation,[34] and MAP did not affect ascorbate peroxidase, the major enzyme involved in ascorbic acid degradation, in broccoli. In Valencia oranges, coating with different commercial waxes that modified their internal O_2 and CO_2 produced no significant difference in ascorbic acid levels between coated and noncoated fruits.[35] However, Valencia oranges showed a decrease in ascorbic acid with increasing storage period.[35] Nevertheless, in the present study, no significant differences were seen in ascorbic acid contents among the three treatments during the storage period.

Carotenoids. β-carotene levels gradually increased in grapefruit pulp during the storage period in all three treatments (Figure 2). At the end of 16 weeks of storage, β-carotene levels were higher in control fruits, followed by fruits stored in MIPB and MAPB. In addition, lycopene was significantly higher in control fruits at 4 and 16 weeks of storage. Fruits stored in MAPB had higher lycopene contents than fruit stored in MIPB at 4 weeks of storage; however, no significant difference was observed between MIPB and MAPB fruits at 8 and 16 weeks of storage. A sharp increase in lycopene levels was observed in the fruits stored in MIPB at 12 weeks of storage, although lycopene decreased after 16 weeks of storage. The current results indicate that MAP delayed color development in peel and carotenoid development, especially β-carotene, in fruit flesh. In plums, storage in MAP delayed anthocyanin and carotenoid development.[13,36] Another study conducted on shredded carrots showed similar results, where MAP (95% O_2 and 5% CO_2) reduced the carotenoid contents of both orange and purple carrots during storage.[37] Being nonclimacteric in nature, mature citrus fruit produce low levels of endogenous ethylene.[38] However, MAP affects ethylene biosynthesis and action and thus may delay carotenoid development.

Limonoids and Furocoumarins. Limonin levels increased sharply after 4 weeks of storage in all three treatments (Figure 3), but limonin was higher in control and in MIPB at 4 and 8 weeks after storage. However, control fruits had lower levels of limonin than MAP-treated fruits at 12 weeks of storage. No significant difference in limonin was observed among the treatments after 16 weeks of storage. LC-MS analysis was conducted to further confirm the increase in limonin observed

DOI: 10.1021/jf505278x
J. Agric. Food Chem. 2015, 63, 1020−1028

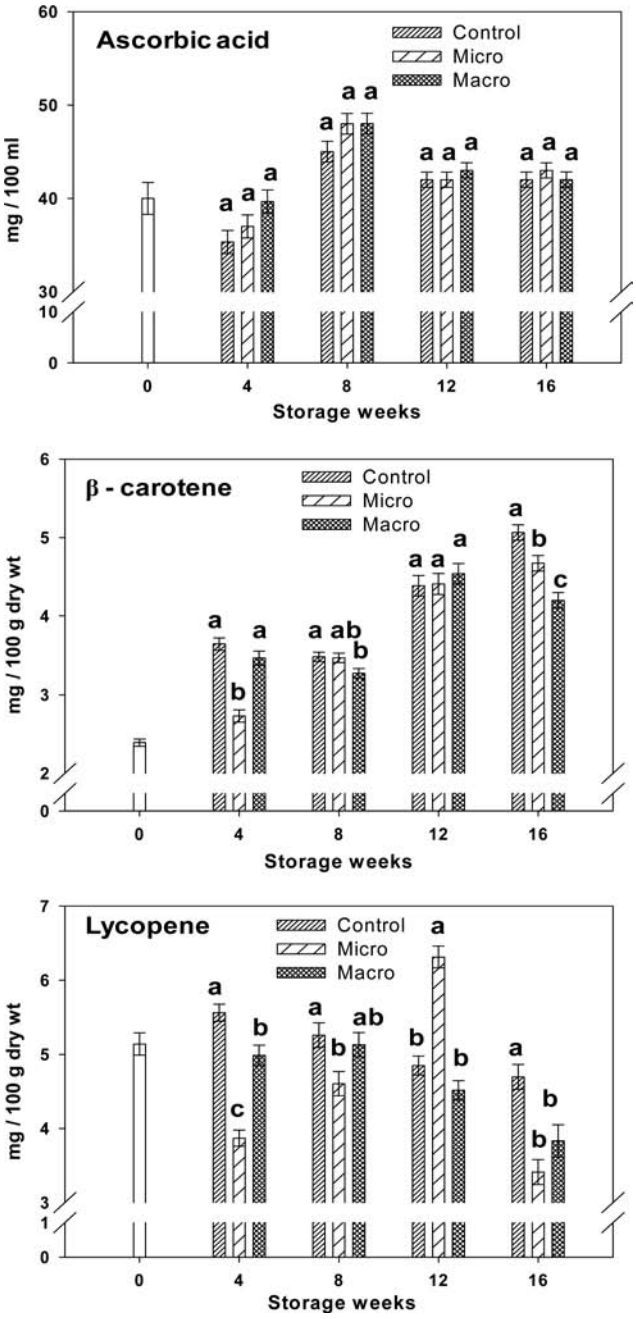

Figure 2. Effect of MAP on ascorbic acid and carotenoid contents of 'Star Ruby' grapefruit. Fruits were stored for 4, 8, 12, and 16 weeks in microperforated and macroperforated bags at 10 °C, followed by 1 week of storage at shelf conditions (20 °C). Data are represented as means ± SE of 3 replications, each from 3 different fruits. Different letters denote significant differences ($P < 0.05$) among treatments at each storage period.

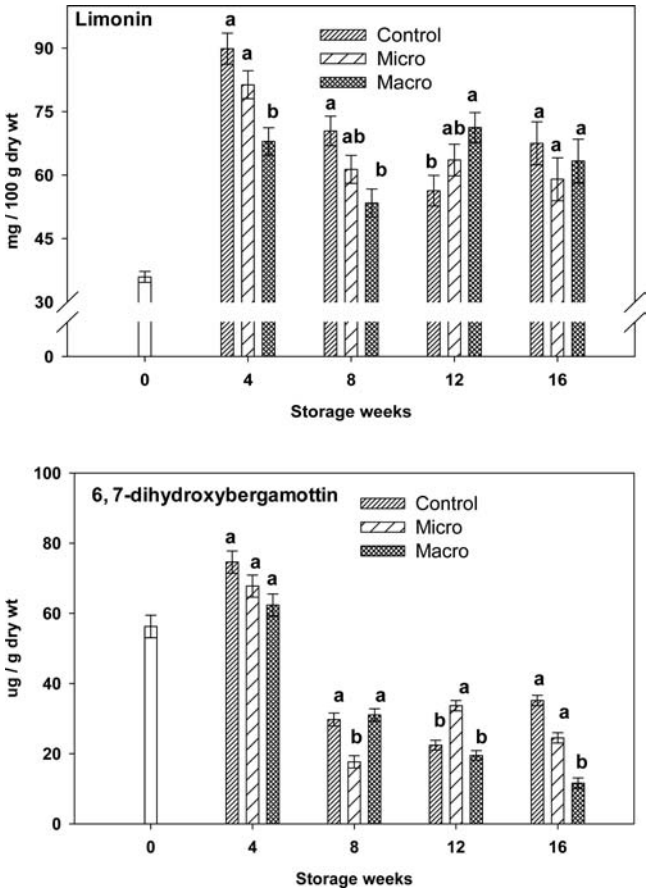

Figure 3. Effect of MAP on limonin (limonoid) and 6,7-dihydroxybergamottin (furocoumarin) contents of 'Star Ruby' grapefruit. Fruits were stored for 4, 8, 12, and 16 weeks in microperforated and macroperforated bags at 10 °C, followed by 1 week of storage at shelf conditions (20 °C). Data are represented as means ± SE of 3 replications, each from 3 different fruits. Different letters denote significant differences ($P < 0.05$) among treatments at each storage period.

at 0 days and 4 weeks. The total ion chromatogram (TIC) of mass spectral analysis of ethyl acetate extracts were illustrated in Figure 4A, and the mass spectrum of limonin shows the negative molecular ion m/z 469.1849 $[M+1]^-$ (mass error 1.39 ppm) (Figure 4B). The limonin levels were found to be more than 2-fold higher at 4 weeks, compared to at 0 days. In citrus fruits, limonin is the most abundant aglycone followed by nomilin.[39] Limonin is one of the compounds responsible for the bitter taste of grapefruit. Nomilin is the precursor of limonin, and limonin is further converted into limonin glucoside.[40]

Furocoumarin, namely, DHB, was quantified in the current study. DHB levels decreased in all three treatments with longer storage, after 4 weeks (Figure 3). No significant difference ($P < 0.05$) was observed in DHB levels among all three treatments up to 4 weeks of storage. At 8 weeks of storage, DHB was significantly lower in fruits stored in MIPB, but control and fruits stored in MAPB showed no difference. Fruits stored in MIPB then showed higher DHB levels at 12 weeks of storage than fruits in the other two treatments. Nevertheless, after 16 weeks of storage, no significant difference was seen between control and the fruits stored in MIPB, while the fruits stored in MAPB showed lower DHB levels. Furocoumarins are derived from the phenylpropanoid pathway, with umbelliferone being their main precursor.[41] Furocoumarins are affected by various factors such as environmental conditions, variety, season, storage period, and postharvest treatment.[19,42,43] A previous study by Girennavar et al.[42] reported a decrease in DHB levels during storage when Rio Red grapefruits were stored at 9 °C for 45 days. The current study is the first to report the effect of MAP on limonoids and furocoumarins in 'Star Ruby' grapefruit.

Flavonoids. The four flavonoids (narirutin, naringin, didymin, and poncirin) showed similar trends during storage

DOI: 10.1021/jf505278x
J. Agric. Food Chem. 2015, 63, 1020−1028

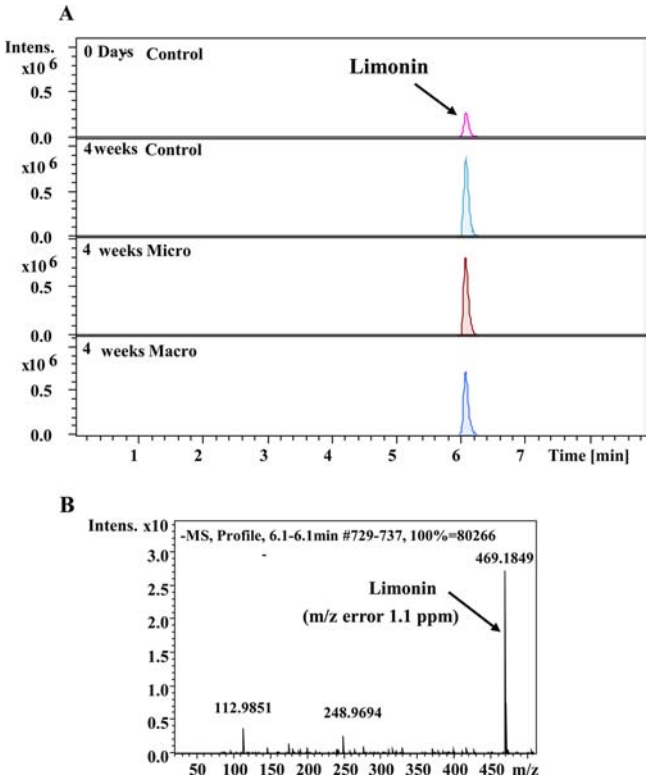

Figure 4. (A). Extracted ion chromatograms of limonin in control grapefruits and fruits stored in microperforated and macroperforated bags at 10 °C for 0 days or 4 weeks, followed by 1 week of storage at shelf conditions (20 °C). (B) ESI−MS spectrum of limonin confirmed by negative ionization mode.

(Figure 5). Their levels decreased gradually with storage up to 8 weeks, with a sharp increase at 12 weeks of storage in all three treatments. However, at the end of the 16-week storage period, initial flavonoid levels were maintained in fruits stored in MAPB, while flavonoids levels decreased slightly in the other two treatments. The sharp increase in flavonoids in all three treatments can be a response to physiological stress during storage. No significant difference was observed in narirutin and didymin levels at 8 weeks of storage in all three treatments. Naringin, didymin, and poncirin levels were higher in the control and in fruits stored in MAPB at 4 weeks of storage. At 8 weeks of storage, controls and fruits stored in MIPB had higher naringin and poncirin levels in comparison to the fruits stored in MAPB. In addition, mass spectral experiments were performed using electrospray ionization operated in negative mode for zero day control and 4-week samples of control and microperforated and macroperforated samples to validate the structural confirmation using high-resolution mass spectra. Figure 6A shows UPLC separation for four flavonoids eluted at 3.8, 3.9, 4.6, and 4.7 min. Figure 6B depicts the negative molecular ion mass spectra of narirutin, m/z 579.1676 (m/z error −5.6 ppm), naringin m/z 579.1705 (m/z error 0.57 ppm), didymin m/z 593.1970 (error 4.7 ppm), and poncirin m/z 593.1860 (error 3.5 ppm). A mass error of the molecular ion of each flavonoid is <5 ppm, which confirms the positive identification of measured mass compared to theoretical mass.

Flavonoids are phenolic compounds derived from the phenylpropanoid pathway, and phenylalanine ammonia lyase (PAL) is the first enzyme in this pathway. Various biotic and abiotic factors including ethylene, chilling injury, irradiation, and low temperature affect the activity of PAL.[44−47] A previous study in plum reported a delay in increase of total phenolics when fruits were stored in MAP for up to 35 days.[13] Delays in

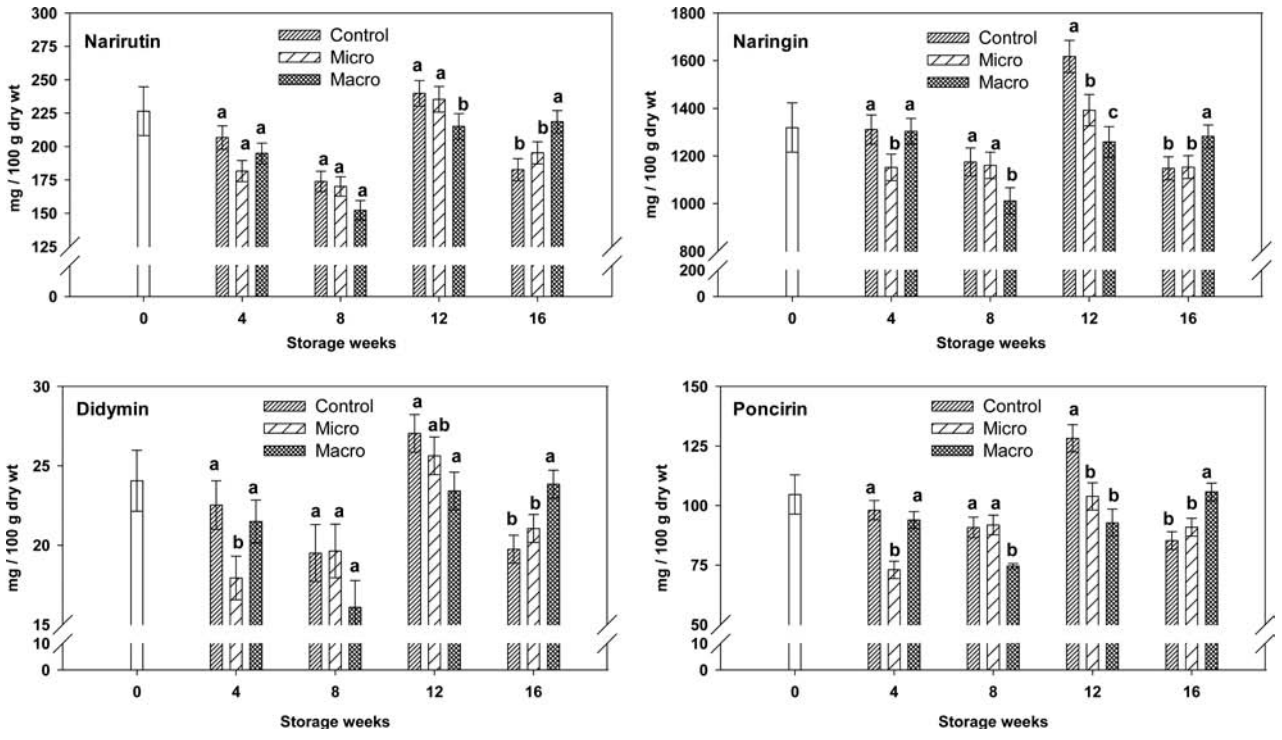

Figure 5. Effect of MAP on flavonoid contents of 'Star Ruby' grapefruit. Fruits were stored for 4, 8, 12, and 16 weeks in microperforated and macroperforated bags at 10 °C, followed by 1 week of storage at shelf conditions (20 °C). Data are represented as means ± SE of 3 replications, each from 3 different fruits. Different letters denote significant differences (P < 0.05) among treatments at each storage period.

DOI: 10.1021/jf505278x
J. Agric. Food Chem. 2015, 63, 1020−1028

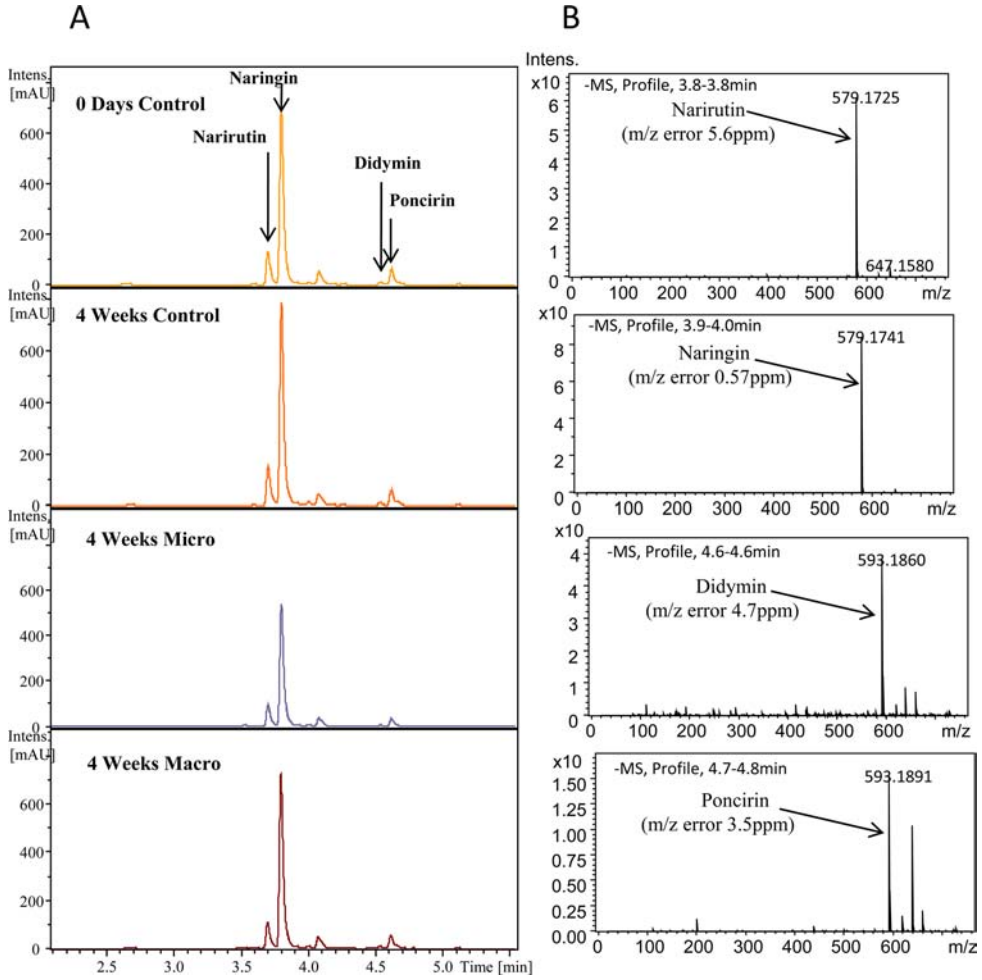

Figure 6. (A). Representative LC-MS total ion chromatogram of flavonoids of control grapefruits and fruits stored in microperforated and macroperforated bags at 10 °C followed by 1 week of storage at shelf conditions (20 °C). (B) Negative mode ESI−MS spectra of narirutin, naringin, didymin, and poncirin. A mass error of the molecular ion is <5 ppm, which confirms the positive identification of measured mass compared to theoretical mass.

ripening or ethylene inhibition due to MAP can affect flavonoid biosynthesis. In addition, grapefruits contain furocoumarins, phenylpropanoid compounds that can influence flavonoid biosynthesis. Further research on biosynthesis of flavonoid and furocoumarins is warranted to help us understand the mechanisms acting under different treatments and storage conditions.

In conclusion MAP can be used as a valuable approach to maintain postharvest quality of grapefruits and reduce the occurrence of disease and rind disorders. The present study demonstrates that, among the different phytochemicals evaluated, MAP has a significant effect on carotenoids, flavonoids, and furocoumarins. Overall, MAP produced no detrimental effects on fruit weight, color development, sensory taste, TSS, acidity, and ripening ratio. In addition, we observed no significant effects of MAP on the levels of ascorbic acid and limonoids among all three treatments at 16 weeks of storage. MIPB is recommended over MAPB, as it modifies the atmosphere and helped to retain certain phytochemicals in comparison to control. Further studies on grapefruits stored at temperatures below 10 °C will examine the effect of MAP on chilling injury and changes in phytochemicals.

AUTHOR INFORMATION

Corresponding Authors

*Department of Postharvest Science, ARO, The Volcani Center, P. O. Box 6, Bet Dagan 50250, Israel. Tel.: +972-3-9683617; fax: +972-3-9683622; e-mail: rporat@volcani.agri.gov.il.

*Vegetable and Fruit Improvement Center, Department of Horticultural Sciences, 1500 Research Parkway, Suite# A120, College Station, Texas 77843, United States. Tel.: +1 979 862 4521; fax: +1 979 862 4522; e-mail: b-patil@tamu.edu.

Funding

This research was supported by Research Grant Award no. TB-8056-08 from the Texas Department of Agriculture, Texas Israel Exchange, and the United States−Israel Binational Agricultural Research and Development Fund.

Notes

The authors declare no competing financial interest.

REFERENCES

(1) Ben-Yehoshua, S.; Fishmant, S.; Fang, D.; Rodov, V. New developments in modified atmosphere packaging and surface coatings for fruits. In *Postharvest Handling of Tropical Fruits*; Champ, B. R., Highley, E., Johnson, G. I., Eds.; Australian Centre for International Agricultural Research: Canberra, Australia, 1993; pp 250−260.

DOI: 10.1021/jf505278x
J. Agric. Food Chem. 2015, 63, 1020−1028

(2) Phillips, C. A. Review: Modified atmosphere packaging and its effects on the microbiological quality and safety of produce. *Int. J. Food Sci. Technol.* **1996**, *31*, 463−479.
(3) Ben-Yeshoshua, S.; Beaudry, R. M.; Fishman, S.; Jayanty, S.; Mir, N. Modified atmosphere packaging and controlled atmosphere storage. In *Environmentally friendly technologies for agricultural produce quality*; Yeshoshua, S. B., Ed.; CRC Press: Boca Raton, FL, 2005; pp 61−112.
(4) Purvis, A. C. Importance of water loss in the chilling injury of grapefruit stored at low temperature. *Sci. Hortic.* **1984**, *23*, 261−267.
(5) Porat, R.; Weiss, B.; Cohen, L.; Daus, A.; Aharoni, N. Reduction of postharvest rind disorders in citrus fruit by modified atmosphere packaging. *Postharvest Biol. Technol.* **2004**, *33*, 35−43.
(6) Kader, A. A.; Zagory, D.; Kerbel, E. L. Modified atmosphere packaging of fruits and vegetables. *Crit. Rev. Food Sci. Nutr.* **1989**, *28*, 1−30.
(7) Patil, B. S.; Jayaprakasha, G. K.; Chidambara Murthy, K. N.; Vikram, A. Bioactive compounds: Historical perspectives, opportunities, and challenges. *J. Agric. Food Chem.* **2009**, *57*, 8142−8160.
(8) Chidambara Murthy, K. N.; Jayaprakasha, G. K.; Kumar, V.; Rathore, K. S.; Patil, B. S. Citrus limonin and its glucoside inhibit colon adenocarcinoma cell proliferation through apoptosis. *J. Agric. Food Chem.* **2011**, *59*, 2314−2323.
(9) Kim, J.; Jayaprakasha, G. K.; Patil, B. S. Limonoids and their anti-proliferative and anti-aromatase properties in human breast cancer cells. *Food Funct.* **2013**, *4*, 258−265.
(10) Perez, J. L.; Jayaprakasha, G. K.; Cadena, A.; Martinez, E.; Ahmad, H.; Patil, B. S. In vivo induction of phase II detoxifying enzymes, glutathione transferase and quinone reductase by citrus triterpenoids. *BMC Complementary Altern. Med.* **2010**, *10*, 51.
(11) Tripoli, E.; Guardia, M. L.; Giammanco, S.; Majo, D. D.; Giammanco, M. Citrus flavonoids: Molecular structure, biological activity and nutritional properties: A review. *Food Chem.* **2007**, *104*, 466−479.
(12) Kim, J.; Jayaprakasha, G. K.; Uckoo, R. M.; Patil, B. S. Evaluation of chemopreventive and cytotoxic effect of lemon seed extracts on human breast cancer (MCF-7) cells. *Food Chem. Toxicol.* **2012**, *50*, 423−430.
(13) Díaz-Mula, H. M.; Zapata, P. J.; Guillén, F.; Valverde, J. M.; Valero, D.; Serrano, M. Modified atmosphere packaging of yellow and purple plum cultivars. 2. Effect on bioactive compounds and antioxidant activity. *Postharvest Biol. Technol.* **2011**, *61*, 110−116.
(14) Zheng, Y.; Wang, S. Y.; Wang, C. Y.; Zheng, W. Changes in strawberry phenolics, anthocyanins, and antioxidant capacity in response to high oxygen treatments. *LWT−Food Sci. Technol.* **2007**, *40*, 49−57.
(15) Odriozola-Serrano, I.; Soliva-Fortuny, R.; Martín-Belloso, O. Effect of minimal processing on bioactive compounds and color attributes of fresh-cut tomatoes. *LWT−Food Sci. Technol.* **2008**, *41*, 217−226.
(16) Simões, A. D. N.; Tudela, J. A.; Allende, A.; Puschmann, R.; Gil, M. I. Edible coatings containing chitosan and moderate modified atmospheres maintain quality and enhance phytochemicals of carrot sticks. *Postharvest Biol. Technol.* **2009**, *51*, 364−370.
(17) Hiromi, K.; Kuwamoto, C.; Ohnishi, M. A rapid sensitive method for the determination of ascorbic acid in the excess of 2,6-dichlorophenolindophenol using a stopped-flow apparatus. *Anal. Biochem.* **1980**, *101*, 421−426.
(18) Chaudhary, P.; Jayaprakasha, G. K.; Porat, R.; Patil, B. S. Degreening and postharvest storage influences 'Star Ruby' grapefruit (*Citrus paradisi* Macf.) bioactive compounds. *Food Chem.* **2012**, *135*, 1667−1675.
(19) Girennavar, B.; Jayaprakasha, G. K.; McLin, S. E.; Maxim, J.; Yoo, K. S.; Patil, B. S. Influence of electron-beam irradiation on bioactive compounds in grapefruits (*Citrus paradisi* Macf.). *J. Agric. Food Chem.* **2008**, *56*, 10941−10946.
(20) McCornack, A. A. Postharvest weight loss of Florida citrus fruits. *Proc. Fla. State Hortic. Soc.* **1975**, *88*, 333−335.
(21) Purvis, A. C. Moisture loss and juice quality from waxed and individually seal-packaged citrus fruits. *Proc. Fla. State. Hortic. Soc.* **1983**, *96*, 327−329.
(22) Kawada, K.; Albrigo, L. G. Effects of film packaging, in-carton air filters, and storage temperatures on the keeping quality of Florida grapefruit. *Proc. Fla. State Hortic. Soc.* **1979**, *92*, 209−212.
(23) Gorny, J. R.; Kader, A. A. Regulation of ethylene biosynthesis in climacteric apple fruit by elevated CO2 and reduced O2 atm. *Postharvest Biol. Technol.* **1996**, *9*, 311−323.
(24) Kader, A. A. Biochemical and physiological basis for effects of controlled and modified atmospheres on fruits and vegetables. *Food Technol.* **1986**, *40* (99−100), 102−104.
(25) Zagory, D.; Kader, A. A. Modified atmosphere packaging of fresh produce. *Food Technol.* **1988**, *42*, 70−77.
(26) Díaz-Mula, H. M.; Martínez-Romero, D.; Castillo, S.; Serrano, M.; Valero, D. Modified atmosphere packaging of yellow and purple plum cultivars. 1. Effect on organoleptic quality. *Postharvest Biol. Technol.* **2011**, *61*, 103−109.
(27) Meir, S.; Akerman, M.; Fuchs, Y.; Zauberman, G. Further studies on the controlled atmosphere storage of avocados. *Postharvest Biol. Technol.* **1995**, *5*, 323−330.
(28) Ramin, A. A.; Khoshbakhat, D. Effects of microperforated polyethylene bags and temperatures on the storage quality of acid lime fruits. *Am.-Eurasian J. Agric. Environ. Sci.* **2008**, 590−594.
(29) Martínez-Romero, D.; Guillén, F.; Castillo, S.; Valero, D.; Serrano, M. Modified atmosphere packaging maintains quality of table grapes. *J. Food Sci.* **2003**, *68*, 1838−1843.
(30) Van de Velde, F.; Güemes, D. R.; Piagentini, A. M.; Pirovani, M. E. Health potential and physicochemical attributes after minimal processing and during refrigerated storage of orange (*Citrus sinensis* L., Osbeck). *Int. J. Fruit Sci.* **2013**, *13*, 285−298.
(31) Miller, N. J.; Rice-Evans, C. A. The relative contributions of ascorbic acid and phenolic antioxidants to the total antioxidant activity of orange and apple fruit juices and blackcurrant drink. *Food Chem.* **1997**, *60*, 331−337.
(32) Wolucka, B. A.; Goossens, A.; Inzé, D. Methyl jasmonate stimulates the de novo biosynthesis of vitamin C in plant cell suspensions. *J. Exp. Bot.* **2005**, *56*, 2527−2538.
(33) Huang, R.; Xia, R.; Lu, Y.; Hu, L.; Xu, Y. Effect of pre-harvest salicylic acid spray treatment on post-harvest antioxidant in the pulp and peel of 'Cara Cara' navel orange (*Citrus sinenisis* L. Osbeck). *J. Sci. Food Agric.* **2008**, *88*, 229−236.
(34) Barth, M. M.; Kerbel, E. L.; Perry, A. K.; Schmidt, S. J. Modified atmosphere packaging affects ascorbic acid, enzyme activity and market quality of broccoli. *J. Food Sci.* **1993**, *58*, 140−143.
(35) Baldwin, E. A.; Nisperos-Carriedo, M.; Shaw, P. E.; Burns, J. K. Effect of coatings and prolonged storage conditions on fresh orange flavor volatiles, degrees brix, and ascorbic acid levels. *J. Agric. Food Chem.* **1995**, *43*, 1321−1331.
(36) Guan, J. F.; Dou, S. The effect of MAP on quality and browning of cold-stored plum fruits. *J. Food Agric. Environ.* **2010**, *8*, 113−116.
(37) Alasalvar, C.; Al-Farsi, M.; Quantick, P. C.; Shahidi, F.; Wiktorowicz, R. Effect of chill storage and modified atmosphere packaging (MAP) on antioxidant activity, anthocyanins, carotenoids, phenolics and sensory quality of ready-to-eat shredded orange and purple carrots. *Food Chem.* **2005**, *89*, 69−76.
(38) Katz, E.; Lagunes, P. M.; Riov, J.; Weiss, D.; Goldschmidt, E. E. Molecular and physiological evidence suggests the existence of a system II-like pathway of ethylene production in non-climacteric Citrus fruit. *Planta* **2004**, *219*, 243−252.
(39) Tundis, R.; Loizzo, M. R.; Menichini, F. An overview on chemical aspects and potential health benefits of limonoids and their derivatives. *Crit. Rev. Food Sci. Nutr.* **2012**, *54*, 225−250.
(40) Hasegawa, S.; Herman, Z.; Orme, E.; Ou, P. Biosynthesis of limonoids in Citrus: Sites and translocation. *Phytochem. Rev.* **1986**, *25*, 2783−2785.
(41) Bourgaud, F.; Hehn, A.; Larbat, R.; Doerper, S.; Gontier, E.; Kellner, S.; Matern, U. Biosynthesis of coumarins in plants: A major

DOI: 10.1021/jf505278x
J. Agric. Food Chem. 2015, 63, 1020−1028

pathway still to be unravelled for cytochrome P450 enzymes. *Phytochem. Rev.* **2006**, *5*, 293−308.
(42) Girennavar, B.; Jayaprakasha, G. K.; Patil, B. S. Influence of pre- and post-harvest factors and processing on the levels of furocoumarins in grapefruits (*Citrus paradisi* Macfed.). *Food Chem.* **2008**, *111*, 387−392.
(43) Girennavar, B.; Jayaprakasha, G. K.; Jifon, J. L.; Patil, B. S. Variation of bioactive furocoumarins and flavonoids in different varieties of grapefruits and pummelo. *Eur. Food Res. Technol.* **2008**, *226*, 1269−1275.
(44) Sanchez-Ballesta, M. T.; Lafuente, M. T.; Zacarias, L.; Granell, A. Involvement of phenylalanine ammonia-lyase in the response of Fortune mandarin fruits to cold temperature. *Physiol. Plant.* **2000**, *108*, 382−389.
(45) Oufedjikh, H.; Mahrouz, M.; Amiot, M. J.; Lacroix, M. Effect of γ-irradiation on phenolic compounds and phenylalanine ammonia-lyase activity during storage in relation to peel injury from peel of *Citrus clementina* Hort. Ex. Tanaka. *J. Agric. Food Chem.* **2000**, *48*, 559−565.
(46) Riov, J.; Monselise, S. P.; Kahan, R. S. Ethylene-controlled induction of phenylalanine ammonia-lyase in citrus fruit peel. *Plant Physiol.* **1969**, *44*, 631−635.
(47) Lafuente, M. T.; Zacarias, L.; Martínez-Téllez, M. A.; Sanchez-Ballesta, M. T.; Granell, A. Phenylalanine ammonia-lyase and ethylene in relation to chilling injury as affected by fruit age in citrus. *Postharvest Biol. Technol.* **2003**, *29*, 309−318.

DOI: 10.1021/jf505278x
J. Agric. Food Chem. 2015, 63, 1020−1028

isomer, and with a consistent ratio of producing strains (70−80%) regardless of where the strains are sampled.[15] Fumonisins originating from *A. niger* have previously been detected in wine and raisins[21−23] as well as Thai coffee beans where the whole fruit is used.[24] *Fusarium xylarioides* causes the Coffee Wilt Disease and thus could be another source of fumonsins because this species belongs to the *Gibberella fujikuroi* species complex that contains many fumonisin producers.[25]

The Quick, Easy, Cheap, Effective, Rugged, and Safe (QuEChERS) extraction method, originally developed for pesticides,[26] has in recent years been adopted for numerous analytical methods for mycotoxins.[1,10,27,28] The popularity lies in (i) fast sample preparation; (ii) the bulk part of contaminants are trapped in the water phase; and (iii) the possibility to mix with water for immuno-affinity or reversed phase column purification. A disadvantage is that basic and acidic mycotoxins cannot be coextracted in one step.[27]

We speculated that it was possible to change to a QuEChERS-based method and also to include the fumonisins in our OTA method for roasted coffee, currently based on immunoaffinity purification and LC-MS/MS. Looking at the functional groups, acidic QuEChERS was tested but it could not meet sensitivity requirements for OTA. Consequently, it was combined with anion exchange solid phase extraction (SPE) where mixed mode anion-exchange was the most promising.

MATERIALS AND METHODS

Chemicals. Acetonitrile (MeCN), methanol, 2-propanol, and formic acid were LC-MS grade and purchased from Sigma-Aldrich (St. Louis, MO). $MgSO_4$, NaCl, H_2PO_4, and KH_2PO_4 were analytical grade and purchased from Sigma-Aldrich. Water was purified with a Milli-Q purification system (Millipore, Bedford, MA). Fumonisin standards (a mixture of FB_1 and FB_2, both at 50 μg/mL), OTA (10 μg/mL), fully ^{13}C-labeled FB_2 ($^{13}C_{34}$−FB_2, 10 μg/mL) and OTA ($^{13}C_{20}$-OTA, 10 μg/mL) were purchased from Romer Laboratories (Tulln, Austria). FB_3 was acquired from Sigma-Aldrich as a 50 μg/mL solution. All toxin solutions were stored at −20 °C.

Roasting of Green Coffee. Selected green coffee samples of about 150 g were roasted in a Helios electrical oven (Struers, Denmark). The oven temperature was set at 200 °C, and the roasting level was controlled by regularly monitoring the coffee color changes for about 20 min until a color similar to medium roasted beans was obtained.

Extraction and Purification. Ground green (5.0 g), roasted (5.0 g), or instant coffee (2.0 g) was shaken with 40 mL of MeCN/water/formic acid (49:49:2, v/v/v) for 15 min at room temperature and centrifuged at 4500*g* for 10 min. The supernatant, approximately 30 mL, was transferred to a new tube, and 4.0 g of $MgSO_4$ and 1 g of NaCl were added. After 10 min of shaking, the tube was centrifuged at 4500*g* for 10 min and filtered through a Whatman No. 4 filter (Brentford, U.K.). From this mixture, 1.9 mL was transferred to a new tube, and 50 μL U−^{13}C-OTA (0.05 μg/mL), 50 μL U−^{13}C-FB_2 (0.05 μg/mL), and 9 mL of water were added, and the tube was centrifuged at 4500*g* for 10 min.

The sample was then transferred to a 200 mg Oasis Max 60 μm cartridge (Waters, Milford, MA, U.S.A.) and passed through the cartridge. The cartridge had previously been conditioned sequentially with 3 mL of methanol and 3 mL of water. Two other brands of mixed mode columns were also tested, also 200 mg: Bond Elute Plexa PAX (Agilent, Waldbronn, Germany) and Evolute AX (Biotage, Uppsala, Sweden).

Columns were sequentially washed by 4 mL of 0.1 M H_2PO_4/$KHPO_4$ (pH 7.2), 4 mL of methanol, and 4 mL of MeCN, and the toxins were eluted by 3 mL of MeCN containing 2% formic acid into a 4 mL acid washed glass vial (Scherf-Präzision Europa GmbH, Meiningen, Germany). Samples were evaporated to dryness with N_2 at 50 °C and kept at −20 °C until analysis.

UHPLC-MS/MS. Samples were vortexed with 400 μL of MeCN/water (1:1, v/v) and transferred directly to a 2 mL autosampler vial. UHPLC-MS/MS was performed on an Agilent 1290 system equipped with a cooled Agilent G4226A auto sampler (tray at 5 °C), a 100 mm × 2 mm inner diameter i.d. 2.6 μm, Poroshell C_6−Phenyl column (Agilent) held at 40 °C and coupled to an Agilent 6490 i-funnel triple quadruple mass spectrometer equipped with the Jet Stream ESI source.

Unless otherwise stated, 1 μL of extract was injected and eluted at a flow rate of 0.4 mL/min using a water (containing 20 mM formic acid)-MeCN (with 20% isopropanol) gradient system starting from 10% MeCN, with a linear increase to 75% in 7.5 min, then to 100% in 1.5 min, holding this for 3 min, then back to 10% MeCN in 0.1 min, holding this for 2.5 min. Other gradient compositions were initially tested.

To avoid carry-over, the Agilent 1290 auto sampler was operated in the flow-through-needle mode and further coupled to an Agilent Flex cube, which was used to back flush the needle seat for 15 s at a flow of 4 mL/min with each of these components: (i) isopropanol-0.2% NH_4OH (1:1 v/v); (ii) MeCN with 2% formic acid; (iii) water with 2% formic acid. To further lower carry-over, the auto sampler valve was switched between main and bypass twice prior to sample injection and further 12 times between 9.5 to 13.5 min while the gradient was at 100% organic and down to 10% at the start conditions.

Ion source conditions were the following: gas temperature 180 °C; gas flow 12 L/min; nebulizer 20 psi; sheath gas temperature 350 °C and flow 12 L/min; capillary 3500 V.

MS was operated in ESI^+ in the dynamic multiple reaction monitoring (MRM) mode using the $[M + H]^+$ ions as the precursor ions. The multiplier was raised 150 V from the autotune value, the ion-funnel fragmentor at 380 V, and all MRM analyses were done at unit resolution for both quadrupoles.

MRM settings were for FB_1, RT 4.48 min, precursor *m*/*z* 722.4 and fragments *m*/*z* 352.3 (collision energy, 37 eV) and *m*/*z* 334.3 (37 eV) ratio 125% (ratio of quantifier and qualifier ion peak areas); FB_6, RT 5.14 min, precursor *m*/*z* 722.4 and fragments *m*/*z* 370.3 (40 eV) and *m*/*z* 352.3 (38 eV) ratio 63%; FB_3, RT 4.97 min, precursor *m*/*z* 706.4 and fragments *m*/*z* 354.3 (35 eV) and *m*/*z* 318.3 (42 eV) ratio 65%; FB_2, RT 5.31 min, precursor *m*/*z* 706.4 and fragments *m*/*z* 354.3 (35 eV) and *m*/*z* 318.3 (42 eV) ratio 90%; U−^{13}C-FB_2, precursor *m*/*z* 740.5 and fragment *m*/*z* 354.3 (35 eV); FB_4, RT 5.79 min, precursor *m*/*z* 690.4 and fragments *m*/*z* 338.3 (34 eV) and *m*/*z* 320.3 (38 eV) ratio 100%; OTA, RT 6.74 min, precursor *m*/*z* 404.2 and fragments *m*/*z* 239.1 (25 eV) and *m*/*z* 102.1 (70 eV) ratio 42%; and U−^{13}C-OTA, precursor 424.2 and fragments 250.1 (25 eV).

Data were integrated in Agilent MassHunter Quant B6.00 Software and copied to Microsoft Excel for quantification. Chromatograms were smoothed using a Gaussian width of 5 scans.

Calibration. Matrix-matched calibration curves were used throughout this study by spiking blank whole samples of roasted, green, and instant coffee. The spike levels including the blank for each coffee type were 0, 2, 5, and 10 μg/kg of OTA and 0, 20, 50, and 100 μg/kg of FB_2, respectively. The spiked samples were stored uncapped overnight at room temperature to allow solvent evaporation and to achieve equilibrium between the analytes and matrix. The following day, all samples were passed through the entire cleanup process as described above. The calibration curves were constructed by plotting the peak area of the analytes divided by the peak area of the respective internal standards of $^{13}C_{20}$-OTA and $^{13}C_{34}$−FB_2 versus the analyte standard concentrations. For determination of OTA and FB_2 in real samples of roasted, green, and instant coffee, the peak area ratio between the analyte and its internal standard was used, and all concentrations were calculated by using the obtained linear calibration equation. The limits of detection (LOD) and quantification (LOQ) were calculated as 3 times and 6 times the standard deviation on the lowest points of the calibration curve for OTA and FB_2, respectively.

The addition of isotope-labeled internal standards before the extraction was not considered as an option in this study for determination of extraction recovery due to the high costs associated with the high amounts of internal standards needed.

Method Performance and Validation. Validation was done for each sample type of roasted, green, and instant coffee at the levels

DOI: 10.1021/jf504254q
J. Agric. Food Chem. 2015, 63, 1029−1034

Table 1. Validation Data (Deviation between Measured and Spiked Levels in %) from Ochratoxin A and Fumonisin B_2 Spiked in Blind Samples of Roasted, Green, and Instant Coffee

		roasted coffee			green coffee			instant coffee		
		deviation (%)			deviation (%)			deviation (%)		
	μg/kg	av	max	*n*	av	max	*n*	av	max	*n*
OTA	2	5.8	6.7	10	1.9	7.0	6	6.8	28	6
	5	4.2	13	10	3.3	13	6	4.4	18	6
	10	1.2	2.0	9	0.9	3.4	5	0.7	3.4	5
	LOQ[a]		1.3 μg/kg			0.46 μg/kg			2.0 μg/kg	
	LOD[b]		0.5 μg/kg			0.3 μg/kg			1 μg/kg	
FB_2	20	5.0	17	9	1.1	6.5	6	5.0	17	6
	50	3.6	14	9	4.0	14	6	4.0	14	6
	100	1.1	3.5	8	1.0	3.1	5	0.6	3.1	5
	LOQ[a]		12 μg/kg			3.2 μg/kg			13 μg/kg	
	LOD[b]		2 μg/kg			2 μg/kg			4 μg/kg	

[a]LOD, limit of detection as estimated by 3 times the standard deviation of the lowest calibration level. [b]LOQ, limit of quantification as estimated by a signal-to-noise ratio of 6:1.

described above, on 5−10 different days for each matrix using three different operators for the sample preparation.

The extraction recovery was assessed in eluates prepared by QuEChERS extraction of blank samples of roasted, green, and instant coffee followed by SPE purification on Oasis Max as described above. The eluates were then spiked with OTA and FB_2 within the same concentration range as for the not purified samples corresponding to the following levels: (i) 3.13 ng/mL of OTA and FB_2; (ii) 6.25 ng/mL of OTA and FB_2; (iii) 9.38 ng/mL of OTA and FB_2; and lastly with (iv) 12.5 ng/mL of OTA and FB_2. These standard calibration curves were used to measure the extraction recovery in each coffee type at the three spiking levels of OTA (2, 5, and 10 μg/kg) and FB_2 (20, 50, and 100 μg/kg), respectively.

Signal suppression and enhancement due to matrix effects was evaluated as the MS signal response areas between standards of OTA and FB_2 dissolved in MeCN containing 2% formic divided by the response area of the standards prepared in the blank eluates as described above.

A roasted coffee sample with a certified level of OTA of 4.36 μg/kg was obtained from the Food Analysis Performance Assessment Scheme (FAPAS, The Food and Environment Research Agency, Sand Hutton, U.K.) and was analyzed on 4 different days and processed in the same way as described for the samples. The Z-score specified by FAPAS is considered as satisfactory for $Z \leq 2$ (numeric value) corresponding to a concentration range between 2.44 and 6.27 μg/kg.

RESULTS AND DISCUSSION

Extraction and Purification. As a start, dry acidic MeCN was tested and it provided very clean extracts, but unfortunately the extraction recoveries were inconsistent. Using an acidic QuEChERS, it was visually apparent that the major part of the colored contaminants were present in the lower discardable water phase. Further initial tests comparing mixed mode versus normal silica based SAX columns showed that the mixed mode columns provided higher recoveries.

A strong ion exchanger compared to a wear anion exchanger was chosen because phospholipids, for example, known to induce ion-suppression,[13,29] are much more strongly bound than the carboxylic acid containing analytes that will become uncharged during elution with formic acid.

During method development, both phosphoric acid and formic acid were tested. The latter gave higher recoveries (>30%) on the Oasis MAX columns. Finally, we also tried to minimize the amount of water added to the QuEChER extract before cleanup on SPE columns. We found that addition of less than 4.5 mL water per mL of MeCN supernatant was the minimum. Thus, addition of less water decreased the recovery of FB_2 significantly, which shows that FB_2 is mainly retained by reversed-phase action. Two other brands of mixed mode columns (Agilent Bond Elute Plexa PAX and Biotage Evolute AX) were also investigated. However, both gave approximately 50% lower recoveries when tested at the same conditions as the Oasis MAX columns (results not shown). During method development, different glass and polypropylene vials were tested for evaporation of the SPE eluate. Loss of up to 75% of FB_2 was observed in single-use glass reagent tubes, whereas less but still up to 40% was lost on 15 mL polypropylene centrifuge tubes, with the lowest on acid washed and silanized glass vials. The loss of FB_2 was about half when the coffee matrix was present and insignificant for OTA with and without matrix. This suggested that the amine group of the fumonisins could be bound to the free silanol groups on the glass surface of the used test tubes. Interestingly, polypropylene was still not as good as acid washed glass and shows that for evaporation of fumonisin solutions, strict control with tubes/vials quality is necessary.

UHPLC-MS/MS Optimization. It was not possible to avoid the SPE purification by direct injection of the QuEChERS extract, but even with a reduced sample load compared to the SPE purified extracts, signal strength was much lower and many interfering peaks were observed. Even with the SPE purification, the relatively flat gradient was needed to elute polar impurities, especially interfering with OTA.

During the SPE fine-tuning, we also tested pure MeCN against MeCN with 20% isopropanol as LC solvent B (kindly suggested by Joachim Thiemann, Agilent Technologies). Here, the 20% isopropanol gave for green coffee 95−113% higher signal for OTA in the range 1−10 μg/kg (n = 8) range) and 55−75% higher signal for FB_2 in the range 10−100 μg/kg (n = 8)). In instant coffee tested at the same concentrations, the effect was less pronounced with 20−30% higher signal for OTA but the same 54−83% for FB_2. Finally, in roasted coffee tested at the same concentrations, the increase was 57−74% for FB_2 but only 20−40% for OTA. Besides better signals, the R^2 for signal versus concentrations of all the above-mentioned comparisons also increased typically from 0.998 to 0.999.

Due to the 50% MeCN in water (v/v) used for redissolving the sample, the maximum injection volume was 1 μL. When higher volumes were used, the eluted peaks were broader and ion-suppression was more pronounced. The elaborate injector

DOI: 10.1021/jf504254q
J. Agric. Food Chem. 2015, 63, 1029−1034

Table 2. Extraction Recoveries for OTA and FB_2 Spiked in Blind Samples of Roasted, Green, and Instant Coffee[a]

	spike level	roasted			green			instant		
	μg/kg	n_{total}	ER (%)	RSD(%)	n_{total}	ER (%)	RSD (%)	n_{total}	ER (%)	RSD (%)
OTA	2	4	79	17	3	82	14	3	90	2
	5	4	76	12	3	90	17	3	81	16
	10	4	76	8	3	86	25	3	93	16
FB_2	20	3	38	8	3	64	4	3	37	4
	50	3	36	10	3	59	8	3	37	6
	100	3	40	12	3	58	6	3	38	4

[a]Number of samples spiked on different levels and days (n_{total}), average extraction recovery (ER), relative standard deviation (RSD).

Table 3. Overview of Analyzed Retail Samples of Roasted, Green, and Instant Coffee Purchased in Denmark, Kenya, Tanzania, and Uganda

		ochratoxin A				fumonisin B_2			fumonisins B_4 + B_6[a]		
	n	positive (%)	av[b] (μg/kg)	above[c] regulatory level (%)	max (μg/kg)	positive (%)	av[b] (μg/kg)	max (μg/kg)	positive (%)	av[b] (μg/kg)	max (μg/kg)
roasted	57	46	2.3	8.8	21	ND[d]	ND	ND	ND	ND	ND
green	18	40	1.7	none	2.8	44	25	134	44	6.3	30
instant	25	56	4.5	none	8.3	ND	ND	ND	ND	ND	ND

[a]Sum of FB_4 and FB_6 assuming same response factor as FB_2. [b]Average of positive samples above LOQ. [c]5 μg/kg in roasted and green coffee, 10 μg/kg in instant coffee. [d]ND, not detected.

cleaning program using the extra Agilent flex-cube module was necessary, as the default methanol cleaning of the needle and flow during the gradient gave a carry-over of >1:5000 of both fumonisins and OTA, presumably the carry-over occurs in the valve system and to some extend in the needle seat. The chromatographic gradient could resolve all the fumonisins FB_1, FB_2, FB_3, FB_4, and FB_6. Standards of FB_4 and FB_6 were only available in very limited amounts and were therefore not validated. In the present study, the two compounds were quantitated using their peak areas relative to the FB_2 peak multiplied with the measured FB_2 amount in the sample. Eluting in a close window with almost the same percent organic solvent, and all having a free amino group where the charge resides,[30] fumonisins ionize almost equally. However, with MS/MS, FB_4 will probably be overestimated by 20−30% because it has one hydroxyl group fewer than FB_2 and thus less possible fragment ions due to one less possible water loss. Conversely, FB_6 can lose one more water molecule than FB_2, resulting in more fragment ions giving a lower response.

Validation. Because most coffee sold in Denmark is roasted ground, this was validated on 10 different days, whereas green and instant coffee were validated for only 5 days.

As seen in Table 1, the average deviation for OTA in roasted coffee was <6%, although with the maximum close to 13% (n = 10), which is fully acceptable. The deviation for fumonisin was very similar and surprisingly comparable to the results of the two other matrices. We have expected a lower amount in the green coffee as it contains fewer impurities.

The deviation can probably be lowered by adding the ^{13}C internal standards to the dry coffee prior to extraction (correcting for differences in losses during the QuEChERS extraction), but this would make the method much more costly due to a higher consumption of internal standards.

The sensitivity did vary considerably over 1 year due to instrument cleaning, a problem with the electronics controlling Q1 (required the unit to be changed), and numerous other projects running on the instrument. The LOD and LOQ values as listed in Table 1 were worst case determined limits. Actual values were in most cases much better (5−10-fold). However, with the regulatory limit of OTA being higher, no problem exists, and the slightly higher limits for fumonisins are not a problem as they are far less toxic than OTA.

Table 2 shows the recoveries of the sample preparation procedure including both the QuEChERS extraction and the SPE purification. As shown, the recovery was independent of the level for both target groups but depended on the matrix for FB_2, as the recovery was significantly lower in instant and roasted coffee than green coffee. This shows that quantification needs to be done from the spiked matrix.[31,32] Overall, the recovery of OTA was very satisfactory with a recovery above 75% in all sample matrices. For FB_2, it was 40% but reproducible, which has also been observed elsewhere.[33] The low recovery is corrected by the matrix-matched calibration, but the value is still below 60%, which is the requirement for EU methods. However, given the lack of regulatory limit for fumonisins in coffee, good recovery for the regulated compound OTA, as well as the possibility of adding ^{13}C-labeled internal standards, the method remains sound and is significantly cheaper than alternatives.

The loss must be due to the zwitterionic nature of FB_2 where it can be speculated that the amine binds to acid interfering substances in the aqueous water phase. In a recent study, QuEChERS combined with cleanup by immuno-affinity columns was described for the analysis of different mycotoxins in green coffee and other food products including OTA, FB_1, and FB_2.[1] The recovery for OTA was very similar to our findings with green coffee. However, no validation data was reported for FB_1 and FB_2 in their green coffee samples.[1]

All three matrices still showed a slight but consistent signal enhancement for OTA. This was 10−40% for instant coffee, 20−50% for roasted coffee, and 10−40% for green coffee. For FB_2, the matrix effect was more variable with −10 to +30% for instant coffee, 10−70% for roasted, and −10 to +60% for green coffee. This shows that it is necessary to use ^{13}C-labeled internal standards to correct for this effect.[31,32]

The trueness of the method was investigated by determining the OTA content in a roasted reference material obtained from FAPAS with an assigned value of 4.36 μg/kg. This sample was analyzed four times over a period of 6 months on different days.

DOI: 10.1021/jf504254q
J. Agric. Food Chem. 2015, 63, 1029−1034

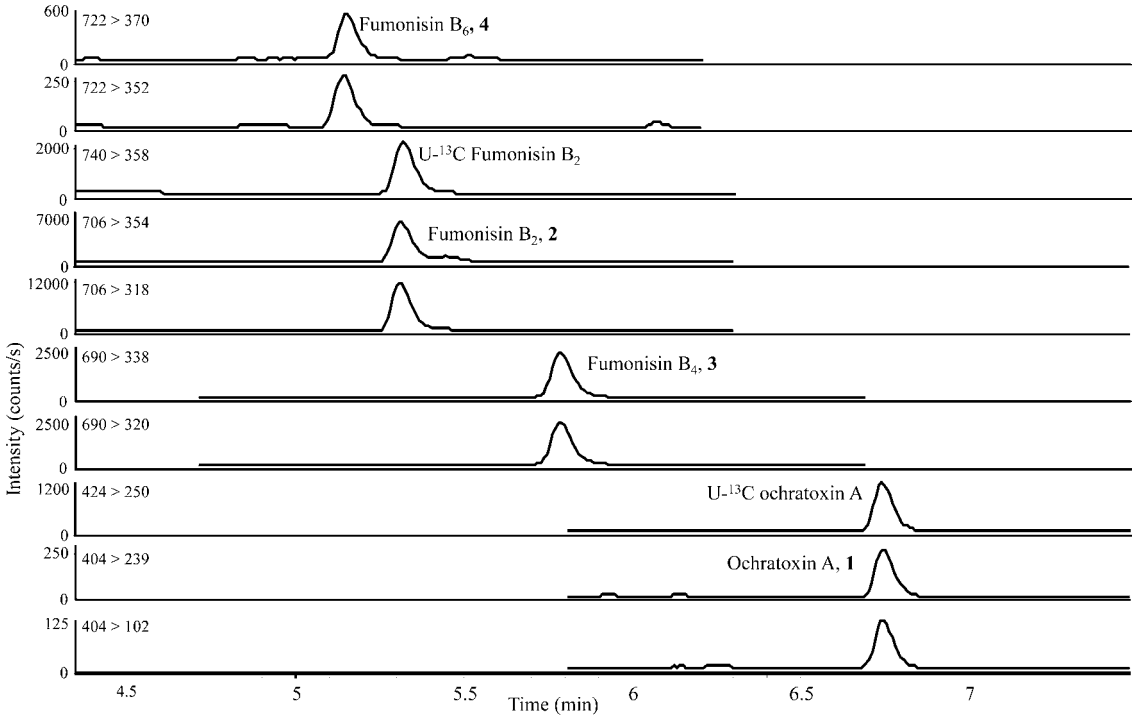

Figure 2. MRM chromatogram from naturally infected green coffee containing fumonisins B_6 (5 μg/kg*), B_2 (134 μg/kg), and B_4 (25 μg/kg) as well as ochratoxin A (2.4 μg/kg). *Below calculated LOQ of fumonisin B_2.

The concentrations of OTA were measured to be 6.04, 5.71, 5.47, and 6.67 μg/kg, respectively. The Z score specified by FAPAS is considered to be satisfactory if the measured result of OTA is between 2.44 and 6.27 μg/kg. This means that three of the results are within this range, whereas the latter was determined to be slightly high.

Retail Samples. In Table 3, an overview of the screened retail samples is listed. For the roasted samples, all purchased in Denmark, about 10% of the samples were above the regulatory level of 5 μg/kg.

Instant coffee did not contain levels above the regulatory limit for OTA and neither did the green coffees, but for the latter, almost half of the samples (purchased in Kenya and Tanzania) contained fumonisins in levels up to 164 μg/kg fumonisins (sum of the three isomers), as illustrated in Figure 2. The fumonisin profile of $FB_2 > FB_4 > FB_6$ and no FB_1 nor FB_3 showed that *A. niger* was the producing organism and not *Fusarium* spp.,[15] and thus, this is the widespread contamination presumably occurring when drying fruits are on/in the soil where *A. niger* is found.[34] This finding combined with the lack of fumonisins in the processed coffee samples suggested that the fumonisins decompose during roasting. This was confirmed by the roasting of a sample containing 164 μg/kg fumonisins, which after 20 min of roasting (medium roast as judged by the color) did not contain any measurable traces of fumonisins. Although the roasting process was not conducted at true production conditions, the OTA content in this sample was reduced from 2.4 to 0.5 μg/kg corresponding to a reduction of approximately 80%. This value is comparable to other studies of OTA reduction during green coffee roasting.[35]

To summarize, a method for the simultaneous analysis of OTA and fumonisins was developed for the three major coffee types using a combination of QuEChERS, mixed-mode anion exchange and UHPLC-MS/MS. Screening of 57 roasted coffee samples from nine countries showed that OTA is present in approximately half of the samples. The regulatory limit of 5 μg/kg was exceeded in five of these samples with a maximum obtained value of 21 μg/kg. Fumonisins were not detected in any of the roasted (n = 25) and instant coffee samples (n = 25). However, in green coffee, fumonisins were found in 44% of the analyzed samples (n = 18) with a maximum value of 164 μg/kg referred to the sum of fumonisin B_2, B_4, and B_6. A roasting study with several samples of the fumonisin-contaminated green coffee showed that they totally decomposed, which also explains the lack of detection in the roasted and instant coffee samples.

AUTHOR INFORMATION

Corresponding Author

*E-mail: phra@food.dtu.dk. Tel.: +45- 3588 7486. Fax: +45-35887448.

Present Address

#Tanganyika Instant Coffee Company Limited, Box 410, Bukoba, Tanzania.

Funding

Funding for this study was provided by the Danish Veterinary and Food Administration (Cocktail- 2011-14) and the EEC project MycoRed (KBBE-2007-222690-2).

Notes

The authors declare no competing financial interest.

ACKNOWLEDGMENTS

We are grateful to Agilent Technologies for the Thought Leader Donation of the UHPLC-QqQ system.

REFERENCES

(1) Desmarchelier, A.; Tessiot, S.; Bessaire, T.; Racault, L.; Fiorese, E.; Urbani, A.; Chan, W. C.; Cheng, P.; Mottier, P. Combining the quick, easy, cheap, effective, rugged and safe approach and clean-up by immunoaffinity column for the analysis of 15 mycotoxins by isotope

DOI: 10.1021/jf504254q
J. Agric. Food Chem. 2015, 63, 1029−1034

dilution liquid chromatography tandem mass spectrometry. *J. Chromatogr. A* **2014**, *1337*, 75−84.
(2) Scott, P. M. Recent research on fumonisins: a review. *Food Addit. Contam., Part A* **2012**, *29*, 242−248.
(3) Monaci, L.; Palmisano, F. Determination of ochratoxin A in foods: state-of-the-art and analytical challenges. *Anal. Bioanal. Chem.* **2004**, *378*, 96−103.
(4) Bandeira, R. D. C. C.; Uekane, T. M.; da Cunha, C. P.; Geaquinto, L. R. O.; Cunha, V. S.; Caixeiro, J. M. R.; Godoy, R. L. O.; de la Cruz, M. H. C. Development and validation of a method for the analysis of ochratoxin A in roasted coffee by liquid Chromatography/electrospray-mass spectrometry in tandem (LC/ESI/MS/MS). *Quim. Nova* **2012**, *35*, 66−71.
(5) Commission regulation (EC) No. 1881/2006 of December 19, 2006 setting maximum levels for certain contaminants in foodstuffs. Revised September 1, 2012. Commission of the European Communities: Brussels. http://eur-lex.europa.eu/LexUriServ/LexUriServ.do?uri=CONSLEG:2006R1881:20120901:EN:PDF (accessed November 29, 2014).
(6) Varga, E.; Glauner, T.; Berthiller, F.; Krska, R.; Schuhmacher, R.; Sulyok, M. Development and validation of a (semi-)quantitative UHPLC-MS/MS method for the determination of 191 mycotoxins and other fungal metabolites in almonds, hazelnuts, peanuts and pistachios. *Anal. Bioanal. Chem.* **2013**, *405*, 5087−5104.
(7) Sulyok, M.; Krska, R.; Schuhmacher, R. Application of an LC-MS/MS based multi-mycotoxin method for the semi-quantitative determination of mycotoxins occurring in different types of food infected by moulds. *Food Chem.* **2010**, *119*, 408−416.
(8) Sørensen, J. L.; Phipps, R. K.; Nielsen, K. F.; Schroers, H. J.; Frank, J.; Thrane, U. Analysis of *Fusarium avenaceum* metabolites produced during wet apple core rot. *J. Agric. Food Chem.* **2009**, *57*, 1632−1639.
(9) Spanjer, M. C.; Rensen, P. M.; Scholten, J. M. LC-MS/MS multi-method for mycotoxins after single extraction, with validation data for peanut, pistachio, wheat, maize, cornflakes, raisins and figs. *Food Addit. Contam., Part A* **2008**, *25*, 472−489.
(10) Yogendrarajah, P.; Van Poucke, C.; De Meulenaer, B.; De Saeger, S. Development and validation of a QuEChERS based liquid chromatography tandem mass spectrometry method for the determination of multiple mycotoxins in spices. *J. Chromatogr. A* **2013**, *1297*, 1−11.
(11) Schenzel, J.; Schwarzenbach, R. ü. P.; Bucheli, T. D. Multi-residue screening method to quantify mycotoxins in aqueous environmental samples. *J. Agric. Food Chem.* **2010**, *58*, 11207−11217.
(12) Herebian, D.; Zuhlke, S.; Lamshoft, M.; Spiteller, M. Multi-mycotoxin analysis in complex biological matrices using LC-ESI/MS: Experimental study using triple stage quadrupole and LTQ-Orbitrap. *J. Sep. Sci.* **2009**, *32*, 939−948.
(13) Sørensen, L. M.; Mogensen, J.; Nielsen, K. F. Simultaneous determination of ochratoxin A, mycophenolic acid and fumonisin B_2 in meat products. *Anal. Bioanal. Chem.* **2010**, *398*, 1535−1542.
(14) Taniwaki, M. H.; Pitt, J. I.; Teixeira, A. A.; Iamanaka, B. T. The source of ochratoxin A in Brazilian coffee and its formation in relation to processing methods. *Int. J. Food Microbiol.* **2003**, *82*, 173−179.
(15) Frisvad, J. C.; Larsen, T. O.; Thrane, U.; Meijer, M.; Varga, J.; Samson, R. A.; Nielsen, K. F. Fumonisin and ochratoxin production in industrial *Aspergillus niger* strains. *PLoS One* **2011**, *6*, e23496.
(16) Accensi, F.; Abarca, M. L.; Cano, J.; Figuera, L.; Cabanes, F. J. Distribution of ochratoxin A producing strains in the A-niger aggregate. *Anton. Leeuwenhoek* **2001**, *79*, 365−370.
(17) Abarca, M. L.; Bragulat, M. R.; Castella, G.; Cabanes, F. J. Ochratoxin A production by strains of *Aspergillus niger* var *niger*. *Appl. Environ. Microbiol.* **1994**, *60*, 2650−2652.
(18) Magnoli, C.; Violante, M.; Combina, M.; Palacio, G.; Dalcero, A. Mycoflora and ochratoxin-producing strains of *Aspergillus* section Nigri in wine grapes in Argentina. *Lett. Appl. Microbiol* **2003**, *37*, 179−184.
(19) Mogensen, J. M.; Frisvad, J. C.; Thrane, U.; Nielsen, K. F. Production of fumonisin B_2 and B_4 by *Aspergillus niger* in raisins and grapes. *J. Agric. Food Chem.* **2010**, *58*, 954−958.
(20) Månsson, M.; Klejnstrup, M. L.; Phipps, R. K.; Nielsen, K. F.; Frisvad, J. C.; Godtfredsen, C. H.; Larsen, T. O. Isolation and characterization of fumonisin B_6, a new fumonisin from *Aspergillus niger*. *J. Agric. Food Chem.* **2010**, *58*, 949−953.
(21) Knudsen, P. B.; Mogensen, J. M.; Larsen, T. O.; Nielsen, K. F. Occurrence of fumonisins B_2 and B_4 in retail raisins. *J. Agric. Food Chem.* **2011**, *59*, 772−776.
(22) Mogensen, J. M.; Larsen, T. O.; Nielsen, K. F. Widespread occurrence of the mycotoxin fumonisin B_2 in wine. *J. Agric. Food Chem.* **2010**, *58*, 4853−4857.
(23) Logrieco, A.; Ferracane, R.; Visconti, A.; Ritieni, A. Natural occurrence of fumonisin B_2 in red wine from Italy. *Food Addit. Contam., Part A* **2010**, *27*, 1136−1141.
(24) Noonim, P.; Mahakarnchanakul, W.; Nielsen, K. F.; Frisvad, J. C.; Samson, R. A. Fumonisin B_2 production by *Aspergillus niger* from Thai coffee beans. *Food Addit. Contam., Part A* **2009**, *26*, 94−100.
(25) Geiser, D. M.; Ivey, M. L. L.; Hakiza, G.; Juba, J. H.; Miller, S. A. *Gibberella xylatioides* (anamorph: *Fusarium xylarioides*), a causative agent of coffee wilt disease in Africa, is a previously unrecognized member of the *G. fujikuroi* species complex. *Mycologia* **2005**, *97*, 191−201.
(26) Anastassiades, M.; Lehotay, S. J.; Stajnbaher, D.; Schenck, F. J. Fast and easy multiresidue method employing acetonitrile extraction/partitioning and "dispersive solid-phase extraction" for the determination of pesticide residues in produce. *J. AOAC Int.* **2003**, *86*, 412−431.
(27) Rasmussen, R. R.; Storm, I. M. L.; Rasmussen, P. H.; Smedsgaard, J.; Nielsen, K. F. Multi mycotoxin analysis in maize silage by LC-MS/MS. *Anal. Bioanal. Chem.* **2010**, *397*, 765−776.
(28) Sospedra, I.; Blesa, J.; Soriano, J. M.; Manes, J. Use of the modified quick easy cheap effective rugged and safe sample preparation approach for the simultaneous analysis of type A- and B-trichothecenes in wheat flour. *J. Chromatogr. A* **2010**, *1217*, 1437−1440.
(29) Chambers, E.; Wagrowski-Diehl, D. M.; Lu, Z. L.; Mazzeo, J. R. Systematic and comprehensive strategy for reducing matrix effects in LC/MS/MS analyses. *J. Chromatogr. B* **2007**, *852*, 22−34.
(30) Nielsen, K. F.; Månsson, M.; Rank, C.; Frisvad, J. C.; Larsen, T. O. Dereplication of microbial natural products by LC-DAD-TOFMS. *J. Nat. Prod.* **2011**, *74*, 2338−2348.
(31) Matuszewski, B. K.; Constanzer, M. L.; Chavez-Eng, C. M. Strategies for the assessment of matrix effect in quantitative bioanalytical methods based on HPLC-MS/MS. *Anal. Chem.* **2003**, *75*, 3019−3030.
(32) Trufelli, H.; Palma, P.; Famiglini, G.; Cappiello, A. An overview of matrix effects in liquid chromatography-mass spectrometry. *Mass Spectrom. Rev.* **2011**, *30*, 491−509.
(33) Sulyok, M.; Berthiller, F.; Krska, R.; Schuhmacher, R. Development and validation of a liquid chromatography/tandem mass spectrometric method for the determination of 39 mycotoxins in wheat and maize. *Rapid Commun. Mass Spectrom.* **2006**, *20*, 2649−2659.
(34) Varga, J.; Frisvad, J. C.; Kocsube, S.; Brankovics, B.; Toth, B.; Szigeti, G.; Samson, R. A. New and revisited species in *Aspergillus* section Nigri. *Stud. Mycol.* **2011**, 1−17.
(35) Blanc, M.; Pittet, A.; Munoz-Box, R.; Viani, R. Behavior of ochratoxin A during green coffee roasting and soluble coffee manufacture. *J. Agric. Food Chem.* **1998**, *46*, 673−675.

NOTE ADDED AFTER ISSUE PUBLICATION

The LOQ and LOD values in Table 1 were in error in the ASAP publication of January 16, 2015, and in the issue publication of January 28, 2015. The values have been corrected as of February 13, 2015.

DOI: 10.1021/jf504254q
J. Agric. Food Chem. 2015, 63, 1029−1034

functions to break down food and nutrients to be absorbed into the body, and the intestinal epithelium is the first physiological barrier after oral intake of the compounds. In order to obtain a more comprehensive insight into the cytotoxicity and apoptotic mechanisms of 7-ketophytosterols, cell viability, cell cycle analysis, and cell apoptosis induced by these compounds were studied. For comparison, the cytotoxic effects of 7-ketocholesterol (7K-CH) were also assessed in the HIC cell line. In addition, several modulators of apoptosis (caspase-3 and Bcl-2) were investigated to determine whether these compounds were responsible for the intrinsic pathway of apoptosis in HIC cancer cells.

MATERIALS AND METHODS

Materials. 7K-CH was purchased from Sigma-Aldrich Company (St. Louis, USA). 7K-ST and 7K-MIX were separately chemically synthesized from stigmasterol (Sigma-Aldrich Company, St. Louis, MO, USA) and phytosterols (Cognis, Saint-Fargeau-Ponthierry, Seine-et-Marne, France) as described by Gao et al.[28] The other three individual POPs (7K-SI, 7K-CA, and 7K-BR) were not commercially available and therefore were separated by semipreparative HPLC and characterized as described in the literature.[28] Except 7K-BR and 7K-MIX, the purity of each individual 7-ketosterol compound was ∼95%. 7K-BR contained 52% 7-ketobrassicasterol and 48% 7-ketoavenasterol, whereas the blend of 7K-MIX contained 45% 7K-SI, 32% 7K-CA, 10% 7K-BR, and 9% 7K-AV. The profile of this mixture reflected the composition of related phytosterol oxides in the plant oil.[28] The chemical structures of these compounds are available in the literature.[28]

Cell Culture and Treatment. The HIC cell line was obtained from Chinese Academy of Medical Sciences Tumor Cell Culture (Beijing, China). HIC cells were cultured in DMEM/high glucose medium (Hyclone, Beijing, China) supplemented with 10% (v/v) fetal bovine serum (FBS), 100 U/mL penicillin G sodium, and 100 μg/mL streptomycin sulfate at 37 °C and 5% CO_2 in a humidified incubator. Cells were routinely harvested by treatment with a 0.25% trypsin-EDTA solution. Cultures were allowed to reach 80% confluence before experiments were performed.

For treatment, all above-mentioned 7-ketosterols were separately dissolved in 100% ethanol and added to the cells to a final concentration of 30, 60, or 120 μM. The concentrations used here were physiologically significant and shown in some published studies.[21,22,29] Equivalent quantities of ethanol were added to the control cells, and the final concentration did not exceed 0.5% (v/v) in the culture medium. Cells were then harvested after 24 h treatment for determination of cell viability, apoptotic effect, cell cycle, caspase-3 activity, and Bcl-2 content analysis.

Cell Viability. Cell viability was determined by using the Cell Counting Kit-8 (CCK8) assay (Dojindo, Kumamoto, Japan), which is based on a reaction catalyzed by dehydrogenase of the mitochondria. Within this assay, cells were adjusted to a density of 2×10^4 cells/well in 96-well plates. After incubation with different concentrations of 7-ketosterol oxides, the culture medium was discarded, cells were washed with PBS, and then 200 μL of 10% CCK8 in culture medium was added and incubated at 37 °C for 2 h. Absorbance was read at 450 nm with a Fluostar Optima microplate reader (BMG Labtech, Ortenberg, Germany) and expressed as the viable cell number as a percentage (%) of control cells. Measurements were made in triplicates.

Cell Apoptosis and Cell Cycle Assay. HIC cells (5×10^5) were seeded in the wells of a 6-well plate and harvested by trypsinization (0.25% trypsin with EDTA) after exposure to different doses of 7-ketosterol oxides for 24 h. With the Annexin V-FITC Apoptosis Detection Kit (BD Biosciences, Franklin Lakes, NJ, USA), cells were stained with fluorescein isothiocyanate (FITC)-conjugated annexin V and propidium iodide (PI) according to the manufacturer's protocol. Apoptotic cells were then analyzed by BD FACScan flow cytometry (BD Biosciences, Franklin Lakes, NJ, USA).

For cell cycle analysis, cells were centrifuged and fixed in 2 mL of methanol/PBS (9:1, v/v) at 0 °C overnight, washed twice in PBS, and resuspended in 200 μL of PBS containing 0.25 mg/mL RNase A for 30 min and then stained in 50 μL of PI (0.2 mg/mL in PBS) with incubation in the dark at 4 °C for 30 min. The fluorescence of 1×10^4 cells was then analyzed by BD FACScan flow cytometry (BD Biosciences, Franklin Lakes, NJ, USA).

Caspase Activity Assay. The measurement of caspase-3 activity was performed using a Caspase-3 Assay Colorimetric Kits (Sigma-Aldrich, Hamburg, Germany) according to the manufacturer's protocol with some modifications. Briefly, HIC cells (1×10^6) were seeded in 60 mm culture dishes and exposed to 7-ketosterol oxides for 24 h and then collected and lysed at 0 °C. Lysates were clarified by centrifugation at 10000*g* (4 °C) for 10 min, and the supernatants were carefully transferred to a new microcentrifuge tube without disturbing the cell-debris pellet in the collection tube. Protein (50−200 ng) was incubated with 50 μL of reaction buffer and 5 μL of caspase-3 (Ac-DEVD-pNA) colorimetric substrate at 37 °C for a further 4 h. The cleavage of the peptide substrate was monitored at 405 nm using a 96-well microplate reader (Bio-Rad, Hercules, CA, USA). The samples were analyzed in triplicate.

Bcl-2 Content. The Bcl-2 level in HIC cells exposed to 7-ketosterol oxides for 24 h was quantified using a Human Bcl-2 Platinum ELISA Kit (BMS244/3, eBioscince, San Diego, CA, USA). The supernatant from cells was removed; cells (5×10^6) were washed once with PBS and harvested by scraping and gentle centrifugation. PBS was aspirated, and an intact cell pellet was frozen at −80 °C for lysis at a later date. The cultured cells were resuspended in lysis buffer and incubated 60 min at room temperature with gentle shaking, and extracts were transferred to microcentrifuge tubes and centrifuged at 1000*g* for 15 min. According to the supplier's instructions, the supernatant was added to the wells of the ELISA plate. The absorbance was measured at 450 nm using a Fluostar Optima Microplate Reader (BMG Labtech, Ortenberg, Germany), and the data were expressed as a percentage of the untreated control sample.

Statistics. All data points represented the mean value (SE) of at least three independent experiments. One-way analysis of variance (ANOVA) and the LSD test were applied to determine differences in cytotoxic effects, apoptosis effects, changes of cell-cycle arrest, and changes in expression of caspase-3 and Bcl-2 between treated and control cultures. Statistical differences were considered significant at a value of $p < 0.05$ and reported as $p < 0.05$ and $p < 0.01$.

RESULTS

Cell Viability Effects of 7-Ketosterols on HIC Cells. CCK8 cell viability assay was used to evaluate the cytotoxicity of the tested compounds after 24 h of exposure. Viability of the control sample was set at 100%. As shown in Figure 1, as the positive control, 30 and 60 μM 7K-CH caused 50% and 38% HIC cell growth inhibition ($p < 0.01$), respectively, whereas 60 μM of five 7-ketophytosterol oxides only caused 10−20% growth inhibition. This indicated that HIC cells were more sensitive to 7-ketocholesterol than 7-ketophytosterols. After treatment with 120 μM 7-ketophytosterol oxides for 24 h, all individual test compounds induced a significant reduction ($p < 0.01$) of cell viability relative to the negative control, and the cell survival was 37%, 39%, 56%, and 79% for 7K-SI, 7K-CA, 7K-BR, and 7K-ST treated cells, respectively. In contrast, 7K-MIX caused no significant change in cell viability at all test concentrations.

7-Ketophytosterols Induce Apoptosis on HIC Cells. We then elucidated whether the cytotoxic effects of 7-ketosterols were mediated through apoptosis. At low dose of 30 μM, all 7-ketophytosterol oxides caused no obvious change in the percentage of apoptotic cells. At 60 μM, there was a significant increase ($p < 0.05$) in apoptotic cells by all tested compounds treatment compared with the control group. At

DOI: 10.1021/jf505079v
J. Agric. Food Chem. 2015, 63, 1035−1041

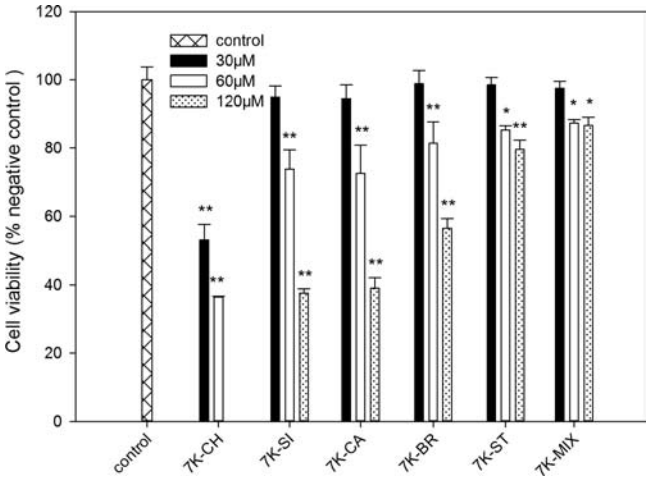

Figure 1. Cell viability measured by the CCK8-test. HIC cells were exposed to 0.5% ethanol (control), 30, 60, and 120 μM of 7-ketophytosterol oxides (7K-SI, 7K-CA, 7K-BR, 7K-ST, and 7K-MIX) or 30 and 60 μM of 7K-CH for 24 h. Values are mean ± SE of three separate experiments and are marked when significantly different from control levels (*p < 0.05, **p < 0.01).

high dose of 120 μM, 7K-SI, 7K-CA, 7K-BR, 7K-ST, and 7K-MIX caused early apoptotic cells to 64.0%, 53.6%, 17.5%, 15.9%, and 14.8%, respectively (Figure 2).

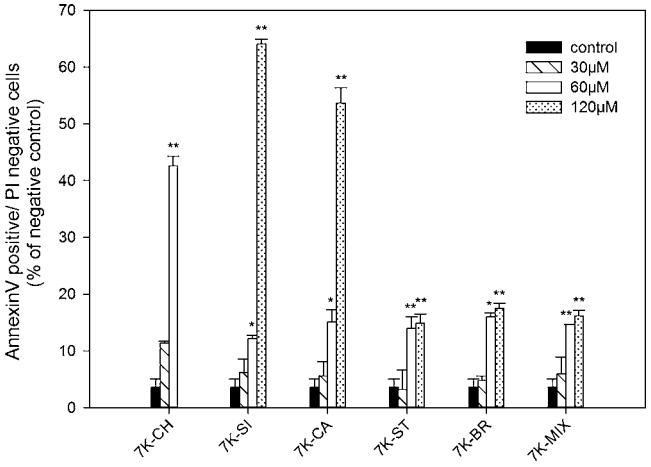

Figure 2. Percentage of apoptosis in HIC cancer cells following exposure for 24 h to 30, 60, and 120 μM of 7-ketophytosterol oxides (7K-SI, 7K-CA, 7K-BR, 7K-ST, and 7K-MIX) or 30 and 60 μM of 7K-CH. All compounds were dissolved in ethanol and equivalent quantities of ethanol were added to control cells. Apoptotic cells were assessed with fluorescein isothiocyanate (FITC)-conjugated annexin V and propidium iodide (PI). Values are mean ± SE of three separate experiments and are marked when significantly different from control levels (*p < 0.05, **p < 0.01).

Effect of 7-Ketophytosterols on Cell Cycle. The effect of 7-ketosterols on cell cycle progression was determined by flow cytometry with PI-based staining. Results showed that after 24 h of 7-ketosterol treatment, the normal cell cycle progression was disrupted in HIC cells (Figure 3). At 60 μM, 7K-CH increased the percentage of cells in G1 phase from 40.5% to 79.4% and decreased the percentage of cells in S phase from 43.5% to 25.8% (p < 0.05) (Figure 3A). In contrast, when the cells were exposed to 120 μM of 7K-SI (Figure 3B), 7K-CA (Figure 3C), or 7K-ST (Figure 3E), the proportion of cells in G1 phase decreased from 40.5% to 26.8%, from 40.2% to 34.5%, and from 39.9% to 35.3%, respectively, whereas 7K-SI and 7K-CA caused the accumulation of cells in S phase from 42.0% to 52.9% and from 41.0% to 51.5% (p < 0.05), respectively. At all concentrations tested, 7K-BR (Figure 3D) and 7K-MIX (Figure 3F) did not show a significant difference (p > 0.05) in G1 and S phases. In addition, all the tested compounds did not lead to increase in the sub-G1 phase population.

Effect of 7-Ketophytosterols on Caspase-3 Activity in HIC Cells. To assess whether 7-ketophytosterols induce caspase activation, which plays an important role in the execution phase of cell apoptosis, caspase-3 activity was evaluated. As shown in Figure 4, relative to the control group, significantly increased caspase-3 activity was observed in HIC cells treated with 60 and 120 μM 7K-SI, 7K-CA, and 7K-BR for 24 h in a dose-dependent manner. Caspase-3 activity was enhanced 3-, 2-, and 1.3-fold relative to control group in response to the incubation with 120 μM 7K-SI, 7K-CA, and 7K-BR, respectively (p < 0.01). In contrast, caspase-3 activity remained at a basal level when HIC cells were treated with 7K-ST and 7K-MIX at all of the concentrations tested.

Effect of 7-Ketosterols on Bcl-2 Protein in HIC Cells. To further verify the apoptotic effect, we investigated the changes in activity of the apoptosis-related proteins triggered by the tested 7-ketosterols. Results showed that, compared with control cells, the HIC cell protein levels of Bcl-2 declined after treatment with 60 μM 7K-CH, 120 μM 7K-SI, and 120 μM 7K-CA, which favors the induction of apoptosis (Table 1). The Bcl-2 protein level was increased after treatment with 7K-BR at 30 μM, while it was decreased after treatment at 120 μM (p < 0.01). Bcl-2 remained at a basal level in cells treated with 7K-ST and 7K-MIX (60 μM and 120 μM) relative to the untreated control.

DISCUSSION

The present study was focused on the biological implications of individual and mixed 7-ketophytosterol oxides on HIC cell line. A further objective was to assess the death pathways related to Bcl-2 and caspase-dependence induced by these phytosterol oxides.

We found that 7-ketophytosterol oxides displayed different cytotoxic and apoptotic effects on HIC cells. Except 7K-ST and 7K-MIX, other 7-ketophytosterol oxides (7K-SI, 7K-CA, and 7K-BR) were capable of inducing growth inhibition and apoptosis on HIC cells in a dose-dependent manner after 24 h treatment. At 120 μM, the order of 7-ketophytosterol oxide toxicity was 7K-SI > 7K-CA > 7K-BR > 7K-ST > 7K-MIX. 7K-SI was the most cytotoxic and apoptotic compound, exerting the strongest reduction in cell viability and inducing cell apoptosis, whereas 7K-ST (120 μM) resulted in decreased cell viability with low level apoptosis in HIC cells. The cytotoxicity of 7K-CA was demonstrated for the first time, in the present study: cell apoptosis was induced when HIC cells were exposed to 7K-CA (60 and 120 μM), but its cytotoxic and apoptotic effects were less than those of 7K-SI. In addition, 60 μM 7K-CH induced even higher cytotoxicity than 120 μM 7K-SI. This finding was in agreement with the results of Maguire et al.[19] and Ryan et al.[20] that β-sitosterol oxides had general toxic effects similar to COPs but higher concentrations of POPs were required to obtain comparable results.

DOI: 10.1021/jf505079v
J. Agric. Food Chem. 2015, 63, 1035−1041

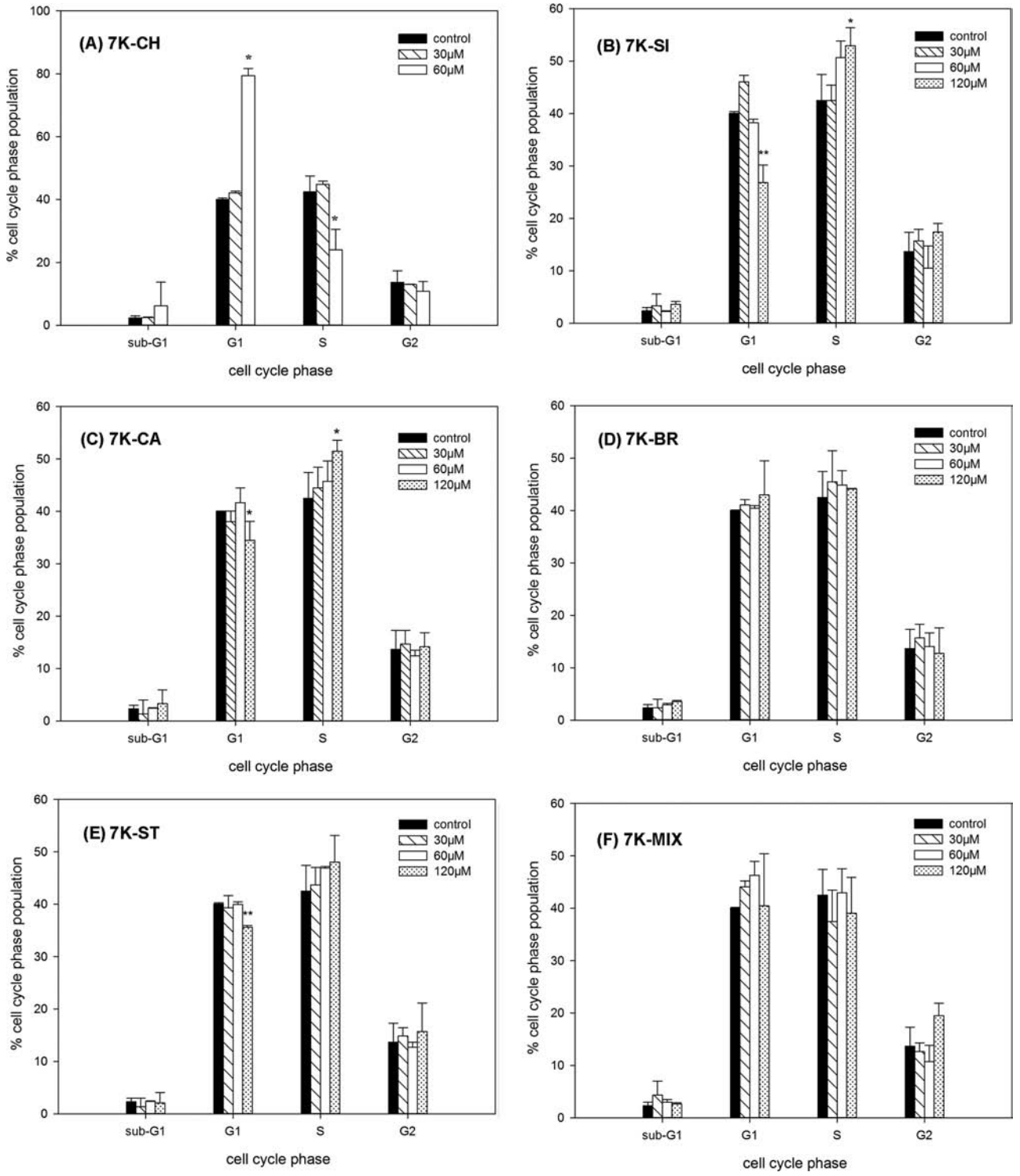

Figure 3. Changes in cell cycle phase populations of HIC cells exposed to 30, 60, and 120 μM of 7-ketophytosterol oxides (7K-SI (B), 7K-CA (C), 7K-BR (D), 7K-ST (E), and 7K-MIX (F)) or 30 and 60 μM of 7K-CH (A) for 24 h. Values are mean ± SE of three separate experiments and are marked when significantly different from control levels (*$p < 0.05$, **$p < 0.01$).

The differences in susceptibility of cells to sterol oxide treatment might be related to the chemical structures of sterol oxides and the genetic background of the cell lines.

7-Ketosterol oxides are structurally similar compounds that possess the same sterol nucleus (one double bond at C5−C6 and a ketone group at C7 in the B-ring) but a small difference in the side chain (such as substitution at C24 or an additional double bond between C22 and C23). We found that, in the present study, HIC cells were more sensitive to the 7-ketosterol oxides that had no double bond in the side chain (7K-CH, 7K-SI, and 7K-CA) than other oxides with a double bond between C22 and C23 in the side chain (7K-ST and 7K-BR). The substitution of the double bond in the side chain (7K-ST) might influence the equilibrium between the ketone form and

DOI: 10.1021/jf505079v
J. Agric. Food Chem. 2015, 63, 1035−1041

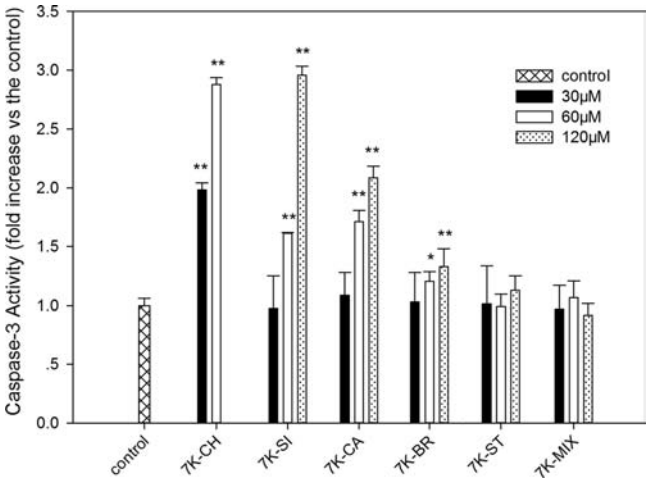

Figure 4. Caspase-3 activity (fold increase vs the control) in HIC cells following 24 h of incubation with 30, 60, and 120 μM of 7-ketophytosterol oxides (7K-SI, 7K-CA, 7K-BR, 7K-ST, and 7K-MIX) or 30 and 60 μM of 7K-CH. Values are mean ± SE of three separate experiments and are marked when significantly different from control levels (*p < 0.05, **p < 0.01).

Table 1. Bcl-2 Content in HIC Cells Following Exposure for 24 h to 30, 60, or 120 μM of Sterol Oxides[a]

		Bcl-2 content (fold increase vs. the control)	
compound	exposure (μM)	mean	SE
	cholesterol oxides		
7K-CH	30	0.80**	0.02
	60	0.68**	0.06
	phytosterol oxides		
7K-SI	30	1.12	0.09
	60	0.91	0.07
	120	0.66**	0.08
7K-CA	30	1.66	0.03
	60	0.98	0.06
	120	0.75**	0.03
7K-BR	30	1.34**	0.08
	60	1.11	0.08
	120	0.82**	0.01
7K-ST	30	1.15	0.01
	60	0.98	0.01
	120	1.03	0.12
7K-MIX	30	1.07	0.04
	60	0.97	0.04
	120	0.93	0.10

[a]Values are mean ± SE of three separate experiments and are marked with when significantly different from control levels (*p < 0.05, **p < 0.01).

hydroxide adducts, which might be shifted by interaction with proteins at the intestinal epithelial level.[23]

Ryan et al. reported that β-sitosterol oxides produced different toxic effects in U937, Caco-2, and HepG2 cell lines, but without inducing apoptosis in either HepG2 or Caco-2 cells.[24] Koschutnig et al. reported a decrease in HepG2 cell viability upon exposure to single β-sitosterol oxide but little effects induced by the mixture of polar oxides.[21] Other studies indicated that 7-ketostigmasterol (30−120 μM) had no cytotoxic effects on U937 cells[24] and Caco-2 cells.[27,29] It is well-known that the U937 cell line can express the Fas antigen and is sensitive to TNF and anti-Fas antibodies.[30,31] Caco-2 cells express retinoic acid binding protein I and retinol binding protein II.[32] HepG2 cells retain many functions of the normal liver cell, express 3-hydroxy-3-methylglutaryl-CoA reductase and hepatic triglyceride lipase activities, have decreased expression of apoA-I mRNA, and have increased expression of catalase mRNA in response to gramoxone (oxidative stress).[33] Combined our experimental results that 7-ketosterol oxides displayed different cytotoxic and apoptotic effects on the HIC cell line, this suggested that the toxicity of sterol oxides on different cell lines depends on the physiological area in which they work.

In addition, synergistic as well as inhibitory effects of individual sterol oxides in mixtures had been noted.[34] Some studies indicated that oxysterols as a mixture did not elicit the same cytotoxic effects and defensive responses as the individual oxysterols.[35−37] They suggested that major oxysterols were not universally cytotoxic and the simultaneous presence of several different oxysterol species might reduce the adverse effects of individual oxysterols.[35] These finding were consistent with our results that 7K-MIX exerted a reduction of the toxic potential compared with the individual phytosterol oxides (7K-SI, 7K-CA, and 7K-BR).

The studies of cytotoxicity were also supplemented with cell cycle assay. Alemany et al. reported that exposure to neither 7K-ST nor 7K-CH led to increases in the sub-G1 phase population in Caco-2 cells.[23] Similar results were found in HIC cells treated by all the tested compounds in the present study. In addition, 7K-CH (60 μM) caused cell cycle arrest in the G1 phase and decreased the percentage of cells in S phases, whereas 7K-SI and 7K-CA (120 μM) led to an accumulation in S phase, and a simultaneous decrease of cells engaged in the G1 phase in HIC cells. Therefore, there is not definite relationship between 7-ketosterol structures and their effect on the cell cycle.

Apoptosis is a highly regulated physiologic cell death process that is critical for development, host defense, and the prevention of malignant transformation and inflammation throughout the body.[38,39] There are two major pathways regulating apoptosis: the intrinsic pathway mediated by the mitochondria,[40] and the extrinsic pathway induced by the death receptor.[41,42] Recently, new apoptotic mechanisms including caspase-independent pathway and granzyme-initiated pathways have been shown to exist in lymphocytes.[42,43]

Regarding the death pathway of oxide derivatives of sterols, Prunet et al. demonstrated that caspase-3 was essential to trigger 7-ketocholesterol- and 7β-hydroxycholesterol-induced apoptosis, and these oxysterols simultaneously activate caspase-3-dependent or -independent modes of cell death.[44] Roussi et al. reported that 7β-hydroxysitosterol and 7β-hydroxycholesterol followed different death pathways despite their structural similarity.[21] In the case of 7β-hydroxysitosterol, the intracellular caspase-9 and -3 was activated in Caco-2 cells. In contrast, 7β-hydroxycholesterol did not activate caspase-3.[21] They caused mitochondrial depolarization but not involve the Bcl-2 family proteins in Caco-2 cells.[21,22] In addition, caspase-8 was not activated in cells treated with both hydroxysterols.[21] Alemany et al. showed that 7K-CH regulate key enzymes HMG-CoA in cholesterol metabolism and cause alterations in mitochondrial membrane potential in Caco-2 cells.[27]

Considering the complexity of the sterol oxides involved in the death way, in our present study, Bcl-2 and caspase-3 were detected to preliminary confirm the intrinsic death pathway of

DOI: 10.1021/jf505079v
J. Agric. Food Chem. 2015, 63, 1035−1041

7-ketosterols. It is becoming clear that the Bcl-2 family proteins play an important role in the regulation of apoptosis at the mitochondrial level. Dysregulation of the Bcl-2 proteins was proved to induce the destruction of mitochondrial membrane, which result in the release of cytochrome *c* and apoptosis-inducing factors from the mitochondria and subsequently induces activation of the caspase cascade.[45,46]

Significant changes were found in expression of the apoptosis related Bcl-2 family proteins after treatment with phytosterol oxides. In the present study, 7K-CH (60 μM) and 7K-SI and 7K-CA (120 μM) caused a significant decrease in the level of antiapoptotic protein Bcl-2, which in turn resulted in the activation of caspase-3. Caspase-3 activity analysis showed that treatment of 7K-CH, 7K-SI, and 7K-CA did activate apoptosis proteins caspase-3 with dose-dependent manner. However, no significant changes in expression of Bcl-2 protein were found after 24 h treatment with 7K-ST and 7K-MIX in HIC cells. It might involve various apoptosis mechanisms or cell death pathway.

In conclusion, our study demonstrated that HIC cells were significantly more sensitive to 7K-CH, 7K-SI, and 7K-CA treatment than other 7-ketophytosterol oxides. The cytotoxicity of 7K-CA was demonstrated at first time and analogue to 7K-SI. 7K-SI and 7K-CA modulated cell viability, proliferation, and expression of apoptosis-related proteins. Since induction of cell cycle arrest was usually accompanied by growth inhibition, the research is required to identify which cell cycle regulators attribute to the alteration of specific phases of cells. Moreover, further study is required to clarify the precise pathway of POPs-induced apoptosis.

AUTHOR INFORMATION

Corresponding Authors

*L.W. Phone/fax: +86 551 65591602. E-mail: ljw@ipp.ac.cn.

*X.Z. Phone/fax: +86 551 65786021. E-mail: xinzhang@ahau.edu.cn.

Funding

This work was supported by the fund of the National Natural Science Foundation of China (Grant 21072002).

Notes

The authors declare no competing financial interest.

ABBREVIATIONS

POPs, phytosterol oxidation products; COPs, cholesterol oxidation products; 7K-CH, 7-ketocholesterol; 7K-SI, 7-ketositosterol; 7K-CA, 7-ketocampesterol; 7K-ST, 7-ketostigmasterol; 7K-BR, 7-ketobrassicasterol; 7K-MIX, mixture of 7-ketophytosterols; HIC, human intestinal cancer epithelial cells; HPLC, high performance liquid chromatography; CCK8, Cell Counting Kit-8

REFERENCES

(1) Jones, P.; AbuMweis, S. Phytosterols as functional food ingredients: Linkages to cardiovascular disease and cancer. *Curr. Opin. Clin. Nutr.* **2009**, *12*, 147−151.

(2) Ostlund, R. E.; Racette, S. B.; Stenson, W. F. Inhibition of cholesterol absorption by phytosterol-replete wheat germ compared with phytosterol-depleted wheat germ. *Am. J. Clin. Nutr.* **2003**, *77*, 1385−1389.

(3) Weber, N.; Weitkamp, P.; Mukherjee, K. D. Cholesterol-lowering food additives: Lipase-catalysed preparation of phytosterol and phytostanol esters. *Food Res. Int.* **2002**, *35*, 177−181.

(4) Shahidi, F. Functional foods: Their role in health promotion and disease prevention. *J. Food Sci.* **2004**, *69*, R146−R149.

(5) Chen, Z. Y.; Ma, K. Y.; Liang, Y.; Peng, C.; Zuo, Y. Role and classification of cholesterol-lowering functional foods. *J. Funct. Foods* **2011**, *3*, 61−69.

(6) Ryan, E.; McCarthy, F. O.; Maguire, A. R.; O'Brien, N. M. Phytosterol oxidation products: Their formation, occurrence, and biological effects. *Food Rev. Int.* **2009**, *25*, 157−174.

(7) O'Callaghan, Y.; McCarthy, F. O.; O'Brien, N. M. Recent Advances in Phytosterol Oxidation Products. *Biochem. Biophys. Res. Commun.* **2014**, *446*, 786−791.

(8) Grandgirard, A.; Martine, L.; Joffre, C.; Juaneda, P.; Berdeaux, O. Gas chromatographic separation and mass spectrometric identification of mixtures of oxyphytosterol and oxycholesterol derivatives: Application to a phytosterol-enriched food. *J. Chromatogr. A* **2004**, *1040*, 239−250.

(9) Conchillo, A.; Cercaci, L.; Ansorena, D.; Rodriguez-Estrada, M. T.; Lercker, G.; Astiasarán, I. Levels of phytosterol oxides in enriched and nonenriched spreads: Application of a thin-layer chromatography-gas chromatography methodology. *J. Agric. Food Chem.* **2005**, *53*, 7844−7850.

(10) Grandgirard, A.; Martine, L.; Demaison, L.; Cordelet, C.; Joffre, C.; Berdeaux, O.; Semon, E. Oxyphytosterols are present in plasma of healthy human subjects. *Br. J. Nutr.* **2004**, *91*, 101−106.

(11) Liang, Y. T.; Wong, W. T.; Guan, L.; Tian, X. Y.; Ma, K. Y.; Huang, Y.; Chen, Z. Y. Effect of phytosterols and their oxidation products on lipoprotein profiles and vascular function in hamster fed a high cholesterol diet. *Atherosclerosis* **2011**, *219*, 124−133.

(12) Menéndez-Carreño, M.; Steenbergen, H.; Janssen, H. G. Development and validation of a comprehensive two-dimensional gas chromatography-mass spectrometry method for the analysis of phytosterol oxidation products in human plasma. *Anal. Bioanal. Chem.* **2012**, *402*, 2023−2032.

(13) Wielkoszyński, T.; Gawron, K.; Strzelczyk, J.; Bodzek, P.; Zalewska-Ziob, M.; Trapp, G.; Srebniak, M.; Wiczkowski, A. Cellular toxicity of oxycholesterols. *Bioessays* **2006**, *28*, 387−398.

(14) Poli, G.; Sottero, B.; Gargiulo, S.; Leonarduzzi, G. Cholesterol oxidation products in the vascular remodeling due to atherosclerosis. *Mol. Aspects Med.* **2009**, *30*, 180−189.

(15) Kanhal, M. A.; Ahmad, F.; Othman, A. A.; Arif, Z.; Orf, S. A.; Murshed, K. A. Effect of pure and oxidized cholesterol-rich diets on some biochemical parameters in rats. *Int. J. Food Sci. Nutr.* **2002**, *53*, 381−388.

(16) Homma, Y.; Kondo, Y.; Kaneko, M.; Kitamura, T.; Nyou, W. T.; Yanagisawa, M.; Yamamoto, Y.; Kakizoe, T. Promotion of carcinogenesis and oxidative stress by dietary cholesterol in rat prostate. *Carcinogenesis* **2004**, *25*, 1011−1014.

(17) Hovenkamp, E.; Demonty, I.; Plat, J.; Lütjohann, D.; Mensink, R. P.; Trautwein, E. A. Biological effects of oxidized phytosterols: A review of the current knowledge. *Prog. Lipid Res.* **2008**, *47*, 37−49.

(18) Adcox, C.; Boyd, L.; Oehrl, L.; Allen, J.; Fenner, G. Comparative effects of phytosterol oxides and cholesterol oxides in cultured macrophage-derived cell lines. *J. Agric. Food Chem.* **2001**, *49*, 2090−2095.

(19) Maguire, L.; Konoplyannikov, M.; Ford, A.; Maguire, A. R.; O'Brien, N. M. Comparison of the cytotoxic effects of β-sitosterol oxides and a cholesterol oxide, 7β-hydroxycholesterol, in cultured mammalian cells. *Br. J. Nutr.* **2003**, *90*, 767−776.

(20) Ryan, E.; Chopra, J.; McCarthy, F.; Maguire, A. R.; O'Brien, N. M. Qualitative and quantitative comparison of the cytotoxic and apoptotic potential of phytosterol oxidation products with their corresponding cholesterol oxidation products. *Br. J. Nutr.* **2005**, *94*, 443−451.

(21) Roussi, S.; Winter, A.; Gosse, F.; Werner, D.; Zhang, X.; Marchioni, E.; Geoffroy, P.; Miesch, M.; Raul, F. Different apoptotic mechanisms are involved in the antiproliferative effects of 7β-hydroxysitosterol and 7β-hydroxycholesterol in human colon cancer cells. *Cell Death Differ.* **2005**, *12*, 128−135.

DOI: 10.1021/jf505079v
J. Agric. Food Chem. 2015, 63, 1035−1041

(22) Roussi, S.; Gosse, F.; Aoude-Werner, D.; Zhang, X.; Marchioni, E.; Geoffroy, P.; Miesch, M.; Raul, F. Mitochondrial perturbation, oxidative stress and lysosomal destabilization are involved in 7β-hydroxysitosterol and 7β-hydroxycholesterol triggered apoptosis in human colon cancer cells. *Apoptosis* **2007**, *12*, 87−96.
(23) Alemany, L.; Laparra, J.; Barberá, R.; Alegría, A. Relative expression of cholesterol transport-related proteins and inflammation markers through the induction of 7-ketosterol-mediated stress in Caco-2 cells. *Food Chem. Toxicol.* **2013**, *56*, 247−253.
(24) Koschutnig, K.; Heikkinen, S.; Kemmo, S.; Lampi, A.-M.; Piironen, V.; Wagner, K.-H. Cytotoxic and apoptotic effects of single and mixed oxides of β-sitosterol on HepG2-cells. *Toxicol. in Vitro* **2009**, *23*, 755−762.
(25) Sato, H.; Nishida, S.; Tomoyori, H.; Sato, M.; Ikeda, I.; Imaizumi, K. Oxysterol regulation of estrogen receptor α-mediated gene expression in a transcriptional activation assay system using Hela cells. *Biosci., Biotechnol., Biochem.* **2004**, *68*, 1790−1793.
(26) Newill, H.; Loske, R.; Wagner, J.; Johannes, C.; Lorenz, R. L.; Lehmann, L. Oxidation products of stigmasterol interfere with the action of the female sex hormone 17β-estradiol in cultured human breast and endometrium cell lines. *Mol. Nutr. Food Res.* **2007**, *51*, 888−898.
(27) Alemany, L.; Laparra, J.; Barberá, R.; Alegría, A. Evaluation of the cytotoxic effect of 7keto-stigmasterol and 7keto-cholesterol in human intestinal (Caco-2) cells. *Food Chem. Toxicol.* **2012**, *50*, 3106−3113.
(28) Gao, J.; Yue, Q.; Ji, Y.; Cheng, B.; Zhang, X. Novel synthesis strategy for the preparation of individual phytosterol oxides. *J. Agric. Food Chem.* **2013**, *61*, 982−988.
(29) O'Callaghan, Y. C.; Foley, D. A.; O'Connell, N. M.; McCarthy, F. O.; Maguire, A. R.; O'Brien, N. M. Cytotoxic and apoptotic effects of the oxidized derivatives of stigmasterol in the U937 human monocytic cell line. *J. Agric. Food Chem.* **2010**, *58*, 10793−10798.
(30) Sundstrom, C.; Nilsson, K. Establishment and characterization of a human histiocytic lymphoma cell line (U-937). *Int. J. Cancer* **1976**, *17*, 565−577.
(31) Ralph, P.; Moore, M. A.; Nilsson, K. Lysozyme synthesis by established human and murine histiocytic lymphoma cell lines. *J. Exp. Med.* **1976**, *143*, 1528−1533.
(32) Trainer, D. L.; Kline, T.; McCabe, F. L.; Faucette, L. F.; Field, J.; Chaikin, M.; Anzano, M.; Rieman, D.; Hoffstein, S.; Li, D. J. Biological characterization and oncogene expression in human colorectal carcinoma cell lines. *Int. J. Cancer* **1988**, *41*, 287−296.
(33) Busch, S. J.; Barnhart, R. L.; Martin, G. A.; Flanagan, M. A.; Jackson, R. L. Differential regulation of hepatic triglyceride lipase and 3-hydroxy-3- methylglutaryl-CoA reductase gene expression in a human hepatoma cell line, HepG2. *J. Biol. Chem.* **1990**, *265*, 22474−22479.
(34) O'Sullivan, A. J.; O'Callaghan, Y. C.; O'Brien, N. M. Differential effects of mixtures of cholesterol oxidation products on bovine aortic endothelial cells and human monocytic U937 cells. *Int. J. Toxicol.* **2005**, *24*, 173−179.
(35) Hall, M. C. The effect of oxysterols, individually and as a representative mixture from food, on in vitro cultured bovine ovarian granulosa cells. *Mol. Cell. Biochem.* **2006**, *292*, 1−11.
(36) Aupeix, K.; Weltin, D.; Mejia, J. E. Oxysterol-induced apoptosis in human monocytic cell lines. *Immunobiology* **1995**, *194*, 4−5.
(37) Leonarduzzi, G.; Sottero, B.; Poli, G. Oxidized products of cholesterol: dietary and metabolic origin, and proatherosclerotic effects. *J. Nutr. Biochem.* **2002**, *13*, 700−710.
(38) Ferri, K. F.; Kroemer, G. Organelle-specific initiation of cell death pathways. *Nat. Cell Biol.* **2001**, *3*, E255−E263.
(39) Bortner, C. D.; Cidlowski, J. A. Cellular mechanisms for repressing apoptosis. *Annu. Rev. Pharmacol. Toxicol.* **2002**, *42*, 259−281.
(40) Hockenbery, D.; Nunez, G.; Millirman, C.; Schreiber, R. D.; Korsmever, S. J. Bcl-2 is an inner mitochondrial membrane protein that blocks programmed cell death. *Nature* **1990**, *348*, 334−336.
(41) Zapata, J. M.; Pawlowski, K.; Hass, E.; Ware, C. F.; Godzik, A.; Reed, J. C. A diverse family of proteins containing tumor necrosis factor receptor-associated factor domains. *J. Biol. Chem.* **2001**, *276*, 24242−24252.
(42) Xu, G.; Shi, Y. Apoptosis signaling pathways and lymphocyte homeostasis. *Cell Res.* **2007**, *17*, 759−771.
(43) Sarin, A.; Williams, M. S.; Alexander-Miller, M. A. Target cell lysis by CTL granule exocytosis is independent of ICE/Ced-3 family proteases. *Immunity* **1997**, *6*, 209−215.
(44) Prunet, C.; Lemaire-Ewing, S.; Menetrier, F.; Neel, D.; Lizard, G. Activation of caspase-3-dependent and -independent pathways during 7-ketocholesterol- and 7β-hydroxycholesterol-induced cell death: A morphological and biochemical study. *J. Biochem. Mol. Toxicol.* **2005**, *19*, 311−326.
(45) Hoetelmans, R. W. M.; van Slooten, H. J.; Keijzer, R.; Erkeland, S.; van de Velde, C. J. H.; van Dierendonck, J. H. Bcl-2 and Bax proteins are present in interphase nuclei of mammalian cells. *Cell Death Differ.* **2000**, *7*, 384−39232.
(46) Youle, R. J.; Strasser, A. The BCL-2 protein family: opposing activities that mediate cell death. *Nat. Rev. Mol. Cell Biol.* **2008**, *9*, 47−59.

DOI: 10.1021/jf505079v
J. Agric. Food Chem. 2015, 63, 1035−1041

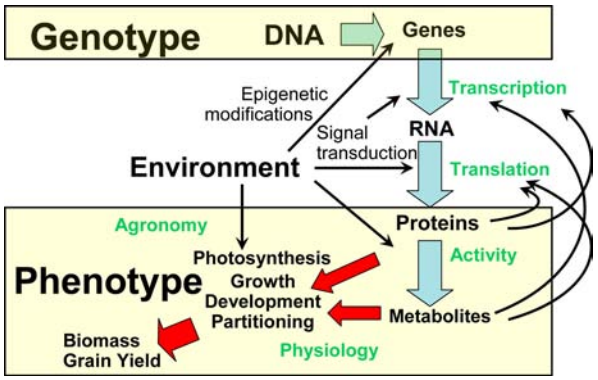

Figure 1. Model showing the large gap between genotype and phenotype. The functional link between DNA and yield is complex because the environment acts at many different levels. Genes can be modified epigenetically by methylation and histone acetylation, which are both affected by the environment. Some epigenetic states can be stably inherited and are therefore relevant for breeding. Multiple feed-forward and feedback signaling loops between metabolites, proteins, and small ribonucleic acids (RNAs) complicate the specific pattern of gene expression. Genes represent "potential", whereas transcripts reveal the short-term "strategy". Proteins and enzymes do the "work", whereas the final "results" are the metabolites that are accumulated in a certain storage organ (e.g., starch in seeds). From this model, it is apparent that metabolites are much closer to grain yield than any DNA sequence, and therefore, selection for biomarker metabolites should be more relevant for breeding than selection for molecular markers [e.g., microsatelites, single nucleotide polymorphisms (SNPs), quantitative trait loci (QTL), etc.].

analytical methods should be retailored to be faster, save reagents, reduce cost, and simplify/automatize data analysis.[6]

Mass spectrometry (MS) allows for the analysis of a large number of chemical compounds and is a promising tool for agricultural research.[5−7] Traditionally, qualitative separation and quantitative detection are performed in two steps: upstream separation, such as liquid chromatography (LC) and gas chromatography (GC) first filters molecules because of physicochemical differences (affinity to a stationary or mobile phase), and then detection of positive or negative ions is performed according to the mass-to-charge ratio (m/z). In GC−MS, post-chromatographic molecular fragmentation is performed by electron impact (EI), a hard ionization method that results in the fragmentation of the molecules.[8] MS methods combining different chromatographic and ionization technologies have been used for phenotyping purposes, such as liquid chromatography−electrospray ionization−mass spectrometry (LC−ESI−MS) and gas chromatography−electron impact−mass spectrometry (GC−EI−MS).[9−12] Metabolic profiling based on GC−EI−MS is the most widely used in plant biology, e.g., for the phenotypic characterization of mutants, transgenic plants, and recombinant inbred line (RIL) populations.[6,13−16] It has also been used to characterize the metabolic response of maize hybrids subjected to drought.[12]

UPLC−MS is too expensive to be implemented for routine breeding in agricultural institutions of the subtropics. GC−EI−MS is more affordable, but unfortunately, it has several technical limitations. Each single chromatographic run requires 30−60 min, and therefore, less than 24−48 samples can be analyzed daily. Besides low throughput, GC−MS-based metabolic profiling depends upon volatility and ionizability of molecules, with both aims being somehow in contrast. On the one hand, ionizable molecules have less propensity to escape from the liquid phase the more charged that they are. On the other hand, uncharged molecules are volatile but do not ionize efficiently. Therefore, GC−EI−MS samples need to be previously derivatized to increase chemical coverage. The most widely used procedure is the addition of trimetylsylyl (TMS) groups,[14] which makes highly hydrophilic compounds, such as amino acids and carboxylic acids, volatile in the gas phase. Unfortunately, biomolecules are derivatized to several possible TMS compounds, each having different retention times (RTs) in the GC column. One single metabolite, such as citric acid, can generate more than 10 different RT peaks in a GC−EI−MS chromatogram. The difficulty is to decide which chromatographic peak should be used to quantify citric acid in the original sample. It becomes even more difficult because GC−EI−MS data are split in two dimensions (RT and m/z). Therefore, sophisticated data processing workflows are needed for data integration and statistical interpretation.[12] Manual processing and intuitive decisions have to be made relying on recommendations of experienced users.[12] Each group may follow particular philosophies, and therefore, GC−EI−MS and LC−ESI−MS data analysis can be considered both mathematics and art.[12,17] The bottleneck of LC−ESI−MS and GC−EI−MS profiling is the manual processing and individual interpretation of chromatographic data by the final user. Typically, a student requires several months for training, and even when it learns to perform GC−EI−MS by himself, a single user cannot fully process and interpret more than 24 samples per day, much less produce publication-ready graphics in less than 1 week (final throughput is very low).

Given the previously mentioned considerations, we decided to implement a metabolic profiling strategy that overcomes the following problems: (1) time-consuming chromatographic separation, (2) limited compound volatility and inefficient ionization of hydrophilic metabolites, (3) generation of multiple peaks because of chemical derivatization (data redundancy), (4) reliable, sensitive, and quantitative detection, (5) manual handling of chromatograms, and (6) complex data workflow and statistical processing (e.g., automatic data reduction and visualization). Inspired by the requirements of plant breeders, we aimed to develop an analytical platform that allows for a high sample throughput, produces a vast amount of quantitative chemical information, and is at the same time cheap, robust, and easy to handle bioinformatically.

Therefore, we compared several analytical methodologies, with particular focus on direct-injection electrospray ionization mass spectrometry (DIESI−MS).[18] We documented the genotypic and environmental effects on the metabolic profile of maize stem extracts. Our leading questions were as follows: Is DIESI−MS data quantitative and repeatable? Can we detect specific ions that have larger variance because of the environment (E) or the genotype (G)? How large is the throughput and how expensive is DIESI−MS profiling compared to other methods? Does this metabolic phenotyping strategy work for other plant samples in addition to maize?

MATERIALS AND METHODS

Plant Materials and Growth Conditions. *Maize Experiments under Nitrogen Stress.* The low nitrogen (LN) and control trial (CT) were performed during the 2011 summer season in El Batán, Texcoco, Mexico [19° 30′ N latitude, 98° 53′ O longitude, 2247 m above sea level (masl) altitude]. It was performed according to the field management standards established by the International Maize and Wheat Improvement Center (CIMMYT).[2] The LN treatment consisted of suppressing nitrogen fertilization during the previous

DOI: 10.1021/jf504853w
J. Agric. Food Chem. 2015, 63, 1042−1052

~4 years (8 cycles), whereas the control field was fertilized chemically with urea at the usual frequency (3 times per growth cycle) and dose (~400 kg/ha). Planting density was 67 000 plants/ha in two rows of 5 m distributed in randomized blocks (α lattice).[2] Six plants were sampled per genotype for each treatment (LN and CT). The CIMMYT field trial HL2011-11-01-PVB-2 was harvested ~10 days after silking (~85 days after sowing), while the field trial HL2011-11-01-PVB-1 was harvested ~12 days after silking (~85 days after sowing). DIESI−MS results are shown for 684 maize samples: 19 genotypes, 2 conditions (LN and CT), and 18 replicates (6 maize plants extracted 3 times each). Figures show the number of n behind each boxplot. Each of the 684 DIESI−MS runs lasted for 60 s, and all MS spectra acquired were averaged to increase accuracy and precision. In total, 4104 individual MS spectra were processed for the maize experiments.

Maize Stem Juice Collection. Representative healthy plants from each genotype and treatment were selected in the field and processed within ~15 min after harvest. Morphological and physiological data were rapidly registered: total plant weight, plant height (up to the flag leaf), number of ears, and ear weight. The tassel and the leaf blades were removed, and the supporting stem (including leaf sheath) was weighted and cut into segments (~30 cm) for tissue homogenization. The stem juice (phloem sap + xylem sap + cellular extracts) was obtained using a mechanical extractor (industrial-scale juice extractor model EXS, International Co., Mexico). The stem juice (~80 mL) was collected in a plastic beaker, weighted accurately (±0.2 g), aliquoted (1 mL), and frozen in dry ice immediately (<30 s). Collected samples were stored at −80 °C for ~4 months in sealed deep well plates (96 well format). For analysis, the stem juice was unfrozen and kept on ice for short time periods (<1 h). Samples were first centrifuged (10 min at 5000g and 4 °C), and the supernatant was used directly for metabolite analysis (see below).

Other Plant Samples. Leaves from different coffee and tea species were obtained as described previously.[18,19] Strawberry fruits were divided in three levels of ripeness (see Figure S1 of the Supporting Information). The level of ripeness was determined according to the following parameters: fruit turgor, fruit color, and peduncle color (see Table S1 of the Supporting Information).

Metabolite Analysis. Analytical methods were evaluated considering costs, sample throughput, and the requirements of chromatographic separation and chemical derivatization. We also evaluated the required workflow for computational and statistical analyses of the generated data. We excluded NIRS because it is well-known that it can simultaneously detect/discriminate only 1−3 different compounds reliably,[20] whereas MS-based methods produce information on more than 300 different metabolites. We also excluded high-end UPLC−MS and nuclear magnetic resonance (NMR) because machine costs are prohibitive for routine plant breeding.

Enzyme-Coupled Spectrophotometry Assays. Soluble sugars were measured in microplate format.[21,22] The insoluble starch pellet was dissolved in 0.5 mL of 10 mM KOH at 99 °C and autoclaved for 30 min. Starch was hydrolyzed in 50 mM *N*-2-hydroxyethylpiperazine-*N*′-2-ethanesulfonic acid (HEPES) (pH 7.5) at 37 °C overnight by the addition of 10 units of α-amylase (EC 3.2.1.1, Roche) and 10 units of amyloglucosidase (EC 3.2.1.3, Roche). Samples were centrifuged (13000g for 5 min); the resulting supernatant was stored at 4 °C; and the pellet was hydrolyzed again for 30 min at 37 °C. Both supernatants were combined, and an aliquot was enzymatically assayed for glucose, as described above.

DIESI−MS. The DIESI−MS assay was performed as described previously,[18,19] with some adjustments (see below). The stem juice supernatant was filtered through a 0.45 μm polyvinylidene difluoride (PVDF) filter and diluted 1:100 with deionized water to avoid saturation of the capillary and cone soiling. To improve ionization, to 475 μL of diluted sample and 25 μL pure formic acid were added [final concentration of 5% (v/v) formic acid]. Control experiments were carried out to determine optimal parameters of sample pretreatment and dilution (data not shown). The diluted and acidified samples were analyzed by DIESI−MS in positive mode, employing a Micromass ZQ 2000 with a quadrupole analyzer (Waters) and MassLynx 4.0 as control software.[18] A constant volumetric flow rate (10 μL/min) was achieved using a syringe pump loaded with 100 μL of sample. Capillary voltage was set to 3 kV; the cone voltage was set to 60 V; the extractor voltage was set to 3 V; and the radio frequency (RF) lens was left at 0.5 V. The source temperature (80 °C) and desolvation temperature (150 °C) were used with a nitrogen gas flow of 250 L/h and a cone gas flow of 50 L/h. In the analyzer section, low-mass (LM) and high-mass (HM) resolution of 15.0 and ion energy of 0.5 were set. The multiplier was adjusted to a value of 650. Continuous spectra were collected in a range of m/z 15−2000, with a total run duration of 1 min, a scan time of 10 s, and a interscan time of 0.1 s, producing six spectra per sample.

Data Analysis and Script Optimization. The raw MS spectra files were converted to *.mzXML using masswolf, version 1.4. Analysis of mass spectra was performed with the OpenMS/TOPP suite, version 1.8.0, and later further processed with the free statistical software R (http://www.r-project.org).[23] A TOPPAS pipeline was written executing the following sequential tasks: file conversion to mzML, spectra merger with a block method (six replicate spectra), NoiseFilter sgolay with a frame length of 21 and polynomial order of 4, followed by a PeakPicker with a signal-to-noise ratio (S/N) of 1 and a peak width of 0.15. Finally, data tables were converted into TOPPAS out files using raw text format, containing tab-separated columns for genotype names, treatment factors, m/z values, and corresponding signal intensities of the individual ions. Individual data files were then automatically imported with a tailored script into R.[23]

Besides sample harvesting and DIESI−MS workflow optimization, other advantages/novelties presented in this paper are the improved algorithms for data processing. The new R script imported all text files from a given directory and allowed for the definition of analysis of variation (ANOVA) experimental factors based on the original file name. Variable assignment was performed inside the R environment and did not require additional software for file merging or renaming. The R script was also optimized to process the data of hundreds of samples in $^1/_{10}$ of the time of previous scripts.[18,19]

Instead of naming peaks by interval boundaries,[18,19] m/z peaks were named by their center of maximal intensities. Instead of defining mass bins across the entire m/z range,[18,19] only real occurring m/z peaks were transferred to the rectangular result matrix used for the heatmap graphics. Instead of defining bin boundaries centered at 0, a mass shift was introduced to reduce bin jumping. The m/z bin boundaries were adjusted according to the observed m/z pattern (metabolic space) in various extracts: in the mass range of 50−400 Da, m/z peaks were centered at +0.2 Da from the unitary mass. In the mass range of 400−700 Da, a mass shift of +0.3 Da was more accurate. Ions were less frequent in the mass range of 800−2000 and had more variability in mass shift, so that it was more convenient to define bin centers based on the occurrence of specific ion peaks (metabolic space).

The improved R script also allowed us to define variably the tolerance of m/z peak assignment (bin size). However, for our plant samples, there was little gain of information by defining mass bins smaller than ±0.25 Da, and therefore, bin size was conveniently defined in 1 Da intervals (±0.5 Da from the center) across the entire m/z range (30−2000 Da).

When double peaks appeared in the same bin (e.g., isotopic peaks), intensities were summed up and not averaged or deleted. The optimized R script produced separate tables documenting the number of peaks per bin, intensity of single peaks, and summed intensity of multiple peaks. Automatic quality control was carried out to detect double-peak occurrence in individual mass bins.

In addition to presenting metabolic data as colored heatmaps, the optimized R script produced gray heatmap biclusters and various boxplot figures showing statistics and quality controls. For example, in addition to reporting the intensity values for given m/z ion bins, the script also ploted the exact m/z value for each sample group. The m/z residual (difference between the real observed mass and the unitary mass) was calculated for each peak and sample and plotted in parallel to the intensity boxplots (e.g., panels D−F of Figure 8). From this approach, users can decide if a given m/z value in one plant sample corresponds to the same metabolite in another plant sample. Ideally,

DOI: 10.1021/jf504853w
J. Agric. Food Chem. 2015, 63, 1042−1052

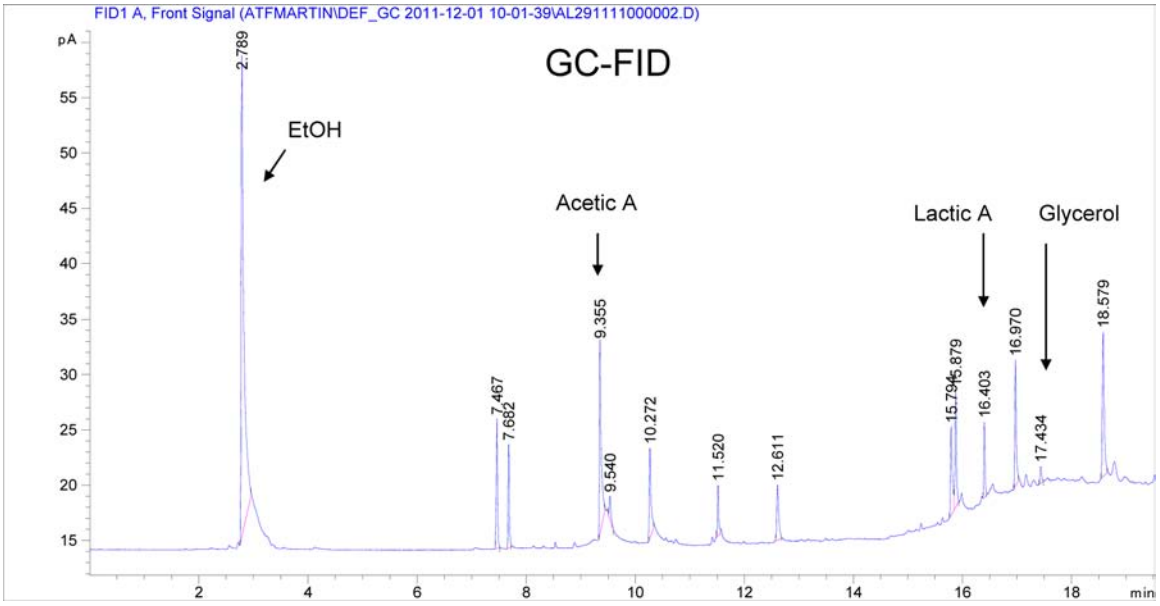

Figure 2. Typical GC−FID chromatogram of juice extracts of maize stem samples. Results correspond to the maize genotype CLQ-RCWQ83 harvested under well-watered conditions. RTs of standards were as follows: methanol, 2.53 min; ethanol, 2.78 min; acetic acid, 9.19 min; lactic acid, 16.38 min; and glycerol, 17.31 min.

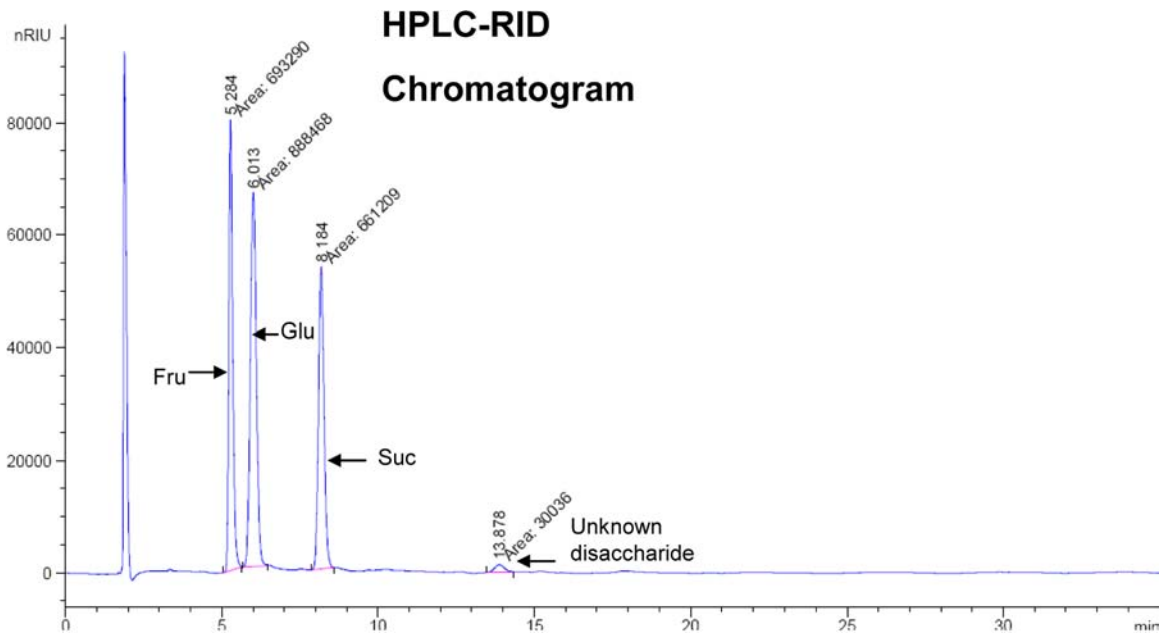

Figure 3. Chromatogram of juice extracts of maize stem samples acquired with HPLC−RID. The three main sugars were fructose, glucose, and sucrose. A fourth minor disaccharide of unknown nature was also observed in maize extracts. Other compounds rather than sugars are not detectable with this method.

m/z values of the same compound across samples should be similar, but in practice, they did vary ±0.2 Da with our quadropole MS equipment.

Overall, the optimized algorithm permitted automatic import of thousands of files, allowed for more rapid data processing, and also significantly increased reliability by diminishing "peak jumping" and eliminating the requirement of manual post-processing of data.

Statistical Procedures. All experiments were conducted using randomized complete block designs with an adequate number of controls and replicas (see the legends). ANOVAs and Tukey's least significant difference (LSD) test were applied with $p \leq 0.05$ (α = 0.05). Mixed effect linear models were used for the analysis of data, with separate factors for the effect of the G, E, development stage (DS), and their respective interactions. Bonferroni correction was used to address the false discovery rate. Statistical analysis was performed with R, version 2.10.[23]

RESULTS AND DISCUSSION

Comparison of Information Density Generated by Different Analytical Methods. Various samples were analyzed with the particular interest of determining the information density of different phenotyping strategies. Maize was grown under different environmental conditions under water and nitrogen stress.[12,18] Plants were harvested at the post-flowering stage, and stem juice aliquots were collected and

DOI: 10.1021/jf504853w
J. Agric. Food Chem. 2015, 63, 1042−1052

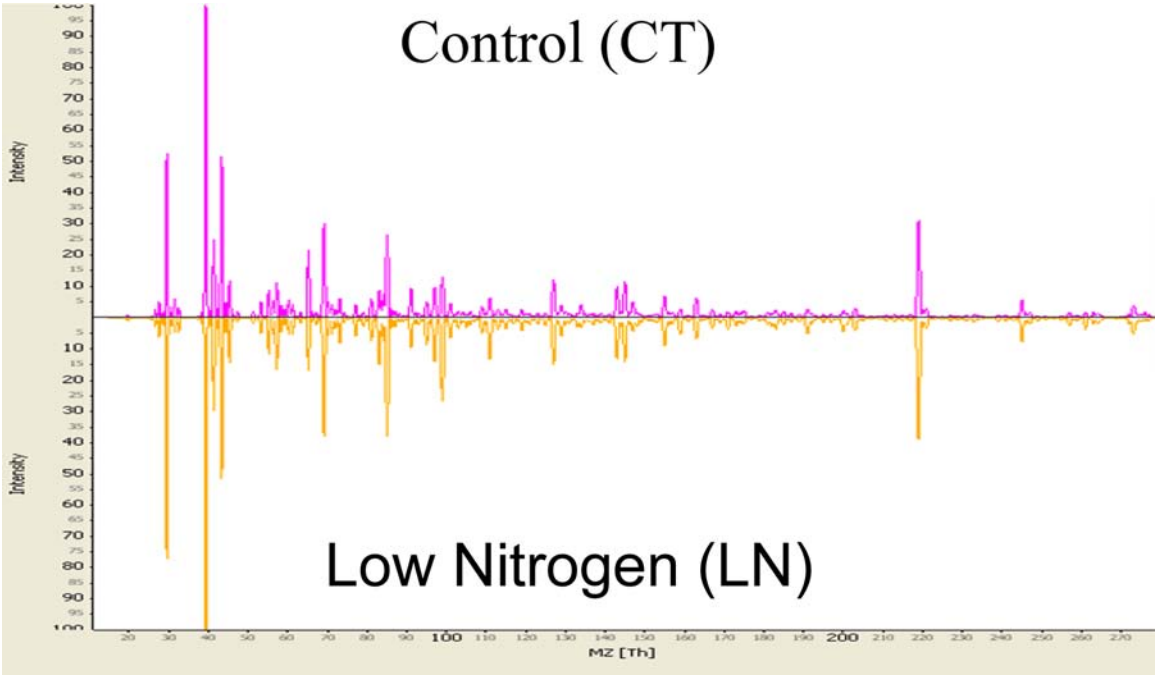

Figure 4. Mass spectrum of stem juice extracts of maize acquired with DIESI−MS showing ∼200 compounds. Maize were grown under normal CT and LN stress, and the stem was harvested ∼12 days after female flowering. Stem juice was extracted mechanically, and aliquots were frozen in liquid nitrogen until analysis. Data from a representative sample (genotype CV-702) are shown.

Table 1. Comparison of Analytical Platforms for Metabolic Phenotyping and Breeding Purposes with Respect to Throughput, Information Density, and Cost[a]

method/analytical platform	sample throughput per day technical/statistical	number of metabolites per assay	cost per sample ($ U.S./sample)	cost per metabolite data point ($ U.S./metabolite)
UV−vis enzymatic	384/384	1−3	∼10.00	3.33−10.00
UV−vis colorimetric	384/500	1	∼0.50	0.50
GC−FID	30/10	5−20	∼50.00	2.50−10.00
GC−EI−MS	24/2	50−100	∼80.00	0.80−1.60
UPLC−MS	48/2	200−1000	∼200.00	0.20−1.00
HPLC−DAD	24/10	3−15	∼80.00	5.30−26.67
NIRS	80/500	1−4	∼2.00	2.00−0.50
DIESI−MS	80/500	100−500	∼10.00	0.02−0.10

[a]Values were estimated from our experiences across several research projects at CINVESTAV and other institutes. Throughput is separated in technical (amount of samples that a laboratory can process) and statistical [amount of data files that an undergraduate student can analyze considering worktime for chromatogram integration, metabolite assignment, statistical analysis, etc. (∼human worktime)] throughput.

frozen for the simultaneous analysis with various analytical procedures [GC, HPLC, ultraviolet−visible (UV−vis), nano-assisted laser desorption ionization time-of-flight mass spectrometry (NALDI−TOF−MS), and DIESI−MS]. The gas chromatography with flame ionization detection (GC−FID) method allowed for the detection of ∼10 different peaks with satisfactory results (Figure 2). The chromatographic peaks had RTs of known alcohols and organic acids that are typically present in plant extracts (e.g., ethanol, acetic acid, lactic acid, glycerol, etc.) (Figure 2).

Using high-performance liquid chromatography with refractive index detection (HPLC−RID), ∼4 different peaks were detected with satisfactory results (Figure 3). The HPLC chromatographic peaks had retention times corresponding to glucose (glu), fructose (fru), and sucrose (suc) (Figure 3). Enzymatic assays coupled to NADPH using a UV−vis spectrophotometer (microplatte reader) specifically detected the three main sugars (glu, fru, and suc) that are typically present in plant samples. From this targeted method, the presence and amount of all sugars were confirmed in the maize stem extracts. The sugar ratio was dependent upon the G but also strongly dependent upon the DS and E conditions in which the maize plants were grown. Using ANOVA, the effects because of E, G, DS, and their interactions were discriminated. The variance effects because of G were in the range of 3−20% of the total phenotypic variance, which is excellent for breeding purposes in maize, because selection is only effective for the genetic variance.

We also employed analytical methods based on MS. NALDI−TOF−MS has the advantage to be relatively cheap if it is implemented routinely and further requires no previous chromatographic separation. With NALDI−TOF−MS we found ∼20 different peaks with a S/N of >10 (data not shown; see also ref 18). The information density generated with NALDI−TOF−MS did nor surpass the previous analytical methods, and therefore, we switched to another MS method that neither employs chromatography nor chemical derivatization: DIESI−MS. Using DIESI−MS in positive-ion mode, more

DOI: 10.1021/jf504853w
J. Agric. Food Chem. 2015, 63, 1042−1052

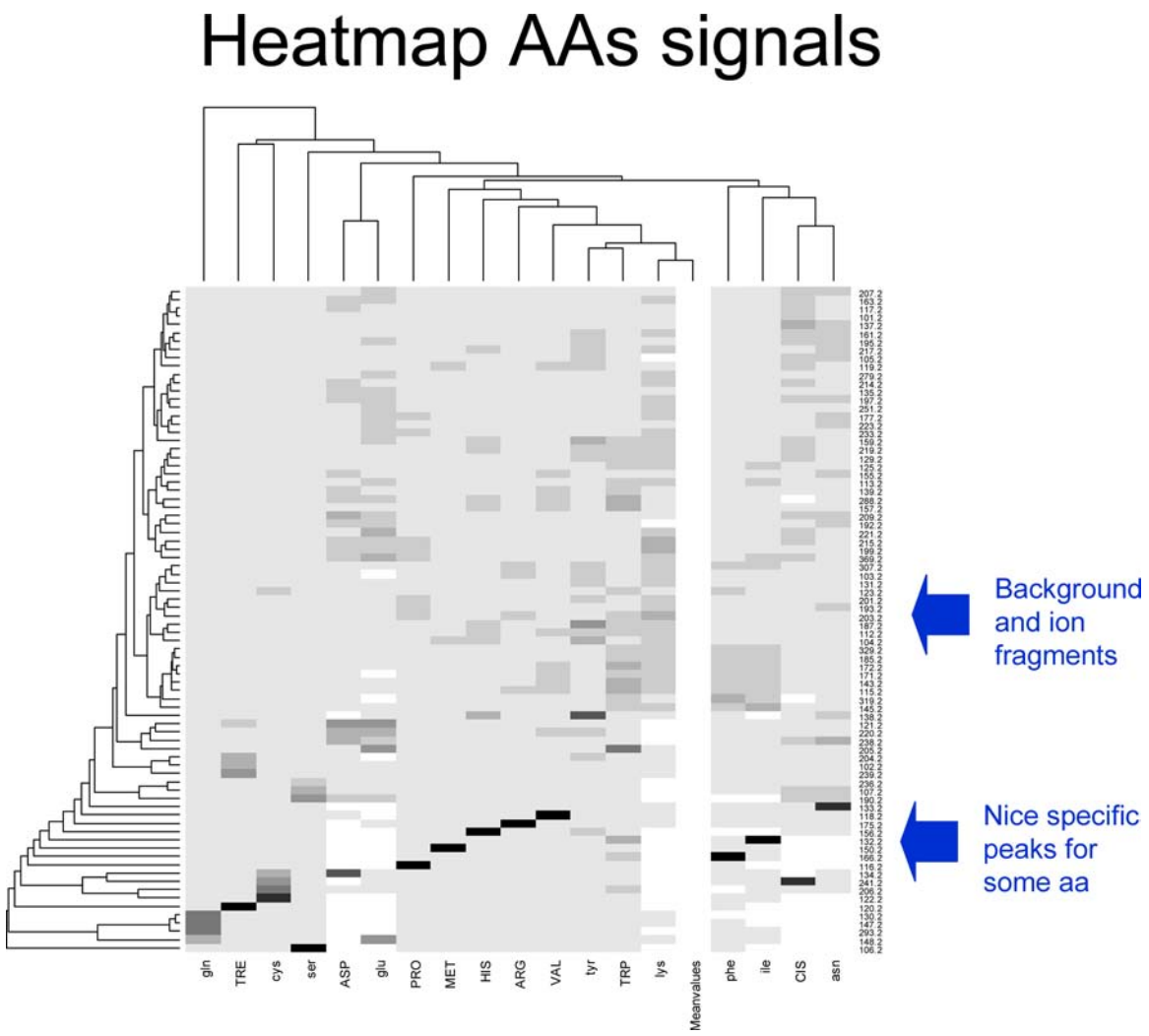

Figure 5. Heatmap profile of amino acid standards. Hierarchical clustering is presented for the ion fragments (horizontal rows) and amino acid standards (vertical rows).

than 200 different peaks were detected with an excellent S/N of >10 (Figure 4). Up to ~600 other ions could also be quantified with acceptable results (S/N > 3). DIESI–MS yielded 1–2 orders of magnitude more biochemical information at a fraction of the cost compared to other methods (Table 1).

DIESI–MS Generates a Metabolic Fingerprint Revealing Specific Ions Differing between Treatments. When samples from maize plants grown under different environmental conditions (normal CT and LN) are compared, many peak intensities were similar, the mass spectra appeared symmetrical, but detailed inspection revealed that there were also specific ions that increased or decreased (Figure 4). A similar response was also observed for maize plants subjected to drought stress and for plants grown at different localities and conditions (data not shown). Overall, the results confirmed our previous report on the possible application of DIESI–MS for the physiological evaluation of maize plants using stem extracts collected at the flowering time.[18]

Method Development and Optimization. The promising results motivated us to further optimize the DIESI–MS platform for high-throughput metabolic phenotyping of maize and other species. We simplified the extraction and sample preparation procedure, but more particularly, we improved the scripts, file handling, statistical procedures, and boxplot figure output compared to previous reports.[18] The statistical analysis of the DIESI–MS data using loop programming and the R scripts were optimized as described extensively in the methods. We also optimized sample treatment and handling, allowing for the realistic measurement of ~80 samples per day (Table 1).

Control Experiments: DIESI–MS Ion Pattern of Standards. We then asked: How repeatable and redundant is the DIESI–MS data? Do standard compounds ionize with the theoretical positive mass, or does our DIESI–MS method produce ions fragmenting other non-standard m/z peaks? To answer those questions, additional control experiments were performed. Candidate primary metabolites that might change under different stress conditions were evaluated. We focused on amino acids, because it could be expected that CT and LN treatments severely affects the nitrogen status of plants. Theoretically, they should all ionize well in positive-ion mode; therefore, the 20 standard amino acids and cistine were injected into the MS quadrupole, and the occurrence and the magnitude of ion fragmentation with electrospray ionization (ESI) was documented using gray heatmaps (Figure 5).

DIESI–MS produced an ion pattern (mass spectrum) that was highly specific for each amino acid (Figure 5). The most intense peaks (black bars) had indeed the expected m/z according to the theoretical mass of non-fragmented proto-

DOI: 10.1021/jf504853w
J. Agric. Food Chem. 2015, 63, 1042–1052

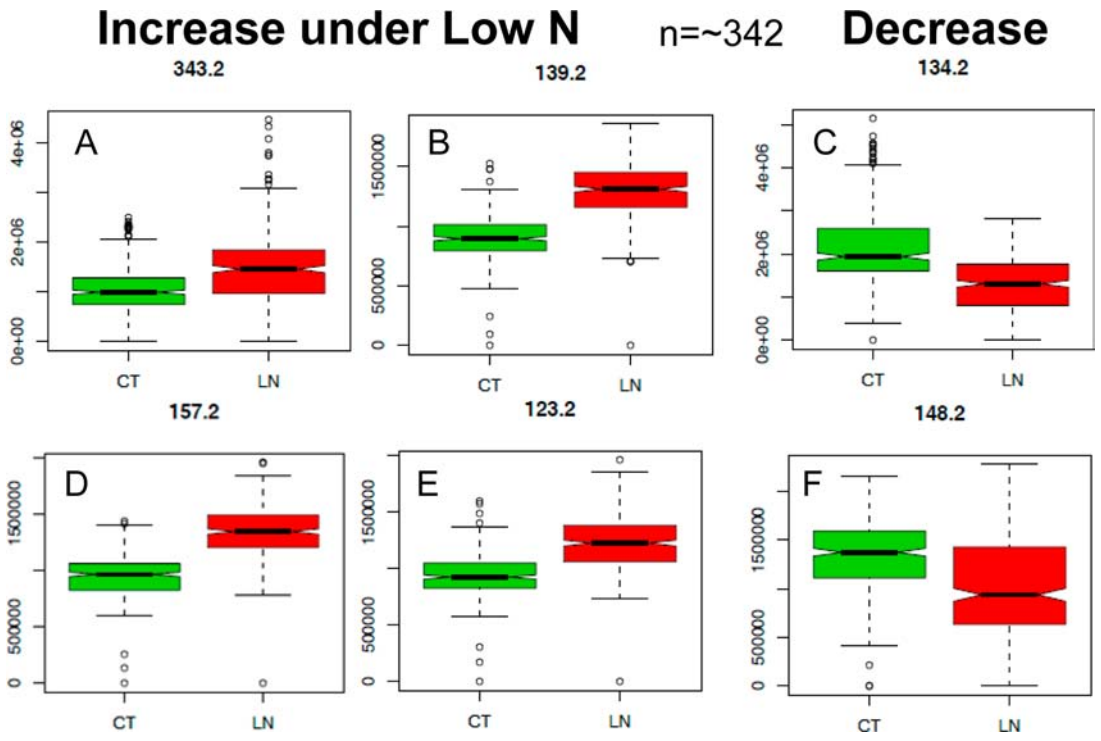

Figure 6. Intensity data of selected m/z ions quantified with DIESI−MS. Maize plants were grown under either normal CT (green) or LN (red) conditions, and stem juice extracts were sampled for DIESI−MS metabolic profiling. Boxplots summarize data from 19 genotypes, 6 biological, and 3 technical replicates (n = 342). Boxplot wiskers are shown for significant differences. (A, B, D, and E) Data from four representative ions that increase under LN conditions. (C and F) Data from two representative ions that decrease under LN conditions.

nated amino acids (AA + 1H) (Figure 5). Most amino acids ionized very well with our DIESI−MS protocol (e.g., Gly, Ser, Thr, Gln, Leu, and Ala). Unfortunately, other amino acids did not ionize equally well (e.g., His, Met, Arg, Asn, Tyr, Trp, Phe, Glu, and Asp), and the reason for this remained unknown. The atomic events that lead to ionization in ESI are complex, so that efficient ionization cannot be theoretically predicted nor explained by the chemical formula but must rather be confirmed by a trial and error approach.

In addition to the expected m/z peaks (main ion fragments), other minor ions of lower intensity also appeared in the DIESI−MS spectra (Figure 5). Minor accompanying peaks were both smaller and larger than the expected molecular mass of the unitary ion. These peaks could be ion fragments (smaller mass) or ion aggregates (larger mass) of the original molecules. Nevertheless, ion fragmentation with ESI was much less than that with EI, and the avoidance of chemical derivatization reduced the problem of data redundancy (e.g., with GC−TOF, citric acid and some amino acids generate more than six RT peaks across several fragmented masses).

Taken together, the control experiments indicated that DIESI−MS efficiently discriminates the chemical profile of samples and that data are repeatable and fairly non-redundant. However, because of fragmentation, aggregation, and matrix interaction, the assignment of a given m/z peak to a given biomolecule should be performed with extreme care. Even if a DIESI−MS peak has a m/z value that is identical to the theoretical mass of a standard known compound, we did not assume that the intensity value corresponded to the concentration of the known compound in the plant sample. In fact, direct-injection spectra provide a numeric phenotype of complex ion mixtures that reveals the physiological status of plants,[18] but it is not the best choice for metabolite identification, chemical discovery, and/or structural assignment as with other high methods, such as UPLC−MS−Orbitrap or NMR. For example, the DIESI−MS peak m/z 106.2 in theory corresponds to positively ionized serine, but other compounds could also generate signals or suppress ionization in that m/z range. A search in chemical databases yielded dozens of chemical compounds for that given m/z value. If the mass tolerance was increased to ±0.5 Da, then hundreds of theoretical compounds were listed. Many molecules are certainly absent in plants or living cells, but unequivocal assignment of m/z values to metabolites requires many control experiments that are out of the focus of the present paper. In the midterm, we will start building a biochemical database of DIESI−MS peaks that are frequently found in various plant extracts (we call it "metabolic space" of each species and tissue) (see also ref 19).

Given the previous limitations, we avoided assigning chemical names to DIESI−MS peaks but only named them by the numerical m/z value (center of maximal intensity of the positive ion). From the practical perspective of metabolic phenotyping for breeding purposes, it does not matter the exact identity or name of the compound but rather the following questions: Is it related to yield? Can we measure it cheaply? Is it quantitative? How much variance depends upon the E, and how much depends upon the G? Will it be useful for plant breeding? Which ions increase or decrease significantly under stress? Which peaks should be used as biomarkers for selection and/or screening?

Discrimination of Phenotypic Variance Because of E and G Effects. To answer above questions, we performed field trials using 18 maize hybrids grown under CT and LN conditions (see the Materials and Methods). The optimized DIESI−MS data analysis pipeline and the novel R scripts

DOI: 10.1021/jf504853w
J. Agric. Food Chem. 2015, 63, 1042−1052

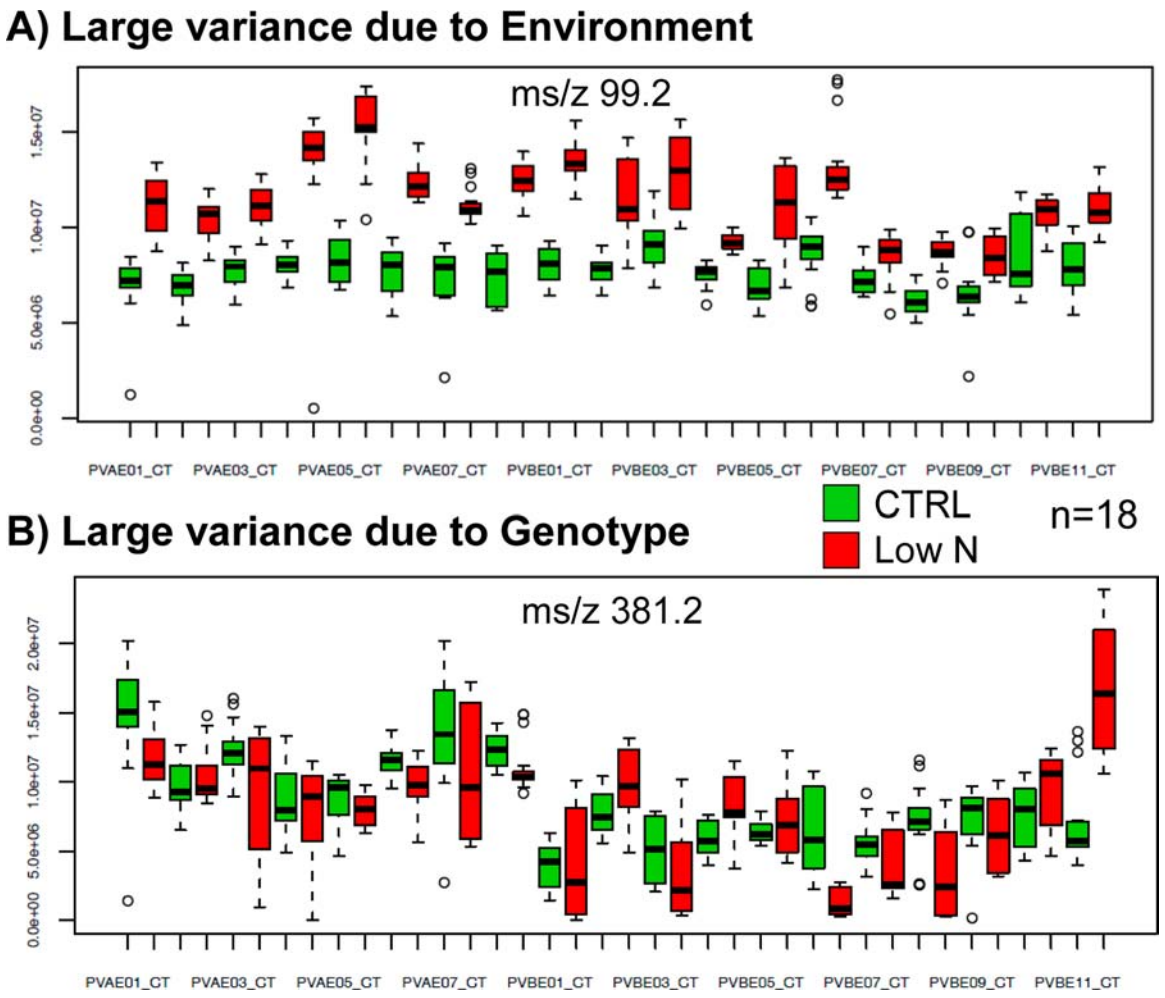

Figure 7. Evaluation of signals that primarily depend upon environmental or genetic factors. Intensity data of selected m/z ions were quantified with DIESI−MS. A total of 19 maize genotypes were grown under either normal CT (green) or LN (red) conditions, and stem juice extracts were sampled for DIESI−MS metabolic profiling. Boxplots summarize data from 6 biological and 3 technical replicates (n = 18). ANOVA was used to discriminate environmental and genotypic variance. (A) Representative m/z ion 99.2 with a large environmental effect. (B) Representative m/z ion 381.2 with a lower environmental effect but larger genetic effect.

allowed us to represent the data of given m/z peaks automatically as boxplots (Figure 6). The pooled data per environmental condition revealed several m/z peaks that significantly increased (panels A, B, D, and E of Figure 6) or decreased (panels C and F of Figure 6) under LN treatment.

When the data for each genotype were analyzed separately (Figure 7), several m/z signals, such as 99.2, displayed a strong dependence upon the environment (Figure 7A), while others, such as 381.2, were less dependent upon the growth conditions but rather presented large variance because of the genotype (Figure 7B). Such information is required for phenotyping purposes because it is important to identify candidate m/z peaks to be used as biomarkers for a given physiological condition or stress. Overall, DIESI−MS allowed for the partitioning of variance of individual peaks according to E and G effects and can be combined with standard agronomic measurements within yield trials to predict hybrid performance under variable conditions.

Comparison of the Cost−Benefit Analysis of Different Metabolic Profiling Strategies. For research purposes, it is attractive to find reliable quantitative biomarkers for genotypic selection, but a maize breeder with limited resources would ask the following questions: How expensive is DIESI−MS profiling? How much training and manual worktime is required? How many samples can a user process per week or season?

Systematic comparison of several analytical platforms revealed that DIESI−MS allowed for a high throughput of samples, required little time for statistical analysis, and was the cheapest method per metabolic data point (Table 1). The cost per metabolic data point was in the range of 2−10 cents in U.S. dollars. Among all metabolic profiling strategies, DIESI−MS had the greatest potential to be extensively used for plant phenotyping.

DIESI−MS Results from Various Plant Extracts. Because DIESI−MS was generating promising results, several colleges asked: does it work for other samples in addition to maize stems? To answer their questions, we combined the DIESI−MS data from different plant samples (Figure 8). We included previously obtained spectra from coffee leaves (*Coffea arabica* and *Coffea canephora*), red and black tea leaves (*Camellia sinensis*), and coca leaves (*Erythroxylum coca*).[18] Novel data were added from maize stem juice extracts (grown under CT and LN conditions) and also strawberry (*Fragaria vesca*) samples of different maturity stages. A pseudo-extract was also included as a blank control (Figure 8).

DOI: 10.1021/jf504853w
J. Agric. Food Chem. 2015, 63, 1042−1052

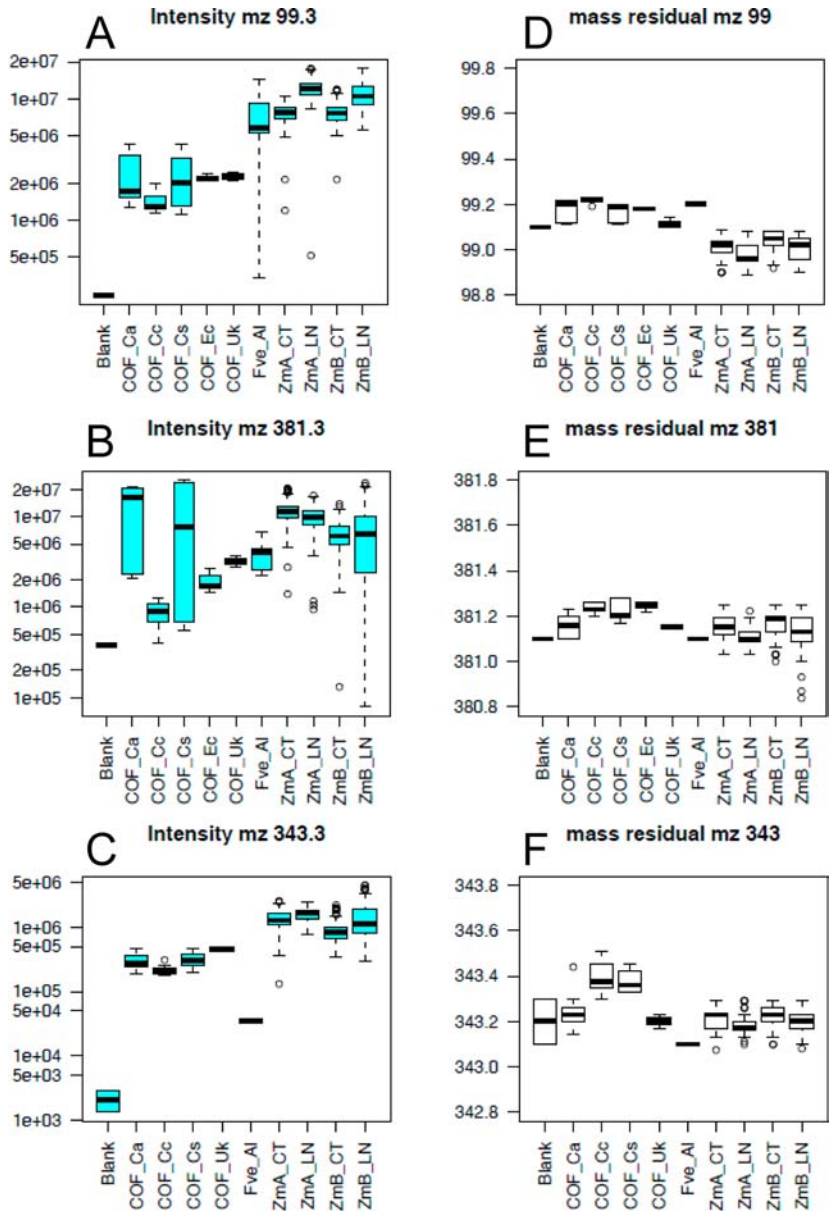

Figure 8. Ion intensity data of nine different plant samples. (A–C) Representative m/z ions. (D–F) Corresponding m/z values. (A) Ion 99.3 was low in leaves of tea samples but was equally abundant in strawberry fruits and maize stem. It increased under LN stress compared to CT but was similar among yellow (ZmA) and white (ZmB) maize hybrids. (B) Ion 381.3 did not change much because of environmental conditions but varied more according to genotype. (C) Ion 343.3 increased slightly because of LN stress in maize but was very low in strawberry fruits. *Zea mays* samples were pooled into white grain genotypes (ZmA) or yellow grain genotypes (ZmB) and grown under either normal CT or LN conditions. Boxplots summarize data from each species or treatment (n = 6–500). Data were from coffee leaves [*C. arabica* (COF-Ca) and *C. canephora* (COF-Cc)], tea leaves [*C. sinensis* (COF-Cs)], and coca leaves [*E. coca* (COF-Ec)][18] as well as strawberry (*F. vesca*) fruit samples of different maturity stages (Fve-Al). A pseudo-extract was used as a blank.

In addition to reporting the intensity values for given m/z ion bins (panels A–C of Figure 8), we also found it relevant to plot the exact m/z values (panels D–F of Figure 8). Peak m/z 99.3 was highest in all maize samples and strawberry fruits, whereas it was lower in all leaf samples (Figure 8A). In maize stem extracts, peak m/z 99.3 increased under LN compared to CT treatment (Figure 8A). The m/z values were similar across leaf samples (Figure 8D). There was a slight tendency that the m/z value was lower in maize, indicating that the metabolite is not necessarily the same in tea leaves or maize stems (Figure 8D).

Peak m/z 381.3 was high in maize stems, intermediate in strawberry fruits, and highly variable in leaves of different species (Figure 8B). It was higher in *C. arabica* than in *C. canephora* (Figure 8B). In maize stem extracts, peak m/z 381.3 did not change significantly under LN or CT conditions (Figure 8B). The m/z values were very similar across all species and treatments (Figure 8E).

Peak m/z 343.3 was high in maize, intermediate in leaves, and rather low in strawberry fruits (Figure 8B). This metabolite was high in maize stem extracts, particularly low in fruits, and totally absent in coca leaves (Figure 8C). No difference was found between LN or CT conditions for peak m/z 343.3 (Figure 8C). The m/z values varied across plant species, so that most likely intensity values correspond to different metabolites in different samples (Figure 8F).

DOI: 10.1021/jf504853w
J. Agric. Food Chem. 2015, 63, 1042–1052

The metabolite detected in *C. arabica* samples probably corresponds to the metabolite detected in maize and strawberry, but it might be different from the metabolite detected in *C. canephora* and *C. sinensis* (Figure 8F).

We conclude from these analyses that the boxplot figures provide useful quality controls for the DIESI−MS results. Our protocol worked for many different plant samples, and it even allowed for the study of phylogenetic relationships. Some specific ions allowed for the identification of plant organs or species. Other ions allowed for the specific identification of environmental variance or the selection according to genetic variance.

Potential Applications of DIESI−MS for Plant Breeding. It can be concluded that, among all metabolic profiling strategies, DIESI−MS generates a vast amount of information at the cheapest price (Table1) and, therefore, has the greatest potential to be routinely implemented for biochemical phenotyping of plant cultivars. Because metabolites are closer related to GY than DNA sequences (Figure 1), we postulate that metabolic phenotyping using DIESI−MS complements genome-wide selection (GWS) strategies.

In summary, DIESI−MS is a great phenotyping tool, which will assist plant research and breeding. We expect it will become common in the near future, because there is still large room for methodological improvements to increase information density, bring down cost, and further simplify procedures. Success will depend upon the establishment of strategic alliances between plant physiologists, biochemical researchers, biostatisticians, breeders, and agronomists.

■ ASSOCIATED CONTENT

Supporting Information

Strawberry batch divided in diferent groups according to their different levels of ripeness, with stage 1 representing the less ripe and stage 3 representing the most riped fruit (Figure S1) and parameters used to identify the different ripeness stages in a strawberry (*F. vesca*) batch (Table S1). This material is available free of charge via the Internet at http://pubs.acs.org.

■ AUTHOR INFORMATION

Corresponding Author

*E-mail: atiessen@ira.cinvestav.mx.

Funding

This work was partially supported by the initiative MASAGRO funded by SAGARPA through Grant IMIC-2012-016 to Axel Tiessen. Axel Tiessen and Robert Winkler acknowledge basic science funding by Consejo Nacional de Ciencia y Tecnología (CONACYT, Mexico). Martín García-Flores, Sheila Juárez-Colunga, and Adrián García-Casarrubias obtained a postgraduate fellowship by CONACYT.

Notes

The authors declare no competing financial interest.

■ ACKNOWLEDGMENTS

The authors thank J. P. Délano and R. Sawers for proofreading the manuscript.

■ ABBREVIATIONS USED

DNA, deoxyribonucleic acid; DIESI−MS, direct-injection electrospray ionization mass spectrometry; GC−FID, gas chromatography with flame ionization detection; GY, grain yield; QTL, quantitative trait loci; *m*/*z*, mass-to-charge ratio; NALDI−TOF−MS, nanoassisted laser desorption ionization time-of-flight mass spectrometry; NIRS, near-infrared reflectance spectroscopy; RNA, ribonucleic acid; UPLC, ultra performance liquid chromatography; UV, ultraviolet

■ REFERENCES

(1) Fiehn, O. Metabolomics—The link between genotypes and phenotypes. *Plant Mol. Biol.* **2002**, *48* (1−2), 155−171.

(2) Monneveux, P.; Sanchez, C.; Tiessen, A. Future progress in drought tolerance in maize needs new secondary traits and cross combinations. *J. Agric. Sci.* **2008**, *146*, 287−300.

(3) Moose, S. P.; Mumm, R. H. Molecular plant breeding as the foundation for 21st century crop improvement. *Plant Physiol.* **2008**, *147* (3), 969−977.

(4) Ribaut, J. M.; de Vicente, M. C.; Delannay, X. Molecular breeding in developing countries: Challenges and perspectives. *Curr. Opin. Plant Biol.* **2010**, *13* (2), 213−218.

(5) Schauer, N.; Fernie, A. R. Plant metabolomics: Towards biological function and mechanism. *Trends Plant Sci.* **2006**, *11* (10), 508−516.

(6) Fernie, A. R.; Schauer, N. Metabolomics-assisted breeding: A viable option for crop improvement? *Trends Genet.* **2009**, *25* (1), 39−48.

(7) Stitt, M.; Fernie, A. R. From measurements of metabolites to metabolomics: An 'on the fly' perspective illustrated by recent studies of carbon−nitrogen interactions. *Curr. Opin. Biotechnol.* **2003**, *14* (2), 136−144.

(8) Cappiello, A.; Famiglini, G.; Palma, P.; Pierini, E.; Termopoli, V.; Trufelli, H. Direct-EI in LC−MS: Towards a universal detector for small-molecule applications. *Mass Spectrom. Rev.* **2011**, *30* (6), 1242−1255.

(9) Geigenberger, P.; Tiessen, A.; Meurer, J. Use of non-aqueous fractionation and metabolomics to study chloroplast function in *Arabidopsis*. *Methods Mol. Biol.* **2011**, *775*, 135−160.

(10) Zwiener, C.; Frimmel, F. H. LC−MS analysis in the aquatic environment and in water treatment—A critical review—Part I: Instrumentation and general aspects of analysis and detection. *Anal. Bioanal. Chem.* **2004**, *378* (4), 851−861.

(11) Bino, R. J.; Hall, R. D.; Fiehn, O.; Kopka, J.; Saito, K.; Draper, J.; Nikolau, B. J.; Mendes, P.; Roessner-Tunali, U.; Beale, M. H.; Trethewey, R. N.; Lange, B. M.; Wurtele, E. S.; Sumner, L. W. Potential of metabolomics as a functional genomics tool. *Trends Plant Sci.* **2004**, *9* (9), 418−425.

(12) Witt, S.; Galicia, L.; Lisec, J.; Cairns, J.; Tiessen, A.; Araus, J. L.; Palacios-Rojas, N.; Fernie, A. R. Metabolic and phenotypic responses of greenhouse-grown maize hybrids to experimentally controlled drought stress. *Mol. Plant* **2012**, *5* (2), 401−417.

(13) Roessner, U.; Luedemann, A.; Brust, D.; Fiehn, O.; Linke, T.; Willmitzer, L.; Fernie, A. R. Metabolic profiling allows comprehensive phenotyping of genetically or environmentally modified plant systems. *Plant Cell* **2001**, *13* (1), 11−29.

(14) Fiehn, O. Metabolite profiling in *Arabidopsis*. *Methods Mol. Biol.* **2006**, *323*, 439−447.

(15) Meyer, R. C.; Steinfath, M.; Lisec, J.; Becher, M.; Witucka-Wall, H.; Torjek, O.; Fiehn, O.; Eckardt, A.; Willmitzer, L.; Selbig, J.; Altmann, T. The metabolic signature related to high plant growth rate in *Arabidopsis thaliana*. *Proc. Natl. Acad. Sci. U. S. A.* **2007**, *104* (11), 4759−4764.

(16) Lisec, J.; Meyer, R. C.; Steinfath, M.; Redestig, H.; Becher, M.; Witucka-Wall, H.; Fiehn, O.; Torjek, O.; Selbig, J.; Altmann, T.; Willmitzer, L. Identification of metabolic and biomass QTL in *Arabidopsis thaliana* in a parallel analysis of RIL and IL populations. *Plant J.* **2008**, *53* (6), 960−972.

(17) Kind, T.; Fiehn, O. Metabolomic database annotations via query of elemental compositions: Mass accuracy is insufficient even at less than 1 ppm. *BMC Bioinf.* **2006**, *7*, 234−243.

(18) Garcia-Flores, M.; Juarez-Colunga, S.; Montero-Vargas, J. M.; Lopez-Arciniega, J. A. I.; Chagolla, A.; Tiessen, A.; Winkler, R.

DOI: 10.1021/jf504853w
J. Agric. Food Chem. 2015, 63, 1042−1052

Evaluating the physiological state of maize (*Zea mays* L.) plants by direct-injection electrospray mass spectrometry (DIESI−MS). *Mol. BioSyst.* **2012**, *8* (6), 1658−1660.
(19) Montero-Vargas, J. M.; Gonzalez-Gonzalez, L. H.; Galvez-Ponce, E.; Ramirez-Chavez, E.; Molina-Torres, J.; Chagolla, A.; Montagnon, C.; Winkler, R. Metabolic phenotyping for the classification of coffee trees and the exploration of selection markers. *Mol. BioSyst.* **2013**, *9* (4), 693−699.
(20) Spielbauer, G.; Armstrong, P.; Baier, J. W.; Allen, W. B.; Richardson, K.; Shen, B.; Settles, A. M. High-throughput near-infrared reflectance spectroscopy for predicting quantitative and qualitative composition phenotypes of individual maize kernels. *Cereal Chem.* **2009**, *86* (5), 556−564.
(21) Tiessen, A.; Hendriks, J. H. M.; Stitt, M.; Branscheid, A.; Gibon, Y.; Farre, E. M.; Geigenberger, P. Starch synthesis in potato tubers is regulated by post-translational redox modification of ADP-glucose pyrophosphorylase: A novel regulatory mechanism linking starch synthesis to the sucrose supply. *Plant Cell* **2002**, *14* (9), 2191−2213.
(22) Angeles-Núñez, J.; Tiessen, A. *Arabidopsis* sucrose synthase 2 and 3 modulate metabolic homeostasis and direct carbon towards starch synthesis in developing seeds. *Planta* **2010**, *232* (3), 701−718.
(23) R Development Core Team, R. *R: A Language and Environment for Statistical Computing*; R Foundation for Statistical Computing: Vienna, Austria, 2008; http://www.R-project.org.

DOI: 10.1021/jf504853w
J. Agric. Food Chem. 2015, 63, 1042−1052

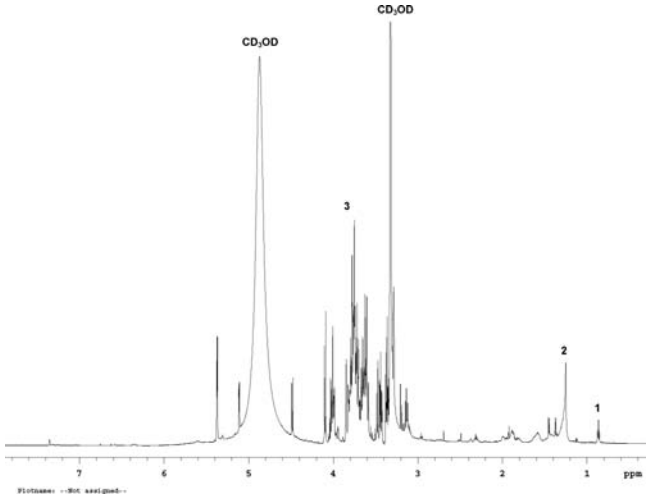

Figure 1. ^{1}H NMR in CD_3OD of the methanolic extract of lyophilized pawpaw fruit pulp. Peaks: 1: $-\mathbf{CH_3}$ 2: $-(\mathbf{CH_2})_n$ 3: **H**CO of sugars and acetogenins.

(ASE, ThermoFisher Scientific, Sunnyvale, CA). Then, methanol (CH_3OH) was added while the temperature and pressure were increased to 23, 60, or 100 °C and 10.3 MPa (1500 psi) over a 3 min time (static time). Next, the solvent was purged into a collection vessel. A total of four cycles were run to statically extract the sample, resulting in a total volume of about 160 mL. The solvent was evaporated off, and the oily residues remaining were weighed.

A portion of the residue remaining after the methanolic extraction at 100 °C was redissolved in methanol for LC-HRMS analysis using a Thermo Scientific HPLC with an Accela 1250 pump and Accela Open AS autosampler. A Waters Acquity UPLC C18 BEH column with 1.7 μm particle size and dimensions of 2.1 × 150 mm was used with a gradient elution. It started with CH_3OH and water containing 0.1% formic acid at a flow rate of 0.300 mL/min. For the first 25 min of the first gradient, an isocratic mobile phase of 4:1 CH_3OH:H_2O (v/v) was used. This was changed linearly to 49:1 CH_3OH:H_2O (v/v) from 25 to 30 min and held at this mixture from 30 to 35 min, followed by a step change back to 4:1 CH_3OH:H_2O (v/v) that was held from 35 to 45 min. An Orbitrap Exactive HRMS (Thermo Scientific, Sunnyvale, CA) was used with heated electrospray ionization (HESI) at 350 °C and a nitrogen gas sheath flow 45 arbitrary units, auxiliary nitrogen gas flow 12 arbitrary units. For negative ionization, the following parameters were used: spray voltage 2.60 kV, capillary temperature 325 °C, capillary voltage −35.00 V, tube lens voltage −80.00 V, skimmer voltage −18.00 V. For positive ionization, the following parameters were used: spray voltage 3.50 V, capillary temperature 325 °C, capillary voltage 32.50 V, tube lens voltage 100.00 V, skimmer voltage 16.00 V. Its resolution at m/z 400 was 100,000 full width at half-maximum peak height (fwhm). It used an internal mass lock. The mass range was 100−1000 m/z with a target of 1,000,000 charges and a maximum ionization time of 250 ms. It was able to rapidly switch between positive and negative ionization, so H^+, Na^+, and formate ($HCOO^-$) adducts could be detected. So, for annonacin, masses in the range of 597.47071−597.47549, 619.45251−619.45747, and 641.46397−641.46911 were monitored for $[M + H]^+$, $[M + Na]^+$, and $[M+HCOO]^-$, respectively. For squamocin, masses in the range of 623.48628−623.49126, 645.46808−645.47324, and 667.47985−667.48519 Da were monitored for $[M + H]^+$, $[M + Na]^+$, and $[M +HCOO]^-$, respectively. Annonacin and squamocin standards from Pierre Champy at the University of Paris were used to identify and quantify the peaks due to annonacin and squamocin that eluted at 19.74 and 22.51, min, respectively.

Calibration curves were obtained using 10−1000 ng/mL annonacin and squamocin, assuming that the standards were 100% pure. Samples were diluted until they produced peaks with areas that fell within the range of the calibration standards.

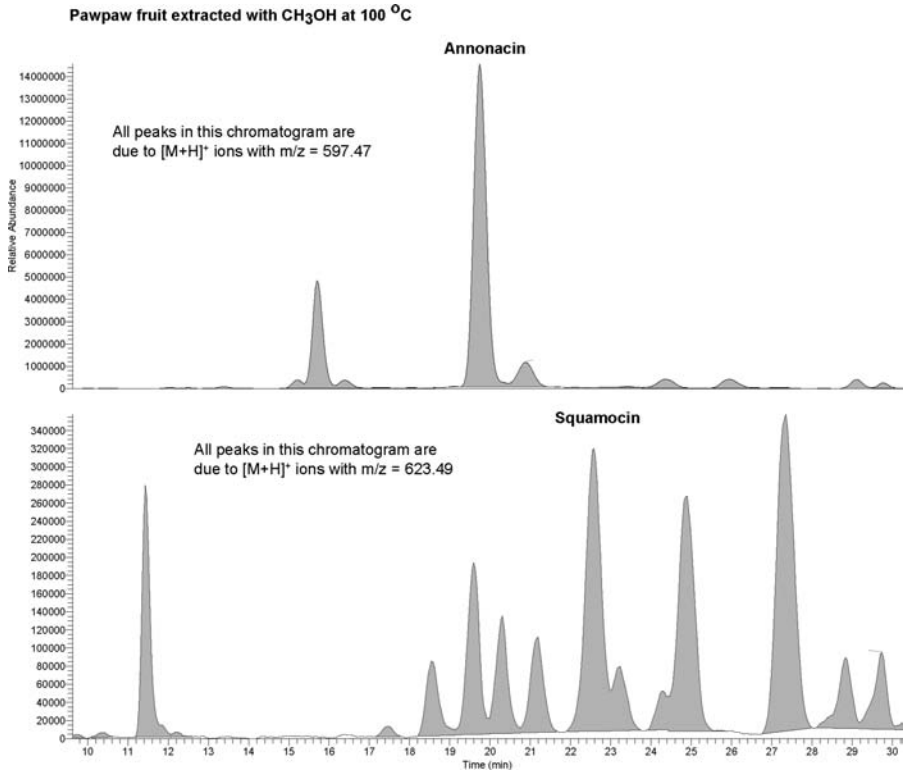

Figure 2. LC-HRMS of methanolic extract of lyophilized whole pawpaw fruits done at 100 °C and 10 MPa pressure in a sealed container. All of the peaks in the top chromatogram are due to $[M + H]^+$ ions that had a mass to charge ratio (m/z) of 597.47, like annonacin. All of the peaks in the bottom chromatogram are due to $[M + H]^+$ ions that had a mass to charge ratio (m/z) of 623.49, like squamocin.

DOI: 10.1021/jf504500g
J. Agric. Food Chem. 2015, 63, 1053−1056

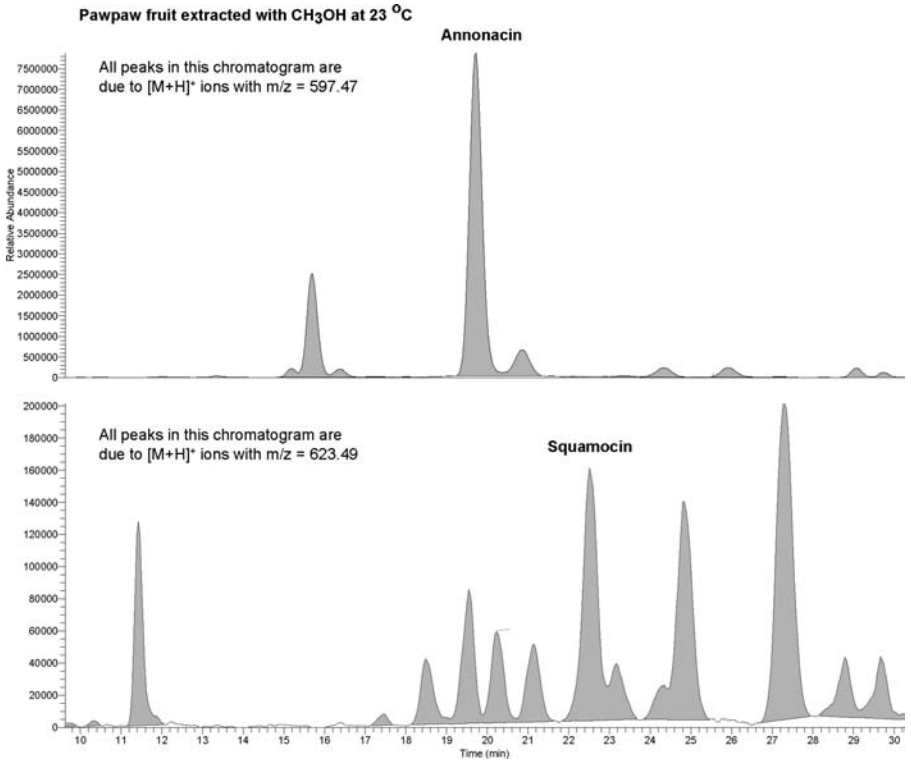

Figure 3. LC-HRMS of methanolic extract of lyophilized whole pawpaw fruits done at 23 °C and 10 MPa pressure in a sealed container. All of the peaks in the top chromatogram are due to $[M + H]^+$ ions that had a mass to charge ratio (m/z) of 597.47, like annonacin. All of the peaks in the bottom chromatogram are due to $[M + H]^+$ ions that had a mass to charge ratio (m/z) of 623.49, like squamocin.

Another portion of the residue remaining after the methanolic extraction at 100 °C was redissolved in CD_3OD for NMR analysis using an Agilent DD2 600 MHz NMR (Santa Clara, CA). A 30° pulse width and 1 s pulse delay were used for the ^1H NMR, while a 30° pulse width and 2 s pulse delay were used for the ^{13}C NMR spectra. Chemical shifts were referenced to the CD_3OD peaks at 3.35 and 4.78 ppm (for ^1H) and 49.3 ppm (for ^{13}C).

RESULTS AND DISCUSSION

About 59.3% of the lyophilized pawpaw fruit was solubilized by dry methanol at 100 °C, compared to 40.4 and 50.1% at 23 and 60 °C. This does not refer to the percent recovery, which is a term that refers to the recovery of standards that are spiked into a sample. It refers to the percentage of material in the fruit that was solubilized. Like the NMR spectra of the methanolic extracts of four other fruits in the Annonaceae family,[18] the pawpaw spectra are dominated by peaks due to fructose and other carbohydrates, as shown in Figure 1. There are no peaks due to triglycerides, which would be strongly retained on a C_{18} column. So, this extract was suitable for LC-HRMS analysis without any sample cleanup being required.

The LC-HRMS chromatograms of the methanolic extract of pawpaw detected not just annonacin and squamocin but also isomers of them, as shown in Figures 2 and 3. The chromatograms of the extracts obtained at 100 and 23 °C look almost identical, indicating that the same compounds were solubilized in about the same ratios. However, the peaks areas were larger in the chromatogram of the extract at 100 °C, and more material was solubilized at this higher temperature. So, the total concentration found in the 100 °C extract was higher than those found in the 23 and 60 °C extracts.

The concentrations of annonacin and squamocin found at each temperature are in Table 1. That is, 7724 and 162 μg/g annonacin and squamocin were found when the extraction was done at 100 °C, while only 3750 and 74 were found at 23 °C and 6370 and 128 were found at 60 °C. This compares to 70.1 μg/g annonacin and no squamocin found by others in fresh (not lyophilized) pawpaw fruit using MALDI-TOF MS analysis.[5] Since pawpaw fruit contains about 77% moisture,[15] this would correspond to about 304 μg annonacin per g of dry weight. There were not enough of the annonacin and squamocin standards to completely validate the method. That is, there was not enough to do the required analyses for percent purity. There was not enough for moisture analysis. Still, each standard produced only one peak in the LC-MS. They were also the same standards used in the previous study that found lower concentrations of them.[5] So, even though the exact concentrations were calculated based on the assumption that the standards were 100% pure (no moisture), they can be compared to the previous study.[5] The main reason why so much less was found in that study was because the extraction was done under ambient conditions and because there was so much moisture in the fresh pawpaw fruit. Annonacin, squamocin, and other acetogenins are lipophilic,[16] so they are extracted best from dry (lyophilized) fruit using dry methanol at 100 °C and 10 MPa pressure. However, if the extraction is

Table 1. Concentrations (in μg/g) of Annonacin and Squamocin Found at Three Different Extraction Temperatures in Lyophilized Whole Pawpaw Fruits from Missouri

temp	annonacin (μg/g)	squamocin (μg/g)
23 °C	3750	74
60 °C	6370	128
100 °C	7724	162

DOI: 10.1021/jf504500g
J. Agric. Food Chem. 2015, 63, 1053−1056

done under these conditions and then the extract is analyzed by MALDI-TOF MS, all the isomers of annonacin would coelute with each other, since no column was used to separate them. This is also true for isomers of squamocin. As a result, the apparent concentrations of annonacin and squamocin would be overestimated. In conclusion, a combination of high pressure liquid extraction using dry methanol at 100 °C and 10 MPa pressure and LC-HRMS is the preferred method.

Robert A. Levine[†]
Kristy M. Richards[†]
Kevin Tran[†]
Rensheng Luo[‡]
Andrew L. Thomas[§]
Robert E. Smith*[,†]

[†]U.S. Food and Drug Administration, Total Diet and Pesticide Research Center, 11510 West 80th Street, Lenexa, Kansas 66214, United States

[‡]University of Missouri − St. Louis, One University Drive, St. Louis, Missouri 63121, United States

[§]Southwest Research Center, University of Missouri, Mt. Vernon, Missouri 65712, United States

AUTHOR INFORMATION

Corresponding Author

*Phone: 913-752-2127. Fax: 913-752-2122. E-mail: robert.smith@fda.hhs.gov.

Notes

This work should not be taken as reflecting FDA policy or regulations.

The authors declare no competing financial interest.

REFERENCES

(1) Templeton, S. B.; Marlette, M.; Pomper, K. W.; Jones, S. C. Favorable taste ratings for several pawpaw products. *Hort. Technol.* **2003**, *13*, 445−448.

(2) Ames, G., Greer, L. *Pawpaw − A "Tropical" Fruit for Temperate Climates*; National Sustainable Agriculture Information Service: Buttte, MT, 2010.

(3) Smith, R. E.; Tran, K.; Richards, K. M. Bioactive annonaceous acetogenins. In *Studies in Natural Products Chemistry*; Atta-ur-Rahman, Ed.; Elsevier: New York, 2014; Chapter 4, pp 93−117.

(4) Adeoye, I. B.; Umeh, U. C.; Ajetunmobi, T. Prospects and problems of marketing pawpaw in the urban environment of Ibadan, Nigeria. *Libyan Agric. Res. Cent. J. Int.* **2012**, *3*, 80−84.

(5) Potts, L. F.; et al. Annonacin in *Asimina triloba* fruit: Implication for neurotoxicity. *Neurotoxicology* **2012**, *33*, 53−58.

(6) Caparros-Lefebvre, D.; Elbaz, A. Possible relation of atypical parkinsonism in the French West Indies with consumption of tropical plants: a case-control study. *Lancet* **1999**, *354*, 281−285.

(7) Escobar-Khondiker, M.; et al. Annonacin, a natural mitochondrial complex I inhibitor, causes tau pathology in cultured neurons. *J. Neurosci.* **2007**, *27*, 7827−7837.

(8) Lannuzel, A.; et al. Atypical parkinsonism in Guadeloupe: a common risk factor for two closely related phenotypes? *Brain* **2007**, *130*, 816−827.

(9) Escobar-Khondiker, M.; et al. Annonacin, a natural mitochondrial complex I inhibitor, causes tau pathology in cultured Neurons. *J. Neurosci.* **2007**, *27*, 7827−7837.

(10) Höllerhage, M.; et al. Natural lipophilic inhibitors of mitochondrial complex I are candidate toxins for sporadic neurodegenerative tau pathologies. *Exp. Neurol.* **2009**, *220*, 133−142.

(11) Champy, P.; et al. Annonacin, a lipophilic inhibitor of mitochondrial complex I, induces nigral and striatal neurodegeneration in rats: possible relevance for atypical parkinsonism in Guadeloupe. *J. Neurochem.* **2004**, *88*, 63−69.

(12) Smith, R. E. *Medicinal Chemistry − Fusion of Traditional and Western Medicine*; Bentham Science: Sharjah, U.A.E., 2013; pp 212−215.

(13) Richter, B. E.; Jones, B. A.; Ezzell, J. L.; Porter, N. L. Accelerated solvent extraction: A technique for sample preparation. *Anal. Chem.* **1996**, *68*, 1033−1039.

(14) Richards, K. M.; et al. Improved extraction of soluble solids from some Brazilian and North American fruits. *Nat. Prod. J.* **2014**, *4*, 201−210.

(15) Champy, P.; et al. Annonacin, a lipophilic inhibitor of mitochondrial complex I, induces nigral and striatal neurodegeneration in rats: possible relevance for atypical parkinsonism in Guadeloupe. *J. Neurochem.* **2004**, *88*, 63−69.

(16) Champy, P.; Guérineau, V.; Laprévote, O. MALDI-TOF MS Profiling of annonaceousa acetogenins in *Annona muricata* products for human consumption. *Molecules* **2009**, *14*, 5235−5246.

(17) Allegrand, J.; et al. Structural study of acetogenins by tandem mass spectrometry under high and low collision energy. *Rapid Commun. Mass Spectrom.* **2010**, *24*, 3602−3608.

(18) Luo, R.; et al. NMR Analysis of Potentially Neurotoxic Annonaceous Fruits. *Nat. Prod. J.* **2013**, 230−241.

DOI: 10.1021/jf504500g
J. Agric. Food Chem. 2015, 63, 1053−1056

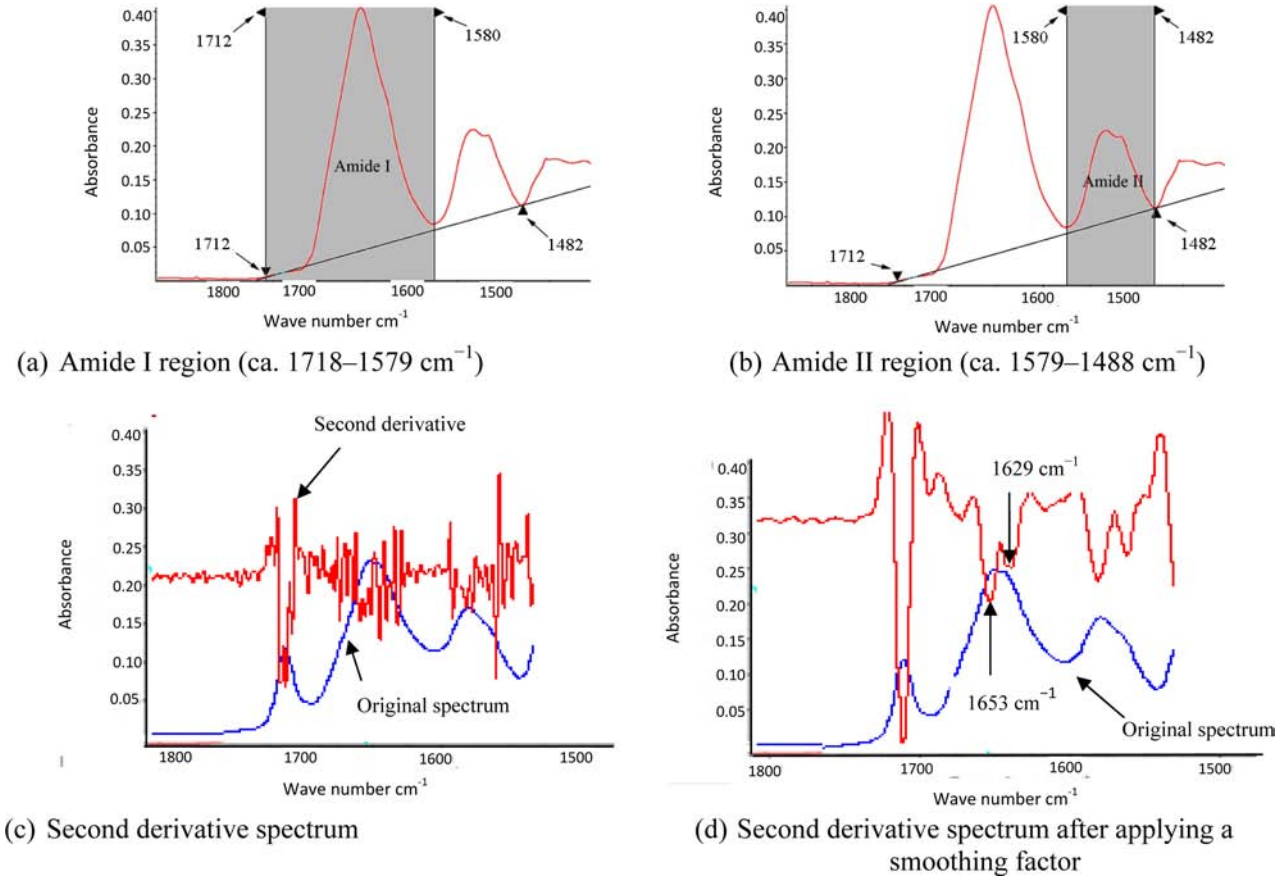

Figure 1. Typical Fourier tansform/infrared-attenuated total reflectance (FT/IR-ATR; Jasco Inc., Easton, MD) spectrum showing (a) amide I region at ca. 1712−1580 cm^{-1}; (b) amide II region 1580−1482 cm^{-1}; (c) original and second-derivative spectrum of the amide I and II region; and (d) second-derivative spectrum of the amide I and II region after applying smoothing factor. The intensities of α-helix (ca. 1653 cm^{-1}) and β-sheet (ca. 1629 cm^{-1}) were measured on the primary spectrum as the height below the first and second negative peak (d).

is vital to establish optimal heating conditions and understanding the changes in CP chemical profile and digestion in dairy cows.[11,14,15] Fourier transform/infrared-attenuated total reflectance (FT/IR-ATR) molecular spectroscopy can be used as a rapid, direct, nondestructive bioanalytical technique to detect heat-induced changes in protein molecular structures.[11,15]

The MIR, dry heating, and moist heating may induce different levels of alteration in feed protein molecular structures. To our knowledge, no systematic study has been conducted on the effect of these different heat-processing methods on protein inherent molecular structures of flaxseed in relation to changes in CP chemical profile, ruminal CP degradation, and intestinal digestibility of RUP. Thus, the objectives of the present study were to (1) determine changes in the protein molecular structure of flaxseed induced by MIR, dry heating, and moist heating, and (2) correlate these structural changes with changes in (a) CP chemical profile, (b) CP subfraction composition, and (c) *in situ* rumen CP degradation and intestinal digestibility of RUP. We hypothesized that these heat processing methods would affect flaxseed protein molecular structures to different extents, resulting in corresponding changes to protein nutritive value and digestibility.

MATERIALS AND METHODS

Chemicals. All the chemicals used for the study were of reagent grade. Sodium hydroxide (purity >99%), trichloroacetic acid (purity 99.6%), sodium tungstate ($Na_2WO_4 \cdot 2H_2O$; purity 100%), sulfuric acid (purity 70%), hydrochloric acid (purity 38%), ethyl ether (purity 99%), sodium borate ($Na_2B_4O_7 \cdot 10H_2O$; purity 99.5%), sodium phosphate ($NaH_2PO_4 \cdot H_2O$; purity 99.5%), kjeltabs (0.15 g $CuSO_4$ and 5.0 g K_2SO_4; $N < 0.005\%$), boric acid (purity >99.5%), acetone (purity ≥99.5%), potassium phosphate (purity >99%), sodium sulphite anhydrous (purity 98.4%), and potassium hydroxide (purity 85%) were purchased from Fisher Scientific (Ottawa, ON, Canada). Thymol ($C_{10}H_{14}O$; purity 99.5%) and enzymes pepsin and pancreatin were purchased from Sigma-Aldrich Co. (St. Louis, MO). Heat-stable α-amylase (17 400 liquefon units/mL); NDF solution containing 30 g of sodium dodecyl sulfate, 18.61 g of ethylenediamine-tetraacetic disodium salt, 6.81 g of sodium borate, 4.56 g of anhydrous sodium phosphate diabasic, and 10 mL of triethylene glycol; and ADF solution containing 20 g of cetyltrimethylammonium bromide in 1 N sulfuric acid were purchased from Ankom Technology (Macedon, NY).

Flaxseed Sample Collection and Heat Processing. Seeds from two varieties (CDC Bethune and CDC Sorrel) of flaxseed were evaluated. Seeds (~3 kg) were sampled from two replicate plots of each variety grown at two different locations: the Kernen Crop Research Farm (52°9′ N and 106°32′ W), managed by the Crop Development Centre (CDC; University of Saskatchewan, Saskatoon, SK, Canada), and Melfort Research Fields (52°8′ N and 104°59′ W; Melfort, SK, Canada), managed by Agriculture and Agri-Food Canada. A subsample (~700 g) of each sample was either kept as raw (control), heated by MIR for 5 min, toasted in an air-draft oven (dry heating) at 120 °C for 60 min, or heated by high pressure (15 lb/in^2) saturated steam (moist heating) in an autoclave (Amsco Eagle SG-3031, Steris Corp., Mentor, OH) at 120 °C for 60 min. The microwave oven (DMW904W, Findlay, OH) was operated at a power of 900 W (1.33 W/g of seeds) and an irradiation frequency of 2450

DOI: 10.1021/jf503575y
J. Agric. Food Chem. 2015, 63, 1057−1066

MHz. To avoid overheating (burning), the seeds were mixed after 2 min of MIR and cooled for 5 min. For dry heating and moist heating, the seeds were spread in aluminum pans (33 × 23 cm^2 area, and 5 cm high) for uniform heating. Heat processing was carried out in two replicate runs, with heated samples subsequently cooled at room temperature (20−22 °C) and stored at 4 °C until further processing.

Both raw and treated samples were ground using a laboratory mill (Retsch ZM-1, Brinkmann Instruments Ltd., Mississauga, ON, Canada) to 0.5 mm for molecular spectral analyses, to 1 mm for all other wet chemical analyses, and to 2 mm for *in situ* studies. Samples were kept cool and slowly fed to the grinder to minimize clumping and sticking, and to make sure that the seeds were crushed and not extruded.

Molecular Spectroscopy. Protein molecular spectral analyses were carried out in the molecular spectroscopy laboratory of the Department of Animal and Poultry Science, University of Saskatchewan (Saskatoon, SK, Canada). Spectral profiles were obtained in the mid-infrared region (ca. 4000−800 cm^{-1}) using a JASCO FT/IR-ATR-4200 (Jasco Inc., Easton, MD). The FT/IR was equipped with a ceramic infrared light source, deuterated L-alanine doped triglycine sulfate detector, and fitted with a MIRacle ATR (Pike Technologies, Madison, WI) sampling accessory equipped with ZnSe crystal plates and a pressure clamp. Each sample was run five times, and each spectrum was collected with 128 coadded scans at a spectral resolution of 4 cm^{-1} in transmission mode. Molecular spectral data were collected and processed (corrected against background and CO_2 noise) using Jasco Spectra Manager II software (Jasco Inc., Easton, MD). Primary protein structures were quantified using two absorbance bands in the amide I (1712−1580 cm^{-1}; Figure 1a) and amide II (1580−1482 cm^{-1}; Figure 1b) regions using OMNIC 7.3 software (Spectra-Tech Inc., Madison, WI). The bands were identified using values reported in the literature.[11] Secondary protein structure (α-helix and β-sheet) intensities were quantified in the amide I region as described by Yu[16] using the second-derivative function of OMNIC 7.3. Briefly, an FTIR/ATR spectrum was selected and corrected for baseline, and then the second derivative function was used to produce a secondary spectrum above the primary spectrum (Figure 1c). Noise in the secondary spectrum was corrected by repeatedly applying a smoothing factor until no further improvement was possible. After smoothing, the intensities of the α-helix and β-sheet were measured on the primary spectrum as the height below the center of the first and second negative peaks (ca. 1653 and 1629 cm^{-1}, respectively; Figure 1d) of the secondary spectrum.

***In Situ* Rumen Incubation.** Four lactating Holstein dairy cows (BW, 680 ± 10 kg), each fitted with permanent rumen fistula (10 cm internal diameter; Bar Diamond Inc., Parma, ID) were used for the *in situ* incubations. The fistulated cows were cared for and handled according to the relevant Canadian Council for Animal Care (CCAC) protocol (#19910012). The cows were individually fed a balanced total mixed ration twice daily (0800 and 1600) in equal portions. The ration contained 31% barley silage, 16% chopped alfalfa hay, and 53% dairy concentrate. The concentrate contained 56% barley grains, 33% dairy supplement pellets, 5% wheat grains, 5% oat grains, and 1% molasses. The dairy supplement pellets were prepared from a mixture of 36.4% soybean meal, 30.3% canola meal, 9.1% mineral and vitamin mixture (University of Saskatchewan), 6% wheat distillers grains, 6.1% corn gluten meal, 3.0% molasses, 2.5% barley, 2.1% canola oil, 1.8% cobalt-iodized salt, 1.8% sodium bicarbonate, and 0.9% Dynamate (K and Mg sulfate, University of Saskatchewan). The cows had 24 h/d access to fresh drinking water.

The standard protocol[17] for *in situ* rumen incubations was adopted to determine rumen degradation characteristics of the control (raw) and heated (dry, moist, MIR) flaxseed. In brief, 7 g of ground (2 mm) sample was weighed into preweighed and coded nylon bags (10 × 20 cm^2) with a pore size of 41 μm (Nitex 03-41/31 monofilament open mesh fabric, Screentec Corp., Mississauga, ON, Canada). The bags were tied ∼2 cm below the top, allowing 19 mg of sample per cm^2 of bag surface area. Each feed was randomly incubated for 48, 24, 12, 8, 4, 2, or 0 h in the four fistulated cows in two replicate runs. To obtain an adequate amount of residue for chemical analysis, multiple replicate bags were used for each incubation period (four bags for 48, 24, and 12 h incubation periods; two bags for 8, 4, 2, and 0 h incubation periods). Bags for different incubation periods were added at appropriately staggered intervals so that all could be extracted together at the end of 48 h (gradual addition, all out method). At the end of the 48 h incubation period, all bags were removed from the rumen and immediately washed (6 times) in a bucket with cold tap water to stop microbial/enzymatic degradation of the residues and remove adhering ruminal contents. The bags were subsequently dried at 55 °C for 48 h, cooled to room temperature (20−22 °C), and reweighed. Residues were pooled together as per incubation time and run, ground to 1 mm particle size, and stored at 4 °C for chemical analysis.

Rumen Degradation Kinetics. The first-order kinetics equation of Ørskov and McDonald,[18] modified for lag time as proposed by Tamminga et al.,[19] was used to compute the degradation kinetics of DM and CP

$$Y(t) = U + (100 - S - U) \times e^{-kd(t-T_0)}$$

where $Y(t)$ is the residue present after t hours of incubation, U is the undegradable fraction, S is the soluble fraction, kd is the degradation rate (%/h) of the potentially degradable fraction, and T_0 is the lag time (h). The nonlinear (PROC NLIN) procedure in Statistical Analysis System (SAS) software[20] was used to estimate degradation parameters from *in situ* data.

The rumen degradability of DM (RDDM) and CP (RDP) were computed from the degradation parameters according to the NRC 2001[21] dairy model

$$\text{RDDM/RDP} = S + D \times \left[\frac{K_d}{(K_d + K_p)}\right]$$

where D is the potentially rumen degradable fraction computed as $D = 100 - S - U$, and K_p is the passage rate of digesta from the rumen (estimate at 6%/h).[19] The rumen undegraded DM (RUDM) and CP (RUP) were calculated according to

$$\text{RUDM/RUP} = U + D \times \left[\frac{K_p}{(K_d + K_p)}\right]$$

Intestinal Protein Digestion Determination. The three-step *in vitro* method of Calsamiglia and Stern[22] was used to analyze the digestibility of RUP. Briefly, ∼0.4 g of dried residues of 16 h rumen incubated samples, containing ∼15 mg N, were transferred to 15 mL centrifuge tubes. Then, 10 mL of 0.1 N HCL solution, containing 1 g/L pepsin, was added to the tubes. The tubes were vortexed and incubated in a shaking water bath at 38 °C for 60 min. Subsequently, 0.5 mL of 1 N NaOH and 13.5 mL of phosphate buffer (pH 7.8) containing 37.5 mg of pancreatin were added to each tube to neutralize the pH. The tubes were vortexed and further incubated at 38 °C for 24 h. At the end of incubation period, 3 mL of 100% (wt/vol) trichloroacetic acid solution was added to precipitate the undigested protein and stop any further enzymatic digestion. The tubes were then vortexed and centrifuged at 10 000 × g for 15 min (at 20 °C), and the supernatant was collected and analyzed for (soluble/digested) N content (AOAC; method 984.13).[23]

Chemical Analysis. The contents of DM (method 930.15), ether extract (EE; method 920.39), CP (method 984.13 using a Kjeltec 2400 autoanalyzer; Foss Analytical A/S, Hillerød, Denmark), ash (method 942.05), acid detergent fiber (ADF; method 973.18), and acid detergent lignin (ADL; ADF method 973.18, followed by digestion with 72% H_2SO_4 for 3 h) were analyzed according to AOAC standard methods.[23] The NDF content was analyzed according to the method of Van Soest et al.[24] with heat-stable α-amylase but without sodium sulfite. The ADF and NDF procedures were adapted for an ANKOM 200 Fiber Analyzer (Ankom Technology Corporation, Fairport, NY) and for the high oil containing seeds as described by Peng et al.[12] Nonprotein nitrogen (NPN), neutral detergent-insoluble CP (NDIP), and acid detergent-insoluble CP (ADIP) content were determined according to methods described by Licitra et al.[25] Soluble protein (SP)

DOI: 10.1021/jf503575y
J. Agric. Food Chem. 2015, 63, 1057−1066

Table 1. Heat Induced Changes in Protein Chemical Profiles[a] of Flaxseeds: Comparison of Heating Methods

		heat treatments (HT)[b]					
	control	MIR	dry heating	moist heating	SEM[c]	contrast[d] control vs HT	p value[d]
Basic Chemical Profile							
dry matter (DM, %)	94.3 b ± 0.21	96.7 a ± 0.57	97.4 a ± 0.64	93.5 b ± 0.26	0.37	**	***
ether extract (EE, % of DM)	41.4 ab ± 1.69	43.0 ab ± 3.30	41.1 b ± 1.86	43.9 a ± 1.56	0.59	ns	*
ash (% of DM)	3.70 ± 0.06	3.75 ± 0.08	3.82 ± 0.09	3.65 ± 0.13	0.05	ns	ns
Protein Chemical Profile[e]							
crude protein (CP, % of DM)	20.9 ± 2.47	21.2 ± 2.07	20.6 ± 1.17	21.3 ± 1.98	1.35	ns	ns
soluble protein (SP, % of DM)	11.9 a ± 1.05	11.2 a ± 0.98	10.9 a ± 1.77	5.47 b ± 1.04	0.58	**	**
NDIP (% of DM)	3.43 b ± 0.23	4.51 b ± 0.51	4.25 b ± 0.59	6.09 a ± 0.67	0.25	**	***
ADIP (% of DM)	0.70 ± 0.32	0.94 ± 0.26	1.28 ± 0.73	1.40 ± 0.56	0.22	ns	ns
NPN (% of DM)	0.83 ± 0.33	0.59 ± 0.23	0.59 ± 0.33	0.98 ± 0.24	0.11	ns	f
SP (% of CP)	56.5 a ± 5.55	51.3 a ± 5.99	54.1 a ± 5.29	25.9 b ± 6.16	1.42	**	***
NDIP (% of CP)	16.5 b ± 1.36	21.5 b ± 2.00	20.7 b ± 2.11	28.7 a ± 2.02	1.47	***	***
ADIP (% of CP)	3.38 ± 1.60	5.04 ± 1.72	6.39 ± 2.72	6.66 ± 3.01	1.12	f	ns
NPN (% of CP)	3.91 ± 1.52	3.08 ± 0.83	2.85 ± 1.81	4.59 ± 0.86	0.47	ns	ns

[a]Means within a row with different letters differ at the $P < 0.05$ level. Values are expressed as the mean ± standard deviation. [b]MIR, microwave irradiation for 5 min; dry heating, heated in an air-draft oven at 120 °C for 60 min.; moist heating, heated in an autoclave by high pressure saturated steam at 120 °C for 60 min. [c]SEM = standard error of the mean. [d]ns, not significant. [e]NDIP = neutral detergent insoluble protein; ADIP = acid detergent-insoluble protein; NPN = nonprotein N. [f]$P < 0.1$; *, $P < 0.05$; **, $P < 0.01$; ***, $P < 0.001$.

Table 2. Heat Induced Changes in Cornell Net Carbohydrate and Protein System (CNCPS) Protein Subfraction Profiles[a] of Flaxseeds: Comparison of Heating Methods

		heat treatment (HT)[b]					
	control	MIR	dry heating	moist heating	SEM[c]	contrast[d] control vs HT	p value[d]
Protein Subfraction (% of Dry Matter)[e]							
PA	0.83 ± 0.33	0.59 ± 0.23	0.59 ± 0.33	0.98 ± 0.24	0.11	ns	f
PB1	11.0 a ± 1.67	10.2 a ± 1.94	10.6 a ± 1.86	4.49 b ± 1.75	0.55	**	***
PB2	5.63 b ± 0.91	5.73 b ± 0.83	5.18 b ± 1.48	9.72 a ± 2.59	0.62	ns	**
PB3	2.73 ± 0.27	3.46 ± 0.23	2.97 ± 1.07	4.70 ± 1.03	0.34	*	*
PC	0.70 ± 0.32	0.94 ± 0.26	1.28 ± 0.73	1.40 ± 0.56	0.22	f	ns
Protein Subfractions (% of Crude Protein)							
PA	3.91 ± 1.52	3.08 ± 0.78	2.85 ± 1.80	4.59 ± 0.87	0.47	ns	ns
PB1	52.6 a ± 4.31	48.2 a ± 5.51	51.3 a ± 6.62	21.3 b ± 8.78	2.62	**	***
PB2	27.1 b ± 4.82	27.3 b ± 4.38	25.1 b ± 6.98	45.4 a ± 8.78	3.57	ns	**
PB3	13.1 b ± 1.00	16.4 ab ± 1.64	14.4 ab ± 1.84	22.1 a ± 2.56	1.75	f	*
PC	3.38 ± 1.60	5.04 ± 1.72	6.39 ± 1.89	6.66 ± 2.42	1.12	f	ns
total true protein	92.7 ± 0.18	91.9 ± 1.42	90.8 ± 3.42	88.8 ± 2.18	0.88	f	f
True Protein Subfraction (% of True Protein)							
PB1	56.7 a ± 4.46	56.3 a ± 5.36	52.4 a ± 4.17	23.9 b ± 5.39	2.79	**	***
PB2	29.2 b ± 5.21	29.7 b ± 5.17	28.0 b ± 5.74	51.3 a ± 5.36	3.69	f	***
PB3	14.1 b ± 1.60	17.9 ab ± 1.64	15.7 b ± 2.21	24.8 a ± 2.71	1.80	*	*

[a]Means within a row with different letters differ at $P < 0.05$ level. Values are expressed as mean ± standard deviation. [b]MIR, microwave irradiation for 5 min; dry heating, heated in an air-draft oven at 120 °C for 60 min; moist heating, heated in an autoclave by high pressure saturated steam at 120 °C for 60 min. [c]SEM = standard error of the mean. [d]ns, not significant. [e]PA = nonprotein N (NPN), the fraction of CP that is instantaneously solubilized at time zero; PB1 = soluble protein-NPN is the rapidly degradable CP fraction; PB2 = CP − (PA + PB1 + PB3 + PC) is the moderately degradable CP fraction; PB3 = NDIP − ADIP is the slowly degradable CP fraction; PC = ADIP is the undegradable fraction of CP, and contains protein associated with lignin and tannins or protein damaged by heat, such as Maillard reaction products. [f]$P < 0.1$; *, $P < 0.05$, **, $P < 0.01$; ***, $P < 0.001$.

was analyzed by the method of Roe et al.[26] with some modifications as described by Peng et al.[27] All samples were analyzed in duplicate and the analyses repeated if error exceeded acceptable levels.

Fractionation of Protein. The Cornell Net Carbohydrate and Protein System (CNCPS) was used to partition the CP into NPN denoted as subfraction PA, true protein as subfraction PB, and unavailable protein as subfraction PC.[28,29] Subfraction PA contains peptides, free amino acids, ammonia, amides, amines, ureides, nucleotides, and nitrates and is considered to degrade in the rumen at a rate of 200%/h.[30] The PB fraction was further fractionated into a rapidly degradable (10−40%/h) subfraction denoted as PB1, a moderately degradable (3−20%/h) subfraction denoted as PB2, and a slowly (4−9%/h) degradable subfraction denoted as PB3.[30] Subfraction PB1 was calculated as SP − PA, PB2 as CP − (PA + PB1 + PB3 + PC), and PB3 as NDIP − ADIP. Subfraction PC is the ADIP.

Statistical Analysis. Data with respect to chemical profile, CP subfractions, and protein molecular spectral characteristics were analyzed using the PROC MIXED procedure of SAS.[20] The model used for analysis was

$$Y_{ijk} = \mu + HT_i + V_j + e_{ijk}$$

DOI: 10.1021/jf503575y
J. Agric. Food Chem. 2015, 63, 1057−1066

Table 3. Heat Induced Changes in *In Situ* Rumen Degradation Kinetics[a] and Intestinal Digestibility[a] of Flaxseeds: Comparison of Heating Methods

		heat treatment (HT)[b]					
	control	MIR	dry heating	moist heating	SEM[c]	contrast[d] control vs HT	*p* value[d]
In Situ Rumen Degradation Kinetics of Dry Matter (DM)[e]							
kd, %/h	9.18 b ± 0.91	9.62 a ± 0.74	9.13 b ± 1.37	8.09 b ± 1.17	0.85	ns	**
lag time (T_0, h)	0.36 b ± 0.10	0.51 ab ± 0.07	1.02 a ± 0.15	0.08 b ± 0.16	0.17	ns	**
S fraction, % DM	11.3 b ± 4.18	11.8 ab ± 4.85	13.2 a ± 3.77	12.0 ab ± 3.22	0.92	*f*	*
D fraction, % DM	76.3 a ± 7.58	71.0 ab ± 5.33	76.2 a ± 9.36	70.4 b ± 6.26	3.47	*	**
U fraction, % DM	12.1 ab ± 3.94	16.8 a ± 2.90	10.2 b ± 2.63	17.3 a ± 5.74	1.32	ns	**
RDDM, % DM	56.3 b ± 4.49	57.5 ab ± 2.59	59.4 a ± 4.33	52.7 c ± 1.66	0.74	ns	***
RUDM, % DM	42.0 bc ± 4.49	43.8 b ± 2.59	40.6 c ± 4.33	47.3 a ± 1.66	0.67	ns	***
In Situ Rumen Degradation Kinetics of Crude Protein (CP)[e]							
kd, %/h	9.90 b ± 0.99	9.67 b ± 1.61	11.7 a ± 2.17	7.53 c ± 1.28	0.42	ns	***
lag time (T_0, h)	0.77 ± 0.32	0.76 ± 0.34	1.19 ± 0.39	0.49 ± 0.43	0.58	ns	ns
S fraction, % CP	15.7 a ± 3.64	11.9 bc ± 4.30	14.5 ab ± 3.92	9.27 c ± 2.12	1.37	***	***
D fraction, % CP	76.4 ± 8.36	76.5 ± 6.85	78.4 ± 8.04	77.5 ± 5.72	2.67	ns	ns
U fraction, % CP	8.35 bc ± 2.04	12.0 ab ± 2.54	7.58 c ± 1.68	13.7 a ± 2.27	1.05	*	***
RDP,% CP	64.0 a ± 5.15	59.6 b ± 4.67	66.4 a ± 5.08	53.1 c ± 2.72	0.72	***	***
RUP, %CP	36.0 c ± 5.15	40.4 b ± 4.67	33.6 c ± 5.08	46.9 a ± 2.72	0.72	***	***
RDP, % DM	14.3 a ± 0.20	13.1 ab ± 0.20	14.4 a ± 0.19	12.1 b ± 0.12	0.35	*	***
RUP, % DM	7.94 bc ± 0.07	8.78 b ± 0.04	7.18 c ± 0.05	10.7 a ± 0.03	0.22	**	***
Intestinal Digestibility of RUP[g]							
IDCP, %RUP	61.0 ab ± 2.28	60.2 ab ± 2.17	56.3 b ± 3.83	63.8 a ± 2.67	3.78	ns	*
IDCP, %CP	20.6 bc ± 1.12	22.9 b ± 1.17	17.8 c ± 1.74	28.2 a ± 1.43	2.47	*	***

[a]Means within a row with different letters differ at $P < 0.05$ level. Values are expressed as mean ± standard deviation. [b]MIR, microwave irradiation for 5 min; dry heating, heated in an air-draft oven at 120 °C for 60 min; moist heating, heated in an autoclave by high pressure saturated steam at 120 °C for 60 min. [c]SEM = standard error of the mean. [d]ns, not significant. [e]K_d = the degradation rate of *D* fraction (%/h); *S* = soluble fraction; *D* = rumen degradable fraction; *U* = rumen undegradable fraction; RDDM = effective degradability of DM in the rumen; RUDM = rumen undegraded DM [f]$P < 0.1$; *, $P < 0.05$, **, $P < 0.01$; ***, $P < 0.001$. [g]IDCP, intestinal digestibility of CP.

Table 4. Heat-Induced Changes in Inherent Molecular Structural Characteristics[a] of Protein Revealed by Fourier Transform/Infrared-Attenuated Total Reflectance (FT/IR-ATR) Molecular Spectroscopy: Comparison of Heating Methods

		heat treatment (HT)[b]					
	control	MIR	dry heating	moist heating	SEM[c]	contrast[d] control vs HT	*p* value[d]
Protein Primary Structure Characteristics[e]							
amide I area	3.68 a ± 0.29	3.37 bc ± 0.38	3.30 c ± 0.15	3.43 b ± 0.06	0.02	***	***
amide II area	1.29 a ± 0.39	1.14 b ± 0.20	1.13 c ± 0.07	1.14 c ± 0.23	0.01	***	***
area ratio (amide I:II)	2.94 a ± 0.39	3.00 a ± 0.21	2.93 ab ± 0.16	2.89 b ± 0.42	0.02	ns	***
amide I height	0.06 a ± 0.01	0.05 ab ± 0.01	0.05 ab ± 0.00	0.05 b ± 0.00	0.00	**	*
amide II height	0.03 ± 0.01	0.02 ± 0.00	0.02 ± 0.00	0.02 ± 0.00	0.00	ns	ns
height ratio (amide I:II)	2.23 a ± 0.20	2.21 ab ± 0.09	2.22 ab ± 0.08	2.04 c ± 0.26	0.05	***	***
Protein Secondary Structure α-Helix and β-Sheet[f]							
α-helix height	0.06 a ± 0.01	0.05 ab ± 0.00	0.06 a ± 0.00	0.05 b ± 0.00	0.00	**	*
β-sheet height	0.05 a ± 0.00	0.05 ab ± 0.00	0.05 ab ± 0.00	0.04 b ± 0.03	0.01	ns	ns
ratio of α-helix:β-sheet	1.22 a ± 0.04	1.08 b ± 0.07	1.12 a ± 0.05	1.00 c ± 0.08	0.01	***	***

[a]Means within a row with different letters differ at $P < 0.05$ level. Values are expressed as mean ± standard deviation. [b]MIR, microwave irradiation for 5 min; dry heating, heated in an air-draft oven at 120 °C for 60 min; moist heating, heated in an autoclave by high pressure saturated steam at 120 °C for 60 min. [c]SEM = standard error of the mean. [d]ns, not significant; *, $P < 0.05$, **, $P < 0.01$; ***, $P < 0.001$. [e]Protein amide bands were measured at ca. 1712−1482 cm^{-1}; measurements are expressed in IR absorbance units. [f]α-helix and β-sheet bands were measured in the amide I region, centered at 1653 and 1630 cm^{-1}, respectively; measurements are expressed in IR absorbance units.

where Y_{ijk} is an observation on the dependent variable *ijk*, μ is the overall population mean, HT_i is the fixed effect of heat treatment (control, MIR, dry heating, and moist heating), V_k is the random effect of variety (CDC Bethune and CDC Sorrel), and e_{ijk} is the random error associated with the observation *ijk*. The plots ($n = 4$) were used as replicates.

The *in situ* rumen degradation and intestinal digestibility data were analyzed using the model

$$Y_{ijkl} = \mu + HT_i + V_j + R_k + e_{ijkl}$$

where Y_{ijkl} is an observation on the dependent variable *ijkl*, μ is the overall population mean, HT_i is the fixed effect of heat treatment, V_k is the random effect of variety, R_k is the random effect of *in situ* experimental run, and e_{ijkl} is the random error associated with the observation *ijkl*. When significant ($P < 0.05$) differences were noted, posthoc analyses were carried out on the least-squares means using the Tukey−Kramer test adjusted for multiple comparisons to compute pairwise differences in the means. Values are presented as mean ± standard deviation.

DOI: 10.1021/jf503575y
J. Agric. Food Chem. 2015, 63, 1057−1066

The strength of relationships between the protein molecular spectral characteristics and chemical profile, CP subfractions, *in situ* CP degradation, and intestinal digestibility were analyzed by the PROC CORR procedure of SAS[20] using the Pearson correlation method. Stepwise multiple regressions analyses were performed using the PROC REG procedure of SAS[20] to obtain regression equations for prediction of chemical profile, CP subfractions, *in situ* degradation characteristics, and intestinal digestibility of RUP. The independent variables tested in the model were the amide I and amide II area, height, and their (height and area) ratio as well as the α-helix and β-sheet height and their ratio. Only variables contributing significantly ($P < 0.05$) to the estimation of the dependent variable were used in the final model.

Multivariate analysis, agglomerative hierarchical cluster analysis (CLA), and principal component analysis (PCA) were performed on the overall spectral data (n = 249 spectral bands) obtained from the fingerprint region (ca. 1732−1483 cm^{-1}) to classify and visualize the heat-induced changes in intrinsic protein molecular structures. Earlier works by our group describe the detailed procedure and concepts for using CLA and PCA for FTIR/ATR spectral analysis.[15]

RESULTS AND DISCUSSION

Heat-Induced Changes in Chemical Profile. Data on the effect of MIR, dry heating, and moist heating on chemical profile of flaxseed compared to the control (raw seed) are provided in Table 1. Microwave irradiation and dry heating significantly increased the DM content, indicating a decrease in the moisture holding capacity of flaxseed, consistent with earlier findings.[12,14] Ether extract content significantly increased with MIR and moist heating. Moist heating is often used to increase oil extraction in the bio-oil industry, and a significant increase in EE has been observed with moist heating of camelina[12] and sunflower[31] seeds. Our results show that MIR for 5 min is as effective as moist heating at 120 °C for 60 min for increasing the ether extractability of flaxseed. This increase could be related to heat-induced physicochemical reactions in the seeds, such as the denaturation of the protein matrix that encapsulates the oil bodies.[32] Moreover, heating can also denature the delicate membranes of oil bodies, thus allowing them to coalesce.[33] These heat-induced physicochemical changes in the protective membrane increase oil body exposure to solvents, resulting in the higher extraction of oil.[12]

Heat processing did not significantly alter the total CP content in flaxseed, in support of earlier findings.[12,31] Among the heating methods, moist heating was more effective in altering the CP chemical profile. Notably, moist heating markedly decreased (56.5% to 25.9% CP) the SP content. Previous studies have reported a similar decrease in the SP fractions of soybean (43.4% to 11.4% CP)[34] and camelina seeds (52.7% to 20.4% CP)[12] after moist heating (120 °C for 60 min). In contrast, dry heating and MIR did not significantly alter the SP content of flaxseed. In agreement with our findings, dry heating also did not alter the SP content of soybean or camelina seeds.[12,34] The NPN content of flaxseed did not significantly change with heat processing. Other studies have reported both increases[12] and decreases[31,34] in NPN content with heat processing of oilseeds. Discrepancies between results may be related to the differences in seed types as well as in the NPN methodology (e.g., trichloroacetic acid vs tungstic acid and filter paper pore size). The NDIP content increased with all heating methods, but only that for moist heating was statistically significant (16.5% to 28.7% CP). Heat induces cross-linkages between amino acids and sugar molecules that can increase the recovery of N in the NDF fraction.[12,34] Our results show that heat-induced changes in chemical profile of flaxseed depend on the type of heating, with moist heating more effective in altering protein chemical profiles than MIR or dry heating. These findings also show that the use of moist heating during oil extraction in the bio-oil industries can improve both oil extractability and the nutritive value of the protein in the coproducts (meals and oil cakes) for dairy cows.

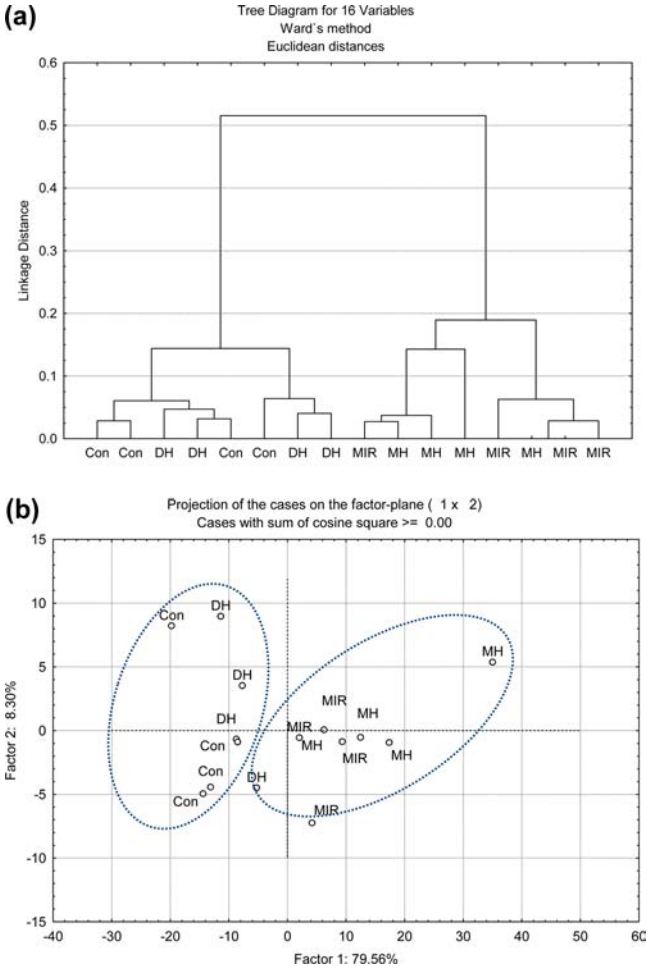

Figure 2. Agglomerative hierarchical cluster analysis (CLA) dendrograms (panel I) and principal component analysis (PCA) scatter plot (panel II) representing the overall spectral (n = 249 spectral bands) differences in the protein primary structures in the amide region (ca. 1712−1482 cm^{-1}) of raw (Con) and heat treated flaxseeds (MIR = microwave irradiation for 5 min; DH = heated in air-draft oven at 120 °C for 60 min; MH = heated in an autoclave by high pressure saturated steam at 120 °C for 60 min).

Heat-Induced Changes in Protein Subfractions. Data with respect to heat-induced changes in CNCPS CP subfractions of flaxseed are presented in Table 2. Moist heating significantly altered the content of PB1, PB2, and PB3 subfractions. The rapidly degradable (PB1) subfraction decreased (52.6% to 21.3% CP) with a subsequent increase (27.1% to 45.4% CP) in the intermediately degradable (PB2) subfraction. The major shift from the rumen degradable PB1 subfraction to the partially rumen degradable PB2 subfraction suggests a decrease in CP degradation in the rumen and a greater supply of RUP to the small intestine. Peng et al.[12] and Samadi and Yu[34] also observed a similar shift from PB1 to PB2 subfractions after moist heating (120 °C for 60 min) of camelina seeds and soybean. Moist heating increased (13.1% to 22.1% CP) the PB3 subfraction of flaxseed. Because of the slow

DOI: 10.1021/jf503575y
J. Agric. Food Chem. 2015, 63, 1057−1066

Table 5. Coefficient of Correlation (Pearson) and Level of Significance between Protein Molecular Structural Characteristics and Nutrients Profile, Protein Subfractions, *in Situ* Degradation Kinetics, and Intestinal Availability As Affected by Different Heat Treatments

	correlation with protein α-helix:β-sheet ratio[a]	
	r	p value[b]
chemical profile (% of crude protein, CP)		
neutral detergent insoluble protein (NDIP)	−0.84	**
soluble crude protein (SP)	0.86	**
protein subfractions (% of CP)[c]		
PB1	0.87	**
PB2	−0.83	**
PB3	−0.74	*
in situ rumen CP degradation		
degradation rate (kd), %/h	0.80	**
undegradable fraction (U), % CP	−0.90	**
effective degradability of CP, % CP (RDP)	0.87	**
rumen undegraded feed CP, % CP (RUP)	−0.87	**
effective degradability of CP, % of dry matter (RDDM)	0.69	*
rumen undegraded feed CP, % of dry matter (RUDM)	−0.72	*
intestinal digestibility, % of RUP	−0.68	*

[a]Only variables with significant ($P < 0.05$) correlation are shown. [b]*, $P < 0.05$; **, $P < 0.01$. [c]PB1 = PB1 = soluble protein − NPN is the rapidly degradable CP fraction; PB2 = CP − (PA + PB1 + PB3 + PC) is the moderately degradable CP fraction; PB3 = NDIP − ADIP is the slowly degradable CP fraction.

ruminal degradation rate (4%/h to 9%/h),[30] a large portion of the PB3 subfraction escapes degradation in the rumen and is instead digested in the small intestine. Therefore, the increase in the PB3 subfraction results in a contribution to the supply of digestible RUP to the postruminal tract. The MIR and dry heating of flaxseed did not significantly alter the CP subfraction profile, suggesting no significant change in ruminal CP degradation characteristics of flaxseed with these treatments. The three heating methods did not alter the PC subfraction. The proteins in the PC subfractions are bound to lignin or are heat damaged, and are thus considered nondegradable in the rumen and nondigestible in the postruminal tract.[28] This means that none of the heat processing method overprotected protein from intestinal digestion. Overall, heat processing method appears to have a major influence on heat-induced changes in CP subfractions.

Heat Induced Changes in Rumen Degradation and Intestinal Digestibility. Data on the effect of heating methods on ruminal DM and CP degradation kinetics and intestinal digestibility of RUP are presented in Table 3. Moist heating significantly increased the content of RUDM. The *S*-fraction of DM did not significantly change with moist heating. Therefore, the higher content of RUDM in the moist heated flaxseed could be related to the significantly lower *D*-fraction (76.3% vs 70.4% DM) and slightly lower kd (9.18% vs 8.09%/h) of the *D*-fraction compared with raw seeds. In agreement with our findings, moist heating (127 °C for 30 min) of sunflower seeds decreased the kd (9.3%/h to 5.2%/h) with a subsequent increase (31.6% to 42.4% DM) in RUDM.[31] The MIR did not alter the DM degradation kinetics. In contrast to our findings, a 5 min MIR increased the RUDM of cottonseed meal (39.7% to 48.3% DM)[35] and canola meal (33.5%/h to 45.9%/h).[36] This discrepancy in DM degradation kinetics could be related to the inherent differences in feed types, and industrial processing such as (defatted)-meals were used in the previous studies compared to full-fat flaxseeds in our study. Dry

Table 6. Multiple Regression Equations, Degree of Fit (R^2), and Standard Error of Estimation (SEE) for Prediction of Heat-Induced Changes in Protein Chemical Profile, Protein Subfractions, and *in Situ* Rumen Crude Protein Degradation from Fourier Transform/Infrared-Attenuated Total Reflectance (FT/IR-ATR) Molecular Spectroscopy Protein Spectral Parameters

predicted variable (Y)	regression equation	R^2	SEE	p value
Protein Chemical Profile[a]				
crude protein, % of dry matter (DM)	68.3−4.49 × amide I:II ratio	0.80	1.00	**
soluble protein, % DM	−34.3 + 25.0 × α-helix:β-sheet ratio	0.62	3.83	*
NPN, % DM	−1.16−1.12 × amide I:II ratio	0.50	0.37	*
NDIP, % DM	27.6−8.54 × α-helix:β-sheet ratio	0.64	1.26	*
Protein Subfraction Profile[b]				
PB1	−79.3+ 56.7 × α-helix:β-sheet ratio	0.64	8.43	*
PB2	110−36.4 × α-helix:β-sheet ratio	0.56	6.34	*
PB3	97.9−30.0 × α-helix:β-sheet ratio	0.60	2.47	*
PC	15.2−93.7 × amide I height	0.47	1.11	*
In Situ Rumen CP Degradation				
degradation rate (kd), %/h	−6.36 + 7.41 × α-helix:β-sheet ratio	0.56	1.29	*
undegradable fraction (U), % CP	38.7−13.0 × α-helix:β-sheet ratio	0.78	1.42	**
effective degradability of CP, % CP (RDP)	2.70 + 26.6 × α-helix:β-sheet ratio	0.71	3.43	**
rumen undegraded feed CP, % CP (RUP)	97.3−26.6 × α-helix:β-sheet ratio	0.71	3.43	**
intestinal digestibility of RUP				
intestinal digestibility, % of RUP	82.3−12.0 × α-helix:β-sheet ratio	0.47	2.45	*
intestinal digestibility, % of CP	68.1−21.2 × α-helix:β-sheet ratio	0.72	2.64	**

[a]NPN, nonprotein N; NDIP, neutral detergent-insoluble protein. [b]Cornell Net Carbohydrate and Protein System (CNCPS) protein subfraction profiles; PA = nonprotein N (NPN), the fraction of CP that is instantaneously solubilized at time zero; PB1 = soluble protein − NPN is the rapidly degradable CP fraction; PB2 = CP − (PA + PB1 + PB3 + PC) is the moderately degradable CP fraction; PB3 = NDIP − ADIP is the slowly degradable CP fraction; PC = ADIP is the undegradable fraction of CP, and contains protein associated with lignin and tannins or protein damaged by heat, such as Maillard reaction products.

DOI: 10.1021/jf503575y
J. Agric. Food Chem. 2015, 63, 1057−1066

heating did not significantly alter the DM degradation kinetics of flaxseed, consistent with earlier findings.[12,34]

With the exception of lag time and *D*-fraction, moist heating significantly altered the contents of all measured CP degradation parameters (Table 3). Notably, the content of RDP decreased (64.0% to 53.1% CP) with a concomitant increase in the supply of RUP (36.0% to 46.9% CP) to the postruminal tract. The higher content of RUP in the moist heated flaxseed could be related to the lower *S*-fraction (15.7% vs 9.27% CP) and lower kd (9.90% vs 7.53% CP) of the *D*-fraction. The higher RUP content in the moist heated flaxseed is also supported by observed changes in CP subfractions, such as the decrease in rapidly rumen degradable (PB1) subfraction and the increase in partially (PB2) and slowly (PB3) degradable subfractions. These results are consistent with the findings of Samadi and Yu[34] and Peng et al.,[12] who observed an increase in RUP content with moist heating (120 °C for 60 min) of soybean meal (13.8% to 33.6% CP) and camelina seeds (24.6% to 42.1% CP). Mustafa et al.[31] also observed a significantly higher RUP content (8.90% to 26.1% CP) with moist heating (127 °C for 30 min) of sunflower seeds. These findings demonstrate that moist heating of flaxseed can shift the site of CP digestion from the rumen to the postruminal tract. Digestion of feed protein in the small intestine results in lower losses of essential amino acids and protein.

Microwave irradiation increased the RUP content (36.0% to 40.4% CP) compared to raw seeds; this increase was not as large as that achieved with moist heating, but MIR requires less energy inputs and processing time. In agreement with our findings, earlier studies report that MIR for 6 min increased the RUP content of canola seeds (17.5% to 34.9% CP),[37] canola meal (34.8% to 53.9% CP),[36] and cottonseed meal (38.9% to 54.6% CP).[35] As MIR did not alter the kd, the higher RUP of the irradiated flaxseed could be related to the lower *S*-fraction and higher *U*-fraction compared to raw seeds. Dry heating did not significantly alter the RUP content (Table 3), consistent with earlier findings.[12,34] Notably, dry heating significantly decreased the intestinal digestibility of RUP, which implies that the seeds were partly overheated. In dry heating, the heat penetrates from the exterior to the interior and can result in the exterior feed being overheated and therefore overprotected from digestion in the postruminal tract.[15] The intestinal digestibility of RUP in the moist heated flaxseed was slightly higher than in the raw seeds (63.8% vs 61.0% RUP). The increase in RUP digestibility with moist heating of soybean and camelina seeds has been reported.[12,34] These results suggest that moist heating can increase the supply of digestible RUP to the postruminal tract. Steam heating, within the scope of the treatment used in this study, can be used for oil extraction in bio-oil industries to decrease CP degradation in the rumen, and improve the supply of metabolizable protein to dairy cows.

Heat Induced Changes in Protein Molecular Structure. Any heat-related processing that can modify the noncovalent interactions in protein molecules can potentially alter their pleated structures,[14] and exposes hydrophobic amino acids that can potentially reduce protein solubility.[36,38] The free (unbounded) amino acids also establish cross-linkages with reducing sugars and other (poly)peptides, resulting in reduced protein solubility and ruminal degradation.[12] Establishment of more complex cross-linkages due to heating for a longer duration or a higher temperature can make the protein molecules more resistant to rumen-microbial degradation and enzymatic hydrolysis.[12,15,38] Therefore, studying the heat-induced changes in protein molecular structures is vital to fully understand the changes in CP chemical profile and digestive behavior.

Amide I and II spectral intensities in terms of peak area and height characterize the protein primary structures.[27,39] Typically, the difference in the amide I and II spectral intensities reflects differences in protein content, whereas the amide I:II and α-helix:β-sheet ratios reflect differences in protein molecular makeup.[39,40] The data in Table 4 show that moist heating significantly decreases the α-helix:β-sheet ratio. This decrease is associated with a decrease in SP (56.5% to 25.9% CP; Table 1) and increases in RUP (36.0% to 46.9% CP; Table 3) and intestinal digestibility of RUP (61.0% to 63.8% RUP). The differences in α-helix:β-sheet ratio affect ruminal CP degradation and intestinal digestibility by altering protein solubility and the access of microbes and proteolytic enzymes.[14,27,41] Dry heating did not significantly alter the α-helix:β-sheet ratio. The lack of change in protein molecular structure with dry heating is associated with a lack of changes in protein subfraction composition and degradation characteristics in the rumen. These findings demonstrate that heat-induced changes in protein chemical profile and digestion are strongly related to heat-induced changes in protein molecular structure.

Multivariate Analysis. The CLA and PCA were performed on overall (n = 249 spectral bands) spectral data from the fingerprint region (ca. 1732−1483 cm^{-1}) to classify and visualize the heat-induced changes in protein molecular structural characteristics. Multivariate analysis is a useful tool for studying molecular structure differences of biopolymers. The CLA dendrograms (Figure 2a) show that protein molecular spectral data from moist heated and irradiated seeds can be distinguished from the raw and dry heated seeds at a linkage distance of <0.6, indicative of structural differences between these two groups. The mixed dendrograms of moist heated and irradiated flaxseed show that their protein molecular makeup is indistinguishable. Similarly, the mixed dendrograms of control (raw) and dry heated seeds show that the protein molecular makeup of dry heated and raw seeds are indistinguishable. The PCA results are presented as a scatter plot of the first two principal factors (Figure 2b). The scatter plot explained 87.9% of the total variation in protein molecular structures of the raw and heat-processed flaxseed. The protein molecular spectra of control and dry heated flaxseed were clustered into one ellipse, and those of MIR and moist heated flaxseed were clustered into another. Similar to the CLA dendrograms, these two groups could be completely distinguished from each other. The multivariate analyses results based on overall spectral data support the conclusion of the univariate spectral analyses (Table 4) that moist heating and MIR significantly alter protein molecular structures compared to raw seed. Moreover, CLA and PCA analysis were able to classify the overall differences in protein molecular makeup.

Correlations between Protein Molecular Structural Characteristics and Protein Availability and Utilization. Table 5 shows the coefficient of correlation (Pearson) and their level of significance between the α-helix:β-sheet ratio and protein chemical profiles, CP subfractions, *in situ* rumen CP degradation, and intestinal digestibility of RUP. Heat-induced changes in the α-helix:β-sheet ratio were negatively correlated with NDIP (r = −0.84), and positively correlated with SP (r = 0.86). These findings suggest that protein denaturation during heating increased the NDF-bound protein and decreased the SP. The α-helix:β-sheet ratio was positively correlated (r =

DOI: 10.1021/jf503575y
J. Agric. Food Chem. 2015, 63, 1057−1066

0.87) with the CNCPS PB1 subfraction, and negatively correlated with PB2 (r = −0.83) and PB3 (r = −0.74) subfractions. Among the *in situ* parameters, heat-induced changes in the α-helix:β-sheet ratio were positively correlated with kd (r = 0.80) and RDP (r = 0.87), and negatively correlated to RUP (r = −0.87) and intestinal digestibility (r = −0.68) of RUP. These results demonstrate the existence of a close relationship between heat-induced changes in α-helix:β-sheet ratio and the changes in protein chemical profile, CP-subfractions, and ruminal CP degradation characteristics.

Using Protein Molecular Spectral Parameters to Predict Protein Subfractions, Rumen Degradation Parameters, and Intestinal Digestibility. Table 6 shows the multiple regression equations, based on protein spectral parameters, and their predictive power for estimation of CP subfractions, *in situ* CP degradation parameters, and intestinal digestibility of RUP. The total CP content can be predicted (R^2 = 0.80) from the area ratio of amide I:II, which reflects differences in protein content of feeds.[38] Heat-induced changes in PB1 (R^2 = 0.64), PB2 (R^2 = 0.56), PB3 (R^2 = 0.60), kd (R^2 = 0.56), U (R^2 = 0.78), RUP (R^2 = 0.71), and intestinal digestibility of RUP (R^2 = 0.47) can be predicted from the α-helix:β-sheet ratio. The relatively high predictive power for estimation of CP subfractions and *in situ* parameters such as RUP could have important practical implications for feed evaluation because FTIR-ATR molecular spectroscopy is a noninvasive and nondestructive analytical technique that can rapidly analyze large numbers of feed samples. The findings of the present study support the suggestion of Yu and Nuez-Ortín[42] and Becker and Yu[43] that the α-helix:β-sheet ratio can be used as an indicator for changes in the protein nutritive value during heat-related processing. For example, the α-helix:β-sheet ratio was strongly correlated with protein solubility, rumen degradability, and intestinal digestibility of RUP. However, it is pertinent to mention that these prediction equations were derived from limited data based on only one type of oilseed. Further studies will be required to obtain predictive equations based on a large number of samples from diverse sources.

Overall, heat induced changes in CP chemical profiles, protein subfractions, rumen degradability, intestinal digestibility, and protein molecular structures of flaxseed clearly depend on the method of heating. Compared to dry heating and MIR, moist heating of flaxseed improves the nutritive value and utilization of protein in flaxseed by decreasing the SP content and the kd of the *D*-fraction, thus causing an increase in the supply of digestible RUP to the postruminal tract. These changes in CP chemical profile and digestive behavior are strongly associated with alterations in intrinsic protein molecular structures as measured by characteristics such as the α-helix to β-sheet ratio. Regression equations based on protein molecular structural features provide relatively good estimations for heat induced changes in SP content (R^2 = 0.62), RUP content (R^2 = 0.71), and intestinal digestibility of RUP (R^2 = 0.47).

AUTHOR INFORMATION

Corresponding Author

*Phone: +1 306 966 4132. Fax: + 1 306 966 4151. E-mail: Peiqiang.yu@usask.ca. Mail: Department of Animal and Poultry Science, College of Agriculture and Bioresources, University of Saskatchewan, 51 Campus Drive, Saskatoon, S7N 5A8, Saskatchewan, Canada.

Funding

Research projects of the feed research chair group of Professor Dr. Peiqiang Yu are supported by grants from the Ministry of Agriculture Strategic Research Chair Program, the Natural Sciences and Engineering Research Council of Canada (NSERC), SaskCanola, the Saskatchewan Agricultural Development Fund (ADF), University Innovation Team "Veterinary Biotechnology" in Tianjin (TD12-5019), and Thousand-Talent-People Program (Tianjin), University Innovation Team "Veterinary Biotechnology" in Tianjin (TD12-5019), Thousand-Talent-People Program (Tianjin), Saskatchewan Forage Network (SFN), and Western Grains Research Foundation (WGRF).

Notes

The authors declare no competing financial interest.

ACKNOWLEDGMENTS

We thank Kenneth Jackle for assistance with seed sampling and Zhiyuan Niu for assistance in laboratory analysis.

REFERENCES

(1) Khan, N. A.; Booker, H.; Yu, P. Molecular structures and metabolic characteristics of protein in brown and yellow flaxseed with altered nutrient traits. *J. Agric. Food Chem.* **2014**, *62*, 6556−6564.

(2) Flax Council of Canada (FCC). *Canadian Flax*. http://www.flaxcouncil.ca/english/index.jsp?p=what2&mp=what. Winnipeg, Manitoba, Canada, 2013. (Accessed February 05, 2014.)

(3) FAOSTAT. *Production and Trade. Food and Agriculture Organization Statistical Database.* http://faostat.fao.org/site/339/default.aspx. FAO: Rome, Italy, 2012. (Accessed February 05, 2014.)

(4) Oomah, B. D.; Mazza, G. Flaxseed proteins-a review. *Food Chem.* **1993**, *48*, 109−114.

(5) Mueller, K.; Eisner, P.; Yoshie-Stark, Y.; Nakada, R.; Kirchhoff, E. Functional properties and chemical composition of fractionated brown and yellow linseed meal (Linum usitatissimum L.). *J. Food Eng.* **2010**, *98*, 453−460.

(6) Petit, H. V.; Twagiramungu, H. Conception rate and reproductive function of dairy cows fed different fat sources. *Theriogenology* **2006**, *66*, 1316−1324.

(7) Ambrose, D. J.; Kastelic, J. P.; Corbett, R.; Pitney, P. A.; Petit, H. V.; Small, J. A.; Zalkovic, P. Lower pregnancy losses in lactating dairy cows fed a diet enriched in α-linolenic acid. *J. Dairy Sci.* **2006**, *89*, 3066−3074.

(8) Petit, H. V. Review: Feed intake, milk production and milk composition of dairy cows fed flaxseed. *Can. J. Anim. Sci.* **2010**, *90*, 115−127.

(9) Mustafa, A. F.; McKinnon, J. J.; Christensen, D. A.; He, T. Effects of micronization of flaxseed on nutrient disappearance in the gastrointestinal tract of steers. *Anim. Feed Sci. Technol.* **2002**, *95*, 123−132.

(10) Habib, G.; Khan, N. A.; Ali, M.; Bezabih, M. In situ ruminal crude protein degradability of by-products from cereals, oilseeds and animal origin. *Livest. Sci.* **2013**, *153*, 81−87.

(11) Yu, P.; Tamminga, S.; Egan, A. R.; Christensen, D. A. Probing equivocal effects of heat processing of legume seeds on performance of ruminants - A review. *Asian-Australas. J. Anim. Sci.* **2004**, *17*, 869−876.

(12) Peng, Q.; Khan, N. A.; Wang, Z.; Yu, P. Moist and dry heating-induced changes in protein molecular structure, protein subfractions, and nutrient profiles in camelina seeds. *J. Dairy Sci.* **2014**, *97*, 446−457.

(13) Sadeghi, A. A.; Shawrang, P. Effects of microwave irradiation on ruminal protein and starch degradation of corn grain. *Anim. Feed Sci. Technol.* **2006**, *127*, 113−123.

(14) Yan, X.; Khan, N. A.; Zhang, F.; Yang, L.; Yu, P. Microwave irradiation induced changes in protein molecular structures of barley grains: relationship to changes in protein chemical profile, protein

DOI: 10.1021/jf503575y
J. Agric. Food Chem. 2015, 63, 1057−1066

subfractions, and digestion in dairy cows. *J. Agric. Food Chem.* **2014**, *62*, 6546−6555.
(15) Peng, Q.; Khan, N. A.; Wang, Z.; Zhang, X.; Yu, P. Effect of thermal processing on estimated metabolizable protein supply to dairy cattle from camelina seeds: relationship with protein molecular structural changes. *J. Agric. Food Chem.* **2014**, *62*, 8263−8273.
(16) Yu, P. Protein secondary structures (α-helix and β-sheet) at a cellular level and protein fractions in relation to rumen degradation behaviours of protein: A new approach. *Br. J. Nutr.* **2005**, *94*, 655−665.
(17) Yu, P.; Christensen, D. A.; McKinnon, J. J. Comparison of the National Research Council-2001 model with the Dutch system (DVE/OEB) in the prediction of nutrient supply to dairy cattle from forages. *J. Dairy Sci.* **2003**, *86*, 2178−2192.
(18) Øskov, E. R.; McDonald, I. The estimation of protein degradability in the rumen from incubation measurements weighted according to rate of passage. *J. Agric. Sci.* **1979**, *92*, 499−503.
(19) Tamminga, S.; Van Straalen, W. M.; Subnel, A. P. J.; Meijer, R. G. M.; Steg, A.; Wever, C. J. G.; Blok, M. C. The Dutch protein evaluation system: the DVE/OEB-system. *Livest. Prod. Sci.* **1994**, *40*, 139−155.
(20) Statistical Analysis System (SAS). *User's Guide: Statistics*, 8th ed.; SAS Institute: Cary, NC, 2009.
(21) National Research Council (NRC). *Nutrient Requirements of Dairy Cattle*, 7th rev. ed.; National Research Council, NRC, Academies Press: Washington, DC, 2001.
(22) Calsamiglia, S.; Stern, M. D. A. three-step *in vitro* procedure for estimating intestinal digestion of protein in ruminants. *J. Anim. Sci.* **1995**, *73*, 1459−1465.
(23) AOAC. *Officials Methods of Analysis*, 15th ed.; Association of Official Analytic Chemists: Arlington, VA, 1990.
(24) Van Soest, P. J.; Mason, V. C. The influence of the Maillard reaction upon the nutritive value of fibrous feeds. *Anim. Feed Sci. Technol.* **1991**, *32*, 45−53.
(25) Lacitra, G.; Hernandez, T. M.; Van Soest, V. J. Standardization of procedures for nitrogen fractionation of ruminant feeds. *Anim. Feed Sci. Technol.* **1996**, *57*, 347−358.
(26) Roe, M. B.; Sniffen, C. J.; Chase, L. E. Techniques for measuring protein fractions in feedstuffs. In *Proceedings—Cornell Nutrition Conference*; Cornell University: Ithaca, NY, 1990; pp 81−85.
(27) Peng, Q.; Khan, N. A.; Wang, Z.; Yu, P. Relationship of feeds protein structural makeup in common prairie feeds with protein solubility, *in situ* ruminal degradation and intestinal digestibility. *Anim. Feed Sci. Technol.* **2014**, *194*, 58−70.
(28) Sniffen, C. J.; O'Connor, J. D.; Van Soest, P. J.; Fox, D. G.; Russell, J. B. A net carbohydrate and protein system for evaluating cattle diets: II. Carbohydrate and protein system availability. *J. Anim. Sci.* **1992**, *70*, 3562−3577.
(29) Tylutki, T. P.; Fox, D. G.; Durbal, V. M.; Tedeschi, L. O.; Russell, J. B.; VanAmburgh, M. E.; Overton, T. R.; Chase, L. E.; Pell, A. N. Cornell Net Carbohydrate and Protein System: A model for precision feeding of dairy cattle. *Anim. Feed. Sci. Technol.* **2008**, *143*, 174−202.
(30) Van Amburgh, M. E.; Chase, L. E.; Overton, T. R.; Ross, D. A.; Recktenwald, E. B.; Higgs, R. J.; Tylutki, T. P. Updates to the Cornell Net Carbohydrate and Protein System v6.1 and Implications for Ration Formulation. In *Proceedings of Cornell Nutrition Conference for Feed Manufacturers*; Syracruse, NY, 2010; pp 144−159.
(31) Mustafa, A. F.; Yu, P.; Chouinard; Ouellet, D. R.; Soita, H. Effects of moist heat treatment on ruminal nutrient degradability of sunflower seed. *J. Sci. Food Agric.* **2003**, *83*, 1059−1064.
(32) Huang, A. H. C. Oleosins and oil bodies in seeds and other organs. *Plant Physiol.* **1996**, *110*, 1055−1061.
(33) Ponne, C. T.; Möller, A. C.; Tijskens, L. M. M.; Bartels, P. V.; Meijer, M. M. T. Influence of microwave and steam heating on lipase activity and microstructure of rapeseed (*Brassica napus*). *J. Agric. Food Chem.* **1996**, *44*, 2818−2824.
(34) Samadi, Yu. P. Dry and moist heating-induced changes in protein molecular structure, protein subfraction, and nutrient profiles in soybeans. *J. Dairy Sci.* **2011**, *94*, 6092−6102.
(35) Sadeghi, A. A.; Shawrang, P. Effects of microwave irradiation on ruminal protein degradation and intestinal digestibility of cottonseed meal. *Livest. Sci.* **2007**, *106*, 176−181.
(36) Sadeghi, A. A.; Shawrang, P. Effects of microwave irradiation on ruminal degradability and in vitro digestibility of canola meal. *Anim. Feed Sci. Technol.* **2006**, *127*, 45−54.
(37) Ebrahimi, S. R.; Nikkhah, A.; Sadeghi, A. A. Changes in nutritive value and digestion kinetics of canola seed due to microwave irradiation. *Asian-Australas. J. Anim. Sci.* **2010**, *23*, 347−354.
(38) Mustafa, A. F.; McKinnon, J. J.; Christensen, D. A. Protection of canola (low glucosinolate rapeseed) meal and seed protein from ruminal degradation-Review. *Asian-Australas. J. Anim. Sci.* **2000**, *13*, 535−542.
(39) Damiran, D.; Yu, P. Molecular basis of structural makeup of hulless barley in relation to rumen degradation kinetics and intestinal availability in dairy cattle: A novel approach. *J. Dairy Sci.* **2011**, *94*, 5151−5159.
(40) Yu, P.; Niu, Z.; Damiran, D. Protein molecular structures and protein fraction profiles of new coproducts from bioethanol production: a novel approach. *J. Agric. Food Chem.* **2010**, *58*, 3460−3464.
(41) Khan, N. A.; Peng, Q.; Xin, H.; Yu, P. Vibrational spectroscopic investigation of heat-induced changes in functional groups related to protein structural conformation in camelina seeds and their relationship to digestion in dairy cows. *Anim. Prod. Sci.* **2014**, *55*, 201−206.
(42) Yu, P.; Nuez-Ortín, W. G. Relationship of protein molecular structure to metabolisable proteins in different types of dried distillers grains with solubles: a novel approach. *Br. J. Nutr.* **2010**, *104*, 1429−1437.
(43) Becker, P. M.; Yu, P. What makes protein indigestible from tissue-related, cellular, and molecular aspects? *Mol. Nutr. Food Res.* **2013**, *57*, 1695−1707.

DOI: 10.1021/jf503575y
J. Agric. Food Chem. 2015, 63, 1057−1066

Table 1. ^{1}H (500 MHz) and ^{13}C NMR (125 MHz) Data for Compound 1 in Pyridine-d_5 and Compounds 2 and 3 in CD_3OD

	1		2			3			3	
no.	δ_H mult (J in Hz)	δ_C	δ_H mult (J in Hz)	δ_C	no.	δ_H mult (J in Hz)	δ_C	no.	δ_H mult (J in Hz)	δ_C
1		167.5		169.6	1a		164.0	1b		167.4
2	6.84 d (15.6)	120.1	6.44 d (15.7)	118.7	2a		140.1	2b	6.53 d (15.7)	119.6
3	8.12 d (15.6)	140.6	7.47 d (15.7)	142.3	3a	7.26 s	124.0	3b	7.49 d (15.7)	139.8
4		127.4		128.5	4a		124.0	4b		130.5
5	7.52 d (8.5)	130.6	7.13 d (1.8)	111.6	5a	7.30 d (1.2)	112.3	5b	7.24 d (2.0)	111.1
6	7.12 d (8.5)	117.3		149.3	6a		147.5	6b		149.1
7		160.8		150.0	7a		148.2	7b		146.1
8	7.12 d (8.5)	117.3	6.82 d (8.2)	116.5	8a	6.73 d (8.0)	115.0	8b	6.72 d (8.0)	113.7
9	7.52 d (8.5)	130.6	7.04 dd (8.2,1.8)	123.3	9a	7.05 dd (8.0,1.2)	124.9	9b	7.02 dd (8.0, 2.0)	120.9
1′	3.86 t (7.2)	42.4	3.48 t (7.4)	42.8	1′a	3.48 br t (7.0)	41.2	1′b	3.48 br t (7.0)	40.9
2′	3.00 t (7.2)	36.0	2.77 t (7.4)	36.1	2′a	2.77 t (7.2)	34.5	2′b	2.65 t (6.7)	34.0
3′		131.0		131.5	3′a		129.4	3′b		129.9
4′	7.24 d (8.4)	130.9	7.07 d (8.4)	130.9	4′a	7.07 d (8.4)	129.3	4′b	6.85 d (8.4)	129.3
5′	7.14 d (8.4)	116.9	6.74 d (8.4)	116.3	5′a	6.61 d (8.4)	115.0	5′b	6.73 d (8.4)	115.0
6′		158.0		157.0	6′a		155.6	6′b		155.4
7′	7.14 d (8.4)	116.9	6.74 d (8.4)	116.3	7′a	6.61 d (8.4)	115.0	7′b	6.73 d (8.4)	115.0
8′	7.24 d (8.4)	130.9	7.07 d (8.4)	130.9	8′a	7.07 d (8.4)	129.3	8′b	6.85 d (8.4)	129.3
OMe			3.89 s	56.7	OMe(a)	3.67 s	54.5	OMe(b)	3.92 s	55.0

studies on the isolation and pharmacological properties of the phenolic amides from the fruits of *L. barbarum* have been reported. In our preliminary chemical investigations on the fruits, phenolic amide constituents were detected. Therefore, the active components from the ethyl acetate part of ethanol extracts, especially the phenolic amides, were isolated and identified from the fruits of this plant with the help of activity-guided chromatography for antioxidants. The antioxidant activities of these phenolic amides isolated from the fruits of *L. barbarum* were also evaluated systematically in scavenging 2,2-diphenyl-1-picrylhydrazyl (DPPH) free radical and inhibiting lipid peroxidation in rat liver microsomes induced by ascorbate/Fe^{2+}, cumine hydroperoxide (CHP), or CCl_4/reduced form of nicotinamide-adenine dinucleotide phosphate (NADPH).

MATERIALS AND METHODS

Animals and Chemicals. Sprague−Dawley rats (male, weight = 180−220 g) were obtained from the Experimental Animal Research Center at the Fourth Military Medical University. All experimental procedures were carried out according to protocols approved by the Ethics Committee for Animal Experimentation of the Fourth Military Medical University (Xi'an, Shaanxi, China) and in accordance with the *National Institutes of Health Guide for the Care and Use of Laboratory Animals*.

CHP (85%), BHA (99%), BHT (99%), bovine serum albumin (BSA, 99%, fraction V, essentially fatty acid free, low endotoxin), and reduced form of nicotinamide-adenine dinucleotide phosphate tetrasodium salt ($NADPHNa_4$, 98%) were purchased from Sigma-Aldrich Chemie (Steinheim, Germany). DPPH was purchased from Fluka (Buchs, Switzerland). Phenolic acids and flavonoid standards, including gallic acid, caffeic acid, *p*-coumaric acid, chlorogenic acid, rutin, quercetin, and kaempferol, with purities of 98, 99, 98, 95, 95, 98, and 99%, respectively, were purchased from Sigma-Aldrich Chemie (Steinheim, Germany). Most of the other solvents and chemicals used in this research were also obtained from Sigma-Aldrich Chemie.

General Experimental Procedures. Optical rotations ($[\alpha]_D$) were measured on a PerkinElmer 343 polarimeter (PerkinElmer Instruments, Norwalk, CT, USA). ^{1}H (500 MHz), ^{13}C (125 MHz), and 2D NMR (500 MHz) spectra were recorded on a Bruker AVANCE-500 NMR spectrometer (Bruker Daltonik GmbH, Rheinstetten, Germany) using pyridine-d_5 or CD_3OD as solvent and tetramethylsilane (TMS) as internal reference. ESIMS, HRESIMS, and ESIMS/MS were carried out on a Micromass Waters Q-Tof Micro Mass Spectrometer Mass Spec QTOF. EIMS was carried out on a Waters AutoSpec Premier. Compounds were separated with a Dionex P680 liquid chromatograph equipped with a UV170 UV−vis detector and a YMC-Pack R&D ODS-A column (20 × 250 mm; YMC Co., Ltd., Japan) and monitored at 225, 250, 275, and 300 nm. Chromatographic materials for low-pressure chromatographies were silica gel (10−40 μm; Qingdao Marine Chemical Inc., China), reversed phase silica gel (Lichroprep RP-18, 40−63 μm; Merck Inc., Germany), and Sephadex LH-20 (GE-Healthcare, USA). Silica gel 60 F_{254} precoated aluminum sheets (0.25 mm, Merck Inc., Germany) were used for thin-layer chromatography (TLC). Fractions were monitored by TLC, and spots were visualized by spraying with 20% H_2SO_4−EtOH solution followed by heating.

Plant Materials. The fruits of *L. barbarum* used in this research were collected from Zhongning county of Ningxia province, the largest planation of goji berry in China, in September 2012. The plant materials were identified by one of the authors (H.T.). A voucher specimen (no. 11485) has been deposited in the Herbarium of the Department of Pharmacy, Xijing Hospital, Fourth Military Medical University, Xi'an, China.

Extraction and Activity-Guided Chromatographic Isolation of Antioxidants. The air-dried fruits of *L. barbarum* (20 kg) were extracted with 80 L of 85% EtOH at 85 °C for 2 h under reflux. This process was repeated three times. The combined extracts were concentrated under vacuum at 60 °C. The residue (540 g) was suspended in H_2O and extracted with petroleum ether and EtOAc (each 2 L × 3), successively. The EtOAc-soluble fraction (120 g) was subjected to column chromatography on silica gel (1400 g, 15 × 120 cm) and eluted with a $CHCl_3$/MeOH/H_2O gradient (100:1:0.1, 50:1:0.1, 20:1:0.1, 10:1:0.1, 8:1:0.1, and 6:4:0.4) to give six major fractions: fraction 1 (17.54 g), fraction 2 (12.83 g), fraction 3 (21.67 g), fraction 4 (20.56 g), fraction 5 (13.42 g), and fraction 6 (20.92 g). The abilities to scavenge the DPPH radical of these six fractions (each 0.1 mg/mL) were evaluated by the DPPH assay (calculated as radical-scavenging percentage, RSP), and the most active fractions were 3 and 4, with RSP values of 48.9 and 47.4%, respectively. The two fractions were evaluated by TLC compared with phenolic acids and flavonoid standards, including gallic acid, caffeic acid, *p*-coumaric acid, chlorogenic acid, rutin, quercetin, and kaempferol standards, and spots were visualized by spraying with 20% H_2SO_4−EtOH solution followed by heating. The TLC results showed that the spots displayed by fraction 3 were similar to those of flavonoids and phenolic acids

DOI: 10.1021/jf5049222
J. Agric. Food Chem. 2015, 63, 1067−1075

standards, but the spots displayed by fraction 4 were distinctively different from them. This suggested that the antioxidants of fraction 3 were mainly composed of flavonoids and phenolic acids,[14] but those of fraction 4 were of a different chemical structure. Accordingly, fraction 4 (20.65 g) was chromatographed on a silica gel column with a $CHCl_3$/MeOH/H_2O gradient (20:1:0.1, 15:1:0.1, 10:1:0.1, and 8:1:01) to give four major fractions: fraction 4.1 (2.24 g), fraction 4.2 (6.13 g), fraction 4.3 (2.68 g), and fraction 4.4 (1.15 g). Among all of these fractions (each 0.1 mg/mL), fraction 4.2 was the most potent in the DPPH assay with an RSP value of 72.3%. Accordingly, fraction 4.2 was submitted to Sephadex LH-20 column chromatography (1000 g, 5 × 120 cm) with MeOH and further purified by open column using reversed phase silica gel (RP-18, 300 g, 2 × 90 cm) eluted with an MeOH/H_2O gradient (4:6 and 7:3) to give two major subfractions: fraction 4.2.1 (3.87 g, 0.1 mg/mL) and fraction 4.2.2 (1.56 g, 0.1 mg/mL); fraction 4.2.1 was the main active part with an RSP value of 86.7%. Purification of fraction 4.2.1 by semipreparative HPLC (MeOH/H_2O, 65:35; 8.0 mL/min) afforded pure compounds **1** (25 mg, t_R 9.3 min), **2** (23 mg, t_R 11.8 min), **3** (15 mg, t_R 19.4 min), **4** (13 mg, t_R 16.6 min), and **5** (12 mg, t_R 14.2 min).

Structural Elucidation of Natural Products. *N-E-Coumaroyl tyramine (**1**):* faint yellow powder; ^{1}H NMR (pyridine-d_5, 500 MHz) and ^{13}C NMR (pyridine-d_5, 125 MHz) data, see Table 1; positive ESIMS m/z 306 $[M + Na]^+$; negative ESIMS m/z 282 $[M - H]^-$; positive HRESIMS m/z 306.1107 $[M + Na]^+$ (calcd for $C_{17}H_{17}NO_3Na$, 306.1106).

*N-E-feruloyl tyramine (**2**):* faint yellow powder; ^{1}H NMR (CD_3OD, 500 MHz) and ^{13}C NMR (CD_3OD, 125 MHz) data, see Table 1; positive ESIMS m/z 336 $[M + Na]^+$; negative ESIMS m/z 312 $[M - H]^-$; positive HRESIMS m/z 336.1213 $[M + Na]^+$ (calcd for $C_{18}H_{19}NO_4Na$, 336.1212).

*Lyciumamide A (**3**):* yellow powder; $[\alpha]^{22}_D$ − 9.4° (*c* 0.21, MeOH); ^{1}H NMR (CD_3OD, 500 MHz) and ^{13}C NMR (CD_3OD, 125 MHz) data, see Table 1; positive ESIMS m/z 647 $[M + Na]^+$; negative ESIMS m/z 623 $[M - H]^-$; positive HRESIMS m/z 647.2370 $[M + Na]^+$ (calcd for $C_{36}H_{36}N_2O_8Na$, 647.2369); negative ESIMS/MS of parent ion at m/z 623, m/z 177, 312, 417, 432, and 460; negative ESIMS/MS of parent ion at m/z 432, m/z 177, 283, 312, and 417; EIMS m/z 120 (41), 149 (16), 165 (8), 177 (100), 193 (81), 254 (23), 296 (16), 312 (34), and 328 (17) (Figure 2A).

*Lyciumamide B (**4**):* yellow powder; $[\alpha]^{22}_D$ − 8.6° (*c* 0.25, MeOH); ^{1}H NMR (CD_3OD, 500 MHz) and ^{13}C NMR (CD_3OD, 125 MHz) data, see Table 2; positive ESIMS m/z 647 $[M + Na]^+$; negative ESIMS m/z 623 $[M - H]^-$; positive HRESIMS m/z 647.2371 $[M + Na]^+$ (calcd for $C_{36}H_{36}N_2O_8Na$, 647.2369); negative ESIMS/MS of parent ion at m/z 623, m/z 283, 296 and 460; negative ESIMS/MS of parent ion at m/z 283, m/z 136 and 255.

*Lyciumamide C (**5**):* yellow powder; $[\alpha]^{22}_D$ − 7.9° (*c* 0.34, MeOH); ^{1}H NMR (CD_3OD, 500 MHz) and ^{13}C NMR (CD_3OD, 125 MHz) data, see Table 2; positive ESIMS m/z 514 $[M + Na]^+$; negative ESIMS m/z 490 $[M - H]^-$; positive HRESIMS m/z 514.1839 $[M + Na]^+$ (calcd for $C_{28}H_{29}NO_7Na$, 514.1842); negative ESIMS/MS of parent ion at m/z 490, m/z 312 and 356; negative ESIMS/MS of parent ion at m/z 356, m/z 163, 179, and 340.

Antioxidant Activities. *DPPH Radical-Scavenging Activity.* Radical-scavenging activities of chromatographic fractions, purified compounds, and reference compounds were determined using a DPPH assay.[23] The RSP was calculated as follows: RSP = $[(A_0 - A_1)/A_0] \times 100$, where A_0 is the absorbance of the control (BHA) at 30 min and A_1 is the absorbance of the sample at 30 min. All samples were analyzed in triplicate.

Preparations of Liver Microsomes. Rat liver microsomes were prepared by standard differential centrifugation techniques as described by the literature.[24] The microsomes were suspended in 0.1 M Tris-HCl buffer (pH 7.4) when used in the experiments. Protein concentration was determined according to the Lowry method[25] using BSA as the standard.

Ascorbate/Fe^{2+}-Induced Lipid Peroxidation. The assay of lipid peroxidation of microsomes was performed as described by the literature.[26] The microsomes (2 mg microsomal protein/mL) were preincubated with (I) or without (I_0) the sample (0.1 mM compounds **1**−**5**, respectively) in the presence of 0.1 M Tris-HCl buffer (pH 7.4) and $FeSO_4$ (50 μM). Lipid peroxidation was initiated by adding ascorbate (5 mM), and the sample was then incubated at 37 °C for 15 min. The extent of lipid peroxidation was detected by the TBA method using trichloroacetic acid (10%, w/v) and TBA (0.67%, w/v) to measure the absorbance at 535 nm. The thiobarbituric acid reactive substances (TBARS) were calculated as malondialdehyde (MDA) equivalents. BHT (0.45 mM) was used as a positive control. The inhibitory effect on vitamin C/Fe^{2+}-induced lipid peroxidation was calculated as (%) inhibition ratio = $(I_0 - I)/I_0 \times 100$.

CHP-Induced Lipid Peroxidation. The microsomes (2 mg microsomal protein/mL) were preincubated with (I) or without (I_0) pure compounds (all 0.1 mM) in the presence of 0.1 M Tris-HCl buffer (pH 7.4). Lipid peroxidation was initiated by CHP (1 mM), and the samples were then incubated at 37 °C for 15 min. Trichloroacetic acid (10%, w/v) was used to stop the reaction. TBARS were determined as described above. BHT (0.45 mM) was used as a positive control. The inhibitory effect on CHP-induced lipid peroxidation was calculated as (%) inhibition ratio = $(I_0 - I)/I_0 \times 100$.

CCl_4/NADPH-Induced Lipid Peroxidation. The reaction mixture contained 2 mg of microsomal proteins and a NADPH-generating system (0.2 mM $NADP^+$, 4 mM glucose 6-phosphate, and 0.8 unit of

Table 2. ^{1}H (500 MHz) and ^{13}C NMR (125 MHz) Data for Compounds 4 and 5 in CD_3OD

	4		5	
no.	δ_H mult (J in Hz)	δ_C	δ_H mult (J in Hz)	δ_C
1a		173.0	3.84 m	65.0
2a	4.16 d (8.3)	58.8	3.54 q (6.2)	55.1
3a	5.90 d (8.3)	90.1	5.58 d (6.4)	90.0
4a		132.8		134.4
5a	6.93 d (1.8)	110.8	6.97 d (1.8)	110.9
6a		149.4		149.3
7a		148.3		147.9
8a	6.81 d (8.2)	116.5	6.80 d (8.2)	116.4
9a	6.79 d (1.8)	120.2	6.84 d (1.8)	120.2
1′a	3.50 t (7.2)	42.4		
2′a	2.79 t (7.2)	35.5		
3′a		131.2		
4′a	7.08 d (8.4)	130.9		
5′a	6.74 d (8.4)	116.4		
6′a		157.0		
7′a	6.74 d (8.4)	116.4		
8′a	7.08 d (8.4)	130.9		
OMe(a)	3.84 s	56.5	3.83 s	56.6
1b		169.2		169.1
2b	6.42 d (15.7)	119.6	6.47 d (15.7)	119.5
3b	7.46 d (15.7)	142.0	7.50 d (15.7)	142.1
4b		130.6		130.3
5b	7.13 d (1.2)	113.4	7.10 d (1.8)	113.7
6b		146.2		145.9
7b		151.4		151.5
8b		129.6		131.0
9b	6.77 s	118.3	7.16 s	118.8
1′b	3.50 t (7.2)	42.7	3.48 t (7.3)	42.7
2′b	2.79 t (7.2)	35.9	2.77 t (7.3)	36.0
3′b		131.4		131.4
4′b	7.03 d (8.4)	131.0	7.07 d (8.4)	130.9
5′b	6.84 d (8.4)	116.6	6.74 d (8.4)	116.4
6′b		157.1		157.0
7′b	6.84 d (8.4)	116.6	6.74 d (8.4)	116.4
8′b	7.03 d (8.4)	131.0	7.07 d (8.4)	130.9
OMe(b)	3.91s	56.8	3.91 s	57.0

DOI: 10.1021/jf5049222
J. Agric. Food Chem. 2015, 63, 1067−1075

glucose-6-phosphate dehydrogenase) in the 0.1 M Tris-HCl buffer (pH 7.4) with (I) or without (I_0) testing samples (all 0.1 mM). Lipid peroxidation was initiated by CCl_4/DMSO (1:4, v/v). After 15 min of incubation at 37 °C, TBARS were determined as described above. BHT (0.45 mM) was used as a positive control. The inhibitory effect on CCl_4/NADPH-induced lipid peroxidation was calculated as (%) inhibition ratio = $(I_0 - I)/I_0 \times 100$.

Statistical Analysis. Data were expressed as the mean ± SD. Statistical analysis was carried out by analysis of variance (ANOVA) followed by the LSD test for multiple comparisons. Data analysis was carried out using the SPSS v.11.0 software package. Differences were considered significant at $P < 0.05$.

RESULTS AND DISCUSSION

Isolation of Compounds from the Fruits of *L. barbarum*. The air-dried fruits of *L. barbarum* were extracted with EtOH under reflux. The petroleum ether extraction allowed removing the nonpolar components that showed low antioxidant activity. The EtOAc extract was fractionated by low-pressure column chromatography on silica gel to yield six major fractions. The six fractions were further purified with the help of activity-guided chromatography. Then the active antioxidants were isolated and identified as *N-E*-coumaroyl tyramine (**1**), *N-E*-feruloyl tyramine (**2**), lyciumamide A (**3**), lyciumamide B (**4**), and lyciumamide C (**5**), respectively (Figure 1). All of the compounds were isolated from the fruits of *L. barbarum* for the first time, and compounds **3**−**5** were identified as new compounds.

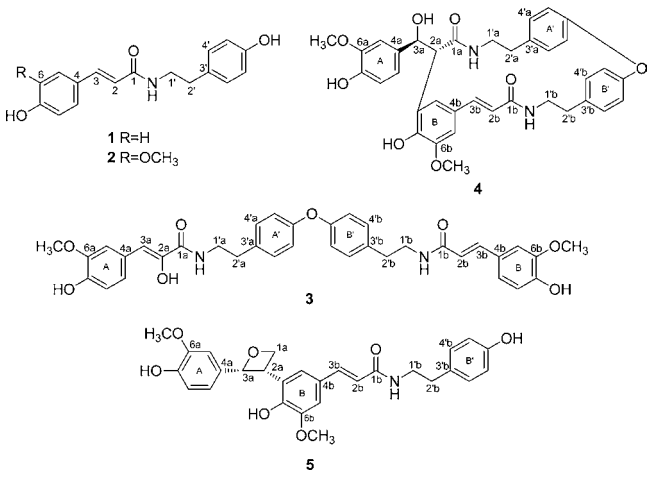

Figure 1. Structures of compounds **1**−**5**.

Structure Elucidation of the Five Purified Compounds. Two known compounds, *N-E*-coumaroyl tyramine (**1**) and *N-E*-feruloyl tyramine (**2**), were identified by comparaison of the observed ^{1}H and ^{13}C NMR data with literature values. The coupling constants between H-2 and H-3 (J = 15.6 and 15.7 Hz, respectively, for **1** and **2**) clearly indicated the *E* configuration of the double bonds. Compound **1** had been identified from *Asimina triloba*[27] and root bark of *Lycium chinense*.[17] Compound **2** had been reported as a natural product from the stem of *Piper argyrophylum*,[28] twigs of *Piper caninum*,[29] roots of *Solanum melongena*,[30] and stem of *Tinospora tuberculata*.[31]

Compound **3** was obtained as a yellow powder. The molecular formula of **3** was established as $C_{36}H_{36}N_2O_8$ from the $[M + Na]^+$ ion at m/z 647.2370 (calcd for $C_{36}H_{36}N_2O_8Na$, 647.2369) in the positive ion mode HRESIMS. This formula corresponded to a phenolic amide dimer consistent with 20 degrees of unsaturation. The ^{1}H and ^{13}C NMR data (Table 1) indicated that it was a dimer consisting of a *N-E*-feruloyl tyramine unit and a unit of its derivative.[32] On the basis of the EIMS fragment ions at m/z 254, 193, 177, and 312 (Figure 2A), the two units were suggested to be linked by an ether bond that was produced by the dehydration of two phenolic hydroxyl groups belonging to the two tyramine parts, that is, −C-6′a−O−C-6′b−. ESIMS data (Figure 2B) provided further evidence that the two tyramine parts were linked by an ether bond. In particular, the ion at m/z 432, which was equivalent to a loss of 191 Da in comparison to an ion at m/z 623, suggested the loss of a ferulic acid fragment, whereas an ion at m/z 283 was assigned as loss of a 2-methoxy-4-vinylphenol unit (149 Da) in comparison to the ion at m/z 432. In addition, the negative ESIMS/MS of parent ion at m/z 623 afforded representative fragmentations at m/z 177, 312, 417, 432, and 460 (Figure 3). The ion at m/z 432, which was equivalent to a loss of 191 Da in comparison to the parent ion at m/z 623, suggested the loss of a ferulic acid fragment, whereas an ion at m/z 417 was assigned as loss of NH (15 Da) in comparison to the ion at m/z 432, etc. The proposed fragmentation pathway of **3** is shown in Figure 3. This was also confirmed by the negative ESIMS/MS of parent ion at m/z 432 (representative fragmentations at m/z 177, 283, 312, and 417, Supporting Information). The assignments of all ^{1}H and ^{13}C NMR signals for the dimer were made by analyzing ^{1}H−^{1}H COSY, HSQC, and HMBC data. After analysis of ^{1}H−^{1}H COSY and HSQC, the ^{1}H NMR spectral data (Table 1) showed the presence of characteristic resonances in two distinct regions. The former, between δ_H 7.5 and 6.0, was produced by two sets of ortho-coupled aromatic protons at δ 7.07 and 6.61 (each 2H, d, J = 8.4 Hz) and δ 6.85 and 6.73 (each 2H, d, J = 8.4 Hz) from the AA′BB′-spin system of two 1,4-disubstituted aromatic rings (A′ and B′), two sets of aromatic protons at δ 7.30 (d, J = 1.2 Hz, H-5a), 6.73 (d, J = 8.0 Hz, H-8a), and 7.05 (dd, J = 8.0 and 1.2 Hz, H-9a) and at δ 7.24 (d, J = 2.0 Hz, H-5b), 6.72 (d, J = 8.0 Hz, H-8b), and 7.02 (dd, J = 8.0 and 2.0 Hz, H-9b), from the ABC-spin system of two 1,3,4-trisubsitituted benzene rings (A and B), two olefinic proton doublets at δ 6.53 and 7.49 (each d, J = 15.7 Hz, H-2b and H-3b), and an olefinic proton singlet at δ 7.26 (H-3a). The second region of the ^{1}H NMR spectrum of the dimer, between δ_H 4.0 and 2.0, indicated two A_2X_2 spin systems (δ 3.48, 4H, H_2-1′a and H_2-1′b; δ 2.77, 2H, H_2-2′a and δ 2.65, 2H, H_2-2′b) corresponding to protons of two isolated and deshielded ethylidene units, and two methoxy groups (δ 3.67, 3H, s, and δ 3.92, 3H, s). The HMBC correlations from protons of the two methoxy groups to C-6a (δ_C 147.5) and C-6b (δ_C 149.1), respectively, showed their positions on rings A and B. Additional ^{13}C NMR resonances in the dimer indicated the presence of two carbonyls of amide (δ 164.0, C-1a and δ 167.4, C-1b). In comparison with the chemical shifts of C-1a, C-2a (δ 140.1, quaternary carbon), C-3a, and C-4a with those of C-1b, C-2b (δ 119.6, tertiary carbon), C-3b, and C-4b, respectively, the variation of the δ values suggested that an active group was linked at C-2a. In consideration of the molecular formula of **3**, it should be a hydroxyl group. This was confirmed by the EIMS fragment ions (Figure 2A) at m/z 193 and 165 and the HMBC correlations H-3a/C-1a, H-5a/C-3a, and H-9a/C-3a. The HMBC interactions (Figure 4) also confirmed the interatomic connectivities and, thus, established the entire structure of **3**, named lyciumamide A.

DOI: 10.1021/jf5049222
J. Agric. Food Chem. 2015, 63, 1067−1075

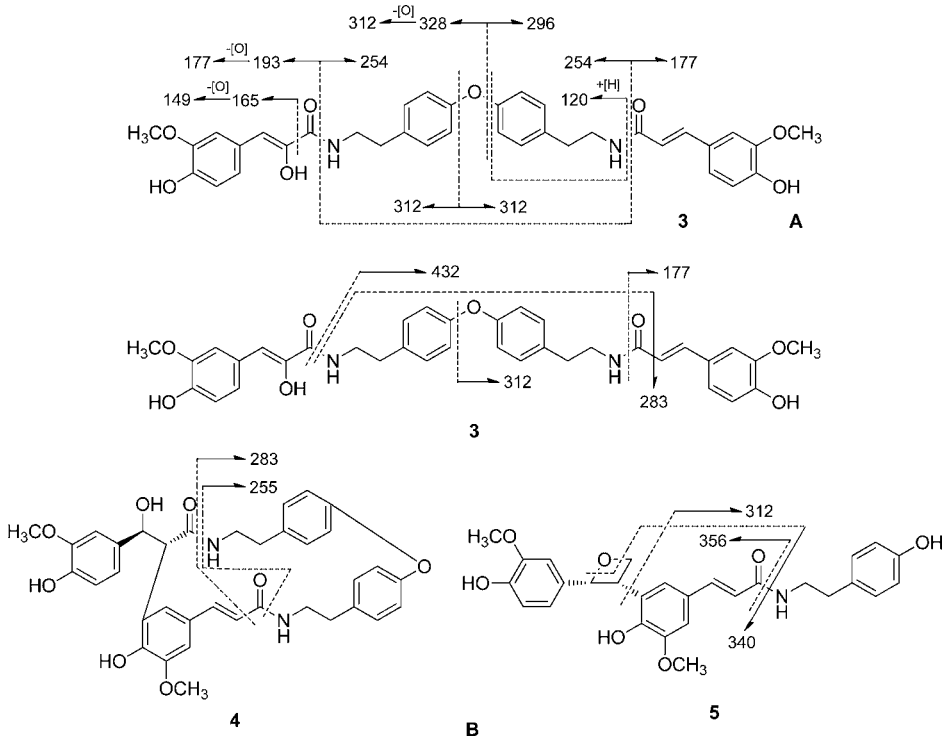

Figure 2. Important EIMS fragments of compound **3** (A) and proposed ESI⁻MS fragmentations of compounds **3**–**5** (B).

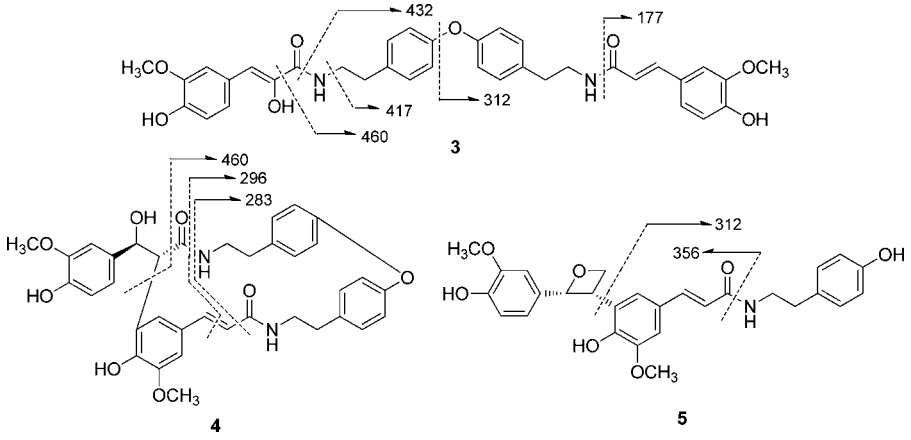

Figure 3. Representative fragmentations of compounds **3**–**5** deduced from ESI⁻MS/MS experiments.

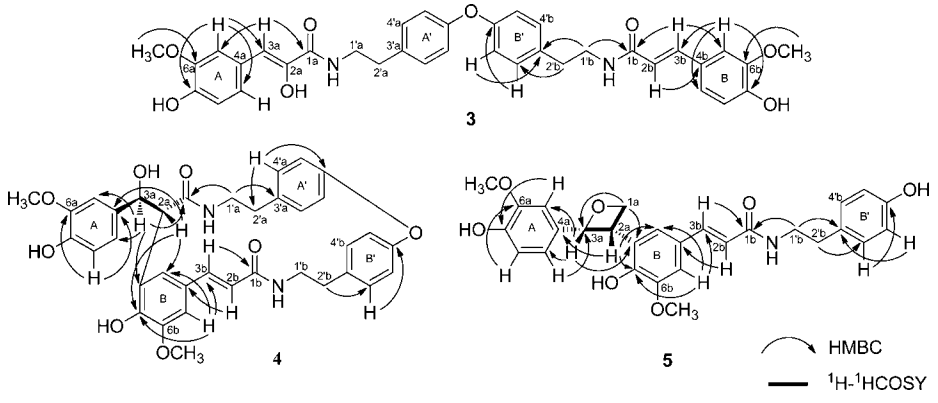

Figure 4. Key $^{1}H-^{1}H$ COSY and HMBC correlations for compounds **3**–**5**.

Compound **4** was obtained as a yellow powder. The molecular formula was established as $C_{36}H_{36}N_2O_8$ from the $[M + Na]^+$ ion at m/z 647.2371 (calcd for $C_{36}H_{36}N_2O_8Na$, 647.2369) in the positive ion mode HRESIMS. The assign-

DOI: 10.1021/jf5049222
J. Agric. Food Chem. 2015, 63, 1067–1075

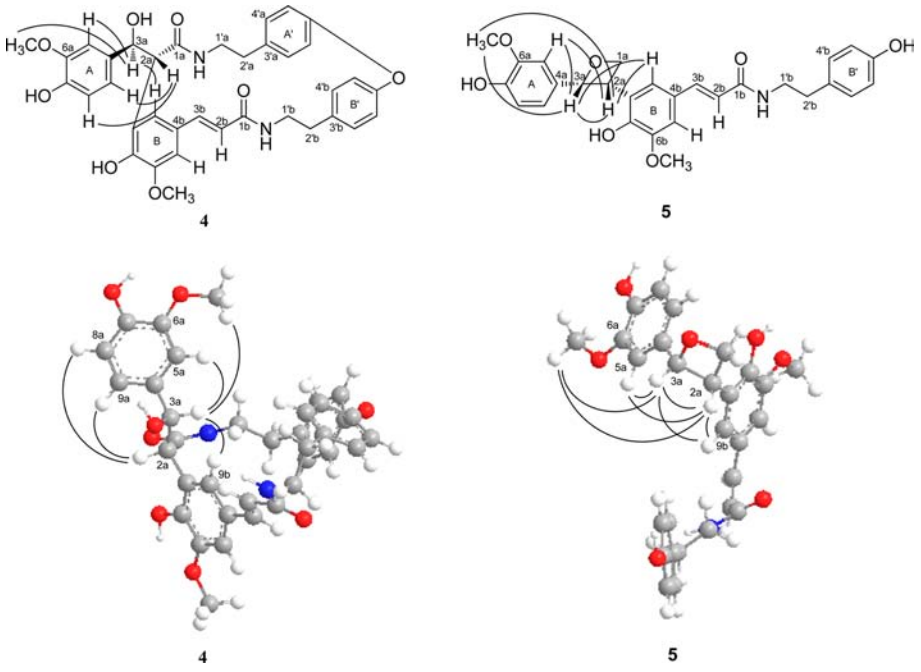

Figure 5. Key NOESY correlations for compounds **4** and **5**.

ments of the NMR signals were secured by analysis of $^{1}H-^{1}H$ COSY, NOESY, HSQC, and HMBC spectra. The ^{1}H and ^{13}C NMR spectral data of **4** (Table 2) were very similar to those of **3**, which indicated that **4** was also a dimer consisting of a *N-E*-feruloyl tyramine unit and a unit of its derivative. The negative ion mode ESIMS (Figure 2B) showed the same daughter ion peak at *m/z* 283 as for compound **3** deduced from the loss of a 340 Da unit (two ferulic acid fragments). Another ion at *m/z* 255, which was equivalent to a loss of 28 Da in comparison to the ion at *m/z* 283, suggested the loss of CO. In addition, the negative ESIMS/MS of parent ion at *m/z* 623 afforded representative fragmentations at *m/z* 283, 296, and 460, which could further confirm the linkage of compound **4**. The ion at *m/z* 296, which was equivalent to a loss of 164 Da in comparison to an ion at *m/z* 460, suggested the loss of CO and a 2-methoxy-4-methylphenol unit. The ion at *m/z* 283 was also assigned as loss of CH (13 Da) in comparison to the ion at *m/z* 296, and the proposed fragmentation pathway of **4** is shown in Figure 3. This was also verified by the negative ESIMS/MS of the parent ion at *m/z* 283 (representative fragmentations at *m/z* 136 and 255, Supporting Information). There were two distinctly distinguishable regions by careful comparison of the NMR data of **4** with **3**. In the former, the signals at C-2a (δ_H 4.16, d, J = 8.3 Hz; δ_C 58.8) in **4** suggested that it was a sp^3 methine instead of the olefinic quaternary carbon atom (δ_C 140.1) in **3**. The signals at C-3a (δ_H 5.90, d, J = 8.3 Hz; δ_C 90.1) in **4** suggested that it was also a sp^3 methine instead of the sp^2 methine (δ_H 7.26, s; δ_C 124.0) in **3**, and the upfield δ values of C-3a and H-3a in **4** indicated that an active group was linked at C-3a. In consideration of the molecular formula of **4**, it should be a hydroxyl group. In the second region, the DEPT and ^{13}C NMR spectra of **4** revealed that C-8b (δ_C 129.6) was a quaternary carbon atom instead of the tertiary carbon atom in **3** (δ_H 6.73, δ_C 115.0). The partial structure from C-1a to C-3a and the linkage of C-8b to C-2a were confirmed from the HMBC correlations from H-2a to C-4a, C-7b, and C-9b and from H-3a to C-1a, C-5a, C-9a, and C-8b, together with the $^{1}H-^{1}H$ COSY correlations between H-2a and H-3a (Figure 4). To infer the relative stereochemistry, a NOESY experiment was conducted (Figure 5). Clear cross peaks of H-2a and H-8a, H-2a and H-9a, H-3a and H-5a, H-3a and the methoxy protons, and H-3a and H-9b were observed. These NOEs indicated that the relative stereochemistry of the two protons H-2a and H-3a was *trans*. Thus, the structure of **4** was established and named lyciumamide B.

Compound **5** was obtained as a yellow powder. The molecular formula was established as $C_{28}H_{29}NO_7$ from the $[M + Na]^+$ ion at *m/z* 514.1839 (calcd for $C_{28}H_{29}NO_7Na$, 514.1842) in the positive ion mode HRESIMS. The assignments of the NMR signals were secured by analysis of $^{1}H-^{1}H$ COSY, NOESY, HSQC, and HMBC spectra. Careful comparison of ^{1}H and ^{13}C NMR data of **4** with those of **5** (Table 2) revealed that the NMR signals from C-1′a to C-8′a could not be observed in **5**, suggesting the absence of the phenethylamine group. Moreover, the NMR spectra of **5** displayed a sp^3 methylene (δ_H 3.84, 2H, m; δ_C 65.0, C-1a) instead of the carbonyl group in **4** ($\delta_{]C}$ 173.0). The upfield δ values of C-1a, H-1a, C-3a (δ_C 90.0), and H-3a (δ_H 5.58) in **5** indicated that C-1a and C-3a were oxygen-bearing atoms. The $^{1}H-^{1}H$ COSY correlations between H-1a and H-2a (δ_H 3.54) and between H-2a and H-3a confirmed the presence of the oxetane segment. The linkages of C-3a to C-4a and C-2a to C-8b were deduced from the HMBC correlations from H-1a to C-3a and C-8b, from H-2a to C-4a, C-7b, and C-9b, and from H-3a to C-5a, C-9a, and C-8b (Figure 4). Meanwhile, the structure of the oxetane segment was further confirmed by the key ESIMS fragmentation at *m/z* 340 and 356 (Figure 2B) and the ESIMS/MS of parent ion at *m/z* 490 (representative fragmentations at *m/z* 312 and 356, Figure 3) and the ESIMS/MS of parent ion at *m/z* 356 (representative fragmentations at *m/z* 163, 179, and 340, Supporting Information). To infer the relative stereochemistry, a NOESY experiment was conducted (Figure 5). Clear cross peaks of H-2a and H-3a, H-3a and H-5a, H-3a and the methoxy protons, H-3a and H-9b, H-2a and the methoxy protons, H-2a and H-5a, and H-2a and H-9b were

DOI: 10.1021/jf5049222
J. Agric. Food Chem. 2015, 63, 1067−1075

observed. These NOEs indicated that the relative stereochemistry of the two protons of oxetane (H-2a and H-3a) was *cis*. Therefore, the structure of **5** was established and named lyciumamide C.

Antioxidant Activities of the Five Purified Compounds. The assessment of antioxidant activity by a single method often underestimates the antioxidant potential of a molecule, and it reflects only the ability to inhibit a precise class of oxidants present.[33] The combination of several complementary analyses can give a clearer idea of the power of an antioxidant extract or a pure molecule. In this context, the antioxidant capacities of the five phenolic amides were evaluated using different antioxidant tests.

Scavenging of DPPH. Figure 6 shows the abilities of these pure compounds in reducing DPPH free radical. It could be noted that all of these pure compounds were effective in scavenging DPPH free radicals, whereas compound **1** showed the most prominent effect (96.3%), followed by compound **2** (96.1%), BHA (93.2%), compound **5** (90.3%), compound **3** (75.6%), and compound **4** (73.2%). In fact, compounds **1** and **2** exhibited better free radical scavenging activity than the reference BHA. The results suggested that phenolic amides isolated from the fruits of *L. barbarum* had good antioxidant activity, similar to that of other phenolic compounds such as phenolic acids and flavonoids from the fruits.[22]

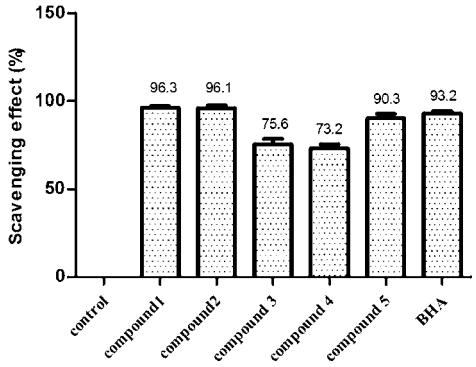

Figure 6. Effects of compounds **1**−**5** (0.1 mM) on DPPH absorption. The values are expressed as the mean ± SD (n = 3). Data with all compounds compared with the control group are significantly different at $P < 0.01$.

Inhibition of Lipid Peroxidation in Rat Liver Microsomes. Lipid peroxidation can be induced rapidly by the incubation of rat liver microsomes with ascorbate/Fe^{2+}, CHP, or CCl_4/NADPH at pH 7.4. Table 3 shows the activities of the pure compounds and BHT against lipid peroxidation. The extent of inhibition of lipid peroxidation was not uniform and varied among different compounds.

The analysis of results (Table 3) showed that the extent of TBARS formation was significantly decreased compared with the control group ($P < 0.01$) in the presence of the pure compounds, which exhibited lipid peroxidation inhibition activity. In the ascorbate/Fe^{2+}-induced lipid peroxidation system, compounds **1** and **2** exhibited the highest inhibiting activity of lipid peroxidation, and no significant difference was found between the two compounds ($P > 0.05$). Compound **5** showed significantly higher inhibitory activity of lipid peroxidation when compared with compounds **3** and **4** ($P < 0.01$), and no significant difference was found between compounds **3** and **4** ($P > 0.05$). In the CHP-induced lipid peroxidation system, compound **5** exhibited the highest inhibitory activity of lipid peroxidation, which was higher than those of the other dimers and the monomers ($P < 0.01$). The monomers **1** and **2** showed significantly higher inhibitory activities of lipid peroxidation when compared with the dimers **3** and **4** ($P < 0.01$). In the CCl_4/NADPH-induced lipid peroxidation system, all of the compounds exhibited excellent inhibiting activity of lipid peroxidation. Compound **5** showed the highest inhibiting activity, whereas there was no significant difference when compared with compounds **1** and **2** ($P > 0.01$). All of the results showed that the inhibition activity of compounds **1**, **2**, and **5** were significantly higher than the two dimers in the lipid peroxidation inhibitory assay.

In summary, the fruits of *L. barbarum* are a new source of natural phenolic amides. Lyciumamides A, B, and C, three new dimers of phenolic amides, along with two monomers, *N-E*-coumaroyl tyramine and *N-E*-feruloyl tyramine, were isolated from the fruits of *L. barbarum* for the first time. Their antioxidant activities were determined in scavenging DPPH free radical and inhibiting lipid peroxidation in rat liver microsomes induced by ascorbate/Fe^{2+}, CHP, or CCl_4/NADPH, and the data supported that these phenolic amides played an important role in the natural antioxidant properties of the fruits of *L. barbarum*, similar to those of other phenolic constituents such as flavonoids and phenolic acids of the fruits.[11] In conclusion, all of the results obtained here complemented the current knowledge of the antioxidative composition of the fruits of *L. barbarum* and confirmed that this agricultural product contained phenolic amide compounds, which might offer interesting potential applications in the food, cosmetic, and pharmaceutical industries.

Table 3. Effects of Compounds 1−5 on Lipid Peroxidation of Rat Liver Microsomes

	ascorbate/Fe^{2+}		CHP		CCl_4/NADPH	
	MDA[a] (μM)	I%[b]	MDA[a] (μM)	I%[b]	MDA[a] (μM)	I%[b]
control	7.16 ± 0.23		3.67 ± 0.18		5.13 ± 0.08	
compound **1**	0.53 ± 0.03**[c]	92.60	0.55 ± 0.04**	85.01	0.21 ± 0.01**	95.91
compound **2**	0.58 ± 0.03**	91.90	0.62 ± 0.04**	83.12	0.18 ± 0.01**	96.49
compound **3**	2.65 ± 0.07**	62.99	1.36 ± 0.07**	62.94	0.95 ± 0.04**	81.48
compound **4**	2.72 ± 0.07**	62.01	1.38 ± 0.08**	62.40	0.93 ± 0.04**	81.87
compound **5**	1.24 ± 0.05**	82.68	0.21 ± 0.02**	94.28	0.17 ± 0.01**	96.69
BHT	0.18 ± 0.01**	97.49	0.06 ± 0.01**	98.37	0.22 ± 0.01**	95.71

[a]Values are expressed as the mean ± SD (n = 3). TBARS (thiobarbituric acid reactive substances) were expressed by MDA (malondialdehyde) produced in the presence of 0.1 mM of pure compounds in the condition assays (see Materials and Methods). [b]Percentage of inhibition (I%) due to the pure compounds was calculated after deducting the basal level of peroxidation. [c]**, $P < 0.01$ compared with the control group (BHT).

DOI: 10.1021/jf5049222
J. Agric. Food Chem. 2015, 63, 1067−1075

■ ASSOCIATED CONTENT

Supporting Information

^{1}H, ^{13}C, and 2D NMR along with ESIMS and ESIMS/MS of the three new compounds **3**, **4**, and **5**; EIMS of compound **3**; possible biosynthesis pathway of **3**−**5**. This material is available free of charge via the Internet at http://pubs.acs.org.

■ AUTHOR INFORMATION

Corresponding Authors

*(H.T.) Phone/fax: +86 29 84774748. E-mail: tanghaifeng71@163.com.

*(J.C.) Phone/fax: +86 29 84775471. E-mail: natprod@163.com.

Notes

The authors declare no competing financial interest.

■ ABBREVIATIONS USED

BHA, *tert*-butyl-4-hydroxyanisole; BHT, 2,6-di-*tert*-butylhydroxytoluene; BSA, bovine serum albumin; CHP, cumine hydroperoxide; DPPH, 2,2-diphenyl-1-picrylhydrazyl; MDA, malondialdehyde; $NADPHNa_4$, nicotinamide-adenine dinucleotide phosphate tetrasodium salt; RSP, radical-scavenging percentage; TBARS, thiobarbituric acid reactive substances

■ REFERENCES

(1) Valko, M.; Leibfritz, D.; Moncol, J.; Cronin, M. T. D.; Mazur, M.; Telser, J. Free radicals and antioxidant in normal physiological function and human disease. *Int. J. Biochem. Cell Biol.* **2007**, *39*, 44−84.

(2) Firuzi, O.; Miri, R.; Tavakkoli, M.; Saso, L. Antioxidant therapy: current status and future prospects. *Curr. Med. Chem.* **2011**, *18*, 3871−3888.

(3) Velioglu, Y. S.; Mazza, G.; Gao, L.; Oomah, B. D. Antioxidant activity and total phenolics in selected fruits, vegetables, and grain products. *J. Agric. Food Chem.* **1998**, *46*, 4113−4117.

(4) Franke, A. A.; Cooney, R. V.; Henning, S. M.; Custer, L. J. Bioavailability and antioxidant effects of orange juice components in humans. *J. Agric. Food Chem.* **2005**, *53*, 5170−5178.

(5) Kranl, K.; Schlesier, K.; Bitsch, R.; Hermann, H.; Rohe, M.; Böhm, V. Comparing antioxidative food additives and secondary plant products − use of different assays. *Food Chem.* **2005**, *93*, 171−175.

(6) Jennings, B. H.; Akoh, C. C. Effectiveness of natural versus synthetic antioxidants in a rice bran oil-based structured lipid. *Food Chem.* **2009**, *114*, 1456−1461.

(7) Jacobsen, C.; Let, M. B.; Nielsen, N. S.; Meyer, A. S. Antioxidant strategies for preventing oxidative flavour deterioriation of foods enriched with *n*-3 polyunsaturated lipids: a comparative evaluation. *Trends Food Sci. Technol.* **2008**, *19*, 76−93.

(8) Le, K.; Chiu, F.; Ng, K. Identification and quantification of antioxidants in *Fructus lycii*. *Food Chem.* **2007**, *105*, 353−363.

(9) Peng, X.; Tian, G. Structural characterization of the glycan part of glycoconjugate LbGp2 from *Lycium barbarum* L. *Carbohydr. Res.* **2001**, *331*, 96−99.

(10) Huang, L.; Tian, G. Y.; Ji, G. Z. Structure elucidation of glycan of glycoconjugate LbGp3 isolated from the fruit of *Lycium barbarum* L. *J. Asian Nat. Prod. Res.* **1999**, *1*, 259−267.

(11) Toyoda-Ono, Y.; Maeda, M.; Nakao, M.; Yoshimura, M.; Sugiura-Tomimori, N.; Fukami, H. 2-*O*-(β-D-Glucopyranosyl) ascorbic acid, a novel ascorbic acid analogue isolated from *Lycium* fruit. *J. Agric. Food Chem.* **2004**, *52*, 2092−2096.

(12) Asano, N.; Kato, A.; Miyauchi, M.; Kizu, H.; Tomimori, T.; Matsui, K.; Nash, R. J.; Molyneux, R. J. Specific α-galactosidase inhibitors, *N*-methylcalystegines. Structure/activity relationships of calystegines from *Lycium chinense*. *Eur. J. Biochem.* **1997**, *248*, 296−303.

(13) Han, S. H.; Lee, H. H.; Lee, I. S.; Moo, Y. H.; Woo, E. R. A new phenolic amide from *Lycium chinense* Miller. *Arch. Pharm. Res.* **2002**, *25*, 433.

(14) Lee, D. G.; Park, Y.; Kim, M. R.; Jung, H. J.; Seu, Y. B.; Hahm, K. S.; Woo, E. R. Antifungal effects of phenolic amides isolated from the root bark of *Lycium chinense*. *Biotechnol. Lett.* **2004**, *26*, 1125−1130.

(15) Funayama, S.; Yoshida, K.; Konno, C.; Hikino, H. Structure of kukoamine A, a hypotensive principle of *Lycium chinense* root barks. *Tetrahedron Lett.* **1980**, *21*, 1355−1356.

(16) Funayama, S.; Zhang, G. R.; Nozoe, S. Kukoamine B, a spermine alkaloid from *Lycium chinense*. *Phytochemistry* **1995**, *38*, 1529−1531.

(17) Xie, L. W.; Atanasov, A. G.; Guo, D. A.; Malainer, C.; Zhang, J. X.; Kopp, B. Activity-guided isolation of NF-κB inhibitors and PPARγ agonists from the root bark of *Lycium chinense* Miller. *J. Ethnopharmacol.* **2014**, *152*, 470−477.

(18) Zhang, J. X.; Guan, S. H.; Feng, R. H.; Wang, Y.; Wu, Z. Y.; Guo, D. A. Neolignanamides, lignanamides, and other phenolic compounds from the root bark of *Lycium chinense*. *J. Nat. Prod.* **2013**, *76*, 51−58.

(19) Potterat, O. Goji (*Lycium barbarum* and *L. chinense*): phytochemistry, pharmacology and safety in the perspective of traditional uses and recent popularity. *Planta. Med.* **2010**, *76*, 7−19.

(20) Chang, R. C.; So, K. F. Use of anti-aging herbal medicine, *Lycium barbarum*, against aging-associated diseases. What do we know so far? *Cell Mol. Neurobiol.* **2008**, *28*, 643−652.

(21) Li, X. M. Protective effect of *Lycium barbarum* polysaccharides on streptozotocin-induced oxidative stress in rats. *Int. J. Biol. Macromol.* **2007**, *40*, 461−465.

(22) Wang, C. C.; Chang, S. C.; Stephen, I. B.; Chen, B. H. Isolation of carotenoids, flavonoids and polysaccharides from *Lycium barbarum* L. and evaluation of antioxidant activity. *Food Chem.* **2010**, *120*, 184−192.

(23) Kao, T. H.; Chen, B. H. Functional components in soybean cake and their effects on antioxidant activity. *J. Agric. Food Chem.* **2006**, *54*, 7544−7555.

(24) Satav, J. G.; Katyare, S. S. Effect of experimental thyrotoxicosis on oxidative phosphorylation in rat liver, kidney and brain. *Mol. Cell. Endocrinol.* **1982**, *28*, 178−189.

(25) Lowry, O. H.; Rosenbrough, N. J.; Farr, A. L.; Randall, R. J. Protein measurement with the Folin phenol reagent. *J. Biol. Chem.* **1951**, *193*, 265−275.

(26) Gutteridge, J. M. C.; Halliwell, B. The measurement and mechanism of lipid peroxidation in biological systems. *Trends Biochem. Sci.* **1990**, *15*, 129−135.

(27) Zhao, Y.; Zhao, Q. S.; Lin, Z. W.; Sun, H. D.; Wu, H. M.; Xu, J. F. Phenolics from *Ceratostigma minus*. *Acta Bot. Sin.* **1998**, *40*, 1035−1039.

(28) Singh, S. K.; Ashok, P. K.; Olsen, C. E.; Jha, A.; Jain, S. C.; Parmar, V. S. Neolignans and alkaloids from *Piper argyrophylum*. *Phytochemistry* **1996**, *43*, 1355.

(29) Jones, M. J. S. H.; Hecht, S. M. Phenolic acid amides: a new type of DNA strand scission agent from *Piper caninum*. *Bioorg. Med. Chem.* **2004**, *12*, 3885−3889.

(30) Yoshihara, T.; Takamatsu, S.; Sakamura, S. Three new phenolic amides from the roots of eggplant (*Solanum melongena* L.). *Agric. Biol. Chem.* **1978**, *42*, 623−627.

(31) Fukuda, N.; Yonemitsu, M.; Kimura, T. Studies on the constituents of the stems of *Tinospora tuberculata* BEUMEE. I. *N-trans*-and *N-cis*-feruloyl tyramine, and a new phenolic glucoside, tinotuberide. *Chem. Pharm. Bull.* **1983**, *31*, 156−161.

(32) Trabelsi, N.; Oueslati, S.; Ksouri, R.; Nassra, M.; Marchal, A.; Krisa, S. The antioxidant properties of new dimer and two monomers of phenolic acid amides isolated from *Limoniastrum guyonianum*. *Food Chem.* **2014**, *146*, 466−471.

(33) Hayouni, E. A.; Abedrabba, M.; Bouix, M.; Hamdi, M. The effects of solvents and extraction method on the phenolic contents and biological activities *in vitro* of Tunisian *Quercus coccifera* L. and

DOI: 10.1021/jf5049222
J. Agric. Food Chem. 2015, 63, 1067−1075

Juniperus phoenicea L. fruit extracts. *Food Chem.* **2007**, *105*, 1126−1134.

DOI: 10.1021/jf5049222
J. Agric. Food Chem. 2015, 63, 1067−1075

Table 1. Varieties from North and South American Field Locations

Variety	North American locations	South American locations
SP Armada	Saskatchewan, Canada; Cass, ND, USA	Maipo, Chile
Q2 Canola	Cass, ND, USA	Maipo, Chile
Magnum	R. M. MacDonald, Manitoba, Canada; Grand Forks, ND, USA	Melipilla, Chile
Trailblazer	R. M. MacDonald, Manitoba, Canada; Grand Forks, ND, USA	Melipilla, Chile
NPV Campino	McHenry, ND, USA	Melipilla, Chile
Python 1651H	R. M. MacDonald, Manitoba, Canada; McHenry, ND, USA; Portage la Prairie, Manitoba, Canada	Maipo, Chile
Ebony	Saskatchewan, Canada; Cass, ND, USA; Grand Forks, ND, USA; McHenry, ND, USA; R. M. MacDonald, Manitoba, Canada; Portage la Prairie, Manitoba, Canada	Maipo, Chile; Melipilla, Chile

Validation Sample Matrix. Canola seed used for method development and validation was purchased from a commercial source. Seed was ground using a centrifugal mill grinder (Retsch, Haan, Germany) to a particle size of ≤0.75 mm. Following preparation, ground seed was stored at approximately −20 °C.

Extraction. Extraction of vitamin K_1 from food matrices has been accomplished primarily via direct extraction with organic solvents or through enzymatic hydrolysis. Because vitamin K_1 is unstable under alkaline conditions, caustic saponification, commonly used for other fat-soluble vitamins such as A and E, is not appropriate.[7] Extraction was accomplished utilizing the procedure recommended by USP24/NF19.[8] Test portions (0.5 g) of ground canola seed were weighed into 15 mL plastic centrifuge tubes. Subsamples designated as laboratory-fortified samples were spiked with 0.07 mL of a 10 μg/mL vitamin K_1 standard solution, producing a fortified concentration of about 1.5 mg/kg. Laboratory-fortified samples were used to assess method accuracy through calculation of percent recovery. All test portions were spiked with 0.1 mL of a 10 μg/mL IS standard solution. To each test portion were added 4 mL of DMSO and 6 mL of hexane, and the contents were mixed on a vortexing apparatus for about 5 s. The samples were placed in an ultrasonic bath at 60 °C and sonicated for 45 min with vigorous hand shaking for 5 s approximately every 10 min. After centrifugation at 1800*g* for 10 min, the upper hexane layer was transferred to a 25 mL volumetric flask. Two additional extractions were performed by adding 6 mL of hexane followed by brief vortex mixing and shaking (sample tubes oriented horizontally) for 5 min at 300 rpm using a platform orbital action shaker. Following centrifugation at 1800*g* for 10 min, the hexane layer was drawn off and combined with the previous extract in the 25 mL volumetric flask. A 2.5 mL aliquot of the hexane extract was transferred to a 15 mL glass culture tube and evaporated to dryness under a stream of nitrogen using a heating block temperature of 30 °C. Sample residues were reconstituted by adding 1 mL of hexane to each culture tube and vortex mixing for about 5 s.

Silica Solid Phase Extraction (SPE) Cleanup. A SPE purification procedure followed recommendations outlined in AOAC method 992.27.[9] Silica SPE Sep-Pak cartridges, 500 mg/6 cm^3 (Waters Corp.), were mounted on a 12- or 24-position SPE vacuum manifold (Supelco, Bellefonte, PA, USA). Each cartridge was washed with 2 mL of hexane and then loaded with the sample solution (1 mL). The extract solution was allowed to drain via gravity flow until reaching the top of the column bed. The SPE cartridge was washed with 1 mL of hexane followed by 2 mL of 5:95 dichloromethane/hexane (v/v). Vacuum (<20 in. Hg) was applied for 5 min to completely dry the cartridge packing. The vacuum was stopped, and a 15 mL glass culture tube was placed under the cartridge inside the manifold. Vitamin K_1 was eluted by adding 2 mL of dichloromethane to the top of each column and allowing the solvent to drain by gravity to the top of the sorbent bed. Vacuum was then applied to remove the remaining dichloromethane from the column bed. The collected eluate was evaporated to dryness under a stream of nitrogen and reconstituted in 1 mL of isopropanol. The isopropanol sample solution was transferred to an amber HPLC autosampler vial and submitted for C_{30} HPLC-MS/MS analysis.

C_{30} HPLC-MS/MS Analysis. The HPLC-MS/MS analysis was based upon the methodology of Huang et al. and Schimpf et al.[10,11] Separation was accomplished on a C30 (3 mm × 150 mm i.d. × 3 μm) reversed phase column (YMC Co., Komatsu, Japan). The column was maintained at a temperature of 30 °C. Elution was carried out at a flow rate of 0.5 mL/min with the following solvent system: A = 0.1% formic acid in deionized water, B = dichloromethane/methanol, 5:95 (v/v). Following injection of 5 μL of sample or calibration standard solution, the solvent composition was held at 5% A/95% B for 0.1 min. A linear gradient to 100% B was then carried out over 5 min and held until 8 min. The mobile phase composition was returned to 5% A/95% B and allowed to equilibrate for an additional 4 min. The total run time was 12 min per injection. Approximate retention times were 7.2 and 7.7 min for *trans*- and *cis*-vitamin K_1, respectively. Mobile phase flow was diverted to waste for the first 6.5 min following injection and then redirected to the MS detector for 2 min to allow detection of the eluted analytes. The flow was again diverted to waste at 8.5 min. The MS detector scanned only during the 2 min retention time range of peak elution. The Quattro micro MS detector was operated in positive ion mode. Multiple reaction monitoring (MRM) was used to detect the vitamin K_1 and d_7-vitamin K_1 isomers. For vitamin K_1, the transition of the precursor ion at a mass to charge ratio (m/z) of 451.6 ($[M + H]^+$) and product ion at m/z 187.2 (451.6 → 187.2) was monitored. For the d_7-vitamin K_1 internal standard, the transition 458.8 → 194.3 was monitored. Source settings were 40 V for the sample cone, 25 (nominal) for the collision cell energy, 4.5 kV for the capillary, 0.00 V for the extractor, and 0.1 V for the RF lens. Source and desolvation temperatures were maintained at 150 and 450 °C, respectively. Cone gas and desolvation nitrogen gas flow rates were 30 and 550 L/h, respectively.

Calculation of Results. Calibration curves were generated for *trans*-vitamin K_1 ranging from 4.5 to 180 ng/mL. Internal standardization was utilized. Each calibration solution contained 90 ng/mL d_7-*trans*-vitamin K_1. A linear regression curve was constructed using peak area ratios (y-axis) and the standard solution concentration ratios (x-axis). A single injection of each calibration standard was carried out over the course of each analysis sequence. Sample solution concentrations (ng/mL) were calculated using the straight-line equation from the calibration curve. A weighting function of $1/x$ was used. Peak areas, calibration curves, and sample solution concentrations were calculated using the data system (Masslynx version 4.1).

Biological Materials. A total of seven conventional canola cultivars were evaluated from Locations in North and South America as listed in Table 1. The South American canola seed materials were grown at two locations (El Monte, Melipilla; and Paine, Maipo) in Chile during 2011/2012. The North American canola seed materials were grown in the United States and Canada (R. M. Corman Park, Saskatchewan, Canada; Portage la Prairie, Manitoba, Canada; R. M. MacDonald, Manitoba, Canada; Cass, ND, USA; Grand Forks, ND, USA; McHenry, ND, USA) during 2012. Various cultivars were planted at each location, with Ebony being planted at each location. Each location was planted in a randomized complete block design with four replicates of each variety. Seed samples were harvested at physiological maturity from all plots and shipped at ambient temperature to Monsanto Co. (Creve Coeur, MO, USA). A subsample for vitamin K_1 analysis was obtained from each sample collected. These subsamples were then ground and stored in a freezer set to maintain a temperature of −20 °C until their shipment on dry ice to EPL Bio Analytical Services for analysis.

DOI: 10.1021/jf503824t
J. Agric. Food Chem. 2015, 63, 1076−1081

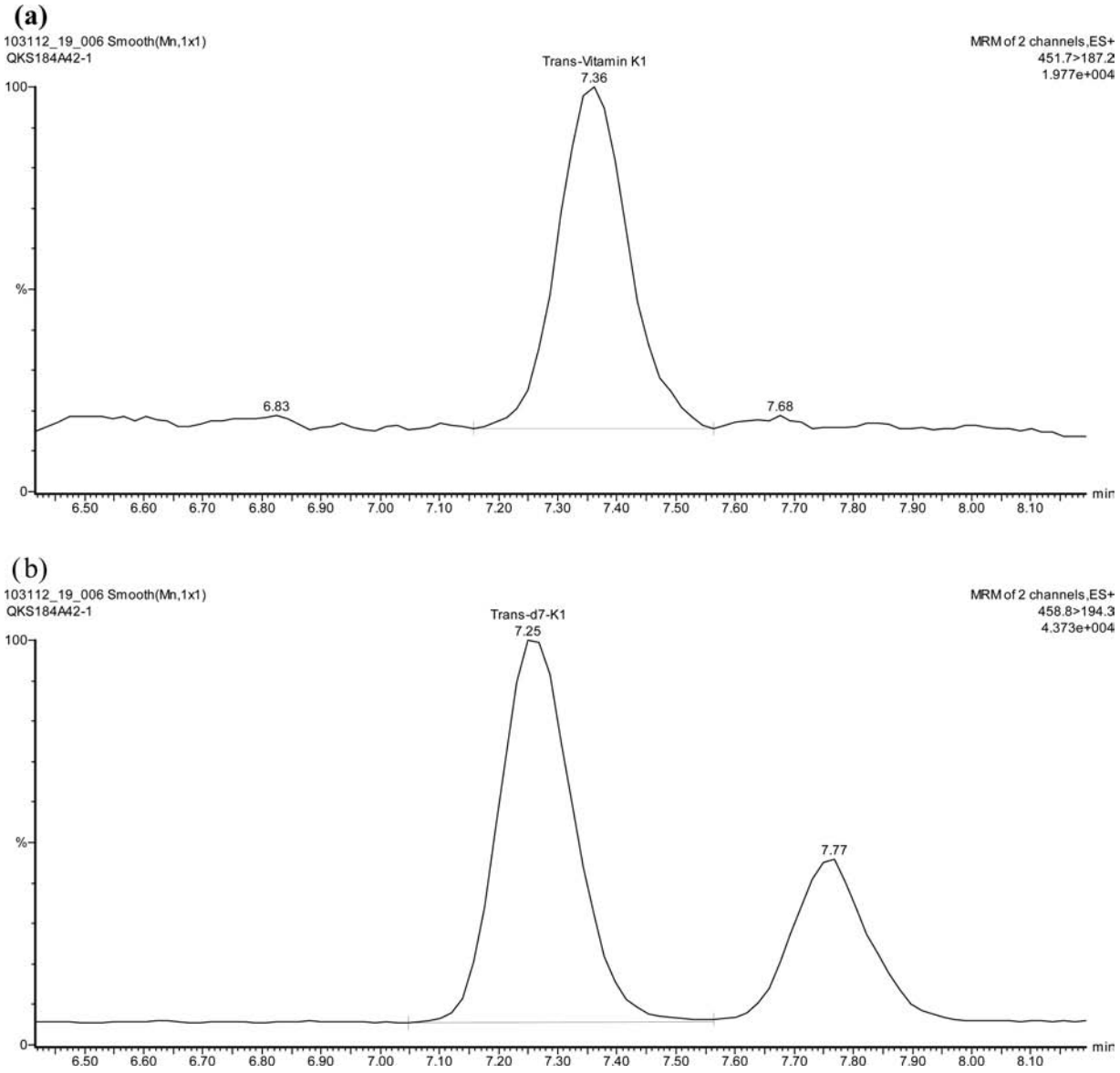

Figure 1. HPLC-MS/MS chromatogram of a canola seed extract showing *trans*-vitamin K_1 (a). *cis*-vitamin K_1 not detected (expected retention time = 7.88 min). HPLC-MS/MS chromatogram of a canola seed extract showing d_7-*trans*-vitamin K_1 internal standard (b). d_7-*cis*-Vitamin K_1 internal standard peak appears at 7.77 min (not integrated).

Statistical Analysis. The vitamin K_1 data were summarized (mean and range) by region (North and South America). In addition, statistical analysis of the data involved a comparison of vitamin K_1 concentrations between the North American sites and the South American sites to determine significant differences ($\alpha = 0.05$) by using the following fixed model to conduct analysis of variance (ANOVA). The model uses the term continent to refer to the North and South American locations.

$$Y_{ijk} = \mu + \tau_i + \lambda_k + (\tau\lambda)_{ik} + \beta_{j(k)} + \varepsilon_{ijk}$$

Y_{ijk} is the value of vitamin K_1 concentration of cultivar i in location j of continent k, μ is the overall mean, τ_i is the random effect of cultivar i, λ_k is the effect of continent k, $(\tau\lambda)_{ik}$ is the random effect of the interaction between cultivar i and continent k, $\beta_{j(k)}$ is the effect of location j nested within continent k, and ε_{ijk} is the residual error. Statistically significant differences between the North American and South American sites were declared at $\alpha = 0.05$.

Variance components analysis (VCA) was also conducted to estimate the proportion of each effect in the model contributing to the total variance. In this application, the effects of cultivar, continent, cultivar × continent interaction, and location (continent) in the ANOVA model were set as random effects. The SAS procedure PROC MIXED was employed to run the analysis. The output table of covariance parameter estimates from SAS PROC MIXED procedure gave estimates of the variance component parameters for each of the model components. The variance component parameters of each model component were divided by the total variance to get the variance proportions for each of the components.

RESULTS AND DISCUSSION

Method Validation. Prior to applying the HPLC-MS/MS methodology to the harvested materials, the method was validated. The method limit of quantitation (LOQ) for *trans*-vitamin K_1 was established at 0.09 mg/kg on the basis of peak signal-to-noise ratios (S/N) for seed extracts (S/N at the LOQ was at least 10). The limit of detection (LOD) was established at a level that was approximately equal to 30% of the LOQ. The LOD concentration was 0.03 mg/kg. It is unlikely that

DOI: 10.1021/jf503824t
J. Agric. Food Chem. 2015, 63, 1076−1081

Table 2. Validation Summary[a]

replicate	initial analysis precision *trans*-vitamin K_1[b] (mg/kg)	analysis accuracy % recovery[c] (1.5 mg/kg spike level)
1	1.79	100
2	1.57	107
3	1.63	107
4	1.63	NA[d]
5	1.85	NA
6	1.51	NA
7	1.62	NA
mean	1.66	105
SD	0.12	4.04
RSD	7.26	3.85

[a]Only three recovery samples analyzed. [b]Concentrations (mg/kg) are expressed on a dry weight basis. [c]Canola seed spiked at 1.5 mg/kg spike level. [d]NA, not applicable.

Table 3. Intermediate Precision

analyst	range[a] (mg/kg)[b]	mean[a] (mg/kg)[b]	SD[a]	RSD[a] (%)
1	1.50−2.03	1.75	0.179	10.2
2	1.78−2.05	1.89	0.0869	4.59
overall (n = 20)	1.50−2.05	1.82	0.156	8.53

[a]n = 10 replicate test portions. Analysts performed extraction and analysis on two different days. [b]Concentrations are expressed on a dry weight basis.

concentrations in canola seed would approach the current LOQ as defined.

The linear concentration range for *trans*-vitamin K_1 was 4.5−180 ng/mL. The minimum acceptable correlation coefficient (r) was 0.990 for each calibration curve; values >0.995 were observed. The use of d_7-vitamin K_1 as an internal standard proved adequate for compensation for matrix-induced ion source suppression. The C30 column provided adequate resolution from any surrounding peaks (Figure 1).

Repeatability precision and spike and recovery accuracy data are presented in Table 2. The repeatability RSD (n = 7) was 7.39% with a mean spike recovery of 105% achieved. Additional analyses were conducted to provide intermediate precision data. Two sets of 10 replicate canola seed test portions were assayed on two different days by two analysts. The overall RSD (n = 20) was 8.53%. Individual analyst RSDs were 10.2 and 4.59% (Table 3). On the basis of these data, the methodology was deemed acceptable (RSD ≤ 15%) for use in determining vitamin K_1 levels in canola seed. Validation acceptance criteria were based on single-laboratory validation guidelines published by AOAC International.[12]

Canola Seed Vitamin K_1 Levels. As previously discussed, canola, soybean, and olive oils are considered to be major sources of vitamin K_1,[2,3] with canola oil containing 0.7−1.5 mg vitamin K_1/kg of oil.[4,5] Vitamin K_1 is a fat-soluble vitamin that is associated with the lipid fraction of the seed. Although there are few data on vitamin K_1, there have been several publications on fat and fatty acid contents of canola seed. Environmental effects on fat content of canola seed have been shown to be large relative to cultivar effects, with high fat levels being shown to be correlated with cooler spring temperatures and higher spring rainfall.[13] The climate of the typical North American canola cultivation region is considered subhumid to semiarid, with mean annual precipitation ranging from 300 to 600 mm

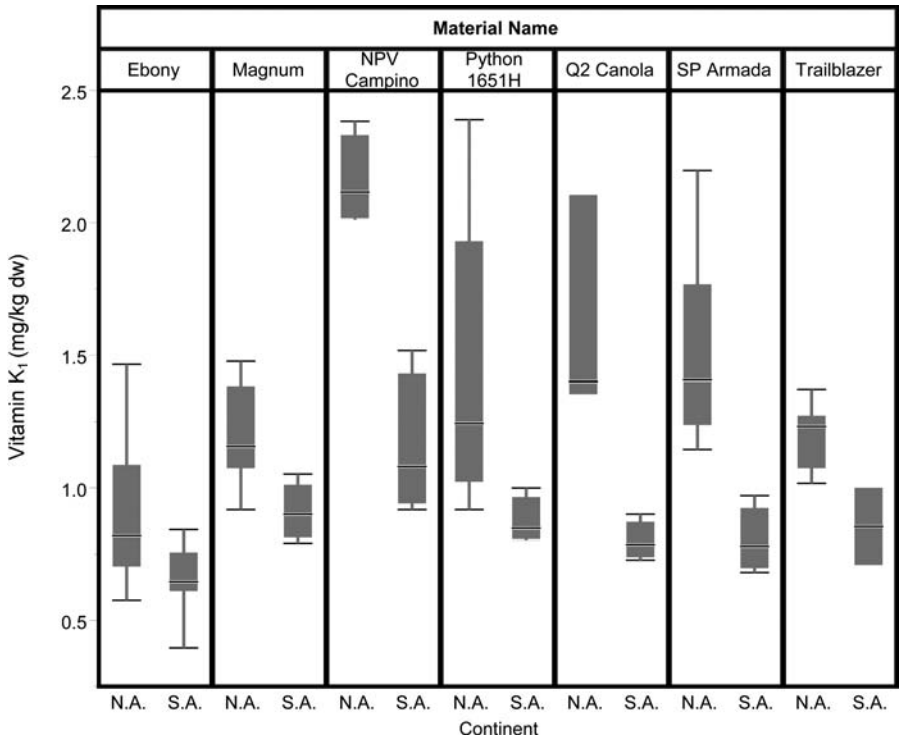

Figure 2. Comparison of vitamin K_1 concentrations in canola seed grown in locations in North America versus South America. Each box plot provides a graphical summary of the distribution of data from all cultivars grown at all locations in either North or South America. The box represents the distribution of the middle 50% of the data, whereas the horizontal line within the box represents the median sample value. Upper and lower lines represent the remaining distribution of the data. Concentrations of vitamin K_1 are expressed on a dry weight basis.

DOI: 10.1021/jf503824t
J. Agric. Food Chem. 2015, 63, 1076−1081

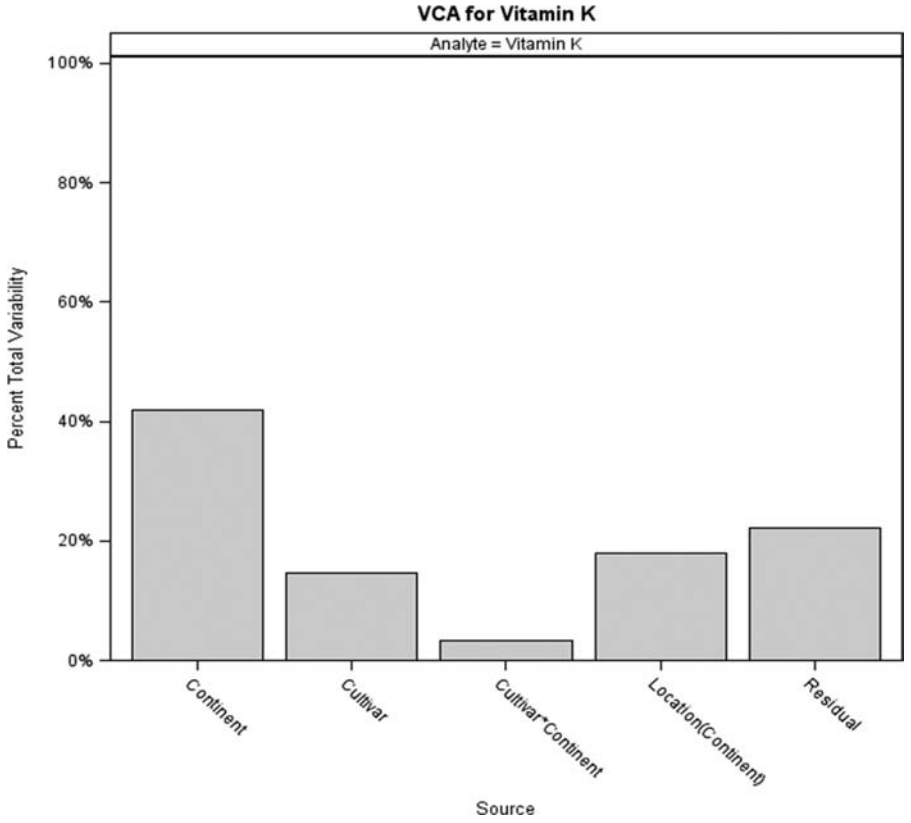

Figure 3. Sources of variation estimates from variance component analysis for vitamin K_1 in canola seed.

per year. In comparison, the climate of the Chilean central region is considered semiarid Mediterranean, with average precipitation of 100−300 mm.[14]

Comparison of mean vitamin K_1 values by cultivar and continent demonstrated that canola grown in locations in North America ranged from 0.25 (Ebony) to 1.01 mg/kg (NPV Campino) higher than the corresponding cultivars grown in locations in South America. The relative difference (difference in means/mean North American value) ranged from 24.2% difference for Magnum to 50.6% difference for Q2 canola. In all cases, numerically higher average vitamin K_1 levels were observed for locations in North America in comparison to those in South America. Figure 2 graphically compares the vitamin K_1 levels for each cultivar grown in locations in both North and South America. Across all cultivars, the individual replicate *trans*-vitamin K_1 values observed for locations in North America were between 0.58 and 2.39 mg/kg and for locations in South America were between 0.40 and 1.52 mg/kg. Statistical analysis included application of VCA to investigate the impacts of environment and cultivar on the variability of vitamin K_1 canola seed composition. Comparisons included data that were combined across all locations for each continent using ANOVA. The results showed there is a significant difference (0.0002, $p < 0.05$) of vitamin K_1 levels in canola seed between locations in North America and South America. These data demonstrated that environment, represented by continent and location effects, was the main contributor to vitamin K_1 level variation (Figure 3). In addition, these data also showed that variation in genetic background represented by cultivar effect to a lesser degree also influenced vitamin K_1 canola seed composition.

An accurate, sensitive, and selective method for the determination vitamin K_1 in canola seed was developed and applied to survey the levels of the biologically active *trans*-vitamin K_1 isomer in several commercial cultivars of canola seed grown in locations in North and South America. The research reported herein provides the first publication describing the variability of vitamin K_1 levels in commercial canola cultivars grown in relevant geographical locations. The data suggest that, similar to other canola components previously evaluated by others,[13] vitamin K_1 levels are influenced by cultivar and environment. Knowing that cultivar and environmental effects influence vitamin K_1 levels provides a context to assess compositional quality of new cultivars developed for market.

■ ASSOCIATED CONTENT

Supporting Information

Supporting data for vitamin K_1 concentrations appearing in Figure 2 and the statistical analysis data represented in Figure 3. This material is available free of charge via the Internet at http://pubs.acs.org.

■ AUTHOR INFORMATION

Corresponding Author

*(F.S.C.) Phone: (217) 963-2143. Fax: (217) 963-2283. E-mail: fclaussen@eplbas.com.

Notes

The authors declare no competing financial interest.

■ REFERENCES

(1) National Academy of Science, Institute of Medicine. *Dietary Reference Intakes for Vitamin A, Vitamin K, Arsenic, Boron, Chromium,*

DOI: 10.1021/jf503824t
J. Agric. Food Chem. 2015, 63, 1076−1081

Copper, Iodine, Iron, Manganese, Molybdenum, Nickel, Silicon, Vanadium, and Zinc; National Academy Press: Washington, DC, USA, 2001.
(2) Commonwealth of Australia. Nutrient Reference Values for Australia and New Zealand Including Recommended Dieatry Intakes; http://www.nrv.gov.au/nutrients/vitamin-K (Sept 9, 2005).
(3) Organization for Economic Cooperation and Development. *Revised Consensus Document on Compositional Considerations for New Varieties of Low Erucic Acid Rapeseed (Canola): Key Food and Feed Nutrients, Anti-Nutrients and Toxicants*; OECD: Paris, France, 2011.
(4) Piironen, V.; Kolvu, T.; Tammisalo, O.; Mattila, P. Determination of phylloquinone in oils, margarines and butter by high performance liquid chromatography with electrochemical detection. *Food Chem.* **1997**, *59*, 473−480.
(5) USDA-ARS, USDA Nutrient Database for Standard Reference, release 23.
(6) Marinova, M.; Lutjohann, D.; Westhofen, P.; Watzka, M.; Breuer, O.; Oldenburg, J. A validated HPLC method for the determination of vitamin K in human serum − first application in a pharmacological study. *Open Clin. Chem. J.* **2011**, *4*, 17−27.
(7) Blake, C. Status of methodology for the determination of fat-soluble vitamins in foods, dietary supplements, and vitamin premixes. *J. AOAC Int.* **2007**, *90* (4), 897−910.
(8) United States Pharmacopeia and National Formulary (USP/NF). *Oil Soluble Vitamins Capsules*; USP 24/NF 19; USP: Rockville, MD, USA, 2000; pp 2321−2322.
(9) AOAC International Official Method 992.27. *trans-Vitamin K_1 in Milk-Based Infant Formula, Liquid Chromatographic Method*; Association of Analytical Chemists International: Gaithersburg, MD, USA, 1995.
(10) Huang, B.; Zheng, F.; Fu, S.; Yao, J.; Tao, B.; Ren, Y. UPLC-ESI-MS/MS for determining *trans*- and *cis*-vitamin K_1 in infant formulas: method and applications. *Eur. Food Res. Technol.* **2012**, *235* (5), 873−879.
(11) Schimpf, K.; Thompson, L.; Schmitz, D. Determination of trans vitamin K_1 in infant and medical nutritional products using AOAC method 999.15 with modified preparation and extraction procedures and C-30 bonded phase chromatography: single-laboratory validation. *J. AOAC Int.* **2010**, *93* (2), 650−662.
(12) AOAC International Guidance Document. *AOAC Guidelines for Single Laboratory Validation of Chemical Methods for Dietary Supplements and Botanicals*; Association of Analytical Chemists International: Gaithersburg, MD, USA, 2002.
(13) Pritchard, F. Environmental effects on seed composition of Victorian canola. *Aust. J. Exp. Agric.* **2000**, *40* (5), 679−685.
(14) Hulbert, M.; Diaz, H. Water governance in Chile and Canada − a comparison of adaptive characteristics; http://www.adaptgov.com/wp-content/uploads/2102/03/Hulbert-Water-governance-Chile-and-Canada-A76-TAction.pdf, 2012.

DOI: 10.1021/jf503824t
J. Agric. Food Chem. 2015, 63, 1076−1081

In general, multiple metal ions, such as Na^+, K^+, Ca^{2+}, and Mg^{2+}, are considered to change some zymogens into active enzymes or accelerate the enzymatic reaction rate. Gibberellin, a type of plant hormone, controls many plant developmental processes, such as germination, growth, and flowering.[30,31] Many studies suggest that aleurone cells could synthesize and secrete a range of hydrolytic enzymes in response to exogenous gibberellin through initiating PCD.[32] This process of PCD can also be initiated by all types of reactive oxygen species (ROS) including hydrogen peroxide.[33−36] Moreover, our previous experiments and previous report[37] revealed that solid−liquid ratio, incubation temperature, and incubation time also have obvious effects on endogenous phytase activity and phytate content in wheat bran.

Hence, we attempted to evaluate the influence of solid−liquid ratio, incubation temperature, and incubation time in this study. Meanwhile, gibberellin and hydrogen peroxide were used to induce PCD and then activate endogenous phytase and reduce phytate level in wheat bran.

MATERIALS AND METHODS

Materials and Reagents. Wheat bran (Xinong 979, hard wheat, harvested in 2014 June, Henan, and stored for 2 months) was purchased from COFCO (Zhengzhou, China). Experiments were performed immediately after milling.

Phytic acid (>95%) was obtained from Sigma-Aladdin (Shanghai, China). Standard sodium phytate were obtained from Sangon Biotech Co., Ltd. (Shanghai, China). Other chemicals were of analytical grade unless stated otherwise.

Incubation. Wheat bran samples (1 g) were incubated in 1−6 mL of working solution of different gibberellin concentrations (0−5000 mg/L), different hydrogen peroxide concentrations (0−1.0%), and different metal ions (0.1 mol/L Na^+, K^+, Ca^{2+}, and Mg^{2+}) in beakers at 4, 20, 38, 55, and 70 °C for 360 min. After 30, 80, 180, and 360 min, the mixtures were used to determine endogenous phytase activity and phytate content. The levels of gibberellin concentration, hydrogen peroxide concentration, and metal ion were chosen according to the previous studies with some modifications.[38−41]

Phytic Acid. Phytic acid was measured according to the bipyridine colorimetric method reported by Buddrick and Jones et al.[23] Phytic acid was used as internal standard. All analyses were carried out in sextuplicate.

Phytase Activity. Phytase activity was measured by determination the inorganic orthophosphate released from the phytic acid by phytase. Standard phytase activity assay was performed at 37 °C according to the method of Huang.[42] Half a gram of wheat bran sample was mixed with 15 mL of acetate buffer A (20.52 g of anhydrous sodium acetate, 0.5 g of Triton X-100, and 0.5 g of bovine serum albumin in 1000 mL of distilled water, pH 5.5 ± 0.01), extracted for 15 min under ultrasonic treatment, and stirred with a magnetic stirrer for 30 min at room temperature. Then the mixture was centrifuged (centrifuge TGL-16G, Shanghai Anting Scientific Instrument Factory, Shanghai, China) at 5000*g* for 4 min. The supernatant (0.2 mL) was incubated at 37 °C with 1.8 mL of buffer A for 5 min and added to 4 mL of 7.5 mmol/L standard sodium phytate. After mixing, the solution was incubated at 37 °C for 30 min, and the enzyme reaction was stopped by the addition of 4 mL of 5% TCA. Inorganic phosphate (P_i) was determined colorimetrically.[43] Two hundred microliters of the resulting solution was added to 5 mL of acetate buffer B (20.52 g of anhydrous sodium acetate in 1000 mL of distilled water, pH 5.5 ± 0.01), 200 μL of 10% ascorbic acid, and 200 μL of 10% ammonium molybdate. Its absorbance was measured at 700 nm after 30 min by a SpectraMax M5Multifunctional microplate reader (Molecular Devices, Sunnyvale, CA, USA). All determinations were performed in sextuplicate. One unit of phytase activity (1 FTU) was defined as the amount of enzyme that liberates 1 μmol of orthophosphate per minute from phytate at 37 °C and pH 5.5.[44]

Optical Microscope Observations. The raw wheat bran and incubated wheat bran were stained with hematoxylin−eosin staining solution and iodine solution and rinsed with distilled water. The samples were subsequently observed with an optical microscope (Nikon, T1-SAM, Japan).

Statistical Analysis. All determinations were performed in sextuplicate. The data obtained are expressed as the mean ± standard deviation. The data obtained in this study were analyzed by one-way analysis of variance (ANOVA), and the differences among means were determined through Dunnet T3 test by using the software SPSS 16.0 for Windows. $p < 0.05$ was considered to be significant.

RESULTS AND DISCUSSION

Solid−Liquid Ratio. Endogenous phytase activity and phytate content of wheat bran samples under various solid−liquid ratios (1:1, 1:2, 1:3, and 1:6) at 55 °C during 360 min of incubation with distilled water are presented in Figure 1. The

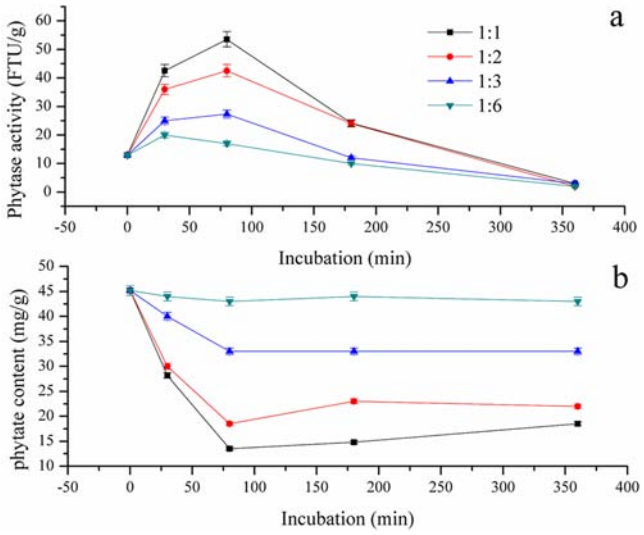

Figure 1. Effect of solid−liquid ratio (1:1, 1:2, 1:3, and 1:6) at 55 °C on endogenous phytase activity and phytate content of wheat bran samples: (a) effect of solid−liquid ratio on endogenous phytase activity; (b) effect of solid−liquid ratio on phytate content. Data values are based on sextuplicate measurements and shown as the mean ± SD.

results show that the solid−liquid ratio had an extremely significant ($p < 0.0001$) effect on endogenous phytase activity and phytate content of wheat bran, which respectively demonstrated an upward or a downward trend with the rising solid−liquid ratio. During incubation, every condition could obtain a better point with a maximum endogenous phytase activity (U^*) and a minimum phytate content (P^*). At high solid−liquid ratio (1:1), U^* (53.54 FTU/g) in wheat bran was higher than those incubated at the other lower solid−liquid ratios, which was about 4.13 times greater than raw material. U^* at solid−liquid ratios of 1:2, 1:3, and 1:6 were 3.28, 2.11, and 1.54 times, respectively, as high as raw material. In addition, P^* (13.52 mg/g) at a solid−liquid ratio of 1:1 was 29.91% of raw material, whereas at solid−liquid ratios of 1:2, 1:3, and 1:6 the values were 40.93, 70.01, and 95.13%, respectively.

Phytase was reported to be inactive in dry conditions, whereas it was activated in wet conditions to degrade phytate.[45] A moderate amount of water could well activate the endogenous phytase activity and reduce phytate, yet a high amount of water probably promoted aleurone cell swelling and rupturing to death. Therefore, a solid−liquid ratio of 1:1 was

DOI: 10.1021/jf504319t
J. Agric. Food Chem. 2015, 63, 1082−1087

selected in follow-up experiments. In addition, this ratio is favorable for subsequent drying.

Incubation Temperature. Endogenous phytase activity and phytate content of wheat bran samples under various temperatures (4, 20, 38, 55, and 70 °C) during 360 min of incubation with distilled water (solid−liquid ratio of 1:1) are shown in Figure 2. It could be found that there was a steadily

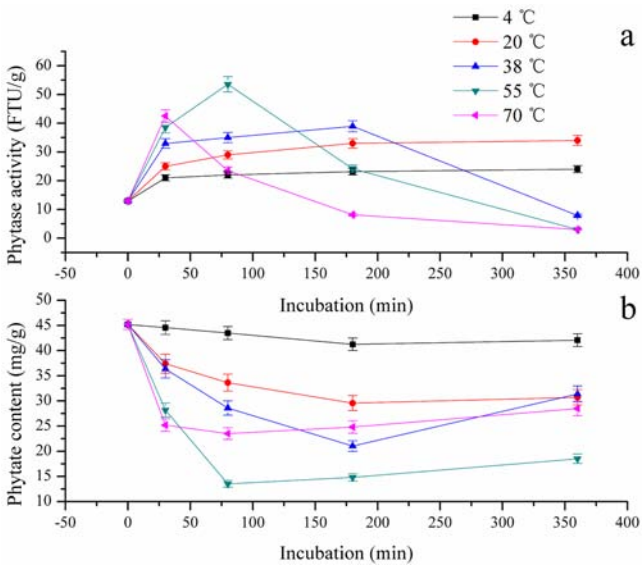

Figure 2. Effect of incubation temperature on endogenous phytase activity and phytate content of wheat bran samples: (a) effect of incubation temperature on endogenous phytase activity; (b) effect of incubation temperature on phytate content. Data values are based on sextuplicate measurements and shown as the mean ± SD.

increasing tendency of *U** from 4 °C (23.15 FTU/g) to 55 °C. However, at 70 °C, *U** revealed a sudden drop (42.51 FTU/g), only 79.40% of that at 55 °C but a little higher than that at 38 °C (38.92 FTU/g). *P**, as well, was extremely significantly ($p < 0.0001$) influenced by incubation temperature. When compared with raw wheat bran, *P** was decreased by 8.74% (41.25 mg/g), 34.60% (29.56 mg/g), 53.50% (21.02 mg/g), 70.09% (13.52 mg/g), and 47.96% (23.52 mg/g) at incubation temperatures of 4, 20, 38, 55, and 70 °C respectively, in comparison with that in raw wheat bran (45.20 mg/g). Obviously, higher incubation temperatures could decrease *P**, but extremely high incubation temperature (70 °C) induced a negative effect.

Appropriate increase in incubation temperature was helpful to promote phytase reaction in aleurone cells, but when the temperature was much higher than ambient temperature, aleurone cell vitality was subject to inhibition and a serious decline in endogenous phytase activity occurred. Loss of endogenous phytase activity at high temperature (70 °C) may be explained by conformational change and irreversible inactivation.[46]

Metal Ions. Four commonly used metal ion activators (Na^+, K^+, Ca^{2+}, and Mg^{2+}) were used to investigate their influence on endogenous phytase activity and phytate content in wheat bran samples during incubation at a solid−liquid ratio of 1:1 and 55 °C (Figure 3). Obviously, all of the metal ions had a negative impact on *U** and *P**. The most significant ($p < 0.0001$) factor was Mg^{2+} (*U**, 19.39 FTU/g; *P**, 39.20 mg/g), which when compared with raw wheat bran just increased the *U** by 49.58%, followed by Na^+ (78.34%), Ca^{2+} (82.19%), and K^+

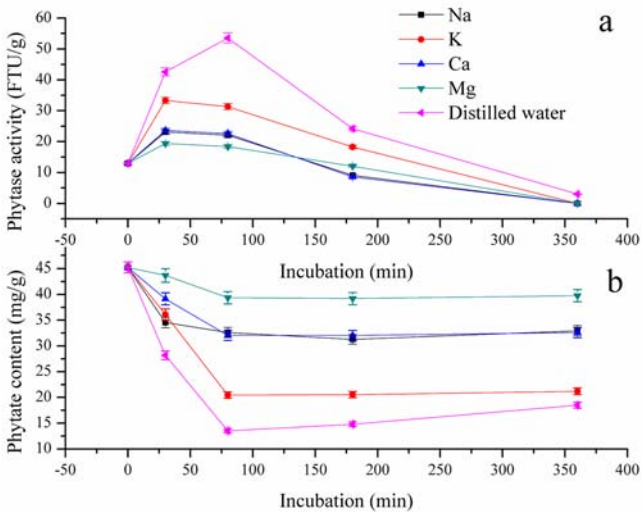

Figure 3. Effect of metal ions on endogenous phytase activity and phytate content of wheat bran samples: (a) effect of metal ions on endogenous phytase activity; (b) effect of metal ions on phytate content. Data values are based on sextuplicate measurements and shown as the mean ± SD.

(157.23%). Accordingly, it decreased the *P** by 13.27%, followed by Ca^+ (29.11%), Na^{2+} (30.78%), and K^+ (54.80%).

Phytate in wheat exists mainly in the form of phytin (calcium magnesium phytate). Thus, adding Ca^{2+} and Mg^{2+} would increase the concentration of enzymatic hydrolysates to inhibit the enzymatic reaction. Moreover, Ca^{2+} competed with phytate for the active site of endogenous phytase and inhibited its activity or formed Ca−phytate complexes that were insoluble and undegradable.[47] The results of this experiment are inconsistent with those from Zhang[48] and Yao,[41] in which the activity of β-propeller phytases (BPPs) were activated by a reasonable concentration of Ca^{2+}. This could be because BPPs were mainly from *Bacillus*, and their degradation mechanism was different from that of wheat endogenous phytase.

Gibberellin Concentration. Under the conditions of incubation temperature at 55 °C, a solid−liquid ratio of 1:1, and in the incubation solution, the effect of gibberellin concentration (0, 5, 50, 500, 2000, and 5000 mg/L) on the endogenous phytase activity and phytate content in wheat bran samples was measured, and the results are displayed in Figure 4. Generally, gibberellin was counterproductive on activation of endogenous phytase and phytate degradation. It was shown that gibberellin had little effect at low concentration (5 mg/L). However, with the increase of the concentration, the deleterious effect of gibberellin began to be revealed. When the gibberellin concentration was 50 and 500 mg/L, *U** fell to around 30 FTU/g and *P** rose to >40 mg/g. When the gibberellin concentration reached 2000 mg/L, *U** dropped to 20.60 FTU/g and *P** went up to 40.67 mg/g. When the gibberellin concentration reached 5000 mg/L, the results improved (*U** was 29.59 FTU/g, and *P** was 25.16 mg/g) but were still worse than those from incubation with distilled water.

Gibberellin was generally regarded as having positive effects on the PCD.[49] The barley aleurone layer and its protoplast treated by gibberellin would secrete large amounts of protease, nuclease, α-amylase, and other hydrolases.[50] However, our results indicated that secretion of endogenous phytase activity by aleurone had nothing to do with gibberellin's induction. This

DOI: 10.1021/jf504319t
J. Agric. Food Chem. 2015, 63, 1082−1087

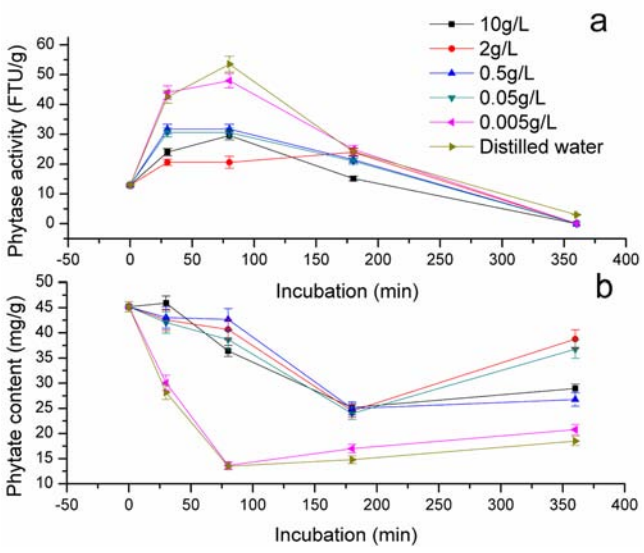

Figure 4. Effect of gibberellin concentration on endogenous phytase activity and phytate content of wheat bran samples: (a) effect of gibberellin concentration on endogenous phytase activity; (b) effect of gibberellin concentration on phytate content. Data values are based on sextuplicate measurements and shown as the mean ± SD.

may be because the main role of gibberellin was to awaken the dormant seed, whereas the selected raw material was fresh and had not yet entered the dormant period or generated adequate germination inhibitors. Thus, the aleurone cells were vital and could produce endogenous phytase by moderate water without gibberellin.[51]

Hydrogen Peroxide Concentration. Under the conditions of incubation temperature at 37 °C and a solid−liquid ratio of 1:1, the effect of hydrogen peroxide concentration (0, 0.2, 0.4, 0.6, 0.8, and 1.0%) on the endogenous phytase activity and phytate content in wheat bran samples was determined (Figure 5). It was found that the effect of hydrogen peroxide on

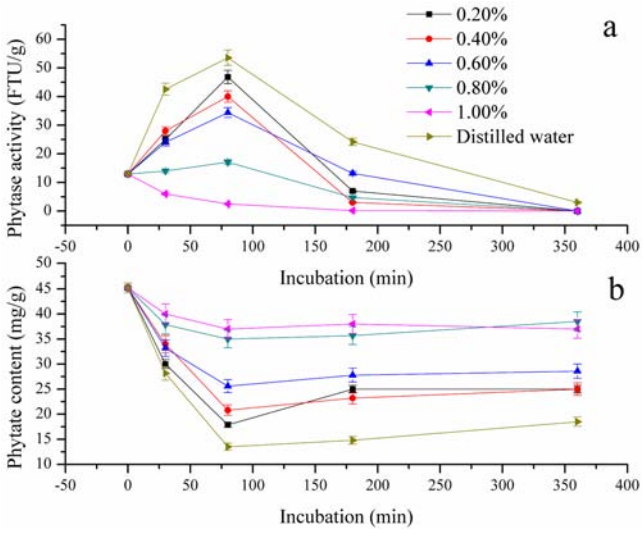

Figure 5. Effect of hydrogen peroxide concentration on endogenous phytase activity and phytate content of wheat bran samples: (a) effect of hydrogen peroxide concentration on endogenous phytase activity; (b) effect of hydrogen peroxide concentration on phytate content. Data values are based on sextuplicate measurements and shown as the mean ± SD.

U^* and P^* was significantly negative ($p < 0.0001$). With the rising hydrogen peroxide concentration, U^* gradually declined and P^* ascended when compared with distilled water. Notably, 1.0% hydrogen peroxide severely inhibited the phytase activity, which decreased rapidly to zero and induced almost no change in phytate content.

According to Golovina's report, reactive oxygen species (ROS) provided by moderate concentration of hydrogen peroxide could induce the PCD process,[52] whereas research carried out in this paper pointed the other way. This may be attributed to the selection of raw materials. In their previous study, wheat kernel was selected, whereas wheat bran was selected in this study.

Incubation Time. From Figures 1−5, it could be found that, in most cases, the endogenous phytase activity rose rapidly and reached the peak at about 80 min of incubation and then steadily declined to zero while the phytate content continuously decreased during the first 80 min of incubation and then slightly increased. The exceptions were the incubations at 4, 20, 38, and 70 °C or the incubation with 1.0% hydrogen peroxide. The lower the temperature was, the later the U^* and P^* occurred. In addition, a high concentration of hydrogen peroxide (1.0%) led to rapid inactivation of endogenous phytase; hence, phytate content had little change with the incubation time.

This study also highlighted that incubation time was a limiting factor for degradation of phytate in wheat bran during incubation. A short period of time might not achieve the peak of endogenous phytase secreted and synthesized by aleurone cells, and there was insufficient phytase in cells, whereas a long period of time would cause the enzyme activity to decrease gradually and lose its utilization value. Research showed that phytase in wheat belongs to 6-purple acid phosphatase (6-PAPhy) and its final enzyme hydrolysates are diphosinositide and phosphate,[53] which would not disturb results of phytate content by bipyridine colorimetric method.[54] Nevertheless, after 80 min of incubation and with the reduction of phytase activity, some substances such as IP3, IP4, and other complexes might be generated and would result in high phytate content.

Optical Microscope Observations. The photomicrographs of raw wheat bran sample and sample incubated with distilled water for 360 min at 55 °C are displayed in Figure 6. As shown in Figure 6a,b, the aleurone cell content had been stained crimson, whereas the cell walls were extremely thick and presented a transparent color. After incubation (Figure 6c−e), the aleurone cells almost disappeared (leaving only a thin layer of pink cell content and a thinner cell wall, Figure 6d), or aleurone cells disappeared completely (Figure 6e), where only neatly arranged long cylindrical transparent cells of intermediate layer were observed.

In cereal aleurone tissue, PCD preceded extensive vacuolation of PSVs. At the time of death, a highly vacuolated status occurred showing a single large vacuole occupied virtually all of the cytoplasm.[55] Then the cell wall became thinner or partial autolysis occurred, plasma membrane integrity was abruptly lost, and cellular autolysis occurred.[56,57] Although there was no vacuolization phenomenon found in this study, the incubated sample still indicated that the PCD and cell autolysis occurred in aleurone cells.

This work showed that endogenous phytase activity could be effectively activated to reduce phytate level in wheat bran during the process of activation for 80 min at 50 °C with a solid−liquid ratio of 1:1. Under this experimental condition,

DOI: 10.1021/jf504319t
J. Agric. Food Chem. 2015, 63, 1082−1087

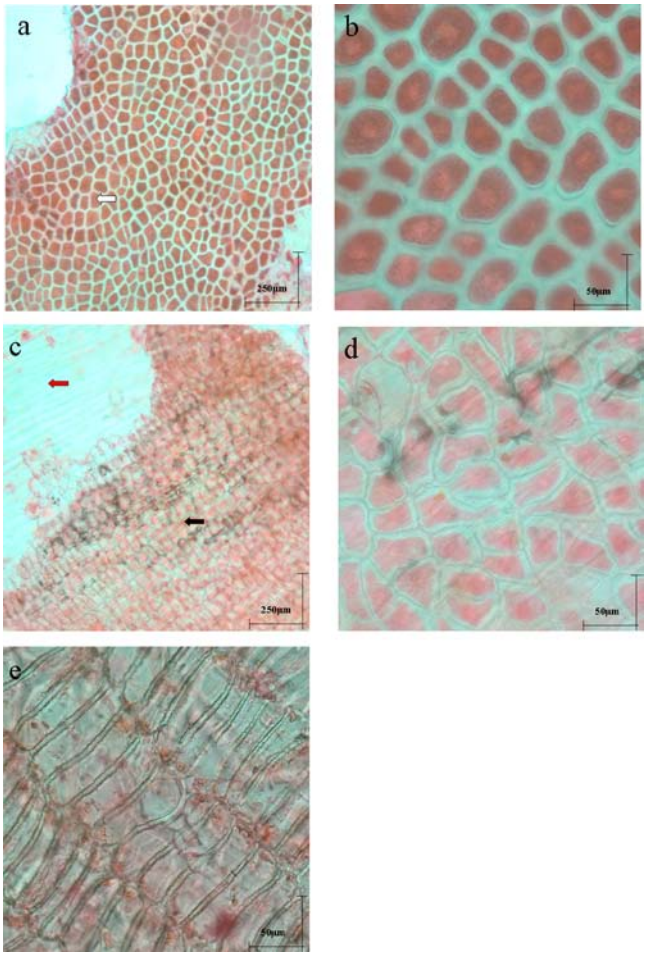

Figure 6. Photomicrographs of raw wheat bran sample and sample incubated with distilled water for 360 min at 55 °C: (a) raw wheat bran; (b) enlarged map of white arrow; (c) incubated sample; (d) enlarged map of black arrow; (e) enlarged map of red arrow.

gibberellin, hydrogen peroxide, and metal ions showed undesirable results. Compared with traditional phytate degradation, the method described in this paper is more effective, efficient, and suitable for industrial production.

AUTHOR INFORMATION

Corresponding Authors

*(K.-X.Z.) Phone/fax: +(86) 510 85329037. E-mail: kxzhu@jiangnan.edu.cn.

*(H.-M.Z.) Phone/fax: +(86) 510 85809610. E-mail: hmzhou@jiangnan.edu.cn.

Funding

This work was sponsored by Qing Lan Project, China Postdoctoral Science Foundation (Grant 2014M560396), Jiangsu Planned Projects for Postdoctoral Research Funds (Grant 1402072C), and the National Key Technology R&D Program (Grant 2012BAD34B01).

Notes

The authors declare no competing financial interest.

ACKNOWLEDGMENTS

We thank Dr. Ben-Guo Liu from Henan Institute of Science and Technology for his corrections.

REFERENCES

(1) Brown, L.; Rosner, B.; Willett, W. W.; Sacks, F. M. Cholesterol-lowering effects of dietary fiber: a meta-analysis. *Am. J. Clin. Nutr.* **1999**, *69*, 30−42.

(2) Keenan, J. M.; Pins, J. J.; Frazel, C.; Moran, A.; Turnquist, L. Oat ingestion reduces systolic and diastolic blood pressure in patients with mild or borderline hypertension: a pilot trial. *J. Fam. Practice* **2002**, *51*, 369−369.

(3) Anderson, J. W.; Randles, K. M.; Kendall, C. W. C.; Jenkins, D. J. A. Carbohydrate and fiber recommendations for individuals with diabetes: a quantitative assessment and meta-analysis of the evidence. *J. Am. Coll. Nutr.* **2004**, *23*, 5−17.

(4) Whelton, S. P.; Hyre, A. D.; Pedersen, B.; Yi, Y.; Whelton, P. K.; He, J. Effect of dietary fiber intake on blood pressure: a meta-analysis of randomized, controlled clinical trials. *J. Hypertens.* **2005**, *23*, 475−481.

(5) Montonen, J.; Knekt, P.; Jarvinen, R.; Aromaa, A.; Reunanen, A. Whole-grain and fiber intake and the incidence of type 2 diabetes. *Am. J. Clin. Nutr.* **2003**, *77*, 622−629.

(6) Lairon, D.; Arnault, N.; Bertrais, S.; Planells, R.; Clero, E.; Hercberg, S.; Boutron-Ruault, M. C. Dietary fiber intake and risk factors for cardiovascular disease in French adults. *Am. J. Clin. Nutr.* **2005**, *82*, 1185−1194.

(7) Steffen, L. M.; Jacobs, D. R.; Stevens, J.; Shahar, E.; Carithers, T.; Folsom, A. R. Associations of whole-grain, refined-grain, and fruit and vegetable consumption with risks of all-cause mortality and incident coronary artery disease and ischemic stroke: the atherosclerosis risk in communities (ARIC) study. *Am. J. Clin. Nutr.* **2003**, *78*, 383−390.

(8) Liu, S. M.; Stampfer, M. J.; Hu, F. B.; Giovannucci, E.; Rimm, E.; Manson, J. E.; Hennekens, C. H.; Willett, W. C. Whole-grain consumption and risk of coronary heart disease: results from the Nurses' Health Study. *Am. J. Clin. Nutr.* **1999**, *70*, 412−419.

(9) Petruzziello, L.; Iacopini, F.; Bulajic, M.; Shah, S.; Costamagna, G. Review article: uncomplicated diverticular disease of the colon. *Aliment. Pharmacol. Ther.* **2006**, *23*, 1379−1391.

(10) Rebello, C. J.; Greenway, F. L.; Finley, J. W. Whole grains and pulses: a comparison of the nutritional and health benefits. *J. Agric. Food Chem.* **2014**, *62*, 7029−7049.

(11) Dost, K.; Tokul, O. Determination of phytic acid in wheat and wheat products by reverse phase high performance liquid chromatography. *Anal. Chim. Acta* **2006**, *558*, 22−27.

(12) Hurrell, R. F.; Reddy, M. B.; Juillerat, M. A.; Cook, J. D. Degradation of phytic acid in cereal porridges improves iron absorption by human subjects. *Am. J. Clin. Nutr.* **2003**, *77*, 1213−1219.

(13) Guttieri, M. J.; Peterson, K. M.; Souza, E. J. Milling and baking quality of low phytic acid wheat. *Crop Sci.* **2006**, *46*, 2403−2408.

(14) Bohn, T.; Davidsson, L.; Walczyk, T.; Hurrell, R. F. Phytic acid added to white-wheat bread inhibits fractional apparent magnesium absorption in humans. *Am. J. Clin. Nutr.* **2004**, *79*, 418−423.

(15) Lin, L.; Ockenden, I.; Lott, J. N. A. The concentrations and distribution of phytic acid-phosphorus and other mineral nutrients in wild-type and low phytic acid 1-1 (lpa1-1) corn (*Zea mays* L.) grains and grain parts. *Can. J. Bot* **2005**, *83*, 131−141.

(16) Liu, B. L.; Rafiq, A.; Tzeng, Y. M.; Rob, A. The induction and characterization of phytase and beyond. *Enzyme Microb. Technol.* **1998**, *22*, 415−424.

(17) Mate, H.; Radomir, L. Phytic acid content of cereals and legumes and interaction with proteins. *Period. Polytech., Chem. Eng.* **2002**, *46*, 59−64.

(18) Isaksen, M. F. Phytic acid effect on endogenous α-amylase activity and starch degradation. *Poult. Sci.* **2006**, *85*, 179−180.

(19) Sharma, A.; Khetarpaul, N. Effect of fermentation on phytic acid content and in vitro digestibility of starch and protein of rice blackgram dhal whey blends. *J. Food Sci. Technol. (Mysore)* **1997**, *34*, 20−23.

(20) Khan, N.; Zaman, R.; Elahi, M. Effect of heat-treatments on the phytic acid content of maize products. *J. Sci. Food Agric.* **1991**, *54*, 153−156.

DOI: 10.1021/jf504319t
J. Agric. Food Chem. 2015, 63, 1082−1087

(21) Skoglund, E.; Larsen, T.; Sandberg, A. S. Comparison between steeping and pelleting a mixed diet at different calcium levels on phytate degradation in pigs. *Can. J. Anim Sci.* **1997**, *77*, 471−477.
(22) Egli, I.; Davidsson, L.; Juillerat, M. A.; Barclay, D.; Hurrell, R. F. The influence of soaking and germination on the phytase activity and phytic acid content of grains and seeds potentially useful for complementary feeding. *J. Food Sci.* **2002**, *67*, 3484−3488.
(23) Buddrick, O.; Jones, O. A. H.; Cornell, H. J.; Small, D. M. The influence of fermentation processes and cereal grains in wholegrain bread on reducing phytate content. *J. Cereal Sci.* **2014**, *59*, 3−8.
(24) Brejnholt, S. M.; Dionisio, G.; Glitsoe, V.; Skov, L. K.; Brinch-Pedersen, H. The degradation of phytate by microbial and wheat phytases is dependent on the phytate matrix and the phytase origin. *J. Sci. Food Agric.* **2011**, *91*, 1398−1405.
(25) Eeckhout, W.; Depaepe, M. Total phosphorus, phytate-phosphorus and phytase activity in plant feedstuffs. *Anim. Feed Sci. Technol.* **1994**, *47*, 19−29.
(26) Schlemmer, U.; Frolich, W.; Prieto, R. M.; Grases, F. Phytate in foods and significance for humans: food sources, intake, processing, bioavailability, protective role and analysis. *Mol. Nutr. Food Res.* **2009**, *53*, S330−S375.
(27) O'Dell, B. L.; Boland, A. R. D.; Koirtyohann, S. R. Distribution of phytate and nutritionally importantelements among the morphological components of cereal grains. *J. Agric. Food Chem.* **1972**, *20*, 718−723.
(28) Cheryan, M. Phytic acid interactions in food systems. *Crit. Rev. Food Sci. Nutr.* **1980**, *13*, 297−335.
(29) Swanson, S. J.; Jones, R. L. Gibberellic acid induces vacuolar acidification in barley aleurone. *Plant Cell* **1996**, *8*, 2211−2221.
(30) Olszewski, N.; Sun, T. P.; Gubler, F. Gibberellin signaling: biosynthesis, catabolism, and response pathways. *Plant Cell* **2002**, *14*, S61−S80.
(31) Sun, T. P.; Gubler, F. Molecular mechanism of gibberellin signaling in plants. *Annu. Rev. Plant Biol.* **2004**, *55*, 197−223.
(32) Mrva, K.; Wallwork, M.; Mares, D. J. α-Amylase and programmed cell death in aleurone of ripening wheat grains. *J. Exp. Bot.* **2006**, *57*, 877−885.
(33) Vranova, E.; Atichartpongkul, S.; Villarroel, R.; Van Montagu, M.; Inze, D.; Van Camp, W. Comprehensive analysis of gene expression in Nicotiana tabacum leaves acclimated to oxidative stress. *Proc. Natl. Acad. Sci. U.S.A.* **2002**, *99*, 10870−10875.
(34) op den Camp, R. G. L.; Przybyla, D.; Ochsenbein, C.; Laloi, C.; Kim, C. H.; Danon, A.; Wagner, D.; Hideg, E.; Gobel, C.; Feussner, I.; Nater, M.; Apel, K. Rapid induction of distinct stress responses after the release of singlet oxygen in arabidopsis. *Plant Cell* **2003**, *15*, 2320−2332.
(35) Dat, J. F.; Pellinen, R.; Beeckman, T.; Van de Cotte, B.; Langebartels, C.; Kangasjarvi, J.; Inze, D.; Van Breusegem, F. Changes in hydrogen peroxide homeostasis trigger an active cell death process in tobacco. *Plant J.* **2003**, *33*, 621−632.
(36) Gechev, T. S.; Van Breusegem, F.; Stone, J. M.; Denev, I.; Laloi, C. Reactive oxygen species as signals that modulate plant stress responses and programmed cell death. *Bioessays* **2006**, *28*, 1091−1101.
(37) Esmaeilipour, O.; Van Krimpen, M. M.; Jongbloed, A. W.; De Jonge, L. H.; Bikker, P. The effects of temperature, moisture, duration of incubation time, calcium level, and soaking with water or citric acid on in vitro phytate degradation in a wheat-barley-rye-soybean meal-based diet. *Anim. Feed Sci. Technol.* **2013**, *183*, 168−174.
(38) Ishibashi, Y.; Tawaratsumida, T.; Kondo, K.; Kasa, S.; Sakamoto, M.; Aoki, N.; Zheng, S. H.; Yuasa, T.; Iwaya-Inoue, M. Reactive oxygen species are involved in gibberellin/abscisic acid signaling in barley aleurone cells. *Plant Physiol.* **2012**, *158*, 1705−1714.
(39) Kondhare, K. R.; Kettlewell, P. S.; Farrell, A. D.; Hedden, P.; Monaghan, J. M. Effects of exogenous abscisic acid and gibberellic acid on pre-maturity α-amylase formation in wheat grains. *Euphytica* **2012**, *188*, 51−60.
(40) Zhang, Z. L.; Shin, M.; Zou, X.; Huang, J.; Ho, T. H. D.; Shen, Q. J. A negative regulator encoded by a rice WRKY gene represses both abscisic acid and gibberellins signaling in aleurone cells. *Plant Mol. Biol.* **2009**, *70*, 139−151.
(41) Yao, M. Z.; Lu, W. L.; Chen, T. G.; Wang, W.; Fu, Y. J.; Yang, B. S.; Liang, A. H. Effect of metals ions on thermostable alkaline phytase from *Bacillus subtilis* YCJS isolated from soybean rhizosphere soil. *Ann. Microbiol.* **2014**, *64*, 1123−1131.
(42) Huang, H.; Luo, H.; Wang, Y.; Fu, D.; Shao, N.; Wang, G.; Yang, P.; Yao, B. A novel phytase from Yersinia rohdei with high phytate hydrolysis activity under low pH and strong pepsin conditions. *Appl. Microbiol. Biotechnol.* **2008**, *80*, 417−426.
(43) Rodriguez, J. B.; Self, J. R.; Soltanpour, P. N. Optimal conditions for phosphorus analysis by the ascorbic acid-molybdenum blue method. *Soil Sci. Soc. Am. J.* **1994**, *58*, 866−870.
(44) Esmaeilipour, O.; Van Krimpen, M. M.; Jongbloed, A. W.; De Jonge, L. H.; Bikker, P. Effects of temperature, pH, incubation time and pepsin concentration on the in vitro stability of intrinsic phytase of wheat, barley and rye. *Anim. Feed Sci. Technol.* **2012**, *175*, 168−174.
(45) Blaabjerg, K.; Poulsen, H. D. Microbial phytase and liquid feeding increase phytate degradation in the gastrointestinal tract of growing pigs. *Livest Sci.* **2010**, *134*, 88−90.
(46) Wyss, M.; Pasamontes, L.; Remy, R.; Kohler, J.; Kusznir, E.; Gadient, M.; Muller, F.; van Loon, A. Comparison of the thermostability properties of three acid phosphatases from molds: *Aspergillus fumigatus* phytase, *A. niger* phytase, and *A. niger* pH 2.5 acid phosphatase. *Appl. Environ. Microbiol.* **1998**, *64*, 4446−4451.
(47) Zyla, K. Phytase applications in poultry feeding: selected issues. *J. Anim. Feed Sci.* **2001**, *10*, 247−258.
(48) Zhang, R.; Yang, P.; Huang, H.; Yuan, T.; Shi, P.; Meng, K.; Yao, B. Molecular and biochemical characterization of a new alkaline β-propeller phytase from the insect symbiotic bacterium *Janthinobacterium* sp TN115. *Appl. Microbiol. Biotechnol.* **2011**, *92*, 317−325.
(49) Pennell, R. I.; Lamb, C. Programmed cell death in plants. *Plant Cell* **1997**, *9*, 1157−1168.
(50) Jones, R. L.; Jacobsen, J. V. Regulation of synthesis and transport of secreted protein in cereal aleurone. *Int. Rev. Cytol.* **1991**, *126*, 49−88.
(51) Evenari, M. Germination inhibitors. *Bot Rev.* **1949**, *15*, 153−194.
(52) Golovina, E. A.; Hoekstra, F. A.; van Aelst, A. C. Programmed cell death or desiccation tolerance: two possible routes for wheat endosperm cells. *Seed Sci. Res.* **2000**, *10*, 365−379.
(53) Schlemmer, U.; Jany, K. D.; Berk, A.; Schulz, E.; Rechkemmer, G. Degradation of phytate in the gut of pigs − pathway of gastrointestinal inositol phosphate hydrolysis and enzymes involved. *Arch. Anim. Nutr.* **2001**, *55*, 255−280.
(54) Sandberg, A.; Carlsson, N.; Svanberg, U. Effects of inositol tri-, tetra-, penta-, and hexaphosphates on in vitro estimation of iron availability. *J. Food Sci.* **1989**, *54*, 159−161.
(55) Bethke, P. C.; Lonsdale, J. E.; Fath, A.; Jones, R. L. Hormonally regulated programmed cell death in barley aleurone cells. *Plant Cell* **1999**, *11*, 1033−1045.
(56) Fath, A.; Bethke, P. C.; Jones, R. L. Barley aleurone cell death is not apoptotic: characterization of nuclease activities and DNA degradation. *Plant J.* **1999**, *20*, 305−315.
(57) Fath, A.; Bethke, P.; Lonsdale, J.; Meza-Romero, R.; Jones, R. Programmed cell death in cereal aleurone. *Plant Mol. Biol.* **2000**, *44*, 255−266.

DOI: 10.1021/jf504319t
J. Agric. Food Chem. 2015, 63, 1082−1087

components and the absorption of light in the infrared region.[27−29]

Ultraviolet−visible (UV−vis) spectroscopy relies on the detection of pi bonding and conjugated double bonds, so the predominant wine matrix does not have a significant signal, although the UV−vis portion of the electromagnetic spectrum contains valuable information regarding phenolic compounds where absorbance features are generated at specific regions. Garcia-Jares and Medina[30] applied UV−vis chemometrics methods in enological research. Despite the limitations of the analytical methods, related to a lack of selectivity,[8,9,31] such as the colorimetric assay used for tannin quantification, and the small sample set (n = 34), the results demonstrated the potential of this technique to predict tannins in red wine.[30] Other authors[32] applied partial least-squares regression (PLS) to the UV−vis spectra of 200 wines at various stages of fermentation. The development and validation of an ultraviolet spectral calibration for the rapid and robust prediction of wine tannin concentration was reported by Dambergs et al.[33] The authors used multiple linear regression (MLR) due its suitability to transfer calibration models between different instruments by means of slope and bias adjustment. The ability to objectively measure wine quality, in which wine tannins play a critical role, is an important requirement for the production of competitively priced high-quality wines by the South African wine industry. Little research has been done on tannin levels in a wide range of South African red wines, including those from different vintages and cultivars and produced on a commercial or experimental scale. It is difficult to compare tannin data from wines elaborated differently, due to the great impact that different locations and/or winemaking techniques have on final tannin concentration. The aim of this work was first to investigate the application of multivariate methods to the UV−vis spectra of South African red wine samples to develop predictive models for determining tannins over a wide range of grape cultivars, growing regions, and vintages. The second aim was to demonstrate the robustness of calibration models across different cultivars and vintages and between commercial and experimental wines to predict tannin concentration. BSA and MCP tannin assays were selected as the reference analytical methods, because they have proven to be robust procedures.[3,4,15,17,34] There also is a lack of studies dealing with PLS calibrations comparing two different wine tannin reference methods (BSA and MCP) and testing the robustness of the tannin concentration prediction by UV−vis spectroscopy in wines.

MATERIALS AND METHODS

Sample Collection. Two hundred and forty South African wine samples were used, including Cabernet Sauvignon (n = 49), Shiraz (60), Merlot (46), Pinotage (13), Sangiovese (5), Nebbiolo (1), Carmenere (2), Pinot Noir (3), Grenache Noir (2), Ruby Cabernet (9), Tempranillo (3), Tinta Barroca (1), Tinta Amarella (2), Monastrell (4), Barbera (1), Durif (4), and some blends (37), ranging in vintage from 2000 to 2012. Samples were from small-lot experimental fermentation trials (n = 121) ,elaborated in the experimental cellar of the Department of Viticulture and Oenology (DVO) at Stellenbosch University, and commercial, bottled wines (n = 119). The sample set was performed with wines from regions having diverse climates and soil types.

Spectral Data Collection. Wine samples were 51-fold diluted in 1 M HCl (Merck, Darmstadt, Germany) (100 μL of sample plus 5 mL of 1 M HCl). The diluted samples were incubated for 1 h in the dark at room temperature and then scanned in an Analytic Jena Specord 50 UV−vis spectrophotometer (Jena, Germany), using a 10 mm path length quartz cuvette, with 1 M HCl as the reference blank. Wine samples were scanned without temperature equilibration at 2 nm intervals over the wavelength range from 200 to 700 nm, therefore yielding 250 data points per spectrum.

Methylcellulose Precipitable Tannin Assay.[4,17] Methylcellulose solution (0.04% w/v; 1500 cP viscosity at 2%) was prepared in accordance with the manufacturer's instructions. Considering the expected high tannin concentration of some samples and with the aim of fitting the absorbance values within the working range (0.1−1.2 AU) for the spectrophotometer used in this study, a modified protocol of the MCP tannin assay was performed on wines using a 2 mL format. In a 2 mL microfuge tube, 600 μL of methylcellulose solution (Sigma-Aldrich Chemie, Steinheim, Germany) was mixed with 50 μL of wine diluted twice (25 μL of wine sample + 25 μL of distilled water), and the tube was capped, inverted several times, and allowed to stand for 2−3 min. Following the addition of 400 μL of saturated ammonium sulfate solution (Merck), the samples were made up to a final volume of 2 mL with distilled water (950 μL). Samples were after 10 min centrifuged at 9279g for 5 min (treatment sample). The same wine solution volume was added to the control sample. Following the addition of 400 μL of saturated ammonium sulfate solution, the sample was made up to final volume with distilled water (1550 μL), mixed, and allowed to stand for 10 min at room temperature before centrifugation. The difference in the A_{280} value obtained by subtracting the A_{280} value of the MCP treated sample from the control A_{280} sample was converted into epicatechin equivalents (mg/L) using a calibration curve (Sigma-Aldrich Chemie). The wine sample had a dilution factor of 80. The wine dilution effect was investigated with the analysis of eight different undiluted and twice-diluted red wine samples. The results showed a small effect of wine dilution on tannin concentration, with diluted samples having slightly higher concentrations. The twice-diluted protocol was therefore used throughout the study after observing that no underestimation of tannin concentration was obtained.

Bovine Serum Albumin Tannin Assay.[18] Wines were diluted twice, three times, and five times, respectively, in a model wine solution of 12% v/v ethanol containing 5 g/L tartaric acid that had been adjusted to pH 3.3 with HCl. The tannin protein precipitate was formed by mixing 0.5 mL of diluted wine and 1 mL of BSA solution (containing 1 mg BSA/mL dissolved in a buffer of aqueous 0.2 M acetic acid and 0.17 M sodium chloride adjusted to pH 4.9 with sodium hydroxide) for 15 min. The precipitate was centrifuged for 5 min at 18188g to form a pellet, and the supernatant was discarded. The pellet was washed twice with 1 mL of the pH 4.9 buffer. After the addition of 0.25 mL of the pH 4.9 buffer to wash the pellet a third time, samples were centrifuged for 1 min at 18188g. The rinsed pellet was redissolved in 0.875 mL of buffer (containing 5% w/v SDS and 5% v/v triethanolamine and adjusted to pH 9.4 with sodium hydroxide). The background (A^{back}) of 0.875 mL redissolved solution was measured in the spectrophotometer at 510 nm and was subsequently mixed with 0.125 mL of ferric chloride solution (10 mM ferric chloride in 10 mM aqueous HCl). The final absorbance at 510 nm (A^{FeCl3}) was measured after 10 min, and the tannin response was calculated as the background absorbance minus 0.875 times the final absorbance. Tannin responses between 0.3 and 0.75 were selected for the different dilutions, as suggested by Jensen et al.,[34] and the tannin concentration was calculated and expressed as milligrams of catechin (Sigma-Aldrich Chemie) equivalents.

Data Analysis. Chemometric analysis was performed using SIMCA version 13.0.3 software (www.umetrics.com). Principal component analysis (PCA) was performed before the PLS regression models were developed. PCA describes the maximal quantity of information present in the data set using a small number of latent variables.[35] Possible sample groupings and outlier visualization were the main aims in applying this technique. Analysis of variance (ANOVA) and coefficient of variation (CV) were also determined to study the variability present in the data set. High variability in the data set means that the data are suitable for PLS calibrations.[36] Calibrations were developed using partial least-squares (PLS) regression with leave-one-out cross-validation. In this way, one object of the training set is removed and a PLS model is built with the remaining objects, and then this model is used to predict the removed object.[37,38]

DOI: 10.1021/jf503412t
J. Agric. Food Chem. 2015, 63, 1088−1098

Of the overall sample set, 50% (n = 120) were used for cross-validation as calibration set, whereas the remaining 50% were used as external validation set. Selection of both the calibration and validation set was performed randomly. Moreover, to develop robust models and to test the effect of seasonal, cultivar, and winemaking (commercial vs experimental) variations on model performance, calibration models were developed on samples from each cultivar or vintage and used further to predict samples from the other remaining cultivars or vintage years. The ability of the tannin concentration of a single variable (single cultivar or year) to be predicted by the model was also determined (ability of the tannin concentration of the cultivar or year to be predicted by the model). The same approach was tested using the classifying variable experimental versus commercial wines. Calibrations for the tannins were developed using various combinations of the data set.

Statistics calculated for the calibrations included the coefficient of determination in calibration (R^2cal), the root mean standard error in cross-validation (RMSECV), the root mean standard error of prediction (RMSEP), and the coefficient of correlation in validation (R^2val). R^2cal estimates the percentage of variation in the training set explained by the model. It is a measure of how well the model fits the data. A large R^2 (close to 1) is a necessary requirement for a good model, but this alone is not sufficient. Poor models can be achieved (models that cannot predict) even with a large R^2cal. Poor R^2cal could be obtained when there is poor reproducibility (much noise) in the training data set or when the spectral information does not explain the chemistry for other reasons.

The RMSECV indicates the fit of the observations to the model estimated using the cross-validation procedure and is a measure of the average difference between the values determined by MCP or BSA and those predicted by the model. It provides an indication of the potential error associated with the future predictions of samples not included in the calibration set. RMSECV is expressed in the same units as the reference values and is influenced by the range of tannin concentrations. R^2val is the percent of variation of the validation set explained by the model. Moreover, the RMSEP, which is also influenced by the reference values range, is a measure of the average difference between the values predicted by the model and values determined by the laboratory method during independent validation of the model (average prediction error).[32] To counteract the effect of range in the RMSEP, the residual predictive deviation (RPD = SD/RMSEP) is used to standardize the predictive accuracy. RPD is defined as the ratio of the standard deviation of the population and the root-mean-square error of prediction. If the RMSEP is large compared to the spread of tannin concentration in all samples (SD), a relatively small RPD is achieved. This means that the model is not able to predict variability. The higher the RPD, the greater the probability of the model to predict chemical composition in samples outside the calibration set.

RESULTS

Reference Values. The tannin concentrations reported here are presented with the aim to compare the analytical methods, although the reported levels may be of interest, as some cultivars have not previously been analyzed for tannin content in South Africa. The data presented here thus offer the first indication of the range of tannin values in South African red wines that might be observed using the MCP and BSA methods (Figure 1). However, the values should be considered indicative, as the wines came from diverse origins, spanned a variety of climates and soil types, and also differed in the winemaking procedure. As has been reported by other authors,[39] a wide range of concentrations was observed for tannin concentrations in both tannin assays. This strengthens the idea that tannin concentration should be considered with caution, as tannin values might differ from site to site, even for the same variety.

ANOVA showed that MCP and BSA varied significantly (p < 0.001) in relation to the classifying variables: variety, commercial/experimental, and vintage for BSA (Table 1).

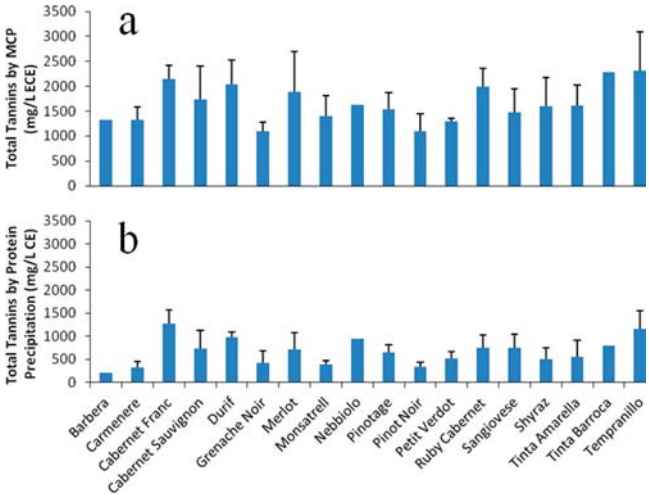

Figure 1. Total tannin levels of the 18 different grape cultivars analyzed, showing standard error bars: (a) tannins determined by methylcellulose precipitation calibrated against an epicatechin standard curve and expressed as mg/L; (b) tannins determined by protein precipitation (BSA) and expressed as mg/L catechin equivalents. The absence of error bars means that only one sample was available.

Significant variation also existed for the variable vintage (p < 0.05) when MCP was used as reference method. It was observed that tannin concentration was affected the most by the experimental/commercial classifying variable (Table 1). Harberston et al.[40] reported exceptional variability in the tannin concentration of commercial wines and stated that winemaking techniques play a critical role in wine tannin levels. A huge overlap in tannin concentrations between populations has also been reported, in agreement with the results observed in our study.

Table 1. ANOVA (ANOVA, F Ratio, and p Values) for MCP and BSA in Relation to Variety, Vintage, and Commercial/Experimental Wines

variable	factor	F ratio	p
MCP	variety	2.74	<0.001
	vintage	2.42	0.0123
	commercial/exptl	73.45	<0.001
BSA	variety	3.75	<0.001
	vintage	6.46	<0.001
	commercial/exptl	52.43	<0.001

Table 2 shows the mean, minimum, maximum, standard deviation, and coefficient of variation of the wines' tannin levels as determined by the reference methods. Tannin levels determined by protein precipitation ranged from 0.05 to 1.72 g/L. The mean of tannins determined by protein precipitation across all samples was 0.62 g/L (%CV = 52.63). The average level of tannins determined by methylcellulose precipitation was 1.64 g/L. The range of tannin values observed was between 0.31 and 3.21 g/L (%CV = 35.56). Although the CV in the samples analyzed by MCP was in accordance with the literature (35.5 vs 37.8%), higher CV values were found in BSA-analyzed samples regarding the study published by Seddon and Downey (52.63 vs 30.5%), even though the analysis was performed in skin grape samples instead of wine.[41] A higher coefficient of variation can also be considered as a source of variability in the tannin

DOI: 10.1021/jf503412t
J. Agric. Food Chem. 2015, 63, 1088−1098

Table 2. Summary Statistics of MCP (g/L Epicatechin Equivalents) and BSA (g/L Catechin Equivalents) Measured in Wines in the Raw Data Set and in both Calibration and Validation Sets[a]

variable	set	N	mean	SD	min	max	CV
MCP	full data	240	1.64	0.58	0.31	3.21	35.56
	calibration	120	1.67	0.60	0.37	3.20	35.88
	validation	120	1.61	0.56	0.31	3.21	34.97
BSA	full data	235	0.62	0.33	0.05	1.72	52.63
	calibration	118	0.65	0.34	0.05	1.72	53.26
	validation	117	0.60	0.31	0.07	1.70	51.32

[a]*N*, number of samples; SD, standard deviation; min, minimum; max, maximum; CV, coefficient of variation.

concentrations of the sample set. The variability in the concentration of tannins in the analyzed samples was considered suitable for developing PLS calibration.

Linear regression analysis showed a good correlation (R^2 = 0.79) between the two tannin quantification techniques for 240 wine samples (Figure 2). The results are similar to those found by

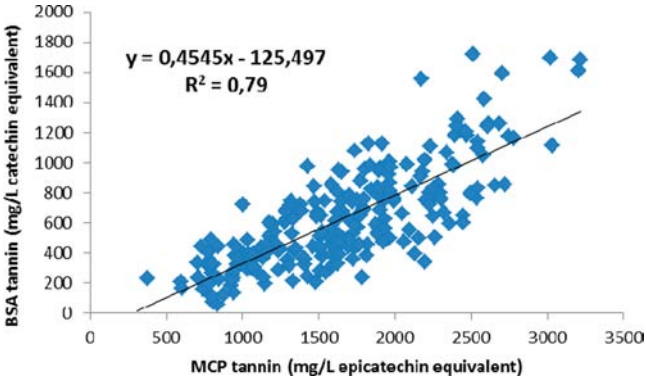

Figure 2. Linear regression analysis of wine tannin concentration determined using the MCP and BSA tannin assays (n = 240).

Mercurio and Smith[16] when 41 wine samples were analyzed by both methods (R^2 = 0.8). MCP and BSA tannin assays showed a slope of 0.45, indicating an almost 2.5-fold difference in tannin concentration. Moreover, the intercept of the line is not close to zero (−125.497), revealing that both methods are not measuring a similar amount of tannin material in the sample. The x-axis intercept of the line is relatively large, showing that the MCP tannin assay was measuring more tannin material, which is in accordance with Mercurio and Smith.[16]

Contradictory results are reported in the literature regarding the magnitude of the tannin concentration determined using both protein and polymer precipitation methods. Mercurio and Smith,[16] in accordance with the results reported here, observed approximately 3-fold higher tannin levels when using the MCP tannin assay in both grape and wine samples. On the other hand, other authors have stated the same magnitude for both analytical procedures in grape skin samples, but lower values were observed for the MCP tannin assay.[41] Furthermore, Harberston and Downey[39] also found lower tannin levels in grape skin and wine samples when the tannin precipitation was carried out with methylcellulose. The variation of the MCP method described by Mercurio et al.,[17] who reported that the methylcellulose concentration used by Sarneckis et al.[4] was suboptimal, may account for the differences in the results observed.

Moreover, the detection step has been proposed in the literature as a key factor that might explain the differences observed in tannin levels when using the two reference methods. The BSA precipitation method involves absorbance at 510 nm after the reaction of precipitated tannins with iron, whereas the MCP tannin assay measures the tannin concentration at 280 nm after precipitation with methylcellulose. Even though both precipitants might not be reacting with the same tannins, it is nowadays widely accepted that they both precipitate the same amount of tannin material.[16,39] Therefore, the detection step rather than the tannin precipitation appears as a crucial factor that could account for the observed differences. At this stage the exact type of tannins precipitated by BSA and MC is not well-known; further work in this area is required with the aim to fully understand the observed differences in tannin values.

The presence of some samples in the higher BSA concentration range that do not fit the regression curve should be highlighted. The spectra of some of the samples farther away from the regression curve were compared with those samples with similar MCP tannin concentrations but that did fit the regression curve, that is, were placed on or close to the regression curve. No differences were observed in the spectra of those samples in the region around 280 nm (the region where tannins show their absorbance features), although higher spectrum values were observed in the region around 520 nm, which corresponds to anthocyanins and polymeric pigments (Figure 3).

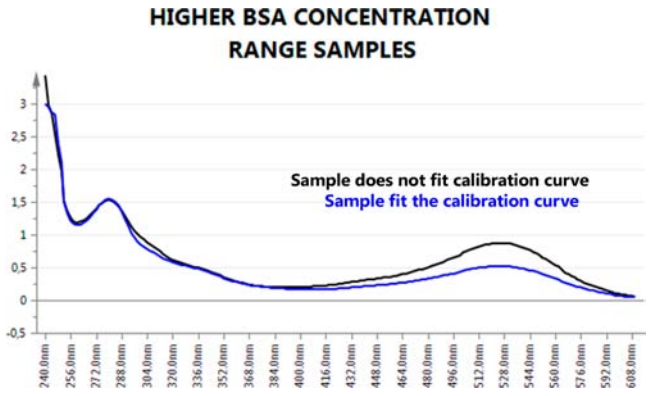

Figure 3. UV−vis spectra comparing a sample that does not fit the calibration curve (black) with a sample that fits the regression curve (blue).

The latter phenomenon of samples deviating at high concentrations could be explained by the inability of the MCP polymer to completely react and precipitate all of the polymeric pigment material in samples containing high levels of these compounds. However, Mercurio and Smith[16] stated that the MCP polymer is able to precipitate all tannins and polymeric pigments, whereas the BSA protein is not. It would seem that the portion of tannins not removed by BSA is representative of small polymeric pigments (SPP).[3] It remains unclear whether the ability to quantify these compounds is related to tannin size or whether other factors, such as difference in detection methods, might also have an effect on tannin quantification.[3] The contradictory results observed lead us to consider the hypothesis of suboptimal concentration, that is, the inability of the MCP to react with all of the polymeric pigments in samples very rich in these compounds.

Descriptive analysis showed that data on both measured tannin parameters (BSA and MCP) were normally distributed

DOI: 10.1021/jf503412t
J. Agric. Food Chem. 2015, 63, 1088−1098

around the mean, as indicated by the skewness. Normally distributed data should have skewness values ranging from −1 to +1, with the absolute of this statistical parameter as close to 0 as possible.[42] MCP and BSA tannin concentrations showed skewness values of 0.224 and 0.915, respectively, which are within the accepted range. Bellon-Maurel et al.[43] stated that RDP values can be affected in highly skewed sample sets because this parameter was developed for data sets showing normal distribution.

Principal Component Analysis. A preliminary study of the information contained in the spectral data set was carried out to detect possible sample grouping and to identify the presence of outliers. To this end, a principal component analysis (PCA-X) of the recorded spectra (260−610 nm) was used to describe the maximal quantity of information present in the data set using a small number of variables (principal components). The information contained in the data set reveals that two principal components explained 94.7% of the spectral variation of the samples (71.8% PC1, 23.9% PC2). No outliers were observed in the score plot (PC1 vs PC2) of the wine samples analyzed using UV−vis spectra. Moreover, PCA of the UV−vis spectra of the wine samples indicates that the variables vintage, variety, and experimental/commercial wines had no clustering effect on the data set. The absence of clustering supports the suitability of the UV−vis calibration for the measurement of tannins (results not shown). On the other hand, it is worth mentioning that a clear sample differentiation appeared in the PCA plot for the variables vintage and commercial/experimental wines (Figure 4).

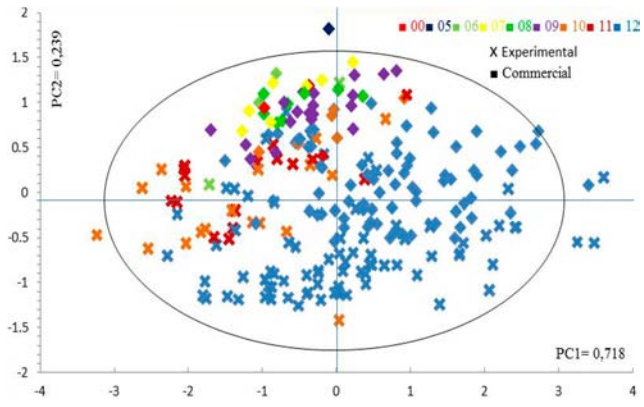

Figure 4. Principal component analyses of the UV−vis spectra of the analyzed wines classified by vintage year and commercial versus experimental wines.

Figure 4 shows the PCA plot for the wine samples identified by vintage (year). Wines included in the study ranged in vintage from 2000 to 2012. Wines elaborated in 2012 are located mostly in the lower right side of the graph, whereas the wines made from older vintages are placed mostly in the upper left side of the graph. The distribution observed in the PCA plot could probably be explained by differences in the phenolic composition, mainly anthocyanin and tannin, of the younger wines compared with that of the older wines. A great number of reactions involving phenolic compounds take place during wine aging. Oxidation and nucleophilic addition reactions, polycondensation with aldehydes, conversion of anthocyanins to pyranoanthocyanins, direct flavan-3-ol anthocyanin reactions, and other nucleophilic addition reactions have been reported in the literature.[44,45] The above-mentioned reactions are responsible for the organoleptic changes observed during wine aging, therefore playing an important role in the color and mouthfeel properties of wines.[46,47] Samples seem to be affected by both first and second components, explaining (PC1 and PC2) 95.7% of the variance. Young samples were positively correlated with PC1, although negatively correlated with PC2. On the other hand, samples of older wine vintages showed the opposite behavior, that is, appear positively correlated with PC2 and negatively correlated with PC1.

Furthermore, the separation of two groups also appeared in the PCA plot when the samples were classified according to commercial or experimental wines (Figure 4). Experimental wines appear in the lower part of the graph, whereas the commercially available wines are placed in the upper part. In this case, samples seem to be influenced more by PC2, where commercial and experimental wines are positively and negatively correlated, respectively. These differences might be due to the effect of winemaking techniques on the phenolic and tannin composition.

As far as we know, very little literature is available on the effect of fermentations at different scales on phenolic composition. It thus is not possible to explain at this stage whether the experimental vinifications carried out at smaller scale had a considerable effect on the phenolic composition. On the other hand, the well-known effect that wood aging and/or oxygen exposure have on phenolic and tannin composition could also explain the differences observed. Moreover, the fact that some of the wines elaborated on the experimental scale did not complete malolactic fermentation (MLF) might also explain some of the observed differences. Some studies have reported the effect of MLF on non-anthocyanin phenolic compounds and found an important decrease in the concentration of hydroxycinnamic acids and an increase in the concentrations of the free forms of caffeic, *p*-coumaric, and ferulic acids,[48] compounds that can act as copigments.[49−53] MLF therefore may influence wine color and phenolic composition.[54] MLF also leads to an increase in pH of between 0.1 and 0.45 unit in wine,[55] leading to subsequent changes in wine color. A decrease in the wine color and anthocyanin concentration takes place during MLF,[56] which could partially explain, together with the mentioned effect of the MLF on the non-anthocyanin phenolic compounds, the different locations of the experimental and commercial wines in the PCA plot.

Analysis of Loadings Plot. The influence of each wavelength on the variance is observed in the loadings plot (Figure 5). As shown in the loadings plot (Figure 5), two main zones highly influence the variance of the samples' spectra. The first region is observed at around 280 nm, a region that should be related to tannins and other phenolic compounds,[33] and the second region appears around 520 nm, where compounds such as anthocyanins or polymeric pigments absorb. Moreover, other regions of the spectra also explain some variance and must be taken into consideration in the development of PLS calibrations. For example, the second component also shows a region around 320 nm, highly influencing the variance of the spectra, and is possibly related to the hydroxycinnamic acids.

Quantitative Analysis: PLS Models. Statistics for the PLS calibrations developed for wine samples using UV−vis spectroscopy (260−610 nm) are shown in Table 3. Three wavelength regions were selected to develop PLS calibrations. First, a region containing all of the recorded spectra was tested (260−610 nm). However, Dambergs et al.[33] reported a robust method for the development and validation of a UV spectrum calibration for the prediction of the tannin concentration in red wines; therefore, a

DOI: 10.1021/jf503412t
J. Agric. Food Chem. 2015, 63, 1088−1098

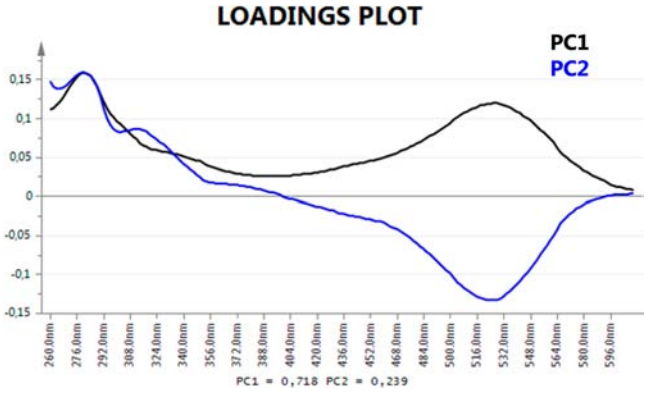

Figure 5. Loadings for the two principal components corresponding to the spectra of the 240 wine samples recorded in the UV−vis region of the electromagnetic spectrum.

section containing only the UV region was also selected. Finally, the region related to the maximum absorbance of anthocyanins and polymeric pigments (480−580 nm) was also considered in combination with the UV region following the results observed in the loadings plot. In addition, and following the study by Dambergs et al.,[33] a model was also built using only the spectral values corresponding to five wavelengths in the UV region (270, 280, 290, 300, and 314 nm). The use of a small number of wavelengths is beneficial when transferability of calibration models between instruments is taken into account. Moreover, wavelengths were selected on the basis of the absorption peak that tannins show in the UV region of the electromagnetic spectrum around 280 nm.

Slightly higher values were observed in the reported statistics when only the UV region (260−310 nm) was considered in the PLS calibrations. R^2val, RMSEP, and RPD were 0.89, 0.16 g/L (epicatechin equivalents), and 3.49 for MCP and 0.93, 0.08 g/L (catechin equivalents), and 4.07 for BSA, respectively. When BSA was used as reference method, slightly higher values were found. These results, together with the higher %CV observed for the BSA method, suggest an increase in the variability of tannins measured by protein precipitation and therefore an increase in the ability of the model to predict new samples outside the calibration set.

It has been reported by several authors that RPD values >2.5 are considered good enough for prediction purposes.[20,33,57,58] Fragoso et al.,[25] however, rated only RPD values >3 as sufficient for prediction purposes, whereas values between 2.5 and 3 were considered suitable only for rough screening.[25] Taking into consideration the complexity of wine tannin molecules, which are more complex than those found in grapes due to the acidic and oxidative nature of the vinification process,[2,39,55] and also the possibly greater variable interaction between wine tannins and methylcellulose or BSA compared to that of grape tannins, we considered RPD values >2.5 valid for prediction purposes.

Moreover, the model built using only five spectral absorbance values in the UV region showed lower RPD vales than those observed when the full UV region was included in the calibrations. In this specific case, MCP presented higher RPD values than BSA, although in both cases the RPD vales were >2.5 and the models were therefore considered suitable for prediction purposes.

Models for Individual Grape Varieties. On the basis of the good results obtained with the full data set (R^2val = 0.88 and 0.9 and RPD = 2.97 and 3.5 for MCP and BSA, respectively), we decided to check the ability of UV−vis spectroscopy to predict tannin concentration by devising models with each grape variety individually. Table 4a shows the statistics for the PLS calibrations developed for wine samples using UV−vis spectroscopy (260−610 nm). The calibration sets were developed using 49 Cabernet Sauvignon samples, 46 Merlot samples, 60 and 57 Shiraz samples, 15 and 14 Pinotage samples, and 60 and 59 samples spanning a wide range of varieties and some blends (called "remaining") for MCP and BSA tannin assays, respectively (five BSA values were missing and therefore were not included in the calibration models). In each case the remainder of the 240 samples was then used as a validation data set.

The ability of Cabernet Sauvignon and Merlot tannin models to predict new samples of all other cultivars was weak, as the RPD values were always <2. On the other hand, the predictive ability of Shiraz and the remaining sample set was relatively strong. Interestingly, although a small range (0.92−0.29 g/L), lower CV (26.61%), and a small calibration set were used (14 samples), the Pinotage model showed strong predictive ability when BSA was used as reference method, whereas weak predictive ability was observed when MCP was used as *Y* variable. A calibration set aimed at predicting the tannin concentration when only Pinotage samples are included therefore probably would need a wider range of Pinotage samples when MCP is used as reference

Table 3. PLS Calibration and Validation Statistics for MCP (g/L Epicatechin Equivalents) and BSA (g/L Catechin Equivalents) in the Set of Red Wine Samples at Different Wavelengths[a]

	*N*cal	*N*val	*A*	R^2cal	RMSECV	R^2val	RMSEP	RPD	wavelength (nm)
MCP	120	120	4	0.90	0.21	0.88	0.20	2.97	260−610
BSA	117	118	4	0.91	0.09	0.9	0.10	3.5	
MCP	120	120	5	0.88	0.21	0.89	0.16	3.49	260−310
BSA	117	118	6	0.93	0.11	0.93	0.08	4.07	
MCP	120	120	4	0.88	0.21	0.88	0.21	2.71	260−310/480−580
BSA	117	118	6	0.91	0.11	0.89	0.10	3.49	
MCP	119	120	3	0.84	0.23	0.9	0.18	3.07	270, 280, 290, 300, 314
BSA	117	118	6	0.89	0.11	0.89	0.11	2.59	

[a] *A*, number of selected components in the PLS model; *N*cal, number of samples in the calibration set; *N*val, number of samples in the validation set; R^2cal, coefficient of determination in calibration; RMSECV, root mean standard error in cross-validation (g/L); R^2val, coefficient of determination in the validation set; RMSEP, root mean standard error of prediction (g/L); RPD; residual predictive deviation.

DOI: 10.1021/jf503412t
J. Agric. Food Chem. 2015, 63, 1088−1098

Table 4. PLS Calibration and Validation Statistics for MCP (g/L Epicatechin Equivalents) and BSA (g/L Catechin Equivalents) in the Set of Red Wine Samples Grouped by the Classifying Variable Cultivar[a]

			calibration								validation			
	calibration	validation	mean	SDEV	range	CV	Ncal	A	R^2cal	RMSECV	Nval	R^2val	RMSEP	RDP
(a) Tannin Concentration Prediction Ability According to Cultivar														
MCP	CS	Me, Sh, Pi, R	1.74	0.66	3.21−0.37	37.93	49	4	0.93	0.22	181	0.78	0.37	1.50
BSA			0.73	0.40	1.72−0.16	54.79	49	4	0.93	0.12	176	0.80	0.24	1.25
MCP	Me	CS, Sh, Pi, R	1.88	0.81	2.78−0.71	43.09	46	3	0.93	0.17	184	0.79	0.30	1.94
BSA			0.71	0.36	1.26−0.16	50.70	46	3	0.91	0.10	179	0.70	0.19	1.74
MCP	Sh	CS, Me, Pi, R	1.61	0.57	2.77−0.70	35.40	30	3	0.87	0.23	170	0.83	0.25	2.29
BSA			0.51	0.24	1.18−0.05	47.06	57	4	0.88	0.10	168	0.90	0.12	2.98
MCP	Pi	CS, Me, Sh, R	1.54	0.33	1.96−1.00	21.43	15	11	1.00	0.26	215	0.55	0.66	0.90
BSA			0.64	0.17	0.92−0.39	26.56	14	5	0.99	0.03	211	0.87	0.14	2.43
MCP	R	CS, Me, Sh, Pi	1.66	0.54	3.21−0.31	32.53	60	4	0.91	0.21	170	0.86	0.22	2.68
BSA			0.68	0.34	1.61−0.12	50.00	59	5	0.93	0.11	166	0.86	0.12	2.64
(b) Ability of the Model To Predict Tannin Concentration of Individual Cultivars														
MCP	Me, Sh, Pi, R	CS	1.61	0.65	3.21−0.31	40.37	181	4	0.87	0.21	49	0.90	0.22	3.07
BSA			0.60	0.30	1.61−0.05	50.00	176	5	0.89	0.10	49	0.96	0.09	4.30
MCP	CS, Sh, Pi, R	Me	1.66	0.57	3.21−0.31	34.34	184	4	0.88	0.22	46	0.89	0.20	3.07
BSA			0.64	0.33	1.72−0.12	51.56	179	4	0.89	0.12	46	0.91	0.10	3.29
MCP	CS, Me, Pi, R	Sh	1.65	0.59	3.21−0.31	35.76	170	4	0.89	0.20	30	0.92	0.22	2.62
BSA			0.66	0.35	1.72−0.12	53.03	168	5	0.91	0.11	57	0.86	0.12	2.72
MCP	CS, Me, Sh, R	Pi	1.65	0.60	3.21−0.31	36.36	215	4	0.89	0.21	15	0.40	0.25	1.28
BSA			0.62	0.34	1.72−0.05	54.84	211	4	0.91	0.11	14	0.85	0.12	1.35
MCP	CS, Me, Sh, Pi	R	1.62	0.60	3.21−0.37	37.04	170	4	0.88	0.22	60	0.85	0.20	2.73
BSA			0.61	0.32	1.72−0.05	52.46	166	5	0.91	0.11	59	0.87	0.12	2.77

[a] Ncal, number of samples in the calibration set; A, number of selected components in the PLS model: Nval, number of samples in the validation set; R^2cal, coefficient of determination in the calibration set; RMSECV, root mean standard error in cross-validation (g/L); R^2val, coefficient of determination in the validation set; RMSEP, root mean standard error of prediction (g/L); RPD; residual predictive deviation; CS, Cabernet Sauvignon; Me, Merlot; Sh, Shiraz; Pi, Pinotage; R, remaining.

method. The differences observed for the Pinotage models could also be related to the different ability of the precipitants, methylcellulose polymer or bovine serum albumin protein, to bind and precipitate tannins from this variety, which is probably due to the unique phenolic composition of Pinotage wines.[59−61] Future work on establishing a MCP model for Pinotage should thus probably take into account the different abilities of both precipitants to react and precipitate tannins.[41] Only the model built with the Shiraz samples using BSA as reference method could be used for prediction purposes (RPD > 2.5). Moreover, the model built with the remaining samples, containing a great number of varieties, showed RPD values >2.5 and therefore is valid for tannin prediction purposes. This gives an idea of the robustness of the models, even though a wide range of varieties, different from Cabernet Sauvignon, Merlot, Syrah, and Pinotage, and a small calibration set were used to build the model (60 and 59 samples for MCP and BSA, respectively).

The results showed a great variability in tannin concentration and composition when building the calibration models. Models built with only single varieties did not cover the tannin variability observed in wines made from different *Vitis vinifera* varieties, therefore being unable to predict new samples. This is supported by the higher ability of the diverse pool of varieties model to predict the tannin concentration of new samples.

Table 4b shows calibration and validation statistics for the PLS models. The models were built with all of the samples from the other cultivars and validated against each individual cultivar; thus, the ability of the model to predict the tannin concentration of each cultivar was tested. The results show slightly higher RPD values where BSA was used as reference method, as has been observed for the full-range calibrations. The model aimed at predicting Cabernet Sauvignon tannin concentrations showed the strongest ability to predict new samples. Merlot and Shiraz, in this order, also showed RPD values considered suitable for prediction purposes, although these were slightly lower than those of the Cabernet Sauvignon model. However, this order was inverted when the ability of each cultivar to predict tannin concentration was tested (Table 4a).

It thus seems that lower variation in tannin composition leads to poorer ability of the cultivar to predict new samples' tannin concentrations. Moreover, the set of samples composed of the remaining cultivars showed R^2val and RPD values of 0.85 and 2.73 for MCP as reference method and 0.87 and 2.77 for BSA as reference method, respectively. These results display the ability

DOI: 10.1021/jf503412t
J. Agric. Food Chem. 2015, 63, 1088−1098

Table 5. PLS Calibration and Validation Statistics for MCP (g/L Epicatechin Equivalents) and BSA (g/L Catechin Equivalents) in the Set of Red Wine Samples Grouped by the Classifying Variable Vintage[a]

			calibration								validation			
	calibration	validation	mean	SDEV	range	CV	*N*cal	*A*	R^2cal	RMSECV	*N*val	R^2val	RMSEP	RDP
(a) Tannin Concentration Prediction Ability According to Cultivar														
MCP	12	11, 10, 09, R	1.57	0.57	3.21−0.37	36.31	140	4	0.87	0.22	97	0.87	0.22	2.71
BSA			0.67	0.35	1.72−0.14	52.24	139	4	0.93	0.10	93	0.82	0.23	1.23
MCP	11	12, 10, 11, R	1.55	0.58	3.21−0.93	37.42	16	3	0.95	0.21	221	0.79	0.30	1.94
BSA			0.61	0.33	1.61−0.25	54.10	15	5	0.95	0.19	217	0.56	0.24	1.39
MCP	10	12, 11, 09, R	1.33	0.55	2.49−0.31	41.35	30	2	0.92	0.17	207	0.92	0.20	2.93
BSA			0.37	0.21	0.80−0.05	56.76	27	2	0.88	0.09	205	0.50	0.29	1.11
MCP	9	12, 11, 10, R	2.06	0.43	3.03−1.29	20.87	27	4	0.88	0.22	210	0.85	0.23	2.49
BSA			0.61	0.25	1.17−0.24	40.98	27	2	0.88	0.09	205	0.42	0.40	0.84
MCP	R	12, 11, 10, 09	2.03	0.47	2.78−1.14	23.15	24	4	0.88	0.23	213	0.53	1.13	0.51
BSA			0.64	0.28	1.16−0.19	43.75	24	4	0.94	0.10	208	0.60	0.37	0.89
(b) Ability of the Model To Predict Tannin Concentration of Individual Cultivars														
MCP	11, 10, 09, R	12	1.74	0.59	3.21−0.31	33.91	97	4	0.92	0.19	140	0.85	0.25	2.28
BSA			0.55	0.28	1.61−0.05	50.91	93	4	0.87	0.12	139	0.90	0.13	2.69
MCP	12, 10, 11, R	11	1.65	0.59	3.21−0.31	35.76	221	4	0.88	0.22	16	0.87	0.20	2.76
BSA			0.63	0.33	1.72−0.05	52.38	217	5	0.91	0.11	15	0.79	0.15	2.23
MCP	12, 11, 09, R	10	1.68	0.58	3.21−0.37	34.52	207	4	0.87	0.22	30	0.90	0.18	3.01
BSA			0.66	0.33	1.72−0.14	50.00	205	4	0.90	0.11	27	0.80	0.12	2.64
MCP	12, 11, 10, R	9	1.59	0.60	3.21−0.31	37.74	210	4	0.85	0.21	27	0.81	0.21	2.00
BSA			0.63	0.34	1.72−0.05	53.97	205	4	0.91	0.11	27	0.80	0.11	2.14
MCP	12, 11, 10, 09	R	1.60	0.58	3.21−0.31	36.25	213	4	0.87	0.21	24	0.85	0.22	2.11
BSA			0.62	0.33	1.72−0.05	53.23	208	4	0.90	0.01	24	0.92	0.10	2.87

[a] *N*cal, number of samples in the calibration set; *A*, number of selected components in the PLS model: *N*val, number of samples in the validation set; R^2cal, coefficient of determination in the calibration set; RMSECV, root mean standard error in cross-validation (g/L); R^2val, coefficient of determination in the validation set; RMSEP, root mean standard error of prediction (g/L); RPD; residual predictive deviation; 12, 2012 vintage samples; 11, 2011 vintage samples; 10, 2010 vintage samples; 09, 2009 vintage samples; R, older vintages (2008, 2007, 2006, 2005, 2000).

of four red varieties (Cabernet Sauvignon, Merlot, Syrah, and Pinotage) to predict samples spanning a wide range of other cultivars. On the other hand, poor statistics were again observed for the cultivar Pinotage for both reference methods. This indicates the poor ability of a diverse calibration set to predict Pinotage wine samples' tannin concentrations, which is probably due to the specific phenolic composition of this variety.[59−61]

Models for Individual Vintage Years. The ability of the 2012 and 2010 tannin model to predict tannin concentrations of samples from other vintages when MCP was used as reference method was considered good enough (RPD > 2.5) for prediction (Table 5a). However, 2011 and 2009 showed lower RPD values. Whereas the 2009 tannin model could be considered for screening purposes, the smaller sample set in the 2011 model could affect the ability of the model to predict tannin concentrations in samples outside the calibration set.

On the other hand, when BSA was used as reference method, the results showed lower accuracy, that is, lower ability to predict new samples, as the model is built with older samples, showing lower predictive ability when models were tested with new samples. A more qualitative interpretation of the RPD is given by other authors, where RPD values <1.5 were considered insufficient for most applications, whereas calibration models with values >2 were considered excellent.[57] In all of the models, RPD values were <1.5 and therefore could not be considered for rough screening.[36,62,63]

The results also show the poor ability of the older sample set (ranging in vintage from 2000 to 2008) to predict the tannin concentration of younger vintage samples. Therefore, when this result is taken into consideration, it is necessary to add samples of younger wines to the model to increase the reliability of the model.

Interestingly, different results were obtained depending on the reference method employed. It seems that BSA protein loses its ability to react with old wine tannins and polymeric pigments, which means that the ability of the models to predict new samples is compromised. However, this effect was not observed when MCP was used as reference method. In this case, the RPD values were 2.71, 1.94, 2.93, and 2.49 for the 2012, 2011, 2010, and 2009 models, respectively. These results, which are reported here for the first time, strengthen the fact that the tannin material is measured differently by MCP and BSA.[39,41]

Older wines exhibit lower astringency intensities together with smaller tannin size.[1,2] Furthermore, an increase in the ability of

DOI: 10.1021/jf503412t
J. Agric. Food Chem. 2015, 63, 1088−1098

Table 6. PLS Calibration and Validation Statistics for MCP (g/L Epicatechin Equivalents) and BSA (g/L Catechin Equivalents) in the Set of Red Wine Samples Grouped by the Classifying Variable Experimental versus Commercial[a]

					calibration						validation			
	calibration	validation	mean	SDEV	range	CV	*N*cal	*A*	R^2cal	RMSECV	*N*val	R^2val	RMSEP	RDP
MCP	C	E	1.96	0.47	3.21−0.94	23.98	121	4	0.81	0.22	119	0.81	0.24	2.11
	E	C	1.32	0.51	3.21−0.31	38.64	119	4	0.86	0.20	121	0.80	0.20	2.29
BSA	C	E	0.74	0.33	1.72−0.19	44.59	120	5	0.89	0.12	115	0.89	0.10	2.75
	E	C	0.51	0.28	1.61−0.05	54.90	115	7	0.94	0.07	120	0.86	0.15	2.28

[a] *N*cal, number of samples in the calibration set; *A*, number of selected components in the PLS model: *N*val, number of samples in the validation set; R^2cal, coefficient of determination in the calibration set; RMSECV, root mean standard error in cross-validation (g/L); R^2val, coefficient of determination in the validation set; RMSEP, root mean standard error of prediction (g/L); RPD; residual predictive deviation; E, experimental samples; C, commercial samples.

the BSA protein to react with tannins based on their molecular size was reported recently.[64] The precipitation of tannin increased with increasing size, up to octamer. The authors report that around 100% of the decamer would be precipitated under the assay conditions. The effect of polymer mixtures for precipitating proteins was also studied, and a different protein precipitation efficacy was observed compared to that of individual polymers.[64] These findings could partially explain the inability of the BSA model composed of young 2012 samples to predict older samples, because lower mDP would be expected in older samples, leading to a decreased ability of the BSA to react and precipitate tannins.[64] In summary, the variability in tannin composition observed in the old samples would probably not be represented in the calibration model based on young samples. This model therefore is unable to predict older samples outside the calibration set. The different ability of tannin polymer mixtures to precipitate BSA could also affect the lower ability of the other models, which contain samples from different vintages, to predict new samples. Unfortunately, a similar study using MCP as a precipitating agent of different polymer size tannins has not yet been conducted.

RPD values between 2 and 3 were observed for all vintages and both reference methods when the model's ability to predict the tannin concentrations of specific years was tested (Table 5b). Wine samples from 2011 and 2010 for MCP as reference method showed satisfactory ability to be predicted by the model containing the remaining set of samples. Moreover, 2010 and the set of remaining vintage years could also be predicted by the model when BSA was taken as reference method (RPD values of 2.64 and 2.87, respectively). Thus, a possible explanation for the differences observed in the calibrations could be caused by the vintage year affecting tannin composition and also by interaction between the two precipitants. When samples from the youngest vintage (2012) were predicted by the model, R^2val and RPD values of 0.85 and 2.59 for MCP and 0.9 and 2.69 for BSA as reference method were achieved, respectively. This shows high predictability when new samples are predicted with a model built with samples from older vintage years. The results show that new samples should probably be added to the model as it becomes older (Table 5a), although new samples do not need to be added every year, because models built with all of the samples except the 2012 wines (latest vintage) and validated against samples from 2012 showed good predictive ability (RPD = 2.59 and 2.69 for MCP and BSA, respectively) (Table 5b).

Models for Commercial/Experimental Wines. Table 6 shows the statistics for the PLS calibrations developed for wine samples using UV−vis spectroscopy (260−610 nm). The calibration set was developed using the 121 commercial wine samples and 119 experimental wine samples for the MCP tannin assay and the 121 commercial and 115 experimental wine samples for the BSA tannin assay, respectively. In each case the remainder of the 240 samples was then used as a validation set. To test the ability of commercial wines to predict experimental wine samples and vice versa, models containing both variables as calibration set were developed. The R^2val and RPD values were 0.81 and 2.11 for MCP as reference method and 0.89 and 2.75 for BSA, respectively, when commercial wines were used as calibration set and experimental samples were used to validate the model. Thus, using BSA as reference method, the commercial wines had sufficient ability (RPD > 2.5) to predict samples outside the calibration set (experimental wines). Otherwise, RPD values <2.5 (2.29 and 2.28 for MCP and BSA, respectively) have been observed when experimental wines were used to predict commercial wines. Models built with experimental wines therefore could be used for the purpose of screening commercial wines, allowing a classification of the wines' tannin levels, but should not be used further for prediction purposes. As we have observed in the PCA-X plot, the effect of barrel aging or oxygen exposure together with the absence of MLF in experimental samples could explain the lower ability of the experimental wines to predict commercial wines, because the changes in the phenolic composition that occur during MLF and wine aging could account for the observed lower accuracy.

Conclusions. The results presented here clearly show the potential and robustness of rapid UV−vis predictive methods to quantify wine tannins in South African red wines. Models built using only the UV region presented slightly higher RPD values and hence better ability to predict new samples and, therefore, should be considered in terms of a reduction in the time of analysis. In addition, differences in the results obtained when the predictive ability of the classifying variables was studied suggest that tannin composition and concentration, and the ability of tannins to react and precipitate with both precipitants MCP and BSA, are affected to a great extent by several factors.

The tested cultivars showed different abilities to predict samples from other, new cultivars. Shiraz, Merlot, and Cabernet Sauvignon, in this order, showed a decreasing ability to predict the tannin concentration of new samples. However, this order was inverted when single-cultivar samples were predicted by a diverse cultivar model. A particular behavior was observed when Pinotage was used as calibration or validation test. The specific phenolic and tannin composition of this variety could perhaps explain the differences in the results observed. The results also showed that models built with older wine samples should also incorporate younger samples to increase their accuracy in predicting samples outside the calibration set when BSA is used

DOI: 10.1021/jf503412t
J. Agric. Food Chem. 2015, 63, 1088−1098

as reference method, an effect that was not observed when MCP was used as the *Y* variable. The different ability of the BSA protein to bind and precipitate tannins with different degrees of polymerization has been proposed as the possible reason for this behavior. Finally, samples from 2012 (last vintage tested) were predicted accurately by models constructed with samples spanning a number of older vintage years. This means that samples from the last vintage should not necessarily be added to the model to achieve prediction accuracy. Furthermore, experimental wines made without MLF and not submitted to barrel aging and oxygen exposure were not able to accurately predict commercial wines. A proposal for future work is that experimental wines subjected to MLF should be also included in the calibration set, as this might be able to increase model predictability. In addition, the distinctive phenolic, especially tannin, composition of Pinotage wines needs to be characterized extensively. Finally, the interaction between Pinotage tannins and BSA protein or MCP polymer needs to be also assessed to understand the ability of Pinotage tannin material and both precipitants to bind and form precipitable aggregates.

AUTHOR INFORMATION

Funding

We are grateful to the National Research Foundation (NRF, Thrip program) and Winetech for financial support.

Notes

The authors declare no competing financial interest.

REFERENCES

(1) Vidal, S.; Francis, L.; Guyot, S.; Marnet, N.; Kwiatkowski, M.; Gawel, R.; Cheynier, V.; Waters, E. J. The mouth-feel properties of grape and apple proanthocyanidins in a winelike medium. *J. Sci. Food Agric.* **2003**, *83*, 564−573.

(2) Cheynier, V.; Duenas-Paton, M.; Salas, E.; Maury, C.; Souquet, J. M.; Sarni-Manchado, P.; Fulcrand, H. Structure and properties of wine pigments and tannins. *Am. J. Enol. Vitic.* **2006**, *57*, 298−305.

(3) Harbertson, J. F.; Picciotto, E. A.; Adams, D. O. Measurement of polymeric pigments in grape berry extracts and wines using a protein precipitation assay combined with bisulfite bleaching. *Am. J. Enol. Vitic.* **2003**, *54*, 301−306.

(4) Sarneckis, C. J.; Dambergs, R. G.; Jones, P.; Mercurio, M.; Herderich, M. J.; Smith, P. A. Quantification of condensed tannins by precipitation with methyl cellulose: development and validation of an optimized tool for grape and wine analysis. *Aust. J. Grape Wine Res.* **2006**, *12*, 1−11.

(5) Silanikove, N.; Shinder, D.; Gilboa, N.; Eyal, M.; Nitsan, Z. Binding of poly(ethylene glycol) to samples of forage plants as an assay of tannins and their negative effects on rumenal degradation. *J. Agric. Food Chem.* **1996**, *44*, 3230−3234.

(6) Antoine, M. L.; Simon, C.; Pizzi, A. UV spectrophotometric method for polyphenolic tannin analysis. *J. Appl. Polym. Sci.* **2004**, *91*, 2729−2732.

(7) Singleton, V. L. Analytical fractionation of the phenolic substances of grapes and wine and some practical uses of such analyses. In *Chemistry of Winemaking*; Webb, A. D., Ed.; ACS Advances in Chemistry Series 137; American Chemical Society: Washington, DC, USA, 1974; pp 184−211.

(8) Porter, L. J.; Hrstich, L. N.; Chan, B. G. The conversion of procyanidins and prodelphinidins to cyanidin and delphinidin. *Phytochemistry* **1986**, *25*, 223−230.

(9) Sun, B. S.; Ricardo-da-Silva, J. M.; Spranger, I. Critical factors of vanillin assay for catechins and proanthocyanidins. *J. Agric. Food Chem.* **1998**, *46*, 4267−4274.

(10) Stevanato, R.; Fabris, S.; Momo, F. Enzymatic method for the determination of total phenolic content in tea and wine. *J. Agric. Food Chem.* **2004**, *52*, 6287−6293.

(11) De Beer, D.; Harbertson, J. F.; Kilmartin, P. A.; Roginsky, V.; Barsukova, T.; Adams, D. O.; Waterhouse, A. L. Phenolics: a comparison of diverse analytical methods. *Am. J. Enol. Vitic.* **2004**, *55* (4), 389−400.

(12) Jones, D. E. Banana tannins and its reaction with polyethylene glycols. *Nature* **1965**, *206*, 299−300.

(13) Montedoro, G.; Fantozzi, P. Dosage des tannins dans les mouts et les vins a l'aide de la methylcellulose et evalution d'autresfractions phenoliques. *Lebensm. Wiss. Technol.* **1974**, *7*, 155−161.

(14) Hagerman, A. E.; Butler, L. G. Protein precipitation method for the quantitative determination of tannins. *J. Agric. Food Chem.* **1978**, *26*, 809−812.

(15) Kennedy, J. A.; Ferrier, J.; Harbertson, J. F.; Peyrot des Gachons, C. Analysis of tannins in red wine using multiple methods: correlation with astringency. *Am. J. Enol. Vitic.* **2006**, *57*, 481−485.

(16) Mercurio, M. D.; Smith, P. A. Tannin quantification in red grapes and wine: Comparison of polysaccharide- and protein-based tannin precipitation techniques and their ability to model wine astringency. *J. Agric. Food Chem.* **2008**, *56*, 5528−5537.

(17) Mercurio, M. D.; Dambergs, R. G.; Herderich, M. J.; Smith, P. A. High throughput analysis of red wine and grape phenolics-adaptation and validation of methyl cellulose precipitable tannin assay and modified Somers color assay to a rapid 96 well plate format. *J. Agric. Food Chem.* **2007**, *55* (12), 4651−4657.

(18) Harbertson, J. F.; Kennedy, J. A.; Adams, D. O. Tannin in skins and seeds of Cabernet Sauvignon, Syrah, and Pinot noir during ripening. *Am. J. Enol. Vitic.* **2002**, *53*, 54−59.

(19) Cozzolino, D.; Kwiatkowski, M. J.; Parker, M.; Cynkar, W. U.; Dambergs, R. G.; Gishen, M.; Herderich, M. J. Prediction of phenolic compounds in red wine fermentations by visible and near infrared spectroscopy. *Anal. Chim. Acta* **2004**, *513*, 73−80.

(20) Cozzolino, D.; Cynkar, W. U.; Dambergs, R. G.; Mercurio, M. D.; Smith, P. A. Measurement of condensed tannins and dry matter in red grape homogenates using near infrared spectroscopy and partial least squares. *J. Agric. Food Chem.* **2008**, *56*, 7631−7636.

(21) Versari, A.; Boulton, R. B.; Parpinello, G. P. Effect of spectral pre-processing methods on the evaluation of the color components of red wines using Fourier-transform infrared spectrometry. *Ital. J. Food Sci.* **2006**, *18*, 423−431.

(22) Fernandez, K.; Agosin, E. Quantitative analysis of red wine tannins using Fourier-transform mid-infrared spectrometry. *J. Agric. Food Chem.* **2007**, *55*, 7294−7300.

(23) Fernandez, K.; Labarca, X.; Bordeu, E.; Guesalaga, A.; Agosin, E. Comparative study of wine tannin classification using Fourier transform mid-infrared spectrometry and sensory analysis. *Appl. Spectrosc.* **2007**, *61*, 1163−1167.

(24) Jensen, J. S.; Egebo, M.; Meyer, A. S. Identification of spectral regions for the quantification of red wine tannins with Fourier transform midinfrared spectroscopy. *J. Agric. Food Chem.* **2008**, *56*, 3493−3499.

(25) Fragoso, S.; Aceña, L.; Guasch, J.; Busto, O.; Mestres, M. Application of FT-MIR spectroscopy for fast control of red grape phenolic ripening. *Food Chem.* **2011**, *59*, 2175−2183.

(26) Van der Merwe, H. *Colour and Phenolic content of Robertson Red Grape Cultivars: Distribution, correlation with wines and analyses*. Ph.D. thesis, Stellenbosch University, South Africa, 2012.

(27) Murray, I. Forage analysis by near infrared spectroscopy. In *Sward Management Handbook*; Davies, A., Baker, R. D., Grant, S. A., Laidlaw, A. S., Eds.; British Grassland Society: Reading, UK, 1993; pp 285−312.

(28) Batten, G. D. Plant analysis using near infrared reflectance spectroscopy: the potential and the limitations. *Aust. J. Exp. Agric.* **1998**, *38*, 697−706.

(29) Deaville, E. R.; Flinn, P. C. Near infrared (NIR) spectroscopy: an alternative approach for the estimation of forage quality and voluntary intake. In *Forage Evaluation in Ruminant Nutrition*; Givens, D. I., Owen, E., Axford, R. F. E., Omedi, H. M., Eds.; CABI Publishing: Wallingford, UK, 2000; pp 301− 320.

(30) Garcia-Jares, C.; Medina, B. Prediction of some physicochemical parameters in red wines from ultraviolet-visible spectra using a partial least-squares model in latent-variables. *Analyst* **1995**, *120*, 1891−1896.

DOI: 10.1021/jf503412t
J. Agric. Food Chem. 2015, 63, 1088−1098

(31) McMurrough, I.; McDowell, J. Chromatographic separation and automated analysis of flavanols. *Anal. Biochem.* **1978**, *91*, 92−100.
(32) Skogerson, K.; Downey, M.; Mazza, M.; Boulton, R. Rapid determination of phenolic components in red wines from UV-visible spectra and the method of partial least squares. *Am. J. Enol. Vitic.* **2007**, *58*, 318−325.
(33) Dambergs, R. G.; Mercurio, M. D.; Kassara, S.; Cozzolino, D.; Smith, P. A. Rapid measurement of methyl cellulose precipitable tannins using ultraviolet spectroscopy with chemometrics: application to red wine and inter-laboratory calibration transfer. *Appl. Spectrosc.* **2012**, *66* (6), 656−664.
(34) Jensen, J. S.; Werge, H. H. M.; Egebo, M.; Meyer, A. S. Effect of wine dilution on the reliability of tannin analysis by protein precipitation. *Am. J. Enol. Vitic.* **2008**, *59*, 103−105.
(35) Wold, S.; Esbensen, K.; Geladi, P. Principal component analysis. *Chemom. Intell. Lab.* **1987**, *2*, 37−52.
(36) Cozzolino, D.; Kwiatkowski, M. J.; Dambergs, R. G.; Cynkar, W. U.; Janik, L. J.; Skouroumounis, G.; Gishen, M. Analysis of elements in wine using near infrared spectroscopy and partial least squares regression. *Talanta* **2008**, *74*, 711−716.
(37) Martens, H.; Naes, T. *Multivariate Calibration*; Wiley: Chichester, UK, 1999.
(38) Wold, S.; Sjostrom, M.; Eriksson, L. PLS regression: a basic tool of chemometrics. *Chemom. Intell. Lab. Syst.* **2001**, *58*, 109−130.
(39) Harbertson, J. F.; Downey, M. O. Investigating differences in tannin levels determinedby methylcellulose and protein precipitation. *Am. J. Enol. Vitic.* **2009**, *60* (2), 246−249.
(40) Harberston, J. F.; Hodgins, R. E.; Thurston, L. N.; Schaffer, L. J.; Reid, M. S.; Landon, J. L.; Ross, C. F.; Adams, D. O. Variability of tannin concentration in red wines. *Am. J. Enol. Vitic.* **2008**, *59* (2), 210−214.
(41) Seddon, T. J.; Downey, M. O. Comparisons of analytical methods for the determination of condensed tannins in grape skins. *Aust. J. Grape Wine Res.* **2008**, *14*, 54−61.
(42) Magwaza, L. S.; Opara, U. L.; Cronje, P. J. R.; Landalh, S.; Nieuwoudt, H. H.; Mouaze, A. M.; Nicolai, B. M.; Terry, L. A. Assessment of rind quality of 'Nules Clementine' mandarin fruit during postharvest storage. 2. Robust Vis/NIR PLS models for prediction of physico-chemical attributes. *Sci. Hortic.* DOI: 10.1016/j-scienta.2013.09.050.
(43) Bellon-Maurel, V.; Fernandez-Ahumada, E.; Palagos, B.; Roger, J. M.; McBratney, A. Critical review of chemometric indicators commonly used for assessing the quality of the prediction of soil attributes by NIR spectroscopy. *Trends Anal. Chem.* **2010**, *29*, 9.
(44) Cheynier, V.; Schneider, R.; Salmon, J. M.; Fulcrand, H. *Chemistry of Wine*; Elsevier: Amsterdam, The Netherlands, 2010; pp 1120−1164.
(45) Du Toit, W. J.; Lisjak, K.; Marais, J.; Du Toit, M. The effect of micro-oxygenation on the phenolic composition, quality and aerobic wine-spoilage microorganisms of different South African red wines. *S. Afr. J. Enol. Vitic.* **2006**, *27*, 57−67.
(46) Linskens, H. F.; Jackson, J. F. Phenolic composition of natural wine types. *Wine Analysis*; Springer-Verlag: Berlin, Germany, 1998.
(47) Scalbert, A. *Phenolics in Fruits and Fruit Products: Progress and Prospects, Polyphenolic Phenomena*; INRA: Paris, France, 1993.
(48) Cabrita, M. J.; Torre, M.; Palma, V.; Alves, E.; Patao, R.; Costa Freitas, A. M. Impact of malolactic fermentation on low molecular weight phenolic compounds. *Talanta* **2008**, *74*, 1281−1286.
(49) Dimitric-Markovic, J. M.; Ignjatovic, L. M.; Markovic, D. A.; Baranac, J. M. Antioxidant capabilities of some organic acids and their co-pigments with malvidin. Part I. *J. Electroanal. Chem.* **2003**, *553*, 169−175.
(50) Dimitric-Markovic, J. M.; Ignjatovic, L. M.; Markovic, D. A.; Baranac, J. M. Antioxidant capabilities of some organic acids and their co-pigments with malvidin. Part II. *J. Electroanal. Chem.* **2003**, *553*, 177−182.
(51) Darias-Martín, J.; Martín, B.; Carrillo, M.; Lamuela, R.; Díaz, C.; Boulton, R. The effect of caffeic acid on the color of red wine. *J. Agric. Food Chem.* **2002**, *50* (7), 2062−2067.
(52) Alvarez, I.; Aleixandre, J. L.; García, M. J.; Lizama, V.; Aleixandre-Tudó, J. L. Effect of the prefermentative addition of copigments on the polyphenolic composition of Tempranillo wines after malolactic fermentation. *Eur. Food Res. Technol.* **2009**, *228*, 201−510.
(53) Aleixandre-Tudo, J. L.; Alvarez, I.; Lizama, V.; Garcia, M. J.; Aleixandre, J. L.; du Toit, W. Impact of caffeic acid addition on phenolic composition of Tempranillo wines from different winemaking techniques. *J. Agric. Food Chem.* **2013**, *61*, 11900−11912.
(54) Hernandez, T.; Estrella, I.; Carlavilla, D.; Martin-Alvarez, P. J.; Moreno-Arribas, M. V. Phenolic compounds in red wine subjected to malolactic fermentation and aging on lees. *Anal. Chim. Acta* **2006**, *563*, 116−125.
(55) Fulcrand, H.; Dueñas, M.; Salas, E.; Cheynier, V. Phenolic reactions during winemaking and aging. *Am. J. Enol. Vitic.* **2006**, *57*, 289−297.
(56) Mazza, G.; Fukumoto, L.; Delaquis, P.; Girard, B.; Ewert, V. Anthocyanins, phenolics and color of Cabernet Sauvignon, Merlot and Pinot Noir from British Columbia. *J. Agric. Food Chem.* **1999**, *47*, 4009−4017.
(57) Williams, P. C. Implementation of near infrared technology. In *Near Infrared Technology in the Agricultural and Food Industries*; Williams, P. C., Norris, K. H., Eds.; American Association of Cereal Chemistry: St. Paul, MN, USA, 2001; pp 145−169.
(58) Fearn, T. Assessing calibrations: SEP, RPD, RER and R2. *NIR News* **2002**, *13*, 12−14.
(59) Rossouw, M.; Marais, J. Pinotage polyphenol profile. *Wynboer* **2003**, *172*, 9−11.
(60) Rossouw, M.; Marais, J. The phenolic composition of South African Pinotage, Shiraz and Cabernet Sauvignon wines. *S. Afr. J. Enol. Vitic.* **2004**, *25*, 94−104.
(61) Minnaar, P. P.; Booyse, M. Differentiation among young and market-ready Cabernet Sauvignon, Pinotage and Shiraz wines: application of canonical discriminant analysis using flavonoid and non-flavonoid compositional data. *S. Afr. J. Enol. Vitic.* **2011**, *32* (2), 251−261.
(62) Chang, C. W.; Laird, D. A.; Mausbach, M. J.; Hurburgh, C. R., Jr. Near-infrared reflectance spectroscopy-principal components regression analysis of soil properties. *Soil Sci. Soc. Am. J.* **2007**, *65*, 480−490.
(63) Dunn, B. W.; Beecher, H. G.; Batten, G. D.; Ciavarella, S. The potential of near-infrared reflectance spectroscopy for soil analysis: a case study from the Riverine Plain of south-eastern Australia. *Aust. J. Exp. Agric.* **2002**, *42*, 607−614.
(64) Harbertson, J. F.; Kilmister, R. L.; Kelm, M. A.; Downey, M. O. Impact of condensed tannin size as individual and mixed polymers on bovine serum albumin precipitation. *Food Chem.* DOI: 10.1016/j.foodchem.2014.03.026.

DOI: 10.1021/jf503412t
J. Agric. Food Chem. 2015, 63, 1088−1098

Table 1. Primary Structural Formulas of CLs

code	new name[a]	old name	amino acid sequence (NαC-)[b]	chemical formula	MW (Da)
1	[1−9-NαC]-CLA	CLA	Ile-Leu-Val-Pro-Pro-Phe-Phe-Leu-Ile	$C_{57}H_{85}N_9O_9$	1040.34
2	[1−9-NαC]-CLB	CLB	Met-Leu-Ile-Pro-Pro-Phe-Phe-Val-Ile	$C_{56}H_{83}N_9O_9S$	1058.38
3	[1−9-NαC],[1-Abu]-CLB[c]	CLB-S	Abu-Leu-Ile-Pro-Pro-Phe-Phe-Val-Ile	$C_{55}H_{81}N_9O_9$	1012.29
4	[1−9-NαC],[1-MetO]-CLB	CLC	MetO-Leu-Ile-Pro-Pro-Phe-Phe-Val-Ile	$C_{56}H_{83}N_9O_{10}S$	1074.38
5	[1−9-NαC],[1-$MetO_2$]-CLB	CLK	$MetO_2$-Leu-Ile-Pro-Pro-Phe-Phe-Val-Ile	$C_{56}H_{83}N_9O_{11}S$	1090.38
6	[1−8-NαC]-CLE	CLP	Met-Leu-Val-Phe-Pro-Leu-Phe-Ile	$C_{51}H_{76}N_8O_8S$	961.26
7	[1−8-NαC],[1-Abu]-CLE[c]	CLP-S	Abu-Leu-Val-Phe-Pro-Leu-Phe-Ile	$C_{50}H_{74}N_8O_8$	915.57
8	[1−8-NαC],[1-MetO]-CLE	CLE	MetO-Leu-Val-Phe-Pro-Leu-Phe-Ile	$C_{51}H_{76}N_8O_9S$	977.26
9	[1−8-NαC],[1-$MetO_2$]-CLE	CLJ	$MetO_2$-Leu-Val-Phe-Pro-Leu-Phe-Ile	$C_{51}H_{76}N_8O_{10}S$	993.26

[a]All new CLs listed are proposed by Shim et al.,[46] except **3** and **7**. [b]The first positions of amino acid sequences are highlighted in Figure 1. Abbreviations are Met for methionine, Abu for 2-aminobutanoic acid, MetO for methionine *S*-oxide, and $MetO_2$ for methionine *S*,*S*-dioxide. [c]This work proposed the use of **3** and **7** for Abu-substituted forms **2** and **6**, respectively.

many physiological roles and pharmacological effects. One of its main functions is to regulate osmotic potential between the blood and tissues. It also plays a role in the maintenance of blood pH. Another very important role of albumin is its function as a transport molecule. This role is based on albumin's unique ability to bind a variety of exogenous and endogenous compounds, such as metal cations, fatty acids, amino acids, and diverse drugs.[24−26] The distribution, free concentration, and metabolism of various drugs can be significantly altered as a result of binding to HSA.[23] HSA has multiple binding sites that bind a wide range of different ligands with high affinity.[22] There are two Sudlow's sites, site I and site II, which have been shown to bind drug molecules, endogenous hormones, and ions.[27] Site I is composed of a pocket with hydrophobic walls and an opening lined with positively charged residues, allowing it to bind a variety of different ligands.[27] It binds dicarboxylic acid or bulky heterocyclic molecules with a negative charge in the middle.[27] Site II is smaller and less flexible than site I. It binds aromatic carboxylic acids with negatively charged acidic groups such as those present on nonsteroidal anti-inflammatory drugs.[27] Because the amino acid residues on CLs are primarily hydrophobic, it is probable that CL interacts with HSA when introduced to the human body.

The interaction of HSA with drugs has been investigated using fluorescence,[28,29] Fourier transform infrared spectroscopy,[30−32] and circular dichroism spectroscopy,[33] but the binding of CLs other than CL **1** to HSA has yet to be investigated. Investigation of the kinetics and equilibrium of CL/HSA binding and release is necessary as cyclic peptides are being considered as drug-delivery molecules.[34] For instance, binding information is essential to understanding how cyclic peptides can be delivered to a target environment or tissue. The information provided by surface plasmon resonance (SPR) is ideal for studying the association/dissociation kinetics of CL/HSA binding. One advantage of SPR is that the different binding kinetics of a number of different analytes to the immobilized ligand can be studied. Comparisons between the association/disassociation kinetics between different analytes can be made easily. The equilibrium constants of association (K_A) and dissociation (K_D) are determined from the association and dissociation rate constants.

MATERIALS AND METHODS

General. HSA (99% purity, fatty acid and globulin free) was purchased from Sigma-Aldrich Canada, Ltd. (Oakville, ON, Canada) and used without further purification. CLs were extracted and purified from flaxseed using previously reported procedures.[5,6,35,36] An amine coupling kit [0.4 M 1-ethyl-3-(3-dimethylaminopropyl)carbodiimide hydrochloride (EDC), 0.1 M *N*-hydroxysuccinimide (NHS), and 1.0 M ethanolamine hydrochloride-NaOH (EA), pH 8.5], HBS-EP buffer [10 mM 4-(2-hydroxyethyl)piperazine-1-ethanesulfonic acid (HEPES), 150 mM NaCl, 0.005% (v/v) surfactant polysorbate 20, and 3.4 mM ethylenediaminetetraacetic acid (EDTA), pH 7.4], and a research-grade CM5 sensor chip were obtained from Biacore (GE Healthcare, Montreal, QC, Canada). The sensor chip CM5 has a 100 nm thick carboxylated dextran layer on a 50 nm thick gold layer surface. All other reagents were of analytical grade, and Milli-Q water (Millipore, Bedford, MA, USA) was used throughout the experiments.

Theoretical Aspects. The kinetic model for a 1:1 interaction is normally represented by eqs 1 and 2

$$A + B \xrightarrow{k_a} AB \quad (1)$$

$$AB \xrightarrow{k_d} A + B \quad (2)$$

where k_a and k_d represent the association and dissociation rates, respectively. The affinity constant K_A is the ratio of k_a and k_d,[37] shown in eq 3.

$$K_A = \frac{k_a}{k_d} = 1/K_D \quad (3)$$

The ligands are immobilized on the SPR sensing surface by passing HSA through a flow cell (Figure 2A). The immobilized ligands have different densities as well as different orientations on the sensor surface. The interactions are measured in real time in the flow cell (Figure 2B).

The affinity of interaction is estimated by first assuming that HSA binding sites are equally available and, second, that only high-affinity sites are occupied in the working concentration range.[38] Plots of the measured response versus different CL concentrations [CLs] are shown in Figure 3 and Figure S1A−H of the Supporting Information, respectively. K_A and the response values at the binding site saturation (R_{max}) were obtained by fitting the measured response values (R_{eq}) obtained with different CL concentrations to eq 4.

$$R_{eq} = R_{max}\frac{K_A[CLs]}{K_A[CLs] + 1} \quad (4)$$

Analyte and Buffer Preparation. Nine CLs with either 8 or 9 amino acids (915.17−1090.38 Da; Table 1 and Figure 1) were used. The CLs were purified to >98% homogeneity using reversed phase high-pressure liquid chromatography (HPLC). Analyte solutions were prepared by diluting CL stock solutions 20-fold into phosphate-buffered saline (PBS; 10 mM phosphate buffer, 2.07 mM KCl, 137 mM NaCl, pH 7.4), giving a final PBS buffer containing 5% (v/v) dimethyl sulfoxide (DMSO). The CL concentrations in the analyte solutions injected on the biosensor ranged from 40 to 150 μM. Preferably, analyte solutions were prepared just before use, but in some cases were stored at 4 °C. Running buffer for all experiments was PBS (pH 7.4) containing 5% (v/v) DMSO. Running buffers were

DOI: 10.1021/jf504811x
J. Agric. Food Chem. 2015, 63, 1099−1106

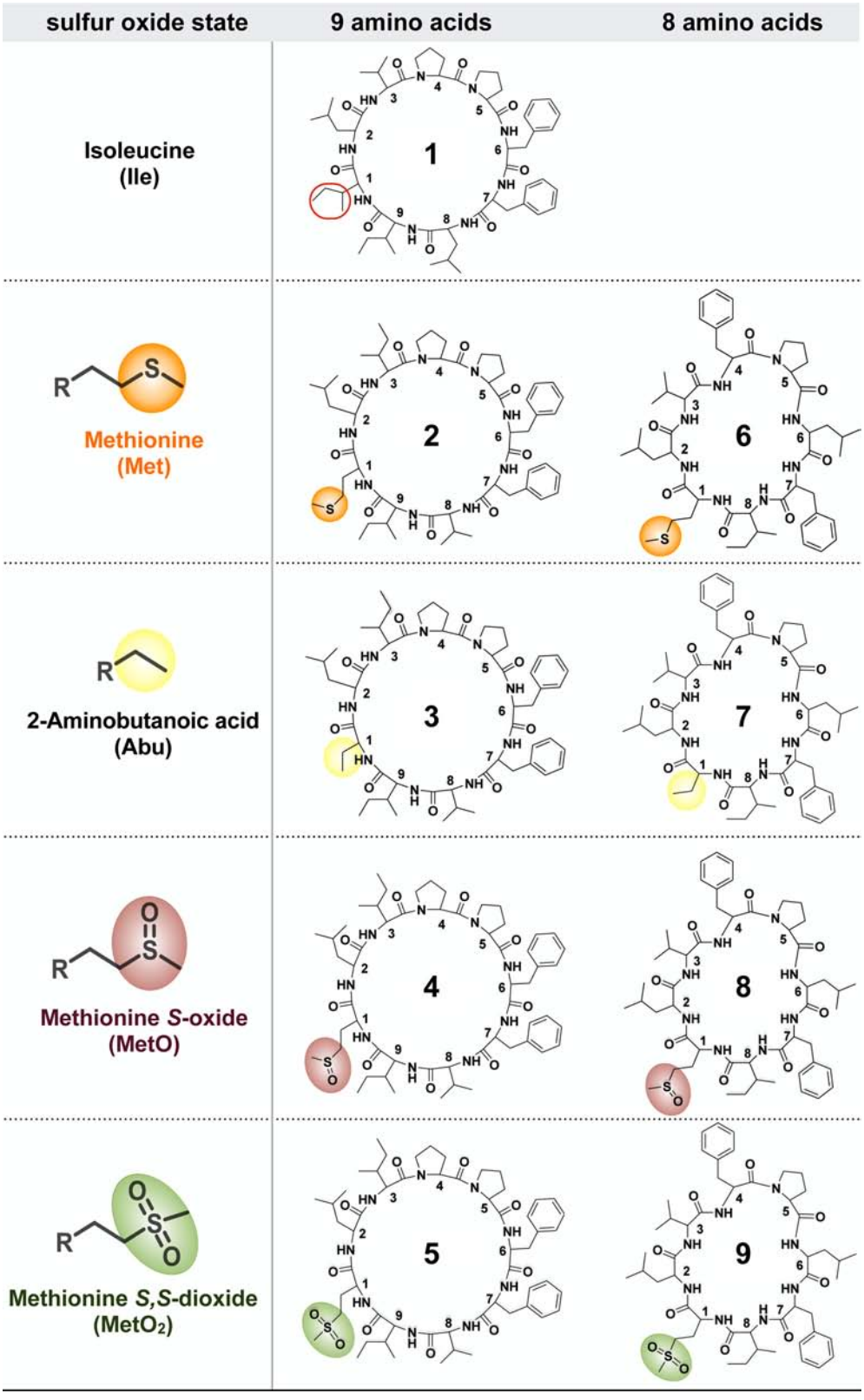

Figure 1. Structure of CLs used in the HSA binding studies.

filtered and degassed daily before use. A 10 mM sodium acetate buffer (pH 5.3) is generally adequate for immobilizing amine ligands onto a CM5 sensor chip and was used in all experiments. All buffer solutions were freshly prepared, degassed, and filtered with a 0.22 μm filter.

Surface Plasmon Resonance Analysis. SPR measurements were performed using a Biacore X instrument (Biacore AB, Uppsala, Sweden) equipped with an internal injection system (500 μL Hamilton syringe). This instrument has a flow injection system to enable real-time measurement of molecular binding. The SPR angle shift is used as a response unit (RU) to quantify the binding of biomolecules to the sensing surface (Figure 2B). The fluidic unit of the instrument was cleaned prior to experiments by injecting 0.5% sodium

DOI: 10.1021/jf504811x
J. Agric. Food Chem. 2015, 63, 1099−1106

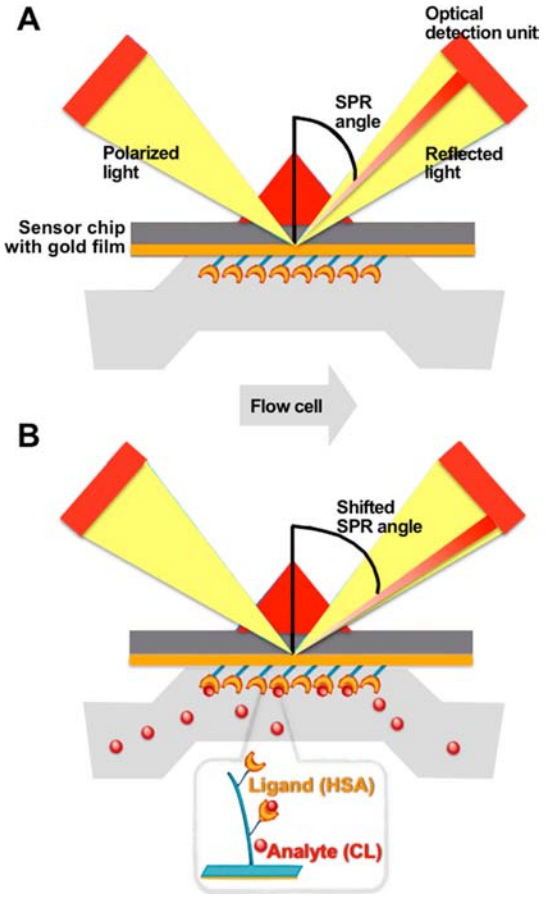

Figure 2. Principle of SPR phenomenon. (A) Polarized light is applied to the surface of the sensor chip and is reflected. The intensity of the reflected light is reduced at a certain incident angle, the SPR angle. (B) Interacting substances near the surface of the sensor chip increase the refractive index, which alters the SPR angle. The optical detection unit detects position changes in the wedge of the reflected light, corresponding to the SPR angle. The signals produced are measured in RU.

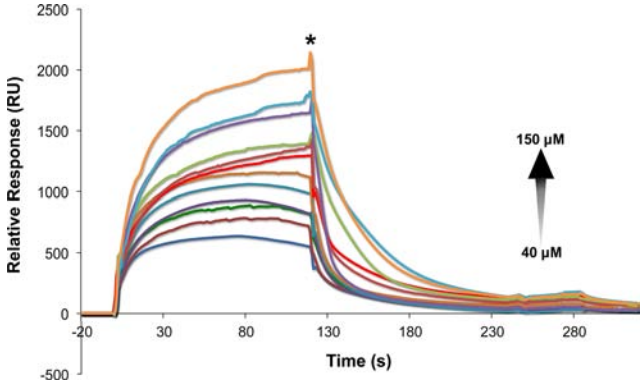

Figure 3. Concentration-dependent analysis of CL **1** complexes binding to HSA. All color plots indicate a spot exposed to 30 μg/mL HSA ligand and with various concentrations of CL **1** on the surface, respectively, with duplicates (omitting the regeneration stage). The response baseline is set to equal the level of HSA whereas time zero is set at the time of injection of CL **1**. One representative experiment is shown. All experiments are performed on the same sensor chip. The asterisk marks the end of the CL **1** injection and the beginning of CL **1** desorption.

dodecyl sulfate, followed by 50 mM glycine (pH 9.5). To reuse a chip for SPR analysis, bound analyte must be regenerated by stripping prior test compounds from the surface after each injection, usually with mild detergents. However, standard regeneration treatments did not effectively remove CLs from the HSA-immobilized chip. The only reagent that reproducibly did so was 6 M guanidine hydrochloride (GdnHCl) applied as a brief pulse (10 μL at 10 μL/min flow rate), followed by continued HBS-EP buffer flow (>5 min at 25 μL/min) to stabilize HSA prior to the next injection.

Immobilization of HSA. HSA was covalently immobilized onto a research-grade CM5 sensor surface at 25 °C using standard amine-coupling chemistry.[37] Briefly, CM5 sensor chips were preconditioned prior to HSA immobilization by priming the instrument three times with HBS-EP buffer, followed by three successive 1 min injections of 50 mM NaOH at 50 μL/min. Flow cell 1 (Fc1) and flow cell 2 (Fc2) were activated by a 7 min injection of a 1:1 mixture of 0.1 M NHS and 0.4 M EDC using a flow rate of 5 μL/min. HSA has an isoelectric point (p*I*) of 5.67 and is positively charged below this pH. Immediately after activation, HSA (30 μg/mL) was diluted in 10 mM acetate buffer (pH 5.3) to impart a positive charge on the HSA (Figure 4). Thereafter, the HSA is attracted to the negatively charged

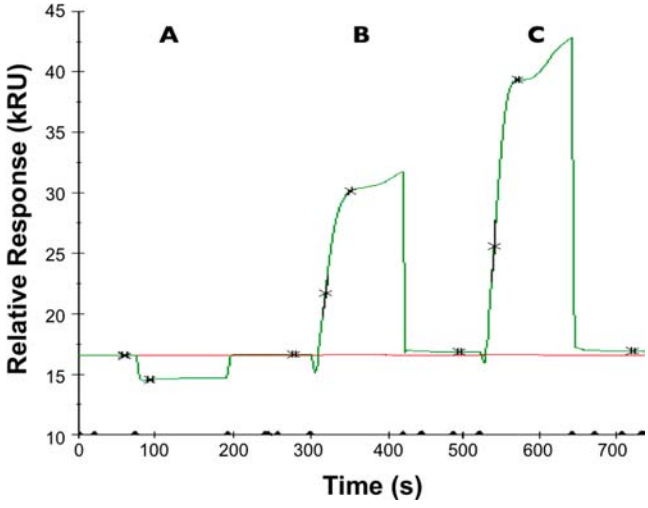

Figure 4. PH scouting of three successive electrostatic preconcentration assays for HSA (66 kDa MW and p*I* 5.67) as ligand. All HSA was diluted in 10 mM sodium acetate to a final concentration of 30 μg/mL, at three different pH values, (A) 5.5, (B) 5.3, and (C) 5.0, respectively.

matrix of the sensor chip and immobilized onto Fc2 (Figure 5). A solution of 10 mM acetate buffer without HSA was passed over Fc1, to act as the reference cell. A 7 min injection of 1.0 M EA (pH 8.5) using a flow rate of 5 μL/min was passed over Fc1 and Fc2 to deactivate unbound areas of the sensor surfaces. The thickness of the bilayer was calculated by assuming that 1 kRU corresponded to a 1 nm thick layer.[39] This bilayer was subsequently used as a model membrane surface to study the CL/HSA interactions. When kinetic analyses are performed, the ligand density should be as low as possible, provided signal-to-noise ratios are adequate. Direct detection of CL (ca. 1.0 kDa) binding to the immobilized HSA ligand (ca. 66 kDa) on a Biacore X generally requires immobilization responses.

CL Binding to HSA. For all CLs, 40 μL of analyte solution (40–150 μM) was injected, in duplicate, and flowed over reference and HSA surfaces for 2 min at a flow rate of 20 μL/min, followed by a dissociation phase of 2 min for all experimental conditions. At the end of the CL injection, the flow solution was switched to the running buffer, and a decrease in the response toward the baseline was observed within minutes. This decrease in response indicated that CLs were dissociating from the HSA immobilized to the sensor surface. All experiments were performed at 25 °C. When the baseline RU was not readily achieved, a short pulse of 50% (v/v) DMSO solution was injected at a high flow rate to remove any remaining CLs. Repeated

DOI: 10.1021/jf504811x
J. Agric. Food Chem. 2015, 63, 1099−1106

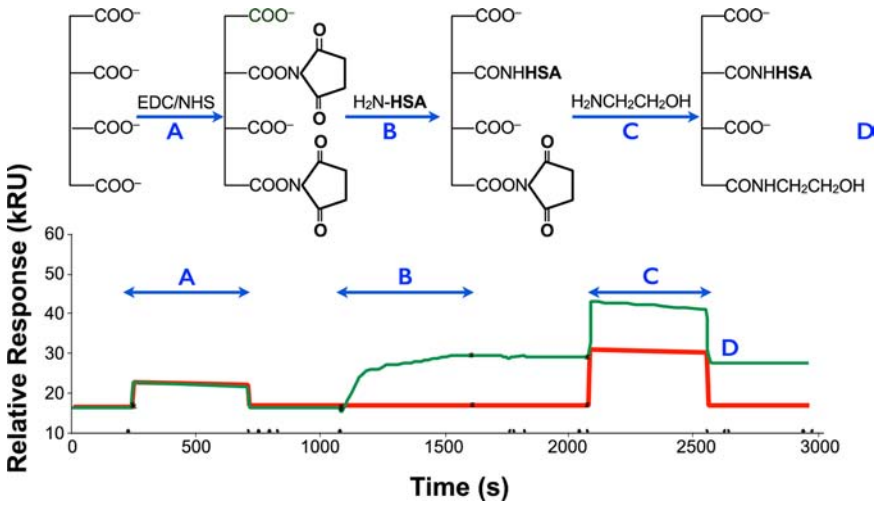

Figure 5. Steps in the immobilization of HSA ligand on a CM5 research-grade sensor chip via the amine coupling reaction (red line, reference surface; green line, HSA surface). The labeled portions of the graph indicate (A) injection of the EDC/NHS mixture (1:1, v/v) onto the surface, activating the carboxymethyl group by forming a highly reactive succinimide ester, followed by termination of the injection; (B) after surface activation, injection of ligand sample diluted in buffer of the appropriate, predetermined pH, with continuation of injection resulting in covalent binding of ligand to the reactive surface to yield; (C) blockage of remaining nonreacted-activated carboxymethyl groups by injection of ethanolamine solution, followed by cessation of injection; and (D) point of attained immobilization of ligand. Small triangles on time line below designate events such as injection, end of injection, and refilling.

Table 2. CL/HSA Equilibrium Binding Constants of Dissociation Determined from SPR Sensorgrams Using a 1:1 Interaction Model with a Drifting Baseline[a]

interaction CL[b]	k_a ($M^{-1}s^{-1}$)	k_d (s^{-1})	K_A (mM^{-1})	K_D (mM)	R_{max} (RU)	χ^2
1	6.55×10^{-1}	2.38×10^{-4}	2.75×10^{0}	3.64×10^{-1}	6.27×10^{3}	7.04×10^{2}
2	5.88×10^{0}	2.62×10^{-2}	2.25×10^{-1}	4.45×10^{0}	1.92×10^{4}	1.94×10^{3}
3	8.47×10^{0}	1.21×10^{-1}	7.01×10^{-2}	1.43×10^{1}	7.86×10^{4}	9.64×10^{2}
4	1.91×10^{2}	5.88×10^{-2}	3.25×10^{0}	3.08×10^{-1}	1.17×10^{3}	5.75×10^{2}
5	1.94×10^{2}	1.60×10^{-2}	1.21×10^{1}	8.27×10^{-2}	2.78×10^{2}	2.00×10^{1}
6	2.78×10^{0}	2.05×10^{-2}	1.35×10^{-1}	7.38×10^{0}	9.05×10^{4}	8.90×10^{3}
7	3.51×10^{0}	2.70×10^{-2}	1.30×10^{-1}	7.68×10^{0}	1.70×10^{4}	5.14×10^{2}
8	1.96×10^{2}	3.47×10^{-2}	5.64×10^{0}	1.77×10^{-1}	4.38×10^{3}	2.99×10^{1}
9	7.06×10^{-1}	1.20×10^{-3}	5.89×10^{-1}	1.70×10^{0}	1.01×10^{4}	1.02×10^{3}

[a]All experiments were performed on the same HSA-immobilized CM5 chip. Values are means of SPR assays performed in duplicate. [b]The slopes were determined from curve-fitting dose-response curves in Figure 3 and Figure S1 of the Supporting Information.

experiments indicated that the regeneration procedure did not change the binding characteristics of the immobilized HSA (data not shown).

The sensorgrams were analyzed by the global fitting procedure using a 1:1 (Langmuir type) drifting baseline model-derived equation[26] available in the BIA evaluation software (version 4.2). RU curves taken from the sensorgrams 10−30 s after association and the dissociation were used in the model. The association rate constant (k_a), the dissociation rate constant (k_d), and the dissociation equilibrium constants (K_D) were determined from the model at the minimal chi-squared (χ^2) value.

RESULTS AND DISCUSSION

Preconcentration Assays. Preconcentration assays were performed to determine the best immobilization buffer. Different preconcentration pH values were used to determine optimal binding of HSA to the sensor chip surface (Figure 4). Using ca. 12 kRU as a reasonable immobilization level for the direct kinetic assay of CL binding to a HSA surface, pH 5.5 produces inefficient preconcentration, resulting in low levels of the ligand binding to the carboxymethyl-dextran matrix of the sensor chip. At pH 5.3, efficient HSA preconcentration occurred, producing a satisfactory final response level (Figure 4B). In contrast, HSA uptake by the surface is too rapid at pH 5.0, resulting in an excessive final response (Figure 4C). Thus, for immobilization of HSA via the amine coupling reaction, a preconcentration pH of 5.3 was chosen.

HSA Covalent Immobilization. Typical SPR response sensorgrams of HSA immobilization are shown in Figure 5. In a first stage (A), the EDC/NHS activating mixture is injected with the consequent increase in the SPR signal due to a change in the bulk refractive index. The HSA solution is then injected, and the binding event (B) can be followed in real time. Once an adequate binding level is reached, the remaining active carboxyl-NHS esters are blocked with ethanolamine hydrochloride (C), causing a significant change in the bulk refractive index. The biospecific HSA surface is then ready to be used (D). The final immobilized HSA response is 12−13 kRU at the sensorgram.

Binding of the Bioactive Compound CLs to HSA. Interactions between **1** and immobilized HSA were measured (Figure 3). As the concentration of **1** increased from 40 to 150 μM, the binding signal steadily increased in RU. This result was similar to that reported by Rempel et al., although the response is significantly stronger in this study.[40] Interestingly, when the chip surface was saturated with analyte, the response

DOI: 10.1021/jf504811x
J. Agric. Food Chem. 2015, 63, 1099−1106

normalized by the concentration-dependent analysis should have yielded equal maximum responses. A CL:HSA (1:1) binding stoichiometry was observed, using a drifting baseline model (Table 2 and Figure S1 of the Supporting Information). Residual values from Figure 6 also support the closeness of this

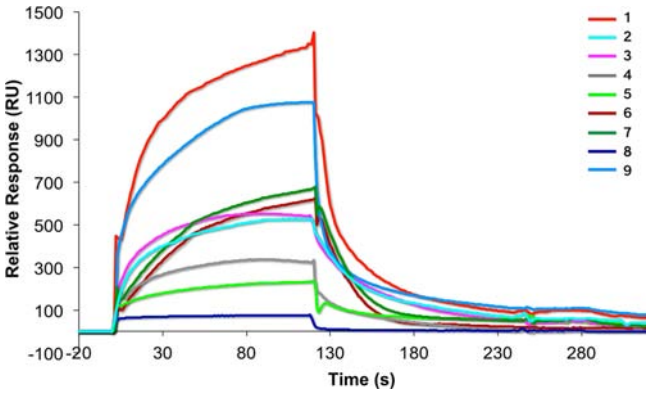

Figure 6. SPR sensorgram responses for 100 μM of different CLs binding to HSA. Colors of sensorgram traces are assigned in the legend.

1:1 ratio between the experimental and theoretical curves. All plots illustrated the experimental curve-fitting methodology for a simple binding model (1:1 Langmuir).

Data Processing and Evaluation. The concentration dependencies of different CLs binding to immobilized HSA for concentrations ranging between 40 and 150 μM were determined (Figure S1 of the Supporting Information). Sensorgrams corresponding to a nonspecific CL **8** injected on a HSA surface are shown in Figure 6 and Figure S1G. The sensorgrams are square-wave shaped due to a refractive index jump, which is confirmed by the fact that no CL **8** is bound to the HSA at the beginning of the dissociation phase: (1) CL **8** did not appreciably bind HSA; (2) the increase in RU caused by an increase in refractive index is largely the result of buffer injection; and (3) all other CLs examined formed HSA complexes as the association curve is relatively higher than observed in CL **8**.

In contrast, other sensorgrams correspond to a specific interaction between an injected CL and the immobilized HSA. Compared to the other CLs tested, CL **1** has slow association kinetics with HSA (Figure 6). At higher concentrations, the steady-state plateau was not reached after 120 s. The gradual increase of response to a steady state during CL **1** injection indicates slow recognition kinetics of CL **1** with the HSA binding site compared to other CLs tested (Figure 6). Quantitative kinetic data were initially extracted using the kinetics profiling within the Biacore Evaluation software. The slow recognition may be due to CL becoming available for interaction with HSA. It is likely that CL **1** has a large hydration sphere, which must dissociate before interaction with HSA is possible.

HSA has seven known fatty acid binding sites, each of which is known to bind other small, hydrophobic molecules. Two of the binding sites for small molecule drugs are known as Sudlow site I (warfarin binding site) and Sudlow site II (indole-benzodiazepine binding site).[41] Site I binds drug molecules that are structurally bulky, heterocyclic compounds with centrally localized negative polar/charges, and hydrophobic substitutions. It has been suggested that binding is through hydrophobic interactions between the analyte and a hydrophobic crevice within the binding cavity of site I.[42] The nature of CL binding was not proven in the present study.

The equilibrium parameters for several CL binding reactions with immobilized HSA were determined (Table 2). The K_A value indicated that the affinity tends to increase as the CL becomes more hydrophobic, although there are significant exceptions. The K_D showed more rapid dissociation of CLs **4**, **5**, and **8** than of CL **1** (Table 2 and Figure 6). This suggests that there is more binding of **1** at the highly hydrophobic crevice. All CLs tested were able to bind, showing more than an order of magnitude increase in the **8**/HSA binding (RU 71.0) and **1**/HSA, which was almost 20-fold higher (RU 1370.6) than **8**/HSA (Figure 6). Also, the oxidation state of the sulfur-containing amino acid residue in position 1 of CLs (**2**−**9**) was a component critical to binding. To examine the importance of this sulfur-containing residue (*S*), we synthesized CLs with 2-aminobutanoic acid (Abu) instead of methionine residues at this position (Table 1 and Figure 1). These modified compounds are named [1−9-NαC],[1-Abu]-CLB (**3**)[35] and [1−8-NαC],[1-Abu]-CLE (**7**)[36] according to established conventions. Each of the S-free [1-Abu]-CLs had similar binding strengths to their 2-Met-containing counterparts (Figure 6). Most strikingly, the conversion of methionine sulfoxide to the sulfone peptide [1−8-NαC],[1-MetO_2]-CLE (**9**) had the greatest effect on binding (Figure 6 and Figure S1 of the Supporting Information). It can be speculated that this was an effect of structural differences between CLs **6** and **9** and CLs **8** and **9** induced by the oxygen−sulfur bonds or the dipole moment of the *S*-oxide group. A similar but less pronounced effect was observed with CLs **2**−**5**. The conservative introduction of an oxygen group to **2** leads to a partial disruption of the HSA interaction and weak binding of compound **4**, whereas the addition of two oxygen groups results in **5** with 4-fold stronger binding than that of **4** (the most polar CL tested).

CLs are produced in plants via expression of genes that code for multiple CLs.[1] The peptides produced in the same reading frame are usually produced in constant ratios in the plant determined by transcription and post-translational modification of the peptide gene. In an attempt to observe the sensorgram of peptides encoded by the same gene after different post-translational modification, we compared three mixtures of three peptides each with a similar modification of methionine. The slow release of the stronger binding groups (CL mixtures **1_2_6**; **1_3_7**; and **1_5_9**) suggested that parameters would also be important in understanding their HSA binding (Figure 7). The fast dissociation of CL mixture **1_4_8** showed weak binding with HSA. This is due to the contribution from breaking of the solution complex and hydrophobic binding. It has been observed that CL mixture **1_2_6** is observed in flaxseed meal products with prolonged storage. This mixture is the major product of a single gene located on scaffold 1198 coded on the 3′ to 5′ strand bases 162067−161526 available via Phytozome portal (version 9.1). Flaxseed oil CLs **2** and **6** become oxidized to **4** and **8**, respectively. Finally, excessive oxidation will produce **5** and **9**.[43]

In conclusion, the K_D of CL/HSA solution is correlated with both the methionine oxidation state and polarity. The binding of methionine-containing CLs with HSA was similar to that of peptides that had Abu in place of methionine but greater than that of peptides with methionine *S*-oxide. The dipole moment of the *S*-oxide likely contributes to decreased affinity.

DOI: 10.1021/jf504811x
J. Agric. Food Chem. 2015, 63, 1099−1106

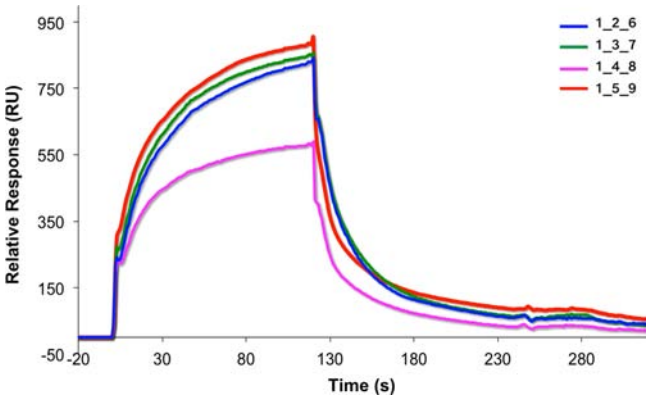

Figure 7. SPR sensorgram responses for 100 μM of each CL mixture binding to HSA.

Conversely, increased oxidation of the methionine *S*-oxide to form the *S*,*S*-dioxide produces a molecule with restored HSA binding. These findings show that cyclic peptides and particularly CLs can be used to study the discrete effects of changing a single amino acid on receptor binding. Other studies on more complex molecules may not allow the examination of a single substitution. For example, oxidation of methionine residues in human IgG2 Fc decreased SPR binding affinities to protein A.[44] Comparison of the equilibrium dissociation constants to other literature compounds indicates that CL binding to HSA is not comparatively strong when compared with that of other drugs, except that the values of K_D for **5** and **8** were similar to those reported for pyrimethamine and rifampicin bindings, respectively.[45] In this study the impact of sulfur oxidation and elimination was observed for orbitides containing methionine and its modified analogues.

■ ASSOCIATED CONTENT

Ⓢ Supporting Information

Concentration-dependent analysis of different CLs (**2**–**9**) binding to immobilized HSA (Figure S1A–H). This material is available free of charge via the Internet at http://pubs.acs.org.

■ AUTHOR INFORMATION

Corresponding Authors

*(Y.Y.S.) Phone: (306) 966-5050. Fax: (306) 966-5015. E-mail: younyoung.shim@usask.ca.

*(M.J.T.R.) Phone: (306) 966-5027. Fax: (306) 966-5015. E-mail: martin.reaney@usask.ca.

Funding

This work was funded by the Saskatchewan Agricultural Development Fund (Saskatchewan Ministry of Agriculture, Project 20080205) and the Natural Sciences and Engineering Research Council (NSERC).

Notes

The authors declare no competing financial interest.

■ ACKNOWLEDGMENTS

We thank Dr. D. J. Craik (Institute for Molecular Bioscience, The University of Queensland) for helpful comments, Dr. R. Sammynaiken of Saskatchewan Structural Sciences Centre (SSSC) for his advise and help with Biacore X studies, and J. Maley of SSSC for performing initial trials with ligand-analyte interactions.

■ REFERENCES

(1) Arnison, P. G.; Bibb, M. J.; Bierbaum, G.; Bowers, A. A.; Bugni, T. S.; Bulaj, G.; Camarero, J. A.; Campopiano, D. J.; Challis, G. L.; Clardy, J.; Cotter, P. D.; Craik, D. J.; Dawson, M.; Dittmann, E.; Donadio, S.; Dorrestein, P. C.; Entian, K. D.; Fischbach, M. A.; Garavelli, J. S.; Goransson, U.; Gruber, C. W.; Haft, D. H.; Hemscheidt, T. K.; Hertweck, C.; Hill, C.; Horswill, A. R.; Jaspars, M.; Kelly, W. L.; Klinman, J. P.; Kuipers, O. P.; Link, A. J.; Liu, W.; Marahiel, M. A.; Mitchell, D. A.; Moll, G. N.; Moore, B. S.; Muller, R.; Nair, S. K.; Nes, I. F.; Norris, G. E.; Olivera, B. M.; Onaka, H.; Patchett, M. L.; Piel, J.; Reaney, M. J. T.; Rebuffat, S.; Ross, R. P.; Sahl, H. G.; Schmidt, E. W.; Selsted, M. E.; Severinov, K.; Shen, B.; Sivonen, K.; Smith, L.; Stein, T.; Sussmuth, R. D.; Tagg, J. R.; Tang, G. L.; Truman, A. W.; Vederas, J. C.; Walsh, C. T.; Walton, J. D.; Wenzel, S. C.; Willey, J. M.; van der Donk, W. A. Ribosomally synthesized and post-translationally modified peptide natural products: overview and recommendations for a universal nomenclature. *Nat. Prod. Rep.* **2013**, *30*, 108–160.

(2) Picur, B.; Cebrat, M.; Zabrocki, J.; Siemion, I. Z. Cyclopeptides of *Linum usitatissimum*. *J. Pept. Sci.* **2006**, *12*, 569–574.

(3) Benedetti, E.; Pedone, C. Cyclolinopeptide A: inhibitor, immunosuppressor or other? *J. Pept. Sci.* **2005**, *11*, 268–272.

(4) Brühl, L.; Matthäus, B.; Fehling, E.; Wiege, B.; Lehmann, B.; Luftmann, H.; Bergander, K.; Quiroga, K.; Scheipers, A.; Frank, O.; Hofmann, T. Identification of bitter off-taste compounds in the stored cold pressed linseed oil. *J. Agric. Food Chem.* **2007**, *55*, 7864–7868.

(5) Jadhav, P. D.; Okinyo-Owiti, D. P.; Ahiahonu, P. W. K.; Reaney, M. J. T. Detection, isolation and characterisation of cyclolinopeptides J and K in ageing flax. *Food Chem.* **2013**, *138*, 1757–1763.

(6) Reaney, M. J. T.; Jia, Y.; Shen, J.; Schock, C.; Tyler, N.; Elder, J.; Singh, S. Recovery of hydrophobic peptides from oils. U.S. Patent 8,383,172, 2013.

(7) Rossi, F.; Saviano, M.; Talia, P. D.; Blasio, B. D.; Redone, C.; Zanotti, G.; Mosca, M.; Saviano, G.; Tancredi, T.; Ziegler, K.; Benedetti, E.; Sons, I. Solution and solid state structure of an aib-containing cyclodecapeptide inhibiting the cholate uptake in hepatocytes. *Biopolymers* **1996**, *40*, 465–478.

(8) Wieczorek, Z.; Bengtsson, B.; Trojnar, J.; Siemion, I. Z. Immunosuppressive activity of cyclolinopeptide A. *Pept. Res.* **1991**, *4*, 275–283.

(9) Morita, H.; Shishido, A.; Matsumoto, T.; Takeya, K.; Itokawa, H.; Hirano, T.; Oka, K. A new immunosuppressive cyclic nonapeptide, cycloinopeptide B from *Linum usitatissimum*. *Bioorg. Med. Chem. Lett.* **1997**, *7*, 1269–1272.

(10) Morita, H.; Shishido, A.; Matsumoto, T.; Itokawa, H.; Takeya, K. Cyclolinopeptides B–E, new cyclic peptides from *Linum usitatissimum*. *Tetrahedron* **1999**, *55*, 967–976.

(11) Gründemann, C.; Koehbach, J.; Huber, R.; Gruber, C. W. Do plant cyclotides have potential as immunosuppressant peptides? *J. Nat. Prod.* **2012**, *75*, 167–174.

(12) Gründemann, C.; Thell, K.; Lengen, K.; Garcia-Kaufer, M.; Huang, Y. H.; Huber, R.; Craik, D. J.; Schabbauer, G.; Gruber, C. W. Cyclotides suppress human T-lymphocyte proliferation by an interleukin 2-dependent mechanism. *PLoS One* **2013**, *8*, No. e68016.

(13) Gaymes, T. J.; Cebrat, M.; Siemion, I. Z.; Kay, J. E. Cyclolinopeptide A (CLA) mediates its immunosuppressive activity through cyclophilin-dependent calcineurin inactivation. *FEBS Lett.* **1997**, *418*, 224–227.

(14) Witkowska, R.; Donigiewicz, A.; Zimecki, M.; Zabrocki, J. New analogue of cyclolinopeptide B modified by amphiphilic residue of α-hydroxymethylmethionine. *Acta Biochim. Polym.* **2004**, *51*, 67–72.

(15) Siemion, I. Z.; Cebrat, M.; Wieczorek, Z. Cyclolinopeptides and their analogs – a new family of peptide immunosuppressants affecting the calcineurin system. *Arch. Immunol. Ther. Exp.* **1999**, *47*, 143–153.

(16) Munter, K.; Mayer, D.; Faulstich, H. Characterization of a transporting system in rat hepatocytes. Studies with competitive and non-competitive inhibitors of phalloidin transport. *Biochim. Biophys. Acta* **1986**, *860*, 91–98.

DOI: 10.1021/jf504811x
J. Agric. Food Chem. 2015, 63, 1099–1106

(17) Kessler, H.; Klein, M.; Müller, A.; Wagner, K.; Bats, J. W.; Ziegler, K.; Frimmer, M. Conformational prerequisites for the *in vitro* inhibition of cholate uptake in hepatocytes by cyclic analogues of antamanide and somatostatin. *Angew. Chem., Int. Ed. Engl.* **1986**, *25*, 997−999.
(18) Ziegler, K.; Frimmer, M.; Kessler, H.; Haupt, A. Azidobenzamido-008, a new photosensitive substrate for the 'multispecific bile acid transporter' of hepatocytes: evidence for a common transport system for bile acids and cyclosomatostatins in basolateral membranes. *Biochim. Biophys. Acta* **1988**, *945*, 263−272.
(19) Münter, K.; Mayer, D.; Faulstich, H. Characterization of a transporting system in rat hepatocytes. Studies with competitive and non-competitive inhibitors of phalloidin transport. *Biochim. Biophys. Acta* **1986**, *860*, 91−98.
(20) Bell, A.; McSteen, P. M.; Cebrat, M.; Picur, B.; Siemion, I. Z. Antimalarial activity of cyclolinopeptide A and its analogues. *Acta Polym. Pharm.* **2000**, *57*, 134−136.
(21) Matsumoto, T.; Shishido, A.; Morita, H.; Itokawa, H.; Takeya, K. Cyclolinopeptides F−I, cyclic peptides from linseed. *Phytochemistry* **2001**, *57*, 251−260.
(22) Fasano, M.; Curry, S.; Terreno, E.; Galliano, M.; Fanali, G.; Narciso, P.; Notari, S.; Ascenzi, P. The extraordinary ligand binding properties of human serum albumin. *IUBMB Life* **2005**, *57*, 787−796.
(23) Peters, T. *All about Albumin: Biochemistry, Genetics and Medical Applications*; Academic: San Diego, CA, USA, 1996; pp 51−54.
(24) Doumas, B. T.; Peters, T., Jr. Serum and urine albumin: a progress report on their measurement and clinical significance. *Clin. Chim. Acta* **1997**, *258*, 3−20.
(25) Kragh-Hansen, U. Molecular aspects of ligand binding to serum albumin. *Pharmacol. Rev.* **1981**, *33*, 17−53.
(26) Liu, J.; Tian, J.; Hu, Z.; Chen, X. Binding of isofraxidin to bovine serum albumin. *Biopolymers* **2004**, *73*, 443−450.
(27) Kragh-Hansen, U.; Chuang, V. T.; Otagiri, M. Practical aspects of the ligand-binding and enzymatic properties of human serum albumin. *Biol. Pharm. Bull.* **2002**, *25*, 695−704.
(28) Gao, H.; Lei, L.; Liu, J.; Kong, Q.; Chen, X.; Hu, Z. The study on the interaction between human serum albumin and a new reagent with antitumour activity by spectrophotometric methods. *J. Photochem. Photobiol., A* **2004**, *167*, 213−221.
(29) Trynda-Lemiesz, L.; Karaczyn, A.; Keppler, B. K.; Kozlowski, H. Studies on the interactions between human serum albumin and transindazolium (bisindazole) tetrachlororuthenate(III). *J. Inorg. Biochem.* **2000**, *78*, 341−346.
(30) Li, Y.; He, W.; Liu, J.; Sheng, F.; Hu, Z.; Chen, X. Binding of the bioactive component jatrorrhizine to human serum albumin. *Biochim. Biophys. Acta* **2005**, *1722*, 15−21.
(31) Pelton, J. T.; McLean, L. R. Spectroscopic methods for analysis of protein secondary structure. *Anal. Biochem.* **2000**, *277*, 167−176.
(32) Min, J.; Meng-Xia, X.; Dong, Z.; Yuan, L.; Xiao-Yu, L.; Xing, C. Spectroscopic studies on the interaction of cinnamic acid and its hydroxyl derivatives with human serum albumin. *J. Mol. Struct.* **2004**, *692*, 71−80.
(33) Trynda-Lemiesz, L. Paclitaxel-HSA interaction. Binding sites on HSA molecule. *Bioorg. Med. Chem.* **2004**, *12*, 3269−3275.
(34) Wang, C. K.; Gruber, C. W.; Cemazar, M.; Siatskas, C.; Tagore, P.; Payne, N.; Sun, G.; Wang, S.; Bernard, C. C.; Craik, D. J. Molecular grafting onto a stable framework yields novel cyclic peptides for the treatment of multiple sclerosis. *ACS Chem. Biol.* **2014**, *9*, 156−163.
(35) Olivia, C. M.; Burnett, P.-G. G.; Okinyo-Owiti, D. P.; Shen, J.; Reaney, M. J. T. Rapid reversed-phase liquid chromatography separation of cyclolinopeptides with monolithic and microparticulate columns. *J. Chromatogr., B* **2012**, *904*, 128−134.
(36) Reaney, M. J. T.; Burnett, P.-G.; Jadhav, P. D.; Okinyo-Owiti, D. P.; Shen, J.; Shim, Y. Y. Cyclic peptide mixtures from flaxseed and uses thereof. World Intellectual Property Organization (WIPO), WO/2013/091070 A1, 2013.
(37) Chaiken, I.; Rose, S.; Karlsson, R. Analysis of macromolecular interactions using immobilized ligands. *Anal. Biochem.* **1992**, *201*, 197−210.
(38) Frostell-Karlsson, Å.; Remaeus, A.; Roos, H.; Andersson, K.; Borg, P.; Hämäläinen, M.; Karlsson, R. Biosensor analysis of the interaction between immobilized human serum albumin and drug compounds for prediction of human serum albumin binding levels. *J. Med. Chem.* **2000**, *43*, 1986−1992.
(39) Biacore. *Real-Time Analysis of Biomolecular Interactions: Applications of Biacore*; Springer: New York, 2000.
(40) Rempel, B.; Gui, B.; Maley, J.; Reaney, M.; Sammynaiken, R. Biomolecular interaction study of cyclolinopeptide A with human serum albumin. *J. Biomed. Biotechnol.* **2010**, *2010*, 1−8.
(41) Sudlow, G.; Birkett, D. J.; Wade, D. N. The characterization of two specific drug binding sites on human serum albumin. *Mol. Pharmacol.* **1975**, *11*, 824−382.
(42) Rich, R. L.; Myszka, D. G. Survey of the year 2005 commercial optical biosensor literature. *J. Mol. Recognit.* **2006**, *19*, 478−534.
(43) Jadhav, P.; Schatte, G.; Labiuk, S.; Burnett, P. G.; Li, B.; Okinyo-Owiti, D.; Reaney, M.; Grochulski, P.; Fodje, M.; Sammynaiken, R. Cyclolinopeptide K butanol disolvate monohydrate. *Acta Crystallogr. Sect. E: Struct. Rep. Online* **2011**, *67*, o2360−o2361.
(44) Pan, H.; Chen, K.; Chu, L.; Kinderman, F.; Apostol, I.; Huang, G. Methionine oxidation in human IgG2 Fc decreases binding affinities to protein A and FcRn. *Protein Sci.* **2009**, *18*, 424−433.
(45) Rich, R. L.; Day, Y. S.; Morton, T. A.; Myszka, D. G. High-resolution and high-throughput protocols for measuring drug/human serum albumin interactions using BIACORE. *Anal. Biochem.* **2001**, *296*, 197−207.
(46) Shim, Y. Y.; Gui, B.; Arnison, P. G.; Wang, Y.; Reaney, M. J. T. Flaxseed (*Linum usitatissimum* L.) bioactive compounds and peptide nomenclature: a review. *Trends Food Sci. Technol.* **2014**, *38*, 5−20.

DOI: 10.1021/jf504811x
J. Agric. Food Chem. 2015, 63, 1099−1106

predominantly pressure, temperature, and solvent type.[10] As a number of factors can influence the course of the extraction, the screening and optimization of the significant factors must be carried out to establish a reliable analytical PLE method. In the study described here, seven extraction factors were evaluated, namely, solvent composition, extraction temperature, pressure, flushing, static time, solvent purge, and sample weight.

In PLE the pressure generally acts by forcing liquid into the solid matrix.[14] In addition, an increase in pressure leads to an increase in the extraction rate because, if sufficient pressure is exerted on the solvent during extractions, temperatures above the boiling point can be reached while the solvent is maintained in the liquid state.[15]

Temperature plays a role in enhancing the extraction yield because higher temperatures can decrease the viscosity of liquid solvents, thus permitting faster diffusion rates and better penetration into the matrix. Furthermore, thermal energy can disrupt the strong interactions between the solute molecules and active sites on the matrix, and this can aid the release of target molecules. However, as melatonin is sensitive to temperature,[16] a preliminary study on its stability under different PLE temperatures was required to define the working temperature range for the optimization.

The extraction yields from plant samples are highly dependent on the nature of the solvent employed[17] because of the effects of both the solvent diffusivity and the solvent polar properties. The polarity of the solvent will affect the extraction depending on the polar properties of the target compound. On the other hand, the enhanced diffusivity of the solvent leads to an increase in extraction speed and efficiency.[18] The amphipathic structure of the melatonin molecule, which is composed of polar and nonpolar moieties, makes it difficult to select a solvent that yields complete recovery.[19] In the study described here, this constraint was therefore taken into account in a preliminary study by screening several solvents, including water, methanol, ethanol, and ethyl acetate, prior to the selection of the extraction solvents to be used in the optimization experiments.

A factorial design with a reduced number of runs is preferable to a full factorial design for more than four factors, particularly when the available resources are limited. Therefore, a chemometrical approach based on a fractional factorial design (FFD) is a reasonable option to evaluate the significance of the studied factors prior to optimization of the PLE conditions.[20,21] The particular focus of this study was on the optimization and validation of PLE for the extraction of melatonin from rice grains using an FFD.

MATERIALS AND METHODS

Chemicals and Reagents. HPLC grade methanol (MeOH), ethanol (EtOH), ethyl acetate (EtOAc), and acetic acid were purchased from Merck (Darmstadt, Germany). Melatonin standard was obtained from Sigma-Aldrich (St. Louis, MO, USA). Water was purified with a Milli-Q purification system (Millipore, Billerica, MA, USA).

Rice Sample Preparation. Red rice samples from Thailand were used in this study. A rice sample (20 g) was placed in a plastic cylinder, and the rice grains were milled with an Ultraturrax homogenizer (IKA T25 Digital, Germany) for 10 min prior to extraction. The milling process was stopped every minute to avoid excessive heating of the sample. The fine powder of rice grain was then homogenized by stirring, and the samples were stored at room temperature in a closed container until analysis (1−5 weeks depending on the sample). No specific humidity conditions were applied during storage. The final extraction method was applied to a wide range of rice products available in the market, and these covered the varieties of polished (short and long) grain, whole (short and semilong) grain, aromatic rice, black rice, black glutinous rice, red rice, and parboiled rice products. Samples were acquired in several different markets in Spain.

Extraction of Melatonin. Pressurized liquid extraction (PLE) of melatonin was performed in a Dionex ASE 200 extractor (Dionex, Sunnyvale, CA, USA) equipped with stainless steel extraction cells (11 mL volume) and collection vials (60 mL capacity). A cellulose filter (Dionex) was inserted at the outlet end of the extraction cell. Rice powder was accurately weighed and loaded into the extraction cell, and washed sea sand was used to complete the extraction cell. The extraction cell was then filled with the extraction solvent (80−100% EtOAc in MeOH), pressurized (100−200 atm), and heated (100−200 °C). The cell was heated for a fixed time to guarantee that the sample reached thermal equilibrium. The sample was then extracted in a static extraction cycle (5−10 min) with the solvent at the experimental temperature and pressure. After the extraction, the cell was rinsed with fresh solvent (50−100% of the extraction cell volume) and purged with a flow of nitrogen for 60−120 s. The extract was dried under vacuum in a rotary evaporator. The residue was reconstituted with methanol and adjusted to a final volume of 5 mL. The liquid was then passed through a 0.45 μm nylon filter prior to injection in the HPLC-FD system.

Determination of Melatonin. High-performance liquid chromatography (HPLC) analyses were carried out on an Alliance HPLC 2695 system with a fluorescence detector (Waters 474 fluorescence detector), controlled by an Empower Pro 2002 data station (Waters, Milford, MA, USA). Separations were performed in a reverse phase RP 18 Lichrospher Column [LiChroCART 250 × 4 (5 μm)] from Merck at a temperature of 25 °C.

The mobile phase was a binary solvent system consisting of phase A (2% acetic acid and 5% methanol in water) and phase B (2% acetic acid and 88% methanol in water) with a flow rate of 0.5 mL min^{-1}. The mobile phase was filtered through a 0.45 μm membrane filter (Millipore) and degassed for 15 min prior to use. The 25 min programmed gradient was as follows: (time, solvent B): 0 min, 0%; 5 min, 35%; 12 min, 40%; 15 min, 40%; 20 min, 45%; 25 min, 50%. After each extraction, the column was washed with 100% B for 5 min and equilibrated with 0% B for 5 min. The established conditions for the fluorescence detector were as follows: excitation wavelength, 290 nm; emission wavelength, 330 nm; gain, 1000; attenuation, 16; injection volume, 10 μL.

Performance of the Method. The chromatographic method used to determine melatonin was performed according to the suggestions of ISO 17025 and the recommendations of ICH Guideline Q2 (R1).[22,23] The range, linearity, recovery, precision, detection, and quantification limits of the method were evaluated.

Linearity was estimated to express how the method provides test results that are directly proportional to the melatonin concentration within the studied range. A series of dilutions from a stock solution of melatonin were carried out to give concentrations ranging from 0.75 to 15 μg L^{-1} and from 15 to 750 μg L^{-1}. Gnumeric 1.12.17 was used to generate the regression analysis of the calibration curves. The standard deviation estimated for the response and the slope from the regression were then used to calculate the limit of detection (LOD) and the limit of quantification (LOQ).

A certified reference material was not available for melatonin in rice matrices and, as a consequence, definitive statements cannot be made with regard to accuracy. Nonetheless, the extraction recovery (%R) was determined by comparing the absolute response of the analytes spiked in control samples before and after the extraction procedure.

The precision of the method was evaluated by studying the repeatability (intraday) and intermediate precision (extraday). Repeatability was assessed by nine independent analyses of the same samples on the same day, whereas intermediate precision was determined by three independent analyses on three consecutive days. Precision was expressed as the coefficient of variance (CV) of the retention time and peak height. The acceptable CV limit is ±10% according to the AOAC manual for the Peer-Verified Methods

DOI: 10.1021/jf505106m
J. Agric. Food Chem. 2015, 63, 1107−1115

Table 1. Analytical Characteristics for the Determination of Melatonin by HPLC-FD

						intraday, CV (%)			
						n = 9		n = 3 × 3	
linear range (μg L^{-1})	observations	linear eq	R^2	LOD (μg L^{-1})	LOQ (μg L^{-1})	RT	height	RT	height
0.75−15	6	y = 580.79x − 1806.8	0.996	1.15	3.84	0.99	0.93	1.23	2.05
15−750	6	y = 615.11x − 961.13	0.999						

program.[24] The CV values with reference to the peak height for both repeatability and intermediate precision were <10%, thus showing that the method has a satisfactory precision. The analytical properties for the chromatographic method for the determination of melatonin are listed in Table 1.

Experimental Design and Optimization. The effects of the tested independent factors on the response within the studied range were evaluated by performing a fractional factorial design (FFD), that is, a 2^{7-2} (quarter fraction) screening design with a central point analysis. The extraction factors included in the design were solvent composition (x_1), extraction temperature (x_2), pressure (x_3), flushing (x_4), static time (x_5), purge (x_6), and sample weight (x_7). Because the variables have different units and ranges, each of the variables was first normalized and forced to range from −1 to +1 to obtain a more even response.[25] Therefore, the factor levels were denoted −1 (low), 0 (central point), and 1 (high). The variables were coded according to the equation

$$x_i = \frac{x_i - x_0}{\Delta x} \quad (1)$$

where x_i is the coded value of the factor x_i, x_0 is the value of x at the center point, and Δx is the increment of x_i corresponding to a variation per unit of x_i. The factors included in the design are shown in Table 2 along with their respective levels. The whole design consisted of 33 runs carried out in random order, and these are presented in Table 3.

Table 2. Coding Table of Experimental Factors and Levels

factor	−1	0	+1	unit
x_1, solvent	80	90	100	% EtOAc in MeOH
x_2, temperature	100	150	200	°C
x_3, pressure	100	150	200	atm
x_4, flushing	50	75	100	%
x_5, static	5	8	10	min
x_6, purge	60	90	120	s
x_7, sample weight	2.5	3.75	5	g

The design of experiment (DOE) matrix was established with the highest possible resolution and the lowest level of aliasing. Thus, resolution (R) of IV and the effects of two factors confounded with high-order interactions between the four other factors was used. The 2^{7-2}_{IV} fractional factorial design allowed the first four variables (x_1−x_4) to be set, and thus the DOE was obtained by establishing the full 2^5 factorial as the basic design (with the four factors x_1, x_2, x_3, and x_4); factors x_6 and x_7 were subsequently equated to the $x_1x_2x_3x_4$ and $x_1x_2x_4x_5$ interactions, respectively. This particular design produced the following defining relationships: $I = x_1x_2x_3x_4x_6 = x_1x_2x_4x_5x_7 = x_3\ x_5\ x_6x_7$. The second order response function for this fractional factorial design is

$$y = \beta_0 + \sum_{k}^{i=1} \beta_i x_i + \sum \sum_{j<i} \beta_{ij} x_i x_j + \varepsilon \quad (2)$$

where β_i (i = 1, 2, ..., 7) is the parameter estimated for the factor i, β_{ij} (i = 1, 2, ..., 7; j = 1, 2, ..., 7) is the parameter estimated for the interaction between variables i and j; x_i is the coded form of factor i that influences the response y; and x_i is the coded form of factor i that influences the response y. This model provides information on only the linear and two-factor interaction effects and assumes that three-factor and higher factor interactions are negligible.

The experimental results in single-factor experiments were analyzed using Gnumeric 1.12.17. The analysis of variance (ANOVA) and least significant difference (LSD) test were used to determine the significance of differences between the means.

RESULTS AND DISCUSSION

Preliminary Study: Stability of Melatonin during the PLE. Extraction temperature is the most crucial factor that affects the stability of melatonin because the extraction process is carried out at high temperature, which can even be above the boiling point of the solvent at atmospheric pressure. The stability of melatonin at different PLE temperatures was evaluated prior to the analytical method development. The level of melatonin in a standard solution was assessed after heating at 50, 100, 150, 175, and 200 °C.

The effect of PLE temperature on the stability of melatonin was analyzed using single-factor ANOVA. The retained melatonin was expressed by the signal height (mV) of the melatonin peak. The ANOVA showed that the different levels of melatonin exposed to different PLE temperatures were all stable. The applied PLE temperatures did not have a significant effect (p = 0.05) on the stability of melatonin because $F_{calculated}$ (0.7) was less than $F_{critical}$ (5.1). As the melatonin levels remained unchanged under the PLE temperatures tested, the optimization range for the temperature factor was defined between 100 and 200 °C.

Solvent Selection. Due to its amphipathic behavior, the extraction of melatonin must be carried out using a specific solvent for a sample with certain characteristics. As a point of reference, the extraction of melatonin from *Juglans regia* L. was achieved using MeOH and chloroform,[26] EtOAc was employed to extract melatonin from *Lupinus albus* L. roots,[27] hot water was used for the extraction from the three flowers from *Tanacetum parthenium*, *Tripleurospermum disciforme*, and *Viola odorata*,[28] and EtOH was employed for extractions from 15 seeds of edible plants including rice.[29] As a result, different solvents have been reported to be useful for the extraction of melatonin from different sources, although previous reports on the extraction of melatonin using PLE were not found. The behavior of solvents during PLE can be rather different from their behavior under regular extraction conditions and, as a consequence, several solvents, namely, MeOH, EtOAc, water, and EtOH, were evaluated to select the most suitable solvent for the PLE of melatonin from rice samples. The extraction efficiencies for melatonin with different solvents are shown in Figure 2.

The results showed that EtOAc as the extraction solvent gave a better yield than MeOH and EtOH. In contrast, water was not a suitable solvent to extract melatonin from rice samples with the PLE system as it can lead to starch gelatinization during the extraction process. This phenomenon occurs due to the presence of starch and water, which, when subjected to heat, leads to swelling of the starch granules as the water is

DOI: 10.1021/jf505106m
J. Agric. Food Chem. 2015, 63, 1107−1115

Table 3. Experimental Factors of the 2_{IV}^{7-2} FFD and the Experimental Yield for the PLE

order	run	solvent, x_1	temperature, x_2	pressure, x_3	flushing, x_4	static, x_5	purge, x_6	sample wt, x_7	rel values to max response (%)
1	22	−1	−1	−1	−1	−1	1	1	0.38
2	17	1	−1	−1	−1	−1	−1	−1	0.50
3	6	−1	1	−1	−1	−1	−1	−1	93.95
4	9	1	1	−1	−1	−1	1	1	52.16
5	28	−1	−1	1	−1	−1	−1	1	0.35
6	16	1	−1	1	−1	−1	1	−1	0.48
7	24	−1	1	1	−1	−1	1	−1	100.00
8	32	1	1	1	−1	−1	−1	1	77.16
9	14	−1	−1	−1	1	−1	−1	−1	0.48
10	20	1	−1	−1	1	−1	1	1	0.39
11	30	−1	1	−1	1	−1	1	1	85.71
12	5	1	1	−1	1	−1	−1	−1	93.39
13	29	−1	−1	1	1	−1	1	−1	0.31
14	1	1	−1	1	1	−1	−1	1	0.30
15	23	−1	1	1	1	−1	−1	1	77.97
16	21	1	1	1	1	−1	1	−1	72.09
17	8	0	0	0	0	0	0	0	12.86
18	7	−1	−1	−1	−1	1	1	−1	0.45
19	26	1	−1	−1	−1	1	−1	1	0.64
20	3	−1	1	−1	−1	1	−1	1	77.13
21	10	1	1	−1	−1	1	1	−1	97.74
22	4	−1	−1	1	−1	1	−1	−1	0.64
23	12	1	−1	1	−1	1	1	1	0.42
24	13	−1	1	1	−1	1	1	1	79.19
25	19	1	1	1	−1	1	−1	−1	88.16
26	15	−1	−1	−1	1	1	−1	1	0.35
27	31	1	−1	−1	1	1	1	−1	0.41
28	25	−1	1	−1	1	1	1	−1	78.05
29	33	1	1	−1	1	1	−1	1	70.33
30	2	−1	−1	1	1	1	1	1	0.32
31	11	1	−1	1	1	1	−1	−1	0.49
32	27	−1	1	1	1	1	−1	−1	92.54
33	18	1	1	1	1	1	1	1	72.66

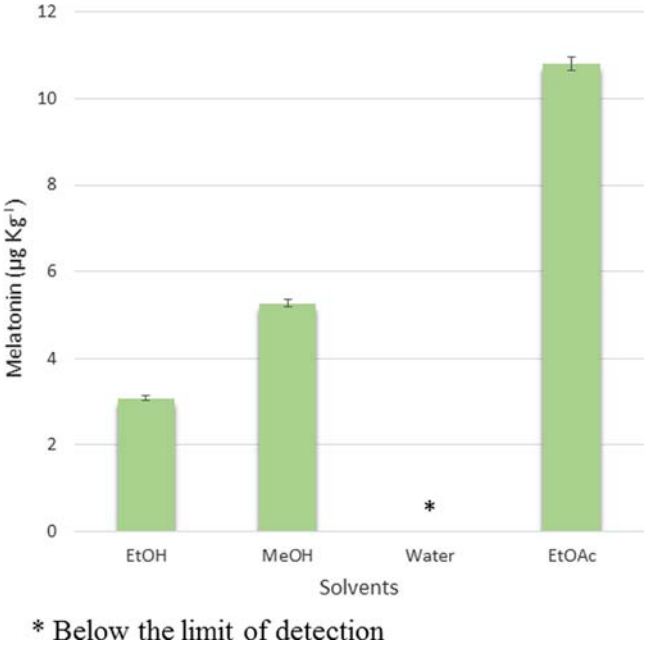

Figure 2. Effect of different solvents on the extraction efficiency.

gradually absorbed by the starch in an irreversible process. As a consequence, the extraction cell became blocked, and this led to an inefficient extraction process. Melatonin can be effectively extracted under PLE conditions using EtOAc, and the optimization was thus focused on obtaining the best concentration of EtOAc for the extraction solution. EtOAc was diluted in MeOH to adjust the concentration used for the optimization, and this was in the range of 80−100%.

2_{IV}^{7-2} Fractional Factorial Design Analysis. Once the working range for the extraction had been established by selecting the appropriate solvent and considering the stability of melatonin, the factors that were likely to influence the melatonin extraction were optimized. The factors considered were solvent composition (x_1; 80−100% EtOAc in MeOH), extraction temperature (x_2; 100−200 °C), pressure (x_3; 100−200 atm), flushing (x_4; 50−100%), static time (x_5; 5−10 min), solvent purge (x_6; 60−120 s), and sample weight (x_7; 2.5−5 g). The main response was the level of melatonin expressed as the value relative to the maximum yield of melatonin obtained (%). On the basis of the experimental design generated by the 2_{IV}^{7-2} fractional factorial design, 33 extraction processes were completed to extract melatonin from rice (Table 3), and the estimated effects of operating factors on the extracted melatonin were subsequently analyzed using the equation

$$\text{effect} = \frac{\Sigma y_+}{n_+} - \frac{\Sigma y_-}{n_-} \quad (3)$$

DOI: 10.1021/jf505106m
J. Agric. Food Chem. 2015, 63, 1107−1115

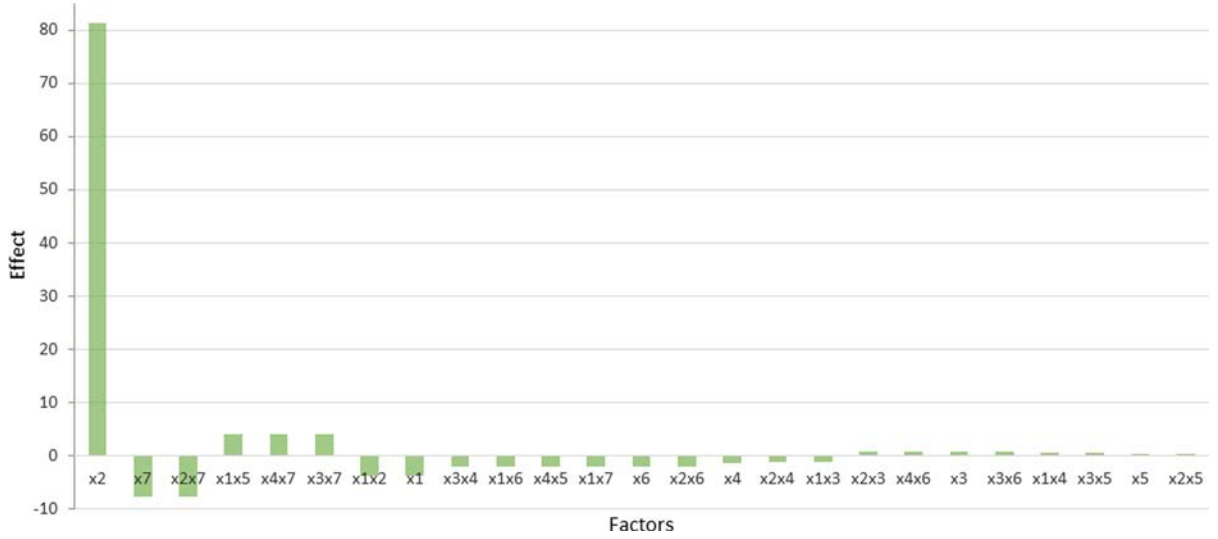

Figure 3. Estimated effects of the main and interaction factors on the recovery.

where n values refer to the number of data points collected at each level and y values refer to the associated responses. The values of the estimated main and interaction effects of factors in decreasing order of importance are plotted in Figure 3. The regression coefficients for the intercept, linear, and interaction terms of the model were calculated, and most of them were <2; only the regression coefficient for temperature showed a value much higher (38.734) than those calculated for the other extraction variables (1.65 as average value). Independent factors with a p value of <0.05 were defined as having a significant effect on the response.

The results shown in the chart for the main and interaction effects indicate that the most significant main effects (p < 0.00001) are extraction temperature (x_2) and sample weight (x_7). Another main factor that was reasonably prominent in terms of the extraction yield was the solvent (x_1) (p < 0.05). Furthermore, several effects caused by interactions of factors, including x_1x_2, x_1x_5, x_2x_7, and x_4x_7, were also found to be important (p < 0.05). Hence, the effects of extraction temperature (x_2) and sample weight (x_7) were the most important because a lower p value indicates a higher significance for the corresponding factors.[30]

The regression coefficients were then used to produce a final predictive equation for melatonin compounds in rice grain extracts by using significant variables. To avoid a high variability, it is advisible to keep the number of factors for an optimized design low by disregarding the nonsignificant factors (p > 0.05). The resulting equation for the fitted model is as follows:

$$y = 38.3273 - 1.82759x_1 + 38.7343x_2 - 3.71909x_7 - 1.84974x_1x_2 + 1.89794x_1x_5 - 3.68268x_2x_7 + 1.89501x_4x_7 \quad (4)$$

The efficiency of the model was checked by ANOVA, and the suitability of the model was judged by considering the coefficient of determination. The R^2 statistic obtained from the regression shows that the as-fitted model explains 0.9641 of the variability in melatonin levels. The adjusted R^2 statistic of 0.9416 indicates a high degree of correlation between the experimental and predicted values, and this is more appropriate when models with different numbers of independent factors are compared.

Optimization of the Significant Main Factors. Significant independent factors are essential to achieve the optimum yield for the melatonin extraction. According to the design analysis, as three main factors were significant, the best way to optimize the extraction yield is by increasing the extraction temperature (*estimated effect* +81.33), decreasing the weight of rice sample (*estimated effect* −7.7), and decreasing the percentage of EtOAc in MeOH (*estimated effect* −3.8).

The use of higher temperature increases the molecular motion and leads to a decrease in the solvent viscosity, resulting in an increase in the diffusivity. Furthermore, the walls of cells are broken more rapidly at higher temperature, and this facilitates the leaching of melatonin into the solvent, thus increasing the extraction efficiency. However, because the tested range includes the highest level (+1) for the maximum working temperature allowed by the system, optimization of the extraction process by increasing the PLE temperature was not possible. Thus, the optimum extraction temperature was set at 200 °C.

The amount of sample was oppositely correlated with the extraction yield, and this confirms that the higher solvent-to-solid ratio provides a higher driving force in transferring the desired analyte into the extraction solvent.[31] Nevertheless, the limitation in reducing the sample weight is the minimum concentration of melatonin in the extract that can be detected by the chromatographic system. Therefore, the lowest level (−1) for the tested optimization range in the design experiment was set as the optimum sample weight (2.5 g) to ensure a reliable quantification by the analytical method.

Solvent Optimization. The composition of the extraction solvent has a significant negative effect on the extraction yield. As a consequence, the solvent optimization should include a lower percentage of EtOAc than the range used in the experimental design. The proportion of EtOAc in MeOH was then examined at 60, 70, and 80% for further optimization (Figure 4). The yield of extracted melatonin increased significantly when the concentration of EtOAc in MeOH was decreased (single-factor ANOVA, p = 0.05) to give a yield of 70%. However, the amount of melatonin extracted was

DOI: 10.1021/jf505106m
J. Agric. Food Chem. 2015, 63, 1107−1115

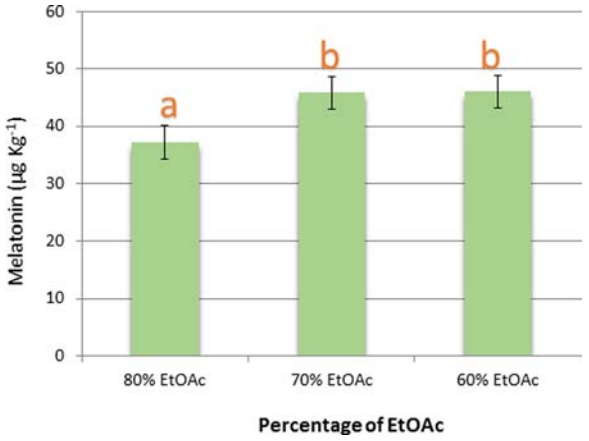

Figure 4. Level of extracted melatonin by different percentages of EtOH in MeOH. Means followed by the same letter are indicated as not significantly different (α = 0.05).

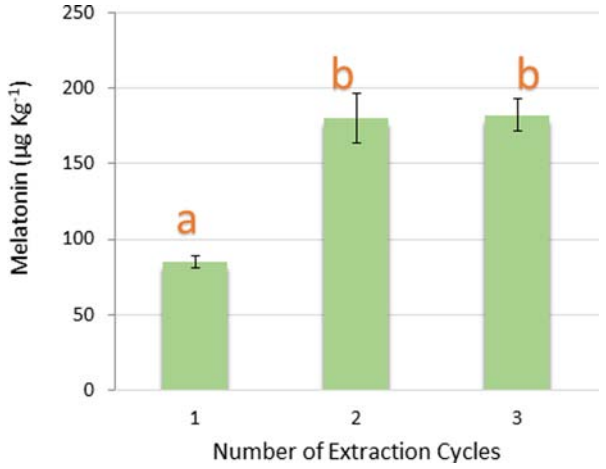

Figure 5. Level of extracted melatonin versus number of extraction cycles. Means followed by the same letter are indicated as not significantly different (α = 0.05).

comparable (LSD, p = 0.05) on decreasing the proportion of EtOAc to 60% in MeOH.

Melatonin has both hydrophilic and lipophilic properties, and it therefore requires a relatively complex solvent for extraction. In general, mixtures of solvents with different polarities lead to more efficient extractions than a single solvent when the analyte to be extracted has a wide range of polarities.[32] The use of solvent mixtures was found to improve the extraction yield by enhancing the solubility and encouraging interactions with the analyte.[33] Furthermore, a binary solvent mixture can effectively improve the extraction efficiency because one solvent may increase the solubility of the analyte, whereas the other may improve the analyte desorption.[10] Ethyl acetate is considered to be a medium-polar solvent that is appropriate for melatonin extraction, but the addition of MeOH to EtOAc increases the polarity of the mixed solvent, and this makes it easier to gain access into the ruptured cells to reach the melatonin. This advantage was exploited by selecting a mixture of 70% EtOAc in MeOH as the optimum PLE solvent for melatonin extraction.

Cycle Optimization. The major shortcoming of the static extraction mode in PLE systems is the limited volume of solvent that can be used to achieve a complete extraction. Nonetheless, an increase in the number of extraction cycles for the static process appears to be a reasonable solution that favors the solvent-to-analyte equilibrium.[34] Additionally, it is emphasized in the literature that the extractions of various compounds by PLE can be completed by employing multiple extraction cycles.[12,35,36] With this constraint taken into account, the number of cycles was also explored in this study to provide an adequate amount of solvent to obtain the maximum extraction efficiency (Figure 5).

The highest level of extracted melatonin was reached with multiple cycles, which increased the extraction yield by up to a factor of 2 when compared to the yield obtained with a single extraction cycle. However, the extraction with three cycles improved the level of extracted melatonin by only 1.15% in comparison to two cycles, and this change is not significantly different (LSD, p = 0.05). The number of extraction cycles dictates the static heating time, and the flushing processes are repeated. Hence, a process with two extraction cycles was selected for the extraction of melatonin with the purpose of saving time, solvent, and energy.

Optimized Conditions. The final conditions in terms of the significant factors ($p < 0.05$) that affect the extraction yield were as follows: extraction solvent (x_1, 70% EtOAc in MeOH), temperature (x_2, 200 °C), and sample weight (x_7, 2.5 g). Because the effects of the remaining factors (pressure, static time, flushing volume, and purging time) were not significant ($p > 0.05$), these operating conditions were set in keeping with the more favorable conditions for the extraction process. Pressure (x_3, 200 atm) was set at its maximum level (+1) to assist the rapid increase of temperature above the boiling point while maintaining the solvent in the liquid state. Flushing volume (x_4, 50% of extraction solvent), static time (x_5, 5 min), and purging time (x_6, 60 s) were selected according to the minimum point (−1) of the experimental domain (see Table 2) because the extraction efficiency was not affected and the extraction time and solvent cost were minimal. In addition, a two-cycle extraction was used to maximize the extraction efficiency.

Method Validation. Under the optimum experimental conditions, the validation of the proposed analytical method involving PLE followed by HPLC-FD was accomplished. The method precision was measured by considering the repeatability and intermediate precision of the analyses. Both measurements were conducted in accordance with ICH guidelines. The precision values, expressed as %CV, of the developed method were as follows: 1.53% for repeatability (n = 9) and 6.54% for intermediate precision ($n = 3 \times 3$). Because the %CV values for precision were lower than the acceptable limit (±10% refers to AOAC), the result confirmed that an excellent precision for the extraction method had been achieved.

On the basis of the calibration curve, LOD and LOQ for the solid sample can be calculated. Values found were LOD = 2.3 μg kg^{-1} and LOQ = 7.68 μg kg^{-1}.

The recovery (%R) of melatonin was evaluated using a standard addition method by comparing the absolute response of the analytes spiked in control samples before and after the extraction process. The average recovery obtained for the developed PLE was 98.9%. These results show that this particular PLE method is applicable for the assessment of melatonin content in real rice samples.

Application to Real Samples. The optimized and validated method was applied to the extraction of a number

DOI: 10.1021/jf505106m
J. Agric. Food Chem. 2015, 63, 1107−1115

Table 4. Concentrations of Melatonin in Tested Rice Grain Samples

Cluster	Rice Sample	Picture	Bran Removal	Melatonin ($\mu g\ Kg^{-1}$)
Pigmented Rice	Black glutinous *Long grain, waxy, Thailand*		No	73.81 ± 0.07
	Black *Long grain, organic farming, Java island, Indonesia*		No	182.04 ± 1.62
	Red *Long grain, Thailand*		No	212.01 ± 1.37
Non-pigmented Rice	Whole short grain *Spain*		No	47.83 ± 0.12
	Whole semi-long grain *Spain*		No	42.95 ± 0.64
	Polished short grain *Spain*		Yes	31.99 ± 0.31
	Polished long grain *Spain*		Yes	27.61 ± 1.16
	Basmati *Aromatic, Long grain, India*		Yes	38.46 ± 0.07
	Parboiled rice *Processed rice, Spain*		Yes	28.33 ± 0.61

of real samples with the intention of evaluating its applicability. Various rice products composed of polished, whole grain, aromatic, black, black glutinous, red, and parboiled rice were extracted, and the melatonin contents were then analyzed in duplicate (Table 4). The results show that the melatonin contents are noticeably different between most of the pigmented and nonpigmented rice samples. The former include black glutinous, black, and red rice, and these have a higher melatonin content than the latter, that is, polished, whole grain, and parboiled rice. Variations in the melatonin contents are reasonable relative to the physical and chemical characteristics of different rice samples.

The cluster of pigmented rice grains has a higher concentration of melatonin as these samples contain a higher level of the vitamin B group.[37] It is widely recognized that niacin (vitamin B_3) prevents the breakdown of the melatonin precursor, whereas pyridoxine (vitamin B_6), a coenzyme in the one-carbon metabolism pathways, is involved in the synthesis of melatonin.[38,39] The level of melatonin may increase by >60% in the presence of pyridoxine during in vivo biosynthesis.[40]

The highest concentration of melatonin present in pigmented rice was 207.79 ± 3.18 $\mu g\ kg^{-1}$ (red rice), and this was followed by black rice (182.04 ± 2.79 $\mu g\ kg^{-1}$) and black glutinous rice (73.81 ± 1.13 $\mu g\ kg^{-1}$). The difference in melatonin contents between black rice and red rice was not as marked as that for black rice and black glutinous rice. Glutinous rice mainly differs from nonglutinous rice in that it has low (<5%) levels of or almost no amylose in its starch but is high in amylopectin.[41] The level of melatonin in black rice was roughly twice as high as that in its glutinous type. This finding is consistent with that reported by Li et al.,[42] who found that plant samples with high amylose contents exhibit better antioxidant activity than their glutinous genotypes. Despite significant research effort, the specific antioxidant enhanced by amylose has not yet been elucidated further, and melatonin is considered as a potential molecule that has a high antioxidant activity.[43]

In nonpigmented rice, the largest difference in the level of melatonin was between whole (from 42.95 ± 0.64 to 47.83 ± 0.12 $\mu g\ kg^{-1}$) and polished (from 28.33 ± 0.61 to 31.99 ± 0.31 $\mu g\ kg^{-1}$) grains. The melatonin content was reduced by as much as 33% on comparison to the whole and polished grains. The merits of the polishing step during rice production are the enhanced palatability and improved product appearance. Conversely, this step includes a bran removal process that causes a disadvantage due to the loss of melatonin from the grain, as shown by studies of the melatonin profile during rice production.[44]

DOI: 10.1021/jf505106m
J. Agric. Food Chem. 2015, 63, 1107−1115

AUTHOR INFORMATION

Corresponding Author

* (M.P.) Phone: +34 956 016 360. Fax: +34 956 016 460. E-mail: miguel.palma@uca.es.

Funding

W.S. is grateful to the CIMB Foundation for a Ph.D. studentship through the CIMB Regional Scholarships 2012.

Notes

The authors declare no competing financial interest.

REFERENCES

(1) OECD-FAO. OECD-FAO agricultural outlook − OECD; http://www.oecd.org/site/oecd-faoagriculturaloutlook/ (accessed Sept 23, 2014).

(2) Hattori, A.; Migitaka, H.; Iigo, M.; Itoh, M.; Yamamoto, K.; Ohtani-Kaneko, R.; Hara, M.; Suzuki, T.; Reiter, R. J.; Ego, M.; Biology, S.; Antonio, S. Identification of melatonin in plants and its effects on plasma melatonin levels and binding to melatonin receptors in vertebrates. *Biochem. Mol. Biol. Int.* **1995**, *35*, 627−634.

(3) Setyaningsih, W.; Palma, M.; Barroso, C. G. A new microwave-assisted extraction method for melatonin determination in rice grains. *J. Cereal Sci.* **2012**, *56*, 340−346.

(4) Byeon, Y.; Park, S.; Lee, H. Y.; Kim, Y.-S.; Back, K. Elevated production of melatonin in transgenic rice seeds expressing rice tryptophan decarboxylase. *J. Pineal Res.* **2014**, *56*, 275−282.

(5) Srikaeo, K.; Sopade, P. A. Functional properties and starch digestibility of instant Jasmine rice porridges. *Carbohydr. Polym.* **2010**, *82*, 952−957.

(6) Giarman, N. J.; Day, M. Presence of biogenic amines in the bovine pineal body. *Biochem. Pharmacol.* **1959**, *1*, 235.

(7) Wang, X. The antiapoptotic activity of melatonin in neurodegenerative diseases. *CNS Neurosci. Ther.* **2009**, *15*, 345−357.

(8) Jung, B.; Ahmad, N. Melatonin in cancer management: progress and promise. *Cancer Res.* **2006**, *66*, 9789−9793.

(9) Hamid, A. A.; Aiyelaagbe, O. O.; Usman, L. A.; Ameen, O. M.; Lawal, A. Antioxidants: its medicinal and pharmacological applications. *Afr. J. Pure Appl. Chem.* **2010**, *4*, 142−151.

(10) Mustafa, A.; Turner, C. Pressurized liquid extraction as a green approach in food and herbal plants extraction: a review. *Anal. Chim. Acta* **2011**, *703*, 8−18.

(11) Shang, Y. F.; Kim, S. M.; Um, B.-H. Optimisation of pressurised liquid extraction of antioxidants from black bamboo leaves. *Food Chem.* **2014**, *154*, 164−170.

(12) Ruiz-Aceituno, L.; Rodríguez-Sánchez, S.; Sanz, J.; Sanz, M. L.; Ramos, L. Optimization of pressurized liquid extraction of inositols from pine nuts (*Pinus pinea* L.). *Food Chem.* **2014**, *153*, 450−456.

(13) Rostagno, M. A.; Palma, M.; Barroso, C. G. Pressurized liquid extraction of isoflavones from soybeans. *Anal. Chim. Acta* **2004**, *522*, 169−177.

(14) Wang, L.; Weller, C. L. Recent advances in extraction of nutraceuticals from plants. *Trends Food Sci. Technol.* **2006**, *17*, 300−312.

(15) Richter, B. E.; Jones, B. A.; Ezzell, J. L.; Porter, N. L. Accelerated solvent extraction: a technique for sample preparation. *Anal. Chem.* **1996**, *68*, 1033−1039.

(16) Agarwal, S. P.; Gonsalves, H. J.; Khar, R. K. HPTLC method for the analysis of melatonin in bulk and phamaceutical formulations. *Asian J. Chem.* **2008**, *20*, 2531−2538.

(17) Sultana, B.; Anwar, F.; Ashraf, M. Effect of extraction solvent/technique on the antioxidant activity of selected medicinal plant extracts. *Molecules* **2009**, *14*, 2167−2180.

(18) Benthin, B.; Danz, H.; Hamburger, M. Pressurized liquid extraction of medicinal plants. *J. Chromatogr., A* **1999**, *837*, 211−219.

(19) Arnao, M. B. Phytomelatonin: discovery, content, and role in plants. *Adv. Bot.* **2014**, *2014*, 1−11.

(20) Yu, H.; Tao, Y.; Chen, D.; Pan, Y.; Liu, Z.; Wang, Y.; Huang, L.; Dai, M.; Peng, D.; Wang, X.; Yuan, Z. Simultaneous determination of fluoroquinolones in foods of animal origin by a high performance liquid chromatography and a liquid chromatography tandem mass spectrometry with accelerated solvent extraction. *J. Chromatogr., B: Anal. Technol. Biomed. Life Sci.* **2012**, *885−886*, 150−159.

(21) Rodriguez, E.; Villoslada, F. N.; Moreno-Bondi, M. C.; Marazuela, M. D. Optimization of a pressurized liquid extraction method by experimental design methodologies for the determination of fluoroquinolone residues in infant foods by liquid chromatography. *J. Chromatogr., A* **2010**, *1217*, 605−613.

(22) ISO. *ISO/IEC 17025:2005 General Requirements for the Competence of Testing and Calibration Laboratories*; Geneva, Switzerland, 2005; Vol. 2005, pp 1−36.

(23) ICH. *ICH Topic Q2 (R1) Validation of Analytical Procedures: Text and Methodology*; Geneva, Switzerland, 2005; Vol. 1994, pp 1−17.

(24) AOAC. *AOAC Peer Verified Methods Program, Manual on Policies and Procedures*; AOAC International: Rockville, MD, USA, 1998; pp 1−35.

(25) Baş, D.; Boyacı, İ. H. Modelling and optimization I: usability of response surface methodology. *J. Food Eng.* **2007**, *78*, 836−845.

(26) Reiter, R. J.; Manchester, L. C.; Tan, D. Melatonin in walnuts: influence on levels of melatonin and total antioxidant capacity of blood. *Nutrition* **2005**, *21*, 920−924.

(27) Arnao, M. B.; Hernández-Ruiz, J. Melatonin promotes adventitious- and lateral root regeneration in etiolated hypocotyls of *Lupinus albus* L. *J. Pineal Res.* **2007**, *42*, 147−152.

(28) Ansari, M.; Yasa, N.; Vardasbi, S.; Naimi, S. M.; Nowrouzi, A. Measurement of melatonin in alcoholic and hot water extracts of *Tanacetum parthenium*, *Tripleurospermum disciforme*, and *Viola odorata*. *DARU J. Pharm. Sci.* **2010**, *18*, 173−178.

(29) Manchester, L. C.; Tan, D. X.; Reiter, R. J.; Park, W.; Monis, K.; Qi, W. High levels of melatonin in the seeds of edible plants: possible function in germ tissue protection. *Life Sci.* **2000**, *67*, 3023−3029.

(30) Mendenhall, W.; Beaver, R. J.; Beaver, B. M. In *Introduction to Probability and Statistics*; Brooks/Cole: Belmont, CA, USA, 2009; pp 447−462.

(31) Meireles, M. A. A. *Extracting Bioactive Compounds for Food Products*; CRC Press: Boca Raton, FL, USA, 2009; p 195.

(32) Carabias-Martínez, R.; Rodríguez-Gonzalo, E.; Revilla-Ruiz, P.; Hernández-Méndez, J. Pressurized liquid extraction in the analysis of food and biological samples. *J. Chromatogr., A* **2005**, *1089*, 1−17.

(33) Ju, Z. Y.; Howard, L. R. Effects of solvent and temperature on pressurized liquid extraction of anthocyanins and total phenolics from dried red grape skin. *J. Agric. Food Chem.* **2003**, *51*, 5207−5213.

(34) Chen, D.; Tao, Y.; Zhang, H.; Pan, Y.; Liu, Z.; Huang, L.; Wang, Y.; Peng, D.; Wang, X.; Dai, M.; Yuan, Z. Development of a liquid chromatography-tandem mass spectrometry with pressurized liquid extraction method for the determination of benzimidazole residues in edible tissues. *J. Chromatogr., B: Anal. Technol. Biomed. Life Sci.* **2011**, *879*, 1659−1667.

(35) Moret, S.; Scolaro, M.; Barp, L.; Purcaro, G.; Sander, M.; Conte, L. S. Optimisation of pressurised liquid extraction (PLE) for rapid and efficient extraction of superficial and total mineral oil contamination from dry foods. *Food Chem.* **2014**, *157*, 470−475.

(36) Ferrer, E.; Santoni, E.; Vittori, S.; Font, G.; Mañes, J.; Sagratini, G. Simultaneous determination of bisphenol A, octylphenol, and nonylphenol by pressurised liquid extraction and liquid chromatography−tandem mass spectrometry in powdered milk and infant formulas. *Food Chem.* **2011**, *126*, 360−367.

(37) Zhang, M.; Guo, B.; Zhang, R.; Chi, J.; Wei, Z.; Xu, Z.; Zhang, Y.; Tang, X. Separation, purification and identification of antioxidant compositions in black rice. *Agric. Sci. China* **2006**, *5*, 431−440.

(38) Fardet, A. New hypotheses for the health-protective mechanisms of whole-grain cereals: what is beyond fibre? *Nutr. Res. Rev.* **2010**, *23*, 65−134.

(39) USA Rice® Federation. Rice nutrition information; http://www.usarice.com/index.php?option=com_content&view=article&id=1727&Itemid=660 (accessed Sept 23, 2014).

(40) Hartvig, P.; Lindner, K. J.; Bjurling, P.; Laengstrom, B.; Tedroff, J. Pyridoxine effect on synthesis rate of serotonin in the monkey brain

DOI: 10.1021/jf505106m
J. Agric. Food Chem. 2015, 63, 1107−1115

measured with positron emission tomography. *J. Neural Transm. Gen. Sect.* **1995**, *102*, 91−97.
(41) Chung, H.-J.; Liu, Q.; Lee, L.; Wei, D. Relationship between the structure, physicochemical properties and in vitro digestibility of rice starches with different amylose contents. *Food Hydrocolloids* **2011**, *25*, 968−975.
(42) Li, W.; Wei, C. V.; White, P. J.; Beta, T. High-amylose corn exhibits better antioxidant activity than typical and waxy genotypes. *J. Agric. Food Chem.* **2007**, *55*, 291−298.
(43) Gulcin, I.; Buyukokuroglu, M. E.; Oktay, M.; Kufrevioglu, I. On the in vitro antioxidative properties of melatonin. *J. Pineal Res.* **2002**, *33*, 167−171.
(44) Setyaningsih, W.; Hidayah, N.; Saputro, I. E.; Lovillo, M. P.; Barroso, C. G. Melatonin profile during rice (*Oryza sativa*) production. *J. Adv. Agric. Technol.* **2014**, *1*, 60−64.

DOI: 10.1021/jf505106m
J. Agric. Food Chem. 2015, 63, 1107−1115

composition of wine lees is subjected to a strong variability and depends on the winery procedures. Once the alcoholic fermentation has ended, autolysis of wine yeast starts, which is characterized by degradation of cell walls and release of some enzymes, mannoproteins, amino acids, and precursors of volatile compounds into wine as well as some phenolic and sulfur compounds that are adsorbed on wine lees.[17,18] Chassagne et al. established that the adsorption phenomenon is directly linked to the degree of autolysis, ethanol concentration, pH of wine, and temperature,[19] while Zea et al. found differences in the concentration of volatile compounds in cells and musts when different yeast races were used.[20−22]

To date, wine lees have been mainly exploited as a source of tartaric acid and calcium tartrate;[15] however, some attempts have also been made to use this raw material for feeding cattle, but these attempts have been discarded in view of the extremely poor nutritional value of wine lees.[23,24] Additionally, their use as a biosorbent for removal of undesirable compounds from wine has also been proposed,[25,26] since wine lees have been reported to retain part of the volatile compounds that oak wood transfers to wine, preventing wine from having an excessive and, thus, unpleasant woody flavor, as well as diminishing the impact of undesirable compounds such as toxins, pesticides, and antifoaming and volatile compounds such as 4-ethylphenol and 4-ethylguaiacol, which have been described as responsible for the associated horsy, medicinal, and spicy aroma of wines.[25−27] From the compositional point of view, some published research has focused on the pigment content of red wine lees, since their intense red coloration suggests a high anthocyanin and anthocyanidin content.[28,29] Some other studies have focused on the production of phenolic extracts from wine lees and the study of their phenolic content and their antioxidant activity.[30,31]

The aim of this research was to study and compare the composition profile of wine lees by independent analysis of imbibed wine from lees obtained by centrifugation and solid dried lees. For this purpose, ethanol−water extracts of solid lees were obtained by microwave-assisted extraction (MAE) as previously done by Pérez et al. and Delgado de la Torre et al.[29,30] Both fractions were subjected to liquid chromatography separation with tandem mass spectrometry detection using a quadrupole time-of-flight (QTOF) hybrid detector. Finally, both fractions were characterized and compared with the aim of studying the potential of these fractions to be recycled together or independently, depending on their composition. Multivariate analysis is a key tool to treat the large data sets provided by the QTOF detector and to understand the similar/dissimilar patterns among a range of samples provided from different wineries pertaining to the most characteristic denomination of origin wines in Spain.

MATERIALS AND METHODS

Samples. Wine lees as semisolid residue were provided in 2010 by 11 Spanish wineries from regions of Spain where different varieties of red grapes are used. The wineries correspond to the two most popular denominations of origin of red wines in Spain, namely, Ribera del Duero and Rioja (see Table 1). In all cases, wine lees were in contact with wine for three months during alcoholic fermentation, after which wine lees were isolated and used for this study. The sample from each winery was homogenized by agitation at room temperature for 15 min and centrifuged at 855*g* for 5 min. The solid phase was dried at 40 °C for 48 h in an oven, milled in a mortar, sieved to a 0.5 mm particle size, and stored at −20 °C until use. The liquid phase was directly stored at −20 °C until use.

Table 1. Samples Provided by Wineries from Two of the Most Characteristic Denominations of Origin in Spain

code	grape	location	denomination of origin
R1	Tempranillo	Azagra (Navarra)	Rioja
R2	Tempranillo	Haro (La Rioja)	Rioja
R3	Tempranillo	Haro (La Rioja)	Rioja
R4	Tempranillo	San Vicente de la Sonsierra (La Rioja)	Rioja
R5	Tempranillo (ecological)	Aldeanueva de Ebro (La Rioja)	Rioja
R6	Tempranillo, Garnacha	Gimileo (La Rioja)	Rioja
R7	Mazuelo	Haro (La Rioja)	Rioja
RD1	92% Tempranillo, 3% Cabernet, 5% Merlot	Gumiel de Mercado (Burgos)	Ribera del Duero
RD2	Tempranillo	Langa del Duero (Soria)	Ribera del Duero
RD3	Tempranillo	Fompedraza (Valladolid)	Ribera del Duero
RD4	Tempranillo	Anguix (Burgos)	Ribera del Duero

Reagents. Acetonitrile (ACN) and formic acid (MS grade) were from Scharlab (Barcelona, Spain). Deionized water (18 MΩ·cm) was obtained by a Milli-Q water purification system from Millipore (Billerica, MA). Ethanol (96%, v/v) PA from Panreac (Barcelona, Spain) and distilled water were used to prepare the extractant.

Apparatus and Instruments. A Microdigest 301 digestor of maximum power 200 W (Prolabo, Paris, France) furnished with a microprocessor programmer (Prolabo) to control the microwave unit was used for MAE.

Shaking and centrifugation of wine lees and extracts were carried out by an MS2 minishaker (IKA, Germany) and a Mixtasel (Selecta, Barcelona, Spain) centrifuge, respectively.

Analysis of the studied compounds was performed in an Agilent 1200 series LC system interfaced to an Agilent UHD accurate-mass QTOF-MS/MS detector (Palo Alto, CA) equipped with an Agilent Technology dual electrospray ion source (dual ESI).

Sample Preparation. A 6 g sample of dried lees was placed into the extraction vessel of the microwave-assisted digestor with 50 mL of 60:40 (v/v) ethanol−water adjusted to pH 4 with formic acid. The vessel was positioned at the suited zone for irradiation with focused microwaves. The auxiliary energy was applied at 140 W irradiation power for 10 min, after which the solid residue was removed by centrifugation and the liquid fraction filtered by a 20 μm pore size filter and 1:2 diluted with 60:40 (v/v) ethanol−water adjusted to pH 4 with formic acid.

LC−QTOF-MS/MS Analysis. Chromatographic separation was performed using a C_{18} Inertsil ODS-2 column (250 mm × 4.6 mm i.d., 5 μm particle size, Análisis Vínicos, Tomelloso, Ciudad Real, Spain) kept at 25 °C. The mobile phases in this case were water (phase A) and ACN (phase B), both LC−MS/MS grade and with 0.1% formic acid as the ionization agent. The LC pump was programmed at a flow rate of 0.9 mL/min, and the following elution gradient was carried out: hold from 0 to 2 min at 4% phase B, 2−7 min 10% phase B, 7−60 min 100% phase B, and hold to 70 min. A postrun of 4 min was included to equilibrate the column. The injection volume was 10 μL, and the injector needle was rinsed five times with 70% methanol. Furthermore, the needle seat back was flushed for 12 s at a flow rate of 4 mL/min with 70% methanol to clean it. The operating conditions of the mass spectrometer were as follows: gas temperature, 325 °C; drying gas, nitrogen at 10 L/min; nebulizer pressure, 40 psi; sheath gas temperature, 380 °C; sheath gas flow, nitrogen at 10 L/min; capillary voltage, 3500 V; skimmer, 65 V; octopole radiofrequency voltage, 750 V; focusing voltage, 175 V. MS and MS/MS data were collected in both polarities using the centroid and the profile modes at a rate of two spectra per second in the extended dynamic range mode (2 GHz). Accurate mass spectra in auto MS/MS mode were acquired in the MS

DOI: 10.1021/jf505331f
J. Agric. Food Chem. 2015, 63, 1116−1125

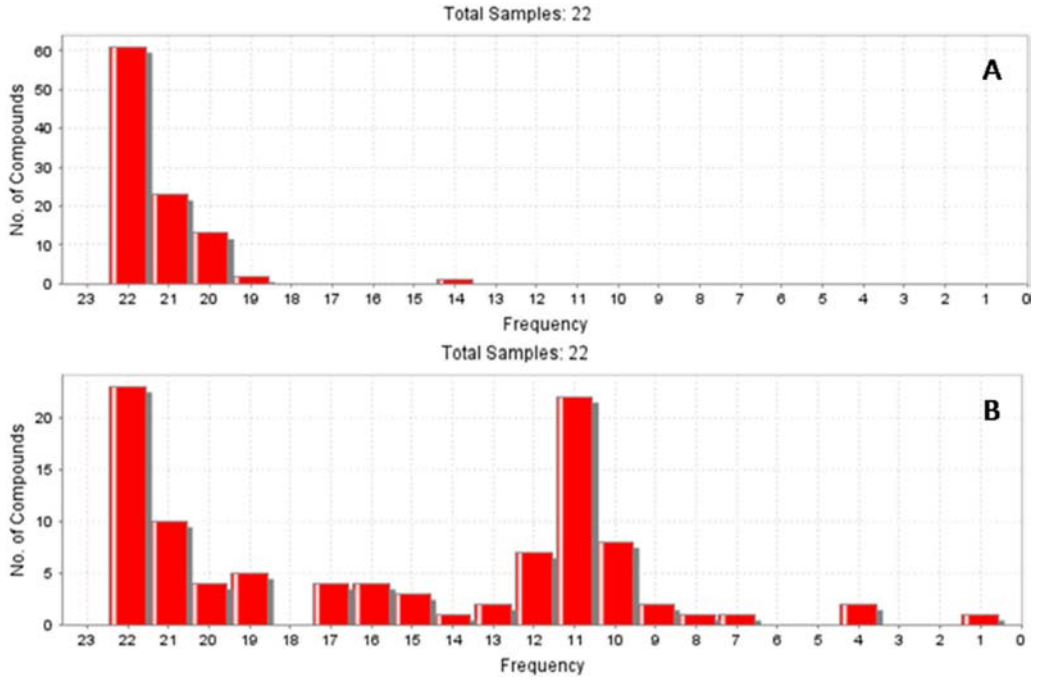

Figure 1. Alignment diagram corresponding to positive (A) and negative (B) ionization modes.

m/*z* range 100−3000 and MS/MS *m*/*z* range 100−3000. The auto MS/MS mode was configured with two maximum precursors per cycle and an exclusion window of 0.25 min after two consecutive selections of the same precursor. The collision energy selected was 22.5 eV. To ensure the desired mass accuracy of recorded ions, continuous internal calibration was performed during analyses by the use of signals at *m*/*z* 121.0509 (protonated purine) and *m*/*z* 922.0098 [protonated hexakis(1*H*,1*H*,3*H*-tetrafluoropropoxy)phosphazine, or HP-921] in positive ionization mode, while ions with *m*/*z* 119.0362 (proton abstracted purine) and *m*/*z* 966.0007 (formate adduct of HP-921) were used in negative ionization mode.

Data Treatment. The MassHunter Workstation software package (B.05.00) and MassHunter Profinder (B.06.00) from Agilent Technologies were used to process all data obtained by LC−QTOF in the auto MS/MS mode. The recursive feature extraction algorithm was used to extract and align potential molecular features in all the injection sets. This algorithm initially deconvolutes the chromatograms and aligns the molecular features across the selected raw data files in terms of *m*/*z* value and retention time; then it uses the mass and retention time of each feature for recursive targeted feature extraction in the raw data files. This two-step procedure reduces the number of both false negatives and false positives in the process of feature extraction. The target parameters for feature extraction included a threshold of 1500 counts and a maximum charge state of 2. In addition, the isotopic distribution for a valid feature had to be defined by two or more ions—with a peak spacing tolerance of 0.0025 *m*/*z*, plus 10.0 ppm. Adduct formation in the positive (+H, +Na) and negative (−H, +HCOO) ionization modes was also used to identify features of the same molecule. Features were aligned by using a tolerance window of 0.30 min and a mass accuracy of 10 ppm for retention times and *m*/*z* values, respectively, across all data files. The minimum absolute height required for feature extraction was set at 3000 counts, which was also used for 100% of samples in the recursive step. Thus, ions with identical elution profiles and related *m*/*z* values (representing different adducts or isotopes of the same compound) were extracted as molecular features (MFs) or entities characterized by RT, intensity in the apex of the chromatographic peak, and accurate mass.

The resulting data files after this treatment were created as comma-separated value files (.csv) for each sample and exported into the Mass Profiler Professional (MPP) software package (version 2.0, Agilent Technologies) for further processing. Compound identification was performed using the METLIN Metabolite and MS/MS (http://metlin.scripps.edu/), Massbank (http://www.massbank.jp/), MetFrag (http://msbi.ipb-halle.de/MetFrag/), and PlantCyc (http://plantcyc.org/) databases.

RESULTS AND DISCUSSION

Data Pretreatment. Wine lees are a complex matrix containing mainly polar and midpolar compounds, as revealed by the LC−MS/MS elution profiles obtained in the positive and negative ionization modes. The elution profiles represented by the base peak chromatograms (BPCs) show the predominance of polar compounds in imbibed wines from lees in both ionization modes, where the peaks were found almost exclusively in the elution time window from 1 to 28 min, while the extracts from the solid residues provided peaks characterized by the presence of less polar compounds, as most of the peaks were associated with compounds eluted at longer times (elution time window from 1 to 60 min), which support the adsorbent role of this residue during wine aging.

With the aim of ensuring the representativeness of the study, the data set obtained after alignment of molecular features was filtered to select a subdata set formed by the molecular features in all the samples of liquid and dried lees. This means that the data sets should contain molecular features present in all the samples analyzed for each class. This data mining operation reduced the data sets to 90 and 68 molecular entities for imbibed wine from lees and extracts, respectively, in the positive ionization mode and 34 and 67 molecular entities in the negative ionization mode. This pretreatment ended with mean-centering of the data set prior to statistical analysis. As the alignment diagram in Figure 1 shows, the positive ionization mode reported a data set formed by molecular features detected in most samples. On the other hand, the profile of molecular features in negative ionization mode allowed deduction of higher variability than in positive mode since a representative proportion of molecular entities were

DOI: 10.1021/jf505331f
J. Agric. Food Chem. 2015, 63, 1116−1125

detected in 50% of the samples. This high proportion of entities detected in half of the samples should be assigned to features detected exclusively in liquid or solid dried lees and, therefore, to differences in their composition.

Multivariate Analysis. The next step was the comparative analysis of samples pertaining to both classes of samples, imbibed wine from lees and extracts of dried lees. Qualitative comparison was carried out by application of Venn diagrams that allow the overlapping in compositional terms between both types of samples to be established. The diagrams illustrated in Figure 2 show a high similarity between the molecular entities found in imbibed wine from lees and in the extracts of dried lees in positive ionization mode, since 61 features were common to the two types of samples, while 7 and 29 features were exclusively detected in the extracts and imbibed wine from lees, respectively. Concerning the negative ionization mode (Figure 2B), the Venn diagram agreed with the alignment diagram (Figure 1B) about the observed variability in the composition of extracts and imbibed wine from lees. Thus, only 23 entities were common to the two types of samples, while 44 entities were exclusively detected in extracts from the solid residue. The different behaviors in positive and negative ionization could be explained by the influence of the chemical structure on the ionization efficiency. Therefore, it is evident that data sets from the two ionization modes should include molecular features corresponding tentatively to different compounds, which are preferentially ionized in one mode.

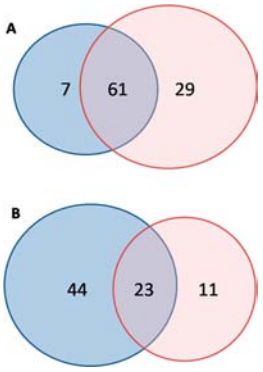

Figure 2. Venn diagram obtained by qualitative comparison of the molecular entities for imbibed wine from lees (right side) and extracts of dried lees (left side) after application of a 100% frequency filter in the positive (A) and negative (B) ionization modes.

Comparison of the compositional profiles of both fractions was made in terms of nonsupervised analysis using principal component analysis (PCA) to evaluate the distribution of the samples according to the variability sources. Figure 3 shows the PCA scores plot obtained for imbibed wine from lees and extracts of dried lees after data pretreatment. As can be seen, both ionization modes led to similar results since a clear discrimination was observed between the samples corresponding to imbibed wine from lees and extracts from dried solid wine lees. In negative ionization mode, PC1/PC2/PC3 explained 54.1% of the total variability, while, in positive mode, the variability explained by the three first components increased to 61.7%. In both cases, discrimination between the two types of samples was ascribed to PC1. Therefore, it is evident that the compositions of both separated materials were quite different. Apart from this discrimination, no trends were observed according to the origin of the wineries such as designation of origin or localization of wineries.

Identification of Compounds in Positive Ionization Mode. Characterization of representative families of compounds in the samples was carried out by tandem mass spectrometry in high-resolution mode. Tentative identification of compounds was supported on mass accuracy measurement of the precursor ion and representative product ions. The isotopic distribution of signals detected in full-scan mode was also taken into account. The combination of these data allowed tentative elucidation of the structure of the compounds listed in

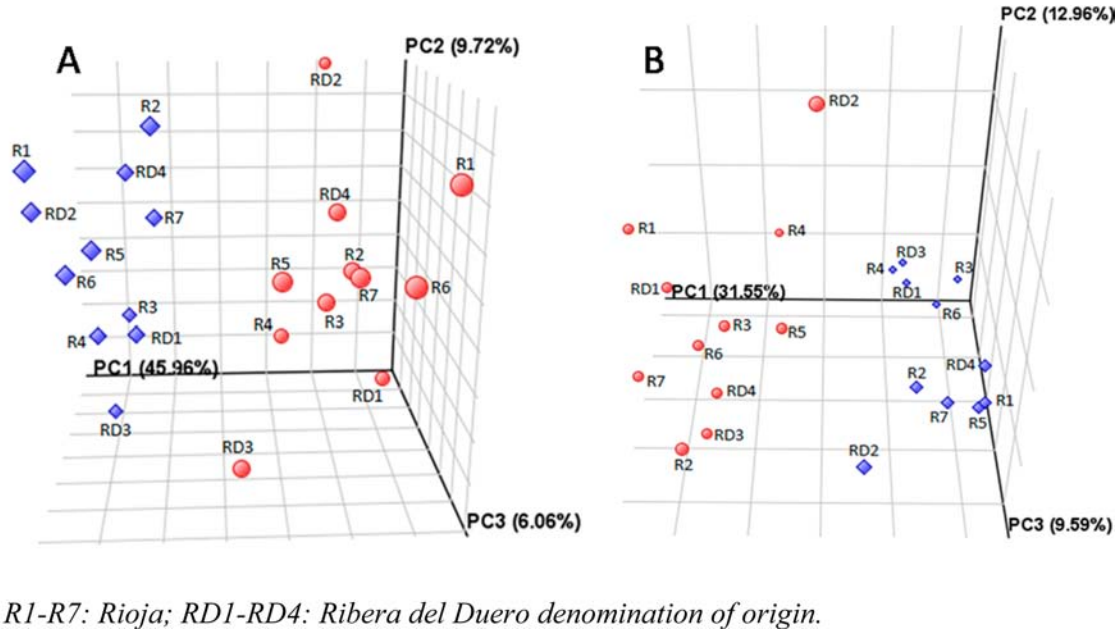

Figure 3. PCA scores plot obtained for imbibed wine from lees (tilted squares) and extracts of dried lees (circles) using the data set formed after data pretreatment for the positive (A) and the negative (B) ionization modes.

DOI: 10.1021/jf505331f
J. Agric. Food Chem. 2015, 63, 1116−1125

Table 2. Compounds Exclusively Found in Imbibed Wine from Lees and Extracts from Dried Lees and Common Compounds Identified by LC−QqTOF-MS/MS Analysis

compd[a]	*m/z*	RT (min)	formula	species	error (ppm)	mass	fragments
			Primary Amino Acids				
3-hydroxy-L-tyrosine[C]	196.0618	3.27	$C_9H_{11}NO_4$	$[M - H]^-$	1.5	197.0688	152.0731
							135.0391
							119.0042
L-valine[C]	118.0857	6.80	$C_5H_{11}NO_2$	$[M + H]^+$	3.1	117.0793	
aminocaproic acid[A]	132.1019	7.21	$C_6H_{13}NO_2$	$[M + H]^+$	0	131.0946	115.0046
L-tyrosine, octadecyl ester[B]	432.3442	40.56	$C_{27}H_{47}NO_3$	$[M - H]^-$	6.5	433.3556	
			Phenolic Compounds				
kaempferol 3-(2′,3′-diacetylrhamnoside)-7″-rhamnoside[A]	661.1820	3.69	$C_{31}H_{34}O_{16}$	$[M - H]^-$	−6.9	662.1847	601.1626
							175.0260
							131.0372
3,4,5-trimethoxyflavone[B]	335.089	7.97	$C_{18}H_{16}O_5$	$[M + Na]^+$	0	312.0998	298.0187
							280.0701
							252.0822
gallic acid[B]	169.0142	11.40	$C_7H_6O_5$	$[M - H]^-$	0	170.0215	125.0281
							107.0159
pelargonidin 3-(6-*p*-coumaryl)glucoside[C]	578.1424	16.25	$C_{30}H_{27}O_{12}$	$[M - H]^-$	1.1	579.1497	289.0687
							407.0733
							125.0229
procyanidin B2[C]	577.1357	17.47	$C_{30}H_{26}O_{12}$	$[M - H]^-$	−1.0	578.1419	425.0932
							407.0767
							289.0731
epicatechin[C]	291.0859	21.13	$C_{15}H_{14}O_6$	$[M + H]^+$	−1.4	290.0790	147.0437
							139.0387
							123.0443
malvidin 3-galactoside[B]	492.1252	18.16	$C_{23}H_{25}O_{12}$	$[M - H]^-$	4.3	493.1346	329.0645
							313.0353
							299.0128
peonidin 3-*O*-glucoside[C]	463.1232	20.96	$C_{22}H_{23}O_{11}$	$[M + H]^+$	2.6	463.1240	301.0723
catechin[C]	291.0856	17.49	$C_{15}H_{14}O_6$	$[M + H]^+$	2.4	290.0790	147.0442
							139.0385
							123.0410
quercetin 3-glucuronide[B]	477.0638	23.24	$C_{21}H_{18}O_{13}$	$[M - H]^-$	2.4	478.0747	300.9973
							151.0065
							178.9983
malvidin 3-(6-*p*-coumarylglucoside)[B]	639.1706	24.59	$C_{32}H_{30}O_{14}$	$[M + H]^+$	0	638.1636	477.1248
							331.0786
							229.1407
myricetin[B]	317.0301	26.62	$C_{15}H_{10}O_8$	$[M - H]^-$	0.6	318.0376	179.0020
							151.0070
							137.0276
quercetin[B]	301.0354	29.81	$C_{15}H_{10}O_7$	$[M - H]^-$	5.2	302.0427	178.9996
							151.0049
							121.0293
			Others				
glycerophosphocholine[B]	258.1104	3.37	$C_8H_{20}NO_6P$	$[M + H]^+$	−1.2	257.1028	184.0723
							124.9994
							104.1067
hexanethiol[C]	119.0977	3.51	$C_6H_{14}S$	$[M + H]^+$	−7.4	118.0816	107.9774
2-carboxy-2,3-dihydro-5,6-dihydroxyindole[A]	194.0400	3.62	$C_9H_9NO_4$	$[M - H]^-$	3.0	195.0532	129.0190
							113.0258
							101.0238
tartaric acid[C]	149.0096	4.57	$C_4H_6O_6$	$[M - H]^-$	−2.7	150.0164	132.6965
							105.0172
2,3-dihydroxy-3-methylbutanoate[C]	135.0543	6.41	$C_5H_{10}O_4$	$[M + H]^+$	7.8	134.0579	119.0429
							107.0455
norfuraneol[C]	115.0392	7.73	$C_5H_6O_3$	$[M + H]^+$	−3.5	114.0317	
hypoxanthine[C]	137.0444	8.48	$C_5H_4N_4O$	$[M + H]^+$	9.2	136.0385	119.0348

DOI: 10.1021/jf505331f
J. Agric. Food Chem. 2015, 63, 1116−1125

Table 2. continued

compd[a]	*m/z*	RT (min)	formula	species	error (ppm)	mass	fragments
			Others				
							110.0346
6-imino-5-oxocyclohexa-1,3-dienecarboxylate[B]	152.0331	9.63	$C_7H_5NO_3$	$[M + H]^+$	7.2	151.0269	106.0607
							118.0605
							135.0048
citric acid[A]	191.0204	9.21	$C_6H_8O_7$	$[M - H]^-$	−3.7	192.027	129.0239
							111.0130
8-oxoguanosine monophosphate[A]	380.0413	11.22	$C_{10}H_{12}N_5O_9P$	$[M + H]^+$	5.6	379.0529	145.9649
							161.0066
							133.0065
1,2-benzoquinone[A]	109.0285	13.47	$C_6H_4O_2$	$[M + H]^+$	−0.9	108.0211	
kasugamycin[A]	362.1589	13.70	$C_{14}H_{25}N_3O_9$	$[M + H - H_2O]^+$	−7.2	379.1591	230.1133
							201.1223
							131.1144
S-adenosylmethioninamine[A]	354.1451	14.23	$C_{14}H_{23}N_6O_3S$	$[M - H]^-$	8.2	355.1552	255.0878
							128.0394
glutathione[B]	306.0783	14.37	$C_{10}H_{17}N_3O_6S$	$[M - H]^-$	−5.9	307.0838	272.0865
							244.0236
							128.0370
5-nitrofurancarboxaldehyde[B]	244.0540	15.26	$C_7H_9N_3O_4$	$[M + FA - H]^-$	−8.6	199.0593	124.0146
2-formamido-N^1-(5-phospho-D-ribosyl)acetamidine[C]	314.0768	15.32	$C_8H_{16}N_3O_8P$	$[M + H]^+$	−6.4	313.0675	136.0600
							153.0146
							107.9478
ureidoglycolate[A]	135.0436	16.75	$C_3H_6N_2O_4$	$[M + H]^+$	−2.7	134.0362	107.0524
							118.9161
							104.0001
cytosine[B]	110.0635	16.83	$C_4H_5N_3O$	$[M - H]^-$	−4.3	111.0433	
phenolic steroid[A]	257.1896	18.77	$C_{18}H_{24}O$	$[M + H]^+$	1.5	256.1724	179.9834
							144.1028
							129.0588
isoquinoline *n*-oxide[A]	146.0597	19.05	C_9H_7NO	$[M + H]^+$	2.1	145.0528	128.0465
							118.0670
benzamide[B]	120.0433	23.15	C_7H_7NO	$[M - H]^-$	−6.6	121.0528	104.0268
5′-deoxy-5-fluorocytidine[B]	244.0758	25.18	$C_9H_{12}FN_3O_4$	$[M - H]^-$	−7.8	245.0812	201.0561
							159.0452
3-hydroxy-6-nonanoyl-CoA[B]	906.2267	31.67	$C_{30}H_{52}N_7O_{17}P_3S$	$[M - H]^-$	1.4	907.2653	811.2179
							359.0944

[a]Key for superscript letters: A, compounds found exclusively in imbibed wine from lees; B, compounds found exclusively in extracts; C, representative compounds common to both fractions.

Table 2, which are organized by families showing information about theoretical and experimental *m/z* values as well as characteristic fragment ions used to support identification.

Concerning the positive ionization mode, it is worth emphasizing the presence of compounds identified exclusively in imbibed wine from lees, those only identified in extracts of dried lees, and those common to both fractions. Few amino acids were identified in the analysis of wine lees. Thus, only one primary amino acid was detected exclusively in imbibed wine from lees in this polarity, aminocaproic acid, an analogue of the amino acid lysine. Two other compounds exclusively identified in imbibed wine from lees were 8-oxoguanosine monophosphate and ureidoglycolate. The former results from degradation of 8-oxoguanosine triphosphate, produced in nucleic acids during cellular metabolic processes and responsible for eliminating oxidized nucleotides in plants, thus preventing replicational and translational errors by misincorporation of 8-oxoguanosine triphosphate into DNA and RNA, which would cause mutation and phenotypic suppression.[32,33] On the other hand, ureidoglycolate is involved in purine metabolism and also in metabolic pathways and microbial metabolism in diverse environments. Particularly, it is present in *Saccharomyces cerevisiae*, where it is produced by degradation of allantoin with the concomitant production of urea.[34]

Concerning compounds found exclusively in extracts of dried lees, only two of them were tentatively identified as phenolic compounds, namely, 3,4,5-trimethoxyflavone and malvidin 3-(6-*p*-coumarylglucoside). The former elutes at 8.0 min with *m/z* at 335.0890 as the precursor ion, which corresponds to the $[M + Na]^+$ adduct. The most abundant fragments were at *m/z* 298.0187, 280.0701, and 252.0822, which is consistent with the results obtained by Huck et al. and explained by the loss of a CH_3 group from the original structure (−15 Da), the subsequent loss of a molecule of water (−18 Da), and the loss of a carbonyl group (−28 Da).[35] Malvidin 3-(6-*p*-coumarylglucoside) was found at 24.6 min, with $[M + H]^+$ as the precursor ion at *m/z* 639.1706. The consecutive loss of the coumaroyl and glucoside moieties explains the characteristic fragments found at *m/z* 477.1248 and 331.0786, respectively,

DOI: 10.1021/jf505331f
J. Agric. Food Chem. 2015, 63, 1116−1125

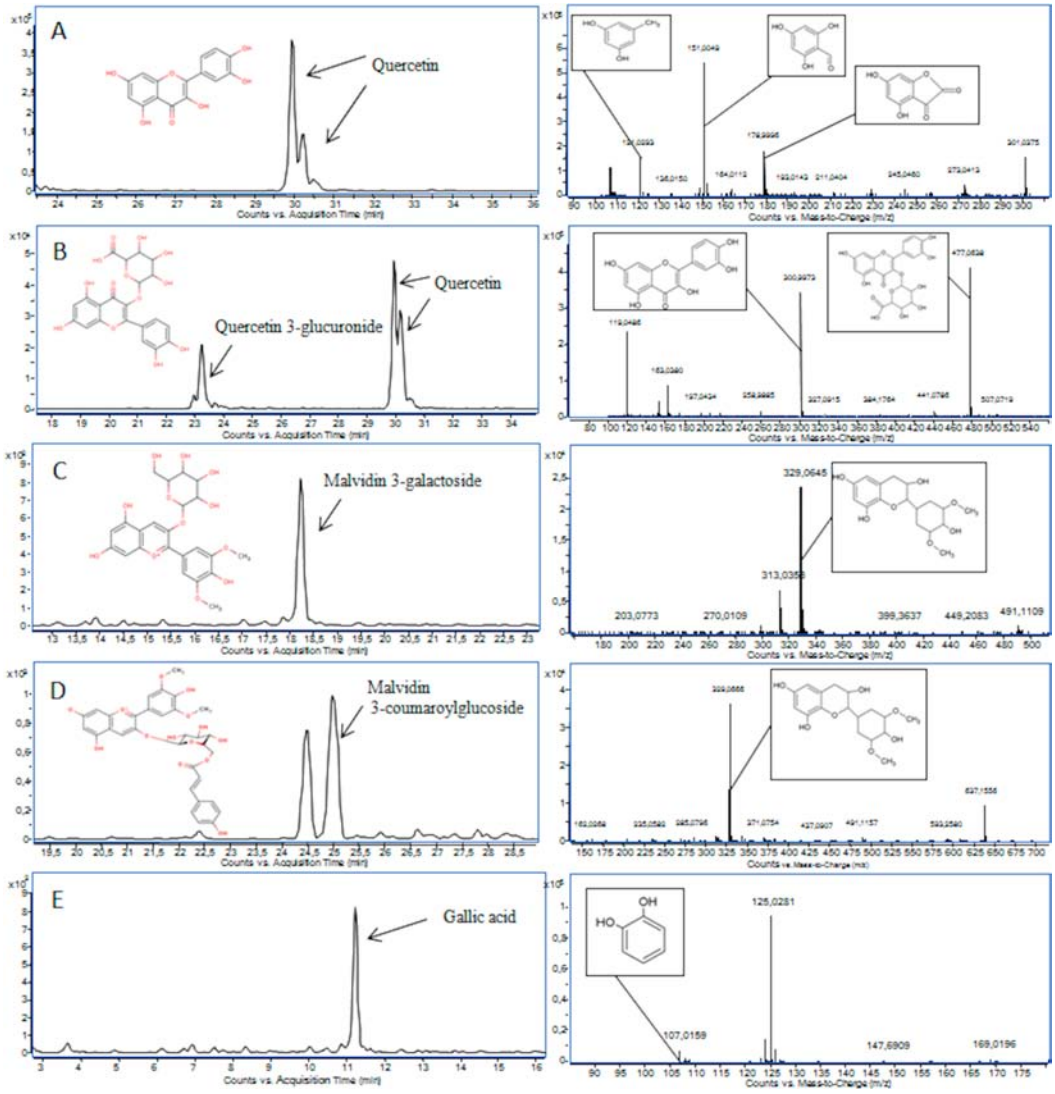

Figure 4. Extracted ion chromatograms for quercetin (A), quercetin 3-glucuronide (B), malvidin 3-galactoside (C), malvidin 3-(6-*p*-coumarylglucoside) (D), and gallic acid (E), with MS/MS spectra obtained by LC−MS/MS analysis in negative ionization mode.

where the fragment at 331.0786 corresponds to the malvidin aglycon.

Valine was the only primary amino acid found in all the samples analyzed in this polarity. It was found at 6.8 min elution time when the m/z ratio at 118.0857 was monitored as the $[M + H^+]$ precursor ion. Two phenolic compounds were tentatively detected in imbibed wine from lees and extracts from the solid residue: two flavanol isomers, catechin and epicatechin, naturally found in diverse plants such as cocoa, tea, apples, and berries, among others. Catechin and epicatechin elute at 17.5 and 21.1 min, respectively, with $[M + H]^+$ precursor ions at m/z 291.0856. Representative fragments supporting the tentative identification of both isomers were detected at m/z 147.0442, 139.0385, and 123.0410. According to Li et al., the fragment at 147.0442 is explained by heterocyclic ring fission and loss of a water molecule, the fragment at 139.0385 is produced by retro-Diels−Alder (RDA) reaction of the original molecule, and that at 123.0410 can be explained either by direct benzofuran-forming fission (BFF) or by loss of a water molecule following BFF.[36]

Other compounds tentatively identified in the positive mode in both types of samples were hypoxanthine, norfuraneol, 2-formamido-N^1-(5-phospho-D-ribosyl)acetamidine, hexanethiol, and 2,3-dihydroxy-3-methylbutanoate. The presence of all them was verified by using the Plantcyc database (www.plantcyc.org). Hypoxanthine is a naturally occurring purine derivative and a reaction intermediate in the metabolism of adenosine and in the formation of nucleic acids. It elutes at 8.5 min with an $[M + H]^+$ precursor ion at 137.0444. The MS/MS fragmentation of this precursor ion produces two characteristic fragments, one at m/z 119.0348 by the loss of a molecule of water (−18 Da) from the original structure and another fragment at 110.0346 by the loss of a CO unit (−28 Da). Norfuraneol is known for being one of the caramel descriptors in wine, together with furaneol and homofuraneol, as supported by Sarrazin et al.[37] This compound was tentatively identified eluting at 7.7 min by monitoring the m/z ratio at 115.0392 as the $[M + H]^+$ precursor ion, with two representative product ions at m/z 113.0244 and 110.9751. 2,3-Dihydroxy-3-methylbutanoate was identified by an $[M + H]^+$ precursor ion at m/z 135.0543 and with representative fragments at m/z 119.0429 produced by the loss of an oxygen unit (−16 Da) and 107.0455 produced by the loss of a CO unit from the original structure (−28 Da). According to the Yeast Metabolome Database (www.ymdb.ca),

DOI: 10.1021/jf505331f
J. Agric. Food Chem. 2015, 63, 1116−1125

2,3-dihydroxy-3-methylbutanoate is present in *S. cerevisiae*, one of the yeast more widely used for winemaking, baking, and brewing. According to Morata et al., the use of different strains of *S. cerevisiae* can have a strong influence on the content of wine in different compounds such as vitisin A and B, pyruvate, and acetaldehyde, among others.[38]

Identification of Compounds in Negative Ionization Mode. As Table 2 shows, only one amino acid derivative and one phenolic compound were tentatively identified as exclusively present in imbibed wine from lees in the negative ionization mode: namely, 3-hydroxy-L-tyrosine and kaempferol 3-(2′,3′-diacetylrhamnoside)-7″-rhamnoside. On the other hand, compounds exclusively detected in imbibed wine from lees were citric acid, *S*-adenosylmethioninamine, and 2-carboxy-2,3-dihydro-5,6-dihydroxyindole. Citric acid is commonly added during the winemaking process to improve the sensory characteristics of wine by increasing acidity to complement a specific flavor or prevent ferric hazes.[39] This acid was found at 9.2 min with an $[M - H]^-$ precursor ion at m/z 191.0240. The MS/MS spectrum associated with this compound presented characteristic fragments at 129.0239 and 111.0130, interpreted by the conversion of citric acid into itaconic acid by decarboxylation following the loss of a molecule of water to form the ion at m/z 111.0130. On the other hand, *S*-adenosylmethioninamine and 2-carboxy-2,3-dihydro-5,6-dihydroxyindole are related to the methionine and tyrosine metabolic pathways, respectively. The former is a precursor of spermine and spermidine, which are undesirable biogenic amines in wine.[40,41]

Regarding compounds exclusively detected in the extracts of wine lees, one other derivative of tyrosine is octadecyl ester, found at 40.6 min with a representative $[M - H]^-$ precursor ion at m/z 432.3442.

The abundance of phenolic compounds tentatively identified in the extracts of dried lees in negative ionization, which is justified by the adsorbent power of wine lees during aging, should be highlighted. As shown in Table 2, most of them are flavonoids, widely spread in wine and grapes, such as quercetin, myricetin, and conjugates such as malvidin 3-galactoside.

Quercetin was identified at 29.8 min with a characteristic $[M - H]^-$ precursor ion at m/z 301.0354 and with MS/MS fragments at 178.9996, 151.0049, and 121.0293 (Figure 4A). The fragment at m/z 151.0049 is produced by RDA reaction of the A ring and is a common product ion from flavonols, flavanones, and flavones. The fragment at m/z 121.0297 is produced by retrocyclation of the original structure of quercetin, with the mechanism proposed by Dubber et al.[41] Another representative fragment for quercetin used for its identification is the ion found at m/z 107.0137, a product of the cleavage of a CO_2 unit after RDA reaction takes place $[M - H - CO - CO_2]^-$. Quercetin was detected in free form, but also as a glucuronide derivative at 23.2 min showing an $[M - H]^-$ precursor ion at m/z 477.0638, as shown in Figure 4B, with a representative ion at m/z 300.9973 produced by the loss of the glucuronide moiety to form the corresponding aglycon.

Following a similar pattern, Figure 4C shows the MS/MS fragmentation pattern of malvidin 3-galactoside, eluted at 18.2 min with precursor ion $[M - H]^-$ at m/z 492.1252. The spectrum was marked by the presence of three representative product ions at m/z 329.0645, 313.0353, and 299.0128, where the ion at 329.0645 corresponds to the malvidin aglycon and the ion at 313.0353 is produced by the complete loss of the galactoside moiety (−179 Da).

Gallic acid was also tentatively detected in lees. This nonflavonoid phenolic compound is a final product in the hydrolysis of ellagitannins, which contribute to the astringent character of wines. Gallic acid elutes at 11.4 min as an $[M - H]^-$ precursor ion at m/z 169.0196. Its fragmentation produces representative product ions at m/z 107.0159 and 125.0281, as shown in Figure 4E, where the ion at m/z 125.0281 is explained by decarboxylation and the ion at 107.0159 is produced by the subsequent loss of an OH unit (−17 Da).

Additionally, two phenolic compounds were tentatively found in the two samples from all wineries, procyanidin B2 and pelargonidin 3-(6-*p*-coumaroylglucoside). Procyanidin B2 reported an $[M - H]^-$ precursor ion at m/z 577.1357, with representative fragments at m/z 407.0767, 289.0731, and 425.0932. This fragmentation pattern is consistent with the scheme proposed by Delgado de la Torre et al., where fragments at m/z 271.0 and 289.0 were explained by a quinone methide (QM) cleavage of the interflavan bond, while those at m/z 407.0 and 425.1 would correspond to the RDA reaction.[29]

Apart from these phenols, tartaric acid was also found in the two fractions of wine lees, a logical finding since this is one of the most concentrated organic acids in grapes and it plays a fundamental role in wine acidity. Tartaric acid was detected at 4.6 min, with an $[M - H]^-$ precursor ion at m/z 149.0086 and representative fragments at m/z 130.9981 and 105.0172. The fragment at m/z 130.9981 is explained by the loss of an OH group and the fragment at 105.0172 is obtained by the loss of a CO unit.

Attending to these results, it can be concluded that both fractions, imbibed wine from lees and extracts from dried lees, can be considered an exploitable source of various interesting compounds, where the former proved to be rich in primary amino acids and phenolic compounds, especially flavonoids, which can be ascribed to its adsorbent characteristics. On the other hand, a similar number of other uncommon compounds have been indentified in both fractions; thus, selection of a fraction for its exploitation would depend on the target product, since, for instance, citric acid was only found in imbibed wine from lees. On the basis of the number of compounds present in both fractions and those existing only in solid lees, this residue is proposed as the most adequate sample for exploitation, since the absence of water facilitates transport and storage. This study complements previous studies on wine lees and other enological byproducts.

AUTHOR INFORMATION

Corresponding Authors

*E-mail: q72prcaf@uco.es. Phone and fax: +34957218615.

*E-mail: qa1lucam@uco.es. Phone and fax: +34957218615.

Funding

The Spanish Ministerio de Economía y Competitividad (MINECO) is thanked for financial support through Project CTQ2012-37428. F.P.C. is also grateful to the Ministerio de Ciencia e Innovación (MICINN) for a Ramón y Cajal contract (RYC-2009-03921).

Notes

The authors declare no competing financial interest.

REFERENCES

(1) Luque-Rodríguez, J. M.; Pérez-Juan, P.; Luque de Castro, M. D. Extraction of polyphenols from vine shoots of *Vitis vinifera* by superheated ethanol−water mixtures. *Agric. Food Chem.* **2006**, *54*, 8875−8781.

DOI: 10.1021/jf505331f
J. Agric. Food Chem. 2015, 63, 1116−1125

(2) Max, B.; Salgado, J. M.; Corte, S.; Domínguez, J. M. Extraction of phenolic acids by alkaline hydrolysis from the solid residue obtained after prehydrolysis of trimming vine shoots. *J. Agric. Food Chem.* **2010**, *58*, 1090−1917.
(3) Moldes, A. M.; Torrado, A. M.; Barral, M. T.; Domínguez, J. M. Evaluation of biosurfactant production from various agricultural residues by *Lactobacillus pentosus*. *J. Agric. Food. Chem.* **2007**, *55*, 4481−4486.
(4) Moldes, A. M.; Torrado, A.; Converti, A.; Domínguez, J. M. Complete bioconversion of hemicellulosic sugars from agricultural residues into lactic acid by *Lactobacillus pentosus*. *Appl. Biochem. Biotechnol.* **2006**, *135*, 219−227.
(5) Bleve, M.; Ciurlia, L.; Erroi, E.; Lionetto, G.; Longo, L.; Rescio; Schettino, T.; Vasapollo, G. An innovative method for the purification of anthocyanins from grape skin extracts by using liquid and sub-critical carbon dioxide. *Sep. Purif. Technol.* **2008**, *64*, 192−197.
(6) Luque-Rodríguez, J. M.; Luque de Castro, M. D.; Pérez-Juan, P. Superheated liquid extraction of anthocyanins and other phenolics from red grape skins of winemaking residues. *Bioresour. Technol.* **2007**, *98*, 2705−2713.
(7) Schieber, A.; Stintzing, F. C.; Carle, R. By-products of plant food processing as a source of functional compounds. Recent developments. *Trends Food Sci. Technol.* **2001**, *12*, 401−413.
(8) Bonilla, F.; Mayen, M.; Mérida, J.; Medina, M. Extraction of phenolic compounds from red grape marc for use as food lipid antioxidants. *Food Chem.* **1999**, *66*, 209−215.
(9) Bagchi, D.; Bagchi, M.; Stohs, S. J.; Das, D. K.; Ray, S. D.; Kuszynki, C. A.; Joshi, S. S.; Pruess, H. G. Free radicals and grape seed proanthocyanidin extract: importance in human health and disease prevention. *Toxicology* **2000**, *148*, 187−197.
(10) Shrikhande, A. J. Wine by-products with health benefits. *Food Res. Int.* **2000**, *33*, 469−474.
(11) Henry, F.; Pauly, G.; Moser, P. Extracts from residues left in the production of wine and usage in cosmetic and pharmaceutical compositions. Int. Patent Appl. WO 2001058412 A2, Aug 16, 2001; 28 pp.
(12) Pykett, M. A.; Craig, A. H.; Galley, E.; Smith, C. Skin care composition against free radicals. Int. Patent Appl. WO 2001017495 A1, March 15, 2001; 59 pp.
(13) Doco, T.; Vuchot, P.; Cheynier, V.; Moutounet, M. Structural modification of arabinogalactan-proteins during aging of red wines on lees. . *Am. J. Enol. Vitic.* **2003**, *54*, 150−157.
(14) Salmon, J. M.; Fornairon-Bonnefond, C.; Mazauric, J. P. Interactions between wine lees and polyphenols: influence on oxygen consumption capacity during simulation of wine aging. *J. Food Sci.* **2002**, *67*, 1604−1609.
(15) Braga, F.; Lencart e Silva, F. G.; Alves, A. Recovery of winery by-products in the Douro demarcated region: production of calcium tartrate and grape pigments. *Am. J. Enol. Vitic.* **2002**, *53*, 41−45.
(16) Pérez-Serradilla, J. A.; Luque de Castro, M. D. Role of lees in wine production: a review. *Food Chem.* **2008**, *111*, 447−456.
(17) Feuillat, M. Spécifité de l'elaboration des grands Vins blancs de Bourgogne. *Rev. Oenologues* **1992**, *65*, 47−50.
(18) Palaces, S.; Vasserot, Y.; Maujean, A. Evidence for sulfur volatile products adsorption by yeast lees. *Am. J. Enol. Vitic.* **1997**, *48*, 525−526.
(19) Chassagne, D.; Guilloux-Benatier, M.; Alexandre, H.; Voilley, A. Sorption of wine volatile phenols by yeast lees. *Food Chem.* **2005**, *91*, 39−44.
(20) Zea, L.; Moreno, J.; Medina, M.; Ortega, J. M. Evolution of C6, C8 and C10 acids and their ethyl esters in cell and must during fermentation with three *Saccaromyces cerevisiae* races. *J. Ind. Microbiol.* **1994**, *13*, 269−272.
(21) Zea, L.; Moreno, J.; Ortega, J. M.; Medina, M. Content of free terpenic compounds in cells and musts during vinification with three *Saccaromyces cerevisiae* races. *J. Agric. Food Chem.* **1995**, *43*, 1110−1114.
(22) Zea, L.; Moreno, J.; Ortega, J. M.; Mauricio, J. C.; Medina, M. Comparative study of the c-butyrolactone and pantolactone contents in cells and musts during vinification by three *Saccaromyces cerevisiae* races. *Biotechnol. Lett.* **1995**, *12*, 1351−1356.
(23) Maugenet, J. Evaluation of the by-products of wine distilleries II. Possibility of recovery of proteins in the vinasse of wine distilleries. *C. R. Seances Acad. Agric. Fr.* **1973**, *59*, 481−487.
(24) Rivas, B.; Torrado, A.; Moldes, A. B.; Domínguez, J. M. Tartaric acid recovery from distilled lees and use of the residual solid as an economic nutrient for *Lactobacillus*. *J. Agric. Food Chem.* **2006**, *54*, 7904−7911.
(25) Mazauric, J. P.; Salmon, J. M. Interactions between yeast lees and wine polyphenols during simulation of wine aging: I. Analysis of remnant polyphenolic compounds in the resulting wines. *J. Agric. Food Chem.* **2005**, *53*, 5647−5836.
(26) Guilloux-Benatier, M.; Chassagne, D.; Alexandre, H.; Feuillat, M. Influence of yeast autolysis after alcoholic fermentation on the development brettanomyces/dekkera in wine. *J. Int. Sci. Vigne Vin* **2001**, *35*, 157−164.
(27) Chassagne, D.; Guilloux-Benatier, M.; Alexandre, H.; Voilley, A. Sorption of wine volatile phenols by yeast lees. *Food Chem.* **2005**, *91*, 39−44.
(28) Morata, A.; Gómez-Cordovés, M. C.; Suberviola, J.; Bartolomé, B.; Colomo, B.; Suárez, J. A. Adsorption of anthocyanins by yeast cell walls during the fermentation of red wines. *J. Agric. Food Chem.* **2003**, *51*, 4084−4088.
(29) Delgado de la Torre, M. P.; Ferreiro-Vera, C.; Priego-Capote, F.; Luque de Castro, M. D. Anthocyanidins, proanthocyanidins, and anthocyanins profiling in wine lees by solid-phase extraction−liquid chromatography coupled to electrospray ionization tandem mass spectrometry with data-dependent methods. *J. Agric. Food Chem.* **2013**, *61*, 12539−12548.
(30) Pérez-Serradilla, J. A.; Luque de Castro, M. D. Microwave-assisted extraction of phenolic compounds from wine lees and spray-drying of the extract. *Food Chem.* **2011**, *124*, 1652−1659.
(31) Alonso, A. M.; Guillén, D. A.; Barroso, C. G.; Puertas, B.; García, A. Determination of antioxidant activity of wine byproducts and its correlation with polyphenolic content. *J. Agric. Food Chem.* **2002**, *50*, 5832−5836.
(32) Yoshimura, K.; Ogawa, T.; Ueda, Y.; Shigeoka, S. AtNUDX1, an 8-oxo-7,8-dihydro-2′-deoxyguanosine 5′-triphosphate pyrophosphohydrolase, is responsible for eliminating oxidized nucleotides in *Arabidopsis*. *Plant Cell Physiol.* **2007**, *48*, 1438−1449.
(33) Ito, R.; Hayakawa, H.; Sekiguchi, M.; Ishibashi, T. Multiple enzyme activities of *Escherichia coli* MutT protein for sanitization of DNA and RNA precursor pools. *Biochemistry* **2005**, *44*, 6670−6674.
(34) Yoo, H. S.; Genbauffe, F. S.; Cooper, T. G. Identification of the ureidoglycolate hydrolase gene in the DAL gene cluster of *Saccharomyces cerevisiae*. *Mol. Cell. Biol.* **1985**, *5*, 2279−2288.
(35) Huck, C. W.; Bonn, G. K. Evaluation of detection methods for the reversed-phase HPLC determination of 3′,4′,5′-trimethoxyflavone in different phytopharmaceutical products and in human serum. *Phytochem. Anal.* **2001**, *12*, 104−109.
(36) Li, H. J.; Deinzer, M. L. Tandem mass spectrometry for sequencing proanthocyanidins. *Anal. Chem.* **2007**, *79*, 1739−1748. Sarrazin, E.; Dubourdieu, D.; Darriet, P. Characterization of key-aroma compounds of botrytized wines, influence of grape botrytization. *Food Chem.* **2007**, *103*, 536−545.
(37) Morata, A.; Gómez-Cordovés, M. C.; Colomo, B.; Suárez, J. A. Pyruvic acid and acetaldehyde production by different strains of *Saccharomyces cerevisiae*: relationship with vitisin A and B formation in red wines. *J. Agric. Food Chem.* **2003**, *51*, 7402−7409.
(38) Ribéreau-Gayon, P.; Glories, Y.; Maujean, A.; Dubourdieu, D. Aging red wines in vat and barrel. Phenomena occurring during aging. *Handbook of Enology Volume 2: The Chemistry of Wine Stabilization and Treatments*; John Wiley & Sons, Ltd.: Chichester, U.K., 1999; pp 99−100.
(39) Bauza, T.; Blaise, A.; Daumas, F.; Cabanis, J. C. Determination of biogenic amines and their precursor amino acids in wines of the Vallée du Rhône by high-performance liquid chromatography with

DOI: 10.1021/jf505331f
J. Agric. Food Chem. 2015, 63, 1116−1125

precolumn derivatization and fluorimetric detection. *J. Chromatogr. A* **1995**, *707*, 373−379.
(40) Kelly, M. T.; Blaise, A.; Larroque, M. Rapid automated high performance liquid chromatography method for simultaneous determination of amino acids and biogenic amines in wine, fruit and honey. *J. Chromatogr. A* **2010**, *1217*, 7385−7392.
(41) Dubber, J. M.; Sewram, V.; Mshicieli, N.; Shephard, G. S.; Kanfer, I. The simultaneous determination of selected flavonol glycosides and aglycones in *Ginkgo biloba* oral dosage forms by high-performance liquid chromatography−electrospray ionisation−mass spectrometry. *J. Pharm. Biomed. Anal.* **2005**, *37*, 723−731.

DOI: 10.1021/jf505331f
J. Agric. Food Chem. 2015, 63, 1116−1125

Facultat de Farmàcia of the Universitat de Barcelona. Animals were kept in an environmentally controlled room with stable humidity (50 ± 10%) and temperature (22 ± 2 °C) and a 12 h light/dark cycle. A commercial diet (2014 Teklad Global 14%, Harlan, Barcelona, Spain) and water were supplied *ad libitum*. Rats were fasted overnight and anesthetized by intraperitoneal injection of 90 mg/kg of ketamine (Imalgene 1000, Merial Laboratorios S.A., Barcelona, Spain) and 10 mg/kg of xylacine (Rompun 2%, Química Farmacéutica Bayer S.A., Barcelona, Spain). All animal manipulations accomplished the requirements set by the European Community guidelines for the care and management of laboratory animals. In addition, the experiments were conducted in the morning to lessen the effects of circadian rhythms. The research protocol (reference 164/10) was approved by the Ethic Committee of Animal Experimentation of the Universitat de Barcelona.

Dose Administration and Sample Collection. Maslinic acid was administered to overnight fasted rats at a dose of 50 mg/kg of body weight by single oral gavage. Pentacyclic triterpene was dissolved in an aqueous solution of (2-hydroxypropyl)-ß-cyclodextrin (40%, w/v) and sodium carboxymethylcellulose (0.5%) as previously described.[12] After oral administration, blood was withdrawn from the saphenous vein[13] at 45 min and placed in tubes containing ethylenediaminetetraacetic acid (EDTA)−K_2 (Microvette CB300, Sarstedt, Granollers, Spain) to avoid coagulation. Samples were maintained on ice until centrifugation at 1500*g* (Centrifuge Megafuge 1.0R, Heraeus, Boadilla, Spain) for 15 min at 4 °C. Plasma was subsequently separated and stored at −20 °C until analysis. At 45 min post-administration, urine samples were directly collected from the urinary bladder of previously anesthetized animals and frozen at −20 °C until processing.

Preparation of Rat Plasma and Urine Samples. Plasma and urine were thawed before analysis, and urine was centrifuged at 25000*g* for 30 min at 2 °C (Centrifuge 5417R, Eppendorf Ibérica S.L.) to obtain a clear supernatant. A total of 200 μL of either plasma or urine was spiked with 10 μL of 50 μM betulinic acid [IS, dissolved in 80:20 (v/v) methanol/water] before being extracted with 2 mL of ethyl acetate. Each sample was strongly stirred in a vortex mixer for 3 min and then centrifuged at 1500*g* for 15 min at 4 °C (Centrifuge Megafuge 1.0R, Heraeus). The ethyl acetate layer was carefully removed and placed in a clean conical tube, and a second extraction of the residue was performed. The organic supernatants were gathered together and evaporated to dryness in a vacuum concentrator (Concentrator 5301, Eppendorf Ibérica S.L., San Sebastián de los Reyes, Spain) at 45 °C. The dry residue was dissolved by adding 100 μL of methanol/water (80:20, v/v), followed by vigorous shaking in a vortex mixer for 5 min. Samples were immediately sonicated for 1 min and centrifuged at 25000*g* for 15 min at 4 °C (Centrifuge 5417R, Eppendorf Ibérica S.L.). Finally, an amber vial was employed to place the clean supernatant before the analysis.

Metabolite Identification by LC−APCI−LTQ−Orbitrap. Samples were analyzed using an Accela liquid chromatograph (Thermo Scientific, Hemel, Hempstead, U.K.) equipped with a thermostated autosampler and a quaternary pump and coupled to a LTQ−Orbitrap Velos mass spectrometer (Thermo Scientific). The equipment was available at the Centres Científics i Tecnològics of the Universitat de Barcelona. Chromatographic separations was carried out on a Luna C_{18} column (150 × 2.0 mm, 5 μm) kept at 40 °C and protected with a security guard cartridge of the same packing material (Phenomenex, Micron Analítica S.A., Madrid, Spain). Gradient elution was performed with water (solvent A) and acetonitrile (solvent B) at a constant flow rate of 0.8 mL/min. The volume of injection was 10 μL. Separation was carried out within 19 min under the following conditions: 0 min, 95% A and 5% B; 4 min, 50% A and 50% B; 8 min, 40% A and 60% B; 12 min, 25% A and 75% B; 15 min, 0% A and 100% B; and 19 min, 0% A and 100% B. An additional period of 8 min was needed for re-equilibration of the column before the ensuing injection.

Mass spectrometric analysis was conducted using an APCI source in the negative-ion mode. Mass calibration was performed daily according to the guidelines of the manufacturer. The LTQ−Orbitrap was tuned to the optimal conditions for maslinic acid. Therefore, a 100 μM standard solution was delivered by the LTQ syringe pump at a constant flow rate of 10 mL/min in the presence of LC mobile phase under isocratic conditions of 25% A and 75% B. Operation parameters were set as follows: vaporizer temperature, 450 °C; sheath gas, 50 arbitrary units (au); auxiliary gas flow, 5 au; sweep gas, 0 au; discharge current, 5 μA; S-lens radio frequency (RF) level, 70%; and capillary gas, 300 °C. The data were acquired using Fourier transform full scan with a resolving power of either 60 000 or 100 000 (at m/z 400) and the microscan count fixed to unity. The automatic gain control (AGC) was set at 1×10^6. The mass spectrometric data were collected in a range of m/z from 100 to 1000.

MS Data Processing. Mass chromatograms and spectral data were acquired with the Xcalibur software 2.0 (Thermo Scientific). Maslinic acid metabolites were searched both manually with Xcalibur Qual Browser and also employing MetWorks software (version 1.3, Thermo Scientific). Qual Browser was employed for MS data processing and calculation of elementary compositions. The elemental composition was selected according to the accurate masses and the isotopic pattern. Mass accuracy was determined by the deviation of measured and theoretical masses relative to theoretical values and was expressed in millidaltons. MetWorks software allowed for the identification of metabolites by comparing the samples to controls, of either blank plasma or urine. The most commonly observed biotransformations in phase I and phase II metabolism were searched to find putative metabolites of maslinic acid with a mass deviation of less than 5 ppm from the predicted values.

Quantification of Maslinic Acid and Its Metabolites by LC−APCI−MS in Rat Plasma and Urine. After the identification of maslinic acid metabolites by LC−APCI−LTQ−Orbitrap, the compounds were quantified by LC−APCI−MS. The liquid chromatograph (PerkinElmer series 200, PerkinElmer, Norwalk, CT) included a quaternary pump and a refrigerated autosampler plate and was coupled to a single quadrupole mass spectrometer (PE Sciex API 150 EX, AB SCIEX, Spain) with an APCI source at 500 °C in negative-ion mode. The LC−MS system was controlled by the 1.4.2 Analyst software supplied by Applied Biosystems (Foster City, CA). The chromatographic conditions were the conditions described for the LC−APCI−LTQ−Orbitrap system. For the mass spectrometer, nitrogen was used as both curtain gas (12 au) and nebulizer gas (10 au) with a nebulizing flow of −3 au. The optimum LC−APCI−MS pre-collision cell voltages were −30 V for declustering potential, −100 V for focusing potential, and −5 V for entrance potential. The selected ion monitoring (SIM) mode was used for quantification of maslinic acid at m/z 471.3 and betulinic acid (IS) at m/z 455.3. The metabolites identified by LC−APCI−LTQ−Orbitrap were quantified at m/z 487.3 (M1−M4), 485.3 (M5), and 501.3 (M6 and M7). The dwell time was set at 165 ms. Concentrations of maslinic acid in plasma and urine samples were calculated from the ratio of the peak area of triterpene to the IS interpolated on an external calibration curve. Because of the absence of synthetic standards, it was assumed that LC−APCI−MS response to derivatives is similar to that of maslinic acid; thus, both plasma and urine metabolites were quantified using the standard curve of the parent compound. Results were expressed as micromoles per liter (μM).

The determination of maslinic acid in plasma and urine was validated for recovery, matrix effect, precision, accuracy, linearity, and sensitivity, according to the European Medicines Agency (EMA) Guideline on Bioanalytical Method Validation.[14] Calibration standards were freshly prepared by spiking 190 μL of rat blank plasma or urine with 10 μL of standard solutions of maslinic acid at different concentrations and were treated as previously indicated for the specimens collected from dosed rats. The post-extraction spiking method proposed by Matuszewski et al.[15] was used to establish the recovery and matrix effect. Briefly, recovery was assessed by comparing the peak areas of calibration standards to the peak areas obtained from blank plasma or urine spiked with maslinic acid after the extraction. The matrix effect was evaluated by comparing the peak areas obtained from blank plasma or urine spiked with pentacyclic triterpene after the extraction to those of a solution of 80% methanol spiked with the expected concentration. Recovery and matrix effect were determined

DOI: 10.1021/jf505379g
J. Agric. Food Chem. 2015, 63, 1126−1132

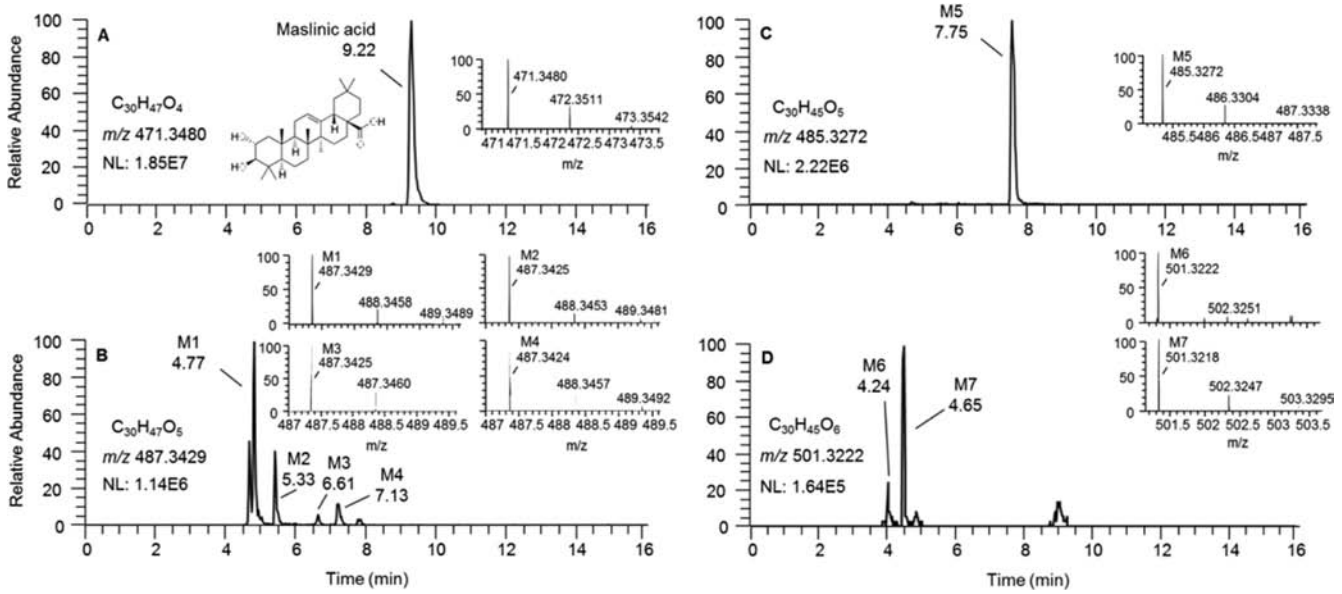

Figure 1. Representative extracted ion chromatograms (EICs) and MS spectra of maslinic acid and its phase I metabolites of the rat plasma sample obtained 45 min after the oral administration of 50 mg/kg of body weight of triterpene. A full-scan analysis was performed by LC−APCI−LTQ−Orbitrap using a scan range from m/z 100.00 to 1000.00. EICs: (A) maslinic acid (m/z 471.32), (B) monohydroxylated metabolites (m/z 487.34), (C) monohydroxylated and dehydrogenated metabolites (m/z 485.32), and (D) dihydroxylated and dehydrogenated metabolites (m/z 501.32). MS spectra: (A1) maslinic acid, (B1−B4) monohydroxylated metabolites, (C1) monohydroxylated and dehydrogenated metabolite, and (D1 and D2) dihydroxylated and dehydrogenated metabolites. NL = normalized level.

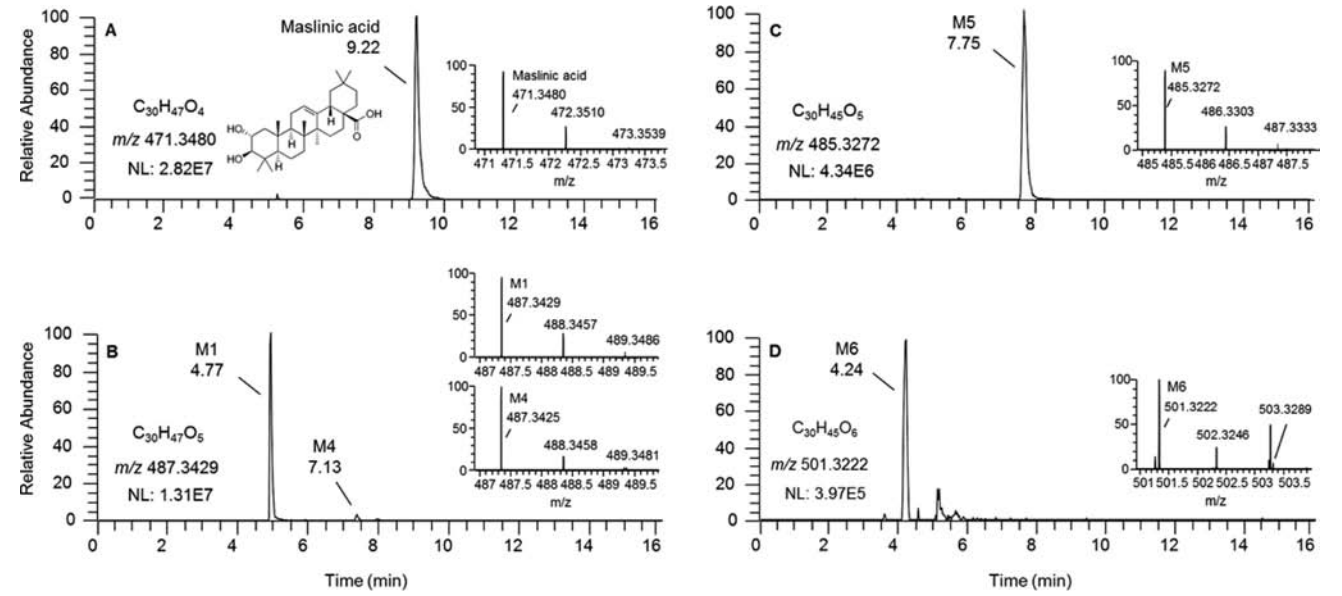

Figure 2. Representative EICs and MS spectra of maslinic acid and its phase I metabolites of the rat urine sample withdrawn 45 min after the oral administration of 50 mg/kg of body weight of triterpene. A full-scan analysis was performed by LC−APCI−LTQ−Orbitrap using a scan range from m/z 100.00 to 1000.00. EIC chromatograms: (A) maslinic acid (m/z 471.32), (B) monohydroxylated metabolites (m/z 487.34), (C) monohydroxylated and dehydrogenated metabolites (m/z 485.32), and (D) dihydroxylated and dehydrogenated metabolites (m/z 501.32). MS spectra: (A1) maslinic acid, (B1 and B2) monohydroxylated metabolites, (C1) monohydroxylated and dehydrogenated metabolite, and (D1) dihydroxylated and dehydrogenated metabolite. NL = normalized level.

at four concentration levels (0.5, 1, 5, and 10 μM), while precision and accuracy were analyzed at 1, 5, and 10 μM. Linearity was assayed in the range of 0.005−10 μM, which included eight concentration levels that covered the expected amounts in the samples. The limit of detection (LOD) was considered as the minimum concentration of maslinic acid that could be recognized by the detector and produced a signal-to-noise ratio of 3:1. The lowest limit of quantification (LLOQ) was defined as the lowest concentration of the standard curve that could be accurately quantified and with a signal at least 10 times above the noise level.

RESULTS

LC−APCI−LTQ−Orbitrap Analysis of Maslinic Acid and Its Metabolites in Rat Plasma and Urine. Maslinic acid ($C_{30}H_{48}O_4$) was unambiguously identified in rat plasma and urine by comparing its retention time (9.22 min) and MS

DOI: 10.1021/jf505379g
J. Agric. Food Chem. 2015, 63, 1126−1132

Table 1. Maslinic Acid and Its Metabolites Identified by LC−APCI−LTQ−Orbitrap in Rat Plasma and Urine Samples Obtained after the Oral Administration of 50 mg/kg of Body Weight of Pentacyclic Triterpene

					error		metabolite appearance	
	retention time (min)	molecular formula	theoretical mass (m/z)	measured mass (m/z)	mDa	ppm	plasma	urine
M0	9.22	$C_{30}H_{48}O_4$	471.3480	471.3479	0.04	−0.22	+	+
			Monohydroxylated Metabolites					
M1	4.77	$C_{30}H_{48}O_5$	487.3429	487.3426	−0.05	−0.30	+	+
M2	5.33	$C_{30}H_{48}O_5$	487.3429	487.3425	0.13	−0.35	+	ND[a]
M3	6.61	$C_{30}H_{48}O_5$	487.3429	487.3425	0.25	−0.80	+	ND[a]
M4	7.13	$C_{30}H_{48}O_5$	487.3429	487.3424	0.9	−0.50	+	+
			Monohydroxylated and Dehydrogenated Metabolites					
M5	7.75	$C_{30}H_{46}O_5$	485.3272	485.3271	0.23	0.03	+	+
			Dihydroxylated and Dehydrogenated Metabolites					
M6	4.24	$C_{30}H_{46}O_6$	501.3222	501.3216	−0.37	0.18	+	+
M7	4.65	$C_{30}H_{46}O_6$	501.3222	501.3218	−0.05	−1.13	+	ND[a]

[a]ND = not detected.

data to the standard reference. In addition, the injection into the high-resolution system LTQ−Orbitrap gave its accurate mass (m/z 471.3480) with an error of 0.4 mDa. The spectra generated for pentacyclic triterpene in plasma and urine showed the deprotonated molecule $[M - H]^-$ without the presence of any fragment (Figures 1A and 2A, respectively).

Possible derivatives of maslinic acid were first predicted on the basis of knowledge of metabolism and then searched in full-scan chromatograms of rat plasma and urine samples. Afterward, the formulas of potential metabolites were compared to that of the parent compound to refer metabolic pathways. The high mass accuracy of the LTQ−Orbitrap analyzer enabled an extraction of individual chromatograms in a narrow interval of the m/z scale (± 5 mDa), which is useful for discarding other compounds with similar masses.[16] The initial screening of plasma and urine samples obtained after the oral administration of maslinic acid revealed the formation of derivatives with mass shifts of +16, +14, and +30 Da in comparison to the parent compound. Mass shifts of +32 Da, which corresponded to a double hydroxylation, were searched but were not found in the analyzed plasma and urine samples. On the other hand, phase II metabolites of maslinic acid were not detected after screening with LC−APCI−LTQ−Orbitrap and MetWorks software, indicating that this compound undergoes mainly phase I metabolism.

Table 1 shows the list of metabolites identified through LTQ−Orbitrap analysis, along with retention times, accurate masses, molecular formulas, and mDa and ppm of error between the mass found and the accurate mass of each derivative. The observed and calculated masses agree to within less than 1 mDa, which demonstrates the high accuracy of the measured masses. Neither maslinic acid nor its metabolites were detected in plasma and urine of the control group at the corresponding retention times.

M1−M4 (m/z 487.3). Four polar metabolites, namely, M1−M4, were detected in plasma as deprotonated molecules at m/z 487.3 and a molecular formula of $C_{30}H_{48}O_5$, according to the Formula Predictor software (Table 1). The mass of these compounds was 15.9949 Da higher than that of maslinic acid, thus indicating that the biotransformation might be the addition of a hydroxyl group. All of the metabolites eluted earlier than the parent compound, showing retention times of 4.77, 5.33, 6.61, and 7.13 min for M1, M2, M3, and M4, respectively. As shown in Figure 1B, the peak of M1 was the most abundant, followed by M2 and M4 peaks, while that of M3 was less intense. The accurate mass of each of these metabolites differed by less than 1 mDa from the theoretical mass, and the respective spectra showed an isotopic distribution that was in accordance with the theoretical spectra of m/z 487.3, indicating a correct identification (panels B1−B4 of Figure 1).

On the other hand, in urine samples, only metabolites M1 and M4 were detected (Figure 2B). The compound M1 was the most abundant, as was observed in plasma. However, M2 and M3 were not present in any of the samples analyzed, and M4 appeared in urine with low intensities. The corresponding spectra are shown in panels B1 and B2 of Figure 2.

M5 (m/z 485.3). A single peak corresponding to a deprotonated molecule at m/z 485.3 was identified as M5. This metabolite had a retention time of 7.75 min and was found in both plasma (Figure 1C) and urine (Figure 2C) samples. The mass increment of 13.9792 Da with respect to maslinic acid (Table 1), together with the molecular formula ($C_{30}H_{46}O_5$) calculated by the Formula Predictor software, suggested that this biotransformation consists of the incorporation of a hydroxyl group and the loss of two hydrogen atoms. M5 was identified with an error of 0.23 mDa (Table 1) and a correct isotopic distribution pattern (Figures 1C1 and 2C1).

M6 and M7 (m/z 501.3). Two additional compounds (M6 and M7) eluting earlier than the parent compound yielded a deprotonated molecule at m/z 501.3. The retention times were 4.24 and 4.65 min for M6 and M7, respectively. Because the molecular formula of both metabolites was $C_{30}H_{46}O_6$, as calculated by the Formula Predictor software (Table 1) and the mass shift was +29.9442 Da, this biotransformation was attributed to dihydroxylation and dehydrogenation of maslinic acid. In plasma samples, M7 showed a higher relative abundance than M6 (Figure 1D), whereas in urine, only M6 was detected and with very low intensities, indicating small concentrations (Figure 2D).

Quantification of Maslinic Acid Metabolites by LC−APCI−MS in Rat Plasma. The mass chromatograms from LC−APCI−LTQ−Orbitrap were consistent with the LC−APCI−MS chromatograms and allowed for the identification of all of the metabolites, taking into account the relative retention times. The method was adequate for the quantification of maslinic acid in plasma samples, as indicated by the results obtained in the validation. The mean recovery and matrix effect

DOI: 10.1021/jf505379g
J. Agric. Food Chem. 2015, 63, 1126−1132

Table 2. Matrix Effect and Recovery of the Analytical Methods To Determine Maslinic Acid in Rat Plasma and Urine by LC–APCI–MS

theoretical concentration (μM)	recovery (%)[a]		matrix effect (%)[a]	
	plasma	urine	plasma	urine
0.5	98.8 ± 1.6 (n = 9)	95.6 ± 2.7 (n = 3)	108.8 ± 3.1 (n = 3)	110.6 ± 1.8 (n = 3)
1	96.8 ± 2.1 (n = 9)	96.7 ± 2.2 (n = 8)	124.7 ± 1.1 (n = 3)	112.0 ± 4.7 (n = 6)
5	100.2 ± 4.2 (n = 8)	98.7 ± 1.8 (n = 8)	116.1 ± 2.2 (n = 3)	111.5 ± 3.0 (n = 10)
10	100.4 ± 5.2 (n = 6)	99.4 ± 2.0 (n = 6)	126.7 ± 2.3 (n = 3)	109.7 ± 2.3 (n = 3)

[a]Values are expressed as means ± standard error of the mean (SEM).

Table 3. Precision and Accuracy of the Analytical Methods To Determine Maslinic Acid in Rat Plasma and Urine by LC–APCI–MS

theoretical concentration (μM)	intraday precision (%)[a]		interday precision (%)[a]		accuracy (%)[a]	
	plasma	urine	plasma	urine	plasma	urine
1	1.30 (n = 3)	5.62 (n = 3)	5.46 (n = 8)	7.59 (n = 12)	0.54 (n = 5)	−4.36 (n = 8)
5	2.64 (n = 3)	6.90 (n = 3)	5.93 (n = 9)	6.91 (n = 10)	2.34 (n = 3)	0.85 (n = 10)
10	3.30 (n = 3)	3.54 (n = 3)	6.42 (n = 9)	5.10 (n = 6)	0.94 (n = 4)	14.5 (n = 3)

[a]Values are expressed as means ± SEM.

at the four concentration levels assayed were 99.1 and 119.1%, respectively (Table 2). The intra- and interday precision and accuracy are summarized in Table 3, showing that, at all concentrations, the results were well below the 15% limit established by the EMA Guideline on Bioanalytical Method Validation.[14] Calibration curves were linear within the concentration range from 0.005 to 10 μM, and a representative curve is $y = 2.39x + 0.25$. Correlation coefficients were above 0.99. The sensitivity was suitable, because the LOD and the LLOQ were 2 and 5 nM, respectively.

Maslinic acid was the main compound in plasma samples withdrawn at 45 min after the oral administration of 50 mg/kg of body weight with a concentration of 4.83 ± 0.85 μM (Figure 3A). The identified metabolites were found in plasma at much lower concentrations than the parent compound. The most abundant derivative was the monohydroxylated and dehydrogenated metabolite M5 (m/z 485.3) at 0.77 ± 0.18 μM, followed by the monohydroxylated metabolite M1 (m/z 487.3) that reached the amount of 0.15 ± 0.03 μM. The other monohydroxylated metabolites were found at concentrations of 57.0 ± 12.7, 22.6 ± 3.8, and 34.2 ± 10.9 nM for M2, M3, and M4, respectively (Figure 3). Similarly, the dihydroxylated and dehydrogenated compounds were present in plasma in minor amounts, of 25.1 ± 4.1 nM for M7 and 10.3 ± 2.3 nM for M6 (Figure 3).

Quantification of Maslinic Acid Metabolites by LC–APCI–MS in Rat Urine. The analytical method for the determination of maslinic acid in urine was also validated to ensure a reliable quantification of both the parent compound and its metabolites. Recovery and matrix effect were analyzed at concentrations of 0.5, 1, 5, and 10 μM (Table 2). The extraction method was appropriate for the analysis of maslinic acid in urine, because it yielded recoveries between 95.6 and 99.4% (Table 2) and matrix effect values from 109.7 to 112%. Table 3 displays the intra- and interday precision and accuracy, which were assayed by spiking blank urine at three concentrations (1, 5, and 10 μM). The method was precise, as evidenced by relative standard deviations (RSDs) of intra- and interday assays lower than 6.90 and 7.59%, respectively, which fall below the 15% limit stipulated by the EMA Guideline on Bioanalytical Method Validation.[14] The accuracy of the method met the same criterion. Linearity was observed over the concentration range assayed (0.005–10 μM), with a representative calibration curve of $y = 0.58x + 0.05$ and correlation coefficients that surpassed 0.99. The LOD was 2 nM, and the LLOQ was 5 nM, meaning appropriate sensitivity.

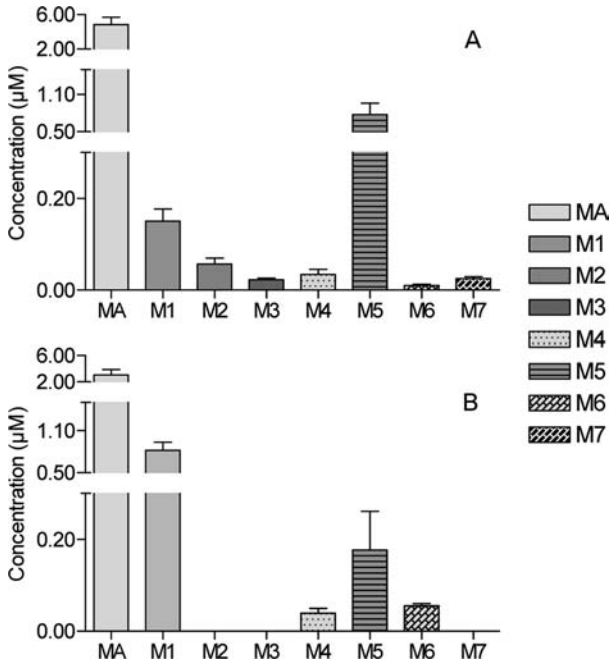

Figure 3. Concentrations of maslinic acid and its metabolites in (A) plasma and (B) urine collected at 45 min after the oral administration of 50 mg/kg of body weight of triterpene. Values are represented as means + SEM (n = 4–5).

Maslinic acid and its metabolites were quantified by LC–APCI–MS in urine samples obtained 45 min after the administration of triterpene (Figure 3B). As previously observed in plasma, maslinic acid was the major compound in urine (73.9%). However, the metabolite profile in this biological fluid differed from that found in plasma. The most abundant compound was the monohydroxylated derivative M1, representing 19.9%, whereas the monohydroxylated and dehydrogenated metabolite (M5) accounted for only 4.30%.

DOI: 10.1021/jf505379g
J. Agric. Food Chem. 2015, 63, 1126–1132

The other monohydroxylated metabolite (M4) and the dihydroxylated and dehydrogenated compound M6 represented only 0.71 and 1.23%, respectively.

DISCUSSION

A large variety of drugs and bioactive compounds from the diet, such as maslinic acid, are considered as xenobiotics by the organism. Consequently, a detoxification process is activated, consisting of the increase of its hydrophilicity via metabolism to facilitate their excretion.[17] The biotransformation of xenobiotics can take place through phase I reactions on the basis of oxidation, reduction, and hydrolysis processes and phase II reactions, which comprise glucuronidation, sulfation, methylation, acetylation, and glutathione conjugation.[1,18] To devise a comprehensive strategy for the detection in plasma and urine of maslinic acid and its metabolites, the derivatives arising from both processes were considered, but only phase I metabolites were found.

The analysis by LTQ−Orbitrap allowed the identification of a monohydroxylated metabolite with four isomers in plasma samples (M1−M4) and two in urine (M1 and M4). The metabolism of pentacyclic triterpenes has been scarcely assessed with only an *in vivo* study for boswellic acids.[19] In agreement with our study, Krüger et al.[19] found in plasma two monohydroxylated derivatives after the oral administration of 12.5 mg/kg of boswellic acids to female albino Wistar rats. The fact that hydroxylation is the principal metabolic route of pentacyclic triterpenes has been confirmed by *in vitro* assays consisting of incubations of oleanolic acid[20] or boswellic acids[19,21] with rat and human liver microsomes. With regard to maslinic acid, the biotransformation of this pentacyclic triterpene has only been investigated *in vitro* with the use of fungi, such as *Cunninghamella*[22] and *Rhizomucor*.[23] These species express cytochrome P450 (CYP) enzymes that enable equivalent phase I reactions to mammalian metabolism, thus being widely used in the assessment of the biotransformation of drugs and xenobiotics.[24] The results obtained with these microbial models of mammalian drug metabolism are in concordance with our findings. Feng et al.[22] described that maslinic acid was transformed by *Cunninghamella blakesleana* into three different monohydroxylated derivatives (7β-hydroxy, 15α-hydroxy, and 13β-hydroxy with double bond migration) and one dihydroxylated metabolite (7β,15α-dihydro derivative). Moreover, the bioconversion of maslinic acid by *Rhizomucor miehei* also yielded a monohydroxylated metabolite, but in this case, the addition of the hydroxyl group took place at the angular methyl group on position 30.[23] Taking into account these published data and considering that, in our study, four isomers of the monohydroxylated maslinic acid were detected in plasma, it could be suggested that the hydroxyl groups were added to the positions 7, 13, 15, and 30.

Maslinic acid underwent a biotransformation that yielded M5, which was detected in both plasma and urine. The mass shift of +14 Da exhibited by this metabolite was compatible with monohydroxylation, followed by dehydrogenation, which could be due to the oxidation of the corresponding secondary alcohol to a ketone. The pentacyclic ring skeleton of maslinic acid has two alcohols at the 2 and 3 positions, respectively, which are likely to be converted to a ketone. Up to now, this modification of maslinic acid has not been reported. However, this reaction has been described *in vitro* for boswellic acids after incubation with rat liver microsomes[19] and also for betulinic acid after incubations with different microbial models of drug metabolism.[25,26] Additionally, metabolites M6 and M7 showed a mass shift of +30 Da, which corresponded to the addition of two hydroxyl groups plus the conversion of a secondary alcohol to a ketone. This result is consistent with the biotransformation observed for boswellic acids[19] as well as ursolic acid after the incubation with the fungus *Pestalotiopsis microspora*.[27] Under our experimental conditions, no metabolites resulting solely from oxidation (−2 Da) or dihydroxylation (+32 Da) reactions were found in either plasma or urine.

Once the metabolites of maslinic acid were identified by LTQ−Orbitrap, their plasmatic concentrations were quantified to know the degree of the biotransformation of this compound by LC−APCI−MS. After the administration of 50 mg/kg of body weight of maslinic acid, this bioactive molecule was the prevalent compound in plasma and urine, where it accounted for 81.8 and 73.9%, respectively. Therefore, although the results indicate that maslinic acid undergoes phase I metabolism, yielding seven derivatives in plasma and four in urine, their contribution to the elimination of this pentacyclic triterpene is not preeminent, because the parent compound is excreted in urine mainly unaltered. These findings are consistent with our previous assessment of the pharmacokinetics of maslinic acid that indicated a low clearance that was attributed to minor hepatic and renal metabolism along with unchanged renal excretion.[10] Moreover, the oral bioavailability of 5.13% observed cannot be mainly attributed to metabolism. At present, experiments on the intestinal absorption of this compound are being conducted in our laboratory, and the results suggest poor absorption from the gastrointestinal tract (data not shown).

In summary, the present study thoroughly characterizes for the first time the metabolite profile of maslinic acid in rat plasma and urine. Although the oral bioavailability of similar pentacyclic triterpenes has been reported and the derivatives of some of them have been identified after incubation with different microorganisms[19,25−27] or rat and human microsomes,[19,20] none of these studies quantified the metabolites in biological fluids. Our results reveal that maslinic acid undergoes mainly phase I metabolism through hydroxylation and oxidation reactions but is not subjected to phase II biotransformations. A total of seven metabolites were identified in plasma, four monohydroxylated derivatives (M1−M4), one monohydroxylated and dehydrogenated metabolite (M5), and two dihydroxylated and dehydrogenated derivatives (M6 and M7). Only M1, M4, M5, and M6 were detected in urine. This study provides comprehensive insight into the metabolite profile of maslinic acid, thus increasing our knowledge about the bioavailability of this bioactive food component.

AUTHOR INFORMATION

Corresponding Authors

*Telephone: +34934024505. Fax: +34934035901. E-mail: mejuan@ub.edu.

*Telephone: +34934024505. Fax: +34934035901. E-mail: jmplanas@ub.edu.

Funding

This work was supported by Grants AGL2009-12866 and AGL2013-41188 from the Ministerio de Economía y Competitividad and 2009SGR471 and 2014SGR1221 from the Generalitat de Catalunya, Spain. Marta Sánchez-González was a recipient of a fellowship from Project 2009SGR471 and Beques Iniciació a Tesi Doctoral (FFAR2012), and Glòria

DOI: 10.1021/jf505379g
J. Agric. Food Chem. 2015, 63, 1126−1132

Lozano-Mena was a recipient of Ajuts de Personal Investigador en Formació (APIF) from the Universitat de Barcelona.

Notes

The authors declare no competing financial interest.

■ ACKNOWLEDGMENTS

The authors thank Dr. Isidre Casals and Dr. Olga Jáuregui from Centres Científics i Tecnològics of the Universitat de Barcelona for excellent technical assistance and advice and Maria Vicente for excellent technical assistance.

■ ABBREVIATIONS USED

LC−MS, liquid chromatography−mass spectrometry; LOD, limit of detection; LLOQ, lowest limit of quantification; RSD, relative standard deviation

■ REFERENCES

(1) Holcapek, M.; Kolárová, L.; Nobilis, M. High-performance liquid chromatography−tandem mass spectrometry in the identification and determination of phase I and phase II drug metabolites. *Anal. Bioanal. Chem.* **2008**, *391*, 59−78.

(2) García-Cañas, V.; Simó, C.; León, C.; Cifuentes, A. Advances in nutrigenomics research: Novel and future analytical approaches to investigate the biological activity of natural compounds and food functions. *J. Pharm. Biomed. Anal.* **2010**, *51*, 290−304.

(3) Romero, C.; García, A.; Medina, E.; Ruiz-Méndez, M. V.; de Castro, A.; Brenes, M. Triterpenic acids in table olives. *Food Chem.* **2010**, *118*, 670−674.

(4) Caligiani, A.; Malavasi, G.; Palla, G.; Marseglia, A.; Tognolini, M.; Bruni, R. A simple GC−MS method for the screening of betulinic, corosolic, maslinic, oleanolic and ursolic acid contents in commercial botanicals used as food supplement ingredients. *Food Chem.* **2013**, *136*, 735−741.

(5) Lin, C. C.; Huang, C. Y.; Mong, M. C.; Chan, C. Y.; Yin, M. C. Antiangiogenic potential of three triterpenic acids in human liver cancer cells. *J. Agric. Food Chem.* **2011**, *59*, 755−762.

(6) Kalogeropoulos, N.; Chiou, A.; Ioannou, M.; Karathanos, V. T.; Hassapidou, M.; Andrikopoulos, N. K. Nutritional evaluation and bioactive microconstituents (phytosterols, tocopherols, polyphenols, triterpenic acids) in cooked dry legumes usually consumed in the Mediterranean countries. *Food Chem.* **2010**, *121*, 682−690.

(7) Li, G. L.; You, J. M.; Song, C. H.; Xia, L.; Zheng, J.; Suo, Y. R. Development of a new HPLC method with precolumn fluorescent derivatization for rapid, selective and sensitive detection of triterpenic acids in fruits. *J. Agric. Food Chem.* **2011**, *59*, 2972−2979.

(8) Sánchez-González, M.; Lozano-Mena, G.; Juan, M. E.; García-Granados, A.; Planas, J. M. Assessment of the safety of maslinic acid, a bioactive compound from *Olea europaea* L. *Mol. Nutr. Food Res.* **2013**, *57*, 339−346.

(9) Lozano-Mena, G.; Sánchez-González, M.; Juan, M. E.; Planas, J. M. Maslinic acid, a natural phytoalexin-type triterpene from olives—A promising nutraceutical? *Molecules* **2014**, *19*, 11538−11559.

(10) Sánchez-González, M.; Colom, H.; Lozano-Mena, G.; Juan, M. E.; Planas, J. M. Population pharmacokinetics of maslinic acid, a triterpene from olives, after intravenous and oral administration in rats. *Mol. Nutr. Food Res.* **2014**, *58*, 1970−1979.

(11) García-Granados, A. Process for the industrial recovery of oleanolic and maslinic acids contained in the olive milling by products. U.S. Patent 6,037,492, 2002.

(12) Lozano-Mena, G.; Juan, M. E.; García-Granados, A.; Planas, J. M. Determination of maslinic acid, a pentacyclic triterpene from olives, in rat plasma by high-performance liquid chromatography. *J. Agric. Food Chem.* **2012**, *60*, 10220−10225.

(13) Hem, A.; Smith, A. J.; Solberg, P. Saphenous vein puncture for blood sampling of the mouse, rat, hamster, gerbil, guinea pig, ferret and mink. *Lab. Anim.* **1998**, *32*, 364−368.

(14) Committee for Medicinal Products for Human Use (CHMP), European Medicines Agency (EMA). *Guideline on Bioanalytical Method Validation*; CHMP, EMA: London, U.K., 2011.

(15) Matuszewski, B. K.; Constanzer, M. L.; Chavez-Eng, C. M. Strategies for the assessment of matrix effect in quantitative bioanalytical methods based on HPLC−MS/MS. *Anal. Chem.* **2003**, *75*, 3019−3030.

(16) Jirásko, R.; Holčapek, M.; Nobilis, M. Identification of phase I and phase II metabolites of benfluron and dimefluron in rat urine using high-performance liquid chromatography/tandem mass spectrometry. *Rapid Commun. Mass Spectrom.* **2011**, *25*, 2153−2162.

(17) Benedetti, M. S.; Whomsley, R.; Poggesi, I.; Cawello, W.; Mathy, F. X.; Delporte, M. L.; Papeleu, P.; Watelet, J. B. Drug metabolism and pharmacokinetics. *Drug Metab. Rev.* **2009**, *41*, 344−390.

(18) Testa, B.; Krämer, S. D. The biochemistry of drug metabolism—An introduction: Part 1. Principles and overview. *Chem. Biodiversity* **2006**, *3*, 1053−1101.

(19) Krüger, P.; Daneshfar, R.; Eckert, G. P.; Klein, J.; Volmer, D. A.; Bahr, U.; Müller, W. E.; Karas, M.; Schubert-Zsilavecz, M.; Abdel-Tawab, M. Metabolism of boswellic acids *in vitro* and *in vivo*. *Drug Metab. Dispos.* **2008**, *36*, 1135−1142.

(20) Jeong, D. W.; Kim, Y. H.; Kim, H. H.; Ji, H. Y.; Yoo, S. D.; Choi, W. R.; Lee, S. M.; Han, C. K.; Lee, H. S. Dose-linear pharmacokinetics of oleanolic acid after intravenous and oral administration in rats. *Biopharm. Drug Dispos.* **2007**, *28*, 51−57.

(21) Gerbeth, K.; Hüsch, J.; Fricker, G.; Werz, O.; Schubert-Zsilavecz, M.; Abdel-Tawab, M. *In vitro* metabolism, permeation, and brain availability of six major boswellic acids from *Boswellia serrata* gum resins. *Fitoterapia* **2013**, *84*, 99−106.

(22) Feng, X.; Luan, J.; Guo, F. F.; Li, D. P.; Chu, Z. Y. Microbial transformation of maslinic acid by *Cunninghamella blakesleana*. *J. Mol. Catal. B: Enzym.* **2012**, *82*, 127−130.

(23) Martinez, A.; Rivas, F.; Perojil, A.; Parra, A.; Garcia-Granados, A.; Fernandez-Vivas, A. Biotransformation of oleanolic and maslinic acids by *Rhizomucor miehei*. *Phytochemistry* **2013**, *94*, 229−237.

(24) Murphy, C. D. Drug metabolism in microorganisms. *Biotechnol. Lett.* **2014**, *37*, 19−28.

(25) Chatterjee, P.; Kouzi, S. A.; Pezzuto, J. M.; Hamann, M. T. Biotransformation of the antimelanoma agent betulinic acid by *Bacillus megaterium* ATCC 13368. *Appl. Environ. Microbiol.* **2000**, *66*, 3850−3855.

(26) Bastos, D. Z.; Pimentel, I. C.; de Jesus, D. A.; de Oliveira, B. H. Biotransformation of betulinic and betulonic acids by fungi. *Phytochemistry* **2007**, *68*, 834−839.

(27) Fu, S. B.; Yang, J. S.; Cui, J. L.; Meng, Q. F.; Feng, X.; Sun, D. A. Multihydroxylation of ursolic acid by *Pestalotiopsis microspora* isolated from the medicinal plant *Huperzia serrata*. *Fitoterapia* **2011**, *82*, 1057−1061.

DOI: 10.1021/jf505379g
J. Agric. Food Chem. 2015, 63, 1126−1132

Table 1. Peptide Sequences for the Endopep-MS Method Listed Along with the Observed $(M + H)^+$ of Substrate and Cleavage Products for Each Serotype[a]

peptide	sequence	m/z observed
SubA	Acetyl-RGSNKPKIDAGNQRATRXLGGR-NH_2	2406
SubA NT product	Acetyl-RGSNKPKIDAGNQ	1427
SubA CT product	RATRXLGGR-NH_2	999
SubB	LSELDDRADALQAGASQFESSAAKLKRKYWWKNLK	4025
SubB NT product	LSELDDRADALQAGASQ	1760
SubB CT product	FESSAAKLKRKYWWKNLK	2283
SubE	WWWAKLGQEIDTRNRQKDhRIMAKADSNKR-NH2	3614
SubE NT product	WWWAKLGQEIDTRNRQKDhR	2501
SubE CT product	IMAKADSNKR-NH2	1133
SubF	TSNRRLQQTQAQVDEVVDIMRVNVDKVLERDQKLSELDDRADAL	5111
SubF NT product	TSNRRLQQTQAQVDEVVDIMRVNVDKVLERDQ	3784
SubF CT product	KLSELDDRADAL	1346

[a]X represents norleucine, and hR represents homoarginine.

Endopep-MS method achieves limits of detection comparable to or below that of the historically used mouse bioassay.[21]

On the basis of our previous success in detecting and differentiating BoNT in clinical specimens and culture supernatants, we sought to extend the utility of the assay to foods. In this work, we used the Endopep-MS method to detect BoNT/A, /B, /E, and /F spiked into more than 50 foods. In all cases, BoNT/A, /B, /E, and /F were detectable at levels spiked below the limit of detection of the mouse bioassay. For 10 diverse types of foods, the limit of detection was determined. Many of the foods evaluated were submitted during suspected botulism outbreaks over the past several years, and the foods account for a wide variety of characteristics such as pH, viscosity, and fat content and are representative of cuisines from varied ethnic cultures.

MATERIALS AND METHODS

Materials. Monoclonal antibodies to BoNT/A (CR2 and RAZ1),[22] BoNT/B (2B18.2 and B12.1),[23] BoNT/E (4E17.1),[24] and BoNT/F (6F5)[25] were obtained from Dr. James Marks at the University of California at San Francisco and used for immunoaffinity purification. Dynabeads (M-280/Streptavidin) were purchased from Invitrogen (Carlsbad, CA). BoNT/A (3.5×10^7 mLD_{50}/mg), BoNT/B (1.1×10^7 mLD_{50}/mg), BoNT/E (3.0×10^7 mLD_{50}/mg), and BoNT/F (3.6×10^6 mLD_{50}/mg) complex toxins at a concentration of 1 mg/mL, where mLD_{50} is the mouse lethal dose, were purchased from Metabiologics (Madison, WI). Botulinum neurotoxin is very toxic and necessitates suitable safety measures (see below). All chemicals were from Sigma-Aldrich (St. Louis, MO) except where indicated. Peptide substrates for evaluation of BoNT activity are listed in Table 1 and were synthesized by Midwest Biotech Inc. (Fishers, IN). Sulfo-NHS-Biotin was purchased from Thermo Fisher Scientific (Waltham, MA). Kingfisher plates (deep well and traditional 96 well) and tip combs were purchased from Thermo Fisher Scientific (Waltham, MA).

Preparation of Food Extracts. Foods were purchased from local stores. For the spiking studies, extracts were made from solid foods prior to analysis. The solid food was weighed and placed into a standard 80 mL stomacher bag. A 1 mL amount of phosphate-buffered saline with 0.05% tween-20 (PBST) was added for every gram of food, with a minimum of 10 g and a maximum of 60 g of processed. Foods were processed using the Stomacher 80 Biomaster (Seward, Port Saint Lucie, FL) at maximum speed for 2 min. The mixture was then centrifuged at 12 000g in a refrigerated centrifuge (4 °C) for 20 min. The supernatant was recovered, and centrifugation continued until a clear supernatant was obtained. The clear supernatant was used for testing. Liquid foods were not processed prior to use. BoNT was pipetted into the clear supernatant or liquid food in volumes varying from 2 to 20 μL.

For foods from outbreak investigations, 5−10 g (or 5−10 mL if liquid) of sample was transferred to a container and 1 mL of gelatin phosphate-buffered collecting fluid (GBS) per 1 g (or 1 mL) of sample was added. After mixing, the sample was centrifuged at 4 °C for 20 min at 23 000 g. The supernatant was then transferred into a 6 or 10 mL sterile syringe and filtered through a 0.45 μm filter.

Preparation of mAb-Coated Beads. The mAbs (20 μg) were biotinylated with 4 μL of the 300 μM sulfo-NHS-biotin in water, prepared immediately before use. The mAb/biotin was incubated overnight at room temperature with no mixing. Biotin-labeled mAb (2 μg) was added to 100 μL of washed (two times with 1 mL of PBST; resuspended in 100 μL of PBST) streptavidin-coated beads and incubated at room temperature for 1 h with constant movement to keep the beads in solution. The beads then were washed twice in 1 mL each of PBST, and then the mAb bound beads were reconstituted in 100 μL of PBST. For a higher number of test samples, the volumes were increased proportionally.

Spiking Liquid Foods and Food Extracts with BoNT. Biosafety Level-2 practices, processes, and facilities were used to ensure safety while working with BoNT. Additionally, toxin stock material and all samples containing BoNT were processed in a Class II biosafety cabinet containing HEPA filters to minimize the potential for aerosol exposure.

An aliquot of the liquid food or food extract of 0.5 or 1 mL was placed into a deep well plate. BoNT/A, /B, /E, or /F complexes were serially diluted in PBST from 1000 mLD_{50}/μL down to 0.001 mLD_{50}/μL immediately prior to spiking using 2 μL of the stock solution and 18 μL of PBST. For milk, the following levels were spiked: 10 mLD_{50}, 1 mLD_{50}, 0.5 mLD_{50}, 0.25 mLD_{50}, 0.1 mLD_{50}, 0.05 mLD_{50}, and 0.01 mLD_{50} of BoNT. For infant formula, yogurt, broccoli, green bean liquid, salami, salmon, liquid egg, orange juice, and tomato juice, the following levels were spiked: 1 mLD_{50}, 0.75 mLD_{50}, 0.5 mLD_{50}, 0.25 mLD_{50}, 0.1 mLD_{50}, 0.05 mLD_{50}, 0.025 mLD_{50}, and 0.01 mLD_{50} of BoNT. The remaining foods were spiked with 0.75 mLD_{50}, 0.5 mLD_{50}, or 0.25 mLD_{50} of BoNT. The limit of detection was defined as the lowest level of toxin which could be detected during five separate analyses performed by a minimum of two analysts. Detection of the toxin consisted of the presence of mass spectrometric peaks with S/N of greater than 3 times above the S/N of the negative control (unspiked sample of same matrix).

Extraction of BoNT from Foods. For spiked foods, 10X PBST was added to achieve a final volume of 0.55 (for 0.5 mL of food extracts) or 1.1 mL (for 1 mL of food extracts). All spiked foods were tested in parallel with the same volume of blank food matrix, diluted to the same level with 10X PBST. For foods from outbreak investigations, an aliquot of 100 μL was placed into a deep well plate along with 400 μL of 1X PBST. A negative control consisting of 100 μL of blank food matrix and 400 μL of 1X PBST and a positive control consisting of 100

DOI: 10.1021/jf505482b
J. Agric. Food Chem. 2015, 63, 1133−1141

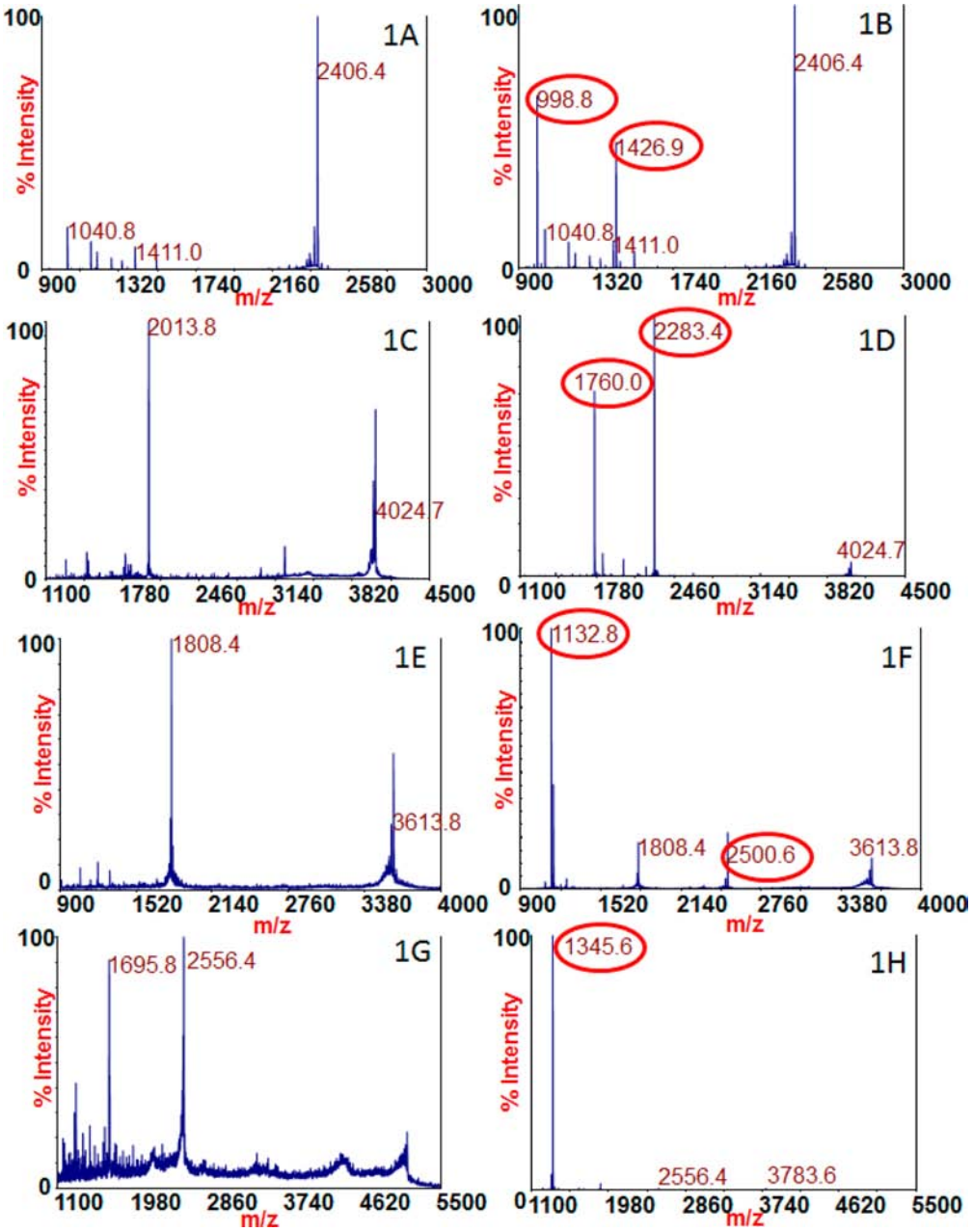

Figure 1. Mass spectra of 10 mLD_{50} of (B) BoNT/A, (D) BoNT/B, (F) BoNT/E, and (H) BoNT/F spiked into 1 mL of milk. Cleavage products indicating the presence of BoNT are circled in red. Negative controls consisted of 1 mL of milk tested for (A) BoNT/A, (C) BoNT/B, (E) BoNT/E, and (G) BoNT/F.

μL of blank food matrix, 400 μL of 1X PBST, and 1 mLD_{50} of BoNT were run in parallel with the food from the outbreak investigation. The foods from outbreak investigations included salmon, kim chi, sofrito, salsa, rice, juice, steak, pebre, corn cake, chili sauce, tomatoes, tomato paste, tofu, soup, fish, sauerkraut, relish, tea grounds, sour cream dip, yogurt, rice, vegemite, chili peppers, and baked potato. In addition, acidic matrices were adjusted to a pH of 7.0 with the addition of ammonium hydroxide unless otherwise noted.

Antibody-coated beads (20 μL) were added to the sample. The deep well plate was capped and placed on a plate shaker for 1 h at the minimal speed necessary to keep the beads in solution. The deep well plate was then uncapped and placed into a KingFisher flex magnetic particle processor (Thermo Fisher Scientific, Waltham, MA) for automated bead washing, which included two washes with 1 mL each of 2 M NaCl (or 1X PBST as specified) followed by two washes with 1 mL each of 1X PBST. The beads were eluted into 80 μL of water and removed from the KingFisher flex. Replicate extracts were incubated with each serotype of mAb coated beads.

Endopep-MS Reaction with MALDI-TOF Analysis. The aqueous extract was removed from the beads, and then the beads were reconstituted in 18 μL of reaction buffer consisting of 0.05 M Hepes (pH 7.3), 25 mM dithiothreitol, and 20 μM $ZnCl_2$ and 2 μL of peptide substrate specific for the antibody extract (SubA, SubB, SubE, or SubF, respectively). The final concentration of each substrate was 50 pmol/μL. All samples were incubated at 37 °C for 4 h with no agitation. A 2 μL aliquot of each reaction supernatant was mixed with 18 μL of matrix solution consisting of α-cyano-4-hydroxy cinnamic acid (CHCA) at 5 mg/mL in 50% acetonitrile, 0.1% trifluoroacetic acid (TFA), and 1 mM ammonium citrate. A 0.5 μL aliquot of this mixture was pipeted onto one spot of a 384-spot matrix-assisted laser desorption/ionization (MALDI) plate (Applied Biosystems, Framingham, MA). Mass spectra of each spot were obtained by scanning from m/z 900 to 5500 in MS-positive ion reflector mode on an Applied

DOI: 10.1021/jf505482b
J. Agric. Food Chem. 2015, 63, 1133−1141

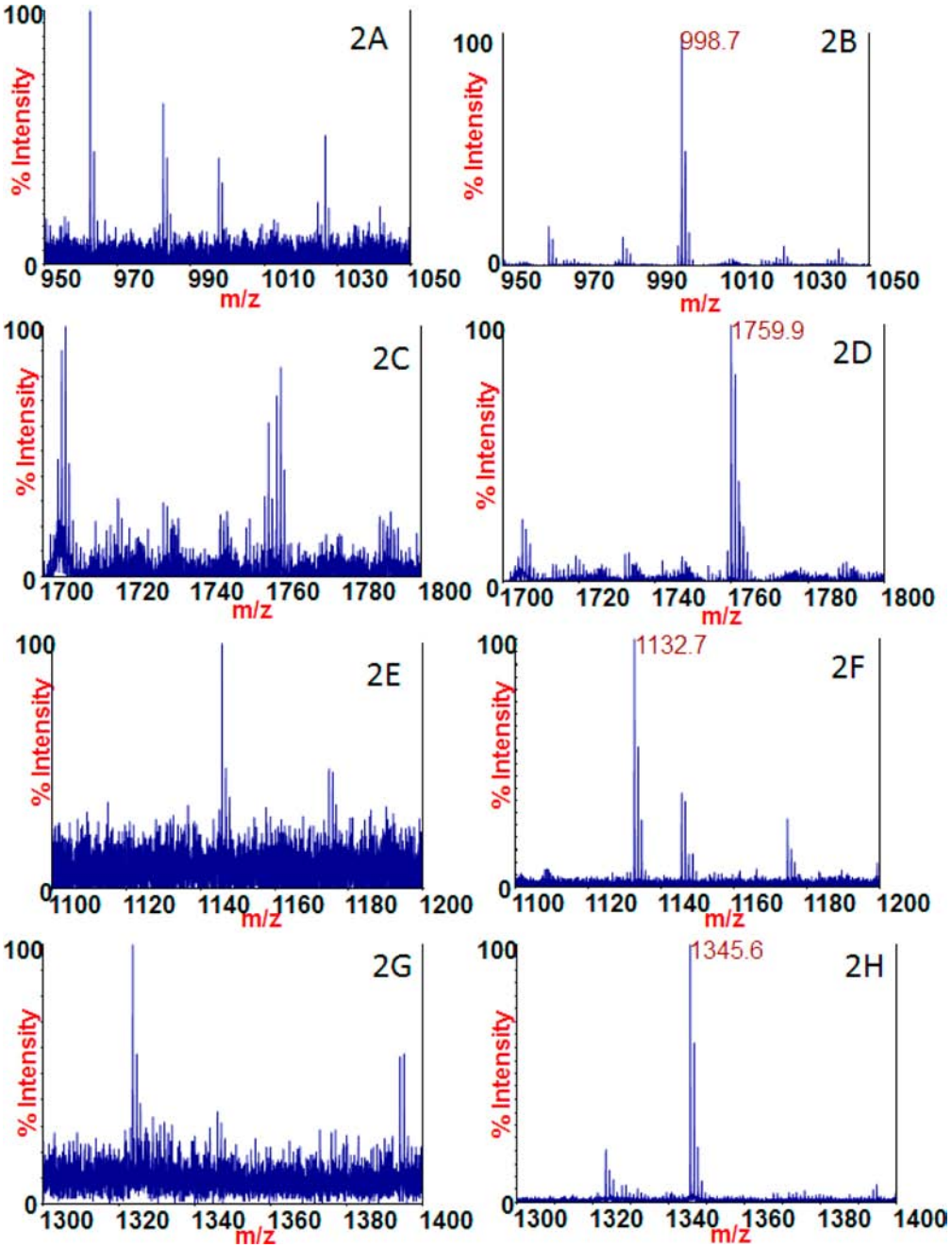

Figure 2. Mass spectra of (B) 0.25 mLD_{50} of BoNT/A, (D) 0.1 mLD_{50} of BoNT/B, (F) 0.25 mLD_{50} of BoNT/E, and (H) 0.01 mLD_{50} of BoNT/F spiked into 1 mL of milk. Negative controls consisted of 1 mL of milk tested for (A) BoNT/A, (C) BoNT/B, (E) BoNT/E, and (G) BoNT/F. Spectra are zoomed to display the dominant cleavage product.

Biosystems 5800 Proteomics Analyzer (Framingham, MA). The instrument uses an Nd:YAG laser at 355 nm, and each spectrum is an average of 2400 laser shots.

RESULTS AND DISCUSSION

Detection of BoNT/A, /B, /E, and /F in Whole Milk. The Endopep-MS method has been used successfully in the analysis of clinical specimens and culture supernatants for BoNT/A, /B, /E, and /F, demonstrating its potential to diagnose botulism, a potentially fatal disease. Although this method has limits of detection in clinical specimens and culture supernatants lower than that of the historically standard assay, the mouse bioassay, until now it was uncertain if the assay could be adapted to examine foods directly for the presence of BoNT/A, /B, /E, and /F. Detection of BoNT in foods is important as it allows for discovery of the vehicle of transmission in foodborne botulism cases, potentially preventing additional outbreaks. Foods represent a wider variety of different characteristics than clinical specimens. For example, foods can be protease rich, low pH, high fat, and very viscous, all properties which could negatively affect any assay for detection of BoNT. We therefore wanted to test the Endopep-MS method on a wide variety of foods with varying properties in addition to foods which have been known to serve as causative agents of botulism in the past.

We began with the analysis of BoNT/A in whole milk. Various levels of BoNT/A were spiked into whole milk and analyzed. Comparison of the mass spectra of whole milk

DOI: 10.1021/jf505482b
J. Agric. Food Chem. 2015, 63, 1133−1141

Table 2. Limit of Detection of BoNT/A, /B, /E, and /F Spiked into 10 Selected Food Matrices

food	food state	BoNT/A	BoNT/B	BoNT/E	BoNT/F
milk	liquid	0.25 mLD_{50}/mL	0.1 mLD_{50}/mL	0.25 mLD_{50}/mL	0.01 mLD_{50}/mL
infant formula	liquid	0.5 mLD_{50}/mL	0.1 mLD_{50}/mL	0.25 mLD_{50}/mL	0.01 mLD_{50}/mL
green bean liquid	liquid	0.5 mLD_{50}/mL	0.1 mLD_{50}/mL	0.25 mLD_{50}/mL	0.01 mLD_{50}/mL
orange juice[a]	liquid	0.25 mLD_{50}/mL	0.25 mLD_{50}/mL	0.5 mLD_{50}/mL	0.025 mLD_{50}/mL
tomato juice[a]	liquid	0.5 mLD_{50}/mL	0.1 mLD_{50}/mL	0.25 mLD_{50}/mL	0.025 mLD_{50}/mL
liquid egg	liquid	0.75 mLD_{50}/mL	0.25 mLD_{50}/mL	0.5 mLD_{50}/mL	0.05 mLD_{50}/mL
yogurt	semisolid	0.25 mLD_{50}/mL	0.1 mLD_{50}/mL	0.25 mLD_{50}/mL	0.01 mLD_{50}/mL
broccoli	solid	0.25 mLD_{50}/mL	0.1 mLD_{50}/mL	0.25 mLD_{50}/mL	0.01 mLD_{50}/mL
salami	solid	0.25 mLD_{50}/mL	0.1 mLD_{50}/mL	0.25 mLD_{50}/mL	0.01 mLD_{50}/mL
salmon	solid	0.25 mLD_{50}/mL	0.1 mLD_{50}/mL	0.25 mLD_{50}/mL	0.01 mLD_{50}/mL

[a]Requires pH adjustment.

Table 3. Detection of BoNT/A, /B, /E, and /F Spiked at Levels Below 1 mLD_{50} in 44 Additional Food Matrices

food	food state	BoNT/A	BoNT/B	BoNT/E	BoNT/F
beef stew	solid	0.5 mLD_{50}	0.5 mLD_{50}	0.25 mLD_{50}	0.25 mLD_{50}
butter beans	solid	0.5 mLD_{50}	0.5 mLD_{50}	0.75 mLD_{50}	0.25 mLD_{50}
carrot juice	liquid	0.25 mLD_{50}	0.25 mLD_{50}	0.25 mLD_{50}	0.25 mLD_{50}
celery	solid	0.25 mLD_{50}	0.25 mLD_{50}	0.5 mLD_{50}	0.25 mLD_{50}
cereal	solid	0.75 mLD_{50}	0.25 mLD_{50}	0.25 mLD_{50}	0.25 mLD_{50}
chicken soup	solid	0.25 mLD_{50}	0.5 mLD_{50}	0.25 mLD_{50}	0.25 mLD_{50}
chili	solid	0.5 mLD_{50}	0.5 mLD_{50}	0.5 mLD_{50}	0.25 mLD_{50}
chili sauce[a]	liquid	0.75 mLD_{50}	0.75 mLD_{50}	0.75 mLD_{50}	0.25 mLD_{50}
collard greens	solid	0.5 mLD_{50}	0.5 mLD_{50}	0.25 mLD_{50}	0.25 mLD_{50}
cooked egg	solid	0.5 mLD_{50}	0.25 mLD_{50}	0.75 mLD_{50}	0.25 mLD_{50}
corn cake	solid	0.75 mLD_{50}	0.25 mLD_{50}	0.75 mLD_{50}	0.25 mLD_{50}
corn syrup	liquid	0.5 mLD_{50}	0.5 mLD_{50}	0.5 mLD_{50}	0.25 mLD_{50}
cranberry juice[a]	liquid	0.5 mLD_{50}	0.25 mLD_{50}	0.5 mLD_{50}	0.25 mLD_{50}
dried beef	solid	0.25 mLD_{50}	0.5 mLD_{50}	0.5 mLD_{50}	0.25 mLD_{50}
figures	solid	0.75 mLD_{50}	0.75 mLD_{50}	0.75 mLD_{50}	0.25 mLD_{50}
garlic	solid	0.5 mLD_{50}	0.25 mLD_{50}	0.25 mLD_{50}	0.25 mLD_{50}
ham	solid	0.5 mLD_{50}	0.75 mLD_{50}	0.5 mLD_{50}	0.25 mLD_{50}
honey	liquid	0.5 mLD_{50}	0.5 mLD_{50}	0.5 mLD_{50}	0.25 mLD_{50}
jelly[a]	semisolid	0.75 mLD_{50}	0.75 mLD_{50}	0.75 mLD_{50}	0.25 mLD_{50}
kim chi[a]	solid	0.75 mLD_{50}	0.5 mLD_{50}	0.5 mLD_{50}	0.25 mLD_{50}
mackerel	solid	0.75 mLD_{50}	0.5 mLD_{50}	0.5 mLD_{50}	0.25 mLD_{50}
molasses	liquid	0.5 mLD_{50}	0.5 mLD_{50}	0.5 mLD_{50}	0.25 mLD_{50}
okra	solid	0.75 mLD_{50}	0.5 mLD_{50}	0.5 mLD_{50}	0.25 mLD_{50}
onions	solid	0.5 mLD_{50}	0.25 mLD_{50}	0.5 mLD_{50}	0.25 mLD_{50}
pebre	semisolid	0.5 mLD_{50}	0.5 mLD_{50}	0.5 mLD_{50}	0.25 mLD_{50}
pickled peppers[a]	solid	0.75 mLD_{50}	0.5 mLD_{50}	0.5 mLD_{50}	0.25 mLD_{50}
potato	solid	0.25 mLD_{50}	0.5 mLD_{50}	0.5 mLD_{50}	0.25 mLD_{50}
potato soup	semisolid	0.5 mLD_{50}	0.5 mLD_{50}	0.5 mLD_{50}	0.25 mLD_{50}
refried beans	semisolid	0.75 mLD_{50}	0.5 mLD_{50}	0.5 mLD_{50}	0.25 mLD_{50}
rice	solid	0.25 mLD_{50}	0.25 mLD_{50}	0.25 mLD_{50}	0.25 mLD_{50}
salad dressing	liquid	0.75 mLD_{50}	0.25 mLD_{50}	0.25 mLD_{50}	0.25 mLD_{50}
salsa[a]	semisolid	0.5 mLD_{50}	0.5 mLD_{50}	0.5 mLD_{50}	0.25 mLD_{50}
sauerkraut[a]	solid	0.5 mLD_{50}	0.25 mLD_{50}	0.5 mLD_{50}	0.25 mLD_{50}
sofrito	semisolid	0.75 mLD_{50}	0.5 mLD_{50}	0.5 mLD_{50}	0.25 mLD_{50}
sour cream dip	semisolid	0.5 mLD_{50}	0.25 mLD_{50}	0.5 mLD_{50}	0.25 mLD_{50}
spaghetti	solid	0.25 mLD_{50}	0.25 mLD_{50}	0.25 mLD_{50}	0.25 mLD_{50}
spaghetti sauce	semisolid	0.25 mLD_{50}	0.25 mLD_{50}	0.5 mLD_{50}	0.25 mLD_{50}
squash	solid	0.25 mLD_{50}	0.25 mLD_{50}	0.25 mLD_{50}	0.25 mLD_{50}
steak	solid	0.25 mLD_{50}	0.25 mLD_{50}	0.25 mLD_{50}	0.25 mLD_{50}
tofu	semisolid	0.5 mLD_{50}	0.5 mLD_{50}	0.75 mLD_{50}	0.25 mLD_{50}
tomatoes[a]	solid	0.25 mLD_{50}	0.25 mLD_{50}	0.25 mLD_{50}	0.25 mLD_{50}
tortillas	solid	0.25 mLD_{50}	0.25 mLD_{50}	0.25 mLD_{50}	0.25 mLD_{50}
vegemite	semisolid	0.75 mLD_{50}	0.5 mLD_{50}	0.5 mLD_{50}	0.25 mLD_{50}
whipping cream	semisolid	0.75 mLD_{50}	0.25 mLD_{50}	0.75 mLD_{50}	0.25 mLD_{50}

[a]Requires pH adjustment.

DOI: 10.1021/jf505482b
J. Agric. Food Chem. 2015, 63, 1133−1141

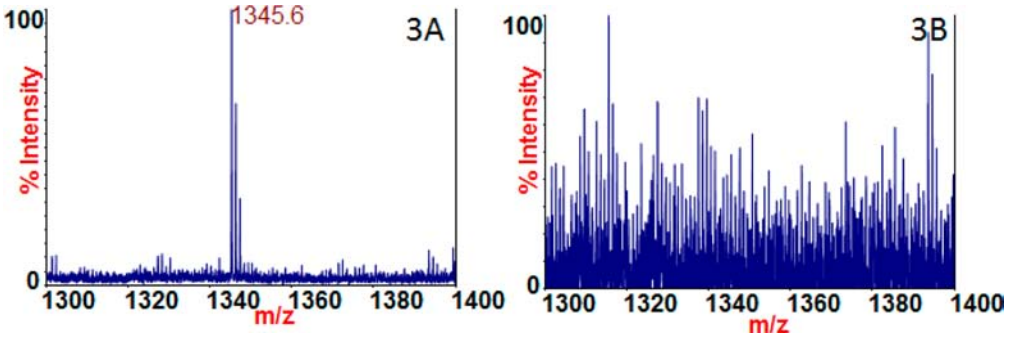

Figure 3. Mass spectra of Endopep-MS reactions containing (A) 0.01 mLD_{50} of BoNT/F spiked into cooked egg and (B) 0.01 mLD_{50} of BoNT/F in raw egg.

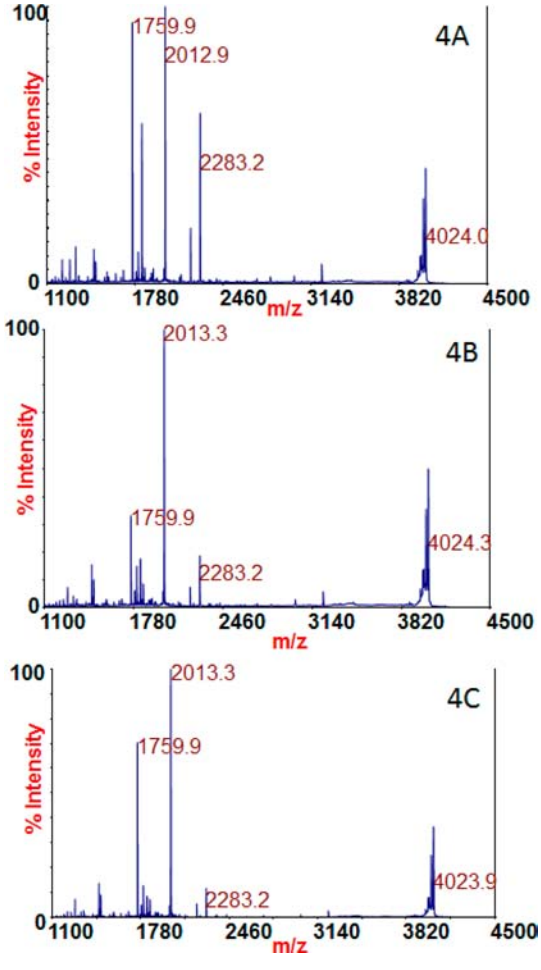

Figure 4. Mass spectra of Endopep-MS reactions containing BoNT/B spiked into (A) PBST, (B) orange juice with no neutralization, and (C) orange juice with neutralization. All were stored for 6 weeks at 4 °C prior to testing.

(Figure 1A) with whole milk spiked with 10 mouse LD_{50} (mLD_{50}) of BoNT/A (Figure 1B) shows two new peaks in the spiked sample which are absent in the untreated sample. These peaks circled in red at m/z 999 and 1427 correspond to the cleavage of SubA by BoNT/A, proving the presence of enzymatically active BoNT/A in the milk. The uncleaved substrate (SubA) is present at m/z 2406. Through repeated analysis, we could reliably detect as little as 0.25 mLD_{50} of BoNT/A spiked into 1 mL of whole milk (Figure 2B).

BoNT/B, /E, and /F were also spiked into whole milk. By examining the differences between untreated whole milk (Figure 1C, 1E, and 1G) and whole milk spiked with 10 mLD_{50} of BoNT/B (Figure 1D), BoNT/E (Figure 1F), and BoNT/F (Figure 1H), the spiked milk can be distinguished from the untreated milk in all cases. In the case of BoNT/B, the two peaks at m/z 1760 and 2283 in Figure 1D correspond to cleavage of SubB by BoNT/B, peaks at m/z 1133 and 2501 in Figure 1F correspond to cleavage of SubE by BoNT/E, and peaks at m/z 1346 and 3784 in Figure 1H correspond to cleavage of SubF by BoNT/F. The uncleaved substrates are present at m/z 4025 for SubB, 3614 for SubE, and 5511 for SubF. Replicate analysis of whole milk spiked with BoNT/B, /E, and /F determined that we could detect as little as 0.1 mLD_{50} of BoNT/B (Figure 2D), 0.1 mLD_{50} of BoNT/E (Figure 2F), or 0.01 mLD_{50} of BoNT/F (Figure 2H) spiked into 1 mL of whole milk. Intact SubF and the N-terminal cleavage product produced by cleavage of the substrate by BoNT/F are long peptides with molecular weights of 5510 and 3783 Da and historically are rarely seen by MALDI-TOF/MS. However, the doubly charged intact SubF is often visible at m/z 2556, using the analytical instrumentation listed here.

Detection of BoNT/A, /B, /E, and /F in Additional Foods. BoNT/A, /B, /E, and /F were spiked into infant formula, yogurt, broccoli, green bean liquid, salami, salmon, liquid egg, orange juice, and tomato juice. Through repeated analysis, we determined that the limits of detection of BoNT/A, /B, /E, and /F spiked into 1 mL of these matrices is below the limit of detection of the mouse bioassay, 1 mLD_{50}, as seen in Table 2. The limits of detection ranged from 0.01 mLD_{50} of BoNT/F in infant formula, yogurt, broccoli, green bean liquid, salami, and salmon up to 0.75 mLD_{50} of BoNT/A in liquid egg.

Additional foods which were of interest as they had been investigated in previous years as suspect agents of foodborne botulism were also tested with the Endopep-MS assay. For these foods, BoNT/A, /B, /E, and /F at levels below the limit of detection of the mouse bioassay were spiked into 0.5 mL of the liquid food or food extract. The results listed in Table 3 indicate that BoNT/A, /B, /E, and /F were successfully detected in 44 additional foods at levels below that of the historical standard, the mouse bioassay.

Many of the food matrices presented no challenges for the Endopep-MS assay. The results from many viscous matrices, such as corn syrup, honey, and molasses, looked identical to the results in PBST. On the basis of the similar results in buffer, it does not appear that the antibody-coated beads lacked sufficient mobility in the viscous matrix to capture the toxin nor does it seem that any of the toxin/antibody-coated beads

DOI: 10.1021/jf505482b
J. Agric. Food Chem. 2015, 63, 1133−1141

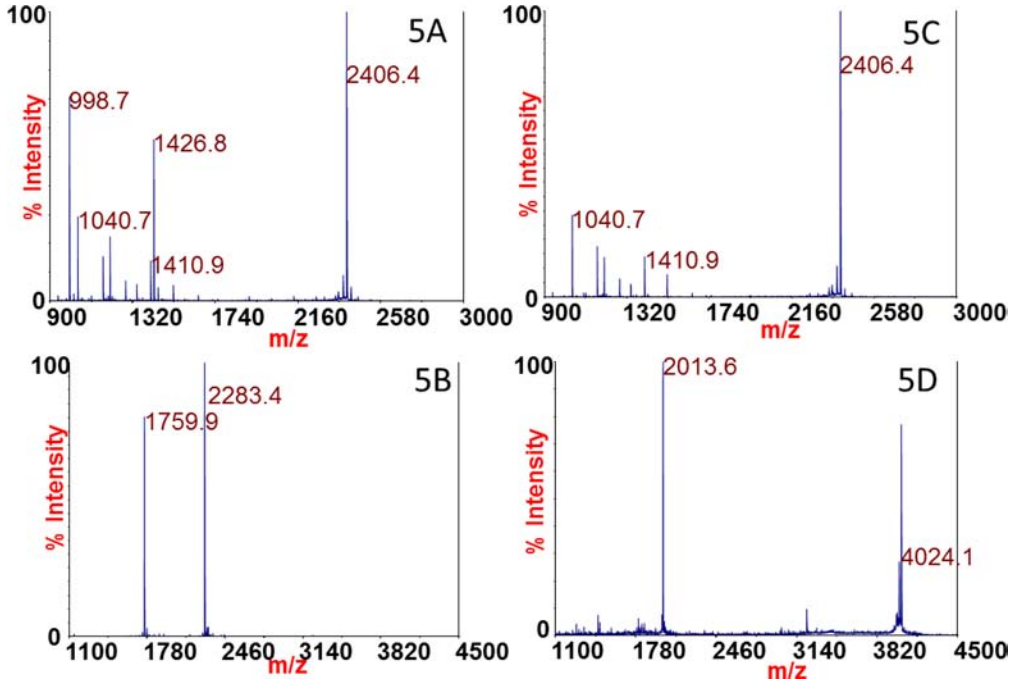

Figure 5. Mass spectra of Endopep-MS reactions testing for (A) BoNT/A and (B) BoNT/B in baked potato. Negative controls of baked potato were also tested for (C) BoNT/A and (D) BoNT/B.

remained in the viscous matrix. Samples with low pH such as tomato juice, salsa, chili sauce, kimchi, pickled peppers, and sauerkraut also looked similar to the results in PBST provided that the sample was neutralized with ammonium hydroxide to physiological pH prior to antibody−bead addition (data not shown).

Foods which were protease rich such as steak, dried beef, beef stew, and ham benefited greatly from washing the antibody-coated beads post toxin capture with 2 M NaCl to remove all nonspecific binding proteases from the antibody-coated beads. This technique was developed for the high protease environment of stool extracts,[26] so it is not surprising that it works for other protease-rich matrices. The high-salt washes however had a negative effect on high-fat matrices. Although it was possible to detect BoNT/A, /B, /E, and /F spiked into high-fat matrices such as mackerel, salami, salad dressing, and salmon when the antibody-coated beads were washed in 2 M NaCl post toxin capture, the limit of detection of the assay with these high-fat matrices was improved by washing the beads in PBST only (data not shown).

One of the more problematic matrices was the liquid egg matrix. Although the Endopep-MS assay could detect BoNT/A, /B, /E, and /F spiked into liquid egg at levels below the limit of detection of the mouse bioassay, the limit of detection in that matrix was elevated when compared to the other matrices for which a limit of detection was established (Table 2). It appeared that some of the antibody-coated beads remained behind in the matrix and the beads which were removed from the matrix had a clumpy appearance similar to the appearance of the beads from high-fat matrices when washed in 2 M NaCl. Altering the wash buffers from 2 M NaCl to PBST did not improve the appearance of the beads when used with the liquid egg matrix.

It was suspected that perhaps the high level of biotin in the liquid egg interfered with the antibody-capture process as the beads used for antibody-capture are streptavidin coated and biotin has a very strong affinity for streptavidin. Upon switching to protein-G-coated beads which do not contain streptavidin, however, similar limits of detection were obtained, indicating that the high level of biotin in eggs did not cause the bead retention or clotted appearance. Additionally, when BoNT was spiked into the extract of cooked eggs, lower levels of toxin could be detected. As little as 0.01 mLD_{50} of BoNT/F spiked into 1 mL of cooked egg extract produced a visible C-terminal cleavage product indicating the presence of active BoNT/F (Figure 3A); however, cleavage product was absent when the same level of toxin was spiked into 1 mL of liquid raw egg (Figure 3B). A level of 0.01 mLD_{50} of BoNT/F could be detected by diluting the liquid egg matrix 1:10 in PBST; however, this step would negatively impact the limit of detection by an order of magnitude in a real outbreak sample as the limit of detection would be increased to 0.1 mLD_{50}/mL of undiluted sample. Because as little as 0.05 mLD_{50} of BoNT/F could be detected in 1 mL of undiluted liquid egg (Table 2), a lower limit of detection was achieved by using 1 mL of liquid egg matrix with no dilution.

Another of the matrices with an increased limit of detection was orange juice (Table 2). Orange juice is very acidic, and it was thought that the low pH of the matrix had an effect on either the enzymatic activity of the toxin or the capture of the toxin by the antibody. An amount of one mLD_{50} of BoNT/B was spiked into 1 mL of orange juice or PBST and stored for 6 weeks at 4 °C. Endopep-MS of the samples proceeded both with and without neutralization of the pH of the orange juice immediately prior to antibody−bead addition. The peaks at m/z 1760 and 2283 in Figure 4 correspond to BoNT/B cleavage of SubB, illustrating that even after being stored for 6 weeks at 4 °C, active toxin remained in all three samples. However, comparison of the intensity of the cleavage product peaks (particularly the peak at m/z 1760) compared to the intensity of the uncleaved SubB peak (at m/z 4024 and especially 2013) indicates that there is either less toxin or less active toxin in the

DOI: 10.1021/jf505482b
J. Agric. Food Chem. 2015, 63, 1133−1141

untreated orange juice sample (Figure 4B) and, to a lesser degree, the neutralized orange juice sample (Figure 4C) when compared to the PBST sample.

Application of Endopep-MS to Foods Suspected of Causing Botulism Outbreaks. Thirty-one food extracts received for testing during botulism outbreak investigations were tested by Endopep-MS for BoNT/A, /B, /E, and /F in parallel with the mouse bioassay. Twenty-nine of these samples were below the limit of detection of BoNT/A, /B, /E, and /F with Endopep-MS as well as the mouse bioassay. One chili pepper sample tested positive for BoNT/B by Endopep-MS, and based on the intensity of the BoNT/B cleavage products, the level of toxin was very low, near the limit of detection for the Endopep-MS assay. This sample tested below the limit of detection of the mouse bioassay. The baked potato sample tested positive for both BoNT/A and /B by Endopep-MS as seen in Figure 5.

Peaks at m/z 999 and 1427 in Figure 5A indicate the presence of active BoNT/A in this sample, and peaks at m/z 1760 and 2283 indicate the presence of active BoNT/B in this same sample (Figure 5B), compared to the negative control of baked potato tested for BoNT/A (Figure 5C) and BoNT/B (Figure 5D). Mouse bioassay results on these food samples were identical to the Endopep-MS results. The finding of two serotypes of BoNT in a single sample is rare, although not completely unique as some strains of *C. botulinum* are known to make more than one BoNT serotype. These are called bivalent toxin producers and are named Ab, Ba, Af, or Bf, with the capital letter representing what is thought to be the main serotype produced. Upon the basis of the intensity of the BoNT/A and /B cleavage products, it would appear that the baked potato contained a Ba strain of *C. botulinum*. Alternatively, the potato could have been contaminated with 2 strains of *C. botulinum*.

In conclusion, we demonstrated that the Endopep-MS method is able to detect enzymatically active BoNT/A, /B, /E, and /F in a wide variety of foods. These foods represent different characteristics such as low pH, high viscosity, high fat, and varied ethnicities. Many of the foods were suspected of causing a botulism outbreak in the past, and others have definitively caused prior botulism outbreaks. The limit of detection varies and is matrix and serotype dependent, but all matrices tested were able to detect BoNT/A, /B, /E, and /F spiked into foods at levels below the limit of the historical standard assay for botulism, the mouse bioassay. The method accurately identified BoNT/A and BoNT/B in a baked potato associated with a recent case of botulism. The combination of the ability to detect BoNT/A, /B, /E, and /F in foods as well as clinical specimens such as stool extracts make this assay a concrete alternative to the mouse bioassay for BoNT detection.

AUTHOR INFORMATION

Corresponding Author

*Tel.: 770-488-7848. Fax: 770-488-0509. E-mail: jbarr@cdc.gov.

Notes

The findings and conclusions in this report are those of the authors and do not necessarily represent the official position of the Centers for Disease Control and Prevention.

The authors declare no competing financial interest.

REFERENCES

(1) Centers for Disease Control and Prevention. *Botulism in the United States, 1899−1996*; Centers for Disease Control and Prevention: Atlanta, GA, 1998.

(2) Schiavo, G.; Matteoli, M.; Montecucco, C. Neurotoxins affecting neuroexocytosis. *Physiol. Rev.* **2000**, *80*, 717−66.

(3) Binz, T.; Blasi, J.; Yamasaki, S.; Baumeister, A.; Link, E.; Sudhof, T. C.; Jahn, R.; Niemann, H. Proteolysis of SNAP-25 by types E and A botulinal neurotoxins. *J. Biol. Chem.* **1994**, *269*, 1617−20.

(4) Blasi, J.; Chapman, E. R.; Link, E.; Binz, T.; Yamasaki, S.; De Camilli, P.; Sudhof, T. C.; Niemann, H.; Jahn, R. Botulinum neurotoxin A selectively cleaves the synaptic protein SNAP-25. *Nature* **1993**, *365*, 160−3.

(5) Foran, P.; Lawrence, G. W.; Shone, C. C.; Foster, K. A.; Dolly, J. O. Botulinum neurotoxin C1 cleaves both syntaxin and SNAP-25 in intact and permeabilized chromaffin cells: correlation with its blockade of catecholamine release. *Biochemistry* **1996**, *35*, 2630−6.

(6) Schiavo, G.; Benfenati, F.; Poulain, B.; Rossetto, O.; Polverino de Laureto, P.; DasGupta, B. R.; Montecucco, C. Tetanus and botulinum-B neurotoxins block neurotransmitter release by proteolytic cleavage of synaptobrevin. *Nature* **1992**, *359*, 832−5.

(7) Schiavo, G.; Malizio, C.; Trimble, W. S.; Polverino de Laureto, P.; Milan, G.; Sugiyama, H.; Johnson, E. A.; Montecucco, C. Botulinum G neurotoxin cleaves VAMP/synaptobrevin at a single Ala-Ala peptide bond. *J. Biol. Chem.* **1994**, *269*, 20213−6.

(8) Schiavo, G.; Rossetto, O.; Catsicas, S.; Polverino de Laureto, P.; DasGupta, B. R.; Benfenati, F.; Montecucco, C. Identification of the nerve terminal targets of botulinum neurotoxin serotypes A, D, and E. *J. Biol. Chem.* **1993**, *268*, 23784−7.

(9) Schiavo, G.; Santucci, A.; Dasgupta, B. R.; Mehta, P. P.; Jontes, J.; Benfenati, F.; Wilson, M. C.; Montecucco, C. Botulinum neurotoxins serotypes A and E cleave SNAP-25 at distinct COOH-terminal peptide bonds. *FEBS Lett.* **1993**, *335*, 99−103.

(10) Schiavo, G.; Shone, C. C.; Rossetto, O.; Alexander, F. C.; Montecucco, C. Botulinum neurotoxin serotype F is a zinc endopeptidase specific for VAMP/synaptobrevin. *J. Biol. Chem.* **1993**, *268*, 11516−9.

(11) Williamson, L. C.; Halpern, J. L.; Montecucco, C.; Brown, J. E.; Neale, E. A. Clostridial neurotoxins and substrate proteolysis in intact neurons: botulinum neurotoxin C acts on synaptosomal-associated protein of 25 kDa. *J. Biol. Chem.* **1996**, *271*, 7694−9.

(12) Yamasaki, S.; Baumeister, A.; Binz, T.; Blasi, J.; Link, E.; Cornille, F.; Roques, B.; Fykse, E. M.; Sudhof, T. C.; Jahn, R.; et al. Cleavage of members of the synaptobrevin/VAMP family by types D and F botulinal neurotoxins and tetanus toxin. *J. Biol. Chem.* **1994**, *269*, 12764−72.

(13) Yamasaki, S.; Binz, T.; Hayashi, T.; Szabo, E.; Yamasaki, N.; Eklund, M.; Jahn, R.; Niemann, H. Botulinum neurotoxin type G proteolyses the Ala81-Ala82 bond of rat synaptobrevin 2. *Biochem. Biophys. Res. Commun.* **1994**, *200*, 829−35.

(14) Sobel, J.; Tucker, N.; Sulka, A.; McLaughlin, J.; Maslanka, S. Foodborne botulism in the United States, 1990−2000. *Emerging Infect. Dis.* **2004**, *10*, 1606−11.

(15) Stanker, L. H.; Scotcher, M. C.; Cheng, L.; Ching, K.; McGarvey, J.; Hodge, D.; Hnasko, R. A monoclonal antibody based capture ELISA for botulinum neurotoxin serotype B: toxin detection in food. *Toxins* **2013**, *5* (11), 2212−26.

(16) Cheng, L. W.; Stanker, L. H. Detection of botulinum neurotoxin serotypes A and B using a chemiluminescent versus electro-chemiluminescent immunoassay in food and serum. *J. Agric. Fooc Chem.* **2013**, *61* (3), 755−60.

(17) Sachdeva, A.; Singh, A. K.; Sharma, S. K. An electro-chemiluminescence assay for the detection of bio threat agents in selected food matrices and in the screening of *Clostridium botulinum* outbreak strains associated with type A botulism. *J. Sci. Food. Agric.* **2014**, *94* (4), 707−12.

(18) Barr, J. R.; Moura, H.; Boyer, A. E.; Woolfitt, A. R.; Kalb, S. R.; Pavlopoulos, A.; McWilliams, L. G.; Schmidt, J. G.; Martinez, R. A.;

DOI: 10.1021/jf505482b
J. Agric. Food Chem. 2015, 63, 1133−1141

Ashley, D. L. Botulinum neurotoxin detection and differentiation by mass spectrometry. *Emerging Infect. Dis.* **2005**, *11*, 1578−83.
(19) Kalb, S. R.; Moura, H.; Boyer, A. E.; McWilliams, L. G.; Pirkle, J. L.; Barr, J. R. The use of Endopep-MS for the detection of botulinum toxins A, B, E, and F in serum and stool samples. *Anal. Biochem.* **2006**, *351*, 84−92.
(20) Kalb, S. R.; Smith, T. J.; Moura, H.; Hill, K.; Lou, J.; Geren, I. N.; Garcia-Rodriguez, C.; Marks, J. D.; Smith, L. A.; Pirkle, J. L.; Barr, J. R. The use of Endopep-MS to detect multiple subtypes of botulinum neurotoxins A, B, E, and F. *Int. J. Mass Spectrom.* **2008**, *278*, 101−108.
(21) Kalb, S. R.; Santana, W. I.; Pirkle, J. L.; Barr, J. R. Detection, differentiation, and subtyping of botulinum toxins A, B, E, and F by mass spectrometry. *Botulinum J.* **2012**, *2*, 119−134.
(22) Kalb, S. R.; Lou, J.; Garcia-Rodriguez, C.; Geren, I. N.; Smith, T. J.; Moura, H.; Marks, J. D.; Smith, L. A.; Pirkle, J. L.; Barr, J. R. Extraction and Inhibition of Enzymatic Activity of BoNT/A1, /A2, and /A3 by a Panel of Monoclonal Anti-BoNT/A Antibodies. *PLoS One* **2009**, *4* (4), e5355.
(23) Kalb, S. R.; Santana, W. I.; Geren, I. N.; Garcia-Rodriguez, C.; Lou, J.; Smith, T. J.; Marks, J. D.; Smith, L. A.; Pirkle, J. L.; Barr, J. R. Extraction and inhibition of enzymatic activity of botulinum neurotoxins/B1, /B2, /B3, /B4, and /B5 by a panel of monoclonal anti-BoNT/B antibodies. *BMC Biochem.* **2011**, *12* (58), 1−12.
(24) Kalb, S. R.; Garcia-Rodriguez, C.; Lou, J.; Baudys, J.; Smith, T. J.; Marks, J. D.; Smith, L. A.; Pirkle, J. L.; Barr, J. R. Extraction of BoNT/A, /B, /E, and /F with a single, high affinity monoclonal antibody for detection of botulinum neurotoxin by Endopep-MS. *PLoS One* **2010**, *5* (8), e12237.
(25) Kalb, S. R.; Baudys, J.; Smith, T. J.; Smith, L. A.; Barr, J. R. Three Enzymatically Active Neurotoxins of Clostridium botulinum Strain Af84: BoNT/A2, /F4, and /F5. *Anal. Chem.* **2014**, *86* (7), 3254−62.
(26) Wang, D.; Baudys, J.; Kalb, S. R.; Barr, J. R. Improved detection of botulinum neurotoxin type A in stool by mass spectrometry. *Anal. Biochem.* **2011**, *412*, 67−73.

DOI: 10.1021/jf505482b
J. Agric. Food Chem. 2015, 63, 1133−1141

Chemicals. We previously reported that the tomato glycoalkaloid referred to as tomatine consists of a 9:1 mixture of α-tomatine and dehydrotomatine.[14] This ratio differs for different parts of the tomato plant, ranging up to 3:1 for tomatine isolated from large stems.[15] The purity of the α-tomatine used in the present study as provided by the supplier is >75%. α-Tomatine ($C_{50}H_{93}NO_{21}$; mol wt 1034.2) has the following chemical name: *O*-[β-D-glucopyranosyl-(1→2)-[β-D-xylopyranosyl-(1→3]-β-D-glucoyranosyl-(1→4)-β-D-galactopyranoside]. Dehydrotomatine has the same structure as α-tomatine except for the presence of a double bond in the steroidal B ring of the aglycone part of the molecule. α-Tomatine has a tetrasaccharide (lycotetraose) attached to the aglycone tomatidine, whereas dehydrotomatine has the lycotetraose moiety attached to the aglycone tomatidenol (Figure 1).

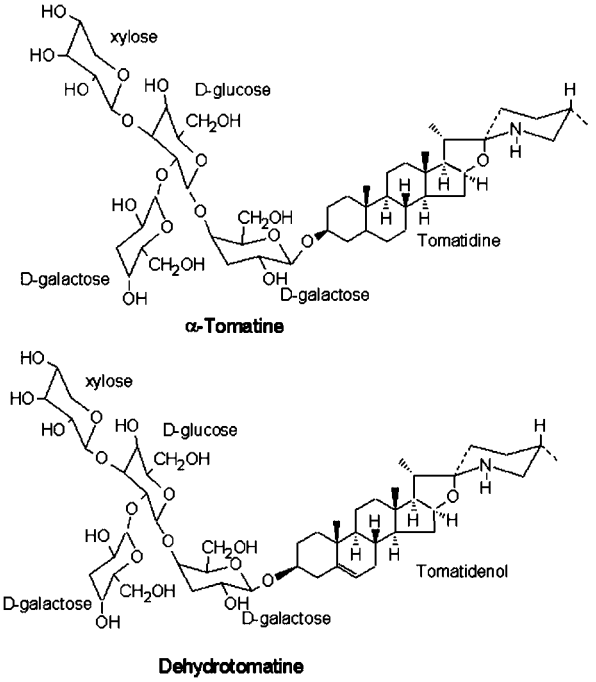

Figure 1. Structures of α-tomatine and dehydrotomatine. In α-tomatine, the tetrasaccharide (lycotetraose) side chain is attached to the aglycone tomatidine and in dehydrotomatine, to the aglycone tomatidenol.

α-Tomatine is soluble in methanol, ethanol, dioxane, and dimethyl sulfoxide (DMSO) and is fairly soluble in water. The experiments were carried out with solutions of 0.1% commercial tomatine in DMSO. This concentration is known not to induce cell toxicity. The term "tomatine" describes a mixture of α-tomatine and dehydrotomatine.

Cancer Cells and Mice. The CT-26 mouse colon cancer cell line from the American Type Tissue Culture Collection (Manassas, VA, USA) was cultured in DMEM supplemented with 10% heat-inactivated FBS containing penicillin (100 U/mL) and streptomycin (100 mg/mL). Cells were cultured at 37 °C in a humidified atmosphere with 5% CO_2.

Cytotoxicity Assay. Cell cytotoxicity was assessed by lactate dehydrogenase (LDH) release upon cell lysis following the method of Nachlas et al.[16] A CytoTox 96 Non-Radioactive Cytotoxicity Assay kit (Promega Corp., Madison, WI, USA) was used following the manufacturer's instructions. Briefly, the CT-26 cancer cells were seeded into a 96-well plate at a density of 1×10^5 cells/well and cultured for 24 h in 37 °C humidified air with 5% CO_2. The cells were then treated with α-tomatine under various concentrations (from 1 to 10 μM final concentration) for various time periods (from 3 to 48 h). After treatments, the supernatant from each well was transferred to the flat-bottom 96-well enzymatic assay plate. Released LDH in culture supernatants was measured with a 30 min coupled enzymatic assay, resulting in the conversion of a tetrazolium salt into a red formazan product. The absorbance of resultant colored products was read in a microplate reader (model 550, Bio-Rad, Hercules, CA, USA) at 490 nm. Cell cytotoxicity was expressed by the following formula:

$$\text{cytotoxicity (\%)} = 100 \times (\text{absorbance of } \alpha\text{-tomatine-treated cells} / \text{absorbance of maximum LDH-released control cells})$$

The concentration that results in ~50% cell death for 24 h treatment was 3.5 μM. We used this concentration and incubation time period to avoid any possible adverse effect of tomatine on the cells. In parallel, α-tomatine-induced cytotoxicity was also assessed by an MTT staining method as described in our previous publication.[3]

Apoptosis Assay by Flow Cytometry. Flow cytometry was carried out according to the method described by Vermes et al.[17] Briefly, CT-26 cancer cells (1×10^6) were seeded into a culture dish and cultivated for 3 h in serum-free DMEM. Serum starvation is needed for all cells to synchronize their cell cycle. This step reduces the background noise of the data. After serum starvation, the serum-free medium was replaced with complete medium. Cells were then treated with 3.5 μM α-tomatine. After incubation for each time period, cells were collected by detaching through trypsin digestion and subsequent centrifugation at 1000*g* for 5 min. Cell pellets were resuspended in a FACS binding buffer (0.1 mL; 10 mM HEPES, 150 mM NaCl, 2.5 mM $CaCl_2$, pH 7.4) with annexin V-FITC (1 μg) and PI (1 μg). After incubation for 15 min in the dark, flow cytometry was carried out in a FACSCaliber (Becton, Dickinson and Co., San Jose, CA, USA).

Mice and Treatments. All experiments were performed in compliance with the relevant laws and institutional guidelines. Pathogen-free female BALB/c mice (6 weeks old), weighing 20−25 g, were purchased from Orient Bio (Seongnam, Korea). The mice were hosted in a stainless steel cage under a 12 h light/dark cycle with a temperature range of 20−22 °C and a relative humidity of 50 ± 10%. The mice were fed pelletized commercial chow diet from Orient Bio (catalog no. 5L79) and sterile tap water ad libitum during the entire experimental period. After acclimation for 1 week, the mice were then randomly divided into two groups (n = 10), avoiding any intergroup difference in body weight. α-Tomatine was dissolved in 0.1% DMSO. After dilution with PBS to an appropriate dose, α-tomatine was given to mice via the intraperitoneal (ip) route at a dose of 5 mg/kg body wt (in 200 μL). Simultaneously, the mice were intracutaneously transplanted with 1×10^6 of CT-26 cancer cells in 200 μL of PBS into the lateral side of the back. The mice were then administered the α-tomatine dose once a day for 2 weeks. Control mice were administered the same volume of vehicle only. Mice were sacrificed by CO_2 inhalation at the end of the experimental periods for excision of tumor masses.

Preliminary experiments indicated that the mice frequently died 4 weeks after tumor transplantation, especially the vehicle-treated control mice without tomatine. To avoid this problem, we carried out the in vivo experiment for 2 weeks.

Tumor Growth. To evaluate the suppressive effect of α-tomatine on tumor growth, removed tumor masses from the control and experimental groups of mice were weighed using an analytical balance. Excised tumor masses were rinsed with ice-cold PBS and stored at −20 °C until use.

Caspase-3, -8, and -9 Activity Assay. Caspase activities were measured using the caspase-3, -8, and -9 activity kits purchased from Millipore (Billerica, MA, USA) according to the manufacturer's instructions. Briefly, α-tomatine-treated cells (1×10^6 cells) or tumor tissues were extracted in an ice-cold lysis buffer (50 mM Tris, 150 mM NaCl, 1 mM EGTA, 1 mM EDTA, 1% NP-40, 1 mM sodium orthovanadate, 1 mM NaF, 1 mM PMSF, 10 μg/mL aprotinin, 10 μg/mL leupeptin) for 30 min, and pulverization of tumor tissues using a homogenizer was conducted for effective protein extraction in a lysis buffer. Lysates were clarified by microcentrifugation at 14000*g* for 10 min. Supernatants (cytosolic extract) containing proteins (50 μg) were incubated in an assay buffer (100 μL) containing colorimetric substances, Ac-Asp-Glu-Val-Asp (DEVD)-*p*-nitroaniline (*p*NA), Ac-Ile-Glu-Thr-Asp (IETD)-*p*-NA), and Ac-Leu-Glu-His-Asp (LEHD)-

DOI: 10.1021/jf5040288
J. Agric. Food Chem. 2015, 63, 1142−1150

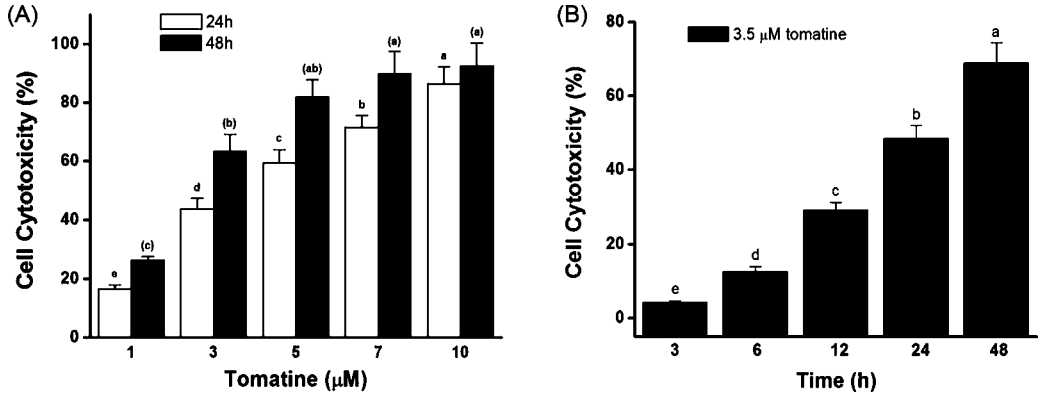

Figure 2. Cytotoxic effect of α-tomatine on CT-26 mouse colon cancer cells. (A) The cells were plated at a density of 1×10^5 cells/well in a 96-well microplate and then treated with the indicated concentrations of α-tomatine for 24 or 48 h at 37 °C, followed by measurement of cell death by LDH activity. (B) The cytotoxicity of α-tomatine was measured for the indicated time periods at a concentration of 3.5 μM. Plotted values are the mean ± SD (n = 3).

Table 1. Changes in Caspase-Independent CT-26 Mouse Colon Cancer Cell Death According to α-Tomatine Incubation Times[a]

	cell viability (%)			
sample	3 h	6 h	12 h	24 h
vehicle	100.0 ± 3.4	100.0 ± 4.7ab	100.0 ± 2.7b	100.0 ± 5.6b
z-VAD-fmk[b]	102.6 ± 6.5	105.7 ± 5.1a	108.4 ± 5.8a	115.3 ± 7.7a
tomatine[c]	98.7 ± 5.3	92.5 ± 3.3b	71.6 ± 3.6c	59.3 ± 3.1c
tomatine + z-VAD-fmk	99.8 ± 4.5	93.1 ± 5.2b	74.0 ± 4.0c	61.9 ± 4.2c

[a]Values are expressed as the mean ± SD of triplicate experiments. Values not sharing the same letter in the column are significantly different at $p < 0.05$. [b]100 μM z-VAD-fmk used as a pan-caspase inhibitor indicates z-Val-Ala-Asp-fluoromethyl ketone. [c]3.5 μM α-tomatine in 200 μL of DMSO was administered once a day. 100 μM z-VAD-fmk used as a pan-caspase inhibitor indicates z-Val-Ala-Asp-fluoromethyl ketone. Vehicle indicates 0.1% DMSO. MTT assay was employed to assess cytotoxicity. Cytotoxicity (%) = 100 × (1 − absorbance of α-tomatine-treated cells/absorbance of vehicle-treated cells).

*p*NA for caspase-3, -8, and -9 activity assays, respectively, at 37 °C for 2 h. Absorbance at 405 nm was quantified in a microplate reader.

Western Blot Analysis of Cell Proteins. α-Tomatine-treated CT-26 cancer cells (10^6 cells/mL) were harvested and then lysed in radioimmunoprecipitation assay (RIPA) buffer (50 mM Tris Cl, 150 mM NaCl, 1% NP-40, 0.5% sodium deoxycholate, 0.1% SDS, and 1 mM EDTA, pH 7.4) to prepare whole cell proteins. For the preparation of nuclear protein fraction, the cells were suspended in hypotonic buffer A (10 mM HEPES, 10 mM KCl, 0.1 mM EDTA, 0.1 mM EGTA, 1 mM DTT, 0.5 mM PMSF, pH7.9) and were allowed to swell on ice. After the addition of NP-40 (final 0.6%), the cells were subjected to vigorous vortexing and centrifugation at 12000*g*. The resultant nuclear pellet was further extracted with hypertonic buffer (20 mM HEPES, 0.4 M NaCl, 1 mM EDTA, 1 mM EGTA, 1 mM DTT, 1 mM PMSF, pH7.9). The extract was centrifuged at 12000*g* to recover the supernatant termed nuclear fraction. Protein concentrations were determined according to the Bradford method using a Bio-Rad Protein kit. Bovine serum albumin (BSA) was used as standard. The cell extract containing proteins (30 μg) was separated on 12% SDS−polyacrylamide gels and electrophoretically transferred onto nitrocellulose membrane (Millipore). The membrane was blocked in 5% skim milk at 4 °C overnight and probed with the primary antibodies as follows: anti-p65 nuclear factor kappa B (NF-κB) monoclonal antibody (catalog no. 6956S, Cell Signaling Technology, Inc., Danvers, MA, USA), anti-β-actin monoclonal antibody (catalog no. 04-1116, Millipore), rabbit anti-mouse apoptosis-inducing factor (AIF) polyclonal antibody (catalog no. 4642S, Cell Signaling Technology, Inc.), anti-survivin monoclonal antibody (catalog no. 2808S, Cell Signaling Technology), 21 monoclonal antibody (catalog no. MAB10072, Millipore), and anti-caspase-3 (catalog no. 9664S), anti-caspase-8 (catalog no. 9429S), and anti-caspase-9 polyclonal antibodies (catalog no. 9509S, Cell Signaling Technology). After allowing the primary antibody reaction for at least 3 h, the secondary antibody reaction with horseradish peroxidase (HRP)-conjugated anti-IgG antibody was performed under the same conditions. Blots were developed using the ECL detection kit (Pierce, Rockford, IL, USA). The intensity of separated protein bands was quantified using a gel documentation system (model LAS-1000CH, Fuji Photo Film Co., Tokyo, Japan). At least three separate replicates were determined for each experiment.

Statistical Analysis. Results are expressed as the mean ± SD of three independent experiments. Significant differences between means were determined by ANOVA test using the Statistical Analysis Software package SAS (Cary, NC, USA). $p < 0.05$ is regarded as significant.

RESULTS

Growth Inhibition of CT-26 Cells. Figure 2 shows the cytotoxicity of α-tomatine on CT-26 mouse colon cancer cells. Treatment with α-tomatine decreased cell viability in a concentration- and time-dependent manner. The maximum inhibitions with α-tomatine at 10 μM were about 86.4 and 92.63% at the end of the 24 and 48 h treatments, respectively. The calculated concentration that results in ∼50% cell death after 24 h was 3.5 μM.

Death Pattern of CT-26 Cells. Next, experiments were carried out to answer the question of whether or not the growth inhibition by α-tomatine resulted from apoptotic cell death. The 3.5 μM α-tomatine treatment for 24 h that induced 48% cell death was used to further treat CT-26 cancer cells. At this concentration, we examined whether the pan-caspase inhibitor,[18] z-VAD-fmk, blocks α-tomatine-induced cell death. The results of the MTT assay (Table 1) show that cell death

DOI: 10.1021/jf5040288
J. Agric. Food Chem. 2015, 63, 1142−1150

was 71.6 and 59.3% at 12 and 24 h of incubation, respectively. z-VAD-fmk (100 μM) failed to reverse α-tomatine-induced cell death; cell viability was not significantly different at $p < 0.05$ between tomatine-treated and tomatine plus the caspase inhibitor-treated groups.

The results of the apoptotic cell death process on α-tomatine-treated CT-26 cancer cells were confirmed by flow cytometric analysis using double staining with annexin V-FITC and PI. This method detects apoptosis by monitoring translocation from the inner membrane to outer cell surface.[19] Indeed, FITC-labeled annexin V can bind to PS to detect apoptotic cells. Figure 3 shows that ~32% of CT-26 cancer cells

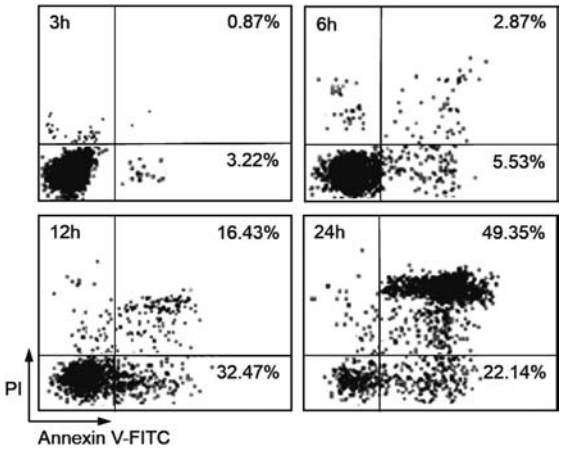

Figure 3. Contour diagram of annexin V-FITC/PI flow cytometry of CT-26 cells after being treated with α-tomatine for the indicated incubation periods. After being treated with 3.5 μM α-tomatine, cells were treated with 1 μg each of annexin V-FITC and PI, respectively, for 15 min. The lower left quadrants of each panel show the viable cells, which exclude PI and are negative for annexin V-FITC binding. The lower right quadrants contain the early apoptotic cells, positive for annexin V-FITC binding and negative for PI uptake, whereas the upper right quadrants contain the later apoptotic/necrotic cells, positive for annexin V-FITC binding and for PI uptake. The figure represents three independent experiments.

treated with α-tomatine for 12 h were stained by annexin V-FITC, which represented the early stage of apoptotic cells, and 16% of the cells were stained by both annexin V and PI, which indicated late-phase apoptosis/necrosis. After treatment for 24 h, 22% of the cells were in the early phase of apoptosis and 49% in the late phase.

CT-26 Cell Death Is Independent of Caspase Activation. Caspase activation is known to play an important role in both intrinsic and extrinsic apoptotic pathways.[20] Among caspases, activation of caspase-3, -8, and -9 is thought to be an important mechanism in the apoptosis pathway (caspase-3 effector caspase, caspase-8 and -9 initiator caspases). Figure 4A shows that the α-tomatine (3.5 μM) treatment failed to increase the initiator caspase activities of caspase-8 and -9 to statistically significant levels. In contrast, the effector caspase-3 activities were significantly induced by α-tomatine treatment during the 12 and 24 h incubations (about 3.2- and 5.0-fold increases during 12 and 24 h incubations, respectively). However, the extent of activity increase was much less than that observed in 50 μM etoposide-treated positive control (18.8- vs 3.2-fold increase during the 12 h incubation).

Etoposide used in the assay is a compound that induces cell apoptosis through the caspase-dependent signal transduction

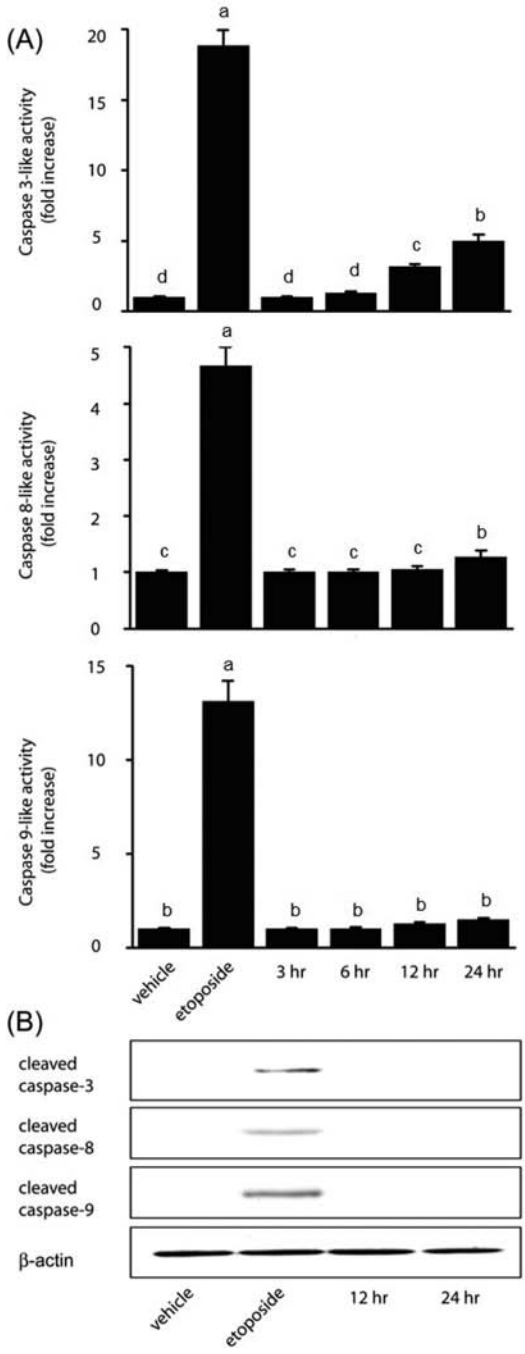

Figure 4. Changes in caspase-3, -8, and -9 activities by treatment with α-tomatine for the indicated incubation times in CT-26 cells. (A) The enzymatic activities of caspase-3, -8, and -9 in the cell lysates were determined by incubation with caspase-specific colorigenic substrates DEVD-*p*NA, IETD-*p*NA and LEHD-*p*NA, respectively. (B) Active forms of caspases produced from pro-forms by proteolytic cleavage. Total cell lysate from α-tomatine-treated cells was subjected to Western blot analysis using caspase-3, -8, and -9 specific antibodies. β-Actin was used as an internal control. Etoposide-treated controls (50 μM) were subjected to incubation for 12 h. Bars not sharing a common letter are significantly different between groups at $p < 0.05$. The figures are representative of three independent experiments.

pathway. It is generally used as a positive control to determine whether cell apoptosis occurs by triggering of caspases. Because etoposide exerts its apoptogenic effect via a caspase-dependent pathway, these findings on α-tomatine-triggered caspase-3-, -8,

DOI: 10.1021/jf5040288
J. Agric. Food Chem. 2015, 63, 1142−1150

and -9 activation modes suggested that CT-26 cell death by α-tomatine largely occurs through a caspase-independent pathway.

Western blot analysis was employed to further examine whether active forms of caspases were produced by proteolytic cleavage from pro-forms in α-tomatine-treated cells due to caspase-dependent apoptosis. Because no detectable protein bands of active forms of caspases were present in Figure 4B, this method confirms that α-tomatine-induced cell death most probably occurred through caspase-independent pathways.

Inhibition of Survivin and NF-κB/p65 Expressions and Induction of AIF Nuclear Translocation. α-Tomatine-induced cell death independent of caspase activation was also supported by the following data (not shown). First, no 4′,6′-diamidino-2-phenylindole (DAPI)-stained chromosomal condensation and apoptotic body appeared during the test conditions. Second, digestion of genomic DNA into a ladder of internucleosomal fragmentation was not observed. Third, there was no evidence that α-tomatine induced release of cytochrome *c* from mitochondria into cytosol.

It has been reported that the permeability of the mitochondrial membrane is regulated by AIF and that AIF-induced cell death bypasses caspase activation.[21] It has also been reported that survivin inhibition promotes cell death independently of cell cycle progression in many types of leukemia cell lines.[22] In addition, survivin has been shown to suppress intracellular translocation of AIF to the nucleus from mitochondria that could induce the caspase-independent apoptotic pathway. We therefore examined the possibility of whether α-tomatine could directly down-regulate the survivin protein level that leads to cell death. The results show that the expression of survivin was down-regulated in CT-26 cancer cells treated with α-tomatine for 24 h (88% reduction compared to control), where marked cell death was observed (Figure 5A and Table 1). Similar results were obtained with NF-κB/p65, in which α-tomatine suppressed nuclear translocation of the p65 subunit from the cytosol, resulting in growth inhibition of the α-tomatine-treated cells.[23] Figure 5B shows that in normal cells, survivin expression blocks nuclear translocation of AIF from mitochondria, suggesting that AIF intracellular translocation and survivin inhibition were strongly involved in α-tomatine-mediated caspase-independent cell death. We examined the translocation of NF-κB because the survivin gene is known to be a target gene regulated by NF-κB.[24]

Antitumor Effects of α-Tomatine in Vivo. To extract the total cell protein, equal amounts of tissue samples were collected and mixed. Relative expression (R.E.) in the figures is an arbitrary value that shows the expression ratio of target protein compared to expressed β-actin as the control protein. Standard deviation does not have statistical significance for R.E. Mean ± SD values were calculated from the average for 10 mice in each group. These values were derived by calculating means ± SD from three independent (separate) experiments.

To examine the antitumor efficacy of α-tomatine in vivo, CT-26 cancer cells were transplanted intracutaneously onto the backs of the mice. The mice were divided into two groups: a vehicle (control) and α-tomatine treatment group (5 mg/kg, ip injection per day). Figure 6 and Table 2 show that compared to the control, α-tomatine inhibited tumor growth by about 38%. Tumor inhibition was not associated with changes in body, heart, lung, stomach, or liver weight. However, there was a significant 29% increase in spleen weight. In addition, there

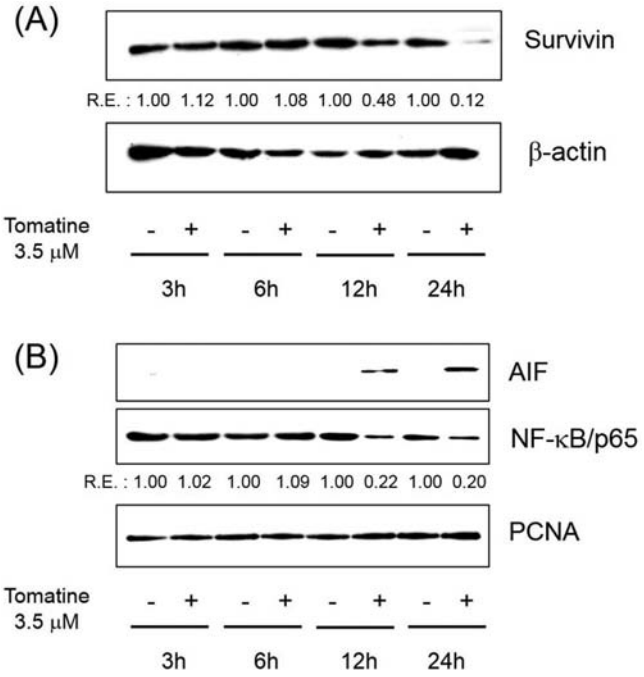

Figure 5. Down-regulation of survivin expression and inhibition of AIF nuclear translocation by α-tomatine treatment on CT-26 mouse colon cancer cells. (A) Total cell lysate from α-tomatine-treated cells was subjected to Western blot analysis using survivin-specific antibodies. β-Actin was used as an internal control for quantifying the modulation rate of survivin expression. (B) Translocation of AIF and NF-κB/p65 to nuclei was assessed by Western blot analysis on nuclear fraction prepared from α-tomatine-treated cells. Each protein expression level was expressed relative expression (R.E.) value calculated from target protein/β-actin or PCNA protein level. The figures represent three independent experiments.

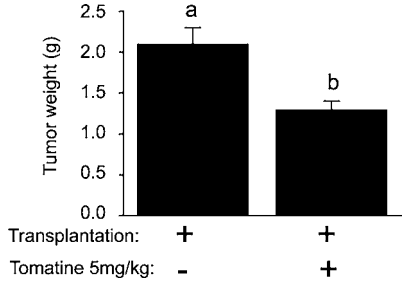

Figure 6. Effects of α-tomatine on tumor growth in vivo. BALB/c mice were intracutaneously transplanted with CT-26 mouse colon cancer cells (1×10^6 cells, 200 μL) and then subjected to intraperitoneal administration of α-tomatine (5 mg/kg body weight in 200 μL of 0.1% DMSO). After 2 weeks, mice were sacrificed and tumors excised to compare tumor growth patterns between experimental and vehicle-treated control group. Tumor weights are expressed as the mean ± SD ($n = 10$). Bars not sharing the same letters are significantly different between groups at $p < 0.05$.

were no associations between tumor regression and caspase-8 and -9 activity increases. However, caspase-3 activity increased in response to α-tomatine administration (Figure 7).

Western blot analysis was used to measure the expression of AIF and survivin (Figure 8). Consistent with the observed effects of α-tomatine in the vitro system, the α-tomatine increased the nuclear-localized AIF protein level and decreased the survivin level. These findings indicate that α-tomatine induced cell death in vitro and inhibited the transplanted tumor

DOI: 10.1021/jf5040288
J. Agric. Food Chem. 2015, 63, 1142−1150

Table 2. Body and Organ Weights of Mice Intraperitoneally Administered α-Tomatine[a]

sample	final body wt (g)	organ wt (g/20 g body wt)				
		heart	lung	stomach	liver	spleen
vehicle	35.7 ± 2.1	0.18 ± 0.01	0.29 ± 0.02	0.28 ± 0.01	1.10 ± 0.12	0.15 ± 0.01b
tomatine 5 mg/kg	35.5 ± 2.3	0.17 ± 0.01	0.28 ± 0.03	0.26 ± 0.02	1.05 ± 0.19	0.21 ± 0.02a

[a]Values are expressed as the mean ± SD of each mouse group (n = 10). Values not sharing the same letters in a column are significantly different at $p < 0.05$. Vehicle indicates 0.1% DMSO treatment only.

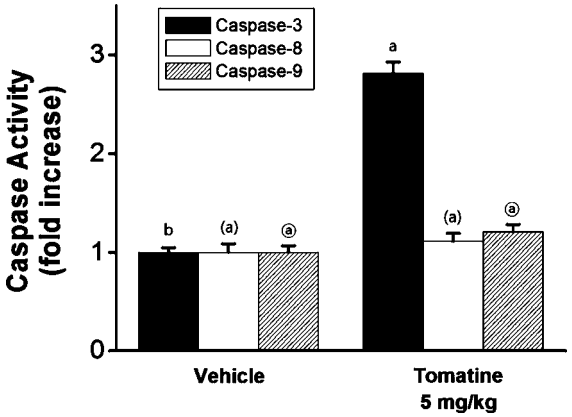

Figure 7. Effects of α-tomatine on caspase-3, -8, and -9 activities on tumor tissues from mice intracutaneously transplanted with CT-26 mouse colon cancer cells. α-Tomatine (5 mg/kg body weight) or vehicle was administered via peritoneal route into mice. The enzymatic activities of caspase-3, -8, and -9 in the tumor tissue lysates were determined by incubation with specific colorigenic substrates DEVD-*p*NA, IETD-*p*NA, and LEHD-*p*NA, respectively. Enzyme activities are expressed as the mean ± SD (n = 10). Bars not sharing a common letter are significantly different between groups at $p < 0.05$. The figures represent three independent experiments.

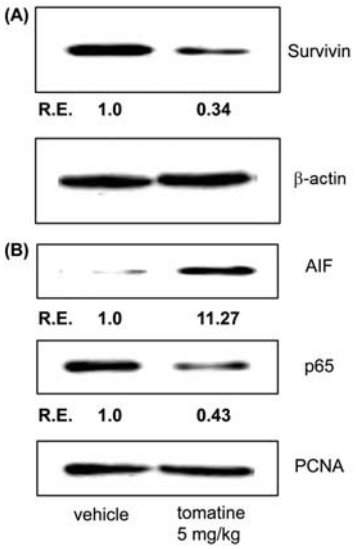

Figure 8. Down-regulation of survivin expression and inhibition of AIF nuclear translocation by α-tomatine treatment on mouse tumors transplanted with CT-26 mouse colon cancer cells. (A) Total tumor tissue lysate from the mice ip administered α-tomatine was subjected to Western blot analysis using survivin-specific antibodies. β-Actin was used as an internal control for quantifying modulation rate of survivin expression. (B) Nuclear translocations of NF-κB/p65 from cytosol and AIF from mitochondria were assessed by Western blot analysis on nuclear fraction prepared from the tumor from the mice administered α-tomatine via peritoneal route. Each protein level was expressed as the R.E. value calculated from target protein/ β-actin or PCNA protein level. The figures represent three independent experiments.

growth in vivo by survivin inhibition and AIF induction, indicating that anticancer effects of α-tomatine might be exerted through caspase-independent pathway in both CT-26 cultured cancer cells and the mice tumor transplanted with the colon cancer cells.

DISCUSSION

Anticarcinogenic Effects of α-Tomatine against CT-26 Cells in Vitro and in Vivo. The cited data imply that α-tomatine induced apoptosis of CT-26 cells and that cell death occurred through caspase-independent pathways. This suggestion is reinforced by the observed failure of a pan-caspase inhibitor, z-VAD-fmk, to block cell death.

A journal reviewer suggested we validate the concentration of z-VA-fmk used in the present study. Table 1 gives the concentration of z-VAD-fmk used. However, we believe that it is not necessary to validate the concentration of z-VAD fmk because this concentration (50−100 μM) was widely used in related earlier studies. We therefore used 100 μM as the working concentration above the saturation point. In addition, increases in the cell viability observed in the control group treated only with z-VAD-fmk might have resulted from suppression of initiation of spontaneous apoptosis.

The cited results show that nuclear localization of AIF and inhibition of survivin expression were strongly involved in the α-tomatine-mediated, caspase-independent cell death and that the tumor-growth-inhibiting effect of α-tomatine was not accompanied by adverse effects such as changes in organ weights, with the possible exception of an increase in spleen weight. In addition, there was no apparent association between tumor regression and increases in caspase-8 and -9 but not caspase-3 activities. We have no obvious explanation for this difference.

Western blot analysis used to measure the in vivo expression of AIF and survivin paralleled the observed effects induced by α-tomatine in vitro; α-tomatine increased the AIF level and decreased the survivin level. Taken together, the described findings indicate that α-tomatine inhibited the cancer cells in vitro and tumor growth in vivo by inhibition of survivin and induction of AIF. It seems that these anticarcinogenic effects of α-tomatine appear to be exerted largely through a caspase-independent pathway in both the CT-26 cultured cancer cells and in the transplanted mouse colon tumor cells.

End Points of Cytotoxicity and FACS Assays. These two assays measure different end points. The two cytotoxicity assays used in this study measure cellular dehydrogenase activities as an indicator of cell viability. The FACS analysis measures the incorporation of PI into nuclei through the gap generated by the collapse of the cell membrane together with staining of phosphatidylserine that is localized on the inner side of the lipid bilayer that flipped over to the outer side. The FACS analysis

DOI: 10.1021/jf5040288
J. Agric. Food Chem. 2015, 63, 1142−1150

data show only the population of cells that are susceptible to apoptosis and not directly associated with cell death. By contrast, the MTT assays measure cell death.

Reported Anticarcinogenic Activities and Mechanisms of α-Tomatine. To place the findings of the present study in proper perspective, we will briefly mention results of reported studies on the anticarcinogenic potential of α-tomatine in vitro and in vivo.

- Using a microculture tetrazolium (MTT) in vitro assay, we previously reported that tomatine is a strong inhibitor of growth for both human colon and liver cancer cell lines, as evidenced by the dose-dependent (0.1−100 μg/mL) inhibition of HT29 colon cancer cells at levels ranging from 38.0 to 81.5% and of human HepG2 cancer cells, from 46.3 to 89.2%.[25] The anticarcinogenic activity against human liver cancer cells at a tomatine concentration of 1 μg/mL was higher than the corresponding activity observed with the commercial anticancer drug doxorubicin.
- We also investigated six green and three red tomato extracts for their ability to induce cell death in human cancer and normal cells using a microculture MTT assay.[26] Compared to untreated controls, the high-tomatine green tomato extracts strongly inhibited the following human cancer cell lines: breast (MCF-7), colon (HT-29), gastric (AGS), and hepatoma (liver) (HepG2), as well as normal human liver cells (Chang).
- α-Tomatine (a) inhibited cell invasion and migration and phosphorylation of Akt and extracellular signal-regulated kinases 1 and 2 (ERK1/2) in human lung adenocarcinoma A549 cells; (b) did not affect phosphorylation of c-Jun N-terminal kinase (JNK) and the p38 gene; (c) decreased nuclear levels of NF-κB, c-Fos, and C-Jun; and (d) inhibited binding abilities of NF-κB and activator protein-1 (AP-1).[27] Inhibition of metastasis occurs by reducing MMP-2, MMP-9, and urokinase-type-plasminogen activator (uPA) activities through the phosphoinositide 3-kinase/Akt (PI3K/Akt or ERK1/2) signaling pathway and inhibition of NF-κB or AP-1 binding activities.
- Another study confirmed that α-tomatine suppressed invasion and migration of human non-small lung cancer NCI-H460 cells through inactivation of the FAK/PI3K/Akt signaling pathway and lowering binding activity of NF-κB.[28] Cytotoxicity occurred through inactivation of the signaling pathway and enhancement of IκBα protein expressions to reduce NF-κB DNA binding activity, resulting in down-regulation of MMP-7 expression, inhibition of cell migration and invasion, and interference with the rearrangement of the actin cytoskeleton by decreasing the expression of the pFAK protein.
- α-Tomatine inhibited PC-3 prostate cancer cells with an IC_{50} value of 1.67 μM.[29,30] Cytotoxicity occurred after an hour of treatment and was mainly due to induction of apoptosis as evidenced by decreased mitochondrial membrane potential and increased nuclear condensation, polarization of F-actin potential, cell membrane permeability, cytochrome *c* expression, induction of activation of caspase-3, -8, and -9, inhibition of NF-κB nuclear translocation, and a decrease in NF-κB/p50 and NF-κBp65 in the nuclear fraction.
- α-Tomatine inhibited human leukemia MOLT-4 cells by activating cell cycle checkpoints without damaging single or double DNA strands in the cells.[31] The slowing of the cell cycle seems to involve caspase-independent cell death associated with an increase in the tumor suppressor protein p53, and the pro-apoptotic protein PUMA (p53 up-regulated modulator of apoptosis), as well as other protein biomarkers associated with cell cycle regulation.
- α-Tomatine-mediated anticancer activity against human chronic myeloid leukemia cells in vitro and in a transplanted mouse tumor operated through cell-cycle and caspase-independent pathways.[32] The mechanism against the leukemia cells seems consistent with that described in the present study for the colon cancer cells.
- We found that feeding 2000 ppm of tomatine and 224 ppm of the multiorgan carcinogen dibenzo[*a*,*l*]pyrene (DBP) to rainbow trout for 9 months resulted in a reduced incidence of liver and stomach tumors by 41.3 and 36.3%, respectively, as compared to the incidence of tumors observed with DBP alone.[33]
- Ip-administered α-tomatine (5−10 mg/kg) significantly attenuated the growth of androgen-independent PC-3 prostate cancer cells in mice.[34] Tumor-suppression was associated with increased apoptosis and by reduced nuclear translocation of the p50 and p65 gene components of the NF-κB signaling pathway. This study seems to provide evidence that α-tomatine can inhibit the growth of prostate cancer tumors in vivo without inducing overt toxicity.
- The activity of α-tomatine generally decreases upon removal of one or more of the four carbohydrate groups of the lycotetraose side chain.[35] For example, the activity of α-tomatine against the PC-3 prostate cancer cells was about 200 times greater than that of the aglycone tomatidine. By contrast, tomatidine was highly active against the foodborne pathogen *Staphylococcus aureus*,[36] suggesting that the two bioactivities are governed by different mechanisms.
- Ip-injected α-tomatine at 1 mg/kg slowed the growth of Ehlich tumor in mice; the combination of α-tomatine (1 mg/kg) and the cancer drug doxorubicin (2 mg/kg) acted synergistically and extended survival of the mice with the Ehrlich tumors.[37] The activity against the tumors, which are derived from adenocarcinoma of the mammary gland, seems to involve the immune system in the inhibition of tumor progression. This suggestion seems plausible on the basis of reports by other investigators that tomatine contributes to the protective immunity of rodents.[38,39]

The results of the present study on the inhibition of tumor growth in mice with implanted colon cancer complement and extend the cited in vitro and in vivo studies by other investigators. It seems that the mechanistic molecular, signaling, biomarker, and immunomodulating events associated with apoptosis and cell migration might not be the same for the different cancer cell lines. Overall, the cited observations imply that both intrinsic and extrinsic pro-apoptosis pathways are involved and that α-tomatine may protect against development and progression of several cancers (multiorgan protection). This is not surprising because carcinogenesis is a sequential multistage cellular process consisting of tumor initiation, tumor

DOI: 10.1021/jf5040288
J. Agric. Food Chem. 2015, 63, 1142−1150

promotion, and tumor progression characterized by dysregulation of multiple genes resulting in multiple adverse symptoms. Each stage involves signaling pathways and associated biomarkers.

Safety of Tomatine. The following reported observations indicate that tomatine does not appear to be toxic to animals or humans.

(a) The following LD_{50} value have been reported for tomatine in mice (in mg/kg body weight): ip, 25–33.5; iv, 18; oral, 500; subcutaneous, >1000.[15,40]

(b) As part of the anticarcinogenic study of feeding tomatine to rainbow trout for 9 months, we found that tomatine did not induce changes in mortality, fish weights, liver weights, or tissue morphology.[33] We also observed a lack of toxicity in hamsters orally fed tomatine.[41]

(c) The apparent nontoxicity of tomatine in animal models is reinforced by the fact that Peruvians consume without deleterious effects high-tomatine red tomatoes grown in the Andes mountains[8] and that high-tomatine "pickled green" and "green-fried" tomatoes are part of the human diet.

(d) The present study shows that except for the spleen, the body and organ weights of the mice were not affected by their exposure to tomatine. Pancreas weights were not determined.

Outlook. Because our previous studies found that dietary tomatine and high-tomatine green tomatoes decreased plasma low-density (bad) cholesterol and plasma triglyceride in hamsters fed a diet high in saturated fat and cholesterol by 41 and 47%,[41,42] chemopreventive effects of α-tomatine and high-tomatine tomatoes against both cancers and cardiovascular disease in humans merit further study. Such studies should evaluate pure tomatine and high-tomatine green tomato diets. A key consideration in cancer prevention and treatment should be the ratio of effective preventive or therapeutic to toxic dose. Combinations of low doses of tomatine with cancer drugs that might act synergistically with reduced side effects also merit study.

There is also a need to develop high-tomatine red tomatoes by suppressing the genes in the tomato plant that govern the biosynthesis of enzymes that degrade most of the tomatine during ripening of tomatoes.[43−46] Such new red tomatoes will contain two highly bioactive health-promoting molecules, α-tomatine and the red pigment lycopene.[40,47,48]

AUTHOR INFORMATION

Corresponding Authors

*(S.H.N.) Phone: 82-31-219-2619. Fax: 82-31-219-1615. E-mail: shnam@ajou.ac.kr.

*(M.F.) Phone: (510) 559-5615. Fax: (510) 559-6162. E-mail: mendel.friedman@ars.usda.gov.

Notes

The authors declare no competing financial interest.

ABBREVIATIONS USED

AIF, apoptosis-inducing factor; Akt, protein kinase B; annexin V-FITC, annexin V conjugated with fluorescein isothiocyanate, for detection of cell apoptosis; AP-1, activator protein-1; BSA, bovine serum albumin; Bcl-2, Bcl-xL, anti-apoptotic proteins; ERK, extracellular signal-regulated kinase; FAK, focal adhesion kinase; IC_{50}, concentration of the test substance that inhibited 50% of the cancer cells; IgG, immunoglobulin; ip, intraperitoneal; HRP, horseradish peroxidase; MMP, matrix metalloproteinase; MTT, a tetrazolium dye, 3-(4,5-dimethylthiazol-2-yl)-2,5-diphenyltetrazolium bromide; NF-κB, nuclear factor kappa B; NP-40, Tergitol-type NP-40 detergent; PI, propidium iodide; PCNA, proliferating cell nuclear antigen; PS, phosphatidylserine; PI3K, phosphoinositide 3-kinase; PI3K/AKT/mTOR, an intracellular signaling pathway; RIPA, radioimmunoprecipitation assay; z-VAD-fmk, pan-caspase inhibitor; XIAP, X-chromosome-linked inhibitor of apoptosis

REFERENCES

(1) Choi, S. P.; Kim, S. P.; Nam, S. H.; Friedman, M. Antitumor effects of dietary black and brown rice brans in tumor-bearing mice: relationship to composition. *Mol. Nutr. Food Res.* **2013**, *57*, 390−400.

(2) Kim, S. P.; Kang, M. Y.; Nam, S. H.; Friedman, M. Dietary rice bran component γ-oryzanol inhibits tumor growth in tumor-bearing mice. *Mol. Nutr. Food Res.* **2012**, *56*, 935−944.

(3) Kim, S. P.; Nam, S. H.; Friedman, M. *Hericium erinaceus* (lion's mane) mushroom extracts inhibit metastasis of cancer cells to the lung in CT-26 colon cancer-transplanted mice. *J. Agric. Food Chem.* **2013**, *61*, 4898−4904.

(4) Friedman, M.; Levin, C. E. α-Tomatine content in tomato and tomato products determined by HPLC with pulsed amperometric detection. *J. Agric. Food Chem.* **1995**, *43*, 1507−1511.

(5) Friedman, M.; Levin, C. E. Dehydrotomatine content in tomatoes. *J. Agric. Food Chem.* **1998**, *46*, 4571−4576.

(6) Friedman, M. Analysis of biologically active compounds in potatoes (*Solanum tuberosum*), tomatoes (*Lycopersicon esculentum*), and jimson weed (*Datura stramonium*) seeds. *J. Chromatogr.* **2004**, *1054*, 143−155.

(7) Iijima, Y.; Watanabe, B.; Sasaki, R.; Takenaka, M.; Ono, H.; Sakurai, N.; Umemoto, N.; Suzuki, H.; Shibata, D.; Aoki, K. Steroidal glycoalkaloid profiling and structures of glycoalkaloids in wild tomato fruit. *Phytochemistry* **2013**, *95*, 145−157.

(8) Rick, C. M.; Uhlig, J. W.; Jones, A. D. High α-tomatine content in ripe fruit of Andean *Lycopersicon esculentum* var. *cerasiforme*: developmental and genetic aspects. *Proc. Natl. Acad. Sci. U.S.A.* **1994**, *91*, 12877−12881.

(9) Kozukue, N.; Yoon, K.-S.; Byun, G.-I.; Misoo, S.; Levin, C. E.; Friedman, M. Distribution of glycoalkaloids in potato tubers of 59 accessions of two wild and five cultivated *Solanum* species. *J. Agric. Food Chem.* **2008**, *56*, 11920−11928.

(10) Kozukue, N.; Han, J.-S.; Lee, K.-R.; Friedman, M. Dehydrotomatine and α-tomatine content in tomato fruits and vegetative plant tissues. *J. Agric. Food Chem.* **2004**, *52*, 2079−2083.

(11) Koh, E.; Kaffka, S.; Mitchell, A. E. A long-term comparison of the influence of organic and conventional crop management practices on the content of the glycoalkaloid α-tomatine in tomatoes. *J. Sci. Food Agric.* **2013**, *93*, 1537−1542.

(12) Nie, C.; Luo, Y.; Zhao, X.; Luo, N.; Tong, A.; Liu, X.; Yuan, Z.; Wang, C.; Wei, Y. Caspase-9 mediates Puma activation in UCN-01-induced apoptosis. *Cell Death Dis.* **2014**, *5*, No. e1495.

(13) Ho, S. T.; Tung, Y. T.; Kuo, Y. H.; Lin, C. C.; Wu, J. H. Ferruginol inhibits non-small cell lung cancer growth by inducing caspase-associated apoptosis. *Integr. Cancer Ther.* **2015**, *14*, 86−97.

(14) Friedman, M.; Levin, C. E.; McDonald, G. M. α-Tomatine determination in tomatoes by HPLC using pulsed amperometric detection. *J. Agric. Food Chem.* **1994**, *42*, 1959−1964.

(15) Friedman, M. Tomato glycoalkaloids: role in the plant and in the diet. *J. Agric. Food Chem.* **2002**, *50*, 5751−5780.

(16) Mosmann, T. Rapid colorimetric assay for cellular growth and survival: application to proliferation and cytotoxicity assays. *J. Immunol. Methods* **1983**, *65*, 55−63.

(17) Vermes, I.; Haanen, C.; Steffens-Nakken, H.; Reutelingsperger, C. A novel assay for apoptosis. Flow cytometric detection of phosphatidylserine expression on early apoptotic cells using fluorescein labelled annexin V. *J. Immunol. Methods* **1995**, *184*, 39−51.

DOI: 10.1021/jf5040288
J. Agric. Food Chem. 2015, 63, 1142−1150

(18) Ryu, D. S.; Kim, S. H.; Kwon, J. H.; Lee, D. S. *Orostachys japonicus* induces apoptosis and cell cycle arrest through the mitochondria-dependent apoptotic pathway in AGS human gastric cancer cells. *Int. J. Oncol.* **2014**, *45*, 459−469.
(19) Stojak, M.; Mazur, L.; Opydo-Chanek, M.; Lukawska, M.; Oszczapowicz, I. In vitro induction of apoptosis and necrosis by new derivatives of daunorubicin. *Anticancer Res.* **2013**, *33*, 4439−4443.
(20) Llambi, F.; Green, D. R. Apoptosis and oncogenesis: give and take in the BCL-2 family. *Curr. Opin. Genet. Dev.* **2011**, *21*, 12−20.
(21) Kim, E. A.; Jang, J. H.; Lee, Y. H.; Sung, E. G.; Song, I. H.; Kim, J. Y.; Kim, S.; Sohn, H. Y.; Lee, T. J. Dioscin induces caspase-independent apoptosis through activation of apoptosis-inducing factor in breast cancer cells. *Apoptosis* **2014**, *19*, 1165−1175.
(22) Yang, Y. W.; Wu, C. A.; Morrow, W. J. The apoptotic and necrotic effects of tomatine adjuvant. *Vaccine* **2004**, *22*, 2316−2327.
(23) Karin, M.; Lin, A. NF-κB at the crossroads of life and death. *Nat. Immunol.* **2002**, *3*, 221−227.
(24) Kwon, H. K.; Hwang, J. S.; So, J. S.; Lee, C. G.; Sahoo, A.; Ryu, J. H.; Jeon, W. K.; Ko, B. S.; Im, C. R.; Lee, S. H.; Park, Z. Y.; Im, S. H. Cinnamon extract induces tumor cell death through inhibition of NFκB and AP1. *BMC Cancer* **2010**, *10*, 392.
(25) Lee, K.-R.; Kozukue, N.; Han, J.-S.; Park, J.-H.; Chang, E.-Y.; Baek, E.-J.; Chang, J.-S.; Friedman, M. Glycoalkaloids and metabolites inhibit the growth of human colon (HT29) and liver (HepG2) cancer cells. *J. Agric. Food Chem.* **2004**, *52*, 2832−2839.
(26) Friedman, M.; Levin, C. E.; Lee, S.-U.; Kim, H.-J.; Lee, I.-S.; Byun, J.-O.; Kozukue, N. Tomatine-containing green tomato extracts inhibit growth of human breast, colon, liver, and stomach cancer cells. *J. Agric. Food Chem.* **2009**, *57*, 5727−5733.
(27) Shih, Y.-W.; Shieh, J.-M.; Wu, P.-F.; Lee, Y.-C.; Chen, Y.-Z.; Chiang, T.-A. α-Tomatine inactivates PI3K/Akt and ERK signaling pathways in human lung adenocarcinoma A549 cells: effect on metastasis. *Food Chem. Toxicol.* **2009**, *47*, 1985−1995.
(28) Shieh, J.-M.; Cheng, T.-H.; Shi, M.-D.; Wu, P.-F.; Chen, Y.; Ko, S.-C.; Shih, Y.-W. α-Tomatine suppresses invasion and migration of human non-small cell lung cancer NCI-H460 cells through inactivating FAK/PI3K/Akt signaling pathway and reducing binding activity of NF-κB. *Cell Biochem. Biophys.* **2011**, *60*, 297−310.
(29) Lee, S.-T.; Wong, P.-F.; Cheah, S.-C.; Mustafa, M. R. α-Tomatine induces apoptosis and inhibits nuclear factor-κB activation on human prostatic adenocarcinoma PC-3 cells. *PLoS One* **2011**, *6*, No. e18915.
(30) Lee, S. T.; Wong, P. F.; Hooper, J. D.; Mustafa, M. R. α-Tomatine synergises with paclitaxel to enhance apoptosis of androgen-independent human prostate cancer PC-3 cells in vitro and in vivo. *Phytomedicine* **2013**, *20*, 1297−1305.
(31) Kúdelová, J.; Seifrtová, M.; Suchá, L.; Tomšík, P.; Havelek, R.; Rezácová, M. α-Tomatine activates cell cycle checkpoints in the absence of DNA damage in human leukemic MOLT-4 cells. *J. Appl. Biomed.* **2013**, *11*, 93−103.
(32) Chao, M. W.; Chen, C. H.; Chang, Y. L.; Teng, C. M.; Pan, S. L. α-Tomatine-mediated anti-cancer activity in vitro and in vivo through cell cycle- and caspase-independent pathways. *PLoS One* **2012**, *7*, No. e44093.
(33) Friedman, M.; McQuistan, T.; Hendricks, J. D.; Pereira, C.; Bailey, G. S. Protective effect of dietary tomatine against dibenzo-[*a*,*l*]pyrene (DBP)-induced liver and stomach tumors in rainbow trout. *Mol. Nutr. Food Res.* **2007**, *51*, 1485−1491.
(34) Lee, S. T.; Wong, P. F.; He, H.; Hooper, J. D.; Mustafa, M. R. α-Tomatine attenuation of in vivo growth of subcutaneous and orthotopic xenograft tumors of human prostate carcinoma PC-3 cells is accompanied by inactivation of nuclear factor-κB signaling. *PLoS One* **2013**, *8*, No. e57708.
(35) Choi, S. H.; Ahn, J.-B.; Kozukue, N.; Kim, H.-J.; Nishitani, Y.; Zhang, L.; Mizuno, M.; Levin, C. E.; Friedman, M. Structure-activity relationships of α-, β1-, γ-, and δ-tomatine and tomatidine against human breast (MDA-MB-231), gastric (KATO-III), and prostate (PC3) cancer cells. *J. Agric. Food Chem.* **2012**, *60*, 3891−3899.
(36) Chagnon, F.; Guay, I.; Bonin, M. A.; Mitchell, G.; Bouarab, K.; Malouin, F.; Marsault, E. Unraveling the structure-activity relationship of tomatidine, a steroid alkaloid with unique antibiotic properties against persistent forms of *Staphylococcus aureus*. *Eur. J. Med. Chem.* **2014**, *80*, 605−620.
(37) Tomsik, P.; Micuda, S.; Sucha, L.; Cermakova, E.; Suba, P.; Zivny, P.; Mazurova, Y.; Knizek, J.; Niang, M.; Rezacova, M. The anticancer activity of α-tomatine against mammary adenocarcinoma in mice. *Biomed. Pap. Med. Fac. Univ. Palacky Olomouc Czech Repub.* **2013**, *157*, 153−161.
(38) Heal, K. G.; Taylor-Robinson, A. W. Tomatine adjuvantation of protective immunity to a major pre-erythrocytic vaccine candidate of malaria is mediated via $CD8^+$ T cell release of IFN-γ. *J. Biomed. Biotechnol.* **2010**, *2010*, No. 834326.
(39) Morrow, W. J. W.; Yang, Y.-W.; Sheikh, N. A. Immunobiology of the tomatine adjuvant. *Vaccine* **2004**, *22*, 2380−2384.
(40) Friedman, M. Anticarcinogenic, cardioprotective, and other health benefits of tomato compounds lycopene, α-tomatine, and tomatidine in pure form and in fresh and processed tomatoes. *J. Agric. Food Chem.* **2013**, *61*, 9534−9550.
(41) Friedman, M.; Fitch, T. E.; Yokoyama, W. E. Lowering of plasma LDL cholesterol in hamsters by the tomato glycoalkaloid tomatine. *Food Chem. Toxicol.* **2000**, *38*, 549−553.
(42) Friedman, M.; Fitch, T. E.; Levin, C. E.; Yokoyama, W. H. Feeding tomatoes to hamsters reduces their plasma low-density lipoprotein cholesterol and triglycerides. *J. Food Sci.* **2000**, *65*, 897−900.
(43) Royer, M.; Larbat, R.; Le Bot, J.; Adamowicz, S.; Robin, C. Is the C:N ratio a reliable indicator of C allocation to primary and defence-related metabolisms in tomato? *Phytochemistry* **2013**, *88*, 25−33.
(44) Ökmen, B.; Etalo, D. W.; Joosten, M. H. A. J.; Bouwmeester, H. J.; de Vos, R. C. H.; Collemare, J.; de Wit, P. J. G. M. Detoxification of α-tomatine by *Cladosporium fulvum* is required for full virulence on tomato. *New Phytol.* **2013**, *198*, 1203−1214.
(45) Ohyama, K.; Okawa, A.; Fujimoto, Y. Biosynthesis of steroidal alkaloids in Solanaceae plants: incorporation of 3β-hydroxycholest-5-en-26-al into tomatine with tomato seedlings. *Bioorg. Med. Chem. Lett.* **2014**, *24*, 3556−3558.
(46) Ohyama, K.; Okawa, A.; Moriuchi, Y.; Fujimoto, Y. Biosynthesis of steroidal alkaloids in Solanaceae plants: involvement of an aldehyde intermediate during C-26 amination. *Phytochemistry* **2013**, *89*, 26−31.
(47) Choi, S. H.; Kim, D.-S.; Kozukue, N.; Kim, H.-J.; Nishitani, Y.; Mizuno, M.; Levin, C. E.; Friedman, M. Protein, free amino acid, phenolic, β-carotene, and lycopene content, and antioxidative and cancer cell inhibitory effects of 12 greenhouse-grown commercial cherry tomato varieties. *J. Food Compos. Anal.* **2014**, *34*, 115−127.
(48) Kozukue, N.; Friedman, M. Tomatine, chlorophyll, β-carotene and lycopene content in tomatoes during growth and maturation. *J. Sci. Food Agric.* **2003**, *83*, 195−200.

DOI: 10.1021/jf5040288
J. Agric. Food Chem. 2015, 63, 1142−1150

2. MATERIALS AND METHODS

2.1. Isolation of the Compound of Interest. *2.1.1. Materials.* Fresh alperujo samples (not stored) were obtained after virgin oil extraction from Picual olive fruits in an experimental mill at the Instituto de la Grasa, Seville, Spain. Samples of wet alperujo were taken from the output of the horizontal centrifuge of the two-phase process. The alperujo (a semi-solid residue composed of olive peels, pulp, seeds, and ground stones) was processed without removal of the stones.

2.1.2. Standard Compounds. Hydroxymethylfurfural, protocatechuic acid, *p*-hydroxybenzoic acid, vanillic acid, 4-methylcatechol, catechol, 3,4-dihydroxyhydrocinnamic acid, and 3,4-dihydroxyphenylglycol were obtained from Sigma-Aldrich (Deisenhofer, Germany). Tyrosol was obtained from Fluka (Buchs, Switzerland). Oleuropein was obtained from Extrasynthese (Lyon Nord, Geney, France). Hydroxytyrosol was obtained by the method described by Fernández-Bolaños et al.[13] Hydroxytyrosol acetate was isolated following the process described by Fernández-Bolaños et al.[14]

2.1.3. Thermal Treatment. The hydrothermal treatment used has been patented[5] and was performed using a prototype designed by our research group at the Instituto de la Grasa (Seville, Spain). The reactor has a stainless-steel reservoir (100 L capacity) that can operate at temperatures between 50 and 190 °C and at a maximum pressure of 1.2 MPa. A total of 20 kg of fresh alperujo was loaded into the reactor and treated for 60 min at 140 and 170 °C, increasing the liquid by steam condensation. The wet material was centrifuged at 4700 *g* (Comteifa, SL, Barcelona, Spain) to separate the solids and liquids. After centrifugation, 10 L of the liquid phase was concentrated to 1 L by rotary evaporation under vacuum at 30 °C.

2.1.4. Phenol Extraction with Refluxing Ethyl Acetate. The liquid portions obtained after treatment were washed with hexane to remove the lipid fraction. A total of 1 L of liquid was mixed with 500 mL of hexane; the mixture was shaken vigorously; and then the phases were separated by decantation and washed twice. Extraction of phenolic compounds was carried out with ethyl acetate. A total of 200 mL of aqueous sample was extracted with 500 mL of ethyl acetate. The liquid−liquid extraction was performed with ethyl acetate (refluxed at 77 °C) in a continuous extractor of a heavier liquid (water) by lighter liquid (ethyl acetate) for 8 h.

2.1.5. Chromatographic Fractionation of the Ethyl Acetate Extract. Approximately 12 g of extract was dissolved in 60 mL of H_2O/MeOH (80:20). The extracts were passed through a column 3.5 cm in diameter and 40 cm in height filled with Amberlite XAD16. The elution was performed with 1 L of H_2O, 30% EtOH (v/v), 50% EtOH (v/v), and 95% EtOH (v/v). A total of 10 fractions of 100 mL each were collected. Fractions were analyzed by high-performance liquid chromatography (HPLC), and those containing the derivative of elenolic acid of interest were mixed and concentrated to 50 mL. The fractions 1 and 2 used in the antimicrobial test were obtained in this step.

2.1.6. HPLC−Diode Array Detector (DAD). The compounds were identified using a Hewlett-Packard 1100 liquid chromatography system with a C_{18} column (Teknokroma Tracer Extrasil ODS-2, 250 × 4.6 mm inner diameter, 5 μm particle size). The system was equipped with a DAD (the wavelengths used for quantification were 254, 280, and 340 nm) and Rheodyne injection valves (20 μL loop). The method used for quantification was described by Rubio-Senent et al.[6] Quantification was performed in triplicate using external standards; standard curves were linear in all cases ($R^2 > 0.99$).

2.1.7. Isolation. The compound of interest was isolated using a semi-preparative system. A HPLC method similar to that described for HPLD−DAD analysis was used. Jasco HPLC (LC-Net II ADC, Kyoto, Japan) equipped with a DAD and a semi-preparative Synergi 4 μm Hydro-RP80A reverse-phase column (25 cm × 21.20 mm inner diameter, 4 μm particle size, Phenomenex, Macclesfield, Cheshire, U.K.) was used. The flow rate was maintained at 12 mL/min, and the injection volume was 600 μL. Before the DAD, the flow was divided with a T connection (0.25 mL/min to the DAD and 11.75 mL/min to the collection port).

2.2. Structural Analysis. *2.2.1. ^1H and ^{13}C NMR, Correlation Spectroscopy (COSY), Heteronuclear Single-Quantum Coherence (HSQC), Nuclear Overhauser Effect Spectrometry (NOESY), and Heteronuclear Multiple-Bond Correlation (HMBC) Experiments.* ^1H (300.1 and 700.2 MHz) and ^{13}C (75.5 and 176.1 MHz) NMR spectra were recorded on Bruker Avance-300 III and Avance-700 III spectrometers using CD_3OD as the solvent. The latter spectrometer was equipped with a cryogenically cooled 5 mm QCI gradient probe. Chemical shifts are reported in δ units (ppm) relative to the solvent peak (3.31 and 49.0 ppm for ^1H and ^{13}C NMR, respectively). The ^{13}C NMR spectrum registered at 75.5 MHz was acquired with the following acquisition parameters: acquisition time, 0.9 s; relaxation delay, 1.5 s; spectral width, 239 ppm; data points, 32 000; number of scans, 1434; and line broadening, 1.0 Hz. The ^{13}C spectrum registered at 176.1 MHz was acquired with the following acquisition parameters: acquisition time, 0.8 s; relaxation delay, 3.0 s; spectral width, 220 ppm; data points, 64 000; number of scans, 14 336; and line broadening, 1.0 Hz. The enhanced sensitivity of NMR at 176.1 MHz with the cryoprobe for the ^{13}C NMR spectrum allowed the signal for the carboxyl groups to be clearly observable, whereas that signal was missing at 75.5 MHz and a shorter relaxation delay (1.5 s).

The assignments of ^1H and ^{13}C signals were confirmed by homonuclear COSY and heteronuclear HSQC spectra (Avance-300 III), respectively. The configuration of the double bond was confirmed by a two-dimensional (2D) NOESY experiment (Avance-300 III). The HMBC (Avance-700 III) experiment confirmed the connection of glutaric acid with the crotonaldehyde moiety through C-3 of the dicarboxylic acid.

2.2.2. Mass Spectrometry (MS). Mass spectra [chemical ionization (CI) and high-resolution chemical ionization (HR-CI)] were recorded on a Micromass AutoSpec-Q mass spectrometer with a resolution of 1000 or 10 000 (10% valley definition).

2.2.3. Infrared (IR) Spectra. IR spectra were recorded on Jasco FT/IR 4100 equipped with an attenuated total reflection (ATR) accessory.

2.3. (*E*)-3-(1-Oxobut-2-en-2-yl)glutaric Acid. IR ν_{max}: 3300−2400, 2727, 1684, 1440, 1405, 1310, 1234, 1160, 982, 932 (br), 844, 801 cm^{-1}. ^1H NMR (700.2 MHz, CD_3OD) δ: 9.28 (d, 1H, $J_{1',3}$ = 2.0 Hz, H-1′), 6.79 (q, 1H, $J_{3',4'}$ = 7.0 Hz, H-3′), 3.59 (m, 1H, H-3), 2.68 (dd, 2H, $J_{2a,2b}$ = 15.5 Hz, $J_{2a,3}$ = 9.1 Hz, H-2a, H-4a), 2.61 (dd, 2H, $J_{2b,3}$ = 6.2 Hz, H-2b, H-4b), 2.08 (d, 3H, $J_{4',3'}$ = 7.0 Hz, H-4′). ^{13}C NMR (176.1 MHz, CD_3OD) δ: 197.0 (C-1′), 176.3 (C-1, C-5), 155.9 (C-3′), 145.3 (C-2′), 38.4 (C-2, C-4), 31.9 (C-3), 15.4 (C-4′). CIMS *m*/*z*: 201 ($[M + H]^+$, 22%), 183 ($[M - H_2O + H]^+$, 66%), 165 ($[M - 2H_2O + H]^+$, 100%). HR-CIMS *m*/*z* calcd for $C_9H_{13}O_5$ ($[M + H]^+$): 201.0763, found: 201.0769.

2.4. Assay of Extraction. Fresh alperujo was submitted to extractions with water, methanol−water, and two hydrothermal treatments. Further phenol extractions from the aqueous fractions were performed with ethyl acetate at 77 °C (hot) and room temperature (cold), to evaluate the optimal conditions for extraction of a high concentration of glutaric acid derivative.

2.4.1. Extraction with Water at Room Temperature. A total of 500 g of fresh alperujo was mixed with 500 mL of water at room temperature for 1 h with stirring. The mixture was filtered, and the liquid was extracted with cold and hot ethyl acetate.

2.4.2. Extraction with Aqueous Methanol at Room Temperature. We used the method reported by Obied et al.[15] for the extraction from 300 g of fresh alperujo with aqueous methanol (80%, v/v; 15 mL/10 g of alperujo) at room temperature for 30 min. The extraction was repeated twice more using 10 mL/10 g of alperujo. The combined organic fractions were filtered, evaporated to dryness in a rotary evaporator (Buchi, Milan, Italy) at 40 °C, and then redissolved in water. The phenols were extracted with cold and hot ethyl acetate.

2.4.3. Thermal Treatment at 140 °C/60 min. A total of 20 kg of fresh alperujo sample was hydrothermally treated at 140 °C for 60 min with saturated steam, obtaining 35 L of aqueous fraction by steam condensation, which was filtered and extracted with cold and hot ethyl acetate.

2.4.4. Thermal Treatment at 170 °C/60 min. A total of 20 kg of fresh alperujo sample was hydrothermally treated at 170 °C for 60 min

DOI: 10.1021/jf5057716
J. Agric. Food Chem. 2015, 63, 1151−1159

with saturated steam, obtaining 41 L of aqueous fraction by steam condensation, which was filtered and extracted with cold and hot ethyl acetate.

2.4.5. Liquid–Liquid Extraction with Ethyl Acetate at 77 °C (Hot). We used the procedure as described in section 2.1.4.

2.4.6. Liquid–Liquid Extraction with Ethyl Acetate at Room Temperature (Cold). The aqueous portions (200 mL) obtained after treatment were mixed with ethyl acetate (250 mL) in a separating funnel, vigorously shaken for 10 min at room temperature, and then allowed to settle for 20 min. The phases were separated, and the extraction was repeated twice. The combined organic phases were evaporated to dryness at a reduced pressure.

2.5. Bactericidal Activity. *P. syringae* CECT 4429T and *A. tumefaciens* CECT 4119T bacterial strains were purchased from the Spanish Type Culture Collection (CECT) at Burjasot, Valencia, Spain. Bactericidal activity of the samples (extracts and pure compound) was tested using 150 μL of the sample inoculated with 10 μL of an overnight broth culture of each microorganism, diluted with saline to obtain an initial population between 5×10^5 and 5.7×10^5 colony-forming units (CFU)/mL. The inoculated samples were incubated at room temperature for 5 min with occasional shaking and plated onto nutrient agar to count the number of survivors after incubation. Experiments were performed in duplicate.[16]

The pH of the extracts (2.8–2.6) and the pure compound (3.1) were adjusted to 5.6 with dilute NaOH and filtered through 0.20 μm pore size cellulose membranes before inoculation. Controls were run with saline.

3. RESULTS AND DISCUSSION

3.1. Isolation and Structural Analysis of Compound 1. The phenolic extract obtained from hydrothermally treated alperujo was characterized as containing different phenolic compounds and various elenolic acid derivatives.[6] In a previous work,[6] these derivatives were called compounds A, B, and C, with derivative A present in the highest proportions and one of the most abundant constituents in ethyl acetate extract after hydroxytyrosol. This compound was purified by HPLC using a C_{18} semi-preparative column (as described in the Materials and Methods). HPLC–DAD analysis revealed the presence of a pure compound at 11 min with an ultraviolet (UV) absorption maximum at 230 nm (Figure 1).

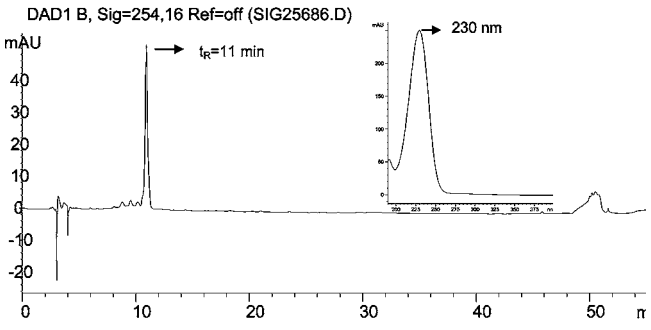

Figure 1. HPLC chromatogram and UV spectrum of compound **1**.

The structure of the compound was elucidated using one-dimensional (1D) ^{1}H and ^{13}C NMR experiments (panels A and B of Figure 2). Structural analysis was completed by using DEPT-45 (see Figure S1 of the Supporting Information) and homonuclear and heteronuclear 2D NMR techniques, such as COSY (see Figure S2 of the Supporting Information), HSQC (see Figure S3 of the Supporting Information), and NOESY and HMBC experiments (panels A and B of Figure 3, respectively). In addition, IR analysis and MS (low-resolution and HR-CI) were also used.

The ^{1}H NMR data showed a doublet at δ 9.28 ppm (J = 2.0 Hz), corresponding to an aldehyde group (H-1′) coupled with H-3 (^4J) of a glutaric acid moiety, as deduced from the COSY experiment. It is remarkable that the aldehyde proton of 2-alkylalk-2-enals, with either *E* or *Z* configuration, do not show any H,H coupling.[17] Furthermore, a quartet at δ 6.79 ppm (J = 7.0 Hz) indicated the presence of an olefinic proton (H-3′) coupled (^3J) to a methyl (H-4′) at δ 2.08 ppm; these data suggest that the compound contains a crotonaldehyde moiety substituted at the α carbon. The ^{1}H NMR spectrum also showed two symmetrical pairs of geminal protons as a doublet of doublets at δ 2.61 ppm (H-2a and H-4a) and δ 2.68 ppm (H-2b and H-4b) (2H each, $^2J_{2a,2b}$ = 15.5 Hz) and a multiplet at δ 3.59 ppm (1H) for protons of the CH_2CHCH_2 fragment, as confirmed by a COSY spectrum (see Figure S2 on the Supporting Information). Furthermore, the HSQC experiment allowed for complete assignments of the carbon signals in the spectrum corresponding to a symmetrical glutaric acid derivative, C-2/C-4 and C-3, for signals at 38.4 and 31.9 ppm, respectively, whereas the crotonaldehyde moiety had carbon signals at 197.0, 155.9, and 15.4 ppm for C-1′, C-3′, and C-4′, respectively (Figure 2). The signals observed at 176.3 and 145.3 ppm in ^{13}C NMR corresponded with the carboxylic carbons (C-1 and C-5) and a quaternary olefinic carbon (C-2′), respectively; this information was corroborated by DEPT-45 experiment, in which quaternary carbon atoms do not appear (see Figure S1 on the Supporting Information).

E configuration of the C=C double bond of compound **1** and the *s-trans* conformation for the C-1′–C-2′ bond were confirmed by a 2D NOESY experiment (Figure 3A), where the off-diagonal cross-peaks, H-1′/H-3′ and H-3/H-4′, indicate through-space interaction, therefore suggesting close proximity of the involved hydrogen atoms (Figure 4A). The planar W pathway between formyl and H-3 protons, depicted in Figure 4A, also explains the long-range coupling (^4J = 2.0 Hz) observed in the ^{1}H NMR spectrum, and it is in agreement with a planar conformation of the crotonaldehyde moiety included in the plane of the C-3–H-3 bond of glutaric acid. No nuclear Overhauser effect (NOE) interactions were observed between H-2/H-4 and crotonadehyde protons, also in agreement with the suggested conformation for compound **1**.

The centrality of C3 was confirmed by the HMBC spectrum (Figure 3B), because it showed correlations between C-3 of glutaric acid with protons H-1′ and H-3′ of the crotonaldehyde moiety and strong correlation with H-2 and H-4 of glutaric acid. Three bond couplings were also observed between aldehydic carbon (C-1′) and both H-3′ of the crotonaldehyde moiety and H-3 of glutaric acid. Furthermore, the carboxylic carbons (C-1) were strongly coupled to H-2/H-4 and weakly coupled to H-3.

Next, we analyzed the CI-MS and IR spectra (see Figures S4 and S5 of the Supporting Information, respectively) to complete the structural deductions for the isolated compound. The pseudo-molecular ion $[M + H]^+$ obtained by HR-CI-MS was in accordance with the assigned molecular formula $C_9H_{13}O_5$ (m/z 201). Additionally, the fragment obtained for the loss of two water molecules successively, $[M + H - H_2O]^+$ and $[M + H - 2H_2O]^+$ with m/z 183 and 165, respectively, was identified. The IR spectrum of the compound revealed an absorption band at 3300–2400 cm^{-1} (vbr), which was attributed to the O–H stretch of hydrogen-bonded carboxylic acids and a band at 930 cm^{-1} associated with the O–H bend. Absorption bands at 2727 and 1684 cm^{-1} can be attributed to

DOI: 10.1021/jf5057716
J. Agric. Food Chem. 2015, 63, 1151–1159

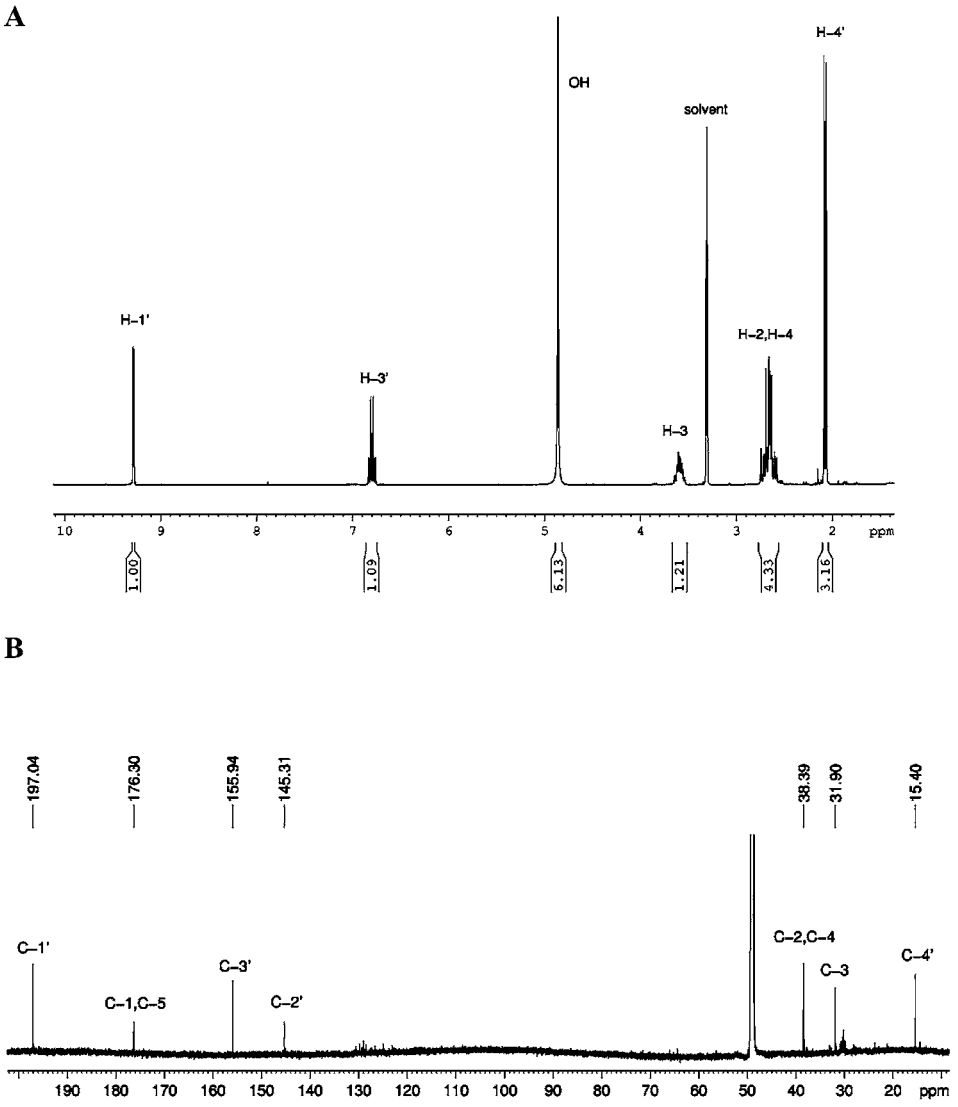

Figure 2. (A) ^{1}H spectrum at 300.1 MHz and (B) ^{13}C NMR spectra at 176.1 MHz, for compound **1** in MeOH-d_4. The signals at 4.85 and 3.31 ppm in panel A and at 49.0 ppm in panel B correspond to the solvent.

C−H(O) and C═O of the conjugated aldehydic group, respectively. Finally, a signal at 1440 cm^{-1} was associated with the asymmetric bending vibrations of the methyl group.

Taking into account the structural descriptions as detailed above, the compound was identified as (*E*)-3-(1-oxobut-2-en-2-yl)glutaric acid (**1**). A similar compound has been described by Gil et al.[18] from olive oil residue, although, in this case, the compound was isolated in its methylated form in the previous treatment of the extract with diazomethane and characterized as its dimethyl ester derivative. Also, Fotinos et al.[19] claimed to have isolated the same compound from oil-press waste of a Greek olive crop variety, the Koroneiki olives, although, in this case, no structural chemical data were reported.

The configuration of this compound was reported to be *Z* (Figure 4B) by the Chemical Abstracts Service (CAS registry number 220007-88-5), the opposite to the configuration described herein, as noted above. Curiously enough, Gil et al.[18] and Fotinos et al.[19] named their isolated compound as the *E* estereoisomer, although they both formulated the compound as *Z*.

3.2. Assay of Extraction. The molecule identified in this paper was obtained and quantified from the ethyl acetate extract, resulting from the hydrothermal treatment of olive oil waste in a previous work.[6] To identify the origin of this molecule, four solid−liquid extractions were realized for fresh alperujo from an olive mill plant. The first was realized with water at room temperature; the second was realized with methanol/water (80:20), followed by methanol elimination; and the other two extractions were performed using a hydrothermal treatment. Subsequent extractions with ethyl acetate were realized in cold and hot conditions for the four aqueous fractions obtained.

The amount of compound **1** measured in the four initial aqueous samples from alperujo and in each of the eight organic fractions is shown in Table 1. To our surprise, the data show that, in the aqueous initial samples obtained after solid−liquid extraction, prior to extraction with ethyl acetate, compound **1** was not detected. However, the compound was identified after extraction with ethyl acetate (in hot and cold), following extractions with H_2O, MeOH:H_2O (80:20), and hydrothermal treatment of 140 °C/60 min. Higher values were obtained in extractions with refluxing ethyl acetate in all cases. These data are in agreement with those obtained by Gil et al.[18] and Fotinos et al.,[19] who, in both cases, isolated their glutaric acid derivative

DOI: 10.1021/jf5057716
J. Agric. Food Chem. 2015, 63, 1151−1159

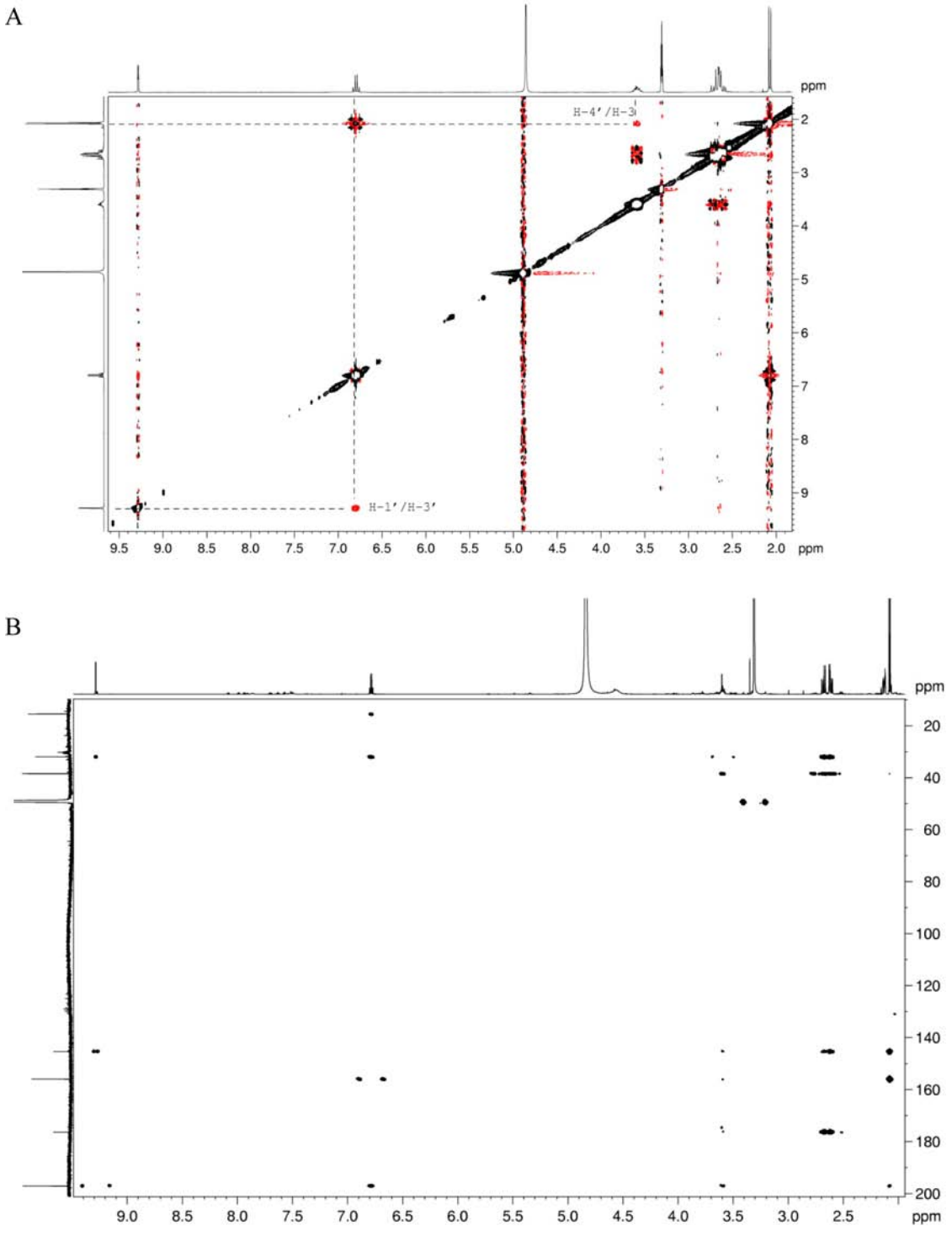

Figure 3. (A) NOESY spectrum for compound **1** in MeOH-d_4 recorded at 300 MHz and (B) HMBC spectrum for compound **1** in MeOH-d_4 recorded at 700 MHz.

from olive products after extraction with ethyl acetate. The fact that, before the extraction with ethyl acetate, compound **1** was not identified and, after extraction, is identified in high concentrations makes us think that the compound **1** is formed during the extraction process, favoring its formation when the process is performed at a temperature of 77 °C. However, in samples of the wastewater from stored alperujo (not ethyl acetate extracted) from a pomace processing mill, a compound named decarboxymethyl elenolic acid (EDA)-like derivative, with a maximum absorbance at 230 nm and MS spectrum with a signal at m/z 199 in the negative mode, was identified,[10] which is present in significant amounts (0.9−1.6 g/kg of alperujo) and matches the compound that we have isolated and identified, although, in this case, after the extraction with ethyl acetate in higher amounts. Thus, these results suggest that the compound could be produced chemically by a hypothetical hydrolytic reaction during the storage and/or processing of the alperujo, in similar conditions that occur when dealing with

DOI: 10.1021/jf5057716
J. Agric. Food Chem. 2015, 63, 1151−1159

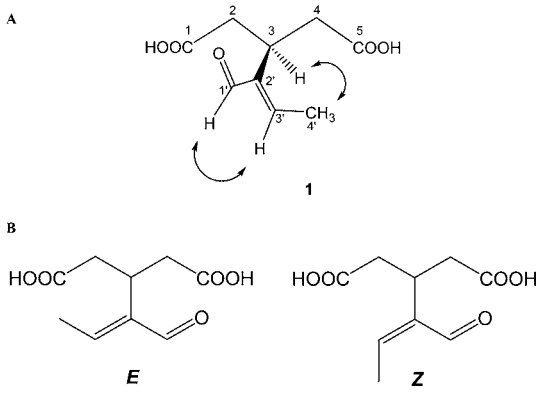

Figure 4. (A) Significant NOE correlations for (*E*)-3-(1-oxobut-2-en-2-yl)glutaric acid (**1**) observed in MeOH-d_4 and (B) possible *E* and *Z* configurations for the cronotonadehyde moiety of compound **1**.

fresh alperujo and ethyl acetate extraction, as described herein. In both cases, the compound likely originates from elenolic acid, the terpenoid skeleton of oleuropein (or ligstroside). Three alternative routes (Figure 5) can be devised for the formation of compound **1** from elenolic acid (**3**), involving ester hydrolysis of compounds **3** or **6**, decarboxylation of β-ketoacid (**4**) or malonic acid derivative (**7**), and oxidation of the formyl group of compounds **3**, **4**, or **5**. Significatively, glutaraldehyde (**5**) is the only intermediate that has been previously described, for example, in stored alperujo[10] and in extra virgin olive oil.[20] Therefore, the pathway through compounds **4** and **5** is the most likely. Nevertheless, two compounds named as "oxidized 3,4-DHPEA-EDA" (oxidized dialdehydic form of decarboxymethyl elenolic acid linked to hydroxytyrosol) with *m*/*z* 335 and 393 (by MS in negative mode) have been recently detected among oxidation products in stored virgin olive oil,[21] which might, in fact, be hydroxytyrosyl esters of compounds **1** and **6**, respectively. These authors have also detected peaks with *m*/*z* 183 and 199, which match with compounds **5** and **1**, respectively.[21]

Table 1 also shows that the highest yield of the compound is obtained by extraction with MeOH:H_2O (80:20), followed by extraction with water, with the yield decreasing with the increasing severity of the solid−liquid extraction process, such that the molecule was not identified in the process of 170 °C/1 h. These results are consistent with the results previously obtained,[6] in which the concentration of the compound herein described as compound **1** decreases at 160 °C with increasing treatment time.

A logical explanation for the absence of compound **1** in aqueous extractions of fresh alperujo and the detection of important amounts of it after extraction with ethyl acetate might be that one or several enzymatic processes (methyl ester hydrolysis, oxidation, or decarboxylation) take place in a faster fashion in ethyl acetate than in aqueous media. Enzymatic oxidation of virgin olive oil (VOO) secoiridoids by enzymes, such as polyphenol oxidase (PPO) and peroxidase (PPP), activated during the oil mechanical extraction process, has been previously described.[22] Furthermore, no detection of compound **1** after the thermal treatment under harsh conditions (170 °C/60 min) might be related to enzyme denaturalization. These results showed that the formation of compound **1** can take place over long storage processes or be accelerated by the extraction with ethyl acetate. In future studies, we will address the origin of compound **1** and will study whether the activity of PPO and PPP is improved in ethyl acetate.

3.3. Antimicrobial Activity. The phenolic ethyl acetate extract obtained from hydrothermally treated alperujo (160 °C/60 min) was fractionated using Amberlite XAD16. This method led to the isolation of two fractions (fractions 1 and 2) that contain the glutaric acid derivative (**1**), together with other phenolic compounds in different ratios (Table 2). Antimicrobial activity against *P. syringae* and *A. tumefaciens* of fractions 1 and 2 and the purified compound were screened. In this work, the antimicrobial ability was determined after only 5 min of contact,[10] because such a bactericidal effect would be of more interest for the application of active compounds for field trials on plants than other methods. The method evaluates the antimicrobial activity considering that the application is performed on the plant and there may be external agents (rain and/or wind) that delimit the most prolonged time of contact. This method is employed by numerous authors to evaluate the antimicrobial activity of different compounds in plants.[10,23]

The bactericidal effect of fraction 1 (Figure 6A) was assessed at concentrations of 50 mg/mL for *P. syringae*, reducing the initial population by 4 log CFU/mL (10 000-fold), and for *A. tumefaciens*, reduced by only 2 log units (100-fold). Fraction 2 (Figure 6B) had the same bactericidal effect on *P. syringae* as fraction 1 at 50 mg/mL; however, 75 mg/mL of this fraction was required to elicit a bactericidal effect against *A. tumefaciens*. The purified glutaric derivative, (*E*)-3-(1-oxobut-2-en-2-yl)-glutaric acid, dramatically decreased the *P. syringae* population by more than 4 log units at the concentration of 18 mg/mL; however, no bactericidal effect was observed at the same concentration for *A. tumefaciens* (Figure 6C).

The concentrations of phenolic compounds in the fractions 1 and 2 are shown in Table 2. After observation of the results obtained for fraction 1, the bactericidal effect on *P. syringae* at 50 mg/mL could be attributed to its high glutaric derivative content (38.9%), corresponding to 19 mg/mL, a concentration that coincides with 18 mg/mL of the purified compound that showed a strong bactericidal effect. Nevertheless, fraction 1 also contained other known antimicrobial compounds, such as hydroxytyrosol (33.7%), representing 16.8 mg/mL of 50 mg/

Table 1. Amount of Compounds Measured in the Initial Aqueous or Hydromethanolic Samples and in Each of the Organic Fractions Isolated after Extraction with Hot and Cold Ethyl Acetate

	initial aqueous or hydromethanolic samples (g of compound/kg of fresh alperujo)	hot extraction (g of compound/kg of fresh alperujo)	cold extraction (g of compound/kg of fresh alperujo)
H_2O	nd[a]	2.85 ± 0.05	1.77 ± 0.05
80:20 MeOH/H_2O	nd	4.06 ± 0.25	2.36 ± 0.18
140 °C/60 min[b]	nd	1.30 ± 0.07	0.82 ± 0.19
170 °C/60 min[b]	nd	nd	nd

[a]nd = not detected. [b]Hydrothermal treatment.

DOI: 10.1021/jf5057716
J. Agric. Food Chem. 2015, 63, 1151−1159

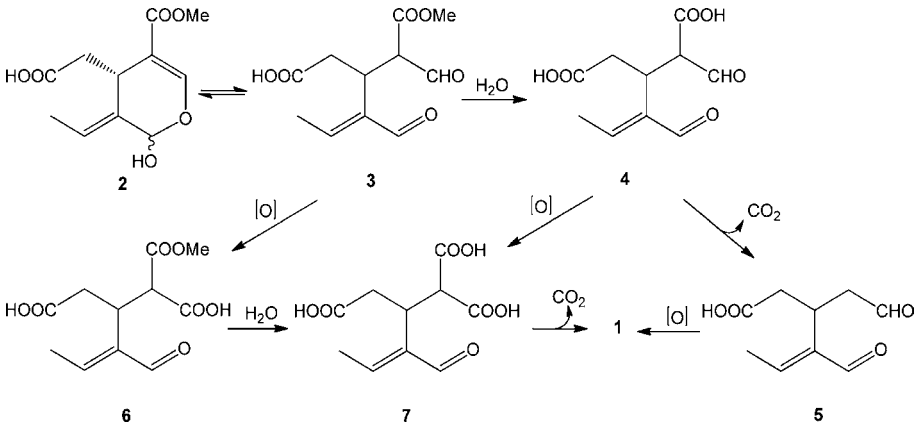

Figure 5. Alternative routes for the formation of the glutaric acid derivative (**1**) from elenolic acids (**2** and **3**) in which demethylation, decarboxylation, and oxidation steps are involved.

Table 2. Phenolic Composition of Fractions 1 and 2 Obtained after the Fractionation of Hydrothermally Treated Alperujo Using Amberlite XAD16

	fraction 1 (g of compound/100 g of dry weight)	fraction 2 (g of compound/100 g of dry weight)
3,4-dihydroxyphenylglycol	0.25 ± 0.02	nd[a]
hydroxymethylfurfural	0.97 ± 0.06	nd
hydroxytyrosol	33.68 ± 0.77	4.53 ± 0.01
protocatechuic acid	0.83 ± 0.02	0.59 ± 0.06
(*E*)-3-(1-oxobut-2-en-2-yl)glutaric acid	38.90 ± 0.57	8.13 ± 0.47
catechol	0.43 ± 0.05	1.25 ± 0.04
tyrosol	2.81 ± 0.03	4.46 ± 0.14
p-hydroxybenzoic acid	nd	0.59 ± 0.01
3,4-dihydroxyhidrocinamic acid	0.45 ± 0.01	1.24 ± 0.04
vanillic acid	nd	0.71 ± 0.01
4-methylcatechol	1.39 ± 0.02	9.85 ± 0.08
oleuropein	0.02 ± 0.01	7.67 ± 0.15
hydroxytyrosyl acetate	nd	4.77 ± 0.05

[a]nd = not detected.

mL that provoked inhibition of microbial growth. We determined that the hydroxytyrosol concentration required to cause an antimicrobial effect on *P. syringae* and *A. tumefaciens* was less than 16.8 mg/mL (data not shown). The effect of purified hydroxytyrosol from aqueous alperujo solution was higher than in the presence of the other substances comprising fraction 1, which would suggest an antagonistic interaction.

Fraction 2 exerted bactericidal activity against *P. syringae* at a concentration of 50 mg/mL, containing 8% of glutaric acid derivative (4 mg/mL) and 4.5% of hydroxytyrosol (2.2 mg/mL), while 75 mg/mL of this fraction were needed to act on *A. tumefaciens*, representing 6 mg/mL of glutaric acid derivatives and 3.3 mg/mL of hydroxytyrosol. In this case, the bactericidal effect of fraction 2 can be explained by the concentration of only hydroxytyrosol, because the effect of purified hydroxytyrosol was detected at a similar concentration (data not shown). However, it could also be explained by the combined effects of hydroxytyrosol, oleuropein, and 4-methylcathecol, with the last compound being the most toxic.[24]

These preliminary studies of antimicrobial activity of compound **1** show that the isolated compound has good antimicrobial activity when compared to hydroxytyrosol. Hydroxytyrosol is a polyphenol found in high concentrations in the alperujo, which present an important antimicrobial activity; its activity has been studied against many bacterial and fungi; and many studies have been realized evaluating this compound.[23,25] Particularly, hydroxytyrosol at 1 mg/mL has bactericidal effect for the two microorganisms evaluated in this paper.[25] Therefore, this first screening opens a new way to study the bactericidal effect of this compound on other pathogens for plants and humans. Furthermore, compound **1** could be used as not only an antimicrobial agent but also a key source of a lactone with significant cytoprotective properties against DNA damage induced by oxidative stress.[19]

Generals Comments. In the present investigation, chemical studies of a phenolic extract obtained from aqueous, methanolic aqueous, or hydrothermically treated fresh alperujo led to the isolation and identification of an elenolic acid derivative, (*E*)-3-(1-oxobut-2-en-2-yl)glutaric acid (**1**). To the best of our knowledge, this is the first time that the structure has been well-established with the spectroscopy data shown. The *s-trans* conformation for the Cα−CHO bond is in agreement with the NOESY experiment. The compound was quantified in large amounts, and synthetic routes to explain its formation involving ester hydrolysis, decarboxylation, and oxidation have been suggested. The role of ethyl acetate as an extracting solvent seems to be key in the process. From a practical point of view, (*E*)-3-(1-oxobut-2-en-2-yl)glutaric acid could be used as an important source of a lactone with significant cytoprotective properties[19] and as an antimicrobial agent against bacteria responsible for plant diseases.

DOI: 10.1021/jf5057716
J. Agric. Food Chem. 2015, 63, 1151−1159

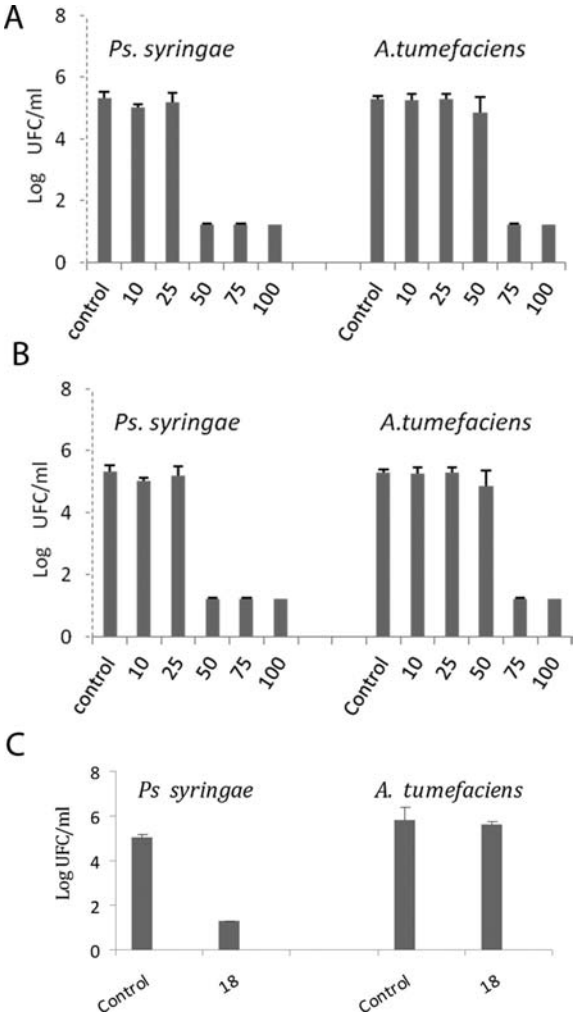

Figure 6. Bactericidal activity of phenolic fraction 1 (A), fraction 2 (B) and isolated (*E*)-3-(1-oxobut-2-en-2-yl)glutaric acid (C) at mg/mL, against *P. syringae* CECT 4429T and *A. tumefaciens* CECT 4119T. Bars indicate the standard deviation of duplicates. Lines indicate the detection limit.

■ ASSOCIATED CONTENT

Supporting Information

DEPT-45 experiment for compound **1** (Figure S1), COSY bidimensional spectrum analysis for compound **1** (Figure S2), HSQC bidimensional spectrum analysis for compound **1** (Figure S3), spectrum of HR-CIMS for compound **1** (Figure S4), and IR spectra for compound **1** (Figure S5). This material is available free of charge via the Internet at http://pubs.acs.org.

■ AUTHOR INFORMATION

Corresponding Author

*Telephone: 34-954691054. Fax: 34-954691262. E-mail: jfbg@cica.es.

Funding

Funding was received from the Spanish Ministry of Economy and Competitiveness and co-funded by the European Social Fund (ESF) (Project AGL2013-48291-R). Guillermo Rodríguez-Gutiérrez (Contract RYC-2012-10456) thanks the "Ramón y Cajal" program, and Fátima Rubio-Senent (JAE-Pre104) thanks the Spanish National Research Council (CSIC) program, for providing financial support, both co-funded by the ESF.

Notes

The authors declare no competing financial interest.

■ REFERENCES

(1) Aragón, J. M.; Palancar, M. C. Present and future of alpeorujo. *Improlive 2000*; Editorial Complutense, S. A.: Madrid, Spain, 2001; pp 242−300.

(2) Lesage-Meessen, L.; Navarro, D.; Maunier, S.; Sigoillot, J.-C.; Lorquin, J.; Delattre, M.; Simon, J.-L.; Asther, M.; Labat, M. Simple phenolic content in olive oil residues as a function of extraction systems. *Food Chem.* **2001**, *75*, 501−507.

(3) López-Miranda, J. Olive oil and health: Summary of the II international conference on olive oil and health consensus report. Jaén and Córdoba (Spain). *Nutr., Metab. Cardiovasc. Dis.* **2010**, *20*, 284−294.

(4) Ghanbari, R.; Anwar, F.; Alkharfy, K. M.; Gilani, A.-H.; Saari, N. Valuable nutrients and functional bioactives in different parts of olive (*Olea europaea* L.)—A review. *Int. J. Mol. Sci.* **2012**, *13*, 3291−3340.

(5) Fernández-Bolaños, J.; Rodríguez-Gutiérrez, G.; Lama-Muñoz, A.; Sánchez, P. Dispositivo y procedimiento para el tratamiento de los subproductos de la obtención del aceite de oliva. ES Patent 2,374,675, 2010.

(6) Rubio-Senent, F.; Rodríguez-Gutiérrez, G.; Lama-Muñoz, A.; Fernández-Bolaños, J. New phenolic compounds hydrothermally extracted from the olive oil byproduct alperujo and their antioxidative activities. *J. Agric. Food Chem.* **2012**, *60*, 1175−1186.

(7) Rubio-Senent, F.; Rodríguez-Gutiérrez, G.; Lama-Muñoz, A.; Fernández-Bolaños, J. Phenolic extract obtained from steam-treated olive oil waste: Characterization and antioxidant activity. *LWT—Food Sci. Technol.* **2013**, *54*, 114−124.

(8) Rubio-Senent, F.; Rodríguez-Gutiérrez, G.; Lama-Muñoz, A.; Fernández-Bolaños, J. Chemical characterization and properties of a polymeric phenolic fraction obtained from olive oil waste. *Food Res. Int.* **2013**, *54*, 2122−2129.

(9) Capasso, R.; Evidente, A.; Schivo, L.; Orru, G.; Marcialis, M. A.; Cristinzo, G. Antibacterial polyphenols from olive oil mill waste waters. *J. Appl. Bacteriol.* **1995**, *79*, 393−398.

(10) Medina, E.; Romero, C.; de los Santos, B.; de Castro, A.; García, A.; Romero, F.; Brenes, M. Antimicrobial activity of olive solutions from stored alperorujo against plant pathogenic microorganisms. *J. Agric. Food Chem.* **2011**, *59*, 6927−6932.

(11) Zampa, A.; Silvi, S.; Servili, M.; Montedoro, G. F.; Orpianese, C.; Cresci, A. In vitro modulatory effects of colonia microflora by olive oil iridoids. *Microb. Ecol. Health Dis.* **2006**, *18*, 147−1532.

(12) Medina, E.; de Castro, A.; Romero, C.; Brenes, M. Comparison of concentration of phenolic compounds in olive oils and other plant oils: correlation with antimicrobial activity. *J. Agric. Food Chem.* **2006**, *54*, 4954−4961.

(13) Fernández-Bolaños Guzmán, J.; Heredia Moreno, A.; Rodríguez Gutiérrez, G.; Rodríguez Arcos, R.; Jiménez Araujo, A.; Guillén Bejarano, R. Method for obtaining purified hydroxytyrosol from products and by-products derived from the olive tree. U.S. Patent 6,849,770 B2, 2005.

(14) Fernández-Bolaños, J.; Rodríguez-Gutiérrez, G.; Lama-Muñoz, A.; Rubio-Senent, F.; Fernández-Bolaños, J. M.; Maya Castilla, I.; López-López, O. Procedimientos para la extracción de extracto de hidroxitirosol, extracto mezcla de hidroxitirosol y 3,4-dihidroxifenilglicol, y extracto de acetato de hidroxitirosol a partir de subproductos del olivo y su purificación. WO Patent 2013/007850 A1, 2011.

(15) Obied, H. K.; Bedgood, D. R., Jr.; Prenzler, P. D.; Robards, K. Chemical screening of olive biophenol extracts by hyphenated liquid chromatography. *Anal. Chim. Acta* **2007**, *603*, 176−189.

(16) National Committee for Clinical Laboratory Standards (NCCLS). *Methods for Determining Bactericidal Activity of Antimicrobial Agents. Approved Guideline M26-A*; NCCLS: Wayne, PA., 1999.

(17) Robert, F.; Héritier, J.; Quiquerez, J.; Simian, H.; Blank, I. Synthesis and sensorial properties of 2-alkylalk-2-enals and 3-(acetylthio)-2-alkyl alkanals. *J. Agric. Food Chem.* **2004**, *52*, 3525−3529.

DOI: 10.1021/jf5057716
J. Agric. Food Chem. 2015, 63, 1151−1159

(18) Gil, M.; Haïdour, A.; Ramos, J. L. Two glutaric acid derivatives from olives. *Phytochemistry* **1998**, *49*, 1311−1315.
(19) Fortinos, S.; Panaitescu, L.; Skaltsounis, A.-L.; Mitakou, S.; Magiatis, P.; Aligiannis, N.; Galaris, D. Compounds and compositions derived from olives and methods of use thereof. U.S. Patent 2003/0185921, 2003.
(20) Pérez-Trujillo, M.; Gómez-Caravaca, A. M.; Segura-Carretero, A.; Fernández-Gutiérrez, A.; Parella, T. Separation and identification of phenolic compounds of extra virgin olive oil from *Olea europaea* L. by HPLC−DAD−SPE−NMR/MS. Identification of a new diastereoisomer of the aldehydic form of oleuropein aglycone. *J. Agric. Food Chem.* **2010**, *58*, 9129−9136.
(21) Di Maio, I.; Esposto, S.; Taticchi, A.; Selvaggini, R.; Veneziani, G.; Urbani, S.; Servili, M. Characterization of 3,4-DHPEA−EDA oxidation products in virgin olive oil by high performance liquid chromatography coupled with mass spectrometry. *Food Chem.* **2013**, *138*, 1381−1391.
(22) Servili, M.; Taticchi, A.; Esposto, S.; Urbani, S.; Selvaggini, R.; Montedoro, G. F. Effect of olive stoning on the volatile and phenolic composition of virgin olive oil. *J. Agric. Food Chem.* **2007**, *55*, 7028−7035.
(23) Brenes, M.; García, A.; de los Santos, B.; Medina, E.; Romero, C.; de Castro, A.; Romero, F. Olive glutaraldehyde-like compounds against plant pathogenic bacteria and fungi. *Food Chem.* **2011**, *125*, 1262−1266.
(24) Capasso, R.; Evidente, A.; Schivo, L.; Orru, G.; Marcialis, M.; Cristinzo, G. Antibacterial polyphenols from olive oil mill waste water. *J. Appl. Bacteriol.* **1995**, *79*, 393−398.
(25) Medina, E.; Brenes, M.; Romero, C.; García, A.; de Castro, A. Main antimicrobial compounds in table olives. *J. Agric. Food Chem.* **2007**, *55*, 9817−9823.

DOI: 10.1021/jf5057716
J. Agric. Food Chem. 2015, 63, 1151−1159

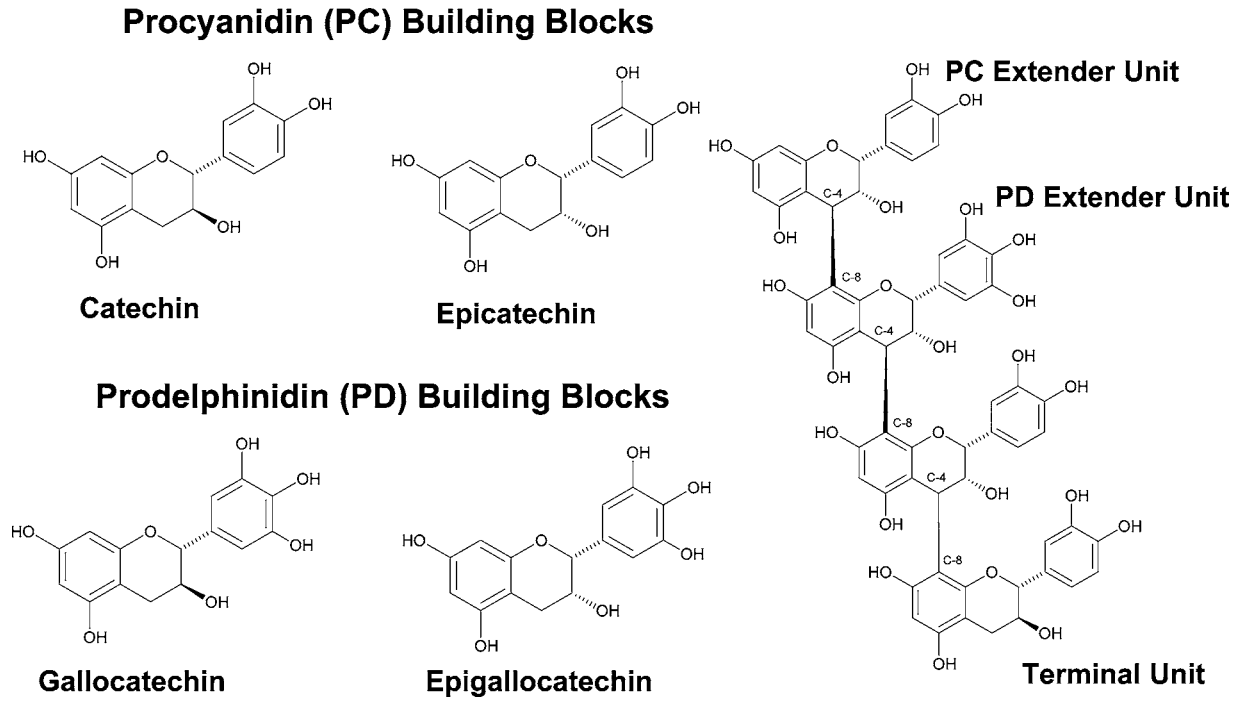

Figure 1. Structures of major flavanol subunits that occur in condensed tannins (left). A condensed tannin tetramer (right) shows a terminal unit with different extender units connected by C4−C8 (B-type) linkages.

tetramer series and beyond. Additional studies leading to the same conclusion include inhibition of methane production parallel with molecular weight increases of CT fractions from *Leucaena* in in vitro rumen fermentation studies[30] and binding to bovine serum albumin (BSA),[31] although in these cases molecular weight did not appear to be the sole factor in determining protein binding affinity.[31,32] To add to the confusion, mixed results of CT size versus protein precipitation capability were seen even across *Leucaena* genotypes.[33] Others have reported conflicting results for protein precipitation. For example, Naumann et al.[34] reported that mDP was not a factor in methane production from in vitro fermentation studies or in protein precipitation studies.[35] Thus, it is clear that the question of the correlation of CT mDP on the formation of CT−protein complexes and precipitates and their ramifications on biological activities remains unresolved.

Progress in this area has been hampered by the difficulty in obtaining sufficient quantities of highly pure and well-characterized CT fractions. Researchers are now starting to perform the necessary purification and characterization of isolated CTs to aid in the unraveling of the intricacies of CT−protein interactions. Noteworthy in this regard is a recent report by Harbertson et al.,[36] which utilized HPLC-purified cocoa CT, consisting entirely of epicatechin (PC) subunits, into singular DP fractions of trimer to octamer oligomers. These authors reported that each individual CT fraction exhibited a linear response in the precipitation of BSA with increasing CT concentration and protein precipitation increased with DP of the CT fractions. In addition, mixtures of the trimer with pentamer through octamer oligomers generally showed an additive effect on precipitation of BSA from solution. However, the authors noted that, in some cases, a synergistic effect was observed for precipitation of BSA when a nonprecipitating level of trimer was added.

Whereas HPLC purification can provide pure CTs or mixtures of CTs sharing the same degree of polymerization up to DP 9,[36−38] and provides insightful information on structure−activity relationships of CT−protein precipitation, the purification process is costly, labor intensive, and quantity limiting. These limitations hamper scale-up preparation of CTs for executing important, next-level in vitro studies, such as rumen and ensiling protein degradation studies and the investigation of ammonia and methane abatement by CTs. Larger quantities of CT are required to execute these studies. At this time and at the current level of purification technology, these limitations force the use of CT mixtures isolated from plant sources containing a range of DP in each fraction to perform these in vitro studies.

When larger quantities of CT fractions have been obtained, the purities of the CT fractions were generally not determined and impurity profiles are often not known. The fact that other plant components can interfere with CT−protein complex formation, especially carbohydrates,[4] incorporates a realm of uncertainty in studies using fractions of unknown purities and may have led to confounding results. McNabb et al.[24] pointed this out, noting that their preparations should be referred to as simply "CT extracts" due to the lack of any purity assessment and their unknown impurity profile. Thus, alternative purification protocols for producing sufficient quantities of well-characterized CTs of high purity are essential for laboratory and in vitro experimentation to obtain unambiguous results.

We have initiated a program directed toward the isolation of highly pure and well-characterized CT fractions with the goal of utilizing information gained in laboratory and in vitro investigations to further our understanding of CT−protein interactions. Here we describe the protein precipitation profiles of two paired sets of purified CT fractions of similar composition against three different protein types. The CT fractions isolated from *Lotus pedunculatus* (big trefoil) leaves and *Trifolium repens* (white clover) flowers possess similar compositions (PC/PD and *cis*/*trans* ratios) but differ 2-fold in

DOI: 10.1021/jf504715p
J. Agric. Food Chem. 2015, 63, 1160−1168

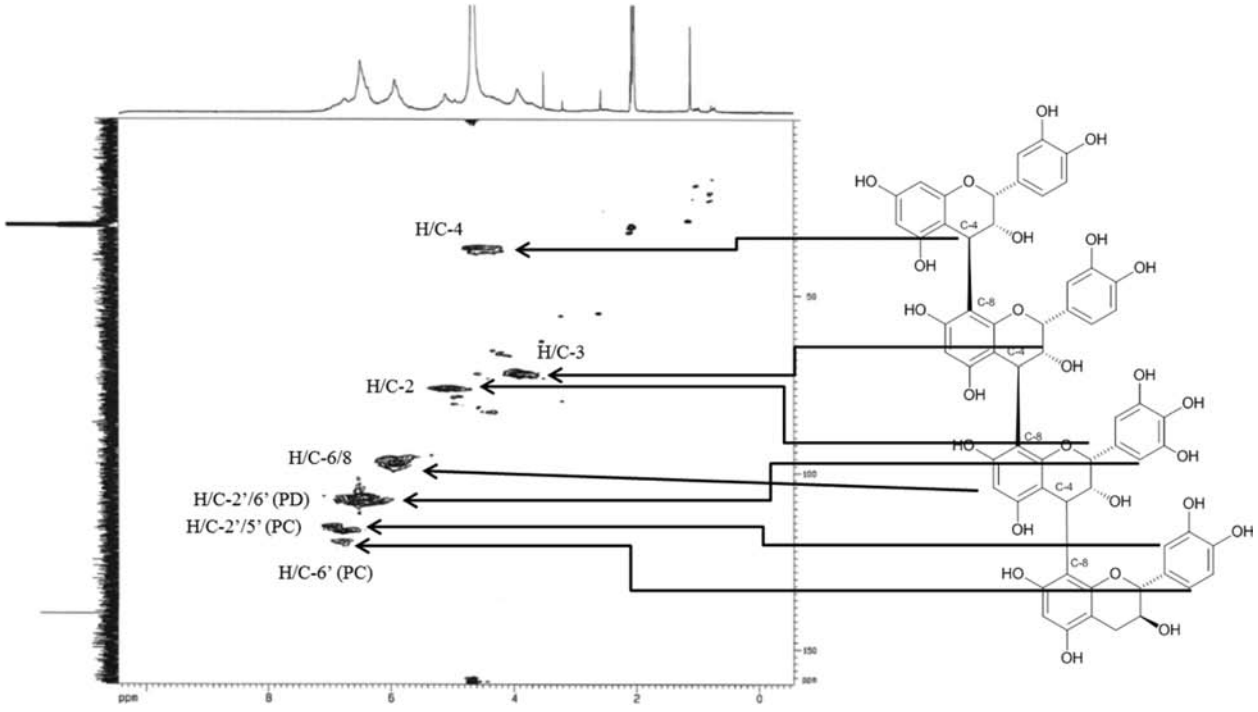

Figure 2. Signal assignments for the $^{1}H-^{13}C$ HSQC NMR spectrum (360/90 MHz, D_2O/acetone-d_6, 4:1) of a large-sized condensed tannin fraction purified from big trefoil (BT-Large). The purity of the fraction was 91.3% by thiolysis.

their mean degrees of polymerization (mDP ~9 versus mDP ~ 18). We selected two commercially available proteins with different p*I* values, BSA and lysozyme (LYS), as test proteins. To provide protein material relevant to ruminant animal production systems, we selected alfalfa leaf protein extract (ALF), the main protein of which is Rubisco.[39]

MATERIALS AND METHODS

Reagents. Lysozyme and bovine serum albumin were purchased from Sigma (St. Louis, MO, USA) and the Pierce 660 nm Protein Assay Reagent from Thermo Scientific (Rockford, IL, USA). Sephadex LH-20 and G-25 were purchased from GE Healthcare Biosciences (Piscataway, NJ, USA).

Plant Materials. In 2013, flowers from naturalized populations of white clover were harvested from lawns in Viroqua, WI, USA, and in Reading, UK, frozen at −20 °C, and subsequently freeze-dried, ground in a cyclone mill (1 mm screen), and stored frozen until used. In 2009, herbage of 45-day-old summer regrowth of big trefoil was harvested from established stands near Prairie du Sac, WI, USA, and frozen at −20 °C. After freeze-drying, herbage was shaken to recover leaves, which were ground with a cyclone mill (0.5 mm screen) and stored frozen until used.

General Procedure for Purification and Analysis of Condensed Tannins. The isolation and purification of condensed tannin fractions BT-Medium and WC-Medium were accomplished by using the previously published procedures.[40,41] Briefly, the ground plant material was extracted with acetone/water (7:3) three times and filtered. The combined filtrates were concentrated on a rotary evaporator (<40 °C) and extracted with dichloromethane to remove nonpolar components, and the resulting aqueous solution was freeze-dried. The freeze-dried extracts were dissolved in water and applied to a Sephadex LH-20 column, and the column was rinsed with water to remove carbohydrates. Then CTs were eluted with acetone/water (3:7, v/v; fraction 1) and acetone/water (1:1; fraction 2), with fraction 2 providing CTs of high purity for the BT-Medium and WC-Medium preparations, from ground big trefoil leaves and white clover flowers, respectively, used in this study. For the isolation of CT fractions BT-Large and WC-Large, the freeze-dried acetone/water (7:3) extracts were obtained in a similar manner, but a different elution scheme was used. This scheme consisted of adsorbing the 7:3 acetone/water extraction residue onto Sephadex LH-20 in methanol/water (1:1) and then eluting the resin with the following series of solvents, first with methanol/water (1:1) and then with a series of acetone/water mixtures (1:1, 7:3, 9:1). As a representative example, details of the purification of CT from big trefoil leaves (BT-Large) are given here. Dried and ground big trefoil leaves (70.2 g) were transferred to a 1 L Erlenmeyer flask, equipped with a large magnetic stir bar. The mixture was rapidly stirred with 7:3 (v/v) acetone/water for 30 min (3 × 700 mL) and filtered through a Buchner funnel. Combined extracts were concentrated on a rotary evaporator at 35 °C to remove acetone and then washed with dichloromethane (2 × 500 mL). Traces of dichloromethane were removed by rotary evaporation, and the material was freeze-dried to yield 19.2 g of solids. The solids were transferred to an 800 mL beaker and dissolved in 1:1 methanol/water (200 mL), and then Sephadex LH-20 (60 g) was added in small portions with stirring until a slurry was formed with the consistency of wet sand. The slurry was transferred to a 600 mL sintered-glass funnel equipped with a filter paper. The Sephadex LH-20 bed was sequentially suspended in the washing solvent, allowed to stand for 5−10 min, and vacuum filtered with the following series of solvents. Solvent washings were pooled into fractions as follows: fraction 1 (BTF1), with methanol/water (1:1; 4 × 250 mL); fraction 2 (BTF2), with methanol/water (1:1; 2 × 250 mL); fraction 3 (BTF3), with methanol/water (1:1; 2 × 250 mL); fraction 4 (BTF4), with acetone/water (1:1; 4 × 250 mL); fraction 5 (BTF5), with acetone/water (7:3; 4 × 250 mL); fraction 6 (BTF6), with acetone/water (9:1; 4 × 250 mL). After removal of volatile organics by rotary evaporation, small aliquots of all of the fractions were freeze-dried and subjected to ^{1}H NMR analysis. Fractions deemed reasonably pure from this analysis (little or no evidence of carbohydrate signals) were forwarded to $^{1}H-^{13}C$ HSQC NMR analysis. Inspection of the $^{1}H-^{13}C$ HSQC NMR spectra of each fraction allowed a qualitative assessment of purity based on the absence of significant non-CT cross-peak signals. On the basis of these evaluations, fraction BTF1 was discarded, fractions BTF2 and BTF3 were set aside pending further purification, and fractions BTF4, BTF5, and BTF6 were freeze-dried. Yields of solids from fractions BTF4, BTF5, and BTF6 were 1.51, 0.809, and

DOI: 10.1021/jf504715p
J. Agric. Food Chem. 2015, 63, 1160−1168

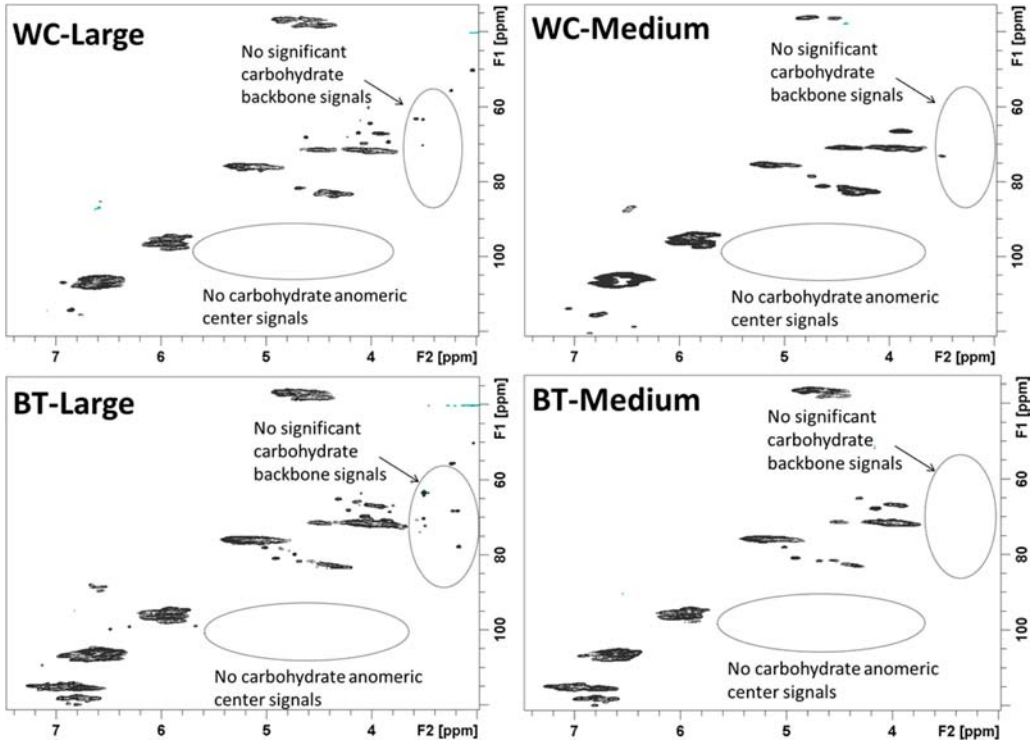

Figure 3. $^{1}H-^{13}C$ HSQC NMR spectra (500/125 MHz, DMSO-d_6/pyridine-d_5, 4:1) of large- and medium-sized condensed tannin fractions purified from white clover (WC) and big trefoil (BT).

0.020 g, respectively. Fractions BTF4 and BTF5 were forwarded to thiolysis[3,40] for purity and compositional analysis. Herewith, fraction BTF5 is referred to as BT-Large (Tables 1 and 2 and Figures 2–4).

NMR Spectroscopy. ^{1}H, ^{13}C, and $^{1}H-^{13}C$ HSQC NMR spectra used for screening of CT fractions were obtained on a Bruker Avance 360 instrument (Bruker Corp., Billerica, MA, USA) operating at 360 MHz (^{1}H) and 90 MHz (^{13}C). Spectra obtained were referenced to the center residual signals of acetone-d_6 contained within the 4:1 D_2O/acetone-d_6 mixture, at 2.04 and 29.8 ppm for ^{1}H and ^{13}C, respectively. Spectra were obtained using standard Bruker pulse programs (programs zg30, zgpg30, and invietgpsi for ^{1}H, ^{13}C, and $^{1}H-^{13}C$ HSQC NMR spectra, respectively). ^{1}H, ^{13}C, and $^{1}H-^{13}C$ HSQC NMR spectra for the CT fractions used in the precipitation studies were recorded at 27 °C on a BrukerBiospin DMX-500 (^{1}H 500.13 MHz, ^{13}C 125.76 MHz) instrument equipped with TopSpin 2.1 software and a cryogenically cooled 5 mm TXI $^{1}H/^{13}C/^{15}N$ gradient probe in inverse geometry. Spectra were recorded in DMSO-d_6/pyridine-d_5 (4:1) mixtures and were referenced to the residual signals of DMSO-d_6 (2.49 ppm for ^{1}H and 39.5 ppm for ^{13}C spectra). ^{13}C NMR spectra were obtained using 5K scans (acquisition time = 4 h and 30 min each). For $^{1}H-^{13}C$ HSQC experiments, spectra were obtained using 128 scans (acquisition time = 18 h and 30 min each) obtained using the standard Bruker pulse program (programs zg30, zgpg30, and hsqcegtpsi for ^{1}H, ^{13}C, and $^{1}H-^{13}C$ HSQC NMR spectra, respectively).

Thiolysis Determination of CT Fraction Composition and Percent Purity. Thiolysis was conducted as previously described.[3,40] Briefly, approximately 8 mg of purified CT fractions was subjected to thiolysis with concentrated HCl in methanol in the presence of benzyl mercaptan providing the extender units of the CT as their benzyl mercaptan adducts and terminal units as underivatized flavan-3-ols. The resulting mixture was then analyzed by LC-MS on an HPLC Agilent 1100 series system and an API-ES instrument Hewlett-Packard 1100 MSD series (Agilent Technologies, Waldbronn, Germany). Separation of mixture components was accomplished on an ACE C_{18} column (3 μm; 250 × 4.6 mm; Hichrom Ltd., Theale, UK) fitted with a guard column at room temperature using a flow rate of 0.75 mL/min. The HPLC eluent consisted of mixtures of 1% acetic acid in water (solvent A) and HPLC grade methanol (solvent B) utilizing the following gradient program: 0–52 min, 36% B; 52–60 min, 36–50% B linear; 60–65 min, 50–100% B linear; 65–73 min, 100–0% B; 73–80 min, 0% B. Chromatograms were recorded at 280 nm, and mass spectra were recorded in the negative ionization scan mode. The percent of each benzyl mercaptan adduct was calculated on the basis of molar response factors determined relative to the internal standard taxifolin. Percent purity was calculated through summation of the total mass of all terminal and extension flavan-3-ol units divided by the initial mass of the analyzed material (g total flavan-3-ols/100 g CT fraction × 100).

Protein Precipitation Assay. BSA and chicken egg white LYS were dissolved in 50 mM 2-[*N*-morpholino]ethanesulfonic acid (MES), pH 6.5 (with NaOH), to a concentration of 10 mg/mL. Alfalfa leaf protein extract was prepared and desalted using Sephadex G-25 spin columns as described previously[42] except that the buffer used for extraction and spin column equilibration was 50 mM MES, pH 6.5. Protein concentration of the desalted alfalfa leaf extract was determined using the Pierce 660 nm Protein Assay Reagent with BSA as the standard and varied from 2.2 to 3.0 mg/mL. Small aliquots of the protein solutions (500 and 1700 μL for the pure proteins and the alfalfa extract, respectively) were flash frozen in liquid nitrogen and stored at −80 °C until needed.

A master stock solution of each CT fraction was prepared by weighing out approximately 20 mg of purified CT and dissolving to a final concentration of 10 mg/mL in ethanol. Further working stock solutions were prepared in ethanol from the master stock to give 5.00, 3.75, 2.50, 1.88, 1.25, 0.95, and 0.62 mg/mL solutions. For each protein tested, 20 μL of each CT working stock solution (or buffer control for no CT) was pipetted into 1.7 mL microfuge tubes in duplicate. A no-protein control series was also carried out for each CT fraction. The CT samples were dried down in a centrifugal vacuum concentrator (Eppendorf Concentrator 5301) and redissolved in 50 mM MES, pH 6.5 (80 μL for BSA and LYS precipitation assays, 10–20 μL for ALF assays depending on the protein concentration of the extract). Previously frozen protein stock solutions were thawed and added to the CT in each tube to give a final reaction volume of 100 μL and a final protein concentration of 2 mg/mL (20 μL for BSA or LYS,

DOI: 10.1021/jf504715p
J. Agric. Food Chem. 2015, 63, 1160–1168

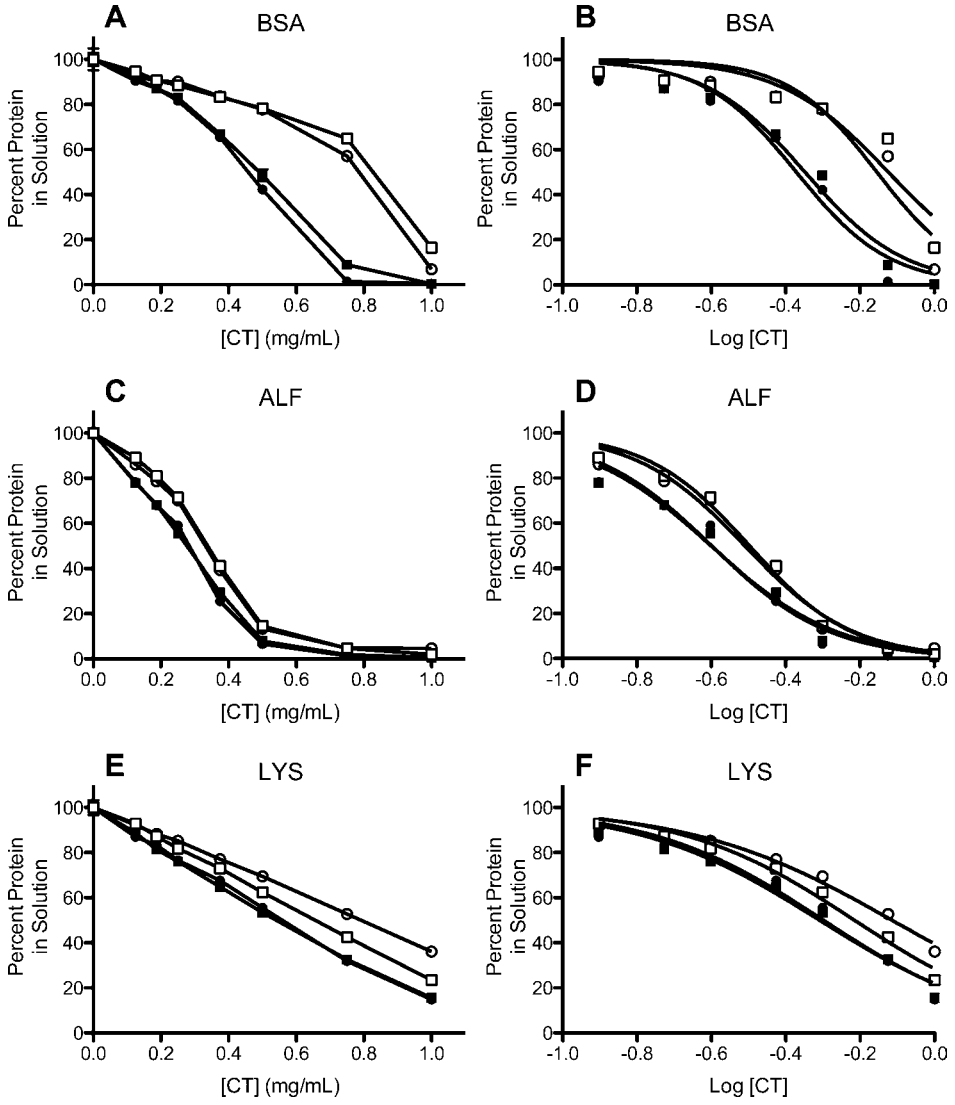

Figure 4. Precipitation of bovine serum albumin (BSA), alfalfa leaf protein extract (ALF), or lysozyme (LYS) by two large- and two medium-sized condensed tannins (CT) isolated from big trefoil and white clover: big trefoil, medium (□); big trefoil, large (BT-Large) (■); white clover, medium (○); white clover, large (●). The concentrations of CT are expressed on a milligram per milliliter basis (left) and a log[CT] basis (right). Graphs depict data from one of two experimental replicates.

80−90 μL for ALF, depending on the protein concentration of the extract). The precipitation reactions were incubated for 10 min on ice and then centrifuged for 5 min at 20000*g*. A sample of each resulting supernatant (20 μL) was added to 30 μL of 50 mM MES (pH 6.5). Protein present in the supernatant samples was determined by adding 750 μL of Pierce 660 nM Protein Assay Reagent and measuring the absorbance at 660 nm using a Beckman DU800 spectrophotometer (Beckman-Coulter, Brea, CA, USA). In pilot experiments we found that the Pierce 660 Protein Assay Reagent was linear over the range of protein concentrations being examined and showed virtually no reactivity with the tannin preparations tested. The duplicate data points were averaged, and data for each tannin/protein combination were analyzed by fitting a curve to the data using Prism (GraphPad Software, La Jolla, CA, USA). Because in pilot experiments protein could be quantitatively precipitated by tannins, an inhibitor dose−response curve (log[tannin concentration] versus normalized response with variable slope) was the nonlinear regression curve-fitting model selected. Fitted curves had *r*-squared values of >0.95, except for BSA with medium mDP CT, which had *r*-squared values of >0.87 and >0.89 for big trefoil and white clover tannins, respectively. This approach allowed determination of an IC_{50} (in this case the tannin concentration at which half the protein was precipitated, hereafter referred to as PP_{50}). The entire experiment was replicated (for $N = 2$) using independently prepared master stock solutions of each tannin.

Statistical Analysis. The replicated PP_{50} values were subjected to a mixed model analysis in a randomized complete block design by running PROC MIXED (SAS, 2014). Protein, CT, and their two-way interactions were considered fixed effects, whereas replicates ($N = 2$) from two independent experiments and their interactions with fixed effects were considered random effects. If *F* tests were significant ($P \leq 0.01$), then least-squares means of fixed effects were compared at $P = 0.01$ using a *t* test performed by a SAS pdmix800 macro.[43] Unless noted otherwise, treatment differences described in the text were significant at $P = 0.01$.

RESULTS AND DISCUSSION

Determinination of Purity and Composition of CT Fractions by NMR and Thiolysis. In previous studies, CTs bound to Sephadex LH-20 or other resins were typically washed with selected polar protic solvent mixtures, eluted with acetone−water, and apparently used in protein precipitation studies without any assessment of purity. Unknown variations in CT purity may therefore account for the conflicting results

DOI: 10.1021/jf504715p
J. Agric. Food Chem. 2015, 63, 1160−1168

Table 1. Composition of Large- and Medium-Sized Condensed Tannin Fractions Purified from White Clover (WC) and Big Trefoil (BT) As Determined by Thiolysis with Benzyl Mercaptan[a]

CT fraction	mDP	SD	PC/PD ratio	SD	*cis*/*trans* ratio	SD
WC-Large	17.4	±0.42	0.8/99.2	±0.01	69.2/30.8	±0.07
WC-Medium	9.3	±0.13	0.9/99.1	±0.04	58.3/41.7	±0.24
BT-Large	18.2	±0.33	16.0/84.0	±0.07	81.8/18.2	±0.22
BT-Medium	9.8	±0.01	26.0/74.0	±0.30	78.7/21.3	±0.23

[a]mDP, mean degree of polymerization; PC/PD, procyanidin/prodelphinidin ratio; *cis*/*trans*, ratio of *cis* (epicatechin and epigallocatechin) and *trans* (catechin and gallocatechin) flavanols.

from previous studies examining the effects of CT structure on protein precipitation. When using such isolation procedures, we have found that acetone−water fractions contain between 30 and 80% CTs (unpublished data) with the balance composed mainly of carbohydrate impurities. As carbohydrates do not possess chromophoric entities, they would not be observed if commonly employed UV detectors were used to track CT elution from chromatography columns. In addition to introducing errors through hitherto unaccounted for variations in CT purity, carbohydrates and carbohydrate derivatives can also bias CT−protein precipitation results by competing with proteins during CT complexation.[44−46] Thus, the need for highly pure CT fractions, free of significant carbohydrate impurities, seems a prerequisite for obtaining meaningful results from CT−protein precipitation studies. Hence, for our protein precipitation studies, we opted to use only CT fractions with purities exceeding 90% as determined by thiolysis. The results of thiolysis analysis for PC/PD and *cis*/*trans* ratios and mDP of the four CT fractions used in the protein precipitation studies are presented in Table 1. The percent purities provided by thiolysis for the CT fractions were BT-Medium, 91.3 ± 0.4; BT-Large, BTF5, 108.0 ± 0.1; WC-Medium,(106.6 ± 5.1; and WC-Large, 120.6 ± 0.9. Occasionally, the purity determined by the thiolysis method exceeds 100%, especially when samples of very high purity are analyzed. This is one identifiable flaw in the method and may be due to the cumulative errors in the summation of multiple HPLC peaks. The presence of coeluting, undetected compounds is unlikely as NMR analysis confirmed the high purity of all fractions. Figure 3 provides the $^{1}H-^{13}C$ HSQC NMR spectra for the CT fractions used in the precipitation studies. The absence of any significant non-CT related cross-peak signals implies high purity of these samples. Cross-peak signals (see Figure 2 for assignments) for H/C-4, H/C-6,8, H/C-2′,6′ (PD), H/C-2′,5′ (PC), and H/C-6′ (PC) appear as compact contours. Clusters of cross-peaks are seen for C-2 and C-3 signals and are not the result of impurities present. These clusters arise from different H/C-2 and H/C-3 chemical shifts for *cis*/*trans* isomers, interflavan (C4−6 vs C4−8) bond isomers, and terminal flavanol subunits. A comprehensive analysis of these spectra is currently underway in an effort to assign specific structural features to these cross-peak signals. On the basis of thiolysis, both plant species yielded a medium-sized CT (mDP ∼9) and a large-sized CT (mDP ∼18). Overall, the compositionally matched pairs of PD-based CTs with mDPs of ∼9 and ∼18 appear ideal for testing whether medium- and large-sized CTs differ in their capacity to precipitate protein.

Protein Precipitation Studies. The three protein preparations used in our precipitation studies were selected because their interaction with CT has direct relevance to protein utilization by ruminants or because they represent proteins with contrasting chemical and structural properties. Alfalfa leaf protein extract (ALF) represents the main group of soluble proteins that react with CT in forage crops consumed by ruminants. The proteins of ALF are composed of approximately 70% Rubisco,[39] which is a large, loose globular protein with an acidic p*I* ∼4.6.[47] The reaction of soluble proteins such as those in ALF with CT limits their degradation by plant proteases and by proteases produced by rumen microflora, and this potentially increases the amount of forage protein digested in the gastrointestinal tract for use in animal growth and production.[48,49] Like Rubisco, BSA is a large, loose globular protein with an acidic p*I* ∼4.7[50] that is commonly used in CT precipitation assays, in part because it is readily available from commercial sources. In contrast to ALF and BSA, LYS is a small basic protein with a p*I* 11.35[51] and has a compact, globular topology. We included LYS in the study to gain some insight into whether the relative reactivity of medium- versus large-sized CTs is markedly affected by the charge, size, and structure of protein.

Precipitation studies were carried out in aqueous buffered solutions at pH 6.5, a value that approximates the pH of freshly chopped or macerated alfalfa[52] and of rumen contents where excessive proteolysis of alfalfa protein commonly occurs. In the assay, proteins were incubated with various quantities of CT, and protein precipitation was estimated by analyzing the supernatants with a protein assay reagent that does not react with CTs. The overall ability of CT to precipitate protein was determined by fitting the data to a dose−response curve to estimate PP_{50} (similar to previously described *b* values),[31,33] which we defined as the amount of CT required to precipitate 50% of the protein from a 2 mg/mL solution.

Overall, PP_{50} values suggested protein precipitation was significantly more effective with large CTs (mDP ∼18) than with medium CTs (mDP ∼9) and with ALF than with BSA or lysozyme (Table 2). The quantity of CT required to precipitate protein was, however, influenced by a highly significant ($P < 0.001$) protein × CT interaction. Within each protein type, large CTs prepared from white clover or big trefoil had similar capacities to precipitate protein, but responses to medium CT from these plant sources differed with protein type. Medium CTs from both plant sources had a similar capacity to precipitate ALF or BSA, but medium CTs from big trefoil were more effective than those from WC for precipitating LYS. The mechanism responsible for these differing protein precipitation responses to medium CT is currently unknown.

All CTs precipitated ALF much more effectively than BSA or LYS, and among the proteins examined, ALF exhibited a smaller, albeit significant, difference in PP_{50} for medium versus large CTs (Table 2). It has been previously shown that leaf protein extracts from white clover precipitate at lower CT concentrations than BSA.[24] The precipitation profiles of ALF in response to increasing CT concentrations were somewhat sigmoidal (Figure 4), suggesting that aggregation of CT−

DOI: 10.1021/jf504715p
J. Agric. Food Chem. 2015, 63, 1160−1168

Table 2. PP_{50} Values[a] of Large- and Medium-Sized Condensed Tannin Fractions Purified from White Clover (WC) and Big Trefoil (BT) for Precipitation of Alfalfa Leaf Protein Extract (ALF), Bovine Serum Albumin (BSA), and Lysozyme (LYS)

	mg CT per mg protein[b]				
protein	WC-Large (mDP 17.4)	WC-Medium (mDP 9.3)	BT-Large (mDP 18.2)	BT-Medium (mDP 9.8)	SE[c]
ALF	0.254 b z	0.305 a z	0.253 b z	0.322 a z	0.0034
BSA	0.433 b y	0.698 a y	0.447 b y	0.731 a y	0.0116
LYS	0.500 c x	0.744 a y	0.490 c x	0.600 b y	0.0131
SE	0.0046	0.0145	0.0022	0.0138	

[a]PP_{50} values are defined as the amount of CT required to precipitate 50% of the protein from a 2 mg/mL solution. [b]Within rows, means with unlike letters (a–c) differ at $P = 0.01$. Within columns, means with unlike letters (x–z) differ at $P = 0.01$. [c]SE, standard error of the mean.

protein complexes may have slightly accelerated the precipitation process. This aggregation effect on CT–protein precipitation has been noted in previous studies.[53,54] Compared to BSA and LYS, Rubisco, the major component of ALF, is relatively unstable, and disruption of its quaternary structure can cause its large subunit to precipitate out of solution even in the absence of tannins.[55] Thus, precipitation of ALF proteins by CT may be facilitated by the disruption of the quaternary structure of Rubisco, as was recently observed with the gallotannin pentagalloylglucose.[56] Although confirmation is needed, the results with ALF might also suggest that CTs aggregate and precipitate a mixed population of proteins more readily than individual proteins.

Differences in the PP_{50} values of BSA and LYS were quite modest considering the greatly differing p*I* and structural characteristics of these proteins. These two proteins, however, had markedly different precipitation profiles in response to increasing CT concentrations (Figure 4). The precipitation profiles of BSA were strongly biphasic or sigmoidal, suggesting that aggregation of CT–protein complexes accelerated the precipitation process. The precipitation profile of LYS, however, exhibited a linear response ($R^2 = 0.99$) to increasing CT concentrations.

Examination of the amino acid sequences for existing lysozyme crystal structures from the Protein Data Bank[57] shows a high ratio of basic/acidic (>2) amino acid residues, translating to a high positive charge density of the resulting CT–lysozyme complex, which is bound to inhibit aggregation. Thus, using lysozyme in protein precipitation studies at pH 6.5 may remove complications in analysis due to aggregation. We did not pursue precipitation studies at higher pH ranges because CT fractions tend to oxidize at pH >8 in aqueous solutions.[58] Because LYS–CT complexes do not appear to undergo accelerated precipitation due to aggregation, CT precipitation studies with LYS might provide a way to more clearly distinguish how CT structural features such as PC/PD ratios, *cis*/*trans* ratios, and different interflavanol linkage types affect the formation of CT–protein complexes. For this reason, additional studies with LYS along with those of ALF and BSA are underway to further investigate how structural features of CT affect protein precipitation.

Coupled with results from Harbertson et al.,[36] these studies clearly show that CT with higher mDP more readily precipitates soluble proteins. The synergy described for protein precipitation using well-defined mixtures of cocoa CTs[36] may indicate that a combination of CTs of various lengths, as present in all CT-containing forages, facilitates precipitation through cooperative complexation and more readily promotes aggregation with the soluble forage proteins. This phenomenon was clearly observed in the current study as nonlinear precipitation profiles for BSA and ALF and is in contrast to the lower DP cocoa CTs' linear precipitation profiles. These results may explain, to some extent, that having mixtures of large and small CTs provides a more powerful combination for generating insoluble protein complexes.

In conclusion, we have demonstrated that BSA, ALF, and LYS proteins are more readily precipitated at pH 6.5 by larger-sized CTs (mDP of ∼18) than by medium-sized CTs (mDP of ∼9) prepared from white clover and big trefoil. The confounding effects of other CT properties on protein precipitation were largely eliminated by using CT pairs that had comparable PD/PC and *cis*/*trans* ratios of subunits and high purity as determined by $^1H–^{13}C$ HSQC NMR and thiolytic degradation with benzyl mercaptan. On the basis of PP_{50} values, all CTs were very efficient at precipitating ALF proteins, possibly because the large subunit of Rubisco has a propensity to dissociate and self-aggregate. Such a dissociation could be facilitated by interactions with CT. The presence of other types of proteins in ALF might further promote aggregation and precipitation by CT. Compared to ALF, the precipitations of BSA and LYS were affected to a larger extent by the mDP of CTs, and both proteins had relatively high PP_{50} values. On the basis of the biphasic or sigmoidal response to increasing CT concentrations, the precipitation of ALF and BSA was likely accelerated by aggregation of CT–protein complexes. By contrast, the linear response of LYS to increasing CT concentration suggests that aggregation was inhibited by the positive charge of this protein at pH 6.5. Studies with high-purity CTs exhibiting a wider range of mDP, PD/PC ratios, and *cis*/*trans* ratios will be pursued to more thoroughly define how compositional and structural features of CTs affect their ability to precipitate various types of proteins under differing pH conditions.

■ ASSOCIATED CONTENT

Supporting Information

^1H and $^1H–^{13}C$ HSQC NMR spectra (360/90 MHz) for residues from purified CT fractions BTF1 through BTF5. This material is available free of charge via the Internet at http://pubs.acs.org.

■ AUTHOR INFORMATION

Corresponding Author

*(W.E.Z.) Phone: (608) 890-0071. Fax: (608) 890-0076. E-mail: Wayne.Zeller@ars.usda.gov.

Funding

This work was funded in part by USDA-ARS Specific Cooperative Agreement 58-3655-0-155F with the University of Reading, UK, and was supported by a European Union Marie Curie Initial Training Network (PITN-GA-2011-289377 ('LegumePlus'). Mention of trade names or commercial products in this paper is solely for the purpose of providing specific information and does not imply recommendation or endorsement by the U.S. Department of Agriculture.

Notes

The authors declare no competing financial interest.

DOI: 10.1021/jf504715p
J. Agric. Food Chem. 2015, 63, 1160–1168

■ ACKNOWLEDGMENTS

We acknowledge the technical assistance of Nicholas Sampalis and Abert Vang as well as Jane Marita for assistance with NMR experiments.

■ REFERENCES

(1) Hagerman, A. E. *Tannin Handbook*; Miami University: Oxford, OH, USA, 2002; available at http://www.users.muohio.edu/hagermae/.
(2) Schofield, P.; Mbugua, D. M.; Pell, A. N. Analysis of condensed tannins: a review. *Anim. Feed Sci. Technol.* **2001**, *91*, 21−40.
(3) Gea, A.; Stringano, E.; Brown, R. H.; Mueller-Harvey, I. *In situ* analysis and structural elucidation of sainfoin (*Onobrychis viciifolia*) tannins for high-throughput germplasm screening. *J. Agric. Food Chem.* **2011**, *59*, 495−503.
(4) Le Bourvellec, C.; Renard, C. M. G. C. Interactions between polyphenols and macromolecules: quantification methods and mechanisms. *Crit. Rev. Food Sci. Nutr.* **2012**, *52*, 213−248.
(5) Hagerman, A. E. Tannin-protein interactions. In *Phenolic Compounds in Foods and Health*; Ho, C. T., Ed.; American Chemical Society: Washington, DC, USA, 1992; pp 236−247.
(6) Asquith, T. N.; Butler, L. G. Interactions of condensed tannins with selected proteins. *Phytochemistry* **1986**, *25*, 1591−1593.
(7) Albrecht, K. A.; Muck, R. E. Proteolysis in ensiled forage legumes that vary in tannin concentration. *Crop Sci.* **1991**, *31*, 464−469.
(8) Min, B. R.; Barry, T. N.; Attwood, G. T.; McNabb, W. C. The effect of condensed tannins on the nutrition and health of ruminants fed fresh temperate forages: a review. *Anim. Feed Sci. Technol.* **2003**, *106*, 3−19.
(9) Waghorn, G. C.; Douglas, G. B.; Niezen, J. H.; McNabb, W. C.; Foote, A. G. Forages with condensed tannins − their management and nutritive value for ruminants. *Proc. N. Z. Grassl. Assoc.* **1998**, *60*, 89−98.
(10) Barry, T. N.; McNabb, W. C. The implications of condensed tannins on the nutritive value of temperate forages fed to ruminants. *Br. J. Nutr.* **1999**, *81*, 263−272.
(11) Patra, A. K.; Saxena, J. A new perspective on the use of plant secondary metabolites to inhibit methanogenesis in the rumen. *Phytochemistry* **2010**, *71*, 1198−1222.
(12) Pellikaan, W. F.; Stringano, E.; Leenaars, J.; Bongers, D. J. G. M.; van Laar-van Schuppen, S.; Plant, J.; Mueller-Harvey, I. Evaluating effects of tannins on extent and rate of in vitro gas and CH_4 production using an automated pressure evaluation system (APES). *Anim. Feed Sci. Technol.* **2011**, *166−167*, 377−390.
(13) Aguerre, M. J.; Wattiaux, M. A.; Capozzolo, M. C.; Lencioni, P.; Cabral, C. Effect of quebracho-chestnut tannin extracts at two dietary crude protein levels on nitrogen partitioning in lactating dairy cows. *J. Dairy Sci.* **2010**, *93* (E-Suppl. 1), 446 (Abstr.).
(14) McMahon, L. R.; McAllister, T. A.; Berg, B. P.; Majak, W.; Acharya, S. N.; Popp, J. D.; Coulman, B. E.; Wang, Y.; Cheng, K.-J. A review of the effects of forage condensed tannins on ruminal fermentation and bloat in grazing cattle. *Can. J. Plant. Sci.* **2000**, *80*, 469−485.
(15) Hoste, H.; Jackson, F.; Athanasiadou, S.; Thamsborg, S. M.; Hoskin, S. O. The effects of tannin-rich plants on parasitic nematodes in ruminants. *Trends Parasitol.* **2006**, *22*, 253−261.
(16) Hagerman, A. E. Fifty years of polyphenol-protein complexes. In *Recent Advances in Polyphenol Research*, 1st ed.; Cheynier, V., Sarni-Manchado, P., Quideau. S., Eds.; Wiley: Hoboken, NJ, USA, 2012; Vol. 3, pp 71−97.
(17) Naumann, H. D.; Muir, J. P.; Lambert, B. D.; Tedeschi, L. O.; Kothmann, M. M. Condensed tannins in the ruminant environment: a perspective on biological activity. *J. Agric. Sci.* **2013**, *1*, 8−20.
(18) Mueller-Harvey, I. Unravelling the conundrum of tannins in animal nutrition and health. *J. Sci. Food Agric.* **2006**, *86*, 2010−2037.
(19) Barbehenn, R. V.; Constabel, C. P. Tannins in plant−herbivore interactions. *Phytochemistry* **2011**, *72*, 1551−1565.
(20) Poncet-Legrand, C.; Edelmann, A.; Putaux, J.-L.; Cartalade, D.; Sarni-Manchado, P.; Vernhet, A. Poly(-proline) interactions with flavan-3-ols units: influence of the molecular structure and the polyphenol/protein ratio. *Food Hydrocolloids* **2006**, *20*, 687−697.
(21) Lorenz, M. M.; Alkhafadji, L.; Stringano, E.; Nilsson, S.; Mueller-Harvey, I.; Udén, P. Relationship between condensed tannin structures and their ability to precipitate feed proteins in the rumen. *J. Sci. Food Agric.* **2014**, *94*, 963−968.
(22) De Freitas, V.; Mateus, N. Nephelometric study of salivary protein-tannin aggregates. *J. Sci. Food Agric.* **2002**, *82*, 113−119.
(23) Hagerman, A. E.; Robbins, C. T. Specificity of tannin-binding salivary proteins relative to diet selection by mammals. *Can. J. Zool.* **1993**, *71*, 628−633.
(24) McNabb, W. C.; Peters, J. S.; Foo, L. Y.; Waghorn, G. C.; Jackson, F. S. Effect of condensed tannins prepared from several forages on the *in vitro* precipitation of ribulose-1,5-*bis*phosphate carboxylase (Rubisco) protein and its digestion by trypsin (EC 2.4.21.4) and chymotrypsin (EC 2.4.21.1). *J. Sci. Food Agric.* **1998**, *77*, 201−212.
(25) Hagerman, A. E.; Butler, L. G. The specificity of proanthocyanidin-protein interactions. *J. Biol. Chem.* **1981**, *256*, 4494−4497.
(26) Hagerman, A. E.; Rice, M. E.; Ritchard, N. T. Mechanisms of protein precipitation for two tannins, pentagalloyl glucose and epicatechin$_{16}$ (4−8) catechin (procyanidin). *J. Agric. Food Chem.* **1998**, *46*, 2590−2595.
(27) Charlton, A. J.; Baxter, N. J.; Khan, M. L.; Moir, A. J. G.; Haslam, E.; Davies, A. P.; Williamson, M. P. Polyphenol/peptide binding and precipitation. *J. Agric. Food Chem.* **2002**, *50*, 1593−1601.
(28) Adamczyk, B.; Salminen, J.-P.; Smolander, A.; Kitunen, V. Precipitation of proteins by tannins: effects of concentration, protein/tannin ratio and pH. *Int. J. Food Sci. Technol.* **2012**, *47*, 875−878.
(29) Bate-Smith, E. C. Haemanalysis of tannins: the concept of relative astringency. *Phytochemistry* **1973**, *12*, 907−912.
(30) Huang, X. D.; Liang, J. B.; Tan, H. Y.; Yahya, R.; Ho, Y. W. Effects of *Leucaena* condensed tannins of differing molecular weights on *in vitro* CH_4 production. *Anim. Feed Sci. Technol.* **2011**, *166− 167*, 373−376.
(31) Huang, X. D.; Liang, J. B.; Tan, H. Y.; Yahya, R.; Long, R.; Ho, Y. W. Protein-binding affinity of *Leucaena* condensed tannins of differing molecular weights. *J. Agric. Food Chem.* **2011**, *59*, 10677−10682.
(32) Huang, X. D.; Liang, J. B.; Tan, H. Y.; Yahya, R.; Khamseekhiew, B.; Ho, Y. W. Molecular weight and protein binding affinity of *Leucaena* condensed tannins and their effects on in vitro fermentation parameters. *Anim. Feed Sci. Technol.* **2010**, *159*, 81−87.
(33) Osborne, N. J. T.; McNeill, D. M. Characterisation of *Leucaena* condensed tannins by size and protein precipitation capacity. *J. Sci. Food Agric.* **2001**, *81*, 1113−1119.
(34) Naumann, H. D.; Tedeschi, L. O.; Muir, J. P.; Lambert, B. D.; Kothmann, M. M. Effect of molecular weight of condensed tannins from warm-season perennial legumes on ruminal methane production *in vitro*. *Biochem. Syst. Ecol.* **2013**, *50*, 154−162.
(35) Naumann, H. D.; Hagerman, A. E.; Lambert, B. D.; Muir, J. P.; Tedeschi, L. O.; Kothmann, M. M. Molecular weight and protein-precipitating ability of condensed tannins from warm-season perennial legumes. *J. Plant Interact.* **2014**, *9*, 212−219.
(36) Harbertson, J. F.; Kilmister, R. L.; Kelm, M. A.; Downey, M. O. Impact of condensed tannin size as individual and mixed polymers on bovine serum albumin precipitation. *Food Chem.* **2014**, *160*, 16−21.
(37) Gu, L.; Kelm, M.; Hammerstone, J. F.; Beecher, G.; Cunningham, D.; Vannozzi, S.; Prior, R. L. Fractionation of polymeric procyanidins from lowbush blueberry and quantification of procyanidins in selected foods with an optimized normal-phase HPLC-MS fluorescent detection method. *J. Agric. Food Chem.* **2002**, *50*, 4852−4860.
(38) Kelm, M. A.; Johnson, J. C.; Robbins, R. J.; Hammerstone, J. F.; Schmitz, H. H. High-performance liquid chromatography separation and purification of cacao (*Theobroma cacao* L.) procyanidins according

DOI: 10.1021/jf504715p
J. Agric. Food Chem. 2015, 63, 1160−1168

to degree of polymerization using a diol stationary phase. *J. Agric. Food Chem.* **2006**, *54*, 1571−1576.
(39) Douillard, R.; de Mathan, O. Leaf proteins for food use: potential of RUBISCO. In *New and Developing Sources of Food Proteins*, 1st ed.; Hudson, B. J., Ed.; Chapman and Hall: Boca Raton, FL, USA, 1994; pp 307−342.
(40) Grabber, J. H.; Zeller, W. E.; Mueller-Harvey, I. Acetone enhances the direct analysis of procyanidin- and prodelphinidin-based condensed tannins in Lotus species by the butanol−HCl−iron assay. *J. Agric. Food Chem.* **2013**, *61*, 2669−2678.
(41) Engström, M. T.; Pälijärvi, M.; Fryganas, C.; Grabber, J. H.; Mueller-Harvey, I.; Salminen, J.-P. Rapid qualitative and quantitative analysis of proanthocyanidin oligomers and polymers by UPLC-MS/MS. *J. Agric. Food Chem.* **2014**, *62*, 3390−3399.
(42) Sullivan, M. L.; Zeller, W. E. Efficacy of various naturally occurring caffeic acid derivatives in preventing post-harvest protein losses in forages. *J. Sci. Food Agric.* **2012**, *93*, 219−226.
(43) Saxton, A. M. A macro for converting mean separation output to letter groupings in proc mixed. *Proceedings, 23rd SAS Users Group International*; SAS Institute: Cary, NC, USA, 1998; pp 1243−1246.
(44) de Freitas, V.; Carvalho, E.; Mateus, N. Study of carbohydrate influence on protein−tannin aggregation by nephelometry. *Food Chem.* **2003**, *81*, 503−509.
(45) Mateus, N.; Carvalho, E.; Luís, C.; de Freitas, V. Influence of the tannin structure on the disruption effect of carbohydrates on protein−tannin aggregates. *Anal. Chim. Acta* **2004**, *513*, 135−140.
(46) Delehanty, J. B.; Johnson, B. J.; Hickey, T. E.; Pons, T.; Ligler, F. S. Binding and neutralization of lipopolysaccharides by plant proanthocyanidins. *J. Nat. Prod.* **2007**, *70*, 1718−1724.
(47) Barbeau, W. E.; Kinsella, J. E. Ribulose bisphosphate carboxylase/oxygenase (rubisco) from green leaves − potentials as a food protein. *Food Rev. Int.* **1988**, *4*, 93−127.
(48) Messman, M. A.; Weiss, W. P.; Albrecht, K. A. *In situ* disappearance of individual proteins and nitrogen from legume forages containing varying amounts of tannins. *J. Dairy Sci.* **1996**, *79*, 1430−1436.
(49) Waghorn, G. C.; Ulyatt, M. J.; John, A.; Fisher, L. J. The effect of condensed tannins on the site of digestion of amino acids and other nutrients in sheep fed on *Lotus corniculatus*. *Br. J. Nutr.* **1987**, *57*, 115−126.
(50) Ge, S.; Kojio, K.; Takahara, A.; Kajiyama, T. Bovine serum albumin adsorption onto immobilized organotrichlorosilane surface: influence of the phase separation on protein adsorption patterns. *J. Biomater. Sci. Polym. Ed.* **1998**, *9*, 131−150.
(51) Wetter, L. R.; Deutsch, H. F. Immunological studies on egg white proteins IV. Immunochemical and physical studies of lysozyme. *J. Biol. Chem.* **1951**, *192*, 237−242.
(52) Sullivan, M. L.; Hatfield, R. D. Polyphenol oxidase and o-diphenols inhibit postharvest proteolysis in red clover and alfalfa. *Crop Sci.* **2006**, *46*, 663−670.
(53) Jöbstl, E.; O'Connell, J.; Fairclough, J. P. A.; Williamson, M. P. Molecular model for astringency produced by polyphenol/protein interactions. *Biomacromolecules* **2004**, *5*, 942−949.
(54) Zanchi, D.; Narayanan, T.; Hagenmuller, D.; Baron, A.; Guyot, S.; Cabane, B.; Bouhallab, S. Tannin-assisted aggregation of natively unfolded proteins. *Europhys. Lett.* **2008**, *82*, No. 58001.
(55) Andrews, T. J.; Ballment, B. The function of the small subunits of ribulose bisphosphate carboxylase-oxygenase. *J. Biol. Chem.* **1983**, *258*, 7514−7518.
(56) Dobreva, M. A.; Frazier, R. A.; Mueller-Harvey, I.; Clifton, L. A.; Gea, A.; Green, R. J. Binding of pentagalloyl glucose to two globular proteins occurs via multiple surface sites. *Biomacromolecules* **2011**, *12*, 710−715.
(57) RCSB Protein Data Bank Web site address: http://www.rcsb.org.
(58) Salminen, J.-P.; Karonen, M.; Sinkkonen, J. Chemical ecology of tannins: recent developments in tannin chemistry reveal new structures and structure−activity patterns. *Chem.−Eur. J.* **2011**, *17*, 2806−2816.

DOI: 10.1021/jf504715p
J. Agric. Food Chem. 2015, 63, 1160−1168

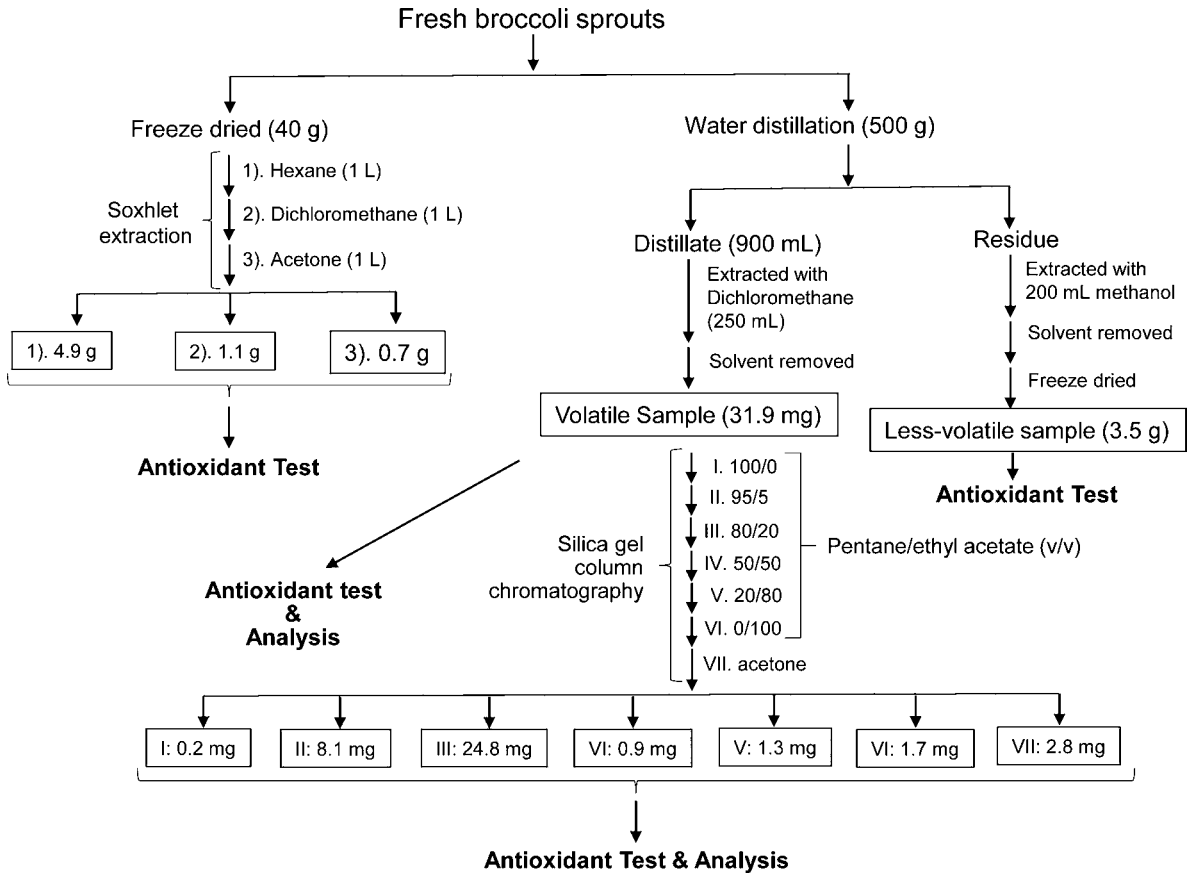

Figure 1. Experimental scheme of sample preparations.

Sample Preparations for Analysis and Antioxidant Assays. The entire scheme of the experimental procedures in the present study is shown in Figure 1.

Water Distillation Samples. Fresh broccoli sprouts (500 g) were placed in a 3 L round-bottom flask with 1 L of deionized water. The aqueous solution was water-distilled at 50 °C for 5 h under reduced pressure (95 mmHg). The distillate (900 mL) was extracted with 250 mL dichloromethane using a liquid–liquid continuous extractor for 6 h. After the extract was dried over anhydrous sodium sulfate, the solvent was removed by a rotary flash evaporator and then placed under a purified nitrogen stream to yield brown viscous material (31.9 mg). This material, labeled the volatile sample, was set aside to be used further for the antioxidant tests and GC-MS analysis.

The residual broccoli sprouts in the distillation flask were mixed with 200 mL of methanol by stirring for 2 h and then filtered. The solvent of the filtrate was removed by rotary flash evaporator, and residual materials were freeze-dried (as the less-volatile sample) and stored at 4 °C until used in the antioxidant tests.

Fractionation of the Volatile Sample. The volatile sample was placed in a glass column (15 cm × 1 cm i.d.) packed with 5 g of silica gel (100–200 mesh, Avantor Performance Materials, Inc., Philipsburg, NJ, USA) and eluted sequentially with the following 100 mL pentane/ethyl acetate solvent fractions: 100/0 (fraction I), 95/5 (fraction II), 80/20 (fraction III), 50/50 (fraction IV), 20/80 (fraction V), 0/100 (fraction VI); finally, elution with 200 mL of acetone yielded fraction VII. The solvent of each fraction was removed by a rotary flash evaporator and then by a purified nitrogen stream to 1 mL in volume. The seven fractions prepared were stored at 4 °C until used for the antioxidant tests and GC-MS analysis.

Freeze-Dried Sample. Fresh broccoli sprouts were freeze-dried at −48 °C for 48 h (FreezOne, Labconco, MO, USA). The freeze-dried broccoli sprouts (40 g) were extracted sequentially with 1 L each of hexane, dichloromethane, and acetone using a Soxhlet extractor. The extracts were dried over anhydrous sodium sulfate. After the solvent of each extract was removed by rotary flash evaporator, they were stored at −5 °C until used for the antioxidant tests.

Analysis of Components in the Volatile Sample. Components in the volatile sample were isolated and identified by GC and GC-MS. Identification was conducted by comparing the Kovats index[20] and MS fragmentation pattern of a GC component with those of an authentic chemical.

The concentration of each compound in broccoli sprouts was calculated according to a previously reported method.[15]

Antioxidant Assays. Three assays were used to examine the antioxidant activity of the samples. Details of the assays used in the present study were described in a previous paper.[21] A standard antioxidant, BHT, was used to validate the assays used.

Malonaldehyde/Gas Chromatography (MA/GC) Assay. This assay is useful for examining the last stage of lipid oxidation.[21]

An aqueous assay solution (5 mL) containing 30 μL of cod liver oil, 0.25 mmol of trizma buffer (pH 7.4), 1 μmol of ferrous chloride, 2 μmol of hydrogen peroxide, 0.75 mmol of potassium chloride, and 1% surfactant sodium dodecyl sulfate was prepared. Various amounts of broccoli sprout samples were added to this assay solution and incubated for 17 h at 37 °C in a 20 mL test tube. After incubation, 50 μL of 4% BHT solution was added to terminate the oxidation of the samples. After MA formed from cod liver oil in the test tube, it was derivatized to 1-methylpyrazole with *N*-methylhydrazine (30 μL). The 1-methylpyrazole formed was eluted with 10 mL of ethyl acetate through an SPE cartridge (MEGA BE-C_{18}, 1 g, 6 mL, Varian, USA). After 20 μL of GC internal standard was added, 2-methylpyrazine was added to the eluate, and the volume of the eluate was adjusted to exactly 10 mL with ethyl acetate. The eluate solution was analyzed for 1-methylpyrazole by GC. All experiments were carried out in triplicate.

2,2-Diphenyl-1-picrylhydrazyl (DPPH) Assay. The DPPH solution (1.52×10^{-4} M) was prepared in ethanol. DPPH solution (4.5 mL) and 0.5 mL of test sample were mixed using a vortex and stored in the dark for 20 min. After the reaction ran to completion, the absorption

DOI: 10.1021/jf504929m
J. Agric. Food Chem. 2015, 63, 1169–1174

activity was measured at 517 nm using a UV−visible spectrophotometer. A solution without the testing sample was used as the control. All experiments were conducted in triplicate.

Aldehyde/Carboxylic Acid Assay. This method is useful to test the long-term antioxidant activity, which is important for determining the shelf life of a product.[21]

Various amounts of the volatile sample (refer to Figure 1) were added to a 2 mL dichloromethane solution of hexanal (3 mg/mL) containing 0.2 mg/mL undecane as a GC internal standard. Standard antioxidant BHT was used to validate the method. Oxidation of the sample solution was initiated by heating at 60 °C for 10 min in a sealed vial and then stored at room temperature. The oxidation of hexanal to hexanoic acid was monitored at 5 day intervals by measuring the amount of hexanal using GC. All experiments were performed in triplicate.

Instruments. An Agilent model 6890 GC equipped with a 60 m × 0.32 mm i.d. (d_f = 0.25 μm) DB-WAX bonded-phase fused-silica capillary column (Agilent, Folsom, CA, USA) and an FID were used for obtaining a Kovats index of components in the volatile sample and its fractions (refer to Figure 1). The linear velocity of the helium carrier gas was 28 cm/s at a split ratio of 10:1. The injector and detector temperatures were 260 and 300 °C, respectively. The oven temperature was programmed to increase from 50 to 210 °C at 2 °C/min and held for 30 min. An Agilent model 6890 GC interfaced to a 5973 mass selective detector (GC-MS) was used for mass spectral identification of the GC components at an MS ionization voltage of 70 eV. GC column conditions were exactly the same as the ones used for GC-FID.

The quantitative analysis of 1-methylpyrazole for the MA/GC assay was performed using an Agilent model 6890 GC equipped with a 30 m × 0.32 mm i.d. (d_f = 0.25 μm) DB-WAX bonded-phase fused silica capillary column (Agilent) and an NPD. The injector and detector temperatures were 250 °C. The oven temperature was programmed to increase from 60 to 160 °C at 4 °C/min and held for 2 min. The linear velocity of the helium carrier gas was 28 cm/s at a split ratio of 20:1.

The quantitative analysis of hexanal for the aldehyde/carboxylic acid assay was conducted by using an Agilent model 6890 GC equipped with a 30 m × 0.25 mm i.d. (d_f = 0.25 μm) DB-1 bonded-phase fused-silica capillary column (Agilent) and a FID. The linear velocity of the helium carrier gas was 30 cm/s at a split ratio of 20:1. The injector and detector temperatures were 300 and 280 °C, respectively. The oven temperature was programmed to rise from 40 to 180 °C at 5 °C/min and then held for 10 min.

Statistical Analyses. The data obtained from the present study were treated with an ANOVA analysis based on the SAS system, and the level of significance was determined using Duncan's multiple-range test at α = 0.05.

RESULTS AND DISCUSSION

Antioxidant Activities of Samples Prepared by Freeze-Drying and Water Distillation. Whereas spectrophotometric methods, such as DPPH assay, cause some difficulties because the absorption of color materials overlaps with that of the target chemical, the MA/GC assay can be applied to samples with dark colors because it measures MA specifically by GC. Therefore, the MA/GC method was used for the preliminary examination of the samples prepared from broccoli sprouts (refer to Figure 1).

Figure 2 shows the antioxidant activity of the samples examined by the MA/GC assay. The values are the mean ± SD (n = 3). BHT showed antioxidant activities of 95.3 ± 0.2% at the level of 500 μg/mL, 92.2 ± 0.4% at the level of 100 μg/mL, and 87.2 ± 3.1% at the level of 20 μg/mL, confirming that the method used was valid. All samples exhibited dose-dependent antioxidant activity. The antioxidant activity ranged from 74.48 ± 0.46% (less volatile sample) to 93.2 ± 0.2% (dichloromethane extract sample) at the level of 500 μg/mL, indicating

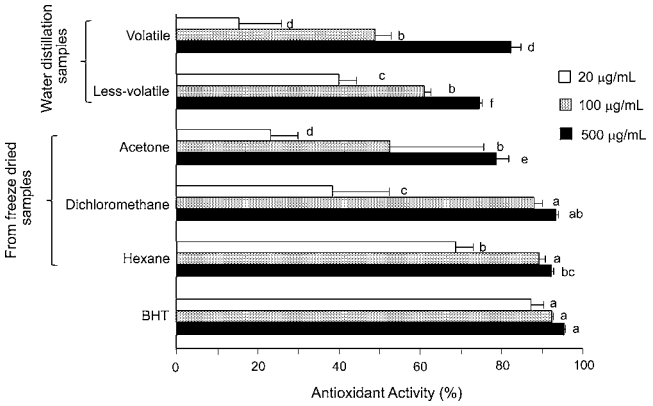

Figure 2. Results of MA/GC assay on the samples prepared from broccoli sprouts by freeze-drying and water distillation.

that all samples contain strong antioxidants. The volatile sample showed 82.1 ± 2.4% at the level of 500 μg/mL. Among the samples tested in this experiment, the sample prepared by Soxhlet extraction with dichloromethane solvent from the freeze-dried sample (refer to Figure 1) exhibited the most potent antioxidant activity. Its antioxidant activities (87.9 ± 1.9% at 100 μg/mL and 93.2 ± 0.6% at 500 μg/mL) were comparable to that of BHT.

Figure 3 shows the results of the DPPH assay. Values are the mean ± SD (n = 3). The results are consistent with those of the

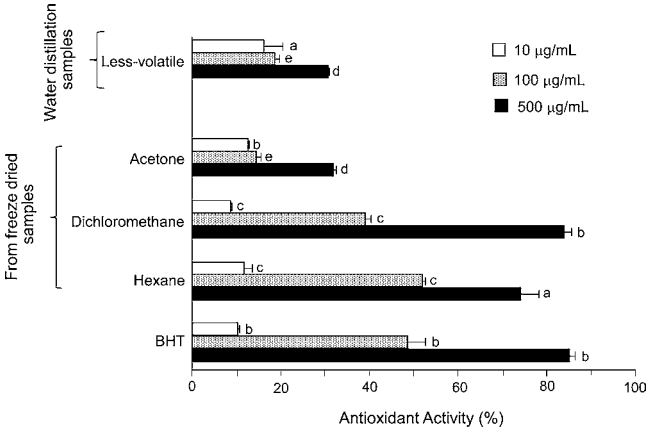

Figure 3. Results of DPPH assay on the samples prepared from broccoli sprouts by freeze-drying and water distillation.

MA/GC assay. The volatile sample was not tested in this experiment because it was tested by the aldehyde/carboxylic acid assay. BHT exhibited clear antioxidant activities with dose response effects: 85.0 ± 1.0% at the level of 500 μg/mL, 47.3 ± 3.9% at the level of 100 μg/mL, and 10.8 ± 0.2% at the level of 20 μg/mL, confirming that this assay is valid. Less volatile samples and acetone samples showed slight dose-dependent antioxidant activities: 30.42 ± 0.17 and 31.7 ± 0.8% at the level of 500 mg/mL, respectively. Dichloromethane samples showed the most potent antioxidant activity among the samples tested in this experiment, which was the same as the results obtained by the MA/GC assay. The antioxidant activity of a dichloromethane sample (83.3 ± 1.7%) was comparable to that of BHT (85.0 ± 1.0%) at the level of 500 μg/mL. Also, dichloromethane and hexane samples exhibited moderate antioxidant activities at the level of 100 μg/mL, which were 39.1 ± 1.2 and

DOI: 10.1021/jf504929m
J. Agric. Food Chem. 2015, 63, 1169−1174

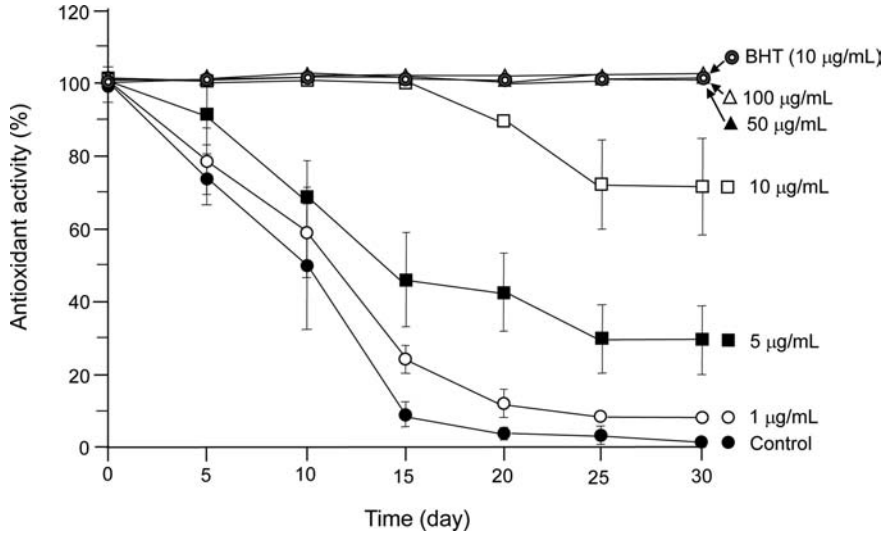

Figure 4. Results of aldehyde/carboxylic acid assay on the volatile sample.

51.8 ± 0.6%, respectively. The less volatile and acetone samples showed only slight antioxidant activities (30.42 ± 0.17 and 31.7 ± 0.8% at the level of 500 mg/mL).

These results from two antioxidant assays suggest that potent antioxidants are present in the dichloromethane and hexane samples and that the amounts of water-soluble antioxidants are less than those of organic solvent extractable (volatile) antioxidants in broccoli sprouts.

Figure 4 shows the antioxidant activity of the volatile sample examined by the aldehyde/carboxylic acid assay over 30 days. This assay is useful in discovering the long-term antioxidant activities of a chemical or a group of chemicals.[21] The values are the mean ± standard deviation (SD) (n = 3). SD ranged from 0.88 (500 μg/mL sample at 10 days) to 34.64 (control sample at 10 days). SDs lower than 1.0 do not appear in the figure. BHT showed >99% antioxidant activity throughout the experiment. The volatile sample exhibited dose-dependent antioxidant activity. The control sample was completely oxidized after 30 days. By the 30th day, the antioxidant activity of the samples was 8% by 1 μg/mL, 29% by 5 μg/mL, 70% by 10 μg/mL, 98% by 50 μg/mL, and 99% by 100 and 500 μg/mL. The 50 and 100 μg/mL samples exhibited antioxidant activity comparable to that of BHT. The results suggest that broccoli sprouts contain antioxidants, the activity of which is maintained for prolonged periods.

Figure 5 shows the antioxidant activity of the fractions obtained from the volatile sample tested by the aldehyde/carboxylic acid assay after 30 days. Values are the mean ± SD (n = 3). BHT exhibited 99.84 ± 2.49% at the level of 10 μg/mL. Fractions I, II, and III exhibited potent dose-dependent antioxidant activity. In particular, fraction II showed activity (95.56 ± 0.22%) comparable with that of BHT at the level of 10 μg/mL. On the other hand, fractions IV, V, VI, and VII exhibited only slight antioxidant activities at the levels tested in this experiment. These results suggest the presence of volatile nonpolar antioxidants in broccoli sprouts.

According to the results obtained in the present study, samples prepared with dichloromethane seem to contain potent antioxidants. Therefore, the volatile sample was analyzed to determine the principal antioxidants in the sprouts.

Compounds Identified in the Volatile Sample. Table 1 shows the compounds identified in the volatile sample from broccoli sprouts, along with their calculated concentrations (μg/g of broccoli sprouts) and Kovats index. Among the over 88 GC peaks observed in the gas chromatogram, 43 compounds were positively identified. The major compounds are 4-methylpentylisothiocyanate (2.48 μg/g), 4-(methylthio)-butylnitrile (10.63 μg/g), 5-(methylthio)pentylnitrile (31.64 μg/g), 3-(methylthio)propylisothiocyanate (3.00 μg/g), and 4-(methylthio)butylisothiocyanate (14.55 μg/g). One recent study reported that these compounds possess strong anti-*Helicobacter* activity.[18]

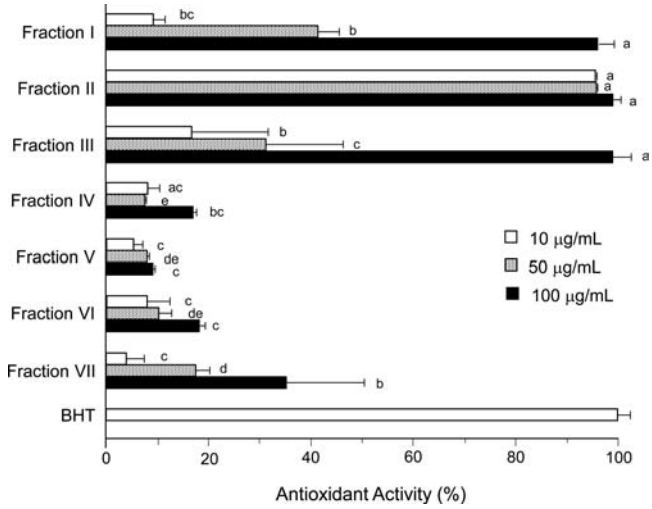

Figure 5. Results of aldehyde/carboxylic acid assay after 30 days on fractions obtained from the volatile sample.

Dimethyl disulfide, 1-penten-3-ol, 2,4,5-trimethylthiazole, 3-(methylthio)propanal, allylisothiocyanate, 2-ethyl-1-hexanol, phenylethyl alcohol, 2-methoxy-4-vinylphenol, and 2-isothiocyanatoethylbenzene have also been reported as volatile components in various vegetables and fruits, including soybeans, mung beans, onions/sprouts, horseradish, cumin, kale sprouts, and persimmon, and some organic solvent extracts of these plants showed certain antioxidant activities.[22−24] When a headspace of raw and cooked broccoli was analyzed, dimethyl sulfide, dimethyl trisulfide, hexanal, and nonanal, which contribute to the characteristic aroma of broccoli, were

DOI: 10.1021/jf504929m
J. Agric. Food Chem. 2015, 63, 1169−1174

Table 1. Compounds Identified in a Volatile Sample

	Kovats index[a]	concentration (μg/g)
alkyl-hydrocarbons, -carbonyls, -alcohols, and esters		
1-penten-3-ol	1163	0.056
(*E*)-2-hexene	1220	0.011
3-hydroxy-2-butanone	1281	0.013
2-penten-1-ol	1314	0.163
1-hexanol	1350	0.016
nonanal	1390	0.008
2-butoxyethanol	1402	0.129
2-ethyl-1-hexanol	1486	0.029
(*E*,*E*)-2,4-heptendienal	1494	0.022
3-hydroxy-2,4,4-trimethylpentyl 2-methylpropanoate	1868	0.115
aromatic compounds		
1,2-dimethoxybenzene	1708	0.013
phenylethyl alcohol	1899	0.024
4-(1-methylpropyl)phenol	2006	0.012
4-methylphenol	2054	0.159
2-methoxy-4-vinylphenol	2166	0.009
thiocyanate and isothiocyanates		
methyl thiocyanate	1264	0.119
isobutyl isothiocyanate	1335	0.003
allylisothiocyanate	1352	0.025
4-methylsulfinylbutylisothiocyanate	1422	0.003
1-isothiocyanate-3-methylbutane	1431	0.007
4-methylpentylisothiocyanate	1549	2.481
3-(methylthio)propylisothiocyanate	1981	3.003
4-methylphenyl isothiocyanate	2090	0.028
4-(methylthio)butylisothiocyanate	2132	14.547
2-phenylethylisothioxyanate	2215	0.798
nitriles		
4-methylpentenenitrile	1244	0.034
3-(methylthio)propanenitrile	1703	0.028
4-(methylthio)butylnitrile	1785	10.627
benzyl nitrile	1915	0.062
benzenepropanenitrile	2030	0.482
5-(methylthio)pentylnitrile	1934	31.639
sulfides		
dimethyl sulfide	1082	0.004
2,4-dithiapentane		
dimethyl trisulfide	1364	0.018
3-(methylthio)propanal	1450	0.080
3-(methylthio)propanol	1713	0.011
4-(methylthio)-1-butanal	1831	0.181
heterocyclic compounds		
tetrahydrothiophene	1152	0.084
pyridine	1186	0.031
1,4,5-trimethylthiazole	1358	0.020
dihydro-2(3)-thiophenone	1638	0.020
1,2,4-trithiolane	1728	0.034

[a]On DB-WAX.

identified.[25] 4-(Methylthio)butylisothiocyanate, 2-phenylethylisothiocyanate, 5-(methylthio)pentylnitrile, and 1,2-dimethoxybenzene were also reported in raw broccoli in a previous study.[26] In broccoli stored under low-oxygen conditions, 3-hydroxybutan-2-one, 2-pentenol, hexanal, hexanol, (*E*,*E*)-2,4-heptadienal, and phenylpropanenitrile were identified.[27]

In this study, 4-methylpentylisothiocyanate, 3-(methylthio)-propylisothiocyanate, and 4-(methylthio)butylnitrile were found as the major compounds found in broccoli sprouts but not in mature broccoli. The functional group −N═C═S in isothiocyanate compounds has been known to possess antioxidant activity, which induces phase II enzymes associated with detoxification of chemical carcinogens.[28]

It is well-known that phenolic compounds found in plants possess antioxidant activity.[29] Possible phenolic antioxidants found in the present study are 4-(1-methylpropyl)phenol, 4-methylphenol, and 2-methoxy-4-vinylphenol. A potent antioxidant activity of 2-methoxy-4-vinylphenol isolated and identified from a persimmon peel was previously reported.[30] Moreover, 2-methoxy-4-vinylphenol found in brewed coffee possessed potent antioxidant activity (>90%) at the level of 200 μg/mL tested by MA/GC assay.[31]

Fraction I (refer to Figure 1) contained isobutylisothiocyanate (0.03 μg/g), allylisothiocyanate (0.02 μg/g), and 2-phenylethylisothiocyanate (0.73 μg/g). A previous study has demonstrated that allylisothiocyanate was found as a volatile compound in Emeraude cauliflower and possessed strong antioxidant activity.[32] Fraction II contained 4-methylpentylisothiocyanate (0.31 μg/g), 4-(methylthio)butylnitrile (3.70 μg/g), 5-(methylthio)pentylnitrile (7.15 μg/g), 3-(methylthio)-propylisothiocyanate (3.20 μg/g), and 4-(methylthio)-butylisothiocyanate (9.98 μg/g). 4-(Methylthio)-butylisothiocyanate has direct antioxidant activity in addition to inducing phase II enzymes. It also oxidizes to sulforaphane, which has anticancer, anti-*Helicobacter*, and antioxidant activities.[18,33] 4-Methylpentylisothiocyanate found in *Raphanus sativus* root induced apoptotic cell death in human cancer cell lines.[34] 4-(Methylthio)butylnitrile, 5-(methylthio)pentylnitrile, and 3-(methylthio)propylisothiocyanate were also reported in Emeraude and Magnifico cauliflower as major volatile compounds.[32] Fraction III also contained high levels of 4-(methylthio)butylnitrile (8.26 μg/g) and 5-(methylthio)-pentylnitrile (24.98 μg/g), which may have contributed to the antioxidant activity of this fraction. These nitrogen/sulfur-containing compounds comprised >90% of the volatile sample and may significantly contribute to the antioxidant activity of broccoli sprouts.

The less volatile sample (refer to Figure 1) also showed relatively moderate antioxidant activity with dose response effects as shown in Figures 2 and 3, suggesting the presence of water-soluble antioxidants. Therefore, the total antioxidant activity of the samples prepared from broccoli sprouts may be comparable to those of known antioxidants such as α-tocopherol and BHT. The present study demonstrated that broccoli sprouts have a strong potential to be a valuable source of antioxidants. Moreover, broccoli sprouts have a short harvest time (2 weeks) and are relatively easy to produce. Therefore, broccoli sprouts could be a good source for natural antioxidants.

AUTHOR INFORMATION

Corresponding Author

*(T.S.) Phone: (530) 752-4523. Fax: (530) 752-3394. E-mail: tshibamoto@ucdavis.edu.

Present Addresses

[†](H.W.J.) Korea Food Research Institute, 1201-62 Anyangpangyoro, Bundanggu, Seongnamsi, Gyeonggido 463-746, Republic of Korea.

[§](J.-K.M.) Department of Plant Life and Environmental Sciences, Hankyong National University, Ansung, Republic of Korea.

DOI: 10.1021/jf504929m
J. Agric. Food Chem. 2015, 63, 1169−1174

Funding

This work was supported in part by a research grant from Hankyong National University in the year of 2012.

Notes

The authors declare no competing financial interest.

■ ABBREVIATIONS USED

BHT, butylated hydroxytoluene; DPPH, 1,1-diphenyl-2-picrylhydrazyl; FID, flame ionization detector; GC, gas chromatography; GC−MS, gas chromatography−mass spectrometry; MA/GC assay, malonaldehyde/gas chromatography assay; NPD, nitrogen−phosphorus detector; SD, standard deviation; SPE, solid phase extraction

■ REFERENCES

(1) Fernandes, F.; de Pinho, P. G.; Valentao, P.; Pereira, J. A.; Andrade, P. B. Volatile constituents throughout *Brassica oleracea* L. var. *acephala* germination. *J. Agric. Food Chem.* **2009**, *57*, 6795−6802.

(2) Mwikya, S. M.; Camp, J. V.; Rodriguez, R.; Huyghebeart, A. Effects of sprouting on nutrient and antinutrient composition of kidney beans (*Phaseolus vulgaris* var. Rose coco). *Eur. Food Res. Technol.* **2001**, *212*, 188−191.

(3) Li, Y.; Zhang, T.; Korkaya, H.; Liu, S.; Lee, H. F.; Newman, B.; Yu, Y.; Clouthier, S. G.; Schwartz, S. J.; Wicha, M. S.; Sun, D. Sulforaphane, a dietary component of broccoli/broccoli sprouts, inhibits breast cancer stem cells. *Clin. Cancer Res.* **2010**, *16*, 2580−2590.

(4) Kurilich, A. C.; Tsau, G. J.; Brown, A.; Howard, L.; Klein, B. P.; Jeffery, E. H.; Kushad, M.; Wallig, M. A.; Juviket, J. A. Carotene, tocopherol, and ascorbate contents in subspecies of *Brassica oleracea*. *J. Agric. Food Chem.* **1999**, *47*, 1576−1581.

(5) Plumb, G. W.; Price, K. R.; Rhodes, M. J.; Williamson, G. Antioxidant properties of the major polyphenolic compounds in broccoli. *Free Radical Res.* **1997**, *27*, 429−435.

(6) Murkovic, M.; Gams, K.; Draxl, S.; Pfannhauser, W. Development of an Austrian carotenoid database. *J. Food Compos. Anal.* **2000**, *13*, 435−440.

(7) Krinsky, N. I. Carotenoids as antioxidants. *Nutrition* **2001**, *17*, 815−817.

(8) Kurilich, A. C.; Jeffery, E. H.; Juvik, J. A.; Wallig, M. A.; Klein, B. P. Antioxidant capacity of different broccoli (*Brassica oleracea*) genotypes using the oxygen radical absorbance capacity (ORAC) assay. *J. Agric. Food Chem.* **2002**, *50*, 5053−5057.

(9) Ford, S. M.; Hook, J. B.; Bond, J. T. The effect of butylated hydroxyanisole and butylated hydroxytoluene on renal function in the rat. *Food Cosmet. Toxicol.* **1980**, *18*, 21−26.

(10) Perez-Jimenez, J.; Diaz-Rubio, M. E.; Saura-Calixto, F. Non-extractable polyphenols, a major dietary antioxidant: occurrence, metabolic fate and health effects. *Nutr. Res. Rev.* **2013**, *26*, 118−129.

(11) Kamiyama, M.; Shibamoto, T. Flavonoids with potent antioxidant activity found in young green barley leaves. *J. Agric. Food. Chem.* **2012**, *60*, 6260−6267.

(12) Singhara, A.; Macku, C.; Shibamoto, T. Antioxidative activity of brewed coffee extracts. In *Functional Foods for Disease Prevention II: Medicinal Plants and Other Foods*; ACS Symposium Series 701; American Chemical Society: Washington, DC, USA, 1998; pp 101−109.

(13) Wei, A.; Shibamoto, T. Antioxidant/lipoxygenase inhibitory activities and chemical compositions of selected essential oils. *J. Agric. Food Chem.* **2010**, *58*, 7218−7225.

(14) Lee, K. G.; Shibamoto, T. Determination of antioxidant potential of volatile extracts isolated from various herbs and spices. *J. Agric. Food Chem.* **2002**, *50*, 4947−4952.

(15) Lee, K. G.; Shibamoto, T. Antioxidant activities of volatile components isolated from *Eucalyptus* species. *J. Sci. Food Agric.* **2001**, *81*, 1573−1579.

(16) Lee, K. G.; Shibamoto, T. Determination of antioxidant properties of aroma extracts from various beans. *J. Agric. Food Chem.* **2000**, *48*, 4817−4820.

(17) Shiratsuchi, H.; Chang, S.; Wei, A.; El-Ghorab, A. H.; Shibamoto, T. Biological activities of low-molecular weight compounds found in foods and plants. *J. Food Drug Anal.* **2012**, *20* (Suppl. 1), 359−365.

(18) Moon, J. K.; Kim, J. R.; Ahn, Y. J.; Shibamoto, T. Analysis and anti-*Helicobacter* activity of sulforaphane and related compounds present in broccoli (*Barassica oleracea* L.) sprouts. *J. Agric. Food Chem.* **2010**, *58*, 6672−6677.

(19) Kamiyama, M.; Shibamoto, T. Increase of bioactive sulforaphane and its related compounds with sulfur compounds in broccoli (*Brassica oleracea* var. *italica*) sprouts during cultivation. *Int. J. Agric. Innovations Res.* **2013**, *2*, 299−306.

(20) Kovàts, E. Gas chromatographic characterization of organic substances in the retention index system. *Adv. Chromatogr.* **1965**, *1*, 229−247.

(21) Moon, J.-K.; Shibamoto, T. Antioxidant assays for plant and food components. *J. Agric. Food Chem.* **2009**, *57*, 1655−1666.

(22) Bettaieb, I.; Bourgou, S.; Wannes, W. A.; Hamrouni, I.; Limam, F.; Marzouk, B. Essential oils, phenolic, and antioxidant activities of different parts of cumin (*Cuminum cyminum* L.). *J. Agric. Food Chem.* **2010**, *58*, 10410−10418.

(23) Lee, K. G.; Shibamoto, T. Antioxidant properties of aroma compounds isolated from soybean and mung bean. *J. Agric. Food Chem.* **2000**, *48*, 4290−4293.

(24) Takahashi, M.; Shibamoto, T. Chemical compositions and antioxidant/anti-inflammatory activities of steam distillate from freeze-dried onion (*Allium cepa* L.) sprout. *J. Agric. Food Chem.* **2008**, *56*, 10462−10467.

(25) Jacobsson, A.; Nielsen, T.; Sjöholm, I. Influence of temperature, modified atmosphere packaging, and heat treatment on aroma compounds in broccoli. *J. Agric. Food Chem.* **2004**, *52*, 1607−1614.

(26) Buttery, R. G.; Guadagni, D. G.; Ling, L. C.; Seifert, R. M.; Lipton, W. Additional volatile components of cabbage, broccoli, and cauliflower. *J. Agric. Food Chem.* **1976**, *24*, 829−832.

(27) Krunbein, A.; Klaring, H. P.; Schonhof, I.; Schreiner, M. Atmospheric carbon dioxide changes photochemical activity, soluble sugars and volatile levels in broccoli (*Brassica oleracea* var. *italica*). *J. Agric. Food Chem.* **2010**, *58*, 3747−3752.

(28) de Figueiredo, S. M.; Fiho, S. A.; Nogueira-Machado, J. A.; Caligiorne, R. B. The anti-oxidant properties of isothiocyanates: a review. *Recent Pat. Endocr. Metab. Immune Drug Discovery* **2013**, *7*, 213−225.

(29) Rubió, L.; Motilva, M. J.; Romero, M. P. Recent advances in biologically active compounds in herbs and spices: a review of the most effective antioxidant and anti-inflammatory active principles. *Crit. Rev. Food Sci. Nutr.* **2013**, *53*, 943−953.

(30) Fukai, S.; Tanimoto, S.; Maeda, A.; Fukuda, H.; Okada, Y.; Nomura, M. Pharmacological activity of compounds extracted from persimmon peel (*Diospyros kaki* THUNB.). *J. Oleo Sci.* **2009**, *58*, 213−219.

(31) Fujioka, K.; Shibamoto, T. Quantitation of volatiles and nonvolatile acids in an extract from coffee beverages: correlation with antioxidant activity. *J. Agric. Food Chem.* **2006**, *54*, 6054−6058.

(32) Podsedek, A. Natural antioxidants and antioxidant capacity of *Brassica* vegetables: a review. *LWT* **2007**, *40*, 1−11.

(33) Barillari, J.; Canistro, D.; Paolini, M.; Ferroni, F.; Pedulli, G. F.; Iori, R.; Valgimigli, L. Direct antioxidant activity of purified glucoerucin, the dietary secondary metabolite contained in rocket (*Eruca sativa* Mill.) seeds and sprouts. *J. Agric. Food Chem.* **2005**, *53*, 2475−2482.

(34) Beevi, S. S.; Mangamoori, L. N.; Subathra, M.; Edula, J. R. Hexane extract of *Raphanus sativus* L. roots Inhibits cell proliferation and induces apoptosis in human cancer cells by modulating genes related to apoptotic pathway. *Plant Foods Hum. Nutr.* **2010**, *65*, 200−209.

DOI: 10.1021/jf504929m
J. Agric. Food Chem. 2015, 63, 1169−1174

Table 1. List of the Detected Compounds from a Sample of the Frantoio Olives from 2012, Collected at 122 DAFB[a]

			lyophilized olive samples			
no.	compd name	MW	mean (mg/kg of dm)	CV (%)	λ_{max} (nm)	major ESI$^-$ peaks
			Secoiridoids			
4	demethyloleuropein	526	359.4	3.76	280	525, 241
11	nuzhenide	686	858.1	5.31	280	685, 523, 223, 179
12	hydroxytyrosyl acyclodihydroelenolate	382	nd		280	381, 363, 349, 245, 227, 153, 151
13	caffeoyl 6′-secologanoside	552	651.4	4.63	280	551, 507, 389, 162
14 + 15 + 17	sum of oleuropein aglycon isomers	378	264.1	7.15	280	377, 307, 275
16	oleuropein	540	32964.0	3.81	280	539, 403, 377, 307, 275, 223
18	comselogoside	536	912.1	4.04	280	535, 491, 389, 345, 145
19	ligstroside	524	1643.8	5.83	280	523
20	oleoside	390	1678.5	5.97	240	389
21	oleoside 11-methyl ester	404	1159.3	5.63	240	807, 403, 179, 224
22	nuzhenide oleoside	1072	1873.0	3.62	240	1071, 909, 685, 523, 299
			Phenylpropanoids			
3	chlorogenic acid	354	162.0	8.97	280	353, 191, 179
6	verbascoside	624	2088.6	6.22	280	623, 461, 161
8 + 9 + 10	sum of isoacteoside isomers	624	101.7	7.80	280	623, 297, 161
			Flavonoids			
5	rutin	610	401.9	2.48	280	609, 301, 300
7	luteolin 7-*O*-glucoside	448	315.5	6.01	280	447, 285
			Phenolic Acids			
1	hydroxytyrosol	154	316.4	7.59	280	153
2	tyrosol	138	nd		280	
			Total Phenolic Content at 280 nm			
	total		63162.3	3.42	280	

[a]The table shows the main fragmentation and the concentration of each compound expressed in milligrams per kilogram of dried matter (dm). The data are the mean of five independent determinations. nd = not detected.

olives harvested in 2011 and fresh with lyophilized fruits from the 2012 season. This research also sheds further light on some biosynthetic aspects of secoiridoids during ripening of the three Tuscan cultivars: Frantoio, Moraiolo, and Leccino. These findings provide a better evaluation of possible applications of the olive flours obtained from unripe freeze-dried fruits for nutraceutical uses.

MATERIALS AND METHODS

Chemicals. All chemicals for the analyses were of analytical reagent grade. The Milli-Q-system (Millipore SA, Molsheim, France) was used to produce deionized water. *n*-Hexane and methanol of HPLC grade were from J.T. Baker (Phillipsburg, NJ), and ethanol and acetonitrile of HPLC grade were purchased from Panreac (Barcelona, Spain). Phosphoric acid was from Merck (Darmstadt, Germany). Tyrosol, syringic acid, verbascoside, and luteolin 7-*O*-*β*-D-glucoside from Sigma-Aldrich (Steinheim, Germany) and oleuropein from Extrasynthese (Genay, France) were used as standard compounds. All the stock solutions containing the standards were prepared in methanol.

Samples. During the 2011 crop season, 10 olive plants of each of the typical Tuscan cultivars Frantoio, Moraiolo, and Leccino were selected from the farm Azienda Agricola Torre Bianca at San Casciano Val di Pesa (Florence). The olive samples were picked from the selected olive plants on a weekly basis, starting from the 109th day after full blooming (DAFB), corresponding to the last week in August. Picking was carried out every Monday morning for 13 weeks until the 193rd DAFB, corresponding to the third week in November. For each of the 13 dates, approximately 500 g of olive fruit of each cultivar was picked from 10 olive plants along their circumference at a height close to 170 cm. As soon as they arrived in the laboratory, some of the olives were used for the fresh fruit analyses while the rest were deep-frozen in liquid nitrogen and stored in a freezer at approximately −20 °C.

During the 2012 crop season, 10 plants of each of the same cultivars were selected from the farm Azienda Agricola Buonamici, Fiesole (Florence). The olive samples were collected on a weekly basis, from the 80th DAFB, corresponding to the first week in September, until the 171th DAFB, corresponding to the first week in December. The conditions of picking were the same as for the 2011 season. As soon as the olives arrived in the laboratory, all samples were analyzed as fresh fruits. On a biweekly basis, part of the sample was freeze-dried.

Freeze-Drying Process. The freeze-drying process was conducted on whole fruits. The olives were deep-frozen in liquid nitrogen, and immediately after, they were subdivided into smaller lots of 125 g and placed in the freeze-dryer at 0.3 atm and −20 °C until they reached a constant weight (5−7 days).

Water Content. The cake/powder obtained by crushing a homogeneous batch of whole olives using a laboratory crusher was used to determine the water content. The procedure consists of placing 60 g of the sample in an oven at 105 °C until it reaches constant weight.

Total Oil Content. The total oil content was determined on fresh olive paste, previously dehydrated in an oven at 103 °C until constant weight, and on freeze-dried olive pastes. In the case of fresh olive paste, the samples were extracted with hexane in an automatic Randall extractor (model 148, VELP Scientifica, Milan, Italy), as previously described.[23] When using lyophilized olive paste, approximately 3 g of sample was weighed in a beaker, and 50 mL of hexane was added. The mixture was stirred at room temperature for 6 h. The results are expressed as grams per kilogram of dry matter (dm).

Extraction of Phenolic Compounds from the Fresh Fruits. Approximately 100 g of fresh olives was crushed with a small laboratory crusher (Zeutec, Germany) to obtain an olive cake as homogeneous as possible within a few hours after collection by applying the extraction method previously described.[18] Briefly, immediately after crushing, 8 g of cake was extracted twice with 30 mL of the EtOH/H_2O (80:20) solution in the presence of 0.5 mL of the internal standard (syringic acid close to 1.5 mg/mL) using a cold ice bath. The obtained solution was concentrated under reduced pressure at 35−40 °C, washed twice with hexane, centrifuged at 7000 rpm and 10 °C, and filtered in a 10 mL flask by a cellulose acetate membrane of 0.45 μm; 5 mL of methanol was

DOI: 10.1021/jf5051359
J. Agric. Food Chem. 2015, 63, 1175−1185

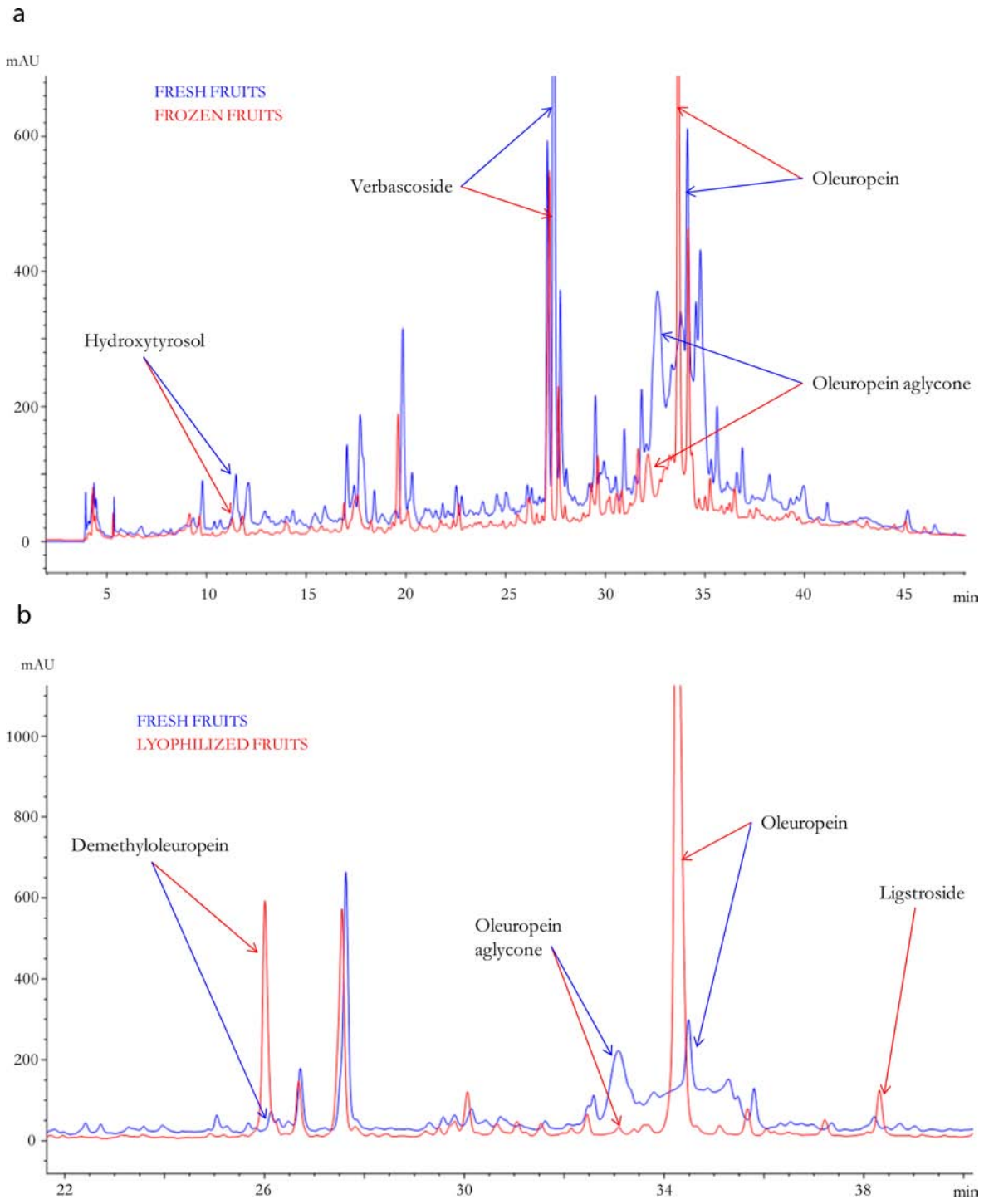

Figure 1. Overlapping of the HPLC profiles at 280 nm of (a) fresh (light blue) and frozen (red) Moraiolo olives at 151 DAFB and (b) fresh (light blue) and freeze-dried (red) Frantoio olives at 150 DAFB.

added, and the final volume was reached with Milli-Q water. The obtained solution was immediately used for chromatographic analysis.

Extraction of Phenolic Compounds from the Frozen Fruits. Five months after collection and freezing, the frozen samples from the 2011 season were used for extraction of the phenolic compounds. The frozen fruits were crushed immediately after they were removed from the freezer (temperature close to −20 °C), and the extraction method used was the same as for the fresh samples. The samples before the addition of the hydroalcoholic solution were kept close to 0 °C.

Extraction of Phenolic Compounds from the Freeze-Dried Fruits. The whole olives were freeze-dried within 6 h after harvest. Five months after collection and freeze-drying, the dried samples of the 2012 season were treated by applying the same extraction method used for the fresh samples, but the weight of each sample was 4 g.

Storage Conditions for the Ground Freeze-Dried Fruits. The olive pastes/powders obtained from milling the whole freeze-dried fruits were stored in conditions of oxidative stress: natural light exposure, temperature higher than 23 °C, and air exposure. Four months after milling, phenolic compounds were extracted again from these olive pastes.

HPLC−DAD−ESI-MS Analysis. Analyses were performed using an HP1100 liquid chromatograph, coupled with DAD and MS detectors, with the HP1100 MSD API-electrospray as the interface (all from

DOI: 10.1021/jf5051359
J. Agric. Food Chem. 2015, 63, 1175−1185

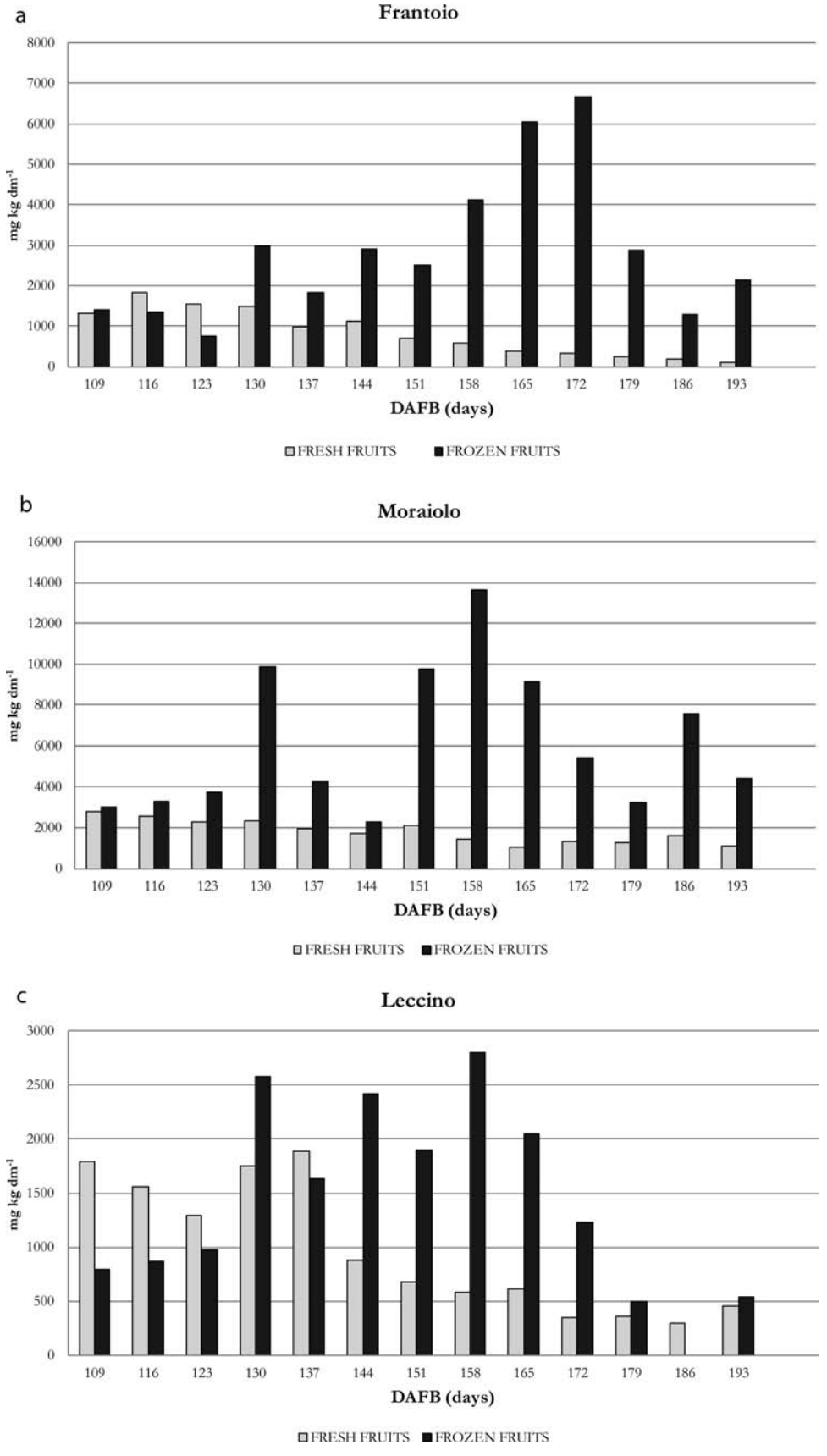

Figure 2. Changes in oleuropein content in fresh and frozen samples harvested in 2011 for Frantoio, Moraiolo, and Leccino olive cultivars.

Agilent Technologies, Palo Alto, CA). A Hypersil Gold QRP-18 (4.6 mm internal diameter, 250 mm length, particle size 3 μm; Thermo Electron Corp., Austin, TX) column was used, associated with a 10 × 4 mm precolumn of the same phase; the oven temperature was 30 °C.

DOI: 10.1021/jf5051359
J. Agric. Food Chem. 2015, 63, 1175−1185

Elution was performed using H_2O at pH 3.2 by formic acid (A), acetonitrile (B), and methanol (C), with a flow rate of 0.8 mL/min with a multistep linear gradient. Both the organic solvents B and C changed as follows: from 2.5% to 27.5% in 45 min and then to 50% in 10 min, with a final plateau of 5 min, with 60 min as the total time of analysis. The following wavelengths were simultaneously selected: 240, 280, and 330 nm.

Quantification of Phenolic Compounds. To quantify each compound, syringic acid was chosen as the internal standard. To evaluate the relative response factor (RRF), the following standards were used: oleuropein for the quantification of oleuropein, oleuropein aglycon, ligstroside, nuzhenide, demethyloleuropein, hydroxytyrosyl acyclodihydroelenolate, comselogoside, caffeoyl 6′-secologanoside, oleoside, oleoside 11-methyl ester, and nuzhenide oleoside (whose values are expressed in milligrams of oleuropein per kilogram of dm); luteolin 7-*O*-glucoside for the quantification of luteolin, rutin, and luteolin 7-*O*-glucoside (whose values are expressed in milligrams of luteolin 7-*O*-glucoside per kilogram of dm); verbascoside for the quantification of chlorogenic acid, verbascoside, and isoverbascoside (whose values are expressed in milligrams of verbascoside per kilogram of dm); tyrosol for the quantification of hydroxytyrosol and tyrosol (whose values are expressed in milligrams of tyrosol per kilogram of dm).

With the aim of also evaluating the minor compounds, the total phenolic content was calculated using only one reference standard and is expressed in milligrams of oleuropein per kilogram of dm. All these molecules were evaluated at 280 nm with the exception of the following secoiridoids: nuzhenide oleoside, oleoside, and oleoside-11-methyl ester. Since these latter molecules do not have the phenol moiety in their molecular structure, their determination was done working at 240 nm.

Precision Parameters. The procedure precision was evaluated only for the lyophilized samples from 2012 because these parameters for fresh and frozen olives had been previously reported.[18] The extraction was repeated five times starting from different shares of olives from the same batch collected at 122 DAFB (about 400 g of fresh olives), and the obtained findings are expressed in terms of the coefficient of variation (CV; %) (Table 1).

RESULTS AND DISCUSSION

Phenolic Profiles of Fresh and Frozen Olives. The phenolic profile of the fresh fruits from the 2011 crop season were compared with that of the corresponding frozen fruits. These two kinds of samples are characterized by similar amounts of water (close to 50% of the total weight), but different temperatures at the moment of milling (room temperature for the fresh fruits, close to 0 °C for the frozen fruits). The overlay of the phenolic profile from fresh and frozen fruits of a sample of Moraiolo shown in Figure 1a highlights some relevant differences. Analyzing the quantitative data of all the fresh and frozen fruits (Supporting Information, Table a), the main differences were related to the secoiridoidic phenols. First, the ligstroside was undetectable, while oleuropein, as expected, was often one of the main compounds.

Oleuropein. In unripe fruits, the oleuropein content was similar in fresh and frozen olives of the Frantoio and Moraiolo cultivars, while it was more abundant in fresh olives of Leccino (Figure 2). During ripening, a strong decrease of oleuropein in all the fresh olives was observed. On the other hand, the content in the corresponding frozen olives increased up to 7-fold in the Frantoio cultivar, 10-fold in Moraiolo, and 5-fold in Leccino. Moraiolo olives were richer in oleuropein (from 1061 to 2758 mg/kg in fresh olives, from 2267 to 13656 mg/kg in frozen olives) than Frantoio (from 113 to 1825 mg/kg in fresh fruit, from 762 to 6677 mg/kg in frozen fruit) or Leccino (from 297 to 1892 mg/kg in fresh fruit, from 501 to 2804 mg/kg in frozen fruit) at all the DAFB.

Demethyloleuropein. This compound, when detectable, was more abundant in frozen olives compared to fresh ones. Low amounts only in the last 3 weeks of sampling (from 55 to 101 mg/kg) were detected in the fresh olives from Frantoio. Increased amounts (from 198 to 4452 mg/kg) were detected in the frozen olives harvested from the middle of the ripening period. Analogous behavior was observed for the fresh Leccino olives with low quantities (from 51 to 258 mg/kg) only in the last 4 weeks of ripening and again higher concentrations (from 487 to 1892 mg/kg) in the frozen fruits harvested in the last 5 weeks of ripening. This molecule was never detectable in the fresh Moraiolo olives, and low content was found in the frozen olives (from 231 to 355 mg/kg) only at the end of the ripening season.

Oleuropein Aglycon. This secoiridoid was more abundant in the fresh olives of the three cultivars at all the DAFB if compared with the corresponding frozen fruits. In particular, Moraiolo was the richest cultivar with values ranging from 4854 to 12386 mg/kg in fresh fruits and less (from 1493 to 10117 mg/kg) in frozen ones. The same behavior but with lower content was true for Frantoio (from 871 to 8553 mg/kg in fresh fruits, from 581 to 4147 mg/kg in frozen fruits) and Leccino (from 1756 to 9164 mg/kg in fresh fruits; from 737 to 7045 mg/kg in frozen fruits).

Nuzhenide. The ratio between nuzhenide levels in frozen olives and that in fresh olives increased during ripening in all three cultivars.

The minor secoiridoids, oleoside, oleoside 11-methyl ester, and nuzhenide oleoside, were greatly increased in frozen olives as shown in the Supporting Information (Table a).

Overall, the main differences between the treatment of the fresh and frozen fruits can be related to the temperature of milling, which is close to 25 °C for fresh fruit and close to 0 °C for frozen fruits. The β-glucosidase hydrolyzes the substrates even when a very short time of milling (30 s) is applied and the time between milling and the addition of the hydroalcoholic mixture (less than 2 min) is strongly reduced. By observing the data related to oleuropein and oleuropein aglycon, it emerges that the low temperature of milling for frozen fruit partially inhibits the enzyme, as confirmed by the lower amounts of the corresponding aglycon (Supporting Information, Table a).

Anyway, the presence of the water's fruit allows a certain activity of this enzyme to also be maintained in the frozen olives. To quantify this effect, we analyzed the phenolic compounds in the freeze-dried fruits of the same cultivar in the 2012 crop season.

Phenolic Profiles in Fresh and Whole Freeze-Dried Olives. In light of the data collected from the 2011 samples, our aim was to use the 2012 crop season to better investigate the role played by the water of the fruits to affect the final phenolic content. Therefore, each sample was divided into two aliquots: one analyzed as fresh and the other as freeze-dried (Supporting Information, Table b). As expected, the choice to lyophilize the olives as whole fruit without any preliminary breaking was crucial. Each pair of samples had different amounts of water during the crushing, close to 50% of the total weight for the fresh olives and a negligible amount in the freeze-dried fruits (Supporting Information, Table c). Unlike the 2011 fruits, the same temperature (close to room temperature) during the milling process was guaranteed for all the 2012 samples.

The overlay of the chromatograms at 280 nm for the phenolic profiles of fresh and freeze-dried fruits (Figure 1b) highlights strong differences. According to the quantitative results (Supporting Information, Table b), the freeze-drying process protects the phenolic compounds against enzymatic degradation

DOI: 10.1021/jf5051359
J. Agric. Food Chem. 2015, 63, 1175−1185

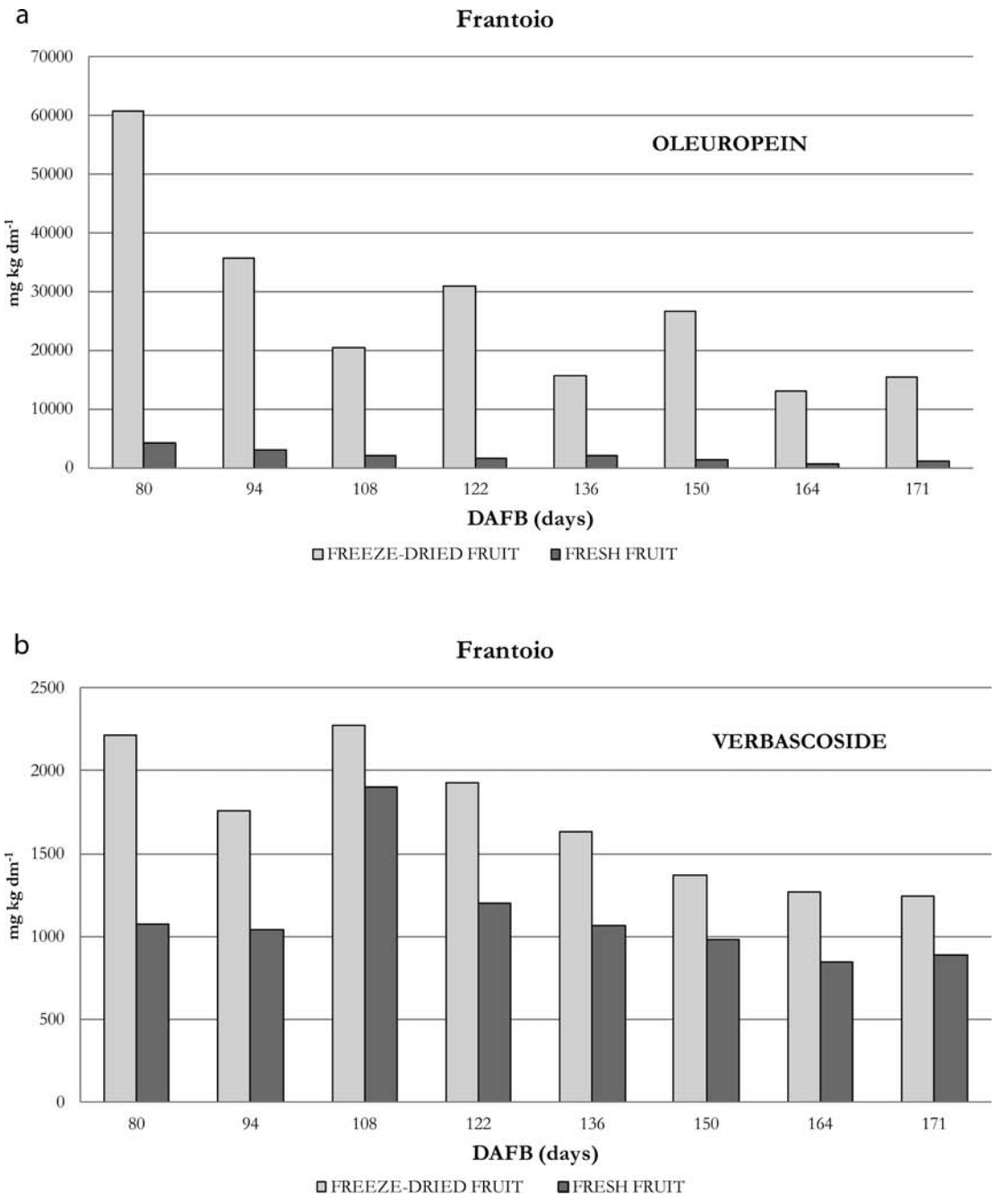

Figure 3. Changes over time for oleuropein and verbascoside in fresh and freeze-dried Frantoio olives.

that occurs during the milling process and/or during the short time before the addition of the hydroalcoholic mixture. The almost complete elimination of the water does prevent endogenous enzyme activity, mainly of the phenol oxidases,[14−17] which during extra virgin olive oil production rapidly induces a decrease in the secoiridoid content.

The novelty of our research is that we have shown that there are huge differences in the contents of the secoiridoids in fresh and whole lyophilized olives. The values of some key molecules such as oleuropein in the dried fruits were several times higher compared with those in the corresponding fresh sample. On the other hand, these differences were consistently lower for other compounds, such as verbascoside (Figure 3). The same results obtained for all the coupled samples harvested during the ripening period confirm that the secoiridoidic compounds are always the main target of enzymatic activity (see also the section "Biosynthetic Considerations Regarding the Secoiridoids").

Oleuropein. This molecule was in very high concentration in freeze-dried olives of the three cultivars at all the DAFB. The values ranged from 12993 to 60679 mg/kg for Frantoio, from 17113 to 80276 mg/kg for Moraiolo, and from 7515 to 79812 mg/kg for Leccino. In the corresponding fresh olives the oleuropein content was up to 30 times lower (from 588 to 4092 mg/kg for Frantoio, from 1001 to 3097 mg/kg for Moraiolo, from 379 to 5745 mg/kg for Leccino).

Oleuropein Aglycon. Although it is shown that the freeze-drying process preserves phenolic compounds, a contrary trend compared to oleuropein was observed for oleuropein aglycon: indeed, in fresh olives, the quantities of this molecule were greater that in freeze-dried olives. In particular, we observed a

DOI: 10.1021/jf5051359
J. Agric. Food Chem. 2015, 63, 1175−1185

decrease (from 3107 mg/kg at 80 DAFB to 740 mg/kg at 122 DAFB) for Frantoio olives followed by an increase in fresh fruits (up to 6278 mg/kg), while in freeze-dried fruits it was initially not detectable and then present but in quantities not over 1379 mg/kg. The amounts of this molecule were higher in Moraiolo than in Frantoio olives with a decrease during ripening in both fresh (from 10139 mg/kg at 80 DAFB to 2787 mg/kg at 171 DAFB) and freeze-dried olives (from 14393 mg/kg at 80 DAFB to 1342 mg/kg at 171 DAFB). Analogously, higher quantities were revealed in fresh Leccino olives and a decrease in lyophilized fruits (Supporting Information, Table b). The very low content of the aglycon in the dried fruit is due to the complete inhibition of the enzyme's activity in the absence of water.

Demethyloleuropein. This secoiridoid was detectable in freeze-dried olives from half of the study period (122 DAFB), with a strong increment over time (up to 8700 mg/kg in Frantoio, 1468 mg/kg in Moraiolo, and 24535 mg/kg in Leccino). In fresh olives, demethyloleuropein was undetectable in Moraiolo at all the DAFB and only in low amounts in Frantoio and Leccino olives (Supporting Information, Table b).

Ligstroside. This precursor of a well-known biologically active compound, namely, oleocanthal,[5] was undetectable in fresh olives of the three cultivars at all the DAFB (Table 2). On the other hand, the freeze-dried fruits had slight amounts of this secoiridoid, with the highest values at the start of sampling. At the 80th DAFB, ligstroside was 3889 mg/kg in Frantoio, 4586 mg/kg in Moraiolo, and 3082 mg/kg in Leccino olives. The concentrations of ligstroside in freeze-dried olives were 20−30 times lower than those of its analogous oleuropein (Figure 4; Supporting Information, Table b).

Table 2. Content of Ligstroside over Time in Fresh and Freeze-Dried Olives from 2012[a]

	Frantoio		Moraiolo		Leccino	
DAFB	fresh fruit	freeze-dried fruits	fresh fruit	freeze-dried fruits	fresh fruit	freeze-dried fruits
80	nd	3888.9	nd	4585.7	nd	3082.0
94	nd	2658.4	nd	2359.6	nd	1645.1
108	nd	1344.6	nd	1174.4	nd	1877.6
122	nd	2206.5	nd	1231.2	nd	984.2
136	nd	943.7	nd	871.5	nd	721.0
150	nd	1361.0	nd	962.5	nd	398.4
164	nd	640.2	nd	881.6	nd	252.4
171	nd	702.3	nd	696.1	nd	372.0

[a]The molecule was not revealed in fresh and frozen olives from 2011. nd = not detected.

Other minor secoiridoids such as nuzhenide, hydroxytyrosyl acyclodihydroelenolate, oleoside, oleoside 11-methyl ester, and nuzhenide oleoside had significantly different quantities in fresh and lyophilized fruits, with a great increment in the latter ones (Supporting Information, Table b).

Biosynthetic Considerations Regarding the Secoiridoids. The results of this research allow us to clarify some biosynthetic aspects of olive phenolic compounds. In a previous work,[24] the researchers hypothesized that demethyloleuropein is both an intermediate in the oleuropein biosynthesis and a degradation product of the oleuropein. In another paper,[20] it was suggested that demethyloleuropein is cultivar-dependent. Our previous data from frozen olives[18] allowed us to hypothesize the existence of two independent biosynthetic pathways for oleuropein and demethyloleuropein.

Our present research sheds light on biosynthetic aspects of the secoiridoidic compounds. In the unripe freeze-dried 2012 olives, demethyloleuropein was undetectable, and then its content consistently increased during ripening while oleuropein decreased in Moraiolo, as shown in Figure 4 (see also the Supporting Information, Table b). This behavior, confirmed for all three cultivars, was in contrast with the hypothesis that this molecule could be an intermediary of oleuropein biosynthesis. On the other hand, demethyloleuropein seems to be a degradation product obtained from the action of an endogenous esterase on oleuropein.

The results relating to ligstroside in the freeze-dried fruits are similar to those observed for oleuropein; the former molecule was undetectable in fresh or frozen fruits (sample of 2011; Supporting Information, Table a) because it was quickly hydrolyzed by enzymes in the presence of the olive's water. This phenomenon had already been described for the secoiridoids by other authors[15,16] and was in agreement with a previous study on these cultivars.[18] As shown in Figure 4, a similar trend was seen for oleuropein and ligstroside over time in freeze-dried Moraiolo olives. The whole lyophilized samples from Frantoio and Leccino confirmed these results. In light of our data, the use of dried fruit can be suggested as a model to study some biosynthetic pathways, taking into account that overall enzymatic degradation is prevented by the lack of water.

Defatting and Stability over Time of Cake/Powder from Whole Dried Fruit. To evaluate the potential use of this matrix in the field of food, several aspects need to be evaluated regarding treatment of higher quantities for industrial purposes. To this aim, the method of production needs to be as easy as possible, the stability over time needs to be controlled, and the final aspect of the material needs to be homogeneous and manageable.

The product obtained by crushing freeze-dried olives has varying consistency: a green homogeneous powder was derived from unripe olives, and a violet-brown cake with muddy consistency due to the increasing oil content was obtained from ripe olives. As discussed above, the phenolic content of lyophilized olives is considerably greater than that obtained from fresh olives, and the greatest differences occur at the beginning of ripening. These latter samples could be particularly useful for preparation of nutraceuticals. To evaluate the feasibility of such an idea, the stability of the cake/powder of three samples of Moraiolo at different ripening stages was controlled after 4 months (Table 3). The storage conditions were under strong oxidative stress: light exposure, room temperature close to 23−28 °C, and free air exposure. After this storage period, the initial green color of the cakes/powder was maintained, confirming the absence of the rapid enzymatic browning typical of fresh fruit.[14] Moreover, we proved that a cold extraction by using *n*-hexane, a widely applied food-grade solvent, compared with the exhaustive Soxhlet extraction, was sufficient to completely remove the fat from the olive cake/powder. In fact, the oil content of the samples reported in Table 3, obtained via Soxhlet and *n*-hexane extraction, were 16.9% and 13.9% for the sample at 80 DAFB, 33.1% and 34.0% for the sample at 122 DAFB, and 45.7% and 44.8% for the sample at 164 DAFB.

Regarding the phenolic content obtained from lyophilized olives at time 0 and after 4 months of storage, Table 3 shows the observed percentage variations for the three selected samples. It is noticeable that the total phenolic amounts were only slightly

DOI: 10.1021/jf5051359
J. Agric. Food Chem. 2015, 63, 1175−1185

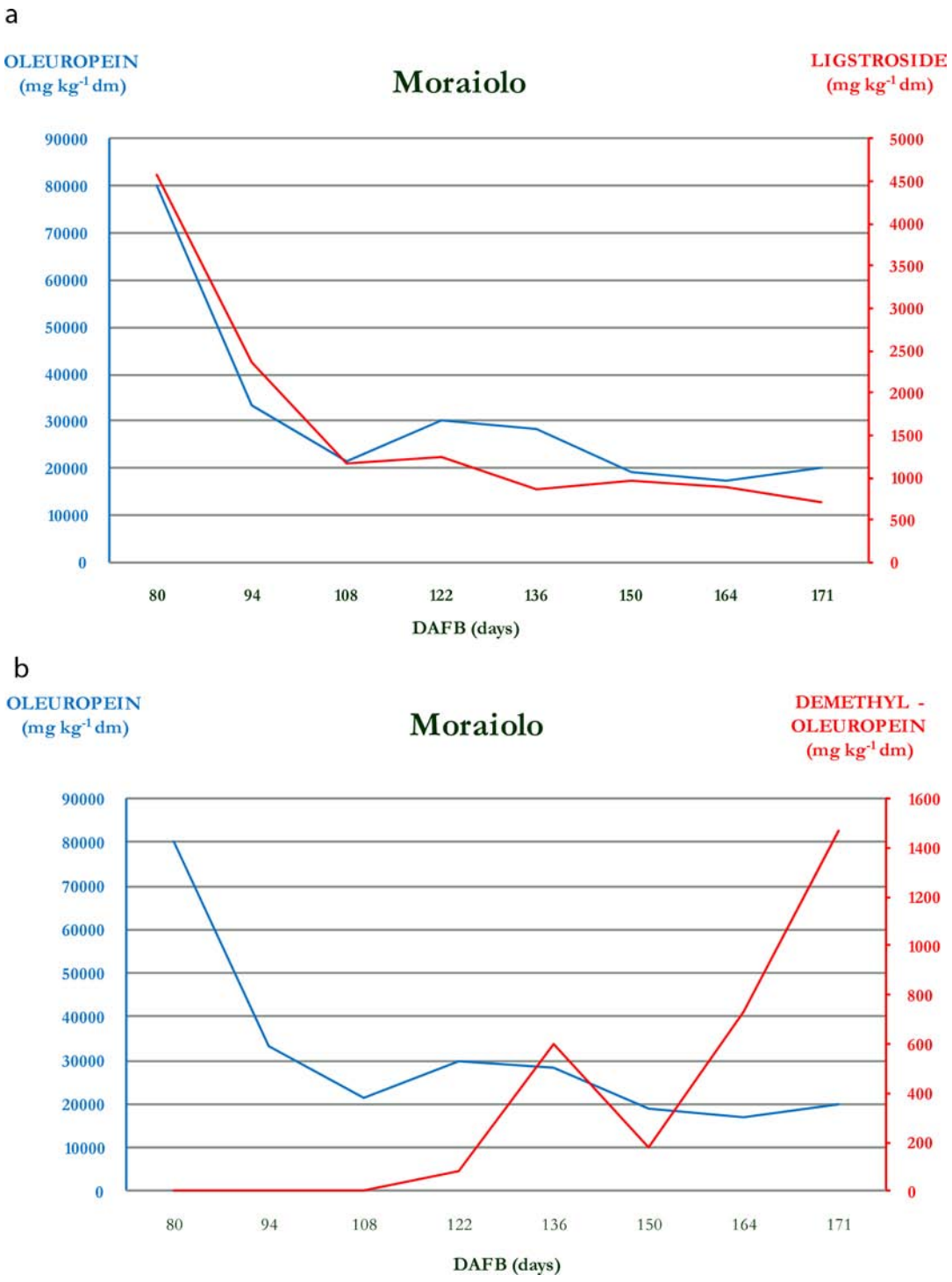

Figure 4. Concentrations of ligstroside and demethyloleuropein in Moraiolo olives during ripening in 2012. To better highlight the relation between each secoiridoid and the oleuropein, the figure shows two different scales (mg/kg of dm).

decreased, even in these stressed storage conditions; the decrease was close to 10% in the unripe sample and was even below 5% in the others.

The main decrease involved oleuropein and oleuropein aglycon. This latter molecule had close to 44% reduction in all studied samples. Oleuropein slightly decreased only in unripe olives (−11.7%), and in correspondence with this change, strong increments of hydroxytyrosol and oleoside 11-methyl ester were observed. It can be hypothesized that the decrease of oleuropein is due to the rupture of the ester bond (Figure 5) mediated by the esterase enzyme, with hydroxytyrosol and oleoside 11-methyl ester formed by this rupture.[15] The results from the other two samples confirmed this hypothesis, because the low variations of oleuropein were related to a nonsimultaneous increase in hydroxytyrosol and oleoside 11-methyl ester.

In light of the recognized benefits of secoiridoid compounds from olive oils in cardiovascular health,[13] the olive powder/cake from dried fruits could be proposed as a new source of these important phenolic compounds.

DOI: 10.1021/jf5051359
J. Agric. Food Chem. 2015, 63, 1175−1185

Table 3. Effect of Storage for up to 4 Months on Powder or Cake Obtained from the Whole Lyophilized Moraiolo Olives at Different Ripening Stages[a]

	DAFB = 80			DAFB = 122			DAFB = 164		
	time 0	time 4 months	Δ (%)	time 0	time 4 months	Δ (%)	time 0	time 4 months	Δ (%)
demethyloleuropein	nd	nd		86.7	nd		732.9	738.6	0.8
nuzhenide	853.7	683.5	−19.9	966.3	946.0	−2.1	933.2	912.8	−2.2
hydroxytyrosyl acyclodihydroelenolate		371.6			158.1			222.3	
caffeoyl 6′-secologanoside	835.2	1007.1	20.6	295.1	303.6	2.9	487.8	338.9	−30.5
sum of oleuropein aglycon isomers	14393.3	8098.7	−43.7	2395.6	1371.8	−42.7	2800.0	1535.6	−45.2
oleuropein	80276.7	70907.9	−11.7	30062.0	29481.3	−1.9	17113.4	16582.6	−3.1
comselogoside	1570.4	1504.8	−4.2	842.8	835.5	−0.9	757.7	659.5	−13.0
ligstroside	4585.7	3683.6	−19.7	1231.2	1292.8	5.0	881.6	973.6	10.4
oleoside	9500.4	8894.2	−6.4	4389.5	4188.2	−4.6	2840.2	2807.2	−1.2
oleoside 11-methyl ester	738.1	1234.8	67.3	6745.8	5733.1	−15.0	7266.1	6077.6	−16.4
nuzhenide oleoside	190.9	194.2	1.7	2038.7	2142.9	5.1	2234.0	1992.1	−10.8
chlorogenic acid	242.4	249.8	3.1	116.0	51.9	−55.3	63.1	33.7	−46.5
verbascoside	605.9	312.3	−48.5	2114.0	2241.8	6.0	1653.0	1679.9	1.6
sum of isoverbascoside isomers	70.5	62.2	−11.8	195.9	175.5	−10.4	95.9	115.1	19.9
rutin	982.6	820.1	−16.5	496.6	607.6	22.4	337.6	470.8	39.5
luteolin 7-*O*-glucoside	571.8	513.3	−10.2	354.7	340.9	−3.9	250.0	229.9	−8.0
hydroxytyros ol	1101.5	2693.9	144.6	492.2	943.6	91.7	492.2	1645.1	234.2
tyrosol	nd	nd		nd	nd		nd	nd	
total	148096.0	131880.4	−10.9	77243.8	79238.7	2.6	62082.8	59467.4	−4.2

[a]The data are expressed in milligrams per kilogram of dry matter. nd = not detected.

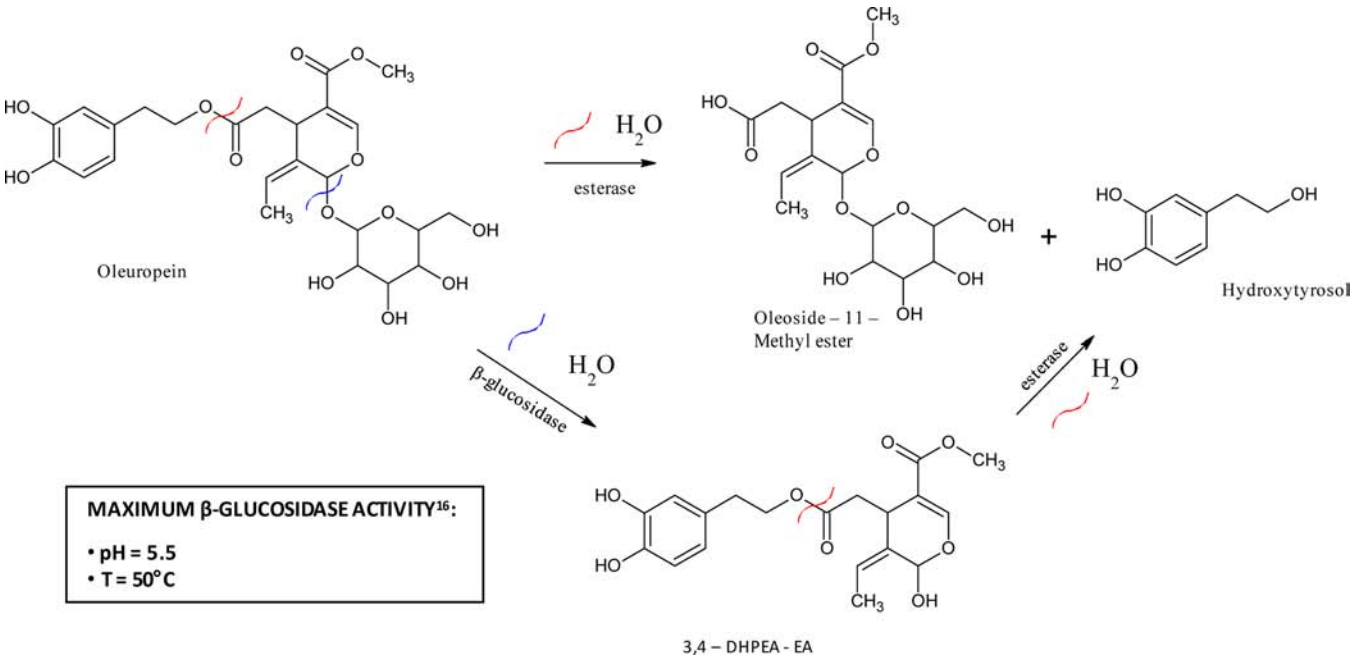

Figure 5. Oleuropein and its relationship with the other main secoiridoids.

In conclusion, the principal novelty of this research is the study of whole freeze-dried olives which turn out to have unexpectedly high concentrations of the secoiridoidic compounds (from 10 to 20 times higher than those in fresh fruits), an observation which has not been previously reported in the literature. The removal of water without previous crushing prevents the rapid enzymatic degradation of this fraction, allowing us to better investigate the real phenolic content in the fruit and providing useful information on some biosynthetic aspects of these secoiridoidic molecules. To the best of our knowledge, this approach has never been applied to whole dried olives to date. Another novelty of this work is the strong stability of the dried cake/powder obtained from whole olives maintained in stress conditions for up to 4 months. In light of these results, it can be hypothesized that unripe olives are a potential source of secoiridoids in the form of a homogeneous powder which is very low in fat and suitable for human consumption. To date, those secoiridoids typical of the olive but also of extra virgin olive oils are not widely present in common foods, as happens for many other phenolic and flavonoid compounds. Several commercial products rich in phenolic compounds derived from different parts (leaves, fruit) of *Olea europaea* or from milling wastes have been marketed, confirming the great interest in these compounds. The freeze-drying process is an expensive method not suitable for work on a

DOI: 10.1021/jf5051359
J. Agric. Food Chem. 2015, 63, 1175−1185

large scale, but the obtained data can be useful to suggest further investigation on most convenient methods to remove the water and/or inhibit the endogenous enzymes in olives. Moreover, this approach can be the best way to exploit this fruit not only as a source of olive oil.

■ ASSOCIATED CONTENT

Supporting Information

Comparison of the phenolic content between fresh and frozen olive samples from the 2011 crop season and between fresh and freeze-dried olive samples from the 2012 crop season and water content in some of the fresh olives from 2012. This material is available free of charge via the Internet at http://pubs.acs.org.

■ AUTHOR INFORMATION

Corresponding Author

*Phone: +39 055 4573773. Fax: +39 055 4573737. E-mail: nadia.mulinacci@unifi.it.

Notes

The authors declare no competing financial interest.

■ ACKNOWLEDGMENTS

Our deepest gratitude goes to the Azienda Agricola Buonamici and to the Azienda Agricola Torre Bianca for providing the olives and to Dr. Marco Mugelli, who recently passed away, for his great contribution to research in the field. We also thank Dr. Aleandro Ottanelli and Prof. Edgardo Giordani for freeze-drying the fruits and Dr. Mary Forrest for final English editing of the manuscript.

■ REFERENCES

(1) Masala, G.; Ceroti, M.; Pala, V.; Krogh, V.; Vineis, P.; Sacerdote, C.; Saieva, C.; Salvini, S.; Sieri, S.; Berrino, F.; Panico, S.; Mattiello, A.; Tumino, R.; Giurdanella, M. C.; Bamia, C.; Trichopoluou, A.; Riboli, E.; Palli, D. A dietary pattern rich in olive oil and raw vegetable is associated with lower mortality in Italian elderly subjects. *Br. J. Nutr.* **2007**, *98*, 406−415.

(2) Frankel, E. N. Nutritional and biological properties of extra virgin olive oil. *J. Agric. Food Chem.* **2011**, *59*, 785−792.

(3) Covas, M. I.; Nyyssonen, K.; Poulsen, H. E.; Kaikkonen, J.; Zunft, H. J.; Kiesewetter, H.; Gaddi, A.; de la Torre, R.; Mursu, J.; Baumler, H.; Nascetti, S.; Salonen, J. T.; Fito, M.; Virtanen, J.; Marrugat, J. The effect of polyphenols in olive oil on heart disease risk factor: a randomized trial. *Ann. Intern. Med.* **2006**, *145*, 333−341.

(4) Salvini, S.; Sera, F.; Caruso, D.; Giovannelli, L.; Visioli, F.; Saieva, C.; Masala, G.; Ceroti, M.; Giovacchini, V.; Pitozzi, V.; Galli, C.; Romani, A.; Mulinacci, N.; Bortolomeazzi, R.; Dolara, P.; Palli, D. Daily consumption of a high-phenol extra-virgin olive oil reduces oxidative DNA damage in postmenopausal women. *Br. J. Nutr.* **2006**, *95*, 742−751.

(5) Beauchamp, G. K.; Keast, R. S. J.; Morel, D.; Lin, J.; Pika, J.; Han, Q.; Lee, C.; Smith, A. B.; Breslin, P. A. S. Phytochemistry: ibuprofen-like activity in extra-virgin olive oil. *Nature* **2005**, *437*, 45−46.

(6) Grossi, C.; Rigacci, S.; Ambrosini, S.; Ed Dami, T.; Luccarini, I.; Traini, C.; Failli, P.; Berti, A.; Casamenti, F.; Stefani, M. The polyphenol oleuropein aglycone protects TgCRND8 mice against Aß plaque pathology. *PLoS One* **2013**, *8* (8), 1−13.

(7) Rigacci, S.; Guidotti, V.; Bucciantini, M.; Parri, M.; Nediani, C.; Cerbai, E.; Stefani, M.; Berti, A. Oleuropein aglycon prevents cytotoxic amyloid aggregation of human amylin. *J. Nutr. Biochem.* **2010**, *21* (8), 726−735.

(8) Rastrelli, L.; Passi, S.; Ippolito, F.; Vacca, G.; De Simone, F. Rate of degradation of α-tocopherol, squalene, phenolics, and polyunsaturated fatty acids in olive oil during different storage conditions. *J. Agric. Food Chem.* **2002**, *50*, 5566−5570.

(9) Visioli, F.; Bellomo, G.; Galli, C. Free radical-scavenging properties of olive oil polyphenols. *Biochem. Biophys. Res. Commun.* **1998**, *247*, 60−64.

(10) Lòpez-Miranda, J.; Perez-Jimenez, F.; Ros, E.; De Caterina, R.; Badimon, L.; Covas, M. I.; Escrich, E.; Ordovas, J. M.; Soriguer, F.; Abia, R.; Alarcon de la Lastra, C.; Battino, M.; Corella, D.; Chamorro-Quiros, J.; Delgado-Lista, J.; Giugliano, D.; Esposito, K.; Estruch, R.; Fernandez-Real, J. M.; Gaforio, J. J.; La Vecchia, C.; Lairon, D.; Lopez-Segura, F.; Mata, P.; Menendez, J. A.; Muriana, F. J.; Osada, J.; Panagiotakos, D. B.; Paniagua, J. A.; Perez-Martinez, P.; Perona, J.; Peinado, M. A.; Pineda-Priego, M.; Poulsen, H. E.; Quiles, J. L.; Ramirez-Tortosa, M. C.; Ruano, J.; Serra-Majem, L.; Sola, R.; Solanas, M.; Solfrizzi, V.; de la Torre-Fornell, R.; Trichopoulou, A.; Uceda, M.; Villalba-Mortoro, J. M.; Villar-Ortiz, J. R.; Visioli, F.; Yiannakouris, N. Olive oil and health: summary of the II International conference on olive oil and health consensus report, Jaen and Cordoba (Spain) 2008. *Nutr., Metab. Cardiovasc. Dis.* **2010**, *20*, 284−294.

(11) Sotiroudis, T. G.; Kyrtopoulos, S. A. Anticarcinogenic compounds of olive oil and related biomarkers. *Eur. J. Nutr.* **2008**, *47*, 69−72.

(12) de la Torre-Carbot, K.; Chavez-Servin, J. L.; Jauregui, O.; Castellote, A. I.; Lamuela-Raventos, R. M.; Nurmi, T.; Poulsen, H. E.; Gaddi, A. V.; Kaikkonen, J.; Zunft, H. F.; Kiesewetter, H.; Fito, M.; Covas, M. I.; Lopez-Sabater, M. C. Elevated circulating LDL phenol levels in men who consumed virgin rather than refined olive oil are associated with less oxidation of plasma LDL. *J. Nutr.* **2010**, *140*, 501−508.

(13) EFSA Panel on Dietetic Products, Nutrition and Allergies (NDA). Scientific opinion on the substantiation of health claims related to polyphenols in olive oil and protection of LDL particles from oxidative damage. *EFSA J.* **2011**, *9* (4), 2033. http://www.efsa.europa.eu/en/efsajournal/pub/2033.htm.

(14) Migliorini, M.; Cecchi, L.; Cherubini, C.; Trapani, S.; Cini, E.; Zanoni, B. Understanding degradation of phenolic compounds during olive oil processing by inhibitor addition. *Eur. J. Lipid Sci. Technol.* **2012**, *114*, 942−950.

(15) Gutierrez-Rosales, F.; Romero, M. P.; Casanovas, M.; Motilva, M. J.; Minguez-Mosquera, M. I. Metabolites involved in oleuropein accumulation and degradation in fruits of *Olea Europaea* L.: Hojiblanca and Arbequina varieties. *J. Agric. Food Chem.* **2010**, *58*, 12924−12933.

(16) Gutierrez-Rosales, F.; Romero, M. P.; Casanovas, M.; Motilva, M. J.; Minguez-Mosquera, M. I. β-Glucosidase involvement in the formation and transformation of oleuropein during the growth and development of olive fruits (*Olea Europaea* L. cv. Arbequina) grown under different farming practices. *J. Agric. Food Chem.* **2012**, *60*, 4348−4358.

(17) Rovellini, P.; Cortesi, N. Liquid chromatography-mass spectrometry in the study of oleuropein and ligstroside aglycons in virgin olive oil: aldehydic, dialdehydic forms and their oxidized products. *Riv. Ital. Sostanze Grasse* **2002**, *79*, 1−14.

(18) Cecchi, L.; Migliorini, M.; Cherubini, C.; Giusti, M.; Zanoni, B.; Innocenti, M.; Mulinacci, N. Phenolic profiles, oil amount and sugar content during olive ripening of three typical Tuscan cultivar to detect the best harvesting time for oil production. *Food Res. Int.* **2013**, *54*, 1876−1884.

(19) Jemai, H.; Bouaziz, M.; Sayadi, S. Phenolic composition, sugar content and antioxidant activity of tunisian sweet olive cultivar with renard to fruit ripening. *J. Agric. Food Chem.* **2009**, *57*, 2961−2968.

(20) Esti, M.; Cinquanta, L.; La Notte, E. Phenolic compound in different olive varieties. *J. Agric. Food Chem.* **1998**, *46*, 32−35.

(21) Damtoft, S.; Franzyk, H.; Jensen, S. R. Biosynthesis of secoiridoid glucosides in oleaceae. *Phytochemistry* **1993**, *34*, 1291−1299.

(22) Damtoft, S.; Franzyk, H.; Jensen, S. R. Biosynthesis of iridoids in *syringe* and *fraxinus*: secoiridoid precursor. *Phytochemistry* **1995**, *40*, 773−784.

(23) Cherubini, C.; Migliorini, M.; Mugelli, M.; Viti, P.; Berti, A.; Cini, E.; Zanoni, B. Towards a technological ripening index for olive oil fruits. *J. Sci. Food Agric.* **2009**, *89*, 671−682.

DOI: 10.1021/jf5051359
J. Agric. Food Chem. 2015, 63, 1175−1185

(24) Amiot, M. J.; Fleuriet, A.; Macheix, J. J. Accumulation of oleuropein derivates during olive maturation. *Phytochemistry* **1989**, *28*, 67−69.

DOI: 10.1021/jf5051359
J. Agric. Food Chem. 2015, 63, 1175−1185

which then reacts with several enzymes in the mevalonate pathway to yield cholesterol.[15] It is well established that HMGCR activity was 3-fold higher in mononuclear blood cells from patients with leukemia, compared with cells from healthy subjects.[16]

We here provide a detailed mechanistic investigation of the apoptotic effect of monacolin K and how it is related to the inhibition of GLO1. In the present study, we hypothesize that monacolin K showed its apoptotic activity through the inhibition of HMGCR, inactivation of Ras translocation, and down-regulation of PI3K/Akt and Raf/ERK1/2 signal pathways, leading to suppression of GLO1 and HMGCR in U937 cells.

MATERIALS AND METHODS

Chemicals and Antibodies. Monacolin K, perchloric acid, 2-methylquinoxaline (2-MQ), *o*-phenylenediamine, 3-(4,5-dimethylthiazol-2-y-l)-2,5-diphenyltetrazolium bromide (MTT), dimethyl sulfoxide (DMSO), and 4,6-diamidino-2-phenylindole (DAPI) were purchased from Sigma-Aldrich (St. Louis, MO, USA). Cell culture media were purchased from Invitrogen (Carlsbad, CA, USA). Antibodies against phospho-p44/42 MAPK (Thr202/Tyr204), phospho-Akt (Ser473), ERK1/2, Akt1/PKBα, and actin, were obtained from Millipore (Billerica, MA, USA). Antibodies against GLO-1, NF-κB (p65), H-Ras, Raf-1, and lamin A were obtained from Santa Cruz Biotechnology (Santa Cruz, CA, USA). Antibodies against K-Ras and N-Ras were obtained from GeneTex (San Antonio, TX, USA). Alexa Fluor 594 goat anti-mouse IgG (H+L) was purchased from Invitrogen. U0126 (MEK1/2 inhibitor), LY294002 (PI3K inhibitor), JSH-23 (NF-κB inhibitor), IgG HRP-conjugated goat anti-mouse and IgG HRP-conjugated goat anti-rabbit were obtained from Chemicon (Temecula, CA, USA).

Cell Culture. U937 cells were purchased from the American Type Culture Collection (Rockville, MD, USA). The cells were cultured in RPMI 1640 medium with 10% fetal bovine serum (GibcoBRL, Grand Island, NY, USA), 5 mM L-glutamine (GibcoBRL), and 1% penicillin/streptomycin (10000 units of penicillin/mL and 10 mg/mL streptomycin) at 37 °C in a humidified 5% CO_2 incubator.

Cell Viability Assay. Cell viability was assessed by MTT assay.[17] Briefly, cells at 1×10^5/mL were treated with various concentrations of monacolin K in 96-well plates for 48 h, followed by treatment with MTT for 4 h at 37 °C. The medium was removed, DMSO was added to dissolve the blue formazan residue, and color intensity was measured using an ELISA reader at 570 nm.

Morphological Assay. After treatment with various concentrations of monacolin K for 48 h, cells were harvested and fixed with 4% paraformaldehyde in PBS for 20 min at room temperature and stained with 2.5 mg/mL DAPI solution for 30 min at room temperature. The cells were washed two more times with PBS and analyzed via a confocal microscope (CARV II Confocal Imager; BD Biosciences).

DNA Fragmentation Assay. After treatment with various concentrations of monacolin K for 48 h and washing with ice-cold PBS, the cells were resuspended in 180 μL of DNA lysis buffer (0.5% lauroylsarcosine, 10 mM EDTA, 0.5 mg/mL proteinase K, and 50 mM Tris-HCl at pH 8.0) overnight at 56 °C and treated with RNaseA (0.5 μg/mL) for 1 h at 37 °C. Total DNA was extracted from the cells with an equal volume of phenol/chloroform/isoamyl alcohol (Sigma-Aldrich). Ten microliters of DNA was analyzed on 1.8% agarose gel.

Image Cytometry Analysis. Cell sub-G1 phase was analyzed by the DNA content using the DAPI staining method. After treatment with various concentrations of monacolin K for 48 h, U937 cells were centrifuged at 1500 rpm for 5 min, and the cell pellets were fixed in 70% ice-cold ethanol overnight at 4 °C. Fixed cells were washed with PBS, incubated with 0.5 mL of hypotonic buffer containing 0.5% Triton X-100 and 0.5 mg/mL RNase A for 30 min at 37 °C, and then stained with 50 μg/mL DAPI, and the sub-G1 phase content was determined on a NucleoCounter NC-3000 cytometer (ChemoMetec, Allerod, Denmark).

RNA Isolation and Reverse Transcription-PCR Amplification (RT-PCR). Total RNA was extracted from U937 cells using a commercially available RNA extraction kit (Favorgen, Pingtung, Taiwan) and following the manufacturer's instruction. First-stranded cDNA was synthesized using 1 μg of total RNA by RT-PCR kit (Roche, Indianapolis). The relative expressions of GLO1 and HMGCR were analyzed using RT-PCR with GAPDH as an internal control. The primers used were GLO1, sense 5′-ATGGCAGAACCGCAGCCCCCGT-3′ and antisense 5′-CTACATTAAGGTTGCCATTTTGTTAG-3′, yielding a product of length 564 bp; HMGCR, sense 5′-TACCATGTCAGGGGTACGTC-3′ and antisense 5′-CAAGCCTAGAGACATAATCATC-3′, yielding a product of length 252 bp; GAPDH, sense 5′-TACCATGTCAGGGGTACGTC-3′ and antisense 5′-CAAGCCTAGAGACATAATCATC-3′, yielding a product of length 248 bp. A 10 μL volume reaction for PCR included 2 μL of cDNA, 1 μL each of sense and antisense primers, and 5 μL of PCR master mix. The conditions were 94 °C for 5 min, 94 °C for 40 s, 60 °C for 35 s (GLO1), 58 °C for 30 s (HMGCR), and 64 °C for 30 s (GAPDH), 72 °C for 40 s, and 72 °C for 7 min, for 26 cycles. The PCR products were separated by electrophoresis on 1.5% agarose gels, and the results were analyzed using a Kodak Gel logic imaging system (Hyland Scientific, Stanwood, WA, USA).

Western Blot Analysis. The whole cell protein was extracted via the addition of 100 μL of gold lysis buffer (50 mM Tris-HCl, 150 mM NaCl, 1 mM EDTA, 1% Triton X-100, and 1% protease inhibitor cocktail at pH 7.4), followed by incubation at 4 °C for 1 h, centrifugation, and collection of cell lysate. A Subcellular Protein Fractionation Kit was used to determine the levels of protein expression in cytosol, nucleus, and membrane. Extract preparation followed instruction of the manufacturer's published protocol (Thermo, Rockford, IL, USA). Protein concentrations were measured with a Bio-Rad protein assay reagent (Bio-Rad Laboratories, Munich, Germany). Equal amounts of lysate protein (30 μg/lane) were subjected to sodium dodecyl sulfate–polyacrylamide gel electrophoresis (SDS-PAGE). After electrophoresis, the proteins were electrotransferred to polyvinylidene difluoride (PVDF) membranes (Millipore, Billerica, MA, USA), blocked at 37 °C for 1 h with 1% BSA in TBST (20 mM/L Tris-base; 125 mM/L NaCl; 0.2% Tween 20; 0.1% sodium azide), then immunoblotted with primary antibodies overnight at 4 °C, and washed with TBST solution (0.05% Tween 20 in TBS). After six washings with TBST buffer, the blot was washed and exposed to horseradish peroxidase conjugated secondary antibodies for 1 h, and immunoreactive proteins were visualized with an enhanced chemiluminescence (ECL) detection system (GE Healthcare, Little Chalfont, UK).

Total Cholesterol Quantitation. The total cholesterol concentration was measured using a Cholesterol/Cholesterol Ester Quantitation Kit (Calbiochem, Novabiochem, Boston, MA, USA). After treatment with monacolin K for 48 h, cells were washed with cold PBS and centrifuged. The pellet was resuspended in 0.2 mL of chloroform/isopropanol/NP-40, homogenized for 3 min, and cleared by centrifugation at 14000 rpm for 10 min. Supernatants were decanted, air-dried at 50 °C, and vacuum-dried for 30 min to remove residual solvents. The dried lipids were dissolved in 0.2 mL of the reaction buffer, and the absorbance was measured at 570 nm for total cholesterol detection.

Methylglyoxal Measurement. MG was measured by using an *o*-phenylenediamine method.[18] MG was derivatized with *o*-phenylenediamine to form the quinoxaline product 2-MQ, which is very specific for MG. Briefly, the supernatant of the cell was incubated with 100 mM *o*-phenylenediamine for 3 h at room temperature. The quantity of the quinoxaline derivative of MG (2-MQ) was measured using a Hitachi L-6200 HPLC system (Hitachi, Ltd., Mississauga, ON, Canada). The mobile phase was generally 68 vol % of 10 mM KH_2PO_4 (pH 2.5) and 32 vol % of HPLC grade acetonitrile. The analysis conditions were as follows: detector wavelength, 315 nm; mobile phase flow rate, 1.0 mL/min; and column temperature, 20 °C. The whole series of samples in a single experiment was run in duplicate.

Immunofluorescence Microscopy. To detect the localization of NF-κB in monacolin K treated U937 cells, the U937 cells were first seeded in a 12-well dish. The cells were fixed with 4% paraformaldehyde

DOI: 10.1021/jf505275s
J. Agric. Food Chem. 2015, 63, 1186−1195

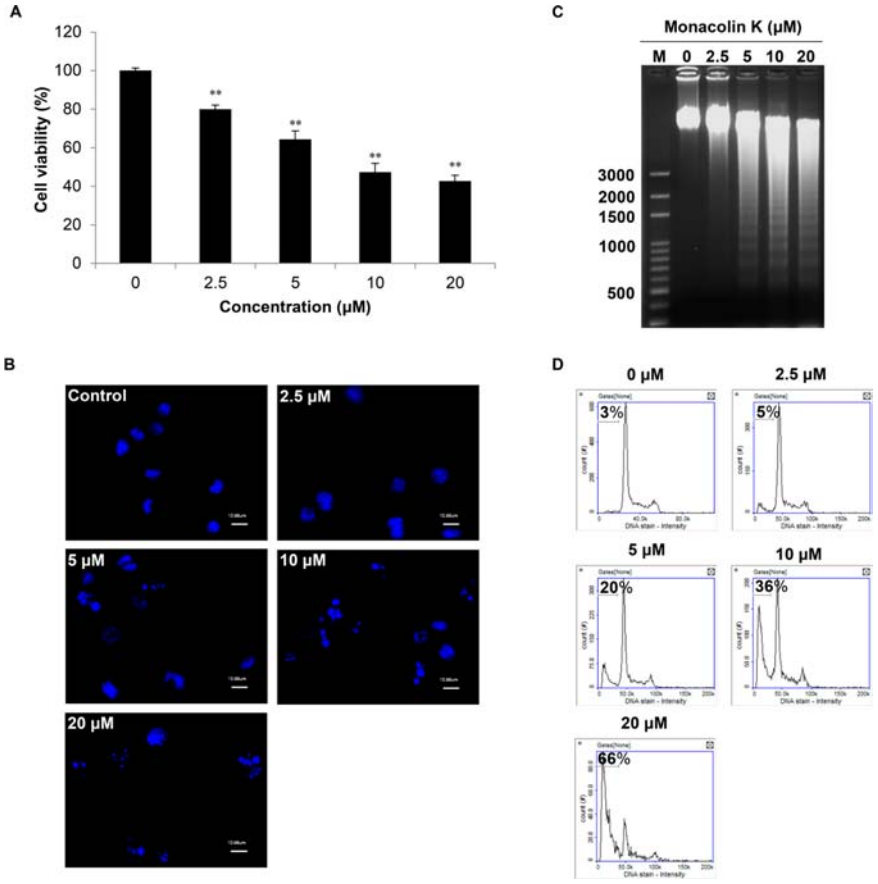

Figure 1. Inhibition of cell viability and apoptosis-inducing effects of monacolin K on U937 cells. (A) U937 cells were seeded (1×10^5 cells/well) in a 96-well plate, the cells were treated with variable concentrations of monacolin K for 48 h, and cell viability was measured by MTT assay. (B) Nuclear condensation in apoptotic cells detected by DAPI staining. U937 cells were treated with various concentrations of monaclin K for 48 h. (C) DNA fragmentation was detected by gel electrophoresis following stimulation with 2.5−20 μM monacolin K for 48 h. (D) Image cytometry analysis shows the percentage of sub-G1 phase in U937 cells treated with monacolin K for 48 h. All data represent means ± SD of triplicates ($n = 3$). In panel A, ** $p < 0.01$, compared with untreated cells (control groups).

for 30 min and permeabilized with PBS containing 0.1% Triton X-100 for 5 min at room temperature. After specimens were blocked with 5% BSA for 1 h at room temperature, they were further incubated with NF-κB (p65) antibody for 2 h. After three washings in TPBS, specimens were then stained with Alexa Fluor 594 goat anti-mouse IgG for 1 h at room temperature. After three washings with TPBS, cells were stained with 0.5 mg/mL of DAPI for 10 min to counterstain the nucleus and then washed three times for 5 min with TPBS. Images were collected by confocal microscope.

Statistical Analysis. The data were analyzed using the SAS program (SAS Institute, Cary, NC, USA). The significance of the difference among mean values was determined by one-way analysis of variance followed by the t test; (*) $p < 0.05$ and (**) $p < 0.01$ were considered statistically significant. Values are the mean ± SD of three independent experiments.

RESULTS

Monacolin K Induced Apoptosis in U937 Cells. MTT assays were performed to evaluate the potential cytotoxic effects of monacolin K. As shown in Figure 1A, U937 cells were incubated with increased concentrations of monacolin K for 48 h. Exposure of monacolin K to U937 cells resulted in a significant decrease in viable cells in a dose-dependent fashion. Treatment with 20 μM monacolin K achieved 57% inhibition ($p < 0.01$). To determine whether an increase in apoptosis was associated with the observed decrease in cell number after monacolin K treatment, the cells were stained with DAPI and analyzed by using a confocal microscope. As shown in Figure 1B, the nuclei of U937 cells exposed to monacolin K exhibited nuclear condensation and fragmented chromatin of typical apoptosis in a dose-dependent manner. Apoptosis was also detected by DNA fragmentation assay. DNA fragmentation was significantly increased after treatment with monacolin K in a dose-dependent manner (Figure 1C). Furthermore, the degree of apoptosis was quantified by analyzing the amount of sub-G1 DNA content in the U937 cells treated with monacolin K using an image cytometer. As shown in Figure 1D, in untreated control, the percentage of untreated control cells with fragmented DNA (sub-G1) was only 3%. Treatment with 20 μM monacolin K increased the percentage of cells with fragmented DNA (sub-G1) to 66%. Taken together, these findings indicated that exposure to monacolin K resulted in the inhibition of cell proliferation and a striking induction of apoptosis in U937 cells.

Monacolin K Down-regulated HMGCR Expression and Reduced Cholesterol Generation. To elucidate the effects of monacolin K on HMGCR production on the transcriptional level, cells were treated with various concentrations of monacolin K for 24 h. The cDNA was amplified by PCR with primers specific for HMGCR or GAPDH (as a control gene), and the results indicated that HMGCR mRNA expression was suppressed in the presence of monacolin K as shown in Figure 2A. The suppression of HMGCR mRNA expression correlated to Western blot analysis. Treatment of U937 cells with monacolin K

DOI: 10.1021/jf505275s
J. Agric. Food Chem. 2015, 63, 1186−1195

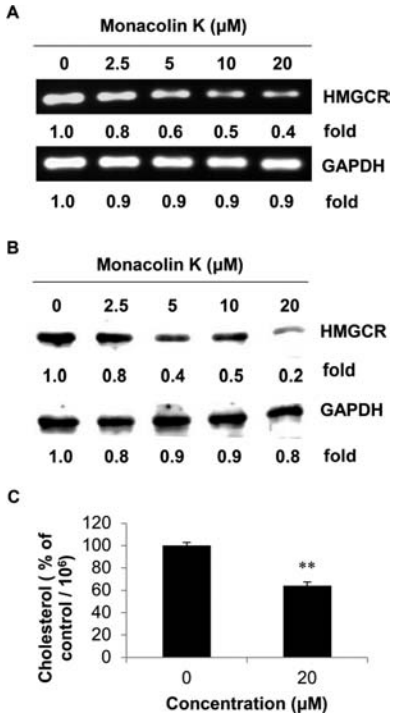

Figure 2. Monacolin K specifically suppresses HMGCR expression and cholesterol level in U937 cells. (A) Cells were incubated with various concentrations of monacolin K for 24 h, and HMGCR and GAPDH mRNA levels were analyzed by RT-PCR. (B) Immunoblots of whole cell lysates were probed with antibodies specific to HMGCR and actin. (C) U937 cells were treated with 20 μM monacolin K for 48 h, and the intracellular total cholesterol content was measured. All data represent means ± SD of triplicates (n = 3). In panel C, ** $p < 0.01$, compared with untreated cells (control groups).

inhibited HMGCR protein expression also in a dose-dependent manner (Figure 2B). After incubation with 20 μM monacolin K, we measured the intracellular total cholesterol content. As shown in Figure 2C, monacolin K showed significant inhibitory effect on cholesterol level at approximately 36% ($p < 0.01$), as compared with control cells.

Monacolin K Down-regulated GLO1 Expression and Increase MG Levels. To understand the critical roles of GLO1 in apoptosis, expression of GLO1 in U937 cells was monitored following treatment with monacolin K. U937 cells were treated with various concentrations of monacolin K for 48 h or 20 μM monacolin K for various times. The cDNA was amplified by PCR with primers specific for GLO1 or GAPDH (as a control gene). As shown in Figure 3A, monacolin K induced time- and dose-dependent down-regulation of GLO1 mRNA levels. Additionally, monacolin K administration resulted in a marked decrease in the GLO1 protein level as compared with control (Figure 3B). To investigate the effect of GLO1 expression blockage on MG level, U937 cells were treated with monacolin K at a concentration of 20 μM for 48 h. A significant increase in MG level was observed in comparison to levels produced by untreated cells (Figure 3C). Monacolin K caused an increase in MG accumulation by 2.7-fold as compared with that of control ($p < 0.05$).

Effects of Monacolin K on Ras Protein Expression and Downstream Signaling Pathways Regulation. Ras is considered a key protein for proliferative, survival, and oncogenic signals. We examined the regulatory effect of monacolin K on membrane protein Ras and its downstream signaling proteins, those being, Raf-1, Akt, and ERK. As shown in Figure 4A, after incubation with 20 μM monacolin K for 24 h, monacolin K significantly decreased the levels of H-Ras, K-Ras, N-Ras, and Raf-1 in cell membrane. In contrast, the H-Ras, K-Ras, N-Ras, and Raf-1 levels in cytosolic fraction were significantly higher in the monacolin K treatments. To assess whether monacolin K mediated and/or inhibited the phosphorylation of Akt and ERK, U937 cells were treated with various concentrations of monacolin K for 24 h. Figure 4B shows that monacolin K significantly inhibited the activation of Akt and ERK as shown by the decrease in the phosphorylation of Akt and ERK.

Monacolin K Abrogated NF-κB Signaling by Blocking the Nuclear Translocation of NF-κB (p65). To explore the underlying mechanism of NF-κB inactivation by monacolin K, we analyzed the protein expression of p65 by immunoblotting. As shown in Figure 5A, treatment of the U937 cells with 20 μM monacolin K for 24 h resulted in a significantly decreased level of p65 in the cell nucleus. In contrast, the p65 levels in cytosolic fraction were significantly increased. Confocal microscope analysis revealed that monacolin K inhibited p65 translocation from cytosol to nucleus (Figure 5B). Therefore, it was possible that the inhibitory effect of monacolin K on the NF-κB translocation was due to inactivation of Akt and ERK pathways, leading to a reduction in GLO1 expression.

Inhibitory Effects of Several Specific Inhibitors on Expression of Akt, ERK, and GLO1 and on Cell Viability in U937 Cells. Several specific inhibitors were used to assess whether a specific signaling pathway was involved in inhibition of monacolin K on GLO1 and other protein expressions. LY294002, U0126, and JSH-23 were used in the treatment of U937 cells. After treatment, cell extracts were prepared to determine the levels of GLO1. As shown in Figure 6A, three LY294002, U0126, and JSH-23 inhibitors could effectively suppress the GLO1 protein expressions. In addition, Figure 6B showed that Akt and ERK phosphorylation decreased after LY294002 and U0126 treatment for 24 h, and JSH-23 had little effect on the phosphorylation of Akt and ERK (Figure 6B). Next, we administered these inhibitors to U937 cells to determine whether suppression of the Ras/PI3K/Akt/NF-κB and Ras/Raf/ERK/NF-κB signaling pathways would inhibit cell viability. As shown in Figure 6C, these inhibitors had a strong inhibitory effect on U937 cell growth ($p < 0.01$). These results confirmed that the apoptotic effect of monacolin K followed the Ras/Akt/NF-κB/GLO-1 and Ras/Raf/ERK/NF-κB/GLO-1 signaling pathways.

Mevalonate Attenuated Monacolin K Induced Apoptosis and Protein Expression in U937 Cells. Accumulation of mevalonate, a precursor of cholesterol, has been reported to be associated with cell survival and proliferation of cancer cells. In the study, the treatment of mevalonate with monacolin K fully reversed its induced apoptosis in U937 cells as evidenced by DNA fragmentation and cell viability analysis ($p < 0.01$) (Figure 7A,B). Next, co-incubation of mevalonate with monacolin K for 24 h reversed monacolin K triggered loss of Akt and ERK phosphorylation (Figure 7C). We further investigated whether mevalonate blocked monacolin K suppresses GLO1 expression. After cells had been pre-incubated with mevalonate for 1 h and then treated with monacolin K for 48 h, as shown in Figure 7D,E, mevalonate prevented the decrease in GLO1 mRNA and protein by monacolin K. These results indicated that down-regulation of the mevalonate pathway is highly associated with monacolin K inhibition on GLO1 as well as the induction of apoptosis in U937 cells.

DOI: 10.1021/jf505275s
J. Agric. Food Chem. 2015, 63, 1186−1195

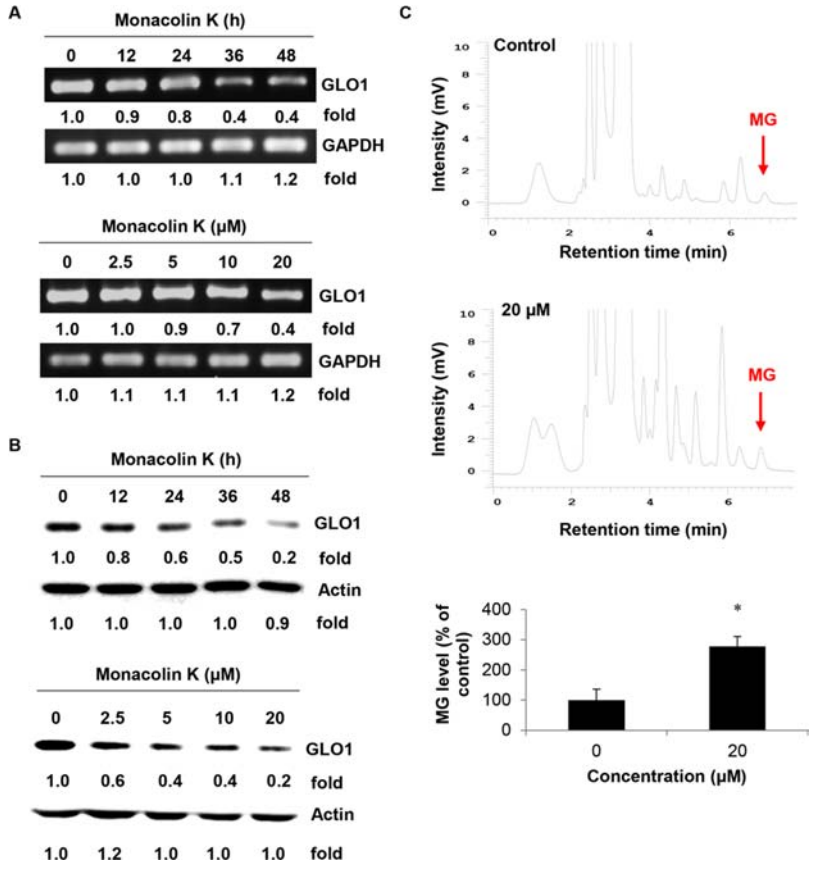

Figure 3. Down-regulation of GLO1 and increase MG levels by monacolin K in U937 cells. U937 cells were incubated with various concentrations of monacolin K for 48 h or with monacolin K (20 μM) for the indicated periods. (A) GLO1 and GAPDH mRNA levels were analyzed by RT-PCR. (B) Immunoblots of whole cell lysates were probed with antibodies specific to GLO1 and actin. (C) MG levels were estimated by HPLC as described under Materials and Methods. Monacolin K caused an increase in MG accumulation by 2.7-fold as compared with that of control (panel C). All data represent means ± SD of triplicates (n = 3). In panel C, ** $p < 0.05$, compared with untreated cells (control groups).

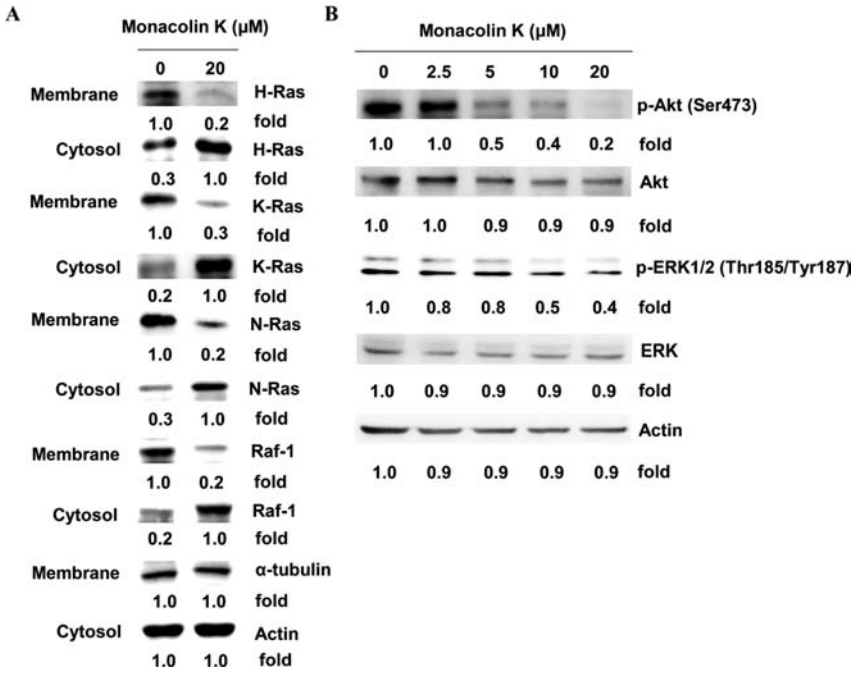

Figure 4. Down-regulation of Ras and its downstream signaling molecules by monacolin K in U937 cells. (A) After treatment with monacolin K for 24 h, membrane and cytosol proteins were extracted and used for immunoblotting of Ras (H, K, and N) and Raf-1. (B) Cells were lysed, and the total protein (30 mg) was submitted to SDS-PAGE and immunodetected with antiphospho- or anti-(ERK or Akt) antibodies. Tests were performed in triplicate and all experiments repeated three times (n = 3).

DOI: 10.1021/jf505275s
J. Agric. Food Chem. 2015, 63, 1186−1195

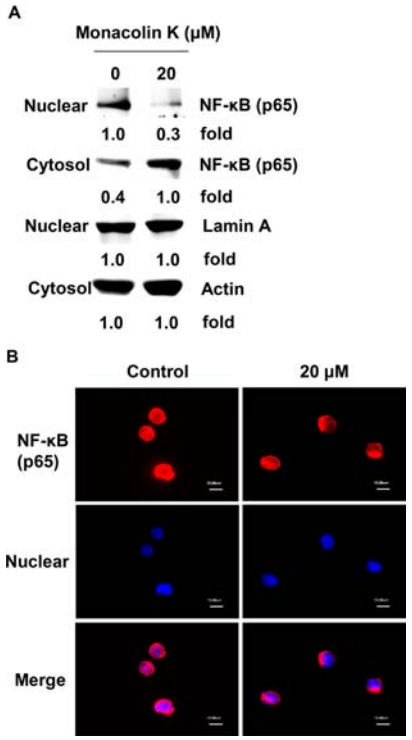

Figure 5. Monacolin K inhibits the translocation of NF-κB (p65) to the nucleus. (A) U937 cells were incubated for 24 h with indicated concentrations of monacolin K, and nuclear extracts were immunoblotted for p65 and the loading control lamin A. (B) After treatment for 24 h, cells were fixed, stained with p65 antibody and Alexa Fluor 594 goat anti-mouse (red), and counterstained with DAPI (blue). Tests were performed in triplicate and all experiments repeated three times (n = 3).

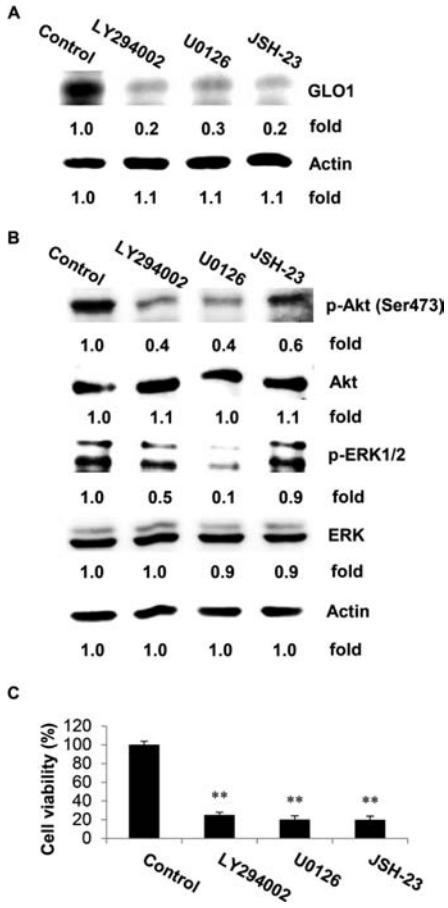

Figure 6. Down-regulation of Ras downstream signaling molecules and cell viability by various inhibitors in U937 cells. (A) U937 cells were treated with 20 μM of various inhibitors for 48 h. Total cell extracts were generated and immunoblotted with antibodies against GLO1. (B) U937 cells were treated with 20 μM of various inhibitors and incubated for 24 h; immunoblots of whole cell lysates were probed with antibodies specific to p-Akt and p-ERK. (C) The cell viabilities of U937 cells treated with 20 μM various inhibitors for 48 h were measured by MTT assay. All data represent means ± SD of triplicates (n = 3). In panel C, ** p < 0.01, compared with untreated cells (control groups).

DISCUSSION

The anticancer effect of monacolin K was demonstrated by its growth inhibitory activity on various cancer cell lines including human acute myeloid leukemia,[19] breast cancer,[20] and pancreatic cancer.[21] A structure−activity relationship analysis showed the alkyl functional group increased the lipophilicity of monacolin K, leading to a direct diffusion through the cell membrane, and affected cell proliferation, survival, and motility.[4] We hypothesize that monacolin K may induce apoptosis in U937 cells by inhibiting the mevalonate pathway and impairing Ras localization to the plasma membrane. It interrupted downstream Akt and ERK pathways, leading to the decreased HMGCR and GLO1 protein expressions.

Tumors, including leukemia, transformed from normal cells alter metabolism. Mutations of oncogenes and tumor-suppressor genes are believed to switch the glucose metabolism from oxidative phosphorylation to glycolysis in cancer cells.[22] Previous papers showed that cancer cells tend to use the glycolysis pathway to metabolize glucose due to lacking or mutated p53 gene.[23] Positron emission tomography (PET) data demonstrated that tumor cells accumulated extraordinary amounts of glucose. Elevated glucose metabolism is seen in activated lymphocytes in the draining lymph nodes of Moloney Murine Sarcoma and Leukemia Virus Complex-challenged mice using a ^{18}F-FDG probe.[24]

MG can be derived nonenzymatically from phosphorylated glycolytic intermediates dihydroxyacetone phosphate and glyceraldehyde-3-phosphate. MG causes DNA fragmentation at physiological concentrations in U937 cells[25] and HL-60 cell lines.[26] Recent studies have shown that MG specifically inhibits mitochondrial respiration in human leukemic leucocytes, leading to a tumoricidal effect.[27] We postulate that U937 cancer cell may use glycolysis to get the required energy and increase the GLO1 expression to eliminate excess MG for surviving and proliferation.

Detoxification of MG is mainly activated via the glyoxalase pathway present in the cytosol of all mammalian cells that use GSH as a cofactor.[28] The apoptotic effects of MG were found in high-glucose-treated VL-17A cells[29] and brain microvascular endothelial cells.[30] It has been shown that GLO1 expression was significantly up-regulated in prostate cancer LNCaP,[31] hepatocellular carcinoma,[32] and human gastric cancer,[33] when compared with adjacent nontumorous tissue. Recently, a novel mechanism of MG cytotoxicity in prostate cancer cells was proposed.[31] The silenced GLO1 in prostate LNCaP and PC3 cancer cells was found to be responsible for the accumulation of excess MG that led to the apoptosis via the cell survival NF-κB signaling pathway.

DOI: 10.1021/jf505275s
J. Agric. Food Chem. 2015, 63, 1186−1195

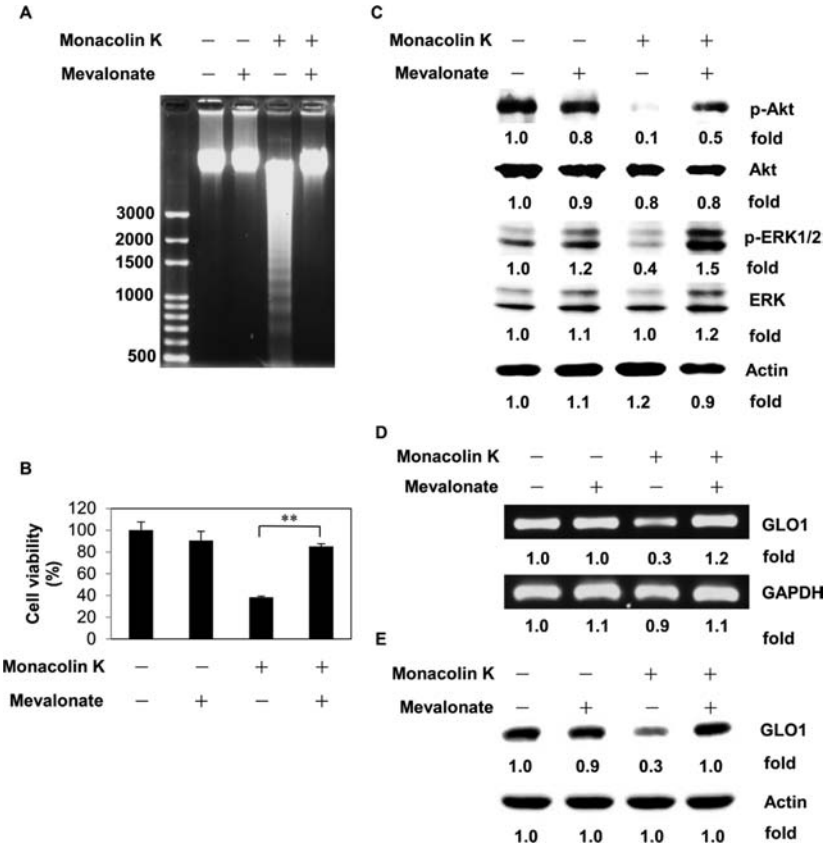

Figure 7. Recovery of monacolin K-induced apoptosis and suppression of Ras downstream signaling molecules in U937 cells by adding mevalonate. Cells were preincubated with 1 mM mevalonate for 1 h and then treated with 20 μM monacolin K for 48 h (A, B). (C) Cells were pretreated with 1 mM mevalonate for 1 h and then treated with 20 μM monacolin K for 24 h; immunoblots of whole cell lysates were probed with antibodies specific to antiphospho- or anti-(ERK or Akt). (D) GLO1 and GAPDH mRNA levels were analyzed by RT-PCR. (E) Immunoblots of whole cell lysates were probed with antibodies specific to GLO1 and actin. All data represent means ± SD of triplicates (n = 3). In panel C, ** $p < 0.01$, compared with untreated cells (control groups).

Ras has been reported to be frequently mutated in patients with AML. *Ras* gene mutation leads to the expression of activated Ras proteins and triggers constitutively overactive signaling inside the cell.[34] A previous study found N-Ras mutations (11%) and K-Ras mutations (5%) in AML patients.[35] Among the Ras isoforms, only H-Ras is palmitoylated and integrated into lipid rafts.[36] Activated Ras recruits Raf family proteins to the lipid raft and activates the subsequent ERK pathway. The constitutively activated Raf/MEK/ERK pathway has been characterized in both AML and acute lymphocytic leukemia (ALL).[37] Down-regulation of activated Raf proteins is closely related to cell cycle arrest in human promyelocytic leukemia and some hematopoietic cells. It is well established that the cross-talk between Ras/Raf/MEK/ERK and Ras/PI3K/PTEN/Akt pathways regulates cell growth and tumorigenesis in many leukemia samples.[38] Both pathways may trigger the phosphorylation of downstream targets and regulate cell survival and proliferation.

PI3K activity is another predominant growth factor activated pathway in varieties of human tumors including leukemia.[39] Accumulated evidence shows that PI3K is heavily involved in the malignant transformation of cells through the activation of the downstream Akt.[40] Blalock et al.[41] reported that MEK-mediated transformation of certain hematopoietic cells requires the activation of the PI3K pathway. Combined treatment with the Chk1 inhibitor 7-hydroxystaurosporine (UCN-01) and lovastatin was found to synergistically disrupt Ras prenylation and its translocation to membrane leading to the inhibition of the phosphorylation of both ERK 1/2 and Akt and enhanced apoptosis in U937 cells.[42] Using immunoprecipitation analysis, Chiu et al.[43] showed that Raf-1, Akt, and Ras can accumulate in the membrane to increase cell migration/invasion through PI3K/Akt and Raf-1/ERK activation. A redox modulated up-regulation of survival signaling, involving the ERK and PI3K/Akt phosphorylation pathways, has been reported in U937 cells.[44] Recent studies demonstrated that monacolin K can inhibit the Akt and ERK pathways leading to the decreased Bcl-2, whereas increased Bax expression in human colon carcinoma HCT-116 cell line.[45]

The expression and activity of the transcription factor NF-κB have been shown to be regulated by the Ras/PI3K/AKT and RAS/MAPK pathways.[46] The transcription factor NF-κB promotes cell proliferation and prevents apoptosis through its regulation of various gene products. Monacolin K and other natural statins were found to reduce NF-κB DNA-binding activity in tumor necrosis factor-α (TNF-α)-stimulated human myeloid leukemia KBM-5 cells.[47]

She et al.[48] reported that farnesyltransferase inhibitor manumycin A (manumycin) induced nitric oxide production and apoptosis in two myeloid leukemia cell lines (U937 and HL-60). Manumycin reduced the amount of functional Ras localized at the cytoplasmic membrane, thus blocking Raf-1 association with Ras. Manumycin inhibits the phosphorylation of both ERK1/2 and Akt and interferes with the association of PI3K and Ras in HepG2 cells.[49]

DOI: 10.1021/jf505275s
J. Agric. Food Chem. 2015, 63, 1186−1195

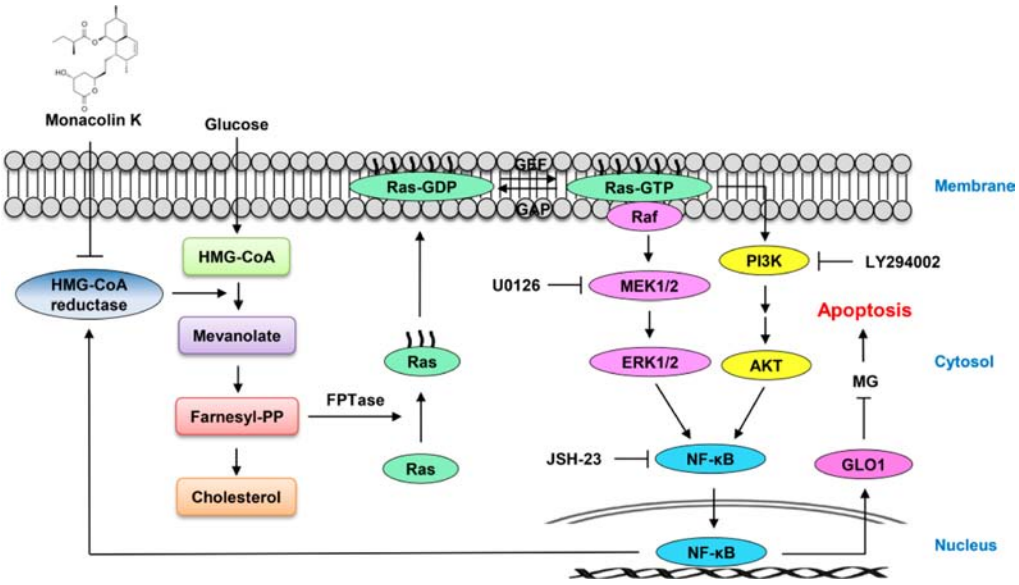

Figure 8. Diagram depicting the hypothesis of signaling regulation on GLO1 expression through both Ras/Raf/ERKNF-κB and Ras/PI3K/Akt/NF-κB pathways following monacolin K exposure in U937 cells. Farnesyl-PP, farnesyl pyrophosphate; FPTase, farnesyl prenyl transferase; GEF, guanine nucleotide exchange factor; GAP, GTPase-activating protein.

Monacolin K and other statins stimulate cell death, which was accompanied by the collapse of the mitochondrial membrane potential (MMP) in isolated Sprague–Dawley rat hepatocytes.[18] This observation indicates that cholesterol levels play a major role in the integrity of cell membranes, and the inactivation of HMGCR activity by monacolin K may be responsible for the apoptotic effect.

Our results reveal that the translocation of both Ras and Raf-1 to membrane and the levels of p-Akt in the PI3K/AKT/mTOR signaling pathway as well as p-ERK in the MAPK signal pathway were down-regulated by monacolin K in the U937 cell line. We postulate that monacolin K, a HMGCR inhibitor, blocks the biosynthesis of mevalonate and the subsequent farnesyl pyrophosphate through the inactivation of HMGCR. Lack of farnesyl pyrophosphate results in the inhibition of the isoprenylation of Ras protein and leads to the repression of accumulation of putative lipid raft-associated proteins. The subsequent phosphorylation of both Akt and ERK pathways will be thus abrogated. Overall, these results provided evidence of the specific molecular pathways by which monacolin K induces apoptosis: it decreases the activation of GLO1 and lowers cholesterol levels through the inhibition of Ras/Raf/ERK/NF-κB and Ras/Akt/NF-κB pathways (Figure 8). These findings provide evidence that it will be worthwhile to investigate the potential of monacolin K for the treatment of leukemia and potentially other types of human cancers.

AUTHOR INFORMATION

Corresponding Author

*(T.-C.H.) Mail: Department of Food Science, National Pingtung University of Science and Technology, 1 Shuehfu Road, Neipu, Pingtung 91201, Taiwan. E-mail: tchuang@mail.npust.edu.tw. Phone: +886-8-7703202, ext. 5196. Fax: +886-8-7740582.

Funding

This work was supported by the Ministry of Science and Technology (Taiwan) (NSC 103-2313-B-020-008-).

Notes

The authors declare no competing financial interest.

ABBREVIATIONS USED

GLO1, glyoxalase 1; HMGCR, HMG-CoA reductase; ERK, extracellular signal regulated kinases; Akt, protein kinase B; NF-κB, nuclear factor kappa-B; MG, methylglyoxal; RYR, red yeast rice

REFERENCES

(1) Ma, J.; Li, Y.; Ye, Q.; Li, J.; Hua, Y.; Ju, D.; Zhang, D.; Cooper, R.; Chang, M. Constituents of red yeast rice, a traditional Chinese food and medicine. *J. Agric. Food Chem.* **2000**, *48*, 5220–5225.

(2) Shamim, S.; Al Badarin, F. J.; DiNicolantonio, J. J.; Lavie, C. J.; O'Keefe, J. H. Red yeast rice for dysipidemia. *Mo. Med.* **2013**, *110*, 349–354.

(3) Hong, M. Y.; Seeram, N. P.; Zhang, Y.; Heber, D. Chinese red yeast rice versus lovastatin effects on prostate cancer cells with and without androgen receptor overexpression. *J. Med. Food* **2008**, *11*, 657–666.

(4) Zhu, L.; Yau, L. F.; Lu, J. G.; Zhu, G. Y.; Wang, J. R.; Han, Q. B.; Hsiao, W. L.; Jiang, Z. H. Cytotoxic dehydromonacolins from red yeast rice. *J. Agric. Food Chem.* **2012**, *60*, 934–939.

(5) Cheng-Qian, Y.; Xin-Jing, W.; Wei, X.; Zhuang-Lei, G.; Hong-Peng, Z.; Songde, X.; Pei-Lin, W. Lovastatin inhibited the growth of gastric cancer cells. *Hepatogastroenterology* **2014**, *61*, 1–4.

(6) van Besien, H.; Sassano, A.; Altman, J. K.; Platanias, L. C. Antileukemic properties of 3-hydroxy-3-methylglutaryl-coenzyme A reductase inhibitors. *Leuk. Lymphoma* **2013**, *54*, 2601–2605.

(7) Goldstein, J. L.; Brown, M. S. Regulation of the mevalonate pathway. *Nature* **1990**, *343*, 425–430.

(8) Swanson, K. M.; Hohl, R. J. Anti-cancer therapy: targeting the mevalonate pathway. *Curr. Cancer Drug Targets* **2006**, *6*, 15–37.

(9) Thornalley, P. J. Glutathione-dependent detoxification of α-oxoaldehydes by the glyoxalase system: involvement in disease mechanisms and antiproliferative activity of glyoxalase I inhibitors. *Chem.–Biol. Interact.* **1998**, *111–112*, 137–151.

(10) Kataoka, S.; Naito, M.; Tomida, A.; Tsuruo, T. Resistance to antitumor agent-induced apoptosis in a mutant of human myeloid leukemia U937 cells. *Exp. Cell Res.* **1994**, *215*, 199–205.

(11) Ranganathan, S.; Tew, K. D. Analysis of glyoxalase-I from normal and tumor tissue from human colon. *Biochim. Biophys. Acta* **1993**, *1182*, 311–316.

DOI: 10.1021/jf505275s
J. Agric. Food Chem. 2015, 63, 1186–1195

(12) Davidson, S. D.; Milanesa, D. M.; Mallouh, C.; Choudhury, M. S.; Tazaki, H.; Konno, S. A possible regulatory role of glyoxalase I in cell viability of human prostate cancer. *Urol. Res.* **2002**, *30*, 116−121.
(13) Hooper, N. I.; Tisdale, M. J.; Thornalley, P. J. Glyoxalase activity during differentiation of human leukaemia cells in vitro. *Leuk. Res.* **1987**, *11*, 1141−1148.
(14) Chaplen, F. W. Incidence and potential implications of the toxic metabolite methylglyoxal in cell culture: a review. *Cytotechnology* **1998**, *26*, 173−183.
(15) Bhattacharya, B. S.; Sweby, P. K.; Minihane, A. M.; Jackson, K. G.; Tindall, M. J. A mathematical model of the sterol regulatory element binding protein 2 cholesterol biosynthesis pathway. *J. Theor. Biol.* **2014**, *349*, 150−162.
(16) Vitols, S.; Norgren, S.; Juliusson, G.; Tatidis, L.; Luthman, H. Multilevel regulation of low-density lipoprotein receptor and 3-hydroxy-3-methylglutaryl coenzyme A reductase gene expression in normal and leukemic cells. *Blood* **1994**, *84*, 2689−2698.
(17) Mosmann, T. Rapid colorimetric assay for cellular growth and survival: application to proliferation and cytotoxicity assays. *J. Immunol. Methods* **1983**, *65*, 55−63.
(18) Wang, X.; Desai, K.; Clausen, J. T.; Wu, L. Increased methylglyoxal and advanced glycation end products in kidney from spontaneously hypertensive rats. *Kidney Int.* **2004**, *66*, 2315−2321.
(19) Park, W. H.; Lee, Y. Y.; Kim, E. S.; Seol, J. G.; Jung, C. W.; Lee, C. C.; Kim, B. K. Lovastatin-induced inhibition of HL-60 cell proliferation via cell cycle arrest and apoptosis. *Anticancer Res.* **1999**, *19*, 3133−3140.
(20) Klawitter, J.; Shokati, T.; Moll, V.; Christians, U.; Klawitter, J. Effects of lovastatin on breast cancer cells: a proteo-metabonomic study. *Breast Cancer Res.* **2010**, *12*, R16.
(21) Kusama, T.; Mukai, M.; Iwasaki, T.; Tatsuta, M.; Matsumoto, Y.; Akedo, H.; Inoue, M.; Nakamura, H. 3-Hydroxy-3-methylglutaryl-coenzyme a reductase inhibitors reduce human pancreatic cancer cell invasion and metastasis. *Gastroenterology* **2002**, *122*, 308−317.
(22) Koppenol, W. H.; Bounds, P. L.; Dang, C. V. Otto Warburg's contributions to current concepts of cancer metabolism. *Nat. Rev. Cancer* **2011**, *11*, 325−337.
(23) Cairns, R. A.; Harris, I. S.; Mak, T. W. Regulation of cancer cell metabolism. *Nat. Rev. Cancer* **2011**, *11*, 85−95.
(24) Shu, C. J.; Guo, S.; Kim, Y. J.; Shelly, S. M.; Nijagal, A.; Ray, P.; Gambhir, S. S.; Radu, C. G.; Witte, O. N. Visualization of a primary anti-tumor immune response by positron emission tomography. *Proc. Natl. Acad. Sci. U.S.A.* **2005**, *102*, 17412−17417.
(25) Okado, A.; Kawasaki, Y.; Hasuike, Y.; Takahashi, M.; Teshima, T.; Fujii, J.; Taniguchi, N. Induction of apoptotic cell death by methylglyoxal and 3-deoxyglucosone in macrophage-derived cell lines. *Biochem. Biophys. Res. Commun.* **1996**, *225*, 219−224.
(26) Kang, Y.; Edwards, L. G.; Thornalley, P. J. Effect of methylglyoxal on human leukaemia 60 cell growth: modification of DNA G1 growth arrest and induction of apoptosis. *Leuk. Res.* **1996**, *20*, 397−405.
(27) Biswas, S.; Ray, M.; Misra, S.; Dutta, D. P.; Ray, S. Selective inhibition of mitochondrial respiration and glycolysis in human leukaemic leucocytes by methylglyoxal. *Biochem. J.* **1997**, *323* (Part 2), 343−348.
(28) Abordo, E. A.; Minhas, H. S.; Thornalley, P. J. Accumulation of α-oxoaldehydes during oxidative stress: a role in cytotoxicity. *Biochem. Pharmacol.* **1999**, *58*, 641−648.
(29) Kumar, S. M.; Swaminathan, K.; Clemens, D. L.; Dey, A. GSH protects against oxidative stress and toxicity in VL-17A cells exposed to high glucose. *Eur. J. Nutr.* **2014**, DOI: 10.1007/s00394-014-0703-2.
(30) Li, W.; Maloney, R. E.; Circu, M. L.; Alexander, J. S.; Aw, T. Y. Acute carbonyl stress induces occludin glycation and brain microvascular endothelial barrier dysfunction: role for glutathione-dependent metabolism of methylglyoxal. *Free Radical Biol. Med.* **2013**, *54*, 51−61.
(31) Antognelli, C.; Mezzasoma, L.; Fettucciari, K.; Talesa, V. N. A novel mechanism of methylglyoxal cytotoxicity in prostate cancer cells. *Int. J. Biochem. Cell Biol.* **2013**, *45*, 836−844.
(32) Zhang, S.; Liang, X.; Zheng, X.; Huang, H.; Chen, X.; Wu, K.; Wang, B.; Ma, S. Glo1 genetic amplification as a potential therapeutic target in hepatocellular carcinoma. *Int. J. Clin. Exp. Pathol.* **2014**, *7*, 2079−2090.
(33) Hosoda, F.; Arai, Y.; Okada, N.; Shimizu, H.; Miyamoto, M.; Kitagawa, N.; Katai, H.; Taniguchi, H.; Yanagihara, K.; Imoto, I.; Inazawa, J.; Ohki, M.; Shibata, T. Integrated genomic and functional analyses reveal glyoxalase I as a novel metabolic oncogene in human gastric cancer. *Oncogene* **2014**, DOI: 10.1038/onc.2014.57.
(34) Beaupre, D. M.; Kurzrock, R. RAS and leukemia: from basic mechanisms to gene-directed therapy. *J. Clin. Oncol.* **1999**, *17*, 1071−1079.
(35) Bowen, D. T.; Frew, M. E.; Hills, R.; Gale, R. E.; Wheatley, K.; Groves, M. J.; Langabeer, S. E.; Kottaridis, P. D.; Moorman, A. V.; Burnett, A. K.; Linch, D. C. RAS mutation in acute myeloid leukemia is associated with distinct cytogenetic subgroups but does not influence outcome in patients younger than 60 years. *Blood* **2005**, *106*, 2113−2119.
(36) Hancock, J. F.; Paterson, H.; Marshall, C. J. A polybasic domain or palmitoylation is required in addition to the CAAX motif to localize p21ras to the plasma membrane. *Cell* **1990**, *63*, 133−139.
(37) Kornblau, S. M.; Womble, M.; Qiu, Y. H.; Jackson, C. E.; Chen, W.; Konopleva, M.; Estey, E. H.; Andreeff, M. Simultaneous activation of multiple signal transduction pathways confers poor prognosis in acute myelogenous leukemia. *Blood* **2006**, *108*, 2358−2365.
(38) McCubrey, J. A.; Steelman, L. S.; Abrams, S. L.; Bertrand, F. E.; Ludwig, D. E.; Basecke, J.; Libra, M.; Stivala, F.; Milella, M.; Tafuri, A.; Lunghi, P.; Bonati, A.; Martelli, A. M. Targeting survival cascades induced by activation of Ras/Raf/MEK/ERK, PI3K/PTEN/Akt/mTOR and Jak/STAT pathways for effective leukemia therapy. *Leukemia* **2008**, *22*, 708−722.
(39) Martinez-Lorenzo, M. J.; Anel, A.; Monleon, I.; Sierra, J. J.; Pineiro, A.; Naval, J.; Alava, M. A. Tyrosine phosphorylation of the p85 subunit of phosphatidylinositol 3-kinase correlates with high proliferation rates in sublines derived from the Jurkat leukemia. *Int. J. Biochem. Cell Biol.* **2000**, *32*, 435−445.
(40) Nicholson, K. M.; Anderson, N. G. The protein kinase B/Akt signalling pathway in human malignancy. *Cell. Signal.* **2002**, *14*, 381−395.
(41) Blalock, W. L.; Navolanic, P. M.; Steelman, L. S.; Shelton, J. G.; Moye, P. W.; Lee, J. T.; Franklin, R. A.; Mirza, A.; McMahon, M.; White, M. K.; McCubrey, J. A. Requirement for the PI3K/Akt pathway in MEK1-mediated growth and prevention of apoptosis: identification of an Achilles heel in leukemia. *Leukemia* **2003**, *17*, 1058−1067.
(42) Dai, Y.; Rahmani, M.; Pei, X. Y.; Khanna, P.; Han, S. I.; Mitchell, C.; Dent, P.; Grant, S. Farnesyltransferase inhibitors interact synergistically with the Chk1 inhibitor UCN-01 to induce apoptosis in human leukemia cells through interruption of both Akt and MEK/ERK pathways and activation of SEK1/JNK. *Blood* **2005**, *105*, 1706−1716.
(43) Chiu, C. F.; Ho, M. Y.; Peng, J. M.; Hung, S. W.; Lee, W. H.; Liang, C. M.; Liang, S. M. Raf activation by Ras and promotion of cellular metastasis require phosphorylation of prohibitin in the raft domain of the plasma membrane. *Oncogene* **2013**, *32*, 777−787.
(44) Vurusaner, B.; Gamba, P.; Testa, G.; Gargiulo, S.; Biasi, F.; Zerbinati, C.; Iuliano, L.; Leonarduzzi, G.; Basaga, H.; Poli, G. Survival signaling elicited by 27-hydroxycholesterol through the combined modulation of cellular redox state and ERK/Akt phosphorylation. *Free Radical Biol. Med.* **2014**, *77*, 376−385.
(45) Guruswamy, S.; Rao, C. V. Synergistic effects of lovastatin and celecoxib on caveolin-1 and its down-stream signaling molecules: implications for colon cancer prevention. *Int. J. Oncol.* **2009**, *35*, 1037−1043.
(46) Amiri, K. I.; Richmond, A. Role of nuclear factor-kappa B in melanoma. *Cancer Metastasis Rev.* **2005**, *24*, 301−313.
(47) Ahn, K. S.; Sethi, G.; Aggarwal, B. B. Reversal of chemoresistance and enhancement of apoptosis by statins through down-regulation of the NF-κB pathway. *Biochem. Pharmacol.* **2008**, *75*, 907−913.

DOI: 10.1021/jf505275s
J. Agric. Food Chem. 2015, 63, 1186−1195

(48) She, M. R.; Li, J. G.; Du, X.; Lin, W.; Niu, X. Q.; Guo, K. Y. [Involvement of mitochondria apoptotic pathway in the manumycin inducing apoptosis of U937 and HL-60]. *Zhonghua Xueyexue Zazhi* **2007**, *28*, 404−406.
(49) Zhou, J. M.; Zhu, X. F.; Pan, Q. C.; Liao, D. F.; Li, Z. M.; Liu, Z. C. Manumycin inhibits cell proliferation and the Ras signal transduction pathway in human hepatocellular carcinoma cells. *Int. J. Mol. Med.* **2003**, *11*, 767−771.

DOI: 10.1021/jf505275s
J. Agric. Food Chem. 2015, 63, 1186−1195

Table 1. ^{1}H and ^{13}C NMR Data for Alternethanoxins C–E (3–5)[a,b]

	3			4			5		
	δC[c]	δH (J in Hz)	HMBC	δC	δH (J in Hz)	HMBC	δC	δH (J in Hz)	HMBC
1	148.9 C			149.3 C		MeCO	155.9 C		H-3
2	126.2 C			128.9 C		H-3	106.2 C		H-3
3	110.1 CH[d]	6.21 (1H) s[d]	MeCO	106.3 CH	6.66 (1H) s	H-6, MeCO	107.2 CH	6.84 (1H) s	MeCO
4	162.8 C[d]		H-3	153.0 C		H-3	148.9 C		MeCO
5	162.8 C[d]		H-3	161.4 C		H-6	158.2 C		H-6
6	110.1 CH[d]	6.21 (1H) s[d]		111.6 CH	6.93 (1H) s		111.2 CH	6.64 (1H) s	
6a	136.3 C		H-8	155.3 C			161.2 C		H-6
7	166.2 C		H-9, H-8, OMe	168.6 C		H-9, MeO	103.3 CH	6.99 (1H) d (2.2)	H-9
8	129.4 CH	7.51 (1H) d (7.3)		112.4 CH	7.06 (1H) s		168.4 C		OMe
9	122.1 CH	7.45 (1H) d (7.3)		156.9 C			112.6 CH	6.91 (1H) d (2.2)	
10	149.8 C		H-9, H-8	165.0 C			168.8 C		H-9
10a	127.7 C		H-9, H-8	133.2 C			135.9 C		
10b	110.0 C			112.7 C			110.1 C		
OMe	53.8 CH_3	3.70 (3H) s		53.3 CH_3	3.90 (3H) s		52.0 CH_3	3.93 (3H) s	
MeCO	21.9 CH_3	2.20 (3H) s	H-3	22.6 CH_3	2.50 (3H) s	H-3	21.5 CH_3	2.45 (3H) s	H-3
MeCO	199.2 C		H-3	179.8 C			179.6 C		
OH		12.19 s			12.10 s			12.14 s	

[a]The chemical shifts are in δ values (ppm) from TMS. [b]2D ^{1}H, ^{1}H (COSY) and 2D ^{13}C, ^{1}H (HSQC) NMR experiments delineated the correlations of all of the protons and the corresponding carbons. [c]Multiplicities were assigned by DEPT spectrum. [d]Signals overlapped.

metabolites, which by preliminary spectroscopic investigation appeared to be closely related to alternethanoxins A and B. This study was designed to establish the chemical and biological characterization of these three new metabolites, named alternethanoxins C–E.

MATERIALS AND METHODS

General Experimental Procedures. UV spectra were taken in MeCN solution on a Beckman Coulter DU800 spectrophotometer (Fullerton, California, USA); ^{1}H and ^{13}C NMR spectra were recorded at 400 and at 100 MHz, respectively, in CD_3COCD_3 on a Bruker AVANCE III 400 MHz spectrometer (Karlsruhe, Germany). The same solvent was used as internal standard. Carbon multiplicities were determined by distortionless enhancement by polarization transfer (DEPT) spectra.[8] DEPT, correlation spectroscopy (COSY)-45, heteronuclear multiple-quantum coherence (HMQC), heteronuclear multiple-bond correlation (HMBC), and nuclear Overhauser enhancement spectroscopy (NOESY) experiments[8] were performed using standard Bruker microprograms. HRESI MS spectra were recorded on an Agilent 6530 Q-TOF LC/MC (ESI-HRMS) spectrometer (Santa Clara, California , USA). Analytical and preparative TLC was performed on silica gel and reverse phase (Kieselgel 60 F_{254} plates, 0.25 and 0.5 mm, and Kieselgel 60 RP-18 F_{254} plates, 0.20 mm, respectively) (Merck, Darmstadt, Germany). The spots were visualized by exposure to UV radiation (254 nm) and/or by spraying first with 10% H_2SO_4 in MeOH and then with 5% phosphomolybdic acid in EtOH, followed by heating at 110 °C for 10 min. Column chromatography was performed on a silica gel column (Kieselgel 60, 0.063–0.200 mm) (Merck, Darmstadt, Germany). Medium-pressure chromatography was performed with Puriflash (Interchim, France, Montluçon, Fr) prepacked normal-phase (Silica HP 30 μm 40G and Silica HP 15 μm 12G) and reverse-phase (C18 HP 15 μm 20G) columns (Interchim, Montluçon, France).

Fungal Strains and Toxins Production and Purification. The strain (S-102) of *A. sonchi* used in this study was deposited in the collection of All-Russian Research Institute of Plant Protection (Pushkin, Saint Petersburg, Russia). The fungus was grown on autoclaved pearl barley, and the solid culture (1.3 kg) was extracted with Me_2CO–H_2O (50:50) according to the procedure previously reported.[7] After evaporation of the Me_2CO, H_2O phase was passed through a column containing 20 g of Diaion HP-20, and then was washed with water, MeOH, EtOAc, and CH_2Cl_2. The dry residue (5.2 g) of the MeOH extract demonstrated phytotoxic activity. It was then subjected to bioassay-guided fractionation through column chromatography (750 mm × 30 mm) on silica gel, eluted with CH_2Cl_2/MeOH (100:0 (800 mL), 95:5 (800 mL), 90:10 (800 mL), and 80:20 (800 mL), v/v) affording four homogeneous fractions. The residue of the second fraction (3.3 g) showing both phytotoxic and antimicrobial activity was further purified by CC on silica gel eluted with $CHCl_3$/*i*-PrOH (90:10, v/v) giving five homogeneous fractions. The residue of the fourth fraction (244 mg) was further purified by MPLC on silica gel, eluted with *n*-hexane/Me_2CO (100:0 to 50:50, v/v), yielding alternethanoxin B, **2** (R_f 0.37, toluene/EtOAc/glacial CH_3COOH (70:30:0.1, v/v/v), R_f 0.35, H_2O/MeOH (20:80, v/v), 8.5 mg), and alternethanoxin E, **5** (R_f 0.45 toluene/EtOAc/glacial CH_3COOH (70:30:0.1, v/v/v), R_f 0.24, H_2O/MeOH (20:80, v/v), 5.0 mg) as a pale yellow homogeneous amorphous solid. The residue of the fifth fraction (470 mg) was further purified by reverse-phase MPLC eluted with MeOH/H_2O (20:80 to 100:0, v/v) and finally by PTLC on silica gel (eluent toluene/EtOAc/glacial CH_3COOH 70:30:0.1) affording alternethanoxin A, **1** (R_f 0.39, toluene/EtOAc/glacial CH_3COOH (70:30:0.1, v/v/v), R_f 0.72, H_2O/MeOH (20:80, v/v) 25.0 mg), alternethanoxin C, **3** (R_f 0.59, toluene/EtOAc/glacial CH_3COOH (70:30:0.1, v/v/v), R_f 0.65, H_2O/MeOH (20:80, v/v), 16.0 mg) as a pale rose homogeneous amorphous solid, and alternethanoxin D, **4** (R_f 0.39, toluene/EtOAc/glacial CH_3COOH (70:30:0.1, v/v/v), R_f 0.36 H_2O/MeOH (20:80, v/v), 7.0 mg), as a pale yellow homogeneous amorphous solid.

Alternethanoxin C (3). Pale rose amorphous solid, UV λ_{max} nm (log ε) 345 (0.1), 280 (0.65), 250 (0.40), 210 (1.75); ^{1}H and ^{13}C NMR, see Table 1; HRESI MS (+) spectrum *m/z*: 695 $[2M + Na]^+$; 375 $[M + K]^+$, 359.0845 $[C_{16}H_{16}NaO_8$ calcd 359.0743, M + Na$]^+$.

Alternethanoxin D (4). Pale yellow amorphous solid, UV λ_{max} nm (log ε) 365 (0.17), 300 (0.50), 243 (1.00); ^{1}H and ^{13}C NMR, see Table 1; HRESI MS (+) spectrum *m/z*: 691 $[2M + Na]^+$; 373 $[M + K]^+$, 357.0574 $[C_{16}H_{14}NaO_8$ calcd 357.0586, M + Na$]^+$.

Alternethanoxin E (5). Pale yellow amorphous solid, UV λ_{max} nm (log ε) 352 (0.16), 305 (0.60) 252 (0.75); 235 (1.14); ^{1}H and ^{13}C NMR, see Table 1; HRESI MS (+) spectrum *m/z*: 623 $[2M + Na]^+$; 339 $[M + K]^+$, 323.0521 $[C_{16}H_{12}NaO_6$ calcd 323.0532, M + Na$]^+$.

Bioassay. *Phytotoxic Activity.* Leaf segments of *Elytrigia repens* (couch-grass) 2 cm length and leaf discs of *Sonchus arvense* (perennial sowthistle) 1 cm in diameter were punctured with a sharp needle in the center and were treated with solutions of isolated compounds in 5% EtOH at the concentration of 2 mg/mL as described previously.[11]

DOI: 10.1021/jf5054595
J. Agric. Food Chem. 2015, 63, 1196–1199

Typically, for this bioassay samples of isolated compounds (400 μg) were dissolved in EtOH (10 μL) ultrasonically, and then water (190 μL) was added and the samples were vortexed. At least 10 replicate leaf segments or discs were used for each treatment.

Antimicrobial Activity. The antimicrobial activity of the isolated compounds was tested against a Gram positive bacterium (*Bacillus subtilis*) and a yeast fungus (*Candida tropicalis*) by using an agar diffusion assay according to the protocol previously reported.[12] Both microorganisms were grown on potato-dextrose agar. Up to 100 μg of each metabolite was applied per disc (6 mm diam) (Macherey-Nagel, Düren, Germany). The cultures were incubated at 30 °C for 24 h before activity was determined by minimum inhibitory concentration (MIC) defined as the lowest concentration of antibiotic that inhibited visible growth.[13]

Statistical Analysis. All bioassays were performed twice with at least three replicates. When appropriate, standard deviation was determined.

RESULTS AND DISCUSSION

The organic extract of the *A. sonchi* solid culture was purified by a combination of column and TLC chromatography, yielding three homogeneous amorphous solids that were closely related to alternethanoxins A and B, as deduced by preliminary investigation of the ^{1}H and ^{13}C NMR spectra, and were named alternethanoxins C−E (**3**−**5**, Figure 1).

Alternethanoxin C, **3** has a molecular formula of $C_{16}H_{16}O_8$ as deduced from its HRESI MS spectrum, which is associated with ten hydrogen deficiencies. In particular, its ^{1}H NMR spectrum (Table 1) differed from that of **1** in the presence of two aromatic protons (H-8 and H-9), which were *ortho*-coupled in the COSY spectrum[8] instead of the typical systems of a 1,2,3-substituted benzene ring.[9] H-8 and H-9 resonated as two doublets (J = 7.3 Hz) at δ 7.51 and 7.45 together with the singlet of H-3 and H-6, which appeared as an overlapped signal as in **1**, the methoxy and the methylcarbonyl at δ 6.21, 3.70, and 2.20. Probably the phenolic hydroxy group at C-1 was hydrogen bonded with the acetyl group at C-2 generating a stable six-membered ring as shown by the singlet observed at the typical chemical shift value of δ 12.19 as in **1**.[6,9] The couplings observed in the HMQC spectrum[8] allowed assignment of the signals of the protonated carbons in the ^{13}C NMR spectrum (Table 1) at δ 129.4, 122.1, 110.1 (an overlapped signal), 53.8, and 21.9 to C-8, C-9, C-3, and C-6, OMe and MeCO. The signals observed in the ^{13}C NMR spectrum at δ 166.2, 162.8 (an overlapped signal), 149.8, 136.3, and 127.7 were assigned to C-7, C-4 and C-5, C-10, and C-10a[10] also on the basis of the couplings observed in the HMBC spectrum[8] between the C-4 and C-5, which gave an overlapped signal, with H-3, C-6a with H-8, C-7 with H-9, H-8 and OMe, and C-10 and C-10a with H-9 and H-8. The signals at δ 148.9, 126.2, and 110.0 were assigned to C-1, C-2, and C-10b by comparison with the values reported for the same carbons in **1**.[6] Finally, the carbonyl group appeared at the typical chemical shift value of δ 199.2.[10] The chemical shifts of all protons and corresponding carbons of **3** were assigned and reported in Table 1.

On the basis of these results, alternethanoxin C appeared to be close to **1**, differing in the hydrolytic opening of the hemiacetal bond between C-6 and C-5 and the hydroxylation of C-10. The structure assigned to **3** was confirmed from the other couplings observed in the HMBC spectrum and from the data of its HRESI MS spectrum. This latter spectrum showed the sodiated dimeric form $[2M + Na]^+$ and the potassium and sodium clusters $[M + K]^+$ and $[M + Na]^+$, at m/z 695, 375, and 359.0845, respectively. Furthermore, a correlation was observed in the NOESY spectrum between H-3 and MeCO.

Therefore, **3** was formulated as 2′-dihydroxymethyl-2,5,6,6′-tetrahydroxy-3′-methoxy-biphenyl-3-carboxylic acid methyl ester.

Alternethanoxin D, **4**, has a molecular formula of $C_{16}H_{14}O_8$ as deduced from its HRESI MS spectrum consistent with nine hydrogen deficiencies. The investigation of its ^{1}H and ^{13}C NMR spectra (Table 1) showed that **4** was also very closely related to **1**. In fact, the ^{1}H NMR spectrum differed from that of **1** in the presence of a proton (H-8) of a pentasubstituted benzene ring appearing as a singlet at δ 7.06; the two adjacent carbons to C-8 (C-10 and C-9) were hydroxylated and resonated in the ^{13}C NMR spectrum at the typical chemical shifts values of δ 165.0 and 156.9.[10] The singlets of H-3, H-6, MeO, and MeCO resonated at the expected δ values of 6.66, 6.93, 3.90, and 2.50. Furthermore, the singlet at δ 12.19 was due to the phenolic hydroxy group at C-6 hydrogen bonded with the methoxy group at C-7 as in **2**, indicating for C-6 the same relative stereochemistry assigned to alternethanoxin B. The couplings observed in the HMQC spectrum allowed assignment of the chemical shifts to the hydrogenated carbons and the signals at δ 112.4, 111.6, 106.3, 53.3, and 22.6 to C-8, C-6, C-3, OMe, and MeCO. In addition, the couplings observed in the HMBC spectrum (Table 1) between C-1 and MeCO, C-2 and C-4 with H-3, C-3 with H-6 and MeCO, C-5 with H-6, and C-7 with H-9 and OMe allowed assignment of the chemical shifts at δ 149.3, 128.9, 153.0, 161.4, and 168.6 to C-1, C-2, C-4, C-5, and C-7. The signals at δ 155.3, 133.2, and 112.7 were assigned to C-6a, C-10a and C-10b by comparison with the values reported for the same carbons in **1**.[6] Finally, the acetyl group appeared at the typical chemical shift value of δ 179.8.[10]

The chemical shifts were attributed to all of the protons and the corresponding carbons as reported in Table 1, and alternethanoxin D, **4** was formulated as 1,4,6,9,10-pentahydroxy-7-methoxy-6*H*-benzo[*c*]chromene-2-carboxylic acid methyl ester. This structure was confirmed by the other long-range couplings observed in the HMBC spectrum (Table 1) and from the data of its HRESI MS spectrum. This latter spectrum showed the sodiated dimeric form $[2M + Na]^+$, and potassium and sodium clusters $[M + K]^+$ and $[M + Na]^+$ at m/z 691, 373, and 357.0574, respectively. Furthermore, a correlation was observed in the NOESY spectrum between H-3 and MeCO.

The absolute configuration at C-6 as depicted in Figure 1, established by comparing the chemical shifts of H-6 and H-3, was different in **2** with respect to **1**, as in the latter they gave an overlapped signal. This was confirmed by the signal at δ 12.10 due to the hemiacetalic hydroxy group at C-6, which was probably hydrogen bonded with the methoxy at C-7 generating a stable six-membered cycle.

Alternethanoxin E, **5**, showed the molecular formula of $C_{16}H_{12}O_6$ deduced from its HRESI MS and consistent with 11 hydrogen deficiencies. The preliminary investigation of ^{1}H and ^{13}C NMR spectra showed that **5** is closely related to **2**. In fact, its ^{1}H NMR spectrum (Table 1) differed from that of **2** only in the location of the methoxy group that was attached to C-8 instead of C-7. This generated the typical system of two *meta*-coupled aromatic protons (H-7 and H-9), resonating as two doublets (J = 2.2 Hz) at δ 6.99 and 6.91.[9] Their carbons resonated in the ^{13}C NMR spectrum (Table 1) at the typical chemical shift values of δ 168.4, 112.6, and 103.3 for C-8, C-9, and C-7. As expected, H-3, H-6, MeO, and MeCO were all observed as singlets at δ 6.84, 6.64, 3.92, and 2.45, respectively.[9] The couplings observed in the HMQC spectrum allowed

DOI: 10.1021/jf5054595
J. Agric. Food Chem. 2015, 63, 1196−1199

assignment of the chemical shifts to the other protonated carbons at δ 111.2, 107.2, 52.0, and 21.5 to C-6, C-3, OMe, and MeCO. The couplings observed in the HMBC (Table 1) between C-1 and C-2 with H-3, C-4 with MeCO, C-5 and C-6a with H-6, C-8 with OMe, and C-10 with H-9 allowed assignment of the signals at δ 155.9, 106.2, 148.9, 158.2, 161.2, 168.4, and 168.8 to C-1, C-2, C-4, C-5, C-6a, C-8, and C-10. The signals at δ 135.9 and 110.1 were assigned to C-10a and C-10b by comparison with the values reported for the same carbons in **1**.[6] Finally, the acetyl group appeared at the typical chemical shift value of δ 179.6.[10]

The chemical shifts were attributed to all of the protons and the corresponding carbons as reported in Table 1, and alternethanoxin E, **5** was formulated as 7,9-dihydroxy-2-methoxy-9*H*-4,8-dioxa-cyclopenta[*def*]phenanthrene-5-carboxylic acid methyl ester. This structure was confirmed by the other long-range couplings observed in the HMBC spectrum and from the data of its HRESI MS spectrum. This latter spectrum showed the sodiated dimeric form $[2M + Na]^+$ and the potassium and sodium clusters $[M + K]^+$ and $[M + Na]^+$ at m/z 623, 339, and 323.0521, respectively. Furthermore, a correlation was observed in the NOESY spectrum between H-3 and MeCO.

The absolute stereochemistry at C-6 of alternethanoxin E as depicted in Figure 1 should be the same as **2** considering the chemical shift values of H3/C3 and H6/C6.

The three new alternethanoxins C−E were assayed together with alternethanoxins A and B for their phytotoxic and antimicrobial activity (Table 2). Among the five compounds tested, only alternethanoxins A and C were toxic to the host plant of the fungus, *S. arvensis*. Alternethanoxin C was more active than alternethanoxin A. Couch-grass was sensitive to 4 of 5 compounds. Alternethanoxins A and C caused significantly stronger necrotic reaction than alternethanoxins B and D. Alternethanoxin E was nontoxic to both plants (Table 2).

Table 2. Biological Activity of Althernethanoxins A−E

	phytotoxic activity[a]		antimicrobial activity[b]	
compound	*Sonchus arvensis*	*Elytrigia repens*	*Bacillus subtilis*	*Candida tropicalis*
1	1.7 ± 0.11	1.2 ± 0.40	100	na
2	0	0.5 ± 0	>100	na
3	2.4 ± 0.23	1.1 ± 0.29	10	25
4	0	0.5 ± 0	10	25
5	0	0	na	na

[a]Necrosis, mm ± std deviation. [b]Minimal inhibitory concentration, μg/disc; na, no activity.

Alternethanoxins A and B showed low antibiotic activity against *B. subtilis*. The yeast fungus was insensitive to them. In the previous study,[6] the absence of this kind activity was reported for these two compounds. As compared to them, alternethanoxins C and D had notable antimicrobial activity against both *B. subtilis* and *C. tropicalis*. Alternethanoxin E was not active at all (Table 2).

■ ASSOCIATED CONTENT

Supporting Information

NMR, UV, and HRESI MS spectra of alternethanoxin C−E. This material is available free of charge via the Internet at http://pubs.acs.org.

■ AUTHOR INFORMATION

Corresponding Author

*Tel.: +39 081 2539178. Fax: +39 081 674330. E-mail: evidente@unina.it.

Funding

The work of the Russian group on production, isolation, and characterization of fungal metabolites was supported by the Russian Scientific Fund (project no. 14-26-00067). This research was carried out in part in the frame of Programme STAR financially supported by UniNA and Compagnia di San Paolo. Prof. Evidente is associated with Istituto di Chimica Biomolecolare CNR, Pozzuoli, Italy.

Notes

The authors declare no competing financial interest.

■ ACKNOWLEDGMENTS

The kind help of Dr. V. Zakharov (Research Institute of Hygiene, Occupational Pathology and Human Ecology, Federal Medical Biological Agency, St. Petersburg, Russia) in NMR experiments is acknowledged. We thank Dr. Andrey Rudenko (Institute of Toxicology, Federal Medical Biology Agency, St. Petersburg, Russia) for HRESIMS spectra.

■ REFERENCES

(1) Donald, W. W. Management and control of Canada thistle (*Cirsium arvense*). *Rev. Weed Sci.* **1990**, *5*, 193−250.

(2) Lemna, W. K.; Messersmith, C. G. The biology of Canada weeds. 94. *Sonchus arvensis* L. *Can. J. Plant Sci.* **1990**, *70*, 509−532.

(3) Vurro, M. *Novel Biotechnologies for Biocontrol Agent Enhancement and Management*; Springer: New York, 2008.

(4) Berestetskiy, A. O. A Review of fungal phytotoxins: from basic studies to practical use. *Appl. Biochem. Microbiol.* **2008**, *44*, 453−465.

(5) Cimmino, A.; Andolfi, A.; Berestetskiy, A.; Evidente, A. Production of phytotoxins by *Phoma exigua* var. *exigua*, a potential mycoherbicide against perennial thistles. *J. Agric. Food Chem.* **2008**, *56*, 6304−6309.

(6) Evidente, A.; Andolfi, A.; Cimmino, A. Fungal phytotoxins for control of *Cirsium arvense* and *Sonchus arvensis*. *Pest Technol.* **2011**, *5*, 1−17.

(7) Evidente, A.; Punzo, B.; Andolfi, A.; Berestetskiy, A.; Motta, A. Alternethanoxin A and B, polyciclic ethanones produced by *Alternaria sonchi*, potential mycoherbicides for *Sonchus arvenis* biocontrol. *J. Agric. Food Chem.* **2009**, *57*, 6656−6660.

(8) Berger, S.; Braun, S. *200 and More Basic NMR Experiments: A Practical Course*, 1st ed.; Wiley-VCH: Weinheim, 2004.

(9) Pretsch, E.; Bühlmann, P.; Affolter, C. *Structure Determination of Organic Compounds-Table of Spectral Data*, 3rd ed.; Springer-Verlag: Berlin, 2000; pp 161−243, 385−404.

(10) Breitmaier, E.; Voelter, W. *Carbon-13 NMR Spectroscopy*; VCH: Weinheim, 1987; pp 183−280.

(11) Berestetskiy, A. O.; Yuzikhin, O. S.; Katkova, A. S.; Dobrodumov, A. V.; Sivogrivov, D. E.; Kolombet, L. V. Isolation, identification, and characteristics of the phytotoxin produced by the fungus *Alternaria cirsinoxia*. *Appl. Biochem. Microbiol.* **2010**, *46*, 75−79.

(12) Bottalico, A.; Capasso, R.; Evidente, A.; Randazzo, G.; Vurro, M. Cytochalasins: structure-activity relationships. *Phytochemistry* **1990**, *29*, 93−96.

(13) Onishi, H. R.; Pelak, B. A.; Gerckens, L. S.; Silver, L. L.; Kahan, F. M.; Chen, M. H.; Patchett, A. A.; Galloway, S. M.; Hyland, S. A.; Derson, M. S.; Raetz, C. R. Antibacterial agents that inhibit lipid A biosynthesis. *Science* **1996**, *274*, 980−982.

DOI: 10.1021/jf5054595
J. Agric. Food Chem. 2015, 63, 1196−1199

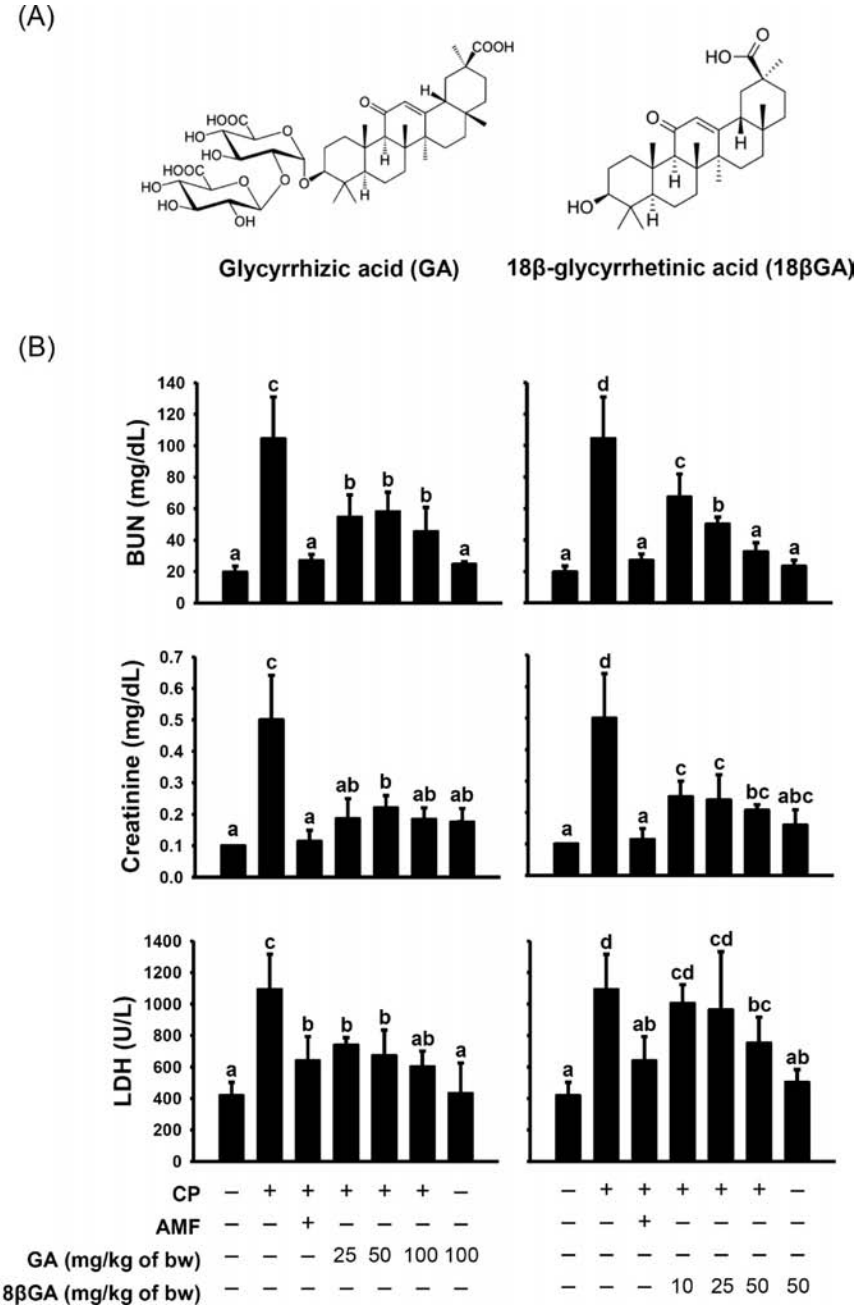

Figure 1. Elevated levels of serum BUN, creatinine, and LDH were reduced by GA and 18βGA in BALB/c mice with CP-induced renal injury. (A) Chemical structures of GA and 18βGA. (B) Mice were gavaged daily with GA (25−100 mg/kg of BW) or 18βGA (10−50 mg/kg of BW) for 8 consecutive days, and a single IP injection of CP (30 mg/kg of BW) was applied on day 6. The positive control group was given a single IP injection of AMF (200 mg/kg of BW) at 0.5 h before the CP challenge. Mice were sacrificed on day 9. Data are presented as the mean ± SD ($n = 8$), and letters (a−c) indicate statistically significant differences in each group ($p < 0.05$). One-way ANOVA tests were used for the statistical analyses.

antioxidant enzyme activities, and reducing inflammatory responses.[1,19] Because oxidative stress and inflammatory responses play key roles in CP-induced nephrotoxicity, this study employed an animal model of CP-induced renal injury to verify the protective effects of GA and 18βGA against chemically induced renal injury and the possible underlying mechanisms of such protective effects.

MATERIALS AND METHODS

Chemicals. CP, GA, 18βGA, Kollisolv PEG E 400, AMF, 1-chloro-2,4-dinitro-benzene (CDNB), glutathione (GSH), glutathione reductase (GSH-Rd), β-nicotinamide adenine dinucleotide phosphate (β-NADPH), sodium azide (NaN_3), and ethanol were obtained from Sigma-Aldrich (St. Louis, MO). The superoxide dismutase (SOD) assay kit was purchased from Faith Technology (Taichung, Taiwan); the GSH assay kit was purchased from Cayman Chemicals (Ann Arbor, MI); the protein assay kit was purchased from Bio-Rad (Hercules, CA); and the anti-nuclear factor E2-related protein (Nrf2), anti-heme oxygenase-1 (HO-1), anti-high-mobility group protein B1 (HMGB1), anti-nuclear factor-κ-light-chain-enhancer of activated B cells (NF-κB), anti-tumor necrosis factor (TNF)-α, anti-interleukin (IL)-1β, and anti-IL-6 antibodies were purchased from Cell Signaling Technology (Beverly, MA).

Experimental Animals and Procedures. The 6-week-old male BALB/c mice were purchased from the National Laboratory Animal

DOI: 10.1021/jf505471a
J. Agric. Food Chem. 2015, 63, 1200−1209

Center (Taipei, Taiwan). The animal experiments in this study were approved by the Institutional Animal Care and Use Committee of the National Chung Hsing University (IACUC approval number 98-76) and followed related regulations of the Animal Care and Use Committee. Animals were housed in animal rooms at the Department of Food Science and Biotechnology of National Chung Hsing University. The temperature and relative humidity (RH) of the animal rooms were maintained at constant levels (22 ± 2 °C and RH of 65 ± 5%). A 12 h light/dark cycle was maintained, and the light cycle was controlled by an automatic timer; the light period was at 06:00−18:00, and the dark period was at 18:00−06:00. After arrival, the experimental mice were immediately weighed, and after a statistical analysis, they were distributed to feeding cages according to a normal distribution. Animals were allowed *ad libitum* access to water and food (laboratory rodent diet 5001, Purina, St. Louis, MO).

The animal groupings and treatments were modified from the methods by Mitazaki et al.[20] and Arjumand et al.[14] After adaptive feeding for 1 week, the 6-week-old male BALB/c mice were continuously fed the sample diets for 8 days (GA at 25, 50, or 100 mg/kg of BW or 18βGA at 10, 25, or 50 mg/kg of BW). After 30 min of sample administration on day 6, an intraperitoneal (IP) injection of CP (30 mg/kg of BW) was given to induce damage, and 30 min prior to the injection of CP on day 6, the positive control group was IP-injected with the chemotherapy protectant, AMF (200 mg/kg of BW). The mice were sacrificed on day 9 to collect samples.

Analysis of Serum Biochemical Values. Serum biochemical values, including BUN, creatinine, and lactate dehydrogenase (LDH), were analyzed using the ADVIA Chemistry Urea Nitrogen Reagent, ADVIA Chemistry Enzymatic Creatinine-2 Reagent, and ADVIA Lactate Dehydrogenase L-P Reagent, respectively (Siemens, NY). The analyses were performed according to protocols in the manuals of the manufacturer.

Histopathological Studies. Renal tissues of BALB/c mice were fixed in 10% formaldehyde immediately following sacrifice, processed for histological examination according to a conventional method, and stained with hematoxylin and eosin (H&E). The morphology of any observed lesions was classified and recorded according to the classification criteria by Shackelford et al.[21]

Analysis of the Activities of Antioxidant Enzymes. Catalase, SOD, glutathione peroxidase (GPx), and glutathione reductase (GRd) activities were measured using an assay kit (Cayman, Ann Arbor, MI) according to the instruction of the manufacturer. The GSH/oxidized glutathione (GSSG) ratio was analyzed using a GSH assay kit purchased from Cayman (Ann Arbor, MI).

Measurement of Malondialdehyde (MDA). The MDA levels in kidney samples of experimental rats were determined using the thiobarbituric acid (TBA) method, with modifications.[22] Briefly, following a preincubation, 0.5 mL of tissue homogenate was mixed with 1 mL of 15% trichloroacetic acid, 0.375% thiobarbituric acid reactive substances (TBARS), and 0.25 mM HCl and then heated in boiling water for 45 min. After centrifugation (2000*g* for 15 min), the absorbance of the butanol phase was read at 535 and 520 nm. The difference between the two values was used to calculate the MDA concentration. An MDA standard was prepared from 1,1,3,3,-tetraethoxypropane. Total protein concentrations were determined by Lowry's method using bovine serum albumin as the standard. The MDA concentration was normalized against the total protein concentration and is expressed in micromoles per milligram of protein.

Immunohistochemical (IHC) Staining. Paraffin blocks of kidney tissues were cut using a microtome into 2 μm thick sections. Sections were floated on water to allow for the tissues to unfold and extend. Tissue sections were placed on 2-aminopropyltriethoxysilane-coated slides, dried at 37 °C, and deparaffinized using xylene. Deparaffinized slides were treated with 3% H_2O_2 and proteinase K (0.5 mg/mL) for 10 min, washed with distilled water 3 times, and incubated in blocking buffer (StartingBlock, Pierce, Rockford, IL) for 5 min. When the slides had slightly dried, they were stained with primary antibodies for 30 min at 40 °C (anti-Nrf2, anti-HO-1, anti-HMGB1, anti-NF-κB, anti-TNF-α, anti-IL-1β, and anti-IL-6 antibodies were used in this study). After the slides were washed with phosphate-buffered saline (PBS) 3 times, they were incubated in EnVision-labeled polymer peroxidase-conjugated anti-immunoglobulin G (IgG, Dako, Glostrup, Denmark) at room temperature for 30 min. Slides were again washed with PBS 3 times and then incubated in diluted 3,3-diaminobenzidine tetrahydrochloride (DAB-4HCl, Dako) for color development. After development, slides were washed with PBS 3 times and counterstained with hematoxylin. Slides were then washed with distilled water 3 times, dehydrated, dried, and mounted. The intensity of antigen expression after staining was quantified using Image-Pro Plus 6.3 image analysis software (Media Cybernetics, Rockville, MD). Results are presented as the positively stained area (%).

Statistical Analysis. All data are expressed as the mean ± standard deviation (SD). An analysis of variance (ANOVA) was used to evaluate differences among multiple groups. Significant differences were subjected to Duncan's test to compare the means of two specific groups. A p value of <0.05 was considered significant.

RESULTS

Evaluation of Renal Function Parameters To Determine the Effects of GA and 18βGA on CP-Induced Renal Injury in BALB/c Mice. The chemical structures of GA and 18βGA are shown in Figure 1A. As shown in Figure 1B, an IP injection of CP (30 mg/kg of BW) induced significant increases in serum BUN, creatinine, and LDH in BALB/c mice. Administration of GA (25, 50, and 100 mg/kg of BW) and 18βGA (10, 25, and 50 mg/kg of BW) significantly reduced CP-induced BUN, creatinine, and LDH levels. The positive control of AMF (200 mg/kg of BW) also showed a protective effect on kidneys exposed to CP-induced acute renal injury. In addition, administration of a high dose of GA or 18βGA alone did not affect levels of BUN, creatinine, or LDH in the kidneys (p < 0.05).

Tissue Pathological Analysis of the Effects of GA and 18βGA on CP-Induced Renal Injury in BALB/c Mice. Acute renal tubular necrosis is an important pathological feature of CP-induced renal injury,[23] and this study used morphological changes in the appearance of the kidneys and renal tubular lesions as indicators to evaluate renal injury. Results showed that CP induced significant lesions that produced whitening of the kidneys in mice. The macroscopic appearances were similar among the GA-, 18βGA-, and AMF-treated sample groups and CP-untreated control group and exhibited a hyperemic dark-maroon color (left panel of Figure 2). The right panel of Figure 2 shows pathological tissue sections with H&E staining (400×) in the GA and 18βGA experimental groups. Changes in tissue morphology indicated that the control group presented a healthy normal morphology of renal glomeruli and tubules, whereas the CP group presented severe renal tubular injury, while the GA and 18βGA groups presented different degrees of protective effects. Further pathological interpretation and classification of the above sections based on the four pathological features of renal tubules, including tubular necrosis, tubular degeneration, hyaline cast, and dilation, were performed according to the classification criteria by Shackelford et al.[21] (Table 1). A statistical analysis of injury scores for the GA and 18βGA experimental groups showed that both compounds significantly protected renal tubules from CP-induced injury (p < 0.05) in dose-dependent manners. In addition, renal tubular injury was found to interfere with the reabsorption of renal filtrate, which might affect BW changes. Administration of a high dose of GA (100 mg/kg of BW) or 18βGA (50 mg/kg of BW) alone did not the affect BW changes in experimental animals (data not shown).

Effects of GA and 18βGA on CP-Induced Lipid Peroxide Accumulation and Alterations of Antioxidant Enzyme

DOI: 10.1021/jf505471a
J. Agric. Food Chem. 2015, 63, 1200−1209

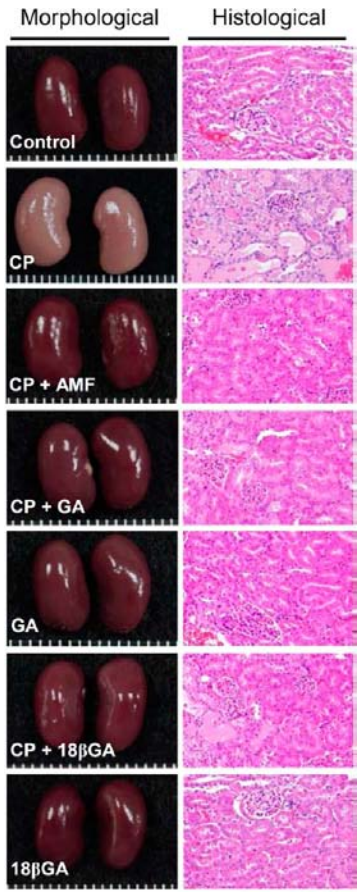

Figure 2. Effects of GA and 18βGA on the kidney morphology and histology in BALB/c mice with CP-induced renal injury. Groups of mice were treated as described in Figure 1, and the data shown are from a representative experiment. Representative macroscopic appearances of the kidneys (left panel) and H&E-stained kidneys (right panel, 400×) were used to assess the renoprotective effects of GA (100 mg/kg of BW) and 18βGA (50 mg/kg of BW) against CP-induced nephrotoxicity in experimental mice.

Activities in the Kidneys of BALB/c Mice. During the pathological process of CP-induced acute renal injury, accumulation of lipid peroxides and reductions in antioxidant enzyme activities in the kidneys play important roles;[24] however, supplementation with antioxidants or activation of the antioxidant defense system can provide a certain degree of protection.[25,26] This study also confirmed that CP promoted formation of MDA and reduced activities of antioxidant enzymes, such as catalase, SOD, and GPx, and the GSH/GSSG ratio in the kidneys. Except for the low dose of GA (25 mg/kg of BW) or 18βGA (10 mg/kg of BW), which showed no effect on GPx activity ($p < 0.05$), AMF and other doses of GA and 18βGA inhibited lipid peroxidation and restored the protective features of the above antioxidant enzymes and GSH/GSSG ratio (Figure 3).

Effects of GA and 18βGA on CP-Induced Antioxidant Protein Expressions in Kidneys of BALB/c Mice. This study used an IHC method to show for the first time that, in a CP-induced renal injury mouse model, the antioxidant transcription factor, Nrf2 (Figure 4A), and its downstream, HO-1 (Figure 4B), were significantly activated in the kidneys. However, GA (50 mg/kg of BW) and 18βGA (25 mg/kg of BW) stimulated antioxidant transcription factor Nrf2 and further stimulated the expression of the above antioxidant proteins in the kidney after CP-induced injury (Figure 4 and Supplementary Figure 1 of the Supporting Information). This result might explain the increased activity of antioxidant enzymes in the kidneys after administration of GA and 18βGA.

Effects of GA and 18βGA on Kidney Inflammation-Related Indicators in BALB/c Mice with CP-Induced Renal Injury. This study also performed IHC analyses and directly used the staining intensity of the detected target molecules in tissues to evaluate alterations in inflammation-related factors in kidney tissues. CP stimulated expression of the NF-κB transcription factor in the kidneys (Figure 5A); however, administration of GA, 18βGA, and AMF all showed a protective effect and significantly inhibited NF-κB (panels A and B of Figure 5). They also had significant inhibitory effects on proinflamma-

Table 1. Histology Injury Scores of CP-Induced Kidney Injury under GA, 18βGA, and AMF Treatment in BALB/c Mice

	injury score[a]			
group[b]	necrosis	hyaline cast	degeneration	dilation
control	0 ± 0 a	0 ± 0 a	0 ± 0 a	0 ± 0 a
CP	2.1 ± 0.8 c	2.2 ± 0.8 c	3.0 ± 0.9 d	1.4 ± 0.5 b
AMF + CP	0.8 ± 0.8 ab	0 ± 0 a	0.8 ± 0.8 ab	0 ± 0 a
GA-10 + CP	1.0 ± 0.6 b	1.0 ± 0.6 b	1.8 ± 0.4 c	0 ± 0 a
GA-25 + CP	0.8 ± 0.4 ab	0.6 ± 0.5 ab	1.4 ± 0.5 bc	0 ± 0 a
GA-100 + CP	0.2 ± 0.4 ab	0.4 ± 0.5 ab	0.2 ± 0.4 a	0 ± 0 a
GA-100	0 ± 0 a	0 ± 0 a	0 ± 0 a	0 ± 0 a
control	0 ± 0 a	0 ± 0 a	0 ± 0 a	0 ± 0 a
CP	2.1 ± 0.8 e	2.2 ± 0.8 b	3.0 ± 0.9 c	1.4 ± 0.5 b
AMF + CP	0.8 ± 0.8 bc	0 ± 0 a	0.8 ± 0.8 ab	0 ± 0 a
18βGA-10 + CP	1.6 ± 0.5 cd	1.8 ± 0.4 b	1.6 ± 0.5 b	0 ± 0 a
18βGA-25 + CP	1.2 ± 0.4 d	1.6 ± 0.5 b	1.2 ± 0.9 b	0.4 ± 0.8 a
18βGA-50 + CP	0.4 ± 0.5 ab	0.6 ± 0.5 a	0 ± 0 a	0 ± 0 a
18βGA-50	0 ± 0 a	0 ± 0 a	0 ± 0 a	0 ± 0 a

[a]Degree of lesions was graded from 0 to 5 depending upon the severity: 0, no significant lesions; 1, minimal (<1%); 2, slight (1−25%); 3, moderate (26−50%); 4, moderate/severe (51−75%); and 5, severe/high (76−100%). Each value is expressed as the mean ± SD ($n = 8$), and letters (a−e) indicate statistically significant differences in each group ($p < 0.05$). One-way ANOVA tests were used for the statistical analysis. [b]CP, 30 mg/kg of BW; AMF, 200 mg/kg of BW; GA-25, 25 mg/kg of BW; GA-50, 50 mg/kg of BW; GA-100, 100 mg/kg of BW; 18βGA-10, 10 mg/kg of BW; 18βGA-25, 25 mg/kg of BW; and 18βGA-50, 50 mg/kg of BW.

DOI: 10.1021/jf505471a
J. Agric. Food Chem. 2015, 63, 1200−1209

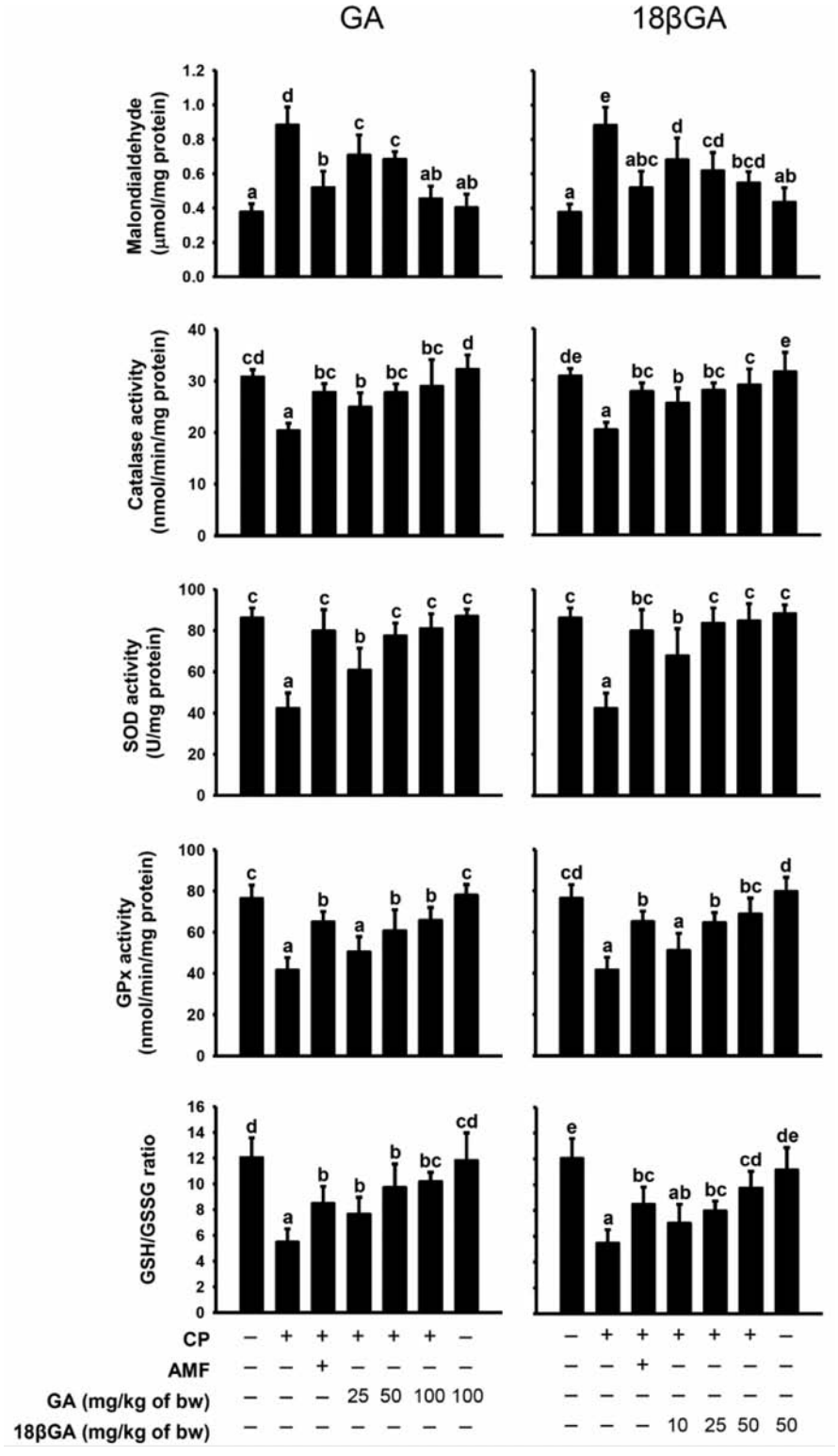

Figure 3. Effects of GA and 18βGA on CP-induced lipid peroxidation and alterations in antioxidant enzyme activities and the GSH/GSSG ratio in renal tissues of BALB/c mice. Groups of mice were treated as described in Figure 1. Data are presented as the mean ± SD (n = 8), and letters (a–e) indicate statistically significant differences in each group ($p < 0.05$). One-way ANOVA tests were used for the statistical analyses.

tory cytokines, including TNF-α (Figure 5C and Supplementary Figure 2 of the Supporting Information), IL-1β (Figure 5D and Supplementary Figure 2 of the Supporting Information), and IL-6 (Figure 5E and Supplementary Figure 2 of the Supporting Information).

Effects of GA and 18βGA on the Expression of HMGB1 in Kidneys of BALB/c Mice with CP-Induced Renal Injury. HMGB1, a nuclear protein that is usually actively or passively released during stress or necrosis in cells, transmits cell injury signals and activates a series of self-protection mechanisms.[27] Results of the IHC analysis shown in the left panel of Figure 6

DOI: 10.1021/jf505471a
J. Agric. Food Chem. 2015, 63, 1200–1209

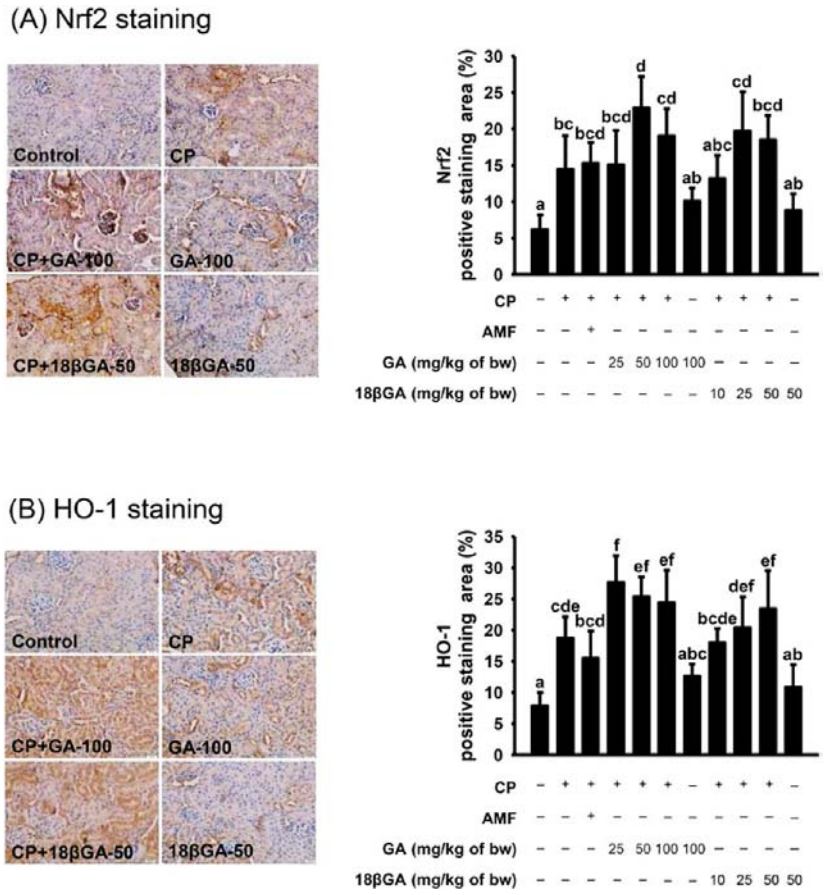

Figure 4. Effects of GA and 18βGA on the IHC expressions of Nrf2 and HO-1 in experimental mice. Groups of mice were treated as described in Figure 1. Renal tissues were analyzed by IHC staining for Nrf2 (A, left panel) and HO-1 (B, left panel). Nrf2- (A, right panel) and HO-1- (B, right panel) stained areas were quantified, and numbers of positively stained areas (%) per 400× field were averaged across eight fields for each section. Each value is expressed as the mean ± SD ($n = 8$), and letters (a−d) indicate statistically significant differences in each group ($p < 0.05$). One-way ANOVA tests were used for the statistical analyses.

indicated that, after CP-induced tissue injury to kidneys of BALB/c mice, HMBG1 showed a typical staining result, indicating diffuse release from nuclei. GA and 18βGA each significantly inhibited the accumulation of HMGB1 in the cytoplasm in a dose-dependent manner, and their inhibitory effects were greater than that of AMF, a known protectant (right panel of Figure 6). In summary, GA and 18βGA were able to decrease expressions of NF-κB, TNF-α, IL-1β, and IL-6 and release of HMGB1; in addition, they provided a protective function by increasing Nrf2 and HO-1 levels.

DISCUSSION

Since approval of CP by the U.S. Food and Drug Administration (FDA) in 1978 as a chemodrug, it has provided great therapeutic contributions to treating solid tumors, such as testicular cancer. Chemotherapy usually causes strong side effects in patients, including serious damage to normal organs, often leading to cessation of treatment; therefore, chemotherapy causes a bottleneck in current cancer treatment. The major clinical side effect of CP is nephrotoxicity, and patients usually show increased serum BUN and creatinine levels in 10 days after an injection.[4] Oxidative stress is the major cause of nephrotoxicity, and CP induces the production of a large amount of ROS in renal tubular cells. Although mitochondria in cells continue to clear ROS by activating antioxidant enzymes (such as catalase, SOD, GPx, and GST), eventually, antioxidant enzyme activities decrease, intracellular GSH is depleted, and mitochondrial dysfunction is induced, which causes cell necrosis and impaired renal function.[28] CP also directly stimulates renal tubular cells to secret TNF-α, which causes severe inflammatory responses, aggravates renal tubular cell damage, directly causes blood vessel injury, reduces blood flow in the kidneys, induces ischemic necrosis of cells, and eventually results in renal failure.[2]

Studies on applying phytochemicals to ameliorate drug side effects are still emerging. The literature shows that quercetin may decrease CP-induced NF-κB and TNF-α expressions and reduce kidney inflammation.[19,29] Lycopene may restore CP-depleted antioxidant enzyme activities through activating the Nrf2/HO-1 signaling pathway.[24] Hesperidin has antioxidant and anti-inflammatory effects and might also decrease CP-induced renal tubular necrosis and high levels of serum BUN and creatinine.[30] Those results show that, during the process of CP-induced renal injury, effective control of excess inflammatory responses and oxidative damage had definite positive effects on renal function maintenance and disease prevention. Previous studies showed that GA and 18βGA have multiple biological activities, such as antioxidant and anti-inflammatory effects,[17,18,31] and are closely associated with the mechanism underlying the aforementioned CP-induced renal injury. Therefore, we speculated that GA and 18βGA might have protective potentials to relieve the nephrotoxicity caused by CP. AMF is a drug currently approved to relieve nephrotoxicity caused by CP treatment. Clinical studies

DOI: 10.1021/jf505471a
J. Agric. Food Chem. 2015, 63, 1200−1209

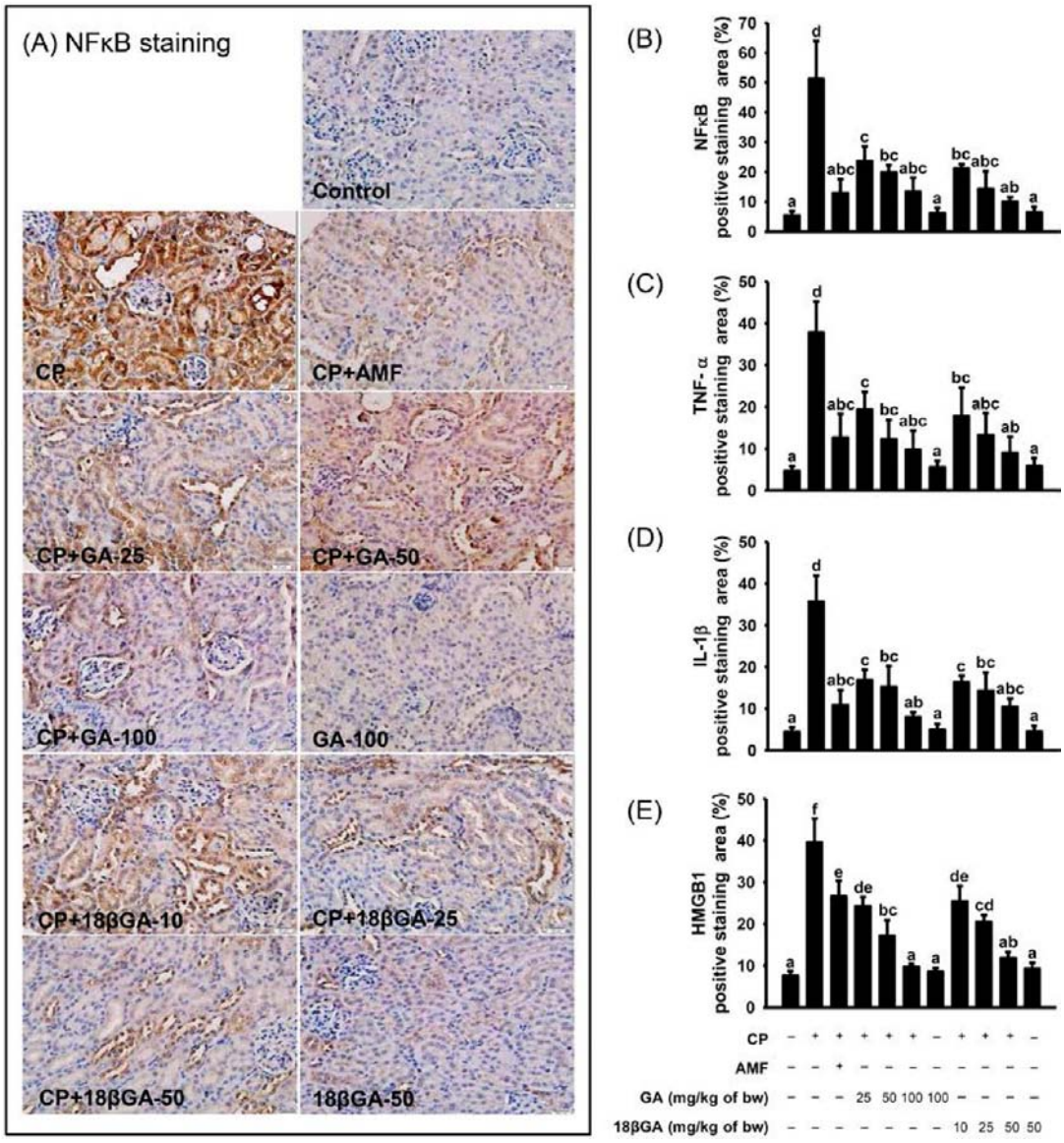

Figure 5. Effects of GA and 18βGA on CP-induced proinflammatory mediator expressions in renal tissues. Groups of mice were treated as described in Figure 1. (A) Renal tissues were analyzed by IHC staining for NF-κB. (B) NF-κB-, (C) TNF-α-, (D) IL-1β-, and (E) IL-6-stained areas were quantified, and numbers of positively stained areas (%) per 400× field were averaged across eight fields for each section. Each value is expressed as the mean ± SD (n = 8), and letters (a–f) indicate statistically significant differences in each group ($p < 0.05$). One-way ANOVA tests were used for the statistical analysis. CP, 30 mg/kg of BW; AMF, 200 mg/kg of BW; GA-25, 25 mg/kg of BW; GA-50, 50 mg/kg of BW; GA-100, 100 mg/kg of BW; 18βGA-10, 10 mg/kg of BW; 18βGA-25, 25 mg/kg of BW; and 18βGA-50, 50 mg/kg of BW.

have confirmed that AMF has inhibitory effects on the accumulation of nephrotoxicity in lung adenocarcinoma patients.[5,6] Therefore, this study selected AMF as the drug in the control group for use as a baseline control of all injury indicators in mice with CP-induced renal injury.

Activation of the Nrf2 is a defense mechanism after toxic insult. In response to CP, the current work also confirmed that expressions of Nrf2 protein were increased (Figure 4A) and the activities of antioxidant enzymes as well as the GSH/GSSG ratio were declined (Figure 3), reflective of more oxidative stress. Instead, not only GA but also 18βGA supplementation was found to significantly improve the changes associated with CP nephrotoxicity, as also evident by the increased level of antioxidant enzymes. A previous study showed that HO-1 expression was upregulated by these two phytochemicals to eliminate ROS formation.[31] Therefore, the expected induction of antioxidant enzymes by GA or 18βGA in CP-treated mice may be at least partly attributed to the functional activation of Nrf2/HO-1 signaling. However, the free radical scavenging ability of GA and 18βGA cannot be ruled out as a mechanism underlying the antioxidant enzyme-inducing effect in response to CP. The protective effects of GA and 18βGA may also be attributable to their ability to scavenge ROS and subsequently ameliorate CP-mediated oxidative stress and appear to be linked to the differential levels of antioxidant enzymes in CP-treated mice.

Previous studies showed that licorice plant extracts can inhibit ochratoxin-A-induced renal injury.[32] GA also showed protective effects against gentamicin-induced acute renal injury in rats.[33] In an ischemic model, GA also decreased neuronal cell apoptosis[17] and acute renal failure in animals.[11] Results of this study also confirmed that GA and 18βGA effectively inhibited CP-induced expressions of proinflammatory agents (NF-κB, TNF-α, IL-1β,

DOI: 10.1021/jf505471a
J. Agric. Food Chem. 2015, 63, 1200–1209

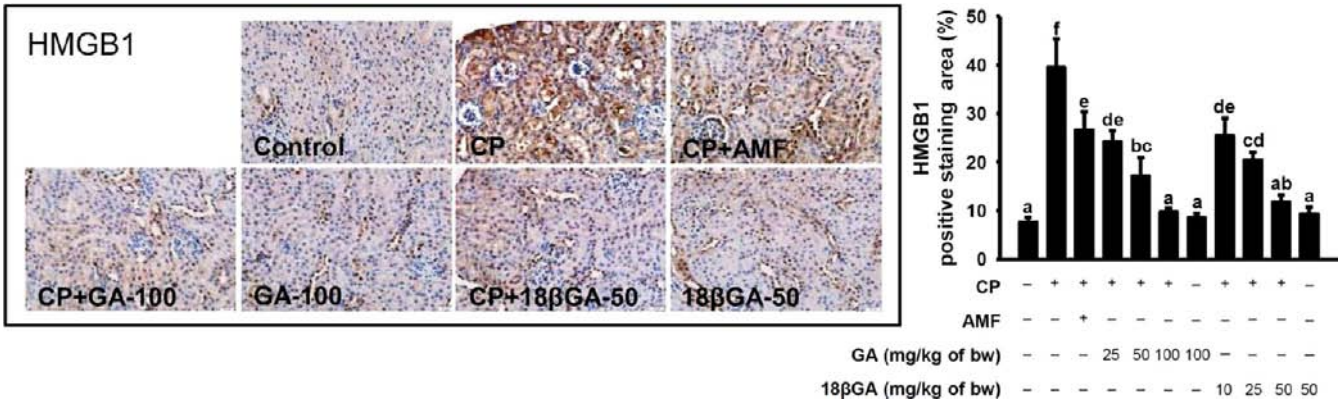

Figure 6. Effects of GA and 18βGA on CP-induced HMGB1 release from nuclei to the cytoplasm in renal tissues. Groups of mice were treated as described in Figure 1. Renal tissues were analyzed by IHC staining for HMGB1 (left panel); HMGB1-stained areas were quantified; and numbers of positively stained areas (%) per 400× field were averaged across eight fields for each section (right panel). Each value is expressed as the mean ± SD (n = 8), and letters (a–f) indicate statistically significant differences in each group ($p < 0.05$). One-way ANOVA tests were used for the statistical analyses. CP, 30 mg/kg of BW; AMF, 200 mg/kg of BW; GA-100, 100 mg/kg of BW; and 18βGA-50, 50 mg/kg of BW.

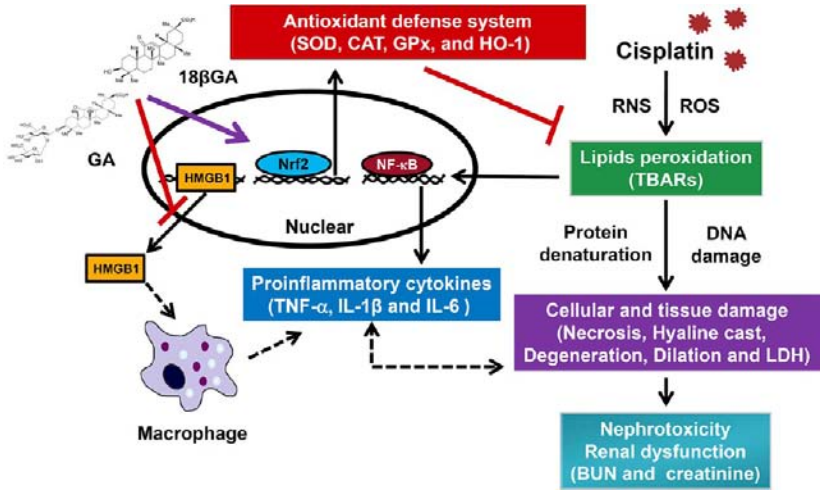

Figure 7. Proposed mechanisms of GA and 18βGA on CP-induced nephrotoxicity in BALB/c mice.

IL-6, and HMGB1) in kidney tissues of BALB/c mice, restored the activities of antioxidant enzymes and the GSH/GSSG ratio, and suppressed CP-induced oxidative stress in the kidneys. Therefore, the conclusion of this study is that GA and 18βGA can be used to relieve CP-induced chemical renal injury because of their antioxidant and anti-inflammatory features.

It is known that HMBG1 is a chaperone protein of nuclear DNA and a secreted protein. HMBG1 can be passively released from necrotic cells or actively released from inflammatory cells, act as an extracellular damage-associated molecular pattern (DAMP) molecule, and is an important mediator of inflammatory responses.[27] Although the association between CP and HMGB1 in cancer treatment is not clear, studies indicated that CP promoted HMGB1 expression in human myeloma cells[34] to produce drug resistance. Sitia et al.[35] suggested that GA interfered with the aggregation of chemotactic neutrophils and other inflammatory cells caused by HMGB1 in hepatitis B virus transgenic mice and relieved hepatic lesions. In addition, GA directly interacts with HMGB1 to inhibit the chemoattractant activity of HMGB1 on inflammatory cells and reduce HMGB1-induced inflammatory responses.[36] The results of this study also found that GA and 18βGA reduced the release of HMGB1 from cell nuclei during CP-induced injury. This result suggests a possible cause of the inhibitory effects of GA and 18βGA on many proinflammatory cytokines during renal injury.

The doses employed in the current work (25–100 mg/kg of BW for GA and 10–50 mg/kg of BW for 18βGA) were based on previous animal studies showing the effectiveness of GA or 18βGA to treat hyperglycemia[16] and chemical-induced hepatotoxicity.[37,38] 18βGA is a metabolic product of GA by way of intestinal bacterial enzymes. Our pilot experiment showed that 100 mg of 18βGA/kg of BW had an unexpected effect of causing a decrease in mice activities and yellowish skin (data not shown). Therefore, this study selected 50 mg of 18βGA/kg of BW, because that dose caused no abnormal conditions in mice. A comparison of the protective effects against renal injury between GA and 18βGA at 50 mg/kg of BW each showed that the biological activity of 18βGA was better than that of GA. This result indicates that 18βGA can possibly be used as an adjuvant factor that has the potential to delay side effects during chemotherapy. Kao et al.[31] indicated that 18βGA had a better anti-inflammatory effect in a cell culture model than GA. GA and 18βGA have different anti-inflammatory mechanisms, with GA mainly activating the PI3K/Akt/GSK3β pathway and 18βGA mainly activating the glucocorticoid receptor. This difference might be explained by the structure of 18βGA, which is much closer to that of steroids; therefore, 18βGA may be able to

DOI: 10.1021/jf505471a
J. Agric. Food Chem. 2015, 63, 1200–1209

activate glucocorticoid receptors to exhibit an improved anti-inflammatory effect.[39]

In addition to GA and 18βGA, there are some constitutes in licorice, such as chalconoids (liquiritin, isoliquiritin, liquiritigenin, and isoliquiritigenin), isoflavonoids (dehydroglyasperin C, dehydroglyasperin D, and glabridin), 18βGA derivative (carbenoxolone), and some unique compounds (licoricidin, licorisoflavan A, and licochalcone A) that have been well-studied and biologically characterized.[10] These effects have been associated with the anti-inflammatory, antioxidative, antimicrobial, antivirus, cell protective, and chemopreventive properties of the compounds, which may also have potential to be developed into a natural chemoprotectant, and they should be analyzed through further investigations in the future.

In summary, CP-induced nephrotoxicity is produced by a combination of interactions among many pathways. GA and 18βGA are phytochemicals in licorice with multiple physiological activities, and a possible mechanism underlying their ability to delay CP-induced physiological renal injury is shown in Figure 7. Our results indicate that GA and 18βGA have the potential to be developed into natural adjuvants to relieve CP side effects in patients undergoing chemotherapy, and they should be analyzed through further clinical validations and investigations in the future.

■ ASSOCIATED CONTENT

Supporting Information

Effects of GA and 18βGA on the IHC expressions of Nrf2 and HO-1 in experimental mice (Supplemental Figure 1) and effects of GA and 18βGA on CP-induced proinflammatory mediator expressions in renal tissues (Supplemental Figure 2). This material is available free of charge via the Internet at http://pubs.acs.org.

■ AUTHOR INFORMATION

Corresponding Author

*Telephone: +886-4-2287-9755. Fax: +886-4-2285-4378. E-mail: gcyen@nchu.edu.tw.

Funding

This research was supported in part by the Ministry of Science and Technology, Taiwan (MOST99-2628-B005-003-MY3).

Notes

The authors declare no competing financial interest.

■ ACKNOWLEDGMENTS

The authors thank Dr. J. W. Liao of the Graduate Institute of Veterinary Pathobiology for his technical assistance on histological examination.

■ ABBREVIATIONS USED

AMF, amifostine; BUN, blood urea nitrogen; CP, cisplatin; GA, glycyrrhizic acid; 18βGA, 18β-glycyrrhetinic acid; HMGB1, high-mobility group protein B1; HO-1, heme oxygenase-1; IHC, immunohistochemical; LDH, lactate dehydrogenase; MDA, malondialdehyde; Nrf2, nuclear factor E2-related protein; ROS, reactive oxygen species

■ REFERENCES

(1) dos Santos, N. A.; Carvalho Rodrigues, M. A.; Martins, N. M.; dos Santos, A. C. Cisplatin-induced nephrotoxicity and targets of nephroprotection: An update. *Arch. Toxicol.* **2012**, *86*, 1233−1250.

(2) Pabla, N.; Dong, Z. Cisplatin nephrotoxicity: Mechanisms and renoprotective strategies. *Kidney Int.* **2008**, *73*, 994−1007.

(3) Lin, Y. H.; Lin, S. F.; Hsiao, H. H.; Liu, Y. C.; Yang, W. C.; Hwang, D. Y.; Hung, C. C.; Hwang, S. J.; Guh, J. Y.; Chen, H. C. Recent update on cisplatin induced acute kidney injury. *J. Int. Med. Taiwan* **2011**, *22*, 416−422.

(4) Arany, I.; Safirstein, R. L. Cisplatin nephrotoxicity. *Semin. Nephrol.* **2003**, *23*, 460−464.

(5) Capizzi, R. L. Amifostine reduces the incidence of cumulative nephrotoxicity from cisplatin: Laboratory and clinical aspects. *Semin. Oncol.* **1999**, *26*, 72−81.

(6) Asna, N.; Lewy, H.; Ashkenazi, I. E.; Deutsch, V.; Peretz, H.; Inbar, M.; Ron, I. G. Time dependent protection of amifostine from renal and hematopoietic cisplatin induced toxicity. *Life Sci.* **2005**, *76*, 1825−1834.

(7) Kouvaris, J. R.; Kouloulias, V. E.; Vlahos, L. J. Amifostine: The first selective-target and broad-spectrum radioprotector. *Oncologist* **2007**, *12*, 738−747.

(8) Blumenthal, M.; Goldberg, A.; Brinckmann, J. In *Herbal Medicine: Expanded Commission E Monographs*; Blumenthal, M., Ed.; American Botanical Council: Newton, MA, 2000; pp 233−236.

(9) Akao, T.; Akao, T.; Hattori, M.; Kanaoka, M.; Yamamoto, K.; Namba, T.; Kobashi, K. Hydrolysis of glycyrrhizin to 18β-glycyrrhetyl monoglucuronide by lysosomal β-D-glucuronidase of animal livers. *Biochem. Pharmacol.* **1991**, *41*, 1025−1029.

(10) Kao, T. C.; Wu, C. H.; Yen, G. C. Bioactivity and potential health benefits of licorice. *J. Agric. Food Chem.* **2014**, *62*, 542−553.

(11) Kang, D. G.; Sohn, E. J.; Mun, Y. J.; Woo, W. H.; Lee, H. S. Glycyrrhizin ameliorates renal function defects in the early-phase of ischemia-induced acute renal failure. *Phytother. Res.* **2003**, *17*, 947−951.

(12) Guo, X. L.; Liang, B.; Wang, X. W.; Fan, F. G.; Jin, J.; Lan, R.; Yang, J. H.; Wang, X. C.; Jin, L.; Cao, Q. Glycyrrhizic acid attenuates CCl_4-induced hepatocyte apoptosis in rats via a p53-mediated pathway. *World J. Gastroenterol.* **2013**, *19*, 3781−3791.

(13) Ni, Y. F.; Kuai, J. K.; Lu, Z. F.; Yang, G. D.; Fu, H. Y.; Wang, J.; Tian, F.; Yan, X. L.; Zhao, Y. C.; Wang, Y. J.; Jiang, T. Glycyrrhizin treatment is associated with attenuation of lipopolysaccharide-induced acute lung injury by inhibiting cyclooxygenase-2 and inducible nitric oxide synthase expression. *J. Surg. Res.* **2011**, *165*, e29−35.

(14) Arjumand, W.; Sultana, S. Glycyrrhizic acid: A phytochemical with a protective role against cisplatin-induced genotoxicity and nephrotoxicity. *Life Sci.* **2011**, *89*, 422−429.

(15) Asl, M. N.; Hosseinzadeh, H. Review of pharmacological effects of *Glycyrrhiza* sp. and its bioactive compounds. *Phytother. Res.* **2008**, *22*, 709−724.

(16) Kalaiarasi, P.; Pugalendi, K. V. Antihyperglycemic effect of 18β-glycyrrhetinic acid, aglycone of glycyrrhizin, on streptozotocin-diabetic rats. *Eur. J. Pharmacol.* **2009**, *606*, 269−273.

(17) Kao, T. C.; Shyu, M. H.; Yen, G. C. Neuroprotective effects of glycyrrhizic acid and 18β-glycyrrhetinic acid in PC12 cells via modulation of the PI3K/Akt pathway. *J. Agric. Food Chem.* **2009**, *57*, 754−761.

(18) Wang, C. Y.; Kao, T. C.; Lo, W. H.; Yen, G. C. Glycyrrhizic acid and 18β-glycyrrhetinic acid modulate lipopolysaccharide-induced inflammatory response by suppression of NF-κB through PI3K p110δ and p110γ inhibitions. *J. Agric. Food Chem.* **2011**, *59*, 7726−7733.

(19) Sanchez-Gonzalez, P. D.; Lopez-Hernandez, F. J.; Perez-Barriocanal, F.; Morales, A. I.; Lopez-Novoa, J. M. Quercetin reduces cisplatin nephrotoxicity in rats without compromising its anti-tumour activity. *Nephrol., Dial., Transplant.* **2011**, *26*, 3484−3495.

(20) Mitazaki, S.; Kato, N.; Suto, M.; Hiraiwa, K.; Abe, S. Interleukin-6 deficiency accelerates cisplatin-induced acute renal failure but not systemic injury. *Toxicology* **2009**, *265*, 115−121.

(21) Shackelford, C.; Long, G.; Wolf, J.; Okerberg, C.; Herbert, R. Qualitative and quantitative analysis of nonneoplastic lesions in toxicology studies. *Toxicol. Pathol.* **2002**, *30*, 93−96.

(22) Ohkawa, H.; Ohishi, N.; Yagi, K. Assay for lipid peroxides in animal tissues by thiobarbituric acid reaction. *Anal. Biochem.* **1979**, *95*, 351−358.

DOI: 10.1021/jf505471a
J. Agric. Food Chem. 2015, 63, 1200−1209

(23) Ali, B. H.; Al Moundhri, M. S. Agents ameliorating or augmenting the nephrotoxicity of cisplatin and other platinum compounds: A review of some recent research. *Food Chem. Toxicol.* **2006**, *44*, 1173−1183.
(24) Sahin, K.; Tuzcu, M.; Sahin, N.; Ali, S.; Kucuk, O. Nrf2/HO-1 signaling pathway may be the prime target for chemoprevention of cisplatin-induced nephrotoxicity by lycopene. *Food Chem. Toxicol.* **2010**, *48*, 2670−2674.
(25) Husain, K.; Morris, C.; Whitworth, C.; Trammell, G. L.; Rybak, L. P.; Somani, S. M. Protection by ebselen against cisplatin-induced nephrotoxicity: Antioxidant system. *Mol. Cell. Biochem.* **1998**, *178*, 127−133.
(26) Ajith, T. A.; Abhishek, G.; Roshny, D.; Sudheesh, N. P. Co-supplementation of single and multi doses of vitamins C and E ameliorates cisplatin-induced acute renal failure in mice. *Exp. Toxicol. Pathol.* **2009**, *61*, 565−571.
(27) Kang, R.; Chen, R.; Zhang, Q.; Hou, W.; Wu, S.; Cao, L.; Huang, J.; Yu, Y.; Fan, X. G.; Yan, Z.; Sun, X.; Wang, H.; Wang, Q.; Tsung, A.; Billiar, T. R.; Zeh, H. J., III; Lotze, M. T.; Tang, D. HMGB1 in health and disease. *Mol. Aspects Med.* **2014**, *40*, 1−116.
(28) Ozbek, E. Induction of oxidative stress in kidney. *Int. J. Nephrol.* **2012**, *2012*, 465897.
(29) Behling, E. B.; Sendao, M. C.; Francescato, H. D.; Antunes, L. M.; Costa, R. S.; Bianchi Mde, L. Comparative study of multiple dosage of quercetin against cisplatin-induced nephrotoxicity and oxidative stress in rat kidneys. *Pharmacol. Rep.* **2006**, *58*, 526−532.
(30) Sahu, B. D.; Kuncha, M.; Sindhura, G. J.; Sistla, R. Hesperidin attenuates cisplatin-induced acute renal injury by decreasing oxidative stress, inflammation and DNA damage. *Phytomedicine* **2013**, *20*, 453−460.
(31) Kao, T. C.; Shyu, M. H.; Yen, G. C. Glycyrrhizic acid and 18beta-glycyrrhetinic acid inhibit inflammation via PI3K/Akt/GSK3β signaling and glucocorticoid receptor activation. *J. Agric. Food Chem.* **2010**, *58*, 8623−8629.
(32) Malekinejad, H.; Farshid, A. A.; Mirzakhani, N. Liquorice plant extract reduces ochratoxin A-induced nephrotoxicity in rats. *Exp. Toxicol. Pathol.* **2011**, *63*, 125−130.
(33) Sohn, E. J.; Kang, D. G.; Lee, H. S. Protective effects of glycyrrhizin on gentamicin-induced acute renal failure in rats. *Pharmacol. Toxicol.* **2003**, *93*, 116−122.
(34) Huang, J.; Ni, J.; Liu, K.; Yu, Y.; Xie, M.; Kang, R.; Vernon, P.; Cao, L.; Tang, D. HMGB1 promotes drug resistance in osteosarcoma. *Cancer Res.* **2012**, *72*, 230−238.
(35) Sitia, G.; Iannacone, M.; Muller, S.; Bianchi, M. E.; Guidotti, L. G. Treatment with HMGB1 inhibitors diminishes CTL-induced liver disease in HBV transgenic mice. *J. Leukocyte Biol.* **2007**, *81*, 100−107.
(36) Mollica, L.; De Marchis, F.; Spitaleri, A.; Dallacosta, C.; Pennacchini, D.; Zamai, M.; Agresti, A.; Trisciuoglio, L.; Musco, G.; Bianchi, M. E. Glycyrrhizin binds to high-mobility group box 1 protein and inhibits its cytokine activities. *Chem. Biol.* **2007**, *14*, 431−441.
(37) Lin, G.; Nnane, I. P.; Cheng, T. Y. The effects of pretreatment with glycyrrhizin and glycyrrhetinic acid on the retrorsine-induced hepatotoxicity in rats. *Toxicon* **1999**, *37*, 1259−1270.
(38) Jeong, H. G.; You, H. J.; Park, S. J.; Moon, A. R.; Chung, Y. C.; Kang, S. K.; Chun, H. K. Hepatoprotective effects of 18β-glycyrrhetinic acid on carbon tetrachloride-induced liver injury: Inhibition of cytochrome P450 2E1 expression. *Pharmacol. Res.* **2002**, *46*, 221−227.
(39) Ploeger, B.; Mensinga, T.; Sips, A.; Seinen, W.; Meulenbelt, J.; DeJongh, J. The pharmacokinetics of glycyrrhizic acid evaluated by physiologically based pharmacokinetic modeling. *Drug Metab. Rev.* **2001**, *33*, 125−147.

DOI: 10.1021/jf505471a
J. Agric. Food Chem. 2015, 63, 1200−1209

monnieri. PXT showed anti-inflammatory activity, but the immune modulation properties of PXT and osthole were found to be different, despite their similar chemical structures. The anti-inflammatory activity of PXT was associated with the unique peroxide group, as the anti-inflammatory activity was reduced when this group was replaced by a hydroxyl group.

MATERIALS AND METHODS

Materials. LPS (from *Escherichia coli* 0111:B4), ATP, and mouse antibodies against mouse phospho-ERK1/2, phospho-JNK1/2, phospho-p38, and actin were purchased from Sigma (St. Louis, MO, USA). Rabbit antibodies against mouse phospho-PKC-α/δ, IL-1β, caspase-1, iNOS, and COX-2 and secondary antibodies were obtained from Santa Cruz Biotechnology (Santa Cruz, CA, USA). Mouse IL-1β, IL-6, and TNF-α ELISA kits were purchased from R&D Systems (Minneapolis, MN, USA). Mouse anti-mouse NLRP3 antibody was purchased from Enzo Life Sciences Inc. (Farmingdale, NY, USA). The AlamarBlue assay kit was purchased from AbD Serotec Ltd. (Oxford, UK). All of the inflammasome inducers and the QUANTI-Blue reagent were purchased from InvivoGen (San Diego, CA, USA).

Compound Extraction and Purification. *C. monnieri* seeds (600 g) were purchased from a traditional Chinese medicine dispensary in Taiwan. The seeds were extracted with 15 L of ethanol (95% v/v) at room temperature for 10 days, and the supernatants were then concentrated to produce an alcoholic extract. PXT and auraptenol were purified by semipreparative high-performance liquid chromatography (HPLC) (D-Star DLC-20 Instruments with a UV−vis detector) with a Phenomenex Luna Silica (2) column (250 mm length, 10 mm i.d., particle shape/size = 5.0 μm) (Figure 1A). The separation conditions were as follows: 500 μL was injected for each separation; flow rate, 4 mL/min; mobile phase, acetone/hexane = 1:6. The structures of PXT and auraptenol were identified by physical and spectral data (mp, EIMS, ^{1}H NMR, UV, IR) compared with previous research values.[4,21]

Cell Cultures. The murine macrophage cell lines RAW 264.7 and J774A.1 were obtained from American Type Culture Collection (Rockville, MD, USA). RAW 264.7 macrophages stably transfected with the NF-κB reporter gene (RAW-Blue cells) were purchased from InvivoGen. Mouse peritoneal macrophages were elicited by intraperitoneal injection of 4% sterile thioglycollate medium (2 mL). After 3 days, the mice were sacrificed by cervical dislocation, and the macrophages were harvested.

AlamarBlue Assay for Cell Viability. RAW 264.7 cells were incubated with or without PXT for 24 h. The AlamarBlue assay was used to determine the cytotoxicity of PXT according to the protocol described in the manufacturer's instructions (AbD Serotec, Oxford, UK).[4]

Detection of Pro-inflammatory Mediators and Protein Phosphorylation. The levels of NO and cytokines (IL-1β, IL-6, and TNF-α) in the culture medium were measured by the Griess reaction and ELISA, respectively. The levels of iNOS, COX-2, and caspase-1 and the phosphorylation levels of ERK1/2, JNK1/2, p38, and PKC-α/δ in cells were measured by Western blotting. The detailed procedures were described in our previous study.[4] The density of the bands of the Western blotting was analyzed by ImageJ software. We selected an identical rectangular area around each lane of the Western blot even there was no band of control lane. The density of the selected area was analyzed by ImageJ, and the relative band density was normalized to actin before fold change was calculated. The densitometry fold change of each group was calculated by comparison to the control group, as the control group had a fold change of 1. The bars accompanying blots are the means of three separate experiments.

Detection of ROS. General ROS production was measured by detecting the fluorescence intensity of 2′,7′-dichlorofluorescein, the oxidation product of 2′,7′-dichlorofluorescein diacetate (Molecular Probes, Eugene, OR USA), at an excitation wavelength of 485 nm and an emission wavelength of 530 nm using a microplate absorbance reader (Bio-Rad Laboratories, Inc.). Mitochondrial ROS generation was measured by detecting the fluorescence intensity of MitoSOX

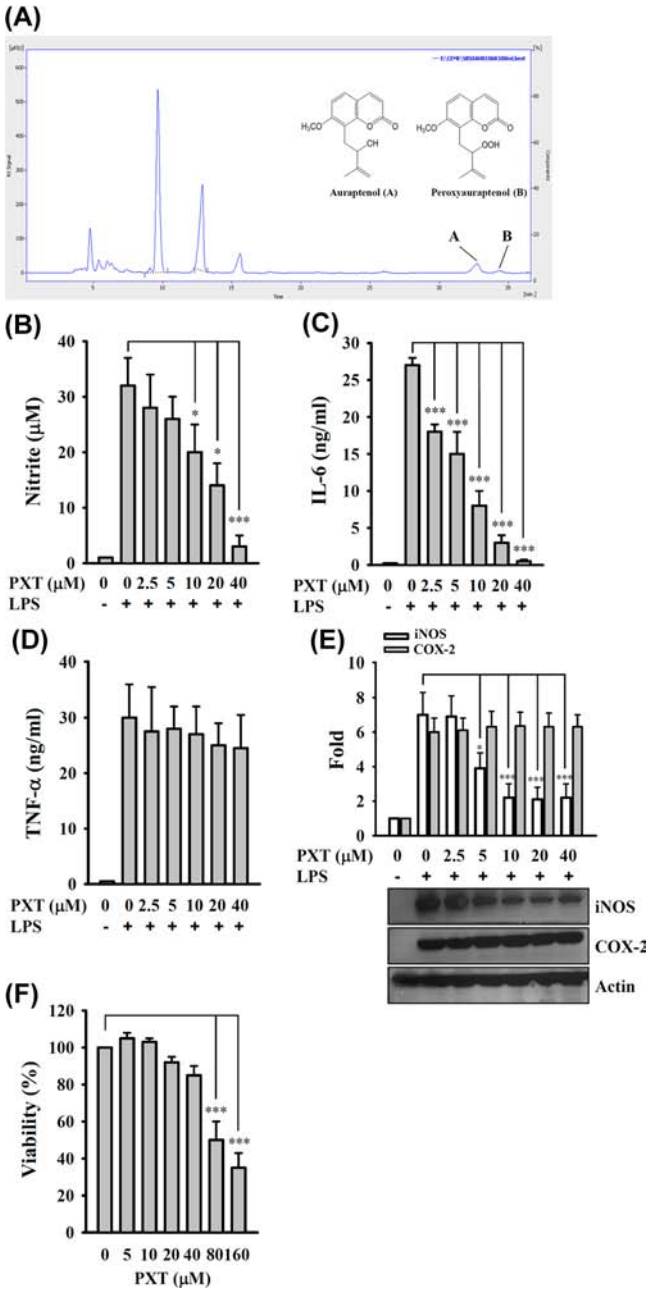

Figure 1. Effect of PXT on the expression levels of inflammatory mediators. (A) Chromatography of alcoholic extract of *C. monnieri* seeds by a silica column. (B−D) RAW 264.7 macrophages were incubated for 30 min with or without PXT and then for 24 h with or without 1 μg/mL LPS. The levels of NO (B), IL-6 (C), and TNF-α (D) in the culture medium were measured by the Griess reaction and ELISA, respectively. (E) RAW 264.7 macrophages were incubated for 30 min with or without PXT and then for 24 h with or without 1 μg/mL LPS. The levels of iNOS and COX-2 were assayed by Western blotting. (F) RAW 264.7 macrophages were incubated for 24 h with or without PXT, and the cell viability was then assayed by the AlamarBlue assay. The data are expressed as the means ± SD of three separate experiments. The Western blotting results are representative of those obtained in three different experiments, and the histograms represent the change in the ratio relative to actin compared to the control group. * and *** indicate a significant difference at the levels of $p < 0.05$ and $p < 0.001$, respectively.

DOI: 10.1021/jf5054436
J. Agric. Food Chem. 2015, 63, 1210−1219

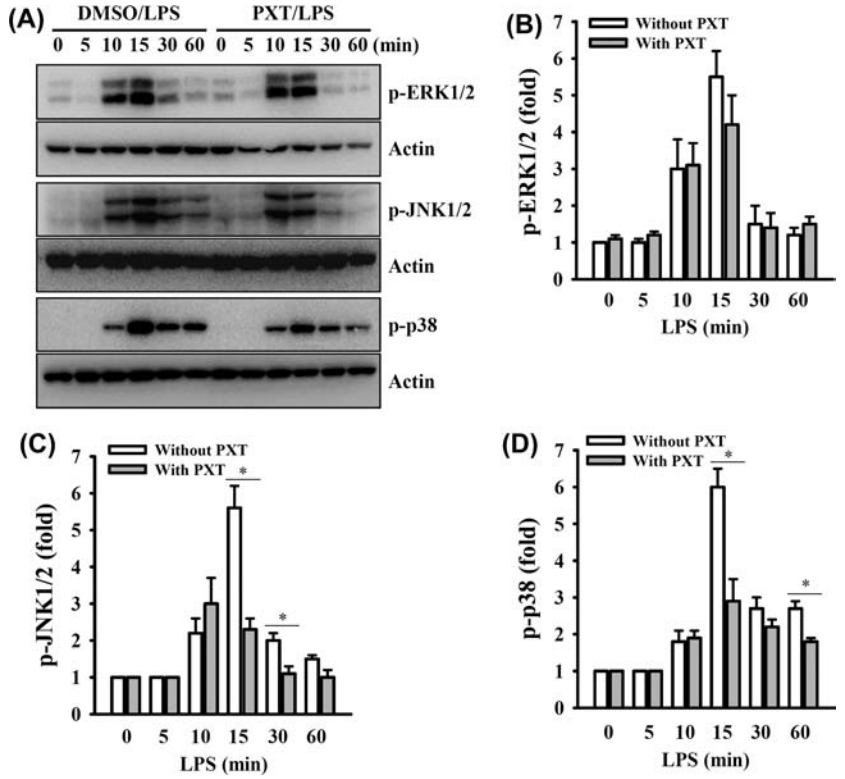

Figure 2. Effect of PXT on the phosphorylation levels of MAPKs. (A) RAW 264.7 macrophages were incubated for 30 min with or without 40 μM PXT and then for 0−60 with or without 1 μg/mL LPS. The phosphorylation levels of ERK1/2, JNK1/2, and p38 were assayed by Western blotting. (B) Quantitation of the phosphorylation levels of ERK1/2. (C) Quantitation of the phosphorylation levels of JNK1/2. (D) Quantitation of the phosphorylation levels of p38. The Western blotting results are representative of those obtained in three different experiments, and the histograms represent the change in the ratio relative to actin compared to the control group. ∗ indicates a significant difference at the level of $p < 0.05$.

(Invitrogen, Carlsbad, CA, USA) at an excitation wavelength of 514 nm and an emission wavelength of 585 nm using a microplate absorbance reader.

Detection of Mitochondrial DNA Release. The detection of mitochondrial DNA (mt-DNA) in the cytosol was performed as described.[22] Briefly, after treatment, cells were homogenized in a protease inhibitor-containing buffer (100 mM, pH 7.4, Tricine−NaOH, 0.25 M sucrose, 1 mM EDTA) and then centrifuged for 10 min at 700*g* and 4 °C. The protein concentration and volume of the supernatant were normalized, and the sample was then centrifuged for 30 min at 10000*g* and 4 °C. The resulting pellets were identified as the mitochondrial fraction, and the supernatants were identified as the cytosolic fraction. DNA was isolated from 200 μL of the cytosolic fraction. The mt-DNA copy number was measured by quantitative PCR and normalized to nuclear DNA (encoding 18S rRNA) levels using a ratio of cytochrome *c* oxidase I DNA to nuclear DNA. The results are expressed as fold changes between the sample and control groups. The quality of the mitochondrial and cytosolic fractions was monitored by detecting the protein expression level of voltage-dependent anion channel (VDAC, a marker protein for mitochondria). We found that VDAC can be detected only in the mitochondrial fraction and is not present in the cytosolic fraction (data not shown), indicating that the cytosolic fraction is free of mitochondria. The primers used were as follows: mouse 18S, forward, 5′-TAGAGG-GACAAGTGGCGTTC-3′, reverse, 5′-CGCTGAGCCAGTCAG-TGT-3′; mouse cytochrome *c* oxidase I, forward, 5′-GCCCCAGAT-ATAGCATTCCC-3′, reverse, 5′-GTTCATCCTGTTCCTGCTCC-3′.

NF-κB Reporter Assay. The medium (20 μL) from treated RAW-Blue cells was mixed with 200 μL of QUANTI-Blue medium (Invitrogen) in 96-well plates and incubated at 37 °C for 15 min. The secreted embryonic alkaline phosphatase activity was assessed by measuring the optical density at 655 nm using a microplate absorbance reader.[4]

Phagocytosis Assay. J774A.1 macrophages were seeded in 96-well flat-bottom plates at a density of 5×10^3 cells in 100 μL of RPMI 1640 medium containing 10% FBS per well and incubated with 1 μg/mL LPS for 6 h. The cells were incubated with or without 40 μM PXT or 10 μM colchicine for 30 min and then incubated for 1 h with or without 100 μg of fluorescence-conjugated *Escherichia coli*. The fluorescence intensity was measured at an excitation wavelength of 509 nm and an emission wavelength of 533 nm. Net phagocytosis was calculated by subtracting the average fluorescence intensity of the no-cell negative-control wells from all of the experimental wells. The percent of phagocytosis was then calculated as a fraction of the net positive control phagocytosis, as follows:

$$\%\ \text{of phagocytosis} = \frac{\text{net experimental phagocytosis} \times 100\%}{\text{net positive control phagocytosis}}$$

Bacterial Infection. J774A.1 macrophages were infected with *Klebsiella pneumoniae* (NTUH K-2044) at a multiplicity of infection (MOI) of 100. The number of viable bacteria used in each experiment was carefully determined by plate counting. One hour after infection, the cells were incubated with penicillin (250 IU/mL)/streptomycin (250 μg/mL) to limit the growth of residual extracellular bacteria. The culture medium was collected at 24 h after infection, and the levels of IL-1β in the medium were measured by ELISA.

Statistical Analysis. All values are the mean ± SD. The data analysis involved one-way ANOVA with a subsequent Scheffé test.

RESULTS

PXT Reduces NO Generation, Inducible NO Synthase Expression, and IL-6 Secretion. The anti-inflammatory activity of PXT was investigated using LPS-activated RAW 264.7 macrophages. We found that NO generation (Figure 1B) and IL-6 secretion (Figure 1C) were inhibited by PXT in a

DOI: 10.1021/jf5054436
J. Agric. Food Chem. 2015, 63, 1210−1219

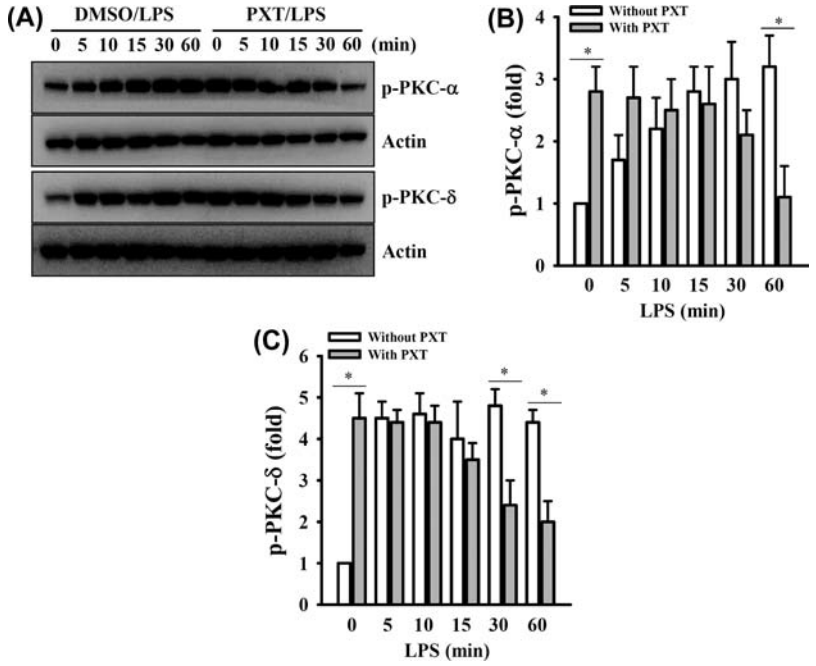

Figure 3. Effect of PXT on the phosphorylation levels of PKC. (A) RAW 264.7 macrophages were incubated for 30 min with or without 40 μM PXT and then for 0−60 with or without 1 μg/mL LPS. The phosphorylation levels of PKC-α and PKC-δ were assayed by Western blotting. (B) Quantitation of the phosphorylation levels of PKC-α. (C) Quantitation of the phosphorylation levels of PKC-δ. The Western blotting results are representative of those obtained in three different experiments, and the histograms represent the change in the ratio relative to actin compared to the control group. $*$ indicates a significant difference at the level of $p < 0.05$.

dose-dependent manner, whereas TNF-α secretion was not reduced significantly (Figure 1D). PXT also reduced iNOS expression in a dose-dependent manner, whereas COX-2 expression was not affected (Figure 1E). To examine whether the reduction in pro-inflammatory mediators resulted from reduced cell viability, the toxicity of PXT toward RAW 264.7 cells was examined, and we found that PXT had no significant effect on cell survival at a concentration of 40 μM (Figure 1F).

PXT Reduces the Phosphorylation Levels of Mitogen-Activated Protein Kinases (MAPKs) and PKC-α/δ. MAPKs, including ERK1/2, JNK1/2, and p38, are activated by LPS and regulate inflammatory mediator expression in macrophages.[2−4,23] In the present study, we found that LPS induced an increase in the phosphorylation levels of ERK1/2, JNK1/2, and p38 and that these effects, except ERK1/2, were reduced by PXT (Figure 2). In addition, PKC, a component of the TLR4 signaling pathway, regulates macrophage activation in response to LPS.[2−4,23] As shown in Figure 3, LPS induced increases in the phosphorylation levels of PKC-α and PKC-δ, and these effects were reduced by PXT. Interestingly, PXT alone increased the phosphorylation levels of PKC-α and PKC-δ; however, the detailed mechanism is unclear.

PXT Reduces NLRP3 Inflammasome Activation by Reducing Mitochondrial Damage. We examined whether PXT is able to inhibit the IL-1β secretion induced by NLRP3 inflammasome activators such as monosodium urate (MSU) crystals, calcium pyrophosphate dihydrate (CPPD), SiO_2 nanoparticles, alum crystals, nigericin, and ATP. We found that IL-1β secretion after treatment with MSU, CPPD, SiO_2 nanoparticles, and alum crystals was significantly reduced by PXT, whereas PXT was not able to inhibit IL-1β secretion induced by nigericin and ATP (Figure 4A). The generation of ROS is a crucial element for NLRP3 activation.[24,25] To determine whether the inhibition of IL-1β secretion by PXT occurs via the inhibition of ROS generation, LPS-primed J774A.1 macrophages were incubated with PXT or the antioxidant *N*-acetylcysteine (NAC) for 30 min before the addition of CPPD, MSU, and ATP. We found that PXT reduced CPPD- and MSU-induced ROS generation; however, PXT was not able to reduce ATP-induced ROS generation (Figure 4B). As damaged and ROS-generating mitochondria activate the NLRP3 inflammasome,[22,26,27] to determine whether PXT inhibits the NLRP3 inflammasome by preventing mitochondrial damage, we used the fluorescent probe MitoSOX to detect ROS released from damaged mitochondria. Mitochondrial ROS (mt-ROS) levels were increased by MSU and CPPD treatments, and PXT reduced the mt-ROS levels in these cells (Figure 4C). The overgeneration of mt-ROS induces the translocation of mitochondrial DNA (mt-DNA) into the cytosol, and this cytosolic mt-DNA is a coactivator of the NLRP3 inflammasome.[27] Thus, we examined whether the translocation of mt-DNA into the cytosol is decreased by PXT and found that the levels of mt-DNA released into the cytosol were increased in MSU- and CPPD-activated macrophages but were significantly reduced by PXT (Figure 4D). These results indicate that PXT protects mitochondria from damage in macrophages. In addition, caspase-11 has been demonstrated to be required to activate caspase-1 in response to bacteria;[28] however, PXT did not affect the expression levels of caspase-11 induced by LPS and interferon-γ (Figure 4E).

PXT Reduces IL-1β Precursor Expression. NLRP3 induction is a critical checkpoint for the priming step of NLRP3 inflammasome activation and is regulated by NF-κB.[29] Therefore, we investigated whether PXT inhibits the LPS-mediated priming step for the NLRP3 inflammasome. We incubated cells with PXT for 30 min before treatment with LPS for 6 h and found that PXT did not inhibit the expression level of NLRP3, although it did reduce the expression level of the IL-

DOI: 10.1021/jf5054436
J. Agric. Food Chem. 2015, 63, 1210−1219

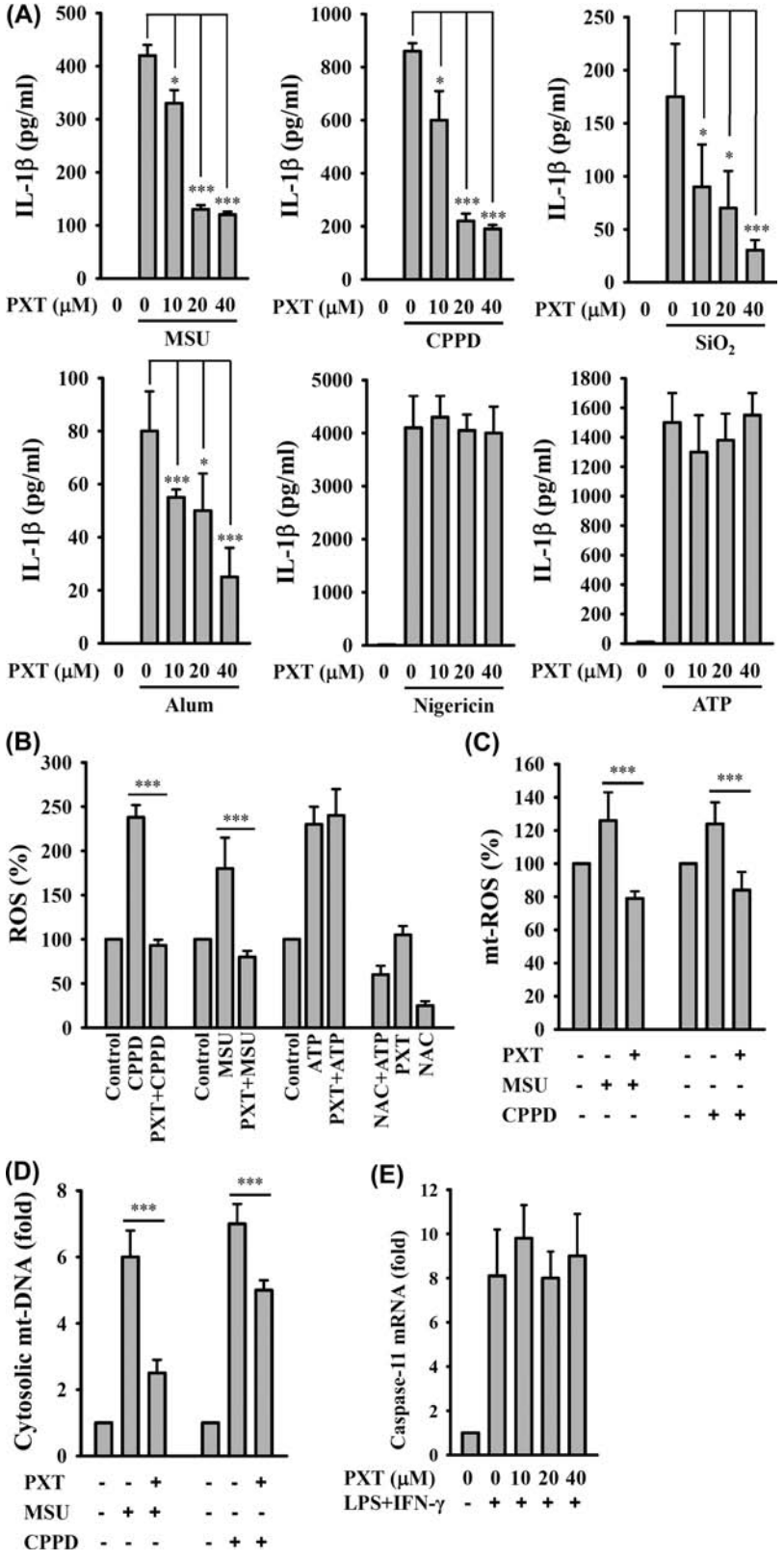

Figure 4. PXT attenuates NLRP3 inflammasome activation. (A) J774A.1 macrophages were incubated for 5.5 h with or without 1 μg/mL LPS, then for 30 min with or without PXT in the continued presence or absence of LPS, and then with or without 100 μg/mL MSU (24 h), 100 μg/mL CPPD crystals (24 h), 200 μg/mL nano SiO_2 (24 h), 500 μg/mL alum crystals (24 h), 5 mM ATP (0.5 h), or 10 μM nigericin (0.5 h). The levels of IL-1β in the culture medium were measured by ELISA. (B) J774A.1 macrophages were incubated for 5.5 h with 1 μg/mL LPS, then for 30 min with or without 40 μM PXT or 10 mM NAC in the continued presence of LPS, and then with or without 100 μg/mL CPPD crystals, 100 μg/mL MSU, or 5 mM ATP for 10 min. The levels of ROS in the cells were measured by 2′,7′-dichlorofluorescein diacetate. (C) J774A.1 macrophages were incubated for 5.5 h with 1 μg/mL LPS, then for 30 min with or without 40 μM PXT in the continued presence of LPS, and then with or without 100 μg/mL MSU or 100 μg/mL CPPD crystals for 10 min. The levels of ROS in the cells were measured by 2′,7′-dichlorofluorescein diacetate. (D) J774A.1

DOI: 10.1021/jf5054436
J. Agric. Food Chem. 2015, 63, 1210−1219

Figure 4. continued

macrophages were incubated for 5.5 h with 1 μg/mL LPS, then for 30 min with or without 40 μM PXT in the continued presence of LPS, and then with or without 100 μg/mL MSU or 100 μg/mL CPPD crystals for 30 min. Mitochondrial DNA release into the cytosol was measured by the detection of cytochrome *c* oxidase I DNA in the cytosol. (E) J774A.1 macrophages were incubated for 6 h with 1 μg/mL LPS and 10 ng/mL IFN-γ. The expression level of caspase-11 mRNA was measured by RT-quantitative PCR. The data are expressed as the means ± SD of three separate experiments. ∗ and ∗∗∗ indicate a significant difference at the levels of $p < 0.05$ and $p < 0.001$, respectively.

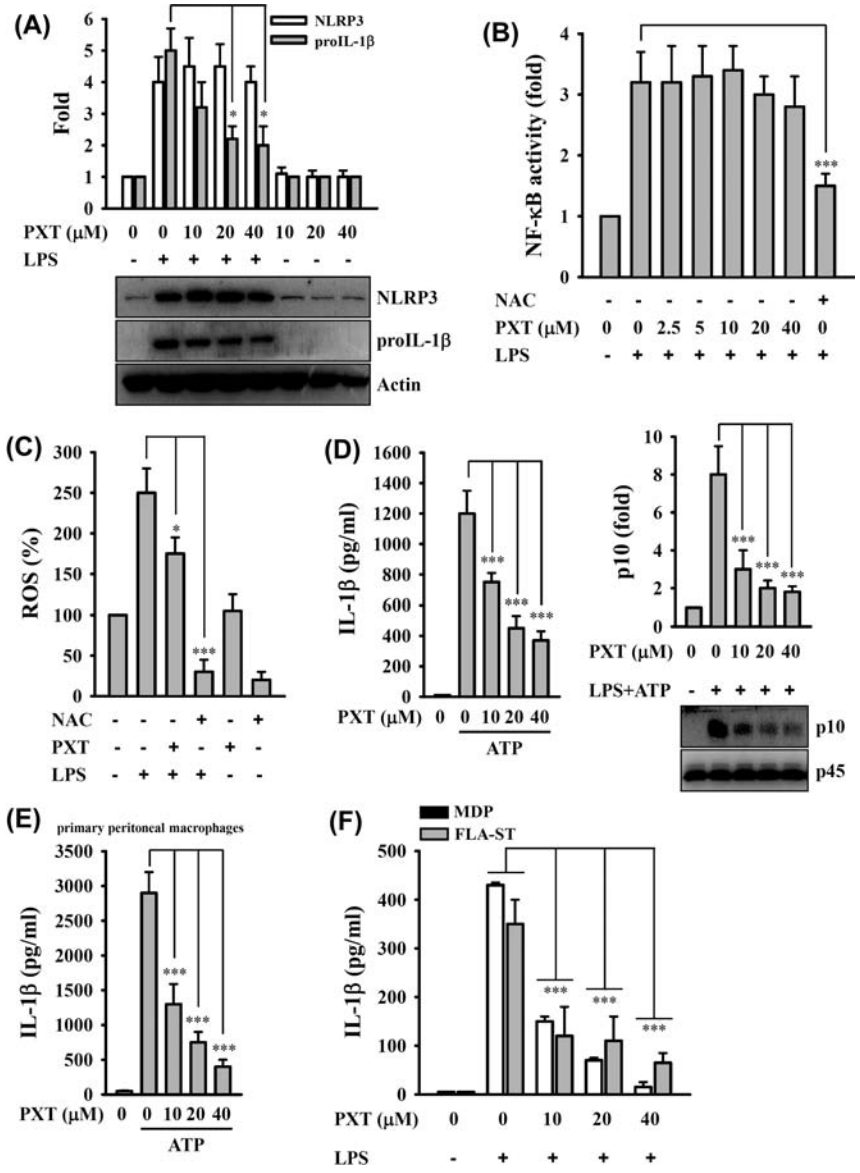

Figure 5. Effect of PXT on the priming step of the NLRP3 inflammasome. (A) J774A.1 macrophages were incubated for 30 min with or without PXT and then for 6 h with or without 1 μg/mL LPS in the continued presence or absence of PXT; the protein expression levels of NLRP3 and proIL-1β in the cells were measured by Western blotting. (B) RAW-Blue cells were incubated for 30 min with or without PXT or 10 mM NAC and then for 24 h with or without 1 μg/mL LPS in the continued presence or absence of PXT or NAC; the activation levels of NF-κB were measured by an NF-κB reporter assay. (C) J774A.1 macrophages were incubated for 30 min with or without 40 μM PXT or 10 mM NAC and then for 10 min with or without 1 μg/mL LPS in the continued presence or absence of PXT or NAC. The levels of ROS in the cells were measured by 2′,7′-dichlorofluorescein diacetate. (D) J774A.1 macrophages were incubated for 30 min with or without PXT, then for 5.5 h with or without 1 μg/mL LPS, and then for 30 min with or without 5 mM ATP. The levels of IL-1β in the culture medium and activated caspase-1 (p10) in the cells were measured by ELISA and Western blotting, respectively. (E) Mouse primary peritoneal macrophages were incubated for 30 min with or without PXT, then for 5.5 h with or without 1 μg/mL LPS, and then for 30 min with or without 5 mM ATP. The levels of IL-1β in the culture medium were measured by ELISA. (F) J774A.1 macrophages were incubated for 5.5 h with or without 1 μg/mL LPS, then for 30 min with or without PXT in the continued presence or absence of LPS, and then with or without 100 μg/mL FLA-ST or 100 ng/mL MDP for 24 h. The levels of IL-1β in the culture medium were measured by ELISA. The data are expressed as the means ± SD for three separate experiments. The Western blotting results are representative of those obtained in three different experiments, and the histograms represent the change in the ratio relative to actin compared to the control group. ∗ and ∗∗∗ indicate a significant difference at the levels of $p < 0.05$ and $p < 0.001$, respectively.

DOI: 10.1021/jf5054436
J. Agric. Food Chem. 2015, 63, 1210−1219

1β precursor proIL-1β (Figure 5A). Using NF-κB-dependent alkaline phosphatase reporter cells (RAW-Blue cells), we then examined whether PXT is able to inhibit NF-κB activation. As shown in Figure 5B, we found that NF-κB transcriptional activity in LPS-stimulated macrophages was not affected by PXT but was markedly inhibited by NAC, which was used as a positive control. These results indicated that PXT does not inhibit the priming signal of the NLRP3 inflammasome. In addition, we investigated the effect of PXT on ROS generation, which plays important roles in the LPS-induced expression of proIL-1β,[30] and found that LPS-induced ROS generation was reduced by PXT and NAC (Figure 5C). Although PXT was not able to reduce the ATP-induced expression of IL-1β in LPS-primed macrophages (Figure 4A), we assessed whether the secretion levels of IL-1β are reduced by PXT if it is added before LPS priming because we observed decreased expression levels of LPS-induced proIL-1β in PXT-treated cells (Figure 5A). We found that ATP-induced IL-1β secretion was significantly inhibited by PXT when it was added before LPS priming (Figure 5D, left); notably, the activation levels of caspase-1 were also inhibited by PXT under the same condition (Figure 5D, right). PXT also inhibited IL-1β secretion in primary peritoneal macrophages under the same condition (Figure 5E). Furthermore, PXT was not selective for NLRP3-dependent inflammasome stimuli, as PXT reduced the IL-1β secretion triggered by FLA-ST (flagellin from *S. typhimurium*) or muramyl dipeptide, which are dependent on the NLRP1 and NLRC4 inflammasomes,[31,32] respectively, and independent of NLRP3 (Figure 5F).

PXT Reduces the Phagocytic Efficiency of Macrophages and Decreases the Expression Levels of IL-1β in Bacteria-Infected Macrophages. PXT reduced the IL-1β secretion induced by crystal NLRP3 inflammasome inducers, including alum crystals, CPPD, and SiO_2 nanoparticles (Figure 4A). As the activation of the NLRP3 inflammasome by these inducers is dependent on their uptake by phagocytosis, we investigated the hypothesis that PXT inhibits crystal-mediated activation of the NLRP3 inflammasome by inhibiting phagocytic activity. To examine whether PXT affects the phagocytic activity of macrophages, LPS-primed J774A.1 macrophages were treated with PXT or colchicine (a microtubule polymerization inhibitor) for 30 min, and the phagocytosis activity was then assessed by measuring the uptake of fluorescence-conjugated *E. coli*. We found that both PXT and colchicine decreased the uptake of fluorescence-conjugated *E. coli* by macrophages (Figure 6A). In addition, we tested whether PXT affects IL-1β secretion by macrophages infected with live *K. pneumoniae* and found that PXT reduced the secretion level (Figure 6B). These results suggest that PXT may modulate macrophage function at *K. pneumoniae*-infected sites by impairing phagocytosis and reducing cytokine production.

The Peroxide Group of PXT Is Important for Its Anti-inflammatory Activity. Because PXT contains a unique peroxide group (−OOH) on its carbon chain, we investigated the hypothesis that this unique group is important for the molecule's anti-inflammatory activity. To this end, we isolated a PXT analogue, auraptenol, which contains a hydroxyl group (−OH) at the corresponding peroxide group position of PXT (Figure 1A), from the ethanol extract of *C. monnieri* fruits. We then compared the anti-inflammatory activities of PXT and auraptenol in LPS-activated macrophages and found that auraptenol reduced LPS-induced IL-6 secretion (23.5 ± 1.5 ng/mL) to 17.5 ± 0.9 ng/mL at 100 μM, whereas 10 μM PXT reduced it to 7.2 ± 1.0 ng/mL (Figure 7A). In addition, 100 μM auraptenol reduced LPS-induced NO production (39 ± 5 μM) to 25 ± 3 μM, although 10 μM PXT reduced it to 5 ± 2 μM (Figure 7B). Furthermore, whereas auraptenol only slightly inhibited the expression levels of iNOS and proIL-1β in LPS-

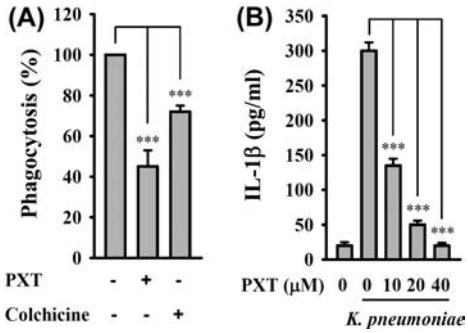

Figure 6. PXT reduces the phagocytic efficiency of macrophages and decreases the expression levels of IL-1β in bacteria-infected macrophages. (A) J774A.1 macrophages were incubated with LPS for 6 h and then for 30 min with or without PXT or colchicine. The cells were incubated with fluorescence-conjugated *E. coli* for 1 h. The phagocytic efficiency was determined by measuring the fluorescence intensity. (B) J774A.1 macrophages were infected with *K. pneumoniae* for 24 h at 100 MOI. The levels of IL-1β in the culture medium were measured by ELISA. The data are expressed as the means ± SD for three separate experiments. *** indicates a significant difference at the level of $p < 0.001$.

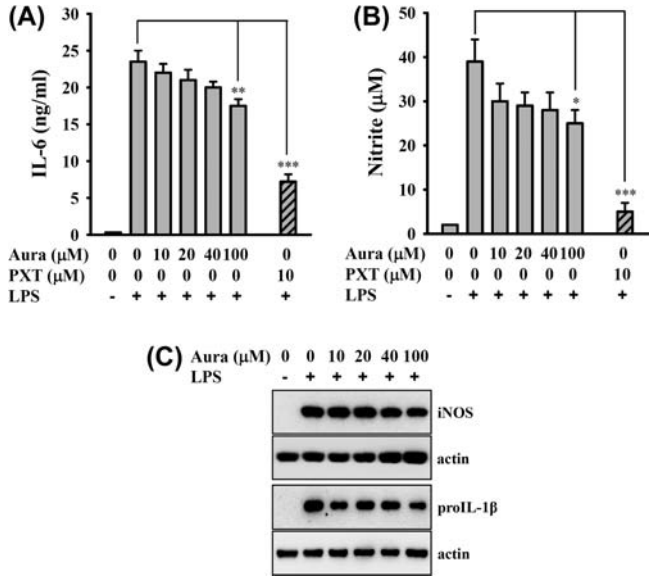

Figure 7. The peroxide group of PXT is important for its anti-inflammatory activity. (A, B) RAW 264.7 macrophages were incubated for 30 min with or without PXT or auraptenol (aura) and then for 24 h with or without 1 μg/mL LPS. The levels of IL-6 (A) and NO (B) in the culture medium were measured by ELISA and the Griess reaction, respectively. (C) RAW 264.7 macrophages were incubated for 30 min with or without aura and then for 6 h (for proIL-1β) and 24 h (for iNOS) with or without 1 μg/mL LPS. The levels of proIL-1β and iNOS in the cells were measured by Western blotting. The data are expressed as the means ± SD for three separate experiments. The Western blotting results are representative of those obtained in three different experiments. *, **, and *** indicate a significant difference at the levels of $p < 0.05$, $p < 0.01$, and $p < 0.001$, respectively.

DOI: 10.1021/jf5054436
J. Agric. Food Chem. 2015, 63, 1210−1219

activated macrophages (Figure 7C), PXT significantly inhibited expression, as shown in Figures 1E and 5A, respectively. These results indicated that the anti-inflammatory activity of auraptenol is lower than that of PXT and suggested that the unique peroxide group is important for the anti-inflammatory activity of PXT.

DISCUSSION

PXT was purified along with osthole from the ethanol extract of *C. monnieri* seeds. The structure of PXT is similar to that of osthole; however, their immune modulation properties in LPS-activated macrophages are quite different.[4] The different biological outcomes between PXT and osthole are as follows: (1) PXT reduces the levels of IL-6, but osthole increases them. (2) PXT does not affect the levels of TNF-α and COX-2, whereas osthole reduces them. (3) PXT does not affect the phosphorylation levels of ERK1/2, yet osthole increases them. (4) PXT does not affect the activation levels of NF-κB, whereas osthole reduces them. (5) PXT reduces the phosphorylation levels of PKC-δ phosphorylation, but osthole does not.

The priming step of the NLRP3 inflammasome is regulated by ROS, which are required for NLRP3 expression.[25] PXT did not affect the priming step of the NLRP3 inflammasome, although PXT did reduce the levels of ROS in LPS-activated macrophages (Figure 5C). ROS is involved in both the priming and activation steps of the NLRP3 inflammasome,[24] and the up-regulation of ROS levels in macrophages results in the activation of PI3K, promoting caspase-1 activation and IL-1β secretion.[33] The inhibition of MSU- and CPPD-induced ROS generation may be responsible for the reduced NLRP3 inflammasome-derived IL-1β secretion caused by PXT. Furthermore, we found that PXT reduced mitochondrial ROS generation, which plays an important role in NLRP3 inflammasome activation.[26,27] The overproduction of mitochondrial ROS promotes a mitochondrial permeability transition that facilitates the cytosolic release of mitochondrial DNA, which stimulates the activation of the NLRP3 inflammasome.[26,27] PXT also reduced the cytosolic release of mitochondrial DNA, indicating that mitochondrial stabilization may be responsible for the reduced activation of the NLRP3 inflammasome mediated by PXT.

PXT did not inhibit either ATP-induced IL-1β secretion (Figure 4A) or ROS generation (Figure 4B) in LPS-primed macrophages; PXT also had no effect on LPS-induced NLRP3 expression (Figure 5A). These results indicated that PXT did not affect the priming or activation signal of the NLRP3 inflammasome due to LPS or ATP, respectively. Notably, however, PXT did reduce ATP-induced caspase-1 activation when it was added before LPS or ATP (Figure 5D). One possible mechanism is that PXT might increase the cellular levels of cAMP, which has been demonstrated to inhibit inflammasome assembly by binding to NLRP3 directly.[34] Osthole was reported to increase the tissue cAMP content by inhibiting the activity of cAMP phosphodiesterase in guinea pig trachea.[35] Another possible mechanism is that PXT might increase autophagy, which limits NLRP3 inflammasome activation by targeting inflammasome components for degradation[36,37] and by inhibiting the release of mitochondrial DNA from damaged mitochondria.[22] Furthermore, caspase-11 induction by LPS or interferon-γ synergizes with the assembled NLRP3 inflammasome to regulate caspase-1 activation;[8] however, PXT did not affect the expression levels of caspase-11 induced by LPS and interferon-γ.

K^+ efflux has a role in the regulation of the NLRP3 inflammasome and can be achieved either directly by nigericin or indirectly by the purinergic receptor for ATP.[38,39] It has been reported that crystal-induced NALP3 inflammasome activation is inhibited by phagocytosis inhibitors.[15] These results indicate that crystal uptake by phagocytosis is a prerequisite for activation of the NARP3 inflammasome. In this study, we demonstrated that PXT reduced phagocytosis, which partially explains why PXT inhibited the NLRP3 inflammasome-mediated IL-1β secretion induced by MSU, CPPD, SiO_2 nanoparticles, and alum crystals. In contrast, PXT did not affect IL-1β secretion induced by nigericin and ATP in LPS-primed macrophages, suggesting that PXT might not affect K^+ efflux induced by these molecules.

PXT is a peroxide (−OOH)-containing coumarin compound. When subjected to acid, base, or temperature increases in the environment, the −OOH group on the compound is likely to degrade into hydroxyl radical ($^{\bullet}$OH), a most destructive free radical that reacts readily with the metallic core atoms of intracellular enzymes and in turn modulates the secretion of certain cytokines. However, when the concentrations of these free radicals are sufficient, they may partake in important intracellular metabolism processes and become a line of defense in preventing or fighting disease. In this study, we found that freshly extracted ethanolic PXT tended to decrease in concentration during storage, which became notable with more than 6 months at room temperature; the situation was much improved by storage at −20 °C. However, storing the ethanolic solution of auraptenol at room temperature for more than 6 months resulted in an unchanged concentration based on HPLC and NMR analyses, indicating that the compound is highly stable.

Although PXT exhibited anti-inflammatory activities in LPS-activated macrophages, it did not cause a general unresponsiveness to LPS, as the expressions of COX-2 and TNF-α were not reduced by PXT. These findings indicate that the administration of PXT might prevent excessive inflammatory response but does not cause immunodeficiency. *C. monnieri* fruits have been used to treat gout in traditional medicine, although there is no scientific evidence supporting this. Here, we demonstrate that PXT reduces MSU-induced activation of the NLRP3 inflammasome by inhibiting ROS generation and mitochondrial DNA release, explaining why *C. monnieri* fruits are able to ameliorate gout.[17] In summary, we demonstrate that PXT possesses anti-inflammatory activity by reducing the expression levels of NO and IL-6, as well as by reducing the activation of the NLRP3 inflammasome. These results suggest that PXT may have a potential use as a natural anti-inflammation agent or nutraceutical for preventing and ameliorating inflammation- and NLRP3 inflammasome-related diseases.

AUTHOR INFORMATION

Corresponding Author

*(K.-F.H.) Phone: +(886)-3-935-7400, ext. 7626. Fax: +(886)-3-931-1526. E-mail: kuofenghua@gmail.com.

Funding

Contract grant sponsor: Ministry of Science and Technology, Taiwan; Contract grant number: NSC 102-2628-B-197-001-MY3; NSC 103-2923-B-197-001-MY3. CMU under the Aim for Top University Plan of the Ministry of Education, Taiwan, and Taiwan Ministry of Health and Welfare Clinical Trial and

DOI: 10.1021/jf5054436
J. Agric. Food Chem. 2015, 63, 1210−1219

Research Center of Excellence (MOHW103-TDU-B-212-113002).

Notes

The authors declare no competing financial interest.

REFERENCES

(1) Goldszmid, R. S.; Trinchieri, G. The price of immunity. *Nat. Immunol.* **2012**, *13* (10), 932−938.

(2) Ho, C. L.; Lin, C. Y.; Ka, S. M.; Chen, A.; Tasi, Y. L.; Liu, M. L.; Chiu, Y. C.; Hua, K. F. Bamboo vinegar decreases inflammatory mediator expression and NLRP3 inflammasome activation by inhibiting reactive oxygen species generation and protein kinase C-α/δ activation. *PLoS One* **2013**, *8* (10), No. e75738.

(3) Hua, K. F.; Chou, J. C.; Lam, Y.; Tasi, Y. L.; Chen, A.; Ka, S. M.; Fang, Z.; Liu, M. L.; Yang, F. L.; Yang, Y. L.; Chiu, Y. C.; Wu, S. H. Polyenylpyrrole derivatives inhibit NLRP3 inflammasome activation and inflammatory mediator expression by reducing reactive oxygen species production and mitogen-activated protein kinase activation. *PLoS One* **2013**, *8* (10), No. e76754.

(4) Liao, P. C.; Chien, S. C.; Ho, C. L.; Wang, E. I.; Lee, S. C.; Kuo, Y. H.; Jeyashoke, N.; Chen, J.; Dong, W. C.; Chao, L. K.; Hua, K. F. Osthole regulates inflammatory mediator expression through modulating NF-κB, mitogen-activated protein kinases, protein kinase C, and reactive oxygen species. *J. Agric. Food Chem.* **2010**, *58* (19), 10445−10451.

(5) Allocca, M.; Jovani, M.; Fiorino, G.; Schreiber, S.; Danese, S. Anti-IL-6 treatment for inflammatory bowel diseases: next cytokine, next target. *Curr. Drug Targets* **2013**, *14* (12), 1508−1521.

(6) Olson, N.; van der Vliet, A. Interactions between nitric oxide and hypoxia-inducible factor signaling pathways in inflammatory disease. *Nitric Oxide* **2011**, *25* (2), 125−137.

(7) Strowig, T.; Henao-Mejia, J.; Elinav, E.; Flavell, R. Inflammasomes in health and disease. *Nature* **2012**, *481* (7381), 278−286.

(8) Rathinam, V. A.; Vanaja, S. K.; Waggoner, L.; Sokolovska, A.; Becker, C.; Stuart, L. M.; Leong, J. M.; Fitzgerald, K. A. TRIF licenses caspase-11-dependent NLRP3 inflammasome activation by Gram-negative bacteria. *Cell* **2012**, *150* (3), 606−619.

(9) Allen, I. C.; Scull, M. A.; Moore, C. B.; Holl, E. K.; McElvania-TeKippe, E.; Taxman, D. J.; Guthrie, E. H.; Pickles, R. J.; Ting, J. P. The NLRP3 inflammasome mediates in vivo innate immunity to influenza A virus through recognition of viral RNA. *Immunity* **2009**, *30* (4), 556−565.

(10) Gross, O.; Poeck, H.; Bscheider, M.; Dostert, C.; Hannesschläger, N.; Endres, S.; Hartmann, G.; Tardivel, A.; Schweighoffer, E.; Tybulewicz, V.; Mocsai, A.; Tschopp, J.; Ruland, J. Syk kinase signalling couples to the Nlrp3 inflammasome for antifungal host defence. *Nature* **2009**, *459* (7245), 433−436.

(11) Masters, S. L.; Dunne, A.; Subramanian, S. L.; Hull, R. L.; Tannahill, G. M.; Sharp, F. A.; Becker, C.; Franchi, L.; Yoshihara, E.; Chen, Z.; Mullooly, N.; Mielke, L. A.; Harris, J.; Coll, R. C.; Mills, K. H.; Mok, K. H.; Newsholme, P.; Nuñez, G.; Yodoi, J.; Kahn, S. E.; Lavelle, E. C.; O'Neill, L. A. Activation of the NLRP3 inflammasome by islet amyloid polypeptide provides a mechanism for enhanced IL-1β in type 2 diabetes. *Nat. Immunol.* **2010**, *11* (10), 897−904.

(12) Duewell, P.; Kono, H.; Rayner, K. J.; Sirois, C. M.; Vladimer, G.; Bauernfeind, F. G.; Abela, G. S.; Franchi, L.; Nuñez, G.; Schnurr, M.; Espevik, T.; Lien, E.; Fitzgerald, K. A.; Rock, K. L.; Moore, K. J.; Wright, S. D.; Hornung, V.; Latz, E. NLRP3 inflammasomes are required for atherogenesis and activated by cholesterol crystals. *Nature* **2010**, *464* (7293), 1357−1361.

(13) Henao-Mejia, J.; Elinav, E.; Jin, C.; Hao, L.; Mehal, W. Z.; Strowig, T.; Thaiss, C. A.; Kau, A. L.; Eisenbarth, S. C.; Jurczak, M. J.; Camporez, J. P.; Shulman, G. I.; Gordon, J. I.; Hoffman, H. M.; Flavell, R. A. Inflammasome-mediated dysbiosis regulates progression of NAFLD and obesity. *Nature* **2012**, *482* (7384), 179−185.

(14) Vandanmagsar, B.; Youm, Y. H.; Ravussin, A.; Galgani, J. E.; Stadler, K.; Mynatt, R. L.; Ravussin, E.; Stephens, J. M.; Dixit, V. D. The NLRP3 inflammasome instigates obesity-induced inflammation and insulin resistance. *Nat. Med.* **2011**, *17* (2), 179−188.

(15) Hornung, V.; Bauernfeind, F.; Halle, A.; Samstad, E. O.; Kono, H.; Rock, K. L.; Fitzgerald, K. A.; Latz, E. Silica crystals and aluminum salts activate the NALP3 inflammasome through phagosomal destabilization. *Nat. Immunol.* **2008**, *9* (8), 847−856.

(16) Heneka, M. T.; Kummer, M. P.; Stutz, A.; Delekate, A.; Schwartz, S.; Vieira-Saecker, A.; Griep, A.; Axt, D.; Remus, A.; Tzeng, T. C.; Gelpi, E.; Halle, A.; Korte, M.; Latz, E.; Golenbock, D. T. NLRP3 is activated in Alzheimer's disease and contributes to pathology in APP/PS1 mice. *Nature* **2013**, *493* (7434), 674−678.

(17) Martinon, F.; Pétrilli, V.; Mayor, A.; Tardivel, A.; Tschopp, J. Gout-associated uric acid crystals activate the NALP3 inflammasome. *Nature* **2006**, *440* (7081), 237−241.

(18) Anders, H. J.; Muruve, D. A. The inflammasomes in kidney disease. *J. Am. Soc. Nephrol.* **2011**, *22* (6), 1007−1018.

(19) Yang, S. M.; Chan, Y. L.; Hua, K. F.; Chang, J. M.; Chen, H. L.; Tsai, Y. J.; Hsu, Y. J.; Chao, L. K.; Yang, F. L.; Tsai, Y. L.; Wu, S. H.; Wang, Y. F.; Tsai, C. L.; Chen, A.; Ka, S. M. Osthole improves an accelerated focal segmental glomerulosclerosis model in the early stage by activating the Nrf2 antioxidant pathway and subsequently inhibiting NF-κB-mediated COX-2 expression and apoptosis. *Free Radical Biol. Med.* **2014**, *73C*, 260−269.

(20) Hua, K. F.; Yang, S. M.; Kao, T. Y.; Chang, J. M.; Chen, H. L.; Tsai, Y. J.; Chen, A.; Yang, S. S.; Chao, L. K.; Ka, S. M. Osthole mitigates progressive IgA nephropathy by inhibiting reactive oxygen species generation and NF-κB/NLRP3 pathway. *PLoS One* **2013**, *8* (10), No. e77794.

(21) Wang, Z. C.; Feng, D. Q.; Ke, C. H. Coumarins from the herb *Cnidium monnieri* and chemically modified derivatives as antifoulants against *Balanus albicostatus* and *Bugula neritina* larvae. *Int. J. Mol. Sci.* **2013**, *14* (1), 1197−1206.

(22) Nakahira, K.; Haspel, J. A.; Rathinam, V. A.; Lee, S. J.; Dolinay, T.; Lam, H. C.; Englert, J. A.; Rabinovitch, M.; Cernadas, M.; Kim, H. P.; Fitzgerald, K. A.; Ryter, S. W.; Choi, A. M. Autophagy proteins regulate innate immune responses by inhibiting the release of mitochondrial DNA mediated by the NALP3 inflammasome. *Nat. Immunol.* **2011**, *12* (3), 222−230.

(23) Su, S. C.; Hua, K. F.; Lee, H.; Chao, L. K.; Tan, S. K.; Lee, H.; Yang, S. F.; Hsu, H. Y. LTA and LPS mediated activation of protein kinases in the regulation of inflammatory cytokines expression in macrophages. *Clin. Chim. Acta* **2006**, *374* (1−2), 106−115.

(24) Tschopp, J.; Schroder, K. NLRP3 inflammasome activation: the convergence of multiple signalling pathways on ROS production? *Nat. Rev. Immunol.* **2010**, *10* (3), 210−215.

(25) Bauernfeind, F.; Bartok, E.; Rieger, A.; Franchi, L.; Núñez, G.; Hornung, V. Cutting edge: reactive oxygen species inhibitors block priming, but not activation, of the NLRP3 inflammasome. *J. Immunol.* **2011**, *187* (2), 613−617.

(26) Kepp, O.; Galluzzi, L.; Kroemer, G. Mitochondrial control of the NLRP3 inflammasome. *Nat. Immunol.* **2011**, *12* (3), 199−200.

(27) Zhou, R.; Yazdi, A. S.; Menu, P.; Tschopp, J. A role for mitochondria in NLRP3 inflammasome activation. *Nature* **2011**, *469*, 221−225.

(28) Kayagaki, N.; Warming, S.; Lamkanfi, M.; Vande Walle, L.; Louie, S.; Dong, J.; Newton, K.; Qu, Y.; Liu, J.; Heldens, S.; Zhang, J.; Lee, W. P.; Roose-Girma, M.; Dixit, V. M. Non-canonical inflammasome activation targets caspase-11. *Nature* **2011**, *479* (7371), 117−121.

(29) Bauernfeind, F. G.; Horvath, G.; Stutz, A.; Alnemri, E. S.; MacDonald, K.; Speert, D.; Fernandes-Alnemri, T.; Wu, J.; Monks, B. G.; Fitzgerald, K. A.; Hornung, V.; Latz, E. Cutting edge: NF-κB activating pattern recognition and cytokine receptors license NLRP3 inflammasome activation by regulating NLRP3 expression. *J. Immunol.* **2009**, *183* (2), 787−791.

(30) Liao, P. C.; Chao, L. K.; Chou, J. C.; Dong, W. C.; Lin, C. N.; Lin, C. Y.; Chen, A.; Ka, S. M.; Ho, C. L.; Hua, K. F. Lipopolysaccharide/adenosine triphosphate-mediated signal transduction in the regulation of NLRP3 protein expression and caspase-

DOI: 10.1021/jf5054436
J. Agric. Food Chem. 2015, 63, 1210−1219

1-mediated interleukin-1β secretion. *Inflamm. Res.* **2013**, *62* (1), 89−96.
(31) Moayeri, M.; Sastalla, I.; Leppla, S. H. Anthrax and the inflammasome. *Microbes Infect.* **2012**, *14* (5), 392−400.
(32) Franchi, L.; Kamada, N.; Nakamura, Y.; Burberry, A.; Kuffa, P.; Suzuki, S.; Shaw, M. H.; Kim, Y. G.; Núñez, G. NLRC4-driven production of IL-1β discriminates between pathogenic and commensal bacteria and promotes host intestinal defense. *Nat. Immunol.* **2012**, *13* (5), 449−456.
(33) Cruz, C. M.; Rinna, A.; Forman, H. J.; Ventura, A. L.; Persechini, P. M.; Ojcius, D. M. ATP activates a reactive oxygen species-dependent oxidative stress response and secretion of proinflammatory cytokines in macrophages. *J. Biol. Chem.* **2007**, *282* (5), 2871−2879.
(34) Lee, G. S.; Subramanian, N.; Kim, A. I.; Aksentijevich, I.; Goldbach-Mansky, R.; Sacks, D. B.; Germain, R. N.; Kastner, D. L.; Chae, J. J. The calcium-sensing receptor regulates the NLRP3 inflammasome through Ca^{2+} and cAMP. *Nature* **2012**, *492* (7427), 123−127.
(35) Teng, C. M.; Lin, C. H.; Ko, F. N.; Wu, T. S.; Huang, T. F. The relaxant action of osthole isolated from *Angelica pubescens* in guinea-pig trachea. *Naunyn Schmiedebergs Arch. Pharmacol.* **1994**, *349* (2), 202−208.
(36) Shi, C. S.; Shenderov, K.; Huang, N. N.; Kabat, J.; Abu-Asab, M.; Fitzgerald, K. A.; Sher, A.; Kehrl, J. H. Activation of autophagy by inflammatory signals limits IL-1β production by targeting ubiquitinated inflammasomes for destruction. *Nat. Immunol.* **2012**, *13* (3), 255−263.
(37) Harris, J.; Hartman, M.; Roche, C.; Zeng, S. G.; O'Shea, A.; Sharp, F. A.; Lambe, E. M.; Creagh, E. M.; Golenbock, D. T.; Tschopp, J.; Kornfeld, H.; Fitzgerald, K. A.; Lavelle, E. C. Autophagy controls IL-1β secretion by targeting pro-IL-1β for degradation. *J. Biol. Chem.* **2011**, *286* (11), 9587−9597.
(38) Pelegrin, P.; Surprenant, A. Pannexin-1 mediates large pore formation and interleukin-1β release by the ATP-gated P2X7 receptor. *EMBO J.* **2006**, *25* (21), 5071−5082.
(39) Pelegrin, P.; Surprenant, A. Pannexin-1 couples to maitotoxin- and nigericin-induced interleukin-1β release through a dye uptake-independent pathway. *J. Biol. Chem.* **2007**, *282* (4), 2386−2394.

DOI: 10.1021/jf5054436
J. Agric. Food Chem. 2015, 63, 1210−1219

Figure 1. Alignment of the internal transcribed spacer (ITS) of the rDNA from several *Delphinium* and *Aconitum* species. Oligonucleotide primers Delph1F and Delph1R are shown.

(AF258718), *D. nuttallianum* (AF258688), *D. ramosum* (AF258687), *D. scaposum* (AF258732), *A. columbianum* (AF258683), and *A. delphiniifolium* (AF258681). An oligonucleotide forward primer Delph1F (5′ GTGAAAAYAAACCGRGACGG 3′) and reverse primer Delph1R (5′ GGGGATGATGAGCACACAACCA 3′) were synthesized by Integrated DNA Technologies, Inc. (Coralville, IA).

Ruminally Cannulated Animals. Three ruminally cannulated Angus cows (510 kg) were maintained on a diet of alfalfa hay at maintenance levels (ca. 10 kg/day). The diet was offered twice daily at 8:30 and 16:00 h. All procedures were approved by the Utah State University IACUC committee and were conducted under veterinary supervision.

Plant Material. Plant material from previous collections representing the following species were used to validate the specificity of the primers: *D. occidentale* (Logan, UT), *D. nuttallianum* (Colbrun, CO), *D. andersonii* (Garrison, UT), *D. glaucesens* (Dillon, MT), *D. scaposum* (Tuweep, AZ), *D. ramosum* (Cuchara, CO), *D. barbeyi* (Crested Butte, CO), *D. occidentale* (Wilsal, MT), *A. columbianum* (Elko, NV), and *Medicago sativa* (Logan, UT). *Delphinium* species were the target species while *A. columbianum* and *M. sativa* were used as negative controls to validate that the primers were specific. Samples when initially collected were placed on dry ice at the time of collection, frozen and freeze-dried upon return to the laboratory, and ground for subsequent DNA extraction.

In Vivo Rumen Digestion. *Delphinium occidentale* leaves collected from Logan, UT, previously frozen, then thawed, were manually cut into pieces with a diameter ranging from 0.5 to 1.5 cm^2. Five grams of cut leaves were placed in each of 27 nylon bags (10 cm × 20 cm and 50 μm pore size) (Ankom Technology, Macedon, NY), respectively.[19] Three bags of material were freeze-dried as control samples. Eight bags each were incubated in the rumen of three ruminally cannulated cows. All eight bags were placed in a larger nylon bag of the same porosity with an inert weight enclosed so the samples would be continually submersed in rumen fluid in the ventral sac, and a 50 cm nylon string attached to allow movement within the rumen yet facilitate the retrieval of the bags. One bag was removed from each animal (n = 3) at the following time points: 4 h, 8 h, 12 h, 16 h, 20 h, 24 h, 36 h, and 48 h. Samples were immediately placed in a −20 °C freezer upon removal and subsequently freeze-dried and ground (1 mm screen).

In Vitro Rumen Digestion. *Delphinium occidentale* leaves, previously frozen, then thawed, from Logan, UT, were cut into pieces with a diameter ranging from 0.5 to 1.5 cm^2. Five grams of cut leaves were placed in each of 21 nylon bags (5 cm × 5 cm, 25 μm pore size, Ankom Technology). Three nylon bags were freeze-dried as control samples. Six bags were placed in each of three nonrotating digestion vessels containing freshly collected and anaerobic rumen inoculum (Daisy II incubator, Ankom Technology) at 39 °C representing a composite rumen fluid sample from the three cannulated cows. One bag was removed from each digestion vessel (n = 3) at the following time points: 8 h, 16 h, 24 h, 32 h, 40 h, and 48 h. Samples were immediately placed in a −20 °C freezer upon removal and subsequently freeze-dried and ground (1 mm screen).

In Vivo and In Vitro Rumen Digestion. *Delphinium occidentale* leaves, previously frozen, then thawed, from Logan, UT, were cut into pieces with a diameter ranging from 0.5 to 1.5 cm^2. Five grams of cut leaves were placed in each of 21 nylon bags as noted above. Three nylon bags were freeze-dried as control samples. Eighteen bags were placed in the rumen of a canulated cow. All 18 bags were placed in a larger bag with the same porosity and an inert weight enclosed so the samples would be continually submersed in rumen fluid in the ventral sac, and a 50 cm string attached to allow movement and to facilitate the retrieval of the bags. All the bags were retrieved at 8 h, and three were immediately frozen. The remaining 15 bags were immediately placed into three nonrotating digestion vessels (Daisy II Incubator, Ankom Technology) containing freshly collected and anaerobic rumen fluid maintained at 39 °C representing a composite sample obtained from the three cannulated cows. One bag was removed from each digestion vessel (n = 3) at the following time points: 16 h (24 h total; 8 h in vivo + 16 h in vitro), 24 h (32 h total), 40 h (48 h total), 48 h (56 h total), and 64 h (72 h total). Samples were immediately placed in a −20 °C freezer upon removal and subsequently freeze-dried and ground.

In Vivo Rumen Digestion Sensitivity. Different ratios of *D. occidentale* leaves from Logan, UT, previously frozen, then thawed, and an alfalfa hay mixture were prepared. Four replicate nylon bags of the following ratios were prepared (g of larkspur:g of alfalfa): 5:0, 1:2.13, 1:5.25, 1:11.5, 1:24, 1:49. One bag of each ratio was freeze-dried as a control sample. One sample of each ratio was placed in the rumen of each of the three cannulated cows. All bags were placed in a larger nylon bag of the same porosity with an inert weight so the samples would be submersed in rumen fluid, and a 50 cm string attached to allow movement within the ventral sac and to facilitate the retrieval of the bags. After 8 h all the samples were retrieved from the cannulated cows. In addition, 3 other ratios were prepared representing the control sample only, namely, 1:99, 1:199, and 1:399. Samples were immediately placed in a −20 °C freezer upon removal and subsequently freeze-dried and ground.

DNA Extraction. DNA was extracted from ∼150 mg of freeze-dried ground tissue using the ZR plant/seed DNA MiniPrep kit (Zymo Research Corp., Irvine, CA). Extractions were performed according to the manufacturer's instructions with one exception: the volume of lysis solution used was increased to 1.2 mL. DNA was quantitated with the ND-1000 spectrophotometer (Nanodrop Technologies, Wilmington, DE).

Polymerase Chain Reaction (PCR). All PCR was performed with a Bio-Rad Dyad PCR detector (Bio-Rad Laboratories Inc., Hercules, CA). Thermal cycling conditions for all material were as follows: (a) an initial denaturation step for 3 min at 94 °C, (b) followed by 10 cycles of 30 s at 94 °C, 45 s at 60 °C, and 30 s at 72 °C, (c) followed by 25 cycles of 30 s at 94 °C, 45 s at 54 °C, and 30 s at 72 °C, and (d) a final extension of 5 min at 72 °C. Each reaction had a total volume of 50 μL containing 500 ng of DNA. GoTaq DNA polymerase (Promega Corporation, Madison, WI) was used following the reaction conditions recommended by the manufacturer. PCR products were resolved on a 1% agarose gel containing ethidium bromide at 118 V for 20 min and visualized under UV illumination. Agarose gels were visualized and analyzed with a Kodak Image Station 2000RT imager and its software (Eastman Kodak, Rochester, NY).

Norditerpene Alkaloid Analysis. Prepared mixtures of plant material were analyzed for larkspur alkaloids by LC−MS.[20] An aliquot

DOI: 10.1021/jf5053496
J. Agric. Food Chem. 2015, 63, 1220−1225

of plant material (100 mg) was extracted with 4.0 mL of methanol for 2 h by mechanical rotation in a sealed (screw cap) test tube. The sample was filtered, and a 0.500 mL aliquot of the extract was diluted with 0.500 mL of 20 mM ammonium acetate in a 1.5 mL autosample vial. LC−ESI-MS analyses was completed using a Thermo Scientific LCQ Advantage system with Surveyor HPLC and autosampler (Thermo Scientific, San Jose, CA). An injection volume of 10 μL was used on a 100 × 2.1 mm i.d., 5 μm, BetaSil C18 column (Thermo Scientific, San Jose, CA) eluted with a mixture of acetonitrile (A) and 0.5% acetic acid/0.05% trifluoroacetic acid (B) at a flow rate of 0.400 mL/min and the following linear gradient: 5−15% A from 0 to 1 min; 15−75% A from 1 to 8 min; 75% A from 8 to 10 min; 75−5% A from 10 to 11 min; and 5% A from 11 to 16 min. The flow from the column was connected directly to the ESI source. The major alkaloid in the *D. occidentale* plant material is deltaline and under the chromatographic conditions eluted with retention time of 4.1 min and gives a strong MH^+ ion (m/z 508). Detection of the alkaloid was targeted by reconstructed ion chromatograms for this select ion.

RESULTS AND DISCUSSION

Primer Specificity. Candidate specific oligonucleotide DNA primers were developed by aligning and comparing the ITS sequence from several *Delphinium* spp. as well as representative *Aconitum* spp. (Figure 1). Oligonucleotide DNA primers were tested to determine if they were specific to representative *Delphinium* taxa of the Western United States. Preliminary experiments were performed to optimize the annealing temperature and reaction conditions that would ensure they were specific to *Delphinium* and not other taxa. The optimal reaction conditions were an annealing temperature of 60 °C for 10 cycles followed by 25 cycles at an annealing temperature of 54 °C. The annealing temperature is critical as lower temperatures will result in amplification of a product from *Aconitum*. A 500 base pair (bp) product was amplified from the seven *Delphinium* species but not from the *Aconitum* or alfalfa sample (Figure 2). The results show that the primers

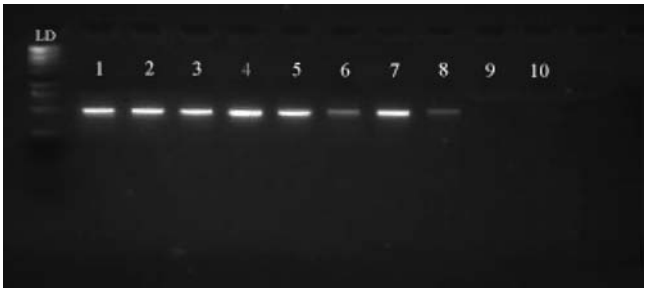

Figure 2. Agarose gel electrophoresis showing specificity of DNA primers. 1000bp marker (LD) shown as a reference. Lanes: 1, *D. occidentale* (Logan, UT); 2, *D. nuttallianum*; 3, *D. andersonii*; 4, *D. glaucescens*; 5, *D. scaposum*; 6, *D. ramosum*; 7, *D. barbeyi*; 8, *D. occidentale*; 9, *A. columbianum*; and 10, *M. sativa*.

amplified a product with all of the *Delphinium* species tested including five of the more important *Delphinium* species in the Western United States in terms of cattle losses. DNA was extracted from all the plant material a second time and PCR performed, and the same results were obtained (data not shown). The alignment of the ITS from the *Delphinium* species (Figure 1) suggests that the primers would also amplify other species including *D. geyeri* and *D. glaucum*. To further demonstrate that the primers amplified a *Delphinium* species, the PCR product could be verified by restriction enzyme digestion or sequencing.

In Vivo Rumen Digestion. An in vivo rumen digestion was performed to determine the length of time one may expect to detect larkspur in a living bovine after the animal ate the plant. A PCR product was amplified from *D. occidentale* samples that had been incubated in the rumen of the three cannulated cows after 4 h, 8 h, 12 h, and 16 h (Figure 3). At the 20 h and 24 h

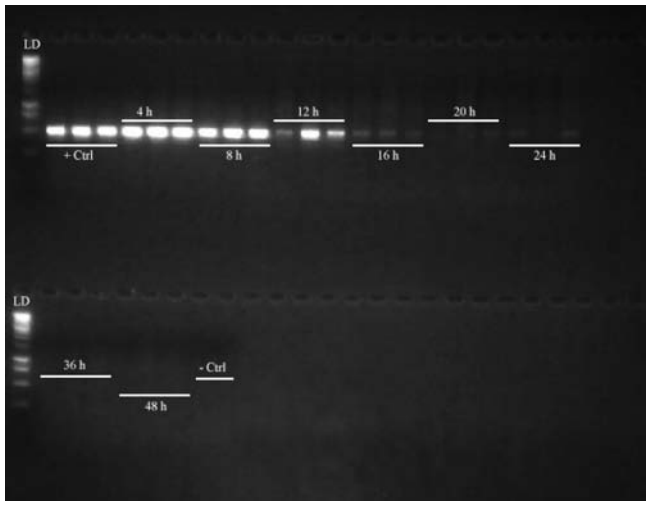

Figure 3. Agarose gel electrophoresis showing amplification of PCR products from the in vivo rumen digestion. 1000bp marker (LD) shown as a reference. Triplicates of undigested positive control (+ctrl) and digested (4−48 h) *D. occidentale*. Negative control (−ctrl) representing *A. columbianum* and *M. sativa*.

time points, a PCR product was detected from 1 or 2 of the replicate samples (Figure 3). No PCR product was amplified from the samples after 36 h and 48 h. As expected, a PCR product was detected from the three control samples but not from the *Aconitum* or alfalfa sample (Figure 3). DNA was extracted from all the plant material a second time and PCR performed, and the same results were obtained (data not shown). These results suggest that the DNA representing *D. occidentale* is degraded over time and that by 36 h post incubation a PCR product is no longer detectable. Studies have shown that plant DNA, particularly naked DNA, may be rapidly degraded by the microbial activity in rumen fluid.[21] Using real-time PCR, Alexander et al.[22] found that digestion of DNA in canola was highly correlated with the digestive activity of intestinal microorganisms. However, DNA from maize has been shown to survive for up to 24 h in the rumen of sheep.[23] Further, Wiedemann et al.[24] reported that survival of corn DNA in the bovine rumen depended on fragment length, previous processing, and the length of time incubated in the rumen.

The in vivo digestion and DNA degradation observed here may have occurred faster than would be expected in a natural grazing scenario, as the starting plant material was initially cut into smaller fragments compared to the large bites consumed by a grazing ruminant.[25] However, biting, mastication, and comminution by a grazing animal may rapidly render grazed larkspur somewhat similar to the chopped material used in this study. Delphinium plants are nutritious and highly digestible;[25,26] as such much of the ingested larkspur probably ends up in the upper layer in the ruminal dorsal sac, part of the raft or mat that is composed primarily of rapidly fermenting, buoyant particles. Digestion and retention time in the rumen

DOI: 10.1021/jf5053496
J. Agric. Food Chem. 2015, 63, 1220−1225

will depend on many complex, interrelated factors, however for comparison ingested larkspur plants are likely to be very similar in retention time to high quality alfalfa hay.[26] Effects of long form (i.e., intact) or chopped alfalfa hay on ruminal retention time were small when high quality alfalfa was used.[27] The retention time in the rumen of high quality alfalfa hay is 18−21 h,[27,28] and larkspur is probably similar.

In Vitro Rumen Digestion. An in vitro rumen digestion was performed to determine the length of time one may expect to detect larkspur in a bovine rumen after a fatal poisoning episode, as the digestion vessels in the Daisy II digestion apparatus were not rotating as is typically done during in vitro experiments (i.e., mimicking a static rumen). A PCR product was detected from *D. occidentale* samples that had been incubated in digestion vessels of rumen fluid in each of the three replicates up to 40 h (Figure 4). At the 48 h time point, a

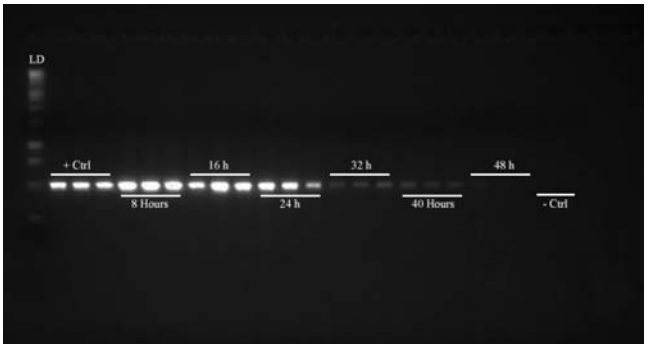

Figure 4. Agarose gel electrophoresis showing amplification of PCR products from the in vitro rumen digestion. 1000bp marker (LD) shown as a reference. Triplicates of undigested positive control (+ctrl) and digested (8−48 h) *D. occidentale*. Negative control (−ctrl) representing *A. columbianum* and *M. sativa*.

PCR product was amplified from one of the replicate samples (Figure 4). As expected a PCR product was detected from the three control samples but not from the *Aconitum* or alfalfa sample (Figure 4). DNA was extracted from all the plant material a second time and PCR performed, and the same results were obtained (data not shown).

Differences were observed in the length of time a PCR product was detected between the in vivo and in vitro rumen digestion of *D. occidentale*. This was evident by the quality and quantity of DNA extracted from the starting material (data not shown). This may be due to the viability of the microflora in the in vitro rumen compared to the in vivo rumen. Further, it may be related to the total ruminal conditions during the in vivo process, including microbial numbers and activity, and rumen fermentation and motility resulting in faster degradation of the target DNA. In the in vitro digestion the rumen fluid was not moving nor was the plant material continually bathed in rumen fluid. The plant material in the nylon bags was buoyant, and moved to the top of the digestion vessel with the other plant material equivalent to the rumen mat. However, there still was evidence of digestion as the nylon bag expanded over time due to the production of gases as the result of fermentation.

In Vivo and In Vitro Rumen Digestion. An in vivo digestion was coupled with an in vitro digestion to determine the length of time one may expect to detect larkspur in a bovine that consumed larkspur and died 8 h later. A PCR product was detected from *D. occidentale* samples that had been incubated in vivo and in vitro from 8 h to 72 h in all three replicates (Figure 5). As expected, a PCR product was detected from the three control samples but not from the *Aconitum* or alfalfa sample

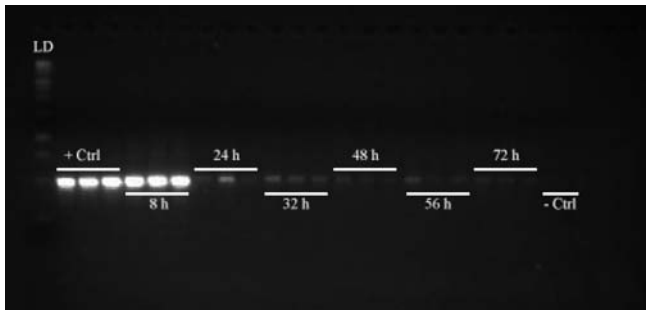

Figure 5. Agarose gel electrophoresis showing amplification of PCR products from the in vivo and in vitro coupled rumen digestion. 1000bp marker (LD) shown as a reference. Triplicates of undigested positive control (+ctrl) and digested (8−72 h) *D. occidentale*. Negative control (−ctrl) representing *A. columbianum* and *M. sativa*.

(Figure 5). DNA was extracted from all the plant material a second time and PCR performed, and the same results were obtained (data not shown). The results from this experiment were similar to the in vitro digestion alone.

In Vivo Rumen Digestion Sensitivity. When collecting rumen samples from poisoned animals, it is not possible to sample the entire rumen. Thus, a rumen from a dead animal has to be randomly sampled with the assumption that the distribution of the plant material is fairly uniform throughout the rumen. Based on research at this Laboratory, we calculate that a minimum of 5−10% of a cow's daily diet needs to be ingested larkspur for the cow to become poisoned.[29−31] Consequently, in the best case scenario, a random sample of rumen contents will contain 5−10% (1:20−1:10) of larkspur plant material. Therefore, different ratios of alfalfa to *D. occidentale* were prepared to determine if it was feasible to detect 5% larkspur, or lower, in the rumen. A PCR product was detected from each undigested control ratio ranging from the *D. occidentale* only sample to 1 g of *D. occidentale* to 399 g of alfalfa (Figure 6). For comparison, the 1:399 sample was analyzed by LC−MS (Figure 7). The norditerpene alkaloids were detected in it and all other ratios. A PCR product was detected from each of the triplicate digested ratios ranging from the *D. occidentale* only sample to 1 g of *D. occidentale* to 49 g of

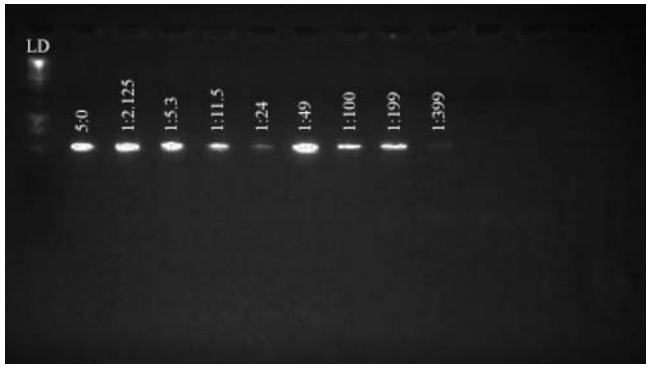

Figure 6. Agarose gel electrophoresis showing amplification of PCR products from different undigested ratios of larkspur to alfalfa. 1000bp marker (LD) shown as a reference. Ratios represent grams of larkspur:grams of alfalfa.

DOI: 10.1021/jf5053496
J. Agric. Food Chem. 2015, 63, 1220−1225

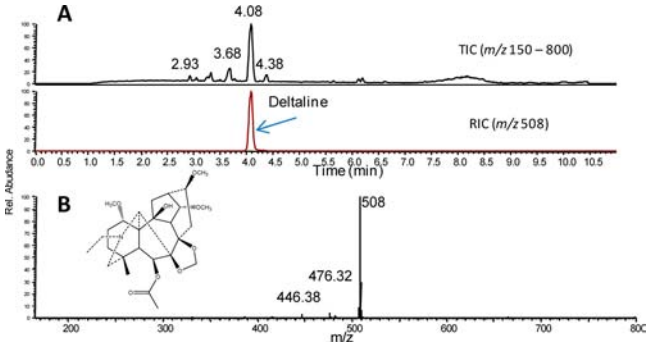

Figure 7. LC–MS analysis of mixture of *D. occidentale* and alfalfa (1 g:399 g). (A) Total ion chromatogram (TIC) and reconstructed ion chromatogram (RIC) (m/z 508) of the methanol extract from the mixed plant material. The alkaloid deltaline eluting at t_R = 4.08 min. (B) Mass spectrum of the peak at 4.1 min.

alfalfa (Figure 8). As expected, a PCR product was not detected from the *Aconitum* or alfalfa sample (Figure 8). DNA was

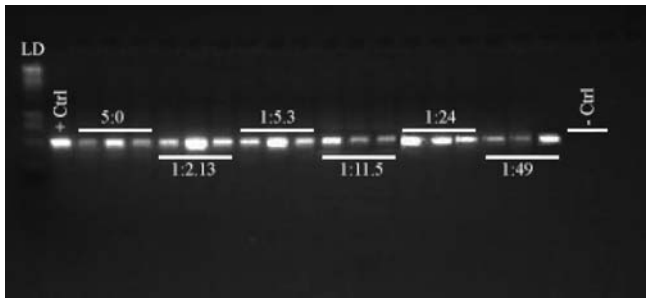

Figure 8. Agarose gel electrophoresis showing amplification of PCR products from undigested positive control (+ctrl) and the in vivo rumen digestion from different ratios of larkspur to alfalfa. 1000bp marker (LD) shown as a reference. Ratios represent grams of larkspur:grams of alfalfa. Negative control (−ctrl) representing *A. columbianum* and *M. sativa*.

extracted from a subset of the plant material a second time and PCR performed, and the same results were obtained (data not shown). These results suggest that, if a rumen from a poisoned animal were sampled from several spots at random, there would likely be sufficient larkspur to detect a PCR product based upon the amount of larkspur one would expect to find in a poisoned animal.

Two principal limitations exist with using PCR as a diagnostic tool. The first is a matter of sampling the rumen from the poisoned animal. How much material would need to be sampled to provide confidence that the sample is representative of the overall rumen contents? The data reported here are promising, as a PCR product was detected at a ratio of 1:399, while larkspur is likely to comprise 5–10% (1:20–1:10) or higher of the rumen contents of a poisoned animal.[2,29,31] However, in the cases of plants that are more acutely toxic such as water hemlock (*Cicuta* spp.), this may not be feasible as there could be much less plant material. The second limiting factor is the integrity of the template DNA. Often there is a lapse in time between the death of an animal and its discovery and the subsequent sampling of rumen contents. The data reported here suggests that up to 48 h after the death of the animal, as mimicked by the coupled in vivo and in vitro samples, larkspur can still be detected by PCR, thus supporting the idea that PCR could be used as a diagnostic tool if the dead animals are found and samples collected within 2 days.

In summary, we developed a pair of oligonucleotide primers specific to *Delphinium* spp. Using these primers, a PCR product was detected in samples from an in vivo, in vitro, and in vivo/in vitro coupled digestion of *D. occidentale*. Lastly, using this method, we were able to detect larkspur in a matrix where the amount of larkspur was far less than what one would expect to find in the rumen contents of a poisoned animal. These data demonstrate that this method and the primers are both specific and sensitive, a characteristic of a good diagnostic tool. This research offers a proof of principle that PCR-based methods could be used as a diagnostic tool to detect a plant of interest in the rumen contents of a poisoned animal. However, further research is needed to validate this method. For example, rumen samples need to be collected and analyzed from actual field cases of poisoned cattle. Also additional research needs to be performed to compare the sensitivity and robustness of this PCR-based method to chemical methods where the norditerpene alkaloids are detected. Finally, hypothetically, a PCR-based method could be developed for diagnosis of poisoning by any other plant species that is acutely toxic such as water hemlock, death camas (*Zigadenus* spp.), and oleander (*Nerium oleander*).

AUTHOR INFORMATION

Corresponding Author

*Tel: (435) 752-2941. Fax: (435) 753-5681. E-mail: daniel.cook@ars.usda.gov.

Notes

The authors declare no competing financial interest.

ACKNOWLEDGMENTS

We thank Kermit Price and Scott Larsen for their technical assistance.

REFERENCES

(1) Marsh, C. D.; Clawson, A. B.; Marsh, H. Larkspur poisoning of livestock. *U.S., Dep. Agric., Bull.* **1916**, No. No.365, 91.

(2) Pfister, J. A.; Gardner, D. R.; Panter, K. E.; Manners, G. D.; Ralphs, M. H.; Stegelmeier, B. L.; Schoch, T. K. Larkspur (*Delphinium* spp.) poisoning in livestock. *J. Nat. Toxins* **1999**, *8*, 81–94.

(3) Pfister, J. A.; Ralphs, M. H.; Gardner, D. R.; Stegelmeier, B. L.; Manners, G. D.; Panter, K. E.; Lee, S. T. Management of three toxic *Delphinium* species based on alkaloid concentrations. *Biochem. Syst. Ecol.* **2002**, *30*, 129–138.

(4) Nielsen, D. B.; Ralphs, M. H.; Evans, J. S. Economic feasibility of controlling tall larkspur on rangelands. *J. Range Manage.* **1994**, *47*, 369–372.

(5) Ewan, J. A synopsis of the North American species of *Delphinium*. *Univ. Colorado Studies, Ser. D* **1945**, *2*, 55–244.

(6) Warnock, M. J. A taxonomic conspectus of North American *Delphinium*. *Physiologia* **1995**, *78*, 73–101.

(7) Warncok, M. J. *Delphinium* Linnaeus. *Flora North Am.* **1997**, *3*, 196–240.

(8) Kingsbury, J. M. *Poisonous plants of the US and Canada*; Prentice Hall: 1964.

(9) Green, B. T.; Gardner, D. R.; Pfister, J. A.; Cook, D. Larkspur poison weed: 100 years of Delphinium research. *Rangelands* **2009**, *31*, 22–27.

(10) Green, B. T.; Welch, K. D.; Cook, D.; Gardner, D. R. Potentiation of the actions of acetylcholine, epibatidine, and nicotine by methyllycaconitine at fetal muscle-type nicotinic acetylcholine receptors. *Eur. J. Pharmacol.* **2011**, *662*, 15–21.

DOI: 10.1021/jf5053496
J. Agric. Food Chem. 2015, 63, 1220–1225

(11) Olsen, J. D.; Manners, G. D.; Pelletier, S. W. Poisonous properties of Larkspur (*Delphinium spp.*). *Collect. Bot. (Barcelona)* **1990**, *19*, 141−151.
(12) Panter, K. E.; Manners, G. D.; Stegelmeier, B. L.; Lee, S. T.; Gardner, D. R.; Ralphs, M. H.; Pfister, J. A.; James, L. F. Larkspur poisoning: alkaloid structure−activity relationships and toxicity. *Biochem. Syst. Ecol.* **2002**, *30*, 113−128.
(13) Stegelmeier, B. L.; Green, B. T.; Panter, K. E.; Welch, K. D.; Hall, J. O. Identifying Plant Poisoning in Livestock. *Rangelands* **2009**, *31*, 5−9.
(14) Sparks, D. R.; Malechek, J. C. Estimating percentage dry weight in diets using a microscopic technique. *J. Range Manage.* **1968**, *21*, 264−265.
(15) Holechek, J. L.; Vavra, M.; Pieper, R. D. Botanical composition determination of range herbivore diets: a review. *J. Range Manage.* **1982**, *35*, 309−315.
(16) Chowdhury, E. H.; Mikami, O.; Murata, H.; Sultana, P.; Shimada, N.; Yoshioka, M.; Guruge, K. S.; Yamamoto, S.; Miyazaki, S.; Yamanaka, N. Fate of maize intrinsic and recombinant genes in calves fed genetically modified maize Bt11. *J. Food Prot.* **2004**, *67*, 365−370.
(17) Einspanier, R.; Lutz, B.; Rief, S.; Berezina, O.; Zverlov, V.; Schwarz, W.; Mayer, J. Tracing residual recombinant feed molecules during digestion and rumen bacterial diversity in cattle fed transgene maize. *Eur. Food Res. Technol.* **2004**, *218*, 269−273.
(18) Koontz, J. A.; Soltis, P. S.; Soltis, D. E. Using phylogeny reconstruction to test hypotheses of hybrid origin in *Delphinium* section Diedropetala (Ranunculaceae). *Syst. Bot.* **2004**, *29*, 345−357.
(19) Ørskov, E. R.; Hovell, F. D.; Mould, F. The use of the nylon bag technique for the evaluation of feedstuffs. *Trop. Anim. Prod.* **1980**, *5*, 195−213.
(20) Gardner, D. R.; Panter, K. E.; Pfister, J. A.; Knight, A. P. Analysis of toxic norditerpenoid alkaloids in Delphinium species by electrospray, atmospheric pressure chemical ionization, and sequential tandem mass spectrometry. *J. Agric. Food Chem.* **1999**, *47*, 5049−5058.
(21) Duggan, P. S.; Chambers, P. A.; Heritage, J.; Forbes, J. M. Survival of free DNA encoding antibiotic resistance from transgenic maize and the transformation activity of DNA in ovine saliva, ovine rumen fluid and silage effluent. *FEMS Microbiol. Lett.* **2000**, *191*, 71−77.
(22) Alexander, T. W.; Sharma, R.; Deng, M. Y.; Whetsell, A. J.; Jennings, J. C.; Wang, Y.; Okine, E.; Damgaard, D.; McAllister, T. A. Use of quantitative real-time and conventional PCR to assess the stability of the cp4 epsps transgene from Roundup Ready® canola in the intestinal, ruminal, and fecal contents of sheep. *J. Biotechnol.* **2004**, *112*, 255−266.
(23) Duggan, P. S.; Chamber, P. A.; Heritage, J.; Forbes, J. M. Fate of genetically modified maize DNA in the oral cavity and rumen of sheep. *Br. J. Nutr.* **2003**, *89*, 159−166.
(24) Wiedemann, S.; Lutz, B.; Kurtz, H.; Schwarz, F.; Albrecht, C. In situ studies on the time-dependent degradation of recombinant corn DNA and protein in the bovine rumen. *J. Anim. Sci.* **2006**, *84*, 135−144.
(25) Pfister, J. A.; Manners, G. D.; Ralphs, M. H.; Hong, Z. X.; Lane, M. A. Effects of phenology, site, and rumen fill on tall larkspur consumption by cattle. *J. Range Manage.* **1988**, *41*, 509−514.
(26) Pfister, J. A.; Adams, D. C.; Arambel, M. J.; Olsen, J. D.; James, L. F. Sublethal levels of toxic larkspur: effects on intake and rumen dynamics in cattle. *Nutr. Rep. Int.* **1989**, *40*, 629−636.
(27) Shaver, R. D.; Nytes, A. J.; Satter, L. D.; Jorgensen, N. A. Influence of amount of feed intake and forage physical form on digestion and passage of prebloom alfalfa hay in dairy cows. *J. Dairy Sci.* **1986**, *69*, 1545−1559.
(28) Shaver, R. D.; Satter, L. D.; Jorgensen, N. A. Impact of forage fiber content on digestion and digesta passage in lactating dairy cows. *J. Dairy Sci.* **1988**, *71*, 1556−1565.
(29) Pfister, J. A.; Panter, K. E.; Manners, G. D. Effective dose in cattle of toxic alkaloids from tall larkspur (*Delphinium barbeyi*). *Vet. Hum. Toxicol.* **1994**, *36*, 10−11.
(30) Pfister, J. A.; Gardner, D. R.; Price, K. W. Grazing risk on tall larkspur-infested ranges. *Rangelands* **1997**, *19*, 12−15.
(31) Welch, K. D.; Green, B. T.; Gardner, D. R.; Cook, D.; Pfister, J. A.; Stegelmeier, B. L.; Panter, K. E.; Davis, T. Z. Influence of 7,8-methylenedioxylycoctonine-type alkaloids on the toxic effects associated with ingestion of tall larkspur (*Delphinium* spp.) in cattle. *Am. J. Vet. Res.* **2010**, *71*, 487−492.

DOI: 10.1021/jf5053496
J. Agric. Food Chem. 2015, 63, 1220−1225

(Tokyo, Japan). *Pfu* DNA polymerase was obtained from Promega (Madison, MI), and T4 DNA ligase was obtained from Biolabs (New England Biolabs, Ipswich, MA). A multifunctional DNA purification kit was purchased from BioTeke (Beijing, China). Chelating Sepharose [nickel−iminodiacetic acid (Ni−IDA)] resin matrix was from GE Life Sciences (Pittsburgh, PA). Q Sepharose Fast Flow was purchased from Pharmacia (Uppsala, Sweden). Debranched arabinan, sugar beet arabinan, arabinoxylan, and arabino-oligosaccharides were purchased from Megazyme (Bray, Wicklow, Ireland). The *p*-nitrophenol (*p*NP) substrates were purchased from Biosynth (Staad, Switzerland). Birchwood xylan, *p*NP-α-L-arabinofuranoside, *p*NP-α-L-arabinopyranoside, and *p*NP-β-D-xylopyranoside were purchased from Sigma (St. Louis, MO). The commercial pectinase was obtained from Sinopharm (Beijing, China). All other chemicals were of analytical grade, unless stated otherwise.

Cloning of an Endo-α-1,5-L-arabinanase Gene and Its Nucleotide Sequence Analysis. Recombinant DNA techniques as described by Sambrook and Russell[22] were employed to perform DNA manipulations. The fungus *R. miehei* CAU 432 used in this study was deposited at the China General Microbiological Culture Collection Center (CGMCC) under number 4967. The strain was grown at 50 °C in the media as described by Tang et al.[20] Genomic DNA was isolated from *R. miehei* CAU432 using the CTAB method.[23] The first and second strands of cDNA were synthesized with PrimeScript RT-PCR kit (TaKaRa, Tokyo, Japan). The specific primers AraDNAF (5′-ATGAAACTATCTTTTGCATTGGCG-3′) and AraDNAR (5′-TTAGTAAGTTGGCCAGCCGTTG-3′) were designed on the basis of the genome sequence of *R. miehei* CAU432[21] to amplify the coding region of endo-α-1,5-L-arabinanase. The polymerase chain reaction (PCR) conditions were as follows: a hot start at 94 °C for 5 min, 30 cycles of denaturation for 30 s at 94 °C, annealing for 30 s at 52 °C, extension for 1 min at 72 °C, and a final extension step for 10 min at 72 °C with LA Taq DNA polymerase (TaKaRa, Tokyo, Japan). After amplification, PCR products were purified, ligated to pMD18-T vector, transformed into *E. coli* DH5α competent cells, and sequenced.

BLAST analysis was performed at National Center for Biotechnology Information (NCBI) server (http://blast.ncbi.nlm.nih.gov/Blast.cgi). Multiple alignment analysis was performed by Clustal W2.0 (http://www.ebi.ac.uk/Tools/clustalw2/index.html), and the alignment figure was produced with ESPript (http://espript.ibcp.fr).[24] Signal peptide was analyzed by SignalP 3.0 server (http://www.cbs.dtu.dk/services/SignalP/). Putative catalytic residues were predicted using Motif Scan (http://myhits.isb-sib.ch/cgi-bin/motif_scan) and CAZY (http://www.cazy.org/).

Expression of the Endo-α-1,5-L-arabinanase Gene in *E. coli*. To express the endo-α-1,5-L-arabinanase gene (*RmArase*) in *E. coli*, the open reading frame (ORF) region of the cDNA gene was amplified by PCR with the primers of RmAraF (5′-ATCATGCCATGGCTTGGGAACTCACAGGTGACATT-3′) and RmAraR (5′-ATTCCGCTCGAGTTAGTAAGTTGGCCAGCCGTTG-3′). *Nco*I and *Xho*I sites (underlined) were added to the forward and reverse primers, respectively, so that the expressed protein carries a N-terminal His tag encoded by the vector. PCR conditions were as follows: 94 °C for 5 min, 30 cycles of 94 °C for 30 s, 58 °C for 30 s, and 72 °C for 1 min, followed by 1 cycle of 72 °C for 10 min. The PCR product was cloned into the *Nco*I/*Xho*I sites of pET30a (+) vector (Novagen) and transformed into *E. coli* BL21 (DE3) for protein expression. A single colony of *E. coli* BL21 (DE3) harboring *RmArase* in pET30a (+) was inoculated into Luria−Bertani broth (LB) medium containing kanamycin (50 μg/mL) and incubated on a rotary shaker (200 rpm at 37 °C) until the optical density OD_{600} reached about 0.8−1.0. Isopropyl-β-D-1-thiogalactopyranoside (IPTG) was added to a final concentration of 1 mM to induce expression, and the culture was further grown at 25 °C for 12 h.

Purification of Recombinant Endo-α-1,5-L-arabinanase. Recombinant cells were harvested from culture broth by centrifugation at 10000*g* for 10 min at 4 °C, resuspended in lysis buffer A (50 mM sodium phosphate at pH 8 containing 500 mM NaCl), and disrupted by sonication. The cell debris was removed by centrifugation at 10000*g* for 10 min at 4 °C, and the supernatant was loaded onto a Ni−IDA column (0.8 × 10 cm) equilibrated with buffer B (buffer A containing 20 mM imidazole). After binding, the column was washed with buffer B followed by buffer C (buffer A containing 50 mM imidazole) at a flow rate of 1.0 mL/min. The bound enzyme was eluted with buffer D (buffer A containing 200 mM imidazole). The protein eluted as a single peak, was pooled, and was further fractionated on a Q-Sepharose column (10 × 1 cm) pre-equilibrated with buffer E (50 mM sodium phosphate at pH 8.0). The column was washed with buffer E at a flow rate of 1 mL/min, and the bound protein was then eluted with a linear gradient from 0 to 500 mM NaCl in buffer E. The elution fractions showing endo-α-1,5-L-arabinanase activity were pooled and dialyzed against 50 mM sodium acetate buffer (pH 5.5). The homogeneity of the purified enzyme was monitored by sodium dodecyl sulfate−polyacrylamide gel electrophoresis (SDS−PAGE).

Enzyme Assay and Protein Determination. The mixture consisting of 10 μL of enzyme and 90 μL of debranched arabinan (10 mg/mL) in 50 mM sodium acetate buffer (pH 5.5) was incubated at 45 °C for 30 min. Activity was assayed by measuring the release of reducing groups according to the method of dinitrosalicylic acid (DNS).[25] The amount of reducing sugars was calculated from a standard plot of L-arabinose. One unit of enzyme activity is defined as the amount of enzyme liberating 1 μmol of reducing sugars per minute under the conditions described. Protein concentrations were measured by the Lowry method[26] using bovine serum albumin (BSA) as a standard.

SDS−PAGE and Size-Exclusion Chromatography. The proteins during the purification process were analyzed on 12.5% SDS−PAGE.[27] The protein bands were stained with Coomassie Brilliant Blue R-250. The molecular mass of the enzyme subunit was determined using a low molecular mass standard (Amersham, London, U.K.) containing phosphorylase B (97.0 kDa), albumin (66.0 kDa), ovalbumin (45.0 kDa), carbonic anhydrase (30.0 kDa), trypsin inhibitor (20.1 kDa), and α-lactalbumin (14.4 kDa).

The native molecular mass of RmArase was determined by size-exclusion chromatography using a Superdex-75 gel filtration column (1 × 40 cm) equilibrated with 50 mM sodium phosphate buffer (pH 8.0) containing 150 mM NaCl at a flow rate of 0.33 mL/min. The molecular mass standards used were phosphorylase B rabbit muscle (97.2 kDa), BSA (66.0 kDa), chicken egg white albumin (45.0 kDa), α-chymotrypsinogen A from bovine pancreas (25.7 kDa), and cytochrome *c* (13.0 kDa).

pH and Temperature Profiles. The optimal pH for endo-α-1,5-L-arabinanase activity was determined in 50 mM different buffers, viz., sodium citrate (pH 3.0−6.0), sodium acetate (pH 4.5−6.0), 2-(*N*-morpholino)ethanesulfonic acid (MES) (pH 5.0−6.5), 4-(*N*-morpholino)propanesulfonic acid (MOPS) (pH 6.5−8.0) and glycine−NaOH (pH 8.5−10.5). pH stability of the enzyme was determined by incubating the enzyme at 45 °C for 30 min in various buffers, as mentioned above, followed by rapid cooling on ice. The residual activity was determined by a standard assay method.

The optimal temperature was determined by the standard assay at temperatures ranging from 30 to 60 °C in 50 mM sodium acetate buffer (pH 5.5). Thermstability was measured by the standard assay after incubating the enzyme in 50 mM sodium acetate buffer (pH 5.5) at different temperatures for 30 min.

Influence of Metal Ions and Other Reagents. The influence of different modulators, such as metal ions and reducing and chelating agents, on enzyme activity was tested. The enzyme was incubated with 1 mM various metal ions and other chemicals [ethylenediaminetetraacetic acid (EDTA), dithiothreitol (DTT), β-mercaptoethanol, SDS] at 45 °C in 50 mM sodium acetate buffer (pH 5.5) for 30 min. The residual activity of the enzyme and the control (without reagents) was determined by the standard assay.

Substrate Specificity and Kinetic Parameters. The substrate specificity of RmArase was determined using different substrates. The enzyme activity toward polysaccharides, including debranched arabinan, sugar beet arabinan, arabinoxylan, and birchwood xylan, was assayed in the presence of 10 mg/mL at 55 °C in 50 mM sodium acetate buffer (pH 5.5) by the DNS method. Activity toward *p*NP derivatives, such as *p*NP-α-L-arabinofuranoside, *p*NP-α-L-arabinopyr-

DOI: 10.1021/jf5058167
J. Agric. Food Chem. 2015, 63, 1226−1233

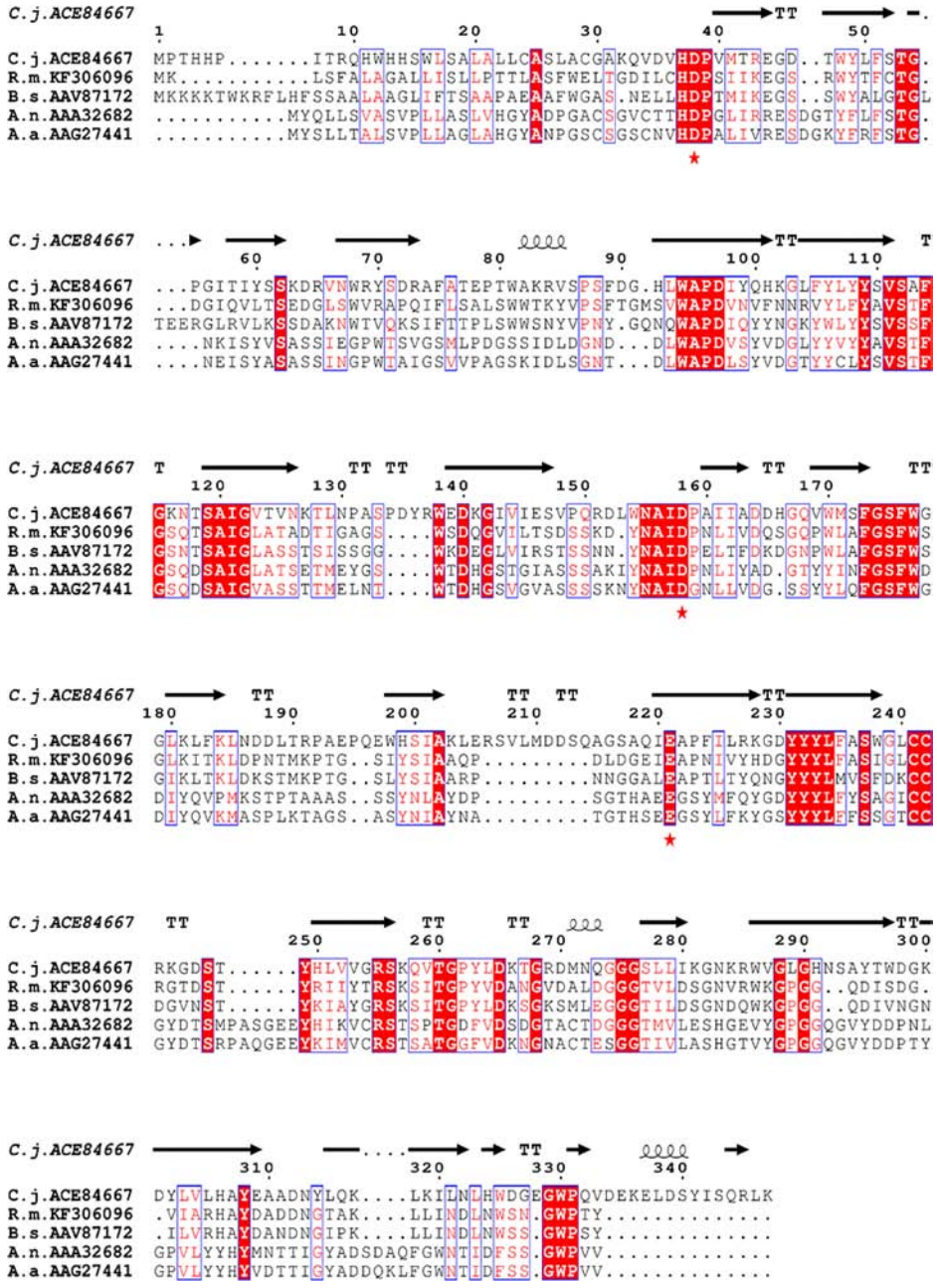

Figure 1. Alignment of homologous endo-α-1,5-L-arabinanases with RmArase sequence. Species for the sequences, with the species abbreviations and GenBank accession numbers in parentheses, are shown as follows: *C. japonicas* (C.j. ACE84667), *R. miehei* (R.m. KF306096), *B. subtilis* (B.s. AAV87172), *A. niger* (A.n. AAA32682), and *A. aculeatus* (A.a. AAG27441). Sequence regions with high similarity are written in red letters and boxed in blue. The secondary structure displayed above the alignment is derived from the three-dimensional structure (PDB code 1GYD) of endo-α-1,5-L-arabinanases (ACE84667) from *C. japonicas* Ueda107. α-Helices are rendered as squiggles, and β-strands are displayed as arrows. The catalytic base (Asp 34), catalytic acid (Glu 202), and another important residue (Asp 150) for enzymatic reaction are denoted by a red star below the residue.

anoside, and *p*NP-β-D-xylopyranoside, was measured by the rate of *p*NP released from 5 mM of the substrate in 50 mM sodium acetate buffer (pH 5.5) at 55 °C after 10 min and detected by spectrophotometry at 410 nm.

For determination of the kinetic parameters for debranched arabinan and sugar beet arabinan, enzyme activities were performed using each substrate with different concentrations at 55 °C in 50 mM sodium acetate buffer (pH 5.5) for 5 min. K_m and V_{max} of the endo-α-1,5-L-arabinanase were calculated using "GraFit" software.

Hydrolysis of Arabinans and Arabino-oligosaccharides. The potential of RmArase in degrading arabinans was analyzed as given below. A total of 1 unit of purified endo-α-1,5-L-arabinanase was incubated in a reaction volume of 1 mL with 10 mg/mL debranched arabinan or sugar beet arabinan at 45 °C in 50 mM sodium acetate buffer (pH 5.5) for 8 h. Samples were withdrawn at various time intervals and boiled for 5 min to terminated the reaction. The hydrolysis products were analyzed by thin-layer chromatography (TLC). The reaction mixtures were spotted on a silica gel plate (Merck Silica Gel 60F254, Darmstadt, Germany) and developed twice in a solvent system containing chloroform/acetic acid/water at 1:1.5:0.1 (v/v/v). Saccharides were detected by heating in an oven after spraying the plates with a mixture of methanol and sulfuric acid (95:5, v/v).

Further, the pattern of RmArase hydrolyzing various arabino-oligosaccharides was assessed. The reaction mixture consisting of 1 unit/mL enzyme and 10 mg/mL different arabino-oligosaccharides

DOI: 10.1021/jf5058167
J. Agric. Food Chem. 2015, 63, 1226−1233

Table 1. Purification Summary of the Recombinant Endo-α-1,5-L-arabinanase (RmArase) Expressed in *E. coli*

purification step	total activity (units)[a]	protein (mg)[b]	specific activity (units/mg)	purification factor (fold)	recovery (%)
crude supernatant	1432	127	11.3	1.0	100.0
Ni–IDA	891	9	100.0	9	62
Q-Sepharose	812	7.5	109	9.7	57

[a]Activity was measured in 50 mM sodium acetate buffer (pH 5.5) at 55 °C using 10 mg/mL debranched arabinan. [b]The protein was measured by the Lowry method,[26] using BSA as the standard.

(arabinobiose, arabinotriose, arabinotetraose, and arabinopentaose) in 50 mM sodium acetate buffer was incubated at 45 °C for 1 h. The hydrolysis products were analyzed by TLC, as described above.

Synergistic Action of RmArase and the Pectinase. Sugar beet pulp (100 g) was soaked in 1 L of water overnight and autoclaved at 121 °C for 60 min. The suspension was filtered and centrifuged. The supernatant pH was adjusted to 5.5 by the addition of $CaCO_3$. The supernatant was treated with 10 units/mL of a single enzyme (RmArase or pectinase) or a combination of enzymes. The reaction mixtures were incubated at 45 °C for 24 h. Reducing sugars released were determined by the DNS method using arabinose as the standard. The arabinose was determined by high-performance liquid chromatography (HPLC) equipped with a BP-800 Pb++ column (Benson Polymeric, Reno, NV). Ultrapure water (Milli-Q, Millipore, Billerica, MA) was used as the mobile phase. Operation conditions for HPLC were 80 °C at a flow rate of 0.6 mL/min. The injection volume was 20 μL, and the elution time was 40 min.

RESULTS AND DISCUSSION

Cloning and Sequence Analysis of an Endo-α-1,5-L-arabinanase Gene from *R. miehei*. The complete coding region of the endo-α-1,5-L-arabinanase gene (*RmArase*) was amplified from cDNA of *R. miehei* CAU432 using the primers AraDNAF and AraDNAR. The nucleotide sequence reported here has been submitted to the GenBank and has been allocated the accession number (KF306096). No intron was found in the coding region when compared to the genomic sequence. The mature protein has 309 amino acids with a predicted molecular mass of 33.5 kDa and a deduced pI value of 4.27. According to the homology search of the deduced amino acid sequences by BLAST (Figure 1), the amino acid sequence of RmArase shared identities of 34, 56, 35, and 35% with the characterized GH family 43 endo-α-1,5-L-arabinanases from *Cellvibrio japonicus* Ueda107 (ACE84667), *B. subtilis* (AAV87172), *A. niger* (AAA32682), and *A. aculeatus* (AAG27441), respectively. Thus, RmArase may be a novel member of GH family 43 endo-α-1,5-L-arabinanases.

To elucidate the secondary structure and catalytic residues of RmArase, the endo-α-1,5-L-arabinanase sequence from *C. japonicus* Ueda107 was added to the alignment because its three-dimensional structure [Protein Data Bank (PDB) code 1GYD] is available. Most of the β-strands are located in the conserved region. Furthermore, Asp 34, Asp 150, and Glu 202 in RmArase match with Asp 38, Asp 158, and Glu 221 in the *C. japonicus* Ueda107 endo-α-1,5-L-arabinanase, which composes the catalytic center.[28] These results suggest that the RmArase should have similar overall molecular folding and catalytic mechanism with the GH family 43 endo-α-1,5-L-arabinanase from *C. japonicus* Ueda107.

Purification of the Recombinant Endo-α-1,5-L-arabinanase (RmArase). The recombinant endo-α-1,5-L-arabinanase (RmArase) expressed in *E. coli* was a soluble, intracellular histidine-tagged protein. The enzyme activity of RmArase was 2.1 units/mL in crude lysate, which is higher than that of *Bacillus licheniformis* (0.25 unit/mL)[31] and *Phanerochaete chrysosporium* (1.66 units/L).[33] The purification summary of RmArase is presented in Table 1. RmArase was purified to homogeneity with an overall yield of 56.7% using affinity chromatography and ion-exchange chromatography. The specific activity of the endo-α-1,5-L-arabinanase increased from 11.3 to 109 units/mg.

It is noted that the purified RmArase exhibited high specific activity against debranched arabinan of 109 units/mg. The high specific activity of RmArase may enhance the degrading ability toward arabinans. The purified enzyme showed a single, homogeneous protein band on SDS–PAGE corresponding to 40.6 kDa (Figure 2), which matches with its native molecular

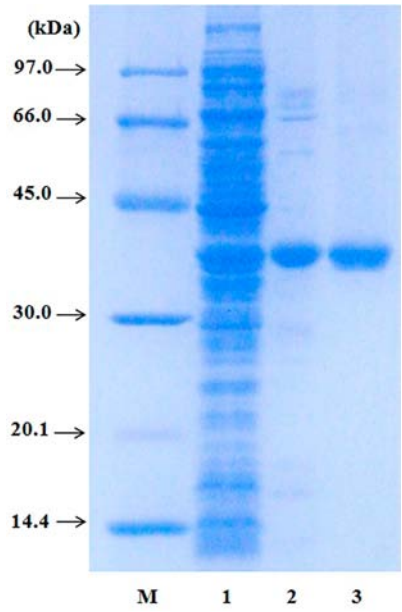

Figure 2. SDS–PAGE analysis of purified RmArase: lane M, low-molecular-weight standard protein markers; lane 1, crude lysate; lane 2, after Ni–IDA; and lane 3, after Q-Sepharose.

mass of RmArase of 38.2 kDa as determined by gel filtration, indicating that the enzyme is a monomer. The molecular mass of RmArase is similar to those of most endo-α-1,5-L-arabinanases from GH family 43. All fungal endo-α-1,5-L-arabinanases are monomeric enzymes with molecular masses in the range of 30–40 kDa.[8,10,16,17,31]

Biochemical Characterization of RmArase. The biochemical properties of the purified RmArase were further determined. RmArase exhibited a maximal activity at pH 5.5 (Figure 3a). The enzyme was stable within pH 5.0–8.5 because it retained more than 90% of its initial activity (Figure 3b). The enzyme showed an optimum temperature at 55 °C (Figure 3c). It was stable up to 45 °C (Figure 3d).

Generally, endo-α-1,5-L-arabinanases from fungi are characterized by their acidic pH optima (pH 5.0–7.0),[5,11,12,19,29] which makes them valuable in application in fruit juice clarification at acidic pH.[12] The optimal pH 5.5 of RmArase

DOI: 10.1021/jf5058167
J. Agric. Food Chem. 2015, 63, 1226–1233

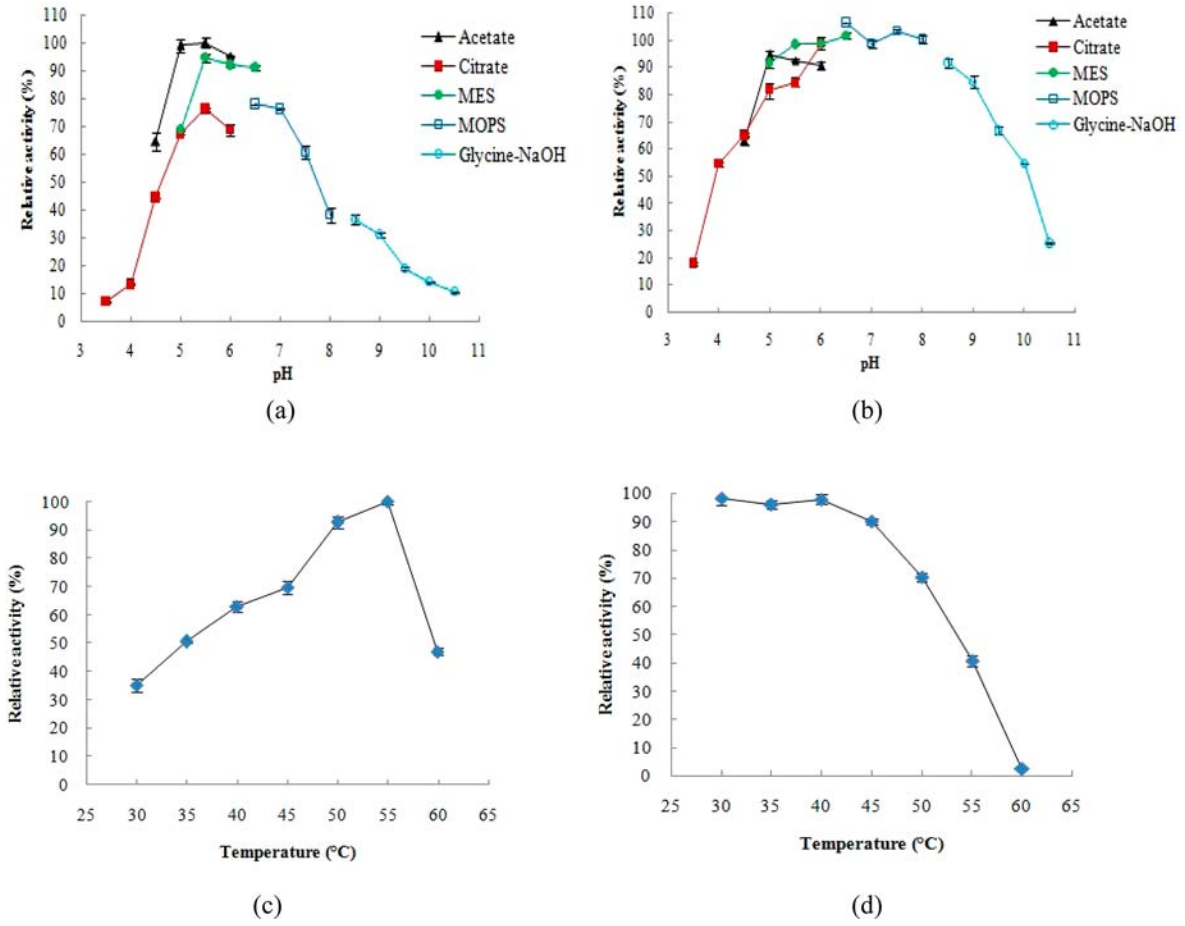

Figure 3. pH and temperature profiles of the purified recombinant endo-α-1,5-L-arabinanase (RmArase). Effect of pH on the (a) activity and (b) stability was performed at 45 °C in 50 mM different buffers. The residual activities were measured after incubation at 45 °C for 30 min over various pH ranges. Effect of the temperature on the (c) activity and (d) thermostability of RmArase were determined at temperatures ranging from 30 to 60 °C in 50 mM sodium acetate buffer (pH 5.5).

is lower than that of two other fungal endo-α-1,5-L-arabinanases from *P. chrysogenum* (pH 6−7).[5,12] Despite its acid pH optimum, RmArase showed good pH stability. RmArase is stable within pH 5.0−9.0, where it retained more than 80% of its activity. In general, fungal endo-α-1,5-L-arabinanases are stable in the acidic to neutral pH range. Thus far, only the endo-α-1,5-L-arabinanase from *P. chrysogenum* is stable up to pH 9.0.[12] The optimal temperature and thermostability of RmArase are comparable to that of the reported recombinant endo-α-1,5-L-arabinanases. RmArase display an optimal temperature of 55 °C, which is higher than that reported from the fungi, such as *A. aculeatus*,[19] and bacteria, such as *B. subtilis*[30] and *B. licheniformis*.[18] RmArase retained about 70% of its activity at 50 °C for 30 min, which is higher than the recombinant endo-α-1,5-L-arabinanase from *B. licheniformis*.[18]

The effects of various metal ions and other reagents on enzyme activity were studied. Among the metal ions tested, Na^+ (113 ± 4.7%), Co^{2+} (108 ± 3.4%), Mg^{2+} (105 ± 2.9%), and K^+ (104 ± 2.0%) slightly activated the enzyme. The activity of RmArase was strongly inhibited by Hg^{2+} (9 ± 2.0%), Cr^{2+} (12 ± 1.0%), Fe^{3+} (18 ± 0.3%), Sn^{2+} (30 ± 2.0%), Ag^+ (34 ± 0.4%), and Zn^{2+} (34 ± 1.3%) and moderately inhibited by Cu^{2+} (65 ± 1.0%), Mn^{2+} (49 ± 1.8%), and Fe^{2+} (46 ± 0.9%). It was slightly affected by DTT (102.5 ± 1.9%), Ca^{2+} (99 ± 1.2%), Ni^{2+} (94 ± 1.6%), and Ba^{2+} (94 ± 4.4%). Additionally, SDS and β-mercaptoethanol enhanced the enzyme activity to 112 and 110%, but the activity was significantly inhibited by EDTA (61.7 ± 3.8%).

The enzyme activity was stimulated by Co^{2+} and Mg^{2+} and inactivated by Fe^{3+}, Sn^{2+}, Zn^{2+}, and Fe^{2+}, similar to endo-α-1,5-L-arabinanases from *Caldicellulorsiruptor saccharolyticus*[15] and *B. licheniformis*.[18] Like most other endo-α-1,5-L-arabinanases, RmArase was inhibited by Hg^{2+} (9%), indicating the presence of free cysteines in the active site.[9,12] Mn^{2+} inhibited the enzyme by 50%, enhanced the enzyme from *C. saccharolyticus*,[15] and slightly affected the enzyme from *P. chrysogenum* 31B.[12] EDTA inhibited the activity of RmArase (60%), suggesting that the recombinant endo-α-1,5-L-arabinanase was a metal-dependent enzyme.

Substrate Specificity and Kinetic Parameters. The substrate specificity of RmArase was determined using various substrates. The enzyme showed highest specific activity toward debranched arabinan (100%), followed by sugar beet arabinan (48.4%). The enzyme, however, did not show any detectable activity toward birchwood xylan, *p*NP-α-L-arabinofuranoside, *p*NP-α-L-arabinopyranoside, and *p*NP-β-D-xylopyranoside.

Most of the GH family 43 endo-α-1,5-L-arabinanases show high activity toward the arabinans, no activity toward arabinoxylan, and no activity toward *p*NP-α-L-arabinofuranoside.[9,11,12,15,18,30−32] In contrast to other endo-α-1,5-L-arabinanases, RmArase exhibits the highest relative specific activity

DOI: 10.1021/jf5058167
J. Agric. Food Chem. 2015, 63, 1226−1233

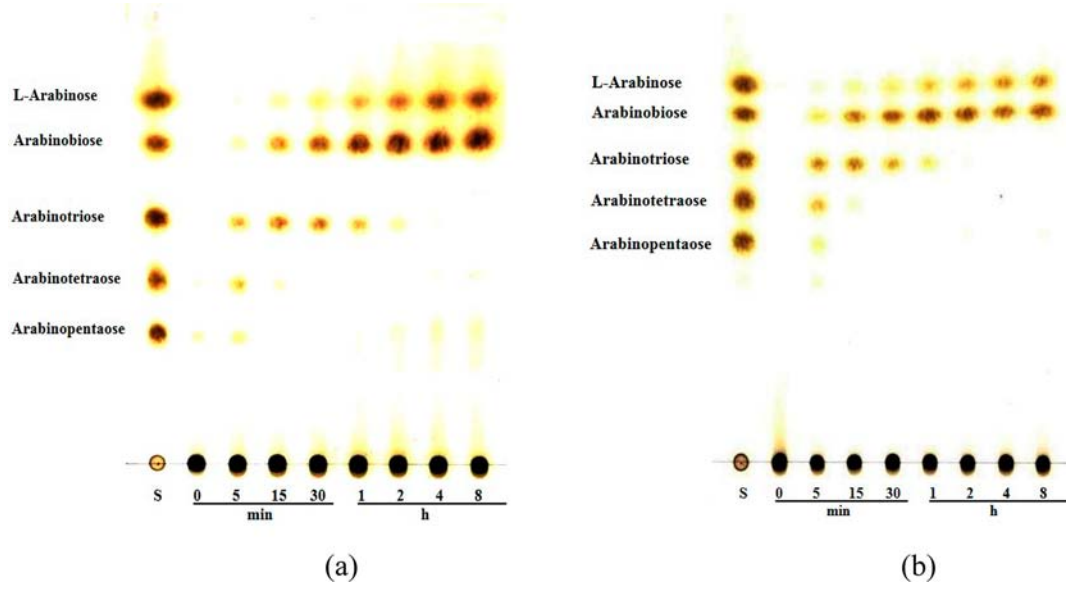

Figure 4. Hydrolysis of (a) debranched arabinan and (b) sugar beet arabinan by RmArase. The reaction mixture containing 10 mg/mL arabinans in 50 mM sodium acetate buffer (pH 5.5) and RmArase (1 unit/ml) was incubated at 45 °C for 8 h. Samples were subjected to TLC. Lane S, a mixture of L-arabinose, arabinobiose, arabinotriose, arabinotetraose, and arabinopentaose.

toward sugar beet arabinan (48.4%) when compared to debranched arabinan (100%).[9,17,31]

The Michaelis−Menten constants were determined for debranched arabinan and sugar beet arabinan (data not shown). The results revealed that RmArase had a higher affinity toward debranched arabinan (K_m = 5.8 mg/mL) than sugar beet arabinan (K_m = 27.5 mg/mL). RmArase shows higher binding affinity for debranched arabinan than that of most reported endo-α-1,5-L-arabinanases.[1,10,15,18,29] However, K_m values of endo-α-1,5-L-arabinanases from *P. chrysosporium* (K_m = 4.3 mg/mL),[33] *B. subtilis* (K_m = 2.0 mg/mL),[29] and *A. nidulans* (K_m = 4.9 mg/mL)[11] are a little lower than that of RmArase.

Hydrolysis of Arabinans and Arabino-oligosacchharides by RmArase. The hydrolysis of arabinans and various α-(1,5)-L-linked arabino-oligosaccharides by the purified RmArase was performed. The degradation of arabinans produced a mixture of arabiose-linked saccharides during the initial hydrolysis, with arabinobiose and arabinose as the end products (Figure 4). Further, degradation of various arabino-oligosaccharides was assessed by TLC (Figure 5). Arabinotetraose was slowly hydrolyzed to produce mainly arabinobiose in 1 h (Figure 5c), whereas arabinopentaose was completely hydrolyzed to yield mainly arabinobiose and arabinotriose in 5 min (Figure 5d). RmArase could slightly hydrolyze arabinotriose to produce arabinobiose and arabinose. However, the recombinant enzyme hardly hydrolyzed arabinobiose. The results revealed that RmArase displayed an endotype mode of action.

RmArase was active on sugar beet arabinan, which is composed of 50% 1,2-α- and 1,3-α-L-arabinofuranosyl side chains linked to a 1,5-α-L-arabinofuranosyl backbone, but the activity was much lower than on debranched arabinan, which is prepared by treatment of sugar beet arabinan with α-L-arabinofuranosidase to remove all 1,2- and 1,3-α-L-arabinofuranosyl branch units. It indicates that RmArase displays internal cleavage of α-1−5-linked L-arabinofuranose residues in the polysaccharide chain.[1] The hydrolysis time-course profiles of two arabinan hydrolysis were detected by TLC (Figure 4). At the beginning of the hydrolysis, RmArase mainly produced a series of arabino-oligosaccharides, a typic feature of endotype enzyme. As time progressed, arabino-oligosaccharides with higher units were hydrolyzed and converted into more arabinobiose and arabinose as the end products. In contrast, the end products produced by other endo-α-1,5-L-arabinanases were arabinobiose and arabinotriose[1,9,11,19] or only arabinotriose.[12,17] The monomeric arabinose was not produced from debranched arabinan by the action of fungal endoarabinanases.[9] RmArase degraded arabinans to produce more arabinose. The property should expand its ability to produce arabinose from arabinans, which is the second most abundant pentose in nature.[34] To understand the details of the hydrolysis mechanism, hydrolysis patterns of linear arabino-oligosaccharides were further investigated by TLC (Figure 5). The enzyme hardly hydrolyzed arabinobiose. However, it could hydrolyze arabinotriose, arabinotetraose, and arabinopentaose to mainly produce arabinotriose and arabinobiose. The hydrolytic properties of the RmArase are similar to the arabinanase from *Pseudomonas fluorescens* subspecies *cellulosa*.[17]

Degradation of Sugar Beet Pulp by RmArase and the Pectinase. The synergistic action of RmArase and pectinase on the degradation of sugar beet pulp was investigated (data not shown). RmArase alone hydrolyzed sugar beet pulp to produce 1.89 g of reducing sugar and 0.43 g of arabinose, respectively. The amounts of reducing sugar and arabinose produced by the pectinase alone were 7.92 and 0.76 g, respectively. Further, RmArase together with the pectinase enhanced the hydrolysis of sugar beet pulp, and the reducing sugar and arabinose were improved up to 9.52 and 1.38 g, respectively. In the previous studies, the sugar beet pulp could be degraded by an enzyme cocktail containing endo-1,5-α-L-arabinanase and α-L-arabinofuranosidase, but no report on the synergistic action of arabinanase and pectinase is available.[10] Sugar beet pulp is a byproduct of sucrose refining, which is mainly used as feed for ruminants, but its biotechnological conversion to value-added products, such as arabinose and arabino-oligosaccharides, is desirable.[5] The RmArase cooper-

DOI: 10.1021/jf5058167
J. Agric. Food Chem. 2015, 63, 1226−1233

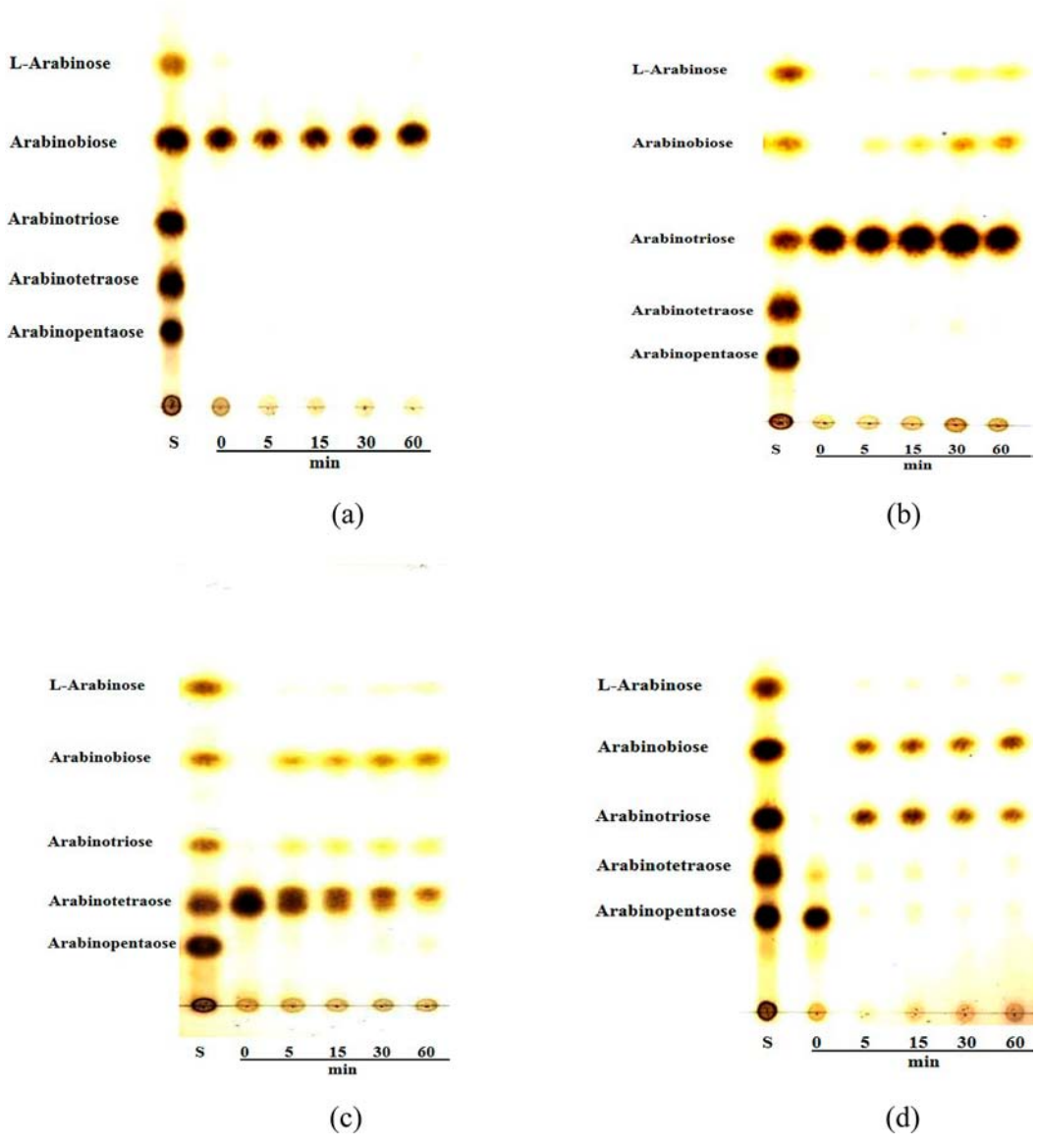

Figure 5. Hydrolysis of (a) arabinobiose, (b) arabinotriose, (c) arabinotetraose, and (d) arabinopentaose by RmArase. The reaction mixture containing 10 mg/mL arabino-oligosaccharides in 50 mM sodium acetate buffer (pH 5.5) and RmArase (1 unit/mL) was incubated at 45 °C for 1 h. Samples were subjected to TLC. Lane S, a mixture of L-arabinose, arabinobiose, arabinotriose, arabinotetraose, and arabinopentaose.

ated with the pectinase can significantly improve the use of sugar beet pulp.

In conclusion, this study reported that the first endo-α-1,5-L-arabinanase gene (*RmArase*) from the thermophilic fungus, *R. miehei*, was expressed in *E. coli*. The recombinant endo-α-1,5-L-arabinanase (RmArase) belonging to GH family 43 was further purified and characterized. RmArase exhibited high specific activity and good pH and thermal stabilities. It exhibited high specificity toward debranched arabinan followed by sugar beet arabinan and hydrolyzed arabinans to mainly produce arabinobiose and arabinose. These results suggest that RmArase has great potential in several industries. Especially, RmArase cooperated with the commercial pectinase may be suitable for arabinose production from sugar beet pulp.

AUTHOR INFORMATION

Corresponding Authors

*Telephone: +86-10-62737689. Fax: +86-10-82388508. E-mail: yanqj@cau.edu.cn.

*Telephone: +86-10-62737689. Fax: +86-10-82388508. E-mail: zhqjiang@cau.edu.cn.

Funding

This work was supported by the Program for Changjiang Scholars and Innovative Research Team in University (IRT1293), the National Science Fund for Distinguished Young Scholars (31325021), and the Program for Changjiang Scholars and the Chinese Universities Scientific Fund (2013YJ007).

Notes

The authors declare no competing financial interest.

DOI: 10.1021/jf5058167
J. Agric. Food Chem. 2015, 63, 1226−1233

ABBREVIATIONS USED

DNS, dinitrosalicylic acid; DTT, dithiothreitol; GH, glycoside hydrolase; IPTG, isopropyl-β-D-1-thiogalactopyranoside; LB, Luria−Bertani broth; MES, 2-(*N*-morpholino)ethanesulfonic acid; MOPS, 4-(*N*-morpholino)propanesulfonic acid; Ni−IDA, nickel−iminodiacetic acid; ORF, open reading frame; PCR, polymerase chain reaction; *p*NP, *p*-nitrophenol; RmArase, GH family 43 endo-1,5-α-L-arabinanase from *Rhizomucor miehei*; SDS−PAGE, sodium dodecyl sulfate−polyacrylamide gel electrophoresis; TLC, thin-layer chromatography

REFERENCES

(1) Squina, F. M.; Santos, C. R.; Ribeiro, D. A.; Cota, J.; de Oliveira, R. R.; Ruller, R.; Mort, A.; Murakami, M. T.; Prade, R. A. Substrate cleavage pattern, biophysical characterization and low-resolution structure of a novel hyperthermostable arabinanase from *Thermotoga petrophila*. *Biochem. Biophys. Res. Commun.* **2010**, *399*, 505−511.

(2) Kim, Y. S.; Lim, Y. R.; Oh, D. K. L-Arabinose production from sugar beet arabinan by immobilized endo- and exo-arabinanases from *Caldicellulosiruptor saccharolyticus* in a packed-bed reactor. *J. Biosci. Bioeng.* **2012**, *113*, 239−241.

(3) Seri, K.; Sanai, K.; Matsuo, N.; Kawakubo, K.; Xue, C. Y.; Inoue, S. L-Arabinose selectively inhibits intestinal sucrase in an uncompetitive manner and suppresses glycemic response after sucrose ingestion in animals. *Metabolism* **1996**, *45*, 1368−1374.

(4) Grootaert, C.; Delcour, J. A.; Courtin, C. M.; Broekaert, W. F.; Verstraete, W.; de Wiele, T. V. Microbial metabolism and prebiotic potency of arabinoxylan oligosaccharides in the human intestine. *Trends Food. Sci. Technol.* **2007**, *18*, 64−71.

(5) Sakamoto, T.; Inui, M.; Yasui, K.; Tokuda, S.; Akiyoshi, M.; Kobori, Y.; Nakaniwaa, T.; Tada, T. Biochemical characterization and gene expression of two endo-arabinanases from *Penicillium chrysogenum* 31B. *Appl. Microbiol. Biotechnol.* **2012**, *93*, 1087−1096.

(6) Coughlan, M. P.; Hazlewood, G. P. β-1,4-D-Xylan-degrading enzyme systems: Biochemistry, molecular biology and applications. *Biotechnol. Appl. Biochem.* **1993**, *17*, 259−289.

(7) Santos, C. R.; Polo, C. C.; Costa, M. C.; Nascimento, A. F.; Meza, A. N.; Cota, J.; Hoffman, Z. B.; Honorato, R. V.; Oliveira, P. S.; Goldman, G. H.; Gilbert, H. J.; Prade, R. A.; Ruller, R.; Squina, F. M.; Wong, D. W.; Murakami, M. T. Mechanistic strategies for catalysis adopted by evolutionary distinct family 43 arabinanase. *J. Biol. Chem.* **2014**, *11*, 7362−7373.

(8) Sakamoto, T.; Yamada, M.; Kawasaki, H.; Sakai, T. Molecular cloning and nucleotide sequence of an endo-1,5-α-arabinase gene from *Bacillus subtilis*. *Eur. J. Biochem.* **1997**, *245*, 708−714.

(9) Fukada, Y.; Koide, O.; Miura, T.; Kobayashi, T.; Inoue, A.; Horikoshi, K. Endo-1,5-α-L-arabinanase from a subseafloor *Bacillus subtilis*: Purification, characterization and nucleotide sequence of its gene. *Jpn. Soc. Appl. Glycosci.* **2011**, *58*, 61−66.

(10) Takao, M.; Akiyama, K.; Sakai, T. Purification and characterization of thermostable endo-1,5-α-L-arabinase from a strain of *Bacillus thermodenitrificans*. *Appl. Environ. Microbiol.* **2002**, *68*, 1639−1646.

(11) de Lima Damásio, A. R.; Pessela, B. C.; Mateo, C.; Segato, F.; Prade, R. A.; Guisan, J. M.; Polizeli, M. L. T. M. Immobilization of a recombinant endo-1,5-arabinanase secreted by *Aspergillus nidulans* strain A773. *J. Mol. Catal. B: Enzym.* **2012**, *77*, 39−45.

(12) Sakamoto, T.; Ihara, H.; Kozaki, S.; Kawasaki, H. A cold-adapted endo-arabinanase from *Penicillium chrysogenum*. *Biochim. Biophys. Acta, Gen. Subj.* **2003**, *1624*, 70−75.

(13) Pitson, S. M.; Voragen, A. G. J.; Gerrit, J. P. V. Action patterns and mapping of the substrate-binding regions of endo-(1→5)-α-L-arabinanases from *Aspergillus niger* and *Aspergillus aculeatus*. *Carbohydr. Res.* **1997**, *303*, 207−218.

(14) Flipphi, M. J. A.; Panneman, H.; van der Veen, P.; Visser, J.; de Graaff, L. H. Molecular cloning, expression and structure of the endo-l,5-α-L-arabinase gene of *Aspergillus niger*. *Appl. Microbiol. Biotechnol.* **1993**, *40*, 318−326.

(15) Hong, M. R.; Park, C. S.; Oh, D. K. Characterization of a thermostable endo-1,5-α-L-arabinanase from *Caldicellulorsiruptor saccharolyticus*. *Biotechnol. Lett.* **2009**, *31*, 1439−1443.

(16) Leal, T. F.; de Sá-Nogueira, I. Purification, characterization and functional analysis of an endo-arabinanase (AbnA) from *Bacillus subtilis*. *FEMS Microbiol. Lett.* **2004**, *241*, 41−48.

(17) Mckie, V. A.; Black, G. W.; Millward-Sadler, S. J.; Hazlewood, G. P.; Laurie, J. I.; Gilbert, H. J. Arabinanase A from *Pseudomonas fluorescens* subsp. *cellulosa* exhibits both an endo- and an exo- mode of action. *Biochem. J.* **1997**, *323*, 547−555.

(18) Seo, E. S.; Lim, Y. R.; Kim, Y. S.; Park, C. S.; Oh, D. K. Characterization of a recombinant endo-1,5-α-L-arabinanase from the isolated bacterium *Bacillus licheniformis*. *Bioprocess Biosyst. Eng.* **2010**, *15*, 590−594.

(19) Skjøt, K.; Kauppinen, S.; Kofod, L. V.; Fuglsang, C.; Pauly, M.; Dalbøge, H.; Andersen, L. N. Functional cloning of an endo-arabinanase from *Aspergillus aculeatus* and its heterologous expression in *A. oryzae* and tobacco. *Mol. Genet. Genomics* **2001**, *265*, 913−921.

(20) Tang, Y. B.; Yang, S. Q.; Yan, Q. J.; Cui, J.; Jiang, Z. Q. Purification and characterization of a novel β-1,3−1,4-glucanase (lichenase) from the thermophilic *Rhizomucor miehei* with high specific activity and its gene sequence. *J. Agric. Food Chem.* **2012**, *60*, 2354−2361.

(21) Zhou, P.; Zhang, G. Q.; Chen, S. W.; Jiang, Z. Q.; Tang, Y. B.; Henrissat, B.; Yan, Q. J.; Yang, S. Q.; Chen, C. F.; Zhang, B.; Du, Z. L. Genome sequence and transcriptome analyses of the thermophilic zygomycete fungus *Rhizomucor miehei*. *BMC Genomics* **2014**, *15*, 294.

(22) Sambrook, J.; Russell, D. W. *Molecular Cloning: A Laboratory Manual*, 3rd ed.; Cold Spring Harbor Laboratory Press: Cold Spring Harbor, NY, 2001.

(23) Lodhi, M. A.; Ye, G. N.; Weeden, N. F.; Reisch, B. I. A simple and efficient method for DNA extractions from grape vine cultivars and *Vitis* species. *Plant Mol. Biol. Rep.* **1994**, *12*, 6−13.

(24) Robert, X.; Gouet, P. Deciphering key features in protein structure with the new ENDscript server. *Nucleic Acids Res.* **2014**, *42*, W320−W324.

(25) Miller, G. L. Use of dinitrosalicylic acid reagent for determination of reducing sugars. *Anal. Chem.* **1959**, *31*, 426−428.

(26) Lowry, O. H.; Rosebrough, N. J.; Farr, A. L.; Randall, R. J. Protein measurement with the folin phenol reagent. *J. Biol. Chem.* **1951**, *193*, 265−275.

(27) Laemmli, U. K. Cleavage of structural proteins during the assembly of the head of bacteriophage T4. *Nature* **1970**, *277*, 680−685.

(28) Nurizzo, D.; Turkenburg, J. P.; Charnock, S. J.; Roberts, S. M.; Dodson, E. J.; McKie, V. A.; Taylor, E. J.; Gilbert, H. J.; Davies, G. J. *Cellvibrio japonicas* α-L-arabinanase 43A has a novel five-blade β-propeller fold. *Nat. Struct. Biol.* **2002**, *9*, 665−668.

(29) Shi, H.; Ding, H.; Huang, Y.; Wang, L.; Zhang, Y.; Li, X.; Wang, F. Expression and characterization in biotechnology. *Biotechnol. Adv.* **2000**, *18*, 403−423.

(30) Inácio, J. M.; de Sá-Nogueira, I. Characterization of abn2 (yxiA), encoding a *Bacillus subtilis* GH43 arabinanase, Abn2 and its role in arabino-polysaccharide degradation. *J. Bacteriol.* **2008**, *190*, 4272−4280.

(31) Park, J. M.; Jang, M. U.; Kang, J. H.; Kim, M. J.; Lee, S. W.; Song, C. S.; Han, T. J. Detailed modes of action and biochemical characterization of endo-arabinanase from *Bacillus licheniformis* DSM13. *J. Microbiol.* **2012**, *50*, 1041−1046.

(32) Wong, D. W. S.; Chan, V. J.; McComack, A. A. Functional cloning and expression of a novel endo-α-1,5-L-arabinanase from a metagenomic library. *Protein Pept. Lett.* **2009**, *16*, 1435−1441.

(33) Huy, N. D.; Thiyagarajan, S.; Choi, Y. E.; Kim, D. H.; Park, S. M. Cloning and characterization of a thermostable endo-arabinanase from *Phanerochaete chrysosporium* and its synergistic action with endo-xylanase. *Bioprocess Biosyst. Eng.* **2013**, *6*, 677−685.

(34) Seiboth, B.; Metz, B. Fungal arabinan and L-arabinose metabolism. *Appl. Microbiol. Biotechnol.* **2011**, *89*, 1665−1673.

DOI: 10.1021/jf5058167
J. Agric. Food Chem. 2015, 63, 1226−1233

for various foods and condiments.[20] Wheat flour tortillas are also a relatively simple food matrix with a short processing time, which thus presents an ideal model for investigating potential impact of gluten-containing food matrix on PA−starch interactions.

In this work, we use a tannin sorghum bran to investigate how the presence of PA influences in vitro starch digestibility in a food matrix containing wheat proteins by using wheat flour tortillas as a model. Nontannin sorghum brans with different phenolic profiles and wheat bran were also used to control for effect of other phenolic components in the bran. Interaction of the polyphenols with proteins and the fate of the PA during processing were also investigated.

MATERIALS AND METHODS

Materials. Three different types of sorghum bran were chosen for their diversity in polyphenolic content and composition. White sorghum (ATxArg-1/*RT*x436, TAMU, College Station, TX, 2008) was decorticated in a PRL mini-dehuller (Nutama Machine Company, Saskatoon, Canada) and separated (Model 6DT4−1, KICE Industries Inc., Wichita, KS) to yield 12% bran. Brown (high tannin) and black sorghum brans were commercial samples (Nu Life Market, Scott City, KS); these two samples were from similar cultivars we previously used.[13] The white sorghum was chosen for its low flavonoid and extractable phenol content; the black sorghum is high in monomeric flavonoids, especially 3-deoxyanthocyanins, and the brown sorghum has PA as the dominant polyphenols. Wheat bran (ADM, Decatur, IL) was also used for comparison. The wheat and white sorghum brans were ground using a WonderMill (The WonderMill Company, Pocatello, ID) to reduce the particle size to closely match to the brown and black sorghum brans.

Catechin and procyanidin B1 were purchased from Sigma (St Louis, MO); procyanidin B1 and C1 were from Extrasynthese (Genay, France).

Tortilla Formulation and Processing. Base wheat flour was substituted with the brans at 10, 15, and 25% (Baker's, i.e., based on flour weight). The base tortilla flour was made from a 1:1 mixture of high gluten bread flour (C. H. Guenther and Son, Inc., San Antonio, TX) and pastry flour (Cargill Inc., Minneapolis, MN). Control tortillas were made with no bran added. Each batch of tortillas was prepared using 1000 g of flour−bran mixture. To compensate for diluting effect of brans on gluten, 12.0, 19.0, and 31.0 g of vital wheat gluten (Cargill Inc., Minneapolis, MN) were added to the 10, 15, and 25% bran substitution levels, respectively. These values were calculated based on the gluten content of the refined flour blend, which was determined by AACC International method 38−10.01.[21] The rest of the tortilla formulation was described previously.[22,23] Briefly, the tortilla formulation included 15.0 g of table salt, 5.0 g of sodium stearoyl lactylate, 4.0 g of potassium sorbate (Caravan Ingredients, Inc., Lenexa, KS), 6.0 g of sodium propionate (Niacet Corporation, Niagara Falls, NY), 6.0 g of baking soda (Church and Dwight Co., Inc., Ewing, NJ), 5.8 g of sodium aluminum sulfate (Budenheim USA, Columbus, OH), 3.3 g of encapsulated fumaric acid (Balchem Inc., New Hampton, NY), 60.0 g of all-purpose shortening (Cargill Inc., Minneapolis, MN), and distilled water.

Dough moisture content was adjusted to account for increased water absorption of the brans as previously described.[20] After mixing, the dough was allowed to rest for 5 min in a proofing chamber (National Manufacturing Co., Lincoln, NE) at 32 °C and 60−70% relative humidity. The dough was then divided and rounded (Duchess Divider and Rounder, Bakery Equipment and Service Co., San Antonio, TX) into 36 pieces, approximately 30 g each. The dough balls were allowed to rest for another 10 min in the proofing chamber under the conditions listed above. Dough balls were hot-pressed (204 °C, 1150 psi, 1.4 s) and baked in a three-tier gas oven (Lawrence Equipment, El Monte, CA) for approximately 40 s at 193−204 °C. Tortillas were cooled to room temperature and packaged in moisture-proof bags for storage.

Sampling. Samples were retained from four different processing stages: dough, hot-pressed but not baked, immediately after baking (day 0), and after 14 days storage at room temperature. Dough, pressed, and day 0 samples were flash frozen in liquid nitrogen and stored at −20 °C until use. Day 14 samples were frozen at −20 °C after 14 days of room temperature storage. Frozen samples (immediately out of the freezer) were ground in a coffee grinder to reduce the particle size, then dried for 2 h in a hot air oven at 45 °C and further ground with a UDY cyclone sample mill (UDY Corp., Fort Collins, CO) to pass through 0.1 mm screen. For phenolic composition analysis (described below), dried, ground samples were defatted by extracting in hexanes (3:1 hexanes:sample, v/w) for 2 h with shaking at room temperature. Samples were centrifuged, the supernatant was discarded, and the extraction repeated. Defatted samples were air-dried in a fume hood until all remaining hexanes had evaporated. The dried, ground, defatted samples were then stored at −20 °C until analysis. Residual moisture content of the dried samples was determined by a moisture analyzer (Model HB43-S, Mettler-Toledo, Columbus, OH).

Phenolic Composition. *Total Phenolic Content.* Total phenols were measured according to the Folin−Ciocalteu method.[24] Samples were extracted in 1% HCl in methanol with shaking for 2 h. Aliquots were diluted with distilled water and reacted with Folin−Ciocalteu reagent (0.4 mL) and ethanolamine (0.9 mL) for 20 min at room temperature. Absorbance at 600 nm was read on a UV−vis spectrophotometer (Shimadzu Scientific Instruments, Columbia, MD). Results were expressed as mg of gallic acid equivalents (GAE)/g based on a standard curve prepared with serial dilutions of gallic acid in methanol.

High-Performance Liquid Chromatography (HPLC) Analysis. Phenolics were profiled using an Agilent 1200 HPLC system (Agilent Technologies, Santa Clara, CA). Phenolic acids and 3-deoxyanthocyanins were analyzed following the method described by Awika et al.[5] at wavelengths of 280, 330, 360, and 480 nm using a diode array detector. A reverse-phase Luna 5u C18[2] column (150 mm × 4.6 mm, 5 μm, Phenomenex, Torrence, CA) was used. Samples were extracted in 1% HCl in methanol (0.5 g in 5 mL) for 2 h and filtered (0.45 μm, nylon) before injection (10 μL). The mobile phase was composed of 1% formic acid in water (A) and 1% formic acid in acetonitrile (B). The elution gradient (B) over the 40 min run time was: 0−3 min, 10% isocratic; 3−5 min, 10−18%; 5−10 min, 18−20%; 10−23 min, 20−26%; 23−25 min, 26−18%; 25−28 min, 28−40%; 28−30 min, 40−60%; 30−32 min, 60% isocratic; 32−34 min, 60−10%; 34−40 min, 10% isocratic. Flow rate was 1 mL/min.

PA were analyzed and separated based on degree of polymerization according to Langer et al.[25] A fluorescence detector with excitation and emission wavelengths of 230 and 321 nm, respectively, and a normal phase Develosil Diol column (250 mm × 4.6 mm, 5 μm particle size, Phenomenex, Torrence, CA) were used. Samples were extracted in 2% acetic acid in 70% aqueous acetone (1 g in 5 mL) for 2 h and filtered (0.45 μm, nylon) before injection (10 μL). The elution gradient (B) over the 83 min run time was: 0−3 min, 7% isocratic; 3−57 min, 7−37.6%; 57−60 min, 37.6−100%; 60−67 min, 100% isocratic; 67−73 min, 100−7%; 73−83 min, 7% isocratic. Flow rate was 0.6 mL/min. Authentic standards (catechin, procyanidins B1 and C1) were used to quantify PA with a degree of polymerization (DP) of 1−3. Quantitative data for PA with a DP greater than or equal to four were based on procyanidin C1 (DP 3) peak response. Results were corrected for molecular weight according to the DP.

Starch Analysis. In vitro starch digestibility was determined on fully baked tortilla samples. The dried, ground samples were removed from the freezer and allowed to equilibrate at room temperature for 1 h before starch analysis.

Total Starch (TS). The K-TSTA assay kit (determination of total starch content of samples containing resistant starch, but no D-glucose or maltodextrins) from Megazyme (Megazyme International, Wicklow, Ireland) was used to determine TS (AACC International method 76−13.01). The sample (~100 mg) and 80% (v/v) ethanol (0.2 mL) were added to a glass test tube and mixed on a vortex mixer. A magnetic stirring rod was added to each tube, and the tubes were

DOI: 10.1021/jf504112z
J. Agric. Food Chem. 2015, 63, 1234−1241

placed in an ice water bath before 2 M KOH (2 mL) was added to each tube with stirring. The tubes were removed after 20 min, and 1.2 M sodium acetate buffer (8 mL) was added to each tube with stirring. Thermostable α-amylase (0.1 mL; 3,000 U/mL) and amyloglucosidase (0.1 mL; 3,300 U/mL) (Megazyme) were added to each tube. The tubes were incubated in a 50 °C water bath for 30 min with intermittent stirring on a vortex mixer. Samples were diluted to 100 mL with distilled water, centrifuged, and the supernatant was retained for analysis. The K-GLUC (GOPOD format) assay kit from Megazyme was used for the determination of D-glucose using glucose oxidase based on absorbance at 510 nm as read on the UV−vis spectrophotometer.

Rapidly Digestible Starch (RDS), Slowly Digestible Starch (SDS), and Resistant Starch (RS). RDS and SDS were determined using the colorimetric version of the procedure described by Englyst et al.[26] as modified by Barros et al.[13] Dried, ground sample (0.20 g) was used for the analysis. The enzyme mixture was prepared from α-amylase (A3176, Sigma-Aldrich, St. Louis, MO) and purified amyloglucosidase (Cat. No. E-AMGDF, Megazyme International) at concentrations of ~300 U/mL and ~95 U/mL, respectively. The K-GLUC (GOPOD format) assay kit from Megazyme was used for the determination of D-glucose using glucose oxidase based on absorbance at 510 nm as read on a UV−vis spectrophotometer (Shimadzu Scientific Instruments). RDS was determined by stopping digestion after 20 min, whereas SDS was based on 120 min of digestion. The K-RSTAR assay kit from Megazyme was used to determine RS (AACC Int. Method 32−40.01,[21]). Results were expressed on a TS basis.

Protein Analysis. *Total Protein Determination.* Nitrogen content of dried samples was determined by combustion using a LECO instrument (LECO Corporation, St. Joseph, MI) and converted to total protein by a factor of 5.7.

Insoluble Protein (IP) Determination. The soluble protein fraction was extracted as described by Schober et al.[27] Samples (100 mg) were extracted three times in 1 mL of 50% 1-propanol for 5 min. This solvent systems was selected because it is known to preserve PA−protein complexes.[28,29] The samples were centrifuged after each extraction. The supernatant from each extraction was discarded. The sample remaining after extraction contained the IP fraction. The pellet was freeze-dried, and its protein content was determined by combustion as mentioned previously.

In Vitro Protein Digestibility. Protein digestibility was measured using the in vitro pepsin digestibility assay of Mertz et al.[30] except that protein was quantified using nitrogen combustion analysis as described above.

Statistical Analysis. All procedures were performed in duplicate. Means and standard deviations were determined using Microsoft Office Excel 2010 (Microsoft Corporation, Redmond, WA). Statistical Analysis Software (SAS) version 9.3 (SAS Institute, Cary, NC) was used for data analysis. Differences in treatments were determined at the 5% significance level (α = 0.05) using the general linear model (GLM) and least significant difference (LSD) for mean separation.

RESULTS AND DISCUSSION

Effect of Processing on Total (Folin) Phenolic Content. The content of phenols present in the dry ingredient mix (dry mix) was determined in a mixture of all dry ingredients without the shortening, and final values were calculated to account for the shortening used in the formulations. As expected, the samples with brown and black sorghum brans had much higher phenols in the dry mix than those made with wheat and white sorghum brans (Figure 1). In the treatments with wheat and white sorghum bran, extractable phenol content initially increased upon dough formation and then decreased with processing and storage ($p < 0.05$) (Figure 1). This may be attributed to increased extractability of phenols from the dough as compared to the bran and flour in the dry mix. Phenolic acids are the predominant phenolic compounds in wheat and white sorghum but are commonly bound to the cell wall.[31,32]

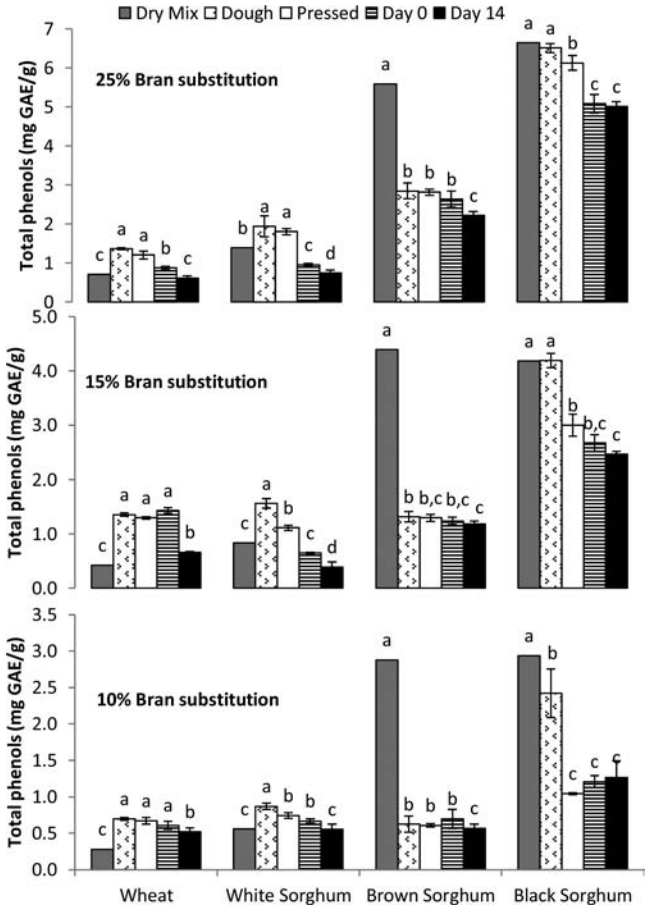

Figure 1. Effect of processing step and bran source on extractable phenols (mg GAE/g) in wheat flour tortillas processing and storage. Bars with the same letter within the same bran treatment category are not statistically different ($p < 0.05$, LSD).

Abdel-Aal and Rabalski[33] observed an increase in free phenolic acids in flat bread dough when prepared with whole grain einkorn wheat flour.

For black sorghum bran treatment, dough formation did not affect extractable phenol content except at 10% bran substitution, where the net change was modest (Figure 1). In general, it appears that the monomeric 3-deoxyanthocyanidins, which are the dominant extractable phenolics in the black sorghum bran, did not significantly interact with dough components. On the other hand, dough formation dramatically decreased the total phenol content in brown sorghum bran treatments (Figure 1). The brown sorghum bran treatments exhibited 58, 69, and 78% decrease in extractable phenols at 25, 15, and 10% substitutions, respectively, in the dough compared to the dry mix.

The large decrease in extractable phenols in dough prepared with brown sorghum bran compared to the other bran treatments suggests that the phenols present in the brown sorghum bran interacted with proteins or starch upon dough formation in a fundamentally different way than the phenols in the other bran treatments. As previously stated, the brown sorghum bran contained the polymeric PA as the dominant polyphenols, which likely accounts for its different behavior. The PA likely formed insoluble complexes with gluten during dough formation.

Interestingly, the changes in extractable phenols in the brown sorghum bran treatments were minimal in subsequent steps

DOI: 10.1021/jf504112z
J. Agric. Food Chem. 2015, 63, 1234−1241

after dough formation (Figure 1). This indicates that the most important chemical interactions that impact the phenolics in the brown sorghum largely occur in the dough. By contrast, significant decreases in extractable phenols were observed in the black sorghum bran treatments postdough formation stage.

Effect of Tortilla Processing on Bran Polyphenol Profile. In general, the phenolic profiles of the black and white sorghum brans were as previously reported,[34] with phenolic acid derivatives dominant in the white sorghum bran treatments and 3-deoxyanthocyanins dominant in the black sorghum bran treatments. The profiles generally did not change during processing, and individual phenolic contents were predictable based on the Folin phenol content trends. An example of 3-deoxyanthocyanin HPLC profile of black sorghum bran treatments is shown in Figure 2. The overall conclusion is

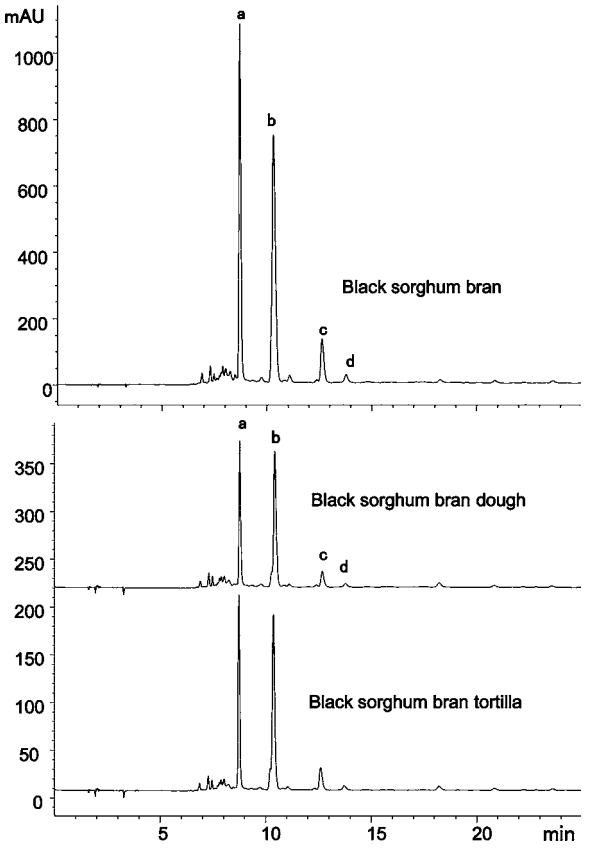

Figure 2. HPLC profile of 3-deoxyanthocyanins in black sorghum bran and dough and tortilla (day 0) made with 25% (baker's) black sorghum bran recorded at 480 nm. The dough and tortilla chromatograms are offset by 100%. Compounds: a = luteolinidin, b = 7-O-methyl luteolinidin, c = 7-O-methyl apigeninidin, d = 5,7-O-dimethyl luteolinidin.

that nonspecific changes in extractability of the monomeric sorghum phenolics are what is impacting the Folin phenols data for white and black sorghum bran treatments and not structural changes (e.g., via thermal degradation) or specific interactions of some of the phenolics in these brans with other ingredients.

The brown sorghum bran treatments, however, presented interesting observations during processing. The brown sorghum bran had a PA profile largely dominated by the high molecular weight polymers (Figure 3), which confirms previous reports.[13] The PA contents of the dry mixes were 0.76, 1.13, and 1.87 mg/g for the 10, 15, and 25% bran substitutions, respectively. In agreement with the Folin phenolic data (Figure 1), the PA, which are the dominant polyphenols in the brown sorghum bran, dramatically declined during dough mixing as determined by normal-phase HPLC (Table 1). The decline in extractable PA in the dough was in the range of 61−72% compared to dry mixes, for the various brown bran substitutions, with the highest decline observed at the lowest bran substitution level. This suggests that the PA in the brown sorghum bran interacted with gluten during dough mixing and thus became less extractable.

We were unable to find any literature reports on interactions of PA with gluten. However, Zhang et al.[35] recently reported that a tannic acid of unspecified source and structure reduced free amino groups in dough when added to flour at 10−30 μg/g. This suggests that the tannic acid participated in cross-linking of the gluten network. It is possible that the PA would participate in similar interactions. Interestingly, after dough mixing, further changes in extractable PA content were relatively small (Table 1), which suggests that most of the "available" or reactive PA constituents in the bran interacted with dough components during mixing. We had previously demonstrated that the PA are relatively stable to thermal processing conditions similar to those used in this study;[13,14] thus, changes during tortilla processing are largely attributable to chemical interactions with other components and not thermal degradation.

Analysis of the PA MW profile during tortilla processing also demonstrated that the most dramatic changes occurred at the dough mixing stage (Figure 3). The higher MW PA decreased the most during dough mixing, which significantly altered the extractable PA MW profile. This suggests specific PA−protein interactions during dough mixing; high MW PA are known to interact more readily with proteins to form insoluble complexes.[10,15] Furthermore, even though the PA can adhere to raw starch and become unextractable,[36] such interaction is limited, nonspecific, and does not affect the MW distribution of the PA.[13] The fact that extractable PA profile remained relatively similar after dough formation (Figure 3) suggests that the protein preferentially bound the high MW PA in the dough, which limited opportunities for PA to interact further during the baking process.

Because the brown sorghum bran itself contained significant amount of proteins, it was important to determine the potential contribution of inherent interactions of the bran PA with the sorghum bran proteins during the dough mixing step to the observed changes in PA profile. The sorghum bran was thoroughly mixed with water (1:0.6, bran:water) and allowed to rest for 2 h at room temperature. The mixture was dried in a convection oven at 45 °C and subjected to PA profiling as described in the Materials and Methods. The PA profile of the wet-mixed sorghum bran was virtually identical to the dry extracted bran (Figures 3 and 4). This suggests that the sorghum bran proteins were not responsible for the dramatic changes in MW profile of the brown sorghum bran dough (Figure 3). More importantly, this provides indirect evidence that the wheat proteins (specifically gluten) are the ones interacting with the PA in the dough. Impact of the above observations on starch and protein properties may provide additional insight.

In Vitro Starch Digestibility. Starch digestibility information is most relevant in final product, thus was only measured in tortillas. None of the bran treatments increased resistant starch content in tortillas relative to refined wheat flour control, and

DOI: 10.1021/jf504112z
J. Agric. Food Chem. 2015, 63, 1234−1241

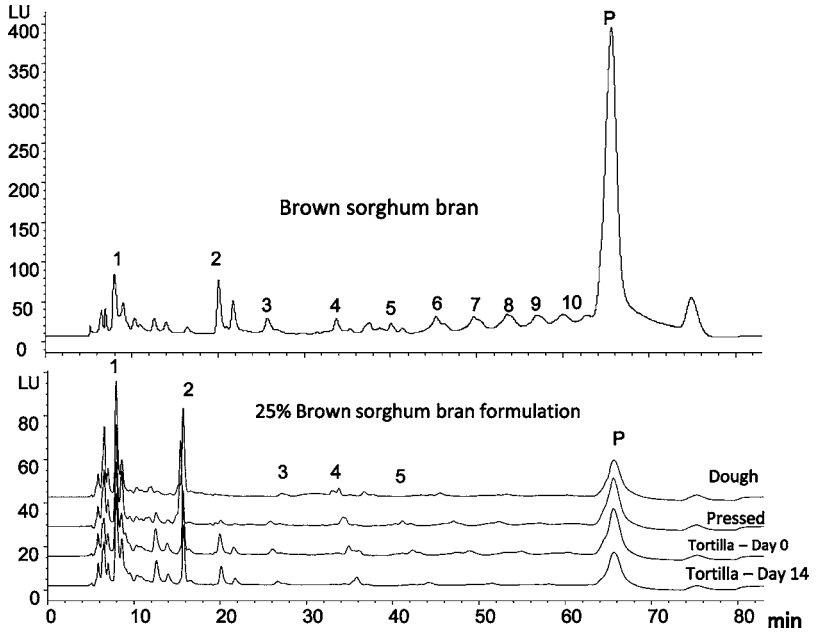

Figure 3. Effect of tortilla processing step on extractable sorghum PA profile. Profiles were obtained using normal-phase HPLC with fluorescence detection. Numbers denote degree of polymerization; *P* = polymers with DP > 10. Profiles of tortilla processing steps offset by 15%.

Table 1. Extractable PA in Brown Sorghum Bran Substituted Sample at Various Steps of Tortilla Processing and Storage Relative to Starting Material[a]

bran substitution (baker's %)	dry mix	dough	pressed	day 0 tortilla	day 14 tortilla
10%	757 ± 12 a	213 ± 13 b	207 ± 5.0 b	191 ± 15 b,c	165 ± 6.2 c
% change from preceding step		−71.9	−2.7	−7.8	−13.7
15%	1132 ± 18 a	336 ± 33 b	296 ± 12 b,c	304 ± 7.0 b	250 ± 2.3 c
% change from preceding step		−70.3	−11.8	2.6	−17.8
25%	1868 ± 30 a	721 ± 102 b	520 ± 25 c	553 ± 24 c	407 ± 10 c
% change from preceding step		−61.4	−27.9	6.2	−26.3

[a]Values are summation of various MW substituents (see Figure 3 for profile), expressed as mean ± standard deviation, μg/g (db), as determined by normal-phase HPLC. Same letter within row not statistically different ($p < 0.05$, LSD).

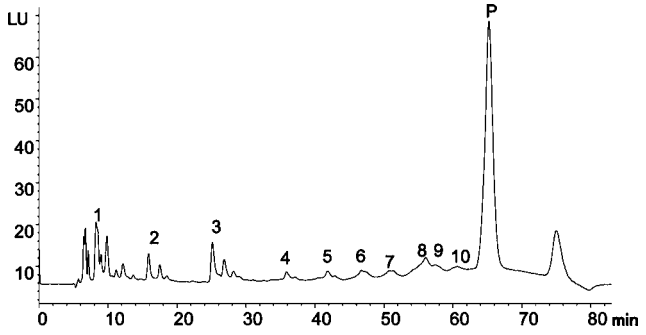

Figure 4. PA profile of brown sorghum bran after mixing with water to imitate dough mixing. Bran was blended with water (0.6 g H_2O/g) and allowed to rest for 2 h before drying in the oven at 45 °C; this was to determine if the PA interaction with the sorghum proteins in the bran contributed to the altered profile observed in the dough (Figure 3). Extraction and analysis followed as described in the Materials and Methods.

all values were below 1% (data not shown). This was contrary to our previous observations using PA and starch in pure systems, where, depending on thermal treatment and starch composition, RS was increased by up to 50% due to interactions with sorghum PA.[14] Thus, the extensive interaction or "binding" of PA observed in the dough (Table 1; Figure 3) likely precluded starch−PA interactions during baking. This further supports the idea that the gluten proteins are the likely components interacting with the PA in the dough.

Contrary to the resistant starch data, significant differences were observed for RDS and the SDS in the tortillas with different bran treatments at 25% substitution level (Table 2). The brown sorghum bran treatment had (as percentage of total starch) the lowest RDS (81.2%) and highest SDS (20.9%) ($p < 0.05$) among all treatments. The rest of the bran treatments were not significantly different from each other or control for RDS (86.1−89.0%) and SDS content (12.2−15.5%) (Table 2). This observation is interesting and somewhat unexpected. We can only hypothesize that the PA likely formed cross-linked networks with gluten during mixing in a way that interferes with amylase enzyme access to starch, likely by physically shielding and slowing, but not blocking, enzyme degradation of starch. Even though the PA can also interfere with starch digestion via enzyme inhibition, the levels used in this study were too low to produce such effect.[17]

The rate and extent of digestion of starch in the small intestine has important implications on glycemic response and calorie impact of starch. RDS causes a rapid peak in blood glucose level as compared to SDS, which takes longer to digest and releases glucose over a prolonged amount of time.[37] Foods that create a moderate glucose response have been shown to

DOI: 10.1021/jf504112z
J. Agric. Food Chem. 2015, 63, 1234−1241

Table 2. In Vitro Starch and Protein Digestibility of Fresh Tortillas Made with 25% (Baker's) Substitutions of Wheat and Sorghum Brans[a]

treatment	rapidly digestible starch (%)	slowly digestible starch (%)	protein content (%)	in vitro protein digestibility (%)
control	87.9 ± 1.23 a	12.1 ± 1.64 b	12.4 ± 0.01 c	93.3 ± 0.37 a
wheat bran	87.3 ± 1.39 a	14.1 ± 2.39 b	14.8 ± 0.23 a	85.3 ± 0.29 b
white sorghum bran	86.1 ± 0.01 a	15.5 ± 1.60 b	13.1 ± 0.35 b	86.8 ± 0.43 b
brown sorghum bran	81.2 ± 1.29 b	20.9 ± 2.25 a	13.3 ± 0.21 b	82.8 ± 0.24 c
black sorghum bran	89.0 ± 3.44 a	12.3 ± 0.68 b	13.5 ± 0.04 b	83.5 ± 0.34 c

[a]Data reported for day 0 tortillas, all values reported on db. RDS and SDS reported on TS basis. TS and RS were determined independently of RDS and SDS; thus, values may not add up to 100%. All RS values were less than 1% and thus are not reported. Same letter within column not statistically different ($p < 0.05$, LSD).

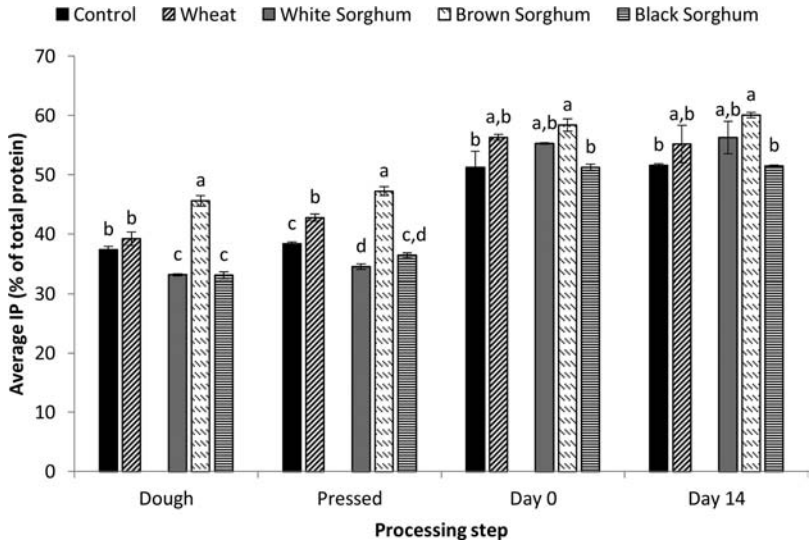

Figure 5. Effect of bran source on IP (% of total protein) content of dough, pressed, day 0, and day 14 tortillas substituted at 25%. Bars with the same letter within the processing step are not statistically different ($p < 0.05$, LSD).

help manage blood glucose levels[38] and may contribute to satiety.[39,40] Thus, the data suggest that sorghum PA may provide a mechanism to modify enzyme degradation kinetics of starch in wheat-based products. However, the PA content of the brown sorghum bran used in this study was relatively low (8.5 mg/g); this may have partly accounted for the less than "dramatic" effect of sorghum PA on starch digestibility in the tortilla matrix. The tannin content is known to affect the feed efficiency of sorghum in vivo, with a minimum tannin threshold needed to produce an effect.[41] In fact, we did not observe any significant difference in starch digestibility among bran substitutions at 15% and 10% levels (data not shown). Thus, it is likely that with a higher level of available PA in the dough formulation, the effect of sorghum PA on starch digestibility would be more significant. Additional work will use purified PA fractions to uncover specific types of interactions of the PA with wheat proteins and how starch digestibility is impacted.

Protein Extractability and in Vitro Digestibility. On the basis of observations for starch digestibility, for protein extractability (in 50% 1-propanol) and digestibility (based on in vitro pepsin assay[30]), only the 25% bran treatments were compared. Protein content of all sorghum bran treatments were similar (Table 2). IP content (as a percent of total proteins) of wheat bran dough was similar to the control but different ($p < 0.05$) from all the sorghum bran treatments (Figure 5).[42] The IP contents of black and white sorghum bran doughs were significantly lower (average 330 mg/g protein) than the wheat bran treatment and control (average 390 mg/g protein) (Figure 5). This may have been due to inherent differences in IP composition of sorghum and wheat brans. Interestingly, the brown sorghum bran dough had significantly higher IP content (456 mg/g protein) than all other treatments. This further suggests that the PA in brown sorghum bran bound to the wheat proteins during dough mixing and formed insoluble complexes, which thus agrees with our hypothesis that the drop in higher MW PA extractability was due to PA–protein complexation.

The fact that the brown sorghum bran dough had proportionately almost 40% higher IP than the other sorghum bran doughs is particularly revealing given that only 1.87 mg extractable PA/g was present in the brown sorghum bran dry formulation at 25% substitution (Table 1). This suggests a rather significant binding capacity of the sorghum PA with the wheat proteins. On the basis of the fact that approximately 1.15 mg PA/g became unextractable at the dough mixing stage (Table 1), we assume this is the amount of PA that complexed with the proteins. If we further assume that the brown sorghum bran dough had similar protein composition as the other sorghum bran treatments, we can estimate that 1.15 mg of PA resulted in the formation of 126 mg of insoluble protein complexes. Furthermore, it is safe to assume that a portion of the PA complexed with native wheat IP; thus, the amount of PA that produced the 126 mg of "new" IP is likely less than 1.15 mg. This suggests a relatively high binding ratio of sorghum PA with the wheat proteins compared to those reported for other protein sources.[3,28]

DOI: 10.1021/jf504112z
J. Agric. Food Chem. 2015, 63, 1234–1241

The large differences in IP between the brown sorghum bran treatment and the other sorghum bran treatments indicate that the PA in the brown sorghum bran were involved in cross-linking with the gluten proteins to form insoluble complexes quantified as IP at the dough mixing stage. This is consistent with the dramatic decline in PA in the brown bran dough previously discussed (Table 1). The fact that the black bran treatment, which had higher Folin phenol content than all other brans and did not differ from white sorghum bran treatment, indicates that the monomeric polyphenols are not involved in protein cross-linking in the dough. Thus, it is apparent that the proline-rich gluten proteins have high affinity for, and readily interact with, the sorghum PA to form insoluble complexes.

For all treatments, IP increased with thermal processing (pressing and baking), with the largest increase observed after baking (Figure 5). The changes in IP during 14 day storage was minimal. Increase in IP after baking was expected; heat is known to reduce solubility of wheat gluten proteins, especially glutenins.[43] Tortillas prepared with brown sorghum bran also had the highest amount of IP after baking (58.4%) and storage for 14 days (60.1%), but were statistically similar to wheat and white sorghum bran treatments ($p < 0.05$) (Figure 5). The day 0 and 14 tortilla samples prepared with white and black sorghum bran were statistically similar to the wheat bran and control ($p < 0.05$). Sorghum proteins, specifically kafirins, have been shown to cross-link upon heat treatment and become insoluble.[44,45] This may have contributed to the larger increase in IP of white and black sorghum bran treatments (23 and 19%, respectively) after baking as compared to the control and wheat bran treatment (14 and 16%, respectively). The increase in IP of brown sorghum bran after baking (14%) was not as large as for the other sorghum bran treatments. Some of the proteins that would contribute to this effect due to cross-linking upon heat treatment were likely already interacted with the PA and became insoluble in the dough formation step.

In vitro protein digestibility of tortillas was lowest for the brown sorghum bran treatment but not significantly different from the black sorghum treatment (Table 2). The control proteins had the highest ($p < 0.05$) digestibility, followed by wheat and white sorghum bran treatments. The evidence points to a potential impact of the PA on protein digestibility in the tortillas, but this is not conclusive based on the data. In general, sorghum tannins are known to reduce protein digestibility, but as previously stated, evidence indicates that a minimum amount of the tannins in a matrix is required to produce this effect.[12,41,46] In this study, only 2.1 mg/g PA was present in the 25% brown sorghum bran dry formulation; this may have been too low to produce a practically significant effect.

The overall data suggest that the interaction of sorghum PA with wheat dough proteins is significant and results in the formation of insoluble complexes. The monomeric polyphenols present in the black and white sorghums do not appear to interact much with gluten. Even more important was the fact that SDS was significantly increased, and RDS decreased, in tortillas made with the sorghum bran with the PA. This suggests that the sorghum PA have a potential as ingredients that can be used to beneficially modify starch digestibility in wheat-based baked foods for populations where excess calorie intake is a problem. We suspect that higher levels or more pure PA inclusion in dough formulation will have a more dramatic effect on starch digestibility profile.

AUTHOR INFORMATION

Corresponding Author

*E-mail: jawika@ag.tamu.edu. Phone: 979-845-2985. Fax: +1 979-845-0456.

Present Address

⊥K.L.D., Pecan Deluxe, 2570 Lone Star Drive, Dallas, Texas 75212, United States. L.Y., Kellogg Company, 2 Hamblin Avenue, Battle Creek, Michigan 49017, United States.

Notes

Names are necessary to report factually on available data; however, the U.S. Department of Agriculture neither guarantees nor warrants the standard of the product, and use of the name by the U.S. Department of Agriculture implies no approval of the product to the exclusion of others that may also be suitable. The authors declare no competing financial interest.

REFERENCES

(1) USDA-ERS.. *United States Department of Agriculture: Economic Research Services Food Consumption Database*. http://www.ers.usda.gov/data/foodconsumption/ (accessed July 20, 2014)..

(2) Hagerman, A. E. Tannin−protein interactions. *Phenolic Compounds in Food and Their Effects on Health I*; American Chemical Society: Washington, DC, 1992; Vol. *506*, pp 236−247.

(3) Riedl, K. M.; Hagerman, A. E. Tannin−protein complexes as radical scavengers and radical sinks. *J. Agric. Food Chem.* **2001**, *49*, 4917−4923.

(4) Tian, Y.; Zou, B.; Li, C. M.; Yang, J.; Xu, S. F.; Hagerman, A. E. High molecular weight persimmon tannin is a potent antioxidant both ex vivo and in vivo. *Food Res. Int.* **2012**, *45*, 26−30.

(5) Awika, J. M.; Yang, L.; Browning, J. D.; Faraj, A. Comparative antioxidant, antiproliferative, and phase II enzyme inducing potential of sorghum (*Sorghum bicolor*) varieties. *LWT—Food Sci. Technol.* **2009**, *42*, 1041−1046.

(6) Jambunathan, R.; Mertz, E. T. Relation between tannin levels, rat growth, and distribution of proteins in sorghum. *J. Agric. Food Chem.* **1973**, *21*, 692−696.

(7) Featherston, W.; Rogler, J. Influence of tannins on the utilization of sorghum grain by rats and chicks. *Nutr. Rep. Int.* **1975**, *11*, 491−497.

(8) Al-Mamary, M.; Molham, A. H.; Abdulwali, A. A.; Al-Obeidi, A. In vivo effects of dietary sorghum tannins on rabbit digestive enzymes and mineral absorption. *Nutr. Res. (N.Y.)* **2001**, *21*, 1393−1401.

(9) Muriu, J.; Njoka-Njiru, E.; Tuitoek, J.; Nanua, J. Evaluation of sorghum (*Sorghum bicolor*) as replacent for maize in the diet of growing rabbits (*Oryctolagus cuniculus*). *Asian-Australas. J. Anim. Sci.* **2002**, *15*, 565−569.

(10) Hagerman, A. E.; Butler, L. G. The specificity of proanthocyanidin−protein interactions. *J. Biol. Chem.* **1981**, *256*, 4494−4497.

(11) Haslam, E. Polyphenol−protein interactions (short communication). *Biochem. J.* **1974**, *139*, 285.

(12) Awika, J. M.; Rooney, L. W. Sorghum phytochemicals and their potential impact on human health. *Phytochemistry* **2004**, *65*, 1199−221.

(13) Barros, F.; Awika, J. M.; Rooney, L. W. Interaction of tannins and other sorghum phenolic compounds with starch and effects on in vitro starch digestibility. *J. Agric. Food Chem.* **2012**, 11609−11617.

(14) Barros, F.; Awika, J.; Rooney, L. W. Effect of molecular weight profile of sorghum proanthocyanidins on resistant starch formation. *J. Sci. Food Agric.* **2014**, *94*, 1212−1217.

(15) Butler, L. G.; Riedl, D. J.; Lebryk, D.; Blytt, H. Interaction of proteins with sorghum tannin: Mechanism, specificity, and significance. *J. Am. Oil Chem. Soc.* **1984**, *61*, 916−920.

(16) Lemlioglu-Austin, D.; Turner, N. D.; McDonough, C. M.; Rooney, L. W. Effects of sorghum [*Sorghum bicolor* (L.) Moench] crude extracts on starch digestibility, estimated glycemic index (EGI), and resistant starch (RS) contents of porridges. *Molecules* **2012**, *17*, 11124−11138.

DOI: 10.1021/jf504112z
J. Agric. Food Chem. 2015, 63, 1234−1241

(17) Mkandawire, N. L.; Kaufman, R. C.; Bean, S. R.; Weller, C. L.; Jackson, D. S.; Rose, D. J. Effects of sorghum (*Sorghum bicolor* (L.) Moench) tannins on α-amylase activity and in vitro digestibility of starch in raw and processed flours. *J. Agric. Food Chem.* **2013**, *61*, 4448−4454.
(18) Austin, D. L.; Turner, N. D.; McDonough, C. M.; Rooney, L. W. Effects of brans from specialty sorghum varieties on in vitro starch digestibility of soft and hard sorghum endosperm porridges. *Cereal Chem.* **2012**, *89*, 190−197.
(19) Woychik, J.; Boundy, J. A.; Dimler, R. Wheat gluten proteins, amino acid composition of proteins in wheat gluten. *J. Agric. Food Chem.* **1961**, *9*, 307−310.
(20) Alviola, J. N.; Jondiko, T. O.; Awika, J. M. Effect of strong gluten flour on quality of wheat tortillas fortified with cross-linked resistant starch. *J. Food Process. Preserv.* **2012**, *36*, 38−45.
(21) Approved methods of analysis. *Methods 26−50.01, 39−11.01, 54−40.02*, 11th ed.; AACC International: St. Paul, MN, 2010.
(22) Jondiko, T. O.; Alviola, N. J.; Hays, D. B.; Ibrahim, A.; Tilley, M.; Awika, J. M. Effect of high molecular weight glutenin subunit allelic composition on wheat flour tortilla quality. *Cereal Chem.* **2012**, *89*, 155−161.
(23) Alviola, J. N.; Jondiko, T.; Awika, J. M. Effect of cross-linked resistant starch on wheat tortilla quality. *Cereal Chem.* **2010**, *87*, 221−225.
(24) Kaluza, W. Z.; McGrath, R. M.; Roberts, T. C.; Schroeder, H. H. Separation of phenolics of *Sorghum bicolor* (L.) Moench grain. *J. Agric. Food Chem.* **1980**, *28*, 1191−1196.
(25) Langer, S.; Marshall, L. J.; Day, A. J.; Morgan, M. R. Flavanols and methylxanthines in commercially available dark chocolate: A study of the correlation with nonfat cocoa solids. *J. Agric. Food Chem.* **2011**, *59*, 8435−8441.
(26) Englyst, K. N.; Hudson, G. J.; Englyst, H. N. Starch analysis in food. *Encyclopedia of Analytical Chemistry*; John Wiley & Sons, Ltd: Hoboken, NJ, 2006.
(27) Schober, T. J.; Bean, S. R.; Kuhn, M. Gluten proteins from spelt *Triticum aestivum* ssp. spelta) cultivars: A rheological and size-exclusion high-performance liquid chromatography study. *J. Cereal Sci.* **2006**, *44*, 161−173.
(28) Kaufman, R. C.; Herald, T. J.; Bean, S. R.; Wilson, J. D.; Tuinstra, M. R. Variability in tannin content, chemistry, and activity in a diverse group of tannin containing sorghum cultivars. *J. Sci. Food Agric.* **2013**, *93*, 1233−1241.
(29) Taylor, J.; Bean, S. R.; Ioerger, B. P.; Taylor, J. R. N. Preferential binding of sorghum tannins with γ-kafirin and the influence of tannin binding on kafirin digestibility and biodegradation. *J. Cereal Sci.* **2007**, *46*, 22−31.
(30) Mertz, E. T.; Hassen, M. M.; Cairns-Whittern, C.; Kirleis, A. W.; Tu, L.; Axtell, J. D. Pepsin digestibility of proteins in sorghum and other major cereals. *Proc. Natl. Acad. Sci. U. S. A.* **1984**, *81*, 1−2.
(31) Kim, K.-H.; Tsao, R.; Yang, R.; Cui, S. W. Phenolic acid profiles and antioxidant activities of wheat bran extracts and the effect of hydrolysis conditions. *Food Chem.* **2006**, *95*, 466−473.
(32) Hahn, D.; Faubion, J.; Rooney, L. Sorghum phenolic acids, their high-performance liquid chromatography separation, and their relation to fungal resistance. *Cereal Chem.* **1983**, *60*, 255−259.
(33) Abdel-Aal, E.-S. M.; Rabalski, I. Effect of baking on free and bound phenolic acids in wholegrain bakery products. *J. Cereal Sci.* **2013**, *57*, 312−318.
(34) Yang, L.; Allred, K. F.; Geera, B.; Allred, C. D.; Awika, J. M. Sorghum phenolics demonstrate estrogenic action and induce apoptosis in nonmalignant colonocytes. *Nutr. Cancer* **2012**, *64*, 419−427.
(35) Zhang, L.; Cheng, L.; Jiang, L.; Wang, Y.; Yang, G.; He, G. Effects of tannic acid on gluten protein structure, dough properties, and bread quality of Chinese wheat. *J. Sci. Food Agric.* **2010**, *90*, 2462−2468.
(36) Davis, A.; Hoseney, R. Grain sorghum condensed tannins. I. Isolation, estimation, and selective adsorption by starch. *Cereal Chem.* **1979**, *56*, 310−313.
(37) Lehmann, U.; Robin, F. Slowly digestible starch—Its structure and health implications: A review. *Trends Food Sci. Technol.* **2007**, *18*, 346−355.
(38) Seal, C. J.; Daly, M. E.; Thomas, L. C.; Bal, W.; Birkett, A. M.; Jeffcoat, R.; Mathers, J. C. Postprandial carbohydrate metabolism in healthy subjects and those with type 2 diabetes fed starches with slow and rapid hydrolysis rates determined in vitro. *Br. J. Nutr.* **2003**, *90*, 853−864.
(39) Sparti, A.; Milon, H.; Di Vetta, V.; Schneiter, P.; Tappy, L.; Jequier, E.; Schutz, Y. Effect of diets high or low in unavailable and slowly digestible carbohydrates on the pattern of 24 h substrate oxidation and feelings of hunger in humans. *Am. J. Clin. Nutr.* **2000**, *72*, 1461−1468.
(40) Alvina, M.; Araya, H. Rapid carbohydrate digestion rate produced lesser short-term satiety in obese preschool children. *Eur. J. Clin. Nutr.* **2004**, *58*, 637−642.
(41) Cousins, B. W.; Tanksley, T. D.; Knabe, D. A.; Zebrowska, T. Nutrient digestibility and performance of pigs fed sorghums varying in tannin concentration. *J. Anim. Sci.* **1981**, *53*, 1524−1537.
(42) Youssef, A. M. Extractability, fractionation, and nutritional value of low and high tannin sorghum proteins. *Food Chem.* **1998**, *63*, 325−329.
(43) Schofield, J. D.; Bottomley, R. C.; Timms, M. F.; Booth, M. R. The effect of heat on wheat gluten and the involvement of sulphydryl−disulphide interchange reactions. *J. Cereal Sci.* **1983**, *1*, 241−253.
(44) Duodu, K. G.; Taylor, J. R. N.; Belton, P. S.; Hamaker, B. R. Factors affecting sorghum protein digestibility. *J. Cereal Sci.* **2003**, *38*, 117−131.
(45) Hamaker, B. R.; Kirleis, A. W.; Butler, L. G.; Axtell, J. D.; Mertz, E. T. Improving the in vitro protein digestibility of sorghum with reducing agents. *Proc. Natl. Acad. Sci. U. S. A.* **1987**, *84*, 626−628.
(46) Lizardo, R.; Peiniau, J.; Aumaitre, A. Effect of sorghum on performance, digestibility of dietary components, and activities of pancreatic and intestinal enzymes in the weaned piglet. *Anim. Feed Sci. Technol.* **1995**, *56*, 67−82.

DOI: 10.1021/jf504112z
J. Agric. Food Chem. 2015, 63, 1234−1241

the tissues of the peduncles and rachises from veraison to harvest for *Vitis vinifera*, coupled with the fact that we have shown peduncle color evolution parallels with the berry ripening process, we wished to further examine the link between grape stem (peduncle and rachis) color change and their associated chemical evolution. Consequently, the aims of this study were 3-fold: (1) to investigate the change in the chemical composition of five key parameters of the peduncles and rachises separately from veraison to harvest over two vintages: these being moisture content, total chlorophylls (including chlorophyll *a* and *b* levels), total carotenoids, total phenolics, and their antioxidant capacity (DPPH) levels; (2) to statistically model the relationships between peduncle chemical compositional change and peduncle color evolution; and (3) to examine the potential codevelopment between peduncle and rachis chemical composition and the corresponding traditional berry ripeness parameters (°Brix, pH, TA, total anthocyanins, and phenolics) from veraison to harvest. Such comparisons between berry ripeness development and grape stem color and associated chemical changes from veraison to harvest may provide for a new opportunity to assess grape quality and maturity over time in a nondestructive manner and consequently assist in the harvest decision making within a certain vineyard.

MATERIALS AND METHODS

Chemicals and Reagents. Methanol and sodium carbonate were purchased from Chem Supply (Australia). 1,1-Diphenyl-2-picrylhydrazyl (DPPH), 6-hydroxy-2,5,7,8-tetramethylchroman-2-carboxylic acid (Trolox), ascorbic acid and magnesium oxide (MgO) were obtained from Sigma-Aldrich (Australia). Hydrochloric acid (HCl) was supplied by VWR (Australia). Folin-Ciocalteau reagent was from Merck (Germany).

Peduncle and Rachis Samples. All 8 patches were coded as Shiraz (SH) followed by position within vineyard with the key viticultural details of each patch such as row orientation, year of planting etc being reported previously.[1] Grape bunches (48) were sampled from each of the 8 Shiraz patches predominantly on a weekly basis from veraison to harvest during the 2011/2012 and 2012/2013 seasons at Longview vineyard (GPS position: 138°49′54″E, 35°11′25″S). Veraison was determined to be on Jan, 24th (DAF 64) in 2012 and Jan, 29th (DAF 67) in 2013 when 50% of the berries showed purple colorization. The samples were transported to the laboratory immediately under a blanket of dry ice. During the 2012 vintage, 24 bunches were randomly selected to obtain 24 peduncles and 24 rachises from the 48 sampled bunches from each patch on each sampling day. The peduncles and rachises were immediately scanned into JPEG images. During the 2013 vintage, 24 peduncles were obtained from each of the 8 patches of Shiraz and scanned for image analysis. Since preliminary data analysis of the 2012 data indicated that the change in color or chemical traits of the rachises showed no significant correlations with berry ripeness parameters and given the logistics of collecting such data, rachis samples were only analyzed from two representative patches (SH 2N and SH 15) in 2013, the results of which would be comparable to all eight patches in 2012. Images containing peduncles and/or rachises were analyzed semi-automatically using a customized code employing Matlab together with its Image Analysis Toolbox (Mathworks Inc., Natick, MA, USA). For each peduncle or rachis, the code extracts the average color values in both RGB (red, blue and green) and CIE$L^*a^*b^*$ color systems. The code for image analysis is available upon request.

Determination of Moisture Content. The fresh weight of the scanned samples was measured in bulk (in 2012, total weights of 24 samples per patch; in 2013, the 24 peduncles from each patch were divided into four groups according to their four sampling row numbers, and the weight of each group of 6 samples was measured at each sampling). After storing the samples at −20 °C overnight, all samples were freeze-dried completely for 24 to 48 h depending on the sample amount utilizing a freeze drier (FreeZone 6, Labconco, USA). The freeze-dried peduncles and rachises were weighed to calculate their moisture levels. Approximately 2 g of each dried sample were ground into a very fine powder employing a Retsch mill at 30 Hz, 2 min for peduncles and 1 min for rachises, with the remaining of the samples sealed and stored at −20 °C for additional analyses.

Determination of Chlorophyll and Carotenoid Contents. Ground samples of peduncle or rachis (100 mg) were mixed with 100 mg of MgO to neutralize plant acids and prevent pheophytin *a* formation.[26] The chlorophylls and carotenoids were extracted in 5 mL of methanol in a glass vial. After mixing rigorously, the samples were shaken at 100 rpm in the dark at 4 °C for 2 h, employing a nitrogen blanket in the vials. The samples were then transferred into 2 mL microtubes for centrifugation (15 min at 14,000 rpm, 15339*g*, 4 °C). Triplicate sample extractions were conducted for each patch on each sampling day. The supernatants were scanned at 750, 665, 652, 520, and 470 nm absorbance (A) using quartz microcuvettes with methanol as blank. The concentrations of chlorophyll *a* (Ca), chlorophyll *b* (Cb), total chlorophylls ($Ca+b$), and total carotenoids ($Cx+c$) in the samples were calculated utilizing the following equations for methanol extracts as detailed elsewhere,[26−28] and the results recorded as microgram/gram sample dry weight.

$$Ca = 16.72A_{665} - 9.16A_{652}$$

$$Cb = 34.09A_{652} - 15.28A_{665}$$

$$Ca + b = 1.44A_{665} + 24.93A_{652}$$

$$Cx + c = (1000A_{470} - 1.63Ca - 104.96Cb)/221$$

Total Phenolics Analysis. A mixture of 10 mL of 80% aqueous methanol with 0.1% HCl was added to 100 mg of either the dried peduncle or dried rachis samples, and the extracts were shaken at 150 rpm at ambient temperature for 2 h under a blanket of nitrogen. They were then transferred into 10 mL centrifuge tubes for centrifugation at 5000 rpm (2370*g*), 4 °C for 15 min. The supernatants were stored at −20 °C before analysis. Triplicate sample extractions were conducted for each patch at each maturation stage, and all samples were prepared in duplicate for the phenolics assay of each of the phenolic extracts. The total phenolics content of the extracts was measured utilizing the Folin-Ciocalteu method in 96 well plates employing a liquid handling robot for sample loading (Corbett Robotics, Australia). In brief, the Folin-Ciocalteu reagent was first diluted by 25:240 with water. To each microplate well, 255 μL of the diluted Folin-Ciocalteu reagent and 4 μL of the phenolic extract were added and mixed well. After 6 min, 45 μL of 200 g/L Na_2CO_3 was added and the solution was mixed thoroughly. After leaving in the dark for 2 h at room temperature, the plates were read at 765 nm using a microplate reader (Tecan infinite M200 Pro, Australia).[29] Gallic acid was employed as a standard, and all standard curves displayed $R^2 > 0.99$ with the results being recorded as mg gallic acid equivalence per gram sample dry weight.

Determination of Antioxidant Capacity—DPPH Assays. The extracted phenolic samples and Trolox standard solutions were diluted 10-fold using 80% aqueous methanol by the liquid handling robot (Corbett Robotics, Australia), and their antioxidant capacity was measured utilizing a microplate DPPH assay, in a similar fashion to that reported previously with some modification.[30] A 180 μM DPPH solution was prepared in 80% aqueous methanol. To each well in the 96-well plate, 200 μL of the DPPH solution was added followed by 22 μL of the diluted phenolic extracts of ground peduncle or rachis or standard solutions of Trolox before mixing thoroughly. All samples were prepared in duplicate for the DPPH assay of each of the phenolic extracts. The plates were placed in the dark at ambient temperature for 6 h and then read at 520 nm absorbance (Tecan infinite M200 Pro). Trolox was used as a standard, and all standard curves displayed $R^2 > 0.99$ with the results being recorded as μM Trolox equivalence per gram sample dry weight. Ascorbic acid solution (80 mg/L) was used as a reference in each plate.

DOI: 10.1021/jf504215e
J. Agric. Food Chem. 2015, 63, 1242−1250

Table 1. Peduncle and Rachis Chemical Composition for 8 Shiraz Patches during the 2012 Season

		sampling date (DAF[a])						
chemical	sample[b]	64	78	92	106	113	120	127
fresh weight (mg)[c]	P	390 ± 14	384 ± 28	366 ± 16	368 ± 30	356 ± 19	345 ± 19	350 ± 30
	R	2058 ± 53	1959 ± 71	1906 ± 51	1898 ± 66	1780 ± 32	1898 ± 79	1744 ± 95
dry weight (mg)[c]	P	143 ± 12	144 ± 29	156 ± 19	166 ± 61	171 ± 28	170 ± 35	165 ± 45
	R	451 ± 10	425 ± 14	419 ± 15	428 ± 32	421 ± 12	446 ± 25	386 ± 24
moisture (%)[c]	P	63 ± 1	62 ± 1	57 ± 1	55 ± 1	52 ± 1	51 ± 1	53 ± 1
	R	78 ± 1	78 ± 1	78 ± 1	78 ± 1	76 ± 1	77 ± 1	78 ± 0.5
chlorophyll *a* (μg/g)	P	231 ± 13	189 ± 11	166 ± 9	151 ± 5	150 ± 9	147 ± 10	136 ± 6
	R	265 ± 18	256 ± 13	236 ± 10	223 ± 10	234 ± 17	215 ± 12	204 ± 9
chlorophyll *b* (μg/g)	P	85 ± 5	68 ± 4	62 ± 3	53 ± 1	53 ± 2	57 ± 3	48 ± 2
	R	96 ± 6	87 ± 4	80 ± 3	74 ± 3	78 ± 6	82 ± 5	78 ± 4
total chlorophylls (μg/g)	P	316 ± 19	258 ± 16	229 ± 12	204 ± 7	203 ± 12	204 ± 13	184 ± 8
	R	361 ± 24	343 ± 17	316 ± 13	298 ± 13	312 ± 23	297 ± 17	283 ± 13
total carotenoids (μg/g)	P	88 ± 4	80 ± 3	75 ± 3	70 ± 2	72 ± 4	69 ± 2	66 ± 2
	R	92 ± 5	94 ± 4	87 ± 3	82 ± 3	87 ± 5	76 ± 3	78 ± 2
total phenolics (mg/g)	P	33 ± 1	33 ± 1	38 ± 1	38 ± 1	38 ± 0.3	41 ± 1	37 ± 1
	R	53 ± 2	58 ± 2	67 ± 1	59 ± 2	61 ± 2	59 ± 2	54 ± 2
DPPH (Trolox equiv. μM/g)	P	30 ± 1	29 ± 1	32 ± 1	32 ± 1	33 ± 1	33 ± 1	31 ± 1
	R	51 ± 2	53 ± 2	54 ± 2	49 ± 2	50 ± 2	50 ± 2	48 ± 2

[a]DAF: days after flowering. All chemical data are predicted means ± standard errors (estimated with REML, GenStat) [sample size: n = 24, measured for 8 patches on each sampling day; except for DPPH (n = 6), measured for the peduncles and rachises from patches SH 2N and SH 15 only on each sampling day]. [b]Sample: P represents peduncles, R represents rachises. [c]All weight and moisture data are means ± standard errors (n = 8, measured for 8 patches on each sampling day).

Table 2. Peduncle and Rachis Chemical Composition for 8 Shiraz Patches during the 2013 Season

		sampling date (DAF[a])						
chemical	sample[b]	67	74	81	88	95	102	109
fresh weight (mg)[c]	P	351 ± 19	316 ± 18	316 ± 16	328 ± 18	318 ± 18	295 ± 17	279 ± 17
	R	1531 ± 75	1362 ± 75	1473 ± 75	1426 ± 75	1370 ± 75	1379 ± 75	1329 ± 75
dry weight (mg)[c]	P	130 ± 8	119 ± 8	125 ± 8	139 ± 8	140 ± 8	140 ± 8	136 ± 8
	R	376 ± 19	338 ± 19	352 ± 19	346 ± 19	332 ± 19	373 ± 19	348 ± 19
moisture (%)[c]	P	63 ± 1	62 ± 1	60 ± 1	58 ± 1	57 ± 1	53 ± 1	51 ± 1
	R	76 ± 1	76 ± 1	77 ± 1	77 ± 1	77 ± 1	74 ± 1	75 ± 1
chlorophyll *a* (μg/g)	P	204 ± 3	186 ± 13	157 ± 9	171 ± 14	141 ± 8	151 ± 12	131 ± 5
	R	233 ± 14	215 ± 14	191 ± 14	211 ± 14	187 ± 14	184 ± 14	171 ± 1
chlorophyll *b* (μg/g)	P	79 ± 6	74 ± 5	58 ± 3	67 ± 6	53 ± 3	58 ± 4	50 ± 2
	R	93 ± 3	85 ± 3	76 ± 3	81 ± 3	70 ± 3	67 ± 3	61 ± 1
total chlorophylls (μg/g)	P	283 ± 19	260 ± 18	215 ± 12	238 ± 20	195 ± 11	209 ± 17	181 ± 7
	R	326 ± 17	300 ± 17	267 ± 17	292 ± 17	257 ± 17	250 ± 17	232 ± 2
total carotenoids (μg/g)	P	75 ± 3	72 ± 3	66 ± 2	71 ± 4	60 ± 2	65 ± 3	61 ± 1
	R	82 ± 3	79 ± 3	73 ± 3	76 ± 3	68 ± 3	69 ± 3	64 ± 1
total phenolics (mg/g)	P	33 ± 1	34 ± 1	36 ± 1	36 ± 1	37 ± 1	36 ± 1	37 ± 1
	R	56 ± 5	58 ± 3	61 ± 4	60 ± 5	60 ± 3	57 ± 3	63 ± 3
DPPH (Trolox equiv μM/g)	P	31 ± 1	32 ± 1	33 ± 1	34 ± 1	35 ± 1	33 ± 1	34 ± 1
	R	51 ± 3	51 ± 2	51 ± 2	50 ± 2	51 ± 3	50 ± 2	52 ± 2

[a]DAF: days after flowering. All chemical data are predicted means ± standard errors (estimated with REML, GenStat) [sample size: n = 24 for peduncles, measured for 8 patches on each sampling day; n = 6 for rachises, measured for 2 patches on each sampling day]. [b]Sample: P represents peduncles for 8 Shiraz patches, R represents rachises for 2 patches (SH 2N and SH 15). [c]All weight and moisture data are predicted means ± standard errors [sample size: n = 32 for peduncles, n = 8 for rachises on each sampling day].

Statistics. Univariate repeated measurement analyses with heterogeneous variance over time were conducted for the 2012 and 2013 seasons separately employing the REML procedure in GenStat (GenStat for Windows 16th edition. VSN International, Hemel Hempstead, UK). In the REML mixed models, time (DAF) was the fixed effect factor, and the random effects were patch and patch by time. Predicted means and their standard errors (reported in the tables herein) were calculated for each parameter separately. For the analysis and estimation of nonlinear models the FITCURVE directive in GenStat was employed.

RESULTS AND DISCUSSION

Peduncle and Rachis Chemical Compositional Change during Ripening. The changes in moisture content (fresh and dried weight), total chlorophylls (including chlorophyll *a* and *b* levels), total carotenoids, total phenolics, and their antioxidant capacity (DPPH) levels occurring in the tissues of the peduncles and rachises from veraison to harvest are summarized in Tables 1 and 2 for the 2012 and 2013 seasons, respectively.

DOI: 10.1021/jf504215e
J. Agric. Food Chem. 2015, 63, 1242−1250

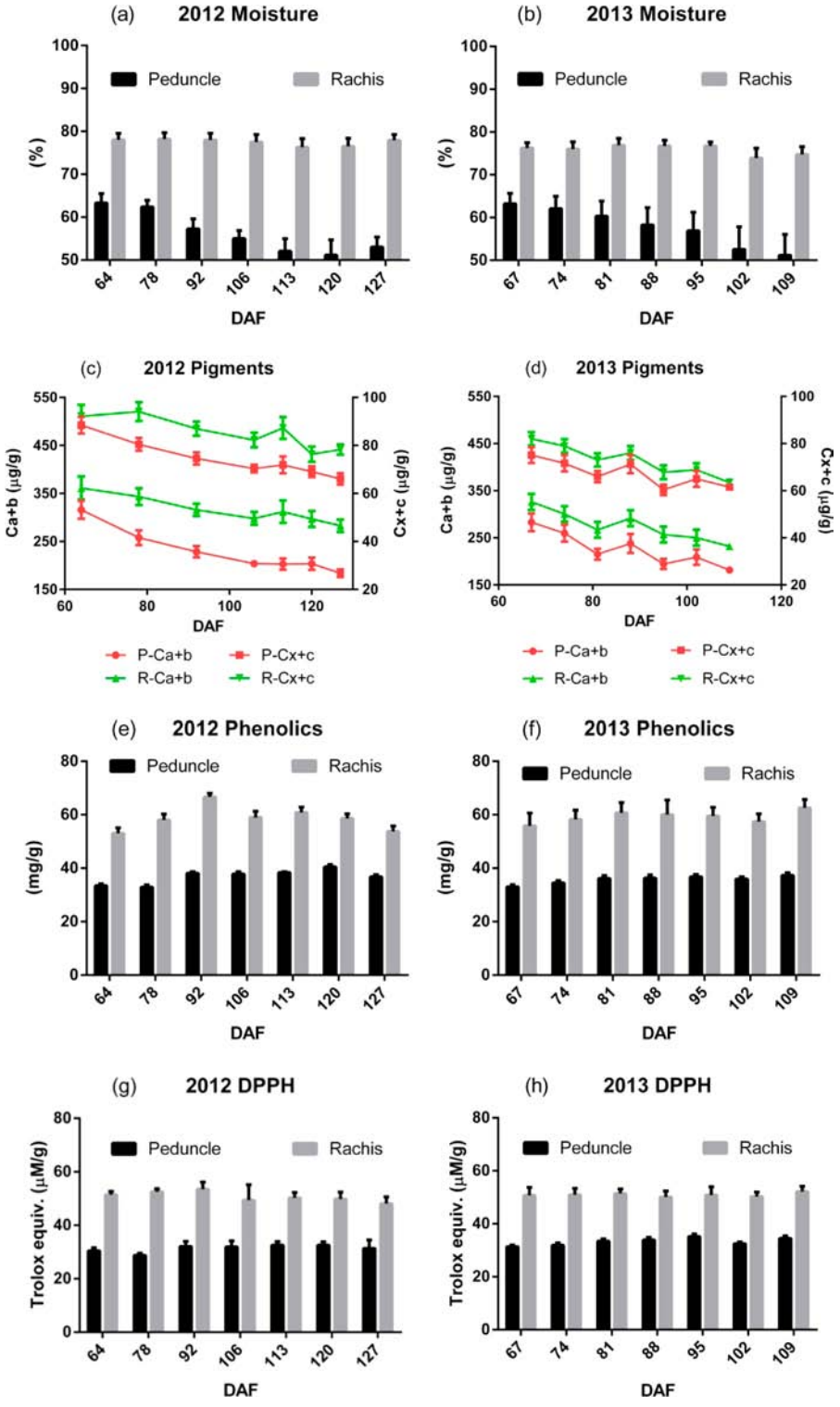

Figure 1. Moisture content, total chlorophylls (*Ca+b*), total carotenoids (*Cx+c*), total phenolics, and antioxidant capacity (DPPH) levels of the peduncles and rachises as a function of time (DAF) from veraison to harvest during the 2012 and 2013 seasons.

Figure 1a displays the change in the average moisture content of the peduncles and rachises over time (DAF). Rachises always contained higher moisture content when compared to the peduncles. Furthermore, it was found that rachis moisture levels remain steady at around 78% from veraison to harvest while the moisture levels of the peduncles decrease by some 10% ± 1.4% from veraison (63%) to harvest. Moisture contents were again measured during the 2013 season (Table 2, Figure 1b), and again the moisture levels of the rachises remained steady from veraison to harvest at around 76% while the peduncles displayed a decrease in moisture content of 12% ± 1.4% over the course of berry ripening. While there are no direct reports in the literature that may be used for comparison, it has been reported on numerous occasions that grape stems (combined peduncle, rachis, and pedicels) from winery waste contain an average of 60−70% moisture.[6,10,31]

DOI: 10.1021/jf504215e
J. Agric. Food Chem. 2015, 63, 1242−1250

From our data, the overall stem moisture content calculated from the combined peduncle and rachis moisture levels fluctuates between 66 and 78% throughout the ripening season and at harvest it can be estimated to be 73% ± 1% in 2012 and 71% ± 2% in 2013, levels which compliment those cited above for winery stem waste. While not directly related to this study, the fresh weight of Shiraz seeds has also been reported to decrease after veraison, with water loss declining until 91−92 DAF before reaching a plateau, a finding also reported by others for Tempranillo seeds.[32,33] Thus, the observed drying out of the peduncles from veraison to harvest may be somewhat related to seed desiccation over time, although further studies would be needed to ascertain this relationship.

Overall, the amount of chlorophyll *a* was found to be some 2.7 times greater in magnitude when compared to that of chlorophyll *b* along the entire veraison to harvest timeline for both seasons (Tables 1 and 2). Consequently and as expected, chlorophyll *a* is the primary pigment and chlorophyll *b* is an accessory pigment in both the peduncles and rachises.[27] Figure 1c and d display the change in total chlorophyll (*Ca*+*b*) and carotenoid levels (*Cx*+*c*) for the 2012 and 2013 seasons, respectively. Overall, the rachises have higher total chlorophyll and carotenoid contents when compared to the peduncles over the entire veraison to harvest ripening period. In terms of total chlorophyll levels, it was observed that the peduncles lost approximately 40% of total chlorophyll from veraison to harvest for both seasons while the rachises lost approximately 25% over the same time frame. Irrespective of whether one is examining total chlorophyll loss for the peduncles or the rachises, there appears to be a concomitant reduction in both the chlorophyll *a* and *b* levels at the same time, as the overall level in total chlorophylls (*Ca*+*b*) over time declines in a steady linear fashion (p-value < 0.01). After the second sampling from veraison (DAF 78 in 2012 and DAF 74 in 2013), the rachises had higher total carotenoid (*Cx*+*c*) levels on average when compared to the peduncles; approximately 14% in the 2012 season (82.2 ± 2.7 in comparison to 70.4 ± 1.9) and 11% in the 2013 season (70.0 ± 2.6 in comparison to 64.6 ± 2.5). Moreover, there is an observed decrease in total carotenoid levels from veraison to harvest for both the peduncles and rachises (p-value < 0.05). Overall, the peduncles lost some 20−25% total carotenoids from veraison to harvest over the two seasons while the rachises display a reduction of some 15−20% total carotenoids over the same time period.

Palliotti and Cartechini measured the pigments within young and old rachises and found that the chlorophyll *a*, chlorophyll *b*, and carotenoid contents were higher in young rachis than old rachis, a finding that correlates with our findings (Tables 1 and 2).[24] On the other hand there are a number of other studies that have examined the total chlorophyll and carotenoid contents of grapes and grapevine leaves over the maturation period. For example, Giovanelli and Brenna observed a decrease in total chlorophylls from fruit-set to harvest for one white and two red Italian grape varieties.[34] Furthermore, Kamffer et al. measured the pigments level in Merlot berries during ripening over two seasons, and they found a decrease in berry chlorophyll and carotenoid levels from veraison to harvest.[35] A number of other studies have reported similar decreasing trends in total chlorophyll and carotenoid levels during the maturation of grape berries.[24,36] Finally, given that leaves are the primary photosynthetic organs of plants, it is not surprising that researchers have investigated the changes in chlorophyll and carotenoid content in leaves during vine growth. For example, Lashbrooke et al. found that the chlorophyll *a* and *b* levels were higher in mature vine leaves when compared to young leaves and their levels dropped post-anthesis.[37] Again, it is too early to determine if our observed changes in total chlorophyll and carotenoid contents of peduncles and rachises are related in any way to those found for grape berries and vine leaves.

Finally, we examined the total phenolics levels and the associated antioxidant capacity (DPPH) of the peduncles and rachises for each patch of Shiraz over the two seasons (Tables 1 and 2). Overall, there was no significant difference (p-value > 0.10) between the amount of total phenolics within the rachises found over the first two sampling time points when compared to the last 5 samplings over both seasons of examination (Figure 1 and f). However, the total amount of phenolics within the peduncles slightly increased after the second sampling date (DAF 78 in 2012 and DAF 74 in 2013, p-value < 0.05) and then remained stable toward harvest in both seasons. The amount of total phenolics was always higher in the rachises (35% in 2012 and 40% in 2013) when compared to the peduncles. Given that the phenolics are the major contributors to the potential antioxidant capacity of the plant tissues, it was not surprising to find that the observed trends in antioxidant capacities of the peduncles and the rachises correlated extremely well with the observed phenolic levels, compare Figure 1g and h with Figure 1e and f. Again, the antioxidant capacity of the rachises was approximately 35% higher after the second sampling (DAF 78 in 2012 and DAF 74 in 2013) when compared to the peduncles over both seasons of examination. For comparison, it has previously been found that the total phenolics levels and overall antioxidant capacity in the stems of Kishmish Chornyi (seedless variety) also remained constant from veraison up until harvest and that the amounts within the stems were greater than those found in the berries or leaves.[23]

Peduncle and Rachis Color and Their Correlations with Moisture and Pigments Levels. Considering that the peduncle and rachis samples in 2012 came from the same bunch stems, it is quite intriguing to see such a significant difference between them in terms of their moisture, total chlorophyll, and carotenoid levels, and total phenolics and antioxidant capacity (DPPH) levels. The rachis tissues displayed higher levels of moisture, total phenolics, and antioxidant capacity (DPPH) throughout the entire maturation process, while the total chlorophyll and carotenoid levels of the peduncles were clearly lower in magnitude after the second sampling, DAF 78 in 2012 and DAF 74 in 2013. Furthermore, our findings above for changes in peduncle and rachis moisture and pigments (total chlorophylls and carotenoids) levels appear to correlate well with our recent findings on the observed color changes of the peduncles and rachises from veraison to harvest for Shiraz. We previously observed that the rachises remain essentially green from veraison to harvest while the overall peduncle color changes from a green soft-unripe state to brittle and brown.[1] We have found herein that the rachis moisture content remains constant while the peduncle moisture content drops during grape maturation. Coupling this observation with the fact that the levels of the pigments (total chlorophylls and carotenoids) of the peduncles dropped to a much greater extent when compared to the rachises, it therefore appears that the observed color change of peduncles from green to brown is primarily driven by a loss of total chlorophyll and carotenoid content coupled with significant dehydration of the peduncle tissue.

DOI: 10.1021/jf504215e
J. Agric. Food Chem. 2015, 63, 1242−1250

Table 3. Color Polar Parameters (chroma and hue) of Peduncle and Rachis for All Patches during the 2012 and 2013 Seasons[a]

		2012 sampling date (DAF)						
color	sample	64	78	92	106	113	120	127
chroma[b]	P	23.36 ± 0.15	22.45 ± 0.35	21.26 ± 0.46	19.63 ± 0.28	17.91 ± 0.42	17.88 ± 0.47	18.04 ± 0.41
	R	23.65 ± 0.25	23.96 ± 0.22	24.98 ± 0.15	24.37 ± 0.27	22.51 ± 0.52	23.49 ± 0.31	23.71 ± 0.13
hue[c]	P	2.01 ± 0.01	1.98 ± 0.01	1.76 ± 0.03	1.69 ± 0.02	1.62 ± 0.03	1.56 ± 0.04	1.60 ± 0.03
	R	1.98 ± 0.01	2.00 ± 0.01	2.02 ± 0.01	2.00 ± 0.01	1.93 ± 0.02	1.94 ± 0.02	1.94 ± 0.01
		2013 sampling date (DAF)						
color	sample	67	74	81	88	95	102	109
chroma[b]	P	22.37 ± 0.20	21.91 ± 0.23	21.14 ± 0.26	19.14 ± 0.40	18.16 ± 0.42	17.07 ± 0.54	15.94 ± 0.26
hue[c]	P	1.99 ± 0.02	1.95 ± 0.02	1.83 ± 0.02	1.71 ± 0.03	1.65 ± 0.03	1.58 ± 0.06	1.51 ± 0.03

[a]All data are predicted means ± standard errors (estimated with REML, GenStat). [Sample size: n = 192, except at DAF 78 in 2012 (n = 96)]. [b]chroma, $C = (a^{*2} + b^{*2})^{0.5}$. [c]hue, $h = arctan2\ (b^*, a^*)$, in this study, $0 < h < \pi$, and when $a^* = 0$, $h = \pi/2$ (1.57).

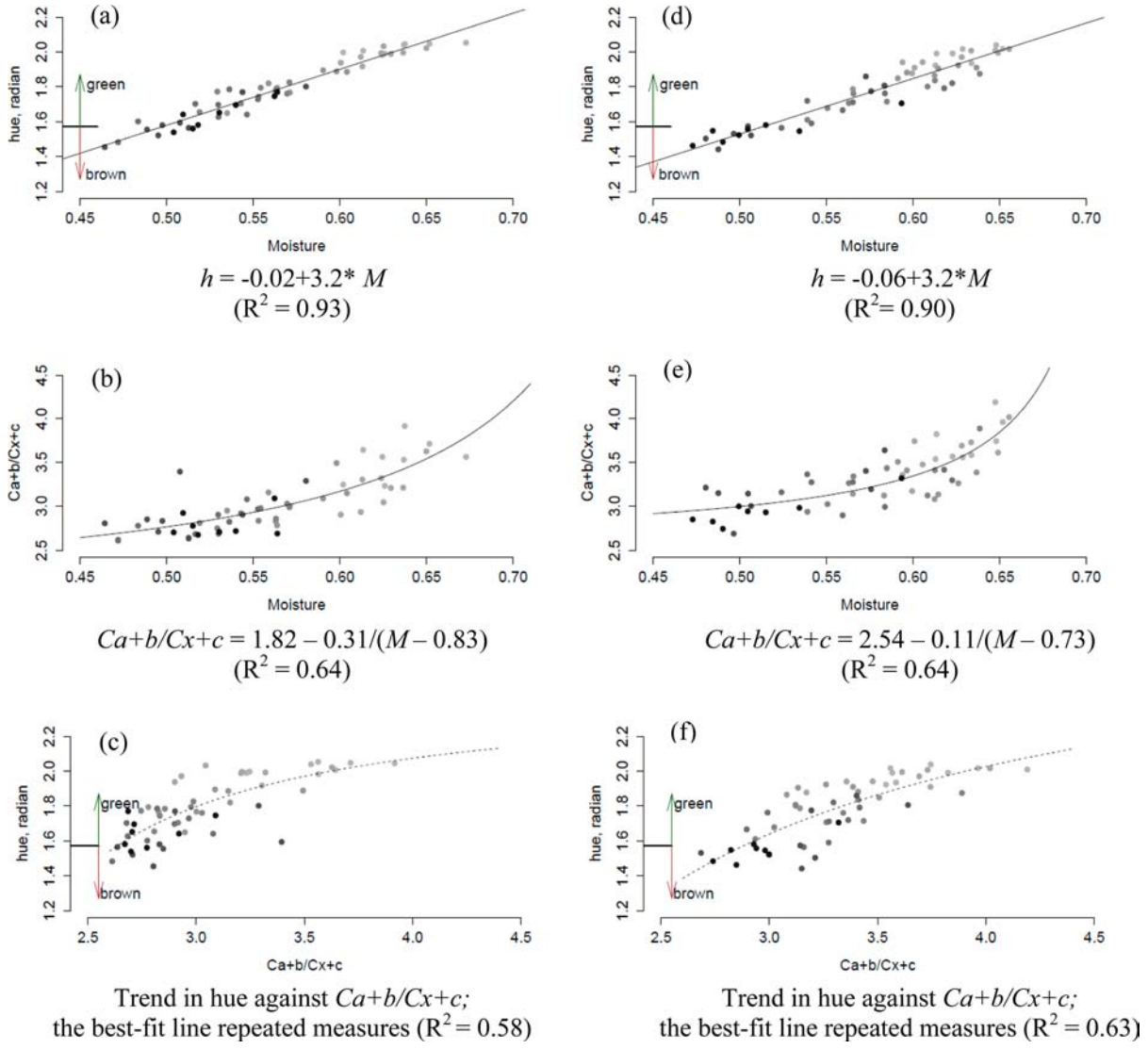

Figure 2. Peduncle chemical and color correlation models with equations for the 2012 and 2013 seasons. (a–c) 2012 data; (d–f) 2013 data. h: hue, $0 < h < \pi$; M: Moisture, $0 < M < 1$; $Ca+b/Cx+c$: weight ratio of pigments, calculated by total chlorophylls/total carotenoids.

Carotenoids serve as an accessory to the light harvesting chlorophylls and aid as photoprotectants during high light conditions or as scavanges during conditions of excessive ROS.[36] The loss or degradation of chlorophylls and carotenoids has been studied and has been shown to increase under conditions of excessive light and oxygen.[38] Consequently, the observed color change of the peduncles from green at veraison to brown at harvest may well be associated with an increase in ROS production which aids pigment destruction in the associated plant tissues. Moreover, lignification of the peduncles may lead to an increase in observed dry weight due to the deposition of starch in the xylem and phloem

DOI: 10.1021/jf504215e
J. Agric. Food Chem. 2015, 63, 1242–1250

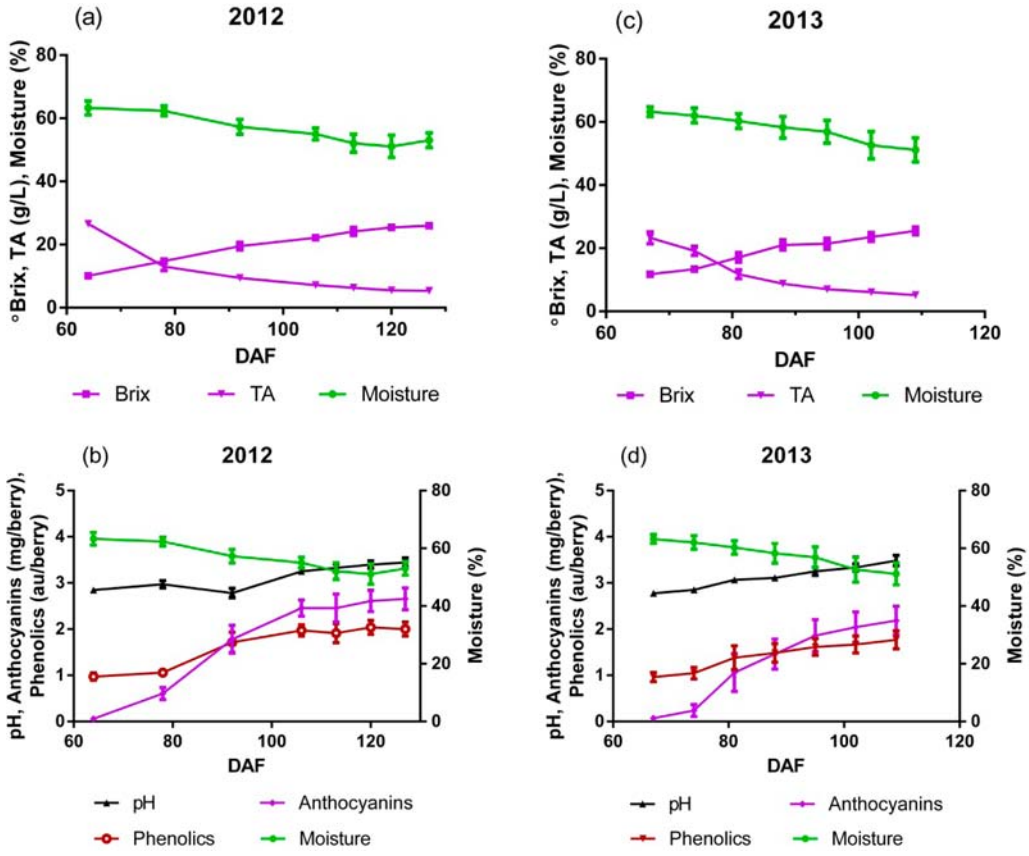

Figure 3. Co-development between peduncle moisture content and prototypical berry ripeness parameters for the 2012 and 2013 seasons.

parenchyma cells as seen in grape stems.[25] Indeed, it appears from the trends in the data that the dry weight of the peduncles increased from veraison toward harvest by more than 10% (17% in 2012 but not significant and 11% in 2013 (p value < 0.01)). When testing this by comparing the first 3 weeks after veraison to the last 3 weeks before harvest, the weight increment was significant (14.0 mg ± 3.8 mg) in 2013 but not significant (25.2 mg ± 26.35 mg) in 2012 (which may be explained by a much larger field variation in the wetter year of 2012 with 100 mm rainfall during vintage compared to 2013 which was considerably drier with 50 mm of rainfall). While at this stage it is clear from these studies that the decrease in moisture content of the peduncles is accompanied by a decrease in total pigments levels, it remains unclear as to why the peduncles indeed initiate such a physiological response in the first place. Several possible hypotheses to explain this observation may include the fact that, as the chlorophyll levels diminish, the requirement for water molecules in the tissues to participate in photosynthesis (i.e., $CO_2 + H_2O +$ photons → sugars + O_2) is lessened; or perhaps it is in some way associated with the known fact that the xylem within the peduncles essentially shuts down after veraison, causing a slowing down of water and solute transport into the berries which may be somehow associated with the dehydration of the peduncle tissues.[39]

With data on the chemical compositional changes for the moisture, total chlorophyll, and carotenoid levels, and total phenolics and antioxidant capacity levels of the peduncles and rachises from veraison to harvest now in hand, we next considered the relationship between these traits and that of the observed color changes seen in the vineyard. In order to do this, we first determined the peduncle and rachis color ($CIEL^*a^*b^*$) change that occurred during ripening in both the 2012 and 2013 seasons. Then the two polar parameters, chroma (C) and hue (h), were calculated from the a^* and b^* color values to quantify the change in peduncle color evolution from veraison to harvest for the 8 Shiraz patches (Table 3).[1]

Independent of which season's data was examined, both the peduncles and rachises had the same green color (same chroma and hue values) at veraison. However, as berry maturation progressed, the peduncles underwent a significant color change, as indicated by a decrease in chroma and hue values (from greenish (over $\pi/2$) to brownish (less than $\pi/2$) based on the color wheel) while the rachises did not change significantly in color intensity and remained essentially green. Statistically, there were no correlations between the color of the rachises over time and the associated moisture and pigments levels and as such the potential use of monitoring rachis color or chemical developmental changes was not considered further herein. However, we found excellent correlations between the change in peduncle color and the associated moisture and pigments levels over time (Figure 2).

Over both seasons of analysis, the average moisture content from a bulk sample of peduncles was predictive ($R^2 > 0.9$) for the average peduncle color hue value with consistent gradient (0.032 rad/(% moisture) in both seasons, Figures 2a, d), and the relationship between peduncle moisture and color existed both between patches and within each patch, suggesting that the relationship was not produced solely from the developmental trends over time. Therefore, if one was to measure the moisture content of a bulk sample of peduncles without knowing their maturation stage, you would still be able to

DOI: 10.1021/jf504215e
J. Agric. Food Chem. 2015, 63, 1242−1250

predict their average color hue value using the equations in Figure 2a and d. Despite the strong correlation between peduncle moisture and color that we have shown herein, there is still a need to further validate this relationship at both overall vineyard level and the individual bunch level.

Moreover, the peduncle moisture level was negatively correlated with peduncle pigments ratio (Figure 2b, e), which could be modeled with a hyperbolic curve but has a weaker prediction power. The relatively low performance of moisture as a predictor for the pigments ratio leads to a loose relationship between peduncle color and the pigments ratio (Figures 2c and f). Even though the peduncle color hue value could also be modeled with a hyperbolic curve against the pigments ratio, the influence of the two parameters on each other was almost at the same extent as the effect of sampling time on peduncle color or pigments ratio. Therefore, although the pigments ratio changed substantially with moisture level and thus affects color, one cannot predict reliably the peduncle color or moisture level from merely the pigments ratio alone; there are obviously other factors influencing peduncle color evolution over time apart from the change in chlorophyll and carotenoid levels. In addition, we also examined the possible relationship between the evolution of peduncle chroma values and moisture content or pigments ratio, but we found that the peduncle chroma values were not as responsive as the hue values to the changes in moisture and were found to be only loosely related to the changes in pigments ratio.

Co-development between Peduncle Moisture Levels and Prototypical Berry Ripeness Parameters. We have previously demonstrated that the change in peduncle color codevelops with the change in berry ripeness parameters, namely °Brix, pH, TA, total anthocyanins, and phenolics from veraison to harvest.[1] Given that peduncle moisture content has a strong linear relationship with peduncle color (Figure 2a and d), it can be speculated that the observed change in peduncle moisture content may also codevelop with berry ripeness parameters. Figure 3 displays an overlay of how peduncle moisture levels and berry °Brix, pH, TA, total anthocyanin, and total phenolics levels changed from veraison to harvest during the 2012 and 2013 seasons. It can clearly be seen that the decrease in peduncle moisture content after veraison parallels with the observed drop in berry TA over both seasons. Furthermore, peduncle moisture content also codeveloped with the observed increase in berry °Brix, pH, total anthocyanin, and total phenolics levels over time. It is also interesting to note that the grapes were determined to be ready for harvest by the viticulturist/winemaker at the time when the peduncle average moisture level dropped to a level close to 50% in both seasons. For example, when the average peduncle moisture level decreased from veraison to harvest to 50%, the berries had an observed 25°Brix, 5.2 g/L of TA, pH 3.49, 2.19 mg of total anthocyanins, and 1.77 au of total phenolics per berry in the 2013 season. In the same way, inspection of the data for the 2012 season also revealed similar codevelopment trends between the changes in peduncle moisture content and the magnitudes of the berry ripeness parameters between veraison and harvest. Given that the grapes were actually defined by the viticulturists and winemakers as ready for harvest, it appears that by utilizing a representative sample of peduncles from an individual patch, one may be able to actually predict the harvest date by just simply measuring their average moisture levels.

Overall we have reported herein the first significant study on how peduncle and rachis moisture content, total chlorophylls (including chlorophyll *a* and *b* levels), total carotenoids, total phenolics, and their antioxidant capacity (DPPH) levels evolve during berry ripening and how this relates to peduncle color change for Shiraz (*Vitis vinifera*). While numerous differences were noted on how the chemical s of the peduncles and rachises change over time, the most significant finding was that there was an excellent linear relationship between the drop in peduncle moisture levels and their associated color hue values. Furthermore, we also found a moderate correlation between peduncle pigment ratio and moisture levels over time. The codevelopment between peduncle moisture level and the corresponding traditional berry ripeness parameters (°Brix, pH, TA, total anthocyanins, and phenolics) from veraison to harvest was also explored, the results of which indicate that monitoring of peduncle moisture levels may be able to be employed to assess grape quality and maturity over time in a nondestructive manner and consequently assist in harvest decision making within a certain vineyard. Since this is the first investigation on how grape peduncle chemistry changes may be linked to berry ripening, further research in the field is needed, with a more extensive sampling procedure that could examine the relationship between berry chemistry and peduncle chemistry at the bunch level.

AUTHOR INFORMATION

Corresponding Author

*E-mail: dennis.taylor@adelaide.edu.au. Phone: +61 8 8313 7239. Fax: + 61 8 8313 7116.

Funding

This research was supported by the School of Agriculture, Food & Wine of The University of Adelaide, and by the Australia's grapegrowers and winemakers through their investment body, formally known as the Grape and Wine Research and Development Corporation (GWRDC) but now known as the Australian Grape and Wine Authority (AGWA). Y.F. thanks the China Scholarship Council for a Ph.D. scholarship.

Notes

The authors declare no competing financial interests.

ACKNOWLEDGMENTS

We thank the staff at Longview Vineyards for allowing access to their vineyards to obtain samples over several vintages.

ABBREVIATIONS USED

Ca, Chlorophyll *a*; Cb, Chlorophyll *b*; Ca+b, total chlorophylls; Cx+c, total carotenoids; DAF, days after flowering; JPEG, Joint Photographic Expert Group; P, peduncle; R, rachis; REML, restricted/residual maximum likelihood; ROS, reactive oxygen species; TA, titratable acidity

REFERENCES

(1) Fang, Y. *Investigating Peduncle Colour Evolution and Chemistry During Ripening in Vitis vinifera L. cv Shiraz*. Ph.D. Thesis, The University of Adelaide, December 2014.

(2) Ribereau-Gayon, P.; Dubourdieu, D.; Doneche, B.; Lonvaud, A. The Grape and its Maturation. *Handbook of Enology*, 2nd ed.; Wiley: West Sussex, England, 2000, Vol.*1*, pp 245−246.

(3) Panouille, M.; Ralet, M.-C.; Bonnin, E.; Thibault, J.-F. Recovery and reuse of trimmings and pulps from fruit and vegetable processing. In *Handbook of waste management and co-product recovery in food processing*; Waldron, K., Eds.; CRC Press: New York, 2007; Vol. *1*, pp 417−447.

DOI: 10.1021/jf504215e
J. Agric. Food Chem. 2015, 63, 1242−1250

(4) Costa, J. M. Aproveitamento de subprodutos da vinificação. O bagaço comomatéria-prima da indústria de óleos e grainha e de fabrico de rações para gado. *1st congresso nacional das indústrias agro-alimentares*; Ministério da Agricultura Comércio e Pescas: Lisboa, 1983.
(5) Prozil, S. O.; Evtuguin, D. V.; Lopes, L. P. C. Chemical composition of grape stalks of *Vitis vinifera* L. from red grape pomaces. *Ind. Crops Products* **2012**, *35*, 178−184.
(6) González-Centeno, M. R.; Rosselló, C.; Simal, S.; Garau, M. C.; López, F.; Femenia, A. Physico-chemical properties of cell wall materials obtained from ten grape varieties and their byproducts: grape pomaces and stems. *LWT—Food Sci. Technol.* **2010**, *43*, 1580−1586.
(7) Llobera, A.; Cañellas, J. Dietary fibre content and antioxidant activity of Manto Negro red grape (*Vitis vinifera*): pomace and stem. *Food Chem.* **2007**, *101*, 659−666.
(8) Llobera, A.; Cañellas, J. Antioxidant activity and dietary fibre of Prensal Blanc white grape (*Vitis vinifera*) by-products. *Int. J. Food Sci. Technol.* **2008**, *43*, 1953−1959.
(9) Doshi, P.; Adsule, P.; Banerjee, K.; Oulkar, D. Phenolic compounds, antioxidant activity and insulinotropic effect of extracts prepared from grape (*Vitis vinifera* L) byproducts. *J. Food Sci. Technol.* **2013**, *Apr*, 1−10.
(10) Makris, D. P.; Boskou, G.; Andrikopoulos, N. K. Polyphenolic content and in vitro antioxidant characteristics of wine industry and other agri-food solid waste extracts. *J. Food Composition Anal.* **2007**, *20*, 125−132.
(11) Gonzalez-Centeno, M. R.; Jourdes, M.; Femenia, A.; Simal, S.; Rossello, C.; Teissedre, P.-L. Proanthocyanidin Composition and Antioxidant Potential of the Stem Winemaking Byproducts from 10 Different Grape Varieties (*Vitis vinifera* L.). *J. Agric. Food Chem.* **2012**, *60*, 11850−11858.
(12) Alonso, A. M.; Guillen, D. A.; Barroso, C. G.; Puertas, B.; Garcia, A. Determination of antioxidant activity of wine byproducts and its correlation with polyphenolic content. *J. Agric. Food Chem.* **2002**, *50*, 5832−5836.
(13) Makris, D. P.; Boskou, G.; Andrikopoulos, N. K. Recovery of antioxidant phenolics from white vinification solid by-products employing water/ethanol mixtures. *Bioresource Technol.* **2007**, *98*, 2963−2967.
(14) Llobera, A. Study on the antioxidant activity of grape stems (*Vitis vinifera*). A preliminary assessment of crude extracts. *Food Nutrition Sci.* **2012**, *3*, 500−504.
(15) Anastasiadi, M.; Pratsinis, H.; Kletsas, D.; Skaltsounis, A.-L.; Haroutounian, S. A. Grape stem extracts: Polyphenolic content and assessment of their in vitro antioxidant properties. *LWT—Food Sci. Technol.* **2012**, *48*, 316−322.
(16) Balik, J.; Kyselakova, M.; Vrchotova, N.; Triska, J.; Kumsta, M.; Veverka, J.; Hic, P.; Totusek, J.; Lefnerova, D. Relations between Polyphenols Content and Antioxidant Activity in Vine Grapes and Leaves. *Czech. J. Food Sci.* **2008**, *26*, S25−S32.
(17) Makris, D.; Boskou, G.; Andrikopoulos, N.; Kefalas, P. Characterisation of certain major polyphenolic antioxidants in grape (*Vitis vinifera* cv. Roditis) stems by liquid chromatography-mass spectrometry. *Eur. Food Res. Technol.* **2008**, *226*, 1075−1079.
(18) Püssa, T.; Floren, J.; Kuldkepp, P.; Raal, A. Survey of Grapevine *Vitis vinifera* Stem Polyphenols by Liquid Chromatography-Diode Array Detection-Tandem Mass Spectrometry. *J. Agric. Food Chem.* **2006**, *54*, 7488−7494.
(19) Rayne, S.; Karacabey, E.; Mazza, G. Grape cane waste as a source of trans-resveratrol and trans-viniferin: High-value phytochemicals with medicinal and anti-phytopathogenic applications. *Ind. Crops Products* **2008**, *27*, 335−340.
(20) Aaviksaar, A.; Haga, M.; Püssa, T.; Roasto, M.; Tsoupras, G. Purification of resveratrol from vine stems. *Proc. Estonian Acad. Sci., Chem.* **2003**, *52*, 155−164.
(21) Melzoch, K.; Hanzlikova, I.; Filip, V.; Buckiova, D.; Smidrkal, J. Resveratrol in parts of vine and wine originating from Bohemian and Moravian vineyard regions. *Agriculturae Conspectus Scientificus* **2001**, *66*, 53−57.
(22) Jordão, A. M.; Ricardo-Da-Silva, J. M.; Laureano, O. Evolution of proanthocyanidins in bunch stems during berry development (*Vitis vinifera* L.). *Vitis* **2001**, *40*, 17−22.
(23) Doshi, P.; Pandurang, A.; Kaushik, B. Phenolic composition and antioxidant activity in grapevine parts and berries (*Vitis vinifera* L.) cv. Kishmish Chornyi (Sharad Seedless) during maturation. *Int. J. Food Sci. Technol.* **2006**, *41*, 1−9.
(24) Palliotti, A.; Cartechini, A. Developmental changes in gas exchange activity in flowers, berries, and tendrils of field-grown Cabernet Sauvignon. *Am. J. Enol. Vitic.* **2001**, *52*, 317−323.
(25) Iland, P.; Dry, P.; Proffitt, T.; Tyerman, S. *The grapevine: from the science to the practice of growing vines for wine*; Patrick Iland Wine Promotions: Adelaide, 2011.
(26) Lichtenthaler, H. K.; Buschmann, C. Extraction of Photosynthetic Tissues: Chlorophylls and Carotenoids. *Current Protocols in Food Analytical Chemistry*; Wrolstad, R. E., Acree, T. E., Decker, E. A, et al., Eds.; John Wiley & Sons: New York, 2001; F4.2.1−F4.2.6.
(27) Lichtenthaler, H. K. Chlorophylls and carotenoids: pigments of photosynthetic biomembranes. *Methods Enzymol.* **1987**, *148*, 350−382.
(28) Lichtenthaler, H. K.; Buschmann, C. Chlorophylls and Carotenoids: Measurement and Characterization by UV-VIS Spectroscopy. *Curr. Protocols Food Anal. Chem.*; Wrolstad, R. E., Acree, T. E., Decker, E. A., et al., Eds.; John Wiley & Sons: New York, 2001; F4.3.1−F4.3.8.
(29) Kwiatkowski, M. J., University of Adelaide, SA, Australia. Personal communication, 2012.
(30) Fukumoto, L. R.; Mazza, G. Assessing antioxidant and prooxidant activities of phenolic compounds. *J. Agric. Food Chem.* **2000**, *48*, 3597−3604.
(31) Pineiro, Z.; Guerrero, R. F.; Fernandez-Marin, M. I.; Cantos-Villar, E.; Palma, M. Ultrasound-Assisted Extraction of Stilbenoids from Grape Stems. *J. Agric. Food Chem.* **2013**, *61*, 12549−12556.
(32) Ristic, R.; Iland, P. G. Relationships between seed and berry development of *Vitis vinifera* L. cv Shiraz: developmental changes in seed morphology and phenolic composition. *Aust. J. Grape Wine Res.* **2005**, *11*, 43−58.
(33) Rubio, M.; Alvarez-Orti, M.; Alvarruiz, A.; Fernandez, E.; Pardo, J. E. Characterization of Oil Obtained from Grape Seeds Collected during Berry Development. *J. Agric. Food Chem.* **2009**, *57*, 2812−2815.
(34) Giovanelli, G.; Brenna, O. V. Evolution of some phenolic components, carotenoids and chlorophylls during ripening of three Italian grape varieties. *Eur. Food Res. Technol.* **2007**, *225*, 145−150.
(35) Kamffer, Z.; Keren, A. B.; Anita, O. Optimization of a method for the extraction and quantification of carotenoids and chlorophylls during ripening in grape berries (*Vitis vinifera* cv. Merlot). *J. Agric. Food Chem.* **2010**, *58*, 6578−6586.
(36) Oliveira, C.; Ferreira, A. C. S.; Pinto, M. M.; Hogg, T.; Alves, F.; Pinho, P. G. D. Carotenoid compounds in grapes and their relationship to plant water status. *J. Agric. Food Chem.* **2003**, *51*, 5967−5971.
(37) Lashbrooke, J. G.; Young, P. R.; Strever, A. E.; Stander, C.; Vivier, M. A. The development of a method for the extraction of carotenoids and chlorophylls from grapevine leaves and berries for HPLC profiling. *Aust. J. Grape Wine Res.* **2010**, *16*, 349−360.
(38) Kowalewska, G.; Szmczak, M. Influence of selected abiotic factors on the decomposition of chlorophylls. *Oceanologia* **2001**, *43*, 315−328.
(39) During, H.; Lang, A. Xylem development and function in the grape peduncle: Relations to bunch stem necrosis. *Vitis* **1993**, *32*, 15−22.

DOI: 10.1021/jf504215e
J. Agric. Food Chem. 2015, 63, 1242−1250

experiments, they were chosen because of their good combining ability with elite inbred testers. The landraces and introduced populations are further being analyzed for macronutrient content[15] and composition, with the aim to identify accessions with drought tolerance and high oil and/or protein quality. The existence of drought tolerance and grain quality in a single accession should enable more effective improvement of commercial genotypes designed to meet the issues of the ongoing climatic changes and increased food demands because of the population growth.

The objectives of the present study were to (1) explore the variability within the drought-tolerant populations previously identified as potentially high oil accessions by near-infrared spectroscopy (NIR) for (a) oil and protein contents determined by standard laboratory methods, (b) FA composition, and (c) tryptophan content, (2) evaluate kernel physical parameters, (3) determine correlations between the traits, and (4) identify genotypes with nutritional value. Because the drought-tolerant mini core collection was selected in field trials performed in both subtropical and temperate zones, the identified genotypes could be used for breeding value-added maize adapted to both environments.

MATERIALS AND METHODS

Plant Material and Field Trials. A total of 25 accessions from the elite drought-tolerant mini core were increased (via pair crossing, i.e., full-sibbing) in two replications, using a completely randomized block design (RCBD), in Zemun Polje, Serbia, during 2010 and 2011 growing seasons. Walter climate diagrams (Figure 1) illustrate temperature and precipitation conditions during the growing season in these 2 years. Standard agronomic practices were used to provide adequate nutrition and keep the fields disease-free. At least 80 ears per population were collected, dried, and shelled, and samples of kernels from the center of each ear were prepared for the grain quality analysis. NIR analysis (Infratec 1241 grain analyzer, FOSS, Sweden) with artificial neural network (ANN) calibrations was used for oil content determination, on non-destructed kernels (300 g/sample) from each replicate (spectra were collected between 800 and 1100 nm). The analyses were performed at the Faculty of Agronomy, Skopje, Macedonia. A total of 13 potentially high oil accessions, with oil content over 4.5% (average content for maize), were selected for further analysis, with 4 of them from Western Balkan, 2 from Iran, 2 from Italy, and 1 each from Bulgaria, France, Pakistan, and the U.S.A. For one introduced population, there are no available data of origin. Information on the 13 analyzed accessions, including agro-ecological group or country of origin, NIR data, kernel type, and color, are given in Table 1. Kernel types were determined according to the CIMMYT/IBPGR descriptor.[16]

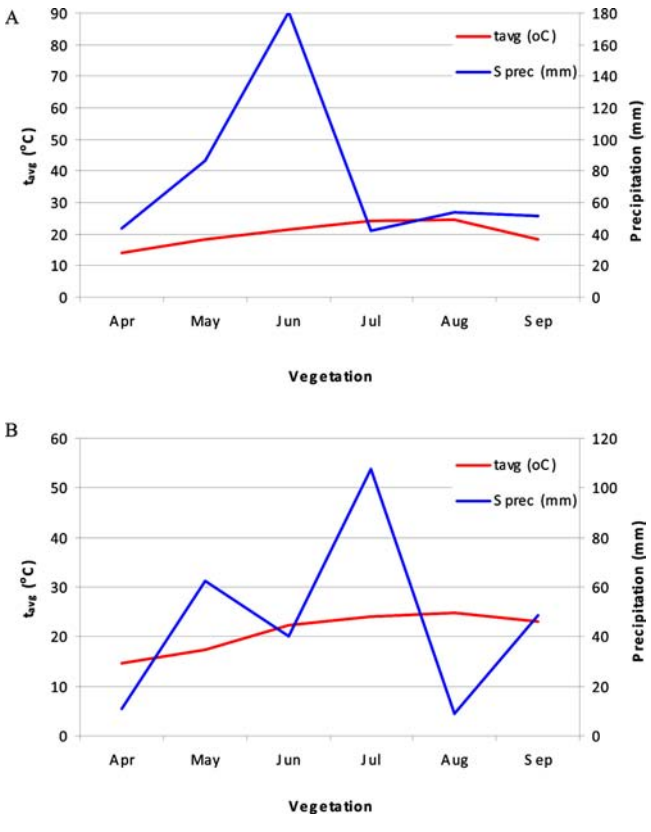

Figure 1. Walter climate diagrams for the years (A) 2010 and (B) 2011 in Belgrade, Serbia. T_{avg}, average temperature (°C); S_{prec}, sum of precipitation (mm).

Determination of the Oil Content and FA Composition. Each accession consisted of 50 g of maize kernels. The oil content was determined by the standard Soxhlet method. Dried kernels were milled in a Cyclotec 1093 lab mill (FOSS Tecator, Sweden) with a particle size of <500 μm, and oil was extracted with hexane in a Soxhlet extractor (INKOLAB, Croatia).

FA composition of the oil samples was determined after transesterification using 0.25 M trimethylsulfonium hydroxide (TMSH, Fluka, Switzerland) in methanol according to EN ISO 5509:2000. Prior to transesterification, 0.05 mL (10 mg mL^{-1}) of the nonadecanoic acid methyl ester (≥99%, Fluka, Switzerland) was added as an internal standard.

The fatty acid methyl esters (FAMEs) were determined by capillary gas chromatography on a GC Shimadzu 2010 (Kyoto, Japan) equipped with a split/splitless injector, fused silica cyanopropyl HP-88 column (length, 100 m; inner diameter, 0.25 mm; film thickness, 0.20 μm; J&W Scientific, Santa Clara, CA), and flame ionization detector. The temperature of the injector was 250 °C, with a split ratio of 1:50, and the detector temperature was 280 °C. Nitrogen was used as the carrier gas at a flow rate of 1.33 mL min^{-1}. The column oven temperature was programmed from 125 to 230 °C. The total analysis time was 50.5 min. FAs were identified by comparing the relative retention time of peaks in the samples to FAME peaks in the Supelco 37 Component FAME mix standard (Supelco, Bellefonte, PA). The chromatographic peak areas were corrected by response factors calculated from the ratios between the peak area of each FA and the internal standard.

Determination of the Protein Content, Tryptophan Content, and Quality Index (QI). Each accession was represented by 60 randomly chosen kernels, divided into two samples of 30 kernels each. Kernels were dried in a controlled oven at 65 °C overnight (16−18 h) and milled in a Cyclotec 1093 lab mill (FOSS Tecator, Sweden) with a particle size of <500 μm. The flour was defatted by hexane treatment for 4 h in a Soxhlet extractor (INKOLAB, Croatia).

The protein content was determined by the standard Kjedahl method using a 2200 Kjeltec auto distillation unit (FOSS, Tecator, Sweden) based on nitrogen determination as explained by Vivek et al.[9] It was estimated from the nitrogen value as percent protein = percent nitrogen × 6.25 (conversion factor for maize).

The tryptophan content was determined using the colorimetric method by Nurit et al.[17] The color was developed in the reaction of flour hydrolysate (obtained by overnight digestion with papain solution at 65 °C) with 2 mL of reagent containing 56 mg of Fe^{3+} dissolved in 1 L of glacial acetic acid and 2 mL of 15 M H_2SO_4. After incubation at 65 °C for 15 min, absorbance was read at 560 nm using an UV-1601 Shimadzu spectrophotometer. The tryptophan content was calculated using a standard calibration curve, developed with known amounts of tryptophan, ranging from 0 to 30 μg mL^{-1}.

QI, defined as the tryptophan/protein ratio in the sample, was calculated as QI = 100(tryptophan content in the sample/protein content in the sample).

Kernel Physical Characteristics. Thousand kernel weight was measured by weighing 5 × 200 unbroken kernels per sample. Flotation

DOI: 10.1021/jf504301u
J. Agric. Food Chem. 2015, 63, 1251−1260

Table 1. High Oil Maize Populations from the Drought-Tolerant Mini Core Collection

	accession[a]	agro-ecological group or country of origin	oil percentage (NIR) (%)	kernel type[b]	kernel color
1	L87	white flinty dents Moravac	5.40	semi-dent	white
2	L244	denty type of U.S.A. Corn Belt dents	4.80	semi-flint	dark yellow
3	L632	denty type of U.S.A. Corn Belt dents	4.75	semi-flint	yellow, red stripes
4	L2033	Mediterranean flints	4.75	flint	yellow
5	IP4347	Iran	4.65	semi-flint	yellow
6	IP4353	Iran	5.05	semi-flint	yellow
7	IP4842	France	5.25	semi-dent	yellow
8	IP6233	Bulgaria	4.90	flint	yellow
9	IP6389	no data	4.65	semi-dent	orange
10	IP6427	Italy	4.85	semi-flint	yellow/white
11	IP6428	Italy	5.35	semi-dent	yellow
12	IP6750	Pakistan	4.65	semi-dent	yellow
13	IP7001	U.S.A.	4.60	semi-flint	yellow

[a]1−4, landraces (L) from Western Balkan; 5−13, introduced populations (IPs). [b]According to the CIMMYT/IBPGR descriptor for maize, semi-dent kernels are intermediate between dent and flint but closer to dent, while semi-flint kernels are flint kernels with soft cup.

Table 2. Oil and Protein Parameters of High Oil Maize Populations from the Drought-Tolerant Mini Core Collection

	oil					protein		
		total FA						
accession	OC[a,b]	SFA[a,c]	MUFA[a,d]	PUFA[a,e]	ω6:3[a]	PC[a,f]	TC[a,g]	QI[a,h]
L87	7.9 a	13.32 h	28.02 g	58.65 b	86.86 b	12.25 b	0.070 bcde	0.58 de
L244	7.7 a	16.40 b	35.00 c	48.60 f	74.52 de	12.25 b	0.075 abcd	0.62 bcd
L632	7.0 bc	12.76 i	45.52 a	41.65 h	60.51 g	11.11 ef	0.077 ab	0.70 a
L2033	6.9 c	15.46 d	31.90 e	52.90 d	67.40 f	11.68 d	0.078 ab	0.67 abc
IP4347	6.6 de	12.65 i	24.19 h	63.15 a	79.40 cd	11.69 d	0.079 ab	0.68 abc
IP4353	7.1 bc	13.55 g	32.21 e	54.22 c	67.47 f	11.02 f	0.076 abc	0.69 a
IP4842	6.5 ef	15.15 e	33.65 d	51.20 e	81.90 bc	11.15 ef	0.066 de	0.60 de
IP6233	6.3 f	16.16 c	32.44 e	51.40 e	98.48 a	11.24 e	0.076 abcd	0.67 abc
IP6389	6.0 g	15.26 de	36.76 b	48.20 f	58.05 g	12.26 b	0.067 cde	0.55 e
IP6427	6.6 ef	16.54 b	32.28 e	51.17 e	72.45 ef	12.37 ab	0.074 abcd	0.61 cde
IP6428	7.3 b	17.91 a	35.00 c	47.10 g	61.66 g	11.93 c	0.081 a	0.68 ab
IP6750	6.8 cd	16.02 c	32.76 de	51.22 e	67.65 f	12.45 a	0.076 abc	0.62 bcde
IP7001	5.8 g	14.30 f	30.82 f	54.89 c	70.19 ef	10.58 g	0.063 e	0.59 de
mean	6.8	15.04	33.12	51.87	73.15	11.69	0.074	0.63
SD[i]	0.87	1.63	4.86	5.32	14.35	1.18	0.01	0.07
CV[j]	2.42	0.91	1.92	1.25	4.92	0.58	5.97	5.92
$LSD_{0.05}$[k]	0.25	0.21	0.98	0.99	5.54	0.15	0.01	0.07

[a]Means followed by the same letter(s) within the same columns are not significantly different ($p < 0.05$). [b]OC = oil content. [c]SFA = saturated fatty acid. [d]MUFA = monounsaturated fatty acid. [e]PUFA = polyunsaturated fatty acid. [f]PC = protein content. [g]TC = tryptophan content. [h]QI = quality index. [i]SD = standard deviation. [j]CV = coefficient of variation. [k]$LSD_{0.05}$ = least significant difference at $p < 0.05$.

index (FI) was measured by soaking 100 randomly selected kernels into an aqueous sodium nitrate solution with a specific weight of 1.25 g cm^{-3} at 35 °C, and values were expressed as a percentage of floating kernels. Kernel dimensions were obtained by measuring thickness, width, and length of a 100 kernels per sample using a digital micrometer. The hull, endosperm, and germ were manually dissected after soaking 50 g of kernels for 2 min in 100 mL of water. After the water was drained, the wet kernels were first manually separated into hull, endosperm, and germ, with the resulting anatomical parts dried in an oven set at 60 °C and weighed to calculate relative percentages. The kernel hardness was measured by a modified Stenvert−Pomeranz method, by milling 20 g of kernels in the micro hammer mill (3600 rpm, 2 mm sieve). Results were expressed as milling response and hard fraction portion (%). The milling response index presents the time (s) necessary for grain grinding until the top level of the material collected in a glass cylinder (125 × 25 mm) reaches the level of 17 mL.

Statistical Methods. All chemical analyses were performed in two replicates, and the results were statistically analyzed. A factorial analysis of variance (ANOVA) for trials was conducted using randomized complete block (RCB) design. Treatment means were tested using Fisher's least significant difference (LSD). All statistical analyses were performed in MSTAT-C software. Pearson's correlation coefficient was used for determining correlations between the estimated traits.

RESULTS AND DISCUSSION

Biochemical Analysis. Laboratory analysis of the oil content in the samples (Table 2) revealed higher values compared to previously performed NIR analysis (Table 1). However, correlation between the two methods was significant at $p < 0.05$ (data not shown). This could be expected, because it was shown that NIR estimation and reference analysis for the oil content in maize kernels were different and that more studies are needed before obtaining accurate measurements using NIR methods.[18] In this context, the oil content determined by the standard Soxhlet method is more accurate.

Populations from the drought-tolerant mini core collection showed significant variability in oil and protein contents as well as in FA composition and tryptophan content (Tables 2 and 3).

DOI: 10.1021/jf504301u
J. Agric. Food Chem. 2015, 63, 1251−1260

Table 3. FA Composition (Percentage of Total Oil) of High Oil Maize Populations from the Drought-Tolerant Mini Core Collection

	FAs											
accession	16:0[a,b]	16:1[a,c]	17:0[a,d]	18:0[a,e]	18:1[a,f]	18:2[a,g]	18:3[a,h]	20:0[a,i]	20:1[a,j]	20:3[a,k]	22:0[a,l]	24:0[a,m]
L87	11.25 g	0.110 a	0.030 a	1.47 l	27.70 h	57.92 b	0.675 ef	0.320 g	0.205 b	0.055 i	0.115 d	0.140 g
L244	13.49 a	0.065 c	0.030 a	2.20 h	34.72 c	47.86 f	0.645 ef	0.435 f	0.210 b	0.095 fg	0.110 d	0.140 g
L632	9.71 j	0.040 d	0.025 a	2.20 h	45.24 a	40.86 h	0.680 def	0.525 cd	0.235 a	0.110 ef	0.135 c	0.160 def
L2033	12.18 de	0.090 b	0.060 a	2.37 f	31.36 fg	52.03 d	0.790 ab	0.510 cde	0.200 b	0.075 h	0.150 bc	0.190 ab
IP4347	10.25 i	0.085 b	0.060 a	1.69 k	23.96 i	62.26 a	0.785 ab	0.330 g	0.145 d	0.105 fg	0.150 bc	0.170 cde
IP4353	10.62 h	0.085 b	0.025 a	2.12 i	31.95 ef	53.33 c	0.795 ab	0.465 ef	0.170 c	0.095 fg	0.140 bc	0.175 bcd
IP4842	11.64 f	0.035 d	0.030 a	2.59 e	33.44 d	50.49 e	0.620 f	0.585 ab	0.170 c	0.090 gh	0.153 b	0.165 cdef
IP6233	12.05 e	0.065 c	0.065 a	3.18 b	32.29 ef	50.72 e	0.515 g	0.540 bcd	0.085 e	0.155 ab	0.155 b	0.170 cde
IP6389	12.34 cd	0.095 ab	0.030 a	1.89 j	36.24 b	47.22 f	0.820 a	0.585 ab	0.200 b	0.165 a	0.210 a	0.205 a
IP6427	12.88 b	0.040 d	0.025a	2.81 c	32.07 ef	50.35 e	0.700 cde	0.505 cde	0.170 c	0.125 de	0.155 b	0.165 cdef
IP6428	13.68 a	0.085 b	0.065 a	3.25 a	34.74 c	46.19 g	0.750 bc	0.610 a	0.170 c	0.155 ab	0.155 b	0.150 fg
IP6750	12.48 c	0.095 ab	0.070 a	2.63 d	32.52de	50.33 e	0.745 bcd	0.545 bc	0.150 d	0.135 cd	0.145 bc	0.155 efg
IP7001	11.07 g	0.085 b	0.060 a	2.35 g	30.58 g	53.97 c	0.770 ab	0.495 de	0.150 d	0.145 bc	0.140 bc	0.180 bc
mean	11.82	0.075	0.044	2.36	32.84	51.04	0.715	0.496	0.174	0.116	0.147	0.167
SD[n]	1.22	0.19	0.03	0.58	4.85	5.32	0.11	0.1	0.05	0.07	0.03	0.02
CV[o]	1.07	13.25	20.95	6.33	1.99	1.28	6.05	7.41	10.69	9.33	9.8	7.09
$LSD_{0.05}$[p]	0.19	0.015	0.049	0.015	1.01	1.01	0.069	0.049	0.015	0.015	0.015	0.015

[a]Means followed by the same letter(s) within the same columns are not significantly different ($p < 0.05$). [b]16:0 = palmitic acid. [c]16:1 = palmitoleic acid. [d]17:0 = heptadecanoic acid. [e]18:0 = stearic acid. [f]18:1 = oleic acid. [g]18:2 = linoleic acid. [h]18:3 = linolenic acid. [i]20:0 = arachidic acid. [j]20:1 = eicosenoic acid. [k]20:3 = eicosatrieonic acid. [l]22:0 = behenic acid. [m]24:0 = lignoceric acid. [n]SD = standard deviation. [o]CV = coefficient of variation. [p]$LSD_{0.05}$ = least significant difference at $p < 0.05$.

However, they can be all considered as high oil and protein genotypes when compared to oil and protein contents of the yellow commodity maize given by Watson;[4] oil content of the analyzed accessions was higher from 35% (IP7001) to 84% (L87), and protein content of the analyzed accessions was higher from 11% (IP7001) to 31% (IP6750). Enhanced nutritional quality of maize with high levels of essential amino acids tryptophan and lysine, such as o2 and QPM, requires tryptophan content and QI (tryptophan/protein ratio) in the whole grain sample to be higher than 0.075 and 0.80%, respectively.[9] Four accessions (L87, IP4842, IP6389, and IP7001) had a low tryptophan content typical for standard maize genotypes. One accession (IP6427) had an elevated tryptophan content of 0.074% (a value close to the threshold of 0.075%) and should be further tested for defining it as a high tryptophan accession. The remaining eight accessions had a tryptophan level over 0.075% and can be considered as high tryptophan genotypes. This also implies that they have high levels of lysine because tryptophan and lysine values are highly correlated and the value of lysine is 3 times that of tryptophan.[9] QI was low in all accessions, with the average value of 0.63.

FA composition for each accession is given in Table 3. Typical dent maize oil has 61.9% linoleic, 24.1% oleic, 11% palmitic, 2% stearic, and 0.7% linolenic acids, while all of the other acids are present only in traces.[12] In our research, palmitoleic (16:1) and heptadecanoic (17:0) acids exhibited less than 0.1% and eicosenoic (20:1), eicosatrieonic (20:3), behenic (22:0), and lignoceric (24:0) acids exhibited less than 0.2% of the total FA content. Arachidic acid (20:0) was the most abundant trace FA, with the average value of 0.49%.

As expected, linoleic (18:2) and oleic (18:1) acids were the most abundant FAs present in the oil samples, accounting for approximately 81−85% of the total FA composition. Their average values were 51.04 and 32.84%, respectively, showing low linoleic acid content and high oleic acid content in comparison to typical dent maize. On average, polyunsaturated linolenic (18:3) and saturated palmitic (16:0) and stearic (18:0) acids were slightly higher than in typical dent maize. Considering saturated fatty acids (SFAs) and unsaturated FAs (Table 2), the most abundant were polyunsaturated fatty acids (PUFAs) with 51.87%, followed by monounsaturated fatty acids (MUFAs) with 33.12% and SFAs with 15.04%. Most of the accessions can be considered high in oleic acid (MUFA) and low in linoleic and linolenic acids (PUFA). Breeding for high oleic acid maize oil can improve the average modern diet rich in saturated fats from animal sources. It was shown that oleic acid has positive effects in reducing serum cholesterol and low-density lipoproteins (LDLs)[7] as well as in preventing degenerative diseases and cancer.[7,19] The same authors found similar positive effects of PUFAs on health, but none of the high oil accessions from the drought-tolerant mini core showed a high content of these FAs. The only exception was accession IP4347, with slightly higher contents of linoleic and linolenic acids than the contents typical for dent maize (62.26 and 0.785% versus 61.9 and 0.70%, respectively). Also, the ω6:3 (linoleic/linolenic) ratios were high, with the average value of 73.15. A significant increase of linolenic acid of over 4% and, thus, a significant decrease in ω6:3 ratio (with values below 10) was achieved in a long-term breeding program through eight cycles of recurrent selection for agronomic traits and high oil content in four subtropical white and yellow maize populations.[20] These changes in linolenic acid content and ω6:3 ratio were achieved from initial populations that had similar contents of linoleic and linolenic acids as our high oil drought-tolerant accessions, suggesting the possibility that they also could be the source for such improvements. This is important because linolenic acid exerts better health benefits but is more prone to oxidation and flavor reversion.

Several accessions can be considered as high SFAs, and some of them had SFAs over 16%. Accession IP6428 proved to be the most prominent high SFA (17.9%), with 13.68% palmitic, 3.20% stearic, and 0.61% arachidic acids. Maize genotypes with high total SFAs can improve manufacturing of margarines and

DOI: 10.1021/jf504301u
J. Agric. Food Chem. 2015, 63, 1251−1260

Table 4. Kernel Physical Characteristics of High Oil Maize Populations from the Drought-Tolerant Mini Core Collection

			kernel dimensions[a]			kernel proportions[a]			kernel hardness[a]	
accession	thousand kernel weight[a] (g)	FI[a] (%)	width (mm)	length (mm)	thickness (mm)	hull (g/100 g)	endosperm (g/100 g)	germ (g/100 g)	hard fraction portion (%)	milling response (s)
L87	305.00 fg	20.44 d	8.7 bcd	8.8 h	4.8 a	9.41 a	77.50 d	13.09 a	64.97 bc	13.44 a
L244	320.00 de	22.44 d	8.1 fg	10.4 c	4.4 cde	6.54 b	83.56 c	9.90 b	63.38 de	11.34 ab
L632	340.00 ab	43.09 ab	8.3 ef	10.5 c	4.2 ef	6.97 ab	83.86 bc	9.17 bc	58.02 g	11.10 ab
L2033	308.08 efg	48.20 a	8.5 cde	9.8 ef	4.5 bcde	5.83 b	87.32 a	6.85 cd	60.62 f	11.82 ab
IP4347	298.05 gh	32.30 c	7.8 h	10.8 ab	4.2 ef	5.61 b	87.01 a	7.40 cd	59.93 f	12.18 ab
IP4353	273.00 i	3.10 f	7.1 i	10.9 a	3.9 f	7.05 ab	85.90 abc	7.03 cd	62.64 e	12.21 ab
IP4842	325.00 cd	3.34 f	8.4 de	10.4 cd	4.3 de	6.03 b	87.27 a	6.70 d	64.84 bc	12.39 ab
IP6233	342.50 ab	10.03 ef	8.8 bc	10.3 cd	4.6 abcd	6.45 b	87.55 a	6.00 d	64.52 bcd	11.15 ab
IP6389	333.13 bc	8.27 ef	8.6 bcd	9.7 efg	4.8 ab	6.88 ab	86.45 a	6.66 d	69.22 a	12.11 ab
IP6427	350.00 a	34.52 bc	9.2 a	10.0 de	4.7 abc	5.40 b	88.16 a	6.44 d	60.84 f	11.92 ab
IP6428	312.50 def	25.94 cd	8.8 b	9.6 fg	4.5 abcd	5.45 b	88.10 a	6.45 d	63.98 cd	11.85 ab
IP6750	288.05 h	16.95 de	8.3 efg	9.4 g	4.4 cde	7.24 ab	86.00 ab	6.75 d	65.53 b	11.70 ab
IP7001	315.00 def	3.19 f	8.0 gh	10.5 bc	4.3 de	6.95 ab	86.67 a	6.38 d	64.86 bc	10.72 b
mean	316.20	20.91	8.4	10.1	4.4	6.60	85.80	7.60	63.33	11.84
SD[b]	2.318	15.401	0.542	0.61	0.299	1.358	2.908	2.138	3.091	1.241
CV[c]	1.86	21.39	1.6	1.8	3.42	17.99	1.28	14.45	2.19	10.53
$LSD_{0.05}$[d]	12.83	9.744	0.3	0.4	0.3	2.59	2.40	2.39	1.17	2.72

[a]Means followed by the same letter(s) within the same columns are not significantly different ($p < 0.05$). [b]SD = standard deviation. [c]CV = coefficient of variation. [d]$LSD_{0.05}$ = least significant difference at $p < 0.05$.

Table 5. ANOVA Mean Squares for Biochemical Components

						principal FAs						
source of variation	df[a]	OC[b]	SFA[c]	MUFA[d]	PUFA[e]	16:0[f]	18:0[g]	18:1[h]	18:2[i]	18:3[j]	PC[k]	TC[l]
year (Y)	1	8.074[m]	4.935[m]	678.204	38.769[n]	1.765	0.449	17.960	38.873[n]	0.093[n]	45.947[o]	0.001[m]
genotype (G)	12	1.509[o]	10.487[o]	604.735[o]	113.938[o]	5.847[o]	1.125[o]	95.762[o]	113.750[o]	0.030[o]	1.519[o]	0.000[o]
$G \times Y$	12	0.957[o]	0.329[o]	158.778[o]	1.873[o]	0.176[o]	0.040	1.172[n]	1.779[m]	0.008[m]	0.625[o]	0.000[o]
error	24	0.027	0.019	12.935	0.418	0.016	0.022	0.429	0.427	0.002	0.005	0.000

[a]df = degrees of freedom. [b]OC = oil content. [c]SFA = saturated fatty acid. [d]MUFA = monounsaturated fatty acid. [e]PUFA = polyunsaturated fatty acid. [f]16:0 = palmitic acid. [g]18:0 = stearic acid. [h]18:1 = oleic acid. [i]18:2 = linoleic acid. [j]18:3 = linolenic acid. [k]PC = protein content. [l]TC = tryptophan content. [m]Significant at the 0.05 level. [n]Significant at the 0.1 level. [o]Significant at the 0.01 level.

shortenings without *trans* fats, which raise LDL−cholesterol and lower high-density lipoprotein (HDL)−cholesterol.[12]

Kernel Physical Parameters. Profiles of grain physical parameters are given in Table 4. These parameters are important for dry milling and food processing industries. Because the accessions analyzed in our work are sources of favorable alleles for breeding genotypes with improved nutritional quality, the kernel parameters are to be understood in that context. Kernels with thousand kernel weights greater than 320 g and FI less than 20% are desirable in food processing.[21] In six accessions, thousand kernel weight was over the desirable 320 g, while the remaining seven accessions had lower values from approximately 2% (IP6428 and IP7001) to 15% (IP4353). Great variability was found for FI among the analyzed accessions. It was below 10% in four accessions and below 20% in another two accessions. In the remaining seven accessions, FI was in the range from 20.44% (L87) to 48.2% (L2033). The hardness classification based on FI proposed by Salinas et al.[22] defined that very hard kernels have values between 0 and 12%, hard kernels have values between 13 and 37%, intermediary hard kernels have values between 38 and 62%, and soft kernels have values over 63%. Results showed that none of the accessions had soft kernels, because the highest detected value was 48.20% (L2033).

Kernel dimensions are important for breakfast cereals and oil crushing.[21] The average values of kernel dimensions as well as kernel proportions were compared to average values of these traits given for high oil populations in Preciado-Ortiza et al.[20] Comparisons were performed with data for C7 cycle of selection of four populations, because their oil content (7.5, 7.6, 6, and 6.3%) coincided with the oil content of the accessions. The average kernel dimensions of the accessions were 8.4, 10.1, and 4.4 mm for width, length, and thickness, respectively. Kernel thickness was in good agreement with this trait value found in high oil populations. However, kernel width and length were lower for 5 and 14%, respectively. Considering kernel proportions, the largest part of the kernels was made of endosperm (85.8% on average), followed by the germ (7.6% on average) and the hull (6.6% on average). Endosperm proportions were in good agreement with the same trait by Preciado-Ortiza et al.,[20] but the germ proportions were smaller for most accessions for approximately 28%, except for accessions L244, L632, and L87.

The hardness of the maize kernel is the most important physical characteristic in dry milling and alkaline cooking industries as well as for feed efficiency. Results obtained for milling response showed low variability among the accessions, while higher variability was found for the hard fraction portion. In comparison to 20 commercial hybrids analyzed by Radosavljevic et al.,[23] the average value of milling response was lower (11.84 versus 12.80 s) and that of the hard fraction portion was higher (63.33 versus 58.80%) among the

DOI: 10.1021/jf504301u
J. Agric. Food Chem. 2015, 63, 1251−1260

Table 6. ANOVA Mean Squares for Kernel Physical Characteristics

				kernel dimensions			kernel proportions			kernel hardness	
source of variation	df[a]	1000KW[b]	FI[c]	KW[d]	KL[e]	KT[f]	HP[g]	GP[h]	EP[i]	HFP[j]	MR[k]
year (Y)	1	5.480	349.718	0.019[l]	0.534	0.425	0.260	0.775	1.908	32.564[l]	7.104[l]
genotype (G)	12	19.912[m]	937.855[m]	1.510[m]	1.162[m]	0.285[m]	4.513[n]	16.007[m]	32.932[m]	32.121[m]	1.913
$G \times Y$	12	2.174	13.804	0.022	0.032	0.015	0.464	0.873	0.963	0.553	1.031
error	24	0.347	20.002	0.033	0.018	0.023	1.411	1.207	1.209	1.921	1.554

[a]df = degrees of freedom. [b]1000KW = thousand kernel weight. [c]FI = flotation index. [d]KW = kernel width. [e]KL = kernel length. [f]KT = kernel thickness. [g]HP = hull proportion. [h]GP = germ proportion. [i]EP = endosperm proportion. [j]HFP = hard fraction portion. [k]MR = milling response. [l]Significant at the 0.1 level. [m]Significant at the 0.01 level. [n]Significant at the 0.05 level.

accessions. The hybrids analyzed by Radosavljevic et al.[23] comprised dent, high oil, waxy, white endosperm, flint, and popcorn hybrids, which showed great variability for hardness. Milling response ranged from 9.4 s (in a dent hybrid) to 19.9 s (in a popcorn hybrid), and the hard fraction portion ranged from 49.6% (in a dent hybrid) to 75.2% (in a popcorn hybrid). The two analyzed oil hybrids showed milling response of 14.1 and 11.6 s, while their hard fraction portion was 63.4 and 58.8%. Because these values coincide with the values obtained for the accessions (Table 4), it can be said that kernel hardness of the high oil accessions is within the range of kernel hardness of the commercial oil hybrids.

Statistical Analysis. Results of the ANOVA for oil content, total FAs, five principal FAs, and protein and tryptophan contents are given in Table 5. Genotype effect was significant for all of the traits analyzed ($p < 0.01$). Year effect was not significant for MUFAs and palmitic, stearic, and oleic acids, while the highest effect was noted for the protein content ($p < 0.01$). Except for stearic acid, all of the other analyzed biochemical components were affected by the genotype × year interaction. Considering trace FAs, the year effect was significant only for eicosenoic ($p < 0.05$) and eicosatrienoic ($p < 0.01$) acids, while genotype and the genotype × year interaction affected all of them (data not shown).

ANOVA for kernel physical characteristics (Table 6) revealed that most of them were not affected by the year, except kernel length, endosperm hardness, and milling response ($p < 0.1$). The genotype effect was significant for all of the traits analyzed at $p < 0.01$, except for hull proportion ($p < 0.05$) and milling response (non-significant). The genotype × year effect was not significant for any of the traits measured. The differences of the values of the traits that were significantly affected by the year are illustrated in Figure 2.

The years differed in total precipitation and number of days, with a maximum temperature over 30 °C during the vegetation period (from April to September), with 2011 having less rainfall and higher temperatures (Figure 1). Biochemical and kernel physical characteristics that were significantly influenced by the year are presented in Figure 2. Although it can be stated that 2010 was optimal and that drought occurred in 2011, oil and protein contents significantly increased in 2011. A significant increase in the same year was also noted for tryptophan, linoleic and linolenic acids, total PUFAs, one monounsaturated trace FA (eicosenoic acid), and two kernel hardness parameters (hard fraction portion and milling response). On the contrary, eicosatrienoic acid, SFAs, and kernel width values were significantly higher in 2010. Most of these results were not expected. It has been shown that drought significantly reduces oil and linoleic acid contents and increases oleic acid content in maize.[24] Similar results were obtained for sunflower[25,26] and in *Moringa oliefera*.[27] However, Petcu et al.[28] found different trends under drought stress, such as an increase in linoleic acid and a decrease in oleic acid of sunflower. This is in accordance with our results, because oleic acid decreased but not significantly (data not shown). Different data on the protein content change under drought stress can be found in the literature. A significant decrease was obtained by Ali et al.,[24] and a significant increase was obtained by Zaidi et al.[29] In the later paper, a significant increase for tryptophan and lysine contents under drought was also recorded. Our results could possibly be explained by rainfall distribution throughout the vegetation period, because total precipitation was not substantially different during the pollination and grain filling period (from July to September) in 2010 and 2011 growing seasons (147 versus 164 mm, respectively). Also, the genotypes analyzed were selected as highly drought tolerant in both subtropical and temperate regions.[14] To precisely determine the effects of drought on the examined kernel traits, an experiment under controlled temperature and water regimes should be performed.

Correlations between biochemical components as well as between biochemical and physical components are given in Table 7. Significant positive correlations were found between oil and protein contents as well as oil and tryptophan contents ($p < 0.01$). Several other studies have shown positive correlations between oil and protein contents in maize kernels.[30−32] Song and Chen[32] reported high positive correlation between lysine and oil, which is in accordance with our results, because lysine and tryptophan values are highly correlated and their ratio is normally 3:1.[9] These positive relationships are important for simultaneous improvement of different nutritional quality traits, because maize is widely used in both human and animal nourishment.

All correlations between oil and principal FA contents were non-significant ($p < 0.05$), but significance was noted with all trace FAs (data not shown). Non-significant correlations between oil and saturated palmitic and stearic acids are in accordance with the results presented in other papers.[33,34] However, in the analysis of elite maize breeding material, Dunlap et al.[35] found small but significant positive correlations between the oil content and levels of stearic and oleic acids. Several other studies representing different genetic backgrounds showed significant positive correlations between oil and oleic acid contents as well as significant negative correlations between oil and PUFA (linoleic and linolenic acids) contents.[33,34,36] In our study, non-significant correlations had the same trend; oleic acid was positively correlated ($r = 0.017$) while linoleic and linolenic acids were negatively correlated ($r = -0.016$ and -0.1363, respectively) with the oil content (data not shown). The lack of significant positive correlations between oil and FAs disables simultaneous selection for increased oil content and FAs, but instead, the

DOI: 10.1021/jf504301u
J. Agric. Food Chem. 2015, 63, 1251−1260

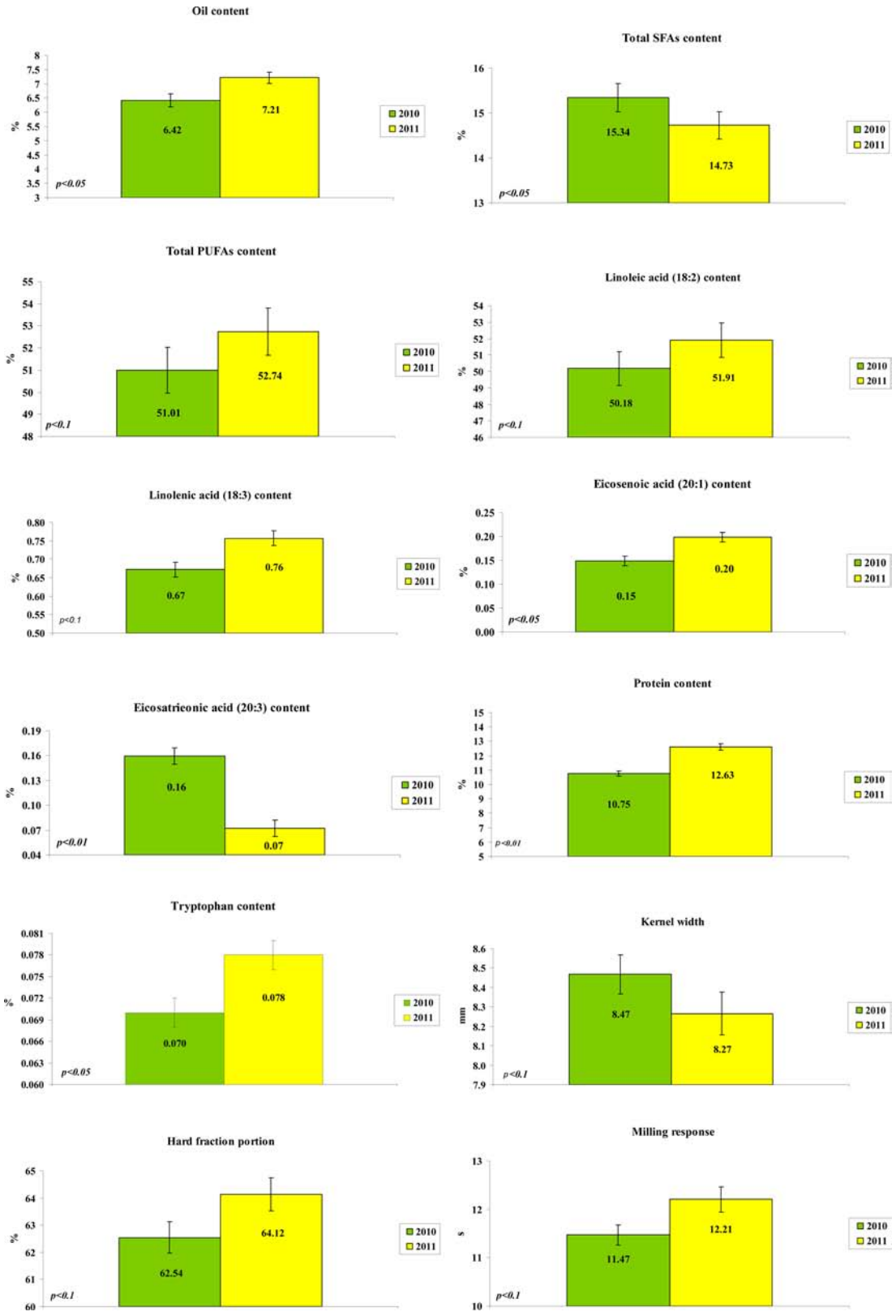

Figure 2. Biochemical and kernel physical characteristics that were significantly influenced by the year. Green bar, optimal temperature and precipitation conditions (2010); yellow bar, drought (2011).

oil content could be increased independently, along with altering FA composition into a desired profile.

Considering correlations between principal FAs, palmitic acid was positively correlated with oleic acid ($p < 0.01$) and negatively correlated with linoleic acid ($p < 0.05$). Correlations between 18-carbon FAs were either non-significant (stearic and oleic, oleic and linolenic, and linoleic and linolenic acids) or significantly negative at $p < 0.01$ (stearic and linoleic, stearic

DOI: 10.1021/jf504301u
J. Agric. Food Chem. 2015, 63, 1251−1260

Table 7. Correlations between Kernel Biochemical and Physical Characteristics

		principal FAs											
	OC[a]	16:0[b]	18:0[c]	18:1[d]	18:2[e]	18:3[f]	SFA[g]	MUFA[h]	PUFA[i]	ω6:3	PC[j]	TC[k]	QI[l]
16:0	ns												
18:0	ns	ns											
18:1	ns	0.433[m]	ns										
18:2	ns	−0.317[n]	−0.402[m]	−0.955[m]									
18:3	ns	ns	−0.453[m]	ns	ns								
SFA	ns	0.927[m]	0.738[m]	ns	ns	−0.290[n]							
MUFA	ns	ns	ns	0.999[m]	−0.953[m]	ns	ns						
PUFA	ns	−0.317[n]	−0.407[m]	−0.955[m]	1[m]	ns	−0.422[m]	−0.953[m]					
ω6:3	ns	ns	ns	−0.380[m]	0.350[n]	−0.800[m]	ns	−0.393[m]	0.334[n]				
PC	0.567[m]	ns	ns	ns	ns	0.376[m]	ns	ns	ns	−0.313[n]			
TC	0.437[m]	ns	ns	ns	ns	ns	ns	ns	ns	ns	0.548[m]		
QI	ns	ns	ns	ns	ns	ns	ns	ns	ns	ns	ns	0.526[m]	
1000KW[o]	ns	ns	0.277[n]	0.407[m]	−0.436[m]	−0.370[n]	ns	0.408[m]	0.443[m]	ns	ns	ns	ns
FI[p]	ns	ns	ns	ns	ns	ns	ns	ns	ns	ns	ns	0.307[n]	0.345[n]
KW[q]	ns	0.512[m]	0.394[m]	ns	−0.309[n]	−0.328[n]	0.548[m]	ns	−0.312[n]	ns	ns	ns	ns
KL[r]	ns	−0.413[m]	ns	ns	ns	ns	−0.302[n]	ns	ns	ns	−0.346[n]	ns	0.278[n]
KT[s]	ns	0.515[m]	ns	ns	ns	ns	0.420[m]	ns	ns	ns	ns	ns	ns
HP[t]	ns	ns	−0.429[m]	ns	ns	ns	−0.346[n]	ns	ns	ns	ns	ns	ns
EP[u]	−0.430[m]	ns	ns	ns	ns	ns	0.426[m]	ns	ns	ns	ns	ns	ns
GP[v]	0.467[m]	ns	−0.446[m]	ns	ns	ns	−0.360[m]	ns	ns	ns	ns	ns	ns
HFP[w]	ns	0.317[n]	ns	ns	ns	ns	ns	ns	ns	ns	0.321[n]	ns	−0.483[m]
MR[x]	0.372[m]	ns	ns	−0.286[n]	0.306[n]	ns	ns	−0.370[m]	0.303[n]	ns	0.381[m]	ns	ns

[a]OC = oil content. [b]16:0 = palmitic acid. [c]18:0 = stearic acid. [d]18:1 = oleic acid. [e]18:2 = linoleic acid. [f]18:3 = linolenic acid. [g]SFA = saturated fatty acid. [h]MUFA = monounsaturated fatty acid. [i]PUFA = polyunsaturated fatty acid. [j]PC = protein content. [k]TC = tryptophan content. [l]QI = quality index. [m]Significant at the 0.01 level. [n]Significant at the 0.05 level. [o]1000KW = thousand kernel weight. [p]FI = flotation index. [q]KW = kernel width. [r]KL = kernel length. [s]KT = kernel thickness. [t]HP = hull proportion. [u]EP = endosperm proportion. [v]GP = germ proportion. [w]HFP = hard fraction portion. [x]MR = milling response.

J. Agric. Food Chem. 2015, 63, 1251−1260 DOI: 10.1021/jf504301u

and linolenic, and oleic and linoleic acids). These results are only partially in accordance with literature data. Wassom et al.[36] found non-significant or weak correlations between palmitic acid and 18-carbon FAs, while all 18-carbon FAs were significantly mutually correlated. On the other hand, Orhun and Korkut[34] reported significant correlations between palmitic acid and 18-carbon FAs and non-significant correlations among 18-carbon FAs. However, a near 1:1 negative correlation between oleic and linoleic acids found within the analyzed accessions was also reported in other studies.[34,36−39] The genetic correlation between oleic and linoleic acids, which is near unity, indicates that most or all of the genes responsible for variation in the accumulation of these two acids are closely linked or pleiotropic.[36]

Correlations between kernel biochemical and physical characteristics revealed, as expected, that the germ proportion was positively correlated with the oil content ($p < 0.01$). This kernel characteristic has been recognized as the most relevant characteristic in high oil breeding programs.[40−43] Among principal FAs, only stearic acid was significantly correlated with germ percent (negatively; $p < 0.01$). This differs from the results presented by Preciado-Ortiza et al.,[20] where all FAs were significantly correlated with germ proportion. In our work, significant correlations with germ were found for all trace FAs (data not presented).

Thousand kernel weight was positively correlated with stearic and oleic acids but negatively correlated with linoleic and linolenic acids. No significant correlation was found between this trait and the oil content, while in the study by Dorsey-Redding et al.,[44] these two traits were correlated at $p < 0.001$. They also noted that the correlation between the protein content and thousand kernel weight was not significant, and this is in accordance with our results for the accessions. Considering other biochemical components analyzed, tryptophan was not significantly correlated with this kernel parameter, while significant positive correlation was found for MUFAs and PUFAs.

The SFA content was significantly correlated with all kernel dimensions and kernel proportions, positively with kernel width, kernel thickness, and endosperm proportion ($p < 0.01$), while negatively with kernel length and hull and germ proportions ($p < 0.01$, $p < 0.01$, and $p < 0.05$, respectively). The hard fraction portion was in positive correlation with palmitic acid and protein content ($p < 0.05$), while milling response was positively correlated with oil, linoleic acid, total PUFAs, and protein content ($p < 0.01$, $p < 0.05$, $p < 0.05$, and $p < 0.01$, respectively) and negatively correlated with oleic acid and total MUFAs ($p < 0.05$ and $p < 0.01$, respectively). These two hardness parameters were also positively correlated with oil and protein contents by Dorsey-Redding et al.[44]

Oil composition and FA concentrations are regulated by more than 40 QTL.[38,45] It is possible that discrepancies in the statistical results of different experiments are due to different genetic backgrounds of the analyzed genotypes and different environmental effects. Differences between our results and results obtained in other studies could also be due to differences in materials analyzed (non-selected populations, versus elite, commercial material). These accessions could harbor alleles not present in commercial germplasm, leading to gene actions involved in oil, FA, and protein metabolic pathways different from the pathways present in elite germplasm.

It was shown that maize kernel nutritional value can be improved by introducing landraces into breeding programs. Genes from exotic germplasm were used for developing maize lines with high total SFAs,[12] and a single cross hybrid was developed from an Italian landrace with high carotenoid content that is being used by an Italian beer industry.[3] The results of biochemical analysis presented in this report indicate considerable potential of the drought-tolerant accessions for improving value-added traits of the commercial genotypes. Moreover, several accessions with multiple nutritional advantages were identified. For example, L632 had high oil and oleic acid contents as well as high tryptophan content, while IP6428 besides high oil and tryptophan contents was also abundant in SFA. On the other hand, positive correlation between palmitic and oleic acids enables the use of IP6428 for improving lines for high contents of these two FAs. Because the drought-tolerant accessions were selected in field trials performed in both subtropical and temperate zones, the identified genotypes could be used for breeding maize with value-added traits adapted to both environments.

AUTHOR INFORMATION

Corresponding Author

*Telephone: +381-11-3756704. Fax: +381-11-3756707. E-mail: idragana@mrizp.rs.

Funding

This research was supported by the Ministry of Education, Science and Technological Development of Republic of Serbia through Project TR31028 "Exploitation of Maize Diversity To Improve Grain Quality and Drought Tolerance".

Notes

The authors declare no competing financial interest.

REFERENCES

(1) FAOSTAT. http://faostat3.fao.org/browse/rankings/commoditiesbyregions/E (accessed Aug 2014).

(2) Pollak, L. M.; Scott, M. P. Breeding for grain quality traits. *Maydica* **2005**, *50*, 247−257.

(3) Berardo, N.; Mazzinelli, G.; Valoti, P.; Lagana, P.; Redaelli, R. Characterization of maize germplasm for the chemical composition of the grain. *J. Agric. Food Chem.* **2009**, *57*, 2378−2384.

(4) Watson, S. A. Description, development, structure and composition of the corn kernel. In *Corn: Chemistry and Technology*, 2nd ed.; White, J., Johnson, L., Eds.; American Association of Cereal Chemists: St. Paul, MN, 2003; pp 69−101.

(5) Weber, E. J. Lipids of the kernel. In *Corn: Chemistry and Technology*; Watson, S. A., Ramstad, P. E., Eds.; American Association of Cereal Chemists: St. Paul, MN, 1987; pp 311−349.

(6) White, P. J.; Weber, E. J. Lipids of the kernel. In *Corn: Chemistry and Technology*; White, P. J., Johnson, L. A., Eds.; American Association of Cereal Chemists: St. Paul, MN, 2002; pp 355−395.

(7) Mattson, F. H.; Grundy, S. M. Comparison of effects of dietary saturated, monounsaturated and polyunsaturated fatty acids on plasma lipids and lipoproteins in man. *J. Lipid Res.* **1985**, *26*, 194−202.

(8) Duvick, S. A.; Pollak, L. M.; Edwards, J. W.; White, P. J. Altering the fatty acid composition of Corn Belt corn through *Tripsacum* introgression. *Maydica* **2006**, *51*, 409−416.

(9) Vivek, B. S.; Krivanek, A. F.; Palacios-Rojas, N.; Twumasi-Afriyie, S.; Diallo, A. O. *Breeding Quality Protein Maize (QPM): Protocols for Developing QPM Cultivars*; CIMMYT: Mexico City, Mexico, 2008.

(10) Prassana, B. M.; Vasal, S. K.; Kassahun, B.; Singh, N. N. Quality protein maize. *Curr. Sci.* **2001**, *81* (10), 1308−1319.

(11) Agrawal, P. K.; Gupta, H. S. Enhancement of protein quality of maize using biotechnological options. *Anim. Nutr. Feed Technol.* **2010**, *10*, 79−91.

DOI: 10.1021/jf504301u
J. Agric. Food Chem. 2015, 63, 1251−1260

(12) White, P. J.; Pollak, L. M.; Duvick, S. A. Improving the fatty acid composition of corn oil by using germplasm introgression. *Lipid Technol.* **2007**, *19*, 35−38.
(13) Flint-Garcia, S. A.; Bodnar, A. L.; Scott, M. P. Wide variability in kernel composition, seed characteristics, and zein profiles among diverse maize inbreds, landraces, and teosinte. *Theor. Appl. Genet.* **2009**, *119*, 1129−1142.
(14) Babic, M.; Andjelkovic, V.; Mladenović Drinić, S.; Konstantinov, K. The conventional and contemporary technologies in maize (*Zea mays* L.) breeding at Maize Research Institute, Zemun Polje. *Maydica* **2011**, *56*, 155−164.
(15) Vancetovic, J.; Ignjatovic-Micic, D.; Bozinovic, S.; Babic, M.; Filipovic, M.; Grcic, N.; Andjelkovic, V. Grain quality of drought tolerant accessions within the MRI Zemun Polje maize germplasm collection. *Span. J. Agric. Res.* **2014**, *12* (1), 186−194.
(16) International Board for Plant Genetic Resources (IBPGR). *Descriptor for Maize*; IBPGR: Rome, Italy, 1991.
(17) Nurit, E.; Tiessen, A.; Pixley, K.; Palacios-Rojas, N. A reliable and inexpensive colorimetric method for determining protein-bound tryptophan in maize kernels. *J. Agric. Food Chem.* **2009**, *57*, 7233−7238.
(18) Egesel, C. Ö.; Kahriman, F. Determination of quality parameters in maize grain by NIR reflectance spectroscopy. *J. Agric. Sci.* **2012**, *18*, 31−42.
(19) Zhang, Y.; Xue, R.; Zhang, Z.; Yang, X.; Shi, H. Palmitic and linoleic acids induce ER stress and apoptosis in hepatoma cells. *Lipids Health Dis.* **2012**, *11*, 1−8.
(20) Preciado-Ortiza, R. E.; García-Larab, S.; Ortiz-Islas, S.; Ortega-Coronaa, A.; Serna-Saldivar, S. O. Response of recurrent selection on yield, kernel oil content and fatty acid composition of subtropical maize populations. *Field Crops Res.* **2013**, *142*, 27−35.
(21) Serna-Saldívar, S. O. *Cereal Grains: Properties, Processing, and Nutritional Attributes*; CRC Press: Boca Raton, FL, 2010.
(22) Salinas, M. Y.; Bustos, F.; Gomez, J. H. Comparación de métodos para medir la dureza del maiz (*Zea mays* L.). *Arch. Latinoam. Nutr.* **1992**, *42*, 59−63.
(23) Radosavljevic, M.; Bekric, V.; Bozovic, I.; Jakovljevic, J. Physical and chemical properties of variuos corn genotypes as a criterion of technological quality. *Genetika* **2000**, *32* (3), 319−329.
(24) Ali, Q.; Ashraf, M.; Anwar, F. Seed composition and seed oil antioxidant activity of maize under water stress. *J. Am. Oil Chem. Soc.* **2010**, *87*, 1179−1187.
(25) Flagella, Z.; Rotunno, T.; Caterina, R. D.; Simone, G. D.; Caro, A. D. Effect of supplementary irrigation on seed yield and oil quality of sunflower (*Helianthus annuus* L.) grown in a sub-arid environment. *Proceedings of the XV International Sunflower Conference*; Toulouse, France, June 12−15, 2000; pp 139−144.
(26) Flagella, Z.; Rotunno, T.; Tarantito, E.; Caterina, R. D.; Caro, A. D. Changes in seed yield and oil fatty acid composition of high oleic sunflower (*Helianthus annuus* L.) hybrids in relation to the sowing date and the water regime. *Eur. J. Agron.* **2002**, *17*, 221−230.
(27) Anwar, F.; Zafar, S. N.; Rashid, U. Characterization of *Moringa oleifera* seed oil from drought and irrigated regions of Punjab, Pakistan. *Grasas Aceites* **2006**, *57*, 160−168.
(28) Petcu, E.; Arsintescu, A.; Stanciu, D. The effect of drought stress on fatty acid composition in some Romanian sunflower hybrids. *Rom. Agric. Res.* **2001**, *15*, 39−43.
(29) Zaidi, P. H.; Vasal, S. K.; Maniselvan, P.; Jha, G. C.; Mehrajjudin; Singh, R. P. Stability in performance of quality protein maize under abiotic stress. *Maydica* **2008**, *53*, 249−260.
(30) Watson, S. A.; Freeman, J. E. Breeding corn for increased oil content. *Proceedings of the 30th Corn and Sorghum Research Conference*; American Seed Trade Association: Washington, D.C., 1975; Vol. *13*, pp 251−257.
(31) Song, T. M.; Zhe, S.; Alexander, D. E. The selection of oil content and the quality improvement of maize (*Zea mays* L.) kernel. *Acta Agric. Univ. Pekin.* **1986**, *12*, 251−256.
(32) Song, T. M.; Chen, S. J. Long term selection for oil concentration in five maize populations. *Maydica* **2004**, *9*, 9−14.
(33) Bilgin, O.; Orak, H. H.; Korkut, K. Z.; Baser, Đ.; Orak, A.; Balkan, A. Interrelationships among some quality characteristics in dent corn (*Zea mays* L.). *Cereal Res. Commun.* **2010**, *38* (2), 233−242.
(34) Orhun, G. E.; Korkut, K. Z. Interrelationships among the oil and fatty acids in maize. *Afr. J. Agric. Res.* **2011**, *6* (9), 2115−2117.
(35) Dunlap, F. G.; White, P. J.; Pollak, L. M.; Brummd, T. J. Fatty acid composition of oil from adapted, elite corn breeding materials. *J. Am. Oil Chem. Soc.* **1995**, *72*, 981−987.
(36) Wassom, J. J.; Mikkelineni, V.; Bohn, M. O.; Rocheford, T. R. QTL for fatty acid composition of maize kernel oil in Illinois High Oil × B73 backcross-derived lines. *Crop Sci.* **2008**, *48*, 69−78.
(37) Cheesbrough, T. M.; Snow, K.; Schneerman, M. C.; Weber, D. F. Fatty acid compositions of maize races from Central and South America. *Maydica* **1997**, *42*, 155−161.
(38) Alrefai, R.; Berke, T. G.; Rocheford, T. R. Quantitative trait locus analysis of fatty acid concentrations in maize. *Genome* **1995**, *38*, 894−901.
(39) Pamin, K.; Compton, W. A.; Walker, C. E.; Alexander, D. E. Genetic variation and selection response for oil composition in corn. *Crop Sci.* **1986**, *26*, 279−282.
(40) Miller, R. L.; Dudley, J. W.; Alexander, D. E. High intensity selection for per cent oil in corn. *Crop Sci.* **1981**, *21*, 433−437.
(41) Lambert, R. J.; Alexander, D. E.; Mejaya, I. J. Single kernel selection for increased grain oil in maize synthetics and high-oil hybrid development. *Plant Breed. Rev.* **2004**, *24*, 153−175.
(42) Val, D. L.; Schwartz, S. H.; Kerns, M. R.; Deikman, J. Development of a high oil trait for maize. In *Molecular Genetic Approaches to Maize Improvement. Biotechnology in Agriculture and Forestry*; Kriz, A. L., Larkins, B. A., Eds.; Springer-Verlag: Berlin, Germany, 2009; Vol. *63*, pp 78−96.
(43) Wang, H. W.; Wu, B. Y.; Song, T. M.; Chen, S. J. Effects of long-term selection for kernel oil concentration in KYHO, a high-oil maize population. *Crop Sci.* **2009**, *49*, 459−466.
(44) Dorsey-Redding, C.; Hurburgh, C. R., Jr.; Johnson, L. A. Relationships among maize quality factors. *Cereal Chem.* **1991**, *68* (6), 602−605.
(45) Yang, X.; Guo, Y.; Yan, J.; Zhang, J.; Song, T.; Rocheford, T.; Li, J. S. Major and minor QTL and epistasis contribute to fatty acid compositions and oil concentration in high-oil maize. *Theor. Appl. Genet.* **2010**, *120*, 665−678.

DOI: 10.1021/jf504301u
J. Agric. Food Chem. 2015, 63, 1251−1260

bicarbonate supplementation represents a promising strategy to stimulate growth and trigger omega-3-enriched oil production in this species.

Several metabolic studies using lipid and fatty acid analysis[14,21,24−26] or radiolabeled fatty acids,[22,27,28] as well as molecular studies,[29−31] have already been performed to investigate the effect of growth conditions on lipid and fatty acid composition in microalgae, as well as to measure at a transcriptional level the expression of different desaturases and elongases involved in n-3 LC-PUFA biosynthesis.[29,32,33] As an example, it has been demonstrated that the expression of the LC-PUFA front-end desaturase from *P. lutheri* (PlDES1, Δ4-desaturase), which converts 22:5 n-3 and 22:4 n-6 into DHA and 22:5 n-6, respectively, was 4-fold higher during the midexponential growth phase compared to late exponential and stationary phases.[29] However, no metabolic study attempted to measure directly in vivo the effects of environmental factors on desaturase and elongase activities in microalgae. Previous work has provided a method for studying microalgal LC-PUFA biosynthesis pathways and desaturase and elongase activities in vivo using externally supplied radiolabeled fatty acids as direct substrates.[28] Using ^{14}C-labeled dihomo-γ-linolenic (DGLA, [1-^{14}C] 20:3 n-6) and arachidonic (ARA, [1-^{14}C] 20:4 n-6) acids as precursors of EPA and DHA, the metabolic relationship between the n-6 and n-3 fatty acid series have been demonstrated in *P. lutheri* by Δ17-desaturation of DGLA and ARA into 20:4 n-3 and EPA.

Herein, using this method, ^{14}C-labeled ARA (^{14}C-ARA) was also used to assess the effect of light intensity on the incorporation of LC-PUFA into total lipids and the regulation of the final metabolic steps involved in EPA and DHA synthesis in *P. lutheri*. Activities of conversion of ARA into EPA (Δ17-desaturation) and of EPA into DHA (Δ5-elongation + Δ4-desaturation) were estimated under three different light intensities through the distribution of radioactivity into longer and more unsaturated fatty acids using short incubation times (1 and 3 h). The results of this study represented the first data investigating the influence of abiotic factors (i.e., light intensity) on desaturase and elongase activities measured on intact microalgal cells "in vivo" using ^{14}C-radiolabeled fatty acids.

MATERIALS AND METHODS

Chemicals and Radiolabeled Fatty Acids. Radiolabeled [1-^{14}C]-eicosa-5,8,11,14-tetraenoic acid ([1-^{14}C] 20:4 n-6; ^{14}C-ARA), specific activity = 2.07 GBq mmol^{-1}, 99.3% radiochemical purity, was purchased from the Radiochemical Center (GE Healthcare, Amersham, Buckinghamshire, UK). All other chemicals were of analytical and HPLC grades and purchased from Fisher Scientific Bioblock (Illkirch-Graffenstaden, Bas-Rhin, France).

Culture and Radiolabeling Conditions. *P. lutheri* (CCAP 931/6) was batch cultivated on artificial seawater as previously described in 500 mL Erlenmeyer flasks using a working volume of 300 mL under controlled temperature (15 ± 1 °C) and a light−dark cycle of 14 h light using three different light intensities (20, 100, or 340 μmol photons m^{-2} s^{-1}).[28] Cultures in midexponential growth phase (day 14) and midlight period were incubated with 0.3 μM ^{14}C-ARA ammonium salt during 1 and 3 h. The availability and/or accessibility of the ^{14}C-radiolabeled fatty acid substrates have been shown to be nonlimiting under such incubation times for *P. lutheri* grown under intermediate conditions (15 ± 1 °C, 100 μmol photons m^{-2} s^{-1}).[28] To avoid any changes of growth conditions (i.e., decrease in light availability per cell), no concentration of the cells has been performed prior to incubation with ^{14}C-ARA. The final cell density on day 14 was determined with a Malassez improved bright-line hemocytometer, after immobilizing the cells with Lugol 5%. The cell density was estimated to be 2.3, 3.1, and 4.4 × 10^6 cells mL^{-1} at the incubation time, for the three light intensities (20, 100, or 340 μmol photons m^{-2} s^{-1}, respectively). After incubation, algal cells were gently harvested by centrifuging at low speed (1200*g*, 10 min), resuspended, and washed three times with fresh medium. The pellets obtained were then frozen and stored at −70 °C prior to lipid extraction and analysis. Three replicate cultures were grown for each incubation time.

Lipid Radiolabeling Determination. The total lipids were extracted using a modified version as previously described,[14,34] and fatty acid methyl esters (FAMEs) were obtained as described[35] for gas chromatography analysis. The distribution of radioactivity between the different labeled fatty acids was determined by the reversed-phase HPLC method,[36] using a P1500 high-pressure pump (Thermo Separation Products, Les Ulis, Essonne, France), equipped with a 410 differential refractometer (Waters, Milford, MA, USA) and a Lichrocart column (Lichrospher 100 RP-18, 5 mm, 250 mm × 4 mm internal diameter; Merck, Darmstadt, Germany). The samples were eluted using acetonitrile/water solvent system (95:5 v/v) with a flow rate of 1 mL min^{-1}, and the FAMEs were collected at the detector outlet. Figure 1 displays a chromatogram of a mixture of FAMEs

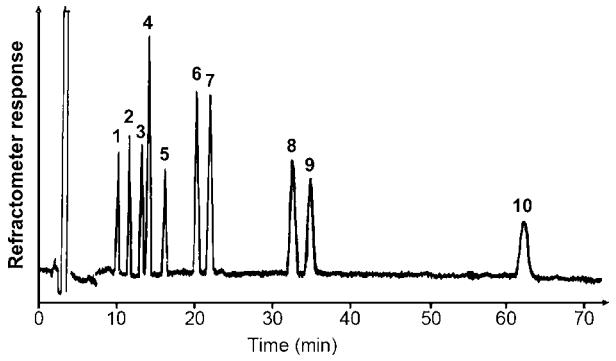

Figure 1. Chromatogram of Mix FAME standards separated using the reversed-phase HPLC method. Peaks: 1, 18:4 n-3; 2, 20:5 n-3 (EPA); 3, 22:6 n-3 (DHA); 4, 18:3 n-3; 5, 20:4 n-6 (ARA); 6, 18:2 n-6; 7, 20:3 n-6; 8, 18:1 n-9; 9, 16:0; 10, 18:0.

separated using the reversed-phase HPLC method described. ^{14}C-Radioactivity incorporated in the total lipid fraction was highly recovered into the FAMEs (percentage of ^{14}C recovered into the FAMEs > 95%). Each individual peak was identified using pure standards (Sigma-Aldrich, St. Quentin Fallavier, Isère, France). The radioactivity levels measured in the total lipid fraction and each individual FAME were expressed in disintegrations per minute (DPM) after correction of the quenching by external standard ratios (ESR) method using a Wallac 1410 liquid scintillation counter (LSC, ECG Instrument, PerkinElmer, Waltham, MA, USA) and liquid scintillation cocktail (ACS, GE Healthcare, Amersham, Buckinghamshire, UK).

Fatty Acid Analysis by GC-FID. Before incubation with ^{14}C-ARA, cultures grown under similar conditions were used to assess the effect of light intensity on *P. lutheri* fatty acid composition. The total lipids were extracted, and FAMEs were prepared as previously described and analyzed with a FOCUS gas chromatography apparatus (Thermo Electron Corp., Les Ulis, Essonne, France) equipped with a flame ionization detector (GC-FID), and a fused-silica capillary column (CP Sil-88, 25 m × 0.25 mm i.d. capillary column, Varian, Les Ulis, Essonne, France). The GC-FID conditions were similar to those used previously.[28] Pure standards (Sigma-Aldrich, St. Quentin Fallavier, Isère, France) were used to identify the fatty acids by comparing the peak retention times of the samples and standards.

Parameters Calculation and Expression. All results and parameters were determined after counting of the radioactivity in DPM. Radioactivity incorporated into the total lipids (Table 1) was expressed in percentage of the radioactivity incorporated into the total lipids in relation to the total radioactivity added in the medium (calculated and expressed in DPM per million cells). According to the

DOI: 10.1021/jf504863u
J. Agric. Food Chem. 2015, 63, 1261−1267

Table 1. Effect of Light Intensity on the Radioactivity Incorporated into the Total Lipids of *P. lutheri* Grown under 20, 100, and 340 μmol Photons m^{-2} s^{-1} and a Temperature of 15 °C after 1 and 3 h of Incubation with 0.3 μM ^{14}C-ARA (37,296 DPM/mL) as Substrate[a]

	light intensity (μmol photons m^{-2} s^{-1}) for 1 h			light intensity (μmol photons m^{-2} s^{-1}) for 3 h		
	20	100	340	20	100	340
% radioactivity	50.4 ± 2.5 c	18.7 ± 0.8 a	21.9 ± 2.0 a	51.7 ± 0.7 c	52.3 ± 1.3 c	27.6 ± 2.9 b
pmol ×10^6 $cell^{-1}$	66.4 ± 0.9 c	17.4 ± 1.0 a	15.1 ± 2.3 a	66.2 ± 1.9 c	52.7 ± 8.3 b	19.2 ± 2.5 a
fmol min^{-1} × 10^6 $cell^{-1}$	1107 ± 14 d	290 ± 16 b	252 ± 39 a	368 ± 11 c	293 ± 46 b	107 ± 14 a

[a]Results are expressed as percentage of incorporated radioactivity, as pmol of incorporated substrate per million cells, and fmol of incorporated substrate per minute per million cells. Values are expressed as the mean ± SD (n = 3). Means assigned different letters are statistically different (p < 0.05), and results are reported in ascending order: a < b < c.

Table 2. Enzymatic Conversion Rate Determinations Involved in n-3 LC-PUFA Synthesis in *P. lutheri* Grown under 20, 100, and 340 μmol Photons m^{-2} s^{-1} and a Temperature of 15 °C after Incubation with 0.3 μM ^{14}C-ARA (37,296 DPM/mL) during 1 and 3 h[a]

	light intensity (μmol photons m^{-2} s^{-1}) for 1 h			light intensity (μmol photons m^{-2} s^{-1}) for 3 h		
	20	100	340	20	100	340
% conversion						
ARA into EPA (Δ17des)	43.9 ± 0.2 a	41.1 ± 4.1 a	40.9 ± 2.4 a	56.6 ± 0.8 b	67.6 ± 1.9 c	52.7 ± 3.0 b
EPA into DHA (Δ5elo + Δ4des)	8.7 ± 0.2 c	6.5 ± 0.2 b	4.6 ± 0.1 a	10.5 ± 0.8 d	9.8 ± 0.7 cd	6.3 ± 0.8 b
conversion rate (fmol min^{-1} 10^6 $cell^{-1}$)						
ARA into EPA (Δ17des)	486.4 ± 8.4 d	119.2 ± 18.4 b	102.7 ± 9.8 b	206.9 ± 2.5 c	200.1 ± 32.8 c	55.9 ± 8.4 a
EPA into DHA (Δ5elo + Δ4des)	95.7 ± 0.4 f	18.8 ± 1.6 c	11.5 ± 1.9 b	38.7 ± 3.2 e	28.4 ± 4.0 d	6.6 ± 1.2 a

[a]Results are expressed as the percentage of conversion of the substrate into longer chain and more unsaturated fatty acids, and in fmol of substrate converted per minute and per million cells. Values are expressed as the mean ± SD (n = 3). Means assigned different letters are statistically different (p < 0.05), and results are reported in ascending order: a < b < c.

moles of ^{14}C-ARA available per million cells in the medium and the percentage of radioactivity incorporated into the total lipids, results were expressed in picomoles per million cells and in femtomoles per minute and per million cells. Distribution of the radioactivity in each FAME (Figure 4) was expressed in percentage of the total DPM radioactivity incorporated into labeled FAMEs. Enzymatic conversion rates (Table 2) were expressed in percentage of conversion of substrate into longer chain and more unsaturated fatty acids as described by the following eqs 1 and 2:

$$\Delta 17\text{des} = [\Sigma(\text{DPM}_{\text{EPA+DHA}})/\Sigma(\text{DPM}_{\text{ARA+EPA+DHA}})] \times 100 \quad (1)$$

$$\Delta 5\text{elo} + \Delta 4\text{des} = [\text{DPM}_{\text{DHA}}/\Sigma(\text{DPM}_{\text{EPA+DHA}})] \times 100 \quad (2)$$

Enzymatic conversion rates expressed in femtomoles of substrate converted per minute and per million cells were determined using the percentage of conversion (Δ17des or Δ5elo + Δ4des) previously calculated and the radioactivity incorporated into the total lipids and expressed in the same units.

Statistical Analyses. One-way analysis of variance (ANOVA) was used to examine the effect of light intensity (n = 3). The Student−Newman−Keuls (SNK) multiple-comparison test was used to test the differences between groups. Differences were considered significant at a probability level of 0.05. All statistics were performed with Statgraphics (version Centurion XV) software (StatPoint Technologies, Warrenton, VA, USA).

RESULTS AND DISCUSSION

Effect of Light Intensity on Total Fatty Acid Composition. Among the abiotic parameters (e.g., light, temperature, CO_2 disponibility, pH, and nutrients), light stands out as a key environmental factor controlling growth and chemical composition of photosynthetic cells. In microalgae, variations in light regimen impose numerous adaptation mechanisms involving changes in pigment content, biochemical composition, and the capacities of the photosynthetic apparatus.[37−39] In particular, changes in lipid content and fatty acid profile are observed in response to changes in the light intensity.[14,40,41] In our work, *P. lutheri* showed a decrease in the proportions of LC-PUFA, in particular stearidonic acid (18:4 n-3) and EPA, associated with an increase in SFA, especially palmitic acid (16:0), with increasing light intensity (Figure 2). These results are similar to those published for *P. lutheri* grown under identical conditions.[14] This previous study showed that the highest PUFA levels, such as those of EPA, were predominantly found in the galactolipid fraction when the cells were grown under low light, and it has been suggested that accumulation of LC-PUFA in the galactolipids may facilitate

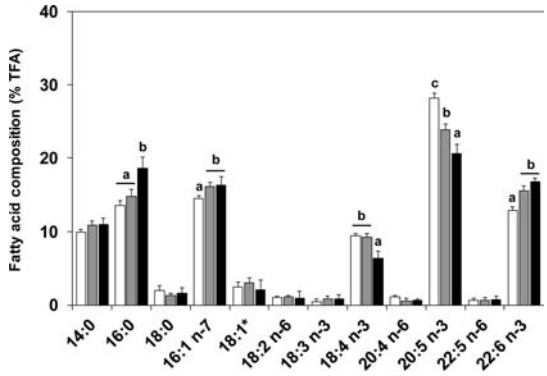

Figure 2. Total lipid fatty acid composition (% TFA) of *P. lutheri* grown under 20, 100, and 340 μmol photons m^{-2} s^{-1} (white, gray, and black bars, respectively), a temperature of 15 °C, and a light−dark cycle of 14 h light and harvested in midexponential growth phase (day 14) and midlight period. Results are expressed as the mean ± SD (n = 3). Means assigned different letters are statistically different (p < 0.05), and results are reported in ascending order: a < b < c.

DOI: 10.1021/jf504863u
J. Agric. Food Chem. 2015, 63, 1261−1267

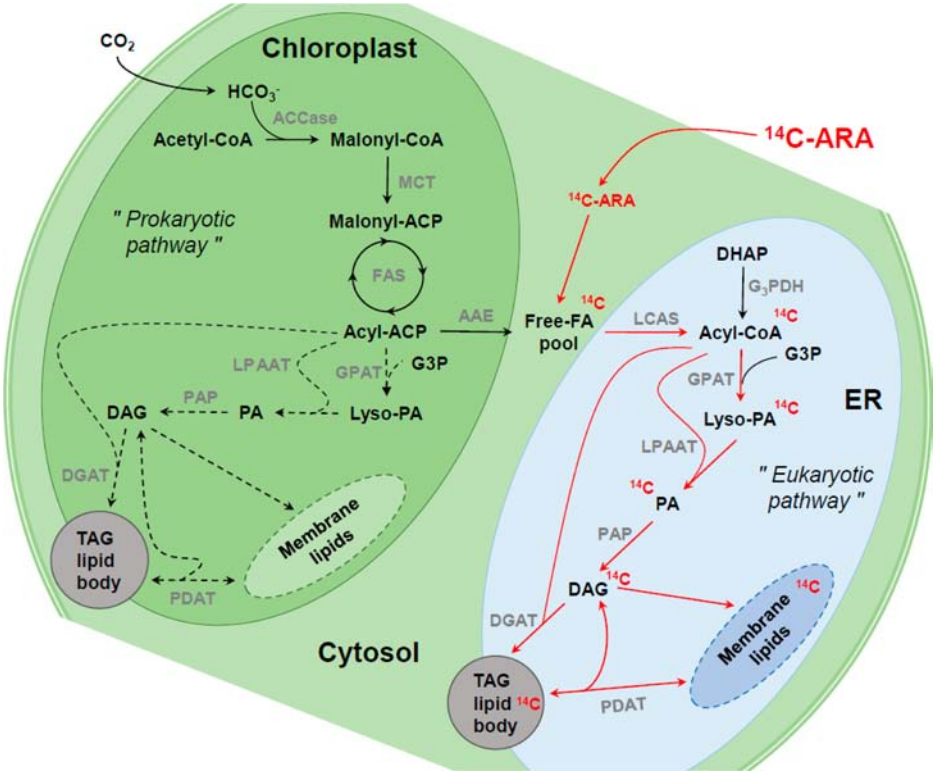

Figure 3. Schematic representation of lipid biosynthesis in microalgae and suggested ways (in red) of incorporation of ^{14}C-ARA into complex lipids of *P. lutheri*. Modified and adapted from previous studies.[42]

thylakoid membrane fluidity and, therefore, the velocity of electron flow involved in photosynthesis during light acclimatization. It is also important to note that ARA accounted for <2% of TFA in *P. lutheri*, suggesting its intermediate metabolic function for longer and more unsaturated LC-PUFA synthesis, whereas EPA and DHA accumulate and reach up to 29% under low light and 18% under high light of TFA, respectively.

Incorporation of ^{14}C-ARA through a Potential Light-Dependent Lipid Biosynthesis Pathway. According to the results reported in Table 1, the incorporation of ^{14}C radioactivity issued from ^{14}C-ARA into total lipids is dependent on the light intensity and the time of incubation. The percentage of ^{14}C incorporated in the total lipid fraction reaches 52% of the radioactivity initially present in the culture medium. After 1 h of incubation and under low light intensity (20 μmol photons m^{-2} s^{-1}), the percentage of ^{14}C incorporated into the total lipid fraction is 2.5 times higher (50% of the radioactivity initially present in the culture medium) than the percentage obtained at 100 and 340 μmol photons m^{-2} s^{-1} (19 and 22%, respectively). Similarly, the amount of ^{14}C incorporated and expressed in picomoles per million cells is highest when the cells are incubated under low light. The average of substrate incorporated per minute and per million cells decreased with increasing light intensity. After 3 h of incubation, the percentages of ^{14}C incorporated were highest at 20 and 100 μmol photons m^{-2} s^{-1} (approximately 52% of the radioactivity initially present in the culture medium), and the amount of ^{14}C incorporated per minute decreased with increasing light intensity. It has been previously demonstrated using [1-^{14}C] 16:0 and [1-^{14}C] 20:3n-6 as radiolabeled fatty acid substrates that 70−80% of the radioactivity incorporated into the cells was recovered in the total lipids of *P. lutheri* whatever the incubation time applied (3, 10, and 24 h).[28] We may assume similar results with ^{14}C-ARA in this study and suggest that the difference may be due to incomplete extraction of the total lipids or losses during this process. The ^{14}C-ARA not incorporated in *P. lutheri* cells was left in the medium, suggesting its nonlimitation over 1 or 3 h of incubation as previously shown.[28]

According to these results, Figure 3 illustrates a suggested way of incorporation of ^{14}C-ARA into complex lipids of *P. lutheri* using a schematic representation of lipid biosynthesis in microalgae. Currently, two locations for de novo lipid biosynthesis have been suggested in microalgae and, more specifically, in *Chlamydomonas reinhardtii*, being the plastid prokaryotic pathway and the endoplasmic reticulum (ER) eukaryotic pathways.[42] The radiolabeled ^{14}C-ARA used in this study may be incorporated into *P. lutheri* cells by diffusion, esterified to CoA by the long chain acyl-CoA synthases (LACS), and therefore associated into the acyl-CoA pool. The LACS gene may be light-dependent and could therefore explained the fast and strong ^{14}C-ARA incorporation into total lipids observed in *P. lutheri* grown under low light. TAG and polar lipids are then assembled using a complex process involving diverse enzymatic activities as presented in Figure 3. As a consequence, ^{14}C-ARA or longer and more unsaturated ^{14}C-radiolabeled fatty acids subsequently synthesized (see the section on LC-PUFA biosynthesis by alternative desaturation and elongation steps), such ^{14}C-EPA and ^{14}C-DHA, may be incorporated into TAG or complex lipids throughout successive acylation steps of the Kennedy pathway.[43,44] Alternatively, fatty acyl donors for production of TAG may also derive from membrane lipids in the acyl-CoA-independent pathway using transacylases or by means of specific lipase activity on membrane lipids, which liberates fatty acyl groups for TAG

DOI: 10.1021/jf504863u
J. Agric. Food Chem. 2015, 63, 1261−1267

synthesis.[42] A similar process using similar enzymes could also be involved in the formation of complex lipids and in the remodeling of fatty acids between membranes. After incubation with ^{14}C-ARA, the high percentage of ^{14}C radioactivity incorporated into total lipids of *P. lutheri* grown under low light could therefore also be explained by an overexpression of all or certain genes encoding acyltransferases or other proteins involved in the process, especially enzymes with strong substrate specificities for lipid membranes containing LC-PUFA such as EPA and DHA. The ability of *P. lutheri* to partition both DHA and EPA to TAG, compared to other microalgal species, raises the question of how this process is regulated.[24] It may involve acyltransferases with different substrate specificities. This could also partially explain the strong ^{14}C-ARA (or other synthesized ^{14}C-LC-PUFA) incorporation into lipids under low light and potentially partitioned to TAGs or complex lipids. Therefore, a high level of expression of specific enzymes, such as acyltransferases, especially under low light conditions, could promote the partitioning of LC-PUFA into complex lipids and could explain the high level of LC-PUFA (e.g., EPA) observed in *P. lutheri* grown under low light intensity and, more specifically, linked to polar lipids (i.e., glycolipids and phospholipids) constituting the membranes.[14,26]

Finally, a strong Δ17-desaturation activity under low light could also explain the high percentage of ^{14}C-ARA incorporated and needed as substrate for the synthesis of longer and more unsaturated fatty acids such as EPA and DHA as described in the following section.

Effect of Light Intensity on the Final Desaturase and Elongase Steps Involved in n-3 LC-PUFA Biosynthesis. In *P. lutheri*, the major radiolabeled fatty acids obtained from ^{14}C-ARA were ^{14}C-EPA and ^{14}C-DHA (Figure 4). After 1 h of incubation, no changes in the percentage of ^{14}C-radioactivity incorporated into EPA and DHA (respectively 38−40 and 2−3% of the total fatty acids labeled) were observed with the level of light. However, after 3 h of incubation, significant variations in the distribution of ^{14}C radioactivity incorporated into the fatty acids were observed with changes in light intensity. The percentage of ^{14}C-EPA was significantly higher when the cells were incubated under 100 μmol photons m^{-2} s^{-1} (61% of the total fatty acids labeled), and the percentage of ^{14}C-DHA decreased under high light (340 μmol photons m^{-2} s^{-1}). Therefore, in addition to the high percentage of ^{14}C-ARA incorporated in the total lipids, the light intensity seems to affect the last desaturation and elongation activities involved in EPA and DHA synthesis in *P. lutheri*. These results are in accordance with several those of other authors and can contribute to the explanation of how the levels of EPA and DHA may vary with light intensity in microalgae.[14,40,45] Whatever the light intensity, the results also show that the proportion of ^{14}C-ARA decreased while those of ^{14}C-EPA and ^{14}C-DHA increased with the time of incubation (data not shown).[28]

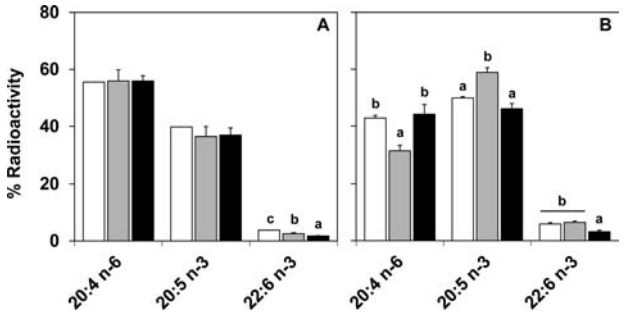

Figure 4. Effect of light intensity on the distribution of radioactivity in the main individual fatty acid fractions of *P. lutheri* grown under 20, 100, and 340 μmol photons m^{-2} s^{-1} (white, gray, and black bars, respectively) and a temperature of 15 °C after incubation with ^{14}C-ARA during 1 h (A) or 3 h (B). Results are expressed as percentage of total radiolabeled fatty acids, mean ± SD (n = 3). Means assigned different letters are statistically different (p < 0.05), and results are reported in ascending order: a < b < c.

The effect of light intensity on the percentage of conversion of ARA into longer and more unsaturated fatty acids and the related conversion rates (expressed in femtomoles of substrate converted per minute and per million cells) are reported in Table 2. The highest percentage of conversion of ARA to EPA was obtained under 100 μmol photons m^{-2} s^{-1} after 3 h of incubation. Under these conditions, 68% of ^{14}C-ARA incorporated in the total lipids was converted to EPA and DHA. The results also show that the highest percentages of conversion of EPA to DHA (Δ5-elongation + Δ4-desaturation) are obtained under 20 and 100 μmol photons m^{-2} s^{-1} after 3 h of incubation (10−11% of the ^{14}C radioactivity were converted to DHA). Meanwhile, whatever the incubation time, the desaturation and elongation conversion rates measured, especially for the Δ17-desaturase, were highest under low light. These rates were also higher after 1 h of incubation compared to those obtained after 3 h of incubation except under 100 μmol photons m^{-2} s^{-1}. The highest conversion rates were consequently obtained under low light (20 μmol photons m^{-2} s^{-1}) after 1 h of incubation (Δ-17 desaturation, 486 fmol min^{-1} 10^6 cell^{-1}; Δ5-elongation + Δ4-desaturation, 96 fmol min^{-1} 10^6 cell^{-1}). Similar to the results obtained during incubation of *P. lutheri* with [1-^{14}C] 16:0 or [1-^{14}C] 20:3 n-6,[28] conversion rates are closely linked to the amount of substrate incorporated. Through photosynthetic mechanisms, the regulatory role played by light regarding gene expression coding for desaturases and elongases could explain the variations of the enzymatic conversion rates observed. Previous study showed that the levels of mRNA transcripts coding for Δ12-, Δ15-, and Δ6-desaturases (*Des*A, *Des*B, and *Des*D, respectively) of the cyanobacteria *Synechocystis* PCC6803 were 10 times higher for cells grown under light conditions compared to those grown in the dark.[46] The desaturation of fatty acids as an adaptive response to shifts in light intensity in five microalga species was also proposed.[37] In that study, the authors suggested that the optimization of photosynthetic process resulted in some increase of the relative content of the most unsaturated fatty acids such as EPA in various unicellular microalgae, which exhibited some similarity in their mechanisms of response to changes in light conditions. Moreover, in their study, the fatty acid desaturation was shown to correlate with the photosynthetic activity, in particular the activity of photosystem (PSI).[37]

In this work, as previously described,[28] the Δ17-desaturation activity involved in the conversion of ARA to EPA was confirmed, as well as the metabolic relationship between the n-6 and n-3 fatty acid series (Figure 5). In addition, microalgal desaturases and elongases are either acyl-CoA dependent or glycerolipid-linked (e.g., phospho-linked) dependent. As examples, acyl-CoA Δ6-desaturases were isolated from microalgae *Ostreococcus tauri* and *Micromonas pusilla*,[47,48] whereas

DOI: 10.1021/jf504863u
J. Agric. Food Chem. 2015, 63, 1261−1267

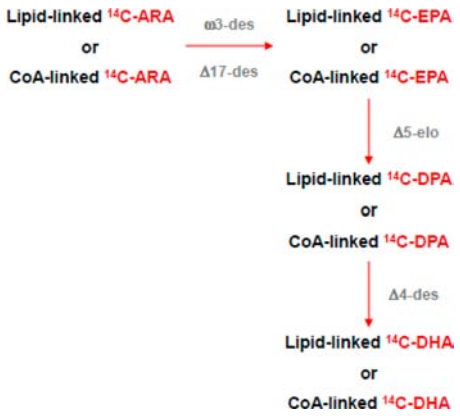

Figure 5. Proposed final steps involved in n-3 LC-PUFA synthesis in *P. lutheri*. Radiolabeled ^{14}C-EPA and ^{14}C-DHA formed by successive desaturation and elongation steps after incubation with ^{14}C-ARA.

two membrane-bound desaturases with Δ6- and Δ5-desaturase activities were isolated from the freshwater microalga *Parietochloris incisa*.[33] As highlighted in Figure 5, the radiolabeled ^{14}C-ARA incorporated in the total lipids of *P. lutheri* may therefore have been converted to ^{14}C-EPA and ^{14}C-DHA before or after esterification to complex lipids by the acyl-CoA dependent or the glycerolipid-linked dependent LC-PUFA biosynthesis pathways, respectively. The strong incorporation of ^{14}C-ARA into total lipids under low light and the strong related Δ17-desaturation activity measured enable us to assume it to be an adaptive response, which provides alterations to lipid−protein interactions in the membrane that may be important for the self-assembly of active chlorophyll−protein complexes for the photosynthetic apparatus. The consequent accumulation of n-3 LC-PUFA such as EPA in *P. lutheri* under low light condition could therefore facilitate thylakoid membrane fluidity and the velocity of electron flow involved in photosynthesis during low light.[14,49]

In conclusion, the present results have confirmed the metabolic relationship between n-6 and n-3 fatty acid series and measured the effect of light intensity on the Δ17-desaturation activity. Our findings also suggested a light-dependent incorporation of LC-PUFA into structured lipids through different enzymes (i.e., acyltransferases) involved in the biosynthesis of lipids (TAGs and membrane lipids), as well as highlight the light-dependent activities of the final desaturation and elongation steps required for n-3 C20/C22 LC-PUFA formation in *P. lutheri*. Therefore, the strong incorporation of ^{14}C-ARA under low light in association with the strong Δ17-desaturation activity could facilitate thylakoid membrane fluidity by LC-PUFA accumulation in the structural lipids (i.e., glycolipids and phospholipids) and, therefore, provide better lipid−protein interactions in the membrane, enhancing the velocity of electron flow involved in photosynthesis during light adaptation.

AUTHOR INFORMATION

Corresponding Author

*(L.U.) Phone: + 33 2 43 59 49 59. Fax + 33 2 43 59 49 58. E-mail: Lionel.Ulmann@univ-lemans.fr.

Funding

This work was financially supported by the French Ministère de l'Enseignement Supérieur et de la Recherche (MESR) and by the FP7-KBBE European Collaborative Project GIAVAP.

Notes

The authors declare no competing financial interest.

ABBREVIATIONS USED

LC-PUFA, long-chain polyunsaturated fatty acid; EPA, eicosapentaenoic acid; DHA, docosahexaenoic acid; TAG, triacylglycerol; SFA, saturated fatty acid; MUFA, monounsaturated fatty acid; TFA, total fatty acids; DGLA, dihomo-γ-linolenic acid; ARA, arachidonic acid; HPLC, high-performance liquid chromatography; FAME, fatty acid methyl ester; ESR, external standard ratios; GC-FID, gas chromatography−flame ionization detector; ANOVA, analysis of variance; ER, endoplasmic reticulum; LACS, long-chain acyl-CoA synthases

REFERENCES

(1) Simopoulos, A. P. N-3 fatty acids and human health: defining strategies for public policy. *Lipids* **2001**, *36*, S83−S89.

(2) Calder, P. C. Very long chain omega-3 (n-3) fatty acids and human health. *Eur. J. Lipid Sci. Technol.* **2014**, *116* (10), 1280−1300.

(3) Meyer, B. J.; Mann, N. J.; Lewis, J. L.; Milligan, G. C.; Sinclair, A. J.; Howe, P. R. C. Dietary intakes and food sources of omega-6 and omega-3 polyunsaturated fatty acids. *Lipids* **2003**, *38* (4), 391−398.

(4) Ward, O. P.; Singh, A. Omega-3/6 fatty acids: alternative sources of production. *Process Biochem.* **2005**, *40* (12), 3627−3652.

(5) Mimouni, V.; Ulmann, L.; Pasquet, V.; Mathieu, M.; Picot, L.; Bougaran, G.; Cadoret, J. P.; Morant-Manceau, A.; Schoefs, B. The potential of microalgae for the production of bioactive molecules of pharmaceutical interest. *Curr. Pharm. Biotechnol.* **2013**, *13* (15), 2733−2750.

(6) Robertson, R.; Guihéneuf, F.; Schmid, M.; Stengel, D. B.; Fitzgerald, G.; Ross, P.; Stanton, C. Algae-derived polyunsaturated fatty acids: implications for human health. In *Polyunsaturated Fatty Acids: Sources, Antioxidant Properties and Health Benefits*; Catalá, A., Ed.; Nova Sciences Publishers: Hauppauge, NY, USA, 2013; pp 45−99.

(7) Khozin-Goldberg, I.; Iskandarov, I.; Cohen, Z. LC-PUFA from photosynthetic microalgae: occurrence, biosynthesis, and prospects in biotechnology. *Appl. Microbiol. Biotechnol.* **2011**, *91* (4), 905−915.

(8) Martins, D. A.; Custódio, L.; Barreira, L.; Pereira, H.; Ben-Hamadou, R.; Varela, J.; Abu-Salah, K. M. Alternative sources of n-3 long-chain polyunsaturated fatty acids in marine microalgae. *Mar. Drugs* **2013**, *11* (7), 2259−2281.

(9) Stengel, D. B.; Connan, S.; Popper, Z. A. Algal chemodiversity and bioactivity: sources of natural variability and implications for commercial application. *Biotechnol. Adv.* **2011**, *29* (5), 483−501.

(10) Reitan, K. I.; Rainuzzo, J. R.; Olsen, Y. Effect of nutrient limitation on fatty acid and lipid content of marine microalgae. *J. Phycol.* **1994**, *30* (6), 972−979.

(11) De Castro Araújo, S.; Tavano Garcia, V. M. Growth and biochemical composition of the diatom *Chaetoceros* cf. *wighamii* brightwell under different temperature, salinity and carbon dioxide levels. I. Protein, carbohydrates and lipids. *Aquaculture* **2005**, *246* (1−4), 405−412.

(12) Liang, Y.; Beardall, J.; Heraud, P. Changes in growth, chlorophyll fluorescence and fatty acid composition with culture age in batch cultures of *Phaeodactylum tricornutum* and *Chaetoceros muelleri* (Bacillariophyceae). *Bot. Mar.* **2006**, *49* (2), 165−173.

(13) Ranga Rao, A.; Dayananda, C.; Sarada, R.; Shamala, T. R.; Ravishankar, G. A. Effect of salinity on growth of green alga *Botryococcus braunii* and its constituents. *Bioresour. Technol.* **2007**, *98* (3), 560−564.

(14) Guihéneuf, F.; Mimouni, V.; Ulmann, L.; Tremblin, G. Combined effects of irradiance level and carbon source on fatty acid and lipid class composition in the microalga *Pavlova lutheri* commonly used in mariculture. *J. Exp. Mar. Biol. Ecol.* **2009**, *369* (2), 136−143.

(15) Renaud, S. M.; Thinh, L. V.; Lambrinidis, G.; Parry, D. L. Effect of temperature on growth, chemical composition and fatty acid

DOI: 10.1021/jf504863u
J. Agric. Food Chem. 2015, 63, 1261−1267

composition of tropical Australian microalgae grown in batch cultures. *Aquaculture* **2002**, *211* (1−4), 195−214.
(16) Jiang, H.; Gao, K. Effects of lowering temperature during culture on the production of polyunsaturated fatty acids in the marine diatom *Phaeodactylum tricornutum* (Bacillariophyceae). *J. Phycol.* **2004**, *40* (4), 651−654.
(17) Hu, Q.; Sommerfeld, M.; Jarvis, E.; Ghirardi, M.; Posewitz, M.; Seibert, M.; Darzins, A. Microalgal triacylglycerols as feedstocks for biofuel production: perspectives and advances. *Plant J.* **2008**, *54* (4), 621−639.
(18) Klok, A. J.; Martens, D. E.; Wijffels, R. H.; Lamers, P. P. Simultaneous growth and neutral lipid accumulation in microalgae. *Bioresour. Technol.* **2013**, *134*, 233−243.
(19) Cohen, Z.; Khozin-Goldberg, I. Searching for PUFA-rich microalgae. In *Single Cell Oils*; Cohen, Z., Ratledge, C., Eds.; American Oil Chemists' Society: Champaign, IL, USA, 2005; pp 53−72.
(20) Alonso, D. L.; Belarbi, E. H.; Rodriguez-Ruiz, J.; Segura, C. I.; Gimenez, A. Acyl lipids of three microalgae. *Phytochemistry* **1998**, *47* (8), 1473−1483.
(21) Tonon, T.; Harvey, D.; Larson, T. R.; Graham, I. A. Long chain polyunsaturated fatty acid production and partitioning to triacylglycerols in four microalgae. *Phytochemistry* **2002**, *61* (1), 15−24.
(22) Bigogno, C.; Khozin-Goldberg, I.; Boussiba, S.; Vonshak, A.; Cohen, Z. Lipid and fatty acid composition of the green oleaginous alga *Parietochloris incisa*, the richest plant source of arachidonic acid. *Phytochemistry* **2002**, *60* (5), 497−503.
(23) Yu, E. T.; Zendejas, F. J.; Lane, P. D.; Gaucher, S.; Simmons, B. A.; Lane, T. W. Triacylglycerol accumulation and profiling in the model diatoms *Thalassiosira pseudonana* and *Phaeodactylum tricornutum* (Baccilariophyceae) during starvation. *J. Appl. Phycol.* **2009**, *21* (6), 669−681.
(24) Guihéneuf, F.; Stengel, D. B. LC-PUFA-enriched oil production by microalgae: accumulation of lipid and triacylglycerols containing n-3 LC-PUFA is triggered by nitrogen limitation and inorganic carbon availability in the marine haptophyte *Pavlova lutheri*. *Mar. Drugs* **2013**, *11* (11), 4246−4266.
(25) Tatsuzawa, H.; Takizawa, E. Changes in lipid and fatty acid composition of *Pavlova lutheri*. *Phytochemistry* **1995**, *40* (2), 397−400.
(26) Guedes, A. C.; Meireles, L. A.; Amaro, H. M.; Malcata, F. X. Changes in lipid class and fatty acid composition of cultures of *Pavlova lutheri*, in response to light intensity. *J. Am. Oil Chem. Soc.* **2010**, *87* (7), 791−801.
(27) Khozin-Goldberg, I.; Shrestha, P.; Cohen, Z. Mobilization of arachidonyl moieties from triacylglycerols into chloroplastic lipids following recovery from nitrogen starvation of the microalga *Parietochloris incisa*. *Biochim. Biophys. Acta* **2005**, *1738* (1−3), 63−71.
(28) Guihéneuf, F.; Ulmann, L.; Mimouni, V.; Tremblin, G. Use of radiolabeled substrates to determine the desaturase and elongase activities involved in eicosapentaenoic acid and docosahexaenoic acid biosynthesis in the marine microalga *Pavlova lutheri*. *Phyochemistry* **2013**, *90*, 43−49.
(29) Tonon, T.; Harvey, D.; Larson, T. R.; Graham, I. A. Identification of a very long chain polyunsaturated fatty acid Δ4-desaturase from the microalga *Pavlova lutheri*. *FEBS Lett.* **2003**, *553* (3), 440−444.
(30) Pereira, S. L.; Leonard, A. E.; Huang, Y. S.; Chuang, L. T.; Mikerji, P. Identification of two novel microalgal enzymes involved in the conversion of the ω3-fatty acid, eicosapentaenoic acid, into docosahexaenoic acid. *Biochem. J.* **2004**, *384* (2), 357−366.
(31) Zhou, X. R.; Robert, S. S.; Petrie, J. R.; Frampton, D. M. F.; Mansour, M. P.; Blackburn, S. I.; Nichols, P. D.; Green, A. G.; Singh, S. P. Isolation and characterization of genes from the marine microalga *Pavlova salina* encoding three front-end desaturases involved in docosahexaenoic acid biosynthesis. *Phytochemistry* **2007**, *68* (6), 785−796.
(32) An, M.; Mou, S.; Zhang, X.; Ye, N.; Zheng, Z.; Cao, S.; Xu, D.; Fan, X.; Wang, Y.; Miao, J. Temperature regulates fatty acid desaturases at a transcriptional level and modulates the fatty acid profile in the Antarctic microalga *Chlamydomonas* sp. ICE-L. *Bioresour. Technol.* **2013**, *134*, 151−157.
(33) Iskandarov, U.; Khozin-Goldberg, I.; Cohen, Z. Identification and characterization of Δ12, Δ6, and Δ5 desaturases from the green microalga *Parietochloris incisa*. *Lipids* **2010**, *45* (6), 519−530.
(34) Bligh, E. G.; Dyer, W. J. A rapid method of lipid extraction and purification. *Can. J. Biochem. Physiol.* **1959**, *37* (8), 911−917.
(35) Slover, H. T.; Lanza, E. Quantitative analysis of food fatty acids by capillary gas chromatography. *J. Am. Oil Chem. Soc.* **1979**, *56* (12), 933−943.
(36) Narce, M.; Gresti, J.; Bezard, J. Method for evaluating the bioconversion of radioactive polyunsaturated fatty acids by use of reversed-phase liquid chromatography. *J. Chromatogr.* **1988**, *448*, 249−264.
(37) Klyachko-Gurvich, G. L.; Tsoglin, L. N.; Doucha, J.; Kopetskii, J.; Shebalina (Ryabykh), I. B.; Semenenko, V. E. Desaturation of fatty acids as an adaptive response to shifts in light intensity. *Physiol. Plant.* **1999**, *107* (2), 240−249.
(38) Mouget, J. L.; Tremblin, G.; Manceau, A.; Morancais, M.; Robert, J. M. Long-term photoacclimation of *Haslea ostrearia* (Bacillariophyta): effect of irradiance on growth rates, pigment content and photosynthesis. *Eur. J. Phycol.* **1999**, *34* (2), 109−115.
(39) Tremblin, G.; Cannuel, R.; Mouget, J. L.; Rech, M.; Robert, J. M. Change in light quality due to a blue-green pigment, mareninne, released in oyster-ponds: effect on growth and photosynthesis in two diatoms, *Haslea ostrearia* and *Skeletonema costatum*. *J. Appl. Phycol.* **2000**, *12* (6), 557−566.
(40) Thompson, P. A.; Harrison, P. J.; Whyte, J. N. C. Influence of irradiance on the fatty acid composition of phytoplankton. *J. Phycol.* **1990**, *26* (2), 278−288.
(41) Tzovenis, I.; De Pauw, N.; Sorgeloos, P. Optimisation of T-ISO biomass production rich in essential fatty acids: I. Effect of different light regimes on growth and biomass production. *Aquaculture* **2003**, *216* (1−4), 203−222.
(42) Klok, A. J.; Lamers, P. P.; Martens, D. E.; Draaisma, R. B.; Wijffels, R. H. Edible oils from microalgae: insights in TAG accumulation. *Trends Biotechnol.* **2014**, *32* (10), 521−528.
(43) Kennedy, E. P. Biosynthesis of complex lipids. *Fed. Proc.* **1961**, *20*, 934−940.
(44) Khozin-Goldberg, I.; Cohen, Z. Unraveling algal lipid metabolism: recent advances in gene identification. *Biochimie* **2011**, *93* (1), 91−100.
(45) Meireles, L. A.; Guedes, A. C.; Malcata, F. X. Lipid class composition of the microalga *Pavlova lutheri*: eicosapentaenoic and docosahexaenoic acid. *J. Agric. Food Chem.* **2003**, *51* (8), 2237−2241.
(46) Kis, M.; Zsiros, O.; Farkas, T.; Wada, H.; Nagy, F.; Gombos, Z. Light-induced expression of fatty acid desaturase genes. *Proc. Natl. Acad. Sci. U.S.A.* **1998**, *95*, 4209−4214.
(47) Domergue, F.; Abbadi, A.; Zähringer, U.; Moreau, H.; Heinz, E. *In vivo* characterization of the first acyl-CoA Δ6-desaturase from a member of the plant kingdom, the microalga *Ostreococcus tauri*. *Biochem. J.* **2005**, *389* (2), 483−490.
(48) Petrie, J. R.; Shrestha, P.; Mansour, M. P.; Nichols, P. D.; Liu, Q.; Singh, S. P. Metabolic engineering of omega-3 long-chain polyunsaturated fatty acids in plants using an acyl-CoA Δ6-desaturase with ω3-preference from the marine microalga *Micromonas pusilla*. *Metab. Eng.* **2010**, *12* (3), 233−240.
(49) Guihéneuf, F.; Ulmann, L.; Tremblin, G.; Mimouni, V. Light-dependent utilization of two radiolabelled carbon sources, sodium bicarbonate and sodium acetate, and relationships with long chain polyunsaturated fatty acids synthesis in the microalga *Pavlova lutheri* (Haptophyta). *Eur. J. Phycol.* **2011**, *46* (2), 143−152.

DOI: 10.1021/jf504863u
J. Agric. Food Chem. 2015, 63, 1261−1267

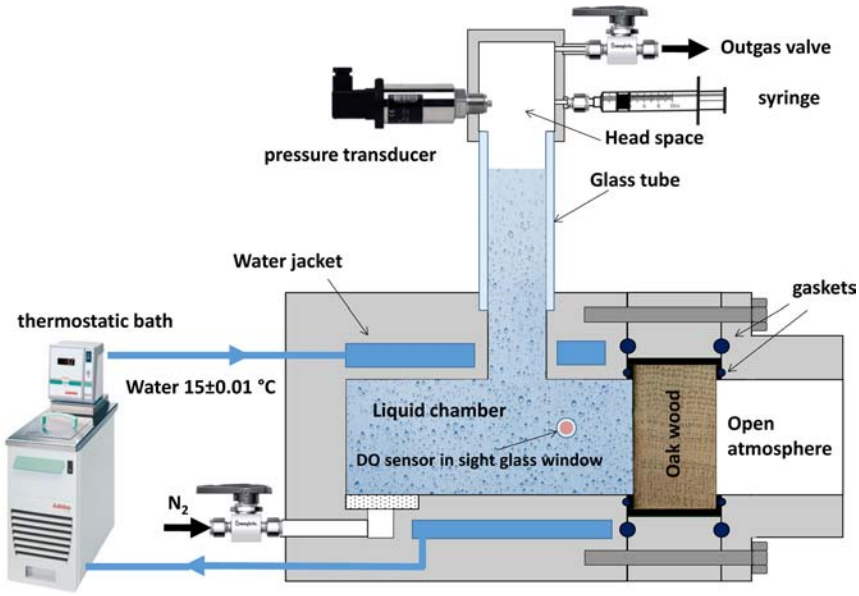

Figure 1. Porous material OTR measuring device.

enological field assessing the measurement of the OTR of oak wood used to build barrels. The limitations of the measurement equipment and those of the gas−wood−gas approach prevented these authors from determining the OTR in oak wood with the same thickness and similar conditions as those found when the wood is part of a barrel containing wine. This work places special importance on the role of moisture content (MC) in the loss of OTR in different wood samples. Other studies have measured oxygen permeability in completely flooded wood in a liquid−wood−liquid setting.[18] In such studies, it was evident that there is oxygen permeation in saturated wood, and the importance of the difference between early wood and late-wood density was highlighted as well as the direction of the diffusion. Likewise, Sorz and Hietz[19] highlight the importance of the MC in oxygen permeation by diffusion in different staves and in different directions. In a previous study,[20] the relationship between oxygen entry through the wood and the increase in its moisture content was demonstrated. For this, the visualization of oxygen diffusion was performed through a French oak stave during moistening in conditions similar to those in a barrel. It was confirmed that the oxygen transmission rate decreases as MC increases with the liquid−wood contact time and that after 40 days, there is still oxygen permeation. This process of progressive moistening of the wood is also reflected in the OTR descending kinetic in new barrels, and this process results in a reduction of up to 40% 2.5 months after being filled.[7]

The aim of this work was to develop a routine method for the classification of rough staves according to their OTR in working conditions similar to those in a barrel, considering the variation in the diffusion coefficient that wood undergoes during aging.

MATERIALS AND METHODS

This study is organized into three phases. The first stage validates the device built for measuring the wood's OTR through the evaluation of the device's airtightness (OTR_{zero}) and the measurement of a material acting as an oxygen barrier with known permeability. In the second phase, rough staves were classified according to their oxygen transmission rates, and from this classification, staves were made from the high- and low-OTR rough stave groups to build two barrels. In the third phase, barrels were built and tested to assess the total OTR of the barrel. Different routes for oxygen entry were also analyzed, hence differentiating between the OTR of the staves after their coopering process and the OTR due to oxygen entry through the joint of the different barrel wood pieces (usually known as gaps).

Measurement Device. A device was developed for the quick measurement of the OTR of porous materials in contact with gas or liquids (Figure 1), including wood for enology applications.[21] The device's dimensions were designed to maintain the same liquid volume/wood surface relationship as in a Bordeaux 225 L barrel. Additionally, the hydrostatic pressure of the liquid in contact with the stave was established to be similar to the pressure of a stave at a barrel's half-height thanks to the glass tube at the top of the device (Figure 1), so the column of liquid was similar to that in a barrel. The study of the diffusion of a gas through a membrane to assess the membrane's permeability to such gas and the gas's diffusivity in said membrane is performed using a classic assay following Crank's diffusion equations.[22] This method, the time lag permeation technique, allows the effective determination of the OTR of different materials in a steady state, under specific circumstances,[23] and in the case of wood, which is considered a porous solid.[19] The method is based on continuous monitoring of the amount of a penetrant diffusing through a solid membrane into a device chamber.[24] The amount of gas recovered in the device chamber as a result of permeation through the membrane is plotted as a function of time. The steady state permeation of gases through a material with thickness d (m) is calculated using the simple equation

$$J = P \times \frac{\Delta p_{O2}}{d} \quad (1)$$

where J (m^3) is the volumetric flow of gas transported per unit of time (s) through a surface area (m^2), which, according to eq 1, is proportional to the constant partial pressure difference Δp_{O2} (Pa) of oxygen between both sides of the solid membrane. The proportionality constant P is called the permeability coefficient ($m^3 \cdot m/m^2 \cdot s \cdot Pa$). The method relies on the measure of the increase in oxygen partial pressure (p_2) over time in an initially oxygen-depleted chamber. Of note, even upon reaching steady state permeation, the partial pressure p_2 of the permeated gas, oxygen, remains negligibly small compared to the partial pressure of the gas at the other side of the membrane, the atmospheric air ($p_2 \ll p_1$). A steady state is reached when the increase in p_2 with time is linear, indicating a constant oxygen entry through the membrane.

DOI: 10.1021/jf505360r
J. Agric. Food Chem. 2015, 63, 1268−1275

OTR_{zero}. The device chamber was tested six times to ensure airtightness before the experiments were conducted by fixing a metal piece to the device in place of the membrane. The device's chamber was filled with N_2, and the dissolved oxygen (DO) entry was monitored for 24 h. Then, the OTR_{zero} was established. Once the device tightness was confirmed and prior to each experiment, the accuracy of the oxygen sensor in the liquid chamber under the measurement conditions was verified with the device's chamber full of nitrogen.

Membrane with Known Permeability. To assess the device's capacity, the oxygen permeability was assessed for a membrane with a known permeability when used as a barrier for oxygen. Repeated measurements were performed using a membrane composed of three layers, polyethylene/polyethylene terephthalate metallized/polyethylene (PE/PETmet/PE) with 50/12/50 μm thicknesses and oxygen permeability ≤ 1 $cm^3/m^2 \cdot 24$ h tested by Smurfit Kappa (Spain) according to ASTM F 1927-07 at 23 °C and 75% relative humidity.[13]

Wood Measurements. The evaluation of rough staves requires the emulation of the conditions of a stave in a full barrel. Therefore, the device was used in a liquid−stave−air configuration. The same relationship between the wood surface and liquid volume was maintained, and the system was given the capacity to control the necessary head space and its pressure according to the operation of a barrel.[25,26]

When a barrel is filled, the wood starts a moistening process, and the MC in the stave is not in a steady state. The variation of the MC in the wood of a 27 mm thick stave maintains a transition state for 82 days, which is the time necessary for the MC in the exterior part of the stave to increase after it contacts the liquid in the interior face.[27] This fact is reflected in the OTR decrease in barrels, which reaches an almost steady point at 2.5 months.[7] For this nonsteady state, the equation proposed by Crank[22] allows the use of the time lag permeation technique, as long as two initial conditions are met by the study. The first condition demands that the membrane be at zero concentration of the gas to be measured, and the second is that the face through which the diffusing substance emerges is effectively maintained at zero concentration. If both conditions are met, the steady state is reached after a specific time (lag). This is the time at which the system reaches the steady state or a constant flow state and can be used to determine the diffusion coefficient of the permeated gas for the material[28] and the OTR. Therefore, to measure a constant OTR, it would be necessary to moisten the wood for 82 days, which is when it reaches the steady state. This length of time would not allow the establishment of a routine method for the measurement of the OTR in wood. Moreover, in the first 2.5 months of aging, the barrel doses close to 40% of all the oxygen that will be incorporated in the barrel contents in a year.[7] Therefore, if the wood was to be tested after the moisture stabilization period, the OTR obtained would not consider almost half of the total annual oxygen input. Bearing this in mind, we decided to condition the rough staves prior to the assay.

Wood Conditioning. In this study, the wood was kept in contact with liquid for a week, which was considered to be the necessary moistening time for its conditioning. Additionally, to accelerate the equilibration transition process of p_{O2} inside the wood and reach a steady state, the device's chamber was completely depleted of oxygen before every assay for at least 2 h to gradually remove any gas from the inner to the outer side of the oak wood sample. With this procedure, desorption phenomenon interference, a process described by other authors in porous materials, was avoided.[29,30] Moreover, we were able to reach the partial pressure gradient of the oxygen inside the wood earlier, similar to that produced in the barrel aging conditions, as reported previously.[20] We decided to work under these conditions to develop a quick routine method, without the requirements of the time lag permeation technique; this method demands great technical complexity and high stabilization times to achieve a stabilized MC and a p_{O2} equal to zero on the inside of a porous material such as wood, with a thickness of a barrel stave (27 mm).

Wood Measuring Conditions. Once depleted of gas, the device's chamber was filled with a previously oxygen-free model wine propelled with nitrogen (99.9992% Carburos Metálicos, Barcelona, Spain). Model wine was used instead of wine because the oxygen-consuming compounds of the wine would not allow the measurement of oxygen delivered to the wine. Wood compounds capable of consuming oxygen are considered to closely reproduce conditions similar to those in an operating barrel; otherwise, the amount of oxygen reaching the wine through wood could be overestimated. To reproduce the conditions under which increased oxygen transmission occurs in a barrel,[26,31] the pressure inside the chamber filled with liquid was adjusted to −100 hPa, using a syringe in the system's head space, controlled with a pressure transducer (Transmitter S-10, Wika, Lawrenceville, GA, USA) in the upper part of the tube (Figure 1).

All of the assays were performed in a climate-controlled barrel room, and the holding temperature was kept constant (15 ± 0.01 °C) using a Julabo FP40-ME thermostatic bath (Seelbach, Germany).

OTR Measurement. The oxygen permeation of wood pieces is performed measuring the increase in the oxygen partial pressure with time (hPa/day), which allows the determination of the OTR using the law of ideal gases[32,33]

$$\mathrm{OTR} = \frac{\Delta n \times V_m}{\Delta t} = \frac{\Delta p_{O2} \times V}{R \times T} \times \frac{V_m}{\Delta t} = \frac{\Delta p_{O2} \times V}{\Delta t \times P_{atm}} \quad (2)$$

where n is the amount of a substance in moles, V_m is the molar volume of oxygen, T is the absolute temperature in K, $((\Delta p_{O2})/(\Delta t))$ is the slope in the linear part of hPa/day, V is the device's chamber volume, and P_{atm} is the atmospheric pressure in hPa during the assay. Henry's law was applied to evaluate the oxygen concentration (mg/L), and the Bunsen absorption coefficient $(cm^3(O_2)/cm^3)$ of oxygen in hydroalcoholic mixtures[34] was used to avoid subestimation measurements when oxygen solubility in water was used.[35]

Rough Staves. For the second part of this study, we worked with Radoux Cooperage personnel (Jonzac, France), who selected 69 French oak rough staves (*Quercus petraea*) of the Allier forest with a greater length (120 cm) than is typical (90 cm). Wood pieces (pieces A and B) were extracted from both ends of the rough stave. A total of 138 pieces were sent to our Center for analysis using the same methodology previously described. The remaining parts of each rough stave, now with the typical dimensions, were stored in the cooperage for the production of staves and further construction of the barrels according to the classification delivered by our Center. The tested wood pieces had effective dimensions of a 40 mm diameter and a thickness of approximately 27 mm. The effective surface area for oxygen transmission was 12.57×10^{-4} m^2. All of the samples were stored under environmental conditions of 15 °C and 75% relative humidity, maintaining the MC of the pieces between 14 and 15%.

Measurement in Barrels. Two barrels of 225 L were built using 25 staves selected from the high- or low-OTR groups. The OTRs of the barrels were measured following the protocol described previously[7] and barrel total OTR (wood + gaps) was obtained. After these tests, the oxygen transmission rate of the barrel wood was also evaluated (wood OTR). For this, all joints and gaps were sealed with epoxy, and before the tests, all barrels were conditioned to ensure that the wood had recovered its initial moisture (14% MC).

All tests were performed following the protocol of the cumulative measurement of dissolved oxygen inside the barrel. Barrels were filled with model wine that was previously deoxygenated according to a previous paper.[7] When the measurements showed the constant absence of dissolved oxygen, the barrels were topped with this solution and were sealed with an expandable modified silicon bung, which ensured airtightness. This bung had a feedthrough for both optical fibers of the submergible oxygen probes introduced in each barrel.

The OTR in barrels is typically expressed in mg/L·year.[17,36] To express the OTR in mL/L·year, we used the parameters of 225 L and 2.01 m^2 of internal wood surface. Bearing in mind the importance of the time of the experiments in the annual OTR measurement, this work expresses the measurement as μg/L·day.

During all tests, the barrels were stored in a climate-controlled cellar, where the room temperature was 15 °C and humidity was 75%, to maintain the typical air physical properties in a real cellar situation, regarding diffusion and permeability.

DOI: 10.1021/jf505360r
J. Agric. Food Chem. 2015, 63, 1268−1275

Table 1. Results of the Tests Performed with the Device for the Evaluation of the Zero Oxygen Transfer Rate (OTR_{zero}) and the Permeability (P) of a Known Membrane (PE/PETmet/PE)

	test							
	1	2	3	4	5	6	mean	SD
$OTR_{zero} \times 10^9$	1.778	1.575	1.755	1.733	1.969	1.477	1.714	0.171
P (cm^3 m^{-2} day^{-1})	0.7227	0.7601	0.7310	0.7393	0.7393	0.6895	0.7303	0.0235

Oxygen Partial Pressure Measurement. The measurement of dissolved oxygen in the device[13] was performed using an Oxytrace device (PreSens GmbH, Germany) equipped with a PSt6 oxygen sensor (measurement range, 0−41.4 hPa; detection limit, 0.002% O_2). This sensor was placed inside the device in direct contact with the fluid of the chamber that, according to the test, was nitrogen or synthetic wine. Luminescent measurements were performed using an optical fiber through a transparent surface where the sensor was attached. For the measurement of the dissolved oxygen levels inside the barrels, we used two submergible oxygen probes in each barrel. The probes were equipped with a PSt6 sensor with a four-channel OXY-4 trace transmitter (PreSens GmbH, Germany) connected to a computer. To determine the representative mean value of the dissolved oxygen concentration in the fluid of each barrel, the arithmetic mean of every barrel was calculated.[7]

Calibration of the oxygen systems in the tonometer[37] was performed using a conventional two-point calibration in the model wine saturated with nitrogen (cal 0) and a second value in the range between 5 and 10% air saturation. A calibration gas mixture with 2.001% (±0.5% rel) pure oxygen gas and nitrogen (9.55% air-sat) was used as a second calibration standard (Carburos Metálicos, Spain). Both gases were pumped into the tonometer for 10 min at a constant 15 °C until stable conditions were achieved. All measurements performed for p_{O2} were corrected to compensate for the interferences introduced by ethanol, according to the model developed in previous studies.[38]

Statistical Analysis. Data were collected using Microsoft Excel 2013 software (Redmond, WA, USA).

RESULTS AND DISCUSSION

Zeros. Initially, six measurements of the oxygen entry rate were performed in the device when it had been hermetically closed with a stainless steel piece. These measurements, called zeros, allowed us to assess the hermeticity of the device, and the mean result was subtracted from the measurements performed. The results are shown in Table 1 and indicate that the device has a mean zero of 0.1714×10^{-9} cm^3/m^2·day. This value was low enough to ensure the airtightness of the device.

Measurement Repeatability. Six assays were performed in the same membrane sample previously described to determine the repeatability. The measurements were performed following the time lag permeation technique[33] to check the accurate performance of the newly designed system, indicated by the zero value and the correct measurement of the reference film.

The results obtained correspond to the manufacturer's indications (<1 cm^3/m^2·day) because the OTR measured in the material varies from 0.689 to 0.760 cm^3/m^2·day. This represents an average permeability (P) of 0.730 cm^3/m^2·day and a repeatability of r = 0.023 cm^3/m^2·day. Therefore, the device meets all of the necessary requirements to evaluate the OTR of materials (Table 1).

Oak Wood OTR. The construction of barrels with different oxygenation levels demands the determination of the OTR of the rough staves. For this, the OTR of 138 wood pieces was evaluated following the protocol of dissolved oxygen cumulative measurement in the device, as described under Materials and Methods.[13] Figure 2 shows the increase in oxygen concentration in the device chamber according to the measurement time in the evaluation of some pieces.

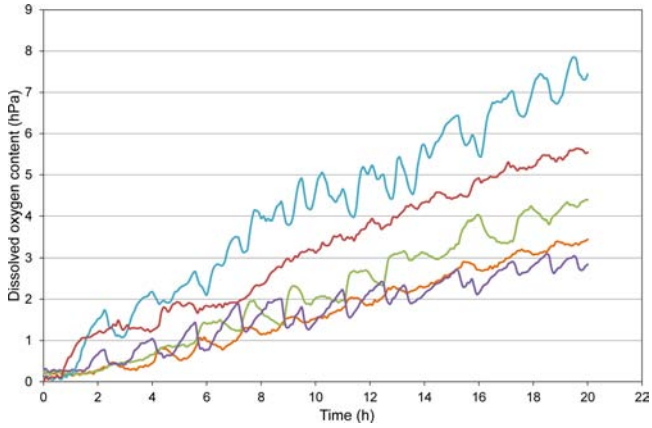

Figure 2. Comparative measurements of the evolution of the dissolved oxygen content (hPa) of five different wood pieces.

Table 2 shows the results obtained expressed as micrograms of oxygen transferred by the wood to each liter of wine during a day (μg/L·day), accumulating the mean of the data obtained from the pieces extracted from each rough stave (piece A, top end; piece B, lower end). These results indicate that in some rough staves, the difference between the pieces of both ends is small, as was the case for rough stave 1 (piece A = 196.41 μg/L·day and piece B = 198.31 μg/L·day) and rough stave 29 (piece A = 113.20 μg/L·day and piece B = 117.11 μg/L·day). However, in other cases, the difference is quite large, such as in the case of rough stave 31 (piece A = 209.86 μg/L·day and piece B = 413.97 μg/L·day) and rough stave 49 (piece A = 150.71 μg/L·day and piece B = 266.23 μg/L·day). This result reflects the wood's natural structural variability throughout the stave, which also affects its physical properties and hence most likely alters its capacity for transmitting oxygen.

The result of the average OTR measured from both ends was considered representative of all of the rough staves and allowed the establishment of the stave classification in two groups. This classification excluded 19 rough staves with values between 180 and 211 μg L·day, which did not clearly belong to either of the two groups. The group of rough staves with a low OTR included staves with an average OTR between 48 and 177 μg/L·day, which represents the group mean OTR of 140 μg/L·day. In contrast, the group of rough staves with a high OTR included staves with an average OTR between 213 and 379 μg/L·day, for a total group mean of 265 μg/L·day (Table 2).

Once a barrel is built, the potential oxygen contribution from the wood must also include the contribution from the gaps. This outcome depends on the assemblage process of each cooperage and on the wood type. Moreover, it is important to bear in mind that the OTR of a rough stave will be modified in the bending and toasting processes performed in the cooperage

DOI: 10.1021/jf505360r
J. Agric. Food Chem. 2015, 63, 1268−1275

Table 2. Mean Values of the OTR in Rough Staves

rough stave	piece	OTR (μg/L·day)	measured grain[a]	grain[b]	rough stave	piece	OTR (μg/L·day)	measured grain[a]	grain[b]
1	A	196.41	2.70	3	36	A	188.25	1.56	3
	B	198.31	1.92	2		B	563.75	1.82	3
2	A	215.94	2.27	3	37	A	136.53	1.20	2
	B	441.82	2.33	3		B	122.42	1.92	3
3	A	163.03	4.76	4	38	A	109.48	1.56	3
	B	275.80	5.26	5		B	428.25	0.98	2
4	A	214.73	4.55	4	39	A	161.85	1.18	2
	B	245.67	3.23	3		B	454.33	1.79	3
5	A	178.48	3.13	3	40	A	123.84	1.72	3
	B	279.60	1.45	2		B	181.92	1.52	3
6	A	178.07	2.08	3	41	A	121.91	1.54	3
	B	236.40	2.94	3		B	191.66	1.59	3
7	A	198.04	2.22	3	42	A	195.71	1.09	2
	B	161.78	2.50	3		B	174.96	1.16	2
8	A	72.38	2.27	3	43	A	125.07	1.14	2
	B	98.75	2.17	3		B	203.98	0.96	2
9	A	118.67	2.27	3	44	A	102.71	1.52	3
	B	337.61	1.47	2		B	137.02	1.82	3
10	A	142.56	2.78	3	45	A	109.00	1.56	3
	B	283.72	1.67	3		B	150.89	1.61	3
11	A	149.92	3.57	3	46	A	215.55	1.67	3
	B	192.65	2.78	3		B	139.50	1.56	3
12	A	103.66	1.59	3	47	A	129.36	1.28	2
	B	200.48	1.96	3		B	179.86	1.52	3
13	A	113.25	1.61	3	48	A	160.49	2.56	3
	B	290.92	2.38	3		B	243.07	3.03	3
14	A	168.39	2.22	3	49	A	150.71	1.37	2
	B	354.34	2.04	3		B	266.23	1.43	2
15	A	153.49	1.96	3	50	A	142.21	1.69	3
	B	176.61	2.00	3		B	233.70	1.47	2
16	A	89.03	2.63	3	51	A	153.01	1.43	2
	B	163.85	1.45	2		B	165.70	1.82	3
17	A	242.12	2.44	3	52	A	122.04	2.17	3
	B	221.50	2.27	3		B	86.86	2.50	3
18	A	161.03	1.79	3	53	A	208.47	2.17	3
	B	223.81	2.00	3		B	346.65	1.92	3
19	A	146.38	1.85	3	54	A	80.38	1.75	3
	B	276.62	2.13	3		B	15.89	1.67	3
20	A	136.89	2.00	3	55	A	147.73	1.69	3
	B	148.16	1.96	2		B	250.25	2.17	3
21	A	197.89	2.17	3	56	A	178.02	2.86	3
	B	130.60	2.00	3		B	212.18	3.03	3
22	A	179.57	2.04	3	57	A	165.96	2.86	3
	B	271.30	1.49	2		B	232.27	2.86	3
23	A	153.81	1.89	3	58	A	358.00	1.05	2
	B	369.39	1.54	3		B	215.54	2.22	3
24	A	161.41	2.08	3	59	A	218.81	1.89	3
	B	494.33	2.08	3		B	234.72	1.56	3
25	A	91.22	2.33	3	60	A	203.60	2.38	3
	B	149.18	2.13	3		B	200.79	1.96	3
26	A	157.37	2.08	3	61	A	436.37	1.39	2
	B	241.05	2.22	3		B	253.51	1.25	2
27	A	329.84	1.41	2	62	A	221.36	2.70	3
	B	213.23	1.56	3		B	214.81	2.63	3
28	A	120.36	2.70	3	63	A	233.76	2.50	3
	B	200.39	2.00	2		B	287.53	2.00	2
29	A	113.20	1.61	3	64	A	110.46	1.64	3
	B	117.11	2.17	3		B	110.06	1.67	3
30	A	199.57	1.89	3	65	A	206.98	1.92	3
	B	288.45	1.52	3		B	109.63	1.79	3
31	A	209.86	1.82	3	66	A	150.84	2.63	3

DOI: 10.1021/jf505360r
J. Agric. Food Chem. 2015, 63, 1268−1275

Table 2. continued

rough stave	piece	OTR (μg/L·day)	measured grain[a]	grain[b]	rough stave	piece	OTR (μg/L·day)	measured grain[a]	grain[b]
	B	413.97	2.50	3		B	188.71	1.64	3
32	A	141.81	2.17	3	67	A	198.59	2.50	3
	B	415.43	2.33	3		B	149.25	2.86	3
33	A	164.88	1.89	3	68	A	266.75	1.85	3
	B	255.65	1.89	3		B	140.68	1.56	3
34	A	294.23	1.64	3	69	A	262.53	3.45	3
	B	310.97	1.61	3		B	147.06	2.94	3
35	A	181.41	2.04	3					
	B	196.72	2.04	3					

[a]Grain value measuring the number of rings in 5 cm of a stave. [b]Grain according to Vivas's classification (1, <1 mm; 2, between 1 and 2 mm; 3, between 2 and 4 mm; 4, between 4 and 5 mm; and 5, >5 mm).

because they modify the shape and maybe also slightly the structure of the wood and therefore most likely affect its OTR.

OTR–Grain Relationship. To assess the relationship between the OTR and the real grain of rough staves, the number of rings present in 5 cm of wood in the transversal section of the rough staves was measured following the medullary rays, yielding the mean width of a growth ring. The results found for the 138 analyzed pieces are shown in Table 2. The classification was also performed according to the method of Vivas,[4] as described previously.

The correlation analysis between the oxygen transmission rate and the measured grain indicates that this relationship is very low (correlation = −0.0216, p = 0.8014). This same result was obtained when the OTR was analyzed with the grain classified according to the method of Vivas (correlation = −0.1172, p = 0.1712).

Barrel Construction. Finally, the barrels were built using 25 staves of each group for each barrel, discarding the staves with an intermediate OTR between the two groups. The barrels were manufactured in the Radoux Cooperage (Jonzac, France), using the regular process with a medium toast.

The results obtained from the assessment of the oxygen entry into the barrels is shown in Figure 3, which displays the

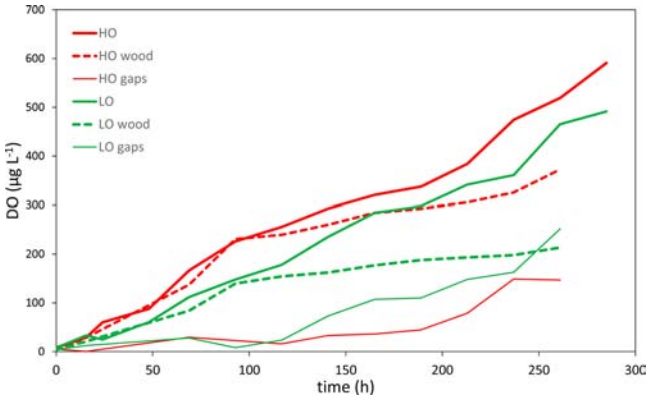

Figure 3. Cumulative measurements of the dissolved oxygen content (μg L^{-1}) inside barrels with a high (HO, in red) and low (LO, in green) OTR, with sealed (dashed) and nonsealed gaps (solid).

increase in dissolved oxygen content in both barrels during 11 days of testing. As expected, the global entrance of oxygen was higher in the barrels that were constructed with rough staves classified with a high OTR than in the barrels constructed with rough staves classified with a low OTR. This experiment was used to assess the aim that was initially proposed. Specifically, it has been found that the high-OTR barrel would supply the aging wine with a total of 116 mg of oxygen (225 L × 519.02 μg/L) in 11 days on average, whereas the low-OTR barrel would supply only 105 mg of oxygen (225 L × 471 μg/L) in 11 days. These global results indicate that the barrel with a high OTR would transfer only 10% more oxygen to the wine than the low-OTR barrel, a result that is not satisfactory in regard to our aim. To perform a comparison of the OTR that is dependent only on the classified staves, it is necessary to analyze in detail the different ways oxygen enters the barrel.

To evaluate the potential of the classification system proposed for the rough staves, the rate of oxygen entry due exclusively to the oxygen transmission process of the wood from the staves of the barrels was evaluated. Figure 3 also shows the oxygen that exclusively enters through the wood, measured in the epoxy-sealed barrels. This procedure allowed us to directly calculate the OTR corresponding to the wood (Table 3). It also permitted us to calculate the oxygen that

Table 3. Cumulative Dissolved Oxygen Content in Barrels with a High or Low OTR, Penetrated by Different Entry Routes after 11 Days

	μg L^{-1}	mg per barrel	%
Low OTR Barrel			
total	465.18	104.7	100
wood	213.31	48.0	46
gaps	251.87	56.7	54
High OTR Barrel			
total	519.02	116.8	100
wood	372.27	83.8	72
gaps	146.75	33.0	28

enters through the gaps as the difference of OTR between the unsealed and the sealed barrel. It was observed that in the case of the barrel with a high OTR, the contribution was 83.8 mg (225 L × 372.27 μg/L) of the 116.8 mg of total oxygen in 11 days. This result indicates that 72% of the oxygen that the aging wine would receive in the high-OTR barrel would enter through the wood, whereas the 33 mg of oxygen (225 L × 146.75 μg/L) that would enter the barrels through the stave gaps would comprise 28% of the total.

In the case of the barrel with a low OTR, it was found that the 48 mg of oxygen (225 L × 213.31 μg/L) that entered the barrel through the wood in 11 days represents 46% of the total oxygen that enters to the barrel, with 54% entering through the gaps. According to the results obtained, the treatment and manufacturing process of the staves from the rough staves classified as having high and low permeability considerably

DOI: 10.1021/jf505360r
J. Agric. Food Chem. 2015, 63, 1268−1275

affected the properties of the wood, as expected. Definitively, the high-OTR staves allowed 1.74 times more oxygen to enter the barrel (372 mg/L) than the low-OTR staves (213 mg/L).

To compare the previously obtained results from the evaluation of the built barrel staves (evaluated for 11 days) with those obtained for rough staves (evaluated for 1 day using the proposed method), an extrapolation was performed to determine the rough stave OTR of 11 days. For this, we included the results of our group's previous studies that were published recently,[7] in which it was demonstrated that the entrance of oxygen to the barrels does not follow a linear variation with time but a potential evolution, such as $y = at^{0.7789}$ in the case of French barrels.[39] Therefore, from the contribution of the first 24 h and considering this model as an approximation of the behavior of French oak barrels, we calculated the constant a for the high- and low-OTR barrels, extrapolating it to 11 days. We found that the high-OTR rough staves would allow 1682.92 μg/L oxygen in and that the low-OTR rough staves would allow 642.23 μg/L oxygen in. These data indicate that the high-OTR rough staves would permit 2.6 times as much oxygen to enter the barrel as the low-OTR rough staves in 11 days.

Analyzing the effect that the bending and toasting processes have on the OTR of rough staves, we found that wood's oxygen permeation decreases between 3 and 4.5 times after these processes. Specifically, after the 11 day evaluation, we found that in the case of high-OTR wood, these changed from dosing 1.68 mg/L in rough staves to 0.37 mg/L in toasted staves, which represents a 4.5-fold decrease in the OTR. In the case of low-OTR wood, they went from 0.64 mg/L in rough staves to 0.21 mg/L in toasted staves. Therefore, wood loses up to 3 times its oxygen transfer rate during the toasting process. This result agrees with previously reported studies,[5,39] which demonstrate the loss of the gas permeability of oak wood after the bending and toasting processes.

From the detailed analysis of the oxygen entrance through the gaps, the results show that the oxygen that enters into the wine in this way greatly varies from one barrel to another. In this case, we found that 56.7 mg (225 L × 251.87 μg/L) of oxygen entered through the gaps of the low-OTR barrels, almost 1.7 times the 33 mg of oxygen entering the high-OTR barrel (225 L × 146.75 μg/L). Bearing in mind that the cooperage is the same (and, therefore, so is the manufacturing system of both barrels), it is possible to conclude that the assembly system makes an important contribution for the variability between barrels.

In conclusion, this study proposes a device and a procedure for the routine measurement of the OTR of oak wood. It is important to highlight that the device has the capacity to reproduce working conditions that are similar to those of the barrel, which allows its use in the classification of rough staves for the manufacturing of barrels. In this way, after the classification of rough staves, two barrels with different oxygen transfer rates were built. Specifically, it was demonstrated that the high-OTR barrel allows almost twice as much oxygen to be transferred throughout the oak wood into the wine as the low-OTR barrel. The results show that the classification of rough stave wood has indeed allowed the construction of barrels with high and low oxygen permeability, accomplishing our aim. The importance of the assembly of staves in the global OTR during barrel construction has been confirmed, a result that requires a deeper study on the factors determining the OTR in this process. Moreover, it was confirmed that the toasting and bending processes are important in the oxygen permeability decrease in oak wood used for barrel making.

AUTHOR INFORMATION

Corresponding Author

*(M.A.-S.) E-mail: delalamo@qa.uva.es.

Funding

This work was financed by Ministerio de Ciencia e Innovacion (AGL2011-26931) and by Junta de Castilla y León (VA-086A11-2) from Spain.

Notes

The authors declare no competing financial interest.

ACKNOWLEDGMENTS

We acknowledge Carlos González Muñoz for data acquisition. We express great appreciation to SA Tonnellerie Radoux (Jonzac, Francia) for their collaboration.

REFERENCES

(1) Ribereau-Gayon, J. Contribution à l'étude des oxydations et réductions dans les vins. Ph.D. thesis, Université de Bordeaux, 1933.

(2) Vivas, N.; Glories, Y. Modélisation et calcul du bilan des apports d'oxygène au cours de l'élevage des vins rouges. II. Les apports liés au passage d'oxygène au travers de la barrique. *Prog. Agric. Vitic.* **1997**, *114*, 315−316.

(3) Feuillat, F.; Huber, F.; Keller. Knowledge on 'grain' used for the classification of stave oak wood, *Quercus robur* L.; *Quercus petraea* Liebl. *Rev. Fr. Oenol.* **1992**, *32*, 65−69.

(4) Vivas, N. Sur la notion de grain en tonnellerie. *J. Sci. Technol. Tonnellerie* **1995**, *1*, 17−32.

(5) Boeglin, N.; Kuzara, S.; Duchanois, G.; Masson, D. Étude du chêne de tonnellerie: perméabilité et cintrage. *Rev. Fr. Oenol.* **1993**, *144*, 35−40.

(6) Pracomtal, G.; Mirabel, M.; Teissier du Cros, R.; Monteau, A. Types of oak grain, wine elevage in barrel. *Pract. Winery Vineyard* **2014**, No. July, 64−69.

(7) del Alamo-Sanza, M.; Nevares, I. Recent advances in the evaluation of the oxygen transfer rate in oak barrels. *J. Agric. Food Chem.* **2014**, *62*, 8892−8899.

(8) Feuillat, F.; Keller, R. Variability of oak wood (*Quercus robur* L., *Quercus petraea* Liebl.) anatomy relating to cask properties. *Am. J. Enol. Vitic.* **1997**, *48*, 502−508.

(9) Hansmann, C.; Gindl, W.; Wimmer, R.; A, T. Permeability of wood − a review. *Wood Res.* **2012**, *47*, 1−16.

(10) Siau, J. F. *Transport Processes in Wood*; Springer-Verlag: Berlin, Germany, 1984; p ix, 245 pp.

(11) ASTM D1434-82(2009)e1. Standard Test Method for Determining Gas Permeability Characteristics of Plastic Film and Sheeting. ASTM International, West Conshohocken, PA, USA, 2009; Vol. 15.10.

(12) ASTM D3985-05(2010)e1. Standard Test Method for Oxygen Gas Transmission Rate Through Plastic Film and Sheeting Using a Coulometric Sensor. ASTM International, West Conshohocken, PA, USA, 2010; Vol. 15.10.

(13) ASTM F1927-14. Standard Test Method for Determination of Oxygen Gas Transmission Rate, Permeability and Permeance at Controlled Relative Humidity Through Barrier Materials Using a Coulometric Detector. ASTM International, West Conshohocken, PA, USA, 2014; Vol. 15.10.

(14) ASTM F1307-14. Standard Test Method for Oxygen Transmission Rate Through Dry Packages Using a Coulometric Sensor. ASTM International, West Conshohocken, PA, USA, 2014; Vol. 15.10.

(15) ISO, 15105-1. Plastics − Film and sheeting − Determination of gas-transmission rate − Part 1: Differential-pressure methods. In International Organization for Standardization, Geneva, Switzerland, 2007; Vol. TC 61 Plastics.

DOI: 10.1021/jf505360r
J. Agric. Food Chem. 2015, 63, 1268−1275

(16) ISO, 15105-2. Plastics − Film and sheeting − Determination of gas-transmission rate − Part 2: Equal-pressure method. International Organization for Standardization, Geneva, Switzerland, 2003; Vol. TC 61 Plastics.
(17) Vivas, N.; Debèda, H.; Ménil, N.; Vivas de Gaulejac, N.; Nonier, M. Mise en évidence du passage de l'oxygène au travers des douelles constituant les barriques par l'utilisation d'un dispositif original de mesure de la porosité du bois. Premiers résultats. *Sci. Aliment.* **2003**, *23*, 655−678.
(18) Huang, H. I.; Sarkanen, K. V.; Johanson, L. N. Diffusion of dissolved oxygen in liquid-saturated Douglas fir sapwood. *Wood Sci. Technol.* **1977**, *11*, 225−236.
(19) Sorz, J.; Hietz, P. Gas diffusion through wood: implications for oxygen supply. *Trees Struc. Funct.* **2006**, *20*, 34−41.
(20) Nevares, I.; Crespo, R.; Gonzalez, C.; del Alamo-Sanza, M. Imaging of oxygen transmission in the oak wood of wine barrels using optical sensors and a colour camera. *Aust. J. Grape Wine Res.* **2014**, *20*, 353−360.
(21) Del Alamo, M.; Nevares, I. PCT/ES2012/070084 Device for measuring the permeability and diffusivity of gases in porous materials and method for measuring said parameters using the device, 2012.
(22) Crank, J. *The Mathematics of Diffusion*; Oxford Science Publications: Oxford, UK, 1986.
(23) Rutherford, S. W. Review of time lag permeation technique as a method for characterisation of porous media and membranes. *Adsorption* **1997**, *3*, 283−312.
(24) Piringer, O. G.; Baner, A. L. Permeation of gases, water vapor and volatile organic compounds. In *Plastic Packaging Materials for Food: Barrier Function, Mass Transport, Quality Assurance, And Legislation*; Wiley: New York, 2000.
(25) Nevares, I.; del Alamo-Sanza, M. Oxygène et barriques Actualisation des connaissances quantité et voies de pénétration de l'oxygène dans la barrique. *Rev. Oenol.* **2014**, *153*, 1−4.
(26) Moutounet, M.; Mazauric, J. P.; Saint-Pierre, B.; Hanocq, J. F. Gaseous exchange in wines stored in barrel. *J. Sci. Technol. Tonnellerie* **1998**, *4*, 131−145.
(27) Feuillat, F. Study on interrelations between wood, wine and atmosphere using a model wooden cask. Relations with the anatomy of oak wood (*Quercus robur* L., *Quercus petraea* Liebl.). Ph.D. thesis, Ecole Nationale du Génie Rural des Eaux et des Forêts, Nancy, France, 1996.
(28) Saikumar, V.; Jaccodine, R. J. Time lag and permeation in multilayer polymer coatings. *IEEE Trans. Compon., Hybrids, Manuf. Technol.* **1993**, *16*, 517−522.
(29) Skouroumounis, G.; Waters, E. Oxygen ingress into bottled wine. *Pract. Winery Vin.* **2008**, No. July−Aug, 1−4.
(30) Lopes, P.; Silva, M. A.; Pons, A.; Tominaga, T.; Lavigne, V. r.; Saucier, C. d.; Darriet, P.; Teissedre, P.-L.; Dubourdieu, D. Impact of oxygen dissolved at bottling and transmitted through closures on the composition and sensory properties of a sauvignon blanc wine during bottle storage. *J. Agric. Food Chem.* **2009**, *57*, 10261−10270.
(31) Moutounet, M.; Mazauric, J. P.; Saint-Pierre, B.; Micaleff, J.; Sarris, J. Causes et conséquences de microdéformations des barriques au cours de l'élevage des vins. *Rev. Oenol.* **1994**, *74*, 34−39.
(32) Diéval, J. B.; Vidal, S.; Aagaard, O. Measurement of the oxygen transmission rate of co-extruded wine bottle closures using a luminescence-based technique. *Packag. Technol. Sci.* **2011**, *7*, 375−385.
(33) Timineri, D.; John, G. T.; Müller, K.; Huber, C. Oxygen permeation measurement with chemical optical sensors. Presented at Meetingpack2013, Valencia, 2013.
(34) Mejane, J. V.; Debailleul, M.; Lecerf, J. Étude sur la solubilité de l'oxygène dans l'alcool. *Ind. Aliment. Agric.* **1973**, *90*, 719−727.
(35) Nevares, I.; del Alamo Sanza, M.; Waters, E.; Day, M. La medida del oxígeno disuelto en vino y mostos, Concentración o presión parcial?: estado actual del conocimiento. Presented at the XIII Congreso Latinoamericano de Viticultura y Enología, Santiago de Chile, Nov 21−23, Santiago de Chile, 2011.
(36) Peterson, R. Formation of reduced pressure in barrels during wine aging. *Am. J. Enol. Vitic.* **1976**, *27*, 80−81.
(37) Proctor, K. G.; Bohlen, H. G. Tonometer for calibration and evaluation of oxygen microelectrodes. *J. Appl. Physiol.* **1979**, *46*, 1016−1018.
(38) del Alamo-Sanza, M.; Pando, V.; Nevares, I. Investigation and correction of the interference of ethanol, sugar and phenols on dissolved oxygen measurement in wine. *Anal. Chim. Acta* **2014**, *809*, 162−173.
(39) Hugi, E.; Wuersch, M.; Risi, W.; Wakili, K. Correlation between charring rate and oxygen permeability for 12 different wood species. *J. Wood Sci.* **2007**, *53*, 71−75.

NOTE ADDED AFTER ASAP PUBLICATION

This paper was published ASAP on January 13, 2015, with an error in Figure 3 and an author's address. The corrected version was reposted on January 26, 2015.

DOI: 10.1021/jf505360r
J. Agric. Food Chem. 2015, 63, 1268−1275

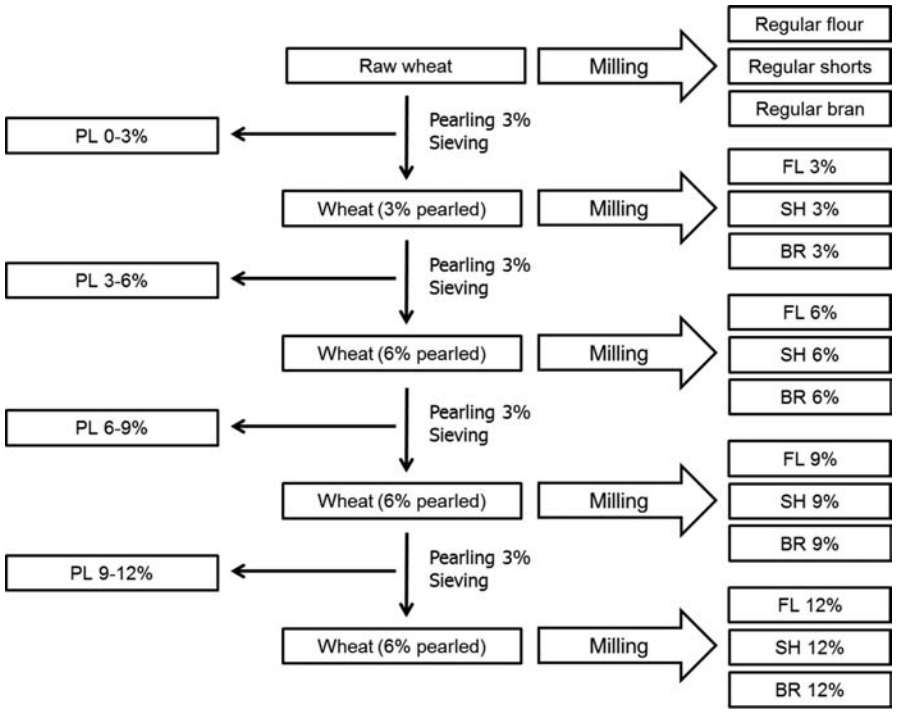

Figure 1. Overview of the production of pearlings, obtained by pearling wheat kernels to 3%, 6%, 9%, and 12%, and flour, shorts, and bran samples, obtained by pearling wheat kernels followed by milling. The pearlings from the sequential pearling process are referred to as PL 0−3%, PL 3−6%, PL 6−9%, and PL 9−12% while flour, shorts, and bran samples produced by (subsequent) roller milling are further referred to as regular flour or flour (FL) *x*%, regular shorts or shorts (SH) *x*%, and regular bran or bran (BR) *x*% respectively, with *x* being the percentage of wheat removed by pearling prior to producing the flour, shorts, and bran samples.

kernels prior to roller milling affects the mineral content of the resulting wheat products. Against this background, this study set out to investigate the distribution of minerals in common wheat and the effect of pearling on the mineral composition of the milled fractions. The resulting knowledge can be used to optimize wheat grain processing methodologies.

MATERIALS AND METHODS

Materials. Wheat grains (cv. Akteur, harvest 2012, moisture content 14.8%) were pearled at Satake Europe (Bredbury, United Kingdom) using PeriTec debranning technology which is based on friction (grain to grain contact) and abrasion (grain to rough surface contact).[19] Wheat was pearled in different successive steps to remove a total of 3.0, 6.0, 9.1, and 11.9% of the grain weight, and pearlings were collected after every pearling step. Broken wheat grains were removed after each pearling step by sieving through a 2.38 mm sieve. The pearlings obtained from this process are referred to as pearlings (PL) 0−3%, PL 3−6%, PL 6−9%, and PL 9−12%, respectively, throughout the remainder of this article. Figure 1 schematically represents pearling and milling fractions. Nonpearled and pearled wheat grains were roller milled with a Bühler (Uzwil, Switzerland) MLU-202 laboratory mill using the diagram described in Delcour et al.[20] Flour, bran, and shorts were produced. The shorts were separated at the end of the milling system using a 150 μm sieve[20] and are essentially bran tissue to which some starchy endosperm is still attached. Flour samples produced by roller milling are further referred to as regular flour or flour (FL) *x*%; where *x* is the percentage of wheat removed by pearling prior to producing the flour under consideration by roller milling. A similar terminology was used for the regular shorts or shorts (SH) *x*%, and regular bran or bran (BR) *x*%, obtained when roller milling wheat from which *x*% had been removed by pearling (Figure 1). Pearling and milling yields of these fractions have been described in De Brier et al.[21]

Sample Digestion and Multielement Analysis. Samples (0.05 g, three analytical replicates) were weighed into glass tubes and digested with 1.00 mL of ultrapure HNO_3 for 4 h followed by dilution to 10.0 mL with Milli-Q water (18.2 U; Milli-Q Plus, Merck Millipore, Darmstadt, Germany) and analysis by ICP-MS (Agilent 7700x, Santa Clara, CA). A reference wheat flour sample with certified mineral composition was included: NIST1567 Wheat (National Institute of Standards and Technology, Gaithersburg, MD). All elements reported were recovered to within 10% of certified values (Supporting Information). For each element, the difference between the concentration in intact (non)pearled wheat kernels and in the weighted average concentration of all corresponding (pearling and) milling fractions did not vary by more than 10% (nonpearled, 3% and 6% pearled) or 20% (9% and 12% pearled). This larger difference is due to the larger number of analyzed pearling fractions needed for the calculations. There was no indication of trace metal contamination (Fe, Cr, Ni, Mo, V) due to kernel pearling or milling from contact with metal parts in the pearling or milling tools (details not shown).

Imaging of Element Distribution. Elemental micro X-ray fluorescence microscopy (μ-XRF) maps were collected at the X-ray fluorescence microscopy beamline (XFM) at the Australian Synchrotron (Melbourne, Victoria, Australia). Thin (80 μm thick) cross-sections of the middle part of the (pearled) wheat grains were made following the method described by Lombi et al.[17] In this way, cross-sections were directly obtained on the Kapton tape without the need for embedding. Two cross-sections from different (pearled) wheat grains were analyzed. The use of thin sections was necessary in order to reduce the distortion of the elemental maps caused by the penetrating nature of the X-rays, as the output is translated into a 2D compression of the illuminated sample volume.[22]

The laterally resolved element maps were collected using the XFM undulator beamline equipped with a Si(111) monochromator and Kirkpatricke−Baez mirrors focusing the beam to a spot size of approximately 3 × 2 μm^2 (horizontal × vertical). An incident beam energy of 10 keV was used, and the fluorescence signal was collected using a 384-element Maia detector system. The detector was placed perpendicularly to the incident beam path and used to collect the full spectra fluorescence signal from the sample. The samples were analyzed continuously in the horizontal direction with steps of 4 μm in

DOI: 10.1021/jf5055485
J. Agric. Food Chem. 2015, 63, 1276−1285

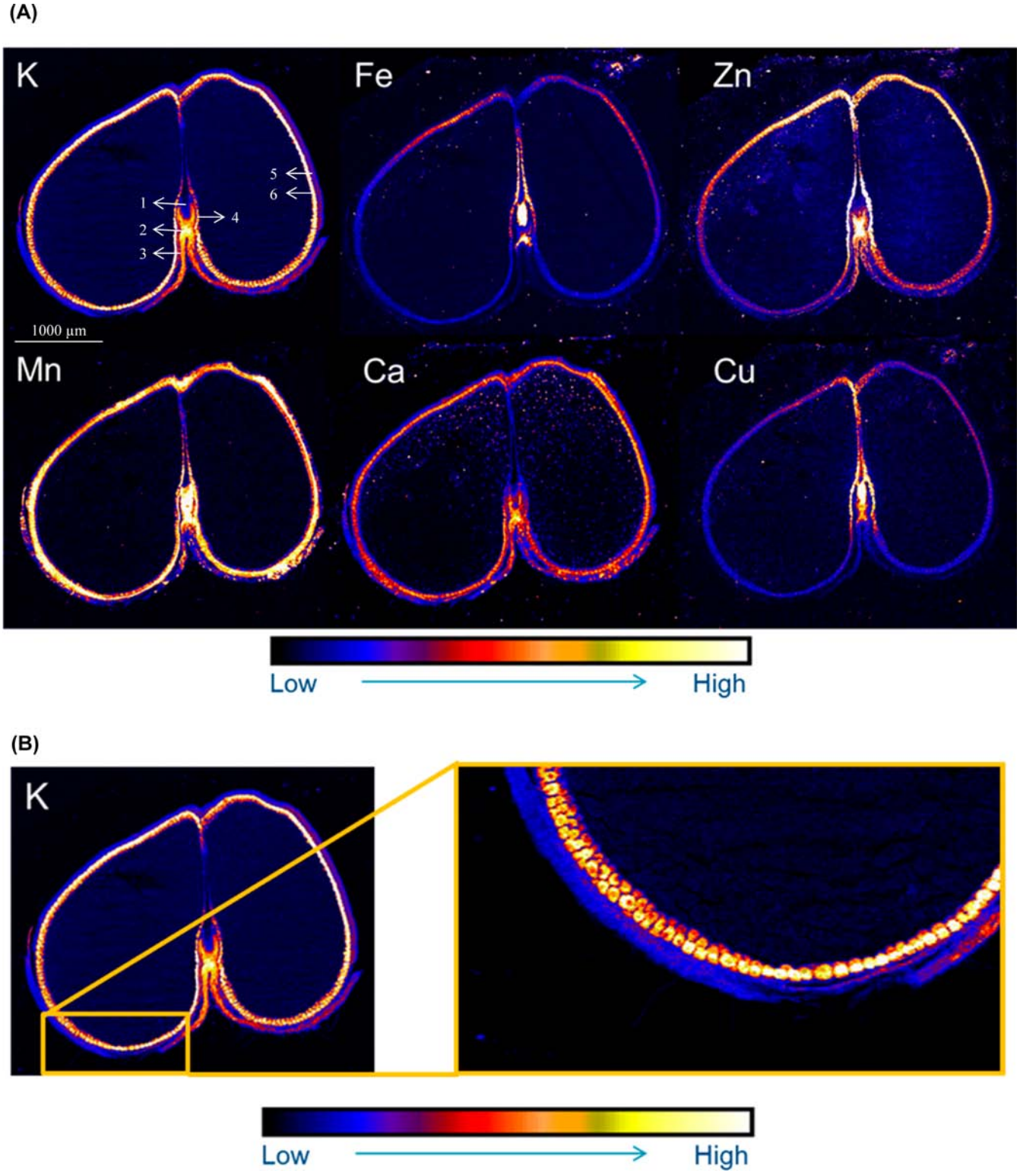

Figure 2. μ-XRF elemental maps of (A) a cross-section of a wheat sample and (B) a detailed picture of individual aleurone cells. The color scale represents different concentrations, with black and white corresponding to the lowest and highest concentration, respectively. The arrows indicate: 1, nucellar projection; 2, transfer cells (vascular bundle); 3, crease pericarp; 4, modified aleurone cells; 5, pericarp; 6, aleurone cells.

the vertical direction. The pixel (4 μm) transit time was approximately 5.2 ms. The full μ-XRF spectra were then analyzed using GeoPIXE.[23] This software uses dynamic analysis to subtract the background and resolves overlapping peaks to generate maps of element concentrations. Using this technique, the distributions of K, Ca, Fe, Zn, Cu, and Mn were imaged (the fluorescence signal for lighter elements cannot be collected using the current version of the Maia detector).

Statistical Analyses. Data was statistically processed using the JMP Pro 11 software (SAS Institute, Cary, NC). One-way analysis of variance (ANOVA) was performed to verify significant differences ($p < 0.05$) between mean values of the analyzed variables. A Dunnett's comparison procedure was used ($p < 0.05$) to test differences in composition, using the milled fractions of nonpearled wheat grains as a control.

DOI: 10.1021/jf5055485
J. Agric. Food Chem. 2015, 63, 1276−1285

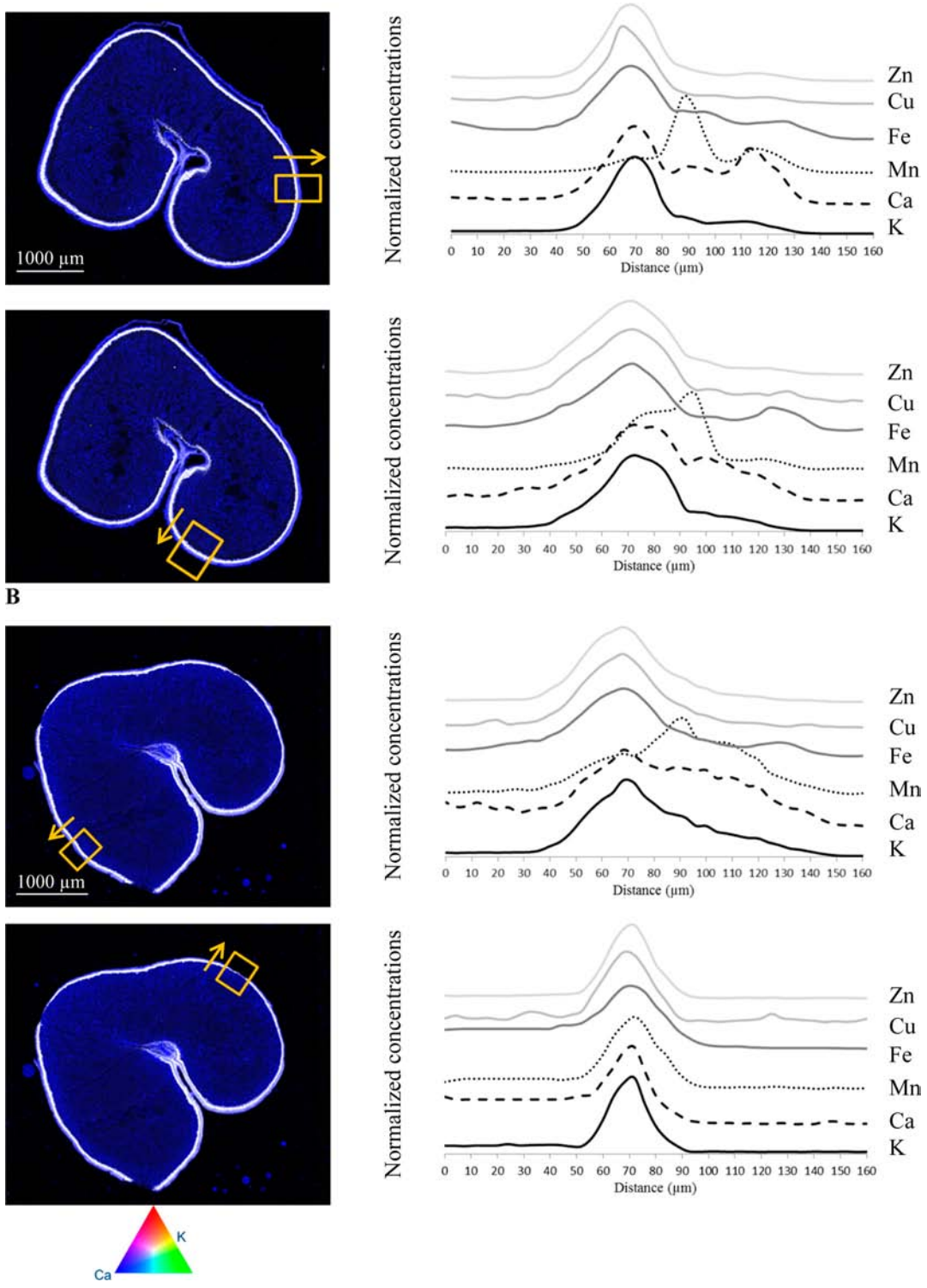

Figure 3. Line scans (from the starchy endosperm to the external surface of the wheat grain) for K, Ca, Mn, Fe, Cu, and Zn for the areas shown in the microphotographs with (A) a map of Ca and K present in a cross-section of nonpearled wheat and (B) 9% pearled wheat. The concentrations in the line scans were normalized against the maximum concentration. Ca is in blue and K in yellow, and the areas where they overlap are given in white.

RESULTS AND DISCUSSION

X-ray Fluorescence Microscopy Mapping of Mineral Distributions in Wheat Grains. Synchrotron μ-XRF is a powerful tool for visualizing the distribution of elements in seeds.[18] Figure 2A shows the distributions of Ca, Cu, K, Fe, Mn, and Zn in a nonpearled wheat kernel cross-section obtained using this technique. Individual cells of the aleurone are distinguishable in the elemental maps (Figure 2A and 2B). Concentrations of Ca and Mn were highest in the outermost bran layers, while the Cu, K, Fe, and Zn concentrations were highest in the aleurone layer. Although K was also mainly confined to the aleurone, a significant proportion was detected

DOI: 10.1021/jf5055485
J. Agric. Food Chem. 2015, 63, 1276−1285

Table 1. Concentrations of Different Elements (mg/kg dry matter) in Wheat Flour As Affected by Different Degrees of Pearling[a]

	regular flour	FL 3%	FL 6%	FL 9%	FL 12%
K	1500 (30)	1610 (20)*	1570 (20)*	1580 (10)	1510 (20)
P	1100 (20)	1200 (20)*	1150 (10)*	1180 (1)*	1090 (10)
Mg	191 (3)	234 (16)*	221 (3)*	220 (7)*	191 (3)
Ca	178 (1)	187 (8)*	179 (3)	181 (1)	173 (4)
Si	9.2 (0.2)	7.4 (0.1)*	7.6 (0.2)*	5.8 (0.7)*	4.4 (0.4)*
Fe	10.8 (0.7)	9.8 (0.6)	8.8 (0.2)*	7.8 (0.1)*	7.4 (0.4)*
Zn	7.8 (0.2)	8.6 (0.1)*	8.3 (0.2)*	8.7 (0.1)*	7.9 (0.2)
Mn	4.4 (0.1)	5.7 (0.1)*	5.2 (0.2)*	5.7 (0.2)*	4.7 (0.1)*
Cu	1.49 (0.04)	1.62 (0.03)*	1.56 (0.02)*	1.60 (0.02)*	1.50 (0.02)
Sr	0.61 (0.01)	0.67 (0.02)*	0.63 (0.01)	0.66 (0.02)*	0.61 (0.02)
Mo	0.11 (0.01)	0.11 (0.01)	0.11 (0.01)	0.12 (0.01)	0.12 (0.01)
Se	0.032 (0.001)	0.030 (0.008)	0.021 (0.002)	0.026 (0.002)	0.033 (0.007)
Cd	0.020 (0.001)	0.022 (0.001)	0.021 (0.001)	0.023 (0.001)*	0.020 (0.001)

[a]Values with an asterix (*) in one row are significantly different ($p < 0.05$, Dunnett's test) from the control sample (regular flour). Flour samples produced by roller milling are further referred to as regular flour or flour (FL) x%, where x is the percentage of wheat removed by pearling prior to producing the flour under consideration by roller milling. Means and standard deviations (in brackets) of three analytical replicates are presented.

in the pericarp. Calcium and, to a lesser extent, Zn were detected in the endosperm, whereas other element concentrations were very low in the endosperm, especially for Mn and Fe (Figures 2A and 3). Low concentrations of Cu were detected in the endosperm parts close to the aleurone and crease. Similar observations have been made for rice (*Oryza sativa* L.) and barley (*Hordeum vulgare* L.) where Fe and Mn mainly occur in bran tissues, while Zn is more evenly distributed in the grain.[16,18]

Although Cu, Fe, and Zn accumulated in the aleurone, their concentrations were highest in the crease region (Figure 2A). The modified aleurone cells surrounding the crease are very rich in these minerals, and Cu, Fe, and Mn are most abundant in the nucellar projection while Zn, K, and Ca mainly occur in the vascular bundle (transfer cells). Manganese, Ca, and K are also present in the crease pericarp. Potassium is more uniformly distributed over the bran tissues than Cu and Zn.

Figure 3A shows line scans, representing the average of the vertical areas indicated by the boxes in the elemental maps, across the bran tissues for intact (nonpearled) wheat grains. Of all the elements investigated, Mn was the one most strongly distributed in the outside parts of the grain. Manganese was highest in the 90−100 μm region. This result is in agreement with Lombi et al.,[18] who found that the highest level of Mn in barley grains was in the testa. Copper, Fe, and Zn were mainly localized within the same band (about 40 to 90 μm) which most probably corresponds to the aleurone layer [as individual cells of this tissue are visible in the elemental maps (Figure 2A and 2B)]. Moreover, the distributions of Ca and, to a lesser degree, those of K were extended over a wider distance (40 to 140 μm), suggesting that these elements may not be limited to the aleurone layer but also extend into the outermost bran layers. In conclusion, these findings show that the different minerals are distributed in different ways across the wheat grain. In plants, the long-distance transport of mineral elements occurs in the vascular system of phloem and xylem. During wheat grain maturation, most mineral elements are transported from the parent plant mainly via the phloem, and they pass into the grain through specialized cells in the crease region.[24,25] Minerals such as Ca and Mn have low mobility in the phloem. They may enter the grain through the vascular system of the pericarp which may have a xylem supply.[25,26]

Investigation of the pearled grains demonstrated that some wheat grain regions are more accessible for abrasion than others, resulting in an inhomogeneous removal of the tissues.[21] In fact, Figure 3B shows that the distribution remained unchanged in the nonabraded regions, whereas, once the outermost bran layers were abraded, all minerals were localized within the same narrow band (50 to 90 μm), i.e., the aleurone. The mineral distribution after pearling depended on the region of the grain. Semiquantification of the minerals by μ-XRF in the grain cross-sections showed that removing the outermost 3% of the wheat grain tissues increased the concentrations of K, Cu, and Zn and decreased those of Fe, Ca, and Mn (results not shown).

Mineral Concentration in Wheat Flour and Shorts As Affected by Pearling. Potassium, P, Mg, and Ca are the most abundant minerals in wheat flour (Table 1). The mineral levels of regular flour are in line with results of Piironen et al.[27] Removing up to 9% of the wheat by pearling prior to milling increased ($p < 0.05$) the K, P, Mg, Ca (only for 3% pearling), Zn, Mn, Cu, and Sr concentrations in flour produced by subsequent roller milling (Table 1). Their concentrations were highest when 3% of the outer layers was abraded prior to milling, and this relative increase in concentration varied from 5% for Ca to about 30% for Mn. This increase is likely due to an increased incorporation of the mineral rich aleurone tissue in the flour milling fractions since the outermost bran layers (the pericarp tissues) were largely removed by pearling prior to milling. We also noted that the levels of some minerals, e.g., Si and Fe, decreased when the peripheral layers were removed prior to milling while the concentrations of some other minerals (e.g., Mo, Se, and Cd) in the flour were rather unaffected by pearling prior to roller milling. Liu et al.[12] also observed a decrease in Fe concentration and an increase in Zn concentration of flour as the pearling degree increased from 5% to 15%. The Cd concentration of wheat flour could not be reduced by pearling prior to milling, which is in line with observations of Cheli et al.[10] for wheat semolina. In conclusion, including pearling in the milling process enriches most minerals in wheat flour on account of loss of the outer tissues (bran).

As for wheat flour, the main minerals present in the shorts are K, P, Mg, and Ca. The effect of pearling on the mineral composition of shorts differs from the effect on flour (Table 2).

DOI: 10.1021/jf5055485
J. Agric. Food Chem. 2015, 63, 1276−1285

Table 2. Concentrations of Different Elements (mg/kg dry matter) in Wheat Shorts As Affected by Different Degrees of Pearling[a]

	regular shorts	SH 3%	SH 6%	SH 9%	SH 12%
K	10140 (410)	10520 (170)	10830 (180)	11330 (590)*	10490 (90)
P	9660 (181)	10220 (90)	10800 (160)*	11150 (450)*	10310 (290)*
Mg	2950 (90)	3160 (100)	3500 (80)*	3580 (210)*	3230 (80)*
Ca	670 (15)	634 (7)*	625 (3)*	632 (22)*	590 (4)*
Si	19 (1)	16 (2)	17 (1)	16 (3)	14 (1)*
Fe	131 (9)	114 (2)	120 (9)	117 (3)	110 (11)
Zn	91 (3)	97 (3)*	95 (3)	98 (3)	94 (1)
Mn	115 (3)	113 (2)	113 (3)	107 (2)*	107 (2)*
Cu	11 (1)	11 (1)	11 (1)	12 (1)	11 (1)
Sr	5.4 (0.1)	4.8 (0.1)*	4.5 (0.4)*	4.8 (0.1)*	4.4 (0.1)*
Mo	0.39 (0.02)	0.46 (0.01)*	0.40 (0.04)	0.41 (0.03)	0.40 (0.01)
Se	0.035 (0.001)	0.043 (0.003)	0.045 (0.010)	0.042 (0.015)	0.035 (0.006)
Cd	0.076 (0.002)	0.080 (0.001)	0.071 (0.006)	0.079 (0.001)	0.074 (0.006)

[a]Values with an asterix (*) in one row are significantly different ($p < 0.05$, Dunnett's test) from the control sample (regular shorts). Short samples produced by roller milling are further referred to as regular shorts or shorts (SH) x%, where x is the percentage of wheat removed by pearling prior to producing the shorts under consideration by roller milling. Means and standard deviations (in brackets) of 3 analytical replicates are presented.

The P and Mg concentrations in the shorts increased when the outer pericarp layers were removed prior to milling, especially at higher pearling degrees. In contrast, the concentrations of Ca, Sr, and, to a lesser extent, those of Mn and Si decreased at higher degrees of pearling, which points to their presence mainly in the outermost wheat bran layers. Once pearling had removed the peripheral bran layers, mainly aleurone-enriched bran fractions were present in the shorts. Selenium, Mo, Cu, Zn, and Cd concentrations in the shorts were not influenced ($p > 0.05$) by the degree of pearling.

Mineral Concentration of Wheat Bran As Affected by Pearling. Abrading the peripheral bran layers prior to milling enriches the bran fractions with aleurone. The aleurone is a mineral-rich tissue as reflected by the increase in the K, P, Mg, Zn, and Cu concentrations of the bran fractions when the degree of pearling prior to milling was increased (Table 3). Highly (K, P, and Mg) and intermediately (Zn and Cu) phloem mobile minerals mainly occur in the aleurone.

The distribution of minerals in the grain depends on their uptake by the roots during grain development and the mineral redistribution to the grain from vegetative tissues via the phloem. Remobilization via the phloem depends greatly on the phloem mobility of each element.[25] The enrichment of minerals in aleurone-dense tissues was reflected by the higher K, P, Mg, Zn, and Cu concentrations in the regular bran than in the PL 0−3%. Such pearlings mainly contain the peripheral bran layers. The P, Mg, Zn, and Cu concentrations in the bran increased with the degree of pearling, as their concentration is higher in the aleurone than in the outer tissues (Table 3). However, the mineral concentration of the pearlings was never as high as that of the bran fractions since significant parts of the less mineral-rich endosperm were removed along with the bran tissues during pearling. Pearlings are increasingly enriched with endosperm as the degree of pearling is increased.[21]

Minerals like Ca, Si, Sr, and (to a lesser extent) Mn are mainly situated in the pericarp as shown for PL 0−3% (Table 3). Such pearlings had higher Ca, Si, and Sr concentrations than did regular bran. These results confirm the μ-XRF data. In contrast to most minerals, Ca and Mn are transported almost exclusively in the xylem.[25] The accumulation of Sr results from its ability to replace Ca to a certain extent. In terms of plant transport mechanisms, Sr and Ca probably have similar properties.[28] Epicarp hairs are the main tissue in wheat for Si deposition,[29] and it is hence logical that the outer peripheral layers are enriched in Si. While the mechanisms of Si uptake and deposition in wheat are largely unknown,[30] Si probably mainly accumulates in older tissues because it is not mobile within higher plants.[30] In rice, Si concentrations are higher than in wheat and the majority of Si is situated in the external parts of the rice husk.[17] Taken together, Ca, Mn, Si, and Sr have low mobility in the phloem which causes them to mainly occur in the dead cells of the pericarp.

The Cd concentration in bran was higher than that in flour. Cheli et al.[10] found for durum wheat (*Triticum turgidum* L. ssp. *durum*) that Cd concentration in bran products was higher than in the grain and its semolina. Its levels in bran were not affected ($p > 0.05$) by pearling although they tended to increase slightly once the peripheral bran layers had been removed prior to milling (Table 3). Moreover, the relatively low Cd level in PL 0−3% when compared to the levels in the (residual) bran fractions shows that Cd is not mainly accumulated in the pericarp and that it may be slightly enriched in the aleurone tissue. This is in contrast to results by Sovrani et al.[31] They only detected Cd in the peripheral bran layers. Cd is similar to Zn in that it can be transported in plants via similar pathways. However, Zn has greater mobility in phloem and can be transported in larger amounts than Cd.[32,33] The Mo concentration of bran was also not affected ($p > 0.05$) by pearling prior to milling (Table 3). Nevertheless, a slight increase in Mo concentration was observed when the bran fractions were more enriched in aleurone, which was also reflected in the lower Mo level of PL 0−3%.

Selenium was the only mineral that was almost homogeneously distributed throughout the whole grain (Table 3). Its concentration in wheat flour was only slightly lower than that in bran. It has been reported[34] that Se is located relatively uniformly throughout the aleurone and the protein matrix surrounding the starch granules in the starchy wheat endosperm. The similar distribution patterns of Se and S in the grain suggest that the two elements are transported to and deposited in the grain via the same pathway.[34] Sulfur and Se have high phloem mobility,[25] and most likely Se metabolism is dominated by the substitution of this element for S in methionine, as reported for rice by Li et al.[35]

DOI: 10.1021/jf5055485
J. Agric. Food Chem. 2015, 63, 1276−1285

Table 3. Concentrations of Different Elements (mg/kg dry matter) in Wheat Bran and Pearlings As Affected by Different Degrees of Pearling[a]

	regular bran	BR 3%	BR 6%	BR 9%	BR 12%	PL 0–3%	PL 3–6%	PL 6–9%	PL 9–12%
K	15840 (40)	17510 (500)*	17270 (490)*	18100 (500)*	16970 (290)	12110 (290)*	11820 (300)*	10140 (270)*	8850 (600)*
P	15150 (140)	16590 (320)*	16320 (510)*	16900 (280)*	16030 (400)	6760 (230)*	9900 (110)*	9100 (230)*	8220 (390)*
Mg	5360 (190)	5950 (100)*	5920 (150)*	6160 (250)*	5920 (170)*	2400 (60)*	3380 (80)*	3140 (80)*	2750 (120)*
Ca	878 (16)	855 (14)	819 (22)*	788 (7)*	807 (15)*	1064 (14)*	817 (15)*	652 (29)*	560 (30)*
Si	24 (2)	20 (2)*	16 (1)*	18 (1)*	18 (1)*	70 (11)*	27 (5)	18 (1)*	14 (1)*
Fe	168 (7)	169 (3)	168 (5)	151 (9)	148 (9)	126 (2)*	115 (3)*	103 (2)*	93 (3)*
Zn	91 (1)	98 (2)	101 (1)	106 (7)*	103 (4)*	53 (1)*	61 (1)*	58 (4)*	56 (2)*
Mn	127 (6)	118 (3)*	118 (4)*	119 (2)*	113 (3)*	121 (4)*	102 (1)*	79 (5)*	68 (4)*
Cu	11.7 (0.7)	13.1 (0.1)*	13.3 (0.1)*	14.4 (0.6)*	14.3 (0.0)*	5.8 (0.1)*	7.3 (0.2)*	6.8 (0.2)*	6.8 (0.9)*
Sr	7.6 (0.6)	6.8 (0.6)	6.4 (0.5)*	6.5 (0.4)	6.3 (0.4)	9.2 (0.5)*	6.4 (0.2)*	4.5 (0.2)*	3.5 (0.1)*
Mo	0.43 (0.03)	0.51 (0.05)	0.48 (0.03)	0.52 (0.01)	0.59 (0.10)	0.30 (0.40)*	0.35 (0.02)*	0.32 (0.02)*	0.31 (0.01)*
Se	0.049 (0.007)	0.049 (0.011)	0.053 (0.013)	0.061 (0.007)	0.047 (0.006)	0.042 (0.007)	0.050 (0.004)	0.065 (0.008)	0.049 (0.007)
Cd	0.063 (0.007)	0.069 (0.001)	0.073 (0.002)	0.074 (0.006)	0.086 (0.012)	0.053 (0.008)	0.053 (0.001)	0.049 (0.003)*	0.043 (0.002)*

[a]Values with an asterix (*) in one row are significantly different ($p < 0.05$, Dunnett's test) from the control sample (regular bran). Bran samples produced by roller milling are further referred to as regular bran or bran (BR) x%, where x is the percentage of wheat removed by pearling prior to producing the bran under consideration by roller milling. The pearlings obtained by the sequential pearling process are referred to as PL 0-3%, PL 3-6%, PL 6-9%, and PL 9-12%. Means and standard deviations (in brackets) of three analytical replicates are presented.

Taken together, pearling hardly affected the Mo, Se, and Cd concentrations of flour. In rice, S, Mo, Cd, and especially Se are almost evenly distributed without a clear transition point between bran layers and endosperm, and their concentrations are only slightly affected by pearling.[16,36]

Mineral Distribution throughout the Different Wheat Milling Fractions. The mineral concentrations in different milling fractions were combined with the milling weight fractions to calculate the mineral distribution as a fraction of total mineral content (Table 4). In contrast to what was noted for the other minerals, about equal portions of the Ca in wheat grains occurs in flour (42%) and bran (40%), while 18% occurs in the shorts (Table 4). This finding is in line with the more homogeneous mineral distribution of Ca in the wheat grain as shown by μ-XRF (Figures 2 and 3). The concentrations of Mg and Mn and to a lesser extent those of P and Fe in regular flour were much lower than their concentrations in regular bran. Only 10% of the total Mg and Mn ended up in flour, whereas 70% and 50% was present in regular bran, respectively (Table 4). For P and Fe, 18−20% occurs in flour and about 60% in bran. Similar observations have been made for rice[16] and barley,[18] with a relatively large proportion of Fe, P, Mg, K, and Mn associated with the outer grain layers which are rapidly lost during pearling. However, the data further show that wheat and rice grains do not have completely the same mineral distribution patterns. In rice grains, a major part of the total amount of Zn is situated in the (outer) endosperm.[17,36] Lombi et al. (2009) found that Zn and S are colocated in the endosperm which suggests that Zn could be complexed by thiol groups like in phytochelatins and metallothionein. Our results for wheat show that 50% of the total Zn is present in wheat bran and 22% in flour. Moreover, wheat bran contains 42% of the total Ca present in wheat (cf. supra) while rice bran contains about 55% of total Ca.[36] The majority (44%) of Cu was present in bran, while 28% ended up in the flour.

Table 4. Fractions of the Total Quantity of Different Minerals in Nonpearled Wheat Grain Present in Its Milling Fractions Bran, Flour, And Shorts

	bran (%)	flour (%)	shorts (%)
K	57	24	19
P	60	20	20
Mg	67	12	21
Ca	40	42	18
Fe	57	19	24
Zn	50	22	28
Mn	55	10	35
Cu	44	28	28

The concentrations of Zn, Cu, and Mn in regular shorts were quite similar to those in regular bran although the shorts contain substantially more endosperm. Taking the milling yields into account,[21] 28%, 28%, and 35% of the total Cu, Zn, and Mn levels were present in the shorts, respectively (which makes up only 8.5% of the total mass) while about 18−20% of the total amount of Fe, Ca, K, Mg, P ended up in the shorts (Table 4). The enrichment of Cu, Zn, and Mn in the shorts indicates that the embryo ends up in the shorts, since the embryo contains the highest concentrations of Zn, Cu, and Mn as has also been shown for barley[22] and wheat.[37] More than 30% of the total Mn in barley grains occurs in the embryo, which represents only 3% of the grain.[18]

DOI: 10.1021/jf5055485
J. Agric. Food Chem. 2015, 63, 1276−1285

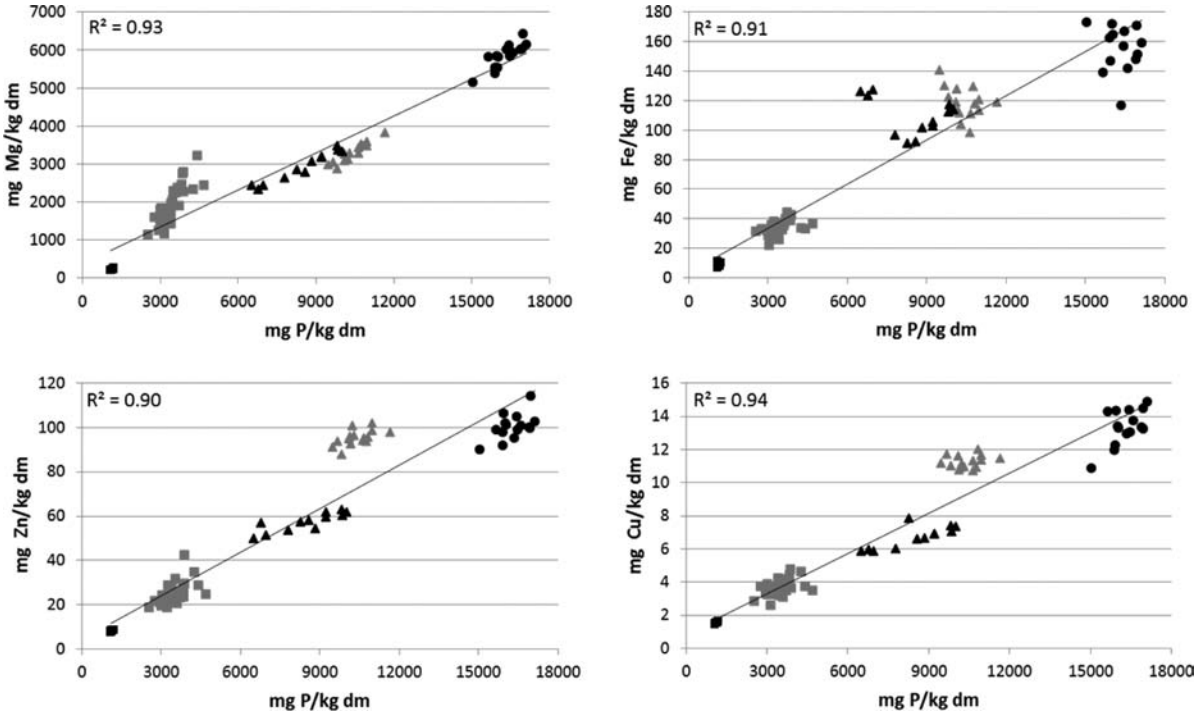

Figure 4. Correlation between P and Mg, Fe, Zn, and Cu in wheat grains (grey square) and its milling [flour (■), shorts (grey triangle), bran (●)] and pearling (▲) fractions.

Taken together, there is good agreement between the quantitative data of the pearling and milling fractions obtained by ICP-MS analysis and the synchrotron μ-XRF images. Both techniques show that Mn is rather confined to the outermost bran layers of the grain while Ca is more homogeneously distributed throughout the wheat grains. Potassium, Fe, Cu, and Zn accumulate mostly in the aleurone.

Correlations between Mineral Element Concentrations in Whole Grains and the Different Pearling and Milling Fractions. The correlation between P and other minerals was investigated across the pearling and milling fraction as P is typically stored as phytate which has a high affinity for minerals such as Mg, Zn, Fe, and Cu and greatly influence their bioavailability. Losses of these minerals during pearling are suggested to be linked to removal of P-containing tissues.[36] A strong positive correlation was observed between P and Mg, Fe, Zn, and Cu (Figure 4). However, not all fractions showed the same behavior when plotting P concentrations as a function of the different mineral concentrations. Zn and Cu concentrations were comparable in shorts and bran and relatively less P ended up in the shorts. This resulted in a higher ratio of Zn/P and Cu/P in the shorts than in the bran fractions. Tang et al.[2] found that shorts contain four times less phytate than bran. The levels of minerals enriched in the peripheral bran layers (Si, Sr, Ca, and Mn in the PL 0−3%) only have a weak correlation with the concentration of P (results not shown).

Furthermore, very good correlations were observed between Cu and Zn concentrations, as they are probably distributed in the same way throughout the wheat grain. As expected (cf. supra), Ca and Sr concentrations and the levels of Cd and Zn also correlated very well with each other (Supporting Information).

In conclusion, this study shows that pearling prior to milling is able to enhance mineral concentrations in pearling and milling products. Pearling increases the mineral concentration of the flour milling products because the bran fractions reaching the flour are probably enriched in aleurone. The highest concentrations of Mn, Si, Ca, and Sr occur in the outer bran layers. In contrast, Mg, Fe, Zn, and Cu accumulate in the aleurone and are probably chelated to phytate, as P is also mostly present in the aleurone-enriched fractions. Removal of the outermost bran layers effectively enriched the residual fractions of most of the essential minerals such as Zn, Cu, P, and Mg but did not change the Fe concentration and did not remove undesired elements such as Cd. The apparent difference in Fe and P may be related to their relative distribution in the scutellum, as this is also known to accumulate these elements. Cadmium, Mo, and especially Se are more uniformly distributed within the wheat grains than the other elements. The μ-XRF images show that Ca and, to lesser extent, Zn are also present in (the outer parts of) the wheat endosperm, while Mn and, to a lesser extent, Fe are more confined to the outer grain parts. This detailed knowledge about mineral distributions in wheat grains may contribute to thorough understanding of the physiological processes responsible for element accumulation. It may also underpin the further development of technologies that preserve or improve the nutritional value contained in wheat grain. Therefore, it would be useful to gain further insights into the mineral distribution in relatively mineral-rich regions such as wheat germ, and the aleurone layer and crease regions.

■ ASSOCIATED CONTENT

Supporting Information

Table S1: Quality control results and certified values of NIST1567 wheat flour (mg/kg dry matter) and the limit of quantification (LOQ) of the procedure (mg/kg). Figure S1: Correlations among different elements present in wheat grains and its milling (flour, shorts, bran) and pearling fractions. This

DOI: 10.1021/jf5055485
J. Agric. Food Chem. 2015, 63, 1276−1285

material is available free of charge via the Internet at http://pubs.acs.org.

AUTHOR INFORMATION

Corresponding Author

*Phone: (+32)-16-376780. Fax: (+32)-16-321997. E-mail: niels.debrier@biw.kuleuven.be.

Funding

This research was conducted in the framework of the W. K. Kellogg Chair in Cereal Science and Nutrition at the KU Leuven (chair holders J. A. Delcour and K. Verbeke), is part of Methusalem programme "Food for the Future" (2007-2021), and was partly undertaken on the X-ray fluorescence microscopy beamline at the Australian Synchrotron, Melbourne, Victoria, Australia. We gratefully acknowledge the "Fonds voor Wetenschappelijk Onderzoek Vlaanderen" (FWO, Brussels, Belgium) for the travel grant for the stay abroad to Niels De Brier.

Notes

The authors declare no competing financial interest.

ACKNOWLEDGMENTS

Fruitful discussions with Drs. C. M. Courtin (KU Leuven), L. Sanders, K. Spence, J. Reid, A. Birkett and R. McDermott (Kellogg Company, Battle Creek, MI) are highly appreciated.

REFERENCES

(1) Delcour, J. A.; Hoseney, R. C. *Principles of Cereal Science and Technology*, 3rd ed.; AACC International: St. Paul, MN, 2010.

(2) Tang, J.; Zou, C.; He, Z.; Shi, R.; Ortiz-Monasterio, I.; Qu, Y.; Zhang, Y. Mineral element distributions in milling fractions of Chinese wheats. *J. Cereal Sci.* **2008**, *48*, 821−828.

(3) Jacobsen, T.; Slotfeldt-Ellingsen, K. D. Phytic acid and metal availability: A study of Ca and Cu binding foodstuffs. *Cereal Chem.* **1983**, *60*, 392−395.

(4) Eeckhout, W.; De Paepe, M. Total phosphorus, phytate-phosphorus and phytase activity in plant feedstuffs. *Anim. Feed Sci. Technol.* **1994**, *47*, 19−29.

(5) Eagling, T.; Neal, A. L.; McGrath, S. P.; Fairweather-Tait, S.; Shewry, P. R.; Zhao, F.-J. Distribution and speciation of iron and zinc in grain of two wheat genotypes. *J. Agric. Food Chem.* **2014**, *62*, 708−716.

(6) Lott, J. N. A.; Randall, P. J.; Goodchild, D. J.; Craig, S. Occurrence of globoid crystals in cotyledonary protein bodies of *Pisum sativum* as influenced by experimentally induced changes in Mg, Ca and K contents of seeds. *Aust. J. Plant Physiol.* **1985**, *12*, 341−353.

(7) Lopez, H. W.; Leenhardt, F.; Coudray, C.; Remesy, C. Minerals and phytic acid interactions: Is it a real problem for human nutrition? *Int. J. Food Sci. Technol.* **2002**, *37*, 727−739.

(8) Dexter, J. E.; Wood, P. J. Recent applications of debranning of wheat before milling. *Trends Food Sci. Technol.* **1996**, *7*, 35−41.

(9) Latunde-Dada, G. O.; Li, X.; Parodi, A.; Edwards, C. H.; Ellis, P. R.; Sharp, P. A. Micromilling enhances iron bioaccessibility from wholegrain wheat. *J. Agric. Food Chem.* **2014**, *62*, 11222−11227.

(10) Cheli, F.; Campagnoli, A.; Ventura, V.; Brera, C.; Berdini, C.; Palmaccio, E.; Dell'Orto, V. Effects of industrial processing on the distributions of deoxynivalenol, cadmium and lead in durum wheat milling fractions. *LWT - Food Sci. Technol.* **2010**, *43*, 1050−1057.

(11) Mousia, Z.; Edherly, S.; Pandiella, S. S.; Webb, C. Effect of wheat pearling on flour quality. *Food Res. Int.* **2004**, *37*, 449−459.

(12) Liu, Z. H.; Wang, H. Y.; Wang, X. E.; Xu, H.; Gao, D.; Zhang, G. P.; Chen, P. D.; Liu, D. J. Effect of wheat pearling on flour phytase activity, phytic acid, iron, and zinc content. *LWT – Food Sci. Technol.* **2008**, *41*, 521−527.

(13) De Brier, N.; Gomand, S. V.; Joye, I. J.; Pareyt, B.; Courtin, C. M.; Delcour, J. A. The impact of pearling as a treatment prior to wheat roller milling on the texture and structure of bran-rich breakfast flakes. *LWT – Food Sci. Technol.* **2014**, DOI: 10.1016/j.lwt.2014.08.015.

(14) Hareland, G. A. Effects of pearling on falling number and alpha-amylase activity of preharvest sprouted spring wheat. *Cereal Chem.* **2003**, *80*, 232−237.

(15) Gys, W.; Gebruers, K.; Sorensen, J. F.; Courtin, C. M.; Delcour, J. A. Debranning of wheat prior to milling reduces xylanase but not xylanase inhibitor activities in wholemeal and flour. *J. Cereal Sci.* **2004**, *39*, 363−369.

(16) Hansen, T. H.; Lombi, E.; Fitzgerald, M.; Laursen, K. H.; Frydenvang, J.; Husted, S.; Boualaphanh, C.; Resurreccion, A.; Howard, D. L.; de Jonge, M. D.; Paterson, D.; Schjoerring, J. K. Losses of essential mineral nutrients by polishing of rice differ among genotypes due to contrasting grain hardness and mineral distribution. *J. Cereal Sci.* **2012**, *56*, 307−315.

(17) Lombi, E.; Scheckel, K. G.; Pallon, J.; Carey, A. M.; Zhu, Y. G.; Meharg, A. A. Speciation and distribution of arsenic and localization of nutrients in rice grains. *New Phytol.* **2009**, *184*, 193−201.

(18) Lombi, E.; Smith, E.; Hansen, T. H.; Paterson, D.; de Jonge, M. D.; Howard, D. L.; Persson, D. P.; Husted, S.; Ryan, C.; Schjoerring, J. K. Megapixel imaging of (micro)nutrients in mature barley grains. *J. Exp. Bot.* **2011**, *62*, 273−282.

(19) McGee, B. The PeriTec process and its application to durum wheat milling. *Bull., Assoc. Oper. Millers* **1995**, 6521−6528.

(20) Delcour, J. A.; Vanhamel, S.; De Geest, C. Physico-chemical and functional properties of rye nonstarch polysaccharides. I. Colorimetric analysis of pentosans and their relative monosaccharide compositions in fractionated (milled) rye products. *Cereal Chem.* **1989**, *66*, 107−111.

(21) De Brier, N.; Hemdane, S.; Dornez, E.; Gomand, S. V.; Delcour, J. A.; Courtin, C. M., Structure, chemical composition and enzymatic activities of pearlings and bran obtained from pearled wheat (*Triticum aestivum* L.) by roller milling. *J. Cereal Sci.* **2015**, DOI: 10.1016/j.jcs.2014.12.009.

(22) Lombi, E.; Scheckel, K. G.; Kempson, I. M. In situ analysis of metal(loid)s in plants: State of the art and artefacts. *Environ. Exp. Bot.* **2011**, *72*, 3−17.

(23) Ryan, C. G. Quantitative trace elements imaging using PIXE and the nuclear microprobe. *Int. J. Imag. Syst. Technol.* **2000**, *11*, 219−230.

(24) Borg, S.; Brinch-Pedersen, H.; Tauris, B.; Holm, P. B. Iron transport, deposition and bioavailability in the wheat and barley grain. *Plant Soil* **2009**, *325*, 15.

(25) White, P. J. Long-distance transport in the xylem and phloem. In *Mineral Nutrition of Higher Plants*, 3rd ed.; Marschner, P., Ed.; Elsevier: London, UK, 2012.

(26) Pearson, J. N.; Rengel, Z.; Jenner, C. F.; Graham, R. D. Transport of zinc and manganese to developing wheat grains. *Physiol. Plant.* **1995**, *95*, 449−455.

(27) Piironen, V.; Lampi, A.-M.; Ekholm, P.; Salmenkallio-Martilla, M.; Liukkonen, K.-H., Micronutrients and phytochemicals in wheat grain. In *Wheat Chemistry and Technology*, 4th ed.; Khan, K.; Shewry, P. R., Eds.; AACC International: St. Paul, MN, 2009.

(28) Birsin, M. A.; Adak, M. S.; Inal, A.; Aksu, A.; Gunes, A. Mineral element distribution and accumulation patterns within two barley cultivars. *J. Plant Nutr.* **2009**, *33*, 267−284.

(29) Bennet, D. M.; Parry, D. W. Electron-probe microanalysis studies of silicon in the epicarp hairs of the caryopses of *Hordeum sativum* Jess., *Avena sativa* L., *Secale cereale* L. and *Triticum aestivum* L. *Ann. Bot.* **1981**, *48*, 645−654.

(30) Ma, J. F.; Yamaji, N. Silicon uptake and accumulation in higher plants. *Trends Plant Sci.* **2006**, *11*, 392−397.

(31) Sovrani, V.; Blandino, M.; Scarpino, V.; Reyneri, A.; Coïsson, J. D.; Travaglia, F.; Locatelli, M.; Bordiga, M.; Montella, R.; Arlorio, M. Bioactive compound content, antioxidant activity, deoxynivalenol and heavy metal contamination of pearled wheat fractions. *Food Chem.* **2012**, *135*, 39−46.

(32) Riesen, O.; Feller, U. Redistribution of nickel, cobalt, manganese, zinc, and cadmium via the phloem in young and maturing wheat. *J. Plant Nutr.* **2005**, *28*, 421−430.

DOI: 10.1021/jf5055485
J. Agric. Food Chem. 2015, 63, 1276−1285

(33) Grant, C. A.; Buckley, W. T.; Bailey, L. D.; Selles, F. Cadmium accumulation in crops. *Can. J. Plant Sci.* **1998**, *78*, 1−17.
(34) Moore, K. L.; Schröder, M.; Lombi, E.; Zhao, F.-J.; McGrath, S. P.; Hawkesford, M. J.; Shewry, P. R.; Grovenor, C. R. M. NanoSIMS analysis of arsenic and selenium in cereal grain. *New Phytol.* **2010**, *185*, 434−445.
(35) Li, H. F.; Lombi, E.; Stroud, J. L.; McGrath, S. P.; Zhao, F. J. Selenium speciation in soil and rice: Influence of water management and Se fertilization. *J. Agric. Food Chem.* **2010**, *58*, 11837−11843.
(36) Wang, K. M.; Wu, J. G.; Li, G.; Zhang, D. P.; Yang, Z. W.; Shi, C. H. Distribution of phytic acid and mineral elements in three indica rice (*Oryza sativa* L.) cultivars. *J. Cereal Sci.* **2011**, *54*, 116−121.
(37) Neal, A. L.; Geraki, K.; Borg, S.; Quinn, P.; Mosselmans, J. F.; Brinch-Pedersen, H.; Shewry, P. R. Iron and zinc complexation in wild-type and ferritin-expressing wheat grain: Implications for mineral transport into developing grain. *J. Biol. Inorg. Chem.* **2013**, *18*, 557−570.

DOI: 10.1021/jf5055485
J. Agric. Food Chem. 2015, 63, 1276−1285

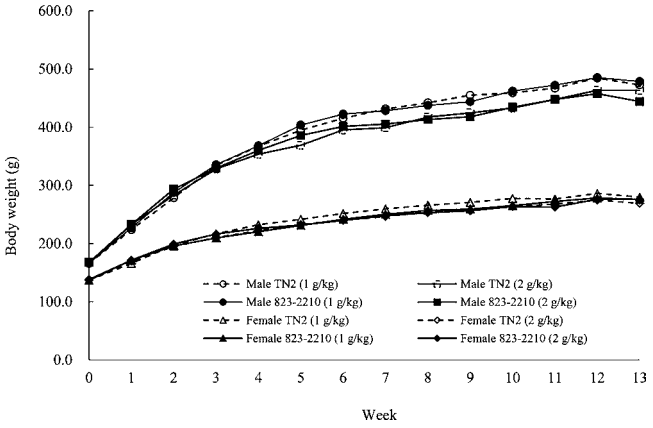

Figure 1. Weekly body weight changes of rats fed with nongenetically modified and genetically modified papaya fruits in the 90 days feeding toxicity trial. TN-2: non-GM papaya of Tainung No. 2. 823-2210: GM papaya fruits. Data expressed as the mean (male and female rats, $n = 10$; except male rats, $n = 9$, and female rats, $n = 11$ in the 2 g/kg 823-2210 groups).

MATERIALS AND METHODS

Samples and Chemicals. The coat protein (CP) gene of *Papaya ringspot virus* (PRSV) was transferred to *Agrobacterium tumefaciens*. Transformation of embryogenic papaya was conducted by liquid-phase wounding with *Agrobacterium tumefaciens*, which contained the CP gene of PRSV.[17] The hybrid line (823-2210) generated by crossing 2210 with 823 was used in this study. Line 2210 was obtained by backcrossing the monoresistant transgenic papaya line 18-2-4 with the non-GM Sunrise. When 18-2-4 was backcrossed with the non-GM Thailand variety, line 823 was obtained. The non-GM control in this study was Tainung No. 2 (TN-2). They were cultivated in a screen house in a certified isolated test field at the Taiwan Agricultural Research Institute. Fresh papaya fruit pulp was harvested and lyophilized (Gold Chia Fong Biotech Co., Wufeng, Taiwan). The ratio of fresh to lyophilized papaya fruit was approximately 8:1. The lyophilized papaya fruits were ground into powder and stored at −20 °C before use. The molecular markers for the characterization of these two GM papaya lines (which were resistant to PRSV) and nontransgenic TN-2 were confirmed in our previous report.[16,17] Isoflurane was obtained from Halocarbon Laboratories (SC, USA), anticoagulative tubes of Vacutainer K3 EDTA syringes were purchased from BD Co. (NJ, USA), and Weigert's iron hematoxylin stain kit was purchased from A.J.P. Scientific (NJ, USA).

Animals. The SPF 5-week-old male and female (nulliparous and nonpregnant) Sprague−Dawley albino rats were obtained from Biolasco Taiwan Co., Ltd. (I-Lan, Taiwan). The same strain of rats was used in the 90-day study as had been used in the previous 28-day and acute toxicity studies.[16] The housing facility was maintained under appropriate environmental conditions at 21 ± 2 °C with 50−70% humidity under a 12-h light/12-h dark cycle. Autoclaved Rat Chow (Purina 5010, MO, USA) and reverse-osmosis water were available ad libitum. This study was approved by the Institutional Animal Care and Use Committee (IACUC) of National Chung Hsing University (IACUC 101-04).

Experimental Design. The 90-day feeding study for the non-GM and GM papaya fruits was performed according to the experimental guidance of EFSA[1] with modification. Tested samples of non-GM TN-2 and GM 823-2210 papaya fruit were prepared in autoclaved reverse-osmosis water. Rats were tagged by picric acid staining on dorsal back with individual cage card as well, randomly assigned and divided into groups that included the low dose of 1 g/kg body weight and high dose of 2 g/kg body weight of non-GM TN-2 and GM 823-2210 papaya fruit lyophilized powder, and gavaged daily for 90 days. For the 10 male and 10 female rats in each group, the body weight did not exceed 20% of the mean weight of each sex in groups at the beginning of the test. However, one female rat was mismatched at day 0 during grouping to make 9 male and 11 female rats in the GM 823-2210 papaya fruit 2 g/kg body weight group.

Table 1. Weekly Feed Consumption and Feed Efficiency of Rats Fed with Nongenetically Modified and Genetically Modified Papaya Fruits for 90 Days[a]

	non-GM line, TN-2		GM lines, 823-2210	
group[b]/day	1 g/kg	2 g/kg	1 g/kg	2 g/kg
male	$n = 10$	$n = 10$	$n = 10$	$n = 9$
1	31.9 ± 2.4[c]	32.4 ± 1.3	31.6 ± 3.4	33.3 ± 2.1
2	28.9 ± 2.6	26.6 ± 4.0	27.5 ± 3.1	28.2 ± 2.6
3	37.9 ± 1.9	35.2 ± 3.5	36.4 ± 2.3	34.9 ± 4.7
4	34.0 ± 3.7	27.8 ± 4.3	30.4 ± 4.6	28.3 ± 5.0
5	31.2 ± 3.3	29.3 ± 4.6	31.3 ± 4.9	29.6 ± 5.0
6	31.9 ± 5.7	28.7 ± 4.0	30.6 ± 6.7	29.4 ± 5.7
7	29.6 ± 5.5	25.2 ± 4.5	27.1 ± 4.2	25.3 ± 3.3
8	32.5 ± 8.6	27.9 ± 6.2	27.5 ± 4.8	25.4 ± 2.2
9	32.0 ± 5.3	25.1 ± 4.1	28.9 ± 5.9	23.6 ± 2.6
10	28.7 ± 6.1	26.9 ± 4.7	31.9 ± 3.5	28.6 ± 3.4
11	31.8 ± 5.3	26.5 ± 4.0	27.4 ± 4.5	25.9 ± 3.2
12	31.4 ± 3.7	25.9 ± 3.3	27.2 ± 3.9[e]	26.3 ± 3.0
13	27.2 ± 5.0	21.4 ± 4.3	21.3 ± 5.7[e]	19.5 ± 4.4
feed efficiency (%)[d]	11.1 ± 1.8	12.0 ± 1.7	12.0 ± 0.9	11.2 ± 1.7
female	$n = 10$	$n = 10$	$n = 10$	$n = 11$
1	22.8 ± 2.1	23.4 ± 3.3	21.2 ± 2.1	21.1 ± 3.3
2	21.0 ± 2.0	20.5 ± 2.2	21.4 ± 3.0	18.4 ± 2.8
3	30.6 ± 3.1	28.4 ± 2.1	25.7 ± 4.6[e]	26.6 ± 3.3
4	23.3 ± 2.1	22.0 ± 2.0	18.8 ± 1.8[e]	20.4 ± 2.9
5	25.4 ± 2.8	24.1 ± 4.3	25.0 ± 3.7	21.2 ± 4.8
6	22.3 ± 1.9	22.4 ± 1.9	19.6 ± 1.4[e]	20.5 ± 3.1
7	22.4 ± 2.0	18.4 ± 2.0	21.7 ± 4.0	20.6 ± 2.5[e]
8	21.2 ± 1.3	20.4 ± 1.3	20.9 ± 2.4	20.6 ± 2.4
9	21.1 ± 2.5	23.4 ± 3.1	21.9 ± 3.3	22.7 ± 2.8
10	22.4 ± 3.0	23.2 ± 2.4	23.0 ± 3.0	21.0 ± 1.6[e]
11	20.8 ± 5.2	23.0 ± 3.0	24.7 ± 4.5	20.6 ± 4.6
12	21.4 ± 4.3	20.3 ± 3.9	22.2 ± 4.7	20.8 ± 3.5
13	16.3 ± 2.3	18.2 ± 3.5	18.3 ± 3.9	17.8 ± 2.6
feed efficiency (%)	7.2 ± 1.1	6.6 ± 1.0	7.1 ± 0.6	7.3 ± 0.7

[a]Data expressed as the mean ± SD. [b]TN-2: Tainung No. 2. 823-2210: GM papaya fruits. [c]Feed consumption (g/day) = [total feed intake (g)/test period (90 days]. [d]Feed efficiency (%) = [daily body weight gain (g)/daily food intake (g)] × 100. [e]Significant difference between the non-GM (TN-2) and GM papaya-treated groups (823-2210) at $p < 0.05$.

Clinical Observations. The health of the animals was observed daily before being gavaged. For the feed consumption record, rats were individually housed in a suspended steel cage with a feeding box. The weekly body weight and feed consumption were recorded. At the end of treatment (day 91), all animals were fasted overnight and sacrificed under 2% isoflurane (Halocarbon Laboratories, USA) anesthesia in an inhalation chamber (MSS 003, Benchtop Small Animal Anesthesia Unit, England).

Hematology and Coagulation. A 0.5 mL amount of whole blood of rats was collected from the abdominal aorta and put it into anticoagulative tubes (K3 EDTA syringes) (Vacutainer, NJ, USA). The red blood cell count (RBC), hemoglobin (HGB), hematocrit (HCT), mean corpuscular volume (MCV), mean corpuscular hemoglobin (MCH), mean corpuscular hemoglobin concentration (MCHC), platelet (PLT), and white blood cell count (WBC) were evaluated with a hematology analyzer (Sysmex K-4500, Toa Medical Electronics, Kobe, Japan). Blood smears were stained by Weigert's iron hematoxylin stain kit (A.J.P. Scientific, NJ, USA), and the differential white blood cell counts (neutrophils, lymphocytes, monocytes, eosinophils, and basophils) were observed by a microscope (Olympus BX50F4Micro-scope, Tokyo, Japan). Prothrombin time (PT), fibrinogen (Fbg), and

DOI: 10.1021/jf5048404
J. Agric. Food Chem. 2015, 63, 1286−1292

Table 2. Hematological and Coagulate Parameters of Rats Fed with Nongenetically Modified and Genetically Modified Papaya Fruits for 90 days

	non-GM line, TN-2		GM lines, 823-2210	
group[a]/day	1 g/kg	2 g/kg	1 g/kg	2 g/kg
male	$n = 10$	$n = 10$	$n = 10$	$n = 9$
RBC ($10^6/\mu L$)	8.8 ± 0.6[b]	9.1 ± 0.6	9.2 ± 0.6	8.9 ± 0.4
HGB (g/dL)	15.5 ± 0.9	16.0 ± 0.4	16.2 ± 0.5[c]	15.7 ± 0.5
HCT (%)	49.0 ± 3.1	51.1 ± 2.1	51.5 ± 2.0[c]	49.9 ± 1.8
MCV (fL)	55.5 ± 0.9	55.9 ± 1.8	56.0 ± 1.8	55.8 ± 1.5
MCH (pg)	17.5 ± 0.4	17.6 ± 0.8	17.6 ± 0.8	17.6 ± 0.7
MCHC (g/dL)	31.5 ± 0.3	31.4 ± 0.7	31.4 ± 0.6	31.5 ± 0.8
PLT ($10^3/\mu L$)	1174 ± 104	1119 ± 135	1145 ± 103	1112 ± 174
PT (s)	11.0 ± 0.1	11.4 ± 0.2	11.3 ± 0.2	12.0 ± 0.5
APTT (s)	28.1 ± 1.7	25.2 ± 1.4	22.1 ± 0.6[c]	23.2 ± 0.9
Fbg (mg/dL)	190 ± 24	187 ± 6	214 ± 5	210 ± 19
female	$n = 10$	$n = 10$	$n = 10$	$n = 11$
RBC ($10^6/\mu L$)	8.2 ± 0.6	8.5 ± 0.3	7.7 ± 1.5	8.3 ± 0.4
HGB (g/dL)	15.0 ± 0.9	15.6 ± 0.6	15.0 ± 0.6	15.4 ± 0.5
HCT (%)	46.3 ± 3.3	48.2 ± 1.8	44.5 ± 9.6	47.6 ± 1.8
MCV (fL)	56.8 ± 1.2	56.8 ± 0.8	57.5 ± 2.4	57.2 ± 1.3
MCH (pg)	18.4 ± 0.6	18.4 ± 0.4	18.8 ± 0.5	18.5 ± 0.6
MCHC (g/dL)	32.4 ± 0.5	32.4 ± 0.4	32.8 ± 1.1	32.3 ± 0.8
PLT ($10^3/\mu L$)	1010 ± 399	1068 ± 198	981 ± 145	993 ± 336
PT (s)	10.3 ± 0.1	10.6 ± 0.2	11.0 ± 0.3[c]	10.5 ± 0.2
APTT (s)	34.0 ± 2.0	32.5 ± 2.3	33.5 ± 1.5	28.7 ± 2.0
Fbg (mg/dL)	187 ± 11	179 ± 9	176 ± 23	174 ± 8

[a]TN-2: Tainung No. 2. 823-2210: GM papaya fruits. RBC: red blood cell. HGB: hemoglobin. HCT: hematocrit. MCV: mean corpuscular volume. MCH: mean corpuscular hemoglobin. MCHC: mean corpuscular hemoglobin concentration. PLT: platelets. PT: prothrombin time. APTT: activated partial prothrombin time. Fbg: fibrinogen. [b]Data expressed as the mean ± SD. [c]Significant difference between the non-GM (TN-2) and the GM papaya-treated groups at $p < 0.05$.

Table 3. White Blood Cell Differentiation of Rats Fed with Nongenetically Modified and Genetically Modified Papaya Fruits for 90 Days

	non-GM line, TN-2		GM lines, 823-2210	
group[a]/day	1 g/kg	2 g/kg	1 g/kg	2 g/kg
male	$n = 10$	$n = 10$	$n = 10$	$n = 9$
WBC ($10^3/\mu L$)	4.8 ± 2.4[b]	4.1 ± 1.3	5.3 ± 1.4	8.2 ± 3.0[c]
lymphocyte (%)	81.8 ± 3.5	82.3 ± 6.0	81.7 ± 4.3	66.1 ± 13.4[c]
neutrophil (%)				
band	1.6 ± 1.2	2.2 ± 0.8	1.4 ± 0.8	2.2 ± 1.6
segment	16.2 ± 2.7	15.3 ± 5.6	16.7 ± 3.8	31.4 ± 12.5[c]
monocyte (%)	0.4 ± 0.5	0.2 ± 0.4	0.2 ± 0.4	0.2 ± 0.4
eosinophil (%)	0.0 ± 0.0	0.0 ± 0.0	0.0 ± 0.0	0.0 ± 0.0
basophil (%)	0.0 ± 0.0	0.0 ± 0.0	0.0 ± 0.0	0.0 ± 0.0
female	$n = 10$	$n = 10$	$n = 10$	$n = 11$
WBC ($10^3/\mu L$)	3.6 ± 1.2	4.4 ± 2.1	3.7 ± 0.8	4.3 ± 1.9
lymphocyte (%)	81.8 ± 7.1	78.4 ± 4.9	72.4 ± 17.0	81.1 ± 6.1
neutrophil (%)				
band	1.0 ± 1.2	0.3 ± 0.5	1.2 ± 1.1	0.9 ± 1.1
segment	17.1 ± 6.9	21.2 ± 4.7	26.3 ± 16.4	18.0 ± 6.3
monocyte (%)	0.1 ± 0.3	0.1 ± 0.3	0.1 ± 0.3	0.0 ± 0.0
eosinophil (%)	0.0 ± 0.0	0.0 ± 0.0	0.0 ± 0.0	0.0 ± 0.0
basophil (%)	0.0 ± 0.0	0.0 ± 0.0	0.0 ± 0.0	0.0 ± 0.0

[a]TN-2: Tainung No. 2; 823-2210: GM papaya fruits. [b]Data expressed as the mean ± SD. [c]Significant difference between the non- GM (TN-2) and GM papaya-treated groups at $p < 0.05$.

activated partial thromboplastin time (APTT) were evaluated with a coagulation analyzer (AMAX 200, Trinity Biotec, Ireland).

Serum Chemistry. Serum albumin, globulin, A/G, alkaline phosphatase (ALKP), amylase, aspartate aminotransferase (AST), alanine aminotransferase (ALT), blood urea nitrogen (BUN), creatinine, creatine kinase (CK), lactate dehydrogenase (LDH), high-density lipoprotein C (HDL-C), total bilirubin (TB), cholesterol, triglycerides (TG), total protein (TP), γ-glutamyltranspeptidase (GGT), glucose, and ions of calcium (Ca^{2+}), sodium (Na^{+}), potassium (K^{+}), chloride (Cl^{+}), magnesium (Mg^{2+}), and inorganic phosphorus (P^{3-}) were evaluated using a Clinical Chemistry Analyzer (Chiron Diagnostics Corp., Oberlin, OH, USA).

Urinalysis. Urinalysis was performed on the day before sacrifice. Urine volume, specific gravity, pH, bilirubin, urobilinogen, protein, glucose, ketones, nitrite, and occult blood (Oc. blood) were evaluated using a Clinitex 100 Urine Chemistry Analyzer (Miles Inc. Diagnostic Division Ellchart, IN, USA). Urinary sediments of leukocytes, red blood cells (RBC), epithelial cells (epithelia), casts, and crystals were evaluated using optical microscopy (Olympus BX50F4 Microscope, Tokyo, Japan).

Gross and Histopathological Examination. A thorough necropsy was performed on all animals, and organs [brain, heart, thymus, liver, spleen, kidneys, adrenal glands, testes (males), and ovaries (females)] were examined grossly, removed, weighed, and fixed in 10% buffered formalin. The organs of the high-dose (2 g/kg) non-GM and GM groups, including the digestive system (liver, esophagus, stomach, duodenum, jejunum, ileum, cecum, colon, rectum, including Peyer's patches, salivary glands, and pancreas), urinary system (kidneys and urinary bladder), respiratory system (lungs, trachea, larynx, and pharynx), cardiovascular system (heart and aorta), hematopoietic system (spleen, thymus, mandibular lymph node, mesenteric lymph node, and bone marrow), endocrine system (pituitary gland, thyroid gland, parathyroid glands, and adrenal glands), nervous system [brain (including cerebrum and cerebellum), spinal cord (cervical, thoracic, and lumbar) and sciatic nerve], musculoskeletal system (skeletal muscle, femur/knee joint, and sternum), reproductive system of males (testes, epididymis, prostate, and seminal vesicles) and females (ovaries, uterus, mammary glands, and vagina), skin, and eyes (including retina and optic nerve) were trimmed based on the revised guidelines for organ sampling and trimming in rats and mice for histopathological examination.[18,19] For semiquantitative grading, lesion severity was graded using the criteria developed by Shackelford et al.[20] Lesion severity was graded as follows: 1 = minimal (<10%); 2 = slight (11−25%); 3 = moderate (26−50%); 4 = moderate/severe (51−75%); and 5 = severe/high (76−100%). The incidence of lesions was expressed as the number of rats affected out of the total number of rats examined.

Statistical Analysis. Data are expressed as mean ± standard deviation. The comparisons were designed to determine whether differences were attributable to the non-GM TN-2 and GM 823-2210 treated groups at the same dosage. All statistical analyses were conducted using Excel software (MicroSoft, WA, USA), and statistical significance levels ($p < 0.05$) were determined by 2-tailed tests with paired comparison in 1 g/kg groups ($n = 10$) and unpaired comparison in 2 g/kg groups for the misidentification of gender ($n = 9$ and 11), respectively.

DOI: 10.1021/jf5048404
J. Agric. Food Chem. 2015, 63, 1286−1292

Table 4. Serum Biochemistry of Male Rats Fed with Nongenetically Modified and Genetically Modified Papaya Fruits for 90 Days

	non-GM line, TN-2		GM lines, 823-2210	
group[a]/day	1 g/kg	2 g/kg	1 g/kg	2 g/kg
	$n = 10$	$n = 10$	$n = 10$	$n = 9$
albumin (g/dL)	3.0 ± 0.4[c]	3.5 ± 0.4	3.2 ± 0.4	2.9 ± 0.2[d]
globulin	2.2 ± 0.4	2.4 ± 0.4	2.3 ± 0.4	2.2 ± 0.3
A/G[b]	1.4 ± 0.2	1.4 ± 0.1	1.4 ± 0.1	1.3 ± 0.1
ALP (U/L)	65.2 ± 19.1	85.0 ± 15.7	61.8 ± 16.4	67.6 ± 11.8[d]
ALT (U/L)	37.5 ± 16.9	49.1 ± 10.3	49.2 ± 23.3	35.1 ± 10.2[d]
AST (U/L)	91.5 ± 21.2	101 ± 25	85.8 ± 17.4	96.3 ± 22.7
amylase (U/Ll)	1148 ± 240	1419 ± 282	1255 ± 211	1095 ± 179[d]
BUN (mg/dL)	17.0 ± 2.6	17.3 ± 2.5	15.7 ± 1.7	18.8 ± 3.0
cholesterol (mg/dL)	43.0 ± 7.0	47.4 ± 8.3	48.5 ± 9.8	46.0 ± 14.6
CK (U/L)	73.5 ± 35.2	78.7 ± 35.2	72.7 ± 27.8	70.7 ± 26.5
creatinine (mg/dL)	0.6 ± 0.1	0.6 ± 0.1	0.6 ± 0.1	0.5 ± 0.1[d]
glucose (mg/dL)	176 ± 28	170 ± 16	161 ± 22	148 ± 23[d]
LDH (U/L)	208 ± 130	173 ± 88	120 ± 58	100 ± 56[d]
total bilirubin (mg/dL)	0.1 ± 0.0	0.2 ± 0.0	0.2 ± 0.0	0.1 ± 0.0
triglyceride (mg/dL)	27.5 ± 4.9	34.9 ± 5.8	38.0 ± 7.8[d]	37.9 ± 8.8
HDL-C (mg/dL)	27.1 ± 4.7	32.5 ± 6.3	32.1 ± 7.2	27.7 ± 8.0
GGT (U/L)	0.1 ± 0.4	0.3 ± 0.7	0.3 ± 0.5	1.0 ± 0.9
TP (g/dL)	5.2 ± 0.8	5.9 ± 0.8	5.6 ± 0.7	5.2 ± 0.5[d]
Ca^{2+} (mg/dL)	9.3 ± 1.1	10.0 ± 0.9	9.4 ± 1.0	9.3 ± 0.9
Cl^- (mEq/dL)	100 ± 18	109 ± 13	100 ± 11	103 ± 11
K^+ (mEq/dL)	5.5 ± 1.0	5.3 ± 0.6	4.8 ± 0.3[d]	4.8 ± 0.5
Mg^{2+} (mEq/dL)	2.2 ± 0.7	2.3 ± 0.4	2.2 ± 0.7	2.0 ± 0.6
Na^+ (mEq/dL)	132 ± 22	145.1 ± 17	134 ± 13	136 ± 12
P^{3-} (mEq/dL)	9.9 ± 1.9	10.8 ± 2.1	10.1 ± 1.9	10.8 ± 1.7

[a]TN-2: Tainung No. 2. 823-2210: GM papaya fruits. [b]A/G: albumin/globulin. AST: aspartate aminotransferase. ALT: alanine aminotransferase. BUN: blood urea nitrogen. CK: creatine kinase. LDH: lactate dehydrogenase. GGT: gamma glutamyltransferase. HDL-C: high-density lipoprotein C. TP: total protein. [c]Data expressed as the mean ± SD. [d]Significant difference between the non-GM (TN-2) and GM papaya-treated groups at $p < 0.05$.

RESULTS

In Life Observation. No deaths or abnormalities occurred in the non-GM TN-2 or GM papaya 823-2210 fruit treatment groups during the test period. No difference in body weight was observed between the groups of non-GM TN-2 and GM papaya 823-2210 groups (Figure 1). Food consumption (g/day) was lower in male rats at weeks 12 and 13 and female rats at weeks 3, 4, and 6 of the GM papaya 823-2210 (1 g/kg) group and female rats at weeks 7 and 10 of the GM papaya 823-2210 (2 g/kg) group when compared with the non-GM TN-2 group ($p < 0.05$), but no significant difference of feed efficacy (%) was observed at the end of treatment (Table 1).

Blood coagulation exhibited lower APTT in male rats and higher PT in female rats of the GM papaya 823-2210 (1 g/kg) group ($p < 0.05$) but no significant difference in the high dose 2 g/kg treated male and female rats (Table 2). A higher count number of WBCs, white blood cell differentiation of segmented neutrophils (%), and decreases of lymphocytes (%) were found in male rats in the GM papaya 823-2210 (2 g/kg) group when compared with the non-GM papaya TN-2 (2 g/kg) group ($p < 0.05$) (Table 3).

Clinical Biochemistry and Urinalysis. For clinical biochemistry, some of the parameters between the non-GM papaya TN-2 and the GM papaya 823-2210 treated groups expressed statistically significant changes, such as a higher number of triglycerides and lower K^+ in the GM papaya 823-2210 (1 g/kg) male rats ($p < 0.05$), lower albumin, ALP, ALT, AST, amylase, creatinine, glucose, TB, and TP levels in the GM papaya 823-2210 (2 g/kg) treated male rats ($p < 0.05$), lower cholesterol, glucose, triglycerides, and HDL-C in the GM papaya 823-2210 (1 g/kg) treated female rats, and GGT and P^{3-} in the GM papaya 823-2210 (2 g/kg) female rats when compared with the non-GM papaya TN-2 2 g/kg female rats. However, these statistical differences have no dose-dependent relationship and ranged within age-matched (17 weeks of age or greater) historical control values.[21] They were not considered biologically significant in male and female rats (Tables 4 and 5).

Parameters in the urinalysis revealed no statistical difference between the GM papaya 823-2210 and the non-GM papaya TN-2 groups (data not shown).

Organ Weight and Pathological Examination. No significant differences of organ weights in male and female rats were observed between the non-GM and the GM papaya treated groups (Table 6). Furthermore, no gross or histopathological lesions were noted in the high-dose (2 g/kg) groups of non-GM and GM papaya 823-2210. Some of the nonspecific lesions that were observed during pathological examination included minimal to slight degrees of mononuclear cell infiltration of the Hadrian gland, heart, kidney, pancreas, prostate gland, and thyroid gland; tubular regeneration, polycystic kidneys, gastric erosion, epithelioid keratinization of the thyroid gland, and minimal to slight foreign body granulomas of the lung that may have been due to accidental inhalation during gavage of the papaya. These lesions were randomly found in both the non-GM TN-2 and the GM papaya fruit treated rats. Finally, there were no significant gross or microscopic lesions in male or female rats attributable to the non-GM and GM papaya 823-2210 fruit treatment.

DOI: 10.1021/jf5048404
J. Agric. Food Chem. 2015, 63, 1286−1292

Table 5. Serum Biochemistry of Female Rats Fed with Nongenetically Modified and Genetically Modified Papaya Fruits for 90 Days

	non-GM line, TN-2		GM lines, 823-2210	
group[a]/day	1 g/kg	2 g/kg	1 g/kg	2 g/kg
	$n = 10$	$n = 10$	$n = 10$	$n = 11$
albumin (g/dL)	3.8 ± 0.3[c]	3.7 ± 0.3	3.6 ± 0.2	3.7 ± 0.4
globulin	2.7 ± 0.3	2.6 ± 0.3	2.7 ± 0.3	2.5 ± 0.3
A/G[b]	1.4 ± 0.2	1.4 ± 0.1	1.3 ± 0.1	1.5 ± 0.2
ALP (U/L)	46.3 ± 11.5	50.8 ± 14.6	47.2 ± 11.3	40.3 ± 6.6
ALT (U/L)	32.7 ± 5.8	41.3 ± 12.3	44.2 ± 31.3	35.8 ± 8.1
AST (U/L)	73.8 ± 11.7	97.7 ± 30.8	126.4 ± 97.4	85.9 ± 25.0
amylase (U/Ll)	956 ± 160	884 ± 155	1016 ± 213	954 ± 210
BUN (mg/dL)	17.8 ± 3.7	20.0 ± 4.7	28.8 ± 24.7	22.5 ± 5.4
cholesterol (mg/dL)	67.3 ± 9.6	63.0 ± 11.0	55.6 ± 9.4[d]	62.1 ± 11.3
CK (U/L)	53.1 ± 7.2	59.9 ± 14.3	67.4 ± 38.4	109.6 ± 185.6
creatinine (mg/dL)	0.6 ± 0.0	0.6 ± 0.0	0.6 ± 0.1	0.6 ± 0.1
glucose (mg/dL)	159 ± 19	144 ± 28	138 ± 16[d]	133 ± 18
LDH (U/L)	88.0 ± 33.7	94.0 ± 39.6	116.7 ± 60.3	116.4 ± 115.7
total bilirubin (mg/dL)	0.2 ± 0.1	0.1 ± 0.0	0.2 ± 0.1	0.2 ± 0.1
triglyceride (mg/dL)	51.4 ± 8.8	38.6 ± 5.7	36.0 ± 8.1[d]	38.4 ± 8.0
HDL-C (mg/dL)	51.5 ± 7.1	47.3 ± 7.1	40.5 ± 7.5[d]	44.3 ± 6.8
GGT (U/L)	0.7 ± 0.7	1.1 ± 0.6	0.9 ± 0.4	0.3 ± 1.0[d]
TP (g/dL)	6.5 ± 0.4	6.3 ± 0.5	6.4 ± 0.4	6.2 ± 0.5
Ca^{2+} (mg/dL)	10.8 ± 0.5	10.0 ± 0.6	9.0 ± 3.4	10.4 ± 0.9
Cl^{-} (mEq/dL)	108 ± 7	108 ± 6	108 ± 8	105 ± 5
K^{+} (mEq/dL)	5.0 ± 0.4	4.7 ± 0.4	4.5 ± 0.5[d]	4.7 ± 0.6
Mg^{2+} (mEq/dL)	1.9 ± 0.3	2.7 ± 0.8	2.0 ± 0.6	2.4 ± 0.6
Na^{+} (mEq/dL)	142 ± 8	142 ± 6	145 ± 7	140 ± 8
P^{3-} (mEq/dL)	8.5 ± 1.3	7.8 ± 1.5	9.9 ± 2.0	10.0 ± 1.8[d]

[a]TN-2: Tainung No. 2. 823-2210: GM papaya fruits. [b]A/G: albumin/globulin. AST: aspartate aminotransferase. ALT: alanine aminotransferase. BUN: blood urea nitrogen.CK: creatine kinase. LDH: lactate dehydrogenase. GGT: gamma glutamyltransferase. HDL-C: high-density lipoprotein C. TP: total protein. [c]Data expressed as the mean ± SD. [d]Significant difference between the non-GM (TN-2) and GM papaya-treated groups at $p < 0.05$.

Table 6. Organ Weight (g) of Rats Fed with Nongenetically Modified and Genetically Modified Papaya Fruits for 90 Days

	non-GM line, TN-2		GM lines, 823-2210	
group[a]/items	1 g/kg	2 g/kg	1 g/kg	2 g/kg
male	$n = 10$	$n = 10$	$n = 10$	$n = 9$
brain	2.2 ± 0.1[b]	2.1 ± 0.1	2.1 ± 0.1	2.1 ± 0.1
heart	1.5 ± 0.2	1.4 ± 0.1	1.4 ± 0.1	1.6 ± 0.5
thymus	0.3 ± 0.1	0.5 ± 0.6	0.5 ± 0.6	0.3 ± 0.06
liver	11.4 ± 1.5	10.5 ± 1.4	11.3 ± 1.3	10.1 ± 1.2
kidney	3.1 ± 0.4	2.9 ± 0.4	3.0 ± 0.2	2.9 ± 0.2
adrenal	0.05 ± 0.01	0.05 ± 0.01	0.06 ± 0.01	0.06 ± 0.01
spleen	0.7 ± 0.1	0.6 ± 0.1	0.7 ± 0.2	0.6 ± 0.1
testis	3.4 ± 0.3	3.3 ± 0.3	3.3 ± 0.3	3.3 ± 0.4
female	$n = 10$	$n = 10$	$n = 10$	$n = 11$
brain	1.9 ± 0.1	1.9 ± 0.1	2.0 ± 0.1	1.9 ± 0.1
heart	0.9 ± 0.1	0.9 ± 0.3	0.9 ± 0.1	0.9 ± 0.1
thymus	0.3 ± 0.1	0.2 ± 0.1	0.3 ± 0.1	0.3 ± 0.1
liver	7.1 ± 0.7	6.5 ± 0.6	6.7 ± 0.7	6.6 ± 0.54
kidney	1.8 ± 0.2	1.7 ± 0.1	1.8 ± 0.2	1.9 ± 0.2
adrenal	0.06 ± 0.01	0.06 ± 0.01	0.06 ± 0.01	0.06 ± 0.01
spleen	0.5 ± 0.1	0.5 ± 0.1	0.5 ± 0.1	0.5 ± 0.1
ovary	0.07 ± 0.01	0.07 ± 0.01	0.07 ± 0.02	0.07 ± 0.01

[a]TN-2: Tainung No. 2. 823-2210: GM papaya fruits. [b]Data expressed as the mean ± SD.

DISCUSSION

The aim of the 90-day feeding study of whole foods from GM crops is to assess the potential for unintended effects in terms of toxicological and/or nutritional relevance and to help establish whether GM food is as safe and nutritious as its traditional counterpart. A 90-day animal feeding trial has a large capacity, in terms of sensitivity and specificity, to detect potential toxicological effects of single, well-defined compounds. This conclusion is based on data from studies investigating whether toxicological effects are adequately identified in 3-month subchronic studies in rodents by comparing findings at 3 and 24 months for a range of different chemicals.[10]

The difference between testing chemicals and whole food/feed is that chemicals can be administered to the test animals at dose levels which are much higher than the human exposure levels; however, such a testing approach is not always possible with whole food or feed as they are bulky. In fact, administering high dose levels of whole food/feed is likely to result in unbalanced diets. In some cases, the administered dose level can be equivalent to a high level of human consumption.[1,10] The daily intake of papaya fruit was investigated to be 0.218 g/kg from 2007 to 2011 in Taiwan. In the present study, we selected the low dose of 1 g/kg and high dose of 2 g/kg of lyophilized papaya fruit to evaluate the food safety in rats. The safety factor of these dosages in rats is higher than that of human consumption in Taiwan.[22]

Following allergenicity assessments, the potential human intake of transgene-derived PRSV coat protein (PRSVCP) was assessed by measuring PRSV-CP levels in Rainbow and SunUp varieties, along with estimating the fruit consumption rates, compared to potential intake estimating PRSV-CP from naturally infected nontransgenic papaya. Results showed that

DOI: 10.1021/jf5048404
J. Agric. Food Chem. 2015, 63, 1286−1292

the transgene-derived PRSV-CP did not pose a risk of food allergy,[23] although the transgenic papaya TPY10-4 did not increase the allergenic potential in ovalbumin-sensitized mice.[5] Whether this would be the same for transgenic papaya line 823-2210 is still not known. For food safety, *C. papaya* leaf extract at a dose of 2 g/kg was investigated for subacute oral toxicity in Sprague−Dawley rats with doses at the levels employed in practical use in traditional medicine in Malaysia that could be considered safe as a agent.[24]

For food safety concerns, regarding the potential for altered nutritional composition and altered expression of inherent allergens and toxic proteins. One of the important safety assessments of GM crops is comparison of the composition with the composition of the appropriate non-GM comparator.[10] A previous study showed that the contents of nutrients benzyl isothiocyanate (BITC) and papain of GM Rainbow papaya are within the range of those of non-GM papaya and concluded that the Rainbow cultivar is substantially similar to the non-GM cultivar.[3] The substantial equivalent rates for both unripe and ripe 823 and 2210 GM papaya fruits including the proximate constituents, microconstituents, antinutrients, toxicants, and other constituents were also evaluated. Results revealed that the substantial equivalent rates for unripe and ripe 823 samples were 82% and 91%, respectively, as well as 100% for both unripe and ripe 2210 samples. There is a little difference between GM to control papaya fruits.[25]

Furthermore, in our previous study, in vitro and in vivo genotoxicity tests and the repeated dose 28-day feeding toxicity test revealed that GM papaya 823-2210 could be considered as an equivalent and safe substitute for conventional non-GM papaya fruit.[16] In the current study of the midterm safety of GM papaya 823-2210, the 90-day feeding toxicity test did not reveal any evidence of adverse health effects in male or female rats following 90 consecutive days of oral exposure to GM papaya fruits. Although some parameters revealed statistically observed differences in feed consumption, hematology, and serum chemistry examinations between the non-GM papaya and the GM papaya 823-2210 fruits groups, no biologically significant differences were considered, although the 90-day feeding test is not long enough to conclude that there were no negative effects from feeding the rats with GM papaya. However, this repeated dose 90-day feeding toxicity test of GM papaya fruit demonstrated that there are no adverse effects in rats. These results provide that midterm (90 days) daily intake of GM papaya fruits can be recognized as an equivalent and safe substitute for conventional non-GM papaya fruit.

AUTHOR INFORMATION

Corresponding Author

*Tel.: +886-4-22840894 ext. 406. Fax: +886-4-22862073. E-mail: jwliao@dragon.nchu.edu.tw.

Funding

The authors would like to thank the Ministry of Health and Welfare, Taiwan, for financially supporting this research under Contract No. MOHW102-FDA-A3002. This work was also supported in part by the Ministry of Education, Taiwan, ROC, under the ATU plan.

Notes

The authors declare no competing financial interest.

REFERENCES

(1) European Food Safety Authority (EFSA). Guidance on conducting repeated-dose 90-day oral toxicity study in rodents on whole food/feed. EFSA Scientific Committee. *EFSA J.* **2011**, *9*, 2438−2459.

(2) Food and Agriculture Organization (FAO). FAO Statistics Database (FAOSTAT), http://faostat.fao.org/, 2013.

(3) Tripathi, S.; Suzuki, J. Y.; Carr, J. B.; McQuate, G. T.; Ferreira, S. A.; Manshardt, R. M.; Pitz, K. Y.; Wall, M. M.; Gonsalves, D. Nutritional composition of Rainbow papaya, the first commercialized transgenic fruit crop. *J. Food Compos. Anal.* **2011**, *24*, 140−147.

(4) Abdullah, M.; Chai, P. S.; Loh, C. Y.; Chong, M. Y.; Quay, H. W.; Vidyadaran, S.; Seman, Z.; Kandiah, M.; Seow, H. F. *Carica papaya* increases regulatory T cells and reduces IFN-γ^+ $CD4^+$ T cells in healthy human subjects. *Mol. Nutr. Food Res.* **2011**, *55*, 803−806.

(5) Chen, Y. N.; Hwang, W. Z.; Fang, T. J.; Cheng, Y. H.; Lin, J. Y. The impact of transgenic papaya (TPY10−4) fruit supplementation on immune responses in ovalbumin-sensitized mice. *J. Sci. Food Agric.* **2011**, *91*, 539−546.

(6) Bau, H. J.; Cheng, Y. H.; Yu, T. A.; Yang, J. S.; Liou, P. C.; Hsiao, C. H.; Lin, C. Y.; Yeh, S. D. Field evaluation of transgenic papaya lines carrying the coat protein gene of *Papaya ringspot virus* in Taiwan. *Plant Dis.* **2004**, *88*, 594−599.

(7) Bau, H. J.; Cheng, Y. H.; Yu, T. A.; Yang, J. S.; Yeh, S. D. Broad-spectrum resistance to different geographic strains of *papaya ringspot virus* in coat protein gene transgenic papaya. *Phytopathology* **2003**, *93*, 112−120.

(8) Harlander, S. K. Safety assessments and public concern for genetically modified food products: The American view. *Toxicol. Pathol.* **2002**, *30*, 132−134.

(9) Food and Agriculture Organization (FAO)/WHO. Biotechnology and food safety. Report of a joint FAO/WHO consultation, FAO Food and Nutrition Paper 61; Food and Agriculture Organization of the United Nations: Rome, Italy, 1996; http://www.fao.org/es/esn/gm/biotec-e.htm.

(10) European Food Safety Authority (EFSA). GMO Panel Working Group on Animal Feeding Trials. Safety and nutritional assessment of GM plants and derived food and feed: the role of animal feeding trials. *Food Chem. Toxicol.* **2008**, *46*, S42−S70.

(11) Dryzga, M.; Yano, B.; Andrus, A.; Mattsson, J. Evaluation of the safety and nutritional equivalence of a genetically modified cottonseed meal in a 90-day dietary toxicity study in rats. *Food Chem. Toxicol.* **2007**, *45*, 1994−2004.

(12) Appenzeller, L. M.; Munley, S. M.; Hoban, D.; Sykes, G. P.; Malley, L. A.; Delaney, B. Subchronic feeding study of herbicide-tolerant soybean DP-356Ø43−5 in Sprague-Dawley rats. *Food Chem. Toxicol.* **2008**, *46*, 2201−2213.

(13) Zhou, X. H.; Dong, Y.; Xiao, X.; Wang, Y.; Xu, Y.; Xu, B.; Shi, W. D.; Zhang, Y.; Zhu, L. J.; Liu, Q. Q. A 90-day toxicology study of high-amylose transgenic rice grain in Sprague−Dawley rats. *Food Chem. Toxicol.* **2011**, *49*, 3112−3118.

(14) Malley, L. A.; Everds, N. E.; Reynolds, J.; Mann, P. C.; Lamb, I.; Rood, T.; Schmidt, J.; Layton, R. J.; Prochaska, L. M.; Hinds, M.; Locke, M.; Chui, C. F.; Claussen, F.; Mattsson, J. L.; Delaney, B. Subchronic feeding study of DAS-59122-7 maize grain in Sprague-Dawley rats. *Food Chem. Toxicol.* **2007**, *45*, 1277−1292.

(15) Liu, P.; He, X.; Chen, D.; Luo, Y.; Cao, S.; Song, H.; Liu, T.; Huang, K.; Xu, W. A 90-day subchronic feeding study of genetically modified maize expressing Cry1Ac-M protein in Sprague-Dawley rats. *Food Chem. Toxicol.* **2012**, *50*, 3215−3221.

(16) Lin, H. T.; Yen, G. C.; Huang, T. T.; Chan, L. F.; Cheng, Y. H.; Wu, J. H.; Yeh, S. D.; Wang, S. Y.; Liao, J. W. Toxicity assessment of transgenic *Papaya ringspot virus* of 823-2210 line papaya fruits. *J. Agric. Food Chem.* **2013**, *61*, 1585−1596.

(17) Fan, M. J.; Chen, S.; Kung, Y. J.; Cheng, Y. H.; Bau, H. J.; Su, T. T.; Yeh, S. D. Transgene-specific and event-specific molecular markers for characterization of transgenic papaya lines resistant to *Papaya ringspot virus*. *Transgenic Res.* **2009**, *18*, 971−986.

(18) MacKenzie, S. A.; Lamb, I.; Schmidt, J.; Deege, L.; Morrisey, M. J.; Harper, M.; Layton, R. J.; Prochaska, L. M.; Sanders, C.; Locke, M.;

DOI: 10.1021/jf5048404
J. Agric. Food Chem. 2015, 63, 1286−1292

Mattsson, J. L.; Fuentes, A.; Delaney, B. Thirteen week feeding study with transgenic maize grain containing event DAS-Ø15Ø7-1 in Sprague-Dawley rats. *Food Chem. Toxicol.* **2007**, *45*, 551−562.
(19) Registry of Industrial Toxicology Animal-data (RITA) and North American Control Animal Database (NACAD). Revised guides for organ sampling and trimming in rats and mice−Part 1. *Exp. Toxic Pathol.* **2003**, *55*, 91−106.
(20) Shackelford, C.; Long, G.; Wolf, J.; Okerberg, C.; Herbert, R. Qualitative and quantitative analysis of nonneoplastic lesions in toxicology studies. *Toxicol. Pathol.* **2002**, *30*, 93−96.
(21) Charles River Laboratories. Clinical laboratory parameters for Crl: WI(Han), United States, 2008; pp 1−14.
(22) Council of Agriculture. Fruit. Food Supply and Utilization Yearbook. 2007−2011; GPN 2009102742, ISSN 0021-8561, Taiwan, 2012.
(23) Fermín, G.; Keith, R. C.; Suzuki, J. Y.; Ferreira, S. A.; Gaskill, D. A.; Pitz, K. Y.; Manshardt, R. M.; Gonsalves, D.; Tripathi, S. Allergenicity assessment of the *papaya ringspot* virus coat protein expressed in transgenic rainbow papaya. *J. Agric. Food Chem.* **2011**, *59*, 10006−12.
(24) Afzan, A.; Abdullah, N. R.; Halim, S. Z.; Rashid, B. A.; Semail, R. H. R.; Abdullah, N.; Jantan, I.; Muhammad, H.; Ismail, Z. Repeated dose 28-days oral toxicity study of *Carica papaya* L. leaf extract in Sprague Dawley rats. *Molecules* **2012**, *17*, 4326−4342.
(25) Lin, J. Y.; Wang, Y. C. Component analysis of backcross genetically modified anti-Papaya ringspot virus domestic papaya fruits. Thesis, Department of Food Science and Biotechnology of National Chung Hsing University, 2011; pp 1−111.

DOI: 10.1021/jf5048404
J. Agric. Food Chem. 2015, 63, 1286−1292

Table 1. Mean Forage Production (t of DM/ha) of the Different Treatments at the Various Cutting Dates[a]

		June		July (a)		July (b)		August		September		October		
treatment	year	x	±se	x	±se	x	±se	x	±se	x	±se	x	±se	sum
1	2007											4.07	0.26	4.07
	2008											3.70	0.61	3.70
	2009											5.48	0.80	5.48
	2010											4.65	0.75	4.65
2	2007	2.33	0.16							1.79	0.19			4.12
	2008	2.52	0.06							2.66	0.16			5.18
	2009	2.17	0.13							2.97	0.22			5.15
	2010	2.85	0.47							2.26	0.26			5.11
3	2007	2.05	0.24			0.93	0.05					0.71	0.09	3.69
	2008	2.25	0.14			0.97	0.03					1.45	0.12	4.67
	2009	2.11	0.11			0.96	0.04					1.83	0.19	4.90
	2010	2.18	0.22			0.98	0.08					1.09	0.17	4.24
4	2007			2.57	0.20							1.00	0.10	3.57
	2008			2.17	0.13							2.50	0.33	4.67
	2009			2.47	0.29							2.97	0.52	5.43
	2010			3.65	0.28							2.09	0.22	5.73
5	2007			2.71	0.22			0.44	0.08			0.71	0.12	3.87
	2008			2.24	0.18			1.04	0.13			1.31	0.22	4.59
	2009			2.30	0.28			1.58	0.11			1.06	0.17	4.93
	2010			2.62	0.24			1.36	0.22			0.74	0.06	4.72
	mean	2.31	0.19	2.59	0.23	0.96	0.05	1.11	0.14	2.42	21.2	2.21	0.30	

[a] x, mean; se, standard error with N = 5.

level (asl)], close to Gmünd. The climate is rather rough, with mean annual temperatures of 6.8 °C and mean annual precipitation of 660 mm. The soil type is acidic pseudogley developed from granite substrate. The experimental site is located in a flat, frequently waterlogged meadow affiliated to the community type Lychnido floris cuculi-Festucetum rubrae Subass. Juncetosum filiformis, typical for this region.[25] Before the experiment was established in 2007, the meadow was mowed once or twice a year after June 15th, without application of fertilizer. A voucher specimen from the toxic plant was deposited in the Herbarium of the University of Vienna (WU) with the accession number WU0079259.[26]

Study Design. A total of 25 permanent plots of 1 m^2 were arranged as a randomized complete block design to apply the five different cutting regimes (treatments) in five pseudo-replicates. The distance from one plot to another was 1 m.

In treatment 1 (standard), cutting was carried out once in early October (Table 1).

Treatment 2 is the common cutting regime for extensive meadows in the Waldviertel. Plots were cut first in early June when all plants were still in the rosette stage, and the second cut took place in early September when the seed set was nearly finished. This treatment allows for full flowering and seed production.

Treatment 3 corresponds to treatment 2, with an additional cut in late July [July (b)], when adult plants are flowering again.

The first cut of treatment 4 took place in early July [July (a)] when marsh ragwort flowered but the seeds were not yet ripened, and the second cut was set in early October.

The plots of treatment 5 were mowed 3 times at full flowering in early July [July (a)], in early August, and in early October. Because the cuttings in July and August took place before the seed set, the seed production is suppressed.

The plots of 1 m^2 were mowed manually to a residual height of 5−10 cm with a scythe from 2007 to 2010. The forage was put into bags; later on, *J. aquatica* was separated. Both *J. aquatica* and the remaining plant material were dried at 50 °C before weighing.

Alkaloid Extraction. A measured aliquot of about 200 mg of the finely powdered plant material of *J. aquatica* was extracted with 25 mL of methanol/0.1 N HCl (30:70, v/v) for 1 h in an ultrasonic bath at room temperature. Exactly 8.0 mL of the filtered resulting extract were reduced under continuous stirring overnight with Zn dust (p.A.). Then, 1.6 mL of 12.5% NH_4OH (diluted from 25% commercially available NH_4OH) and 3 mL (3.96 g) of CH_2Cl_2 were added and vigorously shaken for 5 min. After the separation of the two phases, a measured aliquot (2−3 g) of the CH_2Cl_2 layer was taken and reduced to dryness. Finally, this fraction was made up in 200 μL of methanol containing caffeine (0.25 mg/mL) as an internal standard and subjected to the gas chromatography/mass spectometry (GC/MS) analysis.

GC/MS. The analysis was carried out using a HP 6890 gas chromatograph equipped with a 5972 quadrupole mass selective detector (MSD, Agilent Technologies, Wilmington, DE) and a 30 m × 0.25 mm fused silica column coated with 0.25 μm HP5-MS. The analytical conditions were He carrier gas at 1.3 mL/min constant flow, split ratio of 8:1, and temperature program of heating from 80 to 180 °C at 8 °C/min, then at 4 °C/min up to 280 °C, and held for 10 min at 280 °C. The injector temperature was 275 °C, and the injection volume was 1 μL. The transfer line to the mass spectometer was set at 280 °C, with the detector at 170 °C. The masses were scanned from m/z 40 to 450. The identity of the alkaloids was established according to their mass spectra and retention indices.[27−29]

Quantitative Analysis. For the quantitative analysis, the MSD was operated in the single ion monitoring (SIM) mode recording the mass fragments 109 and 194 for caffeine and 93, 120, and 136 for the alkaloids. Because the macrocyclic pyrrolizidine alkaloids present in *J. aquatica* show similar mass spectra, the calibration graph constructed with senecionine was taken to calculate the concentrations of all alkaloids using the total ion current from the monitored mass fragments.

To construct a calibration graph, seven concentration steps (0.023−0.45 mg/mL) were prepared from a stock solution of 0.45 mg/mL senecionine (Roth, Karlsruhe, Germany) in methanol containing the internal standard caffeine and were each injected 3 times into the GC/MS system. The linear calibration was forced through zero. Repeated injections afforded at most concentrations a coefficient of variation less than 10%. Taking into account the sample preparation, a limit of detection (LOD) of 2 μg/g in the plant material could be calculated.

Statistical Analyses. The SPSS 17.0 software (IBM, Somers, NY) was used to perform the statistical analyses. The data are given as the mean ± standard deviation (SD) for the alkaloid contents and as the mean with the standard error of the mean (SEM) for the growth

DOI: 10.1021/jf5047927
J. Agric. Food Chem. 2015, 63, 1293−1299

Table 2. Percentage of *J. aquatica* DM in Total Dried Fodder of the Different Treatments at the Various Cutting Dates[a]

		June		July (a)		July (b)		August		September		October	
treatment	year	*x*	±se	*x*	±se	*x*	±se	*x*	±se	*x*	±se	*x*	±se
1	2007											2.4	0.8
	2008											3.3	1.0
	2009											0.9	0.3
	2010											0.4	0.1
2	2007	2.6	0.7							12.0	2.8		
	2008	1.5	0.3							7.1	0.8		
	2009	2.2	0.2							4.5	0.8		
	2010	2.3	0.4							4.6	0.9		
3	2007	1.8	0.5			12.9	4.1					5.4	1.2
	2008	2.1	0.8			20.2	4.3					4.2	0.9
	2009	1.8	0.2			4.8	1.2					3.1	0.9
	2010	1.4	0.4			7.0	1.7					2.1	0.5
4	2007			8.8	1.7							7.1	1.3
	2008			7.0	1.1							3.0	0.5
	2009			1.9	0.4							2.2	0.3
	2010			2.1	0.3							2.3	0.5
5	2007			8.5	3.3			14.3	2.4			7.1	1.6
	2008			8.8	2.0			11.9	1.7			4.0	0.8
	2009			2.1	0.4			2.7	0.5			3.9	0.7
	2010			2.8	0.3			5.5	0.6			1.1	0.2
	total *x*	2.0	0.4	5.3	1.2	11.2	2.8	8.6	1.3	7.0	1.3	3.3	0.7

[a] *x*, mean; se, standard error with $N = 5$.

parameters. Significance of treatment effects was tested with an analysis of variation (ANOVA), and Bonferroni post-hoc test was used to determine significant differences between individual means. Pearson correlation coefficients were calculated to test for relations between plant production and alkaloid content data.

RESULTS AND DISCUSSION

The *J. aquatica* population in the meadow near Kleedorf looked well-established and very dense. The growth of forage and ragwort and the alkaloid content of toxic plants were measured for 4 years (2007−2010) at the cutting date of the respective treatments with the exception of the last cutting in October 2010 (Tables 1 and 2). Cutting time and sampling year had a significant influence on plant dry matter production and alkaloid content ($p < 0.01$), and there were interactions between these factors. The productivity of the study site was generally very low, with 4.6 t of dry matter (DM)/ha on average.

The forage of the June cuts of treatments 2 and 3 was less infested with *J. aquatica* (Table 2); *J. aquatica* accounted only for 2% of the DM. If the first cut took place in early July (treatments 4 and 5), the average percentage of *J. aquatica* was 5.3%. We measured the highest proportions of *J. aquatica* in the second cut of treatment 3 (mean = 11.2%) in late July and treatment 5 in early August (mean = 8.6%). The amount of *J. aquatica* in the yield of the second cut of treatment 2 in early September (7.0%) was also quite high. In October, the percentage of *J. aquatica* was low in all treatments. Lowest annual percentages of *J. aquatica* (mean = 1.8% over years 2007−2010) were found in treatment 1. This was significantly lower than in the other treatments (2−5), where annual *J. aquatica* percentages did not differ significantly.

The percentage of *J. aquatica* in the forage was highest in 2007 and 2008, when many individuals flowered (6−7%) and lowest (about 2.5%) in the following years.

Six pyrrolizidine alkaloids could be evaluated in *J. aquatica* (Figure 1). The most abundant alkaloids were *Z*-erucifoline (**1**)

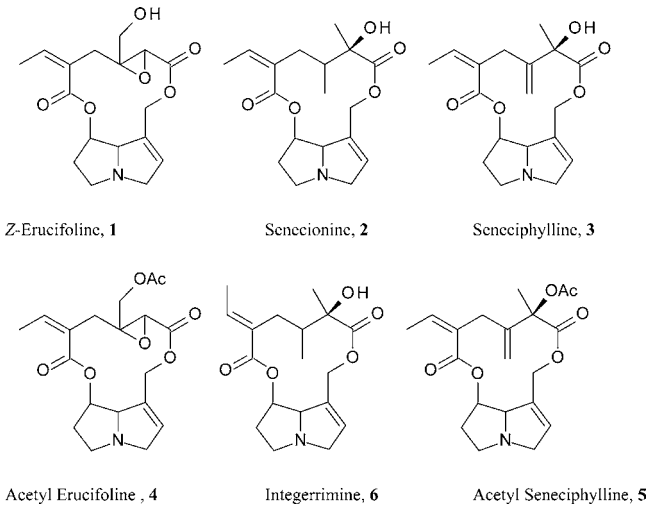

Figure 1. Pyrrolizidine alkaloids from *J. aquatica*.

and senecionine (**2**), followed by seneciphylline (**3**), acetyl-erucifoline (**4**), acetyl-seneciphylline (**5**), and integerrimine (**6**). Table 3 gives the statistical parameters describing the variability in alkaloid concentrations measured in *J. aquatica* plants at the different cutting dates over the 4 years of measurement. The total alkaloid content, as a mean of five plots, varied between 213 and 1979 mg/kg of DM, with *Z*-erucifoline (**1**) and senecionine (**2**) as the main alkaloids. The highest total PA content occurred in August 2010 in treatment 5, and the lowest total PA content occurred in June 2009 in treatment 2.

At certain harvests, some of the alkaloids were below the detection limit of 2 μg/g in the plant material. This was the case

DOI: 10.1021/jf5047927
J. Agric. Food Chem. 2015, 63, 1293−1299

Table 3. Variability in the Alkaloid Concentration in Marsh Ragwort Calculated from All Collection Times

	Z-erucifoline (1) (μg/g)	senecionine (2) (μg/g)	seneciphylline (3) (μg/g)	acetyl-erucifoline (4) (μg/g)	acetyl-seneciphylline (5) (μg/g)	integerrimine (6) (μg/g)	sum (μg/g)
mean	362.3	140.3	118.9	81.7	52.5	33.1	788.8
median	284.9	59.8	103.4	74.1	36.1	21.5	673.3
coefficient of variation (%)	76.5	126.2	57.3	77.2	84.2	92.1	55.3
minimum	13.2	6.1	21.8	<2	5.6	<2	212.5
maximum	1194.5	856.8	320.5	224.2	210.6	127.0	1979.0

for acetyl-erucifoline (**4**), acetyl-seneciphylline (**5**), and integerrimine (**6**).

Cutting time (from June to October) and year (2007−2010) had a significant influence on the alkaloid production ($p < 0.001$), and all alkaloids were affected (Figures 2 and 3). In the early summer (cutting dates from June to early July), the total alkaloid concentration was higher than later in the summer and autumn (cutting dates from late July to October). The differences in alkaloid accumulation were remarkable (Figure 2); between the years, the highest total alkaloid concentrations were reached in 2010 in July [July (b)], whereas the year 2009 was a period with generally low alkaloid levels ($p < 0.001$). Even in this year, the highest alkaloid contents were obtained in July (cutting dates of early July and late July).

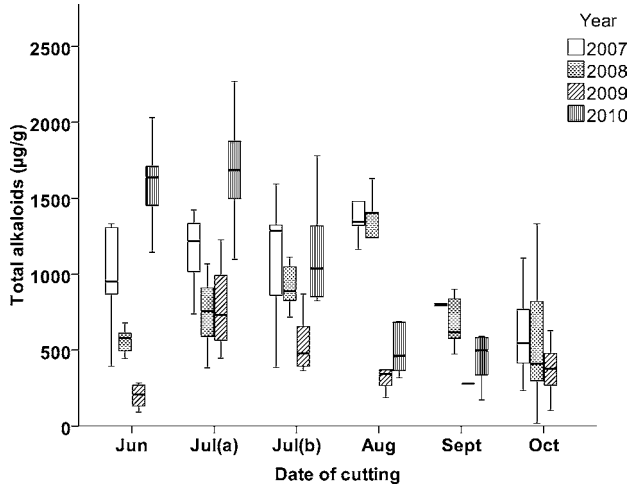

Figure 2. Variability in total alkaloids of *J. aquatica* (box plot, μg/g of DM) at the different cutting dates during the years 2007−2010.

In addition, the different PAs showed a characteristic variation during the vegetation period (panels A−C of Figure 3). The main alkaloid Z-erucifoline (**1**) was higher at the earlier cutting dates, especially in 2010 (Figure 3A; $p < 0.001$), while senecionine (**2**) had its peak instead in midsummer (cutting dates from late July to August) (Figure 3B; $p < 0.001$). Correspondingly, the ratio Z-erucifoline (**1**) to senecionine (**2**) was high at the beginning of the season, and then it decreased and finally increased again slowly. In July and August, there were samples that contained more senecionine (**2**) than Z-erucifoline (**1**). During the year, seneciphylline (**3**) (Figure 3C) followed roughly the distribution of senecionine (**2**), but in July and August, the senecionine (**2**) contents were about 2 times higher; only in June and toward the end of the year, the samples contained more seneciphylline (**3**) than senecionine (**2**).

When the data of the alkaloid concentration, *J. aquatica* growth, and forage production were combined, the alkaloid concentration in the resulting hay was calculated. The variability over the years and the growing season of total alkaloids present in the hay are displayed in Figure 3D. The highest load of alkaloids in the forage could be obtained during midsummer (from late July to August; $p < 0.01$), while the early cutting in early June and the late cuttings in September and October afforded relatively low alkaloid levels in the forage.

Figure 4A compares the alkaloid production in treatments 2 and 5. Treatment 2 representing an early first cutting and a later second cutting is often applied in this region in practice, whereas treatment 5 with two cuttings in July and August is suitable to suppress seed production.[30] Differences between the years became apparent, with the highest alkaloid contents in June and in early July 2010. The July and August cuttings from treatment 5 displayed usually higher alkaloid concentrations than the two cuttings from treatment 2 ($p = 0.027$).

When the alkaloid content is calculated on the basis of fodder (Figure 4B), again the highest contents were obtained in treatment 5 during July and August. At that time, the alkaloid load of the forage was considerably higher during 2007−2008 than during 2009−2010. This was due to the generally lower alkaloid content of *J. aquatica* in 2009 and the lower percentage of this plant in the forage during the last 2 years (Table 2). Finally, for a practical evaluation, the dry matter percentage of *J. aquatica* was correlated with the calculated total alkaloid concentration in the fodder ($R^2 = 0.87$; $p < 0.01$; $N = 28$), while the production of fodder was not correlated with the growth of *J. aquatica*.

Considering the presence of *J. aquatica* on the differently managed meadow plots, this toxic plant was obviously growing vigorously during the summer. Peak flowering took place from July to August, with seed set about 3 weeks later from August to September. The percentage of *J. aquatica* in the forage results from the plants and forage growth, dependent upon the cutting date. The seasonal influence was very high; it is obvious that the percentage of *J. aquatica* DM was lowest in the forage cut in early June, before flowering stems are elongated. The highest percentages were reached in cuts just a few weeks after the previous cut. *J. aquatica* plants regenerate faster than most other plants, and mowed individuals may produce more secondary flower stems and, consequently, more capitulae than undisturbed individuals.[30] Consequently, a few weeks after the last cut, the total forage yield is low and the infestation rate of *J. aquatica* is high. When the meadows are mowed first in autumn (treatment 1), most flowering plants of *J. aquatica* will already have died off. Consequently, the percentage of *J. aquatica* DM in the forage is low, but this cutting regime is not applicable in agricultural practice because of the low quality of hay.

Reports describing the PAs of *J. aquatica* are scarce. Winter et al.[31] reported a *J. aquatica* population with senecionine (**2**) as the main PA, followed by seneciphylline (**3**), integerrimine (**6**),

DOI: 10.1021/jf5047927
J. Agric. Food Chem. 2015, 63, 1293−1299

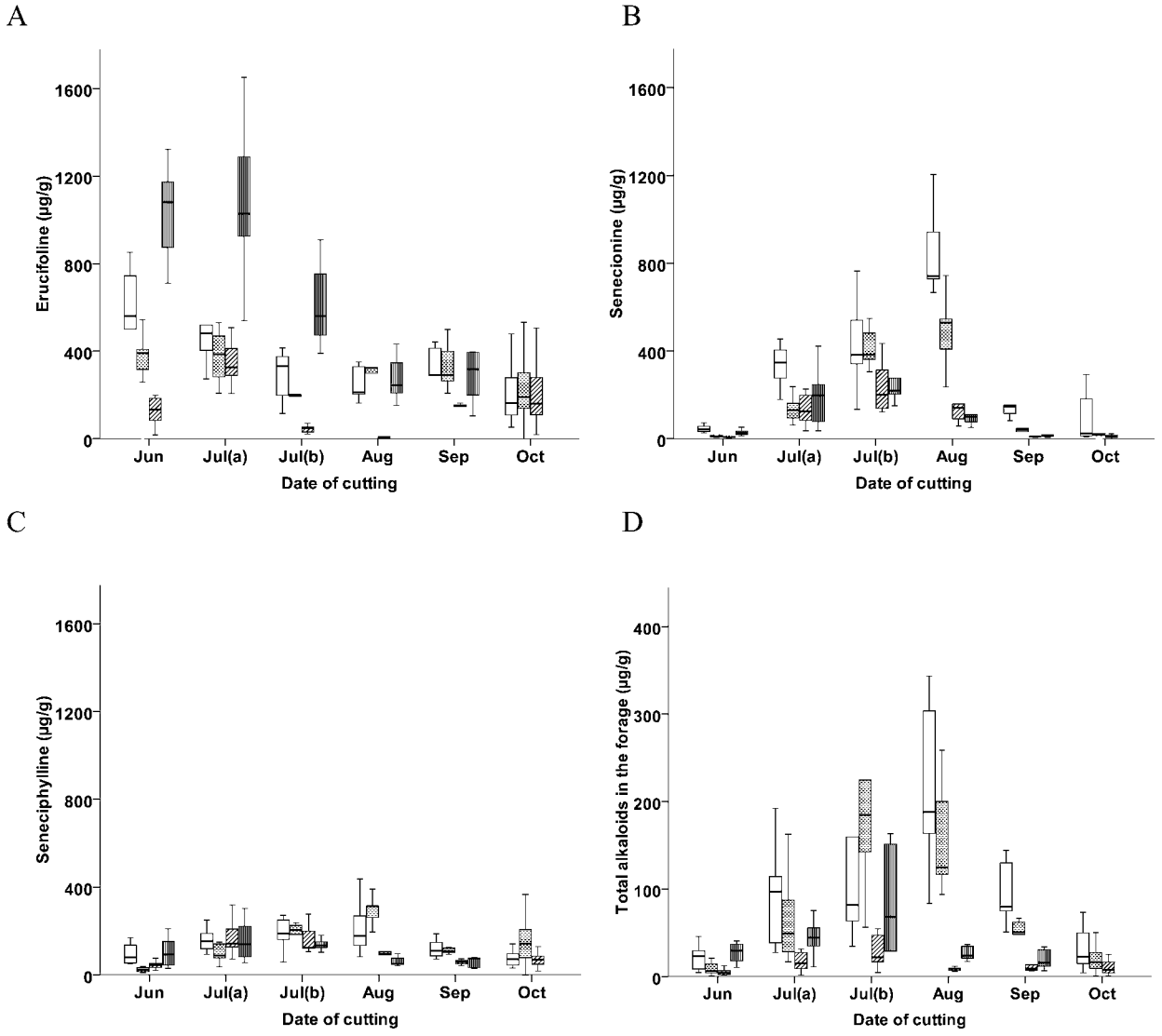

Figure 3. Variability in the content (box plot, µg/g of DM) of (A) *Z*-erucifoline (**1**), (B) senecionine (**2**), and (C) seneciphylline (**3**) of *J. aquatica* and (D) total alkaloid content of forage, at different cutting dates during the years 2007−2010. The legend is the same as in Figure 2.

and *Z*-erucifoline (**1**), from the same Waldviertel region. Erucifoline (**1**) and 9-angeloyl-hastanecine were isolated from *J. aquatica* ssp. *barbareifolius* plants collected in southeast Bulgaria.[22] Senecionine (**2**), integerrimine (**6**), seneciphylline (**3**), *Z*-erucifoline (**1**), and acetyl-erucifoline (**4**) were also found in *J. aquatica* plants in the Netherlands.[3] Additionally, these plants contained jacobine and traces of jacozine, which were not detected in the present study. Further reports from Dutch plants confirmed that these alkaloids for *J. aquatica* as 185 µg/g of senecionine (**2**), 326 µg/g of seneciphylline (**3**), 349 µg/g of integerrimine (**6**), and 29 µg/g of *Z*-erucifoline (**1**) could be measured in the shoots of these plants.[4] In plants, PAs occur as free bases and as *N*-oxides;[24,27,32] for the analysis by GC, the latter must be reduced during clean up.

A systematic analysis of the distribution of the alkaloids within the plant was not carried out in this study. However, in various *Senecio*/*Jacobaea* species, it has been shown that the PAs mostly accumulate in the inflorescences.[32−34] Furthermore, young leaves contain higher alkaloid levels than older leaves.[35] Such a distribution is explained as protecting the plant parts important for further growth.

With regard to the influence of the cutting regime on alkaloid production, we have to take into account different cutting dates. Three treatments were cut in early October. The alkaloid load at that time in the year was generally lower than in earlier cuttings. In comparison to the first year (2007), during 2 years (2008 and 2009), the alkaloid content in the plants from treatment 1, representing a very late first cutting, was lower than in the plants from the other cutting regimes, representing second or third cuttings (data not shown).

The alkaloid accumulation in *J. aquatica* appears to be influenced by several factors, including nutrient supply,[36] water supply,[4] and ontogenetic development.[9,32] Sometimes changes in the PA concentration may be explained by changes in the biomass production rather than true alkaloid production.[36] All of these factors influence the alkaloid levels differently in the various cutting regimes (treatments) tested. Additionally, differences between the years arise from the varying weather conditions. Plants harvested very late in the season (October) were senescent, with their seed production almost completed and the capitulae starting to decay. Thus, they bear lower alkaloid contents in all treatments. Plants cut in late July and August established from individuals that were cut 4−6 weeks

DOI: 10.1021/jf5047927
J. Agric. Food Chem. 2015, 63, 1293−1299

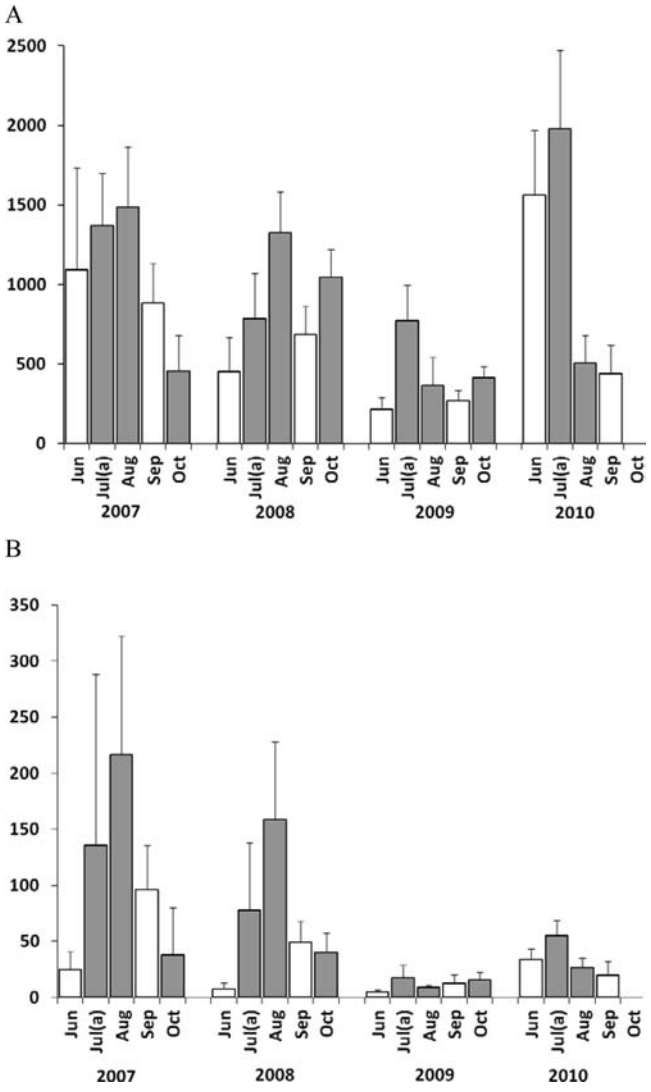

Figure 4. Comparison of the total alkaloid content (μg/g of DM) in (A) *J. aquatica* and (B) fodder, in treatments 2 (white bars) and 5 (gray bars). Mean values with standard deviation (n = 5).

earlier and showed only younger but, nevertheless, flowering shoots with relatively higher alkaloid contents. The samples from treatment 2 cut in September developed from plants that benefited from a longer period for regrowth and, therefore, were already subject to senescence, leading to lower alkaloid contents.

All six monitored PAs are toxic, bearing the structural prerequisites needed to be converted into toxins by cellular cytochrome P450 enzymes. These are (i) a 1,2 double bond, (ii) an esterified allylic hydroxyl group at C-9, and (iii) a second esterified alcoholic hydroxyl group at C-7.[6] During the past few decades, various intoxications of livestock with *Senecio* species have been reported and also feeding experiments with these toxic plants have been carried out to study the toxicity. However, it is difficult to establish toxicity levels because the alkaloid contents of the plants and dosage and duration of toxic plant intake are too variable.[7] Selective food intake may occur because a higher percentage of *J. aquatica* in the remaining material in the manger was left than in the hay. Such a selection was almost impossible in the case of silage.[37] Horses are the most sensitive grazing animals. Among the ruminants, the susceptibility decreases from cattle to goats and to sheep. Levels of 100 μg/g (mg/kg) total alkaloids are easily reached in the fodder cut during July and August (Figures 3D and 4B) when the forage contains more than 5% ragwort. Using this as fodder may provide more than 1−3 mg/kg of body weight PA per day to the animals, a dosage that is considered to induce intoxications,[10] especially when fed during a longer period of time. Therefore, at least the fodder from the July and August cuttings should not be fed to domestic animals.

Great variations occurred in the alkaloid contents of marsh ragwort between the years and the cutting dates. A late cut fodder, which is low in alkaloids, is not useful for agricultural purposes. During the summer, the plants were able to grow quickly, so that they produced flowering stalks 4−5 weeks after a cutting. During this time, marsh ragwort infestation can be high, and therefore, the resulting contamination of forage with toxic PAs may present a health risk for livestock. A long-term management must avoid the seed production of this toxic plant. The following management regime can be a compromise: The forage of a cutting before flowering is best suited for feeding. If it is carried out in early June, it also does not negatively affect biodiversity goals. Further cuttings should be carried out at peak flowering at about 5−7 weeks later. The fodder of these cuttings can be used for non-feeding purposes, such as composting or supply of a biogas plant.

AUTHOR INFORMATION

Corresponding Author

*Telephone: +43-1-250773104. Fax: +43-1-250773190. E-mail: remigius.chizzola@vetmeduni.ac.at.

Funding

This work was funded by the Federal Ministry of Agriculture, Forestry, Environment and Water Management in cooperation with Federal States of Austria and the Jubiläumsfonds of the Austrian Nationalbank.

Notes

The authors declare no competing financial interest.

ACKNOWLEDGMENTS

The authors thank Bernhard Spangl for statistical support, Desirée Bruhin for assistance in the field, and Hanneliese Michitsch for aid in the alkaloid analyses.

REFERENCES

(1) Bassler, G.; Lichtenecker, A.; Karrer, G. Klassifikation des Extensivgrünlandes (Feuchtwiesen, Moore, Bürstlingrasen und Halbtrockenrasen) im Zentralraum des Waldviertels. *Wiss. Mitt. Niederoesterr. Landesmus.* **2003**, *15*, 7−48.

(2) Bartelheimer, M.; Gowing, D.; Silvertown, J. Explaining hydrological niches: The decisive role of below-ground competition in two closely related *Senecio* species. *J. Ecol.* **2010**, *98*, 126−136.

(3) Kirk, H.; Macel, M.; Klinkhamer, P. G. L.; Vrieling, K. Natural hybridization between *Senecio jacobaea* and *Senecio aquaticus*: Molecular and chemical evidence. *Mol. Ecol.* **2004**, *13*, 2267−2274.

(4) Kirk, H.; Vrieling, K.; van der Meijden, E.; Klinkhamer, P. G. L. Species by environment interactions affect pyrrolizidine alkaloid expression in *Senecio jacobaeae*, *Senecio aquaticus*, and their hybrids. *J. Chem. Ecol.* **2010**, *36*, 378−387.

(5) Mattocks, A. R. Toxicity of pyrrolizidine alkaloids. *Nature* **1968**, *217*, 723−728.

(6) Fu, P. P.; Xia, Q.; Lin, G.; Chou, M. W. Pyrrolizidine alkaloids—Genotoxicity, metabolism enzymes, metabolic activation, and mechanism. *Drug Metab. Rev.* **2004**, *36*, 1−55.

DOI: 10.1021/jf5047927
J. Agric. Food Chem. 2015, 63, 1293−1299

(7) Wiedenfeld, H.; Edgar, J. Toxicity of pyrrolizidine alkaloids to humans and ruminants. *Phytochem. Rev.* **2011**, *10*, 137−151.
(8) Candrian, U.; Lüthy, J.; Schmid, P.; Schlatter, C.; Gallasz, E. Stability of pyrrolizidine alkaloids in hay and silage. *J. Agric. Food Chem.* **1984**, *32*, 935−937.
(9) Berendonk, C.; Cerff, D.; Hünting, K.; Wiedenfeld, H.; Becerra, J.; Kuschak, M. Pyrrolizidine alkaloid level in *Senecio jacobaea* and *Senecio erraticus*—The effect of plant organ and forage conservation. *Grassl. Sci. Eur.* **2010**, *15*, 669−671.
(10) Hoogenboom, L. A. P.; Mulder, P. P. J.; Zeilmaker, M. J.; Van Den Top, H. J.; Remmelink, G. J.; Brandon, E. F. A.; Klijnstra, M.; Meijer, G. A. L.; Schothorst, R.; Van Egmond, H. P. Carry-over of pyrrolizidine alkaloids from feed to milk in dairy cows. *Food Addit. Contam.* **2011**, *28*, 359−372.
(11) Boppré, M.; Colegate, S. M.; Edgar, J. A.; Fischer, O. M. Hepatotoxic pyrrolizidine alkaloids in pollen and drying-related implications for commercial processing of bee pollen. *J. Agric. Food Chem.* **2008**, *56*, 5662−5672.
(12) Kempf, M.; Schreier, P.; Reinhard, A.; Beuerle, T. Pyrrolizidine alkaloids in honey and pollen. *J. Consum. Prot. Food Saf.* **2010**, *5*, 393−406.
(13) Korneck, D.; Schnittler, M.; Vollmer, I. Rote Liste der Farn- und Blütenpflanzen (Pteridophyta et Spermatophyta) Deutschlands. *Schriftenr. Veg.* **1996**, *28*, 21−187.
(14) Niklfeld, H.; Schratt-Ehrendorfer, L. Rote Liste Gefährdeter Farn- und Blütenpflanzen (Pteridophyta und Spermatophyta): Österreichs. *Grüne Reihe des Bundesministeriums für Gesundheit und Umweltschutz*; Österreich Bundesministeriums für Gesundheit und Umweltschutz: Vienna, Austria, 1999.
(15) Moser, D. M.; Gygax, A.; Bäumler, B.; Wyler, N.; Palese, R. *Rote Liste der gefährdeten Arten der Schweiz—Farn- und Blütenpflanzen*; Bundesamt für Umwelt, Wald und Landschaft, Bern; Zentrum des Datenverbundnetzes der Schweizer Flora, Chambésy; Conservatoire et jardin botaniques de la Ville de Genève, Eds.; BUWAL-Reihe "Vollzug Umwelt": Chambésy, Switzerland, 2002.
(16) Colling, G. Red List of the vascular plants of Luxembourg. *Ferrentia* **2005**, *42*, 77.
(17) Suter, M.; Lüscher, A. Beeinflusst die Bewirtschaftung das Wasser-Kreuzkraut? *Agrarforschung* **2007**, *14*, 22−27.
(18) Suter, M.; Lüscher, A. Occurrence of *Senecio aquaticus* in relation to grassland management. *Appl. Veg. Sci.* **2008**, *11*, 317−324.
(19) Bosshard, A.; Joshi, J.; Lüscher, A.; Schaffner, U. Jakobs- und andere Kreuzkrautarten: Eine Standortbestimmung. *Agrarforschung* **2003**, *10*, 231−235.
(20) Bohren, C.; Delabays, N.; Rometsch, S. Invasive Pflanzen: Herausforderung für die Landwirtschaft? *Agrarforschung* **2008**, *15*, 314−319.
(21) Suter, M.; Lüscher, A. Measures for the control of *Senecio aquaticus* in managed grassland. *Weed Res.* **2011**, *51*, 601−611.
(22) Christov, V. S.; Mikhova, B. P.; Evstatieva, L. N. Alkaloids from *Senecio aquaticus*. *Fitoterapia* **2002**, *73*, 171−173.
(23) Kirk, H.; Young, H. C.; Hye, K. K.; Verpoorte, R.; van der Meijden, E. Comparing metabolomes: The chemical consequences of hybridization in plants. *New Phytol.* **2005**, *167*, 613−622.
(24) Cheng, D.; Kirk, H.; Mulder, P. P. J.; Vrieling, K.; Klinkhamer, P. G. L. Pyrrolizidine alkaloid variation in shoots and roots of segregating hybrids between *Jacobaea vulgaris* and *Jacobaea aquatica*. *New Phytol.* **2011**, *192*, 1010−1023.
(25) Lichtenecker, A.; Bassler, G.; Karrer, G. Klassifikation der Wirtschaftswiesen (Fettwiesen der Arrhenatheretalia) im Zentralraum des Waldviertels. *Wiss. Mitt. Niederaesterr. Landesmus.* **2003**, *15*, 49−84.
(26) WU-Generale. http:\\herbarium.univie.ac.at.
(27) Hartmann, T.; Dierich, B. Chemical diversity and variation of pyrrolizidine alkaloids of the Senecionine type: Biological need or coincidence? *Planta* **1998**, *206*, 443−451.
(28) Witte, L.; Ernst, L.; Adam, H.; Hartmann, T. Chemotypes of two pyrrolizidine alkaloid containing *Senecio* species. *Phytochemistry* **1992**, *31*, 559−565.
(29) McLafferty, F. W. *Registry of Mass Spectral Data*, 5th ed.; John Wiley and Sons: New York, 1989.
(30) Bassler, G.; Kriechbaum, M.; Karrer, G. The impact of different cutting regimes on the population dynamics of *J. aquatica* (Hill) P. Gaertn., B. Mey. & Scherb. and on the surrounding grassland vegetation. *Weed Res.* **2015**.
(31) Winter, S.; Chizzola, R.; Kriechbaum, M.; Kropf, M. Hybridisation in *Jacobaea*. Characterisation of the hybrids between *Jacobaea aquatica* and *J. vulgaris* in Austria. *Plant Ecol. Diversity* **2013**, *6*, 217−229.
(32) Hartmann, T.; Zimmer, M. Organ specific distribution and accumulation of pyrrolizidine alkaloids during the life history of two annual *Senecio* species. *J. Plant Physiol.* **1986**, *122*, 67−80.
(33) Chizzola, R.; Eckl, D.; Bassler, G.; Kriechbaum, M. Pyrrolizidine alkaloids in *Senecio* species from the urban area of Vienna (Austria). *Planta Med.* **2010**, *76*, 1204.
(34) Wiedenfeld, H. Plants containing pyrrolizidine alkaloids: Toxicity and problems. *Food Addit. Contam.* **2011**, *28*, 282−292.
(35) De Boer, N. J. Pyrrolizidine alkaloid distribution in *Senecio jacobaea* rosettes minimises losses to generalist feeding. *Entomol. Exp. Appl.* **1999**, *91*, 169−173.
(36) Hol, W. H. G.; Macel, M.; Veen, A. V. J. Root damage and aboveground herbivory change concentration and composition of pyrrolizidine alkaloids of *Senecio jacobaea*. *Basic Appl. Ecol.* **2004**, *5*, 253−260.
(37) Hebeisen, H. *Wasserkreuzkraut Bekämpfen: Dran Bleiben*; http://www.lawa.lu.ch/wkk-bek-dran-bleiben.pdf (accessed Sept 10, 2014).

DOI: 10.1021/jf5047927
J. Agric. Food Chem. 2015, 63, 1293−1299

The behavior of pesticides in green tea shoots and the effects of manufacturing on residues in made tea, as well as their transfer rates during tea brewing, have been extensively reported.[17−19] However, few studies have reported on the enantioselective dissipation behavior of chiral pesticides in tea matrix, except for indoxacarb and *cis*-epoxiconazole.[20] In this study, a rapid method has been developed for the separation and determination of acephate and methamidophos enantiomers using gas chromatography with a QuEChERS sample preparation technique. Enantioseletive dissipation of acephate and methamidophos in tea was investigated during cultivation, manufacturing, and infusion.

MATERIALS AND METHODS

Field Trial. The field trial was conducted in a tea plantation (variety, Longjing 43; area, 666.7 m^2; location, Tea Research Institute, Chinese Academy of Agricultural Sciences, Hangzhou, China) from June 9 to July 14, 2014. The plantation was divided equally into six plots for treatment or control, leaving one row of bushes to separate each plot. After being diluted by a factor of 1:400, acephate (30% EC) was sprayed on tea leaf surfaces in five replications with a hand-operated knapsack sprayer. The control was sprayed with a similar amount of water. Before application, fresh tea leaves collected in this plantation were analyzed, and no acephate or methamidophos was found.

Sampling and Sample Preparation. The fresh tea leaves (one bud with two leaves) were collected randomly from tea trees in each plot on 0 (2 h), 1, 3, 5, 7, 10, 14, 21, 28, and 35 days after application to investigate the enantioselective dissipation of acephate and its metabolite during cultivation. Meanwhile, to determine the effects of tea manufacturing on the enantioselective dissipation of acephate and its metabolite, fresh tea leaves were picked from both treatment and control on days 1 and 3 and then made into green and black tea immediately. Samples collected at each stage of manufacturing were analyzed on the day of collection prior to storage.

The tea manufacturing steps were as follows. For green tea manufacturing: (a) spreading, that is, the plucked leaves were spread on a bamboo mat for 5 h at room temperature (23−25 °C) with good ventilation; (b) fixing, that is, the spread leaves were fried in a caldron-type water-removing machine at 220−230 °C to inactivate various enzymes; and (c) drying, that is, fixed leaves were dried by hot air at 110 °C to a final moisture concentration of approximately 3%. For black tea manufacturing: (a) withering, that is, the plucked leaves were spread on withering troughs for approximately 15 h at room temperature (23−25 °C); (b) rolling, that is, withered leaves were rolled by hand for 30−40 min at different pressures; (c) fermentation, that is, rolled leaves were stacked together and covered with a wet nylon net to maintain high relative humidity (about 95%) for 5−6 h to facilitate enzymatic oxidation; and (d) drying, a process similar to that in green tea manufacturing.

A total of 3 g of made tea was brewed with 150 mL of boiling water for 5 min. The infusion was then filtered out, and spent leaves were left. Both infusion and spent leaves were cooled for further analysis in the laboratory.

Chemicals and Reagents. Racemate standards of acephate and methamidophos were obtained from Agro-Environment Protection Institute (1000 mg/L, Tianjin, China). Organic solvents were of analytical grade and purchased from Merk (Darmstadt, Germany). The sorbents of primary−secondary amine (PSA), graphitized carbon black (GCB), and octadecylsilane (C_{18}) were purchased from Agela (Tianjin, China). Analytical grade sodium chloride (NaCl) and anhydrous magnesium sulfate ($MgSO_4$) (Zhejiang, China) were baked for 3 h at 650 °C prior to use. Ultrapure water was made from a Milli-Q water purification system (Bedford, MA, USA) in the laboratory.

Sample Pretreatment. For made tea, samples (2 g) were weighed into a 50 mL centrifuge tube and presoaked with 1 mL of boiled ultrapure water for 15 min. Target pesticides were extracted with 10 mL of acetonitrile by homogenization at 12000 rpm for 2 min. Afterward, 5 g of NaCl and 1 g of $MgSO_4$ were added in the centrifuge tube. The sample was mixed on a vortex mixer immediately for 30 s, followed by a centrifugation at 5000 rpm for 10 min. An aliquot of 2 mL was transferred from the supernatant to a 5 mL centrifuge tube, which contains 200 mg of PSA, 200 mg of C_{18}, 50 mg of GCB, and 100 mg of $MgSO_4$. Then the whole centrifuge tube was vortexed for 30 s before centrifugation (4000 rpm, 10 min). An aliquot of 1 mL was transferred and evaporated to dryness using a nitrogen flow controller. Residues were dissolved in 1 mL of acetone and filtered through a 0.22 μm membrane for final determination by GC-FPD.

For the fresh tea leaves collected within 7 days after acephate application, preparation was similar to the made tea samples mentioned above in addition to presoaking. To reduce the limits of quantification (LOQs) and meet the demand of detection, an additional concentration step was used prior to QuEChERS cleanup for the fresh tea leaves collected on days 10−35. The fresh tea leaves (4 g) were homogenized with 20 mL of acetonitrile in a centrifuge tube at 12000 rpm for 2 min. Then 5 g of NaCl and 2 g of $MgSO_4$ were added. Vortexing was performed for 30 s followed by centrifugation for 10 min at 4000 rpm. An aliquot of 10 mL was transferred and evaporated to 2 mL for further cleanup. Subsequent cleanup steps were similar to those for made tea samples, except the dissolved volume used was 0.5 mL of acetone.

For tea soup, liquid−liquid extraction was used to extract target pesticides from 50 mL of tea soup (dissolved with 10% NaCl) with 50 mL of dichloromethane. The organic phase was evaporated to dryness and dissolved in 2 mL of acetone for final determination.

For spent tea leaves, residues after tea brewing were sheared into pieces and transferred into a centrifuge tube, before the addition of acetonitrile (10 mL). The subsequent steps were similar to those for made tea sample.

Instrumentation. Acephate and methamidophos enantiomers were determined by gas chromatography (Agilent 7890 A, Wilmington, DE, USA) coupled with FPD. Enantiomeric separation was performed by a BGB-176 capillary column (30 m × 0.25 mm × 0.25 μm, BGB, Adiswil, Switzerland), having 20% 2,3-dimethyl-6-*tert*-butyldimethylsilyl-β-cyclodextrin dissolved in BGB-15 (15% phenyl-, 85% methylpolysiloxane). Carrier gas was high-purity nitrogen with a constant flow of 1.2 mL/min, and injection volume was 1 μL. The temperatures of the injector and detector were 230 and 245 °C, respectively. Oven temperature was maintained at 80 °C for 1 min, then increased to 220 °C at 10 °C/min, and held for 5 min.

Data Analysis. To evaluate chromatographic peaks of chiral acephate and methamidophos, the resolution (R) was calculated on the basis of the following equation: $R = 1.18 \times [t_{R(2)} - t_{R(1)}]/[W_{1/2(1)} + W_{1/2(2)}]$. $t_{R(1)}$ and $t_{R(2)}$ here stand for the retention times of the first and second enantiomers eluted from the column, respectively. $W_{1/2(1)}$ and $W_{1/2(2)}$ represent the half-peak width of the first and second enantiomers eluted from the column.

Generally, the dissipation of chiral pesticides hypothetically follows first-order kinetics.[21] In this study, this kinetic was calculated by Sigmaplot 12.5. Enantiomeric fractions (EF), as given by Harner et al.,[22] were used to express the differences between enantiomers, that is, $EF = E_1/(E_1 + E_2)$, where E_1 and E_2 represent the concentrations of the first and second enantiomers eluted from the column, respectively. In this study, E_1 stands for (+)-acephate or (+)-methamidophos. The values of EF ranged from 0.000 to 1.000, wherein EF = 0.500 referred to the racemic mixture.

Transfer rates of acephate or methamidophos enantiomers from made tea to infusion were calculated using eq 1

$$\text{transfer}\,(\%) = (m_1 - m_2)/m_1 \times 100 \quad (1)$$

where m_1 and m_2 stand for the concentrations of the target compounds (mg/kg) in made tea and spent tea leaves, respectively.

Validation Study. This method was validated by analyzing its performance characteristics, such as linearity, recovery, limit of detection (LOD), LOQ, and matrix effect (ME).

For sensitivity evaluation, the linearity was determined using mixed standard solutions at five concentration levels, ranging from 0.08 to 1.6

DOI: 10.1021/jf504916b
J. Agric. Food Chem. 2015, 63, 1300−1308

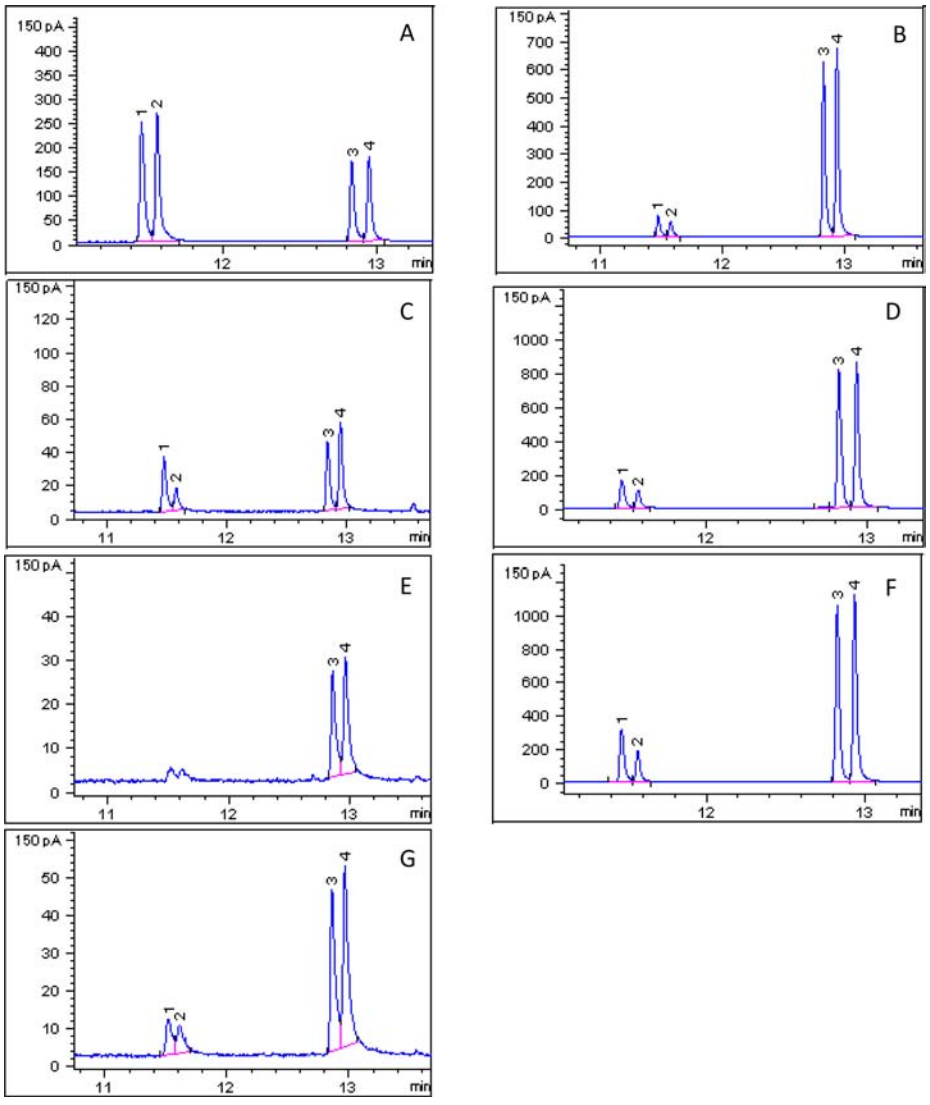

Figure 2. Typical chromatograms of acephate and methamidophos enantiomers in matrix standard solution (fresh tea leaves, 0.8 mg/kg) (A), fresh tea leaves on day 3 (B), fresh tea leaves on day 14 (C), green tea on day 3 (D), spent leaves of green tea on day 3 (E), black tea on day 3 (F), and spent leaves of black tea on day 3 (G). Peaks: 1, (+)-methamidophos; 2, (−)-methamidophos; 3, (+)-acephate; 4, (−)-acephate.

mg/kg for each enantiomer in multiple matrices. The LODs and LOQs for each enantiomer were confirmed on the basis of signal-to-noise (S/N) ratios of 3 and 10, respectively. The matrix effect was calculated by the ratio of the slopes for corresponding matrix-matched and solvent standards. Matrix-matched standard solutions were prepared with blank samples and used for quantification by external standard method.

To evaluate the accuracy and precision of this method, recovery was evaluated by spiking blank materials at two different levels (0.04 and 0.4 mg/kg for fresh tea leaves, whereas 0.4 and 1.6 mg/kg for other matrices).

RESULTS AND DISCUSSION

Method Optimization and Validation. A commercial BGB-176 column was chosen for chiral separation and determination of acephate and methemidophos enantiomers by GC-FPD. Gas chromatographic conditions, such as oven temperature program and flow rate of carrier gas, were optimized step by step for quicker analysis (Supporting Information Tables 1−3). Ultimately, satisfactory capacity ($R_{acephate}$ = 1.37 and $R_{methamidophos}$ = 1.97) was obtained for the whole analysis of each enantiomer within 25 min as described above. According to the previous study by Wang,[23] the (+)-form would be eluted from the column first, followed by the (−)-form for both acephate and methamidophos (Figure 2A).

Addition of water to the tea matrix can significantly improve the extraction efficiency.[24,25] In this study, the effects of adding different levels of water (0, 1, 5 mL) on extraction efficiency were investigated in both spiked made tea and positive made tea. The average recoveries of presoaking with 0, 1, and 5 mL of water were 61.3, 52.5, and 38.2% for acephate and 68.6, 60.0, and 42.5% for methamidophos, respectively. The results indicated that addition of water would reduce the recoveries of both pesticides, which is explained by the pesticides going into the water due to their high polarity.[26] However, extraction yield of acephate in positive samples by presoaking was 11.3−13.9 times that without presoaking. Methamidophos was determined with 0.8−1.0 mg/kg by presoaking, whereas it was not detected without presoaking (Supporting Information Table 4). This indicated that presoaking was necessary to facilitate polar pesticide separation from the matrix. However, it is hard to overcome the great loss of acephate and

DOI: 10.1021/jf504916b
J. Agric. Food Chem. 2015, 63, 1300−1308

Table 1. Linear Regression Equations, Correlation Coefficients (r), Recoveries, Matrix Effect (ME), Limits of Detection (LOD), and Limits of Quantitation (LOQ) for Acephate and Methamidophos Enantiomers in Different Tea Matrices

enantiomer	matrix	regression eq	r	ME[a]	spike level (mg/kg)	recovery[b] (%)	LOD (mg/kg)	LOQ (mg/kg)
(+)-acephate	acetone	$y = 887x - 12$	0.9974					
	fresh tea leaves	$y = 1241x + 3$	0.9993	1.40	0.04	51.6 ± 3.5	0.005	0.015
					0.40	57.3 ± 1.8		
	green tea	$y = 925x - 5$	0.9974	1.04	0.4	50.9 ± 3.3	0.1	0.3
					1.6	54.5 ± 2.7		
	black tea	$y = 1505x + 2$	0.9983	1.70	0.4	52.0 ± 3.4	0.03	0.1
					1.6	54.1 ± 2.7		
	spent leaves of green tea	$y = 973x - 6$	0.9968	1.10	0.4	51.2 ± 3.1	0.1	0.3
					1.6	53.7 ± 3.0		
	spent leaves of black tea	$y = 1749x + 2$	0.9994	1.97	0.4	52.6 ± 2.9	0.03	0.1
					1.6	55.3 ± 2.5		
(−)-acephate	acetone	$y = 955x - 7$	0.9994					
	fresh tea leaves	$y = 1384x + 2$	0.9992	1.45	0.04	51.8 ± 3.4	0.005	0.015
					0.40	57.5 ± 2.0		
	green tea	$y = 1015x - 7$	0.9970	1.06	0.4	50.8 ± 3.3	0.1	0.3
					1.6	54.7 ± 2.7		
	black tea	$y = 1585x + 5$	0.9979	1.66	0.4	52.3 ± 3.5	0.03	0.1
					1.6	55.3 ± 2.8		
	spent leaves of green tea	$y = 1108x - 10$	0.9971	1.16	0.4	51.9 ± 3.6	0.1	0.3
					1.6	55.1 ± 2.9		
	spent leaves of black tea	$y = 1891x + 3$	0.9990	1.98	0.4	53.1 ± 3.4	0.03	0.1
					1.6	55.6 ± 2.7		
(+)-methamidophos	acetone	$y = 1725x - 25$	0.9992					
	fresh tea leaves	$y = 1702x + 4$	0.9995	0.99	0.04	58.4 ± 3.4	0.003	0.01
					0.40	65.0 ± 2.0		
	green tea	$y = 1742x + 5$	0.9974	1.01	0.4	58.7 ± 3.6	0.03	0.1
					1.6	62.9 ± 2.9		
	black tea	$y = 2284x + 1$	0.9989	1.32	0.4	59.8 ± 3.5	0.03	0.1
					1.6	63.8 ± 2.7		
	spent leaves of green tea	$y = 1798x + 4$	0.9977	1.04	0.4	58.5 ± 3.8	0.03	0.1
					1.6	62.8 ± 3.0		
	spent leaves of black tea	$y = 2295x + 2$	0.9988	1.33	0.4	59.9 ± 3.6	0.03	0.1
					1.6	64.1 ± 2.9		
(−)-methamidophos	acetone	$y = 1841x - 9$	0.9993					
	fresh tea leaves	$y = 1877x + 3$	0.9997	1.02	0.04	58.7 ± 3.3	0.003	0.01
					0.40	65.3 ± 2.1		
	green tea	$y = 1901x + 2$	0.9985	1.03	0.4	58.9 ± 3.5	0.03	0.1
					1.6	63.2 ± 2.9		
	black tea	$y = 2416x - 1$	0.9991	1.31	0.4	59.8 ± 3.6	0.03	0.1
					1.6	64.6 ± 2.9		
	spent leaves of green tea	$y = 2038x + 2$	0.9979	1.11	0.4	58.8 ± 3.4	0.03	0.1
					1.6	64.1 ± 3.0		
	spent leaves of black tea	$y = 2502x - 2$	0.9994	1.36	0.4	60.0 ± 2.9	0.03	0.1
					1.6	63.9 ± 3.2		

[a]ME. matrix effect. It was calculated by the ratio of slope of matrix and solvent, where matrix suppression takes place with ME <1.00 and enhancement occurs with ME >1.00. [b]Values are presented as the mean ± SD (n = 5).

methamidophos that occurred during extraction from the dried matrix by water presoaking.[27,28] We also investigated ethyl acetate, dichloromethane, and acetone as extraction solvent, and recoveries of acephate and methamidophos enantiomers ranged from 36.1 to 58.9% (Supporting Information Table 5). This result indicated that acetonitrile was the best choice for sample extraction among these solvents, which was in agreement with Kanrar et al.[29] Thus, 1 mL of water was selected to be the addition volume before extraction by acetonitrile. For other tea matrices with certain amounts of water, there is no need of presoaking, and recoveries are similar to made tea samples.

To overcome the interference of coextraction, a mixture of adsorbents (200 mg of PSA, 200 mg of C_{18}, 50 mg of GCB, and 100 mg of $MgSO_4$) was used as a QuEChERS technique to clean up the tea matrix. We investigated the effect of the

DOI: 10.1021/jf504916b
J. Agric. Food Chem. 2015, 63, 1300−1308

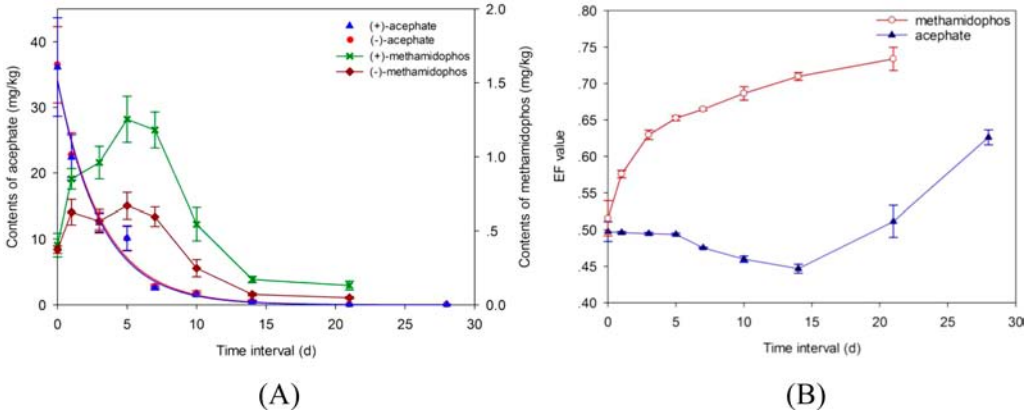

Figure 3. Dissipation of *rac*-acephate in fresh tea leaves (A) and EF value versus time curves of acephate and its metabolite (B). Residues have been corrected with the mean recovery (54% for acephate enantiomers and 62% for methamidophos enantiomers).

proposed adsorbents on the recoveries of acephate and methamidophos enantiomers. Satisfactory recoveries for both pesticides' enantiomers were obtained with the range of 95−98% during cleanup.

The method was validated for fresh tea leaves, made tea, and spent leaves, and the results are presented in Table 1. Recoveries were assessed by spiking the blank samples at two different levels for accuracy evaluation. The recoveries of methamidophos enantiomers spiked in all matrices, which ranged from 58.4 to 65.3%, were higher than those of acephate (50.8−57.5%) ($P < 0.0001$). Low recoveries of acephate (60 ± 10%)[29,30] and methamidophos (26 ± 16%)[30] were also observed in previous studies. All of these studies and our investigation demonstrated that the loss of acephate and methamidophos occurred during extraction, rather than cleanup. The precision was evaluated by the relative standard deviation (RSD) of recoveries for five replications. Acceptable precision for all enantiomers was obtained with RSDs <7%, indicating that this method is consistent. According to European Council No. SANCO 12495-2011,[31] these recoveries could also be acceptable for its consistency. Meanwhile, it is justifiable to correct the results using appropriate recovery factors during quantitation.[32,33] To reflect the actual levels of the residue, data in this study were corrected by the mean recovery of acephate (54%) or methamidophos (62%), respectively, because there is no significant difference of their recoveries among various tea matrices ($P \geq 0.6321$).

Good linearity for each enantiomer was achieved with determination coefficients ≥0.9968. Matrix effects were dependent on enantiomers and tea matrices. Little enhancement or suppression occurred in green tea and its spent leaves for (−)-form enantiomers or in fresh tea leaves for methamidophos enantiomers. Significant matrix enhancement was observed from enantiomers in other matrices. LOQs of enantiomers varied from matrix to matrix. In made tea and spent leaves, although the LOQs (0.1−0.3 mg/kg) were relatively slightly higher, the values have reached the analytical sensitivity in this study because the residues in these samples remained at relatively high levels. Doubled sample amount and lower dissolved volume used in the fresh leaves preparation effectively expanded determination range, resulting in lower LOQs (0.015 mg/kg for acephate enantiomers and 0.01 mg/kg for methamidophos enantiomers). Thus, the proposed method meets the requirements of enantiomer analysis in this study.

Enantioselective Dissipation of Residues in Fresh Tea Leaves. Enantioselective dissipation of acephate and its metabolite, methamidophos, in the tea plantation was investigated, and the results are shown in Figure 3.

Dissipation kinetics of (+)-acephate and (−)-acephate were fitted in a first-order kinetic model with correlation coefficients of 0.9880 and 0.9899, respectively. Half-lives of (+)-acephate and (−)-acephate were about 1.8 and 1.9 days, respectively. The initial deposits of (+)-acephate and (−)-acephate were 36.14 and 36.49 mg/kg, respectively. Then these deposits decreased to 12.50 and 12.76 mg/kg correspondingly 3 days after their field application, which showed a great reduction of approximately 65%. The concentrations of each acephate enantiomer were <10% of initial deposits on day 7, due to the degradation and growth dilution of tea shoots.[34−36]

EF values of acephate decreased from 0.498 to 0.447 in the first 14 days, followed by a significant increase to 0.626 on day 28 ($P < 0.0001$). This phenomenon indicated that faster dissipation of (+)-acephate resulted in a relative enrichment of (−)-acephate in fresh tea leaves within 14 days after application. Acephate would disappear immediately from the surface of the leaves after application and permeated into tissues in 24 h.[37] The enzymatic system was reported to be the most important factor in enantioselective dissipation.[38,39] Therefore, the reduction in the EF curve could be attributed to the effects of various enzymes in the fresh tea leaves. However, it could not be the reason for the increase of EF after day 14, because the enzymatic system in tea fresh leaves should have the same effect on preferential dissipation. Acephate, as a systemic pesticide, can translocate within a tree when it is adsorbed by leaves.[40] Thus, we inferred that enantiotranslocation of acephate was likely to exist and (+)-acephate may prefer to translocate into new leaves during tea growth because new buds have sprouted and grown during this period.

Methamidophos was reported to be one of the most important degradation products of acephate in crops and environments.[37,41] Methamidophos (<1%) is permitted to exist in acephate formulation due to its degradation during storage.[42] Nevertheless, approximately 0.5% of methamidophos was found in acephate formulation (30% EC), from the results obtained from its dilution. Therefore, although 0.40 mg/kg (+)-methamidophos and 0.37 mg/kg (−)-methamidophos in fresh leaves were detected respectively on day 0 (2 h), these compounds most likely originated from the pesticide formulation itself. Subsequently, both (+)-methamidophos

DOI: 10.1021/jf504916b
J. Agric. Food Chem. 2015, 63, 1300−1308

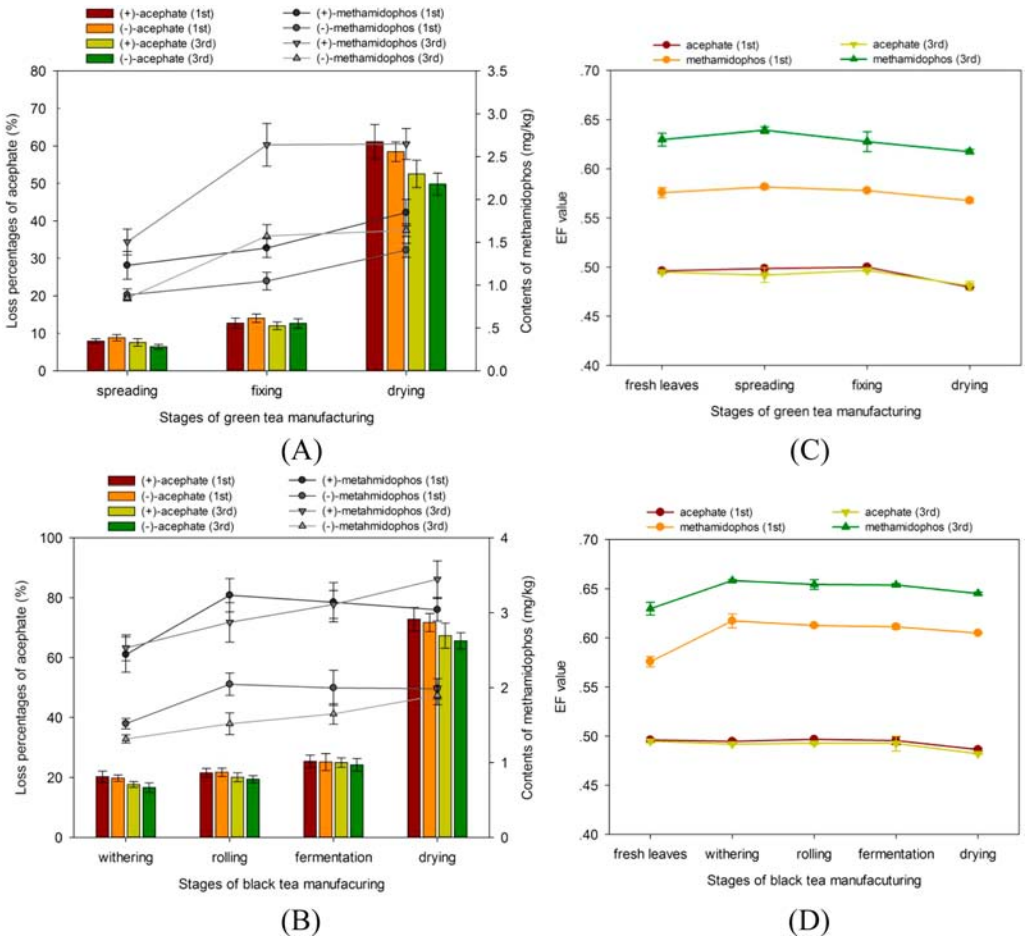

Figure 4. Changes of acephate and its metabolite enantiomers and EF value curves during green tea (A, C) and black tea (B, D) manufacturing. (1) Residues have been corrected with the mean recovery (54% for acephate enantiomers and 62% for methamidophos enantiomers). (2) Moisture content has been taken into account in the loss percentages of acephate enantiomers. (3) First and third stands for the tea manufacturing were conducted on days 1 and 3, respectively.

and (−)-methamidophos reached their highest concentrations (1.25 and 0.67 mg/kg, respectively) on day 5, followed by a gradual dissipation to 0.13 and 0.05 mg/kg on day 21 after application. The increase of methamidophos enantiomers indicated that acephate was degraded into methamidophos in tea cultivation indeed.

The EF value of methamidophos increased with time after application. Wang et al. have reported that there is no interconversion of the (+)-form to the (−)-form or vice versa in soil.[16] In this study, no significant enantioselective dissipation of acephate enantiomers ($P \geq 0.2142$) was found in the first 5 days after application. Thus, compared with its antipode, the higher concentration of (+)-methamidophos during degradation revealed that (−)-methamidophos was preferentially dissipated mainly due to enzyme action.

Effects of Tea Manufacturing on Enantioselective Dissipation. In this study, fresh tea leaves with different deposited pesticides were submitted to green tea and black tea manufacturing. Residues of acephate and methamidophos enantiomer were monitored at each stage of tea manufacturing, and the results are presented in Figure 4. Generally, water evaporation would cause an increase in weight concentration of dry matters, so that residues of pesticides should increase by a similar factor. Thus, the whole amount of residues decreased, although the concentration of the acephate enantiomers showed a slight fluctuation during tea manufacturing. The total loss of acephate enantiomers in black tea was much higher [67.4−72.8 and 65.6−71.8% for (+)-acephate and (−)-acephate, respectively] than green tea [52.6−61.1 and 49.8−58.4% for (+)-acephate and (−)-acephate, respectively]. In addition, fresh leaves collected on day 1 showed a larger loss of enantiomers [61.1−72.8 and 58.4−71.8% for (+)-acephate and (−)-acephate, respectively] than those collected on day 3 [52.6−67.4 and 49.8−65.6% for (+)-acephate and (−)-acephate, respectively].

Among various manufacturing processes, drying made the most important contributions to the dissipation of (+)-acephate and (−)-acephate, leading to a considerable losses of 37.2−48.3%. The loss of acephate enantiomers was much higher than those of carbofuran and carbaryl, which were degraded by 27.0 and 29.0%, respectively, during drying.[43] Drying might facilitate chemical distillation when the water in tea leaves evaporated,[44] wherein the possibility of codistillation depends on the water solubility of the chemicals.[45] Acephate, with extremely high water solubility, is easily absorbed by the water, whether it is inside the leaf tissues or on the surface of tea leaves. Thus, water covolatilization resulted in an impressive reduction of acephate enantiomers. During drying, the EF values of acephate decreased from 0.497−0.500 to 0.479−0.481 when submitted to green tea manufacturing, whereas these values decreased from 0.493−0.495 to 0.482−0.486 in black tea manufacturing. This finding suggested that (+)-acephate was more prone to

DOI: 10.1021/jf504916b
J. Agric. Food Chem. 2015, 63, 1300−1308

Table 2. Residues and EF Values of Acephate and Methamidophos in Made Tea and Corresponding Spent Leaves (n = 5)

		made tea			spent leaves			
matrix[a]	enantiomer	concn ± SD (mg/kg)	corrected concn[b] ± SD (mg/kg)	EF ± SD[c]	concn ± SD (mg/kg)	corrected concn[b] ± SD (mg/kg)	EF ± SD[c]	transfer rate (%)
green tea (first)	(+)-acephate	21.39 ± 1.57	39.61 ± 2.91	0.479 ± 0.002	4.17 ± 0.40	7.72 ± 0.74	0.495 ± 0.003	80.5
	(−)-acephate	23.23 ± 1.28	43.02 ± 2.37		4.26 ± 0.32	7.89 ± 0.59		81.7
	(+)-methamidophos	1.15 ± 0.06	1.85 ± 0.09	0.568 ± 0.002	<LOQ			
	(−)-methamidophos	0.87 ± 0.06	1.40 ± 0.10		<LOQ			
green tea (third)	(+)-acephate	14.60 ± 1.54	27.04 ± 2.85	0.481 ± 0.002	1.79 ± 0.17	3.31 ± 0.31	0.501 ± 0.004	87.7
	(−)-acephate	15.76 ± 1.81	29.19 ± 3.35		1.85 ± 0.15	3.43 ± 0.28		88.3
	(+)-methamidophos	1.64 ± 0.12	2.65 ± 0.19	0.617 ± 0.002	<LOQ			
	(−)-methamidophos	1.02 ± 0.09	1.65 ± 0.15		<LOQ			
black tea (first)	(+)-acephate	14.96 ± 0.92	27.70 ± 1.70	0.486 ± 0.001	1.96 ± 0.05	3.63 ± 0.09	0.492 ± 0.006	86.9
	(−)-acephate	15.80 ± 0.87	29.26 ± 1.61		1.95 ± 0.08	3.61 ± 0.15		87.6
	(+)-methamidophos	1.89 ± 0.49	3.05 ± 0.79	0.605 ± 0.001	0.19 ± 0.02	0.31 ± 0.02	0.610 ± 0.006	89.8
	(−)-methamidophos	1.23 ± 0.14	1.98 ± 0.23		0.12 ± 0.01	0.19 ± 0.02		90.0
black tea (third)	(+)-acephate	10.05 ± 0.42	18.61 ± 0.78	0.482 ± 0.001	1.10 ± 0.09	2.04 ± 0.17	0.487 ± 0.001	89.1
	(−)-acephate	10.80 ± 0.51	20.00 ± 0.94		1.16 ± 0.11	2.15 ± 0.20		89.3
	(+)-methamidophos	2.14 ± 0.12	3.45 ± 0.19	0.645 ± 0.001	0.21 ± 0.01	0.34 ± 0.02	0.621 ± 0.003	90.1
	(−)-methamidophos	1.18 ± 0.09	1.90 ± 0.15		0.13 ± 0.01	0.21 ± 0.01		89.1

[a]First and third in matrix stand for tea manufacturing conducted on days 1 and 3, respectively. [b]These concentrations were corrected by the mean recovery (54% for acephate enantiomers and 62% for methamidophos enantiomers). [c]Enantiometic fractions (EF) = concentration of the (+)-enantiomer/[sum concentrations of the (+)-enantiomer and (−)-enantiomer]. It ranges from 0.000 to 1.000, with EF = 0.500 representing the racemic mixture.

dissipate than its antipode, causing a relative enrichment of (−)-acephate. Such a change in the EF value is similar to that for indoxacarb reported by Zhang et al.,[20] who found that the EF value is much lower in made tea than that in fresh tea leaves collected at the same time. Enantiomers of acephate may demonstrate different distributions inside tea leaves or combinations with compounds of tea leaves. The one close to the surface of leaves or combined lightly would undergo distillation much more easily during water evaporation. However, the reason for the preferential dissipation needs further investigation.

Moreover, compared with spreading in green tea manufacturing, the reduction of (+)-acephate and (−)-acephate during withering in black tea manufacturing (17.6−20.3%) is more than doubled. This finding is in agreement with Hou's suggestion[46] that withering may be the key factor of much lower residues in black tea than in green tea. These two stages resulted in the dissipation of acephate enantiomers because of the physicochemical properties of acephate, such as volatility and water solubility,[19] and residues decreased with increasing time. However, fixing in green tea manufacturing as well as rolling and fermentation in black tea manufacturing did not show much impact on residue concentrations. Little enantioselectivity ($P \geq 0.0619$) was found in all of the stages described above.

By contrast, the concentration of methamidophos enantiomers decreased by 36.4−52.2 and 10.2−30.3% in green tea and black tea, respectively, although an increase in concentration was present during the manufacturing. EF curves of methamidophos demonstrated an increase to 0.582−0.658 during spreading of green tea manufacturing or withering of black tea manufacturing, followed by a slight decrease to 0.568−0.645 during the stages of tea manufacturing. The increase of EF value suggested that (−)-methamidophos was preferentially degraded or dissipated because no enantioselectivity of acephate occurred during withering and spreading. Similar to that on fresh tea leaves, the enantioselectivity of methamidophos was mainly attributed to the effects of enzymes, which had been mentioned above. After spreading, enzymatic activities were inhibited by high temperature of 220−230 °C during fixing, so the key factor of enantioselective dissipation was absent. During rolling, the tea leaf cells were disrupted and chemical compounds, such as polyphenols, started to undergo oxidation, and some competitive effects probably existed among the degradation of methamidophos and other chemical compounds.[47] Thus, methamidophos presented little enantioselectivity ($P \geq 0.0584$) after spreading in green tea manufacturing or withering in black tea manufacturing.

Transfer Rates of Each Enantiomer during Tea Infusion. Residues in made tea would be left in spent leaves during brewing, if they were not transferred into tea infusion, because few of these residues would undergo thermal hydrolysis or escape into atmosphere.[48] In this study, recoveries of acephate and methamidophos enantiomers in tea infusion were too low (<10%; Supporting Information Table 6) for accurate quantification. Therefore, residues in spent tea leaves were analyzed to express the transfer rate indirectly and roughly because satisfactory recoveries of acephate and methamidophos in spent tea leaves were obtained with the range from 51.2 to 64.1% (RSD < 7%). Concentrations and EF values of each enantiomer maintained in made tea and spent leaves are presented in Table 2.

There is a significant difference of EF values for both acephate and methamidiohos between made tea and spent tea leaves ($P \leq 0.0042$). This suggested that significant enantioselectivity of acephate and methamidophos probably occurred during tea infusion. However, the reason for this

DOI: 10.1021/jf504916b
J. Agric. Food Chem. 2015, 63, 1300−1308

change may due to hydrolyzation,[49] which needs further investigation.

Transfer rates of acephate and methamidophos enantiomers were higher than 80.5% and 89.1%, respectively. Theoretically, chemical properties, such as water solubility (W_s) and partition coefficient (K_{ow}), were the key factors of transfer rates of pesticides during tea brewing.[50−52] Therefore, enantiomers of acephate and methamidophos with comparatively high W_s [$W_{s(acephate)}$ = 790 g/L; $W_{s(methamidophos)}$ = 200 g/L] and low K_{ow} [$K_{ow(acephate)}$ = 0.14; $K_{ow(methamidophos)}$ = 0.16] led to a large proportion of 80−90% transferring from made tea to tea infusion.

Interestingly, acephate and methamidophos enantiomers with higher concentration showed lower transfer percentages. Contrary to the present study, Tewary[53] reported that the transfer rate of bifenthrin increased with the residue concentration of made tea, and Chen[54] showed that GA_3 with higher concentration was much more easily extracted during infusion. Such a consequence may be attributed to the high transfer rate, which reached up to approximately 90%. The transfer percentage would no longer be sensitive to W_s when the rate reaches a certain degree.[48] In addition, abundant organic substances, such as polyphenols and caffeine, may promote the saturation of acephate and methamidophos enantiomers in tea infusion, resulting in relatively lower transfer rates.

■ ASSOCIATED CONTENT

Supporting Information

Results of GC optimization for chiral acephate and methamidophos determination (including chiral columns, heating rates, initial temperatures, and flow rates), sample pretreatment optimization for acephate and methamidophos enantiomers (including presoaking and extraction solvent), and recoveries of acephate and methamidophos enantiomers in tea soup using liquid-liquid extraction. This material is available free of charge via the Internet at http://pubs.acs.org.

■ AUTHOR INFORMATION

Corresponding Authors

*(X.L.) Phone: +86 571-86651650. Fax: +86 571-86652004 E-mail: Liuxin@mail.tricaas.com

*(H.C.) E-mail: Thean27@mail.tricaas.com.

Funding

This work was supported by the earmarked fund for Modern Agro-Industry Technology Research System (NYCYTX-26) and Innovative Research Team in Chinese Academy of Agricultural Sciences.

Notes

The authors declare no competing financial interest.

■ REFERENCES

(1) Lambert, J. D.; Elias, R. J. The antioxidant and pro-oxidant activities of green tea polyphenols: A role in cancer prevention. *Arch. Biochem. Biophys.* **2010**, *501*, 65−72.

(2) Basu, A.; Betts, N. M.; Mulugeta, A.; Tong, C.; Newman, E.; Lyons, T. J. Green tea supplementation increases glutathione and plasma antioxidant capacity in adults with the metabolic syndrome. *Nutr. Res. (N.Y.)* **2013**, *33*, 180−187.

(3) Juneja, L. R.; Chu, D. C.; Okubo, T.; Nagato, Y.; Yokogoshi, H. L-Theanine − a unique amino acid of green tea and its relaxation effect in humans. *Trends Food Sci. Technol.* **1999**, *10*, 199−204.

(4) China pesticide information network. http://www.chinapesticide.gov.cn/, 2014.

(5) Kong, Z. Q.; Dong, F. S.; Xu, J.; Liu, X. G.; Li, J.; Li, Y. B.; Tian, Y. Y.; Guo, L. Q.; Shan, W. L.; Zheng, Y. Q. Degradation of acephate and its metabolite methamidophos in rice during processing and storage. *Food Control* **2012**, *23*, 149−153.

(6) Mohapatra, S.; Ahuja, A. K.; Deepa, M.; Sharma, D. Residues of acephate and its metabolite methamidophos in/on mango fruit (*Mangifera indica* L.). *Bull. Environ. Contam. Toxicol.* **2011**, *86*, 101−104.

(7) Wang, Y. S.; Tal, K. T.; Yen, J. H. Separation, bioactivity, and dissipation of enantiomers of the organophosphorus insecticide fenamiphos. *Ecotoxicol. Environ. Saf.* **2004**, *57*, 346−353.

(8) Han, J. J.; Jiang, J. Z.; Su, H.; Sun, M. J.; Wang, P.; Liu, D. H.; Zhou, Z. Q. Bioactivity, toxicity and dissipation of hexaconazole enantiomers. *Chemosphere* **2013**, *93*, 2523−2527.

(9) Zhang, Q.; Wang, C.; Zhang, X. F.; Jin, D. Q.; Huang, C. J.; Zhao, M. R. Enantioselective aquatic toxicity of current chiral pesticides. *J. Environ. Monit.* **2012**, *14*, 465−472.

(10) Nillos, M. G.; Gan, J.; Schlenk, D. Chirality of organophosphorus pesticides: analysis and toxicity. *J. Chromatogr., B* **2010**, *878*, 1277−1284.

(11) Wang, H. Q.; Dong, F. S.; Li, Y. B.; Chen, X.; Cheng, Y. P.; Xiang, W. S.; Zheng, Y. Q. Enantioselective determination of the insecticide indoxacarb in cucumber and tomato by chiral liquid chromatography-tandem mass spectrometry. *Chirality* **2013**, *25*, 350−354.

(12) Sun, D. L.; Pang, J. X.; Qiu, J.; Li, L.; Liu, C. L.; Jiao, B. N. Enantioselective degradation and enantiomerization of indoxacarb in soil. *J. Agric. Food Chem.* **2013**, *61*, 11273−11277.

(13) Celis, R.; Gamiz, B.; Adelino, M. A.; Hermosin, M. C.; Cornejo, J. Environmental behavior of the enantiomers of the chiral fungicide metalaxyl in mediterranean agricultural soils. *Sci. Total Environ.* **2013**, *444*, 288−297.

(14) Miyazaki, A.; Nakamura, T.; Kawaradani, M.; Marumo, S. Resolution and biological activity of both enantiomers of methamidophos and acephate. *J. Agric. Food Chem.* **1988**, *36*, 835−837.

(15) Lin, K.; Zhou, S. S.; Xu, C.; Liu, W. P. Enantiomeric resolution and biotoxicity of methamidophos. *J. Agric. Food Chem.* **2006**, *54*, 8134−8138.

(16) Wang, X. Y.; Li, Z.; Zhang, H.; Xu, J. F.; Qi, P. P.; Xu, H.; Wang, Q.; Wang, X. Q. Environmental behavior of the chiral organophosphorus insecticide acephate and its chiral metabolite methamidophos: enantioselective transformation and degradation in soils. *Environ. Sci. Technol.* **2013**, *47*, 9233−9240.

(17) Satheshkumar, A.; Senthurpandian, V. K.; Shanmugaselvan, V. A. Dissipation kinetics of bifenazate in tea under tropical conditions. *Food Chem.* **2014**, *145*, 1092−1096.

(18) Chen, L.; ShangGuan, L. M.; Wu, Y. N.; Xu, L. J.; Fu, F. F. Study on the residue and degradation of fluorine-containing pesticides in oolong tea by using gas chromatography-mass spectrometry. *Food Control* **2012**, *25*, 433−440.

(19) Gupta, M.; Shanker, A. Fate of imidacloprid and acetamiprid residues during black tea manufacture and transfer into tea infusion. *Food Addit. Contam. Part A* **2009**, *26*, 157−163.

(20) Zhang, X.; Luo, F.; Lou, Z.; Lu, M.; Chen, Z. Simultaneous and enantioselective determination of cis-epoxiconazole and indoxacarb residues in various teas, tea infusion and soil samples by chiral high performance liquid chromatography coupled with tandem quadrupole-time-of-flight mass spectrometry. *J. Chromatogr., A* **2014**, DOI: 10.1016/j.chroma.2014.07.058.

(21) Katagi, T. Isomerization of chiral pesticides in the environment. *J. Pestic. Sci.* **2012**, *37*, 1−14.

(22) Harner, T.; Wiberg, K.; Norstrom, R. Enantiomer fractions are preferred to enantiomer ratios for describing chiral signatures in environmental analysis. *Environ. Sci. Technol.* **2000**, *34*, 218−220.

(23) Wang, X. Y.; Zhang, H.; Xu, H.; Qi, P. P.; Ji, X. F.; Wang, Q.; Wang, X. Q. Direct chiral determination of acephate and its metabolite

DOI: 10.1021/jf504916b
J. Agric. Food Chem. 2015, 63, 1300−1308

methamidophos in vegetables using quechers by gas chromatography-tandem mass spectrometry. *Food Anal. Methods* **2013**, *6*, 133−140.
(24) Cajka, T.; Sandy, C.; Bachanova, V.; Drabova, L.; Kalachova, K.; Pulkrabova, J.; Hajslova, J. Streamlining sample preparation and gas chromatography-tandem mass spectrometry analysis of multiple pesticide residues in tea. *Anal. Chim. Acta* **2012**, *743*, 51−60.
(25) Chen, H. P.; Yin, P.; Wang, Q. H.; Jiang, Y.; Liu, X. A modified quechers sample preparation method for the analysis of 70 pesticide residues in tea using gas chromatography-tandem mass spectrometry. *Food Anal. Methods* **2014**, *7*, 1577−1587.
(26) Obana, H.; Akutsu, K.; Okihashi, M.; Hori, S. Multiresidue analysis of pesticides in vegetables and fruits using two-layered column with graphitized carbon and water absorbent polymer. *Analyst* **2001**, *126*, 1529−1534.
(27) Štajnbaher, D.; Zupančič-Kralj, L. Multiresidue method for determination of 90 pesticides in fresh fruits and vegetables using solid-phase extraction and gas chromatography-mass spectrometry. *J. Chromatogr., A* **2003**, *1015*, 185−198.
(28) Ochiai, N.; Sasamoto, K.; Kanda, H.; Yamagami, T.; David, F.; Tienpont, B.; Sandra, P. Optimization of a multi-residue screening method for the determination of 85 pesticides in selected food matrices by stir bar sorptive extraction and thermal desorption gc-ms. *J. Sep. Sci.* **2005**, *28*, 1083−1092.
(29) Kanrar, B.; Mandal, S.; Bhattacharyya, A. Validation and uncertainty analysis of a multiresidue method for 42 pesticides in made tea, tea infusion and spent leaves using ethyl acetate extraction and liquid chromatography-tandem mass spectrometry. *J. Chromatogr., A* **2010**, *1217*, 1926−33.
(30) Li, H. P.; Li, G. C.; Jen, J. F. Fast multi-residue screening for 84 pesticides in tea by gas chromatography with dual-tower auto-sampler, dual-column and dual detectors. *J. Chin. Chem. Soc.−Taip.* **2004**, *51*, 531−542.
(31) European Council No. SANCO/12495/2011. Method validation and quality control procedures for pesticide residues.
(32) Koesukwiwat, U.; Lehotay, S. J.; Mastovska, K.; Dorweiler, K. J.; Leepipatpiboon, N. Extension of the QuEChERS method for pesticide residues in cereals to flaxseeds, peanuts, and doughs. *J. Agric. Food Chem.* **2010**, *58*, 5950−5958.
(33) Koesukwiwat, U.; Lehotay, S. J.; Leepipatpiboon, N. Fast, low-pressure gas chromatography triple quadrupole tandem mass spectrometry for analysis of 150 pesticide redidues in fruits and vegetables. *J. Chromatogr., A* **2011**, *1218*, 7039−7050.
(34) Chen, Z. M.; Wan, H. B. Degradation of pesticides on plant surfaces and its prediction − a case study on tea plant. *Environ. Monit. Assess.* **1997**, *44*, 303−313.
(35) Bisen, J. S.; Hajra, N. G. Persistence and degradation of some insecticides in darjeeling tea. *J. Plantation Crops* **2000**, *28*, 123−131.
(36) Xia, H.; Ma, X.; Tu, Y. Comparison of the relative dissipation rates of endosulfan pesticide residues between oolong and green tea. *Food Addit. Contam.* **2008**, *25*, 70−75.
(37) Bull, D. L. Fate and efficacy of acephate after application to plants and insects. *J. Agric. Food Chem.* **1979**, *27*, 268−272.
(38) Li, Y.; Dong, F.; Liu, X.; Xu, J.; Han, Y.; Zheng, Y. Chiral fungicide triadimefon and triadimenol: Stereoselective transformation in greenhouse crops and soil, and toxicity to *Daphnia magna*. *J. Hazard. Mater.* **2014**, *265*, 115−123.
(39) Zhang, H.; Wang, X.; Qian, M.; Wang, X.; Xu, H.; Xu, M.; Wang, Q. Residue analysis and degradation studies of fenbuconazole and myclobutanil in strawberry by chiral high-performance liquid chromatography-tandem mass spectrometry. *J. Agric. Food Chem.* **2011**, *59*, 12012−12017.
(40) Gous, S. F.; Richardson, B. Stem injection of insecticides to control herbivorous insects on eucalyptus nitens. *N. Z. Plant Prot.* **2008**, *61*, 174−178.
(41) Kumar, V.; Upadhay, N. Chemical and biochemical mechanistic fate of acephate. *Int. J. Sci. Eng. Res.* **2013**, *4*, 2674−2678.
(42) Lee, H. D.; Kim, K. O.; Rhi, J. H.; Shin, W. C.; Park, H. J.; Lee, S. H.; Park, S. S. Physico-chemical stability of pesticide formulations under different strage conditions. *Korean Pestic. Sci.* **2004**, *8*, 103−106.
(43) Wu, C. C.; Chu, C.; Wang, Y. S.; Lur, H. S. Dissipation of carbofuran and carbaryl on oolong tea during tea bushes, manufacturing and roasting processes. *J. Environ. Sci. Health B* **2007**, *42*, 669−675.
(44) Maguire, R. J. Kinetics of pesticide volatilization from the surface of water. *J. Agric. Food Chem.* **1991**, *39*, 1674−1678.
(45) Karthika, C.; Muraleedharan, N. Influence of manufacturing process on the residues of certain fungicides used on tea. *Toxicol. Environ. Chem.* **2010**, *92*, 1249−1257.
(46) Hou, R. Y.; Hu, J. F.; Qian, X. S.; Su, T.; Wang, X. H.; Zhao, X. X.; Wan, X. C. Comparison of the dissipation behaviour of three neonicotinoid insecticides in tea. *Food Addit. Contam. Part A* **2013**, *30*, 1761−1769.
(47) Lu, Y. L.; Diao, J. L.; Gu, X.; Zhang, Y. F.; Xu, P.; Wang, P.; Zhou, Z. Q. Stereoselective degradation of diclofop-methyl during alcohol fermentation process. *Chirality* **2011**, *23*, 424−428.
(48) Wan, H.; Xia, H.; Chen, Z. Extraction of pesticide residues in tea by water during the infusion process. *Food Addit. Contam.* **1991**, *8*, 497−500.
(49) Zhang, K. K.; Hu, D. Y.; Zhu, H. J.; Yang, J. C.; Wu, J.; He, M.; Jin, L. H.; Yang, S.; Song, B. A. Enantioselective hydrolyzation and photolyzation of dufulin in water. *Chem. Cent. J.* **2013**, *7*, 1−9.
(50) Paramasivam, M.; Chandrasekaran, S. Persistence behaviour of deltamethrin on tea and its transfer from processed tea to infusion. *Chemosphere* **2014**, *111*, 291−295.
(51) Manikandan, N.; Seenivasan, S.; Ganapathy, M. N. K.; Muraleedharan, N. N.; Selvasundaram, R. Leaching of residues of certain pesticides from black tea to brew. *Food Chem.* **2009**, *113*, 522−525.
(52) Jaggi, S.; Sood, C.; Kumar, V.; Ravindranath, S. D.; Shanker, A. Leaching of pesticides in tea brew. *J. Agric. Food Chem.* **2001**, *49*, 5479−5483.
(53) Tewary, D. K.; Kumar, V.; Ravindranath, S. D.; Shanker, A. Dissipation behavior of bifenthrin residues in tea and its brew. *Food Control* **2005**, *16*, 231−237.
(54) Chen, H. P.; Liu, X.; Yang, D.; Yin, P. Degradation pattern of gibberellic acid during the whole process of tea production. *Food Chem.* **2013**, *138*, 976−981.

DOI: 10.1021/jf504916b
J. Agric. Food Chem. 2015, 63, 1300−1308

A metabolomic study can contribute significantly to our understanding of stress in plants and other organisms by identifying various stress-related compounds, such as by-products of stress metabolism, stress signal transducers, and molecules that comprise the acclimation response of plants.[4] This study describes a method that makes use of metabolic profiling and metabolic fingerprinting to obtain a holistic view of stress in plants. This study also includes a detailed pathway analysis. Even with the highest-quality soil and agricultural practices, the impact of stress on a crop can reduce productivity significantly. Thus, diminishing farm land and the potential effects of global climate change on environmental and pathogen or insect-induced stresses provide an increased impetus to understand stress resistance in crop plants.[13] Although much concerning the participation of flavonoids in plant stress is known, the exact function of flavonoid metabolites in a plant's reaction to toxic heavy metals remains a topic of debate.[14] However, it is important to note that not all plants respond to heavy metals in the same manner.[14] This report describes a metabolomic study of burdock roots in response to copper stress.

MATERIALS AND METHODS

Chemicals. Methanol-d_4 (99.8% v/v) and deuterium oxide (99.9% v/v) were obtained from Cambridge Isotope Laboratories, Inc. (Andover, MA). Acetic acid, methylnonadecanoic acid, and 3-(trimethylsilyl)-1-propanesulfonic acid sodium salt were purchased from Sigma–Aldrich (St. Louis, MO). HPLC-grade methanol, water, and methylene chloride were purchased from Burdick & Jackson (Muskegon, MI).

Plant Materials. Burdock plants were cultivated from March to July 2011 in bare ground after seeding. Stress experiments were performed in pots. Eighty plants were transplanted into four pots and allowed to acclimate for 4 weeks. To elicit stress, two pots were spiked with 100 μM $CuCl_2$, while another two pots received a spike of deionized water (DW; control group). Each of the pots received 500 mL of copper solution every 2 days. Plants were harvested after 1 and 6 days, rinsed immediately with water, and divided into groups of eight plants each. Photographs of burdock roots are provided in Supporting Information, Figure S1. Roots cut from the plants were rapidly frozen in liquid nitrogen, chopped into small pieces, freeze-dried, and ground into a fine powder in liquid nitrogen by use of a pestle and mortar. The resulting tissue powder was stored at −80 °C until required for analysis.

Sample Preparation. To obtain a copper-stress-induced metabolic profile, nonpolar and polar metabolites were sequentially extracted from the same sample. This strategy provides a convenient means of replicating the results and performing multivariate data analysis by accounting for the inherent biological variation of independent samples.

For the extraction of nonpolar metabolites, 4 mL of methylene chloride (MC) and 10 μL of 1 mg/mL methylnonadecanoic acid (internal standard) were added to 100 mg of dry, powdered plant material. The mixture was thoroughly mixed at room temperature (RT) for 1 h. The mixtures were centrifuged at 3000 rpm for 10 min at 4 °C. The resulting supernatants were passed through a 0.2-μm poly(tetrafluoroethylene) syringe filter (Merck Millipore, Billerica, MA). The extracts were dried with N_2 gas and dissolved in 200 μL of chloroform for GC–MS analysis. The remaining tissue pellets were extracted with 4 mL of MeOH containing 15 μL of 2 mg/mL sodium 2,2-dimethyl-2-silapentane-5-sulfonate (DSS) in order to profile the polar metabolites. The MeOH extracts were prepared in the same way as the MC phase. Aliquots (500 μL) of the MeOH extracts were transferred to a separate vial for additional analyses. The remaining MeOH extracts were dried with N_2 gas. For NMR analyses, the resulting residue was dissolved in a mixture of 300 μL of methanol-d_4 and 300 μL of 0.2 M sodium phosphate buffer (pH 7) in D_2O. D_2O and DSS provided a field frequency lock and a chemical shift reference (^{1}H, δ 0.00), respectively.

GC–MS Analysis and Data Preprocessing. GC–MS analyses were performed on a 6890 Plus gas chromatograph equipped with a 5973N quadrupole mass spectrometer system (Agilent, Palo Alto, CA). A DB-5 MS capillary column (30 m × 0.25 mm i.d., 0.25 μm film thickness, 5% diphenyl–95% dimethylsiloxane phase) was obtained from J&W Scientific (Folsom, CA). The GC oven temperature was maintained at 60 °C for 2 min, then ramped to 320 °C at 10 °C/min and maintained for 10 min. The sample was injected with a splitting ratio of 1:10. The temperatures of the GC injection port and MS interface were 250 and 280 °C, respectively. Helium was used as the carrier gas at a constant flow rate of 1 mL/min. The mass spectrometer was run in electron impact (EI) mode, with an electron energy of 70 eV. Mass spectra were acquired at 1 scan/s with a full scan range of 50–800 atomic mass units (amu). A freely available mass spectral deconvolution algorithm (automated mass spectral deconvolution and identification system, AMDIS) was used to analyze the data in combination with a filtering algorithm (SpectConnect) for processing of multiple data sets. All GC–MS data were normalized by use of methylnonadecanoic acid as an internal standard.

NMR Analysis and Data Preprocessing. ^{1}H NMR spectra were acquired on a VNMRS 600-MHz NMR spectrometer using a triple-resonance HCN salt-tolerant cold probe (Agilent Technologies Inc., Santa Clara, CA). A NOESYPRESAT pulse sequence was applied to suppress the signals from residual water. For each sample, 64 transients were collected into 67 568 data points with spectral width of 8445.9 Hz, relaxation delay of 2.0 s, acquisition time of 4.00 s, and mixing time of 100 ms. A 0.5-Hz line-broadening function was applied to all spectra prior to Fourier transform (FT). The assignments of NMR signals were based on total correlation spectroscopy (2D ^{1}H–^{1}H TOCSY), heteronuclear single quantum correlations (2D ^{1}H–^{13}C HSQC), and spiking experiments.

All NMR spectra were phased and baseline-corrected by use of Chenomx NMR suite version 7.1 (Chenomx Inc., Edmonton, Alberta, Canada). The regions corresponding to water, methanol, and DSS (4.78–4.85, 3.29–3.37, and 0.00–0.70 ppm, respectively) were excluded, and the remaining spectral regions were divided into 0.005 ppm bins. The spectra were then normalized to the total spectral area and converted to ASCII format. The ASCII files were imported into MATLAB (R2006a; Mathworks, Inc., Natick, MA) and all spectra were aligned by use of the correlation optimized warping method.[15]

NMR Data Processing. The resultant NMR data sets were imported into SIMCA-P version 12.0 (Umetrics, Umeå, Sweden) for chemometric analyses. All imported data were Pareto-scaled for multivariate analyses. Pareto scaling, in which each variable is divided by the square root of the standard deviation, gives greater weight to the variables with larger intensity but gives results that are not as extreme as those obtained with unscaled data. Pareto scaling is typically used when a very large dynamic range exists in the data set.[16,17] Principal component analyses (PCA) were performed to examine the intrinsic variation in the data set and to obtain an overview of the variation among the groups. The quality of the models was described by R^2 and Q^2 values. R^2 is defined as the proportion of variance in the data explained by the models and indicates the goodness of fit. Q^2 is defined as the proportion of variance in the data predictable by the model and indicates predictability.[18]

Metabolites were identified by use of Chenomx Profiler, a module of Chenomx NMR Suite version 7.1, and by analysis of the 2D NMR experimental data. The identities of those metabolites deemed important on the basis of chemometric analyses were confirmed by use of spiking experiments and other references. The quantification of primary metabolites was achieved by use of the 600-MHz library from Chenomx NMR Suite version 7.1, which uses the concentration of a known reference signal (in this case DSS) to determine the concentration of individual compounds. The library is based on a database of 260 individual metabolite spectra acquired with the NOESYPRESAT sequence. Because the secondary metabolites were not contained in this library, their intensities were subjected to two-way analysis of variance (ANOVA).

DOI: 10.1021/jf503193c
J. Agric. Food Chem. 2015, 63, 1309–1317

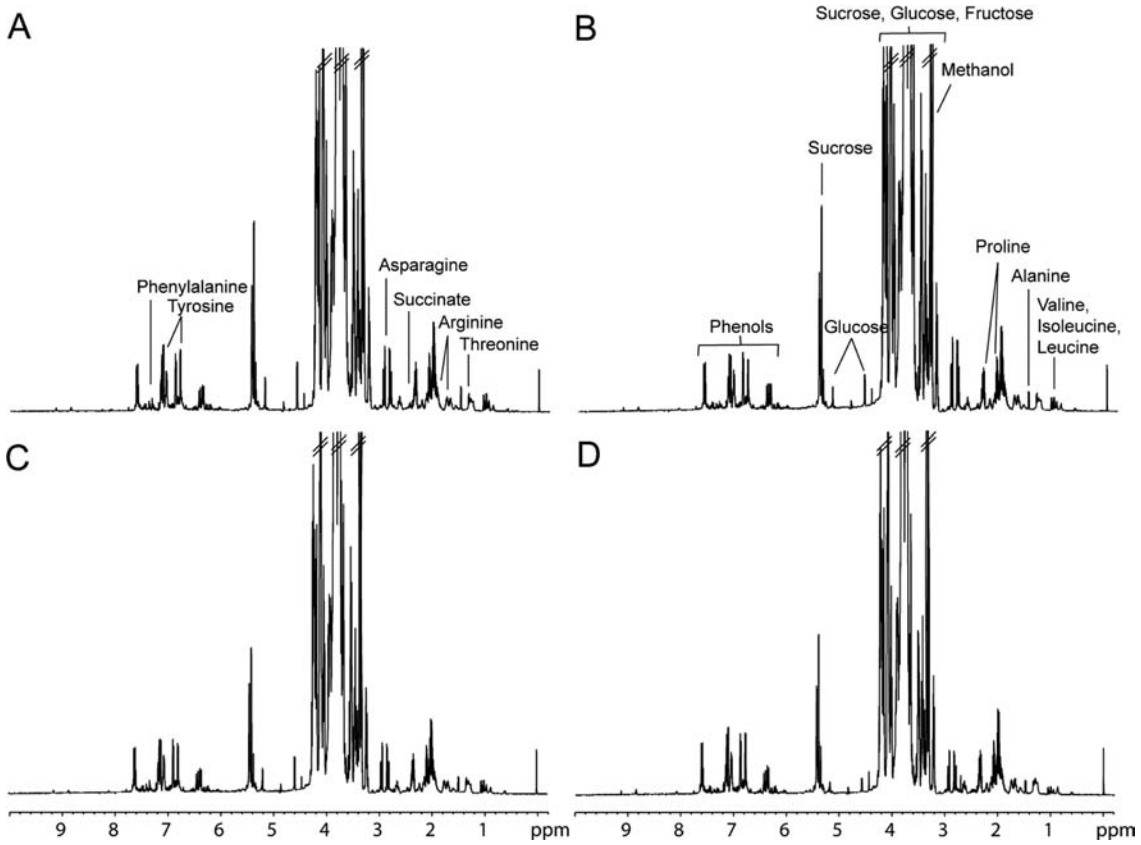

Figure 1. Representative ^{1}H NMR spectra of burdock root extracts. (A) DW treatment for 1 day, (B) DW treatment for 6 days, (C) 100 μM $CuCl_2$ treatment for 1 day, and (D) 100 μM $CuCl_2$ treatment for 6 days.

Targeted Analysis by UPLC/QTRAP-MS. Two plant hormones (jasmonic acid and salicylic acid) and seven fatty acids (myristic acid, palmitic acid, stearic acid, palmitoleic acid, oleic acid, linoleic acid, and linolenic acid) of burdock extracts were analyzed by ultraperformance liquid chromatography (UPLC)/QTRAP-MS. Nine targeted metabolites were prepared by dilution of MC and MeOH fractions of the burdock extracts. Separation of these analytes was performed with an Ekspert ultraLC 100-XL system (Eksigent, Dublin, CA) equipped with a high-strength silica (HSS) T3 C18 column that was 50 × 2.1 mm with a 1.8 μm particle size (Waters, Milford, MA). The column temperature was 40 °C and the autosampler was maintained at 4 °C. Aliquots (5 μL) of sample were injected via the partial loop method. The mobile phase consisted of (A) HPLC-grade water with 0.1% acetic acid and (B) methanol with 0.1% acetic acid. The column was eluted at a flow rate of 0.45 mL/min. For separating plant hormones, the mobile phase was changed from 70% A/30% B at time zero to 1% A/99% B over 3.5 min. To separate the fatty acids, the initial composition of the mobile phase was 15% A/85% B, changing to 1% A/99% B over 3.5 min. In both cases the end gradients remained constant for 0.5 min and then returned to the initial composition over 0.1 min and maintained that mixture for an additional 0.9 min.

This UPLC system was connected to a QTRAP 6500 MS/MS (AB Sciex, Framingham, MA) equipped with an IonDrive Turbo V source operating in negative-ion mode. Two plant hormones and seven fatty acids were detected individually by LC−MS/MS using multiple reaction monitoring (MRM) for the transition of the parent ion to the product ion. The concentration of each compound was then calculated according to calibration curves. The MRM transitions were acquired with the following operational parameters: capillary voltage of −4500 V, nebulizer pressure of 60 psi, drying gas pressure of 60 psi, curtain gas pressure of 30 psi, source temperature of 500 °C, entrance potential (EP) of −10 eV, and dwell time of 20 ms for the monitored transition. To obtain reliable results, specific values of collision energy (CE), declustering potential (DP), and collision cell exit potential (CXP) were used for each targeted metabolite. Data acquisition and processing were performed with Analyst version 1.6 software and MultiQuant version 2.1 software (AB SCIEX, Framingham, MA).

Statistical Methods. Two-way ANOVA was performed with GraphPad Prism version 5.0 (GraphPad Software, Inc., La Jolla, CA) to test the significance of differences in metabolite levels among the control and copper-exposed groups on day 1 versus day 6. Bonferroni's test was performed to determine differences between specific groups. Differences were tested at the 95% probability level ($p < 0.05$).

RESULTS

Polar Metabolite Profiling by Use of NMR. Representative one-dimensional ^{1}H NMR spectra of aqueous burdock extracts are shown in Figure 1. Signals in the sugar region of the NMR spectra were higher than those in the aliphatic and aromatic regions. The majority of the detected metabolites were amino acids and sugars, although some organic acids and phenols were also assigned. The following assignments are based on comparisons with the chemical shifts of standard compounds by use of NMR Suite software (version 7.1; Chenomx) and were confirmed by 2D NMR analyses and spiking experiments: alanine at δ = 1.48 and 3.78; arginine at δ = 1.71, 1.93, 3.22, and 3.76; asparagine at δ = 2.81, 2.94, and 4.02; fructose at δ = 3.48−4.11; glucose at δ = 3.20−3.91, 4.58, and 5.19; isoleucine at δ = 0.95 and 1.02; leucine at δ = 0.97; phenylalanine at δ = 7.33 and 7.38; proline at δ = 2.03, 2.34, 3.32, 3.41, and 4.07; succinate at δ = 2.40; sucrose at δ = 3.41−4.18 and 5.40; threonine at δ = 1.33; tyrosine at δ = 6.79 and 7.12; and valine at δ = 1.00 and 1.05. The characteristic signals in the aromatic region of the spectrum were attributed, by 2D

DOI: 10.1021/jf503193c
J. Agric. Food Chem. 2015, 63, 1309−1317

NMR, to phenols having structures similar to that of caffeic acid (Figure 2).

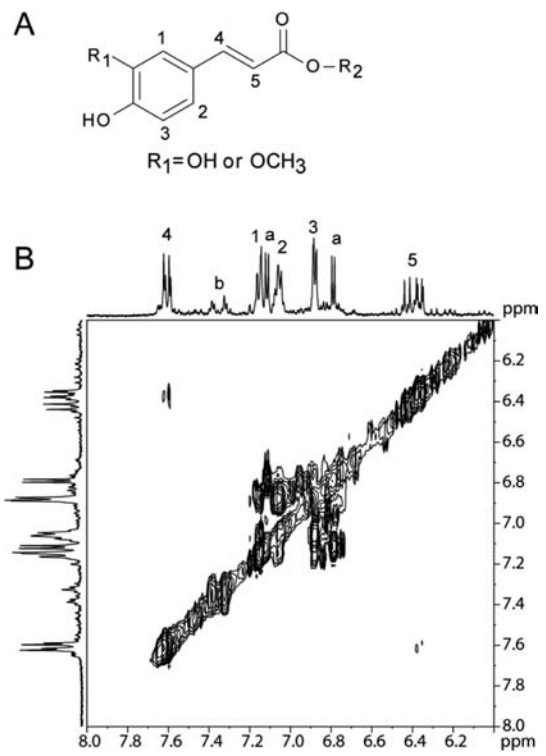

Figure 2. (A) Structure of phenols; (B) expanded TOCSY spectrum. a and b indicate tyrosine and phenylalanine, respectively.

To provide comparative interpretations and a means of visualizing the intrinsic variations and metabolic differences in the burdock root extracts that had been exposed to copper stress, PCA was applied to the ^{1}H NMR data set. The PCA score plot shows significant separation between control and copper-treated groups at different exposure times (Figure 3). The PCA model was established with five components and yielded R^2 and Q^2 values of 0.778 and 0.558, respectively. In this score plot, control groups of burdock root extracts showed no differences between day 1 and day 6. However, groups that had been exposed for 6 days are separated from the other groups by the first component.

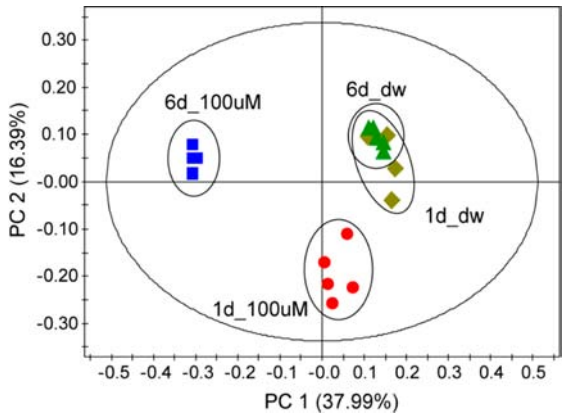

Figure 3. PCA score plot derived from NMR spectra of burdock extracts (R^2 = 0.778, Q^2 = 0.558). The ellipse represents the 95% confidence region for Hotelling's T^2.

To identify the differences in metabolic levels, the aqueous metabolite concentrations were determined by use of the 600-MHz library from Chenomx 7.1. This method compares the integrated intensity of a known reference signal (DSS) with signals derived from a library of compounds containing chemical shifts and peak multiplicities for all of the resonances of that known reference. However, since phenol concentrations could not be determined with Chenomx, peak areas were used instead of compound concentrations.

PCA analyses were performed with quantified metabolites of burdock extracts. The resulting score plot also showed significant separation between control and copper-treated groups (Figure 4). The PCA model was established with three components and yielded R^2 and Q^2 values of 0.926 and 0.803, respectively. In the score plot, control groups of burdock root extracts are separated from copper-treated groups by the first component. Groups with different exposure times (1 or 6 days) are separated by the second component. The loading plot of PCA, in which each data point represents a component (variable), reveals that metabolites that significantly contributed to the intergroup differences were those farthest from the main cluster of metabolites (Figure 4B). Exposure groups were characterized by a lower concentration of all metabolites, except phenols.

Two-way ANOVA was used to assess the significance of observed differences in metabolite levels among the groups. Concentrations of the quantified metabolites and ANOVA results are presented in Table 1. ANOVA showed that, between control and copper-treated groups, all metabolites—with the exception of arginine, proline, and sucrose—were present at significantly different levels.

Nonpolar Metabolite Profiling by Gas Chromatography–Mass Spectrometry. A GC–MS method was used in metabolite profiling of nonpolar extracts. A typical total ion chromatogram of the nonpolar fraction of burdock root extract is shown in Figure 5. Based on spectral similarities and corrections for shifts in retention time, integrated signals of the base peak ions of six major peaks, including the internal standard (IS; methylnonadecanoic acid), were generated by SpectConnect. Identification of the five sample peaks was achieved by searching the NIST05 mass spectral library for compounds matching the experimental fragmented ion to base peak (bp) abundance ratio and retention time. Library matches were validated with standard materials. Thus, the five major peaks were attributed to linoleic acid (9,12-octadecadienoic acid), linolenic acid (9,12,15-octadecatrienoic acid), sitosterol, stigmasterol, and campesterol. The sterol group of the latter three compounds was evidenced by a high-intensity molecular ion. Instead of a molecular ion, compounds containing a fatty acid group yielded an $[M - 15]^+$ ion through the loss of a methyl group.

All mass spectral peaks were normalized by use of methylnonadecanoic acid as an internal standard. Two-way ANOVA was performed to determine the significance of differences in normalized peak intensities. Note that the peak areas used in the ANOVA represented the relative concentration of each metabolite, not the absolute concentration. Nevertheless, relative values can be used to compare among samples. The differences between the copper-treated groups and the controls, determined by Bonferroni post hoc tests, are shown in Figure 6. All five of the metabolites displayed a

DOI: 10.1021/jf503193c
J. Agric. Food Chem. 2015, 63, 1309–1317

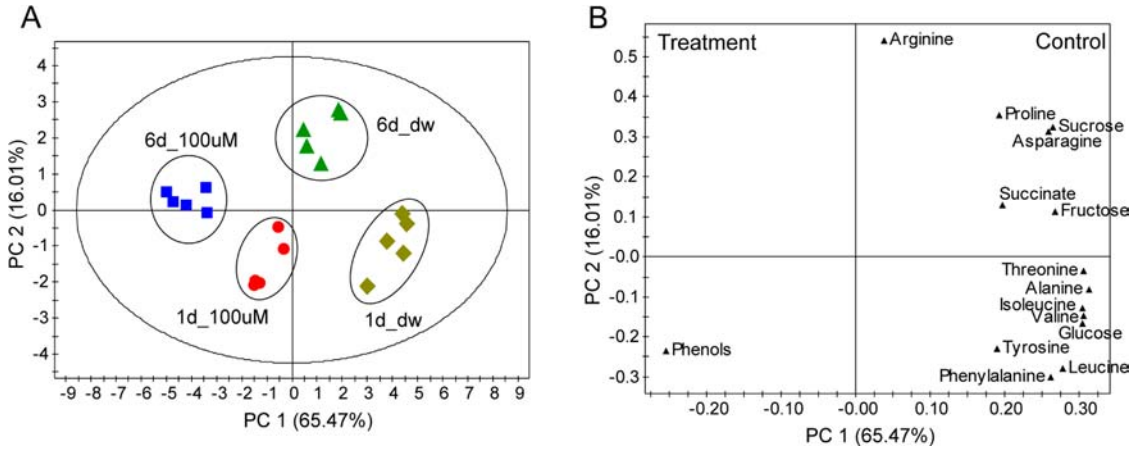

Figure 4. (A) PCA score plot (R^2 = 0.926, Q^2 = 0.803) and (B) loading scatter plot of quantified metabolites in burdock extracts. The ellipse represents the 95% confidence region for Hotelling's T^2.

Table 1. Identification and Quantification of Metabolites from ^{1}H NMR Spectra of Burdock Extracts

	treatment for 1 day			treatment for 6 days					
metabolite[a]	DW[b] (μM)	100 μM $CuCl_2$ (μM)	x-fold change	DW (μM)	100 μM $CuCl_2$ (μM)	x-fold change	interaction (p)[c]	day factor (p)	treatment factor (p)
alanine	591 ± 30.3	382 ± 11.2	0.65***	286 ± 30.2	223 ± 27.4	0.78***	0.0201	<0.0001	<0.0001
arginine	2680 ± 490	2380 ± 432	0.89	3250 ± 316	2890 ± 213	0.89	0.866	0.0056	0.0709
asparagine	7210 ± 353	5360 ± 206	0.74***	8340 ± 345	4290 ± 195	0.51***	<0.0001	0.795	<0.0001
fructose	19000 ± 3230	16600 ± 1310	0.88	20200 ± 1370	7270 ± 456	0.36***	<0.0001	0.0002	<0.0001
glucose	6380 ± 246	4070 ± 391	0.64***	4030 ± 151	1710 ± 156	0.43***	0.981	<0.0001	<0.0001
isoleucine	240 ± 11.9	170 ± 13.5	0.71***	176 ± 14.7	67.9 ± 3.75	0.38***	0.002	<0.0001	<0.0001
leucine	134 ± 18.1	82 ± 11.3	0.61***	64.7 ± 14.4	22.2 ± 7.27	0.34***	0.447	<0.0001	<0.0001
phenylalanine	304 ± 107	259 ± 45	0.85***	207 ± 22.3	147 ± 49.6	0.71**	0.0414	<0.0001	<0.0001
proline	11000 ± 1290	8930 ± 454	0.81	11100 ± 549	9720 ± 643	0.88	0.323	0.251	0.0002
succinate	61.5 ± 1.65	28.5 ± 7.29	0.46***	46.2 ± 4.04	44.5 ± 1.45	0.96***	<0.0001	0.858	<0.0001
sucrose	13300 ± 606	9300 ± 417	0.70	13700 ± 597	9610 ± 718	0.70	0.871	0.210	<0.0001
threonine	345 ± 24.6	283 ± 11.6	0.82*	307 ± 14.2	204 ± 24.6	0.67***	0.0329	<0.0001	<0.0001
tyrosine	3010 ± 110	2300 ± 111	0.77***	2260 ± 69.4	2450 ± 292	1.08	<0.0001	0.0011	0.0034
valine	407 ± 18.1	292 ± 17.1	0.72***	295 ± 10.8	151 ± 14.5	0.51***	0.0510	<0.0001	<0.0001
phenols[d]	4.02 ± 0.107	4.41 ± 0.317	1.10	3.77 ± 0.212	4.92 ± 0.16	1.30**	0.0012	0.165	<0.0001

[a]Identification and quantification of metabolites were performed with the Chenomx software. Concentrations are indicated as mean ± standard deviation. [b]DW, deionized water (control treatment). [c]P values are the result of two-way ANOVA using GraphPad Prism 5.0. [d]Phenols were assigned by use of standard compounds and 2D NMR data with peak intensities instead of actual concentrations.

significance of $p < 0.05$. Levels of fatty acids, including both linoleic acid and linolenic acid, were significantly higher in extracts of burdock roots that had been exposed to copper for 6 days, while levels of sterols such as sitosterol, stigmasterol, and campesterol were significantly lower than those of the control group.

Targeted Analysis by UPLC/QTRAP-MS. Various primary metabolites—including amino acids, organic acids, and sugars—were detected in NMR analyses of methanolic burdock extracts. However, plant hormones that are known to protect plants from oxidative damage associated with a variety of stresses were not evident in the NMR data. Therefore, targeted analyses of jasmonic acid and salicylic acid were conducted by use of UPLC/QTRAP-MS. In addition, among the various fatty acids in the extracts, only linoleic acid and linolenic acid were detected in the GC–MS analyses. To identify not only unsaturated fatty acids but also saturated fatty acids, targeted analyses of myristic acid, palmitic acid, stearic acid, palmitoleic acid, oleic acid, linoleic acid, and linolenic acid were also performed.

MS/MS analyses of standard compounds were first conducted with the QTRAP system with flow injection via syringe pump. The selected fragment ions (Table 2) allowed for selective detection of two plant hormones and seven fatty acids by LC-MS/MS with MRM. MRM transitions were primarily optimized for deprotonated molecular ions $[M - H]^-$. All resulting calibration curves showed high linearity (R^2 > 0.993). The concentrations of metabolites calculated from the calibration curves are presented in Figure 7. A two-way ANOVA test was performed using Prism version 5.0 (GraphPad Software, Inc.) to determine the significance of differences in metabolite levels among the groups. Of the plant hormones, the concentrations of jasmonic acid were lower than the limit of quantitation in all groups and would therefore be less than 5 μg/mL in the original methanolic extract. The concentration of salicylic acid in the copper-treated groups was significantly higher than that of the control groups after the 6-day exposure period. Levels of saturated fatty acids (myristic acid and stearic acid) did not differ significantly between copper-treated and control groups. Only palmitic acid exhibited an increase in

DOI: 10.1021/jf503193c
J. Agric. Food Chem. 2015, 63, 1309–1317

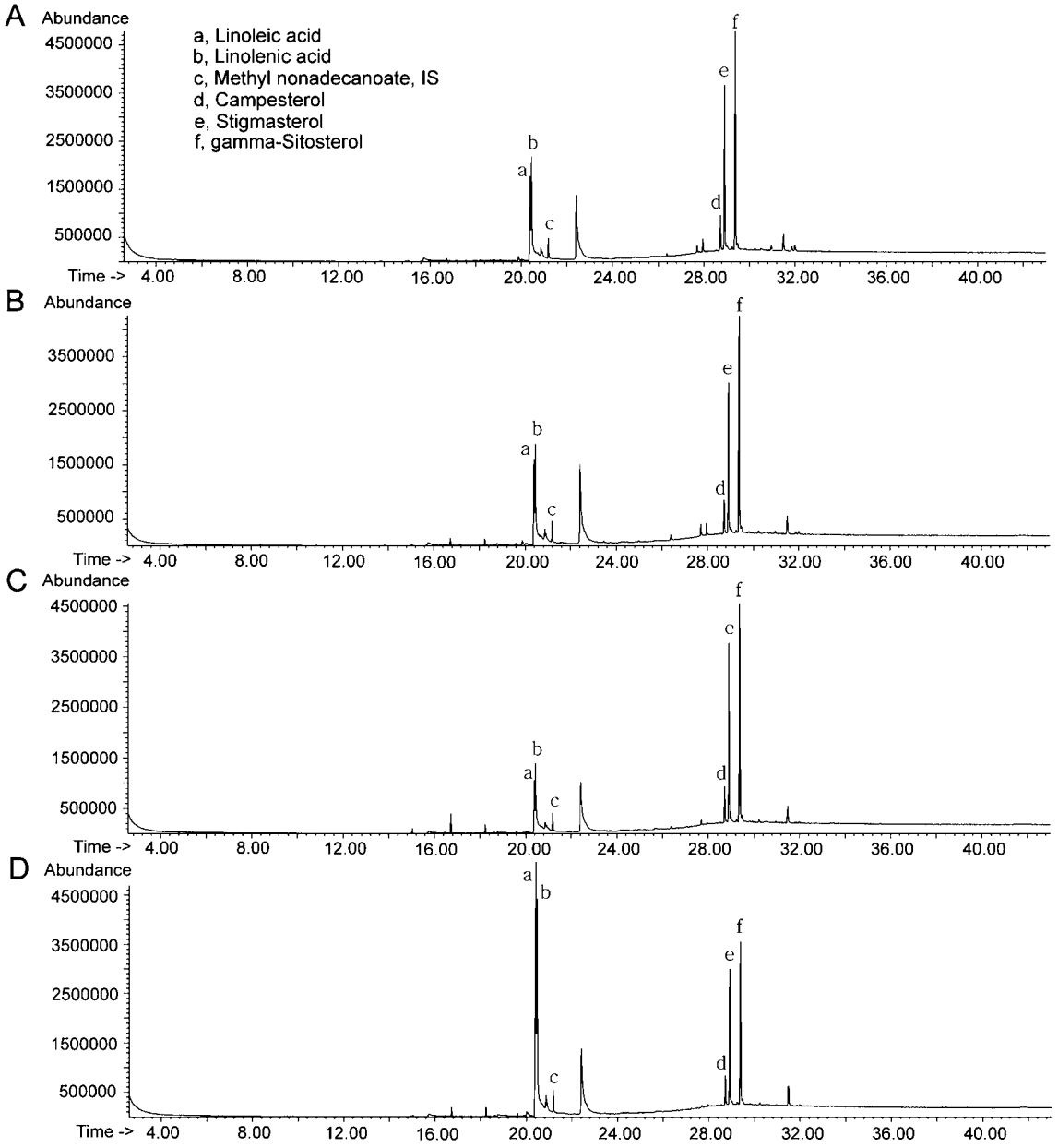

Figure 5. Representative GC−MS chromatograms of burdock extracts. (A) DW treatment for 1 day, (B) 100 μM $CuCl_2$ treatment for 1 day, (C) DW treatment for 6 days, and (D) 100 μM $CuCl_2$ treatment for 6 days.

concentration following copper exposure. Conversely, concentrations of all unsaturated fatty acids (palmitoleic acid, oleic acid, linoleic acid, and linolenic acid) were significantly higher in the copper-treated groups.

DISCUSSION

Generally, the average copper concentration in the dry mass of untreated plant tissue is 10 mg/kg.[19,20] Halasz et al.[21] reported a copper concentration of 21 mg/kg in burdock roots from an uncontaminated site in Hungary. Copper levels above 20−30 mg/kg can be toxic in plants.[20] Roots of *Typha latifolia* contained copper concentrations of 8 and 450−580 mg/kg before and after incubation in a solution of 100 μM copper, respectively.[20] Even though the amount of copper in root extracts was not measured directly, levels of copper concentrations of burdock roots used in this study were expected to be higher than the 20−30 mg/kg toxic level in plants. High copper concentration of 100 μM $CuCl_2$ was selected to induce the metabolic changes in burdock roots under copper stress. It was previously reported that copper concentration of 100 μM or higher was used to identify the effect of copper stress in other plants such as *Vicia faba* L.,[22] *Typha latifolia*,[23] maize,[24] and so on. Growth was significantly inhibited and important cellular processes were impaired in plants containing high copper concentrations. The goals of this study were to examine the metabolic changes in burdock roots in response to copper stress and to understand the metabolic pathway associated with copper stress in burdock roots through polar and nonpolar metabolite profiling.

NMR data acquired on the polar extract showed clear differences between control and exposed groups. In a PCA score plot derived from ^{1}H NMR spectra, the controls were grouped together and the copper-treated groups (6-day exposure) were clearly separated. Conversely, a PCA score

DOI: 10.1021/jf503193c
J. Agric. Food Chem. 2015, 63, 1309−1317

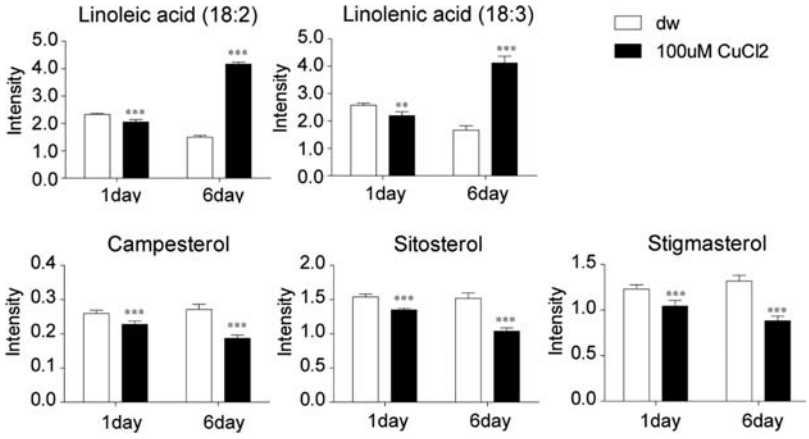

Figure 6. Quantification of identified metabolites by two-way ANOVA of GC−MS data of burdock extracts. Error bars indicate means ± standard deviation. Two-way ANOVA tests (copper treatment × time) yielded significant differences in the levels of all metabolites ($P \leq 0.0002$). ***$p <$ 0.001 as determined by Bonferroni post hoc tests using GraphPad Prism 5.0.

Table 2. Specific Fragment Ions and Calibration Parameters for Targeted Metabolites

targeted metabolites	dilution degree	MRM	DP[a] (eV)	CE[a] (eV)	CXP[a] (eV)	retention time (min)	linear range (μg/mL)	R^2
				Plant Hormones				
jasmonic acid	×10	209/58.9	−25	−16	−7	2.58	0.5−50	0.999
salicylic acid	×10	137/92.9	−20	−22	−11	1.78	0.5−50	0.999
				Fatty Acids				
myristic acid	×10	227/209	−95	−28	−21	1.73	20−500	0.997
palmitic acid	×10	255/237	−95	−28	−15	2.4	20−1000	0.999
stearic acid	×10	283/265	−115	−32	−15	3.11	50−2000	0.997
palmitoleic acid	×100	253/235	−105	−26	−13	1.92	10−2000	0.994
oleic acid	×100	281/263	−125	−28	−19	2.58	20−1000	0.999
linoleic acid	×1000	279/261	−105	−24	−29	2.16	100−2000	0.997
linolenic acid	×1000	277/233	−105	−22	−21	1.83	20−1000	0.997

[a]DP, declustering potential; CE, collision energy; CXP, collision cell exit potential.

plot derived from specific, targeted profiles showed slight differences in the patterns of control groups. On the basis of NMR spectra, sugars accounted for the majority of polar compounds in the burdock extracts. However, only free sugars, such as sucrose, glucose, and fructose, were identified from the Chenomx library. Thus, it is likely that other bound sugars and polyols were detected in the polar extracts but did not affect the separation between control groups.

The levels of most primary metabolites identified in the NMR data decreased after exposure to copper stress. Generally, heavy metals such as Cu are essential for normal plant growth and development.[25] However, excessive concentrations of heavy metals in the soil can lead to toxicity symptoms, inhibit growth, and induce metabolic disorders.[26] High concentrations of heavy metals in plant tissues can disrupt nutrient metabolism, resulting in abnormal growth.[27] The inhibition of growth may result in the observed decrease in the levels of primary metabolites (free sugars, amino acids, and organic acids) in the copper-treated burdock roots. A plant's response to metal toxicity can be expressed in a variety of ways, such as metal ion chelation. Chelation of metals in the cytosol by high-affinity ligands is a potentially important mechanism of heavy-metal detoxification and tolerance.[25] Histidine is particularly important in the chelation of metal.[26]

Phenolic metabolites were detected in polar metabolite profiling based on NMR. The observed phenolic compounds were found to be similar to the structure of caffeic acid through 2D NMR analysis. Caffeic acid derivatives are typically included in phenylpropanoids, which have important functions in stress defense mechanism, and the levels of caffeic acid derivatives in burdock root increased following copper exposure. Increased production of ROS, followed by primary defense reactions, is associated with production of phytoalexin, activation of the general phenylpropanoid pathway, and induction of lignin biosynthesis.[4,26] Phenylpropanoids are precursors of lignins, which are an integral part of the stress defense mechanism, especially at the root level, where such materials can affect cell wall composition and stiffness.[12] Caffeic acid derivatives of phenylpropanoids would be expected to increase as a part of the burdock's defense response. In addition, salicylic acid, methyl salicylate, jasmonic acid, methyl jasmonate, and other small molecules produced as a result of stress can also serve as signaling molecules that activate systemic defense mechanisms and acclimation responses.[4] These plant hormones were not detected in the above NMR analyses because of the low sensitivity of the technique. However, targeted UPLC/QTRAP-MS data showed that levels of jasmonic acid and salicylic acid in the copper-treated groups were twice those of controls.

Nonpolar metabolite profiling of the MC phase of burdock extracts by use of GC−MS showed high levels of two unsaturated fatty acids (linoleic acid and linolenic acid) and three sterols (campesterol, sitosterol, and stigmasterol). Fatty acids and sterols with phospholipids are primary components of the plasma membrane. Because the cell comes into contact with its environment via the plasma membrane, the adaptability and flexibility of the membrane is vital for cell survival.[28] Therefore,

DOI: 10.1021/jf503193c
J. Agric. Food Chem. 2015, 63, 1309−1317

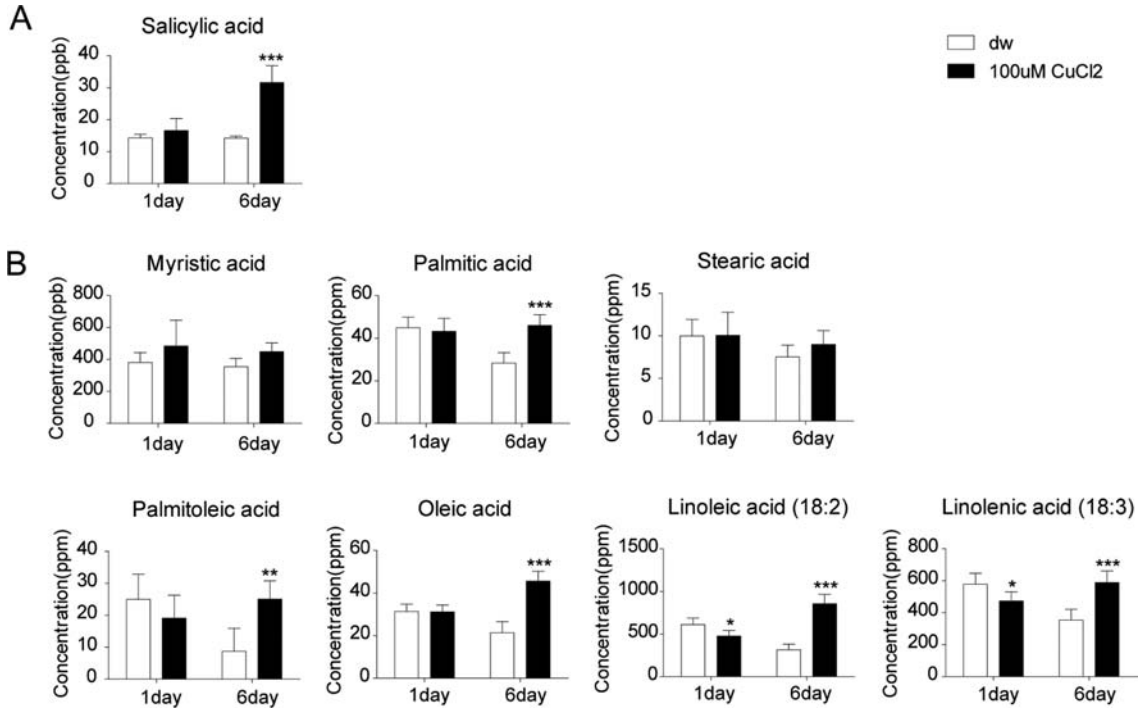

Figure 7. Quantification of identified metabolites by two-way ANOVA on Qtrap-MS data of burdock extracts. Error bars indicate means ± standard deviation. (A) Two-way ANOVA (copper treatment × time) yielded a significant difference in the level of salicylic acid ($P = 0.0001$). (B) Two-way ANOVA revealed significant differences in the levels of five fatty acids ($P \leq 0.0029$). ***$p < 0.001$ as determined by Bonferroni post hoc tests using GraphPad Prism 5.0.

the plant plasma membrane may be regarded as the first "living" structure that is exposed to heavy metal toxicity.[25] The function of the plasma membrane can be rapidly affected by heavy metals, as evidenced by increased cell leakage in the presence of high concentrations of metals, particularly copper.[25] Changes in the composition of the plasma membrane, such as relative levels of sterols and fatty acids, may contribute to changes in membrane fluidity and permeability and can be used as a mechanism of stress adaptation.[28,29]

In the above results, the levels of linoleic acid, linolenic acid, and other unsaturated fatty acids increased following copper exposure, although the presence of other fatty acids was not evident in the GC−MS data. However, targeted UPLC/QTRAP-MS analyses revealed significant changes in the concentrations of various fatty acids as a result of copper exposure. Although the level of palmitic acid increased significantly with copper exposure, the levels of myristic acid and stearic acid were unchanged. However, the levels of all unsaturated fatty acids (palmitoleic acid, oleic acid, linoleic acid, and linolenic acid) increased significantly with copper treatment. This high level of membrane lipid unsaturation is thought to help maintain the fluidity necessary for proper membrane function, which in turn can contribute to cell expansion and plant growth.[29] The ability to adjust membrane lipid fluidity by changing levels of unsaturated fatty acids is a mechanism for stress acclimation in plants. These adjustments are facilitated by the regulated activity of fatty acid desaturases.[13]

Sterol levels (campesterol, sitosterol, and stigmasterol) also decreased following the exposure of burdock roots to copper ion. Sterols are synthesized via the mevalonate pathway of isoprenoid metabolism.[30] The relative levels of stigmasterol, sitosterol, and campesterol have been proposed to influence the properties of cell membranes, particularly in relation to various stresses.[30,31] However, there were no obvious differences in the ratios of these three sterols between the copper-treated and control groups. Although membrane permeability increases according to the relative levels of the three sterols by campesterol < sitosterol < stigmasterol,[30] the observed decrease in concentrations of these three sterols was uniform across all three sterols at approximately 1.5-fold. Therefore, in the copper stress response of burdock roots, sterols may influence the properties of the plasma membrane through changes in their overall levels, not their relative ratios.

In this study, extracts from burdock roots exposed to copper for 1 or 6 days were compared and characterized by metabolite profiling with complementary analyses of ^{1}H NMR, GC−MS, and UPLC/QTRAP-MS data. Changes in primary metabolite and phenol concentrations may result from heavy-metal stress-induced growth inhibition and activation of the phenylpropanoid pathway, respectively. Conversely, changes in levels of salicylic acid and unsaturated fatty acids may result from damage to the cell membrane and/or loss of membrane integrity. This study demonstrates that metabolomic profiling is an effective analytical approach to understand the metabolic pathway(s) associated with copper stress in burdock roots.

■ ASSOCIATED CONTENT

Supporting Information

One figure with pictures of burdock roots following incubation in DW or 100 μM $CuCl_2$ for 1 day or 6 days. This material is available free of charge via the Internet at http://pubs.acs.org.

DOI: 10.1021/jf503193c
J. Agric. Food Chem. 2015, 63, 1309−1317

AUTHOR INFORMATION

Corresponding Authors

*(G.-S.H.) Phone: +82-2-6908-6200, fax: +82-2-6908-6239, e-mail: gshwang@kbsi.re.kr.

*(D.H.R.) Phone: +82-31-290-5931, fax: +82-31-290-5976, e-mail: dhryu@skku.com.

Funding

This study was supported by a grant from the Korea Basic Science Institute (T35622) and the National Research Foundation of Korea Grant, funded by the Korean Government (MSIP).

Notes

The authors declare no competing financial interest.

REFERENCES

(1) Chen, F. A.; Wu, A. B.; Chen, C. Y. The influence of different treatments on the free radical scavenging activity of burdock and variations of its active components. *Food Chem.* **2004**, *86*, 479−484.

(2) Ferracane, R.; Graziani, G.; Gallo, M.; Fogliano, V.; Ritieni, A. Metabolic profile of the bioactive compounds of burdock (*Arctium lappa*) seeds, roots and leaves. *J. Pharm. Biomed. Anal.* **2010**, *51*, 399−404.

(3) Chan, Y. S.; Cheng, L. N.; Wu, J. H.; Chan, E.; Kwan, Y. W.; Lee, S. M.; Leung, G. P.; Yu, P. H.; Chan, S. A review of the pharmacological effects of *Arctium lappa* (burdock). *Inflammopharmacology* **2011**, *19*, 245−254.

(4) Shulaev, V.; Cortes, D.; Miller, G.; Mittler, R. Metabolomics for plant stress response. *Physiol. Plant.* **2008**, *132*, 199−208.

(5) Chaffai, R.; Elhammadi, M. A.; Seybou, T. N.; Tekitek, A.; Marzouk, B.; El Ferjani, E. Altered fatty acid profile of polar lipids in maize seedlings in response to excess copper. *J. Agron. Crop Sci.* **2007**, *193*, 207−217.

(6) Zhang, L.; Liu, X.; You, L.; Zhou, D.; Wu, H.; Li, L. Metabolic responses in gills of Manila clam *Ruditapes philippinarum* exposed to copper using NMR-based metabolomics. *Mar. Environ. Res.* **2011**, *72*, 33−39.

(7) Skórzyńska-Polit, E.; Pawlikowska-Pawlęga, B.; Szczuka, E.; Drążkirwicz, M.; Krupa, Z. The activity and localization of lipogenases in *Arabidopsis thaliana* under cadmium and copper stresses. *Plant Growth Regul.* **2006**, *48*, 29−39.

(8) Cecconi, I.; Scaloni, A.; Rastelli, G.; Moroni, M.; Vilardo, P. G.; Costantino, L.; Cappiello, M.; Garland, D.; Carper, D.; Petrash, J. M.; Del Corso, A.; Mura, U. Oxidative modification of aldose reductase induced by copper ion. *J. Biol. Chem.* **2002**, *277*, 42017−42027.

(9) Jung, Y.; Lee, J.; Kim, H. K.; Moon, B. C.; Ji, Y.; Ryu, D. H.; Hwang, G. S. Metabolite profiling of *Curcuma* species grown in different regions using ^{1}H NMR spectroscopy and multivariate analysis. *Analyst* **2012**, *137*, 5597−5606.

(10) Kim, H. K.; Choi, Y. H.; Verpoorte, R. NMR-based metabolomic analysis of plants. *Nat. Protoc.* **2010**, *5*, 536−549.

(11) Bailey, N. J. C.; Oven, M.; Holmes, E.; Nicholson, J. K.; Zenk, M. H. Metabolomic analysis of consequences of cadmium exposure in *Silene cucunalus* cell cultures via ^{1}H NMR spectroscopy and chemometrics. *Phytochemistry* **2003**, *62*, 851−858.

(12) Arbona, V.; Manzi, M.; de Ollas, C.; Gómez-Cadenas, A. Metabolomics as a tool to investigate abiotic stress tolerance in plants. *Int. J. Mol. Sci.* **2013**, *14*, 4885−4911.

(13) Upchurch, R. G. Fatty acid unsaturation, mobilization, and regulation in the response of plants to stress. *Biotechnol. Lett.* **2008**, *30*, 967−977.

(14) Pawlak-Sprada, S.; Stobiecki, M.; Deckert, J. Activation of phenylpropanoid pathway in legume plants exposed to heavy metals. Part II. Profiling of isoflavonoids and their glycocongugates induced in roots of lupine (*Lupinus luteus*) seedlings treated with cadmium and lead. *Acta Biochim. Polon.* **2011**, *58*, 217−223.

(15) Skov, T.; van den Berg, F.; Tomasi, G.; Bro, R. Automated alignment of chromatographic data. *J. Chemom.* **2006**, *20*, 484−497.

(16) Eriksson, L.; Johansson, E.; Kettaneh-Wold, N.; Trygg, J.; Wikström, C.; Word, S. Centering and scaling. In *Multi- and Megavariate Data Analysis: Basic Principles and Applications*, 2nd ed.; Umetrics Academy: Umea, Sweden, 2006; Vol. *10*, pp 207−219.

(17) Loo, R. L.; Coen, M.; Ebbels, T.; Cloarec, O.; Maibaum, E.; Bictash, M. Metabolic profiling and population screening of analgesic usage in nuclear magnetic resonance spectroscopy-based large-scale epidemiologic studies. *Anal. Chem.* **2009**, *81*, 5119−5129.

(18) Hong, Y. S.; Ahn, Y. T.; Park, J. C.; Lee, J. H.; Lee, H.; Huh, C. S.; Kim, D. H.; Ryu, D. H.; Hwang, G. S. ^{1}H NMR-based metabonomic assessment of probiotic effects in a colitis mouse model. *Arch. Pharm. Res.* **2010**, *33*, 1091−1101.

(19) Marschner, H. *Mineral Nutrition in Higher Plants*, 2nd ed.; Academic Press: San Diego, CA, 1995; pp 379−396.

(20) Lyubenova, L.; Bipuah, H.; Belford, E.; Michalke, B.; Winkler, B.; Schröder, P. Comparative study on the impact of copper suphate and copper nitrate on the detoxification mechanisms in *Typha latifolia*. *Environ. Sci. Pollut. Res.* **2014**, DOI: 10.1007/s11356-014-3402-x.

(21) Halasz, J. L.; Balázsy, S.; Kolesnyk, A.; Krausz, E. The metal uptake of plants on the landfill sites in Bereg County. *Stud. Univ. "Vasile Goldis", Ser. Stiint. Vietii* **2012**, *22*, 217−223.

(22) Kasim, W. A. The correlation between physiological and structural alterations induced by copper and cadmium stress in broad beans (*Vicia faba* L.). *Egypt. J. Biol.* **2005**, *7*, 20−32.

(23) Lyubenova, L.; Bipuah, H.; Belford, E.; Michalke, B.; Winkler, B.; Schröder, P. Comparative study on the impact of copper sulphate and copper nitrate on the detoxification mechanisms in *Typha latifolia*. *Environ. Sci. Pollut. Res.* **2015**, *22*, 657−666.

(24) Doncheva, S.; Stoyanova, Z.; Georgieva, K.; Nedeva, D.; Dikova, R.; Zehirov, G.; Nikolova, A. Exogenous succinate increases resistance of maize plants to copper stress. *J. Plant Nutr. Soil Sci.* **2006**, *169*, 247−254.

(25) Hall, J. L. Cellular mechanisms for heavy metal detoxification and tolerance. *J. Exp. Bot.* **2002**, *53*, 1−11.

(26) Jahangir, M.; Abdel-Farid, I. B.; Choi, Y. H.; Verpoorte, R. Metal ion-inducing metabolite accumulation in *Brassica rapa*. *J. Plant Physiol.* **2008**, *165*, 1429−1437.

(27) Guo, T. R.; Zhang, G. P.; Zhang, Y. H. Physiological changes in barley plants under combined toxicity of aluminum, copper and cadmium. *Colloids Surf., B* **2007**, *57*, 182−188.

(28) Turk, M.; Montiel, V.; Žigon, D.; Plemenitaš, A.; Ramos, J. Plasma membrane composition of *Debaryomyces hansenii* adapts to changes in pH and external salinity. *Microbiology* **2007**, *153*, 3586−3592.

(29) López-Pérez, L.; Martínez-Ballesta, M.; del, C.; Maurel, C.; Carvajal, M. Changes in plasma membrane lipids, aquaporins and proton pump of broccoli roots, as an adaptation mechanism to salinity. *Phytochemistry* **2009**, *70*, 492−500.

(30) Han, P.; Zhou, J.; Yuan, Y. Analysis of phospholipids, sterols, and fatty acids in *Taxus chinensis var. mairei* cells in response to shear stress. *Biotechnol. Appl. Biochem.* **2009**, *54*, 105−112.

(31) Schaller, H. The role of sterols in plant growth and development. *Prog. Lipid Res.* **2003**, *42*, 163−175.

DOI: 10.1021/jf503193c
J. Agric. Food Chem. 2015, 63, 1309−1317

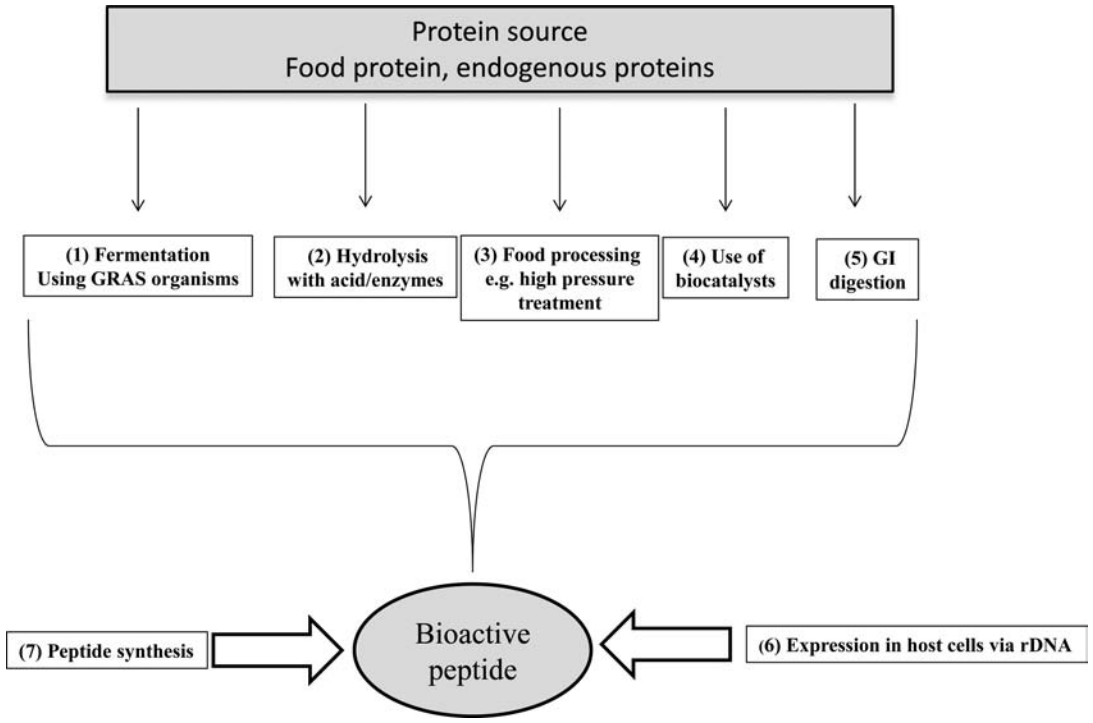

Figure 1. Routes to production of bioactive peptides from food protein sources.

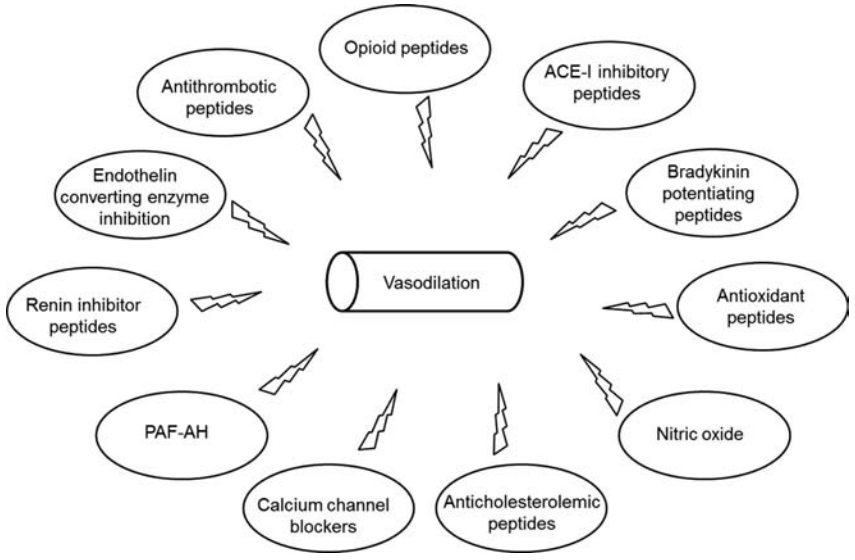

Figure 2. Peptides that can influence blood pressure regulation and vasodilation derived from food protein sources.

economical ACE inhibitors as alternatives to these synthetic drugs. During recent decades, a number of studies have looked at food therapy and dietary approaches for the prevention of chronic, lifestyle-related diseases, including hypertension.[14] Antihypertensive peptides with ACE or renin inhibitory activities are cheaper to produce with less stated side effects.[15] Fish meat consumption is often discussed as a factor in the prevention of heart disease as it is correlated with an increased dietary intake of omega-3 fatty acids.[16] However, fish protein is also a potential source of cardioprotective cryptides with ACE, renin, and phospholipase A_2 (PAF-AH) inhibitory and other activities. This review discusses the different pathways for blood pressure regulation in the circulation system and describes cardioprotective peptide generation from fish proteins. It also discusses the markets and future potential of muscle-derived heart health peptides, and the latest regulations regarding their use and generation.

BLOOD PRESSURE REGULATING ENZYMES AND THE RAAS

The RAAS and the SNS play major roles in the control of blood pressure.[17] In addition, a number of other factors may affect blood pressure due to the action of regulatory peptides including opioid, bradykinin potentiating, calcium channel blockers, and endothelial converting peptides (see Figure 2). Not all opioid or antioxidant peptides affect blood pressure. However, the opioid peptides endomorphin 1 and 2 were found to decrease systemic arterial pressure previously,

DOI: 10.1021/jf505019z
J. Agric. Food Chem. 2015, 63, 1319−1331

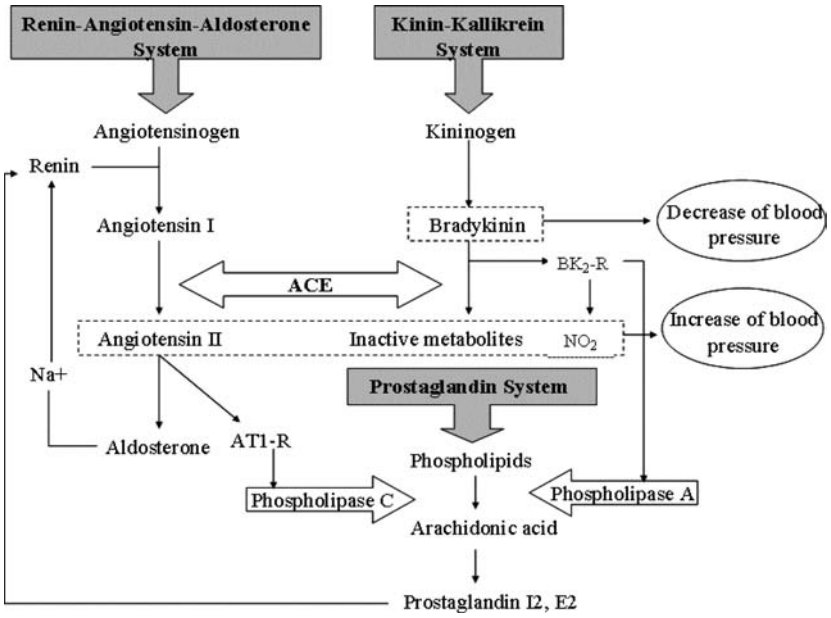

Figure 3. Classical renin–angiotensin aldosterone system (RAAS) and its relationship with the kinin–kallikrein and prostaglandin system. RAAS represents a cascade of enzymatic reactions. The huge precursor molecule of angiotensin II (Ang-II), angiotensinogen, is cleaved by renin, resulting in the still inactive decapeptide angiotensin I (Ang-I), which is then further cleaved by the membrane-bound metalloproteinase angiotensin-converting enzyme (ACE) to give the main effector hormone of the RAAS, the octapeptide Ang-II. In 2000, the first known homologue of ACE, ACE2, was identified. ACE2 catalyzes the generation of Ang-1–9 from An- I and of Ang-7 from An- II. It is not inhibited by ACE inhibitors. ACE2 metabolizes Ang-II to give the vasodilator Ang-1–7, which has been interpreted to mean that ACE2 provides a counterbalance, preventing overactivity of the classic RAAS.

although the mechanism of action is unknown.[18] Furthermore, it is hypothesized that low antioxidant levels may increase coronary heart disease. More research is needed to elucidate the role of antioxidative peptides and their protective functions in humans.[19] The classical RAAS (Figure 3) is a hormonal cascade that functions in the homeostatic control of arterial blood pressure. It was thought to be a straightforward cascade containing one substrate (angiotensinogen), two enzymes (ACE and renin), two peptides, angiotensin I (Ang-I) and angiotensin II (Ang-II), and one receptor (AT1). In reality, RAAS is a multiple effector system that consists of more than two dozen peptidases, a dozen Ang fragments, and at least six receptors.[20] The substrate angiotensinogen is released into the circulation from adipose tissue, and the liver and is degraded by the enzyme renin, which originates in the kidney. This action generates the inactive decapeptide angiotensin I, which is converted at the endothelial surface of blood vessels by the enzyme ACE into angiotensin II, the primary effector molecule of the RAAS.[20] Furthermore, evidence is now available that several RAAS components are expressed in cells from different organs of the body including the kidney.[21] In 2000, a homologue of ACE was discovered and called ACE2. Evidence indicates that ACE2 negatively regulates the activated RAAS by degrading angiotensin II to the heptapeptide Ang-(1–7). The enzymes ACE, renin, and ACE2 are key enzymes in the RAAS and therefore in the control of arterial blood pressure. Furthermore, the peptide Ang-A with the amino acid sequence Ala-Arg-Val-Tyr-Ile-His-Pro-Phe metabolizes Ang-II to Ang-III and causes a vasoconstrictive effect dependent on AT_1 receptors. Furthermore, Ang-M metabolizes Ang-III to Ang-IV and aspartyl aminopeptidase, which metabolizes Ang-I to Ang-2–10. They are suitable targets for functional food therapeutics for potential cardiovascular disease prevention.

ACE (EC 3.4.15.1). ACE, which is also known as kinase II, was first isolated in 1956 and termed the hypertension-converting enzyme.[22] It is a zinc metallopeptidase that requires chlorine for activation.[23] In the RAAS, ACE cleaves the decapeptide angiotensin I (Ang-I) into the octapeptide angiotensin II (Ang-II) by removal of the C-terminal dipeptide His-Leu. Ang-II is a potent vasoconstrictor and stimulates the release of aldosterone and antidiuretic hormone or vasopressin and increases retention of salt and water.[20] These activities raise blood pressure. ACE also inactivates the vasodilatory protein bradykinin and kallidin in the kallikrein–kinin system. ACE cleaves bradykinin (1–7) into the shorter fragment bradykinin (1–5).[24] ACE is also involved in the impairment of nitric oxide bioavailability.[20] Furthermore, ACE is thought to be involved in the functioning of the brain and nervous system as it can hydrolyze neuropeptides including encephalin, substrate P, luteinizing release hormone, and neurotensin.[25] ACE may also play a role in the gastrointestinal system as it hydrolyzes the hormones cholecystokinin and gastrin.[26] Furthermore, the ACE inhibitor perindopril ameliorates cognitive impairment and may have beneficial effects on Alzheimer's disease,[27] although ACE itself is thought to prevent the formation of Alzheimer amyloid β-peptide.[20]

There are over 10 synthetic ACE inhibitors available commercially including Captopril.[20] Drug development of ACE inhibitors is based on the knowledge that somatic ACE has two active sites and that these are not identical. However, ACE inhibitors developed to date show little discrimination between the active sites.[23] A number of studies have looked at isolation of ACE inhibitory peptides from food sources. ACE inhibitory peptides usually have large, bulky side chains, aromatic amino acids at the C-terminal end of the peptide, and nonpolar or positively charged amino acids at the N-terminus.[28] In tripeptides, aromatic amino acids are preferred at

DOI: 10.1021/jf505019z
J. Agric. Food Chem. 2015, 63, 1319–1331

Table 1. Marine- and Food-Derived Cryptide Sequences with Confirmed in Vitro and in Vivo Cardioprotective Effects

source material	bioactive peptide sequence	bioactivity	enzymes or chemicals used	IC_{50} value	ref
marine animal and fish					
dried bonito (katsuobusi)	Ile-Lys-Pro	ACE inhibition	Thermolysin	0.32 μM	39
Branchionus rotundiformis (rotifers)	Asp-Asp-Thr-Gly-His-Asp-Phe-Glu-Asp-Thr-Gly-Glu-Ala-Medt	ACE inhibition	Alcalase	9.64 μM	40
Corbicula fluminea (freshwater clam)	Val-Lys-Pro and Val-Lys-Lys	ACE inhibition	Protamex	0.043 mg/mL	41
Crassostrea gigas (fermented oyster sauce)	not given	ACE inhibition	fermented	2.45 mg/mL	42
Crassostrea talienwhanensis (oyster protein)	Val-Val-Tyr-Pro-Trp-Thr-Gln-Arg-Phe	ACE inhibition	pepsin	66 μmol/L	43
Ctenopharyngodon idella (grass carp fish)	not given	ACE inhibition	desalted fish scale	0.13 mg/mL	44
Limanda aspera (yellowfin sole frame protein)	Met-Ile-Phe-Pro-Gly-Ala-Gly-Gly-Pro-Glu-Leu	ACE inhibition	none	28.7 μg/mL	45
Mytilus edulis (blue mussel)	Glu-Val-Met-Ala-Gly-Asn-Leu-Tyr-Pro-Gly	ACE inhibition	fermented	19.34 μg/mL	46
sardine muscle	not given	ACE inhibition	*Bacillus licheniformis* alkaline protease	0.015 mg protein/mL	47
sea bream scales	Gly-Tyr, Val-Tyr, Gly-Phe, Val-Ile-Tyr	ACE inhibition	alkaline protease	not given	48
shark meat	Cys-Phe, Glu-Tyr, Met-Phe, Phe-Glu, Cys-Phe, Glu-Tyr, Phe-Glu	ACE inhibition	Protease SM98011	0.4 mg/mL	49
Theragra chalcogramma (Alaska pollock skin)	Gly-Pro-Leu, Gly-Pro-Met	ACE inhibition	Alcalase, Pronase, Collagenase	2.6 and 17.13 μM	50
tuna frame protein	Gly-Asp-Leu-Gly-Lys-Thr-Thr-Thr-Val-Ser-Asn-Trp-Ser-Pro-Pro-Lys-Try-Lys-Asp-Thr-Pro	ACE inhibition	pepsin	11.28 μM	51
Barbus callensis (freshwater fish skin)	not given	DPP-IV and PEP inhibition	Esperase	not given	52
macro- and microalgae					
Undaria pinnatifda (wakame)	Ala-Ile-Tyr-Lys, Tyr-Lys-Tyr-Tyr, Lys-Phe-Tyr-Gly, Tyr-Asn-Lys-Leu	ACE inhibition	pepsin	213, 64.2, 90.5, 21 μM	53
Palmaria palmata	Ile-Arg-Leu-Ile-Ile-Val-Leu-Met-Pro-Ile-Leu-Met-Ala	renin inhibition and antihypertensive in SHR	papain	3.34 mM	54
Palmaria palmata	Ile-Leu-Ala-Pro, Leu-Leu-Ala-Pro, Met-Ala-Gly-Val-Asp-His-Ile	DPP-IV inhibition	Corolase PP	43−139 μM	55
Palmaria palmata	Asn-Ile-Gly-Lys	PAF-AH inhibition	papain	2.32 mM	56
Chlorella vulgaris	Val-Glu-Cys-Tyr-Gly-Pro-Asn-Arg-Pro-Gln-Phe	ACE inhibition	pepsin	29.6 μM	57
animal					
Biceps fermoris (beef rump) sarcoplasmic proteins	Val-Leu-Ala-Gln-Tyr-Lys	ACE inhibition	Thermolysin and proteinase A	23.11−24.15 μg/mL	58
bovine brisket sarcoplasmic proteins	multiple peptides	ACE inhibition and antioxidant activity	papain	not given	59
bovine liver sarcoplasmic proteins, 10 kDa fraction	multiple peptides	antioxidant activity	Thermolysin	not given	60
porcine skeletal muscle myosin muscle	Met-Asn-Pro-Pro-Lys, Ile-Thr-Thr-Asn-Pro, Met-Asn-Pro, Asn-Pro-Pro, Pro-Pro-Lys, Ile-Thr-Thr	ACE inhibition	Thermolysin	66.6, 290.5, 1000, 678.2, 672.7 μM	61
dairy and egg					
Bos grunniens (yak) milk casein	Pro-Pro-Glu-Ilu-Asn, Pro-Leu-Pro-Leu-Leu	ACE inhibition	Alcalase	0.25−0.29 mg/mL	62
chicken egg yolk	Arg-Ala-Asp-His-Pro-Phe-Leu, Ile-Val-Phe	antihypertensive in rats		not given	63
fermented dairy drink Calpis	Ile-Pro-Pro, Val-Pro-Pro	ACE inhibition and antihypertensive in humans	*Lactobacillus helveticus* and *Saccharomyces cervisiae*	reported	5
fermented dairy drink Evolus	Ile-Pro-Pro, Val-Pro-Pro	ACE inhibition and reduction of arterial stiffness*	*Lactobacillus helveticus*	reported	5
bovine whey protein isolate BioZate	cysteine peptides	ACE inhibition and antihypertensive	whey hydrolyzed protein	not given	64
bovine casein protein isolate C12 peptide	Phe-Pro-Val-Ala-Pro-Phe-Pro-Glu-Val-Phe-Gly-Lys	antihypertensive in prehypertensive humans	bovine casein hydrolysate	not given	65
plants, legumes, and cereals					
Cicer arietinum (chickpea)	six inhibitory peptides	ACE inhibition	Alcalase	0.011−0.021 mg/mL	66
Amaranth hypochondriacus	Ala-Leu-Gln-Pro, Val-Ile-Lys-Pro	ACE inhibition		6.32, 175 μM	67
Brassica oleracea (broccoli)	Tyr-Pro-Lys	ACE inhibition	organic solvents	10.5 μg protein/mL	68
Allium sativum (garlic)	Ser-Tyr, Gly-Tyr, Phe-Tyr, Asn-Tyr, Ser-Phe, Gly-Phe, Asn-Phe	ACE inhibition	water extraction	66.3, 72.1, 3.74, 32.6, 130.2, 277.9, 46.3 μM	69
Fagopyrum esculentum (buckwheat)	Gly-Pro-Pro	ACE inhibition		6.25 μg protein/mL	70

DOI: 10.1021/jf505019z
J. Agric. Food Chem. 2015, 63, 1319−1331

the C-terminus of the peptide, positively charged amino acids for the central position, and hydrophobic amino acids at the N-terminus for bioactivity. The IC_{50} values obtained for food-derived ACE inhibitors are usually a thousand-fold higher than synthetic Captopril.[29]

ACE2 (EC 3.4.17.23). ACE2 belongs to the metalloproteinase family of enzymes but has a single active site and was discovered in 2000 by two research groups.[30] It has a substrate preference for hydrolysis between proline and a basic or hydrophobic C-terminal residue.[30] It functions to counterbalance ACE and increases Ang-(1−7) formation. ACE2 may regulate blood pressure through bradykinin and apelin, and it is known that ACE2 deficiency accentuates vascular atherosclerosis and inflammation.[31] Compared with ACE inhibitor use, ACE2 is an endogenous regulator of RAAS, and activation of ACE2 would produce Ang-(1−7). ACE2 activity is commonly measured by hydrolysis of quenched fluorescent substrates in the absence or presence of an ACE2-specific inhibitor, such as the commercially available inhibitor DX600.[32] Screening marine and food protein sources for ACE2 activators is a potential option for identification of blood pressure and hypertension regulators.

Renin (EC 3.4.23.15). Renin secretion control is a key and rate-limiting step within the RAAS. Renin cleaves angiotensinogen to form the inert decapeptide Ang-I. Angiotensinogen is produced mainly from the liver but is also found in the brain, heart, adrenal, ovary, and adipose tissue.[33] In 2010 meta-analysis of randomized controlled trials with AT1 receptor blockers found that their use led to an increase in new cancer diagnosis. Direct renin inhibition may be an alternative pharmacological approach to RAAS inhibition. The renin inhibitor Aliskiren has been approved for use in Europe and the United States from 2007.[34] A number of dipeptides with renin inhibitory activities have been isolated previously from pea[35] and seaweed.[54] Their bioactivities were observed in vitro and in animal models. Saponins from soybean have also been documented as having renin inhibitory activities in vitro.[36]

COMMERCIALLY AVAILABLE MARINE PROTEIN HYDROLYSATES WITH HEALTH BENEFITS

Commercialization of cardioprotective food products is dependent on the availability of scientific data from in vivo animals and human models that positively demonstrate their contribution to blood pressure control. In Europe, the European Food Safety Authority (EFSA) governs the use of novel food and health claims made on food products and ingredients. Regulation 1924/2006/EC of December 20, 2006, on nutrition and health claims made on foods is a claim to protect consumers by prohibiting the use of misleading information on packaging. Therefore, food producers have to justify the use of a health claim and need to fully substantiate the claim scientifically. To address this, the bioactivity of functional ingredients needs to be characterized as fully as possible.

Guerard and colleagues[37] provide an overview of commercially available fish protein hydrolysates. Commercially available functional food products for human use developed from fish protein include Stabilium 200, an Atlantic fish autolysate (www.yalacta.com), and PROTIZEN, a white fish hydrolysate (www.copalis.fr), both carrying a relaxing effect. Other products include Nutripeptin, a cod hydrolysate, for lowering glycemic index (www.copalis.fr), Seacure, a fish fillet hydrolysate obtained by fermentation using a marine microorganism for improving gastrointestinal health (www.propernutrition.com (USA)), and Fortidium LIQUAMEN, a fish autolysate of white fish (*Molva molva*) (www.biothalassol.com), which claims to reduce oxidative stress and lower glycemic index. Other fish protein hydrolysates with health benefits include a hydrolyzed sardine protein, VALTYRON, manufactured using enzymatic hydrolysis (a protease) of sardine muscle and subsequent water and ethanol extraction of peptides. The Japanese company Senmi Ekisu Co., Ltd., obtained GRAS status for its hydrolyzed sardine protein from the FDA recently. This hydrolysate contains a dipeptide (Val-Tyr) with known ACE inhibitory and antihypertensive benefits. Furthermore, EFSA issued a positive opinion regarding the safety of the hydrolyzed Californian sardine protein hydrolysate product VALTYRON. EFSA concluded that VALTYRON produced by the Japanese company Senmi Ekisu Co., Ltd., was safe for use as a food ingredient at use levels of up to 0.6 g/serving. Significant reductions in blood pressure were observed following administration of single doses of up to 6 g of a sardine peptide hydrolysate product in subjects that exhibited higher than normal blood pressure at the start of the study and not in normotensive individuals. Indeed, EFSA issued a positive opinion regarding the safety of hydrolyzed sardine protein for use in cereal and other food products in 2010.[71]

Peptide sequences obtained from fish sources, muscle tissue, dairy and eggs, and plants are shown in Table 1.[38−70]

MARINE PROTEIN DERIVED CARDIOPROTECTIVE PEPTIDES

ACE Inhibitory Peptides. ACE inhibitory peptides are extensively used in therapy against hypertension.[72] Many ACE inhibitors have been isolated as enzymatic digestion products from food sources such as milk,[72] wheat,[73] soybean,[74] and maize.[75] Several studies have identified ACE inhibitory peptides from fish muscle proteins including salmon and chum salmon,[76] yellowfin sole,[44] sardine,[46] bonito,[78] tuna,[80] and shrimp.[80] Indeed, the most documented fish product with ACE inhibitory effects is dried bonito bowel, a seasoning used in Japan made from thin slices of boiled, dried bonito.[81,82] The pentapeptide corresponding to the amino acid sequence Leu-Lys-Pro-Asn-Met is responsible for the ACE inhibitory activity, and this peptide demonstrates a prolonged blood pressure lowering effect following oral administration.[82] This peptide is also found in traditional Japanese food known as katsuobushi. Katsuobushi is fermented, smoked skipjack tuna (*Katsuwonus pelamis*).[82] Sardine protein hydrolysate is widely documented as a source of ACE inhibitory peptides. The most active ACE inhibitory sardine peptide is the dipeptide VY. This peptide demonstrated a significant antihypertensive effect on mildly hypertensive patients as well as in spontaneously hypertensive (SPH) rats, previously.[84] Indeed, a thermolysin digest of katsuobushi was approved as a food for special health use (FOSHU) in Japan.[85]

The ACE inhibitory effects of fish sauces developed from salmon, sardine, and/or anchovy have also been reported. For example, Bordenave et al.[76] reported that 50 μg of powder consisting of autohydrolyzed protein of sardine and cod head wastes inhibited ACE by 30%. Shrimp autohydrolyzed waste in a similar quantity inhibited ACE by 57%. Furthermore, a study carried out by Fahmi and colleagues[47] showed that a sea bream hydrolysate showed excellent ACE inhibitory activity, and the peptides responsible for this action were determined as Gly-Tyr, Val-Tyr, Gly-Phe, and Val-Ile-Tyr. Freshwater fish muscle

DOI: 10.1021/jf505019z
J. Agric. Food Chem. 2015, 63, 1319−1331

proteins and their hydrolysates offer huge potential as novel sources of natural bioactive peptides with ACE inhibitory activity.[83] Recently, two ACE inhibitory peptides were isolated from snakehead fish sarcoplasmic protein hydrolysates.[86] Enzymatic hydrolysis of sarcoplasmic protein was performed using commercial enzymes including Alcalase. The peptides had the amino acid sequences Leu-Tyr-Pro-Pro-Pro and Tyr-Ser-Met-Tyr-Pro-Pro with ACE inhibitory IC_{50} values of 1.3 and 2.8 μM, respectively. These peptides showed no cytotoxicity when tested using human embryonic fibroblast cell line (MRC-5) and human hepatocarcinoma cell line (HepG2).[86] ACE inhibitory peptides have also been isolated from fish skin proteins previously. For example, the ACE inhibitory peptide GPL was isolated from Alaska pollock skin gelatin hydrolysate.[49]

Fish-Derived Antioxidant Peptides. The increased production of reactive oxygen species (ROS), reactive nitrogen species (RNS), and free radicals in combination with the outstripping of endogenous antioxidant defense mechanisms is thought to be an important cause of disease development including cancer, gastric ulcers, Alzheimer's, and arthritis. Oxidation of foods is one of the major causes of food deterioration, especially of lipids and proteins. In the food and pharmaceutical industries, many synthetic antioxidants such as butylated hydroxytoluene, butylated hydroxyanisole, *tert*-butylhydroquinone, and propyl gallate are used to retard peroxidation processes. However, the use of these synthetic antioxidants is strictly controlled due to potential health hazards caused by such compounds. This fact has caused an increase in the interest afforded to the isolation and characterization of natural antioxidants.

In relation to heart health, antioxidant peptides may play a positive role as oxidation by ROS and RNS is also thought to play an important role in the initiation or progression of several vascular diseases such as ischemic reperfusion, which is a common occurrence in cardiovascular surgery patients. It results in inflammation and oxidative damage of tissue due to the return of blood supply after a period of ischemia.[58] Several bioactive peptides including carnosine, anserine, L-carnitine, and the lipid conjugated linoleic acid (CLA) were identified as possessing antioxidant regulating properties.[59] Furthermore, commercial enzyme cocktails can be used to generate hydrolysates containing antioxidant peptides from different fish muscle protein sources.[60] These antioxidant peptides can act at different levels in the oxidative sequence, preventing the formation of free radicals or introducing substances that compete for the existing radicals. The antioxidant properties of peptides derived from different proteins are mainly influenced by the antioxidant properties of the amino acids contained in the peptidic sequence, including histidine, tyrosine, methionine, lysine, and tryptophan.

Protein hydrolysates from muscles of several fish species including tuna dark muscle (*Thunnus tonggol*),[61] round scad (*Decapterus maruadsi*),[62] yellow stripe trevally (*Selaroides leptolepis*),[63] Pacific hake (*Merluccius productus*),[64] tilapia (*Oreochromis niloticus*),[65] silver carp (*Hypophthalmichthys molitrix*),[66] grass carp (*Ctenopharyngodon idellus*),[66] houndshark (*Mustelus mustelus*),[67] mackerel (*Scomber austriasicus*),[68] Alaska pollock (*Theregara chalcogramma*),[41] and brown-tripe red snapper (*Lutjanus vitta*),[69] all have reported antioxidant activities. A report comparing the antioxidant activity of Atlantic salmon, Coho salmon, Alaska pollock, and southern blue whiting hydrolysates, generated using pepsin, pancreatin, and thermolysin enzymes, demonstrated antioxidant activities when hydrolysates were assessed using the 1,1-diphenyl-2-picrylhydrazyl (DPPH) radical scavenging activity assay. Alaska pollock pancreatin hydrolysate showed the lowest antioxidant values, whereas all other hydrolysates demonstrated similar antioxidant activities when assayed.[70]

Recently, a peptide identified from a croaker (*Otolithes ruber*) muscle protein hydrolysate with pepsin, trypsin, and α-chymotrypsin, found to contain the bioactive peptide sequence KTFCGRH, exhibited antioxidant activity in vitro against the radical scavenging efficiency of DPPH and hydroxyl radicals.[87] The identified peptide also proved effective when tested in vivo and neutralized ethanol-induced oxidative stress in rats.[87] Peptides VCSV and CAAP were purified and identified from α-chymotrypsin hydrolysate of flounder fish muscle, which showed radical scavenging activity against the DPPH free radical (IC_{50} values of 111.32 and 26.89 μM, respectively) and high cytoprotective activities against 2,2-azobis(2-amidinopropane) dihydrochloride (AAPH) in Vero cells.[88] Recently, Udenigwe and Aluko used partial least-squares (PLS) models to elucidate specific positive and negative contributions of individual amino acid residues and groups to antioxidant activities of proteins. They found that the effects depend on the oxidative assay system used, but on the basis of the results they found that previously reported antioxidant amino acid residues, especially histidine, had a negative effect on the antioxidant properties in the DPPH and H_2O_2 assays.[89]

Opioid Peptides. Opioid peptides bind to opioid receptors to produce morphine-like effects. Opioid receptors exist in the central and peripheral nervous systems, in the endocrine system, and in the immune system of mammals, as well as the intestinal tract. Natural opioid peptides include endorphins, enkephalins, and dynorphins.[90,91]

They are known to regulate various endocrine systems, including the hypothalamic−pituitary−adrenocortical (HPA) axis, and opioid peptides are thought to be responsible for the phenomenon of stress-induced analgesia.[92] Activation of opioid receptors results in adenylate cyclase inhibition, potassium channel activation, and calcium channel inactivation.[93] These receptors are also involved in the regulation of circulation, which can affect blood pressure.[94,95]

The first opioid peptides were identified in the late 1970s and were called "exorphins" due to their structural similarity to the endogenous ligands (endorphins and enkephalins) that interact with the opioid receptors found in the human body (μ-, κ-, and δ-).[96] Individual opioid receptors are responsible for specific bioactivities. For example, the μ-receptor is responsible for emotional behavior and suppression of intestinal motility,[97] the κ-receptor for satiety and food intake, and the δ-receptor for emotional behavior.[97] Opioid peptides derived from foods are of considerable interest as they are considered stable compared to endogenous opioid peptides, which are easily degraded by enzymes. Furthermore, food-derived opioid peptides have weaker bioactivities and therefore fewer side effects than those associated with endogenous opioid peptides, which include addiction and high dependency.[98−101]

The first opioid peptides derived from food proteins were of milk protein origin. The tetrapeptide β-lactorphin (YGLF) was originally released from the milk protein α-lactalbumin by enzymatic hydrolysis and showed an antihypertensive effect after oral administration to spontaneously hypertensive rats (SHR), with maximum reductions of blood pressure (BP) of 23 ± 4 mmHg in systolic BP. The vascular effects of another

DOI: 10.1021/jf505019z
J. Agric. Food Chem. 2015, 63, 1319−1331

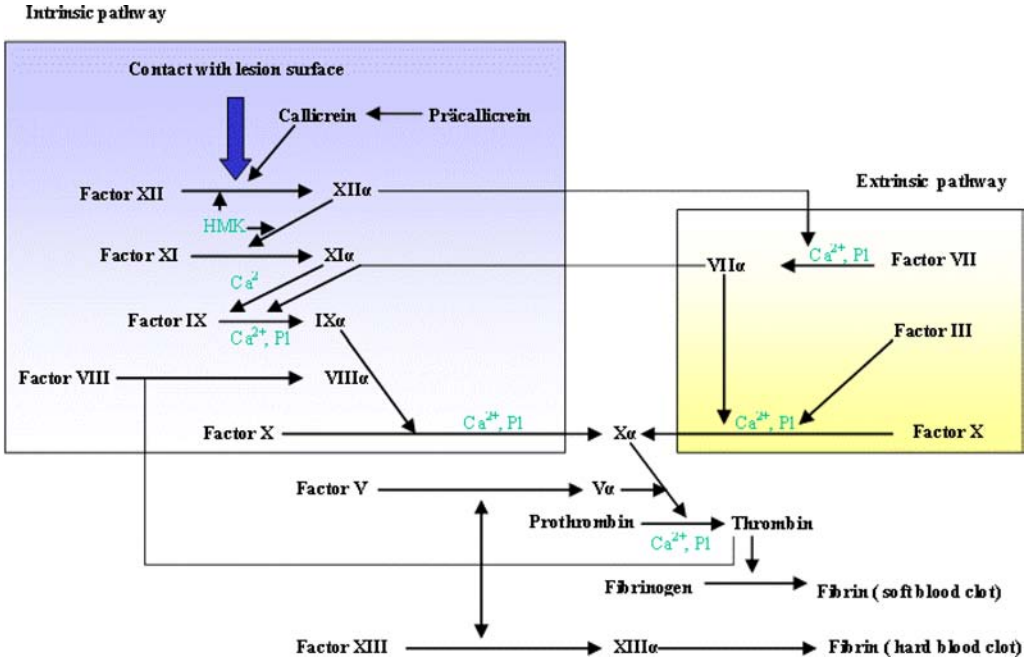

Figure 4. Coagulation cascade. In the intrinsic and extrinsic pathway model, initiation of coagulation is divided into two parts, the extrinsic pathway, which is thought to be responsible for the initial generation of activated factor X (factor Xa), and the intrinsic pathway, which leads to amplification of factor Xa generation. Factor Xa occupies a point where the intrinsic and extrinsic pathways converge and is central to the coagulation cascade.

structurally related tetrapeptide, α-lactorphin (Tyr-Leu-Leu-Phe), which originates from milk protein α-lactoglobulin, were also studied together with α-lactorphin (Tyr-Gly-Leu-Phe) effects. α-Lactorphin produced an endothelium-dependent vasorelaxation effect with nitric oxide synthase (NOS) inhibition. The α-lactorphin peptide also enhanced endothelium-independent vasorelaxation. This study concluded that α-lactorphin may stimulate the opioid receptors, which in turn release NO, causing the vasorelaxative effect.[100,101]

β-Casomorphins are well characterized in the literature.[101] Casomorphins are involved in regulation functions of the gut.[79] They enhance water and electrolyte absorption and act as antidiarrheal agents.[101] The casein-derived peptide casoxin D (Tyr-Val-Pro-Phe-Pro-Pro-Phe) has also been reported to have a hypotensive effect via opioid receptors, causing a vasodilatory relaxing effect in canine mesenteric artery strips.[101] Fish protein hydrolysates are known to accelerate calcium absorption[77] and provide satiety. They include the fish-derived peptide calcitonin/calcitonin gene related peptide (CGRP) and cholecystokinin-like peptides.[102] CGRP is a neuropeptide that acts as a potent arterial and venous vasodilator in humans.[102] Its capacity to increase heart rate as well as its ability to decrease food intake is well documented.[101,102] Guerard and colleagues generated CGRP molecules from a *Pollachius virens* byproduct hydrolyzed with Alcalase and treated with the microbe *Saccharomyces cerevisiae*.[103,104] Indeed, two commercially available products exist that carry relaxing effect claims.[37]

Antithrombotic Effect. An important complication that frequently occurs in patients with heart disease is the predisposition to develop thrombosis. Thrombosis is linked to platelet aggregation and small levels of fibrinolysis. Peptides that inhibit blood platelet aggregation and enhance fibrinolysis are strongly recommended to prevent thrombosis.

Blood coagulation is important in the cessation of blood loss from a damaged blood vessel (also known as hemostasis). A number of factors are involved in blood coagulation. The coagulation cascade consists of two pathways that are interconnected (Figure 4). These include the intrinsic pathway, which is also known as the contact activation pathway, and the extrinsic pathway or tissue factor pathway that leads to fibrin formation. When damaged, a platelet and fibrin-containing clot to prevent further bleeding covers the blood vessel. Both the intrinsic and extrinsic pathways activate the "final common pathway" of factor X, thrombin, and fibrin. Coagulation factors are generally serine proteases, transglutaminases (factor XIII), or glycoproteins (FVIII and FV), helping factors include calcium ions (Ca^{2+}), and phospholipid membranes. Heparin is an important anticlotting agent, which is often isolated from the small intestine of pigs or bovine lung tissue.

Food-derived peptides that inhibit blood platelet aggregation can be useful natural ingredients for the prevention of thrombosis. Thus, the search for new antithrombotic agents has mainly been focused on fruits and vegetables and marine carbohydrates including fucoidans and carrageenan.[105−110] Recently, collagen and its component proteins gelatin, collagen, and gelatin hydrolysates have been examined as potential natural antithrombotic ingredients. Indeed, a tetrapeptide, Asp-Gly-Glu-Ala (D-G-E-A), derived from type I collagen was found to inhibit collagen-induced platelet aggregation.[111] Khiari et al. studied the structure of antithrombotic peptides isolated from mackerel skin gelatin hydrolysates generated with pepsin, and observed antithrombotic activity due to the presence of the tripeptide FGN with a molecular weight of 337 Da.[112]

With regard to muscle sources, a recent study compared the effect of long-term intake of purified vegetable and animal proteins (casein, pork, egg white, chicken, white and red fish, soybean, and potato) and powders from whole vegetable and animal meats (soybean, pork, chicken, and horse mackerel) on thrombotic tendency and found that there was no difference in thrombotic tendency between the vegetable and animal protein diets with the exception of pork protein, which showed a prothrombotic effect.[113] In contrast, soybean powder showed an

DOI: 10.1021/jf505019z
J. Agric. Food Chem. 2015, 63, 1319−1331

antithrombotic effect, which was mainly due to inhibition of atherogenesis rather than to platelet inhibition.[113] More recently, it was published that papain-hydrolyzed pork peptides showed antithrombotic activity using the shear-induced thrombosis test in vivo and a laser-induced thrombosis test in the muscle carotid artery in vivo.[114] However, the amino acid sequence of papain-hydrolyzed peptide responsible for the observed bioactivity was not determined.

Anticholesterolemic Effect. Elevated blood pressure, hypertriglyceridemia, hyperglycemia, and obesity are main factors of metabolic syndrome. These risk factors have a correlation with cardiovascular diseases and are also associated with an increased tendency to develop type 2 diabetes mellitus.[115] Hypercholesterolemia and low levels of high-density lipoprotein cholesterol are strongly associated with increases in blood pressure, which is known to promote atherosclerosis. This process leads to cardiovascular diseases and can cause myocardial infarction, stroke, and peripheral vascular disease. Thus, hypercholesterolemia is usually associated with high levels of low-density lipoprotein (LDL) and lower concentrations of functional, high-density lipoprotein (HDL). These balances are mostly genetically determined but can also be influenced by body build, medications, and food.

The hydrolysis of meat and fish proteins generates peptides that could alter the free and total amount of cholesterol in plasma and, thus, influence blood pressure values and development of cardiovascular diseases. Fish protein hydrolysates have been reported to reduce plasma total cholesterol, increasing the proportion of HDL cholesterol and decreasing the activity of the coenzyme group acetyl coenzyme A (acyl-CoA) in the liver of Zucker rats.[116] Acyl CoA is a group of essential coenzymes in the balance between carbohydrate and fat metabolism. Two acyl CoA molecules can be condensed to create acetoacetyl CoA, which participates in the pathway of cholesterol synthesis. More recently, a combination of fish oil and fish protein hydrolysates in the diet was reported to reduce the plasma cholesterol level and increase the hepatic total cholesterol concentration. This is probably due to the action of the acyl-CoA coenzyme, which increases cholesterol esterification.[117] The hydrolysis of marine waste/byproducts such as freshwater clam residual meat together with insoluble dietary fiber separated from whole *Gracilaria* showed a bile acid-binding capacity and inhibited the micellar solubility of cholesterol in vitro.[118] This study was subsequently conducted in vivo, and results suggested that a combination of the freshwater clam hydrolysate and the insoluble dietary fiber from *Gracilaria* could be used to develop new functional foods for the prevention of hypercholesterolemia.[119]

Calcium Channel Blocking Effects. Calcium channel blockers interact with voltage-gated calcium channels in cardiac muscle and blood vessel walls, reducing intracellular calcium and consequently lowering vasoconstriction. In fact, it has been reported that peptides that bind and solubilize calcium can be considered to be beneficial in the prevention of dental caries, osteoporosis, hypertension, and anemia. During the past decade, some peptides derived from hoki and Alaska pollock frame were reported as calcium channel blockers,[120] and their bioactivities were demonstrated in rat models.[120−122]

Endothelin-1 (ET-1) and Endothelin Converting Enzyme (ECE) Inhibitory Effect. The endothelin system also has an increasingly recognized role in blood pressure regulation. The vasoconstriction peptide ET-1 is released from endothelin-1 by the activation of endothelin converting enzyme. The hyperactivation of the endothelin system has been implicated in the pathogenesis of several cardiovascular disorders such as pulmonary and arterial hypertension, heart failure, myocardial infarction, restenosis, and Chagas cardiopathy.[123]

Indeed, the more potent vasoconstrictive effect of ET-1 over angiotensin II was previously reported. However, only a few studies have focused on the potential effect of food-derived peptides on the endothelin system. Okitsu and colleagues[124] found ECE inhibitory peptides in pepsin digests of bonito pyrolic appendix and beef. Later, the influence of ACE inhibitory peptide Ala-Leu-Pro-Met-His-Ile-Arg, generated through tryptic digestion of bovine β-lactoglobulin, on the release of ET-1 by endothelial cells was investigated,[125] and basal ET-1 release from these cells was reduced by 29% in the presence of 1 mM of the peptide, compared to 42% for 0.1 mM Captopril. More recently, the potential of bovine lactoferrin hydrolysates generated by trypsin and proteinase K digestions as a source of ECE inhibitors was studied.[125,126] The peptides Gly-Ile-Leu-Arg-Pro-Tyr and Arg-Glu-Pro-Tyr-Phe-Gly-Tyr exerted in vitro inhibitory effects on ECE activity.

Useful Computational Methods in the Study of Cryptides. *In Silico Analysis.* Bioinformatics is a useful tool in the study of proteins. Bioinformatics is the computational analysis, modeling, and prediction of biological data. In silico analysis is the use of computational tools and databases to predict the release of bioactive peptides from parent proteins and the prediction of suitable enzymes for the release of bioactive peptides. It is also useful for predicting bioactivities associated with a given peptide sequence. Previously, Vermeirssen and colleagues[127] quantitatively evaluated pea and whey proteins as precursors for ACE inhibitory peptides. This was achieved by means of establishing an ACE inhibitory peptide database, containing about 500 reported sequences and their IC_{50} values. More recently, Iwaniak and Dziuba developed BIOPEP and Pôle Bioinformatique Lyonnais analysis tools.[128,129] These provide valuable data on food protein precursors as sources of bioactive peptides combined with the structural aspects of bioactivities encrypted in proteins. In silico analysis has been used in a number of studies to date to predict the release of bioactive peptides from protein sources including milk[129] cereals,[130] meat,[131] endogenous human proteins,[132] and other food proteins.[133] Bioinformatics and in silico analysis of fish proteins coupled with mass spectrometry technologies could prove useful in the future identification of useful fish-protein derived bioactive peptides.

Computational prediction of peptide bioactivity is also a useful tool for streamlining the search for active peptide sequences. PLS modeling is a widely used descriptive and predictive chemometrics approach for quantitative structure−activity relationship (QSAR) studies. It assists the user in elucidating how variation of molecular structures affects bioactivity of therapeutic agents, especially when working with high numbers of descriptor variables compared to the number of observations. This technique was used in QSAR studies of food-derived peptides and helped to identify bitter peptides[133] and ACE inhibiting peptides[134] previously. The bioactive peptide predictor PeptideRanker can prove useful in identifying among a set of peptides those that are more likely to be bioactive. This allows the focus of experimental screening on this subset.[135]

Technologies for the Identification of Bioactive Peptides. Technologies including mass spectrometry (MS) coupled to

DOI: 10.1021/jf505019z
J. Agric. Food Chem. 2015, 63, 1319−1331

liquid chromatography (LC) are some of the commonly applied technologies for bioactive peptide analysis. Many bioactive peptides contain two or three amino acid residues. These di- and tripeptides are usually identified using de novo sequencing or by matching the accurate mass and retention time to standards. Commonly used database search strategies using MS/MS spectra of peptide ions include SEQUEST and MASCOT, which are designed for proteomics applications. Other commercial databases used include the NIST 12 MS/MS library, the Wiley MS/MS library, and online spectral databases including METLIN (http://metlin.scripps.edu) and MassBank (http://www.massbank.jp/?lang=en). These libraries are suitable for the identification of oligopeptides greater than four amino acids in length. Recently, Tang and colleagues developed a new library suitable for the identification of di- and tripeptides from complex mixtures and untargeted analysis.[135] This method involved the separation of peptides using hydrophilic interaction (HILIC) liquid chromatography. To facilitate di- and tripeptide identification, a database consisting of all the predicted MS/MS spectra from 400 dipeptides and 8000 tripeptides was created, and a search tool, PEP search, was developed and housed at the MyCompoundID Web site (www.mycompoundid.or/PEP).[136] PEP Search in MyCompoundID searches an MS/MS spectrum against a database of di/tripeptides. This database consists of 400 dipeptides and 8000 tripeptides and their theoretical MS/MS fragments. PEP Search also provides an option to use dimethyl labeling confirmation. This option enables the search against the 8400 di/tripeptide database plus a library that consists of 8400 dimethyl-labeled di/tripeptides and their theoretical MS/MS fragments.[136] Peptide databases including BIOPEP are useful for peptide search operations also.

Bioavailability and Safety of Bioactive Peptides. For a bioactive peptide to be delivered to its active site, it is necessary to fully understand the barriers of the GI tract and the blood−brain barrier (BBB). The GI tract has site-specific absorption based on the peptide consumed and regional differences in pH, residence time, surface area, and enzyme activities.[137,138] For cardioprotective peptides to be active and to give a positive effect in the human body, they must be able to cross the intestinal mucosa and reach the systemic circulation. The most well-known antihypertensive and ACE inhibitory peptides, Ile-Pro-Pro and Val-Pro-Pro, contain a double proline at their C-terminal end and can therefore survive GI transit intact and brush border peptidase bioactivities. Transport across the intestinal epithelium may be either active or passive, and the mechanism of transport depends on the physicochemical properties of the peptide and the length of the peptide.[138] Furthermore, the RAAS has been described in the brain, and an interconnection between neurotransmitters and the brain RAS affects behavior and neurological diseases, for example, Parkinson's and Alzheimer's diseases. For a bioactive peptide with cardioprotective capabilities to exert beneficial effects within the brain RAAS, it would need to cross the BBB. The BBB prevents entry into the brain of many substances.[139] This is due to the epithelial-like tight junctions within the brain capillary endothelium.[139] The BBB is anatomically and functionally distinct from the blood−cerebrospinal fluid barrier.[140] However, it is documented that lipid mediated the free diffusion of substances with a molecular mass under 400 Da, which form less than eight hydrogen bonds and may cross the BBB.[139,140]

Protein is an essential part of the human diet. Bioactive peptides encrypted within native fish muscle proteins and released using food-processing methods including fermentation are an attractive option for use in food therapy for the treatment of high blood pressure. Despite their decreased potency, cardioprotective marine-derived peptides offer a suitable alternative to synthetic drugs for the prevention of high blood pressure and the maintenance of normotensive BP. However, further detailed mechanistic studies on how these antihypertensive peptides interact in humans must be carried out to elucidate the blood pressure lowering mechanisms of action involved. Safety issues including potential toxicity also warrant further research. It is important also that complete physicochemical, technofunctional, and bioactive properties, including potential allergic reactions, are considered prior to production of new fish muscle derived antihypertensive food products.

AUTHOR INFORMATION

Corresponding Author

*(M.H.) Phone: +353 (0) 1 8059957. Fax: +353 (0) 1 8059500. E-mail: maria.hayes@teagasc.ie.

Funding

L.M. gratefully acknowledges a JAEDOC−CSIC postdoctoral contract and Fundación Alfonso Martín Escudero. This work was carried out as part of the NutraMara − Marine Functional foods research initiative. This project (Grant-Aid Agreement MFFRI/07/01) is funded under the *Sea Change* Strategy with the support of the Marine Institute and the Department of Agriculture, Food and the Marine, funded by the National Development Plan 2007−2013.

Notes

The authors declare no competing financial interest.

ABBREVIATIONS USED

AAPH, 2,2-azobis(2-amidinopropane) dihydrochloride; Ang-I, angiotensin I; Ang-II, angiotensin II; Ang-A, angiotensin A; Ang-M, angiotensin M; ACE, angiotensin converting enzyme-I; ACE2, angiotensin converting enzyme-2; BBB, blood−brain barrier; BP, blood pressure; CGRP, calcitonin gene-related peptide; CVD, cardiovascular disease; CLA, conjugated linoleic acid; DPPH, 1,1-diphenyl-2-picrylhydrazyl; ET-1, endothelin-1; ECE, endothelin-1 converting enzyme; GI, gastrointestinal; EFSA, European Food Safety Authority; FDA, U.S. Food and Drug Administration; FOSHU, foods of specified health use; GRAS, Generally Recognized As Safe; HDL, high-density lipoprotein; HILC, hydrophilic interaction liquid chromatography; MRC-5, human embryonic fibroblast cell line; HepG2, human hepatocarcinoma cell line; NOS, nitric oxide synthase; PLS, partial least-squares; QSAR, quantitative structure−activity relationship; ROS, reactive oxygen species; RNS, reactive nitrogen species; RAAS, renin angiotensin aldosterone system; SHRs, spontaneously hypertensive rats; SFDA, state food and drug administrations

REFERENCES

(1) Ramakrishnan, V. V.; Ghaly, A. E.; Brooks, M. S.; Budge, S. M. Extraction of proteins from mackerel fish processing waste using Alcalase enzyme. *J. Bioprocess Biotechnol.* **2013**, *3*, 130−135.

(2) Hassan, M.; Javed, M. Studies on muscle protein profile of fish reared in poultry droppings fertilized ponds. *Pak. J. Agric. Sci.* **2000**, *37*, 51−54.

DOI: 10.1021/jf505019z
J. Agric. Food Chem. 2015, 63, 1319−1331

(3) Erdmann, K.; Cheung, B. W.; Schröder, H. The possible role of food-derived bioactive peptides in reducing the risk of cardiovascular disease. *J. Nutr. Biochem.* **2008**, 643−654.
(4) Henda, B. Y.; Labidi, A.; Arnaudin, I.; Bridiau, N.; Delatouche, R.; Maugard, T.; Piot, J. M.; Sannier, F.; Thiéry, V.; Bordenave-Juchereau, S. Measuring angiotensin-I-converting enzyme inhibitory activity by microplate assays: comparison using marine cryptides and tentative threshold determinations with Captopril and Losartan. *J. Agric. Food Chem.* **2013**, *61*, 10685−10690.
(5) Korhonen, H.; Pihlanto, A. Food-derived bioactive peptides − opportunities for designing future foods. *Curr. Pharma Des.* **2003**, 1297−1308.
(6) Lahl, J. W.; Braun, S. D. Enzymatic production of protein hydrolysates for food use. *Food Technol. (Chicago, IL, U.S.)* **1994**, *48*, 61−70.
(7) Escudero, E.; Sentandreu, M. A.; Toldrá, F. Characterisation of peptides released by in vitro digestion of pork meat. *J. Agric. Food Chem.* **2010**, *28*, 5160−5165.
(8) Pihlanto, A.; Virtanen, T.; Korhonen, H. Angiotensin-I converting enzyme (ACE) inhibitory activity and antihypertensive effect of fermented milk. *Int. Dairy J.* **2010**, *20*, 3−10.
(9) Arihara, K.; Nakashima, Y.; Ishikawa, S.; Itoh, M. Antihypertensive activities generated from porcine skeletal muscle proteins by lactic acid bacteria. *Abstracts of 50th International Congress of Meat Science and Technology*; University of Helsinki: Helsinki, Finland, 2005; p 236.
(10) Lewington, S.; Clarke, R.; Qizibash, N.; Peto, R.; Collins, R. Age-specific relevance of usual blood pressure to vascular mortality: a meta-analysis of individual data for one million adults in 61 prospective studies. *Lancet* **2002**, *360*, 1903−1913.
(11) MacMahon, S.; Peto, R.; Cutler, J.; Collins, R.; Sorlie, P.; Neaton, J.; Abbott, R.; Godwin, J.; Dyer, A.; Stanler, J. Blood pressure, stroke and coronary heart disease. Part 1, observational studies corrected from the regression dilution bias. *Lancet* **1990**, *31*, 765−774.
(12) Kumar, R.; Kumar, A.; Sharma, R.; Baruwa, A. Pharmacological review on natural ACE inhibitors. *Pharm. Lett.* **2010**, *2*, 273−293.
(13) Cooper, W. O.; Hernandez-Diaz, S.; Arbogast, P. G.; Dudley, J. A.; Dyer, S.; Gideon, P. S.; Hall, K.; Ray, W. A. Major congenital malformations after first trimester exposure to ACE inhibitors. *New Engl. J. Med.* **2006**, *23*, 2443−2451.
(14) Danquah, M. K.; Agyei, D. Pharmaceutical applications of bioactive peptides. *OA Biotechnol.* **2012**, *29*, 5−6.
(15) Agyei, D.; Danquah, M. K. Industrial scale manufacturing of pharmaceutical grade bioactive peptides. *Biotechnol. Adv.* **2011**, 272−277.
(16) Kris-Etherton, P. M.; Harris, W. S.; Appel, L. T. Fish consumption, fish oil, omega 3 fatty acids and cardiovascular disease. *Circulation* **2002**, *106*, 2747−2757.
(17) De Gasparo, M.; Septh, R. C.; Baltatu, O. C.; Vanderheyden, P. Brain RAS: hypertension and beyond. *Int. J. Hypertens.* **2013**, 157180, DOI: 10.1155/2013/157180.
(18) Czapla, M. A.; Champion, H. C.; Xadina, J. E.; Kastin, A. J.; Hackler, C.; Ge, L. J.; Kadowitz, P. J. Endomorphin 1 and 2, endogenous u-opioid agonists, decrease systemic arterial pressure in the rat. *Life Sci.* **1998**, *62* (13), 175−179.
(19) Sharma, S.; Singh, R.; Rama, S. Bioactive peptides: a review. *Int. J. BIOautomation* **2011**, *15* (4), 223−252.
(20) Guang, C.; Phillips, R. D.; Jiang, B.; Milani, F. Three key proteases − angiotensin-I-converting enzyme (ACE), ACE2 and renin − within and beyond the renin-angiotensin system. *Arch. Cardiovasc. Dis.* **2012**, *105* (6−7), 373−385.
(21) De Mello, W. C. Beyond the circulating renin angiotensin aldosterone system. *Front. Endocrinol.* **2014**, *5*, 104.
(22) Skeggs, L. T.; Kahn, J. R.; Shumway, N. P. The preparation and function of the hypotensin converting enzyme. *J. Exp. Med.* **1956**, *103*, 295−299.
(23) Harrison, C.; Acharya, K. R. ACE for all − a molecular perspective. *J. Cell Commun. Signal* **2014**, *8*, 195−210.
(24) Sivieri, D. O.; Bispo-da-Silva, L. B.; Oliveira, E. B.; Resende, A. C.; Salgado, M. C. Potentiation of bradykinin effect of ACE inhibition does not correlate with ACE activity in the rat mesenteric arteries. *Hypertension* **2007**, *50*, 110−115.
(25) Skidgel, R. A.; Erdös, E. G. Novel activity of human angiotensin I converting enzyme release of the NH_2- and COOH-terminal tripeptides from the luteinizing hormone-releasing hormone. *Proc. Natl. Acad. Sci. U.S.A.* **1985**, *82*, 1025−1029.
(26) Dubreuil, P.; Fulcrand, P.; Rodriguez, M.; Fulcrand, H.; Laur, J.; Martinez, J. Novel activity of angiotensin-converting enzyme. Hydrolysis of cholecystokinin and gastrin analogues with release of the amidated C-terminal dipeptides. *Biochem. J.* **1989**, *262*, 125−130.
(27) Yamada, K.; Uchida, S.; Takahashi, S.; Takayama, M.; Nagata, Y.; Suzuki, N.; Shirakura, S.; Kanda, T. Effect of a centrally active angiotensin-converting enzyme inhibitor, perindopril, on cognitive performance in a mouse model of Alzheimer's disease. *Brain Res.* **2010**, *352*, 176−186.
(28) Wu, J.; Aluko, R. E.; Nakai, S. Structural requirements of angiotensin I-converting enzyme inhibitory peptides: quantitative structure-activity relationship modeling of peptides containing 4−10 amino acid residues. *QSAR Comb. Sci.* **2006**, *25*, 873−880.
(29) Cushman, D. W.; Ondetti, M. A. Design of angiotensin converting enzyme inhibitors. *Nature* **1999**, *5* (10), 1110−1112.
(30) Kuba, K.; Imai, Y.; Ohto-Nakanishi, T.; Penninger, J. M. Trilogy of ACE2: a peptidase in the renin-angiotensin system, a SARS receptor, and a partner for amino acid transporters. *Pharmacol. Ther.* **2010**, *128*, 119−128.
(31) Thomas, M. C.; Pickering, R. J.; Tsorotes, D.; Koitka, A.; Sheehy, K.; Bernardi, S.; Toffoli, B.; Nquyen-Huu, T. P.; Head, G. A.; Fu, Y.; Chin-Dusting, J.; Cooper, M. E.; Tikellis, C. Genetic Ace2 deficiency accentuates vascular inflammation and atherosclerosis in the ApoE knockout mouse. *Circ. Res.* **2010**, *107*, 888−897.
(32) Pedersen, K. B.; Sriramula, S.; Chhabra, K. H.; Xia, H.; Lazartiques, E. Species-specific inhibitor sensitivity of ACE2 and its implication for ACE2 activity assays. *Am. J. Physiol. Regul. Integr. Comp. Physiol.* **2011**, *301*, R1293−R1299.
(33) Atlas, S. A. The renin-angiotensin aldosterone system: pathophysiological role and pharmacologic inhibition. *J. Managed Care Pharm.* **2007**, *13* (Suppl.), S9−S20.
(34) Tabassum, N. Aliskiren: a new renin inhibitor as anti-hypertensive. *J. Appl. Pharm. Sci.* **2011**, 30−33.
(35) Li, H.; Aluko, R. E. Identification and inhibitory properties of multifunctional peptides from pea protein hydrolysate. *J. Agric. Food Chem.* **2010**, *58*, 11471−11476.
(36) Takahashi, S.; Hori, K.; Hokari, M.; Gotoh, T.; Sgiyama, T. Inhibition of human renin activity by saponins. *Biomed. Res.* **2010**, *31*, 155−159.
(37) Guerard, F.; Decourcelle, N.; Sabourin, C.; Floch-laizet, C.; Le Grel, L.; Le Floch, P.; Gowlay, F.; Le Delezir, R.; Jaouen, P.; Bourseau, P. Recent developments of marine ingredients for food and nutraceutical applications: a review. *J. Sci. Hal. Aquat.* **2010**, *2*, 21−27.
(38) Yokoyama, K.; Chiba, H.; Yoshikawa, M. Peptide inhibitors for angiotensin I-converting enzyme from thermolysin digest of dried bonito. *Biosci., Biotechnol., Biochem.* **1992**, *56*, 1541−1545.
(39) Lee, J. K.; Hong, S.; Jeon, J. K.; Kim, S. K.; Byun, H. G. Purification and characterisation of angiotensin I converting enzyme inhibitory peptides from the rotifer, *Brachionus rotundiformis*. *Bioresour. Technol.* **2009**, *100* (21), 5255−5259.
(40) Tsai, J. S.; Lin, T. C.; Chen, J. L.; Pan, B. S. The inhibitory effects of freshwater clam (*Corbicula fluminea*, Muller) muscle protein hydrolysates on angiotensin I converting enzyme. *Process Biochem.* **2006**, *41* (11), 2276−2281.
(41) Je, J.-Y.; Park, P.-J.; Jung, W.-K.; Kim, S.-K. Amino acid changes in fermented oyster (*Crassostrea gigas*) sauce with different fermented periods. *Food Chem.* **2005**, *91*, 15−18.
(42) Wang, J.; Hu, J.; Cui, J.; Bai, X.; Du, Y.; Yuji, M.; Lin, B. Purification and identification of a ACE inhibitory peptide from oyster protein hydrolysate and the antihypertensive effect of hydrolysate in spontaneously hypertensive rats. *Food Chem.* **2008**, *111* (2), 302−308.
(43) Zhang, F. X.; Wang, Z.; Xu, S. Y. Macroporous resin purification of grass carp fish (*Ctenopharyngodon idella*) scale peptides with *in vitro*

DOI: 10.1021/jf505019z
J. Agric. Food Chem. 2015, 63, 1319−1331

angiotensin-I-converting enzyme (ACE) inhibitory ability. *Food Chem.* **2009**, *117* (3), 387.
(44) Jung, W. K.; Mendis, E.; Je, J. Y.; Park, P. J.; Son, B. W.; Kim, H. C.; Choi, Y. K.; Kim, S. K. Angiotensin I converting enzyme inhibitory peptides from yellowfin sole (*Limanda aspera*) frame protein and its antihypertensive effect in spontaneously hypertensive rats. *Food Chem.* **2006**, *94*, 26−32.
(45) Je, J. Y.; Park, P. J.; Byun, H. G.; Jung, W. K.; Kim, S. K. Angiotensin I converting enzyme (ACE) inhibitory peptide derived from the sauce of fermented blue mussel, *Mytilus edulis*. *Bioresour. Technol.* **2005**, *96*, 1624−1629.
(46) Toshiro, M.; Hiroshi, M.; Seki, E.; Osajima, K.; Nakahima, M.; Osajima, Y. Inhibition of Angiotensin-I-converting enzyme by *Bacillus licheniformis* alkaline protease hydrolysate derived from sardine muscle. *Biosci., Biotechnol., Biochem.* **1993**, *57* (6), 922−925.
(47) Fahmi, A.; Morimura, S.; Guo, H. C.; Shigematsu, T.; Kida, K.; Uemura, Y. Production of angiotensin I converting enzyme inhibitory peptides from sea bream scales. *Process Biochem.* **2004**, *39*, 1195−1200.
(48) Wu, H.; He, A. L.; Che, X. L.; Sun, C. Y.; Zhang, Y. Z.; Zhou, B. C. Purification and identification of novel angiotensin-I-converting enzyme inhibitory peptides from shark meat hydrolysate. *Process Biochem.* **2008**, *43*, 457−461.
(49) Byun, H. G.; Kim, S. K. Structure and activity of angiotensin I converting inhibitory peptides derived from Alaska pollack skin. *J. Biochem. Mol. Biol.* **2002**, *35*, 239−243.
(50) Lee, S. H.; Qian, Z. J.; Kim, S. K. A novel angiotensin I converting enzyme inhibitory peptide from tuna frame protein hydrolysate and its antihypertensive effect in spontaneously hypertensive rats. *Food Chem.* **2010**, *118*, 96−102.
(51) Sila, A.; Martinez-Alvarez, O.; Haddar, A.; Gómez-Guillén, M. C.; Nasri, M.; Montero, M. P.; Bougatef, A. Recovery, visoelastic and functional properties of barbel skin gelatine. Investigation of anti-DPP-IV and anti-prolylendopeptidase activities of generated gelatine polypeptides. *Food Chem.* **2015**, *168*, 478−480.
(52) Suetsuna, K.; Nakano, T. Identification of an antihypertensive peptide from peptic digest of wakame (*Undaria pinnatifida*). *J. Nutr. Biochem.* **2000**, *11* (9), 450−454.
(53) Fitzgerald, C.; Mora-Soler, L.; Gallagher, E.; O'Connor, P.; Prieto, J.; Soler-Vila, A.; Hayes, M. Isolation and characterisation of bioactive pro-peptides with in vitro renin inhibitory activities from the macroalga *Palmaria palmata*. *J. Agric. Food Chem.* **2012**, *60*, 7421−7427.
(54) Harnedy, P. A.; O' Keeffe, M. B.; FitzGerald, R. J. Purification and identification of dipeptidyl peptidase (DPP) IV inhibitory peptides from the macroalga *Palmaria palmata*. *Food Chem.* **2015**, *172*, 400−406.
(55) Fitzgerald, C.; Gallagher, E.; O'Connor, P.; Prieto, J.; Mora-Soler, L.; Grealy, M.; Hayes, M. Development of a seaweed derived platelet activating factor acetylhydrolase (PAF-AH) inhibitory hydrolysate, synthesis of inhibitory peptides and assessment of their toxicity using the zebrafish larvae assay. *Peptides* **2013**, *50*, 119−124.
(56) Sheih, I. C.; Fang, T. T.; Wu, T. K. Isolation and characterisation of a novel angiotensin I-converting enzyme inhibitory peptide from the algae protein waste. *Food Chem.* **2009**, *115*, 279−284.
(57) Jang, A.; Lee, M. Purification and identification of angiotensin converting enzyme inhibitory peptides from beef hydrolysates. *Meat Sci.* **2005**, *69* (4), 653−661.
(58) Di Bernardini, R.; Mullen, A. M.; Bolton, D.; Kerry, J.; O'Neill, E.; Hayes, M. Assessment of the angiotensin-I-converting enzyme (ACE-I) inhibitory and antioxidant activities of hydrolysates of bovine brisket sarcoplasmic proteins produced by papain and characterisation of associated bioactive peptide fractions. *Meat Sci.* **2012**, *90*, 226−235.
(59) Di Bernardini, R.; Rai, D. K.; Bolton, D.; Kerry, J.; O'Neill, E.; Mullen, A. M.; Harnedy, P.; Hayes, M. Isolation, purification and characterisation of antioxidant peptidic fractions from a bovine liver sarcoplasmic protein thermolysin hydrolysate. *Peptides* **2011**, *32*, 388−400.
(60) Arihara, K.; Nakashima, Y.; Mukai, T.; Ishikawa, S.; Itoh, M. Peptide inhibitors for angiotensin I converting enzyme from enzymatic hydrolysates of porcine skeletal muscle proteins. *Meat Sci.* **2001**, *57* (3), 319−324.
(61) Jiang, J.; Chen, S.; Ren, F.; Luo, Z.; Zeng, S. S. Yak milk casein as a functional ingredient: preparation and identification of angiotensin-I-converting enzyme inhibitory peptides. *J. Dairy Res.* **2007**, *74* (1), 18−25.
(62) Miguel, M.; Aleixandre, A. Antihypertensive peptides derived from egg protein. *J. Nutr.* **2006**, *136* (6), 1457−1460.
(63) Tidona, F.; Criscione, A.; Guastella, A. M.; Zuccaro, A.; Bordonaro, S.; Marletta, D. Bioactive peptides in dairy products. *Ital. J. Anim. Sci.* **2009**, *8*, 315−340.
(64) Hayes, M.; Stanton, C.; Slattery, H.; O'Sullivan, O.; Hill, C.; Fitzgerald, G. F.; Ross, R. P. Casein fermentate of *Lactobacillus animalis* DPC6134 contains a range of novel propeptide angiotensin-I-converting enzyme inhibitors. *Appl. Environ. Microbiol.* **2007**, *73* (14), 4658−4667.
(65) Cadée, J. A.; Chang, C.-Y.; Chen, C.-W.; Huang, C.-N.; Chen, S.-L.; Wang, C.-K. Bovine casein hydrolysate (C12 peptide) reduces blood pressure in prehypertensive subjects. *Am. J. Hypertens.* **2007**, *1*, 1−5.
(66) Yust, M. M.; Pedroche, J.; Giron-Calle, J.; Alaiz, M.; Millan, F.; Vioque, J. Production of ace inhibitory peptides by digestion of chickpea legumin with alcalase. *Food Chem.* **2003**, *81* (3), 363−369.
(67) Vecchi, B.; Anon, M. C. ACE inhibitory tetrapeptides from *Amaranthus hypochondriacus* 11 S globulin. *Phytochemistry* **2009**, *70*, 864−870.
(68) Lee, J.-E.; Bae, I. Y.; Lee, H. G.; Yang, C.-B. Tyr-Pro-Lys, an angiotensin I-converting enzyme inhibitory peptide derived from broccoli (*Brassica oleracea Italica*). *Food Chem.* **2006**, *99* (1), 143−148.
(69) Suetsuna, K. Isolation and characterisation of angiotensin I-converting enzyme inhibition dipeptides derived from *Allium satiuum* L. (garlic). *J. Nutr. Biochem.* **1998**, *9*, 415−419.
(70) Ma, M. S.; Bae, I. Y.; Lee, H. G.; Yang, C. B. Purification and identification of angiotensin I converting enzyme inhibitory peptides from buckwheat (*Fagopyrum esculentum* Moench). *Food Chem.* **2006**, *90*, 36−42.
(71) EFSA. Scientific opinion on the safety of "Sardine Peptide product". EFSA Panel on Dietetic Products, Nutrition and Allergies (NDA). *EFSA J.* **2010**, *8*, 1684.
(72) Phelan, M.; Kerins, D. The potential role of milk-derived peptides in cardiovascular disease. *Food Funct.* **2011**, *2*, 153−167.
(73) Yang, R.; Zou, Y.; Yu, N.; Zhenxin, G. Accumulation and identification of ACE peptides from wheat germ. *J. Agric. Food Chem.* **2011**, *59*, 3598−3605.
(74) Wang, H.; Zhang, S.; Sun, Y.; Dai, Y. ACE inhibitory peptide isolated from fermented soybean meal as functional food. *Int. J. Food Eng.* **2013**, *9* (1), 1−8.
(75) Parris, N.; Moreau, R. A.; Johnston, D. B.; Dickey, L. C.; Aluko, R. E. Angotensin I converting enzyme inhibitory peptides from commercial wet and dry milled corn germ. *J. Agric. Food Chem.* **2008**, *56*, 2620−2623.
(76) Bordenave, S.; Fruitier, I.; Ballandier, I.; Sannier, F.; Gildberg, A.; Batista, I.; Piot, J. M. HPLC preparation of fish waste hydrolysate fractions. Effect on guinea pig ileum and ACE activity. *Prep. Biochem. Biotechnol.* **2002**, *32*, 65−77.
(77) Jung, W. K.; Lee, B. J.; Kim, S. K. Fish-bone peptide increases calcium solubility and bioavailability in ovariectomised rats. *Br. J. Nutr.* **2006**, *95*, 124−128.
(78) Otani, L.; Ninomiya, T.; Murakani, M.; Osajima, K.; Kato, H.; Murakani, T. Sardine peptide with angiotensin-I-converting enzyme inhibitory activity improves glucose tolerance in stroke prone spontaneously hypertensive rats. *Biosci., Biotechnol., Biochem.* **2009**, *73*, 2203−2209.
(79) Fujita, H.; Yoshikawa, M. LKPNM: a prodrug-type ACE-inhibitory peptide derived from fish protein. *Immunopharmacology* **1999**, *44* (1−2), 123−127.
(80) Huang, J.-S.; Ko, W.-C. Angiotensin I-converting enzyme inhibitory activity of protein hydrolysates from tuna broth. *J. Food Drug Anal.* **2004**, *12*, 232−237.

DOI: 10.1021/jf505019z
J. Agric. Food Chem. 2015, 63, 1319−1331

(81) Fujita, H.; Yokoyama, K.; Yasumoto, R.; Yoshikawa, M. Antihypertensive effect of thermolysin digest of dried bonito in spontaneously hypertensive rat. *Clin. Exp. Pharmacol. Physiol.* **1995**, *22*, S304−S305.
(82) Fujita, H.; Yamagami, T.; Ohshima, K. Effects of an ACE-inhibitory agent, katsuobushi oligopeptide, in the spontaneously hypertensive rat and in borderline and mildly hypertensive subjects. *Nutr. Res. (N.Y.)* **2001**, *21*, 1149−1158.
(83) Vercruysse, L.; Van Camp, J.; Smagghe, G. ACE inhibitory peptides derived from enzymatic hydrolysate of animal muscle protein: a review. *J. Agric. Food Chem.* **2005**, *53*, 8106−8115.
(84) Kawasaki, T.; Seki, E.; Osajima, K.; Yoshida, M.; Asada, K.; Matsui, T.; Osajima, Y. Antihypertensive effect of valyl-tyrosine, a short chain peptide derived from sardine muscle hydrolyzate, on mild hypertensive subjects. *J. Hum. Hypertens.* **2000**, *14*, 519−523.
(85) Iwaniak, A.; Minkiewicz, P.; Darewicz, M. Food originating ACE inhibitors, including antihypertensive peptides as preventative food components in blood pressure reduction. *Compr. Rev. Food Sci. Food Saf.* **2014**, *13*, 114−134.
(86) Ghassem, M.; Babji, A. S.; Said, M.; Mahmoodami, F.; Arihara, K. Angiotensin-I-converting enzyme inhibitory peptides from snakehead fish sarcoplasmic protein hydrolysate. *J. Food Biochem.* **2014**, *38*, 140−149.
(87) Nazeer, R. A.; Kumar, G. *In vitro* and in vivo studies on the antioxidant activity of fish peptide isolated from the croaker (*Otolithes ruber*) muscle protein hydrolysate. *Peptides* **2012**, *35*, 261−268.
(88) Ko, J. Y.; Lee, J. H.; Samarakoon, K.; Kim, J. S.; Jeon, Y. J. Purification and determination of two novel antioxidant peptides from flounder fish (*Paralichthys olivaceus*) using digestive proteases. *Food Chem. Toxicol.* **2013**, *52*, 113−120.
(89) Udenigwe, C. C.; Aluko, R. E. Chemometric analysis of the amino acid requirements of antioxidant food protein hydrolysates. *Int. J. Mol. Sci.* **2011**, *12*, 3148−3161.
(90) Cross, K. J.; Huq, N. L.; Palamara, J. E.; Perich, J. W.; Reynolds, E. C. Physicochemical characterization of casein phosphopeptide-amprphous calcium phosphate nanocomplees. *J. Biol. Chem.* **2005**, *280*, 15362−15369.
(91) Rushen, J.; Boissy, A.; Terlouw, E. M. C.; de Passillé, A. M. B. Opioid peptides and behavioral and physiological responses of dairy cows to social isolation in unfamiliar surroundings. *J. Anim. Sci.* **1999**, *77*, 2918−2924.
(92) Teschemacher, H. Opioid receptor ligands derived from food proteins. *Curr. Pharm. Des.* **2003**, *9*, 1331−1344.
(93) Meisel, H.; FitzGerald, R. J. Opioid peptides encrypted in bovine milk proteins. *Br. J. Nutr.* **2000**, *1*, 27−31.
(94) Jauhiainen, T.; Korpela, R. Milk peptides and blood pressure. *J. Nutr.* **2007**, *137*, 825S−829S.
(95) Hartmann, R.; Meisel, H. Food-derived peptides with biological activity: from research to food applications. *Curr. Opin. Biotechnol.* **2007**, *18*, 163−169.
(96) Pihlanto-Leppälä, A. Bioactive peptides derived from bovine whey proteins: opioid and ACE-inhibitory peptides. *Trends Food Sci. Technol.* **2000**, *11*, 347−356.
(97) Yoshikawa, M.; Takahashi, M.; Yang, S. Delta opioid peptides derived from plant proteins. *Curr. Pharm. Des.* **2003**, *9*, 1325−1330.
(98) Nurminen, M. L.; Sipola, M.; Kaarto, H.; Pihlanto-Leppala, A.; Piilola, K.; Korpela, R.; Tossavainen, O.; Korhonen, H.; Vapaatalo, H. α-Lactorphin lowers blood pressure measured by radiotelemetry in normotensive and spontaneously hypertensive rats. *Life Sci.* **2000**, *66*, 1535−1543.
(99) Sipola, M.; Finckenberg, P.; Vapaatalo, H.; Pihlanto-Leppälä, A.; Korhonen, H.; Korpela, R.; Nurminen, M. L. α-Lactorphin and β-lactorphin improve arterial function in spontaneously hypertensive rats. *Life Sci.* **2002**, *71*, 1245−1253.
(100) Meisel, H. Biochemical properties of peptides encrypted in bovine milk proteins. *Curr. Med. Chem.* **2005**, *12*, 1905−1919.
(101) Yoshikawa, M.; Tani, F.; Shiota, A.; Suganuma, H.; Usui, H.; Kurahashi, K.; Chiba, H. Casoxin D, an opioid antagonist/ileum-contracting/vasorelaxing peptide derived from human α_{s1}-casein. In *β-Casomorphins and Related Peptides: Recent Developments*; Brantl, V., Teschemacher, H., Eds.; Wiley VCH: Weinheim, Germany, 1994; pp 43−48.
(102) Cudennec, B.; Ravallec-Plé, R.; Courois, E.; Fouchereau-Peron, M. Peptides from fish and crustacean by-products hydrolysates stimulate cholecystokinin release in STC-1 cells. *Food Chem.* **2008**, *111* (4), 970−975.
(103) Martínez, O.; Guimas, L.; Delannoy, C.; Fouchereau, M. Use of a commercial protease and yeasts to obtain CGRP-like molecules from saithe protein. *J. Agric. Food Chem.* **2008**, *56*, 7853−7859.
(104) Márquez-Rodas, I.; Longo, F.; Rothlin, R. P.; Balfagon, G. Pathophysiology and therapeutic possibilities of calcitonin gene related peptide in hypertension. *J. Physiol. Biochem.* **2006**, *62*, 45−56.
(105) Yamamoto, J.; Naemura, A.; UraM, I. Y.; Yamashita, T.; Kurioka, A. Testing various fruits for anti-thrombotic effect: I. Mulberries. *Platelets* **2006**, *17*, 555−564.
(106) Yamamoto, J.; Taka, T.; Yamada, K.; Murakami, M.; Hirata, Y. Tomatoes have natural anti-thrombotic effects. *Br. J. Nutr.* **2003**, *90*, 1031−1038.
(107) Yamamoto, J.; Yamada, K.; Naemura, A.; Yamashita, T.; Arai, R. Testing various herbs for anti-thrombotic effect. *Nutrition* **2005**, 80−87.
(108) Yamada, K.; Naemura, A.; Sawashita, N.; Noguchi, Y.; Yamamoto, J. An onion variety has natural anti-thrombotic effect as assessed by thrombosis/thrombolysis. *Thromb. Res.* **2004**, *114*, 213−220.
(109) Naemura, A.; Ohira, H.; Ikeda, M.; Koshikawa, K.; Ishii, H.; Yamamoto, J. An experimentally antithrombotic strawberry variety is also effective in humans. *Pathophysiol. Haemost. Thromb.* **2006**, *35*, 398−404.
(110) Naemura, A.; Mitani, T.; Ijiri, Y.; Tamura, Y.; Yamashita, T.; Yamamoto, J. Antithrombotic effect of strawberries. *Blood Coagul. Fibrinol.* **2005**, *16*, 501−509.
(111) Luzak, B.; Golanski, J.; Rozalski, M.; Boncler, M. A.; Watala, C. Inhibition of collagen-induced platelet reactivity by DGEA peptide. *Acta Biochim. Polym.* **2003**, *50*, 1119−1128.
(112) Khiari, Z.; Rico, D.; Martin-Diana, A. B.; Barry-Ryan, C. Structure elucidation of ACE-inhibitory and antithrombotic peptides isolated from mackerel skin gelatin hydrolysates. *J. Sci. Food Agric.* **2014**, *94*, 1663−1671.
(113) Sawashita, N.; Naemura, A.; Shimizu, M.; Morimatsu, F.; Ijiri, Y.; Yamamoto, J. Effect of dietary vegetable and animal proteins on atherothrombosis in mice. Basic nutritional investigation. *Nutrition* **2006**, *22*, 661−667.
(114) Shimizu, M.; Sawashita, N.; Morimatsu, F.; Ichikawa, J.; Taguchi, Y.; Yoshinobu, I.; Yamamoto, J. Antithrombotic papain-hydrolyzed peptides isolated from pork meat. *Thrombosis Res.* **2009**, *123*, 753−757.
(115) Akintunde, A. A.; Akinwusi, P. O. Metabolic syndrome: comparison of occurrence using three definitions in hypertensive patients. *Clin. Med. Res.* **2011**, *9*, 26−31.
(116) Wergedahl, H.; Liaset, B.; Gudbrandsen, O. A.; Lied, E.; Espe, M.; Muna, Z.; Mørk, S.; Berge, R. K. Fish protein hydrolysate reduces plasma total cholesterol, increases the proportion of HDL cholesterol, and lowers acyl-CoA:cholesterol acyltransferase activity in liver of Zucker rats. *J. Nutr.* **2004**, *134*, 1320−1327.
(117) Wergedahl, H.; Gudbrandsen, O. A.; Røst, T. H.; Berge, R. K. Combination of fish oil and fish protein hydrolysate reduces the plasma cholesterol level with a concurrent increase in hepatic cholesterol level in high-fat-fed Wistar rats. *Nutrition* **2009**, 98−104.
(118) Lin, Y. H.; Tsai, J. S.; Hung, L. B.; Sun-Pan, B. Hypocholesterolemic effect of compounded freshwater clam protein hydrolysate and *Gracilaria*. *Food Chem.* **2010**, *123*, 2395−2399.
(119) Lin, Y. H.; Tsai, J. S.; Hung, L. B.; Sun-Pan, B. Plasma lipid regulatory effect of compounded freshwater clam hydrolysate and *Gracilaria* insoluble dietary fibre. *Food Chem.* **2011**, *125*, 397−401.
(120) Tanaka, M.; Watanabe, S.; Wang, Z.; Matsumoto, K.; Matsui, T. His-Arg-Trp potently attenuates contracted tension of thoracic

DOI: 10.1021/jf505019z
J. Agric. Food Chem. 2015, 63, 1319−1331

aorta of Sprague-Dawley rats through the suppression of extracellular Ca^{2+} influx. *Peptides* **2009**, *30*, 1502−1507.
(121) Jung, W. K.; Kim, S. K. Calcium-binding peptide derived from pepsinolytic hydrolysates of hoki (*Iohnius belengerii*) frame. *Eur. Food Res. Technol.* **2007**, *224*, 763−767.
(122) Jung, W. K.; Lee, B. J.; Kim, S. K. Fish-bone peptide increases calcium solubility and bioavailability in ovariectomised rats. *Br. J. Nutr.* **2006**, *95*, 124−128.
(123) Ivey, M. E.; Osman, N.; Little, P. J. Endothelin-1 signaling in vascular smooth muscle pathways controlling cellular function associated with atherosclerosis. *Atherosclerosis* **2008**, *199*, 237−247.
(124) Okitsu, M.; Morita, A.; Kakitani, M.; Okada, M.; Yokogoshi, H. Inhibition of the endothelinconverting enzyme by pepsin digests of food proteins. *Biosci., Biotechnol., Biochem.* **1995**, *59*, 325−326.
(125) Maes, W.; Van Camp, J.; Vermeirssen, V.; Hemeryck, M.; Ketelslegers, J. M.; Schrezenmeir, J.; Van Oostveldt, P.; Huyghebaert, A. Influence of the lactokinin Ala-Leu-Pro-Met-His-Ile-Arg (ALPMHIR) on the release of endothelin-1 by endothelial cells. *Regul. Pept.* **2004**, *118*, 105−109.
(126) Fernández-Musoles, R.; Salom, J. B.; Martínez-Maqueda, D.; López-Díez, J. J.; Recio, I.; Manzanares, P. Antihypertensive effects of lactoferrin hydrolyzates: inhibition of angiotensinand endothelin-converting enzymes. *Food Chem.* **2013**, *139*, 994−1000.
(127) Vermeirssen, V.; van der Bent, A.; Van Camp, J.; van Amerongen, A.; Verstraete, W. A quantitative in silico analysis calculates the angiotensin I converting enzyme inhibitory activity in pea and whey protein digests. *Biochimie* **2004**, *86*, 231−239.
(128) Iwaniak, A.; Dziuba, J. BIOPEP-PBIL tool for the analysis of the structure of biologically active motifs derived from food proteins. *Food Technol. Biotechnol.* **2011**, *49*, 118−127.
(129) Iwaniak, A.; Minkiewicz, P.; Darewicz, M. Food-originating ACE inhibitors, including antihypertensive peptides, as preventative food components in blood pressure reduction. *Compr. Rev. Food Sci. Food Saf.* **2014**, *13*, 114−134.
(130) Cavazos, A.; Gonzalez de Meja, E. Identification of bioactive peptides from cereal storage proteins and their potential role in prevention of chronic diseases. *Compr. Rev. Food Sci. Food Saf.* **2013**, *12*, 363−380.
(131) Lafarga, T.; O' Connor, P.; Hayes, M. Identification of novel dipeptidyl peptidase-IV and angiotensin-I-converting enzyme inhibitory peptides from meat proteins using in silico analysis. *Peptides* **2014**, *59*, 53−62.
(132) Dziuba, B.; Dziuba, M. New milk protein derived peptides with potential antimicrobial activity: an approach based on bioinformatics studies. *Int. J. Mol. Sci.* **2014**, *15*, 14531−14545.
(133) Wu, J.; Aluko, R. E.; Nakai, S. Structural requirements of angiotensin I-converting enzyme inhibitory peptides: quantitative structure-activity relationship study of di- and tripeptides. *J. Agric. Food Chem.* **2006**, *54*, 732−738.
(134) Mooney, C.; Haslam, N. J.; Pollastri, G.; Shields, D. C. Towards the improved discovery and design of functional peptides: common features of diverse classes permit generalized prediction of bioactivity. *PLoS One* **2012**, *7*, No. e45012.
(135) Tang, Y.; Li, R.; Lin, G.; Li, L. PEP Search in MyCompoundID: detection and identification of dipeptides and tripeptides using dimethyl labeling and hydrophilic interaction liquid chromatography tandem mass spectrometry. *Anal. Chem.* **2014**, *86*, 3568−3574.
(136) Link, A. J.; Eng, J.; Schieltz, D. M.; Carmack, E.; Mize, G. J.; Morris, D. R.; Garvik, B. M.; Yates, J. R. Direct analysis of protein complexes using mass spectrometry. *Nat. Biotechnol.* **1999**, *17*, 676−682.
(137) Scientific Opinion of the Panel on Dietetic Products, Nutrition and Allergies on a request from Valio Ltd. On the scientific substantiation of a health claim related to *Lactobacillus helveticus* fermented Evolus® low-fat milk products and reduction of arterial stiffness. *EFSA J.* **2008**, *824*, 1−12.
(138) Renukuntla, J.; Vadlapudi, A. D.; Patel, A.; Boddu, S. H.; Mitra, A. K. Approaches for enhancing oral bioavailability of peptides and proteins. *Int. J. Pharm.* **2013**, *15*, 75−93.
(139) Pardridge, W. M. Drug transport across the blood-brain barrier. *J. Cerebral Blood Flow Metab.* **2012**, *32*, 1959−1972.
(140) Weksler, B.; Romero, I. A.; Couraud, P. O. The hCMEC/D3 cell line as a model of the human blood brain barrier. *Fluids Barriers CNS* **2013**, *10*, 1−10.

DOI: 10.1021/jf505019z
J. Agric. Food Chem. 2015, 63, 1319−1331

performed. In this paper, in vitro and in vivo methods for predicting the oral bioavailability of bioactive components will be summarized and compared in relation to their relevance to the living system. Later, a discussion of the potential of using in vitro and in vivo methods for the rapid bioavailability screening of future bioactive ingredients and their related oral formulations will also be included.

■ ORAL BIOAVAILABILITY

A sufficient dosage at the target site of action is critical for nutraceuticals to generate the desirable biological activities. That is, until the compound concentration becomes greater than the threshold dose, there could be no desirable health-promoting effect found. To obtain the appropriate concentration at the target site, it is important to determine the bioavailability of the bioactive compounds. Bioavailability is a principal pharmacokinetic term describing the fraction of the administered dose that reaches the system circulation without being altered. As system concentration obtained from intravenous injection was defined as 100% bioavailability, nutraceuticals administered through other delivery routes generally present lower bioavailability with incomplete absorption due to physiological or physiochemical barriers.

In particular, for the system concentration obtained after oral administration, oral bioavailability is greatly dependent on the ability of nutraceuticals to survive structural alteration from preabsorption degradation and postabsorption metabolism. Preabsorption events such as pH instability, ionic interaction, enzymatic degradation, and rapid GI elimination rate could significantly decrease the amount of ingested compound available for gut wall absorption. Once taken up by the intestinal enterocytes, the bioactive compound is then subjected to extensive structural transformation first by intestinal and then by hepatic metabolism. Taking into the account all of the events occurring after oral administration (Figure 1), oral bioavailability (F_{oral}) can be summarized and defined by the following equation:[5,6]

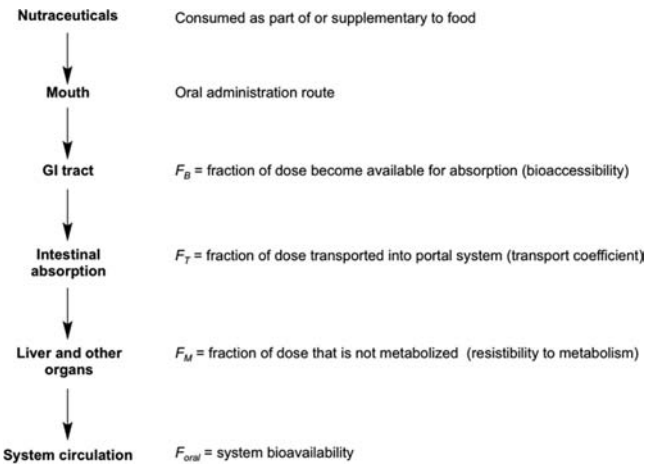

Figure 1. Process of orally ingested compound becoming bioavailable and factors that influence the oral bioavailability.

$$F_{oral} = F_B \times F_T \times F_M \quad (1)$$

In this mathematical expression, F_B is defined as the fraction of ingested dose that becomes accessible for intestinal absorption. The second component of the equation, F_T, describes the fraction of unchanged compound being transported into the portal system. The third component determining the oral bioavailability, F_M, outlines the fraction of ingested dose that survives metabolic activities as it travels to various systemic organs, such as the liver, heart, and lung. Hence, unlike intravenous injection, by which all of the applied dose reaches the system circulation, the system bioavailability of orally ingested nutraceuticals may be reduced to various degrees depending on their specific chemical structure, which influences the above-mentioned physiochemical parameters.

■ IN VITRO MODELS FOR PREDICTING ORAL BIOAVAILABILITY

Oral bioavailability is positively correlated with the bioaccessibility for GI absorption (F_B), the gut wall transport coefficient (F_T), and the resistibility to systemic metabolism (F_M). On the basis of the aforementioned theory, in vitro and in vivo models developed for predicting the oral bioavailability of nutraceuticals generally focus on evaluating one or more of the factors.

Bioaccessibility. Once ingested by mouth, dietary components enter the GI tract, which is essentially a compartment separated from other interior organs and the circulation system with a semipermeable barrier. To get to the inner system, nutraceuticals must be first absorbed by enterocytes. Thus, it is most critical that these bioactives are available at the absorption contact area. The bioaccessibility of a nutraceuitcal is then determined by quantifying the amount of ingested dose reaching the absorption site with its structure intact. The GI tract, specialized for digestion, consists of several sections each having a distinct physical and physiochemical environment responsible for the breakdown of diverse dietary components.

Nutraceuticals, just as all other dietary ingredients, go through the entire GI transition process, during which they may be chemically degraded and/or enzymatically metabolized to a product structure with totally different chemical properties. In other words, nutraceuticals must survive all of the degradation activities within the GI tract while being solubilized, or at least dispersed, in the aqueous lumen to become bioaccessible for absorption. To determine the bioaccessibility of a bioactive component, numbers of in vitro models, from simple to complex, are designed on the basis of the separable nature of the GI tract. Namely, the effect of pH, ionic interaction, enzyme activities, temperature, and luminal solubility on the compound bioaccessibility can be studied individually or systematically using suitable tests.

Chemical tests evaluating the stability of nutraceuticals at physiologically relevant ranges of temperature (37 °C), pH (2−7.5), and ionic composition are commonly performed methodologies to initially assess oral dosage efficiency.[7−14] However, the events occurring in the actual human GI tract comprise a rather complex biochemical process rather than just a few simple chemical reactions. Enzyme activities not only directly cause the structural change, such as bond cleavage and sugar moiety substitution, but also interfere with the absorption kinetics when other dietary components, such as lipids, proteins, and starches, are present.[10,15−18]

As an example, the absorption of hydrophobic compounds is significantly enhanced when lipid is present due to the improved aqueous solubility after being incorporated into the mixed micelle, which is the vehicle-like structure formed after lipid digestion.[5,19−21] An in vitro pH-stat model simulating the digestion environment in the small intestine, the major site for lipid digestion, is an especially suitable analytical tool to evaluate

DOI: 10.1021/jf5047464
J. Agric. Food Chem. 2015, 63, 1332−1338

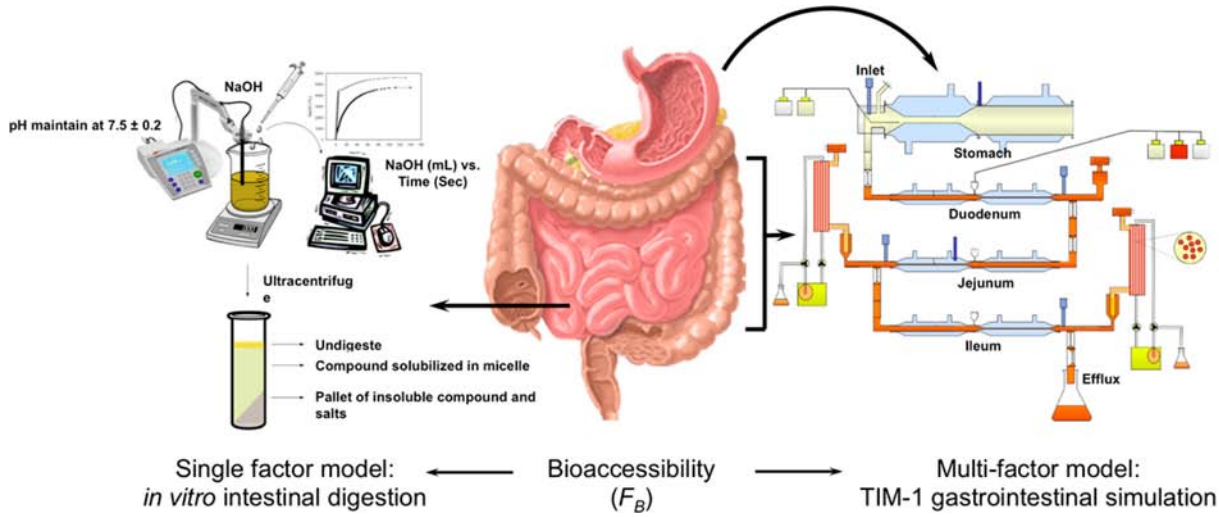

Figure 2. Common in vitro methods to evaluate the bioaccessibility of orally ingested nutraceuticals. The single-factor model simulates only the digestion activity with the small intestine. The multifactor model simulates the dynamic GI digestion events in both the stomach and small intestine.

the change in bioaccessibility for hydrophobic compounds when lipid is ingested either as part of the food matrix or oral formulations.[22,23] The single-factored in vitro chemical model is preferred by many investigators for initial screening of dosing efficiency because it is relatively simple to perform, cost-effective, and rapid and allows large sample throughput.

In addition to methodologies that contain only a single factor, multifactored models that combine two or more bioaccessibility-influential factors are also available (Figure 2). For example, the in vitro digestion model may simulate the physiochemical condition first in the stomach and then in the small intestine.[24] However, the in vitro models discussed above, regardless of number of factors addressed, are considered as static models due to their inability to reproduce the dynamic in vivo physical conditions including the peristalsis motion of the GI tract, integration of all of the influential physiological factors, transitional change in the physiological environment, and elimination from the absorption site. Consequently, the bioaccessibility predicted by static models usually overestimates the oral efficiency.[25]

To take the dynamic factor into account, a sophisticated instrument, a TIM-1 gastrointestinal simulation system, featuring a continuous in vitro digestion process, was developed by TNO Quality of Life, The Netherlands. Physiological and physiochemical factors, such as body temperature, peristalsis movement, gastric and intestinal residence time, pH, luminal composition, and elimination, are closely approximated by an automated computer system.[26] The bioaccessible fraction is determined by continuous sampling from jejunum and ileum sections over a predetermined time period.[25,27] Another advantage of using an open-compartment system, in which the unabsorbed portion is eliminated and collected as efflux, allows estimation of loss due to degradation because it can be quantified by subtracting the total recovered portion from the original input dosage. The TIM system, by far, is the most sophisticated and precise instrument for bioaccessibility estimation of dietary components.

Transport Coefficient. To travel across the intestinal lining, nutraceuticals may undertake either the transcellular or paracellur route. When the transcellular route is assumed, nutraceuticals from the gastric lumen are first absorbed into the enterocytes through either passive diffusion, which is driven by concentration gradient, or active transportation through the transcellular protein channels. During the in-and-out passage through the enterocytes, cellular metabolism significantly reduces the fraction of intact compound being released into the portal circulation.[28] Apart from the transcellular route, small molecules (M_w < 200) permeate through the membrane paracellularly through tight junction and do not go through the enterocytes. Nutraceuticals utilizing the paracellular route escape from the intestinal metabolism and retain the aglycone structure when streaming into the portal blood.[28,29]

Hence, the rate of compound transported from the GI tract into the portal system is dependent on its permeability to the cellular membrane and resistibility to intestinal metabolism. Unlike bioaccessibility, which is determined majorly by the physiochemical events in the GI lumen and can be easily simulated using in vitro chemical studies, the transport coefficient cannot be characterized using only the chemical experiment. A gastrointestinal model that includes a dialysis step after the in vitro digestion is the most simplified in vitro experiment for measuring the membrane transport rate of a dissolved compound.[30] Because no biological system was involved, the dialysis method that allows permeation of small molecules over a concentration gradient can be used only for estimating the fraction of compound that is transported through the paracellualr route.

The intestinal walls composed of a single layer of epithelial cells form the rate-limiting barrier to the transport of bioactive compounds. Cell culture model (Figure 3) of properly differentiated Caco-2 human colon carcinoma cells into phenotype with the characteristic physiochemical functions of the enterocytes is the commonly used in vitro method for elucidating the transport mechanism of nutraceuticals.[31−35] The Caco-2 monolayer allows effective in vitro prediction of compound permeability and absorption while taking into account all of the profound physical, chemical, and biological events during intestinal transportation.[36] Moreover, the Caco-2 monolayer model is also a well-developed model to effectively evaluate lymphatic transport (alterative transport route into the system circulation) of lipid-soluble compounds when included in lipid-based oral formulations.[37−39] However, the transport studies with the Caco-2 monolayer still have a number of disadvantages because the consistency of this study is highly

DOI: 10.1021/jf5047464
J. Agric. Food Chem. 2015, 63, 1332−1338

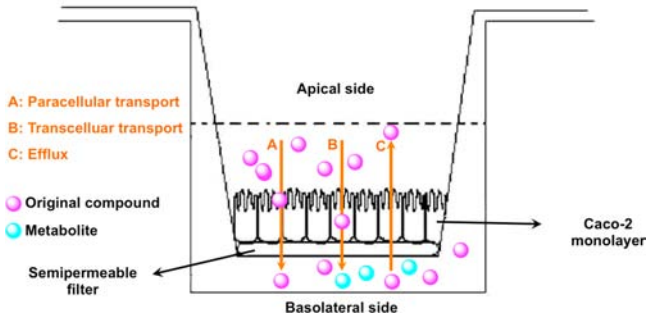

Figure 3. Transport coefficient evaluated using the Caco-2 monolayer model. The Caco-2 monolayer simulated the transport activity of intestinal epithelium utilizing both paracellular and transcellular transport routes.

dependent on the quality of the monolayer. Factors such as cell condition, passage number, length of cultivation, circumstance under which the study is performed, and the transport unit vary among laboratories.[40] Thus, the absolute transport coefficient values generated by different laboratories deviate accordingly and could not be compared directly. Moreover, the fact that Caco-2 human colon carcinoma cells have different physiological characteristics from the normal intestinal cell, such as lacking mucin, biofilm, and other epithelial cell types, can also cause unrealistic prediction of transport coefficient values in humans.[24]

In addition to the cell culture model, single-pass intestinal perfusion (SPIP) is an in situ animal model that provides enhanced approximation of intestinal physiology and allows the study of difference in the absorption behavior at various intestinal regions.[41] The experimental parameters, such as the compound concentration and the flow rate through the perfused section, are closely controlled to ensure the intra- and interexperimental comparabilities. In this model, the compound permeation efficiency is quantified as the concentration difference between the inlet and outlet of perfusate normalized by volume decrease due to water absorption.[42] However, the permeation rate quantified by the loss of compound in the perfusate retains a shortcoming of being unable to differentiate between the metabolized compound and the unchanged fraction, which is the main parameter for calculating the transport coefficient.

Resistibility to Systemic Metabolism. Once transported into the portal system, the absorbed component is then conveyed to the liver, where it will face rigorous first-pass metabolic activities. Due to the high density of the metabolic related cytochromes and enzymes, the liver is the principal facility for biotransformation of xenobiotics and is thought to be one of the major rate-limiting factors that reduce the system bioavailability of orally ingested nutraceuticals.[43] Cytochrome P-450 (CYPs) represents a family of membrane-associated proteins that is variably expressed in different organ tissues[44,45] and is responsible for the metabolism of >75% of endogenous compounds.[46] The major biotransformation of nutraceuticals by CYP450 monooxygenase includes oxidation, hydroxylation, and demethylation.[47,48] The isozymes mainly involved in the metabolism of bioactive compounds are CYP1A1, CYP2B, and CYP3A.[43,49,50]

As CYPs are most abundantly expressed in the liver, isolated liver microsomes are usually employed in the in vitro metabolic model that characterizes the biotransformation of nutraceuticals. During the metabolic test, compounds are incubated with liver microsomes, and the resulting product composition is usually identified by selected analytical instruments. The in vitro metabolism model is an effective method to evaluate the metabolic stability of nutraceuticals as it allows rapid, low-cost, and large throughput sampling. However, the use of animal liver microsomes to predict human metabolite composition is somewhat unreliable because the expression of CYPs is variable among animal species and is also highly dependent on the incubation and sampling interval.

IN VIVO PHARMACOKINETIC MODEL AND CORRELATION TO HUMAN ORAL BIOAVAILABILITY

The bioavailability of orally ingested compounds is the product of a complex process that integrates series of physiological or physiochemical reactions. In vitro methods designed to simulate an aspect of physiochemical process are useful tools for characterization and prediction of the in vivo pharmacokinetics in early screening of bioactive components. Because the bioavailability is affected by multiple factors, in vitro tests conducted in isolation usually present inadequate in vitro−in vivo correlations (IVIVC). Using the combinations of two or more in vitro models, the precision of estimating the oral bioavailability will increase because more influential factors are addressed. However, even the TIM-1 system being the most complex and closest simulation of preabsorption events in the human GI tract still cannot perfectly predict the oral bioavailability due to lack of biological factors, such as enterocyte absorption, systemic metabolism, and volume of body distribution. Thus, even though in vivo pharmacokinetic study is time-consuming, costly, and sometimes inhumane, it is still considered as the best described technique to predict human oral bioavailability. Because completely reproducing the pharmacokinetic process using in vitro models is overly complicated and unrealistic, in vivo animal models offer a living system imitating the full dynamic physiological and physiochemical events during the absorption, distribution, metabo-

Table 1. Pharmacokinetic Profile Different among Animal Species

phenolic	model	dose	t_{max} (h)	C_{max} (μmol/L)	AUC (μmol/L·h)	urinary excretion (%)	ref
quercetin	SD rats	10 mg/kg	0.078	0.69	0.2		57
	SD rats	50 mg/kg		4.9	48.44		58
		100 mg/kg		9.5	80.3		
	dogs	70.6 mg/kg	1.2	0.23	2.59		59
	pigs	50 mg/kg	2	1.19	6.55		60
	humans	50−65 mg/kg		<0.001			61
	humans	10 mg/70 kg	0.5	0.16−0.45		2.9−7.0	62
	humans	500 mg	3	0.05	0.21	1.18	63

DOI: 10.1021/jf5047464
J. Agric. Food Chem. 2015, 63, 1332−1338

lism, and elimination of orally ingested nutraceuticals. Even though the mechanism that underlies the pharmacokinetic process cannot be fully explained, analyzing the timed serum profile from the in vivo studies provides useful information on the oral bioavailability of ingested compounds as well as the metabolite profile.

Although animal data, especially pharmacokinetic profiles of rodents, have been widely used to predict oral bioavailability in humans, the correlation in the absorption of bioactive compounds between animals and humans has not been extensively studied. Variations in body weight, organ size, hepatic and renal blood flow, metabolism, distribution, and elimination rate result in significantly different pharmacokinetic profiles among different animal species. As an example, pharmacokinetic parameters, such as peak concentration time (t_{max}), peak serum concentration (C_{max}), total area under curve (AUC), and urinary excretion, of quercetin deviated accordingly when different in vivo models were used (Table 1). Developed according to the body weight and physiological parameters, allometric scaling was applied to in vivo animal data to better reflect the actual pharmacokinetic process in humans.[51,52] However, due to the complexity of physiological events in living systems, methods of scaling to 100% correlating the in vivo data to human oral bioavailability are still not available.[53]

Besides physiological factors of modeling systems, the pharmacokinetic profile is also significantly affected when different experimental designs were applied. For oral ingestion, the parameter having the most influence on the bioavailability is the physical and chemical characteristic of dosing formulation. By using different dosing media, the absorption of nutraceuticals can deviate appreciably due to changes in the bioaccessibility, a positively correlated parameter to system bioavailability. In particular, for a hydrophobic compound, oral absorption is improved when its solubility, the important factor for the compound to be available for gut wall absorption, becomes higher in the dosing medium.[54−56] In support of this idea, Piskula et al. found the oral bioavailability of quercetin was highest when solubilized in 100% propylene glycol, followed by 25% propylene glycol solution, and then water.[55] Inspired by the finding that better bioaccessibility leads to higher absorption rate, various oral delivery systems were designed to improve the pharmacokinetic profile of nutraceuticals with diverse chemical properties.[5,6] As an example, the oral bioavailability of a hydrophobic compound, such as curcumin (Table 2), is improved by the oral delivery system that enhances its aqueous solubility. On the other hand, delivery systems that could enhance the luminal stability and membrane permeability will lead to better oral bioavailability of EGCG, a hydrophilic compound that could be rapidly degraded in the GI tract (Table 3).

Table 2. Effect of Oral Formulation on the Oral Bioavailability of Curcumin

formulation	functional mechanism	result	ref
liposome	↑ solubility	↑ bioavailability	64
phospholipid complex	↑ solubility	↑ bioavailability	65
microemulsion	↑ solubility	↑ bioavailability	66
nanoemulsion	↑ solubility	↑ bioavailability	67
solid lipid nanoparticle	↑ solubility ↑ stability	↑ bioavailability	68
solid dispersion (with cellulose acetate)	↑ solubility	↑ bioavailability ↑ longer elimination time	69

Table 3. Effect of Oral Formulation on the Oral Bioavailability of EGCG

formulation	functional mechanism	result	ref
phospholipid complex	↑ permeability ↑ stability	↑ bioavailability	70
chitosan−nanoparticle	↑ permeability ↑ stability ↑ paracellular transport	↑ bioavailability	71

Due to the lack of consensus in the selection of animal models, dosing formulation, and delivery system, the in vivo pharmacokinetic data published by different investigators are rarely comparable. Thus, the prediction of human oral bioavailability is difficult without systematic collation of available pharmacokinetic data. Despite being the best preclinical model to evaluate the oral bioavailability of bioactive compounds, pharmacokinetic study itself does not provide enough mechanistic information to allow efficient data organization. In this sense, in vitro tests should be collectively conducted to study the pharmacokinetic behavior of nutraceuticals.

PREDICTION OF HUMAN ORAL BIOAVAILABILITY

To prevent the development of degenerative diseases, it is desirable for nutraceuticals to have good oral dosage efficiency because they are usually consumed either as part of a functional food or as a supplement (dietary supplement) to the diet. Oral bioavailability of bioactive compounds, as discussed in earlier sections, is majorly influenced by their bioaccessibility in the GI lumen, transport rate across the gut wall, and resistibility to the systemic metabolism. To better understand their contribution to the oral bioavailability individually and conjointly, these parameters could be evaluated by using proper in vitro and in vivo modeling systems because evaluating the pharmacokinetic profile using human subjects is expensive and may involve ethical issues. Thus, it is further desirable that these modeling systems could eventually allow accurate prediction of pharmacokinetic events in human body. Even though in vitro studies conveniently examine the factors that contribute to oral bioavailability, they cannot accurately predict human pharmacokinetic profiles without proper correlation to the in vivo system and the application of allometric scaling, which is calculated with regard to the interspecies difference. To take full advantage of the preclinical modeling system to realistically predict human oral bioavailability of nutraceuticals, the mathematical expression of oral bioavailability could be rewritten as follows:

$$F_{oral} = F_B \times F_T \times F_M \times C_A \times C_S \quad (2)$$

The mathematical equation reveals a future perspective, in which the evaluation of human oral bioavailability can be projected using only the in vitro modeling systems. In this equation, the bioaccessibility (F_B), transport rate (F_T), and resistibility to systemic metabolism (F_M) can all be determined with appropriate in vitro studies. The other two components represent the correlation factors of in vitro and in vivo modeling system (C_A) and interspecies scaling (C_S). To determine C_A and

DOI: 10.1021/jf5047464
J. Agric. Food Chem. 2015, 63, 1332−1338

C_S, a consistent experimental procedure is required when pharmacokinetic study using both animal and human subjects is carried out. The in vivo animal models serve as an important bridging factor that links the in vitro data to the actual events occurring in the human body.

To accurately calculate C_A and C_S, much more work needs to be done and problems must be solved. However, the benefits from successfully developing such a mathematical relationship between in vitro measurement and the human pharmacokinetic process are numerous. First, the cost and disadvantages of using models involving living creatures could be minimized. Second, factors that change the pharmacokinetic process can be easily taken into account by conducting in vitro testing of affected parameters. Third, rapid estimation of the required dosage for disease prevention is much more reliable and realistic with regard to the actual value in human subjects. Fourth, the effectiveness of oral formulation to enhance bioavailability can be efficiently determined without going through complicated evaluations. Overall, integration of modeling systems covering all aspects of physiological and physiochemical reactions that contribute to the oral bioavailability of nutraceticals offers the possibility to further elucidate the human pharmacokinetic process via a much more simplified and efficient procedure.

AUTHOR INFORMATION

Corresponding Author

*(Q.H.) Phone: (848) 932-5514. Fax: (732) 932-6776. E-mail: qhuang@aesop.rutgers.edu.

Notes

The authors declare no competing financial interest.

REFERENCES

(1) Tewfik, S.; Tewfik, I. Nutraceuticals, functional foods and botanical dietary supplements; promote wellbeing and underpin public health. *World Rev. Sci. Technol. Sustain. Dev.* **2008**, *5* (2), 104−123.

(2) Go, V. L. W.; Harris, D. M.; Srihari, P. In *Global Overview of the Role of Nutraceuticals in Cancer*; Sarkar, F. H., Ed.; Springer: Dordrecht, The Netherlands, 2012; pp 1−10.

(3) Scheepens, A.; Tan, K.; Paxton, J. W. Improving the oral bioavailability of beneficial polyphenols through designed synergies. *Genes Nutr.* **2010**, *5* (1), 75−87.

(4) Scalbert, A.; Williamson, G. Dietary intake and bioavailability of polyphenols. *J. Nutr.* **2000**, *130* (8), 2073S−2085S.

(5) Ting, Y. W.; Li, S.; Ho, C.-T.; Huang, Q. Emulsion in oral delivery of bioactive lipophilic phytochemicals. In *Nutrition, Functional and Sensory Properties of Foods*; Ho, C.-T., Mussinan, C., Shahidi, F., Colitis, E. T., Eds.; Royal Society of Chemistry: London, UK, 2013; Vol. 344, pp 231−242.

(6) Ting, Y.; Jiang, Y.; Ho, C.-T.; Huang, Q. Common delivery systems for enhancing in vivo bioavailability and biological efficacy of nutraceuticals. *J. Funct. Food* **2014**, *7*, 112−128.

(7) Zhu, Q. Y.; Zhang, A.; Tsang, D.; Huang, Y.; Chen, Z.-Y. Stability of green tea catechins. *J. Agric. Food Chem.* **1997**, *45* (12), 4624−4628.

(8) Zhu, Q. Y.; Holt, R. R.; Lazarus, S. A.; Ensunsa, J. L.; Hammerstone, J. F.; Schmitz, H. H.; Keen, C. L. Stability of the flavan-3-ols epicatechin and catechin and related dimeric procyanidins derived from cocoa. *J. Agric. Food Chem.* **2002**, *50* (6), 1700−1705.

(9) Wen, X.; Walle, T. Methylated flavonoids have greatly improved intestinal absorption and metabolic stability. *Drug Metab. Dispos.* **2006**, *34*, 1786−1792.

(10) Wang, X. Y.; Wang, Y.-W.; Huang, Q. R., Enhancing stability and bioavailability of polyphenols using nanoemulsions. In *Micro/Nano Encapsulation of Active Food Ingredients*; Huang, Q. R., Given, P., Qian, M., Eds.; Oxford University Press: Oxford, UK, 2009; Vol. 1007.

(11) Su, Y. L.; Leung, L. K.; Huang, Y.; Chen, Z. Y. Stability of tea theaflavins and catechins. *Food Chem.* **2003**, *83* (2), 189−195.

(12) McDougall, G. J.; Fyffe, S.; Dobson, P.; Stewart, D. Anthocyanins from red cabbage − stability to simulated gastrointestinal digestion. *Phytochemistry* **2007**, *68* (9), 1285−1294.

(13) Bermudez-Soto, M. J.; Tomas-Barberan, F. A.; Garcia-Conesa, M. T. Stability of polyphenols in chokeberry (*Aronia melanocarpa*) subjected to in vitro gastric and pancreatic digestion. *Food Chem.* **2007**, *102* (3), 865−874.

(14) Bell, L. N. Stability testing of utraceuticals and functional foods. In *Handbook of Nutraceuticals and Functional Foods*; Wildman, R. E. C., Ed.; CRC Press: New York, 2001; pp 501−516.

(15) Yang, X.; Tian, H.; Ho, C.-T.; Huang, Q. Stability of citral in emulsions coated with cationic biopolymer layers. *J. Agric. Food Chem.* **2011**, *60* (1), 402−409.

(16) McClements, D. J.; Decker, E. A.; Park, Y.; Weiss, J. Designing food structure to control stability, digestion, release and absorption of lipophilic food components. *Food Biophys.* **2008**, *3* (2), 219−228.

(17) Kim, M. K.; Park, K. S.; Yeo, W. S.; Choo, H.; Chong, Y. In vitro solubility, stability and permeability of novel quercetin-amino acid conjugates. *Bioorg. Med. Chem.* **2009**, *17* (3), 1164−1171.

(18) Cohen, R.; Schwartz, B.; Peri, I.; Shimoni, E. Improving bioavailability and stability of genistein by complexation with high-amylose corn starch. *J. Agric. Food Chem.* **2011**, *59* (14), 7932−7938.

(19) Trevaskis, N. L.; Charman, W. N.; Porter, C. J. H. Lipid-based delivery systems and intestinal lymphatic drug transport: a mechanistic update. *Adv. Drug Deliver. Rev.* **2008**, *60* (6), 702−716.

(20) Porter, C. J. H.; Trevaskis, N. L.; Charman, W. N. Lipids and lipid-based formulations: optimizing the oral delivery of lipophilic drugs. *Nat. Rev. Drug Discovery* **2007**, *6* (3), 231−248.

(21) Fricker, G.; Kromp, T.; Wendel, A.; Blume, A.; Zirkel, J.; Rebmann, H.; Setzer, C.; Quinkert, R. O.; Martin, F.; Muller-Goymann, C. Phospholipids and lipid-based formulations in oral drug delivery. *Pharm. Res.* **2010**, *27* (8), 1469−1486.

(22) McDougall, G. J.; Dobson, P.; Smith, P.; Blake, A.; Stewart, D. Assessing potential bioavailability of raspberry anthocyanins using an in vitro digestion system. *J. Agric. Food Chem.* **2005**, *53* (15), 5896−5904.

(23) McClements, D. J.; Li, Y. Review of in vitro digestion models for rapid screening of emulsion-based systems. *Food Funct.* **2010**, *1* (1), 32−59.

(24) Failla, M. L.; Huo, T.; Thakkar, S. K. In vitro screening of relative bioaccessibility of carotenoids from foods. *Asia Pac. J. Clin. Nutr.* **2008**, *17* (S1), 200−203.

(25) Ting, Y.; Jiang, Y.; Lan, Y.; Xia, C.; Lin, Z.; Roger, M. A.; Huang, Q. Use of viscoelastic emulsions to increase the oral bioavailability of tangeretin. *Mol. Pharm.* **2015**, submitted for publication.

(26) Blanquet, S.; Zeijdner, E.; Beyssac, E.; Meunier, J.-P.; Denis, S.; Havenaar, R.; Alric, M. A dynamic artificial gastrointestinal system for studying the behavior of orally administered drug dosage forms under various physiological conditions. *Pharm. Res.* **2004**, *21* (4), 585−591.

(27) Zhao, Q.; Lan, Y.; Xia, C.; Rogers, M. A.; Huang, Q. Comparison of in vitro models in determining bioaccessibility of nutraceuticals: the case of coenzyme Q10. *J. Funct. Foods* **2015**, submitted for publication.

(28) Lin, J. H.; Chiba, M.; Baillie, T. A. Is the role of the small intestine in first-pass metabolism overemphasized? *Pharm. Rev.* **1999**, *51* (2), 135−158.

(29) Pelkonen, O.; Boobis, A. R.; Gundert-Remy, U. In vitro prediction of gastrointestinal absorption and bioavailability: an experts' meeting report. *Eur. J. Clin. Pharmacol.* **2001**, *57* (9), 621−629.

(30) Bouayed, J.; Hoffmann, L.; Bohn, T. Total phenolics, flavonoids, anthocyanins and antioxidant activity following simulated gastro-intestinal digestion and dialysis of apple varieties: bioaccessibility and potential uptake. *Food Chem.* **2011**, *128* (1), 14−21.

(31) Zhang, L.; Zheng, Y.; Chow, M. S. S.; Zuo, Z. Investigation of intestinal absorption and disposition of green tea catechins by Caco-2 monolayer model. *Int. J. Pharm.* **2004**, *287* (1−2), 1−12.

(32) Walle, U. K.; Galijatovic, A.; Walle, T. Transport of the flavonoid chrysin and its conjugated metabolites by the human intestinal cell line Caco-2. *Biochem. Pharmacol.* **1999**, *58* (3), 431−438.

DOI: 10.1021/jf5047464
J. Agric. Food Chem. 2015, 63, 1332−1338

(33) Konishi, Y.; Kobayashi, S.; Shimizu, M. Transepithelial transport of *p*-coumaric acid and gallic acid in Caco-2 cell monolayers. *Biosci., Biotechnol., Biochem.* **2003**, *67* (11), 2317−2324.
(34) Chabane, M. N.; Al Ahmad, A.; Peluso, J.; Muller, C. D.; Ubeaud, G. Quercetin and naringenin transport across human intestinal Caco-2 cells. *J. Pharm. Pharmacol.* **2009**, *61* (11), 1473−1483.
(35) Boyer, J.; Brown, D.; Liu, R. H. In vitro digestion and lactase treatment influence uptake of quercetin and quercetin glucoside by the Caco-2 cell monolayer. *Nutr. J.* **2005**, *4*, 1.
(36) Hubatsch, I.; Ragnarsson, E. G. E.; Artursson, P. Determination of drug permeability and prediction of drug absorption in Caco-2 monolayers. *Nat. Protoc.* **2007**, *2* (9), 2111−2119.
(37) Levy, E.; Mehran, M.; Seidman, E. Caco-2 cells as a model for intestinal lipoprotein synthesis and secretion. *FASEB J.* **1995**, *9* (8), 626−635.
(38) Seeballuck, F.; Lawless, E.; Ashford, M. B.; O'Driscoll, C. M. Stimulation of triglyceride-rich lipoprotein secretion by polysorbate 80: in vitro and in vivo correlation using Caco-2 cells and a cannulated rat intestinal lymphatic model. *Pharm. Res.* **2004**, *21* (12), 2320−2326.
(39) Simmons, A. L.; Chitchumroonchokchai, C.; Vodovotz, Y.; Failla, M. L. Isoflavone retention during processing, bioaccessibility, and transport by Caco-2 cells: effects of source and amount of fat in a soy soft pretzel. *J. Agric. Food Chem.* **2012**, *60* (49), 12196−12203.
(40) Bailey, C. A.; Bryla, P.; Malick, A. W. The use of the intestinal epithelial cell culture model, Caco-2, in pharmaceutical development. *Adv. Drug Deliver. Rev.* **1996**, *22* (1−2), 85−103.
(41) Zakeri-Milani, P.; Valizadeh, H.; Tajerzadeh, H.; Azarmi, Y.; Islambolchilar, Z.; Barzegar, S.; Barzegar-Jalali, M. Predicting human intestinal permeability using single-pass intestinal perfusion in rat. *J. Pharm. Pharm. Sci.* **2007**, *10* (3), 368−379.
(42) Fagerholm, U.; Johansson, M.; Lennernas, H. Comparison between permeability coefficients in rat and human jejunum. *Pharm. Res.* **1996**, *13* (9), 1336−1342.
(43) Wilkinson, G. R. Drug metabolism and variability among patients in drug response. *New Engl. J. Med.* **2005**, *352* (21), 2211−2221.
(44) Ding, X. X.; Kaminsky, L. S. Human extrahepatic cytochromes P450: function in xenobiotic metabolism and tissue-selective chemical toxicity in the respiratory and gastrointestinal tracts. *Annu. Rev. Pharmacol.* **2003**, *43*, 149−173.
(45) Botto, F.; Seree, E.; Elkhyari, S.; Desousa, G.; Massacrier, A.; Placidi, M.; Cau, P.; Pellet, W.; Rahmani, R.; Barra, Y. Tissue-specific expression and methylation of the human Cyp2e1 gene. *Biochem. Pharmacol.* **1994**, *48* (6), 1095−1103.
(46) Guengerich, F. P. Cytochrome p450 and chemical toxicology. *Chem. Res. Toxicol.* **2007**, *21* (1), 70−83.
(47) Siess, M. H.; Leclerc, J.; Canivenc-Lavier, M. C.; Rat, P.; Suschetet, M.; Thanou, J. C.; Verhoef; Junginger, H. E. Heterogenous effects of natural flavonoids on monooxygenase activities in human and rat liver microsomes. *Toxicol. Appl. Pharmacol.* **1995**, *130*, 73−78.
(48) Nielsen, S. E.; Breinholt, V.; Justesen, U.; Cornett, C.; Dragsted, L. O. In vitro biotransformation of flavonoids by rat liver microsomes. *Xenobiotica* **1998**, *28* (4), 389−401.
(49) Canivenclavier, M. C.; Brunold, C.; Siess, M. H.; Suschetet, M. Evidence for tangeretin O-demethylation by rat and human liver-microsomes. *Xenobiotica* **1993**, *23* (3), 259−266.
(50) Bursztyka, J.; Perdu, E.; Tulliez, J.; Debrauwer, L.; Delous, G.; Canlet, C.; De, S. G.; Rahmani, R.; Benfenati, E.; Cravedi, J. P. Comparison of genistein metabolism in rats and humans using liver microsomes and hepatocytes. *Food Chem. Toxicol.* **2008**, *46* (3), 939−948.
(51) Boxenbaum, H. Interspecies scaling, allometry, physiological time, and the ground plan of pharmacokinetics. *J. Pharmacokinet. Biopharm.* **1982**, *10* (2), 201−225.
(52) Dedrick, R.; Bischoff, K. B.; Zaharko, D. S. Interspecies correlation of plasma concentration history of methotrexate (NSC-740). *Cancer Chemother. Rep.* **1970**, *54* (2), 95−101.
(53) Obach, R. S.; Baxter, J. G.; Liston, T. E.; Silber, B. M.; Jones, B. C.; MacIntyre, F.; Rance, D. J.; Wastall, P. The prediction of human pharmacokinetic parameters from preclinical and in vitro metabolism data. *J. Pharmacol. Exp. Ther.* **1997**, *283* (1), 46−58.
(54) Vallejo, F.; Larrosa, M.; Escudero, E.; Zafrilla, M. P.; Cerda, B.; Boza, J.; Garcia-Conesa, M. T.; Espin, J. C.; Tomas-Barberan, F. A. Concentration and solubility of flavanones in orange beverages affect their bioavailability in humans. *J. Agric. Food Chem.* **2010**, *58* (10), 6516−6524.
(55) Piskula, M. K.; Terao, J. Quercetin's solubility affects its accumulation in rat plasma after oral administration. *J. Agric. Food Chem.* **1998**, *46* (10), 4313−4317.
(56) Das, S.; Lin, H. S.; Ho, P. C.; Ng, K. Y. The impact of aqueous solubility and dose on the pharmacokinetic profiles of resveratrol. *Pharm. Res.* **2008**, *25* (11), 2593−2600.
(57) Chen, X.; Yin, O. Q.; Zuo, Z.; Chow, M. S. Pharmacokinetics and modeling of quercetin and metabolites. *Pharm. Res.* **2005**, *22* (6), 892−901.
(58) Hou, Y.; Chao, P.; Ho, H.; Wen, C.; Hsiu, S. Profound difference in pharmacokinetics between morin and its isomer quercetin in rats. *J. Pharm. Pharmacol.* **2003**, *55* (2), 199−203.
(59) Reinboth, M.; Wolffram, S.; Abraham, G.; Ungemach, F. R.; Cermak, R. Oral bioavailability of quercetin from different quercetin glycosides in dogs. *Br. J. Nutr.* **2010**, *104* (2), 198−203.
(60) Cermak, R.; Landgraf, S.; Wolffram, S. The bioavailability of quercetin in pigs depends on the glycoside moiety and on dietary factors. *J. Nutr.* **2003**, *133* (9), 2802−2807.
(61) Gugler, R.; Leschik, M.; Dengler, H. Disposition of quercetin in man after single oral and intravenous doses. *Eur. J. Clin. Pharmacol.* **1975**, *9* (2−3), 229−234.
(62) Goldberg, D. M.; Yan, J.; Soleas, G. J. Absorption of three wine-related polyphenols in three different matrices by healthy subjects. *Clin. Biochem.* **2003**, *36* (1), 79−87.
(63) Moon, Y. J.; Wang, L.; DiCenzo, R.; Morris, M. E. Quercetin pharmacokinetics in humans. *Biopharm. Drug Dispos.* **2008**, *29* (4), 205−217.
(64) Li, J.; Jiang, Y. Y.; Wen, J.; Fan, G. R.; Wu, Y. T.; Zhang, C. A rapid and simple HPLC method for the determination of curcumin in rat plasma: assay development, validation and application to a pharmacokinetic study of curcumin liposome. *Biomed. Chromatogr.* **2009**, *23* (11), 1201−1207.
(65) Liu, A. C.; Lou, H. X.; Zhao, L. X.; Fan, P. H. Validated LC/MS/MS assay for curcumin and tetrahydrocurcumin in rat plasma and application to pharmacokinetic study of phospholipid complex of curcumin. *J. Pharm. Biomed.* **2006**, *40* (3), 720−727.
(66) Hu, L. D.; Jia, Y. H.; Niu, F.; Jia, Z.; Yang, X.; Jiao, K. L. Preparation and enhancement of oral bioavailability of curcumin using microemulsions vehicle. *J. Agric. Food Chem.* **2012**, *60* (29), 7137−7141.
(67) Liu, Z. F.; Chiu, M.; Wang, J.; Chen, W.; Yen, W.; Fan-Havard, P.; Yee, L. D.; Chan, K. K. Enhancement of curcumin oral absorption and pharmacokinetics of curcuminoids and curcumin metabolites in mice. *Cancer Chemother. Pharm.* **2012**, *69* (3), 679−689.
(68) Kakkar, V.; Singh, S.; Singla, D.; Kaur, I. P. Exploring solid lipid nanoparticles to enhance the oral bioavailability of curcumin. *Mol. Nutr. Food Res.* **2011**, *55* (3), 495−503.
(69) Wan, S. X.; Sun, Y. Q.; Qi, X. X.; Tan, F. P. Improved bioavailability of poorly water-soluble drug curcumin in cellulose acetate solid dispersion. *AAPS PharmSciTech* **2012**, *13* (1), 159−166.
(70) Pietta, P.; Simonetti, P.; Gardana, C.; Brusamolino, A.; Morazzoni, P.; Bombardelli, E. Relationship between rate and extent of catechin absorption and plasma antioxidant status. *Biochem. Mol. Biol. Int.* **1998**, *46* (5), 895−903.
(71) Dube, A.; Nicolazzo, J. A.; Larson, I. Chitosan nanoparticles enhance the plasma exposure of (−)-epigallocatechin gallate in mice through an enhancement in intestinal stability. *Eur. J. Pharm. Sci.* **2011**, *44* (3), 422−426.

DOI: 10.1021/jf5047464
J. Agric. Food Chem. 2015, 63, 1332−1338

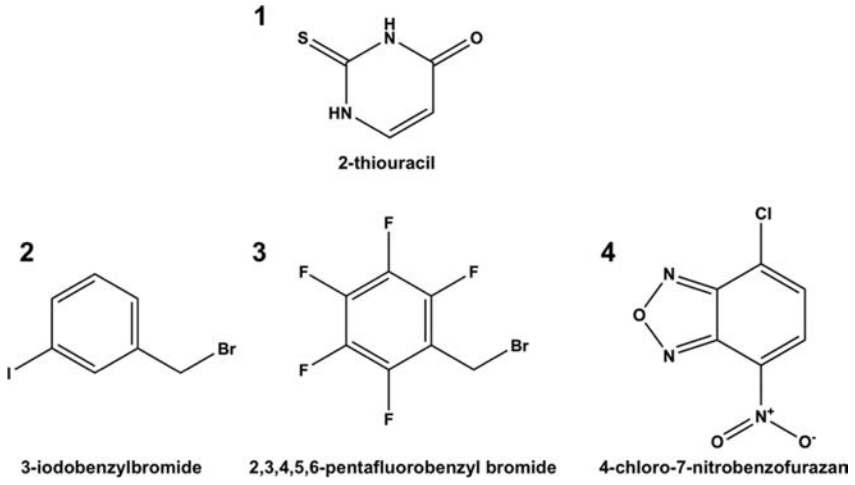

Figure 1. Molecular structure of 2-thouracil, 3-iodobenzyl bromide, 2,3,4,5,6-pentafluorobenzyl bromide, and 4-chloro-7-nitrobenzofurazan.

farms is very unlikely.[15−17] To explain this widely occurring phenomenon, thiouracil was no longer accepted to originate solely from synthetic products. In contrast, the semiendogenous status of thiouracil had to be unraveled.

Pinel et al.[18] performed a first study suggesting species belonging to the family Brassicaceae, commonly used as substantial feed ingredients, as a source of thiouracil. Together with the studies of Vanden Bussche et al.[19,20] and Kiebooms et al.,[21] evidence was gathered on the feed-derived origin of thiouracil. Species in the family Brassicaceae are known to contain glucosinolates, which may be metabolized to thiouracil by the enzymatic interaction with myrosinase at the time of chewing, ingestion, and digestion. A correlation between this particular diet and thiouracil in the urine of livestock was indeed definitely demonstrated.[19−21] However, a relevant concentration of thiouracil was not found in the unprocessed feed itself.[18,19] Additionally, the same correlation could not be demonstrated in a small sample study with humans, despite elevated thiouracil levels in their urine samples, suggesting the existence of additional natural thiouracil sources.[19] Because of these new insights and because of the increasing performance of the newly developed analytical techniques, the zero-tolerance approach of the EU for thiouracil needed revision. As a first step, a guidance paper was published in 2007 by the European Union of Reference Laboratories (EURLs),[22] suggesting a recommended concentration (RC) of 10 μg/L for thiouracil in urine. This RC has no legal value, but it is agreed to be a generally accepted target limit, which should be implemented, wherever possible, by any EU laboratory performing analysis in the light of the thiouracil monitoring programs.

More recently, two member states (France and Poland) suggested new thresholds based on their National Residue Monitoring Plan.[15,17] These studies were performed independently but reported similar outcomes for both countries, suggesting the current RC might be deficient, particularly for certain subgroups of cattle.

To encourage a revision of the existing European guidelines, including the definition of a consensual European threshold for endogenous thiouracil, in this study, a large-scale retrospective epidemiologic study (six member states, 2010−2012) was performed on naturally occurring thiouracil detected by LC-MS/MS in urine samples of bovines, small livestock, and porcines.

Epidemiologic Study Approach: Data Generation, Collection, and Analysis. Retrospective data on urinary thiouracil levels from bovines, small livestock (e.g., sheep, goat), with inclusion of reindeer and porcines, sampled between January 2010 and December 2012, were collected.

Qualified laboratories supplied data from six European countries (i.e., The Netherlands, France, United Kingdom (Great-Britain and Northern-Ireland), Norway, Poland, and Belgium). The contributions of each member state to the total data set of 3894 bovine, 85 small livestock, and 654 porcine records are listed in Table 1. A total of eight laboratories were

Table 1. Overview of Urinary Thiouracil Data Collection

	bovines	small livestock	porcines
The Netherlands	273	0	139
Belgium	244	0	4
France	1718	0	0
United Kingdom	871	5	2
Norway	432	79	124
Poland	356	1	385
total	3894	85	654

involved in the chemical analysis (two laboratories for Belgium and the United Kingdom; the Norwegian samples were outsourced to a third Belgian laboratory). These laboratories participated successfully in the 2013 proficiency test for the detection and quantification of thiouracil in bovine urine organized by the EURL (RIKILT, Wageningen).[23] Equal performances in urinary samples of other species, particularly small livestock and porcines, are assumed.

As previously mentioned, the urine samples arrived at the respective laboratories between January 2010 and December 2012 and were each briefly stored at −20 °C prior to analysis. In one laboratory, urine samples were stabilized by adding HCl (37%) and ethylenediaminetetraacetic acid (EDTA) (0.25 M) to prevent degrading of the compounds while extracting at room temperature. At the start of the extraction protocol, an internal standard was added to 1 mL urine. In most cases (7/8 laboratories), the thyrostatic compounds were derivatized with either 3-iodobenzyl bromide, **2** (5 laboratories), 2,3,4,5,6-pentafluorobenzyl bromide, **3** (1 laboratory), or 4-chloro-7-nitrobenzofurazan, **4** (1 laboratory) (Figure 1), followed by solid phase extraction (SPE), (multiple) liquid liquid extraction

DOI: 10.1021/jf504475f
J. Agric. Food Chem. 2015, 63, 1339−1346

Table 2. Population Parameters for the Total (Six Member States) Dataset of Bovine Urinary Thiouracil

	All Bovines				
	total	<6 months	6−12 months	12−24 months	>24 months
n	3894	426	301	575	1079
mean (μg/L)	1.7	3.4	4.1	1.5	1.5
median (μg/L)	0.0	2.0	2.6	0.0	0.4
SD (μg/L)	4.6	4.5	6.1	4	3.6
min (μg/L)	CC_α	CC_α	CC_α	CC_α	CC_α
max (μg/L)	145.0	25.0	64.5	70.0	77.0
≤CC_α (%)	87.6				
≤RC[a] (%)	96.4				
95% percentile	8.1	14.3	13.3	7.5	6.6
[95% CI[b]] (μg/L)	[7.2−8.9]	[11.0−17.6]	[11.2−14.8]	[5.8−9.4]	[5.0−7.9]
99% percentile	18.2	21.5	28.6	14.8	13.9
[95% CI] (μg/L)	[15.5−20.0]	[18.4−23.2]	[18.2−63.9]	[12.1−17.5]	[11.8−15.3]
	Female Bovines				
	total	<6 months	6−12 months	12−24 months	>24 months
n	1653	136	54	119	947
mean (μg/L)	1.4	2.7	1.3	1.5	1.3
median (μg/L)	0.3	1.6	0.0	0.0	0.4
SD (μg/L)	3.0	4.3	2.3	2.7	2.4
min (μg/L)	CC_α	CC_α	CC_α	CC_α	CC_α
max (μg/L)	34.0	22.1	10.2	15.5	23.1
≤CC_α (%)	90.1				
≤RC (%)	97.4				
95% percentile	6.5	14.5	5.9	8.2	5.8
[95% CI] (μg/L)	[5.1−7.3]	[5.7−19.9]	[4.4−10.2]	[4.7−9.6]	[4.7−6.9]
99% percentile	15.1	22.1	14.3	15.1	12.5
[95% CI] (μg/L)	[13.0−20.0]	[17.6−22.1]	[n.a.]	[9.1−15.5]	[10.9−14.7]
	Male Bovines				
	total	<6 months	6−12 months	12−24 months	>24 months
n	1168	273	205	449	98
mean (μg/L)	3.0	3.9	4.9	1.5	3.67
median (μg/L)	1.1	2.4	3.13	0.0	0.9
SD (μg/L)	5.8	4.6	6.9	4.3	9.1
min (μg/L)	CC_α	CC_α	CC_α	CC_α	CC_α
max (μg/L)	77.0	25.0	64.5	70.0	77.0
≤CC_α (%)	76.0				
≤RC (%)	92.6				
95% percentile	12.3	15.0	14.7	7.6	14.5
[95% CI] (μg/L)	[11.1−14.4]	[11.6−18.2]	[11.9−23.0]	[5.5−9.8]	[7.8−37.0]
99% percentile	25	21.0	35.9	14.8	37.0
[95% CI] (μg/L)	[18.4−32.7]	[18.4−25.0]	[22.3−64.5]	[11.8−19.0]	[n.a.]

[a]RC = recommended concentration. [b]CI = confidence interval.

(LLE), a combination of LLE and SPE, or of LLE with duplicate SPE, adapted from previous reports.[12,14] One participating laboratory did not perform any derivatization but added 1% dithiothreitol (DTT; 1,4-bis(sulfanyl)butane-2,3-diol) to the urine aliquot prior to LLE.[13] Thiouracil (and other thyrostats) was finally detected and identified by triple quadrupole (QqQ-MS/MS) mass analyzers after chromatographic separation on a reversed-phase C18 U(H)PLC column.

For each species (cattle, small livestock, and pigs), statistical analysis was performed on the respective data set. Subpopulations (within one species) were created and compared based on gender (male versus female), age (<6 months, 6−12 months, 12−24 months, and >24 months), the combination of gender and age, or the geographical region (member state). Since these subpopulations clearly deviate from a normal distribution, statistical differences between groups were assessed by either Kruskal−Wallis (multiple comparisons) with a posthoc Dunn's test or by the Mann−Whitney rank sum test (comparison of 2 groups), which is significant if $p < 0.05$. The descriptive statistics (mean, median, standard deviation (SD), minimum, maximum, and percentiles) of each subpopulation were acquired, with special interests for specific population parameters such as the 95 and 99% percentiles. For the latter parameters, a 95% confidence interval (CI) was calculated by nonparametric bootstrapping.[24,25] This confidence interval estimates the uncertainty associated with the population's percentile estimates.

Concentration values below the CCα (decision limit) of the respective (sub)populations were set equal to zero. If analysis was performed on a combination of subpopulations with different CCα values, the CCα of the subpopulation with the highest CCα was used for the entire batch. Clearly, this

DOI: 10.1021/jf504475f
J. Agric. Food Chem. 2015, 63, 1339−1346

Table 3. Member State Specific Population Parameters for Bovine Urinary Thiouracil

	member state					
	The Netherlands	Belgium	France	United Kingdom	Norway	Poland
n	273	244	1718	871	432	356
mean (μg/L)	5.8	2.4	1.6	0.8	1.4	0.9
median (μg/L)	4.3	0.0	0.6	0.0	0.0	0.0
SD (μg/L)	5.4	12.0	2.7	4.4	2.5	2.8
min (μg/L)	CC_α	CC_α	CC_α	CC_α	CC_α	CC_α
max (μg/L)	36.4	145	25	77	29.7	23.1
≤CC_α (%)	46.2	89.8	37.1	94.7	65.7	81.2
≤RC[a] (%)	81.3	93.0	97.8	97.2	99.5	97.2
95% percentile	15.5	14.8	6.2	4.5	5.57	5.24
[95% CI[b]] (μg/L)	[13.5−18.3]	[7.6−29.7]	[4.5−7.1]	[0−7.1]	[4.5−6.2]	[3.9−8.9]
99% percentile	26.4	67.5	14.3	21.56	9.2	15.5
[95% CI] (μg/L)	[18.8−36.4]	[29.0−145.0]	[12.0−16.6]	[13.7−31.0]	[6.9−9.4]	[11.9−20.3]

	Gender					
	France		Norway		Poland	
	male	female	male	female	male	female
n	625	1015	166	218	122	231
mean (μg/L)	2.0	1.4	1.2	1.5	0.9	0.9
median (μg/L)	0.6	0.6	0.0	0.0	0.0	0.0
SD (μg/L)	3.2	2.4	2.0	2.1	2.6	3.0
min (μg/L)	CC_α	CC_α	CC_α	CC_α	CC_α	CC_α
max (μg/L)	25.0	22.1	9.4	8.8	18.2	23.1
≤CC_α (%)	42.2	33.1	71.1	60.1	79.5	82.3
≤RC (%)	97.3	98.0	100	100	97.5	97.0
95% percentile	7.7	5.0	5.5	5.1	5.0	5.9
[95% CI] (μg/L)	[5.8−9.5]	[4.4−6.7]	[4.4−6.7]	[4.4−6.9]	[3.5−10.4]	[3.5−11.7]
99% percentile	18.0	13.5	9.4	7.9	16.9	15.5
[95% CI] (μg/L)	[13.6−20.3]	[10.7−14.8]	[6.3−9.4]	[6.9−8.8]	[8.8−18.1]	[12.3−23.1]

	Age			
	France			
	<6 months	6−12 months	12−24 months	>24 months
95% percentile	8.8	5.7	7.9	6.2
[95% CI] (μg/L)	[6.1−18.0]	[4.5−8.9]	[5.1−9.9]	[4.7−7.9]
99% percentile	22.3	9.4	12.4	13.5
[95% CI] (μg/L)	[19.8−25.0]	[7.3−9.5]	[10.0−14.3]	[10.8−14.7]

[a]RC = recommended concentration. [b]CI = confidence interval.

approach does not influence the percentiles, but particularly, parametric values such as "mean" and "standard deviation" may be slightly influenced. Statistical analysis was performed with SPSS version 22.0 (IBM, Brussels, Belgium).

Occurrence and Evaluation of Thiouracil in Urine. *Total Bovine Data Set.* A detailed overview of the most important population parameters can be seen in Table 2. Considering the highest CCα (3.9 μg/L) throughout the participating laboratories as a cutoff, the presence of thiouracil was identified in 12.4% (n = 483) of the samples (>CCα = 3.9 μg/L), with 3.6% of the data set (n = 140) containing higher thiouracil levels than the RC (=10 μg/L). Consequently, the 95% percentile is characterized by a concentration below the RC (8.1 [7.2−8.9] μg/L) while the 99% percentile is substantially higher (18.2 [15.5−20] μg/L). A maximum value of 145 μg/L (from Belgium), which could not be explained, was observed within this population (Figure 1).

The animals' gender was known in 72.4% of the sample pool, while their age was defined in 61.1% of the samples. Higher thiouracil concentrations were observed for male bovines compared to female bovines, with significantly higher 95% (12.3 [11.1−14.4] μg/L versus 6.5 [5.1−7.3] μg/L, respectively) and 99% (25.0 [18.4−32.7] μg/L versus 15.1 [13.0−20.0] μg/L, respectively) percentiles, both exceeding the RC (p < 0.01).

Young animals ≤12 months were revealed to be another subpopulation with increased urinary thiouracil levels and 95 and 99% percentiles above the RC (Table 2) (p < 0.001). However, if solely female animals were observed, the definition of "young animals" needed to be adapted to "not older than 6 months", while in male animals both the young (≤12 months) and the older (>24 months) bulls had significantly higher thiouracil levels (p < 0.01).

Member State Specific Bovine Data Set. The descriptive statistics of the six participating member states are presented in Table 3. Frequency plots of these member states are illustrated in Figure 2, and more specific population numbers are added in Table 4.

Overall, the data sets of the two smallest member states, Belgium and The Netherlands, were evaluated as statistically different compared to the remaining four data sets (p < 0.01). Both the 95% (14.8 [7.6−29.7] μg/L and 15.5 [13.5−18.3] μg/L, respectively) and 99% (26.4 [18.8−36.4] μg/L and 67.5 [29.0−145.0] μg/L, respectively) percentiles exceeded the RC

DOI: 10.1021/jf504475f
J. Agric. Food Chem. 2015, 63, 1339−1346

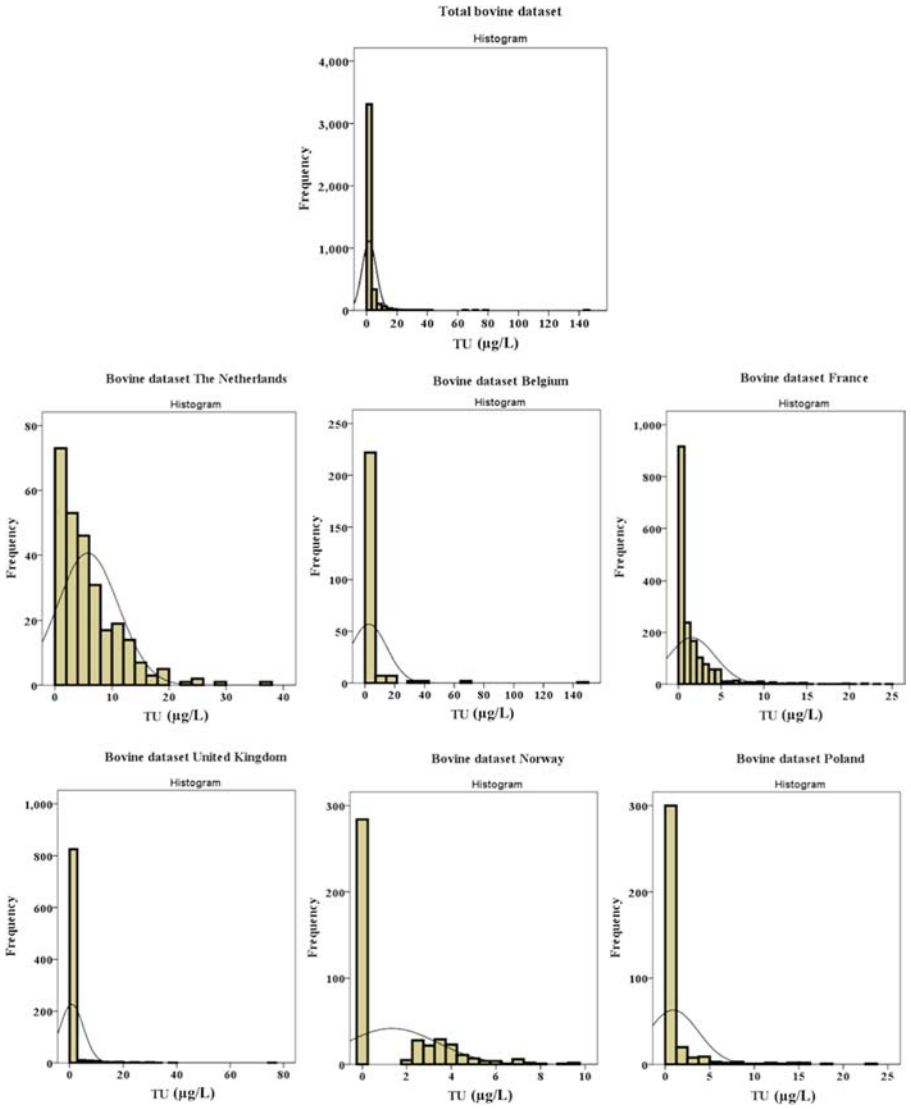

Figure 2. Frequency histograms of the total bovine and member state specific data set indicating the number of samples between given concentrations of urinary thiouracil (μg/L).

Table 4. Member State (Bovine) Population Distributions Based on Age and Gender

	age					gender		
	<6 months	6–12 months	12–24 months	>24 months	unknown	male	female	unknown
The Netherlands	130	143	0	0	0	218	19	36
Belgium	1	1	5	8	229	15	11	218
France	282	121	299	700	316	625	1015	78
United Kingdom	0	0	3	12	856	22	159	690
Norway	4	15	134	178	101	166	218	48
Poland	9	21	134	181	11	122	231	3

substantially, which was not the case for the 95% percentiles of any other member state (max 6.2 μg/L) (nor for the Norwegian 99% percentile (9.2 [6.9–9.4] μg/L)). The Dutch and Belgian data sets are indeed defined by a large sample fraction containing more than 10 μg/L thiouracil (up to 18.7%), while this fraction was limited to 2.8% for the remaining four member states. Due to limited numbers (in one or more subpopulation) and/or lack in detailed information, influences of gender (France, Norway and Poland) and age (France) could only be statistically evaluated in three member states (Table 3). Males and young animals (<6 months) were confirmed to be responsible for higher urinary thiouracil levels, but this could only be statistically confirmed from the largest (French) data set ($p < 0.01$ and $p < 0.01$).

Small Livestock Data Set. Samples ($n = 85$) collected from 63 sheep, 16 goats, and 6 reindeer originating from Norway ($n = 79$), United Kingdom ($n = 5$), and Poland ($n = 1$) were included in this data set (Figure 2). Due to the limited sample group ($n = 85$) with only two samples (2.4%) above the RC, only the 95% percentile (7.3 [4.3–17.0] μg/L) could be defined (Table 5).

DOI: 10.1021/jf504475f
J. Agric. Food Chem. 2015, 63, 1339–1346

Table 5. Population Parameters for the Datasets of Small Livestock and Porcine Urinary Thiouracil

	small livestock	porcines			
	total	total	The Netherlands	Poland	Norway
n	85	654	139	385	124
mean (μg/L)	1.6	1.5	4.4	0.8	0.1
median (μg/L)	0.0	0.0	3.1	0.0	0.0
SD (μg/L)	3.9	2.83	4.0	1.7	0.6
min (μg/L)	CC_α	CC_α	CC_α	CC_α	CC_α
max (μg/L)	27.0	26.4	26.4	16.6	4.5
95% percentile	7.3	7.4	11.3	3.4	0.0
[95% CI[a]] (μg/L)	[4.3−17.0]	[6.4−8.4]	[10.1−14.0]	[3.0−4.7]	[0.0−2.8]
99% percentile	na	13.5	23.8	8.0	4.1
[95% CI] (μg/L)		[10.5−17.0]	[13.4−26.4]	[5.2−10.5]	[2.2−4.5]

[a]CI = confidence interval.

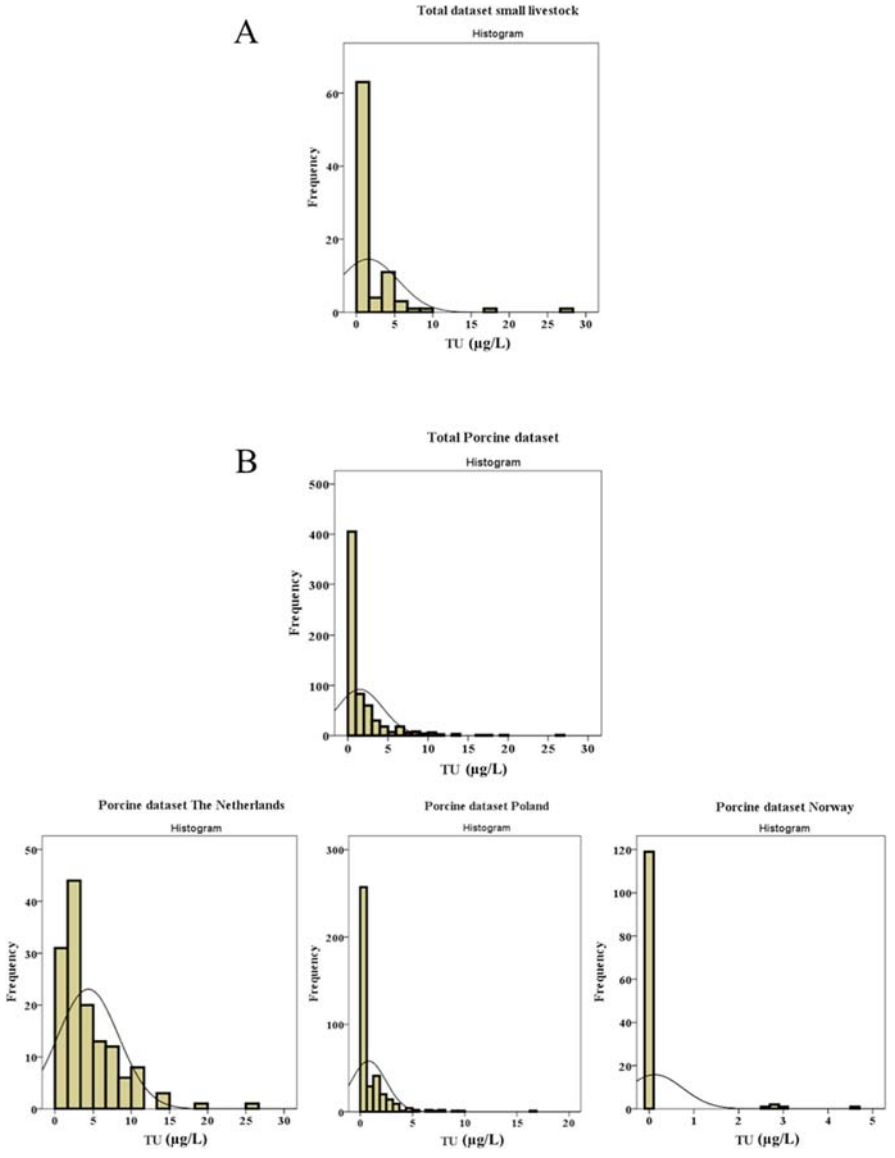

Figure 3. Frequency histograms of (A) the total small livestock population and (B) the total porcine and member state specific data set, indicating the number of samples between given concentrations of urinary thiouracil (μg/L).

Porcine Data Set. The majority of thiouracil data in porcine urine samples was provided by Poland (n = 385), The Netherlands (n = 139), and Norway (n = 124). Limited contributions from Belgium (n = 4) and United Kingdom (n = 2) were included as well.

In 97.7% of the samples, the urinary thiouracil level was below the RC of 10 μg/L, while in 77.1% of the samples,

DOI: 10.1021/jf504475f
J. Agric. Food Chem. 2015, 63, 1339−1346

thiouracil could not be detected (<CC_α). The 95% and 99% percentiles for this database were at 7.4 [6.4−8.4] μg/L and 13.5 [10.5−17.0] μg/L, respectively. These thresholds were not influenced by gender or age. However, data sets differed geographically (exclusion of Belgian and British data set), with significantly higher percentiles for The Netherlands (11.3 [10.1−14.0] μg/L and 23.8 [13.4−26.4] μg/L, for the 95% and 99% percentiles, respectively) compared to Norway (<CC_α [0.0−2.8] μg/L and 4.1 [2.2−4.5] μg/L for the 95% and 99% percentiles, respectively) (Table 5; Figure 3).

DISCUSSION

With this retrospective study, we aimed to evaluate the applicability of the recommended concentration (RC) for monitoring thiouracil in urine samples of bovines, small livestock, and pigs, advised by the EURL,[22] by statistically approaching sample outcomes gained in several European member states from January 2010 to December 2012. A similar epidemiologic threshold-definition has been previously performed on the national level by two participating member states.[15,17] However, combining up to six member states with a rather scattered distribution throughout Europe allows assessing a broader and larger (thus statistically more powerful) sample size and may identify geographical peculiarities.

Due to the obvious lack of homoscedasticity of the data set, analysis was performed integrally by nonparametric analysis. The population "extremes" were hereby described by 95% and 99% percentiles, covered by their bootstrapped 95% confidence intervals (CI), which give an estimation of the uncertainty of the numeric concentration value associated with the percentiles.[24,25] The inclusion of the CI in this study allows comparing results of similar studies, such as the earlier mentioned French and Polish study. The (bovine and porcine) percentiles reported in these studies fit the respective national CI values of the current study, with one exception for the 99% percentiles for French male bovines and the 95% percentiles for Polish porcines, both below their respective CI. The results of these and the current study are therefore (largely) in agreement, leading toward similar reflections.

It depends on the kind of threshold and its application-scope whether the 95% or 99% percentile, or its upper CI limits, should be taken into account for decision-making.[26,27] Although recommendations on this final choice are out of the scope of this study, the current obtained results, and earlier reports, strongly indicate the need to increase (if 99% percentiles are taken into consideration), or at least refine (if 95% percentiles are considered), the RC that is currently suggested.

Indeed, when selecting the 95% percentiles (with CI) as most stringent thresholds, the present RC is inadequate in very young and/or male bovines. The latter might explain the highest percentiles for the Dutch data set, since 80% of the data involved male animals younger than 1 year (no population details are available on the Belgian data set with similar percentiles). However, high thiouracil levels were also observed in urine samples of Dutch pigs with no statistical interference of age and gender. Another feature, unrelated with any population characteristic, might explain these high thiouracil levels in both bovine and porcine urine. The Dutch protocol seems to contrast with the seven other laboratory protocols by an additional thyrostat-stabilizing step. The stability of thyrostatic drugs in bovine and porcine urine has been extensively studied.[28] Urinary thiouracil concentrations were found to decrease rather drastically if inappropriately stored (e.g., short time at room temperature or prolonged at −70 °C), if the pH exceeded a value greater than 3 and if copper was present. Vanden Bussche et al.[28] suggested therefore a successful pretreatment by which the pH was adapted to 1 and EDTA was added to chelated copper. This treatment turned out to delay thyrostat-decay for 24 h at room temperature, in effect controlling degradation while performing the extraction and at least for three months at −70 °C. This is likely to be responsible for the more elevated thiouracil levels in the Dutch data set. Similarly, lower thiouracil levels (with low percentiles) in Norwegian bovine and porcine urine samples may be due to the applied protocol, which discriminates itself by the lack of derivatization. However, this protocol[13] was successfully validated in accordance with Commission Decision 2002/657/EC and fulfilled the performance criteria of the 2013 proficiency test.[23,29] It is therefore more likely that other factors, related to the Norwegian farming style (e.g., feed, pasture type, housing, etc.), have been influencing the data.

The definition of a European threshold for urinary thiouracil to distinct endogenous from administered thiouracil is not straightforward. Two independent national surveys have previously expressed their concerns and have suggested a revision of the existent RC. Considering these and current study results, the urge for a revision of the recommended concentration and/or the definition of the reference points for action for thiouracil residues in urine is obviously demonstrated, with special emphasis on the identified influencing factors, for example, the applied laboratory protocol (all species), gender (cattle), and age (cattle). Consequently, our findings are in agreement with the latest reflection paper of the EURL in which an increase of the RC from 10 to 30 μg/L is suggested.[30]

However, since the endogenous thiouracil levels are clearly multifactorially influenced and the uncertainty related to the threshold approach may still result in incorrect decision-making with major impact on the farmers' activities, future research should not only aim to identify other endogenous sources of thiouracil and related pathways but also investigate potential biomarkers specific for exogenous thiouracil administration or endogenous thiouracil formation. The discovery of a discriminating biomarker might unequivocally alleviate any shortcomings related to the threshold-approach.

ASSOCIATED CONTENT

Supporting Information

Supplementary Table 1: details on the sample extraction and LC-MS/MS detection of urinary thiouracil for the participating laboratories (MeOH = methanol; MeCN = acetonitrile). This material is free of charge via the Internet at http://pubs.acs.org.

AUTHOR INFORMATION

Corresponding Author

*Tel: +3292647457. Fax: +3292647492. E-mail: Lynn.Vanhaecke@ugent.be.

Funding

This research was funded by the Belgian Federal Public Service for Health, Food Chain Safety and Environment with reference number RF12/6260 (THYREOMERK).

Notes

The authors declare no competing financial interest.

DOI: 10.1021/jf504475f
J. Agric. Food Chem. 2015, 63, 1339−1346

■ ACKNOWLEDGMENTS

The authors thank J. Goedgebuer for her technical assistance and M. Andjelkovic, J. Van Loco, and H. van Rhijn for data contributions.

■ ABBREVIATIONS USED

CI, confidence interval; DTT, dithiothreitol; EDTA, ethylenediaminetetraacetate acid; EURLs, European Union reference laboratories; LLE, liquid−liquid extraction; MRLP, minimum required performance limit; QqQ, triple quadrupole; RC, recommended concentration; SPE, solid phase extraction

■ REFERENCES

(1) Astwood, E. B. Treatment of hyperthyroidism with thiourea and thiouracil. *J. Am. Med. Assoc.* **1943**, *122*, 78−81.
(2) Beeson, W. M.; Andrews, F. N.; Brown, P. T. The effect of thiouracil on the growth and fattening of yearling steers. *J. Anim. Sci.* **1947**, *6*, 16−23.
(3) Shirer, J. W.; Cohen, M. The effects of thiouracil on the thyroid gland. *Ann. Int. Med.* **1945**, *23*, 790−799.
(4) Williams, R. H.; Bissell, G. W. Thiouracil in the treatment of thyrotoxicosis. *Science* **1943**, *98*, 156−158.
(5) Williams, R. H.; Clute, H. M. Thiouracil in the treatment of thyrotoxicosis. *Med. Press Egypt* **1946**, *38*, 169−175.
(6) Braude, R.; Cotchin, E. Thiourea and methylthiouracil as supplements in rations of fattening pigs. *Br. J. Nutr.* **1949**, *3*, 171−186.
(7) Courtheyn, D.; Le Bizec, B.; Brambilla, G.; De Brabander, H. F.; Cobbaert, E.; Van de Wiele, M.; Vercammen, J.; De Wasch, K. Recent developments in the use and abuse of growth promotors. *Anal. Chim. Acta* **2002**, *473*, 71−82.
(8) Vanden Bussche, J.; Noppe, H.; Verheyden, K.; Wille, K.; Pinel, G.; Le Bizec, B.; De Brabander, H. F. Analysis of thyreostats: A history of 35 years. *Anal. Chim. Acta* **2009**, *637*, 2−12.
(9) International Agency for Research on Cancer. Some Thyrotropic Agents. *Monographs on the Evaluation of Carcinogenic Risk to Humans* **2001**, *79*, 53−144.
(10) Belgian Government. Koninklijk Besluit betreffende sommige verrichtingen in verband met stoffen met hormonale, anti-hormonale, anabole, β-adrenergische, anti-infectieuze, anti-parasitaire, en anti-inflammatoire werking. *Belgisch Staatsblad* **1974**, 6592.
(11) European Union. Council Directive 81/602/EC concerning the prohibition of certain substances having a hormonal action and of any substances having a thyrostatic action. *Off. J. Eur. Communities: Legis.* **1981**, *222*, 32−33.
(12) Pinel, G.; Bichon, E.; Pouponneau, K.; Maume, D.; Andre, F.; Le Bizec, B. Multi-residue method for the determination of thyreostats in urine samples using liquid chromatography coupled to tandem mass spectrometry after derivatisation with 3-iodobenzylbromide. *J. Chromatogr. A* **2005**, *1085*, 247−252.
(13) Vanden Bussche, J.; Vanhaecke, L.; Deceuninck, Y.; Verheyden, K.; Wille, K.; Bekaert, K.; Le Bizec, B.; De Brabander, H. F. Development and validation of an ultra-high performance liquid chromatography tandem mass spectrometry method for quantifying thyreostats in urine without derivatisation. *J. Chromatogr. A* **2010**, *1217*, 4285−4293.
(14) Wozniak, B.; Zuchowska, I. M.; Zmudzki, J.; Jedziniak, P.; Korycinska, B.; Sielska, K.; Witek, S.; Klopot, A. Liquid chromatography tandem mass spectrometry with ion trap and triple quadrupole analyzers for determination of thyreostatic drugs in urine and muscle tissue. *Anal. Chim. Acta* **2011**, *700*, 155−166.
(15) Le Bizec, B.; Bichon, E.; Deceuninck, Y.; Prevost, S.; Monteau, F.; Antignac, J. P.; Dervilly-Pinel, G. Toward a criterion for suspect thiouracil administration in animal husbandry. *Food Addit. Contam., Part A* **2011**, 1−8.
(16) Pinel, G.; Maume, D.; Deceuninck, Y.; Andre, F.; Le Bizec, B. Unambiguous identification of thiouracil residue in urine collected in non-treated bovine by tandem and high-resolution mass spectrometry. *Rapid Commun. Mass Spectrom.* **2006**, *20*, 3183−3187.
(17) Wozniak, B.; Witek, S.; Zmudzki, J.; Klopot, A. Natural occurrence of thiouracil in urine of livestock in Poland. *Bull. Vet. Inst. Pulawy* **2012**, *56*, 611−615.
(18) Pinel, G.; Mathieu, S.; Cesbron, N.; Maume, D.; De Brabander, H. F.; Andre, F.; Le Bizec, B. Evidence that urinary excretion of thiouracil in adult bovine submitted to a cruciferous diet can give erroneous indications of the possible illegal use of thyrostats in meat production. *Food Addit. Contam.* **2006**, *23*, 974−980.
(19) Vanden Bussche, J.; Kiebooms, J. A.; De Clercq, N.; Deceuninck, Y.; Le Bizec, B.; De Brabander, H. F.; Vanhaecke, L. Feed or food responsible for the presence of low-level thiouracil in urine of livestock and humans? *J. Agric. Food Chem.* **2011**, *59*, 5786−5792.
(20) Vanden Bussche, J.; Vanhaecke, L.; Deceuninck, Y.; Wille, K.; Bekaert, K.; Le Bizec, B.; De Brabander, H. F. Ultra-high performance liquid chromatography coupled to triple quadrupole mass spectrometry detection of naturally occurring thiouracil in urine of untreated livestock, domesticated animals and humans. *Food Addit. Contam., Part A* **2011**, *28*, 166−172.
(21) Kiebooms, J. A.; Vanden Bussche, J.; Hemeryck, L. Y.; Fievez, V.; Vanhaecke, L. Intestinal microbiota contribute to the endogenous formation of thiouracil in livestock. *J. Agric. Food Chem.* **2012**, *60*, 7769−7776.
(22) CRL. CRLs view on state of the art analytical methods for national residue control plans. *CRL guidance paper*, 2007. http://www.bvl.bund.de/SharedDocs/Downloads/09_Untersuchungen/EURL_Empfehlungen_Konzentrationsauswahl_Methodenvalierungen_EN.pdf?__blob=publicationFile&v=2 (accessed Jan. 16, 2015).
(23) Elbers, I. J. W.; Sterk, S. S.; van Ginkel, L. A. Proficiency test for thiouracil in bovine urine. *Confidential Rikilt Report* **2013**, *2013* (520), 1−37.
(24) Carpenter, J.; Bithell, J. Bootstrap confidence intervals: When, which, what? A practical guide for medical statisticians. *Stat. Med.* **2000**, *19*, 1141−1164.
(25) Wood, M. Statistical inference using bootstrap confidence intervals. *Significance* **2004**, *1*, 180−182.
(26) MacLachlan, D. J.; Hamilton, D. Estimation methods for maximum residue limits for pesticides. *Regul. Toxicol. Pharmacol.* **2010**, *58*, 208−218.
(27) Sanquer, A.; Wackowiez, G.; Havrileck, B. Critical review on the withdrawal period calculation for injection site residues. *J. Vet. Pharmacol. Ther.* **2006**, *29*, 355−364.
(28) Vanden Bussche, J.; Sterk, S. S.; De Brabander, H. F.; Blokland, M. H.; Deceuninck, Y.; Le Bizec, B.; Vanhaecke, L. Thyreostatic drugs, stability in bovine and porcine urine. *Anal. Bioanal. Chem.* **2012**, *403*, 2973−2982.
(29) European Union. European Commission Decision 2002/657/EC implementing Council Directive 96/23/EC concerning the performance of analytical methods and the interpretation of results. *Off. J. Eur. Communities: Legis.* **2002**, *221*, 8−36.
(30) EURL. *EURL Reflection Paper: Natural Growth Promoting Substances in Biological Samples*; RIKILT Wageningen UR: Wageningen, 2014; pp 15−21.

DOI: 10.1021/jf504475f
J. Agric. Food Chem. 2015, 63, 1339−1346

nm and recording the emission signals at 485 nm over 120 s using a Cary Eclipse fluorescence spectrophotometer (Varian, USA).

ANS Binding Assay. A 0.4 mM stock solution of ANS was prepared by dissolving ANS in PBS (pH 7.0). The ANS stock solution was stored at 4 °C. Aliquots of cC I66Q solution with or without EGCG taken at different times were mixed with an aliquot of ANS solution, followed by the addition of PBS (pH 7.0) to a final volume of 3 mL. After incubation at room temperature in the dark for 30 min, the samples were subjected to fluorescence assay using an excitation wavelength of 380 nm and an emission wavelength between 400 and 600 nm. Both the ANS fluorescence intensity and the average emission wavelength were recorded to account for the changes in intensity and spectrum.

Transmission Electron Microscopy. Cystatin samples with or without EGCG were diluted 5-fold, and 10 μL of each sample was dispensed onto a coated copper-mesh grid. The grids were negatively stained with 1% (w/v) phosphotungstic acid and then observed under a Hitachi H-7650 transmission electron microscope (Techcomp Ltd., Tokyo, Japan) with an accelerating voltage of 80 kV.

MTT Assay. PC12 cells were purchased from American Type Culture Collection. PC12 cells were maintained in DMEM with 10% horse serum, 5% fetal bovine serum, and 1% penicillin/streptomycin antibiotics. Cells were cultured in a 5% CO_2 atmosphere at 37 °C and then harvested and plated in 96-well plates (Beijing Dingguo Changsheng Biotechnology Co., Ltd.) at a density of 10^4 cells/well. The plates were incubated at 37 °C for 24 h. Subsequently, cC I66Q with and without EGCG was incubated at 65 °C for 35 days, and aliquots of the samples were collected after centrifugation at 6000*g* for 1 h. The concentrated cC I66Q samples were dissolved in PBS buffer (pH 7.0, 50 mM), and the protein concentration in each sample was determined by BCA (a kit bought from Beijing Dingguo Changsheng Biotechnology Co., Ltd.) assay. The cC 166Q samples, with and without ECGC, were separately added to the cells to give a final concentration of cC 166Q in the cells ranging from 0 to 500 ng/mL. The final concentrations of cC I66Q samples (both with and without EGCG) in each well were 0, 1, 5, 50, and 500 ng/mL. The plates were then incubated with the protein samples for 48 h at 37 °C, and cell viability was determined using MTT toxicity assay by adding 10 μL of 5 mg/mL MTT (Beijing Dingguo Changsheng Biotechnology Co., Ltd.) reagent to each well, followed by further incubation for 3 h. After that, the medium was removed and replaced with 100 μL of DMSO. After 10 min of shaking at room temperature, the absorbance of the plate was measured at 490 nm using an iMarkMicroplate Reader (Bio-RAD).

Molecular Dynamic Simulations (MD) and Docking Studies. MD simulations were carried out using the GROMACS 4.0.7 software package.[21] The crystal structure of chicken cystatin (PDB entry 1CEW) was downloaded from the Protein Data Bank.[22] The model of I66Q monomer was constructed using the Swiss-Pdb Viewer software package. Before the docking, MD simulations of cC I66Q monomer at 338 K (65 °C) and pH 2.0 (amyloid fibril forming conditions) were carried out for 20 ns to equilibrate (data not shown).

Docking studies on the interaction between EGCG and cC I66Q were carried out using AutoDock 4.2.5.1 (Molecular Graphics Laboratory, The Scripps Research Institute). The 3D structure of EGCG was downloaded from Chem Spider database (http://www.chemspider.com/). Both cC I66Q and EGCG molecules were prepared using AutoDockTools 1.5.6 (1999–2011 Molecular Graphics Laboratory, The Scripps Research Institute) before docking, The docking was carried out with 60 × 60 × 60 0.375 Å spacing grids covering the entire surface of cC I66Q. The Lamarckian genetic algorithm, which is considered one of the most appropriate docking methods available in AutoDock, was used in the docking analysis.

RESULTS AND DISCUSSION

Analysis of Cystatin Fibril Formation Using ThT Fluorescence. The recombinant variant cC I66Q has been reported to form amyloid fibrils following incubation with continuous agitation at high temperature and low pH.[23] After incubation of cC I66Q with and without EGCG at pH 2.0 and 65 °C, inhibition of cC I66Q fibril formation by EGCG was determined using the ThT-binding fluorescence assay. A consistent increase in the ThT fluorescence intensity occurred when cC I66Q was incubated alone, indicating that the

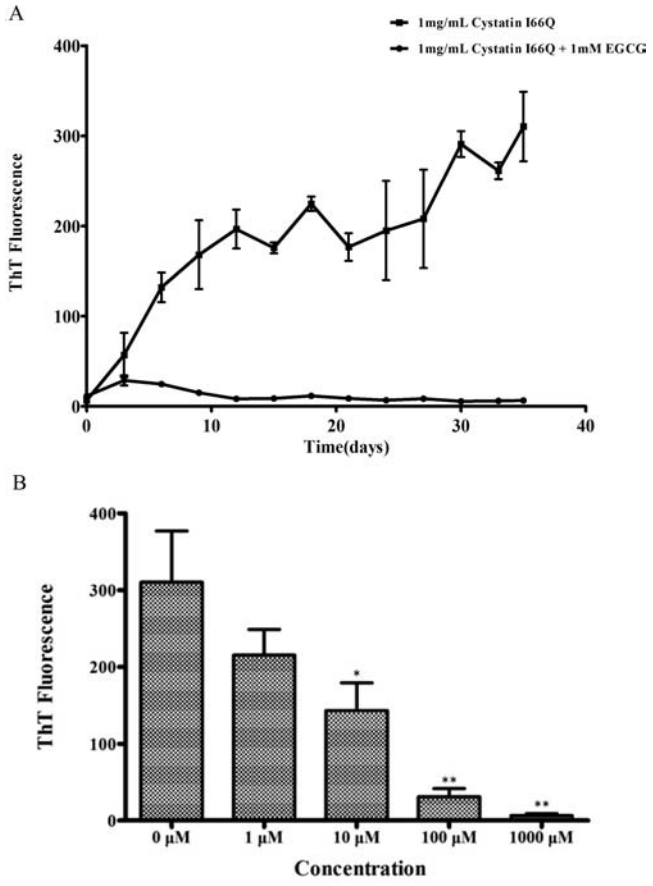

Figure 1. Effects of increasing concentrations of EGCG on amyloid fibril formation by cC I66Q: (A) kinetics of cC I66Q fibril formation in the absence (solid squares) or presence of EGCG (solid circles) as monitored by ThT fluorescence; (B) dose-dependent inhibitory capacity of EGCG toward amyloid formation by cC I66Q following 35 days of incubation at 65 °C and pH 2.0.

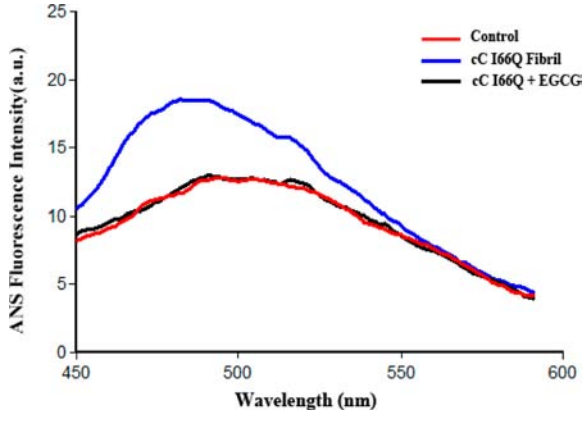

Figure 2. ANS fluorescence emission spectra of cC I66Q with or without EGCG following incubation at 65 °C and pH 2.0 for 35days: (red curve) native cC I66Q; (blue curve) cC I66Q incubated for 35 days; (black curve) cC I66Q incubated for 35 days in the presence of 1 mM EGCG.

DOI: 10.1021/jf505277e
J. Agric. Food Chem. 2015, 63, 1347–1351

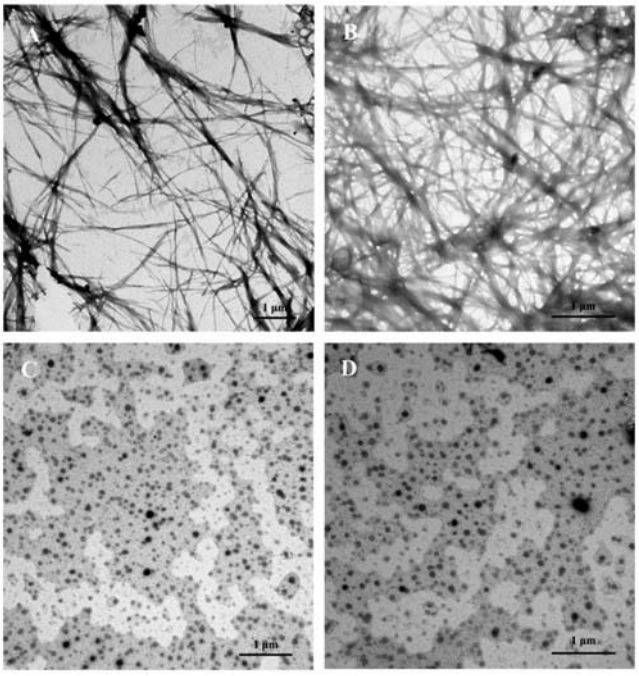

Figure 3. Transmission electron microscopic images of cC I66Q fibrils formed in the absence (A, B) or presence (C, D) of 1 mM EGCG. Data from two independent experiments for each are shown.

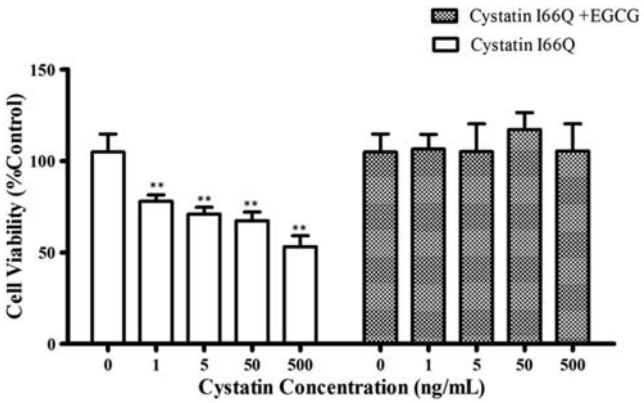

Figure 4. Effect of various concentrations of cC I66Q amyloid fibrils on the viability of PC 12 cells as determined by MTT assay. The concentration of EGCG is 1 mM.

formation of amyloid fibrils proceeded rapidly and without a lag phase (Figure 1A). However, cC I66Q co-incubated with 1 mM EGCG showed a significant decrease in ThT fluorescence across the whole time frame of the experiment. The ThT fluorescence intensity of cC I66Q with EGCG reached a maximum (25.7 au) on the sixth day, indicating that the inhibitory effect exerted by EGCG on the formation of cystatin fibril started from the very beginning of the log phase and continued to the end of the log phase.

To determine the effective concentrations of EGCG for inhibiting cC I66Q fibril formation, the reaction was allowed to occur in the presence of different concentrations (1, 10, 100, and 1000 μM) of EGCG (Figure 1B). Reduction in ThT fluorescence was dependent on EGCG concentration, with significant reduction of fluorescence at 10 μM ($P < 0.05$).

Structural Changes of cC I66Q during Fibril Formation. ANS is a fluorescent dye that probes exposed

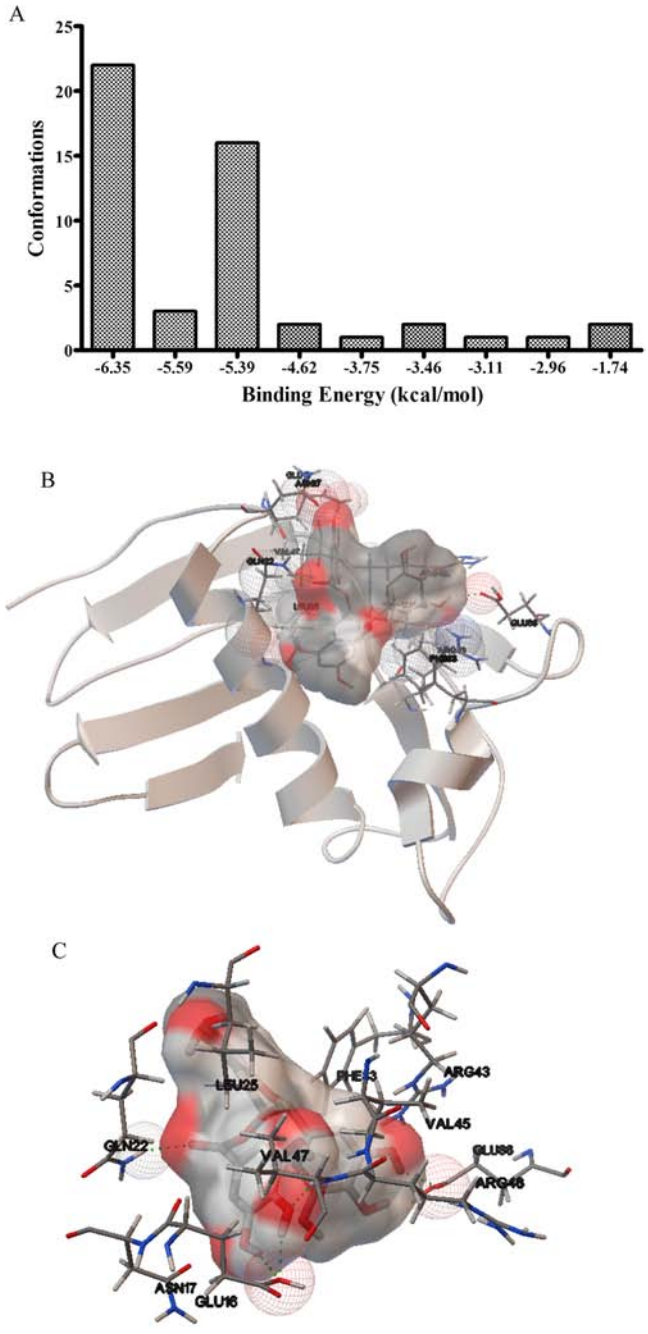

Figure 5. (A) Binding energy of 50 docking models. (B) Panoramic view showing the binding mode between EGCG and cC I66Q at the lowest binding energy of −6.35. (C) Residues of interaction between EGCG and cC I66Q at binding energy of −6.35 (green dots, H-bonds).

hydrophobic surfaces of proteins. Upon binding to the aromatic hydrophobic amino acids of cC, the chemical change of ANS would cause an increase in the intensity of the light to be emitted, with the emission maximum showing a blue shift.[19,24] As shown in Figure 2, the intensity of ANS fluorescence exhibited by cC I66Q fibrils showed a prominent increase in blue shift from 500 to 480 nm. In contrast, the addition of EGCG to cC I66Q resulted in a large reduction in ANS fluorescence intensity and almost no blue shift. This result indicates that the addition of EGCG prevented the accessible exposure hydrophobic regions of cC I66Q. In addition, this

DOI: 10.1021/jf505277e
J. Agric. Food Chem. 2015, 63, 1347−1351

Table 1. Dock Scores and Summary of Molecular Interactions between EGCG and cC I66Q at Binding Energies of −6.35 and −5.39 kcal/mol

intermolecular energy (kcal/mol)	torsional energy (kcal/mol)	binding energy[a] (kcal/mol)	no. of H-bonds	residues of H-bonds	residues of interaction[b]
−9.93	3.58	−6.35	5	Glu86, Val47, Gln22, Glu16 (contains 2 H-bonds)	Glu16, Asn17, Gln22, Leu25, Val45, Arg46, Glu86, Phe83, Arg43, Val47
−8.97	3.58	−5.39	5	Asn17 (contains 3 H-bonds), Glu16 (contains 2 H-bonds)	Glu16, Asn17, Gln22, Leu25, Val45, Arg46, Gln26, Met29

[a]Binding energy is the sum of intermolecular energy and torsional energy. [b]The common residues of interactions are underlined.

result indicated that binding of EGCG to cC probably occurred at the monomeric level.

Physical Analysis of cC I66Q Fibril Formation and Antifibrillogenic Activity of EGCG. TEM was used to observe the inhibitory effect of EGCG on cC I66Q fibril formation. After incubation at 65 °C and in glycine−hydrochloric acid buffer (pH 2.0) for 35 days, cC I66Q formed long and regular mature amyloid fibrils in the absence of EGCG (Figure 3A,B). The width of the detected fibroid material was calculated to be in the range from 50 to 100 Å, which closely matched the widths of the fibers observed for many amyloidogenic proteins, including those of human cystatins.[17] In the presence of EGCG, cC I66Q formed oligomeric aggregates instead of amyloid fibrils, indicating that EGCG either redirected the amyloidogenic cC mutant I66Q toward unstructured off-pathway oligomers or maintained the proteins in the prefibrillar state without redirecting them toward the aggregation pathway, thus inhibiting the process of fibrillation (Figure 3C,D).[23]

MTT Analysis of the Cellular Toxicity of cC I66Q Amyloid Fibril and Oligomers. The mutation of hCC L68Q is associated with massive amyloid deposition within small arteries and arterioles of the leptomeninges, cerebral cortex, basal ganglia, brainstem, and cerebellum, resulting in severe cellular toxicity within the brain.[25] Therefore, after observing the morphology of the cC I66Q amyloid fibril and oligomer formations in the presence of EGCG, we assessed the cellular toxicity of cC I66Q on PC12 cells (neuronal cell model) using the MTT assay. After 48 h of incubation, cell viability decreased significantly ($P < 0.01$) in the presence of increasing concentrations of cC I66Q (Figure 4). However, the complete abrogation of the toxicity of cC I66Q by EGCG indicated that the cC I66Q oligomers formed in the presence of EGCG were nontoxic.

Computational Analysis of the Binding between EGCG and cC I66Q. Both fluorescence and electron microscopy data showed that EGCG could inhibit the formation of amyloid fibrils by cC I66Q, and this occurred at a very early stage in the process. These results suggested that there could be some kind of interaction between EGCG and cC I66Q at the atomic level and at a stage prior to fibril initiation. To investigate this hypothesis, we carried out in silico studies using molecular dynamics (MD) simulations and docking analysis.

MD simulation of cC I66Q was carried out at 338 K and pH 2.0 for 20 ns (data not shown), and we carried out docking simulations to investigate the possible EGCG-binding site on cC I66Q. The binding energy of 50 models in docking is shown in Figure 5A. On the basis of Figure 5A, the interacting residues of the two most possible binding patterns and properties resulting from the binding are listed in Table 1. Compared with the two binding patterns, EGCG probably bound to cC I66Q and was located in a region between the α-domain and the β-domain, as depicted in Figure 5B,C. The possible site on cC I66Q to which EGCG may bind included the appendant structure. The appendant structure of cC I66Q has been demonstrated to play an important role in amyloidogenic cystatin dimerization prior to domain swapping.[26] Consequently, the stabilizing effect contributed by EGCG on the appendant structure of cC I66Q may prevent the occurrence of domain swapping, so as to redirect cC I66Q away from the fibril-forming pathway and into forming nontoxic, unstructured, and off-pathway aggregates.

In this study we show that EGCG can significantly inhibit the fibrillation of amyloidogenic cystatin mutant I66Q (cC I66Q) and that the inhibitory effect is dose-dependent and extremely potent. This observation is of particular significance as there is minimal research available demonstrating the action of small molecule polyphenols (such as EGCG) against proteins that utilize a domain swapping mechanism to initiate amyloid formation.

Na Wang[†]
Jianwei He*[,†]
Alan K. Chang[†]
Yu Wang[†]
Linan Xu[§]
Xiaoying Chong[†]
Xian Lu[†]
Yonghui Sun[†]
Xichun Xia[†]
Hui Li[†]
Bing Zhang[#]
Youtao Song[†]
Akio Kato[⊥]
Gary W. Jones*[,§]

[†]Province Key Laboratory of Animal Resource and Epidemic Disease Prevention, School of Life Science, Liaoning University, Shenyang 110036, China
[§]Department of Biology, National University of Ireland Maynooth, Maynooth, County Kildare, Ireland
[#]Experimental Center of Functional Subjects, China Medical University, 92 BeiEr Road, Heping District, Shenyang 110001, China
[⊥]Department of Biological Chemistry, Faculty of Agriculture, Yamaguchi University, Yamaguchi, Japan

AUTHOR INFORMATION

Corresponding Authors

*(J.H.) E-mail: jwhe@lnu.edu.cn.
*(G.W.J.) E-mail: gary.jones@nuim.ie.

Funding

This publication has emanated from research conducted with the financial support of the Science Foundation Ireland under

DOI: 10.1021/jf505277e
J. Agric. Food Chem. 2015, 63, 1347−1351

International Strategic Cooperation Award Grant SFI/13/ISCA/2845. This work was supported by grants from the Joint Specialized Research Fund for the Doctoral Program of Higher Education.

Notes

The authors declare no competing financial interest.

REFERENCES

(1) Hong, D. P.; Fink, A. L.; Uversky, V. N. Structural characteristics of alpha-synuclein oligomers stabilized by the flavonoid baicalein. *J. Mol. Biol.* **2008**, *383* (1), 214−223.

(2) Zhu, M.; Rajamani, S.; Kaylor, J.; Han, S.; Zhou, F.; Fink, A. L. The flavonoid baicalein inhibits fibrillation of α-synuclein and disaggregates existing fibrils. *J. Biol. Chem.* **2004**, *279* (26), 26846−26857.

(3) Ehrnhoefer, D. E.; Bieschke, J.; Boeddrich, A.; Herbst, M.; Masino, L.; Lurz, R.; Engemann, S.; Pastore, A.; Wanker, E. E. EGCG redirects amyloidogenic polypeptides into unstructured, off-pathway oligomers. *Nat. Struct. Mol. Biol.* **2008**, *15* (6), 558−466.

(4) Ghosh, K. S.; Maiti, T. K.; Debnath, J.; Dasgupta, S. Inhibition of ribonuclease A by polyphenols present in green tea. *Proteins* **2007**, *69* (3), 566−580.

(5) Rambold, A. S.; Miesbauer, M.; Olschewski, D.; Seidel, R.; Riemer, C.; Smale, L.; Brumm, L.; Levy, M.; Gazit, E.; Oesterhelt, D.; Baier, M.; Becker, C. F.; Engelhard, M.; Winklhofer, K. F.; Tatzelt, J. Green tea extracts interfere with the stress-protective activity of PrP and the formation of PrP. *J. Neurochem.* **2008**, *107* (1), 218−229.

(6) Bieschke, J.; Russ, J.; Friedrich, R. P.; Ehrnhoefer, D. E.; Wobst, H.; Neugebauer, K.; Wanker, E. E. EGCG remodels mature α-synuclein and amyloid-β fibrils and reduces cellular toxicity. *Proc. Natl. Acad. Sci. U.S.A.* **2010**, *107* (17), 7710−7715.

(7) Hudson, S. A.; Ecroyd, H.; Dehle, F. C.; Musgrave, I. F.; Carver, J. A. (−)-Epigallocatechin-3-gallate (EGCG) maintains κ-casein in its pre-fibrillar state without redirecting its aggregation pathway. *J. Mol. Biol.* **2009**, *392* (3), 689−700.

(8) Santoso, A.; Chien, P.; Osherovich, L. Z.; Weissman, J. S. Molecular basis of a yeast prion species barrier. *Cell* **2000**, *100* (2), 277−288.

(9) Greenwald, J.; Riek, R. Biology of amyloid: structure, function, and regulation. *Structure* **2010**, *18* (10), 1244−1260.

(10) Hard, T.; Lendel, C. Inhibition of amyloid formation. *J. Mol. Biol.* **2012**, *421* (4−5), 441−465.

(11) Eichner, T.; Radford, S. E. A diversity of assembly mechanisms of a generic amyloid fold. *Mol. Cell* **2011**, *43* (1), 8−18.

(12) Rawlings, N. D.; Barrett, A. J.; Bateman, A. MEROPS: the peptidase database. *Nucleic Acids Res.* **2010**, *38* (database issue), D227−D233.

(13) Grubb, A.; Lofberg, H. Human γ-trace, a basic microprotein: amino acid sequence and presence in the adenohypophysis. *Proc. Natl. Acad. Sci. U.S.A.* **1982**, *79* (9), 3024−3027.

(14) Dubin, G. Proteinaceous cysteine protease inhibitors. *Cell. Mol. Life Sci.* **2005**, *62* (6), 653−669.

(15) Wallin, H.; Bjarnadottir, M.; Vogel, L. K.; Wasselius, J.; Ekstrom, U.; Abrahamson, M. Cystatins − extra- and intracellular cysteine protease inhibitors: high-level secretion and uptake of cystatin C in human neuroblastoma cells. *Biochimie* **2010**, *92* (11), 1625−1634.

(16) Olafsson, I.; Grubb, A. Hereditary cystatin C amyloid angiopathy. *Amyloid: Int. J. Exp. Clin. Invest.: Off. J. Int. Soc. Amyloidosis* **2000**, *7* (1), 70−79.

(17) Staniforth, R. A.; Giannini, S.; Higgins, L. D.; Conroy, M. J.; Hounslow, A. M.; Jerala, R.; Craven, C. J.; Waltho, J. P. Three-dimensional domain swapping in the folded and molten-globule states of cystatins, an amyloid-forming structural superfamily. *EMBO J.* **2001**, *20* (17), 4774−4781.

(18) Jaskolski, M. 3D domain swapping, protein oligomerization, and amyloid formation. *Acta Biochim. Pol.* **2001**, *48* (4), 807−827.

(19) Sanders, A.; Craven, C.; Higgins, L. D.; Giannini, S.; Conroy, M. J.; Hounslow, A. M.; Waltho, J. P.; Staniforth, R. A. Cystatin forms a tetramer through structural rearrangement of domain-swapped dimers prior to amyloidogenesis. *J. Mol. Biol.* **2004**, *336* (1), 165−178.

(20) He, J.; Song, Y.; Ueyama, N.; Harada, A.; Azakami, H.; Kato, A. Characterization of recombinant amyloidogenic chicken cystatin mutant I66Q expressed in yeast. *J. Biochem.* **2005**, *137* (4), 477−485.

(21) Hess, B.; Kutzner, C.; Van Der Spoel, D.; Lindahl, E. GROMACS 4: Algorithms for highly efficient, load-balanced, and scalable molecular simulation. *J. Chem. Theory Comput.* **2008**, *4*, 435−447.

(22) Refaee, M.; Tezuka, T.; Akasaka, K.; Williamson, M. P. Pressure-dependent changes in the solution structure of hen egg-white lysozyme. *J. Mol. Biol.* **2003**, *327* (4), 857−865.

(23) Wahlbom, M.; Wang, X.; Lindstrom, V.; Carlemalm, E.; Jaskolski, M.; Grubb, A. Fibrillogenic oligomers of human cystatin C are formed by propagated domain swapping. *J. Biol. Chem.* **2007**, *282* (25), 18318−18326.

(24) Semisotnov, G. V.; Rodionova, N. A.; Razgulyaev, O. I.; Uversky, V. N.; Gripas, A. F.; Gilmanshin, R. I. Study of the "molten globule" intermediate state in protein folding by a hydrophobic fluorescent probe. *Biopolymers* **1991**, *31* (1), 119−128.

(25) Rostagno, A.; Holton, J. L.; Lashley, T.; Revesz, T.; Ghiso, J. Cerebral amyloidosis: amyloid subunits, mutants and phenotypes. *Cell. Mol. Life Sci.* **2010**, *67* (4), 581−600.

(26) Yu, Y.; Liu, X.; He, J.; Zhang, M.; Li, H.; Wei, D.; Song, Y. Appendant structure plays an important role in amyloidogenic cystatin dimerization prior to domain swapping. *J. Biomol. Struct. Dyn.* **2012**, *30* (1), 102−112.

DOI: 10.1021/jf505277e
J. Agric. Food Chem. 2015, 63, 1347−1351

protein content. This is most likely due to presence of multiple, seed-expressed BBI genes[17,18] and a pronounced environmental effect on BBI protein accumulation.[19] An alternate, successful approach to reduce BBI protein levels was the overexpression of a mutated, inactive BBI transgene, which was able to outcompete endogenous BBI transcripts and significantly reduced BBI protein levels.[20]

By far the largest success in reducing trypsin inhibitor activity in soybean is due to the identification of a soybean accession (PI 157740) with dramatically reduced (~40%) trypsin inhibitor activity.[21] The molecular genetic cause is a frameshift mutation (termed *KTi3*−) that affects one of three seed-expressed *KTi* genes.[22] This accession has been used in extensive backcrossing and feeding trials,[3,23−25] and raw extruded protein meal lacking KTi3 protein is superior for animal weight gain as compared to raw soybeans.[3,23,24] However, weight gain for young animals fed non-heat-treated soybean materials (including *KTi3*−) is inferior to those fed conventional heat-treated soybeans, although soybean seed lacking KTi3 protein has been shown to require less heat processing in comparison to conventional soybeans.[3,23,24]

In this study, we report identification of a *G. max* line with reduced Kunitz trypsin inhibitor protein and decreased trypsin inhibition, which is not due to mutations affecting the previously identified *KTi3* gene. The objectives of this work were (1) to identify the specific genetic cause for this reduction in trypsin inhibition, (2) to evaluate if this reduction was synergistic with the previously identified *KTi3*− mutation, and (3) to ascertain what effect these mutations had on seed proteome and BBI protein accumulation in mature seed.

MATERIALS AND METHODS

Plant Materials. Seed for soybean lines examined was obtained from the USDA-ARS GRIN collection. Out of 520 lines examined, two were Kunitz trypsin inhibitor (KTi) mutants (PI 68679, *KTi1*−, and PI 542044, Kunitz, *KTi3*−). A wild-type line, Williams 82 (PI 518671, *KTi1*, *KTi3*)[26] was used as a control line. The Kunitz trypsin inhibitor 3 (*KTi3*−) mutation in this line is derived from a landrace identified by Theodore Hymowitz (PI 157740) backcrossed to Williams 82 for five generations.[21]

Population Development. PI 68679 (*KTi1*−) and PI 542044 (*KTi3*−) were crossed in the summer of 2012 at the Southfarm experimental research station, and F_1 seed was advanced in greenhouses to produce F_2 seed. Seed chips from individual F_2 seed were examined via SDS−PAGE analysis and two lines were selected for absence of both KTi1 and KTi3 proteins.

***KTi3*− SimpleProbe Assay.** A SimpleProbe assay was developed to track the *KTi3*− allele,[22] designed by use of Lightcycler probe design software, version 1 (Roche Applied Sciences, Indianapolis, IN). Genotyping PCR reactions were performed with a 5:1 asymmetric mix of primers (5′-TTGCAGTTATAATGCTGTGTGTTG-3′, 5′-AA-TACTAATCCCAATATCCCCACA-3′) in the presence of a non-extensible fluorescently labeled SimpleProbe (5′-fluorescein-SPC-TGAATTCATCATCAGAAACTCTCTCAAGTC-phosphate-3′) using Titanium Taq polymerase (Clonetech, Mountain View, CA) and 5−50 ng of genomic DNA in a Lightcycler 480 II instrument (Roche) under the following conditions: 95 °C for 5 min, followed by 45 cycles of 95 °C for 30 s, 60 °C for 30 s, and 72 °C for 30 s. Following amplification (and a 1 min denaturation step at 95 °C and 2 min at 55 °C), melting curve analysis of 20 reads/deg from 50 to 70 °C was performed. For *KTi3*− homozygote samples, a single melting peak was observed at ~56−57 °C, whereas wild-type lines show a single peak at ~64 °C and heterozygotes showed both peaks (Figure S1, Supporting Information).

SDS−PAGE and Immunoblot Analysis of Extracted Soybean Seed Proteins. Protein extraction and SDS−PAGE analysis was performed as previously described.[19] Briefly, mature soybean seed samples were ground with a mortar and pestle, and proteins were extracted from a 10 mg portion (for analysis of F_2 lines, a 10 mg chip from each seed was used instead) in SDS buffer [125 mM Tris-HCl, pH 6.8, 20% glycerol (v/v), 5% (v/v) 2-mercaptoethanol, 4% SDS (w/v), and 0.03 mM bromophenol blue], boiled for 5 min, and centrifuged to remove insoluble material. Protein extract supernatant was separated by SDS−PAGE with 15% (w/v) total acrylamide monomer in the resolving gel for 1 h at 20 mA on a Hoefer SE 260 minigel apparatus. Protein bands were visualized with Coomassie blue R-250. Immunoblots were performed as previously described with a 1:5000 dilution of an anti-BBI antibody[19] or 1:10 000 anti-KTi (non-isoform-specific) antibody[27] in Tris-buffered saline (TBS; 50 mM Tris-HCl, pH 7.5, and 150 mM NaCl). After being washed with TBST buffer (Tris-buffered saline with 0.3% Tween-20), membranes were incubated with goat anti-rabbit IgG−horseradish peroxidase conjugate for 1 h and detected with enhanced chemiluminescent substrate according to manufacturer's recommendations (Pierce, Rockford, IL).

Two-Dimensional Protein Electrophoresis. Two-dimensional electrophoresis was carried out essentially as previously described.[28] Protein samples (300 μg) were initially separated by use of isoelectric focusing IPG strips (pH 3−10, 13 cm in length) in an IPGPhor system (GE Healthcare, Little Chalfont, U.K.). Following electrophoresis, the protein in the IPG strips was resolved in the second dimension with a Hoefer SE 600 Ruby electrophoresis unit according to the manufacturer's specifications (GE Healthcare). After completion of electrophoresis, the gels were removed from the cassette and stained with Coomassie blue R-250. Coomassie-stained gels were scanned on a UMAX PowerLook 2100XL scanner running Adobe Photoshop version 7.0 (Adobe Systems, San Jose, CA), and image files were analyzed via Phoretix 2-D Advanced software, version 6.01 (Nonliner Dynamics Ltd., Newcastle-upon-Tyne, U.K.).

DEAE Anion-Exchange Chromatographic Separation of Extracted Soybean Seed Proteins. Mature soybean seed was ground into a fine powder with a mortar and pestle. To 20 g of seed powder was added 200 mL of 20 mM Tris-HCl/0.1 mM EDTA buffer, pH 6.8, and the mixture was placed in an orbital shaker (150 rpm, 30 °C) for 15 min. The slurry was clarified by centrifugation at 13320*g* for 20 min. To the clear supernatant was added 100 mM $CaCl_2$ stock solution, to a final concentration of 10 mM of calcium chloride. After incubation at room temperature for 10 min, the solution was clarified by centrifugation as stated above. Protein from the supernatant was precipitated by addition of solid $(NH_4)_2SO_4$ to 70%. The resulting protein was recovered by centrifugation, resuspended in 20 mL of 10 mM sodium phosphate/0.1 mM EDTA buffer, pH 6.5, and dialyzed overnight against the same buffer. The concentrated protein solution was loaded onto a column of DEAE-cellulose (2.5 × 20 cm) previously equilibrated with the dialysis buffer. The column was washed with 2 volumes of buffer and then subjected to a step gradient of 50, 100, 200, 300, 400, and 500 mM NaCl, prepared in dialysis buffer. Fractions of 6 mL were collected, and alternate fractions were examined by SDS−PAGE.

Trypsin and Chymotrypsin Inhibitor Assays. Trypsin and chymotrypsin inhibitor assays were done in duplicate as previously described.[29] Briefly, 10−50 μg of seed protein were used in inhibitor assays, using *N*-benzoyl-L-arginine ethyl ester (BAEE) and *N*-benzoyl-L-tyrosine ethyl ester (BTEE; obtained from Sigma) as trypsin and chymotrypsin reaction substrates, respectively. Absorbance at 256 nm was monitored for ~3 min, and trypsin and chymotrypsin inhibitor activities were calculated as the difference between absorbance change in control and samples containing seed protein.

RNA Extraction and qRT-PCR Analysis. F_3 lines were also grown in a growth chamber in a random complete block design with four biological replicates for each genotype. Immature seed was collected and separated into size categories based on fresh weight. Two seed stages representing midmaturation (200−300 mg/seed fresh weight) and late maturation (400−500 mg/seed fresh weight) were selected for mRNA extraction and qRT-PCR analysis.

Each genotype was evaluated with four biological replicates consisting of three pooled immature seeds. RNA isolation, cDNA

DOI: 10.1021/jf505220p
J. Agric. Food Chem. 2015, 63, 1352−1359

production and qRT-PCR were carried out as previously described[28] with 1 μg of DNase-treated total seed RNA. A subsample of $^1/_{20}$ of the total RT reaction was used for qRT-PCR reaction. Samples were compared by the ΔΔ*CT* method,[26] with the *cons6* gene as a reference gene.[31]

Statistical Analyses. JMP version 9 software (SAS Institute Inc., Cary, NC) was used to perform one-way analysis of variance (ANOVA) tests to compare the effect of genotype on gene expression or trypsin/chymotrypsin inhibition activity of seed extracts. For ANOVA tests that displayed significant differences at the $p < 0.05$ level, Tukey's honest significant differences (HSD) ad hoc test was performed ($\alpha = 0.05$ significance level cutoff).

RESULTS AND DISCUSSION

Identification of a Germplasm Line with Reduced Kunitz Trypsin Inhibitor Content. To identify soybean lines with reduced trypsin and chymotrypsin inhibitor content, we screened a total of 520 soybean accessions, obtained from the USDA Soybean Germplasm Collection, Urbana, IL, by SDS–PAGE and Western blot analysis with antibodies raised against purified soybean KTi protein.[27] Among these soybean accessions, one germplasm line, PI 68679, was identified that had reduced KTi protein levels (Figure 1).

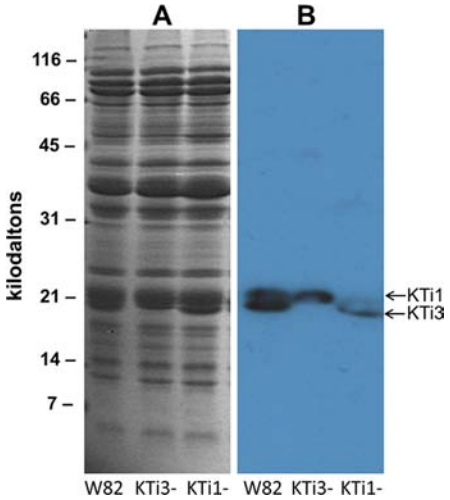

Figure 1. SDS–PAGE protein fractionation of mature soybean seed. Equivalent amounts of protein (50 μg) of clarified seed protein were separated on polyacrylamide gels. (A) Coomassie brilliant blue-stained polyacrylamide gel; (B) Western blot probed with anti-Kunitz trypsin inhibitor antibody (non-isoform-specific). Genotypes are indicated below chart: W82 = Williams 82 (PI 518671, wild type); KTi3– = Kunitz (PI 542044, *KTi3*– mutant); KTi1– = PI 68679 (*KTi1*– mutant). The bands corresponding to KTi1 and KTi3 proteins are indicated by arrows.

Determination of Molecular Genetic Basis for Reduced KTi Levels in PI 68679. In soybean, three *KTi* isoforms (*KTi1*, *KTi2*, and *KTi3*) have been reported to be expressed at the mRNA level in developing seed.[22,32] Cloning of the *KTi3* gene from PI 68679 revealed no mutations that could affect the coding region (Figure 2A). *KTi1/2* were annotated as tightly linked and highly similar (>90%), and were suggested to lack trypsin inhibitor activity based on sequence analysis alone,[32] but this assertion was not experimentally validated. The Williams 82 reference sequence (http://www.phytozome.net/search.php?method=Org_Gmax) does not contain a second locus linked to *KTi1*, which displays high (>90%) similarity reported for *KTi2* in the initial characterization.[22,32] BLAST searches with the *KTi1/KTi2* gene fragment (NCBI accession no. S45035.1), revealed only a single gene (Glyma01g10900/Glyma01G095000) on chromosome 1. Sanger sequencing with cloned *KTi1* PCR products revealed a single-base deletion (GGG356 → 358GG, relative to start codon, NCBI accession no. KC460320), which introduces a frameshift mutation at position 119 (Figure 2B). In concordance with the previously named *KTi3*– allele (Figure 2A), we have termed this new mutant allele *KTi1*–.

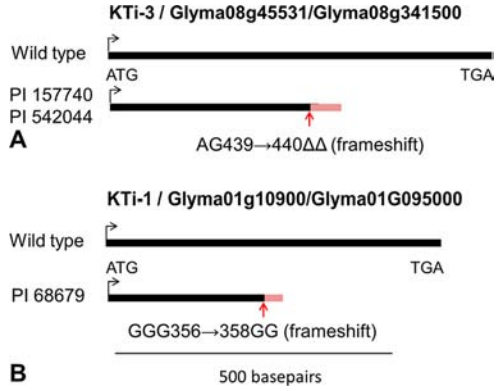

Figure 2. Cartoon depiction of Kunitz trypsin inhibitor genes and the impact of loss-of-function mutations. (A) *KTi3*; (B) *KTi1*.

Development of Lines Containing Two Genetically Distinct Mutations Affecting KTi Encoding Genes. Using traditional hybridization methods, we crossed the line bearing a *KTi1*– mutation (PI 68679) to a line bearing the previously identified *KTi3*– mutation (PI 542044). A SimpleProbe-based genotyping assay for the *KTi3*– mutation was developed (Figure S1, Supporting Information) and this assay was completely predictive for absence/accumulation of KTi3 protein (data not shown). However, attempts to develop a routine molecular marker assay for the novel *KTi1*– mutation were not successful. The mutation is a deletion of one guanine residue within a string of three guanines (GGG > GG), which is extremely difficult to detect by hybridization-based genotyping. We explored other genotyping methods that rely on size polymorphism (e.g., CAPS, dCAPS[33,34]) but no suitable restriction enzymes were identified.

A single F_1 line was advanced and F_2 seed was examined for accumulation of KTi (Figure 3), via SDS–PAGE with seed produced in a greenhouse. Homozygosity for both *KTi1*– and *KTi3*– mutations was completely correlated with absence of both KTi protein bands (Figure 3, lane 8). PCR and sequencing verified that all lines with absent KTi1 and KTi3 protein were homozygous for both *KTi*– mutations and this trait was consistent for at least two generations.

Proteomic Investigations of Mutant Lines Bearing *KTi*– Mutations. Seed of the line homozygous for both the *KTi1*– and *KTi3*– mutations (E16) lacked any KTi protein, as detectable by anti-KTi antibodies. (Figure 4A,B). These results were also concordant with results for F_2 seed chips (Figure 3). However, BBI proteins accumulate to a much greater degree (≥10-fold higher) in mature seed bearing either or both *KTi* mutations, relative to Williams 82 (Figure 4C). Similar seed proteome rebalancing has been documented in previous studies. For example, the silencing of β-conglycinin, 7S seed storage protein, resulted in higher accumulation of the 11S glycinin.[35] Similarly, a soybean β-conglycinin mutant also

DOI: 10.1021/jf505220p
J. Agric. Food Chem. 2015, 63, 1352–1359

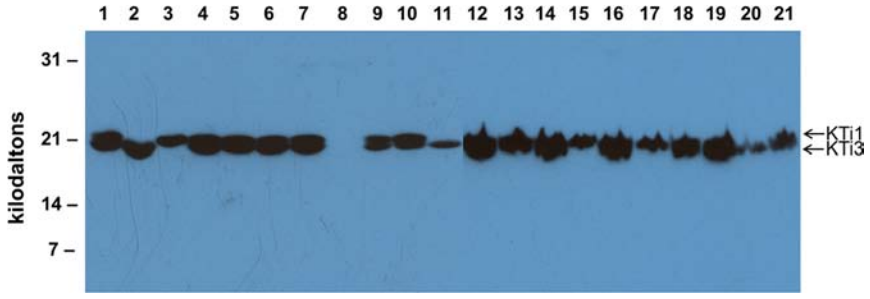

Figure 3. Immunoblot analysis of clarified protein from F_2 seed chips, produced from a single F_1 plant heterozygous for *KTi1*− and *KTi3*−. Immunoblots were probed with a non-isoform-specific anti-Kunitz trypsin inhibitor antibody. Numbers above lanes indicate individual F_2 seed from which seed chips were taken. The bands corresponding to KTi1 and KTi3 proteins are indicated by arrows.

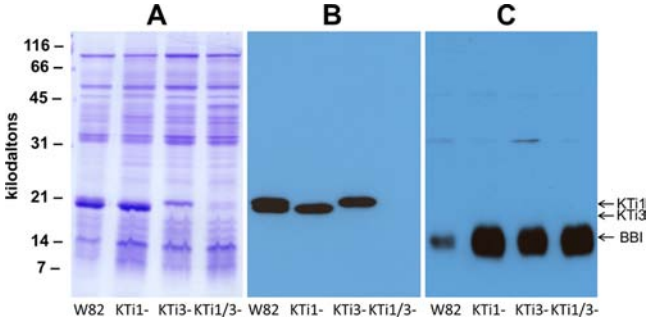

Figure 4. Western blot analysis of Kunitz and Bowman−Birk trypsin inhibitors in soybean seed of selected genotypes. (A) Coomassie brilliant blue R-250-stained PAGE gel. Seed proteins remaining in the supernatant after fractionation with 10 mM calcium were resolved by SDS−15% PAGE and stained with Coomassie brilliant blue. Protein for this analysis was obtained from equal amounts (20 mg) of dry seed powder. (B) Western blot probed with anti-Kunitz trypsin inhibitor antibodies (non-isoform-specific). (C) Western blot probed with anti-Bowman−Birk inhibitor antibody (non-isoform-specific). Bands corresponding to KTi1, KTi3, and BBI proteins are indicated by arrows. Genotypes are indicated below images: W82 = Williams 82 (PI 518671, wild type); KTi3− = Kunitz (PI 542044, *KTi3*− mutant); KTi1− = PI 68679 (*KTi1*− mutant); and KTi1/3− = E16 F_3 progeny of line homozygous for *KTi1*−, *KTi3*− mutant alleles.

exhibited proteome rebalancing by accumulating higher amounts of glycinin.[36]

Proteins extracted from mature seed of Williams 82 or *KTi* mutant lines were separated by DEAE-cellulose chromatography. The elution profile of soybean KTi protein is shown in Figure 5. When DEAE-cellulose-eluted fractions from Williams 82 and *KTi1*− were resolved by SDS−PAGE, an abundant 21 kDa protein was observed in fractions eluted with approximately 250 mM NaCl (Figure 5). Western blot analysis with KTi antibodies reacted strongly with the 21 kDa protein(s), confirming it as KTi (Figure S2, Supporting Information). This abundant protein was drastically reduced in the protein extracts from *KTi3*− and *KTi1/3*− mutant lines (Figure 5). We also fractionated total seed proteins from Williams 82 and *KTi* mutant lines by two-dimensional PAGE (Figure 6). We have previously identified soybean seed proteins resolved by 2D gels by MALDI-TOF-MS.[37] These analyses have demonstrated that the KTi proteins in Williams 82 seed resolves into at least three spots, KTi1/KTi2 and KTi3 (Figure 6, arrows and box indicate KTi protein spots). The protein spot corresponding to KTi3 is much greater in abundance as compared with the KTi1 spots. The *KTi1*− mutant accumulates abundant KTi3 but lacks the KTi1 spot, while the *KTi3*− mutant lacks the abundant KTi3 spot (Figure 6). The homozygote double-mutant line E16 has no detectable KTi protein in mature seed (Figure 6). Although there are at least four *KTi* genes in the soybean genome, the combination of two point mutations (*KTi1*− and *KTi3*−) resulted in complete absence of KTi protein (at a minimum below the threshold level of detection by immunoblot analysis).

Trypsin and Chymotrypsin Activities in Seed of Mutant Lines. The canonical KTi3 protein has been conclusively demonstrated to have trypsin inhibitor activity, and the *KTi3*− nonsense mutation reduces trypsin inhibitory activity by ∼40%.[32] In contrast, the relative contribution of the *KTi1* gene to overall trypsin inhibition activity was unclear.[32] We performed trypsin and chymotrypsin inhibitor assays, and significant genotypic differences were noted by one-way ANOVA (F = 16.8616 and p = 0.0098 for trypsin; F = 7.2156 and p = 0.0432 for chymotrypsin). Seed of all *KTi*− genotypes showed significantly (α = 0.05) decreased trypsin inhibitor activity relative to wild-type seed, and the combination of both mutations in line E16 had the lowest trypsin inhibitor activity (Figure 7A), although the mean trypsin inhibition among *KTi*− genotypes was not significantly different. Soybean genotype E16 revealed only about 50% trypsin inhibitor activity relative to the wild-type Williams 82 (Figure 7A). This observation is consistent with our proteomics data, which show no detectable KTi proteins in E16 (Figure 6). In spite of the complete absence of KTi in E16 genotype, the overall decrease in trypsin inhibitor activity is not significantly different from that of KTi3− mutant. This may be due to E16 seeds compensating for the mutation by overproducing BBI protein (Figures 4C and 8). Mean chymotrypsin activity was lower in all lines bearing *KTi1*− or *KTi3*− mutations, but these differences were significant (α = 0.05) only for the E16 genotype (Figure 7B) as compared to wild-type seed. A previous study has shown that a soybean line lacking KTi3 was nutritionally superior to unheated raw soybean but was inferior to processed soybean meal.[38]Heat treatment reduced trypsin and chymotrypsin inhibitor activities of the KTi3-free soybeans by approximately half and three-fourths in comparison with commercial untoasted soy flour.[38] It will be interesting to compare the effect of heat treatment on trypsin and chymotrypsin inhibitor activities of the E16 genotype created in the current study with those reported for the KTi3− mutant.

qRT-PCR Analysis of Developing Seed of *KTi* Mutant Lines. We examined gene expression in immature seed for all four lines (*KTi1*−, *KTi3*−, *KTi1/3*−, and Williams 82) by qRT-PCR with mRNA isolated from growth-chamber-produced seed at two seed development stages: (1) 200−300 mg/seed fresh weight and (2) 400−500 mg/seed fresh weight. Four of the

DOI: 10.1021/jf505220p
J. Agric. Food Chem. 2015, 63, 1352−1359

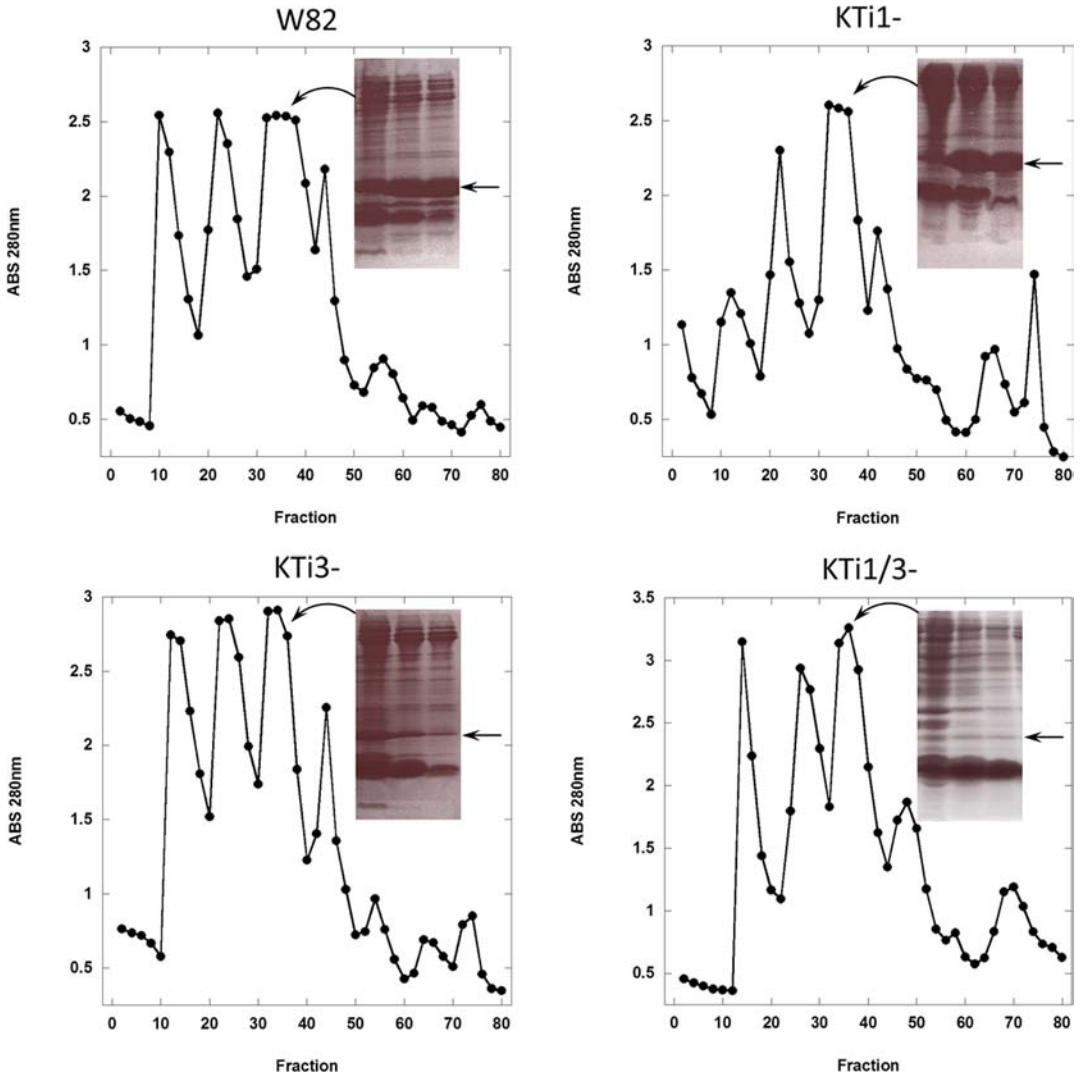

Figure 5. Elution profile of KTi fractionated by DEAE-cellulose chromatography. Soybean KTi was eluted from the column by use of a NaCl step gradient of 50 mM (fractions 1−10), 100 mM (fractions 11−21), 200 mM (fractions 22−31), 250 mM (fractions 32−41), 300 mM (fractions 42−51), 400 mM (fractions 52−61), and 500 mM (fractions 62−82). (Insets) SDS−PAGE images of fractions enriched in KTi. Arrows point to the abundant 21 kDa protein. Genotypes are indicated above each panel as described in the caption for Figure 4.

major seed storage protein-encoding genes present in soybean seed were selected for qRT-PCR analysis: glycinin 4 (*Gy4*), *KTi1*, *KTi3*, and a non-gene-specific primer pair that amplified several BBI genes (full details in Materials and Methods). One-way ANOVA was performed to compare the effect of genotype on each gene's expression level.

We observed no significant differences in *Gy4* mRNA levels between any genotypes at either seed developmental stage (Figure 8A, $F = 0.4091$ and $p = 0.7496$; Figure 8B, $F = 1.0407$ and $p = 0.4127$). No significant differences were noted for *KTi1* at the early developmental stage for any of the genotypes (Figure 8A, $F = 1.5404$ and $p = 0.2591$), and differences at the late developmental stage were not significant (Figure 8B, $F = 2.7633$ and $p = 0.0922$). Significant differences were noted for *KTi3* gene expression at both early and late developmental stages (Figure 8A, $F = 234.9889$ and $p < 0.001$; Figure 8B, $F = 56.8767$ and $p < 0.0001$). We observed significant differences in accumulation of BBI gene transcripts at the early seed developmental stage (Figure 8A, $F = 5.994$ and $p = 0.0113$).

Post hoc analyses were done with the Tukey HSD test ($\alpha = 0.05$) to compare genotype means (Figure 8) for *KTi3* and *BBI*. We noted significant near-absence of *KTi3* gene transcripts in lines bearing the *KTi3*− mutation at both early (Figure 8A) and late (Figure 8B) seed development stages, which is consistent with previous reports.[22] *KTi3* gene expression was similar between Williams 82 and *KTi1*− genotypes and between *KTi3*− and *KTi1/3*− genotypes. BBI gene expression was higher for both the *KTi1*− mutant (~2.75-fold higher) and the *KTi1/3*− mutant (~3.75-fold higher) as compared to Williams 82 at the early seed developmental stage, although only the *KTi1/3*− mutant was significantly different from Williams 82. *BBI* gene expression for Williams 82 and *KTi3*− genotypes were insignificantly different (Figure 8), and no significant differences were found at the later developmental stage for *BBI* gene expression (Figure 8B).

At least 10 BBI isoforms exist in soybean seed, which have been shown to have different specific inhibitory activities on trypsin, chymotrypsin, and/or elastase.[39,40] Some BBI isoforms inhibit only trypsin, or inhibit elastase and trypsin but not chymotrypsin. The specific proportion of these isoforms has been shown to vary from cultivar to cultivar.[41] Enhancement of BBI isoforms that inhibit only trypsin or inhibit elastase and

DOI: 10.1021/jf505220p
J. Agric. Food Chem. 2015, 63, 1352−1359

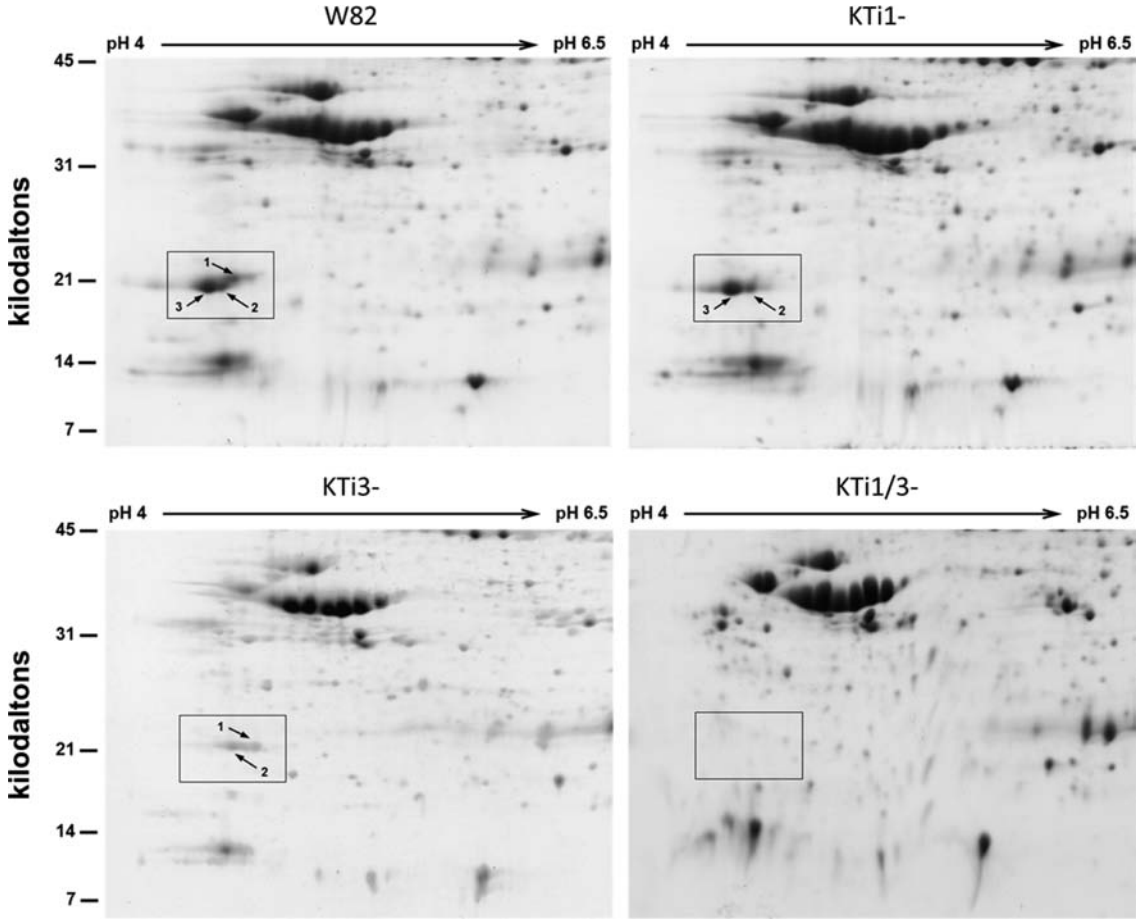

Figure 6. Two-dimensional gel electrophoresis of soybean total seed protein stained with Coomassie brilliant blue. Equivalent amounts of protein (300 μg) were separated on the basis of isoelectric point (p*I*) and then by SDS−PAGE. Genotype is indicated above each image, as described in the caption for Figure 4. The position of KTi proteins is indicated by numbered arrows and box.

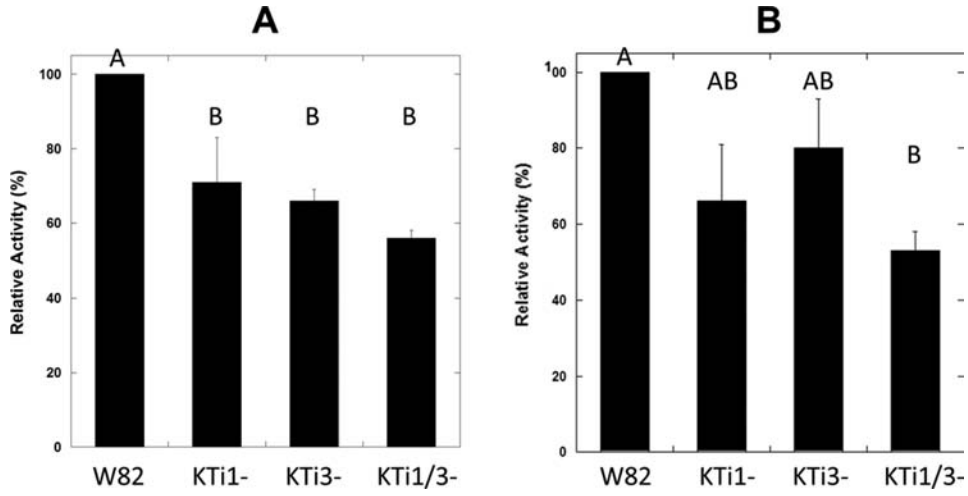

Figure 7. (A) Trypsin and (B) chymotrypsin inhibitor activity levels present in seed of selected genotypes. Letters above columns indicate result of one-way ANOVA ($p < 0.05$) and Tukey's HSD test ($\alpha = 0.05$); common letters indicate insignificant differences between means. Trypsin and chymotrypsin inhibitor activity were measured under standard conditions containing 10−50 μg of soybean seed protein with *N*-benzoyl-L-arginine ethyl ester and *N*-benzoyl-L-tyrosine ester as substrates, respectively. Genotypes are indicated below bars, as described in the caption for Figure 4.

chymotrypsin would compensate for the loss of trypsin inhibitor activity due to the KTi mutations without affecting chymotrypsin inhibitor activity. We observed no change in mRNA abundance of total BBI transcripts in seed of the *KTi3*− mutant (Figure 8A), which suggests that increased BBI protein is not likely due to increased transcription and/or enhanced mRNA stability in *KTi3*− lines. In contrast, we observed significantly higher levels of BBI transcripts in *KTi1*− lines. These results suggest that developing seed responds to *KTi*− lesions to maintain protein homeostasis through two different

DOI: 10.1021/jf505220p
J. Agric. Food Chem. 2015, 63, 1352−1359

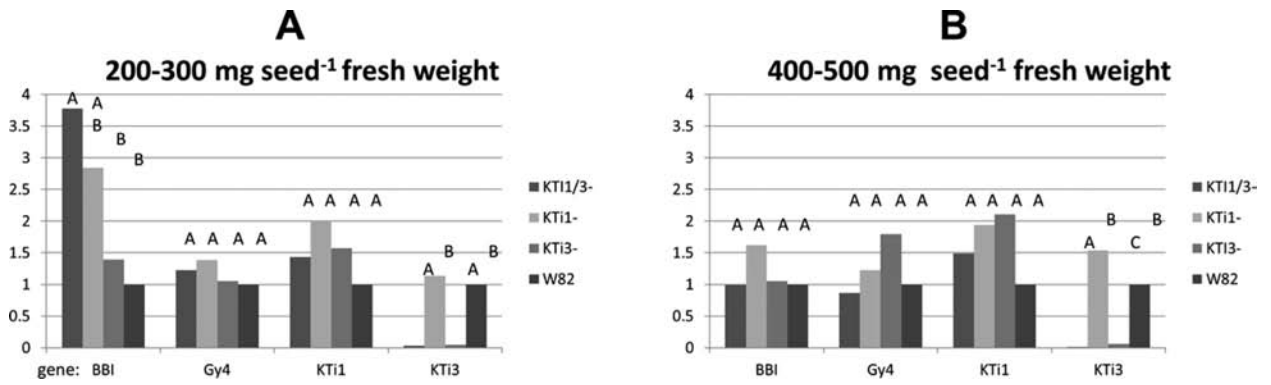

Figure 8. qRT-PCR analysis of mRNA from immature seed of two developmental stages examined with seed storage protein-specific primers: (A) early stage, isolated from immature seed between 200 and 300 mg/seed, and (B) late stage, isolated from immature seed between 400 and 500 mg/seed. Genes examined are *BBI* (non-isoform-specific), *KTi1*, *KTi3*, and glycinin subunit 4 (*Gy4*), and results were normalized to Williams 82 gene expression. Letters above columns indicates result of one-way ANOVA and Tukey's HSD test (α = 0.05); common letters indicate insignificant differences between means.

methods: elevated BBI mRNA levels (*KTi1*−) or proteome rebalancing (*KTi3*−), though the exact mechanisms are still incompletely understood. Enhanced accumulation of BBI proteins, however, does not translate to increased chymotrypsin inhibitor activity, which suggests that only a subset of BBI proteins are upregulated, in contrast to the major BBI isoform, which has functional chymotrypsin inhibition domains.[5] Similar results were obtained by transgenic overexpression of a mutated, nonfunctional BBI transgene, where the nonfunctional version effectively outcompetes translation of an endogenous, chymotrypsin-inhibitory BBI protein.[2016] In this study we have observed a reduction in chymotrypsin inhibitor activity in the KTi mutants (Figure 7B). It has been reported that soybean KTi can inhibit bovine chymotrypsin.[39] The loss of both KTi1 and KTi3 in the E16 genotype could result in greater inhibition of chymotrypsin inhibitor activity.

If substantial reduction in trypsin/chymotrypsin inhibitors can be achieved, beyond that currently possible with the *KTi1*− and/or *KTi3*− mutations, it may be possible to utilize raw soybean derivatives without the pancreatic complications or impaired weight gain issues of conventional soybean seed. This aim is particularly relevant for certain fish species (e.g., salmonoids), which are extremely sensitive to trypsin proteinase inhibitors, as compared to poultry and swine.[12] Even conventional heat-treated soybean meal bears residual trypsin/chymotrypsin inhibitor activity, which has limited inclusion of soybean meal in salmonoid diet mixtures.[42] As the current use of fishmeal is unsustainable in the long term,[43] reducing antinutritional trypsin inhibitory content of soybean seed may facilitate a more sustainable source of protein meal for fish production.

■ ASSOCIATED CONTENT

Supporting Information

Two figures, showing typical genotyping SimpleProbe assay for the *KTi3*− allele and immunoblot confirmation of KTi fractionated by DEAE-cellulose chromatography, and two tables, listing primers used in this work and expression of BBI genes in developing seed, as determined by RNA sequencing analysis. Data are taken from ref 44. This material is available free of charge via the Internet at http://pubs.acs.org.

■ AUTHOR INFORMATION

Corresponding Author

*E-mail Hari.Krishnan@usda.ars.gov; tel 573-882-8151; fax 573-884-7850.

Notes

The authors declare no competing financial interest.

■ ACKNOWLEDGMENTS

We acknowledge the superb technical assistance of Sungchan Jang, Jeremy Mullis, and Nathan Oehrle. This research was supported by the USDA Agricultural Research Service. Mention of a trademark, vendor, or proprietary product does not constitute a guarantee or warranty of the product by the USDA and does not imply its approval to the exclusion of other products or vendors that may also be suitable.

■ ABBREVIATIONS

BBI, Bowman−Birk proteinase inhibitor; DEAE, diethylaminoethyl; EDTA, ethylenediaminetetraacetic acid; *KTi1*, Kunitz trypsin inhibitor isoform 1 gene; *KTi2*, Kunitz trypsin inhibitor isoform 2 gene; *KTi3*, Kunitz trypsin inhibitor isoform 3 gene; PAGE, polyacrylamide gel electrophoresis; qRT-PCR, quantitative real-time polymerase chain reaction; SDS, sodium dodecyl sulfate

■ REFERENCES

(1) Henkel, J. Soy: Health claims for soy protein, questions about other components. *FDA Consum.* **2000**, *34*, 18−20.

(2) Yen, J. T.; Jensen, A. H.; Simon, J. Effect of dietary raw soybean and soybean trypsin inhibitor on trypsin and chymotrypsin activities in the pancreas and in small intestinal juice of growing swine. *J. Nutr.* **1977**, *107*, 156−165.

(3) Palacios, M. F.; Easter, R. A.; Soltwedel, K. T.; Parsons, C. M.; Douglas, M. W.; Hymowitz, T.; Pettigrew, J. E. Effect of soybean variety and processing on growth performance of young chicks and pigs. *J. Anim. Sci.* **2004**, *82*, 1108−1114.

(4) Kunitz, M. Crystallization of a trypsin inhibitor from soybean. *Science* **1945**, *101*, 668−669.

(5) Birk, Y. Purification and some properties of a highly active inhibitor of trypsin and α-chymotrypsin from soybeans. *Biochim. Biophys. Acta* **1961**, *54*, 378−381.

(6) Bowman, D. E. Fractions derived from soy beans and navy beans which retard tryptic digestion of casein. *Exp. Biol. Med.* **1944**, *57*, 139−140.

DOI: 10.1021/jf505220p
J. Agric. Food Chem. 2015, 63, 1352−1359

(7) Kunitz, M. Crystalline soybean trypsin inhibitor II. General properties. *J. Gen. Phys.* **1947**, *30*, 291−310.
(8) Odani, S.; Ikenaka, T. Studies on soybean trypsin inhibitors: X. Isolation and partial characterization of four soybean double-headed proteinase inhibitors. *J. Biochem.* **1977**, *82*, 1513−1522.
(9) Tan-Wilson, A. L.; Cosgriff, S. E.; Duggan, M. C.; Obach, R. S.; Wilson, K. A. Bowman-Birk proteinase isoinhibitor complements of soybean strains. *J. Agric. Food Chem.* **1985**, *33*, 389−393.
(10) Tan-Wilson, A. L.; Chen, J. C.; Duggan, M. C.; Chapman, C.; Obach, R. S.; Wilson, K. A. Soybean Bowman-Birk trypsin isoinhibitors: Classification and report of a glycine-rich trypsin inhibitor class. *J. Agric. Food Chem.* **1987**, *35*, 974−980.
(11) Dia, V. P.; Gomez, T.; Vernaza, G.; Berhow, M.; Chang, Y. K.; de Mejia, E. G. Bowman-Birk and Kunitz protease inhibitors among antinutrients and bioactives modified by germination and hydrolysis in Brazilian soybean cultivar BRS 133. *J. Agric. Food Chem.* **2012**, *60*, 7886−7894.
(12) Krogdahl, Å. Pancreatic proteinases from man, trout, rat, pig, cow, chicken, mink and fox: Enzyme activities and inhibition by soybean and lima bean proteinase inhibitors. *Comp. Biochem. Physiol., Part B: Biochem. Mol. Biol.* **1983**, *74*, 403−409.
(13) DiPietro, C. M.; Liener, I. E. Heat inactivation of the Kunitz and Bowman-Birk soybean protease inhibitors. *J. Agric. Food Chem.* **1989**, *37*, 39−44.
(14) Chang, C. J.; Tanksley, T. D.; Knabe, D. A.; Zebrowska, T. Effects of different heat treatments during processing on nutrient digestibility of soybean meal in growing swine. *J. Anim. Sci.* **1987**, *65*, 1273−1282.
(15) Krishnan, H. B.; Kim, W.-S. A four-nucleotide base-pair deletion in the coding region of the Bowman−Birk protease inhibitor gene prevents its accumulation in the seeds of *Glycine microphylla* PI440956. *Planta* **2003**, *217*, 523−527.
(16) Domagalski, J. M.; Kollipara, K. P.; Bates, A. H.; Brandon, D. L.; Friedman, M.; Hymowitz, T. Nulls for the major soybean Bowman-Birk protease inhibitor in the genus *Glycine*. *Crop Sci.* **1992**, *32*, 1502−1505.
(17) Deshimaru, M.; Yoshimi, S.; Shioi, S.; Terada, S. Multigene family for Bowman-Birk type proteinase inhibitors of wild Soja and soybean: the presence of two BBI-A genes and pseudogenes. *Biosci. Biotechnol. Biochem.* **2004**, *68*, 1279−1286.
(18) de Almeida Barros, B.; da Silva, W.; Moreira, M.; de Barros, E. In silico characterization and expression analysis of the multigene family encoding the Bowman−Birk protease inhibitor in soybean. *Mol. Biol. Rep* **2012**, *39*, 327−334.
(19) Krishnan, H. B.; Jang, S.; Baxter, I.; Wiebold, W. J. Growing location has a pronounced effect on the accumulation of cancer chemopreventive agent Bowman-Birk inhibitor in soybean seeds. *Crop Sci.* **2012**, *52*, 1786−1794.
(20) Livingstone, D.; Beilinson, V.; Kalyaeva, M.; Schmidt, M.; Herman, E.; Nielsen, N. Reduction of protease inhibitor activity by expression of a mutant Bowman-Birk gene in soybean seed. *Plant Mol. Biol.* **2007**, *64*, 397−408.
(21) Orf, J. H.; Hymowitz, T. Inheritance of the absence of the Kunitz trypsin inhibitor in seed protein of soybeans. *Crop Sci.* **1979**, *19*, 107−109.
(22) Jofuku, K. D.; Schipper, R. D.; Goldberg, R. B. A frameshift mutation prevents Kunitz trypsin inhibitor mRNA accumulation in soybean embryos. *Plant Cell* **1989**, *1*, 427−435.
(23) Perez-Maldonado, R. A.; Mannion, P. F.; Farrell, D. J. Effects of heat treatment on the nutritional value of raw soybean selected for low trypsin inhibitor activity. *Br. Poult. Sci.* **2003**, *44*, 299−308.
(24) Cook, D. A.; Jensen, A. H.; Fraley, J. R.; Hymowitz, T. Utilization by growing and finishing pigs of raw soybeans of low Kunitz trypsin inhibitor content. *J. Anim. Sci.* **1988**, *66*, 1686−1691.
(25) Bernard, R. L.; Hymowitz, T.; Cremeens, C. R. Registration of 'Kunitz' soybean. *Crop Sci.* **1991**, *31*, 232−233.
(26) Bernard, R.; Cremeens, C. Registration of 'Williams 82' Soybean. *Crop Sci.* **1988**, *28*, 1027−1028.
(27) Krishnan, H. B. Characterization of a soybean [*Glycine max* (L.) Merr.] mutant with reduced levels of Kunitz trypsin inhibitor. *Plant Sci.* **2001**, *160*, 979−986.
(28) Kim, W.-S.; Gillman, J.; Krishnan, H. Identification of a plant introduction soybean line with genetic lesions affecting two distinct glycinin subunits and evaluation of impacts on protein content and composition. *Mol. Breed.* **2013**, *32*, 291−298.
(29) Palavalli, M. H.; Natarajan, S. S.; Wang, T. T. Y.; Krishnan, H. B. Imbibition of soybean seeds in warm water results in the release of copious amounts of Bowman−Birk protease inhibitor, a putative anticarcinogenic agent. *J. Agric. Food Chem.* **2012**, *60*, 3135−3143.
(30) Livak, K. J.; Schmittgen, T. D. Analysis of relative gene expression data using real-time quantitative PCR and the 2−ΔΔCT method. *Methods* **2001**, *25*, 402−408.
(31) Libault, M.; Thibivilliers, S.; Bilgin, D. D.; Radwan, O.; Benitez, M.; Clough, S. J.; Stacey, G. Identification of four soybean reference genes for gene expression normalization. *Plant Genome (Madison, WI, U. S.)* **2008**, *1*, 44−54.
(32) Jofuku, K. D.; Goldberg, R. B. Kunitz trypsin inhibitor genes are differentially expressed during the soybean life cycle and in transformed tobacco plants. *Plant Cell* **1989**, *1*, 1079−1093.
(33) Konieczny, A.; Ausubel, F. M. A procedure for mapping *Arabidopsis* mutations using co-dominant ecotype-specific PCR-based markers. *Plant J.* **1993**, *4*, 403−410.
(34) Neff, M. M.; Neff, J. D.; Chory, J.; Pepper, A. E. dCAPS, a simple technique for the genetic analysis of single nucleotide polymorphisms: experimental applications in *Arabidopsis thaliana* genetics. *Plant J.* **1998**, *14*, 387−392.
(35) Kinney, A. J.; Jung, R.; Herman, E. M. Cosuppression of the α-subunits of β-conglycinin in transgenic soybean seeds induces the formation of endoplasmic reticulum-derived protein bodies. *Plant Cell* **2001**, *13*, 1165−1178.
(36) Mori, T.; Maruyama, N.; Nishizawa, K.; Higasa, T.; Yagasaki, K.; Ishimoto, M.; Utsumi, S. The composition of newly synthesized proteins in the endoplasmic reticulum determines the transport pathways of soybean seed storage proteins. *Plant J.* **2004**, *40*, 238−249.
(37) Krishnan, H. B.; Nelson, R. L. Proteomic analysis of high protein soybean (*Glycine max*) accessions demonstrates the contribution of novel glycinin subunits. *J. Agric. Food Chem.* **2011**, *59*, 2432−2439.
(38) Liener, I. E.; Tomlinson, S. Heat inactivation of protease inhibitors in a soybean line lacking the Kunitz trypsin inhibitor. *J. Food Sci.* **1981**, *46*, 1354−1356.
(39) Bösterling, B.; Quast, U. Soybean trypsin inhibitor (Kunitz) is doubleheaded. Kinetics of the interaction of alpha-chymotrypsin with each side. *Biochim. Biophys. Acta* **1981**, *657*, 58−72.
(40) Tan-Wilson, A. L.; Chen, J. C.; Duggan, M. C.; Chapman, C.; Obach, R. S.; Wilson, K. A. Soybean Bowman-Birk trypsin isoinhibitors: Classification and report of a glycine-rich trypsin inhibitor class. *J. Agric. Food Chem.* **1987**, *35*, 974−981.
(41) Tan-Wilson, A.; Wilson, K. Relevance of multiple soybean trypsin inhibitor forms to nutritional quality. In *Nutritional and Toxicological Significance of Enzyme Inhibitors in Foods*; Friedman, M., Ed.; Springer: New York, 1986; Vol. *199*, pp 391−411.
(42) Olli, J. J.; Hjelmeland, K.; Krogdahl, Å. Soybean trypsin inhibitors in diets for Atlantic salmon (*Salmo salar, L*): Effects on nutrient digestibilities and trypsin in pyloric caeca homogenate and intestinal content. *Comp. Biochem. Physiol.* **1994**, *109*, 923−928.
(43) Tacon, A. G. J.; Metian, M. Global overview on the use of fish meal and fish oil in industrially compounded aquafeeds: Trends and future prospects. *Aquaculture* **2008**, *285*, 146−158.
(44) Severin, A. J.; et al. RNA-Seq Atlas of *Glycine max*: A guide to the soybean transcriptome. *BMC Plant Biol.* **2010**, *10*, No. 160.

DOI: 10.1021/jf505220p
J. Agric. Food Chem. 2015, 63, 1352−1359

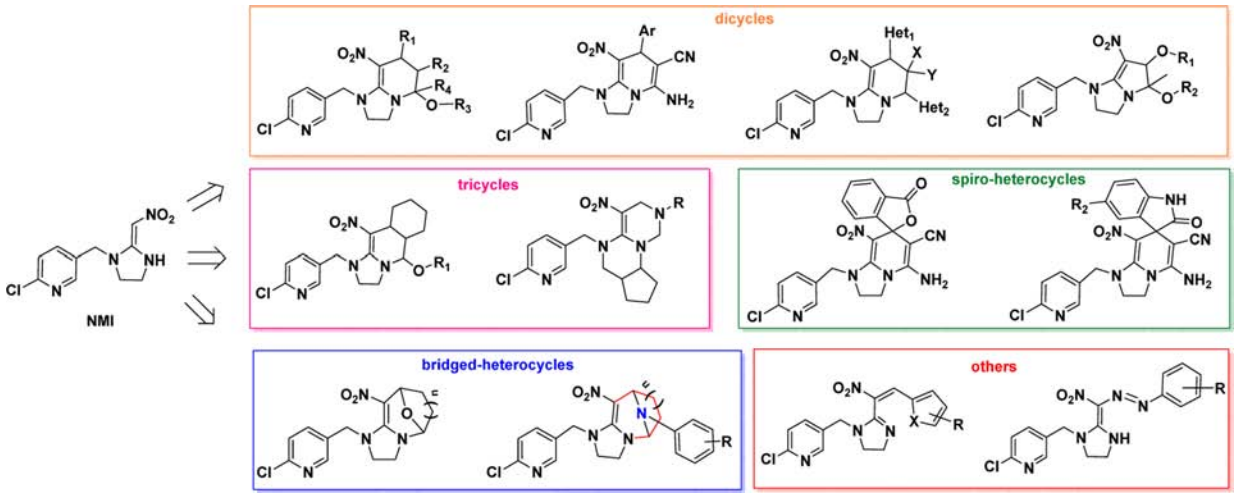

Figure 1. Synthetic variants of neonicotinoids based on NMI.

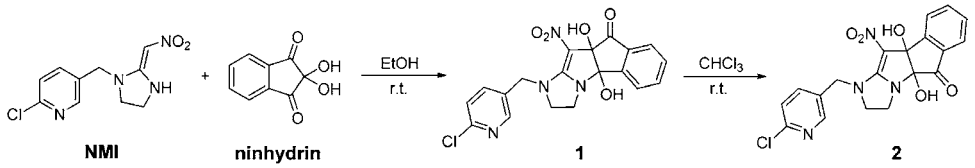

Figure 2. Synthesis and isomerization of NMI-ninhydrin adduct.

General Procedure for the Preparation of 1, 8a, 9a, and 10a. NMI and its analogues were prepared according to our previously reported procedures. To a suspension of NMI or its corresponding analogues (5 mmol) in ethanol (30 mL) was added the solution of ninhydrin (5 mmol) in ethanol (20 mL), and the mixture was stirred at room temperature for 24 h.[35] Then filtration was performed to afford the solid product, which was used directly without further purification.

General Procedure for the Preparation of 2, 8b, 9b, and 10b. Compound **1** or its corresponding analogues (1 mmol) in chloroform (or DMF, 5 mL) were stirred at room temperature for 3 days. Then, the solvent was removed by vacuum, and the solid was further purified by silica gel column chromatography (EtOAc) affording the pure product.[35]

General Procedure for the Preparation of Etherification Products 3a–5d. **3a–3g**: A mixture of **2** (1 mmol) and corresponding alcoholic solvents (10 mL) was stirred at room temperature. Then, TsOH (0.1 mmol) was added to the solution, and the process was monitored by TLC. After completion, the solvent was removed by vacuum, and the solid was further purified by silica gel column chromatography (EtOAc) affording the pure products.

4a–4b: A mixture of **2** (1 mmol) and dry tetrahydrofuran (10 mL) was stirred at room temperature. NaH (1.5 mmol) was added to the solution until no bubbles were produced, then the corresponding alkyl iodide (5 mmol) was added. The process was monitored by TLC. After completion, the solvent was removed by vacuum, and the solid was further purified by silica gel column chromatography (EtOAc) affording the pure products.

5a–5d: A mixture of **2** (1 mmol) and the corresponding alcoholic solvents (10 mL) was stirred at room temperature. Then, TsOH (0.1 mmol) was added to the solution, and the process was monitored by TLC. After completion, the solvent was removed by vacuum, and dry tetrahydrofuran (10 mL) was added. Then, NaH (1.5 mmol) was added to the solution until no bubbles were produced, then the corresponding alkyl iodide (5 mmol) was added. The process was monitored by TLC. After completion, the solvent was removed by vacuum, and the solid was further purified by silica gel column chromatography (EtOAc) affording the pure products.

General Procedure for the Preparation of Chlorine-Substituted Products 6a–6c. A mixture of **2** (1 mmol) and dry chloroform (10 mL) was stirred at reflux. Then $SOCl_2$ (5 mmol) was added to the solution, and the process was monitored by TLC. After completion, to the solution was added the corresponding alcoholic solvents (1 mL), then the solvent was removed by vacuum, and the solid was further purified by silica gel column chromatography (EtOAc) affording the pure products.

General Procedure for the Preparation of Esterification Products 7a–7d. A mixture of **2** (1 mmol), diisopropylethylamine (2.2 mmol), and dry CH_2Cl_2 (10 mL) was stirred at room temperature. Then, the corresponding acyl chloride (2.2 mmol) was added to the solution dropwise, and the process was monitored by TLC. After completion, the solvent was removed by vacuum, and the solid was further purified by silica gel column chromatography (EtOAc) affording the pure products.

*1-((6-Chloropyridin-3-yl)methyl)-4a,9a-dihydroxy-10-nitro-2,3,4a,9a-tetrahydroindeno[2′,1′:4,5]pyrrolo[1,2-a]imidazol-9(1H)-one (**1**).* Yield, 86%; mp, 145.9–146.8 °C; ^{1}H NMR (400 MHz, DMSO-d_6) δ 8.34 (s, 1H), 7.89–7.71 (m, 4H), 7.66 (t, J = 6.9 Hz, 1H), 7.52 (d, J = 8.0 Hz, 1H), 7.09 (s, 1H), 6.43 (s, 1H), 5.41 (d, J = 15.4 Hz, 1H), 4.76 (d, J = 15.4 Hz, 1H), 3.71–4.02 (m, 3H), 3.49–3.72 (m, 1H) ppm; ^{13}C NMR (100 MHz, DMSO-d_6) δ 196.1, 156.3, 149.5, 149.1, 146.0, 139.2, 135.8, 134.2, 131.9, 130.7, 125.1, 124.2, 123.9, 103.8, 88.6, 86.0, 54.0, 48.2, 39.3 ppm; HRMS (ES+) calcd for $C_{19}H_{15}{}^{35}ClN_4O_5Na$ $(M+Na)^+$, 437.0629; found, 437.0623. Calcd for $C_{19}H_{15}{}^{37}ClN_4O_5Na$ $(M+Na)^+$, 439.0599; found, 439.0613.

*1-((6-Chloropyridin-3-yl)methyl)-4a,9b-dihydroxy-10-nitro-2,3,4a,9b-tetrahydroindeno[1′,2′:4,5]pyrrolo[1,2-a]imidazol-5(1H)-one (**2**).* Yield, 85%; mp, 124.3–126.1 °C; ^{1}H NMR (400 MHz, DMSO-d_6) δ 8.27 (d, J = 7.8 Hz, 1H), 7.84 (t, J = 7.4 Hz, 1H), 7.74 (d, J = 7.6 Hz, 1H), 7.58 (t, J = 7.4 Hz, 1H), 7.41 (d, J = 8.2 Hz, 2H), 7.31 (d, J = 8.1 Hz, 2H), 7.10 (s, 1H), 6.43 (s, 1H), 5.40 (d, J = 15.2 Hz, 1H), 4.76 (d, J = 15.2 Hz, 1H), 3.73–3.90 (m, 2H), 3.61–3.73 (m, 1H), 3.47–3.59 (m, 1H) ppm; ^{13}C NMR (100 MHz, DMSO-d_6) δ 195.3, 156.1, 152.9, 136.5, 135.6, 132.4, 132.2, 129.6 (3C), 128.5 (2C), 127.9, 123.4, 106.9, 87.6, 83.7, 53.5, 50.4, 39.3 ppm; HRMS (ES–) calcd for $C_{20}H_{15}{}^{35}ClN_3O_5$ $(M-H)^-$, 412.0700; found, 412.0696. Calcd for $C_{20}H_{15}{}^{37}ClN_3O_5$ $(M-H)^-$, 414.0671; found, 414.0670.

DOI: 10.1021/jf505281p
J. Agric. Food Chem. 2015, 63, 1360–1369

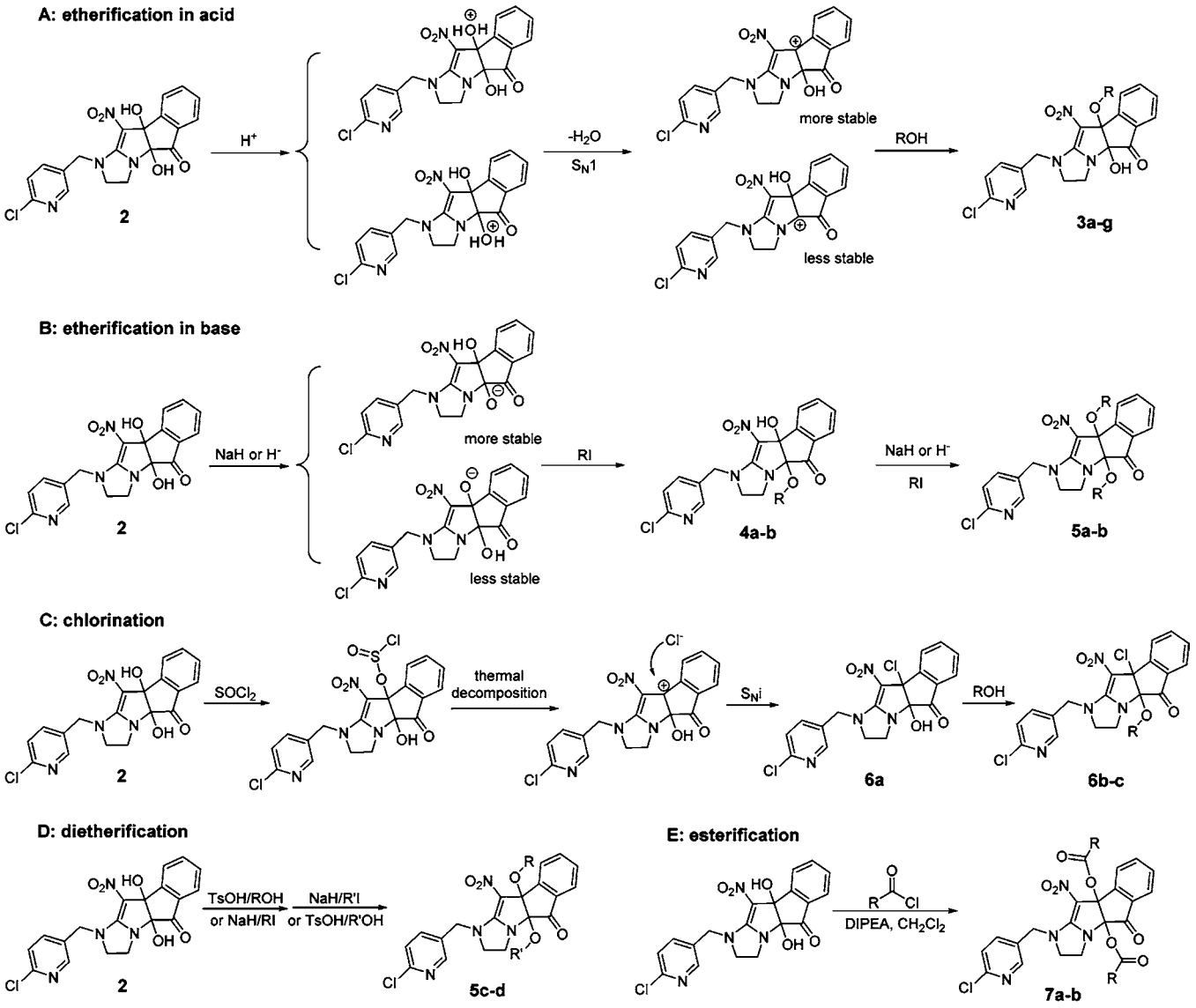

Figure 3. Selective etherification, etherification and chlorination of **2** and the corresponding mechanism.

*1-((6-Chloropyridin-3-yl)methyl)-4a-hydroxy-9b-methoxy-10-nitro-2,3,4a,9b-tetrahydroindeno[1′,2′:4,5]pyrrolo[1,2-a]imidazol-5(1H)-one (**3a**).* Yield, 85%; mp, 108.6−110.1 °C; ^{1}H NMR (400 MHz, DMSO-d_6) δ 8.35 (s, 1H), 8.20 (d, J = 7.8 Hz, 1H), 7.84 (t, J = 7.4 Hz, 1H), 7.78 (d, J = 7.8 Hz, 2H), 7.62 (t, J = 7.4 Hz, 1H), 7.53 (m, 2H), 5.31 (d, J =15.6 Hz, 1H), 4.93 (d, J =15.6 Hz, 1H), 3.84−3.99 (m, 2H), 3.72−3.81 (m, 1H), 3.51−3.63 (m, 1H), 3.35 (s, 3H); ^{13}C NMR (100 MHz, DMSO-d_6) δ 195.4, 156.6, 151.0, 149.5, 149.0, 139.1, 136.4, 133.0, 132.0, 130.0, 128.2, 124.3, 123.7, 103.5, 88.9, 87.8, 54.0, 53.3, 48.4, 39.9; HRMS (ES+) calcd for $C_{20}H_{18}{}^{35}ClN_4O_5$ (M + H)$^+$, 429.0966; found, 429.0964. Calcd for $C_{20}H_{18}{}^{37}ClN_4O_5$ (M + H)$^+$, 431.0936; found, 431.0943.

*1-((6-Chloropyridin-3-yl)methyl)-9b-ethoxy-4a-hydroxy-10-nitro-2,3,4a,9b-tetrahydroindeno[1′,2′:4,5]pyrrolo[1,2-a]imidazol-5(1H)-one (**3b**).* Yield, 81%; mp, 109.7−110.8 °C; ^{1}HNMR (400 MHz, DMSO-d_6) δ 8.35 (s, 1H), 8.23 (d, J = 7.6 Hz, 1H), 7.84 (t, J = 7.4 Hz, 1H), 7.78 (d, J = 7.6 Hz, 2H), 7.61 (t, J = 7.2 Hz, 1H), 7.52 (d, J = 8.2 Hz, 1H), 7.48 (s, 1H), 5.30 (d, J =15.6 Hz, 1H), 4.92 (d, J =15.6 Hz, 1H), 3.83−4.03 (m, 2H), 3.72−3.83 (m, 1H), 3.62−3.72 (m, 1H), 3.52−3.59 (m, 1H), 3.45−3.50 (m, 1H), 1.16 (t, J = 6.6 Hz, 3H); ^{13}C NMR (100 MHz, DMSO-d_6) δ 195.4, 156.5, 151.2, 149.5, 149.0, 139.1, 136.4, 132.9, 132.1, 129.9, 128.3, 124.3, 123.6, 104.2, 88.7, 87.8, 61.0, 54.0, 48.4, 39.8, 15.4; HRMS (ES+) calcd for $C_{21}H_{20}{}^{35}ClN_4O_5$ (M + H)$^+$, 443.1122; found, 443.1118. Calcd for $C_{21}H_{20}{}^{37}ClN_4O_5$ (M + H)$^+$, 445.1093; found, 445.1100.

*1-((6-Chloropyridin-3-yl)methyl)-4a-hydroxy-10-nitro-9b-propoxy-2,3,4a,9b-tetrahydroindeno[1′,2′:4,5]pyrrolo[1,2-a]imidazol-5(1H)-one (**3c**).* Yield, 73%; mp, 99.6−100.3 °C; ^{1}HNMR (400 MHz, DMSO-d_6) δ 8.35 (s, 1H), 8.22 (d, J = 7.8 Hz, 1H), 7.84 (t, J = 7.2 Hz, 1H), 7.77 (d, J = 7.8 Hz, 2H), 7.61 (t, J = 7.2 Hz, 1H), 7.51 (d, J = 8.2 Hz, 1H), 7.45 (s, 1H), 5.29 (d, J = 15.6 Hz, 1H), 4.93 (d, J = 15.6 Hz, 1H), 3.84−4.00 (m, 2H), 3.70−3.83 (m, 1H), 3.48−3.66 (m, 2H), 3.25−3.34 (m, 1H), 1.52−1.61 (m, 2H), 0.88 (t, J = 7.2 Hz, 3H); ^{13}C NMR (100 MHz, DMSO-d_6) δ 195.5, 156.6, 151.3, 149.5, 149.1, 139.1, 136.3, 132.9, 132.1, 129.9, 128.3, 124.3, 123.6, 104.2, 88. 6, 87.9, 67.0, 54.1, 48.4, 39.9, 22.8, 10.5; HRMS (ES+) calcd for $C_{22}H_{22}{}^{35}ClN_4O_5$ (M + H)$^+$, 457.1279; found, 457.1275. Calcd for $C_{22}H_{22}{}^{37}ClN_4O_5$ (M + H)$^+$, 459.1249; found, 459.1250.

*9b-Butoxy-1-((6-chloropyridin-3-yl)methyl)-4a-hydroxy-10-nitro-2,3,4a,9b-tetrahydroindeno[1′,2′:4,5]pyrrolo[1,2-a]imidazol-5(1H)-one (**3d**).* Yield, 58%; mp, 81.0−84.3 °C;^{1}HNMR (400 MHz, DMSO-d_6) δ 8.35 (s, 1H), 8.21 (d, J = 7.8 Hz, 1H), 7.84 (t, J = 7.4 Hz, 1H), 7.77 (d, J = 7.8 Hz, 2H), 7.61 (t, J = 7.4 Hz, 1H), 7.51 (d, J = 8.2 Hz, 1H), 7.44 (s, 1H), 5.29 (d, J =15.6 Hz, 1H), 4.93 (d, J =15.6 Hz, 1H), 3.84−4.01 (m, 2H), 3.70−3.80 (m, 1H), 3.50−3.65 (m, 2H), 3.36−3.42 (m, 1H), 1.44−1.60 (m, 2H), 1.31−1.39 (m, 2H), 0.87 (t, J = 7.0 Hz, 3H); ^{13}C NMR (100 MHz, DMSO-d_6) δ 195.5, 156.6, 151.3,

DOI: 10.1021/jf505281p
J. Agric. Food Chem. 2015, 63, 1360−1369

149.5, 149.0, 139.1, 136.3, 132.9, 132.1, 129.8, 128.3, 124.2, 123.6, 104.2, 88.6, 87.9, 64.9, 54.1, 48.4, 39.8, 31.7, 18.8, 13.8; HRMS (ES+) calcd for $C_{23}H_{24}{}^{35}ClN_4O_5$ (M + H)$^+$, 471.1435; found, 471.1423. Calcd for $C_{23}H_{24}{}^{37}ClN_4O_5$ (M + H)$^+$, 473.1406; found, 473.1403.

*1-((6-Chloropyridin-3-yl)methyl)-4a-hydroxy-9b-(2-hydroxyethoxy)-10-nitro-2,3,4a,9b-tetrahydroindeno[1′,2′:4,5]pyrrolo[1,2-a]imidazol-5(1H)-one (**3e**).* Yield, 87%; mp, 104.9−106.2 °C; ^{1}HNMR (400 MHz, DMSO-d_6) δ 8.36 (s, 1H), 8.22 (d, J = 7.8 Hz, 1H), 7.85 (t, J = 7.4 Hz, 1H), 7.78 (d, J = 7.8 Hz, 2H), 7.62 (t, J = 7.4 Hz, 1H), 7.51 (d, J = 8.4 Hz, 1H), 7.49 (s, 1H), 5.28 (d, J = 15.5 Hz, 1H), 4.89−5.03 (m, 2H), 3.85−4.00 (m, 2H), 3.75−3.83 (m, 1H), 3.68−3.74 (m, 1H), 3.52−3.67 (m, 4H); ^{13}CNMR (100 MHz, DMSO-d_6) δ 195.1, 156.7, 151.0, 149.5, 149.1, 139.2, 136.3, 133.0, 132.0, 130.0, 128.4, 124.3, 123.6, 104.0, 88.8, 87.7, 67.1, 60.3, 54.1, 48.4, 40.1; HRMS (ES+) calcd for $C_{21}H_{20}{}^{35}ClN_4O_6$ (M + H)$^+$, 459.1071; found, 459.1070. Calcd for $C_{21}H_{20}{}^{37}ClN_4O_6$ (M + H)$^+$, 461.1042; found, 461.1042.

*1-((6-Chloropyridin-3-yl)methyl)-4a-hydroxy-9b-(2-methoxyethoxy)-10-nitro-2,3,4a,9b-tetrahydroindeno[1′,2′:4,5]pyrrolo[1,2-a]imidazol-5(1H)-one (**3f**).* Yield, 83%; mp, 134.3−135.8 °C; ^{1}HNMR (400 MHz, DMSO-d_6) δ 8.36 (s, 1H), 8.21 (d, J = 7.8 Hz, 1H), 7.85 (t, J = 7.4 Hz, 1H), 7.78 (d, J = 7.4 Hz, 2H), 7.62 (t, J = 7.4 Hz, 1H), 7.52 (d, J = 8.2 Hz, 1H), 7.40 (s, 1H), 5.27 (d, J = 15.6 Hz, 1H), 4.95 (d, J = 15.6 Hz, 1H), 3.83−4.01 (m, 2H), 3.71−3.82 (m, 2H), 3.48−3.63 (m, 4H), 3.34 (s, 3H); ^{13}CNMR (100 MHz, DMSO-d_6) δ 195.2, 156.6, 151.0, 149.5, 149.1, 139.2, 136.4, 133.0, 132.0, 130.0, 128.3, 124.3, 123.6, 103.8, 88.8, 87.7, 71.2, 64.5, 58.0, 54.1, 48.4, 39.9; HRMS (ES+) calcd for $C_{22}H_{22}{}^{35}ClN_4O_6$ (M + H)$^+$, 473.1228; found, 473.1213. Calcd for $C_{22}H_{22}{}^{37}ClN_4O_6$ (M + H)$^+$, 475.1198; found, 475.1198.

*1-((6-Chloropyridin-3-yl)methyl)-9b-(2-ethoxyethoxy)-4a-hydroxy-10-nitro-2,3,4a,9b-tetrahydroindeno[1′,2′:4,5]pyrrolo[1,2-a]imidazol-5(1H)-one (**3g**).* Yield, 82%; mp, 169.2−170.0 °C; ^{1}HNMR (400 MHz, DMSO-d_6) δ 8.36 (s, 1H), 8.21 (d, J = 7.6 Hz, 1H), 7.85 (t, J = 7.2 Hz, 1H), 7.78 (d, J = 7.2 Hz, 2H), 7.62 (t, J = 7.2 Hz, 1H), 7.52 (d, J = 8.0 Hz, 1H), 7.34 (s, 1H), 5.27 (d, J = 15.6 Hz, 1H), 4.95 (d, J = 15.6 Hz, 1H), 3.83−4.07 (m, 2H), 3.68−3.84 (m, 2H), 3.51−3.67 (m, 4H), 3.40−3.50 (m, 2H), 1.10 (t, J = 6.7 Hz, 3H); ^{13}C NMR (100 MHz, DMSO-d_6) δ 195.1, 156.6, 150.9, 149.5, 149.1, 139.2, 136.4, 133.0, 132.0, 130.0, 128.3, 124.3, 123.6, 103.8, 88.8, 87.7, 69.1, 65.5, 64.7, 54.1, 48.4, 39.9, 15.1; HRMS (ES+) calcd for $C_{23}H_{24}{}^{35}ClN_4O_6$ (M + H)$^+$, 487.1384; found, 487.1371. Calcd for $C_{23}H_{24}{}^{37}ClN_4O_6$ (M + H)$^+$, 489.1355; found, 489.1345.

*1-((6-Chloropyridin-3-yl)methyl)-9b-hydroxy-4a-methoxy-10-nitro-2,3,4a,9b-tetrahydroindeno[1′,2′:4,5]pyrrolo[1,2-a]imidazol-5(1H)-one (**4a**).* Yield, 55%; mp, 179.6−181.0 °C; ^{1}HNMR (400 MHz, DMSO-d_6) δ 8.35 (s, 1H), 8.27 (d, J = 7.8 Hz, 1H), 7.87 (t, J = 7.2 Hz, 1H), 7.77 (d, J = 7.0 Hz, 2H), 7.60 (t, J = 7.2 Hz, 1H), 7.51 (d, J = 8.0 Hz, 1H), 6.66 (s, 1H), 5.36 (d, J =15.6 Hz, 1H), 4.81 (d, J =15.6 Hz, 1H), 3.94−4.09 (m, 2H), 3.81−3.93 (m, 1H), 3.64−3.75 (m, 1H), 3.49−3.61 (m, 1H), 3.45 (s, 3H); ^{13}C NMR (100 MHz, DMSO-d_6) δ 193.5, 155.9, 153.5, 149.5, 149.1, 139.2, 136.9, 132.1, 131.9, 129.8, 127.6, 124.2, 123.5, 106.8, 90.4, 84.4, 54.0, 52.2, 48.3, 40.4; HRMS (ES+) calcd for $C_{20}H_{18}{}^{35}ClN_4O_5$ (M + H)$^+$, 429.0966; found, 429.0951. Calcd for $C_{20}H_{18}{}^{37}ClN_4O_5$ (M + H)$^+$, 431.0936; found, 431.0933.

*1-((6-Chloropyridin-3-yl)methyl)-4a-ethoxy-9b-hydroxy-10-nitro-2,3,4a,9b-tetrahydroindeno[1′,2′:4,5]pyrrolo[1,2-a]imidazol-5(1H)-one (**4b**).* Yield, 47%; mp, 108.5−110.5 °C; ^{1}H NMR (400 MHz, DMSO-d_6) δ 8.35 (s, 1H), 8.27 (d, J = 7.8 Hz, 1H), 7.86 (t, J = 7.6 Hz, 1H), 7.77 (d, J = 7.0 Hz, 2H), 7.60 (t, J = 7.6 Hz, 1H), 7.51 (d, J = 8.2 Hz, 1H), 6.63 (s, 1H), 5.34 (d, J =15.5 Hz, 1H), 4.82 (d, J =15.5 Hz, 1H), 3.78−3.91 (m, 2H), 3.60−3.74 (m, 2H), 3.55 (q, J = 9.3 Hz, 1H), 3.39 (q, J = 7.0 Hz, 1H), 1.15 (t, J = 6.9 Hz, 3H); ^{13}C NMR (100 MHz, DMSO-d_6) δ 193.7, 155.8, 153.4, 149.5, 149.1, 139.2, 136.9, 132.2, 131.9, 129.7, 127.7, 124.2, 123.5, 106.8, 90.5, 84.3, 64.9, 53.9, 48.3, 40.4, 15.3; HRMS (ES+) calcd for $C_{21}H_{20}{}^{35}ClN_4O_5$ (M + H)$^+$, 443.1122; found, 443.1120. Calcd for $C_{21}H_{20}{}^{37}ClN_4O_5$ (M + H)$^+$, 445.1093; found, 445.1099.

*1-((6-Chloropyridin-3-yl)methyl)-4a,9b-dimethoxy-10-nitro-2,3,4a,9b-tetrahydroindeno[1′,2′:4,5]pyrrolo[1,2-a]imidazol-5(1H)-one (**5a**).* Yield, 66%; mp, 152.8−153.6 °C; ^{1}H NMR (400 MHz, DMSO-d_6) δ 8.35 (q, 1H), 8.20 (d, J = 7.8 Hz, 1H), 7.89 (t, J = 7.4 Hz, 1H), 7.84 (d, J = 7.6 Hz, 1H), 7.78 (d, J = 7.2 Hz, 1H), 7.65 (t, J = 7.4 Hz, 1H), 7.51 (d, J = 8.2 Hz, 1H), 5.27 (d, J =15.6 Hz, 1H), 4.93 (d, J =15.6 Hz, 1H), 4.01−4.09 (m, 1H), 3.85−3.94 (m, 1H), 3.69−3.81 (m, 1H), 3.53−3.62 (m, 1H), 3.38 (s, 3H), 3.36 (s, 3H); ^{13}C NMR (100 MHz, DMSO-d_6) δ 193.7, 156.2, 151.1, 149.5, 149.0, 139.1, 136.9, 133.4, 131.9, 130.2, 127.9, 124.2, 123.7, 103.4, 90.7, 89.2, 54.2, 53.3, 53.0, 48.5, 40.6; HRMS (ES+) calcd for $C_{21}H_{20}{}^{35}ClN_4O_5$ (M + H)$^+$, 443.1122; found, 443.1113. Calcd for $C_{21}H_{20}{}^{37}ClN_4O_5$ (M + H)$^+$, 445.1093; found, 445.1101.

*1-((6-Chloropyridin-3-yl)methyl)-9b-ethoxy-4a-methoxy-10-nitro-2,3,4a,9b-tetrahydroindeno[1′,2′:4,5]pyrrolo[1,2-a]imidazol-5(1H)-one (**5b**).* Yield, 50%; mp 88.2−89.0 °C; ^{1}H NMR (400 MHz, DMSO-d_6) δ 8.35 (s, 1H), 8.23 (d, J = 7.8 Hz, 1H), 7.88 (t, J = 7.4 Hz, 1H), 7.83 (d, J = 7.6 Hz, 1H), 7.77 (d, J = 8.0 Hz, 1H), 7.64 (t, J = 7.4 Hz, 1H), 7.50 (d, J = 8.2 Hz, 1H), 5.27 (d, J = 15.6 Hz, 1H), 4.93 (d, J = 15.6 Hz, 1H), 3.95−4.04 (m, 1H), 3.86−3.94 (m, 1H), 3.70−3.81 (m, 1H), 3.52−3.67 (m, 2H), 3.42−3.52 (m, 1H), 3.38 (s, 3H), 1.18 (t, J = 6.8 Hz, 3H); ^{13}C NMR (100 MHz, DMSO-d_6) δ 193.7, 156.1, 151.4, 149.5, 149.1, 139.1, 136.8, 133.3, 131.9, 130.1, 127.9, 124.2, 123.6, 104.1, 90.7, 88.8, 61.4, 54.2, 53.1, 48.5, 40.6, 15.4; HRMS (ES+) calcd for $C_{22}H_{22}{}^{35}ClN_4O_5$ (M + H)$^+$, 457.1279; found,457.1281. Calcd for $C_{22}H_{22}{}^{37}ClN_4O_5$ (M + H)$^+$, 459.1249; found, 459.1251.

*1-((6-Chloropyridin-3-yl)methyl)-4a-ethoxy-9b-methoxy-10-nitro-2,3,4a,9b-tetrahydroindeno[1′,2′:4,5]pyrrolo[1,2-a]imidazol-5(1H)-one (**5c**).* Yield, 43%; mp, 78.2−80.0 °C; ^{1}H NMR (400 MHz, DMSO-d_6) δ 8.35 (s, 1H), 8.20 (d, J = 7.8 Hz, 1H), 7.88 (t, J = 7.6 Hz, 1H), 7.82 (d, J = 7.8 Hz, 1H), 7.78 (d, J = 8.2 Hz, 1H), 7.64 (t, J = 7.4 Hz, 1H), 7.51 (d, J = 8.2 Hz, 1H), 5.29 (d, J =15.6 Hz, 1H), 4.93 (d, J =15.6 Hz, 1H), 3.95−4.05 (m, 1H), 3.83−3.94 (m, 1H), 3.68−3.81 (m, 1H), 3.49−3.66 (m, 3H), 3.39 (s, 3H), 1.15 (t, J = 6.9 Hz, 3H); ^{13}C NMR (100 MHz, DMSO-d_6) δ 193.9, 156.2, 151.2, 149.5, 149.0, 139.1, 136.8, 133.3, 131.9, 130.2, 127.9, 124.2, 123.6, 103.4, 90.7, 89.1, 61.1, 54.1, 53.4, 48.5, 40.6, 15.4; HRMS (ES+) calcd for $C_{22}H_{22}{}^{35}ClN_4O_5$ (M + H)$^+$, 457.1279; found, 457.1271. Calcd for $C_{22}H_{22}{}^{37}ClN_4O_5$ (M + H)$^+$, 459.1249; found, 459.1254.

*1-((6-chloropyridin-3-yl)methyl)-4a,9b-diethoxy-10-nitro-2,3,4a,9b-tetrahydroindeno[1′,2′:4,5]pyrrolo[1,2-a]imidazol-5(1H)-one (**5d**).* Yield, 42%; mp 153.0−151.4 °C; ^{1}H NMR (400 MHz, DMSO-d_6) δ 8.34 (s, 1H), 8.21 (d, J = 7.8 Hz, 1H), 7.87 (t, J = 7.6 Hz, 1H), 7.81 (d, J = 7.8 Hz, 1H), 7.77 (dd, J_1 =1.8 Hz, J_2= 8.2 Hz, 1H), 7.64 (t, J = 7.6 Hz, 1H), 7.51 (d, J = 8.2 Hz, 1H), 5.26 (d, J_1 =15.6 Hz, 1H), 4.92 (d, J_1 =15.6 Hz, 1H), 3.94−4.05 (m, 1H), 3.84−3.94 (m, 1H), 3.71−3.81 (m, 1H), 3.61−3.70 (m, 2H), 3.52−3.61 (m, 2H), 3.44−3.52 (m, 1H), 1.11−1.22 (m, 6H); ^{13}C NMR (100 MHz, DMSO-d_6) δ 194.0, 156.1, 151.4, 149.4, 149.0, 139.1, 136.7, 133.2, 131.9, 130.0, 127.9, 124.2, 123.5, 104.0, 90.7, 88.8, 61.2, 61.0, 54.1, 48.4, 40.7, 15.3, 15.2; HRMS (ES+) calcd for $C_{23}H_{24}{}^{35}ClN_4O_5$ (M + H)$^+$, 471.1435; found, 471.1419. Calcd for $C_{23}H_{24}{}^{37}ClN_4O_5$ (M + H)$^+$, 473.1406; found, 473.1405.

*9b-Chloro-1-((6-chloropyridin-3-yl)methyl)-4a-hydroxy-10-nitro-2,3,4a,9b-tetrahydroindeno[1′,2′:4,5]pyrrolo[1,2-a]imidazol-5(1H)-one (**6a**).* Yield, 82%; mp, 170.3−170.7 °C; ^{1}H NMR (400 MHz, DMSO-d_6) δ 8.37 (s, 1H), 8.28 (d, J = 7.8 Hz, 1H), 7.93 (t, J = 7.6 Hz, 1H), 7.83 (d, J = 7.6 Hz, 1H), 7.80 (d, J = 8.2 Hz, 1H), 7.66 (t, J = 7.6 Hz, 1H), 7.53 (d, J = 8.2 Hz, 1H), 7.21 (s, 1H), 5.34 (d, J =15.6 Hz, 1H), 4.86 (d, J =15.6 Hz, 1H), 3.91−4.02 (m, 1H), 3.82−3.90 (m, 1H), 3.57−3.75 (m, 2H); ^{13}C NMR (100 MHz, DMSO-d_6) δ 189.4, 154.6, 151.6, 149.6, 149.2, 139.3, 137.5, 131.7, 130.8, 130.4, 128.0, 124.4, 124.2, 106.6, 88.8, 86.6, 53.8, 48.3, 40.1; HRMS (ES+) calcd for $C_{19}H_{15}{}^{35}Cl_2N_4O_4$ (M + H)$^+$, 433.0470; found, 433.0462. Calcd for $C_{19}H_{15}{}^{35}Cl\ {}^{37}ClN_4O_4$ (M + H)$^+$, 435.0441; found, 435.0430.

*9b-Chloro-1-((6-chloropyridin-3-yl)methyl)-4a-methoxy-10-nitro-2,3,4a,9b-tetrahydroindeno[1′,2′:4,5]pyrrolo[1,2-a]imidazol-5(1H)-one (**6b**).* Yield, 85%; mp, 169.2−170.6 °C; ^{1}H NMR (400 MHz, DMSO-d_6) δ 8.39 (s, 1H), 8.20 (d, J = 7.8 Hz, 1H), 7.92 (t, J = 7.6 Hz, 1H), 7.86 (d, J = 7.6 Hz, 1H), 7.82 (d, J = 8.2 Hz, 1H), 7.69 (t, J = 7.6 Hz, 1H), 7.52 (d, J = 7.8 Hz, 1H), 5.23 (d, J =15.8 Hz, 1H), 5.05 (d, J =15.8 Hz, 1H), 3.97−4.10 (m, 1H), 3.77−3.97 (m, 2H), 3.67−3.77 (m, 1H), 3.43 (s, 3H); ^{13}C NMR (100 MHz, DMSO-d_6) δ 189.0, 155.7, 149.8, 149.5, 149.1, 139.2, 137.1, 131.7, 131.3, 130.7, 128.3,

DOI: 10.1021/jf505281p
J. Agric. Food Chem. 2015, 63, 1360−1369

Table 1. Insecticidal Activities of All Target Compounds and Cycloxaprid against Cowpea Aphids (*Aphis craccivora*), Brown Planthopper (*Nilaparvata lugens*), and Armyworm (*Mythimna separata*)

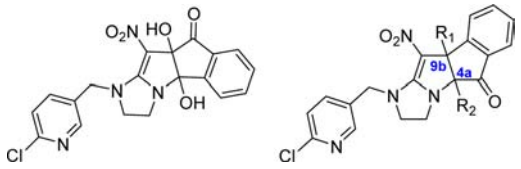

compound			mortality (%)											
			Aphis craccivora (mg L^{-1})				*Nilaparvata lugens* (mg L^{-1})				*Mythimna separata* (mg L^{-1})			
	R_1	R_2	500	100	20	4	500	100	20	4	500	100	20	4
1			100	100	100	100	100	100	100	100	100	0	0	0
2	OH	OH	100	100	100	100	100	100	100	100	100	0	0	0
3a	OCH_3	OH	100	100	0	0	100	100	100	0	0	0	0	0
3b	OC_2H_5	OH	100	100	0	0	100	100	100	60	80	0	0	0
3c	$O(CH_2)_2CH_3$	OH	100	100	0	0	100	100	60	0	0	0	0	0
3d	$O(CH_2)_3CH_3$	OH	100	0	0	0	100	80	0	0	0	0	0	0
3e	$O(CH_2)_2OH$	OH	100	0	0	0	100	100	50	0	0	0	0	0
3f	$O(CH_2)_3OCH_3$	OH	80	0	0	0	100	100	0	0	80	0	0	0
3g	$O(CH_2)_3OC_2H_5$	OH	0	0	0	0	100	100	0	0	0	0	0	0
4a	OH	OCH_3	100	0	0	0	100	80	50	0	0	0	0	0
4b	OH	OC_2H_5	50	0	0	0	100	100	100	80	100	0	0	0
5a	OCH_3	OCH_3	100	0	0	0	100	0	0	0	0	0	0	0
5b	OC_2H_5	OC_2H_5	0	0	0	0	100	80	0	0	0	0	0	0
5c	OC_2H_5	OCH_3	100	0	0	0	100	90	0	0	0	0	0	0
5d	OCH_3	OC_2H_5	100	0	0	0	100	90	70	0	0	0	0	0
6a	Cl	OH	100	100	100	100	100	100	100	95	100	100	100	80
6b	Cl	OCH_3	100	100	100	0	100	100	95	70	100	80	0	0
6c	Cl	OC_2H_5	100	0	0	0	100	100	90	80	100	80	0	0
7a	CH_3COO	CH_3COO	100	100	100	100	100	100	100	100	100	100	100	100
7b	C_2H_5COO	C_2H_5COO	100	100	100	0	100	100	100	95	100	100	100	80
7c	$(CH_3)_2CH_2COO$	$(CH_3)_2CH_2COO$	100	100	50	0	100	100	95	90	0			
7d	$CH_3(CH_2)_2COO$	$CH_3(CH_2)_2COO$	100	100	60	0	100	100	100	80	100	100	100	100
8a			0	0	0	0	0	0	0	0	0	0	0	0
8b			0	0	0	0	0	0	0	0	0	0	0	0
9a			100	100	100	100	100	100	100	90	100	100	50	0
9b			100	100	95	50	100	100	90	50	100	0	0	0
10a			0	0	0	0	80	30	0	0	0	0	0	0
10b			80	0	0	0	80	0	0	0	0	0	0	0
cycloxaprid			100	100	100	100	100	100	100	100	100	100	40	0

124.6, 124.2, 102.9, 91.8, 86.4, 54.2, 53.6, 48.6, 40.6; HRMS (ES+) calcd for $C_{20}H_{17}{}^{35}Cl_2N_4O_4$ $(M + H)^+$, 447.0627; found, 447.0622. Calcd for $C_{20}H_{17}{}^{35}Cl\ {}^{37}ClN_4O_4$ $(M + H)^+$, 449.0597; found, 449.0597.

*9b-Chloro-1-((6-chloropyridin-3-yl)methyl)-4a-ethoxy-10-nitro-2,3,4a,9b-tetrahydroindeno[1′,2′:4,5]pyrrolo[1,2-a]imidazol-5(1H)-one (**6c**).* Yield, 83%; mp, 98.5−100.1 °C; ^{1}H NMR (400 MHz, DMSO-d_6) δ 8.38 (d, J = 2.2 Hz, 1H), 8.21 (d, J = 7.8 Hz, 1H), 7.95−7.88 (m, 1H), 7.85 (d, J = 7.6 Hz, 1H), 7.81 (dd, J_1 =2.4 Hz, J_2= 8.4 Hz, 1H), 7.68 (t, J = 7.6 Hz, 1H), 7.52 (d, J = 8.2 Hz, 1H), 5.20 (d, J =15.8 Hz, 1H), 5.04 (d, J =15.8 Hz, 1H), 3.96−4.08 (m, 1H), 3.85−3.96 (m, 1H), 3.77−3.86 (m, 1H), 3.65−3.76 (m, 2H), 3.48−3.60 (m, 1H), 1.20 (t, J = 7.0 Hz, 3H); ^{13}C NMR (100 MHz, DMSO-d_6) δ 189.0, 155.6, 149.9, 149.5, 149.1, 139.2, 137.1, 131.7, 131.2, 130.6, 128.4, 124.5, 124.2, 103.7, 91.5, 86.5, 61.4, 54.2, 48.6, 40.6, 14.8; HRMS (ES+) calcd for $C_{21}H_{19}{}^{35}Cl_2N_4O_4$ $(M + H)^+$, 461.0783; found, 461.0779. Calcd for $C_{21}H_{19}{}^{35}Cl\ {}^{37}ClN_4O_4$ $(M + H)^+$, 463.0754; found, 463.0750.

*1-((6-Chloropyridin-3-yl)methyl)-10-nitro-5-oxo-1,2,3,4a,5,9b-hexahydroindeno[1′,2′:4,5]pyrrolo[1,2-a]imidazole-4a,9b-diyl diacetate (**7a**).* Yield, 88%; mp 212.0−213.6 °C; ^{1}H NMR (400 MHz, DMSO-d_6) δ 8.36 (s, 1H), 8.19 (d, J = 7.8 Hz, 1H), 7.82−7.94 (m, 2H), 7.77 (d, J = 8.2 Hz, 1H), 7.69 (t, J = 7.4 Hz, 1H), 7.54 (d, J = 8.2 Hz, 1H), 5.63 (d, J =15.6 Hz, 1H), 4.67 (d, J =15.6 Hz, 1H), 3.86−4.07 (m, 2H), 3.73−3.83 (m, 1H), 3.54−3.70 (m, 1H), 2.12 (s, 3H), 2.10 (s, 3H); ^{13}C NMR (100 MHz, DMSO-d_6) δ 188.8, 168.7, 168.4, 154.9, 149.6, 149.1, 147.6, 139.0, 136.9, 132.5, 131.7, 130.6, 126.3, 124.2, 124.1, 103.4, 89.3, 87.7, 54.1, 48.2, 40.2, 20.6, 19.7; HRMS (ES+) calcd for $C_{23}H_{20}{}^{35}ClN_4O_7$ $(M + H)^+$, 499.1021; found, 499.1010. Calcd for $C_{23}H_{20}{}^{37}ClN_4O_7$ $(M + H)^+$, 501.0991; found, 501.0991.

*1-((6-Chloropyridin-3-yl)methyl)-10-nitro-5-oxo-1,2,3,4a,5,9b-hexahydroindeno[1′,2′:4,5]pyrrolo[1,2-a]imidazole-4a,9b-diyl dipropionate (**7b**).* Yield, 91%; mp, 185.5−186.4 °C; ^{1}H NMR (400 MHz, DMSO-d_6) δ 8.36 (s, 1H), 8.19 (d, J = 7.8 Hz, 1H), 7.82−7.96 (m, 2H), 7.78 (d, J = 8.2 Hz, 1H), 7.70 (t, J = 7.4 Hz, 1H), 7.54 (d, J = 8.2 Hz, 1H), 5.59 (d, J =15.6 Hz, 1H), 4.71 (d, J =15.6 Hz, 1H), 4.03 (q, J = 9.8 Hz, 1H), 3.89−3.98 (m, 1H), 3.73−3.87 (m, 1H), 3.64 (q, J = 9.6 Hz, 1H), 2.39−2.50 (m, 2H), 2.23−2.38 (m, 2H), 1.05 (t, J = 7.4 Hz, 3H), 0.96 (t, J = 7.4 Hz, 3H); ^{13}C NMR (100 MHz, DMSO-d_6) δ 188.9, 172.0, 171.6, 155.0, 149.6, 149.1, 147.6, 139.1, 136.9, 132.5, 131.7, 130.5, 126.3, 124.2, 124.1, 103.4, 89.3, 87.6, 54.2, 48.3, 40.2, 26.8, 26.0, 9.1, 8.6; HRMS (ES+) calcd for $C_{25}H_{24}{}^{35}ClN_4O_7$ $(M + H)^+$, 527.1334; found, 527.1310. Calcd for $C_{25}H_{24}{}^{37}ClN_4O_7$ $(M + H)^+$, 529.1304; found, 529.1303.

*1-((6-Chloropyridin-3-yl)methyl)-10-nitro-5-oxo-1,2,3,4a,5,9b-hexahydroindeno[1′,2′:4,5]pyrrolo[1,2-a]imidazole-4a,9b-diyl bis-(2-methylpropanoate) (**7c**).* Yield, 88%; mp, 201.5−202.1 °C; ^{1}H NMR (400 MHz, DMSO-d_6) δ 8.35 (s, 1H), 8.20 (d, J = 7.2 Hz, 1H), 7.62−8.00 (m, 4H), 7.53 (d, J = 7.2 Hz, 1H), 5.52 (d, J = 15.2 Hz,

DOI: 10.1021/jf505281p
J. Agric. Food Chem. 2015, 63, 1360−1369

1H), 4.74 (d, J = 15.2 Hz, 1H), 3.58−4.09 (m, 4H), 2.52−2.66 (m, 2H), 0.97−1.21 (m, 12H); ^{13}C NMR (100 MHz, DMSO-d_6) δ 189.1, 174.2, 174.0, 155.0, 149.6, 149.1, 147.8, 139.1, 136.9, 132.4, 131.7, 130.4, 126.2, 124.2, 124.1, 103.3, 89.2, 87.4, 54.2, 48.3, 40.1, 33.7, 32.7, 19.3, 18.6, 18.4, 18.0; HRMS (ES+) calcd for $C_{27}H_{28}{}^{35}ClN_4O_7$ (M + H)$^+$, 555.1647; found, 555.1632. Calcd for $C_{27}H_{28}{}^{37}ClN_4O_7$ (M + H)$^+$, 557.1617; found, 557.1618.

*1-((6-Chloropyridin-3-yl)methyl)-10-nitro-5-oxo-1,2,3,4a,5,9b-hexahydroindeno[1′,2′:4,5]pyrrolo[1,2-a]imidazole-4a,9b-diyl dibutyrate (**7d**).* Yield, 90%; mp, 116.0−117.0 °C; ^{1}H NMR (400 MHz, DMSO-d_6) δ 8.35 (s, 1H), 8.19 (d, J = 7.8 Hz, 1H), 7.81−7.94 (m, 2H), 7.76 (d, J = 8.2 Hz, 1H), 7.68 (t, J = 7.2 Hz, 1H), 7.53 (d, J = 8.2 Hz, 1H), 5.57 (d, J =15.6 Hz, 1H), 4.71 (d, J =15.6 Hz, 1H), 3.98−4.10 (m, 1H), 3.87−3.97 (m, 1H), 3.72−3.86 (m, 1H), 3.55−3.71 (m, 1H), 2.34−2.47 (m, 2H), 2.18−2.33 (m, 2H), 1.55 (q, J = 14.3, 7.1 Hz, 2H), 1.46 (q, J = 14.2, 7.1 Hz, 2H), 0.91 (t, J = 7.1 Hz, 3H), 0.86 (t, J = 7.1 Hz, 3H); ^{13}C NMR (100 MHz, DMSO-d_6) δ 189.0, 171.1, 170.7, 154.9, 149.6, 149.1, 147.7, 139.1, 136.9, 132.5, 131.7, 130.5, 126.3, 124.2, 124.1, 103.4, 89.3, 87.6, 54.2, 48.2, 40.2, 35.3, 34.3, 17.9, 17.6, 13.4, 13.1; HRMS (ES+) calcd for $C_{27}H_{28}{}^{35}ClN_4O_7$ (M + H)$^+$, 555.1647; found, 555.1631. Calcd for $C_{27}H_{28}{}^{37}ClN_4O_7$ (M + H)$^+$, 557.1617; found, 557.1619.

*4a,9a-Dihydroxy-10-nitro-2,3,4a,9a-tetrahydroindeno[2′,1′:4,5]-pyrrolo[1,2-a]imidazol-9(1H)-one (**8a**).* Yield, 98%; mp, 215.2−216.6 °C; ^{1}H NMR (400 MHz, DMSO-d_6) δ 8.75 (s, 1H), 7.85 (t, J = 7.4 Hz, 1H), 7.78 (d, J = 7.6 Hz, 2H), 7.65 (t, J = 7.3 Hz, 1H), 7.05 (s, 1H), 6.35 (s, 1H), 3.80−3.99 (m, 3H), 3.60−3.65 (m, 1H) ppm; ^{13}C NMR (100 MHz, DMSO-d_6) δ 195.6, 159.1, 145.6, 135.7, 134.3, 130.7, 125.4, 123.8, 102.2, 90.0, 85.8, 47.9, 41.2 ppm; HRMS (ES+) calcd for $C_{13}H_{11}N_3O_5Na$ (M+Na)$^+$, 312.0596; found, 312.0602.

*4a,9b-Dihydroxy-10-nitro-2,3,4a,9b-tetrahydroindeno[1′,2′:4,5]-pyrrolo[1,2-a]imidazol-5(1H)-one (**8b**).* Yield, 37%; mp, 222.2−223.4 °C; ^{1}H NMR (400 MHz, DMSO-d_6) δ 8.80 (s, 1H), 8.22 (d, J = 7.8 Hz, 1H), 7.83 (t, J = 7.0 Hz, 1H), 7.73 (d, J = 7.6 Hz, 1H), 7.57 (t, J = 7.1 Hz, 1H), 7.06 (s, 1H), 6.34 (s, 1H), 3.86−3.96 (m, 1H), 3.78−3.86 (m, 1H), 3.67−3.78 (m, 1H), 3.47−3.61 (m, 1H) ppm; ^{13}C NMR (100 MHz, DMSO-d_6) δ 195.6, 158.9, 152.6, 136.4, 132.4, 129.5, 127.7, 123.4, 105.4, 88.9, 83.2, 47.5, 41.0 ppm; HRMS (ES+) calcd for $C_{13}H_{11}N_3O_5Na$ (M + Na)$^+$, 312.0596; found, 312.0599.

*1-((2-Chlorothiazol-5-yl)methyl)-4a,9a-dihydroxy-10-nitro-2,3,4a,9a-tetrahydroindeno[2′,1′:4,5]pyrrolo[1,2-a]imidazol-9(1H)-one (**9a**).* Yield, 90%; mp, 179.5−180.0 °C; ^{1}H NMR (400 MHz, DMSO-d_6) δ 7.85 (t, J = 7.4 Hz, 1H), 7.78 (t, J = 7.1 Hz, 2H), 7.61−7.71 (m, 2H), 7.14 (s, 1H), 6.46 (s, 1H), 5.43 (d, J = 15.6 Hz, 1H), 4.87 (d, J = 15.6 Hz, 1H), 3.73−4.04 (m, 3H), 3.53−3.69 (m, 1H) ppm; ^{13}C NMR (100 MHz, DMSO-d_6) δ 196.0, 155.7, 151.8, 145.8, 141.3, 136.2, 135.8, 134.2, 130.8, 125.2, 123.9, 104.1, 89.2, 88.7, 86.0, 53.8, 44.1, 39.4 ppm; HRMS (ES−) calcd for $C_{17}H_{12}{}^{35}ClN_4O_5S$ (M − H)$^-$, 419.0217; found, 419.0218. Calcd for $C_{17}H_{12}{}^{37}ClN_4O_5S$ (M − H)$^-$, 421.0187; found, 421.0192.

*1-((2-Chlorothiazol-5-yl)methyl)-4a,9b-dihydroxy-10-nitro-2,3,4a,9b-tetrahydroindeno[1′,2′:4,5]pyrrolo[1,2-a]imidazol-5(1H)-one (**9b**).* Yield, 63%; mp, 193.1−194.2 °C; ^{1}H NMR (400 MHz, DMSO-d_6) δ 8.28 (d, J = 7.8 Hz, 1H), 7.85 (t, J = 7.5 Hz, 1H), 7.74 (d, J = 7.6 Hz, 1H), 7.66 (s, 1H), 7.58 (t, J = 7.4 Hz, 1H), 7.14 (s, 1H), 6.45 (s, 1H), 5.39 (d, J = 15.6 Hz, 1H), 4.94 (d, J = 15.6 Hz, 1H), 3.94−4.01 (m, 1H), 3.84−3.91 (m, 1H), 3.68−3.72 (m, 1H), 3.53−3.63 (m, 1H) ppm; ^{13}C NMR (100 MHz, DMSO-d_6) δ 195.2, 155.7, 152.7, 151.6, 141.1, 136.6, 136.2, 132.3, 129.7, 127.9, 123.5, 107.3, 87.7, 83.6, 53.5, 44.0, 39.4 ppm; HRMS (ES−) calcd for $C_{17}H_{12}{}^{35}ClN_4O_5S$ (M − H)$^-$, 419.0217; found, 419.0219. Calcd for $C_{17}H_{12}{}^{37}ClN_4O_5S$ (M − H)$^-$, 421.0187; found, 421.0193.

*1-Benzyl-4a,9a-dihydroxy-10-nitro-2,3,4a,9a-tetrahydroindeno-[2′,1′:4,5]pyrrolo[1,2-a]imidazol-9(1H)-one (**10a**).* Yield, 82%; mp, 110.9−112.1 °C; ^{1}H NMR (400 MHz, DMSO-d_6) δ 7.84 (td, J_1 = 1.2 Hz, J_2 = 7.4 Hz, 1H), 7.78 (t, J = 7.5 Hz, 2H), 7.66 (t, J = 7.8 Hz, 1H), 7.29−7.38 (m, 3H), 7.22−7.27 (m, 2H), 7.09 (s, 1H), 6.42 (s, 1H), 5.45 (d, J = 15.0 Hz, 1H), 4.73 (d, J = 15.0 Hz, 1H), 3.76−3.88 (m, 3H), 3.52−3.64 (m, 1H) ppm; ^{13}C NMR (100 MHz, DMSO-d_6) δ 196.2, 156.1, 145.9, 136.5, 135.8, 134.3, 130.8, 128.6 (2C), 127.8 (2C), 127.7, 125.2, 123.9, 103.8, 88.6, 86.2, 53.8, 51.1, 39.3 ppm; HRMS (ES−) calcd for $C_{20}H_{16}N_3O_5$ (M − H)$^-$, 378.1090; found, 378.1090.

*1-Benzyl-4a,9b-dihydroxy-10-nitro-2,3,4a,9b-tetrahydroindeno-[1′,2′:4,5]pyrrolo[1,2-a]imidazol-5(1H)-one (**10b**).* Yield, 90%; mp, 155.3−156.8 °C; ^{1}H NMR (400 MHz, DMSO-d_6) δ 8.29 (d, J = 7.8 Hz, 1H), 7.81−7.90 (m, 1H), 7.74 (d, J = 7.6 Hz, 1H), 7.54−7.64 (m, 1H), 7.24−7.38 (m, 5H), 7.10 (s, 1H), 6.44 (s, 1H), 5.43 (d, J = 15.0 Hz, 1H), 4.79 (d, J = 15.0 Hz, 1H), 3.74−3.87 (m, 2H), 3.63−3.73 (m, 1H), 3.47−3.57 (m, 1H) ppm; ^{13}C NMR (100 MHz, DMSO-d_6) δ 195.9, 156.5, 153.4, 137.0, 137.0, 132.8, 130.1, 129.0 (2C), 128.4, 128.2 (2C), 128.1, 123.9, 107.4, 88.1, 84.2, 53.9, 51.4, 39.7 ppm; HRMS (ES−) calcd for $C_{20}H_{16}N_3O_5$ (M − H)$^-$, 378.1090; found, 378.1089.

Biological Assay. Bioassays were performed on representative test organisms grown in the laboratory. The bioassay was repeated at (25 ± 1) °C according to statistical requirements. All compounds were dissolved in *N*,*N*-dimethylformamide (DMF) (AP, Shanghai Chemical Reagent Co., Ltd., Shanghai, China) and diluted with distilled water containing Triton X-100 (0.1 mg L^{-1}) to obtain a series of concentrations of 500.0, 100.0, 20.0, 4.0 mg L^{-1} and others for bioassays. The results of the bioassay are depicted in Table 1.

Insecticidal Test for Cowpea Aphids (Aphis craccivora). The activities of insecticidal compounds against cowpea aphids were tested by the leaf-dip method. The leaves of the horsebean plant with 40−60 apterous adults were dipped in diluted solutions of the chemicals containing Triton X-100 (0.1 mg L^{-1}) for 5 s, and the excess solution was sucked out with filter paper. The burgeoning shoots were placed in a conditioned room ((25 ± 1) °C, 50% RH). Water containing Triton X-100 (0.1 mg L^{-1}) was used as a control. The mortality rates were evaluated 24 h after treatment. Each treatment had three repetitions, and the data were adjusted and subjected to probit analysis as before.

Insecticidal Test for Armyworms (Mythimna separate). The insecticidal activity against armyworms was tested by foliar application. Individual corn (*Zea mays*) leaves were placed on moistened pieces of filter paper in Petri dishes. The leaves were then sprayed with the sample solutions and exposed to dry. The dishes were infested with 10 second-instar larvae and placed in a conditioned room. The mortality rates were evaluated 48 h after treatment. Each treatment had three repetitions, and the data were adjusted and subjected to probit analysis as before.

Insecticidal Test for Brown Planthoppers (Nilaparvata lugens). The activities of insecticidal compounds against *Nilaparvata lugens* were tested using the dipping method. Rice plants at tillering to booting stages were pulled out, and the rice stems (about 10 cm lengths) with roots were cut and air-dried to remove excess water. Three rice stems were dipped in appropriate solutions of tested compound for 30 s. After rice stems had been air-dried, the rice roots was wrapped with moistened cotton and then placed into a tumbler. Thirty *Nilaparvata lugens* were introduced into the tumbler with the treated insects maintained at a temperature of (27 ± 1) °C. Only distilled water only was used as control for each tested chemical. Each process was repeated 3 times, and the mortality rates were evaluated 48 h after treatment. The data were adjusted and subjected to probit analysis as before.

Molecular Docking. The crystal structure of the *Aplysia californica* acetylcholine binding protein (*Ac*-AChBP) complexed with IMI (PDB code: 2WNJ) was selected to construct the binding models,[4] which showed high affinity with neonicotinoids and was a good prototype for investigating the binding mode of neonicotinoids. Compounds were docked into the ligand binding pocket of *Ac*-AChBP by the "Induced Fit Docking" approach, of which the IFDScore scoring function was selected to evaluate the docking results. All atoms within 20 Å around IMI in the 3C79 structure were selected as the binding pocket and considered in the docking study. All computational studies were performed using Maestro 9.0 (Schrödinger, LLC, 2013).

DOI: 10.1021/jf505281p
J. Agric. Food Chem. 2015, 63, 1360−1369

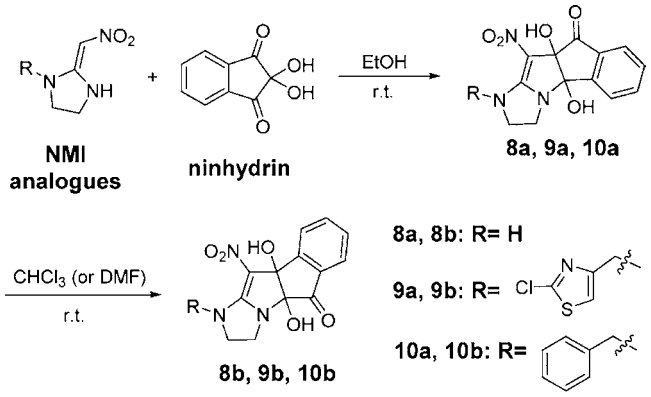

Figure 4. Comparative compounds **8a−b**, **9a−b**, and **10a−b**.

Table 2. LC_{50} and LC_{90} Values of Selected Compounds, Imidacloprid and Cycloxaprid, against Cowpea Aphids (*Aphis craccivora*), Brown Planthopper (*Nilaparvata lugens*), and Armyworm (*Mythimna separata*)

insect	compd	$y = a + bx$	LC_{50} (mg L^{-1})	LC_{90} (mg L^{-1})
Nilaparvata lugens	**1**	$y = 6.375 + 1.565x$	0.132	0.872
	2	$y = 4.961 + 1.549x$	1.06	7.118
	7c	$y = 3.247 + 2.002x$	7.510	32.805
	CYC	$y = 6.965 + 2.400x$	0.152	0.519
	IMI	$y = 4.908 + 2.477x$	1.089	3.586
Aphis craccivora	**6a**	$y = 5.346 + 2.264x$	0.704	2.591
	7a	$y = 5.019 + 1.412x$	0.97	7.837
	CYC	$y = 5.749 + 2.073x$	0.435	1.806
	IMI	$y = 5.402 + 1.672x$	0.634	1.089
Mythimna separata	**6a**	$y = 3.794 + 1.942x$	4.177	19.09
	7a	$y = 3.833 + 1.832x$	4.337	21.708
	7b	$y = 3.885 + 1.911x$	3.833	17.958
	7d	$y = 4.755 + 1.698x$	1.395	7.928
	CYC	$y = 2.261 + 1.909x$	27.214	127.653
	IMI	$y = 1.851 + 2.055x$	34.078	143.219

RESULTS AND DISCUSSION

Synthesis. Our recent reported HKA-ninhydrin reactions allowed for the facile access to novel tetraheterocyclic indeno[2,1-*b*]pyrrol-8(1*H*)-one derivatives. NMI, as a cyclic HKA, reacted with ninhydrin affording two tetracyclic isomers **1** and **2** based on solvent-controlled selectivity (Figure 2). Both isomers have two active hydroxyl groups for further structural derivatizations. Attempts to modify **1** failed due to its easy isomerization to the more thermal stable form **2**. The selective etherification, esterification, and chlorination were explored. Under acidic circumstances, the etherification occurred at the 9b-hydroxyl giving 9b-alkoxy substituted products **3a−g**. While being catalyzed by the base NaH, the etherified products were 4a-alkoxyl substituted compounds **4a−b** (Figure 3B).

This position selectivity upon acid and base can be rationalized by their different catalytic mechanisms. In acid, the stability of the 9b-carbocation is higher than its 4a-counterpart due to the inductive effect of nitro groups and hyperconjugation of the adjacent benzene. While in base, the formed anion at the 9b-oxygen is less stable than that formed at the 4a-position, which preferentially reacts with alkyl iodide.

According to the same or different substituent features, the dietherized compounds **5a−b** were prepared by two methodologies (Figure 3B and D). To introduce the two same alkoxy substituents, **2** was subjected to NaH conditions by adding excess alkyl iodide. In the case of analogues **5c−d** with different alkoxy side chains, a two-step pathway was employed catalyzed by base or acid sequentially. Esterifications of **2** were readily accomplished with acyl chloride in CH_2Cl_2 using DIPEA as the acid capture (Figure 3E). The preparation of mono-ester analogues was unsuccessful due to the high reactivity of acyl chloride. The selectivity mechanism of chlorination is similar to that of etherification in acid conditions. Chlorination by thionyl chloride in $CHCl_3$ was through an S_Ni reaction mechanism in which the carbocation at the 9b-position is more stable (Figure 3C).

Further etherifications of chloride compound **6a** gave **6b−c** with chlorine and alkoxy substituents. All of the compounds were well characterized by ^{1}HNMR, ^{13}CNMR, and HRMS. Furthermore, the structures of **1**, **2**, and **3a** were unambiguously confirmed by X-ray diffraction studies.

Insecticidal Activity. Structure-based design of analogues based on NMI yielded a focused library of compounds leading to clear SAR.[20] Chloropyridinyl, the nitro group, and imidazoline are proved to be the best variations, thus, the modifications of the present study mainly focused on the two hydroxyl groups of compound **2**. To investigate the influence of substituents at the 4a- and 9b-position on activity, commonly

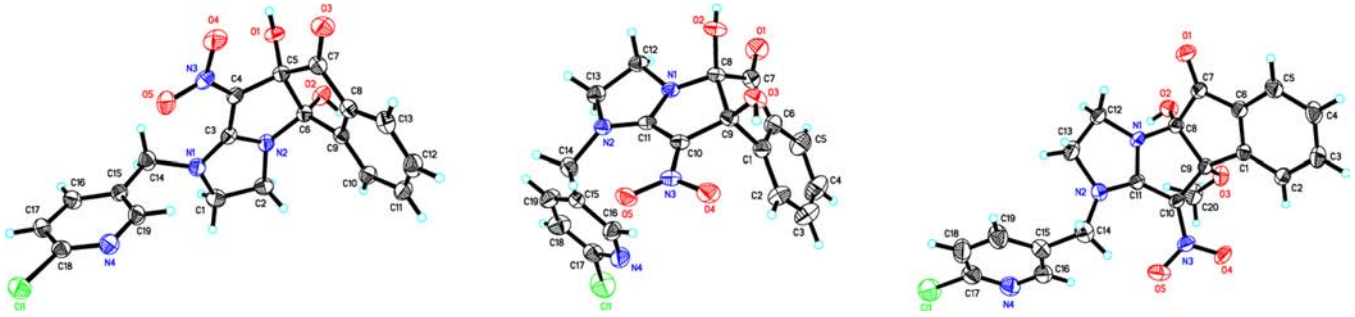

Figure 5. Crystal structure of compounds **1**, **2**, and **3a**.

DOI: 10.1021/jf505281p
J. Agric. Food Chem. 2015, 63, 1360−1369

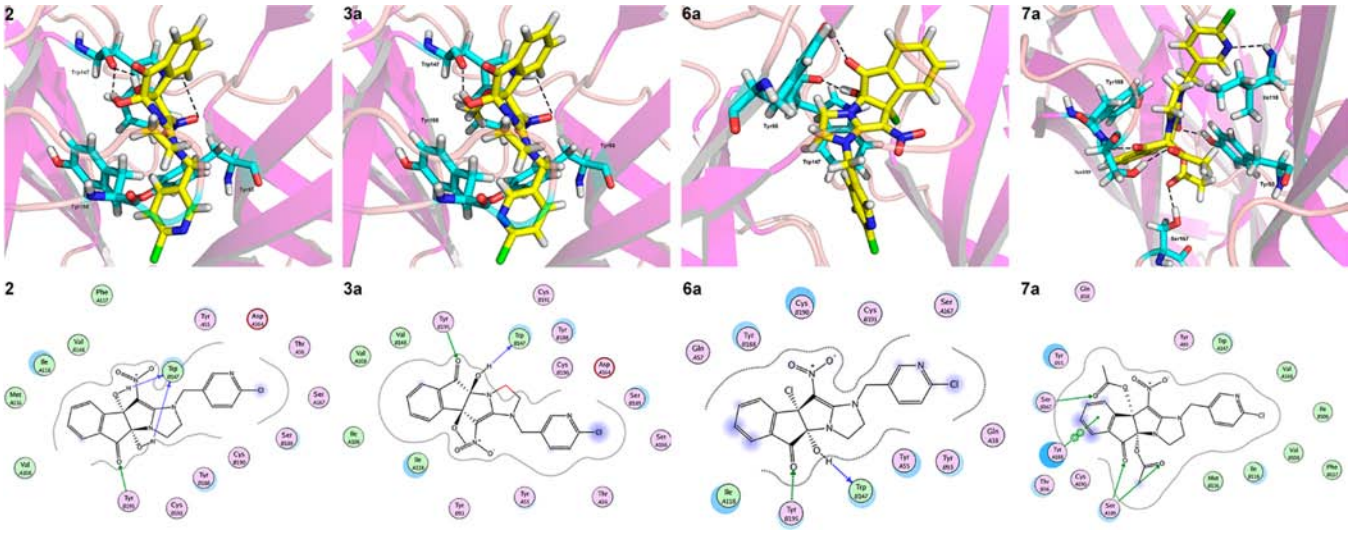

Figure 6. Molecular docking of **2**, **3a**, **6a**, and **7a** with the *Aplysia* acetylcholine binding protein (AChBP).

used derivatization methods such as etherification, chlorination, and esterification were used here to append chemical fragments to this novel chemotype.

Dihydroxy compounds **1** and **2** showed excellent activity against sucking insects, cowpea aphids and brown planthoppers, but very low potency to chewing pests armyworms (Table 1). Compound **1** had slightly higher activity than **2**. Introduction of alkoxy substituents at the 9b-position was unfavorable resulting in a slight decrease of activity. From this set of monoalkoxy substituted compounds, a trend emerged indicating reduced activity with increasing size and hydrophobicity of substituents. Consistent with 9b-alkoxy compounds, insertion of the alkoxy component at the 4a-position also leads to a decrease of the activity. As was expected, dialkoxy compounds **5a**−**d** showed a significant drop in potency compared to that of the corresponding mono- or nonalkoxy substituted analogues, supporting the unfavorable effects of alkoxy substituents at both positions. Chloride compound **6a** maintained high activity but showed much improvement in activity against armyworms. However, etherification of **6a** had a detrimental effect on activity, which agreed with the trend observed above. Encouraged by the interesting results above, we synthesized analogues **7a**−**d** with two ester side chains to increase the activity against the chewing pest armyworm. Satisfyingly, this series had excellent activity against all of the three test insects with the exception of **7c**. Analogues **7a**, **7b**, and **7d** had superior activity even at the concentration of 4 mg L^{-1}.

As a comparison, compounds **8a**−**b**, **9a**−**b**, and **10a**−**b** were prepared with variation at the chloropyridinyl of **2** (Figure 4). Removal of the chloropyridinyl or its replacement with phenyl substantially affected the activity with almost a loss of activity. Bioisoteric replacement of the chloropyridinyl with the chlorothiazolyl group in **1** and **2** maintained the high performance in comparison with that of parent congeners.

Selected compounds were then further evaluated to compare their toxic ratio (Table 2). Imidacloprid and cycloxaprid (CYC), an oxabridged neonicotinoid with outstanding activity discovered in our lab, were used here as a comparison. Against brown planthopper, the activity of **1** (LC_{50} = 0.132 mg L^{-1}) was comparable to that of cycloxaprid (LC_{50} = 0.152 mg L^{-1}), while **2** showed a 7-fold lower activity than CYC. Against cowpea aphids, the activity of **6a**, **7a**, and CYC was almost at the same level. Improvement of activity against armyworms was achieved by attaching an ester or chlorine side chain. Encouragingly, **7d** exhibited a 20-fold enhancement in activity compared to that of CYC, becoming the most potent analogue in this series.

Crystal Structure Analysis. To elucidate the precise three-dimensional structural information for further investigation, crystals of **1**, **2**, and **3a** suitable for X-ray diffraction were obtained by slow evaporation (Figure 5).[35] All of the three compounds showed the common features of our previously reported *cis*-neonicotinoids, such as the delocalization of the electrons in NO_2−C═C−N systems, coplanar olefin-amine network, and fixed *cis*-nitro configuration. The tetracyclic section showed the V-shape feature instead of the planar one with a torsion angle of about 110° between indenone and pyrrolo[1,2-*a*]imidazole. In dihydroxyl compounds **1** or **2**, the indenone part and the pyridine motif were oriented on the same side of the pyrrolo[1,2-*a*]imidazole plane, forming a concave shape, while in monoether analogue **3a**, they pointed in a different direction. This difference in molecular geometry might be one of the causes for the variation in activity.

Molecular Docking. The substituent types at the 4a- or 9b-position showed significant influence on insecticidal potency. In order to understand the activity difference in the target level, the interactions between the tetracyclic derivatives **2**, **3a**, **6a**, and **7a** with the receptor were achieved by a molecular docking study using insect surrogate *Aplysia* AChBP (protein data bank code 2WNJ).[36−38] The most likely binding conformations were selected based on the score and the binding mode (Figure 6). Compounds **2**, **3a**, and **6a** gave the same orientations in the pocket, while **7a** was oriented in a different way. The hydrogen bonds and van der Waals forces are the main features of the interactions of all of the compounds. According to the docking simulations, it appears evident that the chloropyrindyl part is pointing toward a deep hydrophobic hole made by residues Tyr188 and Tyr55 for **2**, **3a**, and **6a**. H-bond formation was found to occur between the nitro oxygen of **2** and **3a** with the hydrogen of H−N of the Trp147 residue (d = 1.76 and 1.90 Å, respectively), indicating a strong interaction of **2** than **3a** in this position. The oxygen of the 4a-hydroxyl in **2** and **3a** participates in a hydrogen-bond interaction with the backbone O−H of Trp147 (d = 1.52 and 2.03 Å, respectively). Meanwhile, the 9b-

DOI: 10.1021/jf505281p
J. Agric. Food Chem. 2015, 63, 1360−1369

hydroxyl in **2** further anchors the ligand by forming a hydrogen bond with the Trp147, which further consolidates the binding. Thus, the comparison between docking **2** and **3a** suggests that the lack of H-bond formation at the 9b-substitutent and the weaker H-bond interaction of the nitro subunit of **3a** attenuate its insecticidal activity. Although the formation of the H-bond between the nitro oxygen with the residue was lacking, an extra H-bond was produced between the carbonyl with Tyr195 (d = 2.0 Å), which contributes to its high activity. The maximum number of H-bond interactions was detected in **7a**-receptor binding, such as the nitro oxygen with Tyr55 (d = 1.90 Å), the pyridyl nitrogen with Ile188 (d = 2.70 Å), carbonyl oxygen of indenone, and in the 4a-ester substituent with Ser189 (d = 1.90 and 2.20 Å, respectively) and carbonyl oxygen in the 9b-ester substituent with Ser167 (d = 1.90 Å). Furthermore, the phenyl ring of **7a** formed the weak $\pi-\pi$ stacking interaction with the Tyr188 residue. All of these interactions made the analogues with two ester side chains the most potent compounds.

In conclusion, the series of tetraheterocyclic tetrahydroindeno[1′,2′:4,5]pyrrolo[1,2-*a*]imidazol-5(1*H*)-one derivatives were synthesized from NMI via cyclization by ninhydrin and etherification, chlorination, or esterification. The etherification showed strong position selectivity upon acid or base catalyzing. Most of the compounds had excellent insecticidal activity against cowpea aphids, brown planthoppers, and armyworms. Crystal structure analysis verified the three-dimensional structural difference in the compounds with different activities. The molecular docking studies indicated that the substituent patterns at the 4a-position play a significant role in the activity. Field trials for high active compounds are in progress.

AUTHOR INFORMATION

Corresponding Authors

*(X.S.) Phone: +86-21-64253967. Fax: +86-21-64252603. E-mail: shaoxusheng@ecust.edu.cn.

*(Z.L.) E-mail: lizhong@ecust.edu.cn.

Funding

We thank the National Natural Science Foundation of China (21372079 and 21472046), National High Technology Research Development Program of China (863 Program, 2011AA10A207), Shanghai Pujiang Program (14PJD012), Key Projects in the National Science & Technology Pillar Program (2011BAE06B05), and the Fundamental Research Funds for the Central Universities (222201414015) for financial support. This work was also partly supported by Australia DC Foundation.

Notes

The authors declare no competing financial interest.

ABBREVIATIONS USED

NMI, nitromethylene analogue of imidacloprid; IMI, imidacloprid; HKA, heterocyclic ketene aminals; CYC, cycloxaprid; DIPEA, *N*,*N*-diisopropylethylamine; DMSO, dimethyl sulfoxide; DMF, *N*,*N*-dimethyl-formamide

REFERENCES

(1) Krämer, W.; Schirmer. U.; Jeschke, P.; Witschel, M. *Modern Crop Protection Compounds*, 2nd ed.; Wiley-VCH: Weinheim, Germany, 2012.

(2) Casida, J. E.; Durkin, K. A. Neuroactive insecticides: targets, selectivity, resistance, and secondary effects. *Annu. Rev. Entomol.* **2013**, *58*, 99−117.

(3) Karaağa, S. U. *Insecticide Resistance in Insecticides-Advances in Integrated Pest Management*; Perveen, F., Ed.; InTech: Rijeka, Croatia, 2012; pp 469−478.

(4) Larramendy, M. L.; Soloneski, S. *Pesticides-Toxic Aspects*; InTech: Rijeka, Croatia, 2014.

(5) Casida, J. E. The greening of pesticide-environment interactions: Some personal observations. *Environ. Health Perspect.* **2012**, *120*, 487−493.

(6) Köhler, H. R.; Triebskorn, R. Wildlife ecotoxicology of pesticides: Can we track effects to the population level and beyond? *Science* **2013**, *341*, 759−765.

(7) Ishaaya, I.; Nauen, R.; Horowitz, A. R. *Insecticides Design Using Advanced Technologies*; Springer-Verlag: Amsterdam, The Netherlands, 2007.

(8) Nauen, F.; Michael, E. B. Nicotinic acetylcholine receptor agonists: A milestone for modern crop protection. *Angew. Chem., Int. Ed.* **2013**, *52*, 9464−9485.

(9) Elbert, A.; Schindler, M.; Nauen, R.; Jeschke, P. Overview of the status and global strategy for neonicotinoids. *J. Agric. Food Chem.* **2011**, *59*, 2897−2908.

(10) Kagabu, S. Discovery of imidacloprid and further developments from strategic molecular designs. *J. Agric. Food Chem.* **2011**, *59*, 2887−2896.

(11) Tomizawa, M.; Casida, J. E. Molecular recognition of neonicotinoid insecticide: The determinants of life or death. *Acc. Chem. Res.* **2009**, *42*, 260−269.

(12) Jeschke, P.; Nauen, R. Neonicotinoids-from zero to hero in insecticide chemistry. *Pest Manag. Sci.* **2008**, *64*, 1084−1098.

(13) Fairbrother, A.; Purdy, J.; Anderson, T.; Fell, R. Risks of neonicotinoid insecticides to honeybees. *Environ. Toxicol. Chem.* **2014**, *33*, 719−731.

(14) Sluijs, J. P.; Simon-Delso, N.; Goulson, D.; Maxim, L.; Bonmatin, J. M.; Belzunces, L. P. Neonicotinoids, bee disorders and the sustainability of pollinator services. *Curr. Opin. Environ. Sustainability* **2013**, *5*, 293−305.

(15) Prisco, G. D.; Cavaliere, V.; Annoscia, D.; Varricchio, P.; Caprio, E.; Nazzi, F.; Gargiulo, G.; Pennacchio, F. Neonicotinoid clothianidin adversely affects insect immunity and promotes replication of a viral pathogen in honey bees. *Proc. Natl. Acad. Sci. U.S.A.* **2013**, *110*, 18466−18471.

(16) Gill1, R. J.; Ramos-Rodriguez, O.; Raine, N. E. Combined pesticide exposure severely affects individual- and colony-level traits in bees. *Nature* **2012**, *491*, 105−109.

(17) Osborne, J. L. Bumblebees and pesticides. *Nature* **2012**, *491*, 43−45.

(18) Henry, M.; Beguin, M.; Requier, F.; Rollin, F.; Odoux, J.; Aupinel, P.; Aptel, J.; Tchamitchian, S.; Decourtype, A. A common pesticide decreases foraging success and survival in honey bees. *Science* **2012**, *336*, 348−350.

(19) Goulson, D. An overview of the environmental risks posed by neonicotinoid insecticides. *J. Appl. Ecol.* **2013**, *50*, 977−987.

(20) Shao, X. S.; Lee, P. W.; Xu, X. Y.; Liu, Z. W.; Li, Z.; Qian, X. H. *cis*-Configuration: A new tactic/rationale for neonicotinoid molecular design. *J. Agric. Food Chem.* **2011**, *59*, 2943−2949.

(21) Shao, X. S.; Ye, Z. J.; Bao, H. B.; Liu, Z. W.; Xu, X. Y.; Li, Z.; Qian, X. H. Advanced research on cis-neonicotinoids. *Chimia* **2011**, *65*, 957−960.

(22) Shao, X. S.; Zhang, W. W.; Peng, Y. Q.; Li, Z. *cis*-Nitromethylene neonicotinoids as new nicotinic family: Synthesis, structural diversity, and insecticidal evaluation of hexahydroimidazo-[1,2-a]pyridine. *Bioorg. Med. Chem. Lett.* **2008**, *18*, 6513−6516.

(23) Shao, X. S.; Xu, Z. P.; Zhao, X. F.; Xu, X. Y.; Tao, L. M.; Li, Z.; Qian, X. H. Synthesis, crystal structure, and insecticidal activities of highly congested hexahydroimidazo[1,2-a]pyridine derivatives: Effect of conformation on activities. *J. Agric. Food Chem.* **2010**, *58*, 2690.

(24) Ren, L. P.; Lou, Y. P.; Chen, N. Y.; Xia, S. S.; Shao, X. S.; Xu, X. Y.; Li, Z. Synthesis and insecticidal activities of tetrahydroimidazo[1,2-a]pyridinones: Further exploration on *cis*-neonicotinoids. *Synth. Commun.* **2014**, *44*, 858−867.

DOI: 10.1021/jf505281p
J. Agric. Food Chem. 2015, 63, 1360−1369

(25) Tian, Z. Z.; Jiang, Z. X.; Li, Z.; Song, G. H.; Huang, Q. C. Syntheses and biological activities of octahydro-1*H*-cyclopenta[*d*]-pyrimidine derivatives. *J. Agric. Food Chem.* **2007**, *55*, 143−147.
(26) Chen, N. Y.; Ren, L. P.; Xu, Z. P.; Zou, M. M.; Shao, X. S.; Xu, X. Y.; Li, Z. Design, synthesis and insecticidal activity of spiro heterocycle containing neonicotinoid analogues. *Chin. Chem. Lett.* **2014**, *25*, 197−200.
(27) Shao, X. S.; Fu, H.; Xu, X. Y.; Xu, X. L.; Liu, Z. W.; Li, Z.; Qian, X. H. Divalent and oxabridged neonicotinoids constructed by dialdehydes and nitromethylene analogues of imidacloprid: design, synthesis, crystal structure, and insecticidal activities. *J. Agric. Food Chem.* **2010**, *58*, 2696−2702.
(28) Chen, N. Y.; Xia, S. S.; Zou, M. M.; Shao, X. S. Bridged heterocyclic neonicotinoid analogues: design, synthesis, and insecticidal activity. *Res. Chem. Intermed.* **2014**, DOI: 10.1007/s11164-014-1631-8.
(29) Zhang, J. W.; Shao, X. S.; Li, Z.; Xu, X. Y. Bis-phenylazoneonicotinoids as divalent insecticides: Design, synthesis and activity. *Lett. Drug Des. Discovery* **2014**, *11*, 150−155.
(30) Shao, X. S.; Li, Z.; Qian, X. H.; Xu, X. Y. Design, synthesis and insecticidal activities of novel analogues of neonicotinoids: replacement of nitromethylene with nitro-conjugated system. *J. Agric. Food Chem.* **2009**, *57*, 951−957.
(31) Xu, X. Y.; Bao, H. B.; Shao, X. S.; Zhang, Y. X.; Yao, X. M.; Liu, Z. W.; Li, Z. Pharmacological of *cis*-ntromethylene neonicotinoids: overlapping one binding site of imidacloprid in the brown planthopper, *Nilaparvata lugens*. *Insect Mol. Biol.* **2010**, *19*, 1−8.
(32) Shao, X. S.; Liu, H. Y.; Bao, H. B.; Xu, X. Y.; Liu, Z. W.; Li, Z. The mode of action of a nitroconjugated neonicotinoid and the effects of target site mutation Y151S on its potency. *Insect Biochem. Mol. Biol.* **2011**, *41*, 440−445.
(33) Shao, X. S.; Swenson, T. L.; Casida, J. E. Cycloxaprid insecticide: Nicotinic acetylcholine receptor binding site and metabolism. *J. Agric. Food Chem.* **2013**, *61*, 7883−7888.
(34) Shao, X. S.; Xia, S. S.; Durkin, K. A.; Casida, J. E. Insect nicotinic receptor interactions in *vivo* with neonicotinoid, organophosphorus and methylcarbamate insecticides and a synergist. *Proc. Natl. Acad. Sci. U.S.A.* **2013**, *110*, 17273−17277.
(35) Chen, N. Y.; Zou, M. M.; Tian, X.; Zhu, F. J.; Jiang, D. P.; Shao, X. S.; Li, Z. Isomerization of ninhydrin-heterocyclic ketene aminals adducts: kinetic versus thermodynamic control, solvents dependency and mechanism. *Eur. J. Org. Chem.* **2014**, *28*, 6210−6218.
(36) Kagabu, S.; Ohno, I.; Tomizawa, M.; Durkin, K. A.; Matsuura, R.; Uchiyama, D.; Nagae, N.; Kumazawa, S. Furan-2,5-dimethylene-tethered bis-imidacloprid insecticide conferring high potency. *J. Agric. Food Chem.* **2010**, *58*, 11832−11836.
(37) Talley, T. T.; Harel, M.; Hibbs, R. E.; Radić, Z.; Tomizawa, M.; Casida, J. E.; Taylor, P. Atomic interactions of neonicotinoids agonist with AChBP: Molecular recognition of the distinctive electronegative pharmacophore. *Proc. Natl. Acad. Sci. U.S.A.* **2008**, *105*, 7606−7611.
(38) Tomizawa, M.; Casida, J. E. Unique neonicotinoid binding conformations conferring selective receptor interactions. *J. Agric. Food Chem.* **2011**, *59*, 2825−2828.

DOI: 10.1021/jf505281p
J. Agric. Food Chem. 2015, 63, 1360−1369

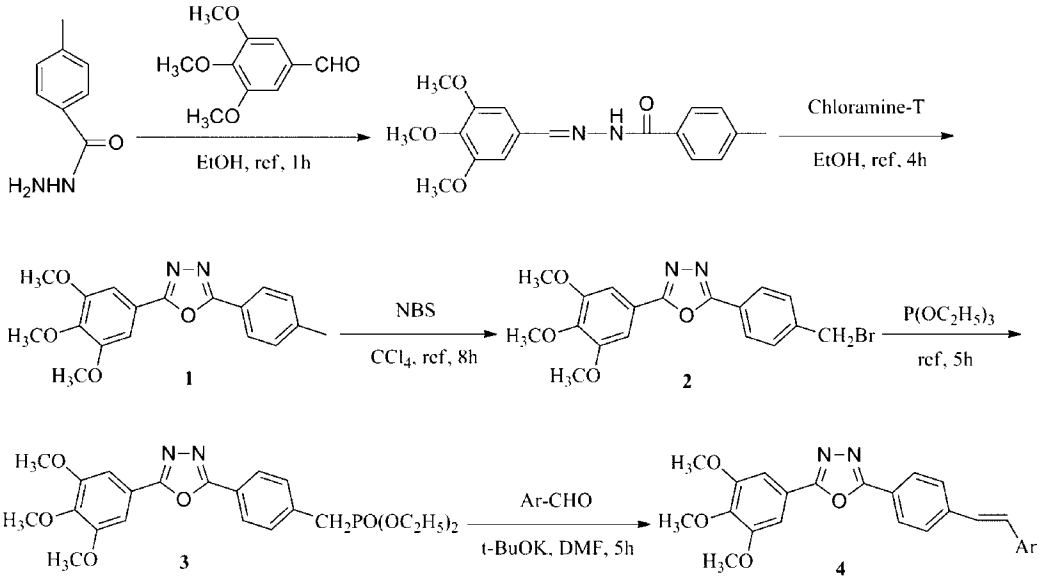

Figure 1. General synthetic route for target compounds: **4a**, Ar = phenyl; **4b**, Ar = 4-F phenyl; **4c**, Ar = 2-Cl phenyl; **4d**, Ar = 3-Cl phenyl; **4e**, Ar = 4-Cl phenyl; **4f**, Ar = 2,4-di-Cl phenyl; **4g**, Ar = 3,4-di-Cl phenyl; **4h**, Ar = 2-Br phenyl; **4i**, Ar = 4-Br phenyl; **4j**, Ar = 2-NO_2 phenyl; **4k**, Ar = 3-NO_2 phenyl; **4l**, Ar = 4-NO_2 phenyl; **4m**, Ar = 2-methoxy phenyl; **4n**, Ar = 3-methoxy phenyl; **4o**, Ar = 4-methoxy phenyl; **4p**, Ar = 3,4,5-trimethoxy phenyl; **4q**, Ar = 1-naphthyl; **4r**, Ar = 9-anthryl; **4s**, Ar = 4-*N*,*N*-dimethylaniline; **4t**, Ar = 2-pyridyl; **4u**, Ar = 3-pyridyl; and **4v**, Ar = 4-pyridyl.

(FTIR) spectra were measured as KBr pellets on a Bruker Vector 33. ^{1}H and ^{13}C nuclear magnetic resonance (NMR) spectra were recorded in $CDCl_3$ on a Bruker AVANCE-400 MHz NMR spectrometer using tetramethylsilane (TMS) as an internal standard. Mass spectra were obtained with a Bruker Esquire HCTplus spectrometer [atmospheric pressure chemical ionization/electrospray ionization (APCI/ESI)]. The purity of the compounds was confirmed by thin-layer chromatography (TLC) on silica gel "G"-coated glass plates, and spots were visualized under ultraviolet (UV) irradiation.

General Synthetic Procedures for Title Compounds 4a−4v. The title compounds were synthesized according to our previously reported procedure.[25] The desired starting materials were prepared by esterification of 4-methylbenzoic acid, followed by treatment with hydrazine hydrate in absolute ethanol. The data for target compounds **4a−4v** are shown below, and the detailed procedures for intermediates **1−3** and target compounds are available in the Supporting Information.

Data for compound **4a**: light yellow solid; yield, 62.5%; melting point (mp), 156−157 °C; ^{1}H NMR (400 MHz, $CDCl_3$) δ, 8.13 (d, J = 8.3 Hz, 2H, C_6H_4 2,6-H), 7.67 (d, J = 8.3 Hz, 2H, C_6H_4 3,5-H), 7.56 (d, J = 7.5 Hz, 2H, C_6H_5 2,6-H), 7.45−7.36 (m, 4H, C_6H_5 3,5-H C_6H_2 2,6-H), 7.32 (t, J = 7.3 Hz, 1H, C_6H_5 4-H), 7.25 (d, J = 16.3 Hz, 1H, CH═CH), 7.15 (d, J = 16.3 Hz, 1H, CH═CH), 4.00 (s, 6H, OCH_3), 3.96 (s, 3H, OCH_3); ^{13}C NMR (101 MHz, $CDCl_3$) δ, 164.42, 153.73, 141.28, 140.76, 136.71, 131.07, 128.81, 128.29, 127.39, 127.28, 127.00, 126.80, 122.56, 119.00, 104.31, 61.04, 56.45; high-resolution mass spectrometry (HRMS) (ESI), m/z calcd for $C_{25}H_{23}N_2O_4$ (M + H)$^+$ 415.1652; found, 415.1650.

Data for compound **4b**: yellow solid; yield, 76.9%; mp, 180−181 °C; ^{1}H NMR (400 MHz, $CDCl_3$) δ, 8.11 (d, J = 8.3 Hz, 2H, C_6H_4 2,6-H), 7.63 (d, J = 8.3 Hz, 2H, C_6H_4 3,5-H), 7.51 (m, 2H, C_6H_4 2,6-H), 7.36 (s, 2H, C_6H_2 2,6-H), 7.18 (d, J = 16.3 Hz, 1H, CH═CH), 7.13−6.97 (3H, C_6H_4 3,5-H, CH═CH), 3.99 (s, 6H, OCH_3), 3.95 (s, 3H, OCH_3); ^{13}C NMR (101 MHz, $CDCl_3$) δ, 164.41, 164.35, 163.92, 153.72, 141.30, 140.57, 132.91, 129.78, 128.34, 127.27, 127.16, 126.91, 122.56, 118.93, 115.79, 115.68, 104.31, 61.02, 56.44; HRMS (ESI), m/z calcd for $C_{25}H_{22}FN_2O_4$ (M + H)$^+$ 433.1558; found, 433.1556.

Data for compound **4c**: light yellow solid; yield, 69.6%; mp, 178−179 °C; ^{1}H NMR (400 MHz, $CDCl_3$) δ, 8.14 (d, J = 8.2 Hz, 2H, C_6H_4 2,6-H), 7.70 (t, 3H, C_6H_4 3,5-H, C_6H_4 5-H), 7.64 (d, J = 16.3 Hz, 1H, CH═CH), 7.42 (d, J = 7.8 Hz, 1H, C_6H_4 2-H), 7.37 (s, 2H, C_6H_2 2,6-H), 7.32−7.21 (m, 2H, C_6H_4 3,4-H), 7.12 (d, J = 16.3 Hz, 1H, CH═CH), 3.98 (s, 6H, OCH_3), 3.96 (s, 3H, OCH_3); ^{13}C NMR (101 MHz, $CDCl_3$) δ, 164.46, 164.33, 153.72, 141.29, 140.40, 134.80, 133.74, 129.95, 129.89, 129.14, 127.32, 127.29, 127.02, 126.99, 126.58, 122.98, 118.96, 104.30, 61.03, 56.44; HRMS (ESI), m/z calcd for $C_{25}H_{22}ClN_2O_4$ (M + H)$^+$ 449.1263; found, 449.1257.

Data for compound **4d**: light yellow solid; yield, 80.6%; mp, 176−177 °C; ^{1}H NMR (400 MHz, $CDCl_3$) δ, 8.11 (d, J = 8.4 Hz, 2H, C_6H_4 2,6-H), 7.64 (d, J = 8.4 Hz, 2H, C_6H_4 3,5-H), 7.52 (s, 1H, C_6H_4 5-H), 7.38 (d, J = 7.5 Hz, 1H, C_6H_4 2-H), 7.35 (s, 2H, C_6H_2 2,6-H), 7.29 (t, J = 7.7 Hz, 1H, C_6H_4 3-H), 7.26 (s, 1H, C_6H_4 4-H), 7.13 (s, 2H, CH═CH), 3.96 (s, 6H, OCH_3), 3.92 (s, 3H, OCH_3); ^{13}C NMR (101 MHz, $CDCl_3$) δ, 164.45, 164.28, 153.71, 141.29, 140.12, 138.58, 134.77, 129.99, 129.45, 128.76, 128.11, 127.28, 127.13, 126.53, 125.01, 122.95, 118.94, 104.29, 61.02, 56.43; HRMS (ESI), m/z calcd for $C_{25}H_{22}ClN_2O_4$ (M + H)$^+$ 449.1263; found, 449.1257.

Data for compound **4e**: light yellow solid; yield, 72.5%; mp, 209−210 °C; ^{1}H NMR (400 MHz, $CDCl_3$) δ, 8.09 (d, J = 8.3 Hz, 2H, C_6H_4 2,6-H), 7.62 (d, J = 8.3 Hz, 2H, C_6H_4 3,5-H), 7.45 (d, J = 8.5 Hz, 2H, C_6H_4 2,6-H), 7.34 (s, 2H, C_6H_2 2,6-H), 7.33 (d, J = 8.5 Hz, 2H, C_6H_4 3,5-H), 7.15 (d, J = 16.3 Hz, 1H, CH═CH), 7.07 (d, J = 16.3 Hz, 1H, CH═CH), 3.97 (s, 6H, OCH_3), 3.94 (s, 3H, OCH_3); ^{13}C NMR (101 MHz, $CDCl_3$) δ, 164.43, 164.32, 153.71, 141.30, 140.34, 135.21, 133.89, 129.64, 128.97, 127.94, 127.27, 127.02, 122.77, 118.93, 104.30, 61.02, 56.43; HRMS (ESI), m/z calcd for $C_{25}H_{22}ClN_2O_4$ (M + H)$^+$ 449.1263; found, 449.1260.

Data for compound **4f**: light yellow solid; yield, 62.7%; mp, 193−194 °C; ^{1}H NMR (400 MHz, $CDCl_3$) δ, 8.15 (d, J = 7.8 Hz, 2H, C_6H_4 2,6-H), 7.70 (d, J = 7.8 Hz, 2H, C_6H_4 3,5-H), 7.65 (d, J = 8.5 Hz, 1H, C_6H_3 5-H), 7.56 (d, J = 16.3 Hz, 1H, CH═CH), 7.44 (d, J = 2.0 Hz, 1H, C_6H_3 2-H), 7.38 (s, 2H, C_6H_2 2,6-H), 7.30 (d, J = 2.0 Hz, 1H, C_6H_3 3-H), 7.11 (d, J = 16.3 Hz, 1H, CH═CH), 4.01 (s, 6H, OCH_3), 3.96 (s, 3H, OCH_3); ^{13}C NMR (101 MHz, $CDCl_3$) δ, 164.52, 164.27, 153.74, 141.36, 140.09, 134.19, 133.44, 130.38, 129.72, 127.45, 127.39, 127.36, 127.30, 125.85, 123.20, 118.89, 104.36, 61.05, 56.48; HRMS (ESI), m/z calcd for $C_{25}H_{21}Cl_2N_2O_4$ (M + H)$^+$ 483.0873; found, 483.0874.

Data for compound **4g**: light green solid; yield, 71.0%; mp, 211−212 °C; ^{1}H NMR (400 MHz, $CDCl_3$) δ, 8.12 (d, J = 8.0 Hz, 2H, C_6H_4 2,6-H), 7.63 (m, 3H, C_6H_4 3,5-H, C_6H_4 2-H), 7.47−7.41 (m, 1H, C_6H_4 3-H), 7.40−7.31 (m, 3H, C_6H_2 2,6-H, C_6H_4 6-H), 7.15−7.06 (m, 2H, CH═CH), 3.99 (s, 6H, OCH_3), 3.96 (s, 3H, OCH_3); ^{13}C NMR (101 MHz, $CDCl_3$) δ, 164.50, 164.24, 153.73, 141.33, 139.85, 136.84, 132.98, 131.85, 130.68, 129.22, 128.36, 128.31, 127.32, 127.18,

DOI: 10.1021/jf5052893
J. Agric. Food Chem. 2015, 63, 1370−1377

125.86, 123.14, 118.91, 104.31, 61.04, 56.46; HRMS (ESI), m/z calcd for $C_{25}H_{21}Cl_2N_2O_4$ $(M + H)^+$ 483.0873; found, 483.0875.

Data for compound **4h**: light yellow solid; yield, 72.6%; mp, 176−177 °C; ^{1}H NMR (400 MHz, $CDCl_3$) δ, 8.16 (d, J = 8.2 Hz, 2H, C_6H_4 2,6-H), 7.72 (d, J = 8.2 Hz, 3H, C_6H_4 3,5-H, C_6H_4 5-H), 7.67−7.58 (m, 3H, CH═CH, C_6H_4 2-H), 7.43−7.32 (m, 3H, C_6H_2 2,6-H, C_6H_4 3-H), 7.18 (t, J = 7.0 Hz, 1H, C_6H_4 4-H), 7.10 (d, J = 16.2 Hz, 1H, CH═CH), 4.01 (s, 6H, OCH_3), 3.97 (s, 3H, OCH_3); ^{13}C NMR (101 MHz, $CDCl_3$) δ, 164.47, 164.33, 153.72, 141.28, 140.34, 136.51, 133.20, 130.07, 129.67, 129.38, 127.66, 127.33, 127.31, 126.82, 124.41, 123.00, 118.96, 104.31, 61.04, 56.45; HRMS (APCI), m/z calcd for $C_{25}H_{22}BrN_2O_4$ $(M + H)^+$ 493.0757; found, 493.0759.

Data for compound **4i**: yellow solid; yield, 80.8%; mp, 213−214 °C; ^{1}H NMR (400 MHz, $CDCl_3$) δ, 8.09 (d, J = 8.3 Hz, 2H, C_6H_4 2,6-H), 7.62 (d, J = 8.3 Hz, 2H, C_6H_4 3,5-H), 7.49 (d, J = 8.4 Hz, 2H, C_6H_4 2,6-H), 7.38 (d, J = 8.4 Hz, 2H, C_6H_4 3,5-H), 7.34 (s, 2H, C_6H_2 2,6-H), 7.13 (d, J = 16.4 Hz, 1H, CH═CH), 7.08 (d, J = 16.4 Hz, 1H, CH═CH), 3.97 (s, 6H, OCH_3), 3.94 (s, 3H, OCH_3); ^{13}C NMR (101 MHz, $CDCl_3$) δ, 164.44, 164.31, 153.72, 141.32, 140.32, 135.64, 131.93, 129.70, 128.21, 128.06, 127.29, 127.04, 122.78, 122.09, 118.90, 104.31, 61.03, 56.45; HRMS (APCI), m/z calcd for $C_{25}H_{22}BrN_2O_4$ $(M + H)^+$ 493.0757; found, 493.0754.

Data for compound **4j**: light green solid; yield, 77.6%; mp, 205−206 °C; ^{1}H NMR (400 MHz, $CDCl_3$) δ, 8.11 (d, J = 8.3 Hz, 2H, C_6H_4 2,6-H), 7.98 (d, J = 8.2 Hz, 1H, C_6H_4 5-H), 7.76 (d, J = 7.7 Hz, 1H, C_6H_4 2-H), 7.73−7.59 (m, 4H, C_6H_4 3,5-H, CH═CH, C_6H_4 3-H), 7.43 (t, J = 7.7 Hz, 1H, C_6H_4 4-H), 7.35 (s, 2H, C_6H_2 2,6-H), 7.08 (d, J = 16.1 Hz, 1H, CH═CH), 3.98 (s, 6H, OCH_3), 3.94 (s, 3H, OCH_3); ^{13}C NMR (101 MHz, $CDCl_3$) δ, 164.51, 164.18, 153.71, 148.02, 141.30, 139.74, 133.25, 132.44, 132.37, 128.53, 128.25, 127.57, 127.30, 125.83, 124.87, 123.45, 118.86, 104.28, 61.01, 56.43; HRMS (APCI), m/z calcd for $C_{25}H_{22}N_3O_6$ $(M + H)^+$ 460.1503; found, 460.1505.

Data for compound **4k**: light yellow solid; yield, 87.5%; mp, 236−237 °C; ^{1}H NMR (400 MHz, $CDCl_3$) δ, 8.39 (s, 1H, C_6H_4 6-H), 8.13 (m, 3H, C_6H_4 3,5-H, C_6H_4 4-H), 7.82 (d, J = 7.8 Hz, 1H, C_6H_4 2-H), 7.68 (d, J = 8.3 Hz, 2H, C_6H_4 3,5-H), 7.55 (t, J = 8.0 Hz, 1H, C_6H_4 3-H), 7.36 (s, 2H, C_6H_2 2,6-H), 7.25 (s, 2H, CH═CH), 3.98 (s, 6H, OCH_3), 3.94 (s, 3H, OCH_3); ^{13}C NMR (101 MHz, $CDCl_3$) δ, 164.55, 164.19, 153.74, 148.77, 141.39, 139.58, 138.52, 132.48, 130.41, 129.73, 128.33, 127.39, 127.36, 123.42, 122.59, 121.10, 118.83, 104.35, 61.04, 56.46; HRMS (APCI), m/z calcd for $C_{25}H_{22}N_3O_6$ $(M + H)^+$ 460.1503; found, 460.1507.

Data for compound **4l**: light green solid; yield, 88.1%; mp, 271−272 °C; ^{1}H NMR (400 MHz, $CDCl_3$) δ, 8.26 (d, J = 8.8 Hz, 2H, C_6H_4 3,5-H), 8.18 (d, J = 8.3 Hz, 2H, C_6H_4 2,6-H), 7.74−7.65 (m, 4H, C_6H_4 2,6-H C_6H_4 3,5-H), 7.38 (s, 2H, C_6H_2 2,6-H), 7.30 (d, J = 5.7 Hz, 2H, CH═CH), 3.99 (s, 6H, OCH_3), 3.95 (s, 3H, OCH_3); HRMS (APCI), m/z calcd for $C_{25}H_{22}N_3O_6$ $(M + H)^+$ 460.1503; found, 460.1507.

Data for compound **4m**: light yellow solid; yield, 60.9%; mp, 145−146 °C; ^{1}H NMR (400 MHz, $CDCl_3$) δ, 8.09 (d, J = 8.0 Hz, 2H, C_6H_4 2,6-H), 7.66 (d, J = 8.1 Hz, 2H, C_6H_4 3,5-H), 7.61 (d, J = 4.5 Hz, 1H, C_6H_4 2-H), 7.58 (d, J = 3.9 Hz, 1H, C_6H_4 5-H), 7.35 (s, 2H, C_6H_2 2,6-H), 7.27 (m, 1H, C_6H_4 4-H), 7.14 (d, J = 16.5 Hz, 1H, CH═CH), 6.98 (t, J = 7.5 Hz, 1H, C_6H_4 3-H), 6.91 (d, J = 8.3 Hz, 1H, CH═CH), 3.97 (s, 6H, OCH_3), 3.94 (s, 3H, OCH_3), 3.90 (s, 3H, OCH_3); ^{13}C NMR (101 MHz, $CDCl_3$) δ, 164.51, 164.35, 157.16, 153.70, 141.45, 141.20, 129.37, 127.75, 127.19, 127.01, 126.68, 125.95, 125.77, 122.25, 120.81, 119.07, 111.02, 104.27, 61.03, 56.43, 55.54; HRMS (ESI), m/z calcd for $C_{26}H_{25}N_2O_5$ $(M + H)^+$ 445.1758; found, 445.1761.

Data for compound **4n**: light yellow solid; yield, 61.5%; mp, 131−132 °C; ^{1}H NMR (400 MHz, $CDCl_3$) δ, 8.11 (d, J = 7.2 Hz, 2H, C_6H_4 2,6-H), 7.64 (d, J = 7.3 Hz, 2H, C_6H_4 3,5-H), 7.37 (s, 2H, C_6H_2 2,6-H), 7.34−7.26 (m, 1H, C_6H_4 3-H), 7.19 (d, J = 16.3 Hz, 1H, CH═CH), 7.16−7.03 (m, 3H, C_6H_4 2-H, C_6H_4 5-H, CH═CH), 6.86 (d, J = 8.1 Hz, 1H, C_6H_4 4-H), 3.99 (s, 6H, OCH_3), 3.95 (s, 3H, OCH_3), 3.86 (s, 3H, OCH_3); ^{13}C NMR (101 MHz, $CDCl_3$) δ, 164.37, 164.34, 159.96, 153.71, 141.39, 140.74, 138.10, 131.00, 129.76, 127.61, 127.29, 127.03, 122.39, 119.50, 118.73, 113.94, 112.06, 104.36, 61.03, 56.45, 55.27; HRMS (ESI), m/z calcd for $C_{26}H_{25}N_2O_5$ $(M + H)^+$ 445.1758; found, 445.1765.

Data for compound **4o**: light yellow solid; yield, 77.3%; mp, 190−191 °C; ^{1}H NMR (400 MHz, $CDCl_3$) δ, 8.08 (d, J = 8.3 Hz, 2H, C_6H_4 2,6-H), 7.61 (d, J = 8.3 Hz, 2H, C_6H_4 3,5-H), 7.47 (d, J = 8.7 Hz, 2H, C_6H_4 2,6-H), 7.35 (s, 2H, C_6H_2 2,6-H), 7.18 (d, J = 16.3 Hz, 1H, CH═CH), 6.99 (d, J = 16.3 Hz, 1H, CH═CH), 6.90 (d, J = 8.7 Hz, 2H, C_6H_4 3,5-H), 3.97 (s, 6H, OCH_3), 3.92 (s, 3H, OCH_3), 3.83 (s, 3H, OCH_3); ^{13}C NMR (101 MHz, $CDCl_3$) δ, 164.48, 164.34, 159.83, 153.70, 141.21, 141.12, 130.59, 129.49, 128.09, 127.22, 126.68, 125.22, 122.09, 119.05, 114.26, 104.26, 61.02, 56.43, 55.33; HRMS (APCI), m/z calcd for $C_{26}H_{25}N_2O_5$ $(M + H)^+$ 445.1758; found, 445.1767.

Data for compound **4p**: light green solid; yield, 81.1%; mp, 187−188 °C; ^{1}H NMR (400 MHz, $CDCl_3$) δ, 8.11 (d, J = 8.1 Hz, 2H, C_6H_4 2,6-H), 7.64 (d, J = 8.1 Hz, 2H, C_6H_4 3,5-H), 7.36 (s, 2H,C_6H_2), 7.15 (d, J = 16.2 Hz, 1H, CH═CH), 7.03 (d, J = 16.2 Hz, 1H, CH═CH), 6.76 (s, 2H, C_6H_2 2,6-H), 3.97 (s, 6H, OCH_3), 3.92 (d, 9H, OCH_3), 3.87 (s, 3H, OCH_3); ^{13}C NMR (101 MHz, $CDCl_3$) δ, 164.40, 164.39, 153.70, 153.47, 141.28, 140.64, 138.56, 132.40, 130.99, 127.25, 126.88, 126.79, 122.46, 118.96, 104.28, 103.97, 61.00, 60.96, 56.43, 56.17; HRMS (ESI), m/z calcd for $C_{28}H_{29}N_2O_7$ $(M + H)^+$ 505.1969; found, 505.1970.

Data for compound **4q**: light yellow solid; yield, 67.3%; mp, 182−183 °C; ^{1}H NMR (400 MHz, $CDCl_3$) δ, 8.21 (d, J = 8.2 Hz, 1H, naphthalene-H), 8.11 (d, J = 8.2 Hz, 2H, C_6H_4 2,6-H), 7.97 (d, J = 16.0 Hz, 1H, CH═CH), 7.86 (d, J = 7.9 Hz, 1H, naphthalene-H), 7.81 (d, J = 8.2 Hz, 1H, naphthalene-H), 7.74 (d, J = 7.1 Hz, 1H, naphthalene-H), 7.70 (d, J = 8.2 Hz, 2H, C_6H_4 3,5-H), 7.59−7.45 (m, 3H, naphthalene-H), 7.33 (s, 2H, C_6H_2 2,6-H), 7.14 (d, J = 16.0 Hz, 1H, CH═CH), 3.97 (s, 6H, OCH_3), 3.96 (s, 3H, OCH_3); ^{13}C NMR (101 MHz, $CDCl_3$) δ, 164.39, 164.35, 153.68, 141.23, 140.89, 134.22, 133.75, 131.33, 130.25, 128.72, 128.65, 127.93, 127.26, 127.14, 126.32, 125.96, 125.65, 123.82, 123.52, 122.66, 118.96, 104.25, 61.02, 56.41; HRMS (APCI), m/z calcd for $C_{29}H_{25}N_2O_6$ $(M + H)^+$ 465.1809; found, 465.1806.

Data for compound **4r**: yellow solid; yield, 76.5%; mp, 191−192 °C; ^{1}H NMR (400 MHz, $CDCl_3$) δ, 8.46 (s, 1H, anthracen-H), 8.41−8.33 (m, 2H, anthracen-H), 8.24 (d, J = 8.3 Hz, 2H, C_6H_4 2,6-H), 8.14−8.01 (m, 3H, CH═CH, anthracen-H), 7.85 (d, J = 8.3 Hz, 2H, C_6H_4 3,5-H), 7.57−7.49 (m, 4H, anthracen-H), 7.42 (s, 2H, C_6H_2 2,6-H), 7.05 (d, J = 16.6 Hz, 1H, CH═CH), 4.02 (s, 6H, OCH_3), 3.98 (s, 3H, OCH_3); HRMS (ESI), m/z calcd for $C_{33}H_{27}N_2O_4$ $(M + H)^+$ 515.1965; found, 515.1964.

Data for compound **4s**: yellow solid; yield, 70.1%; mp, 212−213 °C; ^{1}H NMR (400 MHz, $CDCl_3$) δ, 8.02 (d, J = 8.3 Hz, 2H, C_6H_4 2,6-H), 7.54 (d, J = 8.3 Hz, 2H, C_6H_4 3,5-H), 7.39 (d, J = 8.7 Hz, 2H, C_6H_4 2,6-H), 7.31 (s, 2H, C_6H_2 2,6-H), 7.11 (d, J = 16.2 Hz, 1H, CH═CH), 6.87 (d, J = 16.2 Hz, 1H, CH═CH), 6.67 (d, J = 8.6 Hz, 2H, C_6H_4 3,5-H), 3.94 (s, 6H, OCH_3), 3.91 (s, 3H, OCH_3), 2.95 (s, 6H, CH3); ^{13}C NMR (101 MHz, $CDCl_3$) δ, 164.60, 164.23, 153.68, 150.44, 141.73, 141.14, 131.25, 128.01, 127.17, 126.36, 122.81, 121.45, 119.13, 112.32, 104.23, 61.02, 56.43, 40.34; HRMS (ESI), m/z calcd for $C_{27}H_{28}N_3O_4$ $(M + H)^+$ 458.2074; found, 458.2071.

Data for compound **4t**: light yellow solid; yield, 72.8%; mp, 196−197 °C; ^{1}H NMR (400 MHz, $CDCl_3$) δ, 8.64 (d, J = 4.6 Hz, 1H, pyridine-H), 8.15 (d, J = 8.1 Hz, 2H, C_6H_4 2,6-H), 7.78−7.67 (m, 4H, C_6H_4 3,5-H pyridine-H, CH═CH), 7.45 (d, J = 7.6 Hz, 1H, pyridine-H), 7.37 (s, 2H, C_6H_2 2,6-H), 7.31 (d, J = 16.9 Hz, 1H, CH═CH), 7.26−7.19 (m, 1H, pyridine-H), 3.99 (s, 6H, OCH_3), 3.95 (s, 3H, OCH_3); ^{13}C NMR (101 MHz, $CDCl_3$) δ, 164.51, 164.32, 154.73, 153.73, 149.43, 141.27, 139.91, 137.04, 131.80, 129.62, 127.68, 127.30, 123.33, 122.65, 118.96, 104.29, 61.03, 56.44; HRMS (ESI), m/z calcd for $C_{24}H_{22}N_3O_4$ $(M + H)^+$ 416.1605; found, 416.1610.

Data for compound **4u**: light green solid; yield, 69.3%; mp, 182−183 °C; ^{1}H NMR (600 MHz, $CDCl_3$) δ, 8.77 (d, J = 2.0 Hz, 1H, pyridine-H), 8.53 (d, J = 4.8 Hz, 1H, pyridine-H), 8.14 (d, J = 8.4 Hz, 2H, C_6H_4 2,6-H), 7.88 (d, J = 7.9 Hz, 1H, pyridine-H), 7.68 (d, J = 8.4 Hz, 2H, C_6H_4 3,5-H), 7.37 (s, 2H, C_6H_2 2,6-H), 7.33 (q, 1H, pyridine-H), 7.20 (s, 2H, CH═CH), 3.99 (s, 6H, OCH_3), 3.95 (s, 3H, OCH_3);

DOI: 10.1021/jf5052893
J. Agric. Food Chem. 2015, 63, 1370−1377

HRMS (ESI), m/z calcd for $C_{24}H_{22}N_3O_4$ $(M + H)^+$ 416.1605; found, 416.1606.

Data for compound **4v**: light green solid; yield, 70.2%; mp, 221−222 °C; ^{1}H NMR (600 MHz, $CDCl_3$) δ, 8.63 (d, J = 4.6 Hz, 2H, pyridine-H), 8.18 (d, J = 8.4 Hz, 2H, C_6H_4 2,6-H), 7.71 (d, J = 8.3 Hz, 2H, C_6H_4 3,5-H), 7.44 (d, J = 4.7 Hz, 2H, pyridine-H), 7.37 (d, J = 16.2 Hz, 3H, C_6H_2 2,6-H, CH═CH), 7.16 (d, J = 16.3 Hz, 1H, CH═CH), 4.00 (s, 6H, OCH_3), 3.95 (s, 3H, OCH_3); HRMS (ESI), m/z calcd for $C_{24}H_{22}N_3O_4$ $(M + H)^+$ 416.1605; found, 416.1603.

***In Vivo* Bioassays.** The pot culture test method was adopted to evaluate fungicidal activities of the title compounds against *P. cubensis*, *C. lagenarium*, and *S. cucurbitacearum in vivo* at 600 μg/mL according to the references, with slight modifications.[26,27] Two commercial fungicides, 80% Mancozeb WP and 80% Carbendazim WP, were evaluated as controls against the above-mentioned fungi at the same condition. All compounds were dissolved in dimethylformamide (DMF), and then distilled water (containing 0.1% Tween 80) was added to the solution to generate a tested concentration of 600 μg/mL, in each of which the final concentration of DMF was <1% (v/v). *P. cubensis* sporangia were obtained by washing off the leaves of highly infected cucumber plants that were kept overnight (above 80% relative humidity). *C. lagenarium* and *S. cucurbitacearum* were cultured on the potato dextrose agar (PDA). Spores of those two fungal pathogens were removed from the PDA plates. All of the spore suspensions were adjusted to the desired concentrations prior to use. Germination was conducted by soaking cucurbit seeds in water for 2 h at 50 °C and then keeping the seeds moist for 24 h at 28 °C in an incubator.

When the cucurbit plants used for inoculations were at the stage of two seed leaves, tested compounds and commercial fungicides were sprayed with a hand sprayer on the upper leaf surface of seed leaves at the standard concentration of 600 μg/mL. Distilled water without compounds or commercial fungicide treatments was set as a blank control. After the solution on leaves was air-dried, inoculations of *P. cubensis*, *C. lagenarium*, and *S. cucurbitacearum* were carried out by spraying a spore suspension with the concentrations of 1×10^5, 1×10^6, and 1×10^6 spores/mL of water, respectively. Then, the plants were maintained at 24 ± 1 °C and above 80% relative humidity. Three replicates were used per treatment, and the experiment was repeated 3 times.

The fungicidal activity was evaluated visually when the non-treated cucurbit plant (blank control) fully developed symptoms. The percentage of the diseased area on inoculated treated leaves was assessed and compared to that of non-treated leaves to determine the average disease index. The relative control efficacy of compounds compared to the blank assay was calculated via the following equation:

$$I\ (\%) = [(CK - PT)/CK] \times 100\%$$

where I is the relative control efficacy, CK is the average disease index during the blank assay, and PT is the average disease index after treatment during testing.

Three-Dimensional Quantitative Structure−Activity Relationship (3D-QSAR) Analysis. All molecular modeling studies were performed using the Tripos SYBYL 7.3.5 software package.[28] The CoMFA model was derived from the antifungal activity of 22 compounds (17 compounds for training sets and 5 compounds for test sets) against *C. lagenarium* at 600 μg/mL. The fungicidal activity was converted into D values by the formula $D = \log\{[I/(100 - I)] - MW\}$,[29] where I is the percent control efficacy and MW is the molecular weight of the tested compounds. Compound **4k** was chosen as a template for superimposition because of the highest control efficacy. Each structure was built using the SKETCH option and fully geometry-optimized using a conjugate gradient procedure based on the TRIPOS force field and Gasteiger and Hückel charges.

The steric and electrostatic interaction fields for CoMFA were calculated using the SYBYL default parameters: 2.0 Å grid points spacing, a sp^3 carbon probe atom with a charge of +1.0, and a van der Waals radius of 1.52 Å. Steric and electrostatic fields were scaled by the CoMFA−STD method in SYBYL with a default cutoff energy of 30 kcal/mol. A partial least-squares (PLS) approach was used to derive the 3D-QSAR model, in which the CoMFA descriptors were used as independent variables and the experimental D values were used as dependent variables. The cross-validation with the leave-one-out (LOO) option and the SAMPLS program was carried out to obtain the optimal number of components (N) and cross-validated coefficient (q^2). After the optimal number of components was determined, a non-cross-validated analysis was performed without column filtering to obtain regression coefficients (r^2) and its standard error (S) and F-test value (F) for the model evaluation.

RESULTS AND DISCUSSION

Synthesis. The synthetic route of the title compounds is outlined in Figure 1. A series of novel stilbene derivatives containing a 1,3,4-oxadiazole moiety was synthesized in good yields by bromination of *N*-bromosuccinimide (NBS), Arbuzov reaction, and Wittig−Horner reaction. The key step involved the formation of the stilbenes, which were efficiently generated by the reaction of phosphonate **3** with various aldehydes via Wittig−Horner reaction under mild reaction conditions. The chemical structures of the target compounds were confirmed by FTIR, ^{1}H and ^{13}C NMR, and HRMS. Notably, the ^{1}H NMR spectra of target compounds show two fine doublets as well as a coupling constant (16.7−16.0 Hz) corresponding to the olefinic protons (CH═CH) from *trans*-stilbene, which are further confirmed by the FTIR spectra.[30] All spectral and analytical data are consistent with the assigned structures.

Fungicidal Activity. The *in vivo* fungicidal activities of compounds **4a**−**4v** against *P. cubensis*, *C. lagenarium*, and *S. cucurbitacearum* at a concentration of 600 μg/mL are listed in Table 1. The results of bioassays are compared to those obtained from two commercial fungicides. It was worth noting that all of the tested compounds were found safe for the cucurbit plants. As indicated in Table 1, some of the title compounds showed a broad spectrum and comparable fungicidal activities against the tested fungi. Four main conclusions were drawn from the comparison of the fungicidal activities of title compounds against test fungi to those of commercial fungicides: (a) Compounds **4s** exhibited a significant inhibition effect against cucumber *P. cubensis* with a control efficacy of 71.38 ± 1.47%, which was comparable to that of 80% Mancozeb WP (70.13 ± 3.25%), while compounds **4d**, **4l**, and **4v** showed relatively high antifungal activities against cucumber *P. cubensis* (65.01 ± 1.81 and 63.42 ± 4.60%, respectively) compared to the fungicide 80% Mancozeb WP. (b) Compounds **4b**, **4d**, **4f**, **4i**, **4k**, and **4l** showed prominent activities against *C. lagenarium* compared to the control 80% Carbendazim WP. In particular, the activities of compounds **4d** and **4k** were 82.43 ± 4.66 and 83.82 ± 2.69%, respectively, which were similar to that of 80% Carbendazim WP (81.57 ± 2.19%). (c) Most of the compounds exhibited fair to moderate control efficacy against *S. cucurbitacearum*. Notably, compounds **4b**, **4h**, and **4i**, whose efficacy rates were 72.05 ± 0.96, 69.34 ± 0.93, and 67.68 ± 1.43%, respectively, were found to be almost the same activity level as that of 80% Carbendazim WP (69.02 ± 0.47%). (d) Some compounds showed significant bioactivity variances against the different fungi. For example, compound **4g** exhibited moderate activity (44.81 ± 3.85%) against *C. lagenarium*, whereas the control efficacy of compound **4g** against *S. cucurbitacearum* was only 8.03 ± 2.78% and even showed a negative effect on *P. cubensis*. These results indicated that compounds **4b**, **4d**, **4i**, **4k**, and **4l** were the most promising candidates for crop protection because of their broad spectrum and remarkably high activities against all tested fungi.

DOI: 10.1021/jf5052893
J. Agric. Food Chem. 2015, 63, 1370−1377

Table 1. Chemical Structures and Fungicidal Activities of Compounds 4a−4v at 600 μg/mL *in Vivo*

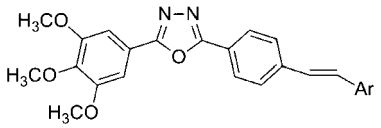

Compd.	Ar	control efficacy (%)[a]		
		P. cubensis	*C. lagenarium*	*S. cucurbitacearum*
4a		58.77 ± 1.97	50.03 ± 4.01	55.17 ± 4.22
4b	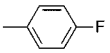	52.20 ± 2.59	65.14 ± 3.52	72.05 ± 0.96
4c		32.66 ± 6.18	31.48 ± 4.10	- 9.34 ± 0.36
4d		65.01 ± 1.81	82.43 ± 4.66	32.03 ± 7.57
4e	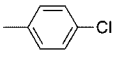	36.96 ± 5.57	47.78 ± 1.15	- 19.08 ± 1.29
4f	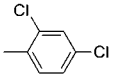	38.52 ± 4.06	63.83 ± 5.38	27.54 ± 8.20
4g	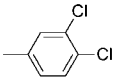	- 4.08 ± 4.17	44.81 ± 3.85	8.03 ± 2.78
4h		8.37 ± 3.03	26.38 ± 1.16	69.34 ± 0.93
4i	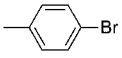	54.87 ± 3.55	64.77 ± 2.10	67.68 ± 1.43
4j		48.34 ± 0.62	56.07 ± 3.45	35.36 ± 2.85
4k	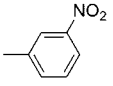	50.13 ± 3.15	83.82 ± 2.69	46.83 ± 4.50
4l	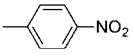	63.42 ± 4.60	66.72 ± 2.83	32.23 ± 1.57
4m		25.28 ± 5.99	33.12 ± 1.66	48.91 ± 1.54
4n	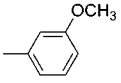	44.13 ± 4.56	37.90 ± 5.83	47.62 ± 3.37
4o	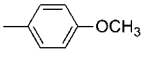	58.21 ± 5.91	56.93 ± 3.04	40.51 ± 4.43
4p	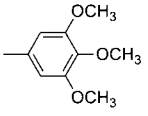	49.57 ± 1.12	61.92 ± 2.69	7.05 ± 1.39
4q		36.01 ± 0.51	37.98 ± 5.48	51.18 ± 4.76
4r	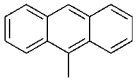	15.3 ± 2.77	14.29 ± 5.50	53.09 ± 4.36

DOI: 10.1021/jf5052893
J. Agric. Food Chem. 2015, 63, 1370−1377

Table 1. continued

Compd.	Ar	control efficacy (%)[a]		
		P. cubensis	*C. lagenarium*	*S. cucurbitacearum*
4s	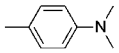	71.38 ± 1.47	30.26 ± 2.38	44.84 ± 4.22
4t		18.38 ± 1.59	52.88 ± 1.06	45.14 ± 6.89
4u		42.67 ± 2.51	37.58 ±1.98	40.27 ± 2.23
4v		62.35 ± 3.09	42.61 ± 1.92	34.24 ± 4.43
Fungicides[b]		70.13 ± 3.25 ^{A}	81.57 ± 2.19 ^{B}	69.02 ± 0.47 ^{B}

[a]Values represent means of three independent replicates ± standard deviation (SD). [b]Control fungicides: A, 80% Mancozeb WP; B, 80% Carbendazim WP.

Table 2. Statistical Parameters of the CoMFA Model

					contribution (%)	
	q^2	r^2	S	F	steric	electrostatic
CoMFA	0.516	0.920	0.114	25.186	56.2	43.8

CoMFA Analysis. The statistical results of the CoMFA model are summarized in Table 2. The internal validation of LOO cross-validated q^2 and non-cross-validated coefficient r^2 are commonly applied as the criterion of robustness and predictive ability of a QSAR model. The statistically recommendatory values for a satisfactory QSAR model are $q^2 > 0.5$ and $r^2 > 0.8$.[31] As listed in Table 2, a good predictive CoMFA model with the LOO cross-validated coefficient $q^2 = 0.516$ and the correlation coefficient $r^2 = 0.920$ was established. The predicted D values are generally in good agreement with the experimental data, as shown in Figure 2. The standard error ($S = 0.114$) and F-test value ($F = 25.186$) further validate the developed model.

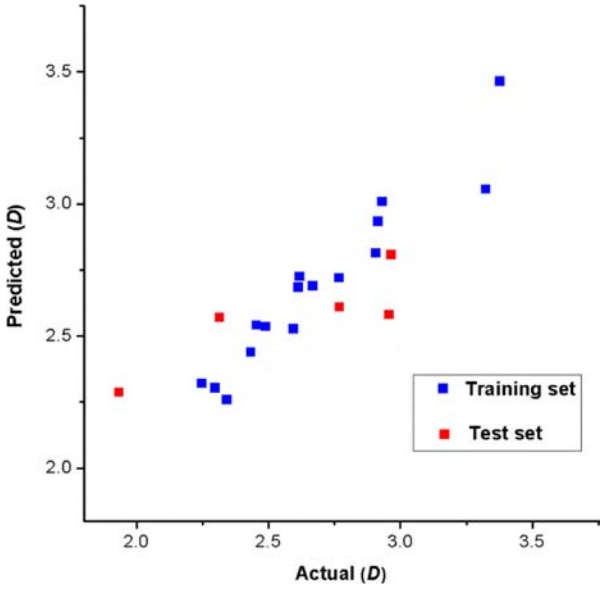

Figure 2. Plot of experimental values versus predicted values for training and test sets based on the CoMFA model.

The contribution steric and electrostatic fields are 56.2 and 43.8% for the QSAR model, respectively. CoMFA contour maps are displayed in Figure 3 to visualize how steric and electrostatic fields contribute to the bioactivity of test compounds.

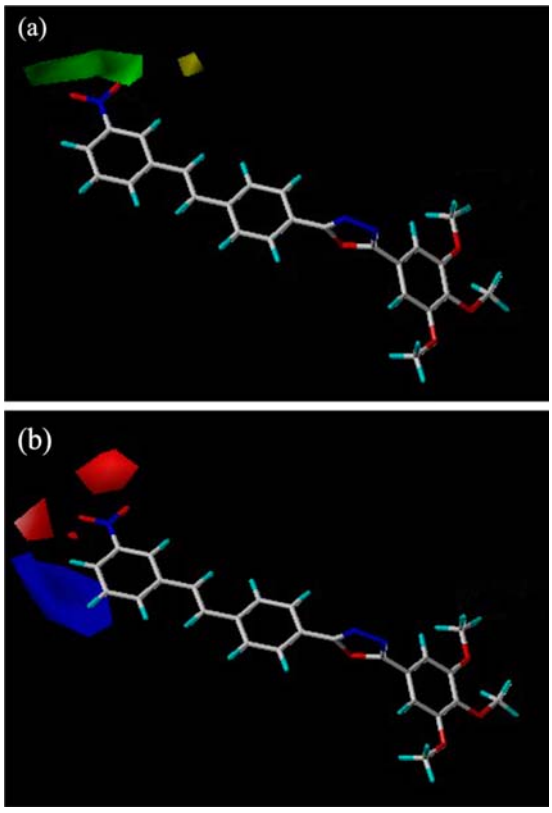

Figure 3. Graphical representation of CoMFA analysis for compound **4k**. (a) Steric contour plots: sterically favored areas are represented by green polyhedra, and sterically disfavored areas are represented by yellow polyhedra. (b) Electrostatic contour plots: positive charge favored areas are represented by red polyhedra, and positive charge disfavored areas are represented by blue polyhedra.

As shown in the steric field contour map (Figure 3a), the green contour surrounding the *meta* position of the benzene ring indicates that a bulky group would be favorable for higher fungicidal activity, while the yellow contour represents the region of unfavorable steric effect. For example, compounds **4k** and **4d** bearing bulkier substituents at the *meta* position displayed higher fungicidal activity. For the electrostatic contour map (Figure 3b), the negatively charged favorable red regions are observed at the *meta* position of the benzene ring, indicating that electron-withdrawing substituents enhance the bioactivity, whereas a positively charged blue region around the *para* position is favored. Compound **4o** (*para* position)

DOI: 10.1021/jf5052893
J. Agric. Food Chem. 2015, 63, 1370−1377

displayed higher activity than those of compounds **4m** (*ortho* position) and **4n** (*meta* position). Analysis of CoMFA contour plots revealed that substitutions at the *meta* position, the bulky groups, and electron-withdrawing groups (e.g., $-NO_2$ and $-Cl$) are favorable to increase the bioactivity.

The results obtained from 3D-QSAR provided reliable clues for mechanistic study and designing of optimized stilbene derivatives. On the basis of the *in vivo* bioassay and 3D-QSAR analysis, it can be concluded that the variances (substituted positions, electronic properties, and steric effects) among substituents (Ar) on stilbenes showed a significant relationship with fungicidal activity against the three fungi. Furthermore, considering that the bioassay of title compounds was evaluated *in vivo*, effects of metabolism and/or biotransformation within the plants or fungi may contribute to the significant variations in fungicidal potency. It is reported that the electron-withdrawing substituents of the phenyl moiety seem to enhance the potency, which may be related to the fact that they tend to retard mechanisms of oxidative metabolism occurring on (or close to) the benzene ring.[32] This assumption is consistent with the higher bioactivity of the title compounds with electron-withdrawing substituents at the *meta* position proposed by the 3D-QSAR analysis.

Discovery of phytopathogenic fungicidal agents with new modes of action and eco-friendly properties is of great importance for crop protection.[33] In the present study, 22 novel stilbene derivatives containing the 1,3,4-oxadiazole moiety and trimethoxybenzene were designed and synthesized. The approach was proven to be an efficient method to implement structural modification by combination of several functional fragments. Bioassay results indicated that compounds **4b**, **4d**, **4i**, **4k**, and **4l** exhibited broad spectrum fungicidal activities *in vivo* against all tested fungi, some of which were comparable to the commercial fungicides. Further field evaluations on their biological efficacies as well as crop toxicities and safety are necessary before they can be developed as fungicide candidates.

■ ASSOCIATED CONTENT

Ⓢ Supporting Information

General procedures for the preparation of key intermediates **1**−**3** and general synthetic procedures for title compounds **4a**−**4v**. This material is available free of charge via the Internet at http://pubs.acs.org.

■ AUTHOR INFORMATION

Corresponding Author

*Telephone/Fax: +86-20-8711-0234. E-mail: cehdh@scut.edu.cn or he16221@163.com.

Funding

This work was financially supported by the Fundamental Research Funds for the Central Universities (2012ZM0035) and the Guangdong Provincial Natural Science Foundation (04300531).

Notes

The authors declare no competing financial interest.

■ REFERENCES

(1) Keinath, A. P.; Holmes, G. J.; Everts, K. L.; Egel, D. S.; Langston, D. B. Evaluation of combinations of chlorothalonil with azoxystrobin, harpin, and disease forecasting for control of downy mildew and gummy stem blight on melon. *Crop Prot.* **2007**, *26*, 83−88.

(2) Lebeda, A.; Cohen, Y. Cucurbit downy mildew (*Pseudoperonospora cubensis*)—Biology, ecology, epidemiology, host-pathogen interaction and control. *Eur. J. Plant Pathol.* **2010**, *129*, 157−192.

(3) Kuan, C. P.; Wu, M. T.; Huang, H. C.; Chang, H. Rapid detection of *Colletotrichum lagenarium*, causal agent of anthracnose of cucurbitaceous crops, by PCR and real-time PCR. *J. Phytopathol.* **2011**, *159*, 276−282.

(4) Zhao, X.; Ren, L.; Yin, H.; Zhou, J.; Han, J.; Luo, Y. Sensitivity of *Pseudoperonospora cubensis* to dimethomorph, metalaxyl and fosetyl-aluminium in Shanxi of China. *Crop Prot.* **2013**, *43*, 38−44.

(5) Chen, Y.; Dai, G. Antifungal activity of plant extracts against *Colletotrichum lagenarium*, the causal agent of anthracnose in cucumber. *J. Sci. Food Agric.* **2012**, *92*, 1937−1943.

(6) Gisi, U.; Sierotzki, H. Fungicide modes of action and resistance in downy mildews. *Eur. J. Plant Pathol.* **2008**, *122*, 157−167.

(7) Feng, J. T.; Wang, H.; Ren, S. X.; He, J.; Liu, Y.; Zhang, X. Synthesis and antifungal activities of carabrol ester derivatives. *J. Agric. Food Chem.* **2012**, *60*, 3817−3823.

(8) Newman, D. J.; Cragg, G. M. Natural products as sources of new drugs over the 30 years from 1981 to 2010. *J. Nat. Prod.* **2012**, *75*, 311−335.

(9) Albert, S.; Horbach, R.; Deising, H. B.; Siewert, B.; Csuk, R. Synthesis and antimicrobial activity of (*E*) stilbene derivatives. *Bioorg. Med. Chem.* **2011**, *19*, 5155−5166.

(10) Iriti, M.; Rossoni, M.; Borgo, M.; Faoro, F. Benzothiadiazole enhances resveratrol and anthocyanin biosynthesis in grapevine, meanwhile improving resistance to *Botrytis cinerea*. *J. Agric. Food Chem.* **2004**, *52*, 4406−4413.

(11) Langcake, P.; Pryce, R. J. A new class of phytoalexins from grapevines. *Experientia* **1977**, *33*, 151−152.

(12) Boulos, R. A.; Man, N. Y.; Lengkeek, N. A.; Hammer, K. A.; Foster, N. F.; Stemberger, N. A.; Skelton, B. W.; Wong, P. Y.; Martinac, B.; Riley, T. V.; McKinley, A. J.; Stewart, S. G. Inspiration from old dyes: Tris(stilbene) compounds as potent Gram-positive antibacterial agents. *Chem.—Eur. J.* **2013**, *19*, 17980−17988.

(13) Cantos, E.; Espin, J. C.; Tomas-Barberan, F. A. Postharvest stilbene-enrichment of red and white table grape varieties using UV-C irradiation pulses. *J. Agric. Food Chem.* **2002**, *50*, 6322−6329.

(14) Seppanen, S. K.; Syrjala, L.; von Weissenberg, K.; Teeri, T. H.; Paajanen, L.; Pappinen, A. Antifungal activity of stilbenes in in vitro bioassays and in transgenic *Populus* expressing a gene encoding pinosylvin synthase. *Plant Cell Rep.* **2004**, *22*, 584−593.

(15) Nopo-Olazabal, C.; Hubstenberger, J.; Nopo-Olazabal, L.; Medina-Bolivar, F. Antioxidant activity of selected stilbenoids and their bioproduction in hairy root cultures of muscadine grape (*Vitis rotundifolia* Michx.). *J. Agric. Food Chem.* **2013**, *61*, 11744−11758.

(16) Sobolev, V. S.; Khan, S. I.; Tabanca, N.; Wedge, D. E.; Manly, S. P.; Cutler, S. J.; Coy, M. R.; Becnel, J. J.; Neff, S. A.; Gloer, J. B. Biological activity of peanut (*Arachis hypogaea*) phytoalexins and selected natural and synthetic stilbenoids. *J. Agric. Food Chem.* **2011**, *59*, 1673−1682.

(17) Garcia, G. X.; Larsen, S. W.; Pye, C.; Galbreath, M.; Isovitsch, R.; Fradinger, E. A. The functional group on (*E*)-4,4′-disubstituted stilbenes influences toxicity and antioxidative activity in differentiated PC-12 cells. *Bioorg. Med. Chem. Lett.* **2013**, *23*, 6355−6359.

(18) Gaonkar, S. L.; Rai, K. M.; Prabhuswamy, B. Synthesis and antimicrobial studies of a new series of 2-[4-[2-(5-ethylpyridin-2-yl)ethoxy]phenyl]-5-substituted- 1,3,4-oxadiazoles. *Eur. J. Med. Chem.* **2006**, *41*, 841−846.

(19) Xu, W. M.; Han, F. F.; He, M.; Hu, D. Y.; He, J.; Yang, S.; Song, B. A. Inhibition of tobacco bacterial wilt with sulfone derivatives containing an 1,3,4-oxadiazole moiety. *J. Agric. Food Chem.* **2012**, *60*, 1036−1041.

(20) Chen, Q.; Zhu, X. L.; Jiang, L. L.; Liu, Z. M.; Yang, G. F. Synthesis, antifungal activity and CoMFA analysis of novel 1,2,4-triazolo[1,5-*a*]pyrimidine derivatives. *Eur. J. Med. Chem.* **2008**, *43*, 595−603.

(21) Zhang, M. Z.; Mulholland, N.; Beattie, D.; Irwin, D.; Gu, Y. C.; Chen, Q.; Yang, G. F.; Clough, J. Synthesis and antifungal activity of 3-(1,3,4-oxadiazol-5-yl)-indoles and 3-(1,3,4-oxadiazol-5-yl)methyl-indoles. *Eur. J. Med. Chem.* **2013**, *63*, 22−32.

DOI: 10.1021/jf5052893
J. Agric. Food Chem. 2015, 63, 1370−1377

(22) Shi, W.; Qian, X. H.; Zhang, R.; Song, G. H. Synthesis and quantitative structure-activity relationships of new 2,5-disubstituted-1,3,4-oxadiazoles. *J. Agric. Food Chem.* **2001**, *49*, 124−130.
(23) Akhter, M.; Husain, A.; Azad, B.; Ajmal, M. Aroylpropionic acid based 2,5-disubstituted-1,3,4-oxadiazoles: Synthesis and their anti-inflammatory and analgesic activities. *Eur. J. Med. Chem.* **2009**, *44*, 2372−2378.
(24) Zhang, S.; Luo, Y.; He, L. Q.; Liu, Z. J.; Jiang, A. Q.; Yang, Y. H.; Zhu, H. L. Synthesis, biological evaluation, and molecular docking studies of novel 1,3,4-oxadiazole derivatives possessing benzotriazole moiety as FAK inhibitors with anticancer activity. *Bioorg. Med. Chem.* **2013**, *21*, 3723−3729.
(25) Li, X. W.; He, D. H. Synthesis and optical properties of novel anthracene-based stilbene derivatives containing an 1,3,4-oxadiazole unit. *Dyes Pigm.* **2012**, *93*, 1422−1427.
(26) Tu, S.; Xu, L. H.; Ye, L. Y.; Wang, X.; Sha, Y.; Xiao, Z. Y. Synthesis and fungicidal activities of novel indene-substituted oxime ether strobilurins. *J. Agric. Food Chem.* **2008**, *56*, 5247−5253.
(27) Cui, Z. N.; Shi, Y. X.; Zhang, L.; Ling, Y.; Li, B. J.; Nishida, Y.; Yang, X. L. Synthesis and fungicidal activity of novel 2,5-disubstituted-1,3,4-oxadiazole derivatives. *J. Agric. Food Chem.* **2012**, *60*, 11649−11656.
(28) TRIPOS, Inc. *SYBYL Molecular Modeling Software Packages, Version 7.3.5*; TRIPOS, Inc.: St. Louis, MO, 2008.
(29) Zhu, Y. Q.; Wu, C.; Li, H. B.; Zou, X. M.; Si, X. K.; Hu, F. Z.; Yang, H. Z. Design, synthesis, and quantitative structure−activity relationship study of herbicidal analogues of pyrazolo[5,1-*d*][1,2,3,5]-tetrazin-4(3*H*)ones. *J. Agric. Food Chem.* **2007**, *55*, 1364−1369.
(30) Lu, H. X.; He, D. H. Asymmetric 1,3,4-oxadiazole derivatives containing naphthalene and stilbene units: Synthesis, optical and electrochemical properties. *Spectrochim. Acta, Part A* **2014**, *124*, 91−96.
(31) Golbraikh, A.; Tropsha, A. Beware of q^2! *J. Mol. Graphics Modell.* **2002**, *20*, 269−276.
(32) Li, M.; Liu, C. L.; Yang, J. C.; Zhang, J. B.; Li, Z. N.; Zhang, H.; Li, Z. M. Synthesis and biological activity of new (*E*)-α-(methoxyimino)benzeneacetate derivatives containing a substituted pyrazole ring. *J. Agric. Food Chem.* **2010**, *58*, 2664−2667.
(33) Qian, X. H.; Lee, P. W.; Cao, S. China: Forward to the green pesticides via a basic research program. *J. Agric. Food Chem.* **2010**, *58*, 2613−2623.

DOI: 10.1021/jf5052893
J. Agric. Food Chem. 2015, 63, 1370−1377

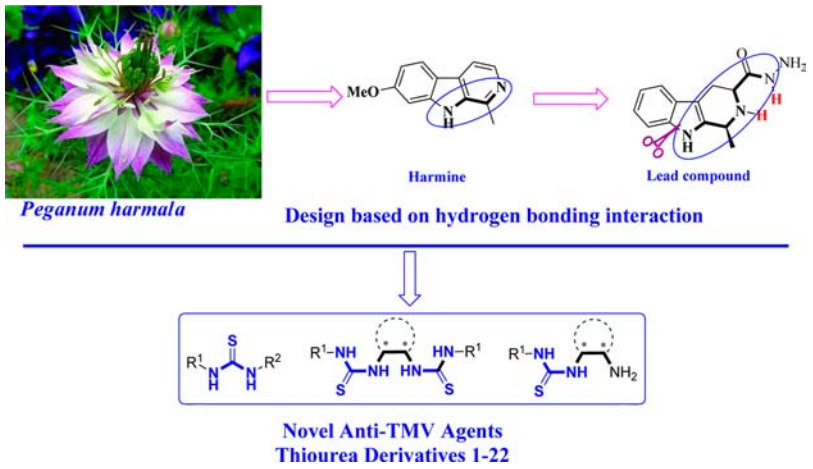

Figure 1. Design of Thiourea Derivatives.

confirmed and assessment for their anti-TMV was systematically evaluated.

MATERIALS AND METHODS

Instruments. The melting points of the products were determined on an X-4 binocular microscope (Gongyi Yuhua Instrument Co., China), and the thermometer was not corrected. NMR spectra were acquired with a Bruker 400 MHz (100 MHz for ^{13}C) instrument at room temperature. Chemical shifts were measured relative to residual solvent peaks of $CDCl_3$ (^1H, δ = 7.26 ppm; ^{13}C, δ = 77.0 ppm) or DMSO-d_6 (^1H, δ = 2.50 ppm; ^{13}C, δ = 39.5 ppm) with tetramethylsilane as internal standards. The following abbreviations were used to designate chemical shift multiplicities: s = singlet, d = doublet, t = triplet, m = multiplet, and bs = broad singlet. All first-order splitting patterns were assigned on the basis of multiplet appearance. Splitting patterns that could not be easily interpreted were designated multiplet (m) or broad (br). HRMS data were obtained with an FT-ICR MS spectrometer (Ionspec, 7.0 T). Analytical TLC was performed on silica gel GF 254. Column chromatographic purification was performed using silica gel. All reagents were of analytical reagent grade or chemically pure and purified prior to use when necessary. Compounds **18**–**22** (Figure 2) were prepared according to our previously reported procedure.[15] The isothiocyanates were prepared according to the literature (±) represented trans-mixture.[16]

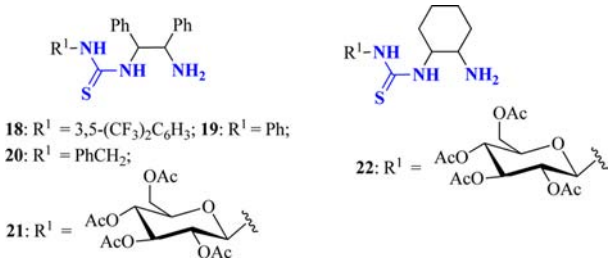

Figure 2. Chemical Structures of **18**–**22**.

General Experimental Procedures. *General Procedures for the Preparation of Compounds **1**–**8**, **13**–**17**, and **20**.*[17] To a mixture of CH_2Cl_2 (10 mL) and amines (5.0 mmol) was added the corresponding isothiocyanate (5.0 or 10 mmol), and the resulting mixture was stirred at room temperature until TLC indicated the reaction was complete. The reaction mixture was evaporated in vacuum. The pure products **1**–**8** and **13**–**17** were obtained by recrystallization from petroleum ether and ether. Compounds **20** were purified by chromatography on a column of silica gel with PE–EtOAc (v/v = 1:1).

*1,3-Diphenylthiourea (**1**).* White solid; yield, 99%; mp 144–145 °C (lit.[18] 140–142 °C). ^1H NMR (400 MHz, $CDCl_3$) δ 8.10 (s, 2H), 7.35–7.40 (m, 10H). ^{13}C NMR (100 MHz, $CDCl_3$) δ 179.8, 137.2, 129.6, 127.1, 125.3. HRMS (ESI) calcd for $C_{13}H_{12}N_2S$ $(M + H)^+$ 229.0794, found 229.0791.

*1,3-Dibenzylthiourea (**2**).* White solid; yield, 98%; mp 142–144 °C (lit.[19] 145–146 °C). ^1H NMR (400 MHz, $CDCl_3$) δ 7.28–7.34 (m, 6H), 7.02 (d, J = 6.8 Hz, 4H), 6.13 (br s, 2H), 4.61 (s, 4H). ^{13}C NMR (100 MHz, $CDCl_3$) δ 181.9, 136.6, 129.0, 128.0, 127.5, 48.6. HRMS (ESI) calcd for $C_{15}H_{16}N_2S$ $(M + H)^+$ 257.1107, found 257.1101.

*1,3-Dicyclohexylthiourea (**3**).* White solid; yield, 99%; mp 176–177 °C (lit.[18] 174–176 °C). ^1H NMR (400 MHz, $CDCl_3$) δ 5.64 (br s, 2H), 3.84 (s, 2H), 1.99–2.02 (m, 4H), 1.60–1.73 (m, 6H), 1.32–1.41 (m, 4H), 1.13–1.24 (m, 6H). ^{13}C NMR (100 MHz, $CDCl_3$) δ 179.0, 52.9, 32.9, 25.4, 24.7. HRMS (ESI) calcd for $C_{13}H_{24}N_2S$ $(M + H)^+$ 241.1733, found 241.1738.

*1-(3,5-Bis(trifluoromethyl)phenyl)-3-phenylthiourea (**4**).* White solid; yield, 99%; mp 135–136 °C (lit.[17] 141–143 °C). ^1H NMR (400 MHz, $CDCl_3$) δ 8.44 (s, 1H), 7.97 (s, 1H), 7.35 (s, 1H), 7.68 (s, 1H), 7.51 (t, J = 6.4 Hz, 2H), 7.40–7.42 (m, 1H), 7.32–7.34 (d, J = 6.8 Hz, 2H). ^{13}C NMR (100 MHz, $CDCl_3$) δ 179.8, 139.5, 135.5, 132.1 (J_{C-F} = 33.6 Hz), 130.6, 128.4, 125.6, 124.7 (J_{C-F} = 2.5 Hz), 124.3, and 121.6 (J_{C-F} = 271.1 Hz), 119.82 (m). HRMS (ESI) calcd for $C_{15}H_{10}F_6N_2S$ $(M + H)^+$ 365.0542, found 365.0546.

*1-(3,5-Bis(trifluoromethyl)phenyl)-3-cyclohexylthiourea (**5**).* White solid; yield, 100%; mp 159–160 °C (lit.[17] 164–165 °C). ^1H NMR (400 MHz, $CDCl_3$) δ 8.39 (s, 1H), 7.76 (s, 2H), 6.13 (s, 1H), 4.20 (s, 1H), 2.04–2.08 (m, 2H), 1.61–1.72 (m, 3H), 1.36–1.45 (m, 2H), 1.17–1.22 (m, 3H). ^{13}C NMR (100 MHz, $CDCl_3$) δ 178.9, 139.1, 132.7 (J_{C-F} = 34.7 Hz), 126.8, 124.1, and 121.4 (J_{C-F} = 271.4 Hz), 118.7, 53.9, 32.3, 25.2, 24.5. HRMS (ESI) calcd for $C_{15}H_{16}F_6N_2S$ $(M + H)^+$ 371.1011, found 371.1017.

*1-(3,5-Bis(trifluoromethyl)phenyl)-3-butylthiourea (**6**).* White solid; yield, 98%; mp 94–97 °C. ^1H NMR (400 MHz, $CDCl_3$) δ 7.76 (s, 2H), 7.70 (s, 1H), 7.60 (s, 1H), 6.13 (br s, 1H), 3.62 (s, 2H), 1.58–1.65 (m, 2H), 1.34 (m, 2H), 0.95 (t, J = 7.6 Hz, 3H). ^{13}C NMR (100 MHz, $CDCl_3$) δ 180.3, 139.1, 132.8 (J_{C-F} = 33.6 Hz), 126.8, 124.1, and 121.4 (J_{C-F} = 271.3 Hz), 118.7, 45.1, 30.7, 20.1, 13.6. HRMS (ESI) calcd for $C_{13}H_{14}F_6N_2S$ $(M + H)^+$ 345.0855, found 345.0852.

*1-(3,5-Bis(trifluoromethyl)phenyl)-3-(tert-butyl)thiourea (**7**).* White solid; yield, 98%; mp 160 °C (dec.). ^1H NMR (400 MHz, $CDCl_3$) δ 8.44 (br s, 1H), 7.77 (s, 2H), 7.72 (s, 1H), 6.13 (s, 1H), 1.55 (s, 9H). ^{13}C NMR (100 MHz, DMSO-d_6) δ 179.7, 142.4, 130.5 (J_{C-F} = 32.4 Hz), 127.8, 125.1, and 122.4 (J_{C-F} = 271.1 Hz), 119.7, 53.6, 28.7. HRMS (ESI) calcd for $C_{13}H_{14}F_6N_2S$ $(M + H)^+$ 345.0855, found 345.0853.

*1,3-Bis(3,5-bis(trifluoromethyl)phenyl)thiourea (**8**).* White solid; yield, 99%; mp 174–176 °C (lit.[20] 170–172 °C). ^1H NMR (400

DOI: 10.1021/jf505355r
J. Agric. Food Chem. 2015, 63, 1378–1384

Table 1. In Vitro Antiviral Activity of Compounds Ribavirin, Harmine, Ningnanmycin, Lead Compound, and 1−22 against TMV

Compd	Concn (μg/mL)	Inhibition rate (%)[a]	compd	Concn (μg/mL)	Inhibition rate (%)[a]
1	500	45±1	(*S*,*S*)-**16**	500	36±1
	100	10±1		100	8±2
2	500	32±2	(±)-**16**	500	41±2
	100	10±2		100	16±1
3	500	18±1	(*R*,*R*)-**17**	500	42±2
	100	0		100	16±1
4	500	45±2	(*R*,*R*)-**18**	500	57±2
	100	5±1		100	29±1
5	500	56±2	(*S*,*S*)-**18**	500	51±1
	100	17±1		100	22±2
6	500	32±2	(±)-**18**	500	53±1
	100	9±1		100	25±2
7	500	45±1	(±)-**19**	500	57±1
	100	10±2		100	23±2
8	500	51±2	(*R*,*R*)-**20**	500	75±2
	100	32±2		100	39±2
9	500	36±1	(*S*,*S*)-**20**	500	70±1
	100	0		100	33±2
10	500	40±2	**(±)-20**	**500**	**73±2**
	100	6±1		**100**	**37±1**
11	500	44±2	(*R*,*R*)-**21**	500	44±2
	100	8±2		100	0
12	500	33±1	(*R*,*R*)-**22**	500	48±1
	100	0		100	13±1
13	500	56±2	**Lead**	500	50±2
	100	23±1	**compound**	100	21±1
14	500	37±1	**Harmine**	500	45±2
	100	15±1		100	20±1
15	500	40±1	**Ribavirin**	**500**	**41±2**
	100	8±1		**100**	**10±1**
(*R*,*R*)-**16**	500	46±2	**Ningnanmycin**	**500**	**61±1**
	100	18±2		**100**	**26±1**

[a]Average of three replicates; All results are expressed as mean ± SD.

MHz, DMSO-d_6) δ 10.65 (s, 2H), 8.21 (s, 4H), 7.85 (s, 2H). ^{13}C NMR (100 MHz, DMSO-d_6) δ 180.5, 141.2, 130.3 (J_{C-F} = 32.9 Hz), 124.4, 124.4, and 121.713 (J_{C-F} = 271.1 Hz), 117.5. HRMS (ESI) calcd for $C_{17}H_8F_{12}N_2S$ (M + H)$^+$ 501.0289, found 501.0293.

*1,1′-((1R,2R)-1,2-Diphenylethane-1,2-diyl)bis(3-phenylthiourea) (**13**).* White solid; yield, 100%; mp 179−181 °C (lit.[21] 198 °C); $[\alpha]_D^{20}$ = +63.2 (c = 0.5, $CHCl_3$). ^{1}H NMR (400 MHz, DMSO-d_6) δ 9.75 (s, 2H), 8.43 (s, 2H), 7.10−7.34 (m, 20H), 5.98 (s, 2H). ^{13}C NMR (100 MHz, DMSO-d_6) δ 180.9, 134.0, 139.6, 129.1, 128.6, 128.5, 127.7, 124.8, 123.5, 62.7. HRMS (ESI) calcd for $C_{28}H_{26}N_4S_2$ (M + H)$^+$ 483.1672, found 483.1669.

*1,1′-((1R,2R)-1,2-Diphenylethane-1,2-diyl)bis(3-benzylthiourea) (**14**).* White solid; yield, 100%; mp 195−196 °C; $[\alpha]_D^{20}$ = +75.4 (c = 0.1, $CHCl_3$). ^{1}H NMR (400 MHz, DMSO-d_6) δ 8.10 (s, 4H), 7.08−7.27 (m, 20H), 5.87 (s, 2H), 4.72 (s, 2H), 4.57 (s, 2H). ^{13}C NMR (100 MHz, DMSO-d_6) δ 182.6, 139.9, 139.0, 128.2, 128.0, 127.7, 127.2, 127.1, 126.8, 62.0, 47.1. HRMS (ESI) calcd for $C_{28}H_{26}N_4S_2$ (M + H)$^+$ 483.1672, found 483.1669.

*1,1′-((1R,2R)-1,2-Diphenylethane-1,2-diyl)bis(3-benzhydrylthiourea) (**15**).* White solid; yield, 93%; mp 109−111 °C; $[\alpha]_D^{20}$ = +84.2 (c = 0.5, $CHCl_3$). ^{1}H NMR (400 MHz, $CDCl_3$) δ 7.06−7.39 (m, 30H), 6.75 (br s, 6H), 5.86 (s, 2H). ^{13}C NMR (100 MHz, $CDCl_3$) δ 180.5, 140.5, 139.5, 137.7, 129.1, 128.4, 128.2, 128.0, 127.8, 127.7, 127.6, 127.1, 65.1, 62.2. HRMS (ESI) calcd for $C_{42}H_{38}N_4S_2$ (M + H)$^+$ 663.2611, found 663.2609.

*1,1′-((1R,2R)-1,2-Diphenylethane-1,2-diyl)bis(3-(3,5-bis(trifluoromethyl)phenyl)thiourea) ((1R,2R)-**16**).* White solid; yield, 92%; mp 192−194 °C (lit.[22] 194−196 °C); $[\alpha]_D^{20}$ = −50.7 (c = 0.5, $CHCl_3$). ^{1}H NMR (400 MHz, DMSO-d_6) δ 10.39 (s, 2H), 8.77 (s, 2H), 8.16 (s, 4H), 7.69 (s, 2H), 7.22−7.38 (m, 10H), 5.97 (s, 2H). ^{13}C NMR (100 MHz, DMSO-d_6) δ 180.2, 141.3, 138.4, 129.8−130.5 (m), 128.3, 128.1, 127.8, 127.6, 126.5, 124.3, 122.0, 121.5, 118.8, 116.0, 62.4. HRMS (ESI) calcd for $C_{32}H_{22}F_{12}N_4S_2$ (M + H)$^+$ 755.1167, found 755.1163.

*1,1′-((1R,2R)-Cyclohexane-1,2-diyl)bis(3-(3,5-bis(trifluoromethyl)-phenyl)thiourea) ((1R,2R)-**17**).* White solid; yield, 95%; mp 132−134 °C (lit.[23] 132−133 °C); $[\alpha]_D^{20}$ = −61.2 (c = 0.5, $CHCl_3$). ^{1}H NMR (400 MHz, DMSO-d_6) δ 10.15 (s, 2H), 8.18 (s, 6H), 7.71 (s, 2H), 4.35 (s, 2H), 2.20 (s, 2H), 1.72 (s, 2H), 1.31 (s, 4H). ^{13}C NMR (100 MHz, DMSO-d_6) δ 180.0, 141.6, 130.1 (J_{C-F} = 32.7 Hz), 127.2, 124.5, and 121.8 (J_{C-F} = 271.0 Hz), 119.1, 56.8, 31.1, 24.2. HRMS (ESI) calcd for $C_{24}H_{20}F_{12}N_4S_2$ (M + H)$^+$ 657.1011, found 657.1016.

*1-((1R,2R)-2-Amino-1,2-diphenylethyl)-3-benzylthiourea ((R,R)-**20**).* White solid; yield, 63%; mp 53−55 °C; $[\alpha]_D^{20}$ = +69.4 (c = 1.0, $CHCl_3$). ^{1}H NMR (400 MHz, $CDCl_3$) δ 7.42 (br s, 1H), 7.12−7.30 (m, 15H), 6.52 (br s, 1H), 5.09 (br s, 1H), 4.59−4.62 (m, 1H), 4.51 (dd, J = 5.2 and 15.2 Hz, 1H), 4.29 (d, J = 4.0 Hz, 1H), 1.50 (br s, 2H). ^{13}C NMR (100 MHz, $CDCl_3$) δ181.8, 141.9, 139.8, 137.2, 128.81, 128.76, 128.6, 127.67, 127.62, 127.4, 126.7, 126.4, 64.0, 60.2, 48.2. HRMS (ESI) calcd for $C_{22}H_{23}N_3S$ (M + H)$^+$ 362.1685, found 362.1684.

*1-((1S,2S)-2-Amino-1,2-diphenylethyl)-3-benzylthiourea ((S,S)-**20**).* White solid; yield, 65%; mp 52−54 °C; $[\alpha]_D^{20}$ = −69.7 (c = 1.0, $CHCl_3$) (lit.[24] $[\alpha]_D^{24}$ = −74.3 (c = 1.0, $CHCl_3$)). ^{1}H NMR (400 MHz,

DOI: 10.1021/jf505355r
J. Agric. Food Chem. 2015, 63, 1378−1384

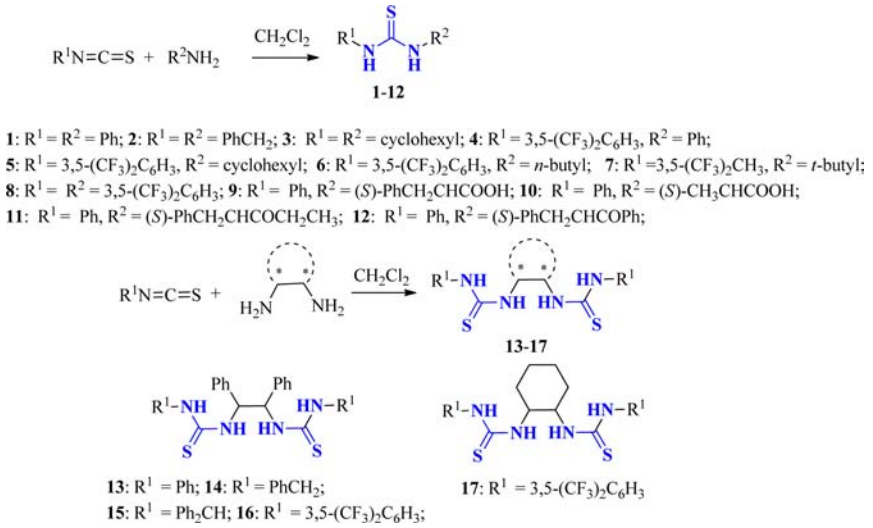

Figure 3. Synthesis of Thiourea Derivatives **1**−**17**.

$CDCl_3$) δ 7.47 (br s, 1H), 7.11−7.27 (m, 15H), 6.58 (br s, 1H), 5.12 (br s, 1H), 4.58−4.62 (m, 1H), 4.50 (dd, J = 4.8 and 14.8 Hz, 1H), 4.28 (d, J = 4.0 Hz, 1H), 1.66 (br s, 2H). ^{13}C NMR (100 MHz, $CDCl_3$) δ 181.8, 141.8, 139.7, 137.2, 128.82, 128.75, 128.6, 127.7, 127.6, 127.4, 126.7, 126.3, 63.9, 60.2, 48.3. HRMS (ESI) calcd for $C_{22}H_{23}N_3S$ $(M + H)^+$ 362.1685, found 362.1683.

General Procedures for the Preparation of Compounds ***9*****−*****12***.[25] In 100 mL three-neck flasks, isothiocyanatobenzene (20 mmol), amino acids or their derivatives (20 mmol), NaOH (22 mmol), water (20 mL), and THF (40 mL) were added and stirred at room temperature for 24 h. After completion of the reaction, the pH of the mixture was adjusted to pH 2−3 with aqueous 25% HCl, and then solvents were removed under vacuum. The remaining residue was recrystallized from absolute methanol to obtain the desired thiourea derivatives **9**−**12**.

*(S)-2-(3-Phenylthioureido)propanoic Acid (****9****).* White solid; yield, 75%; mp 173−175 °C; $[\alpha]_D^{20}$ = −44.2 (c = 0.5, CH_3OH). ^{1}H NMR (400 MHz, $CDCl_3$) δ 7.84 (br s, 1H), 7.46−7.53 (m, 3H), 7.32 (d, J = 8.0 Hz, 2H), 4.35 (q, J = 6.8 Hz, 1H), 1.59 (d, J = 6.8 Hz, 3H). ^{13}C NMR (100 MHz, $CDCl_3$) δ 183.5, 174.1, 132.5, 129.3, 129.2, 128.2, 55.5, 17.0. HRMS (ESI) calcd for $C_{10}H_{12}N_2O_2S$ $(M + H)^+$ 225.0692, found 225.0695.

*(S)-3-Phenyl-2-(3-phenylthioureido)propanoic Acid (****10****).* White solid; yield, 78%; mp 182−184 °C (lit.[25] 184−185 °C); $[\alpha]_D^{20}$ = −43.2 (c = 0.5, CH_3OH). ^{1}H NMR (400 MHz, $CDCl_3$) δ 7.70 (s, 1H), 7.42−7.47 (m, 3H), 7.33−7.39 (m, 3H), 7.26 (d, J = 6.8 Hz, 3H), 7.05 (d, J = 6.8 Hz, 2H), 4.53 (dd, J = 4.0 and 7.6 Hz, 1H), 3.34 (dd, J = 4.0 and 14.0 Hz, 1H), 3.11 (dd, J = 7.6 and 14.0 Hz, 1H). ^{13}C NMR (100 MHz, $CDCl_3$) δ 183.7, 172.9, 133.9, 132.4, 129.7, 129.4, 129.2, 128.2, 127.8, 60.9, 37.4. HRMS (ESI) calcd for $C_{16}H_{16}N_2O_2S$ $(M + H)^+$ 301.1005, found 301.1004.

*(S)-1-(3-Oxo-1-phenylpentan-2-yl)-3-phenylthiourea (****11****).* White solid; yield, 65%; mp 152−154 °C; $[\alpha]_D^{20}$ = −55.0 (c = 0.1, CH_3OH). ^{1}H NMR (400 MHz, DMSO-d_6) δ 8.79 (s, 1H), 7.27−7.39 (m, 10H), 6.68 (s, 1H), 4.06 (t, J = 6.4 Hz, 1H), 3.04−3.07 (m, 1H), 2.89−2.94 (m, 1H), 1.03−1.10 (m, 1H), 0.57 (t, J = 7.2 Hz, 3H). ^{13}C NMR (100 MHz, DMSO-d_6) δ 180.8, 137.8, 137.4, 129.9, 129.4, 128.1, 128.0, 127.0, 126.2, 94.4, 61.2, 34.7, 29.6, 8.0. HRMS (ESI) calcd for $C_{18}H_{20}N_2OS$ $(M + H)^+$ 313.1369, found 313.1368.

*(S)-1-(1-Oxo-1,3-Diphenylpropan-2-yl)-3-phenylthiourea (****12****).* White solid; yield, 68%; mp 152−154 °C; $[\alpha]_D^{20}$ = −58.2 (c = 0.1, CH_3OH). ^{1}H NMR (400 MHz, DMSO-d_6) δ 9.13 (s, 1H), 7.53 (s, 1H), 7.06−7.30 (m, 15H), 4.31 (t, J = 7.2 Hz, 1H), 2.95−3.10 (m, 2H). ^{13}C NMR (100 MHz, DMSO-d_6) δ 181.1, 140.7, 137.9, 137.1, 129.5, 129.1, 128.7, 127.8, 127.6, 127.4, 126.7, 126.4, 125.9, 94.7, 67.9, 33.8. HRMS (ESI) calcd for $C_{22}H_{20}N_2OS$ $(M + H)^+$ 361.1369, found 361.1367.

Antiviral Biological Assay. The procedure of purifying TMV and the method to test the anti-TMV activity of the thiourea derivatives were the same with those reported previously in the literature.[26]

Purification of Tobacco Mosaic Virus. The upper leaves of *Nicotiana tabacum* L. inoculated with TMV were selected and ground in phosphate buffer and then filtered through a double-layer pledget. The filtrate was centrifuged at 10000*g*, treated with PEG twice, and centrifuged again. The whole experiment was processed at 4 °C. Absorbance value was estimated at 260 nm by ultraviolet spectrophotometer.

$$\text{virus concn} = (A_{260} \times \text{dilution ratio}) E^{0.1\%,260\text{nm}}_{1\text{cm}}$$

Antiviral Activity of Compounds against TMV in Vitro. Fresh leaf of the 5−6 growth stage of tobacco inoculated by the juice-leaf rubbing method (concentration of TMV is 5.88 × 10^{-2} μg/mL) was cut into halves along the main vein. The halves were immersed into the solution of different concentrations (see Table 1) of the compounds and double distilled water for 20 min, respectively, and then cultured at 25 °C for 72 h. Every concentration for each compound was replicated at least three times.

Protective Effect of Compounds against TMV in Vivo. The compound solution was smeared on the left side and the solvent serving as control on the right side of growing *N. tabacum* L. leaves of the same ages. The leaves were then inoculated with the virus after 12 h. A brush was dipped in TMV of 6 × 10^{-3} mg/mL to inoculate the leaves, which were previously scattered with silicon carbide. The leaves were then washed with water and rubbed softly along the nervature once or twice. The local lesion numbers appearing 3−4 days after inoculation were counted. There are three replicates for each compound.

Inactivation Effect of Compounds against TMV in Vivo. The virus was inhibited by mixing with the compound solution at the same volume for 30 min. The mixture was then inoculated on the left side of the leaves of *N. tabacum* L., whereas the right side of the leaves was inoculated with the mixture of solvent and the virus for control. The local lesion numbers were recorded 3−4 days after inoculation. There are three replicates for each compound.

Curative Effect of Compounds against TMV in Vivo. Growing leaves of *N. tabacum* L. of the same ages were selected. TMV (concentration of 6.0 × 10^{-3} mg/mL) was dipped and inoculated on the whole leaves. Then the leaves were washed with water and dried. The compound solution was smeared on the left side, and the solvent was smeared on the right side for control. The local lesion numbers were then counted and recorded 3−4 days after inoculation. There are three replicates for each compound. The in vitro and in vivo inhibition rates of the compound were then calculated according to the following formula ("av" means average, and controls were not treated with

DOI: 10.1021/jf505355r
J. Agric. Food Chem. 2015, 63, 1378−1384

Table 2. In Vivo Antiviral Activity of Compounds Ribavirin, Harmine, Ningnanmycin, Lead Compound, and 1−22 against TMV

Compd	Concn (μg/mL)	Inactivation effect (%)[a]	Curative effect (%)[a]	Protection effect (%)[a]	Compd	Concn (μg/mL)	Inactivation effect (%)[a]	Curative effect (%)[a]	Protection effect (%)[a]
1	500	50±1	42±2	40±1	(*S*,*S*)-**16**	500	40±1	46±3	43±1
	100	18±3	13±1	15±1		100	19±1	20±1	13±1
2	500	36±1	43±3	40±1	(±)-**16**	500	46±2	48±1	49±2
	100	9±1	18±2	18±1		100	20±1	21±1	19±1
3	500	17±2	24±1	27±2	(*R*,*R*)-**17**	500	49±2	47±2	50±1
	100	0	0	0		100	16±2	18±2	19±1
4	500	49±1	41±2	42±1	(*R*,*R*)-**18**	500	**57**±1	**55**±1	**60**±1
	100	18±1	12±1	15±1		100	24±2	29±2	27±2
5	500	59±1	53±3	50±1	(*S*,*S*)-**18**	500	55±1	50±1	53±2
	100	20±1	28±1	24±1		100	19±2	25±2	21±2
6	500	38±2	43±1	35±2	(±)-**18**	500	56±2	53±2	58±1
	100	15±1	10±1	9±1		100	22±2	26±2	26±2
7	500	43±2	41±2	39±1	(±)-**19**	500	**61±2**	**63±1**	**61±2**
	100	18±1	11±1	16±1		100	27±1	32±2	26±1
8	500	**60**±1	**56**±1	**58**±1	(*R*,*R*)-**20**	500	**71±2**	**73±1**	**69±2**
	100	25±2	22±2	28±1		100	35±1	37±2	33±1
9	500	49±1	41±1	34±2	(*S*,*S*)-**20**	500	66±2	70±1	64±1
	100	12±1	17±1	11±1		100	29±1	30±2	31±2
10	500	46±2	47±2	42±1	(±)-**20**	500	69±2	70±1	68±2
	100	24±1	23±1	21±1		100	31±1	35±1	33±1
11	500	48±2	49±1	46±2	(*R*,*R*)-**21**	500	44±1	48±1	48±1
	100	13±1	20±2	15±1		100	19±2	18±2	20±1
12	500	41±2	36±1	37±2	(*R*,*R*)-**22**	500	45±1	50±1	48±2
	100	0	9±1	14±1		100	14±2	19±2	22±1
13	500	**58**±1	**61**±2	**60**±1	**Lead**	500	46±2	48±2	50±1
	100	26±1	30±1	24±1	**compound**	100	17±1	20±2	23±1
14	500	33±1	30±3	40±1	**Harmine**	500	41±1	39±1	42±2
	100	0	0	10±2		100	11±1	16±2	16±1
15	500	41±2	47±1	50±2	**Ribavirin**	500	31±2	39±2	47±1
	100	13±2	21±1	20±1		100	12±1	18±2	17±1
(*R*,*R*)-**16**	500	53±1	49±2	54±1	**Ningnanmy**	500	63±2	54±1	64±2
	100	25±1	23±1	20±1	**cin**	100	28±1	22±1	26±1

[a]Average of three replicates; All results are expressed as mean ± SD.

compound). Inhibition rate (%) = [(av local lesion no. of control − av local lesion no. of drug-treated)/av local lesion no. of control] × 100%.

RESULTS AND DISCUSSION

Chemistry. *Synthesis of the Compounds 1−17.* Compounds **1**−**17** were synthesized according to procedures in Figure 3. Amines were reacted with corresponding isothiocyanate to give thioureas **1**−**8** and **13**−**17** in almost quantitatively yields. Compounds **9**−**12** were obtained from isothiocyanatobenzene and amino acids or their derivatives in the presence of NaOH in good yields.

Phytotoxic Activity. Compounds **1**−**22** were first tested for their phytotoxic activity against the test plant.[27] The results indicated that compounds **1**−**22** showed no phytotoxic activity at 500 μg/mL.

Antiviral Activity. The anti-TMV activity of compounds **1**−**22** was tested. The commercial plant virucide Ningnanmycin, perhaps the most successful registered antiplant viral agent, ribavirin, natural product harmine, and lead compound were used as the controls.

In Vitro Anti-TMV Activity. The in vitro antiviral assay results of the synthesized compounds are listed in Table 1. As the control, ribavirin exhibited a 41% inhibitory effect at 500 μg/mL, whereas most of the synthesized compounds **1**−**22** exhibited higher antiviral activity than ribavirin even at the concentration of 100 μg/mL. The optimal compound (*R*,*R*)-**20** exhibited significantly higher inhibitory effect than Ningnanmycin, harmine, and lead compound, emerging as a new lead compound for anti-TMV research. To investigate the influence of the hydrogen bond strength on the anti-TMV activity, compounds **1**, **4**, and **8** were tested. Thiourea **8** with the stronger hydrogen bond did show the best inhibitory effect (inhibitory effect: **8** > **1** ≈ **4**). For studying the influence of the steric effect, thioureas **4**−**7** were synthesized. Compounds **4**−**7** exhibited 45%, 56%, 32%, and 45% inhibitory effect at 500 μg/mL, respectively. Comparing the results of **4**−**7**, the anti-TMV activity was improved by increasing steric hindrance of the thiourea.

Compounds **9**−**12** were prepared from isothiocyanatobenzene and natural amino acids or their derivatives. Compound **11** showed the best in vitro anti-TMV activity among them with 44% inhibitory effect.

Bis-thiourea-type derivatives **13**−**17** displayed in vitro activity ranging from 37% to 56% against TMV at 500 μg/mL. Among them, (*R*,*R*)-**16**, bearing 1,2-diphenylethylenediamine skeleton showed higher activity than (*R*,*R*)-**17** containing 1,2-cyclohexanediamine (46% and 42%, respectively). Compound **13** afforded a good result with an inhibitory rate of 56%. All of primary amine thioureas **18**−**22** exhibited

DOI: 10.1021/jf505355r
J. Agric. Food Chem. 2015, 63, 1378−1384

much higher activity than ribavirin, harmine, and lead compound. Compounds **20** exhibited the best result with an inhibitory rate of >70%. The optical pure compounds **16**, **18**, and **20** were prepared to investigate the effect of configuration on antiviral activity. (*R*,*R*)-Configuration is confirmed to be the optimal in vitro antiviral configuration (inhibitory effect: (*R*,*R*)-**16** > (±)-**16** > (*S*,*S*)-**16**; (*R*,*R*)-**18** > (±)-**18** > (*S*,*S*)-**18**; (*R*,*R*)-**20** > (±)-**20** > (*S*,*S*)-**20**).

As shown in Table 1, most of the compounds **1**−**22** displayed good in vitro activity against TMV. Therefore, these compounds were bioassayed further to investigate their antiviral activity in vivo.

In Vivo Anti-TMV Activity. As shown in Table 2, most of the compounds also displayed higher in vivo activity than that of the Ribavirin. (*R*,*R*)-**20** showed the best result in vivo anti-TMV activity (inactivation activity, 71%/500 μg/mL and 35%/100 μg/mL; curative activity, 73%/500 μg/mL and 37%/100 μg/mL; protection activity, 69%/500 μg/mL and 33%/100 μg/mL), which is significantly higher than that of ribavirin (inactivation activity, 31%/500 μg/mL and 12%/100 μg/mL; curative activity, 39%/500 μg/mL and 18%/100 μg/mL; protection activity, 47%/500 μg/mL and 17%/100 μg/mL) and Ningnanmycin (inactivation activity, 63%/500 μg/mL and 28%/100 μg/mL; curative activity, 54%/500 μg/mL and 22%/100 μg/mL; protection activity, 64%/500 μg/mL and 26%/100 μg/mL).

Just as with the antiviral activity in vitro, compounds **1**−**8** displayed moderate to good in vivo activity, and the results disclosed that the anti-TMV activity related to the hydrogen bond strength and steric effect in molecules. Thiourea **8**, bearing bis-3,5-Bis(trifluoromethyl)phenyl, gave relatively higher activity (60%, 56%, and 58% at 500 μg/mL) than that of **1**−**7**.

Chiral thiourea derivatives **9**−**12** showed moderate antiviral activity ranging from 34%−49% against TMV at 500 μg/mL, and different activity patterns displayed different activity rule (inactivation activity, **9** > **11** > **10** > **12**; curative activity, **11** > **10**> **9** > **12**; protection activity, **11** > **10** > **12** > **9**).

The bis-thiourea derivatives showed relatively lower activity than corresponding single thiourea derivatives (in vivo activity, **19** > **13**; **20** > **14**; **18** > **16**), which indicated that the hydrogen bond is important but not the more the better. All of primary amine thioureas **18**−**22** exhibited much higher in vivo activity than ribavirin, harmine, and lead compound, especially for compounds **20**.

In summary, on the basis of the structures of natural product harmine and lead compound, a series of simple thiourea derivatives were designed and synthesized from amines in one step. The antiviral activity of these compounds were evaluated in vitro and in vivo. Most of them exhibited significantly higher antiviral activity against TMV than commercial plant virucide ribavirin. The optimal compound (*R*,*R*)-**20** showed excellent anti-TMV activity in vitro and in vivo (in vitro activity, 75%/500 μg/mL and 39%/100 μg/mL; inactivation activity, 71%/500 μg/mL and 35%/100 μg/mL; curative activity, 73%/500 μg/mL and 37%/100 μg/mL; protection activity, 69%/500 μg/mL and 33%/100 μg/mL), which is significantly higher than that of ribavirin, Ningnanmycin, harmine, and lead compound. The hydrogen bond is favorable for antiviral activity within a certain range but not the more the better. Present study provides fundamental support for development and optimization of these simple thiourea derivatives as potential inhibitors of plant virus. Further studies on structural optimization and mode of action are currently underway in our laboratories.

■ ASSOCIATED CONTENT

Ⓢ Supporting Information

^{1}H and ^{13}C NMR spectra of compounds **1**−**17** and **20**. This material is available free of charge via the Internet at http://pubs.acs.org.

■ AUTHOR INFORMATION

Corresponding Authors

*For A.L.: phone, 0086-22-60302241 ext 205; fax, 0086-22-60204274; E-mail, luaidang@hebut.edu.cn.

*For Z.W.: phone, 0086-22-23503792; fax, 0086-22-23503792; E-mail, wangziwen2725@163.com.

*forQ.W.: phone, 0086-22-23503952; fax, 0086-22-23503952; E-mail, wangqm@nankai.edu.cn.

Funding

This study was supported by Natural Science Fund of China (21302038, 21402142, 21132003), Natural Science Fund of Hebei Province (B2013202237), and PCSIRT (IRT1059).

Notes

The authors declare no competing financial interest.

■ REFERENCES

(1) Song, B. A.; Yang, S.; Jin, L. H.; Bhadury, P. S. *Environment-Friendly Anti-plant Viral Agents*; Chemical Industry Press (Beijing) & Springer Press: Beijing, 2009; pp 1−305.

(2) Qian, X. H.; Lee, P. W.; Cao, S. China: Forward to the green pesticides via a basic research program. *J. Agric. Food. Chem.* **2010**, *58*, 2613−2623.

(3) Song, H. J.; Liu, Y. X.; Liu, Y. X.; Huang, Y. Q.; Li, Y. Q.; Wang, Q. M. Design, synthesis, anti-TMV, fungicidal, and insecticidal activity evaluation of 1,2,3,4-tetrahydro-b-carboline-3-carboxylic acid derivatives based on virus inhibitors of plant sources. *Bioorg. Med. Chem. Lett.* **2014**, *24*, 5228−5233.

(4) Venkatachalam, T. K.; Vassilev, A. O.; Benyunov, A.; Grigoriants, O. O.; Tibbles, H. E.; Uckun, F. M. Stereochemistry as a determinant of the anti-leukemic potency of halopyridyl and thiazolyl thiourea compounds. *Lett. Drug Des. Discovery* **2007**, *4*, 318−326.

(5) Venkatachalam, T. K.; Sudbeck, E. A.; Mao, C.; Uckun, F. M. Stereochemistry of halopyridyl and thiazolyl thiourea compounds is a major determinant of their potency as nonnucleoside inhibitors of HIV-1 reverse transcriptase. *Bioorg. Med. Chem. Lett.* **2000**, *10*, 2071−2074.

(6) Venkatachalam, T. K.; Mao, C.; Uckun, F. A. Effect of stereo and regiochemistry towards wild and multidrug resistant HIV-1 virus: viral potency of chiral PETT derivatives. *Biochem. Pharmacol.* **2004**, *67*, 1933−1946.

(7) Zou, X. J.; Jin, G. Y.; Yang, Z. Synthesis of the thiosemicarbazides of 1-ary-1,4-dihydro-3-carboxy-6-methyl-4-pyridazinone and their antiviral activity against TMV. *Chem. J. Chin. Univ.* **2002**, *23*, 403−406.

(8) Zang, H. J.; Li, Z. M.; Yang, Y. H.; Zhao, W. G.; Wang, S. H. Synthesis and bioactivity of *N*-(2-methoxylcarbonyl-1-methyl)-ethyl-(*N*′-D-acetyl-pyranosyl)-thiourea. *Chin. J. Appl. Chem.* **2006**, *23*, 242−245.

(9) (a) Chen, M.; Chen, Z.; Song, B.; Bhadury, S. P.; Yang, S.; Cai, X.; Hu, D.; Xue, W.; Zeng, S. Synthesis and antiviral activities of chiral thiourea derivatives containing an α-aminophosphonate moiety. *J. Agric. Food Chem.* **2009**, *57*, 1383−1388. (b) Yan, Z.; Cai, X.; Yang, X.; Song, B.; Chen, Z.; Bhadury, S. P.; Hu, D.; Jin, L.; Xue, W.; Lu, P. Synthesis and antiviral activities of chiral thiourea derivatives. *Chin. J. Chem.* **2009**, *27*, 593−601. (c) Yang, X.; Song, B.; Jin, L.; Wei, X.; Bhadury, S. P.; Li, X.; Yang, S.; Hu, D. Synthesis and antiviral bioactivities of novel chiral bis-thiourea-type derivatives containing α-aminophosphonate moiety. *Sci. China Chem.* **2011**, *54*, 103−109.

DOI: 10.1021/jf505355r
J. Agric. Food Chem. 2015, 63, 1378−1384

(10) Liu, J.; Yang, S.; Li, X.; Fan, H.; Bhadury, S. P.; Xu, W.; Wu, J.; Wang, Z. Synthesis and antiviral bioactivity of chiral thioureas containing leucine and phosphonate moieties. *Molecules* **2010**, *15*, 5112−5123.
(11) Xu, W. P.; Zhang, D. Q.; Li, R. X.; Yang, X. L.; Wang, D. Q.; Yuan, D. K.; Fan, Z. J. Synthesis and anti-TMV activity of novel poly-substituted pyridine-5-amino amide and aryl(thio)urea derivatives. *Chem. J. Chin. Univ.* **2011**, *32*, 1545−1550.
(12) (a) Zhao, P. L.; Wang, L.; Zhu, X. L.; Huang, X. Q.; Zhan, C. G.; Wu, J. W.; Yang, G. F. Subnanomolar inhibitor of cytochrome bc_1 complex designed by optimizing interaction with conformationally flexible residues. *J. Am. Chem. Soc.* **2010**, *132*, 185−194. (b) Hao, G. F.; Wang, F.; Li, H.; Zhu, X. L.; Yang, W. C.; Huang, L. S.; Wu, J. W.; Berry, E. A.; Yang, G. F. Computational discovery of picomolar Q_o site inhibitors of cytochrome bc_1 complex. *J. Am. Chem. Soc.* **2012**, *134*, 11168−11176.
(13) (a) Wang, C. G.; Zhou, Z. H.; Tang, C. C. Novel bifunctional chiral thiourea catalyzed highly enantioselective aza-Henry reaction. *Org. Lett.* **2008**, *10*, 1707−1710. (b) Gao, P.; Wang, C. G.; Wu, Y.; Zhou, Z. H.; Tang, C. C. Sugar-derived bifunctional thiourea organocatalyzed asymmetric Michael addition of acetylacetone to nitroolefins. *Eur. J. Org. Chem.* **2008**, 4563−4566. (c) Lu, A. D.; Gao, P.; Wu, Y.; Wang, Y. M.; Zhou, Z. H.; Tang, C. C. Highly enantio- and diastereoselective Michael addition of cyclohexanone to nitroolefins catalyzed by chiral glucose-based bifunctional secondary amine-thiourea catalyst. *Org. Biomol. Chem.* **2009**, *7*, 3141−3147.
(14) (a) Stanley, W. M.; Loring, H. S. The isolation of crystalline tobacco mosaic virus protein from diseased tomato plants. *Science* **1936**, *83*, 85. (b) Stanley, W. M.; Lauffer, M. A. Disintegration of tobacco mosaic virus in urea solutions. *Science* **1939**, *89*, 345−347. (c) Creager, A. N.; Morgan, G. J. After the double helix: Rosalind Franklin's research on Tobacco mosaic virus. *Isis* June **2008**, *99*, 239−272.
(15) Lu, A.; Hu, K.; Wang, Y.; Song, H.; Zhou, Z.; Fang, J.; Tang, C. Enantioselective synthesis of *trans*-dihydrobenzofurans via primary amine-thiourea organocatalyzed intramolecular Michael addition. *J. Org. Chem.* **2012**, *77*, 6208−6214.
(16) Munch, H.; Hansen, J. S.; Pittelkow, M.; Christensen, J. B.; Boas, U. A new efficient synthesis of isothiocyanates from amines using di-*tert*-butyl dicarbonate. *Tetrahedron Lett.* **2008**, *49*, 3117−3119.
(17) Natarajan, A.; Guo, Y.; Arthanari, H.; Wagner, G.; Halperin, J. A.; Chorev, M. Synthetic studies toward aryl-(4-aryl-4*H*-[1,2,4]-triazole-3-yl)-amine from 1,3-diarylthiourea as urea mimetics. *J. Org. Chem.* **2005**, *70*, 6362−6368.
(18) Wang, F.; Zhao, P.; Xi, C. Copper-catalyzed one-pot synthesis of 2-thioxo-2,3-dihydroquinazolin-4(1*H*)-ones from *ortho*-bromobenzamides and isothiocyanates. *Tetrahedron Lett.* **2011**, *52*, 231−235.
(19) Hisaki, I.; Sasaki, S.; Hirose, K.; Tobe, Y. Synthesis and anion-selective complexation of homobenzylic tripodal thiourea derivatives. *Eur. J. Org. Chem.* **2007**, *2007*, 607−615.
(20) Busschaert, N.; Kirby, I. L.; Young, S.; Coles, S. J.; Horton, P. N.; Light, M. E.; Gale, P. A. Squaramides as potent transmembrane anion transporters. *Angew. Chem., Int. Ed.* **2012**, *51*, 4426−4430.
(21) Touchard, F. O.; Fache, F.; Lemaire, M. Thioureas: new ligands for the metal catalyzed asymmetric reduction of carbonyl compounds. Tetrahedron. *Asymmetry* **1997**, *8*, 3319−3326.
(22) Zhang, Y.; Liu, Y.; Kang, T.; Hu, Z.; Chen, Y. Organocatalytic enantioselective Mannich-type reaction of phosphorus ylides: Synthesis of chiral *N*-Boc-α-amino-γ-methylene carboxylic esters. *J. Am. Chem. Soc.* **2008**, *130*, 2456−2457.
(23) Sohtome, Y.; Tanatani, A.; Hashimoto, Y.; Nagasawa, K. Development of bis-thiourea-type organocatalyst for asymmetric Baylis−Hillman reaction. *Tetrahedron Lett.* **2004**, *45*, 5589−5592.
(24) Isobe, T.; Fukuda, K.; Tokunaga, T.; Seki, H.; Yamaguchi, K.; Ishikawa, T. Modified guanidines as potential chiral superbases. 2. preparation of 1,3-unsubstituted and 1-substituted 2-iminoimidazolidine derivatives and a related guanidine by the 2-chloro-1,3-dimethylimidazolinium chloride-Induced cyclization of thioureas. *J. Org. Chem.* **2000**, *65*, 7774−7778.
(25) Xu, D.; Yue, H.; Luo, S.; Xia, A.; Zhang, S.; Xu, Z. A chiral thioureido acid as an effective additive for enantioselective organocatalytic Michael additions of nitroolefins. *Org. Biomol. Chem.* **2008**, *6*, 2054−2057.
(26) Wang, Z. W.; Wei, P.; Wang, L. Z.; Wang, Q. M. Design, synthesis, and anti-tobacco mosaic virus (TMV) activity of phenanthroindolizidines and their analogues. *J. Agric. Food Chem.* **2012**, *60*, 10212−10219.
(27) Wang, Z. W.; Feng, A.; Cui, M.; Liu, Y.; Wang, L.; Wang, Q. M. First discovery and structure−activity relationship study of phenanthroquinolizidines as novel antiviral agents against tobacco mosaic virus (TMV). *PLoS One* **2012**, *7*, e52933.

DOI: 10.1021/jf505355r
J. Agric. Food Chem. 2015, 63, 1378−1384

popular vegetable in most parts of the world, and it enjoys considerable commercial interest.[30] The prevention or delay of postharvest degreening of broccoli has been addressed in various studies.[18,26] Surprisingly, the nature of the breakdown products of Chl in such a common vegetable is unknown. Identification of Chl-breakdown products may thus be of specific interest from a nutritional point of view, as some Chl-catabolites are suspected to possibly provide health benefits.[9] Earlier work from this group on naturally degreening leaves of spinach (*Spinacia oleracea*) has already addressed the question of the nature of Chl-catabolites in another vegetable.[31,32] As now reported here, we have analyzed degreened florets of broccoli and have identified three main Chl-catabolites in this vegetable, whose structures were elucidated.

MATERIALS AND METHODS

Chemicals and Plant Materials. *Chemicals.* Acetone and methylene chloride (CH_2Cl_2, reagent-grade, commercial) were distilled before use for extractions. HPLC grade HiPerSolv CHROMANORM methanol (MeOH) was from VWR PROLABO. Potassium dihydrogen phosphate and potassium phosphate dibasic anhydrous were from Sigma-Aldrich. Sep-Pak-C18 Cartridges were from Waters Associates. The pH values were measured with a WTW Sentix21 electrode connected to a WTW pH535 digital pH meter.

Plant Material. Fresh, green broccoli (*Brassica oleracea* var. *italica*), produced by Conzorzio APO-FOGGIA S.C., Italy, was typically harvested 5 days before it was sold at the store (Spar Supermarket) in Innsbruck.

Spectroscopy. UV/vis: Hitachi U3000 spectrophotometer, λ_{max} [nm] (relative ε), in H_2O. CD: Jasco J715 spectropolarimeter, λ_{max} and λ_{min} [nm] (Θ), in H_2O. ^1H nuclear magnetic resonance (NMR): Bruker UltraShield 600 MHz or Varian Unity Inova 500 MHz spectrometers, δ[ppm] with δ(HDO) = 4.79 ppm, in D_2O. Electrospray ionization mass spectrometry (ESI-MS): Finnigan MAT 95S, m/z (rel. intensity), positive-ion mode, 1.4 kV spray voltage; signals with >5% rel. intensity are listed.

High Performance Liquid Chromatography (HPLC). Dionex P680 HPLC pump, online UV/vis-spectra: Dionex UVD340U. Column: Phenomenex HyperClone 5 μ ODS 250 mm × 4.6 mm i.d., column at 20 °C, protected with a Phenomenex ODS 4 mm × 3.0 mm i.d. precolumn was used with a flow rate 0.5 mL·min^{-1}. Solvent A: 50 mM aqueous potassium phosphate buffer (pH 7). Solvent B: MeOH, HPLC grade; solvent composition 1:0−5 min, A/B = 80/20; 5−55 min, A/B = 80/20 to 30/70, constant gradient; 55−60 min, 30/70 to 0/100, constant gradient; 60−70 min, A/B = 0/100; 70−75 min:, A/B = 0/100 to 80/20, constant gradient. Analytical HPLC: sample size 50 μL. Semipreparative HPLC: sample size 2 mL.

Preparation and Storage of the Plant Material. Using freshly bought broccoli, green broccoli florets were separated from the stem, their weight was determined, and they were stored up to 6 days at room temperature (about 22 °C), either in the dark or in diffuse day light. On the day of the purchase and on the subsequent 6 days of storage, photographs of the broccoli florets documented their degreening (Figure 2). About 3−6% weight loss was determined at day 1 or day 6, respectively, presumably largely due to loss of water.

Analysis of Chlorophylls and Chlorophyll Catabolites in Senescent Broccoli. The content of Chl in extracts of broccoli florets was determined by an established UV/vis-analytical method.[33] The content of the Chl-catabolites was estimated by quantitative HPLC analysis of the extracts.

Analysis of Chlorophylls. The upper parts of broccoli florets (0.5−1.0 cm; i.e., typically 5−8 g, wet weight) were cut off and were stored for up to 6 days, either in darkness or exposed to diffuse day light. The fresh samples were collected in a mortar then suspended in 10 mL of acetone and ground at room temperature (reduced room light). The suspensions were filtered, and the remaining residues were extracted again with 10 mL of acetone. This procedure was repeated five times until the remaining plant material was practically colorless. Solvents were removed from the collected green filtrates using a rotary evaporator, and green residues were obtained. These were dissolved in 50 mL of a mixture of 80% acetone and 20% 10 mM aqueous ammonium acetate buffer (pH 7); Chl was determined by UV/vis spectroscopy.[33]

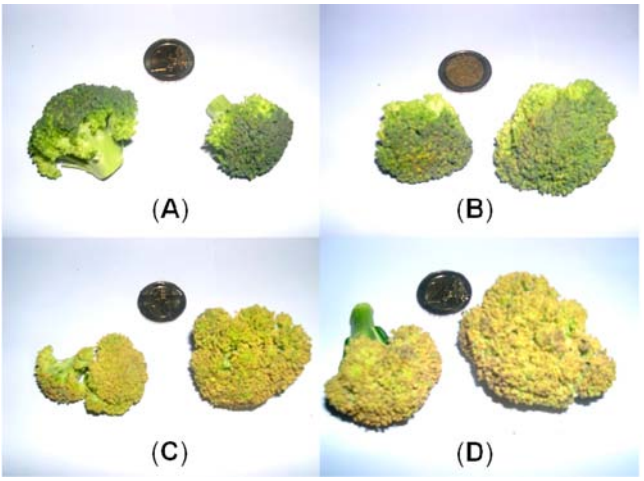

Figure 2. Photographic pictures of broccoli florets at various stages of degreening. (A) On day 1, (B) on day 3, (C) on day 5, and (D) on day 6 of the degreening experiment in the dark.

Analysis of Chlorophyll Catabolites. For analysis of Chl-catabolites, samples of the upper 0.5−1 cm of broccoli florets roughly weighing 3.3 g were likewise collected in a mortar, frozen with liquid nitrogen, crushed, and extracted three times with 3 mL (each) of MeOH. The combined methanolic extracts were mixed 1/1 (v/v) with 50 mM aqueous potassium phosphate buffer (pH 7) and then subjected to analytical HPLC. The catabolites were characterized spectroscopically as described below.

Isolation and Structure Elucidation of Colorless Chlorophyll Catabolites. For structure elucidation, Chl-catabolites were obtained from broccoli florets that were stored for 5 days at room temperature in the dark. The upper 0.5−1 cm of the yellow florets (76.72 g, total wet weight) were cut, frozen with liquid nitrogen, and crushed in a mortar. The cold samples were extracted three times with 100 mL each of MeOH. The combined methanolic extract was analyzed by HPLC (Figure 3) and was concentrated to near dryness under reduced pressure. The residue was taken up in 50 mL of aqueous potassium phosphate buffer (50 mM, pH = 5.1), and the solution was centrifuged (3000 rpm 5 min); a dark-green residue separated, which was extracted two times with 5 mL (each) of aqueous potassium phosphate buffer. The greenish aqueous phases were combined and extracted eight times with 50 mL (each) of CH_2Cl_2. Analyses of the now roughly 50 mL of slightly yellow aqueous phase by HPLC indicated the presence of two Chl-catabolites, of *Bo*-NCC-1 (**1**) and *Bo*-DNCC (**3**). The greenish organic phase contained the less polar *Bo*-NCC-2 (**2**) predominantly.

The greenish CH_2Cl_2 phase was evaporated under reduced pressure, and the remaining residue was resuspended in 25 mL of potassium phosphate buffer (50 mM, pH = 7.0). From the supernatant, *Bo*-NCC-2 (**2**) was isolated by semipreparative HPLC. The fractions containing raw **2** were combined and purified by a second round of semipreparative HPLC. The combined fractions containing pure **2** were desalted by filtration through Sep-Pak-C18 cartridges. Removal of the solvents under reduced pressure gave a sample of *Bo*-NCC-2 (**2**) as an off-white residue that was dried under high vacuum. The sample of pure NCC **2** was dissolved in 0.5 mL of H_2O, and its amount was determined as 0.32 μmol (194 μg) by UV analysis (log $\varepsilon_{(315\ nm)}$ = 3.93).[32]

The yellow aqueous phase that contained *Bo*-NCC-1 (**1**) and *Bo*-DNCC (**3**) was concentrated to about 10 mL using a rotatory evaporator. The now yellow−brownish solution was subjected to semipreparative HPLC in order to isolate raw *Bo*-NCC-1 (**1**) and *Bo*-

DOI: 10.1021/jf5055326
J. Agric. Food Chem. 2015, 63, 1385−1392

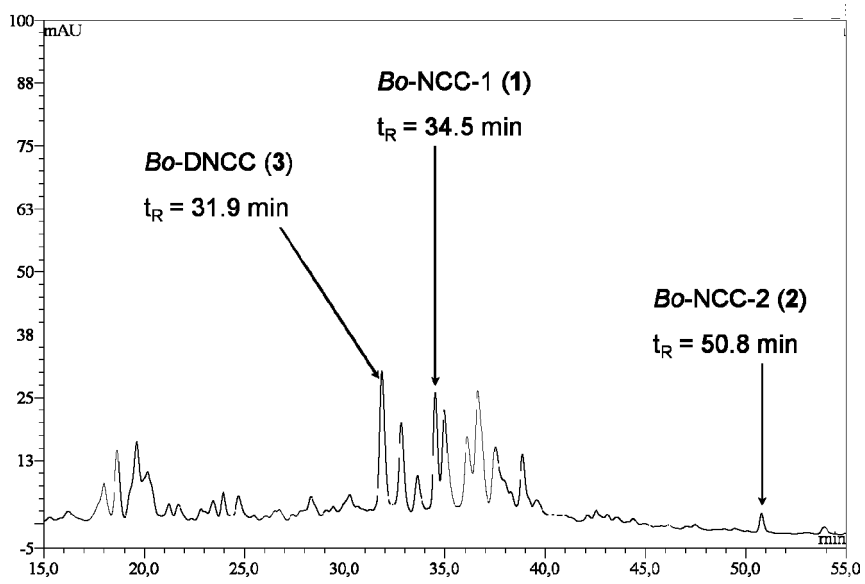

Figure 3. HPLC analysis of a methanolic extract of senescent broccoli florets (online detection at 250 nm). Fractions identified as Chl-catabolites by their UV/vis spectra, are labeled correspondingly as *Bo*-NCC-1 (**1**), *Bo*-NCC-2 (**2**), and *Bo*-DNCC (**3**).

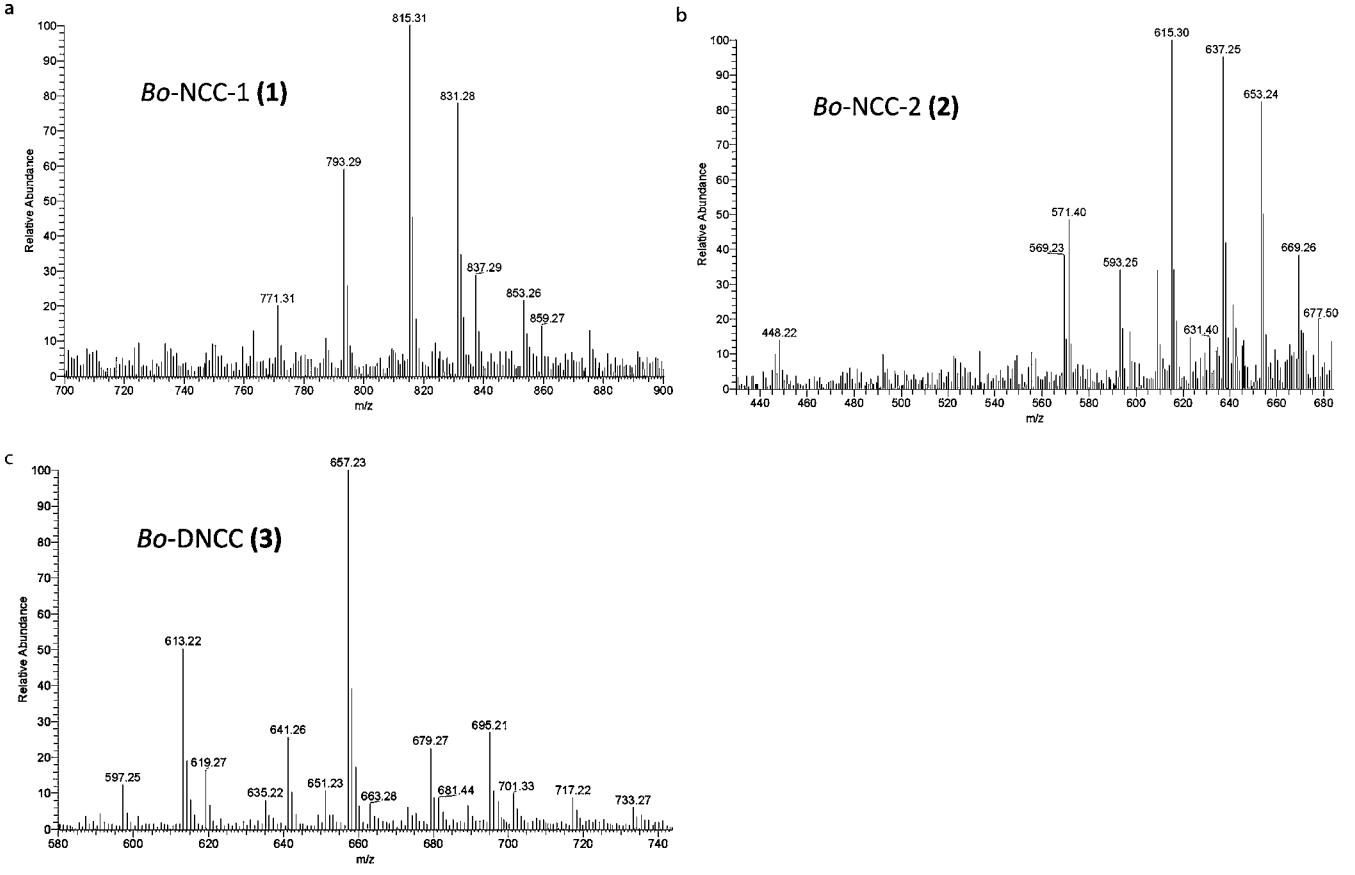

Figure 4. ESI-MS-spectra of *Bo*-NCC-1 (**1**), *Bo*-NCC-2 (**2**), and of *Bo*-DNCC (**3**).

DNCC (**3**). The isolated product fractions were purified by a second round of semipreparative HPLC. Fractions containing **1** or **3** were combined and desalted by filtration through Sep-Pak-C18 cartridges. Solvents were evaporated using a rotatory evaporator, furnishing off-white residues, which were dried at high vacuum, for further analysis. About 0.31 μmol (244 μg) of NCC **1** were obtained (UV-analysis in H_2O[32]). The sample of the DNCC **3** was also analyzed by UV-spectroscopy (log $\varepsilon_{(237\ nm)}$ = 4.49)[16] and was estimated to contain an amount of 0.25 μmol (188 μg).

Spectroscopic Data. *Bo*-NCC-1 (**1**). UV/vis (λ_{max}[nm], rel. ε): 240 (1.22), 250 (1.05), 319 (1.00). CD (λ_{max} and λ_{min} [nm], Θ): 228 (1.6), 245 (−5.3), 257 (−3.8), 282 (−15.0), 321 (8.1). ^{1}H NMR (500 MHz in D_2O, at 293 K): δ = 1.35 (s, H_3C-17^1), 1.87 (s, H_3C-13^1), 2.19 (s, H_3C-2^1), 2.22 (s, H_3C-7^1), 2.26 (m, H_2C-12^2), 2.64 (m, H_2C-12^1), 2.72 (m, H_2C-3^1), 2.74 (m, H_AC-15), 2.86 (m, H_BC-15), 3.26 (t,

DOI: 10.1021/jf5055326
J. Agric. Food Chem. 2015, 63, 1385−1392

J = 8.6 Hz, HC-2′), 3.37 (m, HC-4′), 3.43 (m, HC-5′), 3.49 (t, J = 8.9 Hz, HC-3′), 3.57 (m, H_AC-3^2), 3.59 (m, H_2C-8^2), 3.71 (m, H_AC-6′), 3.72 (m, H_BC-3^2), 3.91 (m, H_BC-6′), 3.97 (s, HC-16), 3.97 (m, J = 17.1 Hz, H_AC-5), 4.09 (m, J = 17.1 Hz, H_BC-5), 4.39 (d, J = 8.1 Hz, HC-1′), 4.72 (m, HC-10, superimposed by signal of HDO), 5.42 (d, J_2 = 11.6 Hz, $H_{cis}C$-18^2), 5.83 (d, J_1 = 18.2 Hz, $H_{trans}C$-18^2), 6.29 (dd, J_1 = 18.0 Hz J_2 = 12.2 Hz, HC-18^1), 9.15 (s, HC-20). ESI-MS: m/z (%) = 859.3 (7, $[M - 2H + 3Na]^+$), 854.3 (11), 853.3 (21, $[M - H + Na + K]^+$); 839.3 (9), 838.31 (11), 837.3 (29, $[M - H + 2Na]^+$); 833.3 (16), 832.3 (44), 831.3 (76, $[M + K]^+$); 818.3 (9) 817.3 (16), 816.3 (46), 815.3 (100, $[M + Na]^+$); 795.3 (9), 794.3 (24), 793.3 (56, $C_{40}H_{49}N_4O_{13}$ $[M + H]^+$); 772.3 (4), 771.3 (16, $[M - CO_2 + Na]^+$) (Figure 4).

Bo-NCC-2 (**2**). UV/vis (λ_{max}[nm], rel. ε): 240 (1.23), 322 (1.00). CD (λ_{max} and λ_{min} [nm], Θ): 226 (−2.3), 244 (−15.6), 259 (−9.4), 282 (−26.8), 325 (18.5). ^{1}H NMR (600 MHz, in D_2O, at 283 K): 0.87 (t, J = 7.55 Hz, H_3C-3^2), 1.29 (s, H_3C-17^1), 1.85 (s, H_3C-13^1), 2.13 (s, H_3C-2^1), 2.21 (s, H_3C-7^1), 2.27 (m, H_2C-12^2), 2.37 (m, H_2C-3^1), 2.63 (m, H_2C-12^1), 2.68 (m, H_AC-15), 2.86 (dd, J_1 = 14.73 Hz J_2 = 5.79 Hz, H_BC-15), 3.88 (m, HC-1 H_AC-5), 4.05 (m, H_BC-5), 4.70 (m, HC-10), 5.42 (d, J_2 = 11.9 Hz, $H_{cis}C$-18^2), 5.82 (d, J_1 = 18.0 Hz, $H_{trans}C$-18^2), 6.28 (dd, J_1 = 18.0 Hz J_2 = 11.9 Hz, HC-18^1), 9.10 (s, HC-20). ESI-MS: m/z (%) = 655.30 (16), 654.24 (48), 653.24 (79, $[M + K]^+$); 639.20 (14), 638.13 (38), 637.25 (94, $[M + Na]^+$); 617.39 (16), 616.28 (34), 615.30 (100, $C_{34}H_{39}N_4O_7$ $[M + H]^+$); 611.19 (7), 610.27 (15), 609.24 (32, $[M - CO_2 + K]^+$); 594.20 (16), 593.25 (34, $[M - CO_2 + Na]^+$); 572.27 (12), 571.40 (50, $[M - CO_2 + H]^+$); 569.21 (36); 492.20 (10, $[M -$ Ring D $+ H]^+$); 448.22 (14, $[M -$ Ring D-$CO_2 + H]^+$) (Figure 4)

Bo-DNCC (**3**). UV/vis (λ_{max}[nm], rel. ε): 250 (1.00); 290 (broad, 0.2). CD (λ_{max} and λ_{min} [nm], Θ): 226 (8.6); 244 (0.6); 259 (−9.4); 282 (−26.8); 325 (18.5). ^{1}H NMR (600 MHz in D_2O by 293 K): 1.68 (s, H_3C-2^1), 1.85 (s, H_3C-13^1), 1.92 (s, H_3C-17^1), 2.02 (s, H_3C-7^1), 2.13 (m, H_2C-12^2), 2.45 (m, H_AC-3^1 H_2C-12^1), 2.61 (m, H_AC-5 H_AC-15), 2.76 (m, H_BC-3^1), 2.95 (dd, J_1 = 15.0 Hz J_2 = 4.8 Hz, H_BC-15), 3.07 (dd, J_1 = 15.0 Hz J_2 = 4.4 Hz, H_BC-5), 3.67 (m, H_2C-3^2), 4.18 (t, J = 6.0 Hz, HC-16), 4.30 (m, HC-4), 4.60 (m, HC-10), 5.30 (d, J_2 = 11.8 Hz, $H_{cis}C$-18^2), 5.72 (d, J_1 = 17.9 Hz, $H_{trans}C$-18^2), 6.28 (dd, J_1 = 17.9 Hz J_2 = 11.7 Hz, HC-18^1). ESI-MS: m/z (%) = 733.27 (6, $[M - 2H + 3K]^+$); 718.19 (6), 717.22 (9, $[M - 2H + Na + 2K]^+$); 701.33 (10, $[M - 2H + 2Na + K]^+$); 697.20 (8), 696.18 (11), 695.21 (26, $[M - H + 2K]^+$); 681.44 (8), 680.26 (8), 679.27 (22, $[M - H + Na + K]^+$); 660.25 (6), 659.24 (18), 658.23 (49), 657.23 (100, $[M + K]^+$); 651.23 (12, $[M -$ H-$CO_2 + 2K]^+$); 642.25 (10), 641.26 (25, $[M + Na]^+$); 635.22 (8, $[M -$ H-$CO_2 + Na + K]^+$); 620.28 (8), 619.27 (16, $C_{33}H_{39}N_4O_8$ $[M + H]^+$); 615.23 (8), 614.22 (19), 613.22 (50, $[M - CO_2 + K]^+$); 598.25 (5), 597.25 (13, $[M - CO_2 + Na]^+$) (Figure 4).

Identification of *Bo*-NCC-1, *Bo*-NCC-2, and *Bo*-DNCC with Known Chlorophyll Catabolites. According to their spectroscopic data, *Bo*-NCC-1 (**1**), *Bo*-NCC-2 (**2**), and *Bo*-DNCC (**3**) had the same molecular constitutions as *Bn*-NCC-2 and *Bn*-NCC-4, two NCCs from oil seed rape (*Brassica napus*).[34] For the purpose of their further identification, the HPL-chromatographic behavior of *Bo*-NCC-1 (**1**) and of *Bn*-NCC-2 was compared, as well as that of *Bo*-NCC-2 (**2**) and of *Bn*-NCC-4. The samples from the two plant sources showed (pairwise) identical chromatographic properties. In a third coinjection experiment, *Bo*-DNCC (**3**) and a DNCC from *A. thaliana*, provisionally named *At*-DNCC-1,[17] also showed the same chromatographic behavior.

RESULTS

Fresh green florets of broccoli (*Brassica oleracea* var. *italica*), which were bought in a super market, were stored in a dry place at ambient temperature for up to 6 days, either in the dark or being exposed to diffuse day light. In both cases, the broccoli florets degreened and developed a faint yellow color (Figure 2). At regular time intervals, a broccoli floret was selected and its upper part (about 3 g wet weight) was then analyzed. In the extracts obtained, residual Chl *a* and Chl *b* were analyzed by UV/vis-spectroscopy, and three colorless Chl-catabolites were tentatively identified by HPLC analysis (Figure 3). In the green, commercially available broccoli florets, the here characterized three colorless Chl-catabolites were already present in small amounts. During storage (in darkness or diffuse day light), the Chl-content in broccoli was seen to decrease to about 50% within roughly 2 days. After 6 days, less than 10% of the original Chl was still present. In the broccoli florets, two NCC fractions were typified, and a DNCC, based on their characteristic UV absorbance properties. In both cases of storage, in the dark and in diffuse daylight, the amount of the most polar NCC, named *Bo*-NCC-1 (**1**), increased strongly until day 3 and decreased upon further storage. The lesser abundant and less polar NCC, *Bo*-DNCC (**3**) displayed a similar profile of its presence in the florets. A small amount of *Bo*-NCC-2 (**2**) was present from the first day onward with a trend to decrease during storage. Other relevant fractions with UV/vis spectral signatures of colorless Chl-catabolites were not found. During the first 2 days of storage, the observed accumulation of Chl-catabolites was estimated to come up for about 30−35%, overall, of the Chls lost due to the degreening process. As was noted elsewhere with respect to the content of Chl-catabolites,[6] storage of broccoli beyond the early stages of degreening and senescence also showed significantly decreased amounts of the recovered Chl-catabolites. Indeed, degradation of organic micronutrients (vitamins and secondary plant metabolites) during storage is a widely observed phenomenon.

For the purpose of isolation and structure analysis of Chl-catabolites, yellow broccoli florets were selected at day 5 of their storage in the dark, and the upper 0.5−1 cm was severed from the stalk, giving a sample of 76.7 g (wet weight), which was crushed and extracted with MeOH (as described in detail in the Materials and Methods section). After a two-stage isolation and purification procedure by HPLC, 0.32 μmol (194 μg) of *Bo*-NCC-2 (**2**), 0.31 μmol (244 μg) *Bo*-NCC-1 (**1**), and 0.25 μmol (188 μg) *Bo*-DNCC (**3**) were obtained.

The samples of the isolated three Chl-catabolites were used for structure determination. UV spectra allowed the classification of two NCCs[4,6] (**1** and **2**) and of a DNCC (**3**).[13,16] The UV-spectra of the NCC fractions **1** and **2** showed absorption maxima at 319 and at 322 nm, respectively, characteristic for the α-formyl-pyrrole moiety (ring A) of NCCs.[6,35] The UV-spectrum of the *Bo*-DNCC (**3**) showed no maxima, but absorption bands near 250 and 290 nm, as is typical for 1,19-dioxobilane-type NCCs (DNCCs).[13,16] CD-spectra of the purified NCCs showed positive and negative extrema at 321 and at 282 nm, respectively, as is characteristic of natural NCCs.[15,36] The CD spectrum of *Bo*-DNCC (**3**) exhibited a very weak maximum at 310 nm, and a pronounced negative extremum at 282 nm, as was described similarly for *At*-DNCC-1,[17] suggesting the configuration at C15 to be the same as in the DNCC from *A. thaliana*.[17]

The molecular formula of *Bo*-NCC-1 (**1**) was deduced as $C_{40}H_{48}N_4O_{13}$ from its electrospray ionization (ESI) mass spectrum (Figure 4), in which the pseudomolecular ions $[M + H]^+$ and $[M + Na]^+$ were found at m/z = 793.29 and at m/z = 815.31, respectively. A signal at m/z = 771.31 $[M\text{-}CO_2 + Na]^+$ indicated loss of CO_2. A 500 MHz ^{1}H NMR spectrum of **1** in D_2O and at 293 K showed signals of 38 H atoms, i.e., of all carbon-bound protons. On the basis of ^{1}H,^{1}H-COSY and ^{1}H,^{1}H-ROESY spectra, the chemical constitution of *Bo*-NCC-1 (**1**) was deduced. At low field, a singlet was present at 9.15 ppm of the α-formyl group (H−C(20) at ring A) and the set of

DOI: 10.1021/jf5055326
J. Agric. Food Chem. 2015, 63, 1385−1392

signals between 5 and 6.5 ppm of the vinyl group at C18. Singlets at 1.35, 2.19, 2.22, and at 1.87 ppm were assigned to the methyl groups at C17, C2, C7, and C13, respectively. The methylene protons at $C12^1$ and $C12^2$ of the propanoic acid group gave rise to multiplets at 2.26 ppm (H_2C12^2) and at 2.64 ppm (H_2C12^1). The methylene protons at $C3^1$ and $C3^2$ gave multiplets at 2.72 ppm ($H_2{-}C3^1$), 3.57 ppm, and at 3.72 ppm ($H_2{-}C3^2$) and coupled with each other. The protons of $H_2{-}$C15 were assigned to the multiplets at 2.74 and 2.86 ppm, both of which coupled with H−C16 at 3.97 ppm. A β-glycopyranosyl unit was identified by ^{1}H,^{1}H-COSY and ^{1}H,^{1}H-ROESY spectra. On the basis of these data, the constitution of *Bo*-NCC-1 (**1**) was deduced as that of a 1-formyl-19-oxo-3^2-(1-ß-glucopyranosyl)-$O8^4$-desmethyl-16,19-dihydrophyllobilane, a Chl-derived 1-formyl-19-oxobilane (Figure 6).

An ESI mass spectrum of *Bo*-NCC-2 (**2**) (Figure 4) indicated the molecular formula $C_{34}H_{38}N_4O_7$ with pseudomolecular ions at m/z = 615.30 $[M + H]^+$, at m/z = 637.25 $[M + Na]^+$ and at m/z = 653.24 $[M + K]^+$. Fragment ions at m/z = 571.40 $[M - CO_2 + H]^+$ and m/z = 593.25 $[M - CO_2 + Na]^+$, corresponding to loss of CO_2, and at m/z = 448.22 $[M - CO_2$-ring D + $H]^+$, were also observed. In the 600 MHz ^{1}H NMR spectrum of **2** in D_2O at 283 K, signals of 32 of the 38 H atoms could be assigned (i.e., of all carbon-bound H atoms). ^{1}H,^{1}H-COSY and ^{1}H,^{1}H-ROESY spectra were used to derive the chemical constitution of the *Bo*-NCC-2 (**2**) (Figure 5). The

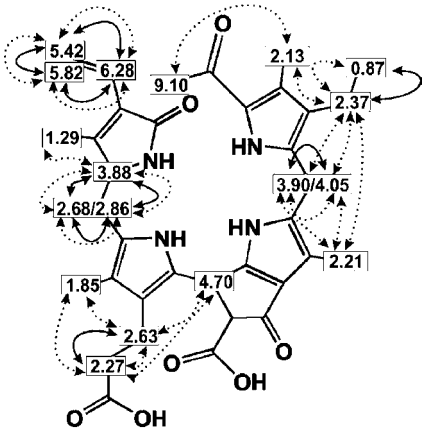

Figure 5. Graphical representation of ^{1}H NMR chemical-shift assignments of signals of carbon-bound H atoms of *Bo*-NCC-2 (**2**) in D_2O (solid arrows represent COSY correlations, dashed arrows represent ROESY correlations).

characteristic singlet of the aldehyde proton H−C20 appeared at 9.10 ppm. In a 600 MHz NMR spectrum of **2** in H_2O/D_2O = 9:1 at 283 K, three additional broad singlets were observed at 7.81, 8.80, and 10.33 ppm of protons bound to pyrrole N-atoms. The signals at 6.28 ppm (dd), at 5.82 ppm (d), and at 5.42 ppm (d) were characteristic of the vinyl group at C18, singlets at 1.29, 1.85, 2.13, and at 2.21 ppm indicated four methyl groups at C17, C13, C2, and C7, respectively. An ethyl group at C3 gave rise to a doublet at 2.37 ppm that coupled with triplet at 0.87 ppm. Multiplets at 2.27 ppm (H_2C12^2) and at 2.63 ppm (H_2C12^1) characterized the propanoic acid group at ring C. H_2C15 gave rise to two multiplets at 2.68 and 2.86 ppm, both showing coupling with a multiplet at 3.88 ppm (HC16). HC10 was seen as a signal at 4.70 ppm. On the basis of mass spectrometric and NMR spectroscopic data, *Bo*-NCC-2 (**2**) was deduced to be a 1-formyl-19-oxo-$O8^4$-desmethyl-16,19-dihydrophyllobilane (Figure 6).

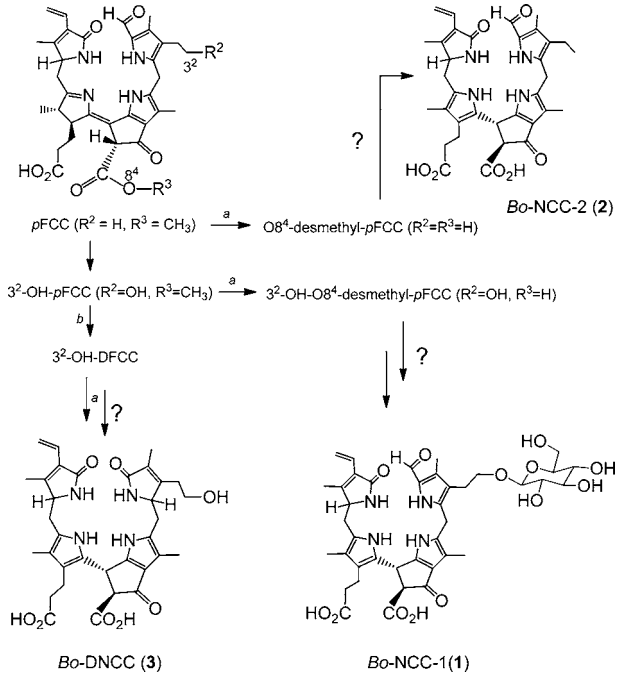

Figure 6. Structures of *Bo*-NCC-1 (**1**), *Bo*-NCC-2 (**2**), and *Bo*-DNCC (**3**), the major Chl-catabolites in senescent broccoli, and possible pathways of their formation from *p*FCC (*a*, methylesterase; *b*, deformylating cytochrome). The hypothetical nonenzymatic isomerization of FCCs and of DFCC to NCCs and to DNCC, respectively, is presumed to take place in the vacuole (see Figure 7).

The colorless catabolite *Bo*-DNCC (**3**) was similarly analyzed by an ESI mass spectrum (Figure 4), which showed pseudo molecular ions at m/z = 619.27 $[M + H]^+$, at m/z = 641.26 $[M + Na]^+$, and at m/z = 657.23 $[M + K]^+$, indicating a molecular formula of $C_{33}H_{38}N_4O_8$. Decarboxylations led to signals at m/z = 651.23 $[M - H\text{-}CO_2 + 2K]^+$, 635.22 $[M - H\text{-}CO_2 + Na + K]^+$, 613.22 $[M - CO_2 + K]^+$, and at m/z = 597.25 $[M - CO_2 + Na]^+$. In the 600 MHz ^{1}H NMR spectrum of **3** in D_2O and at 283 K, signals of 31 C-bound H atoms could be assigned with the help of ^{1}H,^{1}H-COSY and ^{1}H,^{1}H-ROESY spectra. Signals were not found in the low field, consistent with the absence of a formyl group. A vinyl group at C18 gave rise to a characteristic set of signals between 6.5 and 5 ppm. Four singlets of methyl groups (H_3C2^1, H_3C13^1, H_3C17^1, and H_3C7^1 appeared at high field. The methylene protons at $C12^1$ and $C12^2$ of the propanoic acid group gave multiplets at 2.13 ppm (H_2C12^1) and at 2.45 ppm (H_2C12^2). Protons H_2C3^1 coupled with H_2C3^2 and H_AC5 and H_BC5 coupled with HC4. Similarly, an AB system, due to H_AC15 and H_BC15, coupled with HC16. HC10 showed a signal at 4.60 ppm. The mass spectrometric and NMR spectroscopic data established the constitution of the Chl-derived 1,19-dioxobilane **3** as that of a 1,19-dioxo-3^2-hydroxy-$O8^4$-desmethyl-1,4,16,19-tetrahydro-phyllobilane (Figure 6).

The configuration at C10 of the two *Bo*-NCCs **1** and **2** was deduced from the CD spectra to be the same as that of the known natural NCCs, which was tentatively deduced to be (*R*).[36] The absolute configuration of some other stereocenters could not be independently elucidated. However, **1** and **2** were

DOI: 10.1021/jf5055326
J. Agric. Food Chem. 2015, 63, 1385−1392

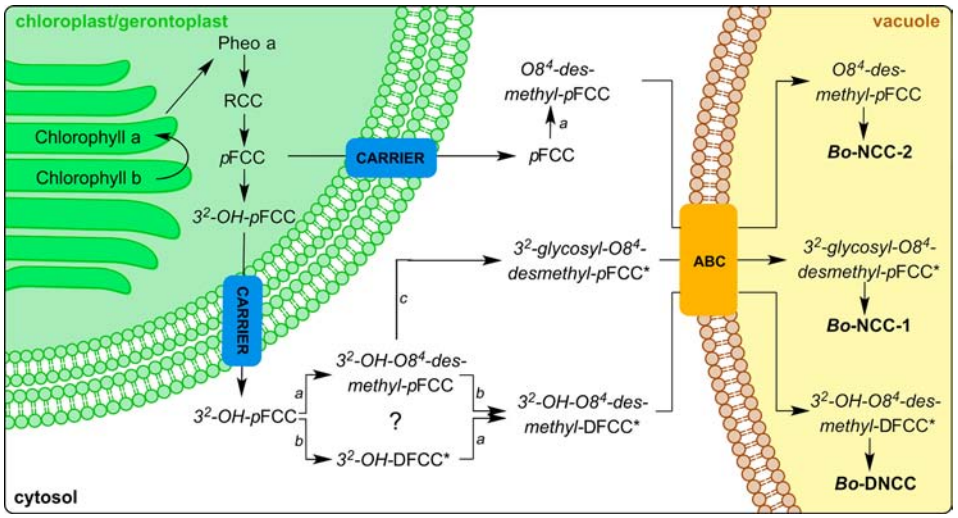

Figure 7. Topographical model of Chl-breakdown in senescent leaves of broccoli, according to the "PAO/phyllobilin-pathway".[7,8] The early steps of this pathway take place in the chloroplast/gerontoplast.[7] The model is based on the current tentative view of the subcellular localization of Chl-catabolites,[41] and Chl-catabolic enzymes of the further pathway are specified, based on presumed modifications of breakdown intermediates, as deduced from the structures of colorless Chl-catabolites identified in the present work. Putative catabolites are labeled with asterisk (*), putative enzyme catalyzed steps are specified by a general label for the enzyme class of a methylesterase (*a*), for a deformylating cytochrome (*b*) and of a glycosidase (*c*) (see Figure 6 for chemical formulas of the suggested intermediate FCCs and of the nonfluorescent catabolites *Bo*-NCC-1 (**1**), *Bo*-NCC-2 (**2**), and *Bo*-DNCC (**3**)).

indicated to have the same constitution as two NCCs from oilseed rape (*Brassica napus*), and named *Bn*-NCC-2[34,37] and *Bn*-NCC-4.[38] The structural identity of **1** and **2**, on one side, and of *Bn*-NCC-2 and Bn-NCC-4, on the other,[34] was established by HPL chromatographic comparison ("coinjection" experiments) of these NCCs. As *Bn*-NCCs were shown earlier to be derived from the "primary" fluorescent Chl-catabolite, *p*FCC[10] (and not from the C1-epimer, *epi*-*p*FCC[11]), the two *Bo*-NCCs **1** and **2** are also indicated to be derived from *p*FCC. In a corresponding experiment, *Bo*-DNCC was identified with *At*-DNCC-1, a prominent Chl-derived dioxobilane from *A. thaliana*.[17] Consistent with these data, the colorless Chl-catabolites of broccoli are all derived from *p*FCC.

DISCUSSION

Degreening is a characteristic sign of breakdown of chlorophyll (Chl) in higher plants, often associated with senescence.[7,39] In this study, the presence of (colorless) Chl-catabolites was investigated in senescent florets of broccoli (*Brassica oleracea* var. *italica*). Two NCCs (1-formyl-19-oxophyllobilanes) and a DNCC (1,19-dioxophyllobilane) could be identified and were structurally characterized. In the early phase of visual degreening of the broccoli florets (days one and two of storage), the amounts of the three colorless Chl-catabolites recovered roughly comes up for about 30−35% of the Chls that disappear during this time. At later stages (days 5 and 6 of storage), not only the green Chls continue to disappear but Chl-catabolites also fade away (by still unknown processes). So far, nongreen Chl-catabolites have been identified only in one other genuine vegetable, in naturally senescing leaves of spinach (*Spinaccia oleracea*).[31,32] A common stereochemical lineage of the catabolites from broccoli with those from oilseed rape (*Brassica napus*)[34] and from *Arabidopsis thaliana*[17] was established, which is consistent with the close phylogenic relationship of the involved *Brassicacea*.

Similar to observations with wild type *A. thaliana*,[17,38] all three catabolites from broccoli carry a free acid function at C8^2, instead of the methyl ester group that is (still) present in their derived common precursor, the "primary" FCC (*p*FCC).[10] An efficient enzyme catalyzed methyl ester hydrolysis is indicated in broccoli. This finding is in line with the recent discovery of the cytosolic methyl esterase Mes16 in *A. thaliana*,[40] which was shown to be crucial in Chl-breakdown path in this plant. Presumably, in broccoli an analogous methyl esterase exists in the cytosol. The occurrence of the now well characterized less polar *Bo*-NCC-2 (**2**) is notable, which was previously identified provisionally in senescent leaves of *A. thaliana*[38] and of spinach.[31] This observation (in broccoli, *A.thaliana*, etc.) suggests export of the "primary" FCC (*p*FCC) into the cytosol, where it is a substrate of the methyl esterase that produces *O*8^4-desmethyl-*p*FCC efficiently (the hypothetical precursor of *Bo*-NCC-2 (**2**), Figures 6 and 7).

Identification of *Bo*-DNCC (**3**), a prominent dioxobilin-type Chl-catabolite in degreened broccoli florets, suggests FCC-deformylation (at C1) to be an important degradation step in broccoli, as was observed in senescent leaves of *A. thaliana*.[17] Thus, similar to the situation in *A. thaliana*, where DNCCs and NCCs were identified,[17] both catabolite lineages occur in broccoli as well. Furthermore, because both hydroxylated DNCC **3** and further glucosylated NCC **1** were found in the extracts of senescent broccoli florets, the enigmatic hydroxylation at the saturated C3^2 position is also indicated to be efficient and to be relevant for both branches of Chl-breakdown. Possibly, this hydroxylation reaction already occurs in the chloroplast, i.e., before export into the cytosol.[7] In contrast, the glycosylation at the OH group at C3^2, observed in the structure of the polar *Bo*-NCC-1 (**1**), would be considered to occur in the cytosol and at the level of the still elusive hypothetical FCCs (Figures 6 and 7). Chl-breakdown in broccoli thus shows the hallmarks of the PaO/phyllobilin pathway,[7,41] and a tentative outline of the Chl-breakdown path in broccoli could be deduced from the structures of the Chl-catabolites found in the degreening florets (see Figures 6 and 7).

DOI: 10.1021/jf5055326
J. Agric. Food Chem. 2015, 63, 1385−1392

In the context of the typical nutritional use of broccoli as a green vegetable, the presence of sizable amounts of colorless Chl-catabolites in the early phase of visual degreening is remarkable. We recently showed NCCs to be excellent antioxidants, such as the ones from apples and pears.[9] Indeed, at present, the physiological effects of the ubiquitous phyllobilanes (NCCs, DNCCs) are unknown that are present in some of our plant-derived nutrition as degradation products of Chl *a*. However, the result with degreening broccoli florets indicates accumulation of such linear tetrapyrroles in this common vegetable, which are also exceptional antioxidants. It will clearly be interesting to learn more about the possible health effects of such colorless Chl-catabolites, as of those that are now known to occur in degreening broccoli florets.

■ ASSOCIATED CONTENT

Supporting Information

Material and methods. Atom numbering of NCCs and of DNCCs used here. Qualitative analyses of the time dependence of the amounts of chlorophyll (Chl) and Chl-catabolites in the raw broccoli plant material during the degreening. HPLC analyses of organic and aqueous phase of the first broccoli extract. Online UV/vis spectra of *Bo*-NCC-1, *Bo*-NCC-2, and *Bo*-NCC-3. CD spectra of *Bo*-NCC-1, *Bo*-NCC-2, and *Bo*-NCC-3. ^{1}H NMR 600 MHz spectra of *Bo*-NCC-1, *Bo*-NCC-2, and *Bo*-NCC-3. Graphical analysis of homonuclear ^{1}H,^{1}H-ROESY, and COSY correlations of *Bo*-NCC-1 and *Bo*-NCC-3. HPLC analyses of Chl-catabolites from broccoli by coinjection experiments. This material is available free of charge via the Internet at http://pubs.acs.org.

■ AUTHOR INFORMATION

Corresponding Author

*Phone: 43-512-507-57700. Fax: +43-512-507-57799. E-mail: bernhard.kraeutler@uibk.ac.at.

Funding

Financial support by the Austrian Science Foundation (FWF project nos. L-472 and I-563) is also gratefully acknowledged.

Notes

The authors declare no competing financial interest.

See formulas and ref 8 for atom-numbering of the chlorophyll catabolites used here.

■ ACKNOWLEDGMENTS

We thank Christoph R. Kreutz and Markus Ruetz for measuring NMR-spectra and Clemens Vergeiner, Barbara Enders, and Iris Süssenbacher for technical advice. We thank Stefan Hörtensteiner (University of Zürich) for helpful discussions.

■ DEDICATION

Dedicated to the memory of Paula Enders.

■ ABBREVIATIONS USED

Chl, chlorophyll; NCC, nonfluorescent chlorophyll catabolite; DNCC, dioxobilane-type chlorophyll catabolite; FCC, fluorescent chlorophyll catabolite; pFCC, "primary" fluorescent chlorophyll catabolite; sFCC, "secondary" fluorescent chlorophyll catabolite; RCC, red chlorophyll catabolite; HPLC, high performance liquid chromatography; UV/vis, ultraviolet/visible absorption; CD, circular dichroism; ^{1}H NMR, proton nuclear magnetic resonance; ESI-MS, electrospray ionization mass spectrometry

■ REFERENCES

(1) Lim, P. O.; Kim, H. J.; Nam, H. G. Leaf Senescence. *Annu. Rev. Plant Biol.* **2007**, *58*, 115−136.

(2) Hörtensteiner, S.; Lee, D. W. Chlorophyll Catabolism and Leaf Coloration. In *Senescence Processes in Plants*; Gan, S., Ed.; Blackwell Publishing Ltd: Oxford, UK, 2007; p 12.

(3) Barry, C. S. The Stay-Green Revolution: Recent Progress in Deciphering the Mechanisms of Chlorophyll Degradation in Higher Plants. *Plant Sci.* **2009**, *176*, 325−333.

(4) Kräutler, B.; Jaun, B.; Bortlik, K.; Schellenberg, M.; Matile, P. On the Enigma of Chlorophyll Degradation—The Constitution of a Secoporphinoid Catabolite. *Angew. Chem., Int. Ed.* **1991**, *30*, 1315−1318.

(5) Kräutler, B. Chlorophyll Breakdown and Chlorophyll Catabolites in Leaves and Fruit. *Photochem. Photobiol. Sci.* **2008**, *7*, 1114−1120.

(6) Moser, S.; Müller, T.; Oberhuber, M.; Kräutler, B. Chlorophyll Catabolites—Chemical and Structural Footprints of a Fascinating Biological Phenomenon. *Eur. J. Org. Chem.* **2009**, 21−31.

(7) Hörtensteiner, S.; Kräutler, B. Chlorophyll Breakdown in Higher Plants. *Biochim. Biophys. Acta, Bioenerg.* **2011**, *1807*, 977−988.

(8) Kräutler, B. Phyllobilins—The Abundant Tetrapyrrolic Catabolites of the Green Plant Pigment Chlorophyll. *Chem. Soc. Rev.* **2014**, *43*, 6227−6238.

(9) Müller, T.; Ulrich, M.; Ongania, K.-H.; Kräutler, B. Colourless Tetrapyrrolic Chlorophyll Catabolites Found in Ripening Fruit are Effective Antioxidants. *Angew. Chem., Int. Ed.* **2007**, *46*, 8699−8702.

(10) Mühlecker, W.; Ongania, K. H.; Kräutler, B.; Matile, P.; Hörtensteiner, S. Tracking Down Chlorophyll Breakdown in Plants: Elucidation of the Constitution of a 'Fluorescent' Chlorophyll Catabolite. *Angew. Chem., Int. Ed.* **1997**, *36*, 401−404.

(11) Mühlecker, W.; Kräutler, B.; Moser, D.; Matile, P.; Hörtensteiner, S. Breakdown of Chlorophyll: A Fluorescent Chlorophyll Catabolite from Sweet Pepper (*Capsicum annuum*). *Helv. Chim. Acta* **2000**, *83*, 278−286.

(12) Kräutler, B.; Hörtensteiner, S. Chlorophyll Breakdown—Chemistry, Biochemistry and Biology. In *Handbook of Porphyrin Science*; Ferreira, G. C., Kadish, K. M., Smith, K. M., Guilard, R., Ed.; World Scientific Publishing, Hackensack, NJ, 2013; Vol. *28*, p 117.

(13) Losey, F. G.; Engel, N. Isolation and Characterization of a Urobilinogenoidic Chlorophyll Catabolite from *Hordeum vulgare*. *J. Biol. Chem.* **2001**, *276*, 8643−8647.

(14) Scherl, M.; Müller, T.; Kräutler, B. Chlorophyll Catabolites in Senescent Leaves of the Lime Tree (*Tilia cordata*). *Chem. Biodiversity* **2012**, *9*, 2605−2617.

(15) Oberhuber, M.; Berghold, J.; Kräutler, B. Chlorophyll Breakdown by a Biomimetic Route. *Angew. Chem., Int. Ed.* **2008**, *47*, 3057−3061.

(16) Müller, T.; Rafelsberger, M.; Vergeiner, C.; Kräutler, B. A Dioxobilane as Product of a Divergent Path of Chlorophyll Breakdown in Norway Maple. *Angew. Chem., Int. Ed.* **2011**, *50*, 10724−10727.

(17) Christ, B.; Süssenbacher, I.; Moser, S.; Bichsel, N.; Egert, A.; Müller, T.; Kräutler, B.; Hörtensteiner, S. Cytochrome P450 CYP89A9 is Involved in the Formation of Major Chlorophyll Catabolites During Leaf Senescence in *Arabidopsis thaliana*. *Plant Cell* **2013**, *25*, 1868−1880.

(18) Fukasawa, A.; Suzuki, Y.; Terai, H.; Yamauchi, N. Effects of Postharvest Ethanol Vapor Treatment on Activities and Gene Expression of Chlorophyll Catabolic Enzymes in Broccoli Florets. *Postharvest Biol. Technol.* **2010**, *55*, 97−102.

(19) King, G. A.; O'Donoghue, E. M. Unravelling Senescence: New Opportunities for Delaying the Inevitable in Harvested Fruit and Vegetables. *Trends Food Sci. Technol.* **1995**, *6*, 385−389.

(20) Gapper, N. E.; Coupe, S. A.; McKenzie, M. J.; Sinclair, B. K.; Lill, R. E.; Jameson, P. E. Regulation of Harvest-induced Senescence in Broccoli (*Brassica oleracea* var. *italica*) by Cytokinin, Ethylene and Sucrose. *J. Plant Growth Regul.* **2005**, *24*, 153−165.

DOI: 10.1021/jf5055326
J. Agric. Food Chem. 2015, 63, 1385−1392

(21) Van Loey, A.; Ooms, V.; Weemaes, C.; Van den Broeck, I.; Ludikhuyze, L.; Indrawati; Denys, S.; Hendrickx, M. Thermal and Pressure−Temperature Degradation of Chlorophyll in Broccoli (*Brassica oleracea* L. *italica*) juice: A Kinetic Study. *J. Agric. Food Chem.* **1998**, *46*, 5289−5294.
(22) Yamauchi, N.; Harada, K.; Watada, A. E. In Vitro Chlorophyll Degradation in Stored Broccoli (*Brassica oleracea* L. var. *italica* Plen.) Florets. *Postharvest Biol. Technol.* **1997**, *12*, 239−245.
(23) Büchert, A. M.; Civello, P. M.; Martínez, G. A. Chlorophyllase versus Pheophytinase as Candidates for Chlorophyll Dephytilation during Senescence of Broccoli. *J. Plant Physiol.* **2011**, *168*, 337−343.
(24) Gomez-Lobato, M. E.; Civello, P. M.; Martinez, G. A. Effects of Ethylene, Cytokinin and Physical Treatments on *BoPaO* Gene Expression of Harvested Broccoli. *J. Sci. Food Agric.* **2012**, *92*, 151−158.
(25) Chen, L. F. O.; Lin, C. H.; Kelkar, S. M.; Chang, Y. M.; Shaw, J. F. Transgenic Broccoli (*Brassica oleracea* var. italicia) with Antisense Chlorophyllase (BoCLH1) Delays Postharvest Yellowing. *Plant Sci.* **2008**, *174*, 25−31.
(26) Aiamla-or, S.; Kaewsuksaeng, S.; Shigyo, M.; Yamauchi, N. Impact of UV-B Irradiation on Chlorophyll Degradation and Chlorophyll-Degrading Enzyme Activities in Stored Broccoli (*Brassica oleracea* L. *italica* Group) Florets. *Food Chem.* **2010**, *120*, 645−651.
(27) Funamoto, Y.; Yamauchi, N.; Shigyo, M. Involvement of Peroxidase in Chlorophyll Degradation in Stored Broccoli (*Brassica oleracea* L.) and Inhibition of the Activity by Heat Treatment. *Postharvest Biol. Technol.* **2003**, *28*, 39−46.
(28) Zhang, X. L.; Zhang, Z. Q.; Li, J.; Wu, L. J.; Guo, J. Y.; Ouyang, L. Q.; Xia, Y. Y.; Huang, X. M.; Pang, X. Q. Correlation of Leaf Senescence and Gene Expression/Activities of Chlorophyll Degradation Enzymes in Harvested Chinese Flowering Cabbage (*Brassica rapa* var. *parachinensis*). *J. Plant Physiol.* **2011**, *168*, 2081−2087.
(29) Gomez, F.; Fernandez, L.; Gergoff, G.; Guiamet, J. J.; Chaves, A.; Bartoli, C. G. Heat Shock Increases Mitochondrial H_2O_2 Production and Extends Postharvest Life of Spinach Leaves. *Postharvest Biol. Technol.* **2008**, *49*, 229−234.
(30) Nath, A.; Bagchi, B.; Misra, L. K.; Deka, B. C. Changes in Post-Harvest Phytochemical Qualities of Broccoli Florets During Ambient and Refrigerated Storage. *Food Chem.* **2011**, *127*, 1510−1514.
(31) Berghold, J.; Breuker, K.; Oberhuber, M.; Hörtensteiner, S.; Kräutler, B. Chlorophyll Breakdown in Spinach: On the Structure of Five Nonfluorescent Chlorophyll Catabolites. *Photosynth. Res.* **2002**, *74*, 109−119.
(32) Oberhuber, M.; Berghold, J.; Mühlecker, W.; Hörtensteiner, S.; Kräutler, B. Chlorophyll Breakdown—On a Nonfluorescent Chlorophyll Catabolite from Spinach. *Helv. Chim. Acta* **2001**, *84*, 2615−2627.
(33) Porra, R. J.; Thompson, W. A.; Kriedemann, P. E. Determination of Accurate Extinction Coefficients and Simultaneous-Equations for Assaying Chlorophyll-a and Chlorophyll-b Extracted with 4 Different Solvents—Verification of the Concentration of Chlorophyll Standards by Atomic-Absorption Spectroscopy. *Biochim. Biophys. Acta* **1989**, *975*, 384−394.
(34) Mühlecker, W.; Kräutler, B. Breakdown of chlorophyll: Constitution of Nonfluorescing Chlorophyll Catabolites from Senescent Cotyledons of the Dicot Rape. *Plant Physiol. Biochem.* **1996**, *34*, 61−75.
(35) Kräutler, B.; Jaun, B.; Amrein, W.; Bortlik, K.; Schellenberg, M.; Matile, P. Breakdown of Chlorophyll—Constitution of a Secoporphinoid Chlorophyll Catabolite Isolated from Senescent Barley Leaves. *Plant Physiol. Biochem.* **1992**, *30*, 333−346.
(36) Oberhuber, M.; Berghold, J.; Breuker, K.; Hörtensteiner, S.; Kräutler, B. Breakdown of Chlorophyll: A Nonenzymatic Reaction Accounts for the Formation of the Colorless 'Nonfluorescent' Chlorophyll Catabolites. *Proc. Natl. Acad. Sci. U. S. A.* **2003**, *100*, 6910−6915.
(37) Mühlecker, W.; Kräutler, B.; Ginsburg, S.; Matile, P. Breakdown of Chlorophyll—A Tetrapyrrolic Chlorophyll Catabolite from Senescent Rape Leaves. *Helv. Chim. Acta* **1993**, *76*, 2976−2980.
(38) Pružinska, A.; Tanner, G.; Aubry, S.; Anders, I.; Moser, S.; Müller, T.; Ongania, K.-H.; Kräutler, B.; Youn, J.-Y.; Liljegren, S. J.; Hörtensteiner, S. Chlorophyll Breakdown in Senescent *Arabidopsis* Leaves. Characterization of Chlorophyll Catabolites and of Chlorophyll Catabolic Enzymes Involved in the Degreening Reaction. *Plant Physiol.* **2005**, *139*, 52−63.
(39) Kräutler, B.; Matile, P. Solving the Riddle of Chlorophyll Breakdown. *Acc. Chem. Res.* **1999**, *32*, 35−43.
(40) Christ, B.; Schelbert, S.; Aubry, S.; Süssenbacher, I.; Müller, T.; Kräutler, B.; Hörtensteiner, S. MES16, a Member of the Methyl Esterase Protein Family, Specifically Demethylates Fluorescent Chlorophyll Catabolites During Chlorophyll Breakdown in Arabidopsis. *Plant Physiol.* **2012**, *158*, 628−641.
(41) Hörtensteiner, S. Update on the biochemistry of chlorophyll breakdown. *Plant Mol. Biol.* **2013**, *82*, 505−517.

DOI: 10.1021/jf5055326
J. Agric. Food Chem. 2015, 63, 1385−1392

Cooking Process. Three pressure cooker pots of 8 L capacity were purchased from Seb (France) and modified in the following way: for an improved process control, temperature and pressure sensors were integrated into the lid. A temperature sensor was additionally added on the bottom of the pots for an ideal control of internal temperature, achieved via autoregulation of the heating system.

Vegetable broths were prepared from boiling 380 g of carrot, 380 g of leek, 300 g of celeriac, and 250 g of turnip in 3275 mL of water. To avoid uneven cooking and obtain ideal heat transfer, all ingredients were maintained entirely immersed during cooking by two grids, one above and one below the vegetable pieces. The lower grid allowed an improved liquid circulation and eliminated nonhomogenous cooking by preventing direct contact between the solid ingredients and the bottom of the pot.

Experimental Considerations. To compare broths prepared from different processes (pressure and boiling temperature), the concept of cooking value (CV) was used to determine the cooking time that should be applied to achieve the identical cooking degree of ingredients or "cookedness" when working at different pressures.[9−11] The formula describing the CV is the following,

$$\mathrm{CV} = 10^{\theta_i - \theta_{ref}/z} \times t_i$$

with θ_i = boiling temperature at pressure P_i, θ_{ref} = reference temperature (100 °C), z = kinetic constant (14−44 °C depending on the food), and t_i = cooking time at boiling point θ_i.

In the current study, the impact of cooking methods (pressure and heating time) was investigated at similar degree of cookedness achieved after boiling ingredients for 1 h at ambient atmosphere, meaning that $\mathrm{CV_{AP1}} = \mathrm{CV_{HP}} = \mathrm{CV_{LP}}$ (AP1 meaning atmospheric pressure (AP) for 1 h; HP and LP are for high- or low-pressure conditions, respectively). This results in the following formula,

$$10^{\theta_{AP1} - \theta_{ref}/z} \times t_{AP1} = 10^{\theta_{LP} - \theta_{ref}/z} \times t_{LP}$$

$$\Leftrightarrow \frac{\theta_{AP1}}{z} + \ln t_{AP1} = \frac{\theta_{LP}}{z} + \ln t_{LP}$$

$$\Leftrightarrow \frac{t_{LP}}{t_{AP1}} = 10^{\theta_{AP1} - \theta_{LP}/z}$$

with θ_{AP1} = 95 °C, t_{AP1} = 1 h, and θ_{LP} = 80 °C.

Using the same formula for determining t_{HP} (θ_{LP} = 110 °C), this leads to

$$\frac{t_{HP}}{t_{AP1}} = 10^{\theta_{AP1} - \theta_{HP}/z}$$

The z-value is generally given between 14 and 44 °C depending on the nature of the food.[10] Because the vegetable soups were prepared from four vegetables of different intrinsic compositions, the exact z-value of our food preparations in the working conditions was not known. To define the z-value (and then the cooking time to be applied at high and low pressures), preliminary kitchen trials were performed. During these trials, sensory assessment on texture showed that high-pressure boiling for 10 min and low-pressure boiling (cook-vide) for 8 h led to a similar degree of cookedness as the reference sample AP1 (the z-value was found to be ∼16.5 °C).

Atmospheric Cooking. Atmospheric cooking was carried out using a thermostatically controlled hot plate to maintain the set boiling temperature at 95 °C. Vegetables were boiled for 1 h at atmospheric pressure to give the broth AP1 (reference broth).

High-Pressure Cooking. High-pressure cooking was carried out using the modified pressure cooker and a thermostatically controlled hot plate to maintain the set boiling temperature at 110 °C. Vegetables were boiled at 1.5 bar for 10 min and 1 h to give broths HP0.6 and HP1, respectively.

Low-Pressure Cooking. Low-pressure boiling was performed using the vacuum system from Gastrovac (International Cooking Concepts, J.P. Selecta S.A., 08630 Abrera, Spain) and the modified pressure cooker. Vegetables were boiled at 480 mbar for 1, 5, and 8 h (LP1, LP5, and LP8, respectively).

Summary of Experimental Plan. Table 1 summarizes the preparation parameters used to produce vegetable broths in this study.

Table 1. Boiling Conditions for the Preparation of Vegetable Broths

name of vegetable broth	pressure (mbar)	cooking time (h)
AP1	926	1
HP0.6	1500	0.6
HP1	1500	1
LP1	480	1
LP5	480	5
LP8	480	8

This experimental plan allowed for assessing the influence of the pressure (HP1 vs AP1 vs LP1), the cooking method at similar CV (HP0.6 vs AP1 vs LP8), and the cooking time when working under reduced pressure (LP1 vs LP5 vs LP8)

Sample Preparation after Cooking. After cooking, the broths were cooled down. Large vegetable chunks were then removed and squeezed manually to extract as much liquid as possible. The liquid was filtered on SEFAR PETEX, 45 μm. Solid and liquid parts were weighed separately, and the pH of the resulting liquids was determined.

Vegetable and Water Weight Loss after Heating (L_{veg} and L_{water}, Respectively). Solid and liquid losses after cooking were calculated according to the following formula,

$$L = \frac{W_{initial} - W_{final}}{W_{initial}} \times 100$$

with L = loss (%) and W = weight (g).

Volatile Analysis. Preparations (4 mL) were introduced in 20 mL solid-phase microextraction (SPME) vials and saturated with NaCl. One-half μL of methyl caprylate solution (5 ppm, in Millipore water) was added to the vials before analysis as the internal standard. The SPME fiber polydimethylsiloxane/divinylbenzene (PDMS-DVB) (65 μm 23-gauge needle, Supelco no. 57345-U), chosen for its good compromise between sensitivity and response linearity, was exposed for 10 min at 40 °C to the headspace above the sample. After sampling, desorption was performed in splitless mode at 250 °C for 10 min to desorb and transfer volatile compounds. The injector was equipped with a 0.75 mm i.d. liner (Supelco). GC separation was performed on a DB-WAX column (Agilent, 30 m length, 0.25 mm internal diameter, and 0.25 μm film thickness). The GC oven temperature program (Agilent Technologies 6890 GC oven) started at 20 °C for 3 min, then heated at 6 °C/min until 240 °C, and held this temperature for 10 min. The GC was coupled to a mass selective (MS) detector (Agilent Technologies 5973) operating in electron ionization/total ion chromatogram (EI/TIC) (70 eV) mode. Peak identification was tentatively done by comparison with theoretical MS spectra and Kovats indices. Experimental retention indices were obtained by the injection of an alkane solution (C_5−C_{18} fraction). The relative quantitation was carried out by calculating the following ratio:

$$R = \frac{\mathrm{Area_{compound}}}{\mathrm{Area_{methylcaprylate}}}$$

Quantitation of Basic Tastants. Broths were freeze-dried using a Lyolab G freeze-drier (LSL Secfroid, 1111 Aclens, CH). The resulting powders were stored in a plastic box at −20 °C until analysis. The samples were diluted in deionized water for quantitation of carbohydrates (1 mg/L), organic acids (0.5 and 0.1 mg/L), and free amino acids (0.5 mg/L).

Organic acids (quinic, pyroglutamic, lactic, formic, acetic, citric, oxalic, butyric, and propionic acids) were quantitated by high-performance ion-exchange chromatography using an ICS-2000 ion chromatography system from Dionex (Thermo Fisher Scientific,

DOI: 10.1021/jf506173m
J. Agric. Food Chem. 2015, 63, 1393−1400

Waltham, MA, U.S.A.) equipped with an autosampler, a OH^- eluent generator, a suppressor, a column oven, and a conductivity detector. The column was an IonPac (AS11-HC, 4 × 250 mm) coupled with a guard column (4 × 50 mm), both from Dionex. The eluent used was deionized water, and the hydroxide (OH^-) was produced by an eluent generator (KOH cartridge EGCII). The following gradient of OH^- was applied: 0.8 mM [OH^-] from 0 to 12.5 min, 0.8−5 mM [OH^-] from 12.5 to 16 min, 5−38.3 mM [OH^-] from 16 to 28 min, 38.3−60 mM [OH^-] from 28 to 30 min, 60 mM [OH^-] from 30 to 33 min, 60−0.8 mM [OH^-] from 33 to 35 min, and 0.8 mM [OH^-] from 35 to 40 min. Each compound was identified by comparing retention times with a corresponding organic acid standard and quantitated using a calibration curve.

Carbohydrates (mannitol, fucose, arabinose, galactose, glucose, sucrose, xylose, mannose, fructose, and lactose) were quantitated by high-performance ion-exchange chromatography using an ICS-5000 ion chromatography system from Dionex (Thermo Fisher Scientific, Waltham, MA, U.S.A.) equipped with an AS-50 autosampler, a OH^- eluent generator, a suppressor, a column oven, and a conductivity detector. The column was a Carbopac (PA1, 2 × 250 mm) coupled with a guard column (2 × 50 mm), both from Dionex. The eluent was deionized water, and the hydroxide (OH^-) gradient was produced by an eluent generator (KOH cartridge EGCIII) (0.4 mL/min). Elution was isocratic, fixed at 20 mM [OH^-] from 0 to 49 min. Each compound was identified by comparing retention times with a corresponding reference standard and quantitated using a calibration curve.

Free amino acids were quantitated by stable isotopic dilution analysis. The freeze-dried broths were dissolved in Millipore water (0.5 mg/mL), filtered (0.45 μm, disposable syringe filter for aqueous sample), and then spiked with the isotope-labeled internal standard (IS) (500 μL of sample + 500 μL of IS) composed of L-alanine-2-d_1, glycine-2,2-d_2, L-phenyl-d_5-alanine, L-proline-2,5,5-d_3, L-serine-2,3,3-d_3, L-threonine-2,3-d_2, and L-valine-d_8 (100 μM). Determination of response factors was done with a standard solution of the amino acids (Pierce NCI0180) diluted in a range from 5 to 50 μM and spiked with the IS (50:50) to create a 10-point calibration curve. Quantitation was performed using an HPLC 1290 Infinity system (Agilent Technologies) consisting of a binary pump (G4202A), a thermostated autosampler (G4226A + G1330B), a column oven (G1316C), and a Triple Quadrupole MS (G6460A). The column was an EC 250/4 Nucleodur 100-3 HILIC from Macherey-Nagel (760530.40), and the guard column a CC 8/4 Nucleodur 100-3 HILIC from the same supplier (761580.40). The column temperature was maintained at 35 °C. Eluent A was a mixture of acetonitrile/water/formic acid f 100:900:5, and eluent B was a mixture of the same solvents of 900:100:5. The injection volume was 1 μL. The flow rate was 0.8 mL/min. The solvent gradient started at 75% B from 0 to 5 min then 75−50% B from 5 to 6 min, 50% B for 4 min, 50−75% for 1 min, and 75% B for 4 min. In the source (ESI) the gas temperature and flow, respectively, were 300 °C and 5.1 L/min; the nebulizer was set at 45 psi. The sheath gas temperature and the gas flow were 255 °C and 11 L/min, respectively. The capillary voltage was set at 3000 V (+) and 2000 V (−), and the nozzle voltage was 500 V for both the positive and negative modes. Table 2 summarizes mass transitions of quantitated amino acids.

Sensory Evaluation. The panel (12 people) had previous experience in the sensory assessment of vegetable broths, and they were trained during 10 sessions on the relevant sensory attributes. The samples were heated before each session and maintained at ∼65 °C in thermostated flasks.

The samples were served warm and directly before evaluation following a balanced and randomized presentation plan. The panelists evaluated the overall intensity, saltiness, umaminess, sweetness, and carrot, leek, and celery notes of each sample on a 10-point sensory scale. They had a 4 min break between samples and were provided with freshly opened Vittel water and white bread as palate cleansers.

Statistical Analyses. *Instrumental Variables.* A one-way analysis of variance (ANOVA), with product as the fixed factor, was performed to detect significant differences between products. For each discriminant variable, the ANOVA was followed by a Fisher's least significant difference (LSD) procedure to identify all pairs of products that were significantly different.

Sensory Data. A two-way ANOVA with the taster as the random factor and the sample as the fixed factor with interaction taster−product was performed to detect significant differences between samples. Then, for each discriminant sensory attribute, the ANOVA was followed by a Fisher's LSD procedure to identify all pairs of products that were significantly different.

Table 2. Mass Transition of Quantitated Amino Acids

substance	MW [Da]	Q1 → Q3 [*m/z*]	frag[a] [V]	CE[b] [V]
L-glutamic acid	147	148 → 84	75	13
L-serine-d_3	108	109 → 63	80	8
L-serine	105	106 → 60	50	4
L-histidine	155	156 → 110	88	9
L-arginine	174	175 → 70	94	10
L-alanine	89	90 → 44	41	5
L-alanine-d_1	90	91 → 45	15	8
L-phenylalanine	165	166 → 120	100	5
L-phenylalanine-d_5	170	171 → 125	110	8
L-threonine	119	120 → 74	50	5
L-threonine-d_2	121	122 → 76	80	8
L-glycine	75	76 → 30	45	1
L-glycine-d_2	77	78 → 32	15	8
L-tyrosine	181	182 → 136	60	9
L-valine	117	118 → 72	45	5
L-valine-d_8	125	126 → 80	80	8
L-leucine	131	132 → 30	55	13
L-isoleucine	131	132 → 69	46	13
L-methionine	149	150 → 56	70	13
L-proline	115	116 → 70	85	13
L-proline-d_3	118	119 → 73	80	8

[a]Fragmentation voltage. [b]Collision energy.

RESULTS AND DISCUSSION

General Characteristics of Vegetable Broths. The pH, solid ingredient/water mass ratios before and after cooking, and the losses in vegetable and water mass (L_{veg} and L_{water}, respectively) are shown in Table 3. The loss of water was dependent on the cooking process. Because low-pressure boiling was carried out in a closed system to maintain a pressure of 480 mbar during boiling, the final water content remained close to the initial one. On the contrary, atmospheric and especially high-pressure cooking allowed water to exit from the system during heating, leading to a higher loss of water. The vegetable mass after cooking decreased by 27.7, 13.1 and 0.3%

Table 3. General Characteristics of Vegetables Broths

name	final pH	initial food/water ratio[a]	final vegetables/broth ratio[b]	L_{veg}[c] (%)	L_{water}[d] (%)
AP1	7.3	0.40	0.38	13.13	9.23
HP0.6	7.0	0.40	0.36	15.5	6.69
HP1	5.6	0.40	0.39	27.73	24.62
LP1	7.4	0.40	0.40	0.35	4.55
LP5	6.4	0.40	0.38	7.63	3.33
LP8	6.1	0.40	0.33	19.8	1.46

[a]Weight ratio between vegetables and water before heating treatment. [b]Weight ratio between vegetables and broth after heating treatment. [c]Vegetables weight loss during heating. [d]Water weight loss after heating.

DOI: 10.1021/jf506173m
J. Agric. Food Chem. 2015, 63, 1393−1400

Table 4. Content of Organic Acids, Sugars, and Amino Acids (mg/L)[a]

compounds (mg/L broth)	taste threshold, mg/L water	AP1	HP0.6	HP1	LP1	LP5	LP8
organic acids							
malic acid	495	926.9 c	996.9 b,c	1393.3 a	765.9 d	1029.3 b,c	1116.1 b
acetic acid	120	327.3 b,c,d	258.9 c,d	472.7 a	236.4 d	341.5 b,c	384.5 a,b
pyroglutamic acid	1264	210.7 c,d	203.9 c,d	514.4 a	124.4 d	278.6 b,c	357.7 b
formic acid[NS]	197	199.9	117.9	221.6	107.2	150.8	170.4
citric acid		47.4 c	63.2 b	84.3 a	37.2 d	59.9 b	59.7 b
oxalic acid[NS]		35.2	35.9	123.9	28.6	42.2	45.6
carbohydrates							
sucrose[NS]	8208	3131.7	2581.3	3328.3	2417.1	3238.3 a	3533.9 a
glucose	16200	2740.4 b,c	2617.8 b,c	3042.1 a,b	2338.6 c	3094.2 a,b	3308.3 a
fructose	9360	2274.4 b,c	2358 b,c	2699.5 a,b	1973.5 c	2673.5 a,b	2968.3 a
mannitol		1158.7 b,c	1135 b,c	1391.6 a,b,c	963.6 c	1492.5 a,b	1694.1 a
amino acids							
leucine	1574	4.2 b,c	3.9 b,c	2.8 c	3.8 b,c	4.7 b	6.9 a
isoleucine	1443	4.1 c,d	3.8 c,d	2.7 d	4.7 b,c	5.9 a,b	7.5 a
phenylalanine	9581	6.8 c	6.9 c	6.8 c	6.1 c	8.3 b	9.9 a
arginine	13065	9.5 c,d	9.2 c,d	10.6 b,c	7.9 d	12.4 a,b	13 a
histidine	7447	11.2 c,d	11.4 b,c,d	12.2 a,b,c	9.4 d	13.4 a,b	14.2 a
valine	2460	16.5 c	16.9 c	16.6 c	16.4 c	22.1 b	24.8 a
tyrosine	906	7.7 c,d	7.8 c,d	8.5 b,c	7 d	9.1 b	11.5 a
methionine	746	2.8 c,d	2.6 d	3 b,c	2.2 e	3.1 a,b	3.5 a
alanine[NS]	712	26.1	21.3	20.4	19	24.2	23.5
glycine	1876	1.7 b	1.86 b	2.05 a	1.5 b	2.2 a	2.2 a
proline	2990	6.4 b	6.2 b	6.3 b	5.8 b	7.5 a	8.1 a
threonine	4764	10.6 d	11.8 c,d	15.2 a,b	8.1 e	13.9 b,c	16.2 a
glutamic acid	220	32.5 b	41.5 a	32.4 b	30.1 b	43.0 a	46.1 a
serine	3150	13.1 b,c	14.9 b	13.9 b,c	12.4 c	18.3 a	19.5 a
aspartic acid	532	19.5 d	24.4 b,c	21.1 c,d	19.8 d	28.4 a	26.9 a,b

[a]Results are expressed as means ($n = 4$); [NS] means nonsignificant statistical difference ($p > 0.05$). a, b, c, and d represent the statistical groups ($p < 0.05$).

for HP1, AP1, and LP1, respectively. Thus, low-pressure boiling implied a reduction in weight loss and therefore increased the yield of vegetables. When boiling at high pressure, the cellular structure of the vegetables might be quickly degraded, leading to the release of water and components of vegetables in the broth. Indeed, after 10 min of boiling at 110 °C under 1.5 bar, a 16% decrease of vegetable mass was observed. At similar CV, the loss of vegetable mass was similar regardless of the pressure (13% for AP1, 15% for HP0.6, and 19% for LP8). Finally, the pH of the vegetable broths ranged from 5.6 to 7.3 and decreased with cooking time (HP0.6 > HP1 and LP1> LP5 > LP8).

Quantitation of Nonvolatile Compounds. During the cooking process, hydrophilic, nonvolatile compounds from the vegetable matter are released into the water. These compounds contribute to the overall flavor of the vegetable broth because they possess their own inherent and specific taste properties. Moreover, they can react with each other to generate new taste-active molecules. Table 4 summarizes the content of organic acids, carbohydrates, and free amino acids in the respective vegetable broths. All carbohydrates and amino acids have been previously detected in leek, carrot, turnip, or celeriac. Sucrose, glucose, and fructose are the most abundant carbohydrates in fresh carrots, celeriac, and leek.[12−15] Mannitol is also present in a relatively high amount in leek and celeriac.[14,15] The main amino acids detected in carrots were aspartic acid and alanine,[12,13] while aspartic and glutamic acids were the most abundant amino acids in leek and celeriac.[15] The occurrence of organic acids in these vegetables is less documented. Phan et al. found that isocitric, citric, malic, and oxalic acids are the most abundant in fresh carrots.[16]

As shown in Table 4, six organic acids were detected and quantitated in vegetable broths (pyroglutamic, acetic, malic, oxalic, citric, and formic acids). Malic acid was the major one with concentrations ranging from 766 to 1393 mg/L. Acetic, formic, and pyroglutamic acids were present at lower concentrations (117−514 mg/L), while the levels of citric and oxalic acids were below 130 mg/L. Malic and acetic acids were present above their respective taste recognition threshold in water, 495 and 120 mg/L,[17] respectively, meaning they contribute to the sourness of the vegetable broths. Significant differences were found for all organic acids except formic and oxalic acids for which the concentrations were similar in all vegetable broths. The highest contents of organic acids were found when the high-pressure cooking process was applied (HP1). On the contrary, the lowest concentrations were found under low-pressure cooking in LP1.

Concentrations of sucrose, glucose, and fructose ranged from 2430 to 3530 mg/L. Mannitol was detected to a smaller extent (963 and 1694 mg/L). Significant differences in their concentrations were found for all carbohydrates except sucrose. However, these sugars were present below their respective taste recognition threshold in water; therefore, they are minor contributors to the taste of broths. The highest levels of carbohydrates were obtained in LP8 cooking, and the lowest ones were obtained in LP1.

Fifteen amino acids were quantitated in the vegetable broths: although significant differences between individual preparations

DOI: 10.1021/jf506173m
J. Agric. Food Chem. 2015, 63, 1393−1400

Table 5. Relative Area Ratios[a] of Volatile Compounds

molecules[b]	exp. R.I.	AP1	HP0.6	HP1	LP1	LP5	LP8	StD[b]
2-thiapropane	720	1.43 b,c	2.29 a,b	0.00 c	1.66 b,c	3.62 a	3.52 a	1.62
propanal	805	0.13 b,c	0.19 b,c	0.00 c	0.31 b	0.56 a	0.62 a	0.26
3-methylbutanal	905	0.13 c	0.37 b	0.90 a	0.00 c	0.13 c	0.11 c	0.34
ethanol[NS]	933	0.35	0.19	0.06	0.62	0.25	0.13	0.33
pentanal[NS]	966	0.17	0.08	0.05	0.36	0.81	0.25	0.42
α-pinene[NS]	1007	0.08	0.24	0.38	0.47	1.68	0.3	1.10
dimethyl disulfide	1057	0.10 b	0.22 b	0.11 b	0.15 b	0.30 b	0.51 a	0.19
hexanal	1071	0.52 c	0.65 b,c	0.53 c	1.12 a,b,c	1.34 a,b	1.55 a	0.60
2-methyl-2-butenal[NS]	1078	0.38	0.32	0.05	1.11	0.41	0.39	0.52
2-β-pinene[NS]	1085	0.53	1.4	1.68	2.32	1.64	1.5	1.11
trans-2-pentenal	1115	0.09 b,c	0.06 b,c	0.00 c	0.20 a,b	0.34 a	0.35 a	0.17
2-methyl-2-pentenal	1144	0.39 c,d	0.65 b,c,d	0.00 d	3.36 a	1.91 a,b,c	1.97 a,b	1.49
β-myrcene[NS]	1149	0.09	0.39	1.02	1.14	0.57	0.42	0.62
limonene[NS]	1179	2.81	5.24	11.28	11.73	7.8	4.67	6.35
methyl propyl disulfide	1215	0.07 c	0.09 b,c	0.00 c	0.08 b,c	0.17 b	0.32 a	0.12
β-ocimene[NS]	1224	0.18	0.46	0.57	0.64	0.35	0.3	0.36
γ-terpinene[NS]	1231	0.71	0.94	1.28	1.93	2.04	1.83	0.83
α-terpinolene[NS]	1269	0.23	0.31	0.18	0.34	1.09	0.71	0.52
octanal[NS]	1281	1.46	1.86	1.88	2.37	2.49	2.72	0.99
trans-2-heptenal[NS]	1312	0.07	0.03	0.21	0.07	0.12	0.08	0.12
6-methyl-5-hepten-2-one[NS]	1328	0.2	0.37	0.36	0.41	0.37	0.38	0.24
dimethyl trisulfide	1365	0.06 c	0.06 b,c	0.18 b,c	0.24 b,c	0.28 b	0.55 a	0.21
nonanal[NS]	1386	1.44	1.99	3	2.43	1.54	1.46	1.10
2-ethyl-1-hexanol	1488	0.47 d	0.65 c,d	0.72 b,c	0.84 b,c	1.16 a,b	1.18 a	0.33
decanal[NS]	1494	0.34	1.6	1.22	1.28	1.07	1.37	0.96
linalol[NS]	1544	0.13	0.06	0.09	0.14	0.19	0.19	0.14
1-octanol[NS]	1557	0.42	0.32	0.38	0.45	0.52	0.29	0.27
trans-caryophyllene[NS]	1592	2.15	9.44	6.45	10.34	11.98	11.93	6.68
4-terpineol	1598	0.29 b	0.57 b	0.59 b	0.40 b	1.60 b	7.34 a	3.62
1-nonanol	1659	0.09 b	0.00 b	0.06 b	0.34 b	0.58 a	0.68 a	0.29
α-humulene[NS]	1665	0.35	0.86	0.64	0.73	0.81	1.18	0.45
trans-geranyl acetone[NS]	1851	0.26	0.48	0.31	0.49	0.43	0.39	0.32
β-ionone[NS]	1936	0.11	0.1	0.06	0.2	0.43	0.34	0.24
(−)-caryophyllene oxide[NS]	1981	0.16	0.17	0.04	0.39	0.39	0.36	0.22
benzenepropanenitrile	2026	1.21 c,d	2.39 c,d	20.67 a	1.00 d	9.63 b,c	16.47 a,b	9.15
2-methoxy-4-vinylphenol	2184	0.12 c	0.18 c	0.54 a,b	0.09 c	0.41 b,c	0.81 a	0.33
2-phenylethylisothiocyanate	2211	1.45 b	3.36 b	3.03 b	29.51 a	3.15 b	1.78 b	11.78
elemicin[NS]	2219	6.05	0.87	0.24	1.2	8.4	3.33	5.80
myristicin[NS]	2254	6.61	0.53	0.98	4.54	5.8	6.08	6.31

[a]Results are expressed as means (n = 3). a, b, c, and d represent the statistical groups ($p < 0.05$). [b]Tentatively identified by comparison with theorical MS spectra and Kovats indices. [b]StD means standard deviation; [NS] means nonsignificant statistical difference ($p > 0.05$).

were found (except for alanine), those might not have an impact on the overall taste as their respective concentration was lower than 50 mg/L, far below their taste recognition threshold. Glutamic and aspartic acids followed by valine and alanine were the amino acids found in the highest concentrations. This is in agreement with the literature data.[12,13,15]

When cooking at different pressures for 1 h (HP1 vs AP1 vs LP1), high-pressure boiling generally led to significantly higher concentrations of carbohydrates (glucose and fructose), amino acids (arginine, histidine, tyrosine, methionine, glycine, and threonine) and organic acids, whereas low-pressure and ambient boiling gave similar results except for malic and citric acids, methionine, and threonine, for which concentrations were higher in broth AP1. However, the differences, even when statistically significant, are too small to modify the taste profile of broth.

When comparing preparations with similar CVs (HP0.6 vs AP1 vs LP8), high-pressure and ambient boiled ones had similar concentrations of nonvolatile compounds. Differences were only observed for citric, aspartic, and glutamic acids (47.4 vs 63.2 mg/L, 19.5 mg/L vs 24.4 g/L, and 32.5 vs 41.5 mg/L, respectively, for AP1 and HP0.6). However, those differences observed should be too minor to influence the taste profile. Generally, significantly higher concentrations of amino acids, carbohydrates, and organic acids were found in LP8, likely due to the longer cooking time required to obtain a comparable CV that allowed nonvolatile molecules to be more greatly extracted from the vegetables.

Cooking time generally had an impact on the release of nonvolatile compounds in broth during boiling: the longer the cooking duration, the higher was the concentration. However, broths LP5 and LP8 led to similar compositions of water-soluble, nonvolatile molecules except for leucine, phenylalanine, valine, tyrosine, and threonine, which were slightly more present in broth LP8. This suggests that the maximum release might be reached after 5 h of cooking.

DOI: 10.1021/jf506173m
J. Agric. Food Chem. 2015, 63, 1393−1400

Semiquantitation of Volatile Compounds. Cooking at different temperatures, under different pressures, and for variable durations can impact release, oxidation, and degradation of aroma compounds and thus influence the aroma profile of the final product. The volatile profile of vegetable broths was investigated by headspace SPME-GC/MS. The relative quantitation of 39 molecules was performed using methyl caprylate as internal standard. Table 5 shows peak area ratios for each tentatively identified volatile compound and vegetable broth. These volatiles mainly belong to the chemical classes of terpenoids, aldehydes, alcohols, and sulfuric compounds. Terpenoids and sesquiterpenes such as β-myrcene, α-terpinolene, limonene, caryophyllene, α-pinene, γ-terpinene, and α-humulene are volatile compounds responsible for the typical aroma of raw carrots.[18,19] Limonene, ocimene, myrcene, γ-terpinene, and pinene have also been found as contributors to the celeriac aroma.[20] Sulfur-derived compounds such as methyl propyl disulfide and dimethyl sulfide have been previously identified as key odorants in leek, while isothiocyanates provide the major part of volatiles in turnip *Brassica rapa* var. *rapa* L.[21−23] Statistical analyses showed significant differences in the relative content of volatile compounds in vegetable broths prepared according to different cooking protocols. Sulfur compounds, aldehydes, and alcohols were the chemical classes most affected by the cooking process. Except the 4-terpineol, no significant difference between vegetable broths was found in other terpernoids concentrations.

When comparing AP1, HP1, and LP1, only a few significant differences in the relative content of volatile compounds were observed. On the one hand, aldehydes tended to be lower in abundance when high pressure was applied. Thus, short-chain aldehydes such as propanal, 2-pentenal, and 2-methyl-2-pentenal were not detected in HP1. On the other hand, boiling under low pressure (LP1) tended to increase the relative content of some aroma molecules: 2-phenylethyl isothiocyanate was present in significantly higher concentration in LP1, as well as pentenal, 2-methyl-2-pentenal, and 1-nonanol. Larger differences were observed when working at similar CVs. In that case, the volatile profiles of HP0.6 and AP1 were comparable, while 13 volatiles out of 39 were detected in higher concentrations in the low-pressure preparation LP8. Interestingly, the content of all sulfide compounds identified and quantitated by HS-SPME GC/MS (HS = headspace) was higher in LP8, namely, dimethyl sulfide (cooked cabbage odor), dimethyl disulfide (cabbage, onion-like odor), methyl propyl sulfide (roasted garlic odor), and dimethyl trisulfide (cabbage-like odor). As previously mentioned, these aroma compounds are known to be key aroma contributors of leek and possess a low odor threshold in water (e.g., 0.3−1 ppb for dimethyl sulfide and 0.005−0.01 ppb for dimethyl trisulfide).[24,25] Moreover, low-pressure boiling increased the content of some aldehydes (e.g., hexanal, pentenal, and propanal) and alcohols (e.g., 2-ethyl-1-hexanol and 1-nonanol).

Increasing the cooking time when boiling under low pressure led to higher concentrations of sulfur compounds (e.g., dimethl sulfide, dimethyl sulfide, methyl propyl sulfide, and dimethyl trisulfide). Other chemical classes of volatiles were not affected by the cooking time.

Sensory Analysis. During the preliminary sensory session, the panel described the broths as sweet, salty with leek/onion, carrots, and celery/savory aroma. An evaluation of the overall flavor intensity of broths was included in the study as well. Results of the sensory analysis are shown in Figures 1, 2, and 3.

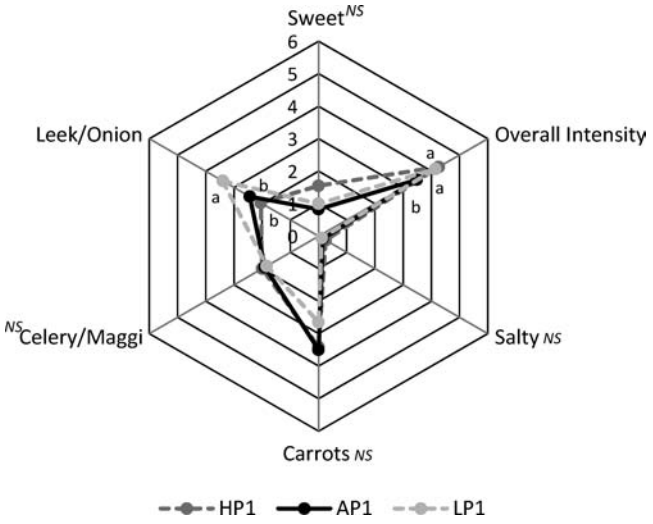

Figure 1. Sensory profile of broths cooked for 1 h. The statistical groups ($p < 0.05$) are represented by [a,b]; [NS] means nonsignificant statistical difference ($p > 0.05$).

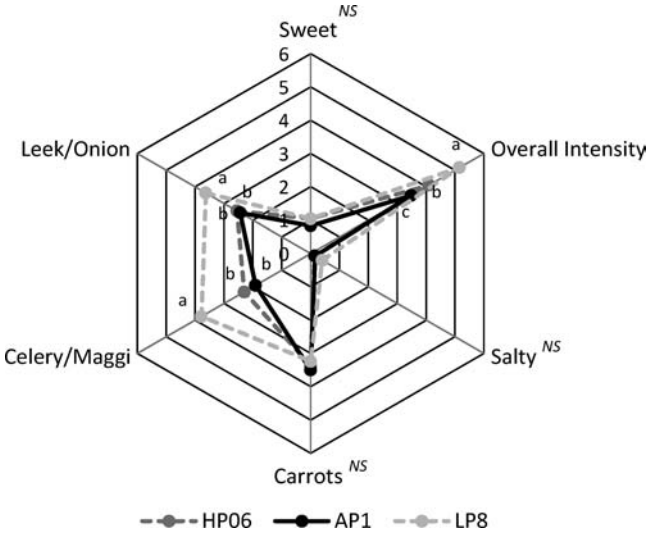

Figure 2. Sensory profile of broths cooked at similar cooking value. The statistical groups ($p < 0.05$) are represented by [a,b]; [NS] means nonsignificant statistical difference ($p > 0.05$).

Sweetness and saltiness were perceived as low with sensory scores below 2 on the 10-point sensory scale, which is explained by the low concentration of sugars as well as the fact that no salt is added to the water. No significant difference for both of these attributes was observed between broths.

As shown in Figure 1, when applying different pressures for an identical cooking time, high and ambient boiling led to broths (AP1 and HP1) with similar sensory profiles. They differed only by the overall flavor intensity, which was greater in HP1. Interestingly, low-pressure cooking for 1 h (LP1) enhanced significantly the overall intensity (compared to AP1) and the leek/onion aroma. Comparing similar CVs (Figure 2), high pressure and ambient boiling (AP1 and HP0.6) consistently gave similar flavor profiles while the greater sensory differences were generated in terms of celery/savory and leek aroma notes when heating under low pressure. Sweet, carrot aroma and saltiness of HP0.6, AP1, and LP8 were found to be similar.

DOI: 10.1021/jf506173m
J. Agric. Food Chem. 2015, 63, 1393−1400

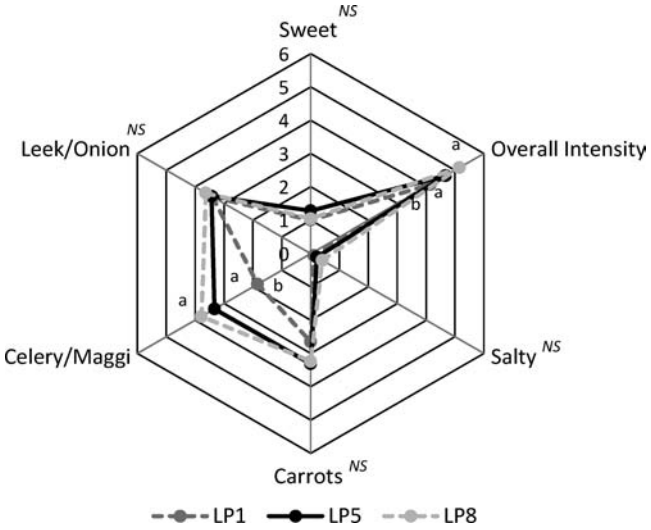

Figure 3. Sensory profile of broths cooked under reduced pressure. The statistical groups ($p < 0.05$) are represented by ^{a,b}; ^{NS} means nonsignificant statistical difference ($p > 0.05$).

Considering the effect of duration when cooking under low pressure, sensory results showed that the maximum intensity of leek/onion aroma was already achieved after 1 h of boiling while celery/savory aroma increased along time and reached a plateau after 5 h, leading to similar flavor profiles of broths LP5 and LP8 (Figure 3).

When assessing the impact of pressure during cooking for 1 h, concentrations of organic acids, amino acids, and sugars were lower when boiling at low pressure; however, no impact on the sweetness or saltiness was observed. Interestingly, the leek/onion note was significantly higher in broth LP1, meaning that some specific aroma might be enhanced by low-pressure cooking. Additionally, the process was found to strongly impact the sensory and chemical profiles of the vegetable broths. Thus, ambient boiling for 1 h or high-pressure cooking for 10 min led to likewise sensory and molecular profiles while low-pressure cooking could be advantageously used to improve the nonvolatile and volatile composition as well as the sensory profiles of broths (especially regarding the overall intensity, leek/onion, and celery/savory notes). Enhancement of sulfur volatiles in the headspace of broths when prepared at low pressure could be correlated to the stronger leek/onion and celery/savory aroma, because those volatiles are known to be the key odorants of leek. The sulfides are known to be highly volatile molecules with low odor thresholds that are sensitive to heat and oxidation. Low-pressure cooking would consequently allow preserving the fragile volatiles even after a long heating time, likely due to the lower boiling point (80 °C in this study) and the reduced level of oxygen. Furthermore, the sensory and chemical profiles of LP vegetable broths seemed to reach a plateau after 5 h, suggesting that cooking time might be reduced to 5 h instead of 8 h while maintaining the same flavor profile of vegetable broths.

Thus, low-pressure boiling might apply to enhance the flavor profiles of culinary preparations and therefore could help to increase consumer preference. The preservative effect of low-pressure boiling might not be restricted to aroma compounds and can be extended to all thermally sensitive compounds like vitamins and coloring molecules. Further work on other culinary preparations and complex dishes is currently being carried out in the laboratory to assess sensorial and nutritional impact of low-pressure cooking.

AUTHOR INFORMATION

Corresponding Author

*E-mail: Candice.smarrito-menozzi@rdls.nestle.com. Phone: +41 21 7885 8868. Fax: +41 21 7885 8554.

Notes

The authors declare no competing financial interest.

REFERENCES

(1) Schellekens, M. New research issues in sous-vide cooking. *Trends Food Sci. Technol.* **1996**, *7*, 256−262.
(2) Baldwin, D. E. Sous vide cooking: A review. *Int. J. Gastronomy Food Sci.* **2012**, *1*, 15−30.
(3) Martinez-Monzo, J.; Andres, J.; Torres, S.; Sanjuan N.; Garcia-Segovia, P. System for vacuum cooking of food. ES 1057342U (A47J27/04), U200400864, 2004 .
(4) García-Segovia, P.; Andrés-Bello, A.; Martínez-Monzó, J. Effect of cooking method on mechanical properties, color and structure of beef muscle (*M. pectoralis*). *J. Food Eng.* **2007**, *80*, 813−821.
(5) Andrés-Bello, A.; García-Segovia, P.; Martínez-Monzó, J. Effect of Vacuum Cooking (Cook-Vide) on the Physical-Chemical Properties of Sea Bream Fillets (*Sparus aurata*). *J. Aquat. Food Prod. Technol.* **2009**, *18*, 79−89.
(6) García-Segovia, P.; Andrés-Bello, A.; Martínez-Monzó, J. Texture properties of potatoes (*Solanum tuberosum* L., cv. Monalisa) as affected by different cooking processes). *J. Food Eng.* **2008**, *88*, 28−35.
(7) Iborra-Bernad, C.; Tarrega, A.; García-Segovia, P. Comparison of Vacuum Treatments and Traditional Cooking Using Instrumental and Sensory Analysis. *Food Anal. Methods* **2014**, *7*, 400−408.
(8) Iborra-Bernad, C.; Philippon, D.; Garcia-Segovia, P.; Martinez-Monzo, J. Optimizing the texture and color of sous vide and cook-vide green bean pods. *LWT −Food Sci. Technol.* **2013**, *51*, 507−513.
(9) Bimbenet, J.-J.; Duquenoy, A.; Trystram, G. Génie des procédés alimentaires. Des bases aux applications. *Le Mensuel de l'Innovation Alimentaire* **2002**, *338*, 286−287.
(10) Holdsworth, S. D. Optimisation of Thermal Processing—A Review. *J. Food Eng.* **1985**, *4*, 86−116.
(11) Mansfield, T. High-temperature-short-time sterilisation. *Proc. 1st Int. Congr. Food Sci. Technol.* **1962**, *4*, 311.
(12) Nyman, E. M.; Svanberg, S. J. M.; Andersson, R.; Nilsson, T. Effects of cultivar, root weight, storage and boiling on carbohydrate content in carrots (Daucus carota L). *J. Sci. Food Agric.* **2005**, *85*, 441−449.
(13) Alabran, D. M.; Mabrouk, A. F. Carrot Flavor. Sugars and free nitrogenous compounds in fresh carrots. *J. Agric. Food Chem.* **1973**, *21*, 205−208.
(14) Brandl, W.; Galensa, R.; Herrmann, K. HPLC-Bestimmung von Sellerieinhaltsstoffen (Hydroxysäureester; Zucker; Mannit; Phtalide). *Z. Lebensm.-Unters. Forsch.* **1983**, *177*, 325−327.
(15) Souci, S. W.; Fachmann, W.; Kraut, H. *Food Composition and Nutrition Tables 1989/90* ; Stuttgart, 1989.
(16) Phan, C. T.; Hsu, H.; Sarkar, S. K. Physical and chemical changes occurring in the carrot root during storage. *Can. J. Plant Sci.* **1973**, *53*, 635−641.
(17) Rotzoll, M.; Dunkel, A.; Hofmann, T. Quantitative studies, taste reconstitution and omission experiements on the key taste compounds in morel mushrooms (*Morchella deliciosa* FR.). *J. Agric. Food Chem.* **2006**, *54*, 2705−2711.
(18) Habegger, R.; Müller, B.; Hanke, A.; Schnitzler, W. H. Aroma compounds in different varieties of carrot. *Gartenbauwissenschaft* **1996**, *61*, 225−229.
(19) Edelenbos, M.; Christensen, L. P.; Kjeldsen, F. Characterisation of aroma volatiles in carrots using GC-olfactometry and aroma extract dilution. *Flavour Research at the Dawn of the Twenty-First Century*; Proceedings of the 10th Weurman Flavour Research Symposium,

DOI: 10.1021/jf506173m
J. Agric. Food Chem. 2015, 63, 1393−1400

Dijon, France, 2002; Le Quéré, J.-L., Étiévant, P. X., Eds.; Intercept: Paris, France, 2003; pp 588−591.
(20) MacLeod, G.; Ames, J. M. Volatile components of celery and celeriac. *Phytochemistry* **1989**, *28*, 1817−1824.
(21) Schreyen, L.; Dirnick, P.; Van Wassenhove, F.; Schamp, N. Analysis of leek volatiles by headspace condensation. *J. Agric. Food Chem.* **1976**, *24*, 1147−1152.
(22) Taveira, M.; Fernandes, F.; Guedes de Pinho, P. G.; Andrade, P. B.; Pereira, J. A.; Valentao, P. Evolution of *Brassica rapa* var. *rapa* L. volatile composition by HS-SPME and GC/IT-MS. *Microchem. J.* **2009**, *93*, 140−146.
(23) Heaney, R. K.; Fenwick, G. R. The glucosinolate content of *Brassica* vegetables. A chemotaxonomic approach to cultivar identification. *J. Sci. Food Agric.* **1980**, *31*, 794−801.
(24) Mulders, J. The odour of white bread. IV. Quantitative determination of constituents in the vapour and their odour values. *Z. Lebensm.-Unters. Forsch.* **1973**, *151*, 310−317.
(25) Buttery, R. G.; Gaudagni, D. G.; Ling, R. M.; Seifert, R. M.; Lipton, W. Additonal volatile components of cabbage, broccoli and cauliflower. *J. Agric. Food Chem.* **1976**, *24*, 829−832.

DOI: 10.1021/jf506173m
J. Agric. Food Chem. 2015, 63, 1393−1400

the composition of volatiles in food has been investigated relative to several factors, including various microorganisms, raw materials, and fermenting and ripening conditions.[5] Moreover, some studies have used fingerprinting analysis or metabolic profiling to obtain the profiles of volatiles of various foods such as tomatoes,[12] green tea,[13] beer,[14] *doenjang*,[4] and pine mushrooms.[15] The application of nontargeted approach has also revealed a correlation between volatile components and sensory attributes in coffee.[16]

The profiles of volatiles of rice-*koji doenjang* inoculated with one or other of three types of *Aspergillus* species (*A. oryzae*, *A. sojae*, and *A. kawachii*) and over a range of fermentation periods were investigated in this study. In addition, the activities of various enzymes were examined to clarify their effects on volatile-compound formation in rice-*koji doenjang*.

MATERIALS AND METHODS

Solvents and Chemicals. The following chemicals were obtained commercially: HPLC grade water (J. T. Baker, Phillipsburg, NJ), methyl cinnamate (Fluka, Buchs, Switzerland), acetonitrile (Merck, Darmstadt, Germany), starch (Samchun, Pyeongtaek Si, Republic of Korea), I_2 (Duksan, Ansan Si, Republic of Korea), and casein (SHOWA, Okayama, Japan). Na_2HPO_4, KH_2PO_4, and Na_2CO_3 were obtained from Daejung (Siheung Si, Republic of Korea). *n*-Paraffins, iodine, KI trichloroacetic acid, Folin and Ciocalteu's phenol, *p*-nitrophenylbutyrate, *p*-nitrophenol, *p*-nitrophenyl palmitate, sodium dodecyl sulfate, Triton X-100, and Tris-HCl buffer were purchased from Sigma-Aldrich (St. Louis, MO).

Preparation of Rice-*koji doenjang*. Polished rice (*Oryza sativa* L., Incheon, Republic of Korea) was steeped in water at 25 °C for 10 h, steamed at 121 °C for 40 min, and then inoculated with three different *Aspergillus* species, including *A. oryzae* (AO), *A. sojae* (AS), and *A. kawachii* (AK), respectively. After that, they were fermented at 30 °C for 40 h to make rice-*koji*. Soybeans (*Glycine max* L.) were soaked in water at 25 °C, cooked at 121 °C for 5 min, and mixed with three different rice-*koji* at the ratio of 4:6 (soybeans:*koji*). Proper amounts of salt and water were added, to the final contents of 17% and 10%, respectively, and then fermented at 30 °C for 8 weeks after yeast strain (*Z. rouxii*) was inoculated at the level of 10^6 CFU/g.

The fermented samples (AO, AS, and AK) were obtained at 0, 1, 2, 4, 5, 7, and 8 weeks, respectively (Table 1), and kept in a deep freezer (below −70 °C) before analysis.

Volatile Components Analysis of Rice-*koji doenjang*. *Extraction of Volatile Components.* Volatile flavor components in rice-*koji doenjang* samples were extracted using the solid-phase microextraction (SPME) method. Each sample (10 g) was mixed with 8 mL of HPLC grade water and 100 μL of methyl cinnamate [200 ppm (w/v) in ethanol] as an internal standard in 60 mL amber SPME vials with a silicon/teflon septum (Supelco, Bellefonte, PA). After that, the mixtures were agitated using a Vortex-Genie 2 (Scientific Industries Inc., Bohemia, NY) at speed 7 for 1 min and maintained at 60 °C, 400 rpm for 30 min with a magnetic stirrer to reach an equilibrium state. The volatiles released into the headspace of the SPME vial were absorbed onto the 75 μm carboxen/polydimethylsiloxane (CAR/PDMS)-coated SPME fiber (Supelco, Bellefonte, PA) that was inserted by 40 mm into the sealed vial for 30 min at the same conditions of equilibrium state. All of the extractions were conducted in triplicate.

GC–MS Analysis. Volatile components extracted were analyzed using a gas chromatograph (6890N) equipped with a mass selective detector (5975) (Agilent Technologies, Palo Alto, CA). The adsorbed volatile compounds onto SPME fiber were desorbed in a GC injector at 230 °C for 5 min, using splitless injection mode with a purge-off time of 5 min and then separated on a DB-FFAP fused silica column (30 m length × 0.25 mm i.d. × 0.25 μm film thickness, J&W Scientific, Folsom, CA).

The oven temperature was maintained at 40 °C for 6 min, increased to 90 °C at a rate of 3 °C/min, raised to 200 °C at 9 °C/min, and then held at 200 °C for 8 min. The temperatures of the transfer line and MS source were 250 and 230 °C, respectively. The other MSD conditions were electronic ionization (EI) mode at 70 eV and scanning range 40–550 amu. Carrier gas was helium at a constant flow rate of 0.8 mL/min.

Table 1. Rice-*koji doenjang* Samples Used in This Study

	Aspergillus sp. inoculated in *koji*-making	permentation periods (weeks)
NA	no *Aspergillus* sp. inoculated (unfermented)	0
AO1	*A. oryzae*	1
AO2		2
AO4		4
AO5		5
AO7		7
AO8		8
AS1	*A. sojae*	1
AS2		2
AS4		4
AS5		5
AS7		7
AS8		8
AK1	*A. kawachii*	1
AK2		2
AK4		4
AK5		5
AK7		7
AK8		8

Identification and Quantification of Volatile Components. The amounts of each volatile component in rice-*koji doenjang* samples were quantified by comparing their peak areas to that of the internal standard compound, 100 μL of methyl cinnamate (200 ppm), on the GC–MS total ion chromatograms. All of the semiquantitative data obtained were mean values of triplicate measurements.

For the identification, each compound was positively confirmed by matching its mass spectral data and retention time to that of an authentic standard chemical. When standards were not available, each volatile compound was tentatively identified by comparing with the Wiley 7n mass spectral data (Agilent Technologies) and Kovats retention index (RI) values in previous literature.[4,17−26] The RI values were calculated with *n*-paraffins from C7 (*n*-heptane) to C22 (*n*-docosane) as external standards.

Enzymatic Activity Assays of Rice-*koji doenjang* during Fermentation. Enzyme activity assays for α-amylase, protease, esterase, and lipase were determined. All experiments were conducted in triplicate.

Preparation of Crude Enzyme Solution from Rice-koji doenjang. Crude enzyme solution from rice-*koji doenjang* was prepared according to the method of Lee et al. with slight modifications.[27] Briefly, 10 g of *doenjang* sample was suspended in 90 mL of distilled water and incubated with gentle shaking for 1 h at 30 °C (JSSI-300C, JSR, Gongju Si, Republic of Korea). After filtration through filter paper (Whatman No. 2), crude enzymes in the filitrate were fractionated with ammonium sulfate ranging from 20% to 80% saturation. The precifitate was centrifuged at 10 000*g* for 15 min, and then the pellet was dissolved in distilled water, followed by dialysis and lyophilization. The resulting crude enzymes were redissolved in the appropriate buffers prior to further analysis of enzyme activities.

Determination of Enzyme Activities. *α-Amylase (EC 3.2.1.1) Assay.* α-Amylase assay was performed with starch solution as substrate. A diluted crude enzyme solution was added to the reaction mixture, which consisted of 2.0 mL of soluble starch substrate solution (1% in the warm water) and 2.0 mL of pH 5.2 buffer (0.1 M citric acid plus 0.2 M Na_2HPO_4), and then at 40 °C for 30 min. After 10 mL of reaction, stopping reagent (1 M CH_3COOH) was added, and 1.0 mL of the mixture was reacted with 10 mL of 0.005% iodine solution,

DOI: 10.1021/jf5056002
J. Agric. Food Chem. 2015, 63, 1401−1418

Table 2. Changes of Volatile Compounds in Three Different Types of Rice-*koji doenjang* Inoculated with *A. oryzae* (AO), *A. sojae* (AS), and *A. kawachii* (AK) during Fermentation

				relative peak areas (mean ± SD)[c]							
				fermentation periods (weeks)							
no.	RI[a]	volatile compounds[b]	Sp.	0	1	2	4	5	7	8	ID[d]
Acids											
ac1	1665	pentanoic acid	AO	nd[e] a[f]	0.04 ± 0.002 c,x[g]	nd a,x	nd a	nd a	nd a	nd a	A
			AS	nd a	0.3 ± 0.01 c,y	0.1 ± 0.008 b,y	nd a	nd a	nd a	nd a	A
			AK	nd a	0.4 ± 0.005 c,z	0.2 ± 0.001 b,z	nd a	nd a	nd a	nd a	A
ac2	1843	hexanoic acid	AO	nd a	0.08 ± 0.004 c,x	0.04 ± 0.002 b,x	nd a	nd a	nd a	nd a	A
			AS	nd a	0.2 ± 0.03 c,y	0.1 ± 0.001 b,z	nd a	nd a	nd a	nd a	A
			AK	nd a	0.1 ± 0.006 c,x	0.1 ± 0.003 b,y	nd a	nd a	nd a	nd a	A
ac3	2056	octanoic acid	AO	nd a	0.04 ± 0.002 b,y	nd a,x	nd a	nd a	nd a	nd a	A
			AS	nd a	0.02 ± 0.002 b,x	nd a,x	nd a	nd a	nd a	nd a	A
			AK	nd a	0.02 ± 0.004 b,x	0.02 ± 0.01 b,y	nd a	nd a	nd a	nd a	A
Alcohols											
al1	1150	butan-1-ol	AO	4.7 ± 0.3 c	0.3 ± 0.02 ab,y	0.4 ± 0.03 b,z	0.3 ± 0.02 ab,y	0.2 ± 0.01 a,z	0.2 ± 0.02 a,y	0.2 ± 0.003 a,y	A
			AS	4.7 ± 0.3 c	nd a,x	0.2 ± 0.006 b,y	0.2 ± 0.005 b,x	0.2 ± 0.01 b,y	0.2 ± 0.006 b,xy	0.2 ± 0.01 b,y	A
			AK	4.7 ± 0.3 c	nd a,x	nd a,x	0.3 ± 0.02 b,y	0.1 ± 0.02 ab,x	0.1 ± 0.02 ab,x	0.1 ± 0.02 ab,x	A
al2	1197	3-methylbutan-1-ol	AO	nd a	18.4 ± 0.9 d,y	23.2 ± 0.6 e,y	7.8 ± 0.5 c,x	4.1 ± 0.3 b,x	4.4 ± 0.06 b,x	4.2 ± 0.6 b,x	A
			AS	nd a	18.6 ± 3.0 d,y	11.6 ± 1.0 c,x	12.1 ± 0.5 c,z	7.1 ± 0.2 b,z	6.4 ± 0.3 b,y	5.0 ± 0.2 b,y	A
			AK	nd a	9.6 ± 0.3 c,x	21.7 ± 1.2 e,y	10.6 ± 0.5 d,y	6.6 ± 0.2 b,y	6.3 ± 0.04 b,y	6.5 ± 0.02 b,z	A
al3	1361	hexan-1-ol	AO	19.8 ± 0.3 e	1.2 ± 0.1 d,x	0.8 ± 0.04 c,x	0.4 ± 0.03 b,y	0.1 ± 0.006 a,x	0.2 ± 0.02 a,x	0.1 ± 0.005 a,x	A
			AS	19.8 ± 0.3 d	4.6 ± 0.3 c,z	1.4 ± 0.06 b,y	0.4 ± 0.02 a,x	0.2 ± 0.02 a,y	0.2 ± 0.006 a,x	0.2 ± 0.008 a,y	A
			AK	19.8 ± 0.3 e	1.9 ± 0.2 d,y	1.5 ± 0.1 c,y	0.5 ± 0.02 b,z	0.2 ± 0.008 a,y	0.2 ± 0.01 a,x	0.2 ± 0.01 a,y	A
al4	1365	(*E*)-hex-3-en-1-ol	AO	0.2 ± 0.01 b	nd a	nd a	nd a	nd a	nd a	nd a	B
			AS	0.2 ± 0.01 b	nd a	nd a	nd a	nd a	nd a	nd a	B
			AK	0.2 ± 0.01 b	nd a	nd a	nd a	nd a	nd a	nd a	B
al5	1383	(*Z*)- hex-3-en-1-ol	AO	0.7 ± 0.1 d	0.5 ± 0.01 c,z	0.3 ± 0.005 b,z	nd a	nd a	nd a	nd a	A
			AS	0.7 ± 0.1 d	0.3 ± 0.005 c,x	0.08 ± 0.002 b,y	nd a	nd a	nd a	nd a	A
			AK	0.7 ± 0.1 c	0.1 ± 0.007 b,y	0.1 ± 0.01 b,x	nd a	nd a	nd a	nd a	A
al6	1396	octan-3-ol	AO	1.9 ± 0.06 f	0.8 ± 0.05 d,x	1.0 ± 0.09 e,x	0.6 ± 0.04 c,x	0.5 ± 0.03 b,y	0.2 ± 0.03 a,y	0.3 ± 0.008 a,x	A
			AS	1.9 ± 0.06 d	2.4 ± 0.4 e,z	1.3 ± 0.07 c,y	0.7 ± 0.03 b,y	0.7 ± 0.05 b,z	0.2 ± 0.02 a,xy	0.7 ± 0.03 b,y	A
			AK	1.9 ± 0.06 f	1.4 ± 0.08 e,y	1.2 ± 0.2 d,xy	0.9 ± 0.005 c,z	0.4 ± 0.05 b,x	0.2 ± 0.02 a,x	0.3 ± 0.03 ab,x	A
al7	1403	(*E*)- hex-2-en-1-ol	AO	0.1 ± 0.01 b	nd a	nd a	nd a	nd a	nd a	nd a	A
			AS	0.1 ± 0.01 b	nd a	nd a	nd a	nd a	nd a	nd a	A
			AK	0.1 ± 0.01 b	nd a	nd a	nd a	nd a	nd a	nd a	A
al8	1454	oct-1-en-3-ol	AO	21.0 ± 1.4 e	11.6 ± 0.6 d,x	9.5 ± 0.5 c,x	3.5 ± 0.2 b,x	1.4 ± 0.09 a,x	1.1 ± 0.09 a,x	0.7 ± 0.06 a,x	A
			AS	21.0 ± 1.4 d	69.8 ± 2.6 f,z	35.2 ± 1.7 e,z	13.0 ± 0.6 c,y	7.7 ± 0.2 b,z	1.6 ± 0.07 a,z	2.7 ± 0.2 a,z	A
			AK	21.0 ± 1.4 d	15.4 ± 0.6 c,y	14.8 ± 1.6 bc,y	13.9 ± 0.1 b,z	2.1 ± 0.1 a,y	1.4 ± 0.002 a,y	1.0 ± 0.1 a,y	A
al9	1455	heptan-1-ol	AO	1.6 ± 0.2 b	nd a,x	nd a,x	nd a	nd a	nd a	nd a	A
			AS	1.6 ± 0.2 d	1.1 ± 0.2 c,y	0.4 ± 0.03 b,y	nd a	nd a	nd a	nd a	A
			AK	1.6 ± 0.2 b	nd a,x	nd a,x	nd a	nd a	nd a	nd a	A
al10	1484	2-ethylhexan-1-ol	AO	0.6 ± 0.03 c	0.2 ± 0.02 b,y	nd a	nd a	nd a	nd a	nd a	A

J. Agric. Food Chem. 2015, 63, 1401−1418
DOI: 10.1021/jf5056002

Table 2. continued

				relative peak areas (mean ± SD)[c]							
				fermentation periods (weeks)							
no.	RI[a]	volatile compounds[b]	Sp.	0	1	2	4	5	7	8	ID[d]
Alcohols											
			AS	0.6 ± 0.03 b	0.7 ± 0.02 c,z	nd a	nd a	nd a	nd a	nd a	A
			AK	0.6 ± 0.03 b	nd a,x	nd a	nd a	nd a	nd a	nd a	A
al11	1555	octan-1-ol	AO	0.5 ± 0.05 d	0.2 ± 0.008 c,y	0.1 ± 0.02 c,x	nd a	nd a,x	0.05 ± 0.003 b,x	nd a,x	A
			AS	0.5 ± 0.05 e	0.5 ± 0.02 e,z	0.3 ± 0.03 d,y	nd a	0.07 ± 0.003 b,y	0.1 ± 0.002 c,z	0.1 ± 0.001 b,y	A
			AK	0.5 ± 0.05 d	nd a,x	0.2 ± 0.04 c,y	nd a	nd a,x	0.06 ± 0.003 b,y	0.08 ± 0.001 b,z	A
al12	1646	nonan-1-ol	AO	0.3 ± 0.006 b	nd a,x	nd a,x	nd a	nd a	nd a	nd a	A
			AS	0.3 ± 0.006 c	0.2 ± 0.03 b,y	0.2 ± 0.005 b,y	nd a	nd a	nd a	nd a	A
			AK	0.3 ± 0.006 b	0.3 ± 0.02 b,z	0.04 ± 0.06 a,x	nd a	nd a	nd a	nd a	A
al13	1868	phenylmethanol	AO	1.3 ± 0.1 b	nd a	nd a	nd a	nd a	nd a	nd a	A
			AS	1.3 ± 0.1 b	nd a	nd a	nd a	nd a	nd a	nd a	A
			AK	1.3 ± 0.1 b	nd a	nd a	nd a	nd a	nd a	nd a	A
al14	1908	2-phenylethanol	AO	4.5 ± 0.4 a	6.0 ± 0.8 a,z	16.3 ± 4.1 bc,y	20.2 ± 0.7 d,y	13.2 ± 0.09 b,x	19.2 ± 0.6 cd,y	26.4 ± 1.9 e,y	A
			AS	4.5 ± 0.4 ab	3.9 ± 0.1 a,y	5.7 ± 0.4 b,x	10.8 ± 1.3 c,x	16.5 ± 1.1 d,y	18.7 ± 1.2 e,y	21.7 ± 0.6 f,x	A
			AK	4.5 ± 0.4 b	0.5 ± 0.009 a,x	4.6 ± 0.09 b,x	11.3 ± 1.7 c,x	13.2 ± 0.1 d,x	15.2 ± 0.6 e,x	21.4 ± 0.8 f,x	A
Benzenes and Benzene Derivatives											
b1	921	benzene	AO	0.7 ± 0.08 d	1.5 ± 0.02 f,x	0.8 ± 0.02 e,z	0.3 ± 0.008 c,y	0.06 ± 0.01 a,x	0.2 ± 0.03 c,y	0.2 ± 0.01 b,y	A
			AS	0.7 ± 0.08 e	0.3 ± 0.002 d,z	0.1 ± 0.004 b,x	0.2 ± 0.002 c,x	0.09 ± 0.003 ab,y	0.06 ± 0.003 ab,x	0.05 ± 0.007 a,x	A
			AK	0.7 ± 0.08 e	0.9 ± 0.04 f,y	0.5 ± 0.002 d,y	0.4 ± 0.03 c,z	0.1 ± 0.01 b,z	0.09 ± 0.003 ab,x	0.05 ± 0.001 a,x	A
b2	1027	methylbenzene	AO	14.7 ± 2.0 d	11.4 ± 0.6 c,y	7.4 ± 0.2 b,z	nd a	nd a	nd a	nd a	A
			AS	14.7 ± 2.0 d	3.6 ± 0.02 c,x	1.9 ± 0.1 b,y	nd a	nd a	nd a	nd a	A
			AK	14.7 ± 2.0 c	4.2 ± 0.3 b,x	3.5 ± 0.3 b,x	nd a	nd a	nd a	nd a	A
b3	1110	ethylbenzene	AO	3.2 ± 0.3 d	1.4 ± 0.2 c,y	0.9 ± 0.07 b,y	0.1 ± 0.009 a,z	0.1 ± 0.008 a,y	0.08 ± 0.002 a,y	nd a	A
			AS	3.2 ± 0.3 d	0.3 ± 0.03 b,x	1.7 ± 0.003 c,z	nd a,x	nd a,x	nd a,x	nd a	A
			AK	3.2 ± 0.3 c	0.5 ± 0.1 b,x	0.4 ± 0.03 b,x	0.08 ± 0.001 a,y	nd a,x	nd a,x	nd a	A
b4	1124	1,4-dimethylbenzene (*p*-xylene)	AO	2.7 ± 0.1 e	1.2 ± 0.1 d,y	0.8 ± 0.03 c,z	0.5 ± 0.006 b,z	0.1 ± 0.008 a,y	0.1 ± 0.007 a,y	0.2 ± 0.001 a,z	A
			AS	2.7 ± 0.1 e	0.7 ± 0.02 d,x	0.5 ± 0.02 c,x	nd a,x	0.1 ± 0.005 b,x	0.1 ± 0.004 b,y	0.07 ± 0.003 ab,x	A
			AK	2.7 ± 0.1 d	0.7 ± 0.05 c,x	0.6 ± 0.07 c,y	0.3 ± 0.006 b,y	0.2 ± 0.006 a,z	0.07 ± 0.002 a,x	0.1 ± 0.010 a,y	A
b5	1129	1,3-dimethylbenzene (*m*-xylene)	AO	5.6 ± 0.7 d	2.6 ± 0.2 c,z	2.2 ± 0.06 c,z	0.9 ± 0.01 b,z	0.3 ± 0.04 a,z	0.3 ± 0.001 a,z	0.6 ± 0.008 ab,z	A
			AS	5.6 ± 0.7 c	1.4 ± 0.2 b,y	1.1 ± 0.04 b,x	nd a,x	0.1 ± 0.007 a,x	0.2 ± 0.007 a,x	0.03 ± 0.002 a,x	A
			AK	5.6 ± 0.7 d	0.9 ± 0.1 b,x	1.6 ± 0.005 c,y	0.4 ± 0.04 a,y	0.3 ± 0.04 a,y	0.2 ± 0.002 a,y	0.1 ± 0.009 a,y	A
b6	1164	1,2-dimethylbenzene (*o*-xylene)	AO	3.8 ± 0.4 c	1.2 ± 0.1 b,y	1.0 ± 0.02 b,z	0.3 ± 0.002 a,y	0.1 ± 0.01 a,y	0.1 ± 0.007 a,z	0.07 ± 0.002 a,z	A
			AS	3.8 ± 0.4 d	0.8 ± 0.03 c,x	0.5 ± 0.02 b,x	0.07 ± 0.001 a,x	0.1 ± 0.01 a,x	0.1 ± 0.006 a,y	0.01 ± 0.001 a,x	A
			AK	3.8 ± 0.358 c	0.7 ± 0.02 b,x	0.8 ± 0.03 b,y	0.07 ± 0.003 a,x	0.1 ± 0.02 a,y	0.04 ± 0.003 a,x	0.03 ± 0.001 a,y	A
b7	1258	ethenylbenzene	AO	1.7 ± 0.1 b	4.7 ± 0.2 e,y	3.4 ± 0.1 d,y	2.0 ± 0.2 c,y	1.02 ± 0.04 a,x	1.0 ± 0.04 a,z	0.9 ± 0.06 a,y	A
			AS	1.7 ± 0.1 b	7.6 ± 0.3 d,z	3.4 ± 0.1 c,y	1.5 ± 0.1 b,x	1.0 ± 0.09 a,x	0.8 ± 0.03 a,y	0.8 ± 0.03 a,x	A
			AK	1.7 ± 0.1 c	4.0 ± 0.1 e,x	3.0 ± 0.1 d,x	1.7 ± 0.01 c,x	1.0 ± 0.05 b,x	0.6 ± 0.05 a,x	0.8 ± 0.02 b,x	A
b8	1277	1,2,4-trimethylbenzene	AO	1.0 ± 0.05 d	0.6 ± 0.08 c,z	0.6 ± 0.07 c,z	0.4 ± 0.01 b,y	0.3 ± 0.02 a,z	0.1 ± 0.01 a,z	0.1 ± 0.006 a,y	A
			AS	1.0 ± 0.05 d	nd a,x	0.04 ± 0.008 b,x	nd a,x	nd a,x	0.09 ± 0.006 c,y	nd a,x	A
			AK	1.0 ± 0.05 e	0.3 ± 0.03 d,y	0.2 ± 0.009 c,y	nd a,x	0.07 ± 0.005 b,y	0.04 ± 0.001 b,x	nd a,x	A

J. Agric. Food Chem. 2015, 63, 1401−1418

DOI: 10.1021/jf5056002

Table 2. continued

no.	RI[a]	volatile compounds[b]	Sp.	relative peak areas (mean ± SD)[c] fermentation periods (weeks) 0	1	2	4	5	7	8	ID[d]
Benzenes and Benzene Derivatives											
b9	1635	methyl benzoate	AO	nd a	0.06 ± 0.002 c,y	nd a,x	nd a	nd a	0.04 ± 0.002 b,y	nd a	B
			AS	nd a	nd a,x	0.06 ± 0.002 b,y	nd a	nd a	nd a,x	nd a	B
			AK	nd	nd x	nd x	nd	nd	nd x	nd	B
b10	1659	ethyl benzoate	AO	nd a	1.1 ± 0.07 b,y	3.2 ± 0.4 c,y	8.5 ± 0.9 f,x	5.7 ± 0.2 d,y	7.5 ± 0.3 e,y	9.8 ± 0.6 g,y	A
			AS	nd a	1.4 ± 0.4 b,y	5.0 ± 0.4 c,z	11.1 ± 1.4 d,y	12.5 ± 0.3 b,z	1.3 ± 0.05 e,x	12.9 ± 0.5 e,z	A
			AK	nd a	nd a,x	0.3 ± 0.06 b,x	12.3 ± 0.4 e,y	0.8 ± 0.03 c,x	1.0 ± 0.006 c,x	1.4 ± 0.02 d,x	A
b11	1786	ethyl 2-phenylacetate	AO	nd a	0.05 ± 0.003 a,x	0.1 ± 0.03 ab,y	1.4 ± 1.8 b,x	0.4 ± 0.06 ab,x	0.4 ± 0.004 ab,y	0.6 ± 0.02 ab,x	A
			AS	nd a	0.08 ± 0.01 b,y	0.3 ± 0.03 c,z	0.7 ± 0.02 e,x	0.7 ± 0.03 f,y	0.4 ± 0.009 d,xy	0.8 ± 0.02 f,y	A
			AK	nd a	0.03 ± 0.008 a,x	0.08 ± 0.01 b,x	0.6 ± 0.03 e,x	0.3 ± 0.03 c,x	0.4 ± 0.04 c,x	0.5 ± 0.03 d,z	A
b12	1815	2-phenylethyl acetate	AO	0.4 ± 0.03 a	1.0 ± 0.15 b,z	2.9 ± 0.3 d,y	2.2 ± 0.02 c,z	3.2 ± 0.08 d,y	4.2 ± 0.4 e,y	9.0 ± 0.2 f,y	A
			AS	0.4 ± 0.03 a	0.4 ± 0.03 a,y	0.6 ± 0.01 a,x	1.5 ± 0.1 b,x	1.9 ± 0.2 c,x	3.8 ± 0.3 d,y	8.5 ± 0.08 e,x	A
			AK	0.4 ± 0.03 b	nd a,x	0.4 ± 0.02 b,x	1.8 ± 0.02 c,y	3.6 ± 0.06 e,z	2.4 ± 0.08 d,x	8.4 ± 0.2 f,x	A
b13	1885	ethyl 3-phenylpropanoate	AO	nd a	0.02 ± 0.003 b,y	0.07 ± 0.004 c,y	0.08 ± 0.002 de,x	0.1 ± 0.01 e,x	0.08 ± 0.006 d,x	0.1 ± 0.01 f,y	A
			AS	nd a	nd a,x	0.07 ± 0.002 ab,y	0.2 ± 0.02 ab,y	0.1 ± 0.004 b,x	0.09 ± 0.004 ab,x	0.1 ± 0.004 ab,x	A
			AK	nd a	nd a,x	0.04 ± 0.002 b,x	0.08 ± 0.008 cd,x	0.07 ± 0.004 c,x	0.08 ± 0.005 d,x	0.2 ± 0.01 e,z	A
Carbonyls											
c1	885	butan-2-one	AO	2.1 ± 0.4 b	0.3 ± 0.01 a,x	nd a,x	nd a,x	nd a	nd a	nd a	A
			AS	2.1 ± 0.4 c	0.6 ± 0.002 b,y	0.1 ± 0.007 a,y	0.01 ± 0.000 a,y	nd a	nd a	nd a	A
			AK	2.1 ± 0.4 c	0.6 ± 0.03 b,y	0.2 ± 0.008 a,z	0.01 ± 0.001 a,y	nd a	nd a	nd a	A
c2	889	2-methylbutanal	AO	nd a	0.2 ± 0.02 e,x	0.2 ± 0.003 f,y	0.1 ± 0.003 d,y	0.05 ± 0.005 b,x	0.05 ± 0.01 b,x	0.08 ± 0.001 c,z	A
			AS	nd a	0.4 ± 0.008 e,y	0.08 ± 0.006 c,x	0.1 ± 0.001 d,y	0.04 ± 0.01 b,x	0.04 ± 0.006 b,x	0.05 ± 0.001 b,x	A
			AK	nd a	0.5 ± 0.03 d,z	0.4 ± 0.01 c,z	0.06 ± 0.004 b,x	0.06 ± 0.001 b,y	0.04 ± 0.000 b,x	0.06 ± 0.002 b,y	A
c3	900	3-methylbutanal	AO	nd a	0.3 ± 0.04 e,x	0.2 ± 0.003 d,y	0.08 ± 0.003 c,y	0.05 ± 0.006 b,y	0.05 ± 0.001 b,xy	0.08 ± 0.005 c,y	A
			AS	nd a	0.5 ± 0.009 e,x	0.1 ± 0.008 c,x	0.1 ± 0.003 c,z	0.2 ± 0.013 d,x	0.06 ± 0.01 b,y	0.05 ± 0.004 b,x	A
			AK	nd a	1.1 ± 0.2 c,y	0.4 ± 0.03 b,z	0.06 ± 0.005 a,x	0.07 ± 0.001 a,z	0.04 ± 0.001 a,x	0.05 ± 0.000 d,x	A
c4	1080	hexanal	AO	3.3 ± 0.2 d	1.3 ± 0.1 c,x	0.2 ± 0.002 b,x	nd a,x	nd a	nd a	nd a	A
			AS	3.3 ± 0.2 d	3.0 ± 0.02 c,y	1.9 ± 0.007 b,z	nd a,x	nd a	nd a	nd a	A
			AK	3.3 ± 0.2 d	1.3 ± 0.2 c,x	0.5 ± 0.009 b,y	0.08 ± 0.001 a,y	nd a	nd a	nd a	A
c5	1133	heptan-3-one	AO	0.2 ± 0.03 c	0.3 ± 0.01 d,y	0.2 ± 0.05 c,x	0.1 ± 0.01 b,z	nd a	nd a	nd a,x	B
			AS	0.2 ± 0.03 b	0.2 ± 0.03 b,x	0.2 ± 0.01 b,x	nd a,x	nd a	nd a	0.020 ± 0.003 a,y	B
			AK	0.2 ± 0.03 c	0.2 ± 0.03 c,x	0.5 ± 0.02 d,y	0.06 ± 0.001 b,y	nd a	nd a	nd a,x	B
c6	1169	heptan-2-one	AO	0.8 ± 0.08 c	1.04 ± 0.06 d,z	0.4 ± 0.04 b,z	nd a	nd a	nd a	nd a,x	A
			AS	0.8 ± 0.08 d	0.7 ± 0.02 c,y	0.2 ± 0.001 b,x	nd a	nd a	nd a	0.013 ± 0.001 a,y	A
			AK	0.8 ± 0.08 d	0.5 ± 0.04 c,x	0.3 ± 0.01 b,y	nd a	nd a	nd a	nd a,x	A
c7	1178	4-methylheptan-2-one	AO	0.3 ± 0.02 d	0.2 ± 0.01 c,xy	0.2 ± 0.004 b,y	nd a	nd a	nd a	nd a	B
			AS	0.3 ± 0.02 d	0.2 ± 0.01 c,x	0.1 ± 0.001 b,x	nd a	nd a	nd a	nd a	B
c8	1296	octan-2-one	AO	0.2 ± 0.02 d	0.2 ± 0.02 e,y	0.1 ± 0.03 c,x	nd a,x	0.05 ± 0.004 b,z	nd a,x	nd a	B
			AS	0.2 ± 0.02 bc	0.2 ± 0.003 c,xy	0.1 ± 0.009 abc,x	1.5 ± 0.2 d,y	0.03 ± 0.007 bc,y	0.02 ± 0.002 bc,y	nd a	B
			AK	0.2 ± 0.02 de	0.2 ± 0.02 e,x	0.1 ± 0.006 d,x	0.04 ± 0.002 bc,x	0.02 ± 0.001 ab,x	0.05 ± 0.002 c,z	nd a	B

J. Agric. Food Chem. 2015, 63, 1401−1418 DOI: 10.1021/jf5056002

Table 2. continued

				relative peak areas (mean ± SD)[c]							
				fermentation periods (weeks)							
no.	RI[a]	volatile compounds[b]	Sp.	0	1	2	4	5	7	8	ID[d]
Carbonyls											
c9	1301	octanal	AO	nd a	0.3 ± 0.03 b,y	nd a,x	nd a	nd a,x	nd a	nd a	A
			AS	nd a	0.6 ± 0.03 b,z	0.3 ± 0.006 c,z	nd a	0.08 ± 0.003 b,y	nd a	nd a	A
			AK	nd a	nd a,x	0.2 ± 0.008 b,y	nd a	nd a,x	nd a	nd a	A
c10	1311	oct-1-en-3-one	AO	0.8 ± 0.01 b	0.4 ± 0.7 ab,x	2.0 ± 0.02 c,t	0.6 ± 0.03 ab,y	0.3 ± 0.03 ab,x	0.4 ± 0.003 ab,x	0.2 ± 0.001 a,x	A
			AS	0.8 ± 0.01 c	5.2 ± 0.02 f,y	3.0 ± 0.1 e,z	0.1 ± 0.02 a,x	1.1 ± 0.07 d,y	0.8 ± 0.03 c,z	0.6 ± 0.02 b,y	A
			AK	0.8 ± 0.01 c	0.3 ± 0.007 a,x	1.0 ± 0.007 d,x	1.7 ± 0.006 f,z	1.1 ± 0.06 e,y	0.8 ± 0.02 b,y	0.8 ± 0.01 c,z	A
c11	1331	(*E*)-hept-2-enal	AO	0.7 ± 0.06 d	0.6 ± 0.04 c,y	0.2 ± 0.05 b,x	0.1 ± 0.009 a,x	0.06 ± 0.006 a,x	0.07 ± 0.005 a,y	0.06 ± 0.003 a,z	B
			AS	0.7 ± 0.06 d	1.0 ± 0.090 e,z	0.3 ± 0.04 c,x	0.1 ± 0.01 b,y	0.09 ± 0.02 ab,xy	0.07 ± 0.003 ab,y	0.04 ± 0.004 a,x	B
			AK	0.7 ± 0.06 e	0.4 ± 0.024 d,x	0.4 ± 0.03 d,y	0.1 ± 0.02 c,xy	0.1 ± 0.01 bc,y	0.06 ± 0.002 ab,x	0.05 ± 0.003 a,y	B
c12	1392	nonanal	AO	nd a	0.6 ± 0.03 e,y	0.5 ± 0.03 d,y	nd a,x	0.06 ± 0.004 b,x	0.1 ± 0.006 c,y	nd a,x	A
			AS	nd a	0.6 ± 0.03 e,y	0.5 ± 0.03 d,y	0.2 ± 0.004 c,y	0.2 ± 0.01 c,y	nd a,x	0.04 ± 0.003 b,y	A
			AK	nd a	nd a,x	0.2 ± 0.04 b,x	nd a,x	0.04 ± 0.003 a,x	0.7 ± 0.05 c,z	0.01 ± 0.02 a,x	A
c13	1429	(*E*)-oct-2-enal	AO	0.3 ± 0.03 b	0.6 ± 0.01 d,x	0.5 ± 0.04 c,x	0.3 ± 0.06 b,x	0.2 ± 0.005 a,x	0.2 ± 0.009 a,x	0.2 ± 0.01 a,x	A
			AS	0.3 ± 0.03 a	1.6 ± 0.01 e,z	1.2 ± 0.2 d,y	0.8 ± 0.06 c,y	0.6 ± 0.01 b,y	0.9 ± 0.01 c,z	0.5 ± 0.01 b,y	A
			AK	0.3 ± 0.03 a	1.1 ± 0.04 d,y	1.08 ± 0.1 d,y	0.9 ± 0.07 c,y	0.6 ± 0.03 b,y	0.6 ± 0.02 b,y	0.6 ± 0.05 b,y	A
c14	1491	decan-2-one	AO	nd a	0.08 ± 0.005 b,y	nd a,x	0.2 ± 0.01 c,z	nd a,x	nd a,x	0.09 ± 0.01 b,x	B
			AS	nd a	0.1 ± 0.026 c,z	0.09 ± 0.08 bc,y	0.1 ± 0.002 c,y	0.03 ± 0.001 ab,y	0.06 ± 0.01 bc,y	0.07 ± 0.01 bc,x	B
			AK	nd a	nd a,x	nd a,x	0.1 ± 0.005 b,x	0.04 ± 0.005 b,z	nd a,x	0.09 ± 0.02 c,x	B
c15	1509	benzaldehyde	AO	2.3 ± 0.070 a	3.4 ± 0.2 c,z	3.8 ± 0.4 c,y	3.3 ± 0.2 c,y	2.0 ± 0.2 a,x	2.3 ± 0.03 a,y	2.7 ± 0.3 b,x	A
			AS	2.3 ± 0.070 a	2.5 ± 0.4 ab,y	2.6 ± 0.1 ab,x	2.7 ± 0.2 b,x	2.4 ± 0.1 a,y	3.5 ± 0.06 c,z	2.4 ± 0.04 a,x	A
			AK	2.3 ± 0.070 c	1.6 ± 0.2 a,x	2.4 ± 0.2 cd,x	2.9 ± 0.02 e,x	2.1 ± 0.02 b,x	2.0 ± 0.02 b,x	2.6 ± 0.2 d,x	A
c16	1528	(*E*)-non-2-enal	AO	0.3 ± 0.020 f	0.1 ± 0.02 d,y	0.1 ± 0.02 d,y	0.3 ± 0.003 e,y	0.1 ± 0.01 c,y	0.05 ± 0.002 b,y	nd a,x	A
			AS	0.3 ± 0.020 e	0.2 ± 0.004 d,z	0.2 ± 0.02 c,y	0.1 ± 0.03 c,x	0.1 ± 0.01 b,x	0.07 ± 0.005 ab,z	0.05 ± 0.007 a,y	A
			AK	0.3 ± 0.020 d	nd a,x	0.08 ± 0.001 b,x	0.1 ± 0.02 c,x	0.1 ± 0.01 c,z	nd a,x	0.07 ± 0.002 b,z	A
c17	1641	2-phenylacetaldehyde	AO	nd a	2.1 ± 0.1 d,x	2.3 ± 0.1 de,y	2.4 ± 0.04 e,z	1.2 ± 0.05 b,z	1.8 ± 0.1 c,y	2.3 ± 0.2 de,z	A
			AS	nd a	2.2 ± 0.1 f,x	1.7 ± 0.05 e,x	0.8 ± 0.04 b,y	1.0 ± 0.04 c,y	1.7 ± 0.1 e,y	1.3 ± 0.1 d,x	A
			AK	nd a	1.9 ± 0.09 d,x	2.4 ± 0.1 e,y	0.7 ± 0.02 b,x	0.6 ± 0.01 b,x	1.3 ± 0.03 c,x	1.9 ± 0.2 d,y	A
c18	1933	(*E*)-2-phenylbut-2-enal	AO	nd a	0.1 ± 0.006 b,y	0.3 ± 0.02 c,y	0.6 ± 0.05 e,y	0.4 ± 0.04 d,x	0.6 ± 0.01 f,x	1.02 ± 0.03 g,y	A
			AS	nd a	0.1 ± 0.003 b,z	0.1 ± 0.001 bc,x	0.4 ± 0.02 c,x	0.6 ± 0.03 d,y	1.7 ± 0.1 f,z	0.8 ± 0.04 e,x	A
			AK	nd a	nd a,x	0.1 ± 0.02 b,x	0.5 ± 0.01 c,y	0.7 ± 0.02 d,z	1.1 ± 0.02 e,y	1.2 ± 0.01 f,z	A
Esters											
e1	867	ethyl acetate	AO	5.6 ± 0.2 c	2.3 ± 0.1 a,y	9.5 ± 0.8 e,y	6.4 ± 0.04 d,y	4.0 ± 0.2 b,x	4.2 ± 0.09 b,z	4.0 ± 0.06 b,y	A
			AS	5.6 ± 0.2 e	3.7 ± 0.4 b,z	5.2 ± 0.1 de,x	4.9 ± 0.1 cd,z	4.6 ± 0.4 c,y	2.6 ± 0.2 a,x	2.8 ± 0.2 a,x	A
			AK	5.6 ± 0.2 d	0.8 ± 0.05 a,x	5.4 ± 0.5 d,x	6.7 ± 0.1 e,x	3.9 ± 0.2 c,x	3.0 ± 0.1 b,y	3.1 ± 0.1 b,x	A
e2	936	ethyl propanoate	AO	nd a	nd a	0.4 ± 0.01 f,y	0.2 ± 0.02 e,x	0.1 ± 0.01 c,x	0.2 ± 0.003 d,z	0.08 ± 0.004 b,x	A
			AS	nd a	nd a	nd a,x	0.3 ± 0.01 e,y	0.3 ± 0.02 d,z	0.1 ± 0.003 c,y	0.08 ± 0.01 b,x	A
			AK	nd a	nd a	0.6 ± 0.007 f,z	0.3 ± 0.01 e,y	0.2 ± 0.01 d,y	0.1 ± 0.02 b,x	0.1 ± 0.002 c,y	A
e3	943	ethyl 2-methylpropanoate	AO	nd a	nd a,x	0.1 ± 0.02 d,x	0.06 ± 0.02 c,x	0.04 ± 0.003 b,x	0.07 ± 0.006 c,y	0.06 ± 0.006 c,x	A
			AS	nd a	0.2 ± 0.006 g,z	0.1 ± 0.003 f,x	0.1 ± 0.01 e,y	0.08 ± 0.006 d,y	0.05 ± 0.005 b,x	0.06 ± 0.006 c,x	A

J. Agric. Food Chem. 2015, 63, 1401−1418
DOI: 10.1021/jf5056002

Table 2. continued

				relative peak areas (mean ± SD)[c]							
				fermentation periods (weeks)							
no.	RI[a]	volatile compounds[b]	Sp.	0	1	2	4	5	7	8	ID[d]
Esters											
			AK	nd a	0.2 ± 0.006 d,y	0.2 ± 0.008 e,y	0.1 ± 0.003 c,z	0.04 ± 0.005 b,x	0.05 ± 0.006 b,x	0.05 ± 0.007 b,x	A
e4	986	methyl 2-methylprop-2-enoate	AO	nd a	1.1 ± 0.02 c,x	1.0 ± 0.04 c,y	0.9 ± 0.02 b,x	1.4 ± 0.01 d,y	2.0 ± 0.07 e,z	1.006 ± 0.05 c,x	A
			AS	nd a	3.1 ± 0.01 f,z	0.6 ± 0.05 b,x	1.3 ± 0.10 d,y	1.5 ± 0.06 e,z	0.5 ± 0.03 b,x	0.9 ± 0.08 c,x	A
			AK	nd a	1.9 ± 0.2 f,y	1.3 ± 0.001 d,z	2.0 ± 0.1 f,z	0.7 ± 0.02 b,x	1.5 ± 0.03 e,y	1.01 ± 0.09 c,x	A
e5	1000	2-methylpropyl acetate	AO	nd a	nd a	0.2 ± 0.2 b,x	0.1 ± 0.01 ab,x	0.06 ± 0.001 a,x	0.09 ± 0.006 ab,y	0.05 ± 0.003 a,x	A
			AS	nd a	nd a	nd a,x	0.1 ± 0.01 d,y	0.1 ± 0.008 c,z	0.06 ± 0.003 b,x	0.06 ± 0.003 b,x	A
			AK	nd a	nd a	nd a,x	0.1 ± 0.01 e,y	0.08 ± 0.008 c,y	0.06 ± 0.006 b,x	0.1 ± 0.01 d,y	A
e6	1027	ethyl butanoate	AO	nd a	nd a	nd a	6.1 ± 0.1 e,y	3.2 ± 0.1 d,x	1.9 ± 0.2 c,z	1.4 ± 0.07 b,z	A
			AS	nd a	nd a	nd a	4.5 ± 0.02 e,x	2.9 ± 0.1 d,x	1.3 ± 0.04 c,y	0.9 ± 0.08 b,x	A
			AK	nd a	nd a	nd a	9.06 ± 0.3 d,z	4.9 ± 0.2 c,y	1.1 ± 0.1 b,x	1.3 ± 0.04 b,y	A
e7	1047	ethyl 2-methylprop-2-enoate	AO	nd a	0.3 ± 0.003 c,z	nd a,x	nd a	nd a	0.3 ± 0.03 b,y	nd a,x	A
			AS	nd a	0.3 ± 0.006 b,y	nd a,x	nd a	nd a	nd a,x	0.4 ± 0.01 c,y	A
			AK	nd a	0.3 ± 0.02 b,x	0.4 ± 0.01 c,y	nd a	nd a	nd a,x	nd a,x	A
e8	1053	ethyl 2-methylbutanoate	AO	nd	nd x	nd x	nd	nd	nd	nd	A
			AS	nd a	0.6 ± 0.03 c,y	0.2 ± 0.03 b,y	nd a	nd a	nd a	nd a	A
			AK	nd	nd x	nd x	nd	nd	nd	nd	A
e9	1060	ethyl 3-methylbutanoate	AO	nd	nd x	nd x	nd	nd	nd	nd	A
			AS	nd a	0.2 ± 0.04 c,z	0.1 ± 0.006 b,y	nd a	nd a	nd a	nd a	A
			AK	nd a	0.09 ± 0.02 b,y	0.2 ± 0.001 c,z	nd a	nd a	nd a	nd a	A
e10	1121	3-methylbutyl acetate	AO	nd a	0.9 ± 0.005 c,y	2.0 ± 0.2 f,z	1.6 ± 0.02 e,y	0.6 ± 0.01 b,x	0.8 ± 0.04 c,y	1.2 ± 0.04 d,y	A
			AS	nd a	0.5 ± 0.01 b,x	1.0 ± 0.1 de,y	1.1 ± 0.05 e,x	0.9 ± 0.09 d,y	0.6 ± 0.04 c,x	0.7 ± 0.1 c,x	A
			AK	nd a	0.5 ± 0.003 b,x	0.6 ± 0.04 c,x	1.0 ± 0.07 f,x	0.9 ± 0.02 e,y	1.2 ± 0.007 g,z	0.8 ± 0.07 d,x	A
e11	1154	ethyl (Z)-but-2-enoate	AO	nd a	0.1 ± 0.005 b,z	0.3 ± 0.01 d,z	0.3 ± 0.007 e,y	0.2 ± 0.006 c,y	0.5 ± 0.02 f,y	0.5 ± 0.01 g,z	A
			AS	nd a	nd a,x	0.1 ± 0.01 b,y	0.2 ± 0.008 e,x	0.2 ± 0.004 d,x	0.1 ± 0.01 c,x	0.3 ± 0.03 f,y	A
			AK	nd a	0.05 ± 0.002 b,y	nd a,x	0.2 ± 0.02 e,x	0.1 ± 0.03 d,x	0.09 ± 0.01 c,x	0.1 ± 0.01 d,x	A
e12	1156	methyl 3-methylbut-2-enoate	AO	nd a	0.1 ± 0.002 c,y	nd a	0.4 ± 0.04 d,z	0.1 ± 0.003 b,z	0.05 ± 0.007 b,y	nd a,x	C
			AS	nd a	nd a,x	nd a	nd a,x	0.03 ± 0.005 d,y	0.02 ± 0.004 b,x	0.03 ± 0.003 c,y	C
			AK	nd a	nd a,x	nd a	0.05 ± 0.002 c,y	nd a,x	0.04 ± 0.002 c,y	0.03 ± 0.002 b,y	C
e13	1227	ethyl hexanoate	AO	nd a	8.8 ± 0.4 d,z	22.5 ± 0.6 e,z	9.6 ± 1.0 d,y	4.5 ± 0.4 c,y	4.1 ± 0.3 bc,y	3.3 ± 0.1 b,z	A
			AS	nd a	2.0 ± 0.01 b,y	9.0 ± 0.5 f,y	6.4 ± 0.3 e,x	3.9 ± 0.1 d,x	2.9 ± 0.2 c,x	2.1 ± 0.1 b,x	A
			AK	nd a	0.4 ± 0.01 b,x	3.0 ± 0.3 c,x	7.0 ± 0.1 e,x	4.1 ± 0.2 d,zy	2.8 ± 0.02 c,x	3.0 ± 0.1 c,y	A
e14	1336	ethyl heptanoate	AO	nd a	1.0 ± 0.03 c,z	2.0 ± 0.4 e,y	1.5 ± 0.1 d,x	0.7 ± 0.07 b,x	0.7 ± 0.04 b,x	0.5 ± 0.03 b,x	A
			AS	nd a	1.0 ± 0.03 d,y	2.1 ± 0.08 g,y	1.7 ± 0.07 f,x	1.2 ± 0.03 e,y	0.7 ± 0.02 c,x	0.5 ± 0.03 b,y	A
			AK	nd a	0.3 ± 0.01 b,x	1.0 ± 0.04 f,x	2.0 ± 0.05 g,y	0.8 ± 0.01 e,x	0.7 ± 0.02 d,x	0.6 ± 0.03 c,z	A
e15	1437	ethyl octanoate	AO	nd a	3.1 ± 0.1 b,z	11.0 ± 1.2 c,z	16.0 ± 4.2 d,y	7.9 ± 0.4 c,z	9.0 ± 0.4 c,z	21.971 ± 1.2 e,y	A
			AS	nd a	0.9 ± 0.003 b,y	4.2 ± 0.2 c,y	7.2 ± 0.7 f,x	5.3 ± 0.3 d,x	6.1 ± 0.6 e,y	14.388 ± 0.7 g,x	A
			AK	nd a	0.1 ± 0.01 a,x	1.1 ± 0.03 b,x	7.1 ± 0.002 d,x	6.3 ± 0.2 d,y	3.5 ± 0.1 c,x	15.431 ± 1.3 e,x	A
e16	1463	3-methylbutyl hexanoate	AO	nd a	nd a	nd a	0.3 ± 0.002 e,z	0.08 ± 0.002 b,y	0.1 ± 0.003 d,z	0.09 ± 0.001 c,y	A
			AS	nd a	nd a	nd a	0.1 ± 0.007 d,y	0.1 ± 0.009 c,z	0.09 ± 0.001 b,y	0.1 ± 0.004 d,z	A

J. Agric. Food Chem. 2015, 63, 1401−1418
DOI: 10.1021/jf5056002

Table 2. continued

				relative peak areas (mean ± SD)[c]							
				fermentation periods (weeks)							
no.	RI[a]	volatile compounds[b]	Sp.	0	1	2	4	5	7	8	ID[d]
Esters											
			AK	nd a	nd a	nd a	0.1 ± 0.001 d,x	0.06 ± 0.002 b,x	nd a,x	0.08 ± 0.005 c,x	A
e17	1486	pentyl propanoate	AO	nd	nd	nd	nd x	nd x	nd	nd	A
			AS	nd a	nd a	nd a	0.1 ± 0.002 c,y	0.09 ± 0.004 b,y	nd a	nd a	A
			AK	nd a	nd a	nd a	0.2 ± 0.003 b,z	nd a,x	nd a	nd a	A
e18	1532	ethyl nonanoate	AO	nd a	0.3 ± 0.01 b,z	0.8 ± 0.03 e,z	1.0 ± 0.02 f,z	0.4 ± 0.004 c,x	0.4 ± 0.01 c,x	0.5 ± 0.02 d,y	A
			AS	nd a	0.1 ± 0.010 b,y	0.6 ± 0.05 d,y	0.7 ± 0.05 e,x	0.6 ± 0.03 e,y	0.4 ± 0.01 c,x	0.5 ± 0.03 c,x	A
			AK	nd a	nd a,x	0.1 ± 0.03 b,x	0.8 ± 0.02 e,y	0.4 ± 0.01 c,x	0.5 ± 0.05 cd,x	0.5 ± 0.04 d,y	A
e19	1618	ethyl decanoate	AO	nd a	0.5 ± 0.04 b,z	1.8 ± 0.2 c,z	4.8 ± 0.1 d,z	1.7 ± 0.06 c,x	1.8 ± 0.1 c,z	7.7 ± 0.2 e,z	A
			AS	nd a	0.2 ± 0.002 a,y	0.7 ± 0.05 b,y	1.9 ± 0.07 c,x	2.3 ± 0.2 d,y	1.0 ± 0.05 e,y	3.2 ± 0.2 f,x	A
			AK	nd a	nd a,x	0.2 ± 0.05 a,x	3.2 ± 0.1 d,y	2.2 ± 0.3 c,y	0.7 ± 0.02 b,x	4.2 ± 0.3 e,y	A
e20	1653	3-methylbutyl octanoate	AO	nd a	nd a	nd a,x	nd a,x	nd a	0.09 ± 0.01 b,x	0.3 ± 0.02 c,x	A
			AS	nd a	nd a	nd a,x	0.1 ± 0.005 b,y	nd a	0.1 ± 0.01 c,y	0.2 ± 0.02 d,x	A
			AK	nd a	nd a	2.2 ± 0.009 d,y	nd a,x	nd a	0.1 ± 0.004 b,x	0.3 ± 0.05 c,x	A
e21	1671	diethyl butanedioate	AO	nd a	nd a	0.3 ± 0.02 b,z	0.9 ± 0.08 d,y	0.7 ± 0.1 c,z	1.0 ± 0.02 d,z	1.7 ± 0.1 e,y	A
			AS	nd a	nd a	0.1 ± 0.02 b,y	0.4 ± 0.03 c,x	0.5 ± 0.03 d,y	0.4 ± 0.03 c,y	0.6 ± 0.007 e,x	A
			AK	nd a	nd a	0.1 ± 0.01 b,x	0.5 ± 0.03 d,x	0.3 ± 0.03 c,x	0.3 ± 0.003 c,x	0.5 ± 0.05 d,x	A
e22	1838	ethyl dodecanoate	AO	nd a	0.1 ± 0.01 a,z	1.2 ± 0.1 b,z	1.8 ± 0.07 d,z	1.2 ± 0.06 b,y	1.4 ± 0.05 c,z	6.5 ± 0.1 e,z	A
			AS	nd a	0.1 ± 0.000 a,y	0.6 ± 0.01 b,y	0.9 ± 0.04 c,x	0.9 ± 0.09 c,x	0.9 ± 0.04 c,y	2.2 ± 0.2 d,x	A
			AK	nd a	nd a,x	0.1 ± 0.01 a,x	1.2 ± 0.04 d,y	0.9 ± 0.05 c,x	0.6 ± 0.02 b,x	3.0 ± 0.2 e,y	A
e23	2045	ethyl tetradecanoate	AO	nd a	0.3 ± 0.03 a,z	4.0 ± 0.7 b,z	8.1 ± 0.4 d,y	6.2 ± 0.4 c,x	7.4 ± 0.4 d,x	9.9 ± 0.5 e,y	A
			AS	nd a	0.3 ± 0.002 a,y	2.7 ± 0.1 b,y	6.0 ± 0.3 c,x	7.7 ± 0.6 d,y	8.5 ± 0.3 e,y	6.7 ± 0.5 f,x	A
			AK	nd a	0.03 ± 0.002 a,x	0.6 ± 0.03 b,x	7.7 ± 0.2 d,y	6.9 ± 0.04 c,xy	7.9 ± 0.02 e,x	11.7 ± 0.1 f,z	A
e24	2145	ethyl pentadecanoate	AO	nd a	0.020 ± 0.001 a,y	0.3 ± 0.06 b,z	0.4 ± 0.03 b,x	0.5 ± 0.04 c,x	0.5 ± 0.04 c,x	0.7 ± 0.05 d,y	A
			AS	nd a	nd a,x	0.2 ± 0.01 b,y	0.5 ± 0.009 d,y	0.7 ± 0.05 e,y	0.9 ± 0.03 f,y	0.4 ± 0.04 c,x	A
			AK	nd a	nd a,x	0.1 ± 0.01 a,x	0.6 ± 0.08 b,z	0.9 ± 0.04 c,z	0.9 ± 0.03 c,y	1.1 ± 0.05 d,z	A
e25	2200	methyl hexadecanoate	AO	nd a	0.05 ± 0.003 a,y	0.2 ± 0.03 b,y	0.3 ± 0.08 d,x	0.1 ± 0.002 bc,x	0.1 ± 0.004 b,y	0.2 ± 0.02 cd,z	A
			AS	nd a	0.1 ± 0.02 d,z	0.2 ± 0.003 e,y	0.2 ± 0.01 f,x	0.2 ± 0.01 e,y	0.06 ± 0.003 b,x	0.08 ± 0.005 c,x	A
			AK	nd a	nd a,x	nd a,x	0.2 ± 0.010 d,x	0.1 ± 0.02 b,x	0.1 ± 0.02 bc,y	0.2 ± 0.04 cd,y	A
e26	2200	ethyl hexadecanoate	AO	nd a	1.9 ± 0.1 a,z	29.2 ± 4.4 b,z	55.8 ± 2.7 d,z	42.8 ± 3.2 c,y	64.7 ± 3.3 e,y	76.9 ± 1.5 f,z	A
			AS	nd a	1.6 ± 0.2 a,y	13.0 ± 1.3 b,y	33.4 ± 1.6 c,x	47.1 ± 3.6 d,y	52.6 ± 1.3 e,x	44.8 ± 4.4 d,x	A
			AK	nd a	0.08 ± 0.01 a,x	2.2 ± 0.3 b,x	44.8 ± 2.5 d,y	33.3 ± 0.4 c,x	50.8 ± 1.4 e,x	67.1 ± 1.0 f,y	A
e27	2200	ethyl hexadecenoate	AO	nd a	nd a	0.2 ± 0.005 b,y	0.3 ± 0.005 c,x	0.7 ± 0.04 d,y	0.7 ± 0.03 d,y	0.9 ± 0.08 e,y	A
			AS	nd a	nd a	nd a,x	0.5 ± 0.03 c,y	0.6 ± 0.09 d,xy	0.4 ± 0.04 c,x	0.3 ± 0.03 b,x	A
			AK	nd a	nd a	nd a,x	0.6 ± 0.03 c,z	0.5 ± 0.02 b,x	0.6 ± 0.03 c,y	0.8 ± 0.01 d,y	A
e28	2200	ethyl hexadec-9-enoate	AO	nd a	nd a	0.04 ± 0.001 a,y	0.7 ± 0.07 d,z	0.1 ± 0.009 b,y	0.1 ± 0.009 b,x	0.2 ± 0.02 c,z	B
			AS	nd a	nd a	nd a,x	0.4 ± 0.03 e,y	0.2 ± 0.02 d,z	0.1 ± 0.01 c,x	0.07 ± 0.007 b,x	B
			AK	nd a	nd a	0.06 ± 0.002 b,z	0.2 ± 0.02 d,x	0.05 ± 0.004 b,x	0.2 ± 0.01 c,y	0.2 ± 0.006 d,y	B
e29	2200	ethyl heptadecanoate	AO	nd a	nd a	0.03 ± 0.001 b,y	0.1 ± 0.006 d,y	0.1 ± 0.009 d,y	0.1 ± 0.01 c,x	0.2 ± 0.02 e,y	B
			AS	nd a	nd a	nd a,x	0.1 ± 0.01 bc,x	0.2 ± 0.02 d,z	0.1 ± 0.01 b,x	0.1 ± 0.009 c,x	B

J. Agric. Food Chem. 2015, 63, 1401−1418 DOI: 10.1021/jf5056002

Table 2. continued

				relative peak areas (mean ± SD)[c]							
				fermentation periods (weeks)							
no.	RI[a]	volatile compounds[b]	Sp.	0	1	2	4	5	7	8	ID[d]
Esters											
			AK	nd a	nd a	nd a,x	0.1 ± 0.01 c,xy	0.09 ± 0.005 b,x	0.2 ± 0.030 d,y	0.3 ± 0.010 e,z	B
e30	2200	butyl hexadecanoate	AO	nd a	nd a	nd a	nd a	0.08 ± 0.01 c,x	0.04 ± 0.001 b,x	0.09 ± 0.009 c,x	C
			AS	nd a	nd a	nd a	nd a	0.1 ± 0.005 d,y	0.04 ± 0.002 b,y	0.08 ± 0.007 c,x	C
			AK	nd a	nd a	nd a	nd a	0.07 ± 0.001 b,x	0.09 ± 0.003 c,z	0.1 ± 0.004 d,y	C
e31	2200	ethyl octadecanoate	AO	nd a	nd a	0.4 ± 0.03 b,y	1.1 ± 0.07 d,z	1.1 ± 1.1 d,y	1.0 ± 0.07 c,y	2.04 ± 0.06 e,z	A
			AS	nd a	nd a	0.4 ± 0.07 b,y	0.7 ± 0.07 c,x	1.07 ± 0.08 d,y	0.7 ± 0.07 c,x	1.05 ± 0.08 d,x	A
			AK	nd a	nd a	0.03 ± 0.001 a,x	0.9 ± 0.04 d,y	0.6 ± 0.01 b,x	0.7 ± 0.03 c,x	1.3 ± 0.06 e,y	A
e32	2200	ethyl octadec-9-enoate	AO	nd a	0.3 ± 0.02 a,y	3.4 ± 0.4 b,z	8.0 ± 0.7 c,z	8.2 ± 0.2 c,z	9.04 ± 0.6 d,y	14.5 ± 0.2 e,z	A
			AS	nd a	0.3 ± 0.02 a,y	2.4 ± 0.001 b,y	4.7 ± 0.2 c,x	7.2 ± 0.6 d,y	7.5 ± 0.6 d,x	7.24 ± 0.8 d,x	A
			AK	nd a	nd a,x	0.4 ± 0.08 b,x	6.6 ± 0.1 d,y	5.3 ± 0.2 c,x	6.9 ± 0.3 e,x	9.7 ± 0.1 f,y	A
e33	2200	ethyl octadeca-9,12-dienoate	AO	nd a	nd a	nd a	nd a,x	nd a	0.3 ± 0.04 b,y	0.9 ± 0.1 c,z	A
			AS	nd a	nd a	nd a	0.8 ± 0.05 c,y	nd a	0.3 ± 0.04 b,y	0.4 ± 0.05 b,x	A
			AK	nd a	nd a	nd a	nd a,x	nd a	0.2 ± 0.001 b,x	0.5 ± 0.02 c,y	A
e34	2200	ethyl octadeca-9,12,15-trienoate	AO	nd a	0.7 ± 0.08 a,z	9.01 ± 0.4 b,z	13.8 ± 1.5 c,z	14.3 ± 0.7 c,z	15.0 ± 1.06 c,y	27.2 ± 2.04 d,z	B
			AS	nd a	0.6 ± 0.01 a,y	4.6 ± 0.01 b,y	8.5 ± 0.5 c,x	12.2 ± 1.1 d,y	11.1 ± 0.9 de,x	10.6 ± 1.4 e,x	B
			AK	nd a	nd a,x	1.1 ± 0.4 b,x	11.3 ± 0.3 e,y	8.2 ± 0.1 c,x	10.5 ± 0.6 d,x	14.9 ± 0.5 f,y	B
e35	2200	methyl octadeca-9,12-dienoate	AO	nd a	nd a	1.1 ± 0.09 b,z	1.4 ± 0.1 b,z	1.7 ± 0.07 d,z	1.1 ± 0.03 c,y	2.9 ± 0.1 e,z	A
			AS	nd a	nd a	0.5 ± 0.002 b,y	0.7 ± 0.08 c,x	1.3 ± 0.06 e,y	0.7 ± 0.05 cd,x	0.8 ± 0.1 d,x	A
			AK	nd a	nd a	0.1 ± 0.002 b,x	1.2 ± 0.01 e,y	0.8 ± 0.01 d,x	0.7 ± 0.05 c,x	1.2 ± 0.1 e,y	A
Furans and Furan Derivatives											
f1	879	2-methylfuran	AO	nd a	0.2 ± 0.02 b,x	nd a	nd a	nd a	nd a	nd a	B
			AS	nd a	0.4 ± 0.006 b,z	nd a	nd a	nd a	nd a	nd a	B
			AK	nd a	0.3 ± 0.02 b,y	nd a	nd a	nd a	nd a	nd a	B
f2	929	2-ethylfuran	AO	22.5 ± 0.6 d	6.2 ± 0.3 c,y	1.6 ± 0.04 b,x	0.2 ± 0.01 a,x	0.2 ± 0.009 a,x	0.2 ± 0.003 a,y	0.1 ± 0.004 a,x	A
			AS	22.5 ± 0.6 d	5.2 ± 0.06 c,x	2.0 ± 0.003 b,y	0.5 ± 0.06 a,y	0.6 ± 0.03 a,y	0.2 ± 0.01 a,y	0.2 ± 0.003 a,y	A
			AK	22.5 ± 0.6 d	7.5 ± 0.4 c,z	3.7 ± 0.02 b,z	0.2 ± 0.01 a,x	0.2 ± 0.02 a,x	0.1 ± 0.01 a,x	0.1 ± 0.021 a,x	A
f3	1073	2-ethenylfuran	AO	1.0 ± 0.08 d	0.4 ± 0.005 c,z	0.3 ± 0.02 b,z	nd a	nd a	nd a	nd a	B
			AS	1.0 ± 0.08 c	0.1 ± 0.09 b,x	0.09 ± 0.006 b,x	nd a	nd a	nd a	nd a	B
			AK	1.0 ± 0.08 d	0.3 ± 0.03 c,y	0.2 ± 0.02 b,y	nd a	nd a	nd a	nd a	B
f4	1200	2-pentylfuran	AO	nd a	6.0 ± 0.3 f,y	4.9 ± 0.2 e,y	2.3 ± 0.3 d,x	1.1 ± 0.08 c,x	0.9 ± 0.02 c,x	0.4 ± 0.02 b,x	A
			AS	nd a	6.5 ± 0.03 g,y	4.1 ± 0.1 f,x	2.0 ± 0.06 e,x	1.4 ± 0.1 d,y	0.9 ± 0.07 c,x	0.5 ± 0.01 b,x	A
			AK	nd a	3.7 ± 0.3 e,x	3.7 ± 0.5 e,x	2.1 ± 0.1 d,x	1.4 ± 0.02 c,y	1.1 ± 0.03 bc,y	0.7 ± 0.04 b,y	A
f5	1469	furan-2-carbaldehyde	AO	0.3 ± 0.03 a	2.4 ± 0.1 f,x	1.7 ± 0.1 e,x	1.2 ± 0.1 d,x	0.5 ± 0.05 b,x	0.7 ± 0.03 c,x	1.2 ± 0.03 a,y	A
			AS	0.3 ± 0.03 a	2.4 ± 0.4 e,x	1.6 ± 0.07 d,x	1.2 ± 0.1 c,x	0.8 ± 0.04 b,y	1.3 ± 0.03 c,z	1.0 ± 0.02 b,x	A
			AK	0.3 ± 0.03 a	2.5 ± 0.1 d,x	3.7 ± 0.1 e,y	1.5 ± 0.04 c,y	1.1 ± 0.06 b,z	1.2 ± 0.009 b,y	1.5 ± 0.04 c,z	A
f6	1652	furan-2-ylmethanol	AO	1.0 ± 0.08 b	nd a	nd a	nd a	nd a	nd a	nd a	A
			AS	1.0 ± 0.08 b	nd a	nd a	nd a	nd a	nd a	nd a	A
			AK	1.0 ± 0.08 b	nd a	nd a	nd a	nd a	nd a	nd a	A
f7	1715	4-methyl-2*H*-furan-5-one	AO	nd a	nd a	0.02 ± 0.001 ab,x	0.04 ± 0.002 b,x	0.1 ± 0.03 d,y	0.1 ± 0.008 c,x	0.2 ± 0.01 e,z	C

J. Agric. Food Chem. 2015, 63, 1401−1418
DOI: 10.1021/jf5056002

Table 2. continued

				relative peak areas (mean ± SD)[c]							
				fermentation periods (weeks)							
no.	RI[a]	volatile compounds[b]	Sp.	0	1	2	4	5	7	8	ID[d]
Furans and Furan Derivatives											
			AS	nd a	nd a	0.05 ± 0.002 b,z	0.07 ± 0.005 bc,y	0.08 ± 0.003 c,x	0.1 ± 0.02 d,x	0.1 ± 0.03 d,y	C
			AK	nd a	nd a	0.04 ± 0.002 b,y	0.1 ± 0.007 d,z	0.2 ± 0.003 e,z	0.1 ± 0.02 d,x	0.07 ± 0.002 c,x	C
f8	2036	5-pentyloxolan-2-one	AO	nd a	0.1 ± 0.01 b,y	0.2 ± 0.01 c,y	0.2 ± 0.01 c,x	0.1 ± 0.004 b,x	0.1 ± 0.009 b,x	0.2 ± 0.003 d,y	B
			AS	nd a	0.2 ± 0.01 c,z	0.2 ± 0.005 e,z	0.2 ± 0.01 d,y	0.2 ± 0.01 c,y	0.1 ± 0.007 b,x	0.2 ± 0.005 c,x	B
			AK	nd a	0.09 ± 0.002 b,x	0.1 ± 0.006 bc,x	0.2 ± 0.02 d,y	0.1 ± 0.006 c,x	0.1 ± 0.008 c,x	0.2 ± 0.02 d,y	B
Hydrocarbons											
hc1	800	octane	AO	nd a	0.2 ± 0.01 c,x	0.06 ± 0.002 b,x	nd a	nd a	nd a	nd a	A
			AS	nd a	0.6 ± 0.08 c,z	0.1 ± 0.006 b,y	nd a	nd a	nd a	nd a	A
			AK	nd a	0.4 ± 0.02 c,y	0.2 ± 0.009 b,z	nd a	nd a	nd a	nd a	A
hc2	833	(*E*)-oct-2-ene	AO	0.4 ± 0.004 b	nd a,x	nd a,x	nd a	nd a	nd a	nd a	B
			AS	0.4 ± 0.004 d	0.2 ± 0.003 c,y	0.05 ± 0.003 b,y	nd a	nd a	nd a	nd a	B
			AK	0.4 ± 0.004 d	0.2 ± 0.006 c,y	0.1 ± 0.008 b,z	nd a	nd a	nd a	nd a	B
hc3	1190	dodecane	AO	nd a	2.8 ± 0.2 d,y	2.9 ± 0.09 d,z	1.6 ± 0.3 c,y	0.8 ± 0.04 b,z	0.9 ± 0.02 b,z	1.0 ± 0.02 b,z	A
			AS	nd a	1.4 ± 0.05 e,x	0.2 ± 0.04 c,x	0.2 ± 0.03 c,x	0.1 ± 0.006 b,x	0.5 ± 0.04 d,x	0.2 ± 0.02 b,x	A
			AK	nd a	1.7 ± 0.2 f,x	1.2 ± 0.1 e,y	0.3 ± 0.01 b,x	0.7 ± 0.06 c,y	0.8 ± 0.05 c,y	1.0 ± 0.03 d,y	A
hc4	1318	tridecane	AO	nd a	4.7 ± 0.2 c,y	10.1 ± 0.5 e,z	9.5 ± 0.1 d,z	3.3 ± 0.7 b,z	3.5 ± 0.3 b,z	3.8 ± 0.2 b,z	A
			AS	nd a	nd a,x	0.2 ± 0.002 b,x	0.07 ± 0.01 ab,x	0.1 ± 0.003 ab,x	1.6 ± 0.2 c,x	0.09 ± 0.008 ab,x	A
			AK	nd a	7.5 ± 0.5 f,z	5.1 ± 0.3 e,y	2.8 ± 0.07 d,y	2.0 ± 0.07 b,y	2.2 ± 0.008 bc,y	2.5 ± 0.2 cd,y	A
hc5	1409	tetradecane	AO	nd a	2.6 ± 1.4 b,y	4.4 ± 0.1 c,z	2.8 ± 0.3 b,y	2.3 ± 1.3 b,y	1.6 ± 0.1 b,z	2.4 ± 0.2 b,z	A
			AS	nd a	0.2 ± 0.003 cd,x	0.3 ± 0.001 d,y	0.1 ± 0.003 b,x	0.2 ± 0.01 bc,x	0.9 ± 0.1 e,x	0.2 ± 0.007 b,x	A
			AK	nd a	1.2 ± 0.105 d,xy	nd a,x	0.2 ± 0.02 b,x	1.0 ± 0.06 c,xy	1.1 ± 0.07 d,y	1.5 ± 0.02 e,y	A
Phenols											
ph1	1862	2-methoxyphenol	AO	nd a	0.1 ± 0.004 d,y	0.1 ± 0.02 d,y	0.2 ± 0.006 e,z	0.1 ± 0.03 cd,y	0.08 ± 0.01 bc,x	0.07 ± 0.008 b,y	A
			AS	nd a	0.1 ± 0.01 d,x	0.07 ± 0.003 c,x	0.1 ± 0.020 e,y	0.03 ± 0.007 b,x	0.08 ± 0.003 cd,x	0.05 ± 0.003 b,x	A
			AK	nd a	0.2 ± 0.01 f,z	0.1 ± 0.004 e,y	0.08 ± 0.003 bc,x	0.07 ± 0.001 b,y	0.09 ± 0.01 c,x	0.1 ± 0.003 d,z	A
ph2	2009	phenol	AO	0.2 ± 0.006 b	0.4 ± 0.03 f,y	0.4 ± 0.02 e,y	0.2 ± 0.010 c,y	0.1 ± 0.01 a,y	0.2 ± 0.003 c,x	0.3 ± 0.01 d,y	A
			AS	0.2 ± 0.006 d	0.1 ± 0.02 c,x	0.1 ± 0.02 c,x	0.06 ± 0.002 a,x	0.09 ± 0.01 b,x	0.3 ± 0.01 e,y	0.07 ± 0.005 ab,x	A
			AK	0.2 ± 0.006 b	0.6 ± 0.03 g,z	0.6 ± 0.02 f,z	0.05 ± 0.004 a,x	0.2 ± 0.02 c,z	0.3 ± 0.02 d,y	0.3 ± 0.05 e,y	A
ph3	2200	4-ethenyl-2-methoxyphenol	AO	0.2 ± 0.004 a	0.3 ± 0.02 b,x	0.4 ± 0.05 d,x	0.3 ± 0.07 c,x	0.2 ± 0.02 b,x	1.3 ± 0.02 e,x	0.4 ± 0.04 d,x	A
			AS	0.2 ± 0.004 a	3.4 ± 0.2 c,z	5.6 ± 0.5 e,z	4.5 ± 0.5 d,y	5.0 ± 0.4 d,z	2.3 ± 0.07 b,y	3.1 ± 0.04 c,y	A
			AK	0.2 ± 0.004 a	1.9 ± 0.2 b,y	3.3 ± 0.2 d,y	4.6 ± 0.2 e,y	2.8 ± 0.04 c,y	3.0 ± 0.1 c,z	3.3 ± 0.1 d,z	A
ph4	2200	4-ethenylphenol	AO	0.2 ± 0.02 c	0.1 ± 0.01 b,x	0.2 ± 0.01 d,x	0.5 ± 0.005 e,y	0.07 ± 0.006 a,x	0.1 ± 0.007 b,x	0.2 ± 0.01 cd,x	C
			AS	0.2 ± 0.02 a	1.3 ± 0.1 d,y	2.2 ± 0.2 e,y	0.3 ± 0.02 a,x	0.6 ± 0.04 b,z	1.01 ± 0.009 c,y	1.0 ± 0.02 c,y	C
			AK	0.2 ± 0.02 a	1.3 ± 0.1 d,y	2.2 ± 0.1 e,y	0.5 ± 0.05 b,y	0.4 ± 0.02 b,y	1.1 ± 0.02 c,z	1.3 ± 0.1 d,z	C
Sulfur-Containing Compounds											
s1	1014	thiophene	AO	4.8 ± 0.5 b	0.4 ± 0.02 a,x	0.2 ± 0.01 a,y	nd a	nd a	nd a	nd a	A
			AS	4.8 ± 0.5 c	0.4 ± 0.001 b,y	0.07 ± 0.001 b,x	nd a	nd a	nd a	nd a	A
			AK	4.8 ± 0.539 c	0.8 ± 0.001 b,z	0.3 ± 0.01 a,z	nd a	nd a	nd a	nd a	A

J. Agric. Food Chem. 2015, 63, 1401−1418
DOI: 10.1021/jf5056002

Table 2. continued

				relative peak areas (mean ± SD)[c]							
				fermentation periods (weeks)							
no.	RI[a]	volatile compounds[b]	Sp.	0	1	2	4	5	7	8	ID[d]
Sulfur-Containing Compounds											
s2	1067	dimethyl disulfide [(methyldisulfanyl) methane]	AO	1.3 ± 0.1 d	0.6 ± 0.1 c,y	0.3 ± 0.02 b,y	nd a	nd a	nd a	nd a,x	A
			AS	1.3 ± 0.1 e	0.6 ± 0.03 d,y	0.2 ± 0.008 c,x	nd a	nd a	nd a	0.1 ± 0.007 b,y	A
			AK	1.3 ± 0.1 d	0.4 ± 0.04 c,x	0.2 ± 0.05 b,x	nd a	nd a	nd a	0.3 ± 0.006 b,z	A
s3	1101	2-methylthiophene	AO	0.9 ± 0.07 d	0.3 ± 0.03 c,x	0.2 ± 0.002 b,xy	nd a	nd a	nd a	nd a	A
			AS	0.9 ± 0.07 d	0.3 ± 0.002 c,xy	0.1 ± 0.02 b,x	nd a	nd a	nd a	nd a	A
			AK	0.9 ± 0.07 d	0.3 ± 0.04 c,y	0.2 ± 0.02 b,y	nd a	nd a	nd a	nd a	A
s4	1369	dimethyl trisulfide [(methyltrisulfanyl) methane]	AO	nd a	0.1 ± 0.002 f,z	0.1 ± 0.02 e,z	0.1 ± 0.01 d,z	0.06 ± 0.004 c,z	0.05 ± 0.002 bc,y	0.04 ± 0.002 b,y	A
			AS	nd a	0.08 ± 0.001 e,y	0.07 ± 0.001 d,y	0.04 ± 0.002 c,x	0.02 ± 0.004 b,x	nd a,x	nd a,x	A
			AK	nd a	nd a,x	nd a,x	0.07 ± 0.002 c,y	0.04 ± 0.001 b,y	nd a,x	nd a,x	A
s5	1710	methionol (3-methylsulfanylpropan-1-ol)	AO	0.2 ± 0.009 a	0.5 ± 0.06 c,z	0.9 ± 0.04 e,z	0.7 ± 0.1 d,y	0.2 ± 0.02 a,x	0.2 ± 0.02 a,x	0.4 ± 0.02 b,y	A
			AS	0.2 ± 0.009 a	0.3 ± 0.07 b,y	0.4 ± 0.02 c,y	0.3 ± 0.03 b,x	0.3 ± 0.03 b,y	0.3 ± 0.007 b,y	0.3 ± 0.01 b,x	A
			AK	0.2 ± 0.009 a	0.1 ± 0.007 a,x	0.3 ± 0.007 b,x	0.3 ± 0.02 b,x	0.2 ± 0.04 b,z	0.2 ± 0.03 a,x	0.3 ± 0.03 cd,x	A
Miscellaneous											
mi1	1269	2-methylpyrazine	AO	0.7 ± 0.03 c	0.1 ± 0.02 b,y	0.1 ± 0.005 b,y	nd a	nd a	nd a	nd a	A
			AS	0.7 ± 0.03 b	nd a,x	nd a,x	nd a	nd a	nd a	nd a	A
			AK	0.7 ± 0.03 c	0.2 ± 0.01 b,z	nd a,x	nd a	nd a	nd a	nd a	A
mi2	1975	3-hydroxy- 2-methylpyran-4-one (maltol)	AO	nd a	1.0 ± 0.007 f,z	0.9 ± 0.05 e,y	0.3 ± 0.04 d,x	0.2 ± 0.03 c,x	0.1 ± 0.008 b,x	0.3 ± 0.03 d,y	A
			AS	nd a	0.6 ± 0.06 e,x	0.5 ± 0.001 d,x	0.2 ± 0.02 c,x	0.3 ± 0.03 c,x	0.2 ± 0.01 b,y	0.2 ± 0.05 b,x	A
			AK	nd a	0.8 ± 0.07 e,y	0.5 ± 0.08 d,x	0.3 ± 0.03 c,x	0.2 ± 0.04 c,x	0.1 ± 0.006 b,y	0.2 ± 0.02 bc,x	A
mi3	2200	1*H*-indole	AO	nd a	nd a,x	nd a,x	nd a	0.05 ± 0.002 b,x	nd a,x	nd a,x	A
			AS	nd a	nd a,x	nd a,x	nd a	0.04 ± 0.008 d,x	0.02 ± 0.01 c,y	0.01 ± 0.002 b,y	A
			AK	nd a	0.04 ± 0.006 d,y	0.05 ± 0.007 d,y	nd a	0.04 ± 0.002 d,x	0.03 ± 0.001 c,y	0.02 ± 0.001 b,z	A

[a]Retention indices (RI) were determined using *n*-paraffins C_7–C_{22} as external standards on DB-FFAP column. [b]All volatile compounds by order of their RI in a chemical class. [c]Average of relative peak areas to that of internal standard ($n = 3$) ± standard deviation. [d]Volatile identification was performed with the following criteria: (A) mass spectrum and retention index were consistent with those of an authentic compound (positive identification); (B) mass spectrum and retention index were consistent with those of the literature;[4,18−27] and (C) mass spectrum was consistent with that of Wiley 7n mass spectral database or by manual interpretation (tentative identification). [e]nd = not detected. [f]Different letters mean significant differences ($p < 0.05$) between seven *doenjang* samples varying with fermentation period by Duncan's multiple range test. [g]Different letters mean significant differences ($p < 0.05$) between three *doenjang* samples according to the different *Aspergillus* sp. inoculated by Duncan's multiple range test.

J. Agric. Food Chem. 2015, 63, 1401−1418
DOI: 10.1021/jf5056002

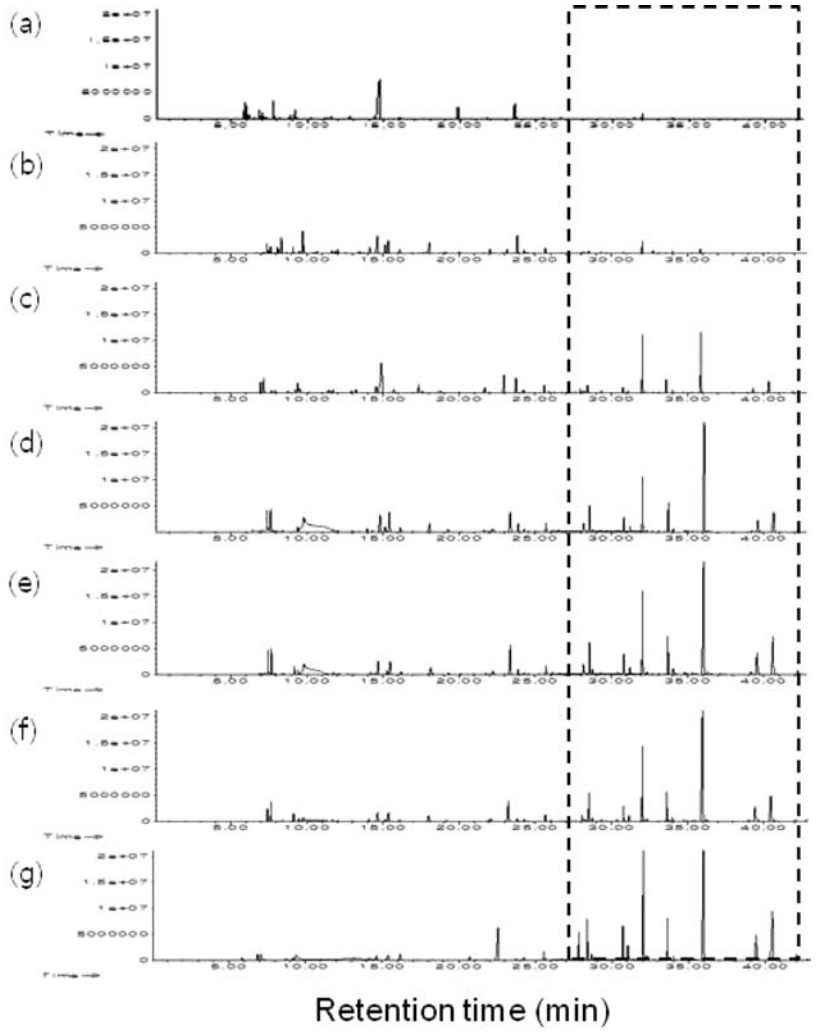

Figure 1. GC−MS total ion chromatograms of volatile components in rice-*koji doenjang* fermented with *Aspergillus oryzae* during fermentation: (a) NA, (b) AO-1 week, (c) AO-2 weeks, (d) AO-4 weeks, (e) AO-5 weeks, (f) AO-7 weeks, and (g) AO-8 weeks.

which was made by mixing KI and I_2 solution, and then measured at 660 nm using a spectrophotometer (Minolta CR-400, Konica Minolta Sensing, Inc., Osaka, Japan).

One unit (U) of α-amylase activity was referred to the quantity of α-amylase that catalyzed the conversion of 1% soluble starch solution to 1.0 mg equivalent of maltose per min under the corresponding conditions.

Protease (EC 3.4.21.19) Assay. To assess protease activity, 2 mL of 2% casein was added to 2 mL of pH 7.0 buffer solution (0.1 M Na_2HPO_4 plus 0.1 M KH_2PO_4) to make substrate solution. One milliliters of crude enzyme solution was mixed, and reacted at 30 °C for 20 min before the reaction was stopped by adding 5 mL of 0.4 M trichloroacetic acid solution for 20 min. The reaction mixture was transferred over filter paper, and then 1 mL of supernatant was mixed with 5 mL of 0.4 M Na_2CO_3 solution and 0.5 M Folin and Ciocalteu's phenol reagent. After reaction ceased, the color change was measured at 660 nm using a spectrophotometer. One unit (U) of protease activity was defined as the quantity of protease inducing a change of 1 μg of tyrosine from 2% casein solution in a minute.

Esterase (EC 3.1.1.1) Assay. The carboxyl ester hydrolase (esterase) activity was determined using a modified spectrometric method,[28] following the hydrolysis of *p*-nitrophenylbutyrate (*p*-NPB) to *p*-nitrophenol at 37 °C for every 5 min. The reaction mixture contained 10 mM *p*-NPB dissolved in acetonitrile and appropriately diluted crude enzyme solution. The instrument was set to zero with Tris-HCl buffer (0.1 M, pH 7.5). The amount of *p*-nitrophenol liberated was measured by a *p*-nitrophenol standard curve at 410 nm (absorbance versus mM of *p*-nitrophenol).

One unit (U) of esterase activity was defined as the amount of esterase needed to liberate 1 μmol of *p*-nitrophenol per minute from *p*-NPB under the specified conditions.

Lipase (EC 3.1.1.3) Assay. A spectrometric method was also performed for the measurement of lipase activity using *p*-nitrophenyl palmitate (*p*-NPP) as a substrate.[29] The substrate solution was prepared by adding 0.0159 g of *p*-NPP, 0.017 g of sodium dodecyl sulfate, and 1.00 g of Triton X-100 into a 100 mL volumetric flask and bringing to volume with distilled water. The assay mixture consisted of 2.5 mL of substrate solution, 2.5 mL of 0.1 M Tris-HCl buffer (pH 7.5), and 1 mL of suitably diluted crude enzyme solution. The release of *p*-nitrophenol from *p*-NPP at 37 °C was continuously monitored at 400 nm using a spectrophotometer every 5 min. The instrument was set to zero with 0.1 M Tris-HCl buffer. To convert absorbance to concentration of substrate hydrolyzed, a *p*-nitrophenol standard curve was used.

One unit (U) of lipase activity was defined as the amount of lipase required to release 1 μmol of *p*-nitrophenol from *p*-NPP in 1 min under the corresponding conditions.

Statistical Analysis. Multivariate analysis of variance (MANOVA) was accomplished using the general linear model procedure in SPSS (version 12.0, Chicago, IL) to assess differences in the volatile components of rice-*koji doenjang*. Duncan's multiple range tests were used when the samples demonstrated significantly different relative peak areas of volatiles according to their fermentation time and fungal

DOI: 10.1021/jf5056002
J. Agric. Food Chem. 2015, 63, 1401−1418

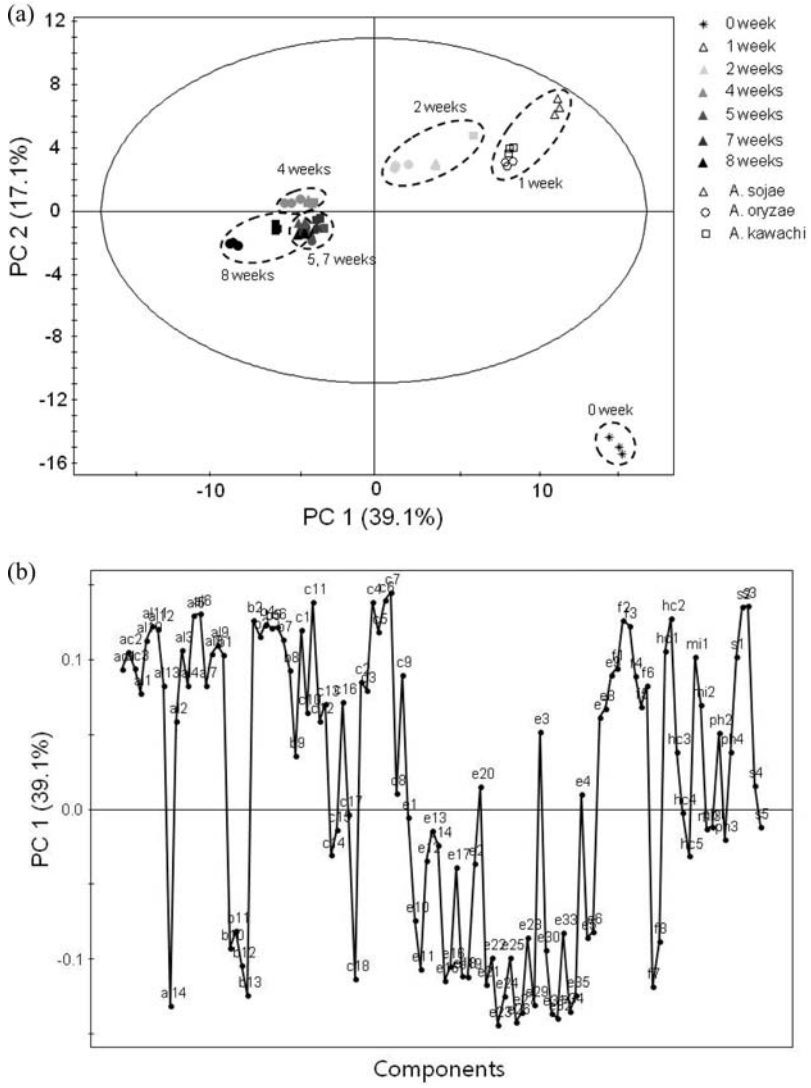

Figure 2. Principal component analysis (PCA) plots for the volatile components isolated from rice-*koji doenjang* according to *Aspergillus* species inoculated and fermentation time: (a) score plot, (b) loading plot.

species inoculated, with the level of significance set at $p < 0.05$ (Table 2). Principal component analysis (PCA) and partial least-squares regression (PLSR) analysis were performed with the aid of SIMCA-P (version 11.0, Umetrics, Umeå, Sweden) software to discriminate different rice-*koji doenjang* samples on the basis of their volatile profiles according to fermentation periods and also clarify the effects of the enzymatic activities originated from *Aspergillus* species inoculated on volatile components formation.

To determine the enzymatic effects on volatiles formation, a bivariate correlation was used, with Pearson's correlation coefficients (r) calculated by SPSS. Also, heatmap was performed using Multiexperiment Viewer (MeV, version 4.8.1, Boston, MA) software to visualize these relationships.

RESULTS AND DISCUSSION

GC−MS Analysis and Assignment of Volatile Components in the Three Sample Types. The 108 volatile components found in the three rice-*koji doenjang* samples during 8 weeks of fermentation are listed in Table 2, with their mean values of relative peak areas and RIs on the DB-FFAP column. These compounds comprised the following 10 classes of compounds: acids (n = 3), alcohols (n = 14), benzene derivatives (n = 13), carbonyls (n = 18), esters (n = 35), furan derivatives (n = 8), hydrocarbons (n = 5), phenols (n = 4), sulfur-containing compounds (n = 5), and miscellaneous compounds (n = 3). Figure 1 shows the GC−MS total ion chromatograms for the volatile compounds of a representative AO sample during 8 weeks of fermentation. The contents of some volatile compounds tended to increase with the fermentation time: most of these compounds were long-chain fatty acid ethyl esters (e22−e35: ethyl dodecanoate, ethyl tetradecanoate, ethyl pentadecanoate, methyl hexadecanoate, ethyl hexadecanoate, ethyl hexadecanoate, ethyl hexadec-9-enoate, ethyl heptadecanoate, butyl hexadecanoate, ethyl octadecanoate, ethyl octadec-9-enoate, ethyl octadeca-9,12-dienoate, ethyl octadeca-9,12,15-trienoate, methyl octadeca-9,12-dienoate), which are considered to be formed via the interaction of acids and ethanol through fermentation, and they affect the quality of fermented rice-*koji doenjang*. In particular, the contents of ethyl tetradecanoate (e23, 33.6 min), ethyl hexadecanoate (e26, 36 min), ethyl octadec-9-enoate (e32, 39.4 min), and ethyl octadeca-9,12,15-trienoate (e34, 40.5 min), which give fatty and oily odor notes, changed considerably with fermentation time.[30] This result indicates that these high-molecular-weight ethyl esters, which are generally related to

DOI: 10.1021/jf5056002
J. Agric. Food Chem. 2015, 63, 1401−1418

Table 3. Changes of Enzymatic Activities in Three Different Types of Rice-*koji doenjang* Inoculated with *Aspergillus oryzae* (AO), *A. sojae* (AS), and *A. kawachii* (AK) during Fermentation

		enzymatic activities (mean ± SD, unit/g protein)[b]		
		fermentation periods (weeks)		
enzymes (EC)[a]	Sp.	2	4	8
α-amylase (EC 3.2.2.1)	AO	271.5 ± 2.3 c,[c]z[d]	255.6 ± 4.0 b,z	167.8 ± 1.2 a,z
	AS	52.0 ± 2.3 c,x	38.8 ± 3.3 b,x	16.0 ± 3.4 a,x
	AK	212.3 ± 0.3 c,y	142.2 ± 0.4 b,y	67.0 ± 3.2 a,y
protease (EC 3.4.21.19)	AO	11.6 ± 2.4 a,x	21.9 ± 0.4 b,x	40.1 ± 2.0 c,x
	AS	16.9 ± 1.0 a,y	49.5 ± 2.0 b,y	101.8 ± 10.1 c,y
	AK	14.3 ± 1.9 a,xy	44.2 ± 4.4 b,y	100.7 ± 11.3 c,y
esterase (EC 3.1.1.1)	AO	27.8 ± 0.8 a,x	31.6 ± 0.2 b,x	44.4 ± 0.5 c,x
	AS	42.1 ± 1.3 a,y	42.7 ± 0.4 a,z	88.3 ± 0.8 b,y
	AK	27.9 ± 0.1 a,x	34.4 ± 0.2 b,y	45.3 ± 0.8 c,x
lipase (EC 3.1.1.3)	AO	21.9 ± 1.5 a,x	32.9 ± 0.9 c,x	28.0 ± 1.7 b,y
	AS	24.9 ± 0.6 b,y	44.5 ± 1.0 c,y	20.0 ± 0.7 a,x
	AK	28.0 ± 0.6 a,z	51.9 ± 0.7 c,z	31.6 ± 1.4 b,z

[a]EC: Enzyme Commission number is a numerical classification scheme for enzymes based on the chemical reactions they catalyze. [b]Average of specific activities (n = 3) ± standard deviation. [c]Different letters mean significant differences ($p < 0.05$) between the *doenjang* samples varying with fermentation period by Duncan's multi range test. [d]Different letters mean significant differences ($p < 0.05$) between the *doenjang* samples varying with *Aspergillus* species inoculated by Duncan's multi range test.

fatty and oily odor notes, influence mainly the latter fermentation stage of rice-*koji doenjang* inoculated with *Aspergillus* species. These compounds could be produced by the actions of enzymes such as lipase and esterase that were excreted by the inoculated *Aspergillus* species.[31]

However, some low molecular weight acids such as acetic acid, butanoic acid, and propanoic acid could not be found in our study, although they had been detected in previous studies on *doenjang* volatiles.[1,2,4−6] We expected those acids could be converted to the corresponding esters in our study.

Principal Component Analysis of Three Types of Rice-*koji doenjang* According to the Inoculated *Aspergillus* Species and Fermentation Time. PCA is an unsupervised method that enables recognition of any inherent sample clustering. It does not require any information on the data sets and represents a multivariate data table as a low-dimensional plane.[32]

PCA was thus used to analyze the data sets of relative peak areas of volatile components to determine whether their fermentation time could be used to differentiate between the three types of rice-*koji doenjang* samples (Figure 2). A total variance of 56.3% was observed, comprising 39.1% from the first principal component (PC1) and 17.2% from the second principal component. Classification of the plots according to fermentation time revealed that the profiles of the volatiles moved from right to left with increasing fermentation period in the PC1 dimension, accounting for the observed steady changes in profiles as fermentation proceeded (Figure 2a).

Overall, rice-*koji doenjang* samples could be differentiated primarily according to their PC1 score with a positioning of the initial stage (0−2 weeks) in the positive dimension, and the middle or latter stages (4−8 weeks) in the negative dimension. As shown in Figure 2b, butan-2-one, hexanal, 4-methyl heptan-2-one, dimethyl disulfide, 2-methyl thiophene, 2-ethyl furan, hexan-1-ol, methylbenzene, and hexanoic acid contributed positively to the PC1 dimension and exhibited marked changes in their contents during the primary stage of fermentation. With the exception of hexanoic acid, the levels of these compounds peaked at 0 weeks of fermentation, and were generally not detected after 4−8 weeks, which would indicate that they originated mainly from the raw materials of the rice-*koji doenjang* and were utilized as precursors for the subsequent fermentation-related reactions. For example, hexanal is a long-chain aldehyde that imparts a green bean note and is known to be derived from long-chain fatty acids as a result of lipoxygenase-catalyzed lipid oxidation in soybeans.[33,34] Volatile sulfur compounds such as dimethyl disulfide and 2-methyl thiophene can affect the flavor of fermented soybean foods because of their low threshold levels and unique aroma notes.[35] Dimethyl disulfide is associated with cooked-cabbage and garlic-like odors,[35] whereas 2-methylthiophene is characterized as a potent cooked odorant. Hexan-1-ol reportedly imparts the green and beany odorant found in raw soybeans,[36] and is formed during the enzymatic oxidation of linoleic acid (C18:2).[37] Hexanoic acid is one of the mid-chain fatty acids related to unpleasant rancid and cheesy odor notes.[38] As with the other acid compounds identified in the present study, hexanoic acid was detected only at 1 and 2 weeks of fermentation.

Conversely, ethyl octanoate and ethyl hexadecanoate contributed to the negative axis of PC1, and their levels tended to increase during fermentation, peaking in 8-week samples. This demonstrates that these ethyl esters, which are generally associated with fatty and oily odor notes, could influence the latter fermentation stage of rice-*koji doenjang*.[31] Furthermore, the PCA score plot in Figure 2a shows the positioning differences among the three species of *Aspergillus* inoculated into the rice-*koji doenjang*. Relatively large differences were observed at 1, 2, and 8 weeks, whereas smaller gaps were found between 5 and 7 weeks. At the early fermentation stage (i.e., 1−2 weeks), there were significant differences in the levels of acids and alcohols, and particularly of hexanoic acid, hexan-1-ol, oct-1-en-3-ol, and heptan-1-ol. The levels of those components were higher in AS than in AO and AK samples.

At 8 weeks of fermentation, there were also noticeable differences in the contents of ethyl octanoate, ethyl decanoate, diethylbutanedioate, ethyl dodecanoate, and ethyl hexadecanoate relative to the microbial species inoculated, with the highest levels being observed in AO. These ethyl ester compounds could be formed by esterification of ethanol and

DOI: 10.1021/jf5056002
J. Agric. Food Chem. 2015, 63, 1401−1418

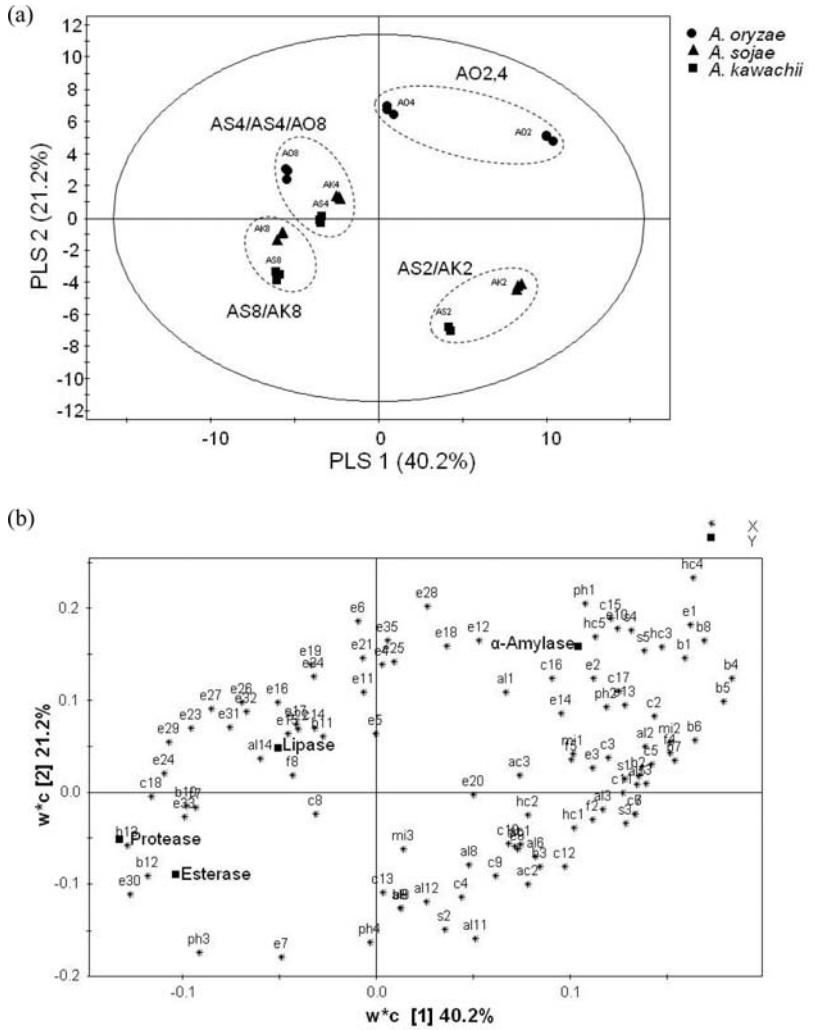

Figure 3. Relationships between the volatile components isolated from rice-*koji doenjang* and enzyme activities (α-amylase, protease, lipase, and esterase) during fermentation using partial least-squares regression (PLSR): score plot (a) and loading plot (b).

fatty acids, which were derived via the Embden−Meyerhof−Parnas pathway by yeast and fungal hydrolysis of soybean lipids, respectively.[38] Lee et al.[25] reported that these high-molecular-weight esters could be detected at much higher levels in *doenjang* samples prepared with *koji* than in traditional *doenjang* samples that were fermented with naturally occurring microorganisms, possibly due to differences in the microbial enzymatic preference for soybean lipid and esterification. These compounds are secondary products formed by reactions after sufficient amounts of ethanol and fatty acids are generated during fermentation, and so differences in enzymatic preferences might be responsible for the differences in the contents of these ester compounds at 8 weeks.

Enzymatic Activities in Three Types of Rice-*koji doenjang* during Fermentation. As described above, rice-*koji doenjang* inoculated with different strains of *Aspergillus* exhibited different volatile-component profiles (Table 2 and Figure 2). This suggests that the *Aspergillus* species exhibit different enzymatic activities, which are in turn directly and/or indirectly related to the formation of volatile components during fermentation.[37] Therefore, the effects of periodic changes in the enzymatic activities of α-amylase, protease, lipase, and esterase on the formation of volatiles of *doenjang* were examined.

Significant differences in the activities of all enzymes according to both fermentation time and microbial species were found (Table 3). α-Amylase activities decreased steadily in all samples over the fermentation period (i.e., at 2, 4, and 8 weeks). The presence of a relatively large amount of carbohydrate, acting as a substrate for α-amylase, in soybean and rice in the early fermentation stage (2 weeks) resulted in the measurement of relatively high levels of enzymatic activity. However, their specific activities gradually declined as the levels of carbohydrate substrate decreased due to its consumption by microorganisms during fermentation. Samples inoculated with *A. oryzae* exhibited the highest α-amylase activity among the samples, ranging from 167.750 to 271.479 units/g of enzyme activity/g protein at 8 to 2 weeks of fermentation, respectively. In contrast, the enzyme activities were lowest in the *A. sojae* samples. α-Amylase catalyzes the breakdown of α-1,4 glucosidic linkages in polysaccharides, such as starches or glycogen, liberating low-molecular-weight sugars.[39] In the present study, it was expected that samples inoculated with *A. oryzae* would exhibit increased formation of mono- or disaccharides and related volatile components in *doenjang* as compared to the other samples.

Conversely, there was a tendency toward a steady increase in protease activities during fermentation. Of particular note was

DOI: 10.1021/jf5056002
J. Agric. Food Chem. 2015, 63, 1401−1418

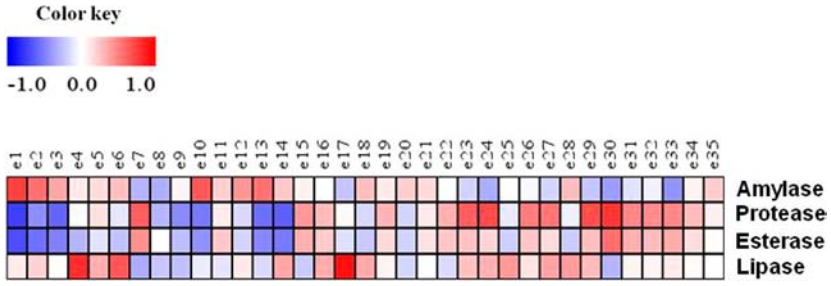

Figure 4. Heatmap representing the relationships between ester compounds identified (e1−e35) and enzymatic activities during rice-*koji doenjang* fermentation: Pearson's correlation coefficients ($-1 \leq r \leq 1$) are shown in each column.

the absence of significant differences in protease activities between samples inoculated with AS and AK (Table 3). It has been shown previously that AS exhibits higher protease activities than AO in solid-state fermentation of soybeans, which are usually used to make soy sauce.[40] In contrast, all AO samples exhibited the lowest protease activity among the samples, the gap between them widening drastically as fermentation proceeded.

Esterase activities increased throughout fermentation, with the highest activities being observed in AS samples. Because esterase catalyzes the formation of ester compounds by condensing alcohols (ethanol) and acids (fatty acids), the increase in esterase activities indicates that there were sufficient amounts of ethanol and fatty acids present in the samples in this study.

All samples exhibited a decreasing tendency of lipase activities after 4 weeks of fermentation in this study, with the greatest change being observed in AK samples. These results concur with those of previous studies.[7,41] Kim et al.[7] reported that lipase activities in soybean pastes prepared with mold-producing protease containing *meju* were increased continuously until 30 days of fermentation, and then decreased gradually thereafter. In addition, Joo et al.[41] demonstrated that soybean/soybean paste fermented with various *Aspergillus* species exhibited a maximum level of lipase activities after 20 days, with the levels increasing dramatically from the beginning of fermentation. The decrease in lipase activities could be attributable to the reduction in triglycerides, which are the substrates of this enzyme, during the fermentation process.

Changes in Enzymatic Activities and Their Effects on the Formation of Volatile Components in Three Types of Rice-*koji doenjang* during Fermentation. The correlations between the formation of volatile components and enzymatic reactions during fermentation were clarified by conducting partial least-squares (PLS) regression analysis. The different enzymatic activities between samples could lead to variance in the profiles of precursors for volatile compounds among them, which may have affected further reactions related to the formation of volatiles throughout the fermentation period.

Figure 3a and b shows the correlations between each of the volatile compounds formed and the activities of each of the associated enzymes (i.e., α-amylase, protease, lipase, and esterase). In terms of microbial types, similar patterns of volatile-components formation were observed for AS and AK, whereas that for AO seemed to differ throughout 8 weeks of fermentation. Figure 3a and b shows that α-amylase was strongly associated with the early stage (2 and 4 weeks) of fermentation in AO, affecting the formation of 2-methylpyrazine, 3-hydroxy-2-methylpyran-4-one, and furan-2-carbaldehyde, which are known to be directly and/or indirectly derived from sugar-degradation products.[4] 2-Methylpyrazine is known to be formed via the Maillard reaction and is found in various foods, such as coffee, cacao bean, and bread, which are manufactured using a heating process.[1,42] It has also been identified in Japanese *natto*,[43] steamed soybeans,[44] and soybean curds,[45] contributing to the nutty and cocoa-like aroma notes.[4] 3-Methyl-2-methyl-4*H*-pyran-4-one is also considered to be formed via the Maillard reaction, and appears to play a role as a sweet enhancer.[46] In *doenjang* production, it is probably formed during the process of steaming the raw materials containing carbohydrates, such as rice and soybeans, which could be exposed to sugar degradation.

There was a close relationship between protease activities and the latter part of the ripening process in AS and AK at 8 weeks. The formation of several compounds, including ethyl 3-phenylpropanoate, 2-phenylethyl acetate, (*E*)-2-phenylbut-2-enal, and 2-phenylethanol, which are known to derive from phenylalanine,[4] could be affected by protease activities. Among these compounds, the formation of two ethyl esters (ethyl 3-phenylpropanoate and 2-phenylethyl acetate) could be influenced by the actions of both protease and esterase, because they were located in the same direction of negative PLS1 and PLS2 (Figure 3b). In the positive dimension of PLS2, most of the ester compounds identified in this study could be more closely related to the activities of lipase and α-amylase than the other enzymes. This indicates that such esters could be more affected by the actions of these enzymes, which involve the hydrolysis of free fatty acids from soybean lipids by fungi and the production of ethanol from sugars by yeasts, respectively. However, because the amount of ethanol in all of the samples increased continuously during fermentation (data not shown), the amount of ethanol was thought to be sufficient to participate in esterification. In other words, lipase activities might have been the rate-limiting step for ethyl ester formation in the present study. Chou et al.[31] also reported that the concentration of ethanol did not affect the fatty-acid profiles in aging Chinese traditional soybean curds, and that ester compound formation was attributed mainly to lipase.

Heatmap of Relationships between the Identified Ester Compounds and Enzymatic Activities during Rice-*koji doenjang* Fermentation. Ester compounds are generally a very important component of many soybean-based fermented foods, mainly due to their characteristic odor notes, including fruity and sweet notes.[30] Given that in the present study, 35 ester compounds (Table 2) were significantly associated with enzyme activities and the levels of some ester compounds quantitatively increased with increasing fermentation time, we focused on the relationship between ester compound formation and enzyme activities.

DOI: 10.1021/jf5056002
J. Agric. Food Chem. 2015, 63, 1401−1418

Figure 4 provides the correlation matrix that summarizes the Pearson's correlation coefficients between the contents of the 35 ester compounds and the activities of 4 enzymes. Among 140 possible ester-enzyme pairs, 8 pairs exhibited strong correlations at $p < 0.05$. Pearson's correlation coefficient, r, provides a measure of strength of the linear relationship between the formation of ester compounds and the four enzymatic activities, and can range from −1 to 1, such that $r = 1$ or −1 indicates a perfect positive or negative linear relationship between two variables, respectively, and $r = 0$ means that there is no linear relationship between them.

Clear correlations were found between lipase activities and levels of methyl 2-methylprop-2-enoate ($r = 0.82$) and pentyl propanoate ($r = 0.91$) during fermentation. The former is known to contribute to sweet, fruity, and apple-like odor notes,[47] and the latter imparts sweet and mixed fruit tropical odor notes,[47] which could be formed by esterification of pentanol and propionic acid. In addition, the levels of ethyl butanoate, ethyl heptanoate, 3-methylbutyl hexanoate, ethyl tetradecanoate, methyl hexadecanoate, ethyl hexadecanoate, and ethyl hexadec-9-enoate were positively correlated with lipase activities. Positive correlations were found for α-amylase, ethyl acetate ($r = 0.74$), ethyl propanoate, 3-methylbutyl acetate ($r = 0.65$), and ethyl hexanoate. Protease and esterase had similar correlation tendencies, being negatively correlated with low-molecular-weight esters including ethyl acetate, ethyl propanoate, ethyl 2-methylpropanoate, 3-methylbutyl acetate, ethyl hexanoate, and ethyl heptanoate. Conversely, positive correlations were observed between protease and esterase enzymatic activities and relatively high-molecular-weight esters such as ethyl heptadecanoate, butyl hexadecanoate, ethyl octadecanoate, ethyl octadec-9-enoate, and ethyl octadeca-9,12-dienoate.

This study investigated differences in the volatile components of rice-*koji doenjang* in samples inoculated with various *Aspergillus* species (AO, AS, and AK) and with fermentation for up to 8 weeks, as well as the effects of specific activities of diverse enzymes on the formation of volatiles. Application of PCA to data sets of the volatiles profiles revealed that the different rice-*koji doenjang* samples could be distinguished according to the specific inoculated *Aspergillus* species and fermentation time. 4-Methylheptan-2-one, heptan-2-one, (*E*)-hept-2-enal, and hexanal contributed to the initial stage of fermentation of rice-*koji doenjang*, regardless of the species of *Aspergillus* inoculated. In contrast, the main components related to the latter stage of fermentation were ethyl esters of long-chain fatty acids, including ethyl tetradecanoate, ethyl hexadecanoate, ethyl octadec-9-enoate, ethyl octadecanoate, ethyl hexadec-9-enoate, and ethyl heptadecanoate. In addition, some esters, including methyl 2-methylprop-2-enoate, ethyl 2-methylprop-2-enoate, 3-methylbutyl acetate, ethyl (*Z*)-but-2-enoate, methyl 3-methylbut-2-enoate, 3-methylbutyl hexanoate, pentyl propanoate, 3-methylbutyl octanoate, ethyl hexadecenoate, ethyl hexadec-9-enoate, butyl hexadecanoate, ethyl octadec-9-enoate, ethyl octadeca-9,12,15-trienoate, and methyl octadeca-9,12-dienoate, were found for the first time in rice-*koji doenjang*, possibly due to high esterase activity in this study.[1,2,4,5,48,49]

The effects of enzymatic activities on the formation of volatile compounds during rice-*koji doenjang* fermentation were evaluated using PLS regression analysis and heatmaps of correlation matrixes between enzymes and volatile components. The formation of volatile esters during soybean-paste fermentation appeared to be strongly associated with protease and esterase activities, which increased as fermentation proceeded.

AUTHOR INFORMATION

Corresponding Author

*Tel.: +82-2-3277-3091. Fax: +82-2-3277-4213. E-mail: yskim10@ewha.ac.kr.

Funding

This research was supported by the High Value-added Food Technology Development Program (no. 311034-3), the Korea Institute of Planning and Evaluation for Technology in Food, Agriculture, Forestry and Fisheries, and the Strategic Initiative for Microbiomes in Agriculture and Food (no. 914007-4), Ministry of Agriculture, Food and Rural Affairs, Republic of Korea.

Notes

The authors declare no competing financial interest.

ABBREVIATIONS USED

A. oryzae and AO, *Aspergillus oryzae*; *A. sojae* and AS, *Aspergillus sojae*; *A. kawachii* and AK, *Aspergillus kawachii*; SPME, solid-phase microextraction; CAR/PDMS, carboxen/polydimethylsiloxane; RI, retention index; *p*-NPB, *p*-nitrophenylbutyrate; *p*-NPP, *p*-nitrophenyl palmitate; MANOVA, multivariate analysis of variance; PCA, principal component analysis; PLSR, partial least-squares regression

REFERENCES

(1) Park, J.; Lee, M.; Kim, K. S.; Lee, T. Volatile flavor components of soybean paste(*doenjang*) prepared from different types of strains. *Korean J. Food Sci. Technol.* **1994**, *26*, 255−260.

(2) Namgung, H.; Park, H.; Cho, I. H.; Choi, H.; Kwon, D.; Shim, S.; Kim, Y. Metabolite profiling of *doenjang*, fermented soybean paste, during fermentation. *J. Sci. Food Agric.* **2010**, *90*, 1926−1935.

(3) Park, M. K.; Cho, I. H.; Lee, S.; Choi, H.; Kwon, D.; Kim, Y. Metabolite profiling of *Cheonggukjang*, a fermented soybean paste, during fermentation by gas chromatography-mass spectrometry and principal component analysis. *Food Chem.* **2010**, *122*, 1313−1319.

(4) Jo, Y.; Cho, I. H.; Song, C. K.; Shin, H. W.; Kim, Y. Comparison of fermented soybean paste (*doenjang*) prepared by different methods based on profiling of volatile compounds. *J. Food Sci.* **2011**, *76*, C368−C379.

(5) Hong, Y.; Jung, H.; Kim, H. Aroma characteristics of fermented Korean soybean paste (*Doenjang*) produced by Bacillus amyloliquefaciens. *Food Sci. Biotechnol.* **2012**, *21*, 1163−1172.

(6) Lee, H. D.; Lee, C. H.; Lee, G. G. Changes in sensory characteristics during salt aging of *Doenjang* (fermented soybean paste) made by different starters. *Food. Eng. Prog.* **2003**, *7*, 13−19.

(7) Kim, J. H.; Yoo, J. S.; Lee, C. H.; Kim, S. Y.; Lee, S. K. Quality properties of soybean pastes made from *Meju* with mold producing protease isolated from traditional *Meju*. *J. Korean Soc. Appl. Biol. Chem.* **2006**, *49*, 7−14.

(8) Ham, S. N.; Kim, S. W.; Lee, J. H.; Chang, P. S. Changes in enzymatic activities during *Eoyukjang* fermentation. *Korean J. Food Sci. Technol.* **2008**, *40*, 251−256.

(9) Wishart, D. S. Metabolomics: applications to food science and nutrition research. *Trends Food Sci. Technol.* **2008**, *19*, 482−493.

(10) Yang, S.; Shin, Y.; Hyun, S.; Cho, S.; Bang, K.; Lee, D.; Choi, S. P.; Choi, H. NMR-based metabolic profiling and differentiation of ginseng roots according to cultivation ages. *J. Pharm. Biomed. Anal.* **2012**, *58*, 19−26.

(11) Watkins, S. M.; German, J. B. Metabolomics and biochemical profiling in drug discovery and development. *Curr. Opin. Mol. Ther.* **2002**, *4*, 224−228.

DOI: 10.1021/jf5056002
J. Agric. Food Chem. 2015, 63, 1401−1418

(12) Tikunov, Y.; Lommen, A.; de Vos, C. H.; Verhoeven, H. A.; Bino, R. J.; Hall, R. D.; Bovy, A. G. A novel approach for nontargeted data analysis for metabolomics. Large-scale profiling of tomato fruit volatiles. *Plant Physiol.* **2005**, *139*, 1125−1137.
(13) Pongsuwan, W.; Fukusaki, E.; Bamba, T.; Yonetani, T.; Yamahara, T.; Kobayashi, A. Prediction of Japanese green tea ranking by gas chromatography/mass spectrometry-based hydrophilic metabolite fingerprinting. *J. Agric. Food Chem.* **2007**, *55*, 231−236.
(14) Inui, T.; Tsuchiya, F.; Ishimaru, M.; Oka, K.; Komura, H. Different beers with different hops. Relevant compounds for their aroma characteristics. *J. Agric. Food Chem.* **2013**, *61*, 4758−4764.
(15) Cho, I. H.; Choi, H.; Kim, Y. Difference in the volatile composition of pine-mushrooms (*Tricholoma matsutake* Sing.) according to their grades. *J. Agric. Food Chem.* **2006**, *54*, 4820−4825.
(16) Lindinger, C.; Pollien, P.; de Vos, R. C.; Tikunov, Y.; Hageman, J. A.; Lambot, C.; Fumeaux, R.; Voirol-Baliguet, E.; Blank, I. Identification of ethyl formate as a quality marker of the fermented off-note in coffee by a nontargeted chemometric approach. *J. Agric. Food Chem.* **2009**, *57*, 9972−9978.
(17) Münch, P.; Hofmann, T.; Schieberle, P. Comparison of key odorants generated by thermal treatment of commercial and self-prepared yeast extracts: influence of the amino acid composition on odorant formation. *J. Agric. Food Chem.* **1997**, *45*, 1338−1344.
(18) Guth, H. Identification of character impact odorants of different white wine varieties. *J. Agric. Food Chem.* **1997**, *45*, 3022−3026.
(19) Jagella, T.; Grosch, W. Flavour and off-flavour compounds of black and white pepper (*Piper nigrum* L.) I. Evaluation of potent odorants of black pepper by dilution and concentration techniques. *Eur. Food Res. Technol.* **1999**, *209*, 16−21.
(20) Wanakhachornkrai, P.; Lertsiri, S. Comparison of determination method for volatile compounds in Thai soy sauce. *Food Chem.* **2003**, *83*, 619−629.
(21) Steinhaus, P.; Schieberle, P. Characterization of the key aroma compounds in soy sauce using approaches of molecular sensory science. *J. Agric. Food Chem.* **2007**, *55*, 6262−6269.
(22) Lozano, P. R.; Drake, M.; Benitez, D.; Cadwallader, K. R. Instrumental and sensory characterization of heat-induced odorants in aseptically packaged soy milk. *J. Agric. Food Chem.* **2007**, *55*, 3018−3026.
(23) Poisson, L.; Schieberle, P. Characterization of the most odor-active compounds in an American bourbon whisky by application of the aroma extract dilution analysis. *J. Agric. Food Chem.* **2008**, *56*, 5813−5819.
(24) Steinhaus, M.; Sinuco, D.; Polster, J.; Osorio, C.; Schieberle, P. Characterization of the aroma-active compounds in pink guava (*Psidium guajava* L.) by application of the aroma extract dilution analysis. *J. Agric. Food Chem.* **2008**, *56*, 4120−4127.
(25) Lee, S.; Ahn, B. Comparison of volatile components in fermented soybean pastes using simultaneous distillation and extraction (SDE) with sensory characterisation. *Food Chem.* **2009**, *114*, 600−609.
(26) Madrera, R. R.; Valles, B. S. Determination of volatile compounds in apple pomace by stir bar sorptive extraction and gas chromatography-mass spectrometry (SBSE-GC-MS). *J. Food Sci.* **2011**, *76*, C1326−C1334.
(27) Lee, J. S.; Kwon, S. J.; Chung, S. W.; Choi, Y. J.; Yoo, J. Y.; Chung, D. H. Changes of microorganisms, enzyme activities and major components during the fermentation of korean traditional *doenjang* and *kochujang*. *Korean J. Microbiol. Biotechnol.* **1996**, *24*, 247−253.
(28) Lopes, D. B.; Fraga, L. P.; Fleuri, L. F.; Macedo, G. A. Lipase and esterase: to what extent can this classification be applied accurately? *Food Sci. Technol.* **2011**, *31*, 603−613.
(29) Park, S.; Kim, J.; Kang, S. G.; Woo, J.; Lee, J.; Choi, H.; Kim, S. A new esterase showing similarity to putative dienelactone hydrolase from a strict marine bacterium, Vibrio sp. GMD509. *Appl. Microbiol. Biotechnol.* **2007**, *77*, 107−115.
(30) Qin, L.; Ding, X. Formation of taste and odor compounds during preparation of douchiba, a chinese traditional soy fermented appetizer. *J. Food Biochem.* **2007**, *31*, 230−251.
(31) Chou, C.; Hwan, C. Effect of ethanol on the hydrolysis of protein and lipid during the ageing of a Chinese fermented soya bean curd-sufu. *J. Sci. Food Agric.* **1994**, *66*, 393−398.
(32) Carraro, S.; Giordano, G.; Reniero, F.; Perilongo, G.; Baraldi, E. Metabolomics: a new frontier for research in pediatrics. *J. Pediatr.* **2009**, *154*, 638−644.
(33) Vandamme, E. J. Bioflavours and fragrances via fungi and their enzymes. *Fungal Diversity* **2003**, *13*, 153−166.
(34) Rowan, D. D.; Allen, J. M.; Fielder, S.; Hunt, M. B. Biosynthesis of straight-chain ester volatiles in Red Delicious and Granny Smith apples using deuterium-labeled precursors. *J. Agric. Food Chem.* **1999**, *47*, 2553−2562.
(35) Landaud, S.; Helinck, S.; Bonnarme, P. Formation of volatile sulfur compounds and metabolism of methionine and other sulfur compounds in fermented food. *Appl. Microbiol. Biotechnol.* **2008**, *77*, 1191−1205.
(36) Boué, S. M.; Shih, B. Y.; Carter-Wientjes, C. H.; Cleveland, T. E. Identification of volatile compounds in soybean at various developmental stages using solid phase microextraction. *J. Agric. Food Chem.* **2003**, *51*, 4873−4876.
(37) Borjesson, T.; Stollman, U.; Schnurer, J. Volatile metabolites produced by six fungal species compared with other indicators of fungal growth on cereal grains. *Appl. Environ. Microbiol.* **1992**, *58*, 2599−2605.
(38) Reineccius, G. *Flavor Chemistry and Technology*; CRC Press: London, England, 2004; pp 123−124.
(39) Yoo, Y. J.; Hong, J.; Hatch, R. T. Comparison of α-amylase activities from different assay methods. *Biotechnol. Bioeng.* **1987**, *30*, 147−151.
(40) Sardjono; Zhu, Y.; Knol, W. Comparison of fermentation profiles between lupine and soybean by *Aspergillus oryzae* and *Aspergillus sojae* in solid-state culture systems. *J. Agric. Food Chem.* **1998**, *46*, 3376−3380.
(41) Joo, H. K.; Kim, N. D.; Yoon, K. S. Changes of enzymatic activities during the fermentation of soybean-soypaste by *Aspergillus* spp. *J. Korean Soc. Appl. Biol. Chem.* **1989**, *32*, 295−302.
(42) Shin, M. R.; Joo, K. J. Fractionated volatile flavor components of soybean paste by dynamic headspace method. *J. Korean Soc. Food Sci. Nutr.* **1999**, *28*, 305−311.
(43) Sugawara, E.; Ito, T.; Odagiri, S.; Kubota, K.; Kobayashi, A. Comparison of compositions of odor components of natto and cooked soybeans. *Agric. Biol. Chem.* **1985**, *49*, 311−317.
(44) Kim, G. E.; Kim, M. H.; Lee, J. H.; Choi, B. D.; Kim, T. S. Flavor compounds of domestic *Meju* and *Doenjang*. *J. Korean Soc. Food Sci. Nutr.* **1992**, *21*, 557−565.
(45) Chung, H. Y. Volatile components in fermented soybean (*Glycine max*) curds. *J. Agric. Food Chem.* **1999**, *47*, 2690−2696.
(46) Yaylayan, V. A.; Mandeville, S. Stereochemical control of maltol formation in Maillard reaction. *J. Agric. Food Chem.* **1994**, *42*, 771−775.
(47) Mosciano, G. Organoleptic characteristics of flavor materials. *Perfum. Flavor.* **1998**, *23*, 55−57.
(48) Giri, A.; Osako, K.; Okamoto, A.; Okazaki, E.; Ohshima, T. Effect of meat washing on the development of impact odorants in fish *miso* prepared from spotted mackerel. *J. Sci. Food Agric.* **2011**, *91*, 850−859.
(49) Giri, A.; Osako, K.; Ohshima, T. Identification and characterisation of headspace volatiles of fish *miso*, a Japanese fish meat based fermented paste, with special emphasis on effect of fish species and meat washing. *Food Chem.* **2010**, *120*, 621−631.

DOI: 10.1021/jf5056002
J. Agric. Food Chem. 2015, 63, 1401−1418

Germany). Dichloromethane, diethyl ether, and pentane were distilled prior to use.

Reference Odorants. Propane-1-thiol, butane-1-thiol, pentane-1-thiol, hexane-1-thiol, heptane-1-thiol, octane-1-thiol, nonane-1-thiol, decane-1-thiol, butane-2-thiol, 2-methylbutane-1-thiol, 3-methylbutane-2-thiol, propane-1,3-dithiol, butane-1,4-dithiol, hexane-1,6-dithiol, octane-1,8-dithiol, and nonane-1,9-dithiol were obtained from Sigma-Aldrich. 2-Methylbutane-2-thiol, decane-1,10-dithiol, 1-(methylthio)-pentane, 1-(methylthio)heptane, 1-(methylthio)-octane, and 1-(methylthio)decane were purchased from TCI Europe Laboratory Chemicals (Eschborn, Germany). Pentane-1,5-dithiol, 1-(methylthio)-butane, and 2-(methylthio)butane were supplied by Alpha-Aesar.

Syntheses. In total 40 sulfur compounds were newly synthesized. All reactions were carried out in oven-dried glassware under argon atmosphere unless otherwise noted.

Primary and Secondary Thiols. The primary and secondary thiols were prepared from the corresponding alcohols in a three-step synthesis following a previously described method[8] with slight modifications. If the respective alcohol was not commercially available (e.g., 2-methylhexan-1-ol and 2-methylheptan-1-ol), these were synthesized from the corresponding carboxylic acid by reduction with $LiAlH_4$.

Tosylation of Primary and Secondary Alcohols. To a solution of the alcohol (30 mmol) in anhydrous pyridine (20 mL) was slowely added *p*-toluenesulfonyl chloride (6.29 g; 33 mmol) at 0 °C. The solution was allowed to reach room temperature, and the mixture was stirred overnight. Hexane (30 mL) was added, the solution was filtered, and the residue was washed with hexane (30 mL). The combined organic layers were washed with aqueous hydrochloric acid (5 mol/L; 2 × 30 mL). After drying over anhydrous sodium sulfate, the solvent was removed by rotary evaporation.

Thioacetylation of the p-Tosylderivates. Potassium thioacetate (5.71 g; 50 mmol) was dissolved in DMF (20 mL). The tosylated alcohol (20 mmol) was added, and the solution was stirred at 80 °C for 2 h. Then, a saturated aqueous sodium chloride solution (100 mL) was added, the aqueous solution was extracted with diethyl ether (3 × 100 mL), and the combined organic layers were washed with a saturated aqueous sodium chloride solution (5 × 50 mL). After drying over anhydrous sodium sulfate, the solvent was removed by rotary evaporation. Purification of the compound was performed by column chromatography on silica gel (silica 60, 0.040−0.063 mm) (Merck, Darmstadt, Germany) using pentane/diethyl ether (99/1; v/v) as the eluent.

Reduction with $LiAlH_4$. The acetylthio derivative (10 mmol) obtained was dissolved in anhydrous diethyl ether (15 mL) and added slowly to a suspension of lithium aluminum hydride (0.76 g; 20 mmol) in anhydrous diethyl ether (20 mL) at 0 °C. The solution was stirred for 2 h at room temperature, and a saturated aqueous ammonium chloride solution (20 mL) was added slowly at 0 °C. Then, aqueous hydrochloric acid (2 mol/L; 50 mL) was added to dissolve the precipitate formed, the ethereal layer was separated, and the aqueous layer was extracted with diethyl ether (3 × 70 mL). The combined organic layers were washed with a saturated aqueous sodium bicarbonate solution (50 mL), followed by water (50 mL). After drying over anhydrous sodium sulfate, the solvent was distilled off by means of a Vigreux column (50 × 1 cm). Purification of the compound was performed by column chromatography on silica gel using pentane as the eluent.

Synthesis of Tertiary Thiols. Tertiary thiols were prepared in a three-step synthesis from the corresponding alcohols by bromination,[9] followed by substitution of the bromine with zinc thioacetate[10] and reduction of the thioacetates with $LiAlH_4$. If the respective alcohol was not commercially available (e.g., 2-methyloctan-2-ol, 2-methylnonan-2-ol, and 2-methyldecan-2-ol), these were synthesized from the respective methyl ketone by a Grignard reaction with methylmagnesium bromide.

Tertiary Alcohols. To a solution of the respective methyl ketone (40 mmol) in diethyl ether (100 mL) was added a methylmagnesium bromide solution (3.0 mol/L in diethyl ether; 19 mL; 56 mmol) at 0 °C, and the mixture was refluxed for 2 h. The mixture was cooled to 0 °C, and water (50 mL) was slowly added, followed by an aqueous saturated ammonium chloride solution (40 mL) to dissolve the precipitate. The organic layer was separated, and the aqueous layer was extracted with diethyl ether (3 × 50 mL). The combined organic layers were washed with saturated aqueous sodium bicarbonate solution (50 mL), followed by water (50 mL). After drying over anhydrous sodium sulfate, the solvent was removed by rotary evaporation.

Bromination of the Tertiary Alcohol. Bromination was done as previously reported.[9] To a mixture of the tertiary alcohol (30 mmol) and lithium bromide (3.91 g; 45 mmol) was slowly added aqueous HBr (10.1 g; 60 mmol; 48%) at room temperature. The organic layer was separated, washed with ethylene glycol (3 × 10 mL), and dried over anhydrous sodium sulfate.

Thioacetylation of the Bromo Derivatives. Following the method by Gurudutt et al.[10] zinc sulfide (1.95 g; 20 mmol) was added to a solution of thioacetic acid (3.04 g; 40 mmol) in dichloromethane (40 mL), and stirred for 2 h at room temperature. The tertiary bromo derivative (20 mmol) was added, and the solution was refluxed for 10 h. The filtrate was washed with dichloromethane (50 mL), and the combined organic solutions were washed with aqueous hydrochloric acid (2 mol/L; 30 mL), followed by a saturated aqueous sodium bicarbonate solution (30 mL). After drying over anhydrous sodium sulfate, the solvent was removed by rotary evaporation. Purification of the compound was performed by column chromatography on silica gel using pentane/diethyl ether (99/1; v/v) as the eluent.

Reduction with $LiAlH_4$. Reduction with $LiAlH_4$ was performed as described above for the primary and secondary thiols.

Synthesis of Alkanedithiols. Alkanedithiols were prepared from the respective dibromoalkanes in a two-step procedure, that is, by thioacetylation with potassium thioacetate, followed by reduction with $LiAlH_4$ as described above.

Preparation of the Methylthioethers. Methylation of the thiols was done as previously reported.[11] To a solution of the thiol (4 mmol) in anhydrous tetrahydrofuran (12 mL) was added *n*-butyllithium (2.5 mol/L in hexane; 2 mL, 5 mmol) at 0 °C. The solution was allowed to warm to room temperature, and the mixture was stirred for 10 min. Then, methyl iodide (568 mg; 4 mmol) was added slowly at 0 °C, and the reaction mixture was stirred for 20 min at room temperature. After the addition of water (20 mL), the mixture was extracted with pentane (3 × 30 mL), and the combined organic layers were washed with water and dried over anhydrous sodium sulfate. The solvent was distilled off by means of a Vigreux column (50 × 1 cm). Purification of the compound was performed by column chromatography on silica gel using pentane as the eluent.

Gas Chromatography−Flame Ionization Detection (GC-FID) and Gas Chromatography−Olfactometry (GC-O). GC-FID and GC-O analyses were performed by means of a gas chromatograph 8160 (Fisons Instruments, Mainz, Germany) using helium as the carrier gas. Samples were applied by the cold-on-column injection technique. Capillaries used were DB-5 and DB-FFAP (each 30 m × 0.32 mm i.d., 0.25 μm film thickness, 70 kPa head pressure) (J&W Scientific, Chromatographie-Handel Mueller, Fridolfing, Germany). The temperature programs were adapted to the respective volatility of each analyte. For GC-O applications, the ends of the capillaries were connected to a deactivated Y-shaped glass splitter (Chromatographie Handel Mueller) dividing the effluent into two equal parts, which were transferred via two deactivated fused silica capillaries (50 cm × 0.25 mm) to a sniffing port and an FID, respectively. The sniffing port consisted of a cylindrically shaped aluminum device (80 mm × 25 mm i.d.) with a beveled top and a central drill hole (2 mm) housing the capillary. It was mounted on a detector base of the GC and heated to 200 °C. The FID was operated at 250 °C with hydrogen (20 mL/min) and air (200 mL/min). Nitrogen (30 mL/min) was used as the makeup gas. The injection volume was 1.0 μL. During a GC-O run, the nose of the panelist was placed closely above the top of the sniffing port, and the odor of the effluent was evaluated. If an odor was recognized, the retention time was marked in the chromatogram, and the odor quality was assigned. The evaluation was performed by three panelists, and the results were averaged. Panelists were trained on a

DOI: 10.1021/jf506135c
J. Agric. Food Chem. 2015, 63, 1419−1432

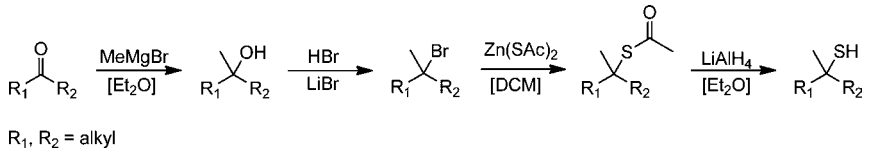

Figure 1. Synthetic route used in the preparation of tertiary thiols.

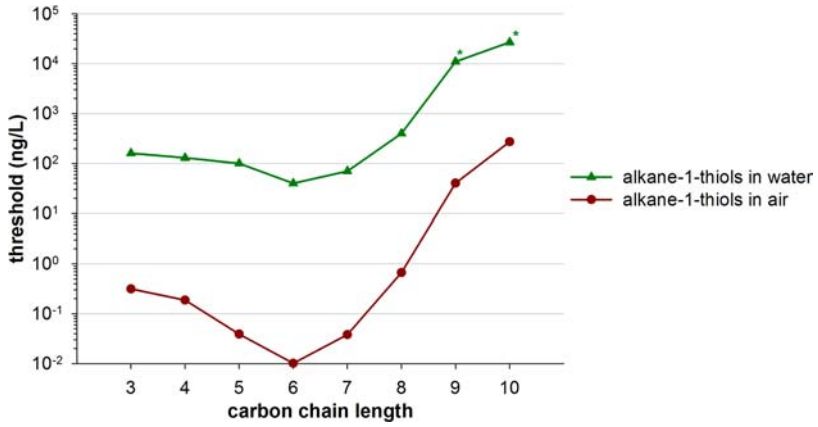

Figure 2. Comparison of odor thresholds in air and in water (*, minimum threshold, due to aroma-active impurities exact quantitation not possible).

"flavor language" in weekly training sessions for at least 6 months, in which pure reference odorants were used.[14]

Gas Chromatography–Mass Spectrometry (GC-MS). Mass spectra were recorded after chromatography on a gas chromatograph 5890 series II (Hewlett-Packard, Waldbronn, Germany) connected to a sector field mass spectrometer MAT 95 S (Finnigan, Bremen, Germany). Mass spectra in the electron ionization mode (MS-EI) were recorded at 70 eV ionization energy and mass spectra in the chemical ionization mode (MS-CI) at 115 eV with isobutane as the reactant gas.

Determination of Odor Thresholds and Odor Qualities in Air. Thresholds were determined by aroma extract dilution analysis of a mixture containing known amounts of the target odorant and (*E*)-2-decenal as the internal standard. Thresholds were calculated from the flavor dilution (FD) factors determined by using the method previously described[12] and a threshold of 2.7 ng/L for (*E*)-2-decenal.[13] Odor qualities were assigned during GC-O at the threshold level.

Determination of Odor Thresholds in Water. Odor thresholds were determined following a procedure published previously.[14]

NMR Spectroscopy. The ^{1}H, ^{13}C, and 2D NMR experiments were performed using a Bruker 400 MHz DMX spectrometer (Bruker, Rheinstetten, Germany). Samples were dissolved in $CDCl_3$, and chemical shifts were determined using tetramethylsilane as the internal standard (0.03%) in the proton dimension and from the carbon signal of $CDCl_3$ (77.0 ppm) in the carbon dimension.

Molecular Modeling and Alignment. All molecular modeling studies, CoMFA, and partial least-squares (PLS) approaches were performed using the SYBYL-X 1.2 program package.[15] Initial template structures were built using Sybyl's Concord module. Energy minimizations were carried out using Tripos force field, and Gasteiger–Hückel charges were calculated for all molecules. For molecular alignment, 2-methylpentane-2-thiol, showing the lowest odor thresholds of all investigated sulfur-containing compounds, was used as the reference molecule. Superimposition was performed with the main focus on maximal alignment of the SH group.

Comparative Molecular Field Analysis (CoMFA). For CoMFA, the aligned molecules were positioned inside a three-dimensional grid box with a grid spacing of 2 Å. Steric and electrostatic fields were calculated using an sp^3 carbon probe atom with a van der Waals radius of 1.52 Å and a +1.0 charge. Steric and electrostatic cutoff values were set to 30 kcal/mol.

Partial Least Squares Regression. PLS regression was conducted to establish and validate the 3D-QSAR model. Thereby, the optimal number of principal components was determined using leave-one-out cross-validation.

RESULTS AND DISCUSSION

Syntheses. If not commercially available, primary and secondary thiols were synthesized according to a method described by Simian et al.[8] for the preparation of heptane-2-thiol from the respective primary and secondary alcohols, respectively. If the corresponding alcohols were not available, these were first synthesized by reduction of the corresponding carboxylic acids.

Because of the S_N1 activity of tertiary alcohols, tertiary thiols were prepared according to a different procedure (Figure 1). First, tertiary alcohols were synthesized from the respective methyl ketones by a Grignard reaction with methylmagnesium bromide. After bromination of the tertiary alcohol under S_N1 conditions,[9] followed by an S_N1 substitution of the bromine with zinc thioacetate,[10] the reduction of the thioacetate finally resulted in the targeted thiol in good yields.

Determination of Odor Thresholds. Although several methods for the determination of odor thresholds are available, the results of different methods are not necessarily comparable and may differ by several orders of magnitude.[16,17] Therefore, prior to the study of structure–odor correlations, the selection of an appropriate method for threshold determination was essential. For the following reasons a previously published[12] GC-O method was applied: First, the use of GC before sniffing removes odor-active impurities, which might influence the odor threshold of the target analyte. Second, during elution from the hot column, the compound is completely volatilized and can easily be compared to the threshold of a reference compound. Thus, the influence of different volatilities of the compounds depending on matrices when determined in water or oil, respectively, is negligible.

However, in comparison to a determination of odor thresholds in air, the determination of odor thresholds in water is rather quick and easy. Therefore, most of the odor thresholds published so far were measured in water. To show

DOI: 10.1021/jf506135c
J. Agric. Food Chem. 2015, 63, 1419–1432

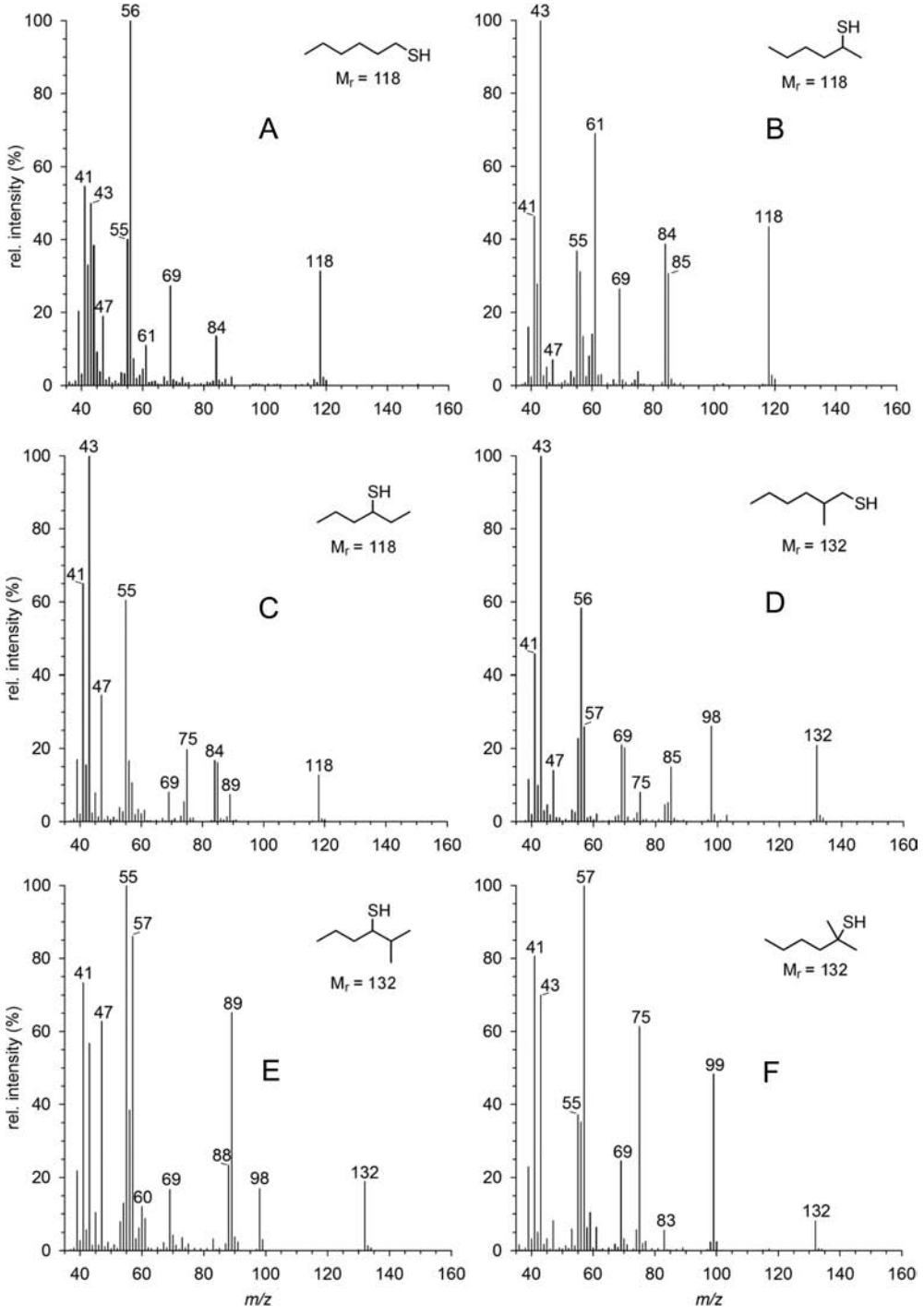

Figure 3. Selected mass spectra (MS-EI) of alkanethiols.

the correlation of odor thresholds in air and in water, thresholds of alkane-1-thiols were determined in both media. For the determination of odor thresholds in water, the thiols had to be purified by column chromatography on silica gel using *n*-pentane as the eluent. In Figure 2, the thresholds of the alkane-1-thiols are plotted versus the number of carbon atoms between 3 and 10. Interestingly, both curves showed a similar shape; however, thresholds in air were by a factor of 1000 lower than those in water. Clearly, in both media, a minimum in odor thresholds was found for hexane-1-thiol, and the highest odor threshold was measured for decane-1-thiol. These results suggest a similar potency of a single thiol independently from the method applied.

Alkane-1-thiols. The mass spectra of the alkane-1-thiols, illustrated by hexane-1-thiol (Figure 3A), revealed strong signals for M^+ (m/z 118). The presence of sulfur in the molecule was clearly indicated by the intensity of $[M + 2]^+$ and by the loss of H_2S (m/z 84). Further significant fragments resulted from an α- (CH_3S^+, m/z 47) and a β-cleavage ($C_2H_5S^+$, m/z 61) as well as from the loss of H_2S and ethylene ($[M - H_2S - C_2H_4]^+$, m/z 56). The fragments at m/z 69 ($C_5H_9^+$), m/z 55 ($C_4H_7^+$), m/z 43 ($C_3H_7^+$), and m/z 41 ($C_3H_5^+$) are formed by fragmentation of the alkyl chain. The

DOI: 10.1021/jf506135c
J. Agric. Food Chem. 2015, 63, 1419−1432

Table 1. Retention Indices, MS-EI Data, and Sensory Properties of Alkane-1-thiols

compound	RI FFAP	RI DB-5	m/z (intensity in %)[a]	odor quality[b]	odor threshold[c] (ng/L in air)	reported as food constituent[d]
propane-1-thiol	<900	622	76 (100, M^+), 43 (90), 47 (85), 42 (85), 41 (76), 39 (26), 46 (20), 45 (18), 61 (12), 48 (9)	garlic, sulfury	0.32	onion[20]
butane-1-thiol	930	712	56 (100), 90 (89, M^+), 41 (87), 47 (39), 61 (24), 57 (18), 39 (15), 55 (15), 45 (12), 43 (11)	garlic, sulfury, burned	0.19	cheese[21]
pentane-1-thiol	1031	816	42 (100), 55 (53), 41 (48), 70 (39), 104 (38, M^+), 43 (29), 47 (23), 39 (23), 61 (13), 44 (13)	burned, rubber, sulfury	0.039	flour model[22]
hexane-1-thiol	1138	917	56 (100), 41 (55), 43 (50), 55 (40), 44 (38), 42 (33), 118 (31, M^+), 69 (27), 39 (20), 47 (19)	burned, roasty, mushroom-like	0.010	chicken[23]
heptane-1-thiol	1243	1021	70 (100), 56 (89), 55 (73), 41 (71), 69 (54), 42 (48), 43 (44), 132 (44, M^+), 57 (30), 47 (27)	burned, mushroom-like	0.038	beef[24]
octane-1-thiol	1343	1163	56 (100), 55 (81), 70 (76), 41 (74), 69 (70), 43 (59), 146 (58, M^+), 84 (56), 83 (56), 42 (39)	roasty, mushroom-like	0.67	beef[25]
nonane-1-thiol	1443	1230	56 (100), 55 (86), 70 (80), 41 (72), 69 (69), 43 (64), 160 (53, M^+), 83 (48), 97 (45), 84 (42)	mushroom-like, fatty	40	beef[25]
decane-1-thiol	1555	1328	55 (100), 70 (90), 41 (86), 56 (81), 43 (80), 69 (76), 83 (63), 57 (48), 84 (42), ..., 174 (32, M^+)	fatty, soapy	270	

[a]For further spectroscopic data (MS-CI, NMR) see the Supporting Information. [b]Odor quality as perceived at the sniffing port during GC-O at threshold level. [c]Odor thresholds in air were determined as previously reported.[12] Data are mean values obtained by three panelists. [d]First report.

Table 2. Retention Indices, MS-EI Data, and Sensory Properties of Alkane-2-thiols

compound	RI FFAP	RI DB-5	m/z (intensity in %)[a]	odor quality[b]	odor threshold[c] (ng/L in air)	reported as food constituent[d]
butane-2-thiol	<900	656	57 (100), 41 (94), 61 (80), 90 (73, M^+), 56 (23), 39 (20), 47 (14), 55 (11), 60 (10), 35 (10)	garlic, burned, sulfury	0.035	oysters[26]
pentane-2-thiol	993	753	43 (100), 55 (59), 61 (57), 41 (57), 42 (39), 70 (38), 39 (36), 71 (32), 104 (29, M^+), 47 (13)	burned, roasty, sulfury	0.0032	guava[27]
hexane-2-thiol	1044	856	43 (100), 61 (69), 41 (46), 118 (43, M^+), 84 (39), 55 (37), 56 (31), 85 (31), 42 (28), 69 (26)	burned, roasty	0.013	
heptane-2-thiol	1148	962	57 (100), 56 (74), 61 (62), 41 (55), 98 (54), 132 (41, M^+), 55 (40), 69 (34), 43 (33), 70 (32)	roasty, mushroom-like	0.018	bell pepper[8]
octane-2-thiol	1248	1066	41 (100), 70 (88), 57 (85), 55 (85), 61 (83), 43 (77), 71 (60), 56 (56), 112 (55), ..., 146 (24, M^+)	mushroom-like, roasty	0.098	beef[24]
nonane-2-thiol	1350	1168	55 (100), 43 (98), 126 (92), 41 (90), 61 (88), 56 (88), 70 (66), 57 (66), 71 (64), ..., 160 (39, M^+)	mushroom-like, soapy	2.3	bell pepper[28]
decane-2-thiol	1457	1269	43 (100), 41 (97), 55 (92), 56 (82), 57 (80), 61 (66), 70 (63), 69 (59), 140 (44), ..., 174 (12, M^+)	fatty, soapy	130	

[a]For further spectroscopic data (MS-CI, NMR) see the Supporting Information. [b]Odor quality as perceived at the sniffing port during GC-O at threshold level. [c]Odor thresholds in air were determined as previously reported.[12] Data are mean values obtained by three panelists. [d]First report.

Table 3. Retention Indices, MS-EI Data, and Sensory Properties of Alkan-3-thiols

compound	RI FFAP	RI DB-5	m/z (intensity in %)[a]	odor quality[b]	odor threshold[c] (ng/L in air)	reported as food constituent[d]
pentane-3-thiol	938	764	43 (100), 41 (97), 75 (52), 47 (44), 71 (36), 104 (33, M^+), 39 (28), 55 (28), 42 (18), 45 (13)	burned, sulfury, roasty	0.0028	
hexane-3-thiol	1040	859	43 (100), 41 (65), 55 (60), 47 (35), 75 (20), 39 (17), 84 (17), 56 (17), 85 (16), ..., 118 (13, M^+)	burned, sulfury, roasty	0.0053	
heptane-3-thiol	1136	960	57 (100), 41 (93), 69 (83), 56 (74), 75 (61), 43 (57), 98 (55), 55 (50), 132 (40, M^+), 47 (36)	burned, roasty	0.21	
octane-3-thiol	1237	1063	41 (100), 55 (97), 57 (95), 71 (81), 112 (71), 83 (71), 43 (67), 75 (66), 56 (59), ..., 146 (35, M^+)	roasty, mushroom-like	1.6	
nonane-3-thiol	1342	1165	55 (100), 41 (88), 43 (85), 71 (63), 126 (63), 75 (56), 57 (53), 70 (50), 56 (47), ..., 160 (23, M^+)	mushroom-like	12	
decane-3-thiol	1446	1269	41 (100), 55 (99), 69 (96), 43 (94), 57 (91), 56 (69), 75 (62), 140 (56), 70 (51), ..., 174 (15, M^+)	fatty	200	

[a]For further spectroscopic data (MS-CI, NMR) see the Supporting Information. [b]Odor quality as perceived at the sniffing port during GC-O at threshold level. [c]Odor thresholds in air were determined as previously reported.[12] Data are mean values obtained by three panelists. [d]First report.

determination of the odor thresholds by GC-O revealed a significant decline from propane-1-thiol to pentane-1-thiol to reach a minimum for hexane-1-thiol (Table 1). With an increasing number of carbon atoms, the thresholds clearly increased with decane-1-thiol, showing a 27,000 fold higher odor threshold than hexane-1-thiol.

DOI: 10.1021/jf506135c
J. Agric. Food Chem. 2015, 63, 1419−1432

Table 4. Retention Indices, MS-EI Data, and Sensory Properties of 2-Methylalkane-1-thiols

compound	RI FFAP	RI DB-5	m/z (intensity in %)[a]	odor quality[b]	odor threshold[c] (ng/L in air)	reported as food constituent[d]
2-methylbutane-1-thiol	1000	781	41 (100), 55 (72), 70 (70), 57 (58), 39 (37), 104 (35, M^+), 42 (33), 56 (29), 47 (29), 43 (21)	garlic, burned	0.39	beef[29]
2-methylpentane-1-thiol	1081	879	43 (100), 41 (45), 56 (35), 55 (25), 84 (23), 42 (20), 118 (20, M^+), 69 (19), 71 (18), 39 (16)	burned, roasty	0.37	
2-methylhexane-1-thiol	1186	979	43 (100), 56 (58), 41 (46), 98 (26), 57 (26), 55 (23), 69 (21), 132 (21, M^+), 70 (20), 85 (15)	burned, roasty	0.32	
2-methylheptane-1-thiol	1284	1079	57 (100), 41 (42), 56 (33), 70 (29), 43 (29), 112 (28), 55 (25), 146 (18, M^+), 83 (16), 69 (16)	roasty, burned	21	

[a]For further spectroscopic data (MS-CI, NMR) see the Supporting Information. [b]Odor quality as perceived at the sniffing port during GC-O at threshold level. [c]Odor thresholds in air were determined as previously reported.[12] Data are mean values obtained by three panelists. [d]First report.

Table 5. Retention Indices, MS-EI Data, and Sensory Properties of 2-Methylalkane-3-thiols

compound	RI FFAP	RI DB-5	m/z (intensity in %)[a]	odor quality[b]	odor threshold[c] (ng/L in air)	reported as food constituent[d]
2-methylbutane-3-thiol[e]	924	745	43 (100), 61 (76), 41 (48), 55 (38), 39 (30), 60 (26), 71 (19), 104 (12, M^+), 70 (11), 42 (9)	burned	0.46	beef[29]
2-methylpentane-3-thiol	1029	844	41 (100), 43 (88), 75 (67), 55 (37), 74 (36), 47 (31), 39 (27), 85 (25), 118 (23, M^+), 69 (21)	burned, roasty	0.32	
2-methylhexane-3-thiol	1109	937	55 (100), 57 (86), 41 (73), 89 (65), 47 (63), 43 (57), 56 (38), 88 (23), 39 (22), 132 (19, M^+)	burned, roasty	0.35	
2-methylheptane-3-thiol	1202	1036	69 (100), 41 (65), 55 (44), 43 (39), 57 (36), 60 (24), 56 (22), 71 (21), 103 (17), ..., 146 (11, M^+)	burned, roasty, mushroom-like	11	

[a]For further spectroscopic data (MS-CI, NMR) see the Supporting Information. [b]Odor quality as perceived at the sniffing port during GC-O at threshold level. [c]Odor thresholds in air were determined as previously reported.[12] Data are mean values obtained by three panelists. [d]First report. [e]Correct IUPAC name is 3-methylbutane-2-thiol.

In agreement with the change in odor thresholds, also a change in odor qualities was observed. The short-chain homologues (C_3, C_4) showed garlic-like odors (Table 1). At the minimum level (C_5–C_7) the odor changed to burned, roasty aroma notes, and with increasing number of carbon atoms (C_9, C_{10}) the odor quality changed to fatty, soapy. All alkane-1-thiols except decane-1-thiol have already been reported as food constituents (Table 1).

Alkane-2-thiols. The mass spectra of the alkane-2-thiols, for example, hexane-2-thiol (Figure 3B), also revealed a strong signal for the molecular ion (m/z 118). In addition to the fragment at m/z 84 $[M - H_2S]^+$, also a signal at m/z 85 $[M - SH]^+$ appeared. A further characteristic fragment for the alkane-2-thiols resulted from an α-cleavage at m/z 61 ($C_2H_5S^+$). The odor thresholds of the alkane-2-thiols showed a similar dependency on the chain length as found for the alkane-1-thiols (Table 2). With a minimum at C_5, odor thresholds significantly increased up to 41,000 for C_{10}. As found for the alkane-1-thiols, also for the alkane-2-thiols a change in odor qualities to fatty, soapy odor notes was observed with increasing carbon number (Table 2), and most of these thiols have been reported in foods before. The odor thresholds and odor qualities of the racemic mixtures were determined without differentiation of the single enantiomers.

Alkane-3-thiols. The mass spectra of the alkane-3-thiols, illustrated by hexane-3-thiol (Figure 3C), also showed strong signals for M^+ (m/z 118), $[M - H_2S]^+$ (m/z 84), and $[M - SH]^+$. Characteristic fragments for the alkane-3-thiols at m/z 89 ($C_4H_9S^+$) and m/z 75 ($C_3H_7S^+$) resulted from an α-cleavage. The odor thresholds of the alkane-3-thiols rose exponentially with increasing length of the alkyl chain (Table 3), and the odor threshold of decane-3-thiol was 71,000 times higher than that of pentane-3-thiol.

With the change in odor thresholds, also a change in odor qualities from burned, roasty odors to fatty aroma notes occurred (Table 3). Interestingly, none of these alkane-3-thiols have ever been reported as food constituents.

2-Methylalkane-1-thiols. Mass spectra of the 2-methylalkane-1-thiols, for example, for 2-methylhexane-1-thiol (Figure 3D), again revealed strong signals for M^+ (m/z 132) and $[M - H_2S]^+$ (m/z 98). Typical fragments for primary thiols with a methyl group in the α-position to the thiol function were $C_3H_7S^+$ (β-cleavage, m/z 75) and $C_5H_{10}^+$ (m/z 70). The 2-methylalkane-1-thiols showed rather constant threshold values between C_4 and C_6 (Table 4). However, a further extension of the alkyl chain (2-methylheptane-1-thiol) resulted in a clear increase in odor thresholds by a factor of 75. All homologues exhibited burned, roasty aroma notes (Table 4).

2-Methylalkane-3-thiols. Mass spectra of the 2-methylalkane-3-thiols, represented by 2-methylhexane-3-thiol (Figure 3E), displayed typical signals for the molecular ion M^+ (m/z 132) as well as $[M - H_2S]^+$ (m/z 98). A further characteristic fragment for this homologous series of thiols was $[M - C_3H_7]^+$ (m/z 89). As with the 2-methylalkane-2-thiols, also the 2-methylalkane-3-thiols revealed rather constant threshold values between C_4 and C_6 followed by a significant increase in odor thresholds starting at C_7 (Table 5).

2-Methylalkane-2-thiols. Because of the stability of the tertiary carbenium cation, the 2-methylalkane-2-thiols, in contrast to the primary and secondary thiols, showed considerably higher signals for $[M - SH]^+$ (m/z 99; shown for 2-methylhexane-2-thiol, Figure 3F), whereas the fragment $[M - H_2S]^+$ (m/z 98) showed only a very weak intensity. A

DOI: 10.1021/jf506135c
J. Agric. Food Chem. 2015, 63, 1419–1432

Table 6. Retention Indices, MS-EI Data, and Sensory Properties of 2-Methylalkane-2-thiols

compound	RI FFAP	RI DB-5	m/z (intensity in %)[a]	odor quality[b]	odor threshold[c] (ng/L in air)	reported as food constituent[d]
2-methylbutane-2-thiol	<900	716	43 (100), 71 (89), 41 (81), 55 (77), 75 (61), 39 (53), 104 (44, M^+), 47 (19), 59 (18), 42 (10)	burned, catty, sulfury	0.0023	beef[24]
2-methylpentane-2-thiol	960	806	43 (100), 85 (89), 41 (84), 75 (69), 69 (49), 39 (33), 57 (29), 55 (23), 118 (22, M^+), 61 (17)	catty, black currant	0.00053	
2-metylhexane-2-thiol	1062	905	57 (100), 41 (81), 43 (70), 75 (61), 99 (48), 55 (37), 56 (35), 69 (25), 39 (23), ..., 132 (8, M^+)	catty, black currant	0.0026	
2-methylheptane-2-thiol	1160	1002	57 (100), 71 (92), 41 (88), 43 (83), 75 (81), 113 (73), 56 (61), 55 (57), 69 (40), ..., 146 (8, M^+)	roasty, sulfury, catty	0.23	
2-methyloctane-2-thiol	1261	1107	43 (100), 41 (90), 57 (87), 71 (78), 56 (56), 75 (54), 69 (42), 55 (40), 85 (36), ..., 160 (2, M^+)	roasty, mushroom-like	0.16	
2-methylnonane-2-thiol	1365	1209	57 (100), 43 (95), 41 (80), 56 (61), 75 (44), 55 (41), 71 (40), 69 (39), 85 (36), ..., 174 (1, M^+)	mushroom-like, fatty	40	
2-methyldecane-2-thiol	1470	1314	57 (100), 43 (62), 41 (60), 56 (58), 55 (37), 69 (37), 75 (32), 71 (32), 85 (23), ..., 188 (1, M^+)	fatty, soapy	160	

[a]For further spectroscopic data (MS-CI, NMR) see the Supporting Information. [b]Odor quality as perceived at the sniffing port during GC-O at threshold level. [c]Odor thresholds in air were determined as previously reported.[12] Data are mean values obtained by three panelists. [d]First report.

further characteristic fragment for the 2-methylalkane-2-thiols resulted from the α-cleavage at m/z 75 ($C_3H_7S^+$). The odor thresholds of the tertiary 2-methylalkane-2-thiols also revealed a strong dependency on the length of the alkyl chain (Table 6). After a minimum in the odor threshold of 2-methylpentane-2-thiol, threshold values exponentially increased with increasing carbon number by a factor of 290,000 between C_5 and C_{10}. With an extremely low odor threshold and an exceptional black currant-like aroma note, 2-methylpentane-2-thiol and 2-methylhexane-2-thiol were the most remarkable compounds in this homologous series. Neither compound has ever been detected in foods. With increasing chain length ($\geq C_7$), however, again roasty, fatty aroma notes occurred (Table 6).

Alkane-1,ω-dithiols. The presence of two sulfur atoms in the mass spectra of the alkane-1,ω-dithiols, illustrated by hexane-1,6-dithiol (Figure 4A), was indicated by the intensity of $[M + 2]^+$ (m/z 154, 8.5% in comparison to M^+). Further characteristic fragments were $[M - H_2S]^+$ (m/z 116) and the base peak at m/z 87. The odor thresholds of the alkanedithiols were also strongly influenced by the length of the carbon chain (Table 7). Propane-1,3-dithiol, butane-1,4-dithiol, and pentane-1,5-dithiol showed almost identical odor thresholds, but with increasing carbon numbers, the thresholds of the alkanedithiols increased exponentially. Propane-1,3-dithiol showed a garlic-like odor note, whereas the other homologues revealed a cabbage-like aroma quality (Table 7). Compounds with carbon numbers three to six have previously been identified only in beef meat.

To study the influence of an S-alkylation, the thiols reported above were methylated to obtain the respective thioethers.

1-(Methylthio)alkanes. Besides strong signals for the molecular ion, mass spectra of the 1-(methylthio)alkanes, for example, 1-(methylthio)hexane (Figure 4B), revealed characteristic fragments resulting from methyl elimination (m/z 117) and an α-cleavage (m/z 61, $C_2H_5S^+$). The 1-(methylthio)-alkanes showed a minimum in their odor thresholds for 1-(methylthio)heptane (Table 8), but with increasing chain length threshold values increased to 490 ng/L air for C_{10}. The compounds in this homologous series showed predominantly metallic, sweet, and garlic-like aroma qualities, except the long-chain homologues (C_9, C_{10}) exhibiting fatty odor qualities (Table 8).

2-(Methylthio)alkanes. As illustrated for 2-(methylthio)-hexane (Figure 4C), mass spectra of the 2-(methylthio)alkanes showed signals for M^+ (m/z 132) and $[M - CH_3]^+$ (m/z 117). A further characteristic fragment resulted from the β-cleavage yielding m/z 75.

Up to a carbon number of eight, odor thresholds for the 2-(methylthio)alkanes remained relatively constant (Table 9). By contrast, the longer homologues (C_9/C_{10}) showed considerably higher thresholds. For the C_4–C_6 homologues burned, garlic-like aroma qualities were dominant, whereas in C_7–C_{10} compounds mushroom-like odors were detected (Table 9).

3-(Methylthio)alkanes. As for the 2-(methylthio)alkanes, mass spectra of the 3-(methylthio)alkanes revealed a distinct signal for M^+ (Figure 4D), as for 3-(methylthio)hexane, and a weak signal for $[M - CH_3]^+$ (m/z 117). Characteristic signals for the methylthio group in the 3-position, resulting from an α-cleavage, were at m/z 103 ($C_5H_{11}S^+$) and m/z 89 ($C_4H_9S^+$). Odor thresholds of the 3-(methylthio)alkanes increased exponentially with increasing carbon number (Table 10). However, in particular, the thresholds of 3-(methylthio)nonane and 3-(methylthio)decane were too high (>1500 ng/L) to be accurately measured by GC-O. The compounds of this homologous series showed predominantly metallic, sweet aroma qualities (Table 10).

2-Methyl-2-(methylthio)alkanes. In contrast to the primary and secondary methylthioalkanes, the mass spectra of the tertiary 2-methyl-2-(methylthio)alkanes, shown for 2-methyl-2-(methylthio)hexane (Figure 4E), revealed a signal for $[M - SCH_3]^+$ (m/z 99). Further characteristic fragments were M^+ (m/z 146), $[M - CH_3]^+$ (m/z 131), and a fragment ion at m/z 89 resulting from the α-cleavage. As for the 3-(methylthio)alkanes an extension of the alkyl chain resulted in exponentially increasing odor thresholds (Table 11). The thresholds of the C_9 and C_{10} homologues were also too high (>1500 ng/L) to be accurately measured by GC-O. From C_4 to C_6, spicy odor qualities were dominant, which were replaced by mushroom-like odors for compounds with seven to eight carbons (Table 11).

Influence of Thiol Exchange or Modification on Odor Thresholds. *Chain Length.* The biggest effect on odor thresholds of all examined alkanethiols was observed for the length of the alkyl chain. Primary and secondary as well as tertiary thiols showed a very similar dependency on the chain

DOI: 10.1021/jf506135c
J. Agric. Food Chem. 2015, 63, 1419–1432

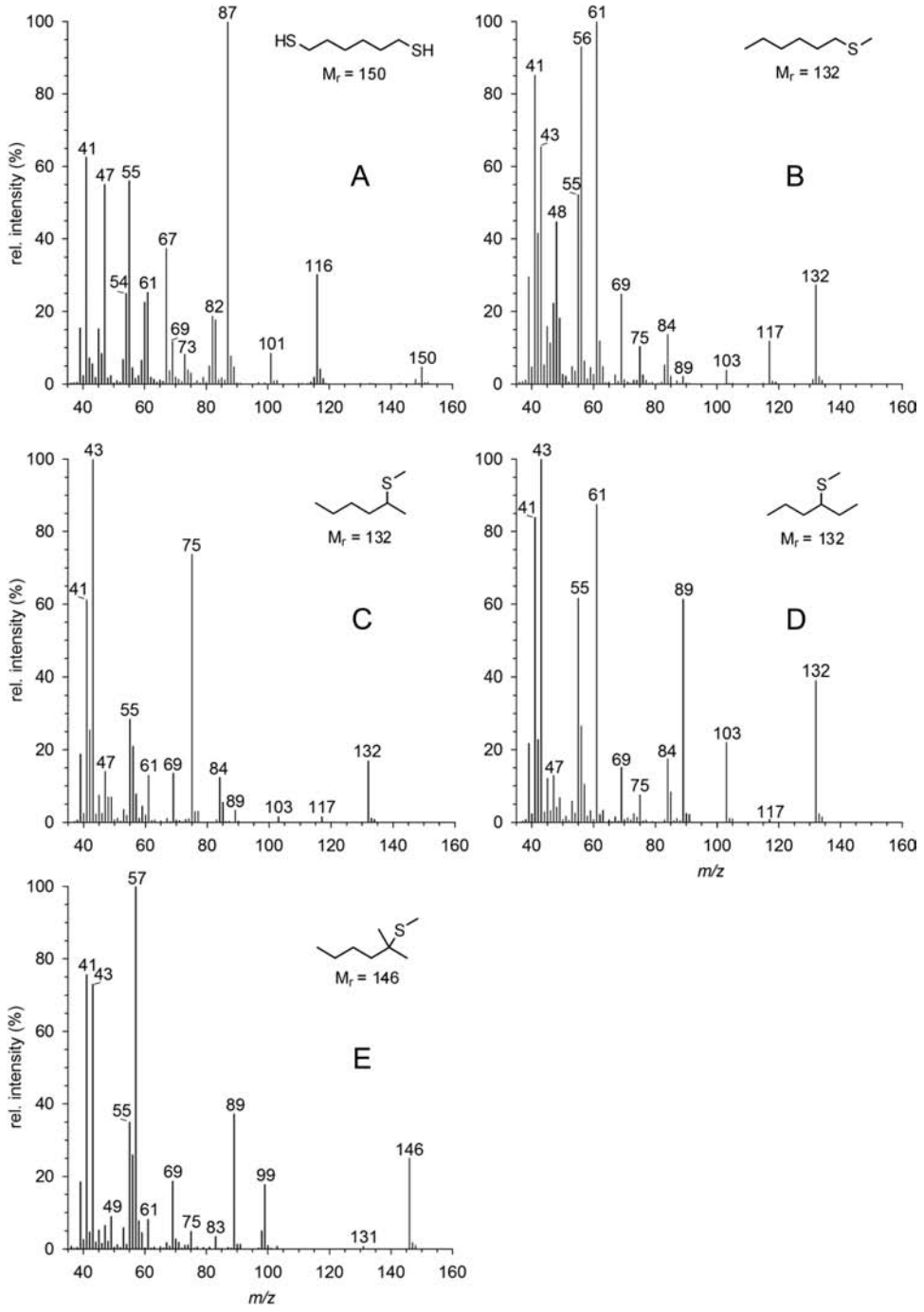

Figure 4. Selected mass spectra (MS-EI) of alkanedithiols and (methylthio)alkanes.

length (Figure 5): After a decline by a factor of ~10 from C_3–C_4 or C_4–C_5, all four homologous series showed a minimum in odor thresholds for thiols with five to seven carbon atoms, but with increasing chain length the thresholds considerably increased. The alkanethiols at minimum level, for example, 2-methylpentane-2-thiol or pentane-3-thiol, with odor thresholds in the range of pico- or femtograms per liter air, belong to the most potent odorants reported so far in the literature. By contrast, the corresponding C_{10} homologues, showing by factors of 27,000 (alkane-1-thiols) or 290,000 (2-methylalkane-2-thiols) higher thresholds than these two thiols, were almost odorless. These results suggest that, besides the importance of the mercapto group on the odor activity of thiols, the odor perception of mercaptans is also strongly influenced by steric effects.

With increasing substitution at the mercapto-containing carbon atom, the thresholds at minimum level decreased. For example, the primary alkane-1-thiols showed by a factor of 20 higher odor thresholds at minimum level than tertiary 2-methylalkane-2-thiols. This is in accordance with the results of Meilgaard,[1] who determined the odor thresholds of, for example, butane-1-thiol, butane-2-thiol, and 2-methylbutane-2-thiol occurring in beer. Furthermore, this is consistent with the theories of Wang et al.[18] and Duan et al.,[19] who found some evidence that metal ions such as zinc(II) or copper(II) may be involved in olfactory perception of thiols at the receptor level.

DOI: 10.1021/jf506135c
J. Agric. Food Chem. 2015, 63, 1419–1432

Table 7. Retention Indices, MS-EI Data, and Sensory Properties of Dithiols

compound	RI FFAP	RI DB-5	m/z (intensity in %)[a]	odor quality[b]	odor threshold[c] (ng/L in air)	reported as food constituent[d]
propane-1,3-dithiol	1429	930	41 (100), 74 (87), 47 (63), 108 (49, M^+), 45 (32), 61 (30), 46 (22), 39 (17), 59 (9), 73 (6)	garlic	0.075	beef[24]
butane-1,4-dithiol	1559	1047	47 (100), 88 (79), 60 (75), 55 (57), 45 (25), 46 (20), 122 (19, M^+), 41 (18), 54 (15), 39 (14)	cabbage-like, burned	0.088	beef[24]
pentane-1,5-dithiol	1665	1156	102 (100), 41 (68), 47 (66), 69 (58), 68 (48), 87 (46), 55 (34), 61 (29), 67 (26), ..., 136 (3, M^+)	cabbage-like, burned, fatty	0.075	beef[24]
hexane-1,6-dithiol	1773	1263	87 (100), 41 (62), 55 (56), 47 (55), 67 (37), 116 (30), 61 (25), 54 (25), 60 (22), ..., 150 (5, M^+)	cabbage-like, burned, fatty	0.35	beef[24]
heptane-1,7-dithiol	1887	1372	101 (100), 55 (97), 87 (65), 41 (44), 47 (43), 67 (34), 68 (30), 61 (24), 81 (21), ..., 164 (4, M^+)	cabbage-like, burned, fatty	0.32	
octane-1,8-dithiol	1997	1480	55 (100), 87 (95), 101 (84), 41 (75), 115 (69), 67 (67), 69 (66), 47 (60), 61 (35), ..., 178 (4, M^+)	fatty, cabbage-like	1.3	
nonane-1,9-dithiol	2112	1589	55 (100), 87 (90), 101 (75), 41 (74), 47 (53), 67 (52), 69 (51), 157 (49), 68 (39), ..., 192 (8, M^+)	fatty, cabbage-like	5.4	
decane-1,10-dithiol	2222	1695	87 (100), 55 (98), 101 (79), 41 (66), 67 (57), 69 (49), 47 (44), 68 (43), 81 (38), ..., 206 (14, M^+)	fatty, cabbage-like	38	

[a]For further spectroscopic data (MS-CI, NMR) see the Supporting Information. [b]Odor quality as perceived at the sniffing port during GC-O at threshold level. [c]Odor thresholds in air were determined as previously reported.[12] Data are mean values obtained by three panelists. [d]First report.

Table 8. Retention Indices, MS-EI Data, and Sensory Properties of Homologous 1-(Methylthio)alkanes

compound	RI FFAP	RI DB-5	m/z (intensity in %)[a]	odor quality[b]	odor threshold[c] (ng/L in air)
1-(methylthio)-butane	1014	813	61 (100), 56 (87), 41 (84), 104 (50, M^+), 47 (29), 48 (28), 45 (21), 39 (19), 75 (17), 49 (16)	metallic, sulfury	2.0
1-(methylthio)-pentane	1116	917	61 (100), 42 (73), 41 (53), 70 (50), 55 (44), 118 (37, M^+), 48 (36), 43 (29), 39 (20), 47 (18)	metallic, garlic, sulfury	30
1-(methylthio)-hexane	1218	1019	61 (100), 56 (93), 41 (85), 43 (65), 55 (52), 48 (45), 42 (42), 39 (30), 132 (27, M^+), 69 (25)	metallic, garlic, sulfury	1.8
1-(methylthio)-heptane	1363	1121	61 (100), 41 (81), 56 (71), 55 (63), 70 (56), 146 (34, M^+), 42 (34), 69 (32), 48 (32), 43 (27)	mushroom-like	0.94
1-(methylthio)-octane	1426	1223	61 (100), 41 (98), 56 (64), 55 (63), 43 (60), 69 (44), 70 (40), 42 (38), 48 (36), 160 (23, M^+)	metallic, garlic, sulfury	15
1-(methylthio)-nonane	1533	1329	61 (100), 41 (87), 55 (71), 56 (68), 43 (57), 69 (47), 70 (40), 48 (27), 174 (27, M^+), 159 (25)	fatty, soapy	120
1-(methylthio)-decane	1640	1434	61 (100), 41 (99), 55 (87), 43 (68), 56 (58), 69 (50), 70 (50), 57 (36), 83 (35), ..., 188 (26, M^+)	fatty, sweaty	490

[a]For further spectroscopic data (MS-CI, NMR) see the Supporting Information. [b]Odor quality perceived at the sniffing port during GC-O at threshold level. [c]Odor thresholds in air were determined as previously reported.[12] Data are mean values obtained by three panelists.

Table 9. Retention Indices, MS-EI Data, and Sensory Properties of Homologous 1-(Methylthio)alkanes

compound	RI FFAP	RI DB-5	m/z (intensity in %)[a]	odor quality[b]	odor threshold[c] (ng/L in air)
2-(methylthio)-butane	947	778	41 (100), 75 (48), 56 (30), 39 (24), 57 (23), 104 (22, M^+), 47 (20), 43 (16), 45 (14), 55 (11)	garlic, sulfury, metallic	8.0
2-(methylthio)-pentane	1047	867	43 (100), 75 (68), 41 (67), 55 (49), 70 (29), 42 (28), 39 (26), 118 (20, M^+), 47 (19), 61 (18)	garlic, sulfury, metallic	14
2-(methylthio)-hexane	1143	968	43 (100), 75 (74), 41 (61), 55 (28), 42 (25), 56 (21), 39 (19), 132 (17, M^+), 47 (14), 69 (14)	burned, sulfury, asparagus	13
2-(methylthio)-heptane	1245	1069	41 (100), 75 (98), 57 (69), 56 (53), 43 (50), 55 (39), 39 (25), 69 (21), 146 (20, M^+), 42 (18)	mushroom-like, metallic	11
2-(methylthio)-octane	1347	1173	75 (100), 41 (75), 43 (53), 55 (42), 57 (38), 70 (27), 56 (24), 42 (22), 71 (19), ..., 160 (14, M^+)	mushroom-like	13
2-(methylthio)-nonane	1451	1272	75 (100), 41 (72), 43 (67), 55 (42), 56 (30), 57 (24), 42 (19), 69 (18), 70 (16), ..., 174 (12, M^+)	mushroom-like	110
2-(methylthio)-decane	1558	1375	75 (100), 41 (62), 43 (58), 55 (44), 57 (36), 56 (31), 69 (21), 70 (20), 42 (17), 188 (14, M^+)	mushroom-like, fatty	590

[a]For further spectroscopic data (MS-CI, NMR) see the Supporting Information. [b]Odor quality as perceived at the sniffing port during GC-O at threshold level. [c]Odor thresholds in air were determined as previously reported.[12] Data are mean values obtained by three panelists.

With increasing substitution at the mercapto-containing carbon atom, also the Lewis basicity of the SH group and, thus, the binding affinity to metal ions are increased. Therefore, tertiary thiols are able to link more strongly to metal ions in the active

DOI: 10.1021/jf506135c
J. Agric. Food Chem. 2015, 63, 1419−1432

Table 10. Retention Indices, MS-EI Data, and Sensory Properties of Homologous 3-(Methylthio)alkanes

compound	RI FFAP	RI DB-5	m/z (intensity in %)[a]	odor quality[b]	odor threshold[c] (ng/L in air)
3-(methylthio)pentane	1044	867	41 (100), 43 (93), 89 (87), 55 (43), 118 (36, M^+), 70 (27), 61 (25), 39 (22), 42 (21), 47 (14)	sweaty, metallic, fatty	28
3-(methylthio)hexane	1139	959	43 (100), 61 (88), 41 (84), 55 (62), 89 (61), 132 (39, M^+), 56 (27), 42 (23), 103 (22), 39 (22)	sweaty, metallic, fatty	52
3-(methylthio)heptane	1224	1058	41 (100), 57 (63), 61 (38), 43 (36), 89 (32), 56 (31), 69 (28), 55 (23), 39 (18), 146 (10, M^+)	mushroom-like, fatty	200
3-(methylthio)octane	1322	1157	41 (100), 43 (57), 55 (51), 89 (47), 57 (41), 61 (38), 56 (27), 39 (21), 71 (20), ..., 160 (15, M^+)	mushroom-like	640
3-(methylthio)nonane	1426	1258	41 (100), 43 (80), 55 (78), 89 (59), 61 (39), 57 (30), 56 (26), 42 (21), 71 (20), ..., 174 (14, M^+)		>1500
3-(methylthio)decane	1573	1360	89 (100), 41 (97), 43 (77), 55 (69), 69 (52), 57 (46), 61 (40), 56 (31), 159 (31), 188 (20, M^+)		>1500

[a]For further spectroscopic data (MS-CI, NMR) see the Supporting Information. [b]Odor quality as perceived at the sniffing port during GC-O at threshold level. [c]Odor thresholds in air were determined as previously reported.[12] Data are mean values obtained by three panelists.

Table 11. Retention Indices, MS-EI Data, and Sensory Properties of Homologous 2-Methyl-2-(methylthio)alkanes

compound	RI FFAP	RI DB-5	m/z (intensity in %)[a]	odor quality[b]	odor threshold[c] (ng/L in air)
2-methyl-2-(methylthio)-butane	1009	833	43 (100), 71 (76), 118 (50, M^+), 55 (47), 41 (26), 89 (20), 39 (16), 70 (15), 45 (11), 42 (10)	metallic, fruity, spicy	2.1
2-methyl-2-(methylthio)-pentane	1086	921	43 (100), 41 (34), 85 (31), 57 (11), 89 (11), 132 (11, M^+), 39 (10), 69 (10), 55 (8), 56 (5)	spicy, coriander	4.8
2-methyl-2-(methylthio)-hexane	1182	1021	57 (100), 41 (76), 43 (73), 89 (37), 55 (35), 56 (26), 146 (25, M^+), 69 (19), 39 (18), 99 (18)	sweaty, spicy, metallic	9.0
2-methyl-2-(methylthio)-heptane	1280	1120	57 (100), 71 (93), 43 (90), 41 (85), 89 (67), 55 (62), 56 (53), 160 (36, M^+), 69 (34), 113 (22)	sweaty, mushroom-like	35
2-methyl-2-(methylthio)-octane	1382	1223	43 (100), 57 (76), 41 (71), 71 (68), 55 (34), 85 (33), 56 (33), 89 (29), 69 (26), 174 (15, M^+)	mushroom-like, metallic	250
2-methyl-2-(methylthio)-nonane	1485	1326	57 (100), 43 (74), 41 (60), 71 (54), 85 (53), 56 (45), 55 (42), 89 (41), 69 (34), 188 (24, M^+)		>1500
2-methyl-2-(methylthio)-decane	1591	1428	57 (100), 43 (59), 71 (45), 41 (42), 56 (36), 55 (35), 85 (35), 89 (33), 69 (28), 202 (16, M^+)		>1500

[a]For further spectroscopic data (MS-CI, NMR) see the Supporting Information. [b]Odor quality as perceived at the sniffing port during GC-O at threshold level. [c]Odor thresholds in air were determined as previously reported.[12] Data are mean values obtained by three panelists.

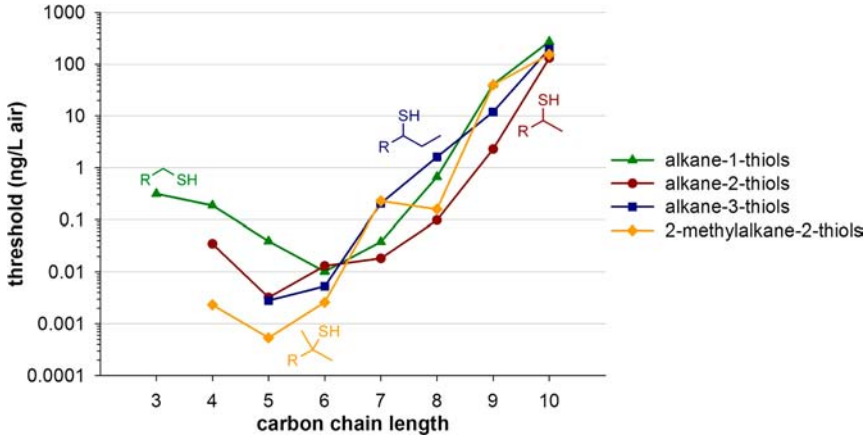

Figure 5. Influence of the chain length on odor thresholds of homologous primary, secondary, and tertiary alkanethiols.

center of a hypothetical olfactory receptor than primary thiols, leading to a more sensitive detection resulting in lower odor thresholds. In agreement with this hypothesis, methyl substitution in the α-position to the SH group, in contrast to a tertiary methyl substitution, did not lower the odor thresholds (Figure 6). The 2-methylalkane-1-thiols as well as 2-methylalkane-3-thiols showed almost the same dependency on the chain length, but exhibited even higher thresholds at minimum level than the respective alkane-1-thiols.

Odor Quality. Because sensory properties of sulfur compounds are often strongly dependent on their concentrations, all odor qualities were determined at threshold level. Nevertheless, with the change in odor thresholds also a change in odor qualities was observed among the members of the

DOI: 10.1021/jf506135c
J. Agric. Food Chem. 2015, 63, 1419−1432

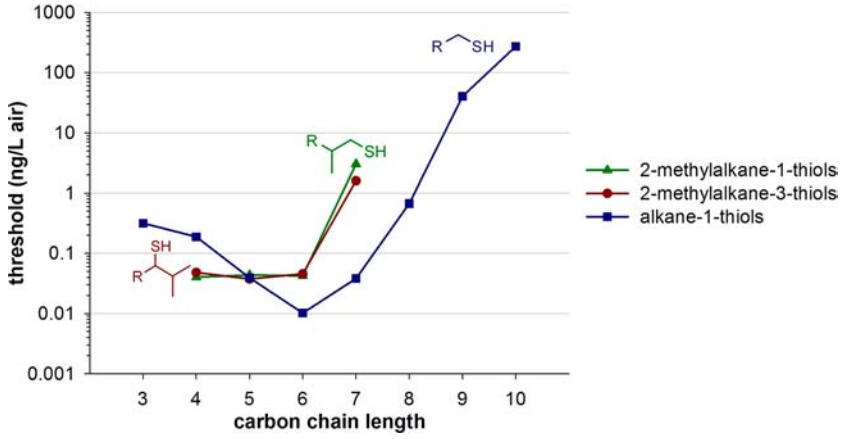

Figure 6. Influence of α-methyl substitution on odor thresholds of thiols.

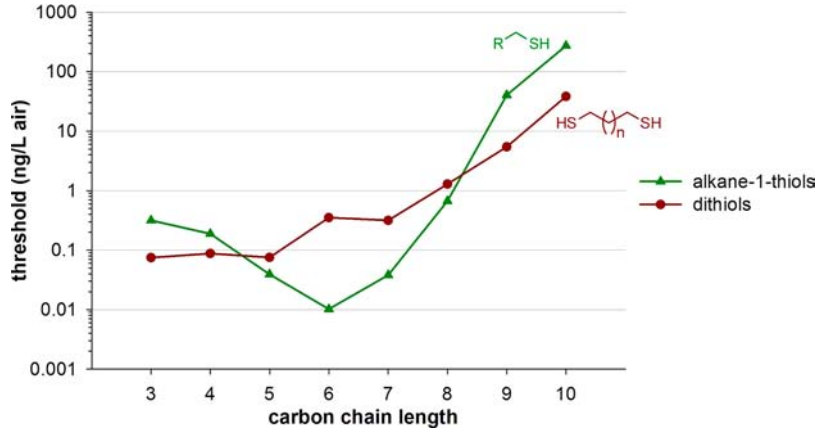

Figure 7. Comparison of odor thresholds of homologous alkane-1-thiols and alkanedithiols.

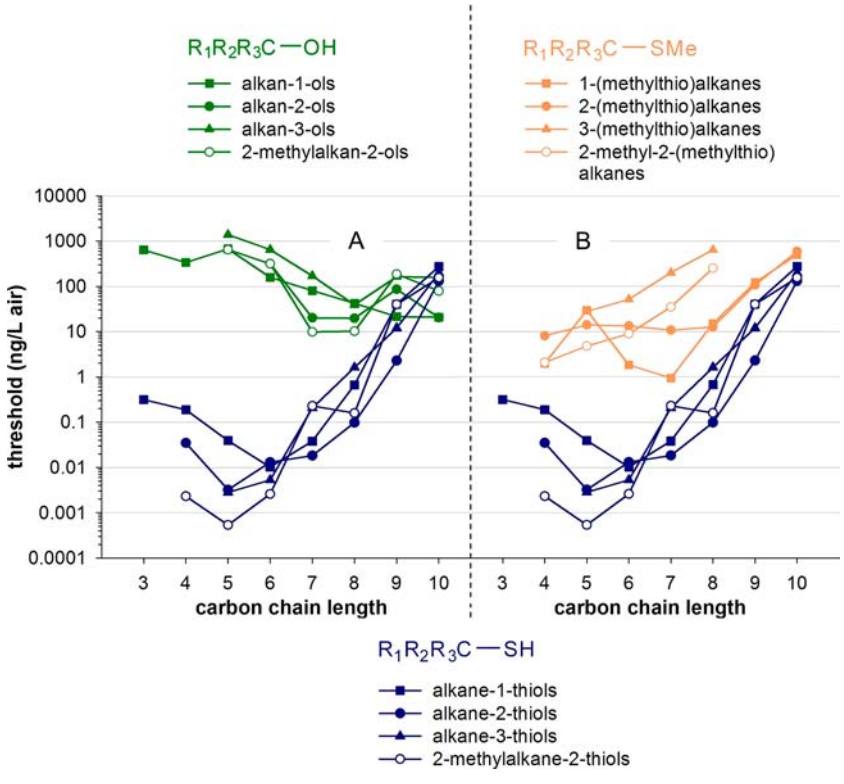

Figure 8. Comparison of odor thresholds of alkanethiols with (A) corresponding alkanols and (B) (methylthio)alkanes.

DOI: 10.1021/jf506135c
J. Agric. Food Chem. 2015, 63, 1419−1432

homologous series, whereas compounds with identical chain length of different homologues series often showed similar odor qualities. The C_3 and C_4 homologues of primary and secondary thiols showed garlic-like, burned odor notes. At minimum level, for the C_5 and C_6 homologues, burned, roasty odors were detected, but with increasing carbon numbers (C_9 and C_{10} homologues) the odor changed to fatty, soapy notes. By contrast, short-chain tertiary thiols (C_4–C_7) showed exceptional catty, black currant-like aroma notes. 2-Methylpentane-2-thiol and 2-methylhexane-2-thiol displayed the most attractive odor of all examined mercaptans in this study, and both thiols were previously not identified in foods. With a threshold of 0.00053 ng/L, 2-methylpentane-2-thiol also showed the lowest value of all thiols examined. Surprisingly, with increasing chain length (>C_7) tertiary thiols revealed odor qualities similar to those of the corresponding primary and secondary thiols.

Influence of a Second Mercapto Group. To study the influence of a second thiol group on odor perception, odor thresholds of some alkane-1,ω-dithiols were determined. In contrast to the alkane-1-thiols, the alkanedithiols did not show a clear minimum (Figure 7). Propane-1,3-dithiol, butane-1,4-dithiol, and pentane-1,5-dithiol showed almost identical odor thresholds. With increasing carbon numbers also the thresholds of alkanedithiols increased exponentially as found for the alkane-1-thiols. Altogether, the thresholds of alkane-1-thiols at minimum level were clearly lower than those of the alkane-1,ω-dithiols; for example, hexane-1-thiol had a 35 times lower odor threshold than hexane-1,6-dithiol. Thus, it can be concluded that a second mercapto group in the molecule does not result in an additional activation of SH-specific odorant receptors leading to a lower odor threshold.

Importance of the Mercapto Group. To show the influence of the free mercapto group on odor thresholds, on the one hand the SH group was replaced by the chemically related OH group. On the other hand, the mercapto group was blocked by S-methylation and the thresholds obtained were compared to the thresholds of the alkanethiols.

In comparison to the alkanethiols, the corresponding alcohols showed a completely different dependency of odor thresholds with respect to chain length (Figure 8A). In contrast to the thiols, the odor thresholds of the alcohols clearly decreased with increasing carbon number from C_3 to C_8. The thresholds of some of the short-chain homologues (butan-2-ol, pentan-2-ol, and 2-methylbutan-2-ol) were very high and exceeded the measurement range of GC-O (Table 12). From C_9 to C_{10} the thresholds of the alcohols stayed relatively constant with a weak maximum at C_9 for the secondary and tertiary alcohols. From C_3 to C_8 all alcohols showed much higher odor thresholds than the corresponding thiols. The thresholds of the alcohols were by factors of 16,000 (primary thiols) and 1,200,000 (tertiary thiols), respectively, higher than those of the corresponding thiols at minimum level. With increasing chain length, the odor thresholds of alcohols and thiols were nearly identical, and, finally, for the C_9/C_{10} homologues some alcohols even showed lower thresholds than the corresponding thiols.

This different behaviors of alcohols and thiols indicate that chemoreception of thiols should occur by different mechanisms or at different olfactory receptors than the perception of alcohols, also, because the alcohols showed mainly fruity odors (Table 12). Correlations between the odor qualities of alcohols and thiols, as described by Sakoda and Hayashi[4] for alkane-2-ols and alkane-2-thiols, could not be confirmed.

Table 12. Odor Qualities and Odor Thresholds of Alkanols

compound	odor quality[a]	odor threshold[b] (ng/L in air)
propan-1-ol	pungent, solvent, ethanolic	635
butan-1-ol	pungent, solvent, fruity	336
pentan-1-ol	solvent, fruity, flowery	673
hexan-1-ol	fruity, green	158
heptan-1-ol	fruity, flowery, soapy	81
octan-1-ol	fruity, soapy	42
nonan-1-ol	green, soapy, fatty	21
decan-1-ol	fatty, soapy	21
butan-2-ol		>1500
pentan-2-ol		>1500
hexan-2-ol	fruity, flowery, solvent	317
heptan-2-ol	fruity, flowery	20
octan-2-ol	fruity, soapy	20
nonan-2-ol	fruity, green	87
decan-2-ol	soapy, sour	20
pentan-3-ol	pungent, solvent	1385
hexan-3-ol	fruity, soapy	645
heptan-3-ol	fruity, flowery	169
octan-3-ol	fruity, flowery	39
nonan-3-ol	fruity, fatty	164
decan-3-ol	fatty, soapy	158
2-methylbutan-2-ol		>1500
2-methylpentan-2-ol	fruity, sweet	646
2-methylhexan-2-ol	fruity, flowery, coriander	315
2-methylheptan-2-ol	fruity, flowery, coriander	9.9
2-methyloctan-2-ol	fruity, soapy, mushroom-like	10
2-methylnonan-2-ol	fruity, soapy	186
2-methyldecan-2-ol	soapy, fatty	79

[a]Odor quality as perceived at the sniffing port during GC-O at threshold level. [b]Odor thresholds in air were determined as previously reported.[12] Data are mean values obtained by three panelists.

Methylation of the SH group also resulted in an increase in odor thresholds (Figure 8B). Like the thiols, the (methylthio)-alkanes showed higher odor thresholds with increasing chain length, and the thresholds of 2-methyl-2-(methylthio)nonane and 3-(methylthio)decane were even too high to be accurately measured by GC-O. In contrast to the thiols, the (methylthio)-alkanes did not show clear minima within their homologous series. Apart from the 1-(methylthio)alkanes, all homologous series exhibited their lowest thresholds at C_4. Up to a carbon number of seven, methylation of the thiol group led to a strong increase in odor thresholds, and the thresholds of the corresponding (methylthio)alkanes differed by factors of 180 (primary thiols) to 9000 (tertiary thiols), respectively. Therefore, blocking of the SH group by methylation clearly reduced the olfactory power of the thiols. The data highlight that the free thiol group is an important structural feature for the low odor thresholds of sulfur compounds. Most of the short-chain (methylthio)alkanes showed typical sulfury odors, often with additional metallic or garlic-like odor notes. With increasing chain length (C_7/C_8) odor qualities changed to mushroom-like odors, and finally at C_9/C_{10} also fatty odor notes occurred, as also found for the thiols.

3D-QSAR Studies. To get a first insight into the odotope structure defining the space for a low odor threshold in mercaptans, 3D-QSAR calculations were performed. Using CoMFA, 3D-QSAR models were established to correlate the

DOI: 10.1021/jf506135c
J. Agric. Food Chem. 2015, 63, 1419–1432

threshold data of the 44 thiols analyzed with their molecular structures. The calculation of positive (resulting in lower thresholds) and negative (resulting in higher thresholds) steric and electrostatic fields showed that most of the differences in odor thresholds can be explained by steric effects, whereas electrostatic fields had only little influence on odor thresholds. The thresholds simulated by the theoretical model were in good agreement with the experimentally determined data (Figure 9). Statistical validation showed a reliable model with a

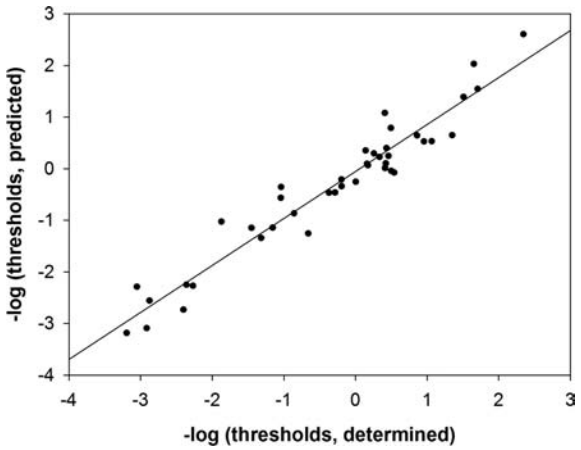

Figure 9. Correlation of determined and predicted odor thresholds of alkanethiols.

coefficient of correlation (r^2) of 0.89 (q^2 = 0.63) at a number of 10 principal components and a standard deviation (s) of 0.52. However, more data are needed to validate this model.

In conclusion, the results have revealed that odor perception of alkanethiols is strongly influenced by steric effects, such as the length of the carbon chain or an additional methyl group in the carbon chain, but in particular only one free SH group is essential for the low odor thresholds of sulfur compounds. Blocking this SH group by alkylation clearly reduced the olfactory power, whereas a second mercapto group in the molecule did not lower the odor thresholds.

■ ASSOCIATED CONTENT

Ⓢ Supporting Information

Experimental procedures and spectral data (NMR, MS) of the synthesized compounds and intermediates. In Figures S1−S5, the synthesis pathways of the conducted reactions are illustrated. Figures S6−S85 show the NMR spectra of the synthesized sulfur compounds. This material is available free of charge via the Internet at http://pubs.acs.org.

■ AUTHOR INFORMATION

Corresponding Author

*(P.S.) E-mail: peter.schieberle@lrz.tum.de. Phone: +49 8161 712932. Fax: +49 8161 712970.

Notes

The authors declare no competing financial interest.

■ ABBREVIATIONS USED

CoMFA, comparative molecular field analysis; GC-O, gas chromatography−olfactometry; PLS, partial least-squares regression; q^2, cross-validated correlation coefficient; QSAR, quantitative structure−activity relationship; r^2, correlation coefficient; *s.d.*, standard deviation; M_r, relative molecular mass

■ REFERENCES

(1) Meilgaard, M. C. Flavor chemistry of beer. II. Flavor and threshold of 239 aroma volatiles. *Tech. Q. Master Brew. Assoc. Am.* **1975**, *12*, 151−168.

(2) Wannagat, U.; Damrath, V.; Schliephake, A.; Harder, U. Sila-substituted perfumes and isosteric compounds of perfumes. XI. Comparison of carbinols and silanols with thiocarbinols and silanethiols. *Monatsh. Chem.* **1987**, *118*, 779−788.

(3) Polak, E.; Fetison, G.; Fombon, A. M.; Skalli, A. Structure-odor relationships for "catty"-smelling mercapto compounds in humans. *J. Agric. Food Chem.* **1988**, *36*, 355−359.

(4) Sakoda, Y.; Hayashi, S. Relationship of odour and chemical structure in 1- and 2-alkyl alcohols and thiols. *Spec. Publ.−R. Soc. Chem.* **2002**, *277*, 15−24.

(5) Polster, J.; Schieberle, P. Structure/odor relationships in homologous series of primary, secondary and tertiary thiols. In *State-of-the-Art in Flavour Chemistry and Biology*, Proceedings of the 9th Wartburg Symposium on Flavor Chemistry and Biology; Hofmann, T., Meyerhof, W., Schieberle, P., Eds.; Deutsche Forschungsanstalt für Lebensmittelchemie: Freising, Germany, 2011; pp 69−74.

(6) Wakabayashi, M.; Wakabayashi, H.; Nörenberg, S.; Reichardt, B.; Kubota, K.; Engel, K. H. Analytical and sensory characterization of chiral 4-mercapto-2-alkanones, 4-acetylthio-2-alkanones, and the corresponding alcohols. In *Recent Advances in the Analysis of Food and Flavors*; Toth, S., Mussinan, C. J., Eds.; American Chemical Society: Washington, DC, USA, 2012; Vol. 1098, pp 27−39.

(7) Noerenberg, S.; Reichardt, B.; Andelfinger, V.; Eisenreich, W.; Engel, K.-H. Influence of the stereochemistry on the sensory properties of 4-mercapto-2-heptanol and its acetyl-derivatives. *J. Agric. Food Chem.* **2013**, *61*, 2062−2069.

(8) Simian, H.; Robert, F.; Blank, I. Identification and synthesis of 2-heptanethiol, a new flavor compound found in bell peppers. *J. Agric. Food Chem.* **2004**, *52*, 306−310.

(9) Masada, H.; Murotani, Y. A convenient method for the preparation of highly pure *tert*-alkyl bromides and iodides. *Bull. Chem. Soc. Jpn.* **1980**, *53*, 1181−1182.

(10) Gurudutt, K. N.; Rao, S.; Srinivas, P.; Srinivas, S. Nucleophilic substitution of SN1-active halides using zinc salts: preparation of thiolacetates. *Tetrahedron* **1995**, *51*, 3045−3050.

(11) Yin, J.; Pidgeon, C. A simple and efficient method for preparation of unsymmetrical sulfides. *Tetrahedron Lett.* **1997**, *38*, 5953−5954.

(12) Ullrich, F.; Grosch, W. Identification of the most intense volatile flavor compounds formed during autoxidation of linoleic acid. *Z. Lebensm. Unters. Forsch.* **1987**, *184*, 277−282.

(13) Teranishi, R.; Buttery, R. G.; Guadagni, D. G. Odor quality and chemical structure in fruit and vegetable flavors. *Ann. N.Y. Acad. Sci.* **1974**, *237*, 209−216.

(14) Czerny, M.; Christlbauer, M.; Christlbauer, M.; Fischer, A.; Granvogl, M.; Hammer, M.; Hartl, C.; Hernandez, N. M.; Schieberle, P. Re-investigation on odour thresholds of key food aroma compounds and development of an aroma language based on odour qualities of defined aqueous odorant solutions. *Eur. Food Res. Technol.* **2008**, *228*, 265−273.

(15) Tripos SYBYL-X 1.2; Tripos International, St. Louis, MO, USA, 2012.

(16) Amoore, J. E.; Hautala, E. Odor as an aid to chemical safety: odor thresholds compared with threshold limit values and volatilities for 214 industrial chemicals in air and water dilution. *J. Appl. Toxicol.* **1983**, *3*, 272−290.

(17) Vermeulen, C.; Gijs, L.; Collin, S. Sensorial contribution and formation pathways of thiols in foods: a review. *Food Rev. Int.* **2005**, *21*, 69−137.

(18) Wang, J.; Luthey-Schulten, Z. A.; Suslick, K. S. Is the olfactory receptor a metalloprotein? *Proc. Natl. Acad. Sci. U.S.A.* **2003**, *100*, 3035−3039.

(19) Duan, X.; Block, E.; Li, Z.; Connelly, T.; Zhang, J.; Huang, Z.; Su, X.; Pan, Y.; Wu, L.; Chi, Q.; Thomas, S.; Zhang, S.; Ma, M.; Matsunami, H.; Chen, G.-Q.; Zhuang, H. Crucial role of copper in

DOI: 10.1021/jf506135c
J. Agric. Food Chem. 2015, 63, 1419−1432

detection of metal-coordinating odorants. *Proc. Natl. Acad. Sci. U.S.A.* **2012**, *109*, 3492−3497.
(20) Challenger, F.; Greenwood, D. Sulfur compounds of the genus *Allium*. Detection of propylthiol in the onion. The fission and methylation of diallyl disulfide in cultures of *Scopulariopsis brevicaulis*. *Biochem. J.* **1949**, *44*, 87−91.
(21) Libbey, L. M.; Bills, D. D.; Day, E. A. Technique for the study of lipid-soluble food flavor volatiles. *J. Food Sci.* **1963**, *28*, 329−333.
(22) Parker, J. K.; Hassell, G. M. E.; Mottram, D. S.; Guy, R. C. E. Sensory and instrumental analyses of volatiles generated during the extrusion cooking of oat flours. *J. Agric. Food Chem.* **2000**, *48*, 3497−3506.
(23) Minor, L. J.; Pearson, A. M.; Dawson, L. E.; Schweigert, B. S. Chicken flavor. Identification of some chemical components and the importance of sulfur compounds in the cooked volatile fraction. *J. Food Sci.* **1965**, *30*, 686−696.
(24) Garbusov, V.; Rehfeld, G.; Woelm, G.; Golovnia, R. V.; Rothe, M. Volatile sulfur compounds contributing to meat flavor. Part I. Components identified in boiled meat. *Nahrung* **1976**, *20*, 235−241.
(25) Golovnja, R. V.; Rothe, M. Sulfur containing compounds in the volatile constituents of boiled meat. *Nahrung* **1980**, *24*, 141−154.
(26) Ronald, A. P.; Thomson, W. A. B. Volatile sulfur compounds of oysters. *J. Fish. Res. Board Can.* **1964**, *21*, 1481−1487.
(27) Bassols, F.; Demole, E. P. The occurrence of pentane-2-thiol in guava fruit. *J. Essent. Oil Res.* **1994**, *6*, 481−483.
(28) Naef, R.; Velluz, A.; Jaquier, A. New volatile sulfur-containing constituents in a simultaneous distillation-extraction extract of red bell peppers (*Capsicum annuum*). *J. Agric. Food Chem.* **2008**, *56*, 517−527.
(29) Wilson, R. A.; Mussinan, C. J.; Katz, I.; Sanderson, A. Isolation and identification of some sulfur chemicals present in pressure-cooked beef. *J. Agric. Food Chem.* **1973**, *21*, 873−876.

DOI: 10.1021/jf506135c
J. Agric. Food Chem. 2015, 63, 1419−1432

scopic characteristics that facilitate collection of information which is complementary to the infrared techniques. These include its relative insensitivity to water and ability to reveal significant information on composition and structure of macromolecules, especially protein, in foods. On the contrary, fluorescence can be a problem, especially with biological materials, and Raman signals are weak. However, fluorescence can be minimized by both appropriate laser wavelength selection and mathematical processing of collected spectra while weak Raman signals are no longer a serious disadvantage due to improved detector sensitivity and the technical feasibility of using longer collection times.

Raman spectroscopy has been reported to predict the sensory quality of beef silverside,[20] to quantify saturated and unsaturated fatty acids in pork adipose tissue,[21] to predict water-holding capacity in meat,[22] to detect protein contents in meat and fish,[23−25] and to predict meat spoilage.[26] Only a small number of studies have reported the use of Raman spectroscopic methods to detect meat adulteration. These have included the use of Raman spectroscopy combined with multivariate analysis to classify adipose tissue in different meat species,[27] to confirm authenticity of poultry species,[28] and to detect and quantify horse meat content in minced beef.[29]

Beefburgers, a classic type of minced beef product, are regularly consumed in the developed world. A typical beefburger is produced as a homogenized item composed of minced beef, water, added fat, certain cereal products (e.g., rusk), and flavoring agents. Some vegetables (spring onion, onion etc.) may be present in greater or lesser amounts in particular formulations. Furthermore, beefburgers may be produced in higher or lower quality variants and sold in either the fresh or frozen state. In this study, an experimental design was undertaken to cover the widest possible range of formulations involving beef offal types (i.e., kidney, liver, heart, and lung) and other ingredients (i.e., water and rusk) in the least number of experiments. Both classification and class-modeling approaches were studied to try to distinguish between the authentic and offal-adulterated beefburgers manufactured. Quantitative models for total offal incorporation and added fat prediction were also developed. The present study investigated detection of beef offal (i.e., kidney, liver, heart, and lung) adulteration in frozen-then-thawed beefburgers using Raman spectroscopy and multivariate data analysis. The main aim of the study was to explore the potential of Raman spectroscopy for addressing authentication issues in processed meat products with complex formulations.

MATERIALS AND METHODS

Beefburger Formulation and Manufacture. *Beefburger Formulation.* Authentic beefburgers comprised two groups, so-called lean burgers and fat burgers, which correspond to higher and lower quality grades. Higher quality burgers contained only lean beef and beef fat; lean meat content was varied between 80 and 100% w/w of burger in 2.5% increments, with fat accounting for the remainder. Lower quality burgers contained rusk (5% w/w) and water (20% w/w) in addition to lean beef (45−65% w/w in 2.5% increments) and beef fat (30−10% w/w in 2.5% increments). These compositional ranges were based on market intelligence concerning those typically used in the butchery trade. Burgers in each of the two groups were made on separate occasions, beginning with the highest lean meat content and moving to the lowest. Depending particularly on the quality of the lean meat purchased, production of either group could require more than 1 day. Each group of beefburgers was produced on two separate occasions; therefore, a total of 36 (18 higher quality and 18 lower quality) authentic beefburgers was prepared.

Adulterated beefburgers were formulated with lean beef, beef fat, water, rusk, and offal (liver, lung, kidney, and heart). Formulations were produced using a D-optimal experimental design (Design Expert v. 7.6.1, Stat-Ease Inc., Minneapolis, MN, USA) with minimum and maximum incorporation levels of meat (0−75% w/w), fat (0−25% w/w), water (0−15% w/w), and rusk (0−5% w/w) set by the operator; each formulation also contained liver, lung, kidney, and heart, each at concentrations between 0 and 20% w/w. A total of 46 different beefburger formulations was generated by the software to efficiently represent the design space for the multitude of possible combinations of ingredients. These beefburgers were produced in random order over a period of several days; because of time constraints, each formulation was produced only once. Variability in this data set was maximized by sourcing meat and offal from several suppliers and on different occasions. Adulterated beefburger formulations are shown in Table 1.

Beefburger Manufacture. Fresh beef (brisket), beef offal (kidney, liver, lungs, and heart), and beef fat were purchased from local stores and stored overnight at 4 °C at Teagasc Food Research Centre Ashtown. Skin, fatty tissue, connective tissue, visible blood vessels, and cartilage were removed to ensure the highest possible quality of the raw materials. Raw materials were cut into cubes, weighed, and mixed according to each formulation before mincing; mixed meat samples were minced twice (Mainca meat mincer, Cheshire, England) through a mesh plate (5 mm diameter holes). In between the two mincing occasions and when required by the formulation, sifted pinhead rusk (Redbrook, Damastown, Dublin) and iced water were blended into the minced meat by hand for 2−3 min. After the second mincing step, the mixture was pressed into a standard beefburger mold. Between each formulation, the meat mincer was washed with warm water and detergent, rinsed with warm water, and then wiped dry with tissue paper. Ten burgers were made for each formulation; two out of the ten were randomly picked and placed in storage at −20 °C.

In total, 82 beefburger samples (36 authentic, 46 adulterated) were prepared. It should be noted that one of the adulterated formulations generated by the experimental design software required the incorporation of no offal, i.e., it was in fact an authentic formulation. To avoid complications in data analysis, it was removed from the data set; therefore, 36 authentic and 45 adulterated samples were studied.

Spectroscopic Measurements. Before spectroscopic analysis, frozen beefburgers were removed from −20 °C storage and allowed to thaw at room temperature for ∼16 h. Each frozen-then-thawed sample was homogenized using a Robot Coupe R301 ultra (Vincennes, France) for 1 min and transferred into a sterile plastic container. The Robot Coupe mincing bowl was washed with detergent, rinsed with tap water, and wiped dry after each sample.

Raman spectra were collected on a DXR SmartRaman spectrometer (ThermoFisher Scientific UK Ltd., Loughborough, UK) equipped with a diode laser operating at 780 nm to minimize sample fluorescence issues and a charge coupled device (CCD) detector operating at −50 °C. For analysis, approximately 10 g of homogenized beefburger was wrapped in PVC clingfilm to form a ball. A smooth side of the wrapped sample was then placed over the aperture of the universal platform sampling (UPS) accessory. All spectra of each sample were accumulated for 3 min (i.e., 15 s exposure time × 20 exposures) using a 100 mW laser power setting. Samples were scanned in random order at ambient temperature (∼20 °C). Raman intensity counts per second (cps) were recorded over the wavelength range 250−3380 cm^{-1} at 2 cm^{-1} intervals). Cosmic spikes were removed automatically by supplied software, while fluorescence correction of spectra was performed using a fifth-order polynomial. Instrument control, spectral acquisition, and file conversion were performed using supplied OMNIC software (v 9.2.98; Thermo Fisher Scientific Inc., USA). Each sample was scanned three times, once each at three different scan sites on the sample ball; the mean of these replicate spectra was used in subsequent chemometric operations.

Chemometric Operations. *Data Pretreatments.* Spectra were exported from OMNIC software as JCAMP.DX files and imported directly into The Unscrambler software (version 9.7; Camo,

DOI: 10.1021/jf5041959
J. Agric. Food Chem. 2015, 63, 1433−1441

Table 1. Adulterated Beefburger Formulations Generated by D-Optimal Experimental Design

sample	% meat	% fat	% water	% rusk	% heart	% liver	% kidney	% lung
1	0	25	10	5	20	20	20	0
2	32.5	12.5	15	0	20	0	0	20
3	30	0	15	5	0	20	20	10
4	75	0	0	5	0	0	20	0
5	75	25	0	0	0	0	0	0
6	20	25	0	5	0	10	20	20
7	47.5	12.5	0	0	0	0	20	20
8	60	0	0	0	0	20	0	20
9	42.5	25	7.5	5	0	0	0	20
10	20	25	15	0	0	20	0	20
11	0	5	15	0	20	20	20	20
12	22.5	12.5	0	5	0	20	20	20
13	55	0	15	0	10	0	20	0
14	65	0	0	5	0	0	10	20
15	17.5	25	15	2.5	20	0	20	0
16	60	0	0	0	20	20	0	0
17	30	25	15	0	20	10	0	0
18	60	0	0	0	20	0	0	20
19	10	10	15	5	20	0	20	20
20	45.5	10.4	6.4	0	9.4	9.4	9.4	9.5
21	45.5	10.4	6.4	0	9.4	9.4	9.4	9.5
22	52.5	25	0	2.5	0	20	0	0
23	0	25	15	0	0	20	20	20
24	25	0	0	5	20	20	20	10
25	37.5	0	0	2.5	20	0	20	20
26	30	0	15	5	20	20	10	0
27	60	0	0	0	0	20	20	0
28	55	0	15	0	10	0	20	0
29	50	0	15	5	20	0	0	10
30	75	0	2.5	2.5	20	0	0	0
31	30	0	15	5	0	20	20	10
32	60	0	0	0	20	0	20	0
33	40	25	0	5	20	0	10	0
34	20	25	15	0	0	20	20	0
35	30	0	15	5	10	20	0	20
36	30	0	15	5	10	20	0	20
37	0	25	15	5	20	20	0	15
38	45	25	15	5	0	10	0	0
39	37.5	25	15	2.5	0	0	20	0
40	65	0	15	0	0	20	0	0
41	0	25	15	0	20	0	20	20
42	65	0	15	0	0	0	0	20
43	20	25	0	5	20	10	0	20
44	40	25	0	5	20	0	10	0
45	0	20	0	0	20	20	20	20
46	52.5	0	7.5	0	0	0	20	20

Trondheim, Norway), which was used for all preprocessing and chemometric analyses. Spectral data in the fingerprint range 900−1800 cm^{-1} (which is rich in information on water, protein, fat, and glycogen species in meat matrices[22]) were used in all chemometric operations; they were used either without modification (raw) or after preprocessing by normalization to unit vector length (u.v.nor) or Savitzky−Golay derivatisation (note: first derivatives with 5, 9, or 13 points, second derivatives with 5, 9, 13, or 17 points were employed for the trials; eventually first derivatives with 9 points and second derivative with 17 points were selected for use in this study due to their better performances than the others). Additionally, models were developed after both a baseline correction (Savitzky−Golay derivatives) and subsequent normalization step in that order as previously recommended for quantitative Raman applications.[30] These pretreatments have the potential to remove undesirable systematic variation in the data and thus facilitate the development of classification models with best performance; moreover, Savitzky−Golay derivatives can reveal otherwise hidden structure in the spectral data which may make it easier to uncover the chemical basis of the observed signals.

Principal Component Analysis (PCA). Principal component analysis (PCA) of the raw spectral data was used to compress the Raman spectral data via orthogonal constructions. In this study, PCA was used to visually examine the distribution of frozen-then-thawed authentic and offal-adulterated beefburgers in PC space to (i) detect any relevant sample clustering and (ii) identify any unusual or outlying samples.[31]

Partial Least-Squares-Discriminant Analysis (PLS-DA) Models. To discriminate between authentic and offal-adulterated beefburgers, PLS-DA calibration models were developed and evaluated on separate calibration and validation sample sets. Each such set represented approximately 50% of the total sample numbers. In the case of adulterated samples, odd-numbered samples were selected as calibration samples while the remainder were used for validation. In the case of authentic samples, both examples of half of the formulated beefburgers were used for calibration development and the other 50% used in validation. This was to avoid overoptimistic model statistics which would likely arise if one example of each formulation were to be used in calibration and the other in validation. Calibration models were developed using full, i.e., leave-one-out cross-validation; optimum model complexity was determined using the first local minimum in PLS residual variance plots. For PLS-DA models, a dummy *Y*-value was given to each sample, viz. 0 for adulterated samples and 1 for authentic samples. During validation, samples with a predicted value ≥ 0.5 were identified as authentic while those with a value <0.5 were identified as adulterated. Model performance was evaluated on the basis of correct classification rates.

Soft Independent Modeling of Class Analogy (SIMCA) Models. In a class-modeling approach, SIMCA models of authentic beefburgers were developed using 50% of the authentic samples as described above; model performance was estimated using all remaining samples, i.e., the remaining 50% of the authentic samples plus all of the adulterated material. A 5% significance value was utilized for membership determination. The characteristic limitation of SIMCA relates to the fact that principal components are calculated on the basis of variability in spectroscopic measurements alone and individual PCs may not be clearly related to chemical data of specific relevance in any class model. Principal components describe decreasing amounts of variability in spectral data, and the calculated components may not be directly linked to membership of any given class. In contrast, PLS regression involves *Y*-values in the calculation of PLS factors and therefore includes a targeted contribution to PLS scores from *Y*. In an attempt to improve SIMCA modeling, therefore, PLS scores were input to the SIMCA modeling process in a separate exercise. Model performances were evaluated on the basis of sensitivity, specificity, and efficiency. Sensitivity is defined as the fraction of samples belonging to the modeled class which is correctly accepted by the respective model; specificity is that fraction of samples not belonging to the modeled class that is correctly rejected by the model.[32] Efficiency summarizes the sensitivity and specificity of model performance by calculating the geometric mean of their values. Index values of efficiency vary between 0 and 1.[32] In our case, sensitivity was described as the fraction of authentic samples correctly identified by the authentic beefburger model; specificity was the fraction of adulterated samples correctly rejected by the same model; efficiency was calculated as

$$\text{Efficiency} = (\text{Sensitivity} \times \text{Specificity})^{0.5} \quad (1)$$

Partial Least-Squares Regression (PLSR) Models. To quantify offal and added fat adulteration in adulterated beefburgers, PLSR linear models were developed. In the case of offal, *Y*-values were ascribed to each sample according to the total quantity (%w/w) of offal (i.e., heart + liver + kidney + lung) in each formulation. PLS regression models were also developed to quantify added fat in all samples. Half of the

DOI: 10.1021/jf5041959
J. Agric. Food Chem. 2015, 63, 1433−1441

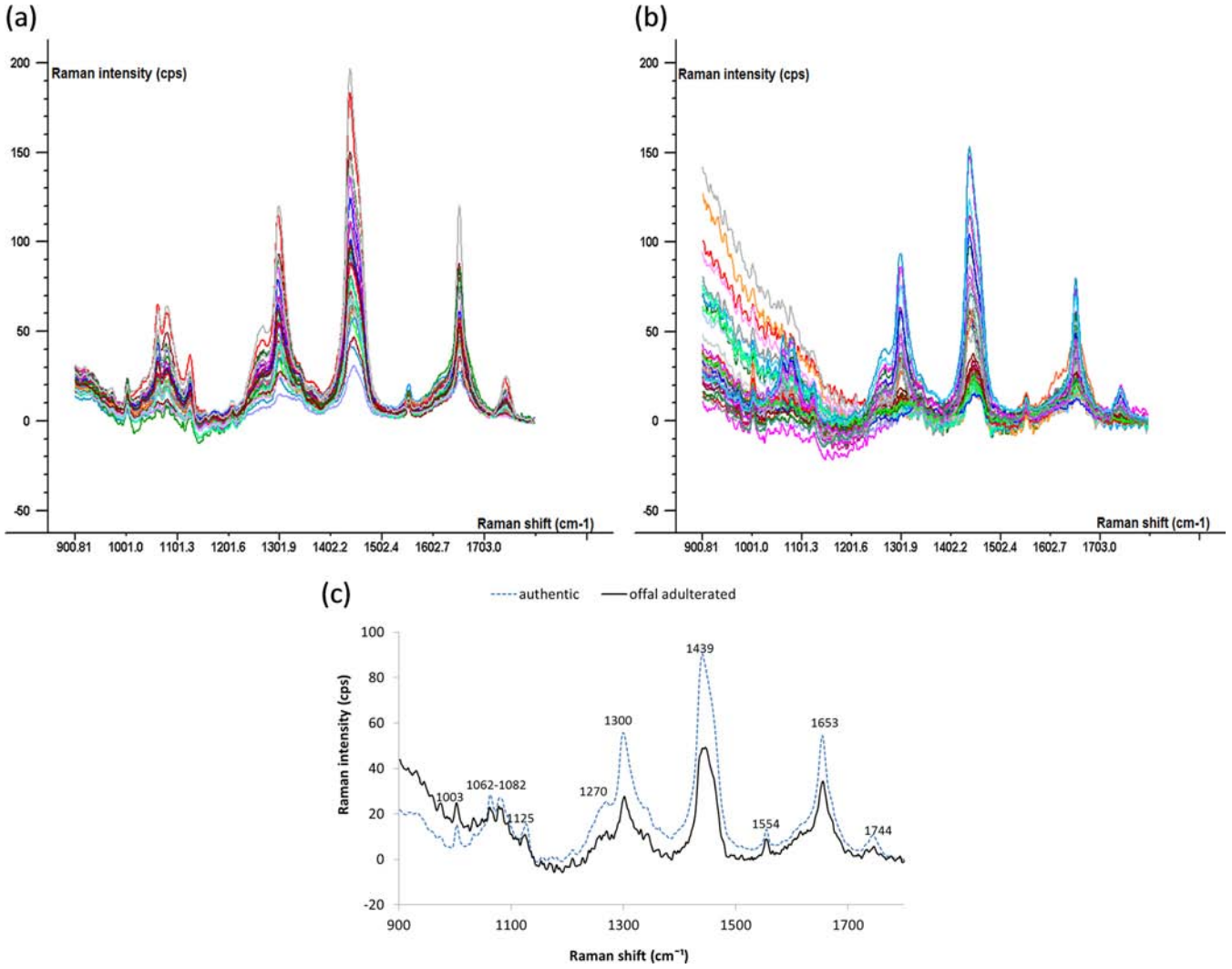

Figure 1. Spectra of (a) authentic beefburgers, (b) adulterated beefburgers, and (c) average spectra of authentic and adulterated beefburgers.

samples were randomly selected as the calibration data set to develop PLS models; the other half was used as the validation data set.

Model performances were evaluated by the correlation coefficients and root-mean-square errors in the calibration (i.e., R^2CV, RMSECV) and the validation (i.e., R^2P, RMSEP) exercises with the bias value calculated. In this case, these values were calculated based on the reference and predicted values of offal or added fat adulteration in beefburger samples. R^2, RMSE, and bias were calculated as follows:

$$R^2 = 1 - \frac{\sum_{i=1}^{n} (\hat{y}_i - y_i)^2}{\sum_{i=1}^{n} (\hat{y}_i - \bar{y})^2} \quad (2)$$

$$\text{RMSE} = \left(\frac{\sum_{i=1}^{n} (y_i - \hat{y}_i)^2}{n} \right)^{0.5} \quad (3)$$

$$\text{Bias} = \frac{\sum_{i=1}^{n} y_i - \hat{y}_i}{n} \quad (4)$$

Where $\hat{y}_i$ and y_i are the predicted and reference values of one sample (i); $\bar{y}$ is the mean of the reference values of all the samples. The value of R^2 is expected to be close to 1 while values of RMSE and bias are expected to be close to 0. A value of R^2 above 0.82 indicates good or excellent performance of a model while a value of R^2 below 0.81 reveals imprecise performance of model.[31]

RESULTS AND DISCUSSION

Raman Spectral Data. Raman spectra (900−1800 cm^{-1}) of frozen-then-thawed authentic and offal-adulterated samples are shown in Figure 1a,b. The major features of these two sets of spectra occur at the same or similar peak positions, although there is an obviously larger and more variable Raman intensity spread over the 900−1231 cm^{-1} range in offal-adulterated samples than is the case for authentic material. Average raw Raman spectra acquired from authentic and offal-adulterated beefburger samples are shown in Figure 1c. Spectra in this wavelength range provide information on some of the main biochemical components of beefburgers; peaks at 1645−1685 and 1200−1350 cm^{-1} have been related to the secondary and tertiary structure of proteins, i.e., amide I and amide III bands, respectively. The peak at 1653 nm is probably due to α-helical structures, while those at 1270 and 1300 cm^{-1} have been attributed to $\alpha_{globular}$- and $\alpha_{fibrous}$-helix formations.[20] Phenylalanine is a strong absorber at 1003 cm^{-1}, tryptophan shows a specific peak at 1554 cm^{-1}, and the peak at 1439 cm^{-1} has been attributed to a CH_2 scissoring vibration in proteins.[20] Bands in the 1062−1082 cm^{-1} region have been reported as originating in the C−O stretching of aspartic and glutamic acids.[25,33] It should be noted, however, that Raman spectral peaks at some of these wavenumbers (i.e., 1744, 1653, 1439, 1300, 1270,

DOI: 10.1021/jf5041959
J. Agric. Food Chem. 2015, 63, 1433−1441

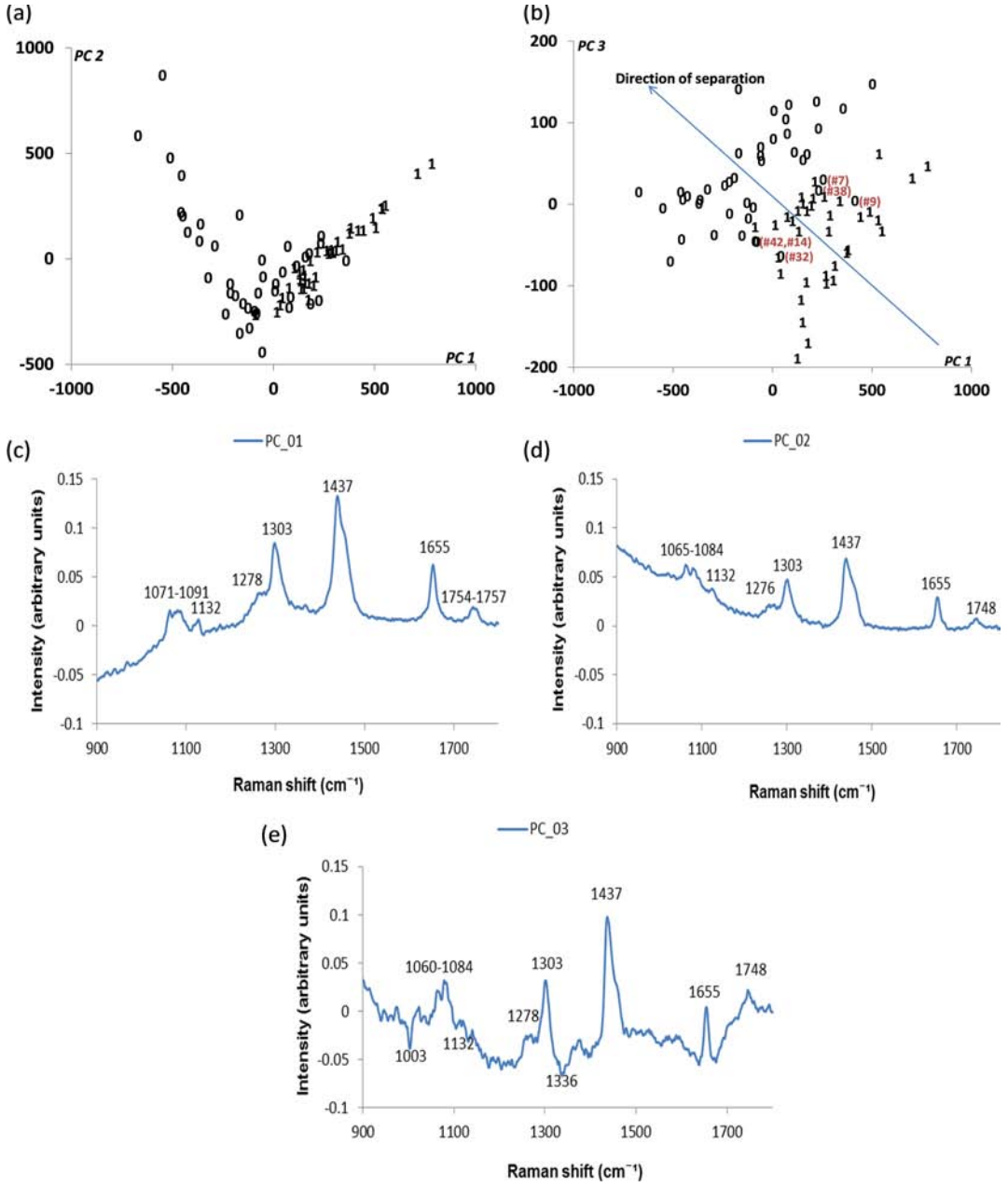

Figure 2. PCA score plots of all beefburger samples (a) PC1 vs PC2, (b) PC1 vs PC3, loading plots of all beefburger samples, (c) PC1, (d) PC2, and (e) PC3 (# = number of adulterated beefburger formulation in Table 1).

1125, and 920 cm^{-1}) have also been assigned to the C═O, C═C stretching bonds, CH_2 scissoring or twisting bonds, and C−H in-plane deformation bonds of aliphatic chains in lipids.[25,34] Thus, the main spectral features can be explained by the major beefburger components, although it is not possible to be prescriptive about actual band assignments given that many species absorb at the same or similar wavenumber locations. Indeed, given the relative range of protein and added fat contents in the formulations used, lipid may arguably be expected to contribute more variation to the spectral collection than protein.

Principal Component Analysis (PCA). Following PCA, three offal-adulterated samples were recognized as potential outliers. Close examination of their spectra revealed them to be faulty; the problem may have arisen from saturation of the CCD detector which occurred during spectral collection but, on the basis of the spectra, their removal was felt justified.

PCs 1−3 described 61%, 34%, and 3%, respectively, of variance in the frozen-then-thawed beefburger spectral data set. PCA score plots (i.e., PC1 vs PC2, PC1 vs PC3) for authentic and offal-adulterated spectra are shown in Figure 2a,b. In these figures, there is no clear separation visible between authentic (labeled as 1) and offal-adulterated (labeled as 0) samples but two discernible although overlapping, extended clusters can be identified. PC1 contributes significantly to the partial separation of the two sample groups which is visible (Figure 2a), while PC2 appears to describe variation within each sample group, especially in the case of the adulterated samples. In Figure 2b, group separation is almost complete along a direction from bottom right to top left of the plot. It is also notable that the samples adulterated at low level were located close to authentic

DOI: 10.1021/jf5041959
J. Agric. Food Chem. 2015, 63, 1433−1441

Table 2. Summary of PLS-DA Classification Model Results (900−1800 cm^{-1})

		% correct classification of calibration sample set		% correct classification of validation sample set	
data pretreatment	no. of PLS loadings	authentic	adulterated	authentic	adulterated
none	3	89 (16/18)	95 (20/21)	100 (18/18)	90 (19/21)
u.v.nor[a]	**3**	**100 (18/18)**	**100 (21/21)**	**100 (18/18)**	**90 (19/21)**
1der.9 Savitzky-Golay	4	94 (17/18)	100 (21/21)	94 (17/18)	86 (18/21)
2der.17 Savitzky-Golay	4	94 (17/18)	90 (19/21)	94 (17/18)	90 (19/21)
1der.9 plus u.v.nor	5	100 (18/18)	90 (19/21)	100 (18/18)	81 (17/21)
2der.17 plus u.v.nor	5	100 (18/18)	90 (19/21)	100 (18/18)	81 (17/21)

[a]Unit vector normalization.

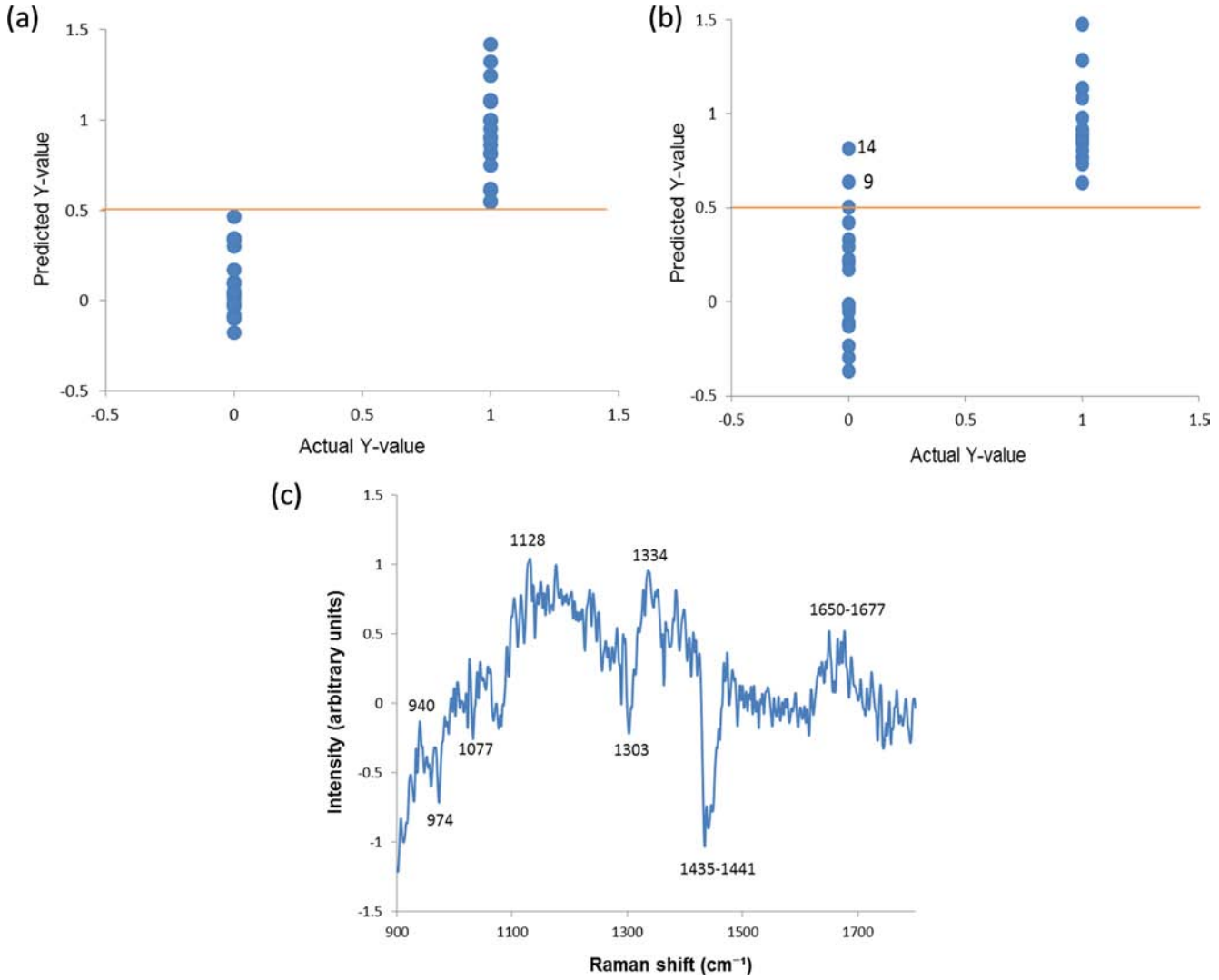

Figure 3. Best PLS-DA model result: (a) predicted *Y*-values in calibration samples, (b) predicted *Y*-values in validation samples, (c) regression vectors for PLS-DA model (3 loadings) (note: all input spectra were normalized on unit vectors).

samples; moreover, six adulterated samples (i.e., nos. 9, 38, 7, 32, 42, and 14) were located at the edge of the adulterated sample (label 0) cluster, merging into the authentic sample (label 1) cluster (Figure 2b). These six adulterated samples all contained a high content of total lean beef and beef fat. Three samples (nos. 9, 38, and 7) individually contained 67.5%, 70%, and 60% total lean beef and beef fat with 20%, 10%, and 40% offal, respectively. The other three samples (nos. 32, 42, and 14) separately contained a high level of lean beef (i.e., 60%, 65%, and 65%) without beef fat but adulterated with 40%, 20%, and 30% offal (Table 1).

Loading plots of PCs 1−3 (Figure 2c−e) show major intensity maxima at similar wavelengths. Maxima at 1303, 1437, 1655, and 1748 cm^{-1} are indicative of lipid contents; other features are located in spectral regions generally related to protein, i.e., 1000−1360 and 1645−1685 cm^{-1}.[25,34] In the plot of PC1 (Figure 2c), the main features mirror those in the mean spectra of beefburgers shown in Figure 1c, although certain features in the original mean spectra are absent, i.e., small peaks at 1554 and 1003 cm^{-1}, and the relative heights of peaks have changed. The plot of PC2 (Figure 2d) shows a general decline in intensity from 900 to 1360 cm^{-1} but reveals maxima at

DOI: 10.1021/jf5041959
J. Agric. Food Chem. 2015, 63, 1433−1441

wavelengths ascribed to lipid structures (1132, 1276, 1303, and 1437 cm^{-1}) with a small contribution from protein at 1655 cm^{-1}. Interestingly, two small maxima at 1065−1084 cm^{-1}, previously noted as originating in aspartic and glutamic acids, are quite obvious. PC 1 and 2 loadings are responsible for locating authentic and adulterated sample clusters in this two-dimensional space; PC2 plays a role in extending the adulterated sample pattern in a different direction from that of the authentic material. Regarding the PC3 loading, some minima appear at 1003, 1336, and 1645−1685 cm^{-1}, which are related to some specific protein structures and separate to some degree the adulterated samples from the authentic. Absorbance by lipid structures is also important in this PC.

PLS Discriminant Analysis (PLS-DA). PLS discriminant models were assessed on the basis of the percentage correct classification of both calibration and validation sample sets; a summary of their performance is shown in Table 2. Results reveal that models required between 3 and 5 loadings; in the calibration sample set, 89−100% of authentic and 90−100% of offal-adulterated beefburgers were correctly classified by the various models. For the validation sample set, the percentage correct classification of authentic samples remained within the range 94−100% but that of adulterated samples decreased to 81−90%. The most accurate classification model was based on data pretreated only by normalization on unit vectors. In this case, all authentic and offal-adulterated samples in the calibration set were predicted correctly; in prediction, all (n = 18) authentic samples and 19 out of 21 (90%) adulterated samples were correctly identified.

PLS scores for this model are shown in Figure 3a,b. In Figure 3b, two adulterated samples (formulations no. 9 and 14 of Table 1) were misclassified. Sample no. 9 contained 42.5% lean beef, 25% beef fat, 7.5% water, 5% rusk, and 20% lung; number 14 contained 65% lean beef, 5% rusk, 10% kidney, and 20% lung. These two samples both contained 20% lung and 65−67.5% beef and beef fat combined. However, these similarities cannot explain the misclassification because other similar formulations have been correctly classified (e.g., no. 42 of Table 1). A regression coefficient plot of the model is shown in Figure 3c. Interpretation of regression plots is difficult and potentially misleading, but it seems that certain features in Figure 3c can be attributed to protein (940, 974, 1077, and 1128 cm^{-1}) and lipid (1303, 1334, 1435−1441, and 1650−1677 cm^{-1}) components.[25,34]

It is interesting that models developed using two pretreatments (baseline correction followed by normalization) were not overall the most accurate; while identification of authentic samples in both calibration and validation had 100% accuracy, classification of the adulterated samples proved more problematic than when a normalization step alone was used. This is despite the fact that one of the most significant sources of systematic error in Raman spectra arises from total intensity variations. In a previous report,[30] the use of such a two-step pretreatment emerged as most successful in the prediction of a specific constituent, i.e., carotenoid in salmon meat. The lack of success of this procedure in our hands may be evidence of the problem specific nature of quantitative solutions using Raman spectra.

SIMCA Modeling. Results of SIMCA modeling (Table 3) based on PCA scores of spectral variables show that models developed using raw and pretreated data exhibited high sensitivity (0.95−1) but lower specificity (0.64−0.89); efficiency values of 0.80−0.94 were recorded. The best model, i.e., that with the highest efficiency value, involved data pretreated by normalization on unit vectors, required five principal components, and produced values of sensitivity, specificity, and efficiency of 1, 0.89, and 0.94, respectively. These results indicated that SIMCA modeling was able to accurately identify authentic beefburgers (i.e., sensitivity value of 1) but did not identify offal-adulterated beefburgers with complete accuracy (i.e., specificity value <1), resulting in some false positive classifications (n = 5).

Table 3. Summary of PCA and PLS Scores-Based SIMCA Model Results (900−1800 cm^{-1}) on Beefburger Validation Sample Set

			model performance		
scores source	data pretreatment	factors[a] used	sensitivity	specificity	efficiency
PCA	none	4	1	0.84	0.92
	u.v.nor[b]	**5**	**1**	**0.89**	**0.94**
	1der.9 plus u.v.nor	4	0.95	0.67	0.80
	2der.17 plus u.v.nor	4	1	0.64	0.80
PLS	none	3	0.94	0.82	0.88
	u.v.nor	4	0.94	0.95	0.95
	1der.9 plus u.v.nor	3	1	0.81	0.90
	2der.17 plus u.v.nor	**2**	**0.94**	**1**	**0.97**

[a]Principal components or PLS loadings. [b]Unit vector normalization pretreatment.

In an attempt to improve on these results, SIMCA models were also developed using PLS scores extracted from the first 20 PLS loadings of the PLS-DA models derived using the appropriate data pretreatments. SIMCA models based on PLS scores contain information relating to both spectral variables (X-values) and the memberships of specific sample categories (Y-values). Compared to SIMCA models using PCA scores, performance of those based on PLS scores (Table 3) revealed slight improvements regarding specificity (0.81−1.0) and efficiency (0.88−0.97). In the particular case of models using normalization on unit vector pretreated data, specificity values increased from 0.89 to 0.95 although this was accompanied by a drop (from 1 to 0.94) in sensitivity. Efficiency increased marginally from 0.94 to 0.95; 17 of 18 authentic samples and 40 of 42 adulterated samples were identified correctly. The misclassified samples included one sample in the lower quality range of authentic beefburgers and formulations 9, 38, and 44 of the adulterated beefburgers. In Table 3, models based on PCA scores required the involvement of four or five principal components; in the case of models developed using PLS scores, the corresponding number was between 2 and 4 PLS loadings. In general, the use of different data pretreatments or none had only a minor effect on model sensitivity values; in the case of specificity, however, between-model variations were much larger, thus justifying exploration of pretreatment options. SIMCA modeling may therefore play a useful role in quality control of industrial authentic beefburger production based on the formulations used in this work. To improve classification accuracy further, SIMCA models developed using PLS scores could be applied to test samples in parallel to PLS-DA models. Using such an approach, samples identified as adulterated by both types of models may be accepted as offal-adulterated samples with greater confidence than if only one model or the

DOI: 10.1021/jf5041959
J. Agric. Food Chem. 2015, 63, 1433−1441

Table 4. Summary of PLS Quantitative Models (900−1800 cm^{-1}) for (A) Prediction of Total Offal and (B) Added Fat Content in Both Calibration and Validation Sets of Beefburger Samples

data pretreatment	no. of loadings	R^2CV[b]	RMSECV[c]	R^2P[d]	RMSEP[e]	bias
(A) Offal Adulteration						
none	1	0.27	14.8	0.16	14.0	−2.04
u.v.nor[a]	3	0.35	13.9	0.17	15.3	−4.63
1der.9	3	0.49	12.4	0.29	15.0	−5.51
2der.17	3	0.39	13.6	0.31	13.9	−4.12
1der.9+u.v.nor	2	0.52	12.0	0.27	13.7	−4.47
2der.17+u.v.nor	2	0.43	13.1	0.18	14.3	−4.03
(B) Added Fat						
none	5	0.76	5.27	0.47	7.21	0.94
u.v.nor[a]	4	0.84	4.25	0.7	5.39	1.28
1der.9	2	0.73	5.56	0.68	5.59	−0.22
2der.17	3	0.71	5.78	0.63	6.06	−0.06
1der.9+u.v.nor	**2**	**0.85**	**4.18**	**0.85**	**3.80**	**0.39**
2der.17+u.v. nor	2	0.82	4.56	0.82	4.16	0.13

[a]unit vector normalization. [b]coefficient of determination in cross-validation. [c]root-mean-square error of cross-validation. [d]coefficient of determination in prediction. [e]root-mean-square error of prediction.

other was used. However, it should be noted that in this work, formulation no. 9 (Table 1) was incorrectly identified by each model.

PLS Quantitation. Table 4A shows that performance of PLS quantitative calibration models for total offal adulteration was poor; R^2CV values at only 0.27−0.52 were very low, while RMSECV values were relatively high. In prediction, correlations between reference and predicted values were similarly low and accompanied by quite large bias values; therefore, none of these models was suitable for practical application. Possible reasons for modeling failure involve the chemical complexity of the matrix studied, the likely spectral similarity of offal and lean meat, and other effects including structural changes in macromolecular moieties after the freezing and thawing procedure.

A performance summary of PLS models for predicting added fat in all samples is shown in Table 4B. R^2CV values (0.71−0.85) of the calibration data set were generally higher than their validation set counterparts (R^2P; 0.47−0.85); root-mean-square errors of the calibration and validation data sets were 4.2−5.8 (RMSECV) and 3.8−7.2 (RMSEP), respectively. Calibration statistics indicated that the best model was based on data pretreated by a combination of first derivative and subsequent normalization on unit vectors using 2 PLS loadings with values for R^2CV, RMSECV, R^2P, and RMSEP of 0.85, 4.2, 0.85, and 3.8, respectively; however, the model exhibited a bias value of 0.39. Overall prediction accuracy of models for added fat prediction will be compromised by the inclusion of errors arising from the intramuscular fat content of the lean beef that was used in beefburger production because this was a variable and unaccounted for quantity.

In this feasibility study, Raman spectroscopy was studied to (a) discriminate between authentic and offal-adulterated beefburgers in the frozen-then-thawed state and (b) to quantify total offal and added fat contents of these samples. Classification (PLS-DA), class-modeling (SIMCA), and quantitative models (PLS1) have been developed separately on Raman spectra of frozen-then-thawed beefburgers. Results showed that (1) using PLSDA models for offal-adulterated beefburgers, correct predictions of 90−100% of calibration samples and 81−90% of validation samples was achieved; for authentic beefburgers, 94−100% of both calibration and validation samples were predicted correctly; (2) in the case of the SIMCA class-modeling approach, sensitivity values (1.0) of models based on PCA scores were generally slightly higher than those (0.94) of models based on PLS scores; conversely, specificity values (0.81−1.0) for models based on PLS scores were much higher than those (0.64−0.89) of models based on PCA scores; (3) prediction of offal content proved not to be possible, as might be expected given the unlikely possession of a unique spectral signal by this material; (4) performance of quantitative models for added fat prediction was not satisfactory. Compared with previous work of this research team using infrared (i.e., near-infrared (NIR) and Fourier transform mid-infrared (FT-IR)) spectroscopy on frozen-then-thawed offal adulterated beefburgers,[18,19] the correct classification rate of PLS-DA models for adulterated samples (based on the same validation sample group) ranged from 74−91% (NIR), 73−100% (FT-IR), and 81−100% (Raman); the efficiency of SIMCA models varied from 0.62−0.91(NIR), 0.81−0.94 (FT-IR) to 0.88−0.97 (Raman). It therefore seems, on the basis of this specific set of samples at any rate, that Raman spectroscopy may provide higher levels of classification accuracy than either of the two infrared spectral ranges.

In conclusion, the potential of Raman spectroscopy in the analysis of formulated meat products has been examined in this work. Using Raman spectroscopy to study a complex meat formulation has shown some misclassification and quantification errors. One potential strategy to minimize sample misclassification would be the use of multispectroscopic methods (e.g., near-infrared, mid-infrared)[18,19] combined with Raman spectroscopy because these spectra contain complementary information. In future work, the focus will be on such a strategy to improve quantification and qualification outcomes in this adulteration problem.

AUTHOR INFORMATION

Corresponding Author

*Phone: +353(0)18059752. Fax: +353(0)18059550. E-mail: ming.zhao@teagasc.ie.

Notes

The authors declare no competing financial interest.

DOI: 10.1021/jf5041959
J. Agric. Food Chem. 2015, 63, 1433−1441

■ ACKNOWLEDGMENTS

We are grateful to the Food Safety Authority of Ireland for funding for this work; opinions expressed in this paper are those of the authors solely. We thank Derek Keenan, Eugene Vesey, and Astrid Malechaux for skilled technical assistance. Ming Zhao is a Teagasc Walsh Fellow.

■ REFERENCES

(1) McElhinney, J.; Downey, G.; Fearn, T. Chemometric processing of visible and near infrared spectra for species identification in selected raw homogenised meats. *J. Near Infrared Spectrosc.* **1999**, *7*, 145−154.
(2) Ballin, N. Z. Authentication of meat and meat products. *Meat Sci.* **2010**, *86*, 577−587.
(3) Downey, G. Non-invasive and non-destructive percutaneous analysis of farmed salmon flesh by near infra-red spectroscopy. *Food Chem.* **1996**, *55*, 305−311.
(4) *Labelling and Composition of Meat Products*; European Food Standards Agency (EFSA), 2003; http://tna.europarchive.org/20110615133801/http://www.food.gov.uk/multimedia/pdfs/meatguidance.pdf.
(5) Macedo-Silva, A.; Shimokomaki, M.; Vaz, A. J.; Yamamoto, Y. Y.; Tenuta-Filho, A. Textured soy protein quantification in commercial hamburger. *J. Food Compos. Anal.* **2001**, *14*, 469−478.
(6) Flores-Munguia, M. E.; Bermudez-Almada, M. C.; Vázquez-Moreno, L. A research note: detection of adulteration in processed traditional meat products. *J. Muscle Foods* **2000**, *11*, 319−325.
(7) Hsieh, Y. H. P.; Woodward, B. B.; Ho, S. H. Detection of species substitution in raw and cooked meats using immunoassays. *J. Food Prot.* **1995**, *58*, 555−559.
(8) Ayaz, Y.; Ayaz, N. D.; Erol, I. Detection of species in meat and meat products using enzyme-linked immunosorbent assay. *J. Muscle Foods* **2006**, *17*, 214−220.
(9) Gremaud, G.; Karlen, S.; Hulliger, K. Analytical methods for the authentication of meat and meat products: recent developments. *Mitt Geb Lebensmittelunters Hyg.* **2002**, *93*, 481−502.
(10) Reuters, 2013; http://www.theguardian.com/uk/2013/may/10/horsemeat-scandal-timeline-investigation (accessed 2013).
(11) McCarthy, M.; Barton, J. *Beef Consumption, Risk Perception and Consumer Demand for Traceability along the Beef Chain*; Agribusiness Discussion Paper No. 21; Department of Food Economics, University College Cork: Cork, Ireland, 1998.
(12) Al-Jowder, O.; Defernez, M.; Kemsley, E. K.; Wilson, R. H. Mid-Infrared spectroscopy and chemometrics for the authentication of meat products. *J. Agric. Food Chem.* **1999**, *47*, 3210−3218.
(13) McElhinney, J.; Downey, G.; O'Donnell, C. Quantitation of lamb content in mixtures with raw minced beef using visible, near and mid-Infrared spectroscopy. *J. Food Sci.* **1999**, *64*, 587−591.
(14) Ding, H. B.; Xu, R. J. Near-infrared spectroscopic technique for detection of beef hamburger adulteration. *J. Agric. Food Chem.* **2000**, *48*, 2193−2198.
(15) Prieto, N.; Roehe, R.; Lavín, P.; Batten, G.; Andrés, S. Application of near infrared reflectance spectroscopy to predict meat and meat products quality: a review. *Meat Sci.* **2009**, *83*, 175−186.
(16) Meza-Márquez, O. G.; Gallardo-Velázquez, T.; Osorio-Revilla, G. Application of mid-infrared spectroscopy with multivariate analysis and soft independent modeling of class analogies (SIMCA) for the detection of adulterants in minced beef. *Meat Sci.* **2010**, *86*, 511−519.
(17) Morsy, N.; Sun, D.-W. Robust linear and nonlinear models of NIR spectroscopy for detection and quantification of adulterants in fresh and frozen-thawed minced beef. *Meat Sci.* **2013**, *93*, 292−302.
(18) Zhao, M.; O'Donnell, C. P.; Downey, G. Detection of offal adulteration in beefburgers using near infrared reflectance spectroscopy and multivariate modelling. *J. Near Infrared Spectrosc.* **2013**, *21*, 237−248.
(19) Zhao, M.; Downey, G.; O'Donnell, C. P. Detection of adulteration in fresh and frozen beefburger products by beef offal using mid-infrared ATR spectroscopy and multivariate data analysis. *Meat Sci.* **2014**, *96*, 1003−1011.
(20) Beattie, R. J.; Bell, S. J.; Farmer, L. J.; Moss, B. W.; Patterson, D. Preliminary investigation of the application of Raman spectroscopy to the prediction of the sensory quality of beef silverside. *Meat Sci.* **2004**, *66*, 903−913.
(21) Olsen, E. F.; Rukke, E.-O.; Flåtten, A.; Isaksson, T. Quantitative determination of saturated-, monounsaturated- and polyunsaturated fatty acids in pork adipose tissue with non-destructive Raman spectroscopy. *Meat Sci.* **2007**, *76*, 628−634.
(22) Pedersen, D. K.; Morel, S.; Andersen, H. J.; Bolling Engelsen, S. Early prediction of water-holding capacity in meat by multivariate vibrational spectroscopy. *Meat Sci.* **2003**, *65*, 581−592.
(23) Tuma, R. Raman spectroscopy of proteins: from peptides to large assemblies. *J. Raman Spectrosc.* **2005**, *36*, 307−319.
(24) Sikorski, Z. E.; Kolakowska, A. Changes in proteins in frozen stored fish. In *Seafood Proteins*; Sikorski, Z. E., Sun Pan, B., Shahidi, R., Eds.; Chapman and Hall: New York, 1994; pp 99−231.
(25) Li-Chan, E. C. Y. The applications of Raman spectroscopy in food science. *Trends Food Sci. Technol.* **1996**, *7*, 361−370.
(26) Argyri, A. A.; Jarvis, R. M.; Wedge, D.; Xu, Y.; Panagou, E. Z.; Goodacre, R.; Nychas, G.-J. E. A comparison of Raman and FT-IR spectroscopy for the prediction of meat spoilage. *Food Control* **2013**, *29*, 461−470.
(27) Beattie, J. R.; Bell, S. J.; Borggaard, C.; Fearon, A.; Moss, B. Classification of adipose tissue species using Raman spectroscopy. *Lipids* **2007**, *42*, 679−685.
(28) Ellis, D. I.; Broadhurst, D.; Clarke, S. J.; Goodacre, R. Rapid identification of closely related muscle foods by vibrational spectroscopy and machine learning. *Analyst* **2005**, *130*, 1648−1654.
(29) Zając, A.; Hanuza, J.; Dymińska, L. Raman spectroscopy in determination of horse meat content in the mixture with other meats. *Food Chem.* **2014**, *156*, 333−338.
(30) Afseth, N. K.; Segtnan, V. H.; Wold, J. P. Raman spectra of biological samples: a study of preprocessing methods. *Appl. Spectrosc.* **2006**, *60*, 1358−1367.
(31) Williams, P. Implementation of near-infrared technology. In *near Infrared Technology in the Agriculture and Food Industries*, 2nd ed.; Williams, P., Norris, K., Eds.; American Association of Cereal Chemists: St. Paul, MN, 2001; pp 161−163.
(32) Oliveri, P.; Downey, G. Multivariate class-modelling for the verification of food authenticity claims. *Trends Anal. Chem.* **2012**, *35*, 74−86.
(33) Careche, M.; Herrero, A. M.; Rodriguez-Casado, A.; Del Mazo, M. L.; Carmona, P. Structural changes of Hake (*Merluccius merluccius* L.) fillets: effects of freezing and frozen storage. *J. Agric. Food Chem.* **1999**, *47*, 952−959.
(34) Socrates, G. *Infrared and Raman Characteristic Group Frequencies, Tables and Charts*, 3rd ed.; John Wiley & Sons Ltd.: Chichester, West Sussex, England, 2000.

■ NOTE ADDED AFTER ASAP PUBLICATION

This paper was published ASAP on January 28, 2015, with an error in equation 4. The corrected version was reposted on January 30, 2015.

DOI: 10.1021/jf5041959
J. Agric. Food Chem. 2015, 63, 1433−1441

desirable for the detailed analysis of a complex PL mixture. Off-line NPLC × RPLC/MS was first used for the study of PL molecular species. In general, the PL extract was first separated by NPLC, then each fraction was collected off-line and injected onto a RPLC column separately for further molecular species elucidation.[13,14] In order to solve the possible immiscibility problem between the mobile phases from NPLC and RPLC, a solvent-evaporating interface was used for online NPLC × RPLC/MS analysis.[15] In the lipid profiling of a biological sample, Liu et al. used a vacuum pump at the interface of the NPLC and RPLC; in this way, the mobile phase from the NPLC was evaporated; then the mobile phase from RPLC passed through the interface and transferred the fraction into the second dimension C18 column for further molecular species separation.[16] Later, HILIC was used as the first dimension LC for online 2D-LC separation of PLs.[18,25] HILIC is a versatile tool for the separation of polar compounds; in addition, the aqueous−organic (usually acetonitrile) mobile phase used during HILIC separation is miscible with the second dimension RPLC mobile phase.[17] For the analysis of a milk PL extract, 23 fractions from the first dimension HILIC column were collected and injected onto a C18 column for species separation via a 100 μL sample loop under the stop-flow mode.[18] Further improvement of the stop-flow 2D-LC method was made by using an intermediate column to trap the components eluting from the HILIC column; these components were then eluted from the trap using a makeup flow.[19]

In general, 2D-LC/MS and -MS/MS analyses have revealed a large diversity in both PL classes and molecular species within each class. However, the identification of an specific molecular species may rely on a combination of LC/MS analysis with the separate identification of the overall fatty acid profile, as determined by gas chromatography coupled to a flame ionization detector (GC-FID)[20,21] or from the literature.[18,22,23] A necessary part of the full identification of fatty acids is the specific assignment of double bond positions. In GC-FID, this can often be achieved via the retention times of fatty acid methyl ester (FAME) derivatives. In other cases, the fatty acids from hydrolysis of PLs have been converted into dimethyloxazolines (DMOX) derivatives. Under electron ionization mass spectrometry, DMOX derivatives of fatty acids undergo charge remote fragmentations, and these fragmentation patterns can reveal double bond locations.[11,24] However, in these GC/MS analyses of DMOX or FAME derivatives, the complete PL molecular structure is lost, and the derivatization procedures add additional complexity to the analysis.

Recently, we successfully coupled online 2D-LC with in-line ozonolysis-MS (O_3-MS) to allow the detailed structure determination of PC molecular species, as demonstrated for the identification of PC molecules in the PL extract from rat liver.[25] The fraction containing PC species eluted from the first dimension HILIC column at between 8.2 and 9.0 min was directly injected onto the second dimension C18 column through a 10-port 2-position switching valve. The PC molecular species, eluting from the HILIC × C18 LC separation, then passed through the ozonolysis device that was connected between the C18 column and the ESI source. The ozonolysis device is a length of gas-permeable Teflon tube that passes through a chamber filled with ozone vapor, as described in detail by our previous study.[26] The ozonolysis reaction occurred to all double bonds in the PC molecules, resulting in the formation of diagnostic ozonolysis product aldehydes that were used for the direct assignment of double bond positions in unsaturated PC species.

In this study, the online 2D-LC method is further developed in order to allow for molecular species separation within the PI and PE classes, in addition to that already described for the PC class.[25] In addition, we have also demonstrated for the first time the application of the in-line O_3-MS method to the direct assignment of double bond positions in PI, PE, SM, lyso-PE (LPE), and LPC molecules. Overall, this approach can allow the structural characterization of PL molecules, including the definitive determination of each significant molecular species, as demonstrated here for the PLs extracted from chicken egg yolk.

MATERIALS AND METHODS

Material. HPLC grade water, tetrahydrofuran (THF), chloroform, methanol, acetonitrile (ACN), and isopropanol (IPA) were purchased from Fisher Scientific Company (Ottawa, ON, Canada). HPLC grade ammonium formate and formic acid were obtained from Sigma (St. Louis, MO, USA). All of the standards PI(18:0/20:4 (*n*-6,9,12,15)), PE(18:0/20:4 (*n*-6,9,12,15)), SM(d18:1/18:1(*n*-9)) ("d" means dihydroxy base), LPE(18:1(*n*-9)), and LPC(18:1(*n*-9)) were purchased from Avanti polar lipids, Inc. (Alabaster, AL, USA). Each standard solution was prepared in methanol at a concentration of 200 μg/mL. The Teflon AF-2400 tubing (0.020″ OD, 0.010″ ID) was purchased from Biogeneral Inc. (San Diego, CA, USA).

Nomenclature. We adopted as much as possible the nomenclature and abbreviation conventions from Liebisch et al.[27] In this study, it is advantageous to locate the double bond by counting from the terminal methyl group, thus the "*n*-" terminology is used. For example, 1-octadecanoyl-2-(9*Z*,12*Z*-octadecadienoyl)-*sn*-glycero-3-phosphocholine is expressed as PC(18:0/18:2 (*n*-6,9)). If the *sn*-position of the fatty acids is not known, the separator "_" is used, for example, PC(18:0_18:2 (*n*-6,9)).

Extraction of PLs from Egg Yolk. Fresh eggs were purchased from local markets. The egg yolk was separated from the egg white, and was rolled on the filter membrane in order to completely remove the egg white. Six egg yolks were mixed well together and used for PL extraction according to a modified Bligh and Dyer method.[23] In brief, 100 mg of egg yolk was mixed with 2 mL of extraction solvent (chloroform/methanol/water, 1:2:0.8) and homogenized at 10,000 rpm for 5 min on a Polytron PT1300D homogenizer (Kinematica AG, Switzerland) and then centrifuged at 3000 rpm for 5 min. The extraction procedure was repeated three times, and all of the supernatants were combined and made up to 10 mL using methanol. The extract was further diluted 10-fold with methanol prior to analysis.

LC and MS Instrument. An Agilent 1200 series HPLC system (Agilent Technologies Inc., Palo Alto, CA, USA) coupled to a hybrid quadrupole time-of-flight mass spectrometer (QSTAR Elite, Applied Biosystems/MDS Sciex, Concord, ON, Canada) with ESI source was used for all of the LC-MS analysis. The ion source temperature was kept at 375 °C and the ionspray voltage was at 5500 V for ESI (+) and −4500 V for ESI (−). Source region nitrogen gas flows in arbitrary units assigned by the data system were as follows: curtain gas 25; auxiliary gas 10, and nebulizing gas 50. The declustering potential (DP), focus potential (FP), and DP2 were 40 V, 150 V, 10 V, and −40 V, and −150 V and −10 V for ESI (+) and ESI (−), respectively. Analyst QS 2.0 software was used for data acquisition and analysis.

HILIC × C18 LC/MS Analysis. The 2D-LC configuration was the same as that in our previous study[25] using a 10-port 2-position switching valve (Rheodyne, Rohnert Park, CA) as the interface between the HILIC column and the C18 column (see Figure S1, Supporting Information). Separation conditions were modified for the shorter analysis time. The Ascentis Express HILIC column (2.1 mm i.d. × 150 mm, 2.7 μm particles) (Sigma, St. Louis, MO) was used as the first dimension LC for PL class separation. Mobile phase A was ACN, and B was 10 mM ammonium formate in water at pH 3.0, and the flow rate was at 0.2 mL/min. The gradient was as follows: 0−10 min, from 8% to 30% B; 10.0−10.1 min, from 30% to 95% B; 10.1−

DOI: 10.1021/jf5049595
J. Agric. Food Chem. 2015, 63, 1442−1451

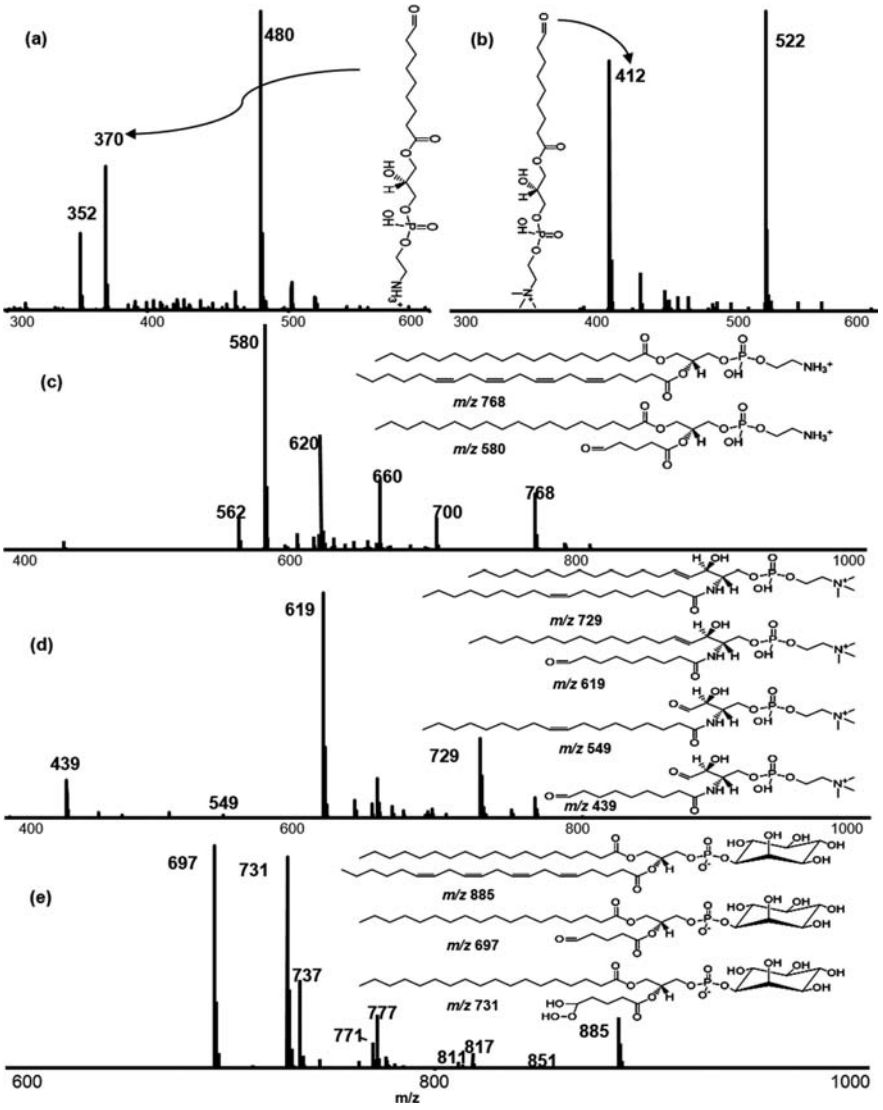

Figure 1. In-line O_3-MS spectrum of PL standard (a) LPE(18:1(*n*-9)) (+ve); (b) LPC(18:1(*n*-9)) (+ve); (c) PE(18:0/20:4 (*n*-6,9,12,15))(+ve); (d) SM(d18:1/18:1(*n*-9)) (+ve); and (e) PI(18:0/20:4 (*n*-6,9,12,15)) (−ve).

15.0 min, held at 95% B; 15.0−15.1 min, from 95% to 8% B; and 15.1−20.0 min, held at 8% B. The Ascentis Express C18 column (2.1 mm i.d. × 75 mm, 2.7 μm particles, Supelco, Bellefonte, PA USA) was used as the second dimension RPLC. The mobile phase at 0.475 mL/min was composed of THF/ACN/IPA/water with 10 mM ammonium formate at pH 3.0 (5:20:16:9, v/v/v) at 45 °C.

The injection of the eluent from the HILIC column to the C18 column was achieved by switching the valve from the A to B position and back to the A position (Figure S1, Supporting Information). For the PI class, the fraction between 4.0 and 4.8 min from the first dimension HILIC column was transferred to the second dimension C18 column and detected under ESI (−). For PE and PC, the fractions between 5.6 and 6.4 min and 8.2−9.0 min were transferred onto the C18 column and analyzed under ESI (+). In this study, LPE, LPC, and SM were analyzed by one dimension HILIC/MS instead of 2D-LC/MS, as described below.

In-line O_3-MS Analysis. The method development of the in-line O_3-MS approach for double bond position determination has been described in detail in our previous study.[26] In this study, a 20 cm length of gas permeable and liquid impermeable Teflon tube passed through a 0.5 L glass chamber filled with oxygen and ozone gas (ozone concentration 56.2 g/m^3) at room temperature. This ozonolysis device was placed in-line between 2D-LC and ESI source of the mass spectrometer for the analysis of PI, PE, and PC molecular species. For the analysis of LPE, LPC, and SM species, the ozonolysis device was coupled in-line with the HILIC column. In this way, each PL species eluting from either the second dimension C18 column or the HILIC column passed through the semipermeable tube, ozone vapor immediately reacted with carbon−carbon double bonds existing in the molecules, and the ozonolysis products would be directly detected by ESI-MS.

RESULTS AND DISCUSSION

In this study, ESI-MS, MS/MS, and in-line O_3-MS analyses were performed on PE, SM, PI, LPE, and LPC standards in order to demonstrate how these can yield similar structural information as was achieved for the analysis of PC in our previous study.[25] Then we further developed the 2D-LC and 2D-LC/O_3-MS methods for the direct identification of the PE, PI, SM, LPC, and LPE molecular species. Finally, these methods were applied to the characterization of the PL extracted from egg yolk.

ESI-MS and MS/MS Analysis of PE, SM, LPE, LPC, and PI Standards. Flow injection analysis (FIA) was performed on PI(18:0/20:4 (*n*-6,9,12,15)), PE(18:0/20:4 (*n*-6,9,12,15)), SM(d18:1/18:1(*n*-9)), LPE(18:1(*n*-9)), and LPC(18:1(*n*-9))

DOI: 10.1021/jf5049595
J. Agric. Food Chem. 2015, 63, 1442−1451

standards in positive ion mode using a mobile phase of ACN/water with 10 mM ammonium formate (85/15, v/v). The PE, SM, LPE, and LPC standards were observed as $[M + H]^+$ ions with high abundance, whereas the PI $[M + H]^+$ ion at m/z 887 appeared at very low intensity, and instead, the ion at m/z 627 generated from the neutral loss of 260 Da was the dominant ion. For PE and SM, mass measurements of the $[M + H]^+$ ions were used to deduce their elemental compositions. However, the ESI (+)-MS/MS analyses of PE and SM $[M + H]^+$ ions failed to provide fragment ions that could be used for the determination of fatty acyl chain composition. The dominant product ions in these MS/MS spectra arise due to the fragmentation of the headgroup, such as phosphocholine ions at m/z 184 for SM or the product ions from neutral loss of phosphoethanolamine (141 Da) from $[M + H]^+$ ions of PE. This has also been observed by other studies.[8,23,28]

ESI(−)/MS analysis of PE(18:0/20:4 (*n*-6,9,12,15)) resulted in $[M - H]^-$ ions at m/z 766. MS/MS analysis of the ion at m/z 766 generated carboxylate anions at m/z 283 and 303 that are characteristic of 18:0 and 20:4 fatty acyl chains (Figure S2a, Supporting Information). For SM(d18:1/18:1(*n*-9)), $[M + HCOO]^-$ ions at m/z 773 were observed, and the following MS/MS analysis of these ions (Figure S2b, Supporting Information) resulted in the demethylated molecular ion $[M - CH_3]^-$ at m/z 713 as the dominant product ions. However, fragment ions directly corresponding to the N-acyl chain did not appear in the MS/MS spectrum. Instead, the ion at m/z 449 was observed, which was formed by the neutral loss of the N-acyl chain (18:1 ketene) from the demethylated molecular ion at m/z 713. Thus, the mass difference between the ion $[M - CH_3 - R_1CO]^-$ (m/z 449 in this case) and the demethylated molecular ion $[M - CH_3]^-$ (m/z 713 in this case) can be used to assign the N-acyl chain. A similar fragmentation pattern to the SM $[M + HCOO]^-$ ion was also observed by another study and used for molecular species assignment of SM.[9]

In contrast to the weak $[M + H]^+$ ions seen under positive ion mode, the PI(18:0/20:4 (*n*-6,9,12,15)) deprotonated molecule $[M - H]^-$ at m/z 885 was seen with high intensity under ESI (−). Thus, with the PI class, mass measurements of $[M - H]^-$ ions can be used for the determination of elemental compositions. The MS/MS spectrum of the ions at m/z 885 is presented in Figure S2c (Supporting Information). The $[RCOO]^-$ ions at m/z 283 and 303 correspond to the 18:0 and 20:4 fatty acyl chains, and in addition, the inositol phosphate ion at m/z 241 is present with high intensity. Other product ions at m/z 599 ([lysostearoyl PI−H]$^-$) and 581 $[\text{lysostearoyl PI} - H - H_2O]^-$) are also observed, probably formed by the loss of the 20:4 acyl chain and the further loss of H_2O. The product ion at m/z 419 is due to the further loss of inositol from the $[\text{lysostearoyl PI} - H]^-$ ion at m/z 599. A similar fragmentation pattern for PI under ESI(−)-MS/MS was also observed by other studies.[10,29]

In-line O_3-MS Analysis of LPE, LPC, PE, SM, and PI Standards. For LPE and LPC, even though the chain length and number of double bonds can already be determined by the mass measurement of $[M + H]^+$ ions, the position of double bonds along the chain cannot be assigned. Hence, in-line O_3-MS analyses of LPE(18:1(*n*-9)) and LPC(18:1(*n*-9)) standards were performed under ESI (+) (Figure 1a and b). The ozonolysis product of LPE(18:1(*n*-9)) was observed at m/z 370 as well as the intact $[M + H]^+$ ion at m/z 480 (Figure 1a). The ion at m/z 370 corresponds to the characteristic ozonolysis product aldehyde that was formed by oxidative cleavage of the *n*-9 double bond in LPE. The mass loss of 110 Da after ozonolysis has also been observed in other lipids with double bonds located at the *n*-9 position such as methyl oleate[26] and PC(16:0/18:1(*n*-9)).[25] The ion at m/z 352 was probably due to the neutral loss of one H_2O molecule from the ion at m/z 370. For the LPC(18:1(*n*-9)) standard, a similar mass loss of 110 Da from the intact molecular ion at m/z 522 was observed resulting in the ion at m/z 412 after in-line ozonolysis (Figure 1b).

In the O_3-MS spectrum of the PE(18:0/20:4 (*n*-6,9,12,15)) standard (Figure 1c), the ozonolysis product aldehyde ions at m/z 700, 68 Da mass lower than that of intact $[M + H]^+$ ion at m/z 768, were generated by the ozonolysis of the double bond at the *n*-6 position. The product ions at m/z 660, 620, and 580 corresponded to the further oxidative cleavage of successive methylene interrupted double bonds. In addition, the neutral loss of one H_2O molecule from the aldehyde ion at m/z 580 was observed at m/z 562.

The O_3-MS spectrum of the SM(d18:1/18:1(*n*-9)) standard (Figure 1d) contained the intact $[M + H]^+$ ions at m/z 729 and the high intensity ozonolysis product ions at m/z 619, which resulted from ozonolysis of the double bond at the *n*-9 position in the N-18:1 chain. The low intensity ions at m/z 549, 180 Da lower mass than that of the $[M + H]^+$ ions at m/z 729, were formed by ozonolysis of the 4,5-*trans* double bond located along the sphingosine (d18:1) chain. The ozonolysis of both double bonds in SM(d18:1/18:1(*n*-9)) resulted in the ions at m/z 439. The ozonolysis product aldehydes formed by oxidative cleavage of double bonds located along the N-acyl chain (m/z 619 in this case) can be used for the direct assignment of the double bond positions within the N-acyl chain.

The in-line ozonolysis products of the PI(18:0/20:4 (*n*-6,9,12,15)) standard were detected in negative ion mode, since the PI can be observed as $[M - H]^-$ ions. In the resulting O_3-MS spectrum (Figure 1e), intact $[M - H]^-$ ions at m/z 885 were still observed along with the ozonolysis product aldehydes ions at m/z 817, 777, 737, and 697, due to the oxidative cleavage of double bonds at the *n*-6,-9,-12,-15 positions. The same group of ozonolysis product aldehyde ions were also reported from the OzID-MS analysis of PI(18:0/20:4 (*n*-6,9,12,15)) under ESI (−).[30] Along with these characteristic ozonolysis aldehyde ions, another set of ions at m/z 851, 811, 771, and 731 were also observed. These ions have 34 Da higher mass than the corresponding deprotonated aldehydes ions at m/z 817, 777, 737, and 697. These ions might be attributed to the further reaction of "Criegee intermediates" that are zwitterions formed during the oxidative cleavage of each double bond. They are probably formed by the addition of a H_2O molecule to the Criegee intermediates, resulting in the formation of hydroperoxide groups. As an example, a possible structure of the product ion at m/z 731 is shown in the inset of Figure 1e. The Criegee intermediates themselves were observed during the OzID-MS analysis of PI under ESI (−) as the carbonyl oxide ions at 16 Da are higher in mass than their corresponding aldehyde ions.[30] Whether the Criegee intermediate adducts observed in the present study were generated during the in-line ozonolysis reaction or during the negative electrospray ionization is not clear, but they do not diminish the use of the ozonolysis product aldehydes for the definitive assignment of double bond positions in PI molecules.

In summary, for LPE, LPC, PE and SM, both the intact molecules and the ozonolysis product aldehydes that are

DOI: 10.1021/jf5049595
J. Agric. Food Chem. 2015, 63, 1442−1451

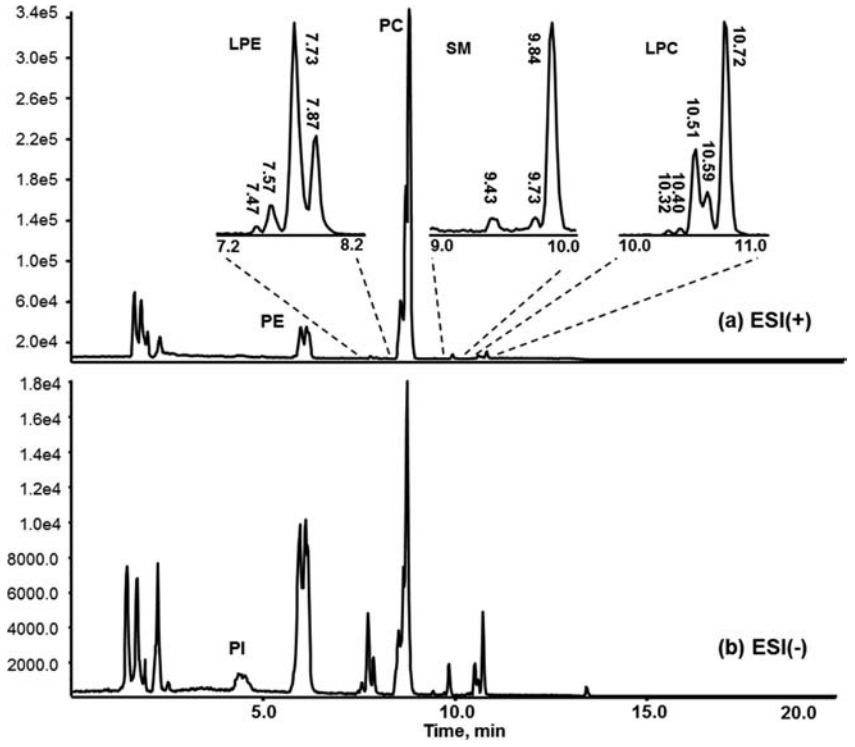

Figure 2. TIC of HILIC/MS analysis of egg yolk PL extract: (a) detected under ESI (+ve); (b) detected under ESI (−ve).

characteristic of double bond positions are detected as $[M + H]^+$ ions during O_3-ESI(+)/MS analysis. For PI, the deprotonated molecule can only be observed as $[M - H]^-$ ions under negative ion mode. The in-line ozonolysis products of PI are also detected under ESI (−) from which the aldehydes can still be used for the unambiguous assignment of double bond locations.

Characterization of Egg Yolk PL Extract. Egg yolk is a good source of dietary PL, and recently, PL extracted from egg yolk has been introduced as a novel food in the EU.[3] In addition, it is known that the egg yolk fatty acid profile can be modified through the hen's diet. For example, the abundance of *n*-3 PUFA in egg yolk can be increased by enriching seal blubber oil in the diet of layers.[10] The main classes of PLs in chicken egg yolk that have been reported include PI, PE, LPE, PC, SM, and LPC.[10,23,31] In the following sections, HILIC/MS and HILIC/MS/MS analyses are used for PL class separation and for the determination of elemental and fatty acyl chain composition. Additionally, online 2D-LC/MS analyses were carried out for the separation of molecular species within each PI, PE, and PC class, and 2D-LC/O_3-MS analysis was also performed to assign the double bond positions directly. Finally, HILIC was coupled to O_3-MS (HILIC/O_3-MS) in order to determine the double bond positions in LPE, LPC, and SM classes since the molecular species within these three classes are relatively simple and can be adequately separated on a HILIC column.

HILIC/MS and HILIC/MS/MS Analysis. We have previously demonstrated the separation of PL classes using a HILIC column with gradient elution.[10,23,31] Here, the egg yolk PL extract was analyzed by HILIC/ESI-MS under both positive and negative ion modes (Figure 2). As can be seen in the total ion current chromatogram (TIC) of HILIC/ESI(+)-MS (Figure 2a), the egg yolk PLs were well separated into PE, LPE, PC, SM, and LPC classes which formed abundant $[M + H]^+$ ions. Under ESI(−) (Figure 2b), the PI class was also observed as $[M - H]^-$ ions at elution times between 4.0 and 5.0 min. The PE, LPE, PC, SM, and LPC classes could still be observed under negative mode but with about half of the intensity of that seen under ESI (+). Hence, the mass measurements of PE, LPE, PC, SM, and LPC $[M + H]^+$ ions and PI $[M - H]^-$ ions were used to determine their elemental compositions. From the mass measurements of LPE and LPC $[M + H]^+$ ions, the fatty acyl chain compositions could be directly assigned.

In order to obtain information on the fatty acyl chain composition for PI, PE, PC, and SM, information dependent acquisition (IDA) mode was used during HILIC/ESI(−) analyses. During IDA, which is used to automatically trigger MS/MS scans, CID with CE of −35 and −42 eV were applied to ions with intensity higher than 10 cps. This results in the formation of fragment ions that are the deprotonated fatty acid residues $[R_1COO]^-$ and $[R_2COO]^-$. Thus, the MS/MS spectra of $[M - H]^-$ ions of PE, PI, and the $[M + HCOO]^-$ ions of PC were used for the determination of their fatty acyl chain compositions. For SM, the mass difference between the fragment ions $[M - CH_3]^-$ and $[M - CH_3 - R_1CO]^-$ in the MS/MS spectrum of $[M + HCOO]^-$ was used to determine the composition of the N-acyl chain. Following this, the composition of the sphingosine group in SM could be deduced.

In this way, the fatty acid residue chain lengths and numbers of double bonds in PI, PE, PC, and SM were assigned even for isomeric species such as PE(18:0_18:3) and PE(18:1_18:2). These are listed in Table 1.

2D-LC/MS and 2D-LC/O_3-MS Analysis of PI, PE, and PC Classes. In our previous study, HILIC × C18 LC, achieved by using a 10-port 2-position switching valve as the interface, was developed for online PC molecular species separation of a rat liver extract. In the present study, a C18 column with the same

DOI: 10.1021/jf5049595
J. Agric. Food Chem. 2015, 63, 1442−1451

Table 1. PL Species Identified in Egg Yolk PL Extract

observed ions (m/z)	formula	mass accuracy (ppm)	molecular species		ECN	t_R (min)	double bond position *n*-	ozonolysis product aldehyde ions (m/z)
			PI $[M - H]^-$					
833.52	$C_{43}H_{78}O_{13}P$	−0.50	34:2	16:0_18:2	30	7.37	*n*-6,9	765,725
857.52	$C_{45}H_{78}O_{13}P$	−0.50	36:4	16:0_20:4	28	7.16	N/A	N/A[a]
859.53	$C_{45}H_{80}O_{13}P$	−4.10	36:3	16:0_20:3	30	7.60	*n*-6,9,12	791,751,711
861.55	$C_{45}H_{82}O_{13}P$	4.40	36:2	18:0_18:2	32	8.30	*n*-6,9	793,753
863.57	$C_{45}H_{84}O_{13}P$	3.40	36:1	18:0_18:1	34	9.43	*n*-9	753
885.55	$C_{47}H_{82}O_{13}P$	−1.50	38:4	18:0_20:4	30	8.11	*n*-6,9,12,15	817,777,737,697
887.57	$C_{47}H_{84}O_{13}P$	0.20	38:3	18:0_20:3	32	8.60	*n*-6,9,12	819,779,739
			PE $[M + H]^+$					
716.52	$C_{39}H_{75}NO_8P$	−0.30	34:2	16:0_18:2	30	10.14	*n*-6,9	648,608
718.54	$C_{39}H_{77}NO_8P$	−3.50	34:1	16:0_18:1	32	11.36	*n*-9	608
740.52	$C_{41}H_{75}NO_8P$	0.80	36:4	16:0_20:4	28	9.91	*n*-6,9,12,15	672,632,592,552
				18:2_18:2	28	9.39	N/A	N/A[a]
742.54	$C_{41}H_{77}NO_8P$	−0.60	36:3	18:0_18:3	30	10.53	*n*-6,9,12	674,634,594
				18:1_18:2	30	10.21	N/A	N/A[a]
744.55	$C_{41}H_{79}NO_8P$	−0.30	36:2	18:0_18:2	32	11.73	*n*-6,9	676,636
746.57	$C_{41}H_{81}NO_8P$	1.20	36:1	18:0_18:1	34	13.58	*n*-9	636
764.53	$C_{43}H_{75}NO_8P$	4.80	38:6	16:0_22:6	26	9.56	*n*-3,6,9,12,15,18	738,698,658,618,578,538
768.56	$C_{43}H_{79}NO_8P$	1.80	38:4	18:0_20:4	30	11.38	*n*-6,9,12,15	700,660,620,580
792.55	$C_{45}H_{79}NO_8P$	−0.50	40:6	18:0_22:6	28	10.89	*n*-3,6,9,12,15,18	766,726,686,646,606,566
			PC $[M + H]^+$					
732.55	$C_{40}H_{79}NO_8P$	−0.10	32:1	16:0_16:1	30	11.86	*n*-9	622
734.57	$C_{40}H_{81}NO_8P$	−3.00	32:0	16:0_16:0	32	12.86	saturated	saturated
756.56	$C_{42}H_{79}NO_8P$	1.60	34:3	16:0_18:3	28	11.43	*n*-3,6,9	730,690,650
758.57	$C_{42}H_{81}NO_8P$	−1.50	34:2	16:0_18:2	30	12.02	*n*-6,9	690,650
760.59	$C_{42}H_{83}NO_8P$	1.20	34:1	16:0_18:1	32	12.93	*n*-9	650
762.60	$C_{42}H_{85}NO_8P$	−1.20	34:0	16:0_18:0	34	14.52	saturated	saturated
780.55	$C_{44}H79NO_8P$	−0.40	36:5	16:0_20:5	26	10.95	N/A	N/A[a]
782.57	$C_{44}H_{81}NO_8P$	−0.10	36:4	16:0_20:4	28	11.84	*n*-6,9,12,15	714,674,634,594
784.58	$C_{44}H_{83}NO_8P$	−2.40	36:3	16:0_20:3	30	12.27	*n*-6,9,12	636,676,716
				18:1_18:2	30	12.07	*n*-9/*n*-9,12	674/606,566
786.60	$C_{44}H_{85}NO_8P$	−2.50	36:2	18:1_18:1	32	13.01	*n*-9/*n*-9	676/566
				18:0_18:2	32	13.26	*n*-6,9	718,678
788.62	$C_{44}H_{87}NO_8P$	3.90	36:1	18:0_18:1	34	14.68	*n*-9	678
806.57	$C_{46}H_{81}NO_8P$	0.20	38:6	16:0_22:6	26	11.57	*n*-3,6,9,12,15,18	780,740,700,660,620,580
808.58	$C_{46}H_{83}NO_8P$	−2.60	38:5	18:0_20:5	28	12.21	N/A	N/A[a]
				18:1_20:4	28	11.88	N/A	N/A[a]
810.60	$C_{46}H_{85}NO_8P$	0.20	38:4	18:0_20:4	30	12.98	*n*-6,9,12,15	742,702,662,622
812.62	$C_{46}H_{87}NO_8P$	−1.60	38:3	18:0_20:3	32	13.67	*n*-6,9,12	744,704,664
834.60	$C_{48}H_{85}NO_8P$	−2.00	40:6	18:0_22:6	28	12.59	*n*-3,6,9,12,15,18	808,768,728,688,648,608
			LPE $[M + H]^+$					
454.29	$C_{21}H_{45}NO_7P$	0.40	*sn*-2−16:0			7.72	saturated	saturated
			sn-1−16:0			7.87	saturated	saturated
466.33	$C_{23}H_{49}NO_6P$	0.60	18:1-eLPE			7.47	*n*-9	356
480.31	$C_{23}H_{47}NO_7P$	−1.20	18:1			7.78	*n*-9	370
482.32	$C_{23}H_{49}NO_7P$	−0.40	*sn*-2−18:0			7.57	saturated	saturated
			sn-1−18:0			7.73	saturated	saturated
			SM $[M + H]^+$					
703.57	$C_{39}H_{80}N_2O_6P$	−1.70	d18:1/16:0			9.84	saturated	saturated
705.59	$C_{39}H_{82}N_2O_6P$	3.10	d18:0/16:0			9.73	saturated	saturated
731.61	$C_{41}H_{84}N_2O_6P$	2.10	d18:1/18:0			9.72	saturated	saturated
813.68	$C_{47}H_{94}N_2O_6P$	0.20	d18:1/24:1			9.43	*n*-9	703
			LPC $[M + H]^+$					
496.34	$C_{24}H_{51}NO_7P$	0.40	*sn*-2−16:0			10.54	saturated	saturated
			sn-1−16:0			10.72	saturated	saturated
522.35	$C_{26}H_{53}NO_7P$	−0.50	*sn*-2−18:1			10.40	*n*-9	412
			sn-1−18:1			10.60	*n*-9	412
524.37	$C_{26}H_{55}NO_7P$	−1.10	*sn*-2−18:0			10.32	saturated	saturated
			sn-1−18:0			10.50	saturated	saturated

[a]The intensity of ozonolysis product aldehyde ions is too low to observe.

DOI: 10.1021/jf5049595
J. Agric. Food Chem. 2015, 63, 1442−1451

stationary phase but only half the length (75 mm) was used along with a modified gradient (see Materials and Methods) in order to shorten the second dimension separation time from 30 to 20 min, with only minor effect on the efficiency of separation. Using this arrangement, 2D-LC/MS analysis was applied to the molecular species separation of PI, PE, and PC classes from egg yolk PL extract. 2D-LC/MS analysis coupled to in-line ozonolysis was also performed for more detailed structural investigation of each eluting molecule within these 3 classes.

In the 2D-LC separation of PI molecular species, the PI fraction eluting from the HILIC column was transferred onto the C18 column by switching the valve to position B at 4.0 min and back to position A at 4.8 min (see Materials and Methods and Figure S1, Supporting Information). Compared to the first dimension HILIC separation (Figure 2b), the molecular species of PI were much better separated on the second dimension C18 column (Figure 3a). The observed molecular species and

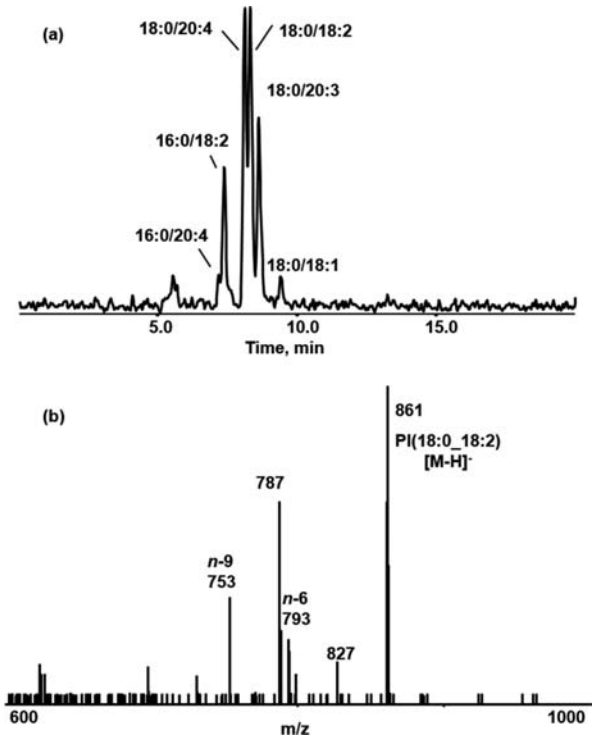

Figure 3. (a) TIC of 2D-LC/MS analysis of the PI class in egg yolk PL extract in negative ion mode; (b) O_3-MS spectrum of PI(18:0_18:2) in the egg yolk sample.

their corresponding t_R are listed in Table 1. The elution order of these PI species was consistent with their equivalent carbon number (ECN), meaning the PI molecules with higher ECN were retained longer on the C18 column. In order to assign the specific fatty acyl chains in these PI species, 2D-LC was coupled to O_3-MS in the negative ion mode. As an example of the results, the O_3-MS spectrum of PI(18:0_18:2) in this egg yolk PL extract is shown in Figure 3b. In addition to the intact $[M - H]^-$ ions at m/z 861, ozonolysis product ions appeared at m/z 753, 787, 793, and 827. The ions at m/z 787 and 827, that are 34 Da higher in mass than the ions at m/z 753 and 793, were generated by H_2O addition to the corresponding Criegee intermediates, consistent with results from the example of in-line ozonolysis of a PI(18:0/20:4) standard (Figure 1e). The ions at m/z 793 and 753 corresponded to ozonolysis product aldehydes from the oxidative cleavage of double bonds at n-6 and −9 positions along the 18:2 acyl chain. For other PI molecular species in this sample, the ozonolysis product aldehydes along with the products at 34 Da or higher are also observed and used for the determination of all double bond positions (Table 1).

For the molecular species separation of the PE class, the fraction eluting at between 5.6 and 6.4 min from the HILIC column (Figure 2a) was transferred onto the C18 column. Although a small degree of PE species separation was achieved on the HILIC column (Figure 2a), the diversity of the PE molecular species was far better resolved after 2D-LC separation (Figure 4a). Since PE $[M + H]^+$ ions under ESI

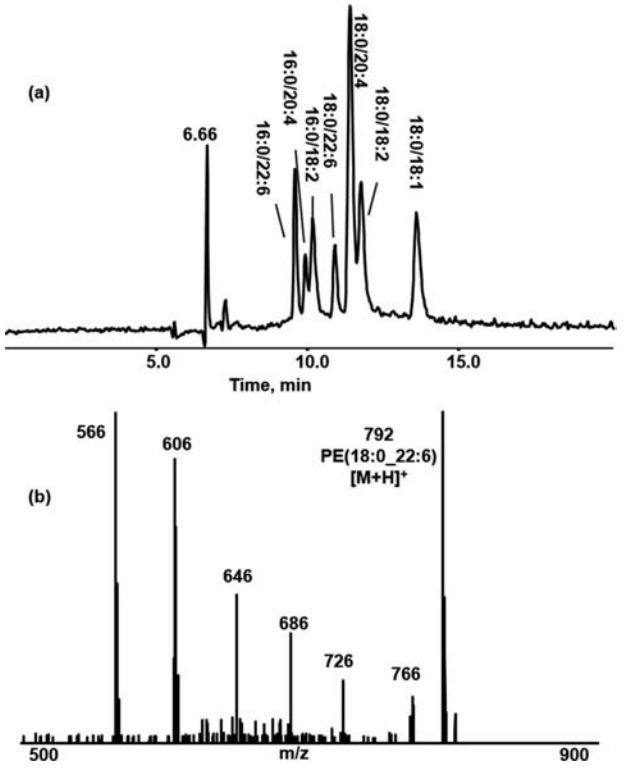

Figure 4. (a) TIC of 2D-LC/MS analysis of the PE class in egg yolk PL extract in positive ion mode; (b) O_3-MS spectrum of PE(18:0_22:6) in the egg yolk sample.

(+) have higher intensity than the $[M - H]^-$ ions seen under ESI (−), 2D-LC/MS analysis was carried out in positive ion mode. The first eluting species was PE(16:0_22:6) (ECN = 26) at 9.56 min, and the rest of the PE molecular species eluted generally according to their ECN, ranging from 26 to 34. However, one exception was observed for PE(18:0_22:6) with an ECN of 28 eluting at 10.89 min, which was retained longer than PE(16:0_18:2) (t_R 10.14 min) with an ECN of 30. Similar retention order exceptions for PLs containing a PUFA chain were also observed during 2D-LC separation of PC in rat liver in our previous study.[25] Even though the PE species containing PUFA such as PE(16:0_22:6), PE(18:0_22:6), PE(16:0_20:4), and PE(18:0_20:4) can be relatively well separated from other species, no more detailed structure information can be derived from just the 2D-LC/MS analysis to identify them as n-3 or n-6 PUFA. Therefore, 2D-LC/O_3-MS analysis was also performed on these PE species. As an example, the O_3-MS spectrum of

DOI: 10.1021/jf5049595
J. Agric. Food Chem. 2015, 63, 1442−1451

PE(18:0_22:6) in the sample is shown in Figure 4b. The mass difference of 26 Da between the intact PE(18:0_22:6) $[M + H]^+$ ion at m/z 792 and the ozonolysis product ion at m/z 766 directly assigns the first double bond at the n-3 position. The successive ozonolysis product ions at m/z 726, 686, 646, 606, and 566, with 40 Da mass differences between each other, demonstrate that as expected, all of the double bonds are separated only by a methylene group. Thus, PE(18:0_22:6) in egg yolk contains the n-3 docosahexaenoic acid chain.

The PC class eluting at between 8.2 and 9.0 min from the HILIC column was also directed onto the C18 column for the further separation of molecular species. The major PC species are indicated in Figure 5a; other minor PC species are listed in Table 1 due to their partial coelution with the major species. Compared to PI and PE, the PC class has an even higher level of species diversity, with ECNs that ranged from 26 to 34. PC molecular species also elute based on their ECN, with the exception of the PC molecule with PUFA such as PC(16:0_22:6) and PC(18:0_22:6), which have greater retention than some PC species with higher ECNs.

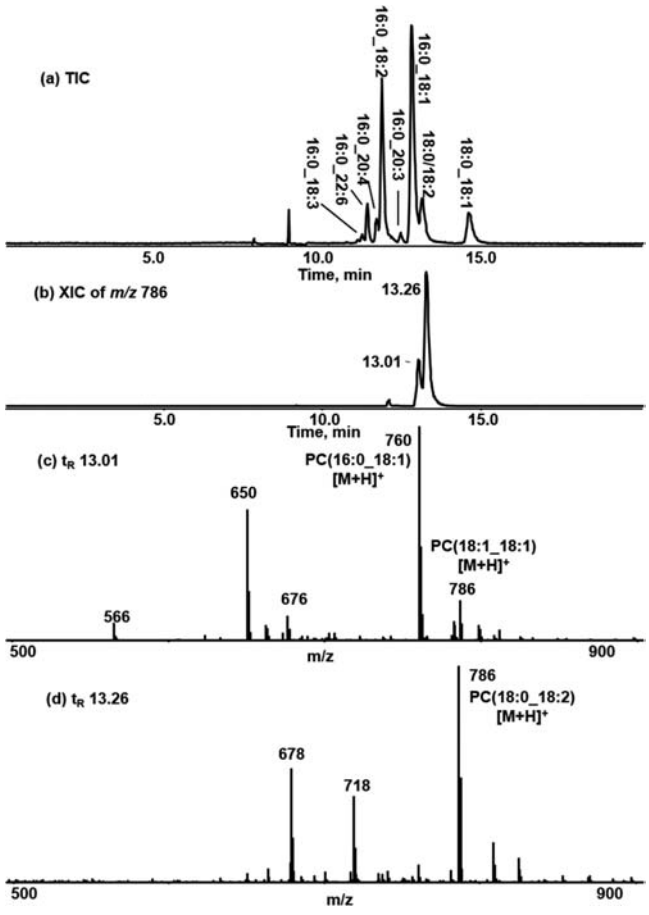

Figure 5. (a) TIC of 2D-LC/MS analysis of PC class in egg yolk PL extract in positive ion mode; (b) XIC of m/z 786 from (a); (c) O_3-MS spectrum of the peak at 13.01 min; (d) O_3-MS spectrum of the peak at 13.26 min.

In-line ozonolysis was also performed on PC species separated by 2D-LC, and the diagnostic ozonolysis product aldehydes were detected as $[M + H]^+$ ions. The isomers of PC 36:2 in the egg yolk is used as an example to illustrate how the double bond positions were assigned using in-line ozonolysis. In the extracted ion chromatogram (XIC) of m/z 786 (Figure 5b), two peaks appear at 13.01 and 13.26 min, indicating that they are PC(18:1_18:1) and PC(18:0_18:2) isomers. In the O_3-MS spectrum of the peak at 13.01 min (Figure 5c), ozonolysis product ions were observed at m/z 676 along with the intact molecular ion at m/z 786, which directly assigned the double bond at n-9 in one of the 18:1 acyl chains. The other ozonolysis product ion at m/z 566 was generated from the further ozonolysis of the double bond in the other chain, and the mass loss of 110 Da from m/z 676 also located the second double bond at the n-9 position in the second 18:1 acyl chain. Also seen in the O_3-MS spectrum of the peak eluting at 13.01 min (Figure 5c) is an abundant $[M + H]^+$ ion at m/z 760 from PC(16:0_18:1), along with its ozonolyis product ion at m/z 650. However, the partial coelution of this species does not affect the assignment of double bond positions in PC(18:1_18:1) at 13.01 min. In Figure 5d, the O_3-MS spectrum of the isomeric species at m/z 786 which elutes at 13.26 min is shown. From this spectrum, the ozonolysis product ions at m/z 718 and 678 allow assignment of the double bond positions at n-6 and 9 in PC(18:0_18:2).

HILIC/MS Analysis of LPE, LPC, and SM Class. Initially, similar to the 2D-LC/MS analysis of PI, PE, and PC classes, LPE eluting between 7.2 and 8.0 min and LPC eluting between 10.2 and 11.0 min from the HILIC column were also switched onto the C18 column and eluted using the same isocratic conditions. However, all of the species in both the LPE and LPC classes had very little retention and almost eluted as one single peak on the C18 column. The low retention of the LPE and LPC classes on the C18 column was also observed in the off-line 2D-LC study, in which LPE and LPC classes from the HILIC column were collected and injected onto a C18 column separately for molecular species separation.[32] However, it can be seen by the insets of Figure 2a that significant molecular species separation of LPE and LPC has already been achieved on the HILIC column. The accurate mass measurement of the ion at m/z 454 identified it as LPE(16:0). In the XIC of the ion at m/z 454 from Figure 2a (not shown), two peaks at 7.73 and 7.87 min are present, representing regio-isomers with the 16:0 acyl chain at either sn-1 or sn-2 position. The regio-isomers of LPE(18:0) at m/z 482 were also observed at 7.57 and 7.73 min. Although unambiguous assignment of regio-isomers cannot be achieved by our study, it was shown earlier that sn-1 LPE and LPC were retained longer than the corresponding sn-2 isomers on a HILIC column.[32] Thus, the assignment of sn-isomers presented is solely based on the retention time on the HILIC column in our study (Table 1). We also observed low intensity ions at m/z 466 from LPE species eluting at a t_R of 7.47 min. The accurate mass measurement at m/z 466.3295 assigned the elemental composition of these LPE molecules as $C_{23}H_{49}NO_6P^+$, which excluded the possibility that this ion represented the isobaric LPE(17:1). Therefore, this LPE species was tentatively identified as either eLPE(18:1) which has the long alkyl chain bound as a 1-O-alkyl ether, or as pLPE(18:0) with the chain bound as 1-O-alk-1′-enyl (note that plasmenyl- or p(18:0) refers to the vinyl ether form, which is derived from the saturated 18:0 but includes a double bond at C-1 and hence is isobaric with eLPE(18:1)). However, the exact structure of this LPE species could not be determined because the MS/MS spectra in both positive and negative ionizations failed to provide product ions that could be used for this specific assignment. In order to differentiate between these two ether lipids, other work has used acidic hydrolysis performed on the ether PL before MS analysis since the double bond in 1-O-

DOI: 10.1021/jf5049595
J. Agric. Food Chem. 2015, 63, 1442−1451

alk-1′-enyl linkage is unstable to acid treatment.[33] It was also previously reported that product ions from the loss of R_1OH can only be observed from the MS/MS analysis of the *p*LPC $[M+Li]^+$ ions and not from the MS/MS analysis of *e*LPC $[M + Li]^+$ ions.[34] For the LPC class, regio-isomers of LPC(16:0), LPC(18:0), and LPC(18:1) were also observed in their XIC traces of *m*/*z* 496, 524, and 522, respectively. As with LPE, the identification of regio-isomers only relied on their retention time on the HILIC column (Table 1).

For the SM class, even though there are two substituents in the molecules besides the polar headgroup, the SM fraction eluting at between 9.2 and 10.0 min from the HILIC column had poor retention and resolution under the current C18 separation. However, the SM molecular species were separated well on the HILIC column (the inset of Figure 2a). SM(d18:1/24:1) eluted at 9.43 min and was separated from SM(d18:1/16:0) (t_R 9.84 min) and SM(d18:1/18:0) (t_R 9.72 min); only SM(d18:0/16:0) coeluted with SM(d18:1/18:0) at 9.73 min.

HILIC/O_3-MS Analysis of LPE, LPC, and SM Class. While molecular species separation of LPE, LPC, and SM classes was achieved on the HILIC column, the double bond positions in unsaturated species such as LPE(18:1), LPC(18:1), and SM(d18:1/24:1) could still not be assigned. Therefore, the in-line ozonolysis device was coupled with the HILIC column (HILIC/O_3-MS). In this way, the ozonolysis products from each eluting LPE, LPC, and SM molecule was detected by ESI (+)-MS. For example, in Figure S3a (Supporting Information) an ion at *m*/*z* 370 appeared in the O_3-MS spectrum of LPE(18:1) along with the intact $[M + H]^+$ ions at *m*/*z* 480. This mass loss of 110 Da allows the assignment of the only double bond in this LPE to the *n*-9 position. Also seen in Figure S3a (Supporting Information) is an ion at *m*/*z* 454, which is due to the coelution of LPE(16:0). However, this does not compromise the value of the diagnostic ozonolysis product ion for the determination of double bond position in LPE(18:1). In the O_3-MS spectrum averaged at between 7.45 and 7.50 min (see Figure 2a and Table 1), the $[M + H]^+$ ion at *m*/*z* 466 was still observed but was accompanied by an ozonolysis product ion at *m*/*z* 356. The latter ion locates the double bond to the *n*-9 position, which in turn confirms that the ion at *m*/*z* 466 corresponds to the $[M + H]^+$ ion of *e*LPE(18:1(*n*-9)) rather than to *p*LPE(18:0). Hence, in this study the differentiation between possible *e*LPE and *p*LPE isomers was achieved using O_3-MS analysis, although further experiments would be needed in order to validate this as a general approach.

Figure S3b (Supporting Information) is the O_3-MS spectrum of the SM (d18:1/24:1) at *m*/*z* 813 from the egg yolk sample. The double bond along the N-24:1 chain was assigned to the *n*-9 position based on the observation of the ozonolysis product ion at *m*/*z* 703, 110 Da below the $[M + H]^+$ ion at *m*/*z* 813. The ion observed at *m*/*z* 523 is the ozonolysis product aldehyde generated by the subsequent oxidative cleavage of the 4,5-*trans* double bond located along the 18:1 sphingosine group. An analogous pattern of ozonolysis product ions was seen in the O_3-MS spectrum of the SM(d18:1/18:1(*n*-9)) standard (Figure 1d).

In the above discussions, it has been demonstrated that for the egg yolk PL extract, all of the molecular species in PI, PE, and PC can be unambiguously identified using HILIC/MS and MS/MS analysis followed by 2D-LC/O_3-MS. It has also been shown that LPE, LPC, and SM molecular species can be accurately assigned using HILIC/MS and HILIC/O_3-MS analyses. Our findings have revealed even more of the diversity of PL species that are present in egg yolk, compared to that in previous reports.[10,23] Furthermore, the methods that we have used have allowed for the definitive identification of each PL species with the position of the double bond directly assigned.

In summary, we have developed a comprehensive PL characterization method which involves using a combination of HILIC/MS, HILIC/MS/MS, 2D-LC/MS, and O_3-MS analyses. The use of in-line ozonolysis coupled with a HILIC column and 2D-LC is necessary for the elucidation of the structure of the chains within the molecules. The experimental setup is very easily adapted to a range of LC and MS configurations, which is especially helpful for the characterization of PL, a group of chemically diverse compounds. While the use of shotgun lipidomics can reveal a great diversity of lipid structures, the minor species and most isomers can only be observed with chromatographic separation prior to MS detection, and other analytical techniques are often required to confirm species identification. The comprehensive method demonstrated here has shown great success, as exemplified by the detailed structure elucidation of egg yolk PL molecules. The additional level of structural detail for lipid analyses that can be generated by this approach will be complementary to other experimental methods used in lipidomics.

■ ASSOCIATED CONTENT

Ⓢ Supporting Information

HILIC×C18 LC/O3-MS configuration; ESI (−)-MS/MS analysis of PL standard; and O_3-MS spectrum of LPE(18:1) and SM(d18:1/24:1). This material is available free of charge via the Internet at http://pubs.acs.org.

■ AUTHOR INFORMATION

Corresponding Author

*Clinical Science Building 10-102, Department of Laboratory Medicine & Pathology, University of Alberta, Edmonton, Alberta T6G 2G3, Canada. Tel: 780-492-5096. E-mail: chenxing@ualberta.ca

Funding

This work was supported by an NSERC Discovery grant 197273 awarded to J.M.C. and by a Quality Food for Health grant to J.M.C. and coinvestigators jointly funded by Alberta Livestock and Meat Agency, Alberta Innovates Biosolutions, and the Alberta Egg Producers.

Notes

The authors declare no competing financial interest.

■ REFERENCES

(1) Vance, D. E.; Vance, J. E. *Biochemistry of Lipids, Lipoproteins and Membranes*; Elsevier Science B.V.: Amsterdam, The Netherlands, 2008.

(2) Amate, L.; Gil, A.; Ramirez, M. Feeding infant piglets formula with long-chain polyunsaturated fatty acids as triacylglycerols or phospholipids influences the distribution of these fatty acids in plasma lipoprotein fractions. *J. Nutr.* **2001**, *131*, 1250−1255.

(3) Küllenberg, D.; Taylor, L. A.; Schneider, M.; Massing, U. Health effects of dietary phospholipids. *Lipids Health Dis.* **2012**, *11*, 1−16.

(4) Bunea, R.; El, F. K.; Deutsch, L. Evaluation of the effects of Neptune Krill Oil on the clinical course of hyperlipidemia. *Altern. Med. Rev.* **2004**, *9*, 420−428.

(5) Han, X.; Gross, R. W. Structural determination of picomole amounts of phospholipids via electrospray ionizaion tandem mass spectrometry. *J. Am. Soc. Mass Spectrom.* **1995**, *6*, 1202−1210.

(6) Smith, M.; Jungalwala, F. B. Reversed-phase high performance liquid chromatography of phosphatidylcholine: a simple method for

DOI: 10.1021/jf5049595
J. Agric. Food Chem. 2015, 63, 1442−1451

determining relative hydrophobic interaction of various molecular species. *J. Lipid Res.* **1981**, *22*, 697−704.
(7) Pulfer, M.; Murphy, R. C. Electrospay mass spectrometry of phospholipids. *Mass Spectrom. Rev.* **2003**, *22*, 332−364.
(8) Ekroos, K.; Chernushevich, I. V.; Simons, K.; Shevchenko, A. Quantitative profiling of phospholipids by multiple precursor ion scanning on a hybrid quadrupole time-of-flight mass spectrometer. *Anal. Chem.* **2002**, *74*, 941−949.
(9) Houjou, T.; Yamatani, K.; Nakanishi, H.; Imagawa, M.; Shimizu, T.; Taguchi, R. Rapid and selective identification of molecular species in phosphatidylcholine and sphingomyelin by conditional neutral loss scanning and MS^3. *Rapid Commun. Mass Spectrom.* **2004**, *18*, 3123−3130.
(10) Pacetti, D.; Boselli, E.; Hulan, H. W.; Frega, N. G. High performance liquid chromatography-tandem mass spectrometry of phospholipid molecular species in eggs from hens fed diets enriched in seal blubber oil. *J. Chromatogr., A* **2005**, *1097*, 66−73.
(11) Berdeaux, O.; Juaneda, P.; Martine, L.; Cabaret, S.; Bretillon, L.; Acar, N. Identification and quantification of phosphatidylcholines containing very-long-chain polyunsaturated fatty acid in bovine and human retina using liquid chromatography/tandem mass spectrometry. *J. Chromatogr., A* **2010**, *1217*, 7738−7748.
(12) Brouwers, J. F. Liquid chromatographic−mass spectrometric analysis of phospholipids. Chromatography, ionization and quantification. *Biochim. Biophys. Acta* **2011**, *1811*, 763−775.
(13) Houjou, T.; Yamatani, K.; Imagawa, M.; Shimizu, T.; Taguchi, R. A shotgun tandem mass spectrometric analysis of phospholipids with normal-phase and/or reverse-phase liquid chromatography/electrospray ionization mass spectrometry. *Rapid Commun. Mass Spectrom.* **2005**, *19*, 654−666.
(14) Sato, Y.; Nakamura, T.; Aoshima, K.; Oda, Y. Quantitative and wide-ranging profiling of phospholipids in human plasma by two-dimensional liquid chromatography/mass spectrometry. *Anal. Chem.* **2010**, *82*, 9858−9864.
(15) Tian, H.; Xu, J.; Xu, Y.; Guan, Y. Multidimensional liquid chromatography system with an innovative solvent evaporation interface. *J. Chromatogr., A* **2006**, *1137*, 42−48.
(16) Nie, H.; Liu, R.; Yang, Y.; Bai, Y.; Guan, Y.; Qian, D.; Wang, T.; Liu, H. Lipid profi ling of rat peritoneal surface layers by online normal- and reversed-phase 2D LC QToF-MS. *J. Lipid Res.* **2010**, *51*, 2833−2844.
(17) Jandera, P. Stationary and mobile phases in hydrophilic interaction chromatography: a review. *Anal. Chim. Acta* **2011**, *692*, 1−25.
(18) Dugo, P.; Fawzy, N.; Cichello, F.; Cacciola, F.; Donato, P.; Mondello, L. Stop-flow comprehensive two-dimensional liquid chromatography combined with mass spectrometric detection for phospholipid analysis. *J. Chromatogr., A* **2013**, *1278*, 46−53.
(19) Shi, X.; Qiao, L.; Lu, X.; Xu, G. A novel stop-flow two-dimensional liquid chromatography−massspectrometry method for lipid analysis. *J. Chromatogr., A* **2013**, *1321*, 65−72.
(20) Grandois, J. L.; Marchiono, E.; Zhao, M.; Giuffrida, F.; Ennahar, S.; Bindler, F. Investigation of natural phosphatidylcholine sources: Separation and identification by liquid chromatography-electrospray ionization-tandem mass spectrometry (LC -ESI-MS^2) of molecular species. *J. Agric. Food Chem.* **2009**, *57*, 6014−6020.
(21) Montealegre, C.; Verardo, V.; Gómez-Caravaca, A. M.; García-Ruiz, C.; Marina, M. L.; Caboni, M. F. Molecular characterization of phospholipids by high-performance liquid chromatography combined with an evaporative light scattering detector, high-performance liquid chromatography combined with mass spectrometry, and gas chromatography combined with a flame ionization detector in different oat varieties. *J. Agric. Food Chem.* **2012**, *60*, 10963−10969.
(22) Shen, Q.; Wang, Y.; Gong, L.; Guo, R.; Dong, W.; Cheung, H. Shotgun lipidomics strategy for fast analysis of phospholipids in fisheries waste and its potential in species differentiation. *J. Agric. Food Chem.* **2012**, *60*, 9384−9393.
(23) Zhao, Y.; Xiong, Y.; Curtis, J. M. Measurement of phospholipids by hydrophilic interaction liquid chromatography coupled to tandem mass spectrometry: The determination of choline containing compounds in foods. *J. Chromatogr., A* **2011**, *1218*, 5470−5479.
(24) Spitzer, V. Structure analysis of fatty acids by gas chromatography-low resolution electron impact mass spectrometry of their 4,4-dimethyloxazoline derivatives - a review. *Prog. Lipid Res.* **1997**, *35*, 387−408.
(25) Sun, C.; Zhao, Y.; Curtis, J. M. Elucidation of phosphatidylcholine isomers using two dimensional liquid chromatography coupled in-line with ozonolysis mass spectrometry. *J. Chromatogr., A* **2014**, *1351*, 37−45.
(26) Sun, C.; Zhao, Y.; Curtis, J. M. The direct determination of double bond positions in lipid mixtures by liquid chromatography/in-line ozonolysis/mass spectrometry. *Anal. Chim. Acta* **2013**, *762*, 68−75.
(27) Liebisch, G.; Vizcaíno, J. A.; Köfeler, H.; Trötzmüller, M.; Griffiths, W. J.; Schmitz, G.; Spener, F.; Wakelam, M. J. O. Shorthand notation for lipid structures derived from mass spectrometry. *J. Lipid Res.* **2013**, *54*, 1523−1530.
(28) Norris, C.; Fong, B.; MacGibbon, A.; McJarrow, P. Analysis of phospholipids in rat brain using liquid chromatography-mass spectrometry. *Lipids* **2009**, *44*, 1047−1054.
(29) Hus, F. F.; Turk, J. Characterization of phosphatidylinositol,-phosphatidylinositol-4-phosphate, and phosphatidylinositol-4,5-bisphosphate by electrospray ionization tandem mass spectrometry: A mechanistic study. *J. Am. Soc. Mass Spectrom.* **2000**, *11*, 986−999.
(30) Thomas, M. C.; Mitchell, T. W.; Harman, D. G.; Deeley, J. M.; Nealon, J. R.; Blanksby, S. J. Ozone-induced dissociation: Elucidation of double bond position within mass-selected lipid ions. *Anal. Chem.* **2008**, *80*, 303−311.
(31) Xiong, Y.; Zhao, Y.; Goruk, S.; Oilund, K.; Field, C. J.; Jacobs, R. L.; Curtis, J. M. Validation of an LC−MS/MS method for the quantification of choline-related compounds and phospholipids in foods and tissues. *J. Chromatogr., B* **2012**, *911*, 170−179.
(32) Lísa, M.; Cífková, E.; Holcapek, M. Lipidomic profiling of biological tissues using off-line two dimensional high-performance liquid chromatography−mass spectrometry. *J. Chromatogr., A* **2011**, *1218*, 5146−5156.
(33) Chen, S.; Li, K. W. Mass Spectrometric Identification of molecular species of phosphatidylcholine and lysophosphatidylcholine extracted from shark liver. *J. Agric. Food Chem.* **2007**, *55*, 9670−9677.
(34) Hus, F. F.; Turk, J.; Thukkani, A. K.; Messner, M. C.; Wildsmith, K. R.; Ford, D. A. Characterization of alkylacyl, alk-1-enylacyl and lyso subclasses of glycerophosphocholine by tandem quadrupole mass spectrometry with electrospray ionization. *J. Mass Spectrom.* **2003**, *38*, 752−763.

DOI: 10.1021/jf5049595
J. Agric. Food Chem. 2015, 63, 1442−1451

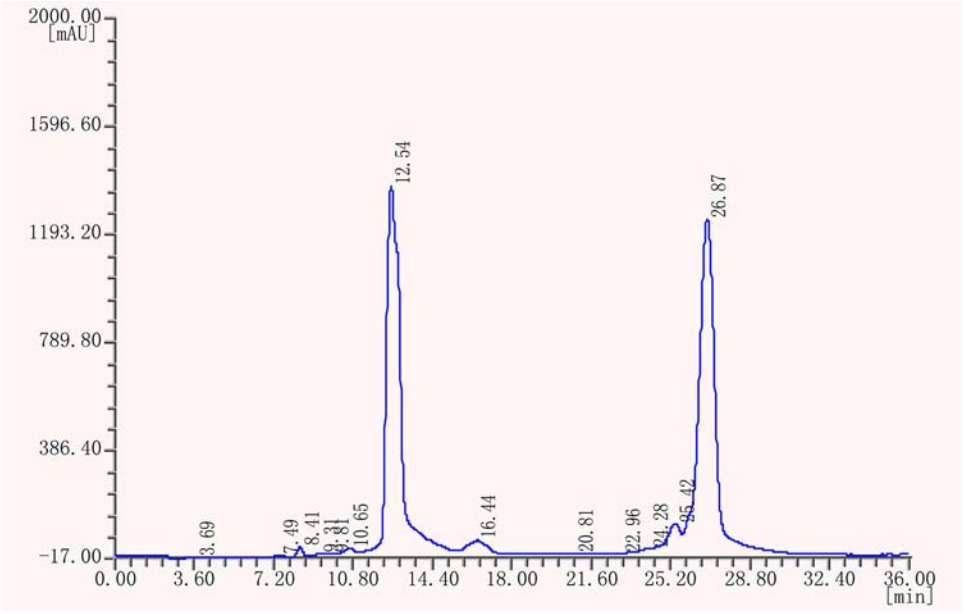

Figure 1. Subfraction $B_{3\text{-}4}$ chromatogram of preparative HPLC. The retention times of kuwanon G (K_1) and kuwanon O (K_2) were 12.5 and 26.9 min, respectively.

a 21.2 × 250 mm XB-C_{18} column (Welch, Ellicott City, MD). Spectra data from ESI−MS were recorded on a 4000 QTRAP liquid chromatography−tandem mass spectrometry (LC−MS/MS) instrument (Allen-Bradley, Milwaukee, WI). Nuclear magnetic resonance (NMR) spectra were obtained from a Bruker Avance III 500 spectrometer (Bruker, Karlsruhe, Germany) operating at 500 MHz for ^{1}H and at 125 MHz for ^{13}C with the samples dissolved in methanol-d_4. An inverted microscope (Nikon, Tokyo, Japan) was used to observe and count the treated theronts.

Plant Material Preparation. *M. alba* was planted by farmers in Guangxi province and identified by a plant taxonomist before the root bark (10 kg) of *M. alba* was purchased from the Chinese medicinal market at Guangzhou, China. The plant was kept in an oven at 55 °C until completely dried before usage.

Extraction, Isolation, and Identification. The dried root bark of *M. alba* was powdered with a pulverizer that contained a 50 mesh strainer. The root bark powder was extracted 3 times with 25 L of 95% ethanol at 78 °C for 2 h each. The ethanol extract was gathered and evaporated in a vacuum rotary evaporator. Subsequently 1.14 kg of the medium dry concentrate was suspended in 1.2 L of water and extracted with petroleum ether, ethyl acetate, and *n*-butanol. Then, the organic solvent extracts were evaporated to dryness by a vacuum rotary evaporator at 40 °C. The water-soluble fraction was freeze-dried. The ethyl acetate extract showed the highest efficacy against *I. multifiliis* theronts among all extracts; therefore, it was used for further separation.

The mixture of 750 g of ethyl acetate extract and 750 g of silica gel (200−300 mesh) was used for column chromatography on a normal-phase silica gel column (7500*g*, 100−200 mesh) and eluted with (A) petroleum ether, (B) petroleum ether/ethyl acetate (1:1, v/v), (C) ethyl acetate, or (D) methanol to obtain four crude fractions. Because fraction B exhibited the strongest anti-Ich activity, the mixture of 350 g of fraction B and 350 g of silica gel (200−300 mesh) was continuously eluted in column chromatography containing silica gel (7000*g*, 100−200 mesh). A polarity gradient of petroleum ether/ethyl acetate (from 10:0 to 0:10, v/v) and ethyl acetate/methanol (1:0, 1:1, and 0:1, v/v) was used in the elution to yield active fraction B_3 on the basis of TLC. A third silica column chromatography (1600*g*, 100−200 mesh) was conducted for the mixture of 80 g of silica gel (200−300 mesh) and 80 g of active fraction B_3 from the elution of 2:1 petroleum ether/ethyl acetate. After repeated column chromatography from 10:0 to 0:10 petroleum ether/ethyl acetate (v/v), fraction B_3 was divided into 10 subfractions ($B_{3\text{-}1}$−$B_{3\text{-}10}$) based on the TLC patterns. $B_{3\text{-}4}$ (18 g) was the most active subfraction against *I. multifiliis* and then used for purification of active compounds with HPLC using a preparative HPLC column. HPLC was performed with a mobile-phase methanol/H_2O (75:25, v/v) at a flow rate of 10 mL/min at room temperature with UV detection at 210 nm. The subfraction $B_{3\text{-}4}$ chromatogram of preparative HPLC is shown in Figure 1. Two active compounds K_1 (3.9 g) and K_2 (4.3 g) were purified. The major purification procedure is shown in Figure 2.

The chemical structures of active compounds were identified on the basis of the physicochemical properties, ESI−MS, ^{1}H NMR spectrum, and ^{13}C NMR spectrum.

Fish and Parasite. Grass carp with an average weight of 22.0 ± 1.3 g were purchased from a commercial fish hatchery at Huadu, Guangzhou, Guangdong, China. All fish were acclimated for 2 weeks in 100 L of aquaria equipped with an aerator and a water suction pump before usage. A light/dark period of 12:12 h was maintained throughout the whole trial. Fish were fed daily at 1% body weight with commercial granule feeds manufactured by Guangdong Haid Group Co., Ltd. One quarter of tank water was exchanged with dechlorinated freshwater every day. The dissolved oxygen, water temperature, and pH were detected with a Professional Plus handheld multiparameter instrument (YSI, Yellow Springs, OH). The water temperature and dissolved oxygen were maintained at 23.0 ± 0.5 °C and 7.1 ± 0.45 mg/L, respectively, and pH was 7.2 ± 0.4 daily.

I. multifiliis was isolated from a goldfish obtained from an ornamental fish market at Guangzhou, China. The parasite was cultured and collected as previously described.[14,23] Theront numbers were enumerated in five 10 μL of 1% formalin-fixed theront suspensions on a glass slide under a microscope (10×) and expressed as the mean number of theronts per milliliter.

Antiparasitic Activity and Toxicity Bioassay. The anti-theront activity was evaluated for two compounds with the methods described by Fu et al.[22] and Buchmann et al.[23] Each purified compound was dissolved in 1 mL of ethanol and adjusted with distilled water to a 100 mg/L stock solution for the bioassay. A 2-fold serial dilution was made from each compound stock solution into working concentrations. There were two negative controls for the trials: one containing only 0.1% ethanol and the other containing only water.

I. multifiliis theronts were considered dead if they were motionless without cilia beating. The lethal exposure duration and mortality were recorded for all theronts in each well of a 96 well plate during 4 h of exposure. The infectivity was evaluated for theronts pretreated with low concentrations of compounds as described by Fu et al.[22] Briefly,

DOI: 10.1021/jf505544e
J. Agric. Food Chem. 2015, 63, 1452−1459

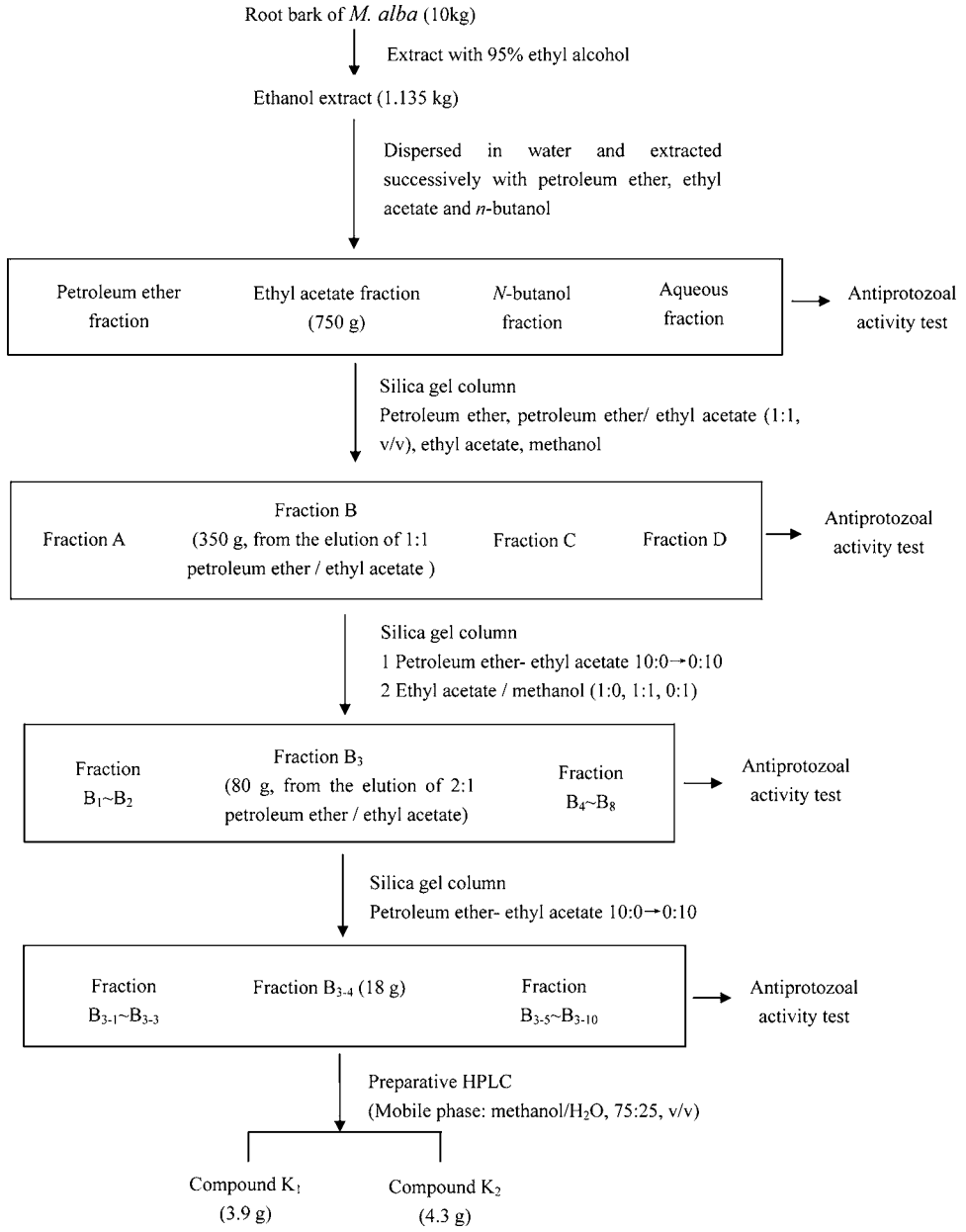

Figure 2. Isolation and purification of parasiticidal compounds.

theronts were treated in 10 mL of kuwanon G or O solution at concentrations of 0 (control), 0.125, 0.25, 0.5, and 1 mg/L for 2 h and then incubated with 10 naive grass carps at 20 000 theronts per fish in 4 L of dechlorinated water for another 2 h. Subsequently, 10 fish were maintained in 10 L of water at 23 ± 0.5 °C for 7 days. Infection prevalence (number of infected fish/total number of fish) and infection intensity (total number of white spots/number of infected fish) were determined 7 days post-exposure in each aquarium after the fish were anesthetized with 150 mg/L tricaine methanesulfonate (MS-222).

In a preliminary acute toxicity trial, kuwanon G or O at 0, 20, 40, 60, and 80 mg/L was used to determine the concentrations, which resulted in 0 or 100% fish mortality. Kuwanon G at 60 mg/L or kuwanon O at 40 mg/L caused 100% fish mortality, but both compounds caused no fish death (0% mortality) at 20 mg/L. On the basis of the result from the preliminary trial, acute toxicity trials were conducted for grass carp with kuwanon G at the concentrations of 0 (control), 20, 25, 30, 40, 50, and 60 mg/L or kuwanon O at the concentrations of 0 (control), 20, 25, 30, and 40 mg/L. Each concentration had three replicated tanks, and each tank contained 10 fish and 5 L of dechlorinated water. Fish were randomly taken from acclimation tank and put into each tank for acute toxicity trial. No feed was given to the fish during the period of acute toxicity trial. Air was provided to each tank by an aerator, and the water temperature was maintained at 23.0 ± 0.5 °C. The compound solution in each tank was replaced daily with fresh solution at the same concentration. Fish behavior and mortality were recorded, and dead fish were removed daily during the 96 h trial. The median lethal concentration (LC_{50}) to fish was determined 96 h post-exposure to each antiparasitic compound.

Statistical Analysis. Data were analyzed with Statistical Product and Service Solutions software (SPSS 17.0) and expressed as the mean ± standard deviation (SD). Mortality, lethal duration, and infectivity of theronts treated at different concentrations of compounds were analyzed by the double-factor variance analysis and Student−Newman−Keuls test. EC_{50} and LC_{50} were calculated by probit analysis.

DOI: 10.1021/jf505544e
J. Agric. Food Chem. 2015, 63, 1452−1459

RESULTS

Structure Identification of Active Compounds. The anti-*I. multifiliis* compounds were isolated from the alcohol extract of *M. alba* root bark by means of bioassay-guided fractionation. A series of fractions were obtained during the isolation and showed various antiparasitic effects (Table 1).

Table 1. Effects of Fractions against *I. multifiliis* Theronts

	anti-theront efficacy (mg/L)			
fraction	0	6.25	12.5	25
petroleum ether fraction	−[a]	−	−	−
ethyl acetate fraction	−	−	−	+[b]
n-butanol fraction	−	−	−	−
aqueous fraction	−	−	−	−
fraction A	−	−	−	−
fraction B	−	−	−	+
fraction C	−	−	−	−
fraction D	−	−	−	−
fraction B_1	−	−	−	−
fraction B_2	−	−	−	+
fraction B_3	−	+	+	+
fraction B_4		−	−	+
fraction B_5−B_8	−	−	−	−
fraction $B_{3\text{-}1}$−$B_{3\text{-}3}$	−	−	−	+
fraction $B_{3\text{-}4}$	−	+	+	+
fraction $B_{3\text{-}5}$− $B_{3\text{-}6}$	−	−	−	+
fraction $B_{3\text{-}7}$−$B_{3\text{-}10}$	−	−	−	+

[a]− = fraction at the listed concentration could not kill 100% theronts by 30 min of exposure. [b]+ = fraction at the listed concentration killed 100% theronts by 30 min of exposure.

The fraction $B_{3\text{-}4}$ demonstrated the best anti-theront effect (Table 1) and was further isolated by preparative HPLC (Figure 1). Finally, two active compounds (K_1 and K_2) were purified and identified according to following data.

Compound K_1 was a yellow brown to reddish brown amorphous powder. ESI−MS *m/z*: 691.5 $[M - H]^-$, 727.5 $[M + Cl]^-$, 693.5 $[M + H]^+$, 715.5 $[M + Na]^+$. ^{1}H NMR (500 MHz, MeOD) *δ*: 7.28 (1H, d, *J* = 8.0 Hz, H-6′), 7.10 (1H, d, *J* = 7.8 Hz, H-14″), 6.70 (1H, d, *J* = 8.1 Hz, H-20″), 6.46 (1H, s, H-3′), 6.43 (1H, d, *J* = 2.0 Hz, H-5′), 6.10 (1H, br s, H-17″), 6.03 (1H, dd, *J* = 8.3 and 2.4 Hz, H-19″), 5.90 (1H, s, H-11″), 5.85 (1H, d, *J* = 8.6 Hz, H-13″), 5.15 (1H, s, H-2″), 5.13 (1H, d, *J* = 7.0 Hz, H-10), 4.54 (1H, s, H-4″), 4.30 (1H, d, *J* = 9.7 Hz, H-3″), 3.17 (1H, br s, H-5″), 3.13 (2H, m, H-9), 1.92 (1H, d, *J* = 14.1 Hz, H-6″), 1.66 (1H, m, H-6″), 1.60 (3H, s, H-12), 1.44 (3H, s, H-7″), 1.42 (3H, s, H-13). ^{1}C NMR (125 MHz, MeOD) *δ*: 210.2 (C-8″), 183.9 (C-4), 165.9 (C1-0″), 165.8 (C1-2″), 163.3 (C-8a), 162.5 (C-4′), 161.9 (C-2), 161.8 (C-7), 161.1 (C-5), 157.8 (C-2′), 157.8 (C-18″), 157.0 (C-16″), 134.4 (C-14″), 134.1 (C-1″), 132.7 (C-11), 132.7 (C-6′), 132.7 (C-20″), 124.7 (C-2″), 123.0 (C-10), 123.0 (C-15″), 121.7 (C-3), 116.0 (C-9″), 113.8 (C-1′), 108.6 (C-5′), 108.2 (C-19″), 108.0 (C-8), 107.9 (C-13″), 105.7 (C-4a), 103.7 (C-3′), 103.6 (C-17″), 102.9 (C-11″), 98.5 (C-6), 49.8 (C-4″), 39.1 (C-3″), 39.1 (C-5″), 39.1 (C-6″), 25.9 (C-12), 24.7 (C-9), 23.2 (C-7″), 17.7 (C-13). The data were identical to those of early studies.[24,25] Compound K_1 was identified as kuwanon G with a molecular formula of $C_{40}H_{36}O_{11}$ and a flavone structure (Figure 3).

Compound K_2 was also a yellow brown to reddish brown amorphous powder. ESI−MS *m/z*: 693.5 $[M - H]^-$, 729.5 $[M + Cl]^-$, 695.5 $[M + H]^+$, 717.5 $[M + Na]^+$. ^{1}H NMR (500 MHz, MeOD) *δ*: 7.60 (1H, d, *J* = 8.8 Hz, H-14″), 7.17 (1H, d, *J* = 8.1 Hz, H-6′), 6.87 (1H, d, *J* = 8.7 Hz, H-20″), 6.36 (3H, m, H-17″, 13′, 5′), 6.06 (1H, d, *J* = 2.4 Hz, H-19″), 6.05 (1H, d, *J* = 2.2 Hz, H-8), 5.97 (1H, d, *J* = 6.7 Hz, H-6), 5.72 (1H, d, *J* = 11.8 Hz, H-2), 5.52 (1H, s, H-2″), 5.21 (1H, m, H-22″), 4.58 (1H, s, H-4″), 4.28 (1H, d, *J* = 8.1 Hz, H-3″), 3.46 (1H, m, H-5″), 3.34 (2H, d, *J* = 8.6 Hz, H-21″), 2.96 (1H, m, H-3), 2.67 (1H, dd, *J* = 16.0 and 2.3 Hz, H-3), 2.15 (1H, m, H-6″), 2.06 (1H, m, H-6″), 1.83 (3H, s, H-7″), 1.70 (3H, s, H-24″), 1.63 (3H, s, H-25″). ^{1}C NMR (125 MHz, MeOD) *δ*: 210.7 (C-8″), 198.6 (C-4), 167.0 (C-7), 165.8 (C-8a), 164.0 (C-5), 163.3 (C-12″), 162.5 (C-10″), 159.6 (C-18″), 157.1 (C-16″), 156.7 (C-2′), 156.6 (C-4′), 134.2 (C-1″), 132.2 (C-20″), 132.1 (C-14″), 131.9 (C-23″), 131.9 (C-6′), 128.8 (C-2″), 125.6 (C-22″), 125.2 (C-15″), 122.8 (C-1′), 117.9 (C-9″), 116.2 (C-11″), 110.6 (C-3′), 110.4 (C-19″), 107.8 (C-13″), 107.3 (C-5′), 103.8 (C-17″), 102.9 (C-4a), 96.1 (C-6), 95.1 (C-8), 76.0 (C-2), 47.4 (C-4″), 43.2 (C-3), 38.8 (C-3″), 38.7 (C-5″), 38.6 (C-6″), 27.5 (C-24″), 26.0 (C-7″), 20.9 (C-21″), 17.8 (C-25″). The data were consistent with those reported previously.[26] Compound K_2 was identified as kuwanon O with a molecular formula of $C_{40}H_{38}O_{11}$ and a flavonone structure (Figure 3).

Anti-*I. multifiliis* Theront Effects of Active Compounds. The anti-theront efficacy of the two compounds was significantly correlated with the tested concentrations (Table 2). The two compounds resulted in 70.1% mortality of theronts by kuwanon O and 59.8% mortality of theronts by kuwanon G at 1 mg/L after 4 h of exposure. Both compounds

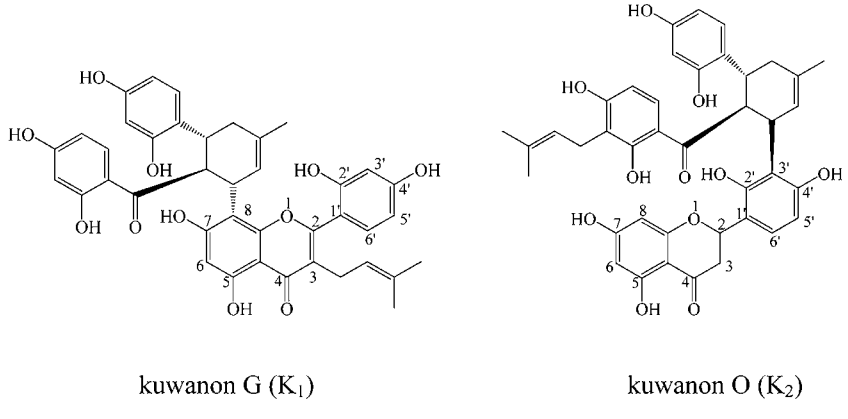

Figure 3. Chemical structures of kuwanon G (K_1) and kuwanon O (K_2).

DOI: 10.1021/jf505544e
J. Agric. Food Chem. 2015, 63, 1452−1459

Table 2. Lethal Duration (min) and Mortality of Various Concentrations of Kuwanons G and O against Theronts of *I. multifiliis* in 4 h of Exposure[a]

	lethal duration (min)		4 h of mortality (%, mean ± SD)	
concentration (mg/L)	kuwanon G	kuwanon O	kuwanon G	kuwanon O
0 (D H_2O)[b]	+[c]	+	0 a	0 a
0 (0.1% ethanol)[b]	+	+	0 a	0 a
0.125	+	+	16.8 ± 3.9 b	9.2 ± 5.8 b
0.25	+	+	24.3 ± 2.0 c	13.9 ± 2.7 b
0.5	+	+	29.1 ± 2.3 d	20.5 ± 8.2 c
1	+	+	59.8 ± 3.8 e	70.1 ± 5.9 d
2	30.7 ± 3.7 a	13.2 ± 3.0 a	100 f	100 e
4	1.3 ± 0.3 b	1.0 ± 0.2 b	100 f	100 e
8	0.7 ± 0.2 b	0.4 ± 0.1 b	100 f	100 e

[a]Values are expressed as the mean ± standard deviation of 10 replicates. In the same column, values with different letters are significantly different ($p < 0.05$). [b]Negative control groups include distilled water (D H_2O) and 0.1% ethanol. [c]+ = there are still live theronts after 4 h of exposure.

Table 3. Infection Prevalence and Intensity of Theronts Pretreated for 2 h with Various Concentrations of Kuwanon G or O on Grass Carp at 7 Days[a]

			kuwanon G		kuwanon O	
concentration (mg/L)	theronts per fish	number of fish per tank	infection prevalence[b] (%)	infection intensity[c]	infection prevalence[b] (%)	infection intensity[c]
0 (D H_2O)	20000	10	100 a	500 ± 82.6 a	100 a	500 ± 82.6 a
0 (0.1% ethanol)	20000	10	100 a	513 ± 34.5 a	100 a	513 ± 34.5 a
0.125	20000	10	100 a	238 ± 107 b	100 a	368 ± 51.2 b
0.25	20000	10	100 a	96.4 ± 20.4 c	100 a	120 ± 14.7 c
0.5	20000	10	13.3 ± 11.5 b	8.2 ± 7.8 d	23.3 ± 5.8 b	12.4 ± 8.7 d
1	20000	10	3.3 ± 5.8 b	0.5 ± 0.8 e	13.3 ± 5.8 c	1.3 ± 2.2 e

[a]Values are expressed as the mean ± SD of three replicates. In the same column, values with different letters are significantly different ($p < 0.05$). [b]Infection prevalence (%) = number of infected fish/number of total fish. [c]Infection intensity = number of white spots on fish/number of infected fish.

Table 4. Acute Toxicity of Kuwanons G and O to Grass Carp[a]

			number of dead fish in a treated group				
compound	concentration (mg/L)	number of fish per tank	24 h	48 h	72 h	96 h	mortality[b] (%, mean ± SD)
kuwanon G	0	10	0	0	0	0	0
	20	10	0	0	0	0	0
	25	10	0	0	0	0	0
	30	10	0	3	0	0	10.0 ± 10.0
	40	10	11	4	3	0	60.0 ± 17.3
	50	10	17	13	0	0	100
	60	10	30	0	0	0	100
kuwanon O	0	10	0	0	0	0	0
	20	10	0	0	0	0	0
	25	10	2	0	1	0	10.0 ± 10.0
	30	10	22	8	0	0	100
	40	10	30	0	0	0	100

[a]Each treatment group contained triplicate tanks. [b]Mortality (%) = dead fish number during 96 h/total fish number.

caused 100% mortality of theronts at the concentration of 2 mg/L between 13.2 and 30.7 min of exposure. The lethal duration was significantly shortened to less than 2 min when the concentration of each compound was increased to 4 mg/L.

Infectivity of Theronts Pretreated with Active Compounds. The theront infectivity was significantly reduced after the theronts were exposed to a low concentration of kuwanon G or O for 2 h (Table 3). Kuwanon G or O at 1 and 0.5 mg/L could protect a majority of grass carps from infestation of theronts. The infection prevalences were 3.3 and 13.3% for kuwanon G or 13.3 and 23.3% for kuwanon O at 1 and 0.5 mg/L, respectively. The infection prevalence was 100% in control groups. Meanwhile, fish showed low infection intensities of 0.5 and 8.2 for kuwanon G or 1.3 and 12.4 for kuwanon O after exposure to 1 and 0.5 mg/L for 2 h, respectively. The two compounds at 0.25 or 0.125 mg/L could not prevent infestation of *I. multifiliis* on grass carps but significantly decreased infection intensity compared to those in negative controls (Table 3).

Acute Toxicity to Grass Carp. In the acute toxicity assay, both kuwanons G and O showed external stimulation to the skin and gills of grass carp. Fish increased mucus secretion and respiratory frequency. The fish died at the concentration of ≥30 mg/L kuwanon G or ≥25 mg/L kuwanon O (Table 4). A

DOI: 10.1021/jf505544e
J. Agric. Food Chem. 2015, 63, 1452−1459

Table 5. Anti-theront Efficacy and Acute Toxicity of Kuwanons G and O to Grass Carp

	anti-theront efficacy at 4 h		acute toxicity at 96 h	
compound	EC_{50}[a] (mg/L, mean ± SD)	95% CI[b]	LC_{50}[c] (mg/L, mean ± SD)	95% CI[b]
kuwanon G	0.80 ± 0.04	0.59−1.18	38.0 ± 0.82	36.1−40.1
kuwanon O	0.80 ± 0.04	0.65−1.06	26.9 ± 0.51	25.9−28.0

[a]EC_{50} = median effective concentration. [b]95% CI = 95% confidence interval. [c]LC_{50} = median lethal concentration.

100% fish mortality was observed at 50 mg/L kuwanon G or 30 mg/L kuwanon O after 48 h of exposure. There was no fish death in the control groups during the experiments. The 96 h LC_{50} values of kuwanons G and O to grass carp were 38.0 ± 0.82 and 26.9 ± 0.51 mg/L (Table 5).

DISCUSSION

Medical plants contain natural products with a large number of pharmacologically active compounds. In previous studies, crude extracts of some medical plants showed antiprotozoal activity against *I. multifiliis*.[11−13,22,23,27] However, there is an information limit on the purification and identification of the compounds responsible for the antiparasitic activity.[14−17,28] In this study, ethanol extracts of the root bark of *M. alba* were used for bioassay-guided isolation. The ethyl acetate fraction showed strong anti-Ich activity and was used for further separation and purification. Finally, two active flavonoids were identified as kuwanons G and O with similar structural skeletons and owning the same substituent groups. Kuwanon G is a flavone, but kuwanon O is a flavonone, which is from a flavone hydrogenated at the second and third positions of a double carbon−carbon bond. The similar structure and same substituent groups may be responsible for the similar anti-*I. multifiliis* activity of the two compounds. However, the substituent groups are at different positions of the basic structural skeletons. This may be the reason for difference on antiparasitic efficiency between the two compounds. The phenomenon was also found for other compounds in publications.[29−34] The data above suggest that the compound structure may determine its activity against *I. multifiliis*.

Recent studies suggest that flavonoids with phenolic hydroxyl groups or an isopentene group usually show cytotoxicity and antimicrobial activity because they can easily penetrate the cell membrane and result in perforation and leakage.[35−39] Both kuwanons G and O have eight phenolic hydroxyl groups and one isopentene group; therefore, these two compounds might damage the cell membrane of *I. multifiliis* and finally kill the parasite. The exact anti-*I. multifiliis* mechanism of these two flavonoids needs further study.

In previous studies, kuwanon G was reported to possess various biological activities, including antibacterial,[20] hypotensive,[40] and antinociceptive[41] activities. Kuwanon O, another active compound, was found to have antioxidant[42] and tyrosinase inhibitory[43] activities. To the best of our knowledge, this study is the first report to demonstrate the antiparasitic efficacy of kuwanons G and O. The bioassay results showed that kuwanons G and O caused 100% mortality of *I. multifiliis* theronts at 2 mg/L or higher after a short exposure. The lethal exposure time was dramatically reduced with increment of the compound concentrations. However, the 4 h mortality of theronts was significantly reduced with the decrease of treatment concentrations when the dose of the two compounds was less than 2 mg/L. This indicated that 2 mg/L was the lowest lethal dose for kuwanon G or O to kill 100% of *I. multifiliis* theronts. In comparison to the published data, the anti-Ich efficacies of kuwanons G and O were better than those of compounds isolated from *Galla chinensis* and *Cinnamomum cassia*. Pentagalloylglucose killed all theronts at 2.5 mg/L within 228.0 min,[14] and cinnamaldehyde killed all theronts at 8 mg/L within 208.4 min.[28] In addition, the lethal exposure durations and concentrations of kuwanons G and O for killing all theronts were shorter and lower than those of some crude plant extracts and chemicals. Ethyl acetate or acetone extracts from *M. alba* root bark killed all theronts at 8 mg/L within 36.0 or 38.7 min.[22] Garlic (*Allium sativum*) extract killed all theronts at 62.5 mg/L within 15 h.[23] *Psoralea corylifolia* methanol extract killed all theronts at 5 mg/L within 4 h.[27] *Magnolia officinalis* and *Sophora alopecuroides* extracts killed all theronts at 10 mg/L within 3 or 4 h.[12] Potassium ferrate killed all theronts at 24 mg/L within 30 min.[44] Sodium percarbonate killed all theronts at 12.5 mg/L within 3 h.[23] A hydrogen peroxide, peracetic, acetic, and peroctanoic acid-based formulation (HPPAPA) killed all theronts at 8 mg/L within 60 min.[45]

Although kuwanons G and O at the concentrations of 1 mg/L or less for 4 h exposure could not kill all theronts, pretreatment of *I. multifilliis* by exposing theronts at 1, 0.5, 0.25, or 0.125 mg/L for 2 h significantly reduced theront infectivity and partially protected grass carp from infestation. Similar phenomena were observed in several previous studies. When live theronts were pretreated with pentagalloylglucose at low concentrations ranging from 0.5 to 10 mg/L for 1 h, the infectivity of the theronts on catfish was lost or greatly decreased.[14] Bronopol at a concentration of 1 mg/L could not kill 100% theronts within a 12 h exposure but significantly reduced the infection ability of theronts on rainbow trout (*Oncorhynchus mykiss*).[4] Methanol extract from *P. corylifolia* at 2.5 mg/L could not kill all theronts in 4 h but showed an adverse effect on the infectivity of *I. multifiliis*.[27] Kuwanons G and O exhibited the strongest anti-*I. multifiliis* activity compared to the agents mentioned above.

The trial result showed that kuwanons G and O had similar efficacy against *I. multifiliis* theronts. However, the LC_{50} values of the two compounds were different to fish, indicating that kuwanons G and O had various toxicity to fish. These two compounds belong to flavonoids. They are usually absorbed into blood and other tissues and then transferred to the liver for metabolism in humans.[46] Overdose of flavonoids can result in hepatotoxicity and cause liver damage.[47] No information on the metabolism and toxicity of kuwanons G or O has been reported in fish. Kuwanons G and O might have different hepatotoxicity to fish because of their different structure and positions of substituent groups. Different flavonoids have been noted to possess various metabolism ways in liver.[48] However, the toxicity mechanism between kuwanons G and O to grass carp is not clear and needs further study.

The LC_{50} values of kuwanon G (38.0 mg/L) and kuwanon O (26.9 mg/L) to grass carp were higher than those of some reported antiparasitic phytochemicals and chemotherapeutants to fish, such as dihydrochelerythrine (18.2 mg/L), dihydro-

DOI: 10.1021/jf505544e
J. Agric. Food Chem. 2015, 63, 1452−1459

sanguinarine (13.3 mg/L),[16] malachite green (0.05 mg/L),[49] copper sulfate (6.89 mg/L),[50] and potassium permanganate (17.6 mg/L).[51] The LC_{50} values of kuwanons G and O to grass carp were approximately 50−35 times the EC_{50} (0.8 mg/L for both compounds) for killing the theronts. Therefore, kuwanons G and O are safe for fish at an effective treatment concentration.

Because malachite green has been prohibited for use in food fish due to its carcinogenicity,[10,52] extensive research has been conducted to investigate alternatives to control ichthyophthiriasis in recent years.[4,6,11−17,27,28,45] Ideally, the alternative agents are safe to fish and effective to kill the parasite with low environmental impact.[53,54] This study demonstrated that kuwanons G and O from the root bark of *M. alba* possessed good anti-*I. multifiliis* activity and low toxicity to grass carp. In our previous studies, several compounds with anti-Ich activity were obtained by bioassay-guided isolation from *G. chinensis* (pentagalloylglucose),[14] *C. cassia* (cinnamaldehyde),[28] and *Cynanchum atrium* (cynatratoside-C).[17] The antiparasitic efficacy of kuwanons G and O was better than that of pentagalloylglucose or cinnamaldehyde. However, cynatratoside-C was demonstrated to have similar anti-*I. multifiliis* effects as malachite green[17] and show better anti-Ich activity than kuwanons G and O. Approximately 0.039% kuwanon G and 0.043% kuwanon O could be isolated and purified from dried *M. alba* root bark. However, only 0.0031% cynatratoside-C was isolated and purified from dried *C. atrium*. The yield of kuwanons G and O from *M. alba* root bark was 13 and 14 times that of cynatratoside-C from *C. atrium*. The cost would be lower for producing the same amount of kuwanons G and O than that for cynatratoside-C. Moreover, the market price of *M. alba* root bark was about $^1/_3$ of the price for *C. atrium*. The overall costs for producing kuwanons G and O will be cheaper than that for cynatratoside-C. The cheaper product will be easier to be commercialized. Therefore, kuwanons G and O are promising agents to become new, safe, and efficacious anti-Ich drugs. Further evaluation is needed for the effectiveness of kuwanons G and O to control ichthyophthiriasis under fish farm conditions before these two flavonoids become commercial drugs against *I. multifiliis*.

AUTHOR INFORMATION

Corresponding Author

*Telephone: +86-20-85225808, Fax: +86-20-85226263. E-mail: zhangqzdr@126.com.

Author Contributions

†Jing-Han Liang and Yao-Wu Fu contributed equally to this work.

Funding

This research was supported financially by the National High Technology Research and Development Program of China (863 Program, 2011AA10A216), the Guangzhou Science and Technology Project (2013J4100047), the Marine and Fishery Special Project of Science and Technology in Guangdong Province (A201301B05), and the Fundamental Research Funds for the Central Universities (21612111 and 21613105).

Notes

The authors declare no competing financial interest.

REFERENCES

(1) Abowei, J. F. N.; Briyai, O. F.; Bassey, S. E. A review of some basic parasite diseases in culture fisheries flagellids, dinoflagellides and ichthyophthriasis, ichtyobodiasis, coccidiosis trichodiniasis, heminthiasis, hirudinea infestation, crustacean parasite and ciliates. *Br. J. Pharmacol. Toxicol.* **2011**, *2*, 213−226.

(2) Matthews, R. A. *Ichthyophthirius multifiliis* Fouquet and ichthyophthiriosis in freshwater teleosts. *Adv. Parasitol.* **2005**, *59*, 159−241.

(3) Dickerson, H. W. *Ichthyophthirius multifiliis*. In *Fish Parasites: Pathobiology and Protection*; Woo, P. T. K., Buchmann, K., Eds.; CAB International: Wallingford, U.K., 2012; pp 55−72, ISBN: 978-1-84593-806-2.

(4) Shinn, A. P.; Picón-Camacho, S. M.; Bron, J. E.; Conway, D.; Yoon, G. H.; Guo, F. C.; Taylor, N. G. The anti-protozoal activity of bronopol on the key life-stages of *Ichthyophthirius multifiliis* Fouquet, 1876 (Ciliophora). *Parasitol. Res.* **2012**, *186*, 229−236.

(5) Schmahl, G.; Ruider, S.; Mehlhorn, H.; Schmidt, H.; Ritter, G. Treatment of fish parasites. 9. Effects of a medicated food containing malachite green on *Ichthyophthirius multifiliis* Fouquet, 1876 (Hymenostomatida, Ciliophora) in ornamental fish. *Parasitol. Res.* **1992**, *78*, 183−192.

(6) Ling, K.; Sin, Y.; Lam, T. Effect of copper sulphate on ichthyophthiriasis (white spot disease) in goldfish (*Carassius auratus*). *Aquaculture* **1993**, *118*, 23−35.

(7) Schlenk, D.; Gollon, J. L.; Griffin, B. R. Efficacy of copper sulfate for the treatment of ichthyophthiriasis in channel catfish. *J. Aquat. Anim. Health* **1998**, *10*, 390−396.

(8) Rowland, S. J.; Mifsud, C.; Nixon, M.; Read, P.; Landos, M. Use of formalin and copper to control ichthyophthiriosis in the Australian freshwater fish silver perch (*Bidyanus bidyanus* Mitchell). *Aquacult. Res.* **2008**, *40*, 44−54.

(9) Rintamaki-Kinnunen, P.; Rahkonen, M.; Mannermaa-Keranen, A. L.; Suomalainen, L. R.; Mykra, H.; Valtonen, E. T. Treatment of ichthyophthiriasis after malachite green. I. Concrete tanks at salmonid farms. *Dis. Aquat. Org.* **2005**, *64*, 69−76.

(10) Alderman, D. Malachite green: A review. *J. Fish Dis.* **1985**, *8*, 289−298.

(11) Ekanem, A. P.; Obiekezie, A.; Kloas, W.; Knopf, K. Effects of crude extracts of *Mucuna pruriens* (Fabaceae) and *Carica papaya* (Caricaceae) against the protozoan fish parasite *Ichthyophthirius multifiliis*. *Parasitol. Res.* **2004**, *92*, 361−366.

(12) Yi, Y. L.; Lu, C.; Hu, X. G.; Ling, F.; Wang, G. X. Antiprotozoal activity of medicinal plants against *Ichthyophthirius multifiliis* in goldfish (*Carassius auratus*). *Parasitol. Res.* **2012**, *111*, 1771−1778.

(13) Ling, F.; Wang, J. G.; Lu, C.; Wang, G. X.; Lui, Y. H.; Gong, X. N. Effects of aqueous extract of *Capsicum frutescens* (Solanaceae) against the fish ectoparasite *Ichthyophthirius multifiliis*. *Parasitol. Res.* **2012**, *111*, 841−848.

(14) Zhang, Q. Z.; Xu, D. H.; Klesius, P. H. Evaluation of an antiparasitic compound extracted from *Galla chinensis* against fish parasite *Ichthyophthirius multifiliis*. *Vet. Parasitol.* **2013**, *198*, 45−53.

(15) Yao, J. Y.; Shen, J. Y.; Li, X. L.; Xu, Y.; Hao, G. J.; Pan, X. Y.; Wang, G. X.; Yin, W. L. Effect of sanguinarine from the leaves of *Macleaya cordata* against *Ichthyophthirius multifiliis* in grass carp (*Ctenopharyngodon idella*). *Parasitol. Res.* **2010**, *107*, 1035−1042.

(16) Yao, J. Y.; Zhou, Z. M.; Li, X. L.; Yin, W. L.; Ru, H. S.; Pan, X. Y.; Hao, G. J.; Xu, Y.; Shen, J. Y. Antiparasitic efficacy of dihydrosanguinarine and dihydrochelerythrine from *Macleaya microcarpa* against *Ichthyophthirius multifiliis* in richadsin (*Squaliobarbus curriculus*). *Vet. Parasitol.* **2011**, *183*, 8−13.

(17) Fu, Y. W.; Zhang, Q. Z.; Xu, D. H.; Liang, J. H.; Wang, B. Antiparasitic effect of cynatratoside-C from *Cynanchum atratum* against *Ichthyophhirius multifiliis* on grass carp. *J. Agric. Food Chem.* **2014**, *62*, 7183−7189.

(18) National Pharmacopoeia Committee. *Pharmacopoeia of the People's Republic of China*; Chemical Industry Press: Beijing, China, 2010; Vol. *1*, p 26.

(19) El-Beshbishy, H. A.; Singab, A. N. B.; Sinkkonen, J.; Pihlaja, K. Hypolipidemic and antioxidant effects of *Morus alba* L. (Egyptian mulberry) root bark fractions supplementation in cholesterol-fed rats. *Life Sci.* **2006**, *78*, 2724−2733.

DOI: 10.1021/jf505544e
J. Agric. Food Chem. 2015, 63, 1452−1459

(20) Park, K.; You, J.; Lee, H.; Baek, N.; Hwang, J. Kuwanon G: An antibacterial agent from the root bark of *Morus alba* against oral pathogens. *J. Ethnopharmacol.* **2003**, *84*, 181−185.
(21) Dat, N. T.; Binh, P. T. X.; Quynh, L. T. P.; Van Minh, C.; Huong, H. T.; Lee, J. J. Cytotoxic prenylated flavonoids from *Morus alba*. *Fitoterapia* **2010**, *81*, 1224−1227.
(22) Fu, Y. W.; Zhang, Q. Z.; Xu, D. H.; Xia, H.; Cai, X. X.; Wang, B.; Liang, J. H. Parasiticidal effects of *Morus alba* root bark extracts against *Ichthyophthirius multifiliis* infecting grass carp. *Dis. Aquat. Org.* **2014**, *108*, 113−127.
(23) Buchmann, K.; Jensen, P. B.; Kruse, K. D. Effects of sodium percarbonate and garlic extract on *Ichthyophthirius multifiliis* theronts and tomocysts: *In vitro* experiments. *N. Am. J. Aquacult.* **2003**, *65*, 21−24.
(24) Takasugi, M.; Ishikawa, S.; Nagao, S.; Masamune, T.; Shirata, A.; Takahashi, K. Albanins F and G, natural Diels−Alder adducts from mulberry. *Chem. Lett.* **1980**, *(12)*, 1577−1580.
(25) Nomura, T.; Fukai, T.; Hano, Y.; Nemoto, K.; Terada, S.; Kuramochi, T. Constituents of cultivated mulberry tree. *Planta Med.* **1983**, *47*, 151−156.
(26) Hano, Y.; Hirakura, K.; Nomura, T.; Terada, S.; Fukushima, K. Components of root bark of *Morus lhou* 1. Structures of two new natural Diels−Alder adducts, kuwanons N and O. *Planta Med.* **1984**, *50*, 127−130.
(27) Ling, F.; Lu, C.; Tu, X.; Yi, Y. L.; Huang, A. G.; Zhang, Q. Z.; Wang, G. X. Antiprotozoal screening of traditional medicinal plants: Evaluation of crude extract of *Psoralea corylifolia* against *Ichthyophthirius multifiliis* in goldfish. *Parasitol. Res.* **2013**, *112*, 2331−2340.
(28) Liang, J. H.; Zhang, Q. Z.; Fu, Y. W.; Wang, B. Effect of cinnamaldehyde from *Cinnamomum cassia* on killing *Ichthyophthirius multifiliis in vitro*. *J. Fish. China* **2014**, *38*, 457−463 (in Chinese with an English abstract).
(29) Song, H.; Liu, Y.; Liu, Y.; Wang, L.; Wang, Q. Synthesis and antiviral and fungicidal activity evaluation of β-carboline, dihydro-β-carboline, tetrahydro-β-carboline alkaloids, and their derivatives. *J. Agric. Food Chem.* **2014**, *62*, 1010−1018.
(30) Zhou, Z. Y.; Liu, W. X.; Pei, G.; Ren, H.; Wang, J.; Xu, Q. L.; Xie, H. H.; Wan, F. H.; Tan, J. W. Phenolics from *Ageratina adenophora* roots and their phytotoxic effects on *Arabidopsis thaliana* seed germination and seedling growth. *J. Agric. Food Chem.* **2013**, *61*, 11792−11799.
(31) Zhang, Y.; Wang, J.-S.; Wang, X.-B.; Gu, Y.-C.; Wei, D.-D.; Guo, C.; Yang, M.-H.; Kong, L.-Y. Limonoids from the fruits of *Aphanamixis polystachya* (Meliaceae) and their biological activities. *J. Agric. Food Chem.* **2013**, *61*, 2171−2182.
(32) Wang, K. P.; Zhang, Q. L.; Liu, Y.; Wang, J.; Cheng, Y.; Zhang, Y. Structure and inducing tumor cell apoptosis activity of polysaccharides isolated from *Lentinus edodes*. *J. Agric. Food Chem.* **2013**, *61*, 9849−9858.
(33) Kim, M. G.; Yang, J. Y.; Lee, H. S. Acaricidal potentials of active properties isolated from *Cynanchum paniculatum* and acaricidal changes by introducing functional radicals. *J. Agric. Food Chem.* **2013**, *61*, 7568−7573.
(34) Demirkiran, O.; Sabudak, T.; Ozturk, M.; Topcu, G. Antioxidant and tyrosinase inhibitory activities of flavonoids from *Trifolium nigrescens* subsp. *petrisavi*. *J. Agric. Food Chem.* **2013**, *61*, 12598−12603.
(35) Mun, S. H.; Joung, D. K.; Kim, S. B.; Park, S. J.; Seo, Y. S.; Gong, R.; Choi, J. G.; Shin, D. W.; Rho, J. R.; Kang, O. H.; Kwon, D. Y. The mechanism of antimicrobial activity of sophoraflavanone B against methicillin-resistant *Staphylococcus aureus*. *Foodborne Pathog. Dis.* **2014**, *11*, 234−239.
(36) Thabti, I.; Elfalleh, W.; Tlili, N.; Ziadi, M.; Campos, M. G.; Ferchichi, A. Phenols, flavonoids, and antioxidant and antibaterial activity of leaves and stem bark of *Morus* species. *Int. J. Food Prop.* **2014**, *17*, 842−854.
(37) Yin, S.; Fan, C. Q.; Wang, Y.; Dong, L.; Yue, J. M. Antibacterial prenylflavone derivatives from *Psoralea corylifolia*, and their structure−activity relationship study. *Bioorg. Med. Chem.* **2004**, *12*, 4387−4392.
(38) Tsuchiya, H.; Iinuma, M. Reduction of membrane fluidity by antibacterial sophoraflavanone G isolated from *Sophora exigua*. *Phytomedicine* **2000**, *7*, 161−165.
(39) Sohn, H. Y.; Son, K. H.; Kwon, C. S.; Kwon, G. S.; Kang, S. S. Antimicrobial and cytotoxic activity of 18 prenylated flavonoids isolated from medicinal plants: *Morus alba* L., *Morus mongolica* Schneider, *Broussnetia papyrifera* (L.) Vent, *Sophora flavescens* Ait and *Echinosophora koreensis* Nakai. *Phytomedicine* **2004**, *11*, 666−672.
(40) Nomura, T. The chemistry and biosynthesis of isoprenylated flavonoids from moraceous plants. *Pure Appl. Chem.* **1999**, *71*, 1115−1118.
(41) Santos, A. R. S.; Yunes, R. A.; Cechinel-Filho, V.; Ferrari, F.; Delle-Monache, F.; Messana, I.; Calixto, J. B. Mechanisms underlying the antinociceptive actions of the Diels−Alder adduct kuwanon G isolated from *Morus bombycis*. *Phytomedicine* **2000**, *7* (Supplement 2), 98−98.
(42) Kang, J.; Chen, R. Y.; Yu, D. Q. Five new Diels−Alder type adducts from the stem and root bark of *Morus mongolica*. *Planta Med.* **2006**, *72*, 52−59.
(43) Zheng, Z. P.; Tan, H. Y.; Wang, M. Tyrosinase inhibition constituents from the roots of *Morus australis*. *Fitoterapia* **2012**, *83*, 1008−1013.
(44) Ling, F.; Wang, J. G.; Liu, Q. F.; Li, M.; Ye, L. T.; Gong, X. N. Prevention of *Ichthyophthirius multifiliis* infestation in goldfish (*Carassius auratus*) by potassium ferrate(VI) treatment. *Vet. Parasitol.* **2010**, *168*, 212−216.
(45) Picón-Camacho, S. M.; Marcos-Lopez, M.; Beljean, A.; Debeaume, S.; Shinn, A. P. *In vitro* assessment of the chemotherapeutic action of a specific hydrogen peroxide, peracetic, acetic, and peroctanoic acid-based formulation against the free-living stages of *Ichthyophthirius multifiliis* (Ciliophora). *Parasitol. Res.* **2012**, *110*, 1029−1032.
(46) Aheme, S. A.; Nora, M. O. B. Dietary flavonols chemistry, food content, and metabolism. *J. Nutr.* **2002**, *18*, 75−81.
(47) Galati, G.; O' Brien, P. J. Potential toxicity of flavonoids and other dietary phenolics: Significance for their cemopreventive and anticancer properties. *Free Radical Biol. Med.* **2004**, *37* (3), 287−303.
(48) Kim, S. H.; Lee, M. G. Phamacokinetics of ipriflavone, an isoflavone derivative, after intravenous and oral administration to rats hepatic and intetinal first-pass effects. *Life Sci.* **2002**, *70*, 1299−1315.
(49) Bills, T. D.; Marking, L. L.; Chandler, J. H., Jr. Malachite green: Its toxicity to aquatic organisms, persistence and removal with activated carbon. *Invest. Fish Control* **1977**, *75*, 1−6.
(50) Straus, D. L. Species sensitivity to copper: Acute toxicity to channel catfish, *Ictalurus punctatus* and sunshine bass, *Morone chrysops* × *M. saxatilis*. *J. Appl. Aquacult.* **2006**, *18*, 89−99.
(51) Tucker, C. S. Acute toxicity of potassium permanganate to channel catfish fingerlings. *Aquaculture* **1987**, *60*, 93−98.
(52) Wahli, T.; Schmitt, M.; Meier, W. Evaluation of alternatives to malachite green oxalate as a therapeutant for ichthyophthiriosis in rainbow trout *Oncorhynchus mykiss*. *J. Appl. Ichthyol.* **1993**, *9*, 237−249.
(53) Kim, M. G.; Jeon, J. H.; Lee, H. S. Larvicidal activity of the active constituent isolated from *Tabebuia avellanedae* bark and structurally related derivatives against three mosquito species. *J. Agric. Food Chem.* **2013**, *61*, 10741−10745.
(54) Tabanca, N.; Bernier, U. R.; Ali, A.; Wang, M.; Demirci, B.; Blythe, E. K.; Khan, S. I.; Baser, K. H.; Khan, I. A. Bioassay-guided investigation of two *Monarda* essential oils as repellents of yellow fever mosquito *Aedes aegypti*. *J. Agric. Food Chem.* **2013**, *61*, 8573−8580.

DOI: 10.1021/jf505544e
J. Agric. Food Chem. 2015, 63, 1452−1459

Table 1. Sequences of PCR Primers

target	primer pair	sequences (5′ to 3′)	bacterial strains for standard curve
Lactobacillus spp.	forward	AGCAGTAGGGAATCTTCCA	*Lactobacillus delbrueckii* subsp. *Bulgaricus* (KCTC3635)[56,57]
	reverse	CACCGCTACACATGGAG	
Bifidobacterium spp.	forward	CTCCTGGAAACGGGTGG	*Bifidobacterium animalis* subsp. *Lactis* (KCTC 5854)[58]
	reverse	GGTGTTCTTCCCGATATCTACA	
Enterococcus spp.	forward	CCCTTATTGTTAGTTGCCATCATT	*Enterococcus faecalis* (KCTC 3206)[59]
	reverse	ACTCGTTGTACTTCCCATTGT	
Clostridium letpum	forward	GCACAAGCAGTGGAGT	*Clostridium leptum* (KCTC 5155)[60]
(cluster IV)	reverse	CTTCCTCCGTTTTGTCAA	
Enterobacteriaceae	forward	TGCCGTAACTTCGGGAGAAGGCA	*Escherichia coli* (KCTC1682)[61]
	reverse	TCAAGGCTCAATGTTCAGTGTC	
Bacteroides fragilis	forward	CTGAACCAGCCAAGTAGCG	*Bacteroides fragilis* (KCTC1322)[62]
	reverse	CCGCAAACTTTCACAACTGACTTA	
total bacteria	forward	TCCTACGGGAGGCAGCAGT	*Escherichia coli* (KCTC1682)[63]
	reverse	GGACTACCAGGGTATCTAATCCTGTT	
Bacteroidetes	forward	CATGTGGTTTAATTCGATGAT	*Bacteroides fragilis* (KCTC1322)[64]
	reverse	AGCTGACGACAACCATGCAG	
Firmicutes	forward	ATGTGGTTTAATTCGAAGCA	*Lactobacillus delbrueckii* subsp. *Bulgaricus* (KCTC3635)[64]
	reverse	AGCTGACGACAACCATGCAC	
Proteobacteria	forward	CATGACGTTACCCGCAGAAGAAG	*Escherichia coli* (KCTC1682)[38,65]
	reverse	CTCTACGAGACTCAAGCTTGC	

gene	primer pair	5′ primer sequence 3′	product size (bp)
FGF15/19	forward	ACCCGCCTGCAGTACCTGT	224
	reverse	GCCGAGTAATGAATCAGCC	
OCLN	forward	GGAATACCCACCTATCACTTC	186
	reverse	TCATCAGCGGCAGCCATGTA	
ZO-1	forward	GGTGTGTTGAGTTCCATAGAAAC	236
	reverse	CAGGTTTTAGGGTCACAGTGT	

diet did not induce obesity.[17] Germ-free mice on a HF diet did not become obese.

Several lines of research have suggested that the regulation of a host's metabolism by its intestinal microbiota occurs through alteration of the host's nuclear receptor signaling via production of secondary metabolites by bacteria. Intestinal bacteria have been shown to produce short chain fatty acids (SCFAs), which reduce insulin-stimulated fat accumulation via the SCFA receptor GPR43.[18] Trimethylamine-N-oxide (TMAO), another metabolite produced by intestinal bacteria, was associated with cardiovascular risk factors via multiple macrophage scavenger receptors.[19] Reduction of the genus *Lactobacillus* following treatment with the antioxidant, tempol (4-hydroxy-2,2,6,6-tetramethylpiperidin-1-oxyl), caused accumulation of tauro-β-muricholic acid (T-β-MCA) and inactivation of the intestinal farnesoid X (nuclear) receptor (FXR).[20] Gut microbiota modulation of fasting-induced adipocyte factor (Fiaf) gene expression in the intestine and cytochrome P450 7A1 (CYP7A1) gene expression in the liver indicates a role of gut microbiota in host lipid and bile acid metabolism.[21,22] Taken together, these findings suggest that restoration of the healthy phenotypic intestinal microbiota through diet may be a preferred strategy for preventing or treating obesity-related metabolic diseases.

Our previous work[23] has shown that hamsters fed a HF and hypercholesterolemic diet supplemented with white wine grape seed flour (ChrSd diet) exhibited significantly lowered plasma low density lipoprotein (LDL)-, very low density lipoprotein (VLDL)-, total-cholesterol concentrations, abdominal adipose tissue weight, and body weight gain compared to those fed a control diet. To date, the prebiotic effects of whole grape seed itself are largely unknown since most studies have utilized aqueous or alcoholic polyphenolic grape seed extracts. To our knowledge, the effect of wine varietal grape seed flour on intestinal microbiota composition has not been evaluated. In this study, we extended our previous research to evaluate a select number of bacteria from hamster feces by reverse transcription quantitative polymerase chain reaction (RT-qPCR) of 16S rRNA and correlated their relative abundances with physiological changes in order to determine whether metabolic effects were associated with intestinal microbiota in male Syrian Golden hamsters fed HF diets supplemented with grape seed flours from red and white wine production.

MATERIALS AND METHODS

Animals and Diets. Male Syrian Golden hamsters (approximately 80 g, LVG strain, Charles River Laboratories, Wilmington, MA) were randomized into three groups of 10 hamsters each and fed HF diets (37% of energy as fat, 18% as protein, and 45% as carbohydrate) *ad libitum* containing 10% (w/w) grape seed flour (Chardonnay or Cabernet Sauvignon from Sonomaceuticals, LLC/WholeVine Products, Santa Rosa, CA) and a control diet containing 5% microcrystalline cellulose (MCC; Dyets Inc. Bethlehem, PA) for 3 weeks as shown in our previous study.[23] Microcrystalline cellulose (MCC), an insoluble fiber, has little effect on energy or sterol metabolism.[24] Grape pomace was obtained from coastal vineyards in Sonoma County, California. Seeds from the 2010 vintage were screened and dried using heated air (55−70 °C) to be separated from skins and stems. Oil was pressed from the seed, and the residual press cake was then milled to pass through an 85 mesh sieve. Body weights were monitored weekly, and food intake was recorded twice per week. Feces were collected during the last 3 consecutive days of the feeding period and were lyophilized, milled, and stored at −20 °C. Blood was collected by cardiac puncture with syringes previously rinsed with potassium EDTA solution (15 wt %/v) after hamsters were feed-deprived for 12 h and anesthetized with isoflurane (Phoenix

DOI: 10.1021/jf5026373
J. Agric. Food Chem. 2015, 63, 1460−1467

Pharmaceutical, St. Joseph, MO). The plasma was separated after centrifugation at 2000 × *g* for 30 min at 4 °C. Livers, intestines, and adipose tissues (epididymal and perirenal adipose tissues) were collected, weighed, and immediately frozen in liquid nitrogen for later analysis. The protocol, #P-04−02, was reviewed and approved by the Animal Care and Use Committee, Western Regional Research Center, Albany, CA. The male Syrian hamster was used since its hepatic cholesterol and bile acid metabolism is more similar to humans compared to mice and rats.[25,26]

Plasma Lipoproteins and Hepatic and Fecal Lipids Analysis. Cholesterol in plasma lipoproteins was determined by size-exclusion chromatography as previously described.[23,27] Liver and fecal total lipid contents were determined gravimetrically as described before.[23,30]

Fecal Microbiota Analysis. A 200 mg sample of lyophilized fecal samples was added to 10 volumes of RNA later-ICE (Applied Biosystems, Foster City, CA, USA) for 24 h for RNA stabilization. Total RNA from fecal samples was extracted using a Stool Total RNA purification kit (Norgen Biotek Inc., Thorold, ON, Canada), and cDNA was synthesized using a PrimeScript RT reagent kit (TaKaRa Biotechnology, Shiga, Japan) per the manufacturer's protocol. Quantitative PCR was performed on an AB 7500 real-time PCR system (Applied Biosystems) using SYBR Premix Ex Taq (TaKaRa Biotechnology). Individual bacteria strains for generation of standard curve were obtained from Korean Collection for Type Cultures (KCTC), grown in pure culture media, and then isolated cDNA was serially diluted to generate the standard curve. The bacteria number from each sample was calculated by comparing the Ct value derived from the standard curve with the 7500 Software 2.01. Standard curves were generated by a serial 10-fold dilution of DNA from pure cultures, 10^1−10^{12} copies/g feces. The data represented the mean values of duplicate qPCR analysis. Bacterial groups reported to impart health benefits or prevent obesity-related metabolic disorders were selected for this study. The bacterial primer sequences are shown in Table 1. The cycle conditions were as follows: 30 s at 95 °C followed by 40 cycles of incubation at 95 °C for 5 s and 60 °C for 34 s. The experimental data were analyzed with the 7500 Software v2.0.1 (Applied Biosystems).

Hepatic and Intestinal Gene Expression by Real-Time (RT)-PCR. Total RNA from livers and intestines was extracted using a TRIzol plus RNA purification kit (Invitrogen, Life Technologies, Carlsbad, CA), and cDNA was synthesized using a GeneAmpRNA PCR kit (Applied Biosystems, Foster City, CA) per the manufacturer's protocol. One microliter of diluted cDNA (1:10) was used in each real-time RT-PCR using SYBR Green Supermix (Bio-Rad, Hercules, CA) with an Mx3000P instrument (Stratagene, Cedar Creek, TX). The cycle conditions were as follows: 5 min at 95 °C followed by 40 cycles of incubation at 94 °C for 15 s, then 58−60 °C for 1 min and 72 °C for 30 s. The sequences of the primers used for this study are shown in Table 1 and our previous study.[28,29] The primers were validated by size and sequencing of PCR products. No accumulation of nonspecific products and primer dimers was observed in a gel electrophoresis test of the PCR products. The results were analyzed using the software provided with the Stratagene Mx3000P QPCR system. Differences in mRNA expression for intestines and livers were calculated after normalizing to β-Actin or 36B4 mRNA expression.

Statistical Analysis. All data are expressed as means ± SE. One-way analysis of variance (ANOVA) was performed to examine the effect of treatment on plasma biomarkers, lipid levels, and body and tissue weights using the JMP7 statistical program (SAS Institute, Cary, NC). Tukey−Kramer honestly significant difference (HSD) tests were used to determine the significant differences in group means. Pearson correlation coefficients were calculated to investigate relationships between the abundance of intestinal bacteria and plasma cholesterol concentrations as well as liver, adipose tissue, and body weights. Significance was defined at $P < 0.05$.

RESULTS

Metabolic Effects of Grape Seed Flour Supplementation on Hamsters. Plasma VLDL-, LDL-, and total-cholesterol concentrations of hamsters fed the ChrSd diet were 73, 56, and 38%, respectively, lower compared with the control diet ($P < 0.05$) (Table 2). The CabSd diet did not lower plasma cholesterol concentration when compared to the control diet (Table 2). The ChrSd diet also significantly lowered hepatic total lipid concentration by 24% compared to the control diet ($P < 0.05$) (Table 2). Fecal percent total lipid of the grape seed diets did not significantly differ from the control diet (Table 2).

Table 2. Plasma Lipid Concentrations and Hepatic and Fecal Total Lipid Contents in Hamsters Fed HF Control, ChrSd, and CabSd Diets for 3 Weeks[a,b]

	control	ChrSd	CabSd
Plasma Lipid (mg/dL)			
VLDL-cholesterol	23.6 ± 3.5[a]	6.5 ± 1.3[b]	25.6 ± 5.2[a]
LDL-cholesterol	75.2 ± 12.4[a]	33.4 ± 6.6[b]	85.7 ± 7.2[a]
HDL-cholesterol	90.3 ± 4.2[a]	77.6 ± 4.0[ab]	75.4 ± 3.7[b]
total-cholesterol	189.1 ± 14.9[a]	117.6 ± 6.7[b]	186.7 ± 8.9[a]
LDL/HDL	0.8 ± 0.1[a]	0.5 ± 0.1[b]	1.2 ± 0.1[a]
hepatic percent total lipid content (g/100g)	23.9 ± 1.0[a]	18.1 ± 1.0[b]	21.6 ± 1.4[a]
fecal percent total lipid content (g/100g)	2.6 ± 0.5[a]	2.9 ± 0.9[a]	2.3 ± 0.4[a]

[a]ChrSd, Chardonnay seed; CabSd, Cabernet Sauvignon seed. [b]Values are means ± SE, $n = 10$. Different letters indicate significant difference at $P < 0.05$.

The total methanol extractable flavonoid content of the CharSd was 1.4-fold greater than that of CabSd as described in our previous study.[23] The higher levels of flavonoids in red wines and lower levels in seeds are partly due to the ethanol extraction of flavonoids during fermentation. Different processing methods for white and red wine account for some of the differences in flavonoid content; the whole fruit including seed is fermented for the production of red wines; however, only the juice is fermented in typical white wine production.

Fecal Microbiota Profiles by Chardonnay and Cabernet Grape Seed Flour Supplementation. ChrSd supplementation significantly lowered numbers of total bacteria in feces compared to the HF control diet (Figure 1A). Relative abundance of *Bifidobacterium* spp. and *Lactobacillus* spp. in feces was significantly lowered by the ChrSd diet compared to the HF control diet (Figure 1B). In contrast, relative abundance of *Bacteroides fragilis* was significantly greater in feces of the ChrSd diet than the control diet (Figure 1B). The CabSd diet significantly lowered relative abundance of *Enterobacteriaceae* in feces compared to the control diet (Figure 1B). At a phylum level, relative abundance of *Bacteroidetes* tended to be greater, and *Firmicutes* were markedly lower in the ChrSd diet compared to the control diet; this resulted in a significant reduction in the ratio of *Firmicutes*/*Bacteroidetes* (F/B) (Figure 2A,B). Relative abundance of *Proteobacteria* numbers was significantly lower in the CabSd diet than in the control diet (Figure 2A).

Expression of Hepatic and Intestinal Genes following Chardonnay Grape Seed Flour Supplementation. The expression of FGF15/19, a downstream target gene of FXR, in the intestine of hamsters fed the ChrSd diet was one-tenth that of hamsters fed the control diet (Figure 3). The mRNA levels of ZO-1 (zonula occludens 1) and OCLN (occludin), genes that encode intestinal tight junction proteins, were not significantly affected by the ChrSd diet (Figure 3). The

DOI: 10.1021/jf5026373
J. Agric. Food Chem. 2015, 63, 1460−1467

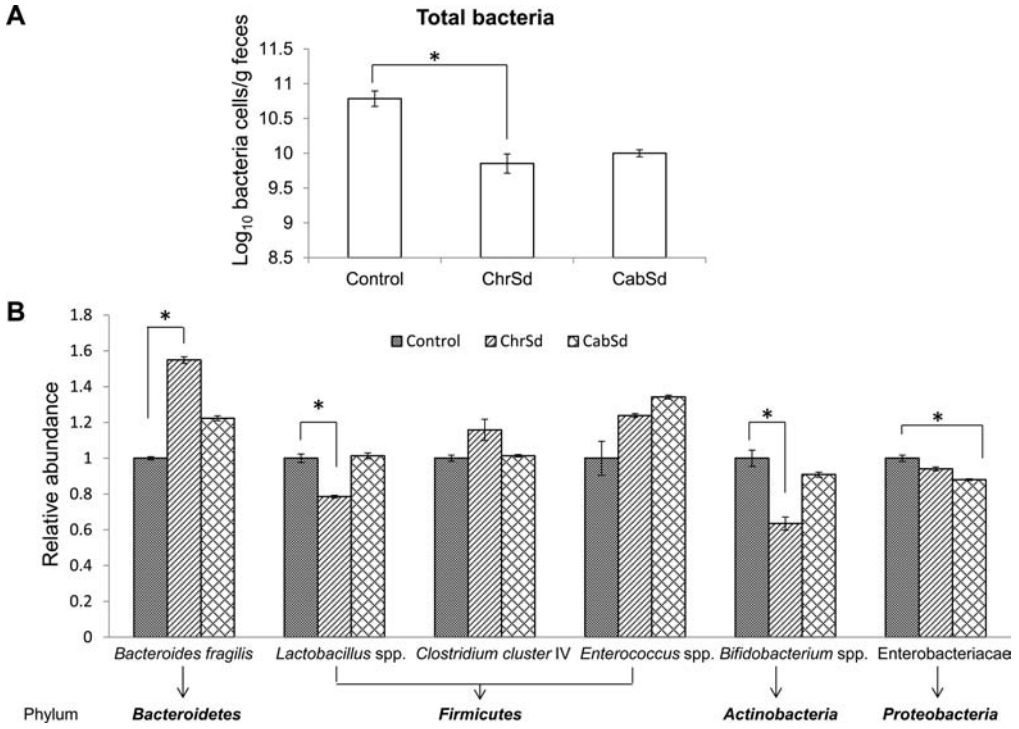

Figure 1. Effect of grape seed flour diets on numbers of total bacteria (A) and relative abundance of specific intestinal bacteria (B). Male Golden Syrian hamsters were fed HF diets containing 10% (w/w) Chardonnay (ChrSd), Cabernet Sauvignon (CabSd) grape seed flours, and 5% MCC (control) for 3 weeks. Data are expressed as means ± SE; n = 4/group. ∗ indicates significant difference at $P < 0.05$.

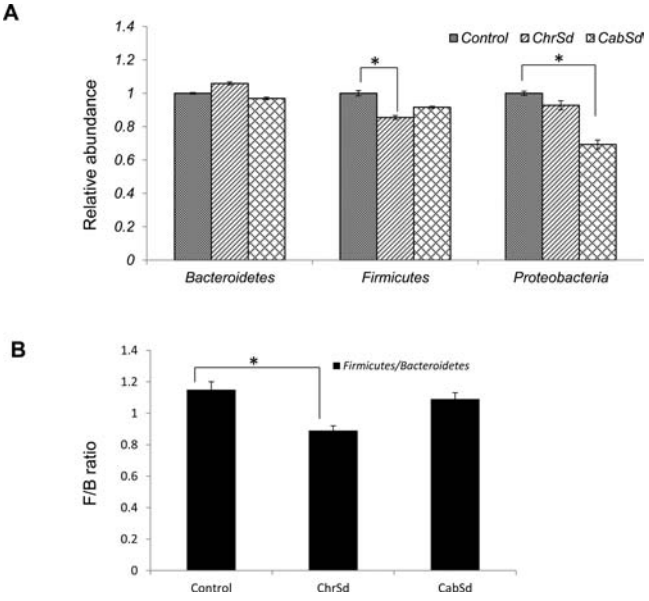

Figure 2. Effect of grape seed flour diets on relative phylum abundance of intestinal bacteria (A) and ratio of *Firmicutes* to *Bacteroidetes* (B). Male Golden Syrian hamsters were fed HF diets containing 10% (w/w) Chardonnay (ChrSd), Cabernet Sauvignon (CabSd) grape seed flours, and 5% MCC (control) for 3 weeks. Data are expressed as means ± SE; n = 4/group. ∗ indicates significant difference at $P < 0.05$.

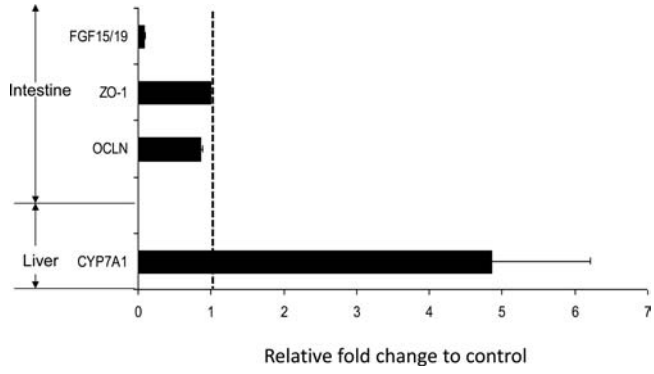

Figure 3. Relative expression of FGF15/19, ZO-1, and OCLN genes in ileum and CYP7A1 in liver of hamsters fed HF diet supplemented with 10% (w/w) Chardonnay (ChrSd) grape seed flours and 5% MCC (control) for 3 weeks. Data are expressed as mean ± SE; n = 5/group.

mRNA level of CYP7A1, the gene that controls the rate-limiting step of bile acid synthesis from cholesterol, was 4.9-fold greater in the livers of hamsters fed the ChrSd diet compared to those fed the control diet (Figure 3).

Correlation of Intestinal Microbiota–Host Metabolic Effects. Correlations of specific genus/species and phylum of intestinal microbiota with plasma cholesterol concentrations, liver, adipose tissue, and body weight were calculated to determine if the changes of the host physiological characteristics were associated with changes in the microbiota after grape seed flavonoid intake (Table 3). Relative abundance of *Lactobacillus* spp. and the F/B ratio showed strong positive correlations to plasma total-, LDL-cholesterol concentrations, and liver weights ($P < 0.05$). Relative abundance of *Bifidobacterium* spp. ($P < 0.01$) and *Firmicutes* ($P < 0.05$) both showed significant positive relationships with liver weights. Relative abundance of *B. fragilis* showed a significant negative relationship with liver weights ($P < 0.01$).

DISCUSSION

The association between the health benefits of grape flavonoids, such as amelioration of cardiovascular and obesity risk factors,

DOI: 10.1021/jf5026373
J. Agric. Food Chem. 2015, 63, 1460−1467

Table 3. Correlations between Plasma Cholesterol Concentrations, Body and Organ Weights, and Fecal Microbiota[a,b]

type of bacteria	total-C	VLDL-C	LDL-C	HDL-C	liver	adipose tissue	body weight
Phylum *Bacteroidetes*	−0.47	−0.51	−0.46	0.00	−0.56	−0.49	−0.57
Species *Bacteroides fragilis*	−0.36	−0.24	−0.41	0.00	−0.87**	−0.41	−0.49
Phylum *Firmicutes*	0.54	0.22	0.57	0.22	0.65*	0.14	0.28
Species *Clostridium Cluster IV*	−0.24	−0.26	−0.20	0.26	−0.36	−0.32	−0.40
Genus *Lactobacillus* spp.	0.62*	0.40	0.69*	0.00	0.62*	0.39	0.49
Genus *Enterococcus* spp.	0.00	0.36	−0.20	0.26	0.00	0.26	0.10
Phylum *Actinobacteria*							
Genus *Bifidobacterium* spp.	0.53	0.36	0.56	0.10	0.78**	0.46	0.55
Phylum *Proteobacteria*	0.14	0.60*	0.10	0.39	0.20	0.66*	0.36
Family *Enterobacteriaceae*	0.00	0.35	0.00	0.36	0.10	0.44	0.00
Ratio of F/B[c]	0.63*	0.41	0.66*	0.14	0.73**	0.33	0.46
Total bacteria	0.44	0.35	0.46	0.26	0.45	0.00	0.00

[a]Total-C, total cholesterol; VLDL-C, very low density lipoprotein cholesterol; LDL-C, low density lipoprotein cholesterol; HDL-C, high density lipoprotein cholesterol. [b]Values are Pearson correlation, $n = 12$; $*P < 0.05$; $**P < 0.01$. [c]Ratio of *Firmicutes*/*Bacteroidetes*.

and changes in intestinal microbiota composition has profound implications for the relationship between diet and chronic metabolic disease. The present study provides further indirect evidence for the potential role of the intestinal microbiota in metabolic dyslipidemia. Quantification of selected species/genera and phylum of fecal bacteria from obese and hypercholesterolemic hamsters revealed that supplementation of flavonoid-rich Chardonnay grape seed flour (ChrSd diet) significantly altered intestinal microbiota composition and total number. These modifications were correlated to the prevention of ectopic HF-induced hepatic fat deposition, decreased adipose tissue accumulation and body weight gain, and reduced plasma LDL-, VLDL-, and total-cholesterol concentrations by supplementation of the HF diet with Chardonnay grape seed flour.

The ChrSd diet significantly lowered numbers of total bacteria and relative abundance of *Bifidobacterium* spp. and *Lactobacillus* spp. compared to control. It has been previously shown that there is a positive relationship between total flavonoid content in grape-derived products (pomace or grape seed extract) with selective antimicrobial activity.[30−36] Calculated intakes of flavonoids from our previous study[23] by the hamsters from ChrSd and CabSd diets are about 1000 and 700 mg/kg body wt/d, respectively, and total epicatechin intakes of about 138 and 21 mg/kg body wt/d, respectively. Therefore, lower numbers of total bacteria were associated with higher total catechin content in the grape seed diets, which supports the role of flavonoids as the potential bioactive component responsible for selective antimicrobial effects of Chardonnay grape seed flour on these bacteria. However, other studies reported either no effect or stimulation of growth of *Lactobacillus* spp. or *Bifidobacterium* spp. in the presence of grape or related flavonoids. Tea flavonoids, for example, did not affect growth of these bacteria.[37] Flavonoid intake from red wine or procyanidin-rich grape seed extract was found to stimulate growth of *Bifidobacterium* spp. in human studies.[13,38] Consumption of red wine polyphenols significantly increased numbers of *Bifidobacterium* as well as *Enterococcus*, *Prevotella*, and *Bacteroides*, while it reduced total- and HDL-cholesterol concentrations in a small ($n = 10$) human study.[38] Phenolic extracts from grape pomace increased the growth of *Lactobacillus acidophilus* in an *in vitro* study.[39] Malvidin, an anthocyanidin extracted from grape pomace, and enocianin, an anthocyanin extracted from grape skin, both significantly enhanced the growth of *Bifidobacterium* spp. and *Lactobacillus*−*Enterococcus* spp. in human fecal slurries.[40] At low (150 mg/L) but not high (1000 mg/L) levels, (+)-catechin itself was shown to significantly stimulate growth of *Bifidobacterium* spp. in an *in vitro* study.[11] These discrepancies with our results may be due to *in vivo* versus *in vitro* models, different species (rat, hamster, or human), gut biotype, and dosage threshold. Nonetheless, our observed effect of the ChrSd diet on intestinal bacteria may possibly represent the effects of multiple constituents specific to Chardonnay grape seed flour.

The hypocholesterolemic properties of probiotic bacteria are still unclear.[41] Previously, probiotic *Lactobacillus* and *Bifidobacteria* have been shown to possess bile salt hydrolase (BSH) activity that promotes bile acid excretion by increasing deconjugation of bile acids.[42] Excretion of bile acids leads to a reduction of plasma cholesterol concentration by a compensatory mechanism since cholesterol is the precursor of bile acids in the liver.[43] However, the present study exhibited no significant change in fecal lipid excretion after the ChrSd diet was consumed. Alternatively, studies suggest that intestinal microbiota regulate bile acid metabolism via intestinal FXR signaling and hepatic expression of genes related to bile acid pathway.[22] It has been shown that germ-free mice had lower expression of FGF15 in the intestine, which attenuated FGF15-mediated down-regulation of CYP7A1 in the liver compared to conventional mice.[22] This effect was not observed in FXR-deficient mice. Furthermore, treatment of mice with a strong antioxidant (tempol) inactivated intestinal FXR, which led to a significant reduction in the genus *Lactobacillus* and caused down-regulation of FGF15 expression in the intestine.[20] Our results are similar to these previous reports in that the ChrSd diet lowered the relative abundance of genus *Lactobacillus* in the intestine and that mRNA levels for both FGF15/19 in the intestine and CYP7A1 in the liver were altered compared to the control diet. These findings suggest that a modification of gut microbiota, such as reduction of *Lactobacillus* spp., by the ChrSd diet affects hepatic bile acid metabolism and improved plasma cholesterol concentrations in hypercholesterolemic hamsters possibly by activation of intestinal FXR.

Recent studies have brought light to alterations in gut microbiota that are linked to the development of obesity in both animal models and humans.[44] Our previous study showed that ChrSd supplementation of the HF diet for 3 weeks significantly reduced body weight gain and adipose tissue weights by 31 and 23%, respectively, compared to the control diet.[23] Body weight gains (g) in control, ChrSd, and CabSd

DOI: 10.1021/jf5026373
J. Agric. Food Chem. 2015, 63, 1460−1467

diets were 34.7 ± 1.9, 23.9 ± 1.9, and 38.8 ± 1.9, respectively.[23] Here we observed that reduction of adipose tissue and body weight was accompanied by an increased relative abundance of *B. fragilis* and reduced relative abundance of *Lactobacillus* spp. and *Firmicutes*. The F/B ratio was also lowered by ChrSd supplementation. Consistent to our study, previous studies have shown that *Bacteroidetes* numbers including the *B. fragilis* group were increased with weight loss in obese human subjects undergoing dietary or surgical interventions.[45] Several studies such as a recent report have shown that on HF diets, obese-prone rats had a higher F/B ratio compared to obese-resistant rats.[46] However, other studies, for example, in obese humans, have not shown a causative relationship between the ratio of intestinal F/B and obesity.[47] We have also found similar percentage levels of *Firmicutes* and *Bacteroidetes* compared to total number of bacteria in feces of mice fed ChrSd diets by next generation sequencing (NGS, data not shown). *Lactobacillus* numbers were elevated in obese humans and animals.[48−50] The converse was demonstrated when a reduction of the genus *Lactobacillus* contributed to inactivation of FXR signaling in the intestine via accumulation of intestinal T-β-MCA, a FXR antagonist, and subsequently decreased intestinal FXR-mediated obesity.[20] Interestingly, the present study also correlated a significant reduction of intestinal *Lactobacillus* spp. with the down-regulation of FGF15/19 in the intestine, which supports inactivation of FXR signaling following a ChrSd diet. These data suggest that the antiobesity effect of ChrSd diet may be in part associated with reduced abundance of *Lactobacillus* in the intestine. Other factors in the antiobesity effects of the flavonoid-rich ChrSd diet may be the antioxidant effect of the flavonoids themselves, playing a preventive role in the development of obesity by regulating adipocyte differentiation,[51] or the suppression of PPAR γ2 expression, adipogenesis, and lipid accumulation.[52,53]

Increased abundance of probiotics (*Lactobacillus* spp. and *Bifidobacterium* spp.) may reduce HF-induced plasma lipopolysaccharide (LPS, endotoxin) concentration and inflammatory markers and lead to decreased hepatic steatosis.[54,55] Our previous work showed that ChrSd supplementation of the HF diet for 3 weeks significantly reduced liver weight by 38% compared to the control diet.[23] In the current study, liver weight was positively correlated with relative abundance of *Lactobacillus* spp. and *Bifidobacterium* spp. as well as the F/B ratio. The reduction of liver weight is mainly due to decreased lipid content after ChrSd feeding. Therefore, these results suggest that improvement of hepatic steatosis following ChrSd feeding may be mediated via alteration of the intestinal microbiota independent of the relative abundances of *Lactobacillus* spp. and *Bifidobacterium* spp.

In summary, numbers of total bacteria and relative abundances of *Bifidobacterium* spp., *Lactobacillus* spp., and *Firmicutes* were all lowered in feces from hamsters fed diets supplemented with the ChrSd diet. The ChrSd diet prevented HF and hypercholesterolemic diet-induced increases of plasma LDL-, VLDL-, total-cholesterol concentrations, hepatic steatosis, abdominal adipose tissue weight, and body weight gain. The hypocholesterolemic effect of the ChrSd diet may be mediated, in part, by up-regulation of hepatic CYP7A1 via decreased expression of intestinal FGF15/19 and is associated with lowered relative abundance of *Lactobacillus* spp. There was a significant positive correlation between *Lactobacillus* spp., the F/B ratio, and plasma total- and LDL-cholesterol. Reduction of HF-diet induced adipose tissue and body weight gain was accompanied by an increased relative abundance of *B. fragilis* and other *Bacteroidetes* and by reduced *Lactobacillus* spp. and *Firmicutes*, as represented in the F/B ratio. The antiobesity effect of the ChrSd diet may partially act through a change in the abundance of *Lactobacillus* spp. and subsequent inhibition of intestinal FXR-mediated signaling. In conclusion, although our study did not provide evidence for direct interaction of Chardonnay grape seed flour with intestinal microbiota, these findings suggest that the effect of Chardonnay grape seed flour on ameliorating HF- and high cholesterol-induced metabolic disorders is closely linked to modulation of intestinal microbiota. These data must be considered cautiously because only a few species and genera were quantified. In-depth analysis of intestinal microbiota composition following consumption of Chardonnay grape seed flour warrants further investigation.

AUTHOR INFORMATION

Corresponding Author

*E-mail: hyunsk13@konkuk.ac.kr. Phone: +82 2 450 4154. Fax: +82 2 450 3037.

Author Contributions

Many thanks to Sonomaceuticals, LLC/WholeVine Products, and their sister company for their contribution of grape seed flours and compositional analysis.

Funding

Hyunsook Kim was supported by the KU-Research Professor Program of Konkuk University.

Notes

The authors declare no competing financial interest.

REFERENCES

(1) Hervert-Hernández D, G. I. Dietary Polyphenols and Human Gut Microbiota: A Review. *Food Rev. Int.* **2011**, *27*, 154−169.

(2) Puupponen-Pimiä R, A. A.; Oksman-Caldentey, K. M.; Myllärinen, P.; Saarela, M.; Mattila-Sandholm, T.; Poutanen, K. Development of Functional Ingredients for Gut Health. *Trends Food Sci. Technol.* **2002**, *13*, 3−11.

(3) Etxeberria, U.; Fernandez-Quintela, A.; Milagro, F. I.; Aguirre, L.; Martinez, J. A.; Portillo, M. P. Impact of Polyphenols and Polyphenol-Rich Dietary Sources on Gut Microbiota Composition. *J. Agric. Food Chem.* **2013**, *61*, 9517−9533.

(4) Tremaroli, V.; Backhed, F. Functional Interactions between the Gut Microbiota and Host Metabolism. *Nature* **2012**, *489*, 242−249.

(5) Laparra, J. M.; Sanz, Y. Interactions of Gut Microbiota with Functional Food Components and Nutraceuticals. *Pharmacol. Res.* **2010**, *61*, 219−225.

(6) Cavaliere, C.; Foglia, P.; Gubbiotti, R.; Sacchetti, P.; Samperi, R.; Lagana, A. Rapid-Resolution Liquid Chromatography/Mass Spectrometry for Determination and Quantitation of Polyphenols in Grape Berries. *Rapid Commun. Mass Spectrom.* **2008**, *22*, 3089−3099.

(7) Pastrana-Bonilla, E.; Akoh, C. C.; Sellappan, S.; Krewer, G. Phenolic Content and Antioxidant Capacity of Muscadine Grapes. *J. Agric. Food Chem.* **2003**, *51*, 5497−5503.

(8) Beecher, G. R. Overview of Dietary Flavonoids: Nomenclature, Occurrence, and Intake. *J. Nutr.* **2003**, *133*, 3248S−3254S.

(9) Hellstrom, J. K.; Mattila, P. H. HPLC Determination of Extractable and Unextractable Proanthocyanidins in Plant Materials. *J. Agric. Food Chem.* **2008**, *56*, 7617−7624.

(10) Tabasco, R.; Sanchez-Patan, F.; Monagas, M.; Bartolome, B.; Victoria Moreno-Arribas, M.; Pelaez, C.; Requena, T. Effect of Grape Polyphenols on Lactic Acid Bacteria and Bifidobacteria Growth: Resistance and Metabolism. *Food Microbiol.* **2011**, *28*, 1345−1352.

(11) Tzounis, X.; Vulevic, J.; Kuhnle, G. G.; George, T.; Leonczak, J.; Gibson, G. R.; Kwik-Uribe, C.; Spencer, J. P. Flavanol Monomer-

DOI: 10.1021/jf5026373
J. Agric. Food Chem. 2015, 63, 1460−1467

Induced Changes to the Human Faecal Microflora. *Br. J. Nutr.* **2008**, *99*, 782−792.
(12) Pozuelo, M. J.; Agis-Torres, A.; Hervert-Hernandez, D.; Elvira Lopez-Oliva, M.; Munoz-Martinez, E.; Rotger, R.; Goni, I. Grape Antioxidant Dietary Fiber Stimulates *Lactobacillus* Growth in Rat Cecum. *J. Food Sci.* **2012**, *77*, H59−H62.
(13) Yamakoshi J, T. S.; Kikuchi, M.; Kubota, Y.; Konishi, H.; Mitsuoka, T. Effect of Proanthocyanidin-Rich Extract from Grape Seeds on Human Fecal Flora and Fecal Odor. *Microb. Ecol. Health Dis.* **2001**, *13*, 25−31.
(14) Gauffin Cano, P.; Santacruz, A.; Moya, A.; Sanz, Y. *Bacteroides uniformis* CECT 7771 Ameliorates Metabolic and Immunological Dysfunction in Mice with High-Fat-Diet Induced Obesity. *PLoS One* **2012**, *7*, e41079.
(15) Park, D. Y.; Ahn, Y. T.; Park, S. H.; Huh, C. S.; Yoo, S. R.; Yu, R.; Sung, M. K.; McGregor, R. A.; Choi, M. S. Supplementation of *Lactobacillus curvatus* HY7601 and *Lactobacillus plantarum* KY1032 in Diet-Induced Obese Mice Is Associated with Gut Microbial Changes and Reduction in Obesity. *PLoS One* **2013**, *8*, 1−12.
(16) Everard, A.; Belzer, C.; Geurts, L.; Ouwerkerk, J. P.; Druart, C.; Bindels, L. B.; Guiot, Y.; Derrien, M.; Muccioli, G. G.; Delzenne, N. M.; de Vos, W. M.; Cani, P. D. Cross-Talk Between *Akkermansia muciniphila* and Intestinal Epithelium Controls Diet-Induced Obesity. *Proc. Natl. Acad. Sci. U. S. A.* **2013**, *110* (22), 9066−9071.
(17) Fei, N.; Zhao, L. An Opportunistic Pathogen Isolated from the Gut of an Obese Human Causes Obesity in Germfree Mice. *ISME J.* **2013**, *7*, 880−884.
(18) Kimura, I.; Ozawa, K.; Inoue, D.; Imamura, T.; Kimura, K.; Maeda, T.; Terasawa, K.; Kashihara, D.; Hirano, K.; Tani, T.; Takahashi, T.; Miyauchi, S.; Shioi, G.; Inoue, H.; Tsujimoto, G. The Gut Microbiota Suppresses Insulin-Mediated Fat Accumulation via the Short-Chain Fatty Acid Receptor GPR43. *Nat. Commun.* **2013**, *4*, 1829.
(19) Wang, Z.; Klipfell, E.; Bennett, B. J.; Koeth, R.; Levison, B. S.; Dugar, B.; Feldstein, A. E.; Britt, E. B.; Fu, X.; Chung, Y. M.; Wu, Y.; Schauer, P.; Smith, J. D.; Allayee, H.; Tang, W. H.; DiDonato, J. A.; Lusis, A. J.; Hazen, S. L. Gut Flora Metabolism of Phosphatidylcholine Promotes Cardiovascular Disease. *Nature* **2011**, *472*, 57−63.
(20) Li, F.; Jiang, C.; Krausz, K. W.; Li, Y.; Albert, I.; Hao, H.; Fabre, K. M.; Mitchell, J. B.; Patterson, A. D.; Gonzalez, F. J. Microbiome Remodelling Leads to Inhibition of Intestinal Farnesoid X-Receptor Signalling and Decreased Obesity. *Nat. Commun.* **2013**, *4*, 2384.
(21) Backhed, F.; Ding, H.; Wang, T.; Hooper, L. V.; Koh, G. Y.; Nagy, A.; Semenkovich, C. F.; Gordon, J. I. The Gut Microbiota As an Environmental Factor That Regulates Fat Storage. *Proc. Natl. Acad. Sci. U. S. A.* **2004**, *101*, 15718−15723.
(22) Sayin, S. I.; Wahlstrom, A.; Felin, J.; Jantti, S.; Marschall, H. U.; Bamberg, K.; Angelin, B.; Hyotylainen, T.; Oresic, M.; Backhed, F. Gut Microbiota Regulates Bile Acid Metabolism by Reducing the Levels of Tauro-Beta-Muricholic Acid, A Naturally Occurring FXR Antagonist. *Cell Metab.* **2013**, *17*, 225−235.
(23) Kim, H.; Bartley, G. E.; Arvik, T.; Lipson, R.; Nah, S. Y.; Seo, K.; Yokoyama, W. Dietary Supplementation of Chardonnay Grape Seed Flour Reduces Plasma Cholesterol Concentration, Hepatic Steatosis, and Abdominal Fat Content in High-Fat Diet-Induced Obese Hamsters. *J. Agric. Food Chem.* **2014**, *62*, 1919−1925.
(24) Horton, J. D.; Cuthbert, J. A.; Spady, D. K. Regulation of Hepatic 7 Alpha-Hydroxylase Expression by Dietary Psyllium in the Hamster. *J. Clin. Invest.* **1994**, *93*, 2084−2092.
(25) Zhang, Z.; Wang, H.; Jiao, R.; Peng, C.; Wong, Y. M.; Yeung, V. S.; Huang, Y.; Chen, Z. Y. Choosing Hamsters but Not Rats as a Model for Studying Plasma Cholesterol-Lowering Activity of Functional Foods. *Mol. Nutr. Food Res.* **2009**, *53*, 921−930.
(26) Turley, S. D.; Spady, D. K.; Dietschy, J. M. Role of Liver in the Synthesis of Cholesterol and the Clearance of Low Density Lipoproteins in the Cynomolgus Monkey. *J. Lipid Res.* **1995**, *36*, 67−79.
(27) German JB, X. R.; Walzem, R.; Kinsella, J. E.; Knuckles, B.; Nakamura, M.; Yokoyama, W. H. Effect of Dietary Fats and Barley Fiber on Total Cholesterol and Lipoprotein Cholesterol Distribution in Plasma of Hamsters. *Nutr. Res. (N.Y.)* **1996**, *16*, 1239−1249.
(28) Bartley, G. E.; Yokoyama, W.; Young, S. A.; Anderson, W. H.; Hung, S. C.; Albers, D. R.; Langhorst, M. L.; Kim, H. Hypocholesterolemic Effects of Hydroxypropyl Methylcellulose Are Mediated by Altered Gene Expression in Hepatic Bile and Cholesterol Pathways of Male Hamsters. *J. Nutr.* **2010**, *140*, 1255−1260.
(29) Kim, H.; Bartley, G. E.; Young, S. A.; Seo, K. H.; Yokoyama, W. Altered Hepatic Gene Expression Profiles Associated with Improved Fatty Liver, Insulin Resistance, and Intestinal Permeability after Hydroxypropyl Methylcellulose (HPMC) Supplementation in Diet-Induced Obese Mice. *J. Agric. Food Chem.* **2013**, *61*, 6404−6411.
(30) Shi, J.; Yu, J.; Pohorly, J. E.; Kakuda, Y. Polyphenolics in Grape Seeds—Biochemistry and Functionality. *J. Med. Food* **2003**, *6*, 291−299.
(31) Brown, J. C.; Huang, G.; Haley-Zitlin, V.; Jiang, X. Antibacterial Effects of Grape Extracts on *Helicobacter pylori*. *Appl. Environ. Microbiol.* **2009**, *75*, 848−852.
(32) Su, X.; D'Souza, D. H. Grape Seed Extract for Control of Human Enteric Viruses. *Appl. Environ. Microbiol. 77*, 3982−3987.
(33) Alexa, E.; Poiana, M. A.; Sumalan, R. M. Mycoflora and Ochratoxin a Control in Wheat Grain Using Natural Extracts Obtained from Wine Industry Byproducts. *Int. J. Mol. Sci.* **2012**, *13*, 4949−4967.
(34) Baydar, N. G.; Sagdic, O.; Ozkan, G.; Cetin, S. Determination of Antibacterial Effects and Total Phenolic Contents of Grape (*Vitis vinifera* L.) Seed Extracts. *Int. J. Food Sci. Technol.* **2006**, *41*, 799−804.
(35) Baydara, N. G.; Özkanb, G.; Sağdiçç, O. Total Phenolic Contents and Antibacterial Activities of Grape (*Vitis vinifera* L.) Extracts. *Food Control* **2004**, *15*, 335−339.
(36) Mahboubi, M.; Kazempour, N.; Reza, A.; Nazar, B. Total Phenolic, Total Flavonoids, Antioxidant, and Antimicrobial Activities of Scrophularia Striata Boiss Extracts. *Jundishapur J. Nat. Pharmaceutical Prod.* **2013**, *8*, 15−19.
(37) Lee, H. C.; Jenner, A. M.; Low, C. S.; Lee, Y. K. Effect of Tea Phenolics and Their Aromatic Fecal Bacterial Metabolites on Intestinal Microbiota. *Res. Microbiol.* **2006**, *157*, 876−884.
(38) Queipo-Ortuno, M. I.; Boto-Ordonez, M.; Murri, M.; Gomez-Zumaquero, J. M.; Clemente-Postigo, M.; Estruch, R.; Cardona Diaz, F.; Andres-Lacueva, C.; Tinahones, F. J. Influence of Red Wine Polyphenols and Ethanol on the Gut Microbiota Ecology and Biochemical Biomarkers. *Am. J. Clin. Nutr.* **2012**, *95*, 1323−34.
(39) Hervert-Hernandez, D.; Pintado, C.; Rotger, R.; Goni, I. Stimulatory Role of Grape Pomace Polyphenols on *Lactobacillus acidophilus* Growth. *Int. J. Food Microbiol.* **2009**, *136*, 119−122.
(40) Hidalgo, M.; Oruna-Concha, M. J.; Kolida, S.; Walton, G. E.; Kallithraka, S.; Spencer, J. P.; de Pascual-Teresa, S. Metabolism of Anthocyanins by Human Gut Microflora and Their Influence on Gut Bacterial Growth. *J. Agric. Food Chem.* **2012**, *60*, 3882−3890.
(41) Kumar, M.; Nagpal, R.; Kumar, R.; Hemalatha, R.; Verma, V.; Kumar, A.; Chakraborty, C.; Singh, B.; Marotta, F.; Jain, S.; Yadav, H. Cholesterol-Lowering Probiotics As Potential Biotherapeutics for Metabolic Diseases. *Exp. Diabetes Res.* **2012**, *2012*, 1−14.
(42) Huang, Y.; Wang, X.; Wang, J.; Wu, F.; Sui, Y.; Yang, L.; Wang, Z. *Lactobacillus plantarum* Strains As Potential Probiotic Cultures with Cholesterol-Lowering Activity. *J. Dairy Sci.* **2013**, *96*, 2746−2753.
(43) Sanders, T. A. Food Production and Food Safety. *BMJ* **1999**, *318*, 1689−1693.
(44) Delzenne, N. M.; Neyrinck, A. M.; Cani, P. D. Modulation of the Gut Microbiota by Nutrients with Prebiotic Properties: Consequences for Host Health in the Context of Obesity and Metabolic Syndrome. *Microb. Cell Fact* **2011**, *10* (Suppl. 1), S10.
(45) Ley, R. E.; Turnbaugh, P. J.; Klein, S.; Gordon, J. I. Microbial Ecology: Human Gut Microbes Associated with Obesity. *Nature* **2006**, *444*, 1022−1023.
(46) Duca, F. A.; Sakar, Y.; Lepage, P.; Devime, F.; Langelier, B.; Dore, J.; Covasa, M. Replication of Obesity and Associated Signaling Pathways through Transfer of Microbiota from Obese Prone Rat. *Diabetes* **2014**, *63*, 1624−1636.

DOI: 10.1021/jf5026373
J. Agric. Food Chem. 2015, 63, 1460−1467

(47) Santacruz, A.; Collado, M. C.; Garcia-Valdes, L.; Segura, M. T.; Martin-Lagos, J. A.; Anjos, T.; Marti-Romero, M.; Lopez, R. M.; Florido, J.; Campoy, C.; Sanz, Y. Gut Microbiota Composition Is Associated with Body Weight, Weight Gain, and Biochemical Parameters in Pregnant Women. *Br. J. Nutr.* **2010**, *104*, 83−92.
(48) Armougom, F.; Henry, M.; Vialettes, B.; Raccah, D.; Raoult, D. Monitoring Bacterial Community of Human Gut Microbiota Reveals an Increase in *Lactobacillus* in Obese Patients and Methanogens in Anorexic Patients. *PLoS One* **2009**, *4*, e7125.
(49) Khan, M.; Raoult, D.; Richet, H.; Lepidi, H.; La Scola, B. Growth-Promoting Effects of Single-Dose Intragastrically Administered Probiotics in Chickens. *Br. Poult. Sci.* **2007**, *48*, 732−735.
(50) Million, M.; Thuny, F.; Angelakis, E.; Casalta, J. P.; Giorgi, R.; Habib, G.; Raoult, D. *Lactobacillus reuteri* and *Escherichia coli* in the Human Gut Microbiota May Predict Weight Gain Associated with Vancomycin Treatment. *Nutr. Diabetes* **2013**, *3*, e87.
(51) Kanda, Y.; Hinata, T.; Kang, S. W.; Watanabe, Y. Reactive Oxygen Species Mediate Adipocyte Differentiation in Mesenchymal Stem Cells. *Life Sci.* **2011**, *89*, 250−258.
(52) Furuyashiki, T.; Nagayasu, H.; Aoki, Y.; Bessho, H.; Hashimoto, T.; Kanazawa, K.; Ashida, H. Tea Catechin Suppresses Adipocyte Differentiation Accompanied by Down-Regulation of PPARgamma2 and C/EBPalpha in 3T3-L1 Cells. *Biosci. Biotechnol. Biochem.* **2004**, *68*, 2353−2359.
(53) Hung, P. F.; Wu, B. T.; Chen, H. C.; Chen, Y. H.; Chen, C. L.; Wu, M. H.; Liu, H. C.; Lee, M. J.; Kao, Y. H. Antimitogenic Effect of Green Tea (−)-Epigallocatechin Gallate on 3T3-L1 Preadipocytes Depends on the ERK and Cdk2 Pathways. *Am. J. Physiol. Cell Physiol.* **2005**, *288*, C1094−C1108.
(54) Griffiths, E. A.; Duffy, L. C.; Schanbacher, F. L.; Qiao, H.; Dryja, D.; Leavens, A.; Rossman, J.; Rich, G.; Dirienzo, D.; Ogra, P. L. In Vivo Effects of *Bifidobacteria* and *Lactoferrin* on Gut Endotoxin Concentration and Mucosal Immunity in Balb/c Mice. *Dig. Dis. Sci.* **2004**, *49*, 579−589.
(55) Fukunishi, S.; Sujishi, T.; Takeshita, A.; Ohama, H.; Tsuchimoto, Y.; Asai, A.; Tsuda, Y.; Higuchi, K. Lipopolysaccharides Accelerate Hepatic Steatosis in the Development of Nonalcoholic Fatty Liver Disease in Zucker Rats. *J. Clin. Biochem. Nutr.* **2014**, *54*, 39−44.
(56) Heilig, H. G.; Zoetendal, E. G.; Vaughan, E. E.; Marteau, P.; Akkermans, A. D.; de Vos, W. M. Molecular Diversity of *Lactobacillus* spp. and Other Lactic Acid Bacteria in the Human Intestine As Determined by Specific Amplification of 16S Ribosomal DNA. *Appl. Environ. Microbiol.* **2002**, *68*, 114−123.
(57) Walter, J.; Hertel, C.; Tannock, G. W.; Lis, C. M.; Munro, K.; Hammes, W. P. Detection of *Lactobacillus*, *Pediococcus*, *Leuconostoc*, and *Weissella* Species in Human Feces by Using Group-Specific PCR Primers and Denaturing Gradient Gel Electrophoresis. *Appl. Environ. Microbiol.* **2001**, *67*, 2578−2585.
(58) Matsuki, T.; Watanabe, K.; Fujimoto, J.; Miyamoto, Y.; Takada, T.; Matsumoto, K.; Oyaizu, H.; Tanaka, R. Development of 16S rRNA-Gene-Targeted Group-Specific Primers for the Detection and Identification of Predominant Bacteria in Human Feces. *Appl. Environ. Microbiol.* **2002**, *68*, 5445−5451.
(59) Rinttila, T.; Kassinen, A.; Malinen, E.; Krogius, L.; Palva, A. Development of an Extensive Set of 16S rDNA-Targeted Primers for Quantification of Pathogenic and Indigenous Bacteria in Fecal Samples by Real-Time PCR. *J. Appl. Microbiol.* **2004**, *97*, 1166−1177.
(60) Matsuki, T.; Watanabe, K.; Fujimoto, J.; Takada, T.; Tanaka, R. Use of 16S rRNA Gene-Targeted Group-Specific Primers for Real-Time PCR Analysis of Predominant Bacteria in Human Feces. *Appl. Environ. Microbiol.* **2004**, *70*, 7220−7228.
(61) Matsuda, K.; Tsuji, H.; Asahara, T.; Kado, Y.; Nomoto, K. Sensitive Quantitative Detection of Commensal Bacteria by rRNA-Targeted Reverse-Transcription PCR. *Appl. Environ. Microbiol.* **2007**, *73*, 32−39.
(62) Liu, C.; Song, Y.; McTeague, M.; Vu, A. W.; Wexler, H.; Finegold, S. M. Rapid Identification of the Species of the *Bacteroides fragilis* Group by Multiplex PCR Assays Using Group- and Species-Specific Primers. *FEMS Microbiol. Lett.* **2003**, *222*, 9−16.
(63) Nadkarni, M. A.; Martin, F. E.; Jacques, N. A.; Hunter, N. Determination of Bacterial Load by Real-Time PCR Using a Broad-Range (Universal) Probe and Primers Set. *Microbiology* **2002**, *148*, 257−266.
(64) Guo, X.; Xia, X.; Tang, R.; Zhou, J.; Zhao, H.; Wang, K. Development of a Real-Time PCR Method for *Firmicutes* and *Bacteroidetes* in Feces and Its Application to Quantify Intestinal Population of Obese and Lean Pigs. *Lett. Appl. Microbiol.* **2008**, *47*, 367−373.
(65) Bartosch, S.; Fite, A.; Macfarlane, G. T.; McMurdo, M. E. Characterization of Bacterial Communities in Feces from Healthy Elderly Volunteers and Hospitalized Elderly Patients by Using Real-Time PCR and Effects of Antibiotic Treatment on the Fecal Microbiota. *Appl. Environ. Microbiol.* **2004**, *70*, 3575−33581.

DOI: 10.1021/jf5026373
J. Agric. Food Chem. 2015, 63, 1460−1467

is important in the management of chronic respiratory symptoms. Therefore, there is a need to develop new and effective therapies for mucus hypersecretion.

We evaluated the inhibitory effects of CKS or PA on airway inflammation in ovalbumin-induced mice and PMA-exposed A549 cells. Our findings indicated that CKS or PA inhibited the development of airway inflammation, hyperresponsiveness, and remodeling by reducing the allergic responses. This may provide an effective alternative therapy in the treatment of allergy-induced respiratory diseases.

MATERIALS AND METHODS

Chemicals. Chicken egg ovalbumin (OVA) (Grade II), aluminum hydroxide gel, Giemsa solution, and hematoxylin-eosin Y (H&E) staining solution were obtained from Sigma Chemical Co. (St. Louis, MO, USA). Enzyme-linked immunosorbent assay kits were obtained from R&D Systems (Minneapolis, MN, USA) and BD Biosciences (San Diego, CA, USA). Alcian blue periodic acid-Schiff (PAS) staining solution was obtained from Merck KGaA (Darmstadt, Germany).[3] All other chemicals and solvents were of the highest grade available commercially.

Preparation of CKS from the Roots Extract of *Platycodon grandiflorum*. *Platycodon grandiflorum* root (CK) was supplied by Jangsaeng Doraji Co., Ltd. (Jinju, Korea). CK was extracted with MeOH. Concentration of the MeOH solution gave a brown syrupy extract which was suspended in H_2O and then divided successively with ethyl acetate and *n*-butanol. The *n*-butanol layer was suspended in H_2O and put into a Diaion HP20 column. The column was washed with H_2O and then eluted with MeOH. Also, eluted solution was concentrated in reduced pressure to give a crude saponin mixture (CKS).[23]

Preparation of Platycosides by HPLC and NMR Analysis. CKS extracted from the roots of *Platycodon grandiflorum* was analyzed by HPLC. The extracts were dissolved in H_2O and then put into a solid-phase-extraction cartridge (RP-C18, CREEX 600-3506). The cartridge was washed with H_2O and eluted with MeOH. The elution solution was injected into an OptimaPak column (4.6 × 250 mm, 5 μm, 100 Å) maintained at 40 °C on a Futecs NS-3000*i* system equipped with a light scattering detector (ELSD). Platycosides such as deapioplatycoside E, platycoside E, platyconic acid A, platycodin D, 2″-*O*-acetylpolygalacin D_2, and platycodin D_3 were purified from CKS, and then their chemical structures were identified by direct comparison of their physical and spectral data (^{1}H NMR and ^{13}C NMR).[22,23]

Cell Culture. A549 cells were purchased from the American Type Culture Collection (Manassas, VA, USA). A549 cells were cultured in RPMI 1640 supplemented with 10% fetal bovine serum, 100 U/mL penicillin, and 100 μg/mL streptomycin at 37 °C in a humidified chamber with 5% CO_2.[4] PA was dissolved in DMSO and added into the medium.

Animals and Treatment. Six-week-old female ICR mice were obtained from Samtako (Osan, Korea). The animals were allowed free access to Purina rodent chow (Seoul, Korea) and tap water, and were maintained under specific pathogen-free conditions. The animals were acclimated to the temperature (22 ± 2 °C) and humidity (55 ± 5%) of the control rooms with a 12-h light/dark cycle for at least 1 week prior to experimentation.[3] All experimental protocols in the use of the animals were performed according to the rules and regulations of the Animal Ethics Committee, Chungnam National University (Daejeon, Korea).

Immunization and Challenge. Mice were immunized on days 1, 7, and 14 by intraperitoneal (i.p.) injection of 50 μg of chicken OVA emulsified in 1 mg of aluminum hydroxide adjuvant, in a total volume of 100 μL of PBS. The CKS was dissolved in saline. The mice were intragastrically (i.g.) administered 0.5, 1, or 2 mg/kg/day (in 100 μL) CKS each day from days 12 to 16, consecutively. The control and OVA group were administered saline (i.g.). The animals were challenged with OVA on the final day by inhalation of 1 mg/mL OVA in PBS. The control group was immunized and challenged with PBS without CKS administration (Figure 1).[3]

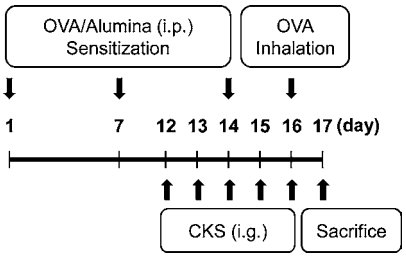

Figure 1. Schematic diagram of the experimental protocol in mice. Mice were divided into five groups. Mice were immunized on days 1, 7, and 14 by intraperitoneal (i.p.) injection of 50 μg of chicken OVA emulsified in 1 mg of aluminum hydroxide adjuvant in a total volume of 100 μL of PBS. CKS was dissolved in saline. Mice were intragastrically (i.g.) administered 0.5, 1, or 2 mg/kg/day (in 100 μL) CKS each day from days 12 to 16, consecutively. The control and OVA group were administered saline (i.g.) without CKS. The animals were challenged with OVA on the final day by inhalation of 1 mg/mL OVA in PBS. The control group was immunized and challenged with PBS without drug administration.

Bronchoalveolar Lavage (BAL) Fluid Collection and Leukocyte Count. Each mouse was anesthetized and the trachea was cannulated by gentle massaging of the throat. BAL fluid was collected by flushing 1 mL of PBS into the lungs via the trachea immediately after sacrifice; approximately 0.8 mL of BAL fluid was recovered after five lavages. The BAL fluid was centrifuged (400*g*, 4 °C, 5 min) and the supernatant was stored at −20 °C until measurement of cytokines. Cells from the BAL fluid were washed three times with PBS, and the pellet was resuspended in 100 μL of PBS. The total cell number was counted by cytospin, and a differential cell count was performed after staining with Giemsa solution.[3]

Enzyme-Linked Immunosorbent Assay (ELISA). The levels of cytokines in the BAL fluid were measured by sandwich ELISA using the OptEIA Set mouse IL-4, IL-5, MCP-1, and IgE kits from BD Biosciences and DuoSet mouse TNF-α, IFN-γ, and IL-13 kits from R&D Systems, according to the manufacturer's instructions. Each concentration was calculated using a linear-regression equation obtained from the standard absorbance values.[3]

Histopathological Studies. Right lung tissues were sliced and fixed in 10% buffered-neutral formalin for 24 h. The fixed lung tissue slices were embedded in paraffin, sectioned, deparaffinized, and rehydrated using standard techniques. Sections 4 μm thick were subjected to H&E staining for general morphological analysis. Airway mucus hypersecretion was evaluated using alcian blue-PAS to stain infiltrated goblet cells. Pulmonary histopathological changes were assessed on a five-point score by three independent examiners. The scores were as follows: 0, no inflammatory cells; 1, minimal accumulation of inflammatory cells; 2, moderate accumulation of inflammatory cells; 3, severe accumulation of inflammatory cells; 4, extreme accumulation of inflammatory cells. Infiltrated goblet cells were also assessed on a five-point score by three independent examiners. The scores were as follows: 0, no goblet cells; 1, minimal infiltration of goblet cells; 2, moderate infiltration of goblet cells; 3, severe infiltration of goblet cells; 4, extreme infiltration of goblet cells.[3,24] All lung tissue was processed according to the histopathological protocols of the pathological laboratory, College of Veterinary Science, Chungnam National University (Daejeon, Korea).

Western Blot Analysis. Western blot analysis was performed as described previously.[3] The intensity of the Western blot bands was measured using the ImageJ software (NIH ImageJ program).

Semiquantitative Reverse Transcription–Polymerase Chain Reaction (RT-PCR) Analysis. Total RNA was extracted from the left lung tissues or A549 cells using RNAiso reagent (Takara, Kyoto, Japan), according to the manufacturer's instructions. RT-PCR analysis was performed as described previously.[3,25] The intensity of the RT-PCR bands was measured using the ImageJ software (NIH ImageJ program). The PCR primer sequences are listed in Table 1.

DOI: 10.1021/jf5043954
J. Agric. Food Chem. 2015, 63, 1468−1476

Table 1. Primer Sequences for Semiquantitative RT-PCR and qRT-PCR

gene	primer sequence (5′→3′)	gene bank no.
mMUC5AC	(F) AAA GAC ACC AGT AGT CAC TCA GCA A	NM_010844.1
	(R) CTG GGA AGT CAG TGT CAA ACC A	
mMMP-2	(F) AGA TCT TCT TCT TCA AGG ACC GGT T	NM_008610.2
	(R) GGC TGG TCA GTG GCT TGG GGT A	
mMMP-9	(F) GTA TGG TCG TGG CTC TAA GC	NM_013599.3
	(R) AAA ACC CTC TTG GTC TGC GG	
mTIMP-1	(F) CAC CAC CTT ATA CCA GCG TT	NM_001044384.1
	(R) GTC ACT CTC CAG TTT GCA AG	
mTIMP-2	(F) CCA GGT CCT TTT CAT CCT GA	NM_011594.3
	(R) TCC ATT CGC TGA AGT CTG TG	
mGAPDH	(F) CAT CTT CCA GGA GCG AGA CC	NM_008084.2
	(R) TCC ACC ACC CTG TTG CTG TA	
hMUC5AC	(F) CTG AGG GTC TCA GGA ATG ACG C	XM_006726526.1
	(R) TTT ATG CAA CAG ATT GGC CGT G	
hGAPDH	(F) CCA CAT CGC TCA GAC ACC AT	NM_002046.5
	(R) CCA GGC GCC CAA TAC G	

Quantitative Real-Time RT-PCR (qRT-PCR). Cells were pretreated with PA (0.5, 1, or 2 μM) and then treated with PMA (20 nM). PCR product formation was monitored continuously during amplification using the Sequence Detection System software, version 1.7 (Applied Biosystems, Foster City, CA, USA). The accumulated products were detected directly by monitoring the signal from the SYBR Green reporter dye. MUC5AC mRNA expression was compared between the treated and control cells at each time point using the comparative cycle threshold (Ct) method. The quantity of each transcript was calculated as described in the instrument manual, and normalized to the GAPDH mRNA expression.[34] The PCR primer sequences are listed in Table 1.

Transient Transfection and Luciferase Assays. To determine the promoter activity, a dual-luciferase reporter assay system (Promega, WI, USA) was used. The cells were seeded into 48-well plates and incubated at 37 °C. At 70−80% confluence, the cells were incubated with RPMI1640 without serum or antibiotics for 6 h. The cells were transiently cotransfected with a wild-type MUC5AC promoter luciferase construct, NF-κB reporter vector, and pRL-SV plasmid (Promega, WI, USA) using LipofectAMINE 2000 reagent (Invitrogen, CA, USA), according to the manufacturer's instructions. After 5 h, the medium was replaced with basal medium. The cells were pretreated with PA for 1 h and then treated with PMA for 24 h. After incubation, the cells were lysed and luciferase activity was measured using a luminometer (Luminoscan Ascent, Thermo Electron, Waltham, MA, USA). For each sample, the luciferase signal was normalized to Renilla luciferase activity and expressed relative to the control value.[4]

Statistical Analyses. All experiments were repeated at least three times. Results reported are means ± the standard error of the mean (SEM). Statistical significance was determined using a one-way analysis of variance (ANOVA) followed by the Tukey−Kramer test, with $p < 0.05$ or $p < 0.01$ indicating significance.

RESULTS

CKS Inhibited OVA-induced Leukocyte Recruitment and Histopathological Changes in Mice. Leukocytes play an important role in airway inflammation. To evaluate the effectiveness of CKS in airway inflammation, OVA-induced leukocytes were counted in bronchoalveolar lavage (BAL) fluid. As shown in Table 2, repeated ovalbumin (OVA) application increased the numbers of total and differential leukocytes (i.e., eosinophils, basophils, lymphocytes, and macrophages) in the BAL fluid. The numbers of OVA-induced total and differential leukocytes were reduced by CKS administration in a dose-dependent manner. Continuously, we determined the inhibitory effect of CKS on OVA-induced histopathological changes in the lung tissue. Repeated OVA application increased bronchoconstriction in sensitized mice, with the trachea characterized by goblet cell hyperplasia and mucus hypersecretion from the goblet cells.[26,27] Histopathological analysis by H&E and alcian blue-PAS staining of the lung tissue showed inflammatory cell infiltration and goblet cell hyperplasia in the OVA-treated mice. CKS inhibited these OVA-induced pathological changes in the lung tissue (Figure 2A, B).

CKS Inhibited OVA-Induced IgE, Th1/Th2 Cytokines, and MCP-1 Secretion in Mice. Mast cells are key effector cells in IgE-mediated allergic disorders. IgE-mediated allergic disorders are regulated by mast cells. During mast cells activation, mast cells undergo degranulation and secrete a variety of biologically active substances, which play an important role in the development of airway inflammation.[28,46] We evaluated the effectiveness of CKS against total IgE secretion in BAL fluid. CKS reduced OVA-induced IgE level in a dose-dependent manner (Table 3). Furthermore, airway inflammation is associated with the secretion of Th1/Th2 cytokines and monocyte chemoattractant protein-1 (MCP-1) chemokine.[29] We examined the effectiveness of CKS against OVA-induced TNF-α, IFN-γ, IL-4, -5, -13, and MCP-1 secretion in BAL fluid. Repeated OVA application increased TNF-α, IFN-γ, IL-4, -5, -13, and MCP-1 secretion levels. CKS reduced OVA-elevated Th1/Th2 cytokines and MCP-1 secretion in a dose-dependent manner (Table 3). These results demonstrated that CKS decreased the OVA-induced inflammatory response, affecting leukocyte recruitment and secretion of IgE, Th1 and Th2 cytokines, and MCP-1 chemokine in mice.

CKS Inhibited OVA-Increased MUC5AC and MMP-2/-9 mRNA Expression in Mice. Airway mucus hypersecretion is associated with goblet cell hyperplasia in mice.[30] We determined the inhibitory effects of CKS on OVA-increased MUC5AC

Table 2. Effects of CKS on OVA-Induced Total and Differential Leukocytes in BAL Fluid[a]

	control	OVA	OVA + CKS 0.5	OVA + CKS 1.0	OVA + CKS 2.0
total cells (1×10^4 cells/mL)	14.0 ± 1.00	59.3 ± 6.43[b]	26.0 ± 2.65[c]	21.3 ± 2.31[c]	15.0 ± 2.00[c]
eosinophils (1×10^4 cells/mL)	5.00 ± 1.00	57.0 ± 5.57[b]	27.0 ± 3.61[c]	18.3 ± 2.52[c]	11.7 ± 1.53[c]
basophils (1×10^4 cells/mL)	5.30 ± 1.53	24.0 ± 2.00[b]	16.0 ± 2.00[c]	12.3 ± 2.08[c]	9.70 ± 1.53[c]
lymphocytes (1×10^4 cells/mL)	14.3 ± 1.53	46.0 ± 2.00[b]	35.7 ± 2.52[c]	26.3 ± 3.21[c]	18.7 ± 1.53[c]
macrophages (1×10^4 cells/mL)	11.0 ± 1.00	26.0 ± 2.65[b]	17.7 ± 2.08[c]	14.7 ± 2.08[c]	13.0 ± 1.00[c]

[a]Recovered total cells or differential leukocytes were counted using standard morphological criteria for cytospin (cells number $\times 10^4$). At least 200 cells were examined in each cytospin. PBS-inhaled mice administered saline (control), OVA-inhaled mice administered saline (OVA), OVA-inhaled mice administered CKS 0.5 mg/kg/day (OVA + CKS 0.5), OVA-inhaled mice administered CKS 1.0 mg/kg/day (OVA + CKS 1.0), and OVA-inhaled mice administered CKS 2.0 mg/kg/day (OVA + CKS 2.0). Results represent the means ± SEM of five mice per group. [b]$p < 0.05$, significantly different from the control group. [c]$p < 0.05$, significantly different from the OVA-treated group.

DOI: 10.1021/jf5043954
J. Agric. Food Chem. 2015, 63, 1468−1476

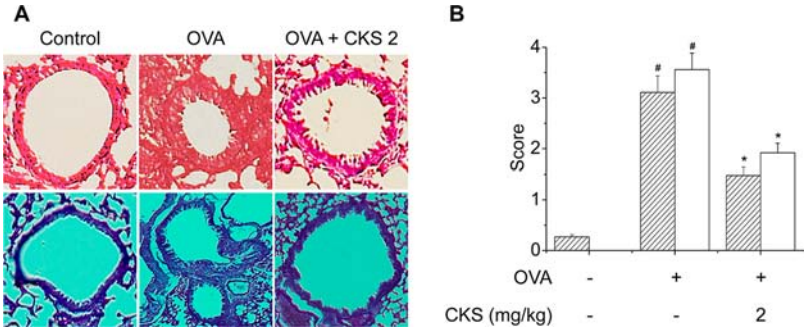

Figure 2. Inhibitory effects of CKS on OVA-induced leukocytes and goblet cells infiltration in mice. (A) Histopathological changes in the lung tissues. Lung tissue was cut and stained with H&E or alcian blue-PAS. Lung tissue was obtained from PBS-inhaled mice administered saline (control), OVA-inhaled mice administered saline (OVA), and OVA-inhaled mice administered CKS2 (OVA + CKS2). (B) Inflammatory cell infiltration (closed bar) and mucus production (open bar) in the lung tissue were scored as described in the Materials and Methods section. Results shown are representative of five observations. Results are presented as means ± SEM of three independent experiments. Magnification ×100; $^{\#}p < 0.05$, significantly different from the control group; $^{*}p < 0.05$, significantly different from the OVA-treated group.

Table 3. Effect of CKS on OVA-Induced Levels of IgE, Th1 and Th2 Cytokines, and MCP-1 Chemokine in BAL Fluid[a]

	control	OVA	OVA + CKS 0.5	OVA + CKS 1.0	OVA + CKS 2.0
IgE (ng/mL)	2.80 ± 0.50	16.3 ± 0.52[b]	7.90 ± 0.70[c]	5.80 ± 0.31[c]	4.60 ± 0.54[c]
TNF-α (pg/mL)	141 ± 3.40	538 ± 56.2[b]	254 ± 15.4[c]	203 ± 17.8[c]	150 ± 14.0[c]
IFN-γ (pg/mL)	49.7 ± 1.35	66.4 ± 4.04[b]	59.4 ± 2.37[c]	53.6 ± 1.81[c]	49.9 ± 3.04[c]
IL-4 (pg/mL)	6.50 ± 0.75	35.4 ± 2.38[b]	21.3 ± 2.50[c]	17.3 ± 1.12[c]	12.1 ± 1.75[c]
IL-5 (pg/mL)	83.9 ± 5.11	562 ± 17.7[b]	287 ± 21.6[c]	224 ± 11.7[c]	163 ± 8.86[c]
IL-13 (pg/mL)	231 ± 17.8	789 ± 81.3[b]	493 ± 54.4[c]	316 ± 27.0[c]	264 ± 8.62[c]
MCP-1 (pg/mL)	72.9 ± 1.63	237 ± 28.3[b]	107 ± 10.2[c]	88.8 ± 6.37[c]	74.8 ± 5.98[c]

[a]Cytokine levels in the BAL fluid were measured using ELISA kits. PBS-inhaled mice administered saline (control), OVA-inhaled mice administered saline (OVA), OVA-inhaled mice administered CKS 0.5 mg/kg/day (OVA + CKS 0.5), OVA-inhaled mice administered CKS 1.0 mg/kg/day (OVA + CKS 1.0), and OVA-inhaled mice administered CKS 2.0 mg/kg/day (OVA + CKS 2.0). Results represent the means ± SEM of five mice per group. [b]$p < 0.05$, significantly different from the control group. [c]$p < 0.05$, significantly different from the OVA-treated group.

mRNA expression in lung tissues. Repeated OVA application increased MUC5AC mRNA expression, similar to the histopathological changes observed. CKS inhibited OVA-increased MUC5AC mRNA expression in a dose-dependent manner (Figure 3A, B). Airway remodeling is associated with MMPs and TIMPs modulation in mice.[25] We also determined the inhibitory effects of CKS on OVA-mediated MMP-2/9 and TIMP-1/2 mRNA expression in lung tissues. MMP-2/-9 mRNA expression increased with OVA application, but TIMP-1/-2 mRNA expression decreased with OVA application. CKS significantly inhibited OVA-increased MMP-2/-9 mRNA expression and OVA-decreased TIMP-1/-2 mRNA expression (Figure 3A, B). These results demonstrated that CKS inhibited OVA-induced mucus hypersecretion- and airway remodeling-related MUC5AC and MMPs mRNA expression in mice.

CKS Inhibited OVA-Increased NF-κB Activation in Mice. Nuclear factor-kappa B (NF-κB) activation plays an important role in airway inflammation. Various stimuli lead to the phosphorylation, ubiquitination, and proteolytic degradation of IκBα, resulting in the release of NF-κB from its inhibitory protein and its translocation to the nucleus.[31] NF-κB activation has been observed in allergic airway inflammation in human and animal.[33] We determined the inhibitory effect of CKS on NF-κB p65 level during OVA-increased allergic airway inflammation in lung tissues. OVA-sensitized and -challenged mice showed a notably increased NF-κB p65 nuclear protein and a decreased cytoplasmic NF-κB p65 cytosolic protein compared to control mice. CKS treatment inhibited OVA-increased these alterations in a dose dependent manner (Figure 4A, B).

Platyconic Acid A Inhibited PMA-Induced MUC5AC Expression by Inhibiting the Activation of NF-κB in A549 Cells. We determined the inhibitory effects of CKS triterpenoid saponins, platycosides, on PMA-induced MUC5AC expression in A549 cells. First, the cytotoxicity of CKS triterpenoid saponins, platycosides, such as deapioplatycoside E, platycoside E, platyconic acid A (PA), platycodin D, 2″-*O*-acetylpolygalacin D_2, and platycodin D_3 was determined in A549 cells (Supporting Information Supplementary Figure 2). Treatment with each platycoside at concentrations of 0−8 μM for 24 h showed that platycoside concentrations <4 μM did not affect cell viability, and cytotoxicity was determined by MTT reduction and LDH release assays. We further evaluated the inhibitory effects of platycosides on PMA-increased MUC5AC expression in cells. Among the platycosides tested, PA significantly decreased PMA-increased MUC5AC mRNA expression in the cells (Table 4). The chemical structure of platyconic acid A (PA) is shown in Figure 5A. PA is the most potent CKS platycoside, which improves glucose homeostasis by enhancing insulin sensitivity in type 2 diabetic mice.[10] To assess the inhibitory effects of PA on MUC5AC expression, A549 cells were treated with PMA in the presence of PA for 24 h, and MUC5AC mRNA expression was then evaluated by qRT-PCR. PA treatment inhibited PMA-increased MUC5AC mRNA expression in the cells in a concentration-dependent manner (Figure 5B). PA also inhibited PMA-induced MUC5AC luciferase activity by inhibiting the NF-κB promoter-driven luciferase reporter activity (Figure 5C, D). PA inhibited PMA-induced NF-κB p65 phosphorylation, IκBα phosphorylation, and degradation in a concentration-dependent manner (Figure 5E, F). These results demonstrated that PA

DOI: 10.1021/jf5043954
J. Agric. Food Chem. 2015, 63, 1468−1476

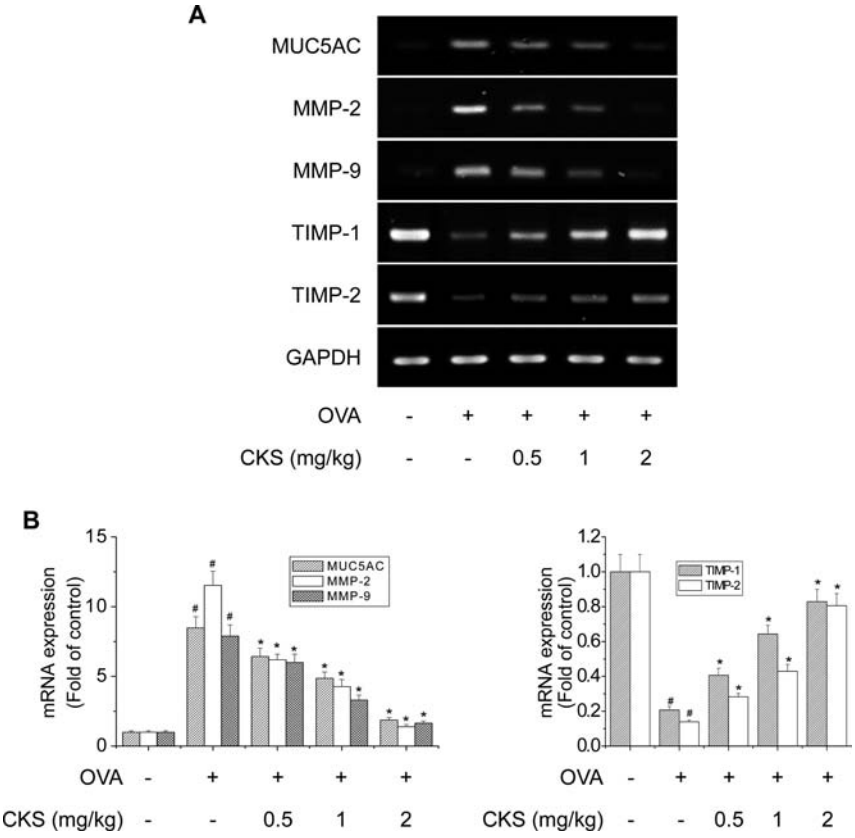

Figure 3. Inhibitory effects of CKS on OVA-induced airway remodeling in mice. (A) Total RNA was extracted from the lung tissue and mRNA expression of MUC5AC, MMP-2, MMP-9, TIMP-1, TIMP-2, and GAPDH were determined by semiquantitative RT-PCR. (B) Intensities of the PCR bands were calculated using the ImageJ software. Results shown are representative of five observations. Results are presented as means ± SEM of three independent experiments. $^{\#}p < 0.05$, significantly different from the control group; $^{*}p < 0.05$, significantly different from the OVA-treated group.

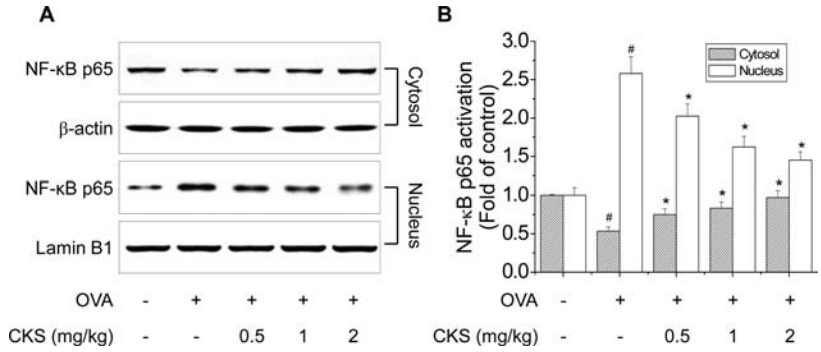

Figure 4. Inhibitory effects of CKS on OVA-induced NF-κB activation in mice. (A) Mice were pretreated with CKS (0.5, 1, or 2 mg/kg) for 1 h and then treated with OVA for 2 h. Cytosolic and nuclear protein was extracted from lung tissue treated with OVA, and NF-κB activation was determined by Western blotting. (B) The intensities of the Western blot bands were calculated using the ImageJ software. Results shown are representative of five observations. Results are presented as means ± SEM of three independent experiments. $^{\#}p < 0.05$, significantly different from the control group; $^{*}p < 0.05$, significantly different from the OVA-treated group.

inhibited PMA-increased MUC5AC expression by suppressing NF-κB activation in cells.

Platyconic Acid A Inhibited PMA-Induced MUC5AC Expression by Inhibiting the Activation of Akt in A549 cells. We demonstrated that PA inhibited NF-κB activity of PMA-treated cells at the transcriptional level (Figure 5). Akt pathway is a well-known upstream regulator of NF-κB signaling in MUC5AC transcription factor.[40] We evaluated the inhibitory effect of PA on PMA-induced Akt phosphorylation in cells. PA inhibited PMA-induced Akt phosphorylation in a concentration-dependent manner (Figure 6A, B).

■ DISCUSSION

There is widespread interest in developing new, and less toxic, anti-inflammatory agents from natural sources. Natural immune modulators from herbal extracts or herbal derivatives have been reported to have inhibitory effects on inflammation.[21,34,41−45] We investigated the inhibitory effects of *Platycodon grandiflorum* root-derived saponins (CKS), especially platyconic acid

DOI: 10.1021/jf5043954
J. Agric. Food Chem. 2015, 63, 1468−1476

Table 4. Effect of Platycosides and CKS on PMA-Induced MUC5AC mRNA Expression in A549 Cells[a]

treatment	relative MUC5AC mRNA to GAPDH (fold of control)
control	1.0 ± 0.11
PMA	2.1 ± 0.22[b]
PMA + deapioplatycoside E	2.0 ± 0.19
PMA + platycoside E	2.0 ± 0.20
PMA + platyconic acid A	1.2 ± 0.11[c]
PMA + platycodin D	1.6 ± 0.17[c]
PMA + 2″-*O*-acetylpolygalacin D_2	1.5 ± 0.16[c]
PMA + platycodin D_3	1.4 ± 0.15[c]
PMA + CKS	1.3 ± 0.14[c]

[a]A549 cells were pretreated with platycosides (1 μM) or CKS (1 μg/mL) and then treated with PMA (each 20 nM). After 24 h, total RNA was extracted from the cells and MUC5AC mRNA levels were determined by qRT-PCR. Results represent the means ± SEM of three independent experiments. [b]$p < 0.01$, significantly different from the control group. [c]$p < 0.01$, significantly different from the PMA-treated group.

A (PA), on airway inflammation in ovalbumin-induced mice and PMA-exposed A549 cells.

Asthma is one of the most common respiratory inflammatory diseases worldwide, and is characterized by airway hyperresponsiveness. Asthma is caused by inappropriate responses to inhaled allergens, and the strength of the hyperresponsiveness correlates with the level of airway inflammation, which is predominated by inflammatory cell infiltration, mucus hypersecretion, allergen-specific IgE, and overproduction of Th1/Th2-mediated cytokines and chemokines.[32]

Allergen exposure in the airway induces a Th2-dominant response by activating inflammatory cells and increasing Th2 cytokines. IL-4, IL-5, and IL-13 play important roles in causing the symptoms, such as airway hyperresponsiveness, airway inflammation, and goblet cell hyperplasia via eosinophil activation and IgE secretion.[33] Th2 cytokines are important therapeutic targets for the inhibition of airway inflammation. We evaluated the inhibitory effects of CKS on the secretion of Th1/Th2 cytokines in OVA-induced mice. OVA-induced

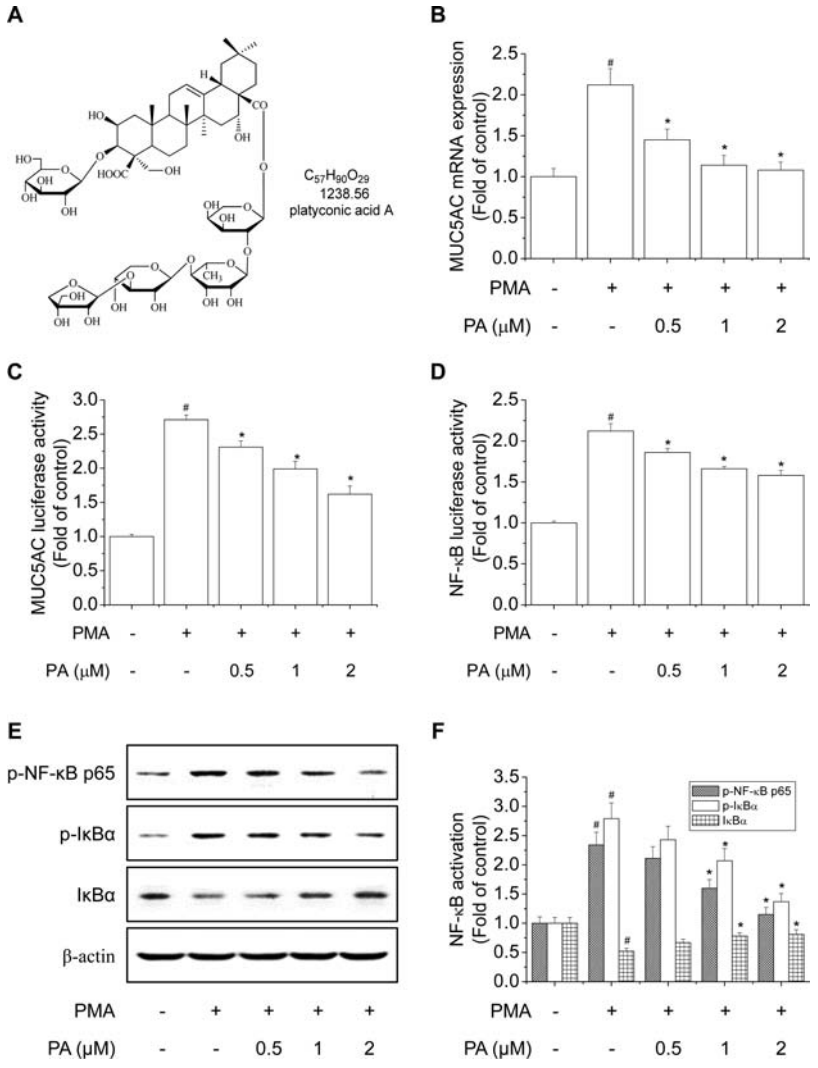

Figure 5. Inhibitory effects of PA on PMA-induced MUC5AC mRNA expression in cells. (A) Chemical structure of platyconic acid A. (B) Total RNA was extracted from the cells, and MUC5AC mRNA expression was measured by qRT-PCR. (C and D) MUC5AC or NF-κB luciferase activity was measured by a promoter construct. (E) Cells were pretreated with PA (0.5, 1, and 2 μM) and then treated with PMA (20 nM). After 30 min, total protein was extracted from the cells, and phospho-NF-κB p65, phospho-IκBα, and IκBα level was measured by Western blotting. (F) Intensities of the Western blot bands were calculated using the ImageJ software. Results are presented as means ± SEM of three independent experiments. #$p < 0.01$, significantly different from the control group; * $p < 0.01$, significantly different from the PMA-treated group.

DOI: 10.1021/jf5043954
J. Agric. Food Chem. 2015, 63, 1468−1476

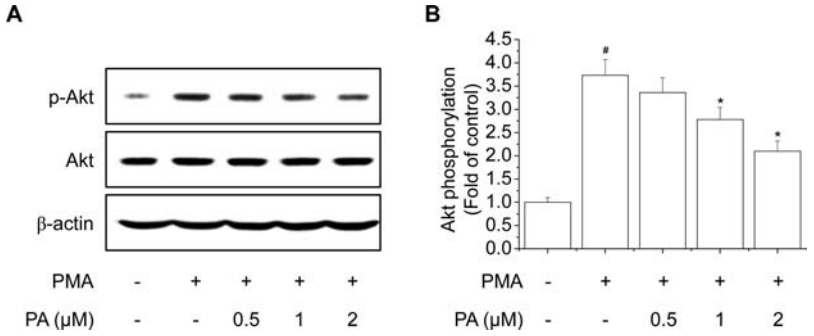

Figure 6. Inhibitory effect of PA on PMA-induced Akt activation in cells. (A) Cells were pretreated with PA (0.5, 1, and 2 μM) and then treated with PMA (20 nM). After 30 min, total protein was extracted from the cells and phospho-Akt and Akt level was measured by Western blotting. (B) Intensities of the Western blot bands were calculated using the ImageJ software. Results are presented as means ± SEM of three independent experiments. $^{\#}p < 0.01$, significantly different from the control group; * $p < 0.01$, significantly different from the PMA-treated group.

secretion of Th2 cytokines (IL-4, IL-5, and IL-13), as well as secretion of Th1 cytokines (TNF-α and IFN-γ), was reduced by CKS treatment. The Th2 immune response is associated with IgE hypersecretion. In IgE-mediated airway inflammation, IgE released from B cells binds to mast cells, leading to degranulation of the mast cells and the release of various biological mediators.[14] We confirmed that OVA-induced IgE production was reduced by CKS treatment, and we previously reported on the inhibitory effects of CKS on IgE-mediated allergic responses in mast cells.[34] Chemokines play an important role in the development of airway inflammation through their participation in leukocyte recruitment. MCP-1 plays a role in the recruitment and activation of leukocytes in response to various stimuli.[35] We demonstrated that CKS treatment reduced OVA-induced MCP-1 secretion. These results suggest that CKS reduced OVA-induced development of airway inflammation by suppressing IgE-mediated mast cell activation, Th1/Th2 inflammatory cytokines, and MCP-1 chemokine release.

Airway inflammation occurs due to an infiltration of leukocytes into the bronchial and lung tissues. It is associated with the production of Th2 cytokines, which play a critical role in the differentiation, infiltration, and activation of eosinophils.[25] We evaluated the inhibitory effects of CKS on the number of leukocytes in OVA-inhaled mice. We demonstrated that the number of total and differential inflammatory cells was reduced by CKS treatment. Asthma is characterized by the infiltration of inflammatory cells, as well as hyperplasia of goblet cells into the lung tissues. Goblet cell hyperplasia is associated with bronchial inflammation and narrowing of the airways.[36] Pathological changes showed that CKS treatment inhibited OVA-induced inflammatory cell infiltration and goblet cell hyperplasia in the lung tissue.

Airway remodeling often occurs during the initial stages of asthma and may facilitate the continuation of damage to tissues and the inflammatory response. Airway remodeling is characterized by inflammatory cell infiltration, goblet cell hyperplasia, and MMP-2/-9 production.[37] MMPs are proteases that cleave components of the extracellular matrix. MMPs play an important role in tissue remodeling associated with pathological processes such as morphogenesis, angiogenesis, tissue repair, and migration.[37] A recent study reported that MMP-2/-9 overexpression was related to an accumulation of airway inflammatory cells in an animal model.[37] We evaluated OVA-induced MMP-2/9 and MUC5AC mRNA expression associated with airway remodeling in lung tissues. We demonstrated that OVA-induced MMP-2/9 and MUC5AC mRNA expression was reduced by CKS treatment. However, OVA-reduced TIMP-1/-2 mRNA recovered with CKS treatment. Expression of MUC5AC and MMP-2/-9 is controlled by a NF-κB transcription factor. We examined the OVA-induced NF-κB nuclear translocation in lung tissues. OVA-induced NF-κB nuclear translocation was reduced by CKS treatment. We previously reported the inhibitory effects of CKS on cellular MMP-2/-9 and MUC5AC expression via inhibition of NF-κB activity.[4,38] CK inhibited OVA-induced MMP-2/-9 production via inhibition of NF-κB nuclear translocation.[3] Finally, we evaluated the effects of PA, a component of the CKS triterpenoid saponins, on MUC5AC expression via NF-κB activation in the cells. The inhibition of iNOS and COX-2 mRNA expression by PA, through blocking of NF-κB activation, has been reported previously.[39] We showed that PA treatment inhibited PMA-induced MUC5AC expression by suppressing NF-κB activity. These results suggested that CKS reduced OVA-induced airway remodeling by suppression of MMP-2/-9 and MUC5AC expression via inhibition of NF-κB activity. PA potentially inhibited MUC5AC expression through the inactivation of NF-κB.

In conclusion, we demonstrated that CKS and its active component, PA, reduced the severity of airway inflammation in an experimental animal model and in cells. CKS inhibited OVA-induced airway inflammation symptoms, including infiltration of inflammatory cells, hypersecretion of goblet cells, levels of IgE, Th1/Th2, and MCP-1, mRNA expression of MMP-2/-9 and MUC5AC, and NF-κB activation in mice. PA inhibited MUC5AC expression via suppression of NF-κB activation in cells. These results demonstrated that CKS and PA have a potent preventive effect against the progression of airway inflammation related to mucin production.

■ ASSOCIATED CONTENT

Supporting Information

Supplemental figures and table. This material is available free of charge via the Internet at http://pubs.acs.org.

■ AUTHOR INFORMATION

Corresponding Authors

*Tel: +82-53-810-2819. E-mail: taecheon@ynu.ac.kr. College of Pharmacy, Yeungnam University, Gyeongsan 712-749, Republic of Korea.

*Tel: +82-42-821-5936. Fax: +82-42-825-4936. E-mail: hgjeong@cnu.ac.kr. Department of Toxicology, College of Pharmacy, Chungnam National University, Daejeon 305-764, Republic of Korea.

DOI: 10.1021/jf5043954
J. Agric. Food Chem. 2015, 63, 1468−1476

Author Contributions

[¶]Authors J.H.C. and S.W.J. contributed equally to this work.

Funding

This research was supported by Basic Science Research Program through the National Research Foundation of Korea (NRF) funded by the Ministry of Education (2009-0093815) and Technology Commercialization Support Program, Ministry of Agriculture, Food and Rural Affairs (MAFRA) (113039-2), Republic of Korea.

Notes

The authors declare no competing financial interest.

■ ABBREVIATIONS USED

IgE, immunoglobin E; MMP, matrix metalloproteinase; MCP-1, monocyte chemoattractant protein-1; MUC5AC, mucin 5 subtype A and C; NF-κB, nuclear factor kappaB; PMA, phorbol 12-myristate 13-acetate; Th, T helper; TIMP, tissue inhibitor of metalloprotease

■ REFERENCES

(1) Kim, J. Y.; Hwang, Y. P.; Kim, D. H.; Han, E. H.; Chung, Y. C.; Roh, S. H.; Jeong, H. G. Inhibitory effect of the saponins derived from roots of *Platycodon grandiflorum* on carrageenan-induced inflammation. *Biosci. Biotechnol. Biochem.* **2006**, *70*, 858−864.

(2) Kim, J. Y.; Kim, D. H.; Kim, H. G.; Song, G. Y.; Chung, Y. C.; Roh, S. H.; Jeong, H. G. Inhibition of tumor necrosis factor-alpha-induced expression of adhesion molecules in human endothelial cells by the saponins derived from roots of *Platycodon grandiflorum*. *Toxicol. Appl. Pharmacol.* **2006**, *210*, 150−156.

(3) Choi, J. H.; Hwang, Y. P.; Lee, H. S.; Jeong, H. G. Inhibitory effect of *Platycodi radix* on ovalbumin-induced airway inflammation in a murine model of asthma. *Food Chem. Toxicol.* **2009**, *47*, 1272−1279.

(4) Choi, J. H.; Hwang, Y. P.; Han, E. H.; Kim, H. G.; Park, B. H.; Lee, H. S.; Park, B. K.; Lee, Y. C.; Chung, Y. C.; Jeong, H. G. Inhibition of acrolein-stimulated MUC5AC expression by *Platycodon grandiflorum* root-derived saponin in A549 cells. *Food Chem. Toxicol.* **2011**, *49*, 2157−2166.

(5) Lee, K. J.; Choi, C. Y.; Chung, Y. C.; Kim, Y. S.; Ryu, S. Y.; Roh, S. H.; Jeong, H. G. Protective effect of saponins derived from roots of *Platycodon grandiflorum* on tert-butyl hydroperoxide-induced oxidative hepatotoxicity. *Toxicol. Lett.* **2004**, *147*, 271−282.

(6) Lee, K. J.; Choi, J. H.; Kim, H. G.; Han, E. H.; Hwang, Y. P.; Lee, Y. C.; Chung, Y. C.; Jeong, H. G. Protective effect of saponins derived from the roots of *Platycodon grandiflorum* against carbon tetrachloride induced hepatotoxicity in mice. *Food Chem. Toxicol.* **2008**, *46*, 1778−1785.

(7) Khanal, T.; Choi, J. H.; Hwang, Y. P.; Chung, Y. C.; Jeong, H. G. Saponins isolated from the root of *Platycodon grandiflorum* protect against acute ethanol-induced hepatotoxicity in mice. *Food Chem. Toxicol.* **2009**, *47*, 530−535.

(8) Khanal, T.; Choi, J. H.; Hwang, Y. P.; Chung, Y. C.; Jeong, H. G. Protective effects of saponins from the root of *Platycodon grandiflorum* against fatty liver in chronic ethanol feeding via the activation of AMP-dependent protein kinase. *Food Chem. Toxicol.* **2009**, *47*, 2749−2754.

(9) Noh, J. R.; Kim, Y. H.; Gang, G. T.; Yang, K. J.; Kim, S. K.; Ryu, S. Y.; Kim, Y. S.; Lee, C. H.; Lee, H. S. Preventative effects of *Platycodon grandiflorum* treatment on hepatic steatosis in high fat diet-fed C57BL/6 mice. *Biol. Pharm. Bull.* **2010**, *33*, 450−454.

(10) Kwon, D. Y.; Kim, Y. S.; Ryu, S. Y.; Choi, Y. H.; Cha, M. R.; Yang, H. J.; Park, S. Platyconic acid, a saponin from *Platycodi radix*, improves glucose homeostasis by enhancing insulin sensitivity in vitro and in vivo. *Eur. J. Nutr.* **2012**, *51*, 529−540.

(11) Corry, D. B. Emerging immune targets for the therapy of allergic asthma. *Nat. Rev. Drug Discovery* **2002**, *1*, 55−64.

(12) Berkman, N.; Krishnan, V. L.; Gilbey, T.; Newton, R.; O'Connor, B.; Barnes, P. J.; Chung, K. F. Expression of RANTES mRNA and protein in airways of patients with mild asthma. *Am. J. Respir. Crit. Care Med.* **1996**, *154*, 1804−1811.

(13) Zimmermann, N.; Hershey, G. K.; Foster, P. S.; Rothenberg, M. E. Chemokines in asthma: cooperative interaction between chemokines and IL-13. *J. Allergy Clin. Immunol.* **2003**, *111*, 227−242.

(14) Cheng, C.; Ho, W. E.; Goh, F. Y.; Guan, S. P.; Kong, L. R.; Lai, W. Q.; Leung, B. P.; Wong, W. S. Anti-malarial drug artesunate attenuates experimental allergic asthma via inhibition of the phosphoinositide 3-kinase/Akt pathway. *PLoS One* **2011**, *6*, e20932.

(15) Galli, S. J.; Tsai, M.; Piliponsky, A. M. The development of allergic inflammation. *Nature* **2008**, *454*, 445−454.

(16) Medoff, B. D.; Thomas, S. Y.; Luster, A. D. T cell trafficking in allergic asthma: the ins and outs. *Annu. Rev. Immunol.* **2008**, *26*, 205−232.

(17) Kim, H. J.; Park, Y. D.; Moon, U. Y.; Kim, J. H.; Jeon, J. H.; Lee, J. G.; Bae, Y. S.; Yoon, J. H. The role of Nox4 in oxidative stress-induced MUC5AC overexpression in human airway epithelial cells. *Am. J. Respir. Cell Mol. Biol.* **2008**, *39*, 598−609.

(18) Barnes, P. J. Reactive oxygen species and airway inflammation. *Free Radical Biol. Med.* **1990**, *9*, 235−243.

(19) Wanner, A.; Salathé, M.; O'Riordan, T. G. Mucociliary clearance in the airways. *Am. J. Respir. Crit. Care Med.* **1996**, *154*, 1868−1902.

(20) Rogers, D. F. Physiology of airway mucus secretion and pathophysiology of hypersecretion. *Respir. Care* **2007**, *52*, 1134−1146.

(21) Verza, S. G.; Silveira, F.; Cibulski, S.; Kaiser, S.; Ferreira, F.; Gosmann, G.; Roehe, P. M.; Ortega, G. G. Immunoadjuvant activity, toxicity assays, and determination by UPLC/Q-TOF-MS of triterpenic saponins from *Chenopodium quinoa* seeds. *J. Agric. Food Chem.* **2012**, *60*, 3113−3118.

(22) Kim, Y. S.; Kim, J. S.; Choi, S. U.; Kim, J. S.; Lee, H. S.; Roh, S. H.; Jeong, Y. C.; Kim, Y. K.; Ryu, S. Y. Isolation of a new saponin and cytotoxic effect of saponins from the root of *Platycodon grandiflorum* on human tumor cell lines. *Planta Med.* **2005**, *71*, 566−568.

(23) Choi, Y. H.; Yoo, D. S.; Choi, C. W.; Cha, M. R.; Kim, Y. S.; Lee, H. S.; Lee, K. R.; Ryu, S. Y. Platyconic acid A, a genuine triterpenoid saponin from the roots of *Platycodon grandiflorum*. *Molecules* **2008**, *13*, 2871−2879.

(24) Ip, W. K.; Wong, C. K.; Lam, C. W. Interleukin (IL)-4 and IL-13 up-regulate monocyte chemoattractant protein-1 expression in human bronchial epithelial cells: involvement of p38 mitogen-activated protein kinase, extracellular signal-regulated kinase 1/2 and Janus kinase-2 but not c-Jun NH2-terminal kinase 1/2 signalling pathways. *Clin. Exp. Immunol.* **2006**, *145*, 162−172.

(25) Kim, D. Y.; Park, B. S.; Hong, G. U.; Lee, B. J.; Park, J. W.; Kim, S. Y.; Ro, J. Y. Anti-inflammatory effects of the R2 peptide, an inhibitor of transglutaminase 2, in a mouse model of allergic asthma, induced by ovalbumin. *Br. J. Pharmacol.* **2011**, *162*, 210−225.

(26) Yamauchi, K.; Piao, H. M.; Nakadate, T.; Shikanai, T.; Nakamura, Y.; Niisato, M.; Ito, H.; Mouri, T.; Kobayashi, H.; Maesawa, C.; Sawai, T.; Ohtsu, H.; Inoue, H. Progress in allergy signal research on mast cells: the role of histamine in goblet cell hyperplasia in allergic airway inflammation - a study using the Hdc knockout mouse. *J. Pharmacol. Sci.* **2008**, *106*, 354−360.

(27) Cowden, J. M.; Riley, J. P.; Ma, J. Y.; Thurmond, R. L.; Dunford, P. J. Histamine H4 receptor antagonism diminishes existing airway inflammation and dysfunction via modulation of Th2 cytokines. *Respir. Res.* **2010**, *11*, 1−12.

(28) Chung, M. J.; Park, J. K.; Park, Y. I. Anti-inflammatory effects of low-molecular weight chitosan oligosaccharides in IgE-antigen complex-stimulated RBL-2H3 cells and asthma model mice. *Int. Immunopharmacol.* **2012**, *12*, 453−459.

(29) Amin, K. The role of mast cells in allergic inflammation. *Respir. Med.* **2012**, *106*, 9−14.

(30) Liu, D. S.; Liu, W. J.; Chen, L.; Ou, X. M.; Wang, T.; Feng, Y. L.; Zhang, S. F.; Xu, D.; Chen, Y. J.; Wen, F. Q. Rosiglitazone, a peroxisome proliferator-activated receptor-gamma agonist, attenuates acrolein-induced airway mucus hypersecretion in rats. *Toxicology* **2009**, *260*, 112−119.

DOI: 10.1021/jf5043954
J. Agric. Food Chem. 2015, 63, 1468−1476

(31) Shi, Y.; Dai, J.; Liu, H.; Li, R. R.; Sun, P. L.; Du, Q.; Pang, L. L.; Chen, Z.; Yin, K. S. Naringenin inhibits allergen-induced airway inflammation and airway responsiveness and inhibits NF-kappaB activity in a murine model of asthma. *Can. J. Physiol. Pharmacol.* **2009**, *87*, 729−735.
(32) Ci, X.; Chu, X.; Wei, M.; Yang, X.; Cai, Q.; Deng, X. Different effects of farrerol on an OVA-induced allergic asthma and LPS-induced acute lung injury. *PLoS One* **2012**, *7*, e34634.
(33) Bao, Z.; Guan, S.; Cheng, C.; Wu, S.; Wong, S. H.; Kemeny, D. M.; Leung, B. P.; Wong, W. S. A novel antiinflammatory role for andrographolide in asthma via inhibition of the nuclear factor-kappaB pathway. *Am. J. Respir. Crit. Care Med.* **2009**, *179*, 657−665.
(34) Han, E. H.; Park, J. H.; Kim, J. Y.; Chung, Y. C.; Jeong, H. G. Inhibitory mechanism of saponins derived from roots of *Platycodon grandiflorum* on anaphylactic reaction and IgE-mediated allergic response in mast cells. *Food Chem. Toxicol.* **2009**, *47*, 1069−1075.
(35) Kita, T.; Fujimura, M.; Myou, S.; Watanabe, K.; Waseda, Y.; Nakao, S. Effects of KF19514, a phosphodiesterase 4 and 1 Inhibitor, on bronchial inflammation and remodeling in a murine model of chronic asthma. *Allergol. Int.* **2009**, *58*, 267−275.
(36) Ci, X.; Chu, X.; Chen, C.; Li, X.; Yan, S.; Wang, X.; Yang, Y.; Deng, X. Oxytetracycline attenuates allergic airway inflammation in mice via inhibition of the NF-κB pathway. *J. Clin. Immunol.* **2011**, *31*, 216−227.
(37) Shin, I. S.; Lee, M. Y.; Lim, H. S.; Ha, H.; Seo, C. S.; Kim, J. C.; Shin, H. K. An extract of *Crataegus pinnatifida* fruit attenuates airway inflammation by modulation of matrix metalloproteinase-9 in ovalbumin induced asthma. *PLoS One* **2012**, *7*, e45734.
(38) Lee, K. J.; Hwang, S. J.; Choi, J. H.; Jeong, H. G. Saponins derived from the roots of *Platycodon grandiflorum* inhibit HT-1080 cell invasion and MMPs activities: regulation of NF-kappaB activation via ROS signal pathway. *Cancer Lett.* **2008**, *268*, 233−243.
(39) Ahn, K. S.; Noh, E. J.; Zhao, H. L.; Jung, S. H.; Kang, S. S.; Kim, Y. S. Inhibition of inducible nitric oxide synthase and cyclooxygenase II by *Platycodon grandiflorum* saponins via suppression of nuclear factor-kappaB activation in RAW 264.7 cells. *Life Sci.* **2005**, *76*, 2315−2328.
(40) Yang, J.; Li, Q.; Zhou, X. D.; Kolosov, V. P.; Perelman, J. M. Naringenin attenuates mucous hypersecretion by modulating reactive oxygen species production and inhibiting NF-κB activity via EGFR-PI3K-Akt/ERK MAPKinase signaling in human airway epithelial cells. *Mol. Cell. Biochem.* **2011**, *351*, 29−40.
(41) El-Gamal, Y. M.; Elmasry, O. A.; El-Ghoneimy, D. H.; Soliman, I. M. Immunomodulatory effects of food. *Egypt. J. Pediatr. Allergy Immunol.* **2011**, *9*, 3−13.
(42) Cherng, J. M.; Chiang, W.; Chiang, L. C. Immunomodulatory activities of edible beans and related constituents from soybean. *Food Chem.* **2007**, *104*, 613−618.
(43) Lee, S. H.; Lillehoj, H. S.; Jang, S. I.; Lee, K. W.; Bravo, D.; Lillehoj, E. P. Effects of dietary supplementation with phytonutrients on vaccine-stimulated immunity against infection with *Eimeria tenella*. *Vet. Parasitol.* **2011**, *181*, 97−105.
(44) Yang, X.; Lv, Y.; Tian, L.; Zhao, Y. Composition and systemic immune activity of the polysaccharides from an herbal tea (*Lycopus lucidus* Turcz). *J. Agric. Food Chem.* **2010**, *58*, 6075−6080.
(45) Hsu, Y. J.; Weng, C. F.; Lin, K. W.; Lin, K. C. Suppression of allergic reactions in ovalbumin-sensitized mice by yam storage proteins dioscorins. *J. Agric. Food Chem.* **2013**, *61*, 11460−11467.
(46) Choi, J. H.; Kim, H. G.; Jin, S. W.; Han, E. H.; Khanal, T.; Do, M. T.; Hwang, Y. P.; Choi, J. M.; Chun, S. S.; Chung, Y. C.; Jeong, T. C.; Jeong, H. G. Topical application of *Pleurotus eryngii* extracts inhibits 2,4-dinitrochlorobenzene-induced atopic dermatitis in NC/Nga mice by the regulation of Th1/Th2 balance. *Food Chem. Toxicol.* **2013**, *53*, 38−45.

DOI: 10.1021/jf5043954
J. Agric. Food Chem. 2015, 63, 1468−1476

Table 1. Identification of Phenolic Compounds in Different Extracts of Elderflowers in Negative Ionization with HPLC-MS and MS^2/MS^3

Peak No.[a]	t_R (min)[b]	λ (nm)	Tentative identification	$[M-H]^-$ (m/z)	MS^2 (m/z)	MS^3 (m/z)	Analyzed in		
							methanol	syrup	sabesa
1	11.82	234, 326	3-Caffeoylquinic acid (neochlorogenic acid)	353	191, 179, 135		X	X	X
2	13.84	316, 287, 234	*p*-Coumaric acid hexoside	325	163		X	X	X
3	14.59	312	3-*p*-Coumaroylquinic acid	337	163, 191, 173		X	X	X
3	14.59	234, 279	Catechin	289	245		X		
4	15.09	234, 328	5-Caffeoylquinic acid 1 (chlorogenic acid)	353	191, 179, 173, 135		X	X	X
5	15.84	234, 328	4-Caffeoylquinic acid (cryptochlorogenic acid)	353	173, 179, 191, 135		X	X	X
5	15.84	322	3-Feruloylquinic acid	367	193, 134		X	X	X
6	16.39	266, 348	Kaempferol dihexoside 1	609	447	285	X	X	
7	17.05	234, 328	5-Caffeoylquinic acid 2	353	191, 179		X	X	X
8	18.05	234, 279	Epicatechin	289	245		X	X	
9	18.42	234, 278	Procyanidin trimer	865	577, 425, 407, 289		X	X	X
10	18.72	312	5-*p*-Coumaroylquinic acid 1	337	191, 173, 163		X	X	X
11	19.76	322	5-Feruloylquinic acid	367	191, 173		X	X	X
12	20.31	312	5-*p*-Coumaroylquinic acid 2	337	191, 163, 173		X	X	X
13	19.76	257, 354	Quercetin dihexoside	625	463	301	X	X	X
14	19.95	265, 347	Kaempferol triglycoside	755	285		X	X	X
15	21.13	254, 358	Quercetin hexoside pentoside 1	595	301		X	X	X
16	21.56	266, 346	Kaempferol dihexoside 2	609	447	285	X	X	X
16	21.56	255, 356	Isorhamnetin dihexoside	639	315		X	X	X
16	21.56	255, 358	Quercetin hexoside pentoside 2	595	301		X	X	X
17	22.21	255, 355	Quercetin-3-rutinoside	609	301		X	X	X
18	22.57	256, 356	Quercetin-3-galactoside	463	301		X		
19	23.21	255, 355	Quercetin-3-glucoside	463	301		X	X	X
20	23.86	264, 345	Kaempferol-3-rutinoside	593	285		X	X	X
21	24.05	256, 354	Isorhamnetin-3-rutinoside	623	315		X	X	X
22	24.77	265, 352	Kaempferol-3-glucoside	447	285		X	X	X
23	24.94	256, 354	Isorhamnetin-3-glucoside	477	315		X	X	X
24	25.29	255, 355	Quercetin-acetylglucoside	505	463	301	X	X	X
25	25.32	246, 316	Dicaffeoylquinic acid 1	515	353	173, 179	X	X	X
26	25.56	247, 321	Dicaffeoylquinic acid 2	515	353	191, 179, 173	X	X	X
27	25.84	247, 328	Dicaffeoylquinic acid 3	515	353	173, 179, 191	X		
28	26.18	255, 367	Isorhamnetin pentoside	447	315		X		
29	26.96	265, 346	Kaempferol acetylhexoside	489	285		X	X	X
30	27.26	254, 346	Isorhamnetin acetylhexoside	519	315		X	X	X
31	27.56	312	*p*-Coumaroyl-caffeoylquinic acid 1	499	353	191, 179	X	X	X
32	27.75	316	*p*-Coumaroyl-caffeoylquinic acid 2	499	353	191, 179	X	X	X
33	33.03	213, 225, 289	Naringenin	271	151		X	X	X

[a]Peak No. = peak number. [b]t_R = retention time.

primary aim of the present study was the separation, comprehensive identification and quantification of phenolic compounds and antioxidant properties in three different elderflower extracts (methanol and two water extracts prepared as fresh drinks according to local recipes). Moreover, the effect of extraction solution, duration of extraction and method of juice preparation on the content of phenolic compounds has been evaluated. Methanol was used as a standard solvent for phenolic extraction to enable maximum levels of extracted compounds. Additionally, the study aims to underline qualitative and quantitative differences between two types of elderflower beverages: a local drink known as "sabesa" and elderflower syrup. The results are indicative of the potential value of elderflower extracts in the processing industry (juices, syrups, beverages) as well as important for further studies monitoring the effects of plant-based product intake on human health.

MATERIALS AND METHODS

Chemicals. The following standards were used for the quantification of phenolic compounds: neochlorogenic acid (3-caffeoylquinic acid), chlorogenic acid (5-caffeoylquinic acid), naringenin and quercetin-3-rutinoside from Sigma-Aldrich Chemie GmbH (Steinheim, Germany), caffeic and ferulic acid, (−)-epicatechin, quercetin-3-galactoside, quercetin-3-glucoside, *p*-coumaric acid, procyanidin B1 and kaempferol-3-glucoside from Fluka Chemie GmBH (Buchs, Switzerland); isorhamnetin-3-*O*-glucoside from Extrasynthese (Genay Cedex, France) and (+)-catechin from Roth (Karlsruhe, Germany). Methanol for the extraction of phenolics was acquired from Sigma. The chemicals for the mobile phases were HPLC-MS grade acetonitrile and formic acid from Fluka Chemie

DOI: 10.1021/jf506005b
J. Agric. Food Chem. 2015, 63, 1477−1487

GmbH. Water for mobile phase was double distilled and purified with the Milli-Q system (Millipore, Bedford, MA, USA). For the total phenolic content, Folin-Ciocalteu phenol reagent (Fluka Chemie GmBH), sodium carbonate (Merck, Darmstadt, Germany), gallic acid (Sigma) and ethanol (Sigma) were used. For the antioxidant activity 6-hydroxy-2,5,7,8-tetramethylchroman-2-carboxylic acid (Trolox), 2,2′azinobis(3-ethylbenzthiazoline-6-sulfonic acid ($ABTS^{\bullet+}$); potassium persulfate, acetic acid, 2,4,6-tripyridyl-1,3,5-triazine (TPTZ), $FeCl_3 \cdot 6H_2O$, hydrochloric acid, sodium acetate and methanol were purchased from Sigma-Aldrich.

Plant material. Mature elderberry umbels were hand-picked from wild-growing elderberry shrubs growing near Ljubljana (latitude 46° 08′ 19″ N, longitude 14° 30′ 27″ E) on May 19th 2014. Umbels were picked from the middle and top branches of several elderberry bushes in the morning hours. Approximately 200 umbels were collected and transferred into the laboratory. Stalks were shortened to about 2 cm from the center of the umbel and pedicles and flowers were further processed into different elderflower products.

Processing of elderflower extracts. Three different extracts (in six replications each) were prepared from fresh elderflowers. The first extraction was prepared by extracting 2 g of elderflowers with 15 mL of methanol. Tubes were placed in a cooled ultrasonic bath for 1 h. After extraction, flower extracts were centrifuged for 10 min at 12.857 g. Each supernatant was filtered through a Chromafil AO-20/25 polyamide filter produced by Macherey-Nagel (Düren, Germany), transferred into a vial and stored at −20 °C prior to injection into the HPLC (high performance liquid chromatography) system.

The remaining two extraction procedures utilized tap water for elderflower extraction and were based on traditional recipes for syrup and sabesa beverage preparation. These elderflower beverages are frequently made in Slovenia. The syrup was prepared according to the following procedure: one (1) kg of sugar (sucrose) and 16.7 g of citric acid were dissolved in one (1) L of water. To the sweet liquid 140 g of elderflowers were added to produce syrup. The second type of a local drink, known as sabesa, was prepared by adding 150 g of sucrose, 1 g of citric acid, 50 mL of acetic acid and 14 g of fresh elderflowers to one (1) L of water.

Elderflowers were extracted in a dark cool room (10 °C) for 1, 3, or 7 days and the liquid was stirred several times each day. Original recipe for preparing sabesa is extracting flowers for 3 days and for syrup just 1 day. After the extraction the beverages were filtered through gauze, the extracts were centrifuged for 10 min at 12.857 g and filtered through a polyamide filter (Macherey-Nagel, AO-20/25) into a vial. The samples were stored at −20 °C prior to injection into the HPLC system.

Determination of individual phenolic compounds using HPLC-DAD-MS^n analysis. Phenolic compounds were analyzed on a Thermo Finnigan Surveyor HPLC system (Thermo Scientific, San Jose, USA) with a diode array detector at 280 nm (flavanols, hydroxycinnamic acid derivatives, flavanone) and 350 nm (flavonols). Spectra of the compounds were recorded between 200 and 600 nm. The column was a Gemini C_{18} (150 × 4.6 mm 3 μm; Phenomenex, Torrance, USA) operated at 25 °C. The elution solvents were aqueous 0.1% formic acid in double distilled water (A) and 0.1% formic acid in acetonitrile (B). Samples were eluted according to a linear gradient from 5% to 20% B in the first 15 min, followed by a linear gradient from 20% to 30% B for 5 min, then an isocratic mixture for 5 min, followed by a linear gradient from 30% to 90% B for 5 min, and then an isocratic mixture for 15 min before returning to the initial conditions.[14] The injection amount was 20 μL and flow rate 0.6 mL min^{-1}.

All phenolic compounds were identified using a mass spectrometer (Thermo Scientific, LCQ Deca XP MAX) with electrospray ionization (ESI) operating in negative ion mode. The analyses were carried out using full scan data-dependent MS^n scanning from m/z 115 to 1500 (Table 1). The injection volume was 10 μL and the flow rate maintained at 0.6 mL min^{-1}. The capillary temperature was 250 °C, the sheath gas and auxiliary gas were 60 and 15 units, respectively; the source voltage was 3 kV and normalized collision energy was between 20−35%. Spectral data were elaborated using the Excalibur software (Thermo Scientific).

Contents of phenolic compounds were calculated from peak areas of the sample and the corresponding standards and expressed in mg/L of elderflower extract or in mg/kg elderflowers. For compounds lacking standards, quantification was carried out using similar compounds as standards. Thus, coumaric acid derivatives were quantified in equivalents of *p*-coumaric acid, caffeic acid derivatives in equivalents of caffeic acid, ferulic acid derivatives in equivalents of ferulic acid, procyanidin trimer in equivalents of procyanidin B1, quercetin-glycosides in equivalents of quercetin-3-galactoside, isorhamnetin glycosides in equivalents of isohamnetin-3-glucoside and kaempferol glycosides in equivalents of kaempferol-3-glucoside.

Determination of total phenolic content. Total phenolic content (TPC) of extracts was assessed by the Folin-Ciocalteau phenol reagent method.[15] To 100 μL of the sample extracts (methanolic extracts were diluted 1 to 4 (v/v) with MeOH), 6 mL of double distilled water and 500 μL of Folin-Ciocalteau reagent were added; after resting between 8 s and 8 min at room temperature, 1.5 mL of sodium carbonate (20% w/v) was added. The extracts were mixed and allowed to stand for 30 min at 40 °C before measuring the absorbance on a spectrophotometer (PerkinElmer, UV/vis Lambada Bio 20) at 765 nm. A mixture of water and reagents was used as a blank sample. Total phenolic content was expressed as gallic acid equivalents (GAE) in mg/L of extract or in mg/kg fresh flowers. Absorption was measured in three replications.

Determination of $ABTS^{\bullet+}$ radical cation scavenging activity. The free-radical scavenging activity was determined by ABTS radical cation decolourization assay according to the method of Re et al.[16] ABTS was dissolved in water to a 7-mM concentration. ABTS radical cation ($ABTS^{\bullet+}$) was produced after the reaction of $ABTS^{\bullet+}$ stock solution with 2.45 mM potassium persulfate (final concentration) and the mixture was left in the dark at room temperature for 12−16 h before use. The radical remains stable in this form for more than 2 days. In the following step, $ABTS^{\bullet+}$ solution was diluted with double distilled water to an absorbance of 0.700 (±0.02) measured at 734 nm. Thirty μL of the extract were added to 3.0 mL of diluted $ABTS^{\bullet+}$ solution and the absorbance was assessed exactly 6 min after the initial mixing. All measurements were performed in triplicate. The results of the assay were expressed relative to mM Trolox/L of extract or in mM Trolox per kg of fresh flowers in terms of trolox equivalent antioxidant capacity (TEAC).

Determination of ferric reducing antioxidant power (FRAP) assay. Total antioxidant potential of the extracts was determined using a ferric reducing ability of plasma (FRAP) assay by Benzie and Strain[17] as a measure of antioxidant power. The assay is based on the reducing power of a compound (antioxidant). A potential antioxidant will reduce the ferric ion (Fe^{3+}) to ferrous ion (Fe^{2+}); the latter forms a blue complex (Fe^{2+}/TPTZ), which increases the absorption at 593 nm. Briefly, the FRAP reagent was prepared by mixing acetate buffer (300 μM, pH 3.6), a solution of 10 μM TPTZ in 40 μM HCl, and 20 μM $FeCl_3$ at 10:1:1 (v/v/v). The FRAP reagent (300 μL) and sample solutions (10 μL) were added to each well and mixed thoroughly. The absorbance was measured at 593 nm after 10 min. Standard curve was prepared using different concentrations of Trolox. All solutions were used on the day of preparation. All determinations were performed in triplicate. The results were expressed in mM Trolox/L of extract or in mM Trolox per kg of fresh flowers.

Statistical analysis. The content of individual phenolic in mg/kg of fresh flowers were compared among three treatments (methanol extract, sabesa after 72 h of extraction and syrup after 24 h of extraction) using one-way ANOVA. The effect of extraction time (three levels), type of elderflower beverage (two levels) and their interaction on the content of individual phenolic compound in mg/L was investigated using linear mixed effects model with the extraction vessel as the random factor. The model assumptions tests (variance check, normality check) were performed graphically (plot of residuals vs fitted values and Q-Q plot, respectively). After the overall tests planned contrasts were performed to determine significant differences between extraction times for sabesa and syrup separately. All the analyses were performed in R environment (R Core Team, 2013); for linear mixed models the package nlme was used.

DOI: 10.1021/jf506005b
J. Agric. Food Chem. 2015, 63, 1477−1487

Table 2. Content of Individual Phenolic Compounds,[b] Total Phenolic Content[c] and Antioxidant Activity[d] in Elderflower Methanolic Extract, in Sabesa after 72 h Extraction and Syrup after 24 h Extraction[a]

	Methanol		Sabesa 72 h		Syrup 24 h	
Phenolic compound[b]	Mean ± SE	Hom.gr.	Mean ± SE	Hom.gr.	Mean ± SE	Hom.gr.
3-Caffeoylquinic acid	510.57 ± 18.84	c	360.27 ± 18.66	b	162.54 ± 6.20	a
4-Caffeoylquinic acid	31.37 ± 0.99	c	23.86 ± 0.50	b	8.3 ± 0.16	a
5-Caffeoylquinic acid 1	2779.34 ± 48.40	c	1962.71 ± 35.93	b	775.31 ± 6.51	a
5-Caffeoylquinic acid 2	187.24 ± 3.27	b	180.08 ± 5.56	b	37.15 ± 0.41	a
p-Coumaric acid hexoside	28.88 ± 0.73	b	30.19 ± 0.69	b	11.58 ± 0.13	a
3-*p*-Coumaroylquinic acid	40.47 ± 2.70	b	42.79 ± 0.89	b	11 ± 0.21	a
5-*p*-Coumaroylquinic acid 1	80.93 ± 2.99	b	79.9 ± 1.51	b	20.61 ± 0.40	a
5-*p*-Coumaroylquinic acid 2	14.64 ± 0.64	b	21.2 ± 0.28	c	5.78 ± 0.14	a
3-Feruloylquinic acid	717.26 ± 22.55	c	545.71 ± 11.45	b	189.7 ± 3.72	a
5-Feruloylquinic acid	370.58 ± 10.30	c	264.37 ± 10.06	b	78.48 ± 3.36	a
Dicaffeoylquinic acid 1	217.42 ± 6.01	b	41.65 ± 3.89	a	24.16 ± 2.13	a
Dicaffeoylquinic acid 2	64.63 ± 2.56	b	5.46 ± 0.21	a	1.65 ± 0.08	a
Dicaffeoylquinic acid 3	43.06 ± 3.29		n.d.[e]		n.d.	
p-Coumaroyl-caffeoylquinic acid 1	11.71 ± 0.61	b	0.23 ± 0.01	a	0.18 ± 0.03	a
p-Coumaroyl-caffeoylquinic acid 2	10.64 ± 0.55	b	0.31 ± 0.02	a	0.07 ± 0.01	a
Total hydroxycinnamic acids	5108.73 ± 91.61	c	3558.74 ± 67.42	b	1326.5 ± 18.31	a
Catechin	6.84 ± 0.46		n.d.		n.d.	
Epicatechin	254.28 ± 8.21		n.d.		58.91 ± 1.70	
Procyanidin trimer	155.64 ± 4.04	c	82.88 ± 2.89	b	31.46 ± 0.91	a
Total flavanols	416.75 ± 8.71	b	82.88 ± 2.89	a	90.37 ± 1.03	a
Kaempferol dihexoside 1	40.24 ± 1.03		n.d.		13.36 ± 0.23	
Kaempferol dihexoside 2	33.49 ± 1.57	b	34.45 ± 0.69	b	10.66 ± 0.22	a
Kaempferol triglycoside	44.25 ± 2.37	b	36.43 ± 1.29	b	13.76 ± 0.26	a
Kaempferol-3-rutinoside	646.91 ± 18.49	b	118.46 ± 2.72	a	34.07 ± 0.50	a
Kaempferol-3-glucoside	3.54 ± 0.20	b	1.03 ± 0.04	a	1.1 ± 0.06	a
Kaempferol acetylhexoside	13.49 ± 0.37	b	1.44 ± 0.05	a	0.57 ± 0.04	a
Quercetin hexoside pentoside 1	15.06 ± 0.59	b	28.9 ± 0.86	c	7.09 ± 0.30	a
Quercetin hexoside pentoside 2	2.04 ± 0.10	b	2.1 ± 0.04	b	0.65 ± 0.01	a
Quercetin-3-rutinoside	3265.13 ± 32.46	b	4144.43 ± 114.69	c	471.16 ± 4.78	a
Quercetin-3-galactoside	10.28 ± 0.49		n.d.		n.d.	
Quercetin-3-glucoside	20.2 ± 0.47	c	12.31 ± 1.24	b	3.58 ± 0.23	a
Quercetin dihexoside	12.26 ± 0.34	a	34.99 ± 1.33	b	10.39 ± 0.45	a
Quercetin acetylglucoside	94.78 ± 2.62	b	4.54 ± 0.42	a	2.63 ± 0.23	a
Isorhamnetin dihexoside	24.5 ± 1.15	b	25.21 ± 0.51	b	7.8 ± 0.16	a
Isorhamnetin-3-rutinoside	887.99 ± 17.76	c	694.31 ± 17.96	b	208.87 ± 2.95	a
Isorhamnetin-3-glucoside	61.64 ± 4.85	b	10 ± 0.61	a	5.69 ± 0.57	a
Isorhamnetin pentoside	3.35 ± 0.14		n.d.		n.d.	
Isorhamnetin acetylhexoside	37.8 ± 1.15	c	7.26 ± 0.11	b	0.98 ± 0.05	a
Total flavonols	5216.95 ± 58.94	b	5155.86 ± 134.68	b	792.37 ± 5.69	a
Naringenin	734.15 ± 30.01	b	3.59 ± 0.13	a	0.38 ± 0.03	a
Total phenolic content[c]	10217.1 ± 219.14	b	14962.63 ± 709.56	c	2396.02 ± 53.01	a
Antioxidant activity (ABTS)[d]	35.83 ± 0.56	c	27.97 ± 0.79	b	8.9 ± 0.15	a
Antioxidant activity (FRAP)[d]	43.83 ± 0.47	b	31.22 ± 2.39	b	14.74 ± 0.24	a

[a]The letters indicate homogeneous groups of treatments at the 0.05 significance level. [b]The content of phenolic compounds was expressed as mean ± SE in mg per kg fresh flowers. [c]Total phenolic content as mean ± SE in mg GAE per kg flowers. [d]Antioxidant activity as mean ± SE in mM trolox per kg flowers. [e]n.d. = not detected.

RESULTS AND DISCUSSION

Traditionally beverages (sabesa and syrup) are prepared with different amounts of elderflowers in water. To directly compare the extractability of phenolics between the two beverages and those with standard solvent methanol, results should be express in mg per kg of fresh flowers (Table 2). However, when comparing both traditional drinks, regardless of the quantity of elderberry flowers added, the concentration was expressed in mg per liter (Table 3). Additionally, it should be taken into account that syrup is usually diluted in the ratio 1:5. The traditional extraction time of elderflowers for preparing syrup is 24 h and that for sabesa is 72 h.

Phenolic composition in elderflower extracts. 37 different phenolic compounds have been identified in the methanolic extract of elderflowers with the use of HPLC-MS (Table 1, Figure 1). Four hydroxycinnamic acid derivatives and different flavonol glycosides have been tentatively identified in elderflowers for the first time. Specific information on LC-MS ions and subsequent fragmentation patterns of the dominant ions in MS^2 enabled the identification of compounds based on the molecular masses of conjugates, the masses of the sugars

DOI: 10.1021/jf506005b
J. Agric. Food Chem. 2015, 63, 1477−1487

Table 3. Content of Individual Phenolic Compounds,[b] Total Phenolic Content[c] and Antioxidant Activity[d] in Two Elderflower Beverages at Three Extraction Durations[a]

	SABESA						SYRUP					
	24 h		72 h		168 h		24 h		72 h		168 h	
Phenolic compound[b]	Mean ± SE	Hom.gr.	Mean ± SE	Hom.gr.	Mean ± SE	Hom.gr.	Mean ± SE	Hom.gr.	Mean ± SE	Hom.gr.	Mean ± SE	Hom.gr.
3-Caffeoylquinic acid	3.65 ± 0.19	a	5.04 ± 0.26	a	5.21 ± 0.28	a	22.75 ± 0.87	a	46.47 ± 0.84	b	52.70 ± 1.01	b
4-Caffeoylquinic acid	0.22 ± 0.01	a	0.33 ± 0.01	b	0.30 ± 0.02	ab	1.16 ± 0.02	a	2.35 ± 0.01	b	2.75 ± 0.03	c
5-Caffeoylquinic acid 1	18.51 ± 0.66	a	27.48 ± 0.50	b	27.05 ± 0.59	b	108.54 ± 0.91	a	283.93 ± 4.36	b	279.90 ± 3.19	b
5-Caffeoylquinic acid 2	1.45 ± 0.03	a	2.52 ± 0.08	b	3.48 ± 0.09	c	5.20 ± 0.06	a	12.92 ± 0.12	b	17.20 ± 0.23	c
p-Coumaric acid hexoside	0.31 ± 0.01	a	0.42 ± 0.01	b	0.48 ± 0.01	b	1.62 ± 0.02	a	2.14 ± 0.02	b	2.46 ± 0.03	c
3-*p*-Coumaroylquinic acid	0.37 ± 0.01	a	0.60 ± 0.01	b	0.70 ± 0.02	b	1.54 ± 0.03	a	3.24 ± 0.00	b	3.80 ± 0.02	c
5-*p*-Coumaroylquinic acid 1	0.71 ± 0.02	a	1.12 ± 0.02	b	1.19 ± 0.02	b	2.89 ± 0.06	a	6.25 ± 0.07	b	7.41 ± 0.09	c
5-*p*-Coumaroylquinic acid 2	0.17 ± 0.00	a	0.30 ± 0.00	b	0.47 ± 0.01	c	0.81 ± 0.02	a	1.66 ± 0.04	b	2.20 ± 0.03	c
3-Feruloylquinic acid	5.04 ± 0.15	a	7.64 ± 0.16	b	6.86 ± 0.39	ab	26.56 ± 0.52	a	53.74 ± 0.27	b	62.81 ± 0.61	c
5-Feruloylquinic acid	1.80 ± 0.14	a	3.70 ± 0.14	b	4.26 ± 0.14	b	10.99 ± 0.47	a	22.77 ± 0.71	b	22.82 ± 0.53	b
Dicaffeoylquinic acid 1	0.35 ± 0.06	a	0.58 ± 0.05	a	8.68 ± 0.31	b	3.38 ± 0.30	a	2.46 ± 0.09	a	11.61 ± 0.10	b
Dicaffeoylquinic acid 2	0.06 ± 0.00	a	0.08 ± 0.00	a	0.53 ± 0.02	b	0.23 ± 0.01	a	0.55 ± 0.03	b	2.85 ± 0.05	c
p-Coumaroyl-caffeoylquinic acid 1	0.00 ± 0.00	a	0.00 ± 0.00	a	0.08 ± 0.00	b	0.02 ± 0.00	a	0.04 ± 0.01	a	0.39 ± 0.01	b
p-Coumaroyl-caffeoylquinic acid 2	0.01 ± 0.00	a	0.00 ± 0.00	a	0.08 ± 0.00	b	0.01 ± 0.00	a	0.04 ± 0.00	a	0.44 ± 0.01	b
Total hydroxycinnamic acids	**32.67 ± 1.07**	**a**	**49.82 ± 0.94**	**b**	**59.37 ± 1.32**	**b**	**185.71 ± 2.56**	**a**	**438.54 ± 5.32**	**b**	**469.33 ± 3.72**	**b**
Epicatechin							8.25 ± 0.24	a	12.50 ± 0.18	b	14.42 ± 0.30	b
Procyanidin trimer	0.81 ± 0.05	a	1.16 ± 0.04	a	2.21 ± 0.14	b	4.40 ± 0.13	a	12.58 ± 0.37	b	17.18 ± 0.19	c
Total flavanols	**0.81 ± 0.05**	**a**	**1.16 ± 0.04**	**a**	**2.21 ± 0.14**	**b**	**12.65 ± 0.14**	**a**	**25.07 ± 0.29**	**b**	**31.61 ± 0.25**	**c**
Kaempferol dihexoside 1							1.87 ± 0.03	a	3.04 ± 0.06	b	3.87 ± 0.04	c
Kaempferol dihexoside 2	0.35 ± 0.02	a	0.48 ± 0.01	b	0.57 ± 0.01	b	1.49 ± 0.03	a	2.13 ± 0.03	b	2.43 ± 0.02	c
Kaempferol triglycoside	0.40 ± 0.01	a	0.51 ± 0.02	ab	0.58 ± 0.02	b	1.93 ± 0.04	a	2.53 ± 0.02	a	2.33 ± 0.18	a
Kaempferol-3-rutinoside	0.77 ± 0.07	a	1.66 ± 0.04	b	1.94 ± 0.06	b	4.77 ± 0.07	a	37.18 ± 0.57	c	10.79 ± 0.14	b
Kaempferol-3-glucoside	0.02 ± 0.00	a	0.01 ± 0.00	a	0.08 ± 0.00	b	0.15 ± 0.01	a	0.09 ± 0.00	a	0.32 ± 0.01	b
Kaempferol acetylhexoside	0.02 ± 0.00	a	0.02 ± 0.00	a	0.12 ± 0.00	b	0.08 ± 0.01	a	0.21 ± 0.01	b	0.65 ± 0.02	c
Quercetin hexoside pentoside 1	0.25 ± 0.02	a	0.40 ± 0.01	b	0.49 ± 0.01	b	0.99 ± 0.04	a	1.67 ± 0.05	b	1.98 ± 0.04	b
Quercetin hexoside pentoside 2	0.02 ± 0.00	a	0.03 ± 0.00	b	0.03 ± 0.00	b	0.09 ± 0.00	a	0.13 ± 0.00	b	0.15 ± 0.00	c
Quercetin-3-rutinoside	15.34 ± 1.63	a	58.02 ± 1.61	b	64.25 ± 1.51	b	65.96 ± 0.67	a	288.00 ± 5.16	b	316.37 ± 2.36	b
Quercetin-3-glucoside	0.08 ± 0.01	a	0.17 ± 0.02	a	1.31 ± 0.05	b	0.50 ± 0.03	a	1.66 ± 0.03	b	4.11 ± 0.11	c
Quercetin dihexoside	0.24 ± 0.02	a	0.49 ± 0.02	b	0.56 ± 0.02	b	1.22 ± 0.04	b	0.75 ± 0.02	a	0.76 ± 0.02	a
Quercetin acetylglucoside	0.04 ± 0.01	a	0.06 ± 0.01	a	0.95 ± 0.03	b	0.37 ± 0.03	a	1.07 ± 0.04	b	5.06 ± 0.04	c
Isorhamnetin dihexoside	0.26 ± 0.02	a	0.35 ± 0.01	b	0.42 ± 0.01	b	1.09 ± 0.02	a	1.56 ± 0.02	b	1.77 ± 0.02	c
Isorhamnetin-3-rutinoside	4.46 ± 0.48	a	9.72 ± 0.25	b	11.14 ± 0.27	b	29.24 ± 0.41	a	64.69 ± 1.40	b	66.27 ± 0.82	b
Isorhamnetin-3-glucoside	0.10 ± 0.01	a	0.14 ± 0.01	a	0.81 ± 0.01	b	0.80 ± 0.08	a	2.12 ± 0.07	b	3.49 ± 0.08	c
Isorhamnetin acetylhexoside	0.07 ± 0.01	a	0.10 ± 0.00	a	0.20 ± 0.01	b	0.14 ± 0.01	a	0.60 ± 0.03	b	1.29 ± 0.08	c
Total flavonols	**22.41 ± 2.27**	**a**	**72.18 ± 1.89**	**b**	**83.45 ± 1.89**	**b**	**110.70 ± 0.77**	**a**	**407.43 ± 6.99**	**b**	**421.65 ± 3.08**	**b**
Naringenin	0.04 ± 0.00	a	0.05 ± 0.00	a	0.31 ± 0.01	b	0.05 ± 0.00	a	0.12 ± 0.01	a	4.03 ± 0.07	b
Total phenolic content[c]	**91.09 ± 1.63**	**a**	**209.48 ± 9.93**	**ab**	**310.74 ± 21.45**	**b**	**335.44 ± 7.42**	**a**	**672.72 ± 5.40**	**b**	**746.63 ± 7.99**	**c**
Antioxidant activity (ABTS)[d]	0.36 ± 0.01	a	0.39 ± 0.01	a	0.51 ± 0.01	b	1.25 ± 0.02	a	1.91 ± 0.02	b	2.34 ± 0.02	c
Antioxidant activity (FRAP)[d]	0.49 ± 0.01	a	0.44 ± 0.03	a	1.99 ± 0.09	b	2.06 ± 0.03	a	2.97 ± 0.01	b	8.20 ± 0.02	c

J. Agric. Food Chem. 2015, 63, 1477−1487

DOI: 10.1021/jf506005b

Table 3. continued

[a]Letters indicate homogeneous groups of extraction durations for each beverage separately at the 0.05 significance level. [b]The content of phenolic compounds was expressed as mean ± SE in mg per kg fresh flowers. [c]Total phenolic content as mean ± SE in mg GAE per kg flowers. [d]Antioxidant activity as mean ± SE in mM trolox per kg flowers.

bonded to the aglycons, and the structures of aglycons (Table 1).

Methanol is widely used to extract phenolics from plant material, as these compounds are often more soluble in organic solvents less polar than water.[18] Alcohols, particularly methanol and ethanol, proved more efficient compared to water in extracting phenolics from different natural sources, such as coffee, onion and grape.[19−21] For this reason, elderflowers were extracted in methanol—a standard solvent for phenolic compounds. In the present study, a second extraction method was employed utilizing water as a solvent because, traditionally, elderflower beverages are prepared at home with tap water. As expected, methanol proved a superior solvent of elderflowers, as higher content levels of phenolic groups have been determined in methanol-extracted samples compared to water-extracted elderflowers (Table 2).

The major group of phenolic compounds in elderflowers comprised hydroxycinnamic acids (HC) representing almost 50% of total analyzed phenolic compounds (TAP) in elderflower syrup. In sabesa, their share accounted for up to 40% TAP and in methanolic extract less than 35% TAP. These results suggest a better extraction of hydroxycinnamic acids in water. Correspondingly, studies report that water is an ideal solvent for extraction of phenolic acids.[22] The main hydroxycinnamic acid detected in elderflower samples was 5-caffeoylquinic acid (chlorogenic acid), representing from 50 to 60% total hydroxycinnamic acids analyzed (TAH). 3-Caffeoylquinic acid (neochlorogenic acid), 3- and 5-feruloylquinic acid and dicaffeoylquinic acid 1, 2, and 3 (diCQA) have also been quantified in elderflower extracts. Three peaks with m/z 515 have been identified as dicaffeoylquinic acids based on the fragment MS^2 ion at m/z 353, and MS^3 ions at m/z 191, 179 (diCQA 1); the second had MS^3 ions at m/z 191, 179, and 173 (diCQA 2); and the last one had MS^3 ions at m/z 173, 179, and 191 (diCQA3). Numbers from 1 to 3 were appointed to these compounds according to their elution or retention time. The fragmentation patterns suggest these dicaffeoylquinic acids to be 1,5-dicaffeoylquinic acid, 3,5-dicaffeoylquinic acid and 4,5-dicaffeoylquinic acid described by Clifford et al.[23] and previously detected in elderflowers.[9]

Fifteen (15) different hydroxycinnamic acid derivatives have been analyzed in elderflower methanolic extracts (Table 1). All except dicaffeoylquinic acid 3 have also been quantified in water-extracted elderflower samples. For nearly all analyzed phenolic compound treatments (sabesa, syrup), the duration of extraction and their interactions were highly significant ($p < 0.001$). TAH increased with the duration of water extraction (Table3; $p < 0.001$). Specifically, a 1.5-fold increase from 24 h (1 day) extraction to 72 h (3 day) extraction time has been determined in sabesa and a 2.3-fold increase in elderflower syrup (Figure 2). An additional 7−20% increase has been measured between the third and seventh days of extraction. Significantly higher levels of individual and total hydroxycinnamic acids have been determined in elderflower syrup compared to sabesa. Despite the fact that the syrup is diluted with water prior to consumption (usually 1:5, v/v), the intake of phenolic acids in the diluted syrup is still much higher compared to sabesa. Some references report a dietary role of hydroxycinnamic acids.[24] Dietary antioxidants may protect the body against oxidative stress-related diseases. Caffeic acid derivatives (e.g., dicaffeoylquinic acid) have been shown to be potent and selective inhibitors of some viruses[25,26] and have antitumor activity.[27] To our knowledge, 3- and 5-feruloylquinic

DOI: 10.1021/jf506005b
J. Agric. Food Chem. 2015, 63, 1477−1487

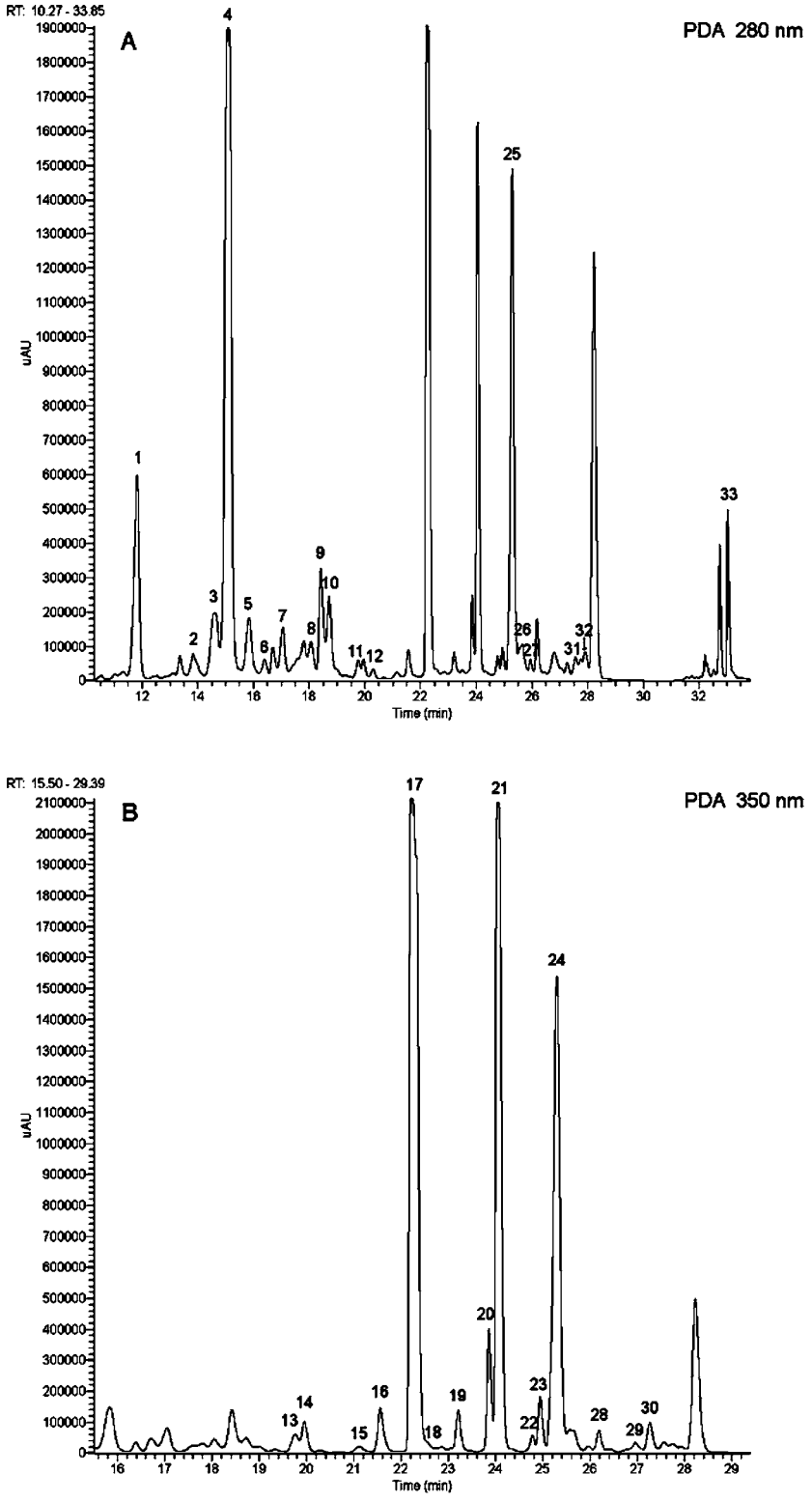

Figure 1. Phenolic chromatogram of elderflower methanolic extract recorded at (A) 280 nm and (B) 350 nm. Peak numbers are described in Table 1

acid and two *p*-coumaroyl-caffeoylquinic acids have not been detected in elderflower extracts prior to the present research.

Flavonols represented the subsequent principal phenolic group and together with hydroxycinnamic acids accounted for up to 98% total analyzed phenolic compounds in water-extracted samples. Eighteen (18) different glycosides of kaempferol, quercetin and isorhamnetin have been identified in elderflower methanolic extract (Table 1). All except kaempferol dihexoside 1, quercetin-3-galactoside and isorhamnetin-pentoside have also been determined in water-extracted samples. Two peaks with $[M - H]^-$ value at m/z 609 have been detected and determined as kaempferol dihexosides based on the MS^3 fragment at m/z 285 obtained after the loss of 2 hexoses. The second unknown peak with $(M - H)^-$ at m/z 447

DOI: 10.1021/jf506005b
J. Agric. Food Chem. 2015, 63, 1477−1487

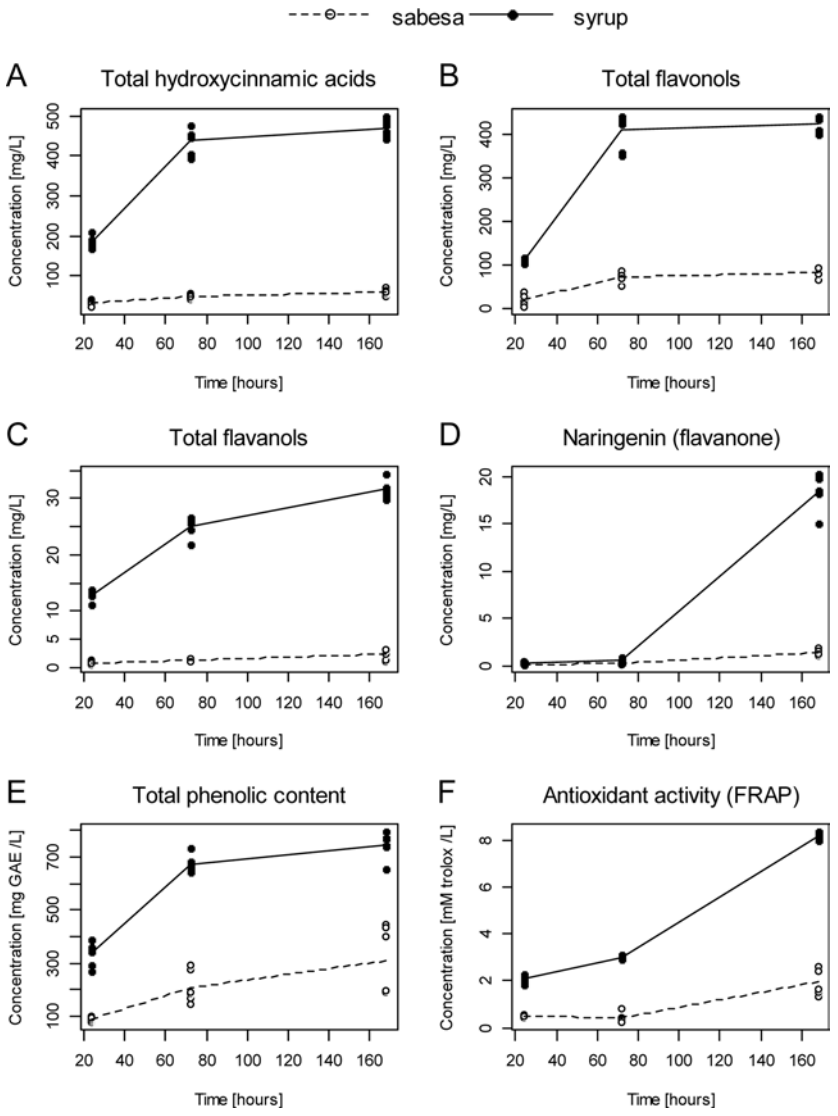

Figure 2. Content of different phenolic groups (mg/L), total phenolic content (mg GAE/L) and antioxidant activity (mM trolox/L) of two elderflower beverages (sabesa and syrup) at different extraction periods.

and MS^2 fragment ion at m/z 315, corresponding to a fragmental loss of a pentose moiety, was identified as isorhamnetin pentoside.

Several glycosides of quercetin and kaempferol have been identified in elderflower extracts representing 5−10% total analyzed flavonols. Additionally, isorhamnetin glycosides accounted for 15−25% total analyzed flavonols. Derivatives of quercetin, kaempferol and isorhamnetin are the most abundant flavonols in plant-based foods.[28] Information on the conjugation of sugar to the polyphenolic section may provide additional knowledge on their nutritional significance, since the sugar moiety is an important determinant of flavonol bioavailability.[29]

In elderflower extracts, quercetin-3-rutinoside (rutin) represented almost 75% of all flavonols. Previous research also reports rutin as the major polyphenol in elderberry.[30,31] Rutin content increased from day 1 to day 3 of water extraction (p < 0,001); in sabesa the increase was 3.8-fold and in syrup 4.4-fold (Table 3). After 7 days of extraction the content of rutin additionally increased for 10%. The results suggest that the majority of rutin is extracted during the first 3 days. This is in accordance with the report of Machavarapu et al.[20] Reis et al.[22] determined that water readily extracts quercetin aglycone but is a poor solvent for quercetin glycosides. Instead, 40% methanol proved to be the best solvent to extract quercetin glycosides. Quercetin-glycosides are probably linked to cell walls with hydrophobic bonds and are therefore difficult to extract from the plant material with water. Similarly, Machavarapu et al.[20] studied the extraction of rutin in onion and reported that methanol was a superior solvent compared to ethanol or water. In our study, better extraction effect of mostly all quercetin glycosides was in beverage sabesa and the lowest in elderflower syrup (Table 2). Statistically the highest content of rutin was analyzed in sabesa after 72 h of extraction (Table 2).

In the present study several flavonol derivatives have been detected, which have not been reported in other studies.[8−10,32,33] Two kaempferol-dihexosides ($[M - H]^-$ at m/z 609), kaempferol triglycoside ($[M - H]^-$ at m/z 755), kaempferol acetylhexoside ($[M - H]^-$ at m/z 489), isorhamnetin-pentoside ($[M - H]^-$ at m/z 447), isorhamentin acetylhexoside ($[M - H]^-$ at m/z 519), isorhamnetin dihexoside ($[M - H]^-$ at m/z 639), quercetin-3-galactoside ($[M - H]^-$ at m/z 463), quercetin dihexoside ($[M - H]^-$ at

DOI: 10.1021/jf506005b
J. Agric. Food Chem. 2015, 63, 1477−1487

m/z 625) and two quercetin hexoside-pentosides ($[M - H]^-$ at m/z 595) have been quantified in elderflower extracts.

Elderflower syrup contained up to 5.6-fold levels of total flavonols (110.7−421.65 mg total flavonols per L) compared to sabesa (Table 3, Figure 2). But we must take into account that syrup is diluted with water (1:5, v/v) for consumption, so the differences between both beverages in flavonol levels are not so high. The content levels of individual and total flavonols make these beverages ideal for daily consumption. Several health beneficial activities have namely been attributed to naturally occurring plant flavonols, including antioxidant, anticarcinogenic, anti-inflammatory, neurodegenerative and antidiabetic properties. In recent years, the antioxidant potential of flavonols has become the main topic of investigation, as these compounds exhibited a positive effect on reducing the progression of major diseases. Epidemiological studies indicating that the high dietary intake of flavonols reduces the risk of mortality due to coronary heart disease have provoked interest in the mechanism of their cardioprotective effects.[12,13]

From the group of flavanols, catechin, epicatechin and procyanidin trimer have been identified in elderflower methanolic extract (Table 1). The latter has been detected in sabesa and in elderflower syrup, which also contained epicatechin. Elderflower syrup contained 14- to 21-fold higher levels of total flavanols (12.65 to 31.61 mg/L) compared to sabesa (Table 3, Figure 2). This means that even as the syrup is consumed diluted with water, the prepared beverage still contains significantly higher levels of total flavanols compared to the sabesa beverage. Flavanols can cause astringency (dry and pucker feeling in the mouth) and bitter taste in plant-based foods and drinks. They are mainly the constituents of unripe fruit and have been linked to its bitterness and astringent taste,[34] preventing herbivores consuming and disseminating immature seed. Other researchers reported that adding sugars or other sweeteners reduces bitterness and astringency of plant-based products.[35]

Flavanone naringenin represented as much as 23% total analyzed phenolic compounds (TAP) in methanol-extracted samples. However, water extraction yielded different results. This compound accounted for approximately 0.08% TAP in elderflower syrup and 0.4% TAP in sabesa after 24 h of extraction. The results are indicative of a better solubility of naringenin in methanol, previously stated in several studies. For example, Wilcox et al.[36] report that naringenin is almost insoluble in water and only soluble in organic solvents such as alcohol. Naringenin is the main flavanone naturally occurring in citrus fruits.[11] The role of naringenin in the prevention and treatment of disease has recently received considerable attention, with particular interest as a potential anticancer compound.[11] Therefore, elderflower beverages and extracts can represent important sources of this bioactive compound in the daily diet, but the extraction method must enable naringenin solubility. It has been reported that naringenin enantiomers inhibit several important drug-metabolizing CYP isoforms.[37] Moreover, it has been reported that naringenin present in elderflower extracts is one of the most potent compounds with a major effect on the enhancement of glucose uptake and reduction of fat accumulation.[7] Elderflower extracts have been found to activate peroxisome proliferator-activated receptors and enhance insulin-dependent glucose uptake (GU) in adipocytes.[38] In addition to a decreased blood glucose level, the reduction of body fat is also an important goal for combating obesity and diabetes type 2.[7]

Total phenolic content (TPC) increased in the following order: syrup (water extraction), methanolic extract and sabesa (water extraction) (Table 2). The largest effect of rutin extraction was in sabesa, which was probably the reason for significantly higher TPC in this beverage (Table 2). Contrary to our results, Tai et al.[39] reported that alcoholic extracts of *Sophora viciifolia* flowers had higher TPC in comparison to water extracts. When it comes to duration of total phenolic extraction, the highest total phenolic content (TPC) was measured in elderflower syrup after 7 days and the lowest in sabesa after 1 day of the extraction (Table 3, Figure 2). In water-extracted beverages, TPC significantly increased after 7 days of extraction, 2.2-fold in elderflower syrup and 3.4-fold in sabesa in comparison to the first day (Table 3). Furthermore, water-extracted elderflower beverages had similar TPC as mandarin[40] and orange juice.[41]

Antioxidant activity of elderflower extracts. Two in vitro assays ($ABTS^{\bullet+}$ and FRAP) were used as complementary methods to evaluate the antioxidant activity of the samples. The $ABTS^{\bullet+}$ scavenging activity of various elderflower drinks differed significantly and ranged from 0.36 to 2.34 mM TE (trolox equivalents) per liter. The comparison of the antioxidant activity of elderflower beverages to other juices reveals a high antioxidant activity of the former: 0.206−0.285 mM TE was measured for apple juice[42] and 0.694 to 0.886 mM TE for strawberry juice.[43] The highest antioxidant activity was measured for elderflower syrup after 7 days of water extraction and the lowest for sabesa after 1 day of extraction (Table 3, Figure 2). Prolonged extraction of elderflowers in water solvent caused higher $ABTS^{\bullet+}$ antioxidant activity. The ferric reducing antioxidant power (FRAP) showed a similar pattern. A 4-fold increase of FRAP antioxidant activity has been measured in elderflower syrup and sabesa after 7 days of extraction compared to the first sampling. FRAP antioxidant activity ranged from 0.49 to 1.99 mM TE for sabesa and 2.06 to 8.20 mM TE for elderflower syrup. Both beverages exhibited significantly higher FRAP activity compared to apple juice (0.15−0.21 mM TE) and blackcurrant juice (0.37 mM TE).[42] On the other hand, higher FRAP antioxidant activity has been reported for sweet lemon juice[44] and quince juice.[45]

Total antioxidant activity measured by FRAP and $ABTS^{\bullet+}$ assays was significantly correlated with total phenolic content (r = 0.807 and 0.942). A strong correlation between antioxidant activity and phenolic compounds has been reported in several juices.[46,47] A strong correlation has also been observed between the content of flavonols and total phenolic content (r = 0.954).

The present study focuses on the analysis of a wide spectrum of phenolic compounds in elderflower beverages and compares their contents in three different types of extracts. 37 phenolic compounds have been identified in elderflower methanolic extracts. A smaller diversity of phenolic components has been detected in water-extracted traditional elderflower beverages. Elderflower syrup also contained higher levels of phenolics compared to sabesa. Generally, a longer extraction period caused higher contents of phenolic compounds in traditional beverages. Elderflower beverages were characterized by high total phenolic content (from 91.09 to 746.63 mg GAE/L), which has been linked to high antioxidant activity of the extracts. The $ABTS^{\bullet+}$ antioxidant activity of sabesa ranged from 0.36 to 0.51 mM TE (trolox equivalents), and even higher values have been recorded for elderflower syrup (1.25−2.34 mM TE). Both traditional elderflower drinks should therefore be recommended as a potent source of natural health agents.

DOI: 10.1021/jf506005b
J. Agric. Food Chem. 2015, 63, 1477−1487

The consumption of these natural beverages may significantly contribute to the dietary intake of phenolic compounds, which are believed to have a positive effect on human health. The results of the present study can hopefully lead to increased utilization of elderflowers and production of traditional beverages on a larger scale. Not only are the traditional elderflower beverages easy and cheap to make, but they should be promoted due to their pleasing taste characteristics and high levels of health-promoting compounds.

AUTHOR INFORMATION

Corresponding Author

*E-mail: maja.mikulic-petkovsek@bf.uni-lj.si, Fax: +386 1 423 10 88, Tel: +386 1 320 31 41.

Notes

The authors declare no competing financial interest.

REFERENCES

(1) Kaack, K.; Christensen, L. P.; Hughes, M.; Eder, R. The relationship between sensory quality and volatile compounds in raw juice processed from elderberries (*Sambucus nigra* L.). *Eur. Food Res. Technol.* **2005**, *221*, 244−254.

(2) Kaack, K.; Christensen, L. P.; Hughes, M.; Eder, R. Relationship between sensory quality and volatile compounds of elderflower (*Sambucus nigra* L.) extracts. *Eur. Food Res. Technol.* **2006**, *223*, 57−70.

(3) Jorgensen, U.; Hansen, M.; Christensen, L. P.; Jensen, K.; Kaack, K. Olfactory and quantitative analysis of aroma compounds in elder flower (*Sambucus nigra* L.) drink processed from five cultivars. *J. Agric. Food Chem.* **2000**, *48*, 2376−2383.

(4) Jensen, K.; Christensen, L. P.; Hansen, M.; Jorgensen, U.; Kaack, K. Olfactory and quantitative analysis of volatiles in elderberry (*Sambucus nigra* L.) juice processed from seven cultivars. *J. Sci. Food Agric.* **2001**, *81*, 237−244.

(5) Cejpek, K.; Malouskova, I.; Konecny, M.; Velisek, J. Antioxidant activity in variously prepared elderberry foods and supplements. *Czech. J. Food Sci.* **2009**, *27*, S45−S48.

(6) Frokiaer, H.; Henningsen, L.; Metzdorff, S. B.; Weiss, G.; Roller, M.; Flanagan, J.; Fromentin, E.; Ibarra, A., Astragalus root and elderberry fruit extracts enhance the IFN-beta stimulatory effects of *Lactobacillus acidophilus* in murine-derived dendritic cells. *PLoS One* **2012**, *7*, (10).

(7) Bhattacharya, S.; Christensen, K. B.; Olsen, L. C. B.; Christensen, L. P.; Grevsen, K.; Faergeman, N. J.; Kristiansen, K.; Young, J. F.; Oksbjerg, N. Bioactive components from flowers of *Sambucus nigra* L. increase glucose uptake in primary porcine myotube cultures and reduce fat accumulation in *Caenorhabditis elegans*. *J. Agric. Food Chem.* **2013**, *61*, 11033−11040.

(8) Kaack, K.; Christensen, L. P. Phenolic acids and flavonoids in tea processed from flowers of black elder (*Sambucus nigra* L.) stored in different packing materials. *Eur. J. Horticul. Sci.* **2010**, *75*, 214−220.

(9) Christensen, L. P.; Kaack, K.; Frette, X. C. Selection of elderberry (*Sambucus nigra* L.) genotypes best suited for the preparation of elderflower extracts rich in flavonoids and phenolic acids. *Eur. Food Res. Technol.* **2008**, *227*, 293−305.

(10) Rieger, G.; Muller, M.; Guttenberger, H.; Bucar, F. Influence of altitudinal variation on the content of phenolic compounds in wild populations of *Calluna vulgaris*, *Sambucus nigra*, and *Vaccinium myrtillus*. *J. Agric. Food Chem.* **2008**, *56*, 9080−9086.

(11) Im, S. J.; Kim, J. H.; Kim, M. Y. Evaluation of bioactive components and antioxidant and anticancer properties of citrus wastes generated during bioethanol production. *Nat. Prod. Commun.* **2014**, *9*, 483−486.

(12) Di Castelnuovo, A.; Di Giuseppe, R.; Iacoviello, L.; de Gaetano, G. Consumption of cocoa, tea and coffee and risk of cardiovascular disease. *Eur. J. Int. Med.* **2012**, *23*, 15−25.

(13) Peterson, J. J.; Dwyer, J. T.; Jacques, P. F.; McCullough, M. L. Associations between flavonoids and cardiovascular disease incidence or mortality in European and US populations. *Nutr. Rev.* **2012**, *70*, 491−508.

(14) Wang, S. Y.; Zheng, W.; Galletta, G. J. Cultural system affects fruit quality and antioxidant capacity in strawberries. *J. Agric. Food Chem.* **2002**, *50*, 6534−6542.

(15) Singleton, V. L.; Orthofer, R.; Lamuela-Raventos, R. M., Analysis of total phenols and other oxidation substrates and antioxidants by means of Folin-Ciocalteu reagent. In *Oxidants and Antioxidants, Pt A*; Packer, L., Ed.; Elsevier Academic Press Inc.: San Diego, 1999; Vol. *299*, pp 152−178.

(16) Re, R.; Pellegrini, N.; Proteggente, A.; Pannala, A.; Yang, M.; Rice-Evans, C. Antioxidant activity applying an improved ABTS radical cation decolorization assay. *Free Radical Biol. Med.* **1999**, *26*, 1231−1237.

(17) Benzie, I. F. F.; Strain, J. J. The ferric reducing ability of plasma (FRAP) as a measure of "antioxidant power": The FRAP assay. *Anal. Biochem.* **1996**, *239*, 70−76.

(18) Hosseinzadeh, R.; Khorsandi, K.; Hemmaty, S. Study of the effect of surfactants on extraction and determination of polyphenolic compounds and antioxidant capacity of fruits extracts. *PLoS One* **2013**, *8* (3), No. e57353.

(19) Mussatto, S. I.; Ballesteros, L. F.; Martins, S.; Teixeira, J. A. Extraction of antioxidant phenolic compounds from spent coffee grounds. *Sep. Purif. Technol.* **2011**, *83*, 173−179.

(20) Machavarapu, M.; Sindiri, M. K.; Vangalapati, M. Optimization of physico-chemical parameters for the extraction of flavonoids and phenolic components from the skin of *Allium cepa*. *Int. J. Innovat. Res. Sci. Eng. Technol.* **2013**, *2* (7), 3125.

(21) Pinelo, M.; Rubilar, M.; Jerez, M.; Sineiro, J.; Nunez, M. J. Effect of solvent, temperature, and solvent-to-solid ratio on the total phenolic content and antiradical activity of extracts from different components of grape pomace. *J. Agric. Food Chem.* **2005**, *53*, 2111−2117.

(22) Reis, S. F.; Rai, D. K.; Abu-Ghannam, N. Water at room temperature as a solvent for the extraction of apple pomace phenolic compounds. *Food Chem.* **2012**, *135*, 1991−1998.

(23) Clifford, M. N.; Knight, S.; Kuhnert, N. Discriminating between the six isomers of dicaffeoylquinic acid by LC-MSn. *J. Agric. Food Chem.* **2005**, *53*, 3821−3832.

(24) El-Seedi, H. R.; El-Said, A. M. A.; Khalifa, S. A. M.; Goransson, U.; Bohlin, L.; Borg-Karlson, A. K.; Verpoorte, R. Biosynthesis, natural sources, dietary intake, pharmacokinetic properties, and biological activities of hydroxycinnamic acids. *J. Agric. Food Chem.* **2012**, *60*, 10877−10895.

(25) Shen, H.; Yamashita, A.; Nakakoshi, M.; Yokoe, H.; Sudo, M.; Kasai, H.; Tanaka, T.; Fujimoto, Y.; Ikeda, M.; Kato, N.; Sakamoto, N.; Shindo, H.; Maekawa, S.; Enomoto, N.; Tsubuki, M.; Moriishi, K. Inhibitory effects of caffeic acid phenethyl ester derivatives on replication of hepatitis C virus. *PLoS One* **2013**, *8* (12), No. e82299.

(26) Xie, Y. C.; Huang, B.; Yu, K. X.; Xu, W. F. Further discovery of caffeic acid derivatives as novel influenza neuraminidase inhibitors. *Bioorgan. Med. Chem.* **2013**, *21*, 7715−7723.

(27) Xu, R. S.; Kang, Q. M.; Ren, J.; Li, Z. K.; Xu, X. P. Antitumor molecular mechanism of chlorogenic acid on inducting genes GSK-3 beta and APC and inhibiting gene beta-catenin. *J. Anal. Methods Chem.* **2013**, No. 951319.

(28) Riihinen, K.; Jaakola, L.; Kärenlampi, S.; Hohtola, A. Organ-specific distribution of phenolic compounds in bilberry (*Vaccinium myrtillus*) and 'northblue' blueberry (*Vaccinium corymbosum* × *V. angustifolium*). *Food Chem.* **2008**, *110*, 156−160.

(29) Vrhovsek, U.; Masuero, D.; Palmieri, L.; Mattivi, F. Identification and quantification of flavonol glycosides in cultivated blueberry cultivars. *J. Food Compos. Anal.* **2012**, *25*, 9−16.

(30) Lee, J.; Finn, C. E. Anthocyanins and other polyphenolics in American elderberry (*Sambuclus canadensis*) and European elderberry (*S. nigra*) cultivars. *J. Sci. Food Agric.* **2007**, *87*, 2665−2675.

(31) Maatta-Riihinen, K. R.; Kamal-Eldin, A.; Mattila, P. H.; Gonzalez-Paramas, A. M.; Torronen, A. R. Distribution and contents of phenolic compounds in eighteen Scandinavian berry species. *J. Agric. Food Chem.* **2004**, *52*, 4477−4486.

DOI: 10.1021/jf506005b
J. Agric. Food Chem. 2015, 63, 1477−1487

(32) Barros, L.; Duenas, M.; Carvalho, A. M.; Ferreira, I.; Santos-Buelga, C. Characterization of phenolic compounds in flowers of wild medicinal plants from Northeastern Portugal. *Food Chem. Toxicol.* **2012**, *50*, 1576−1582.
(33) Celik, S. E.; Ozyuerek, M.; Guclu, K.; Capanoglu, E.; Apak, R. Identification and anti-oxidant capacity determination of phenolics and their glycosides in elderflower by on-line HPLC-CUPRAC Method. *Phytochem. Anal.* **2014**, *25*, 147−154.
(34) Lesschaeve, I.; Noble, A. C. Polyphenols: factors influencing their sensory properties and their effects on food and beverage preferences. *Am. J. Clin. Nutr.* **2005**, *81*, 330S−335S.
(35) Sun-Waterhouse, D.; Wadhwa, S. S. Industry-relevant approaches for minimising the bitterness of bioactive compounds in functional foods: a review. *Food Bioprocess Technol.* **2013**, *6*, 607−627.
(36) Wilcox, L. J.; Borradaile, N. M.; Huff, M. W. Antiatherogenic properties of naringenin, a citrus flavonoid. *Cardiovasc. Drug Rev.* **1999**, *17*, 160−178.
(37) Lu, W. J.; Ferlito, V.; Xu, C.; Flockhart, D. A.; Caccamese, S. Enantiomers of naringenin as pleiotropic, stereoselective inhibitors of cytochrome P450 isoforms. *Chirality* **2011**, *23*, 891−896.
(38) Christensen, K. B.; Minet, A.; Svenstrup, H.; Grevsen, K.; Zhang, H. B.; Schrader, E.; Rimbach, G.; Wein, S.; Wolffram, S.; Kristiansen, K.; Christensen, L. P. Identification of plant extracts with potential antidiabetic properties: effect on human peroxisome proliferator-activated receptor (PPAR), adipocyte differentiation and insulin-stimulated glucose uptake. *Phytother. Res.* **2009**, *23*, 1316−1325.
(39) Tai, Z. G.; Cai, L.; Dai, L.; Dong, L. H.; Wang, M. F.; Yang, Y. B.; Cao, Q. E.; Ding, Z. T. Antioxidant activity and chemical constituents of edible flower of *Sophora viciifolia*. *Food Chem.* **2011**, *126*, 1648−1654.
(40) Kelebek, H.; Selli, S. Identification of phenolic compositions and the antioxidant capacity of mandarin juices and wines. *J. Food Sci. Technol. Mys.* **2014**, *51*, 1094−1101.
(41) Stella, S. P.; Ferrarezi, A. C.; dos Santos, K. O.; Monteiro, M. Antioxidant activity of commercial ready-to-drink orange juice and nectar. *J. Food Sci.* **2011**, *76*, C392−C397.
(42) Oszmianski, J.; Wojdylo, A. Effects of blackcurrant and apple mash blending on the phenolics contents, antioxidant capacity, and colour of juices. *Czech J. Food Sci.* **2009**, *27*, 338−351.
(43) Oszmianski, J.; Wojdylo, A. Comparative study of phenolic content and antioxidant activity of strawberry puree, clear, and cloudy juices. *Eur. Food Res. Technol.* **2009**, *228*, 623−631.
(44) Barreca, D.; Bellocco, E.; Caristi, C.; Leuzzi, U.; Gattuso, G. Flavonoid profile and radical-scavenging activity of Mediterranean sweet lemon (*Citrus limetta* Risso) juice. *Food Chem.* **2011**, *129*, 417−422.
(45) Wojdylo, A.; Teleszko, M.; Oszmianski, J. Antioxidant property and storage stability of quince juice phenolic compounds. *Food Chem.* **2014**, *152*, 261−270.
(46) Tezcan, F.; Gultekin-Ozguven, M.; Diken, T.; Ozcelik, B.; Erim, F. B. Antioxidant activity and total phenolic, organic acid and sugar content in commercial pomegranate juices. *Food Chem.* **2009**, *115*, 873−877.
(47) Yang, J.; Gadi, R.; Paulino, R.; Thomson, T. Total phenolics, ascorbic acid, and antioxidant capacity of noni (*Morinda citrifolia* L.) juice and powder as affected by illumination during storage. *Food Chem.* **2010**, *122*, 627−632.

DOI: 10.1021/jf506005b
J. Agric. Food Chem. 2015, 63, 1477−1487

The purified fraction with the highest hemagglutinating activity was Chinese leek seed lectin, designated as CLSL.

Assay of Hemagglutinating Activity. Hemagglutinating activity was performed using the method reported by Silva et al.[22] with modifications. Two-fold serial dilutions of the sample (25 μL) were mixed with erythrocyte buffer solution (25 μL) and 2% (v/v) supernatant of red blood cells (50 μL) at 25 °C in the 96-well microtiter plate. Saline was used as the blank control, and the results were recorded after incubation at 25 °C for 1 h. The maximum number of a serial two-fold dilution of the sample showing hemagglutinating activity was defined as the hemagglutinating titer (U).

Gel Electrophoresis. Sodium dodecyl sulfate–polyacrylamide gel electrophoresis (SDS-PAGE) was carried out in a 15.0% separating gel and 5.0% stacking gel under nonreducing and reducing conditions according to the modified method of Zhu et al.[23] The molecular weight of CLSL was determined by the migration rate with reference to the standard molecular weight marker.

Analysis of *N*-Terminal Amino Acid Sequence. The purified CLSL was loaded to SDS-PAGE on 4–12% gradient NuPAGE Bis–Tris gel and then mobilized onto a polyvinylidene difluoride (PVDF) membrane by electroblotting. *N*-Terminal sequencing by Edman degradation was performed by using an Applied Biosystems model 471A protein sequenator (Applied Biosystems, Shanghai, China).

Carbohydrate-Binding Specificity. To confirm the specificity of CLSL for sugars, the inhibition of hemagglutination was performed using a method described by Takahashi et al. with modifications.[24] The 2-fold serial dilution samples (25 μL) were incubated with 25 μL sugar solutions (20 mmol/L) for 30 min at room temperature, and hemagglutination was analyzed as described above. The beginning protein concentration was 0.5 mg/mL, and its hemagglutinating activity was 128 U.

Measurement of Carbohydrate Content. The total sugar content of purified CLSL was measured by the anthrone–sulfuric acid method with reference to glucose, according to the modified method of Alberto Leyva et al.[25]

Effect of pH, Temperature, and Metal Ions. The pH stability of CLSL was measured by incubating 50 μL of CLSL (1.0 mg/mL) in buffers with different pH values (pH 2.0–11.0, 50 μL) for 1 h at room temperature. The temperature stability of CLSL was determined by incubating 50 μL of CLSL at different temperature (20–100 °C) for 60 min. The effect of metallic compounds ($BaCl_2$, $CaCl_2$, LiCl, $CuCl_2$, $FeCl_2$, and $K_2Cr_3O_4$) was measured by incubating 50 μL of CLSL in equivalent volume of metallic compounds buffer.

Circular Dichroism. Circular dichroism (CD) is an effective physical technique for evaluating structures and structural changes of proteins.[26] For the analysis of the secondary structure of purified CLSL, the CD spectra were measured in 2.0 mM acetic acid–sodium acetate buffer (pH 5.0), using a J-810 spectropolarimeter at the room temperature in a wavelength range of 190–260 nm. The spectrum was recorded with the response time of 1 s and scan speed of 100 nm/min. Each data point was an average of three accumulations.

Fluorescence Spectroscopy. The purified CLSL (20 mmol) dissolved in 2.0 mL of deionic water was analyzed using a 970 CRT spectrofluorometer (Shanghai, China) at room temperature, with both the excitation and the emission band-pass filters set at 5 nm. Samples were irradiated at excitation wavelength of 295 nm, and emission spectra were recorded in the range 290–400 nm. Quenching of the protein intrinsic fluorescence was performed by addition of micro-aliquots of the quenchers (10 mmol/L $BaCl_2$ solutions) to the protein.

The synchronous fluorescence spectra, focused on investigating the influence of Ba^{2+} on conformation of CLSL, was carried out at the wavelength interval ($\Delta\lambda$) of 15 and 60 nm between the excitation and emission wavelengths, respectively, with both the excitation and the emission band-pass filters set at 5 nm.

Antiproliferative Activity. The cell lines HepG2, LO2, and Caco-2 were cultivated in 1640 medium supplemented with 10% fetal bovine serum (FBS), 100 mg/L of streptomycin, and 100 U/mL of penicillin at 37 °C in a humidified atmosphere of 5% CO_2. Cells (1.5×10^4/well) were seeded into a 96-well culture plate in their exponential growth phase and added to different concentrations of sample after being maintained for 24 h. Incubation was carried out for another 24 h, and the cell viability of each well was measured by MTT assay.[27]

Statistical Analysis. All experiments were carried out in triplicate ($n = 3$), and all data were expressed as means ± standard deviation. Analysis of variance (ANOVA) was performed using SPSS 19.0 (SPSS, Chicago, IL, USA). The significance in differences was determined by Duncan's multiple range test ($P < 0.05$).

RESULTS

Purification of CLSL. Chinese leek seed extract was purified with two chromatographic steps, namely ion exchange chromatography with a SP Sephadex C-25 column and size exclusion chromatography with a Sephadex G-50 column. As shown in Figure 1A, the extract was resolved into seven peaks after the SP Sephadex C-25 column, but only fraction A7 showed stronger hemagglutinating activity (Table S1, Supporting Information). Purification of fraction A7 was examined with SDS-PAGE, and two bands were observed (Figure 1B). Subsequently, fraction A7 was concentrated and applied onto a Sephadex G-50 column for further purification. As shown in Figure 1C, fraction A7 was resolved into two peaks (G1 and G2),

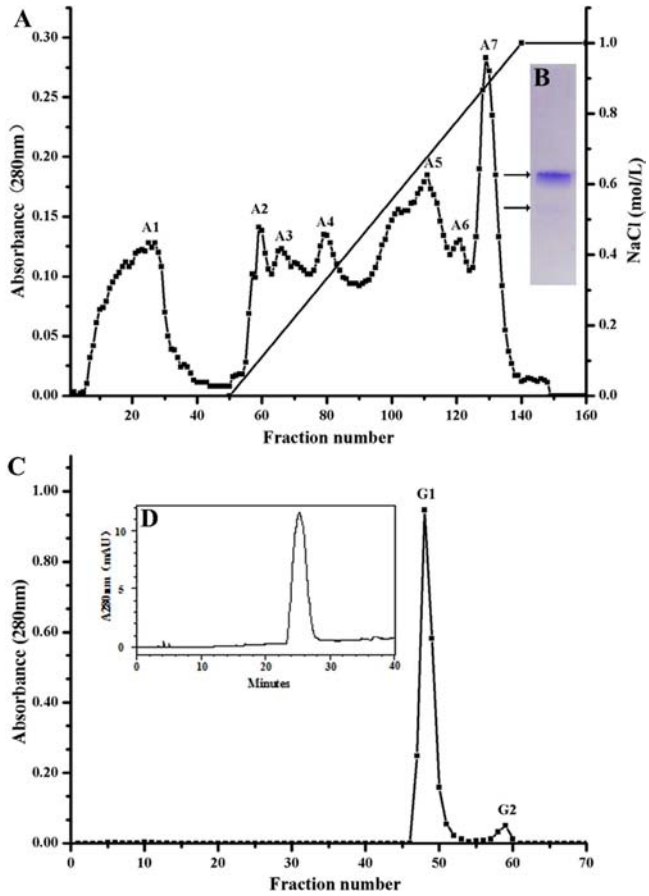

Figure 1. Purification of lectin (CLSL) from Chinese leek seeds. (A) Purification of CLSL using ion exchange chromatography on SP-Sephadex C25 column and fraction A7 showed the higher hemagglutinating activity. (B) Purity of fraction A7 from SP-Sephadex C25 column identified by SDS-PAGE. (C) Further purification of fraction A7 from SP-Sephadex C25 column using gel filtration chromatography on a Sephadex G50 column and fraction G1 exerted the higher agglutinating activity. (D) Purity of fraction G1 from Sephadex G50 column determined by RP-HPLC.

DOI: 10.1021/jf5046014
J. Agric. Food Chem. 2015, 63, 1488–1495

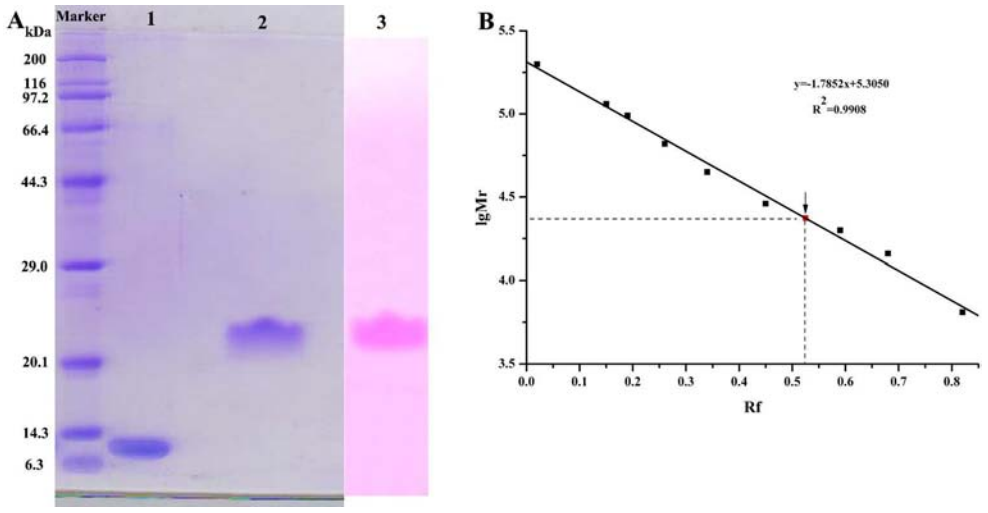

Figure 2. Molecular weight of CLSL calculated by SDS-PAGE and its standard curve. (A) Lanes: Marker, molecular weight marker; 1 and 2, experiment performed under reduced and nonreduced condition stained by Coomassie brilliant blue; 3, CLSL stained by the periodic acid Schiff's reagent. (B) Calculated standard curve of CLSL. The position of CLSL on the regression curve was represented as a red dot.

Table 1. Summary of Purification Process for CLSL and Its Hemagglutinating Activity

fractions	total protein (mg)	extraction yield (%)	HA[a] (U)	purification fold
crude extraction[b]	554.00 ± 0.15	11.08 ± 0.03		
SP Sephadex C-25	215.68 ± 0.35	4.31 ± 0.02	64	1.0
Sephadex G-50	23.04 ± 0.10	0.46 ± 0.02	128	18.7

[a]HA: hemagglutinating activity. The tested concentration of sample was 1.0 mg/mL. [b]Crude extraction was gained from 5.0 g Chinese leek seed powder. SD: standard deviation. All the values were mean ± SD.

and only fraction G1 was identified as the desired fraction. Purification of fraction G1 was confirmed by the elution of single peak from reverse phase-high performance liquid chromatography (RP-HPLC) and a single band on SDS-PAGE (Figures 1D and 2A). The above process resulted in an 18.7-fold purification (Table 1).

Structural Characterization. CLSL appeared as a single band on SDS-PAGE. Molecular weights of the bands under reducing and nonreducing conditions were 11.7 and 23.6 kDa, respectively, suggesting that CLSL was a dimer consisting of two identical subunits connected by disulfide bonds (Figure 2A). A brick-red band was observed after PAS staining, indicating CLSL was a glycoprotein (Figure 2A). The sugar content of CLSL was 3.6 ± 0.25%, measured by anthrone–sulfuric acid method.

The CD spectrum of CLSL was characterized by one positive peak near 195 nm, two negative peaks near 210 and 223 nm, respectively, and a positive to negative crossover at 200 nm (Figure 3), which was characteristic of an α-helical protein. The secondary structure content estimated by Yang's method[28] was 35.8% α-helixes, 8.6% β-sheets, 18.3% β-turns, and 37.3% random coils.

***N*-Terminal Amino Acid Sequences of CLSL.** *N*-Terminal amino acid sequences of CLSL were determined by Edman degradation. The results showed that the seven *N*-terminal residues of CLSL were Cys-Val-Ile-Ala-Pro-Val-Ala (CVIAPVA).

Characterization of Hemagglutinating Activity. The hemagglutinating activity of CLSL was partly inhibited by D-fructose, sorbose, and mannitol at the concentration of 20 mmol/L with the inhibition ratios of 75%, 25%, and 75%,

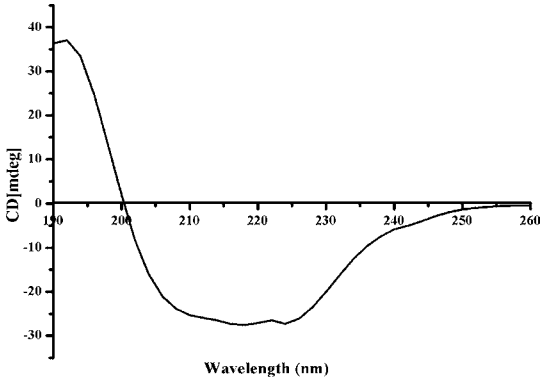

Figure 3. CD spectrum of CLSL in acetate buffer (20 mM, pH 5.0). The concentration of CLSL was 0.4 mg/mL. The positive peak near 195 nm and two negative peaks near 210 and 223 nm, respectively, indicated an α-helical structure of CLSL.

Table 2. Effect of Various Carbohydrates on CLSL (Initial Hemagglutination Activity: 128 U)

carbohydrate (20 mM)	residual activity (titer/U)
raffinose	128
lactose	128
D-glucose	128
D-fructose	32
sucrose	128
D-xylose	128
D-mannose	128
D-galactose	128
maltose	128
sorbose	64
mannitol	32
fucose	128

respectively. Other sugars studied did not affect the hemagglutinating activity of CLSL (Table 2), indicating complex sugar specificity of CLSL.[29]

As Table 3 shows, temperatures in the range 20–100 °C did not have significant effects on the hemagglutinating activity of CLSL, implying that CLSL possessed strong thermostability

DOI: 10.1021/jf5046014
J. Agric. Food Chem. 2015, 63, 1488–1495

Table 3. Effect of Temperature on CLSL (Initial Hemagglutination Activity: 128 U)

temperature (°C)	20	30	40	50	60	70	80	90	100
residual activity (titer/U)	128	128	128	128	128	128	256	128	128

Table 4. Effect of pH on CLSL (Initial Hemagglutination Activity: 128 U)

pH	2	3	4	5	6	7	8	9	10	11
residual activity (titer/U)	128	128	128	128	128	32	0	0	0	0

Table 5. Effect of Metal Ions on CLSL (Initial Hemagglutination Activity: 128 U)

metal ions (10 mmol/L)	$CuCl_2$	$CaCl_2$	$BaCl_2$	$K_2Cr_3O_4$	LiCl	$FeCl_2$
residual activity (titer/U)	2^{12}	2^{12}	0	8	128	2^{12}

like a lectin from *Moringa oleifera*.[30,31] The hemagglutinating activity was retained at acidic pH values ranging from 2.0 to 6.0. However, the activity began to decrease at neutral pH and was completely lost in the alkaline pH range 8.0−11.0 (Table 4).

The influence of metal ions on the hemagglutinating activity was studied. The hemagglutinating activity of CLSL was completely inhibited by Ba^{2+} but was greatly enhanced in the present of Ca^{2+}, Fe^{2+}, and Cu^{2+} at a concentration of 10 mmol/L (Table 5).

Antiproliferative Activity. Inhibition of proliferations of HepG2 cells was observed in the presence of CLSL, and its IC_{50} value was 30 μM. In contrast, proliferation of Caco-2 cells and the normal cells LO2 were only slightly affected by up to 40 μM CLSL (Figure 4), suggesting that the antiproliferative potential of CLSL was selective.

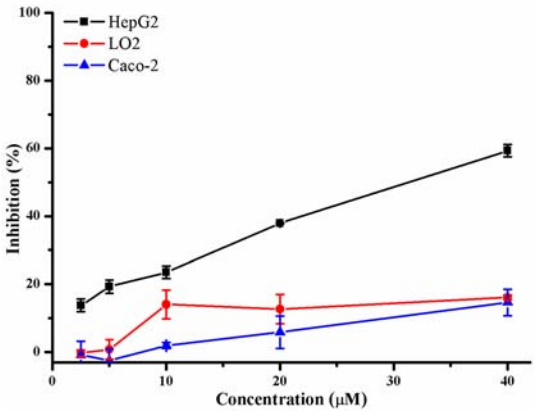

Figure 4. Inhibitory effect of CLSL on proliferation of HepG2, LO2, and Caco-2. Proliferation of HepG2 cells was inhibited with an IC_{50} of 30 μM. Cell proliferation was determined by MTT assay (data represent means ± SD, n = 3).

Effect of Ba^{2+} on the Hemagglutinating Activity of CLSL. To investigate the mechanism of Ba^{2+}-mediated inhibition of hemagglutinating activity, the fluorescence spectra of CLSL quenched by Ba^{2+} at different concentrations were analyzed (Figure 5A). Quenching of the intrinsic fluorescence of CLSL and a slight blue shift of the maximum emission fluorescence peak (about 2 nm) were observed.

The synchronous fluorescence spectra of CLSL in the presence of Ba^{2+} were also shown in Figure 5. The synchronous fluorescence was characteristic of tyrosine residues (Tyr) and tryptophan residues (Trp) at the wavelength interval ($\Delta\lambda$) of 15 and 60 nm between the excitation and emission wavelengths, respectively.[32] It was obvious that the maximum emission peak intensities of both tyrosine and tryptophan decreased with increased Ba^{2+} concentrations. A slight blue shift of the maximum emission wavelength was observed at the wavelength interval of 15 nm, and it did not show significant shift at the wavelength interval of 60 nm (Figure 5B,C).

To further investigate the influence of Ba^{2+} on the CLSL conformation, CD spectroscopy of CLSL was carried out with the addition of Ba^{2+} (Figure 6). A positive peak at 195 nm and two negative peaks near 210 and 225 nm shifted toward the zero graduation with the increase of Ba^{2+} concentrations. Moreover, an apparent change of its ellipticity was observed at the Ba^{2+} concentration of 5.0 μmol/L, and no significant difference was observed at higher Ba^{2+} concentrations, suggesting that the reaction was under saturation conditions.

DISCUSSION

In the present work, a novel lectin (CLSL) was purified from Chinese leek seeds and displayed activity against rat erythrocytes. The purity of CLSL was confirmed by SDS-PAGE and RP-HPLC.

CLSL was a dimeric glycoprotein consisting of two identical subunits linked by disulfide bonds with a molecular weight of 23.6 kDa. It produced a smear on SDS-PAGE, similar to that of some reported lectins.[22,29] The smear was probably because glycoproteins possessed the heterogeneous glycosylation pattern and stronger hydration in water solution due to the presence of carbohydrate units and disulfide bonds.[33,34]

Similar to CLSL, a mannose-binding protein (ATL) from Chinese *Allium tuberosum* was also a dimeric protein.[35,36] ATL had an *N*-terminal sequence of RNVLLNGEGLYAGQS, different from that of CLSL (CVIAPVA). The seven residue sequence of CLSL was submitted to a blast search in the NCBI database. Although some similarities to the sequences of other reported lectins were observed, they were far away from the *N*-terminus (Table 6), which inferred that CLSL was a novel lectin. CLSL was identified to be an α-helix protein with CD spectroscopy. Compared with CLSL, different lectins possessed different contents of secondary structures (Table 7). For example,

Table 6. *N*-Terminal Amino Acid Sequence Alignment of CLSL in NCBI Database

Content	Starting amino acid	Sequences	Ending amino acid	Reference
CLSL	**1**	**C V I A P V A**	**7**	The present
Fucose-specific lectin	9	V I A A V A	14	49
Lectin-domain containing receptor kinase A4.3	321	C V I A V V	326	50

DOI: 10.1021/jf5046014
J. Agric. Food Chem. 2015, 63, 1488−1495

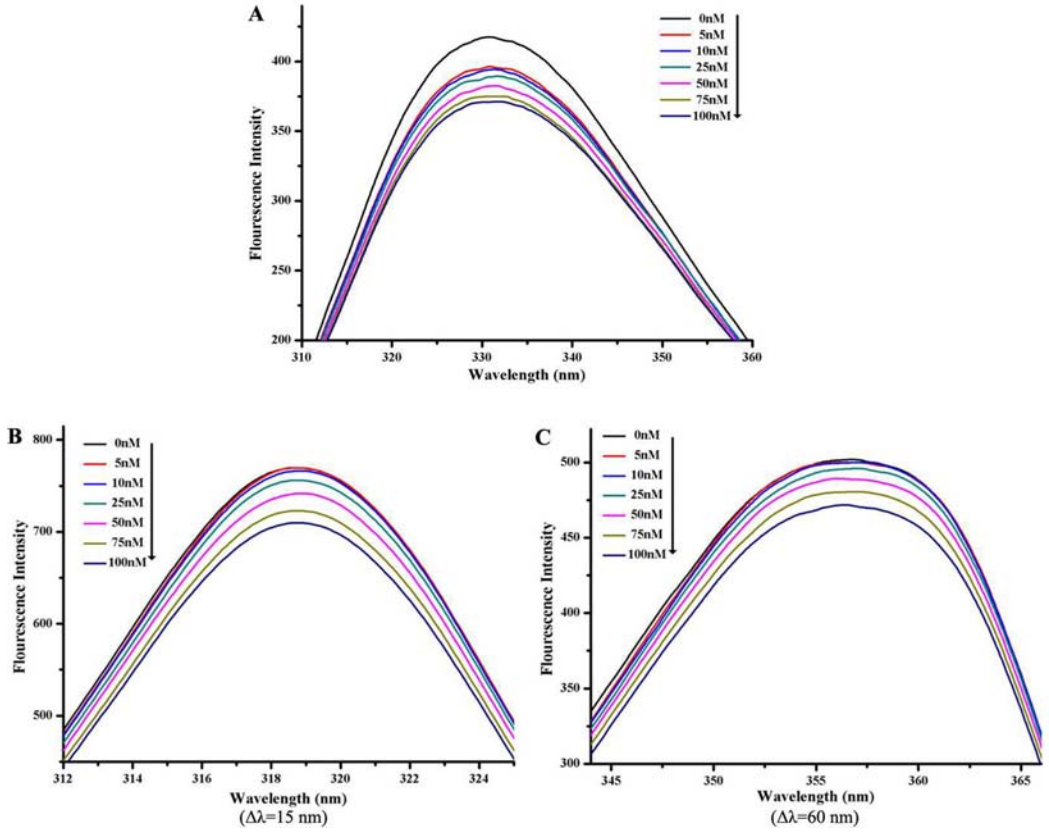

Figure 5. Fluorescence spectra of CLSL and fluorescence quenching spectra of CLSL quenched by barium ions. (A) Synchronous fluorescence spectra of CLSL at different concentrations of barium ions in acetate buffer (20 mM, pH 5.0). (B) and (C) CLSL concentration (20 μM) and final concentrations of barium ions (0, 5, 10, 25, 50, 75, and 100 nM, separately).

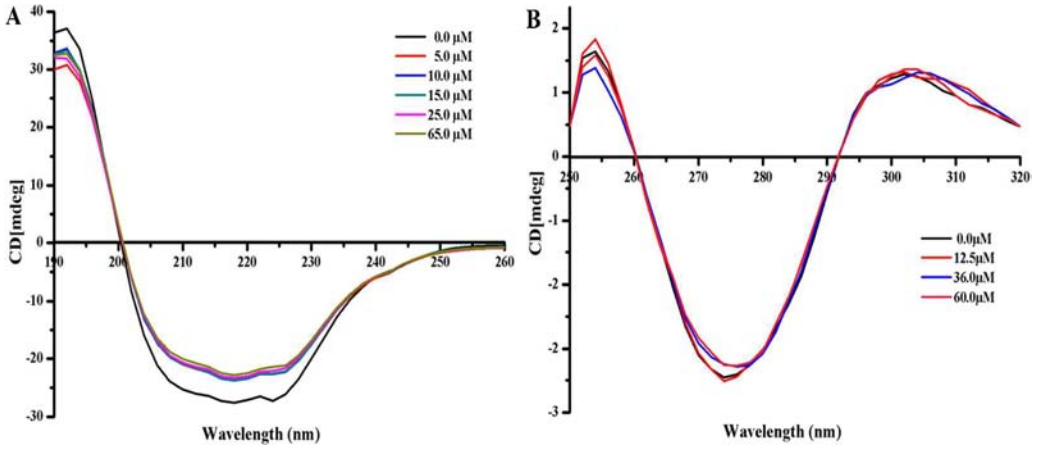

Figure 6. Superimposition of far-UV (A) and near-UV (B) CD spectra of CLSL recorded at presence of different barium ions concentrations in acetate buffer (20 mM, pH 5.0).

Table 7. Secondary Structure Contents of CLSL Compared with Other Lectins

	secondary structure				
	α-helixes (%)	β-sheets (%)	β-turns (%)	random coils (%)	reference
CLSL	35.8	8.6	18.3	37.3	the present
LAA	6	46	17	31	37
cMoL	46	12	17	25	31
BfL	19	27	22	32	22
MoL	28	23	20	28	41

an α/β lectin contains 46% α-helixes, 12% β-sheets, 17% β-turns, and 25% unordered structures, as reported by Luz et al.[31] A cotyledonary lectin from *Luetzelburgia auriculata* is composed of 6% α-helixes, 46% β-sheets, 17% β-turns, and 31% unordered structures.[37]

CLSL exerted strong thermostability similar to lectins reported by Oliveira et al.,[38] Ngai et al.,[39] and Santos et al.[30] The hemagglutinating activity of CLSL was stable at 100 °C for 60 min. The intramolecular disulfide bonds may be responsible for its thermostability.[40,41] However, CLSL was only active in acidic conditions and rapidly inactivated in neutral and

DOI: 10.1021/jf5046014
J. Agric. Food Chem. 2015, 63, 1488−1495

basic conditions. This might be because the hydroxyl ions increased with pH, induced changes of ionization state on the lectin surface, and affected the interaction between lectin and the cell membrane.[42−44] A similar phenomenon was observed with an *Archidendron jiringa* Nielsen-derived lectin.[6]

Lectins are a class of highly specific carbohydrate-binding proteins. Their multiple function (e.g., recognition and defense against pathogens) is closely related to the types of carbohydrate-binding.[45] The activities of lectins are often inhibited by monosaccharide and oligosaccharides.[46] In the present study, CLSL exhibited complex carbohydrate specificity, and the activity could be inhibited by carbohydrates including D-fructose, sorbitol, and mannitol, the binding of which likely prevented attachment of lectins to cell membranes.[46]

To the best of our knowledge, there has been no evidence demonstrating that hemagglutinating activity is related to antiproliferative activity. Despite that, both hemagglutinating and antiproliferative activities are related to the high binding specificity of lectins to oligosaccharides, and it is well-known that malignant transformation is accompanied by aberrant glycosylation of surface structures that may affect tumor invasion and metastasis.[47] Lectins could recognize the specific conformation of a cell surface due to specific binding of oligosaccharides and affect proliferation of cells. In the present paper, CLSL showed a selective antiproliferation activity against HepG2 cells but not Caco-2 and LO2 cells. The reason for the selectivity might be the discrepant oligosaccharides on HepG2, Caco-2, and LO2 cell surfaces.

Divalent metal compounds (e.g., $CuCl_2$, $CaCl_2$, and $FeCl_2$) could dramatically improve the activity of CLSL, one reason for which might be that some divalent metal ions (e.g., Ca^{2+} and Mn^{2+}) contribute to maintaining the conformation of lectin and stabilize amino acid residues in specific sugar-side-chain-binding sites.[42,43] However, inhibition of the hemagglutinating activity of CLSL by Ba^{2+} was noteworthy. The slight blue shift on fluorescence spectra demonstrated that Ba^{2+} interacted with CLSL and quenched its intrinsic fluorescence.[48] Moreover, synchronous fluorescence spectra also showed that not only was fluorescence intensities of tyrosine and tryptophan residues decreased but there was also a slight blue shift of tyrosine residues, suggesting the increase in hydrophobicity around tyrosine residues.[32,48] The most likely reason for the above changes was that conformation of CLSL had changed.

Notably, we also found that the α-helix content of CLSL gradually increased, accompanied by an equal decrease of its β-fold content when the Ba^{2+} concentration increased (Figure S1, Supporting Information), which hinted that the interaction between CLSL and Ba^{2+} resulted in transformation of its β-fold to α-helical conformations, destroying the conformation of its glycosylation active domains. Therefore, pathways of Ba^{2+}-mediated inactivation of CLSL speculated that the binding of Ba^{2+} changed the conformation of CLSL, leading to conformational changes of glycosylation domains and inhibition of activity. It was also likely that by directly binding to glycosylation domains, Ba^{2+} hindered the recognition and interaction between CLSL and sugar side chains on cell surface (Figure 7).

In conclusion, we reported purification and characterization of a novel lectin, CLSL from Chinese leek seeds, and its interaction with Ba^{2+}. The blood clotting parameters and biological functions of CLSL as a potential anticoagulant and platelet antiaggregation protein were examined in detail. The possible mechanism of interaction between CLSL and Ba^{2+} was deduced.

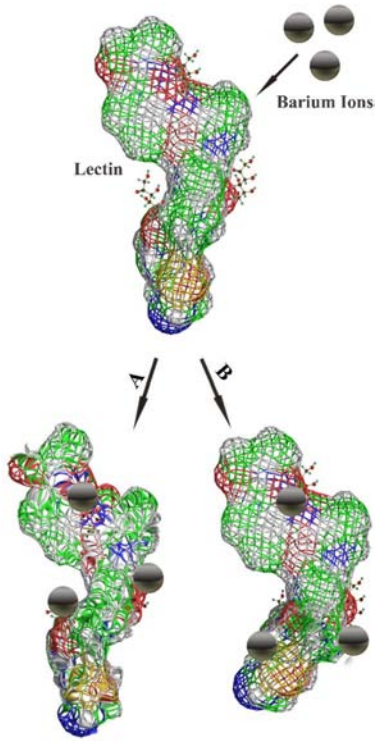

Figure 7. Sketch of the mechanism of interaction between CLSL and barium ions. Pathway A: Barium ions directly bound to carbohydrate-binding sites and caused the overall structural shrinkage of CLSL. Pathway B: The binding of barium ions caused the critical conformation change of CLSL and blocked the active sites. Both of the above pathways could destroy the conformation of its glycosylation domain, leading to the inactivation of CLSL.

Although further experiments should be conducted to elucidate the mechanism of CLSL interaction with sugars and explore its applications in the pharmaceutical industry, the present study provided a valuable basis for future research.

■ ASSOCIATED CONTENT

Supporting Information

Secondary structural content of CLSL titrated with different concentrations of Ba^{2+} and hemagglutinating activity of the different fractions from SP Sephadex C-25 column. This material is available free of charge via the Internet at http://pubs.acs.org.

■ AUTHOR INFORMATION

Corresponding Author

*S.W. telephone: +86-591-22866375. Fax: +86-591-22866278. E-mail: shywang@fzu.edu.cn.

Funding

This research was supported by grants from the National Natural Science Foundation of China (No. 31000335) and the Fujian Province Natural Science Foundation (No. 2013J05050).

Notes

The authors declare no competing financial interest.

■ ABBREVIATIONS USED

CLSP, Chinese leek seed protein; CLSL, Chinese leek seed lectin; SDS-PAGE, sodium dodecyl sulfate polyacrylamide gel electrophoresis; CD, circular dichroism; RP-HPLC, reverse phase-high performance liquid chromatography

DOI: 10.1021/jf5046014
J. Agric. Food Chem. 2015, 63, 1488−1495

REFERENCES

(1) Van Damme, E. J.; Peumans, W. J.; Pusztai, A.; Bardocz, S. *Handbook of Plant Lectins: Properties and Biomedical Applications*; Wiley: West Sussex, England, 1998.

(2) Darville, L. N. F.; Merchant, M. E.; Maccha, V.; Siddavarapu, V. R.; Hasan, A.; Murray, K. K. Isolation and determination of the primary structure of a lectin protein from the serum of the American alligator (Alligator mississippiensis). *Comp. Biochem. Physiol., Part B: Biochem. Mol. Biol.* **2012**, *161*, 161−169.

(3) Peumans, W. J.; Damme, E. J. M. Lectins as Plant Defense Proteins. *Plant Physiol.* **1995**, *109*, 347−352.

(4) Ding, J.; Bao, J.; Zhu, D.; Zhang, Y.; Wang, D. C. Crystal structures of a novel anti-HIV mannose-binding lectin from Polygonatum cyrtonema Hua with unique ligand-binding property and super-structure. *J. Struct. Biol.* **2010**, *171*, 309−317.

(5) Santi-Gadelha, T.; Rocha, B. A. M.; Gadelha, C. A. A.; Silva, H. C.; Castellon, R. E. R.; Gonçalves, F. J. T.; Toyama, D. O.; Toyama, M. H.; De Souza, A. J. F.; Beriam, L. O. S.; Martins, J. L.; Joazeiro, P. P.; Cavada, B. S. Effects of a lectin-like protein isolated from Acacia farnesiana seeds on phytopathogenic bacterial strains and root-knot nematode. *Pestic. Biochem. Phys.* **2012**, *103*, 15−22.

(6) Charungchitrak, S.; Petsom, A.; Sangvanich, P.; Karnchanatat, A. Antifungal and antibacterial activities of lectin from the seeds of Archidendron jiringa Nielsen. *Food Chem.* **2011**, *126*, 1025−1032.

(7) Alencar, V. B. M.; Alencar, N. M. N.; Assreuy, A. M. S.; Mota, M. L.; Brito, G. A. C.; Aragão, K. S.; Bittencourt, F. S.; Pinto, V. P. T.; Debray, H.; Ribeiro, R. A.; Cavada, B. S. Pro-inflammatory effect of Arum maculatum lectin and role of resident cells. *Int. J. Biochem. Cell Biol.* **2005**, *37*, 1805−1814.

(8) Wu, Y.; Wang, H.; Ng, T. B. Purification and characterization of a lectin with antiproliferative activity toward cancer cells from the dried fruit bodies of Lactarius flavidulus. *Carbohydr. Res.* **2011**, *346*, 2576−2581.

(9) Ota, E.; Tsuchiya, W.; Yamazaki, T.; Nakamura, M.; Hirayama, C.; Konno, K. Purification, cDNA cloning and recombinant protein expression of a phloem lectin-like anti-insect defense protein BPLP from the phloem exudate of the wax gourd, Benincasa hispida. *Phytochemistry* **2013**, *89*, 15−25.

(10) Lis, H.; Sharon, N. Lectins Carbohydrate-Specific Proteins That Mediate Cellular Recognition. *Chem. Rev.* **1998**, *98*, 637−674.

(11) Vasconcelos, I. M.; Oliveira, J. T. A. Antinutritional properties of plant lectins. *Toxicon* **2004**, *44*, 385−403.

(12) Lee, C. F.; Han, C. K.; Tsau, J. L. In vitro inhibitory activity of Chinese leek extract against Campylobacter species. *Int. J. Food Microbiol.* **2004**, *94*, 169−174.

(13) Mau, J. L.; Chen, C. P.; Hsieh, P. C. Antimicrobial effect of extracts from Chinese Chive, Cinnamon, and Corni Fructus. *J. Agric. Food Chem.* **2001**, *49*, 183−188.

(14) Shao, J.; Dai, J.; Ma, J. K. H. A pilot study on anticancer activities of Chinese leek. *J. Altern. Complement. Med.* **2001**, *7*, 517−522.

(15) Hu, G. H.; Lu, Y. H.; Mao, R. G.; Wei, D. Z.; Ma, Z. Z.; Zhang, H. Aphrodisiac properties of Allium tuberosum seeds extract. *J. Ethnopharmacol.* **2009**, *122*, 579−582.

(16) Clement, F.; Pramod, S. N.; Venkatesh, Y. P. Identity of the immunomodulatory proteins from garlic (Allium sativum) with the major garlic lectins or agglutinins. *Int. Immunopharmacol.* **2010**, *10*, 316−324.

(17) Smeets, K.; Van Damme, E. J.; Van Leuven, F.; Peumans, W. J. Isolation, characterization and molecular cloning of a leaf-specific lectin from ramsons (Allium ursinum L.). *Plant Mol. Biol.* **1997**, *35*, 531−535.

(18) Mo, H.; Vandamme, E.; Peumans, W.; Goldstein, I. Purification and Characterization of a Mannose-Specific Lectin from Shallot (*Allium ascalonicum*) Bulbs. *Arch. Biochem. Biophys.* **1993**, *306*, 431−438.

(19) Hu, G. H.; Mao, R. G.; Ma, Z. Z. A new steroidal saponin from the seeds of Allium tuberosum. *Food Chem.* **2009**, *113*, 1066−1068.

(20) Ikeda, T.; Tsumagari, H.; Nohara, T. Steroidal Oligoglycosides from the Seeds of Allium tuberosum. *Chem. Pharm. Bull.* **2000**, *48*, 362−365.

(21) Hu, G. H.; Lu, Y. H.; Wei, D. Z. Fatty acid composition of the seed oil of Allium tuberosum. *Bioresour. Technol.* **2005**, *96*, 1630−1632.

(22) Silva, M. C. C.; Santana, L. A.; Mentele, R.; Ferreira, R. S.; De Miranda, A.; Silva-Lucca, R. A.; Sampaio, M. U.; Correia, M. T. S.; Oliva, M. L. V. Purification, primary structure and potential functions of a novel lectin from Bauhinia forficata seeds. *Process Biochem.(Oxford, U. K.)* **2012**, *47*, 1049−1059.

(23) Zhu, Z. C.; Chen, Y.; Ackerman, M. S.; Wang, B.; Wu, W.; Li, B.; Obenauer-Kutner, L.; Zhao, R.; Tao, L.; Ihnat, P. M.; Liu, J.; Gandhi, R. B.; Qiu, B. Investigation of monoclonal antibody fragmentation artifacts in non-reducing SDS-PAGE. *J. Pharm. Biomed. Anal.* **2013**, *83*, 89−95.

(24) Takahashi, K. G.; Kuroda, T.; Muroga, K. Purification and antibacterial characterization of a novel isoform of the Manila clam lectin (MCL-4) from the plasma of the Manila clam, Ruditapes philippinarum. *Comp. Biochem. Physiol., Part B: Biochem. Mol. Biol.* **2008**, *150*, 45−52.

(25) Leyva, A.; Quintana, A.; Sánchez, M.; Rodríguez, E. N.; Cremata, J.; Sánchez, J. C. Rapid and sensitive anthrone−sulfuric acid assay in microplate format to quantify carbohydrate in biopharmaceutical products: Method development and validation. *Biologicals* **2008**, *36*, 134−141.

(26) Li, R.; Nagai, Y.; Nagai, M. Changes of tyrosine and tryptophan residues in human hemoglobin by oxygen binding: near- and far-UV circular dichroism of isolated chains and recombined hemoglobin. *J. Inorg. Biochem.* **2000**, *82*, 93−101.

(27) Twentyman, P. R.; Luscombe, M. A study of some variables in a tetrazolium dye (MTT) based assay for cell growth and chemosensitivity. *Br. J. Cancer* **1987**, *56*, 279−285.

(28) Yang, J. T.; Wu, C. C.; Martinez, H. M. Calculation of protein conformation from circular dichroism. *Methods Enzymol.* **1986**, *130*, 208−269.

(29) Chumkhunthod, P.; Rodtong, S.; Lambert, S. J.; Fordham-Skelton, A. P.; Rizkallah, P. J.; Wilkinson, M. C.; Reynolds, C. D. Purification and characterization of an N-acetyl-d-galactosamine-specific lectin from the edible mushroom Schizophyllum commune. *Biochim. Biophys. Acta, Gen. Subj.* **2006**, *1760*, 326−332.

(30) Santos, A. F. S.; Luz, L. A.; Argolo, A. C. C.; Teixeira, J. A.; Paiva, P. M. G.; Coelho, L. C. B. B. Isolation of a seed coagulant Moringa oleifera lectin. *Process Biochem.(Oxford, U. K.)* **2009**, *44*, 504−508.

(31) Luz, L. D. A.; Silva, M. C. C.; Ferreira, R. d. S.; Santana, L. A.; Silva-Lucca, R. A.; Mentele, R.; Oliva, M. L. V.; Paiva, P. M. G.; Coelho, L. C. B. B. Structural characterization of coagulant Moringa oleifera Lectin and its effect on hemostatic parameters. *Int. J. Biol. Macromol.* **2013**, *58*, 31−36.

(32) Zhang, H. X.; Huang, X.; Mei, P.; Gao, S. Interaction between Glyoxal-bis-(2-hydroxyanil) and Bovine Serum Albumin in Solution. *J. Solution Chem.* **2008**, *37*, 631−640.

(33) Geyer, H.; Geyer, R. Strategies for analysis of glycoprotein glycosylation. *Biochim. Biophys. Acta, Proteins Proteomics* **2006**, *1764*, 1853−1869.

(34) Zhu, K.; Zhou, H. Purification and characterization of a novel glycoprotein from wheat germ water-soluble extracts. *Process Biochem. (Oxford, U. K.)* **2005**, *40*, 1469−1474.

(35) Hu, G. H.; Lu, Y. H.; Wei, D. Z. Chemical characterization of Chinese chive seed. *Food Chem.* **2006**, *99*, 693−697.

(36) Ooi, L. S. M.; Yu, H.; Chen, C. M.; Sun, S. S. M.; Ooi, V. E. C. Isolation and Characterization of a Bioactive Mannose-Binding Protein from the Chinese Chive Allium tuberosum. *J. Agric. Food Chem.* **2002**, *50*, 696−700.

(37) Oliveira, J. T.A.; Melo, V. M. M.; Camara, M. F. L.; Vasconcelos, I. M.; Beltramini, L. M.; Machado, O. L. T.; Gomes, V. M.; Pereira, S. P.; Fernandes, C. F.; Nunes, E. P.; Capistrano, G. G. G.; Monteiro-Moreira, A. C. O. Purification and physicochemical characterization of

DOI: 10.1021/jf5046014
J. Agric. Food Chem. 2015, 63, 1488−1495

a cotyledonary lectin from Luetzelburgia auriculata. *Phytochemistry* **2002**, *61*, 301−310.
(38) Oliveira, M. D. L.; Andrade, C. A. S.; Santos-Magalhães, N. S.; Coelho, L. C. B. B.; Teixeira, J. A.; Carneiro-da-Cunha, M. G.; Correia, M. T. S. Purification of a lectin from Eugenia uniflora L. seeds and its potential antibacterial activity. *Lett. Appl. Microbiol.* **2008**, *46*, 371−376.
(39) Ngai, P. H. K.; Ng, T. B. A mushroom (Ganoderma capense) lectin with spectacular thermostability, potent mitogenic activity on splenocytes, and antiproliferative activity toward tumor cells. *Biochem. Biophys. Res. Commun.* **2004**, *314*, 988−993.
(40) Liu, Q.; Wang, H.; Ng, T. B. Isolation and characterization of a novel lectin from the wild mushroom Xerocomus spadiceus. *Peptides* **2004**, *25*, 7−10.
(41) Katre, U. V.; Suresh, C. G.; Khan, M. I.; Gaikwad, S. M. Structure−activity relationship of a hemagglutinin from Moringa oleifera seeds. *Int. J. Biol. Macromol.* **2008**, *42*, 203−207.
(42) Eretan, K.; Eretan, O. B. Purification and Partial Characterization of a Lectin from the Fresh Leaves of Kalanchoe crenata (Andr.) Haw. *J. Biochem. Mol. Biol.* **2004**, *37*, 229−233.
(43) Ahmad, S.; Khan, R. H.; Ahmad, A. Physicochemical characterization of Cajanus cajan lectin: effect of pH and metal ions on lectin carbohydrate interaction. *Biochim. Biophys. Acta* **1999**, *1427*, 378−384.
(44) Adolph, L.; Lorenz, R. *Enzyme Diagnosis in Diseases of the Heart, Liver, and Pancreas*; Karger: Basel, Switzerland, New York, 1982.
(45) Francis, F.; Jaber, K.; Colinet, F.; Portetelle, D.; Haubruge, E. Purification of a new fungal mannose-specific lectin from Penicillium chrysogenum and its aphicidal properties. *Fungal Biol.* **2011**, *115*, 1093−1099.
(46) Shao, B.; Wang, S.; Zhou, J.; Ke, L.; Rao, P. A novel lectin from fresh rhizome of Alisma orientale (Sam.) Juzep. *Process Biochem. (Oxford, U. K.)* **2011**, *46*, 1554−1559.
(47) Hakomori, S. Glycosylation defining cancer malignancy: New wine in an old bottle. *Proc. Natl. Acad. Sci. U. S. A.* **2002**, *99*, 10231−10233.
(48) Zhang, J.; Chen, L.; Zeng, B.; Kang, Q.; Dai, L. Study on the binding of chloroamphenicol with bovine serum albumin by fluorescence and UV−vis spectroscopy. *Spectrochim. Acta, Part A* **2013**, *105*, 74−79.
(49) Chen, L.; Yue, Q.; Zhang, M.; Wang, C.; Li, S.; Che, Y.; Ortiz-Lopez, F. J.; Bills, G. F.; Liu, X.; An, Z. Genomics-driven discovery of the pneumocandin biosynthetic gene cluster in the fungus Glarea lozoyensis. *BMC Genomics* **2013**, *14*, 339−339.
(50) Jia, J.; Zhao, S.; Kong, X.; He, W.; Appels, R.; Pfeifer, M.; Tao, Y.; Zhang, C.; Ma, Y.; Gao, L.; Gao, C.; Spannagl, M.; Mayer, K. F. X.; Li, D.; Pan, S.; Zheng, F.; Hu, Q.; Xia, X.; Liang, Q.; Chen, J.; Wicker, T.; Gou, C.; Kuang, H.; He, G.; Luo, Y.; Keller, B.; Xia, Q.; Lu, P.; Wang, J.; Zou, H.; Zhang, R.; Xu, J.; Gao, J.; Middleton, C.; Quan, Z.; Liu, G.; Wang, J.; Yang, H.; Liu, X.; He, Z.; Mao, L.; Wang, J. Aegilops tauschii draft genome sequence reveals a gene repertoire for wheat adaptation. *Nature* **2013**, *496*, 91−95.

DOI: 10.1021/jf5046014
J. Agric. Food Chem. 2015, 63, 1488−1495

The immune system is a complex biochemical process that enables efficient detection and removal of pathogens that threaten host viability. Immune processes have traditionally been divided into two broad, but interconnected, subsystems on the basis of their functions in host defense: the adaptive immune system and the innate immune system. Innate immunity is composed of those immunological effectors that provide robust, immediate, and nonspecific immune responses. Phagocytosis by neutrophils and complement system are two key factors of the innate immunity.

Neutrophils are the first line of the host defense mechanism against microbial infection. They are recruited to the site of infection and are capable of phagocytosis and killing a wide range of bacteria. Phagocytosis is an actin-dependent mechanism by which cells ingest large particles that are usually >0.5 μm in diameter.[6]

Complement system is a major effector mechanism of the innate immune system. It is a complex network of plasma and membrane-associated serum proteins, which can elicit highly efficient and tightly regulated inflammatory and cytolytic immune responses to infectious organisms, tissue damaged by physical, chemical, or neoplasm insults, and other surfaces identified as "nonself". The complement can be activated by a cascade mechanism of the classical pathway (CP), the alternative pathway (AP), or the mannan binding lectin (MBL) associated serine protease pathway. Inappropriate activation of the system may lead to pathologic reactions in a variety of inflammatory and degenerative diseases such as dermatological diseases, rheumatoid arthritis, and gout.

Although other activities of essential oils have been deeply researched, few studies have examined the influence of essential oils over phagocytosis. From a literature review on the subject, it appears that essential oils of *Houttuynia cordata*, *Allium sativum*, *Cinnamomum zeylanicum*, *Eucalyptus globulus*, and *Rheum palmatum* are capable of stimulating phagocytosis in experiments developed either in vitro or in vivo.[7−11] An inhibitory effect on phagocytosis was found in *Ocimum basilicum* essential oil,[12] whereas those from *Salvia officinalis*, *Lavandula angustifolia*, *Melaleuca alternifolia*, and *Origanum minutiflorum* showed no effect at all.[10,13,14]

Pure compounds have also been examined. 3-Carene was found to be a phagocytosis inhibitor in vitro.[15] On the other hand, limonene, citronellyl acetate, linalyl acetate, and methyl nonyl ketone clearly stimulated phagocytosis,[7,16−18] whereas camphor, menthol, and eucalyptol were found to be rather inactive.[19] The activity of eugenol on phagocytosis has not been tested on untreated cells. Nevertheless, it produced a recovery in the phagocytic function in nicotine-treated mouse peritoneal macrophages.[20] Additionally, mixtures containing eugenol, either in endodontic sealers or mixed with formaldehyde and cresol, showed some phagocytosis inhibitory activity, which cannot be unambiguously assigned to eugenol.[21,22]

Literature on the influence of the essential oils on complement activity is even more scarce. In fact, only one retracted paper[23] has been found on this topic.

The aim of the present study was to investigate the in vitro phagocytic and complement system modulating activities of 15 well-characterized essential oils, 4 essential oil fractions, and 3 pure compounds.

MATERIALS AND METHODS

Chemicals and Reagents. Water was freshly taken daily from a Milli-Q system (Millipore, Bedford, MA, USA). Sodium chloride (NaCl), ethylenediaminetetraacetic acid (EDTA), trypan blue, propidium iodide, Hanks' balanced salt solution (HBSS) with Ca^{2+} and Mg^{2+} or without Ca^{2+} and Mg^{2+}, Alsever's solution, gelatin veronal buffer, ammonium chloride (NH_4Cl), potassium bicarbonate ($KHCO_3$), ethylenediaminetetraacetic acid tetrasodium salt dihydrate (EDTA-Na_4·$2H_2O$), dimethyl sulfoxide (DMSO), paraformaldehyde, quercetin, ethylene glycol bis(2-aminoethyl ether)-*N*,*N*,*N*′,*N*′-tetra-acetic acid (EGTA), sodium 5,5-diethylbarbiturate, lipopolysaccharides (LPS) from *Escherichia coli* O127:B8, and human sera were obtained from Sigma Chemical Co. (St. Louis, MO, USA). Fluorescent microspheric hydrophilic particles (FluoSpheres) were purchased from Invitrogen, Molecular Probes (Carlsbad, CA, USA). Red blood cell polyclonal antibody anti-sheep were bought at ICN ibérica SA (Barcelona, Spain). Sheep red blood cells in Alsever's solution and rabbit red blood cells in Alsever's solution were obtained from the animal facilities of the Faculty of Veterinary of the Autonomous University of Barcelona and the Faculty of Pharmacy of the University of Barcelona, respectively.

Essential Oils and Compounds Studied. Essential oils from nutmeg (*Myristica fragrans* Houtt.), niaouli (*Melaleuca quinquenervia* (Cav.) S. T. Blake), clove (*Syzygium aromaticum* (L.) Merr. & L. M. Perry), tarragon (*Artemisia dracunculus* L.), coriander (*Coriandrum sativum* L.), juniper (*Juniperus communis* L.), tea tree (*Melaleuca alternifolia* (Maiden & Betche) Cheel), ginger (*Zingiber officinale* Roscoe), rosemary (*Rosmarinus officinalis* L.), bay laurel (*Laurus nobilis* L.), palmarosa (*Cymbopogon martini* (Roxb.) Will. Watson), cajuput (*Melaleuca cajuputi* Powell), lemon (*Citrus limon* (L.) Burm. f.), red thyme (*Thymus zygis* L.), and Spanish oregano (*Coridothymus capitatus* (L.) Rchb. f. = *Thymbra capitata* (L.) Cav.) were tested. The terpenic fractions from nutmeg, clove, and lemon were also included in our research. Finally, the pure compounds eugenol, carvacrol, and thymol, as well as a mixture of bornyl (76.8%) and isobornyl (21.7%) acetates, were also investigated. All samples except eugenol (Sigma-Aldrich) were supplied by Lidervet S.L. (Tarragona, Spain) and obtained from commercial sources (Lluch Essence S.L., Barcelona, Spain, and Ernesto Ventós S.A., Barcelona, Spain). All samples were kept in sealed airtight glass vials, protected from the light, at 4 °C.

Characterization and Analysis of the Essential Oils. The essential oils and fractions were characterized by their composition and some physical constants. The analyses of the composition of the oils were carried out by gas chromatography (GC-FID) and gas chromatography coupled to mass spectrometry (GC-MS), using a fused silica Supelcowax 10 capillary column (60 m × 0.25 mm i.d.; 0.25 μm film thickness). GC-FID analyses were performed on a Hewlett-Packard 6890 instrument, equipped with a HP ChemStation data processor software. Helium was used as carrier gas, and a split ratio of 1:80 was employed. Samples were injected undiluted (0.1 μL). Chromatographic conditions were different depending on the essential oil and, whenever possible, were based on the methods stated in the European Pharmacopeia.[24] Mass spectra were obtained using a Hewlett-Packard GC-MS instrument constituted by a GC HP 6890 coupled to a mass selective detector HP 5973N. The same analytical conditions employed in the GC-FID were applied in the GC-MS. Mass spectra were taken over m/z 35−400, using an ionizing voltage of 70 eV. Identification of the constituents of the oils and fractions was achieved by means of their linear retention indexes calculated in relation to a homologous series of *n*-alkanes (C8−C23) from the GC-FID analysis and by comparison of fragmentation patterns in their mass spectra with those stored in our own library, in the GC-MS database (Wiley 6), and with literature data.[25,26] Percentages of constituents were determined on the basis of their GC-FID peak areas using the normalization procedure without corrections for response factor.

Relative density, optical rotation, and refractive index of the essential oils and fractions were determined according to the European Pharmacopoeia.[24]

Sample Preparation for Biological Testing. Samples of the essential oil, fractions, and pure compounds were prepared at 1.0% (v/v) in HBSS supplemented with 10% (v/v) DMSO and 1.5% (v/v) E-484 (glyceryl polyethylene glycol ricinoleate). All solvents were

DOI: 10.1021/jf504761m
J. Agric. Food Chem. 2015, 63, 1496−1504

previously assayed to rule out any possible intrinsic activity. Samples were emulsified through exhaustive vortexing (10 min) and sonication (5 min, in ice). In the phagocytosis assay, nine dilutions that ranged from 5.0×10^{-3} to 7.8×10^{-7} % (v/v) in HBSS with Ca^{2+} and Mg^{2+} were tested. For the complement system assays, eight successive 2-fold dilutions (ranging from 6.67×10^{-2} to 5.21×10^{-4} % (v/v)) were prepared in barbital gelatin buffer with EGTA (for the AP essay) or barbital gelatin buffer with Ca^{2+} and Mg^{2+} (for the CP essay). Each dilution was thoroughly vortexed (10 min) immediately before use.

Isolation of Human Leukocytes. Leukocytes were isolated through a controlled hemolytic shock with an ammonium chloride solution from buffy coats obtained from blood of healthy donors at the Blood and Tissue Bank of Catalonia. The pellet was suspended in HBSS without Ca^{2+} and Mg^{2+}.

Phagocytosis Evaluation by Flow Cytometry. The phagocytosis assay was carried out following a modification of the method described by Risco et al.[27] A suspension (5.5×10^7 particles/mL) of fluorescent microspheric hydrophilic particles (2 μm in diameter) of modified carboxylate with a yellow-green fluorescence (505/515 nm), and opsonized using human serum (30 min at 37 °C), were used for the phagocytic test.

In a microtiter plate, 200 μL of a suspension of human leukocytes (approximately 10^6 cells) was incubated with 20 μL of different treatments for 10 min at 37 °C. Treatments included a positive control of LPS (1 mg/mL). Fluorescent particles (20 μL) were added to all wells. To manage nonspecific adhesion, 50 μL of paraformaldehyde (1% w/v) was added to wells designated as nonspecific adhesion controls. Microtiter plates were again incubated for 45 min in a stirred thermally controlled chamber at 37 °C. Fifty microliters of stop solution (0.9% w/v NaCl and 0.02% w/v of disodium EDTA) at 0 °C were added to all wells. The EDTA captures cations necessary for the phagocytic process. With the purpose of discriminating viable cells, 2 μL of a propidium iodide solution (10 μg/mL) was added. Finally, 20 μL of quenching solution (trypan blue solution, 2.25 mg/mL) and 50 μL of paraformaldehyde (1% w/v) were added to all wells.

A flow cytometer Cytomics FC 500 MPL system (Beckman Coulter, Inc., Brea, CA, USA) and Summit software v4.2 were employed for the analysis. Cellular viability was well over 95% in all experiments. The gate for neutrophils was established on the basis of the size and granularity. The acquisition process was stopped when 20000 viable neutrophils (negative to propidium iodide) were acquired and the green fluorescence histogram (515−548 nm) was obtained. Activity on phagocytosis (stimulation or inhibition) is calculated as percentage from phagocytic capacity (percentage of cells that ingested one or more particles), which is determined from the fluorescence distributions. Phagocytic capacity was corrected by taking in account the fluorescence due to nonspecific adhesion (particles adhered to the cell surface but not phagocyted). Examples of histograms are given as Supporting Information.

Hemolytic Assay for Human Complement Activity. A hemolytic assay was used to determine the inhibition of the alternative pathway (AP) and classical pathway (CP) of complement activation as described by Klerx et al.,[28] in human pooled serum. Assays were carried out in a microtiter plate, using barbital gelatin buffer with Ca^{2+} and Mg^{2+} (CP) or barbital gelatin buffer with EGTA (AP). Sensitized sheep erythrocytes (CP) or nonsensitized rabbit erythrocytes (AP) were incubated with the test samples for 30 min at 37 °C. Human pooled serum was added and incubated for 30 min (AP) or 60 min (CP) at 37 °C. The reaction was stopped by adding barbital buffer containing 10 mM EDTA. Erythrocytes were removed by centrifugation at 700*g* for 5 min, and the supernatant was transferred to a new flat-bottom microtiter plate. Absorbance was measured at 405 nm using a Benchmark Plus spectrophotometer (Bio-Rad, Hercules, CA, USA). Positive controls used were quercetin (CP) and an aqueous extract from *Azadirachta indica* (AP). Inhibition (%) was calculated from absorbance values of treated samples in relation to untreated controls.

Statistical Analysis. The results were expressed as the mean ± standard deviation (SD) of at least four independent experiments. One-way analysis of variance (ANOVA) followed by a Dunnett's test was used to compare means of untreated controls to each treatment. In all cases, a difference was considered significant when $p < 0.05$. Fifty percent inhibitory concentration (IC_{50}) was calculated by interpolation in a concentration/effect curve when possible. For data analysis, software Graph Pad Prism version 5.0 for Windows (San Diego, CA, USA) was used.

RESULTS AND DISCUSSION

The in vitro activity of 15 essential oils, 4 essential oil fractions, and 3 pure compounds (thymol, carvacrol, and eugenol) on phagocytosis by human neutrophils and complement system was investigated. As will be shown in the present section, tested essential oils were mainly phagocytosis inhibitors, whereas some of them showed a moderate but significant complement inhibitory activity in the classical pathway. Those properties might be related in some measure to the anti-inflammatory activity attributed to essential oils.[29] Because inflammation is a pathogenic factor in the evolution and origin of many diseases, essential oil consumption linked to culinary herbs and spices may prevent or at least alleviate the onset of various pathologies.

Characterization of the Essential Oils and Fractions. The composition of the oils and fractions analyzed is shown in Table 1. Eugenol, carvacrol, and thymol had a purity that was well over 99.0%. The mixture of bornyl acetate and isobornyl acetate contained 76.8% of the former and 21.7% of the latter, together with 1.0% of α-terpineol. The oils were also characterized by physical data, such as relative density, optical rotation, and refractive index (see the Supporting Information).

Activity on Phagocytosis by Human Neutrophils. Results on the activity of essential oils, fractions, and compounds tested on phagocytosis by human neutrophils are shown in Table 2. Most of the volatile oils tested inhibited phagocytosis, although the mixture of bornyl and isobornyl acetates showed a mild stimulating activity (21.3%) at the highest concentration tested (55.90 μg/mL). Some authors have also found stimulatory effects on phagocytosis for a few essential oils, such as those of *Rheum palmatum* L. and *Allium sativum* L., and for some pure constituents, such as citronellyl acetate and linalyl acetate.[8,11,18] Essential oils from cajuput, tarragon, and coriander showed no activity whatsoever on phagocytosis at the concentrations tested.

At the highest concentration tested, essential oils of nutmeg, clove, niaouli, tea tree, bay laurel, lemon, red thyme, and ginger, as well as nutmeg terpenes, eugenol, and thymol, met or exceeded the 25% inhibition of phagocytosis. Thymol was the most active inhibitor of phagocytosis, giving an IC_{50} of 1.5 μg/mL (Figure 1). In an early study, thymol appeared as a moderate promoter of phagocytosis, but results were produced through an in vivo experiment.[30] Red thyme essential oil, with thymol as its main constituent, caused an inhibition of phagocytosis greater than 25% ($p < 0.05$) at the highest evaluated concentration (47.15 μg/mL). Carvacrol and eugenol, the other two phenols tested in the present study, showed weak and mild inhibitory activity (Figure 1). Eugenol inhibited phagocytosis (29% at 57.6 μg/mL, $p < 0.05$) with a concentration−activity profile very similar to that of clove oil (Figure 2), suggesting that it is the major compound responsible for the activity of the oil. Literature reports on this compound have shown dissimilar results. In vitro evaluations of eugenol by different authors resulted in a reduction of phagocytosis.[21,22] In other in vitro experiments, it was found that eugenol was able to recover macrophage

DOI: 10.1021/jf504761m
J. Agric. Food Chem. 2015, 63, 1496−1504

Table 1. Composition of the Essential Oils and Fractions Investigated

	percentages in the essential oils and fractions[a]																	
constituent	BL[a]	CA	CL	CLT	CO	GI	JU	LE	LET	NI	NU	NUT	PA	RT	RO	SO	TA	TT
α-pinene	5.6	1.8			5.1	2.2	54.8	1.9	3.0	10.9	14.3	50.9		1.2	9.9	0.8	0.8	2.5
α-thujene								0.4	0.6		2.0	3.7		0.6	0.4	1.4		1.2
camphene					0.9	7.3	0.4		0.1			0.7		0.8	4.3			
6-methyl-5-hepten-2-one						0.4												
β-pinene	4.4	1.4			0.4	1.0	29.2	12.0	16.6	2.7	11.4	17.2		0.4	9.7	1.9		0.8
sabinene	7.5						0.5	2.1	2.7		40.8	22.1						0.7
Δ3-carene							0.5				1.1				1.3			
myrcene		1.4			0.5		7.6	1.6	1.7		3.3		0.2	1.8	2.1	1.4		
α-phellandrene							0.2											
α-terpinene	0.6										2.1			1.2		0.3		5.9
limonene	1.1	5.7			2.1	7.9	4.1	70.3	69.1	7.1	4.1	0.5		0.6		0.8	2.5	1.1
β-phellandrene								0.4	0.3		2.6							
1,8-cineole	65.6	67.8								58.3				0.6	49.7			4.5
cis-*β*-ocimene													0.4				4.8	
γ-terpinene	0.7				3.7			6.8	1.4	1.2	3.4			4.6	0.4	5.4		16.5
trans-*β*-ocimene													1.2				3.2	
p-cymene	2.2	1.6			1.8		0.5	1.6	4.3	2.4	1.3	0.7		23.2	1.7	8.1		9.3
terpinolene					0.5			0.3		0.9	1.5							2.9
α-cubebene				0.8														
trans-sabinene hydrate														0.2		0.2		
γ-elemene						0.6	0.3											
linalool oxide					0.3													
α-copaene				1.6		0.7												
camphor					5.7										9.6			
linalool		3.1			74.0	0.4							3.1	4.5	0.8	1.2		
cis-sabinene hydrate																0.4		
β-elemene						1.1												
bornyl acetate						0.5									1.3			
β-caryophyllene		1.0	14.9	83.0			0.4	0.3					2.0	1.2	3.9	0.7		
isosativene						0.4												
terpinen-4-ol	2.8	1.0								2.4	4.4				0.7	3.3		44.5
myrtenal	0.6																	
sativene																		0.5
trans-carveol									0.1									
trans-pinocarveol	0.7						0.4					0.7						
trans-verbenol												0.7						
β-farnesene						0.4												
aromadendrene														1.6				1.7
ar-curcumene						19.0												
estragole																	87.8	
δ-terpineol	0.6																	
α-humulene		0.7	1.7	9.1											1.0			

J. Agric. Food Chem. 2015, 63, 1496−1504
DOI: 10.1021/jf504761m

Table 1. continued

constituent	percentages in the essential oils and fractions[a]																	
	BL[a]	CA	CL	CLT	CO	GI	JU	LE	LET	NI	NU	NUT	PA	RT	RO	SO	TA	TT
neral								0.3					0.2					
geranyl formate													0.2					
α-terpenyl acetate	1.3									1.2								
α-terpineol	6.4	11.6			0.5	0.5		0.3		6.0					1.7			3.3
borneol						0.9								2.0	1.5			
ledene																		0.6
selinene		0.8																
germacrene D						0.6												
geranial								0.8					0.9					
zingiberene						22.3												
valencene								0.3										
β-bisabolene						9.2		0.4										
bicyclogermacrene																		1.4
E,*E*-α-farnesene						3.7												
δ-cadinene				0.8														1.5
geranyl acetate					3.2								8.1					
γ-cadinene						2.9												
mirtenol							0.3					0.6						
β-sesquiphellandrene						12.2												
cis-α-bisabolene								0.2								0.3		
nerol													0.2					
cis-calemenene				0.4														
geraniol					1.5								80.3					
safrole											1.1							
geranyl butyrate													0.2					
geranyl valerate													0.2					
caryophyllene oxide			0.5															
β-caryophyllene oxide				2.7									0.4	0.4		0.7		
guaiol		0.6																
nerolidol						0.6				2.3			0.7					
viridiflorol										4.9								
α-cedrol							0.5											
eugenol			81.5											0.4				
elemol						0.4												
thymol														50.0		0.4		0.6
elemicin											2.3							
carvacrol														4.3		72.7		
α-eudesmol		0.4																
β-eudesmol		0.5																
myristicin											4.3							
eugenyl acetate			1.3															
farnesol													1.1					

J. Agric. Food Chem. 2015, 63, 1496−1504
DOI: 10.1021/jf504761m

Table 1. continued

constituent	percentages in the essential oils and fractions[a]																	
	BL[a]	CA	CL	CLT	CO	GI	JU	LE	LET	NI	NU	NUT	PA	RT	RO	SO	TA	TT
identified (%)	100.0	99.3	99.9	98.4	100.0	95.4	99.7	100.0	99.9	100.0	100.0	97.8	99.5	99.6	100.0	100.0	99.1	99.5

[a]Essential oils and fractions: BL, bay laurel; CA, cajuput; CL, clove; CLT, clove terpenes; CO, coriander; GI, ginger; JU, juniper; LE, lemon; LET, lemon terpenes; NI, niaouli; NU, nutmeg; NUT, nutmeg terpenes; PA, palmarosa; RT, red thyme; RO, rosemary; SO, Spanish oregano; TA, tarragon; TT, tea tree.

phagocytic capacity previously diminished by treatment with nicotine.[20] Other volatile compounds and essential oils, such as 3-carene and basil oil, have been dubbed in the literature as phagocytic inhibitors.[12,15] In in vivo and in vitro experiments, limonene (the main constituent of lemon oil and lemon terpenes) showed a stimulating effect over phagocytosis or the recuperation of the macrophages phagocytic capacity previously reduced.[16−18] Those results differ from ours, although it is important to highlight that employed cells and methodologies were different. Essential oils from juniper, rosemary, palmarosa, and Spanish oregano, lemon terpenes, and carvacrol showed a significant inhibition of phagocytosis, but it was lower than 25% at the highest tested concentration. The measured activity of carvacrol was lower than that of its isomer, thymol (Figure 1).

In some situations, a decreased phagocytic activity caused by essential oils could be a good strategy to reduce viral and bacterial infection. There is evidence that certain microbes subvert neutrophil protective functions and that neutrophils could, in fact, promote susceptibility to infection. This is due to the fact that intracellular invasion achieved with the phagocytic process can allow, in certain infections, pathogen proliferation and protection. This could be the case with leishmania parasites, *Chlamydia pneumoniae* or *Mycobacterium tuberculosi*, Epstein−Barr, and cytomegaloviruses.[31] It has been shown that a selective depletion, in vivo, of neutrophils by monoclonal antibody administration did provide a protective effect against *Chlamydia pneumoniae* in infected mice.[32]

Moreover, antibiotics are also known for their modulating effects on many components of the human immune system, in addition to their direct antimicrobial effects. For example, macrolide antibiotics cause a significant reduction in the chemotactic response of neutrophils to chemokines, resulting in a markedly decreased airway neutrophilia in patients with various inflammatory pulmonary diseases.[33] More than four decades earlier Forsgren and Schmeling[34] had reported a similar inhibition of neutrophil chemotaxis by rifampin, tetracyclines, and chloramphenicol.

Certainly, a body of evidence has emerged indicating that both antibiotics and essential oils possess modes of action which are independent of their antimicrobial activity when facing an infection.

In addition, neutrophils express Fc receptors, which are responsible for phagocytosis and intracellular killing of opsonized microbial pathogens, and it has been reported that this response can be blocked by inhibitors of ROS and by inhibitors of the H_2O_2−myeloperoxidase−chloride system.[35] Both activities have been reported in many of these essential oils in preliminary studies of our group,[36] showing consistency of the relationship between ROS inhibition and phagocytosis reduction.

Activity on Human Complement System. Results of the hemolytic assay for human complement activity are shown in Table 2. Different degrees of inhibitory activity were evident on the classical pathway of the complement system, whereas all essential oils were found inactive in the alternative pathway experiment. No other results on essential oils activity on complement system have been found in the literature. Nevertheless, a similar pattern of activity has also been described for other extracts or substances of terpenoid nature.[37] A closer look at individual results of the classical pathway shows that eugenol and clove oil had similar moderate IC_{50} values (78.3 and 74.9 μg/mL, respectively). This, together with the fact that clove terpenes showed almost no activity, points to

DOI: 10.1021/jf504761m
J. Agric. Food Chem. 2015, 63, 1496−1504

Table 2. Activity of Essential Oils, Their Fractions, and Constituents on Phagocytosis by Human Neutrophils and on Complement System

	phagocytosis		complement system inhibition IC_{50} (μg/mL)	
essential oils, fractions, and constituents	concentration[a] (μg/mL)	activity[b] (% ± SD)	classical pathway[c]	alternative pathway[d]
bay laurel	45.75	−38.7 ± 3.1*	155.4 ± 3.5	na
bornyl acetate + isobornyl acetate	55.90	21.3 ± 2.6*	126.1 ± 4.1	na
cajuput	46.75	4.1 ± 8.7	97.3 ± 4.6	na
clove	50.40	−36.1 ± 15.5*	74.9 ± 3.2	na
clove terpenes	45.35	−14.6 ± 1.7*	nc	na
coriander	45.55	−12.8 ± 2.2	154.4 ± 3.5	na
eugenol	57.60	−29.4 ± 5.2*	78.3 ± 3.9	na
ginger	47.00	−28.5 ± 1.4*	nc	na
juniper	22.40	−24.3 ± 10.5*	nc	na
lemon	45.05	−41.0 ± 14.2*	nc	na
lemon terpenes	43.50	−9.7 ± 6.4*	nc	na
niaouli	46.70	−39.1 ± 28.3*	91.3 ± 4.2	na
nutmeg	46.35	−33.8 ± 2.7*	nc	na
nutmeg terpenes	43.85	−38.5 ± 2.0*	nc	na
palmarosa	47.75	−22.1 ± 1.9*	75.2 ± 3.0	na
red thyme	47.15	−38.0 ± 1.0*	67.8 ± 2.9	na
thymol	55.80	−72.2 ± 25.0*	125.5 ± 4.4	na
rosemary	48.40	−11.3 ± 2.5*	nc	na
Spanish oregano	49.15	−16.2 ± 2.2*	118.1 ± 7.8	na
carvacrol	52.05	−14.9 ± 4.1*	78.1 ± 4.7	na
tarragon	46.80	−12.9 ± 1.4	64.8 ± 3.4	na
tea tree	48.00	−35.2 ± 20.2*	97.0 ± 4.2	na

[a]Highest concentration tested. [b]$n = 4$; *, statistically significant ($p < 0.05$). [c]$n = 6$; nc, activity did not allaw calculation of IC_{50}; positive control, quercetin (IC_{50} = 33.7 μg/mL). [d]$n = 4$; na, not active; positive control, aqueous extract from *Azadirachta indica* (IC_{50} = 226.4 μg/mL).

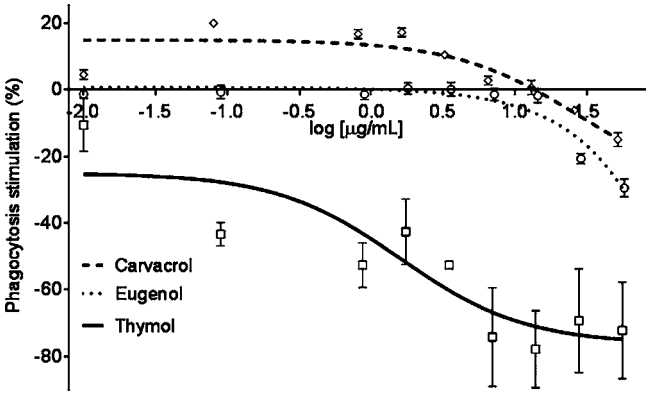

Figure 1. Activity of eugenol, thymol, and carvacrol on phagocytosis by human neutrophils (stimulation %, mean ± SD).

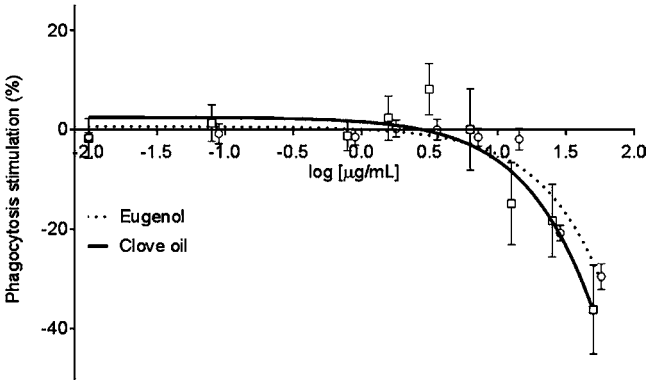

Figure 2. Activity of clove oil and eugenol on phagocytosis by human neutrophils (stimulation %, mean ± SD).

eugenol as the source of activity in clove oil (Figure 3). Other phenol-rich essential oils (red thyme, Spanish oregano, and

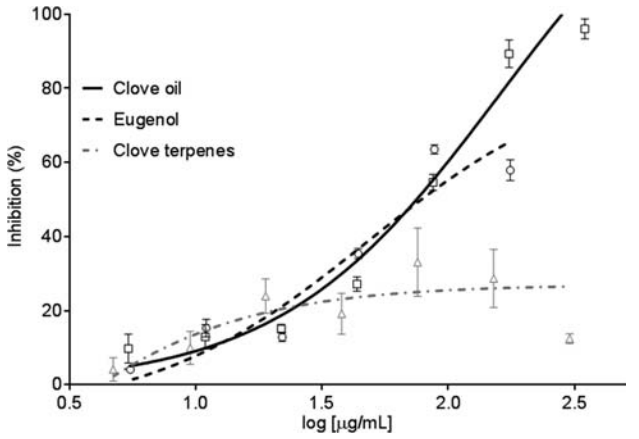

Figure 3. Activity of clove oil, clove terpenes, and eugenol on the classic pathway of the human complement system (inhibition %, mean ± SD).

tarragon) also displayed a similar mild inhibitory activity. It is interesting to highlight that carvacrol, the main constituent of the Spanish oregano oil, was more active that the essential oil, whereas thymol, the major component of red thyme oil, was less active than the essential oil. Maybe in red thyme essential oil other substances take part in its activity, whereas carvacrol remains as the main source of activity for Spanish oregano. All phenols tested, either monoterpenes (thymol and carvacrol) or phenylpropanoids (eugenol), had a similar behavior (Figure 4). In the essential oils tested from the *Melaleuca* genus, some activity was found, although it was moderate. This was the case

DOI: 10.1021/jf504761m
J. Agric. Food Chem. 2015, 63, 1496−1504

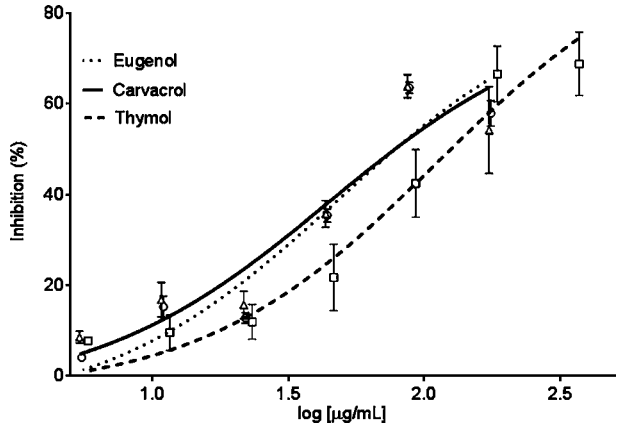

Figure 4. Activity of eugenol, carvacrol, and thymol on the classic pathway of the human complement system (inhibition %, mean ± SD).

of niaouli, tea tree, and cajuput oils. Tea tree oil is rich in terpinen-4-ol (44.5%), whereas in niaouli and cajuput oils 1,8-cineole is the major constituent (58.3 and 67.8%, respectively). Essential oils of bay laurel (IC_{50} = 155.4 μg/mL) and rosemary (showing a 27% inhibition at 154.7 μg/mL, $p < 0.01$) were also rich in 1,8-cineole (49.7 and 65.6%, respectively), which suggests a possible role of this compound in the anticomplementary activity. Other oxygenated monoterpene-rich oils and fractions showed moderate to weak activities, with IC_{50} values of 75.2 μg/mL for palmarosa oil (with 80.3% of geraniol), 126.1 μg/mL for the mixture of bornyl and isobornyl acetates, and 1540.4 μg/mL for coriander oil (with 74.0% of linalool). Results confirm that oxygen-containing compounds (either phenylpropanoids or monoterpenes) confer higher inhibitory activity of the classical pathway of the complement system than monoterpene hydrocarbons. Among oxygen-containing compounds, phenols, especially eugenol and carvacrol, showed the best profile.

Hemolytic effects of the essential oils tested were also examined. In vitro testing for hemolytic action has been used as one of the methods of triage for different toxic agents. Hemolysis tests are a simple tool to detect membrane toxicity and cytotoxicity. Most of the essential oils studied caused erythrocyte lysis at concentrations >200 μg/mL, showing thus a low toxicity toward membranes. The most noticeable action on erythrocyte membrane integrity was rendered by juniper oil and nutmeg terpenes, which caused erythrocyte membrane lysis at concentrations <100 μg/mL. Both of them are very rich in α-pinene and β-pinene. Those monoterpenes seem to increase erythrocyte lysis, a process that could be related to their capacity to affect cell membrane integrity with the sequential loss of control over chemio-osmotic processes and finally cell lyses and death.[38]

■ ASSOCIATED CONTENT

Supporting Information

The essential oils studied were characterized, in part, by physical data, such as relative density, optical rotation, and refractive index. This material is available free of charge via the Internet at http://pubs.acs.org.

■ AUTHOR INFORMATION

Corresponding Author

*(S.C.) Phone: +34 934 024531. Fax: +34 934 035982. E-mail: s.canigueral@ub.edu.

Present Address

⊥(E.R.) Phytonexus S.L.

Funding

This work was financially supported by Lidervet S.L. (Tarragona, Spain). R.P.-R. enjoyed a grant from the Generalitat de Catalunya and the European Social Fund during the development of this research.

Notes

All biological samples, either from animals or humans, were obtained under the relevant ethical approval, by the Ethical Committees of the Faculty of Pharmacy of the University of Barcelona and the Blood and Tissue Bank of Catalonia.

The authors declare the following competing financial interest(s): Pedro Peñalver is shareholder of the company Lidervet S.L. (Tarragona, Spain). The work presented in this paper was financially supported by Lidervet S.L.

■ REFERENCES

(1) Brenes, A.; Roura, E. Essential oils in poultry nutrition: main effects and modes of action. *Anim. Feed Sci. Technol.* **2010**, *158*, 1−14 http://dx.doi.org/10.1016/j.anifeedsci.2010.03.007.

(2) Burt, S. Essential oils: their antibacterial properties and potential applications in foods − a review. *Int. J. Food Microbiol.* **2004**, *94*, 223−253 http://dx.doi.org/10.1016/j.ijfoodmicro.2004.03.022.

(3) Peñalver, P.; Huerta, B.; Borge, C.; Astorga, R.; Romero, R.; Perea, A. Antimicrobial activity of five essential oils against origin strains of the *Enterobacteriaceae* family. *Acta Pathol., Microbiol. Immunol. Scand.* **2005**, *113*, 1−6 http://dx.doi.org/10.1111/j.1600-0463.2005.apm1130101.x.

(4) Ordóñez, G.; Llopis, N.; Peñalver, P. Efficacy of eugenol against a *Salmonella enterica* serovar enteritidis experimental infection in commercial layers in production. *J. Appl. Poult. Res.* **2008**, *17*, 376−382 http://dx.doi.org/10.3382/japr.2007-00109.

(5) Trichet, V. V. Nutrition and immunity: an update. *Aquacult. Res.* **2010**, *41*, 356−372 http://dx.doi.org/10.1111/j.1365-2109.2009.02374.x.

(6) Kerrigan, A. M.; Brown, G. D. C-type lectins and phagocytosis. *Immunobiology* **2009**, *214*, 562−575 http://dx.doi.org/10.1016/j.imbio.2008.11.003.

(7) Jin, J. Methyl *n*-nonylketone as an active principle of Herba Houtltuyniae and its mechanism. *Zhongguo Linchuang Yaoxue Zazhi* **2012**, *21* (1), 23−26.

(8) Gu, B.; You, J.; Li, Y.; Duan, C.; Fang, M. Enteric-coated garlic supplement markedly enhanced normal mice immunocompetence. *Eur. Food Res. Technol.* **2010**, *230*, 627−634 http://dx.doi.org/10.1007/s00217-009-1202-1.

(9) Faix, Š.; Faixová, Z.; Plachá, I.; Koppel, J. Effect of *Cinnamomum zeylanicum* essential oil on antioxidative status in broiler chickens. *Acta Vet. Brno* **2009**, *78*, 411−417 http://dx.doi.org/10.2754/avb200978030411.

(10) Serafino, A.; Vallebona, P. S.; Andreola, F.; Zonfrillo, M.; Mercuri, L.; Federici, M.; Rasi, G.; Garaci, E.; Pierimarchi, P. Stimulatory effect of eucalyptus essential oil on innate cell-mediated immune response. *BMC Immunol.* **2008**, *9* (17), http://dx.doi.org/10.1186/1471-2172-9-17.

(11) Zhang, B.; Chen, H.; Xu, A.; Chen, J.; Sheng, S. Effects of volatile oil from *Rheum palmatum* on immunologic function in mice. *Zhongyaocai* **1997**, *20*, 85−88.

(12) Courrèges, M. C.; Benencia, F. *In vitro* antiphagocytic effect of basil oil on mouse macrophages. *Fitoterapia* **2002**, *73*, 369−374 http://dx.doi.org/10.1016/S0367-326X(02)00117-X.

DOI: 10.1021/jf504761m
J. Agric. Food Chem. 2015, 63, 1496−1504

(13) Ryzner, M.; Takáčová, J.; Čobanová, K.; Plachá, I.; Venglovská, K.; Faix, Š. Effect of dietary *Salvia officinalis* essential oil and sodium selenite supplementation on antioxidative status and blood phagocytic activity in broiler chickens. *Acta Vet. Brno* **2013**, *82*, 43−48 http://dx.doi.org/10.2754/avb201382010043.
(14) Karagouni, E.; Athanassopoulou, F.; Lytra, A.; Komis, C.; Dotsika, E. Antiparasitic and immunomodulatory effect of innovative treatments against *Myxobolus* sp. infection in *Diplodus puntazzo*. *Vet. Parasitol.* **2005**, *134*, 215−228 http://dx.doi.org/10.1016/j.vetpar.2005.07.020.
(15) Johansson, A.; Lundborg, M. Effects of low concentrations of 3-carene on alveolar macrophages *in vitro*. *Toxicology* **1997**, *120*, 99−104 http://dx.doi.org/10.1016/S0300-483X(97)03641-X.
(16) Del Toro-Arreola, S.; Flores-Torales, E.; Torres-Lozano, C.; del Toro-Arreola, A.; Tostado-Pelayo, K.; Ramirez-Dueñas, M. G.; Daneri-Navarro, A. Effect of D-limonene on immune response in BALB/c mice with lymphoma. *Int. Immunopharmacol.* **2005**, *5*, 829−838 http://dx.doi.org/10.1016/j.intimp.2004.12.012.
(17) Hamada, M.; Uezu, K.; Matsushita, J.; Yamamoto, S.; Kishino, Y. Distribution and immune responses resulting from oral administration of D-limonene in rats. *J. Nutr. Sci. Vitaminol.* **2002**, *48*, 155−160 http://dx.doi.org/10.3177/jnsv.48.155.
(18) Gözsy, B.; Kátó, L. Reticuloendothelial system-stimulating compounds and their mechanism of action. *Can. J. Biochem. Physiol.* **1958**, *36*, 319−326.
(19) Goldstein, E.; Cooper, A. D.; Tarkington, B. Effect of inhaling medication vapors from a colds preparation on murine pulmonary bacterial defense systems. *J. Toxicol. Environ. Health* **1976**, *2*, 371−388 http://dx.doi.org/10.1080/15287397609529440.
(20) Mahapatra, S. K.; Bhattacharjee, S.; Chakraborty, S. P.; Majumdar, S.; Roy, S. Alteration of immune functions and Th1/Th2 cytokine balance in nicotine-induced murine macrophages: immunomodulatory role of eugenol and *N*-acetylcysteine. *Int. Immunopharmacol.* **2011**, *11*, 485−495 http://dx.doi.org/10.1016/j.intimp.2010.12.020.
(21) De Oliveira-Mendes, S. T.; Ribeiro-Sobrinho, A. P.; Teixeira de Carvalho, A.; de Souza-Cortes, M. I.; Quercia-Vieira, L. *In vitro* evaluation of the cytotoxicity of two root canal sealers on macrophage activity. *J. Endodontics* **2003**, *29*, 95−99 http://dx.doi.org/10.1097/00004770-200302000-00002.
(22) Segura, J. J.; Jimenez-Rubio, A.; Guerrero, J. M.; Calvo, J. R.; Feito, J. J. Effect in vitro of Tifell (formocresol-eugenol) on macrophage adhesion. *Int. Endodontic J.* **1998**, *31*, 112−116 http://dx.doi.org/10.1046/j.1365-2591.1998.00121.x.
(23) Chung, I. M.; Yeo, M.-A.; Kim, S.-J.; Moon, H.-I. RETRACTED: Anti-complement activity of essential oils from red and black rice bran. *Int. J. Food Sci. Nutr.* **2011**, *62*, 215−218 http://dx.doi.org/10.3109/09637486.2010.503187.
(24) EDQM. *European Pharmacopoeia*, 8th ed.; Council of Europe: Strasbourg, France, 2013.
(25) McLafferty, F. W.; Stauffer, D. B.; Stenhagen, E.; Heller, S. R. *The Wiley/ MBS Registry of Mass Spectral Data*; Wiley: New York, 1993.
(26) Adams, R. P. In *Identification of Essentials Oils by Gas Chromatography/Mass Spectrometry*; Adams, R. P., Ed.; Allured Publishing: Carol Stream, IL, USA, 2007.
(27) Risco, E.; Ghia, F.; Vila, R.; Iglesias, J.; Álvarez, E.; Cañigueral, S. Immunomodulatory activity and chemical characterisation of Sangre de drago (dragon's blood) from *Croton lechleri*. *Planta Med.* **2003**, *69*, 785−794 http://dx.doi.org/10.1055/s-2003-43208.
(28) Klerx, J. P. M. A.; Beukelman, C. J.; Van Dijk, H.; Willers, J. M. N. Microassay for colorimetric estimation of complement activity in guinea pig, human and mouse serum. *J. Immunol. Methods* **1983**, *63*, 215−220 http://dx.doi.org/10.1016/0022-1759(83)90425-8.
(29) Miguel, M. G. Antioxidant and anti-inflammatory activities of essential oils: a short review. *Molecules* **2010**, *15*, 9252−9287 http://dx.doi.org/10.3390/molecules15129252.
(30) Kátó, L.; Gözsy, B. Stimulation of the cell-linked defense forces of the skin. Mechanism of action of certain topical agents. *Can. Med. Assoc. J.* **1955**, *73*, 31−34.
(31) Appelberg, R. Neutrophils and intracellular pathogens: beyond phagocytosis and killing. *Trends Microbiol.* **2007**, *15*, 87−92 http://dx.doi.org/10.1016/j.tim.2006.11.009.
(32) Rodríguez, N.; Fend, F.; Jennen, L.; Schiemann, M.; Wantia, N.; Prazeres da Costa, C. U.; Dürr, S.; Heinzmann, U.; Wagner, H.; Miethke, T. Polymorphonuclear neutrophils improve replication of *Chlamydia pneumoniae in vivo* upon MyD88-dependent attraction. *J. Immunol.* **2005**, *174*, 4836−4844 http://dx.doi.org/10.4049/jimmunol.174.8.4836.
(33) Altenburg, J.; de Graaff, C. S.; van der Werf, T. S.; Boersma, W. G. Immunomodulatory effects of macrolide antibiotics − part 1: biological mechanisms. *Respiration* **2011**, *81*, 67−74 http://dx.doi.org/10.1159/000320319.
(34) Forsgren, A.; Schmeling, D. Effect of antibiotics on chemotaxis of human leukocytes. *Antimicrob. Agents Chemother.* **1977**, *11*, 580−584 http://dx.doi.org/10.1128/AAC.11.4.580.
(35) Fialkow, L.; Wang, Y.; Downey, G. P. Reactive oxygen and nitrogen species as signaling molecules regulating neutrophil function. *Free Radical Biol. Med.* **2007**, *42*, 153−164 http://dx.doi.org/10.1016/j.freeradbiomed.2006.09.030.
(36) Pérez-Rosés, R.; Risco, E.; Vila, R.; Peñalver, P.; Cañigueral, S. Effect of essential oils on the activity of human neutrophil myeloperoxidase in vitro. *Planta Med.* **2012**, *78*, No. PF61, http://dx.doi.org/10.1055/s-0032-1320608.
(37) Min, B.-S.; Lee, I.-S.; Chang, M.-J.; Yoo, J. K.; Na, M.-K.; Hung, T. M.; Thuong, P. T.; Lee, J.-P.; Kim, J.-H.; Kim, J. C.; Woo, M. H.; Choi, J. S.; Lee, H.-K.; Bae, K.-H. Anticomplementary activity of triterpenoids from the whole plant of *Aceriphyllum rossii* against the classical pathway. *Planta Med.* **2008**, *74*, 726−729 http://dx.doi.org/10.1055/s-2008-1074534.
(38) Uribe, S.; Ramirez, J.; Peña, A. Effects of β-pinene on yeast membrane functions. *J. Bacteriol.* **1985**, *161*, 1195−1200.

DOI: 10.1021/jf504761m
J. Agric. Food Chem. 2015, 63, 1496−1504

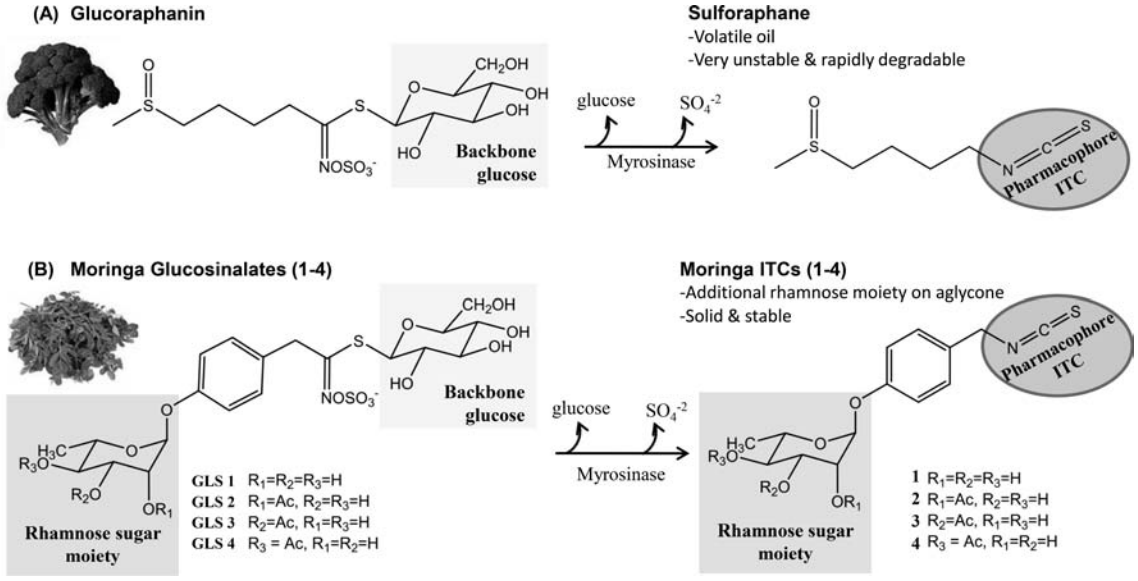

Figure 1. Enzymatic conversion of (A) glucorophanin from broccoli to sulforaphane (SF) and of (B) moringa glucosinolates (GLSs) to isothiocyanates (ITCs) **1**−**4**.

content from the leaves of *M. oleifera* has shown that GLS **1** (see Figure 1B for the structure) is present in significant concentrations (ranging between 33.9 and 59.4 mg/g dry weight of the tissue). However, the concentration of its monoacetyl isomers, especially GLSs **2** and **3**, are relatively less abundant (ranging between 1.2 and 5.0 mg/g dry weight of the tissue).[12] The occurrence of these compounds at relatively low levels makes isolation of them and their corresponding ITCs a purification challenge. Herein, we accomplished a large-scale fractionation of moringa leaf extract to yield ITC-rich fractions by fast partition counter current chromatography (FCPC) using a three-phase solvent system, which has been previously used to separate a mixture of plant compounds having a broad range of polarity in a one-step operation.[13] We applied this system followed by solid phase extraction (SPE) to further enrich the ITC content of the fractions, thus enabling the isolation of other, less abundant monoacetyl isomers. The methanolic extract of moringa was prepared from finely chopped and crushed fresh leaves to activate plant myrosinase for the efficient conversion of GLSs to corresponding ITCs.

The use of moringa leaves as traditional medicine dates back to ancient times. Growing scientific evidence has suggested the effectiveness of moringa in treating inflammation, hyperlipidemia, hyperglycemia, hypertension, bacterial and viral infections, ulcers, and cancer.[14−16] It is now well-known that many of these conditions are brought on and/or exacerbated by oxidative and electrophilic stress.[17] Thus, moringa's ability to prevent and treat such conditions may be due to the high level of antioxidant/bioactive compounds present in the leaves including vitamins, micronutrients, and polyphenols.[14,18] To date, moringa ITCs have not been well studied for their antioxidant activity. Therefore, this study was designed to evaluate and distinguish the role of moringa polyphenols and ITCs in both direct and indirect antioxidant capacities.

Generally, direct antioxidants are redox active, short-lived small molecules that directly scavenge reactive oxygen and/or nitrogen species.[17] On the other hand, indirect antioxidants induce a battery of phase II xenobiotic metabolizing enzymes (XMEs) through a shared Keap1/Nrf2/ARE pathway resulting in increased antioxidant capacity and long-lived protective effect compared to direct antioxidants.[17] Among phase II XMEs, NAD(P)H quinone oxidoreductase 1 [NQO1, EC 1.6.99.2] serves as a cytoprotective marker enzyme to evaluate indirect antioxidant potential of various phytochemicals including ITCs.[19,20] NQO1 catalyzes a two-electron reduction of highly reactive quinone molecules that are found in automobile exhaust, cigarette smoke, and many foods.[21] Numerous studies have shown associations between elevated NQO1 activity and protection against cancer and inflammatory diseases.[22,23]

Assaying NQO1 inducer potency has been used to isolate several chemoprotective agents from plant materials, leading to the synthesis of more effective ITCs and curcumin derivatives.[24] SF was first isolated from broccoli by monitoring NQO1 inducer potency.[25] In the current work, polyphenol-rich fractions, ITC-enriched fractions, compounds **1** and **4**, and SF were tested and compared for indirect antioxidant activity by measuring induction of NQO1 activity in murine hepatoma cells and direct antioxidant activity by measuring the oxygen radical absorbance capacity (ORAC). This study also demonstrates the effectiveness of FCPC and solid phase extraction (SPE) to concentrate polyphenols and ITCs from moringa leaves.

MATERIALS AND METHODS

Chemicals. Acetonitrile, 2,2′-azobis(2-methylpropionamidine) dihydrochloride (AAPH), 3-(4,5-dimethylthiazol-2-yl)-2,5-diphenyltetrazolium bromide (MTT), fluorescein sodium salt, Folin−Ciocalteu phenol reagent, gallic acid, *n*-hexane, methanol, methyl acetate, *β*-naphthoflavone (BNF), phosphate-buffered saline (PBS) 10× concentrate, L-sulforaphane (SF), and trolox [(±)-6-hydroxy-2,5,7,8-tetramethylchromane-2-carboxylic acid, 97%] were purchased from Sigma-Aldrich (St. Louis, MO, USA). Fetal bovine serum and *α*-minimum essential medium (MEM) were purchased from Invitrogen (Carlsbad, CA, USA). All solvents were of analytical grade. Water used in the experiments was purified using a Millipore water purification system with a minimum resistivity of 18.2 MΩ·cm (Bedford, MA, USA).

Compounds **1** and **4** were previously purified in our laboratory from a methanolic extract of fresh moringa leaves by HPLC as described by Waterman et al.[8] The chemical purity of isolated ITCs was confirmed by LC-MS and ^{1}H NMR analyses.[8]

DOI: 10.1021/jf505014n
J. Agric. Food Chem. 2015, 63, 1505−1513

Plant Material and Preparation of Crude Extract. Fresh leaves from moringa (Indian PKM variety) were shipped overnight from Moringa Farms, Sherman Oaks, CA, USA. A voucher specimen (CW1) was prepared and deposited at the Chrysler Herbarium of Rutgers University (CHRB). The leaves were extracted on the day of arrival. Briefly, 200 g of fresh leaves was finely chopped and crushed by using a pestle and mortar to activate myrosinase enzymes and conversion of GLSs into corresponding ITCs by tissue damaging. The resulting material was extracted in methanol (3 × 300 mL, overnight) at room temperature by continuous shaking. Solvent was removed from extract under reduced pressure by rotary evaporation. The moringa methanol extract (ME) was frozen at −80 °C, lyophilized, and stored at −20 °C.

Selection and Preparation of the Solvent System. The following three-phase solvent system was selected according to the partition coefficient (K) of compounds **1** and **4**: *n*-hexane/methyl acetate/acetonitrile/water (4:4:3:4). K values were determined as follows: 1 mg of ME was dissolved in 500 μL of a pre-equilibrated two- or three-phase solvent system in a vial with vigorous shaking. After equilibration, equal amounts (100 μL) of upper and lower/middle (in the case of the three-phase solvent system) phases were analyzed by LC-MS using the conditions described under LC-MS Analysis and Quantification of ITCs. The K value is defined as the ratio between the peak area of each ITC in the upper phase (UP) and lower phase (LP), ($K_{UP/LP}$) for a two-phase solvent system or as the ratio between the peak area of each ITC in the middle phase (MP) and lower phase ($K_{MP/LP}$) for a three-phase solvent system.

The selected three-phase solvent system of FCPC was equilibrated in a separatory funnel and left for equilibration at room temperature overnight. The three phases were separated and degassed by sonication for 15 min shortly before use.

Fractionation of ME by FCPC. Counter current chromatography was performed by a bench-scale fast centrifugal partition chromatography sytem FCPC1000, v 1.0, from Kromaton (Annonay, France) with a rotor volume of 1000 mL and maximum pressure of 860 psi. For fractionation, the column was first filled with MP and LP in a ratio of (7:3) at a flow rate of 80 mL/min while rotating at 300 rpm. The system was then equilibrated with UP at a flow rate of 10 mL/min and 750 rpm. A 3 g sample of ME was suspended in 10 mL of each phase of the solvent system used for separation. ME was sonicated briefly and filtered through a 0.45 μm pore. As the UP was pumped at 10 mL/min at 750 rpm, the sample was injected through the Rheodyne valve. UV detection was performed at 227 nm, and 20 mL fractions were collected every 2 min with a CHF122 SC Advantec fraction collector (Dublin, CA, USA).

Enrichment of Fractions by SPE. FCPC fractions, particularly C, D, and E (50−100 mg), were dissolved in 1 mL of water containing 1% acetic acid and sonicated for 10−15 min. A 3 mL SPE column with C18 absorbents (J. T. Baker, Bakerbond) was equilibrated by 3 mL of methanol followed by 3 mL of water containing 1% acetic acid. The sample solution (1 mL) was loaded into the SPE column. The aliquots (1 mL × 3) of water (1% acetic acid) and methanol (1 mL × 3) were successively applied into the SPE tube, and two elutes were collected separately and evaporated to dryness. The methanol elute was used for further characterization of fractions in terms of ITC content, total polyphenol content (TPC), ORAC, and NQO1 activity assays.

LC-MS Analysis and Quantification of ITCs. LC-MS analysis was performed using the Dionex UltiMate 3000 RSLC ultrahigh-pressure liquid chromatography system, consisting of a workstation with Dionex Chromeleon v. 6.8 software package, solvent rack/degasser SRD-3400, pulseless chromatography pump HPG-3400RS, autosampler WPS-3000RS, column compartment TCC-3000RS, and photodiode array detector DAD-3000RS. After the photodiode array detector, the eluent flow was guided to a Varian 1200L (Varian Inc., Palo Alto, CA, USA) triple-quadrupole mass detector with electrospray ionization interface, operating in the negative ionization mode. The voltage was adjusted to −4.5 kV, heated capillary temperature was 280 °C, and sheath gas (zero grade compressed air) was used for the negative ionization mode. The mass detector was used in scanning mode from 65 to 1500 atomic mass units. Data from the the Varian 1200L mass detector were collected, compiled, and analyzed using Varian's MS Workstation, v. 6.9, SP2. Compounds were separated on a Phenomenex Luna C8 reversed phase column, size 150 × 2 mm, particle size = 3 μm, pore size = 100 Å. The mobile phase consisted of two components: solvent A (0.5% ACS grade acetic acid in double-distilled deionized water, pH 3−3.5), and solvent B (acetonitrile). The initial conditions of the gradient were 95% A and 5% B. The gradient progressed linearly to 5% A and 95% B over 30 min and then remained isocratic for the next 8 min. During the following 4 min, the ratio of solvents A and B was brought to initial conditions linearly. An 8 min equilibration interval was included between subsequent injections.

ITCs were characterized on the basis of their retention times, UV maxima, and MS fragmentation patterns. The MS data obtained for the ITCs (**1**−**4**) gave the expected m/z values and fragment ions that were characteristic for these compounds.[8] In the current study, the quantification of ITCs in the fractions were done by using standard curves generated for pure **1** and **4**, which were purified (>98%) previously as described by Waterman et al.[8] Briefly, 1 μL LC-MS injections of compound **1** at 20, 100, and 200 ng/μL generated a standard curve ($y = 123x - 0.098$, $R^2 = 1$), and injections of compound **4** at 10, 50, and 100 ng/μL generated a standard curve ($y = 104.32x - 0.098$, $R^2 > 0.99$). The concentrations of compounds **2** and **3** in the fractions and crude extract were estimated by using the standard curve of compound **4**. All injections were repeated at least three times for either standard curve generation or determination of ITC content in the fractions. Therefore, results are represented as means ± SD of three independent measurements.

Analyses of TPC and ORAC. TPC was quantified according to a modified Folin−Ciocalteu method[26] as previously described[27] and expressed as mean gallic acid equivalents (GAE) of at least three independent experiments. ORAC was determined by using fluorescein as the fluorescent probe and AAPH as a peroxyl radical generator in a procedure adapted from a previously published method.[28] ORAC results for fractions and ME were expressed as μM Trolox equiv (TE)/g and directly expressed as TE for **1**, **4**, and SF. All samples were assayed in triplicate. Results are presented as means ± SD.

NQO1 Induction Assay: Cell Culture and Treatment. Hepa1c1c7 mouse hepatoma cells (CRL-2026, American Type Culture Collection, Manassas, VA, USA) were plated in 24-well tissue culture plates (Greiner Bio One, Frickenhausen, Germany) and grown at 37 °C in a humidified incubator with 5% CO_2 to near confluence in α-MEM without ribonucleosides or deoxyribonucleosides (Invitrogen Corp., Carlsbad, CA, USA) supplemented with 100 IU/mL penicillin, 100 mg/mL streptomycin (Cellgro, Manassas, VA, USA), and 10% (v/v) fetal bovine serum. Confluent cells were washed two times with PBS (1×) and incubated in serum-free α-MEM overnight (18 h). Cells were treated in triplicate with BNF (0.05−5 μM), SF (5 μM), extract/fractions (ME, A−C, F, 1, 5, and 10 μg/mL; D, E, 1, 2.5, and 5 μg/mL), and compounds **1** (1, 5, and 10 μM) and **4** (1, 2.5, and 5 μM) in serum-free media for 48 h. The NQO1 activity in the cultured cells was assayed in duplicate at the end of the incubation by using an Abcam NQO1 activity assay kit (Abcam, Cambridge, MA, USA). Briefly, cells were washed with PBS (1×) twice and solubilized in 0.2 mL of extraction buffer supplied by the manufacturer. Cells were scraped and incubated on ice for 15 min. Then, lysates were centrifuged at 18000*g* for 20 min at 4 °C. Supernatant was assayed immediately or stored at −80 °C. The protein concentration in the supernatant was quantified by the Pierce BCA Protein Assay Kit (Thermo Scientific, Rockford, IL, USA). The NQO1 activity was measured at 440 nm for 5 min. The linear rate of increase in absorbance was examined over time. The NQO1 activity was normalized to total protein content of each sample to eliminate sample-to-sample variability. NQO1 fold induction was expressed as specific activity of treatment over those of control. Results are means ± SD of three independent experiments.

Cell Viability. Hepa1c1c7 cells were plated into 24-well plates at 1 × 10^5 cells/well and grown for 48 h (90% confluent), and then confluent cells were washed two times with PBS (1×) and incubated in serum-free α-MEM overnight (18 h). ME (1−25 μg/mL), fractions

DOI: 10.1021/jf505014n
J. Agric. Food Chem. 2015, 63, 1505−1513

(A, B, 10 and 25 μg/mL; C−F, 1−25 μg/mL), and compounds **1** and compound **4** (both 5 and 10 μM), dissolved in ethanol (0.25% v/v final concentrations), were added to cells together with vehicle control (ethanol alone) and incubated for an additional 48 h. The effect of treatments on cell viability was examined by using MTT (TCI, Portland, OR, USA).[29] MTT working solution (5 mg/mL in 1× PBS) was filtered through a 0.22 μm cellulose membrane (Corning, Corning, NY, USA) and added to treated cells during the last 3 h of treatment (48 h). Media were carefully aspirated; cells were dissolved in DMSO, and the absorbance was read at 570 nm. Results are means ± SD of three independent experiments.

Statistical Analysis. Data were analyzed by one-way ANOVA followed by a Dunnett or Wilcoxon test as indicated. Pearson's correlation coefficients for ORAC results with TPCs were calculated using means of triplicate measurements. For statistical analysis GraphPad Prism version 6.02 for Windows (GraphPad Software, Inc.) was used.

RESULTS AND DISCUSSION

Optimization of FCPC Solvent System. Various two-phase solvent systems for FCPC separations were tested and *K* values measured for compounds **1** and **4** (Table 1). Three two-phase solvent systems *n*-butanol/ethyl acetate/water, methanol/ethyl acetate/water, and *n*-hexane/ethyl acetate/methanol/water at different volume ratios could not provide acceptable partition coefficients, ideally 0.5−2.0 for efficient separation.[30] The three-phase solvent system composed of *n*-hexane/methyl acetate/acetonitrile/water (4:4:3:4) was selected for the current study as the best solvent system on the basis of the optimal partition coefficient of ITCs between the MP and LP. Accordingly, the ideal $K_{MP/LP}$ value obtained for **1** (1.61) together with a larger value for **4** (5.14) suggest that relatively less hydrophilic **4** should be eluted first by MP, followed by more hydrophilic **1** by LP. With this strategy, **1** and **4** were separated completely within a single FCPC run even though their structure differed only by the presence of one acetyl group.

Table 1. Partition Coefficients (*K*) of 1 and 4 in Various Solvent Systems

		partition coefficient[a] (*K*)	
solvent system	ratio	**1**	**4**
n-butanol/ethyl acetate/water	1:1.5:2.5	28.5	74.5
methanol/ethyl acetate/water	1:3:2	3.97	9.66
	1:2:2	3.97	8.24
n-hexane/ethyl acetate/methanol/water	4:6:4:6	0.01	0.03
	3:7:4:6	0.09	0.37
	3:7:3:7	0.02	0.10
	35:100:35:100	0.02	0.07
n-hexane/methyl acetate/acetonitrile/water[b]	4:4:3:4	1.61[c]	5.14[c]

[a]Expressed as concentration at upper phase/concentration at lower phase. [b]Solvent system used in the current study. [c]Three-phase solvent system: concentration at middle phase/concentration at lower phase.

Separation by FCPC. The UV absorption of compounds separated by FCPC in ME is shown in Figure 2. The starting mobile UP was eluted for 100 min to obtain hydrophobic compounds and then switched to MP to elute moderately hydrophilic compounds for 100 min. Finally, the highly polar compounds were separated by eluting the column with LP for 150 min. LC-MS analyses revealed that fractions A, collected between 0 and 92 min (393 mg; 13.1%), and B, collected between 94 and 172 min (231 mg; 7.7%), were composed of nonpolar compounds such as fatty acids and chlorophylls. Fractions C, collected between 176 and 196 min (111 mg; 3.7%), D, collected between 198 and 204 min (123 mg; 4.1%), and E, collected between 206 and 224 min (108 mg; 3.6%), contained high levels of compounds **1**−**4** (Figure 3). The UV profile of fraction C showed compound **4** representing 94% of the total peak area (Figure 3A) and fraction E with compound **1** at 87% of total peak area (Figure 3C), demonstrating efficient separation of these two structurally similar compounds by FCPC. Fraction D contained all ITCs (**1**−**4**) together with niazicin A (see enlarged representation in Figure 3B). Fraction F (2.014 g, 67%), eluted between 226 and 360 min (Figure 2), contained the majority of polyphenolic compounds.

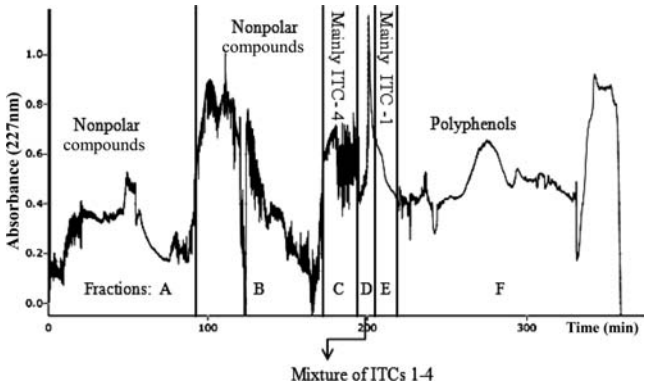

Figure 2. Fractionation chromatogram of moringa methanolic leaf extract (ME) by fast centrifugal partition chromatography (FCPC) using *n*-hexane/methyl acetate/acetonitrile/water (4:4:3:4) three-phase solvent system.

Enrichment by SPE. ITCs **1**−**4** were quantified in fractions C, D, and E before and after SPE by LC-MS analysis as previously described[6] and expressed as percent of fraction dry weight (DW). There was significant enrichment in the total concentration of ITCs (**1**−**4**), after SPE in all three fractions (Figure 4). The concentration of ITCs (**1**−**4**) was increased by 3.7-fold in fraction C-SPE, yielding concentrations of 1.62 ± 0.07% (**1**), 1.50 ± 0.01% (**2**), 1.66 ± 0.11% (**3**), and 5.4 ± 0.08% (**4**) of fraction DW. Fraction D-SPE was enriched by 2.1-fold yielding concentrations of 6.41 ± 0.01% (**1**), 4.00 ± 0.05% (**2**), 1.85 ± 0.05% (**3**), and 5.18 ± 0.06% (**4**) of fraction DW. The highest enrichment (15-fold) was observed in fraction E, initially containing 2.0% (±0.14) of **4** and increasing to 30% (±0.43) of fraction DW after SPE. Overall, fractions obtained by FCPC/SPE contained higher percentage values of **1**−**4** when compared to the crude extract, which contained 1.46% (±0.05) of **1**, 1.36% (±0.07) of **4**, and undetectable amounts of **2** and **3**. These results demonstrated an efficient method to concentrate ITCs for bioassay applications or for further purification by HPLC.

TPC and ORAC. Generally, phenolic compounds are direct antioxidants, which can effectively scavenge and/or chelate readily oxidizable reactive compounds. Moringa extracts and fractions containing phenolic acids (chlorogenic acid, ellagic acids) and flavonoids (mostly quercetin, kaempferol, and rutin) possess direct antioxidant activity in several in vitro assays including β-carotene bleaching, ferric reducing, DPPH/super-

DOI: 10.1021/jf505014n
J. Agric. Food Chem. 2015, 63, 1505−1513

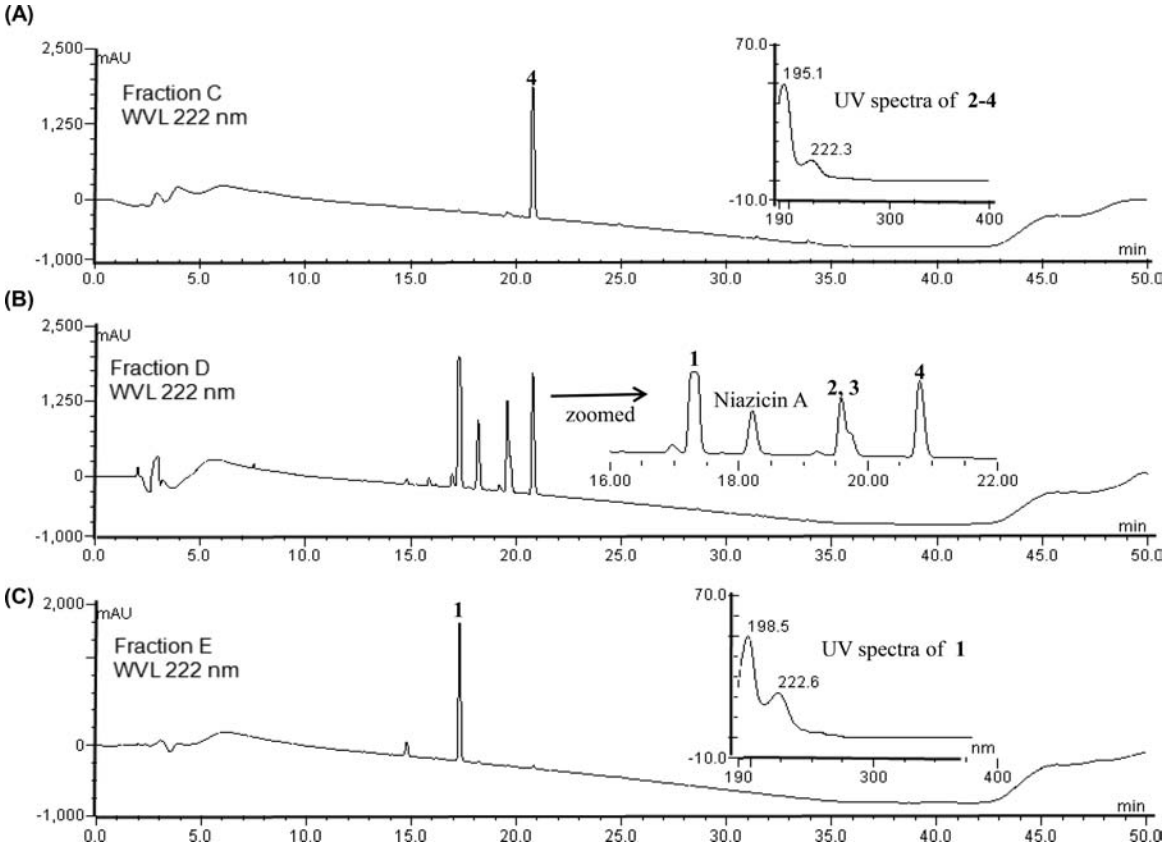

Figure 3. LC-MS analysis of fractions C, D, and E. (A) Fraction C. Elution peak corresponds to compound **4**; UV spectra of ITCs **2**−**4** (isomers) are also presented on the right. (B) Fraction D. Elution peaks seen in the inset correspond to **1**, niazicin A, and **2**−**4**, respectively. (C) Fraction E. Elution peak corresponds to compound **1**; UV spectra are also presented on the right.

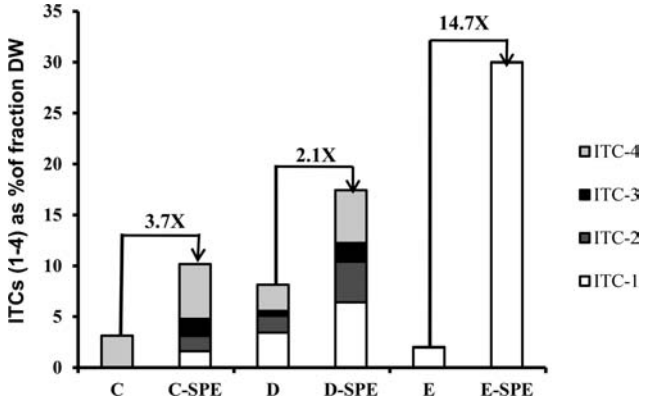

Figure 4. ITCs (**1**−**4**) as percent of fraction dry weight (DW) before and after solid phase extraction (SPE).

oxide/hydroxyl radical scavenging, and lipid peroxidation.[18,31] However, there have not been any studies evaluating the role of moringa ITCs in direct antioxidant activity. Therefore, we evaluated the direct antioxidant capacity of moringa FCPC fractions containing different classes of compounds ranging from essential oils and chlorophylls to ITCs and polyphenols by using the in vitro ORAC assay. ORAC provides an improved analysis technique for direct antioxidant capacity by measuring the inhibition of the peroxyl radical (predominant free radical in biological system) damage over a time course and combining these factors into a single "area under curve" (AUC) quantity.[32] We also measured TPC of each fraction to establish the contribution of polyphenol components of moringa to direct antioxidant capacity (Figure 5A).

As seen in Figure 5A, the highest ORAC value was obtained for ME (12721 ± 310 μmol TE/g extract) with the highest TPC (18.1 ± 0.3 mg GAE/100 mg). The ORAC of ME was higher than reported values for coffee powder (10007 μmol TE/g), black tea leaves (1566−1629 μmol TE/g), grape seeds (11681−11889 μmol TE/g), and blueberry extracts (2441−2792 μmol TE/g), which have been noted for their high antioxidant values.[32,33] Although TPC of fraction F was 2.6 times less than TPC of ME, the ORAC of fraction F (12452 ± 488 TE/g) was not significantly different from the ORAC of the ME. The LC-MS analysis of fraction F showed much higher peak areas of rutin, chlorogenic acid, and quercetin-malonyl-glucoside compared to the ME, suggesting these polyphenols concentrated in fraction F play a significant role in the observed high direct antioxidant activity.

In SPE-enriched ITC fractions C, D, and E, the ORAC values were found to be moderate, almost 2−3 times less than that of fraction F. Statistical analyses performed for these fractions revealed that, although ORAC values were significantly correlated ($r = 0.99$, $p < 0.05$) with TPC, they did not correlate with total ITC content. These findings support the role of moringa polyphenols as direct antioxidants, however, leaving the role of ITCs uncertain. For further investigation, we determined the ORAC of compounds **1** and **4** in comparison to SF, which has no direct antioxidant activity.[34] Figure 5B reports the linear regression analyses of trolox, compounds **1** and **4** (ranging from 1.25 to 12.5 μM), and SF (12.5−62.5 μM) with respect to their net AUC value. SF was found to have the

DOI: 10.1021/jf505014n
J. Agric. Food Chem. 2015, 63, 1505−1513

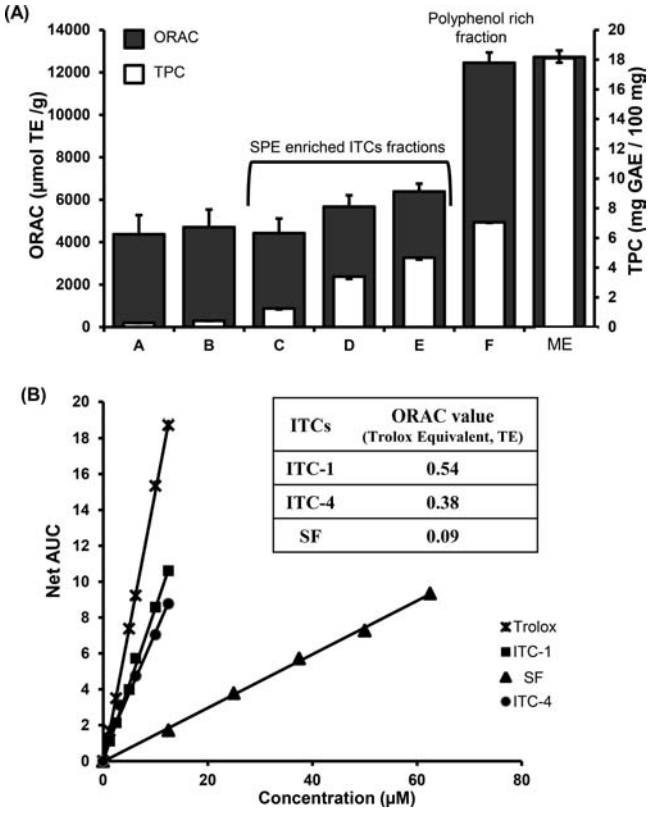

Figure 5. (A) Oxygen radical absorbance capacity (ORAC) and total polyphenol content (TPC) of fractions (A–F) and moringa methanol extract (ME). ORAC was determined as μmol Trolox equiv (TE)/g. TPC was determined as mg gallic acid equiv/100 mg extract or fractions. (B) Linear regression of ORAC value as a function of the concentration (μM) of Trolox ($y = 1.534x \pm 0.017$; $r = 0.999$), **1** ($y = 0.824x \pm 0.042$; $r = 0.989$), **4** ($y = 0.576x \pm 0.042$; $r = 0.989$), and SF ($y = 0.1494x \pm 0.0048$; $r = 0.996$). The table on the graph shows TE values of each ITC calculated by slope of compound/slope of trolox. The net AUCs were calculated by subtracting AUC of blank (75 mM potassium phosphate buffer at pH 7.4) from AUC of sample. Data represent the mean of three independent experiments.

lowest ORAC value (0.09 TE); however, both **1** (0.54 TE) and **4** (0.38 TE) had 6 and 4.2 times higher ($p < 0.0001$) ORAC compared to SF. This relatively high antioxidant capacity of compounds **1** and **4** most likely can be attributed to the presence of an aromatic side chain and increased stability of molecules due to the presence of a rhamnose sugar moiety (Figure 1B). On the basis of previous papers, ORAC values of **1** and **4** are considerably lower than those of other direct acting phenolic compounds such as quercetin (7.28 TE), rutin (6.01 TE), and chlorogenic acid (3.14 TE).[33] On the other hand, the similarity of our data to the ORAC of some physiologically active endogenous antioxidants such as glutathione (0.57 TE) and ascorbic acid (0.75 TE)[35] suggests that moringa ITCs may act as direct antioxidants.

Effects of ME, Fractions, and ITCs on NQO1 Catalytic Activity. Up-regulation of phase II XMEs by indirect antioxidants has been widely accepted as one of the preventive mechanisms of action against several pathological conditions. Among these enzymes, NQO1 has been accepted as a biomarker in the discovery of natural chemopreventive and anti-inflammatory agents due its widespread presence in all mammalians, high magnitude of response toward inducers, and ease of enzymatic detection.[36] The measurement of NQO1 activity in Hepa1c1c7 mouse hepatoma cells provides a reliable, specific, and reproducible method for determining inducer potency of pure[25,37,38] as well as complex bioactive (mixtures or plant extracts) compounds.[39,40] In the current work, cell viability was tested over a range of 1–25 μg/mL for fractions/ME and 5–10 μM for pure ITCs to determine doses that maintain cell viability of >95% (see Figure S1 in the Supporting Information), confirming that the observed induction was due to potency of inducers rather than an artifact of cytotoxicity in the NQO1 assay. Accordingly, ME, SPE fractions, and pure ITCs were all tested at at least three noncytotoxic doses (Figures 6A and 7). The ME (1, 5, and 10 μg/mL) significantly ($p < 0.001$) induced NQO1 activity up to 4.8-fold compared to untreated-control cells in the mouse Hepa1c1c7 cell line (Figure 6A). The three SPE-enriched ITC fractions, C (1–10 μg/mL), D, and E (both at 1–5 μg/mL), also significantly ($p < 0.001$) elevated NQO1 activity. Figure 6B represents induction level of fractions and ME at a fixed dose of 5 μg/mL (common noncytotoxic dose for all) together with total ITC yield. The highest level of induction in NQO1 activity was detected in fraction E containing the highest total ITC yield (30%, ITCs), followed by fractions D (17.4% ITCs) and C (11.5% ITCs). The correlation of ITC yields in the fractions with their NQO1 induction capacity confirms that the compounds with ITC pharmacophore (–N═C═S group) are highly effective in inducing indirect antioxidant activity. Fractions A and B, which do not contain ITCs, showed NQO1 activity at the same low level as the control, indicating the fatty acids and chlorophylls do not have any indirect antioxidant activity.

Similarly, fraction F did not induce NQO1 activity even at the relatively high dose (10 μg/mL; Figure 6A), indicating polyphenols present in this fraction (predominantly hydroxylated flavones, quercetin 3-*O*-rutinoside, quercetin 3-*O*-(6″-malonylglucoside), and 5-caffeoylquinic acid) do not possess indirect antioxidant capacity, confirming a recent study which showed that hydroxylated flavones are ineffective at inducing cytoprotective enzymes, despite having substantial direct antioxidant activity.[41] However, other classes of polyphenols, including methoxylated flavones, have been shown to significantly increase NQO1 and elicit cytoprotective enzyme activity.[20,38] Accordingly, we observed a clear dose-dependent induction pattern in cells treated with β-naphthoflavone (5,6-benzoflavone, BNF) (Figure 6B), a classical phenolic inducer of NQO1,[42] confirming the sensitivity of the cells to certain polyphenols under our experimental conditions.

As seen in Figure 7, in addition to the ME and FCPC fractions, compounds **1** (1–10 μM) and **4** (1–5 μM) were tested for their NQO1 inducer capacities in comparison to SF (5 μM). Previously, it was shown that SF is the most potent inducer of NQO1 activity, reaching a maximum induction of 3–5-fold between 2.5 and 8 μM concentrations.[25,37,43] In accordance with these studies, the current work showed 5 μM SF induced NQO1 activity 4.2-fold. At this concentration, compounds **1** and **4** induced NQO1 activity 4.3- and 3.9-fold, respectively, showing that SF and ITCs (**1**, **4**) from moringa are equipotent inducers of NQO1. For compound **1**, concentrations of 10 μM did not cause any greater induction than 5 μM did. Similarly, a dose response could not be observed from 1 to 5 μM for compound **4**, indicating that a clear dose-dependent response occurs under 1 μM dose range. To our knowledge, this is the first study demonstrating that moringa ITCs can significantly induce NQO1 activity at such low concentrations; therefore, it may be a practical dietary

DOI: 10.1021/jf505014n
J. Agric. Food Chem. 2015, 63, 1505–1513

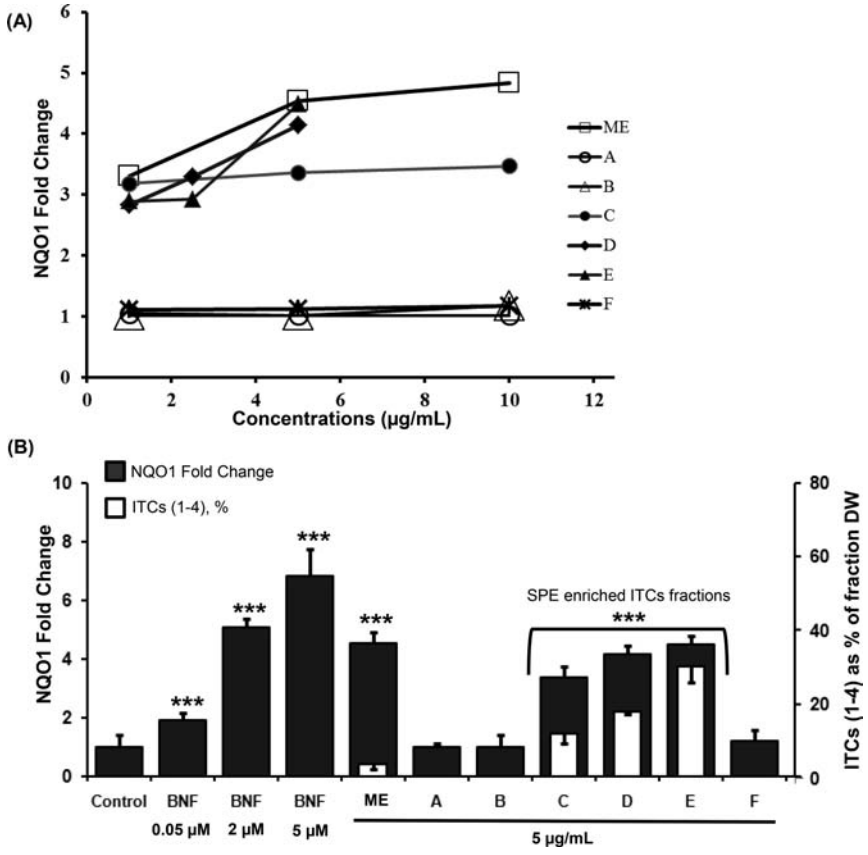

Figure 6. Effect of moringa methanol extract (ME) and its FCPC fractions (A–F) on the induction of NQO1 catalytic activity (treated/untreated) in Hepa1c1c7 cells (A) at three different noncytotoxic doses and (B) at fixed common noncytotoxic doses (5 μg/mL) in comparison with corresponding ITC concentration (**1**–**4**, % by DW) in each fraction. β-Naphthoflavone was used as a positive control. Data represent the mean of three experiments ± SD; ***, $p < 0.001$.

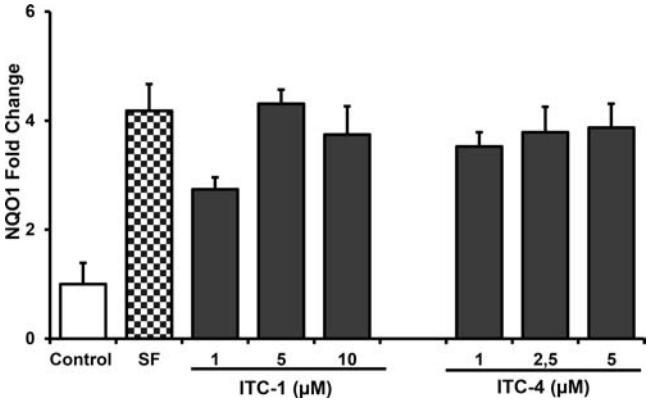

Figure 7. Effect of compounds **1** and **4** and sulforaphane (SF) on the induction of NQO1 catalytic activity (treated/untreated) in Hepa1c1c7 cells. Data represent the mean of three experiments ± SD, which are significantly different (***, $p < 0.001$) for all compared to control.

alternative to SF from broccoli due to increased stability as previously shown.

In summary, the separation and concentration of distinct classes of compounds in moringa leaves, namely, phenolics and ITCs, were successfully achieved through FCPC fractionation followed by SPE. These enriched fractions allowed direct and indirect antioxidant analysis, distinguishing which phytochemicals are responsible for differential antioxidant mechanism. We determined that the polyphenol-rich fraction had high ORAC, indicating strong direct antioxidant activity, whereas ITC-enriched fractions, compounds **1** and **4**, effectively induced NQO1 activity, representing their potent indirect antioxidant activity.

The unique combination of direct (polyphenols) and indirect (ITCs) antioxidant compounds in moringa provides justification and support for the therapeutic uses of polyphenol- and ITC-enriched moringa products. One of the major findings of this study is that compounds **1** and **4** are as potent as SF in inducing NQO1 activity. This indirect antioxidant potency of moringa ITCs, combined with their unique chemical stability and anti-inflammatory activity, makes them attractive food-based therapeutic alternatives to unstable ITCs such as SF. Health-related applications will require the purification of ITCs (**1**–**4**) in significant quantities. The large-scale fractionation followed by SPE enrichment techniques reported here may provide an efficient strategy for ITC isolation.

■ ASSOCIATED CONTENT

Supporting Information

Figure S1 presenting results of MTT assay in Hepa1c1c7 cells. This material is available free of charge via the Internet at http://pubs.acs.org.

■ AUTHOR INFORMATION

Corresponding Author

*(T.B.T.) Mail: Department of Molecular Biology and Genetics, Faculty of Arts and Sciences, Çanakkale Onsekiz

DOI: 10.1021/jf505014n
J. Agric. Food Chem. 2015, 63, 1505–1513

Mart University, Terzioglu Campus, Çanakkale, Turkey 17100. Phone: +90 286 2180018-1844. E-mail: tumerb@gmail.com or tumertb@comu.edu.tr.

Funding

This study was supported by a Botanical Research Center Pilot Program Sub award 5P50AT002776-08 S12-50318 and P50AT002776-01 from the National Center for Complementary and Alternative Medicine (NCCAM) and the Office of Dietary Supplements (ODS). C.W. was also supported by NIH Training Grant T32:5T32AT004094-04. P.R.-S. was supported by the SENESCYT 2011 Fellowship from Ecuador. T.B.T. was supported by a postdoctoral research grant of the Higher Education Council of Turkey.

Notes

IR has equity in Nutrasorb LLC, which licensed *Moringa*-related intellectual property from Rutgers University.
The authors declare no competing financial interest.

REFERENCES

(1) Dinkova-Kostova, A. T.; Kostov, R. V. Glucosinolates and isothiocyanates in health and disease. *Trends Mol. Med.* **2012**, *18*, 337−347.
(2) Traka, M.; Mithen, R. Glucosinolates, isothiocyanates and human health. *Phytochem. Rev.* **2009**, *8*, 269−282.
(3) Sønderby, I. E.; Geu-Flores, F.; Halkier, B. A. Biosynthesis of glucosinolates − gene discovery and beyond. *Trends Plant. Sci.* **2010**, *15*, 283−290.
(4) Koroleva, O. A.; Gibson, T. M.; Cramer, R.; Stain, C. Glucosinolate-accumulating S-cells in *Arabidopsis* leaves and flower stalks undergo programmed cell death at early stages of differentiation. *Plant J.* **2010**, *64*, 456−469.
(5) Siegfried, J. Cyanogenic plants. In *Poisonous Plant Contamination of Edible Plants*, 1st ed.; Rizk, A. M., Ed.; CRC Press: Boca Raton, FL, USA, 1991.
(6) Kawakishi, S.; Kaneko, T. Interaction of proteins with allyl isothiocyanate. *J. Agric. Food Chem.* **1987**, *35*, 85−88.
(7) Franklin, S. J.; Dickinson, S. E.; Karlage, K. L.; Bowden, G. T.; Myrdal, P. B. Stability of sulforaphane for topical formulation. *Drug Dev. Ind. Pharm.* **2014**, *40*, 494−502.
(8) Waterman, C.; Cheng, D. M.; Rojas-Silva, P.; Poulev, A.; Dreifus, J.; Lila, M. A.; Raskin, I. Stable, water extractable isothiocyanates from *Moringa oleifera* leaves attenuate inflammation in vitro. *Phytochemistry* **2014**, *103*, 114−122.
(9) Brunelli, D.; Tavecchio, M.; Falcioni, C.; Frapolli, R.; Erba, E.; Iori, R.; Rollin, P.; Barillari, J.; Manzotti, C.; Morazzoni, P.; D'Incalci, M. The isothiocyanate produced from glucomoringin inhibits NF-κB and reduces myeloma growth in nude mice in vivo. *Biochem. Pharmacol.* **2010**, *79*, 1141−1148.
(10) Cheenpracha, S.; Park, E. J.; Yoshida, W. Y.; Barit, C.; Wall, M.; Pezzuto, J. M.; Chang, L. C. Potential anti-inflammatory phenolic glycosides from the medicinal plant *Moringa oleifera* fruits. *Bioorg. Med. Chem.* **2010**, *18*, 6598−6602.
(11) Park, E. J.; Cheenpracha, S.; Chang, L. C.; Kondratyuk, T. P.; Pezzuto, J. M. Inhibition of lipopolysaccharide-induced cyclooxygenase-2 and inducible nitric oxide synthase expression by 4-[(2′-*O*-acetyl-α-L-rhamnosyloxy)benzyl]isothiocyanate from *Moringa oleifera*. *Nut. Cancer* **2011**, *63*, 971−982.
(12) Bennett, R. N.; Mellon, F. A.; Foidl, N.; Pratt, J. H.; Dupont, M. S.; Perkins, L.; Kroon, P. A. Profiling glucosinolates and phenolics in vegetative and reproductive tissues of the multi-purpose trees *Moringa oleifera* L. (horseradish tree) and *Moringa stenopetala* L. *J. Agric. Food Chem.* **2003**, *51*, 3546−3553.
(13) Shibusawa, Y.; Yamakawa, Y.; Noji, R.; Yanagida, A.; Shindo, H.; Ito, Y. Three-phase solvent systems for comprehensive separation of a wide variety of compounds by high-speed counter-current chromatography. *J. Chromatogr., A* **2006**, *10*, 119−125.
(14) Mbikay, M. Therapeutic potential of *Moringa oleifera* leaves in chronic hyperglycemia and dyslipidemia: a review. *Front. Pharmacol.* **2012**, *3*, 1−12.
(15) Fahey, J. W. *Moringa oleifera*: a review of the medical evidence for its nutritional, therapeutic, and prophylactic properties. *Trees Life J.* **2005**, *1*, 5.
(16) Jung, I. L. Soluble extract from *Moringa oleifera* leaves with a new anticancer activity. *PLoS One* **2014**, *9* (4), No. e95492, DOI: 10.1371/journal.pone.0095492.
(17) Dinkova-Kostova, A. T.; Talalay, P. Direct and indirect antioxidant properties of inducers of cytoprotective proteins. *Mol. Nutr. Food Res.* **2008**, *52*, S128−S138.
(18) Verma, A. R.; Vijayakumar, M.; Mathela, C. S.; Rao, C. V. In vitro and in vivo antioxidant properties of different fractions of *Moringa oleifera* leaves. *Food Chem. Toxicol.* **2009**, *47*, 2196−2201.
(19) Fahey, J. W.; Stephenson, K. K. Pinostrobin from honey and Thai ginger (*Boesenbergia pandurata*): a potent flavonoid inducer of mammalian phase 2 chemoprotective and antioxidant enzymes. *J. Agric. Food Chem.* **2002**, *50*, 7472−7476.
(20) Dinkova-Kostova, A. T.; Massiah, M. A.; Bozak, R. E.; Hicks, R. J.; Talalay, P. Potency of Michael reaction acceptors as inducers of enzymes that protect against carcinogenesis depends on their reactivity with sulfhydryl groups. *Proc. Natl. Acad. Sci. U.S.A.* **2001**, *98*, 3404−3409.
(21) Ernster, L.; Navazio, F. Soluble diaphorases in animal tissues. *Acta Chem. Scand.* **1958**, *12*, 595−602.
(22) Iskander, K.; Jaiswal, A. K. Quinone oxido reductases in protection against myelogenous hyperplasia and benzene toxicity. *Chem.−Biol. Interact.* **2005**, *153−154*, 147−157.
(23) Smith, M. T.; Wang, Y.; Skibola, C. F.; Slater, D. J.; LoNigro, L.; Nowell, P. C.; Lange, B. J.; Felix, C. A. Low NAD(P)H: quinone oxidoreductase activity is associated with increased risk of leukemia with MLL translocations in infants and children. *Blood* **2002**, *100*, 4590−4593.
(24) Fahey, J. W.; Dinkova-Kostova, A. T.; Stephenson, K. K.; Talalay, P. The "Prochaska" microtiter plate bioassay for inducers of NQO1. *Methods Enzymol.* **2004**, *382*, 243−258.
(25) Zhang, Y. S.; Talalay, P.; Cho, C. G.; Posner, G. H. A major inducer of anticarcinogenic protective enzymes from broccoli − isolation and elucidation of structure. *Proc. Natl. Acad. Sci. U.S.A.* **1992**, *89*, 2399−2403.
(26) Singleton, V.; Rossi, J. A. Colorimetry of total phenolics with phosphomolybdic-phosphotungstic acid reagents. *Am. J. Enol. Vitic.* **1965**, *16*, 144−158.
(27) Cheng, D. M.; Kuhn, P.; Poulev, A.; Rojo, L. E.; Lila, M. A.; Raskin, I. In vivo and in vitro antidiabetic effects of aqueous cinnamon extract and cinnamon polyphenol-enhanced food matrix. *Food Chem.* **2010**, *135*, 2994−3002.
(28) Prior, R. L.; Hoang, H.; Gu, L.; Wu, X.; Bacchiocca, M.; Howard, L.; Hampsch-Woodill, M.; Huang, D.; Ou, B.; Jacob, R. Assays for hydrophilic and lipophilic antioxidant capacity (oxygen radical absorbance capacity (ORAC(FL))) of plasma and other biological and food samples. *J. Agric. Food Chem.* **2003**, *51*, 3273−3279.
(29) Mosmann, T. Rapid colorimetric assay for cellular growth and survival: application to proliferation and cytotoxicity assays. *J. Immunol. Methods* **1983**, *65*, 55−63.
(30) Ito, Y. Golden rules and pitfalls in selecting optimum conditions for high-speed counter-current chromatography. *J. Chromatogr., A* **2005**, *1065*, 145−168.
(31) Siddhuraju, P.; Becker, K. Antioxidant properties of various solvent extracts of total phenolic constituents from three different agroclimatic origins of drumstick tree (*Moringa oleifera* Lam.) leaves. *J. Agric. Food Chem.* **2003**, *51*, 2144−2155.
(32) Huang, D.; Ou, B.; Hampsch-Woodill, M.; Flanagan, J. A.; Prior, R. L. High-throughput assay of oxygen radical absorbance capacity (ORAC) using a multichannel liquid handling system coupled with a microplate fluorescence reader in 96-well format. *J. Agric. Food Chem.* **2002**, *50*, 4437−4444.

DOI: 10.1021/jf505014n
J. Agric. Food Chem. 2015, 63, 1505−1513

(33) Ou, B.; Hampsch-Woodill, M.; Prior, R. L. Development and validation of an improved oxygen radical absorbance capacity assay using fluorescein as the fluorescent probe. *J. Agric. Food Chem.* **2001**, *49*, 4619−4626.
(34) Fahey, J. W.; Talalay, P. Antioxidant functions of sulforaphane: a potent inducer of phase II detoxication enzymes. *Food Chem. Toxicol.* **1999**, *37*, 973−979.
(35) Benedetti, S.; Benvenuti, F.; Scoglio, S.; Canestrari, F. Oxygen radical absorbance capacity of phycocyanin and phycocyanobilin from the food supplement *Aphanizomenon flos-aquae*. *J. Med. Food* **2010**, *13*, 223−227.
(36) Talalay, P.; Fahey, J. W. Phytochemicals from cruciferous plants protect against cancer by modulating carcinogen metabolism. *J. Nutr.* **2001**, *131*, 3027S−3033S.
(37) Matusheski, N. V.; Jeffery, E. H. Comparison of the bioactivity of two glucoraphanin hydrolysis products found in broccoli, sulforaphane and sulforaphane nitrile. *J. Agric. Food Chem.* **2001**, *49*, 5743−5749.
(38) Uda, Y.; Price, K. R.; Williamson, G.; Rhodes, M. J. Induction of the anticarcinogenic marker enzyme, quinone reductase, in murine hepatoma cells in vitro by flavonoids. *Cancer Lett.* **1997**, *120*, 213−216.
(39) Hashimoto, K.; Kawamata, S.; Usui, N.; Tanaka, A.; Uda, Y. In vitro induction of the anticarcinogenic marker enzyme, quinone reductase, in human hepatoma cells by food extracts. *Cancer Lett.* **2002**, *180*, 1−5.
(40) Chandra, S.; De Mejia Gonzalez, E. Polyphenolic compounds, antioxidant capacity, and quinone reductase activity of an aqueous extract of *Ardisia compressa* in comparison to mate (*Ilex paraguariensis*) and green (*Camellia sinensis*) teas. *J. Agric. Food Chem.* **2004**, *52*, 3583−3589.
(41) Tsuji, P. A.; Stephenson, K. K.; Wade, K. L.; Liu, H.; Fahey, J. W. Structure-activity analysis of flavonoids: direct and indirect antioxidant, and antiinflammatory potencies and toxicities. *Nutr. Cancer* **2013**, *65*, 1014−1025.
(42) Kohle, C.; Bock, K. W. Activation of coupled Ah receptor and Nrf2 gene batteries by dietary phytochemicals in relation to chemoprevention. *Biochem. Pharmacol.* **2006**, *72*, 795−805.
(43) Gerhäuser, C.; You, M.; Liu, J.; Moriarty, R. M.; Hawthorne, M.; Mehta, R. G.; Moon, R. C.; Pezzuto, J. M. Cancer chemopreventive potential of sulforamate, a novel analogue of sulforaphane that induces phase 2 drug-metabolizing enzymes. *Cancer Res.* **1997**, *57*, 272−278.

DOI: 10.1021/jf505014n
J. Agric. Food Chem. 2015, 63, 1505−1513

Protean precast gels, and Precision Plus Protein Standards (recombinant proteins expressed by *E. coli* with molecular masses of 10, 15, 20, 25, 37, 50, 75, 100, 150, and 250 kDa) (all from Bio-Rad-Laboratories (Hercules, CA)) were employed for the separation of proteins by SDS-PAGE. Quick Start Bradford-1xDye reagent from Bio-Rad-Laboratories was employed for the estimation of proteins by Bradford assay. Hydrochloric acid, sodium dihydrogen phosphate, sodium hydroxide (all from Merck), sodium tetraborate, and Thermolysin enzyme (both from Sigma-Aldrich) were used for the digestion of proteins. Alcalase 2.4 L FG and Flavourzyme 1000 L were kindly donated by Novozymes Spain S.A. (Madrid, Spain). Sodium chloride (Merck), angiotensin converting enzyme (ACE), ethanol (EtOH), 2-[4-(2-hydroxyethyl)-1-piperazinyl]-ethanesulfonic acid (HEPES), hippuryl-histidyl-leucine (HHL), 1,10-phenanthroline, 2-mercaptoethanol, 6-hydroxy-2,5,7,8-tetramethylchroman-2-carboxylic acid (Trolox), 2,2′-azino-bis(3-ethylbenzothiazoline-6-sulfonic acid) (ABTS), albumin from bovine serum, ammonium thiocyanate, hydrogen peroxide, ferrous sulfate, iron(II) sulfate, iron(II) chloride, iron(III)chloride, L-gluthathion (GSH), linolenic acid, methanol, *ortho*-phthalaldehyde, potassium ferricyanide, trichloroacetic acid, and potassium persulfate (all from Sigma-Aldrich) were used to carry out in vitro assays. Acetonitrile (ACN) HPLC gradient grade (Scharlab), trifluoroacetic acid (TFA), and acetic acid (both from Sigma-Aldrich) were employed in the preparation of mobile phases in HPLC and HPLC-Q-TOF experiments.

Protein Extraction. The extraction procedure was similar to the described by Esteve et al.[12] with some modifications. Cherry pulp was removed, and the stone was broken to extract cherry seeds. Seeds were milled, and fat was removed by extracting three times with hexane (25 mL per 0.5 g of seeds). Seeds moisture was determined keeping them at 103 ± 2 °C until constant weight. Defatted seeds were stored at −20 °C until use. The procedure used to extract proteins from cherry seeds consisted of mixing 30 mg of defatted seeds with 5 mL of 100 mM Tris-HCl buffer (pH 7.5) containing 1% SDS and 0.5% DTT. Extraction was carried out using high intensity focused ultrasounds (HIFU) for 5 min and an amplitude of 30% followed by centrifugation at 4000*g* for 20 min. Proteins from the supernatant were next precipitated with 10 mL of cold acetone at 4 °C for 1 h. After centrifugation at 4000*g* for 10 min, precipitated proteins were dried overnight at 37 °C. Pellets were weighed and then dissolved in the previous Tris-HCl buffer (without DTT) using HIFU for 5 min at 30% amplitude. The solution was filtrated through 0.45 μm and stored at 4 °C until use. The protein content in this solution was estimated by Bradford assay.[13]

Protein Separation. Proteins were separated by SDS-PAGE and RP-HPLC. SDS-PAGE separation was carried out in a Mini-Protean from Bio Rad. Samples were prepared by mixing 15 μL of the cherry seed protein isolate with 15 μL of Laemmli buffer containing 5% (v/v) β-mercaptoethanol and by heating for 5 min at 100 °C. Electrophoresis was carried out on commercial Ready Gel Precast Gels using Tris/glycine/SDS as running buffer and applying 80 V for 5 min and 200 V for 30 min. For the estimation of molecular weights, peptide standards (10, 15, 20, 25, 37, 50, 75, 100, 150, and 250 kDa) were used as a ladder. After separation, proteins were fixed with 50 mL of 10% (v/v) glacial acetic acid/40% (v/v) MeOH gently shaking for 30 min and stained with 50 mL of Bio-Safe Coomassie stain by slightly shaking for 1 h. Finally, the gel was washed with Milli-Q water for 2 h.

RP-HPLC separation of the cherry seed protein isolate was performed in a modular Agilent Technologies liquid chromatograph (Pittsburgh, PA). All samples were prepared twice and measured by duplicate. A Poros R2/10 Perfusion column (4.6 mm D × 50 mm) at a flow-rate of 2 mL/min and a temperature of 25 °C were used. The gradient was 30−40% B in 13 min, 40−60% B in 6 min, 60−80% B in 1 min, and 80−30% B in 2 min. Mobile phase A was water with 0.1% (v/v) of TFA, and mobile phase B consisted of ACN with 0.1% (v/v) TFA. Detection was carried out with a fluorescent detector at λ_{exc} = 280 and λ_{em} = 360 nm.

Protein Digestion and Fractionation. Digestion of extracted proteins was carried out using three different enzymes: Alcalase (borate buffer (pH 8.5), 0.10 AU enzyme/g protein), Thermolysin (phosphate buffer (pH 8.0), 0.4 g enzyme/g protein), and Flavourzyme (bicarbonate buffer (pH 6.0), 75 AU enzyme/g protein). In all cases, a protein concentration of 2.5 mg/mL, a digestion temperature of 50 °C, and a digestion time of 7 h were selected. Additionally, blank digestions without proteins prepared by mixing buffer and enzyme were carried out. Digestions were carried out by slight mixing (600 rpm) at a controlled temperature in a Thermomixer Compact (Eppendorf AG, Hamburg, Gernmany). Digestions were stopped by heating to 100 °C for, at least, 10 min, and then they were centrifuged (5 min at 7000 rpm).

Hydrolysates were fractionated by ultrafiltration using Vivaspin 500 PES molecular weight (Mw) cutoff filters (5 kDa) (Sartorius Stedim biotech, Goettingen, Germany) and Amicon Mw cutoff filters (3 kDa) (Millipore).

Degree of Hydrolysis (% DH). The degree of hydrolysis was determined by the OPA assay following the method of Wang et al.[14] with modifications. OPA mixture (5 mL) consisted of 2.5 mL of 100 mM sodium tetraborate, 1 mL of 5% (w/v) SDS, 100 μL of 40 mg/mL OPA dissolved in MeOH, 10 μL of β-mercaptoethanol, and 1.39 mL of water. The assay consisted of mixing 2.5 μL of sample with 100 μL of OPA mixture and measuring the absorbance at 340 nm (spectrophotometer Lambda 35, PerkinElmer, Waltham, MA) after 8 min at room temperature. The peptide content was calculated by interpolation in a calibration curve obtained using GSH (0−5 mg/mL). The degree of hydrolysis was calculated by the following equation:

$$\mathrm{DH} = \frac{\text{peptide content}}{\text{protein content}} \times 100 \quad (1)$$

where the protein content was determined by the Bradford assay.

Antioxidant Capacity. Four different in vitro antioxidant assays were carried out for the evaluation of the antioxidant capacity of hydrolysates from the cherry seed protein isolate.

ABTS Radical Scavenging Assay. The scavenging capacity against ABTS radicals was evaluated according to the method of Wiriyaphan et al.[15] with modifications. $ABTS^{\bullet+}$ stock solution was prepared by mixing a 7.4 mM ABTS solution with 2.6 mM potassium persulfate in 10 mM phosphate buffer (pH 7.4) for, at least, 16 h kept in the dark. $ABTS^{\bullet+}$ working solution was daily prepared by mixing the stock solution with 10 mM phosphate buffer (pH 7.4). The assay was carried out by mixing 1 μL of sample with 100 μL of $ABTS^{\bullet+}$ working solution for 6 min at room temperature. The absorbance corresponding to $ABTS^{\bullet+}$ was measured at 734 nm. $ABTS^{\bullet+}$ scavenging capacity was calculated using the following equation:

$$\text{ABTS radical scavenging capacity (\%)} = \left(\frac{\mathrm{Abs_{blank}} - \mathrm{Abs_{sample}}}{\mathrm{Abs_{blank}}}\right) \times 100 \quad (2)$$

where Abs_{sample} was the absorbance of 1 μL of sample with 100 μL of $ABTS^{\bullet+}$ working solution and Abs_{blank} was the absorbance of 1 μL of digestion buffer with 100 μL of $ABTS^{\bullet+}$ working solution. Trolox (1 mM) was employed as positive control.

Hydroxyl Radical Scavenging Assay. The capacity to scavenge hydroxyl radicals was evaluated by the method of Ajibola et al.[16] with modifications. Hydroxyl radicals were obtained by the oxidation of Fe(II) with hydrogen peroxide. Antioxidant compounds inhibit the oxidation of Fe(II) and the formation of hydroxyl radicals. The assay was monitored by measuring the absorbance corresponding to the colored complex resulted from the reaction between Fe(II) and 1,10-phenanthroline. The assay consisted of mixing 50 μL of 3 mM 1,10-phenanthroline in 0.1 M phosphate buffer (pH 7.4), 50 μL of 3 mM ferrous sulfate, 50 μL of sample, and 50 μL of 0.01% (v/v) hydrogen peroxide. The mixture was incubated for 1 h at 37 °C, and the absorbance of the Fe(II) complex was measured at 536 nm. The hydroxyl radical scavenging capacity was evaluated according to the following equation:

DOI: 10.1021/jf505037p
J. Agric. Food Chem. 2015, 63, 1514−1520

hydroxyl radical scavenging capacity (%)

$$= \left(\frac{\text{Abs}_{\text{sample}} - \text{Abs}_{\text{blank}}}{\text{Abs}_{\text{control}} - \text{Abs}_{\text{blank}}}\right) \times 100 \quad (3)$$

where $\text{Abs}_{\text{sample}}$ was the absorbance of the sample, $\text{Abs}_{\text{blank}}$ was the absorbance of the digestion buffer, and $\text{Abs}_{\text{control}}$ was the absorbance of the solution resulting when adding the digestion buffer instead of sample and water instead of hydrogen peroxide. GSH (1 mg/mL) was employed as positive control.

Ferric Ion Reducing Antioxidant Power (FRAP) Assay. This assay measures the capacity of the sample to reduce Fe(III) from ferricyanide, and it was evaluated according to the method proposed by Ajibola et al.[16] with modifications. The assay consisted of incubating 12.5 μL of sample with 12.5 μL of 0.2 M phosphate buffer (pH 6.6) and 25 μL of 1% potassium ferricyanide solution for 20 min at 50 °C in the Thermomixer. The reaction was stopped with 25 μL of 10% (w/v) trichloroacetic acid solution. This solution (50 μL) was mixed with 60 μL of water and 15 μL of 2.5% iron(III) chloride solution, and after 3 min, the absorption at 700 nm was measured. The reducing power was calculated according to the following equation:

$$\text{reducing power} = \frac{\text{Abs}_{\text{sample}}}{\text{peptide content}} \quad (4)$$

where $\text{Abs}_{\text{sample}}$ was the absorbance obtained for the hydrolyzate, and the peptide content was that calculated by the OPA assay. The positive control was GSH (0−1 mg/mL). The percentage of inhibition was calculated considering the reducing power corresponding to 1 mg/mL GSH as the maximum reduction.

Capacity To Inhibit Lipid Peroxidation. This assay was carried out by the method developed by Chen et al.[17] with modifications. The assay involved mixing 20 μL of sample, 20 μL of 0.13% (v/v) linoleic acid in EtOH, and 10 μL of water at 40 °C for 144 h (6 days) in the dark. The degree of oxidation was monitored by mixing 2.5 μL of that solution with 175 μL of 75% (v/v) EtOH, 2.5 μL of 30% (w/v) ammonium thiocyanate, and 2.5 μL of 20 mM Fe(II) chloride in 3.5% (v/v) HCl for 3 min at room temperature and measuring the absorbance of the resulting ferric thiocyanate at 500 nm. The capacity to inhibit lipid peroxidation of linoleic acid was calculated using the following equation:

lipid peroxidation inhibition capacity

$$= \left(1 - \frac{\text{Abs}_{\text{sample,144h}} - \text{Abs}_{\text{sample,0h}}}{\text{Abs}_{\text{blank,144h}} - \text{Abs}_{\text{blank,0h}}}\right) \times 100 \quad (5)$$

where $\text{Abs}_{\text{sample,144h}}$ and $\text{Abs}_{\text{blank,144h}}$ were the absorbances of the sample and digestion buffer for 144 h, respectively; and $\text{Abs}_{\text{sample,0h}}$ and $\text{Abs}_{\text{blank,0h}}$ were the initial absorbances of the sample and digestion buffer, respectively.

ACE Inhibition Capacity. ACE inhibition capacity was expressed as the peptide concentration needed for the 50% inhibition of ACE activity (IC_{50}). For that purpose, an assay developed by Geng et al.[18] based on the hydrolysis of the tripeptide HHL into hippuric acid (HA) by the action of ACE was employed. The assay measures the capacity of hydrolyzates to inhibit ACE activity by monitoring the signal corresponding to HA. To calculate the IC_{50} value, the whole peptide extract and dilutions up to 1:10 ratio were measured for every hydrolysate. All measurements were made by duplicate. In every case, 2.5 μL of sample was mixed with 10 μL of ACE (0.05 U/mL), 17.5 μL of 50 mM HEPES buffer (pH 8.3) with 300 mM NaCl, and 5 μL of HHL (1.25 mg/mL). For the controls, 2.5 μL of the corresponding digestion buffer was used. The mixture was kept at 37 °C (in the Thermomixer), and the reaction was stopped by the addition of 50 μL of cold ACN (−20 °C). Separation and detection of HA was performed by HPLC using a Chromolith Performance RP-18e column (100 mm × 4.6 mm ID) from Merck. Separation was carried out at 25 °C, and mobile phases consisted of water with 0.025% (v/v) TFA (mobile phase A) and ACN with 0.025% (v/v) TFA (mobile phase B). The injection volume was 10 μL. A linear gradient from 5% to 95% B in 10 min followed by 95% to 5% B in 2 min was used. Detection was made at 228 nm. Percentage of ACE inhibition was calculated using the following expression where A_{control} was the area under the peak of HA in the control sample and A_{sample} was the area under the peak of HA in the sample.

$$\%\ \text{ACE inhibition} = \frac{A_{\text{control}} - A_{\text{sample}}}{A_{\text{control}}} \quad (6)$$

For every hydrolysate, the % of ACE inhibition of the undiluted and diluted sample was plotted against the peptide concentration (determined by OPA assay), and the IC_{50} value was determined from the signal corresponding to an inhibition of 50% of ACE.

HPLC-Q-TOF-MS Identification of Bioactive Peptides. Identification of peptides was carried out by MS/MS detection using a quadrupole time-of-flight (Q-TOF) series 6530 coupled to a HPLC (model 1100) both from Agilent Technologies. An Ascentis Express peptide ES-C18 (100 mm × 2.1 mm, 2.7 μm particle size, 160 Å pore size) analytical column with a guard column Ascentis Express peptide ES-C18 (5 mm × 2.1 mm), both from Sigma-Aldrich, was employed for the separation of peptides. Elution gradient employed for the separation of peptides in fraction >5 kDa was: 3% B for 6 min, followed by 3−43% B in 20 min, 43−55% B in 2 min, 55−74% B in 9 min, 74−95% B in 2 min, 1 min at 95% B, and 95−3% B in 2 min. Separation of peptides in the fraction <3 kDa was carried out with an elution gradient at 3% B for 7 min, 3−60% B in 28 min, 60−95% B in 3 min, 95% B for 2 min, and 95−3% B in 2 min. The rest of the parameters were: separation temperature, 25 °C; injection volume, 15 μL; and flow rate, 0.3 mL/min. Mobile phases A and B consisted of water and ACN, both containing 0.3% (v/v) acetic acid. Electrospray ionization in the positive ion mode at a capillary voltage of 3500 V and a MS-range from m/z 200 to 2200 were employed. Other MS conditions were: dry gas flow, 12 L/min; dry gas temperature, 350 °C; nebulizer pressure, 50 psig; sheath gas flow, 12 L/min; and sheath gas temperature, 400 °C. The fragmentation energy was calculated taking into account 5 V per 100 Da molecular weight.

In all cases, two independent extracts were analyzed by duplicate. Peaks software (Bioinformatics Solutions Inc., Waterloo, ON, Canada) was employed for the treatment of MS/MS data and de novo peptide sequencing using an error tolerance of 50.0 ppm for the precursor and 0.5 kDa for the fragment. Peptide identification was accepted if peptides appeared in the two independent samples analyzed by duplicate and presented an average local confidence (ALC (%), expected percentage of correct amino acids in the peptide sequence) above 90%. Moreover, because the equipment is not able to distinguish between I and L amino acids due to their equal molecular masses, both amino acids must be considered.

Statistical Analysis. Statistical analysis was performed using Statgraphics Software Plus 5.1 (Statpoint Technologies, Inc., Warranton, VA).

RESULTS AND DISCUSSION

To obtain peptides from cherry seeds, it is necessary to extract first cherry seed proteins. Despite that there is no method previously developed for the extraction of cherry seeds proteins, the group experience on the extraction of proteins from other seeds like olive[12] and plum[19] was very useful. Using extraction conditions described in the Materials and Methods, the protein content, estimated by Bradford assay, was 39.2 ± 5.8 g protein/100 g in defatted and dried seeds. This content is similar to the observed previously for plum seeds.[19] Extracted proteins were next separated by SDS-PAGE (see Figure 1) observing numerous bands below 75 kDa. It was important to highlight the bands appearing around 10, 15, and 20 kDa. Additionally, the RP-HPLC separation of the extract using fluorescent detection at wavelengths corresponding to tryptophan and tyrosine amino acids also showed many signals that could correspond to proteins (results not shown). All of these results

DOI: 10.1021/jf505037p
J. Agric. Food Chem. 2015, 63, 1514−1520

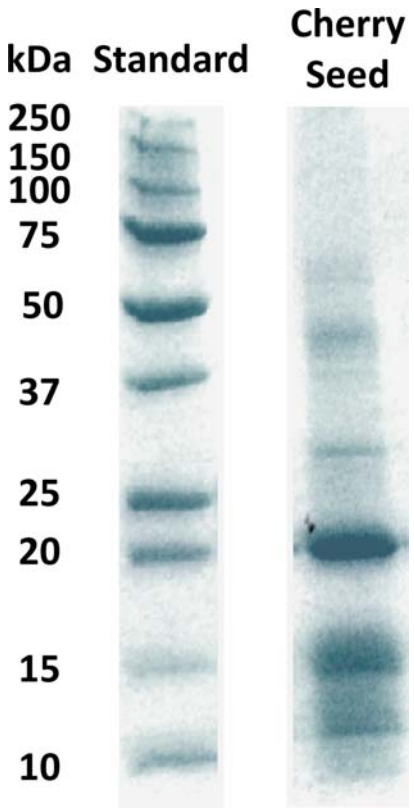

Figure 1. SDS-PAGE separation of proteins from the cherry seed protein isolate.

demonstrated that the procedure enabled the extraction of proteins from cherry seeds.

To obtain peptides from this cherry seed protein isolate, extracted proteins have to be digested with suitable enzymes.

Optimization of the Digestion of the Cherry Seed Protein Isolate. Taking into account bibliographic data and research group experience, Alcalase, Thermolysin, and Flavourzyme were the enzymes chosen for the hydrolysis of the cherry seed protein isolate. To obtain the highest digestion efficiency, different parameters were optimized with every enzyme: pH, protein concentration, enzyme:protein ratio, and digestion time. Digestion temperature was always 50 °C, corresponding to the highest enzymes activity. The optimization of the digestion was monitored by the determination of the degree of hydrolysis. Table 1 groups the conditions tested in every case.

There was not any significant variation ($P > 0.05$) in the hydrolysis degree when using Alcalase enzyme at pH's 8.0 and 8.5, while Flavourzyme showed a higher hydrolysis degree at pH 6.0 than at higher pH's. In the case of Thermolysin, a pH 8.0 was selected taking into account previous results from our research group.[19,20] Regarding the substrate concentration, as expected, the degree of hydrolysis decreases when increasing the substrate concentration, and a concentration of 2.5 mg/mL was selected for the three enzymes. Moreover, different enzyme:substrate ratios were tried. There was no significant variation ($P > 0.05$) in the hydrolysis degree when using Alcalase enzyme at different enzyme:substrate ratios, and the lowest value tried (0.10 AU/g proteins) was chosen. In the case of Flavourzyme, the enzyme:substrate ratio yielding the highest hydrolysis degree was 75 AU/g protein. Finally, the hydrolysis degree when using Thermolysin varied from 34% (at 0.03 g enzyme/g protein) to 49% (at 0.4 g enzyme/g protein), this being the enzyme:substrate ratio first chosen. Nevertheless, further investigations revealed that a high enzyme:substrate ratio resulted in enzyme autolysis, and, thus, a lower enzyme:substrate ratio (0.05 g enzyme/g protein) was finally selected. In all cases, hydrolysis degree increased rapidly in the first hours of digestions, and then it showed a slow increase up to 24 h. Nevertheless, black digestions performed at 24 h also showed the enzyme autolysis, and, to prevent it, a digestion time of 7 h was chosen for the three enzymes. Finally, Table 1 shows the hydrolysis degree obtained under optimal conditions for the three enzymes. In comparison with olive[20] and plum[19] seed proteins, these hydrolysis degrees were slightly lower. There was no significant difference among the hydrolysis degrees observed with the three enzymes ($P > 0.05$).

Evaluation of the In Vitro Antioxidant Capacity of Hydrolysates Obtained from Cherry Seed Protein Isolate. Antioxidant properties were evaluated in hydrolysates obtained using the three enzymes under optimal conditions. For that purpose, four different assays evaluating different antioxidant capabilities were applied: radical scavenging capacity, reduction capacity, and capacity to inhibit lipid peroxidation. Figure 2 shows the antioxidant capacity obtained

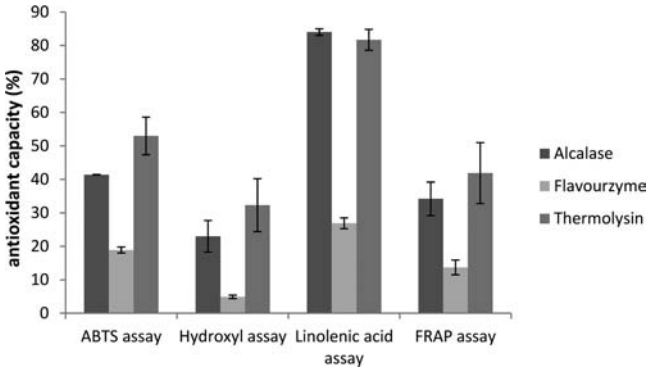

Figure 2. Antioxidant capacity of the cherry seed protein isolate digested with Alcalase, Flavourzyme, and Thermolysin and evaluated using different assays.

Table 1. Parameters Optimized in the Digestion of the Cherry Seed Protein Isolate with Alcalase, Flavourzyme, and Thermolysin Enzymes[a]

enzyme	pH	protein concentration (mg/mL)	enzyme:protein ratio	digestion time (h)	hydrolysis degree (%)[b]
Alcalase	8.0, **8.5**	**2.5**, 5.0, 7.5, 10	**0.10**, 0.15, 0.30, 0.50, 0.90 AU enzyme/g protein	0.5, 1, 1.5, 2, 3, 4, 7, 24	51 ± 2
Flavourzyme	**6.0**, 6.5, 7.0	**2.5**, 5.0, 7.5, 10	25, 50, **75**, 100 AU enzyme/g protein	0.5, 1, 1.5, 2, 3, 4, 7, 24	49 ± 4
Thermolysin	**8.0**	**2.5**, 5.0, 7.5, 10	0.03, **0.05**, 0.10, 0.40 mg enzyme/g protein	0.5, 1, 1.5, 2, 3, 4, 7, 24	55 ± 5

[a]Selected conditions are in bold. [b]Hydrolysis degrees obtained under optimal digestion conditions.

DOI: 10.1021/jf505037p
J. Agric. Food Chem. 2015, 63, 1514−1520

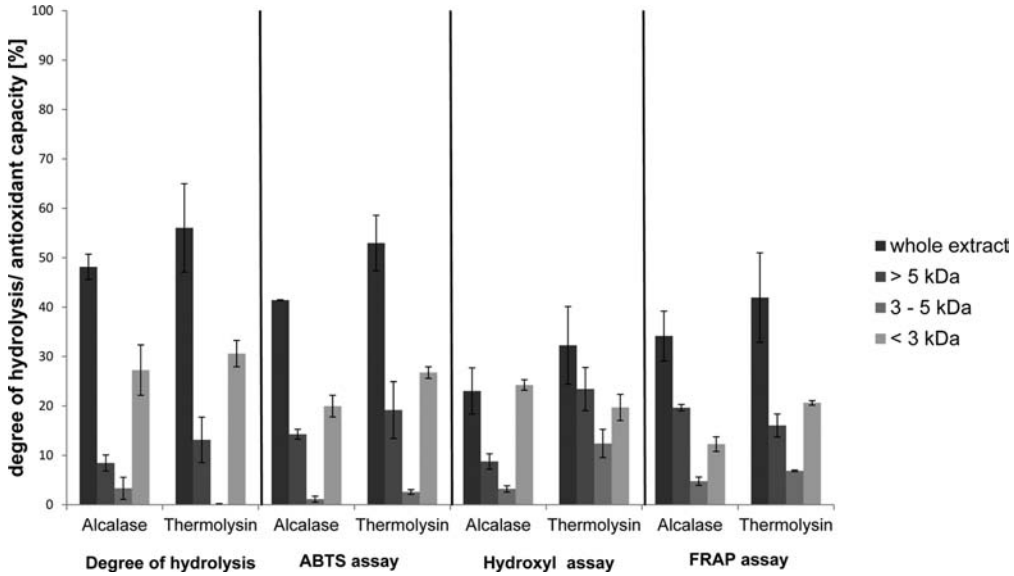

Figure 3. Comparison of hydrolysis degree and antioxidant capacity of fractions obtained from the cherry seed peptide extracts using Alcalase and Thermolysin with those corresponding to the whole extract.

by the two radical scavenging assays (ABTS and hydroxyl radical scavenging assays), by the assay measuring the reduction capacity of peptides (FRAP assay), and by the assay evaluating the capacity to inhibit lipid peroxidation. In all cases, Flavourzyme was the enzyme yielding the peptides with the lowest antioxidant capacity, while Alcalase and Thermolysin resulted in the peptides with the highest antioxidant capacities. These results were similar to those observed with peptides obtained from plum[19] and olive[20] seed proteins. Nevertheless, in comparison with olive and plum seeds, antioxidant capacity of cherry seed peptides was lower when using the ABTS and the hydroxyl radical assays. To obtain a fraction containing most antioxidant peptides, whole peptide extracts obtained with Alcalase and Thermolysin enzymes were fractionated according to their molecular weights within fractions above 5 kDa, from 5 to 3 kDa, and below 3 kDa. Figure 3 shows the antioxidant capacity of the whole peptide extracts and fractions. In all cases, the whole peptide extract showed a higher antioxidant capacity than the fractions, with the fraction from 3 to 5 kDa the one that always yielded the lowest antioxidant capacity, while fractions above 5 kDa and below 3 kDa showed higher values. These results were compared to the amount of peptides determined by OPA assay in the whole peptide extract and in every fraction. As expected, the fraction showing the highest peptide amount was the fraction below 3 kDa, while the fraction above 5 kDa presented a much lower peptide content. This situation was also observed in olive seed peptide fractions.[20] Taking into account these data, the fraction containing peptides with the highest antioxidant capacities seemed to be the fraction above 5 kDa for both Alcalase and Thermolysin enzymes. Therefore, these fractions were selected for the identification of peptides by MS.

Evaluation of the Antihypertensive Capacity of Hydrolysates Obtained from the Cherry Seed Protein Isolate. Antihypertensive capacity of whole peptide extracts was evaluated by measuring the capacity to inhibit ACE activity. Figure 4A shows no ACE inhibition in the case of the Flavourzyme peptide extract, while the Thermolysin peptide extract showed the lowest IC_{50} value (0.31 ± 0.07 mg/mL) and, thus, the highest inhibition capacity. Results obtained were

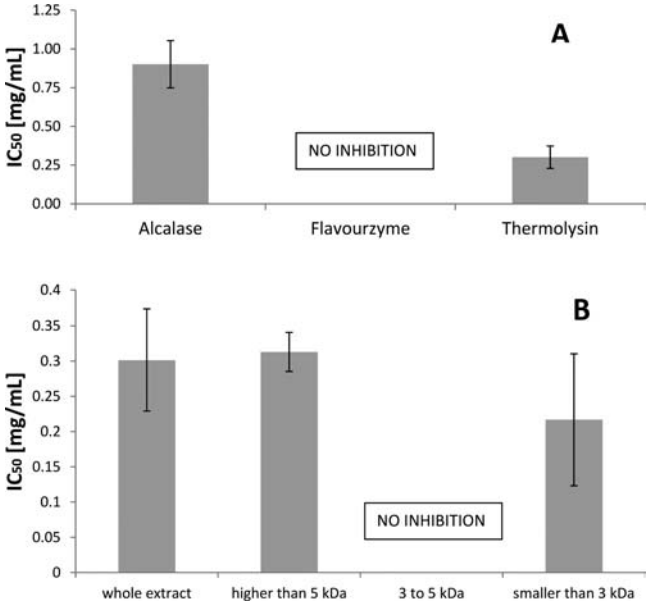

Figure 4. IC_{50} values (mg/mL) of the cherry seed protein isolate digested with Alcalase, Flavourzyme, and Thermolysin (A) under optimal conditions and of the peptide fractions obtained from the Thermolysin peptide extract (B).

again compared to those from plum[19] and olive[20] seed proteins. ACE inhibition activity of cherry seed peptides was similar to the observed in plum seed peptides but lower than that observed in olive seeds peptides. Thermolysin fractions were next obtained by ultrafiltration, and ACE inhibition capacity was evaluated in every fraction (see Figure 4B). The fraction below 3 kDa yielded the highest capacity to inhibit ACE activity, while the fraction from 3 to 5 kDa showed no ACE inhibition.

Peptide Identification in Most Bioactive Fractions by RP-HPLC-ESI-Q-TOF. Peptide identification was carried out in the fractions yielding the highest antioxidant capacity (fractions above 5 kDa obtained with Alcalase and Thermolysin enzymes)

DOI: 10.1021/jf505037p
J. Agric. Food Chem. 2015, 63, 1514−1520

and antihypertensive capacity (fraction below 3 kDa obtained with the Thermolysin enzyme).

Peptide Identification in the Fraction above 5 kDa from the Alcalase Peptide Extract. A total of 51 different peptides were identified in the two independent samples of cherry seed peptides injected by duplicate. Nevertheless, only six common peptides were observed in the four analyses. To increase the number of identified peptides, more concentrated peptide extracts were next analyzed (10-fold more concentrated). Using these concentrated samples, eight additional peptides were observed, although one peptide (TELAL), originally observed in the diluted sample, was not identified in the concentrated one. Ionization of this peptide could have been suppressed by other peptides in the concentrated sample. Identified peptides have been grouped in Table 2. Identified peptides showed molecular weights below 5 kDa in all cases (M_w < 1.3 kDa).

Table 2. Peptides Identified by RP-HPLC-Q-TOF in Fractions above 5 kDa from the Alcalase or Thermolysin Peptide Extracts (Fractions Showing the Highest Antioxidant Capacity) and in the Fraction below 3 kDa from the Thermolysin Digestion Extract (Fraction Showing the Highest Antihypertensive Capacity)

fraction	peptide sequence	ALC (%)	mass
fraction >5 kDa obtained from the Alcalase peptide extract	DGDPLLDQ	96	871.392
	NLPLL	95	568.359
	NGDPLLDQ	95	870.408
	ESGAVTE	94	691.302
	QLPLL	93	582.374
	QLPEPDNRLQ	94	1208.615
	AFGPE	93	519.233
	DEVPR	94	614.302
	NLGNPE	91	642.297
	NLGDPS	92	601.271
	FVLGL	93	547.337
	QLNEPDNRLQ	91	1225.605
	VVNE	91	459.233
	TELAL[a]	92	545.306
fraction >5 kDa obtained from the Thermolysin peptide extract	LYSPH	97	615.302
	LYTPH	96	629.317
	FDAVGVK	96	734.396
	LLPGANH	96	720.392
	LAGNPENE	94	842.377
	LLNDE	95	602.291
	LLNDEVKEGQ	95	1143.577
	LAGNPQDE	95	842.377
	LLES	94	460.253
	LLAQA	93	514.312
	YGPQQQE	91	848.366
	VTYDYYKN[a]	96	1061.481
	LTPTSN[a]	96	631.318
	LQAE[a]	93	459.233
	FGPEMEQ[a]	95	836.338
	LLMQ[a]	94	503.278
	LFSPR[a]	91	618.349
fraction <3 kDa obtained from the Thermolysin peptide extract	LYSPH	96	615.302
	LYTPH	94	629.317
	LTPTSN	94	631.318
	LLPGANH	94	720.392
	LLMQ	92	503.278

[a]Peptides only observed in the diluted sample.

These results could suggest a very low selectivity in the ultrafiltration process as it was observed previously.[21] No common peptide was observed with peptides identified in the olive seed[20] peptide extract, while one common peptide (NLPLL) was identified when comparing with peptides in plum seed[19] peptide extract.

Peptide Identification in the Fraction above 5 kDa from the Thermolysin Peptide Extract. In this case, 50 different peptides were identified in the two independent samples of cherry seed peptides injected by duplicate. Among them, 14 common peptides were observed. When more concentrated samples were analyzed, three new peptides were identified, but there were six peptides, observed in the diluted samples, that could not be detected in the concentrated ones probably due to ionization suppression. All identified peptides are listed in Table 2. Again, the low efficiency of the ultrafiltration procedure could be the reason for the low molecular weight of identified peptides. All peptides observed in the fractions above 5 kDa, showing antioxidant ability (see Table 2), presented common features. Indeed, all peptides showed a high percentage of hydrophobic (V, I, L) and aromatic amino acids (H, F, W, Y), common features within antioxidant peptides.[22]

Peptide Identification in the Fraction below 3 kDa from the Thermolysin Peptide Extract. A total of 21 different peptides were identified in the two independent samples of cherry seed peptides injected by duplicate, with just five being the number of common peptides. Some of these peptides presented proline (P) in its sequence that is a characteristic feature within antihypertensive peptides.[11] All of these peptides were previously observed in the fraction above 5 kDa, confirming the low selectivity of ultrafiltration filters. Many of these peptides were also observed in plum seed[19] peptide extract (LYSPH, LYTPH, LLAQA, LAGNPENE, LLNDE, LLMQ), but no common peptide was detected when comparing with olive seed peptides.[20]

In conclusion, it has been possible to extract proteins from a waste material derived from the processing of cherry. Protein content of cherry seeds was close to 39% of the dried and defatted seed. The digestion of extracted proteins with different enzymes enabled one to obtain peptides showing antioxidant and antihypertensive properties. Flavourzyme was the enzyme yielding the peptides with the lowest antihypertensive and antioxidant capacity, while Thermolysin was the enzyme showing the peptides with the highest antihypertensive capacity. Fractionation of peptides by ultrafiltration allowed one to obtain fractions with high antioxidant or antihypertensive capacities. HPLC-ESI-Q-TOF enabled one to identify the peptides in most active fractions, which are potentially responsible for the observed bioactivities. Identified peptides in antioxidant fractions showed less than 10 amino acids and a high number of hydrophobic and aromatic amino acids, which are characteristic features for antioxidant peptides. Some identified peptides in antihypertensive fraction contained proline, which is a characteristic amino acid within antihypertensive peptides. These results open a new pathway for the recovery of this waste material, its revalorization, and reuse.

AUTHOR INFORMATION

Corresponding Author

*Tel.: (+34) 918854915. Fax: (+34) 918854971. E-mail: concepcion.garcia@uah.es.

DOI: 10.1021/jf505037p
J. Agric. Food Chem. 2015, 63, 1514−1520

Funding

This work was supported by the Ministry of Economy and Competitiveness (ref AGL2012-36362), the University of Alcalá (ref CCG2013/EXP-028), and the Comunidad Autónoma de Madrid and European funding from FEDER program (S2009/AGR-1464, ANALISYC-II). E.G.-G. thanks the University of Alcalá for her predoctoral grant.

Notes

The authors declare no competing financial interest.

■ ACKNOWLEDGMENTS

We acknowledge Novozymes Spain S.A. for the kind donation of Alcalase and Flavourzyme enzymes.

■ REFERENCES

(1) United Nations Environment Programme, http://www.unep.org, Jan. 13, 2014.

(2) Rodríguez, G.; Lama, A.; Rodríguez, R.; Jiménez, A.; Guillén, R.; Fernández-Bolaños, J. Olive stone an attractive source of bioactive and valuable compounds. *Bioresour. Technol.* **2008**, *99*, 5261−5269.

(3) Restrepo, M. Cleaner production in food industry. *Prod. + Limpia* **2006**, *1*, 87−101.

(4) Panchaud, A.; Affolter, M.; Kussmann, M. Mass spectrometry for nutritional peptidomics: how to analyze food bioactives and their health effects. *J. Proteomics* **2012**, *75*, 3546−3559.

(5) Lee, J.; Koo, N.; Min, D. B. Reactive oxygen species, aging, and antioxidative nutraceuticals. *Compr. Rev. Food Sci. Food Saf.* **2004**, *3*, 21−33.

(6) Dhole, S. N.; Kuchekar, B. S. Comparative study of antihypertensive activity of telmisartan with telmisartan-hydroxypropyl-*β*-cyclodextrin inclusion complexes. *Pharm. Globale* **2011**, *2*, 1−5.

(7) Sakat, S. S.; Wankhede, S. S.; Juvekar, A. R.; Mali, V. R.; Bodhankar, S. L. Antihypertensive effect of aqueous extract of *Elaeocarpusganitrus* Roxb. seeds in renal artery occluded hypertensive rats. *Int. J. Pharm. Technol. Res.* **2009**, *1*, 779−782.

(8) Lobo, V.; Patil, A.; Phatak, A.; Chandra, N. Free radicals, antioxidants and functional foods: Impact on human health. *Pharmacogn. Rev.* **2010**, *4*, 118−126.

(9) Sakanaka, S.; Tachibana, Y.; Ishihara, N.; Juneja, L. R. Antioxidant activity of egg-yolk protein hydrolysates in a linoleic acid oxidation system. *Food Chem.* **2004**, *86*, 99−103.

(10) Sakanaka, S.; Tachibana, Y.; Ishihara, N.; Juneja, L. R. Antioxidant properties of casein calcium peptides and their effects on lipid oxidation in beef homogenates. *J. Agric. Food Chem.* **2005**, *53*, 464−468.

(11) Puchalska, P.; Marina, M. L.; García, M. C. Isolation and characterization of peptides with antihypertensive activity in foodstuffs. *Cri. Rev. Food Sci. Nutr.*, DOI: 10.1080/10408398.2012.664829.

(12) Esteve, C.; Del Rio, C.; Marina, M. L.; García, M. C. First ultraperformance liquid chromatography based strategy for profiling intact proteins in complex matrices: application to the evaluation of the performance of olive (*Olea europaea* L.) stone proteins for cultivar fingerprinting. *J. Agric. Food Chem.* **2010**, *58*, 8176−8182.

(13) Bradford, M. M. A rapid and sensitive method for the quantitation of microgram quantities of protein utilizing the principle of protein-dye binding. *Anal. Biochem.* **1976**, *72*, 248−254.

(14) Wang, D.; Wang, L.; Zhu, F.; Zhu, J.; Chen, X. D.; Zou, L.; Saito, M.; Li, L. In vitro and in vivo study of the antioxidant activities of the aqueous extracts of Douchi (a traditional Chinese salt-fermented soybean food). *Food Chem.* **2008**, *107*, 1421−1428.

(15) Wiriyaphan, C.; Chitsomboon, B.; Yongsawadigul, J. Antioxidant activity of protein hydrolysates derived from threadfin bream surimi byproducts. *Food Chem.* **2012**, *132*, 104−111.

(16) Ajibola, C. F.; Fashakin, J. B.; Fagbemi, T. N.; Aluko, R. E. Effect of peptide size on antioxidant properties of african yam bean seed (*Sphenostylis stenocarpa*) protein hydrolysate fractions. *Int. J. Mol. Sci.* **2011**, *12*, 6685−6702.

(17) Chen, H. M.; Muramoto, K.; Yamauchi, F.; Nokihara, K. Antioxidant activity of design peptides based on the antioxidative peptide isolated from the digests of a soybean proteins. *J. Agric. Food Chem.* **1996**, *44*, 2619−2623.

(18) Geng, F.; He, Y.; Yang, L.; Wang, Z. A rapid assay for angiotensin-converting enzyme activity using ultra-performance liquid chromatography−mass spectrometry. *Biomed. Chromatogr.* **2010**, *24*, 312−317.

(19) González-García, E.; Marina, M. L.; García, M. C. Plum (*Prunus Domestica L.*) by-product as a new and cheap source of bioactive peptides: extraction method and peptides characterization. *J. Funct. Foods*, **2014**, *11*, 428−437.

(20) Esteve, C.; Marina, M. L.; García, M. C. Novel strategy for the revalorization of olive (*Olea europaea*) residues based on the extraction of bioactive peptides. *Food Chem.* **2015**, *167*, 272−280.

(21) Puchalska, P.; García, M. C.; Marina, M. L. Identification of native angiotensin-I converting enzyme inhibitory peptides in commercial soybean based infant formulas using HPLC-Q-TOF-MS. *Food Chem.* **2014**, *157*, 62−69.

(22) Sarmadi, B. H.; Ismail, A. Antioxidative peptides from food proteins: a review. *Peptides* **2010**, *31*, 1949−1956.

DOI: 10.1021/jf505037p
J. Agric. Food Chem. 2015, 63, 1514−1520

cancer chemoprevention,[14−18] antivirus,[19] antiobesity,[20,21] and anti-inflammation.[15,22] Nevertheless, the investigation of this pleiotropic molecule on the neuronal system has only been limitedly cultivated,[23] and the underlying mechanism of the action has not been well elucidated.

As our continued efforts in discovering and developing novel redox-active small molecules as potential therapeutic agents,[24−30] we synthesized Xn and investigated its cytoprotection and the underlying mechanism in a neuronlike rat pheochromocytoma cell line, PC12. Xn was prepared from the readily available starting materials in seven steps with a total yield of 5.0%. As a polyphenolic compound, Xn moderately scavenges free radicals in vitro. Moreover, Xn efficiently activates the Nrf2−ARE signaling pathway at submicromolar concentrations in PC12 cells, leading to upregulation of a panel of phase II enzyme expression and remarkable protection of the cells from hydrogen peroxide (H_2O_2)- or 6-hydroxydopamine (6-OHDA)-induced neurotoxicity. We further clarified that the potential neuroprotection of Xn is dependent on both the α,β-unsaturated ketone moiety within Xn and the activation of transcription factor Nrf2. Our results demonstrate, for the first time, that Xn is a small-molecule activator of the Nrf2−ARE pathway in neuronal cells and suggest that Xn might be a potential candidate for the prevention of neurodegeneration. The structural determinant of such cytoprotection sheds light on designing and developing novel therapeutic agents.

MATERIALS AND METHODS

Materials. Dulbecco's modified Eagle's medium (DMEM), *N*-acetyl-Asp-Glu-Val-Asp-*p*-nitroanilide (Ac-DEVD-pNA), G418 disulfate salt, dimethyl sulfoxide (DMSO), yeast glutathione reductase (GR), Hoechst 33342, and 2′,7′-dichlorfluorescein diacetate (DCFH-DA) were obtained from Sigma-Aldrich (St. Louis, MO). NADPH was obtained from Roche (Mannheim, Germany). 2,2′-Azinobis(3-ethylbenzthiazoline-6-sulfonic acid) (ABTS), 2,6-dichlorophenol indophenol (DCPIP), 2,2′-azobis(2-methylpropionamidine) dihydrochloride (AAPH), *tert*-butylhydroquinone (tBHQ), and β-NADH were purchased from Sigma-Aldrich. Fetal bovine serum (FBS) was obtained from HyClone, Thermo Fisher Scientific (Waltham, MA). The recombinant rat TrxR1, which has a specific activity of 50% of that of the wild-type rat TrxR1 with the DTNB assay, was a gift from Prof. Arne Holmgren at Karolinska Institute, Sweden. *Escherichia coli* Trx was purchased from IMCO (Stockholm, Sweden, www.imcocorp.se). Anti-TrxR1 antibody was obtained from Santa Cruz Biotechnology (Santa Cruz, CA). 3-(4,5-Dimethylthiazol-2-yl)-2,5-diphenyltetrazolium bromide (MTT), penicillin, and streptomycin were obtained from Amresco (Solon, OH). Bovine serum albumin (BSA), phenylmethanesulfonyl fluoride (PMSF), sodium orthovanadate (Na_3VO_4), and antilamin and antiactin antibodies were obtained from Beyotime (Nantong, China). 5,5′-Dithiobis(2-nitrobenzoic acid) (DTNB) was obtained from J&K Scientific (Beijing, China). 6-Hydroxydopamine hydrobromide (6-OHDA), anti-TrxR1 antibody, anti-Trx1 antibody, and anti-Nrf2 antibody were from Santa Cruz Biotechnology. Anti-HO-1 antibody and anti-NQO1 antibody were obtained from Sangon Biotech (Shanghai, China). The shRNA plasmids targeting coding regions of the rat Nrf2 gene (shNrf2) and the control nontargeting shRNA (shNT) were purchased from GenePharma Co., Ltd. (Shanghai, China). GeneTran III transfection reagent was obtained from Biomiga (San Diego, CA). All other reagents were of analytical grade.

In Vitro Antioxidant Activity of Xn. *ABTS Free-Radical-Scavenging Activity.* The $ABTS^{\bullet+}$ scavenging capacity was determined according to the published method.[27] The $ABTS^{\bullet+}$ radical cation solution, which was prepared from oxidation of ABTS (7 mM) by potassium persulfate (2.5 mM) for 12−16 h in the dark at room temperature, was diluted to an absorbance of 0.700 ± 0.020 at 734 nm. The $ABTS^{\bullet+}$ solution (2 mL) and the antioxidant solution (100 μL) were mixed and incubated at room temperature. After 30 min, the absorbance at 734 nm was determined. The absorbance of the free radical solution without Xn was divided by that with 40 μM Xn to give the percentage of the remaining free radicals.

Assay of Thiobarbituric Acid Reactive Substances (TBARSs). The erythrocyte ghost, prepared following the published procedures,[27] was diluted to a final protein concentration of 0.96 mg/mL and incubated at 37 °C in 0.1 M PBS (pH 7.4). The lipid peroxidation was initiated by the addition of AAPH in the presence or absence of Xn (40 μM). The reaction mixture was gently shaken at 37 °C for 30 min. The reaction mixture was taken out, and a TCA−TBA−HCl stock solution (15% (w/v) trichloroacetic acid, 0.375% (w/v) TBA, 0.25 M HCl) was added, together with 0.02% (w/v) BHT. This amount of BHT completely prevents the formation of any nonspecific TBARS from the decomposition of AAPH during the subsequent boiling. The resulting mixture was heated in a boiling water bath for 15 min. After cooling, the precipitate was removed by centrifugation. TBARS in the supernatant was quantified at 532 nm using an extinction coefficient of $1.56 \times 10^5\ M^{-1}\ cm^{-1}$.[27]

Cell Cultures. The rat adrenal pheochromocytoma cell line PC12 was obtained from the Shanghai Institute of Biochemistry and Cell Biology, Chinese Academy of Sciences. The cells were cultured in DMEM medium supplemented with 10% FBS, 2 mM glutamine, and 100 units/mL penicillin/streptomycin and maintained in a humidified atmosphere with 5% CO_2 at 37 °C. The generation of Nrf2-knockdown PC12 cells is described in the following section.

Cytotoxicity Assays. *MTT Assay.* To investigate the cytotoxicity of Xn on PC12 cells, the cells were seeded at a density of 1×10^4 cells/well in 96-well plates for 24 h followed by incubation with Xn or other agents for 24 h at 37 °C in a final volume of 100 μL. For the H_2O_2 or 6-OHDA injury model, PC12 cells (1×10^4 cells/well) were plated in a 96-well plate and allowed to adhere for 24 h. After the cells were further treated with the indicated concentrations of Xn or DMSO (control) for 24 h, the medium was removed and replaced with fresh medium containing 600 μM H_2O_2 for 12 h or 200 μM 6-OHDA for 24 h. At the end of the treatments, 10 μL of MTT (5 mg/mL) was added to each well followed by incubation for an additional 4 h at 37 °C. An extraction buffer (100 μL, 10% SDS, 5% isobutanol, 0.1% HCl) was added, and the cells were incubated overnight at 37 °C. The absorbance was measured at 570 nm using a microplate reader (Thermo Scientific Multiskan GO, Finland).

Lactate Dehydrogenase (LDH) Release Assay. PC12 cells were seeded in 12-well plates at a density of 2×10^5 cells/well. On the following day, the cells were exposed to various concentrations of Xn for 24 h, followed by addition of 600 μM H_2O_2 for an additional 12 h or 200 μM 6-OHDA for an additional 24 h. The leakage of LDH from cultured cells was quantified by measuring LDH activity in the culture medium. Briefly, 50 μL of the culture medium was mixed with 110 μL of 100 mM Tris−HCl buffer (pH 7.4), 20 μL of 2 mM NADH, and 20 μL of 20 mM pyruvate, and the change of absorbance at 340 nm due to the consumption of NADH was monitored every 20 s for 5 min. The content of LDH release was calculated by normalizing the LDH activity of samples to that measured in culture medium from the control cells.

Hoechst 33342 Staining. PC12 cells were plated in 12-well plates at a density of 2×10^5 cells/well. On the following day, the cells were incubated with the indicated concentrations of Xn for 24 h. After replacement with the fresh medium containing 600 μM H_2O_2 or 200 μM 6-OHDA, the cells were allowed to continue growing for 12 h (H_2O_2) or for 24 h (6-OHDA). After the treatments, Hoechst 33342 was subsequently added to a final concentration of 5 μg/mL to stain the nuclei. The cells were visualized and photographed with a Leica inverted fluorescent microscope.

Measurement of Caspase-3 Activity. PC12 cells were seeded in 60 mm dishes at a density of 2×10^6 cells/well for 24 h and then treated with different concentrations of Xn or DMSO for another 24 h. After replacement with the fresh medium containing 600 μM H_2O_2 or 200 μM 6-OHDA for 24 h, the cells were harvested, washed with PBS, and lysed with RIPA buffer (50 mM Tris−HC,l pH 7.5, 2 mM EDTA, 0.5% deoxycholate, 150 mM NaCl, 1% Triton X-100, 0.1% SDS, 1 mM

DOI: 10.1021/jf505075n
J. Agric. Food Chem. 2015, 63, 1521−1531

Na_3VO_4, and 1 mM PMSF) for 30 min on ice. The protein concentration was quantified using the Bradford procedure. A cell extract containing 15 μg of total proteins was incubated with the assay mixture (50 mM Hepes, 2 mM EDTA, 5% glycerol, 10 mM DTT, 0.1% CHAPS, 0.2 mM Ac-DEVD-pNA, pH 7.5) for 4 h at 37 °C in a final volume of 100 μL. The absorbance at 405 nm was measured using a microplate reader. The caspase-3 activity was expressed as the percentage of the control cells that grow with DMSO treatment.

Assessment of the Intracellular ROS. PC12 cells (2×10^5 cells/well) were seeded into 12-well plates and allowed to adhere for 24 h. Then the cells were treated with Xn or DMSO for another 24 h, followed by replacement with the fresh medium containing 600 μM H_2O_2 for 3 h or 200 μM 6-OHDA for 6 h. After removal of the culture medium, the ROS indicator DCFH-DA (10 μM) in fresh FBS-free medium was added to each well, and incubation was continued for 30 min at 37 °C in the dark. The cells were visualized and photographed under a fluorescent microscope. Intracellular ROS were quantified in PC12 cells using the green fluorescent probe DCFH-DA. Cells were seeded at 1×10^4 cells/well in black 96-well plates for 1 d. The cells were exposed to 600 μM H_2O_2 for 3 h or 200 μM 6-OHDA for 6 h after a 24 h pretreatment with or without Xn. After removal of the medium and staining of the cells with DCFH-DA (10 μM) for 30 min, the cells were washed with PBS and the fluorescence intensity at 525 nm excited at 488 nm in each well was read by an Infinite M200 (Tecan). The ROS levels are expressed as the percentage of treated cells compared to the control.

Real-Time Reverse Transcription PCR (RT-PCR). PC12 cells were seeded in 60 mm dishes at a density of 2×10^6 cells/well for 24 h, followed by treatment with 0.5 μM Xn for 0, 6, and 12 h. As a positive control, the cells were treated with tBHQ (20 μM) for 6 h. For the injury models, the cells were further exposed to 600 μM H_2O_2 for 6 h or 200 μM 6-OHDA for 12 h after the cells were pretreated with Xn for 6 h. Total RNA was isolated from cells using an RNAiso Plus (TaKaRa, Dalian, China) according to the manufacture's protocol and quantified through 260 nm/280 nm wavelength measurement. Reverse transcription was performed using a Primescript RT reagent kit according to the manufacture's protocol (TaKaRa). RT-PCR was performed on an Agilent Technologies Stratagene Mx3005P RT-PCR system using SYBR Premix Ex Taq II (Tli RNaseH Plus). PCR primers specific to each gene were as follows: glyceraldehyde-3-phosphate dehydrogenase (GAPDH), 5′-cagtgccagcctcgtctcat-3′ (forward, F) and 5′-aggggccatccacagtcttc-3′ (reverse, R); heme oxygenase 1 (HO-1), 5′-gccctggaagaggagatagag-3′ (F) and 5′-tagtgctgtgtggct-ggtgt-3′ (R); NAD(P)H:quinone oxidoreductase 1 (NQO1), 5′-tcaccactctactttgctccaa-3′ (F) and 5′-ttttctgctcctcttgaacctc-3′ (R); thioredoxin 1 (Trx1), 5′-ccttctttcattccctctgtgac-3′ (F) and 5′-cccaa-ccttttgacccttttttat-3′ (R); thioredoxin reductase 1 (TrxR1), 5′-actgc-tcaatccacaaacagc-3′ (F) and 5′-ccacggtctctaagccaatagt-3′ (R); catalytic subunit of glutamate−cysteine ligase (GCLC), 5′-caaggacaagaacac-accatct-3′ (F) and 5′-cagcactcaaagccataacaat-3′ (R); modifier subunit of glutamate−cysteine ligase (GCLM), 5′-ggcacaggtaaaacccaatagt-3′ (F) and 5′-ttcaatgtcagggatgctttct-3′ (R). The GAPDH was used as an internal control. Target gene expression was measured and was normalized to the GAPDH expression level.

Measurement of Total Glutathione. Quantification of the total glutathione was based on the enzymatic recycling method.[31] PC12 cells were seeded in 60 mm dishes at a density of 2×10^6 cells/well for 24 h and treated with different concentrations of Xn or vehicle for 24 h. For each sample, cells were collected and resuspended using ice-cold extraction buffer containing 0.1% Triton X-100 and 0.6% sulfosalicyclic acid in 0.1 M potassium phosphate buffer with 5 mM EDTA disodium salt, pH 7.5 (KPE buffer) . The cell suspension was sonicated in ice every 30 s for 2−3 min. After the cell suspension was centrifuged at 3000*g* for 4 min at 4 °C, the supernatant was immediately transferred to a new Eppendorf tube. A 120 μL solution containing 0.33 mg/mL DTNB and 1.66 units/mL glutathione reductase was added to each sample (20 μL). β-NADPH (60 μL, 0.66 mg/mL) was then added quickly, and the absorbance at 412 nm was measured every 15 s for 2 min. The same amounts of DMSO were added to the control experiments, and the activity is expressed as a percentage of the control.

Measurement of NQO1 Activity. The NQO1 activity was determined spectrophotometrically by monitoring the reduction of the electron acceptor 2,6-DCPIP at 600 nm.[27] In brief, PC12 cells were seeded in 60 mm dishes at a density of 2×10^6 cells/well for 24 h and treated with different concentrations of Xn or DMSO for another 24 h. The cells were harvested and lysed in RIPA buffer. The total protein concentration was quantified using the Bradford procedure. The enzymatic reaction was initiated by the addition of cell lysate (5 μg of total protein) to the reaction mixture (2 mM Tris−HCl, pH 7.4, 200 μM NADH, and 40 μM DCPIP), and the decrease in absorbance at 600 nm was measured every 15 s for 2 min at room temperature in the presence or absence of 20 μM dicoumarol, a known NQO1 inhibitor. The dicoumarol-inhibitable part of DCPIP's reduction was used to calculate the NQO1 activity. The same amounts of DMSO were added to the control experiments, and the activity is expressed as a percentage of the control.

Determination of Trx and TrxR Activity. After PC12 cells were treated with different concentrations of Xn for 24 h, the cells were harvested and washed twice with PBS. Total cellular proteins were extracted by RIPA buffer for 30 min on ice. The total protein content was quantified using the Bradford procedure. Trx and TrxR activity in cell lysates was measured by the end point insulin reduction assay.[32] Briefly, the cell extract containing 20 μg of total proteins was incubated in a final reaction volume of 50 μL containing 100 mM Tris−HCl (pH 7.6), 0.3 mM insulin, 660 μM NADPH, 3 mM EDTA, and 15 μM *E. coli* Trx (for assaying the activity of TrxR) or 250 nM recombinant rat TrxR1 (for assaying the activity of Trx) for 30 min at 37 °C. The reaction was terminated by adding 200 μL of 1 mM DTNB in 6 M guanidine hydrochloride, pH 8.0. A blank sample, containing everything except TrxR or Trx, was treated in the same manner. The absorbance at 412 nm was measured, and the blank value was subtracted from the corresponding absorbance value of the sample. The same amounts of DMSO were added to the control experiments, and the activity is expressed as a percentage of the control.

Western Blot Analysis. PC12 cells (4×10^6 cells/well) seeded in 100 mm dishes for 1 d and subsequently treated with Xn (0.5 μM) for 0, 2, 4, 6, 8 h were harvested, and different cell extracts were prepared according to the published procedure.[27] For the whole cell protein extraction, PC12 cells were washed with ice-cold PBS three times and then with RIPA buffer for 30 min on ice. Cell lysates were centrifuged at 12000*g* for 20 min at 4 °C, and the supernatant was collected for analysis or stored at −80 °C.

For the cytosolic and nuclear extracts, the cells were rinsed with ice-cold PBS, and the pellet was dissolved in 100 μL of buffer A (10 mM Hepes, pH 7.9, 10 mM KCl, 0.1 mM EDTA, 0.1 mM EGTA, 1 μM DTT, and 1 μM protease inhibitor cocktail freshly added to buffer A). After 15 min of incubation, 10 μL of Nonidet-P40 (10%) was added, and the lysate was vortexed for 15 s. Thereafter, the lysate was repeatedly centrifuged for 10 min (1000*g*, 4 °C) to separate the nuclei from the cytosolic fraction. The supernatant (cytosolic fraction) was stored on ice. The pellet was resuspended in 100 μL of buffer B (20 mM Hepes, pH 7.9, 0.4 M NaCl, 1 mM EDTA, 1 mM EGTA, 1 μM DTT, and 1 μM protease inhibitor cocktail freshly added to buffer B) and incubated on ice for 15 min with vortexing for 10−15 s every 2 min. After a final centrifugation step for 10 min (20000*g*, 4 °C), the supernatant (nuclear extract) and the cytosolic extract were used for analysis or stored at −80 °C. For Western blot analysis, equal amounts of protein in each lysate sample were separated by SDS−PAGE and electroblotted onto a PVDF membrane (Millipore, United States). After blocking with 2.5% nonfat milk at room temperature for 2 h, the membranes were incubated with primary antibodies at 4 °C overnight. The membranes were washed with TBST three times and then incubated with horseradish peroxidase-conjugated secondary antibodies at room temperature for 1 h. The signal was detected using an enhanced chemiluminescence (ECL) kit from GE Healthcare. The band intensity was quantified by Image Pro Plus 6.0

Generation of Nrf2-Knockdown PC12 Cells Using Short Hairpin RNAs. The short hairpin RNAs specifically targeting the rat

DOI: 10.1021/jf505075n
J. Agric. Food Chem. 2015, 63, 1521−1531

Scheme 1. Synthesis of Xn and TH-Xn

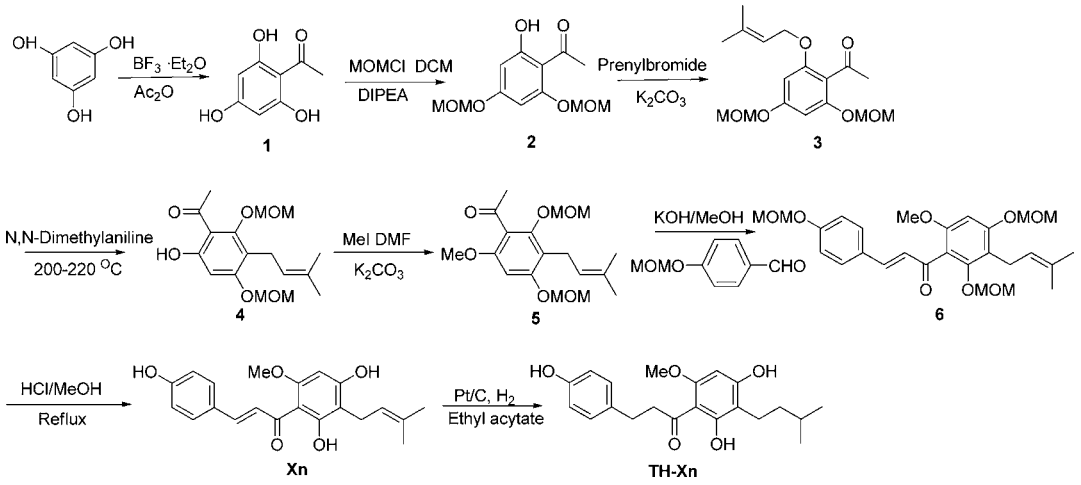

Nrf2 gene (shNrf2) and with a scrambled sequence (shNT) as the control were used for Nrf2-knockdown experiments.[27] The exponentially growing PC12 cells were transfected with different shRNAs using GeneTran III transfection reagent according to the manufacture's instructions. After 48 h of transfection, the cells were maintained in DMEM, 10% FBS, 2 mM glutamine, and 100 units/mL penicillin/streptomycin at 37 °C in a humidified atmosphere of 5% CO_2 and selected by supplementation with 0.5 mg/mL G418. Knockdown of the Nrf2 expression in the cells was analyzed by Western blotting.

Statistics. Data are presented as the mean ± SE. Statistical differences between two groups were assessed by Student's *t* test. Comparisons among multiple groups were performed using one-way analysis of variance (ANOVA), followed by a post hoc Scheffe test. $P < 0.05$ was used as the criterion for statistical significance.

RESULTS AND DISCUSSION

Chemical Synthesis. Xn and TH-Xn described in this study were prepared according to the published procedures.[30,33] The synthetic routes are illustrated in Scheme 1 and afforded a total yield of 5.0% in seven steps. Analysis of the chemical structure of Xn reveals it belongs to chalcones, the structure of which could be easily constructed by the base-catalyzed Claisen−Schmidt condensation of an aldehyde and ketone in a polar solvent such as ethanol or methanol. The key intermediate **4** was prepared from **3** via para-Claisen rearrangement. The skeleton of Xn was afforded by reaction of **5** with *p*-hydroxybenzaldehyde employing KOH as a catalyst in anhydrous methanol. Removal of the methoxymethyl protecting groups under acidic conditions furnishes the desired Xn. TH-Xn was prepared by the Pt/C-catalyzed hydrogenation of Xn. Xn and TH-Xn were fully characterized by ^1H and ^{13}C NMR and MS (Figures S2−S6 in the Supporting Information). The detailed chemical syntheses are described in the Supporting Information. The stability of Xn was determined in DMEM cell culture medium by scanning its absorbance spectra, and >90% of the compound remained after 6 h (Figure S1, Supporting Information).

Scavenging Free Radicals in Vitro. Xn is a polyphenol, and thus, we first investigated its antioxidant activity in vitro. ABTS radical cation is a stable radical with a characteristic absorbance at 734 nm. Neutralization of ABTS free radicals could be easily determined by following the decrease of optical density at 734 nm. As shown in Figure 1A, Xn displays moderate efficiency to scavenge ABTS free radicals. We also employed a model of free-radical-mediated lipid peroxidation to assay the antioxidant activity of Xn. Thermal decomposition of AAPH in aqueous solution under aerobic conditions constantly generates peroxyl radicals, which attack membrane unsaturated lipids to induce lipid peroxidation. Xn remarkably protects the erythrocyte ghost from AAPH-induced formation of TBARS (Figure 1B), a biomarker of lipid peroxidation. Taken together, Xn could directly scavenge free radicals in vitro.

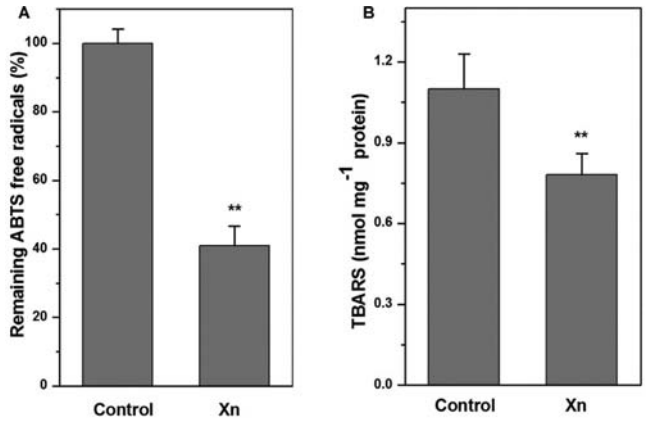

Figure 1. Scavenging of free radicals by Xn in vitro. (A) Neutralization of ABTS free radicals by Xn. (B) Prevention of the free-radical-mediated formation of TBARS in erythrocyte ghost by Xn. Key: **, $P < 0.01$ vs the control group.

Protecting PC12 Cells from H_2O_2- and 6-OHDA-Induced Damage. As Xn was reported to have cytotoxicity,[16,18] we first determined this effect in PC12 cells. Xn shows little cytotoxicity toward PC12 cells at submicromolar concentrations, and significant cytotoxicity was observed only at concentrations greater than 2 μM (Figure 2A). Thus, the concentrations of Xn used in the following protection experiments are no more than 1 μM. Next, we asked if Xn has cytoprotection at nontoxic concentrations in PC12 cells. Hydrogen peroxide, an endogenous cellular signaling molecule, has been extensively used as an inducer of oxidative stress in many cellular models. As shown in Figure 2B, PC12 cells treated with H_2O_2 only showed about 50% cell death compared with the control group. However, if the cells were pretreated with Xn (0.5 μM) for 24 h followed by H_2O_2 insult, the population of viable cells increased to about 75%. This protection was significant even at 0.1 μM Xn. 6-OHDA is a

DOI: 10.1021/jf505075n
J. Agric. Food Chem. 2015, 63, 1521−1531

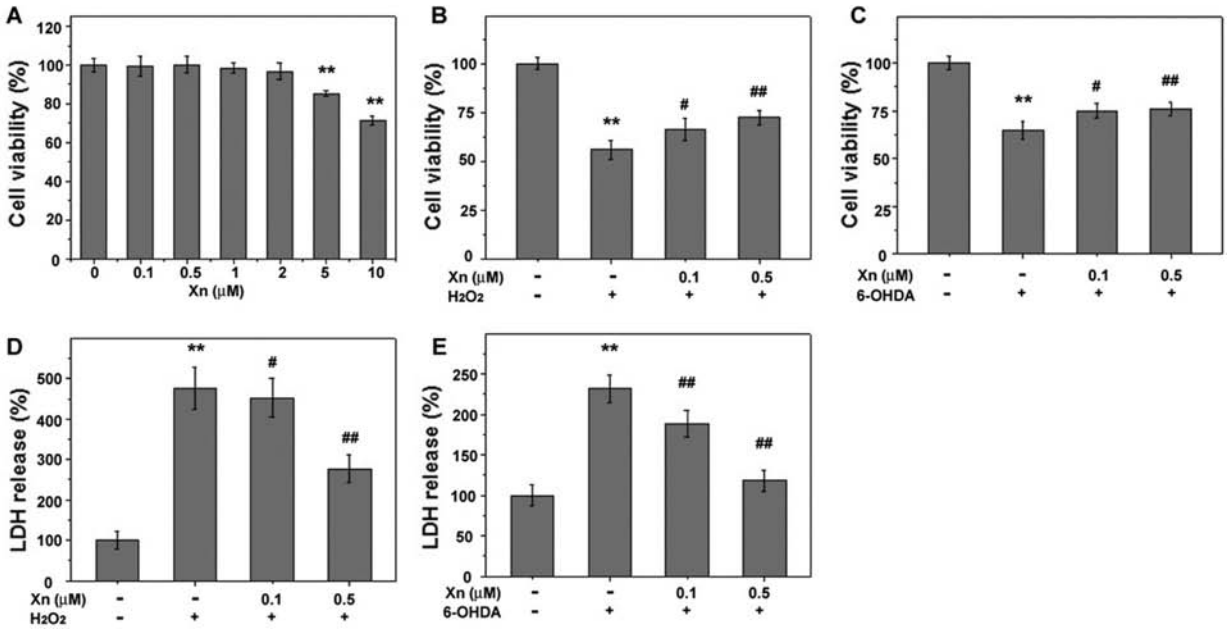

Figure 2. Protection of Xn against H_2O_2- or 6-OHDA-induced PC12 cell damage. (A) Cytotoxicity evaluation of Xn toward PC12 cells. The cells were treated with the indicated concentrations of Xn for 24 h, and the cytotoxicity of Xn was determined by the MTT assay. Protection against (B) H_2O_2-induced and (C) 6-OHDA-induced PC12 cell damage. PC12 cells (1×10^4 cells/well) were plated in a 96-well plate for 1 d and subsequently treated with Xn for another 24 h. After replacement with the fresh medium containing H_2O_2 and 6-OHDA and after incubation was continued for the indicated times, the cell viability was measured by MTT assay. The content of LDH in the medium after H_2O_2 (D) or 6-OHDA (E) treatment was determined as described in the Materials and Methods. All data represent the means ± SE of three independent experiments. Key: **, $P < 0.01$ vs the vehicle group; #, $P < 0.05$ vs the H_2O_2- or 6-OHDA-treated group; ##, $P < 0.01$ vs the H_2O_2- or 6-OHDA-treated group.

potent neurotoxin and is widely used to generate an experimental model of Parkinson's disease. 6-OHDA-mediated neurotoxicity is engendered, at least in part, by its ability to generate ROS.[34] As shown in Figure 2C, 6-OHDA treatment reduced cell viability to about 60% of that of the control. Similarly, addition of Xn, at either 0.1 or 0.5 μM, also markedly promoted cell viability to more than 75%. Lactate dehydrogenase (LDH) is a soluble cytosolic enzyme that is released into the culture medium following loss of membrane integrity resulting from cell damage. To confirm the cytoprotection of Xn, we further determined the content of LDH leakage after H_2O_2 or 6-OHDA insult. As shown in Figure 2D,E, H_2O_2 and 6-OHDA cause ~4.7-fold and ~2.4-fold increases of LDH release, respectively. Pretreatment of PC12 cells with Xn significantly reduces the leakage of LDH in a dose-dependent manner. Taken together, Xn at nontoxic concentration can significantly protect PC12 cells from H_2O_2- or 6-OHDA-induced cell damage.

Alleviating H_2O_2- and 6-OHDA-Induced PC12 Cell Apoptosis. Nuclear condensation and caspase-3 activation are hallmarks of cell apoptosis. The morphologic changes of the nuclei were revealed by Hoechst staining. As shown in Figure 3A,B, both H_2O_2 and 6-OHDA elicit apoptosis in PC12 cells evidenced by the appearance of apoptotic nuclei as highly fluorescent, condensed bodies (indicated by arrows), while no apparent apoptotic nuclei were observed in control cells. Pretreatment of PC12 cells with nontoxic concentrations of Xn remarkably lowers the population of apoptotic nuclei. Activation of caspase-3 is a biochemical character in all apoptotic cells. We thus further quantified the level of caspase-3 activation. Both H_2O_2 and 6-OHDA activate the cellular caspase-3, but with different potencies (Figure 3C,D). Again, Xn significantly alleviates the extent of caspase-3 activation in a concentration-dependent manner. Collectively, Xn alleviates H_2O_2- and 6-OHDA-induced apoptotic cell death in PC12 cells.

Preventing ROS Accumulation in PC12 Cells. DCFH-DA is a cell-permeable, nonfluorescent probe. After diffusing into cells, DCFH-DA is deacetylated by cellular esterases to nonfluorescent 2′,7′-dichlorodihydrofluorescin (DCFH), which is rapidly converted to highly fluorescent 2′,7′-dichlorofluorescein (DCF) upon reacting with ROS. Stimulation of the cells with H_2O_2 or 6-OHDA leads to intracellular burst of ROS, while the control cells display a negligible ROS level, as revealed by DCFH-DA staining (Figure 4A,B), and the quantifying results are shown in Figure 4C,D. Pretreatment of the cells with Xn remarkably reduces the ROS accumulation induced by either H_2O_2 or 6-OHDA. As oxidative stress, arising from the overproduction of ROS beyond the cellular capacity to remove them, has been implicated in a common pathway of neurotoxicity in a wide variety of acute and chronic neurologic disorders, the inhibition of ROS accumulation in neuronal cells might be the molecular basis of the neuroprotective action of Xn.

Inducing Phase II Gene Expression. Xn belongs to the chalcone family, which bears an α,β-unsaturated ketone structure. Due to the electron-deficient character of the double bond, this structure is renowned as a Michael acceptor moiety, which is a core structure of many reported small-molecule ARE inducers.[7] In analogy to known ARE activators, we thus hypothesized that Xn might activate the cellular ARE response. We measured the expression of Nrf2-driven antioxidant/detoxifying genes (HO-1, NQO1, Trx1, TrxR1, GCLC, and GCLM) at 0, 6, and 12 h after treatment with Xn (0.5 μM) in PC12 cells (Figure 5). Although the positive control tBHQ displays more potency, the induction of these genes by Xn is

DOI: 10.1021/jf505075n
J. Agric. Food Chem. 2015, 63, 1521−1531

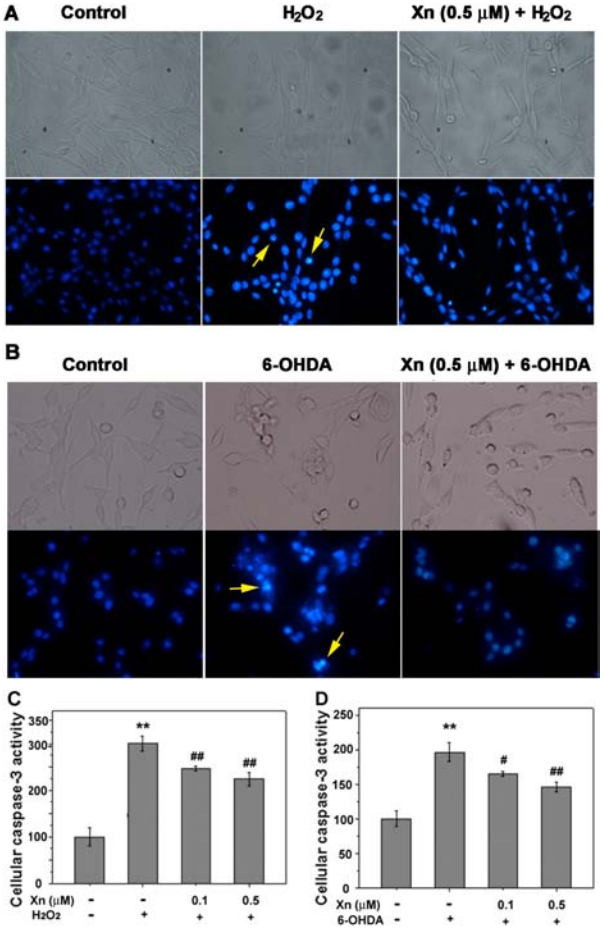

Figure 3. Inhibition of H_2O_2- or 6-OHDA-induced apoptosis in PC12 cells. PC12 cells were treated as described in the Materials and Methods, and the morphological changes of the nuclei were determined by Hoechst 33342 staining (A, B). Activation of the cellular caspase-3 (C, D) was determined by a colorimetric assay as described in the Materials and Methods. The data represent the means ± SE of three independent experiments. Key: **, $P < 0.01$ vs the vehicle group; #, $P < 0.05$ vs the H_2O_2- or 6-OHDA-treated group; ##, $P < 0.01$ vs the H_2O_2- or 6-OHDA-treated group.

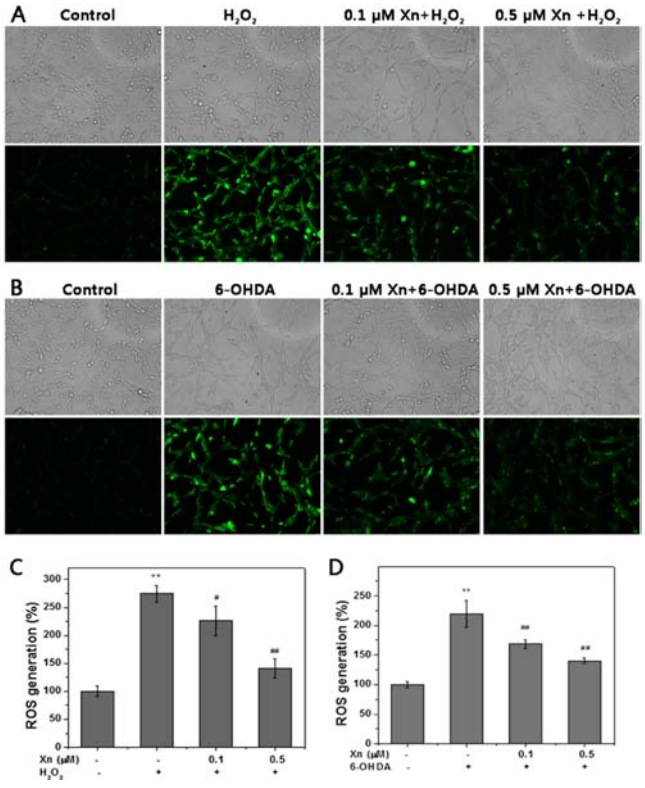

Figure 4. Prevention of ROS accumulation in PC12 cells by Xn. Pretreatment of the cells with Xn significantly alleviates ROS accumulation induced by H_2O_2 (A, C) or 6-OHDA (B, D) determined by DCFH-DA staining as described in the Materials and Methods. The fluorescence images (A, B) were acquired by inverted fluorescence microscopy. The ROS level was quantified in (C) and (D) by a fluorescence microplate reader, Infinite M200 (Tecan). Key: **, $P < 0.01$ vs the vehicle group; #, $P < 0.05$ vs the H_2O_2- or 6-OHDA-treated group; ##, $P < 0.01$ vs the H_2O_2- or 6-OHDA-treated group.

significant. The time-course studies showed the highest induction of the genes at 6 h after stimulation with Xn. The HO-1 and TrxR1 mRNAs were highly transcribed by ∼2.8- and 2.3-fold increases, respectively, after treatment with Xn for 6 h. The induction of other genes is moderate but sustainable, and this induction could last for 12 h. The phase II genes were also induced if the cells were pretreated with Xn followed by the oxidant insults. Our data suggest that Xn treatment can effectively promote the transcription of Nrf2-driven antioxidant/detoxifying genes.

Upregulating the Antioxidant Defense System in PC12 Cells. The induction of phase II enzymes is an important defense mechanism against exogenous stress. As a series of phase II genes have been upregulated at different levels, we then examined the corresponding gene products. Xn dose-dependently elevated HO-1, NQO1, TrxR1, and Trx1 protein expression (Figure 6). The glutamate cysteine ligase, composed of a GCLC and a GCLM subunit, is a rate-limiting enzyme for cellular GSH synthesis. As a consequence of the elevation of GCLC gene expression, the total GSH level in PC12 cells was increased by ∼1.6-fold (Figure 6C). By adopting the

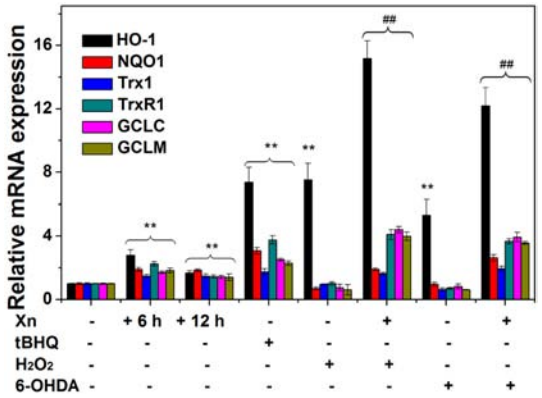

Figure 5. Induction of cytoprotective genes in PC12 cells by Xn. The cells were treated, and the mRNA levels of different genes were analyzed and normalized using GAPDH as an internal standard by qRT-PCR as described in the Materials and Methods. Pretreatment of the cells with Xn significantly elevates phase II gene expression under H_2O_2 or 6-OHDA conditions determined by qRT-PCR. PC12 cells were pretreated with Xn for 6 h or cotreated with H_2O_2 or 6-OHDA for another 6 or 12 h. tBHQ was used as a positive control. The data represent the means ± SE of three independent experiments. Key: *, $P < 0.05$ vs the control group (0 h); **, $P < 0.01$ vs the control group (0 h); #, $P < 0.05$ vs the H_2O_2- or 6-OHDA-treated group; ##, $P < 0.01$ vs the H_2O_2- or 6-OHDA-treated group.

DOI: 10.1021/jf505075n
J. Agric. Food Chem. 2015, 63, 1521−1531

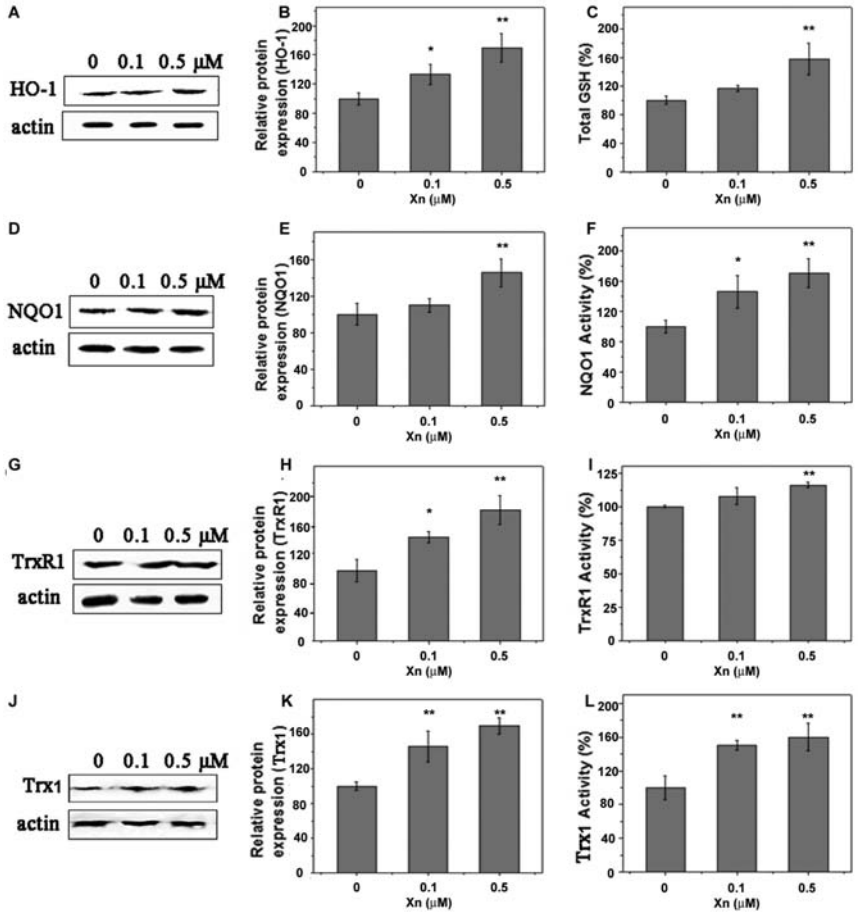

Figure 6. Upregulation of antioxidant enzymes by Xn in PC12 cells. (A) Induction of HO-1 protein expression by Xn. (B) Quantification of the band intensity in (A). (C) Xn induces upregulation of GSH in PC12 cells. The total intracellular GSH was measured as described in the Materials and Methods. Induction of NQO1 expression (D) and enzyme activity (F) by Xn. (E) Quantification of the band intensity in (D). Induction of TrxR1 expression (G) and total TrxR1 enzyme activity (I) by Xn. (H) Quantification of the band intensity in (G). Induction of Trx1 protein expression (J) and total Trx enzyme activity (L) by Xn. (K) Quantification of the band intensity in (J). Data are expressed as the means ± SE of three experiments. Key: *, $P < 0.05$ vs the vehicle group; **, $P < 0.01$ vs the vehicle group.

convenient assays, we further determined the cellular activity of NQO1, TrxR1, and Trx1. In line with the upregulation of protein expression, all the enzymes' activities were significantly increased (Figure 6F,I,L). After Xn (0.5 μM) treatment, the NQO1 activity (Figure 6F), TrxR1 activity (Figure 6I), and Trx1 activity (Figure 6L) were increased by ∼1.7-, ∼1.2-, and ∼1.5-fold, respectively. Our data demonstrate that Xn at submicromolar concentration could efficiently boost various endogenous cytoprotective molecules.

Promoting Nrf2 Nuclear Localization. Induction of antioxidant gene expression via the Nrf2-dependent cytoprotective pathway requires translocation of Nrf2 from the cytosol to the nucleus. We therefore examined whether Xn could promote Nrf2 to accumulate in the nuclei. After isolation of the nuclei from the cells, the total Nrf2, the cytosolic Nrf2, and the nuclear Nrf2 were determined by immunoblots. Upon Xn treatment, immunoblotting results revealed that the total Nrf2 expression increased, peaking at 4 h, and decreased to the basal level at 8 h (Figure 7A). Notably, the cytosolic Nrf2 decreased gradually, coincident with its continuous accumulation in the nuclei (Figure 7B,C), indicating the translocation of Nrf2 from the cytosol to the nuclei. We also analyzed the change of nuclear Nrf2 under H_2O_2 or 6-OHDA treatment conditions. As shown in Figure 7D, H_2O_2 or 6-OHDA alone has a marginal effect on the Nrf2 nuclear accumulation. However, after pretreatment with Xn followed by the oxidant insult, the amount of Nrf2 in the nucleus remarkably increased. The presence of Nrf2 in the nuclei would facilitate its binding to ARE and thus subsequently initiates the transcription process to induce the phase II gene expression.

Requiring the α,β-Unsaturated Ketone Structure in Xn and Nrf2 for Cytoprotection. As aforementioned, we speculated that the α,β-unsaturated ketone moiety in Xn and the transcription factor Nrf2 are key determinants for the action of Xn in PC12 cells. We prepared TH-Xn, a molecule without the α,β-unsaturated ketone structure, and generated Nrf2-knockdown PC12 cells to validate the molecular mechanism underlying the cytoprotection of Xn. Hydrogenation of Xn to TH-Xn almost completely abolishes the protective effect (Figure 8A), indicating the importance of the α,β-unsaturated ketone structure in Xn. Next, we compared the protection of Xn in PC12 cells with different Nrf2 expressions. After confirmation of the knockdown efficiency of Nrf2 (Figure 8B), we evaluated the effect of Xn against oxidative insult toward different cells. As shown in Figure 8C,D, Xn displays a protective pattern in PC12 cells transfected with shNT similar to that observed in wild-type PC12 cells. However, this protection is drastically lost in PC12 cells transfected with

DOI: 10.1021/jf505075n
J. Agric. Food Chem. 2015, 63, 1521−1531

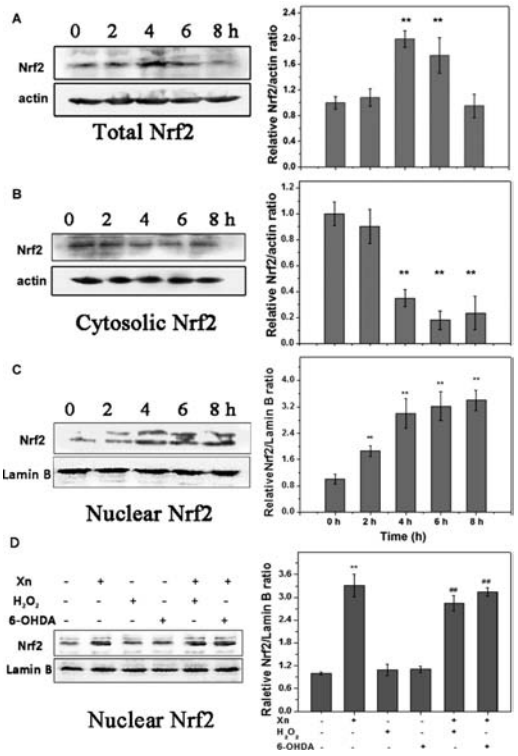

Figure 7. Promotion of Nrf2 nuclear accumulation by Xn. After the cells were treated with Xn (0.5 μM) for 0, 2, 4, 6, and 8 h, they were harvested, and different cell extracts were prepared as described in the Materials and Methods. The total Nrf2 (A), cytosolic Nrf2 (B), and nuclear Nrf2 (C) were analyzed by Western blotting. (D) Pretreatment of the cells with Xn promotes nuclear Nrf2 accumulation under H_2O_2 or 6-OHDA treatment conditions. PC12 cells were pretreated with Xn for 6 h and cotreated with H_2O_2 or 6-OHDA for another 6 or 12 h. Actin or lamin B was used as a loading control. Quantification of the blots is presented in the right panel. The data are expressed as the means ± SE of three experiments. Key: *, $P < 0.05$ vs the control group (0 h); **, $P < 0.01$ vs the control group (0 h). #, $P < 0.05$ vs the H_2O_2- or 6-OHDA-treated group; ##, $P < 0.01$ vs the H_2O_2- or 6-OHDA-treated group.

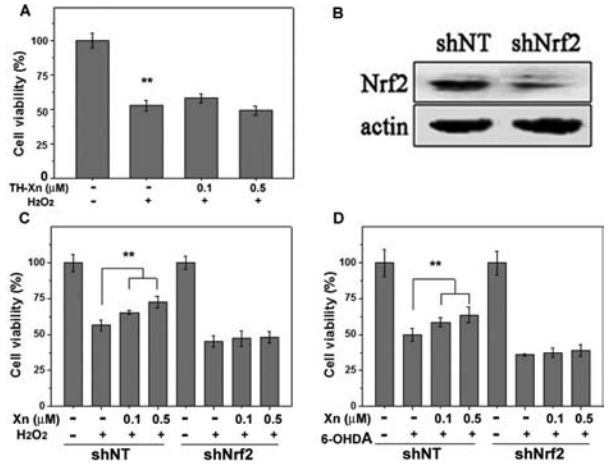

Figure 8. Involvement of Nrf2 in the cytoprotection of Xn in PC12 cells. (A) Protection of TH-Xn against H_2O_2-induced PC12 cell damage. (B) Evaluation of Nrf2-knockdown efficiency by different shRNAs. PC12 cells were transfected with shRNAs specifically targeting the rat Nrf2 gene (shNrf2s) or nontargeting shRNA (shNT), and the efficiency of silencing Nrf2 was evaluated by Western blots. (C, D) Impairment of cytoprotection of Xn in Nrf2-knockdown cells. Different PC12 cells were treated with Xn for 24 h followed by treatment with 600 μM H_2O_2 for 12 h or 200 μM 6-OHDA for 24 h. The cell viability was determined by MTT assay. The results are expressed as the means ± SE. Key: **, $P < 0.01$; *, $P < 0.05$.

shNrf2 (Figure 8C,D), demonstrating the definite involvement of Nrf2 in cytoprotection of Xn in PC12 cells.

Common targets and mechanisms of neurodegenerative diseases have been elegantly summarized in a recent paper.[35] Among various pathogenic hypotheses, increasing evidence has supported that oxidative stress is a causal, or at least an ancillary, factor in the progressive degeneration of a subset of neurons, which is the pathologic hallmark of adult-onset neurodegenerative diseases.[1,36] Surgical operation to replace the dying or dead neurons in these diseases has been demonstrated only with limited success.[37] Therefore, pharmacological management intended to assuage the oxidative stress is one promising strategy to protect loss of neurons, which is expected to eventually lead to retardation or blockage of the neurodegenerative progression. Tactics against oxidative stress include direct antioxidative action by supplying exogenous antioxidants and indirect defense by activating the pathway(s) involved in expression of endogenous cytoprotective molecules. In this regard, accumulating enthusiasm has been devoted to discovering and developing novel antioxidants or molecules that may prompt endogenous antioxidant defense as potential therapeutic agents for neurodegenerative disorders.[7]

Preceding studies have suggested that Xn could promote neuronal differentiation as well as neurite outgrowth[23] and prevent middle cerebral artery occlusion-induced cerebral ischemia in rats[38] to confer neuroprotective function. We revealed in this work for the first time that Xn displayed potent cytoprotection against H_2O_2- or 6-OHDA-mediated cell damage in PC12 cells via the induction of phase II antioxidant/detoxifying enzymes. Treatment of PC12 cells with Xn significantly upregulates a set of Nrf2-driven phase II genes as well as the corresponding gene products, including the antioxidant enzymes (HO-1, NQO1, Trx1, and TrxR1) and small peptide antioxidant GSH. Activation of Nrf2 by Xn in different types of cells, including microglial BV2 cells,[22] human hepatocytes,[39] and Hepa 1c1c7 cells,[40] and even in vivo,[41] has been reported. Besides, Xn has been demonstrated to possess diverse functions in a variety of cellular assays, such as anticancer[14−18] and anti-inflammation.[15,22] However, there has been no study on induction of Nrf2 in neuronal cells prior to this work, and most of the activity in these cellular assays requires higher concentrations of Xn (>1 μM). We demonstrated that Xn, as low as 0.1 μM, could significantly protect neuronal cells from oxidative insult. This concentration could be easily reached in vivo by daily intake of Xn-containing products, such as beers. The pharmacokinetics and metabolites of xanthohumol in rats have been evaluated by giving the rats intravenous injection or oral administration.[20,42] The highest plasma concentration of 2.97 mg/L (~8 μM) could be reached after intravenous injection at a dose of 1.86 mg/kg. Oral administration of Xn also leads to a significant amount of plasma circulation. One major challenge for most neuroprotective agents is their ability to pass through the blood−brain barrier (BBB). There are no available BBB penetration data for the flavonoid Xn. However, there is strong evidence showing that structurally different flavonoids are able to traverse the BBB.[43] The prenyl group further increases the

DOI: 10.1021/jf505075n
J. Agric. Food Chem. 2015, 63, 1521−1531

lipophilicity of Xn, which favors BBB penetration. It is much like Xn having the ability to pass through the BBB in vivo. Thus, our finding, i.e., the induction of endogenous cytoprotective enzymes by Xn to confer potential neuroprotection, is of physiological significance.

The Keap1−Nrf2−ARE regulatory pathway plays a central role in protecting cells against oxidative or electrophilic insult. Under unstressed conditions, Nrf2 is bound to the repressor protein Keap1, which anchors Nrf2 in the cytoplasm and targets it for ubiquitination and proteasome degradation. Upon exposure to stressors, the Nrf2−Keap1 complex dissociates and Nrf2 translocates to the nucleus. The mechanisms underlying the activation of the Keap1−Nrf2−ARE pathway are not well understood but may involve oxidation/alkylation of key thiol(s) in Keap1 and/or phosphorylation of Nrf2. Upon exposure to electrophiles or oxidants, the Cys-rich protein Keap1 is modified by forming covalent adduct or disulfide bond(s) within the protein, and it is this Cys-based modification of Keap1 that allows dissociation of Nrf2 from Keap1 and subsequent nuclear translocation of Nrf2. Analysis of the chemical structure of Xn reveals that the molecule contains one α,β-unsaturated ketone moiety, a thiol-reactive electrophilic center that may covalently modify the Cys thiols. Many natural or synthetic molecules bearing such a structure are known effective inducers of phase II genes.[6,44] Thus, alkylation of certain Cys residue(s) might be the molecular basis for the activation of the Keap1−Nrf2−ARE pathway by Xn, which was evidenced by the liquid chromatography−tandem mass spectrometry analysis[40] and our observation that removal of the electrophilic center from Xn blocks such protection (Figure 8A). Abrogating the protection of Xn by silencing Nrf2 expression in PC12 cells further supports the involvement of Nrf2 in the cellular action of Xn. Our findings suggest a novel neuroprotective mechanism of Xn shown schematically in Figure 9. The lipophilic character of Xn allows it to easily

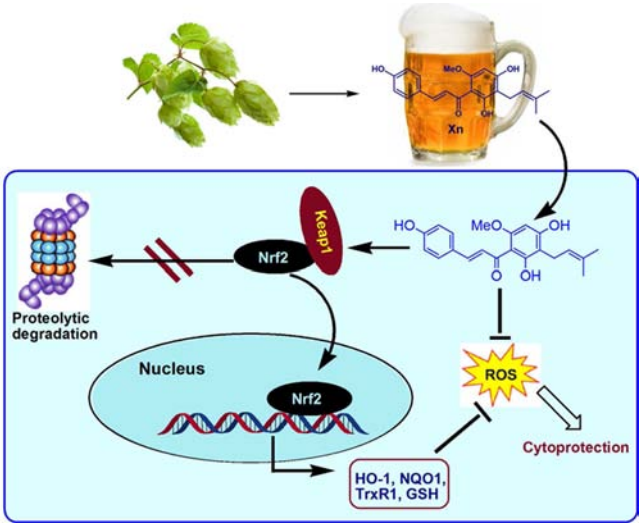

Figure 9. A neuroprotective mode of Xn in PC12 cells.

penetrate the cell membrane and accumulate within cells. As a polyphenol, Xn could directly neutralize ROS. Furthermore, the α,β-unsaturated ketone structure in Xn allows it to bind covalently to the Cys residue(s) in the cytosolic inhibitory protein Keap1, thus breaking the Keap1−Nrf2 complex to prevent proteasome degradation of Nrf2 and release Nrf2. Subsequently, Nrf2 is translocated into the nucleus, where it binds to ARE and initiates the transcription of a variety of cytoprotective genes to confer protection against oxidative stress.

In summary, we conclude that Xn is effective in preventing oxidative-stress-induced neuronal cell damage. Xn displays a moderate capacity to directly neutralize ROS in vitro. More importantly, this cytoprotection is mediated by the induction of endogenous antioxidant defense molecules, which relies on the α,β-unsaturated ketone structure in Xn and the transcription factor Nrf2 in PC12 cells as removal of such a chemical structure or knockdown of Nrf2 abolishes the protection. Our discovery discloses that Xn is a novel small-molecule activator of the Keap1−Nrf2 pathway and provides deep insights into understanding the molecular mechanism underlying the cytoprotection of Xn. This mechanism of action could lead to the design and development of novel small molecules as potential neuroprotective agents.

■ ASSOCIATED CONTENT

Supporting Information

Stability of Xn determined by its absorbance spectrum and synthesis and original spectra of Xn and TH-Xn. This material is available free of charge via the Internet at http://pubs.acs.org.

■ AUTHOR INFORMATION

Corresponding Author

*E-mail: fangjg@lzu.edu.cn. Fax: +86 931 8915557.

Funding

Financial support from Lanzhou University (Fundamental Research Funds for the Central Universities, Grant lzujbky-2014-56) and Natural Science Foundation of Gansu Province (Grant 145RJZA225) is greatly acknowledged.

Notes

The authors declare no competing financial interest.

■ ACKNOWLEDGMENTS

We express heartfelt appreciation to Prof. Arne Holmgren for recombinant rat TrxR1 and *E. coli* Trx.

■ REFERENCES

(1) Halliwell, B.; Gutteridge, J. In *Free Radicals in Biology and Medicine*, 4th ed.; Oxford University Press: Oxford, U.K., 2007.

(2) Sauer, H.; Wartenberg, M.; Hescheler, J. Reactive oxygen species as intracellular messengers during cell growth and differentiation. *Cell Physiol. Biochem.* **2001**, *11*, 173−186.

(3) Barnham, K. J.; Masters, C. L.; Bush, A. I. Neurodegenerative diseases and oxidative stress. *Nat. Rev. Drug Discovery* **2004**, *3*, 205−214.

(4) Kobayashi, M.; Yamamoto, M. Nrf2-Keap1 regulation of cellular defense mechanisms against electrophiles and reactive oxygen species. *Adv. Enzyme Regul.* **2006**, *46*, 113−140.

(5) McMahon, M.; Itoh, K.; Yamamoto, M.; Hayes, J. D. Keap1-dependent proteasomal degradation of transcription factor Nrf2 contributes to the negative regulation of antioxidant response element-driven gene expression. *J. Biol. Chem.* **2003**, *278*, 21592−21600.

(6) Satoh, T.; McKercher, S. R.; Lipton, S. A. Nrf2/ARE-mediated antioxidant actions of pro-electrophilic drugs. *Free Radical Biol. Med.* **2013**, *65*, 645−657.

(7) Magesh, S.; Chen, Y.; Hu, L. Small molecule modulators of Keap1-Nrf2-ARE pathway as potential preventive and therapeutic agents. *Med. Res. Rev.* **2012**, *32*, 687−726.

DOI: 10.1021/jf505075n
J. Agric. Food Chem. 2015, 63, 1521−1531

(8) Stevens, J. F.; Page, J. E. Xanthohumol and related prenylflavonoids from hops and beer: to your good health! *Phytochemistry* **2004**, *65*, 1317−1330.
(9) Stevens, J. F.; Taylor, A. W.; Deinzer, M. L. Quantitative analysis of xanthohumol and related prenylflavonoids in hops and beer by liquid chromatography-tandem mass spectrometry. *J. Chromatogr. A* **1999**, *832*, 97−107.
(10) Jain, M. G.; Hislop, G. T.; Howe, G. R.; Burch, J. D.; Ghadirian, P. Alcohol and other beverage use and prostate cancer risk among Canadian men. *Int. J. Cancer* **1998**, *78*, 707−711.
(11) Magalhaes, P. J.; Carvalho, D. O.; Cruz, J. M.; Guido, L. F.; Barros, A. A. Fundamentals and health benefits of xanthohumol, a natural product derived from hops and beer. *Nat. Prod. Commun.* **2009**, *4*, 591−610.
(12) Miranda, C. L.; Stevens, J. F.; Ivanov, V.; McCall, M.; Frei, B.; Deinzer, M. L.; Buhler, D. R. Antioxidant and prooxidant actions of prenylated and nonprenylated chalcones and flavanones in vitro. *J. Agric. Food Chem.* **2000**, *48*, 3876−3884.
(13) Doddapattar, P.; Radovic, B.; Patankar, J. V.; Obrowsky, S.; Jandl, K.; Nusshold, C.; Kolb, D.; Vujic, N.; Doshi, L.; Chandak, P. G.; Goeritzer, M.; Ahammer, H.; Hoefler, G.; Sattler, W.; Kratky, D. Xanthohumol ameliorates atherosclerotic plaque formation, hypercholesterolemia, and hepatic steatosis in ApoE-deficient mice. *Mol. Nutr. Food Res.* **2013**, *57*, 1718−1728.
(14) Harikumar, K. B.; Kunnumakkara, A. B.; Ahn, K. S.; Anand, P.; Krishnan, S.; Guha, S.; Aggarwal, B. B. Modification of the cysteine residues in IkappaBalpha kinase and NF-kappaB (p65) by xanthohumol leads to suppression of NF-kappaB-regulated gene products and potentiation of apoptosis in leukemia cells. *Blood* **2009**, *113*, 2003−2013.
(15) Monteiro, R.; Calhau, C.; Silva, A. O.; Pinheiro-Silva, S.; Guerreiro, S.; Gartner, F.; Azevedo, I.; Soares, R. Xanthohumol inhibits inflammatory factor production and angiogenesis in breast cancer xenografts. *J. Cell. Biochem.* **2008**, *104*, 1699−1707.
(16) Monteghirfo, S.; Tosetti, F.; Ambrosini, C.; Stigliani, S.; Pozzi, S.; Frassoni, F.; Fassina, G.; Soverini, S.; Albini, A.; Ferrari, N. Antileukemia effects of xanthohumol in Bcr/Abl-transformed cells involve nuclear factor-kappaB and p53 modulation. *Mol. Cancer Ther.* **2008**, *7*, 2692−2702.
(17) Gerhauser, C.; Alt, A.; Heiss, E.; Gamal-Eldeen, A.; Klimo, K.; Knauft, J.; Neumann, I.; Scherf, H. R.; Frank, N.; Bartsch, H.; Becker, H. Cancer chemopreventive activity of xanthohumol, a natural product derived from hop. *Mol. Cancer Ther.* **2002**, *1*, 959−969.
(18) Miranda, C. L.; Stevens, J. F.; Helmrich, A.; Henderson, M. C.; Rodriguez, R. J.; Yang, Y. H.; Deinzer, M. L.; Barnes, D. W.; Buhler, D. R. Antiproliferative and cytotoxic effects of prenylated flavonoids from hops (*Humulus lupulus*) in human cancer cell lines. *Food Chem. Toxicol.* **1999**, *37*, 271−285.
(19) Buckwold, V. E.; Wilson, R. J.; Nalca, A.; Beer, B. B.; Voss, T. G.; Turpin, J. A.; Buckheit, R. W., 3rd; Wei, J.; Wenzel-Mathers, M.; Walton, E. M.; Smith, R. J.; Pallansch, M.; Ward, P.; Wells, J.; Chuvala, L.; Sloane, S.; Paulman, R.; Russell, J.; Hartman, T.; Ptak, R. Antiviral activity of hop constituents against a series of DNA and RNA viruses. *Antiviral Res.* **2004**, *61*, 57−62.
(20) Legette, L. L.; Luna, A. Y.; Reed, R. L.; Miranda, C. L.; Bobe, G.; Proteau, R. R.; Stevens, J. F. Xanthohumol lowers body weight and fasting plasma glucose in obese male Zucker fa/fa rats. *Phytochemistry* **2013**, *91*, 236−241.
(21) Kirkwood, J. S.; Legette, L. L.; Miranda, C. L.; Jiang, Y.; Stevens, J. F. A metabolomics-driven elucidation of the anti-obesity mechanisms of xanthohumol. *J. Biol. Chem.* **2013**, *288*, 19000−19013.
(22) Lee, I. S.; Lim, J.; Gal, J.; Kang, J. C.; Kim, H. J.; Kang, B. Y.; Choi, H. J. Anti-inflammatory activity of xanthohumol involves heme oxygenase-1 induction via NRF2-ARE signaling in microglial BV2 cells. *Neurochem. Int.* **2011**, *58*, 153−160.
(23) Oberbauer, E.; Urmann, C.; Steffenhagen, C.; Bieler, L.; Brunner, D.; Furtner, T.; Humpel, C.; Baumer, B.; Bandtlow, C.; Couillard-Despres, S.; Rivera, F. J.; Riepl, H.; Aigner, L. Chroman-like cyclic prenylflavonoids promote neuronal differentiation and neurite outgrowth and are neuroprotective. *J. Nutr. Biochem.* **2013**, *24*, 1953−1962.
(24) Zhang, L.; Duan, D.; Cui, X.; Sun, J.; Fang, J. A selective and sensitive fluorescence probe for imaging endogenous zinc in living cells. *Tetrahedron* **2013**, *69*, 15−21.
(25) Duan, D.; Zhang, B.; Yao, J.; Liu, Y.; Sun, J.; Ge, C.; Peng, S.; Fang, J. Gambogic acid induces apoptosis in hepatocellular carcinoma SMMC-7721 cells by targeting cytosolic thioredoxin reductase. *Free Radical Biol. Med.* **2014**, *69*, 15−25.
(26) Duan, D.; Zhang, B.; Yao, J.; Liu, Y.; Fang, J. Shikonin targets cytosolic thioredoxin reductase to induce ROS-mediated apoptosis in human promyelocytic leukemia HL-60 cells. *Free Radical Biol. Med.* **2014**, *70*, 182−193.
(27) Yao, J.; Ge, C.; Duan, D.; Zhang, B.; Cui, X.; Peng, S.; Liu, Y.; Fang, J. Activation of the phase II enzymes for neuroprotection by ginger active constituent 6-dehydrogingerdione in PC12 cells. *J. Agric. Food Chem.* **2014**, *62*, 5507−5518.
(28) Liu, Y.; Duan, D.; Yao, J.; Zhang, B.; Peng, S.; Ma, H.; Song, Y.; Fang, J. Dithiaarsanes induce oxidative stress-mediated apoptosis in HL-60 cells by selectively targeting thioredoxin reductase. *J. Med. Chem.* **2014**, *57*, 5203−5211.
(29) Cai, W.; Zhang, L.; Song, Y.; Wang, B.; Zhang, B.; Cui, X.; Hu, G.; Liu, Y.; Wu, J.; Fang, J. Small molecule inhibitors of mammalian thioredoxin reductase. *Free Radical Biol. Med.* **2012**, *52*, 257−265.
(30) Cai, W.; Zhang, B.; Duan, D.; Wu, J.; Fang, J. Curcumin targeting the thioredoxin system elevates oxidative stress in HeLa cells. *Toxicol. Appl. Pharmacol.* **2012**, *262*, 341−348.
(31) Rahman, I.; Kode, A.; Biswas, S. K. Assay for quantitative determination of glutathione and glutathione disulfide levels using enzymatic recycling method. *Nat. Protoc.* **2006**, *1*, 3159−3165.
(32) Zhang, L.; Duan, D.; Liu, Y.; Ge, C.; Cui, X.; Sun, J.; Fang, J. Highly selective off-on fluorescent probe for imaging thioredoxin reductase in living cells. *J. Am. Chem. Soc.* **2014**, *136*, 226−233.
(33) Khupse, R. S.; Erhardt, P. W. Total synthesis of xanthohumol. *J. Nat. Prod.* **2007**, *70*, 1507−1509.
(34) Saito, Y.; Nishio, K.; Ogawa, Y.; Kinumi, T.; Yoshida, Y.; Masuo, Y.; Niki, E. Molecular mechanisms of 6-hydroxydopamine-induced cytotoxicity in PC12 cells: involvement of hydrogen peroxide-dependent and -independent action. *Free Radical Biol. Med.* **2007**, *42*, 675−685.
(35) Trippier, P. C.; Jansen Labby, K.; Hawker, D. D.; Mataka, J. J.; Silverman, R. B. Target- and mechanism-based therapeutics for neurodegenerative diseases: strength in numbers. *J. Med. Chem.* **2013**, *56*, 3121−3147.
(36) Klein, J. A.; Ackerman, S. L. Oxidative stress, cell cycle, and neurodegeneration. *J. Clin. Invest.* **2003**, *111*, 785−793.
(37) Freed, C. R.; Greene, P. E.; Breeze, R. E.; Tsai, W. Y.; DuMouchel, W.; Kao, R.; Dillon, S.; Winfield, H.; Culver, S.; Trojanowski, J. Q.; Eidelberg, D.; Fahn, S. Transplantation of embryonic dopamine neurons for severe Parkinson's disease. *N. Engl. J. Med.* **2001**, *344*, 710−719.
(38) Yen, T. L.; Hsu, C. K.; Lu, W. J.; Hsieh, C. Y.; Hsiao, G.; Chou, D. S.; Wu, G. J.; Sheu, J. R. Neuroprotective effects of xanthohumol, a prenylated flavonoid from hops (*Humulus lupulus*), in ischemic stroke of rats. *J. Agric. Food Chem.* **2012**, *60*, 1937−1944.
(39) Krajka-Kuzniak, V.; Paluszczak, J.; Baer-Dubowska, W. Xanthohumol induces phase II enzymes via Nrf2 in human hepatocytes in vitro. *Toxicol. Vitro* **2013**, *27*, 149−156.
(40) Dietz, B. M.; Kang, Y. H.; Liu, G.; Eggler, A. L.; Yao, P.; Chadwick, L. R.; Pauli, G. F.; Farnsworth, N. R.; Mesecar, A. D.; van Breemen, R. B.; Bolton, J. L. Xanthohumol isolated from *Humulus lupulus* inhibits menadione-induced DNA damage through induction of quinone reductase. *Chem. Res. Toxicol.* **2005**, *18*, 1296−1305.
(41) Dietz, B. M.; Hagos, G. K.; Eskra, J. N.; Wijewickrama, G. T.; Anderson, J. R.; Nikolic, D.; Guo, J.; Wright, B.; Chen, S. N.; Pauli, G. F.; van Breemen, R. B.; Bolton, J. L. Differential regulation of detoxification enzymes in hepatic and mammary tissue by hops (*Humulus lupulus*) in vitro and in vivo. *Mol. Nutr. Food Res.* **2013**, *57*, 1055−1066.

DOI: 10.1021/jf505075n
J. Agric. Food Chem. 2015, 63, 1521−1531

(42) Legette, L.; Ma, L.; Reed, R. L.; Miranda, C. L.; Christensen, J. M.; Rodriguez-Proteau, R.; Stevens, J. F. Pharmacokinetics of xanthohumol and metabolites in rats after oral and intravenous administration. *Mol. Nutr. Food Res.* **2012**, *56*, 466−474.
(43) Youdim, K. A.; Shukitt-Hale, B.; Joseph, J. A. Flavonoids and the brain: interactions at the blood-brain barrier and their physiological effects on the central nervous system. *Free Radical Biol. Med.* **2004**, *37*, 1683−1693.
(44) Wilson, A. J.; Kerns, J. K.; Callahan, J. F.; Moody, C. J. Keap calm, and carry on covalently. *J. Med. Chem.* **2013**, *56*, 7463−7476.

DOI: 10.1021/jf505075n
J. Agric. Food Chem. 2015, 63, 1521−1531

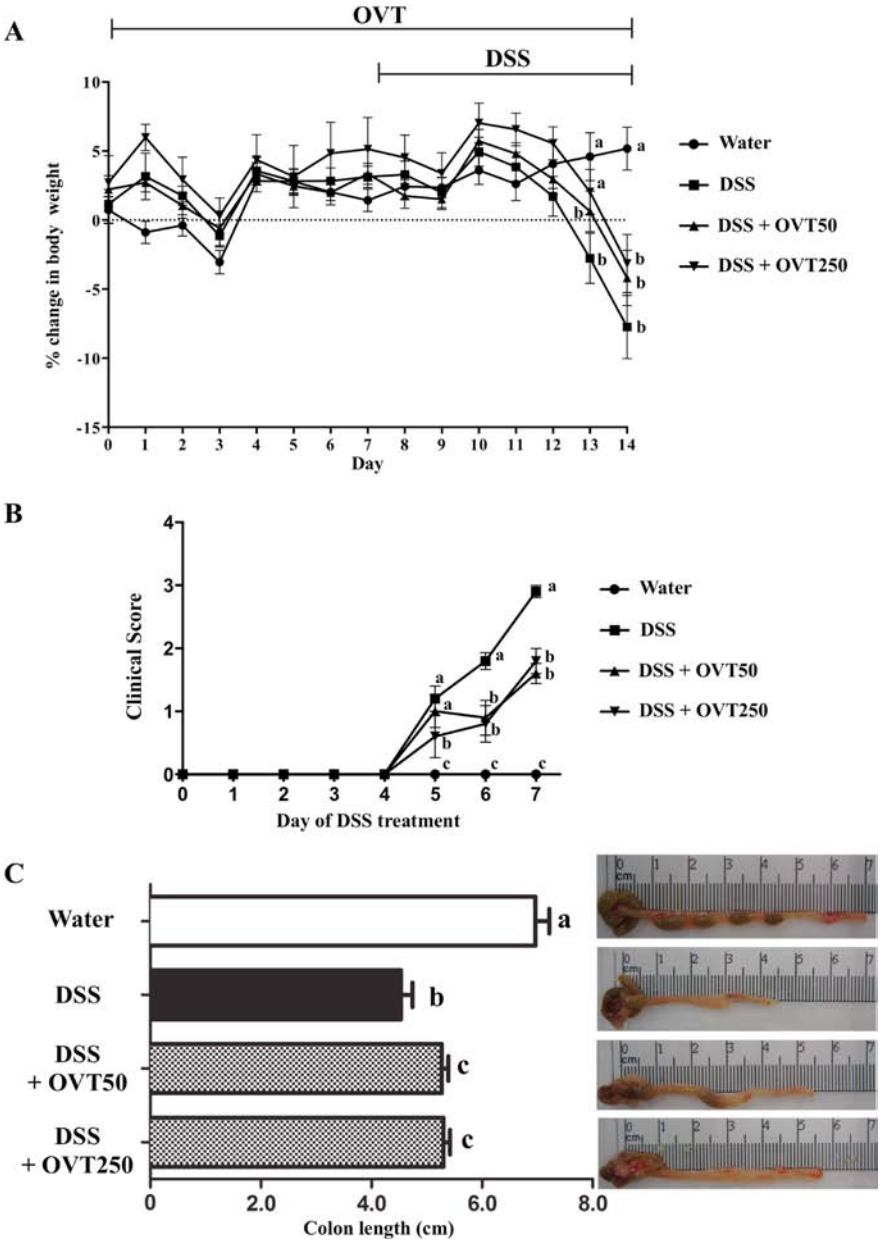

Figure 1. OVT ameliorates DSS-induced colitis. Mice were given 50 or 250 mg/kg BW OVT for 14 days. On day 7, colitis was induced with 5% DSS water. (A) Mice were weighed daily, and changes in body weight are reported as percent change relative to the initial weight. (B) Mice were scored daily for clinical signs of DSS-induced colitis. (C) After 14 days, the extracted colons were measured from the end of cecum to the anus. Data represent the mean ± SEM of n = 10/group. Unless indicated, no significance difference was observed between groups. Values without a common letter are significantly different at $P < 0.05$.

1.0 mL/min for 40 min. The purified OVT was dialyzed (MWCO 8000 tubing) against Milli-Q water and lyophilized. The purity was determined by sodium dodecyl sulfate−polyacrylamide gel electrophoresis (SDS-PAGE) and confirmed as >90% (data not shown).

Induction of Colitis and Sample Treatment. All animal experiments were approved by the University of Guelph Animal Care Committee and carried out in accordance with the Canadian Council of Animal Care Guide to the Care and Use of Experimental Animals (eAUP no. 1536). The experiments for induction of DSS-induced colitis in mice were performed as previously described.[11] Briefly, 40 female BALB/c mice (6−8 weeks; Charles River Laboratories, Montreal, QC, Canada) were randomly divided into four groups (n = 10/group) and housed with a 12 h light/dark cycle with access to standard food and water ad libitum. OVT (50 or 250 mg/kg BW/day) was given by oral gavage for 14 days. On the seventh day, 5% (w/v) DSS (MW 36−50 kDa; MP Biomedical, Solon, OH, USA) was added to drinking water to induce acute colitis for 7 days. The DSS solution was replaced every other day. The negative control group received water only. The positive group received water with DSS for 7 days. Body weights were measured on a daily basis. The daily weight changes were calculated by percent in relation to the initial weight measured. After 14 days, mice were humanely euthanized, and colons were collected and sectioned longitudinally. Colon samples were flash frozen and stored at −80 °C until further analysis.

Clinical Evaluation of Colitis. Mice were examined daily for stool consistency, presence of blood in stool, and general appearance. The clinical scoring was performed as described earlier by Maxwell et al.[20] and defined as follows: stool score, 0 = normal, 1 = moist/sticky stool, 2 = soft stool, 3 = diarrhea; stool blood score, 0 = no blood, 1 = evidence of blood in stool or around anus, 2 = severe bleeding; mouse

DOI: 10.1021/jf505248n
J. Agric. Food Chem. 2015, 63, 1532−1539

appearance, 0 = normal, 1 = ruffled fur or altered gait, 2 = lethargic or moribund.

Cytokine Concentration in Colon Samples. The colons were excised and homogenized in ice-cold phosphate-buffered saline (PBS) containing proteinase inhibitors (1 mM phenylmethanesulfonyl fluoride (PMSF), 0.1 mM ethylenediaminetetraacetic acid (EDTA), 10 μg/mL aprotinin, 10 μg/mL leupeptin, and 10 μg/mL pepstain A; Sigma-Aldrich) for 3 min using a homogenizer (Polytron PT 1200, Kinematica AG, Luzern, Switzerland). The supernatants were collected following centrifugation at 10000*g* for 10 min. The concentration of protein was determined by using a DC protein assay (Bio-Rad), according to the manufacturer's instruction. Tumor necrosis factor (TNF)-α and interleukin (IL)-6 cytokine concentration were determined by ELISA as described earlier.[11] IL-17A was measured using an IL-17A ELISA kit (eBioscience, San Diego, CA, USA), according to the manufacturer's protocol. The following antibodies and standard proteins for ELISA were obtained from BD Bioscience (San Jose, CA, USA): anti-mouse TNF-α, biotin anti-mouse TNF-α, recombinant mouse TNF-α, anti-mouse IL-6, biotin anti-mouse IL-6, recombinant mouse IL-6, and avidin–horseradish peroxidase (Av-HRP). Briefly, 96-well ELISA plates (Corning, Corning, NY, USA) were coated with anti-mouse TNF-α antibody (1:500, diluted in 0.2 M sodium phosphate buffer, pH 6.5) or anti-mouse IL-6 antibody (1:250, diluted in 0.1 M sodium phosphate buffer, pH 9.0) overnight at 4 °C. The plate was blocked with PBS containing 1% bovine serum albumin (BSA; Fisher Scientific, Ottawa, ON, Canada) for 1 h at 37 °C. Colon supernatant samples and diluted standards were added to the plate and incubated for 2 h at 37 °C. Biotin anti-mouse TNF-α (1:500, v/v) or anti-mouse IL-6 antibody (1:500, v/v) was further added and incubated for 1 h at 37 °C. Av-HRP (1:2000, v/v) was added for 0.5 h at 37 °C. The plate was washed three times with PBS-0.05% Tween 20 (PBS-T). Then, 100 μL of 3,3′,5,5′-tetramethylbenzidine (TMB; Sigma-Aldrich) was added to each well, and the reaction was stopped by adding 0.5 N H_2SO_4 (50 μL/well). The absorbance was measured at 450 nm by a plate reader (iMark model 550, Bio-Rad). The concentration of these cytokines was determined from the standard calibration curves and reported as picograms of cytokine relative to protein concentration in the supernatant.

RNA Isolation, cDNA Synthesis, and Real-Time PCR. Total RNA from the colon was extracted according to a previous study.[11] Briefly, the colon was homogenized in Trizol reagent (Life Technologies, Carlsbad, CA, USA) and total RNA was extracted by using an Aurum Total RNA Mini Kit (Bio-Rad) according to the manufacturer's instructions. The quantity and quality of RNA were determined by Nano Drop ND-1000 (Thermo Scientific, Waltham, MA, USA). The cDNA was synthesized using the qScript cDNA synthesis kit (Quanta BioSciences, Gaithersburg, MD, USA), according to the manufacturer's instructions. Real-time quantitative PCR was carried out using PerfeCTa SYBR Green Supermix (Quanta Biosciences) on a MyiQ single-color real-time PCR detection system (Bio-Rad) using the following conditions: denaturation for 15 s at 95 °C, annealing for 15 s at 58 °C, and extension for 30 s at 72 °C. The mouse primers used were as follows: β-actin, forward, 5′-GAAATC-GTGCGTGACATCAAAG-3′, reverse, 5′-TGTAGTTCATGGATG-CCACAG-3′; TNF-α, forward, 5′-CCCCAAAGGGATGAGAAGTT-3′, reverse, 5′-CACTTGGTGGTTTGCTACGA-3′; IL-6, forward, 5′-CCGGAGAGGAGACTTCACAG-3′, reverse, 5′-CAGAATTGC-CATTGCACAAC-3′; IL-1β, forward, 5′-GGATGAGGACATGAG-CACCT-3′, reverse, 5′-AGCTCATATGGGTCCGACAG-3′; interferon (IFN)-γ, forward, 5′-GCTCTTCCTCATGGCTGTTT-3′, reverse, 5′-GTCACCATCCTTTTGCCAGT-3′; monocyte chemoattractant protein (MCP)-1, forward, 5′-CCCAATGAGTAGGCTGGAGA-3′, reverse, 5′-TCTGGACCCATTCCTTCTTG-3′, IL-17A, forward, 5′-CCAGGGAGAGCTTCATCTGT-3′, reverse, 5′-AGGAAGTCC-TTGGCCTCAGT-3′; IL-10, forward, 5′-GCCTTATCGGAAATG-ATCCA-3′, reverse, 5′-AGGGGAGAAATCGATGACAG-3′. These primers were obtained from the University of Guelph Laboratory Services Molecular Biology Section (Guelph, ON, Canada). Relative gene expression was calculated according to the $2^{-\Delta\Delta Ct}$ method[21] using mouse β-actin as an endogenous control for normalization. Results were expressed as fold changes relative to the negative control samples.

Histological Analysis. A section of the distal colon was fixed in 10% (w/v) buffered formalin (Fisher Scientific). Paraffin-embedded sections were stained with hematoxylin and eosin (H&E) (Animal Health Laboratory, University of Guelph, Guelph, ON, Canada). The stained samples were examined using a Leica DMR microscope (Leica Microsystems, Wetzlar, Germany). Histological scoring of the colitic lesions was evaluated in a double-blinded fashion by a pathologist using the previously reported scoring system[11] with respect to the degree, extent, and depth of inflammation and the severity of damage of the glands and epitheliums. The total sum of histologic score ranged from 0 to 19.

Statistical Analysis. The results were expressed as the mean ± SEM. Statistical analyses were performed using GraphPad Prism version 5.0 (GraphPad, San Diego, CA, USA). Statistical differences between curves were analyzed using two-way analysis of variance (ANOVA) followed by Tukey's multiple-comparison test. Statistical differences between individual group were determined using one-way ANOVA followed by Tukey's multiple-comparison test. $P < 0.05$ was considered statistically significant.

RESULTS

Effects of OVT on the Development of DSS-Induced Colitis in Mice. To determine a possible dose-dependent effect of OVT, OVT was administered by oral gavage at two different doses: 50 and 250 mg/kg BW. The DSS treatment for 7 days exacerbated the progression of acute colitis characterized by weight loss, the presence of blood in stool, and diarrhea. As shown in Figure 1A, the ratio of changing body weight in the positive (DSS) group was significantly decreased in the last 2 days of DSS treatment (days 13 and 14 of the study, $P < 0.001$), compared with the negative control (water) group. The high-dose OVT (DSS + OVT250) group had significantly lower body weight loss than the DSS group on the sixth day of DSS treatment (day 13, $P = 0.048$ vs DSS) and tended to be lower on the seventh day (day 14, $P = 0.064$ vs DSS) (Figure 1A). In the low-dose OVT group (DSS + OVT50), the decrease in the ratio of weight change between days 12 and 13 tended to be lower than that in the DSS treatment (DSS, 1.7 ± 1.4 to −2.8 ± 1.8%; DSS + OVT50, 3.0 ± 1.1 to 0.6 ± 1.5%); however, no significant improvement of DSS-induced weight loss was observed (day 13, $P = 0.256$; day 14, $P = 0.221$ vs DSS) (Figure 1A). The average of initial weights did not differ among each group (water group, 17.3 ± 0.4 g; DSS group, 17.0 ± 0.3 g; DSS + OVT50 group, 17.1 ± 0.3 g; DSS + OVT250 group, 16.9 ± 0.3 g). The increase of clinical scores was also observed in the DSS group on the fifth day of DSS treatment ($P < 0.001$), compared with the control group. As shown in Figure 1B, low-dose OVT treatment significantly decreased the severity of DSS-induced clinical signs on the sixth and seventh days of DSS treatment (day 6, $P < 0.001$; day 7, $P < 0.001$ vs DSS) and high-dose treatment also reduced the signs on the fifth, sixth, and seventh days (day 5, $P = 0.003$; day 6, $P < 0.001$; day 7, $P < 0.001$ vs DSS). The consumption of water among groups showed no significant differences during the whole experiment, and no clinical signs were observed in mice before the start of DSS treatment (data not shown). The colon shortening induced by DSS has already been shown to be inversely linked with the severity of DSS-induced colitis in mice.[22] As shown in Figure 1C, the significant shortening of the colon length was confirmed in the DSS group (water, 7.0 ± 0.3 cm; DSS, 4.6 ± 0.2 cm; $P < 0.001$ vs water), whereas both doses of OVT treatment remarkably improved the colon length

DOI: 10.1021/jf505248n
J. Agric. Food Chem. 2015, 63, 1532−1539

(DSS + OVT50, 5.3 ± 0.1 cm, $P = 0.039$; DSS + OVT250, 5.3 ± 0.1 cm, $P = 0.030$ vs DSS).

Effects of OVT on the Expression of Inflammatory Cytokines in DSS-Treated Mice. The anti-inflammatory effects of OVT in the colon were investigated by measuring protein and mRNA expression of the inflammatory cytokines in the colon. As shown in Figure 2, DSS treatment remarkably

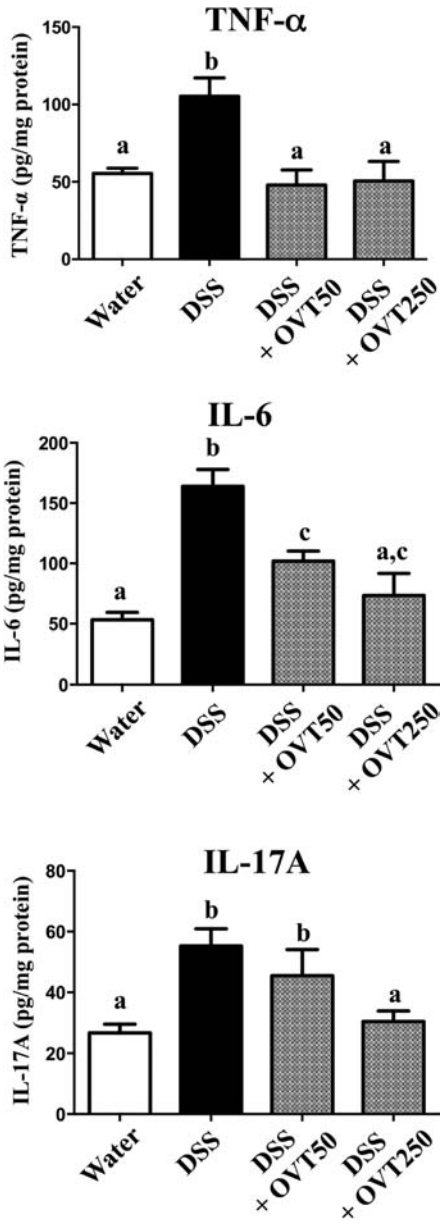

Figure 2. Effect of OVT on inflammatory cytokine protein expression in the colon of DSS-treated mice. Protein expression of TNF-α, IL-6, and IL-17A was determined by ELISA. Results were expressed as picograms of cytokine relative to protein concentration in the colon supernatant. Data represent the mean ± SEM of $n = 10$/group. Values without a common letter are significantly different at $P < 0.05$.

increased the protein expression of TNF-α, IL-6, and IL-17A, compared to the water group (TNF-α, water, 55.4 ± 3.4 pg/mg protein, DSS, 105.4 ± 11.8 pg/mg protein, $P = 0.014$; IL-6, water, 53.2 ± 6.2 pg/mg protein, DSS, 163.9 ± 14.0 pg/mg protein, $P < 0.001$; IL-17A, water, 26.7 ± 2.9 pg/mg protein, DSS, 55.3 ± 5.6 pg/mg protein, $P = 0.010$ vs water). Both doses of OVT significantly inhibited the DSS-induced expression of TNF-α and IL-6 (TNF-α, DSS + OVT50, 47.9 ± 9.8 pg/mg protein, $P = 0.005$; DSS + OVT250, 50.6 ± 12.6 pg/mg protein, $P = 0.007$; IL-6, DSS + OVT50, 102.0 ± 8.4 pg/mg protein, $P = 0.009$; DSS + OVT250, 73.5 ± 16.3 pg/mg protein, $P < 0.001$ vs DSS); high-dose OVT treatment also significantly decreased IL-17A expression (DSS + OVT50, 45.5 ± 8.6 pg/mg protein, $P = 0.561$; DSS + OVT250, 30.5 ± 3.4 pg/mg protein, $P = 0.024$ vs DSS). In addition, as shown in Figure 3, both doses of OVT significantly inhibited the mRNA expression of pro-inflammatory cytokines TNF-α ($P < 0.001$ vs DSS), IL-6 ($P < 0.05$ vs DSS), IL-1β ($P < 0.05$ vs DSS), IFN-γ ($P < 0.01$ vs DSS), MCP-1 ($P < 0.05$ vs DSS), and IL-17A ($P < 0.01$ vs DSS). However, the expression of IL-10, an anti-inflammatory cytokine, was not affected by OVT treatment, suggesting that the anti-inflammatory action of OVT is likely not associated with its ability to inhibit the expression of anti-inflammatory cytokines in the colon.

Effect of OVT on the Histological and Morphological Damage in DSS-Treated Mice. The treatment effects of OVT on histological and morphological damages in the colons were examined following the histological grading system as described before.[11] The observations were confirmed by estimation of biological parameters relevant to colonic inflammation. Colonic inflammation is characterized by severe lesions in the mucosa, alteration of epithelial structure, increase in neutrophil population and lymphocyte infiltration into the mucosal and submucosal areas, and loss of crypts. The colons from the negative control group displayed typical characteristic features of normal glands, abundant goblet cells in epithelium, no mucosal hyperplasia, and a small amount of infiltrated immune cells (Figure 4A). In contrast, the DSS-treated colons displayed severe epithelial damage with extensive loss of glands, depletion of the goblet cells, thickening of the mucosa, cellular infiltration into the submucosa and lamina propria, and destruction of the architecture (Figure 4B), resulting in a high histological score (Figure 4E). Both doses of OVT remarkably ($P < 0.05$) reduced the total histological score (Figure 4E) compared with the DSS group. As shown in Figure 4C,D, OVT-treated colons displayed a decrease in inflammatory cellular infiltration of cells with mild loss of epithelial cells and less expansion of the lesion area. These data suggested that OVT treatment improved the colonic inflammation based on histological analysis, which confirms beneficial preventative effects of OVT on colitis progression.

DISCUSSION

In the present study, we have made progress toward elucidating the mechanism of action of OVT in the amelioration of DSS-induced colitis in mice. Currently, most conventional medical treatments for IBD are mainly based on the use of anti-inflammatory drugs such as 5-aminosalicylates or biological agents such as anti-TNF-α antibody. However, the long-term use of these immunosuppressive agents is associated with strong side effects, including infectious complications that weaken the immune system, resulting in malignancies and severe heart failure.[4] Therefore, complementary and effective treatments for IBD are needed. Several dietary intervention trials have reported beneficial effects in maintaining remission or improving recovery of lesion in IBD patients.[23−28] Our previous in vivo and in vitro studies demonstrated that some egg proteins or peptides[5−9] could ameliorate the colonic inflammatory responses and the development of colitis. OVT

DOI: 10.1021/jf505248n
J. Agric. Food Chem. 2015, 63, 1532−1539

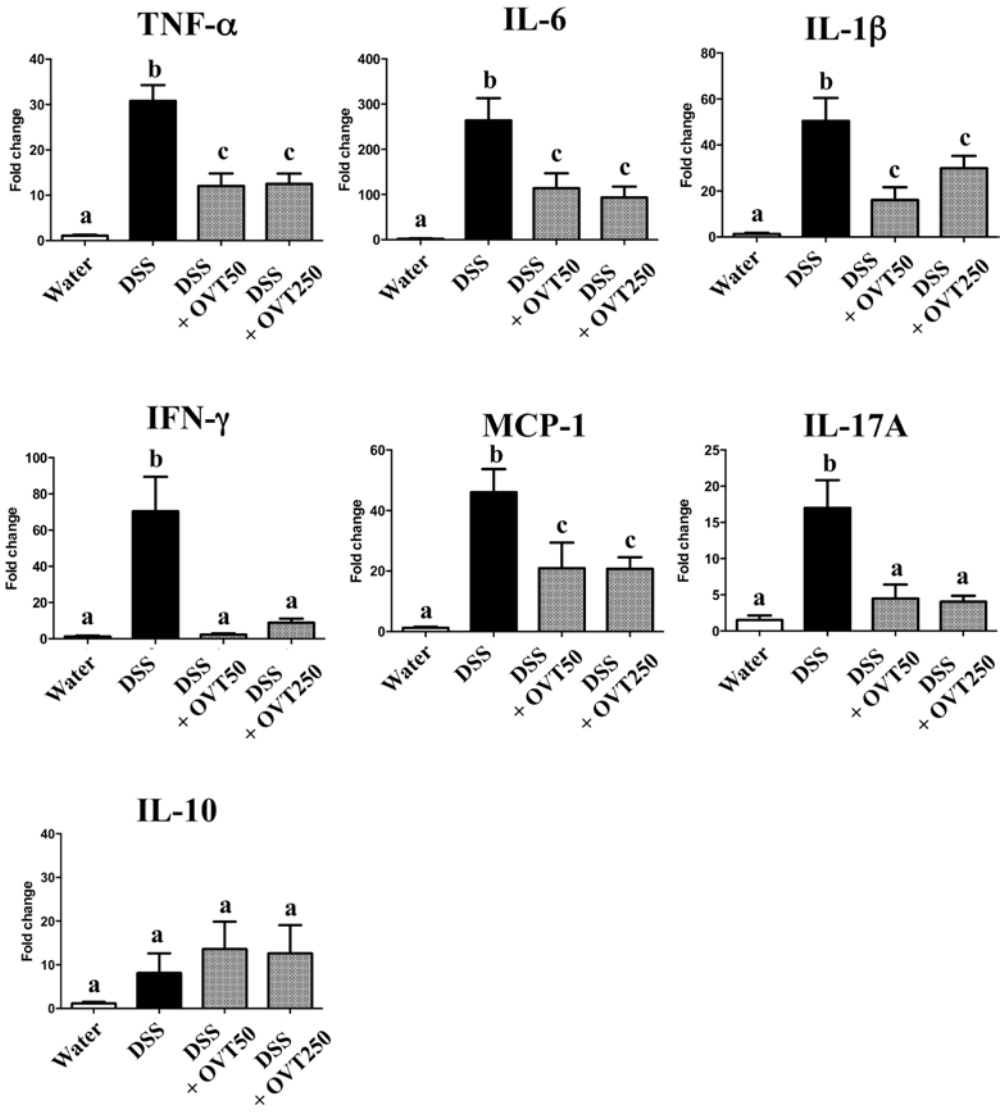

Figure 3. Effect of OVT on inflammatory cytokine gene expression in the colon of DSS-treated mice. Relative mRNA expressions of TNF-α, IL-6, IL-1β, IFN-γ, MCP-1, IL-17A, and IL-10 were measured by real-time PCR. Results were expressed as fold change relative to negative control mice. Data represent the mean ± SEM of n = 10/group. Values without a common letter are significantly different at $P < 0.05$.

has been shown earlier to possess antibacterial activity and antioxidant activity,[17] but the anti-inflammatory effect of OVT on IBD has not been performed yet. To the best of our knowledge, the present study is the first of its kind to demonstrate that OVT (50 or 250 mg/kg BW) successfully attenuated DSS-induced intestinal inflammation in mice. In macroscopic and clinical evaluation analyses, both doses of OVT significantly inhibited clinical signs and colon shortening in DSS-induced colitis mice. In addition, OVT significantly suppressed local expression of cytokines (TNF-α, IL-6, IL-1β, IFN-γ, MCP-1, and IL-17A) in the colon. These results suggested that OVT would block the pathological progress of UC by inhibiting cytokine production. Likewise, histological analysis revealed that OVT improved the function of colon impaired by DSS induction, suggesting OVT was able to attenuate clinical symptoms of colitis in the present study, even at low dose (50 mg/kg BW).

The present study demonstrated that OVT significantly decreased the clinical score and prevented the colon shortening induced by DSS treatment. In addition, the improvement of weight loss was shown in the high-dose group. Cytokines play a crucial role in developing the perpetuating inflammation in IBD. The recruitment of macrophages, neutrophils, and T cells are enhanced by cytokines, resulting in dysregulated immune response and chronic inflammation.[29] Increases in the expression of cytokines, such as TNF-α, IL-6, IL-1β, IFN-γ, and MCP-1, have been shown in both mouse models of DSS-induced colitis[30,31] and IBD patients.[32,33] TNF-α and IL-6 are key cytokines involved in the amplification of mucosal inflammation, including the activation of macrophages, neutrophils, and T cells, in IBD patients.[32] IL-1β is produced by activated macrophages partially through ROS generation[34] and plays a key role in the onset of IBD.[35] IFN-γ is involved in the perpetuation of intestinal inflammation, which increases the severity of IBD in the colon.[36] MCP-1 is involved in the infiltration of immune cells from the bloodstream into the mucosa and submucosa during chronic IBD.[37] Moreover, the involvement of IL-17A in the pathogenesis of IBD has recently been explored. IL-17A was known to be produced mainly in a subset of T lymphocytes named Th17. Jiang et al.[38] reported that the increase of Th17 cells and Th17-related cytokines was correlated with the elevation of disease activity in IBD patients.

DOI: 10.1021/jf505248n
J. Agric. Food Chem. 2015, 63, 1532−1539

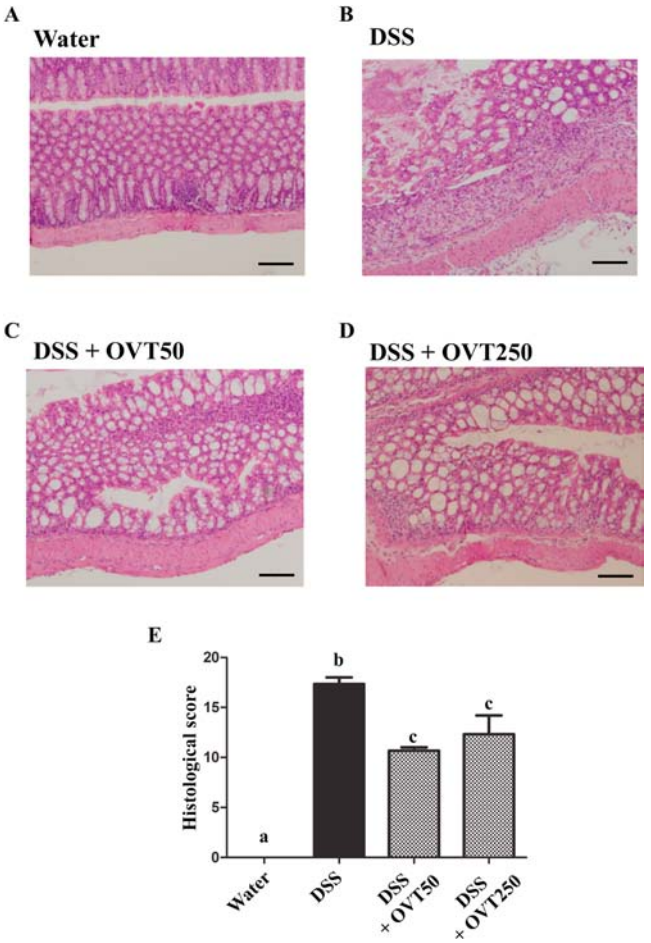

Figure 4. Effect of OVT on colon histology. (A–D) Representative H&E-stained colon sections are shown at 4× magnification. Black scale bar indicates 100 μm for all panels. (E) Colon sections were scored for DSS-induced colonic inflammation and tissue injury as previously described.[11] Data represent the mean ± SEM of $n = 3$. Values without a common letter are significantly different at $P < 0.05$.

Ito et al.[39] demonstrated that deficient IL-17A gene expression contributed to the prevention of the progression of colitis in DSS-treated mice through the inhibition of MCP-1 expression and neutrophil infiltration. IL-1β,[40] IL-6, and transforming growth factor-β (TGF-β)[41] were shown to be involved in the induction of Th17 differentiation, which in turn accelerated the secretion of IL-17A associated with neutrophil infiltration. Here, we have demonstrated that OVT treatment significantly reduced the expression of the cytokine proteins (TNF-α and IL-6) and mRNA (TNF-α, IL-6, IL-1β, IFN-γ, MCP-1, and IL-17A) in the colonic tissue. The significant decrease of IL-17A protein was not observed in low-dose OVT, but this low dose significantly inhibited the mRNA expression of IL-17A, IL-1β, IL-6, and MCP-1 that might be involved in Th17-related inflammatory pathways and improved the colitic histological score. These results are consistent with other recent studies which demonstrated that dipeptide Ala-Gln[42] or the immune milk[43] treatment could reduce the Th17-related inflammation responses and improve the histological damage in the colon of DSS-treated mice, suggesting OVT may be involved in the regulation of IL-17A-related inflammatory responses.

The OVT hydrolysates produced by acidic or enzymatic digestion have been indicated to possesses higher antioxidant activity than the native protein.[19] In addition, tripeptides Ile-Arg-Trp and Ile-Gln-Trp, derived from OVT, were found to attenuate TNF-α-induced inflammatory responses and oxidative stress in vascular endothelial cells.[44] The underlying molecular mechanisms of anti-inflammatory effect by OVT were not fully investigated, but these findings suggested the possibility of involvement in the prevention of IBD by OVT-derived peptides. Further experiments to examine the anti-inflammatory effects and underlying mechanisms of OVT and OVT hydrolysates are in progress.

In conclusion, we demonstrated for the first time the potent immune-modulating property of the egg white protein ovotransferrin. The administration of OVT prevented the progression of DSS-induced colitis in mice and had a preventative effect by inhibiting the epithelial dysfunction and modulating the cytokine profile. We suggest that OVT may be validated as a potential effective agent in the management of chronic intestinal inflammatory diseases.

AUTHOR INFORMATION

Corresponding Author

*(Y.M.) Phone: (519) 824-4120. Fax: (519) 824-6631. E-mail: ymine@uoguelph.ca.

Funding

This study was supported in part by the Advanced Foods and Materials Network (AFMNet), part of the Networks of Centre of Excellence (NCE), Canada, to Y.M., by a grand-in-aid from the Ministry of Education, Science, Sports and Culture of Japan (No. 22248014) to T.M., and by the JSPS Research Fellowship for Young Scientists to Y.K.

Notes

The authors declare no competing financial interest.

ACKNOWLEDGMENTS

We thank Annette Morrison, Maka Natsvlishvili, and Jackie Rombeek for their assistance with the animal studies.

ABBREVIATIONS USED

OVT, ovotransferrin; IBD, inflammatory bowel disease; DSS, dextran sodium sulfate; CD, Crohn's disease; UC, ulcerative colitis; SDS-PAGE, sodium dodecyl sulfate–polyacrylamide gel electrophoresis; PBS, phosphate-buffered saline; PMSF, phenylmethanesulfonyl fluoride; EDTA, ethylenediaminetetraacetic acid; TNF, tumor necrosis factor; IL, interleukin; Av-HRP, avidin–horseradish peroxidase; BSA, bovine serum albumin; TMB, 3,3′,5,5′-tetramethylbenzidine; IFN, interferon; MCP, monocyte chemoattractant protein; H&E, hematoxylin and eosin; TGF, transforming growth factor

REFERENCES

(1) Calder, P. C.; Albers, R.; Antoine, J. M.; Blum, S.; Bourdet-Sicard, R.; Ferns, G. A.; Folkerts, G.; Friedmann, P. S.; Frost, G. S.; Guarner, F.; Lovik, M.; Macfarlane, S.; Meyer, P. D.; M'Rabet, L.; Serafini, M.; Eden, W. V.; Loo, J. V.; Dias, W. V.; Virdy, S.; Winklhofer-Roob, B. M.; Zhao, J. Inflammatory disease processes and interactions with nutrition. *Br. J. Nutr.* **2009**, *101* (Suppl.), S1–S45.

(2) Kim, E. R.; Chang, D. K. Colorectal cancer in inflammatory bowel disease: the risk, pathogenesis, prevention and diagnosis. *World J. Gastroenterol.* **2014**, *20*, 9872–9881.

(3) Pithadia, A. B.; Jain, S. Treatment of inflammatory bowel disease (IBD). *Pharmacol. Rep.* **2011**, *63*, 629–642.

(4) Stallmach, A.; Hagel, S.; Bruns, T. Adverse effects of biologics used for treating IBD. *Best Pract. Res. Clin. Gastroenterol.* **2010**, *24*, 167–182.

DOI: 10.1021/jf505248n
J. Agric. Food Chem. 2015, 63, 1532–1539

(5) Lee, M.; Kovacs-Nolan, J.; Yang, C.; Archbold, T.; Fan, M. Z.; Mine, Y. Hen egg lysozyme attenuates inflammation and modulates local gene expression in a porcine model of dextran sodium sulfate (DSS)-induced colitis. *J. Agric. Food Chem.* **2009**, *57*, 2233−2240.
(6) Katayama, S.; Xu, X.; Fan, M. Z.; Mine, Y. Antioxidative stress activity of oligophosphopeptides derived from hen egg yolk phosvitin in Caco-2 cells. *J. Agric. Food Chem.* **2006**, *54*, 773−778.
(7) Katayama, S.; Ishikawa, S.; Fan, M. Z.; Mine, Y. Oligophosphopeptides derived from egg yolk phosvitin up-regulate gamma-glutamylcysteine synthetase and antioxidant enzymes against oxidative stress in Caco-2 cells. *J. Agric. Food Chem.* **2007**, *55*, 2829−2835.
(8) Young, D.; Fan, M. Z.; Mine, Y. Egg yolk peptides up-regulate glutathione synthesis and antioxidant enzyme activities in a porcine model of intestinal oxidative stress. *J. Agric. Food Chem.* **2010**, *58*, 7624−7633.
(9) Young, D.; Nau, F.; Pasco, M.; Mine, Y. Identification of hen egg yolk-derived phosvitin phosphopeptides and their effects on gene expression profiling against oxidative stress-induced Caco-2 cells. *J. Agric. Food Chem.* **2011**, *59*, 9207−9218.
(10) Young, D.; Ibuki, M.; Nakamori, T.; Fan, M.; Mine, Y. Soy-derived di- and tripeptides alleviate colon and ileum inflammation in pigs with dextran sodium sulfate-induced colitis. *J. Nutr.* **2012**, *142*, 363−368.
(11) Kovacs-Nolan, J.; Zhang, H.; Ibuki, M.; Nakamori, T.; Yoshiura, K.; Turner, P. V.; Matsui, T.; Mine, Y. The PepT1-transportable soy tripeptide VPY reduces intestinal inflammation. *Biochim. Biophys. Acta* **2012**, *1820*, 1753−1763.
(12) Kim, C. J.; Kovacs-Nolan, J.; Yang, C.; Archbold, T.; Fan, M. Z.; Mine, Y. L-Cysteine supplementation attenuates local inflammation and restores gut homeostasis in a porcine model of colitis. *Biochim. Biophys. Acta* **2009**, *1790*, 1161−1169.
(13) Kim, C. J.; Kovacs-Nolan, J.; Yang, C.; Archbold, T.; Fan, M. Z.; Mine, Y. L-Tryptophan exhibits therapeutic function in a porcine model of dextran sodium sulfate (DSS)-induced colitis. *J. Nutr. Biochem.* **2010**, *21*, 468−475.
(14) Ibuki, M.; Fukui, K.; Kanatani, H.; Mine, Y. Anti-inflammatory effects of mannanase-hydrolyzed copra meal in a porcine model of colitis. *J. Vet. Med. Sci.* **2014**, *76*, 645−651.
(15) Lee, I. A.; Park, Y. J.; Yeo, H. K.; Han, M. J.; Kim, D. H. Soyasaponin I attenuates TNBS-induced colitis in mice by inhibiting NF-κB pathway. *J. Agric. Food Chem.* **2010**, *58*, 10929−10934.
(16) Giner, E.; Andu, I.; Recio, M. C.; Luis, J.; Cerda, J. M.; Giner, R. M. Oleuropein ameliorates acute colitis in mice. *J. Agric. Food Chem.* **2011**, *59*, 12882−12892.
(17) Kovacs-Nolan, J.; Phillips, M.; Mine, Y. Advances in the value of eggs and egg components for human health. *J. Agric. Food Chem.* **2005**, *53*, 8421−8431.
(18) Rupa, P.; Nakamura, S.; Katayama, S.; Mine, Y. Effects of ovalbumin glycoconjugates on alleviation of orally induced egg allergy in mice via dendritic-cell maturation and T-cell activation. *Mol. Nutr. Food Res.* **2014**, *58*, 405−417.
(19) Kim, J.; Moon, S.; Ahn, D.; Paik, H.; Park, E. Antioxidant effects of ovotransferrin and its hydrolysates. *Poult. Sci.* **2012**, 2747−2754.
(20) Maxwell, J. R.; Brown, W. A.; Smith, C. L.; Byrne, F. R.; Viney, J. L. Methods of inducing inflammatory bowel disease in mice. *Curr. Protoc. Pharmacol.* **2009**, *47*, 5.58.1−5.58.37.
(21) Livak, K. J.; Schmittgen, T. D. Analysis of relative gene expression data using real-time quantitative PCR and the 2(-ΔΔCt) method. *Methods* **2001**, *25*, 402−408.
(22) Okayasu, I.; Hatakeyama, S.; Yamada, M.; Ohkusa, T.; Inagaki, Y.; Nakaya, R. A novel method in the induction of reliable experimental acute and chronic ulcerative colitis in mice. *Gastroenterology* **1990**, *98*, 694−702.
(23) Jonkers, D.; Stockbrugger, R. Probiotics and inflammatory bowel diseases. *J. R. Soc. Med.* **2003**, *96*, 167−171.
(24) Baroja, L.; Kirjavainen, P.; Hekmat, S.; Reid, G. Anti-inflammatory effects of probiotic yogurt in inflammatory bowel disease patients. *Clin. Exp. Immunol.* **2007**, *149*, 470−479.
(25) Olendzki, B. C.; Silverstein, T. D.; Persuitte, G. M.; Ma, Y.; Baldwin, K. R.; Cave, D. An anti-inflammatory diet as treatment for inflammatory bowel disease: a case series report. *Nutr. J.* **2014**, *13*, 5.
(26) Jang, S. E.; Jung, J. J.; Hyan, S. R.; Han, M. J.; Kim, D. H. Ursolic acid isolated from the seed of *Cornus officinalis* ameliorates colitis in mice by inhibiting the binding of lipopolysaccharide to Toll-like receptor 4 on macrophages. *J. Agric. Food Chem.* **2014**, *62*, 9711−9721.
(27) Algieri, F.; Rodríguez-Nogales, A.; Garrido-Mesa, N.; Vezza, T.; Garrido-Mesa, J.; Utrilla, M. P.; Montilla, A.; Cardelle-Cobas, A.; Olano, A.; Corzo, N.; Guerra-Hernández, E.; Zarzuelo, A.; Rodriguez-Cabezas, M. E.; Julio Galvez, J. Intestinal anti-inflammatory effects of oligosaccharides derived from lactulose in the trinitrobenzenesulfonic acid model of rat colitis. *J. Agric. Food Chem.* **2014**, *62*, 4285−4297.
(28) Kiyono, T.; Hirooka, K.; Yamamoto, Y.; Kuniishi, S.; Ohtsuka, M.; Kimura, S.; Young Park, E. Y.; Nakamura, Y.; Sato, K. Identification of pyroglutamyl peptides in Japanese rice wine (sake): presence of hepatoprotective PyroGlu-Leu. *J. Agric. Food Chem.* **2013**, *61*, 11660−11667.
(29) Sartor, R. B. Mechanisms of disease: pathogenesis of Crohn's disease and ulcerative colitis. *Nat. Clin. Pract. Gastroenterol. Hepatol.* **2006**, *3*, 390−407.
(30) Dutra, R. C.; Claudino, R. F.; Bento, A. F.; Marcon, R.; Schmidt, E. C.; Bouzon, Z. L.; Pianowski, L. F.; Calixto, J. B. Preventive and therapeutic euphol treatment attenuates experimental colitis in mice. *PLoS One* **2011**, *6*, No. e27122.
(31) Mishra, S. K.; Kang, J. H.; Kim, D. K.; Oh, S. H.; Kim, M. K. Orally administered aqueous extract of *Inonotus obliquus* ameliorates acute inflammation in dextran sulfate sodium (DSS)-induced colitis in mice. *J. Ethnopharmacol.* **2012**, *143*, 524−532.
(32) Beck, P. L.; Wallace, J. L. Cytokines in inflammatory bowel disease. *Mediators Inflamm.* **1997**, *6*, 95−103.
(33) Banks, C.; Bateman, A.; Payne, R.; Johnson, P.; Sheron, N. Chemokine expression in IBD. mucosal chemokine expression is unselectively increased in both ulcerative colitis and Crohn's disease. *J. Pathol.* **2003**, *199*, 28−35.
(34) Kwon, K. H.; Ohigashi, H.; Murakami, A. Dextran sulfate sodium enhances interleukin-1β release via activation of p38 MAPK and ERK1/2 pathways in murine peritoneal macrophages. *Life Sci.* **2007**, *81*, 362−371.
(35) Kwon, K. H.; Murakami, A.; Hayashi, R.; Ohigashi, H. Interleukin-1β targets interleukin-6 in progressing dextran sulfate sodium-induced experimental colitis. *Biochem. Biophys. Res. Commun.* **2005**, *337*, 647−654.
(36) Obermeier, F.; Kojouharoff, G.; Hans, W.; Schölmerich, J.; Gross, V.; Falk, W. Interferon-gamma (IFN-γ)- and tumour necrosis factor (TNF)-induced nitric oxide as toxic effector molecule in chronic dextran sulphate sodium (DSS)-induced colitis in mice. *Clin. Exp. Immunol.* **1999**, *116*, 238−245.
(37) Grimm, M.; Elsbury, S.; Pavil, P.; Doe, W. Enhanced expression and production of monocyte chemoattractant protein-1 in inflammatory bowel disease mucosa. *J. Leukocyte Biol.* **1996**, *59*, 804−812.
(38) Jiang, W.; Su, J.; Zhang, X.; Cheng, X.; Zhou, J.; Shi, R.; Zhang, H. Elevated levels of Th17 cells and Th17-related cytokines are associated with disease activity in patients with inflammatory bowel disease. *Inflamm. Res.* **2014**, *63*, 943−950.
(39) Ito, R.; Kita, M.; Shin-Ya, M.; Kishida, T.; Urano, A.; Takada, R.; Sakagami, J.; Imanishi, J.; Iwakura, Y.; Okanoue, T.; Yshikawa, T.; Kataoka, K.; Mazda, O. Involvement of IL-17A in the pathogenesis of DSS-induced colitis in mice. *Biochem. Biophys. Res. Commun.* **2008**, *377*, 12−16.
(40) Coccia, M.; Harrison, O. J.; Schiering, C.; Asquith, M. J.; Becher, B.; Powrie, F.; Maloy, K. J. IL-1β mediates chronic intestinal inflammation by promoting the accumulation of IL-17A secreting innate lymphoid cells and $CD4^+$ Th17 cells. *J. Exp. Med.* **2012**, *209*, 1595−1609.
(41) Iwakura, Y.; Nakae, S.; Saijo, S.; Ishigame, H. The roles of IL-17A in inflammatory immune responses and host defense against pathogens. *Immunol. Rev.* **2008**, *226*, 57−79.

DOI: 10.1021/jf505248n
J. Agric. Food Chem. 2015, 63, 1532−1539

(42) Hou, Y. C.; Liu, J. J.; Pai, M. H.; Tsou, S. S.; Yeh, S. L. Alanyl-glutamine administration suppresses Th17 and reduces inflammatory reaction in dextran sulfate sodium-induced acute colitis. *Int. Immunopharmacol.* **2013**, *17*, 1−8.
(43) Wang, Y.; Lin, L.; Yin, C.; Othtani, S.; Aoyama, K.; Lu, C.; Sun, X.; Yoshikai, Y. Oral administration of bovine milk from cows hyperimmunized with intestinal bacterin stimulates lamina propria T lmphocytes to produce Th1-biased cytokines in mice. *Int. J. Mol. Sci.* **2014**, *15*, 5458−5471.
(44) Majumder, K.; Chakrabarti, S.; Davidge, S. T.; Wu, J. Structure and activity study of egg protein ovotransferrin derived peptides (IRW and IQW) on endothelial inflammatory response and oxidative stress. *J. Agric. Food Chem.* **2013**, *61*, 2120−2129.

DOI: 10.1021/jf505248n
J. Agric. Food Chem. 2015, 63, 1532−1539

IV colorectal adenocarcinoma, in which cancer cells have spread to nearby lymph nodes and other organs or tissues (common destinations: liver and lungs). The irinotecan-resistant (CPT-11-R) LoVo colon cancer cell line was originally constructed by challenging parental LoVo cells with increasing doses of CPT-11.[11]

CPT-11-R cells were previously shown to activate the EGFR/IKKα/β/NF-κB pathway, leading to increased basal autophagy.[11] NF-κB mediates chemoresistance and activates autophagy in cancer cells.[12−15] In addition, NF-κB is a molecular target in treatments of a variety of cancers, including colon cancer.[16]

TQ is a 164.2 g/mol phytochemical from *Nigella sativa* and displayed different pharmaceutical functions, such as analgesic, anticancer, and antioxidation in the heart.[17−19] TQ was shown to have anticancer effects against a variety of cancers, such as brain, breast, colon, liver, lung, and prostate cancers.[20−23] Moreover, TQ was shown to alter activity of different mitogen-activated protein kinases (MAPKs) in treating cancers.[24−26]

Certain cancer treatments, such as curcumin, genistein, and resveratrol, are able to activate autophagy, leading to caspase-independent cancer cell death.[27] Under stressful conditions, the mitochondrial outer membrane can become permeabilized, leading to abnormal mitochondrial membrane potential, namely, MOMP.[28] MOMP has been known to result in apoptosis. In addition, MOMP also causes mitophagy, a special type of autophagy that involves engulfment of permeabilized mitochondria into autophagosomes and subsequent degradation of the cargos and mitochondrial proteins. LAMP2 is a lysosomal protein that mediates fusion of lysosome and autophagosome,[29] and SQSTM1/p62 is a receptor for mitophagy.[30] These two serve as mitophagy markers. In addition, some phytochemicals, such as sulforaphane[31] and pentagalloylglucose (PGG),[32] were reported to induce caspase-independent, autophagic cell death (ACD) in cancer cells.

The purpose of this study was to investigate the mechanism through which TQ induces death of CPT-11-R LoVo colon cancer cells.

MATERIALS AND METHODS

Cell Culture. The LoVo colon cancer cell line was purchased from Bioresource Collection and Research Center (BCRC, Hsinchu, Taiwan). The CPT-11-R LoVo colon cancer cell line was constructed by stepwise challenges of CPT-11 (described previously).[11] CPT-11-R cells were cultured in Dulbecco's modified Eagle's medium (DMEM,Sigma-Aldrich, St. Louis, MO) with 10% cosmic calf serum (CCS, HyClone, Logan, UT) in humidified air with 5% CO_2 at 37 °C. The cell medium was changed 48 h after sub-cultivation. A total of 3.5 mL of Dulbecco's phosphate-buffered saline (PBS, GIBCO, Auckland, New Zealand) was used to wash each 10 cm culture plate or vessel. CPT-11-R cells were treated with bafilomycin-A1 (Baf-A1, lysosome inhibitor, Calbiochem, Billerica, MA), LY294002 (class I and III PI3K inhibitor, Promega, Madison, WI), 3-methyladenine (3-MA, class III PI3K inhibitor, Sigma, St. Louis, MO), SB230580 (p38 inhibitor, Promega, Madison, WI), SP600125 (JNK inhibitor, Sigma-Aldrich, St. Louis, MO), TQ (Sigma-Aldrich, St. Louis, MO), or *Z*-DEVD-fluoromethylketone (*Z*-DEVD-fmk, caspase 3 inhibitor, BioVision, Milpitas, CA) for later experiments.

Immunofluorescence Microscopy. CPT-11-R cells were grown in a 12 well plate (1×10^5 cells/well) containing DMEM (10% CCS). After 12 h, different doses of TQ (2, 4, 6, and 8 μM) were added to appropriate wells. After 24 h of administration of TQ, the plates were washed with 1× PBS (0.5 mL/well) 3 times. Then, 0.5 mL of fixation solution (4% paraformaldehyde in 1× PBS) was added to each well to fix the cells for 1 h at room temperature (RT). In the process of cell permeabilization, 0.5 mL of permeabilization solution (0.1% Triton X-100 in 0.1% sodium citrate) was added to cells in each well and the plate was rest on ice for 2 min without shaking. A 10% CCS was added to wells to prevent non-specific binding. Stock primary antibody solution was diluted 100× with 1× PBS, and the diluted solution was added to each well (500 μL/well). Then, the plate was sealed in a plastic wrap, shaken for 20 s at RT, and stored at 4 °C for at least 24 h. The diluted primary antibody solution was then recycled. Stock secondary antibody solution was diluted 100× with 1× PBS, and the diluted solution was added to each well (500 μL/well). Then, the plate was sealed in a tin foil, shaken for 20 s at RT, and stored at RT. The diluted secondary antibody solution was discarded. A total of 500 μL of 10000× diluted DAPI was added to each well. The plate was covered with a tin foil and rested for 30 min at RT. Then, each well was washed with 0.5 mL of 1× PBS 3 times at RT and added with 0.6 mL of 1× PBS. Finally, the cells were observed under a confocal microscope.

The following primary antibody was used in this assay for different experiments: anti-LC3 (Cell Signaling, Boston, MA). The following fluorescent secondary antibody was used in this assay for different experiments: Alexa Fluor488 goat anti-rabbit IgG (H+L), 2 mg/mL (green, Invitrogen, Carlsbad, CA).

JC-1 Staining Assay. CPT-11-R cells were grown in 12 well plates (1×10^5 cells/well) containing DMEM (10% CCS). After 12 h, different doses of TQ (2, 4, 6, and 8 μM) were added to appropriate wells. After 24 h of administration of TQ, 25 μL of 200× JC-1 stock solution (1 mg/mL, Sigma, St. Louis, MO) was mixed with 4 mL of deionized distilled water (DDW) and 1 mL of 5× JC-1 staining buffer (avoiding light, Sigma, St. Louis, MO) to make the JC-1 staining mixture. A total of 0.5 mL of JC-1 staining mixture per well was added. The plates were covered with tin foils and placed in humidified air with 5% CO_2 at 37 °C for 30 min. During incubation, 5× JC-1 staining buffer was mixed with DDW in a 1:4 ratio (washing buffer). Each well was washed with 0.5 mL of washing buffer 3 times after incubation. Finally, 3 mL of DMEM (10% CCS) was added to each well, and then cells were observed under a fluorescent microscope using Cy3 (red; excitation, 525 nm; emission, 590 nm) and FITC (green; excitation, 490 nm; emission, 530 nm).

TUNEL Assay. CPT-11-R cells were grown in a 12 well plate (1×10^5 cells/well) containing DMEM (10% CCS). After 12 hours, different doses of TQ (2, 4, 6, and 8 μM) were added to appropriate wells. After 24 h of administration of TQ, each well was washed with 1× PBS (1 mL/well) and incubated with fixation solution (1 mL/well, 4% paraformaldehyde in 1× PBS at pH 7.4) at RT for 1 h. Blocking buffer (3% H_2O_2 in 100% methanol) was added (1 mL/well), and the plate was rested for 10 min at RT. Permeabilization solution (0.1% Triton X-100 in 0.1% sodium citrate) was added (0.5 mL/well), and the 12 well plate was placed on ice for 2 min without shaking. A 10× diluted TUNEL reagent [Enzyme Solution and Label Solution (In Situ Cell Death Detection Kit), Roche, Indianapolis, IN] was added (200−250 μL/well), and the plate was placed in humidified air at 37 °C, avoiding light for 1 h for the reagent to react with cell nuclei. A 10000× diluted DAPI per well was added (200 μL/well), and the plate was covered with tin foil and rested for 25 min. Finally, the cells were observed under a fluorescent microscope.

Western Blotting. CPT-11-R LoVo colon cancer cells were grown in 10 cm culture dishes containing DMEM (10% CCS) at 80−90% confluency. After 12 h, different doses of TQ (2, 4, 6, and 8 μM) were added to appropriate plates. After 24 h of administration of TQ, cells from each plate were collected with cell lysis buffer [50 mM Tris base (pH 7.5), 0.5 M NaCl, 1 mM EDTA (pH 8.0), 1 mM β-mercaptoethanol, 1% NP40, 1% glycerol, and protease inhibitor] (100 μL/plate). Equal amounts of protein samples (40 μg) were separated by 12% sodium dodecyl sulfate−polyacrylamide gel electrophoresis (75 V, 2.5 h) in running buffer (0.3% Tris base, 1.47% glycine, and 0.1% SDS) and then transferred to polyvinylidene difluoride (PVDF) membranes (100 V, 2 h) in transfer buffer (0.3% Tris base, 1.44% glycine, and 20% methanol), which were incubated in blocking buffer [5% milk in 1× TBS (0.13% Tris base, 0.9% NaCl, and 0.05% Tween-20)] for 1 h at RT. PVDF membranes were rocked in 1:1000 primary antibody solutions at least once overnight at 4 °C. Then, PVDF membranes were incubated in 1:1000 secondary antibody solutions for 1 h at RT. Finally, the results were detected with a LAS-3000 luminescent image analyzer (Fujifilm, Tokyo, Japan).

DOI: 10.1021/jf5054063
J. Agric. Food Chem. 2015, 63, 1540−1546

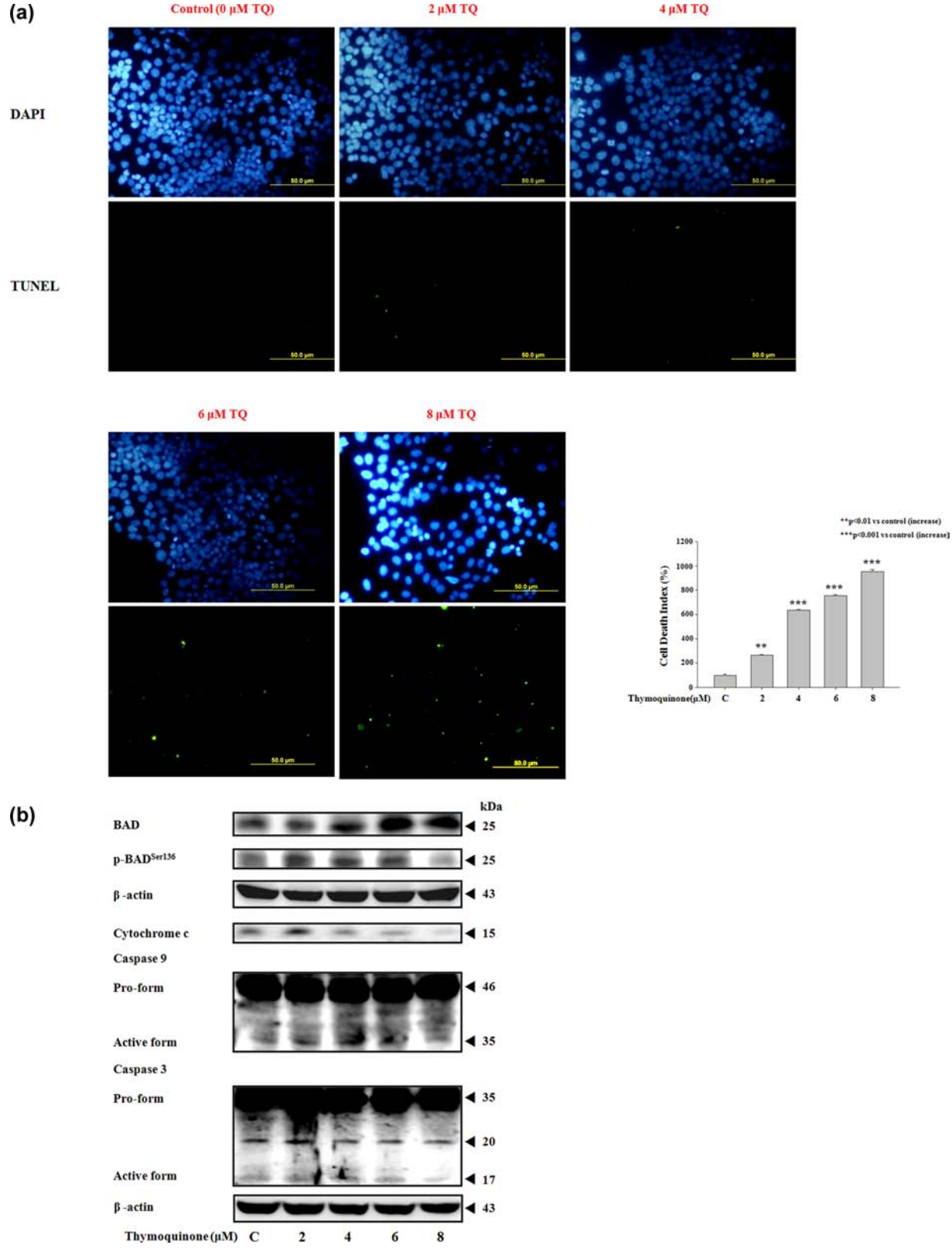

Figure 1. TQ resulted in increasing total cell death index but did not upregulate apoptosis at increasing doses. (a) After 12 h of seeding CPT-11-R LoVo colon cancer cells in 12 well culture plates, different doses of TQ were added. The TUNEL assay was conducted 24 h after administration of TQ. TQ elevated the percentage of TUNEL-positive cells/total cell death index of CPT-11-R cells. (b) After 12 h of seeding CPT-11-R cells in 10 cm culture plates, different doses of TQ were added. Western blotting was conducted 24 h after administration of TQ. TQ resulted in an initial activation of apoptosis, which decreased at increasing doses of the phytochemical.

Statistical Analysis. Each sample was analyzed on the basis of results that were repeated at least 3 times, and SigmaPlot 10.0 software and standard *t* test were used to analyze each numeric data. In all cases, differences at $p < 0.05$ were regarded as statistically significant; differences at $p < 0.01$ or $p < 0.001$ were considered to have higher statistical significance.

DOI: 10.1021/jf5054063
J. Agric. Food Chem. 2015, 63, 1540−1546

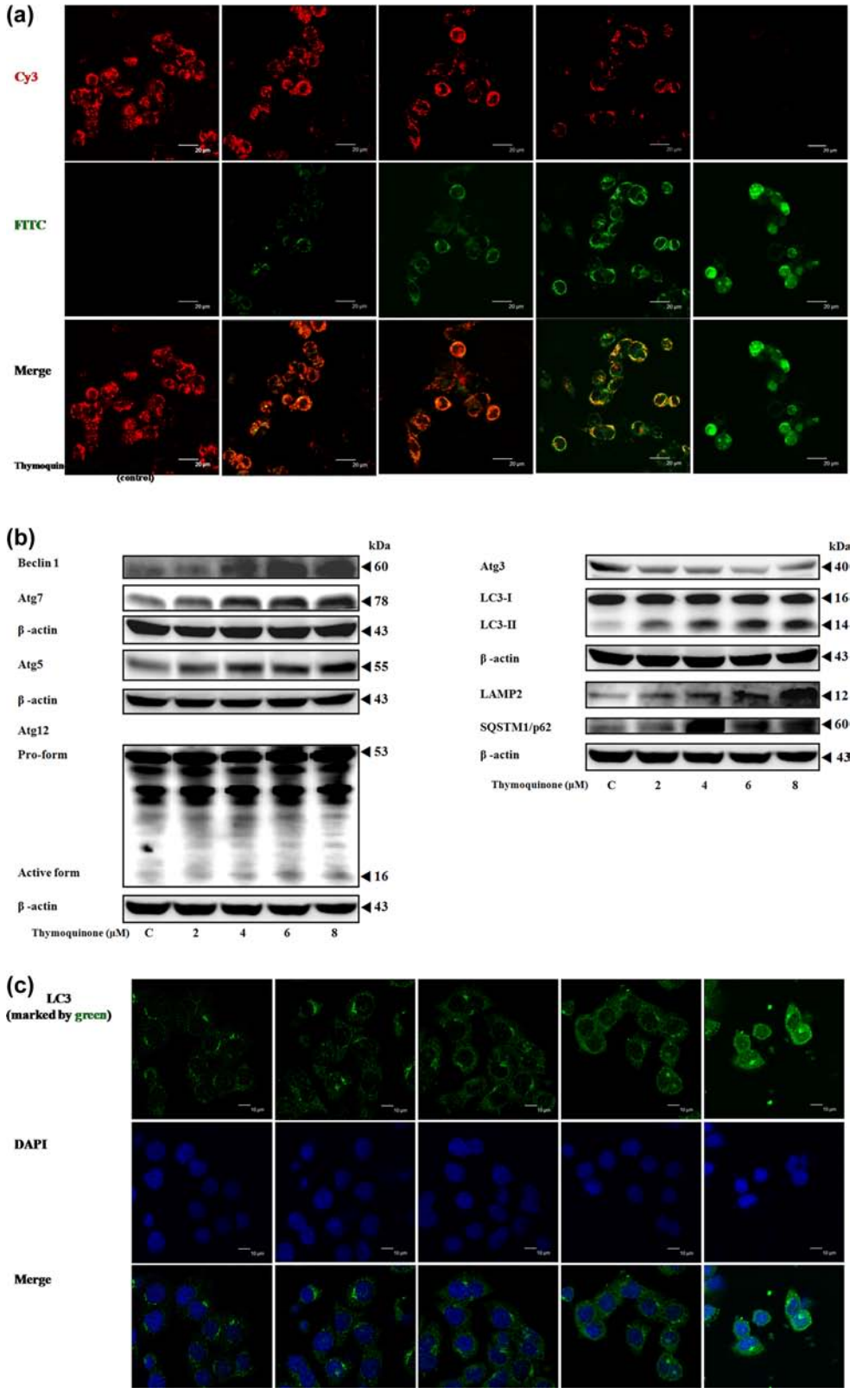

Figure 2. TQ induced ACD of CPT-11-R cells involving MOMP. (a) After 12 h of seeding CPT-11-R cells in 10 cm culture plates, different doses of TQ were added. JC-1 staining was conducted 24 h after administration of TQ. TQ increased the FITC (JC-1 monomer) signal and reduced the Cy3 (JC-1 aggregate) signal dose-dependently. (b) After 12 h of seeding CPT-11-R cells in 10 cm culture plates, different doses of TQ were added. Western blotting was conducted 24 h after administration of TQ. TQ caused increased Atg5, Atg7, Atg12, Beclin-1, LC3-II, LAMP2, and SQSTM1/p62 and reduced Atg3. (c) After 12 h of seeding CPT-11-R cells in 12 well culture plates, different doses of TQ were added. Immunofluorescence microscopy was conducted 24 h after administration of TQ. TQ increased cellular expression of LC3 in a dose-dependent manner.

DOI: 10.1021/jf5054063
J. Agric. Food Chem. 2015, 63, 1540−1546

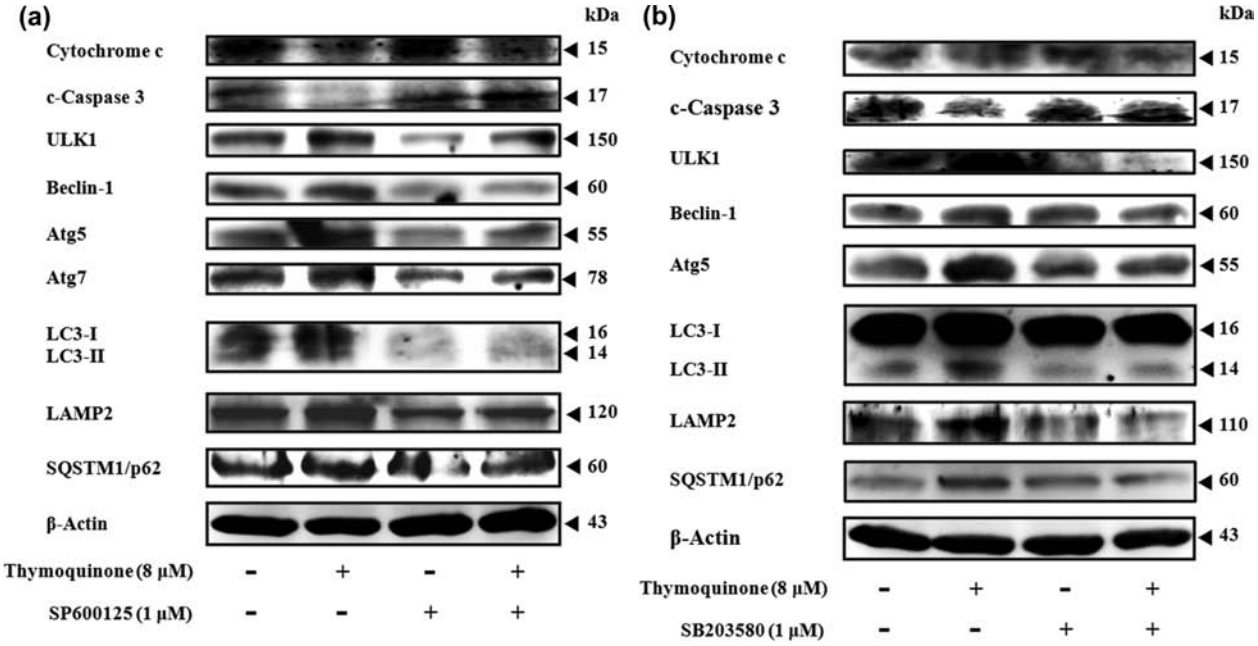

Figure 3. TQ induced ACD of CPT-11-R cells via activation of JNK and p38. (a) After 12 h of seeding CPT-11-R cells in 10 cm culture plates, 1 μM SP600125 was added first, followed by 8 μM TQ at 2 h later. Western blotting was conducted 24 h after administration of TQ. SP600125 reversed TQ-induced cell death. (b) After 12 h of seeding CPT-11-R cells in 10 cm culture plates, 1 μM SB203580 was added first, followed by 8 μM TQ at 2 h later. Western blotting was conducted 24 h after administration of TQ. SB203580 reversed TQ-induced ACD.

RESULTS

TQ Resulted in ACD in CPT-11-R Cells via Activation of JNK and p38 and MOMP. In a traditional view, cancer treatments are known to cause apoptosis in cancer cells. However, certain phytochemicals were shown to induce caspase-independent ACD in cancers. Therefore, the authors investigated which type of cell death (i.e., apoptosis or ACD) was caused by TQ in CPT-11-R cells.

First, TQ dose-dependently elevated the total cell death index (166.4, 534.54, 653.79, and 853.94% increase compared to the control) (Figure 1a). TQ increased unphosphorylated BAD and reduced phosphorylated BAD (Figure 1b). However, TQ only caused increased cytochrome *c*, caspase 9, and caspase 3 at 2 μM, which then decreased at increasing doses. The effect of TQ on mitochondrial membrane potential and autophagy in CPT-11-R cells was investigated. The JC-1 staining assay was conducted to access TQ-induced MOMP, and western blotting was conducted to investigate TQ-induced autophagy. TQ caused a dose-dependent increase in the FITC (JC-1 monomer) signal and a dose-dependent decrease in the Cy3 (JC-1 aggregate) signal (Figure 2a). Further, TQ upregulated protein levels of Atg5, Atg7, Atg12, Beclin-1, LAMP2, LC3-II, and SQSTM1/p62, while that of Atg3 was reduced (Figure 2b). TQ also dose-dependently increased cellular expression of LC3 (Figure 2c). Therefore, TQ induced ACD via MOMP.

Finally, TQ was found to activate JNK and p38, which are stress-activated protein kinases; it was assumed that JNK or p38 mediated TQ-induced ACD. The 8 μM TQ reduced cytochrome *c* and cleaved caspase 3 but increased Atg5, Atg7, Beclin-1, LAMP2, LC3, SQSTM1/p62, and ULK1 (Figure 3a). The 1 μM SP600125 restored protein levels of cytochrome *c* and cleaved caspase 3 while deducting those of Atg5, Atg7, Beclin-1, LAMP2, LC3, SQSTM1/p62, and ULK1, which were lower than the control. SP600125 also reversed TQ-induced ACD. SB203580 also had similar effects on TQ-induced ACD in CPT-11-R LoVo colon cancer cells (Figure 3b) and, therefore, reversed the effect of TQ. Therefore, JNK and p38 mediated TQ-induced ACD in CPT-11-R cells.

Relationship between TQ-Induced Apoptosis and ACD. In Figures 1 and 2, TQ resulted in increased total cell death, initial activation of apoptosis, increased autophagy activity, and increased expression of mitophagy markers (LAMP2 and SQSTM1/p62). TQ induced apoptosis and autophagy at 2 μM, and then at increasing doses, apoptosis was decreased, while autophagy was elevated. Therefore, the authors attempted to determine the relationship between and TQ-induced apoptosis and ACD.

TQ activated Atg7, Beclin-1, caspase 3, and LC3 at 2 μM (Figure 4). Co-treating with 50 μM 3-MA resulted in decreased Atg7, Beclin-1, and LC3 and increased caspase 3 activation. Baf-A1 caused increased accumulation of Atg7, Beclin-1, and LC3 but did not increase caspase 3 in the presence of 2 μM TQ. The 1 μM LY294002 resulted in reduced Beclin-1 and LC3 but did not reduce Atg7 or increase caspase 3 when co-administered with TQ. Finally, 2 μM *Z*-DEVD-fmk caused increased Atg7 and LC3, decreased caspase 3, but did not upregulate Beclin-1. Therefore, TQ activated apoptosis prior to initiation of ACD in CPT-11-R LoVo cells, and the key switching step must had occurred early in the formation of autophagosome.

DISCUSSION

Besides eliminating tumor cells, chemotherapeutic drugs cause side effects and result in chemoresistant tumors in patients.[3] Therefore, there is a need for alternative cancer treatments.[4] Phytochemicals serve as an alternative method to treat colon cancer and are by means of targeted therapy.[7,8] CPT-11-R LoVo colon cancer cells were generated by challenging parental cells with increasing doses of CPT-11 and activate the NF-κB pathway to promote basal autophagy.[11] TQ is a phytochemical that was applied to treat different cancers, including colon cancer.[20] In addition, TQ altered activity of MAPKs in treating cancers.[24−26]

DOI: 10.1021/jf5054063
J. Agric. Food Chem. 2015, 63, 1540−1546

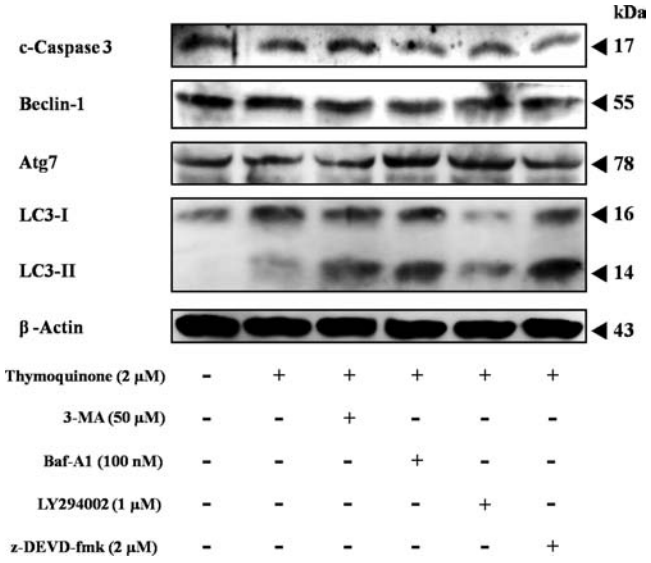

Figure 4. TQ induced apoptosis before inducing ACD in CPT-11-R LoVo cells. After 12 h of seeding CPT-11-R cells in 10 cm culture plates, 50 μM 3-MA, 100 nM Baf-A1, 1 μM LY294002, and 2 μM *Z*-DEVD-fmk were added to separate plates, followed by 2 μM TQ to appropriate plates at 2 h later. Western blotting was conducted 24 h after administration of TQ. Apoptosis was induced by TQ before ACD.

Traditionally, cancer treatments usually cause apoptosis of tumor cells. Therefore, the authors first investigated whether TQ caused apoptosis in CPT-11-R cells. TQ caused a dose-dependent increase in the cell death index. However, although apoptosis was initially activated TQ, it still decreased at increasing doses of the phytochemical. Therefore, the possibility of ACD was considered. First TQ resulted in a dose-dependent increase in MOMP, and then TQ elevated protein levels of Atg5, Atg7, Atg12, Beclin-1, LAMP2, LC3-II, and SQSTM1/p62, while that of Atg3 was reduced. Furthermore, TQ also increased LC3 intracellular expression dose-dependently. In addition, autophagy is a context-dependent process; its outcomes in terms of cellular response are different.[33] In CPT-11-R cells, NF-κB activation resulted in increased basal autophagy.[11] However, TQ was previously shown to inhibit NF-κB in CPT-11-R cells (unpublished result). In this study, it resulted in increased autophagy and decreased cell viability. Together these results showed that TQ induced ACD via MOMP (mitophagy). In a review by Tait et al., MOMP can result in caspase-dependent (apoptosis) or caspase-independent (autophagy) cell death.[28] In this study, TQ induced, in an initial activation of mitochondria-dependent cell death, a dose-dependent increase in autophagy and MOMP in CPT-11-R cells. Finally, TQ was found to induce ACD by activation of JNK and p38 in CPT-11-R LoVo colon cancer cells. Therefore, TQ resulted in autophagic cell death via MOMP and activation of JNK and p38.

Finally, because TQ initially resulted in activation of apoptosis and autophagy and the latter took over cell death at increasing doses, it was necessary to determine which TQ-induced apoptosis and autophagy occurred earlier than the other. TQ at 2 μM activated both apoptosis and autophagy (Figure 4); however, 3-MA co-administration pointed the direction of cell death toward apoptosis, and that of *Z*-DEVD-fmk pointed to ACD. In addition, TQ caused elevated MOMP and protein levels of mitophagy markers, LAMP2 and SQSTM1/p62. TQ also caused increased Atg7 and Atg12 while reducing Atg3. Therefore, it was concluded that apoptosis was induced by TQ before activating ACD and the key switching step occurred at initiation of autophagosome formation. Therefore, TQ initially activated both apoptosis and ACD; however, at increasing doses, intracellular damages must be increasingly more severe (such as a number of dysfunctional mitochondria), and therefore, the upregulated autophagic process functioned to clear damaged organelles and other intracellular components, resulting in caspase-independent ACD (Figure 5). In other studies, different phytochemicals induced ACD at increasing doses with or without an initial apoptosis, such as dihydrocapsaicin, PGG, resveratrol, SAHA, and sulforaphane.[31,32,34−36]

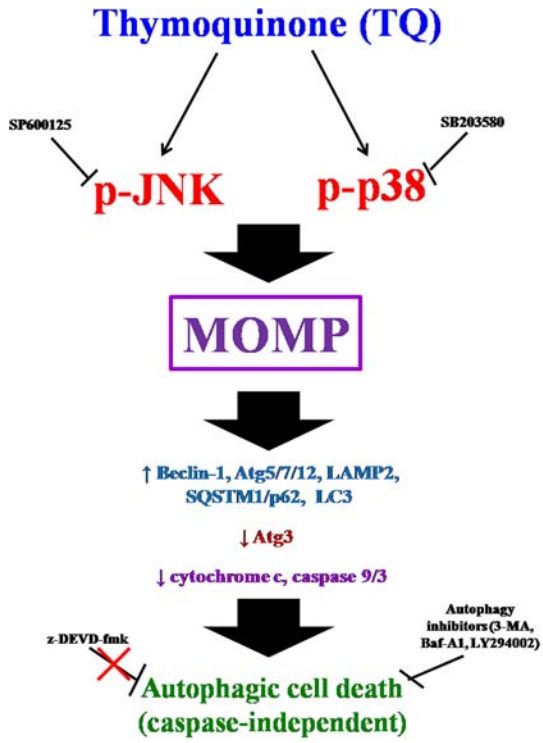

Figure 5. Schematic representation of TQ-induced caspase-independent, autophagic cell death via MOMP and activation of JNK and p38 in CPT-11-R LoVo colon cancer cells.

To summarize, TQ caused in autophagic cell death via MOMP and activation of JNK and p38 in CPT-11-R LoVo colon cancer cells. This activation of ACD occurred after induction of apoptosis by TQ. Furthermore, the key switching event occurred at early autophagosome formation. Therefore, TQ causes mitochondrial-dependent ACD via MOMP and JNK and p38 activation in CPT-11-R LoVo colon cancer cells.

AUTHOR INFORMATION

Corresponding Author

*E-mail: cyhuang@mail.cmu.edu.tw.

Author Contributions

[&]Wei-Wen Kuo and Chih-Yang Huang contributed equally to this work.

Funding

This study is supported in part by Taiwan Ministry of Health and Welfare Clinical Trial and Research Center of Excellence (MOHW104-TDU-B-212-113002).

Notes

The authors declare no competing financial interest.

DOI: 10.1021/jf5054063
J. Agric. Food Chem. 2015, 63, 1540−1546

REFERENCES

(1) http://globocan.iarc.fr/.

(2) *SEER Cancer Statistics Review*; Altekruse, S. F., Kosary, C. L., Krapcho, M., Neyman, N., Aminou, R., Waldron, W., Ruhl, J., Howlader, N., Tatalovich, Z., Cho, H., Mariotto, A., Eisner, M. P., Lewis, D. R., Cronin, K., Chen, H. S., Feuer, E. J., Stinchcomb, D. G., Edwards, B. K., Eds.; National Cancer Institute: Rockville, MD, 1975−2007.

(3) Luqmani, Y. A. Mechanisms of drug resistance in cancer chemotherapy. *Med. Princ. Pract.* **2005**, *14*, 35−48.

(4) Yim, K. L.; Cunningham, D. Targeted drug therapies and cancer. *Recent Res. Cancer* **2011**, *185*, 159−171.

(5) Chen, H. W.; Lee, J. Y.; Huang, J. Y.; Wang, C. C.; Chen, W. J.; Su, S. F.; Huang, C. W.; Ho, C. C.; Jeremy, W.; Chen, J. W.; Tsai, M. F.; Yu, S. L.; Yang, P. C. Curcumin inhibits lung cancer cell invasion and metastasis through the tumor suppressor HLJ1. *Cancer Res.* **2008**, *68*, 7428−7438.

(6) Hsu, S. C.; Chung, J. G. Anticancer potential of emodin. *Biomedicine* **2012**, *2*, 108−116.

(7) Pan, M. H.; Lai, C. S.; Wu, J. C.; Ho, C. T. Molecular mechanisms for chemoprevention of colorectal cancer by natural dietary compounds. *Mol. Nutr. Food Res.* **2011**, *55*, 32−45.

(8) Ruhul Amin, A. R. M.; Kucuk, O.; Khuri, F. R.; Shin, D. M. Perspectives for cancer prevention with natural compounds. *J. Clin. Oncol.* **2009**, *27*, 2712−2725.

(9) Pommier, Y. Topoisomerase I inhibitors: Camptothecins and beyond. *Nat. Rev. Cancer* **2006**, *6*, 789−802.

(10) Drewinko, B.; Romsdahl, M. M.; Yang, L. Y.; Ahearn, M. J.; Trujillo, J. M. Establishment of a human carcinoembryonic antigen-producing colon adenocarcinoma cell line. *Cancer Res.* **1976**, *36*, 467−475.

(11) Chen, M. C.; Lee, N. H.; Ho, T. J.; Hsu, H. H.; Kuo, C. H.; Kuo, W. W.; Lin, Y. M.; Tsai, F. J.; Tsai, C. H.; Huang, C. Y. Resistance to irinotecan (CPT-11) activates epidermal growth factor receptor/nuclear factor kappa B and increases cellular metastasis and autophagy in LoVo colon cancer cells. *Cancer Lett.* **2014**, *349*, 51−60.

(12) Baldwin, A. S. Regulation of cell death and autophagy by IKK and NF-κB: Critical mechanisms in immune function and cancer. *Immunol. Rev.* **2012**, *246*, 327−345.

(13) Cusack, J. C.; Liu, R.; Baldwin, A. S. NF-κB and chemoresistance: Potentiation of cancer drugs via inhibition of NF-κB. *Drug Resist. Update* **1999**, *2*, 271−273.

(14) Marin, J. J.; Briz, O.; Monte, M. J.; Blazquez, A. G.; Macias, R. I. Genetic variants in genes involved in mechanisms of chemoresistance to anticancer drugs. *Curr. Cancer Drug Targets* **2012**, *12*, 402−438.

(15) Uetsuka, H.; Haisa, M.; Kimura, M.; Gunduz, M.; Kaneda, Y.; Ohkawa, T.; Takaoka, M.; Murata, T.; Nobuhisa, T.; Yamatsuji, T.; Matsuoka, J.; Tanaka, N.; Naomoto, Y. Inhibition of inducible NF-κB activity reduces chemoresistance to 5-fluorouracil in human stomach cancer cell line. *Exp. Cell Res.* **2003**, *289*, 27−35.

(16) Aggarwal, B. B.; Sethi, G.; Nair, A.; Ichikawa, H. Nuclear factor-κB: A holy grail in cancer prevention and therapy. *Curr. Signal Transduction Ther.* **2006**, *1*, 25−52.

(17) Abdel-Fattah, A. M.; Matsumoto, K.; Watanabe, H. Antinociceptive effects of *Nigella sativa* oil and its major component, thymoquinone, in mice. *Eur. J. Pharmacol.* **2000**, *400*, 89−97.

(18) Al-Shabanah, O. A.; Badary, O. A.; Nagi, M. N.; Al-Gharably, N. M.; Al-Rikabi, A. C.; Al-Bekairi, A. M. Thymoquinone protects against doxorubicin-induced cardiotoxicity without compromising its antitumor activity. *J. Exp. Clin. Cancer Res.* **1998**, *17*, 193−198.

(19) Gali-Muhtasib, H.; Roessner, A.; Schneider-Stock, R. Thymoquinone: A promising anti-cancer drug from natural sources. *Int. J. Biochem. Cell Biol.* **2006**, *38*, 1249−1253.

(20) Attoub, S.; Sperandio, O.; Raza, H.; Arafat, K.; Al-Salam, S.; Sultan, M. A. A.; Safi, M. A.; Takahashi, T.; Adem, A. Thymoquinone as an anticancer agent: Evidence from inhibition of cancer cells viability and invasion in vitro and tumor growth in vivo. *Fundam. Clin. Pharmacol.* **2013**, *27*, 557−569.

(21) Gurung, R. L.; Lim, S. N.; Khaw, A. K.; Soon, J. F. F.; Shenoy, K.; Ali, S. M.; Jayapal, M.; Sethu, S.; Baskar, R.; Hande, M. P. Thymoquinone induces telomere shortening, DNA damage and apoptosis in human glioblastoma cells. *PLoS One* **2010**, *5*, No. e12124.

(22) Jafri, S. H.; Glass, J.; Shi, R. H.; Zhang, S. L.; Prince, M.; Kleiner-Hancock, H. Thymoquinone and cisplatin as a therapeutic combination in lung cancer: In vitro and in vivo. *J. Exp. Clin. Cancer Res.* **2010**, *29*, 87.

(23) Yi, T. F.; Cho, S. G.; Yi, Z. F.; Pang, X. F.; Rodriguez, M.; Wang, Y.; Sethi, G.; Aggarwal, B. B.; Liu, M. G. Thymoquinone inhibits tumor angiogenesis and tumor growth through suppressing AKT and extracellular signal-regulated kinase signaling pathways. *Mol. Cancer Ther.* **2008**, *7*, 1789−1796.

(24) El-Najjar, N.; Chatila, M.; Hiba Moukadem, H.; Vuorela, H.; Ocker, M.; Gandesiri, M.; Schneider-Stock, R.; Gali-Muhtasib, H. Reactive oxygen species mediate thymoquinone-induced apoptosis and activate ERK and JNK signaling. *Apoptosis* **2010**, *15*, 183−195.

(25) Muniz, V. P.; Askeland, R. W.; Zhang, X. F.; Reed, S. M.; Tompkins, V. S.; Hagen, J.; McDowell, B. D.; Button, A.; Smith, B. J.; Weydert, J. A.; Mezhir, J. J.; Quelle, D. E. RABL6A promotes oxaliplatin resistance in tumor cells and is a new marker of survival for resected pancreatic ductal adenocarcinoma patients. *Genes Cancer* **2013**, *4*, 273−284.

(26) Torres, M. P.; Ponnusamy, M. P.; Chakraborty, S.; Smith, L. M.; Das, S.; Arafat, H. A.; Batra, S. K. Effects of thymoquinone in the expression of mucin 4 in pancreatic cancer cells: Implications for the development of novel cancer therapies. *Mol. Cancer Ther.* **2010**, *9*, 1419−1431.

(27) Singletary, K.; Milner, J. Diet, autophagy, and cancer: A review. *Cancer Epidemiol., Biomarkers Prev.* **2008**, *17*, 1596−1610.

(28) Tait, S. W. G.; Green, D. R. Mitochondria and cell death: Outer membrane permeabilization and beyond. *Nat. Rev. Mol. Cell Biol.* **2010**, *11*, 621−631.

(29) González-Polo, R. A.; Boya, P.; Pauleau, A. L.; Jalil, A.; Larochette, N.; Souquère, S.; Eskelinen, E. L.; Pierron, G.; Saftig, P.; Kroemer, G. The apoptosis/autophagy paradox: Autophagic vacuolization before apoptotic death. *J. Cell Sci.* **2005**, *118*, 3091−3102.

(30) Ishihara, N.; Mizushima, N. A receptor for eating mitochondria. *Dev. Cell* **2009**, *17*, 1−2.

(31) Herman-Antosiewicz, A.; Johnson, D. E.; Singh, S. V. Sulforaphane causes autophagy to inhibit release of cytochrome *c* and apoptosis in human prostate cancer cells. *Cancer Res.* **2006**, *66*, 5828−5835.

(32) Hu, H. B.; Chai, Y. B.; Wang, L.; Zhang, J. H.; Lee, H. J.; Kim, S. H.; Lu, J. X. Pentagalloylglucose induces autophagy and caspase-independent programmed deaths in human PC-3 and mouse TRAMP-C2 prostate cancer cells. *Mol. Cancer Ther.* **2009**, *8*, 2833−2843.

(33) White, E. Deconvoluting the context-dependent role for autophagy in cancer. *Nat. Rev. Cancer* **2012**, *12*, 401−410.

(34) Kueck, A.; Opipari, A. W., Jr.; Griffith, K. A.; Tan, L. J.; Choi, M. H.; Huang, J.; Wahl, H.; Liu, J. R. Resveratrol inhibits glucose metabolism in human ovarian cancer cells. *Gynecol. Oncol.* **2007**, *107*, 450−457.

(35) Oh, S. H.; Kim, Y. S.; Lim, S. C.; Hou, Y. F.; Chang, I. Y.; You, H. J. Dihydrocapsaicin (DHC), a saturated structural analog of capsaicin, induces autophagy in human cancer cells in a catalase-regulated manner. *Autophagy* **2008**, *4*, 1009−1019.

(36) Shao, Y. F.; Gao, Z. H.; Marks, P. A.; Jiang, X. J. Apoptotic and autophagic cell death induced by histone deacetylase inhibitors. *Proc. Natl. Acad. Sci. U. S. A.* **2004**, *101*, 18030−18035.

DOI: 10.1021/jf5054063
J. Agric. Food Chem. 2015, 63, 1540−1546

Table 1. Results of the Stability Experiments of Various Classes of Polyphenols (Initial Concentration 10 μM) in DMEM under the Cell Culture Condition (37 °C, 5% CO_2)[a]

Subclass	Name	Substitutions			$^{10}T_{10}$	$^{10}T_{50}$	Concentration at 3h / μM
		OH	OCH_3	others	min	min	
Flavones	7,8-dihydroxyflavone	7,8			104.1	>180	8.81±0.18
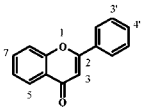	chrysin	5,7			>180	>180	11.3±0.3
	baicalein	5,6,7			<1	3.04	0
	baicalin	5,6		7-*O*-β-D-glucuronide	<1	27.31	0.1±0.06
	apigenin	5,7, 4'			>180	>180	9.1±0.36
	aposide	5, 4'		7-*O*-glucoside	>180	>180	9.6±0.36
	vitexin	5,7		8-*C*-glucoside	>180	>180	9.8±0.39
	luteolin	5,7,3', 4'			56.35	>180	7.4±0.13
	luteolin 7-*O*-glucoside	5, 3', 4'		7-*O*-glucoside	111.70	>180	8.3±0.13
	wogonoside	5	8	7-*O*-β-D-glucuronide	>180	>180	9.6±0.41
Multi-hydroxyflavonols	galangin	3,5,7			>180	>180	9.8±0.37
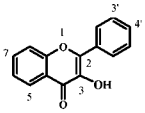	kaempferol	3,5,7, 4'			46.68	119.47	2.0±0.43
	kaempferide	3,5,7	4'		150.02	>180	8.6±0.034
	quercetin	3,5,7,3', 4'			4.66	17.96	0.043±0.16
	quercitrin	5,7,3', 4'		3-*O*-β-D-glucoside	>180	>180	9.9±0.42
	isorhametin	3,5,7, 4'	3'		6.73	21.77	0
	rutin	5,7,3', 4'		3-*O*-α-L-rhamnopyranosyl-(1→6)-β-D-glucopyranose	>180	>180	10.1±0.43
	myricetin	3,5,7,3',4',5'			<1	<1	0
	myricitrin	5,7,3', 4', 5'		3-*O*-β-D-glucoside	20.66	63.95	0
Less-hydroxyflavonols	fisetin	3,7,3', 4'			<1	14.40	0
	3,4'-dihydroxyflavone	3,4'			>180	>180	7.1±0.32
	3-hydroxy-4'-methoxyflavone	3	4'		>180	>180	7.2±0.27
	3-hydroxyflavone	3			>180	>180	7.9±0.13
	3-methoxyflavone		3		>180	>180	6.9±0.09
Isoflavones	formononetin	7	4'		>180	>180	9.92±0.14
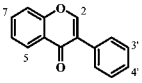	formononetin7-*O*-glucoside		4'	7-*O*-glucoside	>180	>180	9.11±0.13
	genistein	5,7,4'			>180	>180	10.30±0.26
	genistin	5,4'		7-*O*-glucoside	>180	>180	9.67±0.10
	daidzein	7,4'			>180	>180	10.28±0.16
	daidzin	4'		7-*O*-glucoside	>180	>180	9.01±0.02
	biochanin A	5,7	4'		>180	>180	10.81±0.22
	puerarin	7,4'		8-*C*-glucoside	>180	>180	10.04±0.13
Flavanones	naringenin	5,7, 4'			>180	>180	10.25±0.33
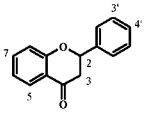	naringin	5,4'		7-*O*-neohesperidose	>180	>180	9.90±0.10
	narirutin	5,4'		7-*O*-α-L-rhamnopyranosyl-(1→6)-β-D-glucopyranose	>180	>180	10.23±0.09
	hesperetin	5,7, 3'	4'		>180	>180	9.83±0.10
	hesperidin	5,3'	4'	7-*O*-α-L-rhamnopyranosyl-(1→6)-β-D-glucopyranose	>180	>180	10.85±0.18
	dihydromyricetin	3,5,7,3',4',5'			<1.0	1.91	0
	liquiritigenin	7, 4'			>180	>180	10.00±0.11
	liquiritin			4'-*O*-glucoside	>180	>180	9.96±0.10
Stilbenoids	resveratrol	3,5,4'			165.92	>180	8.7±0.09
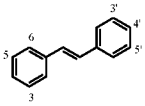	isorhapontigenin	3,5,4'	5'		81.14	>180	7.9±0.20
	oxyresveratrol	3,5,4',6'			11.57	59.12	1.8±0.22
	pinostilbene	3, 4'	5		>180	>180	10.4±0.04
	pterostilbene	4'	3,5		>180	>180	10.7±0.9
	piceid	3, 4'		5-*O*-glucoside	>180	>180	10.8±0.6
	piceatannol	3,5,4', 5'			5.68	22.51	0
Catechins	GCG (2,3-trans)	5,7,3',4',5'		3-gallate	<1	<1	0
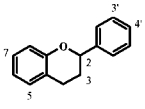	EGCG (2,3-cis)	5,7,3',4',5'		3-gallate	<1	<1	0
	ECG (2,3-cis)	5,7,4',5'		3-gallate	114.42	>180	8.2±1.2
	EC (2,3-cis)	3,5,7,4',5'			21.26	104.91	2.4±0.52
	EGC (2,3-cis)	3,5,7,3',4',5'			<1	<1	0
	C (2,3-trans)	3,5,7,4',5'			<1	<1	0

[a]Results depict mean and SD of n = 3 samples.

DOI: 10.1021/jf505514d
J. Agric. Food Chem. 2015, 63, 1547−1557

wogonoside (>98.0%), galangin (>97.0%), gallocatechin-3-gallate (GCG) (>98.0%), epicatechin (EC) (>98.0%), epigallocatechin (EGC) (>98.0%), kaempferide (>97.0%), quercetin (>97.0%), catechin (C) (96.0%), quercitrin (>98.0%), isorhametin (>98.0%), myricitrin (>98.0%), formononetin 7-*O*-glucoside (>98.0%), genistin (>98.0%), daidzin (>96.0%), biochanin A (>98.0%), naringin (>95.0%), narirutin (>97.0%), hesperidin (>97.0%), liquiritigenin (>98.0%), and liquiritin (>98.0%) were obtained from Aladdin Chemistry Co. Ltd. (Shanghai, China). Methanol and acetonitrile (HPLC grade) were purchased from Baker (J.T. Baker). Penicillin, streptomycin, L-glutamine, and fetal bovine serum (FBS) were all purchased from Biochrom AG (Berlin, Germany). Dulbecco's modified Eagle's medium (DMEM) was obtained from Sigma (St Louis, MO). MiliQ water was used throughout the experiments. Other organic solvents and reagents were of analytical reagent grade.

Instrumentation and Chromatographic Conditions. The high performance liquid chromatography (HPLC) system consisted of a Waters 1525 Binary HPLC pump, a Waters 2487 Dual λ absorbance detector, and a Waters 717 autosampler. Separation was carried out on a YMC America C_{18} column (4.6 mm × 150 mm; 5 μm) (Pennsylvania). The polyphenols were classified into seven groups: flavones, multihydroxyflavonols, flavonols, flavanones, isoflavones, catechins, and stilbenoids (Table 1). The mobile phase consisted of 0.1% phosphoric acid (A) and acetonitrile (B) and was degassed prior to use (Table 2). The flow rate was 1.0 mL/min.

Stability of Polyphenols in Cell Culture Medium. Polyphenols were dissolved in methanol or DMSO to obtain a 10^{-2} mol/L standard stock solutions. DMEM was supplemented with 10% FBS, 50 U/mL penicillin, 100 mg/L streptomycin, and L-glutamine. The standard stock solutions of polyphenols were diluted to 1×10^{-3} mol/L with DMEM before testing. 50 μL of the diluted polyphenol solution was added to 4950 μL DMEM (prewarmed to 37 °C in a 5% CO_2 atmosphere 30 min prior to experiments); then, the mixtures were incubated at 37 °C in 5% CO_2. At 1, 10, 30, 60, 90, 120, and 180 min, a sample of 500 μL was withdrawn and immediately mixed with 1000 μL cold methanol (−20 °C) and kept at −20 °C for 30 min to precipitate the proteins. After centrifugation at 12 000 × *g* for 10 min at 4 °C, a 50 μL aliquot was injected to the HPLC system.

Stability of Polyphenols in Human Plasma. Human plasma from three volunteers was obtained from a local blood bank (Bayerisches Rotes Kreuz, München, Germany). The standard stock solutions of flavonols (myricetin, myricitrin, quercetin, and kaempferol) were diluted to 1×10^{-3} mol/L with MiliQ water before testing. A 50 μL portion of the diluted flavonol solution was added to 4950 μL of the pooled human plasma (prewarmed to 37 °C for 30 min prior to experiments); then, the mixtures were incubated at 37 °C. After 1, 10, 30, 60, 90, 120, and 180 min, a sample of 500 μL was withdrawn and immediately mixed with 1000 μL cold methanol (−20 °C) and kept at −20 °C for 30 min to precipitate the proteins. After centrifugation at 12 000 × *g* for 10 min at 4 °C, a 50 μL aliquot was injected to the HPLC system.

Determination of Protein Concentrations in DMEM and Human Plasma. The protein concentrations in DMEM and human plasma were determined using the BCA protein assay (Thermo Scientific).[22] For calibration curves BSA (125 μg/mL to 2000 μg/mL) was used as standard. DMEM and human plasma were diluted with PBS before testing.

Data Analysis. An early degradation time ($^{C}T_{10}$) and a half degradation time ($^{C}T_{50}$) have been defined to characterize the stability of a compound (initial concentration of C μM) in a specific biological or biochemical system. $^{C}T_{10}$ and $^{C}T_{50}$ represent the time that is required for 10% and 50%, respectively, degradation of an individual compound *in vitro*. The $^{C}T_{10}$ and $^{C}T_{50}$ of each compound were derived from time-response curves. The time−concentration curve was fitted using linear, polynomial, or exponential data regression. $^{C}T_{10}$ and $^{C}T_{50}$ values were defined as the time when the concentration of polyphenol decreased to 10% or 50% of the initial concentration.

Table 2. Composition of Gradient Mobile Phases for HPLC Separations

time/min	0.1% phosphoric acid	acetonitrile
	Flavones (280 nm)	
0	90%	10%
3	90%	10%
10	85%	15%
15	85%	15%
30	75%	25%
35	70%	30%
40	65%	35%
45	52%	48%
50	90%	10%
	Multihydroxyflavonols (360 nm)	
0	90%	10%
5	90%	10%
10	85%	15%
20	77%	23%
30	75%	25%
40	60%	40%
50	50%	50%
55	50%	50%
60	90%	10%
	Less-hydroxyflavonols (280 nm)	
0	85%	15%
5	85%	15%
10	75%	25%
20	60%	40%
30	55%	45%
40	52%	48%
45	85%	15%
	Flavanones (280 nm) Isoflavones (280 nm)	
0	95%	5%
3	90%	10%
10	85%	15%
20	85%	15%
30	80%	20%
35	75%	25%
45	70%	30%
55	60%	40%
60	95%	5%
	Catechins (270 nm)	
0	95%	5%
10	95%	5%
15	90%	10%
20	80%	20%
25	75%	25%
27	70%	30%
30	95%	5%
	Stilbenoids (280 nm)	
0	92%	8%
5	90%	10%
10	80%	20%
22	75%	25%
25	75%	25%
33	50%	50%
42	50%	50%
45	92%	8%

DOI: 10.1021/jf505514d
J. Agric. Food Chem. 2015, 63, 1547−1557

Statistical Analysis. All experiments were repeated three times. All values were expressed as means ± standard deviations.

RESULTS

Stability of Polyphenols in Cell Culture Medium. After incubation with DMEM at 37 °C for 1, 10, 30, 60, 90, 120, and 180 min, the concentrations of polyphenols were determined to compile time−concentration response curves. The $^{10}T_{10}$ and $^{10}T_{50}$ values of polyphenols (initial concentration 10 μM) in DMEM at 37 °C varied considerably (Table 1). Some polyphenols, such as myricetin, C, EGCG, GCG, and EGC, were significantly degraded within 10 min of incubation ($^{10}T_{10}$ < 1 min, $^{10}T_{50}$ < 1 min). However, most polyphenols such as isoflavones flavanones and less-hydroxyflavonols were very stable even after 3 h incubation ($^{10}T_{10}$ > 180 min, $^{10}T_{50}$ > 180 min).

Flavonols. *Hydroxylation. 1. Hydroxylation on Ring B.* The hydroxylation at the ring B of flavonols significantly affected the stability (Figure 1). Myricetin (3′,4′,5′-OH) ($^{10}T_{10}$ < 1 min and $^{10}T_{50}$ < 1 min; Table 1) was highly instable, degraded to 26% within 1 min, and completely disappeared within 10 min. Quercetin (3′,4′-OH) ($^{10}T_{10}$ = 4.66 min and $^{10}T_{50}$ = 17.96 min) decreased to 25% of the initial concentration within 30 min and almost disappeared after 120 min incubation. Kaempferol (4′-OH) ($^{10}T_{10}$ = 46.68 min and $^{10}T_{50}$ = 119.47 min) was more stable than myricetin and quercetin. Moreover, kaempferol was found to degrade linearly while quercetin degraded exponentially. Galangin without any hydroxyl groups on ring B appeared to be most stable over a 3 h time course ($^{10}T_{10}$ > 180 min and $^{10}T_{50}$ > 180 min). Likewise, 3,4′-dihydroxyflavone was more stable than 3-hydroxyflavone (Figure 3).

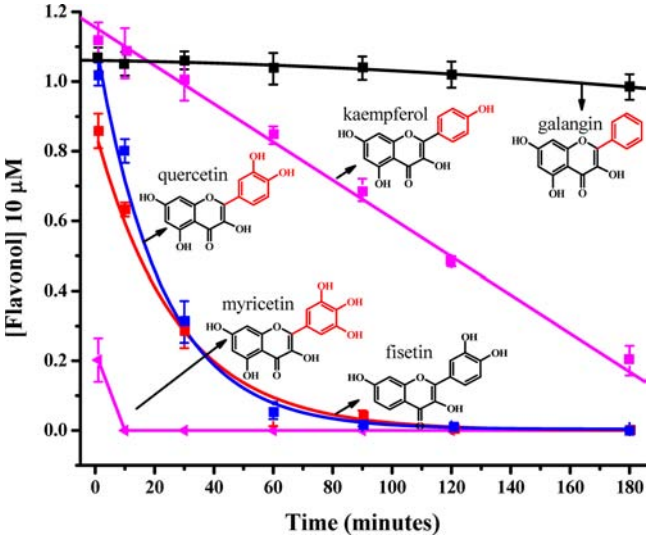

Figure 1. Stability of multihydroxyflavonols (initial concentration 10 μM) in DMEM incubated at 37 °C in 5% CO_2. These results are the mean of three independently performed experiments.

2. Hydroxylation on Ring A. Quercetin (3,5,7,3′,4′-OH) ($^{10}T_{10}$ = 4.66 min and $^{10}T_{50}$ = 17.96 min) exhibited slightly higher stability as compared to fisetin (3,7,3′,4′-OH) ($^{10}T_{10}$ < 1 min and $^{10}T_{50}$ = 14.40 min; Figure 1).

Methoxylation. The methoxylation at ring B of multihydroxyflavonols apparently improved their stability (Figure 2). Isorhametin revealed a slightly higher stability than quercetin ($^{10}T_{10}$ < 1 min and $^{10}T_{50}$ = 14.40 min versus $^{10}T_{10}$ < 1 min and $^{10}T_{50}$ = 14.40 min); the methoxylation at the C-4′ position of kaempferol ($^{10}T_{10}$ = 46.68 min and $^{10}T_{50}$ = 119.47 min) significantly enhanced its stability (kaempferide, $^{10}T_{10}$ = 150.02 min and $^{10}T_{50}$ > 180 min). However, the methoxylation of less hydroxylated flavonols such as 3-hydroxyflavonol slightly compromised their stability (Figure 3). 3,4′-Dihydroxyflavone and 4′-hydroxyflavone showed a slightly higher stability than 3-hydroxy-4′-methoxyflavone and 4′-methoxyflavone (Table 1).

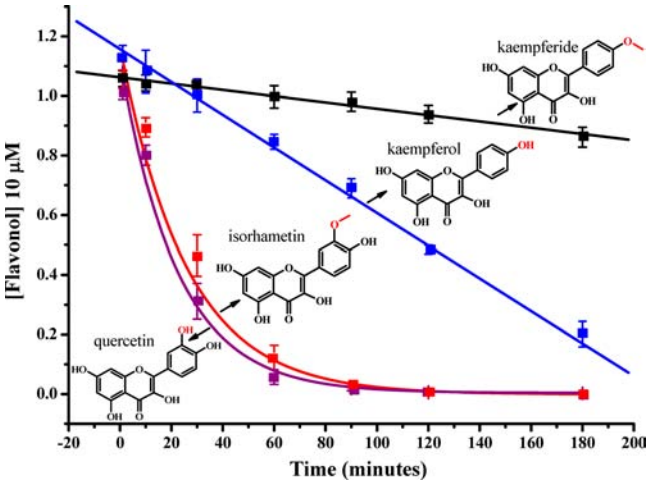

Figure 2. Methoxylation on ring B of multihydroxyflavonols (initial concentration 10 μM) improved the stability in DMEM incubated at 37 °C in 5% CO_2. These results are the mean of three independently performed experiments.

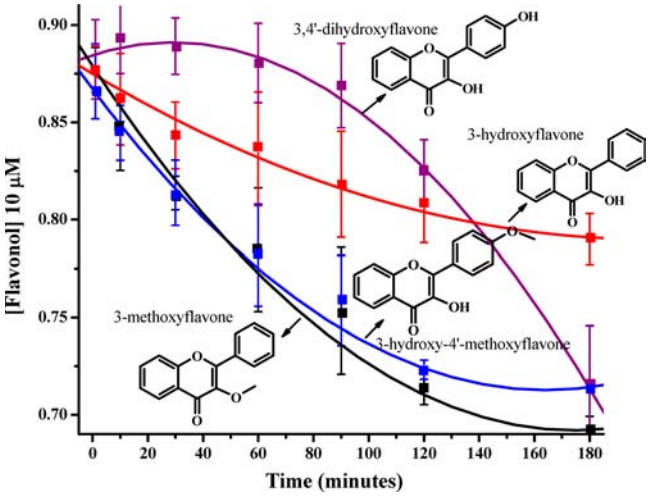

Figure 3. Methoxylation of flavonols (initial concentration 10 μM) slightly weakened the stability in DMEM incubated at 37 °C in 5% CO_2. These results are the mean of three independently performed experiments.

Glycosylation. In the present study, the glycosylation of flavonols significantly enhanced their stability. Compared with quercetin ($^{10}T_{10}$ = 4.66 min and $^{10}T_{50}$ = 17.96 min; Figure 4), quercitrin and rutin were more stable during 3 h of incubation in DMEM medium with T_{10} > 180 min and T_{50} > 180 min. After 3 h of incubation, quercetin almost completely disappeared, but quercitrin and rutin barely degraded (Figure 4). Myricitrin ($^{10}T_{10}$ = 20.66 min and $^{10}T_{50}$ = 63.95 min) also showed higher stability than myricetin ($^{10}T_{10}$ < 1 min and $^{10}T_{50}$

DOI: 10.1021/jf505514d
J. Agric. Food Chem. 2015, 63, 1547−1557

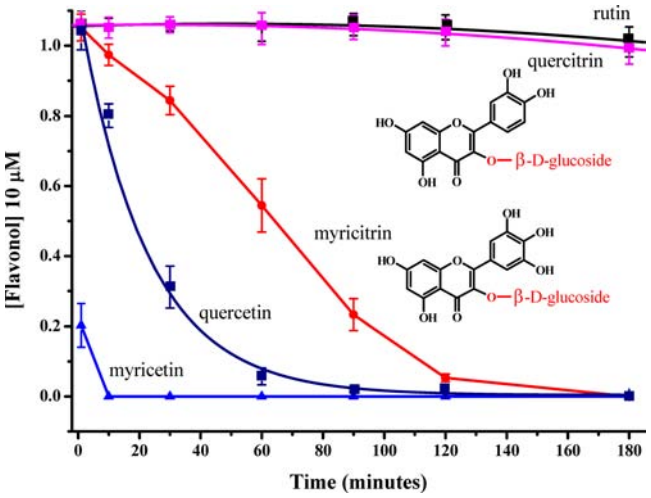

Figure 4. Glycosylation of flavonols (initial concentration 10 μM) improved the stability in DMEM incubated at 37 °C in 5% CO_2. These results are the mean of three independently performed experiments.

< 1 min). Even with the glycoside attached at the C-3 positon of myricitrin, it was still instable and entirely vanished after 3 h incubation. Apparently, the pyrogallol moiety in myricetin and myricitrin were the key structures influencing the stability.

Flavones. *Hydroxylation. 1. Hydroxylation in Ring B.* The hydroxylation at the ring B of flavones obviously influenced the stability (Figure 5). Chrysin (no hydroxyl group in the B-ring)

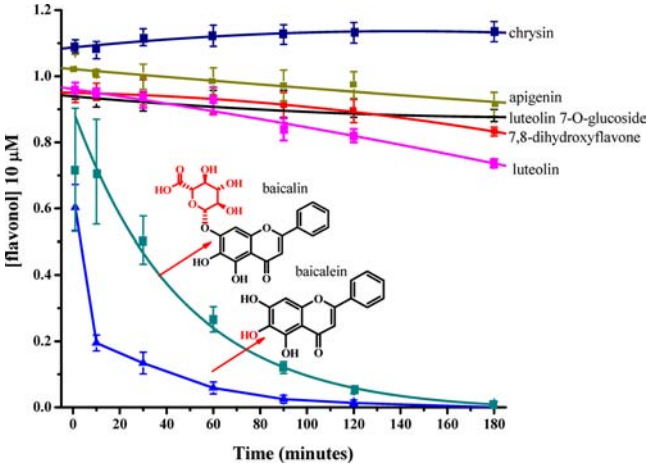

Figure 5. Stability of flavones (initial concentration 10 μM) in DMEM incubated at 37 °C in 5% CO_2. These results are the mean of three independently performed experiments.

and apigenin (4′-OH in ring B) were very stable during 3 h incubation in DMEM ($^{10}T_{10}$ > 180 min and $^{10}T_{50}$ > 180 min). Compared with chrysin and apigenin, luteolin (3′,4′-OH on ring B) showed a slightly lower stability (T_{10} = 56.35 min and T_{50} > 180 min). The general pattern of flavone stability was determined as chrysin > apigenin > luteolin. Apparently, the hydroxylation on ring B of flavones would slightly increase the stability.

2. Hydroxylation in Ring A. Baicalein (5,6,7-OH) ($^{10}T_{10}$ < 1 min and $^{10}T_{50}$ = 3.04 min) showed significantly lower stability than chrysin (5,7-OH) ($^{10}T_{10}$ > 180 min and T_{50} > 180 min) and 7,8-dihydroxyflavone (7,8-OH) ($^{10}T_{10}$ = 104.1 min and $^{10}T_{50}$ > 180 min, Figure 5), which suggested that the hydroxylation in ring A of flavones decreased the stability of flavones. The influence of various substitutions in ring A on the stability of flavones was determined as resorcinol-type (chrysin) > catechol-type (7,8-dihydroxyflavone) > pyrogallol-type (baicalein).

3. Hydroxylation in Ring C (C-3 Position). Galangin (5,7-dihydroxyflavonol) and chrysin (5,7-dihydroxyflavone) without any hydroxyl groups at ring B were all very stable in DMEM ($^{10}T_{10}$ > 180 min and T_{50} > 180 min). Compared to flavonols with hydroxyl groups on ring B [kaempferol ($^{10}T_{10}$ = 46.68 min and $^{10}T_{50}$ =119.47 min), and quercetin ($^{10}T_{10}$ = 4.66 min and $^{10}T_{50}$ =17.96 min)], flavones [apigenin ($^{10}T_{10}$ > 180 min and $^{10}T_{50}$ > 180 min), and luteolin ($^{10}T_{10}$ = 56.35 and $^{10}T_{50}$ > 180)] were found to be more stable during 3 h incubation in DMEM (Table 1 and Figures 1 and 5). Obviously, a hydroxylation in the ring C (C-3 position) of flavones with hydroxyl groups on ring B reduced their stability.

Glycosylation. The sugar moieties are in C-7 or C-8 position of ring A (Table 1). Luteolin 7-*O*-glucoside obviously exhibited higher stability than luteolin. Baicalin ($^{10}T_{10}$ < 1 min and $^{10}T_{50}$ = 27.31 min) also showed a higher stability than baicalein ($^{10}T_{10}$ < 1 min and $^{10}T_{50}$= 3.04 min). Even a glycoside attached at the C-7 positon of baicalein was still instable and entirely decomposed after 3 h incubation in DMEM.

Isoflavones. All the isoflavones tested were very stable during 3 h incubation in DMEM ($^{10}T_{10}$ > 180 min and $^{10}T_{50}$ > 180 min), which might be due to their few hydroxyl groups in the rings A and B. The concentrations of isoflavones after 3 h incubated in DMEM (initial concentration 10 μM) (Table 1) were determined as biochanin A (10.81 ± 0.22 μM) > genistein (10.30 ± 0.26 μM) > daidzein (10.28 ± 0.16 μM) > puerarin (10.04 ± 0.13 μM) > formononetin (9.92 ± 0.14 μM) > genistin (9.67 ± 0.10 μM) > formononetin 7-*O*-glucoside (9.11 ± 0.13 μM) > daidzin (9.01 ± 0.02 μM).

Hydrogenation of the C_2=C_3 Double Bond. Naringenin, naringin, narirutin, hesperetin, hesperidin, liquiritigenin, and liquiritin were stable during 3 h incubation in DMEM ($^{10}T_{10}$ > 180 min and $^{10}T_{50}$ > 180 min; Table 1). In contrast, dihydromyricetin was degraded during the incubation period ($^{10}T_{10}$ < 1.0 min and $^{10}T_{50}$ = 1.91 min). Compared with the flavonoid apigenin, the flavanoid naringenin displayed a slightly higher stability ($^{10}T_{10}$ > 180 min and $^{10}T_{50}$ > 180 min). However, dihydromyricetin was very instable ($^{10}T_{10}$ < 1 min and $^{10}T_{50}$ = 1.91 min) with more than 90% being decomposed within 10 min incubation. However, dihydromyricetin was more stable than myricetin ($^{10}T_{10}$ < 1 min and $^{10}T_{50}$ < 1 min).

Catechins. Catechins are the major polyphenols in green tea leaves. The major catechins of green tea extract are C, EC, EGC, EGCG, EGC, and GCG. The order of stability of catechins was determined as ECG> EC > EGCG> GCG > EGC ≈ C (Figure 6 and Table 1). EGC and C were extremely instable and completely decomposed within 1 min. EGCG and GCG revealed significant instability within 10 min. The initial concentrations (10 μM) of catechins decreased within 10 min: ECG (9.8 ± 1.1 μM) > EC (9.6 ± 0.1 μM) > EGCG (2.1 ± 0.3 μM) > GCG (0.76 ± 0.8 μM) > EGC = C (0) (Figure 7). Apparently, the pyrogallol-type catechins showed lower stability than the catechol-type catechins. The galloylation of catechins obviously improved their stability. However, specific to various substitutions on ring B, the degree of influence was quite different. For the pyrogallol-type catechins, a galloylation

DOI: 10.1021/jf505514d
J. Agric. Food Chem. 2015, 63, 1547−1557

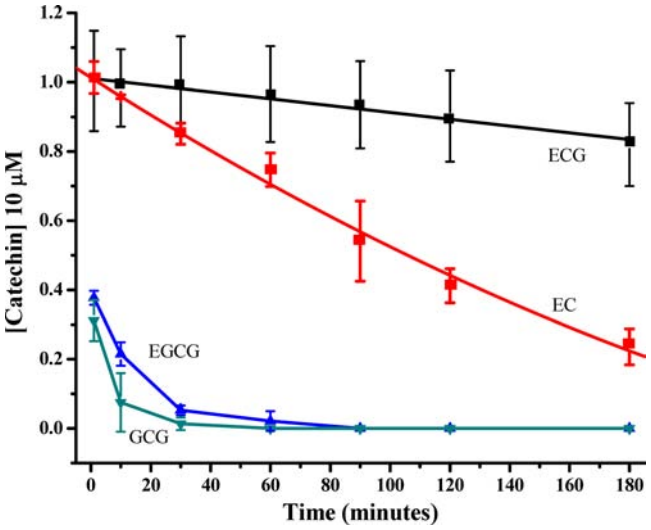

Figure 6. Stability of catechins (initial concentration 10 μM) in DMEM incubated at 37 °C in 5% CO_2. These results are the mean of three independently performed experiments.

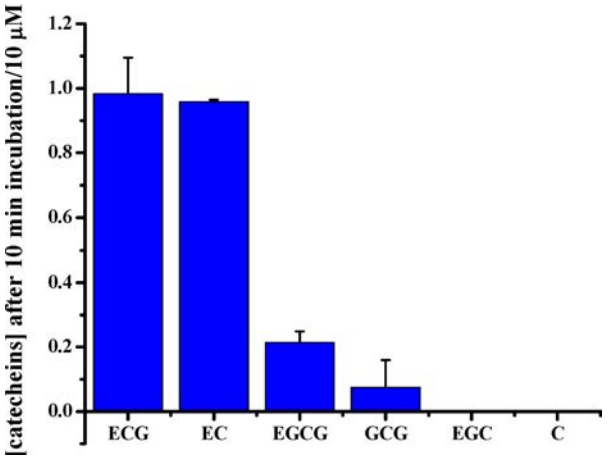

Figure 7. Concentration of catechins after 10 min incubated in DMEM. These results are the mean of three independently performed experiments.

significantly enhanced the stability. For catechol-type catechins, a galloylation only slightly increased the stability. Moreover, the catechins with 2,3-*cis* structure exhibited higher stability than the catechins with 2,3-*trans* structure.

Stilbenoids. A hydroxylation, glycosylation, and methylation of resveratrol significantly influenced the stability of its derivatives isorhapontigenin, oxyresveratrol, pinostilbene, pterostilbene, and piceid (Table 1, Figure 8). Compared with resveratrol (3,5,4′-OH) ($^{10}T_{10}$ = 165.92 min and $^{10}T_{50}$ > 180 min), piceatannol (3,5,4′,5′-OH) ($^{10}T_{10}$ = 5.68 min and $^{10}T_{50}$= 22.51 min) and oxyresveratrol (3,5,4′,6′−OH) ($^{10}T_{10}$ = 11.57 min and $^{10}T_{50}$= 59.12 min) with an additional hydroxyl group on ring B were instable during the 3 h incubation. The stability of resorcinol-type stilbenoids was higher than that of catechol-type stilbenoids. The 5′-methoxylation of piceatannol to isorhapontigenin (3,5,4′-OH,5′-OCH_3) ($^{10}T_{10}$ = 81.14 min and $^{10}T_{50}$ > 180 min) clearly improved the stability. The methoxylation on ring A of resveratrol to pinostilbene (3,4′-OH,5-OCH_3) ($^{10}T_{10}$ > 180 min and T_{50} > 180 min) and pterostilbene (4′-OH,3,5-OCH_3) ($^{10}T_{10}$ > 180 min and $^{10}T_{50}$ > 180 min) slightly enhanced the stability. Piceid (3, 4′-OH,5-O-glucoside) ($^{10}T_{10}$ > 180 min and $^{10}T_{50}$ > 180 min) was the most stable compound among stilbenoids tested: it was more stable than resveratrol (3,5,4′-OH). The concentrations of stilbenoids after 3 h incubated in DMEM (initial concentration 10 μM) (Figure 9) were determined as piceid (10.8 ± 0.6 μM) > pterostilbene (10.7 ± 0.9 μM) > pinostilbene (10.4 ± 0.04 μM) > resveratrol (8.7 ± 0.09 μM) > isorhapontigenin (7.9 ± 0.2 μM) > oxyresveratrol (1.8 ± 0.22 μM) > piceatannol (0). It was concluded that the glycosylation and methoxylation of OH moiety on stilbenoids would enhance the stability and the hydroxylation of stilbenoids decreases the stability.

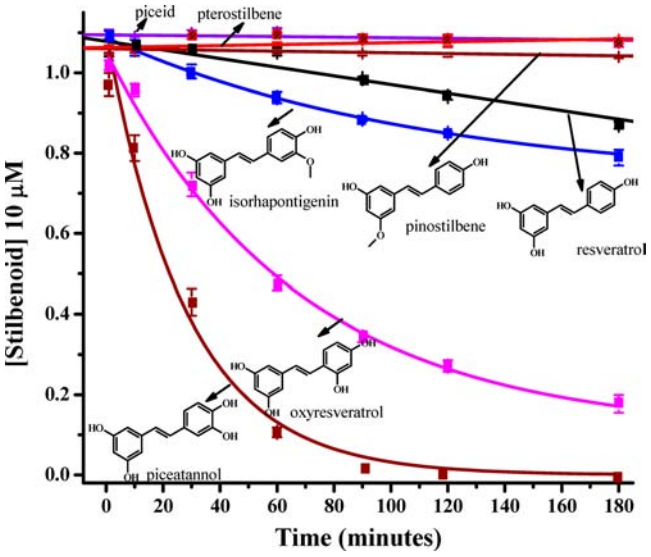

Figure 8. Stability of stilbenoids (initial concentration 10 μM) in DMEM incubated at 37 °C in 5% CO_2. These results are the mean of three independently performed experiments.

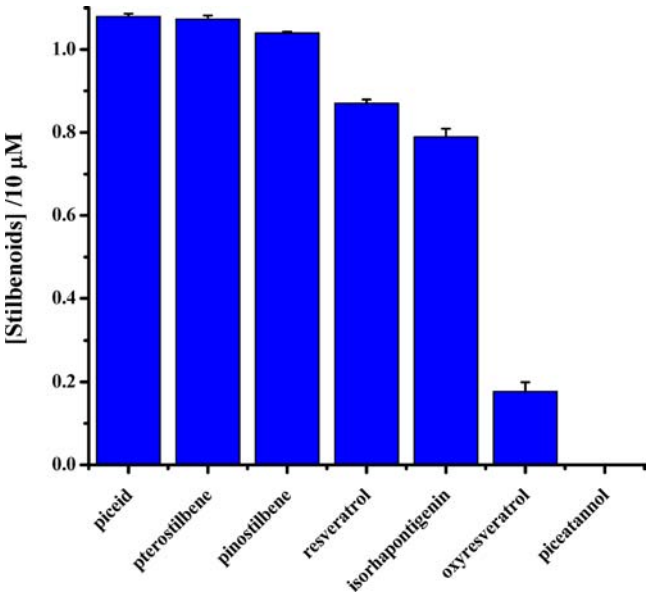

Figure 9. Concentration of stilbenoids after 3 h incubated in DMEM at 37 °C in 5% CO_2. These results are the mean of three independently performed experiments.

Correlation of the Stability with the Antioxidant Potential of the Compounds. The correlation between the stability and the antioxidant properties of polyphenols was

DOI: 10.1021/jf505514d
J. Agric. Food Chem. 2015, 63, 1547−1557

analyzed using published data of the antioxidant potential.[23] There was a weak linear relationship between the stability and antioxidant potential (Figure 10, $R^2(^{10}T_{10})$=0.5399, $R^2(^{10}T_{50})$=0.6336). For example, the TEAC values (ABTS) of flavonols were determined as quercetin > kaempferol > myricetin > galangin,[23] which is different from the following order of stability: galangin > kaempferol > quercetin > myricetin. Rutin ($TEAC_{ABTS}$ = 2.02 mM; $TEAC_{DPPH}$ = 2.33 mM) showed much higher antioxidant potential than baicalin ($TEAC_{ABTS}$ = 1.55 mM; $TEAC_{DPPH}$ = 1.79 mM).[23] However, rutin ($^{10}T_{10}$ > 180 min and $^{10}T_{50}$ > 180 min) was much more stable than baicalin under the cell culture conditions.

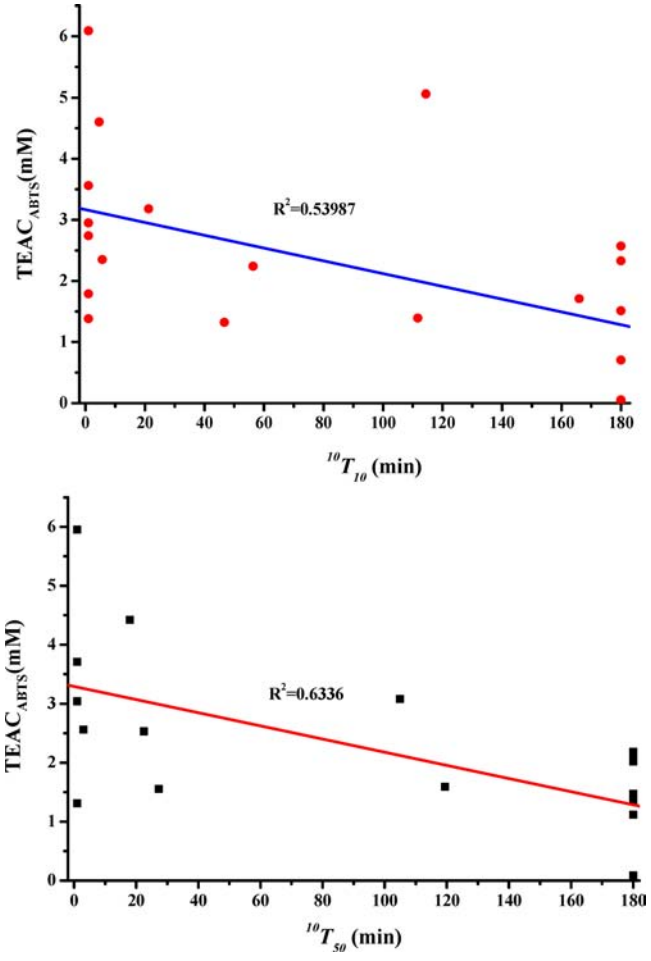

Figure 10. Correlation between the stability of polyphenols in DMEM and their antioxidant properties. The data of the antioxidant potential of polyphenols are expressed as TEAC values (mM) based on the ABTS assay and DPPH assay.[23]

Stability of Flavonols in Human Plasma. The stablility of flavonols such as myricetin, myricitrin, quercetin, and kaempferol, which were particularly instable under the cell culture conditions, was further investigated. It was found that myricetin was still highly instable in human plasma; however, myricetin revealed increased stability in human plasma as compared to DMEM. After incubation with DMEM at 37 °C for 10 min, there was no more myricetin detectable (Figure 1), but when incubated with human plasma at 37 °C for 180 min, myricetin was still present (Figure 11). The stability of myricitrin, quercetin, and kaempferol (initial concentration 10 μM) in human plasma at 37 °C was determined as $^{10}T_{50}$ > 180 min. The $^{10}T_{50}$ values of myricitrin, quercetin, and kaempferol (initial concentration 10 μM) in DMEM at 37 °C were determined as 119.47, 17.96, and 63.95 min (Table 1).

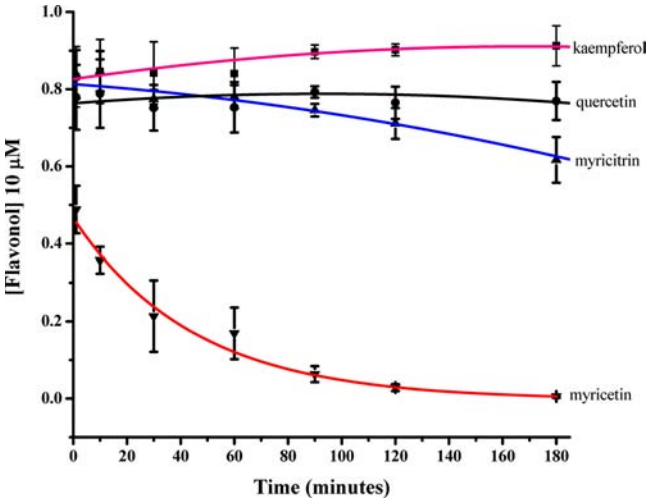

Figure 11. Stability of flavonols (initial concentration 10 μM) in human plasma incubated at 37 °C in 5% CO_2. These results are the mean of three independently performed experiments.

Protein Concentrations in DMEM and Human Plasma. The protein concentration in DMEM supplemented with 10% FBS was determined as 0.41 g/L; the total protein concentration in human plasma was 61.7 g/L.

DISCUSSION

Numerous researchers in biological and medicinal areas use cell cultures for their experiments, which provide information on cell proliferation and apoptosis, cell signaling, and regulation of gene expression and protein synthesis under controlled and reproducible conditions.[24] However, when working with polyphenols it must be taken into consideration that these compounds might not be stable under the cell culture conditions and that artifacts might arise.[24] The results of our study revealed that the factors influencing the stability of polyphenol in cell culture medium include the initial concentration of polyphenol, temperature, the presence and concentration of proteins, and the pH value. In contrast, the polyphenols' stability in organic solvents depends mainly on their initial concentration and the temperature. Thus, the stability of polyphenols in cell culture medium differs from that in organic solvents.

Several groups have investigated the stability of selected tea catchins under the cell culture conditions.[15,25] However, the structure−stability relationship of dietary polyphenols has not been systematically and comprehensively investigated for the main groups of polyphenols and their major representatives. The present study revealed a systematic influence of the chemical stucture of polyphenols on their stability under the cell culture conditions (Figure 12). We defined and used for the first time an early degradation ($^{C}T_{10}$) and a half degradation time ($^{C}T_{50}$) to characterize and compare the stability of the individual compounds. It was concluded that polyphenols with divergent structure significantly differed regarding their stability in cell culture medium. The stability of flavonoids was mainly correlated with structural motifs of the molecules, which also frequently affect their reactivity and bioactivity in a variety of physiological processes.[26] Important structural motifs were

DOI: 10.1021/jf505514d
J. Agric. Food Chem. 2015, 63, 1547−1557

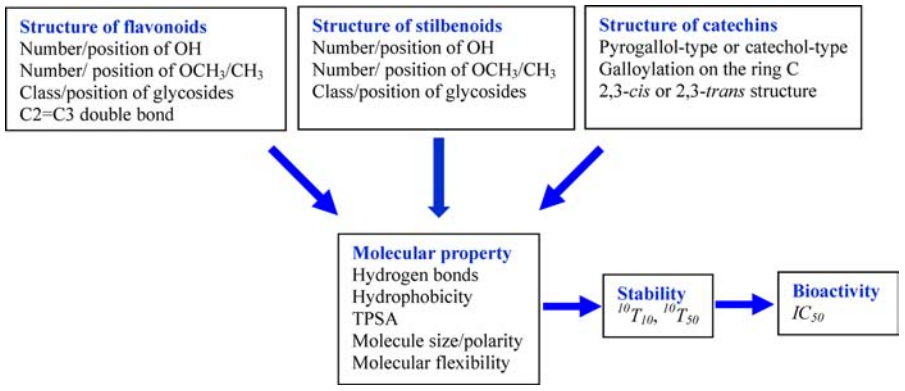

Figure 12. Structural and molecular properties of polyphenols that influence the stability of polyphenols.

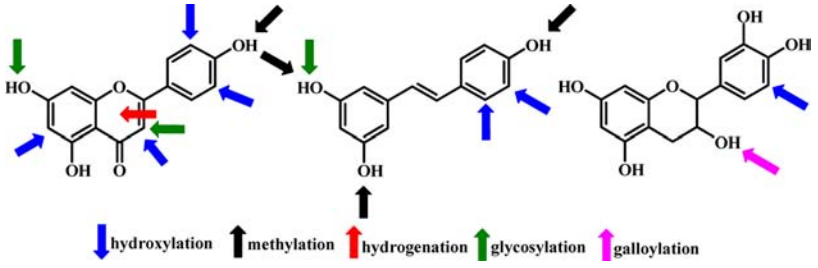

Figure 13. Potential sites of polyphenols affecting the stability are schematically illustrated. The up arrows represent increasing the stability; the down arrows represent decreasing the stability.

determined as follows (1) for flavonoids: (a) the number and position of the hydroxyl groups on the rings A, B, and C; (b) the methoxyl or methyl groups in the rings A and B; (c) the class and position of the glycosides; (d) the degree of saturation of the ring C (the presence or absence of a C_2=C_3 double bond). Motifs follow (2) for silbenoids: (a) the number and position of the hydroxyl and methoxyl moieties on the rings A and B; (b) the class and position of the glycosides. Motifs follow (3) for catechins: pyrogallol-type or catechol-type for ring B; (b) galloylation on the ring C; (c) 2,3-*cis* or 2,3-*trans* structure.

The structure−stability relationships of polyphenols determined under the cell culture conditions were summarized (Figure 13). Hydroxylation on flavonoids usually weakened the stability. The hydroxyl substitutions on the nucleus rings of flavonoids influencing the stability were determined as resorcinol-type > catechol-type > pyrogallol-type. Maini et al. investigated the UVA-light and aqueous stability of galangin, kaempferol, quercetin, and myricetin and analyzed the stability of these flavonols in DMEM at room temperature (25 °C).[27] They also observed a lower stability of these compounds under the cell culture conditions compared to in aqueous solution. As expected, the temperature is also an important factor affecting the stability. The lower stability of catechol-type and pyrogallol-type flavonols is likely due to more hydrogen-bond donating hydroxyl groups and the formation of an ortho-quinone on ring B, which favors the formation of a critical carbocation intermediate on ring C during the oxidative decomposition.[28,29] The hydroxyl group at C-5 position can form a hydrogen bond with the carbonyl group at C-5 position, which may enhance the stability. However, hydroxylation on ring A of flavonols is not the key factor influencing the stability.

Natural dietary flavonols are found mainly as 3- and 7-*O*-glycosides, and the plant flavones are mainly found as 4′- and 7-*O*-glycosides.[5,30,31] Even though the effect of glycosylation on the stability of flavonoids has been discussed previously,[32] there is limited information on the stability of flavonoid *O*-glycosides in DMEM. Herein, the influence of glycosylation of dietary flavonols and flavones on the stability in DMEM medium was investigated. *C* or *O*-Glycosylation of flavonoids obviously enhanced the stability. It was reported that *C*-glycosylated flavonoids are more stable in comparison with aglycones or *O*-glycosylated flavonoids.[33] However, we found that apigenin *C*- and *O*-glycosides were very stable during 3 h incubation in DMEM (T_{10} > 180 min and T_{50} > 180 min), which were similar to the aglycone. It has been reported that the glycosylation of flavonoids decreases antioxidant activity,[34] and this negative effect may result from the properties of sugar itself, rather than from the loss of a free hydroxyl group.[35] Plumb et al. have also reported that antioxidant capacities of flavonol glycosides present in tea decrease as the number of glycosidic moieties increased.[36] Moreover, the glycosylation is not the crucial factor deciding the stability of flavones and flavonols, which depends on the substitutions on the nucleus rings of flavonoids.

In the present study it was found that the hydrogenation of the C2=C3 double bond of flavonoids to corresponding flavanoids increased the stability. However, along with disparate substitutions on the nucleus rings, the degree of influence is not identical. Planarity of the C ring in flavonoids maybe important for the stability, as the molecules with saturated C2—C3 bonds (flavanones and certain others) permit more twisting of ring B with reference to ring C. A C2=C3 double bond increases the delocalization of π-electrons across those conjugated systems and the *p*-conjugation of the bond linking the rings B and C, which favors near-planarity of the two rings.[37]

Stilbenoids are phytoalexins become activated when plants are stressed and are important polyphenols with the C_6−C_2−C_6 structure.[38] The typical natural stilbenoids are resveratrol and its 3-glucoside, piceid.[39] We found that the glycosylation and methoxylation of stilbenoids enhanced the stability, and the

DOI: 10.1021/jf505514d
J. Agric. Food Chem. 2015, 63, 1547−1557

hydroxylation of stilbenoids decreased the stability. Long et al. found that pyrogallol-type compounds decompose in cell culture media to generate significant amounts of H_2O_2.[40] 3,4,5,4′-Tetrahydroxystilbene and 3,3′,4,4′,5,5′-trihydroxystilbene, but not resveratrol, generate measurable amounts of H_2O_2 when incubated in DMEM at a concentration of 50 μM.[41]

Some polyphenols displayed instability in cell culture medium. It has been reported that reactive oxygen species are formed under most cell culture conditions.[14] For example, EGCG has been shown to be instable and subject to oxidation and polymerization, resulting in the formation of reactive oxygen species.[14,15] It appears that also different cell culture media might have a different influence on the stability of polyphenols. In the present study, it was found that EGCG (initial concentration 10 μM) was very instable in DMEM without cells ($^{10}T_{10}$ < 1 min and $^{10}T_{50}$ < 1 min). It was reported that in McCoy's 5A culture media, the $^{25}T_{50}$ of EGCG (initial concentration 10 μM) was less than 30 min; surprisingly, the stability was prolonged to 130 min in the presence of HT-29 cells.[15] In contrast, it was reported that quercetin (initial concentration 25 μM) was very instable when incubated with DMEM in the presence of HT29 cells ($^{25}T_{50}$ = 30 min).[42] In the present study, the $^{10}T_{50}$ of quercetin (initial concentration 10 μM) was 17.96 min with DMEM in the absence of cells, which is not consistent with the notion that cells enhance the stability of quercetin. It needs further investigations to clarify the stability of polyphenols in the presence of cells. Generally, it seems possible that various cellular enzymes compromise the compounds' stability via degradation or metabolism. On the other side, adsorption of polyphenols to cellular proteins might enhance the stability of the compounds. Such a stabilizing effect has been described for polpyphenols attached to plasma proteins.[43,44]

Several factors, such as pH, proteins, antioxidant levels, and the presence of metal ions, might influence the stability of polyphenols, and pH is possibly the most critical determinant.[15,45] In DMEM, quercetin was shown to be very stable at pH of 6 and decomposed under pH of 7 and 8.[45] Other constituents in DMEM obviously also influenced its stability because quercetin was reported to be more stable in H_2O than in DMEM. However, most supplements for cell culture media, such as HEPES, glucose, sodium pyruvate, antibiotics, and FBS, had a neglible influence on the stability of quercetin.[45] Yet, it is not clear for how these factors influence other polyphenols.

Kosińska et al. investigated the stability of polyphenol extracts from cocoa, green tea, and strawberries in HBSS buffer.[46] They found that most of the polyphenols decomposed during 2 h of incubation. EGCG and EGC were very vulnerable in HBSS both at pH 6.5 and 7.4; their specific molecular structure was discussed to be responsible for this phenomenon.[46] The flavan-3-ols from cocoa were more stable at pH 6.5 than at pH 7.4. The major oxidative products of EGCG in McCoy's 5A culture media were theasinensin and its dimer.[15] However, the mechanism should be further elucidated. Autooxidation was observed for EGCG in air-saturated Tris buffer, which may generate $\bullet O_2^-$ and quinones to form H_2O_2.[47] It was reported that the stability of EGCG was significantly enhanced in the presence of SOD in the cell culture medium, which prolonged the T_{50} of EGCG to 24 h. The presence of 5% serum in the medium also prolonged the T_{50} of EGCG to 1 h.[47]

On the basis of many previous and recent findings,[48−52] it appears that favorable structures required for radical scavenging of polyphenols follow these requirements: (a) the *o*-dihydroxyl (3′,4′-diOH, i.e., catechol) structure in the B-ring, (b) the C_2−C_3 double bond (in conjugation with the 4-oxo group), (c) the presence of both 3-OH and 5-OH groups for the maximal radical scavenging capacity and the strongest radical absorption. (d) In the absence of *o*-dihydroxyl structure in the B ring, the hydroxyl substituents in a catechol structure on the A ring are able to compensate and become a larger determinant of flavonoid antiradical activity. These summarized structural features are partially similar to the partial structures that make the molecule more prone to instability under the cell culture conditions.

It was obvious to speculate that the polyphenols' degree of stability in cell culture medium merely reflected their antioxidant properties. However, in the present study it was found that there was no strong correlation between the antioxidant potential of polyphenols and their stability. Consequently, it can be assumed that oxidation processes are not the only factor governing the stability of polyphenols in biological systems. Other influences such as polyphenol−protein interactions or complex formation might play an important role, too. It has been reported that binding to human plasma proteins improved the polyphenols' stability and protected against oxidation.[43] Our results are consistent with that observation. We found that polyphenols revealed a higher stability in human plasma as compared to DMEM. The protein concentration determined in human plasma was 150-fold higher than in DMEM which suggested that the adsorption of polyphenols to plasma proteins contributed to their enhanced stability in this matrix. The degree of plasma protein binding has been shown to be highly variable among individual polyphenolic compounds,[44] and it needs to be investigated how strong the extent of protein binding correlates with the compounds' stability in plasma or cell culture medium.

At this point, it is not clear whether similar degraded or oxidized polyphenol products can be found in human plasma and cell culture medium. The compounds may exhibit different degradation or oxidation patterns, which might also help explaining the different results from cell experiments *in vitro* and animal/human experiments *in vivo*.[53] It also has to be considered that the degraded or metabolized polyphenol might exhibit a bioactivity which might be different from the parent compound.[21] In 2010, D'Archivio et al. criticized that a large number of *in vitro* studies tested polyphenols rather than their active metabolites.[54] So, we might be looking at the wrong compounds when investigating the mechanisms contributing to the health benefits of polyphenols. Recently, it was shown that metabolites of resveratrol (resveratrol 3-*O*-sulfate, resveratrol 3-*O*-glucuronide, and resveratrol 4′-*O*-glucuronide) inhibited human colon carcinoma and metastatic cell proliferation through an accumulation of cells in DNA replication phase and by inducing DNA damage.[55] Further investigations should clarify the precise mechanisms of degradation of polyphenols in cell culture medium and plasma and take the bioactivity of the resulting derivatives into consideration. In the case that an individual polyphenol displays pronounced instability in cell culture medium while exerting significant cellular effects, it should be considered that not the mother compound but a degradation product or metabolite is the actual bioactive principle.[56,57] Further isolation and identification of the final degraded products is necessary to explore the mechanism, as well as to investigate the bioactivity of the derivatives and metabolites of polyphenols. To summarize, it is essential to

DOI: 10.1021/jf505514d
J. Agric. Food Chem. 2015, 63, 1547−1557

account for polyphenol stability in cell culture experiments to avoid erroneous conclusions.

In conclusion, the influence of cell culture conditions on the stability and fate of polyphenols is rarely considered, which might result in misleading conclusions about the compound's bioactivity or the active principle. In the current investigation, the structure−stability relationship of polyphenols incubated with the cell culture medium DMEM was comprehensively investigated. Some polyphenols, especially aglycones with catechol or pyrogallol structures and pyrogallol-type glycosides, were evidently instable. The additional hydroxyl moieties attached to ring B of flavonols obviously weakened the compound's stability under the cell culture conditions. The glycosylation of a hydroxyl group of the pyrogallol moiety in flavones slightly enhanced the stability. It appears that the glycosylation of isoflavones decreased and the methoxylation of isoflavones increased their stability. The C2═C3 double bond in conjugation with a 4-oxo group is also considered as an important role for the stability. The hydrogenation of the C2═C3 double bond of flavanoids to corresponding flavonoids increased the stability. We suggest that the stability of polyphenols in a biological system is not solely governed by the oxidation processes, because the degradation tendency of these polyphenols was not highly correlated with their antioxidant potential. Polyphenols were considerably more stable in human plasma as compared to DMEM, which may be based on polyphenol−protein interactions enhancing the compounds' stability.[10] Our results might be used to further investigate the mechanism of degradation or metabolism of polyphenols in cell culture and human plasma, which might stimulate the search for the actual bioactive compounds derived from polyphenols.

AUTHOR INFORMATION

Corresponding Author

*Phone: +49 (0) 17681574937. E-mail: jianboxiao@yahoo.com.

Funding

The authors are grateful for financial support by the Alexander von Humboldt Foundation (Germany).

Notes

The authors declare that they have no conflict of interests.

The authors declare no competing financial interest.

REFERENCES

(1) Xiao, J. B.; Ni, X. L.; Kai, G. Y.; Chen, X. Q. Advance in dietary polyphenols as aldose reductases inhibitors: Structure-activity relationship aspect. *Crit. Rev. Food Sci. Nutr.* **2015**, *55*, 16−31.

(2) Schluesener, J. K.; Schluesener, H. Plant polyphenols in the treatment of age-associated diseases: Revealing the pleiotropic effects of icariin by network analysis. *Mol. Nutr. Food Res.* **2014**, *58*, 49−60.

(3) Ayissi, V. B. O.; Ebrahimi, A.; Schluesenner, H. Epigenetic effects of natural polyphenols: A focus on SIRT1-mediated mechanisms. *Mol. Nutr. Food Res.* **2014**, *58*, 22−32.

(4) Xiao, J. B.; Högger, P. Dietary polyphenols and type 2 diabetes: Current insights and future perspectives. *Curr. Med. Chem.* **2015**, *22*, 23−38.

(5) Pugliese, A. G.; Tomas-Barberan, F. A.; Truchado, P.; Genovese, M. I. Flavonoids, proanthocyanidins, vitamin C, and antioxidant activity of *Theobroma grandiflorum* (Cupuassu) pulp and seeds. *J. Agric. Food Chem.* **2013**, *61*, 2720−2728.

(6) Andrae-Marobela, K.; Ghislain, F. W.; Okatch, H.; Majinda, R. Polyphenols: A diverse class of multi-target anti-HIV-1 agents. *Curr. Drug Metab.* **2013**, *7*, 392−413.

(7) Manach, C.; Scalbert, A.; Morand, C.; Rémésy, C.; Jiménez, L. Polyphenols: Food sources and bioavailability. *Am. J. Clin. Nutr.* **2004**, *79*, 727−747.

(8) Clifford, M. N. Diet-derived phenols in plasma and tissues and their implications for health. *Planta Med.* **2004**, *70*, 1103−1114.

(9) Xiao, J. B.; Högger, P. Influence of diabetes on the pharmacokinetic behavior of natural polyphenols. *Curr. Drug Metab.* **2014**, *15*, 23−29.

(10) Xiao, J. B.; Kai, G. Y. A review of dietary polyphenol-plasma protein interactions: Characterization, influence on the bioactivity, and structure-affinity relationship. *Crit. Rev. Food Sci. Nutr.* **2012**, *52*, 85−101.

(11) Xiao, J. B.; Högger, P. Advance in pharmacokinetics of bioactive polyphenols. *Curr. Drug Metab.* **2014**, *15*, 1−2.

(12) Kanakis, C. D.; Hasni, I.; Bourassa, P.; Tarantilis, P. A.; Polissiou, M. G.; Tajmir-Riahi, H. A. Milkbeta-lactoglobulin complexes with tea polyphenols. *Food Chem.* **2011**, *127*, 1046−1055.

(13) Dubeau, S.; Samson, G.; Tajmir-Riahi, H. A. Dual effect of milk on the antioxidant capacity of green, Darjeeling, and English breakfast teas. *Food Chem.* **2010**, *122*, 539−545.

(14) Sang, S.; Lambert, J. D.; Yang, C. S. Bioavailability and stability issues in understanding the cancer preventive effects of tea polyphenols. *J. Sci. Food Agric.* **2006**, *86*, 2256−2265.

(15) Hong, J.; Lu, H.; Meng, X.; Ryu, J. H.; Hara, Y.; Yang, C. S. Stability, cellular uptake, biotransformation, and efflux of tea polyphenol (−)-epigallocatechin-3-gallate in HT-29 human colon adenocarcinoma cells. *Cancer Res.* **2002**, *62*, 7241−7246.

(16) Yuan, L.; Wei, S. P.; Wang, J.; Liu, X. B. Isoorientin induces apoptosis and autophagy simultaneously by reactive oxygen species (ROS)-related p53, PI3K/Akt, JNK, and p38 signaling pathways in HepG2 cancer cells. *J. Agric. Food Chem.* **2014**, *62*, 5390−5400.

(17) Yuan, L.; Wang, J.; Xiao, H. F.; Wu, W. Q.; Wang, Y. T.; Liu, X. B. MAPK signaling pathways regulate mitochondrial-mediated apoptosis induced by isoorientin in human hepatoblastoma cancer cells. *Food Chem. Toxicol.* **2013**, *53*, 62−68.

(18) Lee, W. C.; Peng, C. C.; Chang, C. H.; Huang, S. H.; Chyau, C. C. Extraction of antioxidant components from *Bidens pilosa* flowers and their uptake by human intestinal Caco-2 cells. *Molecules* **2013**, *18*, 1582−1601.

(19) Boyer, J.; Brown, D.; Liu, R. H. Uptake of quercetin and 1uercetin 3-glucoside from whole onion and apple peel extracts by Caco-2 cell monolayers. *J. Agric. Food Chem.* **2004**, *52*, 7172−7179.

(20) Uhlenhut, K.; Högger, P. Facilitated cellular uptake and suppression of inducible nitric oxide synthase (iNOS) by a metabolite of maritime pine bark extract (Pycnogenol). *Free Radic. Biol. Med.* **2012**, *53*, 305−313.

(21) Kurlbaum, M.; Mülek, M.; Högger, P. Facilitated uptake of a bioactive metabolite of maritime pine bark extract (Pycnogenol) into human erythrocytes. *PLoS One* **2013**, *8*, e63197.

(22) Walker, J. M. *The Bicinchoninic Acid (BCA) Assay for Protein Quantitation. The Protein Protocols Handbook*; Humana Press: Totowa, NJ, 1996.

(23) Cai, Y. Z.; Sun, M.; Xing, J.; Luo, Q.; Corke, H. Structure−radical scavenging activity relationships of phenolic compounds from traditional Chinese medicinal plants. *Life Sci.* **2006**, *78*, 2872−2888.

(24) Halliwell, B. Cell culture, oxidative stress, and antioxidants, avoiding pitfalls. *Biomed. J.* **2014**, *37*, 99−105.

(25) Sang, S.; Lee, M. J.; Hou, Z.; Ho, C. T.; Yang, C. S. Stability of tea polyphenol (−)-epigallocatechin-3-gallate and formation of dimers and epimers under common experimental conditions. *J. Agric. Food Chem.* **2005**, *53*, 9478−9484.

(26) Kumar, S.; Pandey, A. K. Chemistry and biological activities of flavonoids, an overview. *Sci. World J.* **2013**, 162750.

(27) Maini, S.; Hodgson, H. L.; Krol, E. S. The UVA and aqueous stability of flavonoids is dependent on B-ring substitution. *J. Agric. Food Chem.* **2012**, *60*, 6966−6976.

(28) Krishnamachari, V.; Levine, L. H.; Zhou, C.; Pare, P. W. *In vitro* flavon-3-ol oxidation mediated by a B ring hydroxylation pattern. *Chem. Res. Toxicol.* **2004**, *17*, 795−804.

DOI: 10.1021/jf505514d
J. Agric. Food Chem. 2015, 63, 1547−1557

(29) Krishnamachari, V.; Levine, L. H.; Pare, P. W. Flavonoid oxidation by the radical generator AIBN, a unified mechanism for quercetin radical scavenging. *J. Agric. Food Chem.* **2002**, *50*, 4357−4363.
(30) Xiao, J. B.; Muzashvili, T. S.; Georgiev, M. I. Advance on biotechnology for glycosylation of high-value flavonoids. *Biotechnol. Adv.* **2014**, *32*, 1145−1156.
(31) Davis, B. D.; Brodbelt, J. S. Determination of the glycosylation site of flavonoid monoglucosides by metal complexation and tandem mass spectrometry. *J. Am. Soc. Mass. Spectrom.* **2004**, *15*, 1287−1299.
(32) Plaza, M.; Pozzo, T.; Liu, J.; Ara, K. Z. G.; Turner, C.; Karlsson, E. N. Substituent effects on *in vitro* antioxidizing properties, stability, and solubility in flavonoids. *J. Agric. Food Chem.* **2014**, *62*, 3321−3333.
(33) Rawat, P.; Kumar, M.; Sharan, K.; Chattopadhyay, N.; Maurya, R. Ulmosides A and B, flavonoid 6-*C*-glycosides from *Ulmus wallichiana*, stimulating osteoblast differentiation assessed by alkaline phosphatase. *Bioorg. Med. Chem. Lett.* **2009**, *19*, 4684−4687.
(34) Mora, A.; Paya, M.; Rios, J. L.; Alcaraz, M. J. Structure-activity relationships of polymethoxyflavones and other flavonoids as inhibitors of non-enzymic lipid peroxidation. *Biochem. Pharmacol.* **1990**, *40*, 793−797.
(35) Heim, K. E.; Tagliaferro, A. R.; Bobilya, D. J. Flavonoid antioxidants, chemistry, metabolism and structure-activity relationships. *J. Nutr. Biochem.* **2002**, *13*, 572−584.
(36) Plumb, G. W.; Price, K. R.; Williamson, G. Antioxidant properties of flavonol glycosides from tea. *Redox Rep.* **1999**, *4*, 13−16.
(37) Edenharder, R.; von Petersdorff, I.; Rauscher, R. Antimutagenic effects of flavonoids, chalcones and structurally related compounds on the activity of 2-amino-3-methylimidazo(4,5-f)quinoline (IQ) and other heterocyclic amine mutagens from cooked food. *Mutat. Res.* **1993**, *287*, 261−274.
(38) Wang, T. T. Y.; Schoene, N. W.; Kim, Y. S.; Mizuno, C. S.; Rimando, A. M. Differential effects of resveratrol and its naturally occurring methylether analogs on cell cycle and apoptosis in human androgen-responsive LNCaP cancer cells. *Mol. Nutr. Food Res.* **2010**, *54*, 335−344.
(39) Zhou, S. Y.; Yang, R. T.; Teng, Z. H.; Zhang, B. L.; Hu, Y. Z.; Yang, Z. F.; et al. Dose-dependent absorption and metabolism of transpolydatin in rats. *J. Agric. Food Chem.* **2009**, *57*, 4572−4579.
(40) Long, L. H.; Hoi, A.; Halliwell, B. Instability of, and generation of hydrogen peroxide by, phenolic compounds in cell culture media. *Arch. Biochem. Biophys.* **2010**, *501*, 162−169.
(41) Kucinska, M.; Piotrowska, H.; Luczak, M. W.; Mikula-Pietrasik, J.; Ksiazek, K.; Wozniak, M.; et al. Effects of hydroxylated resveratrol analogs on oxidative stress and cancer cells death in human acute T cell leukemia cell line. Prooxidative potential of hydroxylated resveratrol analogs. *Chem.-Bio. Interact.* **2014**, *209*, 96−110.
(42) Skrbek, S.; Rüfer, C. E.; Marko, D.; Esselen, M. Quercetin and its microbial degradation product 3,4-dihydroxyphenylacetic acid generate hydrogen peroxide modulating their stability under in vitro conditions. *J. Food Nutr. Res.* **2009**, *48*, 129−140.
(43) Kragh-Hansen, U.; Chuang, V. T. G.; Otagiri, M. Practical aspects of the ligand-binding and enzymatic properties of human serum albumin. *Biol. Pharm. Bull.* **2002**, *25*, 695−704.
(44) Kurlbaum, M.; Högger, P. Plasma protein binding of polyphenols from maritime pine bark extract (USP). *J. Pharm. Biomed. Anal.* **2011**, *54*, 127−132.
(45) Hu, J.; Chen, L.; Lei, F.; Tian, Y.; Xing, D. M.; Chai, Y. S.; et al. Investigation of quercetin stability in cell culture medium, role in *in vitro* experiment. *Afr. J. Pharm. Pharmacol.* **2012**, *6*, 1069−1076.
(46) Kosińska, A.; Xie, Y. L.; Diering, S.; Héritier, J.; Andlauer, W. Stability of phenolic compounds isolated from cocoa, green tea and strawberries in Hank's balanced salt solution under cell culture conditions. *Polym. J. Food Nutr. Sci.* **2012**, *62*, 91−96.
(47) Mochizuki, M.; Yamazaki, S.; Kano, K.; Ikeda, T. Kinetic analysis and mechanistic aspects of autoxidation of catechins. *Biochim. Biophys. Acta* **2002**, *1569*, 35−44.
(48) Amic, D.; Davidovic-Amic, D.; Beslo, D.; Rastija, V.; Lucic, B.; Trinajstic, N. SAR and QSAR of the antioxidant activity of flavonoids. *Curr. Med. Chem.* **2007**, *14*, 827−845.
(49) Farkas, O.; Jakus, J.; Héberger, K. Quantitative structure-antioxidant activity relationships of flavonoid compounds. *Molecules* **2004**, *9*, 1079−1088.
(50) Om, A. S.; Ryu, J. C.; Kim, J. H. Quantitative structure-activity relationships for radical scavenging activities of flavonoid compounds by GA-MLR technique. *Mol. Cell. Toxicol.* **2008**, *4*, 170−176.
(51) Seyoum, A.; Asres, K.; El-Fiky, F. K. Structure−radical scavenging activity relationships of flavonoids. *Phytochemistry* **2006**, *67*, 2058−2070.
(52) Sarkar, A.; Middya, T. R.; Jana, A. D. A QSAR study of radical scavenging antioxidant activity of a series of flavonoids using DFT based quantum chemical descriptors−the importance of group frontier electron density. *J. Mol. Model.* **2012**, *18*, 2621−2631.
(53) Lambert, J. D.; Hong, J.; Yang, G. Y.; Liao, J.; Yang, C. S. Inhibition of carcinogenesis by polyphenols, evidence from laboratory investigations. *Am. J. Clin. Nutr.* **2005**, *81*, 284S−91S.
(54) D'Archivio, M.; Filesi, C.; Varì, R.; Scazzocchio, B.; Masella, R. Bioavailability of the polyphenols, status and controversies. *Int. J. Mol. Sci.* **2010**, *11*, 1321−1342.
(55) Aires, V.; Limagne, E.; Cotte, A. K.; Latruffe, N.; Ghiringhelli, F.; Delmas, D. Resveratrol metabolites inhibit human metastatic colon cancer cells progression and synergize with chemotherapeutic drugs to induce cell death. *Mol. Nutr. Food Res.* **2013**, *57*, 1170−1181.
(56) Zamin, L. L.; Filippi-Chiela, E. C.; Dillenburg-Pilla, P.; Horn, F.; Salbego, C.; Lenz, G. Resveratrol and quercetin cooperate to induce senescence-like growth arrest in C6 rat glioma cells. *Cancer Sci.* **2009**, *100*, 1655−1662.
(57) Amiri, F.; Zarnani, A. H.; Zand, H.; Koohdani, F.; Jeddi-Tehrani, M.; Vafa, M. Synergistic anti-proliferative effect of resveratrol and etoposide on human hepatocellular and colon cancer cell lines. *Eur. J. Pharmacol.* **2013**, *718*, 34−40.

DOI: 10.1021/jf505514d
J. Agric. Food Chem. 2015, 63, 1547−1557

Table 1. Enzyme-Mediated PS Synthesis in Various [Ch][AA] ILs

Entry	ILs	Side chain of amino acid	Viscosity (mPa·s)[19]	V_0 (μmol PS/min)	PS yield (%)[a]	Time (h)	PA content[b]
1	[Ch][Gly]		121	0.64	78.1	12	-
2	[Ch][Ala]		163	0.62	76.2	15	-
3	[Ch][Val]		372	0.58	70.9	36	-
4	[Ch][Ser]		402	0.57	73.3	36	-
5	[Ch][Thr]		454	0.56	71.6	36	-
6	[Ch][Leu]		476	0.56	60.4	36	-
7	[Ch][Ile]		480	0.56	57.5	36	-
8	[Ch][Pro]		500	0.45	50.1	42	-
9	[Ch][Phe]		520	0.50	45.2	42	-
10	[Ch][His]		980	0.49	46.7	48	-
11	[Ch][Asp]		2060	0.36	84.3	60	-
12	[Ch][Glu]		2308	0.36	86.5	60	-

[a]Maximum yield. [b]PA was not detected during the sample analysis by HPLC.

0.5% water (based on the total weight of the reaction system). Samples (50 μL) were taken from the reaction mixture at specified time intervals, centrifuged to obtain the upper layer, and analyzed by HPLC.

Analysis of the Samples.[20] The sample was analyzed by a Waters e2695 HPLC system (Waters, Milford, U.S.A.) with an evaporative light scattering detector (ELSD). External standards of PC, PS, and PA were used to prepare calibration solutions at five different concentrations. Two microliter sample and 1 mL hexane−isopropane (1/1, v/v) were precisely measured and mixed thoroughly. Ten microliters of the aforementioned mixture was injected. HPLC separation was on a Lichrospher 100 Diol column (5 μm, 250 mm × 4.6 mm, Merck). Mobile phase A was *n*-hexane/2-propanol/methanol (38:1:1, v/v). Mobile phase B was 2-propanol/methanol (2:3, v/v). Each mobile phase contained 1 mM ammonium acetate. The flow rate was 1.5 mL min^{-1}, and the gradient was as follows: 0−18.7% B from 0 to 20 min, 18.7−100% B from 20 to 20.2 min, 100% B from 20.2 to 25 min, 100−0% B from 25 to 25.1 min, and 0% B from 25.1 to 30 min. The column temperature and drift pipe temperature were controlled at 25 and 65 °C, respectively, and the nitrogen pressure was controlled at 40 psi. The retention times were 2.52, 2.95, and 23.83 min for PA, PS, and PC, respectively. PS yield was calculated from the HPLC data. The average error for this assay is less than 0.5%. All the reported data are averages of experiments performed at least in duplicate.

Operational Stability (Reusability) of PLD in [Ch][Glu]. The operational stabilities of PLD in [Ch][Glu] during batch reactions were evaluated. After each batch reaction, PLD was separated by filtration using Whatman #1 filter paper, washed with isopropyl alcohol three times, and then added into the fresh reaction mixtures for the next batch.

RESULTS AND DISCUSSION

In this work, 12 [Ch][AA] ILs, i.e., [Ch][Gly], [Ch][Ala], [Ch][Val], [Ch][Ser], [Ch][Thr], [Ch][Leu], [Ch][Ile], [Ch][Pro], [Ch][Phe], [Ch][His], [Ch][Asp], and [Ch][Glu], were successfully applied to enzymatic synthesis of PS. Table 1 shows that the prepared ILs had an obvious effect on the enzymatic reaction for PS synthesis. The reaction initial rate (V_0), PS yield, and the reaction time were measured to evaluate the enzymatic reaction.

As can be seen from Table 1, the initial reaction rates were remarkably influenced by the ILs employed. The minimum V_0 (0.36 μmol PS/min) was obtained in [Ch][Asp] and [Ch][Glu], while the maximum V_0 (0.64 μmol PS/min) was achieved when [Ch][Gly] was used as the reaction medium. It is clear that the V_0 values varied with the viscosity of the [Ch][AA] ILs used. Generally, the viscosity is one of the most important factors affecting the applications of the solvent for catalysis. It is well-known that an increase in solvent viscosity can augment the diffusion resistance of substrates, thus enhancing the mass transfer limitations and impairing the interactions between enzyme particles and substrates. Accordingly, the increase in the viscosity of the [Ch][AA] ILs resulted in the decrease of the V_0 value with the exception of [Ch][Pro].

Also, the V_0 values showed a clear dependence on the anion structures of the [Ch][AA] ILs. An increase in the number of carbon atoms in the side chain of amino acid generally resulted in a lower V_0 value (Table 1, entries 1, 2, 3, 6, and 7). Of the ILs tested, [Ch][Gly], with the anion being the simplest amino acid, displayed the highest V_0 value (0.64 μmol PS/min). In addition to the molecular size of the anion, the introduction of extra hydroxyl, phenyl ring, or carboxylic acid group

DOI: 10.1021/jf505296k
J. Agric. Food Chem. 2015, 63, 1558−1561

significantly decreased the V_0 value (Table 1, entries 4, 5, 8−12). In the [Ch][AA] ILs containing hydroxyl group in the side chain of amino acid ([Ch][Ser] and [Ch][Thr]), the V_0 values were slightly lower, while the ILs with aromatic group in the anions displayed relatively lower V_0 values (i.e., 0.45, 0.50, and 0.49 μmol PS/min for [Ch][Pro], [Ch][Phe], and [Ch][His], respectively). Unfortunately, the lowest V_0 values of 0.36 μmol PS/min were recorded for [Ch][Asp] and [Ch][Glu] in which the acidic amino acids served as the anions. A reason for the substantial correlation between V_0 values and the anion structures of the [Ch][AA] ILs may be that the efficiency of the enzyme action during PS synthesis was affected by the solvent used. Particularly, the intermolecular forces of the ILs such as van der Waals, hydrogen bond, and π-stacking interactions might contribute to this effect.

Moreover, the maximal PS yields of the PLD-mediated reaction and the time they consumed in all the [Ch][AA] ILs employed are presented in Table 1 columns 6 and 7, respectively. As can be observed, although the PS yield value in [Ch][Gly] was only 78.1%, the reaction time (12 h) it needed was the shortest. By contrast, the reaction in [Ch][Glu] proceeded slowest but constantly increased up to the highest PS yield value of 86.5% after 60 h. Obviously, the lowest PS yield (45.2%) was found in [Ch][Phe].

In Table 1, we found that the PS yield has no apparent dependence on the viscosity of the [Ch][AA] ILs used. Similarly, it was shown that the PS yields showed a close correlation to the anion structures of the [Ch][AA] ILs as well. When the side chain of amino acid was alkyl group, elongation of the side chain generally led to lower PS yield (Table 1, entries 1, 2, 3, 6, and 7). The [Ch][AA] ILs containing basic amino acids as the anions displayed relatively lower PS yields, i.e., 73% and 71% for [Ch][Ser] and [Ch][Thr], respectively. The introduction of an additional carboxylic acid group to the side chain of the amino acid substantially increased the PS yields (Table 1, entries 12 and 13). Higher PS yields of 84% and 86% were exhibited in [Ch][Asp] and [Ch][Glu], respectively. To be noted was that the introduction of a phenyl ring exerted drastic effect on the PS yields (Table 1, entries 8−10). The PS yields obtained in three [Ch][AA] ILs with aromatic group were much lower. In particular, the lowest PS yield (45%) was found in [Ch][Phe]. As we all know, the maximal PS yield value was attributable to the thermodynamic equilibrium of the enzymatic transphosphatidylation of PC with L-serine for PS synthesis. Consequently, as far as the dependence of PS yield on the [Ch][AA] ILs was concerned, a speculative explanation could be that the thermodynamic equilibrium of the enzyme-mediated reaction may be affected by the ILs used. Furthermore, the [Ch][AA] ILs effects on the thermodynamic equilibrium of the reaction may be due to their specific structures, especially the anions structures.

From a practical viewpoint, the reusability of the biocatalyst is one of essential factors for the cost-efficiency. If the biocatalyst can be reused, the economical sustainability is increased. Encouraged by the excellent experiment results above, the operational stability of PLD in [Ch][Glu] was investigated to further examine the potential of the enzyme as a catalyst for PS production. After each batch reaction, the enzyme was recovered by filtration, and the next batch was carried out with fresh substrates. Figure 1 presents the plot of the activity of the enzyme as a function of the number of reaction batches. Batch 0 corresponds to the activity of the fresh enzyme employed in the first reaction trial which was taken as 100%. It was worth noting that PLD displayed excellent operational stability, and 75% of its original activity was maintained after being used for 10 batches, highlighting the presumable cost-effectiveness of the enzyme.

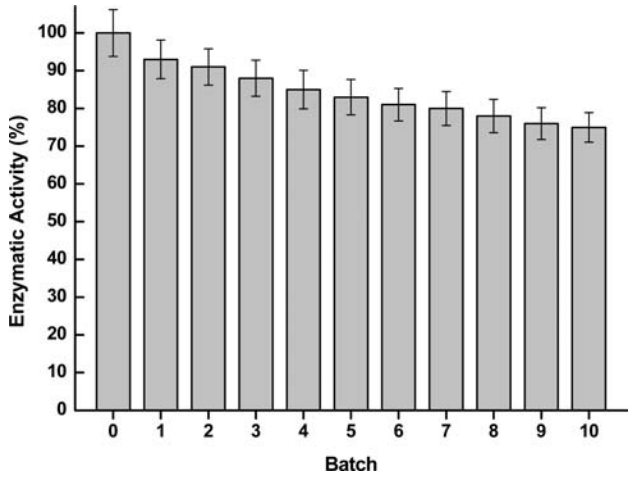

Figure 1. Operational stability of PLD in [Ch][Glu]. Reaction conditions: 3.0 mL of [Ch][Glu], 0.05 mmol PC, 0.15 mmol L-serine, 60 U PLD, 0.5% water (based on the total weight of the reaction system), 40 °C.

In general, the whole synthesis process for PS is highlighted by the application of eco-friendly solvents [Ch][AA] ILs as the reaction media. An efficient, cost-effective, and easy-to-use "green chemistry" method for the enzymatic PS preparation was provided. Additionally, the excellent results make the biobased ionic liquids promising candidates for use as environmentally friendly solvents in biocatalysis applications.

AUTHOR INFORMATION

Corresponding Author

*Tel.: +86-517-83591044. Fax: +86-517-83591165. E-mail: zhaoyu_wang@126.com.

Funding

The authors express their thanks for the support from Qing Lan Project of Jiangsu Province, Natural Science Foundation of Jiangsu Province (No. BK2012243), Natural Science Research Project of Higher Education of Jiangsu Province (No. 10KJB530001), and National Natural Science Foundation of China (No. 21102027).

Notes

The authors declare no competing financial interest.

REFERENCES

(1) Leiros, I.; McSweeney, S.; Hough, E. The reaction mechanism of phospholipase D from *Streptomyces* sp. strain PMF snapshots along the reaction pathway reveal a pentacoordinate reaction intermediate and an unexpected final product. *J. Mol. Biol.* **2004**, *339*, 805−820.

(2) Vance, J. E.; Steenbergen, R. Metabolism and functions of phosphatidylserine. *Prog. Lipid Res.* **2005**, *44*, 207−234.

(3) Hellhammer, J.; Fries, E.; Buss, C.; Engert, V.; Tuch, A. Effects of soy lecithin phosphatidic acid and phosphatidylserine complex (PAS) on the endocrine and psychological responses to mental stress. *Stress* **2004**, *7*, 119−126.

(4) Hirayama, S.; Masuda, Y.; Rabeler, R. Effect of phosphatidylserine administration on symptoms of attention-deficit/hyperactivity disorder in children. *Agro Food Ind. Hi-Technol.* **2006**, *17*, 16−20.

(5) Hashioka, S.; Han, Y. H.; Fujii, S.; Kato, T.; Monji, A.; Utsumi, H.; Sawada, M.; Nakanishi, H.; Kanba, S. Phosphatidylserine and

DOI: 10.1021/jf505296k
J. Agric. Food Chem. 2015, 63, 1558−1561

phosphatidylcholine-containing liposomes inhibit amyloid β and interferon-γ-induced microglial activation. *Free Radical Biol. Med.* **2007**, *42*, 945−954.
(6) Vaisman, N.; Kaysar, N.; Zaruk-Adasha, Y.; Pelled, D.; Brichon, G.; Zwingelstein, G.; Bodennec, J. Correlation between changes in blood fatty acid composition and visual sustained attention performance in children with inattention: Effect of dietary n-3 fatty acids containing phospholipids. *Am. J. Clin. Nutr.* **2008**, *87*, 1170−1180.
(7) Hosokawa, M.; Shimatani, T.; Kanada, T.; Inoue, Y.; Takahashi, K. Conversion to docosahexaenoic acid-containing phosphatidylserine from squid skin lecithin by phospholipase D-mediated transphosphatidylation. *J. Agric. Food Chem.* **2000**, *48*, 4550−4554.
(8) Zhang, Y. N.; Lu, F. P.; Chen, G. Q.; Li, Y.; Wang, J. L. Expression, purification, and characterization of phosphatidylserine synthase from *Escherichia coli* K_{12} in *Bacillus subtilis*. *J. Agric. Food Chem.* **2009**, *57*, 122−126.
(9) Dittrich, N.; Ulbrich-Hofmann, R. Transphosphatidylation by immobilized phospholipase D in aqueous media. *Biotechnol. Appl. Biochem.* **2001**, *34*, 189−194.
(10) Iwasaki, Y.; Mizumoto, Y.; Okada, T.; Yamamoto, T.; Tsutsumi, K.; Yamane, T. An aqueous suspension system for phospholipase D-mediated synthesis of PS without toxic organic solvent. *J. Am. Oil Chem. Soc.* **2003**, *80*, 653−657.
(11) Klibanov, A. M. Improving enzymes by using them in organic solvents. *Nature* **2001**, *409*, 241−246.
(12) van Rantwijk, F.; Sheldon, R. A. Biocatalysis in ionic liquids. *Chem. Rev.* **2007**, *107*, 2757−2785.
(13) Tavares, A. P. M.; Rodriguez, O.; Macedo, E. A. New generations of ionic liquids applied to enzymatic biocatalysis. In *Ionic liquids—New aspects for the future*; Kadokawa, J. I., Ed.; InTech: Rijeka, Croatia, 2013; pp 537−556.
(14) Petkovic, M.; Seddon, K. R.; Rebelo, L. P.; Silva Pereira, C. Ionic liquids: A pathway to environmental acceptability. *Chem. Soc. Rev.* **2011**, *40*, 1383−1403.
(15) Fukumoto, K.; Yoshizawa, M.; Ohno, H. Room temperature ionic liquids from 20 natural amino acids. *J. Am. Chem. Soc.* **2005**, *127*, 2398−2399.
(16) Hu, S.; Jiang, T.; Zhang, Z.; Zhu, A.; Han, B.; Song, J.; Xie, Y.; Li, W. Functional ionic liquid from biorenewable materials: Synthesis and application as a catalyst in direct aldol reactions. *Tetrahedron Lett.* **2007**, *48*, 5613−5617.
(17) Moriel, P.; Garcia-Suarez, E. J.; Martinez, M.; Garcia, A. B.; Montes-Moran, M. A.; Calvino-Casilda, V.; Banares, M. A. Synthesis, characterization, and catalytic activity of ionic liquids based on biosources. *Tetrahedron Lett.* **2010**, *51*, 4877−4881.
(18) Petkovic, M.; Ferguson, J. L.; Gunaratne, H. Q.; Ferreira, R.; Leitao, M. C.; Seddon, K. R.; Rebelo, L. P.; Silva Pereira, C. Novel biocompatible cholinium-based ionic liquids—Toxicity and biodegradability. *Green Chem.* **2010**, *12*, 643−649.
(19) Liu, Q. P.; Hou, X. D.; Li, N.; Zong, M. H. Ionic liquids from renewable biomaterials: Synthesis, characterization, and application in the pretreatment of biomass. *Green Chem.* **2012**, *14*, 304−307.
(20) Duan, Z. Q.; Hu, F. Highly efficient synthesis of phosphatidylserine in the eco-friendly solvent γ-valerolactone. *Green Chem.* **2012**, *14*, 1581−1583.

DOI: 10.1021/jf505296k
J. Agric. Food Chem. 2015, 63, 1558−1561

rice starch, amylose, and amylopectin of 16 rice cultivars are isolated after the rice powder is hydrolyzed by lipase and protease first. The main retrogradation-related properties of starches are identified by correlating their retrogradation rates with average molecule weight (amylopectin), chain-length distribution (amylopectin), wavelength of maximum visible absorption (λ_{max}), IR, X-ray diffraction, and DSC of the native rice starches, amylose and amylopectin.

MATERIALS AND METHODS

Materials. Rice seeds were offered by Tianjin Crops Research Institute. Thermostable α-amylase (12 000 units/mL) from *Bacillus licheniformis*, microbial lipase from *Rhizopus chinensis*, and alkali protease from *Bacillus pumilus* were purchased from Tianjin Nuoao Technology Development Co., Ltd. Pullulanase microbial from *Bacillus subtilis* (Enzyme Commission Number 3.2.1.41; 5000 units/mL), maltose, maltotriose, maltotetrose, maltopentaose, maltohexaose, and maltoheptaose were purchased from Sigma-Aldrich Co., LLC. Butanol and ethanol were purchased from Tianjin Fuyu Fine Chemical Co., Ltd.

Methods. *Preparation of Rice Starch from Rice Seeds.* The rice seeds were first ground into a fine powder with a grinder, and the brans were removed by sieving with 80 mesh. Then, the rice powder (20 g) was dispersed in 0.085 M NaOH solution (100 mL) with rapid stirring, and the starch was extracted at 40 °C for 180 min, after which the crude starch was obtained by centrifugation at 5000*g* for 15 min. Purification of the crude starch was carried out by washing with deionized water for more than 3 times at room temperature. The purified rice starch was dried at 45 °C in the oven until a constant weight.

Hydrolysis of Rice Starches by Lipase and Alkali Protease. Hydrolysis of lipid and protein in rice starches were performed by dissolving 5 g of starch in 100 mL of water with stirring; after gelatinization at 95 °C for 30 min, the pH of the mixtures was adjusted to 7.0 for lipase and 8.0 for alkali protease by 2.0 M NaOH. Then, 10 mg of lipase (1500 units/g) or alkali protease (20 000 units/g) was added, and the starch solutions were kept for 24 h. The hydrolysis temperatures were set at 37 °C for lipase and 65 °C for alkali protease. The lipase and alkali protease were inactivated by being boiled for 10 min. Then, the starches hydrolyzed were obtained by centrifugation (3040*g* for 10 min). The dried starches for visible absorbance, IR, average molecule weight (amylopectin), chain-length distribution (amylopectin), X-ray diffraction, and DSC were obtained by removing water with hot air at the temperature of 55−60 °C in a drying oven until a constant weight.[16]

Preparation of Rice Amylose and Amylopectin from Rice Starch. The rice starch (10 g) was dispersed in deionized water (100 mL) with continuous stirring, and the slurry was poured into 0.15 M NaOH solution (1.3 L) slowly and kept for 5 min. Then, NaCl (5%) with a volume of 360 mL was added to the solution, and the pH of the solution was adjusted to 6.5−7.5 by 1.0 M NaOH with stirring. The solution was separated into two sections, and the up and down sections were crude rice amylose and amylopectin, respectively. Then, 100% *n*-butanol (at one-third the volume of the supernatant) was added to the up section. The mixture was stirred and held at room temperature for 4 h before centrifuging for 10 min at 5000*g* to precipitate amylose. The crude rice amylopectin was obtained by centrifugation at 5000*g* for 15 min and further purified by washing with 1% NaCl 4 times. The precipitates of amylose and amylopectin were washed with absolute alcohol, and the purified starches were dried in an oven at 45 °C until a constant weight.

Determination of Retrogradation Rates of Rice Starches. The retrograded rice starch was prepared according to our previous method.[17] A total of 10 g of rice starch blended with 100 mL of distilled water was gelatinized for 20 min at 95 °C by continuous stirring. Gelatinized starches were autoclaved at 120 °C for 30 min and retrograded at 4 °C for 24 h. Then, 0.6 mL of α-amylase (12 000 units/mL) was added to hydrolyze non-retrograded starch into soluble carbohydrates for 6 h at 90 °C. Crude retrograded rice starch was precipitated with a centrifuge (3040*g* for 5 min), and the supernatant fraction was discarded. The crude retrograded rice starch was washed with deionized water 3 times to remove soluble impurities, and the purified retrograded starches were dried with hot air at the temperature of 55−60 °C on an oven until a constant weight. The retrogradation rate (%) was calculated according to the following equation:

$$\text{retrogradation rate (\%)} = (m/m_0) \times 100\%$$

where m and m_0 are the weights of purified retrograded starch and native starch, respectively. All of the samples are duplicated 3 times.

Scanning of the Wavelengths of Maximum Absorbance (λ_{max}) of Samples. I_2/KI (1:3) solutions were prepared with a total of 5% (w/v) total iodine. A total of 5.0 mg of samples was first dissolved in 4.0 M NaOH with magnetic stirring, and then the pH of the solutions was adjusted to 7.0. After that, 0.25 mL of I_2/KI (1:3) solutions was added rapidly, and the solutions were sent to scan λ_{max} after 30 min. λ_{max} of samples was determined by UV-2501pc, ultraviolet−visible (UV−vis)-recording spectrophotometer (Shimadzu, Japan).

IR Spectra. All samples have been dried at 120 °C for 2 h first. Then, each sample was mixed with potassium bromide (KBr) at the rate of 1:60, and the mixture was compressed into slices by equipment. After that, samples were loaded on a slide holder, and spectral curves were obtained in transmission mode using a Bio-Rad FES135 IR spectrometer at 27 °C. The IR instrument is equipped with a deuterated triglycine sulfate (DTGS) detector using the Digilab attenuated total reflectance (ATR) accessory at 4 cm^{-1} resolution by 64 scans.

Molecular Weight Distribution (MWD) Profiles. MWD was determined by the method described in ref 18. Sweet potato amylose or amylopectin (100 mg) was added to 80 mL of deionized water and heated in boiling water with stirring for 20 min to make the samples dissolve. After filtration through 5 μm cellulose acetate filters, the dissolved samples were injected into a high-performance size-exclusion column chromatography system (HPSEC) with a multi-angle laser light scattering detector (MALS), a refractive index detector (RI), a pump (LC-10AT, Shimadzu Corporation, Kyoto, Japan), and an injector valve with a 100 μL loop (Rheodyne, Cotati, CA). Two series tandem columns (300 × 7.5 mm, PL aquagel-OH MIXED, 8 μm, Polymer Laboratories, Ltd., Shropshire, U.K.), a DAWN DSP-F laser photometer fitted with He−Ne laser (k = 623.8 nm) with a K-5 flow cell (Wyatt Technology, Santa Barbara, CA), and a RID-10A differential refractive detector (Shimadzu Corporation, Kyoto, Japan) were used. The flow rate was 0.5 mL/min. The mobile phase was $NaNO_3$ solution (0.1 M) containing 0.02% NaN_3, which had been passed through a 0.4 μm membrane filter (Membrane Solutions, LLC). A dn/dc value of 0.150 was used in molecular weight calculation, and data handling was carried out using ASTRA software (version 4.73.04, Wyatt Technology, Santa Barbara, CA).

Chain-Length Distribution Profiles. The chain-length distribution of sweet potato amylose or amylopectin was determined by high-performance anion-exchange chromatography with pulsed amperometric detection (HPAEC−PAD).[19] The samples (100 mg) were dissolved in 30 mL of 4.0 M KOH solution, and the pH of the solution was 6.0. Then, pullulanase (0.5 unit) was added to each solution for hydrolysis at 45 °C for 24 h with stirring. After that, the solution was heated in a boiling water bath for 10 min to deactivate the enzyme. The debranched sample solutions were first centrifuged at 21500*g* and filtered through a 0.45 μm membrane filter before being injected into the HPAEC−PAD system. The HPAEC−PAD system included a Dionex DX 600 equipped with an ED 50 electrochemical detector with a gold working electrode, a GP 50 gradient pump, a LC 30 chromatography oven, and an AS40 automated sampler (Dionex Corporation, Sunnyvale, CA). The standard triple potential waveform was used with the following period and pulse potentials: T1 = 0.40 s, with 0.20 s sampling time, E1 = 0.05 V; T2 = 0.20 s, E2 = 0.75 V; and T3 = 0.40 s, E3 = −0.15 V. The data were collected using Chromeleon software (version 6.50, Dionex Corporation, Sunnyvale, CA). The eluents were prepared in distilled deionized water with helium sparging, with eluent A consisted of 200 mM NaOH and eluent B consisted of 50 mM sodium acetate in 200 mM NaOH.

X-ray Diffraction Patterns. The X-ray patterns of the starches were obtained with copper, nickel foil filtered, Kα radiation using a diffractometer (D-500 Siemens, Madison, WI). The diffractometer was operated at 27 mA and 50 kV. The scanning region of the diffraction angle (2θ) was from 4° to 60° at 0.05° step size with a count time of 2 s.

DOI: 10.1021/jf503203r
J. Agric. Food Chem. 2015, 63, 1562−1572

Table 1. Correlation between the Starch Retrogradation Rates and the Proportion of Amylopectin (DP > 10) of Different Varieties of Rice[a]

mark	sample	retrogradation rate of starches (%) (Y)	percentage of DP > 10 in their amylopectins (%) (X)	coefficient of correlation
o	ZP-35	0.82 ± 0.02	0	$Y = 10.219X + 13.595$; $R^2 = 0.8568$ ($r = 0.926$; $p < 0.01$)
p	ZP-36	1.13 ± 0.01	19.91 ± 0.02	
i	ZP-15	1.36 ± 0.03	21.40 ± 0.01	
j	ZP-19	1.88 ± 0.01	29.46 ± 0.03	
f	ZP-12	2.34 ± 0.04	35.67 ± 0.02	
e	ZP-11	2.38 ± 0.03	*b*	
a	IZDP-30	2.51 ± 0.01	*b*	
h	ZP-14	2.63 ± 0.03	44.64 ± 0.04	
l	ZP-31	2.75 ± 0.02	50.0 ± 0.05	
k	ZP-26	3.08 ± 0.01	52.94 ± 0.02	
b	IZP-8	3.71 ± 0.04	*b*	
n	ZP-33	3.90 ± 0.05	57.72 ± 0.01	
g	ZP-13	4.57 ± 0.01	58.44 ± 0.03	
c	ZP-3	4.72 ± 0.02	*b*	
m	ZP-32	4.71 ± 0.03	*b*	
d	ZP-8	6.63 ± 0.02	75.10 ± 0.04	

[a]Values are means ± standard deviations. Where given, means and standard deviations are calculated from three samples. [b]The data are absent for a limited amount of rice seeds.

Retrograded starches were equilibrated at 100% relative humidity for 24 h at 25 °C prior to examination.

DSC. Thermal analysis of the complex was carried out with DSC (Q20, TA Instruments, New Castle, DE). The complex (6.0 mg) was placed in an aluminum DSC pan, and scanning was performed from 25 to 230 °C at a heating rate of 5 °C/min, with an empty pan as a reference. For each endothermic curve, the onset (T_o), peak (T_p), and conclusion (T_c) temperatures as well as the corresponding enthalpy changes (ΔH) associated with these transitions were computed with the universal analysis 2000 software (version 4.5A, TA Instruments—Waters, LLC, New Castle, DE).

Statistical Analysis. All samples were analyzed in triplicate. The statistical significance of observed differences among treatment means was evaluated by analysis of variance (ANOVA) and a least significant difference (LSD) test (Excel). The coefficients of correlation were calculated by Microsoft Excel. Regression equations were developed between retrogradation rates and λ_{max}, proportions of chains, molecular weight, and thermal index. Significance of correlations (r) was examined by SPSS 12.0 for Windows software using Pearson's correlation.

RESULTS AND DISCUSSION

Chain-Length Distribution Profiles. To reduce adverse effects of lipids, protein, and association of amylose and amylopectin on analysis of main retrogradation-related properties, all 16 rice starches have been hydrolyzed by lipase and protease and their amylopectin has been isolated to determine profiles of chain-length distribution. The results in Table 1 and Figure 1 show the correlation between retrogradation rate of rice starch and chain-length distribution of corresponding amylopectin. There is significant positive correlation (R^2 = 0.85; r = 0.926; $p < 0.01$) between proportions of chains with degree of polymerization (DP) > 10 of amylopectin from different rice cultivars and their corresponding starch retrogradation rates, which verifies the speculation in ref 20. Cereal cultivars having amylopectin structures with a lower proportion of long B chains are speculated to give improved quality products with lower rates of retrogradation and stalling. Such a coefficient of correlation (R^2) will decrease to 0.65 if proportions of chains with DP > 5 are investigated. Gidley and Bulpin[21] indicate that a minimum chain length of DP of 10 is required for formation of double helices. The results in the paper indicate that the minimum chain length of DP of 10 is also probably necessary for the occurrence of retrogradation. Such a chain length might be the minimum length for nucleation of starch retrogradaton, which might offer the stability of association among those chains in starch solutions. In other words, double helix (not too long) formation is probably necessary during the nucleation stage of starch retrogradation. The finding in the paper suggests that we can screen rice cultivars with a low rate of retrogradation by seeking the gene or enzyme in rice to control the proportions of chains with DP > 10 of amylopectin. Furthermore, the low-retrogradation cultivar will be obtained by transferring the identical gene to normal rice. There are similar cultivars in the ethnic residential area in China, called "soft rice", which have attracted the attention of many rice breeders. The cultivars ZP-35 and ZP-36 in the paper are of this kind. The average chain length is related to the melting temperature of retrograded waxy starch[22] but not to the retrogradation rate of rice starches. The results in Figure 1 and Table 1 also negate the speculation that the amylopectin molecule with a narrower chain-length distribution has a higher retrogradation tendency,[23] because the rice cultivars ZP-14, ZP-19, and ZP-35 have narrower chain-length distributions and a relatively low retrogradation rate.

The MWDs of amylopectin, as the main property of rice starch, are also measured to investigate their relationships with retrogradation rates. Such results are described in Figure 2 and Table 2. The results in Table 2 and Figure 2 show that there are various quantities of the distribution interval of molecule weights for those 16 rice cultivars: four intervals for ZP-32, ZP-33, and ZP-35, three intervals for ZP-3, ZP-12, ZP-13, ZP-15, and ZP-36, two intervals for ZP-26, and one interval for ZP-14 and ZP-19. The coefficient of correlation between those quantities and retrogradation rates is 0.0356 (R^2) (r = 0.189). Other coefficients between the weight-average molecular weights (M_w) in the first to the fourth intervals and retrogradation rates are 0.1445, 0.064, 0.0429, and 0.0091 (R^2) (r = −0.380, 0.253, 0.096, and 0.207), respectively, in Table 2. The results of the significant test suggest that there is no correlation between retrogradation rates and quantities of intervals or M_w. The polydispersity index (PDI) is another index that represents the weight distribution of macromolecules.

DOI: 10.1021/jf503203r
J. Agric. Food Chem. 2015, 63, 1562−1572

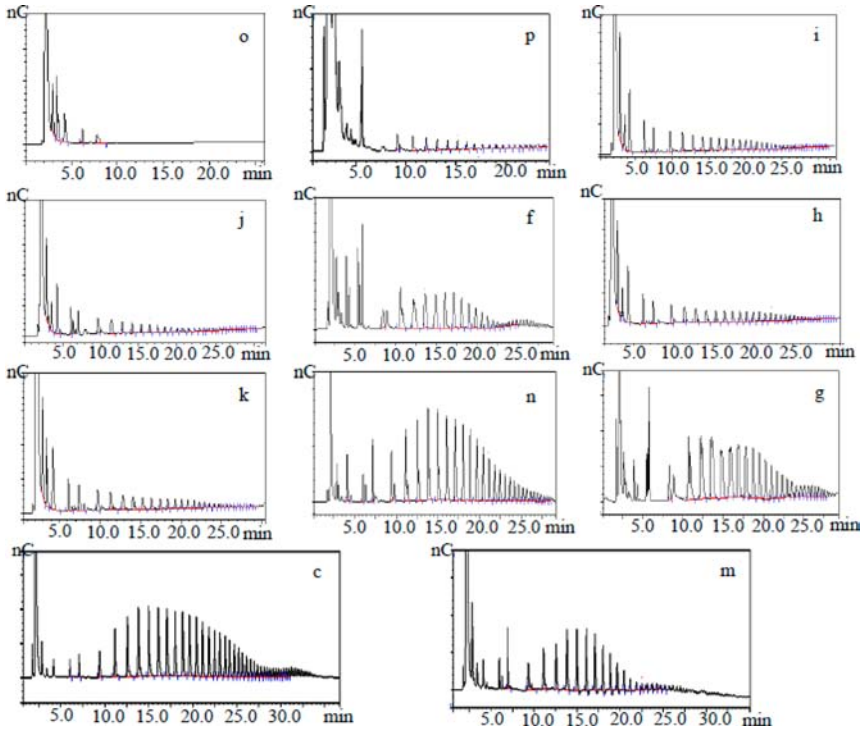

Figure 1. Chain-length distributions of different varieties of rice: (o) ZP-36, (p) ZP-35, (i) ZP-15, (j) ZP-19, (f) ZP-12, (e) ZP-11, (a) IZDP-30, (h) ZP-14, (l) ZP-31, (k) ZP-26, (b) IZP-8, (n) ZP-33, (g) ZP-13, (c) ZP-3, and (m) ZP-32.

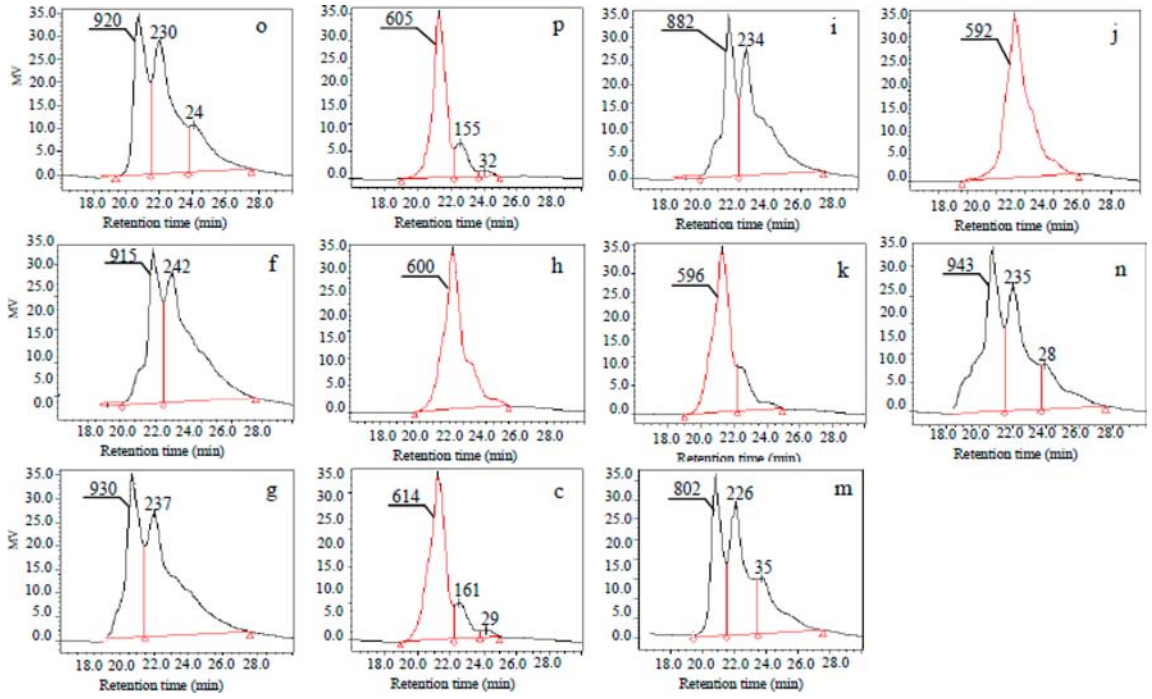

Figure 2. MWD of different varieties of rice: (o) ZP-36, (p) ZP-35, (i) ZP-15, (j) ZP-19, (f) ZP-12, (e) ZP-11, (a) IZDP-30, (h) ZP-14, (l) ZP-31, (k) ZP-26, (b) IZP-8, (n) ZP-33, (g) ZP-13, (c) ZP-3, and (m) ZP-32.

It can be calculated by M_w/M_n, M_n is the number-average molecular weight. Table 3 shows the correlation between rice starch retrogradation rates and corresponding PDI in different intervals. The coefficients in the first to the fourth intervals are 0.062, 0.021, 0.009, and 0.027 (R^2) (r = 0.249, −0.167, −0.095, and 0.244), respectively, in Table 3. Also, the correlation between them is not significant. Such results infer that the main factor to determine rice starch retrogradaion rates is proportions of chains with DP > 10 of amylopectin and not the narrowness or width of the MWD of rice starch. Such results also suggest that retrogradation is in essence the formation of crystals and the nucleation is the main factor to influence the extent of retrogradation.[24]

DOI: 10.1021/jf503203r
J. Agric. Food Chem. 2015, 63, 1562−1572

Table 2. Correlation between the Starch Retrogradation Rates and the MWD of Rice Amylopectin of Different Varieties of Rice[a]

mark	sample	retrogradation rate of starches (%) (Y)	quantities of distribution interval (X)	M_w (X) in the first interval (DP)	M_w (X) in the second interval (DP)	M_w (X) in the third interval (DP)	M_w (X) in the fourth interval (DP)	coefficient of correlation
o	ZP-35	0.82 ± 0.02	4 ± 0	2341519 ± 11	855 ± 8	177 ± 4	20 ± 12	$Y = 0.1384X + 2.4263$; $R^2 = 0.0356$ (for quantities of distribution interval) ($r = 0.189$, not significant)
p	ZP-36	1.13 ± 0.01	3 ± 0		693 ± 8	139 ± 5	29 ± 2	
i	ZP-15	1.36 ± 0.03	3 ± 0	53875 ± 7	1249 ± 13	148 ± 3		
j	ZP-19	1.88 ± 0.01	1 ± 0		732 ± 8			$Y = -179471X + 1000000$; $R^2 = 0.1445$ [for M_w (X) in the first interval] ($r = -0.380$, not significant)
f	ZP-12	2.34 ± 0.04	3 ± 0	839438 ± 6	1024 ± 5	153 ± 9		
e	ZP-11	2.38 ± 0.03	*b*	*b*	*b*	*b*	*b*	
a	IZDP-30	2.51 ± 0.01	*b*	*b*	*b*	*b*	*b*	$Y = 48.637X + 814.04$; $R^2 = 0.064$ [for M_w (X) in the second interval] ($r = 0.253$, not significant)
h	ZP-14	2.63 ± 0.03	1 ± 0		687 ± 5			
l	ZP-31	2.75 ± 0.02	*b*	*b*	*b*	*b*	*b*	
k	ZP-26	3.08 ± 0.01	2 ± 0		775 ± 8	120 ± 3		$Y = 1.411X + 150.6$; $R^2 = 0.0091$ [for M_w (X) in the third interval] ($r = 0.096$, not significant)
b	IZP-8	3.71 ± 0.04	*b*	*b*	*b*	*b*	*b*	
n	ZP-33	3.90 ± 0.05	4 ± 0	413535 ± 15	1581 ± 3	186 ± 4	22 ± 2	
g	ZP-13	4.57 ± 0.01	3 ± 0	584244 ± 12	1191 ± 8	149 ± 5		$Y = 0.397X + 23.587$; $R^2 = 0.0429$ [for M_w (X) in the fourth interval] ($r = 0.207$, not significant)
c	ZP-3	4.72 ± 0.02	3 ± 0		813 ± 6	134 ± 5	27 ± 3	
m	ZP-32	4.71 ± 0.03	4 ± 0	978506 ± 13	869 ± 9	187 ± 8	26 ± 7	
d	ZP-8	6.63 ± 0.02	*b*	*b*	*b*	*b*	*b*	

[a]Values are means ± standard deviations. Where given, means and standard deviations are calculated from three samples. [b]The data are absent for a limited amount of rice seeds.

Figure 3. Visible absorbance of different rice (left) starches, (middle) amyloses, and (right) amylopectins: (o) ZP-36, (p) ZP-35, (i) ZP-15, (j) ZP-19, (f) ZP-12, (e) ZP-11, (a) IZDP-30, (h) ZP-14, (l) ZP-31, (k) ZP-26, (b) IZP-8, (n) ZP-33, (g) ZP-13, (c) ZP-3, (m) ZP-32, and (d) ZP-8.

The wavelength of maximum absorption (λ_{max}) of starch combined with iodine is sensitive to the presence and length of double helices in starches, which represents another important property of starch. λ_{max} of different rice starches, amyloses, and amylopectins with iodine in complex is shown in Figure 3 and Table 4. The coefficients of correlation between retrogradation rates and λ_{max} of different rice starches, amylose, and amylopectin are 0.2736, 0.3232, and 0.1573 (R^2) (r = 0.523, −0.386, and −0.809), respectively. The results of the significant test in Table 4 suggest that there is no correlation between λ_{max} of those starches and the corresponding retrogradation rates. There are no λ_{max} for the samples ZP-35 and ZP-36 with a low proportion of chains with DP > 10 of amylopectin and low retrogradation rates, verifying that a lot of amylopectin in those two cultivars is too short to form double helices. The absence and presence of λ_{max} in sample ZP-26 starch and amylose in Figure 3 indicate that the interaction of amylose and amylopectin in the sample might greatly influence the formation of double helices of the rice starch. The results of λ_{max} of different samples support the above point of view that the distribution of rice amylopectin determines the retrogradation rate of rice starches.

Although the degree of short-range molecular order in the retrograded state can be determined by FTIR,[4,25] few papers report the prediction of retrogradation tendency by IR spectra of native starch, amylose, or amylopectin. The IR spectra of

DOI: 10.1021/jf503203r
J. Agric. Food Chem. 2015, 63, 1562−1572

Table 3. Correlation between the Starch Retrogradation Rates and the PDI of Rice Amylopectin of Different Varieties of Rice[a]

mark	sample	retrogradation rate of starches (%) (Y)	PDI (X) in the first interval (DP)	PDI (X) in the second interval (DP)	PDI (X) in the third interval (DP)	PDI (X) in the fourth interval (DP)	coefficient of correlation
o	ZP-35	0.82 ± 0.02	12.63 ± 0.5	1.14 ± 0.1	1.55 ± 0.1	1.17 ± 0.1	$Y = 0.806X + 8.9474$; $R^2 = 0.062$ [for PDI (X) in the first interval] ($r = 0.249$, not significant)
p	ZP-36	1.13 ± 0.01		1.23 ± 0.2	1.15 ± 0.1	1.07 ± 0.1	
i	ZP-15	1.36 ± 0.03	2.08 ± 0.2	1.42 ± 0.1	2.64 ± 0.2		
j	ZP-19	1.88 ± 0.01		3.62 ± 0.1			$Y = -0.089X + 1.9018$; $R^2 = 0.0279$ [for PDI (X) in the second interval] ($r = -0.167$, not significant)
f	ZP-12	2.34 ± 0.04	18.21 ± 0.3	1.23 ± 0.2	2.83 ± 0.1		
e	ZP-11	2.38 ± 0.03	*b*	*b*	*b*	*b*	
a	IZDP-30	2.51 ± 0.01	*b*	*b*	*b*	*b*	$Y = -0.0411X + 1.9562$; $R^2 = 0.009$ [for PDI (X) in the third interval] ($r = -0.095$, not significant)
h	ZP-14	2.63 ± 0.03		2.68 ± 0.1			
l	ZP-31	2.75 ± 0.02	*b*	*b*	*b*	*b*	
k	ZP-26	3.08 ± 0.01		1.36 ± 0.2	1.51 ± 0.3		$Y = -0.0501X + 0.7365$; $R^2 = 0.0217$ [for PDI (X) in the fourth interval] ($r = 0.244$, not significant)
b	IZP-8	3.71 ± 0.04	*b*	*b*	*b*	*b*	
n	ZP-33	3.90 ± 0.05	9.04 ± 0.4	1.61 ± 0.1	1.51 ± 0.1	1.15 ± 0.1	
g	ZP-13	4.57 ± 0.01	12.00 ± 0.6	1.37 ± 0.3	2.75 ± 0.2		
c	ZP-3	4.72 ± 0.02		1.35 ± 0.1	1.18 ± 0.1	1.08 ± 0.1	
m	ZP-32	4.71 ± 0.03	13.99 ± 0.7	1.14 ± 0.1	1.39 ± 0.2	1.23 ± 0.1	
d	ZP-8	6.63 ± 0.02	*b*	*b*	*b*	*b*	

[a]Values are means ± standard deviations. Where given, means and standard deviations are calculated from three samples. [b]The data are absent for a limited amount of rice seeds.

Table 4. Correlation between the Starch Retrogradation Rates and λ_{max} of Different Rice Starches[a]

mark	sample	retrogradation rate of starches (%) (Y)	starch (X)	amylose (X)	amylopectin (X)	coefficient of correlation
o	ZP-35	0.82 ± 0.02	*b*	*b*	*b*	$Y = 4.1894X + 546.25$; $R^2 = 0.2736$ [starch (X)] ($r = 0.523$, not significant)
p	ZP-36	1.13 ± 0.01	*b*	*b*	*b*	
i	ZP-15	1.36 ± 0.03	549 ± 2	585 ± 5	601 ± 3	
j	ZP-19	1.88 ± 0.01	564 ± 3	*b*	593 ± 6	$Y = 93.594X + 141.29$; $R^2 = 0.3232$ [amylose (X)] ($r = -0.386$, not significant)
f	ZP-12	2.34 ± 0.04	555 ± 5	583 ± 3	585 ± 5	
e	ZP-11	2.38 ± 0.03	576 ± 1	*b*	*b*	
a	IZDP-30	2.51 ± 0.01	543 ± 3	583 ± 1	*b*	$Y = -71.759X + 403.8$; $R^2 = 0.1573$ [amylopectin (X)] ($r = -0.809$, not significant)
h	ZP-14	2.63 ± 0.03	559 ± 7	579 ± 2	570 ± 4	
l	ZP-31	2.75 ± 0.02	555 ± 2	564 ± 5	587 ± 7	
k	ZP-26	3.08 ± 0.01	*b*	552 ± 4	*b*	
b	IZP-8	3.71 ± 0.04	550 ± 6	587 ± 3	*b*	
n	ZP-33	3.90 ± 0.05	558 ± 8	557 ± 7	*b*	
g	ZP-13	4.57 ± 0.01	575 ± 5	583 ± 2	*b*	
c	ZP-3	4.72 ± 0.02	568 ± 4	559 ± 6	*b*	
m	ZP-32	4.71 ± 0.03	552 ± 5	558 ± 3	*b*	
d	ZP-8	6.63 ± 0.02	582 ± 7	568 ± 5	*b*	

[a]Values are means ± standard deviations. Where given, means and standard deviations are calculated from three samples. [b]The data are absent for a limited amount of rice seeds.

different rice starches (up), amyloses (middle), and amylopectins (down) are shown in Figure 4 to discern their correlation with retrogradation property. The results show that no special peaks are present for low retrogradation rate or high retrogradation rate cultivars and all of the IR spectra of different rice starches are the same. Also, the difference of the intensities of different peaks in all of the samples is not obvious. Therefore, IR spectra are not suitable for discerning rice cultivars with a low or high retrogradation rate. The results agree well with ref 26.

Different starches fall into four crystal types, showing the strong reflections (2θ) at around 15°, 17°, 18°, 20°, and 23° for A-type crystallinity, 5.5°, 17°, 22°, and 24° for B-type crystallinity, 7.8°, 13.5°, and 20.7° for V-type crystallinity, and the mixture of reflections of A- and B-types for C-type X-ray diffraction pattern.[27−29] X-ray diffractions of different rice starches, amyloses, and amylopectins were determined to discern the correlation of those patterns and retrogradation rates of rice starches. Figure 5 shows the X-ray diffractions of different rice starches (up), amyloses (middle), and amylopectins (down). All of the native rice starches exhibit A-type X-ray pattern, which shows the strong diffraction peaks at about 15° and 23° (2θ) and an unresolved doublet at around 17° and 18° (2θ).[27] All rice amylose and amylopectin samples show ambiguous diffraction peaks between 15° and 23° (2θ) and an obvious peak at about 29° (2θ). They are not attributed to any types of X-ray pattern, inferring that the rice amylose/amylopectin forms crystals different from those of native rice starch. These results are also different from those in ref 30, which is probably caused by the presence of lipids and protein in those starches. There are no identical peaks or intensities of diffraction for rice cultivars with a low or high retrogradation rate in Figure 5; therefore, no correlation exists between the retrogradation rate and intensities of diffraction of different rice cultivars. Such results suggest that the patterns for crystal formation of native starch in the growth of plants are different from those of amylose/amylopectin in drying.

DOI: 10.1021/jf503203r
J. Agric. Food Chem. 2015, 63, 1562−1572

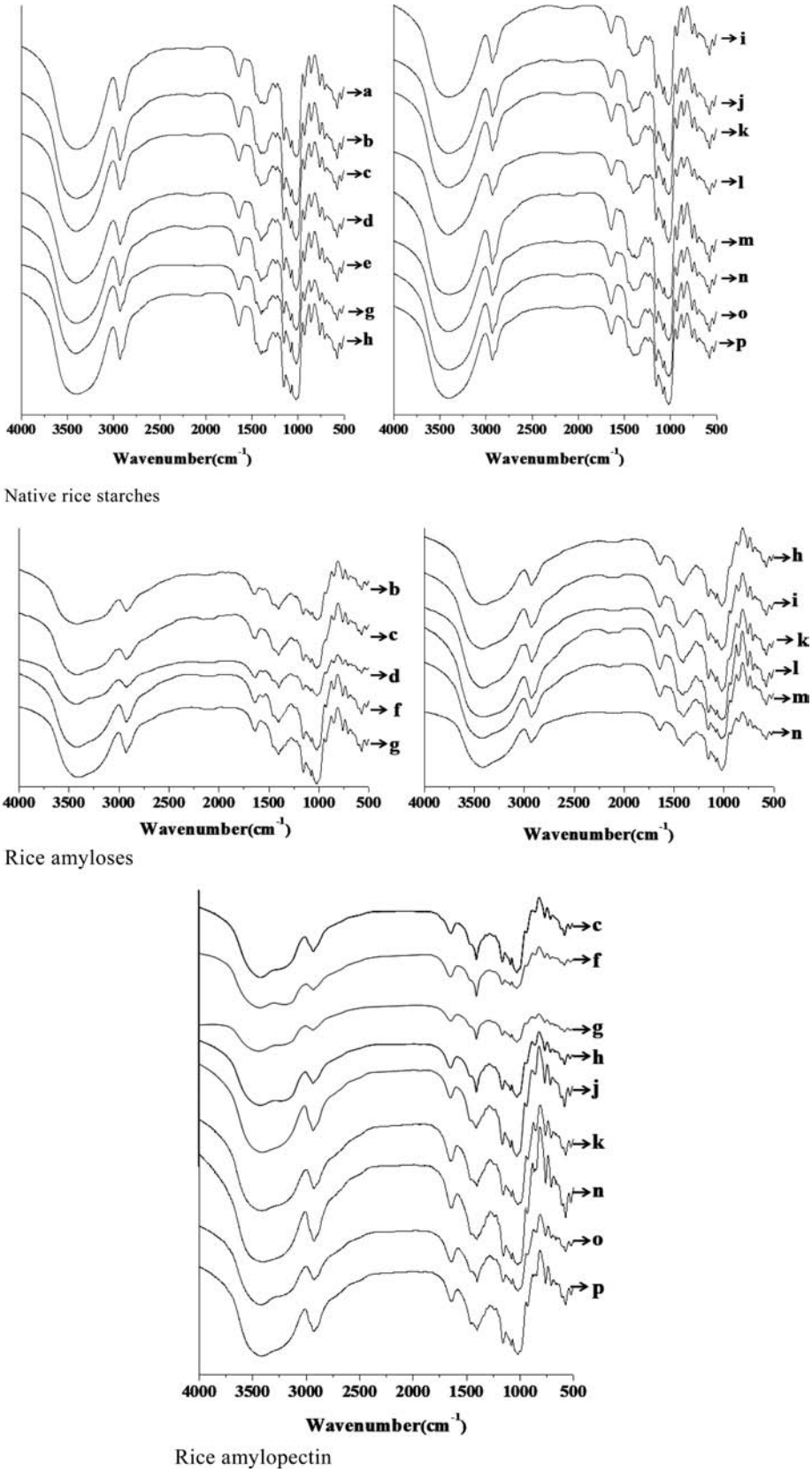

Figure 4. IR spectra of different rice (up) starches, (middle) amyloses, and (down) amylopectins: (o) ZP-36, (p) ZP-35, (i) ZP-15, (j) ZP-19, (f) ZP-12, (e) ZP-11, (a) IZDP-30, (h) ZP-14, (l) ZP-31, (k) ZP-26, (b) IZP-8, (n) ZP-33, (g) ZP-13, (c) ZP-3, (m) ZP-32; and (d) ZP-8.

A DSC thermogram reveals the detailed information on the structure of a starch granule.[31] To gain an understanding of the contribution of structural aspects to the retrogradation behavior of rice starch, the DSC thermogram of the rice starches, amyloses, and amylopectins from the 16 rice cultivars is determined and analyzed for its relation with retrogradation

DOI: 10.1021/jf503203r
J. Agric. Food Chem. 2015, 63, 1562−1572

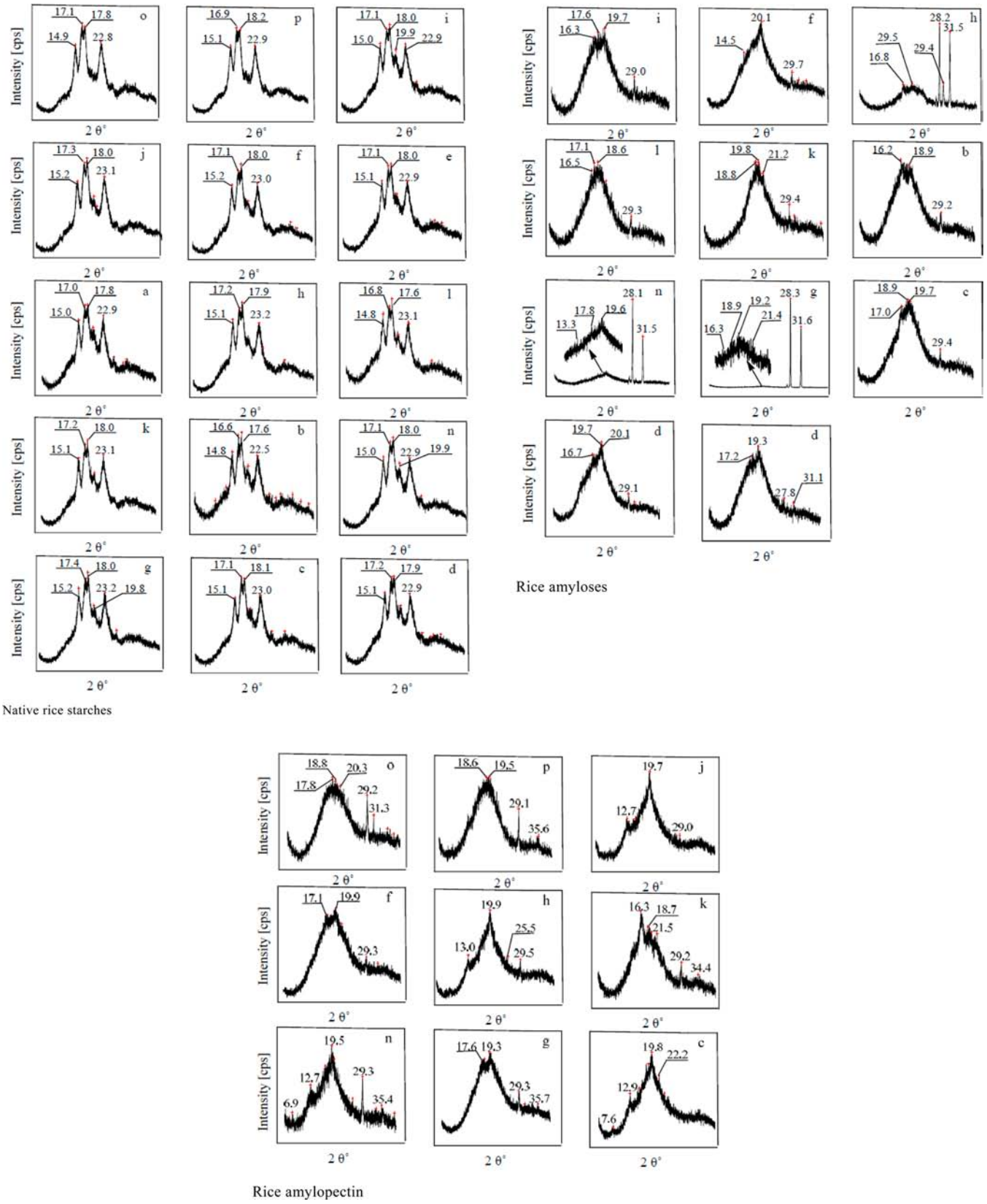

Figure 5. X-ray diffractions of different rice (up) starches, (middle) amyloses, and (down) amylopectins: (o) ZP-36, (p) ZP-35, (i) ZP-15, (j) ZP-19, (f) ZP-12, (e) ZP-11, (a) IZDP-30, (h) ZP-14, (l) ZP-31, (k) ZP-26, (b) IZP-8, (n) ZP-33, (g) ZP-13, (c) ZP-3, (m) ZP-32, and (d) ZP-8.

properties. Four parameters, including onset, peak, and offset temperatures and enthalpy of melting (ΔH), are usually determined to analyze the property of starch. Figure 6 and Tables 5−7 show the DSC results of different rice starches, amyloses, and amylopectins. The coefficient of correlation (R^2) between retrogradation rates and the thermal properties of different rice

DOI: 10.1021/jf503203r
J. Agric. Food Chem. 2015, 63, 1562−1572

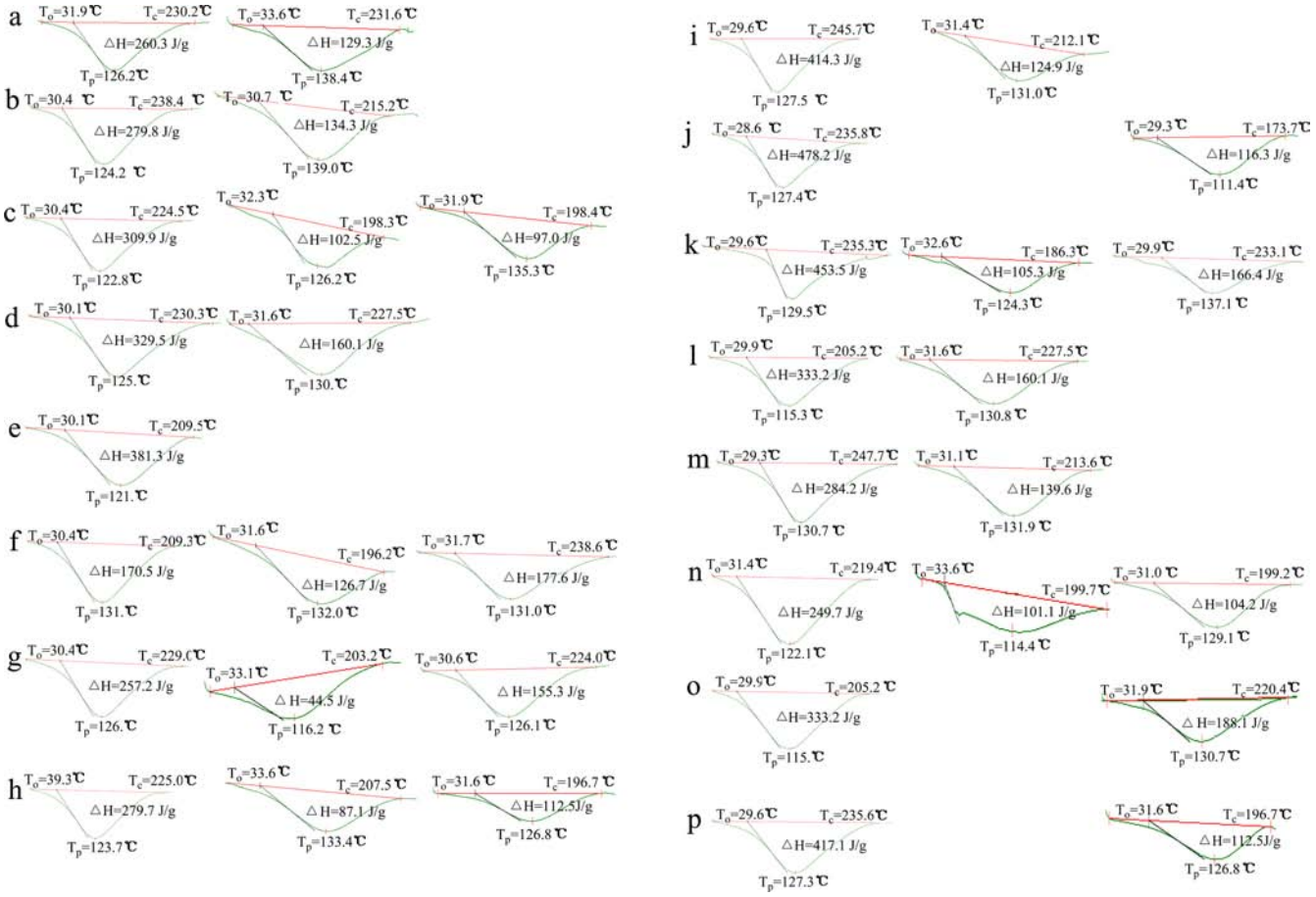

Figure 6. DSC of different rice (left) starches, (middle) amyloses, and (right) amylopectins: (o) ZP-36, (p) ZP-35, (i) ZP-15, (j) ZP-19, (f) ZP-12, (e) ZP-11, (a) IZDP-30, (h) ZP-14, (l) ZP-31, (k) ZP-26, (b) IZP-8, (n) ZP-33, (g) ZP-13, (c) ZP-3, (m) ZP-32, and (d) ZP-8.

Table 5. Correlation between the Starch Retrogradation Rates and the Thermal Properties of Rice Starches of Different Varieties of Rice[a]

mark	sample	retrogradation rate of starches (%) (Y)	onset (X) temperature (°C)	peak (X) temperature (°C)	offset (X) temperature (°C)	enthalpy of melting (X) (ΔH) (J/g)	coefficient of correlation
o	ZP-35	0.82 ± 0.02	29.9 ± 0.1	115.3 ± 0.5	205.2 ± 0.2	333.2 ± 0.5	$Y = 0.1092X + 29.571$; $R^2 = 0.0366$ (for onset temperature) ($r = 0.191$, not significant)
p	ZP-36	1.13 ± 0.01	29.6 ± 0.3	127.3 ± 0.4	235.6 ± 0.6	417.1 ± 0.4	
i	ZP-15	1.36 ± 0.03	29.6 ± 0.2	127.5 ± 0.2	245.7 ± 0.3	414.3 ± 0.5	
j	ZP-19	1.88 ± 0.01	28.6 ± 0.1	127.4 ± 0.1	235.8 ± 0.1	478.2 ± 0.3	
f	ZP-12	2.34 ± 0.04	30.1 ± 0.2	121.1 ± 0.3	209.5 ± 0.4	381.3 ± 0.8	$Y = 0.364X + 123.58$; $R^2 = 0.0156$ (for peak temperature) ($r = 0.125$, not significant)
e	ZP-11	2.38 ± 0.03	30.4 ± 0.1	131.1 ± 0.2	209.3 ± 0.7	170.5 ± 0.6	
a	IZDP-30	2.51 ± 0.01	31.9 ± 0.3	126.2 ± 0.1	230.2 ± 0.5	260.3 ± 0.4	
h	ZP-14	2.63 ± 0.03	28.6 ± 0.1	122.9 ± 0.6	225.7 ± 0.4	240.5 ± 0.1	$Y = 1.2219X + 221.6$; $R^2 = 0.0215$ (for offset temperature) ($r = 0.147$, not significant)
l	ZP-31	2.75 ± 0.02	29.3 ± 0.2	121.6 ± 0.4	217.9 ± 0.3	313.4 ± 0.3	
k	ZP-26	3.08 ± 0.01	29.6 ± 0.4	129.5 ± 0.3	235.3 ± 0.1	453.5 ± 0.2	
b	IZP-8	3.71 ± 0.04	29.3 ± 0.1	117.4 ± 0.4	210.3 ± 0.5	268.5 ± 0.9	
n	ZP-33	3.90 ± 0.05	31.4 ± 0.3	122.1 ± 0.6	219.4 ± 0.4	249.7 ± 0.6	$Y = -18.343X + 378.9$; $R^2 = 0.1105$ (for ΔH) ($r = -0.356$, not significant)
g	ZP-13	4.57 ± 0.01	30.4 ± 0.1	126.8 ± 0.2	229.0 ± 0.3	257.2 ± 0.7	
c	ZP-3	4.72 ± 0.02	30.4 ± 0.2	122.8 ± 0.7	224.5 ± 0.1	309.9 ± 0.3	
m	ZP-32	4.71 ± 0.03	29.3 ± 0.4	130.7 ± 0.5	247.7 ± 0.8	284.2 ± 0.1	
d	ZP-8	6.63 ± 0.02	30.1 ± 0.1	125.5 ± 0.3	230.3 ± 0.6	329.5 ± 0.5	

[a]Values are means ± standard deviations. Where given, means and standard deviations are calculated from three samples.

starches are 0.0366 (r = 0.191, not significant) (for onset temperature), 0.0156 (r = 0.125, not significant) (for peak temperature), 0.0215 (r = 0.147, not significant) (for offset temperature), and 0.1105 (r = −0.356, not significant) (for ΔH) in Table 5. For rice amylose, they are 0.0156 (r = −0.125, not significant) (for onset temperature), 0.0154 (r = −0.124, not significant) (for peak temperature), 0.0188 (r = −0.137, not significant) (for offset temperature), and 0.04 (r = 0.200, not significant) (for ΔH) in Table 6. For rice amylopectin, they are 0.076 (r = −0.087, not significant) (for onset temperature),

DOI: 10.1021/jf503203r
J. Agric. Food Chem. 2015, 63, 1562−1572

Table 6. Correlation between the Starch Retrogradation Rates and the Thermal Properties of Rice Amyloses of Different Varieties of Rice[a]

mark	sample	retrogradation rate of starches (%) (Y)	onset (X) temperature (°C)	peak (X) temperature (°C)	offset (X) temperature (°C)	enthalpy of melting (X) (ΔH) (J/g)	coefficient of correlation
o	ZP-35	0.82 ± 0.02	*b*	*b*	*b*	*b*	$Y = -0.1002X + 32.645$; $R^2 = 0.0156$ (for onset temperature) ($r = -0.125$, not significant)
p	ZP-36	1.13 ± 0.01	*b*	*b*	*b*	*b*	
i	ZP-15	1.36 ± 0.03	31.4 ± 0.1	131.0 ± 0.6	212.1 ± 0.7	124.9 ± 0.4	
j	ZP-19	1.88 ± 0.01	31.1 ± 0.3	131.9 ± 0.3	213.6 ± 0.4	139.6 ± 0.3	
f	ZP-12	2.34 ± 0.04	33.6 ± 0.2	133.4 ± 0.4	207.5 ± 0.2	87.1 ± 0.8	$Y = -0.7157X + 130.1$; $R^2 = 0.0154$ (for peak temperature) ($r = -0.124$, not significant)
e	ZP-11	2.38 ± 0.03	33.1 ± 0.1	116.2 ± 0.2	203.2 ± 0.6	44.5 ± 0.2	
a	IZDP-30	2.51 ± 0.01	33.6 ± 0.4	138.4 ± 0.5	231.6 ± 0.2	129.3 ± 0.9	
h	ZP-14	2.63 ± 0.03	33.6 ± 0.2	133.4 ± 0.4	207.5 ± 0.5	87.1 ± 0.4	
l	ZP-31	2.75 ± 0.02	30.9 ± 0.3	120.6 ± 0.8	201.0 ± 0.3	121.7 ± 0.5	$Y = 1.1348X + 204.77$; $R^2 = 0.0188$ (for offset temperature) ($r = -0.137$, not significant)
k	ZP-26	3.08 ± 0.01	32.6 ± 0.2	124.3 ± 0.7	186.3 ± 0.6	105.3 ± 0.3	
b	IZP-8	3.71 ± 0.04	30.7 ± 0.5	139.0 ± 0.3	215.2 ± 0.8	134.3 ± 0.7	
n	ZP-33	3.90 ± 0.05	33.6 ± 0.1	114.4 ± 0.2	199.7 ± 0.5	101.1 ± 0.9	
g	ZP-13	4.57 ± 0.01	33.1 ± 0.2	116.2 ± 0.1	203.2 ± 0.2	44.51 ± 0.5	$Y = 4.845X + 92.362$; $R^2 = 0.04$ (for ΔH) ($r = 0.200$, not significant)
c	ZP-3	4.72 ± 0.02	32.3 ± 0.4	126.2 ± 0.6	198.3 ± 0.1	102.5 ± 0.2	
m	ZP-32	4.71 ± 0.03	31.1 ± 0.3	131.9 ± 0.4	213.6 ± 0.8	139.6 ± 0.1	
d	ZP-8	6.63 ± 0.02	31.6 ± 0.1	130.8 ± 0.9	227.5 ± 0.1	160.1 ± 0.7	

[a]Values are means ± standard deviations. Where given, means and standard deviations are calculated from three samples. [b]The data are absent for a limited amount of rice seeds.

Table 7. Correlation between the Starch Retrogradation Rates and the Thermal Properties of Rice Amylopectin of Different Varieties of Rice[a]

mark	sample	retrogradation rate of starches (%) (Y)	onset (X) temperature (°C)	peak (X) temperature (°C)	offset (X) temperature (°C)	enthalpy of melting (X) (ΔH) (J/g)	coefficient of correlation
o	ZP-35	0.82 ± 0.02	31.9 ± 0.1	130.7 ± 0.2	220.4 ± 0.4	188.1 ± 0.3	$Y = -0.0582X + 31.218$; $R^2 = 0.0076$ (for onset temperature) ($r = -0.087$, not significant)
p	ZP-36	1.13 ± 0.01	31.6 ± 0.3	132.2 ± 0.1	186.0 ± 0.3	48.5 ± 0.2	
i	ZP-15	1.36 ± 0.03	*b*	*b*	*b*	*b*	
j	ZP-19	1.88 ± 0.01	29.3 ± 0.2	111.4 ± 0.3	173.7 ± 0.1	116.3 ± 0.4	
f	ZP-12	2.34 ± 0.04	31.7 ± 0.1	131.0 ± 0.1	238.6 ± 0.2	177.6 ± 0.5	
e	ZP-11	2.38 ± 0.03	*b*	*b*	*b*	*b*	$Y = 1.0224X + 126.01$; $R^2 = 0.0373$ (for peak temperature) ($r = -0.125$, not significant)
a	IZDP-30	2.51 ± 0.01	*b*	*b*	*b*	*b*	
h	ZP-14	2.63 ± 0.03	31.6 ± 0.2	126.8 ± 0.4	196.7 ± 0.5	112.5 ± 0.2	
l	ZP-31	2.75 ± 0.02	*b*	*b*	*b*	*b*	$Y = 2.4398X + 200.99$; $R^2 = 0.0241$ (for offset temperature) ($r = 0.193$, not significant)
k	ZP-26	3.08 ± 0.01	29.9 ± 0.3	137.1 ± 0.4	233.1 ± 0.1	166.4 ± 0.3	
b	IZP-8	3.71 ± 0.04	*b*	*b*	*b*	*b*	
n	ZP-33	3.90 ± 0.05	31.0 ± 0.1	129.1 ± 0.5	199.2 ± 0.3	104.2 ± 0.6	
g	ZP-13	4.57 ± 0.01	30.6 ± 0.2	126.1 ± 0.1	224.0 ± 0.4	155.3 ± 0.2	$Y = -1.3834X + 133.4$; $R^2 = 0.0018$ (for ΔH) ($r = -0.043$, not significant)
c	ZP-3	4.72 ± 0.02	31.9 ± 0.1	135.3 ± 0.2	198.4 ± 0.1	97.04 ± 0.1	
m	ZP-32	4.71 ± 0.03	*b*	*b*	*b*	*b*	
d	ZP-8	6.63 ± 0.02	*b*	*b*	*b*	*b*	

[a]Values are means ± standard deviations. Where given, means and standard deviations are calculated from three samples. [b]The data are absent for a limited amount of rice seeds.

0.0373 ($r = -0.125$, not significant) (for peak temperature), 0.0241 ($r = 0.193$, not significant) (for offset temperature), and 0.018 ($r = -0.043$, not significant) (for ΔH) in Table 7. The results of the significant test suggest that the correlation between rice starch retrogradation rates and their DSC characteristics, such as onset, offset, and peak temperatures or melting enthalpy ΔH (J/g) of different starches, is not significant at all.

The findings in the paper provide us with a new way to solve the retrogradation problem. On the basis of knowledge of rice starch synthesis,[32,33] we can easily screen those genes controlling synthesis of the starch branching enzyme and transfer them to proper cultivars to obtain the rice cultivars with a low retrogradation rate, high yield, and better taste.

AUTHOR INFORMATION

Corresponding Authors

*Telephone: +86-13312101772. Fax: +86-20-87110249. E-mail: lianliu2002@163.com.

*Telephone: +86-18981731925. Fax: +86-20-87110249. E-mail: kanghq@126.com.

*Telephone: +86-13602864341. Fax: +86-20-87110249. E-mail: felinli@scut.edu.cn.

Funding

This work is supported by the State Key Program of the National Natural Science of China (31130042), the National Key Technology Research and Development Program (2012BAD37B01), the National Natural Science Foundation of China (31271935), and the Tianjin Research Program of

DOI: 10.1021/jf503203r
J. Agric. Food Chem. 2015, 63, 1562−1572

Application Foundation and Advanced Technology (14JCYBJC30800).

Notes

The authors declare no competing financial interest.

■ ACKNOWLEDGMENTS

The authors thank Liu Yufang and Liu Yuhui for their kind help in the experiments.

■ REFERENCES

(1) Hizukuri, S. Polymodal distribution of the chain lengths of amylopectins, and its significance. *Carbohydr. Res.* **1986**, *147*, 342−347.
(2) Yao, Y.; Zhang, J.; Ding, X. Partial β-amylolysis retards starch retrogradation in rice products. *J. Agric. Food Chem.* **2003**, *51*, 4066−4071.
(3) Kim, J. O.; Kim, W. S.; Shin, M. S. A comparative of rice starch and α-amylase study on retrogradation gels by DSC, X-ray methods. *Starch/Staerke* **1997**, *49*, 71−75.
(4) Flores-Morales, A.; Jiménez-Estrada, M.; Mora-Escobedo, R. Determination of the structural changes by FT-IR, Raman, and CP/MAS ^{13}C NMR spectroscopy on retrograded starch of maize tortillas. *Carbohydr. Polym.* **2012**, *87*, 61−68.
(5) Sar, S.; Tizzotti, M. J.; Hasjim, J.; Gilbert, R. G. Effects of rice variety and growth location in Cambodia on grain composition and starch structure. *Rice Sci.* **2014**, *21*, 47−58.
(6) Ibáñez, A. M.; Wood, D. F.; Yokoyama, W. H.; Park, I. M.; Tinoco, M. A.; Hudson, C. A.; McKenzie, K. S.; Shoemaker, C. F. Viscoelastic properties of waxy and nonwaxy rice flours, their fat and protein-free starch, and the microstructure of their cooked kernels. *J. Agric. Food Chem.* **2007**, *55*, 6761−6771.
(7) Fredriksson, H.; Silverio, J.; Andersson, R.; Eliasson, A. C.; Åman, P. The influence of amylose and amylopectin characteristics on gelatinization and retrogradation properties of different starches. *Carbohydr. Polym.* **1998**, *35*, 119−134.
(8) Lawal, O. S. Composition, physicochemical properties and retrogradation characteristics of native, oxidised, acetylated and acid-thinned new cocoyam (*Xanthosoma sagittifolium*) starch. *Food Chem.* **2004**, *87*, 205−218.
(9) Ali, T. M.; Hasnain, A. Effect of emulsifiers on complexation and retrogradation characteristics of native and chemically modified white sorghum (*Sorghum bicolor*) starch. *Thermochim. Acta* **2013**, *552*, 46−53.
(10) Jinsong, B.; Mei, S.; Harold, C. Analysis of genotypic diversity in starch thermal and retrogradation properties in nonwaxy rice. *Carbohydr. Polym.* **2007**, *67*, 174−181.
(11) Hongsheng, L.; Long, Y.; Zhen, T.; Ling, C. Retrogradation of waxy cornstarch studied by DSC. *Starch/Staerke* **2010**, *62*, 524−529.
(12) Vandeputtea, G. E.; ermeylen, R.; Geeroms, V. J.; Delcour, J. A. Rice starches. III. Structural aspects provide insight in amylopectin retrogradation properties and gel texture. *J. Cereal Sci.* **2003**, *38*, 61−68.
(13) Harinder, S.; Jheng-Hua, L.; Wei-Hsiang, H.; Yung-Ho, C. Influence of amylopectin structure on rheological and retrogradation properties of waxy rice starches. *J. Cereal Sci.* **2012**, *56*, 367−373.
(14) Fredriksson, H.; Silverio, J.; Andersson, R.; Elliason, A. C.; Åman, P. The influence of amylose and amylopectin characteristics on gelatinization and retrogradation properties of different starches. *Carbohydr. Polym.* **1998**, *35*, 119−134.
(15) Chang, Y.-H.; Lin, J.-H. Effects of molecular size and structure of amylopectin on the retrogradation thermal properties of waxy rice and waxy cornstarches. *Food Hydrocolloids* **2007**, *21*, 645−653.
(16) Xijun, L.; Haibo, S.; Lin, L.; Hong, W.; Nan, Z. Characterizing the chemical features of the lipid and protein in sweet potato and maize starches. *Starch/Staerke* **2014**, *66*, 361−368.
(17) Xijun, L.; Kunsheng, Z.; Qingfeng, L.; Chen, W.; Xueyan, L. A possible structure of retrograded maize starch speculated by UV and IR spectra of it and its components. *Int. J. Biol. Macromol.* **2012**, *50*, 119−124.
(18) Philpot, K.; Martin, M.; Butardo, V.; Willoughby, D.; Fitzgerald, M. Environmental factors that affect the ability of amylose to contribute to retrogradation in gels made from rice flour. *J. Agric. Food Chem.* **2006**, *54*, 5182−5190.
(19) Ming, M.; Shanshan, X.; Fan, Y.; Bo, J.; Steve, W. C.; Tao, Z. Development of maize starch with a slow digestion property using maltogenic α-amylase. *Carbohydr. Polym.* **2014**, *103*, 164−169.
(20) Matalanis, A. M.; Campanella, O. H.; Hamaker, B. R. Storage retrogradation behavior of sorghum, maize and rice starch pastes related to amylopectin fine structure. *J. Cereal Sci.* **2009**, *50*, 74−81.
(21) Gidley, M. J.; Bulpin, P. V. Crystallisation of malto-oligosaccharides as models of the crystalline forms of starch: minimum chain-length requirement for the formation of double helices. *Carbohydr. Res.* **1987**, *161*, 291−300.
(22) Yung-Ho, C.; Jheng-Hua, L. Effects of molecular size and structure of amylopectin on the retrogradation thermal properties of waxy rice and waxy cornstarches. *Food Hydrocolloids* **2007**, *21*, 645−653.
(23) Man, J.; Yang, Y.; Zhang, C.; Zhang, F.; Wang, Y.; Gu, M.; Liu, Q.; Wei, C. Morphology and structural characterization of high-amylose rice starch residues hydrolyzed by porcine pancreatic α-amylase. *Food Hydrocolloids* **2013**, *31*, 195−203.
(24) Baik, M. Y.; Kim, K. J.; Cheon, K. C.; Ha, Y. C.; Kim, W. S. Recrystallization kinetics and glass transition of rice starch gel system. *J. Agric. Food Chem.* **1997**, *45*, 4242−4248.
(25) Ottenhof, M. A.; Hill, S. E.; Farhat, I. A. Comparative study of the retrogradation of intermediate water content waxy maize, wheat, and potato starches. *J. Agric. Food Chem.* **2005**, *53*, 631−638.
(26) Jinsong, B.; Yun, S.; Liang, J. Determination of thermal and retrogradation properties of rice starch using near-infrared spectroscopy. *J. Cereal Sci.* **2007**, *46*, 75−81.
(27) Wenhao, L.; Yulin, S.; Xinlong, X.; Qingui, L.; Jianmei, Z.; Shaohui, O.; Guoquan, Z. Physicochemical properties of A- and B-starch granules isolated from hard red and soft red winter wheat. *J. Agric. Food Chem.* **2013**, *61*, 6477−6484.
(28) Xuanxuan, L.; Zhigang, L.; Xiong, F.; Zhigang, X. Two-step method of enzymatic synthesis of starch laurate in ionic liquids. *J. Agric. Food Chem.* **2013**, *61*, 9882−9891.
(29) Feng, Z.; Fei, M.; Qunyu, G.; Shujuan, Y.; Fansheng, K.; Siming, Z. Debranching and temperature-cycled crystallization of waxy rice starch and their digestibility. *Carbohydr. Polym.* **2014**, *113*, 91−96.
(30) Lesmes, U.; Beards, E. J.; Gibson, G. R.; Tuohy, K. M.; Shimoni, E. Effects of resistant starch type III polymorphs on human colon microbiota and short chain fatty acids in human gut models. *J. Agric. Food Chem.* **2008**, *56*, 5415−5421.
(31) Lamberts, L.; Gomand, S. V.; Derycke, V.; Delcour, J. A. Presence of amylose crystallites in parboiled rice. *J. Agric. Food Chem.* **2009**, *57*, 3210−3216.
(32) Schwall, G. P.; Safford, R.; Westcott, R. J.; Jeffcoat, R.; Tayal, A.; Shi, Y. C.; Gidley, M. J.; Jobling, S. A. Production of very-high-amylose potato starch by inhibition of SBE A and B. *Nat. Biotechnol.* **2000**, *18*, 551−554.
(33) Lee, C. K.; Le, Q. T.; Kim, Y. H.; Shim, J. H.; Lee, S. J.; Park, J. H.; Lee, K. P.; Song, S. H.; Auh, J. H.; Lee, S. J.; Park, K. H. Enzymatic synthesis and properties of highly branched rice starch amylose and amylopectin cluster. *J. Agric. Food Chem.* **2008**, *56*, 126−131.

DOI: 10.1021/jf503203r
J. Agric. Food Chem. 2015, 63, 1562−1572

1. The formation of insoluble and unstable dicalcium phosphate in water results in the formation of intermediate calcium phosphate phases and ultimately apatite (e.g., hydroxyapatite, HAP), the most stable form of calcium phosphate. The following equations[9] show the compounds formed between free calcium and phosphoric acid under slightly alkaline conditions:

$$Ca^{2+}(aq) + HPO_4^{2-}(aq) \rightarrow CaHPO_4(s)$$
(dicalcium phosphate) (1)

$$Ca^{2+}(aq) + 2H_2PO_4^{-}(aq) \rightarrow Ca(H_2PO_4)_2(s)$$
(monocalcium phosphate) (2)

$$3Ca^{2+}(aq) + 2PO_4^{3-}(aq) \rightarrow Ca_3(PO_4)_2(s)$$
(tricalcium phosphate) (3)

$$2CaHPO_4(aq) + 2Ca_3(PO_4)_2(s) \rightarrow Ca_8H_2(PO_4)_4(s)$$
(octacalcium phosphate) (4)

$$Ca_3(PO_4)_2(aq) + 2Ca^{2+}(aq) + HPO_4^{2-}(aq) + H_2O(l) \rightarrow Ca_5(PO_4)_3OH(s) + 2H^{+}(aq)$$ (hydroxyapatite) (5)

Amorphous tricalcium phosphate is the main compound that forms flocs in aqueous systems, including sugar solutions.[9]

The physicochemical properties of flocs influence the efficacy of solid−liquid separation processes. Colloidal particles in an aqueous solution are charged as a result of the dissociation of surface groups or adsorption of ions in solution, resulting in the electrical double layer surrounding the particle.[10] The electrical double layer of particles governs the electrostatic attraction between charged particles and determines the extent of floc formation. The nature and structure of flocs formed in an aqueous solution dictate how effective the solid−liquid separation process is in relation to floc size and settling velocity.[11] Loosely held or more open floc structures have fractal dimensions in the range of 1.6−2.4.[12] On the other hand, compact structures have fractal dimension values in the range of 2.5−3.0.[13,14] Generally, flocs with fractal dimension in the range of 2.0−2.5[13,14] are effective in trapping suspended particles and the adsorption of particles onto the floc network[13,14] (Figure 1), if the effect of impurities in the matrix

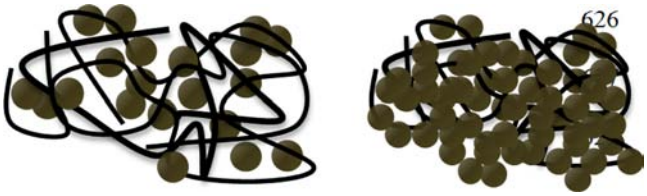

Figure 1. Formation of disordered, loosely attached, fine flocs (left) and tightly bound bridged flocs (right).

is neglected. As such, it was hypothesized that examining the effect of impurities on floc structure and size would provide information on strategies that could be adopted to improve solid−liquid separation processes in sugar and other systems. Typically, the floc structure is characterized by the fractal dimension; however, the measurement of size of primary particles is not directly proportional to the wavelength of the incident light, which consequently voids the Rayleigh−Gans−Debye (RGD) theory. In the current study, the term "scattering exponent" is used.

Studies on the various phases of calcium phosphate precipitates formed in sugar solutions have been reported to provide information on the mechanism of calcium phosphate formation and on the clarification process.[15−17] Greenwood et al.[15] studied the size and structural properties of calcium phosphate flocs formed in simple synthetic juice solutions using light scattering techniques. These flocs were reported to have scattering exponents (which are qualitative representations of the floc structures)[15] between 1.97 and 2.76 and average sizes of between 10.4 and 17.5 μm. Following the work conducted by Greenwood et al.,[15] the present study examined the effect of starch, Na^+ ions, SiO_2, and phosphate ion concentrations on floc structure and size of calcium phosphate particles formed in synthetic sugar solutions. These constituents were examined using small-angle laser light scattering technique, X-ray powder diffraction (XRD), and attenuated total reflectance Fourier transformed infrared (ATR-FTIR) spectroscopy. The investigations were conducted to provide explanations on how certain impurities influence the properties of calcium phosphate flocs and, hence, the clarification process of sugar cane juice. On the basis of the information derived from the initial study, further clarification studies were conducted using both cold and cold/intermediate liming techniques on juice expressed from prepared WC. These two liming techniques produce calcium phosphate flocs with different properties.[18] In addition, one-stage (i.e., conventional) and two-stage clarification processes using these techniques were examined.

MATERIALS AND METHODS

Preparation of Synthetic Cane Juices. The composition of the synthetic juice solution used in the study is shown in Table 1. Sucrose

Table 1. Composition of Synthetic Cane Juice Solutions

concentration (mg/kg)	substance	added as
120000	sucrose	white sugar
125	dextran	dextran
500	starch	soluble starch
75	SiO_2	sodium silicate pentahydrate
300	CaO	calcium hydroxide
1000	organic acid	*trans*-aconitic acid
265	P_2O_5	potassium dihydrogen phosphate
400	MgO	magnesium sulfate heptahydrate

(Sigma-Aldrich, Castle Hill, NSW, Australia), equivalent to 120 mg/kg, and Milli-Q water were used to prepare the solutions. Also, proportions of $Ca(OH)_2$, $Mg(SO)_4{\cdot}7H_2O$, KH_2PO_4, and aconitic acid (Chem-Supply, Gillman, SA, Australia); dextran, NaCl, and $NaSiO_3{\cdot}5H_2O$ (Sigma-Aldrich, Sydney, Australia); and AR grade soluble starch (Ajax Finechem, Seven Hills, NSW, Australia) were added to prepare the synthetic juice solution. Varying amounts of Na^+ ions, SiO_2, phosphate ions, and starch were added to the synthetic juice solution prior to liming to examine the influence of each component on the structure and size of calcium phosphate. For the addition of SiO_2, a correction was made to account for the total amount of Na^+ ions, as it was added in the form of $NaSiO_3{\cdot}5H_2O$. Lime saccharate was prepared with 725 mg/kg of sucrose and 50 mg/kg of $Ca(OH)_2$. This solution was used in the synthetic juice solution studies.

Preparation of Raw Cane Juices. Tully Sugar factory (Queensland, Australia) processed mechanically harvested green cane with all of the trash removed during the August−September 2012 crushing season. Factory juice (SJ) was collected directly from the incubator

DOI: 10.1021/jf502229f
J. Agric. Food Chem. 2015, 63, 1573−1581

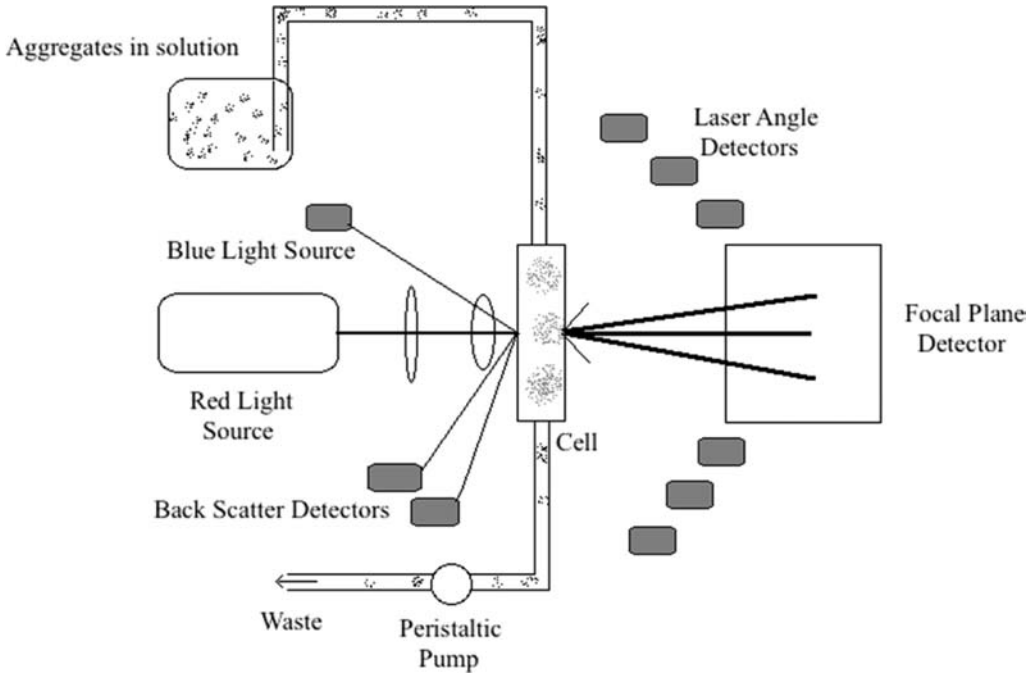

Figure 2. Schematic diagram of the Malvern Mastersizer S Particle Analyzer.

tank (76 °C) prior to the clarification process. Juice samples were collected every 0.5 h for 3 h, and composite samples were prepared to reduce the variability of the data. It was necessary to maintain the temperature of the collected juices at 76 °C to avoid changes in juice properties.

None of the sugar factories in Australia were processing WC at the time of the present study; thus, WC juice was not available. As a result, synthetic WC juice was prepared by mixing 850 mL of SJ juice with 150 mL of juice expressed from trash, for each clarification test. Several sugar cane plants in the fields in the vicinity of the Tully Sugar factory were hand-cut to obtain sugar cane trash. The trash was fibrillated using a cutter grinder, and the juice was expressed using a 20 tonne hydraulic press unit (Carolina Industrial Equipment, Charlotte, NC, USA).

Clarification Procedure. Clarification experiments (by sedimentation) were conducted using settling tubes (60 mm diameter, 460 mm high) in a Sugar Research Institute (SRI) designed heated illuminated batch settling kit.[19] Each tube was calibrated 0−400 mm with a 400 mm settling depth and volume of ∼1.0 L. Samples of sugar cane juices were clarified immediately after collection from the sugar factory. One-stage (i.e., conventional) and two-stage clarification processes were conducted to determine which process produces juice of better quality and fast-settling juice flocs. The lime saccharate used was a mixture of 100 g of a 200 g/kg solution of calcium oxide and 100 g of 68 °Brix factory syrup. The pH of the juices was measured using a portable pH meter (Hach H160, Cleveland, CO, USA) with a glass probe (model 93×218814, Eutech Instruments, Singapore) and a high-temperature probe (EC-FG-7350401B, Eutech Instruments).

Two liming techniques (cold and cold/intermediate) were selected for this study. Cold liming for the one-stage process was performed as follows: Lime saccharate was added to juice (50−55 °C) to provide free calcium ions, which reacted with the inorganic phosphates in the juice to form the calcium phosphate flocs. Enough lime saccharate was added to neutralize the juice to pH 7.1/7.8 (to examine the effect pH on turbidity and Ca^{2+} ion levels). The juice was heated to 76 °C and then boiled at ∼100 °C to remove entrained air, which can interfere with floc settling. A dose of 5 mg/kg of flocculant, poly(acrylamide-*co*-sodium acrylate) polymer (Magnafloc LT27 with a degree of hydrolysis of 27%, TD Chemicals, Robina, QLD, Australia), was added to the juice to bridge the calcium phosphate flocs, enhance agglomeration, and improve sedimentation. After 30 min of quiescent settling, the samples of clarified juice (CJ) were siphoned from the settling tubes for subsequent analyses. The experiments were performed in duplicate. For the cold/intermediate liming technique, the following modifications were made: juice was limed to pH 6.2 at 52 °C, then heated 76 °C, and further limed to pH 7.1/7.8. The limed juice was then boiled at ∼100 °C. The juice was then processed in a similar fashion as the cold liming technique.

The two-stage clarification process involved heating the juice (60 °C) followed by lowering the juice pH to 3.5 using 2 M H_2SO_4 (Ajax Finechem, Seven Hills, NSW, Australia) to facilitate precipitation of proteins and polysaccharides. A highly charged cationic coagulant (10 mg/kg, Magnafloc LT525 with a degree of hydrolysis of 46%, Chemiplas Australia Pty Ltd., East Melbourne, VIC, Australia) was also added to aid the precipitation process. After sedimentation, the supernatant, stage 1 juice, was collected for further clarification. The stage 1 juice was clarified using the process described for the one-stage normal clarification process. The pH of the juice was limed to pH 7.1/7.8. Both the cold liming and the cold/intermediate liming techniques were performed for the one-stage clarification process. All clarified juice samples were stored at −20 °C and thawed prior to compositional analyses.

The settling rate of calcium phosphate flocs provides a good indication of how effectively the flocs settle. It was determined by measuring the level of the mud interface at 0.5, 1.0, 2.0, 3.0, 4.0, and 5 min. The initial settling rate (cm/min) was obtained from the graphical analysis of the initial linear slope.

The final mud level was determined after 30 min of sedimentation by visual assessment, recording the height of the interface where the boundary line between the solid and liquid phase is evident. As the settled flocs were unstirred, the final mud levels were not indicative of values obtained in commercial clarifiers.

The turbidity of CJ was determined by measuring the absorbance (A) at 900 nm in 1 cm cuvette cells against Milli-Q water[20] using a Cintra 40 double-beam UV−visible spectrophotometer (GBC Scientific Equipment Pty. Ltd., Braeside, VIC, Australia). The turbidity was measured in triplicate and calculated as 100A. The error for turbidity determination was ±0.5%.

Compositional Analyses. The total soluble solids (i.e., the °Brix of the juice) was determined using a digital refractometer (RFM 342, Bellingham and Stanley Ltd., London, UK) accurate to ±0.01 °Brix. Total soluble polysaccharides were calculated according to the

DOI: 10.1021/jf502229f
J. Agric. Food Chem. 2015, 63, 1573−1581

procedure described by Roberts.[21] Proteins were isolated from the organic sugar cane juice by gel filtration using PD-10 desalting columns prepacked with Sephadex G-25 (GE Healthcare, Rydalmere, NSW, Australia), and the concentration was measured using the BCA protein assay kit (Thermo Scientific, Scoresby, VIC, Australia). Percentages of sucrose, glucose, and fructose present in the samples were determined using a Waters (Milford, MA, USA) high-performance ion chromatography system coupled to an electrochemical detector (model 2465, Waters), a pump (model 626, Waters), and a controller (model 600S, Waters). The carbohydrates were separated using a CarboPac PA-1 column (4 × 250 mm, Dionex, Idstein, Germany). The samples for HPIC analysis were prepared using ICUMSA method GS7/8/4-24.[22] Inorganic ions were determined using a Varian Vista-MPX CCD simultaneous inductively coupled argon plasma optical emission spectrometer (ICP-OES; Varian Inc., Mulgrave, VIC, Australia). All measurements were conducted in triplicate.

Floc Size and Structure. The synthetic juice test solutions were heated to 76 °C in a temperature-controlled water bath. Once the temperature was stabilized, lime saccharate was added to raise the pH to 7.8 ± 0.05. Floc size and structure measurements were conducted online using the small-angle laser light scattering instrument (Malvern Mastersizer S Particle Analyzer, Malvern Instruments, Southborough, MA, USA) using a circulation system (Figure 2). The inlet and outlet tubes were placed in the beaker of hot synthetic sugar solution. A peristaltic pump was used to deliver the solution through the tubes to flow through the flow cell. The gentle action of the peristaltic pump ensured minimum breakup of the aggregates while maintaining them in suspension. Pure sugar solution (maintained at 94 °C) was used to preheat the instrument. The silicon lines and top of the flow cell were insulated.

Prior to measurements, the alignment and background readings for the Mastersizer were conducted using Milli-Q water. Measurements were taken every 30 s for 5 min, and all measurements were repeated 10 times during each sequence to ensure that consistent results were obtained.

The floc structure (i.e., compactness), represented as the scattering exponent, was calculated (please refer to the Supporting Information) using the RGD scattering theory and by constructing a log−log plot of scattered light intensity versus scattering momentum.[23]

The measurement of particle size was within the range of 0.05−900 μm. The instrument consisted of a He−Ne laser light (λ = 632.8 nm) as the light source, an optic lens, and photosensitive detectors. The scattered light was collected at angles between 0° and 46°. An integration time of 40 s per curve was selected to provide both optimum rate of measurement and data quality. The light obscuration level of the samples was maintained between 10% and 30% to enhance the reliability of the measurements, and aliquots of the samples were injected into a small dispersion unit containing Milli-Q water. The variability in the scattering exponent for these measurements was generally ≤0.05, and for the average size distribution, the variability was ≤50 μm.

The XRD patterns were obtained for the calcium phosphate flocs using a PANalytical X'Pert MPD with Cu Kα radiation of wavelength 1.5418 Å.

Infrared spectra were collected using a Nicolet 870 Nexus Fourier transform infrared (FTIR) spectrometer equipped with an attenuated total reflection accessory (Madison, WI, USA). Spectra were collected in the spectral range from 4000 to 440 cm^{-1} and were the average of 64 scans at a resolution of 4 cm^{-1}. The spectra were plotted using the Galactic 187 Industries Corp. GRAMS/32 software package (Salem, NH, USA). The final FTIR spectra were normalized with respect to the reference peak located at 1007 cm^{-1}.

RESULTS AND DISCUSSION

Effect of Sodium on Calcium Phosphate Flocs. The scattering exponent and average size of the flocs formed in the presence of Na^+ ions are shown in Table 2. A linear decrease in the scattering exponent (from 2.50 to 2.25) with increasing Na^+ ion concentration is attributable to the increasing formation of looser flocs. Looser flocs exhibit lower packing density and, hence, slower settling rates. The changes in floc structure with increasing Na^+ concentration may be associated with the dispersive properties of Na^+ ions.[24] The floc size increased to a maximum of 280 μm before slightly dropping and leveling off. The general increase in size may be due to electrostatic repulsion between calcium phosphate particles and or electrostatic repulsion between the microflocs because of the dispersive action of Na^+ ions.[24]

Table 2. Scattering Exponent (±5%) and Average Size (±5%) of Flocs under the Influence of Na^+ Ions, Silica, Phosphate, and Starch Concentrations

	scattering exponent	av size (μm)
Na (mg/kg)		
2.5	2.50	150
3.2	2.45	280
4.2	2.30	220
5.1	2.25	240
SiO_2 (mg/kg)		
50	2.65	350
80	2.60	350
90	2.65	375
100	2.55	380
120	2.58	360
150	2.58	310
phosphate (mg/kg)		
150	2.70	220
250	2.72	190
300	2.69	230
350	2.69	380
450	2.68	370
starch (mg/kg)		
100	2.56	390
200	2.58	290
300	2.58	260
400	2.60	310
500	2.55	270

Effect of Silica on Calcium Phosphate Flocs. The effects of SiO_2 on the size and structure of the primary flocs formed in the synthetic cane juice solutions are also presented in Table 2. Increasing the SiO_2 concentration generally decreased the scattering exponent. This trend is similar to that obtained with the Na^+ ions. However, the drop in the scattering exponent value with increasing SiO_2 concentration was not as distinct as that obtained with Na^+ ions. The decline in the scattering exponent is likely to be, in part, due to increasing Na^+ concentration in solution, as SiO_2 was added in the form of $NaSiO_3 \cdot 5H_2O$. However, the absolute scattering exponent values were higher with the addition of SiO_2 relative to situations when Na^+ ions were added, possibly indicating that SiO_2 has less of an impact than Na^+ ions on floc structure. The size of the calcium phosphate flocs peaked at approximately 380 μm at 100 mg/kg and then declined with increasing SiO_2 concentration. The reason for this is not known.

Effect of Phosphate on Calcium Phosphate Flocs. Floc structure was not influenced by phosphate addition; however, the size of calcium phosphate flocs significantly increased from approximately 220 to 380 μm when >350 mg/kg P_2O_5 was added compared to the addition of 300 mg/kg P_2O_5 (Table 2). Supplying phosphoric acid to the sugar solution provided

DOI: 10.1021/jf502229f
J. Agric. Food Chem. 2015, 63, 1573−1581

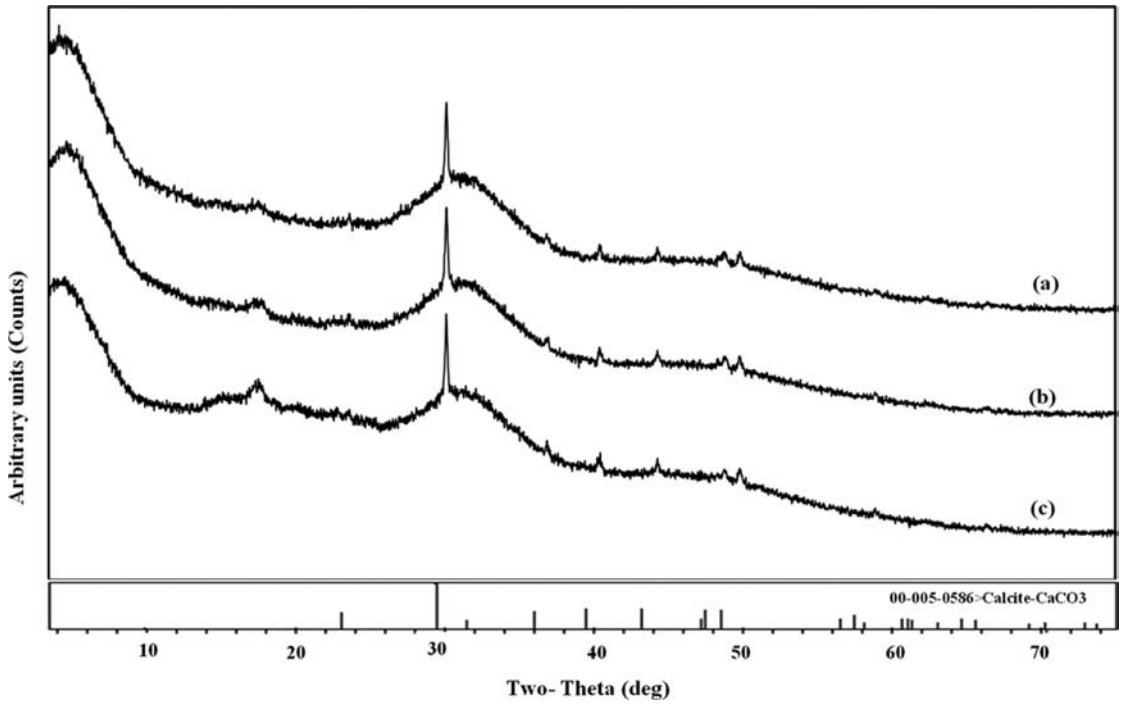

Figure 3. X-ray powder diffraction patterns of calcium phosphate flocs: (a) 5 mg/kg of NaCl added to synthetic juice; (b) synthetic juice; (c) 200 mg/kg starch added to synthetic juice.

additional phosphate ions, which interacted with calcium ions from lime saccharate and resulted in an increase in the growth of calcium phosphate particles. The results show that there is a wide P_2O_5 range over which there is stabilization of floc structure. It is unclear whether the stabilization is due to the changes in surface charge of the calcium phosphate, via changes in proportion of the phases that constitute the floc.[9] In a typical clarification process in a sugar factory, juice phosphate concentration >300 mg/kg as P_2O_5 does not influence clarification performance significantly.[9]

Effects of Starch on Calcium Phosphate Flocs. As shown in Table 2, increasing the amount of starch did not change the floc structure, but slightly affected the floc size. At the lowest dosage of starch (100 mg/kg), the floc size of the formed flocs was 390 μm. Increasing starch concentration to 500 mg/kg dropped the size to approximately 270 μm. The reduction in floc size may be associated with starch molecules adhering to the surface of microflocs inhibiting growth, without affecting packing arrangement.[25] Starch molecules when present to a significant extent in juice do affect sugar crystallization, so the same may occur with calcium phosphate.[25]

X-ray Powder Diffraction Results. XRD was used to identify the phases of calcium phosphate precipitates formed in the presence of Na^+ ions and starch, as these two components were shown to most strongly influence the scattering exponent and size of flocs. The XRD patterns of selected precipitates are shown in Figure 3. Calcite (2θ, 23.06°, 29.46°, 35.98°, 39.46°, 43.18°, 47.54°, 48.56°, and 57.40°) is the main crystal phase in all of the samples. The prominent halo in the 2θ region between 26° and 36° is characteristic of an amorphous compound,[26] which is presumably calcium phosphate, because energy dispersive spectroscopy gave a mass ratio of Ca to P similar to that of tricalcium phosphate. As was reported for SiO_2, the variation in the size of the halo may be a representation of the variation of the interatomic distances between P−O−P structural units, which is related to the arrangement of the phosphorus molecules.[14]

The addition of phosphate broadens the XRD halo relative to the control, indicating that the calcium phosphate phase is far less ordered (smaller particles, i.e., more amorphous) than that of the control. The increased amorphous nature of the calcium phosphate particles will increase the amount of impurities removed because of an increase in surface area.[18]

The crystalline peaks associated with starch at 2θ values of 15° and 17°, which is typical of the A-type pattern,[25] are highest when an increasing amount of starch was added prior to lime neutralization and lowest when the Na^+ level was increased prior to neutralization. Starch is electronegative, so cations attract starch hydroxyl groups and destabilize starch granules, whereas anions tend to repel starch hydroxyl groups and stabilize starch granules.[27] Chiotelli[27] and co-workers postulated that Na^+ ions tend to penetrate starch granules and replace hydrogen ions, which reduces the water phase. When the electrostatic driving force of the anions in solution exceeds the repulsive force associated with the Na^+ ions, the anions enter the starch granule and rupture the hydrogen bond between starch molecules. This results in gelatinization, and so the amount of starch trapped (or rather removed) by the calcium phosphate flocs is reduced. The presence of starch in sugar cane juice processed in the factory can create boiling and viscosity problems, filterability impairment, and poor molasses exhaustion.[28] As a consequence, high levels of Na^+ ions in juice have two negative effects on clarification: (i) increasing the amount of starch molecules present in the CJ and (ii) loosening the floc structure, thereby reducing the amount of suspended particles not trapped by the flocs.[12]

Attenuated Total Reflectance Fourier Transform Infrared spectroscopy. The ATR-FTIR spectra of calcium phosphate precipitate formed in the control synthetic juice and

DOI: 10.1021/jf502229f
J. Agric. Food Chem. 2015, 63, 1573−1581

in the presence of starch, SiO_2, NaCl, and phosphate are shown in Figure 4. The broad band observed at 3325 cm^{-1} is

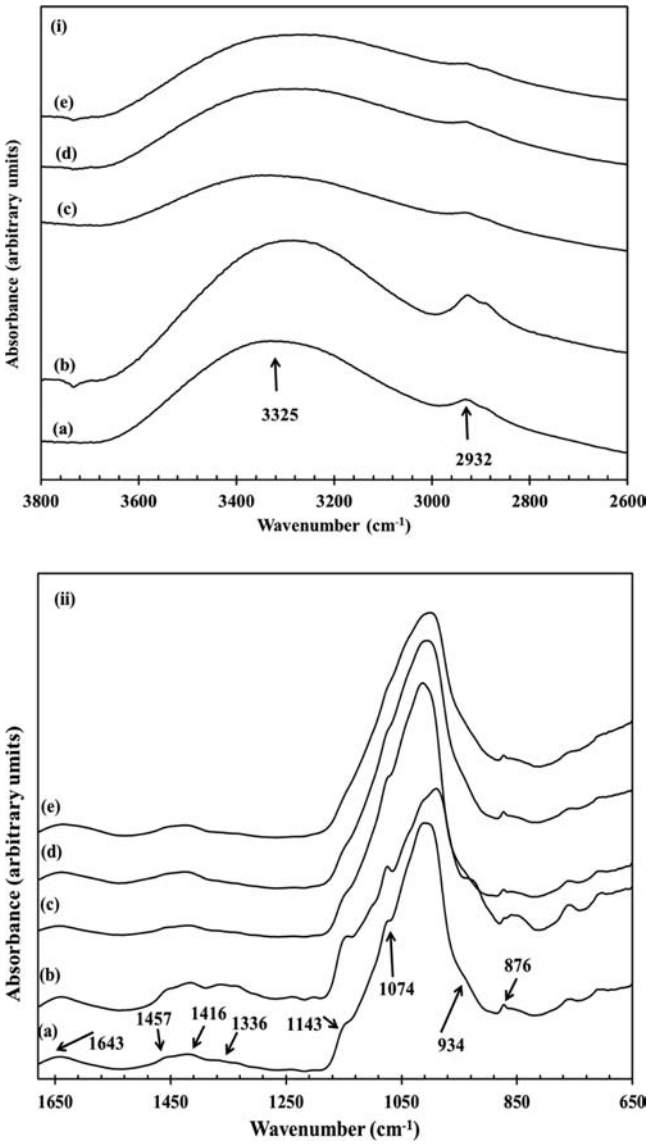

Figure 4. ATR-FTIR spectra ((i) 3800−2600 cm^{-1} and (ii) 1650−650 cm^{-1}) of calcium phosphate precipitate formed during juice flocculation of synthetic juice: (a) control; (b) 200 mg/kg starch; (c) 25 mg/kg SiO_2; (d) 5 mg/kg NaCl; (e) 250 mg/kg phosphate.

associated with the O−H group stretch vibration of calcium phosphate.[29] The presence of adsorbed water may also be associated with this peak. Figure 4I shows that the addition of SiO_2 significantly reduced the intensity of this broad peak. This peak was also reduced, albeit to a lesser extent, for the calcium phosphate precipitates derived from the synthetic juice in the presence of NaCl and phosphate ions. It is therefore likely that these added compounds affect the properties of calcium phosphate at differing extents. The band at 2932 cm^{-1} is related to the C−H stretching vibration of methyl groups, which is related to the presence of starch and/or dextran.[30] From Figure 4i, the intensity of this peak is highest in the synthetic juice obtained in the presence of starch (Figure 4i(b) followed by the control (Figure 4i(a) in comparison to the intensities of the other samples. This confirms that the addition of phosphate, NaCl, and SiO_2 reduces the amount of starch trapped by the calcium phosphate flocs.

The peak detected at 1643 cm^{-1} in the spectra (Figure 4ii) is correlated to the H−O−H symmetric bending vibration.[31] The bands observed at 1457, 1416, and 876 cm^{-1} are derived from two antisymmetric stretching and bending vibrations of CO_3^{2-}, respectively. The presence of these peaks is due to the formation of $CaCO_3$.[32] The partially resolved shoulder at 1336 cm^{-1} detected from the control and synthetic juice, in which starch was added, is assigned to the C−H bending of CH_2 groups in starch.[30] This peak was not detected in the spectra obtained from the analysis of other samples. The other peaks present as shoulders at 1143, 1074, and 934 cm^{-1}, characteristic of starch, were detected in the control (Figure 4ii(a) and calcium phosphate sample (Figure 4ii(b)). These peaks are associated with C−O, C−C stretching, C−O−H bending, and C−O−C vibrations in starch molecular structure, respectively.[29] Each spectrum shown in Figure 4ii reveals an intense peak between 1200 and 896 cm^{-1}, which is related to P−O stretching derived from the phosphate group.[32] The position of this peak shifted in the spectra of the samples, which may be related to the salt added during flocculation and the change in crystallinity of the calcium phosphate floc. In summary, the results obtained using ATR-FTIR correlate with the XRD data, in terms of the relative proportions of starch in the various calcium phosphate samples. The calcium phosphate flocs are not effective in trapping starch molecules. However, increasing the concentration of phosphate increases the floc size and presumably the amount of flocs formed to improve clarification performance.[6] Thai et al.[6] investigated the clarification performance of sugar cane juice derived from burnt cane (BE) and green cane with half of the trash removed (GE) and concluded that the latter can be clarified with acceptable juice turbidity when up to 100 mg/kg of P_2O_5 is added.

Clarification of Sugar Cane Juice Derived from Whole Sugar Cane Crop. The compositions of sugar cane juices obtained from the factory (SJ) and those prepared from factory juice and hand-cut trash material (prepared WC) are shown in Table 3. The inclusion of juice derived from trash contributed significantly to the level of soluble proteins, polysaccharides, reducing sugars, calcium, phosphate, magnesium, and silicon ions.

The polysaccharide content of juice derived from WC was higher than that of SJ by ∼36% (Table 3). Starch, polysaccharides, and proteins are polar and thus would influence the coagulation and flocculation processes of juice particles and their floccing ability.[18] Furthermore, if a higher proportion of these impurities is carried through the various processing stages, they would increase the viscosity of molasses (sugar syrup), reduce the rate of sucrose crystallization, and produce colored compounds.[33]

The results of the soluble inorganic ions (Table 3) show that Ca^{2+} and phosphate contents in the WC juices were higher than those in the SJ by ∼30% and ∼52%, respectively. As a result, Ca^{2+} and phosphate ions are expected to increase the coagulation of WC juice particles and hence improve clarification compared to juice expressed from SJ. However, it is important to note that the proportion of Ca^{2+} ions in WC juice that takes part in particle aggregation is not known.[24]

Clarification Performance. As shown in Table 3, the one-stage (i.e., conventional) clarification processes using cold and cold/intermediate liming resulted in relatively high CJ turbidities of 15.7 and 29.0 NTU, respectively. For good

DOI: 10.1021/jf502229f
J. Agric. Food Chem. 2015, 63, 1573−1581

Table 3. Clarification Results of Prepared WC Juice[a] at Tully Mill

description/liming technique	SJ	prepared WC	cold liming	cold/ intermediate	cold liming	cold/ intermediate	cold liming	cold/intermediate
clarification	not treated	not treated	normal	normal	two-stage	two-stage	two-stage	two-stage
juice pH	5.8	5.5	5.5	5.6	5.2	5.3	5.3	5.3
additives					H_2SO_4, pH 3.5	H_2SO_4, pH 3.5	H_2SO_4, pH 3.5 10 mg/kg LT525	H_2SO_4, pH 3.5 10 mg/kg LT525
pH after liming			7.1	6.2/7.8	7.1	6.2/7.8	7.1	6.2/7.8
alkali vol (mL)			9.8	3.8/12.0	13.9	11.1/14.2	13.4	5.0/13.2
floc size (visual)			small	small	large	large	large	large
settling rate, cm/min			30	10	flocs floated	flocs floated	flocs floated	flocs floated
final mud level (%)			30	15.0				
turbidity (NTU)			15.7	29.0	5.2	6.7	4.8	8.1
polysaccharides (mg/kg)[b]	47300	64300	41700	52600	44000	46700	42900	44700
proteins (mg/kg)[b]	2460	15400	6220	7080	3000	5290	2800	5170
Ca (mg/kg)[b]	1010	1310	2120	3380	5000	5850	4960	5570
Mg (mg/kg)[b]	924	1560	1240	1220	1270	1300	1240	1220
P (mg/kg)[b]	924	1400	387	460	246	220	240	214
Si (mg/kg)[b]	773	533	314	338	262	276	256	260
S (mg/kg)[b]	840	1150	1170	1220	3490	3660	3490	3510

[a]Composite juice samples. [b]Units are on dry solids.

clarification, this value is usually <20 NTU under Australian conditions.[34] In the two-stage clarification process (with or without LT525 addition), the cold liming technique improved CJ turbidity by 67−69% in comparison to the one-stage clarification process. With this process, cold liming gave lower CJ turbidities than the cold/intermediate liming technique.

The one-stage clarification process (both cold and cold/intermediate liming techniques) resulted in the formation of fine and small flocs (Table 3), which led to slow to moderate settling rates of the particles during sedimentation, similar to the results obtained by Kent et al.[35] Mud compaction was very poor at 30% for the cold liming technique. This will have implications with the clarifier size and the pol loss during mud filtration. If this liming process is to be adopted, then a suitable flocculant must be identified to improve mud compaction and reduce juice turbidity. However, the level of mud compaction reduced by half when the juice was treated using cold/intermediate liming. Again, a suitable flocculant should be identified if the process is to be used commercially.

In the two-stage process, the flocs formed in the second stage were significantly larger in size (than those formed in the one-stage process) but floated, rather than settled. The reason for this is that a significant portion of heavy insoluble impurities was removed during the first stage of the two-stage process, which would have assisted floc densification in the second stage of the process. An alternative method to gravity sedimentation is to use dissolved air flotation (DAF) system. This will readily remove the floating flocs. The DAF method is used in syrup clarification and is an efficient, practical, and reliable separation method for the removal of impurities.[36]

Significant protein removal was achieved when the juice was cold-limed as part of a two-stage clarification process (Table 3). The protein level in the CJ was remarkably low with 82% removed using the two-stage clarification process and 60% with the one-stage clarification process. The significantly higher amount of proteins removed in CJ obtained by the two-stage clarification process was a result of their partial removal during the pretreatment step (i.e., stage one). Polysaccharide removal was highest when the juice was cold limed. Liming to a lower pH level of 7.1 (instead of 7.8) reduced the proportion of the protein and polysaccharide contents in CJ. The reason for this is not known. It was observed that there was no benefit in using the coagulant during the first stage of the two-stage process.

Amino acids formed by protein denaturation in sugar cane juice react with reducing sugars (e.g., glucose and fructose) via the Maillard reaction to form undesirable high molecular weight dark colored compounds that become incorporated into the sucrose crystals.[37] Thus, the two-stage process, which reduced proteins (and polysaccharides) may thus affect the proportions of colored bodies formed during sugar manufacturing. Previous studies by Lindeman and O'Shea[38,39] revealed a strong association between colored compounds and polysaccharides in sucrose crystals.

In comparison to the one-stage clarification process, the two-stage clarification process resulted in CJ with higher reducing sugar content by ≤28% (≥2.0% on dry solids) and sucrose levels were lower by ≤4.5% (∼93% on dry solids) (please refer to the Supporting Information for glucose, fructose, and sucrose concentrations in WC juices). The results showed that sucrose degradation occurred, due to the use of acid to drop the juice pH to 3.5 during the pretreatment step.

Table 3 shows that lime consumption was notably higher using the cold/intermediate liming technique than cold liming because additional lime saccharate was required for neutralization. There were no changes in the proportion of Mg^{2+} ion concentrations irrespective of liming technique or clarification process. In general, cold liming resulted in lower inorganic ion levels than the cold/intermediate liming technique. For both cold and cold/intermediate liming techniques, there was an improved removal of phosphate and silicon using the two-stage clarification process compared to the one-stage clarification process by ≤53% and ≤23%, respectively, whereas, Ca^{2+} and sulfur levels were considerably higher by ≤136% and ≤200%, respectively. The higher the sulfur content in juice treated using the dual clarification process is due to the addition of H_2SO_4 during pretreatment.

The high levels of these inorganic components, particularly Ca^{2+}, phosphate, silicon, and sulfur, will cause severe scaling in

DOI: 10.1021/jf502229f
J. Agric. Food Chem. 2015, 63, 1573−1581

the evaporators,[40] as they are significantly higher than those present in burnt cane or green cane with the trash removed.[6] With the one-stage clarification process, predominantly calcium phosphate and silica scale (neglecting the contribution from calcium oxalate) will be deposited in the evaporators, and the proportion will be significantly higher with the juice obtained with cold/intermediate liming. However, the proportion of scale formed from the juice using the cold liming technique may be only marginally higher than the scale derived from juice expressed from green cane with half the trash extracted (GE).[6] This is because of the higher proportion of phosphorus and suspended particles (i.e., higher turbidity). As mentioned in the previous work by the authors, the cost of cleaning the evaporators increases if phosphate scale coprecipitates with calcium oxalate and amorphous SiO_2 in the no. 4 and 5 evaporators of a quintuple evaporator set.[41] A high proportion of phosphate level in CJ is usually associated with high raw sugar filterability.[4]

On the basis of the inorganic constituents of the CJ obtained by the two-stage process, the main scale compounds apart for calcium oxalate will be calcium phosphate, calcium sulfate, and SiO_2. The CJ obtained by the two-stage process contains 2 and 3 times as much Ca^{2+} and sulfur, respectively, than the CJ obtained in the one-stage clarification process. As such, an increase in scaling propensity will occur if this juice is processed compared to the juice obtained by the one-stage clarification process. As, the CJ obtained with the two-stage process resulted in significantly lower turbidity than that of the one-stage clarification process, scaling in the no. I and 2 evaporators of a quintuple evaporator set will be expected to be significantly less.[42]

An approach that needs to be explored to reduce Ca^{2+} ions present in the CJ obtained by the two-stage process is to use an inorganic acidic salt (e.g., alum) instead of H_2SO_4 to lower the juice pH and then use an alkali (e.g., soda ash or dolomite) to slightly raise it to the original value prior to liming. The removal of the flocs can be achieved with either the DAF process or the addition of higher density material microsilica or even dirt prior to the clarification via sedimentation. To reduce sucrose inversion, the pH level of the first stage should be lowered to between 4 and 4.5, not to 3.5 as was done in the present study. The removal of significant quantities of proteins and polysaccharides will reduce not only color bodies in sugar process streams but also the proportion that ends up in the sucrose crystal. This will reduce the color of the product sugar.

■ ASSOCIATED CONTENT

Supporting Information

Information on RGD theory and equations associated with scattering momentum; information on the glucose, fructose, and sucrose contents of WC juices. This material is available free of charge via the Internet at http://pubs.acs.org.

■ AUTHOR INFORMATION

Corresponding Author

*(C.C.D.T.) Phone: +61 421 543 692. E-mail: caroline.thai@connect.qut.edu.au.

Funding

We thank the Sugar Research and Development Corporation, Sugar Research Limited, and Queensland University of Technology for funding this project.

Notes

The authors declare no competing financial interest.

■ ACKNOWLEDGMENTS

We thank Darryn Rackemann and Hakan Bakir, both at the Centre for Tropical Crops and Biocommodities, Queensland University of Technology, Brisbane, Australia, for their technical assistance.

■ ABBREVIATIONS USED

ATR-FTIR, attenuated total reflectance Fourier transformed infrared; BE, burnt cane; CJ, clarified juice; DAF, dissolved air flotation; GE, green cane with half the trash extracted; HAP, hydroxyapatite; ICPOES, inductively coupled argon plasma optical emission spectroscopy; MJ, mixed juice; RGD, Rayleigh−Gans−Debye; SJ, secondary juice; XRD, X-ray powder diffraction; WC, whole crop

■ REFERENCES

(1) Rainey, T. J. A study into the permeability and compressibility properties of Australian bagasse pulp. Ph.D. thesis, Queensland University of Technology, 2009.

(2) Kent, G. A.; Allen, W. J.; Hoare, C. P.; Dixon, T. F. The effect of extraneous matter on factory throughput and performance. *Proc. Aust. Soc. Sugar Cane Technol.* **1999**, *21*, 38−43.

(3) McGuire, P. J.; Inderbitzin, M.; Rich, B.; Kent, G. A. The effect on whole crop harvesting on crop yield. *Proc. Aust. Soc. Sugar Cane Technol.* **2011**, *33*, 1−12.

(4) Bennett, M. C.; Regnauth, J. M. The effects of calcium and phosphate in cane juice clarification. *Int. Sugar J.* **1960**, *62*, 13−16.

(5) East, C. P.; Doherty, W. O. S.; Fellows, C. M.; Yu, H. Characterization of sugar juice heat exchanger tube deposit. *Surf. Interface Anal.* **2011**, *43*, 1231−1239.

(6) Thai, C. C. D.; Bakir, H.; Doherty, W. O. S. Insights to the clarification of sugar cane juice expressed from sugar cane stalk and trash. *J. Agric. Food. Chem.* **2012**, *60*, 2916−2923.

(7) Thai, C. C. D.; Doherty, W. O. S. Characterisation of sugarcane juice particles that influence the clarification process. *Int. Sugar J.* **2012**, *114*, 719−724.

(8) Doherty, W. O. S.; Edye, L. A. An overview on the chemistry of clarification of cane sugar juice. *Proc. Aust. Soc. Sugar Cane Technol.* **1999**, *21*, 381−388.

(9) Deben, J. G. The chemistry of calcium phosphate precipitation in cane sugar juice clarification, parts I, II and III. *Int. Sugar J.* **1976**, *78*, 35−39 and 73−75.

(10) Kopeliovich, D. Stabilization of colloids. 2009 [cited 2011 June 2011]; available from http://www.subtech.com.

(11) Vahedi, A.; Gorczyca, B. Application of fractal dimensions to study the structure of flocs formed in lime softening process. *Water Res.* **2011**, *45*, 545−556.

(12) Witten, T. A.; Cates, M. E. Tenuous structures from disorderly growth processes. *Science* **1986**, *232*, 1607−1612.

(13) Schaefer, D. W. Polymers, fractals and ceramic materials. *Science* **1989**, *243*, 1023−1027.

(14) Nakamura, T.; Sameshima, K.; Okunaga, K.; Sugiura, Y. Determination of amorphous phase is quartz powder by X-ray powder diffractometry. *Powder Diffr.* **1989**, *4*, 9−16.

(15) Greenwood, J.; Rainey, T. J.; Doherty, W. O. S. Light scattering study on the size and structure of calcium phosphate/hydroxyapatite flocs formed in sugar solutions. *J. Colloid Interface Sci.* **2007**, *306*, 66−71.

(16) Tang, P.; Chan, H. K.; Raper, J. A. Validation of computation method to predict aerodynamic diameter of particles with rough surface. *Powder Technol.* **2009**, *192*, 74−84.

(17) Thai, C. C. D.; Doherty, W. O. S. Effect of trash on the coagulation and flocculation of sugarcane juice. *Int. Sugar J.* **2013**, *114*, 719−724.

DOI: 10.1021/jf502229f
J. Agric. Food Chem. 2015, 63, 1573−1581

(18) Doherty, W. O. S.; Greenwood, J.; Pilaski, D.; Wright, P. G. The effect of liming conditions in juice clarification. *Proc. Aust. Soc. Sugar Cane Technol.* **2002**, *24*, 443−451.
(19) SRI. *Operating Procedure for the SRI Settling Test Kit*; Sugar Research Institute: Mackay, QLD, Australia, 1999.
(20) BSES. *Laboratory Manual for Australian Sugar Mills*; Bureau of Sugar Experiment Stations: Indooropily, QLD, Australia2001; Method 10, Vol. 2.
(21) Roberts, E. J. Estimation of the soluble polysaccharides in sugar − a rapid test for total polyaccharides. In *Proceedings of the 1980 Technical Session on Cane Refining Research*; Sugar Processing Research Institute: New Orleans, LA, USA, 1981; pp 130−133.
(22) ICUMSA. The determination of glucose, fructose and sucrose in cane juices, syrups and molasses, and sucrose in beet molasses by high performance ion chromatography method GS7/8/4-24, 1998.
(23) Selomulya, C.; Amal, R.; Bushell, G.; Waite, T. D. Evidence of shear rate dependence on restructuring and breakup of latex aggregates. *J. Colloid Interface Sci.* **2001**, *236*, 67−77.
(24) Doherty, W. O. S. Improved sugar cane juice clarification by understanding calcium oxide-phosphate-sucrose systems. *J. Agric. Food Chem.* **2011**, *59*, 1829−1836.
(25) Cheetham, N. W. H.; Tao, L. Variation in crystalline type with amylase content in maize starch granules: an X-ray powder diffraction study. *Carbohydr. Polym.* **1998**, *36*, 277−284.
(26) Jondhale, S.; Bhise, S.; Pore, Y. Physicochemical investigations and stability studies of amorphous gliclazide. *AAPS PharmSciTechnol.* **2012**, *13*, 448−459.
(27) Chiotelli, E.; Pilosio, G.; Le Meste, M. Effect of sodium chloride on the gelatinization of starch: a multi-measurement study. *Biopolymers* **2002**, *63*, 41−58.
(28) Meade, G. P.; Chen, J. C. P. In *Cane Sugar Handbook*, 10th ed.; Wiley-Interscience: Hoboken, NJ, USA, 1977; p 27.
(29) Cael, J. J.; Koenig, J. L.; Blackwell, J. Infrared and Raman spectroscopy of carbohydrates Part VI: Normal coordinate analysis of V-amylose. *Biopolymers* **1975**, *14*, 1885−1903.
(30) Kizil, R. J.; Irudayaraj, J.; Seetharaman, K. Characterization of irradiated starches by using FT-Raman and FTIR spectroscopy. *J. Agric. Food Chem.* **2002**, *50*, 3912−3918.
(31) Podstawka, E.; Ozaki, Y.; Proniewicz, L. M. Part I: Surface-enhanced Raman spectroscopy investigation of amino acids and their homodipeptides adsorbed on colloidal silver. *Soc. Appl. Spectrosc.* **2004**, *58*, 570−580.
(32) Salma, K.; Borodajenko, N.; Plata, A.; Berzina-Cimdina, L.; Stunda, A. Fourier transform infrared spectra of technologically modified calcium phosphates. In *14th Nordic-Baltic Conference on Biomedical Engineering and Medical Physics*; Katashev, A., Dekhtyar, Y., Spigulis, J., Eds.; Springer: Berlin, Germany, 2008; pp 68−71.
(33) Clarke, M. A.; Roberts, E. J.; Godshall, M. A.; Brannan, M. A.; Carpenter, F. G.; Coll, E. E. Sucrose loss in the manufacture of the cane sugar. *Proc. Int. Soc. Sugar Cane Technol.* **1980**, *17*, 2192−2203.
(34) Steindl, R. J. Clarification of cane juice for fermentation. *Proc. Int. Soc. Sugar Cane Technol.* **2010**, *27*, 1−10.
(35) Kent, G. A.; Moller, D. J.; Scroope, P. D.; Broadfoot, R. The effect of whole crop processing on sugar recovery and sugar quality. *Proc. Aust. Soc. Sugar Cane Technol.* **2010**, *32*, 559−572.
(36) Rein, P. W.; Cox, M. G. S.; Montocchio, G. Syrup clarification in raw sugar mills. *Proc. S. Afr. Sugar Technol. Assoc.* **1987**, *61*, 22−31.
(37) Painter, T. J. Carbohydrate polymers in food preservation: an integrated view of the Maillard reaction with special reference to discoveries of preserved foods in sphagnum-dominated peat bogs. *Carbohydr. Polym.* **1998**, *36*, 335−347.
(38) Lindeman, P. F.; O'Shea, M. G. Colorant removal during clarification and decolourisation processes. *Proc. Aust. Soc. Sugar Cane Technol.* **2004**, *26*, 51−64.
(39) Lindeman, P. F.; O'Shea, M. G. High molecualr weight (HMW) colorants and their impact on the refinability of raw sugar. A study of Australian and overseas raw sugars. *Proc. Aust. Soc. Sugar Cane Technol.* **2001**, *23*, 322−329.
(40) Walthew, D. C.; Khan, F.; Whitelaw, R. Some factors affecting the concentration of silica in cane juice evaporators. *Proc. S. Afr. Sugar Technol. Assoc.* **1998**, *72*, 223−227.
(41) Rackemann, D. W.; Doherty, W. O. S.; East, C. P. Development of descriptor tools for the characterization of Australian sugar mill evaporator scale. *Int. Sugar J.* **2011**, *113*, 44−51.
(42) East, C. P.; Doherty, W. O. S.; Fellows, C. M.; Yu, H. Deposition of hydroxyapatite and calcium oxalate dihydrate on a heat exchanger tub. *Asia−Pac. J. Chem. Eng.* **2011**, *6*, 921−932.

DOI: 10.1021/jf502229f
J. Agric. Food Chem. 2015, 63, 1573−1581

Also, the role of sucrose (apart from its free radical scavenging ability) in the degradation process of these acids in a mixture has not been reported.[22]

CaA, *p*CoA, and FeA are also the main color precursors present in sugar cane juice and are known to participate in reactions producing color that results in the raw sugar (sucrose) product.[23,24] In this study, a comprehensive investigation on the degradation of CaA, *p*CoA, and FeA in aqueous sucrose solutions containing the mixture of these HCAs was conducted. The degradation efficiencies and behaviors of individual HCAs were studied. The degradation conditions were optimized using central composite design (CCD) and multiresponse surface methodology (MRSM). Models were developed to predict the degradation of HCA mixtures in synthetic sugar cane juice solutions and examined by regression analysis.

MATERIALS AND METHODS

Reagents and Solvents. CaA, *p*CoA, FeA, fructose, glucose, lactose, and sucrose were obtained from Sigma-Aldrich (St. Louis, MO). Ferrous sulfate heptahydrate ($FeSO_4{\cdot}7H_2O$), glacial acetic acid, hydrogen peroxide (H_2O_2; 30%, w/w), sodium acetate, sodium hydroxide, and sulfuric acid were purchased from APS Ajax Finechem (Seven Hills, NSW, Australia). Ethanol (absolute) was supplied from Merck (Darmstadt, Germany). All chemicals were purchased of the highest purity grade available and used as supplied without any further purification. Stock solutions of HCAs (i.e., CaA, *p*CoA, and FeA, 10 mg/mL) were prepared individually by dissolution in degassed aqueous ethanol solution (50%, v/v) and stored at 4.0 °C in the absence of UV light.

Fenton Oxidation Reactions. Reactions were carried out in 10 mL glass scintillated reaction vessels housed in a Pierce Reacti-Therm heating/stirring module (Rockford, IL) with continuous magnetic stirring (280 rpm). In each run, predetermined amounts of high-purity water (18.2 MΩ·cm), sucrose, and each HCA were added to the reaction vessel. Consistent amounts of $FeSO_4{\cdot}7H_2O$ and H_2O_2 solutions were added to achieve a final volume of 5.0 mL and final concentrations of 0.5 and 7.50 mM, respectively. The optimum working molar ratio (Fe(II):H_2O_2) determined for the Fenton reaction by the authors was 1:15.[25] The reaction was initiated as soon as H_2O_2 was added. After 2 min, 3 mL of the solution was taken, diluted 10-fold to quench the reaction, and kept frozen. Table 1 gives the operating conditions used in the Fenton oxidation process. The reaction time was kept to 2 min to minimize sucrose degradation to allow treatment of sugar cane process streams, where the main objective is to preserve the sucrose content.

Table 1. Coded and Actual Values of the Experimental Design

			coded levels of parameters				
notation	factor	unit	−2	−1	0	+1	+2
A (X_1)	total HCA concn	mg/L	20	65	110	155	200
B (X_2)	sucrose concn	mass %	0	3.75	7.50	11.25	15
C (X_3)	pH		4.5	4.75	5.0	5.25	5.5
D (X_4)	temp	°C	25	31.25	37.5	43.75	50

Although it is well-known that ethanol is a scavenger for hydroxyl radical, in this study, ethanol had to be used for the dissolution of HCAs due to the low solubility of HCAs in water. As the ethanol concentration was at least 11 times higher than the concentrations of Fe (II) and H_2O_2 (0.5 and 7.5 mM, respectively), it was assumed that the effect of ethanol on the Fenton reaction was similar.

Instrumental Procedures and Analyses. The proportion of each HCA degraded was monitored by reversed-phase HPLC with UV/vis diode-array detection (DAD). The analysis was performed on a Hewlett-Packard HP/Agilent 1100 series HPLC system (Germany) using a Waters Symmetry C18 column (150 mm length × 3.9 mm diameter) with a Waters Guard-Pak Resolve C18 guard insert (10 μm) (Milford, MA). The mobile phase consisted of 1.0% (v/v) acetic acid in water (as eluent A) and methanol (as eluent B). The gradient program was as follows: 20% B to 25% B (5 min), 25% B to 50% B (15 min), and 50% B to 20% B (5 min). Simultaneous detection at specific wavelengths (280 and 320 nm) was subtracted against a reference wavelength (620 nm). The column temperature was ambient (25 °C), and the flow rate of the mobile phase was 1.0 mL/min. Aliquots of samples were membrane filtered (0.45 μm) prior to injection into the HPLC system. Sucrose and reducing sugar contents in the reaction mixtures were monitored by a Waters HPLC system (Milford, MA) equipped with a 626 pump, a 600S controller, a 717plus autosampler, and a 2465 electrochemical detector. A Dionex CarboPac PA-1 anion exchange column (250 mm × 4 mm) with a Dionex CarboPac PA-1 guard column (50 mm length × 4 mm diameter) (Waltham, MA) was used to separate the sugars at 27 °C with 150 mM sodium hydroxide as the mobile phase (a flow rate of 1.0 mL/min). The samples were diluted 100-fold and filtered through 0.45 μm membrane disk filters prior to HPLC analysis.

The efficiency of the Fenton process on the degradation of CaA, *p*CoA, and FeA was determined individually on the basis of the change in absorbance of the corresponding HPLC peak using the following equation:

$$\text{CaA, } p\text{CoA, or FeA degradation (\%)} = \left(\frac{A_0 - A_t}{A_0}\right) \times 100 \quad (1)$$

where A_0 is the initial absorbance of HCA (mAU) (i.e., t = 0 min) and A_t is the absorbance of HCA (mAU) at the time the aliquot was taken (i.e., t = 2 min).

Experimental Design and Statistical Analysis. The design of the experiments, mathematical modeling, and optimization of process parameters were evaluated using the Stat-Ease Inc. Design-Expert 7.0.0 software package (Minneapolis, MN). A rotatable circumscribed CCD was used to evaluate the main effect for each condition and the possible interactive effects on the residual stresses between two variables. The process parameters (independent variables) used in this study are the initial total HCA concentration (A), the initial sucrose concentration (B), the solution pH (C), and the reaction temperature (D). The selected response factors (dependent variables) for optimization are CaA degradation (y_1, %), *p*CoA degradation (y_2, %), FeA degradation (y_3, %), and total HCA degradation (y_4, %). The coded and actual values of each variable and their levels for the experimental design used in the study are shown in Table 1. The ranges for each parameter were determined by preliminary experiments based on previous work by the authors[23] and were selected to closely mimic operating parameters during the processing of sugar cane juice for raw sugar manufacture. Concentrations of HCAs varied from 20 to 200 mg/L to mimic the range of HCA and phenolic compound concentrations in sugar cane juice, which depends on the season, region, and type of cane and the method of harvesting (e.g., burnt cane, green cane, whole crop cane).

Analysis of variance (ANOVA) was used for model adequacy and analysis of the experimental data. The quality of the fit polynomial model was expressed by the regression coefficient R^2, and its statistical significance was checked using Fisher's F test.

Evaluation of the Interactions between Fe(II) and HCAs. Studies were conducted to investigate the interaction between Fe(II) and each of the HCAs in the presence and absence of sucrose using UV/vis and attenuated total reflectance Fourier transform infrared (ATR-FTIR) spectroscopy. Sodium acetate (100 mM) and acetic acid (100 mM) solutions were used to make buffer solutions having pH values of 4.0−6.0. For each analysis, predetermined amounts of buffer, sucrose, and $FeSO_4{\cdot}7H_2O$ were added to achieve a final HCA concentration of 5.50 mM. Samples were diluted to the desired concentration and immediately membrane disk filtered (0.45 μm) for analysis. The pH of each solution was checked before and after dilution. The UV/vis spectra were recorded on a PerkinElmer Lambda

DOI: 10.1021/jf504184u
J. Agric. Food Chem. 2015, 63, 1582−1592

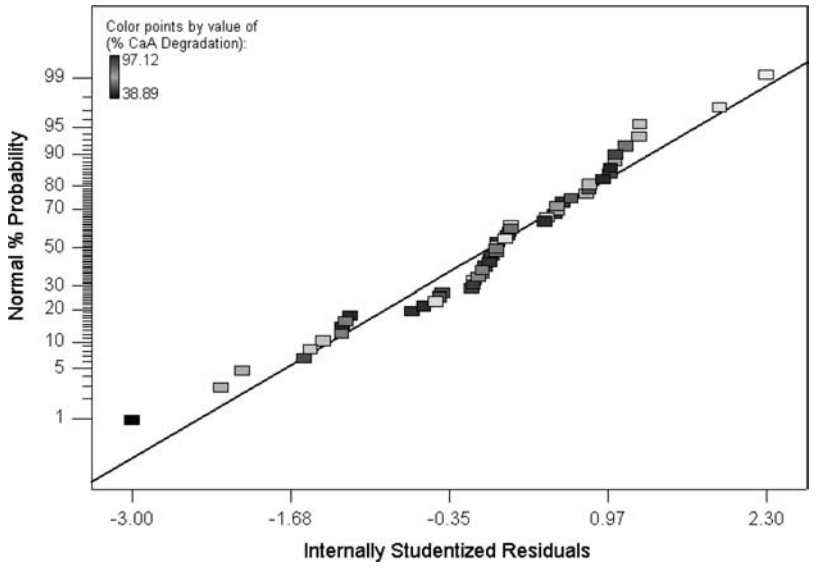

Figure 1. Normal probability plot of residuals for the fitted model using CaA degradation data before power transformation.

35 double-beam UV/vis spectrophotometer (Shelton, CT) using cells of 1.0 cm path length and at a wavelength range of 190−450 nm in 1.0 nm increments. Data acquisition was performed using the PerkinElmer UV WinLab (version 2.85.04) software package.

Infrared absorbance spectra were obtained using a Thermo Electron Nicolet Nexus 870 FT-IR instrument fitted with a deuterated triglycine sulfate (DTGS) detector (Madison, WI). Spectra were recorded over the 4000−650 cm^{-1} range at 4 cm^{-1} resolution for 64 scans with an optical path difference (OPD) velocity of 0.6329 cm/s. Data acquisition and processing was performed using the OMNIC 7.3 software package. The FTIR peaks were normalized with respect to the main peak at 1045 cm^{-1}.

A light brown precipitate was formed at pH ≥ 5 for all the acids with iron. No recoverable amount of precipitate was obtained at lower pH. This precipitate was filtered using a poly(vinyl chloride) (PVC) membrane filter (5 μm), and the retentate was analyzed by X-ray powder diffraction (XRD). Sample analysis was performed on a PANalytical X'Pert PRO multipurpose X-ray diffractometer (MPD) (Almelo, The Netherlands) using Cu Kα radiation (λ = 1.5406 Å) at 40 kV and 40 mA. Patterns were recorded in the 2θ range from 3.5° to 75° with a scan step size of 0.017° and a count time per step of 50 s. Data were acquired and processed using the X'Pert Data Collector 2.2 and MDI Jade 9.0 software packages, respectively.

RESULTS AND DISCUSSION

Optimal Data Transformation and Test for Normality. CCD and response surface methodology (RSM) were used to investigate the relationships between the response factors (dependent variables) and the process parameters (independent variables). To achieve this, an empirical second-order polynomial function for each response investigated with respect to the four process parameters was used to fit the experimental results obtained, as described in ref 26.

A normal probability plot of residuals based on the experimental data obtained for CaA degradation (Figure 1) indicates a nonlinear pattern in the middle of the trend line and short tails with the first and last few points showing increasing departure from the trend line. To address the nonlinearity of these plots, the Box−Cox power transformation was used to improve linearity. The power transformation on the predicted response can be described as follows:[27]

$$y^{\lambda} = \begin{cases} \dfrac{y^{\lambda} - 1}{\lambda} & \lambda \neq 0 \\ \ln(y) & \lambda = 0 \end{cases} \quad (2)$$

where λ indicates the power to which all data should be raised. The initial value of λ in the standard quadratic function (i.e., eq 2) is 1.00.

To determine the λ value for each response, a Box−Cox plot was used as a guide for the selection of the optimized λ value for the power transformation of the experimental data. Supplementary Figure 1 (Supporting Information) shows the Box−Cox plots for each response investigated. From the Box−Cox plots for the *p*CoA (Supplementary Figure 1b) and FeA (Supplementary Figure 1c) degradation data, the recommended λ values ranged from 0.70 to 2.40 and from 0.59 to 2.23, respectively, at a 95% confidence interval. On the other hand, the λ value range within the 95% confidence interval is not shown for CaA (Supplementary Figure 1) and total HCA (Supplementary Figure 1d) degradation data, due to the values being outside the λ = ±3.00 limits. Hence, the optimum λ values used to transform the CaA and total HCA degradation were both maximized at λ = 3.00. For *p*CoA and FeA degradation, the optimum λ values were determined by observing the minima of the curves, which were 1.56 and 1.43, respectively. Using the optimized λ values, the normal probability plot for each response surface model shown in Supplementary Figure 2 (Supporting Information) indicates improved linearity of data points. There are only a minimal number of data points deviating from the line of fit. The data for all fitted response surface models show good correspondence to a normal distribution and validate the normality assumption.

Regression Modeling and Statistical Analysis. On the basis of the sequential model sum of squares (type I), the power transformed response surface models for CaA (y_1), *p*CoA (y_2), FeA (y_3), and total HCA (y_4) degradation were selected on the basis of the highest order polynomial, where the additional model terms were significant and the models were not aliased. The data obtained for all four responses fit a quadratic polynomial function.

DOI: 10.1021/jf504184u
J. Agric. Food Chem. 2015, 63, 1582−1592

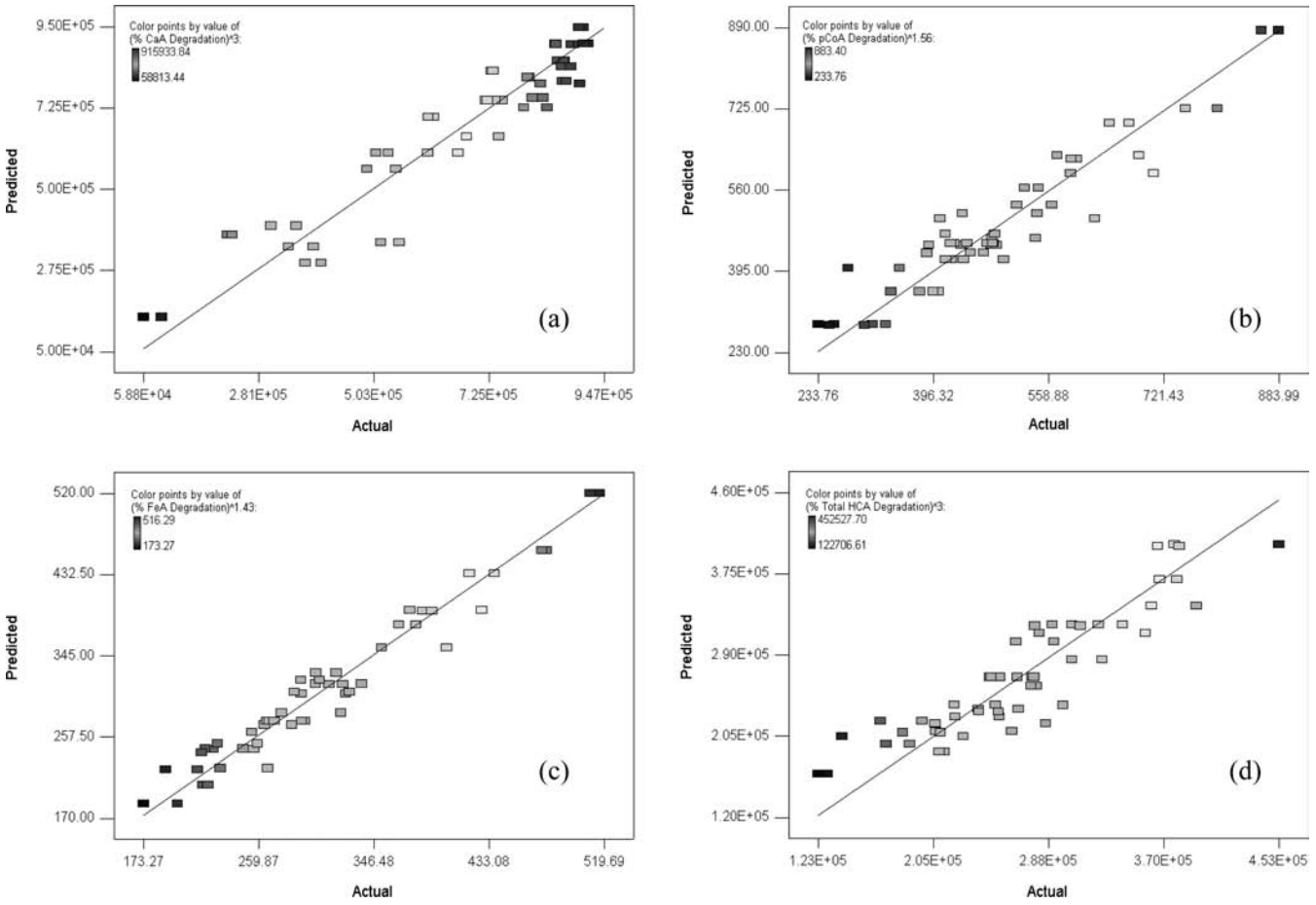

Figure 2. Predicted response and experimental (actual) values for the degradation (%) of (a) CaA, (b) *p*CoA, (c) FeA, and (d) total HCAs.

The ANOVA results for the partial sum of squares (type III) for the four response surface reduced quadratic models after stepwise regression are shown in Supplementary Table 1 (Supporting Information). The analysis indicates that most independent variables and some of the interactions are significant and contribute to the degradation of the HCAs. Model terms with a p value of <0.0500 are significant at the 95% confidence level. Values of >0.1000 indicate the model terms are insignificant at the 90% confidence level and are removed from the proposed models via stepwise regression, with the exception of the first-order temperature model term for all models. Temperature was regarded as statistically insignificant but was added to all models to make each model hierarchical. In other words, parent (i.e., first-order) model terms are added to the model to complete the family of any significant higher order (i.e., second-order) model terms.

The independent variables in the models were initial total HCA concentration, initial sucrose concentration, solution pH, and reaction temperature and were coded A, B, C, and D, respectively. The final empirical quadratic equations in terms of coded factors for each response are as follows:

CaA degradation (%)

$$y_1^{\,3} = 7.459 \times 10^5 - 22685.04A + 87649.64B - (1.893 \times 10^5)C - 2787.88D + 38875.43BC + 25613.66BD - 48866.47B^2 - 55229.82C^2 + 21771.66D^2 \quad (3)$$

*p*CoA degradation (%)

$$y_2^{\,1.56} = 452.03 - 25.39A - 112.96B + 56.46C - 9.29D + 25.34AB + 24.11CD + 51.51B^2 - 13.11C^2 \quad (4)$$

FeA degradation (%)

$$y_3^{\,1.43} = 274.79 - 14.82A - 69.60B + 25.99C - 3.36D + 24.97AB - 9.36BD + 6.34CD + 26.42B^2 + 9.46D^2 \quad (5)$$

total HCA degradation (%)

$$y_4^{\,3} = 2.670 \times 10^5 - 22911.69A - 49869.11B - 10752.76C - 4168.93D + 19018.79AB + 17344.68BC + 14113.81CD + 9351.73B^2 - 19861.54C^2 + 11289.82D^2 \quad (6)$$

The predicted R^2 values of all response surface models are in reasonable agreement with the adjusted R^2 values, which show that the fitted models are adequate. The accuracy of the models is shown in Figure 2, which compares the predicted responses against the experimental data. Reasonable linear relationships were obtained for predicting the degradation of *p*CoA and FeA (Figure 2b,c) but not CaA and total HCAs (Figure 2a,d), respectively. This may be related to complex formation as discussed in the section "Complex Formation".

DOI: 10.1021/jf504184u
J. Agric. Food Chem. 2015, 63, 1582−1592

On the basis of the coefficients of the first-order model terms in eqs 3−6, it is evident that the degradation efficiency of all HCAs decreases with the increase of the initial total HCA concentration (A). Sucrose concentration (B) is the most influential parameter with the highest coefficient in all equations and shows a negative influence on *p*CoA and FeA degradation but a positive influence on CaA degradation. Also, the degradation efficiency of *p*CoA and FeA increases with the solution pH (C), but the opposite is observed for CaA (refer to the section on complex formation). Temperature (D) has a negative effect on all responses, but its minuscule coefficient has little effect on the respective response. Hence, this model term is statistically insignificant and was only included in all of the equations to make the models hierarchical.

For the degradation of the mixture (i.e., the combined acids), there are strong interactions between total HCA concentration and sucrose concentration (AB), between sucrose concentration and pH (BC), and between pH and temperature (CD).

Perturbation Analysis. Perturbation plots were analyzed to further identify the most influential variables on the degradation of each HCA investigated in this study (Figure 3). Sucrose concentration and solution pH appeared to be the most influential parameters. Temperature showed an insignificant effect as expected, while the initial total HCA concentration exhibited a consistent effect for the degradation of each HCA.

As shown in Figure 3, the higher the initial total HCA concentration, the lower the amount of each HCA degraded. The reason behind the decrease in degradation efficiency is simply due to a higher uptake of $^{\bullet}$OH radicals by the increased amounts of HCA molecules.

The presence of sucrose significantly affected the degradation efficiency of the HCAs. The fate of sucrose during the degradation process was evaluated by high-performance anion-exchange chromatography with pulsed amperometric detection (HPAEC-PAD). The results showed up to 0.01% sucrose loss due to complete mineralization, as no glucose and/or fructose are detected. This is related to the effective scavenging ability of sucrose in removing $^{\bullet}$OH radicals[22] and accounts for the decrease in degradation efficiency with increasing sucrose concentration for *p*CoA and FeA (Figure 3b,c), but not for CaA (Figure 3a). The reason for the increased degradation efficiency of CaA with increasing sucrose concentration may be related, as will be shown in the next section, to a strong association between CaA and sucrose, which increased with increasing sucrose concentration, and precipitation of CaA out of solution.

Degradation of CaA decreases with increasing pH, whereas the opposite was observed for *p*CoA and FeA degradation. The reason for the results obtained with *p*CoA and FeA is not known but may be related to the various species that exist in the acid−base equilibria that influence the logarithmic acid dissociation constants (pK_a values) of these acids. The results obtained with CaA with increasing pH are again related to the precipitation of the latter as shown later.

Complex Formation. To obtain insights into the apparent differences in the behavior among the three HCAs, the UV/vis spectra of the individual acids, mixtures of each acid with Fe(II), and mixtures of each acid with Fe(II) and sucrose at pH 4.0−6.0 were obtained. The UV/vis spectra obtained with mixtures of FeA or mixtures of *p*CoA were not dissimilar compared to those of their corresponding acids. However, as Figure 4 shows, there is a significant difference between the

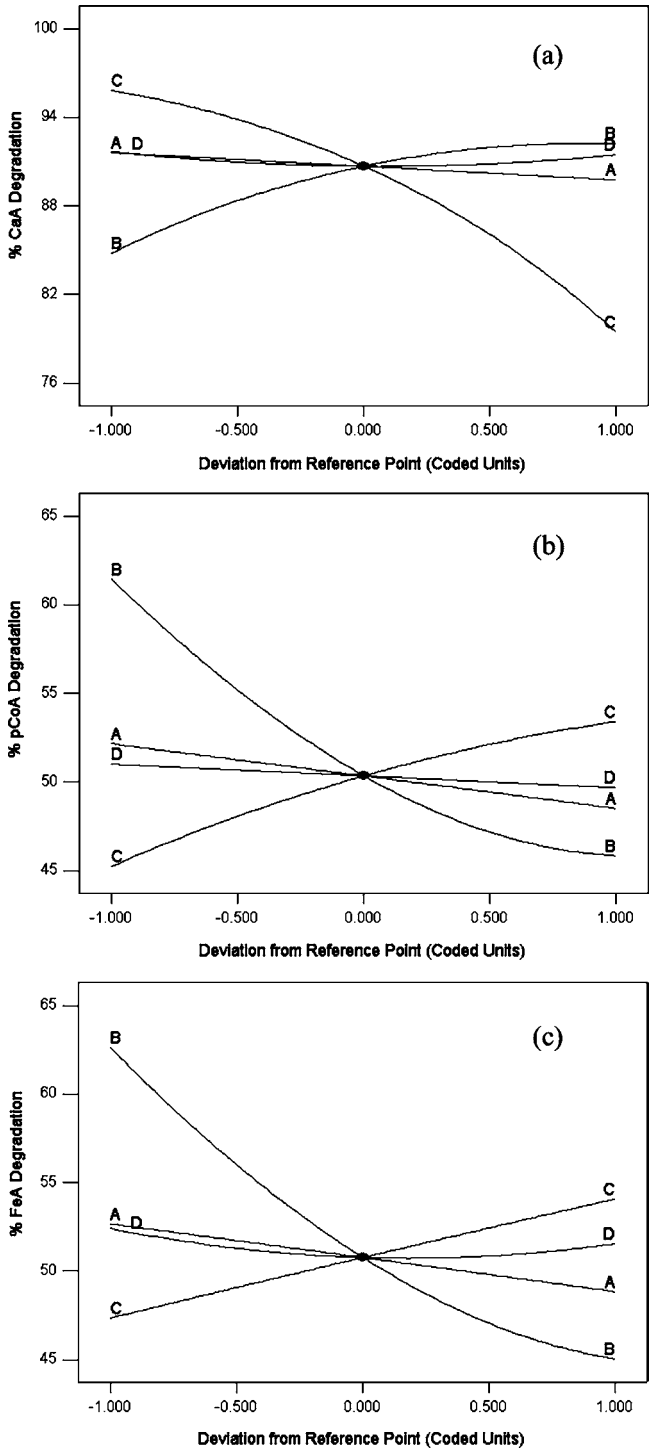

Figure 3. Perturbation plot for the degradation (%) of (a) CaA, (b) *p*CoA, and (c) FeA. Coded values are shown for each factor, total HCA concentration (A), sucrose concentration (B), pH (C), and temperature (D), and refer to actual values listed in Table 1.

spectra of CaA with Fe(II) and the spectra of CaA without Fe(II). In these acidic conditions, Fe(II) and Fe(III) will be present in equilibrium.[28] The change in the profile of the spectra is likely due to complexation between Fe(III) and CaA, as shown in the spectra obtained for Al(III)−CaA in aqueous acidic solutions by Cornard and co-workers.[29] In fact, Hynes and O'Coinceanainn[30] have reported the formation of a 1:1 complex between Fe(III) and CaA at pH between 1 and 2.5

DOI: 10.1021/jf504184u
J. Agric. Food Chem. 2015, 63, 1582−1592

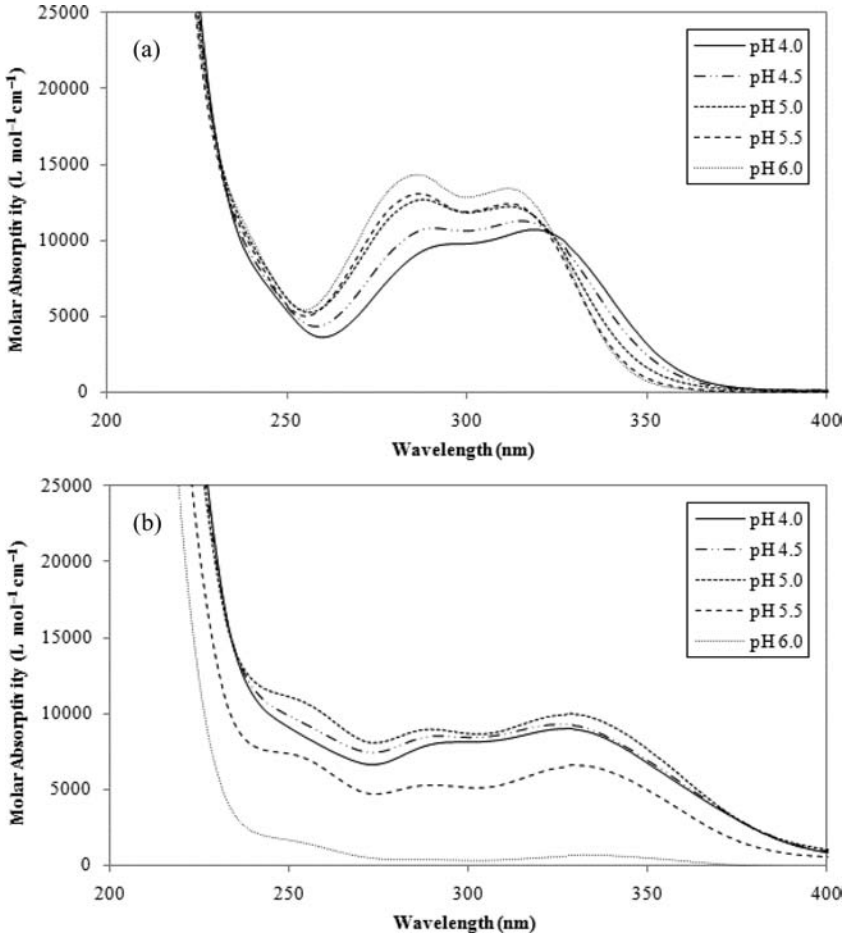

Figure 4. Effect of pH (4.0−6.0) on the absorption spectra of CaA (0.055 mM): (a) in the absence and (b) in the presence of Fe(II) (0.04 mM).

Scheme 1

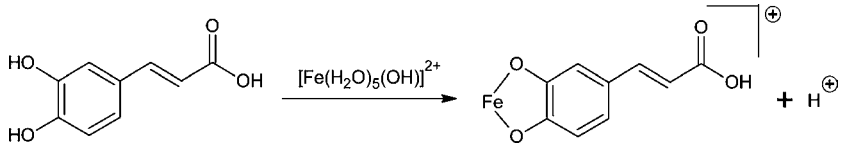

(Scheme 1). Moreover, previous studies have shown the accelerated decomposition of H_2O_2 to $^{\bullet}OH$ radicals by Fe(III) complexes of analogous phenolic acids.[31]

There is a shape drop in peak intensities at pH ≥ 5 for CaA and Fe(III) mixtures (Figure 4b), likely associated with increased complex formation due to increasing amounts of caffeate ions with pH rise. As the pK_{a1} of CaA is 4.38, there is an increasing amount of deprotonation with increasing pH.[32] The drop in intensity may also be due to the removal of CaA by adsorption onto the iron precipitate formed under these pH conditions. The spectra of Figure 4b also show that there was no change in the shape of the curves with increasing pH, so it is probable that only one type of complex is formed between Fe(III) and CaA under the conditions investigated.

The CaA mixtures were further characterized using ATR-FTIR spectroscopy. From the FTIR data, a number of bands were used to monitor changes in CaA as a result of the presence of Fe(II) and the presence of Fe(II) and sucrose. The spectral bands of CaA and sucrose solutions and CaA mixtures containing Fe(II) or Fe(II) and sucrose are given in Table 2. Spectral bands were assigned on the basis of literature data for CaA,[33−36] similar phenolic acids,[37−40] and sucrose.[41−45] Bands attributable to aromatic ring vibrations are numbered using the Wilson notation adapted by Varsányi[46] The main differences between the spectrum of CaA and that of Fe(II)−CaA are shown in Figure 5. The $\nu(CC)_{ar}$ aromatic bands (i.e., 8a and 19a) that occur at 1554 and 1483 cm^{-1} [36] are of increased intensity in the Fe(II)−CaA mixture compared to CaA (Figure 5). The peak at ∼1386 cm^{-1} associated with $\nu(CC) + \beta(OH)_{ar}$ (i.e., 14)[36] is also of higher intensity in the spectrum containing both Fe(II) and CaA. These increases in intensity may be attributed to complex formation between the aromatic −OH group in CaA and Fe(III).[39] The peak at 1275 cm^{-1} attributable to ν(C−OH) for CaA[35,47] has shifted to a lower wavelength of 1265 cm^{-1} with an increase in intensity. This is a further confirmation of a strong association between Fe(III) and CaA and that the complex formed is between Fe(III) and the phenolic hydroxyl group.[30,31] There was no change in the band at 1672 cm^{-1} associated with ν(C═O), implying no evidence of Fe(III) bonding to the carboxylic acid group of CaA. Previous works have shown that, with other phenolic acids, linkages are formed with their carboxylic acid groups.[37−39]

DOI: 10.1021/jf504184u
J. Agric. Food Chem. 2015, 63, 1582−1592

Table 2. Wavenumbers (cm^{-1}) of Selected Bands from ATR-FTIR Spectra of CaA Solution and CaA Mixtures Containing Fe(II) and/or Sucrose at pH 5.5

CaA mixtures					
CaA	Fe(II)	Fe(II) and sucrose	sucrose	band assignment[a]	
		3401	3495	ν(OH)	
3274	3247			$\nu(OH)_{ar}$	
		3182	3113	ν(OH)	
2981	2981	2980	2980	$\nu(CH)_{C=C} + \nu(CH)$	
2921		2933	2933	ν(CH)	20a
		2900	2900	ν(CH)	
2854	2852			ν(OH)	
1672	1672	1669	1674	ν(C═O)	
1618	1608	1611	1619	$\nu(CC)_{C=C}$	
1554	1550	1567	1578	$\nu(CC)_{ar}$	8a
1524	1524			$\nu(CC)_{ar}$	8b
1483	1483			$\nu(CC)_{ar}$	19a
1454	1454	1454	1454	$\nu(CC)_{ar}$	19b
		1426	1426	β(COH)	
1386	1388	1377	1377	$\nu(CC) + \beta(OH)_{ar}$	14
1328	1329	1332	1332	$\beta(CH)_{C=C}$	
1275	1265	1274	1266	ν(C−OH)	
		1210	1210	β(CH)	
1160	1160			β(CH)	18a
1118	1118			β(CH)	18b
1085	1085			β(OH)	
1045	1045	1045	1045	$\gamma(CH)_{C=C} + \gamma$(CH)	17b
		1018	1018	ν(C−O)	
		998	998	β(COH)	
		927	927	ν(CC)	
877	877	876	876		
		830	830	β(CCH)	

[a]Symbols are denoted as follows: ν, stretching vibrations; β, in-plane bending modes; γ, out-of-plane bending modes.

The spectra for CaA, Fe(II), and sucrose (Figure 6) show that the broad band that occurs at 3495 cm^{-1} [ν(OH)][45] which is associated with sucrose has shifted by 94 cm^{-1} to a lower wavenumber of 3401 cm^{-1}. This implies hydrogen-bonding interactions between CaA, Fe(III), and sucrose and could well explain why CaA degradation increases with increasing sucrose concentration.[48] These interactions provide supporting evidence of the differences in the degradation behavior of CaA and the other two HCAs (viz., *p*CoA and FeA). It is also probable that sucrose−Fe(III)−CaA complex formation may result in the coprecipitation of CaA, causing its reduction in the system, and not due to its oxidation. As reported in the next section, XRD data showed the coprecipitation of CaA.

Response Surface Analysis. Graphical representations of the regression model in the form of three-dimensional surface plots were used to provide a pictorial view of the interactions between the independent variables on total HCA degradation. These plots are shown in Figure 7, where two independent variables were varied within the experimental ranges investigated while the remaining variables were kept constant. The interactions are significant as the curvature of the surfaces is obvious.

The variables of sucrose concentration and initial total HCA concentration were varied as shown in Figure 7a, while the other variables, namely, pH and temperature, were kept constant at 5.0 and 35 °C, respectively. These fixed values were chosen as they were similar to those typical of process sugar cane juice.[23] The total HCA degradation efficiency decreases with increasing sucrose concentration and the initial total HCA concentration. Increasing the initial total HCA concentration did not significantly decrease the degradation efficiency of the HCAs. This can be seen both by the coefficient of the first- and second-order model terms (eq 6) for total HCA concentration (i.e., A) and in Figure 7a where there was only a 5.9% discrepancy between 65 and 155 mg/L initial total HCA at 3.75 mass % sucrose. This discrepancy is not noticeable

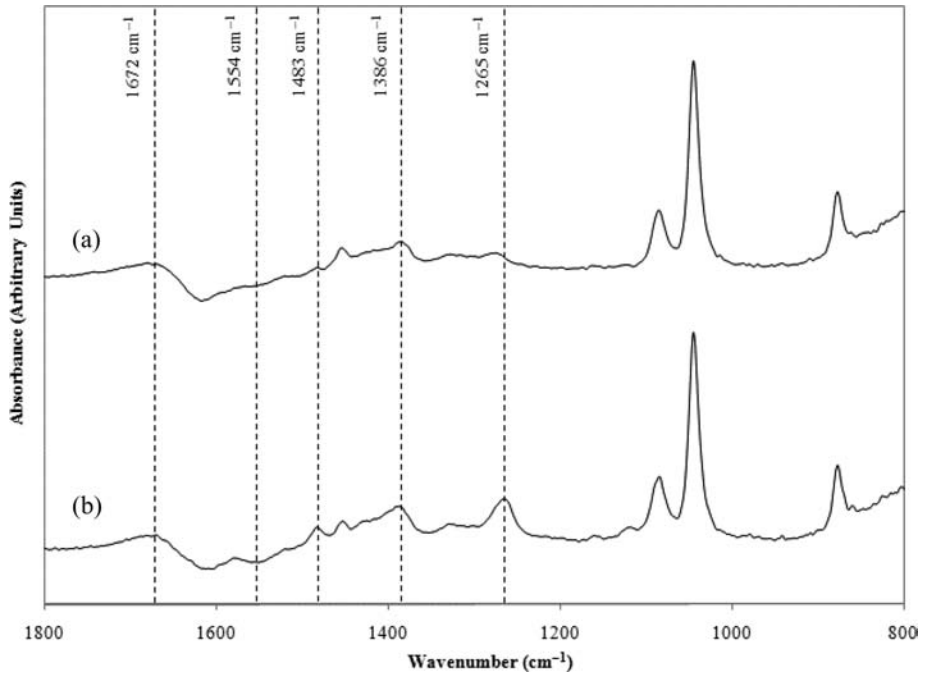

Figure 5. Normalized ATR-FTIR spectra of CaA solutions after subtraction of acetate buffer (pH 5.5): (a) in the absence and (b) in the presence of Fe(II).

DOI: 10.1021/jf504184u
J. Agric. Food Chem. 2015, 63, 1582−1592

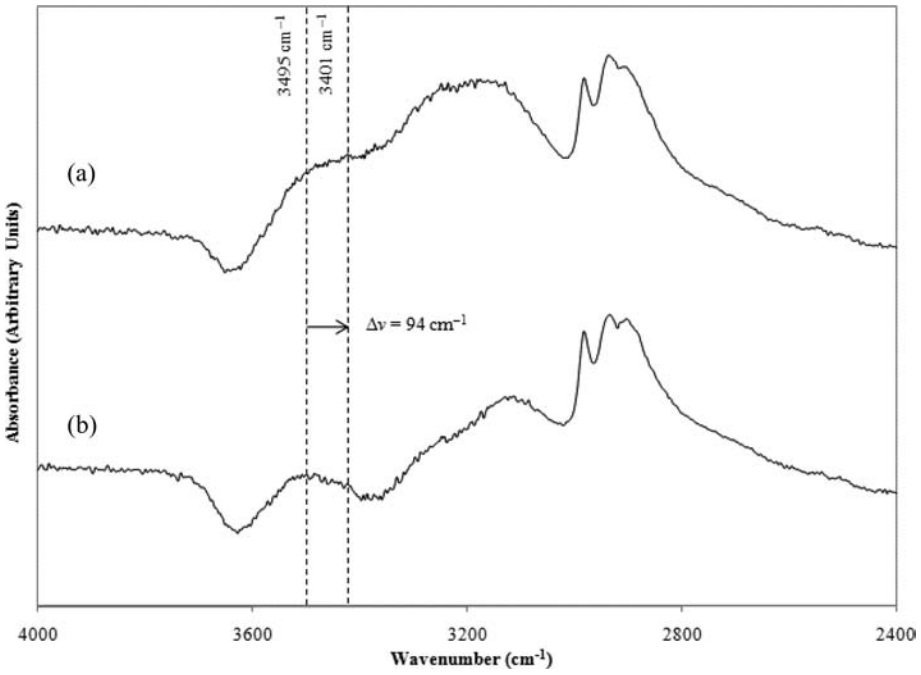

Figure 6. Normalized ATR-FTIR spectra of CaA solutions containing sucrose after subtraction of acetate buffer (pH 5.5): (a) in the absence and (b) in the presence of Fe(II).

at higher sucrose concentrations. It can be said from these observations that the optimal Fenton dosage is capable of degrading higher concentrations of HCAs and other components (similar to that of HCAs) than at the highest concentration studied (i.e., >200 mg/L).

Sucrose concentration showed a significant effect on the degradation of the HCAs (Figure 7b). Degradation increases smoothly with an increase in pH from 4.75 to 5.0 but decreases gradually when the pH exceeds 5.0 at any given concentration of sucrose. The negative effect on total HCA degradation at lower pH than the optimal may be attributed to the scavenging effect of H^+ or $^\bullet OH$ radicals, which can inhibit the reduction of Fe(III) to Fe(II) and prevent the further generation of $^\bullet OH$ radicals.[49,50] On the other hand, the negative effect at pH above the optimal may be attributable to the deactivation of the Fe(II) catalyst with the formation of iron(III) oxyhydroxide in lieu of being regenerated back to Fe(II).[51] The formation of iron(III) oxyhydroxides in the present study was confirmed by analyzing the precipitates obtained at pH 5.5 and 25 °C by XRD (Table 3). The *d* spacing values 6.21, 3.28, 2.46, and 2.36 Å correspond to lepidocrocite (i.e., iron(III) oxide hydroxide), FeO(OH), while the peaks at 5.20 and 2.04 Å are associated with CaA.[52] The formation of oxyhydroxide is derived from the following reaction equation:

$$Fe^{2+} + {}^1/_4O_2 + 2OH^- \rightarrow FeOOH + {}^1/_2H_2O \quad (7)$$

Figure 7c shows the interaction effects of pH and temperature on HCA degradation. The nonsignificance of the temperature variable is evident by the narrow range on the response axis (i.e., 57−64%). Despite this, the degradation trend on the HCAs in terms of temperature is still observable. Increasing temperature leads to less degradation of the HCAs. The decomposition of H_2O_2 by Fe(II) is not directly linked to the amount of HCA degraded. In addition to the formation of $^\bullet OH$ radicals by the Fenton process, nonreactive species such as H_2O and O_2 are also formed at higher temperatures (>40 °C).[53] The Fenton process was the only contributor to the degradation of HCAs as there was no thermal decomposition of any of the HCAs within the temperature range studied (25−50 °C).

Process Optimization and Model Validation. Numerical optimization was performed on the basis of the desirability function to determine the optimum process parameters for the degradation of the HCAs. The desirability function is expressed numerically from a scale of 0−1 (lowest to highest desirability) and denotes the degree of importance in obtaining the desired response value.[54] A desirability function value can be constructed by using five different goal optimization constraints: none, maximum, minimum, target, and within range. On the basis of the fitted quadratic models, an optimized response value can then be predicted by using the chosen goal optimization criteria that maximize the desirability function. To simultaneously optimize numerous responses (i.e., multi-response optimization), the desirability function values for each response (i.e., CaA, *p*CoA, and FeA) are combined into an overall desirability function by computing their geometric mean of different desirability values, as shown in the following equation:[55]

$$D = (d_1 d_2 d_3 ... d_n)^{1/n} = \left(\prod_{i=1}^{n} d_1\right)^{1/n} \quad (8)$$

where D is the overall desirability function, d_i is the desirability of the response, and n is the number of responses investigated.

To confirm the accuracy and robustness of the predicted models and assess their reliability to predict the degradation (%) of HCAs, additional experiments were carried out under those conditions, as well as selected conditions of process streams close to that of a typical Australian sugar mill.

For this study, the desirability functions for the three individual HCA degradation models were combined into one value and compared to the desirability function of the total HCA model (Table 4). The combined desirability function

DOI: 10.1021/jf504184u
J. Agric. Food Chem. 2015, 63, 1582−1592

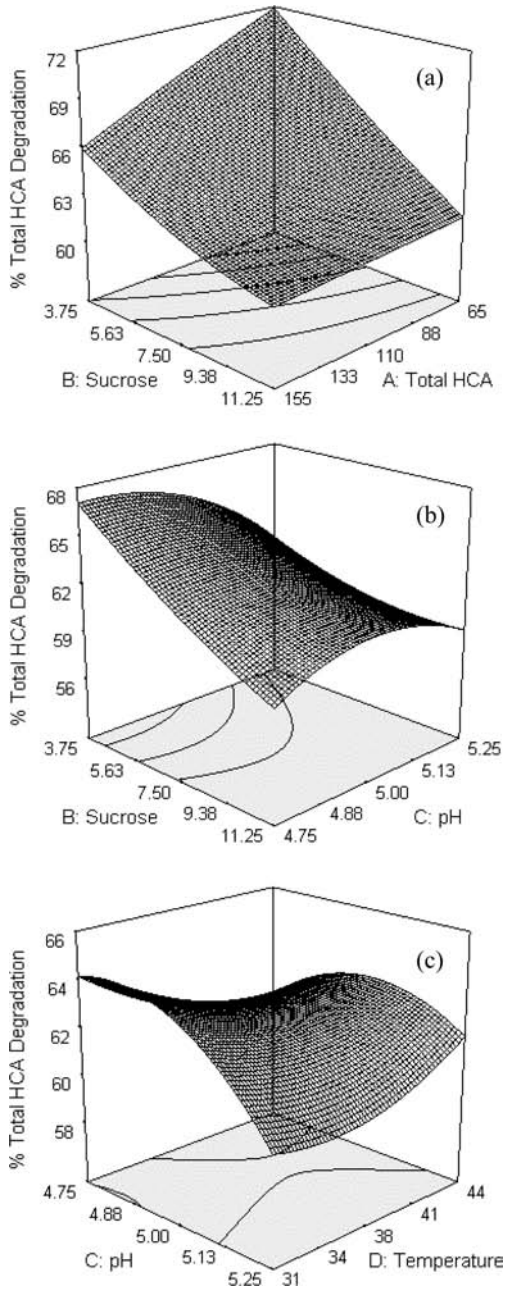

Figure 7. Three-dimensional surface plots of total HCA degradation (%) as a function of (a) total HCA and sucrose concentrations, (b) sucrose concentration and pH, and (c) pH and temperature (bottom). Variables: total HCA concentration (155 mg/L), sucrose concentration (7.5 mass %), pH (5.0), and temperature (35 °C).

values of the three individual HCA models for the experiments were relatively close to the desirability values produced for the single total HCA degradation model. This indicates that there is little variation between the simultaneously predicted values of each HCA degraded and the predicted value for the total HCAs degraded.

Table 4 shows the experimental and predicted (in parentheses) values for the degradation of each HCA and the total HCAs under specified constraints. The optimum conditions for maximum degradation of HCAs (200 mg/L) using the Fenton process (2.49 mM $FeSO_4 \cdot 7H_2O$ and 7.5 mM H_2O_2) are 0 mass % sucrose (i.e., aqueous), pH 4.73, and 25.15 °C. Under these conditions 92% CaA, 69% *p*CoA, and 70% FeA (total degradation of 77%) were degraded. The experimental values of the optimum conditions agree well with the predicted values deduced from each of the four models. The low error in the experimental and predicted values indicates good agreement of the results. The experimental values obtained for the worst conditions were also in good agreement with the predicted values. The good agreement between values is attributable to the high combined desirability function value. It is worth mentioning that the sum of the predicted degradation values of the individual HCA degradation models (i.e., CaA, *p*CoA, and FeA) is not equal to the predicted total HCA degradation value. Hence, the individual degradation models should only be used as a guide to predict the degradation of the total HCAs present in a mixture.

The best results for the synthetic juices are obtained with solutions having sucrose contents and operating temperatures similar to those of factory-mixed juice (synthetic juice 1) followed by factory no. 1 mill juice (i.e., juice expressed from the first mill of a quintuple set of mills) (synthetic juice 2). Despite a low desirability function value predicted under the synthetic juice 1 conditions, the experimental results were in close agreement with the predicted values for all four models. The lower desirability may be due to some of the constraints not being close to any of the design points of the CCD. On the other hand, a higher error was observed for synthetic juice 2, despite a reasonable desirability value. In addition, the experimental values obtained for *p*CoA and FeA degradation were significantly lower than the predicted values. Then again, the calculated total HCA degradation (76%) based on the predicted degradation values of CaA (68%), *p*CoA (75%), and FeA (84%) degradation models is higher than the model-predicted total HCA degradation (67%). It is highly probable therefore that the presence of sucrose may have contributed to the inaccuracy of this prediction as its concentration was outside the range used to develop the proposed models. Therefore, it is not recommended to use constraints outside the ranges studied for multiresponse optimization, as the responses are all dependent on each other.

From these results, the Fenton process can successfully be used to degrade HCAs (i.e., color precursor compounds) in a raw sugar manufacturing factory, as minimum sucrose breakdown occurred. However, the effectiveness of the Fenton process will be expected to be dependent on the type of sugar cane cultivar, harvesting conditions, cane maturity, and location. This is also because the proportion and ratio of free and conjugated phenolics will influence degradation. Despite this, the Fenton process will be particularly useful in processing juice expressed from the whole sugar cane biomass (instead of the stalk) because of the prevalence of color precursors in such

Table 3. XRD Data of the Precipitate Formed between CaA and Fe(II) at pH 5.5 and 25 °C

	d spacing (Å)			*d* spacing (Å)	
intensity (counts)	precipitate	FeO(OH)[a]	intensity (counts)	precipitate	FeO(OH)[a]
126.31	6.2164	6.2580	543.59	2.0409	
80.550	5.2003		78.600	1.9320	1.9365
204.48	3.2821	3.2933	36.960	1.7282	1.7350
161.52	2.4644	2.4737	28.340	1.5252	1.5360
138.89	2.3609	2.3635	112.57	1.2941	1.2990

[a]Based on an FeO(OH) reference pattern from the International Centre for Diffraction Data (ICDD PDF card 04-010-4300).

DOI: 10.1021/jf504184u
J. Agric. Food Chem. 2015, 63, 1582−1592

Table 4. Optimized Conditions under Specified Constraints for the Degradation of Total HCAs (200 mg/L) and Model Verification

				degradation[a] (%)				desirability	
experiment	sucrose concn (mass%)	pH	T (°C)	CaA	*p*CoA	FeA	total HCAs	combined	total HCAs
water	0	4.73	25.15	92 (90)	69 (68)	70 (64)	77 (73)	0.720	0.743
worst case	14.47	4.52	39.68	87 (90)	33 (37)	40 (46)	53 (49)	0.542	0.632
synthetic juice 1	13.00	5.39	35.98	73 (72)	48 (52)	51 (56)	57 (58)	0.383	0.332
synthetic juice 2	21.00	4.86	29.97	78 (68)	52 (75)	54 (84)	61 (67)	0.655	0.621

[a]Values in parentheses indicate the model-predicted degradation (%) of each individual HCA/total HCAs. Measurements were conducted in triplicate. The RSD was <5.0%.

juice types. As the sugar cane industry around the world is looking toward diversification by value-adding with the excess biomass produced from whole crop processing, the use of the Fenton or similar processes will allow juice expressed from the whole sugar cane plant to be cost-effectively processed. The advantages of the use of the Fenton process in the sugar manufacturing process include its simplicity, its nonspecific oxidation property, and the use of inexpensive equipment. Also, the sludge that is produced has the potential to remove colorants and other impurities (including proteins and polysaccharides), improving the quality of the juice feedstock.

■ ASSOCIATED CONTENT

Supporting Information

ANOVA for model terms of the response surface reduced quadratic models, Box−Cox plots of CaA, *p*CoA, FeA, and total HCA degradation data for the determination of the optimized power transformed response surface model, and normal probability plots of residuals for fitted models using CaA, *p*CoA, FeA, and total HCA degradation data after power transformation. This material is available free of charge via the Internet at http://pubs.acs.org.

■ AUTHOR INFORMATION

Corresponding Author

*E-mail: w.doherty@qut.edu.au.

Funding

We thank Sugar Research Development and Corp. (Brisbane, Australia) and Sugar Research Ltd. (Brisbane, Australia) for financial assistance in the project.

Notes

The authors declare no competing financial interest.

■ ACKNOWLEDGMENTS

We thank Tony Raftery of the IFE Central Analytical Research Facility at the Queensland University of Technology for his assistance in the XRD analyses.

■ REFERENCES

(1) Ho, C. T. Phenolic compounds in food: an overview. In *Phenolic Compounds in Food and Their Effects on Health I: Analysis, Occuurence, and Chemistry*; Ho, C. T., Lee, C. Y., Huang, M. T., Eds.; American Chemical Society: Washington, DC, 1992; Vol. *506*, pp 2−7.

(2) Lucas, M. S.; Peres, J. A.; Amor, C.; Prieto-Rodríguez, L.; Maldonado, M. I.; Malato, S. Tertiary treatment of pulp mill wastewater by solar photo-Fenton. *J. Hazard. Mater.* **2012**, *225−226*, 173−181.

(3) Kuo, C. Y.; Pai, C. Y.; Wu, C. H.; Jian, M. Y. Effects of oxidant concentration and temperature on decolorization of azo dye: comparisons of UV/Fenton and UV/Fenton-like systems. *Water Sci. Technol.* **2012**, *65*, 1970−1974.

(4) Wang, Y.; Li, X.; Zhen, L.; Zhang, H.; Zhang, Y.; Wang, C. Electro-Fenton treatment of concentrates generated in nanofiltration of biologically pretreated landfill leachate. *J. Hazard. Mater.* **2012**, *229−230*, 115−121.

(5) Babuponnusami, A.; Muthukumar, K. Degradation of phenol in aqueous solution by Fenton, sono-Fenton and sono-photo-Fenton methods. *Clean: Soil, Air, Water* **2011**, *39*, 142−147.

(6) Nichela, D.; Haddou, M.; Benoit-Marquié, F.; Maurette, M.-T.; Oliveros, E.; García Einschlag, F. S. Degradation kinetics of hydroxy and hydroxynitro derivatives of benzoic acid by Fenton-like and photo-fenton techniques: a comparative study. *Appl. Catal., B* **2010**, *98*, 171−179.

(7) Li, Y.; Bachas, L. G.; Bhattacharyya, D. Selected chloro-organic detoxifications by polychelate (poly(acrylic acid)) and citrate-based Fenton reaction at neutral pH environment. *Ind. Eng. Chem. Res.* **2007**, *46*, 7984−7992.

(8) Catrinescu, C.; Arsene, D.; Apopei, P.; Teodosiu, C. Degradation of 4-chlorophenol from wastewater through heterogeneous Fenton and photo-Fenton process, catalyzed by Al−Fe PILC. *Appl. Clay Sci.* **2012**, *58*, 96−101.

(9) Segura, Y.; Martínez, F.; Melero, J. A.; Molina, R.; Chand, R.; Bremner, D. H. Enhancement of the advanced Fenton process (Fe^0/H_2O_2) by ultrasound for the mineralization of phenol. *Appl. Catal., B* **2012**, *113−114*, 100−106.

(10) Arsene, D.; Musteret, C. P.; Catrinescu, C.; Apopei, P.; Barjoveanu, G.; Teodosiu, C. Combined oxidation and ultrafiltration processes for the removal of priority organic pollutants from wastewaters. *Environ. Eng. Manage. J.* **2011**, *10*, 1967−1976.

(11) Üstün, G. E.; Solmaz, S. K. A.; Birgül, A. Regeneration of industrial district wastewater using a combination of Fenton process and ion exchange—a case study. *Resour., Conserv. Recycl.* **2007**, *52*, 425−440.

(12) Elías-Maxil, J. A.; Rigas, F.; Orta De Velásquez, M. T.; Ramírez-Zamora, R.-M. Optimization of Fenton's reagent coupled to dissolved air flotation to remove cyanobacterial odorous metabolites and suspended solids from raw surface water. *Water Sci. Technol.* **2011**, *64*, 1668−1674.

(13) Khoddami, A.; Wilkes, M. A.; Roberts, T. H. Techniques for analysis of plant phenolic compounds. *Molecules* **2013**, *18*, 2328−2375.

(14) Herrmann, K. Occurrence and content of hydroxycinnamic and hydroxybenzoic acid compounds in foods. *Crit Rev. Food Sci.* **1989**, *28*, 315−347.

(15) Heredia, J. B. D.; Torregrosa, J.; Dominguez, J. R.; Peres, J. A. Kinetic model for phenolic compound oxidation by Fenton's reagent. *Chemosphere* **2001**, *45*, 85−90.

(16) Du, Y.; Zhou, M.; Lei, L. Role of the intermediates in the degradation of phenolic compounds by Fenton-like process. *J. Hazard. Mater.* **2006**, *B136*, 859−865.

(17) Amat, A. M.; Arques, A.; Beneyto, H.; García, A.; Miranda, M. A.; Seguí, S. Ozonisation coupled with biological degradation for treatment of phenolic pollutants: a mechanistically based study. *Chemosphere* **2003**, *53*, 79−86.

(18) Azabou, S.; Najjar, W.; Gargoubi, A.; Ghorbel, A.; Sayadi, S. Catalytic wet peroxide photo-oxidation of phenolic olive oil mill wastewater contaminants. Part II. Degradation and detoxification of

DOI: 10.1021/jf504184u
J. Agric. Food Chem. 2015, 63, 1582−1592

low-molecular mass phenolic compounds in model and real effluent. *Appl. Catal., B* **2007**, *77*, 166−174.
(19) Gernjak, W.; Krutzler, T.; Glaser, A.; Malato, S.; Caceres, J.; Bauer, R.; Fernández-Alba, A. R. Photo-Fenton treatment of water containing natural phenolic pollutants. *Chemosphere* **2003**, *50*, 71−78.
(20) Kusvuran, E.; Samil, A.; Atanur, O. M.; Erbatur, O. Photocatalytic degradation kinetics of di- and tri-substituted phenolic compounds in aqueous solution by TiO_2/UV. *Appl. Catal., B* **2005**, *58*, 211−216.
(21) Monteagudo, J. M.; Durán, A.; Aguirre, M.; San Martín, I. Optimization of the mineralization of a mixture of phenolic pollutants under a ferrioxalate-induced solar photo-Fenton process. *J. Hazard. Mater.* **2011**, *185*, 131−139.
(22) Morelli, R.; Russo-Volpe, S.; Bruno, N.; Lo Scalzo, R. Fenton-dependent damage to carbohydrates: free radical scavenging activity of some simple sugars. *J. Agric. Food Chem.* **2003**, *51*, 7418−7425.
(23) Nguyen, D. M. T.; Doherty, W. O. S. Phenolics in sugar cane juice: potential degradation by hydrogen peroxide and Fenton's reagent. *Int. Sugar J.* **2012**, *114*, 309−315.
(24) Paton, N. H. The origin of colour in raw sugar. *Proc. Aust. Soc. Sugar Cane Technol.* **1992**, 8−17.
(25) Nguyen, D. M. T.; Doherty, W. O. S. Optimisation of process parameters for the removal of hydroxycinnamic acids in sugar solutions. *Int. Sugar J.* **2013**, *1377*, 642−647.
(26) Montgomery, D. C. *Design and Analysis of Experiments*, 7th ed.; John Wiley & Sons: New York, 2008.
(27) Box, G. P. E.; Cox, D. R. An analysis of transformations. *J. R. Stat. Soc.* **1964**, *B26*, 211−243.
(28) Morgan, B.; Lahav, O. The effect of pH on the kinetics of spontaneous Fe(II) oxidation by O_2 in aqueous solution—basic principles and a simple heuristic description. *Chemosphere* **2007**, *68*, 2080−2084.
(29) Cornard, J.-P.; Caudron, A.; Merlin, J.-C. UV−visible and synchronous fluorescence spectroscopic investigations of the complexation of Al(III) with caffeic acid, in aqueous low acidic medium. *Polyhedron* **2006**, *25*, 2215−2222.
(30) Hynes, M. J.; O'Coinceanainn, M. The kinetics and mechanisms of reactions of iron(III) with caffeic acid, chlorogenic acid, sinapic acid, ferulic acid and naringin. *J. Inorg. Biochem.* **2004**, *98*, 1457−1464.
(31) Rivas, F. J.; Beltrán, F. J.; Garcia-araya, J. F.; Navarrete, V.; Gimeno, O. Co-oxidation of *p*-hydroxybenzoic acid and atrazine by the Fenton's like system Fe(III)/H_2O_2. *J. Hazard. Mater.* **2002**, *B91*, 143−157.
(32) Adams, M. L.; O'Sullivan, B.; Downard, A. J.; Powell, K. J. Stability constants for aluminum(III) complexes with the 1,2-dihydroxyaryl ligands caffeic acid, chlorogenic acid, DHB, and DASA in aqueous solution. *J. Chem. Eng. Data* **2002**, *47*, 289−296.
(33) Sánchez-Cortés, S.; García-Ramos, J. V. Photoinduced coupling and adsorption of caffeic acid on silver surface studied by surface-enhanced Raman spectroscopy. *Spectrochim. Acta, Part A* **1999**, *55*, 2935−2941.
(34) Dürüst, N.; Özden, S.; Umur, E.; Dürüst, Y.; Küçükislamoğlu, M. The isolation of carboxylic acids from the flowers of *Delphinium formosum*. *Turk. J. Chem.* **2001**, *25*, 93−97.
(35) Machado, N. F. L.; Calheiros, R.; Gaspar, A.; Garrido, J.; Borges, F.; Marques, M. P. M. Antioxidant phenolic esters with potential anticancer activity: solution equilibria studied by Raman spectroscopy. *J. Raman Spectrosc.* **2009**, *40*, 80−85.
(36) Świsłocka, R. Spectroscopic (FT-IR, FT-Raman, UV absorption, ^{1}H and ^{13}C NMR) and theoretical (in B3LYP/6-311++G** level) studies on alkali metal salts of caffeic acid. *Spectrochim. Acta, Part A* **2013**, *100*, 21−30.
(37) Świsłocka, R.; Kowczyk-Sadowy, M.; Kalinowska, M.; Lewandowski, W. Spectroscopic (FT-IR, FT-Raman, ^{1}H and ^{13}C NMR) and theoretical studies of *p*-coumaric acid and alkali metal *p*-coumarates. *J. Spectrosc. (N.Y., NY, U.S.)* **2012**, *27*, 35−48.
(38) Kalinowska, M.; Świsłocka, R.; Lewandowski, W. Zn(II), Cd(II) and Hg(I) complexes of cinnamic acid: FT-IR, FT-Raman, ^{1}H and ^{13}C NMR studies. *J. Mol. Struct.* **2011**, *993*, 404−409.
(39) Hanna, K.; Quilès, F. Surface complexation of 2,5-dihydroxybenzoic acid (gentisic acid) at the nanosized hematite−water interface: an ATR-FTIR study and modeling approach. *Langmuir* **2011**, *27*, 2492−2500.
(40) Dobson, K. D.; McQuillan, A. J. In situ infrared spectroscopic analysis of the adsorption of aromatic carboxylic acids to TiO_2, ZrO_2, Al_2O_3, and Ta_2O_5 from aqueous solutions. *Spectrochim. Acta, Part A* **2000**, *56*, 557−565.
(41) Vasko, P. D.; Blackwell, J.; Koenig, J. L. Infrared and raman spectroscopy of carbohydrates: part I: identification of O−H and C−H-related vibrational modes for D-glucose, maltose, cellobiose, and dextran by deuterium-substitution methods. *Carbohydr. Res.* **1971**, *19*, 297−310.
(42) Huvenne, J. P.; Vergoten, G.; Fleury, G.; Legrand, P. Champ de forces de symetrie locale de molecules cycliques: III. Interprétation des spectres de vibration du glucose cristallisé sous les deux formes α et β. *J. Mol. Struct.* **1981**, *74*, 169−180.
(43) Kodad, H.; Mokhlisse, R.; Davin, E.; Mille, G. Étude IRTF par réflexion totale atténuée (ATR) de sucres en solution aqueuse. *Can. J. Appl. Spectrosc.* **1994**, *39*, 107−112.
(44) Kačuráková, M.; Mathlouthi, M. FTIR and laser-Raman spectra of oligosaccharides in water: characterization of the glycosidic bond. *Carbohydr. Res.* **1996**, *284*, 145−157.
(45) Max, J.-J.; Chapados, C. Sucrose hydrates in aqueous solution by IR spectroscopy. *J. Phys. Chem. A* **2001**, *105*, 10681−10688.
(46) Varsányi, G. *Assignments for Vibrational Spectra of Seven Hundred Benzene Derivatives*; Adam Hilger: London, 1974; Vol. *1*.
(47) Yost, E. C.; Tejedor-Tejedor, M. I.; Anderson, M. A. In situ CIR-FTIR characterization of salicylate complexes at the goethite/aqueous solution interface. *Environ. Sci. Technol.* **1990**, *24*, 822−828.
(48) Gilfillan, W. N.; Nguyen, D. M. T.; Sopade, P. A.; Doherty, W. O. S. Preparation and characterisation of composites from starch and sugar cane fibre. *Ind. Crops Prod.* **2012**, *40*, 45−54.
(49) Rivas, F. J.; Frades, J.; Alonso, M. A.; Montoya, C.; Monteagudo, J. M. Fenton's oxidation of food processing wastewater components. Kinetic modeling of protocatechuic acid degradation. *J. Agric. Food Chem.* **2005**, *53*, 10097−10104.
(50) Deng, Y. Physical and oxidative removal of organics during Fenton treatment of mature municipal landfill leachate. *J. Hazard. Mater.* **2007**, *146*, 334−340.
(51) Bigda, R. J. Consider Fenton's chemistry for Fenton wastewater treatment. *Chem. Eng. Prog.* **1995**, *91*, 62−66.
(52) Dong, W.; Xu, Y.; Ren, J.; Chu, H.; Li, J.; Liu, X.; Chen, M. Synthesis and characterization of biodegradable polymers composed of 3,4-dihydroxycinnamic acid and poly(ethylene glycol). *J. Appl. Polym. Sci.* **2012**, *125*, 1657−1662.
(53) Rodrigues, C. S. D.; Madeira, L. M.; Boaventura, R. A. R. Treatment of textile effluent by chemical (Fenton's Reagent) and biological (sequencing batch reactor) oxidation. *J. Hazard. Mater.* **2009**, *172*, 1551−1559.
(54) Harrington, E. C. The desirability function. *Ind. Qual. Control* **1965**, *21*, 494−498.
(55) Derringer, G.; Suich, R. Simultaneous optimization of several response variables. *J. Qual. Technol.* **1980**, *12*, 214−219.

DOI: 10.1021/jf504184u
J. Agric. Food Chem. 2015, 63, 1582−1592

Table 1. Regimens Used for Oak Maturation of 2009 and 2011 Cabernet Sauvignon Wines

wine sample	code	maturation vessel	volume (L)	oak maturation regimen
trial 1 2009 Padthaway Cabernet Sauvignon	SSVAT	stainless steel vat	900	2 g/L toasted French oak chips
	P1VAT	stainless steel vat with two 4.5 mm HDPE panels	900	2 g/L toasted French oak chips
	P2VAT[a]	stainless steel vat with two 1.5 mm HDPE panels	900	2 g/L toasted French oak chips
	FOVAT	stainless steel vat with two French oak panels	900	1.6 m^2 French oak panels
trial 2 2011 Eden Valley Cabernet Sauvignon	barrel[a]	barrel	225−300[b]	French oak (22% new, 16% 1-year-old, and 62% 2-year-old), medium toast
	SS + OAK[a]	stainless steel	4550	French oak staves (1.4 m^2/kL), medium toast
	SS − OAK	stainless steel	4550	no oak treatment
	P1 + OAK[a]	plastic tank (with 12 g/L/year O_2 ingress)	1000	French oak staves (1.4 m^2/kL), medium toast
	P1 − OAK[a]	plastic tank (with 12 g/L/year O_2 ingress)	1000	no oak treatment
	P2 + OAK	plastic tank (with 4 g/L/year O_2 ingress)	1000	French oak staves (1.4 m^2/kL), medium toast
	P2 − OAK	plastic tank (with 4 g/L/year O_2 ingress)	1000	no oak treatment

[a]Wines retained for consumer acceptability and expert panel testing. [b]Blend of wines aged in 4 × 300 L hogsheads and 26 × 225 L barriques.

traditional and alternative oak maturation regimens on the composition, sensory properties, quality, and consumer acceptability of wine. The knowledge gained from this study can be used by wine producers to both inform and justify their use of oak alternatives, in particular for the production of wines at certain price points and/or targeted toward specific segments of the wine market.

MATERIALS AND METHODS

Oak Maturation Trials. Two South Australian Cabernet Sauvignon wines were sourced from industry-based trials, involving a range of different oak maturation regimens (Table 1). Trial 1 involved a 12 month maturation of a 2009 Padthaway Cabernet Sauvignon in four types of 900 L Stakvats (Ausvat Pty. Ltd., Willunga, Australia), being (i) stainless steel, hereafter referred to as "SSVAT"; (ii) stainless steel with two 4.5 mm high-density polyethylene (HDPE) panels, hereafter referred to as "P1VAT"; (iii) stainless steel with two 1.5 mm HDPE panels, hereafter referred to as "P2VAT"; and (iv) stainless steel with two French oak wood panels, hereafter referred to as "FOVAT". French oak chips (medium toast) sourced from the same batch of oak wood were inserted in each of the stainless steel and plastic Stakvats (SSVAT, P1VAT, P2VAT), but not the oak-sided Stakvat (FOVAT), at a rate of 2 g/L. Trial 2 involved a 4 month maturation of a 2011 Eden Valley Cabernet Sauvignon in four different vessels, being (i) 1000 L plastic tanks with oxygen ingress of 17 mg O_2/L/year, hereafter referred to as "P1"; (ii) 1000 L plastic tanks with oxygen ingress of 12.6 mg O_2/L/year, hereafter referred to as "P2"; (iii) 4550 L stainless steel tanks, hereafter referred to as "SS"; and (iv) a combination of new, 1- and 2-year-old French oak barrels (medium plus toast), which were blended after maturation, hereafter referred to as "barrel". Maturation in plastic and stainless steel tanks comprised treatments with and without the addition of French oak staves (medium toast), sourced from the same batch of oak wood (hereafter designated "+ OAK" and "− OAK", respectively). Staves were added to achieve an area-to-volume ratio of 1.4 m^2/kL.

Following completion of each maturation trial, wines were bottled (using 750 mL bottles fitted with metal screw-cap closures for trial 1 and 375 mL bottles fitted with plastic screw-cap closures for trial 2) and stored at 15 °C prior to sensory and chemical analysis. Trial 1 wines were bottle aged for 3 years prior to analysis, whereas trial 2 wines were analyzed approximately 4 months after bottling.

Chemical Analysis of Wine. Wines were analyzed (in duplicate) to determine pH, titratable acidity (TA, as tartaric acid equivalents to an end point of pH 8.2), volatile acidity (VA, as acetic acid equivalents to an end point of pH 8.2), free and total SO_2 content (by the aspiration method), wine color density, and total phenolics, according to methods described previously.[19] Glucose and fructose concentrations were determined enzymatically (Boehringer-Mannheim/R-BioPharm, Darmstadt, Germany). Ethanol content (as % alcohol by volume) was measured with an alcolyzer (Anton Paar, Graz, Austria). Oak volatiles were quantified by gas chromatography−mass spectrometry (GC-MS) using stable isotope dilution analysis (SIDA) methods reported previously.[20−22] These publications describe the preparation of deuterated internal standards, method validation, and instrumental operating conditions. Analysis of oak volatiles was performed by the Australian Wine Research Institute (AWRI) Commercial Services Laboratory using an Agilent 6890 gas chromatograph coupled to a 5973 mass selective detector.

Sensory Analysis of Wine. Wines were equilibrated at 21 °C for 24 h prior to each sensory experiment. Wines were assigned a random three-digit code for descriptive analysis (DA), expert and consumer sensory assessments. Wine aliquots (30 mL) were presented in covered Viticole XL5 (ISO standard) 215 mL stemmed wine tasting glasses, using a randomized presentation order.

Descriptive Analysis. DA was undertaken using a panel comprising 10 University of Adelaide staff and students (seven females, three males). Panelists were recruited on the basis of their availability and previous participation on DA panels involving analysis of red wine. Prior to formal assessment, panelists underwent 9 h of training (comprising 6 × 1.5 h sessions held over 6 weeks) involving detection, identification, evaluation, and intensity rating of red wine aroma and palate (i.e., flavor, taste and mouthfeel) attributes. During the training sessions, the panel evaluated each wine at least twice, to generate appropriate aroma and palate terms and to gain familiarity in recognizing and scoring their intensity, according to previously published protocols.[23] The training sessions also included three practice evaluation sessions conducted in sensory booths, under the conditions used during formal assessment. Data were evaluated after each practice evaluation to assess panelist-by-sample interactions, to determine when formal assessment should commence. The panel agreed upon 15 aroma attributes and 16 palate attributes; when reference standards were used, their preparation is shown in Table 2. Because panelists were unable to perceive any differences in wine color, appearance was not evaluated. Three formal assessment sessions were held, with all 11 wines presented in each session, such that all wines were assessed in triplicate. Panelists assessed each wine in an isolated tasting booth at 22−23 °C under red lights, with a light temperature of 6500 K, and rated the intensity of each sensory

DOI: 10.1021/jf5044025
J. Agric. Food Chem. 2015, 63, 1593−1600

Table 2. Reference Standards Used in Descriptive Analysis of Cabernet Sauvignon Wines after Oak Maturation

descriptor[a]	reference standard
red fruit	two McCain frozen raspberries and one fresh strawberry
confectionary	$^1/_2$ Allens strawberries and cream lolly + 0.5 cm piece Coles banana lolly
dark fruit	two McCain frozen blackberries and two McCain frozen blueberries
herbaceous	0.5 cm cube of green capsicum, two small tomato plant leaves
mint/menthol	$^1/_2$ tsp eucalyptus solution (1 drop of eucalyptus oil (Bosisto's, Australia) in 2 L of water)
dusty[b]	3 cm square of Hessian, 3 sticks of white chalk crushed
earthy	1 tsp wet earth with moss
charry	1 tsp 4-ethylguaiacol solution (1 drop of 4-ethylguaiacol in 50 mL of water) and 2 tsp of oak solution (medium-toasted American oak wood (Oak Chips Inc., Waverly, OH, USA) prepared in 10% ethanol)
leather[b]	3 cm × 10 cm piece of leather
mocha	1 tsp of mocha solution (100 g of 70% Lindt chocolate + 20 coffee beans in 250 mL of water)
licorice	0.5 cm piece of Darrell Lea licorice
sweet oak	$^1/_8$ tsp of vanillin powder (Sigma-Aldrich) + $^1/_2$ tsp of oak solution
spice	$^1/_4$ tsp of McKenzie's mixed spice + $^1/_4$ tsp of freshly ground black pepper + 3 cloves
woody[b]	1 cm × 9 cm × 0.5 cm untoasted French oak wood (Oak Chips Inc.) + $^1/_2$ tsp of pencil shavings

[a]Samples prepared in 30 mL of Cabernet Sauvignon cask wine, unless otherwise stated. [b]Denotes samples that were prepared dry.

descriptor using a 15 cm unstructured line scale with anchor points of "low" and "high" placed at 10 and 90% on the scale, respectively. Sensory reference standards (Table 2) were developed during training sessions and provided to panelists at each formal assessment session in covered, opaque black glasses. Panelists were required to reacquaint themselves with the sensory reference standards and written definitions of attributes several times during each evaluation. Distilled water and crackers were provided as palate cleansers, and panelists were required to have a 1 min break between samples and a 5 min break every three samples. Sensory data were collected using FIZZ software (version 2.47b, Biosystemes, Couternon, France).

Consumer Acceptance and Expert Panel Testing. On the basis of the outcomes of DA, five wines (barrel, SS + OAK, P1 + OAK, P1 − OAK, and P2VAT), with distinct sensory profiles were selected for consumer acceptance and expert panel testing. Consumer acceptability tests were carried out in a sensory laboratory at a central location, with each participant assigned a random "taster" number and allocated to an individual booth. Participants were recruited using a variety of methods, including social networking sites (e.g., Facebook, LinkedIn, Twitter), distribution of a flyer (via a mailbox drop within a 6 km radius of the University of Adelaide's Waite campus, and distribution at local wine retail outlets) and e-mail. Participants were screened against inclusion criteria requiring consumption of red wine at least once a month and being of legal drinking age (i.e., ≥18 years of age); exclusion criteria precluded participation by wine industry professionals and university staff and students. One hundred and sixteen consumers were recruited and acceptability tests were performed in October 2012, approximately 3 months after DA was completed. Consumers were asked to rate their hedonic liking of each wine using a 9-point scale with anchors from 1 (dislike extremely) to 9 (like extremely). Prior to evaluation of wines, consumers were instructed on how to assess the wine and use the hedonic scale. Coded samples were presented monadically with consumers signaling the researchers for their next sample using a switch in the sensory booth. Crackers and distilled water were provided as palate cleansers. After wines were evaluated, consumers answered demographic questions regarding gender, age, education, household income, and wine consumption. Consumers also indicated their average spend per bottle of wine for home consumption.

The expert panel comprised 10 wine industry personnel (9 males and 1 female), who met the criteria of "expert" defined by Parr and co-workers.[24] Each panelist assessed 10 wines, that is, the subset of 5 wines in duplicate. Participants were asked to assess each wine according to the 20-point scoring system used in Australian wine show judging[25] and to provide informal comments describing what they liked or disliked about each wine. Tasting was conducted 4 months after consumer acceptability testing in an open-plan tasting room at a winery in the Barossa Valley.

Data Analysis. Data were analyzed using Senpaq v5.01 (Qi Statistics, 2012) and XLSTAT 2013.1.01 (Addinsoft, 2012). Consumer acceptance data were analyzed using a combination of descriptive and multivariate techniques, including analysis of variance (ANOVA) with post hoc Tukey's test, partial least-squares regression (PLSR), internal preference mapping, and principal component analysis (PCA). Hedonic clusters were identified using cluster analysis.

RESULTS AND DISCUSSION

Cabernet Sauvignon wines (a 2009 Padthaway and a 2011 Eden Valley) were matured using a range of traditional and/or alternative oak maturation regimens (Table 1). Various chemical and sensory analyses were subsequently performed to compare the influence of each maturation regimen on the composition, sensory properties, quality and consumer acceptability of wines.

Influence of Oak Maturation Regimen on Chemical Composition of Wine. The wine color density, wine hue, total phenolics, alcohol content, pH, TA and VA of wines are reported in Table 3. Wines from trial 1 (i.e., 2009 Padthaway wines) had slightly lower pH, TA and VA and slightly higher alcohol content than wines from trial 2 (i.e., 2011 Eden Valley wines). There were no meaningful differences between the basic wine parameters of trial 1 wines, but trial 2 wines showed greater variation, in particular for wine color density and phenolic content, which ranged from 9.7 to 10.2 and from 51 to 57 au, respectively. Increased phenolic content can influence the perception of astringency by enhancing the drying sensation,[26] but the relatively small differences observed

Table 3. Wine Color Density, Wine Hue, Phenolics, Alcohol Content, pH, Titratable Acidity (TA), and Volatile Acidity (VA) of Cabernet Sauvignon Wines after Oak Maturation

		wine color density	wine hue	phenolics (au)	alcohol (% v/v)	pH	TA[a] (g/L)	VA[a] (g/L)
trial 1, 2009 Padthaway Cabernet Sauvignon	mean	12.6 ± 0.3	0.84 ± 0.01	61 ± 1	14.6 ± 0.01	3.43 ± 0.01	6.1 ± 0.05	0.42 ± 0.02
	range	12.4−12.8	0.83−0.86	60−62	14.5−14.6	3.43−3.45	6.0−6.2	0.41−0.42
trial 2, 2011 Eden Valley Cabernet Sauvignon	mean	9.9 ± 0.4	0.77 ± 0.01	53 ± 2	14.2 ± 0.05	3.51 ± 0.01	6.4 ± 0.07	0.52 ± 0.15
	range	9.7−10.2	0.76−0.80	51−57	14.1−14.3	3.50−3.53	6.4−6.6	0.54−0.62

[a]TA measured as g/L of tartaric acid; VA measured as g/L of acetic acid.

DOI: 10.1021/jf5044025
J. Agric. Food Chem. 2015, 63, 1593−1600

Table 4. Oak Volatile Composition of Cabernet Sauvignon Wines after Oak Maturation[a]

		concentration (μg/L)							
treatment		*cis*-oak lactone	*trans*-oak lactone	guaiacol	4-methyl guaiacol	eugenol	vanillin	furfural	5-methyl furfural
trial 1, 2009 Padthaway Cabernet Sauvignon	SSVAT	128 ± 1 a	23 ± 0	7 ± 0 b	4 ± 0 b	12 ± 1	54 ± 1 b	121 ± 0	nd
	P1VAT	121 ± 1 b	27 ± 3	8 ± 0 a	11 ± 0 a	5 ± 7	153 ± 12 a	123 ± 1	nd
	P2VAT	121 ± 1 b	29 ± 0	8 ± 0 a	10 ± 0 a	nd	128 ± 42 ab	119 ± 3	nd
	FOVAT	122 ± 4 b	29 ± 3	8 ± 0 a	11 ± 1 a	10 ± 0	131 ± 19 ab	119 ± 2	nd
	P value	0.048	0.107	<0.001	<0.001	0.096	0.052	0.243	
trial 2, 2011 Eden Valley Cabernet Sauvignon	barrel	99 ± 1 a	79 ± 4 a	4 ± 1 c	1 ± 0 c	6 ± 9	123 ± 3 b	261 ± 24 c	32 ± 1 d
	SS + OAK	39 ± 1 c	30 ± 1 c	28 ± 1 b	15 ± 0 b	nd	242 ± 5 a	1877 ± 2 b	282 ± 1 b
	SS − OAK	nd	nd	4 ± 1 c	nd	nd	18 ± 7 c	173 ± 1 cd	nd
	P1 + OAK	30 ± 1 d	46 ± 2 b	27 ± 1 b	16 ± 0 a	nd	281 ± 64 a	32 ± 1 e	54 ± 1 c
	P1 − OAK	nd	nd	4 ± 1 c	nd	nd	6 ± 8 c	121 ± 4 de	nd
	P2 + OAK	47 ± 1b	24 ± 2 d	33 ± 1 a	16 ± 0 a	6 ± 8	313 ± 98 a	2633 ± 141 a	368 ± 13 a
	P2 − OAK	nd	nd	3 ± 0 c	nd	nd	20 ± 11 c	116 ± 4 de	nd
	P value	<0.001	<0.001	<0.001	<0.001	0.580	<0.001	<0.001	<0.001

[a]Values are the mean of two technical replicates (± standard deviation). Means within a column (per trial) followed by different letters are significantly different (P = 0.05, one-way ANOVA, Tukey's LSD post hoc).

Table 5. Mean Intensity Ratings for Sensory Attributes of Cabernet Sauvignon Wines after Oak Maturation[a]

	trial 1 2009 Padthaway Cabernet Sauvignon				trial 2 2011 Eden Valley Cabernet Sauvignon						
attribute[b]	SSVAT	P1VAT	P2VAT	FOVAT	barrel	SS + OAK	SS − OAK	P1 + OAK	P1 − OAK	P2 + OAK	P2 − OAK
A-red fruit	4.8	5.2	5.5	5.2	7.1 ab	6.8 ab	8.3 a	6.2 b	7.8 a	5.9 b	7.8 a
A-confectionary	4.5	5.3	5.2	4.2	5.7 ab	6.0 ab	6.9 ab	5.5 b	7.0 ab	5.7 ab	7.1 a
A-dark fruit	6.8	7.6	7.2	6.9	6.8 b	6.7 b	7.1 ab	7.3 ab	7.0 ab	6.9 ab	8.2 a
A-herbaceous	3.5	3.3	3.9	3.5	4.1 ab	3.4 b	4.0 ab	4.3 ab	4.9 a	3.2 b	5.2 a
A-mint/menthol	4.1	4.1	4.0	3.6	4.3 bc	4.1 bc	4.4 bc	4.1 bc	5.4 ab	4.0 c	5.9 a
A-dusty	6.7	6.1	6.2	6.7	4.1 abc	4.3 abc	3.5 c	4.9 a	3.7 bc	4.5 ab	4.2 abc
A-charry	4.1 b	4.8 ab	5.1 ab	5.9 a	3.2 b	4.5 a	2.7 b	5.6 a	3.0 b	4.6 a	3.2 b
A-leather	5.2 b	5.0 b	5.4 ab	6.6 a	3.2 ab	3.3 ab	2.5 b	3.6 ab	3.0 ab	3.7 a	3.1 ab
A-mocha	3.5	4.3	4.0	4.2	3.0 c	3.8 bc	3.6 bc	5.0 a	3.5 bc	4.4 ab	3.5 bc
A-sweet oak	4.4	5.1	4.9	4.7	4.8 ab	5.1 ab	4.6 b	5.8 a	5.1 ab	5.7 ab	4.9 ab
A-woody	5.1	5.9	6.4	5.8	4.0 b	4.9 ab	3.9 b	5.4 a	4.0 b	5.2 ab	4.2 ab
P-red fruit	6.5	6.0	6.2	7.2	8.1 ab	7.0 ab	8.2 ab	6.9 b	7.9 ab	7.0 b	8.3 a
P-earthy	3.3	3.8	3.5	3.6	2.8 b	3.5 a	2.8 ab	3.3 ab	3.0 ab	3.2 ab	3.4 ab
P-charry	3.3 b	5.2 a	4.9 a	5.0 a	3.7 bc	4.4 ab	3.0 c	5.0 a	3.3 c	4.6 ab	3.7 bc
P-mocha	3.5	4.3	4.2	4.3	3.8 ab	4.2 ab	3.7 ab	4.4 a	3.4 b	4.3 a	3.4 b
P-licorice	3.7	3.9	3.2	3.6	3.5 bcd	2.9 d	4.4 a	3.9 abc	4.3 ab	3.5 cd	3.9 abc
P-sweet oak	4.7 ab	5.4 a	4.4 b	4.9 ab	4.7 bc	4.7 bc	4.2 c	5.6 ab	4.4 c	6.5 a	4.9 bc
P-woody	5.6 b	7.4 a	6.6 ab	6.4 ab	4.8 b	6.7 a	5.3 ab	5.9 ab	5.5 ab	5.9 ab	5.1 ab
tannins	7.9 b	8.5 ab	9.4 a	9.0 ab	7.2 ab	7.3 a	6.7 ab	7.2 ab	7.4 a	6.0 b	7.3 ab

[a]Values are mean scores from one wine replicate (per treatment) presented to 10 judges in three replicate sessions. Means within a row (per trial) followed by different letters are significantly different (P = 0.05, one way ANOVA, Tukey's LSD post hoc). [b]A, aroma attribute; P, palate attribute.

between phenolic measurements obtained in the current study (i.e., 5−10%) would not be expected to lead to perceptible sensory differences.

Similar concentrations of oak volatiles were observed in each of the trial 1 wines, albeit SSVAT wines contained significantly lower levels of vanillin than the other wines from trial 1 (Table 4). Of the oak volatiles measured, only *cis*-oak lactone and eugenol occurred at concentrations above their detection thresholds, of 23 and 5 μg/L, respectively.[27,28] More significant differences were observed between trial 2 wines. Wines aged using maturation regimens without the addition of oak wood (i.e., SS − OAK, P1 − OAK, and P2 − OAK) contained low or undetectable (<1 μg/L) levels of oak volatiles, as expected. The barrel-aged wine contained the highest concentrations of *cis*- and *trans*-oak lactones (99 and 79 μg/L respectively), but comparatively lower levels of other oak-derived volatiles. The maturation regimens involving addition of oak staves yielded similar oak volatile concentrations, albeit P1 + OAK wines contained extremely low levels of furfural and 5-methylfurfural (i.e., <100 μg/L) compared to SS + OAK and P2 + OAK wines (which contained >1800 μg/L) and even the unoaked wines. Again, *cis*-oak lactone was detected (in oaked wines) at concentrations above its detection threshold. The guaiacol and vanillin levels of trial 2 wines aged using alternative oak maturation regimens also exceeded threshold concentrations, being 10 and 200 μg/L, respectively.[28]

DOI: 10.1021/jf5044025
J. Agric. Food Chem. 2015, 63, 1593−1600

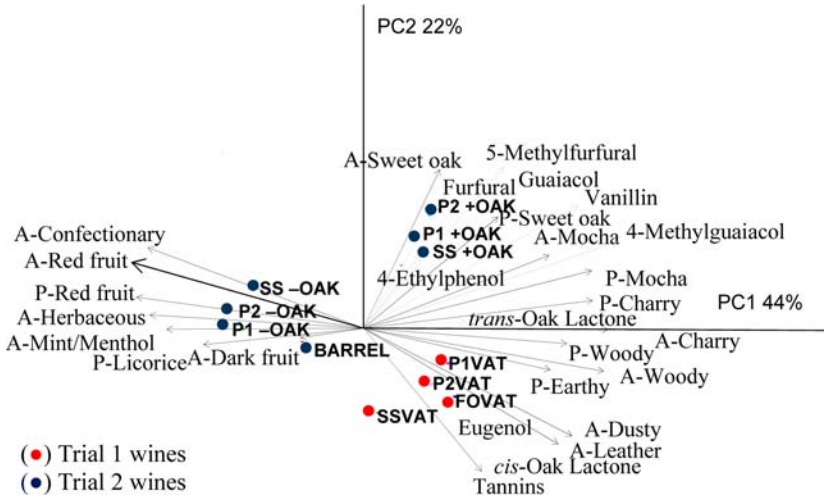

Figure 1. PCA biplot of oak volatile concentrations and sensory attribute ratings for Cabernet Sauvignon wines after oak maturation.

The differences observed between the oak volatile profiles of wines from trial 1 compared to those from trial 2 likely reflect differences in oak composition, in agreement with previous studies.[29−31] Interestingly, the oak wood used in trial 1 yielded a considerably higher proportion of *cis*-oak lactone (i.e., approximately 4-fold higher levels) than *trans*-oak lactone, whereas the oak used in trial 2 gave approximately equal concentrations of each isomer. Compositional differences can also be attributed to differences in the rate of oak addition, the surface area available for extraction, and the duration of oak maturation. Surprisingly, meaningful differences in wine color, phenolic and oak volatile profiles were not observed for the different maturation regimens, even when oxygen ingress varied considerably (Table 1).

Influence of Oak Maturation Regimen on Sensory Properties of Wine. ANOVA was performed on the DA data, and 19 of 31 attributes were found to significantly differentiate ($P < 0.05$) wines within each trial (Table 5).

Wines from trial 1 were generally rated higher in *dusty*, *charry*, *leather*, and *woody* characters than trial 2 wines, with FOVAT receiving the highest ratings for *charry* and *leather* aromas. Similar ratings were given to varietal attributes, that is, *red fruit*, *dark fruit*, and *herbaceous* attributes. That wines from this trial were perceived to be more complex, that is, to exhibit more intense oak- and age-related sensory attributes, reflects the extended period of oak maturation (12 months) and bottle aging (24 months) prior to sensory analysis. The duration of oak maturation directly influences the concentration of volatiles extracted from oak wood into wine,[32] but biochemical reactions continue to occur, for example, the conversion of furanic aldehydes into their corresponding alcohols.[33,34] This likely explains the lower levels of furfural (i.e., approximately 120 μg/L) and the absence of 5-methylfurfural observed in trial 1 wines, compared to trial 2 wines, in particular SS + OAK and P2 + OAK (Table 4).

The unoaked wines from trial 2 received similar ratings for most attributes and tended to exhibit more intense varietal characteristics, for example, *red fruit*, *dark fruit*, *herbaceous*, and *mint/menthol* attributes, than the oaked wines; the prominence of varietal characters is due to the absence of oak influence. Of the oak-treated wines, the barrel-aged wine received the lowest scores for most oak-related attributes, which was not surprising given the low levels of oak volatiles observed in this wine. The ratings for oak attributes in the barrel wine more closely resembled scores given to the unoaked wines, and instead, the barrel wine displayed more intense *red fruit* and *mint/menthol* aromas and *red fruit* on the palate. P1 + OAK exhibited the highest *charry*, *mocha*, *sweet oak*, and *woody* aromas and *charry*, *licorice* flavor, whereas P2 + OAK displayed *leather* and *sweet oak* on the palate. Previous studies have investigated the impact of micro-oxygenation (MOX) on wine sensory attributes, including the development of aged notes in MOX wines. For example, Cejudo-Bastante and colleagues observed an increase in nutty, tobacco, and spice notes in MOX-treated wines compared to wines stored in stainless steel tanks without oxygen addition.[35] Several of the maturation regimens used in trial 2 deliberately enabled oxygen ingress (Table 1), but the resulting wines did not exhibit overly apparent aged notes.

PCA was performed on the mean intensity ratings obtained for the sensory attributes that were perceived to be significantly different across the two trials (Figure 1), with PC1 and PC2 accounting for 44 and 22% of variation between wines, respectively. Clear separation was observed between oaked wines, which were predominantly located in the right quadrants, and unoaked wines, which were located in the left quadrants. The barrel-aged wine was located in close proximity to the unoaked wines, which again was not surprising given its relatively low levels of oak volatiles (Table 4). PC1 suggests separation of oaked and unoaked wines is primarily driven by the intensity of varietal (i.e., *fruit/green*) versus oak-related sensory attributes. Discrimination of trial 1 and 2 wines was also observed, with wines aged in vats clustered together in the bottom right quadrant and wines aged in stainless steel or plastic tanks (containing oak) clustered in the top right quadrant. Trial 1 wines were in part differentiated on the basis of *dusty* and *leather* aromas, which reflect the increased age of these wines. SS + OAK, P1 + OAK, and P2 + OAK each contained higher levels of vanillin (being 242−313 μg/L) than trial 1 wines (Table 4). These concentrations exceed the detection threshold reported for vanillin in red wine, that is, 200 μg/L.[28] Vanillin might therefore contribute to the *sweet oak* and *mocha* attributes that helped differentiate these wines. Differentiation of trial 1 and 2 wines may also have been influenced by guaiacol, *cis*-oak lactone, and eugenol, that is, the other volatiles observed in selected wines at concentrations above their threshold levels (Table 4).

DOI: 10.1021/jf5044025
J. Agric. Food Chem. 2015, 63, 1593−1600

Influence of Oak Maturation Regimen on Quality and Consumer Acceptance of Wines. A subset of five wines was selected for quality and acceptability ratings by wine experts and consumers, respectively. The expert panel used a 20-point scoring system to rate wine quality (Table 6); mean scores ranged from 13.8 (for the barrel-aged wines) to 14.8 (for P1 − OAK), which indicates all wines were technically sound. The experts informally described the unoaked sample as having "*varietal characters, fresh cherry nose, forest fruits, confectionary*" but "*lacking complexity and palate length*". The barrel-aged wine was considered to display "*dull, manufactured oak*" and "*lack fruit intensity*". P2VAT was described as "*savory, chocolate, dusty, earthy, lacking fruit flavor*" with "*softer tannins*" and "*more complex than the other wines*". In general, these comments were in good agreement with DA results.

Table 6. Consumer Liking and Expert Quality Ratings for Selected Cabernet Sauvignon Wines after Oak Maturation[a]

	hedonic ratings[b]				quality ratings[b]
treatment	total sample (n = 116)	cluster 1 (n = 35)	cluster 2 (n = 55)	cluster 3 (n = 26)	wine experts (n = 10)
barrel	5.7	5.11 b	6.35 a	4.85 b	13.75
SS + OAK	5.8	4.49 b	6.45 a	6.12 a	14.42
P1 − OAK	5.9	4.31 b	6.60 a	6.23 a	14.82
P1 + OAK	5.9	3.91 b	6.73 a	6.58 a	13.92
P2VAT	5.9	5.80 b	7.00 a	3.42 c	14.65

[a]Means within a row followed by different letters are significantly different (P = 0.05, one-way ANOVA, Tukey's LSD post hoc). [b]Hedonic ratings were determined using a 9-point scale and quality ratings using a 20-point scoring system.

One hundred and sixteen consumers participated in the acceptance test, and their demographic data are reported in Table 7. A similar proportion of male and female participants and a relatively even distribution of ages were achieved. Most consumers were regular wine drinkers and consumed wine at least once per week (i.e., 86%). There were no significant differences in the hedonic ratings given by the consumer cohort for the five wines (Table 6), with mean scores ranging from 5.7 to 5.9. However, as in previous research,[17] disparity in consumers' wine preferences was observed, and cluster analysis based on individual hedonic scores enabled the identification of three distinct consumer segments (Tables 6 and 7). The first cluster comprised 35 consumers, who were not overly accepting of any wine, but who liked P2VAT most and P1 + OAK least. Cluster 2, the largest cluster (n = 55), gave similar scores to each wine and quite closely resembled the total sample. Cluster 3 comprised 26 consumers, who did not like the barrel-aged or P2VAT wines, but equally liked the other wines. Surprisingly, the wine produced using traditional barrel maturation was not favored by any segment and actually received the lowest overall score, whereas P1 − OAK, the wine made without oak contact, was quite well liked by clusters 2 and 3.

Internal preference mapping was undertaken to investigate the sensory attributes driving consumer liking. PLSR was performed on the DA data and hedonic ratings for each consumer segment and the total sample (Figure 2). Sensory attributes with regression coefficients > ±0.2 are generally considered to influence consumer liking.[6] In the current study, there were neither positive nor negative drivers for either the total consumer sample or cluster 2. In contrast, strong positive drivers were observed for cluster 1, including *leather* aroma (0.34) and flavor (0.33), *licorice* flavor (0.24), and *astringent/dry* mouthfeel (0.26), whereas strong negative drivers included *mocha* (−0.47) and *charry* (−0.30) aromas. This explains cluster 1's preference for P2VAT, which exhibited more apparent aged characters relative to other wines. Positive drivers for cluster 3 included *red fruit* (0.42), *charry* (0.27), and *mocha* (0.56) aromas and *earthy* (0.61) and *woody* (0.31) flavors. The strong negative drivers for cluster 3 were *dusty* (−0.44) and *leather* (−0.64) aromas and *leather* flavor on the palate (−0.57). Consumers within this cluster tended to be younger, from households with higher incomes, who were willing to spend more for wine on average than consumers from clusters 1 and 2 (Table 7). On the basis of demographic data, hedonic scores, and the sensory attributes driving wine preferences, consumers from clusters 2 and 3 would be most likely to be receptive to wines made using alternate oak maturation regimens; indeed, consumers from cluster 2 were generally accepting of all wines (Table 6).

Table 7. Consumer Demographics for Total Sample (n = 116) and Consumer Segments

	total sample[a] (n = 116)	cluster 1[a] (n = 35)	cluster 2[a] (n = 55)	cluster 3[a] (n = 26)
gender				
male	50.9	42.9	63.6	34.6
female	49.1	57.1	36.4	65.4
age (years)				
18−34	27.6	37.1	20.0	30.8
35−54	31.9	28.6	27.3	46.2
55+	40.5	34.3	52.7	23.1
education				
high school	10.3	17.1	7.3	7.7
technical/trade	15.5	5.7	21.8	15.4
bachelor's degree	29.3	28.6	30.9	26.9
postgraduate	44.8	48.6	40.0	50.0
household income ($AUD)				
<$25000	8.6	11.4	7.3	7.7
$25001−50000	11.2	5.7	14.5	11.5
$50001−75000	18.1	25.7	16.4	11.5
$75001−100000	21.6	25.7	18.2	23.1
$100001−150000	28.4	20.0	32.7	30.8
$150001−200000	7.8	5.7	7.3	11.5
>$200000+	4.3	5.7	3.6	3.8
wine consumption				
4+ times/week	22.2	22.9	27.3	11.5
2−3 times/week	35.9	28.6	40.0	38.5
once a week	27.4	28.6	23.6	34.6
once every 2 weeks	11.1	17.1	7.3	11.5
once a month	2.6	2.9	1.8	3.8
average price/bottle for home consumption ($AUD)				
<$10	2.6	2.9	1.8	3.8
$11−15	26.5	25.7	27.3	26.9
$16−20	37.6	40.0	41.8	26.9
$21−30	28.2	28.6	25.5	34.6
$31−50	3.4	2.9	1.8	7.7
$51+	0.9	0	1.8	0

[a]Values expressed as percentages.

This study demonstrates consumer acceptance of wines made using alternative oak maturation regimes. The presence of key oak-derived volatile compounds and perceptible oak aromas and flavor in oak-aged wines was confirmed by chemical

DOI: 10.1021/jf5044025
J. Agric. Food Chem. 2015, 63, 1593−1600

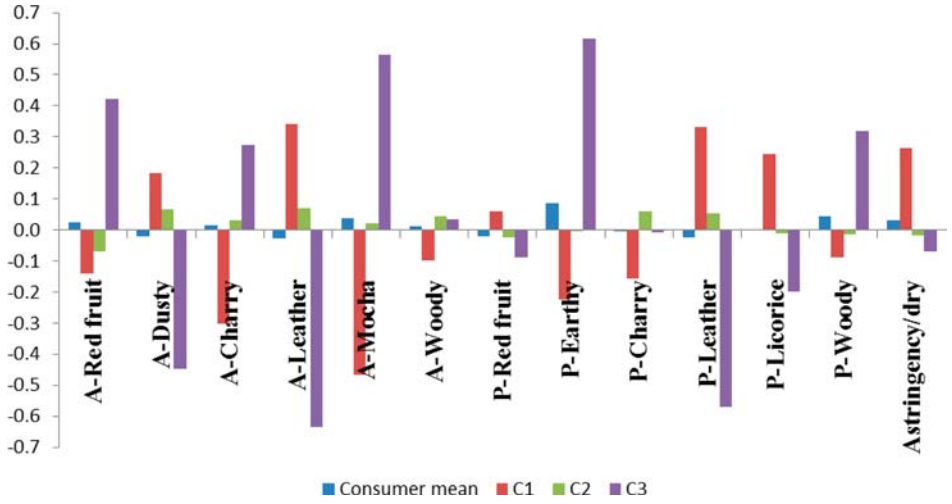

Figure 2. PLSR plot of consumer liking against wine sensory attributes for selected Cabernet Sauvignon wines.

and sensory analysis. Differences observed in the oak volatile concentrations and intensity of varietal versus oak-derived aromas and flavors of wines reflect differences in oak treatment, including the duration of oak maturation and the use of different oak woods. Quality rating scores ranged from 13.8 to 14.8, indicating wines were considered technically sound, but because wines aged using oak alternatives tend not to be premium quality wines, quality scores were always expected to be modest. Segmentation based on consumers' hedonic ratings demonstrated the variation in wine preferences of different consumers, but importantly, also demonstrated the appeal of wines made using alternative maturation regimens to consumers within different segments. These results justify wine producers' use of alternative oak maturation regimens, in particular for the production of wines targeted at certain price points and/or toward specific segments of the wine market. Furthermore, this study highlights the importance of combining compositional and descriptive sensory analyses with consumer research (e.g., hedonic ratings) to achieve a more substantial overview of the drivers of wine quality and acceptability.

AUTHOR INFORMATION

Corresponding Author

*(K.L.W.) Fax: + 61 8 8313 7116. E-mail: kerry.wilkinson@adelaide.edu.au.

Funding

A.M.C. thanks the Australian Grape and Wine Authority for provision of a research scholarship.

Notes

The authors declare no competing financial interest.

ACKNOWLEDGMENTS

We thank the producers who kindly donated the wines used in this study; without their support this research would not have been possible. We acknowledge the technical support provided by industry partners and the panelists who participated in the DA, expert, and consumer tastings.

REFERENCES

(1) Mueller, S.; Szolnoki, G. The relative influence of packaging, labelling, branding and sensory attributes on liking and purchase intent: consumers differ in their responsiveness. *Food Qual. Pref.* **2010**, *21*, 774−783.

(2) Marin, A. B.; Jorgensen, E. M.; Kennedy, J. A.; Ferrier, J. Effects of bottle closure type on consumer perceptions of wine quality. *Am. J. Enol. Vitic.* **2007**, *58*, 182−191.

(3) Johnson, T. E.; Bastian, S. E. P. A preliminary study of the relationship between Australian wine consumers' expertise and their wine purchasing and consumption behaviour. *Aust. J. Grape Wine Res.* **2007**, *13*, 186−197.

(4) Chrea, C.; Melo, L.; Evans, G.; Forde, C.; Delahunty, C.; Cox, D. N. An investigation using three approaches to understand the influence of extrinsic product cues on consumer behaviour: an example of Australian wines. *J. Sens. Stud.* **2011**, *26*, 13−24.

(5) Bruwer, J.; Li, E. Wine-related lifestyle (WRL) market segmentation: demographic and behavioural factors. *J. Wine Res.* **2007**, *18*, 19−34.

(6) Lattey, K. A.; Bramley, B. R.; Francis, I. L. Consumer acceptability, sensory properties and expert quality judgements of Australian Cabernet Sauvignon and Shiraz wines. *Aust. J. Grape Wine Res.* **2010**, *16*, 189−202.

(7) Mueller, S.; Lockshin, L.; Saltman, Y.; Blanford, J. Message on a bottle: the relative importance of wine back label information on wine choice. *Food Qual. Pref.* **2010**, *21*, 22−32.

(8) Arfelli, G.; Sartini, E.; Corzani, C.; Fabiani, A.; Natali, N. Impact of wooden barrel storage on the volatile composition and sensorial profile of red wine. *Food Sci. Technol. Int.* **2007**, *13*, 293−299.

(9) Chatonnet, P.; Boidron, J. N.; Pons, M. Maturation of red wines in oak barrels: evolution of some volatile compounds and their aromatic impact. *Sci. Aliments* **1990**, *10*, 565−587.

(10) Ortega-Heras, M.; Rivero-Perez, M. D.; Pérez-Magariño, S.; González-Huerta, C.; González-Sanjosé, M. L. Changes in the volatile composition of red wines during aging in oak barrels due to microoxygenation treatment applied before malolactic fermentation. *Eur. Food Res. Technol.* **2008**, *226*, 1485−1493.

(11) Ortega-Heras, M.; González-Huerta, C.; Herrera, P.; González-Sanjosé, M. L. Changes in wine volatile compounds of varietal wines during ageing in wood barrels. *Anal. Chim. Acta* **2004**, *513*, 341−350.

(12) Lockshin, L. S.; Rhodus, W. T. The effect of price and oak flavor on perceived wine quality. *Int. J. Wine Market* **1993**, *5*, 13−25.

(13) Cano-López, M.; Bautista-Ortín, A. B.; Pardo Mínguez, F.; López-Roca, J. M.; Gómez-Plaza, E. Sensory descriptive analysis of a red wine aged with oak chips in stainless steel tanks or used barrels: effect of the contact time and size of the oak chips. *J. Food Qual.* **2008**, *31*, 645−660.

(14) Gutiérrez-Afonso, V. L. Sensory descriptive analysis between white wines fermented with oak chips and in barrels. *J. Food Sci.* **2002**, *67*, 2415−2419.

(15) Bozalongo, R.; Carillo, J. D.; Torroba, M. A. F.; Tena, M. T. Analysis of French and American oak chips with different toasting

DOI: 10.1021/jf5044025
J. Agric. Food Chem. 2015, 63, 1593−1600

degrees by headspace solid-phase microextraction-gas chromatography-mass spectrometry. *J. Chromatogr., A* **2007**, *1173*, 10−17.
(16) Arfelli, G.; Sartini, E.; Corzani, C.; Fabiani, A. Chips, lees, and micro-oxygenation: influence on some flavours and sensory profile of a bottles red Sangiovese wine. *Eur. Food Res. Technol.* **2011**, *233*, 1−10.
(17) Pérez-Magariño, S.; Ortega-Heras, M.; González-Sanjosé, M. L. Wine consumption habits and consumer preferences between wines aged in barrels or with chips. *J. Sci. Food Agric.* **2011**, *91*, 943−994.
(18) Crump, A. M.; Johnson, T. E.; Bastian, S. E. P.; Bruwer, J.; Wilkinson, K. L. Consumers' knowledge of and attitudes towards the role of oak in winemaking. *Int. J. Wine Res.* **2014**, *6*, 21−30.
(19) Iland, P.; Bruer, N.; Edwards, G.; Weeks, S.; Wilkes, E. *Chemical Analysis of Grapes and Wine: Techniques and Concepts*; Patrick Iland Wine Promotions Pty. Ltd.: Campbelltown, Australia, 2004.
(20) Pollnitz, A. P.; Pardon, K. H.; Sefton, M. A. Quantitative analysis of 4-ethylphenol and 4-ethylguaiacol in red wine. *J. Chromatogr., A* **2000**, *874*, 101−109.
(21) Pollnitz, A. P.; Pardon, K. H.; Sykes, M.; Sefton, M. A. The effects of sample preparation and gas chromatograph injection techniques on the accuracy of measuring guaiacol, 4-methylguaiacol and other volatile oak compounds in oak extracts by stable isotope dilution analyses. *J. Agric. Food Chem.* **2004**, *52*, 3244−3252.
(22) Pollnitz, A. P. *The Analysis of Volatile Wine Components Derived from Oak Products during Winemaking and Storage*; The University of Adelaide, Australia, 2000.
(23) Lawless, H. T.; Heymann, H. Acceptance and preferance testing. In *Sensory Evaluation of Food: Principles and Practices*; Heldman, D. R., Ed.; Chapman & Hall, International Thomson Publishing: New York, 1999; pp 430−479.
(24) Parr, W. V.; Heatherbell, D.; White, K. G. Demystifying wine expertise: olfactory threshold, perceptual skill and semantic memory in expert and novice wine judges. *Chem. Sens.* **2002**, *27*, 747−755.
(25) Gawel, R.; Godden, P. W. Evaluation of the consistency of wine quality assessments from expert wine tasters. *Aust. J. Grape Wine Res.* **2008**, *14*, 1−8.
(26) Gawel, R. Red wine astringency: a review. *Aust. J. Grape Wine Res.* **1998**, *4*, 74−95.
(27) Wilkinson, K. L.; Elsey, G. M.; Prager, R. H.; Tanaka, T.; Sefton, M. A. Precursors to oak lactone. Part 2: Synthesis, separation and cleavage of several *β*-D-glucopyranosides. *Tetrahedron* **2004**, *60*, 6091−6100.
(28) Guth, H. Quantitation and sensory studied of character impact odorants of different white wine varieties. *J. Agric. Food Chem.* **1997**, *45*, 3027−3032.
(29) Spillman, P. J.; Iland, P. G.; Sefton, M. A. Accumulation of volatile oak compounds in a model wine stored in American and Limousin oak barrels. *Aust. J. Grape Wine Res.* **1998**, *4*, 67−73.
(30) Pollnitz, A. P.; Jones, G. P.; Sefton, M. A. Determination of oak lactones in barrel aged wines and in oak extracts by stable isotope dilution analysis. *J. Chromatogr., A* **1999**, *857*, 239−246.
(31) Mosedale, J. R.; Puech, J. L.; Feuillat, F. The influence on wine flavour of the oak species and natural variation of heartwood components. *Am. J. Enol. Vitic.* **1999**, *50*, 503−512.
(32) Garde-Cerdán, T.; Ancín-Azpilicueta, C. Effect of oak barrel type on the volatile composition of wine: storage time optimization. *LWT−Food Sci. Technol.* **2006**, *39*, 199−205.
(33) Spillman, P. J.; Pollnitz, A. P.; Liacopoulos, D.; Pardon, K. H.; Sefton, M. A. Formation and degradation of furfuryl alcohol, 5-methylfurfuryl alcohol, vanillyl alcohol, and their ethyl ethers in barrel aged wines. *J. Agric. Food Chem.* **1998**, *46*, 657−663.
(34) Garde-Cerdán, T.; Ancín-Azpilicueta, C. Review of quality factors on wine ageing in oak barrels. *Trends Food Sci. Technol.* **2006**, *17*, 438−447.
(35) Cejudo-Bastante, M. J.; Hermosín-Gutiérrez, I.; Peréz-Coello, M. S. Micro-oxygenation and oak chip treatments of red wines: effects on colour-related phenolics, volatile composition and sensory characteristics. Part II: Merlot wines. *Food Chem.* **2011**, *124*, 738−748.

DOI: 10.1021/jf5044025
J. Agric. Food Chem. 2015, 63, 1593−1600

patterns of these flavonoids during fruit development. In this study, anthocyanins, flavonols, and PAs were identified, quantified, and localized over fruit development in four pigmented-fruited (blue-purple) cultivars and one white-fruited cultivar of saskatoon. This study furthers our understanding of the developmental regulation of these three branches of the flavonoid pathway during saskatoon fruit development. Furthermore, these data can aid breeding efforts to optimize flavonoid content and specific flavonoid composition for the production of fruit with higher levels of health-beneficial flavonoids and aid in the targeting of specific developmental stages with an optimal flavonoid profile for the production of health-beneficial products.

MATERIALS AND METHODS

Plant Material. Saskatoon fruits from four purple-fruited cultivars (Northline, Pembina, Thiessen, and Honeywood) and one white-fruited cultivar (Altaglo) were collected from the University of Alberta Experimental Farm, Edmonton, Alberta, Canada. Fruit samples for chemical analyses were harvested onto dry ice in the field and were then sorted on dry ice in the laboratory into maturity classes according to a nine-stage system[10,11] (see Figure 1). After sorting, the fruits were immediately stored at −80 °C. Fruits for the histological studies were harvested onto ice in the field, transported on ice to the laboratory, and dissected immediately in the laboratory for tissue fixation.

Anthocyanin, Flavonol, and PA Analysis. For anthocyanin and flavonol quantitation, fruits were removed from −80 °C storage, and approximately 2−4 g of fruit per sample (with a minimum of four fruits per sample; see Table 1 for fruit size within each developmental stage) was ground in a commercial blender (New Hartford, CT). The ground tissue was weighed and then immediately extracted with 8 mL of an HPLC-grade solvent mixture (acetone/methanol/water/formic acid, 40:40:20:0.1, v/v/v/v), and further extraction and purification of anthocyanins and flavonols from saskatoon fruit were performed using a C18 column high-performance liquid chromatography (HPLC) diode array detector (DAD) method as outlined by Ozga et al.[7] and fully described in the Supplementary Materials and Methods in the Supporting Information. The quantitation of anthocyanins and flavonols was determined using absorption at 520 nm for anthocyanins and 350 nm for flavonols. Commercial authentic standards of anthocyanins and flavonols were used for comparison of HPLC retention times, and UV−vis absorption spectra and for construction of standard curves at the HPLC step for quantitation. Anthocyanin and flavonol quantitation data are the means of independent biological replicates (i.e., each replicate consists of a different fruit sample; the number of replicates ranged from 2 to 4, but in most cases, $n = 3$) ± the standard error of the mean (SE). Further identification of the putative quercetin triglycosides (HPLC peaks 2c and 2g, retention times of 10.5 and 32.7 min; Figure 2) was conducted using an Agilent 1100 liquid chromatography−mass spectrometry (LC−MS) system fitted with an electrospray ionization (ESI) interface. The LC−MS column and conditions were as reported by Ozga et al.[7]

For PA extraction, frozen fruit was ground to a fine powder in liquid nitrogen using a mortar and pestle. Ground samples (5−10 g with a minimum of four fruits per sample) were weighed and then immediately extracted with 66% (v/v) aqueous acetone (10 mL/g of tissue) as outlined by Kennedy and Jones[19] and fully described in the Supplementary Materials and Methods in the Supporting Information. The phloroglucinolysis reaction procedure was similar to that reported by Koerner et al.[18] with minor modifications as described in the Supplementary Materials and Methods in the Supporting Information. The phloroglucinolysis reaction times for monitoring free flavan-3-ols and flavan-3-ol−phloroglucinol adducts were as follows: 20 min for B-type and A-type (A_2; dimer made up of two flavan-3-ols linked together with an A-type linkage) terminal units, B-type phloroglucinol adducts, and grape skin PA standard extracts (no A-type PA linkages present), 120 min for A_2−phloroglucinol adducts for saskatoon fruit PA extracts, and 135 min for cranberry fruit PA standard extracts (containing abundant A-type PA linkages).

A 20 μL aliquot of the diluted reaction mixture was injected onto two Chromolith RP-18e (4.6 × 100 mm; Merck, Germany) columns connected in series, protected by a guard column (Chromolith RP-18e 4.6 × 10 mm; Merck, Germany), stabilized at 30 °C, using an Agilent 1200 HPLC system equipped with an Agilent G1315B DAD. The HPLC conditions were similar to that of Kennedy and Taylor[20] with minor modifications. The samples were eluted at 3 mL min^{-1} using a linear gradient with 1% (v/v) aqueous acetic acid (solvent A) and acetonitrile with 1% acetic acid (v/v; solvent B) as follows: isocratic at 3% B from 0 to 4 min, 3% to 18% B by 14 min, and 80% B from 14 to 18 min. Free flavan-3-ols, A_2 dimers, flavan-3-ol−phloroglucinol adducts (from extension subunits), and A_2−phloroglucinol adducts (from extension subunits) were monitored at 280 nm. PA terminal subunits were identified by comparison of HPLC-DAD retention times and absorbance spectra with commercially available flavan-3-ol standards. Phloroglucinol−PA adducts were identified by comparison of HPLC retention times with grape skin and cranberry fruit PA reaction products that were previously characterized by Koerner et al.[18] The mean degree of polymerization and conversion yields were calculated according to the method of Kennedy and Jones.[19] PA quantitation data are the means of independent biological replicates (the number of replicates ranged from 2 to 4, but in most cases, $n = 3$) ± SE.

To confirm the identification of the phloroglucinolysis products, LC−MS analysis was performed on the products using a 4000 Q-TRAP LC−MS/MS mass spectrometer (MDS SCIEX, Applied Biosystems) connected to an Agilent 1200 HPLC system as described by Zifkin et al.[21] PA terminal subunits (except for the terminal unit dimer, A_2) were identified by comparison of HPLC-DAD retention times, LC−MS fragmentation spectra, and absorbance spectra with commercially available flavan-3-ol standards. (−)-Epicatechin-(4β→2)-phloroglucinol (EC−P) was identified by comparison of HPLC retention times and the LC−MS fragmentation pattern with grape skin PA phloroglucinolysis reaction products. A_2 and the A_2−phloroglucinol (A_2−P) adducts were characterized by comparison of HPLC retention times and LC−MS spectra with cranberry fruit PA phloroglucinolysis products, which have been previously characterized.[18,19] The (+)-catechin-(4α→2)-phloroglucinol (C−P) standard was synthesized using taxifolin (see the Supplementary Materials and Methods in the Supporting Information). (−)-Epicatechin was used as an external standard for quantification of the free PA terminal subunits [(+)-catechin, (−)-epicatechin, and A_2] and phloroglucinol adducts. The relative molar and mass response factors from previous publications[18,19] were used for calculating PA subunit concentration, mDP, and conversion yield.

Histochemical Localization of PAs and Flavonols. Whole fruits were fixed for stages 1−4. For stages 5, 7, and 9, the top (pedicel end) and bottom (calyx end) parts of the fruit were removed, and approximately 5−10 mm of the central fruit tissue was used for tissue fixation. The fresh fruit sections were fixed, dehydrated, infiltrated, and embedded in Paraplast tissue embedding medium (Fisher Scientific, Houston, TX) as described by Zifkin et al.[21] Tissue blocks were sectioned to 10 or 20 μm thickness and affixed onto clean glass slides for microscopy.

For PA localization, the paraffin was removed from the tissue sections using two toluene (100%) washes at 5 min intervals. Tissue sections were stained with 0.1% 4-(dimethylamino)cinnamaldehyde (DMACA)/0.5 M H_2SO_4/1-butanol solution prepared as described by Gutmann and Feucht[22] (see the Supplementary Materials and Methods in the Supporting Information). For tissue staining, slides with fruit sections were covered with the DMACA solution and incubated at 60 °C on a hot plate for 15 min. The slides were subsequently washed with 100% ethanol to remove the excess staining solution and then dipped into two fresh toluene (100%) baths for 5 min each to remove moisture from the tissues. Cover slides were placed on slide-mounted tissue sections using DPX mounting media (BDH Chemicals, New York). Tissue sections were observed using a Zeiss AXIO scope A1 light microscope (Zeiss, Germany), and

DOI: 10.1021/jf504722x
J. Agric. Food Chem. 2015, 63, 1601−1614

micrographs were taken with a microscope-mounted Optronics camera (Optronics, United States) controlled by Picture Frame Application 2.3 software.

For flavonol localization, tissue sections were stained with 0.1% (w/v) diphenylboric acid 2-aminoethyl ester (DPBA) staining solution (containing 0.025% Triton X-100) for 5 min. The nearly dried sections were covered with cover slides using Fluoro Mount G (Electron Microscopy Sciences, United States) mounting medium. The micrographs of whole-fruit cross sections were taken with a Nikon camera (DXM1200, Japan) mounted on a Leica DMRXA microscope (Leica, Germany) (bright-field option). The fruit pericarp, placenta, and seed fluorescence micrographs were obtained using the same equipment described above under the fluorescence microscopy configuration (green; excitation filter, BP, 420–490 nm; dichromatic mirror, 510 nm; suppression filter, LP, 515 nm).

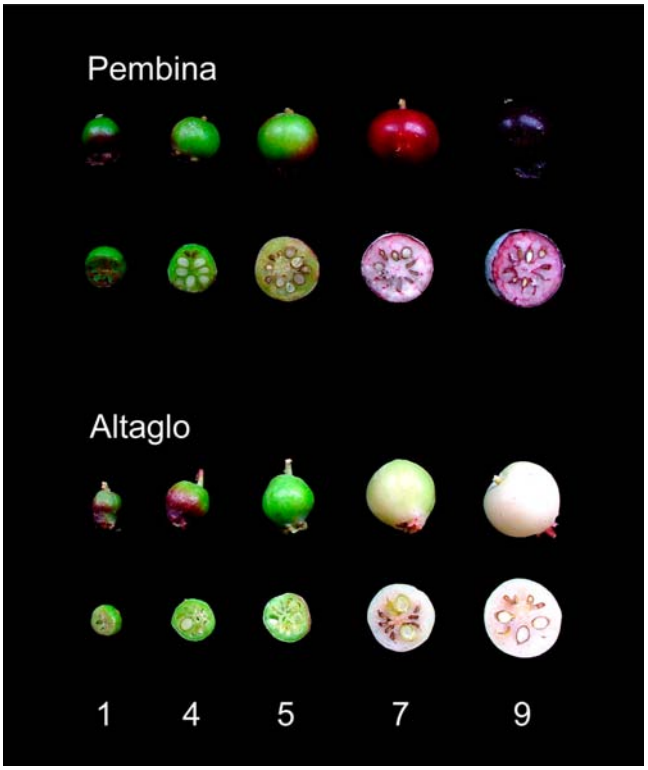

Figure 1. Whole and bisected saskatoon fruits (cultivars Pembina and Altaglo) over development. Stages for 'Pembina' fruit: 1, small green fruit; 4, larger green fruit; 5, light green fruit with slight pink mottling; 7, red fruit; 9, mature blue-purple fruit. Stages for 'Altaglo' fruit: 1, 4, and 5, green fruit in the order of ascending fruit size; 7, light green to white fruit; 9, white fruit. The fruit and pigment developmental patterns of saskatoon cultivars Honeywood, Northline, and Thiessen were similar to that of Pembina.

Chemicals. All HPLC-grade organic solvents (acetone, acetonitrile, methanol, ethyl acetate), acetic acid (ACS grade), and 1-butanol were purchased from Fisher Scientific (Ottawa, ON, Canada).The anthocyanin and flavonol standards (cyanidin 3-*O*-galactoside chloride, cyanidin 3-*O*-glucoside chloride, quercetin 3-*O*-glucoside, quercetin 3-*O*-galactoside, quercetin 3-*O*-rutinoside, and quercetin 3-*O*-arabinoglucoside) were purchased from Extrasynthese (Genay, France). (+)-Catechin hydrate, (−)-epicatechin, (−)-epicatechin gallate, (−)-epigallocatechin, (−)-gallocatechin, (−)-catechin gallate, (−)-epigallocatechin gallate, (−)-gallocatechin gallate, taxifolin, phloroglucinol, trifluoroacetic acid (TFA), L-(+)-ascorbic acid, hydrochloric acid (HCl; 36.5–38%), 5-*O*-caffeoylquinic acid (chlorogenic acid), diphenylboric acid 2-aminoethyl ester (DPBA), 4-(dimethylamino)cinnamaldehyde (DMACA), Triton X-100, and TOYOPEARL resin (HW-40F) were from Sigma (Oakville, ON, Canada). Glutaraldehyde and paraformaldehyde were purchased from Electron Microscopy Sciences (Hatfield, PA). The crude cranberry PA and grape skin PA standards were kindly provided by Dr. James Kennedy (Oregon State University).

RESULTS AND DISCUSSION

Fruit Development. Among the nine defined stages of saskatoon fruit development,[10] stages 1, 4, 5, 7, and 9 were selected to represent the major stages of fruit development (Figure 1). Saskatoon fruit increased in size throughout development, with the greatest increases in fruit fresh weight occurring at the latter stages of fruit development[23] (Table 1). Of the cultivars studied, Honeywood and Thiessen had the largest fruit fresh weight at maturity (Table 1). For the pigmented-fruit cultivars, from stages 1 to 4, the mainly green fruit increased in size. Stage 5 fruits were lighter green, and intermittent pink color occurred on the fruit surface. By stage 7, the fruit turned red and transitioned into the ripening stage. Fully mature fruits at stage 9 were blue-purple (Figure 1). For 'Altaglo', the early stages of fruit development (stages 1–5) were similar to those of the pigmented-fruit cultivars except for the substantially smaller fruit size at stage 1 (Figure 1, Table 1). However, with the transition to ripening (stage 7), minimal coloration occurred in 'Altaglo' fruits, and the fruits were white at maturity (stage 9; Figure 1). Saskatoon fruits have five locules as do other pome fruits such as apple, and each locule

Table 1. Fresh Fruit Weight and Diameter of Northline, Honeywood, Pembina, Thiessen, and Altago Saskatoon Fruit Cultivars over Development

cultivar	stage 1	stage 4	stage 5	stage 7	stage 9
			Fresh Fruit Diameter (mm)		
Northline	6.9 ± 0.3[a]	9.1 ± 0.1	10.4 ± 0.4	12.2 ± 0.3	13.4 ± 0.3
Honeywood	6.5 ± 0.2	8.7 ± 0.4	11.7 ± 0.1	13.2 ± 0.2	15.5 ± 0.4
Pembina	6.9 ± 0.2	7.6 ± 0.2	9.5 ± 0.3	11.5 ± 0.5	12.9 ± 0.2
Thiessen	7.8 ± 0.2	8.3 ± 0.4	11.1 ± 0.3	12.8 ± 0.3	13.8 ± 0.3
Altaglo	4.2 ± 0.0	9.2 ± 0.2	10.6 ± 0.3	11.6 ± 0.3	13.3 ± 0.3
			Fresh Fruit Weight (mg)		
Northline	181.3 ± 9.0	327.9 ± 23.2	475.3 ± 27.2	830.3 ± 14.1	1122.4 ± 27.4
Honeywood	153.7 ± 2.8	291.1 ± 23.2	642.8 ± 40.7	981.4 ± 66.8	1865.8 ± 19.2
Pembina	188.3 ± 4.2	242.3 ± 14.0	373.8 ± 21.6	666.3 ± 76.7	957.6 ± 27.5
Thiessen	234.2 ± 3.6	387.1 ± 61.5	623.2 ± 45.8	948.6 ± 23.1	1522.4 ± 126.3
Altaglo	52.0 ± 3.1	345.7 ± 17.7	521.4 ± 34.9	667.6 ± 35.2	1030.0 ± 92.1

[a]Data are the means ± SE, $n = 5$.

DOI: 10.1021/jf504722x
J. Agric. Food Chem. 2015, 63, 1601–1614

can produce up to two seeds; however, at maturity the number of developed seeds is usually substantially lower than 10 (between 3 and 5; Figure 1).[23]

Anthocyanin Profiles in Developing Fruit. A typical HPLC-DAD chromatogram of a flavonoid extract from 'Pembina' stage 9 fruit monitored at 520 nm for anthocyanin detection is presented in Figure 2A. Four anthocyanin peaks were detected, cyanidin 3-*O*-galactoside (cyn-gal; 1a), cyanidin-3-*O*-glucoside (cyn-glu; 1b), cyanidin 3-*O*-arabinoside (cyn-arb; 1c), and cyanidin 3-*O*-xyloside (cyn-xyl; 1d), as previously determined for cultivars Honeywood and Smoky.[7] Cyn-gal, cyn-glu, and cyn-arb were detected throughout development in fruits from all pigmented-fruit cultivars tested (stages 1−9), with cyn-gal predominating in the profile throughout development (Figure 3B−E). Thus, cyn-gal is mainly responsible for the red coloration on the largely green-colored fruit skin early in development (Figure 1). As the fruit transitioned into the ripening phase (stage 7), the anthocyanin content dramatically increased, and cyn-xyl was detected (Figure 3B−E). Anthocyanin levels peaked at fruit maturity (stage 9) in all pigmented-fruit cultivars tested. Anthocyanin localization was carried out by cross sectioning whole fruits and visually observing tissue coloration. The typical red color of anthocyanins appeared on some parts of the fruit exocarp (skin) throughout the earlier developmental stages (stages 1−5; Figure 1). The red color on the fruit skin intensified as the fruit transitioned into the ripening stage (stage 7), and red-purple pigmentation was also observed in the cells of the mesocarp, vascular traces, and fruit locule margins. The fruit skin was dark purple at maturity (stage 9), with some purple coloration throughout the mesocarp tissue (Figure 1). The total anthocyanin concentration in the mature fruits of cultivars Honeywood, Pembina, Thiessen, and Northline ranged from 154 to 201 mg/100 g of fresh fruit weight (Table 2).

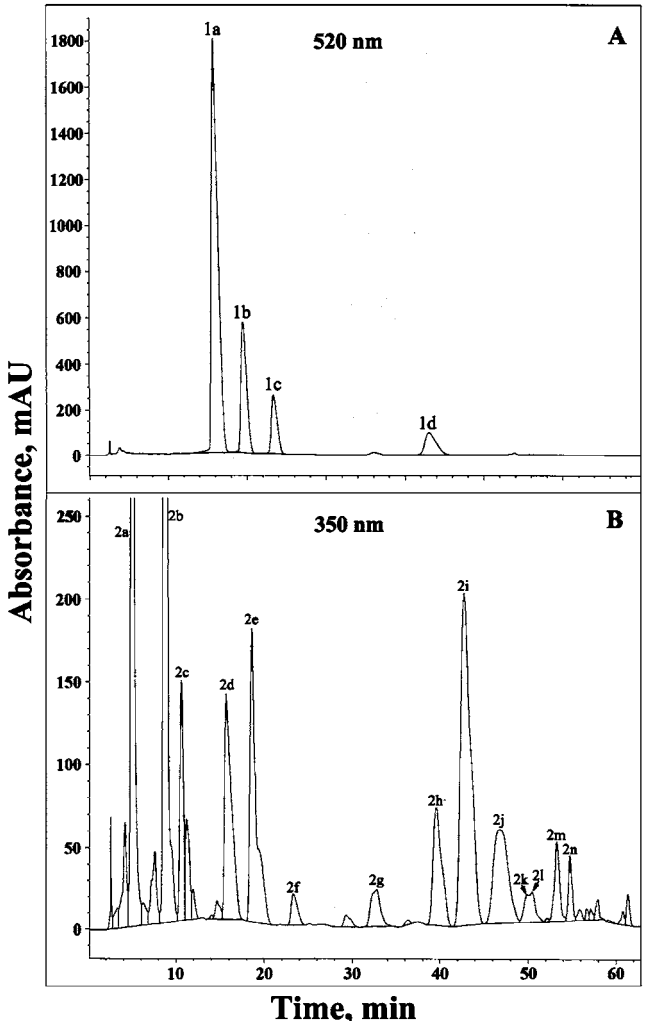

Figure 2. HPLC-DAD profiles of a stage 9 'Pembina' saskatoon fruit flavonoid extract. (A) Profile of anthocyanins monitored at 520 nm: peak 1a (15.7 min), cyanidin 3-*O*-galactoside; peak 1b (19.4 min), cyanidin 3-*O*-glucoside; peak 1c (23.3 min), cyanidin 3-*O*-arabinoside; peak 1d (43.0 min), cyanidin 3-*O*-xyloside. (B) Profile of flavonols and phenolics monitored at 350 nm: peak 2a (4.9 min), 3-*O*-caffeoylquinic acid; peak 2b (8.7 min), 5-*O*-caffeoylquinic acid; peak 2c (10.6 min), putative quercetin triglycoside; peak 2d (15.7 min), cyanidin 3-*O*-galactoside; peak 2e (18.6 min), unknown chlorogenic acid isomer; peak 2f (23.3 min), cyanidin 3-*O*-arabinoside; peak 2g (32.7 min), putative quercetin triglycoside; peak 2h (39.6 min), quercetin 3-*O*-arabinoglucoside; peak 2i (42.7 min), quercetin 3-*O*-galactoside; peak 2j (46.8 min), quercetin 3-*O*-glucoside; peak 2k + peak 2l (50.4 min), quercetin 3-*O*-robinobioside + quercetin 3-*O*-rutinoside; peak 2m (53.3 min), quercetin 3-*O*-arabinoside; peak 2n (54.7 min), quercetin 3-*O*-xyloside.

In the pigmented-fruit saskatoon cultivars, anthocyanin levels in the mature fruit were comparable to those found in other small fruits such as blackberry, cranberry, and sweet cherry (Table 2).[24] In general, saskatoon fruits have a relatively simple anthocyanin profile (four major anthocyanins that are monoglycosides of cyanidin) compared with blueberry fruits.[25] The dramatic increase in anthocyanin levels as the fruit transitions into ripening suggests that, as part of the ripening process, there is increased expression of transcription factors that up-regulate transcription of genes in the anthocyanin biosynthesis pathway, as observed in grape berries.[26,27]

In 'Altaglo' fruits (white fruit at maturity), cyn-gal and cyn-arb were found at levels comparable to those of the pigmented-fruit cultivars during early fruit development (stage 4; Figure 3, Table 2), demonstrating that the structural genes in the flavonoid pathway required to produce these anthocyanins are present during this developmental phase. However, as 'Altaglo' fruit continued to develop and transition into the ripening phase (stage 7), the dramatic increase in anthocyanin levels did not occur as observed in the pigmented-fruit cultivars, and only minimal levels of anthocyanins were detected in 'Altaglo' fruit at maturity (stage 9; Figure 3, Table 2). It is unlikely that the white fruits produced by 'Altaglo' at maturity are the result of a mutation in a key enzyme(s) for anthocyanin biosynthesis, as anthocyanins were detected in 'Altaglo' fruit at levels similar to those of the pigmented-fruit cultivars at earlier developmental stages. Furthermore, the presence of cyn-xyl in all the pigmented-fruit cultivars at stage 7 when the fruit is transitioning into ripening and subsequent cyn-xyl accumulation in these fruits through stage 9, and the lack of cyn-xyl in white-fruited 'Altaglo', lend support to the hypothesis that 'Altaglo' fruits lack a functional transcription factor(s) that up-regulates the transcription of genes for anthocyanin production as the fruit transitions into the ripening phase.

Flavonol Profiles in Developing Fruit. A representative HPLC-DAD chromatogram of a flavonoid extract from 'Pembina' stage 9 fruit monitored at 350 nm for flavonol detection is presented in Figure 2B. Seven main flavonols were detected in all pigmented-fruit cultivars studied (as previously determined in cultivars Honeywood and Smoky fruits by Ozga et al.[7]) as

DOI: 10.1021/jf504722x
J. Agric. Food Chem. 2015, 63, 1601−1614

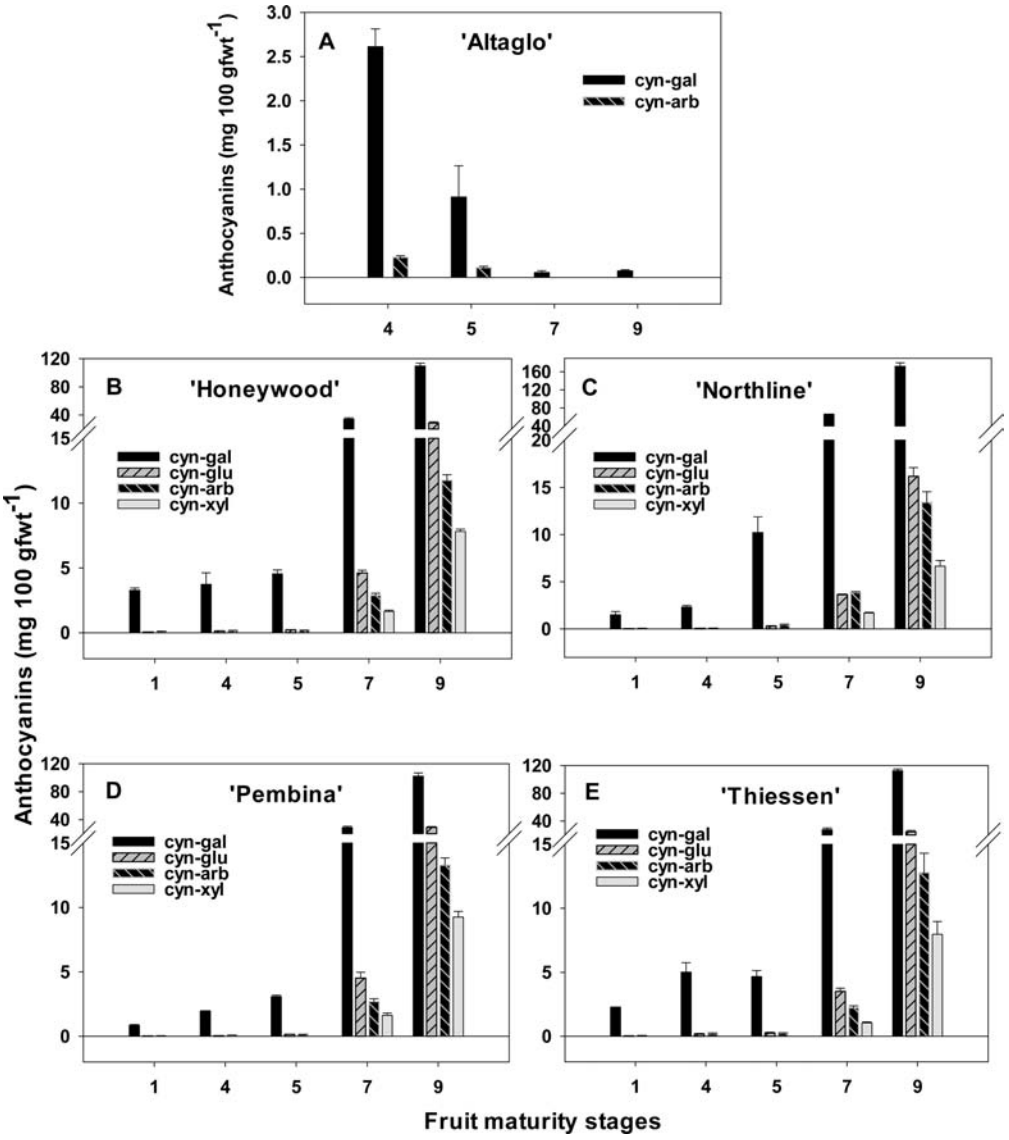

Figure 3. Type and content of anthocyanins in the fruits of cultivars (A) Altaglo, (B) Honeywood, (C) Northline, (D) Pembina, and (E) Thiessen over development (stages 1, 4, 5, 7, and 9). Abbreviations: cyn-gal, cyanidin 3-*O*-galactoside; cyn-glu, cyanidin 3-*O*-glucoside; cyn-arb, cyanidin 3-*O*-arabinoside; cyn-xyl, cyanidin 3-*O*-xyloside. Cyn-glu and cyn-arb were detected in cultivars Northline stages 1 and 4, Pembina stages 1 and 4, and Thiessen stage 1 fruits at <0.2 mg 100 gfwt^{-1}. Data are the means of independent biological replicates ± SE, n = 2−4.

follows: quercetin 3-*O*-arabinoglucoside (peak 2h), quercetin 3-*O*-galactoside (peak 2i), quercetin 3-*O*-glucoside (peak 2j), quercetin 3-*O*-robinobioside (peak 2k), quercetin 3-*O*-rutinoside (peak 2l), quercetin 3-*O*-arabinoside (peak 2m), and quercetin 3-*O*-xyloside (peak 2n). Additionally, in ripening and mature fruit (stages 7 and 9) of the pigmented-fruit cultivars, the presence of a strongly hydrophilic flavonol-type compound was observed (peak 2c; Figures 2B and 4) that had maximum absorbance at 343 nm (data not shown). LC−MS analysis was performed on HPLC fraction 2c. The MS fragmentation pattern suggested that peak 2c was a quercetin derivative with the characteristic quercetin aglycon ion mass of 303 (quercetin + H^+ ion; Table S1 and Figure S1, Supporting Information). Strongly polar quercetin triglycosides have been reported in Italian red onion and cauliflower.[28,29] These quercetin triglycosides were glycosylated at carbon 3, 7, or 4′. As the polarity of the peak 2c quercetin-type flavonol was much stronger than that of the other flavonols detected (eluted at 10.5 min in our HPLC system; Figure 2B), it is reasonable to propose that the glycosylation pattern of the peak 2c flavonol likely differs from that of the other saskatoon fruit flavonols identified, with a hexose sugar attached at carbons 3 and 7 or 4′. Another flavonol-type compound (peak 2g, Figure 2 B) was detected in cultivars Honeywood stage 1 fruits and Pembina fruits throughout development (Figure 4). This flavonol was further identified by LC−MS analysis as a quercetin triglycoside of rhamnose, hexose, and pentose with a molecular ion mass of 743 (302 + 146 + 162 + 132 + 1 = quercetin + rhamnose + hexose + pentose + H; Table S1 and Figure S2, Supporting Information). This compound (eluted at 32.7 min in the HPLC system) had a polarity similar to that of quercetin 3-*O*-arabinoglucoside; therefore, it is reasonable to postulate that this compound is a quercetin 3-*O*-triglycoside. The exact linkage of the three sugar units to quercetin cannot be determined by LC−MS analysis since internal monosaccharide loss might happen during the electrospray ionization process.[30] In general, the flavonol profiles of the pigmented-fruit cultivars were relatively similar, with quercetin 3-*O*-galactoside, quercetin

DOI: 10.1021/jf504722x
J. Agric. Food Chem. 2015, 63, 1601−1614

Table 2. Developmental Profile of the Total Anthocyanin Content of Cultivars Altaglo, Honeywood, Northline, Pembina, and Thiessen Saskatoon Fruits

	total anthocyanin content[a] (mg 100 gfwt^{-1})				
cultivar	stage 1	stage 4	stage 5	stage 7	stage 9
Altaglo	nd[b]	2.8 ± 0.2[c]	1.0 ± 0.4	0.06 ± 0.02	0.08 ± 0.01
Honeywood	3.4 ± 0.2	4.0 ± 0.9	4.9 ± 0.3	43.3 ± 2.2	157.9 ± 5.6
Northline	1.6 ± 0.4	2.5 ± 0.2	11.0 ± 1.8	75.4 ± 0.5	200.9 ± 14.5
Pembina	0.90 ± 0.07	2.1 ± 0.0	3.4 ± 0.1	37.4 ± 2.8	153.5 ± 6.9
Thiessen	2.4 ± 0.0	5.4 ± 0.8	5.2 ± 0.6	34.4 ± 2.9	157.5 ± 7.2

[a]Content estimated as cyanidin 3-*O*-galactoside (cyn-gal, cyn-arb, and cyn-xyl) and cyanidin 3-*O*-glucoside (cyn-glu) equivalents at the HPLC step. [b]nd = not determined. [c]Data are the means of independent biological replicates ± SE, n = 2−4.

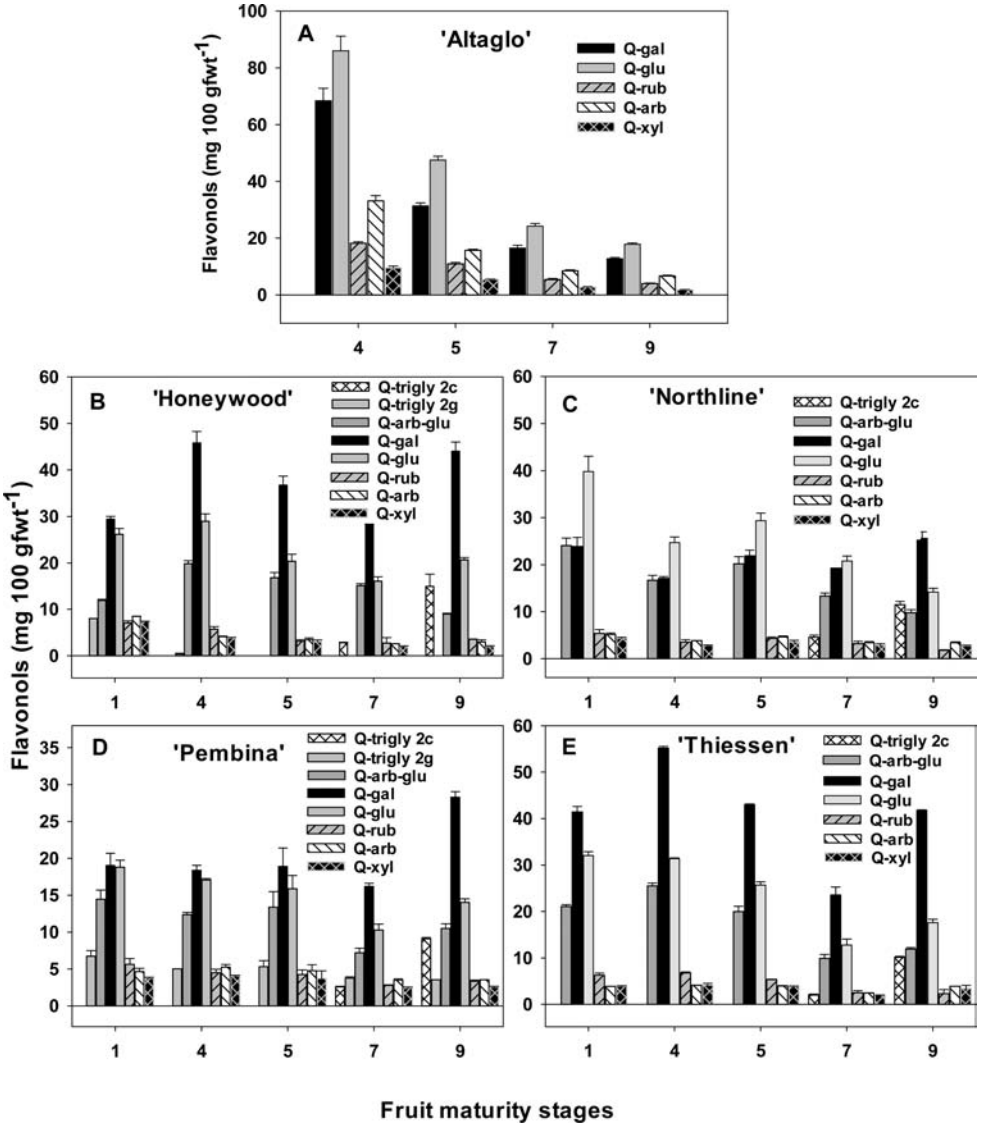

Figure 4. Type and content of flavonols in the fruits of cultivars (A) Altaglo, (B) Honeywood, (C) Northline, (D) Pembina, and (E) Thiessen over development (stages 1, 4, 5, 7, and 9). Abbreviations: Q-trigly 2c, putative quercetin triglycoside; Q-trigly 2g, putative quercetin triglycoside; Q-arb-glu, quercetin 3-*O*-arabinoglucoside; Q-gal, quercetin 3-*O*-galactoside; Q-glu, quercetin 3-*O*-glucoside; Q-rub, quercetin 3-*O*-robinobioside + quercetin 3-*O*-rutinoside; Q-arb, quercetin 3-*O*-arabinoside; Q-xyl, quercetin 3-*O*-xyloside. Data are the means of independent biological replicates ± SE, n = 2−4.

3-*O*-glucoside, and quercetin 3-*O*-arabinoglucoside dominating the flavonol profile throughout development (Figure 4). The flavonol profile of 'Altaglo' fruit differed from those of the pigmented-fruit cultivars in several ways. Quercetin 3-*O*-arabinoglucoside was not detected in 'Altaglo' fruits over development (Figure 4A), while this flavonol was relatively abundant in the other pigmented-fruit cultivars (Figure 4). Also, quercetin 3-*O*-glucoside was in greater abundance in 'Altaglo' fruits relative to other flavonols (Figure 4). In contrast, quercetin 3-*O*-galactoside was the most abundant flavonol in

DOI: 10.1021/jf504722x
J. Agric. Food Chem. 2015, 63, 1601−1614

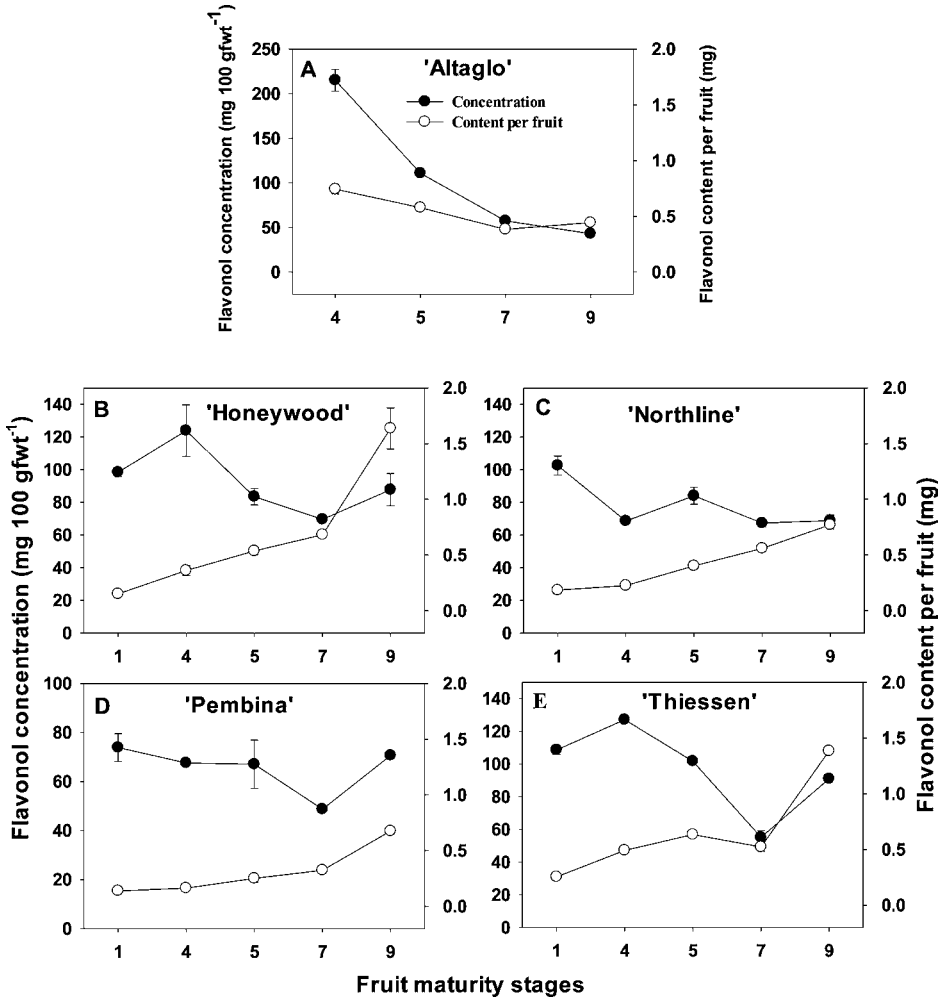

Figure 5. Total flavonol concentration and content of cultivars (A) Altaglo, (B) Honeywood, (C) Northline, (D) Pembina, and (E) Thiessen saskatoon fruits over development (stages 1, 4, 5, 7, and 9) expressed as milligrams per 100 g of fresh weight and milligrams per fruit. Data are the means of independent biological replicates ± SE, n = 2–4. Where standard error is minimal, error bars may be obscured by the symbols.

most pigmented-fruit cultivars (Figure 4). In flavonol biosynthesis, the glycosyltransferases, which catalyze the transfer of sugars to the flavonol aglycons, may have different preferences for sugars as substrates. The variation in flavonol type between the cultivars and over development within a cultivar may reflect the type and activities of specific glycosyltransferases.[31]

In the pigmented-fruit cultivars, in general, higher fruit flavonol concentration occurred earlier in fruit development (Figure 5B–E). In three of the four pigmented-fruit cultivars, the minimal flavonol concentration occurred as the fruit transitioned into ripening (stage 7; Figure 5B–E), followed by an increase in the flavonol concentration as the fruit completed development (stage 9; Figure 5B–E). The increase in flavonol concentration after transitioning into ripening may be related to the activity of transcription factors that up-regulate specific parts of the flavonoid biosynthesis pathway.[32] In blueberry (*Vaccinium corymbosum* L.) and bilberry (*Vaccinium myrtillus*) fruits, flavonol concentration decreased with increasing fruit maturity, with no increase in flavonol concentration following the transition to ripening.[21,33,34]

As the saskatoon fruit continued to increase in size throughout development, the total flavonol content per fruit increased during development in the pigmented-fruit cultivars (Figure 5B–E). This was not the case for 'Altaglo' fruits, where the total flavonol content decreased as the fruit matured (stages 4–9; Figure 5 A). In contrast, pink bilberry fruit (color mutant, pink fruits at maturity) had greater flavonol content at maturity compared with that in wild-type bilberry (dark-colored fruits at maturity).[34] The reduction in flavonol content per fruit in 'Altaglo' over development is consistent with the loss of function of a ripening-related transcription factor(s) that could act to up-regulate flavonoid biosynthesis, leading to flavonol accumulation over development in this cultivar. In addition to the flavonols, chlorogenic acid isomers were detected (peak 2a, neochlorogenic acid; peak 2b, chlorogenic acid; peak 2e, an unknown chlorogenic acid isomer), as previously described (Figure 2B).[7]

Flavonol Localization during Fruit Development. Flavonols autofluoresce, and the autofluorescence (yellow color) can be intensified by a flavonol-specific staining reagent, DPBA.[35,36] For flavonol localization, flavonol autofluorescence within fruit cross sections after histological fixation was monitored using fluorescence microscopy. To verify that the yellow-colored fluorescence signal was derived from flavonols, we stained sections with DPBA. After DPBA staining, the yellow-colored fluorescence signal dramatically intensified but retained the same pattern, confirming that the yellow autofluorescence was specific to the flavonols (Figure 6). Furthermore, we previously confirmed the autofluorescence emission wavelength range of

DOI: 10.1021/jf504722x
J. Agric. Food Chem. 2015, 63, 1601–1614

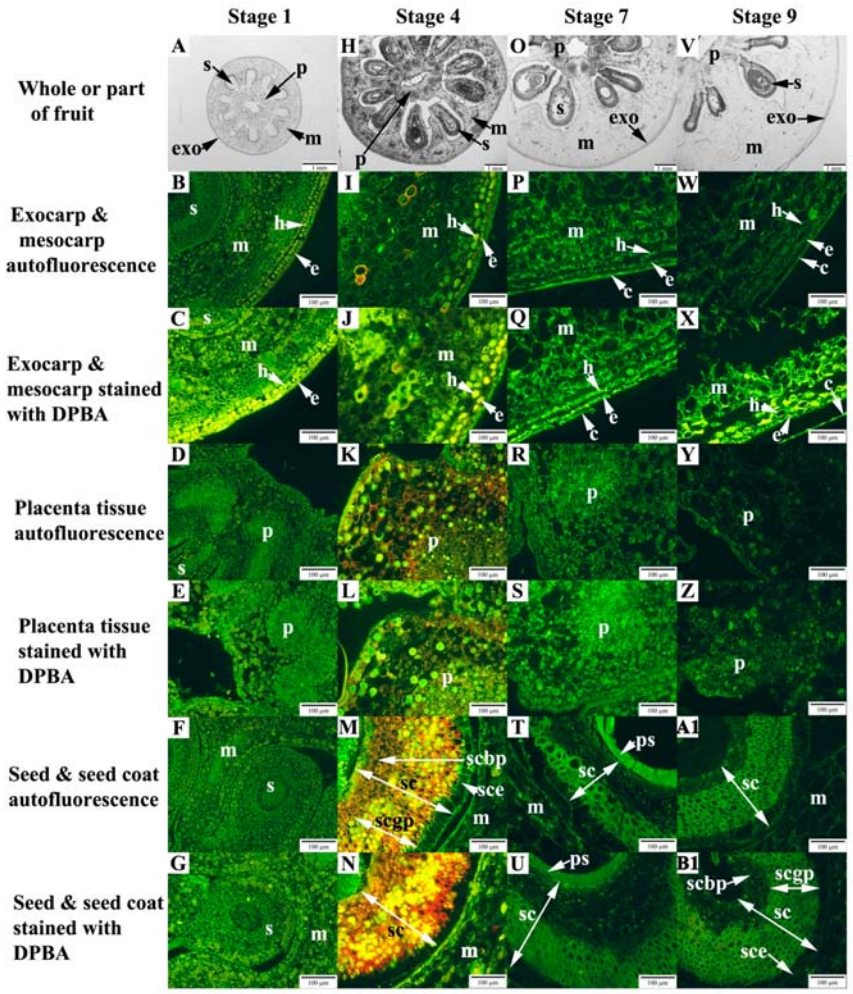

Figure 6. Fluorescence light micrographs showing flavonol localization in 'Altaglo' saskatoon fruit cross sections over development. Flavonols were visualized by autofluorescence and enhanced fluorescence after DPBA staining (yellow color). Panels are paired vertically, with the autofluorescence panel and corresponding DBPA-enhanced fluorescence panel shown immediately below. Micrographs from fruit stages 1 (A–G), 4 (H–N), 5 (O–U), and 9 (V–B1) are shown as columns. Panels A, H, O, and V are light micrographs that depict the entire fruit over development (size bar 1 mm). Exocarp and mesocarp tissues are depicted as autofluorescence (panels B, I, P, and W) and after staining with DPBA (panels C, J, Q, and X). Placental tissues are shown as autofluorescence (panels D, K, R, and Y) and after staining with DPBA (panels E, L, S, and Z). Seed tissues are shown as autofluorescence (panels F, M, T, and A1) and after staining with DPBA (panels G, N, U, and B1). Bars for fluorescence micrographs are 100 mm. Abbreviations: c, cuticle; e, epidermis; exo, exocarp; h, hypodermis; m, mesocarp; p, placenta; ps, perisperm; s, seed; sc, seed coat; scbp, seed coat branch parenchyma; sce, seed coat epidermis; scgp, seed coat ground parenchyma.

flavonols and the enhancement of the flavonol-specific fluorescence emission by DPBA using commercial standards of flavonols and a spectrofluorometer with an excitation wavelength within the range used for the fluorescence micrographs (420–490 nm).[21] These controls confirmed that flavonols autofluoresence and that DPBA enhances the fluorescence of flavonols within the expected wavelength range. This enhancement was not observed for chlorogenic acids, which are abundant nonflavonoid phenolic acids of saskatoon and blueberry fruits.[7,21]

Flavonol localization was determined over development in 'Pembina' and 'Altaglo' fruits. The same general pattern of flavonol localization was observed in the fruit of both cultivars. However, the minimal anthocyanin content of 'Altaglo' fruits throughout development allowed for better flavonol localization resolution. As demonstrated in 'Altaglo', flavonols were localized intracellularly (most likely in the vacuole) in the fruit (epidermis and hypodermis of the exocarp, mesocarp, and placental tissues) and the developing seed tissues of stage 1 fruits (Figure 6B–G). As the fruits and seeds developed, flavonol localization differed among the tissue types. The most intense flavonol staining was detected in the epidermal and hypodermal layers of stage 1 fruit (Figure 6B,C). At stage 4, flavonol localization remained high in the epidermal and hypodermal layers, but was substantially reduced in the mesocarp layer of the fruit wall (Figure 6I,J). As the fruit continued to mature, flavonols were observed mainly in the epidermal/hypodermal layer and cuticle of the fruit wall (Figure 6P,Q,W,X). Flavonol localization in the cuticle layer may be the result of flavonol migration from the epidermal to the cuticle layer to provide protection to fruits from UV light damage.[37]

Flavonols were detected in the placental tissues at all stages, with particularly intense staining in specific placental cells in stage 4 fruit (Figure 6D,E,K,L,R,S,Y,Z). In seed tissues, flavonols localized to the vacuoles of the ground parenchyma cells of the developing seed coats during early fruit development (stage 4; Figure 6M,N). As the seed coat matures, seed

DOI: 10.1021/jf504722x
J. Agric. Food Chem. 2015, 63, 1601–1614

coat cells undergo a programmed cell death.[38,39] Flavonols from the vacuoles are likely deposited on the cell walls of the seed coat ground parenchyma layer (Figure 6T,U,A1,B1) during this process, potentially to provide protection to the embryo from potential microbial attack during germination. This hypothesis is supported by the report that flavonols accumulated in the vacuoles and the cell walls of lisianthus (*Eustoma grandiflorum*) flower petals.[40] In addition, saskatoon seeds with viable embryos were found to contain a perisperm layer that also stained for the presence of flavonols (Figure 6T,U).

Characterization and Quantitation of PAs. Phloroglucinolysis (the method of HPLC analysis following acid catalysis in the presence of phloroglucinol)[41] was used to determine PA subunit composition and concentration by comparison of product retention properties with those of known products. Flavan-3-ols in the extension units form phloroglucinol adducts at their C-4 position, while terminal flavan-3-ol units are released as flavan-3-ol monomers or dimers (depending on subunit linkages). To determine the type of PA subunit linkages present in saskatoon fruit, we followed a procedure based on the property that PA polymers with a higher portion of A-type linkages are more resistant to the acid-catalyzed cleavage reaction than the PA polymers with only B-type linkages between the flavan-3-ol subunits.[18,42] Resistance to acid-catalyzed cleavage is likely due to the enhanced intermolecular forces resulting from the double linkages between the flavan-3-ol subunits characteristic of the A-type linkage group.[18,19] A kinetic study was conducted to determine the phloroglucinolysis reaction products produced over reaction time for saskatoon fruit PA extracts (from 'Thiessen' stage 1 fruits). The optimal reaction time was 20 min for the production of free A_2 dimer and epicatechin (EC) from terminal subunits and epicatechin-(4β→2)-phloroglucinol (EC−P) from the extension units of PAs from saskatoon fruits (the levels of these compounds were reduced at longer reaction times; Figure S3B−D, Supporting Information; see Figure S4 in the Supporting Information for depolymerized product structures). These data are consistent with PAs with B-type linkages from grape skin and seed, where a 20 min reaction time was optimal for releasing terminal subunits and production of phloroglucinol adducts (longer reaction times for PA extracts resulted in epicatechin terminal units forming undesirable C-2 phloroglucinol adducts).[19] Formation of A_2 dimer−phloroglucinol adducts (A_2−P) from the PA extension units was also detected in the phloroglucinolysis reaction products of saskatoon fruits, with approximately 80% of A_2−P production occurring within a 120 min reaction time (Figure S3A). In cranberry juice PA extracts, which contain higher levels of A-type PA linkages, 135 min was found to be the optimal reaction time for production of A_2−P in the phloroglucinolysis reaction.[18]

Typical HPLC chromatograms of the phloroglucinolysis products of PA extracts of saskatoon fruit ('Northline' stage 1) and grape skin and cranberry fruit standards are presented in Figure 7. The chemical structures of PA phloroglucinolysis products detected in the HPLC chromatograms are presented in Figure S4 in the Supporting Information. The major products from a 20 min phloroglucinolysis reaction in the saskatoon fruit and grape skin PA extracts are EC−P (peak 3), A_2−P (peak 5), EC (peak 7), and A_2 (peak 8) (Figure 7A). After the 120 min phloroglucinolysis reaction, the amount of EC (peak 7) was reduced, while that of A_2−P (peak 5) increased (compare 'Northline' chromatograms in panels A and B of Figure 7). These data demonstrate that the 120 min phloroglucinolysis reaction

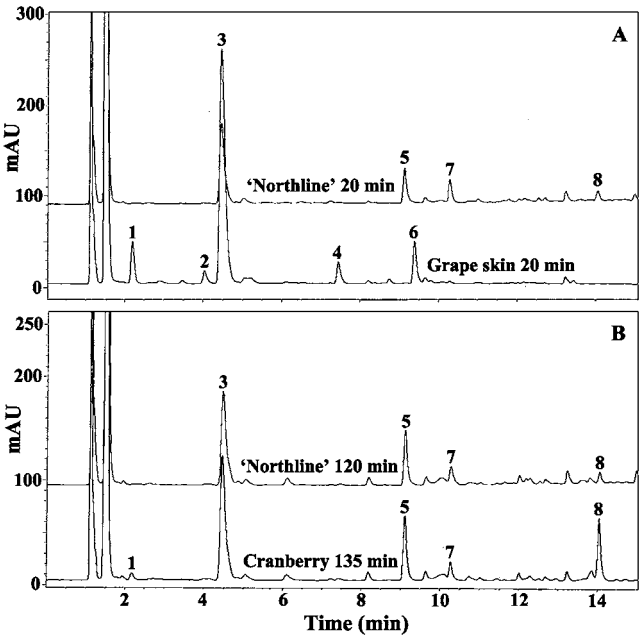

Figure 7. Reversed-phase HPLC chromatograms (monitored at 280 nm) of PA phloroglucinolysis products from 'Northline' stage 1 saskatoon fruit, cranberry fruit, and grape skin extracts: (A) comparison of 'Northline' 20 min reaction products with grape skin standard 20 min reaction products, (B) comparison of 'Northline' 120 min reaction products with cranberry standard 135 min reaction products. Peaks: 1, (−)-epigallocatechin-(4β→2)-phloroglucinol (EGC−P); 2, (+)-catechin-(4α→2)-phloroglucinol (C−P); 3, (−)-epicatechin-(4β→2)-phloroglucinol (EC−P); 4, (+)-catechin (C); 5, A_2−phloroglucinol (A_2−P); 6, (−)-epicatechin gallate-(4β→2)-phloroglucinol (ECG−P); 7, (−)-epicatechin (EC); 8, A_2. The two peaks detected prior to peak 1 are the reaction components ascorbic acid and phloroglucinol.

time is optimal for A_2−P quantitation but not for epicatechin quantitation. By comparing HPLC retention times and UV absorption spectra (data not shown) with those of known grape skin and cranberry fruit standards, saskatoon fruit PA flavan-3-ol extension units were confirmed to be nearly exclusively procyanidin (epicatechin; Figure 7, Table 3).

Our saskatoon PA composition data are consistent with those reported using fractionation with normal-phase semi-preparative HPLC followed by electrospray ionization coupled with tandem mass spectrometry (ESI-MS/MS) analysis of each PA oligomer fraction[43] and direct thiolysis of PA extracts with benzyl mercaptan followed by RP-HPLC analysis.[8] In the above-mentioned studies, PAs from mature saskatoon fruits were found to consist mainly of (−)-epicatechin subunits, with only B-type linkages reported. In this study, we found (−)-epicatechin−flavan-3-ol subunits were linked together by both B-type (peak 3, EC−P) and A-type (peak 5, A_2−P) linkages in the extension units, as well as the terminal units (peak 7, EC; peak 8, A_2) (Figure 7, Table 3). The abundance of A-type PA linkages varies with the cultivars, with 'Pembina' fruit having the greatest abundance of PA A-type linkages at most stages of fruit development (Table 3). Additionally, minimal amounts of (+)-catechin were detected in the PA extension subunits over fruit development in most cultivars (Table 3). The terminal subunits of PAs from saskatoon fruits consisted mainly of (−)-epicatechin (peak 7, Figure 7; Table 3), with a minor portion of (−)-epicatechin dimer in the A-type configuration (A_2, peak 8, Figure 7; Table 3). Only minimal

DOI: 10.1021/jf504722x
J. Agric. Food Chem. 2015, 63, 1601−1614

Table 3. Developmental Profile of Saskatoon Fruit PA Subunit Composition Following Phloroglucinolysis of Cultivars Altaglo, Honeywood, Northline, Pembina, and Thiessen[a]

	EGC−P	C−P	EC−P	A_2−P	C	EC	A_2	mDP	total PA content[b]
				'Altaglo'					
stage 4	nd[c]	1.9 ± 0.1[d]	78.4 ± 0.2	4.9 ± 1.3	1.1 ± 0.1	11.9 ± 2.1	1.8 ± 0.4	6.8 ± 0.7	321.2 ± 66.5
stage 5	nd	1.9 ± 0.1	79.3 ± 3.6	3.1 ± 2.5	0.8 ± 0.1	13.7 ± 0.7	1.2 ± 0.4	6.4 ± 0.5	316.6 ± 93.7
stage 7	nd	2.0 ± 0.1	71.4 ± 0.2	8.3 ± 0.0	1.0 ± 0.0	14.5 ± 0.4	2.8 ± 0.3	5.5 ± 0.0	86.4 ± 28.8
				'Honeywood'					
stage 1	nd	1.1 ± 0.1	75.8 ± 0.9	8.3 ± 0.0	1.1 ± 0.0	11.6 ± 0.7	2.1 ± 0.2	6.8 ± 0.4	484.8 ± 45.7
stage 4	nd	1.1 ± 0.1	73.4 ± 1.9	8.6 ± 1.2	0.9 ± 0.1	13.1 ± 1.0	2.9 ± 0.3	6.0 ± 0.3	253.2 ± 51.2
stage 5	nd	1.4 ± 0.2	75.3 ± 0.6	6.8 ± 0.3	0.9 ± 0.0	13.0 ± 0.0	2.6 ± 0.1	6.1 ± 0.2	147.1 ± 7.4
stage 7	nd	1.2 ± 0.1	74.1 ± 1.1	8.9 ± 1.1	0.5 ± 0.3	11.4 ± 0.0	3.9 ± 0.4	6.4 ± 0.5	71.3 ± 5.4
stage 9	nd	1.3 ± 0.0	81.5 ± 2.0	2.9 ± 1.1	1.2 ± 0.1	9.5 ± 1.0	3.5 ± 0.0	7.0 ± 0.4	104.2 ± 15.0
				'Northline'					
stage 1	nd	0.1 ± 0.1	72.6 ± 7.4	11.1 ± 4.6	0.7 ± 0.3	12.5 ± 2.0	3.1 ± 1.1	6.7 ± 1.4	246.2 ± 138.8
stage 4	nd	0.7 ± 0.1	85.0 ± 0.8	2.4 ± 0.4	1.2 ± 0.0	9.1 ± 0.1	1.6 ± 0.1	8.4 ± 0.2	327.0 ± 11.0
stage 5	nd	0.4 ± 0.2	77.8 ± 3.4	6.8 ± 2.1	0.8 ± 0.4	11.4 ± 1.0	2.7 ± 0.5	6.9 ± 0.7	140.2 ± 35.1
stage 7	nd	0.6 ± 0.1	80.6 ± 4.1	5.7 ± 2.7	1.1 ± 0.1	8.4 ± 0.9	2.2 ± 0.4	7.7 ± 0.8	73.7 ± 20.0
stage 9	nd	0.7 ± 0.1	82.8 ± 2.8	5.2 ± 1.8	1.0 ± 0.0	8.2 ± 0.9	2.2 ± 0.2	8.8 ± 0.8	62.0 ± 16.1
				'Pembina'					
stage 1	nd	0.4 ± 0.0	80.8 ± 0.6	5.9 ± 0.3	0.9 ± 0.0	10.6 ± 0.1	1.6 ± 0.2	7.7 ± 0.2	436.5 ± 64.6
stage 4	nd	nd	66.9 ± 2.2	14.8 ± 0.9	nd	13.6 ± 1.0	4.6 ± 0.4	5.5 ± 0.4	72.2 ± 16.6
stage 5	nd	nd	64.8 ± 4.5	16.1 ± 2.4	nd	13.6 ± 1.1	5.5 ± 1.1	5.4 ± 0.6	64.7 ± 13.9
stage 7	nd	nd	58.7 ± 5.2	18.1 ± 2.6	nd	17.5 ± 2.1	5.8 ± 0.9	4.5 ± 0.6	17.7 ± 4.5
stage 9	nd	nd	63.4 ± 0.7	18.2 ± 0.3	nd	13.0 ± 1.3	5.4 ± 0.3	5.4 ± 0.3	27.1 ± 0.1
				'Thiessen'					
stage 1	2.3 ± 0.4	1.0 ± 0.0	80.9 ± 0.3	2.5 ± 0.1	0.9 ± 0.0	11.8 ± 0.4	0.6 ± 0.1	7.5 ± 0.2	414.4 ± 83.8
stage 4	1.5 ± 0.8	1.4 ± 0.1	76.0 ± 1.6	5.7 ± 1.1	0.9 ± 0.0	13.0 ± 0.6	1.5 ± 0.6	6.5 ± 0.5	243.1 ± 5.0
stage 5	1.8 ± 0.2	1.2 ± 0.1	75.6 ± 0.9	7.3 ± 0.4	0.9 ± 0.1	12.0 ± 0.3	1.3 ± 0.2	7.1 ± 0.3	126.7 ± 21.7
stage 7	1.6 ± 0.9	1.4 ± 0.1	77.2 ± 2.8	6.2 ± 2.2	0.8 ± 0.1	11.2 ± 0.7	1.6 ± 0.7	7.5 ± 0.7	103.5 ± 12.7
stage 9	3.8 ± 1.5	0.7 ± 0.7	83.0 ± 1.8	2.4 ± 0.9	0.4 ± 0.4	9.3 ± 0.4	0.6 ± 0.1	9.7 ± 0.1	108.1 ± 12.7

[a]Abbreviations: EGC−P, (−)-epigallocatechin-(4β→2)-phloroglucinol; C−P, (+)-catechin-(4α→2)-phloroglucinol; EC−P, (−)-epicatechin-(4β→2)-phloroglucinol; C, (+)-catechin; A_2−P, A_2−phloroglucinol; EC, (−)-epicatechin; mDP, mean degree of polymerization. [b]Total PA content in milligrams per 100 g of fresh fruit weight. [c]nd = not detected. [d]Value of proportional composition (mol %). Data are the means of independent biological replicates ± SE, n = 2−4.

amounts of (+)-catechin (peak 4) from the terminal subunits were detected in saskatoon fruit over development (Table 3). These PA composition results suggest that either the flavonoid biosynthesis enzymes for synthesizing both (+)-catechin (leucoanthocyanidin reductase, LAR) and (−)-epicatechin (anthocyanidin synthase, ANS, anthocyanidin reductase, ANR) from leucocyanidin are present in saskatoon fruits or that (+)-catechin is produced by ANR epimerase activity.[44,45] Interestingly, the presence of (−)-epigallocatechin in the PA extension subunits was detected only in 'Thiessen' fruits, and it occurred at all developmental stages studied (Table 3). (−)-Epigallocatechin has three hydroxyl groups attached to the B-ring, whereas (−)-epicatechin has two (see Figure S4 in the Supporting Information). This suggests that both B-ring hydroxylases, flavonoid 3′-hydroxylase (F3′H) and flavonoid 3′,5′-hydroxylase (F3′5′H),[46] are present and active in 'Thiessen' fruits, where only F3′H is active in the other cultivars studied.

PA concentration (mg/100 g of fresh fruit weight) was higher during early fruit development and decreased as the fruit ripened in the saskatoon cultivars studied (Table 3, Figure 8). Similar PA accumulation patterns were observed over fruit development in bilberry,[34] strawberry,[47] and grape.[41] As supported by flavonoid gene expression data in blueberry fruit over development,[21] a likely scenario is that PA synthesis is limited to the early fruit developmental stages of saskatoon fruit, resulting in decreasing PA concentration as the fruit matures. The average PA polymer length (mDP) was relatively constant at 5−10 among all cultivars tested and over fruit development (Table 3). Our fruit PA mDP data are consistent with those of Bakowska-Barczak and Kolodziejczyk[8] for pigmented-fruit saskatoon cultivars at maturity. The PA composition and concentration of the white-fruited 'Altaglo' were similar to those of the pigmented-fruit cultivars (Table 3), suggesting that PA synthesis is not affected by the genetic modification(s) that result in the white fruit in 'Altaglo'. With respect to organoleptic properties, in general, PA polymers impart astringency to the fruit, while PA monomers are perceived as bitter.[48] The saskatoon PA mDP range is similar to that reported for blueberry fruit (7)[21] and apple fruit (4−8 in 14 of 16 varieties of French cider apples).[49]

The phloroglucinolysis reaction products of PAs from saskatoon fruit were further characterized by LC−MS/MS analysis. Saskatoon fruit C−P (RP-HPLC peak 2) and EC−P (RP-HPLC peak 3) had similar retention times, the same molecular ion mass of 413, and similar fragment ions compared to C−P and EC−P in the grape skin and cranberry fruit PA standards (Table 4). A_2−P (RP-HPLC peak 5) from saskatoon fruit had the same retention time and molecular ion mass of 699 and similar fragment ions compared to A_2−P in the cranberry fruit standard (Table 4), and these data are consistent with the RP-HPLC and positive ion mode LC−MS data for

DOI: 10.1021/jf504722x
J. Agric. Food Chem. 2015, 63, 1601−1614

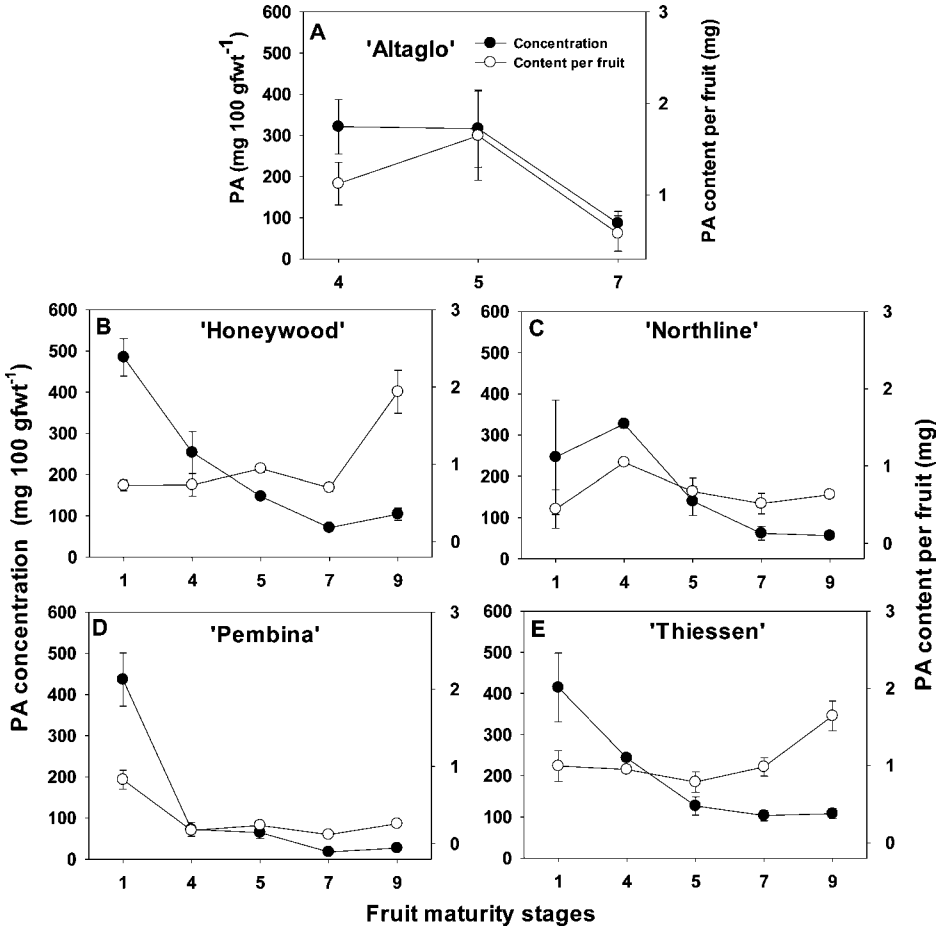

Figure 8. Total proanthocyanidin (PA) concentration and content of cultivars (A) Altaglo, (B) Honeywood, (C) Northline, (D) Pembina, and (E) Thiessen saskatoon fruits over development (stages 1, 4, 5, 7, and 9) expressed as milligrams per 100 g of fresh weight and milligrams per fruit. Data are the means of independent biological replicates ± SE, n = 2−4.

A_2−P in cranberry fruit extracts.[18] A_2 (HPLC peak 8) from saskatoon fruit also had the same retention time, molecular ion mass of 575, and fragment ions as A_2 in the cranberry fruit standard (Table 4). Possible A_2−P and A_2 ion fragmentation patterns in negative ion mode LC−MS are presented in Figure S5 in the Supporting Information according to the major fragment ions we observed (Table 4).

Localization of PAs in Saskatoon Fruit. 'Altaglo' fruit PA levels were similar to those in the pigmented-fruit cultivars (Table 3), but Altaglo fruits do not accumulate high levels of anthocyanins in the later stages of development. Therefore, PA localization was performed in 'Altaglo' fruits to avoid anthocyanin interference in the later stages of fruit development, as the PA-specific stain DMACA changes PAs to a dark-blue color, similar to that of anthocyanins. PAs accumulated in all the fruit tissues of stage 1 'Altaglo' fruit (Figure 9A,B,F), with intense staining in the exocarp (hypodermal layer), seed coat, and placental tissues. By stage 4, PA accumulation was the greatest in the hypodermal layer of the exocarp and seed coat tissues (Figure 9C,D). At fruit maturity (stage 9), PA staining was still clearly observed in the exocarp, placenta, and seed coat tissues (Figure 9E). Interestingly, in the hypodermal, mesocarp, and placental stage 1 fruit tissue of 'Altaglo', small DMACA-staining vesicles were observed within some cells, along with cells that stained for PAs within one large vacuole (Figure 9B,F). Similar small DMACA-staining vesicles were observed in the same fruit tissues in 'Altaglo' stage 4 fruit and 'Pembina' stage 1 and stage 4 fruit (data not shown). Small PA vesicles have also been observed via transmission electron microscopy (TEM) in the endothelial cells of *tds4-1* mutant seeds.[50] The occurrence of small DMACA-staining vesicles in the cells of young saskatoon fruit tissue (stages 1 and 4) is consistent with the hypothesis that the process of vacuolar formation involves a combination of specific vacuolar docking and fusion events and that vacuolar formation and PA biosynthesis may be coupled processes in the cell.[50]

In young seed coats (stage 1), PAs were localized mainly intercellularly in the cells of the innermost cell layer of the seed coat, around vascular bundle tissue, and in the ground parenchyma layers of the seed coat (Figure 10A). At seed maturity, the PAs in the seed coat ground parenchyma cell layers were localized within or adjacent to the cell wall region (Figure 10B). In *Arabidopsis* seeds, flavonols are localized in proximity to PAs, where they both become imbedded into the mature seed coat by enzyme-catalyzed oxidative polymerization.[51]

Additionally, as noted in the fluorescence light micrographs (Figure 6T,U), a perisperm layer (residual endosperm) was observed in mature saskatoon seeds (Figure 10B).

Overall, saskatoon fruits have a relatively simple anthocyanin profile that consists of four major anthocyanins that are monoglycosides of cyanidin. The dramatic increase in anthocyanins in all pigmented-fruited cultivars contrasts with the lack of this ripening-associated increase in anthocyanins in the white-fruited 'Altaglo'. This difference is consistent with the

DOI: 10.1021/jf504722x
J. Agric. Food Chem. 2015, 63, 1601−1614

Table 4. Characterization of Proanthocyanidin Phloroglucinolysis Products of 'Northline' Stage 1 Saskatoon Fruits and Cranberry Fruit and Grape Skin Standards by LC−MS

compd[a]	t_R[b] (min)	sample	$[M-H]^-$[c]	fragment ions
EC−P	23.8	'Northline'	413	287, 261
	23.6	grape skin[d]	413	287, 261
	23.7	cranberry[e]	413	287, 261
C−P	22.6	'Northline'	413	287, 261
	22.6	grape skin	413	287, 261
	21.9	synthesized	413	287, 261
A_2−P	32.3	'Northline'	699	547, 285
	32.3	cranberry	699	547
epicatechin	45.5	'Northline'	289	245, 137
	45.5	cranberry	289	245, 137
	45.5	grape skin	289	245, 137
catechin	34.7	'Northline'	289	245, 137
	34.7	grape skin	289	245, 137
	34.7	cranberry	289	245, 137
	33.2	standard	289	245, 137
A_2	53.3	'Northline'	575	423, 285
	53.2	cranberry	575	423, 285

[a]Abbreviations: EC−P, (−)-epicatechin-(4β→2)-phloroglucinol; C−P, (+)-catechin-(4α→2)-phloroglucinol; A_2−P, A_2−phloroglucinol. [b]Retention time. The blueberry, grape skin, and cranberry samples were run at different times, leading to some variation in t_R between the same compounds in the different samples. [c]MS was run in the negative mode, and all the molecular ions are $[M-H]^-$. [d]The grape skin PA sample was processed as described by Kennedy and Taylor.[20] Fraction 5 was used (eluent from the solvent system consisting of (v/v/v) 20% acetone, 65% methanol, and 15% water with the solvent−water mixture containing 0.2% (v/v) formic acid). [e]The cranberry PA sample was processed as described by Koerner et al.[18]

loss of transcription factor activity in 'Altaglo' fruit that up-regulates the transcription of genes for anthocyanin production as the fruit transitions into the ripening phase, as documented in the flavonoid pathways of fruits of other plant species such as grape and apple.[26,27,34,52] High anthocyanin levels in the mature fruit might function to alleviate oxidative stress as the fruit ripens,[53] and the intense fruit coloration may function to attract animals for seed dispersal.[12]

Flavonols identified in saskatoon fruits were glycosides of quercetin. Previously identified flavonols in saskatoon fruit were confirmed, and two quercetin triglycosides were newly identified. PAs were composed mainly of (−)-epicatechin, with not only B-type, but also A-type, subunit linkages. Variation in PA flavan-3-ol subunit composition was also detected among the cultivars tested ['Thiessen' fruit PAs contained both (−)-epigallocatechin (three hydroxyl groups attached to the B-ring) and (−)-epicatechin (two hydroxyl groups attached to the B-ring), and only (−)-epicatechin was detected in the other four cultivars], making saskatoon fruit an interesting model for further understanding and manipulating flavonol B-ring hydroxylases for production of flavonoids with a specific compositional structure.

Flavonols and PAs were quantified and localized in saskatoon fruit over development. Our studies suggest that both flavonols and PAs are localized to similar tissues within the fruit, with higher levels, in general, observed during early fruit development. In the seed, both flavonols and PAs localized mainly to the seed coat. Flavonols and PAs are noted for their protective/defense function in plants. Our studies support that these

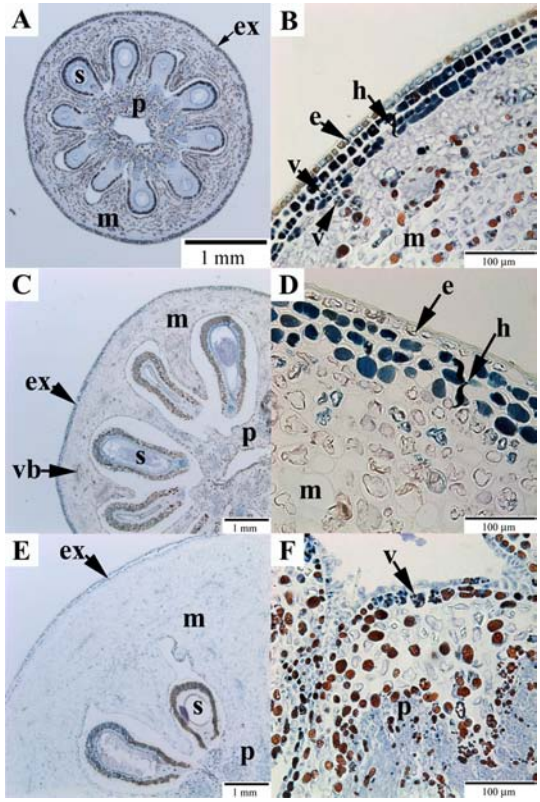

Figure 9. Light microscopic images of 'Altaglo' saskatoon fruit cross sections stained with DMACA for PA visualization: (A) stage 1 fruit, (B) stage 1 exocarp and mesocarp at 40× magnification, (C) stage 4 fruit, (D) stage 4 exocarp and mesocarp at 40× magnification, (E) stage 9 fruit, (F) stage 1 placenta at 40× magnification. Scale bars in panels A, C, and E are 1 mm, and panels B, D, and F are 100 μm. Abbreviations: e, epidermis; ex, exocarp (including cuticle, epidermis, and hypodermis); h, hypodermis; m, mesocarp; p, placenta; s, seed; v, small DMACA-staining vesicles with a cell; vb, vascular bundle.

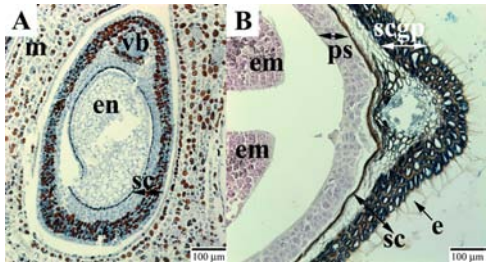

Figure 10. Light microscopic images of 'Pembina' saskatoon seed cross sections stained with DMACA for PA visualization: (A) Stage 1 seed at 20× magnification, (B) stage 7 seed at 20× magnification. Abbreviations: sc, seed coat; em, embryo; en, endosperm; ps, perisperm; vb, vascular bundle; m, mesocarp of fruit wall; e, epidermis of seed coat; scgp, ground parenchyma layers of seed coat staining for PAs.

compounds are developmentally regulated and tissue localized in the fruits and seeds of saskatoons to provide protection/defense during the reproductive and germination phase of this species. Also, their greater presence in immature fruit may also, through their astringency, help deter frugivores from consuming fruit prior to ripening.

The accumulation of anthocyanins, flavonols, and PAs in ripe saskatoon fruit, particularly in the fruit exocarp (skin) and the seed coats of seeds within the fruit, makes the consumption of these fruits a good source for flavonoids purported to impart

DOI: 10.1021/jf504722x
J. Agric. Food Chem. 2015, 63, 1601−1614

health-beneficial effects.[54] Future studies to understand the transcriptional mechanisms of the regulation of the flavonoid pathway during fruit ripening would be beneficial to provide further insight for further enhancing health-beneficial flavonoid content in saskatoon fruits.

■ ASSOCIATED CONTENT

Supporting Information

(Table S1) characteristic retention time and fragment ion masses of quercetin triglycosides in saskatoon fruit extracts as determined by LC−MS analysis, (Figure S1) full mass spectrum (from 100 to 1500 amu) of the flavonol-type compound 2c, (Figure S2) full mass spectrum (from 100 to 1250 amu) of the flavonol-type compound 2g, (Figure S3) effect of the phloroglucinolysis reaction time on the production of flavan-3-ols and flavan-3-ol−phloroglucinol adducts from fruit extracts, (Figure S4) chemical structures of depolymerized products following phloroglucinolysis of saskatoon fruit, grape skin, and cranberry fruit PA extracts, (Figure S5) possible fragmentation patterns of A_2−P and A_2 in a negative ion mode LC−MS system, and text describing anthocyanin and flavonol analysis and histochemical localization of PAs and flavonols. This material is available free of charge via the Internet at http://pubs.acs.org.

■ AUTHOR INFORMATION

Corresponding Author

*Phone: 780-492-2653. Fax: 780-492-4265. E-mail: jocelyn.ozga@ualberta.ca.

Present Addresses

[§]J.A.K.: Department of Viticulture and Enology, California State University, Fresno, CA 93740.

[∥]J.L.K.-S.: Research & Development, Betty Lou's Inc., 750 SE Booth Bend Road, McMinnville, OR 97128.

Funding

This work was funded in part by an Alberta BioSolutions grant to J.A.O. and D.M.R.

Notes

The authors declare no competing financial interest.

■ ACKNOWLEDGMENTS

We thank Randall Weselake (University of Alberta) and his group for help with the HPLC-DAD for flavonoid identification and quantitation.

■ ABBREVIATIONS USED

A_2−P, A_2−phloroglucinol; ANS, anthocyanidin synthase; ANR, anthocyanidin reductase; C, catechin; C−P, catechin-(4α→2)-phloroglucinol; cyn-arb, cyanidin 3-*O*-arabinoside; cyn-gal, cyanidin 3-*O*-galactoside; cyn-glu, cyanidin 3-*O*-glucoside; cyn-xyl, cyanidin 3-*O*-xyloside; DAD, diode array detector; DMACA, 4-(dimethylamino)cinnamaldehyde; DPBA, diphenylboric acid 2-aminoethyl ester; EC, epicatechin; EC−P, epicatechin-(4β→2)-phloroglucinol; EGC−P, epigallocatechin-(4β→2)-phloroglucinol; ECG−P, epicatechin gallate-(4β→2)-phloroglucinol; ESI, electrospray ionization; F3′H, flavonoid 3′-hydroxylase; F3′5′H, flavonoid 3′,5′-hydroxylase; FFW, fresh fruit weight; HPLC, high-performance liquid chromatography; LC−MS, liquid chromatography−mass spectrometry; LC−MS/MS, liquid chromatography−tandem mass spectrometry; mDP, mean degree of polymerization; NMR, nuclear magnetic resonance spectroscopy; PA, proanthocyanidin; PEM, Paraplast tissue embedding medium; Q-arb-glu, quercetin 3-*O*-arabinoglucoside; Q-arb, quercetin 3-*O*-arabinoside; Q-gal, quercetin 3-*O*-galactoside; Q-glu, quercetin 3-*O*-glucoside; Q-rub, quercetin 3-*O*-robinobioside + quercetin 3-*O*-rutinoside; Q-xyl, quercetin 3-*O*-xyloside; RP, reversed phase; TEM, transmission electron microscopy; TFA, trifluoroacetic acid

■ REFERENCES

(1) Prior, R. L., Absorption and metabolism of anthocyanins: potential health effects. In *Phytochemicals: Mechanisms of Action*; CRC Press-Taylor & Francis Group: Boca Raton, FL, 2004; pp 1−19.

(2) Martineau, L. C.; Couture, A.; Spoor, D.; Benhaddou-Andaloussi, A.; Harris, C.; Meddah, B.; Leduc, C.; Burt, A.; Vuong, T.; Le, P. M.; Prentki, M.; Bennett, S. A.; Arnason, J. T.; Haddad, P. S. Anti-diabetic properties of the Canadian lowbush blueberry *Vaccinium angustifolium* Ait. *Phytomedicine* **2006**, *13*, 612−623.

(3) Crozier, A.; Jaganath, I. B.; Clifford, M. N. Dietary phenolics: chemistry, bioavailability and effects on health. *Nat. Prod. Rep.* **2009**, *26*, 1001−1043.

(4) St-Pierre, R. G. *Growing Saskatoons—A Manual for Orchardists*, 5th ed.; Department of Horticulture Science, University of Saskatchewan: Saskatoon, Canada, 1997; p 338.

(5) Spencer, R., Saskatoon Berry Production: Alberta Farm Fresh School, 2014. http://www.agric.gov.ab.ca/crops/hort/bv2014/saskatoon-berry-production.pdf. (accessed online on September 1, 2014).

(6) Lavola, A.; Karjalainen, R.; Julkunen-Tiitto, R. Bioactive polyphenols in leaves, stems, and berries of saskatoon (*Amelanchier alnifolia* Nutt.) cultivars. *J. Agric. Food Chem.* **2012**, *60*, 1020−1027.

(7) Ozga, J. A.; Saeed, A.; Wismer, W.; Reinecke, D. M. Characterization of cyanidin- and quercetin-derived flavonoids and other phenolics in mature saskatoon fruits (*Amelanchier alnifolia* Nutt.). *J. Agric. Food Chem.* **2007**, *55*, 10414−10424.

(8) Bakowska-Barczak, A. M.; Kolodziejczyk, P. Evaluation of saskatoon berry (*Amelanchier alnifolia* Nutt.) cultivars for their polyphenol content, antioxidant properties, and storage stability. *J. Agric. Food Chem.* **2008**, *56*, 9933−9940.

(9) Mazza, G. Anthocyanins and other phenolic-compounds of saskatoon berries (*Amelanchier Alnifolia* Nutt). *J. Food Sci.* **1986**, *51*, 1260−1264.

(10) Rogiers, S. Y.; Knowles, N. R. Physical and chemical changes during growth, maturation, and ripening of saskatoon (*Amelanchier alnifolia*) fruit. *Can. J. Bot.* **1997**, *75*, 1215−1225.

(11) McGarry, R.; Ozga, J. A.; Reinecke, D. M. The effects of ethephon on saskatoon (*Amelanchier alnifolia* Nutt.) fruit ripening. *J. Am. Soc. Hort. Sci.* **2005**, *130*, 12−17.

(12) Schaefer, H. M.; Schaefer, V.; Levey, D. J. How plant-animal interactions signal new insights in communication. *Trends Ecol. Evol.* **2004**, *19*, 577−584.

(13) Hosseinian, F. S.; Beta, T. Saskatoon and wild blueberries have higher anthocyanin contents than other Manitoba berries. *J. Agric. Food Chem.* **2007**, *55*, 10832−10838.

(14) Middleton, E. M.; Teramura, A. H. The role of flavonol glycosides and carotenoids in protecting soybean from ultraviolet-B damage. *Plant Physiol.* **1993**, *103*, 741−752.

(15) Kolb, C. A.; Kopecky, J.; Riederer, M.; Pfundel, E. E. UV screening by phenolics in berries of grapevine (*Vitis vinifera*). *Funct. Plant Biol.* **2003**, *30*, 1177−1186.

(16) Aron, P. M.; Kennedy, J. A. Flavan-3-ols: nature, occurrence and biological activity. *Mol. Nutr. Food Res.* **2008**, *52*, 79−104.

(17) Gu, L. W.; Kelm, M. A.; Hammerstone, J. F.; Beecher, G.; Holden, J.; Haytowitz, D.; Prior, R. L. Screening of foods containing proanthocyanidins and their structural characterization using LC−MS/MS and thiolytic degradation. *J. Agric. Food Chem.* **2003**, *51*, 7513−7521.

(18) Koerner, J. L.; Hsu, V. L.; Lee, J. M.; Kennedy, J. A. Determination of proanthocyanidin A2 content in phenolic polymer isolates by reversed-phase high-performance liquid chromatography. *J. Chromatogr. A* **2009**, *1216*, 1403−1409.

DOI: 10.1021/jf504722x
J. Agric. Food Chem. 2015, 63, 1601−1614

(19) Kennedy, J. A.; Jones, G. P. Analysis of proanthocyanidin cleavage products following acid-catalysis in the presence of excess phloroglucinol. *J. Agric. Food Chem.* **2001**, *49*, 1740−1746.
(20) Kennedy, J. A.; Taylor, A. W. Analysis of proanthocyanidins by high-performance gel permeation chromatography. *J. Chromatogr. A* **2003**, *995*, 99−107.
(21) Zifkin, M.; Jin, A.; Ozga, J. A.; Zaharia, L. I.; Schernthaner, J. P.; Gesell, A.; Abrams, S. R.; Kennedy, J. A.; Constabel, C. P. Gene expression and metabolite profiling of developing highbush blueberry (*Vaccinium corymbosum* L.) fruit indicates transcriptional regulation of flavonoid metabolism and activation of abscisic acid metabolism. *Plant Physiol.* **2012**, *158*, 200−224.
(22) Gutmann, M.; Feucht, W. A new method for selective localization of flavan-3-ols in plant tissues involving glycolmethacrylate embedding and microwave irradiation. *Histochemistry* **1991**, *96*, 83−86.
(23) McGarry, R.; Ozga, J. A.; Reinecke, D. M. Patterns of saskatoon (*Amelanchier alnifolia* Nutt.) fruit and seed growth. *J. Am. Soc. Hort. Sci.* **1998**, *123*, 26−29.
(24) Wu, X. L.; Beecher, G. R.; Holden, J. M.; Haytowitz, D. B.; Gebhardt, S. E.; Prior, R. L. Concentrations of anthocyanins in common foods in the United States and estimation of normal consumption. *J. Agric. Food Chem.* **2006**, *54*, 4069−4075.
(25) Prior, R. L.; Lazarus, S. A.; Cao, G. H.; Muccitelli, H.; Hammerstone, J. F. Identification of procyanidins and anthocyanins in blueberries and cranberries (*Vaccinium* spp.) using high-performance liquid chromatography/mass spectrometry. *J. Agric. Food Chem.* **2001**, *49*, 1270−1276.
(26) Deluc, L.; Bogs, J.; Walker, A. R.; Ferrier, T.; Decendit, A.; Merillon, J. M.; Robinson, S. P.; Barrieu, F. The transcription factor VvMYB5b contributes to the regulation of anthocyanin and proanthocyanidin biosynthesis in developing grape berries. *Plant Physiol.* **2008**, *147*, 2041−2053.
(27) Kobayashi, S.; Ishimaru, M.; Hiraoka, K.; Honda, C. Myb-related genes of the Kyoho grape (*Vitis labruscana*) regulate anthocyanin biosynthesis. *Planta* **2002**, *215*, 924−933.
(28) Llorach, R.; Gil-Izquierdo, A.; Ferreres, F.; Tomas-Barberan, F. A. HPLC-DAD-MS/MS ESI characterization of unusual highly glycosylated acylated flavonoids from cauliflower (*Brassica oleracea* L. var. *botrytis*) agroindustrial byproducts. *J. Agric. Food Chem.* **2003**, *51*, 3895−3899.
(29) Bonaccorsi, P.; Caristi, C.; Gargiulli, C.; Leuzzi, U. Flavonol glucoside profile of southern Italian red onion (*Allium cepa* L.). *J. Agric. Food Chem.* **2005**, *53*, 2733−2740.
(30) Cuyckens, H.; Claeys, M. Mass spectrometry in the structural analysis of flavonoids. *J. Mass Spectrom.* **2004**, *39*, 1−15.
(31) Offen, W.; Martinez-Fleites, C.; Yang, M.; Kiat-Lim, E.; Davis, B. G.; Tarling, C. A.; Ford, C. M.; Bowles, D. J.; Davies, G. J. Structure of a flavonoid glucosyltransferase reveals the basis for plant natural product modification. *EMBO J.* **2006**, *25*, 1396−1405.
(32) Bovy, A.; de Vos, R.; Kemper, M.; Schijlen, E.; Pertejo, M. A.; Muir, S.; Collins, G.; Robinson, S.; Verhoeyen, M.; Hughes, S.; Santos-Buelga, C.; van Tunen, A. High-flavonol tomatoes resulting from the heterologous expression of the maize transcription factor genes LC and C1. *Plant Cell* **2002**, *14*, 2509−2526.
(33) Castrejon, A. D. R.; Elchholz, I.; Rohn, S.; Kroh, L. W.; Huyskens-Keil, S. Phenolic profile and antioxidant activity of highbush blueberry (*Vaccinium corymbosum* L.) during fruit maturation and ripening. *Food Chem.* **2008**, *109*, 564−572.
(34) Jaakola, L.; Maatta, K.; Pirttila, A. M.; Torronen, R.; Karenlampi, S.; Hohtola, A. Expression of genes involved in anthocyanin biosynthesis in relation to anthocyanin, proanthocyanidin, and flavonol levels during bilberry fruit development. *Plant Physiol.* **2002**, *130*, 729−739.
(35) Schnitzler, J. P.; Jungblut, T. P.; Heller, W.; Kofferlein, M.; Hutzler, P.; Heinzmann, U.; Schmelzer, E.; Ernst, D.; Langebartels, C.; Sandermann, H. Tissue localization of UV-B screening pigments and of chalcone synthase mRNA in needles of Scots pine seedlings. *New Phytol.* **1996**, *132*, 247−258.
(36) Peer, W. A.; Brown, D. E.; Tague, B. W.; Muday, G. K.; Taiz, L.; Murphy, A. S. Flavonoid accumulation patterns of transparent testa mutants of Arabidopsis. *Plant Physiol.* **2001**, *126*, 536−548.
(37) Solovchenko, A.; Merzlyak, M. Optical properties and contribution of cuticle to UV protection in plants: experiments with apple fruit. *Photochem. Photobiol. Sci.* **2003**, *2*, 861−866.
(38) Haughn, G.; Chaudhury, A. Genetic analysis of seed coat development in Arabidopsis. *Trends Plant Sci.* **2005**, *10*, 472−477.
(39) Wada, S.; Kennedy, J. A.; Reed, B. M. Seed-coat anatomy and proanthocyanidins contribute to the dormancy of *Rubus* seed. *Sci. Hort.* **2011**, *130*, 762−768.
(40) Markham, K. R.; Ryan, K. G.; Gould, K. S.; Rickards, G. K. Cell wall sited flavonoids in lisianthus flower petals. *Phytochemistry* **2000**, *54*, 681−687.
(41) Kennedy, J. A.; Hayasaka, Y.; Vidal, S.; Waters, E. J.; Jones, G. P. Composition of grape skin proanthocyanidins at different stages of berry development. *J. Agric. Food Chem.* **2001**, *49*, 5348−5355.
(42) Kimura, H.; Ogawa, S.; Akihiro, T.; Yokota, K. Structural analysis of A-type or B-type highly polymeric proanthocyanidins by thiolytic degradation and the implication in their inhibitory effects on pancreatic lipase. *J. Chromatogr. A* **2011**, *1218*, 7704−7712.
(43) Hellstrom, J.; Sinkkonen, J.; Karonen, M.; Mattila, P. Isolation and structure elucidation of procyanidin oligomers from saskatoon berries (*Amelanchier alnifolia*). *J. Agric. Food Chem.* **2007**, *55*, 157−164.
(44) Gargouri, M.; Chaudiere, J.; Manigand, C.; Mauge, C.; Bathany, K.; Schmitter, J. M.; Gallois, B. The epimerase activity of anthocyanidin reductase from *Vitis vinifera* and its regiospecific hydride transfers. *Biol. Chem.* **2010**, *391*, 219−227.
(45) Pang, Y. Z.; Abeysinghe, I. S. B.; He, J.; He, X. Z.; Huhman, D.; Mewan, K. M.; Sumner, L. W.; Yun, J. F.; Dixon, R. A. Functional characterization of proanthocyanidin pathway enzymes from tea and their application for metabolic engineering. *Plant Physiol.* **2013**, *161*, 1103−1116.
(46) Winkel-Shirley, B. Flavonoid biosynthesis. A colorful model for genetics, biochemistry, cell biology, and biotechnology. *Plant Physiol.* **2001**, *126*, 485−493.
(47) Halbwirth, H.; Puhl, I.; Haas, U.; Jezik, K.; Treutter, D.; Stich, K. Two-phase flavonoid formation in developing strawberry (*Fragaria* x *ananassa*) fruit. *J. Agric. Food Chem.* **2006**, *54*, 1479−1485.
(48) Robichaud, J.; Noble, A. Astringency and bitterness of selected phenolics in wine. *J. Sci. Food Agric.* **1990**, *53*, 343−353.
(49) Sanoner, P.; Guyot, S.; Marnet, N.; Molle, D.; Drilleau, J. Polyphenol profiles of French cider apple varieties (*Malus domestica* sp.). *J. Agric. Food Chem.* **1999**, *47*, 4847−4853.
(50) Abrahams, S.; Lee, E.; Walker, A. R.; Tanner, G. J.; Larkin, P. J.; Ashton, A. R. The *Arabidopsis* TDS4 gene encodes leucoanthocyanidin dioxygenase (LDOX) and is essential for proanthocyanidin synthesis and vacuole development. *Plant J.* **2003**, *35*, 624−636.
(51) Pourcel, L.; Routaboul, J.-M.; Kerhoas, L.; Caboche, M.; Lepiniec, L.; Debeaujon, I. *TRANSPARENT TESTA10* encodes a laccase-like enzyme involved in oxidative polymerization of flavonoids in *Arabidopsis* seed coat. *Plant Cell* **2005**, *17*, 2966−2980.
(52) Espley, R. V.; Hellens, R. P.; Putterill, J.; Stevenson, D. E.; Kutty-Amma, S.; Allan, A. C. Red colouration in apple fruit is due to the activity of the MYB transcription factor, MdMYB10. *Plant J.* **2007**, *49*, 414−427.
(53) Rogiers, S. Y.; Kumar, G. N. M.; Knowles, N. R. Maturation and ripening of fruit of *Amelanchier alnifolia* Nutt. are accompanied by increasing oxidative stress. *Ann. Bot.* **1998**, *81*, 203−211.
(54) Juríková, T.; Balla, S.; Sochor, J.; Pohanka, M.; Mlcek, J.; Baron, M. Flavonoid profile of saskatoon berries (*Amelanchier alnifolia* Nutt.) and their health promoting effects. *Molecules* **2013**, *18*, 12571−12586.

DOI: 10.1021/jf504722x
J. Agric. Food Chem. 2015, 63, 1601−1614

(PEG 400), dimethyl sulfoxide (DMSO), ethanol (EtOH), methanol (MeOH), sodium dihydrogen orthophosphate ($NaH_2PO_4 \cdot 2H_2O$), anhydrous disodium hydrogen phosphate (Na_2HPO_4), and dichloromethane (CH_2Cl_2) were all purchased from Sinopharm Chemical Reagent Co., Ltd. (China). (+)-Limonene was purchased from J&K Scientific (New Jersey, USA). Mushroom tyrosinase (3130 units/mg), L-tyrosine, kojic acid, ascorbic acid (V_C), and 4-hexylresorcinol (4-HR) were purchased from Sigma Chemical Co (St. Louis, MO, USA). HPLC grade solvents were purchased from J&K Scientific. Norartocarpetin (NorA) was isolated from the wood of *A. heterophyllus* in our previous study.[3]

HPLC-DAD Analysis of NorA. The analytical HPLC system consisted of a Shimadzu LC-20AT series pumping system, an SIL-20A automatic injector, an SPD-M20A UV−visible detector, and Class-Vp chromatography data station software. All samples were analyzed by HPLC using a reverse-phase GraceSmart column (4.6 μm, 2.1 × 250 mm, Ryss Tech Ltd., China) at 25 °C with a Shimadzu HPLC system. Norartocarpetin was detected at 352 nm by a gradient elution with water containing 0.5% formic acid (solvent A) and methanol (solvent B) as a mobile phase. For the elution program, the gradient elution was as follows: initial, 20% B; 0−10 min, 20−60% B; 10−20 min, 60−100% B; 20−25 min, 100% B; 25−30 min, 100−20% B. The flow rate was set at 1.0 mL/min. The sample injection volume was 10 μL. Three injections were performed for each sample. The calibration curve of NorA in the concentration range of 3.125−50.0 μg/mL was linear with a correlation coefficient of 0.9995.

Solubility Studies. The solubility of NorA was determined in different oils, surfactants, and cosurfactants to find the appropriate constituents of microemulsions. An excess amount of NorA was added in 2 mL of ethyl butyrate, ethyl oleate, (+)-limonene, peppermint oil, Tween 80, Tween 40, Tween 20, ethanol, glycerin, PEG 400, 1,2-propanediol, and *n*-octanol. The mixtures were shaken reciprocally at 25 °C for 48 h to reach equilibrium using a magnetic stirrer (Genius 3 vortex and RW 20D magnetic stirrer, IKA Laboratory Technology, Germany). Each sample was centrifuged at 10000*g* for 20 min (Jintanshi Jinchengguosheng Shiyanyiqichang, Jiangsu, China), followed by filtering through a 0.45 μm membrane filter. The concentration of NorA was determined by HPLC analysis at appropriate dilution with methanol. The solubility was determined in triplicate.

Construction of Pseudoternary Phase Diagrams. Pseudoternary phase diagrams were constructed to obtain the concentration of all components of ME. Pseudoternary phase diagrams were constructed according to the water titration method.[18] Different weight ratios (S_{mix}) of surfactants and cosurfactants were mixed first, the S_{mix} ratio varying from 1:1 to 2:1 to 3:1. For each S_{mix} ratio, a pseudoternary phase diagram was elaborated by testing the weight ratios of oil/S_{mix} of 5:95, 10:90, 20:80, 30:70, 40:60, 50:50, 60:40, 70:30, 80:20, 90:10, and 95:5. Water was added drop by drop to each oily mixture under magnetic stirring (Genius 3 vortex and RW 20D magnetic stirrer, IKA Laboratory Technology) at room temperature. After being equilibrated, each sample was visually checked and determined as a clear microemulsion. The pseudoternary phase diagram was drawn by OriginPro for Windows version 9.0.

Preparation and Solubility Determination of NorA-Loaded ME. The selected formulas based on phase diagram and NorA solubility were prepared by mixing ethyl oleate, Tween 80, and PEG 400 together, and then the required quantity of water was added and stirred to form a clear and transparent dispersion. All ME were stored to achieve equilibrium at room temperature for at least 24 h before further investigation. To determine the maximum loading capacity of NorA in ME, increasing amounts of NorA were loaded to the base ME.[18,23] The mixture was stirred for 24 h at 25 ± 1 °C. The undissolved NorA was removed by centrifugation at 10000*g* (DL-5-B table model large capacity centrifuge, Shanghai Anting Scientific Instrument Factory, Shanghai, China) for 20 min, and then supernatant was taken and the encapsulation efficiency was quantified by HPLC-DAD at 352 nm after 100-fold dilution with methanol. The analyses were performed in triplicate.

Characterization of MEs. The appearance of ME was determined by visual inspection of clarity, turbidity, phase separation, and color. The conductivity, mean particle size, and polydispersity index (PI) were determined by three independent experiments.

Physical Properties. Physical properties of blank ME and NorA ME were characterized for pH and conductivity using a pH meter (Mettler Toledo, Shanghai, China) and conductivity meter (Mettler Toledo) at 25 ± 1 °C.

Particle Size Analysis. The mean particle diameter of the ME was determined by photon correlation spectroscopy using a Zetasizer Nano ZS (Marvern Instruments, Worcestershire, UK). Each size analysis lasted 180 s and was performed with an angle detection of 90°. The measurements of samples without dilution were performed at 25 ± 0.1 °C.

Morphology. Morphology of NorA ME was observed using a transmission electron microscope (TEM, JEOL JEM2100, Eindhoven, The Netherlands). One drop of NorA ME sample was deposited on a formvar film-coated copper grid and allowed to dry before TEM observation.

Stability Studies. The thermodynamic stability of ME systems was investigated visually for phase separation after their centrifugation at 10000*g* for 20 min at room temperature (25 ± 1 °C). Stability tests using accelerated condition by cooling−heating wee conducted at 4 and 40 °C for 24 h for six cycles. Long-term stability testing at room temperature (20−37 °C) for 8 weeks was also performed. Their chemical and physical stabilities were studied and recorded by monitoring the occurrence of phase separation, dispersed phase size, and NorA content before and after the stability tests. The particle size of the ME was evaluated by laser light scattering technique at 25 ± 0.1 °C. NorA content was measured by HPLC-DAD method.

Tyrosinase Inhibition Activity of NorA ME. The tyrosinase inhibitory activity of NorA ME was determined by spectrophotometric method (UV-5300PC spectrophotometer, Metash Instrument Co., Ltd., Shanghai, China) as described in our previous study.[3] Briefly, the prepared ME were first diluted to 20, 10, 5, 2.5, 1.25, and 0.625 μg/mL with deionized water. Each of the sample solutions (300 μL) was diluted with 700 μL of 0.05 mM sodium phosphate buffer (pH 6.8) in the test tubes, followed by the addition of 1 mL of 0.1 mg/mL L-tyrosine and finally 1.0 mL of mushroom tyrosinase solution (200 units/mL). Thirty microliters of DMSO and a kojic acid solution was used as the blank reference and positive control, respectively. The reaction mixtures (3.0 mL) were mixed by vortex, and the initial absorbance at 492 nm was measured. After incubation for 20 min at 37 °C, the final absorbance at the same wavelength was taken. The IC_{50} values, which represent the concentrations of ME at which 50% of the tyrosinase activity was inhibited, were determined. The percent inhibition of tyrosinase activity was calculated as follows:

$$\%\ \text{inhibition} = [(A_2 - A_1) - (B_2 - B_1)]/(A_2 - A_1) \times 100$$

A_1 is the absorbance at 492 nm of the blank at 0 min, A_2 is the absorbance at 492 nm of the blank at 20 min, B_1 is the absorbance at 492 nm of test sample at 0 min, and B_2 is the absorbance at 492 nm of test sample at 20 min.

Antibrowning Effects of NorA ME on Fresh-Cut Apple Slices. Apples of comparable size were cleaned and cut into 4 mm thick slices and then treated by dipping in 500 mL of the corresponding test solutions for 5 min and drained. Samples were then placed in plastic Petri dishes, sealed with parafilm, and stored at room temperature for 24 h. Replicate samples were prepared for each treatment, and the experiment was repeated three times. Test solutions used for the above samples included aqueous solutions of blank ME, 0.5% V_C, 0.01% NorA ME, 0.01% 4-HR + 0.5% V_C, and 0.01% NorA ME + 0.5% V_C. Visual assessment of color development in the samples was performed with a digital camera, whereas the relative extents of browning were measured with a tristimulus reflectance colorimeter. The center of the apple slices was in touch with the lens of the Minolta CR-400 Chroma meter (Konica Minolta Sensing, Inc., Japan) when the readings (a^* values) were taken. Measurements were made immediately following each treatment and at timed intervals of 3, 6, 12, and 24 h thereafter.

DOI: 10.1021/jf5048805
J. Agric. Food Chem. 2015, 63, 1615−1621

Statistical Analysis. All of the measurements were carried out in triplicate. An analysis of variance (ANOVA) of the data was performed using the SPSS 13.0 statistical analysis system. The treatments were considered to be significantly different at $p < 0.05$.

RESULTS AND DISCUSSION

Solubility Study in Various Vehicles. The solubility of NorA in different vehicles was determined and is listed in Table 1. On the basis of the results, NorA showed the highest solubility in ethyl oleate among four oils. It is considerably higher than its solubility in water, although the solubility in oils is limited. Among the three surfactants, Tween 80 showed the best solubility for NorA relative to Tween 20 and Tween 40, up to 3.63 mg/mL. The solubility values of NorA in surfactants are much higher compared to oils. Tween 80 is one of the polysorbates (ethoxylated sorbitan esters) belonging to a nonionic surfactant; it is widely used as an emulsifier and dispersing agent for pharmaceutical products and as an emulsifier in food products. Meanwhile, it is reported that the concentration of Tween 80 in the systems greatly affected the appearance and stability of the systems.[24] Low concentrations of Tween 80 (1−4% w/w) resulted in a milky white layer and relatively large droplets of the system, whereas higher concentrations of Tween 80 (>15% w/w) led to homogeneous transparent liquids and very small particles.[24] Although the content of Tween 80 is not clearly defined, it is necessary to reduce the content of surfactant to obtain ideal ME without potential side effects.[20,25] The content of Tween 80 was controlled in the range of 10−20% in this study to form the transparent ME. Among all of the cosurfactants, PEG 400 has the best solubility values of NorA. PEG 400 is a low-molecular-weight grade of polyethylene glycol. It is a clear, colorless, and odorless liquid, it is strongly hydrophilic, and it can be soluble in water, acetone, alcohols, benzene, glycerin, glycols, and aromatic hydrocarbons.[26] Due to its low toxicity, it is widely used in foods, pharmaceuticals, and personal and home care products as a solvent or solubilizing agent.[27] On the basis of these advantages and great solubility for NorA, PEG 400 was chose as cosurfactant for NorA ME. On the basis of solubility results, ethyl oleate, Tween 80, and PEG 400, which showed maximal solubilizing capacity for NorA, were selected for further NorA ME formulations.

Table 1. Solubility of Norartocarpetin in Various Vehicles (25 °C)[a]

vehicle	solubility ± SD (mg/mL)
water	ND[b]
oils	
ethyl butyrate	0.22 ± 0.03
ethyl oleate	0.36 ± 0.07
(+)-limonene	0.16 ± 0.04
peppermint oil	0.28 ± 0.05
surfactants	
Tween 20	2.59 ± 0.03
Tween 40	0.89 ± 0.01
Tween 80	3.63 ± 0.02
cosurfactants	
ethanol	24.46 ± 0.18
glycerol	(14.50 ± 0.03) × 10^{-3}
PEG 400	72.72 ± 0.09
1,2-propanediol	6.93 ± 0.03
n-octanol	6.09 ± 0.02

[a]Results are presented as the mean ± SD ($n = 3$). [b]Not detected.

Pseudoternary Phase Diagram Study and Determination of ME Formulation. To figure out the optimal proportion of the components in ME, pseudoternary phase diagrams were constructed using a water titration method.

The pseudoternary phase diagrams of ME systems contained ethyl oleate, Tween 80, PEG 400 at fixed ratios (w/w, S_{mix}) of 1:1, 2:1, and 3:1), and water. In the pseudoternary phase diagrams, the left area along the curve was referred to as the turbid region, whereas the right region was the ME region (Figure 1). All ME were isotropic, transparent dispersions, and no phase separation could be observed with all the ratios of oil/surfactant−cosurfactant/water after centrifugation at 10000*g* for 20 min at 25 °C. The previous study showed that the cosurfactant was arranged exactly among surfactant molecules and resulted in the formation of ME with maximum solubilizing capacity at the optimum ratio of surfactant and cosurfactant.[28] Therefore, the ratio of surfactant and cosurfactant (S_{mix}) was very important in the formation of stable ME. In this study, when the same oil phase (ethyl oleate) was fixed, the area of ME regions existing in various ratios of surfactant and cosurfactant in pseudoternary phase diagrams were in the order 2:1 > 3:1 > 1:1 (Figure 1).

On the basis of the above optimization, the formulation of NorA ME was composed of ethyl oleate (2% w/w), Tween 80 (12% w/w), PEG 400 (6% w/w), with a ratio of 2:1 of

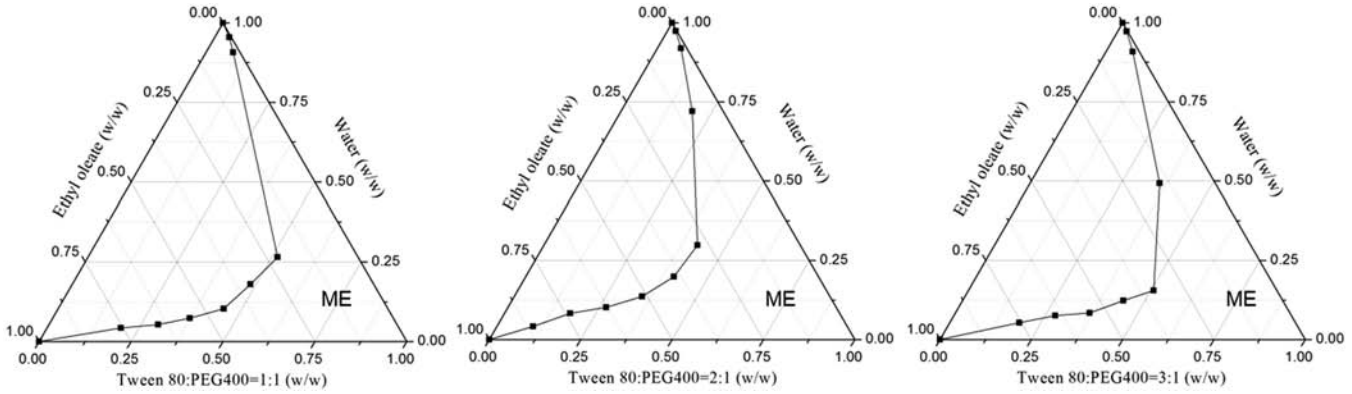

Figure 1. Construction of pseudoternary phase diagram of ethyl oleate/Tween 80/PEG 400/water system at a ratio of surfactant and cosurfactant (w/w) of 1:1, 2:1, or 3:1.

DOI: 10.1021/jf5048805
J. Agric. Food Chem. 2015, 63, 1615−1621

surfactant/cosurfactant, and water (80% w/w). The ME formulation exhibited the maximum solubility for NorA, up to 1.73 ± 0.21 mg/mL, increasing at least 1000 times its solubility in water.

Physicochemical Properties of ME. The selected ME base showed a colorless and transparent appearance, whereas NorA ME exhibited a light yellow and transparent appearance (Figure 2). The pH values of blank ME and NorA ME were

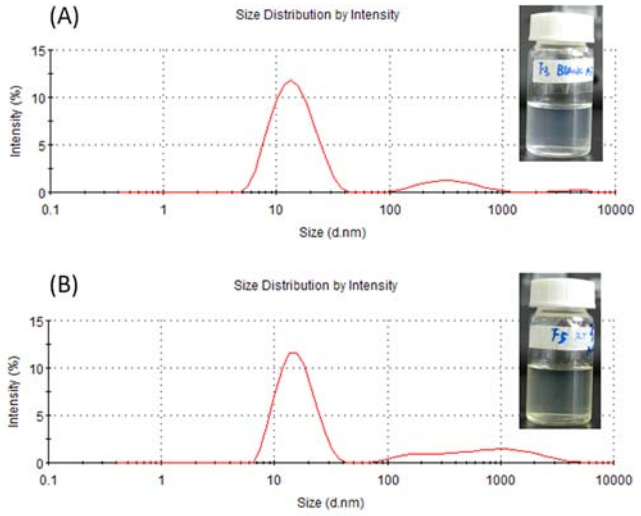

Figure 2. Particle size distribution and visual appearance of blank ME (A) and NorA ME (B).

5.56 and 5.51, respectively, a slight decrease after incorporation of NorA into ME. This may be induced by the phenolic hydroxyl groups in the structure of NorA. The mean particle sizes determined by the dynamic light scattering (DLS) measurements were 15.84 ± 0.02 and 16.01 ± 0.16 nm for the blank ME and NorA ME (Table 2), respectively. It can be

Table 2. Physical Properties and Solubility Determination of NorA ME (25 °C)[a]

characteristic	B ME[b]	NorA ME[c]
transparent	found[d]	found
phase separation	not found[e]	not found
color	colorless	light yellow
pH value	5.56	5.51
conductivity (μS/cm)	126.13 ± 0.21	129.13 ± 0.06
particle size (nm)	15.84 ± 0.02	16.01 ± 0.16
polydispersity index	0.270 ± 0.004	0.340 ± 0.020
concentration (mg/mL)		1.73 ± 0.21

[a]Results are presented as the mean ± SD (n = 3). [b]Blank microemulsion. [c]NorA ME norartocarpetin-loaded ME. [d]Transparent appearance was found after centrifugation. [e]No phase separation was found after centrifugation.

seen that the droplet sizes of ME and their homogeneity remain unchanged after the addition of NorA. The values of polydispersity indices were 0.270 ± 0.004 and 0.340 ± 0.020 for blank ME and NorA ME, respectively. The low values of PI indicated that the formulas had uniformity of narrow size distribution.[18] A lower diameter of the drops of oil (<100 nm) and the transparency of the system confirm the presence of microemulsions.[23] Conductivity is a certain correlation with the water content of ME, which can be used to categorize the ME area to w/o, o/w, and the bicontinuous structure between them.[29] The conductivity values of blank ME and NorA ME were 126.13 ± 0.21 and 129.13 ± 0.06 μS/cm, respectively. The results of high conductivity suggested that the ME were in o/w systems.[18,29]

TEM results confirmed the presence of droplets with size <30 nm (Figure 3). TEM analysis of NorA ME showed the presence of small spherical drops of oil with a mean diameter of 15−27 nm, coherent with particle sizes obtained by DLS.

Solubility Determination of NorA-Loaded ME. The solubility of NorA in the selected ME was 1.73 ± 0.21 mg/mL, which was improved considerably by loading it in ME. The solubility of NorA in the optimization ME was much higher than in water. On the other hand, it was found that the solubility of NorA showed little improvement when it was added in the oil phase first rather than directly adding it in the blank ME (Supporting Information). However, the latter was found to have a slight decrease in stability relative to the former one during long-term storage, and a trace of precipitate was found after 8 weeks of storage.

Stability Studies. Phase transitions are known to occur in ME structures as a result of changes in appearance, particle size, dilution, and so on, as well as the presence of guest molecules. To determine physical stability, the formulation was characterized by visual inspection, determinations of concentration, and particle size.

In stability tests, blank ME and NorA ME were stable during cooling−heating for six cycles (accelerated conditions) and long-term storage at room temperatures (20−37 °C) for 8 weeks (Table 3). Incorporation of NorA into ME did not affect the structure and the physical stability of the blank ME, because no significant changes in phase separation, clarity, and precipitation were observed after accelerated and long-term conditions. After accelerated and long-term conditions, the color and transparency of the blank ME and NorA ME were still the same as those freshly prepared. In addition, pH values decreased a lot after accelerated and long-term conditions for both blank ME and NorA ME. The decrease of pH values of NorA ME could be explained due to the large number of hydrogen protons ionized from phenolic hydroxyl groups, but it was strange that the pH values of blank ME also decreased by about 2−3 units. The optimum pH for PPO activity was between 5 and 7.[30] When pH values were <3, the enzyme activity could be effectively inhibited because hydrogen ions are noncompetitive inhibitors of apple PPO at pH <5.[31,32] The conductivities increased much from 126.13 to 208.67 and 294.0 μS/cm for blank ME and from 129.13 to 170.87 and 337.67 μS/cm for NorA ME after accelerated and long-term conditions, respectively. Both blank ME and NorA ME increased their conductivities about 2−4 times. The particle sizes of blank ME, after accelerated and long-term storage, slightly increased (from 15.84 to 17.36 and 21.62 nm) when compared with those of freshly prepared ME. However, the particle size of NorA ME slightly decreased compared to the fresh preparation after accelerated storage (from 16.01 to 15.44 nm), whereas it slightly increased after long-term storage (from 16.01 to 17.89 nm). All of the particle sizes were below 30 nm, suggesting both base and NorA ME were stable ME. The NorA contents of formulations were 1.71 ± 0.15 and 1.63 ± 0.14 mg/mL after accelerated and long-term stability testing, respectively, which were not significantly different compared with that of freshly prepared NorA ME (1.73 ± 0.21 mg/mL). These

DOI: 10.1021/jf5048805
J. Agric. Food Chem. 2015, 63, 1615−1621

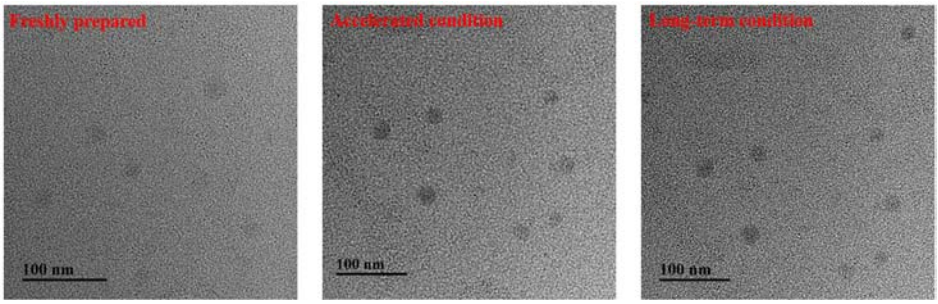

Figure 3. Morphology of NorA MEs, observed using a transmission electron microscope.

Table 3. Physical Properties, Solubility Determination, and Stability of NorA ME under Accelerated Conditions and Long-Term Storage[a]

	characteristics							
conditions	transparent	phase separation	color	pH value	conductivity (μS/cm)	particle size (nm)	polydispersity index	concentration (mg/mL)
accelerated								
B ME[b]	found[d]	not found[e]	colorless	3.56	208.67 ± 0.47	17.36 ± 0.31	0.297 ± 0.004	
NorA ME[c]	found	not found	light yellow	4.26	170.87 ± 0.62	15.44 ± 0.03	0.225 ± 0.010	1.71 ± 0.15
long term								
B ME	found	not found	colorless	2.86	294.0 ± 2.0	21.62 ± 0.05	0.392 ± 0.001	
NorA ME	found	not found	light yellow	3.08	337.67 ± 1.15	17.89 ± 0.60	0.312 ± 0.001	1.63 ± 0.14

[a]Results are presented as the mean ± SD (n = 3). [b]Blank microemulsion. [c]NorA ME norartocarpetin-loaded ME. [d]Transparent appearance was found after centrifugation. [e]No phase separation was found after centrifugation.

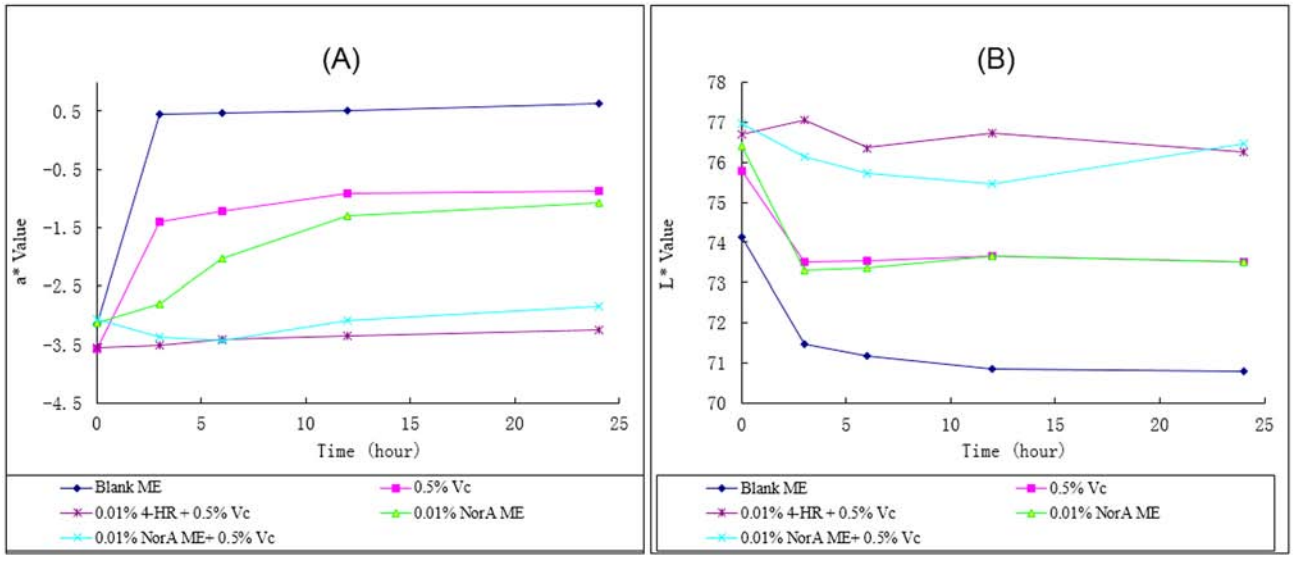

Figure 4. Reflectance measurement of a^* (A) and L^* (B) of apple slices treated with the different tested solutions and stored at room temperature.

results suggested that NorA was chemically stable in selected ME.

Tyrosinase Inhibition Activity and Antibrowning Effects of NorA ME on Fresh-Cut Apple Slices. To study whether the prepared NorA ME maintained good tyrosinase inhibitory activity and antibrowning effects, the NorA ME was diluted to different concentrations and tested for their inhibitory activities on tyrosinase. The IC_{50} of NorA ME was 1.43 ± 0.06 μM, which is similar to the IC_{50} obtained from using DMSO as a solubilizer,[3] suggesting the tyrosinase inhibitory activity of NorA does not decrease due to incorporation into ME.

Until today, there is still not a unified standard quantitative method for measurement of the extent of browning in foods. Usually, ΔE (total color difference), L^*, a^*, and b^* have been used as parameters for measuring the extent of browning reactions in fruits and vegetables. A decrease in L^* and an increase in a^* or ΔE indicate the occurrence of browning. Among them, the a^* value was reported to be more sensitive to browning and had been used to effectively monitor browning in fresh-cut pear and apple.[33−35] Moreover, it was found that plant extracts or compounds needed to be used in combination with V_C to exhibit better antibrowning effects.[35−37] In the present study, a^* and L^* values were chosen as parameters for estimation of the antibrowning activity of NorA ME on apple

DOI: 10.1021/jf5048805
J. Agric. Food Chem. 2015, 63, 1615−1621

slices, in addition to visual observation. Except for blank ME, V_C, and NorA ME alone, NorA ME and 4-HR combination with V_C were assayed for antibrowning effects on fresh-cut apple slices. According to the change of a^* value, blank ME almost did not show antibrowning effects even at 3 h in room temperature, whereas NorA ME and 4-HR in combination with 0.5% V_C, respectively, showed similarly better antibrowning effects than NorA ME and V_C alone, even at 3 h (Figure 4). NorA ME in combination with 0.5% V_C were not significantly different from apple slices treated with 0.01% 4-HR in combination with 0.5% V_C dipping solution in 24 h. The results of L^* values displayed the same trend according to the results obtained for the a^* values. The solutions of 0.01% NorA ME + 0.5% V_C and 0.01% 4-HR + 0.5% V_C exhibited higher L^* values than the solutions of NorA ME and V_C alone and much higher L^* values than base ME solution. According to the decrease in L^* value normally associated with browning, 0.01% NorA ME + 0.5% V_C and 0.01% 4-HR + 0.5% V_C could better inhibit browning for fresh-cut apple slices than NorA ME or V_C alone. Although the inhibitory effect of norartocarpetin on tyrosinase has been reported in our previous studies,[2,4] the mechanism of browning inhibition is still unknown. The above findings suggest that browning inhibition of norartocarpetin was achieved possibly through a mechanism similar to that of 4-HR. These results preliminarily suggest that NorA may be a potential candidate for 4-HR and V_C as antibrowning agents for fresh-cut fruit products. The visual assessment agreed with colorimetric measurements.

In conclusion, the results of this study suggest that the solubility of NorA was improved greatly in the food grade MEs. NorA ME retains good physicochemical stability after accelerated and long-term conditions. NorA ME still showed strong tyrosinase inhibitory activities and antibrowning effects on apple slices. On the basis of physicochemical characterization and antibrowning effect studies, the ME formulation may be employed to improve the solubility of insoluble tyrosinase inhibitors such as NorA. However, further studies on texture, sensory, nutritional values, aroma, and flavor of apple slices need to be performed before this formulation can be commercially exploited.

■ ASSOCIATED CONTENT

Supporting Information

Additional experimental details, figures, and tables. This material is available free of charge via the Internet at http://pubs.acs.org.

■ AUTHOR INFORMATION

Corresponding Author

*(J.C.) E-mail: chenjie@jiangnan.edu.cn. Phone: +86-51085329032. Fax: +86-51085329065.

Funding

This work was supported by grants from the National Basic Research Program of China (973 Program, 2012CB720801), a grant from the Natural Science Foundation of Jiangsu Province (BK20141110), the Fundamental Research Funds for the Central Universities (JUSRP11220), and the Hangzhou Bureau of Science and Technology Project (20120433B03).

Notes

The authors declare no competing financial interest.

■ REFERENCES

(1) Artés, F.; Castañer, M.; Gil, M. I. Revisión: El pardeamiento enzimático en frutas y hortalizas mínimamente procesadas [Review: Enzymatic browning in minimally processed fruit and vegetables]. *Food Sci. Technol. Int.* **1998**, *4*, 377−389.

(2) Zheng, Z. P.; Cheng, K. W.; Zhu, Q.; Wang, X. C.; Lin, Z. X.; Wang, M. Tyrosinase inhibitory constituents from the roots of *Morus nigra*: a structure-activity relationship study. *J. Agric. Food Chem.* **2010**, *58*, 5368−5373.

(3) Zheng, Z. P.; Chen, S.; Wang, S.; Wang, X. C.; Cheng, K. W.; Wu, J. J.; Yang, D.; Wang, M. Chemical components and tyrosinase inhibitors from the twigs of *Artocarpus heterophyllus*. *J. Agric. Food Chem.* **2009**, *57*, 6649−6655.

(4) Zheng, Z. P.; Cheng, K. W.; To, J. T. K.; Li, H.; Wang, M. Isolation of tyrosinase inhibitors from *Artocarpus heterophyllus* and use of its extract as antibrowning agent. *Mol. Nutr. Food Res.* **2008**, *52*, 1530−1538.

(5) Zheng, Z. P.; Tan, H. Y.; Chen, J.; Wang, M. Characterization of tyrosinase inhibitors in the twigs of *Cudrania tricuspidata* and their structure-activity relationship study. *Fitoterapia* **2013**, *84*, 242−247.

(6) Lan, W. C.; Tzeng, C. W.; Lin, C. C.; Yen, F. L.; Ko, H. H. Prenylated flavonoids from *Artocarpus altilis*: antioxidant activities and inhibitory effects on melanin production. *Phytochemistry* **2013**, *89*, 78−88.

(7) Fozing, C. D. A.; Ali, Z.; Ngadjui, B. T.; Choudhary, M. I.; Kapche, G. D. W. F.; Abegaz, B. M.; Khan, I. A. Phosphodiesterase I-inhibiting Diels-Alder adducts from the leaves of *Morus mesozygia*. *Planta Med.* **2012**, *78*, 154−159.

(8) Kesisoglou, F.; Panmai, S.; Wu, Y. H. Application of nanoparticles in oral delivery of immediate release formulations. *Curr. Nanosci.* **2007**, *3*, 183−190.

(9) Spernath, A.; Aserin, A. Microemulsions as carriers for drugs and nutraceuticals. *Adv. Colloid Interface Sci.* **2006**, *128−130*, 47−64.

(10) Xiao, Y.; Chen, X.; Yang, L.; Zhu, X.; Zou, L.; Meng, F.; Ping, Q. Preparation and oral bioavailability study of curcuminoid-loaded microemulsion. *J. Agric. Food Chem.* **2013**, *61*, 3654−3660.

(11) Amar, I.; Aserin, A.; Garti, N. Solubilization patterns of lutein and lutein esters in food grade nonionic microemulsions. *J. Agric. Food Chem.* **2003**, *51*, 4775−4781.

(12) Gulotta, A.; Saberi, A. H.; Nicoli, M. C.; McClements, D. J. Nanoemulsion-based delivery systems for polyunsaturated (ω-3) oils: formation using a spontaneous emulsification method. *J. Agric. Food Chem.* **2014**, *62*, 1720−1725.

(13) Yang, X.; Tian, H.; Ho, C. T.; Huang, Q. Inhibition of citral degradation by oil-in-water nanoemulsions combined with antioxidants. *J. Agric. Food Chem.* **2011**, *59*, 6113−6119.

(14) Karadag, A.; Yang, X.; Ozcelik, B.; Huang, Q. Optimization of preparation conditions for quercetin nanoemulsions using response surface methodology. *J. Agric. Food Chem.* **2013**, *61*, 2130−2139.

(15) Helgason, T.; Awad, T. S.; Kristbergsson, K.; Decker, E. A.; McClements, D. J.; Weiss, J. Impact of surfactant properties on oxidative stability of β-carotene encapsulated within solid lipid nanoparticles. *J. Agric. Food Chem.* **2009**, *57*, 8033−8040.

(16) Zhang, Q. F.; Nie, H. C.; Shangguang, X. C.; Yin, Z. P.; Zheng, G. D.; Chen, J. G. Aqueous solubility and stability enhancement of astilbin through complexation with cyclodextrins. *J. Agric. Food Chem.* **2013**, *61*, 151−156.

(17) Tan, C.; Xue, J.; Abbas, S.; Feng, B.; Zhang, X.; Xia, S. Liposome as a delivery system for carotenoids: comparative antioxidant activity of carotenoids as measured by ferric reducing antioxidant power, DPPH assay and lipid peroxidation. *J. Agric. Food Chem.* **2014**, *62*, 6726−6735.

(18) Sasivimolphan, P.; Lipipun, V.; Ritthidej, G.; Chitphet, K.; Yoshida, Y.; Daikoku, T.; Sritularak, B.; Likhitwitayawuid, K.; Pramyothin, P.; Hattori, M.; Shiraki, K. Microemulsion-based oxyresveratrol for topical treatment of herpes simplex virus (HSV) infection: physicochemical properties and efficacy in cutaneous HSV-1 infection in mice. *AAPS PharmSciTech* **2012**, *13*, 1226−1275.

DOI: 10.1021/jf5048805
J. Agric. Food Chem. 2015, 63, 1615−1621

(19) Solanki, S. S.; Sarkar, B.; Dhanwani, R. K. Microemulsion drug delivery system: for bioavailability enhancement of ampelopsin. *ISRN Pharm.* **2012**, *108164*, 1−4.
(20) Flanagan, J.; Singh, H. Microemulsions: a potential delivery system for bioactives in food. *Crit. Rev. Food Sci. Nutr.* **2006**, *46*, 221−237.
(21) Vicentini, F. T. M. C.; Vaz, M. M. O. L. L.; Fonseca, Y. M.; Bentley, M. V. L. B.; Fonseca, M. J. V. Characterization and stability study of a water-in-oil microemulsion incorporating quercetin. *Drug Dev. Ind. Pharm.* **2011**, *37*, 47−55.
(22) Rogerio, A. P.; Dora, C. L.; Andrade, E. L.; Chaves, J. S.; Silva, L. F.C.; Lemos-Senna, E.; Calixto, J. B. Anti-inflammatory effect of quercetin-loaded microemulsion in the airways allergic inflammatory model in mice. *Pharmacol. Res.* **2010**, *61*, 288−297.
(23) Bergonzi, M. C.; Hamdouch, R.; Mazzacuva, F.; Isacchi, B.; Bilia, A. R. Optimization, characterization and in vitro evaluation of curcumin microemulsions. *LWT−Food Sci. Technol.* **2014**, *59*, 148−155.
(24) Rao, J.; McClements, D. J. Formation of flavor oil microemulsions, nanoemulsions and emulsions: influence of composition and preparation method. *J. Agric. Food Chem.* **2011**, *59*, 5026−5035.
(25) You, X.; Xing, Q.; Tuo, J.; Song, W.; Zeng, Y.; Hu, H. Optimizing surfactant content to improve oral bioavailability of ibuprofen in microemulsions: just enough or more than enough? *Int. J. Pharm.* **2014**, *471*, 276−284.
(26) Ma, T. Y.; Hollander, D.; Krugliak, P.; Katz, K. PEG 400, a hydrophilic molecular probe for measuring intestinal permeability. *Gastroenterology* **1990**, *98*, 39−46.
(27) Yuan, Q.; Williams, R. A.; Biggs, S. Surfactant selection for accurate size control of microcapsules using membrane emulsification. *Colloid Surf. A: Physicochem. Eng. Asp.* **2009**, *347*, 97−103.
(28) Kawakami, K.; Yoshikawa, T.; Moroto, Y.; Kanahashi, K.; Nishihara, Y.; Masuda, K. Microemulsion formulation for enhanced absorption of poorly soluble drugs. II. In vivo study. *J. Controlled Release* **2002**, *81*, 65−74.
(29) Bumajdad, A.; Eastoe, J. Conductivity of water-in-oil microemulsions stabilized by mixed surfactants. *J. Colloid Interface Sci.* **2004**, *274*, 268−276.
(30) Fan, X.; Sokorai, K. J. B.; Liao, C. H.; Cooke, P.; Zhang, H. Q. Antibrowning and antimicrobial properties of sodium acid sulfate in apple slices. *J. Food Sci.* **2009**, *74*, M485−M492.
(31) McEvily, A. J.; Lyengar, R. Inhibition of enzymatic browning in foods and beverages. *Crit. Rev. Food Sci. Nutr.* **1992**, *32*, 253−273.
(32) Janovitz-Klapp, A. H.; Richard, F. C.; Goupy, P. M.; Nicolas, J. J. Inhibition studies on apple polyphenol oxidase. *J. Agric. Food Chem.* **1990**, *38*, 926−931.
(33) Abbott, J. A.; Buta, J. G. Effect of anti-browning treatment on color and firmness of fresh-cut pears. *J. Food Qual.* **2000**, *25*, 333−341.
(34) Sapers, G. M.; Miller, R. L. Browning inhibition in fresh-cut pears. *J. Food Sci.* **1998**, *63*, 342−346.
(35) Rojas-Graü, M. A.; Soliva-Fortuny, R.; Martín-Bellsos, O. Effect of natural antibrowning agents on color and related wnzymes in fresh-cut Fuji apples as an alternative to the use of ascorbic acid. *J. Food Sci.* **2008**, *73*, s267−s272.
(36) Luo, Y.; Barbosa-Canovas, G. V. Enzymic browning and its inhibition in new apple cultivars slices using 4-hexylresorcinol in combination with ascorbic acid. *Int. J. Food Sci. Technol.* **1997**, *3*, 195−201.
(37) Li, H. T.; Cheng, K. W.; Cho, C. H.; He, Z. A.; Wang, M. Oxyresveratrol as an antibrowning agent for cloudy apple juices and fresh-cut apples. *J. Agric. Food Chem.* **2007**, *55*, 2604−2610.

DOI: 10.1021/jf5048805
J. Agric. Food Chem. 2015, 63, 1615−1621

Table 1. ^{1}H (500 MHz) NMR Data for Compounds 3, 6, and 7 and ^{13}C (125 MHz) NMR Data for Compound 6

	3		6			7	
position	^{1}H	mult (J in Hz)[a]	^{13}C	^{1}H	mult (J in Hz)	^{1}H	mult (J in Hz)
1			131.8				
2	2.46	overlapped	124.3	5.12	m	5.12	m
3	~1.84, 1.86	each m	22.1	2.12	m	2.12	m
4	~1.84, 1.86	each m	38.8	1.54	t (7)	1.54	t (7)
5			75.0				
6	2.46	overlapped	78.9	4.04	dd (7.5, 3[b])	4.02	dd (7.5, 3)
7	5.50	dd (15, 8)	126.2	5.70	dd (15.5, 7.5)	5.74	dd (15.5, 7.5)
8	6.20	d (15)	138.1	6.38	d (15.5)	6.38	d (15.5)
9			134.3				
10	6.14	d (11)	132.8	6.20	d (11)	6.20	d (11)
11	6.60	dd (15, 11)	124.5	6.59	dd (15, 11)	6.59	dd (15, 11)
12	6.35	d (15)	138.1	6.38	d (15)	6.38	d (15)
13			136.3				
14	6.26	d (11)	133.2	6.26	d (11)	6.26	d (11)
15	6.64	m	129.9	6.64	m	6.64	m
16	4.69 and 4.71	each br s	25.7	1.69	s	1.69	s
17	1.68	s	17.7	1.62	s	1.62	s
18	1.19	s	21.5	1.14	s	1.22	s
19	1.92	s	12.6	1.93	s	1.93	s
20	1.97	s	12.8	1.97	s	1.97	s
1′			131.6				
2′	5.12	m	123.9	5.12	m	5.12	m
3′	2.12	m	26.7	2.12	m	2.12	m
4′	2.12	m	40.2	2.12	m	2.12	m
5′			138.6				
6′	5.96	d (11)	125.7	5.96	d (11)	5.96	d (11)
7′	6.50	dd (15, 11)	124.8	6.50	dd (15, 11)	6.50	dd (15, 11)
8′	6.25	d (15)	135.4	6.25	d (15)	6.25	d (15)
9′			136.1				
10′	6.19	d (11)	131.6	6.19	d (11)	6.19	d (11)
11′	6.64	dd (15, 11)	125.2	6.64	dd (15, 11)	6.64	dd (15, 11)
12′	6.35	d (15)	136.2	6.35	d (15)	6.35	d (15)
13′			136.3				
14′	6.26	d (11)	132.5	6.26	d (11)	6.26	d (11)
15′	6.64	m	129.9	6.64	m	6.64	m
16′	1.69	s	25.7	1.69	s	1.69	s
17′	1.63	s	17.7	1.63	s	1.63	s
18′	1.82	s	17.0	1.82	s	1.82	s
19′	1.93	s	12.6	1.93	s	1.93	s
20′	1.97	s	12.8	1.97	s	1.97	s
OH				2.07	br s	2.07	br s

[a]s, singlet; d, doublet; dd, doublet of doublets; t, triplet; m, multiplet; br s, broad singlet. [b]Coupling with OH.

and a 250 × 10 mm i.d., 10 μm Cosnosil 5SL-II (Nacalai Tesque, Kyoto, Japan).

Plant Materials. Gac fruits were purchased at a local vegetable market in Vietnam.

Quantitative Analysis of Carotenoids. The total carotenoid content and the amount of carotenoids eluted by column chromatography were calculated using the extinction coefficient of $E^{1\%}_{cm}$ = 3450 at λ_{max}.[21] In the HPLC analysis, the relative amounts of individual carotenoids were calculated from the peak area detected at 470 nm.

Isolation of Carotenoids. The aril (980 g) of gac was extracted with acetone (Me_2CO) at room temperature. The Me_2CO extract was evaporated to dryness. The reddish residue was subjected to silica gel 60 (Nacalai Tesque, Kyoto, Japan) column chromatography (300 × 20 mm). The fraction (fr) eluted with 200 mL of ether−hexane (1:9 v/v, fr 1) was subjected to preparative HPLC on ODS (Cosmosil 5C18-II) with a CH_3CN flow rate of 2.0 mL/min to yield α-carotene, β-carotene, 9Z-β-carotene, γ-carotene, lycopene (**1**), 9Z-lycopene, and 13Z-lycopene.

The fraction eluted with ether-hexane (5:5 v/v, fr 2) was subjected to preparative HPLC on silica gel (Cosmosil 5Si) with acetone−hexane (15:85 v/v) to yield new carotenoid **3** (retention time 18.4 min) and 1,16-dehydro-2,6-cyclolycopene-5-ol A (rt 20.5 min).

The fraction eluted with ether−hexane (8:2 v/v, fr 3) was subjected to preparative HPLC on silica gel (Cosmosil 5Si) with acetone−hexane (25:75 v/v) to yield isocryptoxanthin (rt 9.4 min), β-cryptoxanthin (rt 10.4 min), and new carotenoids **11** (rt 12.0 min), **12** (rt 14.0 min), **6** (rt 16.0 min), and **7** (rt 17.0 min). The fraction eluted with ether (fr 4) was subjected to preparative HPLC on silica gel (Cosmosil 5 Si) with acetone−hexane (25:75 v/v) to yield new carotenoids **10** (rt 12.0 min) and **9** (rt 14.0 min), 2,6-cyclolycopene-1,5-diol B (rt 17.0 min) and 2,6-cyclolycopene-1,5-diol A (rt 20.0 min), lutein (25.0 min), and zeaxanthin (27.0 min).

Identification and Characterization of Carotenoids. α-Carotene, β-carotene, 9Z-β-carotene, γ-carotene (**8**), lycopene (**1**),

DOI: 10.1021/jf505008d
J. Agric. Food Chem. 2015, 63, 1622−1630

Table 2. ^{1}H (500 MHz) NMR Data for Compounds 9−12 in $CDCl_3$

	9		10		11		12	
position	^{1}H	mult (J in Hz)[a]	^{1}H	mult (J in Hz)	^{1}H	mult (J in Hz)	^{1}H	mult (J in Hz)
2	∼1.46	m	∼1.46	m	∼1.46	m	∼1.46	m
3	∼1.62	m	∼1.62	m	∼1.62	m	∼1.62	m
4	2.02	t (7)	2.02	t (7)	2.02	t (7)	2.02	t (7)
7	6.16	d (15)	6.16	d (15)	6.16	d (15)	6.16	d (15)
8	6.15	d (15)	6.15	d (15)	6.15	d (15)	6.15	d (15)
10	6.15	d (11)	6.15	d (11)	6.15	d (11)	6.15	d (11)
11	6.65	dd (15, 11)	6.65	dd (15, 11)	6.65	dd (15, 11)	6.65	dd (15, 11)
12	6.35	d (15)	6.35	d (15)	6.35	d (15)	6.35	d (15)
14	6.26	d (11)	6.26	d (11)	6.26	d (11)	6.26	d (11)
15	6.64	m	6.64	dd (15, 11)	6.64	dd (15, 11)	6.64	dd (15, 11)
16	1.03	s	1.03	s	1.03	s	1.03	s
17	1.03	s	1.03	s	1.03	s	1.03	s
18	1.71	s	1.71	s	1.71	s	1.71	s
19	1.96	s	1.96	s	1.97	s	1.97	s
20	1.97	s	1.97	s	1.97	s	1.97	s
2′	2.31	m	∼1.96	m	5.12	m	5.12	m
3′	1.53 and 2.21	m	1.78 and 1.80	m	2.12	m	2.12	m
4′	1.67 and 1.80	m	1.68 and 1.71	m	1.54	t (7)	1.54	t (7)
6′	2.24	d (10, 6)	2.52	dd (10, 6)	4.04	dd (7.5, 3)	4.02	dd (7.5, 3)
7′	5.73	dd (16, 10)	5.48	dd (15, 11)	5.70	dd (15.5, 7.5)	5.74	dd (15.5, 7.5)
8′	6.25	d (16)	6.15	d (15)	6.38	d (15.5)	6.38	d (15.5)
10′	6.18	d (11)	6.13	d (11)	6.20	d (11)	6.20	d (11)
11′	6.60	dd (15, 11)	6.60	dd (15, 11)	6.59	dd (15, 11)	6.59	dd (15, 11)
12′	6.36	d (15)	6.36	d (15)	6.38	d (15)	6.38	d (15)
14′	6.24	d (11)	6.26	d (11)	6.26	d (11)	6.26	d (11)
15′	6.64	m	6.64	m	6.64	m	6.64	m
16′	1.24	s	1.21	s	1.69	s	1.69	s
17′	1.17	s	1.25	s	1.62	s	1.62	s
18′	1.18	s	1.17	s	1.14	s	1.22	s
19′	1.94	s	1.91	s	1.93	s	1.93	s
20′	1.98	s	1.97	s	1.97	s	1.97	s

[a] s, singlet; d, doublet; dd, doublet of doublets; t, triplet; m, multiplet.

9*Z*-lycopene, 13*Z*-lycopene, 1,16-didehydro-2,6-cyclolycopene-5-ol A (**2**), 2,6-cyclolycopene-1,5-diol A (**4**), and 2,6-cyclolycopene-1,5-diol B (**5**) were identified based on UV/vis, ^{1}H NMR, and FAB MS data.[14−18,21,22]

*1,16-Didehydro-2,6-cyclolycopene-5-ol B (**3**).* Yield: 1 mg. UV/vis (Et_2O): 431, 455, 486 nm. HR FAB MS m/z: 552.4344 [M+] (calcd for $C_{40}H_{56}O$, 552.4331). ^{1}H NMR (Table 1).

*(threo)-Lycopene-5,6-diol (**6**).* Yield: 3 mg. UV/vis (Et_2O): 431, 455, 486 nm. HR FAB MS m/z: 570.4436 [M+] (calcd for $C_{40}H_{58}O_2$, 570.4437). FAB MS/MS m/z 552 [M-18] $^+$, 501 [M-69] $^+$, 478 [M-92] $^+$, 443 [M-127] $^+$, 374 [M-96−127] $^+$. ^{1}H and ^{13}C NMR (Table 1). Acetylation of **6** with acetic anhydride in pyridine at room temperature for 1 h gave a monoacetate of **6**. FAB MS m/z 612 [M^+].

*(erythro)-Lycopene-5,6-diol (**7**).* Yield: 1 mg. UV/vis (Et_2O): 431, 455, 486 nm. HR FAB MS m/z: 570.4437 [M+] (calcd for $C_{40}H_{58}O_2$, 570.4437). ^{1}H NMR (Table 1). Acetylation of **7** with acetic anhydride in pyridine at room temperature for 1 h gave a monoacetate of **7**. FAB MS m/z 612 [M^+].

*2′,6′-cyclo-γ-Carotene-1′,5′-diol A (**9**).* Yield: 0.2 mg. UV/vis (Et_2O): 420, 445, 472 nm. HR FAB MS m/z: 570.4430 [M+] (calcd for $C_{40}H_{58}O_2$, 570.4437). ^{1}H NMR (Table 2).

*2′,6′-cyclo-γ-Carotene-1′,5′-diol B (**10**).* Yield: 0.2 mg. UV/vis (Et_2O): 420, 445, 472 nm. HR FAB MS m/z: [M^+] calcd for $C_{40}H_{58}O_2$, 570.4437; found 570.4429. ^{1}H NMR (Table 2).

*(threo)-γ-Carotene-5′,6′-diol (**11**).* Yield: 0.1 mg. UV/vis (Et_2O): 420, 445, 472 nm. HR FAB MS m/z: [M^+] calcd for $C_{40}H_{58}O_2$, 570.4437; found 570.4440. ^{1}H NMR (Table 2).

*(erythro)-γ-Carotene-5′,6′-diol (**12**).* Yield: 0.2 mg. UV/vis (Et_2O): 420, 445, 472 nm. HR FAB MS m/z: [M^+] calcd for $C_{40}H_{58}O_2$, 570.4437; found 570.4439. ^{1}H NMR (Table 2).

Ab Initio Molecular Orbital Calculation. Ab initio molecular orbital calculations were performed using the Gaussian 03 program (Gaussian, Inc., Wallingford, CT). The starting coordinates were generated by inspection of the molecular model and were fully optimized using a Fujitsu HX600 supercomputer at the Information Technology Center of Nagoya University. The position of methyl group and hydroxyl group were represented as follows. The position of methyl group was represented by the average of coordinates of three hydrogens that were obtained by the ab initio molecular orbital calculations. Similarly, the position of the hydroxyl group was represented by the coordinates of the base of a perpendicular line drawn from the hydrogen atom to the extension of the C-6 and O bond.

In Vitro Epstein−Barr Virus (EBV) Early Antigen Activation Induction Effect. EBV genome-carrying lymphoblastoid cells (Raji cells) derived from Burkitt's lymphoma were cultivated in RPMI-1640 medium with 10% fetal bovine serum (FBS). The Raji cells were incubated for 48 h at 37 °C in a medium containing *n*-butyric acid (4 nmol), TPA (32 pmol), and various amounts of test compounds. Smears were made from the cell suspension, and we employed an indirect immunofluorescence technique. Details of the in vitro assay on EBV-EA induction have been reported previously.[23,24]

DOI: 10.1021/jf505008d
J. Agric. Food Chem. 2015, 63, 1622−1630

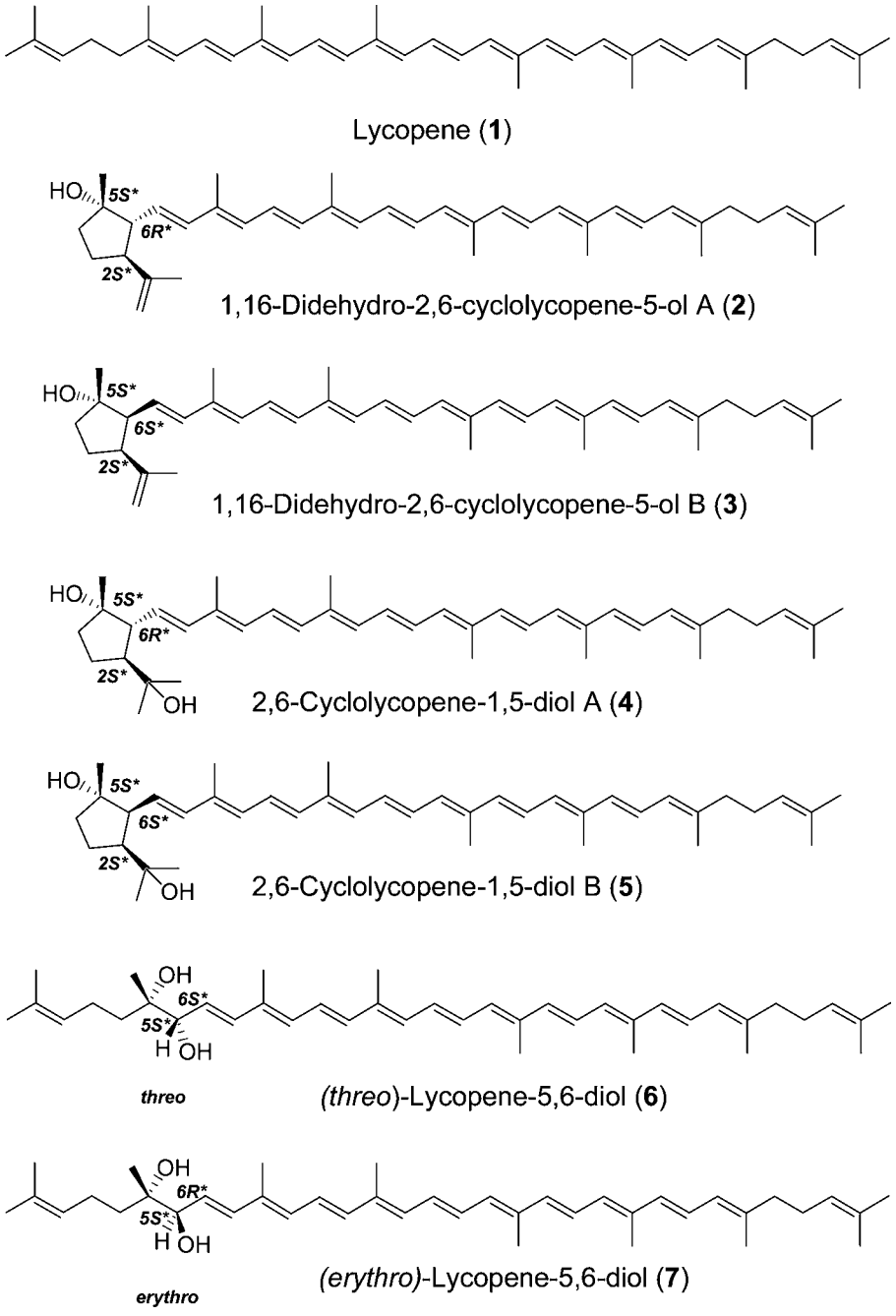

Figure 1. Lycopene (**1**) and its oxidative metabolites (**2**–**7**) in gac. The relative stereochemistry was indicated as *R** and *S**.

RESULTS AND DISCUSSION

Three new carotenoids, **3**, **6**, and **7**, were isolated as minor components along with lycopene (**1**), 1,16-didehydro-2,6-cyclolycopene-5-ol A (**2**), 2,6-cyclolycopene-1,5-diol A (**4**), and 2,6-cyclolycopene-1,5-diol B (**5**) from the aril of gac, as shown in Figure 1. Relative stereochemistry of these compounds is indicated as *R** and *S**.

The new carotenoid **3** showed absorption maxima at 431, 455, and 486 nm, indicating the presence of a decene conjugated double bond system.[22] The molecular formula of **3** was determined as $C_{40}H_{56}O$ by HR FAB MS. The ^{1}H NMR spectral data for **3**, assigned by COSY and NOESY analyses, are shown in Table 1. The ^{1}H NMR spectroscopic data were almost the same as those of 1,16-didehydro-2,6-cyclolycopene-5-ol A (**2**),[18] except for the H-5, H-6, H-7, and H-18 positions. This suggested that **3** might be an epimer of 1,16-didehydro-2,6-cyclolycopene-5-ol A (**2**), having a (2*S**,5*S**,6*R**) configuration. The relative configuration of **3** was elucidated by performing a NOESY experiment. In the case of **2**, a NOESY correlation for CH_3-18/H-7 was not noted. However, a NOESY correlation for CH_3-18/H-7 was observed in the case of **3** (Figure 2). This clearly indicated that **3** is a 6-epimer of **2**. Therefore, a (2*S**,5*S**,6*S**) configuration was postulated for **3**. Thus, compound **3** was named 1,16-didehydro-2,6-cyclolycopene-5-ol B ((2*S**,5*S**,6*S**)-1,16-didehydro-1,2,5,6-tetrahydro-2,6-cyclo-*ψ*,*ψ*-carotene-1′,5′-diol). This stereostructure was also confirmed using the ab initio molecular orbital method employing the Gaussian 03 program.

Both new carotenoids **6** and **7** showed the same absorption maxima at 431, 455, and 486 nm, indicating the presence of a

DOI: 10.1021/jf505008d
J. Agric. Food Chem. 2015, 63, 1622−1630

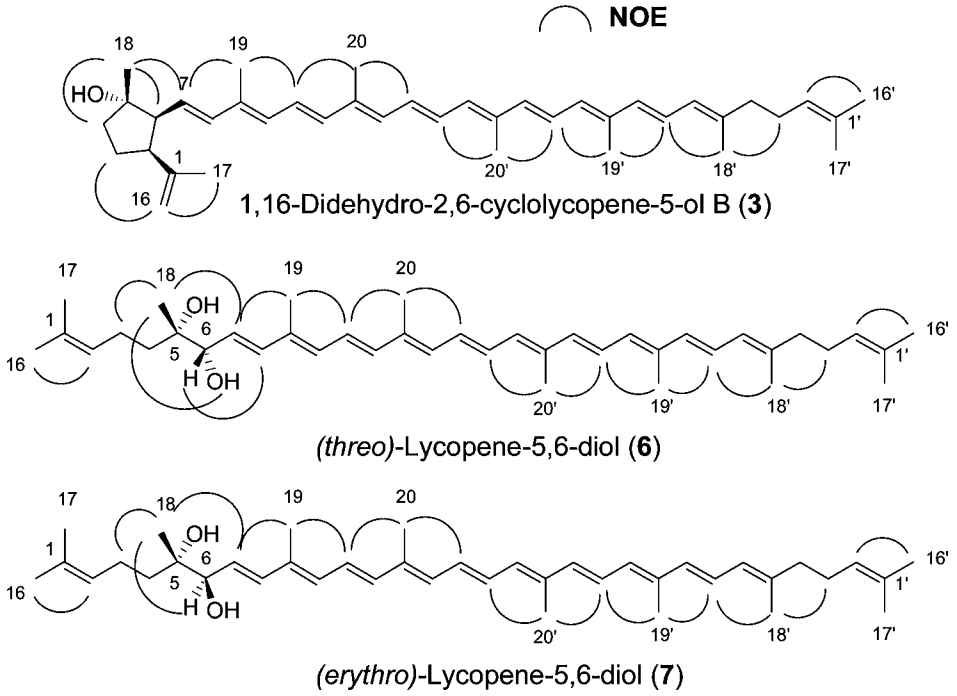

Figure 2. NOESY correlations of **3**, **6**, and **7**.

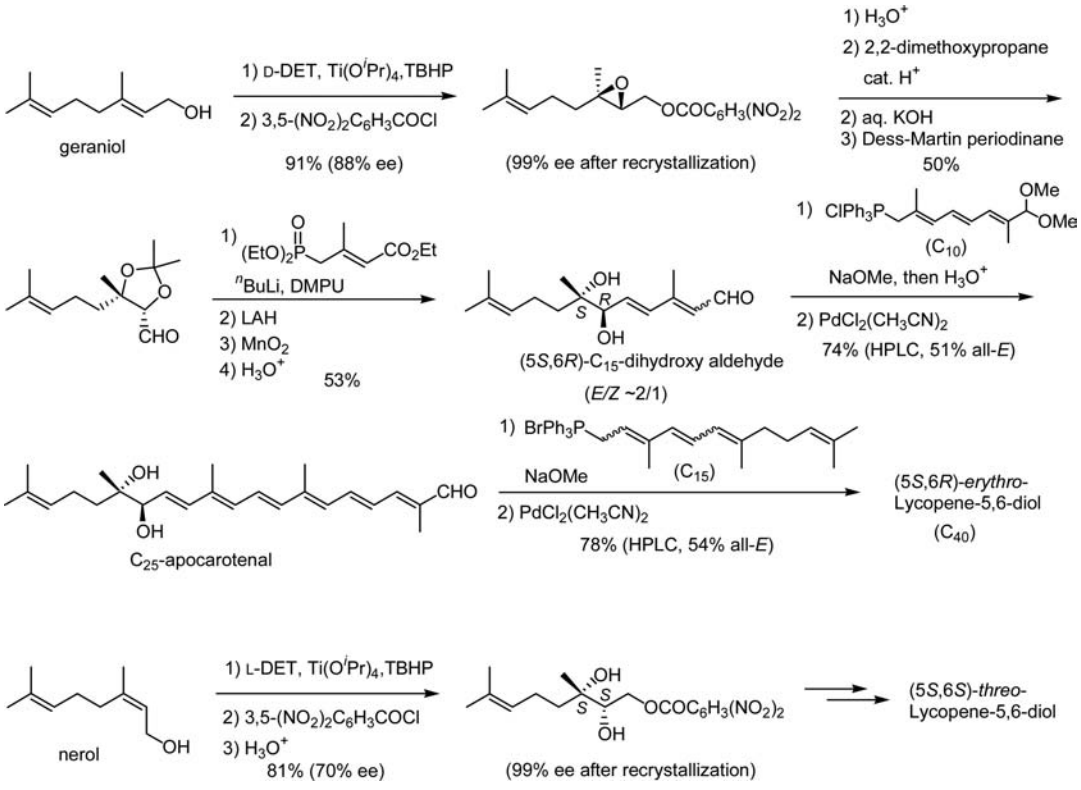

Figure 3. Outline of the total synthesis of (5*S*,6*R*)- and (5*S*,6*S*)-lycopene-5,6-diol.

decene conjugated double bond system.[22] The molecular formulas of both **6** and **7** were determined as $C_{40}H_{58}O_2$ by HR FAB MS. Acetylation of both compounds yielded a monoacetate. The ^{1}H and ^{13}C NMR data for **6**, which were assigned by COSY, NOESY, HSQC, and HMBC analyses, are shown in Table 1. These ^{1}H and ^{13}C NMR spectroscopic data were almost the same as those of lycopene (**1**), except for the C-5, C-6, and C-18 positions. The presence of one secondary hydroxy group (δ_C 78.9 and δ_H 4.04) and tertiary hydroxy group (δ_C 75.0) in **6** was revealed by NMR data. The presence of a tertiary hydroxy group at C-5 and secondary hydroxy group at C-6 was determined by HMBC data. HMBC correlations for CH_3-18/C-5, CH_3-18/C-6, H-3/C-5, and H-7/C-6 were in agreement with this structure. Thus, the planar structure of **6**

DOI: 10.1021/jf505008d
J. Agric. Food Chem. 2015, 63, 1622−1630

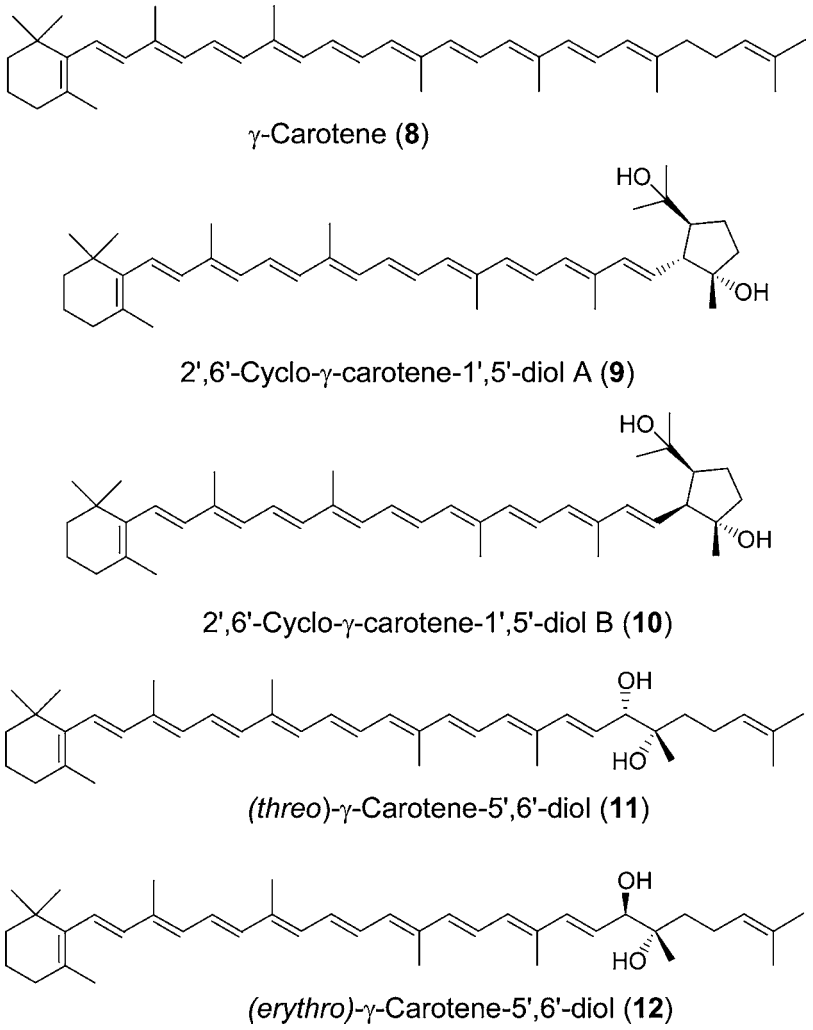

Figure 4. γ-Carotene (**8**) and its oxidative metabolites (**9**−**12**) in gac.

was determined as 5,6-dihydro-ψ,ψ-carotene-5,6-diol. The ^{1}H NMR data for **7** were almost the same as those for **6**, except for the H-6 and H-18 positions. The COSY experiment also revealed the planar structure 5,6-dihydro-ψ,ψ-carotene-5,6-diol for **6**. We decided on lycopene-5,6-diol to refer to the carotenoid of 5,6-dihydro-ψ,ψ-carotene-5,6-diol. Concerning the relative stereochemistry of lycopene-5,6-diol, the *threo* form (indicated as 5*S**,6*S** configuration) and *erythro* form (indicated as 5*S**,6*R** configuration) can be considered (Figure 1). The relative stereochemistry of **6** and **7** was elucidated by NOESY and NOE difference experiments. Strong NOE (>5%) was observed between protons of CH_3-18 and OH-6 in compound **6**, and NOE was not noted between protons of CH_3-18 and OH-6 in compound **7**. Furthermore, strong NOE between protons of CH_3-18 and H-6 was not observed in compound **6** but it was observed in compound **7**. Molecular calculation using the ab initio molecular orbital method employing the Gaussian 03 program indicated that, in the case of the *threo* isomer, distances of CH_3-18 to H-6 and CH_3-18 to OH-6 are 3.81 and 3.28 Å, respectively. Additionally, in the case of the *erythro* isomer the distances of CH_3-18 and H-6 and CH_3-18 and OH-6 are 3.16 and 3.91 Å, respectively. It has been reported that NOE is observed at both protons pairs, located within 3.5 Å.[25] Therefore, *threo* stereochemistry for **6** and *erythro* stereochemistry for **7** could be postulated. These stereochemistries were also confirmed with a synthetic approach. Namely, (5*S*,6*R*)-(*erythro*)-lycopene-5,6-diol was synthesized by a stepwise C_{15} + C_{10} + C_{15} double Wittig reaction. The key compound, (5*S*,6*R*)-C_{15}-dihydroxy aldehyde, was prepared via Sharpless asymmetric epoxidation of geraniol and subsequent acidic hydrolysis of the epoxide as shown in Figure 3. The enantiomeric purity of the epoxy geraniol was improved by recrystallization of its dinitrobenzoate. In the same procedure, (5*S*,6*S*)-(*threo*)-lycopene-5,6-diol was synthesized starting from nerol. The enantiomerically enriched compound was obtained by recrystallization of the dihdroxy dinitrobenzoate instead of the epoxy dinitrobenzoate. The outline of the total synthesis of (5*S*,6*R*)- and (5*S*,6*S*)- lycopene-5,6-diol is shown in Figure 3. The detailed synthetic procedures of these compounds will be described elsewhere.

The ^{1}H NMR and ^{13}C NMR data of **6** were identical to those of synthetic (*threo*)-lycopene-5,6-diol, and the ^{1}H NMR data of **7** were identical to those of (*erythro*)-lycopene-5,6-diol. Therefore, structures of **6** and **7** were determined to be (*threo*-) and (*erythro*)-lycopene-5,6-diol, respectively.

Four oxidative metabolites of γ-carotenes, **9**, **10**, **11**, and **12**, were isolated as very minor components. The new carotenoid **9** showed absorption maxima at 420, 445, and 472 nm. The molecular formula of **9** was determined as $C_{40}H_{58}O_2$ by HR FAB MS. The ^{1}H NMR data for **9** are shown in Table 2. The

DOI: 10.1021/jf505008d
J. Agric. Food Chem. 2015, 63, 1622−1630

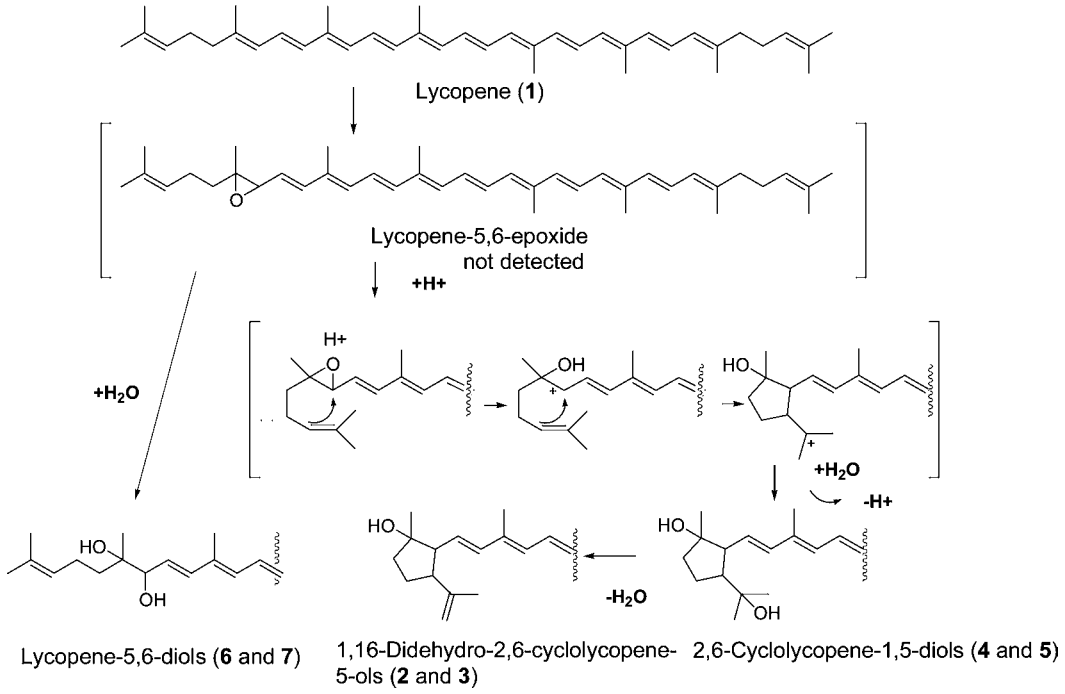

Figure 5. Possible metabolic conversion pathways of lycopene in gac.

Table 3. Percent Relative Rate of EBV-EA Activation[a] with Respect to the Positive Control in the Presence of Carotenoids 1, 4, 6, 8, 9, and 11[b]

	concentration (mol ratio/TPA)[c]				
compounds	1000	500	100	10	IC_{50}[e]
lycopene (**1**)	15.5 (60)[d]	43	86.7	100	406
2,6-cyclolycopene-1,5-diol A (**4**)	9.6 (60)	31.8	79.8	100	355
lycopene-5,6-diol (**6**)	11.3 (60)	34.4	80.8	100	374
γ-carotene (**8**)	12.0 (70)	34.9	81.2	100	379
2,6-cyclo-γ-carotene-1′,5′-diol A (**9**)	9.2 (70)	31.9	78.6	100	349
γ-carotene-5′,6′-diol (**11**)	6.2 (70)	32.0	79.8	100	352

[a]Values represent the percentage relative to the positive control values (100%). [b]There are significant differences ($P < 0.01$) in inhibitory capacity in treatment groups of carotenoids **1**, **4**, **6**, **8**, **9**, and **11** with the control group. [c]TPA concentration was 20 ng (32 pmol/mL). [d]Values in parentheses are percentage viability of Raji cells. [e]Units are nmol.

^{1}H NMR spectroscopic data showed the presence of a β-carotene moiety (H-2 to H-20). The signals of the remaining part (H-2′ to H-20′) were the same as those of H-2 to H-20 positions of 2,6-cyclolycopene-1,5-diol A (**4**), having a (2*S**,5*S**,6*R**) configuration.[14] This structure was confirmed by COSY and NOESY experiments. Therefore, the structure of **9** was determined as (2′*S**,5′*S**,6′*R**)-1′,2′,5′,6′-tetrahydro-2′,6′-cyclo-β,ψ-carotene-1′,5′-diol. Like 2,6-cyclolycopene-1,5-diol, this structure corresponds to a cyclic oxidative metabolite of γ-carotene. Therefore, we referred to **9** as 2′,6′-cyclo-γ-carotene-1′,5′-diol A (Figure 4).

The new carotenoid **10** showed the same UV/vis and MS spectra as those of **9**. The ^{1}H NMR spectroscopic data were almost the same as those of **9** except for the H-2′ to H-6′ and H-16′ to H-18′ positions. This suggested that **10** might be an epimer of 2′,6′-cyclo-β,ψ-carotene-1′,5′-diol A (**9**). The ^{1}H NMR spectroscopic data of H-2′ to H-6′ and H-16 to H-18 were the same as those of H-2 to H-6 and H-16′ to H-18′ of 2,6-cyclolycopene-1,5-diol B (**5**), having a (2′*S**,5′*S**,6′*S**) configuration.[14] Therefore, the structure of **10** was determined as (2′*S**,5′*S**,6′*S**)-1′,2′,5′,6′- tetrahydro-2′,6′-cyclo-β,ψ-carotene-1′,5′-diol and was named 2′,6′-cyclo-β,ψ-carotene-1′,5′-diol B (Figure 4). Very recently, Crawford et al. synthesized 1,2,5,6-tetrahydro-2,6-cyclo-γ-carotene-1,5-diol, an oxidation product of γ-carotene.[26] This compound has the same relative stereochemistry as that of **9** and the spectral data of 1,2,5,6-tetrahydro-2,6-cyclo-γ-carotene-1,5-diol synthesized by Crawford et al. were identical to those of **9**.

Both compounds **11** and **12** showed the same absorption maxima at 420, 445, and 472 nm and the same molecular formula of $C_{40}H_{58}O_2$. ^{1}H NMR data of both compounds were similar to each other except for H-5′ and H-18′. ^{1}H NMR data of **11** indicated the presence of a β-carotene moiety (H-2 to H-20) and (*threo*)-lycopene-5,6-diol moiety (H-2′ to H-20′). Therefore, the structure of **11** was determined as (*threo*)-5′,6′-dihydro-β,ψ-carotene-5′,6′-diol, which was confirmed by COSY and NOESY experiments, and was named (*threo*)-γ-carotene-5′,6′-diol (Figure 4).

Similarly, the structure of **12** was determined as (*erythro*)-5′,6′-dihydro-β,ψ- carotene-5′,6′-diol by comparison of the ^{1}H NMR data with β-carotene and (*erythro*)-lycopene-5,6-diol (**7**), and was named (*erythro*)-γ-carotene-5′,6′-diol (Figure 4).

Based on the results of the present investigation and the previous literature,[13−18] possible metabolic conversion path-

DOI: 10.1021/jf505008d
J. Agric. Food Chem. 2015, 63, 1622−1630

Table 4. Carotenoid Compositions in Aril of Gac

carotenoid	% composition
α-carotene	3.6
β-carotene	7.7
9Z-β-carotene	1.2
γ-carotene (**2**)	4.1
lycopene (**1**)	40.7
9Z-lycopene	11.8
13Z-lycopene	4.5
1,16-didehydro-2,6-cyclolycopene-5-ol A (**2**)	2.5
1,16-didehydro-2,6-cyclolycopene-5-ol B (**3**)	1.4
2,6-cyclolycopene-1′,5′-diol A (**4**)	4.5
2,6-cyclolycopene-1,5-diol B (**5**)	2.5
(*threo*)-lycopene-5,6-diol A (**6**)	6.0
(*erythro*)-lycopene-5,6-diol B (**7**)	2.0
2′,6′-cyclo-γ-carotene-1′,5′-diol A (**9**)	0.8
2′,6′-cyclo-γ-carotene-1′,5′-diol B (**10**)	0.8
(*threo*)-γ-carotene-5′,6′-diol (**11**)	0.5
(*erythro*)-γ-carotene-5′,6′-diol (**12**)	0.5
other carotenoids[a]	4.9

[a]β-Cryptoxanthin, isocryptoxanthin, zeaxanthin, lutein. Carotenoid content 0.61 mg/g.

ways of 1,16-didehydro-2,6-cyclolycopene-5-ols (**2** and **3**), 2,6-cyclolycopene-1,5-diols (**4** and **5**), and lycopene-5,6-diols (**6** and **7**) from lycopene (**1**) are proposed, as shown in Figure 5. Nevertheless, lycopene-5,6-epoxide was not detected in gac, and it was assumed that compounds **2**−**7** might be formed through lycopene-5,6-epoxide. Epoxidation of lycopene provided lycopene-5,6-epoxide. Lycopene-5,6-epoxide was reported as a reaction product of lycopene with MCPB,[14] but it has not been isolated and characterized by spectroscopy including NMR.[14−18] Lycopene-5,6-epoxide might be a very unstable compound and soon converted to other metabolites. Immediately, lycopene-5,6-epoxide was converted to 2,6-cyclolycopene-1,5-diols (**4** and **5**) through epoxy ring cleavage and cyclization of the end group by acid catalysis. Subsequently, dihydroxylation of the hydroxy group at C-1 in **4** and **5** yielded 1,16-didehydro-2,6-cyclolycopene-5-ols (**2** and **3**). However, hydrolytic cleavage of the epoxide ring in lycopene-5,6-epoxide led to two diastereomeric pairs of lycopene-5,6-diols, **6** and **7**. Similarly, 2′,6′-cyclo-γ-carotene-1′,5′-diols (**9** and **10**) and γ-carotene-5′,6′-diols (**11** and **12**) were assumed to be formed from γ-carotene through γ-carotene-5′,6′-epoxide, which was not detected in gac, like lycopene-5,6-diol.

The antitumor-promoting activity of lycopene (**1**), 2,6-cyclolycopene-1,5-diol A (**4**), lycopene-5,6-diol (**6**), γ-carotene (**8**), 2′,6′-cyclo-γ-carotene-1′,5′-diol (**9**), and γ-carotene-5′,6′-diol (**11**) was examined using the Epstein−Barr virus (EBV) activation assay in Raji cells. The results are shown in Table 3. These compounds showed inhibitory effects on the EBV-EA induction of Raji cells without significant cytotoxicity (more than 60% viability of Raji cells) in this assay. The lycopene oxidative metabolites 2,6-cyclolycopene-1,5-diol A (**4**) and lycopene-5,6-diol (**6**) showed slightly higher activity than lycopene (**1**), which is a well-known and excellent antitumor-promoter.[5−8] Similarly, 2′,6′-cyclo-γ-carotene-1′,5′-diol (**9**) and γ-carotene-5′,6′-diol (**11**) also showed slightly higher activity than γ-carotene (**8**). These results revealed that oxidative metabolites of lycopene and γ-carotene exhibit anticarcinogenic activity as well as lycopene and γ-carotene. Carotenoid contents and compositions in gac are shown in Table 4. Gac is a good dietary source of lycopene, as is tomato.[19,20]

AUTHOR INFORMATION

Corresponding Author

*T.M. telephone: +81-75-781-1107. Fax: +81-75-791-7659. E-mail: maoka@mbox.kyoto-inet.or.jp.

Notes

The authors declare no competing financial interest.

ACKNOWLEDGMENTS

We thank Mitani Sangyo Co., Ltd. for providing gac fruits.

REFERENCES

(1) Di Mascio, P.; Kaiser, S.; Sies, H. Lycopene is the most efficient biological carotenoid singlet oxygen quencher. *Arch. Biochem. Biophys.* **2000**, *72*, 990−997.

(2) Oshima, S.; Ojima, F.; Sakamato, H.; Ishiguro, Y.; Terao, J. Supplementation with carotenoids inhibits singlet oxygen-mediated oxidation of human plasma low-density lipoprotein. *J. Agric. Food Chem.* **1999**, *44*, 2306−2309.

(3) Böhm, F.; Tinkler, J. H.; Truscott, T. G. Carotenoids protect against cell membrane damage by the nitrogen dioxide radical. *Nat. Med. (N. Y., NY, U. S. A.)* **1995**, *1*, 98−99.

(4) Böhm, F.; Edge, R.; Burk, M.; Truscott, T. G. Dietary uptake of lycopene protects human cells from singlet oxygen and nitrogen dioxide - ROS components from cigarette smoke. *J. Photochem. Photobiol., B* **2001**, *64*, 176−179.

(5) Levy, J.; Danilenko, M.; Shatoi, Y. The Tomato Carotenoid Lycopene and Cancer. In *Food Factors for Cancer Prevention*; Ohigashi, H., Osawa, T., Terao, J., Watanabe, S., Yoshikawa, T., Eds.; Springer: Tokyo, 1997; pp 209−212.

(6) Nishino, H.; Tokuda, H.; Satomi, Y.; Masuda, M.; Bu, P.; Onozuka, M.; Yamaguchi, S.; Okuda, Y.; Takayama, Y.; Tsuruta, J.; Okuda, M.; Ichiishi, E.; Murakoshi, M.; Yano, M. Cancer prevention by carotenoids. *Pure. Appl. Chem.* **1999**, *71*, 2273−2278.

(7) Nishino, H.; Murakoshi, M.; Ii, T.; Takemura, M.; Kuchide, M.; Kanazawa, M.; Mou, Y. M.; Wada, S.; Masuda, M.; Ohsaka, Y.; Yogosawa, S.; Satomi, Y.; Jinno, K. Carotenoids in cancer chemoprevention. *Cancer Metastasis Rev.* **2002**, *21*, 257−264.

(8) Nishino, H.; Murakoshi, M.; Tokuda, H.; Satomi, Y. Cancer prevention by carotenoids. *Arch. Biochem. Biophys.* **2009**, *483*, 165−168.

(9) Gann, P. H.; Ma, J.; Giovannucci, E.; Willett, W.; Sacks, F. M.; Hennekens, C. H.; Stampfer, M. J. Lower prostate cancer risk in men with elevated plasma lycopene levels: results of a prospective analysis. *Cancer Res.* **1999**, *59*, 1225−1230.

(10) Giovannucci, E. Tomatoes, tomato-based products, lycopene, and cancer: Review of the epidemiologic literature. *J. Natl. Cancer Inst.* **1999**, *91*, 317−331.

(11) Giovannucci, E.; Ascherio, A.; Rimm, E. B.; Stamofer, M. J.; Colditz, G. A.; Willett, W. C. A prospective study on tomato products, lycopene, and prostate cancer risk. *J. Natl. Cancer Inst.* **1995**, *94*, 391−398.

(12) Gerster, H. The potential role of lycopene for human health. *J. Am. Coll. Nutr.* **1997**, *176*, 109−126.

(13) Khachik, F.; Beecher, G. R.; Goli, M. B.; Lusby, W. R.; Smith, J. C., Jr. Separation and identification of carotenoids and their oxidation products in the extracts of human plasma. *Anal. Chem.* **1992**, *64*, 2111−2122.

(14) Khachik, F.; Steck, A.; Niggli, U. A.; Pfander, H. Partial synthesis and structural elucidation of the oxidative metabolites of lycopene identified in tomato paste, tomato juice and human serum. *J. Agric. Food Chem.* **1998**, *46*, 4885−4874−4884.

(15) Khachik, F.; Pfander, H.; Traber, B. Proposed mechanism for the formation of synthetic and naturally occurring metabolites of

DOI: 10.1021/jf505008d
J. Agric. Food Chem. 2015, 63, 1622−1630

lycopene in tomato products and human serum. *J. Agric. Food Chem.* **1998**, *46*, 4885−4890.
(16) Lu, Y.; Etoh, H.; Watanabe, N.; Ina, K.; Ukai, N.; Oshima, S.; Ojima, F.; Sakamato, H.; Ishiguro, Y. A new carotenoid, hydrogen peroxide oxidation products from lycopene. *Biosci., Biotechnol., Biochem.* **1995**, *59*, 2153−2155.
(17) Yokota, T.; Etoh, H.; Ukai, N.; Oshima, S.; Sakamoto, H.; Ishiguro, Y. 1,5-Dihydroxyiridanyl-lycopene in tomato puree. *Biosci., Biotechnol., Biochem.* **1997**, *61*, 549−550.
(18) Yokota, T.; Etoh, H.; Oshima, S.; Hayakawa, K.; Ishiguro, Y. Oxygenated lycopene and dehydrated lutein in tomato puree. *Biosci., Biotechnol., Biochem.* **2003**, *67*, 2644−2647.
(19) Aoki, H.; Kieu, T. M.; Kuze, N.; Tomisaka, K.; Chuene, N. V. Carotenoid pigments in gac fruit (*Momordica cochinchinensis* Spreng). *Biosci., Biotechnol., Biochem.* **2002**, *66*, 2479−2482.
(20) Ishida, B. K.; Turner, C.; Chapman, M. H.; McKeron, T. A. Fatty acid and carotenoid composition of gac (*Momordica cochinchinensis* Spreng) fruit. *J. Agric. Food Chem.* **2004**, *52*, 274−279.
(21) Schiedt, K.; Liaaen-Jensen, S. Isolation and Analysis. In *Carotenoids*; Britton, G., Liaaen-Jensen, S., Pfander, H., Eds.; Birkhäuser: Basel, 1995; Vol. *1A*, pp 81−108.
(22) Britton, G. UV/Visible Spectroscopy. In *Carotenoids*; Britton, G., Liaaen-Jensen, S., Pfander, H., Eds.; Birkhäuser: Basel, 1995; Vol. *1B*, pp 13−62.
(23) Tsushima, M.; Maoka, T.; Katsuyama, M.; Kozuka, M.; Matsuno, T.; Tokuda, H.; Nishino, H.; Iwashima, A. Inhibitory effect of natural carotenoids on Epstein-Barr virus activation activity of a tumor promoter in Raji cells. A screening study for anti-tumor promoters. *Biol. Pharm. Bull.* **1995**, *18*, 227−233.
(24) Maoka, T.; Mochida, K.; Kozuka, M.; Ito, Y.; Fujiwara, Y.; Hashimoto, K.; Enjo, F.; Ogata, M.; Nobukuni, Y.; Tokuda, H.; Nishino, H. Cancer chemopreventive activity of carotenoids in the fruits of red paprika *Capsicum annuum* L. *Cancer Lett.* **2001**, *172*, 103−109.
(25) Englert, G. NMR Spectroscopy. In *Carotenoids*; Britton, G., Liaaen-Jensen, S., Pfander, H., Eds.; Birkhäuser: Basel, 1995; Vol. *1B*, pp147−160.
(26) Crawford, K.; Mazzola, E.; Khachik, F. Total synthesis of 1,2,5,6-tetrahydro-2,6-cyclo-γ-carotene-1,5-diol, an oxidation product of γ-carotene. *Synthesis* **2014**, *46*, 635−645.

DOI: 10.1021/jf505008d
J. Agric. Food Chem. 2015, 63, 1622−1630

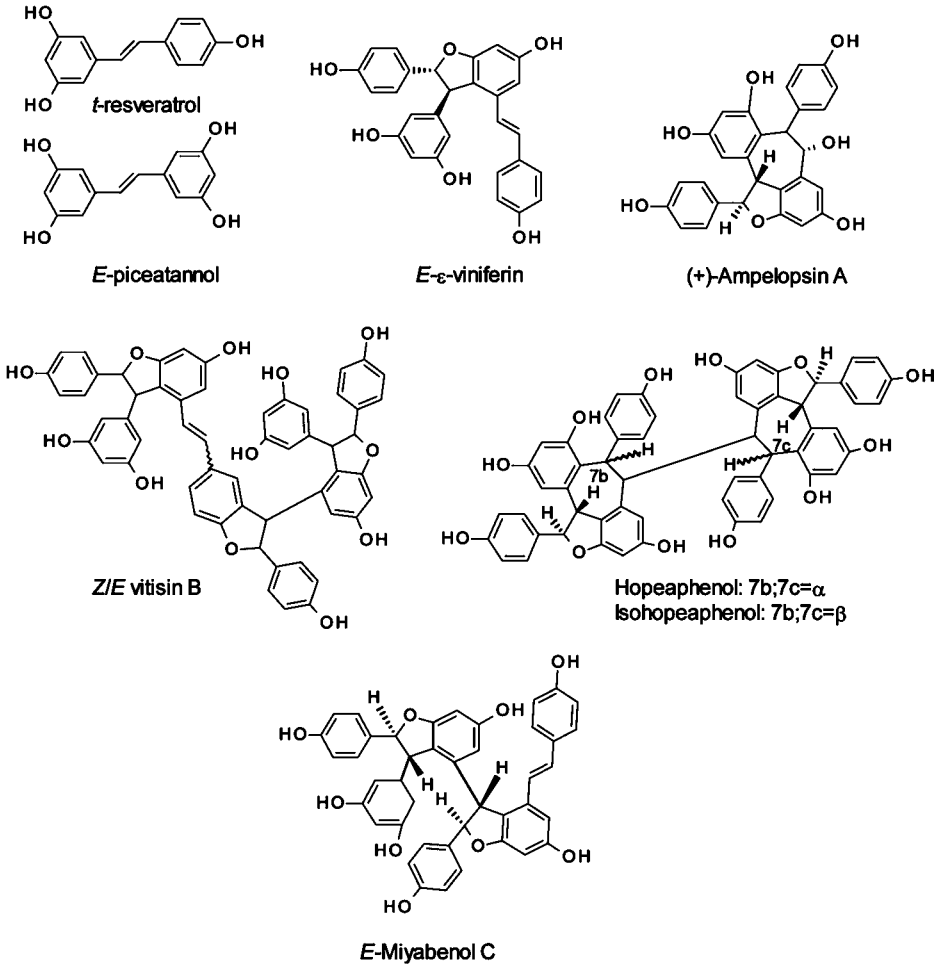

Figure 1. Selected structures of typical stilbenoids present in grape canes.

pharmacological properties of stilbenoids[31] and in agriculture as an alternative source of anti-phytopathogenic substances.[12]

Despite recent advances in the evaluation of stilbenoid composition of grape canes,[31−33] varying results have been reported. Several factors can explain this variability. First, the variety and provenance of the grape can greatly influence stilbenoid composition.[11,30,34] To note, *E*-resveratrol ranged from 0.022 mg kg^{-1} of dry weight (DW) in Turkish cultivars[35] to 6533 mg kg^{-1} of DW in canes from Chile.[30] Second, the extraction method is critical to ensure a good recovery of stilbenoids,[32,36] and the range of extraction methods tends to bias the results. Furthermore, an accurate quantification of stilbenoids relies on calibration curves with pure stilbenoid standards because the quantification of stilbenoids as a resveratrol equivalent leads to an underestimation of the concentrations of resveratrol oligomers.[11] Additionally, a disparity in stilbenoid composition of "Pinot Noir" grape canes has been observed during storage, i.e., the time elapsed between vine pruning and the phytochemical analyses.[37] An increase in the stilbenoid concentration (up to 5-fold) after 6 months at 20 °C was observed. Canes were enriched in *E*-resveratrol, whereas the level of *E*-ε-viniferin did not vary. Although an increase in stilbenoid concentrations has been found in "Pinot Noir" canes in response to storage, the determining factors controlling this accumulation remain unknown and the effect of storage on other grape varieties has not been determined systematically.

The aim of this study was to better characterize stilbenoid accumulation in pruned grape canes and particularly to (i) determine the optimal storage period for 8 grape varieties representative of the Loire valley, (ii) evaluate the influence of temperature storage on stilbenoid accumulation, and (iii) assess the potential biosynthetic activity in pruned grape wood.

MATERIALS AND METHODS

Plant Material. Grape canes of *Vitis vinifera* varieties, "Cabernet Franc", "Chardonnay", "Chenin", "Malbec" (Côt), "Gamay", "Grolleau", "Pinot Noir", and "Sauvignon Blanc", were collected in vineyards at the wine school of Amboise (France) in December 2012. The canes were cut into 10 cm long sections and stored in a controlled chamber at 20 °C for 10 weeks in the dark. In the same way, grape canes of *V. vinifera* var. "Malbec" were stored in additional controlled chambers at −20, 5, 15, 20, and 28 °C for 10 weeks in the dark. Heat shock treatment with intent to denature enzymes consisted of a treatment at 65 °C for 2 h immediately after cane harvest, followed by storage at 20 °C. After storage, samples were ground for 2 min with a cooled analytical grinder (Ika-Werke, Staufen, Germany), frozen in liquid nitrogen, and stored at −80 °C for stilbenoid and gene expression analysis. For time point zero, canes were cut in the vineyards, transported to the laboratory (1 h), and immediately ground, as described above.

Chemicals. *E*-Resveratrol, *E*-piceatannol, catechin, and epicatechin were purchased from Sigma-Aldrich (St. Louis, MO). *E*-ε-Viniferin, *Z*/*E*-vitisin B, ampelopsin A, and hopeaphenol were extracted from grape canes.[19] Acetonitrile and ethanol were purchased from Thermo Fisher

DOI: 10.1021/jf505316a
J. Agric. Food Chem. 2015, 63, 1631−1638

Scientific (Courtaboeuf, France). Ultrapure water was obtained from a Millipore Milli-Q water purification system.

Stilbenoid Analysis. A second grinding step was performed to obtain a powder with an average particle size of 1 mm using a cutting mill (Polymix PX-MFC 90 D, Kinematica AG, Switzerland). Stilbenoid extraction was adapted from the study by Karacabey and Mazza.[33] A total of 50 mg of lyophilized powder were extracted in 1 mL of ethanol/water solution (60:40; v/v), shaken for 30 min at 1400 rpm at 83 °C, and centrifuged at 18000*g* for 5 min. A high-performance liquid chromatography (HPLC) apparatus consisted of a Waters system equipped with a gradient pump (Waters 600 controller, Milford, MA), a cooled autosampler (Waters 717 plus), and a UV−vis photodiode array detector (Waters 996) set to acquire data from 200 to 400 nm. Empower 2 software from Waters was used for instrument control, data acquisition, and data processing. Analyses were performed on a column packed with 3 μm particles (250 × 4 mm, Multospher 120 RP18HP, CS-Service, Langerwehe, Germany) at 24 °C. The mobile phase consisted of aqueous phosphoric acid (0.1%, w/v, eluent A) and acetonitrile (eluent B) pumped at 0.5 mL min^{-1} into the HPLC system. The gradient started at 5% B and increased linearly to 72.5% in 60 min, followed by washing and reconditioning the column. Compounds in extracts were identified according to their UV spectra and retention time by comparison to external standards. Quantification was performed using pure reference standards of *E*-resveratrol, *E*-piceatannol, *E*-ε-viniferin, *Z*/*E*-vitisin B, ampelopsin A, and hopeaphenol and five-point calibration curves (0−100 ppm) using the Maxplot detection mode.

Gene Expression Analysis. Total RNA extractions were performed on ground grape canes (approximately 100 mg) using the improved RNA extraction protocol for woody plants,[38] with RNeasy Plant Mini Kit (Qiagen, U.K.). RNA quality and concentration were assessed both spectrophotometrically and on agarose gel. Reverse transcription of RNA was carried out using ThermoScript RT (Invitrogen) according to the instructions of the manufacturer. First-strand cDNA was synthesized using total RNA (200 ng) and oligo dT_{20} primer (2.5 μM) in the presence of RNaseOUT (Invitrogen). Gene expression was analyzed by quantitative real-time PCR on retro-transcribed RNA using the following primer pairs: 5′-GAAACCCAT-CAATTCCGAACC-3′ (forward) and 5′-GCACTGAGACAATCCA-GAAGAG-3′ (reverse) for phenylalanine ammonia lyase (PAL), 5′-AAAGCTCTGTTAGCGGTGTTCTG-3′ (forward) and 5′-TCAGGTGGTTCAAGTCATCCC-3′ (reverse) for cinnamate 4-hydroxylase (C4H), 5′-CCTGAAATTCCCATCTCCAACC-3′ (forward) and 5′-GACTTTGCGAGAAATGAGGTG-3′ (reverse) for 4-coumaric acid:CoA ligase (4CL), 5′-CAGCAGCCCAAACATT-TATTCC-3′ (forward) and 5′-GTTCCAATCGCTAATAC-CAAGTG-3′ (reverse) for stilbene synthase (STS), and 5′-CTTCTCCTGTATGGGAGCTGCG-3′ (forward) and 5′-GCCA-TAACAACTGGTACAATCGAC-3′ (reverse) for VATP16 reference gene, chosen according to Gamm et al.[39] A real-time polymerase chain reaction (PCR) was run on a CFX96 Touch real-time PCR system (Bio-Rad) using the SYBR Green I technology. Each PCR mixture of 15 μL of total reaction volume contained an equal amount of cDNAs, 0.2 μM forward and reverse primers, and 1× SsoAdvanced SYBR Green Supermix (Bio-Rad). The reaction was initiated by a denaturation step (95 °C for 7 min), followed by 40 cycles at 95 °C for 10 s and 60 °C for 30 s. Melt curve analysis was performed on the end products of PCR, to determine the specificity of reactions. Absolute quantification of the transcript copy number was performed using calibration curves (plasmid dilution series from 10^8 to 10^4 copies). The results are expressed as the copy number of cDNA normalized using VATP16 reference gene.

Statistical Analysis. Data were analyzed with Statistica, version 6.0 (StatSoft, Inc., Tulsa, OK). Statistical significance from different treatments was revealed after one-way analysis of variance (ANOVA), followed by Tukey's test.

RESULTS AND DISCUSSION

A total of 10 compounds were identified in grape cane extracts from the varieties "Cabernet Franc", "Chardonnay", "Chenin", "Malbec" (Côt), "Gamay", "Grolleau", "Pinot Noir" and "Sauvignon Blanc", corresponding to the flavonoids, catechin and epicatechin, and the stilbenoids, ampelopsin A, *E*-piceatannol, *E*-resveratrol, hopeaphenol, isohopeaphenol, *E*-ε-viniferin, *E*-miyabenol C, and *Z*/*E*-vitisin B (Figure 1). HPLC chromatograms of "Sauvignon Blanc" grape cane extracts before and after a 6 week storage period show striking changes in stilbenoid composition, particularly for *E*-resveratrol and *E*-piceatannol (Figure 2). To confirm those observations, a survey

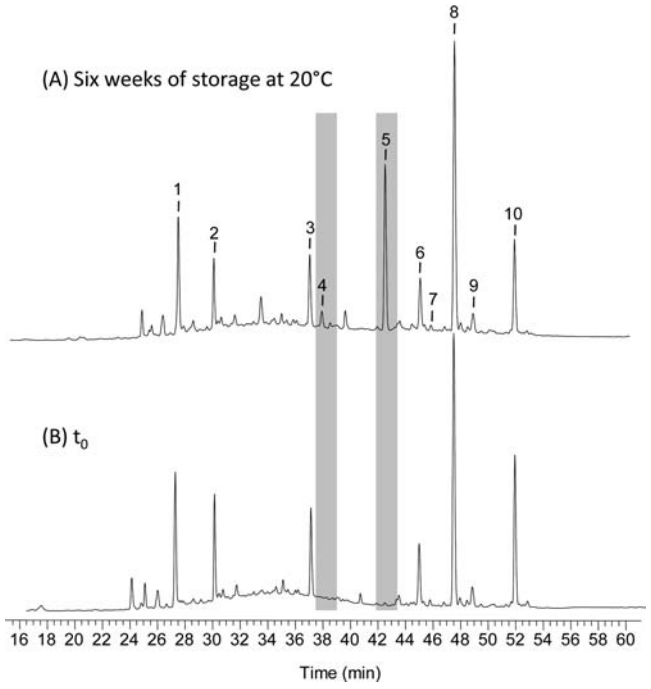

Figure 2. HPLC chromatograms measured in Maxplot detection of hydroalcoholic cane extracts of *V. vinifera* "Sauvignon Blanc". Grape canes were harvested in the vineyard and stored for 6 weeks at 20 °C (A) or were immediately ground for stilbenoid extraction (B). (1) Catechin, (2) epicatechin, (3) ampelopsin A, (4) *E*-piceatannol, (5) *E*-resveratrol, (6) hopeaphenol, (7) isohopeaphenol, (8) *E*-ε-viniferin, (9) *E*-miyabenol C, and (10) *Z*/*E*-vitisin B.

of stilbenoid accumulation in pruned wood was expanded to eight grape varieties stored for 8 weeks at 20 °C (Figure 3). The initial concentration of *E*-resveratrol contained in branches before any treatment was determined prior to storage. For this, the grape canes were ground and frozen at −80 °C within 1 h (maximum) after pruning in the vineyards. The *E*-resveratrol contents measured at t_0 in all varieties were shown to be very low (101 ± 77 mg kg^{-1} of DW) and corresponded to the values previously reported for unstored grape canes.[37] In contrast, an accumulation of *E*-resveratrol was observed in the eight tested grape varieties during storage, reaching a peak after 6 weeks (Figure 3A). On average, a 40-fold increase in *E*-resveratrol was observed with a range from 19-fold for "Pinot Noir" to 102-fold for "Chenin" (Table 1). At the same time, *E*-piceatannol increased in a similar fashion but on a smaller scale (Figure 3B). The accumulation of *E*-resveratrol during storage in these eight varieties confirms previous results obtained for "Pinot Noir",[37] with an additional increase in *E*-piceatannol (3-hydroxyresver-

DOI: 10.1021/jf505316a
J. Agric. Food Chem. 2015, 63, 1631−1638

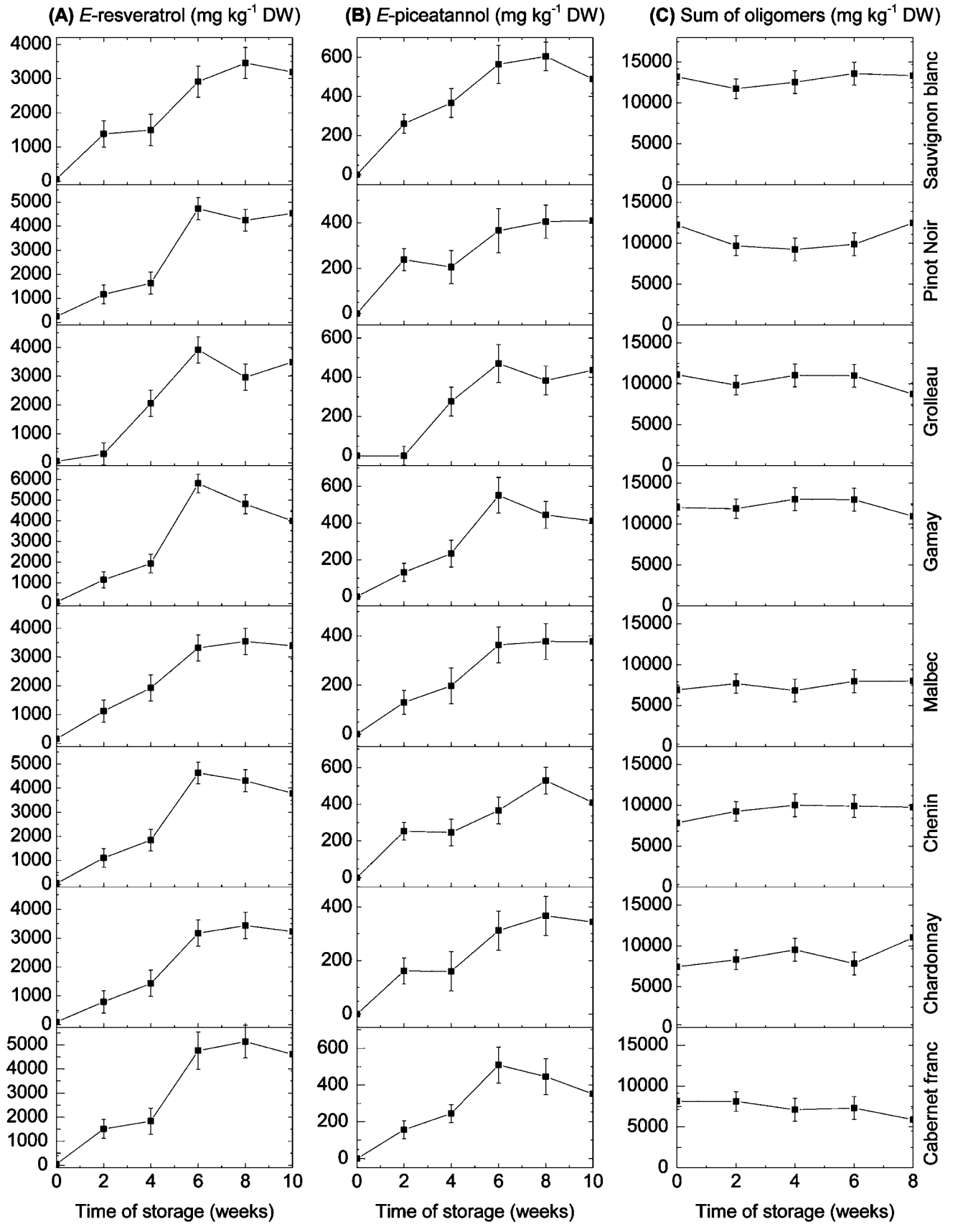

Figure 3. Changes in the stilbene concentration during storage of grape canes from eight varieties. The grape varieties are presented by lines with "Cabernet Franc", "Chardonnay", "Chenin", "Malbec", "Gamay", "Grolleau", "Pinot Noir", and "Sauvignon Blanc". The stilbene compounds are presented by columns with (A) *E*-resveratrol, (B) *E*-piceatannol, and (C) sum of oligomers (i.e., addition of concentrations of ampelopsin A, hopeaphenol, isohopeaphenol, *E*-ε-viniferin, *E*-miyabenol C, and *Z*/*E*-vitisin B).

DOI: 10.1021/jf505316a
J. Agric. Food Chem. 2015, 63, 1631−1638

Table 1. Changes in the *E*-Resveratrol Concentration in Grape Canes from Eight Varieties after a 6 Week Storage Period at 20 °C

	E-resveratrol concentration (mg kg^{-1} of DW)		
variety	0 weeks	6 weeks	fold induction
Sauvignon Blanc	60 (31)	2908 (552)	48
Chardonnay	96 (16)	3175 (508)	33
Côt	158 (23)	3316 (762)	21
Grolleau	41 (18)	3913 (704)	95
Chenin	45 (15)	4631 (926)	106
Pinot Noir	250 (112)	4725 (897)	19
Cabernet Franc	57 (15)	4762 (952)	83
Gamay	100 (33)	5100 (867)	51
Means	101	4066	40

atrol). Such an induction of monomeric stilbenoids was also observed in other postharvest plant materials.[40] Indeed, *E*-resveratrol and *E*-piceatannol were shown to accumulate in sugar cane billets within 7 days after harvest. Furthermore, it has been shown that red wines and table grapes can be enriched in stilbenoids by postharvest UV-C irradiation of grapes.[41−43] As for other stilbenoid-rich products, the present results highlight the importance of the postharvest process to obtain grape canes with enriched contents in *E*-resveratrol and *E*-piceatannol.

Nevertheless, the origin of the accumulated stilbenoids was not elucidated. They might be formed from the degradation of oligomeric stilbenoids or a biosynthetic activity. For this reason, the concentrations of resveratrol oligomers (ampelopsin A, hopeaphenol, isohopeaphenol, *E*-ε-viniferin, *E*-miyabenol C, and *Z*/*E*-vitisin B) were individually quantified during the storage period but no significant changes were observed (data not shown). In summary, Figure 3C presents the total concentration of resveratrol oligomers, which do not significantly vary during storage in any of the varieties tested. Therefore, the possibility that *E*-resveratrol and *E*-piceatannol originated from the degradation of resveratrol oligomers was ruled out. To test the hypothesis that the accumulation of *E*-resveratrol originated from a *de novo* biosynthesis, the influence of temperature storage on *E*-resveratrol accumulation was tested on the "Cabernet Franc" variety over 10 weeks (Figure 4). First, when the canes were stored at either 5, 15, or 20 °C, the *E*-resveratrol concentration increased to approximately 6384 ± 456 mg kg^{-1} of DW; however, the accumulation rate of *E*-resveratrol was shown to be delayed at lower temperatures. Second, at 28 °C, *E*-resveratrol accumulated rapidly during the first 2 weeks up to a peak of 3923 ± 584 mg kg^{-1} of DW; however, no further accumulation was observed in the weeks after. Finally, when a short heat-shock treatment (2 h at 65 °C) was applied to grape canes, no *E*-resveratrol accumulation was observed. Such a treatment with intent to denature proteins inhibits the accumulation of *E*-resveratrol during the storage period and suggests the involvement of active enzymes in this phenomenon. Similarly, when canes were stored at −20 °C, *E*-resveratrol was not induced. The temperature during the storage process of grape canes is therefore a determining factor for optimal *E*-resveratrol accumulation (observed at 20 °C). Moreover, whereas an excessive temperature (up to 28 °C) rapidly inhibits *E*-resveratrol accumulation, a decrease in the storage temperature only slows the induction rate and the optimal *E*-resveratrol content is still achieved, albeit at a later

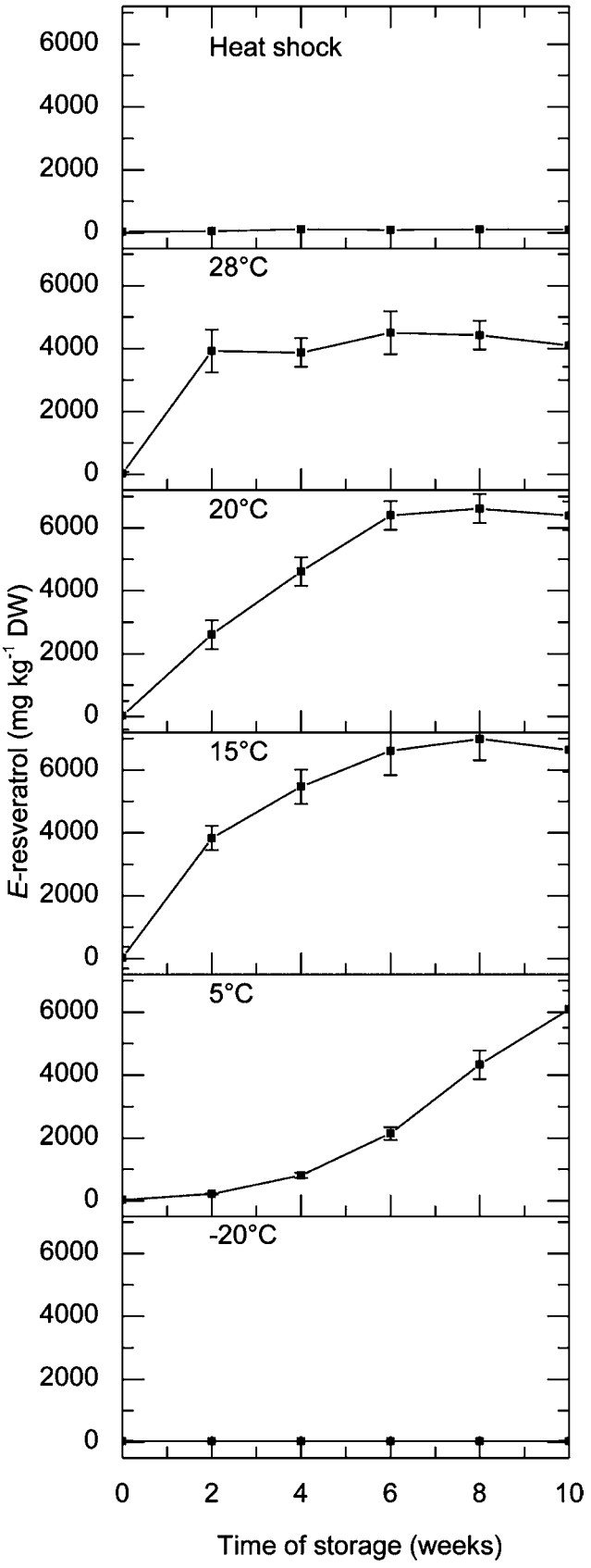

Figure 4. Effect of the temperature on *E*-resveratrol accumulation during cane storage of *V. vinifera* "Cabernet Franc". Grape canes were stored for a period of 10 weeks at −20, 5, 15, 20, and 28 °C. Heat shock consisted of a treatment at 65 °C for a period of 2 h immediately after harvest, followed by storage at 20 °C.

DOI: 10.1021/jf505316a
J. Agric. Food Chem. 2015, 63, 1631−1638

time period (Figure 4). These data prompt us to assume that the biosynthetic enzyme activities and, particularly, those involved in the stilbene pathway persist during storage and that the optimal period of storage is directly related to the storage temperature.

Given these data, we investigated by real-time PCR the transcriptional activity of key genes involved in the stilbene biosynthesis during the 6 weeks of *E*-resveratrol accumulation in pruned grape wood of the "Cabernet Franc" variety stored at 20 °C (Figure 5). The transcript abundance of the structural

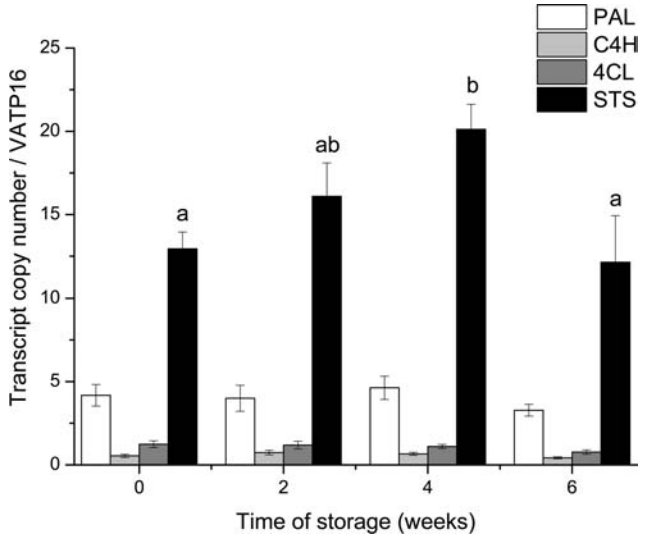

Figure 5. Transcript abundance of the stilbene biosynthesis pathway genes PAL, 4CL, C4H, and STS measured by quantitative real-time PCR during cane storage of *V. vinifera* "Cabernet Franc". Grape canes were collected in the vineyard and directly frozen at −80 °C (t_0) or stored at 20 °C for 2, 4, and 6 weeks. Transcript abundance of each gene was normalized against VATP16 reference gene. Different letters in the same group of bars indicate significant differences ($p < 0.05$).

genes PAL, 4CL, C4H, and STS were assayed by quantitative real-time PCR (Figure 5). PAL, 4CL, and C4H, the three genes of the general phenylpropanoid pathway, were constitutively expressed over the 6 weeks of storage, and in addition, STS (forming *E*-resveratrol) was induced during the first 4 weeks of storage. These results suggest that grape pruned wood is still transcriptionally active during the storage period.

In planta, *E*-resveratrol is a well-known phytoalexin, i.e., an antimicrobial substance that rapidly accumulates at the pathogen infection site. *E*-Resveratrol is induced in response to biotic and abiotic stresses, such as elicitors,[44] UV-C light,[45] ozone,[46] anoxia,[47] and wounding.[48] Following pathogenic infection, the STS transcripts are induced within 16−48 h[3,39] and the peak value for *E*-resveratrol accumulation occurs around 24−72 h.[6] In contrast, the induction of stilbene metabolism in postharvest material is poorly documented, and available data are restricted to grape berries. Pioneering work showing the induction of stilbene metabolism during the drying process of postharvest grape berries was reported by Versari et al.[49] Recently, complementary studies showed that both STS transcripts and *E*-resveratrol biosynthesis are induced in the epicarp of postharvest grape berries and the induction level depends upon the dehydratation rate.[50] Our study highlights a similar induction of stilbene biosynthesis in postharvest grape canes where the drying process during storage might be perceived as a stress signal by living tissues. Stilbene metabolism is thus induced, and *E*-resveratrol and *E*-piceatannol accumulate until the tissues are dry. Further investigations will help to evaluate the influence of the hygrometric conditions in relation to temperature on stilbenoid accumulation during grape cane storage.

In conclusion, at the pruning stage, grape canes contain high levels of oligomeric stilbenoids previously accumulated during the growing season but almost no monomeric stilbenoids. During the first 6 weeks of storage, *E*-resveratrol and *E*-piceatannol accumulate at various rates depending upon the storage temperature. This *E*-resveratrol accumulation resulted from a *de novo* biosynthesis with induction of STS expression during storage. Grape canes appear to be an original plant byproduct containing valuable stilbenoids. Because this pruned wood is still metabolically active during the drying process, the storage conditions have to be controlled to obtain stilbene-enriched material for further medicinal or agronomical applications. To further characterize the variability of stilbenoids in grape canes, the impact of grape diseases during the growing season will be required.

AUTHOR INFORMATION

Corresponding Author

*Telephone: +33-0-2-47-36-72-14. Fax: +33-0-2-47-36-72-32. E-mail: arnaud.lanoue@univ-tours.fr.

Funding

This work was supported by the Région Centre Grants ACTISARM 201100068678 and VITITERROIR 201300083172.

Notes

The authors declare no competing financial interest.

ACKNOWLEDGMENTS

The authors thank Aurélie Mançois and Frédéric Fourmont (Lycée Viticole d'Amboise, France) for providing the grape canes.

REFERENCES

(1) Riviere, C.; Pawlus, A. D.; Merillon, J.-M. Natural stilbenoids: Distribution in the plant kingdom and chemotaxonomic interest in Vitaceae. *Nat. Prod. Rep.* **2012**, *29*, 1317−1333.

(2) Vannozzi, A.; Dry, I. B.; Fasoli, M.; Zenoni, S.; Lucchin, M. Genome-wide analysis of the grapevine stilbene synthase multigenic family: Genomic organization and expression profiles upon biotic and abiotic stresses. *BMC Plant Biol.* **2012**, *12*, 130.

(3) Chong, J.; Poutaraud, A.; Hugueney, P. Metabolism and roles of stilbenes in plants. *Plant Sci.* **2009**, *177*, 143−155.

(4) Jeandet, P.; Clement, C.; Courot, E.; Cordelier, S. Modulation of phytoalexin biosynthesis in engineered plants for disease resistance. *Int. J. Mol. Sci.* **2013**, *14*, 14136−14170.

(5) Jeandet, P.; Hebrard, C.; Deville, M.-A.; Cordelier, S.; Dorey, S.; Aziz, A.; Crouzet, J. Deciphering the role of phytoalexins in plant−microorganism interactions and human health. *Molecules* **2014**, *19*, 18033−18056.

(6) Pezet, R.; Gindro, K.; Viret, O.; Richter, H. Effects of resveratrol, viniferins and pterostilbene on *Plasmopara viticola* zoospore mobility and disease development. *Vitis* **2004**, *43*, 145−148.

(7) Schnee, S.; Viret, O.; Gindro, K. Role of stilbenes in the resistance of grapevine to powdery mildew. *Physiol. Mol. Plant Pathol.* **2008**, *72*, 128−133.

(8) Adrian, M.; Jeandet, P. Effects of resveratrol on the ultrastructure of *Botrytis cinerea* conidia and biological significance in plant/pathogen interactions. *Fitoterapia* **2012**, *83*, 1345−1350.

DOI: 10.1021/jf505316a
J. Agric. Food Chem. 2015, 63, 1631−1638

(9) Yang, M.-H.; Kuo, C.-H.; Hsieh, W.-C.; Ku, K.-L. Investigation of microbial elicitation of *trans*-resveratrol and *trans*-piceatannol in peanut callus led to the application of chitin as a potential elicitor. *J. Agric. Food Chem.* **2010**, *58*, 9537−9541.
(10) Ku, K. L.; Chang, P. S.; Cheng, Y. C.; Lien, C. Y. Production of stilbenoids from the callus of *Arachis hypogaea*: A novel source of the anticancer compound piceatannol. *J. Agric. Food Chem.* **2005**, *53*, 3877−3881.
(11) Lambert, C.; Richard, T.; Renouf, E.; Bisson, J.; Waffo-Teguo, P.; Bordenave, L.; Ollat, N.; Merillon, J.-M.; Cluzet, S. Comparative analyses of stilbenoids in canes of major *Vitis vinifera* L. cultivars. *J. Agric. Food Chem.* **2013**, *61*, 11392−11399.
(12) Schnee, S.; Queiroz, E. F.; Voinesco, F.; Marcourt, L.; Dubuis, P.-H.; Wolfender, J.-L.; Gindro, K. *Vitis vinifera* canes, a new source of antifungal compounds against *Plasmopara viticola*, *Erysiphe necator*, and *Botrytis cinerea*. *J. Agric. Food Chem.* **2013**, *61*, 5459−5467.
(13) Cottart, C.-H.; Nivet-Antoine, V.; Beaudeux, J.-L. Review of recent data on the metabolism, biological effects, and toxicity of resveratrol in humans. *Mol. Nut. Food Res.* **2014**, *58*, 7−21.
(14) Smoliga, J. M.; Baur, J. A.; Hausenblas, H. A. Resveratrol and health—A comprehensive review of human clinical trials. *Mol. Nutr. Food Res.* **2011**, *55*, 1129−1141.
(15) Vang, O.; Ahmad, N.; Baile, C. A.; Baur, J. A.; Brown, K.; Csiszar, A.; Das, D. K.; Delmas, D.; Gottfried, C.; Lin, H.-Y.; Ma, Q.-Y.; Mukhopadhyay, P.; Nalini, N.; Pezzuto, J. M.; Richard, T.; Shukla, Y.; Surh, Y.-J.; Szekeres, T.; Szkudelski, T.; Walle, T.; Wu, J. M. What is new for an old molecule? Systematic review and recommendations on the use of resveratrol. *PLoS One* **2011**, *6*, No. e19881.
(16) Piotrowska, H.; Kucinska, M.; Murias, M. Biological activity of piceatannol: Leaving the shadow of resveratrol. *Mutat. Res., Rev. Mutat.* **2012**, *750*, 60−82.
(17) Fu, J.; Jin, J.; Cichewicz, R. H.; Hageman, S. A.; Ellis, T. K.; Xiang, L.; Peng, Q.; Jiang, M.; Arbez, N.; Hotaling, K.; Ross, C. A.; Duan, W. *trans*-(−)-ε-Viniferin increases mitochondrial sirtuin 3 (SIRT3), activates AMP-activated protein kinase (AMPK), and protects cells in models of Huntington disease. *J. Biol. Chem.* **2012**, *287*, 24460−24472.
(18) Gonzalez-Sarrias, A.; Gromek, S.; Niesen, D.; Seeram, N. P.; Henry, G. E. Resveratrol oligomers isolated from *Carex* species inhibit growth of human colon tumorigenic cells mediated by cell cycle arrest. *J. Agric. Food Chem.* **2011**, *59*, 8632−8638.
(19) Houille, B.; Papon, N.; Boudesocque, L.; Bourdeaud, E.; Besseau, S.; Courdavault, V.; Enguehard-Gueiffier, C.; Delanoue, G.; Guerin, L.; Bouchara, J.-P.; Clastre, M.; Giglioli-Guivarc'h, N.; Guillard, J.; Lanoue, A. Antifungal activity of resveratrol derivatives against *Candida* species. *J. Nat. Prod.* **2014**, *77*, 1658−1662.
(20) Richard, T.; Poupard, P.; Nassra, M.; Papastamoulis, Y.; Iglesias, M.-L.; Krisa, S.; Waffo-Teguo, P.; Merillon, J.-M.; Monti, J.-P. Protective effect of ε-viniferin on β-amyloid peptide aggregation investigated by electrospray ionization mass spectrometry. *Bioorg. Med. Chem.* **2011**, *19*, 3152−3155.
(21) Zghonda, N.; Yoshida, S.; Ezaki, S.; Otake, Y.; Murakami, C.; Mliki, A.; Ghorbel, A.; Miyazaki, H. ε-Viniferin is more effective than its monomer resveratrol in improving the functions of vascular endothelial cells and the heart. *Biosci., Biotechnol., Biochem.* **2012**, *76*, 954−960.
(22) Zhang, Y.; Yu, B.; Sui, Y.; Gao, X.; Yang, H.; Ma, T. Identification of resveratrol oligomers as inhibitors of cystic fibrosis transmembrane conductance regulator by high-throughput screening of natural products from chinese medicinal plants. *PLoS One* **2014**, *9*, No. e94302.
(23) Donnez, D.; Jeandet, P.; Clement, C.; Courot, E. Bioproduction of resveratrol and stilbene derivatives by plant cells and micro-organisms. *Trends Biotechnol.* **2009**, *27*, 706−13.
(24) Snyder, S. A.; Gollner, A.; Chiriac, M. I. Regioselective reactions for programmable resveratrol oligomer synthesis. *Nature* **2011**, *474*, 461−466.
(25) Shen, T.; Wang, X.-N.; Lou, H.-X. Natural stilbenes: An overview. *Nat. Prod. Rep.* **2009**, *26*, 916−935.
(26) Kang, S.-Y.; Lee, J. K.; Choi, O.; Kim, C. Y.; Jang, J.-H.; Hwang, B. Y.; Hong, Y.-S. Biosynthesis of methylated resveratrol analogs through the construction of an artificial biosynthetic pathway in *E. coli*. *BMC Biotechnol.* **2014**, *14*, 67.
(27) Jeandet, P.; Delaunois, B.; Aziz, A.; Donnez, D.; Vasserot, Y.; Cordelier, S.; Courot, E. Metabolic engineering of yeast and plants for the production of the biologically active hydroxystilbene, resveratrol. *J. Biomed. Biotechnol.* **2012**, 579089.
(28) Rayne, S.; Karacabey, E.; Mazza, G. Grape cane waste as a source of *trans*-resveratrol and *trans*-viniferin: High-value phytochemicals with medicinal and anti-phytopathogenic applications. *Ind. Crops Prod.* **2008**, *27*, 335−340.
(29) Devesa-Rey, R.; Vecino, X.; Varela-Alende, J. L.; Barral, M. T.; Cruz, J. M.; Moldes, A. B. Valorization of winery waste vs. the costs of not recycling. *Waste Manage.* **2011**, *31*, 2327−2335.
(30) Vergara, C.; von Baer, D.; Mardones, C.; Wilkens, A.; Wernekinck, K.; Damm, A.; Macke, S.; Gorena, T.; Winterhalter, P. Stilbene levels in grape cane of different cultivars in southern Chile: Determination by HPLC−DAD−MS/MS method. *J. Agric. Food Chem.* **2012**, *60*, 929−933.
(31) Pawlus, A. D.; Waffo-Teguo, P.; Saver, J.; Merillon, J.-M. Stilbenoid chemistry from wine and the genus *Vitis*, a review. *J. Int. Sci. Vigne Vin* **2012**, *46*, 57−111.
(32) Karacabey, E.; Bayindirli, L.; Artik, N.; Mazza, G. Modeling solid−liquid extraction kinetics of *trans*-resveratrol and *trans*-ε-viniferin from grape cane. *J. Food Process Eng.* **2013**, *36*, 103−112.
(33) Karacabey, E.; Mazza, G. Optimisation of antioxidant activity of grape cane extracts using response surface methodology. *Food Chem.* **2010**, *119*, 343−348.
(34) Zhang, A.; Fang, Y.; Li, X.; Meng, J.; Wang, H.; Li, H.; Zhang, Z.; Guo, Z. Occurrence and estimation of *trans*-resveratrol in one-year-old canes from seven major Chinese grape producing regions. *Molecules* **2011**, *16*, 2846−2861.
(35) Cetin, E. S.; Altinoz, D.; Tarcan, E.; Baydar, N. G. Chemical composition of grape canes. *Ind. Crops Prod.* **2011**, *34*, 994−998.
(36) Karacabey, E.; Mazza, G. Optimization of solid−liquid extraction of resveratrol and other phenolic compounds from milled grape canes (*Vitis vinifera*). *J. Agric. Food Chem.* **2008**, *56*, 6318−6325.
(37) Gorena, T.; Saez, V.; Mardones, C.; Vergara, C.; Winterhalter, P.; von Baer, D. Influence of post-pruning storage on stilbenoid levels in *Vitis vinifera* L. canes. *Food Chem.* **2014**, *155*, 256−263.
(38) MacKenzie, D. J.; McLean, M. A.; Mukerji, S.; Green, M. Improved RNA extraction from woody plants for the detection of viral pathogens by reverse transcription-polymerase chain reaction. *Plant Dis.* **1997**, *81*, 222−226.
(39) Gamm, M.; Heloir, M.-C.; Kelloniemi, J.; Poinssot, B.; Wendehenne, D.; Adrian, M. Identification of reference genes suitable for qRT-PCR in grapevine and application for the study of the expression of genes involved in pterostilbene synthesis. *Mol. Genet. Genomics* **2011**, *285*, 273−285.
(40) Boue, S. M.; Shih, B. Y.; Burow, M. E.; Eggleston, G.; Lingle, S.; Pan, Y.-B.; Daigle, K.; Bhatnagar, D. Postharvest accumulation of resveratrol and piceatannol in sugarcane with enhanced antioxidant activity. *J. Agric. Food Chem.* **2013**, *61*, 8412−8419.
(41) Cantos, E.; Espin, J. C.; Fernandez, M. J.; Oliva, J.; Tomas-Barberan, F. A. Postharvest UV-C-irradiated grapes as a potential source for producing stilbene-enriched red wines. *J. Agric. Food Chem.* **2003**, *51*, 1208−1214.
(42) Crupi, P.; Pichierri, A.; Basile, T.; Antonacci, D. Postharvest stilbenes and flavonoids enrichment of table grape cv Redglobe (*Vitis vinifera* L.) as affected by interactive UV-C exposure and storage conditions. *Food Chem.* **2013**, *141*, 802−808.
(43) Gonzalez-Barrio, R.; Beltran, D.; Cantos, E.; Gil, M. I.; Espin, J. C.; Tomas-Barberan, F. A. Comparison of ozone and UV-C treatments on the postharvest stilbenoid monomer, dimer, and trimer induction in var. 'Superior' white table grapes. *J. Agric. Food Chem.* **2006**, *54*, 4222−4228.

DOI: 10.1021/jf505316a
J. Agric. Food Chem. 2015, 63, 1631−1638

(44) Chang, X.; Heene, E.; Qiao, F.; Nick, P. The phytoalexin resveratrol regulates the initiation of hypersensitive cell death in *Vitis* cell. *PLoS One* **2011**, *6*, No. e26405.
(45) Adrian, M.; Jeandet, P.; Douillet-Breuil, A. C.; Tesson, L.; Bessis, R. Stilbene content of mature *Vitis vinifera* berries in response to UV-C elicitation. *J. Agric. Food Chem.* **2000**, *48*, 6103−6105.
(46) Grimmig, B.; Gonzalez-Perez, M. N.; Welzl, G.; Penuelas, J.; Schubert, R.; Hain, R.; Heidenreich, B.; Betz, C.; Langebartels, C.; Ernst, D.; Sandermann, H. Ethylene- and ozone-induced regulation of a grapevine resveratrol synthase gene: Different responsive promoter regions. *Plant Physiol. Biochem.* **2002**, *40*, 865−870.
(47) Jimenez, J. B.; Orea, J. M.; Gonzalez Urena, A.; Escribano, P.; Lopez de la Osa, P.; Guadarrama, A. Short anoxic treatments to enhance *trans*-resveratrol content in grapes and wine. *Eur. Food Res. Technol.* **2007**, *224*, 373−378.
(48) Chung, I. M.; Park, M. R.; Chun, J. C.; Yun, S. J. Resveratrol accumulation and resveratrol synthase gene expression in response to abiotic stresses and hormones in peanut plants. *Plant Sci.* **2003**, *164*, 103−109.
(49) Versari, A.; Parpinello, G. P.; Tornielli, G. B.; Ferrarini, R.; Giulivo, C. Stilbene compounds and stilbene synthase expression during ripening, wilting, and UV treatment in grape cv. Corvina. *J. Agric. Food Chem.* **2001**, *49*, 5531−5536.
(50) Bonghi, C.; Rizzini, F. M.; Gambuti, A.; Moio, L.; Chkaiban, L.; Tonutti, P. Phenol compound metabolism and gene expression in the skin of wine grape (*Vitis vinifera* L.) berries subjected to partial postharvest dehydration. *Postharvest Biol. Technol.* **2012**, *67*, 102−109.

NOTE ADDED AFTER ASAP PUBLICATION

This article published January 27, 2015 with errors in the "fold induction" column of Table 1. The corrected version published February 11, 2015.

DOI: 10.1021/jf505316a
J. Agric. Food Chem. 2015, 63, 1631−1638

pathway is strictly regulated by Wnt antagonists, including Wnt inhibitory protein 1 (WIF1), Frizzled related protein (sFRP), and Dickkopf (Dkk). Binding of WIF to Wnts and binding of sFRP to both Wnts and Fzs cause negative modulation in both the canonical and noncanonical Wnt pathways. Binding of Dkks to the Fz−LRP complex impairs its function, acting as specific inhibitors of the canonical Wnt pathway.[18] Abnormal Wnt gene expression is associated with the epithelial-to-mesenchymal transition (EMT). Importantly, many oncogenic pathways may activate EMT, thus causing EMT metastatic potential in epithelial cancer cells,[19] which is related to the upregulation of mesenchymal markers, including Twist and fibronectin, in the majority of premetastatic tumors.[20] However, tissue fibrosis is tight EMT activation, which may also be initiated by tissue damage and inflammatory processes.[21] Furthermore, EMT has been suggested to result in the increases in the levels of fibroblasts, collagen, and other matrix components at chronic inflammatory sites, involving progressive organ fibrosis.[22] Furthermore, changes in the expression of Wnts, their receptors, and antagonists were demonstrated to be associated with renal interstitial fibrosis induced by unilateral ureteral obstruction.[14] Therefore, we hypothesized that nano-TiO_2-induced chronic renal inflammation may subsequently lead to renal fibrosis and is associated with the Wnt pathway in mouse kidney.

Nano-TiO_2 is a common additive in food and personal care products, and their presence in daily life is increasing. Dietary exposure to TiO_2 in Western populations is 1−3 mg of TiO_2 [kg of body weight (bw)]$^{-1}$ day^{-1} on average for children under the age of 10 years and approximately 0.2−1 mg of TiO_2 (kg of bw)$^{-1}$ day^{-1} for other age groups. Several reports (e.g., NIOSH) recommend exposure limits of 2−3 mg/m^3 for fine TiO_2 and 0.3−1 mg/m^3 for ultrafine (including nanoscale engineered) TiO_2.[22] Assuming that 36% of food-grade TiO_2 is smaller than 100 nm in at least one dimension, this exposure limit decreases to approximately 0.1 mg of nanoscale TiO_2 person^{-1} day^{-1}.[23] Therefore, the long-term oral ingestion of the smaller dose of TiO_2 may be associated with potential kidney toxicity. In this study, female mice were continuously exposed to 1.25, 2.5, or 5 mg of nano-TiO_2/kg administered by gavage according to FDA guidelines for 9 consecutive months. The expression levels of Wnt pathway-related markers and EMT markers in mouse kidney were investigated to determine the mechanism of renal fibrosis caused by chronic exposure to nano-TiO_2.

MATERIALS AND METHODS

Chemicals. The preparation of nano-anatase TiO_2 was described by Yang.[24] It was fully characterized as previously described by Yang et al.[24] and in our previous studies[25] and is listed in Table 1.

Table 1. Characteristics of Nano-TiO_2[24,25]

phase	particle size (nm)	surface area (m^2/g)	Man hydrodynamic diameter (nm)	ζ potential (mV)
anatase	5−6	174.8	208−330 (mainly 294)	9.28

Animals and Treatment. CD-1 (ICR) female mice (4 weeks old, 20 ± 2 g), obtained from the Animal Center of Soochow University (China), were used in this study and were fed with sterilized food and distilled water *ad libitum* and housed in stainless steel cages (five mice per cage). All mice were kept at standardized laboratory conditions (24 ± 2 °C, 60 ± 10% humidity, and a 12 h light/dark cycle). After being acclimated to the laboratory conditions for one week, the mice were fasted for 3 h prior to nano-TiO_2 administration. All experiments were conducted using the recommendations for the ethical conditions approved by the Care and Use of Animals Committee of Soochow University, which are consistent with international ethics for handling experimental animals.

One hundred mice were divided into four groups (n = 25 in each group): a control group treated with 0.5% (w/v) hydroxypropylmethylcellulose (HPMC) K4M (Sigma-Aldrich, St. Louis, MO) solvent and three experimental groups treated with 1.25, 5, or 5 mg of nano-TiO_2/kg of bw suspended in HPMC solvent. All mice were weighed, and the nano-TiO_2 suspensions of different doses were administered to mice by intragastric feeding every day for 9 months. Food and water intake was carefully recorded during the last week of the 9th months. Food and water intake was calculated according to the Drozdz method.[26]

Kidney Indices. After the 9 month study period, all mice were weighed and urine was collected in 50 mL conical tubes over 24 h. Urine volumes were measured, and the samples were stored at −80 °C. All mice were lightly anesthetized with ether; blood samples were collected from the heart, and the kidneys were quickly removed and placed on ice. After the kidneys had been weighed, the kidney indices were calculated as the ratio of kidney (wet weight, milligrams) to body weight (grams). Fresh kidneys from five mice in each group were quickly soaked in a 10% formaldehyde solution for histopathological examination. The remaining fresh kidneys were quickly stored in liquid nitrogen and subsequently assayed for titanium content and cytokine expression. Serum was collected by centrifuging the blood samples at 1200g for 10 min.

Analysis of Titanium Content. The frozen kidney tissues (n = 5 from each group) were thawed; approximately 0.3 g samples were digested, and titanium, sodium, magnesium, potassium, calcium, zinc, and iron concentrations were determined using inductively coupled plasma mass spectrometry (ICP-MS) (Thermo Elemental X7, Thermo Electron Co., Waltham, MA).[11,12]

Analysis of Kidney Toxicity Biomarkers. Urinary levels of kidney injury molecule-1 (KIM-1), clusterin (CLU), osteopontin (OPN), β2-microglobulin, and cystatin C were performed by enzyme-linked immunosorbent assays (ELISAs) using commercial kits (R&D Systems, Minneapolis, MN), following the manufacturer's instructions.

Analysis of Serum Biochemical Parameters. Uric acid (UA), blood urea nitrogen (BUN), creatinine (CR), and urinary protein excretion in serum (n = 10 in each group) were assessed using a clinical automatic chemistry analyzer (type 7170A, Hitachi, Tokyo, Japan).

Histopathological Observation of Kidneys. After being fixed in 10% neutral formalin and embedded in paraffin, kidney specimens from five mice in each group were sliced at a thickness of 5 μm, and the slices were placed on separate glass slides. After being stained with hematoxylin and eosin, the renal samples were routinely evaluated by a histopathologist unaware of the treatments for light microscopy (U-III Multipoint Sensor System, Nikon, Tokyo, Japan).

Assay of Cytokine Expression. Total RNA was extracted from individual kidneys (n = 5 in each group) with Tripure Isolation Reagent (Roche) according to the manufacturer's protocol. According to MIQE guidelines, probes and cycling conditions were optimized for polymerase chain reaction (PCR).[27] cDNA was reverse transcribed (RT) from total RNA samples using the TaqMan RT reagents (Applied Biosystems) and used for real-time PCR by employing primers designed using Primer Express Software according to its guidelines. Primer sets were used for real-time PCR assays and are listed in Table 2. The probes for *Wnt1*, *Wnt2*, *Wnt3*, *Wnt4*, *Wnt5a*, *Wnt6*, *Wnt7a*, *Wnt9a*, *Wnt10a*, *Wnt11*, *Gsk3β*, *Fz1*, *Fz5*, *Fz7*, *LRP5*, *LRP6*, *Dkk1*, *Dkk2*, *Dkk3*, *Dkk4*, *SFRP/FrzB*, *Abcb1b*, *cyclin D1*, *Myc*, *Col1a1*, *Fn* (fibronectin), *Twist*, and *α-SMA* in the kidneys (n = 5 in each group) were designed by the manufacturer and purchased from Shinegene Co. (Shanghai, China). As an endogenous reference for these PCR quantification studies, GAPDH gene expression was measured. According to the method of Schefe et al.,[28] the RT-qPCR data were processed with sequence detection software version 1.3.1.

DOI: 10.1021/jf5034834
J. Agric. Food Chem. 2015, 63, 1639−1647

Table 2. Real-Time PCR Primer Pairs Used in Gene Expression Analysis

gene name	description	primer sequence	primer size (bp)
Refer-GAPDH	mGAPDH-F	5′-TGTGTCCGTCGTGGATCTGA-3′	
	mGAPDH-R	5′-TTGCTGTTGAAGTCGCAGGAG-3′	150
Wnt1	mWnt1-F	5′-CCGAGAAACAGCGTTCATCT-3′	
	mWnt1-R	5′-GCCTCGTTGTTGTGAAGGTT-3′	252
Wnt2	mWnt2-F	5′-ATCTCTTCAGCTGGCGTTGT-3′	
	mWnt2-R	5′-AGCCAGCATGTCCTCAGAGT-3′	326
Wnt3	mWnt3-F	5′-CGCTCAGCTATGAACAAGCA-3′	
	mWnt3-R	5′-AAAGTTGGGGGAGTTCTCGT-3′	303
Wnt4	mWnt4-F	5′-AACGGAACCTTGAGGTGATG-3′	
	mWnt4-R	5′-GGACGTCCACAAAGGACTGT-3′	345
Wnt5a	mWnt5a-F	5′-CTGGCAGGACTTTCTCAAGG-3′	
	mWnt5a-R	5′-CTCTAGCGTCCACGAACTCC-3′	388
Wnt6	mWnt6-F	5′-GCAGCAGGACATCCGAGAG-3′	
	mWnt6-R	5′-TCCAGGAGTGCCCAGAAGG-3′	166
Wnt7a	mWnt7a-F	5′-ACGCCATCATCGTCATAGGA-3′	
	mWnt7a-R	5′-CACAGTCGCTCAGGTTGCC-3′	225
Wnt9a	mWnt9a-F	5′-GGGTGTGAAGGTGATAAAGGC-3′	
	mWnt9a-R	5′-CAGTGGCTTCATTGGTAGTGC-3′	179
Wnt10a	mWnt10a-F	5′-AGCCTGGAGACTCGGAACAA-3′	
	mWnt10a-R	5′-CGCAAGCCTTCAGTTTACCC-3′	148
Wnt11	mWnt11-F	5′-AAGTTTTCCGATGCTCCTATGA-3′	
	mWnt11-R	5′-ATGGCATTTACACTTCGTTTCC-3′	129
Gsk3β	m Gsk3*β*-F	5′-GCCACCATCCTTATCCCTCC-3′	
	m Gsk3*β*2-R	5′-GTTATTGGTCTGTCCACGGTCT-3′	111
Fz1	mFz1-F	5′-TGTTTTGTGGGGCTCAACAAC-3′	
	mFz1-R	5′-CTTCTCTGTCTTGGTGCCGTC-3′	159
Fz5	mFz5-F	5′-GGCAATGAAGCCATCGCA-3′	
	mFz5-R	5′-GCCCAAGACAAAGCCTCGTA-3′	174
Fz7	mFz7-F	5′-AGAGGAGAGACGGTTCGCC-3′	
	mFz7-R	5′-CAGGAAGATGATGGGTCGC-3′	136
LRP5	mLRP5-F	5′-AAGACCCTGCTTGAGGACAA-3′	
	mLRP5-R	5′-GAGTGGGATAGCCACATCGT-3′	402
LRP6	mLRP6-F	5′-GAGCTCATCGGTGACATGAA-3′	
	mLRP6-R	5′-GCTCGAGGACTGTCAAGGTC-3′	400
Dkk1	mDkk1-F	5′-GAGGGGAAATTGAGGAAAGC-3′	
	mDkk1-R	5′-GGTGCACACCTGACCTTCTT-3′	230
Dkk2	mDkk2-F	5′-CATCCTCACCCCACATATCC-3′	
	mDkk2-R	5′-GTAGGCATGGGTCTCCTTCA-3′	155
Dkk3	mDkk3-F	5′-TGTTTGAAGGGAGAGGATGG-3′	
	mDkk3-R	5′-TTGTGTAGCCACTGCCTCAG-3′	158
Dkk4	mDkk4-F	5′-TAGAGTTCGCAGGAGGTGTCA-3′	
	mDkk4-R	5′-TCCCCTGAGGTCTGTTTTCC-3′	182
FrzB	mFrzB-F	5′-GCTGCCTCTGTCCTCCACTTA-3′	
	mFrzB-R	5′-TCCAAGGTGTCGGAGTTTCA-3′	167
Abcb1b	mAbcb1b-F	5′-CCAGGCTCGCCAGTGATG-3′	
	mAbcb1b-R	5′-GCCCAATACAATGAGCGGTA-3′	167
cyclin D1	mcyclin D1-F	5′-TGAGGAGCAGAAGTGCGAAGA-3′	
	mcyclin D1-R	5′-CGGCAGTCAAGGGAATGGT-3′	161
Myc	mc-Myc-F	5′-CACAACTACGCCGCACCC-3′	
	mc-Myc-R	5′-GCTTCAGCTCGTTCCTCCTCT-3′	196
Col1a1	mCol1a1-F	5′-GAGGGCGAGTGCTGTGCT-3′	
	mCol1a1-R	5′-GTCCAGGGATGCCATCTCG-3′	145
Fn	mFn-F	5′-GCAATCCTCTGACGGCACA-3′	
	mFn-R	5′-CAGTCGGTAGCCTGCTATACG-3′	131
α-SMA	m*α*-SM-F	5′-CCCTGAAGAGCATCCGACA-3′	
	m*α*-SM-R	5′-CTCCAGAGTCCAGCACAATACC-3′	1791
Twist	mTwist-F	5′-AGCGGGTCATGGCTAACG-3′	
	mTwist-R	5′-GCCGCCAGTTTGAGGGTC-3′	133

DOI: 10.1021/jf5034834
J. Agric. Food Chem. 2015, 63, 1639−1647

The levels of Wnt1, Wnt2, Wnt3, Wnt4, Wnt5a, Wnt6, Wnt7a, Wnt9a, Wnt10a, Wnt11, Gsk3β, Fz1, Fz5, Fz7, LRP5, LRP6, Dkk1, Dkk2, Dkk3, Dkk4, SFRP/FrzB, Abcb1b, cyclin D1, Myc, Col1a1, Fn, Twist, and α-SMA in mouse kidney tissues were measured by an ELISA using commercial kits that were selective for each respective protein (R&D Systems), following the manufacturer's protocols.

Statistical Analysis. Values are presented as means ± the standard deviation (SD). One-way analysis of variance (ANOVA) was performed to compare the differences in means from the multigroup data using SPSS 19 software (SPSS, Inc., Chicago, IL). Dunnett's test was performed when each data set was compared with the solvent control data. The statistical significance for all tests was judged at the $P < 0.05$ probability level.

RESULTS

Food and Water Intake. The quantitative data regarding food and water intake of female mice after intragastric feeding with nano-TiO_2 during the last week of the 9 months are presented in Figure 1. It can be observed that the values of daily food and water intake from nano-TiO_2-exposed groups were decreased compared with those of the control, suggesting

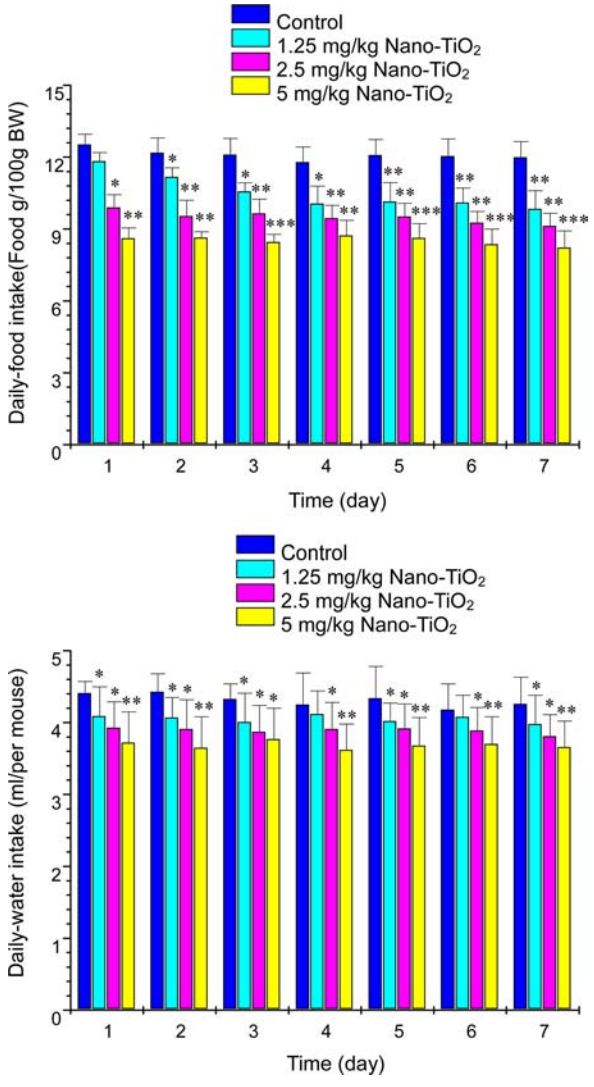

Figure 1. Daily food intake and water intake of female mice after intragastric feeding with nano-TiO_2 during the last week of the 9 months. *$P < 0.05$. **$P < 0.01$. ***$P < 0.001$. Values represent means ± SD ($n = 10$).

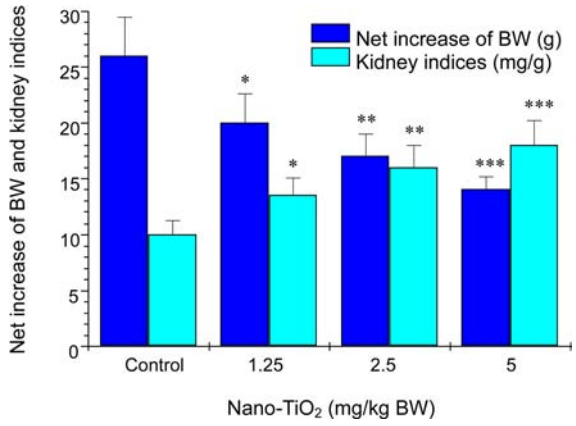

Figure 2. Body weight and kidney indices of female mice after intragastric feeding with nano-TiO_2 for 9 consecutive months. *$P < 0.05$. Values represent means ± SD ($n = 25$).

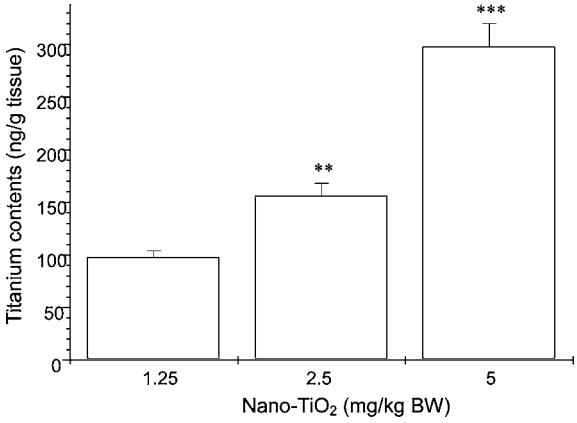

Figure 3. Titanium content of mouse kidneys after intragastric feeding with nano-TiO_2 for 9 consecutive months. **$P < 0.01$. ***$P < 0.001$. Values represent means ± SD ($n = 5$).

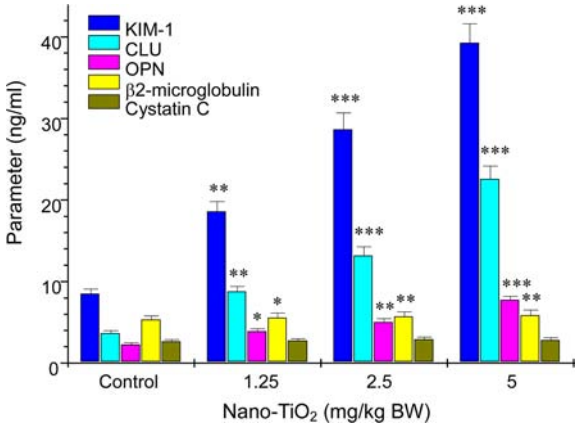

Figure 4. Alterations in nephrotoxicity biomarkers in mouse urine after intragastric feeding with nano-TiO_2 for 9 consecutive months. *$P < 0.05$. **$P < 0.01$. ***$P < 0.001$. Values represent means ± SD ($n = 5$).

reductions of 5.6−31.42% for daily food intake and 2.39−17.61% for daily water intake.

Body Weight, Renal Indices, and Titanium Content of Mouse Kidneys. Figure 2 shows the net increase in body weight and renal indices in female mice caused by exposure to nano-TiO_2. Nano-TiO_2 exposure led to significant decreases in

DOI: 10.1021/jf5034834
J. Agric. Food Chem. 2015, 63, 1639−1647

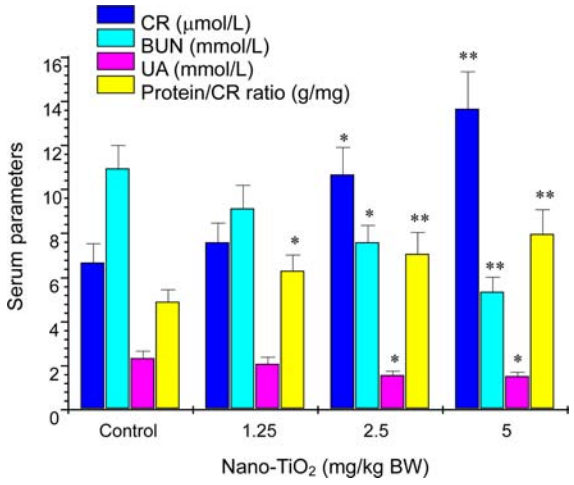

Figure 5. Changes in serum parameters in mice after administration of TiO_2 NPs by intragastric feeding for 9 consecutive months. *$P < 0.05$. **$P < 0.01$. Values represent means ± SD ($n = 10$).

body weight and increases in renal indices compared with those of the control group ($P < 0.05$). Furthermore, significant titanium accumulation occurred with an increased nano-TiO_2 dose (Figure 3; $P < 0.05$). The increased renal indices following exposure to nano-TiO_2 may be related to nephrotoxicity and renal injury.

Table 3. Effect of Nano-TiO_2 on the Level of mRNA Expression of Wnt Ligand Genes in Mouse Kidney after Intragastric Feeding with Nano-TiO_2 for 9 Consecutive Months

	x-fold change in the level of mRNA expression (treatment vs control)		
	1.25 mg of nano-TiO_2/kg of bw	2.5 mg of nano-TiO_2/kg of bw	5 mg of nano-TiO_2/kg of bw
Wnt1	2.08 ± 0.21^b	2.34 ± 0.27^b	5.02 ± 0.51^c
Wnt2	1.88 ± 0.19^a	2.61 ± 0.25^b	4.51 ± 0.47^c
Wnt3	1.12 ± 0.15	1.66 ± 0.18^b	2.40 ± 0.22^c
Wnt4	1.15 ± 0.16	1.83 ± 0.20^a	2.15 ± 0.22^b
Wnt5a	1.09 ± 0.14	1.63 ± 0.18^a	1.77 ± 0.19^a
Wnt6	1.13 ± 0.11	1.85 ± 0.21^a	2.24 ± 0.23^b
Wnt7a	1.58 ± 0.16^a	1.74 ± 0.18^a	1.90 ± 0.20^a
Wnt9a	1.76 ± 0.18	2.94 ± 0.31	3.96 ± 0.41
Wnt10a	1.98 ± 0.22^b	2.38 ± 0.25^b	4.13 ± 0.41^c
Wnt11	1.10 ± 0.11	1.78 ± 0.19^a	3.29 ± 0.34^b
Gsk3β	0.86 ± 0.10	0.53 ± 0.07^a	0.36 ± 0.05^b

$^a P < 0.05$. Values represent means ± SD ($n = 5$). $^b P < 0.01$. Values represent means ± SD ($n = 5$). $^c P < 0.001$. Values represent means ± SD ($n = 5$).

Nephrotoxicity Biomarkers. Changes in nephrotoxicity biomarkers in mouse urine induced by exposure to nano-TiO_2 are presented in Figure 4. With an increasing nano-TiO_2 dose, levels of KIM-1, CLU, and OPN were significantly increased by 1.18−3.60-, 1.40−5.14-, and 0.71−2.41-fold ($P < 0.05$),

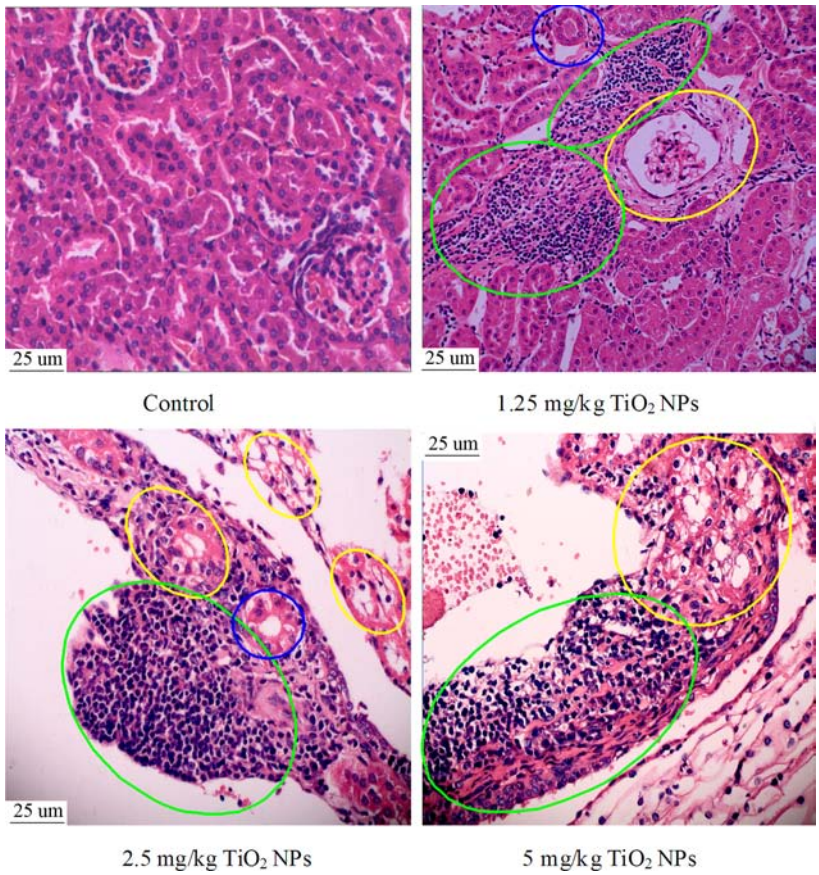

Figure 6. Histopathological observation of kidneys of male mice after intragastric feeding with nano-TiO_2 for 9 consecutive months ($n = 5$). The green ovals denote infiltration of inflammatory cells; the yellow ovals suggest tissue fibrosis or mesh in renal glomerulus, and blue ovals denote the proteinic liquid in the renal tubule.

DOI: 10.1021/jf5034834
J. Agric. Food Chem. 2015, 63, 1639−1647

Table 4. Effect of Nano-TiO_2 on the Level of Protein Expression of Wnt Ligand Genes in Mouse Kidney after Intragastric Feeding with Nano-TiO_2 for 9 Consecutive Months

	level of protein expression (ng/g of tissue)			
	control	1.25 mg of nano-TiO_2/kg of bw	2.5 mg of nano-TiO_2/kg of bw	5 mg of nano-TiO_2/kg of bw
Wnt1	42.3 ± 3.12	88.7 ± 6.44^b	136 ± 11.55^c	220 ± 18.0^c
Wnt2	54.1 ± 5.71	102 ± 10.2^b	170 ± 16.3^c	316 ± 25.9^c
Wnt3	140 ± 12.35	207 ± 21.4^a	304 ± 29.7^b	408 ± 38.2^c
Wnt4	169 ± 15.8	268 ± 25.8^b	454 ± 41.3^c	653 ± 52.5^c
Wnt5a	206 ± 18.4	326 ± 29.9^a	553 ± 49.3^b	799 ± 70.2^c
Wnt6	29.6 ± 2.51	53.9 ± 4.31^a	99.7 ± 10.1^c	141 ± 12.6^c
Wnt7a	63.5 ± 6.27	100 ± 8.53^a	132 ± 14.1^b	193 ± 20.2^c
Wnt9a	145 ± 15.7	257 ± 26.1^a	426 ± 39.8^b	574 ± 52.6^c
Wnt10a	38.2 ± 4.08	68.5 ± 7.37^a	113 ± 10.8^b	158 ± 16.2^c
Wnt11	83.0 ± 7.71	164 ± 15.1^b	249 ± 21.3^c	418 ± 40.7^c
Gsk3β	262 ± 24.5	211 ± 20.8^a	180 ± 15.3^b	131 ± 12.2^c

$^a P < 0.05$. Values represent means ± SD ($n = 5$). $^b P < 0.01$. Values represent means ± SD ($n = 5$). $^c P < 0.001$. Values represent means ± SD ($n = 5$).

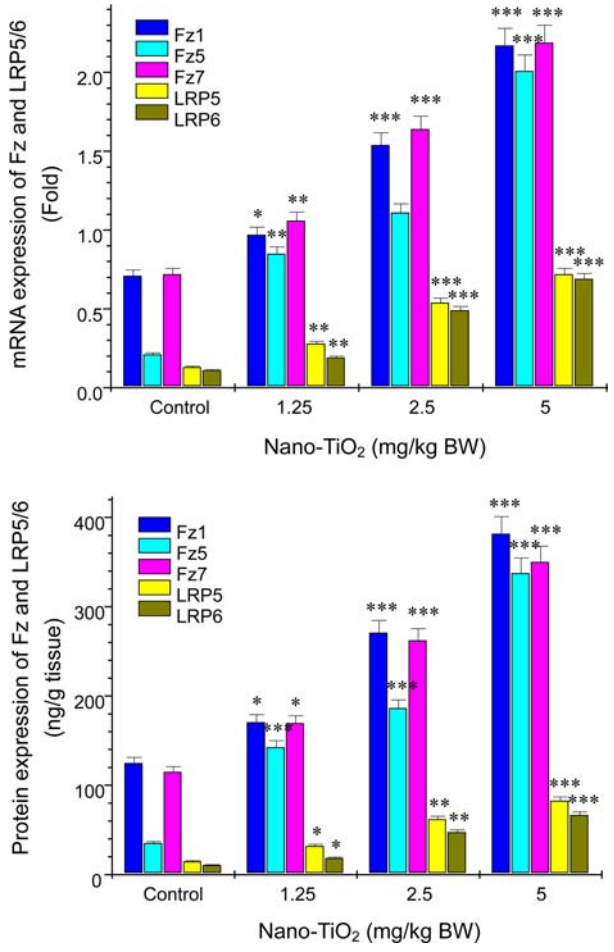

Figure 7. Effect of exposure to nano-TiO_2 on Fz and LRP5 and -6 expression in mouse kidney after intragastric feeding with nano-TiO_2 for 9 consecutive months. *$P < 0.05$. **$P < 0.01$. ***$P < 0.001$. Values represent means ± SD ($n = 5$).

respectively, whereas levels of β2-microglobulin and cystatin C showed no statistically significant change ($P > 0.05$).

Serum Biochemical Parameters. To confirm the effects of nano-TiO_2 on renal function, serum levels of CR, UA, and BUN were examined and are shown in Figure 5. It can be seen that the level of CR and the protein/CR ratio increased by 11.32−20.40 and 2.66−62.19%, respectively, and those of UA and BUN declined by 16.62−50.96 and 11.06−34.94% due to nano-TiO_2 ($P < 0.05$ or 0.01), respectively, compared with the control.

Table 5. Effects of Nano-TiO_2 on the Level of mRNA Expression of the Wnt Pathway- and EMT-Related Genes in Mouse Kidney after Intragastric Feeding with Nano-TiO_2 for 9 Consecutive Months

	x-fold change in the level of mRNA expression (treatment vs control)		
	1.25 mg of nano-TiO_2/kg of bw	2.5 mg of nano-TiO_2/kg of bw	5 mg of nano-TiO_2/kg of bw
Dkk1	0.93 ± 0.11	0.55 ± 0.06^a	0.38 ± 0.04^b
Dkk2	0.94 ± 0.13	0.57 ± 0.07^a	0.34 ± 0.04^b
Dkk3	0.56 ± 0.06^a	0.71 ± 0.07^a	0.59 ± 0.06^a
Dkk4	0.65 ± 0.07^a	0.61 ± 0.05^a	0.36 ± 0.03^b
sFRP/FrzB	0.51 ± 0.05^b	0.40 ± 0.04^b	0.29 ± 0.02^c
Abcb1b	1.52 ± 0.15^a	1.78 ± 0.19^a	2.78 ± 0.29^b
cyclin D1	1.63 ± 0.16^a	1.80 ± 0.19^a	1.94 ± 0.20^a
Myc	1.03 ± 0.13	1.44 ± 0.16^a	2.08 ± 0.23^c
Col1a1	2.52 ± 0.28^b	2.67 ± 0.29^b	4.64 ± 0.45^c
Fn	1.28 ± 0.14	1.78 ± 0.18^a	2.08 ± 0.23^b
Twist	2.29 ± 0.22^b	2.71 ± 0.26^b	2.93 ± 0.31^b
α-SMA	1.25 ± 0.12	1.88 ± 0.20^a	2.62 ± 0.28^b

$^a P < 0.05$. Values represent means ± SD ($n = 5$). $^b P < 0.01$. Values represent means ± SD ($n = 5$). $^c P < 0.001$. Values represent means ± SD ($n = 5$).

Histopathological Evaluation. The histological changes in the kidney specimens are shown in Figure 6. Unexposed kidney samples presented intact architecture and regularly arranged renal cells, while those from the mice exposed to increasing concentrations of nano-TiO_2 exhibited severe pathological changes, including infiltration of inflammatory cells, dilatation and filling proteinic liquids in the renal tubule, degeneration of tubular cells, tubular dilatation, fibrosis, cell abscission, and tissue necrosis. The results suggested that chronic exposure to TiO_2 NPs resulted in significant pathological changes in the kidneys, which may be related to expression of renal fibration-related markers.

Expression of Wnt Ligands. The effects of nano-TiO_2 on the expression of Wnt ligands are listed in Tables 3 and 4. The results suggested that the level of expression of all Wnt ligands in the nano-TiO_2-exposed kidneys, including Wnt1, Wnt2, Wnt3, Wnt4, Wnt5a, Wnt6, Wnt7a, Wnt9a, Wnt10a, and

DOI: 10.1021/jf5034834
J. Agric. Food Chem. 2015, 63, 1639−1647

Table 6. Effects of Nano-TiO_2 on the Level of Protein Expression of the Wnt Pathway- and EMT-Related Genes after Intragastric Feeding with Nano-TiO_2 for 9 Consecutive Months

	level of protein expression (ng/g of tissue)			
	control	1.25 mg of nano-TiO_2/kg of bw	2.5 mg of nano-TiO_2/kg of bw	5 mg of nano-TiO_2/kg of bw
Dkk1	84.6 ± 7.05	63.2 ± 5.35[a]	59.6 ± 4.76[a]	43.4 ± 3.49[b]
Dkk2	77.9 ± 8.01	67.9 ± 5.76	52.4 ± 4.03[a]	35.7 ± 3.29[b]
Dkk3	63.9 ± 6.57	44.2 ± 4.69[a]	32.7 ± 3.21[b]	28.9 ± 2.65[b]
Dkk4	115 ± 8.08	101 ± 7.67	79.1 ± 5.51[a]	51.8 ± 4.22[b]
sFRP/FrzB	79.5 ± 6.73	32.4 ± 3.49[a]	28.9 ± 2.82[a]	10.1 ± 1.45[c]
Abcb1b	15.1 ± 1.27	16.9 ± 1.38	27.4 ± 2.55[b]	29.7 ± 3.77[b]
cyclin D1	19.6 ± 1.61	29.1 ± 2.72[a]	45.6 ± 4.27[b]	73.2 ± 6.73[c]
Myc	88.5 ± 7.59	98.8 ± 10.3	120 ± 11.5[a]	252 ± 23.9[c]
Col1a1	35.8 ± 2.91	51.5 ± 4.76[a]	94.0 ± 8.59[b]	243 ± 23.1[c]
Fn	165 ± 13.78	192 ± 18.1[a]	289 ± 26.7[b]	318 ± 30.9[b]
Twist	7.84 ± 0.59	16.3 ± 1.79[a]	19.7 ± 2.05[a]	35.8 ± 5.75[c]
α-SMA	77.3 ± 6.56	81.7 ± 8.42	142 ± 13.05[b]	216 ± 19.4[c]

[a]$P < 0.05$. Values represent means ± SD ($n = 5$). [b]$P < 0.01$. Values represent means ± SD ($n = 5$). [c]$P < 0.001$. Values represent means ± SD ($n = 5$).

Wnt11, was significantly elevated by 0.09−4.84-fold, whereas the level of Gsk3β expression was reduced by 14−64% with an increased nano-TiO_2 dose ($P < 0.05$).

Expression of Fz and Coreceptors LRP5 and -6. Figure 7 shows that exposure to nano-TiO_2 significantly induced the expression of all Wnt receptors Fz- and coreceptors LRP5 and -6-related markers in the kidneys, including Fz1, Fz5, Fz7, and LRP5 (0.37−8.57-fold) and LRP6 (0.73−5.27-fold).

Expression of Wnt and EMT Target Genes. Tables 5 and 6 show that with an increased nano-TiO_2 dose, the expression of all Wnt antagonist-related markers, such as Dkk1, Dkk2, Dkk3, Dkk4, and sFRP/FrzB, was notably inhibited by −0.06- to −0.87-fold. In addition, the levels of expression of Wnt and EMT target genes, such as Abcb1b, cyclin D1, Myc, Col1a1, Fn, Twist, and α-SMA, were markedly elevated by 0.03−2.73- and 0.06−5.80-fold in the kidneys with an increased nano-TiO_2 dose, respectively.

DISCUSSION

The FDA's Critical Path Initiative sought to identify more sensitive and predictive biomarkers of nephrotoxicity that can specifically detect adverse changes in renal integrity before kidney function is compromised. ELISA measurements can identify numerous urinary protein biomarkers (such as KIM-1, CLU, OPN, cystatin C, and β2-microglobulin) and serum parameters, including CR, UA, and BUN, which were qualified by the FDA and European Medicines Agency (EMA) as prognostic prepathological indicators of nephrotoxicity in preclinical rat studies.[29,30] The study presented here suggests that administration of 1.25, 2.5, and 5 mg of nano-TiO_2/kg of bw by intragastric feeding for 9 consecutive months increased the level of nano-TiO_2 accumulation in mouse kidney. This led to severe nephrotoxicity, shown by significant elevations in levels of urinary KIM-1, CLU, and OPN, serum CR and proteinuria, and reductions in serum UA and BUN, together with decreased body weight, inflammatory responses, fibrosis, and tissue necrosis. Reductions in levels of eating, drinking, and activity in mice caused by nano-TiO_2 were also observed; therefore, loss of body weight may be associated with loss of appetite. A decreased level of food intake is due to excessive ROS,[30] and exposure to nano-TiO_2 promoted the over-production of ROS in mouse kidney.[10−13] Our previous studies indicated that exposure to nano-TiO_2 for 3 or 6 consecutive months resulted in renal inflammation in mice; however, renal fibrosis was not observed.[9−13] Renal inflammation and fibrosis in mice following exposure to nano-TiO_2 for 9 consecutive months may be due to modulation of the Wnt pathway.[14]

The Wnt pathway has been shown to play an important role in kedney development; in adult mouse kidney, however, Wnts and their receptors (Fzs) are also expressed.[14] Therefore, we examined the alterations in Wnt ligands and Wnt receptors (Fzs) in mouse kidney following exposure to nano-TiO_2. Levels of all Wnt ligands, including Wnt1, Wnt2, Wnt3, Wnt4, Wnt5a, Wnt6, Wnt7a, Wnt9a, Wnt10a, and Wnt11, were elevated following exposure to nano-TiO_2. As suggested, Wnt3a may be involved in various cancers[31] and is associated with β-catenin activation, thus driving transcription from the LEF-1 promoter.[32] As secretory proteins, Wnts proteins can bind to their respective receptors and execute their function in a paracrine or autocrine manner. He et al. observed that Fz receptors are expressed in tubular epithelial cells in vivo and guessed that these receptors may be the main targets of Wnt signaling in renal fibrosis.[14] Our findings suggest that exposure to nano-TiO_2 markedly upregulated the expression of Fz1, Fz5, and Fz7 in the kidneys. These results support the hypothesis that nano-TiO_2 promotes renal inflammation and fibrosis by triggering the Wnt pathway as chronic exposure to nano-TiO_2 caused significant alterations in these Wnts and Fzs.

In this study, our data suggest that chronic exposure to nano-TiO_2 significantly decreased the level of expression of Dkk1, Dkk2, Dkk3, Dkk4, and sFRP/FrzB as antagonists of the Wnt pathway in the kidneys. As suggested, epigenetic silencing of Wnt antagonistic genes such as sFRP/FrzB,[33] Dkks,[34] and WIF1 is closely associated with poor prognosis in renal cell carcinoma patients.[35] The reduction in the level of antagonist expression in the kidneys caused by exposure to nano-TiO_2 may promote renal inflammation and fibrosis in mice.

As the expression of all Wnts and Fzs was greatly induced in the kidneys by nano-TiO_2, the question of whether β-catenin modulated transcription and the canonical Wnt pathway activated by nano-TiO_2 was also examined. Our findings indicate that nano-TiO_2 significantly elevated the level of expression of the Wnt genes c-Myc, cyclin D1, and Abcb1b in mouse kidney. It was previously demonstrated that both cyclin D1 and Abcb1b expression was involved in renal cancer and the aberrant Wnt/'β-catenin pathway.[36] As EMT markers, fibronectin, collagen I, and α-SMA are closely related to tissue regeneration or fibrosis; in particular, these EMT markers play

DOI: 10.1021/jf5034834
J. Agric. Food Chem. 2015, 63, 1639−1647

pivotal roles in the development of renal fibrosis under various stresses and chronic inflammation, while Twist is associated with cancer generation and cancer cell metastasis.[37−39] Expression of Twist and fibronectin was demonstrated to be modulated by the β-catenin pathway.[40,41] Because of the activation of the Wnt/β-catenin pathway caused by exposure to nano-TiO_2, we observed significantly increased levels of expression of fibronectin, α-SMA, and Twist in the kidneys. Importantly, collagen I has been shown to be very abundant in renal fibrosis[14] and to be a critical modulator of kidney fibrosis.[41] Our data also suggest that nano-TiO_2 significantly elevated the level of collagen I expression in the kidney.

In conclusion, this study shows that administration of nano-TiO_2 resulted in significant increases in urinary KIM-1, CLU, and OPN levels in mice. Furthermore, exposure to nano-TiO_2 activated the Wnt pathway through directly increasing the levels of expression of Wnts, Fz receptors, and EMT markers and decreasing the levels of expression of Wnt antagonists, thus resulting in renal inflammation and fibrosis.

AUTHOR INFORMATION

Corresponding Author

*Telephone: 86-13915553751. E-mail: hfshui666@126.com.

Funding

This work was supported by the National Natural Science Foundation of China (Grants 81473007, 81273036, and 30901218) and the Jiangsu Collaborative Innovation Center of Regional Modern Agriculture & Environmental Protection.

Notes

The authors declare no competing financial interest.

REFERENCES

(1) Hendren, C. O.; Mesnard, X.; Droge, J.; Wiesner, M. R. Estimating production data for five engineered nanomaterials as a basis for exposure assessment. *Environ. Sci. Technol.* **2011**, *45*, 2562−2569.

(2) Skocaj, M.; Filipic, M.; Petkovic, J.; Novak, S. Titanium dioxide in our everyday life; is it safe? *Radiol. Oncol.* **2011**, *45*, 227−247.

(3) Weir, A.; Westerhoff, P.; Fabricius, L.; Hristovski, K.; von Goetz, N. Titanium dioxide nanoparticles in food and personal care products. *Environ. Sci. Technol.* **2012**, *46*, 2242−2250.

(4) Elsaesser, A.; Howard, C. V. Toxicology of nanoparticles. *Adv. Drug Delivery Rev.* **2012**, *64*, 129−137.

(5) Sang, X. Z.; Li, B.; Ze, Y. G.; Hong, J.; Ze, X.; Gui, S. X.; Sun, Q. Q.; Liu, H. T.; Zhao, X. Y.; Sheng, L.; Liu, D.; Yu, X. H.; Hong, F. S. Toxicological effects of nanosized titanium dioxide-induced spleen injury in mice. *J. Agric. Food Chem.* **2013**, *61*, 5590−5599.

(6) Hong, J.; Wang, L.; Zhao, X. Y.; Yu, X. H.; Sheng, L.; Xu, B. Q.; Liu, D.; Zhu, Y. T.; Long, Y.; Hong, F. S. Th2 factors may be involved in the TiO_2 NP-induced hepatic inflammation. *J. Agric. Food Chem.* **2014**, *62*, 6871−6878.

(7) Wang, J. X.; Zhou, G. Q.; Chen, C. Y.; Yu, H. W.; Wang, T. C.; Ma, Y. M.; Jia, G.; Gao, Y. X.; Li, B.; Sun, J.; Li, Y. F.; Jia, F.; Zhao, Y. L.; Chai, Z. F. Acute toxicity and biodistribution of different sized titanium dioxide particles in mice after oral administration. *Toxicol. Lett.* **2007**, *168*, 176−185.

(8) Chen, J. Y.; Dong, X.; Zhao, J.; Tang, G. P. In vivo acute toxicity of titanium dioxide nanoparticles to mice after intraperitoneal injection. *J. Appl. Toxicol.* **2009**, *29*, 330−337.

(9) Liu, H. T.; Ma, L. L.; Zhao, J. F.; Liu, J.; Yan, J. Y.; Ruan, J.; Hong, F. S. Biochemical toxicity of mice caused by nano-anatase TiO_2 particles. *Biol. Trace Elem. Res.* **2009**, *129*, 170−180.

(10) Zhao, J. F.; Wang, J.; Wang, S. S.; Zhao, X. Y.; Yan, J. Y.; Ruan, J.; Li, N.; Duan, Y. M.; Wang, H.; Hong, F. S. The mechanism of oxidative damage in nephrotoxicity of mice caused by nano-anatase TiO_2. *J. Exp. Nanosci.* **2010**, *5* (5), 447−462.

(11) Gui, S. X.; Zhang, Z. L.; Zheng, L.; Sun, Q. Q.; Sang, X. Z.; Liu, X. R.; Gao, G. D.; Cui, Y. L.; Cheng, Z.; Cheng, J.; Tang, M.; Hong, F. S. The molecular mechanism of kidney injury of mice caused by exposure to titanium dioxide nanoparticles. *J. Hazard. Mater.* **2011**, *195*, 365−370.

(12) Gui, S. X.; Li, B. Y.; Zhao, X. Y.; Sheng, L.; Hong, J.; Yu, X. H.; Sang, X. Z.; Sun, Q. Q.; Ze, Y. G.; Wang, L.; Hong, F. S. Renal injury and Nrf2 modulation in mouse kidney following exposure to titanium dioxide nanoparticles. *J. Agric. Food Chem.* **2013**, *61*, 8959−8968.

(13) Lee, S. B.; Kalluri, R. Mechanistic connection between inflammation and fibrosis. *Kidney Int.* **2010**, *78* (Suppl.119), S22−S26.

(14) He, W.; Dai, C.; Li, Y.; Zeng, G.; Monga, S. P.; Liu, Y. Wnt/β-catenin signaling promotes renal interstitial fibrosis. *J. Am. Soc. Nephrol.* **2009**, *20*, 765−776.

(15) Banumathy, G.; Cairns, P. Signaling pathways in renal cell carcinoma. *Cancer Biol. Ther.* **2010**, *10*, 658−664.

(16) McCoy, K. E.; Zhou, X.; Vize, P. D. Non-canonical wnt signals antagonize and canonical wnt signals promote cell proliferation in early kidney development. *Dev. Dyn.* **2011**, *240*, 1558−1566.

(17) Vlad, A.; Rohrs, S.; Klein-Hitpass, L.; Muller, O. The first five years of the Wnt targetome. *Cell. Signalling* **2008**, *20*, 795−802.

(18) Niehrs, C. Function and biological roles of the Dickkopf family of Wnt modulators. *Oncogene* **2006**, *25*, 7469−7481.

(19) Kalluri, R. EMT: When epithelial cells decide to become mesenchymal-like cells. *J. Clin. Invest.* **2009**, *119*, 1417−1419.

(20) Yang, J.; Mani, S. A.; Donaher, J. L.; Ramaswamy, S.; Itzykson, R. A.; Come, C.; Savagner, P.; Gitelman, I.; Richardson, A.; Weinberg, R. A. Twist, a master regulator of morphogenesis, plays an essential role in tumor metastasis. *Cell* **2004**, *117*, 927−939.

(21) Lee, J. M.; Dedhar, S.; Kalluri, R.; Thompson, E. W. The epithelial−mesenchymal transition: New insights in signaling, development, and disease. *J. Cell Biol.* **2006**, *172*, 973−981.

(22) Outlines Guidance on Handling Titanium Dioxide (TiO_2); National Institute for Occupational Safety and Health: Atlanta, 2011.

(23) Baan, R.; Straif, K.; Grosse, Y.; Secretan, B.; El Ghissassi, F.; Cogliano, V. Carcinogenicity of carbon black, titanium dioxide, and talc. *Lancet Oncol.* **2006**, *7*, 295−296.

(24) Yang, P.; Lu, C.; Hua, N.; Du, Y. Titanium dioxide nanoparticles co-doped with Fe^{3+} and Eu^{3+} ions for photocatalysis. *Mater. Lett.* **2002**, *57*, 794−801.

(25) Hu, R. P.; Zheng, L.; Zhang, T.; Cui, Y. L.; Gao, G. D.; Cheng, Z.; Chen, J.; Tang, M.; Hong, F. S. Molecular mechanism of hippocampal apoptosis of mice following exposure to titanium dioxide nanoparticles. *J. Hazard. Mater.* **2011**, *191*, 32−40.

(26) Drozdz, A. Food habits and food assimilation in mammals. In *Methods for ecological bioenergetics*; Grodzinki, W., Klekowski, R. Z., Duncan, A., Eds.; Blackwell: Oxford, U.K., 1975; pp 333−337.

(27) Bustin, S. A.; Benes, V.; Garson, J. A.; Hellemans, J.; Huggett, J.; Kubista, M.; Mueller, R.; Nolan, T.; Pfaffl, M. W.; Shipley, G. L.; Vandesompele, J.; Wittwer, C. T. The MIQE guidelines: Minimum information for publication of quantitative real-time PCR experiments. *Clin. Chem.* **2009**, *55* (4), 611−622.

(28) Schefe, J. H.; Lehmann, K. E.; Buschmann, I. R.; Unger, T.; Funke-Kaiser, H. Quantitative real-time RT-PCR data analysis: Current concepts and the novel "gene expression's CT difference" formula. *J. Mol. Med.* **2006**, *84*, 901−910.

(29) FDA, European Medicines Agency to Consider Additional Test Results When Assessing New Drug Safety Collaborative Effort by FDA and EMEA Expected to Yield Additional Safety Data. U.S. Food and Drug Administration: Silver Spring, MD, 2008.

(30) Benani, A.; Troy, S.; Carmona, M. C.; Fioramonti, X.; Lorsignol, A.; Leloup, C.; Casteilla, L.; Pénicaud, L. Role for mitochondrial reactive oxygen species in brain lipid sensing: Redox regulation of food intake. *Diabetes* **2007**, *56*, 152−160.

(31) Katoh, M. WNT3-WNT14B andWNT3A-WNT14 gene clusters (review). *Int. J. Mol. Med.* **2002**, *9*, 579−584.

(32) Filali, M.; Cheng, N.; Abbott, D.; Leontiev, V.; Engelhardt, J. F. Wnt-3A/β-catenin signaling induces transcription from the LEF-1 promoter. *J. Biol. Chem.* **2002**, *277*, 33398−33410.

DOI: 10.1021/jf5034834
J. Agric. Food Chem. 2015, 63, 1639−1647

(33) Kawakami, K.; Yamamura, S.; Hirata, H.; Ueno, K.; Saini, S.; Majid, S.; Tanaka, Y.; Kawamoto, K.; Enokida, H.; Nakagawa, M.; Dahiya, R. Secreted frizzled-related protein-5 is epigenetically downregulated and functions as a tumor suppressor in kidney cancer. *Int. J. Cancer* **2011**, *128*, 541−550.
(34) Hirata, H.; Hinoda, Y.; Nakajima, K.; Kawamoto, K.; Kikuno, N.; Ueno, K.; Yamamura, S.; Zaman, M. S.; Khatri, G.; Chen, Y.; Saini, S.; Majid, S.; Deng, G.; Ishii, N.; Dahiya, R. Wnt antagonist DKK1 acts as a tumor suppressor gene that induces apoptosis and inhibits proliferation in human renal cell carcinoma. *Int. J. Cancer* **2011**, *128*, 1793−1803.
(35) Kawakami, K.; Hirata, H.; Yamamura, S.; Kikuno, N.; Saini, S.; Majid, S.; Tanaka, Y.; Kawamoto, K.; Enokida, H.; Nakagawa, M.; Dahiya, R. Functional significance of Wnt inhibitory factor-1 gene in kidney cancer. *Cancer Res.* **2009**, *69*, 8603−8610.
(36) Alao, J. P. The regulation of cyclinD1 degradation: Roles in cancer development and the potential for therapeutic invention. *Mol. Cancer* **2007**, *6*, 24.
(37) Kalluri, R.; Neilson, E. G. Epithelial−mesenchymal transition and its implications for fibrosis. *J. Clin. Invest.* **2003**, *112*, 1776−1784.
(38) Polyak, K.; Weinberg, R. A. Transitions between epithelial and mesenchymal states: Acquisition of malignant and stemcell traits. *Nat. Rev. Cancer* **2009**, *9*, 265−273.
(39) Zeisberg, M.; Neilson, E. G. Biomarkers for epithelial−mesenchymal transitions. *J. Clin. Invest.* **2009**, *119*, 1429−1437.
(40) Gradl, D.; Kuhl, M.; Wedlich, D. The Wnt/Wg signal transducer β-catenin controls fibronectin expression. *Mol. Cell. Biol.* **1999**, *19*, 5576−5587.
(41) Howe, L. R.; Watanabe, O.; Leonard, J.; Brown, A. M. Twist is up-regulated in response toWnt1 and inhibits mouse mammary cell differentiation. *Cancer Res.* **2003**, *63*, 1906−1913.

DOI: 10.1021/jf5034834
J. Agric. Food Chem. 2015, 63, 1639−1647

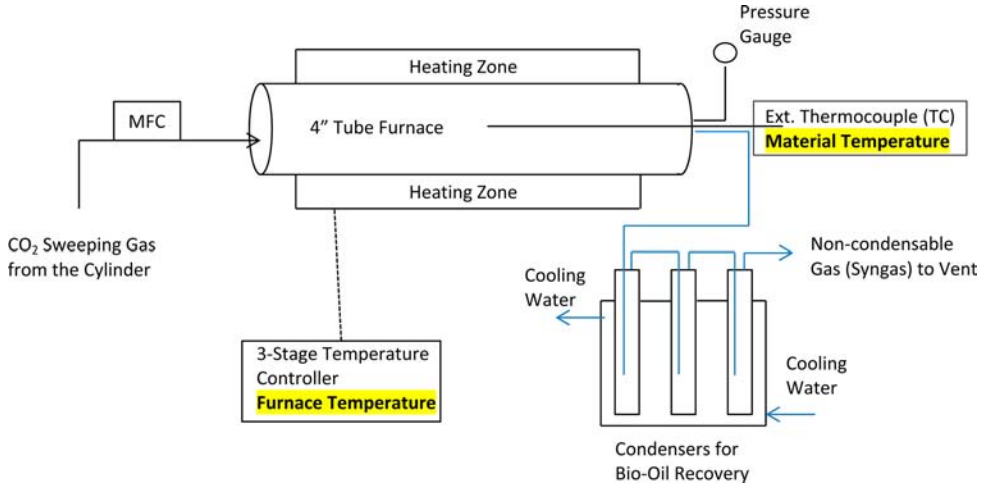

Figure 1. Slow pyrolysis experimental setup.

conditions, specifically temperature range and residence time, to obtain biochars with negligible PAH content. The impetus behind this work is the prospect of the existence and bioavailability of PAHs in the biochar, which are pyrolytic compounds produced during pyrolysis. This valid concern is hindering biochar's market acceptance with greenhouse growers and cooperators. This study will provide the applied knowledge required to ensure confidence (of cooperators/greenhouse growers) in biochar as a consistent, high-quality, well-documented, locally made greenhouse growing medium (substrate). This aspect has not been sufficiently studied or documented before, and the existing knowledge gap in the information is vital for commercial adoption of biochar as a benign growing medium for the greenhouse industry. The results of the proposed study will help fill the gap of assuring consistency in the quality and safety of biochar use for food production in greenhouses. The overall objective of this project is to make recommendations to the biochar producers and biochar end users (greenhouse growers) on what criteria biochars derived from thermomechanical pulp sludge (TMPS) can be considered safe for use in greenhouses for food production.

For this study the TMPS feedstock was sourced from Alberta Newsprint Co. (ANC), which was considering installing a 5000 tonne/year commercial biochar production facility at White Court, Alberta, Canada. ANC employs a thermomechanical pulping (TMP) process, wherein the wood chips are heated using steam to mechanically separate fibers (pulp) in a refiner. Wastewater generated from the pulping process is directed to a wastewater treatment system, where the remnant solids, termed sludge (TMPS), are separated. TMPS is essentially a combination of primary and secondary sludges. The primary sludge consists mainly of cellulose, hemicellulose, and lignin, whereas the secondary sludge is mainly composed of proteins, cellulose fibers, and lignin. Approximately 12000 oven-dried (OD) tonnes of sludge is produced by ANC annually. The main recycling and disposal routes for sludge are land-spreading or incineration. The conversion of TMPS, a negative-value effluent, into biochar, a high-value greenhouse growing medium, would be economically favorable to ANC.

MATERIALS AND METHODS

Feedstock. One hundred liters of TMPS was supplied by ANC, White Court, AB, Canada.

Feedstock Preprocessing. TMPS was manually delumped to improve heat transfer efficiency during drying and carbonization. It was dried at 110 °C overnight to obtain bone-dry homogeneous material, which was subsequently characterized and used in biochar production.

Feedstock Characterization. Proximate (volatile, ash, and fixed carbon), ultimate (CHNSO), and trace metal (36 element scan) analyses of TMPS were performed using the standard American Standard for Testing Materials (ASTM) and U.S. Environmental Protection Agency (EPA) methods.[11−20] All of the results and discussion in this study are presented on a dry weight basis (db).

Biochar Production. The laboratory-scale experimental setup employed to generate slow pyrolysis biochars from the TMPS feedstock is depicted in Figure 1. It comprises three components: (1) a tube furnace;,(2) a 4 in. stainless steel reactor, and (3) a three-stage programmable temperature controller.

To maintain uniform process conditions all through the TMPS feedstock, about 800 g of bone-dry TMPS was packed between two perforated metallic plates in the center of a tube reactor, which created a 10 in. void space on both/either ends of the reactor. The sealed reactor was inspected for leaks and placed in a split hinge tubular furnace. The tube furnace is equipped with three programmable temperature zones (left, center, right), which are regulated with the help of three thermocouples (TCs). In addition, a calibrated TC was placed directly into the center of the sludge sample, which was employed to measure the actual material temperature and was used to determine the process temperature and residence time in all of the experiments. In a typical run, the furnace was heated to a desired (material) temperature and maintained at that desired temperature for a desired time (residence time). Nine different kinds of biochars were made from TMPS by treating it at three different material temperatures (450, 500, 550 °C) and for three different residence times (30, 60, 120 min) under anoxic conditions (CO_2 purge). At the end of each experiment the tubular reactor was removed from the furnace and quenched rapidly (20 min) to cool the biochar to room temperature. Subsequently, the biochar was collected and weighed to calculate its yields.

Biochar Characterization. A composite aliquot of each biochar generated in this study was first ground and sieved to 0.25 mm size and then dried in the oven at 105 °C overnight. The dried samples were characterized by various techniques using standard ASTM and EPA methods,[11−23] with the exception of bioassays,[21] wherein as-produced biochars were employed. PAHs in biochar were extracted by Soxhlet extraction following EPA method 3540C. Extracts were further cleaned up using silica gel column according to EPA method 3630C prior to analysis by GC-MS operated in SIM as described in EPA methods 625 and 8270.[22] Soxhlet extraction employed 1 g of biochar and 10 g of sodium sulfate with hexane/DCM overnight (18 h). The extracts were concentrated to 1 mL and analyzed GC-MS (SIM) to determine PAH concentrations. Analyte recovery was determined by the addition of surrogate standards [2-fluorobiphenyl, 4-terphenyl, benzo(*g*,*h*,*i*)-

DOI: 10.1021/jf502556t
J. Agric. Food Chem. 2015, 63, 1648−1657

perylene] to the biochar sample prior to the Soxhlet extraction; typically recovery varies from 60 to 120%. Due to variability of the sample matrix the MDL was set at 1 ng/g to provide a high level of confidence in the data. The biochar exhibiting highest PAH content was submitted to PCDDs/PCDFs analyses, which was performed in accordance with EPA methods 1613 and 1668.[23]

Bioassay of Biochar Phytotoxicity and Effect on Plant Performance. A 5 day germination bioassay was performed to compare phytotoxicity differences on radish seeds between the various carbonized TMPS biochars, uncarbonized (raw) coconut coir (greenhouse industry standard growing medium), Sunshine (SS) commercial potting mix, and quartz sand by adapting the standard Organisation for Economic Co-operation and Development (OECD) methodology (1984).[21] Radish seeds (11) were plated on the substrate in a Petri plate, and each sample was tested in three replicated plates that were incubated in a humidity chamber at room temperature with 12 h of light for 5 days. Germination rate and root/shoot length were recorded for each treatment.

To assess the biochar's phytotoxicity and its effects on plant performance and human health, a growth chamber trial was conducted on a rapid-growing lettuce vegetable crop from July 31 to August 30, 2013. Six different biochar samples, coconut coir, and SS mix (controls) with six replicates each were employed in a 30 day growth chamber trial. Lettuce seeds (Burgia variety) were sown in 1 in. rockwool cubes and incubated in a growth chamber programed at 20/16 °C, day/night, and 16 h of light for 2 weeks. Seedlings were transplanted to biochar or coconut coir or SS mix in 4 in. plastic pots, one seedling per pot and six pots per treatment, watered with nutrient solution daily, and incubated under the same conditions for 30 days. The pH and EC of leachates were monitored and measured once a week. The foliage biomass yield was recorded, and lettuce tissue samples were subjected to Soxhlet extraction, cleanup, and PAH analysis as per EPA methods 3540C, 3630C, 8270, and 625, respectively (GC-MS analyses).[23]

RESULTS AND DISCUSSION

Feedstock Characterization. As-received TMP sludge contained about 65 wt % moisture content. It was manually delumped and dried overnight at 110 °C to obtain bone-dry TMPS feedstock, which was analyzed to evaluate its quality and was employed in the biochar production runs. The proximate composition, ultimate composition, and inorganic constituents of the TMPS are shown in Tables 1 and 2, respectively. In the TMP process, chipped soft woods (spruce, fir, pine) are pulped thermomechanically to extract cellulose fibers (pulp). During pulping most of the hemicellulose fraction of the wood is extracted into the liquid phase. The concentration of chemical compounds in TMP mill waste streams is usually rather low and constitutes a complex mixture of various substances such as hemicelluloses, extractives, inorganic ions, and suspended matter. These waste waters are directed to the waste treatment plant, where the remnant solids are separated, termed sludge, which is predominantly lignin, hemicellulose, protein, and cellulose remnants.[10] Table 1 compares the proximate and ultimate analyses values of typical clean wood and TMPS feedstock. As noted, it is evident that TMPS has characteristics similar to those of wood, except for high ash and lower oxygen contents. Removal of hemicellulose with significantly high oxygen content[24] during pulping results in lowering the oxygen content of TMPS, as evidenced from Table 1.[24] As noted from Table 2, the concentrations of specified metals such as As, Cd, Co, Cr, Cu, Hg, Mo, Ni, Pb, Se, and Zn were far below the stipulated guideline for maximum permissible metal concentration in biomass ashes, processed sewage, compost, and biosolids for land applications as regulated by European Union (EU) and Canadian Food Inspection Agency (CFIA) guidelines.[25] Furthermore, the TMPS also meets the specifications of clean biomass commonly employed in combustion and co-firing applications.[25] On the basis of the above finding TMPS can be designated a clean feedstock suitable for multiple applications ranging from land spreading to thermochemical processing (torrefaction, pyrolysis, combustion) applications. A recent study by Parikh's group[26] investigated trends in the biochar properties in relation to its feedstock material to develop guidelines for biochar use in agronomic systems. Special emphasis was given to ash content, C/N ratio, and surface area measurements. The overall exercise was intended to guide end users with feedstock selection tool for specific soil functions.[26]

Table 1. TMPS Feedstock Basic Analyses

feedstock[a]	TMPS	typical clean wood[b]	hemicellulose[24]
proximate analysis			
moisture content wt % (wb)	64.5	18.2	
volatile matter (VM) content wt % (db)	82.5	85.4	
ash content wt % (db)	3.0	0.4	
fixed carbon (FC) content wt % (db) (by difference)	14.5	14.2	
ultimate analysis			
C wt % (db)	52.2	49.6	39.05
H wt % (db)	6.2	6.4	5.73
N wt % (db)	1.6	0.15	
S wt % (db)	0.3	0.1	0.003
O wt % (db) (by difference)	36.7	43.75	55.22

[a]db, dry basis; wb, wet basis. FC was computed by the following equation: FC (%) = 100 − [VM (%) + ash (%)]. Oxygen was computed by the following equation: O (%) = 100 − [N (%) + C (%) + H (%) + S (%) + ash (%)]. [b]For comparison, proximate/ultimate analyses of typical wood feedstock were referenced from *The Handbook of Biomass Combustion & Co-firing*, edited by Sjaak van Loo and Jaap Koppejan in 2008.

Biochar Production. Nine different biochars were generated by carbonizing the TMPS at three different material temperatures for three different residence (retention) times. The observed biochar yields are shown in Figure 2. As noted in Figure 2, biochar yields decrease with increasing carbonization (material) temperature and residence (material retention) time on account of a higher degree of devolatilization. The results reveal that the temperature increment has a more pronounced effect on the degree of devolatilization and associated weight loss than residence time.

Generally, in the demonstration-scale continuous operation, the feedstock is conveyed using augers or rakes and gravity and is under constant agitation and could also experience air penetration, which would potentially raise the material temperatures to ≥600 °C. In the current study, laboratory-scale batch equipment was selected for producing biochars at specific temperatures and residence times as it offers more accurate control over the process parameter than demonstration-scale equipment operated in continuous mode. In the current investigation, the biochar material temperatures were precisely regulated within ±5 °C tolerance and air infiltration/penetration was prevented by regulating a continuous CO_2 purge through the tube furnace.

Biochar Basic Characterization. All of the biochars generated in this study were analyzed for gross and elemental compositions by ASTM methods. The measurements obtained are presented in Table 3. As noted, the volatile matter decreases, whereas fixed carbon and elemental carbon contents increase

DOI: 10.1021/jf502556t
J. Agric. Food Chem. 2015, 63, 1648−1657

Table 2. TMPS Feedstock Trace Metal Analyses

	current study		ref[25]	recommended guidelines (μg/g)[25]			
						max permissible heavy metal concn in biosolids for land application in Canada and USA (compiled from MENV, 2002; anonymous, 1998[d]	
	element	concn (μg/g)	typical clean wood[a] (μg/g)	EU guideline for max concn of heavy metals in biomass ashes added to agricultural land[b]	processed sewage, compost, and other byproducts, T-4-093, Standards for Metals in Fertilizers and Supplements, Plants, Canadian Food Inspection Agency (CFIA)[c]	Ontario	EPA
1	aluminum	460					
2	antimony	0.0653					
3	arsenic	0.243	<1.5		75	170	75
4	barium	43.8					
5	beryllium	0.0083					
6	bismuth	0.0133					
7	boron	21.5					
8	cadmium	0.822	<0.4	5	20	34	85
9	calcium	6290					
10	chlorine	297	<400				
11	chromium	3.36	<17	250		2800	3000
12	cobalt	0.364	<0.7		150	340	
13	copper	6.97		250		1700	4300
14	iron	414					
15	lead	0.249	<2.7	250	500	1100	840
16	lithium	0.172					
17	magnesium	285					
18	manganese	498					
19	mercury	0.0229	<0.17		5	11	57
20	molybdenum	1.17	<1.5		20	94	75
21	nickel	1.76	<11	100	180	420	420
22	phosphorus	1870					
23	potassium	378					
24	selenium	0.13			14		
25	silicon	340					
26	silver	0.325					
27	sodium	243					
28	strontium	15.2					
29	sulfur	3480					
30	thallium	0.0285					
31	thorium	0.0476					
32	tin	0.534					
33	titanium	14.4					
34	uranium	0.093					
35	vanadium	0.685					
36	zinc	73.5		1000	1850		

[a]Feedstock comparison data was referenced from *The Handbook of Biomass Combustion & Co-firing* edited by Sjaak van Loo and Jaap Koppejan in 2008. [b]*The Handbook of Biomass Combustion & Co-firing* edited by Sjaak van Loo and Jaap Koppejan in 2008, p 367. [c]CFIA T-4-093, Standards for Metals in Fertilizers and Supplements. [d]MENV 2002. Interim criteria for the reclamation of fertilizing residuals B: land application, storing, composting, manufacture,and use of soil mixes, Ministry of Environment, Quebec, Canada, 128 pp

with increase in temperature and residence time. The effect is more pronounced in the case of temperature increment rather than with the residence time increment; these findings are in-line with a similar study reported on poultry manure biochars.[27] It is also evident from Table 3 that as the volatile matter content of biochars decreases so does their O/C atomic ratio. Furthermore, all of the biochars generated in this study possess O/C atomic ratios <0.2, with predicted half-lives of >1000 years from the literature.[28] From the data presented in Table 3, it is clear that all of the biochars except the one generated at 450 °C with 1 h residence time fall under the IBI class I biochar on account of their fixed carbon being >60 wt % (db) and H/C atomic ratio being <0.7.[7] The biochar generated at 450 °C temperature with a 60 min residence time exhibits H/C = 0.8 and therefore fails to meet the IBI biochar classification criterion.[7]

DOI: 10.1021/jf502556t
J. Agric. Food Chem. 2015, 63, 1648−1657

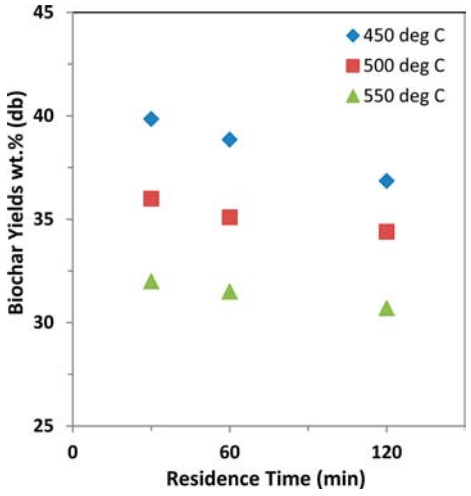

Figure 2. TMPS biochar yields versus process conditions.

Biochar Toxicity Characterization. *Polycyclic Aromatic Hydrocarbons (PAHs).* PAHs are a group of chemicals that are formed during the incomplete burning of coal, oil, gas, wood, garbage, or other organic substances. There are more than 100 different PAHs. PAHs generally occur as complex mixtures, not as single compounds. They can have a faint, pleasant odor. They are found throughout the environment in the air, water, and soil. They can occur in the air, attached to dust particles, or as solids in soil or sediment.[29,30]

Although the health effects of individual PAHs are not exactly alike, the following 17 PAHs are considered as a group in this profile:[29] acenaphthene, acenaphthylene, anthracene, benzo(*a*)-anthracene, benzo(*a*)pyrene, benzo(*e*)pyrene, benzo(*b*)-fluoranthene, benzo(*g*,*h*,*i*)perylene, benzo(*j*)fluoranthene, benzo(*k*)fluoranthene, chrysene, dibenzo(*a*,*h*)anthracene, fluoranthene, fluorene, indeno(1,2,3-*cd*)pyrene, phenanthrene, and pyrene.

These 17 PAHs were chosen to be included in this profile because[29] (1) more information is available on these than on the others; (2) they are suspected to be more harmful than some of the others, and they exhibit harmful effects that are representative of the PAHs; (3) there is a greater chance that you will be exposed to these PAHs than to the others; (4) of all the PAHs analyzed, these were the PAHs identified at the highest concentrations at hazardous waste sites; and (5) some of them are listed in EPA's Priority Chemical list such as benzo(*a*)pyrene, which is the most studied polycyclic aromatic hydrocarbon and is considered the most toxic and it is listed as a group 2a carcinogen by the International Agency for Research in Cancer (IARC).[31] The Group 2a carcinogenic chemical agent (or mixture) is probably carcinogenic to humans. This category is used when there is limited evidence of carcinogenicity in humans and sufficient evidence of carcinogenicity in experimental animals.[15] Benzo(*a*)pyrene [B(a)P] is often used as a human health risk indicator for PAH exposure and as a marker for the overall PAH exposure. The toxicity of dibenzo(*a*,*h*)anthracene is similar to that of benzo(*a*)pyrene; therefore, both have been assigned a TEF = 1.[32] The toxicity of other PAHs is converted into B(a)P equivalents by using their relative toxicity equivalency factors (TEFs). The EPA TEF values for the select PAHs available in the literature are presented in Table 4.[29]

The potentially toxic compounds in the biochars such as PAHs were determined by using a GC-MS technique. In all, 27 different PAHs were detected, and the corresponding results are shown in Table 4. The content of PAHs generated depended on the biochar production parameters (temperature and time) and varied from 0.4 to 236 μg/g biochar (Table 4). Per IBI guidelines, the maximum allowable threshold of PAHs in biochar should not exceed the 20 mg/kg biochar limit (≅20 μg/g biochar).[7] According to the above guideline, the biochars generated at 500 °C, 30 min; 500 °C, 120 min; 550 °C, 30 min; and 550 °C, 120 min meet the IBI criterion (Figure 3).[7]

Further insight into the relative compositions of PAHs revealed that the PAH in most detected quantities was retene (7-isopropyl-1-methylphenanthrene), which is a common combustion product of wood, a biotransformation product of a conifer resin (dehydroabietic acid) found in pulp and paper mill effluents. The detection of retene in high concentrations can be attributed to the origin of TMPS. It is not listed in the EPA 17 PAHs and does not have an assigned toxicity equivalency factor (TEF) associated with it, pointing to no toxicity in human health. After ignoring the retene content, the PAHs sum varied from 0.09 to 27.2 μg/g biochar as presented in Table 4. Per IBI guidelines, the maximum allowable threshold of PAHs in biochar should not exceed the 20 mg/kg biochar limit.[7] Among the nine biochars generated in the course of this study, except the one generated at 450 °C and 60 min, all other biochars pass the IBI criterion[7] if the retene content is ignored (Table 4).

Table 3. TMPS Biochars Proximate and Ultimate Analyses[a]

carbonization process parameters			proximate analyses wt % (db)			ultimate analyses wt % (db)					atomic ratios	
material temp (°C)	furnace temp (°C)	residence time (min)	VM	ash	FC[b]	C	H	N	S	O[b]	H/C	O/C
450	360	30	32.6	7.4	60.0	72.8	3.6	2.5	0.4	13.3	0.59	0.137
		60	29.4	6.7	63.9	73.1	4.9	2.4	0.3	12.6	0.80	0.129
		120	25.6	8.0	66.4	73.3	3.5	2.5	0.4	12.3	0.57	0.126
500	410	30	26.2	7.8	66.0	73.9	3.3	2.6	0.4	12	0.54	0.122
		60	19.1	10.7	70.2	74.6	3.3	2.6	0.4	8.4	0.53	0.084
		120	17.7	9.6	72.7	76.3	3.0	2.5	0.4	8.2	0.47	0.081
550	455	30	24.4	9.2	66.4	74.0	2.6	2.6	0.4	11.2	0.42	0.114
		60	15.3	9.7	75.0	75.3	3.1	2.6	0.4	8.9	0.49	0.089
		120	12.7	11.4	75.9	79.3	2.7	2.6	0.4	3.6	0.41	0.034

[a]db, dry weight basis; VM, volatile matter; FC, fixed carbon. [b]Computed by difference.

DOI: 10.1021/jf502556t
J. Agric. Food Chem. 2015, 63, 1648−1657

Table 4. TMPS Biochar Polycyclic Aromatic Hydrocarbon (PAH) Analyses[a]

		450 °C			500 °C			550 °C		
PAHs (ng/g)[b]	EPA TEF[c]	RT = 30 min	RT = 60 min	RT = 120 min	RT = 30 min	RT = 60 min	RT = 120 min	RT = 30 min	RT = 60 min	RT = 120 min
1-methylnaphthalene		187	3860	31.1	13.6	84.7	41.3	15.4	69.8	13.5
2-methylnaphthalene		180	3080	31.5	12.3	68.5	33.7	10.5	58.3	8
3-methylchloranthrene		0	0	0	0	0	0	0	0	0
7,12-dimethylbenz(*a*)anthracene		637	8830	1830	56.7	457	26.7	11.3	324	20.9
acenaphthene	0.001	43.4	184	0	0	19.7	0	0	13.9	0
acenaphthylene	0.001	41	0	0	0	0	0	0	0	0
acridine		0	0	8.7	0	0	0	0	0	0
anthracene	0.01	408	606	99.9	10.2	137	16	7.2	55.8	8.1
benzo(*a*)anthracene	0.1	734	1050	223	0	66.5	0	0	40.7	0
benzo(*a*)pyrene	1	373	591	128	14.2	30.8	13.8	0	25.2	0
benzo(*b,j,k*)fluoranthene	0.1	460	292	117	0	17.5	0	0	0	0
benzo(*c*)phenanthrene		143	0	0	0	0	0	0	0	0
benzo(*e*)pyrene		262	362	127	12	28.2	9.8	0	23.9	0
benzo(*ghi*)perylene	0.01	67.8	204	31.2	10.4	10.9	8.4	0	11.1	8.1
chrysene	0.01	623	1720	198	0	72.6	0	0	36.5	0
dibenzo(*a,h*)pyrene		0	0	0	0	0	0	0	0	0
dibenzo(*a,i*)pyrene		0	0	0	0	0	0	0	0	0
dibenzo(*a,l*)pyrene		51.1	218	0	0	0	0	0	0	0
dibenzo(*ah*)anthracene	1	63	188	602	0	0	0	11.6	0	0
fluoranthene	0.001	1720	1280	529	12.6	194	26.3	6.1	104	0
fluorene	0.001	206	794	47.7	0	131	21.1	0	65.9	0
indeno(1,2,3-*cd*)pyrene	0.1	92	0	33.9	13.1	0	0	11.7	15.1	0
naphthalene		91.4	933	8.3	6.8	21.6	28.8	9.5	24.6	9.8
perylene		89.9	374	46.2	0	22	12	0	20.3	0
phenanthrene	0.001	1970	2100	417	16.6	519	56.8	8.5	200	8.2
pyrene	0.001	1690	540	450	11.8	180	22.8	0	94.7	0
retene		73700	209000	143000	2010	56200	2780	345	24300	1070
total (ng/g biochar)		83832	236206	147959	2200.3	58261	3097	436	25483	1146
total − retene (ng/g)		10132	27206	4959.5	190.3	2061	317	91	1183	76.6
B(a)P TEF (ng/g)		575.5	938.5	770.6	15.7	41.4	14.0	12.8	31.8	0.16

[a]db, dry basis; RT, retention time. [b]EPA method 625, 8270. [c]EPA toxicity equivalency factor. Provisional guidance for quantitative risk assessment of polycyclic aromatic hydrocarbons. Environmental Criteria and Assessment Office, Cincinnati, OH, Final Draft ECAO-CIN-842, March 1993.

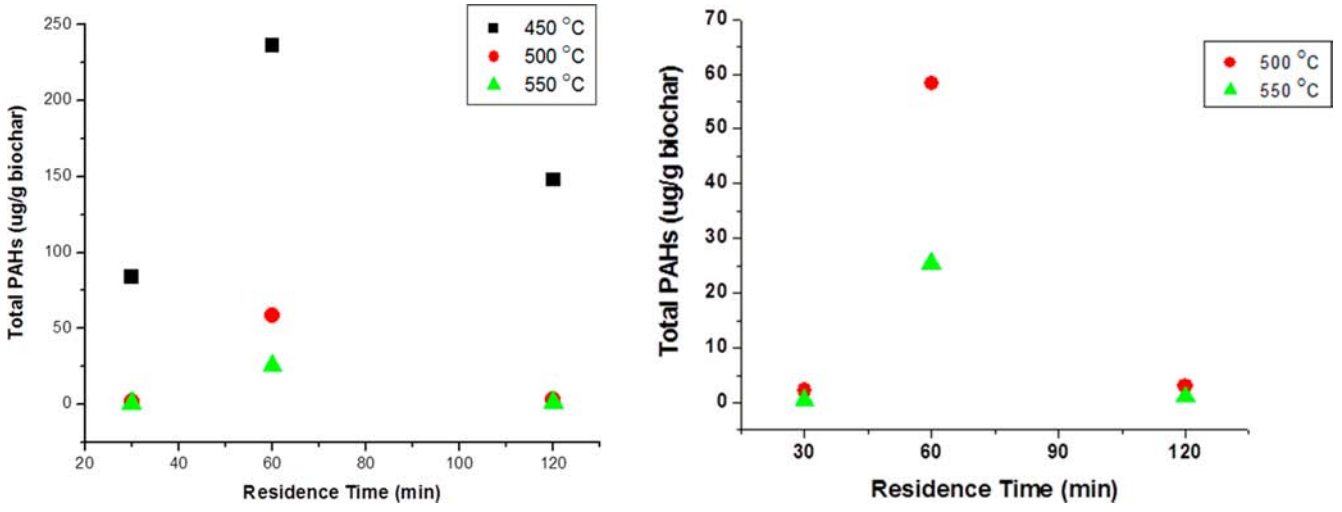

Figure 3. Cumulative PAHs (including retene) versus process conditions.

In a comprehensive study,[33] researchers evaluated four different biochars derived from wood, elephant grass (miscanthus), and coniferous/deciduous wood residues (carbonized at 600−750 °C) for 16 EPA PAHs (Σ16 EPA PAHs) and reported PAH concentrations ranging from 9 to 355 mg/kg biochar (db). According to their observation, both naphthalene (40−60%) and phenanthrene (10−30%) detected in high concentrations among the 16 EPA PAHs were produced during

DOI: 10.1021/jf502556t
J. Agric. Food Chem. 2015, 63, 1648−1657

Table 5. Radish Germination Bioassay and Lettuce Growth Trials

biochar production parameters		radish germination bioassay[a]				lettuce growth chamber trials
material temperature (°C)	residence time (min)	pass/fail	germination	shoot length (mm)	root length (mm)	lettuce yield (g/head)
450	30	pass	10.7 a	63.0 cde	27.1 bc	65.3
	60	**fail**	**2.3 c**	**22.8 g**	**10.0 d**	**15.5**
	120	pass	10.0 a	47.3 efg	26.0 bc	n/a
500	30	pass	11.0 a	109.7 ab	38.8 a	67.6
	60	pass	7.7 b	58.2 def	21.9 c	n/a
	120	pass	10.7 a	90.4 bc	27.4 bc	68.3
550	30	pass	10.7 a	99.5 ab	30.9 ab	63.5
	60	pass	9.7 a	87.2 bcd	27.8 bc	n/a
	120	pass	10.3 a	85.1 bcd	26.2 bc	61.8
controls						
sand		pass	9.7 a	93.8 ab	27.7 bc	n/a
Sunshine mix 1		pass	10.7 a	121.9 a	33.2 ab	98.2
coconut coir		pass	9.7 a	30.8 fg	21.7 c	88.3

[a]Means followed by the same letter in a column are not significantly different according to Fisher's least significant difference test ($p = 0.05$). n/a, not applicable (not tested).

pyrolysis process conditions and were not originally present in the feedstocks.[33]

The toxicity of the TMPS-derived biochars depended on the production (process) parameters such as material temperature and residence time. A significant correlation between the content of PAHs content and toxicity was noted and was matched to their production conditions. The total benzo(*a*)pyrene equivalents in each biochar sample was estimated on the basis of the detected probable carcinogenic PAHs[31] in the given biochar sample per the EPA TEF methodology (U.S. EPA 1993)[29] and is presented in the form of process toxicity relationships (PTRs) as detailed in a later section.

Polychlorinated Dibenzo Dioxins/Difurans (PCDDs/PCDFs). The biochar sample generated at 450 °C and 60 min was found to contain the highest concentration of PAHs (236 μg/g biochar) in this study. These detected high levels of PAHs prompted the need for PCDDs/PCDFs (dioxins/furans) analyses. The test results (not shown) indicate the absence of both PCDDs and PCDFs within the minimum detection limit (MDL) (0.1 pg/g) of the analytical method employed.[23] The nonformation of dioxins and furans can be attributed to the cleaner nature of the feedstock (free of chlorine and heavy metals).

Swift Radish Germination Bioassay. A 5 day radish germination test[34] was conducted to compare toxicity differences between the carbonized sludge feedstocks (biochars), uncarbonized coconut coir, SS mix, and quartz sand (controls). The germination test measures the effect of substrates on plant performance by measuring seed germination, initial shoot growth, and root development. Results in terms of number of germinated seeds, shoot length, and root length are shown in Table 5. Except for one biochar (produced at 450 °C for 60 min), all other biochars passed the radish seedling germination bioassay, and so did the quartz and coconut coir controls. The best radish performance, with the highest germination and root growth, was observed on seeds placed on biochar produced at 500 °C for 30 min. Interestingly, root zone development in biochar was different from the one noted in coconut coir and quartz. Extensive branching of roots was noted in the seedlings germinated in biochar, whereas long thin and unbranched roots were noted in seedlings germinated in quartz. In the current trials, substrate materials tested (biochar, coco, SS mix, and quartz) were not rinsed/washed in water (intentionally), which could be the reason behind the poor performance of coconut coir in comparison to other controls in this germination test. Coir media is known to contain high alkali content as most of it is sourced from coastal regions of Southeast Asia. Rinsing or washing could have potentially led to PAHs leaching, thus skewing the bioassay.

Growth Chamber Trial. To assess the biochar's phytotoxicity and its effects on plant performance, a 30 day growth chamber trial was conducted on a rapid-growing lettuce vegetable crop. The results obtained are presented in Table 5 and Figure 4. As noted from Table 5 and Figure 4, all of the

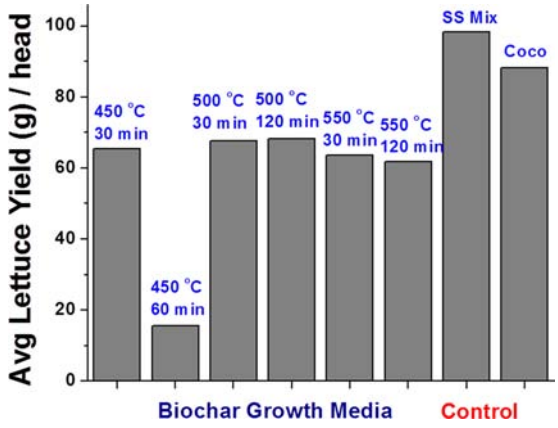

Figure 4. Average lettuce yield in TMPS biochars and controls.

biochar samples display very similar results in terms of lettuce growth and yield, except for the lettuce vegetable grown in biochar produced at 450 °C with a 60 min residence time. These results corroborate well the radish germination bioassay results, wherein except for the biochar produced at 450 °C with 60 min residence time, all other biochars passed the germination bioassay. Lettuce yields per head varied in the following order: commercial SS potting mix 1 (~100 g/head) > coconut coir (~90 g/head) > biochar (~65 g/head). Most of the lettuce plants grown (except those grown with 450 °C, 60 min medium) in the biochar display similar growth pattern and yielded similar weights of lettuce heads (average 65 g/head). The lettuce plants grown in biochar generated at 450 °C and 60 min exhibited stunted growth (~15 g/head), which is due to high

DOI: 10.1021/jf502556t
J. Agric. Food Chem. 2015, 63, 1648−1657

Table 6. Lettuce Tissue Ecotoxicity Analyses

		biochar						control	
		450 °C		500 °C		550 °C			
NAME (ng/g lettuce)	EPA TEF[a]	30 min	60 min	30 min	120 min	30 min	120 min	SS mix	CoCo
2-methylnaphthalene		0.18	0.62	1.7	1.9	1.4	1.5	0.28	0.18
anthracene	0.01	0	0	0	0	0	0	0	0
benzo(*a*)anthracene	0.1	0	0	0	0	0	0	0	0
benzo(*a*)pyrene	1	0	0	0	0	0	0	0	0
benzo(*b,j,k*)fluoranthene	0.1	0	0	0	0	0	0	0	0
benzo(*ghi*)perylene	0.01	0	0	0	0	0	0	0	0
chrysene	0.01	0	0	0	0	0	0	0	0
dibenzo(*ah*)anthracene	1	0.24	0.5	0	0	0	0	0	0.17
fluoranthene		0.21	0.62	0.96	1	1.1	0.98	0	0.14
indeno(1,2,3-*cd*)pyrene	0.1	0.15	0	0	0	0	0	0.18	0
naphthalene		0.57	1.6	5	8.4	3	6.3	1.4	0.89
perylene		0	0	0	0	0	0	0	0
phenanthrene		0.33	1	1.7	1.6	1.8	1.8	0.36	0.21
pyrene		0.24	0.49	0.96	0.99	1	0.96	0.27	0.16
retene		8.4	83.1	19.4	16.4	15.2	14.2	7.6	4.7
total (ng/g lettuce)		10.3	87.9	29.7	30.3	23.5	25.7	10.1	6.5
total − retene (ng/g lettuce)		1.9	4.8	10.3	13.9	8.3	11.5	2.5	1.8

[a]EPA. Provisional guidance for quantitative risk assessment of polycyclic aromatic hydrocarbons. Environmental Criteria and Assessment Office, Cincinnati, OH, Final Draft. ECAO-CIN-842, March 1993.

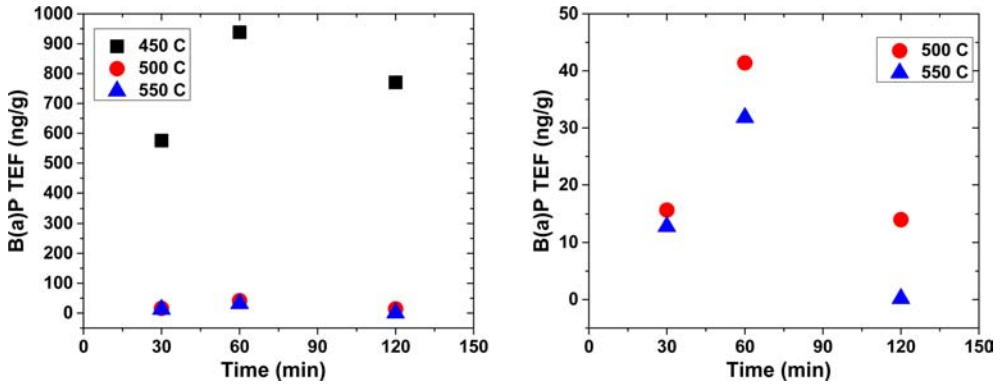

Figure 5. Biochar toxicity [B(a)P TEF] versus process conditions.

concentrations of PAHs identified in the biochar and their plausible bioavailability and translocatability.

The pH of leachate from biochar media was initially high (~8), but it was monitored, controlled, and maintained at about 6 throughout the test. The high initial pH (~8) of biochar is an important issue that may affect plant growth. A pretreatment, such as washing, is needed to reduce the pH of biochar and make it suitable and comparable with coco and SS mix growth substrates, which exhibit neutral pH (~7). Another option is to avoid prewash; instead, let the normal nutrient leaching as practiced with soilless production practices bring the pH down. Research trials conducted so far have shown that normal leaching practices with several daily watering cycles may be adequate for plants nutrient uptake needs.[3−5] As this study was focused on characterizing biochar toxicity, no attempts such as presoaking the biochar in nutrient solution (precharging) or water/nutrient washing (flashing) were done to improve the lettuce yields. In commercial greenhouses coconut coir bags are always presoaked in a calcium nitrate solution for 24−48 h so as to buffer it and replace sodium and potassium ions, which are present in high concentrations. In the early stages, fresh biochar has a high adsorption capacity for nutrients and there is a competition between the plant roots and the biochar media for the available nutrients, which initially hinders plant growth. Precharging the biochar with nutrients prior to its use in a greenhouse would likely bring lettuce yields up to levels similar to those seen with coconut coir media, but such work was beyond the scope of this study.

Lettuce Tissue Toxicity Analyses. Lettuce tissue samples were analyzed for the existence of PAHs; the results thus obtained are documented in Table 6. The results show the existence of PAHs in very minute proportions in the lettuce grown in the various biochars. Interestingly, PAHs were also detected in lettuce grown in commercial SS potting mix and coconut coir, however, in extremely low amounts. The PAH in greatest detected quantities is retene (7-isopropyl-1-methylphenanthrene), which is a common combustion product of wood. It is not listed in the EPA 17 PAHs and does not have an assigned toxicity equivalency factor (TEF) associated with it, pointing to its negligible toxicity to human health. The total benzo(*a*)pyrene equivalents in each lettuce tissue analyzed were estimated on the basis of the detected PAHs with probable human carcinogenicity

DOI: 10.1021/jf502556t
J. Agric. Food Chem. 2015, 63, 1648−1657

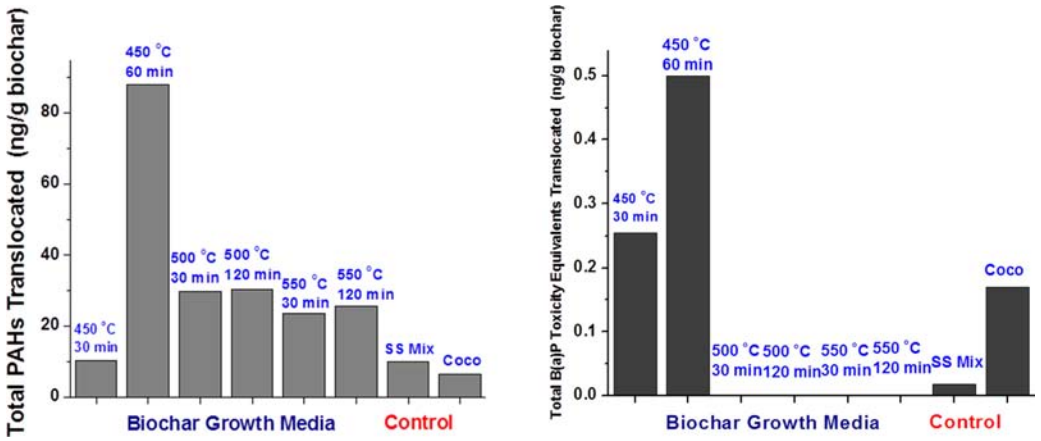

Figure 6. Total translocatable PAHs in lettuce (left) and total toxicity [B(a)P TEF] in lettuce (right).

(IARC class 2a)[31] using the U.S. EPA TEF methodology[29] (Table 6) and are presented in the form of process toxicity relationships (PTRs) as detailed in a later section.

Process Toxicity Relationships. All of the data generated during the course of the study were used in developing meaningful and realistic (slow pyrolysis) process/(biochar) toxicity relationships (PTRs). The PTRs would form the core applied knowledge base for developing future standards for biochar quality programs. PTRs generated in this study are shown in Figures 5 and 6. Figure 5 correlates toxicity in biochar to production (process) conditions. It can be observed from Figure 5 that biochars generated at 500 °C and beyond with an optimum residence time of 30 min exhibit very low B(a)P TEFs, which increase with prolonging the residence time to 60 min, on account of further breakdown of the lignin component of TMPS feedstock causing further PAH enrichment in the biochar. Prolonging the residence time to 120 min leads to thermal degradation/breakdown of the PAHs formed at 60 min as observed in Figure 5 (and also in Table 4). From process optimization and economic perspectives, minimal residence time would be favored for increased throughput. Figure 6 documents the translocatable PAH contents and the resulting toxicity in the lettuce tissue grown in the various TMPS-derived biochars generated at different process conditions. It is evident that the B(a)P TEFs noted in lettuce are extremely small and insignificant. From the learning garnered in this study, it is recommended that TMPS feedstock will yield benign quality biochar when processed at a minimum 500 °C material temperature for an optimum residence time of 30 min. The current study strengthens the fact that "*not all biochars are created equal*" and with proper feedstock selection and process optimization, it is possible to create a benign quality biochar suitable for safe greenhouse-based food production.

AUTHOR INFORMATION

Corresponding Author

*(A.K.) E-mail: ataullahkhan.mohammed@albertainnovates.ca. Phone: (780) 632-8206. Fax: (780) 632-4567.

Funding

This collaborative project between the Alberta Greenhouse Growers Association (AGGA) and Alberta Innovates – Technology Futures (AITF) was funded through Agriculture and Agri-Food Canada's Canadian Agricultural Adaptation Program (CAAP) by Agriculture and Food Council of Alberta Grant CAAP AB1314. Industry support from Alberta Newsprint Co. (ANC), White Court, AB, is kindly acknowledged.

Notes

The authors declare no competing financial interest.

REFERENCES

(1) Lehmann, J. A handful of carbon. *Nature* **2007**, *447*, 143–144.

(2) Anyia, A.; Gibson, G.; Wang, S. *Biochar – a Potential Technology to Sequester Carbon and Sustainably Improve Agricultural and Horticultural Productivity in Alberta*; AITF Report, 2010.

(3) Anyia A.; Anderson, T.; Dobson, J.; Yang J.; Drozdowski, B. *High Value Biochar for Horticultural Crops and Carbon Sequestration*; AITF Report to Alberta Newsprint Co., 2011.

(4) Savidov, N. A. *Supergrow – Greenhouse Trials and Commercial Applications*; Alberta Agriculture Report to ACIDF (Alberta Crop Industry Development Fund Ltd.), 2013.

(5) Zhang, J. W.; Mohammed, N.; Cote, P.; Dalpe, S.; Dufresne, G. *Greenhouse Trials on Biochar As Growth Media for Cucumber, Tomato and Pepper Hydroponic Vegetable Production*; Alberta Agriculture Report, 2014.

(6) Brick, S.; Lyutse, S. *Biochar*; NRDC Issue Paper, Nov 2010.

(7) International Biochar Initiative. *Biochar Testing Guidelines*, version 1.1, April 2013.

(8) Spokas, K. A.; Cantrell, K. B.; Novak, J. M.; Archer, D. A.; Ippolito, J. A.; Collins, H. P.; Boateng, A. A.; Lima, I. M.; Lamb, M. C.; McAloon, A. J.; Lentz, R. D.; Nichols, K. A. Biochar: a synthesis of its agronomic impact beyond carbon sequestration. *J. Environ. Qual.* **2012**, *41*, 973–989.

(9) Hale, S. E.; Lehmann, J.; Rutherford, D.; Zimmerman, A. R.; Bachmann, R. T.; Shitumbanuma, V.; O'Toole, A.; Sundqvist, K. L.; Arp, H. P. H.; Cornelissen, G. Quantifying the total and bioavailable polycyclic aromatic hydrocarbons and dioxins in biochars. *Environ. Sci. Technol.* **2012**, *46*, 2830–2838.

(10) *Standards and Guidelines for the Land Application of Mechanical Pulp Mill Sludge to Agricultural Land*; Alberta Environmental Protection, Environmental Sciences Division, publication 0-7785-0426-3, Feb 1999.

(11) ASTM E871-82(2006). *Standard Test Method for Moisture Analysis of Particulate Wood Fuels*; ASTM International, West Conshohocken, PA, USA, 2006.

(12) ASTM E1755-01(2007). *Standard Test Method for Ash in Biomass*; ASTM International, West Conshohocken, PA, USA, 2007.

(13) ASTM E1534-93(2013). *Standard Test Method for Determination of Ash Content of Particulate Wood Fuels*; ASTM International, West Conshohocken, PA, 2013.

(14) ASTM E872-82(2013). *Standard Test Method for Volatile Matter in the Analysis of Particulate Wood Fuels*; ASTM International, West Conshohocken, PA, 2013.

DOI: 10.1021/jf502556t
J. Agric. Food Chem. 2015, 63, 1648–1657

(15) ASTM E777-08. *Standard Test Method for Carbon and Hydrogen in the Analysis Sample of Refuse-Derived Fuel*; ASTM International, West Conshohocken, PA, 2008.
(16) ASTM E778-08. *Standard Test Methods for Nitrogen in the Analysis Sample of Refuse-Derived Fuel*; ASTM International, West Conshohocken, PA, 2008.
(17) ASTM E775-87(2008)e1. *Standard Test Methods for Total Sulfur in the Analysis Sample of Refuse-Derived Fuel*; ASTM International, West Conshohocken, PA, USA, 2008.
(18) ASTM E776-87(2009). *Standard Test Method for Forms of Chlorine in Refuse-Derived Fuel*; ASTM International, West Conshohocken, PA, USA, 2009.
(19) ASTM D1762-84(2013). *Standard Test Method for Chemical Analysis of Wood Charcoal*; ASTM International, West Conshohocken, PA, USA, 2013.
(20) EPA Method 6020A. Inductively Coupled Plasma-Mass Spectrometry.
(21) OECD guideline for testing of chemicals, OECD methodology, 1984.
(22) EPA method 8270D semi-volatile organic compounds by gas chromatography/mass spectrometry (GC/MS), Feb 2007; EPA method 625 — base/neutrals and acids: methods for organic chemical analysis of municipal and industrial wastewater.
(23) EPA Method 1613: Tetra- through octa-chlorinated dioxins and furans by isotope dilution HRGC/HRMS, Oct 1994.
(24) Lv, G.-j.; Wu, S.-b.; Lou, R. Hemicellulose pyrolysis. *BioResources* **2010**, *5*, 2051−2062.
(25) *The Handbook of Biomass Combustion and Co-firing*; Koppejan, J.; Sjaak van Loo, S., Eds.; Earth Scan: London, UK, 2008; p 367; CFIA T-4-093 − Standards for Metals in Fertilizers and Supplements; MENV. 2002; Guidelines For the Beneficial Use of Fertilising Residuals: Reference Criteria and Regulatory Standards (Interim criteria for the reclamation of fertilizing residuals B: land application, storing, composting, manufacture and use of soil mixes, 1997). Ministry of Environment, Quebec, Canada, 2008.
(26) Mukome, F. N. D.; Zhang, X.; Silva, L. C. R.; Six, J.; Parikh, S. J. Use of chemical and physical characteristics to investigate trends in biochar feedstocks. *J. Agric. Food Chem.* **2013**, *61*, 2196−2204.
(27) Cimo, G.; Kucerik, J.; Berns, A. E.; Schaumann, G. E.; Alonzo, G.; Conte, P. Effect of heating time and temperature on the chemical characteristics of biochar from poultry manure. *J. Agric. Food Chem.* **2014**, *62*, 1912−1918.
(28) Spokas, K. A. Review of the stability of biochar in soils: predictability of O:C molar ratios. *Carbon Manage.* **2010**, *1*, 289−296. Crombie, K.; Mašek, O.; Sohi, S. P.; Brownsort, P.; Cross, A. The effect of pyrolysis conditions on biochar stability as determined by three methods. *GCB Bioenergy* **2013**, *5*, 122−131.
(29) U.S. EPA, Provisional guidance for quantitative risk assessment of polycyclic aromatic hydrocarbons. Environmental Criteria and Assessment Office. Cincinnati, OH. Final Draft. ECAO-CIN-842. March 1993.; Polycyclic Aromatic Hydrocarbons, Canadian Soil Quality Guidelines for the Protection of Environmental and Human Health, Canadian Environmental Quality Guidelines, Canadian Council of Ministers of the Environment, 2008, rev. 2010, pp 19. Safe, S. Hazard and risk assessment of chemical mixtures using the toxic equivalency factor approach. *Environ. Health Perspect.* **1998**, *106*, 1051−1058.
(30) Fabbri, D.; Rombola, A. G.; Torri, C.; Spokas, K. A. Determination of PAHs in biochar and biochar amended soils. *J. Anal. Appl. Pyrolysis* **2013**, *103*, 60−67.
(31) *IARC Monographs on the Evaluation of the Carcinogenic Risk of Chemicals to Man: Certain Polycyclic Aromatic Hydrocarbons and Heterocyclic Compounds*; IARC: Lyon, France, 1973; Vol. 3.
(32) NEPM B3 Guideline on Laboratory Analysis of Potentially Contaminated Soils − May 2013, (F2013L00768); NEPM B1 Guideline on Investigation levels for Soil and Groundwater − May 2013 (F2013L00768).
(33) Hilber, I.; Blum, F.; Leifeld, J.; Schmidt, H.-P.; Bucheli, T. D. Quantitative determination of PAHs in biochar: a prerequisite to ensure its quality and safe application. *J. Agric. Food Chem.* **2012**, *60*, 3042−3050.
(34) Rogovska, N.; Laird, D.; Cruse, R. M.; Trabue, S.; Heaton, E. Germination tests for assessing biochar quality. *J. Environ. Qual.* **2011**, *41*, 1014−1022.

DOI: 10.1021/jf502556t
J. Agric. Food Chem. 2015, 63, 1648−1657

provided by Santa Cruz Biotechnology Co. (Paso Robles, CA). The purity of these standards is greater than 98.0%. Nonafluoropentanoic acid (NFPA, purity over 97%), HPLC grade methanol, and acetonitrile were obtained from J&K Chemical Co., Ltd. (Shanghai, China). Pure CML (purity over 95%) was synthesized by Qiangdao Vochem Co., Ltd. (Shandong, China). Ultrapure water was produced by a Superpure Water System (Shanghai, China). All other chemicals were of analytical grade and were provided by Sinopharm Chemical Reagent Co. Ltd. (Shanghai, China).

Sample Collection. Fourteen Sprague−Dawley rats were housed in a specific pathogen-free room (temperature: 22−24 °C, 55−70% humidity, and a 12-h light-dark cycle). After 1 week of acclimatization, the rats were randomly divided into Control group and CML group (n = 7 each). Rats in the CML group were given pure CML by stomach gavage (60 mg kg^{-1} per day, dissolved in ultrapure water in the form of CML inner salt (10 mg/mL)), whereas rats in the Control group received an equivalent volume of water. All of the treatments were for 12 consecutive weeks. During the experimental period, rats were allowed free access to a normal diet and to water except as otherwise noted. The fasting body weight (FBW) and 24-h food and water intake of all rats were recorded every 2 weeks. Furthermore, fasting blood glucose (FBG) was measured with an Accu-Check Performa glucometer (Roche Diagnostics, Mannheim, Germany) at the same time each week. At the end of the experiment, all rats were weighed and anesthetized intraperitoneally with 40 mg kg^{-1} pentobarbital sodium after an overnight fast. Blood samples were collected from the heart and centrifuged at 1400g for 20 min. Each serum sample obtained was divided into two portions: one portion for measuring serum biochemical markers and the other stored at −80 °C for later determination of the serum protein-bound CML level. The kidney, liver, heart, lung, spleen, and pancreas were immediately removed, weighed, and frozen at −80 °C for determination of the protein-bound CML levels.

All study management and experimental procedures adhered to the Guide for the Care and Use of Laboratory Animals (issued by the Ministry of Science and Technology of the People's Republic of China in 2006 [398]) and were approved by the Ethics Committee of Jiangnan University, China (JN no. 28 2013).

Determination of Serum Biochemistry Values.[33] Serum samples were run on a Roche Modular-P800 automatic biochemistry analyzer (Roche Diagnostics GmbH, Mannheim, Germany) for measuring the following serum biochemistry values: (1) kidney function markers: blood urea nitrogen (BUN), creatinine (CREA); and (2) liver function markers: alanine aminotransferase (ALT), aspartate aminotransferase (AST).

Sample Preparation for Protein-Bound CML Analysis. All tissue samples were lyophilized and powdered by mortar. The protein-bound CML was extracted by means of a modified method developed by Zhang et al.[18] and Teerlink et al.[22] Approximately 100 mg of tissue sample was extracted three times with hexane to remove the sample fat. For each extraction, 2 mL of hexane was added to the tube, the mixture was vortexed for 1 min and centrifuged at 5000g for 5 min, and the hexane layer was removed with a Pasteur pipet. After the three extractions, the residue was dried with nitrogen gas and then reduced with 1 mL of 0.1 M sodium borohydride (dissolved in 0.2 M borate buffer, pH 9.2) at room temperature for 4 h. After reduction, 2 mL of 60% (w/v) trichloroacetic acid (TCA) was added to the reduced sample to a final concentration of 20% (w/v), the mixture was vortexed vigorously for 1 min and centrifuged at 4000g for 10 min. This step ensured the determination of only protein-bound CML. The protein pellet was washed twice with 2 mL of 20% (w/v) TCA, dissolved in 5 mL of 6 M HCl, and then incubated at 110 °C for 24 h for hydrolysis. The acid hydrolysate was then filtered with Whatman no. 1 qualitative filter paper (70 mm) and volumed with ultrapure water in a 10 mL volumetric flask. Five hundred microliters of diluted acid hydrolysate was evaporated to dryness under nitrogen gas at 50 °C, and the residue was reconstituted in 2 mL of 0.1 M HCl and spiked with 150 μL of CML-d_4 (475 ng/mL in ultrapure water) for solid phase extraction (SPE).

For the SPE, an Oasis MCX cartridge (3 mL, 60 mg; Waters, Milford, MA) was preconditioned with 3 mL of methanol and 3 mL of ultrapure water, followed by 3 mL of 0.1 M HCl at a flow rate of 1 mL/min. The reconstituted sample was loaded onto the preconditioned cartridge at a flow rate of <0.5 mL/min. The cartridge was washed, in sequence, with 3 mL of 0.1 M HCl and 3 mL of ultrapure water. Finally, the analyte was eluted with 3 mL of 5% ammonia/methanol (v/v) at a flow rate of <0.5 mL/min. The eluant was dried gently with nitrogen gas at 50 °C, reconstituted in 300 μL of 5 mM NFPA in ultrapure water, vortexed for 30 s, and then microfiltered through a 0.22 μm syringe needle membrane prior to analysis by LC-MS/MS.

A 80 μL amount of serum sample was directly reduced in accordance with the above procedures. All samples were performed in triplicate or duplicate if they were limited.

CML was quantified using standard addition methods employing CML-d_4. The peak area ratio of CML standard/CML-d_4 internal standard was used to establish the standard curve. Recovery studies were performed by six tissues samples (each sample from each tissue) and one serum sample. Each sample was spiked with a certain level of CML standard before SPE cleanup. All samples were performed in triplicate. Limit of detection (LOD) and limit of quantification (LOQ) were determined by diluting the same calibrator to a specified signal-to-noise (S/N) ratio (S/N = 3 and 10 for the LOD and LOQ, respectively).

LC-MS/MS Analysis. Chromatographic separation was performed on a Waters 2690 LC system equipped with a degasser, a binary pump, and an autosampler, coupled with an X-Bridge C18 column (Waters) at 35 °C. The binary mobile phase consisted of solvent A (100% acetonitrile) and solvent B (5 mM NFPA in ultrapure water). Five microliters of sample solution was injected with an autoinjector. The flow rate of the mobile phase was set to 300 μL/min. The gradient elution was performed as follows: mobile phase A was increased from 5% to 60% within 5 min and then to 100% within 2 min and was held for 2 min; it was changed to 5% over 1 min and was held for 10 min to equilibrate the column prior to the next injection.

The LC was directly interfaced to an electrospray ionization (ESI) source of a Micromass Quattro Micro triple quadrupole mass spectrometer (Waters). The triple quadrupole was operated in positive ESI mode with a capillary voltage of 3.55 kV. Temperatures of the source block and desolvation capillary were 110 °C and 400 °C, respectively. Nitrogen (99.9% purity) was used as the cone and desolvation gases, the flow rates of which were 50 L/h and 600 L/h, respectively. Argon (99.99% purity) was used as the collision gas. Data were acquired in multiple reaction monitoring (MRM) mode for quantitation and analyzed by MassLynx V 4.1 software. Optimized cone voltages and collision energy are as follows: cone voltages (CML: 25 V; CML-d_4: 20 V), collision energy (CML: m/z 130−12 eV, m/z 84.1−14 eV; CML-d_4: m/z 130−12 eV, m/z 88.1−15 eV). For CML, the product ion at m/z 84.1 was used for quantification and the other for confirmation (m/z 130).

Statistical Analysis. Data are expressed as mean ± standard deviation (SD). After confirmation of their normal distribution, between-group differences in measured variables were tested by one-way analysis of variance (ANOVA). Statistical significance for all analyses was accepted at a level of $p < 0.05$. All statistical analyses were performed with the SPSS statistical program (version 20.0 for Windows).

RESULTS AND DISCUSSION

Analytical Performance of the Method. LC-MS/MS chromatograms of standards solutions and a kidney sample are shown in Figure 1. The retention time of CML in the kidney sample was almost consistent with that in CML standard solution (Figure 1A,C). However, a split peak of CML appeared for the kidney sample compared with CML standard solution. This might be due to matrix effects, because when CML-d_4 was added into the kidney sample solution the same

DOI: 10.1021/jf505063t
J. Agric. Food Chem. 2015, 63, 1658−1663

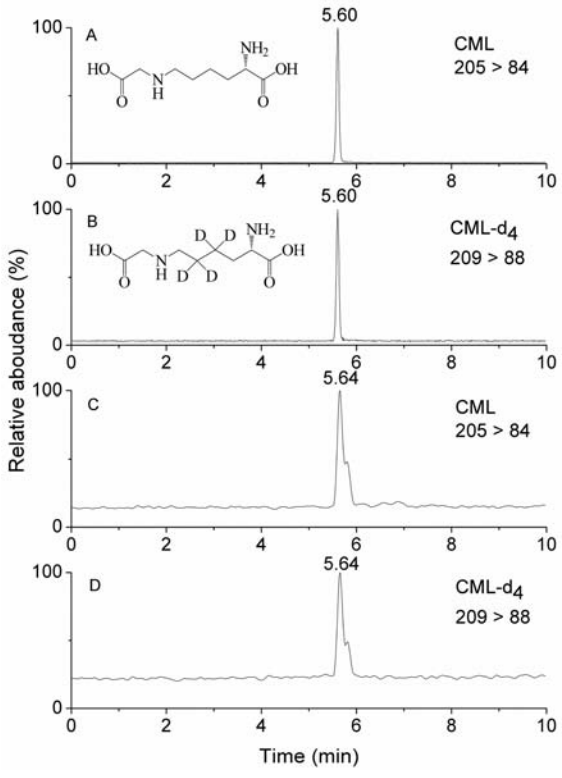

Figure 1. Typical LC-MS/MS chromatogram of CML standard solution (A), CML-d_4 internal standard solution (B), CML in kidney sample solution (C), and CML-d_4 added to kidney sample solution (D).

split peak also appeared compared with CML-d_4 standard solution (Figure 1B,D).

The method used in this work was verified by calibration, sensitivity, and recovery test. The correlation coefficient (R^2) of the CML calibration curve was 0.9995, and the linear range (41.21−5275 ng/mL) was wide enough to assess CML in biological samples. The LOD and LOQ were 8.5 and 28.34 ng/mL, respectively. The recoveries for CML were 94.93−105.74% for tissues and 107.22% for serum (Table 1). These data show that this method is suitable for determining the protein-bound CML level in biological samples.

Protein-Bound CML Levels in Serum and Tissue Samples. The dose of CML in this study was based on the studies of Somoza et al.,[26,32] aiming to reveal a potential biological effect of dietary CML on healthy tissues over a short period of time. Noteworthy, this dose is not representative of a normal exposure (0.034−0.252 mg kg^{-1} per day for adults).[34] In the present study, the protein-bound CML level in serum in CML-rats did not differ significantly from that in the Control group (CML: 1.40 ± 0.33; Control: 1.60 ± 0.52 μg/mL serum, $p > 0.05$). This finding was in good agreement with the results of recent studies,[29,31] further confirming that protein-bound CML in serum mainly comes from the in vivo glycation rather than the dietary intake of CML.

Up to now, a correlation between serum CML content and pathophysiological outcomes has not been found based on up-to-date methodology,[35,36] but it is reported that dietary AGE restriction could attenuate insulin resistance, oxidative stress, and endothelial dysfunction.[37] Therefore, tissue CML levels might be of greater relevance to chronic diseases.[36] Figure 2 shows the protein-bound CML levels in the tissues of rats in different groups. After oral CML administration for 12 consecutive weeks, the protein-bound CML contents in tissues of rats were increased in different degrees. In the kidney and liver (Figure 2A,B), the protein-bound CML levels were increased by 107% and 56%, respectively (kidney: CML 202 ± 17, Control 98 ± 1 μg/g dry matter, $p < 0.05$; liver: CML 217 ± 44, Control 140 ± 42 μg/g dry matter, $p < 0.05$). Liver and kidneys are the essential metabolic and blood-filtering organs, respectively.[38] In addition, kidneys also play a major role in AGE excretion.[26] Therefore, it is hypothesized that after entering the bloodstream, exogenous free CML is primarily transported to the liver and then partially transferred to the kidneys and other organs, which is consistent with Bergmann et

Table 1. Recovery Data for LC-MS/MS Analysis of Protein-Bound CML[a]

	protein-bound CML[b]			
sample	control sample	spiked sample	amount added	recovery (%)
kidney	97.7 ± 1.50	185 ± 10.8	83.7	106 ± 12.8
liver	99.9 ± 0.55	186 ± 8.11	91.6	94.9 ± 8.86
heart	158 ± 3.92	292 ± 11.0	138	98.9 ± 7.94
lung	92.0 ± 0.11	165 ± 4.48	74.6	97.6 ± 6.00
spleen	153 ± 0.98	300 ± 1.63	148	99.7 ± 1.10
pancreas	28.7 ± 0.21	58.1 ± 5.78	29.1	102 ± 19.9
serum	1.02 ± 0.02	2.07 ± 0.04	0.97	107 ± 4.37

[a]Values are mean ± SD ($n = 3$). [b]Protein-bound CML in tissues and serum expressed as μg/g dry matter and μg/mL serum, respectively.

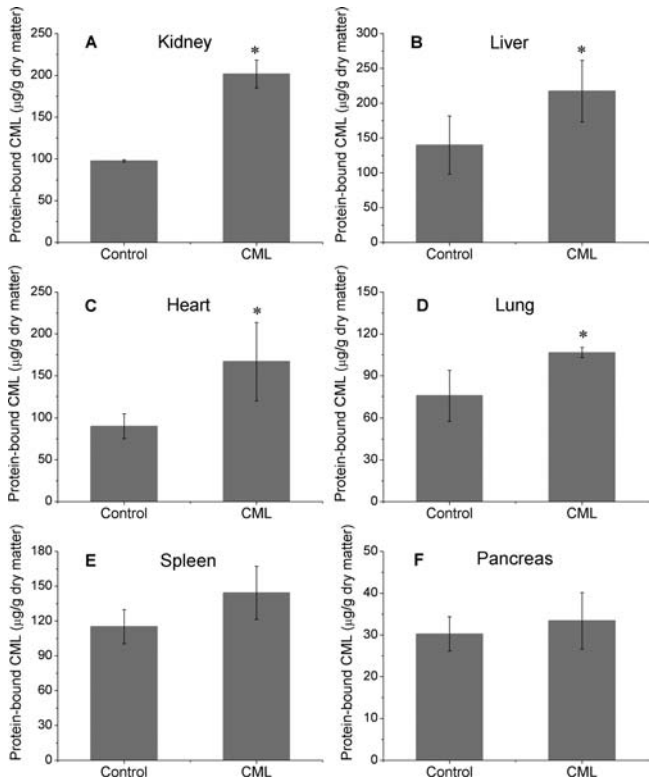

Figure 2. Protein-bound CML in tissues expressed as μg/g dry matter (mean ± SD, $n = 7$). A: Kidney, B: liver, C: heart, D: lung, E: spleen, F: pancreas. All samples were performed in triplicate or duplicate when sample was limited. *$p < 0.05$ indicates a significant difference between the Control and CML groups.

DOI: 10.1021/jf505063t
J. Agric. Food Chem. 2015, 63, 1658−1663

al.[39] When the free CML is conveyed to these organs, it would accumulate and bind to tissue certain proteins, thus elevating the protein-bound CML levels in these tissues. This study proved that the elevated protein-bound CML is due to exogenous free CML binding to tissue proteins. Since protein-bound CML is not cleared by the liver scavenger cells,[40] it would not be catabolized further in the organism.[39] Furthermore, it is reported that protein-bound CML is not easily excreted through the kidneys.[8] These factors explain the marked elevation in the protein-bound CML levels in the kidneys and liver.

In the heart (Figure 2C), the protein-bound CML level increased by 85% over that in the Control group (CML 167 ± 47, Control 90 ± 15 μg/g dry matter). This significant increase was consistent with the findings of Roncero-Ramos et al.,[29] who reported that CML in the rat heart increased significantly after rats were fed bread crust. In the lung (Figure 2D), the protein-bound CML level increased by 41% (CML 107 ± 4, Control 76 ± 18 μg/g dry matter). Protein-bound CML is reported to form only under aerobic conditions.[41] Thus, we suggested that the abundant oxygen in the lungs could accelerate the absorbed exogenous free CML binding to tissue proteins and thus elevate the protein-bound CML in vivo. However, in the spleen and pancreas (Figure 2E,F), there was no significant difference in the protein-bound CML levels between the two groups (spleen: CML 144 ± 23, Control 115 ± 15 μg/g dry matter; pancreas: CML 33 ± 7, Control 30 ± 4 μg/g dry matter), although the level tended to be higher in the CML group. Why did protein-bound CML increase markedly in the heart and lungs rather than the spleen and pancreas? One possibility is that blood flowing into the heart and lungs comes from aorta, while blood flowing into the spleen and pancreas comes from arterial branches. Thus, in the same time, more exogenous free CML is carried to the heart and lungs along with bloodstream. Another possibility is that the rate at which CML and proteins combine in the spleen and pancreas is slow, and thus protein-bound CML does not quickly accumulate in these tissues.

Notably, the formation of protein-bound CML generally reflects the level of oxygen stress in vivo;[42] therefore, we suggest that the oxygen stress level might have been higher in the tissues of the CML group rats than in those of the Control group rats, particularly in the kidney, heart, and liver tissues, which might induce chronic diseases in these organs.[43]

Serum Markers. Because the clearly accumulated protein-bound CML in body tissues might be a threat to the kidneys and liver, several serum markers of kidney and liver function were measured in this work. As shown in Figure 3, after oral CML treatment for 12 consecutive weeks, the serum BUN, CREA, ALT, and AST levels were all significantly elevated over those in the Control group. It is reported that serum BUN and CREA are regarded as diagnostic markers of renal function,[44] and the significantly elevated levels of BUN and CREA indicate renal dysfunction.[45] Similarly, serum ALT and AST are generally used to assess liver damage,[46] and a significant increase usually indicates abnormal liver function.[47] Therefore, we believe that chronic intake high level of CML contributes to functional impairment of the kidneys and liver in healthy individuals.

FBW, Food, and Water Intake and FBG Levels. To investigate the effect of chronic oral intake of CML on healthy rats, the FBW and food and water intake of all rats were recorded every other week. As shown in Figure 4A–C, there were no significant differences between the CML and Control

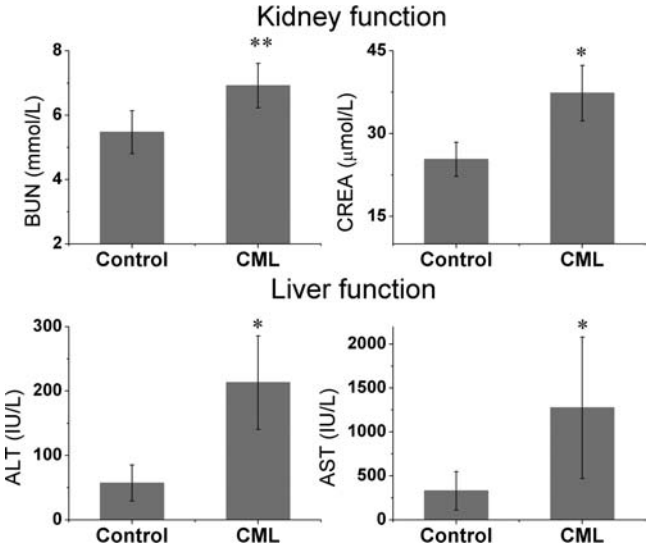

Figure 3. Serum markers of kidney and liver function (mean ± SD, n = 5). *p < 0.05 indicates a significant difference between Control and CML groups and **p < 0.01 indicates a highly significant difference between both groups.

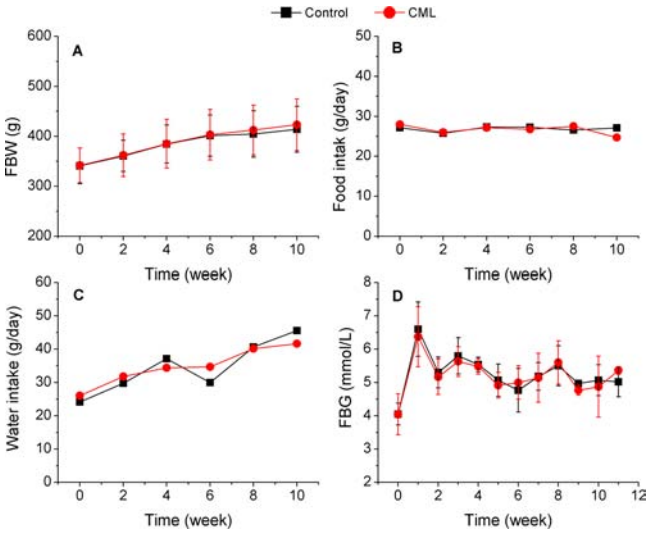

Figure 4. Biweekly FBW (A), 24-h food intake (B), 24-h water intake (C), and weekly FBG levels (D) in the Control and CML groups.

groups, indicating that chronic oral CML intake did not affect the appetite or weight of the rats. In addition, the FBG level was measured every week during the experiment (Figure 4D). During the first week, the FBG levels of the rats in both groups were elevated, which could have been caused by poor adaptation of the rats to stomach gavage. During the following week, the FBG levels were back to normal, indicating that the rats had adapted to the procedure. As time went on, no significant difference was observed between the CML and Control groups, and the trends in both groups were similar. Thus, we suggest that chronic oral CML administration does not affect the FBG levels of rats fed a normal diet.

In summary, the distribution of protein-bound CML in tissues of healthy rats after chronic oral administration of pure CML was investigated in this work. After entering the bloodstream, exogenous free CML is conveyed and accumulated in tissues along with the blood circulation and binds to

DOI: 10.1021/jf505063t
J. Agric. Food Chem. 2015, 63, 1658–1663

tissue proteins to form protein-bound CML, especially in the kidneys, heart, and liver, followed by the lungs. Conversely, no statistically excess protein-bound CML accumulated in the spleen or pancreas. Furthermore, serum BUN, CREA, ALT, and AST increased significantly. Our findings might be clinically meaningful, i.e., chronic intake of high level of CML could lead to kidney and liver toxicology and induce kidney and liver dysfunction in healthy individuals. In addition, chronic oral CML did not induce a rise in the FBG level. Thus, we emphasize that long-term consumption of CML-rich foods is a potential risk for healthy humans, especially in terms of kidney or liver function. This finding is of vital importance. We must realize the harm that can come from a daily diet rich in AGEs, and we must also realize the implications of an AGE-rich diet for timely prevention and diagnosis AGE-related chronic diseases.

AUTHOR INFORMATION

Corresponding Author

*Tel: +86 139 6176 1357. Fax: +86 510 85919065. E-mail: chenjie@jiangnan.edu.cn.

Funding

This work was supported financially by the National Basic Research Program of China (973 Program, 2012 CB720801).

Notes

The authors declare no competing financial interest.

ABBREVIATIONS USED

AGEs, advanced glycation end products; CML, N^{ϵ}-(carboxymethyl)lysine; CML-d_4, N^{ϵ}-(carboxy[$^2H_4$]methyl)-lysine; NFPA, nonafluoropentanoic acid; FBW, fasting body weight; FBG, fasting blood glucose; BUN, blood urea nitrogen; CREA, creatinine; ALT, alanine aminotransferase; AST, aspartate aminotransferase; TCA, trichloroacetic acid; SPE, solid-phase extraction; LOD, limit of detection; LOQ, limit of quantification; S/N, signal-to-noise; ESI, electrospray ionization; MRM, multiple reaction monitoring; SD, standard deviation; ANOVA, analysis of variance

REFERENCES

(1) Singh, R.; Barden, A.; Mori, T.; Beilin, L. Advanced glycation end-products: A review. *Diabetologia* **2001**, *44*, 129−146.

(2) Vitek, M. P.; Bhattacharya, K.; Glendening, J. M.; Stopa, E.; Vlassara, H.; Bucala, R.; Manogue, K.; Cerami, A. Advanced glycation end products contribute to amyloidosis in Alzheimer disease. *Proc. Natl. Acad. Sci. U. S. A.* **1994**, *91*, 4766−4770.

(3) Takeuchi, M.; Yamagishi, S. I. Possible involvement of advanced glycation end-products (AGEs) in the pathogenesis of Alzheimer's disease. *Curr. Pharm. Des.* **2008**, *14*, 973−978.

(4) Basta, G.; Schmidt, A. M.; De Caterina, R. Advanced glycation end products and vascular inflammation: Implications for accelerated atherosclerosis in diabetes. *Cardiovasc. Res.* **2004**, *63*, 582−592.

(5) Vlassara, H.; Palace, M. R. Diabetes and advanced glycation endproducts. *J. Int. Med.* **2002**, *251*, 87−101.

(6) Schalkwijk, C. G.; Baidoshvili, A.; Stehouwer, C. D.; van Hinsbergh, V. W.; Niessen, H. W. Increased accumulation of the glycoxidation product N^{ϵ}-(carboxymethyl)lysine in hearts of diabetic patients: Generation and characterisation of a monoclonal anti-CML antibody. *Biochim. Biophys. Acta, Mol. Cell Res.* **2004**, *1636*, 82−89.

(7) Heijst, J. W.; Niessen, H. W.; Hoekman, K.; Schalkwijk, C. G. Advanced glycation end products in human cancer tissues: Detection of N^{ϵ}-(carboxymethyl) lysine and argpyrimidine. *Ann. N.Y. Acad. Sci.* **2005**, *1043*, 725−733.

(8) Thornalley, P.; Battah, S.; Ahmed, N.; Karachalias, N.; Agalou, S.; Babaei-Jadidi, R.; Dawnay, A. Quantitative screening of advanced glycation endproducts in cellular and extracellular proteins by tandem mass spectrometry. *Biochem. J.* **2003**, *375*, 581−592.

(9) Goldberg, T.; Cai, W.; Peppa, M.; Dardaine, V.; Baliga, B. S.; Uribarri, J.; Vlassara, H. Advanced glycoxidation end products in commonly consumed foods. *J. Am. Diet. Assoc.* **2004**, *104*, 1287−1291.

(10) Uribarri, J.; Peppa, M.; Cai, W.; Goldberg, T.; Lu, M.; Baliga, S.; Vassalotti, J. A.; Vlassara, H. Dietary glycotoxins correlate with circulating advanced glycation end product levels in renal failure patients. *Am. J. Kidney Dis.* **2003**, *42*, 532−538.

(11) Vlassara, H.; Cai, W.; Crandall, J.; Goldberg, T.; Oberstein, R.; Dardaine, V.; Peppa, M.; Rayfield, E. J. Inflammatory mediators are induced by dietary glycotoxins, a major risk factor for diabetic angiopathy. *Proc. Natl. Acad. Sci. U. S. A.* **2002**, *99*, 15596−15601.

(12) Koschinsky, T.; He, C. J.; Mitsuhashi, T.; Bucala, R.; Liu, C.; Buenting, C.; Heitmann, K.; Vlassara, H. Orally absorbed reactive glycation products (glycotoxins): An environmental risk factor in diabetic nephropathy. *Proc. Natl. Acad. Sci. U. S. A.* **1997**, *94*, 6474−6479.

(13) Delgado-Andrade, C. Maillard reaction products: Some considerations on their health effects. *Clin. Chem. Lab. Med.* **2014**, *52*, 53−60.

(14) Liardon, R.; De Weck-Gaudard, D.; Philippossian, G.; Finot, P. A. Identification of N^{ϵ}-carboxymethyllysine: A new Maillard reaction product in rat urine. *J. Agric. Food Chem.* **1987**, *35*, 427−431.

(15) Ames, J. M. Determination of N^{ϵ}-(carboxymethyl) lysine in foods and related systems. *Ann. N.Y. Acad. Sci.* **2008**, *1126*, 20−24.

(16) Chao, P. C.; Hsu, C. C.; Yin, M. C. Analysis of glycative products in sauces and sauce-treated foods. *Food Chem.* **2009**, *113*, 262−266.

(17) Uribarri, J.; Woodruff, S.; Goodman, S.; Cai, W.; Chen, X.; Pyzik, R.; Yong, A.; Striker, G. E.; Vlassara, H. Advanced glycation end products in foods and a practical guide to their reduction in the diet. *J. Am. Diet. Assoc.* **2010**, *110*, 911−916.

(18) Zhang, G.; Huang, G.; Xiao, L.; Mitchell, A. E. Determination of advanced glycation endproducts by LC-MS/MS in raw and roasted almonds (*Prunus dulcis*). *J. Agric. Food Chem.* **2011**, *59*, 12037−12046.

(19) Hull, G. L.; Woodside, J. V.; Ames, J. M.; Cuskelly, G. J. N^{ϵ}-(Carboxymethyl) lysine content of foods commonly consumed in a Western style diet. *Food Chem.* **2012**, *131*, 170−174.

(20) Wagner, Z.; Wittmann, I.; Mazák, I.; Schinzel, R.; Heidland, A.; Kientsch-Engel, R.; Nagy, J. N^{ϵ}-(carboxymethyl) lysine levels in patients with type 2 diabetes: Role of renal function. *Am. J. Kidney Dis.* **2001**, *38*, 785−791.

(21) Friess, U.; Waldner, M.; Wahl, H. G.; Lehmann, R.; Haring, H. U.; Voelter, W.; Schleicher, E. Liquid chromatography-based determination of urinary free and total N^{ϵ}-(carboxymethyl) lysine excretion in normal and diabetic subjects. *J. Chromatogr., B* **2003**, *794*, 273−280.

(22) Teerlink, T.; Barto, R.; Herman, J.; Schalkwijk, C. G. Measurement of N^{ϵ}-(carboxymethyl) lysine and N^{ϵ}-(carboxyethyl) lysine in human plasma protein by stable-isotope-dilution tandem mass spectrometry. *Clin. Chem.* **2004**, *50*, 1222−1228.

(23) Faist, V.; Müller, C.; Drusch, S.; Erbersdobler, H. F. Selective fortification of lysinoalanine, fructoselysine and N^{ϵ}-carboxymethyllysine in casein model systems. *Food (Weinheim, Germany)* **2001**, *45*, 218−221.

(24) Kislinger, T.; Fu, C.; Huber, B.; Qu, W.; Taguchi, A.; Yan, S. D.; Hofmann, M.; Yan, S. F.; Pischetsrieder, M.; Stern, D.; Schmidt, A. M. N^{ϵ}-(Carboxymethyl) lysine adducts of proteins are ligands for receptor for advanced glycation end products that activate cell signaling pathways and modulate gene expression. *J. Biol. Chem.* **1999**, *274*, 31740−31749.

(25) Uribarri, J.; Cai, W.; Peppa, M.; Goodman, S.; Ferrucci, L.; Striker, G.; Vlassara, H. Circulating glycotoxins and dietary advanced glycation endproducts: Two links to inflammatory response, oxidative stress, and aging. *J. Gerontol., Ser. A* **2007**, *62*, 427−433.

DOI: 10.1021/jf505063t
J. Agric. Food Chem. 2015, 63, 1658−1663

(26) Somoza, V.; Lindenmeier, M.; Hofmann, T.; Frank, O.; Erbersdobler, H. F.; Baynes, J. W.; Thorpe, S. R.; Heidland, A.; Zill, H.; Bek, S.; Huber, J.; Weigle, T.; Scheidler, S.; Busch, A. E.; Šebeková, K. Dietary bread crust advanced glycation end products bind to the receptor for AGEs in HEK-293 kidney cells but are rapidly excreted after oral administration to healthy and subtotally nephrectomized rats. *Ann. N.Y. Acad. Sci.* **2005**, *1043*, 492−500.
(27) Tanji, N.; Markowitz, G. S.; Fu, C.; Kislinger, T.; Taguchi, A.; Pischetsrieder, M.; Stern, D.; Schmidt, M.; D'agati, V. D. Expression of advanced glycation end products and their cellular receptor RAGE in diabetic nephropathy and nondiabetic renal disease. *J. Am. Soc. Nephrol.* **2000**, *11*, 1656−1666.
(28) Nerlich, A. G.; Schleicher, E. D. N^{ϵ}-(Carboxymethyl) lysine in atherosclerotic vascular lesions as a marker for local oxidative stress. *Atherosclerosis* **1999**, *144*, 41−47.
(29) Roncero-Ramos, I.; Delgado-Andrade, C.; Tessier, F. J.; Niquet-Léridon, C.; Strauch, C.; Monnier, V. M.; Navarro, M. P. Metabolic transit of N^{ϵ}-carboxymethyl-lysine after consumption of AGEs from bread crust. *Food Funct.* **2013**, *4*, 1032−1039.
(30) Roncero-Ramos, I.; Niquet-Leridon, C.; Strauch, C.; Monnier, V. M.; Tessier, F. J.; Navarro, M. P.; Delgado-Andrade, C. An advanced glycation endproduct (AGE)-rich diet promotes N^{ϵ}-carboxymethyl-lysine accumulation in the cardiac tissue and tendons of rats. *J. Agric. Food Chem.* **2014**, *62*, 6001−6006.
(31) Alamir, I.; Niquet-Leridon, C.; Jacolot, P.; Rodriguez, C.; Orosco, M.; Anton, P. M.; Tessier, F. J. Digestibility of extruded proteins and metabolic transit of N^{ϵ}-carboxymethyllysine in rats. *Amino Acids* **2013**, *44*, 1441−1449.
(32) Somoza, V.; Wenzel, E.; Weiss, C.; Clawin-Rädecker, I.; Grübel, N.; Erbersdobler, H. F. Dose-dependent utilisation of casein-linked lysinoalanine, N(epsilon)-fructoselysine and N(epsilon)-carboxymethyllysine in rats. *Mol. Nutr. Food Res.* **2006**, *50*, 833−841.
(33) Dhar, A.; Dhar, I.; Jiang, B.; Desai, K. M.; Wu, L. Chronic methylglyoxal infusion by minipump causes pancreatic β-cell dysfunction and induces type 2 diabetes in Sprague-Dawley rats. *Diabetes* **2011**, *60*, 899−908.
(34) Tessier, F. J.; Birlouez-Aragon, I. Health effects of dietary Maillard reaction products: The results of ICARE and other studies. *Amino Acids* **2012**, *42*, 1119−1131.
(35) Schwedler, S. B.; Metzger, T.; Schinzel, R.; Wanner, C. Advanced glycation end products and mortality in hemodialysis patients. *Kidney Int.* **2002**, *62*, 301−310.
(36) Busch, M.; Franke, S.; Wolf, G.; Brandstädt, A.; Ott, U.; Gerth, J.; Stein, G. The advanced glycation end product N^{ϵ}-carboxymethyllysine is not a predictor of cardiovascular events and renal outcomes in patients with type 2 diabetic kidney disease and hypertension. *Am. J. Kidney Dis.* **2006**, *48* (4), 571−579.
(37) Kellow, N. J.; Savige, G. S. Dietary advanced glycation end-product restriction for the attenuation of insulin resistance, oxidative stress and endothelial dysfunction: A systematic review. *Eur. J. Clin. Nutr.* **2013**, *67*, 239−248.
(38) Higuchi, H.; Gores, G. J. Mechanisms of liver injury: An overview. *Curr. Mol. Med.* **2003**, *3*, 483−490.
(39) Bergmann, R.; Helling, R.; Heichert, C.; Scheunemann, M.; Mäding, P.; Wittrisch, H.; Johannsen, B.; Henle, T. Radio fluorination and positron emission tomography (PET) as a new approach to study the in vivo distribution and elimination of the advanced glycation endproducts N^{ϵ}-carboxymethyllysine (CML) and N^{ϵ}-carboxyethyllysine (CEL). *Food (Weinheim, Germany)* **2001**, *45*, 182−188.
(40) Svistounov, D. N.; Berg, T. J.; McCourt, P. A.; Zykova, S. N.; Elvevold, K. H.; Nagai, R.; Horiuchi, S.; Smedsrod, B. H. Lack of recognition of N^{ϵ}-(carboxymethyl) lysine by the mouse liver reticulo-endothelial system: Implications for pathophysiology. *Biochem. Biophys. Res. Commun.* **2003**, *309*, 786−791.
(41) Schleicher, E. D.; Wagner, E.; Nerlich, A. G. Increased accumulation of the glycoxidation product N^{ϵ}-(carboxymethyl) lysine in human tissues in diabetes and aging. *J. Clin. Invest.* **1997**, *99*, 457−468.
(42) Baynes, J. W. Role of oxidative stress in development of complications in diabetes. *Diabetes* **1991**, *40*, 405−412.
(43) Cai, W.; He, J. C.; Zhu, L.; Chen, X.; Zheng, F.; Striker, G. E.; Vlassara, H. Oral glycotoxins determine the effects of calorie restriction on oxidant stress, age-related diseases, and lifespan. *Am. J. Pathol.* **2008**, *173*, 327−336.
(44) Finco, D. R.; Duncan, J. R. Evaluation of blood urea nitrogen and serum creatinine concentrations as indicators of renal dysfunction: A study of 111 cases and a review of related literature. *J. Am. Vet. Med. Assoc.* **1976**, *168*, 593−601.
(45) Williams, P.; Lopez, H.; Britt, D.; Chan, C.; Ezrin, A.; Hottendorf, R. Characterization of renal ischemia-reperfusion injury in rats. *J. Pharmacol. Toxicol. Methods* **1997**, *37*, 1−7.
(46) Ramaiah, S. K. A toxicologist guide to the diagnostic interpretation of hepatic biochemical parameters. *Food Chem. Toxicol.* **2007**, *45*, 1551−1557.
(47) Solter, P. F. Clinical pathology approaches to hepatic injury. *Toxicol. Pathol.* **2005**, *33*, 9−16.

DOI: 10.1021/jf505063t
J. Agric. Food Chem. 2015, 63, 1658−1663

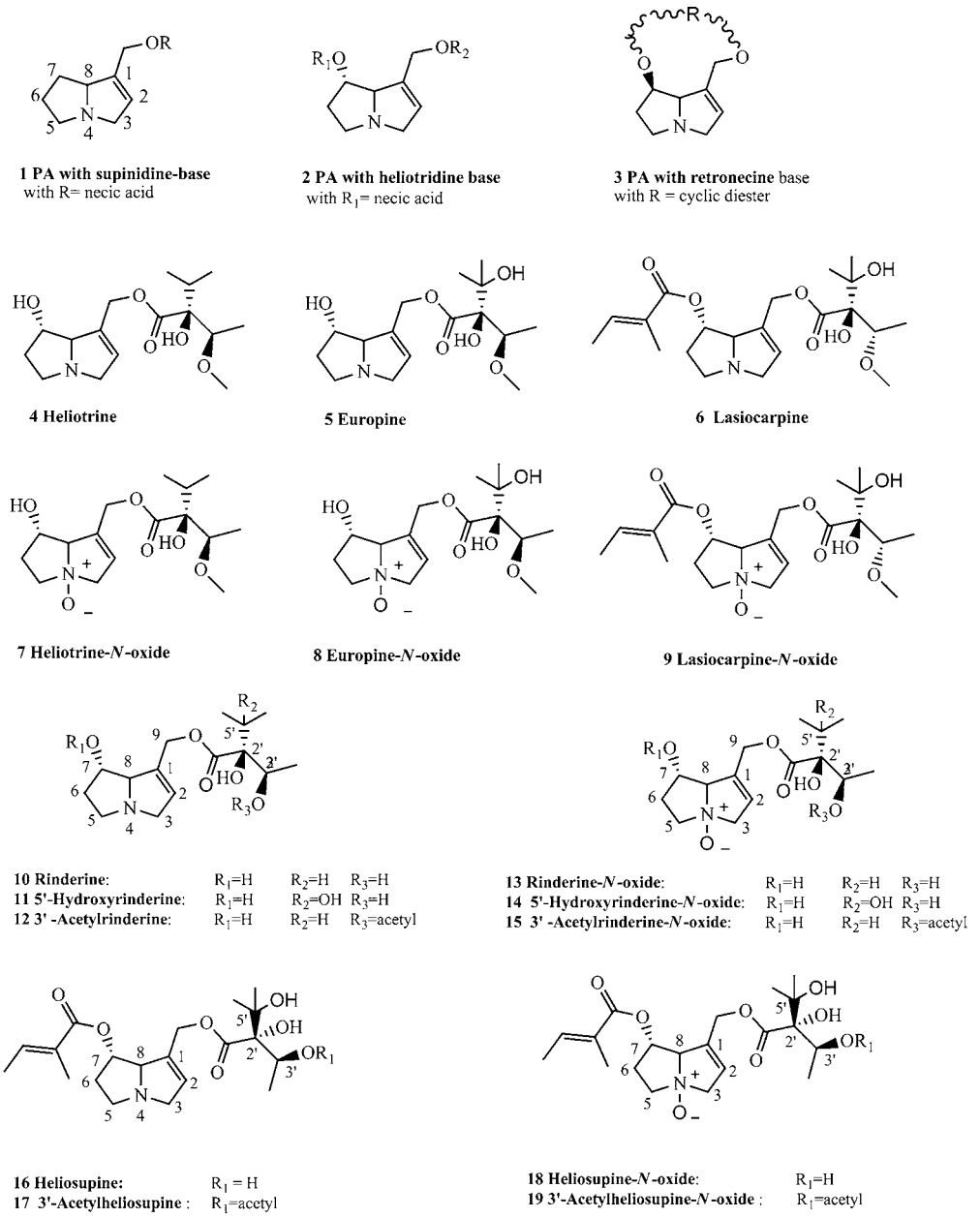

Figure 1. Classification of 1,2-unsaturated PA, commonly found in *Heliotropium* spp., into four subgroups according to their PA base-type and the number/type of ester bonds. The generic names are indicated in bold below each chemical structure.

literature.[9] A mortality rate of about 30% was recorded over a time period of 26 weeks. The surviving animals were eventually slaughtered after it was shown that some clinically normal calves had striking pathological lesions. Between March 14 and May 15, 2014, in a herd of 15−18-month-old replacement mixed-breed beef cattle (n = 73) from the Galilee region in Israel, a 33% mortality rate occurred, following ingestion of total mixed ration (TMR) containing hay that turned out to be contaminated with *H. europaeum*. The aims of the present work were to provide a detailed description of the chronic PA poisoning in cattle, including clinical signs, pathology, and histopathology in association with the total PA levels found in the feed, and to characterize the PA/PA-*N*-oxide composition in the contaminated hay in comparison to the PA and PA-*N*-oxide profile of the aerial portions of *H. europaeum* collected under similar conditions.

MATERIALS AND METHODS

Toxicosis Event. History of the herd: the affected cattle consisted of 73 mixed-breed beef cattle (15−18 months old, weighting 340−390 kg), which were reared in Kibbutz Gazit located in the Galilee region in Israel. The herd was held in a semiopen pen with a yard. The herd was fed from the beginning of February 2014 a TMR supplied by a local private company composed of 50% hay accidently contaminated with *H. europaeum*, 47.5% poultry litter, and 2.5% *Stevia rebaudiana*. Neither the feed producer, the farmer, nor the farm veterinarian considered the dried green plant material present in the hay a noxious weed. After 42 days of contaminated TMR consumption, followed by 1 week of rearing on a nearby pasture, as commonly practiced at the beginning of spring, two cows were found dead (March 14, 2014), and 2 days later two additional cows were found dead (Figure 2). The mortality cases were immediately reported to the Israeli Veterinary Institute, and of the four dead cows, three were submitted to the Department of Pathology for full necropsy and histopathological as well as parasitological and virological examination. Furthermore,

DOI: 10.1021/jf5052199
J. Agric. Food Chem. 2015, 63, 1664−1672

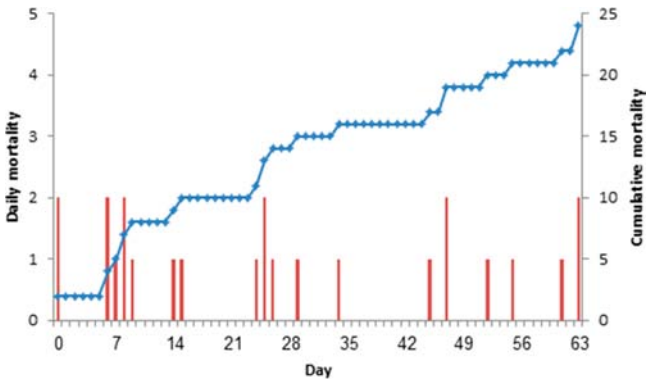

Figure 2. Daily mortality and cumulative mortality curve of mixed-breed beef cattle (15−18 months old) poisoned with *H. europaeum*. The time scale begins with the first mortality events (day 0) following 42 days of consumption of *H. europaeum*-contaminated feed and 7 days after cessation of feeding the affected herd with the contaminated hay.

leftovers of the suspected feed material were submitted to the Department of Toxicology and Bacteriology for toxicological and bacteriological evaluation. The sudden deaths occurred without any previously noticeable clinical signs according to the farmer's testimony. Noticeable clinical signs appeared only about 1 week after the first sudden death events and affected only a small proportion of the herd and included lethargy, staggering with dragging of the hind quarters, and tenesmus, invariably accompanied by varying degrees of rectal prolapse. In some cases, restlessness was a marked feature, sometimes coupled with circling within the perimeter of the yard. The course of all these manifestations was short, with affected animals invariably dying within 48 h with a significant loss of weight during this period. Over a period of 63 d counted from the first mortality event, 24 cows were found dead, yielding a mortality rate of 33%. As clinically normal cows revealed marked pathological liver lesions, the remaining 49 cows were slaughtered. The Israeli Veterinary Services decided to incinerate the meat of the affected cattle, due to an unknown risk associated with meat products possibly contaminated with PA residues. The suspected contaminated hay was stored for inspection in a closed confinement within the kibbutz.

Laboratory Investigations. *Total Mixed Ration (TMR) Analysis.* Samples of the TMR ingredients (hay, poultry litter, and *Stevia*) were screened for a wide range of pesticides, including organophosphates, carbamates, pyrethroids, and organochlorides as well as PAs by GC−MS (Agilent Technologies, Santa Clara, CA), according to an in-house-validated screening method published recently.[18] The TMR ingredients were also analyzed for doxycycline and oxytetracycline, as well as the ionophores monensin, lasalocid, salinomycin, maduramicin, semduramicin, and narasin by LC−MS/MS according to the previously described method.[19] The analysis of the TMR ingredients for aflatoxins B_1, B_2, G_1, and G_2 was performed by HPLC with postcolumn photochemical derivatization and fluorescence detection. Moreover, the TMR ingredients were analyzed for the elements As, Cd, Co, Zn, Cu, Fe, Pb, Mn, Hg, Mo, Se, Tl, and Zn by utilizing an ARCOS ICP-AES (Spectro Analytical Instruments, Kleve, Germany) according to the EPA method 6010c.[20]

LC−MS/MS Analysis for PA and PA-N-Oxides in Animal Feed and H. europaeum. Dried, ground plant material was extracted using a slightly adapted procedure.[21] Powdered material was extracted with 2% formic acid (Merck, Darmstadt, Germany) solution in a 1:100 ratio (w/v). The extract was then filtered and 5 μL was diluted 200 times with 2 mM NH_4OH solution (Merck). The contaminated hay material was extracted the same way, but in this case, 50 μL was diluted 20 times with 20 mM NH_4OH solution. PA composition and content of the samples were determined using an Acquity chromatographic system coupled to a Quattro Premier XE tandem mass spectrometer (Waters, Milford, MA), run in multiple reaction monitoring mode (MRM) with positive electrospray ionization. Cone voltage was set at 30 V, desolvation gas temperature at 450 °C, source block temperature at 120 °C, and the argon collision gas pressure at 4.0×10^{-3} mbar. Dwell time of the selected transitions was 10 ms with an interscan delay of 0.5 ms. The column used was a 150 × 2.1 mm i.d., 1.7 μm Acquity BEH RP-18 (Waters, Milford, MA), kept at 50 °C and run at 0.4 mL/min. A mobile phase consisting of 6.5 mM NH_4OH in water and 6.5 mM NH_4OH in acetonitrile was used. The gradient started at 100% water and was changed linearly to 50% acetonitrile in 12 min. After 0.2 min the composition was returned to the starting condition and the column was allowed to equilibrate for another 2.5 min. Mass spectrometric data were processed using Masslynx 4.1 software (Waters, Milford, MA).

Representative *H. europaeum* samples were screened for the presence of known and new PAs using parent ion scanning. Typical product fragments were selected, such as m/z 120, 122, 138, 156, 172, and 254. The mass scanning range was from m/z 200 to 500 with a mass resolution of 0.1 Da and a scan time of 800 ms. Spectra were recorded using a fixed cone voltage of 30 V and fixed collision energy of 30 eV. Compounds producing a protonated molecular ion with an even mass and displaying fragmentation behavior typical for specific types of PAs were tentatively identified as PAs. These potential PAs were further identified by collecting individual fragmentation spectra at a collision energy range of 20−40 eV. On the basis of their fragmentation spectra, tentative structures could be derived. These compounds have been included in the MRM method, by selecting two product ions, typically the most abundant ones. See Table 1 for the mass spectrometric settings selected for each compound. PAs were quantitated against a range of calibrant samples (0−500 ng/mL) containing available PA standards [heliotrine (**4**), europine (**5**), lasiocarpine (**6**), their corresponding *N*-oxides (**7**−**9**), lycopsamine, and echimidine (Phytoplan, Heidelberg, Germany)]. Echimidine-*N*-oxide was synthesized in-house by *N*-oxidation of echimidine. For a number of PAs, no reference standard was available. For those PAs, a semiquantitative result was obtained by comparison of the peak area with that of a structurally related standard, as indicated in Table 1. The available PA standards accounted for approximately 90% of the PA content in the hay and plant material. The limit of quantification in the *H. europaeum* plant material was 1 μg/g and in the hay approximately 0.1 μg/g.

Aflatoxin B_1, B_2, G_1, and G_2 Analysis by HPLC with Postcolumn Photochemical Derivatization and Fluorescence Detection. Homogenized hay was extracted and analyzed according to a previously published method with slight modifications.[22] In brief, a 5 g sample was extracted with 15 mL of acetonitrile:water 80:20 (v/v) and shaken for 1 h. The sample was centrifuged for 10 min at 4000*g* and 13 mL of organic supernatant was transferred into a new 15 mL Falcon tube and evaporated to dryness in a water bath (40 °C) under a stream of N_2. The dried residue was reconstituted with 0.5 mL of methanol:water 60:40 (v/v) in water and subjected to centrifugation for 10 min at 14 000*g* and finally injected into a HPLC-FLD equipped with a PHRED photochemical derivatization system (AURA Industries, New York, NY) installed before the fluorescence detector. The method utilized a model 1100 (Agilent Technologies, Waldbronn, Germany) liquid chromatography system (equipped with binary pump, degasser, column compartment, and autosampler) combined with a fluorescence detector with excitation and emission wavelengths of 360 and 455 nm, respectively. The column used was a 150 × 4.5 mm i.d., 3.5 μm, ZORBAX RP-18 (Agilent Technologies, Santa Clara, CA), and the following gradient program was utilized: separation was started with 70% water, 17% methanol, and 13% acetonitrile (0−7 min), followed by an increase of the organic phase to 55% water, 30% methanol, and 15% acetonitrile (7−10 min), holding at the latter conditions for an additional 6 min, and eventually returning to the initial mobile phase conditions (16−19 min). The flow rate was 1.0 mL/min and the injection volume 40 μL. A limit of quantitation of 1 and 0.3 μg/kg was achieved for AFB_1 and AFG_1, and AFB_2 and AFG_2, respectively.

Blood Samples. Blood samples were collected from the jugular vein of 27 randomly chosen live cattle during the intoxication event, counted from the first mortality event, over a time period of 63 d. Samples for complete blood count were collected in potassium-EDTA

DOI: 10.1021/jf5052199
J. Agric. Food Chem. 2015, 63, 1664−1672

Table 1. Mass Spectrometric Conditions Used and Indicative Retention Times of Utilized Standards and Pyrrolizidine Alkaloids Detected in *H. europaeum*.

pyrrolizidine alkaloid	precursor ion (m/z)	fragment 1 (m/z)	collision energy (eV)	fragment 2 (m/z)	collision energy (eV)	retention time (min)	standard used for quantification
supinine	284.2	122	20	140	25	8.95	lycopsamine
supinine-*N*-oxide	300.2	120	30	156	30	5.55	lycopsamine-*N*-oxide
heleurine	298.2	122	30	140	25	10.75	heliotrine
heleurine-*N*-oxide	314.2	120	30	156	25	6.65	heliotrine-*N*-oxide
lycopsamine[a]	300.2	94	35	156	30	6.35	lycopsamine
lycopsamine-*N*-oxide[b]	316.2	94	40	172	30	4.76	lycopsamine-*N*-oxide
echinatine	300.2	138	30	156	30	6.95	lycopsamine
echinatine-*N*-oxide	316.2	111	40	172	30	4.89	lycopsamine-*N*-oxide
rinderine	300.2	138	30	156	30	7.05	lycopsamine
rinderine-*N*-oxide	316.2	111	40	172	30	4.95	lycopsamine-*N*-oxide
heliotrine	314.2	138	25	156	25	8.32	heliotrine
heliotrine-*N*-oxide	330.2	111	35	172	25	5.95	heliotrine-*N*-oxide
5′-hydroxyrinderine[c]	316.2	94	40	138	30	5.63	lycopsamine
5′-hydroxyrinderine-*N*-oxide[c]	332.2	111	35	172	30	3.85	lycopsamine-*N*-oxide
europine	330.2	94	35	138	30	6.72	europine
europine-*N*-oxide	346.2	172	30	256	25	4.81	europine-*N*-oxide
3′-acetylrinderine[c]	342.2	120	30	138	20	8.16	lycopsamine
3′-acetylrinderine-*N*-oxide[c]	358.2	172	30	298	25	5.92	lycopsamine-*N*-oxide
5′-acetyleuropine	372.2	156	25	254	25	8.19	europine
5′-acetyleuropine-*N*-oxide	388.2	172	30	328	20	6.18	europine-*N*-oxide
7-angeloylheliotrine-*N*-oxide	412.2	136	30	330	25	9.30	lasiocarpine-*N*-oxide
echimidine	398.2	120	25	220	20	9.92	echimidine
echimidine-*N*-oxide	414.2	254	30	352	25	7.27	echimidine-*N*-oxide
heliosupine	398.2	120	25	220	20	9.74	echimidine
heliosupine-*N*-oxide	414.2	94	30	254	30	7.08	echimidine-*N*-oxide
lasiocarpine	412.2	120	25	220	20	11.10	lasiocarpine
lasiocarpine-*N*-oxide	428.2	138	30	254	25	7.92	lasiocarpine-*N*-oxide
iso-lasiocarpine[c]	412.2	120	25	220	20	10.96	lasiocarpine
iso-lasiocarpine-*N*-oxide[c]	428.2	138	30	254	25	7.76	lasiocarpine-*N*-oxide
3′-acetylheliosupine	440.2	120	25	220	20	10.95	echimidine
3′-acetylheliosupine-*N*-oxide	456.2	254	30	338	25	7.95	echimidine-*N*-oxide
5′-acetyllasiocarpine	454.2	120	30	336	25	12.56	lasiocarpine
5′-acetyllasiocarpine-*N*-oxide	470.2	352	20	410	20	9.18	lasiocarpine-*N*-oxide
iso-acetyllasiocarpine[c]	454.2	120	30	336	25	12.41	lasiocarpine
iso-acetyllasiocarpine-*N*-oxide[c]	470.2	352	20	410	20	9.02	lasiocarpine-*N*-oxide

[a]Coelutes with its structural isomer intermedine. [b]Coelutes with its structural isomer intermedine-*N*-oxide. [c]Tentative identification, based on fragmentation spectra, MW, retention time, and the presence/absence of *N*-oxides. The prefix iso indicates the presence of a structural isomer (e.g., 7-tigloyl or 7-senecioyl) instead of the 7-angeloyl ester moiety.

tubes and analyzed within 2 h of collection using an Advia 120 hematology analyzer (Siemens Medical Solutions Diagnostics, Erfurt, Germany). Samples for serum chemistry were collected in plain tubes with gel separators. Samples were centrifuged within 2 h of collection, and harvested sera were analyzed immediately using a Cobas Integra 400 Plus wet chemistry analyzer (Roche, Mannheim, Germany) at 37 °C, and reagents were supplied by the manufacturer. The serum was assayed for the enzymes creatine phosphokinase (CK), aspartate aminotransferase (AST), alkaline phosphatase (ALP), and γ-glutamyltransferase (GGT) and for the concentrations of albumin, total protein, globulin, calcium, phosphate, magnesium, and urea. Whole blood was examined to determine the values of the red blood-cell count (RBC), mean cell volume (MCV), mean corpuscular hemoglobin concentration (MCHC), and white blood cell count (WBC).

Bacteriology and Virology. Fresh samples of lung, liver, spleen, and kidney from three dead cows were examined for evidence of bacteriological and viral infections. The analysis for botulism neurotoxin from feed, stomach content, and plasma was performed by the Israeli Reference Laboratory, Department of Bacteriology, The Kimron Veterinary Institute, Israel, utilizing in-house-validated mouse lethality assay.[23] Brain tissues were tested for rabies virus (RABV) at the Israeli Reference Laboratory, Department of Rabies, The Kimron Veterinary Institute, Israel, utilizing the direct fluorescent antibody test according to an in-house-validated method.[24]

Necropsy and Gross Pathology. Three cows were submitted to the Kimron Veterinary Institute for full necropsy on the first week of the intoxication event.

Histopathology. Tissues collected for histopathological examination from three cows included the entire heart, lung, liver, kidney, spleen, brain, both ventricular walls and the interventricular septum, and small intestine and were preserved in 10% buffered formalin. In addition, liver samples from 49 slaughtered cows were collected for

DOI: 10.1021/jf5052199
J. Agric. Food Chem. 2015, 63, 1664−1672

histopathological evaluation. Tissues were embedded in paraffin, sectioned at a 5 μm thickness, and stained with hematoxylin and eosin.

Ethical Animal Use. Blood sampling for diagnostic purpose was performed by the farm veterinarian in compliance with the Animal Disease Order, Article 11, 1985.[25] Cattle slaughtering was performed according to the Israeli Livestock Slaughter Regulations, Article 30, 1964.[26]

Statistical Analysis. The results of the blood tests were analyzed for differences between healthy (standard reference values) (Table 2) and intoxicated cows by Student's t test, with a level of significance of $p < 0.05$. The biochemical values of the healthy mixed breed cattle were provided by the Veterinarian Hospital, The Hebrew University, Beit-Dagan, Israel. The biochemical reference values were determined from dozens of healthy mixed-breed cattle over a time period of 5 years, weighting 300−400 kg.

Table 2. Serum Biochemical Markers of Intoxicated Mixed-Breed Beef Cattle in Comparison to Reference Values of Healthy Mixed-Breed Beef Cattle of the Same Age

biochemical marker[a]	mean (range) values of intoxicated cows	blood values outside the normal range[b] (%)	mean (range) values of healthy cows
AST	180 (68−811) U/L[c]	48	75 (45−110) U/L
CK	749 (124−4128) U/L[c]	100	57 (14−107) U/L
GGT	58 (17−232) U/L[c]	70	12 (5−25) U/L
ALP	224 (51−439) U/L[c]	62	80 (17−152) U/L
albumin	3.2 (2.3−4.5) g/dL	33	2.9 (2.5−4) g/dL
total protein	8 (6.1−10.7) g/dL	62.5	6.8 (6−8) g/dL
globulin	5.3 (2.7−6.6) g/dL	66	3.6 (3−5) g/dL
urea	13 (6−28) mg/dL	18.7	15 (8−24) mg/dL
Ca^{2+}	9 (8−10.7) mg/dL	12.5	10.2 (8−11) mg/dL
phosphate	6.9 (3−9.5) mg/dL	37.5	5.6 (4−7) mg/dL
Mg^{2+}	2.4 (2−3.6) mg/dL	13	2.3 (1.7−3) mg/dL

[a]AST = aspartate aminotransferase, CK = creatinine kinase, GGT = γ-glutamyl transferase, and ALP = alkaline phosphatase. [b]The percent values are related to the number of cattle being outside the normal range. [c]Mean enzyme activity values of healthy vs intoxicated cows are significantly different according to the Student's t test ($p < 0.05$).

RESULTS

Necropsy and Gross Pathology. Necropsy was performed on three cows that were found dead 7−9 d after being allocated to a nearby grazing field free of any visible *Heliotropium* weeds. The findings in the three dead cows were consistent. Pathological abnormalities were mostly confined to the liver, which was pale-yellowish, firm, and smaller than normal, with fibrotic streaks in most cases (Figure 3). Furthermore, mild to moderate ascites and mesenteric edema were observed. The kidneys were mildly congested but retained normal architecture. The rest of the necropsy revealed no gross abnormalities within the rest of the body.

Histopathology. Histopathological examination of the livers revealed similar changes in all animals, with hyperplasia of bile ductulus and prominent periportal fibrosis. Megalocytosis was not consistently seen in all liver samples. Cirrhosis was observed in all livers, with fibroblasts infiltrating the liver parenchyma (Figure 4). Nodules of regeneration of hepatocytes were also recorded. No pathological changes were observed in the other organs examined.

Blood Analysis. Biochemical tests of blood samples collected from 27 live cows during the mortality event revealed extraordinarily high CK levels in all animals tested (125−4128 U/L), whereas the enzyme activities for AST (68−811 U/L), GGT (17−232 U/L), and ALP (51−439 U/L) were significantly elevated in more than 47% of all animals examined (Table 2). Serum urea, Ca^{2+}, Mg^{2+}, phosphate, albumin, total protein, and globulin were within the normal range (Table 2). Blood hemoglobin, hematocrit, red blood-cell count (RBC),

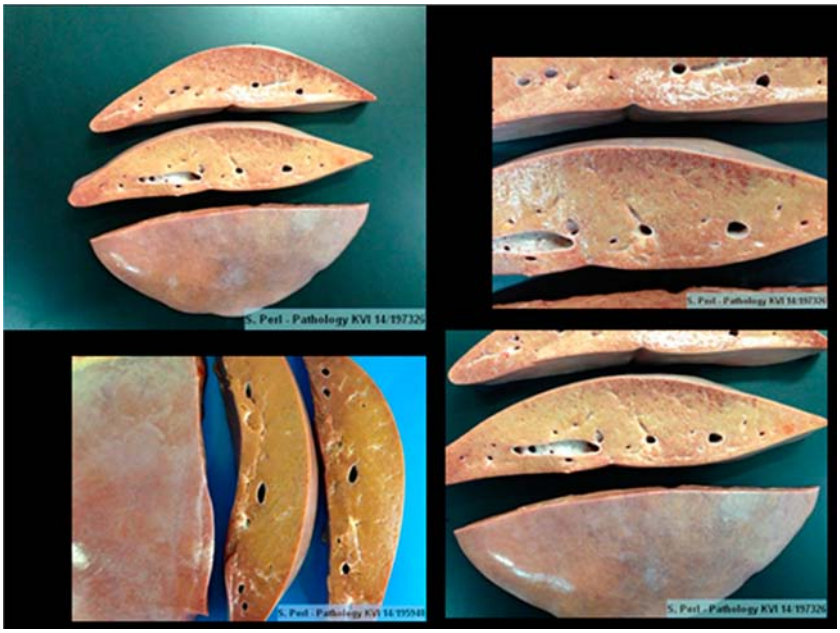

Figure 3. Macroscopic depiction of a liver of mixed-breed cattle (15 months old) following chronic PA toxicity due to *H. europaeum* ingestion. Depicted is a pale-yellowish, firm liver with diffuse fibrosis.

DOI: 10.1021/jf5052199
J. Agric. Food Chem. 2015, 63, 1664−1672

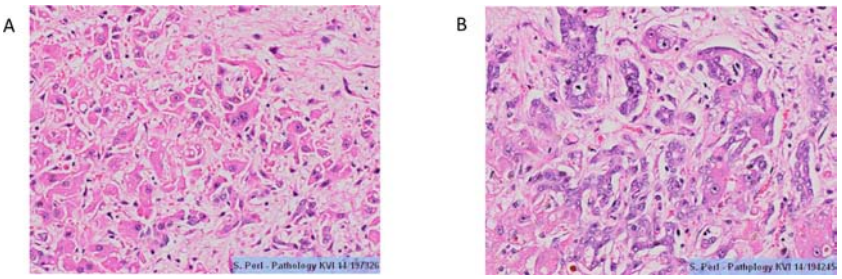

Figure 4. Histopathological liver sample of mixed-breed cattle (15 months old) following chronic PA toxicity due to *H. europaeum* ingestion (A) revealing extensive hepatocellular necrosis and moderate megalocytosis and fibrosis and (B) extensive biliary epithelial hyperplasia (paraffin embedded, hematoxylin and eosin stained, ×100).

Table 3. Total PA Profile of Hay Contaminated with *H. europaeum* in Comparison to the Total PA Profile of Aerial Plant Parts of *H. europaeum*

pyrrolizidine alkaloid-type classification[a]	pyrrolizidine alkaloid[b]	contaminated hay (μg/g dry wt)[c]	*H. europaeum* (μg/g dry wt)
supinine-type (**1**)	supinine	0.5 ± 0.2	10.5 ± 6.9
	supinine-*N*-oxide	9.4 ± 0.7	66 ± 24
	heleurine	1.4 ± 0.1	35 ± 10
	heleurine-*N*-oxide	75 ± 20	540 ± 100
heliotrine-type (**2**)	heliotrine (**4**)	170 ± 45	1180 ± 290
	europine (**5**)	90 ± 33	830 ± 470
	heliotrine-*N*-oxide (**7**)	950 ± 54	9340 ± 1050
	europine-*N*-oxide (**8**)	990 ± 210	9680 ± 3400
	rinderine (**10**)	1.5 ± 0.8	8.4 ± 4.4
	5′-hydroxyrinderine[d] (**11**)	1.4 ± 0.8	6.0 ± 2.6
	3′-acetylrinderine[d] (**12**)	0.2 ± 0.1	0.6 ± 0.3
	rinderine-*N*-oxide (**13**)	31 ± 16	260 ± 110
	5′-hydroxyrinderine-*N*-oxide[d] (**14**)	17.1 ± 0.4	100 ± 74
	3′-acetylrinderine-*N*-oxide[d] (**15**)	0.5 ± 0.4	3.6 ± 2.5
	5′-acetyleuropine	1.6 ± 0.9	11.4 ± 3.1
	5′-acetyleuropine-*N*-oxide	60 ± 20	760 ± 250
	echinatine-*N*-oxide	5.9 ± 2.5	37 ± 13
lasiocarpine-type (**3**)	7-angeloylheliotrine-*N*-oxide	4.4 ± 0.7	9.1 ± 7.0
	lasiocarpine (**6**)	56 ± 5	240 ± 200
	lasiocarpine-*N*-oxide (**9**)	715 ± 43	3800 ± 1740
	iso-lasiocarpine[d]	4.9 ± 1.1	18 ± 21
	iso-lasiocarpine-*N*-oxide[d]	51 ± 1	180 ± 190
	5′-acetyllasiocarpine	3.8 ± 0.0	22 ± 15
	5′-acetyllasiocarpine-*N*-oxide	100 ± 10	440 ± 270
	iso-acetyllasiocarpine[d]	0.4 ± 0.1	1.9 ± 2.1
	iso-acetyllasiocarpine-*N*-oxide[d]	9.7 ± 0.8	41 ± 42
	heliosupine (**16**)	1.1 ± 0.2	8.3 ± 4.1
	3′-acetylheliosupine (**17**)	0.3 ± 0.1	1.6 ± 1.6
	heliosupine-*N*-oxide (**18**)	10.7 ± 1.6	92 ± 52
	3′-acetylheliosupine-*N*-oxide (**19**)	4.1 ± 0.2	13.8 ± 8.1
total PA content		3370 ± 410	27700 ± 5900
% PA bases		9.8 ± 1.4	8.4 ± 1.4
% PA-*N*-oxides		90.2 ± 1.4	91.6 ± 1.4
% supinine-type		2.5 ± 0.2	2.3 ± 0.4
% heliotrine-type		68.8 ± 3.0	80.0 ± 7.9
% lasiocarpine-type		28.7 ± 2.2	17.7 ± 7.7

[a]Classification according to the PA necine base and the number and type of esterifying necic acids (Figure 1). [b]The chemical structure of the PAs without a bold compound number can be found in ref 5. [c]*n* = 3. [d]Tentative identification. The prefix iso indicates the presence of a structural isomer (e.g., 7-tigloyl or 7-senecioyl) instead of the 7-angeloyl ester moiety.

packed cell volume (PCV), and white blood cell count (WBC) were within normal limits.

Liver Analysis for Trace Elements. The elements analyzed in the liver samples by ICP-AES (As, Cd, Co, Zn, Cu, Fe, Pb, Mn, Hg, Mo, Se, Tl, and Zn) were within the normal limits.[27]

Bacteriology and Virology. No pathogenic bacteria (aerobic, anaerobic and *Salmonella*, *Clostridium*) and viruses of epidemiological significance were detected in the tissues examined.

Feed Analysis. The feed ingredients were concomitantly analyzed for ionophores, tetracycline antibiotics, pesticides, and aflatoxins. Only ionophore and tetracyclines, approved by the Ministry of Agriculture for use in farm animals, were included in the analysis.[19] The antibiotics and ionophores analyzed by LC−MS/MS were below the detection limit of 60 μg/kg. The feed ingredients analyzed for aflatoxins by HPLC-FLD were below the limit of quantitation (1 μg/kg).

Our routine qualitative multiresidue screening analysis utilizing GC−MS of the TMR ingredients did not reveal any pesticide contamination. However, in the hay samples analyzed, GC−MS clearly indicated the presence of three PAs, heliotrine (**4**), europine (**5**), and lasiocarpine (**6**). Hay inspection by the Department of Toxicology and by a certified botanist revealed the presence of aerial parts of dried *H. europaeum*, and therefore, a subsequent qualitative and quantitative PAs analysis of the contaminated hay samples together with the aerial parts

DOI: 10.1021/jf5052199
J. Agric. Food Chem. 2015, 63, 1664−1672

of *H. europaeum* collected in the fields used for the aforementioned hay harvest was carried out by LC−MS/MS.

The PA and PA-*N*-oxide composition and relative concentrations of the individual PAs in the contaminated hay and in *H. europaeum* overlapped strongly, yielding in both sample types 30 structurally different PAs [16 *N*-oxides and 14 tertiary amines containing supinidine (**1**) and heliotridine (**2**) as necine bases; see Table 3 and Figure 1]. PAs containing a heliotridine necine base (**2**) were classified into two subtypes, according to the number of esterifying necic acids [monoester heliotrine-type PAs (**4**) and diester lasiocarpine-type PAs (**6**); Figure 1]. The total PA content in the contaminated hay was 3.4 mg/g dried hay, while the aerial plant parts of *H. europaeum* contained 27.7 mg PA/g dried plant (Table 3). The most abundant tertiary PA bases found in *H. europaeum* and the contaminated hay were heliotrine (**4**) (170 and 1180 μg/g, respectively), followed by europine (**5**) (90 and 830 μg/g, respectively) and lasiocarpine (**6**) (56 and 240 μg/g, respectively) (Table 3). The PA-*N*-oxides constituted the major part of the total PA composition in the hay and in *H. europaeum* (90 and 91%, respectively), with heliotrine-*N*-oxide (**7**) and europine-*N*-oxide (**8**) being the most prevalent *N*-oxides (28−29% and 33−34%, respectively), followed by lasiocarpine-*N*-oxide (**9**) (21% and 13.6%, respectively) (Table 3).

The LC−MS/MS analysis of *H. europaeum* revealed the presence of trace amounts of 10 PAs containing rinderine (**10**−**15**) and heliosupine structures (**16**−**19**) (Figure 1). Putative assignments were made on the basis of retention time, protonated precursor mass, fragmentation behavior (such as the loss of characteristic fragments), the oxidation state of the nitrogen atom; and comparison with literature data and with additional plant extracts available at RIKILT. In this way, rinderine (**10**), 5′-hydroxyrinderine (**11**), 3′-acetylrinderine (**12**), rinderine-*N*-oxide (**13**), 5′-hydroxyrinderine-*N*-oxide (**14**), 3′-acetylrinderine-*N*-oxide (**15**), heliosupine (**16**), 3′-acetylheliosupine (**17**), heliosupine-*N*-oxide (**18**), and 3′-acetylheliosupine-*N*-oxide (**19**) could be identified (Figure 1 and Table 3). The supinidine-type PAs (**1**) exhibited low abundances in both the hay and the *H. europaeum* samples (Table 3).

DISCUSSION

Chronic PA poisoning of cattle in Israel due to consumption of hay contaminated with *H. europaeum* was first reported about 30 years ago.[9] The clinical manifestations and histopathological findings were similar to those described previously.[9] In general, the clinical manifestation of PA toxicosis is not pathognomonic and might have been indicative of aflatoxicosis, lead poisoning, or rabies. Rabies was eliminated by examination of brain slices, and lead poisoning was ruled out by liver lead determination; neither latter poisonings are associated with characteristic liver lesions. Aflatoxicosis, which in cattle often displays histopathological signs similar to those of PA toxicosis, was ruled out by the results of the feed analysis by HPLC-FLD. Routine bacteriological examinations eliminated possible causative infective bacteria, while chemical analysis of TMR ingredients excluded the involvement of common causes of poisoning previously reported in Israel (organophosphorus, carbamate, organochlorine pesticides). However, the inspection of the TMR ingredients by GC−MS led to the identification of three PAs in the hay: heliotrine (**4**), europine (**5**), and lasiocarpine (**6**). The discovery of PAs in the hay led us to examine the suspected hay, eventually revealing the presence of *H. europaeum*. Subsequent analysis of the contaminated hay and native *H. europaeum* by LC−MS/MS resulted in the identification of 30 different PA and PA-*N*-oxides, at a total level of 3.4 mg/g dry weight in the hay (Table 3).

In the literature there have been a number of descriptions of the histopathological changes of PA toxicosis, among which megalocytosis was often stated to be pathognomonic. However, the histopathological results of the present study indicate that megalocytosis was not a prominent and consistent feature, appearing only in one liver specimen and at a very low intensity, in agreement with the experimental trial results on cattle published previously.[17,28] The differences reported regarding the prominence of megalocytosis might arise due to intra- and interspecies variation in PA composition and duration of exposure, as well as varying degrees of susceptibility to PA toxicities among different cattle breeds. From the results of this study together with previous studies, the inconsistent appearance of megalocytosis in a biopsy specimen does not rule out PA toxicosis in a clinical situation.[17,28]

Measurement of specific serum enzyme activities, in conjunction with markers of renal activity and complete blood count, is a very useful tool in the diagnosis of hepatobilliary injury due to hepatotoxic xenobiotics such as PAs and aflatoxins. Concomitant increases of ALP with GGT raises the suspicion of hepatobilliary disease, as was demonstrated in more than 70% of all cows tested in the present study ($n = 27$) (Table 2). Elevated serum GGT activity can be found in liver, biliary system, and pancreas disorders. In this respect, it is similar to ALP in indicating biliary tract diseases. The main value of GGT over ALP is in verifying that ALP elevations are due to biliary disease, as ALP may increase in certain bone diseases, while GGT does not.[17] Increased AST activity in the serum is indicative of liver damage; however, in the present study only 48% of all examined cows revealed values above the normal AST range (Table 2); hence, according to the results presented herein, GGT and ALT are potentially more sensitive biomarkers for hepatobilliary injury due to PA toxicity.

CK is generally very useful in diagnosing skeletal or cardiac muscle degeneration.[17] In all examined cows, CK levels were substantially above the normal range over a time period of 63 d, indicating muscle trauma, most probably due to prolonged recumbancy, as histologically no marked myocardial damage was observed (Table 2).

Measuring serum GGT and ALP as diagnostic enzymes could be useful as a first screening test in suspected cases of PA toxicosis.[17] These enzymes, together with a histopathological examination of the liver, provide important information in diagnosing lethal exposure to hepatotoxic compounds such as PAs or aflatoxins. However, a differentiation between various hepatotoxic xenobiotics is only possible by direct determination of the noxious compound and/or its metabolites in the feed and/or organ tissues, such as the liver. The main obstacle in establishing a diagnosis of PA or aflatoxin intoxication is that in both cases the clinical symptoms and sudden death occur weeks or several months after chronic exposure, depending on the exposure level and animal species, age, and sex, so that often no samples of contaminated feed are available for chemical analysis.[9,29] Moreover, since PAs and aflatoxins are quickly metabolized to their corresponding reactive intermediates, the ability even of highly sensitive instruments such as LC−MS/MS to identify parent compounds as well as major metabolites

DOI: 10.1021/jf5052199
J. Agric. Food Chem. 2015, 63, 1664−1672

thereof diminishes rapidly within a few days.[12,30] On the other hand, protein and/or DNA adducts of PAs and aflatoxins have far longer tissue half-lives and therefore are currently the most promising biomarkers for establishing a conclusive diagnosis, even after several months of washout period.[12]

The average feed intake of 15−18-month-old mixed-breed cattle weighting 350 kg was estimated to be 7 kg feed/d, hence 20 g feed/d/kg body weight (BW). Taking into account an average total PA content of 3.4 mg/g hay and a dilution ratio of 1:2 with the other feed ingredients, the total mean PA intake leading to the observed high mortality rate and clinical and pathological signs was 34 mg/kg BW/d. This value is about twice as high as the lethal doses (15 mg PAs/kg BW/d) given as dried *Senecio jacobaea* for 14 d to four lactating cows and administered for 20 d to three calves in the form of dried *Senecio riddellii* (17 mg PAs/kg BW/d).[11,31] LD_{50} values reported for various PAs vary widely, but macrocyclic and diester PAs tend to be somewhat more toxic than monoester PAs.[5]

Careful inspection of weed species likely to thrive in pastures and meadows under certain environmental conditions, such as drought, could prevent future cases of PA intoxications both in livestock and humans. An inspection protocol must include collection and retention specimens of the suspected feed and feed analysis, preferably by utilizing highly sensitive instruments such as GC−MS or LC−MS/MS. Furthermore, the establishment of a future database of MS spectra and corresponding retention times together with the availability of sufficient PAs standards would facilitate rapid diagnosis.

To the best of our knowledge, this is the first study utilizing LC−MS/MS for qualitative and quantitative analysis of the PA content in *H. europaeum*. The high sensitivity of the LC−MS/MS analysis utilized for the determination of the PA and PA-*N*-oxide composition in the contaminated hay, as well as the possibility of measuring both forms of PAs simultaneously and the ease of sample preparation, enabled us to markedly expand the known PA profile of *H. europaeum* from 12 to 30 different PA and PA-*N*-oxides (Table 3).[3] A total of 10 PAs of the rinderine and heliosupine classes are reported for the first time to be present in this species. To the best of our knowledge, PAs derivatives of rinderine (**10**−**16**, Figure 1) and heliosupine (**16**−**19**, Figure 1) have so far been reported only in *Heliotropium indicum*, *Heliotropium peruvianum*, *Heliotropium transalpinum*, and *Heliotropium supinum*.[3] The definite assignment of the rinderine derivatives could not be made, because the obtained mass fragmentation spectra do not exclude the presence of echinatine structures. However, on the basis of the fact that (+)-trachelanthic acid, the necic acid in rinderine, has the same stereochemistry as heliotric acid, the necic acid in heliotrine, its presence was considered more likely than the echinatine structure, which is esterified with (−)-viridifloric acid and for which no heliotrine counterpart is known.

Utilizing LC−MS/MS analysis techniques is expected to expand substantially the PA composition of known PA-producing plants.[33]

In agreement with previous studies, the most abundant PAs found in *H. europaeum* were heliotrine (**4**), europine (**5**), and lasiocarpine (**6**).[3,32] In the investigated *H. europaeum*, the total PA level was 2.7%, being comparable to the levels found in *H. europaeum* grown in southeastern Australia at the same flowering stage.[34]

The total PA profiles of *H. europaeum* and of the contaminated hay strongly overlapped in terms of composition and relative abundance, with heliotrine-*N*-oxide (**7**) and europine-*N*-oxide (**8**) being the most abundant alkaloids in both samples (Table 3). This finding suggests that a selection of abundant PA and PA-*N*-oxides may be used as a fast and reliable tool for species identification.

In conclusion, a mortality rate of 33% in mixed-breed cattle was recorded, following ingestion of TMR contaminated with *H. europaeum* at a level of 12% dry weight. The toxicosis event was characterized by typical clinical and histopathological signs of PA toxicosis. LC−MS/MS analysis of the PA and PA-*N*-oxide profile in *H. europaeum* enabled a comprehensive composition determination, including 10 PAs of the rinderine and heliosupine classes reported for the first time in *H. europaeum*.

■ ASSOCIATED CONTENT

Ⓢ Supporting Information

Blood parameters from intoxicated mixed-breed beef cattle (Table S1) and additional information about the elemental composition, molecular weight, and chemical structures of PAs determined in the present study (Table S2). This material is available free of charge via the Internet at http://pubs.acs.org.

■ AUTHOR INFORMATION

Corresponding Author

*Tel. +972-3-9688911. E-mail: jakobshimshoni@gmail.com. Fax: +972-3-9681730.

Notes

The authors declare no competing financial interest.

■ ACKNOWLEDGMENTS

We gratefully thank Dr. Yotam Zipper at the Hebrew University of Jerusalem, for the assistance in determining the *Heliotropium* species. The authors thank Mr. Yossi Hofi and David Ochana, for their excellent technical assistance.

■ REFERENCES

(1) Bull, L. B.; Culvenor, C. C. J.; Dick, A. T. The pyrrolizidine alkaloids: Their chemistry, pathogenicity and other biological properties. In *Frontiers of Biology Series*; North-Holland Publishing Co.: Amsterdam, 1968.

(2) Mattocks, A. R. *Chemistry and Toxicology of Pyrrolizidine Alkaloids*; Academic Press: London, 1986.

(3) El-Shazly, A.; Wink, M. Diversity of pyrrolizidine alkaloids in the Boraginaceae structures, distribution and biological properties. *Diversity* **2014**, *6*, 188−282.

(4) Rizk, A. M. *Naturally Occurring Pyrrolizidine Alkaloids*; CRC Press: Boca Raton, FL, 1991; p 234.

(5) EFSA Panel on Contaminants in the Food Chain (CONTAM). Scientific opinion on pyrrolizidine alkaloids in food and feed. *EFSA J.* **2011**, *9*, 2406. Available online: http://www.efsa.europa.eu/en/efsajournal/doc/2406.pdf.

(6) Zohary, M. *Plant Life of Palestine: Israel and Jordan*; Ronald Press: New York, 1962.

(7) Hill, B. D.; Gaul, K. L.; Noble, J. W. Poisoning of feedlot cattle by seeds of *Heliotropium europaeum*. *Aust. Vet. J.* **1997**, *75*, 360−361.

(8) Harper, P. A. W.; Krahenbuhl, R. E.; Christie, B. M. Pyrrolizidine alkaloid poisoning in calves due to contamination of straw by *Heliotropium europaeum*. *Aust. Vet. J.* **1985**, *62*, 382−383.

(9) Shlosberg, A.; Egyed, M. N.; Nobel, T. A.; Klopfer, U.; Perl, S.; Yakobson, B. First cases in Israel of chronic poisoning in calves caused by ingestion of *Heliotropium europaeum*. *Refuah Vet.* **1981**, *38*, 80−88.

(10) Kakar, F.; Akbarian, Z.; Leslie, T.; Mustafa, M. L.; Watson, J.; van Egmond, H. P.; Omar, M. F.; Mofleh, J. An outbreak of hepatic veno-occlusive disease in Western Afghanistan associated with

DOI: 10.1021/jf5052199
J. Agric. Food Chem. 2015, 63, 1664−1672

exposure to wheat flour contaminated with pyrrolizidine alkaloids. *J. Toxicol.* **2010**, *2010*, 1−7.
(11) Molyneux, R. J.; Gardner, D. L.; Colegate, S. M.; Edgar, J. A. Pyrrolizidine alkaloid toxicity in livestock: A paradigm for human poisoning? *Food Addit. Contam. Part A* **2011**, *28*, 293−307.
(12) Ruan, J.; Yang, M.; Fu, P.; Ye, Y.; Lin, G. Metabolic activation of pyrrolizidine alkaloids: Insights into the structural and enzymatic basis. *Chem. Res. Toxicol.* **2014**, *27*, 1030−1039.
(13) Fu, P.; Xia, Q.; Lin, G.; Chou, M. W. Pyrrolizidine alkaloids—Genotoxicity, metabolism enzymes, metabolic activation and mechanisms. *Drug Metab. Rev.* **2004**, *36*, 1−55.
(14) Schmeller, T.; El-Shazly, A.; Wink, M. Allelochemical activities of pyrrolizidine alkaloids: Interactions with neuroreceptors and acetylcholine related enzymes. *J. Chem. Ecol.* **1997**, *23*, 399−416.
(15) Gardner, D. R.; Thorne, M. S.; Molyneux, R. J.; Pfister, J. A.; Seawright, A. A. Pyrrolizidine alkaloids in *Senecio madagascariensis* from Australia and Hawaii and assessment of possible livestock poisoning. *Biochem. System. Ecol.* **2006**, *34*, 736−744.
(16) Molyneux, R. J.; Johnson, E. A.; Stuart, L. D. Delayed manifestation of *Senecio*-induced pyrrolizidine alkaloidosis in cattle: Case reports. *Vet. Hum. Toxicol.* **1988**, *30*, 201−205.
(17) Craig, A. M.; Pearson, E. G.; Meyer, C.; Schmitz, J. A. Serum liver enzyme and histopathologic changes in calves with chronic and chronic-delayed *Senecio jacobaea* toxicosis. *Am. J. Vet. Res.* **1991**, *52*, 1969−1978.
(18) Shimshoni, J. A.; Evgeny, E.; Lublin, A.; Cuneah, O.; King, R.; Horowitz, I.; Shlosberg, A. Determination of brain choline esterase activity in normal and pesticide exposed wild birds. *Isr. J. Vet. Med.* **2012**, *67*, 214−219.
(19) Shimshoni, J. A.; Britzi, M.; Pozzi, S. P.; Edery, N.; Berkowitz, A.; Bouznach, A.; Cuneah, O.; Soback, S.; Bellaiche, M.; Younis, A.; Blech, E.; Oren, P.; Galon, N.; Shlosberg, A.; Perl, S. Acute maduramicin toxicosis in pregnant gilts. *Food Chem. Toxicol.* **2014**, *68*, 283−389.
(20) EPA method, 6010c. http://www.epa.gov/osw/hazard/testmethods/sw846/pdfs/6010c.pdf (accessed on October 14, 2014).
(21) Cheng, D. D.; Kirk, H.; Mulder, P. P. J.; Vrieling, K.; Klinkhamer, P. G. L. Pyrrolizidine alkaloid variation in shoots and roots of segregating hybrids between *Jacobaea vulgaris* and *Jacobaea aquatica*. *New Phytol.* **2011**, *192*, 1010−1023.
(22) Rahman, A.; Jinap, S. Validation of the procedure for the simultaneous determination of aflatoxins ochratoxin A and zearalenone in cereals using HPLC-FLD. *Food Addit. Contam. Part A* **2010**, *24*, 1683−1693.
(23) Elad, D.; Yas-Natan, E.; Aroch, I.; Shamir, M. H.; Kleinbart, S.; Hadash, D.; Chaffer, M.; Greenberg, K.; Shlosberg, A. Natural *Clostridium botulinum* type C toxicosis in a group of cats. *J. Clin. Microbiol.* **2004**, *42*, 5406−5408.
(24) David, D.; Yakobson, B.; Rotenberg, D.; Dveres, N.; Davidson, I.; Stram, Y. Rabies virus detection by RT-PCR in decomposed naturally infected brains. *Vet. Microbiol.* **2002**, *87*, 111−118.
(25) Animal Disease Order, Article 11, 1985. http://www.sviva.gov.il/InfoServices/ReservoirInfo/DocLib/%D7%98%D7%91%D7%A2/teva40.pdf (accessed on October 14, 2014).
(26) Israeli Livestock Slaughter Regulations, Article 30, 1964. http://www.sviva.gov.il/InfoServices/ReservoirInfo/DocLib/%D7%98%D7%91%D7%A2/teva68.pdf (accessed on October 14, 2014).
(27) Puls, R. *Mineral Levels in Animal Health. Diagnostic Data*, 2nd ed.; Sherpa International: Aldergrove, Canada, 1994.
(28) Johnson, A. E. Tolerance of cattle to tansy ragwort (*Senecio jacobaea*). *Am. J. Vet. Res.* **1978**, *39*, 1542−1544.
(29) McLennan, M. W.; Dodson, M. E. *Heliotropium* poisoning in cattle. *Aust. Vet. J.* **1972**, *48*, 480.
(30) Hoogenboom, L. A. P.; Mulder, P. P. J.; Zeilmaker, M. J.; Top, H. J.; van den Remmelink, G. J.; Brandon, E. F. A.; Klijnstra, M.; Meijer, G. A. L.; Schothorst, R.; van Egmond, H. P. Carry-over of pyrrolizidine alkaloids from feed to milk in dairy cows. *Food Addit. Contam. Part A* **2011**, *28*, 359−372.
(31) Dickinson, J. O.; Cooke, M. P.; King, R. R.; Mohamed, P. A. Milk transfer of pyrrolizidine alkaloids in cattle. *J. Am. Vet. Med. Assoc.* **1976**, *169*, 1192−1196.
(32) Crowley, H. C.; Culvenor, C. C. J. Alkaloid assays of *Heliotropium europaeum* L. *Aust J. Appl. Sci.* **1956**, *7*, 359−364.
(33) Crews, C.; Berthiller, F.; Krska, R. Update on analytical methods for toxic pyrrolizidine alkaloids. *Anal. Bioanal. Chem.* **2010**, *396*, 327−338.
(34) O'Dowd, D. J.; Edgar, J. A. Seasonal dynamics in the pyrrolizidine alkaloids of *Heliotropium europaeum*. *Aust. J. Ecol.* **1989**, *14*, 95−105.

DOI: 10.1021/jf5052199
J. Agric. Food Chem. 2015, 63, 1664−1672

The aim of this study was to evaluate the influence of climatic variables such as temperature, solar radiation, relative humidity, and precipitation on the phenolic composition and color of three pigmented baby leaf lettuce varieties sampled during 16 consecutive weeks from February to May. In addition, possible color−anthocyanin composition relationships were studied by applying multivariate statistical analysis.

MATERIALS AND METHODS

Plant Material. Three pigmented baby leaf lettuces (*Lactuca sativa*), two Batavia cultivars (B1 and B2) and one red oak leaf (R), were cultivated under commercial conditions in Fuente Alamo (Murcia, Spain) by a commercial grower (Langmead, Murcia, Spain). The growing fields were located within an area of 20 km^2. The type of soil in the selected fields was mainly clay and clay loam. Sowing was performed directly from seeds on elevated beds using a density of 700 plants m^{-2}. Baby leaves at the commercial maturity stage (10−12 cm) were mechanically harvested during 16 consecutive weeks from February (week 5) to May (week 20) in 2012. Supplemental information regarding the dates of plantation and harvesting and the crop cycle schedule has been provided by Medina-Martínez et al.[24] After harvest, baby leaves were transported under refrigeration (approximately 35 km) to the CEBAS-CSIC laboratory (Murcia, Spain). On arrival, samples were characterized by measuring fresh weight, dry matter content, leaf area, and color, and the remaining leaves were frozen within 2 h of harvest and stored at −80 °C for the analysis. Twenty leaves per cultivar were characterized for fresh weight, dry matter content, leaf area, and color. Dry matter content was measured after drying the leaves in a ventilated oven at 70 °C until constant weight. Leaf area was measured by a horizontal photography and image treatment (ImageJ, Bethesda, MD, USA) of each leaf.

Color Measurements. Color was measured using a compact tristimulus colorimeter (Minolta CR-300, Ramsey, NJ, USA) with an 8 mm diameter viewing aperture. The parameters L^*, a^*, and b^* were used to calculate the hue angle $[\tan^{-1}(b^*/a^*)]$ and the chroma index $[(a^{*2} + b^{*2})^{1/2}]$. Hue angle was expressed on a 360° color wheel where 0° and 360° represents red, 90° represents yellow, 180° represents green, and 270° represents blue. Chroma indicates color purity or saturation (high values are more vivid).[25] Twenty leaves per cultivar and sampling date were measured.

Extraction, Identification, and Quantification of Phenolic Compounds. For the analysis of phenolic compounds, 100 g of leaves per cultivar were lyophilized. For the identification and characterization of phenolic compounds, 0.02 g of lyophilized leaf powder was extracted with 2 mL of methanol:water:formic acid (50:49:1,v/v) by sonication for 1 h. The resulting extract was centrifuged and filtered through a 0.45 PVDF filter. Chromatographic analyses were carried out on a Luna C18 100 Å column (150 × 1.0 mm, 3 μm particle size; Phenomenex, Macclesfield, U.K.). The mobile phase consisted of two solvents: water (1% formic acid) (A) and methanol (B). Elution was performed with a flow rate of 20 μL min^{-1} and an injection volume of 3 μL. The elution profile was as follows: gradient from 5 to 30% solvent B for 15 min, gradient from 30 to 50% solvent B for 15 min, isocratic solution 50% for 5 min, gradient from 50 to 60% solvent B for 1 min, gradient from 60 to 70% for 4 min, gradient from 70 to 90% solvent B for 5 min, and isocratic solution 90% for 5 min. Spectral data from all peaks were accumulated in the 200−400 nm range. Chromatograms were recorded at 320, 340, and 520 nm. The analyses were carried out by high-performance liquid chromatography (HPLC) coupled to diode array detection (DAD) and mass spectrometry (MS−MS) with an ion trap detector equipped with an electrospray ionisation interface (ESI). The HPLC−DAD−MS−MS/ESI analyses were carried out in an Agilent HPLC 1200 series (Agilent Technologies, Waldbronn, Germany) equipped with a binary pump (model G1376A), an autosampler (model G1377A) refrigerated at 4 °C (model G1330B), a degasser (model G1379B), and a photodiode array detector (model G1315D). The HPLC system was controlled by ChemStation software (Agilent, v. B.01.03-SR2). The mass detector was a Bruker ion trap spectrometer (model HCT Ultra) equipped with an electrospray ionization interface controlled by software (LCMSD, Agilent, v. 6.1). The ionization conditions were 300 °C and 4.0 kV for capillary temperature and voltage, respectively. The nebulizer pressure and flow rate of nitrogen were 5.0 psi and 3 L/min^{-1}, respectively. The full scan mass covered the range from m/z 100 up to m/z 1200, and the target mass was adjusted to m/z 350. Collision-induced fragmentation experiments were performed in the ion trap using helium as the collision gas, with voltage ramping cycles from 0.3 up to 2 V. Mass spectrometry data were acquired in the negative mode for phenolic acids and flavonoids and in the positive ionization mode for anthocyanins. MSn was carried out in the Selected Ion Monitoring (SIM) mode.

The identification of the peaks was carried out by the extracted-ion chromatograms of the ion current at m/z values corresponding to the $[M-H]^-$ ions of the individual investigated compounds, as well as their fragmentation. Quantification of the identified analytes was performed by HPLC-DAD using the external standard method with calibration graphs, as a function of concentration based on peak area, detected at the wavelength corresponding to the maximum absorbance (320 nm for phenolic acids, 360 nm for flavonoids, and 520 nm for anthocyanins). Phenolic acids were quantified as chlorogenic acid (5-*O*-caffeoylquinic acid) (Sigma, St Louis, MO, USA), flavonoids as quercetin-3-rutinoside (Sigma, St. Louis, MO, USA), and anthocyanins as cyanidin-3-glucoside (Polyphenols Laboratories AS Hanaveien, Sandnes, Norway). Three replicates per cultivar and sampling date were analyzed.

Climatic Variables. Climate data were obtained from the nearby Balsapintada climate station (37° 44′ 53,89″ N, 1° 7′ 45,14″ W) and El Campillo climate station (37° 41′ 56,52″ N, 1° 14′ 16,96″ W), located within 10 km of the fields, using the local climatological database.[26] Relevant climatic variables such as temperature, solar radiation, precipitation, and relative humidity were collected daily from the start to the end of the growing season. The climatic variables and their abbreviations are listed in Table 1.

Table 1. Climatic Variables Investigated and Their Abbreviations

abbreviations	climatic variable	units
Rw	radiation in the last week before harvest	MJ m^{-2}
Rgh	radiation from the start of the growing until harvest	MJ m^{-2}
Tw	temperature in the last week before harvest	°C
Tgh	temperature from the start of the growing until harvest	°C
T0w	hours with temperature below 0 °C in the last week before harvest	h
T0gh	hours with temperature below 0 °C from the start of the growing until harvest	h
T7w	temperature below 7 °C in last week before harvest	h
T7gh	hours with temperature below 7 °C from the start of the growing until harvest	h
RHw	humidity in last week before harvest	%
RHgh	humidity from the start of the growing until harvest	%
Pw	precipitation in last week before harvest	mm
Pgh	precipitation from the start of the growing until harvest	mm

Statistical Analysis. Two-way analysis of variance (ANOVA) was carried out to detect significant differences between cultivars and harvest weeks on the color and phenolic composition and content. Tukey's HSD test for the population with equal variances was used to carry out the multiple comparisons at $p < 0.05$. Principal component analysis (PCA) and Pearson's correlation coefficient analysis were carried out to study the influence of seasonal variability in the three pigmented baby leaf lettuces. Statistical analyses were performed using SPSS 20.0.0 (SPSS Inc., Chicago, IL, USA).

DOI: 10.1021/acs.jafc.5b00120
J. Agric. Food Chem. 2015, 63, 1673−1681

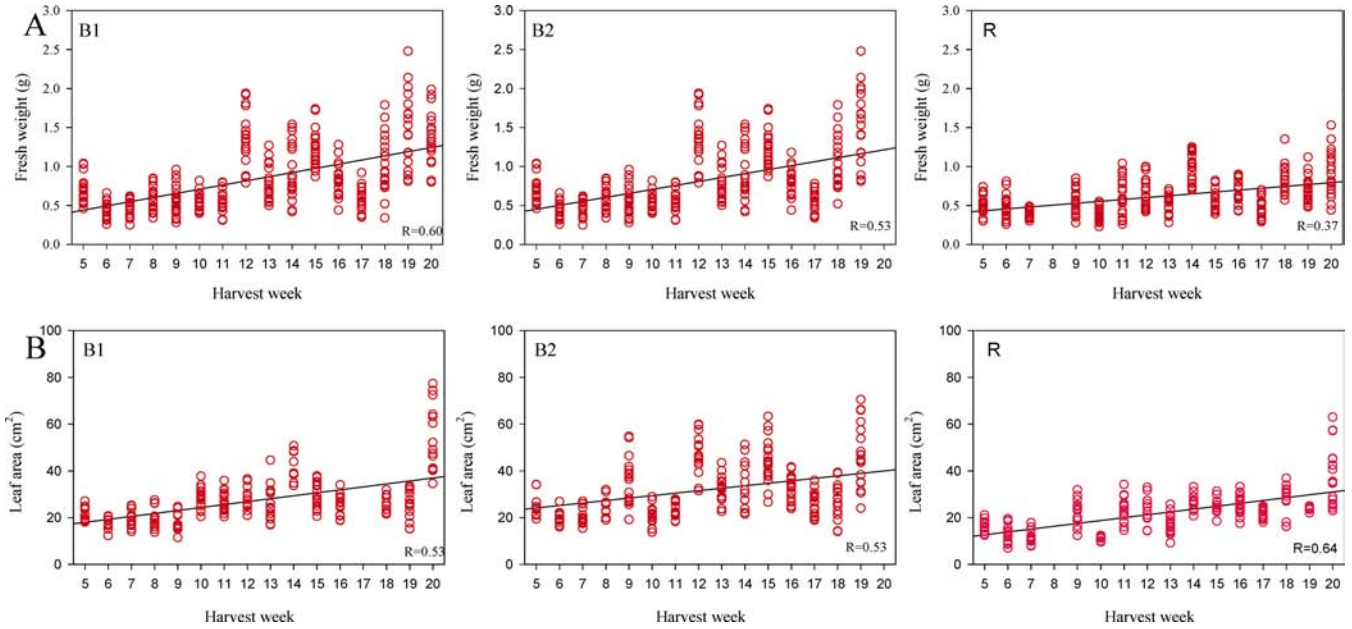

Figure 1. Scatter plots of growth parameters vs harvest week of baby leaf Batavia (B1 and B2) and red oak leaf (R) lettuces. (A) Fresh weight and (B) leaf area.

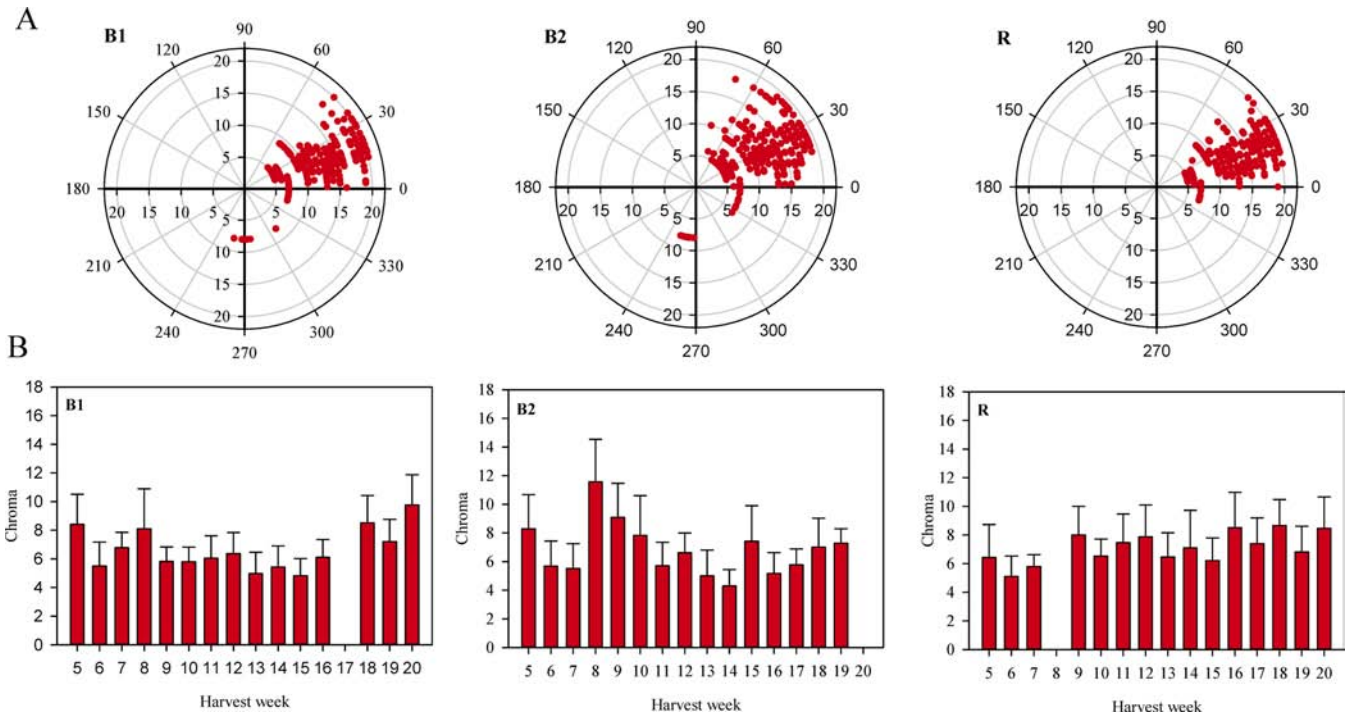

Figure 2. Hue angle vs harvest week (A) and chroma values vs harvest week (B) of baby leaf Batavia (B1 and B2) and red oak leaf (R) lettuces. In polar plot (A) 0° and 360° indicate red, 90° indicates yellow, 180° indicates green, and 270° indicates blue.

RESULTS

Effect of Seasonal Variability on Growth and Color Characteristics. Growth characteristics were significantly ($P \leq 0.001$) influenced by the cultivar and harvest week (Supporting Information, Table SI.1). In detail, the fresh weight and leaf area were higher in Batavia B2 (0.81 g and 32.27 cm^2), followed by Batavia B1 (0.72 g and 27.7 cm^2) and red oak leaf (0.67 g and 22.3 cm^2) (Figure 1). However, the fresh weight and leaf area increased slightly with harvest week for the three pigmented lettuce cultivars.

To determine which cultivar presented the reddest and most intense color, data of the three cultivars were combined and analyzed (Figure 2). Batavia B1 showed the lowest hue value (15.22°) followed by red oak leaf and Batavia B2, which had hue angles of 18.01° and 23.16°, respectively (Figure 2A). These data indicated that Batavia B1 showed the reddest color followed by red oak leaf and Batavia B2. The changes in the hue angle indicated the fluctuation with the growing season, and together with other genetic and agricultural implements, weather variability might be responsible for the lack in color

DOI: 10.1021/acs.jafc.5b00120
J. Agric. Food Chem. 2015, 63, 1673−1681

consistency as it was observed for the hue angle values of B1 and B2 for the harvest week 8. Regarding chroma values, red oak leaf showed the highest value (7.1) whereas Batavia B1 and B2 had the lowest values (6.6 and 6.7, respectively) with no significant differences between them (Figure 2B). With respect to the influence of harvest week on the hue angle, Batavia B1 and red oak leaf showed lower dispersion of hue angle values than Batavia B2 and therefore more homogeneous color throughout the season (Figure 2A). Moreover, Batavia B2 showed the highest chroma value for the harvest weeks 8 and 9 (Figure 2B).

Effect of Seasonal Variability on Individual Composition and Content of Phenolic Compounds. Figure 3 shows

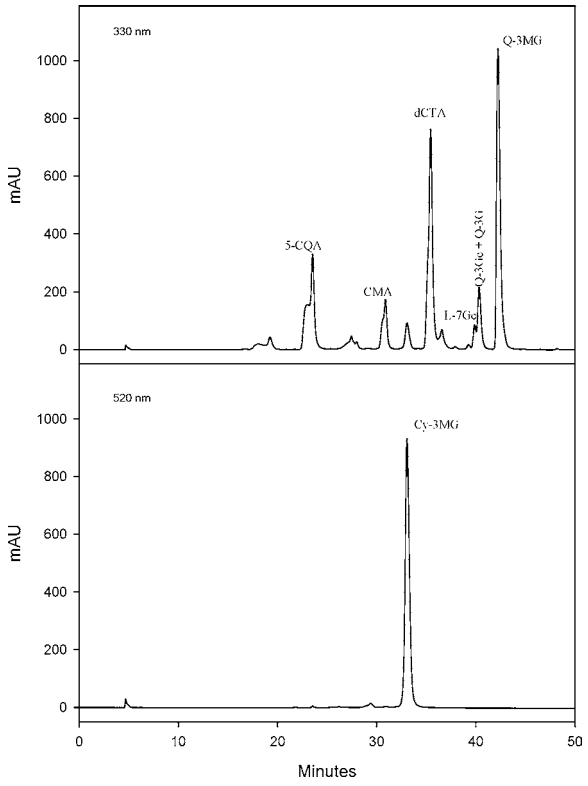

Figure 3. HPLC chromatograms of Batavia B1. Hydroxycinamics acids, flavonols, and flavone at 330 nm and anthocyanins at 520 nm. Abbreviations: Cy−3MG, cyanidin-3-*O*-(6″-*O*-malonyl)-glucoside; 5-CQA, 5-caffeoylquinic acid; CMA, caffeolylmalic acid; dCTA, dicaffeoyltartaric acid; L−7Gc, luteolin-3-*O*-glucuronide; Q−3Gc, quercetin-3-*O*-glucuronide; Q−3G, quercentin-3-*O*-glucoside; Q−3MG, quercetin-3-*O*-(6″-*O*-malonyl)-glucoside.

the HPLC chromatograms of Batavia B1 recorded at 330 and 520 nm. Identification of phenolic compounds was based on the chromatographic and mass spectral characteristics as well as the previous literature descriptions.[8] Three hydroxycinnamic acids were confirmed as 5-*O*-caffeoylquinic acid (5-CQA), *O*-caffeoylmalic acid (CMA), and di-*O*-caffeoyltartaric acid (dCTA), three quercetin glycosides (quercetin-3-*O*-glucuronide, quercetin-3-*O*-glucoside, and quercetin-3-*O*-(6″-malonyl)-glucoside), one luteolin glycoside (luteolin-7-*O*-glucuronide), and one cyanidin glycoside (cyanidin-3-*O*-(6″-malonyl)-glucoside). See legend of Figure 3 for abbreviations.

Throughout the season, the phenolic content was significantly ($P \leq 0.001$) influenced by cultivar and harvest week (Supporting Information, Table SI.1). Among the three pigmented lettuce cultivars, the same individual phenolic constituents were observed but with significant ($P \leq 0.001$) differences in their individual content (Supporting Information, Table SI.2). The flavonol Q−3MG was the main phenolic compound in the three cultivars, followed by Cy−3MG and the phenolic acids 5-CQA, dCTA, and CMA. The flavonols Q−3Gc and Q−3G coeluted and were quantified as the sum and the flavone L−7Gc was present at the lowest concentration. When the contents of the individual phenolic compounds for all the harvest weeks were combined, Batavia B1 and red oak leaf had similar but higher phenolic acid contents, except for CMA, than Batavia B2, which showed the highest phenolic acid content for dCTA (Supporting Information, Table SI.2).

To create an overview of the changes in the content of phenolic compounds with harvest week, the data of the three cultivars were combined and analyzed together (Figure 4). The three cultivars showed the same trend for phenolic acids throughout the season; the content of 5-CQA and dCTA increased while the content of CMA slightly decreased as the harvest week progressively advanced. Concerning flavonoids, Q−3MG showed marked differences between consecutive harvest weeks, particularly Batavia B2, but in general it increased as the growing season advanced. The content of Cy−3MG in Batavia cultivars was maintained or increased slightly throughout the season while this pigment tended to decrease slightly in red oak leaf (Figure 4).

Effects of Climatic Variables on Phenolic Compounds and Color. Principal component analysis (PCA) was conducted to give an overview of the impact of climatic variables on the content of phenolic compounds and color of the pigmented baby leaf lettuces (Figure 5). PCA resulted in five uncorrelated principal components (PC) for Batavia B1 and B2 and four PC for red oak leaf that accounted for 88.4, 90.2, and 85.6% of the total variability, respectively. Eigenvalues, loadings, and accumulated percentage of data variation of each PC are shown in Table SI.3 (Supporting Information). PC1 and PC2 explained 66.7, 67.1, and 64.1% of the variation in the content of phenolic compounds and color by climatic variables for B1, B2, and R cultivars, respectively. As it can be observed in Figure 5, phenolic compounds were located close to each other in the PCA plot arrangement and responded in a similar way to the changes in the climatic variables. PC1, which accounted for 45.6%, 47.7%, and 40.7% for B1, B2, and R cultivars, respectively, separated the different phenolic compounds by their sensitivity to the changes in temperature and radiation doses. PC2, which accounted for 20.8%, 19.4%, and 23.4% for B1, B2, and R cultivars, respectively, separated the different phenolic compounds by their sensitivity to the changes in humidity, precipitation, and the number of hours below 0 and 7 °C in the last week before harvest.

In addition to the general correlations observed via PCA analysis, correlations between climatic variables and individual phenolic compounds were also detected via Pearson's correlation coefficient analysis (Table 2). Batavia cultivars had similar correlations between climatic variables and individual phenolic compounds. Temperature and radiation during the growing cycle was positively correlated with Cy−3MG, 5-CQA, dCTA, L−7Gc, and Q−3MG (Table 2). However, a CMA showed higher correlation with the number of hours below 7 °C the week before harvest (correlation coefficients $r = 0.73$ and $r = 0.74$ for B1 and B2, respectively). In red oak leaf, the content of Cy−3MG showed a good correlation with the

DOI: 10.1021/acs.jafc.5b00120
J. Agric. Food Chem. 2015, 63, 1673−1681

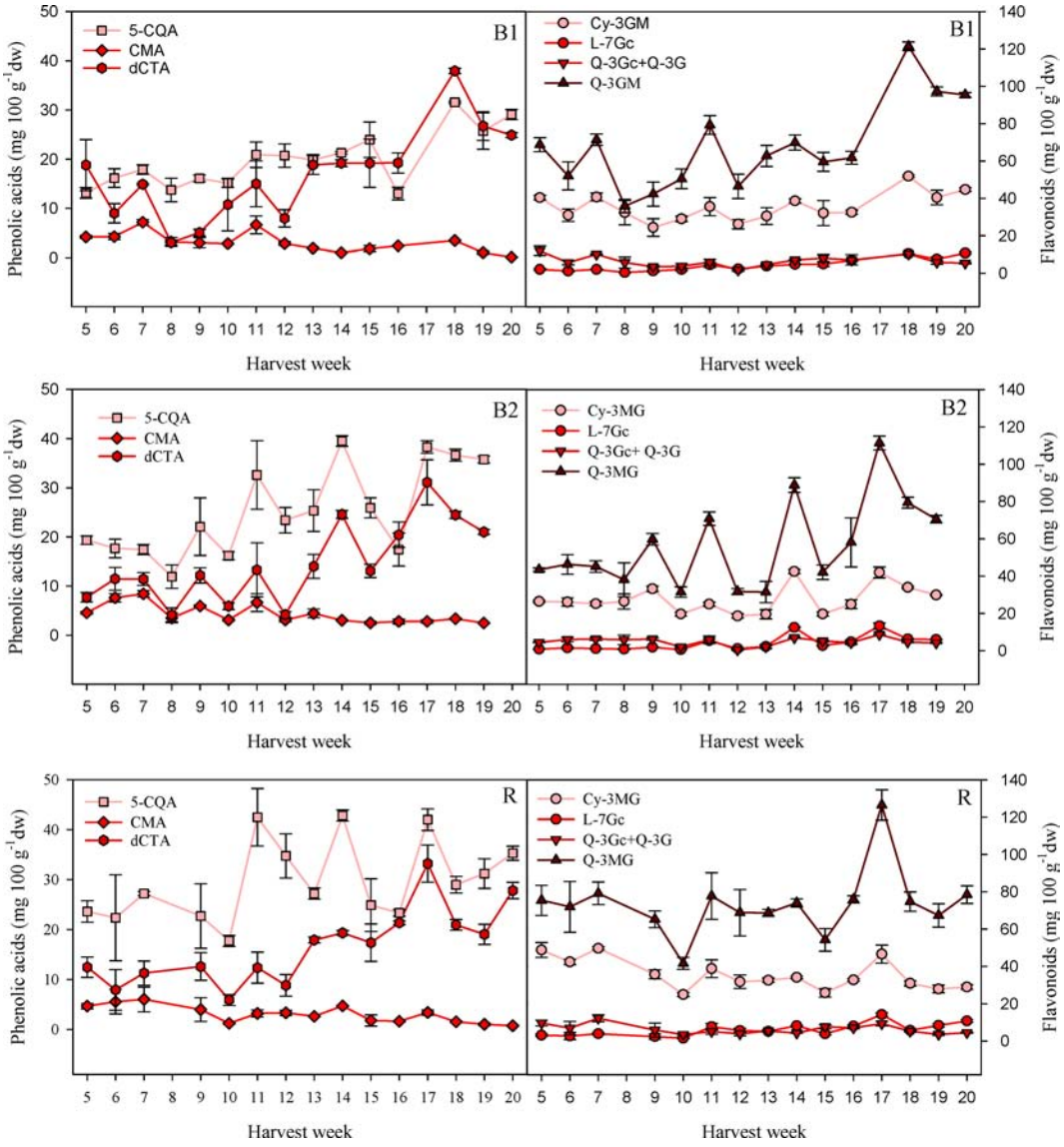

Figure 4. Phenolic compounds vs harvest week of baby leaf Batavia (B1 and B2) and red oak leaf (R) lettuces. Symbols represent the mean ± standard deviation of three replicates. See Figure 3 for abbreviations.

number of hours at a temperature below 0 and 7 °C (r = 0.50 and r = 0.62, respectively). At the end of the growing season, red oak leaf showed the lowest concentration of Cy−3MG. The same trend observed for the anthocyanin Cy−3MG was shown for CMA and the flavonols Q−3Gc + Q−3G (r = 0.44 and r = 0.59, respectively). With respect to the color, the hue angle was the parameter that best represented the color changes of these cultivars. PCA analysis showed that there was no correlation between anthocyanin content and hue angle in any of the cultivars studied (Figure 5). However, the hue angle was related with cold temperatures during the weeks before harvest and therefore showed the same trend as the CMA.

■ DISCUSSION

The changes observed in the phenolic content throughout the season agree with other studies in which the effect of variety, processing, and storage has been studied in whole pigmented lettuce heads.[27] We have previously observed that the individual phenolic composition depends on the genetic information[8,11] although the content is very much influenced by the growing conditions.[13,14,28] In the present study, we also observed that the climatic variables influenced the content of phenolic compounds; in particular, the increase in temperature and radiation during the season promoted the increase in the content of phenolic acids and flavonoids. In another study by Bunning et al.[29] it was observed that differences among lettuce cultivars appear to have a larger impact on sensory and phenolic profiles than environmental variation during the growing season. However, in green and white currants high radiation and temperature have been associated with low content of the major phenolic compounds.[30] In lettuce, most of the studies have evaluated the influence of light quality, light intensity, and temperature on the changes in the phenolic compounds but always under controlled conditions far from the environmental conditions in open fields. In previous studies under controlled conditions, light experiments have been carried out using different plastic films to allow the filtration of different doses of ultraviolet radiation.[12,21,31] In other studies, the influence of light quality was also studied but by using different supplemental light qualities such as UV-A, blue, green, red,

DOI: 10.1021/acs.jafc.5b00120
J. Agric. Food Chem. 2015, 63, 1673−1681

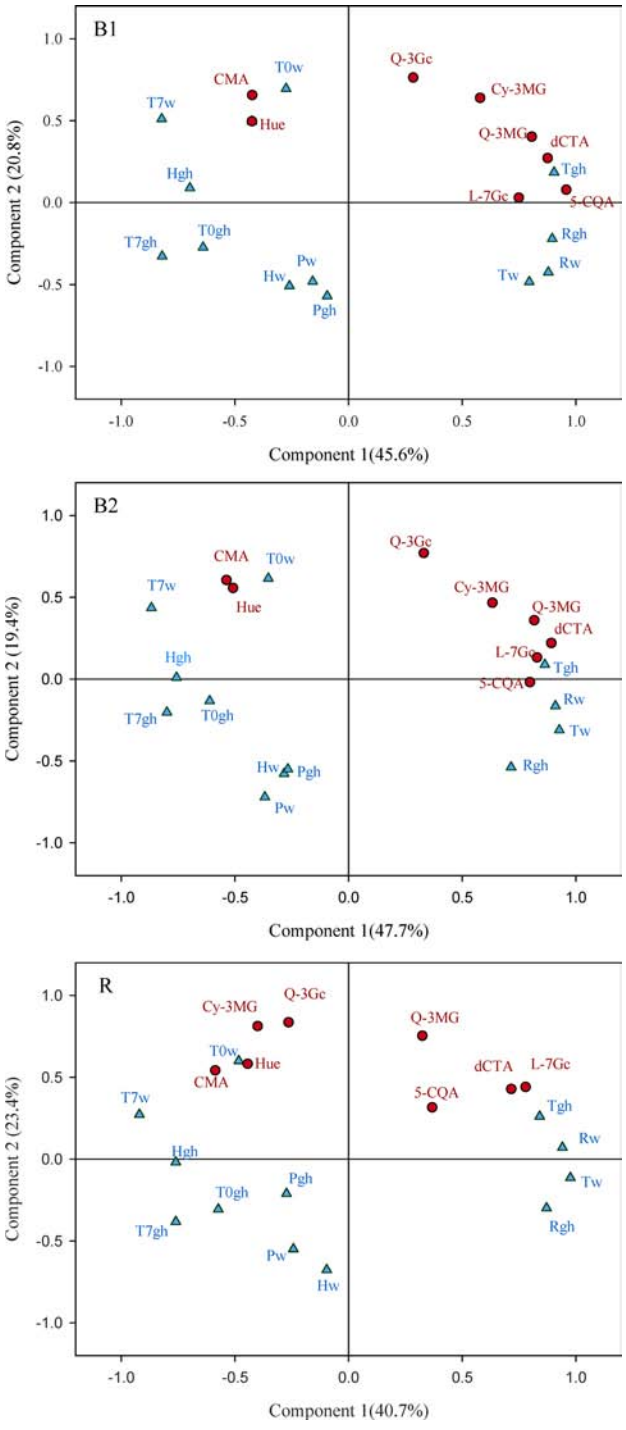

Figure 5. PCA plots of the correlations between phenolic compounds and hue angle and climatic variables. See Figure 3 and Table 1 for abbreviations.

and far-red-light-emitting diodes (LEDs).[23,32] In summary, radiation intensity has a definite influence increasing the phenolic metabolism in accordance with our results. The biosynthesis of flavonoids in pigmented leaf lettuce is enhanced by growing under plastic films that allows a higher exposure to UV radiation.[19] These authors observed that there was not a significant impact on the phenolic acids whereas the glycosides of quercetin and luteolin were significantly affected by the different radiation treatments. With the same approach, García-Macías et al.[12] showed that exposure to increased levels of UV radiation during cultivation caused the lettuce leaves to redden and increased the concentrations of total phenolics, particularly the main flavonoids, quercetin and cyanidin glycosides, as well as luteolin conjugates and phenolic acids. In a previous study, we could not study the variability of the content of anthocyanins among red-leafed lettuce genotypes because of the lack of color development when lettuces were protected by the greenhouse compared to that of lettuce grown in open fields.[13] Generally, the flavonoid content is much higher in field-grown than in glasshouse-grown plants, as in the case of a New Asia Salad (*Gynura bicolor*).[33]

Anthocyanin accumulation in plants is sensitive to environmental conditions, but depending on the crop, their impact can be different. In strawberries[34] and black currant[35] the content of the anthocyanins increases as temperature and radiation increase. In pomegranate, however, anthocyanins accumulate with cold temperatures.[36] In addition, foliar anthocyanin accumulation has been reported to be induced at high light intensities, in particular high-UV light, and low growth temperatures.[37,38] Our results showed that the climatic conditions prior to harvest had a great influence on pigmentation. The content of Cy−3MG increased with temperature and radiation in Batavia cultivars, and in red oak leaf it increased with cold temperatures. In lettuce, several studies have shown that low temperatures lead to an increase in anthocyanins due to the biosynthesis of phenylpropanoids by the increase in the PAL activity.[10,22] In the present study, the different response of Cy−3MG in Batavia and red oak leaf to the temperature and radiation may indicate genetic differences for the regulation of anthocyanin biosynthesis. Recently, Becker et al.[17]cdescribed that the light-related increase of flavonoid glycosides was structure- and growth-stage-dependent. In detail, an interaction was detected between plant age and low-level photosynthetic photon flux density (PPFD) regarding the cyanidin-3-*O*-(6″-*O*-malonyl)-glucoside concentration: the increase was strongest before head formation. Becker et al.[39] observed that the content of Cy−3MG was higher in cool-cultivated than in warm-cultivated lettuce heads. All major phenolic compounds decreased with plant age. Nevertheless, in our study baby leaves were harvested at the immature stage. The pigmented baby lettuces were harvested at the commercial maturity stage for baby leaves that varied between 8 and 12 cm leaf length depending on the season.[3] As expected, samples harvested in May showed shorter growing cycles than the ones harvested in winter. There was an increase mainly in the solar radiation and temperature with the transition from winter to spring. It is well-known that plant growth and development are regulated by light quality, light intensity, and photoperiod.[40] Our results showed that baby leaves harvested in May presented higher fresh weight and leaf area but lower dry matter content than those harvested in February. Researchers have reported that increased light intensity and extended photoperiods usually promoted the growth.[41] Li and Kubota[32] demonstrated that the growth of red baby leaf lettuce was significantly affected by light quality as fresh weight, dry weight, and leaf area increased with supplemental far-red light compared to those of plants grown in white light.

A clear seasonal variability was observed by the grower in agreement with the analytical results that showed the seasonal fluctuations in the content of individual phenolic compounds. However, our results indicate that it was not possible to establish a relationship between color measured by hue angle and the content of anthocyanins and, therefore, hue angle

DOI: 10.1021/acs.jafc.5b00120
J. Agric. Food Chem. 2015, 63, 1673−1681

Table 2. Pearson's Correlation Coefficients between Phenolic Compounds and Climatic Variables of Baby Leaf Batavia (B1 and B2) and Red Oak Leaf (R) Lettuces[a]

	Climatic Variables											
	Rw	Rgh	Tw	Tgh	T0w	T0gh	T7w	T7gh	RHw	RHgh	Pw	Pgh
Batavia B1												
Anthocyanin Glycosides												
Cy−3MG	**0.43**[b]	**0.52****	**0.34****	**0.61****	0.20	**−0.47****	0.21	**−0.62****	0.20	**−0.40****	**−0.44****	**−0.36***
Phenolic Acids												
5-CQA	**0.80****	**0.72****	**0.67****	**0.65****	−0.12	**−0.36***	**−0.58****	**−0.54****	**−0.54****	**−0.66****	−0.15	−0.13
CMA	**−0.54****	**−0.60****	**−0.73****	**−0.50****	**0.57****	**0.32***	**0.73****	**0.40****	−0.10	**0.48****	−0.10	0.01
dCTA	**0.73****	**0.75****	**0.61****	**0.74****	−0.05	**−0.62***	**−0.62****	**−0.75****	−0.19	**−0.51****	**−0.36***	−0.14
Flavonol and Flavone Glycosides												
L−7Gc	**0.89****	**0.93****	**0.86****	**0.89****	−0.21	**−0.61****	−0.77	**−0.81****	**−0.31***	**−0.77****	−0.28	−0.27
Q−3Gc + Q−3G	−0.04	−0.16	−0.12	**−0.32***	**−0.37***	**−0.42****	0.10	**−0.38****	−0.16	0.18	**0.52****	0.17
Q−3MG	0.70	**0.71****	**0.56****	**0.74****	0.04	**−0.52****	−0.47	**−0.71****	−0.26	**−0.56****	**−0.38***	**0.32***
Batavia B2												
Anthocyanin Glycosides												
Cy−3MG	**0.36***	**0.35***	**0.39****	**0.39****	−0.09	−0.20	**−0.32**	**−0.39****	−0.19	**−0.41****	**0.56****	−0.28
Phenolic Acids												
5-CQA	**0.62****	**0.75****	**0.68****	**0.53****	0.25	0.24	**−0.65****	**−0.44****	−0.06	**−0.60****	−0.21	−0.07
CMA	**−0.62****	**−0.56****	**−0.73****	**−0.48****	−0.57**	**0.32***	**0.74****	**0.39****	**−0.30***	**0.90****	−0.08	−0.09
dCTA	**0.75****	**0.75****	**0.72****	**0.71****	−0.13	**−0.49****	**−0.68****	**−0.70****	**−0.36***	**−0.67***	**−0.37***	−0.21
Flavonol and Flavone Glycosides												
L−7Gc	**0.68****	**0.54****	**0.68****	**0.51****	−0.22	−0.27	**−0.64****	**−0.47****	−0.17	**−0.57***	**−0.35***	0.03
Q−3Gc + Q−3G	0.11	−0.19	0.06	0.17	0.16	−0.19	0.03	−0.26	**−0.43****	−0.10	**−0.74****	−0.28
Q−3MG	**0.63****	**0.36****	**0.61****	**0.58****	−0.15	**−0.35***	**−0.52****	**−0.55****	**−0.31***	**−0.58****	**0.54****	−0.27
Red Oak Leaf												
Anthocyanin Glycosides												
Cy−3MG	**0.44****	**−0.44****	**−0.51****	**−0.52****	**0.50****	0.03	**0.62****	0.11	−0.25	**−0.43****	−0.24	0.11
Phenolic Acids												
5-CQA	**0.46****	**0.40****	**0.36***	**0.11**	−010	0.75	−0.29	−0.11	−0.02	**−0.40****	0.15	0.12
CMA	**0.63****	**−0.61****	**0.65****	**−0.53****	**0.44****	**0.33***	**0.65****	**0.42****	−0.10	**0.56****	0.05	**0.36***
dCTA	**0.79****	**0.78****	**−0.68****	**0.72****	−0.20	**−0.55****	**−0.68****	**−0.73****	**−0.31***	**−0.65****	**−0.34***	**−0.34***
Flavonol and Flavone Glycosides												
L−7Gc	**0.68****	**0.74****	**−0.58****	**0.62****	−0.19	**−0.36***	**−0.58****	**−0.57****	−0.29	**−0.65****	−0.24	−0.30
Q−3Gc + Q−3G	−0.25	**−0.48****	**−0.36***	**−0.02**	**0.59****	−0.16	**0.43****	−0.07	**−0.41****	**0.35***	−0.29	0.02
Q−3MG	**0.30***	0.04	0.23	**0.34****	0.09	−0.29	−0.12	**−0.38***	**−0.37***	−0.22	−0.26	−0.06

[a]See Figure 3 and Table 1 for abbreviations. Bold indicates values with significance. [b]* represents $P < 0.05$; ** represents $P < 0.01$.

DOI: 10.1021/acs.jafc.5b00120
J. Agric. Food Chem. 2015, 63, 1673−1681

cannot be considered a good indicator for anthocyanin accumulation. These results disagree with a previous publication that shows the good correlations between analytic, instrumental, and visual assessment of coloration in red lettuce.[15] These authors measured the pigment extract by spectrophotometer at 530 nm. However, in plant material where two or more pigments are present, close examinations of individual constituents are needed.[42] Other phenolic compounds (copigmentation) as well as the amounts and distribution of chlorophylls and carotenoids contribute significantly to leaf color. Therefore, it is very difficult to find a good correlation between color measurements and pigment content.

Lettuce breeders need to be assisted by agricultural and food chemistry specialists to select cultivars with improved color and phenolic constituents grown under commercial environmental conditions.

■ ASSOCIATED CONTENT

Supporting Information

Tables showing ANOVA assessment of the influence of cultivar and harvest schedules, phenolic composition of baby Batavia and red oak leaf plants during growth, and loadings, eigenvalues, and percent of cumulative variance for the two main principal components of Batavia B1 and B2 and red oak leaf cultivars. This material is available free of charge via the Internet at http://pubs.acs.org.

■ AUTHOR INFORMATION

Corresponding Author

*M.I.G. phone: +34-968396315. Fax: +34-968396213. E-mail: migil@cebas.csic.es.

Funding

This work was financed by the MINECO (AGL2013-48529-R).

Notes

The authors declare no competing financial interest.

■ ACKNOWLEDGMENTS

The authors are grateful to Langmead Spain, S. L. for providing the plant material for the study.

■ REFERENCES

(1) Clydesdale, F. M. Color as a factor in food choice. *Crit. Rev. Food Sci. Nutr.* **1993**, *33* (1), 83−101.

(2) Kader, A. A.; Lipton, W. J.; Morris, L. L. Systems for scoring quality of harvested lettuce. *HortScience* **1973**, *8*, 408−409.

(3) Gil, M. I.; Tudela, J. A.; Martínez-Sánchez, A.; Luna, M. C. Harvest maturity indicators of leafy vegetables. *Stewart Posthar. Rev.* **2012**, *1* (2), 1−9.

(4) Ferrer, J. L.; Austin, M. B.; Stewart, C., Jr.; Noel, J. P. Structure and function of enzymes involved in the biosynthesis of phenylpropanoids. *Plant Physiol. Biochem.* **2008**, 356−370.

(5) Petroni, K.; Tonelli, C. Recent advances on the regulation of anthocyanin synthesis in reproductive organs. *Plant Sci.* **2011**, *181*, 219−229.

(6) Cheynier, V.; Comte, G.; Davies, K. M.; Lattanzio, V.; Martens, S. Plant phenolics: Recent advances on their biosynthesis, genetics, and ecophysiology. *Plant Physiol. Biochem.* **2013**, *72*, 1−20.

(7) Ferreres, F.; Gil, M. I.; Castañer, M.; Tomás-Barberán, F. A. Phenolic metabolites in red pigmented lettuce (Lactuca sativa). Changes with minimal processing and cold storage. *J. Agric. Food Chem.* **1997**, *45*, 4249−4254.

(8) Llorach, R.; Martínez-Sanchez, A.; Tomás-Barberán, F. A.; Gil, M. I.; Ferreres, F. Characterization of polyphenols and antioxidant properties of five lettuce varieties and escarole. *Food Chem.* **2008**, *108*, 1028−1038.

(9) Harbone, J. B.; Willians, C. A. Advances in flavonoid research since 1992. *Phytochemistry* **2000**, *55*, 481−504.

(10) Gazula, A.; Kleinhenz, M. D.; Streeter, J. G.; Miller, A. R. Temperature and cultivar effects on anthocyanin and chloropyll b concentration in three related *Lolla Rosso* lettuce cultivar. *HortScience* **2005**, *40*, 1731−1733.

(11) Martínez-Sanchez, A.; Gil-Izquierdo, A.; Gil, M. I.; Ferreres, F. A comparative study of flavonoid compounds, vitamin C and antioxidant properties of baby leaf *Brassicaceae* species. *J. Agric. Food Chem.* **2008**, *56*, 2330−2340.

(12) García-Macías, P.; Ordidge, M.; Vysini, E.; Waroonphan, S.; Battey, N. H.; Gordon, M. H.; Hadley, P.; John, P.; Lovegrove, J. A.; Wagstaffe, A. Changes in the flavonoid and phenolic acid contents and antioxidant activity of red leaf lettuce (Lollo Rosso) due to cultivation under plastic films varying in ultraviolet transparency. *J. Agric. Food Chem.* **2007**, *55*, 10168−10172.

(13) Selma, M. V.; Luna, C.; Martínez-Sánchez, A.; Tudela, J. A.; Beltrán, D.; Baixauli, C.; Gil, M. I. Sensory quality, bioactive constituents and microbiological quality of green and red fresh-cut lettuces (*Lactuca sativa* L.) are influenced by soil and soilless agricultural production systems. *Postharvest Biol. Technol.* **2012**, *63*, 16−24.

(14) Luna, C.; Martínez-Sánchez, A.; Selma, M. V.; Tudela, J. A.; Beltrán, D.; Baixauli, C.; Gil, M. I. Influence of nutrient solutions in open field soilless system on the quality characteristics and shelf life of fresh-cut red and green lettuces (*Lactuca sativa* L.) in different seasons. *J. Sci. Food Agric.* **2013**, *93*, 415−421.

(15) Gazula, A.; Kleinhenz, M. D.; Streeter, J. G.; Ling, P. P. Anthocyanin levels in nine lettuce (*Lactuca sativa*) cultivars: Influence of planting date and relations among analytic, instrumented, and visual assessments of color. *HortScience* **2007**, *42*, 232−238.

(16) Martínez-Sánchez, A.; Luna, C.; Selma, M. V.; Tudela, J. A.; Abad, J.; Gil, M. I. Baby-leaf and multi-leaf of green and red lettuces are suitable raw materials for the fresh-cut industry. *Postharvest Biol. Technol.* **2012**, *63*, 1−10.

(17) Becker, C.; Klaering, H. P.; Schreiner, M.; Kroh, L. W.; Krumbein, A. Unlike quercetin glycosides, cyanidin glycoside in red leaf lettuce responds more sensitively to increasing low radiation intensity before than after head formation has started. *J. Agric. Food Chem.* **2014**, *62*, 6911−6917.

(18) Behn, H.; Schurr, U.; Ulbrich, A.; Noga, G. Development-dependent UV-B responses in red oak leaf lettuce (*Lactuca sativa* L.): physiological mechanisms and significance for hardening. *Eur. J. Hortic. Sci.* **2011**, *76*, 33−40.

(19) Becker, C.; Klaering, H. P.; Kroh, L. W.; Krumbein, A. Temporary reduction of radiation does not permanently reduce flavonoid glycosides and phenolic acids in red lettuce. *Plant Physiol. Biochem.* **2013**, *72*, 154−160.

(20) Oh, M. M.; Carey, E. E.; Rajashekar, C. B. Environmental stresses induce health-promoting phytochemicals in lettuce. *Plant Physiol. Biochem.* **2009**, *47*, 578−583.

(21) Tsormpatsidis, E.; Henbest, R. G. C.; Battey, N. H.; Hadley, P. The influence of ultraviolet radiation on growth, photosynthesis and phenolic levels of green and red lettuce: potential for exploiting effects of ultraviolet radiation in a production system. *Ann. Appl. Biol.* **2010**, *156*, 357−366.

(22) Boo, H. O.; Heo, B. G.; Gorinstein, S.; Chon, S. U. Positive effects of temperature and growth conditions on enzymatic and antioxidant status in lettuce plants. *Plant Sci.* **2011**, *181*, 479−484.

(23) Samuolienė, G.; Sirtautas, R.; Brazaitytė, A.; Duchovskis, P. LED lighting and seasonality effects antioxidant properties of baby lettuce. *Food Chem.* **2012**, *134*, 1494−1499.

(24) Medina-Martínez, M. S.; Allende, A.; Barberá, G. G.; Gil, M. I. Climatic variations influence the dynamic of epiphyte bacteria of baby lettuce. *Food Res. Int.* **2014**, in press (Special Issue in Climate Change).

(25) McGuire, R. G. Reporting of objective color measurements. *HortScience* **1992**, *27*, 1254−1255.

DOI: 10.1021/acs.jafc.5b00120
J. Agric. Food Chem. 2015, 63, 1673−1681

(26) SIAM, Sistema de Información Agraria de Murcia. IMIDA. http://siam.imida.es/apex/f?p=101:1:219250110726293 (accessed 09-2014).
(27) Dupont, S. M.; Mondin, Z.; Williamson, G.; Prince, K. R. Effect of variety, processing and storage on the flavonoids glycoside content and composition of lettuce and endive. *J. Agric. Food Chem.* **2000**, *48*, 3957−3964.
(28) Romani, A.; Pinelli, P.; Galardi, C.; Sani, G.; Cimato, A.; Heimier, D. Polyphenol in greenhouse and open-air grown lettuce. *Food Chem.* **2002**, *79*, 337−342.
(29) Bunning, M. L.; Kendall, P. A.; Stone, M. B.; Stonaker, F. H.; Stushnoff, C. Effects of seasonal variation on sensory properties and total phenolic content of 5 lettuce cultivars. *J. Food Sci.* **2010**, *75*, S156−S161.
(30) Yang, B.; Zheng, J.; Laaksonen, O.; Tahvonen, R.; Kallio, H. Effects of latitude and weather conditions on phenolic compounds in currant (*Ribes* spp.) cultivars. *J. Agric. Food Chem.* **2013**, *61*, 3517−3532.
(31) Tsormpatsidis, E.; Henbest, R. G. C.; Battey, N. H.; Hadley, P.; Wagstaffe, A. UV irradiance as a major influence on growth, development and secondary products of commercial importance in Lollo Rosso lettuce 'Revolution' grown under polyethylene films. *Environ. Exp. Bot.* **2008**, *63*, 232−239.
(32) Li, Q.; Kubota, C. Effects of supplemental light quality on growth and phytochemicals of baby leaf lettuce. *Environ. Exp. Bot.* **2009**, *67*, 59−64.
(33) Rouphael, Y.; Cardarelli, M. T.; Bassal, A.; Leonardi, C.; Giuffrida, F.; Colla, G. Vegetable quality as affected by genetic, agronomic and environmental factors. *J. Food, Agric. Environ.* **2012**, *10* (3−4), 680−688.
(34) Wang, S.; Zheng, W. Effect on plant growth temperature on antioxidant capacity in strawberry. *J. Agric. Food Chem.* **2001**, *49*, 4977−4982.
(35) Zheng, J.; Yang, B.; Ruusunen, V.; Laaksonen, O.; Tahvonen, R.; Hellsten, J.; Kallio, H. Compositional differences of phenolic compounds between black currant (*Ribes nigrum* L.) cultivars and their response to latitude and weather conditions. *J. Agric. Food Chem.* **2012**, *60*, 6581−6593.
(36) Borochov-Neori, H.; Judeinstein, S.; Harari, M.; Bar-Ya'akov, I.; Patil, B. S.; Lurie, S.; Holland, D. Climate effects on anthocyanin accumulation and composition in the pomegranate (*Punica granatum* L.) fruit arils. *J. Agric. Food Chem.* **2011**, *59*, 5325−5334.
(37) Leyva, A.; Jarillo, J. A.; Salinas, J.; Martinez-Zapater, J. M. Low temperatures induces the accumulation of phenylalanine ammonia lyase and chalcone synthase Messenger RNAs of Arabidopsis thaliana in a light-dependent manner. *Plant Physiol.* **1995**, *108*, 39−46.
(38) Chalker-Scott, L. Enviromental significance of anthocyanins in plant stress responses. *Photochem. Photobiol.* **1999**, *70*, 1−9.
(39) Becker, C.; Klaering, H. P.; Kroh, L. W.; Krumbein, A. Cool-cultivated red leaf lettuce accumulates cyanidin-3-*O*-(6″-*O*-malonyl)-glucoside and caffeoylmalic acid. *Food Chem.* **2014**, *146*, 404−411.
(40) Inada, K.; Yabumoto, Y. Effects of light quality, daylength and periodic temperature variation on the growth of lettuce and radish plants. *Jpn. J. Crop Sci.* **1989**, *58*, 689−694.
(41) Kang, J. H.; Krishnakumar, S.; Sua Atulba, S. L.; Jeong, B. R.; Hwang, S. J. Light intensity and photoperiod influence the growth and development of hydroponically grown leaf lettuce in a closed-type plant Factory system. *Hortic., Environ. Biotechnol.* **2013**, *54* (6), 501−509.
(42) Santos-Buelga, C.; Mateus, N.; De Freitas, V. Anthocyanins. Plant pigments and beyond. *J. Agric. Food Chem.* **2014**, *62*, 6879−6884.

DOI: 10.1021/acs.jafc.5b00120
J. Agric. Food Chem. 2015, 63, 1673−1681

including organoclays,[14,15,20,23,25,26] polymer−clays,[16,17,24,27] and micelle−clays.[28−31] Several of the clay-based formulations were tested and found to reduce herbicide leaching through soils. However, these formulations were designed for herbicides with high solubility and extensive leaching to reduce their leaching of 10−100 cm, unlike the case of pendimethalin where the goal is to eliminate its leaching of 1−2 cm. A pendimethalin organoclay formulation was designed for enhanced herbicidal activity, but reduced leaching was not tested.[32]

Hence, the main goal of this study was to develop and examine slow-release formulations of pendimethalin for the reduction of root penetration into subsurface irrigation drippers. The formulations developed were based on pendimethalin solubilization in octadecyltrimethylammonium bromide (ODTMA) micelles adsorbed and unadsorbed on montmorillonite. We have characterized in detail the ODTMA (as monomer and as micelles)−clay interactions in previous studies applying adsorption isotherms, modeling, X-ray diffraction, freeze−fracture electron microscopy, herbicide solubilization measurements,[29] fluorescence studies,[19] and FTIR analysis.[33] The solubilization of several herbicides was further explored in our more recent studies.[25,34]

The novelty of this investigation covers three different aspects; formulation design, bioassay design, and application. More specifically the originality of this study involves the development of (1) two-mode formulations (in the past, unadsorbed micelles were considered not adequate for slow release[31,34] because the release was too fast, but here we demonstrate the advantage of having both modes of micelles, adsorbed and unadsorbed), (2) a bioassay to study herbicide migration at a refined scale of 1−2 cm, and (3) the application of slow release herbicide formulations for the reduction of root penetration into subsurface irrigation drippers.

MATERIALS AND METHODS

Materials. Wyoming sodium montmorillonite (SWy-2) (cation exchange capacity, 0.76 mmol/g; surface area, 700 m^2/g) was obtained from the Source Clays Repository of the Clay Mineral Society (Columbia, MO, USA). Octadecyltrimethylammonium bromide (ODTMA) and Triton X-100 were purchased from Sigma-Aldrich (Stenheim, Germany). Pendimethalin *N*-(1-ethylpropyl)-3,4-dimethyl-2,6-dinitrobenzenamine (technical grade 96%) and Stomp 330 (a commercial formulation containing 330 g/L pendimethalin) were from BASF Agro, Germany. Rehovot sandy soil (95.5% sand, 3.3% silt, 1.2% clay, 0.2% OM) was collected (top 20 cm) from the Faculty's experimental farm.The test plant for the bioassay was *Sorghum bicolor*.

Methods. *ODTMA Adsorption on Montmorillonite: Temperature Effect.* Throughout the study, the preparation of ODTMA micelle solutions included heating the solutions to a temperature exceeding the Krafft temperature, T_K (36 °C), and reaching a clear solution. The adsorption of ODTMA from a micelle solution (20 mL) to montmorillonite (10 mL) was studied in batch experiments (in duplicates) reaching final concentrationd of 1−10 mM and 0.56 or 1.67 g/L. The adsorption was studied at temperatures of 40 and 60 °C by agitating the tubes in a hot tub for 24 h (reaching equilibrium). Supernatants were separated by centrifugation at 15000*g* for 20 min (at 40 and 60 °C), and the precipitates were lyophilized. The percent of carbon in the precipitates was measured using a CHNSO analyzer, Carlo-Erba 1108. The concentration of ODTMA adsorbed was calculated by taking into account full cation exchange at concentrations above the cation exchange capacity of the clay.

ODTMA−clay samples were prepared (as described above) for scanning electron microscopy (SEM) analysis by adsorbing ODTMA (5 mM) to montmorillonite (0.56−5 g/L) at 27 °C and at 40 °C on 0.56 g/L montmorillonite (all concentrations are final).

The morphology of montmorillonite and the ODTMA−clay samples was studied by SEM and elemental analysis. Samples were prepared on Akulon stubs using double-sided sticky tape. The microphotographs are recorded using scanning electron microscope JEOL model JSM-5410 LV. The images were taken with an accelerating voltage of 20 kV, at low vacuum mode (28 Pa), and backscattered electron detection.

Pendimethalin Solubilization in Micelles and Adsorption to Montmorillonite. The solubilization of pendimethalin (50−900 mg/L, 0.18−3.2 mM) in ODTAM micelles (10 mM) was studied in batch experiments (final concentrations). The solutions were stirred for 24 h in covered glass tubes (to avoid photodegradation) at 40 °C. If complete solubilization of pendimethalin was not reached, its precipitation was observed. This precipitate was separated by centrifugation at 15000*g* for 20 min at 40 °C. The concentration of pendimethalin in solution was determined by using a UV−vis spectrophotometer (Evolution 300, Thermo Scientific, Waltham, MA, USA). For herbicide concentrations <50 mg/L the measurement was with a 1 cm glass cuvette at 200−800 nm with λ_{max} = 423 nm. For herbicide concentrations >50 mg/L the measurement was with a 0.2 cm glass cuvette (to avoid dilution and micelle decomposition). Pendimethalin solubilization was calculated by subtracting the solution concentration from the initial concentration. The contribution of pendimethalin in water, 0.275 mg/L, not solubilized in micelles, is negligible.

Pendimethalin (300 mg/L) adsorption on montmorillonite (3−10 g/L) via its solubilization in ODTMA micelles (10 mM) was studied at 40 °C in batch experiments in triplets. Pendimethalin solubilization was performed as described above. The herbicide−micelle solution was added to a clay suspension (final concentrations of 3−10 g/L) at 40 °C. The tubes were agitated for 24 h (equilibrium reached) in a hot tub, supernatants were separated by centrifugation at 15000*g* for 20 min, and pendimethalin concentration was measured by UV−vis spectrophotometer as described. The concentration of adsorbed pendimethalin was then calculated.

Herbicide−Micelle−Clay Formulation Preparation. Pendimethalin (300 mg/L) was solubilized in ODTMA (10 mM) as described above. To prepare the one-mode formulation the herbicide−micelle solution was added to a high clay concentration (7 g/L) at 40 °C, and to prepare the two-mode formulation the solution was added to a low clay concentration (2 g/L) at 27 °C. The tubes were agitated for 24 h (equilibrium reached) in a hot tub with the relevant temperatures, supernatants were separated by centrifugation at 15000*g* for 20 min, and the precipitates were lyophilized. For the greenhouse study a larger scale preparation included adding pendimethalin (800 mg/L 10 mLin acetone) to ODTMA (20 mM) and adsorbing the solubilized herbicide to a high clay concentration (16 g/L) at 40 °C and to a low clay concentration (4 g/L) at 27 °C for the preparation of the one- and two-mode formulations, respectively. The suspension was left to settle, and the concentrated suspension was centrifuged. Pendimethalin concentrations in the supernatants were determined by UV−vis spectrophotometer measurements, and the adsorbed pendimethalin was calculated. The percentages of active ingredient in the one- and two-mode formulations were 1.6−2.7 and 3.2−4.8%, respectively.

Pendimethalin Desorption from the Formulations. The one- and two-mode formulations were suspended in 20 mL for 24 h at 27 °C in batch experiments in triplets. Supernatants were separated by centrifugation at 15000*g* for 20 min, and pendimethalin concentration was measured by UV−vis spectrophotometer as described.

Pendimethalin Desorption and Leaching through Thin Soil Layers. The release and leaching of pendimethalin from the one- and two-mode formulations and from the commercial formulation, Stomp 330, was measured by applying the formulations on a thin sandy soil layer (160 g and approximately 1 cm) deposited on a filter paper (Whatman 1442-125) in a Buchner funnel (area of 7.85×10^{-3} m^2). No herbicide adsorption was detected on the filter paper. The formulations were applied in 30 mL of water at a rate of 1.4 mg of active ingredient (ai) per funnel, equivalent to 1.8 kg ai/ha. Water was applied as a control. A second filter paper was placed on top of the soil to ensure uniform water distribution and to minimize disruption of the

DOI: 10.1021/jf504839q
J. Agric. Food Chem. 2015, 63, 1682−1688

soil surface. The funnels were irrigated five times with 50 mm of water (40 mL per funnel) at uniform intervals between irrigations. The leachates were collected after each irrigation, and herbicide concentrations were measured by UV−vis spectrophotometer. Each treatment was performed in triplicate.

Bioactivity and Reduced Leaching of Pendimethalin in the Soil: Laboratory Essays. The release, leaching, and bioactivity of pendimethalin applied as Stomp 330 or one- and two-mode formulations were measured by applying the formulations (0.3 kg ai/ha) on sandy soil columns of 10 cm diameter and 5 cm height. Water was applied as control. Each treatment was performed in triplicates. The columns were irrigated with 60 mL of water, covered with paper to prevent photodegradation, and after 60 h, each centimeter of the top 3 cm was pushed from the bottom up and removed. The soil from each depth was transferred to Petri plates (in triplets). Ten *Sorghum* seeds were sown in each plate, and plates were covered, sealed with tape, and placed in a 27 °C dark room at a 45° angle to force roots to grow downward along the Petri dish cover. After 60 h, root length was measured for each treatment. Pendimethalin leaching and bioactivity were calculated by measuring the degree of root growth inhibition at each depth, which was calculated by comparison to untreated control.

Bioactivity and Reduced Leaching of Pendimethalin in Soil: Greenhouse Assays. The efficiency of the micelle−clay formulation and of Stomp 330 to reduce root penetration into the drippers was studied in a greenhouse setup. The study was conducted in large pots (1 m × 0.5 m and a depth of 0.35 m total volume of 175 L) filled with a soilless matrix of sand mix with compost 70/30% (Givat Adda, Israel). The subsurface irrigation drippers were buried at a depth of 15 cm, two rows per pot including 10 drippers per pot. Lettuce (*Lactuca sativa* L.) seedlings at the 13−14 BBCH growth stage were transplanted, 10 per pot, and grown by regular protocol. Each treatment was repeated five times. Three weeks from planting irrigation was reduced gradually to induce root penetration into the drippers. Five weeks after planting the two-mode formulation, Stomp 330, or water (as control) was applied at 0.06 g ai per dripper (10 g from the two-mode formulation in 100 mL of water or 2 mL of Stomp 330 in 100 mL of water). Three weeks after pendimethalin application, the drippers were removed and root penetration was evaluated. The penetration was ranked from 0 to 3 (low to high) and compared to the control.

A second greenhouse scale test (same setup) was performed to test an earlier application of the formulations. In this study tomato (*Lycopersicon esculentum* Mill.) seedlings at the 12−13 BBCH growth stage were planted and the growth period was extended to 4 months to increase the probability of root penetration into drippers. Three weeks from planting the one- and two-mode formulations were injected through the irrigation system (early application). Eight weeks after planting, irrigation was reduced gradually to induce root penetration. Ten weeks after planting, the one-mode and Stomp formulations were injected through the irrigation system (regular application).

Data Analysis. The statistical analysis was carried out using JMP 7.0.1 (SAS 2007) and $p = 0.05$. The bioactivity study at the laboratory scale was subjected to a two-way ANOVA model in a "split-plot" design, where the treatment (formulation), the depth, and root length were used as the main effects. Multiple comparisons were done using a *t* test. The bioactivity study at the greenhouse scale was subjected to the same analysis with treatment (formulation and application timing) and root penetration as main effects.

RESULTS AND DISCUSSION

Effect of Temperature on ODTMA Adsorption to Montmorillonite. The effect of temperature on ODTMA adsorption from a micelle solution (concentrations above the critical micelle concentration (CMC) and at temperatures above the T_k) to montmorillonite was explored (Figure 1). As previously reported for ODTMA adsorption from a micelle solution, adsorption was extremely high, reaching loadings of >2-fold the cation exchange capacity (CEC) of the clay, which

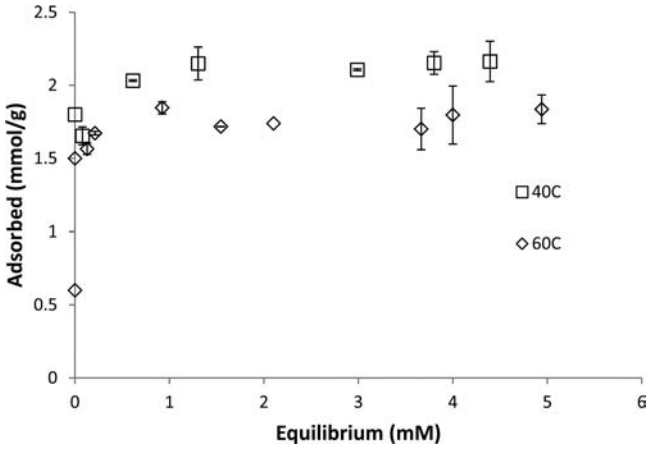

Figure 1. ODTMA (1−10 mM) adsorption on montmorillonite (0.56 and 1.67 g/L).

was explained in terms of micelle adsorption.[29] The adsorption was complete up to the CEC of the clay at both temperatures but decreased with temperature at adsorbed concentrations exceeding the CEC. These trends indicate that the adsorption reaction, exceeding the CEC, is most likely exothermic.[28] The adsorption reaction below the CEC, under the current experimental conditions, is complete and therefore cannot be determined; that is, it may be endothermic or exothermic.

Enthalpies of adsorption of organic molecules to clay minerals are generally exothermic,[28] because the molecules leaving the solution and attaching to the surface lead to a decrease in the dispersion of the energy, a decrease in the entropy.[32,35] Processes with decreasing entropy might be spontaneous only if they are exothermic (definition of Gibb's free energy). However, sorption of organic cations to montmorillonite are usually exchange processes, and the release of inorganic cations with their hydration shells may bring on an overall increase in entropy,[27] and endothermic adsorption processes have been reported in a few cases.[24,27,29] The adsorption of ODTMA monomers to the clay surface below the CEC is indeed due to cation exchange, that is, possibly an endothermic reaction. The adsorption of ODTMA from a micelle solution is driven by two forces; cation exchange (up to the CEC) and a bilayer that is formed on the surface due to hydrophobic interactions between the surfactants, which involve only confinement. The release of exchangeable cations (with their hydration shell) increases entropy, but this increase may be smaller than the loss of entropy due to both electrostatic and hydrophobic confinement, explaining the total decrease in enthalpy, that is, an exothermic reaction at adsorbed concentrations exceeding the CEC.

Little has been reported in the literature on the effect of temperature on monomer and micelle adsorption. Nevertheless, trends similar to those found in this study were reported for micelle adsorption of sodium dodecyl sulfate micelle to hydrotalcite.[36]

The effect of temperature on monomer versus micelle adsorption is expressed not only by their different reaction enthalpies but also by the adsorption mode, monomer conformation, and orientation.[37] It is well-known that a surfactant solution will spontaneously form micelles when prepared at concentrations above the CMC and above the T_k. The adsorption to montmorillonite of ODTMA at a concentration above the CMC (5 mM) and above (40 °C)

DOI: 10.1021/jf504839q
J. Agric. Food Chem. 2015, 63, 1682−1688

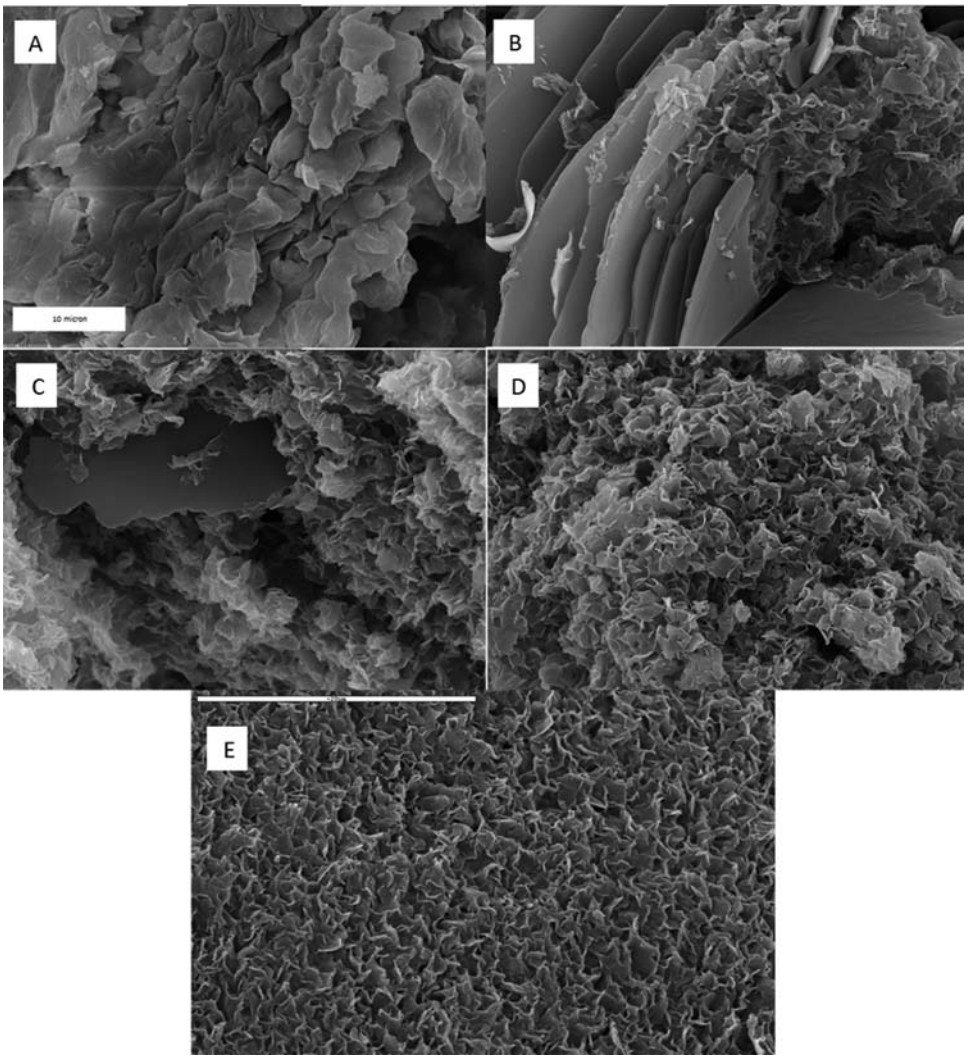

Figure 2. SEM images of (A) montmorillonite and ODTMA (5 mM) adsorption, (B) at 27 °C on 0.56 g/L montmorillonite, (C) at 27 °C on 4 g/L montmorillonite, (D) at 27 °C on 5 g/L montmorillonite, and (E) at 40 °C on 0.56 g/L montmorillonite.

or below (27 °C) the T_k was studied, and images of the precipitates were collected by SEM measurements (Figure 2).

ODTMA adsorption at 27 °C to a low clay concentration (0.56 g/L) resulted in high concentrations of ODTMA, which do not adsorb, and because the solution temperature is below T_k, the excess surfactant precipitates as an ODTMA salt with a platter morphology (Figure 2B). In contrast, ODTMA adsorption at 40 °C from a micelle solution resulted in homogeneous surfactant adsorption, and clay exfoliation was observed (Figure 2E). Because the temperature was above the T_k, the excess surfactant remained in the supernatant (was removed) and did not precipitate.

To increase ODTMA (5 mM) adsorption at temperatures below the T_k, the clay concentration was increased (0.56−5 g/L). As expected, fewer ODTMA platters were observed as the clay concentration increased, and uniform organoclay composites were observed upon the addition of ODTMA (5 mM) to high clay concentrations 5 g/L (Figure 2C,D).

Elemental analysis (eds) supports the identification of the platters as ODTMA salt precipitation with significant amounts of carbon, nitrogen, and bromine (55, 5, and 30%, respectively) The "fluffier" material was identified as organic−clay composite samples, containing carbon and nitrogen (of the surfactant) and aluminum and silica (characteristic of the clay) (55, 7, and 12%, respectively).

The identification of two modes of ODTMA in the samples, precipitate and adsorbed to clay, was further utilized to design two-mode pendimethalin formulations.

Pendimethalin Solubilization in Micelles and Adsorption to Montmorillonite. The first step to design pendimethalin−micelle−clay formulations was solubilizing pendimethalin, which has extremely low water solubility (0.275 mg/L), in a micelle solution of ODTMA (10 mM) to enhance its solubility (Figure 3). Pendimethalin solubilization in a 10 mM ODTMA solution was complete up to a concentration of 300 mg/L, and above this concentration the degree of solubilization decreased but the concentration increased, reaching 550 mg/L. Pendimethalin solubility increased by 3 orders of magnitude at a herbicide/surfactant ratio of only 0.2 mol/mol. High pendimethalin solubilization in ODTMA micelles enabled high active ingredient adsorption on the clay (via micelle adsorption).

Pendimethalin (300 mg/L) adsorption on montmorillonite (3−10 g/L) via its solubilization in ODTMA micelles (10 mM) was studied at 40 °C (Table 1). Surfactant/clay molar ratio (taking the cation exchange capacity into account) has a

DOI: 10.1021/jf504839q
J. Agric. Food Chem. 2015, 63, 1682−1688

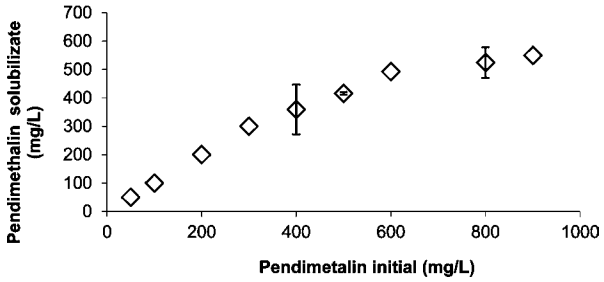

Figure 3. Pendimethalin (50–900 mg/L) solubilization in ODTMA micelles (10 mM) at 40 °C.

Table 1. Pendimethalin (300 mg/L) Adsorption on Montmorillonite (3–10 g/L) via Its Solubilization in ODTMA Micelles (10 mM)

	pendimethalin adsorbed	
clay (g/L)	mg/g clay	%
3	35.5 ± 2.0	35
5	48.2 ± 1.6	80
6	47.3 ± 0.5	95
7	42.7 ± 0.0	99
8	37.3 ± 0.0	99
10	29.9 ± 0.0	99

pronounced effect on surfactant loading and adsorption/precipitation mode. A high ratio will result in unadsorbed micelles (as obtained for a clay concentration of 3 g/L), whereas a slightly low ratio, with complete surfactant adsorption, will decrease the loading (mg/g) of pendimethalin (as obtained for clay concentration of 8–10 g/L). At a very low surfactant/clay ration, below 1, micelle decomposition and active ingredient release may occur.[19,34]

Complete pendimethalin adsorption on the clay (via micelle adsorption) and high herbicide loading were reached upon the addition of 10 mM ODTMA to 7 g/L montmorillonite. This surfactant/clay molar ratio of ~1.9 is in within the suggested optimal range.[34]

On the basis of the results of ODTMA adsorption on low and high clay concentrations and at temperatures above and below T_k (Figure 2) two types of micelle–clay formulations were designed. A one-mode formulation was prepared at 40 °C (above the T_k) by fully solubilizing the herbicide (300 mg/L) in micelles (10 mM) and at a surfactant/clay ratio in which surfactant adsorption is complete (7 g clay/L). A two-mode formulation was prepared by fully solubilizing the herbicide in micelles (like the one-mode) but at a surfactant/clay ratio at which surfactant adsorption is not complete (2 g clay/L) and the adsorption was at 27 °C. Due to the low temperature the unabsorbed pendimethalin, solubilized in micelles, precipitates. We hypothesized that the release from the one-mode formulation will be slower than from the two-mode and at a lower rate. The release from the two-mode formulation will be in two phases: a relatively fast phase, when the herbicide will release from nonadsorbed micelles, and a slower phase, when the herbicide solubilized in micelles adsorbed on clay will be released.

Pendimethalin Desorption from the Formulations. Pendimethalin desorption, in suspension, at 27 °C, after 24 h from the one-mode formulation was 0.13 ± 0.01%, whereas the release from the two-mode formulation was 10-fold higher, reaching 1.5 ± 0.3%. Higher desorption from the two-mode formulation was also observed when the desorption and leaching of pendimethalin through a thin layer of sand were studied (Figure 4). After irrigation of 5 pore volumes, 0.56 and

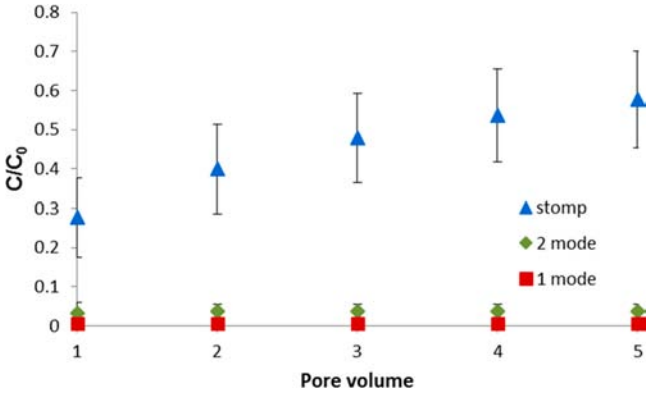

Figure 4. Pendimethalin desorption and leaching through a thin layer of sand applied as a commercial formulation or as the one- and two-mode micelle–clay formulations.

4% of the pendimethalin applied as one- and two-mode formulations leached through the soil, respectively. The leaching from the commercial formulation (Stomp) was significantly higher, reaching 57%.

Bioactivity and Reduced Leaching of Pendimethalin in the Soil: Laboratory Essays. Herbicide leaching in soil columns of several centimeters (10–100 cm) has been widely explored in bioassays. The challenge in the current study was to reach a leaching resolution of 1–2 cm. To test pendimethalin release from the formulations and leaching through 0–3 cm of soil, the formulations (and water as control) were applied to soil columns, irrigated, allowed to settle, and then sliced to depths of 0–1, 1–2, and 2–3 cm. Each soil layer was placed in a Petri dish, the test plants were sown, and root growth inhibition was measured (compared to the control) (Figure 5).

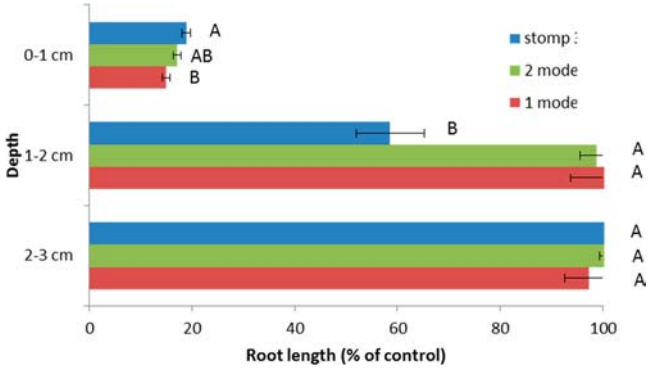

Figure 5. Effect of pendimethalin, applied as formulations one-mode, two-mode, and Stomp, on root growth of sorghum as a function of soil depth.

Pendimethalin did not leach beyond 2 cm. Its release and leaching from the commercial formulation to 1–2 cm depth was significant, resulting in nearly 60% root growth (percent of control), whereas no release and leaching from the micelle–clay formulations were observed (Figure 5). Efficient root growth inhibition was obtained for all three formulations at the top of the soil. Root growth inhibition by the one-mode formulation was significantly higher than by Stomp. This

DOI: 10.1021/jf504839q
J. Agric. Food Chem. 2015, 63, 1682–1688

leaching experiment indicates that the micelle−clay formulations demonstrate good root inhibition at the target location <1 cm from the point of application (in the case of the one-mode even better than the commercial formulation) while reducing pendimethalin leaching.

Bioactivity and Reduced Leaching of Pendimethalin: Greenhouse Assay. The efficiency of the micelle−clay formulation to reduce root penetration into the drippers was demonstrated in greenhouse studies (Figure 6). The

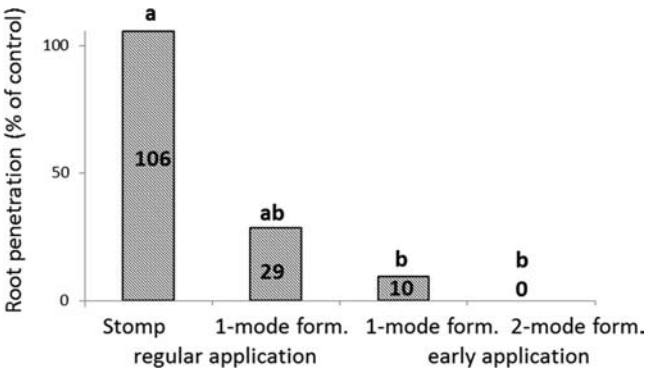

Figure 6. Root penetration (percent of control) in drippers treated with Stomp, one-mode, and two-mode formulations applied 3 weeks after tomato planting (early application) or 10 weeks after tomato planting (regular application).

commercial formulation and the two-mode formulation were applied as usually practiced, a few days (~14 days) after irrigation was gradually ceased. Lettuce root penetration (measured 8 weeks after planting) reached 50 and 37% (of control) for drippers treated with Stomp and the two-mode formulation. However, the difference was not significant.

In the second greenhouse study (Figure 7) tomatoes were planted and the growth period was extended to 4 months,

Figure 7. Image of greenhouse study.

increasing the probability of root penetration. In addition, an early application of the micelle−clay formulations (one- and two-mode formulations) was explored to test whether the activity and efficiency of the formulations indeed are for a longer period. The commercial and the one-mode formulations were applied as usually practiced. Prolonging the growth period indeed increased root penetration for the drippers treated with Stomp, reaching 100% (compared to control) penetration. In contrast, only 30% penetration was observed for the drippers treated with the one-mode formulation. An early application was extremely efficient with 10 and 0% penetration for drippers treated with the one- and two-mode formulations (between them, the difference was not significant).

To conclude, with the aim of inhibiting root penetration, slow-release pendimethalin formulations based on its solubilization in micelles adsorbed and unadsorbed to clay were developed (one- and two-mode formulations, respectively). The novelty of this investigation covers three different aspects: formulation design, bioassay design, and application. The two formulations were designed by controlling the temperature and ratio between the surfactant and clay. Although unadsorbed micelles were considered inadequate for slow release (release was too fast), we demonstrated the advantage of a two-mode release formulation. A bioassay to study pendimethalin leaching at a refined scale of 1−2 cm was developed, and reduced leaching from the micelle−clay formulations in comparison to the commercial formulation (Stomp) was exhibited. In a greenhouse study the application of the formulations by injection into the irrigation system was extremely efficient with 0−10% root penetration in comparison to 100% penetration upon Stomp injection. Reductions in root penetration and herbicide leaching upon application of the designed formulation were demonstrated.

AUTHOR INFORMATION

Corresponding Author

*(Y.G.M.) Phone: 972-8-948-9171. Fax: 972-8-948-9856. E-mail: yael.mishael@mail.huji.ac.il.

Funding

This research was supported by The Magneton Grant for innovative technologies from the Israeli Ministry of Economics.

Notes

The authors declare no competing financial interest.

ABBREVIATIONS USED

ai, active ingredient; ODTMA, octadecyltrimethylammonium; SEM, scanning electron microscopy

REFERENCES

(1) Ayars, J. E.; Phene, C. J.; Hutmacher, R. B.; Davis, K. R.; Schoneman, R. A.; Vail, S. S.; Mead, R. M. *Agric. Water Manag.* **1999**, *42*, 1−27.
(2) Camp, C. R. *Trans. ASAE* **1998**, *41*, 1353−1367.
(3) Oliveira, M. R. G.; Calado, A. M.; Portas, C. A. M. *J. Am. Soc. Hortic. Sci.* **1996**, *121*, 644−648.
(4) Phene, C. J.; Davis, K. R.; Hutmacher, R. B.; Bar-Yosef, B.; Meek, D. W.; Misaki, J. *Irrig. Sci.* **1991**, *12*, 135−140.
(5) Yu, Y.; Shihong, G.; Xu, D.; Jiandong, W.; Ma, X. *Agric. Water Manag.* **2010**, *97*, 723−730.
(6) Suarez-Rey, E. M.; Choi, C. Y.; McCloskey, W. B.; Kopec, D. M. *Irrig. Drain.* **2006**, *55*, 501−509.
(7) Zoldoske, D. F.; Genito, S.; Jorgensen, C. *Calif. Agric. Technol. Inst. Publ.* **1995**, 1−4.
(8) Russo, D.; Zaidel, J.; Laufer, A.; Gerstl, Z. *Soil Sci. Soc. Am. J.* **2001**, *65*, 1648−1658.
(9) Lee, Y. D.; Kim, H. J.; Chung, J. B.; Jeong, B. R. *J. Agric. Food Chem.* **2000**, *48*, 5376−5382.
(10) Chopra, I.; Kumari, B.; Sharma, S. K. *Environ. Monit. Assess.* **2010**, *160*, 123−126.
(11) Simmons, L. D.; Derr, J. F. *Weed Technol.* **2007**, *21*, 873−876.

DOI: 10.1021/jf504839q
J. Agric. Food Chem. 2015, 63, 1682−1688

(12) Lin, H. T.; Chen, S. W.; Shen, C. J.; Chu, C. *Bull. Environ. Contam. Toxicol.* **2007**, *79*, 84−86.
(13) Franklin, R. E.; Quisenberry, V. L.; Gossett, B. J.; Murdock, E. C. *Weed Technol.* **1994**, *8*, 6−16.
(14) Undabeytia, T.; Mishael, Y. G.; Nir, S.; Papahadjopoulos-Sternberg, B.; Rubin, B.; Morillo, E.; Maqueda, C. *Environ. Sci. Technol.* **2003**, *37*, 4475−4480.
(15) Undabeytia, T.; Nir, S.; Rubin, B. *J. Agric. Food Chem.* **2000**, *48*, 4767−4773.
(16) Sánchez-Verdejo, T.; Undabeytia, T.; Nir, S.; Maqueda, C.; Morillo, E. *Environ. Sci. Technol.* **2008**, *42*, 5779−5784.
(17) Radian, A.; Mishael, Y. G. *Environ. Sci. Technol.* **2008**, *42*, 1511−1516.
(18) Bojemueller, E.; Nennemann, A.; Lagaly, G. *Appl. Clay Sci.* **2001**, *18*, 277−284.
(19) Mishael, Y. G.; Undabeytia, T.; Rabinovitz, O.; Rubin, B.; Nir, S. *J. Agric. Food Chem.* **2003**, *51*, 2253−2259.
(20) El-Nahhal, Y.; Nir, S.; Serban, C.; Rabinovitz, O.; Rubin, B. *J. Agric. Food Chem.* **2001**, *49*, 5364−5371.
(21) Celis, R.; Hermosín, M. C.; Carrizosa, M. J.; Cornejo, J. *J. Agric. Food Chem.* **2002**, *50*, 2324−2330.
(22) Bakhtiary, S.; Shirvani, M.; Shariatmadari, H. *Chemosphere* **2013**, *90*, 699−705.
(23) Carrizosa, M.; Calderon, M.; Hermosin, M.; Cornejo, J. *Sci. Total Environ.* **2000**, *247*, 285−293.
(24) Li, J.; Jiang, M.; Wu, H.; Li, Y. *J. Agric. Food Chem.* **2009**, *57*, 2868−2874.
(25) Ziv, D.; Mishael, Y. G. *J. Agric. Food Chem.* **2008**, *56*, 9159−9165.
(26) Undabeytia, T.; Nir, S.; Gomara, M. J. *Langmuir* **2004**, *20*, 6605−6610.
(27) Li, J.; Li, Y.; Dong, H. *J. Agric. Food Chem.* **2008**, *56*, 1336−1342.
(28) Huh, K. M.; Min, H. S.; Lee, S. C.; Lee, H. J.; Kim, S.; Park, K. *J. Controlled Release* **2008**, *126*, 122−129.
(29) Mishael, Y. G.; Undabeytia, T.; Rytwo, G.; Papahadjopoulos-Sternberg, B.; Rubin, B.; Nir, S. *J. Agric. Food Chem.* **2002**, *50*, 2856−2863.
(30) Polubesova, T.; Nir, S.; Rabinovitz, O.; Borisover, M.; Rubin, B. *J. Agric. Food Chem.* **2003**, *51*, 3410−3414.
(31) Mishael, Y. G.; Undabeytia, T.; Rabinovitz, O.; Rubin, B.; Nir, S. *J. Agric. Food Chem.* **2002**, *50*, 2864−2869.
(32) Rytwo, G.; Gonen, Y.; Afuta, S.; Dultz, S. *Appl. Clay Sci.* **2005**, *28*, 67−77.
(33) Radian, A.; Carmeli, M.; Zadaka-Amir, D.; Nir, S.; Wakshal, E.; Mishael, Y. G. *Appl. Clay Sci.* **2011**, *54*, 258−263.
(34) Katz, H.; Mishael, Y. G. *J. Agric. Food Chem.* **2014**, *62*, 50−57.
(35) Kumar, J.; Nisar, K.; Shakil, N. a; Walia, S.; Parsad, R. *J. Environ. Sci. Health B* **2010**, *45*, 330−335.
(36) Pavan, P. C.; Crepaldi, E. L.; de A. Gomes, G.; Valim, J. B. *Colloids Surfaces A: Physicochem. Eng. Asp.* **1999**, *154*, 399−410.
(37) Galán-Jiménez, M. D. C.; Mishael, Y.-G.; Nir, S.; Morillo, E.; Undabeytia, T. *PLoS One* **2013**, *8*, No. e59060.

DOI: 10.1021/jf504839q
J. Agric. Food Chem. 2015, 63, 1682−1688

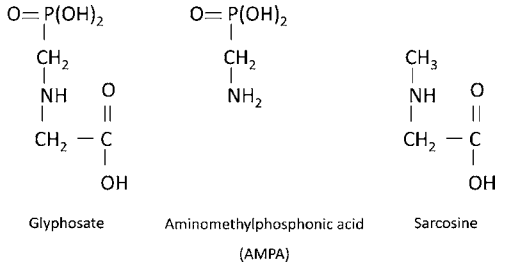

Figure 1. Chemical structure of glyphosate and its metabolites aminomethylphosphonic acid and sarcosine.

no established proof that metabolic degradation plays a role in either glyphosate tolerance or resistance in nontransgenic plants.

Enhanced metabolic degradation of herbicides is a common mechanism of resistance to many herbicide classes.[18] Because several plant species, including all *Ipomoea* species thus far studied, can metabolize glyphosate, we hypothesized that enhanced metabolism of glyphosate would be a likely response to strong selection with glyphosate (resistance) and could also explain biotype differences in susceptibility to glyphosate that are not due to selection with glyphosate (tolerance). The objectives of this research were to investigate (i) the variability in tolerance to glyphosate among *I. lacunosa* accessions, (ii) if there is any correlation between metabolism of glyphosate to AMPA or sarcosine and the level of tolerance, and (iii) the role of differential translocation as a potential mechanism of tolerance to glyphosate.

MATERIALS AND METHODS

Plant Material and General Experimental Conditions. During 2004 through 2006, seeds from *I. lacunosa* were randomly collected at multiple locations across the U.S. that had or had not been exposed to glyphosate for several years in GR crop management systems.[19] *I. lacunosa* seeds were stored at 10 °C until used. Germination of seed, transplanting of seedlings, growth of plants, and all experiments were conducted under greenhouse growing conditions (30/22 °C day/night, 12 h photoperiod under natural sunlight) unless otherwise described. Seeds were planted at 1 cm depth in 50 × 20 × 6 cm plastic trays with drain holes containing a commercial Metro-Mix 360 potting mix (Sun Gro Horticulture, Bellevue, WA). Two weeks after emergence, seedlings were transplanted into 6 × 6 × 6 cm pots containing the same soil mix. Plants were watered as needed. Plants were fertilized once by subirrigating the pots with a Miracle-Gro nutrient solution (The Scotts Company, Marysville, OH) containing 200 mg/L each of N, P_2O_5, and K_2O at 4 weeks after transplanting. All herbicide treatments were applied with an air-pressurized indoor spray chamber equipped with an 8002E flat-fan nozzle (Spraying Systems Company, Wheaton, IL) delivering 140 L/ha at 280 kPa and were made on plants of each accession at the four- to five-leaf stage (beginning to vine).

Glyphosate Dose Response in *I. lacunosa* Accessions. Fourteen *I. lacunosa* accessions were selected strictly on the basis of their response to preliminary screening, being the seven most tolerant (MS-WAS-8, MS-VJ, MS-SCO-1, MS-PAN-1, MS-YAZ-2, MS-COA-1, and MS-ITA-1) and the seven least tolerant (MS-LEE-2, MS-WAS-2, MS-MAR-1, MS-99, MS-90, MS-QUI-1, and MS-YAZ-1) accessions, among 76 initial accessions. Plants of each of the 14 accessions were treated with the Roundup WeatherMAX formulation of glyphosate (Monsanto Company, St. Louis, MO) at 0, 105, 210, 420, 840, and 1680 g of ae (acid equivalent)/ha. Shoot fresh weights were recorded at 2 weeks after treatment (WAT) only, as the separation of vines between control plants becomes problematic at later growth stages. Shoot fresh weight was expressed as a percent of nontreated plants. There were four replications per treatment, one plant per replication, in a completely randomized design, and the experiment was conducted twice.

Glyphosate Metabolism Studies in Intact Plants. The most tolerant (MT) (MS-WAS-8) and least tolerant (LT) (MS-YAZ-1) accessions were selected on the basis of the dose response assay described above and were analyzed for metabolism of glyphosate to AMPA and sarcosine as well as shikimate, the precursor of aromatic amino acids. Two experiments were conducted. In the first, five plants were treated with glyphosate at 420 g of ae/ha (0.5 × field rate) and harvested at 2 WAT, and the experiment was conducted twice. In the second, three plant replications were treated at their respective GR_{50} doses (MT, 151 g of ae/ha; LT, 58 g of ae/ha) and at 1, 3, and 6 days after treatment (DAT) plants were harvested. The GR_{50} rate for each plant accession was selected so that the two accessions would have the same level of phytotoxicity interfering with metabolism of glyphosate. There was one plant per replication in a completely randomized design, and the experiment was repeated over time. At harvesting, plants from both experiments were excised at the soil surface, washed with running water, rinsed with distilled water to remove glyphosate remaining on the leaf surface, and blotted dry with paper towels. Each sample consisted of all leaves from each single plant (replicate) and leaves were predried in a greenhouse and then oven-dried at 80 °C for 2 weeks, ground with a mortar and pestle, and analyzed for glyphosate, AMPA, shikimate, and sarcosine.

Extraction and derivation were performed for glyphosate and AMPA analysis according to previously reported procedures,[20,21] with modifications. Ground tissue (0.25 g) was extracted with 8 mL of water in a 20 mL scintillation vial, shaken, placed in a sonicating bath for 20 min, and then centrifuged at 5000*g*, 20 °C, for 20 min. The supernatant was collected, the remaining tissue sample pellet was extracted a second time by adding 4 mL of water, and procedures were performed as in the first extraction. The volume of the combined supernatant was measured and syringe-filtered (0.45 μm) into a new 20 mL plastic vial. Then, 45 μL of 12.1 N HCl was added to the supernatant and shaken. Four milliliters was transferred to a 20 mL scintillation vial with a Teflon-lined cap, shaken with 2 mL of CH_2Cl_2, and centrifuged at 300*g*, 25 °C, for 10 min. A portion (1.8 mL) of the top water layer was taken, and 200 μL of acidic modifier [(16 g of KH_2PO_4:160 mL of H_2O):13.4 mL of 12.1 N HCl] was added and vortexed. One milliliter was loaded to a cation exchange (CAX) resin column, 0.8 × 4 cm AG 50W-X8 Resin 200−400 mesh, H^+ (Bio-Rad Laboratories, Hercules, CA), previously equilibrated with two 5 mL portions of water. The sample was eluted until the column bed was reached. Seven hundred microliters of CAX mobile phase (160 mL of H_2O:40 mL of MeOH:2.7 mL of HCl) was added, eluted, and discarded. Twelve milliliters of CAX mobile phase was again added to the column to elute the analytes. The eluate was collected in a 20 mL vial and evaporated to dryness using a Savant speed vac. A 1.5 mL volume of CAX mobile phase was added to the dried sample, and then the vial was placed in a sonicating bath for 30 min. A 20 μL aliquot was syringe-filtered (0.2 μm) and added to 640 μL of a solution of 2,2,3,3,4,4,4-heptafluoro-1-butanol and trifluoroacetic anhydride (1:2, v/v) in a chilled 4 mL vial with a Teflon-lined lid in a duplicate extraction experiment. The mixture was equilibrated at room temperature for 10 min. The vial was transferred to a heating block at 90 °C for 1 h and then allowed to cool to room temperature. The solvent was evaporated under a stream of nitrogen at 50 °C, and the residue was dissolved in 80 μL of ethyl acetate containing 0.2% citral.

For the analysis of shikimate and sarcosine, a 1 g powdered sample was placed in a 20 mL scintillation vial and extracted with 15 mL of water, shaken, placed in a sonicating bath for 20 min, and then centrifuged at 5000*g*, 20 °C, for 20 min. A 4 mL aliquot of supernatant was removed to a new 20 mL vial. The tissue sample pellet was extracted a second time by adding 5 mL of water, and procedures were performed as in the first extraction. A 2 mL aliquot of supernatant was removed and combined with the previous 4 mL aliquot, totaling 6 mL of supernatant. Then, 30 μL of HCl was added to supernatant and shaken. One half of the total supernatant was transferred to a tared vial, frozen, and lyophilized. The dry product was recovered, and 5 mg of lyophilized extract was transferred to gas chromatography (GC)

DOI: 10.1021/jf5055722
J. Agric. Food Chem. 2015, 63, 1689−1697

vial, in a duplicate extraction experiment, to be treated with 50 μL of *N*,*O*-bis(trimethylsilyl)trifluoroacetamide and *N*,*N*-dimethylformamide (1:1, v/v) and vortexed. The vial was transferred to a heating block at 70 °C for 30 min, allowed to cool to room temperature, and centrifuged at 300*g*, 25 C, for 10 min. Then, 25 μL of clear liquid was transferred to a GC vial and analyzed by GC−mass spectrometry (MS).

Analysis of glyphosate and AMPA was performed by GC−MS on a 6890 GC gas chromatograph (Agilent, Santa Clara, CA) coupled to a JEOL GCMateII mass spectrometer (JEOL USA, Peabody, MA), using a 30 m length × 0.25 mm i.d., 0.25 μm film, DB-5 capillary column (Agilent Technologies, Foster City, CA). The GC temperature program: initialized at 80 °C, held for 2.5 min, raised to 160 °C at 30 C/min rate, raised to 270 °C at 40 C/min rate, raised to 300 °C at 35 °C/min rate, and kept at this temperature for 1.5 min. The carrier gas was ultrahigh purity helium at a 1 mL/min flow rate. The injection port was kept at 250 °C, and the GC−MS interface and the ionization chamber were kept at 230 °C. The volume of injection was 1 μL (splitless injection). The mass spectrum was acquired in the positive, low resolution, selected ion monitoring mode, with electron impact of 70 eV. AMPA was monitored using *m*/*z* 571, 502, 446, and 372 (t_R 5.97 min); glyphosate was monitored using *m*/*z* 611, 584, 486, and 460 (t_R 6.77 min). Glyphosate and AMPA in the samples were quantitated from a calibration curve of the respective standards: glyphosate, purity 99.5% (Chem Service, West Chester, PA), and AMPA, purity 99% (Sigma-Aldrich, Saint Louis, MO). Analysis was performed in duplicate. The LOD and LOQ for glyphosate were 19.9 and 160 pg on column (1 μL injection), respectively. The LOD and LOQ for AMPA were 4.16 and 12.61 pg on column (1 μL injection), respectively.

Analysis of sarcosine and shikimate was performed by GC-MS using the same conditions as in the analysis of glyphosate and AMPA, except the GC temperature program: initialized at 120 °C, held for 2 min and raised to 300 °C at 17 °C/min rate, and then held at this temperature for 0.5 min. Sarcosine was monitored using *m*/*z* 233, 218, 190, and 160 (t_R 5.58 min); shikimate was monitored at *m*/*z* 462, 447, 372, and 255 (t_R 8.67 min). Sarcosine and shikimic acid in the samples were quantitated from a calibration curve of the respective standards: shikimic acid, purity 99% (Sigma-Aldrich), and sarcosine (Sigma-Aldrich). Analysis was performed in duplicate. Sarcosine was not detected in any of the samples. The LOD and LOQ for shikimate were 929 and 2815 pg on column (1 μL injection), respectively.

Glyphosate Metabolism Studies in Leaf Discs. In a study to eliminate uptake and translocation effects, 4 mm diameter leaf discs were cut with a cork borer from uniform leaves of 18-day-old, greenhouse-grown-MT and LT plants. Three hundred discs were floated on 20 mL of aqueous solutions of technical grade glyphosate for 1 day in 10 cm diameter polystyrene Petri dishes. Treatments were quadruplicated. After incubation, samples were taken for analysis of shikimate, AMPA, and glyphosate content. The 300 discs from each dish were washed in a total of 1 L of Millipore filtered water and then frozen at −80 °C in 50 mL centrifuge tubes until analysis by the methods above. Relative shikimate content was also determined by the method of Shaner et al.[22]

Glyphosate Absorption and Translocation. MT and LT *I. lacunosa* plants were treated with glyphosate as described before at a rate of 840 g of ae/ha, except that the second youngest fully expanded leaf was covered with a water-resistant paper sleeve. This sleeve was removed immediately after herbicide treatment for subsequent (within 30 min of overspray) application of solutions containing ^{14}C-glyphosate, ^{14}C-methyl labeled with 2.0 GBq/mmol specific activity, 99.5% radiochemical purity in an aqueous stock solution of 7.4 MBq/mL (American Radiolabeled Chemicals, Inc., St. Louis, MO). A solution containing glyphosate at a final concentration equivalent to 0.84 kg/ha in 140 L was prepared using ^{14}C-glyphosate, a commercial formulation of glyphosate, and distilled water. A 10 μL volume of the treatment solution, containing 5 kBq of ^{14}C-glyphosate, was applied to the adaxial surface of the not oversprayed second true leaf of 15 cm tall plants in the form of 25 droplets with a microapplicator. Plants were harvested at 1, 4, 24, 48, 96, and 168 h after ^{14}C-glyphosate treatment (HAT) for absorption measurements carried out as described previously.[6]

MT and LT plants were processed for phosphorimaging prior to translocation analysis. The treated leaves from the plants were removed at respective harvest times to wash off unabsorbed radioactivity and set aside. The remaining above ground part of the plant was excised from the roots and mounted on a 27 × 21.25 cm piece of plain white paper. Shoot parts were evenly spread and kept in place with thin strips of clear office tape. Care was taken to avoid contact of the washed treated leaf with other parts of the plant. Roots were gently rinsed with water to remove soil, blotted dry with paper towels, and mounted on a separate sheet as with the shoot. The mounted plant parts were pressed between one or more layers of newspaper, and bookended with two hard cardboard sections. The assembled plant press was held together with large binder clips and stored at −20 °C for later drying. The plant samples were dried in a gravity convection oven set at 60 °C for 24 h. Phosphorimaging was used to develop an image of the plant samples. After the dried sample was cooled to room temperature, the plant was placed in a 20 × 40 cm exposure cassette (GE Healthcare Bio-Sciences Corp., Piscataway, NJ) and brought into contact with a BAS IPSR 2025 E storage phosphor screen (GE Healthcare Bio-Sciences Corp.) under diffused lighting. The apparatus was placed in a dark cabinet for 24 h. A Typhoon FLA 7000 phosphorimager (GE Healthcare) was used to detect distribution of ^{14}C-glyphosate and develop an image. Phosphorimaged plants were carefully removed from the mounting paper and divided into treated leaf, shoot above treated leaf (SATL), shoot below treated leaf (SBTL), and roots, and translocation was measured according to previously described procedures.[6] There were five replications per treatment (harvest) time per plant type (MT/LT).

Statistical Analysis. All data were analyzed by ANOVA via the PROC GLM statement using SAS software version 9.3 (SAS Institute, Cary, NC) to determine the main effects and interactions of the factors at $P < 0.05$. No significant experimental effect was observed in repeated experiments; therefore, data from experiments were pooled. Treatment means in selected experiments were separated using Fisher's Protected LSD test at $P < 0.05$.

Glyphosate dose response data were subjected to nonlinear regression analysis, and a sigmoidal log−logistic curve[23] of the form

$$y = L + \frac{U - L}{\left[1 + \left(\frac{D}{GR_{50}}\right)^{s}\right]} \quad (1)$$

where *y* represents shoot fresh weight reduction as compared to that of nontreated plants in percentage at herbicide rate *D*, *L* is the mean response at very high herbicide rate (lower limit), *U* is the mean response when the herbicide rate is zero (upper limit), *s* is the slope of the line at GR_{50}, and GR_{50} is the glyphosate rate required for 50% growth reduction of *I. lacunosa* plants, was fit to the data. The estimate of the four regression parameters was obtained using Sigma Plot version 11 (Systat Software, San Jose, CA) and tested for significance using the *t*-test method ($P < 0.05$). GR_{50} values of tolerant accessions were compared to that of the least tolerant accession according to the Student *t*-test at $P < 0.05$ with the open-source R software version 2.15.2 (R Foundation for Statistical Computing) using the drc package and drm function, and the comparisons were given by means of the selectivity index (SI) function.

In the glyphosate metabolism study, data variance was visually inspected by plotting residuals to confirm the homogeneity of variance prior to statistical analysis using SAS. The Shapiro−Wilk test was applied to verify if the data among accessions were normally distributed, and Hartley's F_{max} test was applied to verify if different populations have a similar variance using SAS. Means separation was performed using Fisher's Protected LSD test at $P < 0.05$.

RESULTS AND DISCUSSION

Glyphosate Dose Response in *I. lacunosa* Accessions. The F-test in the ANOVA was significant ($P < 0.0035$) for the pairing of dependent variable (fresh weight reduction) with

DOI: 10.1021/jf5055722
J. Agric. Food Chem. 2015, 63, 1689−1697

Table 1. Effect of Glyphosate and GR_{50} Rate on Shikimate, Glyphosate, and Aminoethylphosphonic Acid (AMPA) Concentrations in the Most Tolerant (MT) and Least Tolerant (LT) *I. lacunosa* Accessions

accession[a]	glyphosate rate, g of ae/ha	DAT	shikimate (SE),[b,c] μg/g of tissue	glyphosate (SE),[c] μg/g of tissue
MT	420	14	683.94 (554.37) b	3.57×10^{-5} (2.02×10^{-5}) b
LT			9868.30 (10 793.31) a	9.78×10^{-5} (3.63×10^{-5}) a
MT	151[d]	1	190.85 (16.87) A	14.87 (2.66) B
		3	148.16 (40.42) AB	11.55 (3.01) BC
		6	97.44 (22.28) B	22.66 (7.48) A
LT	58[d]	1	135.94 (34.93) AB	5.40 (2.62) C
		3	133.35 (27.20) AB	5.19 (1.61) C
		6	118.39 (40.23) B	4.77 (3.78) C
accession[a]	glyphosate rate, g of ae/ha	DAT	glyphosate/AMPA ratio (SE)[c]	
MT	420	14	1.28×10^{-5} (0.46×10^{-5}) b	
LT			3.76×10^{-5} (1.11×10^{-5}) a	
MT	151[d]	1	23.55 (2.69) A	
		3	20.35 (6.02) AB	
		6	26.26 (9.06) A	
LT	58[d]	1	17.69 (5.61) AB	
		3	10.82 (5.03) BC	
		6	6.91 (5.01) C	

[a]The most tolerant (MT) was MS-WAS-8 and least tolerant (LT) was MS-YAZ-1. [b]SE represents the standard error of the mean where $n = 10$ (pooled data from two experiments of glyphosate at 420 g of ae/ha) and $n = 6$ (pooled data from two experiments of glyphosate at GR_{50} rate). [c]Values followed by the same letter (lowercase when MT and LT were treated with glyphosate at 420 g ae/ha, uppercase when MT and LT were treated with glyphosate at 151 and 58 g ae/ha, respectively) within each column are not significantly different at the 5% level as determined by the LSD test. [d]GR_{50} indicates the glyphosate dose required to cause a 50% reduction in plant growth, 151 g of ae/ha for the MT accession, and 58 g of ae/ha for the LT accession.

main effect terms (accessions and glyphosate dose) and interaction terms, indicating that the response to glyphosate varied among the 14 *I. lacunosa* accessions (data not shown). The accessions with less previous exposure to glyphosate in GR crops were the ones with numerically smaller GR_{50} values (MS-99 106, MS-90 91, MS-QUI-1 59, and MS-YAZ-1 58 g/ha glyphosate) (data not shown). Thus, the higher GR_{50} values of some accessions could be due to selection with glyphosate. If so, these more "tolerant" accessions may actually be categorized as resistant (genetically changed by selection with glyphosate). *I. lacunosa* went from the fifth to the second most common weed in Mississippi soybean six years after the introduction of GR soybean.[24] Therefore, it appears that the emergence of *I. lacunosa* as a major weed problem has coincided with the widespread adoption of GR crops. The tolerance/resistance of *I. lacunosa* may be a consequence of a mutation(s) arising after the introduction of the herbicide, or the resistance gene(s) may predate the widespread use of the herbicide with selection from preexisting genetic variation in the population.[11] Also, localized adaptations have probably resulted in the evolution of several variably glyphosate tolerant *I. lacunosa* ecotypes in North America, which could, in turn, be unrelated to exposure of the population to glyphosate.

Intersimple sequence repeat (ISSR) markers were used to study intraspecific population structure in *I. lacunosa*.[25] Subpopulation differentiations were detected in those accessions from proximal locations and clustered together populations with high similarity of agricultural environments, like Arkansas and Mississippi. However, intraspecific accessions almost always clustered together among various *Ipomoea* species.[26] Moreover, it is possible that the colonization of *I. lacunosa* in the southern U.S. started with only one genotype and evolved with time due to localized adaptations and hybridization with compatible species. Consequently, the morphological and genetic variance of *I. lacunosa* in the southern U.S. may impact the efficacy of weed management strategies.

The MS-YAZ-1 accession had the lowest GR_{50} value of 58 g/ha glyphosate and MS-WAS-8 accession had the highest GR_{50} value of 151 kg/ha glyphosate, resulting in a R/S (proportion of GR_{50} values of most and least tolerant accessions) ratio of 2.6. The 2.6-fold R/S ratio of glyphosate tolerance is more than that reported for other *I. lacunosa* accessions from the southern U.S., which was 1.9-fold less when their most tolerant and least tolerant populations were compared.[19] In weed species that have evolved glyphosate resistance, the resistance mechanisms thus far elucidated are target-site-based and non-target-site-based.[27,28] The following processes have been reported to provide different levels of resistance to glyphosate: reduced glyphosate absorption (~3-fold),[29,30] impaired glyphosate translocation (~3- to 13-fold),[31−34] sequestration to the vacuole (2.9−5.6-fold),[35] EPSPS mutations (~2- to 15-fold),[36,37] and overproduction of target enzyme (6−8-fold)[38] in weedy species.

Because legume species have been reported to metabolize glyphosate,[7,39] different sensitivities to glyphosate in certain populations of *I. lacunosa* may be due to differences in the levels of degradation of glyphosate to the much less phytotoxic metabolite of glyphosate, AMPA, or even sarcosine. To test this hypothesis, glyphosate, shikimate, AMPA, and sarcosine levels were measured in glyphosate-treated leaves of the MT and LT accessions.

Glyphosate Metabolism Studies. Two experiments were performed. In the first, the LT and MT accessions were each treated with 420 g/ha glyphosate (half the recommended field rate), after which shikimate, glyphosate, and AMPA levels in the entire plant shoot were determined at 14 DAT (Table 1). In the second experiment, the LT and MT bioptyes were treated with GR_{50} doses (58 and 151 g/ha, respectively), after which shikimate, glyphosate, and AMPA shoot contents were

DOI: 10.1021/jf5055722
J. Agric. Food Chem. 2015, 63, 1689−1697

measured at 1, 3, and 6 DAT (Table 1). Sarcosine was not detected in either accession in either experiment.

In the first experiment, shikimate levels were much more elevated (ca. 15-fold more) in the LT than the MT accession. There were no differences in AMPA levels between the two accessions, but glyphosate levels were more than twice as high in the LT than the MT accession. Such an experiment provides only pool sizes at one time point, without any information on flux of compounds through those pools. The higher glyphosate pool in the LT could be due to a slower rate of glyphosate metabolism in the LT than the MT accession. An alternative explanation could be the reduced metabolism of glyphosate in the LT accession caused by metabolic dysfunction, due to the fact that this accession was more severely affected by the herbicide. Also, reduced growth during the 14 DAT would mean that the glyphosate would be more concentrated in the LT accession.

The second experiment in which the two accessions should have been equally affected by the glyphosate treatment was designed to better assess whether glyphosate metabolism differs in the two accessions, as the higher rates used in the first experiment may have disrupted metabolic processes. By blocking EPSPS, glyphosate causes many-fold increases in shikimate levels in non-GR plants and, consequently, elevated shikimate levels are used as an early and highly sensitive indicator of glyphosate effects on glyphosate-sensitive plant tissue.[40,41] The nonsignificantly different levels of shikimate between the two accessions at 1, 3, and 6 DAT indicated that the GR_{50} doses for the two accessions had similar physiological effects (Table 1). The only signficant difference between the two accessions was a higher shikimate level at 1 DAT of the MT accession than at 6 DAT in the LT accession. Shikimate levels decreased from 1 to 6 DAT for both accessions, but the only statistically significant change with time for an accession was a reduction for the MT accession between 1 and 6 DAT (Table 1).

AMPA levels were the same in both accessions at all times after treatment (Table 1). Although AMPA levels trended upward from 1 to 6 DAT for both accessions, the increase was not statistically significant. However, glyphosate concentrations were higher at 1 and 6 DAT (ca. 3-fold and 5-fold, respectively) in the MT than the LT accession. Under different growth conditions, Reddy et al.[21] found that AMPA levels in treated soybean leaves were highest 1 DAT and decreased over a period of 22 days.

If there were enhanced metabolism of glyphosate in the MT accession, one would not expect the higher levels of glyphosate than LT observed above. If the uptake and translocation as a percentage of glyphosate applied were the same in the two accessions, one would expect about 2.6-fold more glyphosate in the MT than the LT accession when each is treated with their respective GR_{50} dose. This is approaching the 1 DAT result for both glyphosate and AMPA (2.75-fold and 2.13-fold more in the MT than the LT) (Table 1). The nonsignficant differences in the glyphosate to AMPA ratio between the two accessions at 1 and 3 DAT suggest similar levels of metabolism as a percent of glyphosate taken up. However, the 6 DAT glyphosate to AMPA ratio was significantly higher in the MT than the LT (ca. 3.7 fold), indicating that metabolism could be higher as a percent of glyphosate taken up in the LT accession (Table 1). Again, these data are only a snapshot in time of pool sizes that do not take into account flux through the pools due to the translocation of glyphosate and AMPA to roots and metabolic degradation of AMPA. Nevertheless, these data do not support the theory that metabolism of glyphosate explains the relative sensitivities to glyphosate in the two *I. lacunosa* accessions tested.

There has been no conclusive evidence of metabolic degradation as an important mechanism of evolved resistance to glyphosate.[8] The fact that *I. lacunosa* accessions with variable levels of tolerance accumulated the same amount of AMPA does not support the view that enhanced metabolism of glyphosate is involved in the tolerance of the MT accession. Gene mutation or amplification of plant genes for GOX-like enzyme activity or horizontal transfer of microbial genes for glyphosate-degrading enzymes could result in GR weeds.[16] This mechanism of tolerance could be combined with another mechanism such as differential absorption or translocation of glyphosate. This is supported by our results of increased glyphosate concentration from 1 to 6 DAT in the MT, suggesting that glyphosate may be slowly taken up in this accession. This hypothesis of single or multiple mechanisms of glyphosate tolerance was investigated using studies of absorption and translocation of glyphosate in the *I. lacunosa* accessions.

Metabolism in cut leaf discs was determined to avoid effects of potential differences in uptake and translocation between the two accessions. Glyphosate content was slightly higher in the MT than the LT accession at each glyphosate treatment concentration (Figure 2). AMPA levels rose with glyphosate dose for both accessions (Figure 2), but the percentage of AMPA as a fraction of glyphosate as glyphosate dose increased was 3.5, 7.2, and 8.7% for the MT accession vs 13, 9.7, and 10.4% for the LT accession. These data do not support the view that differences in glyphosate metabolism have anything to do with the differences in tolerance to glyphosate between these two accessions. Shikimate levels after 24 h of incubation in 0.1, 0.33, or 1 mM glyphosate were the same or slightly higher in the LT accession at the three concentrations (Figure 2). The differences in shikimate levels between MT and LT plants were not as great as in whole plants (Table 1). These results provide further support for the view that metabolism is not involved in the difference between the LT and MT accessions.

^{14}C-Glyphosate Absorption and Translocation. The absorption pattern of ^{14}C-glyphosate in the MT and LT accessions of *I. lacunosa* was similar throughout the time course of 168 HAT (Figure 3A). Glyphosate absorption amounts reported here (21−25%, 42−43%, and 45−46% of applied at 24, 48, and 96 HAT, respectively) are similar to previously reported estimates (23% and 43% of applied at 24 and 96 HAT, respectively),[6] but lower than levels (57−63%, 52−58%, and 53−59% of applied at 26, 50, and 74 HAT, respectively) reported for three different formulations of glyphosate in *I. lacunosa*.[42] In *I. cordatotriloba* Dennstedt (sharppod morningglory), glyphosate absorption was much higher (75% of absorbed at 72 HAT)[43] than for MT and LT accessions of *I. lacunosa* reported here.

The amount of ^{14}C-glyphosate that translocated out of the treated leaves of the MT and LT plants was similar up to 4 HAT (Figure 3B). Thereafter, the LT accession translocated more (41 and 53% of absorbed at 24 and 48 HAT, respectively) ^{14}C-glyphosate than the MT accession (26 and 38% of absorbed at 24 and 48 HAT, respectively) out of the treated leaf, with translocated amounts leveling off to similar levels in both populations by 96 HAT (49 and 51% of absorbed in LT and MT, respectively) and 168 HAT (48 and 49% of absorbed

DOI: 10.1021/jf5055722
J. Agric. Food Chem. 2015, 63, 1689−1697

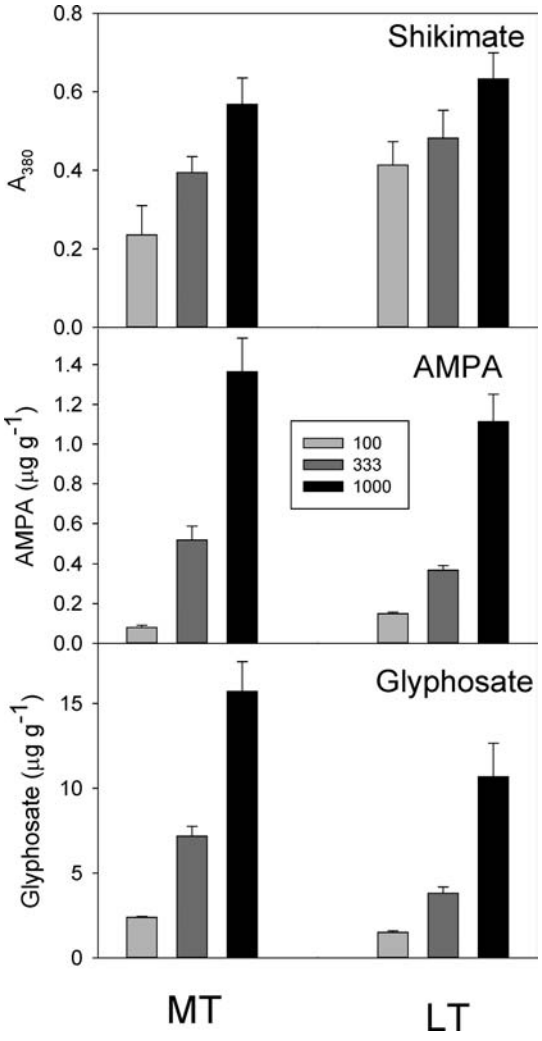

Figure 2. Shikimate, glyphosate, and AMPA levels in leaf discs of MT and LT *I. lacunosa* floating on 0.100, 0.333, and 1.000 mM glyphosate for 24 h.

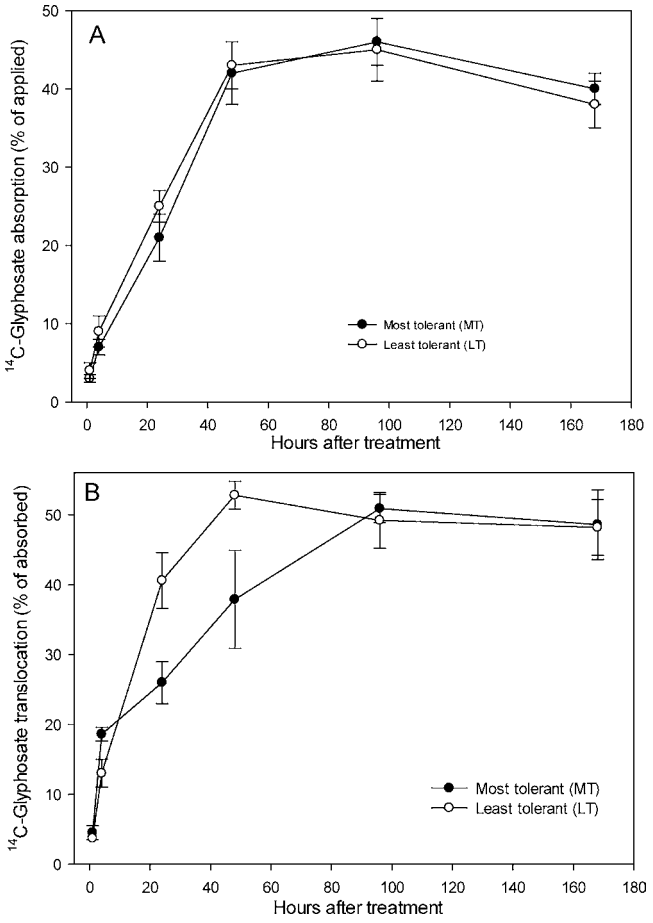

Figure 3. Absorption (A) and translocation (B) of ^{14}C-glyphosate in most (MT, closed circles) and least (LT, open circles) tolerant *Ipomoea lacunosa* accessions. Vertical bars represent standard error of mean (n = 5).

in LT and MT, respectively). The translocation levels of ^{14}C-glyphosate out of the treated leaf reported here (26–41%, 38–53%, and 49–51% of absorbed at 24, 48, and 96 HAT, respectively) are greater than those reported previously in *I. lacunosa* (5 and 23% of absorbed at 24 and 96 HAT, respectively)[6] and *I. cordatotriloba* (13% of absorbed at 72 HAT),[43] with the same formulation of the potassium salt of glyphosate used in all cases.

Distribution of absorbed ^{14}C-glyphosate in the MT and LT accessions is summarized in Table 2. The quantity of ^{14}C-glyphosate that remained in the treated leaf was higher in the LT (87% of absorbed) than in the MT plants (81% of absorbed) at 4 HAT. Thereafter, the MT accession retained more glyphosate in the treated leaf (74 and 62% of absorbed at 24 and 48 HAT, respectively) than the LT accession (59 and 47% of absorbed at 24 and 48 HAT, respectively). A similar trend was reflected in the SATL where the level of glyphosate in the MT plants was higher (15% vs 5% of absorbed at 4 HAT) and lower (14% vs 20% and 19% vs 25% of absorbed at 24 and 48 HAT, respectively) than the LT plants. The MT accession retained more ^{14}C-glyphosate in SBTL (12% of absorbed) than the LT accession (8% of absorbed) at 48 HAT. However, the LT accession roots contained more glyphosate (20% of absorbed) than those of the MT accession (7% of absorbed) at 48 HAT. Distribution of ^{14}C-glyphosate in the treated leaf and other parts of the plant was generally lower and higher, respectively, across the LT and MT accessions compared to previous reports in *I. lacunosa*[6] and *I. cordatotriloba*[43] within 24–96 HAT, which is an extension of translocation observations.

Phosphorimaging was used to generate autoradiographs of MT and LT plants treated with ^{14}C-glyphosate to visualize ^{14}C-glyphosate translocation patterns. ^{14}C-glyphosate movement was discernible in the SATL of the LT accession (Figure 4) at 24 HAT, but not the MT accession (Figure 5). The intensity of the autoradiograph of SATL was greater in the LT accession (Figure 4) at 48 HAT compared to that of the MT accession (Figure 5), reflecting the translocation and distribution data at 48 HAT. A closer examination of the colored plant specimen of the LT accession at 168 HAT indicated extensive chlorosis compared to the case of the MT population (data not shown) at the same harvest time. Inhibition of the apical meristems in the LT population may have caused a feedback inhibition of glyphosate loading, thereby resulting in numerically reduced glyphosate levels in SATL of LT plants (22 and 23% of absorbed at 96 and 168 HAT, respectively) compared to the level of the MT plants (30 and 34% of absorbed at 96 and 168 HAT, respectively). The progressive increase in intensity of the root in LT (data not shown) could be partly due to a switch to

DOI: 10.1021/jf5055722
J. Agric. Food Chem. 2015, 63, 1689–1697

Table 2. Distribution of ^{14}C-Glyphosate (% Absorbed) in Most Tolerant (MT) and Least Tolerant (LT) *Ipomoea lacunosa* Accessions[a,b],

	hours after treatment											
accession	1	4	24	48	96	168	1	4	24	48	96	168
	TL						SATL					
MT	96	81	74	62	49	51	1	15	14	19	30	34
LT	96	87	59	47	51	55	2	5	20	25	22	23
LSD (0.05)[c]	ns	5	12	4	ns	ns	ns	4	4	3	ns	ns
	SBTL						Root					
MT	1	2	8	12	8	5	2	2	4	7	13	10
LT	1	4	7	8	6	6	1	4	14	20	21	16
LSD (0.05)	ns	ns	ns	4	ns	ns	ns	ns	ns	4	ns	ns

[a]Abbreviations: LT, least tolerant; MT, most tolerant; ns, not significant; SATL, shoot above treated leaf; SBTL, shoot below treated leaf; TL, treated leaf. [b]Distribution represents partitioning of absorbed ^{14}C-glyphosate between the treated leaf, shoot above treated leaf, shoot below treated leaf, and root. [c]Number indicates significance at the 5% level of probability and ns indicates no significant difference between means within the same column and within the same plant part.

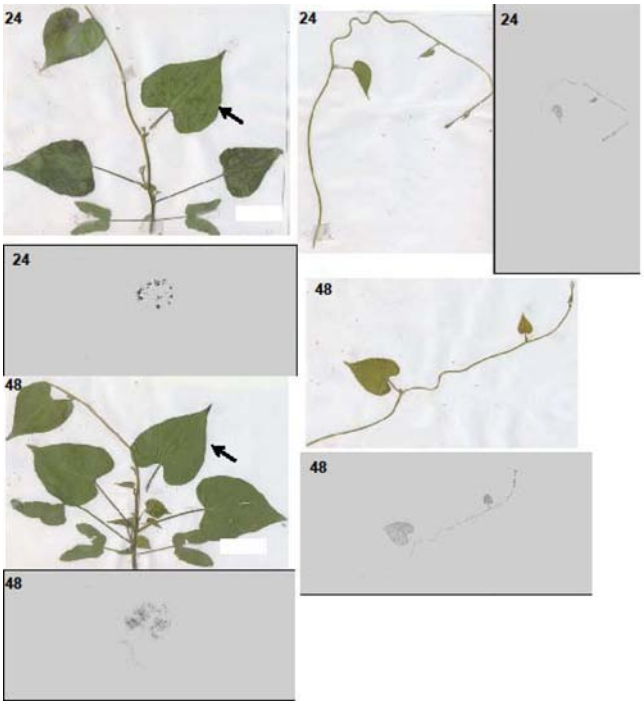

Figure 4. Above ground plant parts and corresponding phosphor-images of least tolerant (LT) *Ipomoea lacunosa* accession. Arrow indicates TL. A part of the SATL appears above the TL. Numbers indicate hours after treatment (HAT) with ^{14}C-glyphosate.

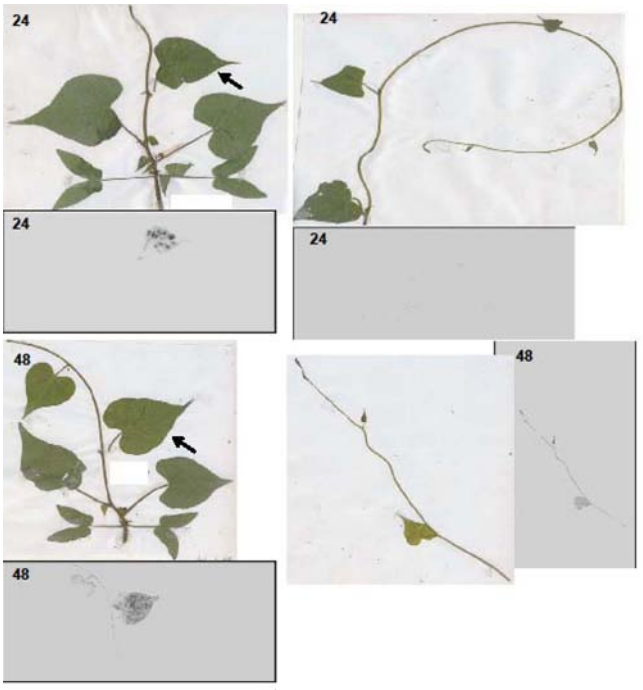

Figure 5. Above ground plant parts and corresponding phosphor-images of most tolerant (MT) *Ipomoea lacunosa* accession. Arrow indicates treated leaf. A part of the SATL appears above the TL. Numbers indicate hours after treatment (HAT) with ^{14}C-glyphosate.

basipetal translocation brought about by inhibition of aerial sinks by glyphosate.

In summary, glyphosate dose response studies were conducted on selected *I. lacunosa* accessions suspected to be tolerant to glyphosate. Results indicated variable tolerance with the most tolerant (MT) and least tolerant (LT) accessions exhibiting GR_{50} values of 151 and 58 g of ae/ha of glyphosate, with a resistance index of 2.6. Contrary to our hypothesis, metabolism of glyphosate to AMPA did not explain the tolerance mechanism. The absence of enhanced metabolic degradation of glyphosate as a resistance or tolerance mechanism of any case of resistance or tolerance thus far studied remains unresolved. ^{14}C-glyphosate absorption patterns were similar in the MT and LT accessions, but the LT accession translocated more glyphosate at 24 and 48 HAT than the MT accession. Differential glyphosate translocation may explain, at least in part, tolerance in the MT accession.

■ ASSOCIATED CONTENT

Supporting Information

A table summarizing regression parameters from glyphosate dose response curves of 14 *I. lacunosa* accessions. This material is available free of charge via the Internet at http://pubs.acs.org.

■ AUTHOR INFORMATION

Corresponding Author

*V.N. tel: 662-686-3760. Fax: 662-686-5422. Email: vijay.nandula@ars.usda.gov.

Present Address

[‖]Monsanto Co., 700 Chesterfield Pkwy West, Chesterfield, MO 63017, USA.

DOI: 10.1021/jf5055722
J. Agric. Food Chem. 2015, 63, 1689−1697

Funding

This work was supported by the United States Department of Agriculture-Agricultural Research Service (USDA-ARS) project number 6402-21000-050-00D. Funding was also provided by Monsanto Co.

Notes

The authors declare no competing financial interest.

■ ACKNOWLEDGMENTS

The authors thank Earl Gordon, Bob Jones, Gloria Hervey, and Robert Johnson for technical support.

■ ABBREVIATIONS USED

AMPA, aminomethylphosphonic acid; DAT, days after treatment; GOX, glyphosate oxidoreductase; GR, glyphosate-resistant; GR_{50}, glyphosate rate required for 50% growth reduction of *I. lacunosa* plants; HAT, hours after treatment; LT, least tolerant; MT, most tolerant; SATL, shoot above treated leaf; SBTL, shoot below treated leaf; WAT, weeks after treatment

■ REFERENCES

(1) Duke, S. O. Biotechnology: Herbicide-Resistant Crops. In *Encyclopedia of Agriculture and Food Systems*; Van Alfen, N., Ed.; Elsevier: San Diego, 2014; Vol. 2, pp 94−116.

(2) Duke, S. O.; Powles, S. B. Glyphosate: A once-in-a-century herbicide. *Pest Manage. Sci.* **2008**, *64*, 319−325.

(3) Heap, I. *The International Survey of Herbicide Resistant Weeds*. http://www.weedscience.org (accessed October 23, 2014).

(4) Owen, M. D. K. Weed species shifts in glyphosate-resistant crops. *Pest Manage. Sci.* **2008**, *64*, 377−387.

(5) Webster, T. M.; Nichols, R. L. Changes in the prevalence of weed species in the major agronomic crops of the southern United States: 1994/1995 to 2008/2009. *Weed Sci.* **2012**, *60*, 145−157.

(6) Koger, C. H.; Reddy, K. N. Glyphosate efficacy, absorption, and translocation in pitted morningglory (*Ipomoea lacunosa*). *Weed Sci.* **2005**, *53*, 277−283.

(7) Reddy, K. N.; Rimando, A. M.; Duke, S. O.; Nandula, V. K. Aminomethylphosphonic acid accumulation in plant species treated with glyphosate. *J. Agric. Food Chem.* **2008**, *56*, 2125−2130.

(8) Starke, R. J.; Oliver, L. R. Interaction of glyphosate with chlorimuron, fomesafen, imazethapyr, and sulfentrazone. *Weed Sci.* **1998**, *46*, 652−660.

(9) Koger, C. H.; Poston, D. H.; Reddy, K. N. Effect of glyphosate spray coverage on control of pitted morningglory (*Ipomoea lacunosa*). *Weed Technol.* **2004**, *18*, 124−130.

(10) Baucom, R. S.; Mauricio, R. Fitness costs and benefits of novel herbicide tolerance in a noxious weed. *Proc. Natl. Acad. Sci. U. S. A.* **2004**, *101*, 13386−13390.

(11) Baucom, R. S.; Mauricio, R. Defense against the herbicide RoundUp® registered predates its widespread use. *Evol. Ecol. Res.* **2010**, *12*, 131−141.

(12) Baucom, R. S.; Mauricio, R. Constraints on the evolution of tolerance to herbicide in the common morning glory: resistance and tolerance are mutually exclusive. *Evolution* **2008**, *62*, 2842−2854.

(13) Leslie, T.; Baucom, R. S. *De novo* assembly and annotation of the transcriptome of the agricultural weed *Ipomoea purpurea* uncovers gene expression changes associated with herbicide resistance. *G3: Genes, Genomes, Genet.* **2014**, DOI: 10.1534/g3.114.013508.

(14) Weed Science Society of America. Herbicide resistance and tolerance defined. *Weed Technol.* **1998**, *12*, 789.

(15) Sandberg, C. L.; Meggitt, W. F.; Penner, D. Absorption, translocation and metabolism of ^{14}C-glyphosate in several weed species. *Weed Res.* **1980**, *20*, 195−200.

(16) Duke, S. O. Glyphosate degradation in glyphosate-resistant and -susceptible crops and weeds. *J. Agric. Food Chem.* **2011**, *59*, 5835−5841.

(17) Green, J. M. Evolution of glyphosate-resistance crop technology. *Weed Sci.* **2009**, *57*, 108−117.

(18) Powles, S. B. Evolution in action: Plants resistant to herbicides. *Annu. Rev. Plant Biol.* **2010**, *61*, 317−347.

(19) Burke, I. C.; Reddy, K. N.; Bryson, C. T. Pitted and hybrid morningglory accessions have variable tolerance to glyphosate. *Weed Technol.* **2009**, *23*, 592−598.

(20) Alferness, P. L.; Wiebe, L. A. Determination of glyphosate and aminomethylphosphonic acid in crops by capillary gas chromatography with mass-selective detection: collaborative study. *J. AOAC Int.* **2001**, *84*, 823−846.

(21) Reddy, K. N.; Rimando, A. M.; Duke, S. O. Aminomethylphosphonic acid, a metabolite of glyphosate, causes injury in glyphosate-treated, glyphosate-resistant soybean. *J. Agric. Food Chem.* **2004**, *52*, 5139−5143.

(22) Shaner, D. L.; Nadler-Hassar, T.; Henry, W. B.; Koger, C. H. A rapid in vivo shikimate accumulation assay with excised leaf discs. *Weed Sci.* **2005**, *53*, 769−774.

(23) Seefeldt, S. S.; Jensen, J. E.; Fuerst, E. P. Log-logistic analysis of herbicide dose-response relationships. *Weed Technol.* **1995**, *9*, 218−227.

(24) Koger, C. H.; Poston, D. H.; Reddy, K. N. Effect of glyphosate spray coverage on control of pitted morningglory (*Ipomoea lacunosa*). *Weed Technol.* **2004**, *18*, 124−130.

(25) Burgos, N. R.; Stephenson, D. O.; Agrama, H. A.; Oliver, L. R.; Bond, J. A. A survey of genetic diversity of the weedy species *Ipomoea lacunosa* L. in the USA mid-south. *Am. J. Plant Sci.* **2011**, *2*, 396−407.

(26) Huang, J. C.; Sun, M. Genetic diversity and relationships of sweet potato and its wild relatives in *Ipomoea* series Batatas (Convolvulaceae) as revealed by inter-simple sequence repeat (ISSR) and restriction analysis of chloroplast DNA. *Theor. Appl. Genet.* **2000**, *100*, 1050−1060.

(27) Perez-Jones, A.; Mallory-Smith, C. Biochemical mechanisms and molecular basis of evolved glyphosate resistance in weed species. In *Glyphosate Resistance in Crops and Weeds*; Nandula, V. K., Ed.; John Wiley & Sons, Inc.: Hoboken, NJ, 2010; 119−140.

(28) Powles, S. B.; Preston, C. Evolved glyphosate resistance in plants: Biochemical and genetic basis of resistance. *Weed Technol.* **2006**, *20*, 282−289.

(29) Michitte, P.; De Prado, R.; Espinoza, N.; Ruiz-Santaella, J. P.; Gauvrit, C. Mechanisms of resistance to glyphosate in a ryegrass (*Lolium multiflorum*) biotype from Chile. *Weed Sci.* **2007**, *55*, 435−440.

(30) Nandula, V. K.; Reddy, K. N.; Poston, D. H.; Rimando, A. M.; Duke, S. O. Glyphosate tolerance mechanism in Italian ryegrass (*Lolium multiflorum*) from Mississippi. *Weed Sci.* **2008**, *56*, 344−349.

(31) Dinelli, G.; Marotti, I.; Bonetti, A.; Catizone, P.; Urbano, J. M.; Barnes, J. Physiological and molecular bases of glyphosate resistance in *Conyza bonariensis* biotypes from Spain. *Weed Res.* **2008**, *48*, 257−265.

(32) Dinelli, G.; Marotti, I.; Bonetti, A.; Minelli, M.; Catizone, P.; Barnes, J. Physiological and molecular insight on the mechanisms of resistance to glyphosate in *Conyza canadensis* (L.) Cronq. biotypes. *Pestic. Biochem. Physiol.* **2006**, *86*, 30−41.

(33) Feng, P. C. C.; Tran, M.; Chiu, T.; Sammons, R. D.; Heck, G. R.; CaJacob, C. A. Investigations into glyphosate-resistant horseweed (*Conyza canadensis*): retention, uptake, translocation, and metabolism. *Weed Sci.* **2004**, *52*, 498−505.

(34) Lorraine-Colwill, D. F.; Powles, S. B.; Hawkes, T. R.; Hollinshead, P. H.; Warner, S. A. J.; Preston, C. Investigations into the mechanism of glyphosate resistance in *Lolium rigidum*. *Pestic. Biochem. Physiol.* **2003**, *74*, 62−72.

(35) Ge, X.; d'Avignon, D. A.; Ackerman, J. J. H.; Sammons, R. D. Rapid vacuolar sequestration: the horseweed glyphosate resistance mechanism. *Pest Manage. Sci.* **2010**, *66*, 345−348.

(36) Baerson, S. R.; Rodriguez, D. J.; Tran, M.; Feng, Y.; Best, N. A.; Dill, G. M. Glyphosate-resistant goosegrass: identification of a

DOI: 10.1021/jf5055722
J. Agric. Food Chem. 2015, 63, 1689−1697

mutation in the target enzyme 5-enolpyruvylshikimate-3-phosphate synthase. *Plant Physiol.* **2002**, *129*, 1265−1275.
(37) Perez-Jones, A.; Park, K. W.; Polge, N.; Colquhoun, J.; Mallory-Smith, C. Investigating the mechanisms of glyphosate resistance in *Lolium multiflorum*. *Planta* **2007**, *226*, 395−404.
(38) Gaines, T. A.; Zhang, W.; Wang, D.; Bukun, B.; Chisholm, S. T.; Shaner, D. L.; Nissen, S. J.; Patzoldt, W. L.; Tranel, P. J.; Culpepper, A. S.; Grey, T. L.; Webster, T. M.; Vencill, W. K.; Sammons, R. D.; Jiang, J.; Preston, C.; Leach, J. E.; Westra, P. Gene amplification confers glyphosate resistance in *Amaranthus palmeri*. *Proc. Natl. Acad. Sci. U. S. A.* **2010**, *107*, 1029−1034.
(39) Duke, S. O.; Rimando, A. M.; Pace, P. F.; Reddy, K. N.; Smeda, R. J. Isoflavone, glyphosate, and aminomethylphosphonic acid levels in seeds of glyphosate-treated, glyphosate-resistant soybean. *J. Agric. Food Chem.* **2003**, *51*, 340−344.
(40) Harring, T.; Streibig, J. C.; Husted, S. Accumulation of shikimic acid: A technique for screening glyphosate efficiency. *J. Agric. Food Chem.* **1998**, *46*, 4406−4412.
(41) Lydon, J.; Duke, S. O. Glyphosate induction of elevated levels of hydroxybenzoic acids in higher plants. *J. Agric. Food Chem.* **1988**, *36*, 813−818.
(42) Li, J.; Smeda, R. J.; Sellers, B. A.; Johnson, W. G. Influence of formulation and glyphosate salt on absorption and translocation in three annual weeds. *Weed Sci.* **2005**, *53*, 153−159.
(43) Steele, G. L.; Senseman, S. A.; Sciumbato, A. S.; Chandler, J. M. Diuron reduces absorption and translocation of glyphosate in sharppod morningglory (*Ipomoea codatotriloba*). *Weed Technol.* **2008**, *22*, 414−419.

DOI: 10.1021/jf5055722
J. Agric. Food Chem. 2015, 63, 1689−1697

new groups of water protons according to their relaxation characteristics. In this work, the effect of freezing and thawing on water relaxation was followed as a means to probe the extent of nano-/microstructural changes resulting from seed germination. An interest was to assess the ability of relaxometry to distinguish the different phases of seeds' germination, particularly the onset of embryonic axis elongation.

In the present study, the model legume *Medicago truncatula* was chosen as an example because several of its germination characteristics are known.[32−34] Radicle protrusion is achieved within ∼20 h. It mobilizes proteins and reserves carbohydrates and involves cell wall loosening.[34] The endosperm cells of *M. truncatula* seeds contain cell wall galactomannan that is metabolized at the end of germination during radicle growth. Due to its hydrophilic nature, galactomannan likely participates in the water balance of the seed during imbibition.[35,36] In this work, NMR relaxometry was evaluated as a means to detect minor developmental perturbations during seed germination. Among the many small chemicals affecting plant biological processes, the growth modulators fusicoccin and oryzalin were added to the imbibition medium to test if relaxometry could differentiate seed germination alterations due to perturbed cell expansion or cell division and elongation.[37−40]

MATERIALS AND METHODS

Plant Material. Seeds of *M. truncatula* cv. Jemalong A17, harvested in 2009 were obtained from INRA UMR 1334 AGAP (Amélioration Génétique et Adaptation des Plantes méditerranéennes et tropicales).

For all conditions, seeds were germinated at 25 °C in darkness in 9 cm diameter Petri dishes on Whatman paper soaked with 4 mL of imbibition solution at pH 5.8. The latter was composed of 0.5 g L^{-1} of a salt solution (1 mM $CaCl_2$ (2 H_2O), 1 mM $MgSO_4$ (7 H_2O), 2 mM KH_2PO_4, 1 mM NH_4NO_3, 4 mM KNO_3, 100 μM $MnSO_4$ (H_2O), 30 μM $ZnSO_4$ (7 H_2O), 0.1 μM $CuSO_4$ (5 H_2O), 1 μM $NaMo_4$ (2 H_2O), 100 μM H_3BO_3, 5 μM KI, 0.1 μM $CoCl_2$ (6 H_2O), 25 μM Na_2Fe−EDTA). This salt solution was used alone (MS) or was complemented with 10 μM oryzalin (OR; Sigma-Aldrich) or 2 μM fusicoccin (FU; Sigma-Aldrich).

Different imbibition times were studied: 0, 1, 2.5, 5, 15, 21, 24, 38, and 48 h.

NMR Measurements. Seeds were packed in 10 mm diameter NMR tubes to reach 1 cm height. For measurement at 20 °C on the fresh seeds, the NMR tubes were immediately placed in the spectrometer and left 10 min for temperature stabilization. For measurement at −20 °C, NMR tubes were immersed in liquid nitrogen for 10 min, transferred to the spectrometer at −20 °C and allowed to equilibrate for 10 min. The frozen seeds were allowed to thaw in the NMR tubes at room temperature for about 4 h prior to measurement at 20 °C. For each condition (time of imbibition, temperature, and growth modulators), NMR measurements were made on five biological replicates. NMR analyses were done using a Minispec mq20 (Bruker) at 0.47 T (20 MHz proton resonance frequency) equipped with a thermostated (±0.1 °C) ^{1}H probe.

The longitudinal (T_1) relaxation times were determined using an inversion−recovery sequence. Recycle delay varied from 0.5 to 5 s, depending on temperature of measurement and imbibition time. Sixteen data points were acquired by incrementing (geometric series) the 180°−90° pulse spacing. Scans acquisition varied from 8 to 64 according to an experiment time of ∼15 min.

The transverse (T_2) relaxation times were determined using a Carr−Purcell−Meiboom−Gill (CPMG) sequence. Only even echoes were collected from 600 to 16000. The 180° pulse separation was 0.08 ms, and the acquisition was from 128 to 512 scans according to an acquisition time of about 15 min.

NMR Data Analysis. Relaxation curves obtained from T_1 and T_2 measurements were subjected to multiexponential nonlinear least-squares fitting (which minimizes the sum of quadratic deviations between fitted and experimental values) of signal amplitude $A_1(t)$ and $A_2(t)$ according to eqs 1 and 2, respectively,

$$A_1(t) = \sum_n P_{1n}(1 - C\exp(-t/T_{1n})) \quad (1)$$

$$A_2(t) = \sum_n P_{2n}\exp(-t/T_{2n}) \quad (2)$$

where P_{in} (i = 1 or 2) is the normalized amplitude/proportion ($\Sigma_n P_{in} = 1$) of the nth component, C is a constant that depends on the 180° pulse efficiency (ideally, $C = 2$), and T_{in} is the T_i value associated with the nth component. A standard F test was used to discriminate between models with different numbers (n) of exponentials.

Free Sugar Extraction. For each imbibition time, the five seed samples studied by NMR were pooled and then divided in three lots to have analytical repetitions. The three lots of seeds at each set of imbibition conditions were frozen and lyophilized. Each dried sample was ground to a fine powder (CryoMill, Retsch). Soluble sugars were extracted from 5 mg powders in 1 mL of deionized water at room temperature overnight with agitation. After filtration through 0.33 μm pore membranes (Millipore), the contents of α-galactosides, sucrose, fructose, and glucose in the filtrate were analyzed by HPAEC.

High-Performance Anionic Exchange Chromatography (HPAEC). Raffinose, stachyose, sucrose, fructose, and glucose were separated by anionic exchange chromatography using a ICS-3000 system (Dionex, Voisin Le Bretonneux, France) controlled by the Chromeleon software. The column used was a Carbopac PA1 analytical column (2 × 250 mm). The column was placed in an oven at 30 °C during the analysis. All mobile phases were sparged and pressurized with helium to prevent adsorption of atmospheric carbon dioxide and subsequent production of carbonate. The flow rate was set at 0.250 mL min^{-1}. The mobile phase consisted of a binary gradient of solvents A (water) and B (sodium hydroxide, 500 mM). Detection of eluted sugars was performed by amperometry using a pulsed electrochemical detector. Eluent B was constant (16%) during the 30 min of the whole process. Five external standards containing a mixture of glucose, fructose, sucrose, raffinose and stachyose in similar concentrations ranging from 0.1 to 50 μg mL^{-1} were used to calibrate the linear response of the detector.

Radicle Length Measurement. To follow the radicle growth, images were taken using a camera at the different imbibition times, inserting a ruler for length calibration, and processed with ImageJ software. The average length of 25 radicles was carried out for each imbibition time.

Statistical Analyses. Statistical analyses were performed using *R*.[41] Exploratory statistics consisted of principal component analysis (PCA). Significant differences between imbibition conditions were evaluated by a Student test from NMR and were set at a probability value of below 5%.

RESULTS

Water Uptake, Radicle Development and Unfreezable Water Evolution in MS Seeds. Water uptake during imbibition showed different events (Figure 1). A very fast uptake was observed up to about 2.5−5 h imbibition with significantly lower water contents for oryzalin-treated seeds. Water uptake of MS-imbibed seeds was constant from 5 h imbibition until the end of the observation after 48 h, with a rate of ∼0.6% h^{-1}. In the presence of fusicoccin and oryzalin, deviations in the water uptake rate were observed, although they were significant for the oryzalin-treated seeds only at 5 (p = 0.011), 21 (p = 0.046), and 48 h (p = 0.002) imbibition. At these times, the oryzalin-treated seeds contained less water than MS-imbibed seeds. After 48 h imbibition, fusicoccin-treated seeds also contained significantly less water than MS-imbibed seeds (p = 0.001). Irrespective of the medium of germination, the water content represented ∼69% (w/w) after 15 h of imbibition. Then a significant increase from 69% to 77% was observed for fusicoccin-treated seeds between

DOI: 10.1021/jf505515n
J. Agric. Food Chem. 2015, 63, 1698−1710

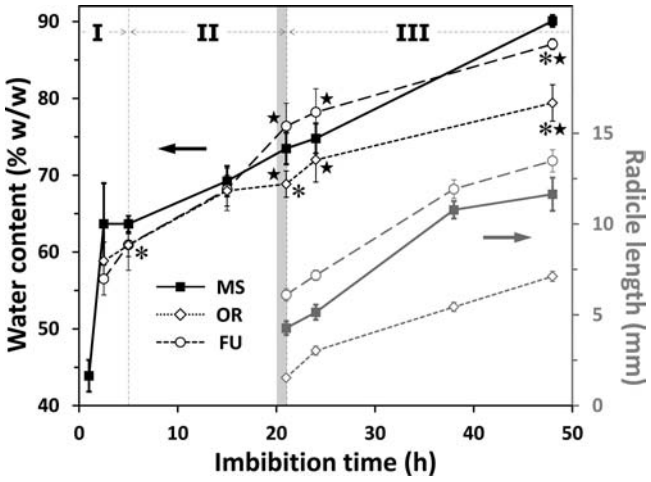

Figure 1. Water uptake and length of radicle after germination of seeds during imbibition in Murashig and Skog (MS) medium and supplemented by oryzalin (OR) or fusicoccin (FU). Bar: standard deviation, $n = 5$; symbols * and ★ indicate significant difference (t-test; $p < 0.05$) between OR and FU media with MS medium and between the two growth modulators, respectively. The shaded area corresponds to the radicle emergence period. At each time of imbibition, radicle length of oryzalin- and fusicoccin-treated seeds differed significantly from MS and between them (t-test, $p < 0.05$, $n = 8–25$). Vertical dashed lines mark the three imbibition phases (I, II, and III) as defined in the text.

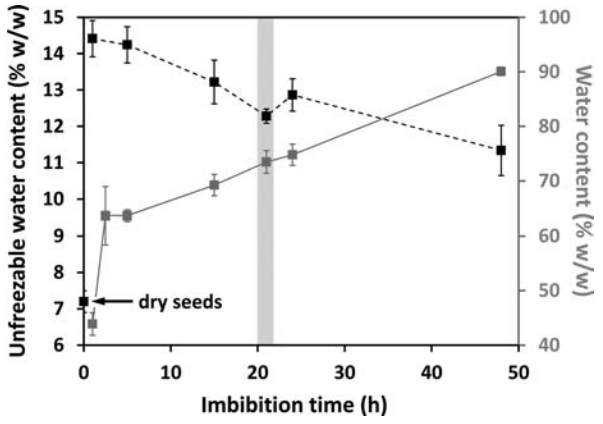

Figure 2. Unfreezable water content (black squares) and water content (gray squares) evolutions during MS seed imbibition. Bar: standard deviation, $n = 3$. The shaded area corresponds to the radicle emergence period.

15 and 21 h, but no major change was observed for oryzalin-treated seeds. This delay in water uptake was partially made up after 24 h of imbibition to reach a value of 76%, comparable to the 78.5% obtained at the same imbibition time for fusicoccin.

As previously reported, germination occurred after ∼20 h of imbibition.[34] Radicle length after emergence was significantly ($p < 0.01$) shorter for all seeds treated with oryzalin and longer under fusicoccin treatment (Figure 1). The rate of radicle development under MS medium was similar to that under fusicoccin medium, with a reduction of the growth rate after 38 h of imbibition, whereas under oryzalin medium, this growth rate was higher until 24 h, reduced during the 24–38 h period, and then similar until 48 h compared with the two other media.

The unfreezable water content was determined from the residual NMR signal obtained at −20 °C after freezing, compared with the fresh one and normalized to the total weight of the seeds. Between 1 and 48 h of imbibition, the unfreezable water content of MS-imbibed seeds decreased from about 14.5% to 11% w/w (Figure 2). A small increase (from 12.3% to 12.9% w/w) of this unfreezable water content was observed after the radicle emergence.

Water Dynamics in MS Seeds. *M. truncatula* seed germination phases were followed by NMR relaxometry. Longitudinal (T_1) and transverse (T_2) relaxation times were registered at 20, −20, and 20 °C after thawing. It was assumed that over the 4 h thawing period, enzymatic activities affected the composition and microstructure of seeds similarly for all imbibition conditions. Differences observed in the relaxation results from thawed seeds were attributed to the imbibition conditions. The results obtained at 20 °C on fresh, frozen, and freeze–thawed MS seeds are shown in Figure 3. The different relaxation time components and their normalized proportions resulting from the multiexponential fitting of T_1 and T_2 relaxation curves (with eq 1 and eq 2, respectively) are defined as follows: the three groups of letters a, b, c, d; i, j, k, l; and α, β, γ, used for T_2 and the three other groups x, y, z; q, r, s; and λ, μ, ν used for T_1 referred to the relaxation time components of fresh, freeze–thawed, and frozen seeds, respectively. In each group, the relaxation time values are sorted in alphabetical order in increasing order of value. The results are thereafter set out in terms of imbibition phases subdivided in noteworthy periods.

Dry seeds. Water in fresh dry seeds at 20 °C (about 9% w/w) gave two components for T_1 ($T_{1x,y}$) and three for T_2 ($T_{2a,b,c}$; Figure 3A,B, respectively). The latter corresponds to three pools of water molecules with different mobilities and environments. T_1 being more sensitive to molecular diffusion and chemical exchange than T_2 can be represented by a lower number of T_1 components than T_2.[42] As a consequence, the merged T_1 values partly lose specific physical/chemical environment information attached to the different proton populations. In the present case, it can explain the two components' behavior of T_1 instead of the three obtained for T_2. In the frozen state, two components for T_1($T_{1\mu,\nu}$) and three for T_2 ($T_{2\alpha,\beta,\gamma}$) were also observed (Figure 3E,F, respectively). The proportions' similarity to those obtained at 20 °C reflected that the three water pools in dry seeds were very little affected by freezing; however, compared with fresh dry seeds, the long $T_{1\nu}$ component was reduced by a factor of ∼2 while the short one remained unchanged ($T_{1\nu} \approx T_{1x}$). The two longest T_2 components, $T_{2\beta}$ and $T_{2\gamma}$, were reduced by a factor 10 compared with $T_{2b,k}$ and $T_{2c,l}$ and the shortest one, $T_{2\alpha}$, by a factor of 3 compared with $T_{2a,i}$ (Figure 3). The unfreezable water, tightly associated, was determined from the residual NMR signal after freezing to represent ∼80% of the water content of fresh dry seeds; that is, ∼7% w/w (see Figure 2). Compared with fresh seeds, no significant changes in the relaxation times values and proportions were observed for thawed seeds (Figure 3C,D), suggesting that the tissue structures of the seeds were essentially intact after the freezing process as a result of a negligible ice nucleation at this low water content.

Phase I: 0–2.5 h Imbibition Period. The first hour of imbibition induced marked changes in relaxation distribution. For fresh seeds, an additional water component appeared with long T_1 and T_2 values of about 950 and 850 ms for T_{1z} and T_{2d}, respectively, with similar proportions of about 43% (Figure 3A,B). A marked increase in time and proportion was observed for the short T_1 relaxation time (T_{1x}) until 2.5 h imbibition; T_2 values were less affected, except the significant increase and decrease in the proportions P_{2a} and P_{2d} of the shortest and longest T_2 components, respectively. The freeze–thawing process induced

DOI: 10.1021/jf505515n
J. Agric. Food Chem. 2015, 63, 1698–1710

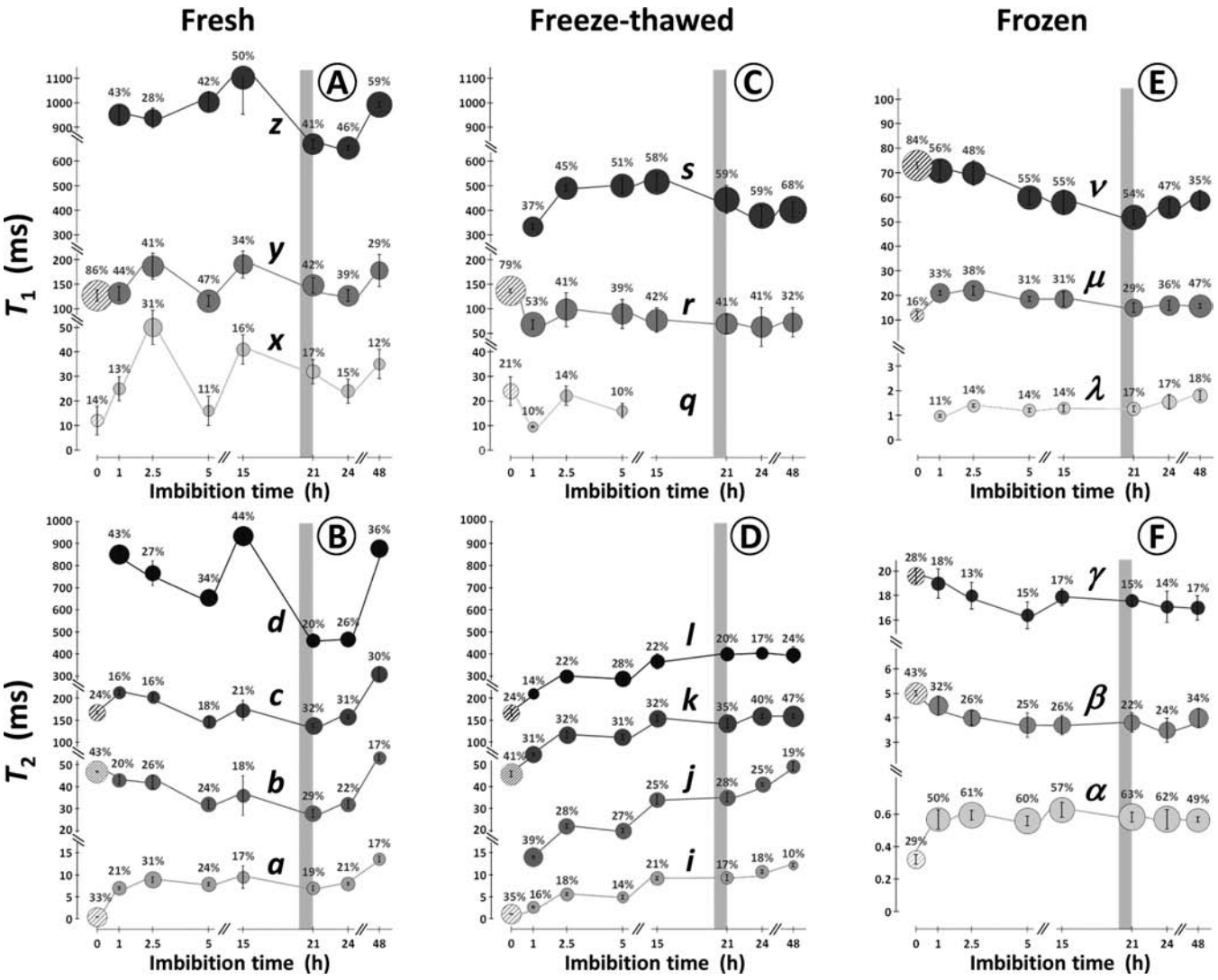

Figure 3. T_1 (A, C, E) and T_2 (B, D, F) components of germinating *M. truncatula* seeds on Murashig and Skog (MS) medium registered at 20 °C on fresh (A, B) and freeze−thawed (C, D) seeds and at −20 °C on frozen seeds (E, F) for different imbibition times. Circles of different gray densities denote different T_1 and T_2 components, indicated by different groups of letters: from the shortest to the longest relation time, T_1 components are identified by letters *x, y, z*; *q, r, s*; and *λ, μ, ν* for fresh, freeze−thawed and frozen seeds, respectively. In the same way, T_2 components are identified by letters *a, b, c, d*; *i, j, k, l*; and *α, β, γ*. The circle area and percentage refer to the proportion (P_1 or P_2) of the component to the overall T_1 or T_2 signal. The standard error on these proportions does not exceed an absolute value of 3% ($n = 5$). A bar represents standard error of time ($n = 5$). The striated circles are associated with fresh dry seeds, and the shaded area corresponds to the radicle emergence period. For each relaxation time component, the line is a guide to the eye.

an overall decrease in relaxation times by a factor of ∼2 (Figure 3C,D) by comparison with those of the fresh sample (Figure 3A,B), and an overall increase in relaxation times was observed until 2.5 h imbibition. At the frozen state, a short T_1 component of 1 ms ($T_{1\lambda}$), with a proportion of 11%, appeared (Figure 3E), and the shortest T_2 component ($T_{2\alpha}$) increased in value and markedly in proportion (Figure 3F).

Phase I: 2.5−5 h Imbibition Period. For the fresh seeds, all T_2 values decreased significantly as well as the two shortest T_1 components. Concerning the proportions P_1 and P_2 (circle area and percentage in Figure 3) of the T_1 and T_2 components, respectively, the major events were the increase in P_{1z} and P_{2d}, and the concomitant decrease in P_{1x} and P_{2a}. The freeze−thawed seeds showed no significant changes. In the frozen state, the only marked change consisted in the decrease in the longest $T_{1\nu}$ component.

Phase II: 5−15 h Imbibition Period. During this period, all relaxation time values of fresh seeds (Figure 3A,B) increased, as well as the contribution of more mobile water fractions (P_{1z} and P_{2d}). The T_2 values of freeze−thawed seeds also increased, but without marked changes in proportions, and the shortest T_{1q} component disappeared (Figure 3D). No noticeable changes were detected in the frozen state.

Phase II: 15−21 h Imbibition Period. The most significant changes concerned the fresh seeds (Figure 3A,B). With emergence of the radicle, the longest components T_{1z} and T_{2d} decreased markedly while the others decreased slightly. A marked redistribution of component proportions was also observed, with a decrease in the longest (P_{1z} and P_{2d}) and an increase in the intermediate (P_{1y}, P_{2c} and P_{2b}) ones.

Phase III: 21−48 h Imbibition. Whatever the temperature conditions, all relaxation time components remained relatively stable in values and proportions from the radicle emergence to 24 h of imbibition. For fresh seeds, a global increase in the water mobility was observed between 24 and 48 h, with a significant increase in the proportions P_{1z} and P_{2d} of the longest T_1 and T_2

DOI: 10.1021/jf505515n
J. Agric. Food Chem. 2015, 63, 1698−1710

Table 1. T_1 and T_2 Component Relaxation Times and Proportions[a] for Frozen (−20°C) Seeds Imbibed in MS Medium Alone or Complemented by Oryzalin (OR) or Fusicoccin (FU) as a Function of Imbibition Time (IT)[b]

			T_1						T_2					
			Component (ms)			Proportion (%)			Component (ms)			Proportion (%)		
	IT (h)	Φ	$T_{1\lambda}$	$T_{1\mu}$	$T_{1\nu}$	$P_{1\lambda}$	$P_{1\mu}$	$P_{1\nu}$	$T_{2\alpha}$	$T_{2\beta}$	$T_{2\gamma}$	$P_{2\alpha}$	$P_{2\beta}$	$P_{2\gamma}$
MS	2.5	I	1.4 (0.1)	22 (2)	70 (5)	14 (1)	38 (2)	48 (2)	0.59 (0.02)	4.0 (0.3)	18 (1)	61 (3)	26 (2)	13 (1)
	5	I	1.2 (0.1)	19 (1)	60 (3)	14 (1)	31 (3)	55 (3)	0.55 (0.02)	3.7 (0.5)	16 (1)	60 (2)	25 (1)	15 (1)
	15	II	1.3 (0.1)	19 (3)	58 (5)	14 (1)	31 (6)	55 (7)	0.63 (0.03)	3.7 (0.4)	18 (1)	57 (3)	26 (2)	17 (1)
	21	II	1.3 (0.1)	15 (2)	52 (3)	17 (1)	29 (2)	54 (3)	0.57 (0.02)	3.8 (0.4)	18 (1)	63 (1)	22 (2)	15 (1)
	24	III	1.6 (0.3)	16 (2)	56 (3)	17 (1)	36 (3)	47 (3)	0.56 (0.04)	3.5 (0.5)	17 (1)	62 (3)	24 (2)	14 (1)
	48	III	1.8 (0.2)	16 (1)	59 (4)	18 (1)	47 (5)	35 (6)	0.57 (0.01)	3.3 (0.1)	18 (1)	47 (2)	40 (1)	13 (1)
OR	2.5	I	**1.8 (0.1)**	23 (1)	67 (5)	13 (1)	38 (4)	48 (4)	0.57 (0.03)	3.9 (0.4)	17 (1)	56 (4)	28 (2)	**16 (1)**
	5	I	1.3 (0.3)	20 (3)	59 (3)	13 (1)	34 (6)	53 (6)	**0.47 (0.02)**	3.9 (0.1)	16 (1)	62 (2)	24 (1)	14 (1)
	15	II	**1.8 (0.1)**	23 (2)	65 (4)	14 (1)	40 (4)	46 (4)	0.62 (0.02)	3.6 (0.3)	17 (1)	60 (2)	25 (1)	**15 (1)**
	21	II	**1.5 (0.1)**	**20 (2)**	**64 (6)**	**15 (1)**	**39 (5)**	**46 (5)**	0.57 (0.04)	3.3 (0.4)	17 (1)	61 (2)	**26 (2)**	**13 (1)**
	24	III	1.3 (0.1)	15 (1)	**50 (1)**	**14 (1)**	**28 (2)**	**58 (2)**	**0.44 (0.01)**	3.4 (0.2)	**15 (1)**	**66 (2)**	**21 (1)**	13 (1)
	48	III	1.6 (0.2)	**14 (1)**	**50 (3)**	**16 (1)**	**38 (2)**	**46 (2)**	0.55 (0.02)	3.6 (0.3)	16 (1)	**56 (2)**	**30 (1)**	14 (2)
FU	2.5	I	**1.7 (0.1)**	23 (1)	64 (2)	13 (1)	38 (1)	49 (1)	0.59 (0.03)	**3.5 (0.2)**	17 (1)	61 (3)	25 (2)	14 (1)
	5	I	**1.6 (0.2)**	**24 (1)**	**73 (2)**	14 (1)	**43 (2)**	**43 (2)**	**0.48 (0.04)**	3.2 (0.2)	15 (1)	**66 (3)**	**22 (2)**	**12 (2)**
	15	II	**1.7 (0.1)**	23 (2)	**66 (4)**	13 (1)	**41 (4)**	45 (4)	0.59 (0.04)	3.6 (0.2)	17 (1)	**62 (2)**	24 (2)	**14 (1)**
	21	II	**1.6 (0.1)**	17 (2)	51 (4)	**15 (1)**	**35 (4)**	50 (4)	0.54 (0.05)	**3.1 (0.3)**	16 (1)	61 (3)	**28 (3)**	**11 (1)**
	24	III	1.3 (0.2)	15 (2)	51 (4)	16 (1)	39 (4)	45 (4)	0.51 (0.04)	3.3 (0.3)	16 (2)	**55 (2)**	**32 (2)**	13 (1)
	48	III	**1.4 (0.2)**	**12 (2)**	**45 (3)**	**15 (1)**	43 (3)	42 (4)	0.55 (0.06)	**3.9 (0.3)**	17 (1)	47 (6)	36 (2)	17 (4)

[a]Standard deviations are indicated in parentheses. [b]In bold and bold underlined, significantly ($p < 0.05$) higher and lower values than MS ones, respectively. Φ denotes the three phases of imbibition (see Figure 1). The values associated with the radicle emergence at the end of phase II (21 h of imbibition) appear on a grey background.

components at the expense of others (Figure 3A,B). The latter was also observed for the freeze−thawed seeds, but without significant changes in relaxation time values (Figure 3C,D). At −20 °C, changes in relaxation time values were minor after 48 h of imbibition. The only significant differences lie in the component proportions with a marked decrease in $P_{1\nu}$ and $P_{2\alpha}$ and an increase in $P_{1\mu}$ and $P_{2\beta}$ (Figure 3E,F).

Growth Modulator Effects on Water Dynamics. Oryzalin and fusicoccin were used to modify cell division and development and consequently change tissue microstructure. These were expected to lead to different water relaxation behaviors in the freeze−thawed germinating seeds. Significant differences ($p < 0.05$) observed for relaxometry data between treated seeds compared with MS-imbibed seeds are specified in Tables 1 and 2 for frozen and freeze−thawed seeds, respectively.

Comparison with MS Medium in Frozen Seeds. Compared with MS-imbibed seeds, oryzalin-treated seeds showed the first main significant changes at radicle emergence (Table 1). The three T_1 relaxation time components were longer, with their first and third proportions ($P_{1\lambda}$ and $P_{1\nu}$) lower and the intermediate one ($P_{1\mu}$) higher. A very similar event was observed with fusicoccin treatment but at an earlier imbibition time (5 h), and it lasted up to 15 h. After radicle emergence (phase III), oryzalin-treated seeds differed from MS-imbibed seeds essentially by a shorter $T_{1\mu}$ and $T_{1\nu}$; higher $P_{1\nu}$ and lower $P_{1\lambda}$ and $P_{1\mu}$; shorter $T_{2\alpha}$ and $T_{2\gamma}$; and proportions $P_{2\beta}$ and $P_{2\gamma}$ that were higher and lower, respectively. For fusicoccin-treated seeds, differences were less marked. As for the oryzalin-treated seeds, $T_{1\mu}$ and $T_{1\nu}$ were shorter at 48 h of imbibition (as well as $T_{1\nu}$). In contrast, proportions $P_{2\alpha}$ and $P_{2\beta}$ at 24 h of imbibition were lower and higher, respectively. As illustrated in Figure 4, the $P_{2\alpha}$ and $P_{2\beta}$ proportions proved to be very closely correlated with the radicle length (removing the shortest value of radicle length associated with oryzalin-treated seeds at 21 h of imbibition), irrespective of the germination medium used (MS, oryzalin, or fusicoccin).

Comparison with MS Medium in Freeze−Thawed Seeds. Oryzalin treatment essentially affected the transverse relaxation parameters after radicle protrusion (Table 2). From 21 to 48 h of imbibition, the T_{2i} and T_{2j} components became shorter than those of MS seeds, with an increase in their proportions at 48 h, at the expense of P_{2k} and P_{2l}, which decreased.

Thawed fusicoccin-treated seeds showed significantly longer T_{1q} and T_{1r} during phase I of imbibition, with an increase in the proportion P_{1q} and at 21 and 24 h with longer T_{1r} values. Concerning transverse relaxation parameters, except for the longer T_{2k} at 48 h, fusicoccin treatment affected only the proportions P_2, with a decrease in P_{2l} and an increase in P_{2j} and P_{2k} at the early imbibition time of 2.5 h and, during the third phase, a decrease in P_{2i} at 24 h and then, as observed for oryzalin-treated seeds, higher P_{2j} and lower P_{2l} proportions at 48 h.

Furthermore, pooling the T_2 relaxation results obtained during phase III of imbibition for the three germination media, the three components $T_{2i,j,k}$ and their proportions $P_{2i,j,k}$ showed relatively good correlation, with radicle length as displayed in Figure 5A,B, respectively.

Direct Comparison between Oryzalin and Fusicoccin Media. The comparison between relaxation parameters obtained with oryzalin and fusicoccin treatments is reported in Figure 6 for frozen (Figure 6A,B) and freeze−thawed seeds (Figure 6C,D). No significant differences were noticed at 2.5 and 15 h of imbibition, whatever the relaxation parameter or the temperature considered. At the end of phase I (5 h), the two treatments differed only by their longitudinal relaxation parameters. Thawed fusicoccin-treated seeds revealed systematically significant higher T_1 values than those of oryzalin-treated seeds. At the frozen state, fusicoccin-treated seeds differ only by a longer $T_{1\nu}$ value and lower $P_{1\nu}$ and higher $P_{1\mu}$ proportions. Following the radicle

DOI: 10.1021/jf505515n
J. Agric. Food Chem. 2015, 63, 1698−1710

Table 2. T_1 and T_2 Component Relaxation Times and Proportions[a] for Freeze-Thawed (20°C) Seeds Imbibed in MS Alone or Complemented by Oryzalin (OR) or Fusicoccin (FU) as a Function of Imbibition Time (IT)[b]

			T_1						T_2							
			Component (ms)			Proportion (%)			Component (ms)				Proportion (%)			
	IT (h)	Φ	T_{1q}	T_{1r}	T_{1s}	P_{1q}	P_{1r}	P_{1s}	T_{2i}	T_{2j}	T_{2k}	T_{2l}	P_{2i}	P_{2j}	P_{2k}	P_{2l}
MS	2.5	I	21 (4)	99 (7)	494 (15)	14 (2)	41 (1)	45 (3)	5.7 (0.3)	22 (1)	117 (8)	299 (17)	18 (1)	28 (1)	32 (2)	22 (3)
	5		15 (3)	90 (6)	504 (32)	10 (2)	39 (2)	51 (3)	4.9 (0.4)	20 (1)	112 (6)	288 (12)	14 (2)	27 (2)	31 (2)	28 (5)
	15	II		77 (5)	520 (35)		42 (2)	58 (2)	9.2 (0.4)	34 (2)	154 (7)	367 (35)	21 (2)	25 (2)	32 (2)	22 (3)
	21			70 (4)	447 (58)		41 (4)	59 (4)	9.3 (0.7)	35 (2)	143 (11)	400 (30)	17 (2)	27 (4)	35 (1)	21 (6)
	24	III		63 (8)	383 (41)		41 (3)	59 (3)	10.7 (0.4)	41 (1)	159 (6)	404 (16)	18 (1)	25 (1)	40 (2)	17 (3)
	48			73 (6)	406 (32)		32 (3)	68 (3)	12.2 (0.4)	49 (2)	159 (5)	396 (38)	10 (1)	19 (1)	47 (1)	24 (2)
OR	2.5	I	30 (8)	111 (12)	530 (29)	15 (5)	43 (2)	42 (4)	5.8 (0.6)	21 (1)	110 (6)	330 (22)	19 (4)	30 (2)	34 (1)	17 (5)
	5		10 (3)	83 (4)	487 (15)	9 (1)	42 (2)	49 (2)	5.7 (0.3)	22 (1)	106 (2)	275 (7)	15 (1)	27 (1)	34 (2)	24 (3)
	15	II		75 (7)	551 (18)		43 (3)	57 (3)	8.5 (0.5)	33 (2)	164 (10)	399 (22)	20 (2)	26 (2)	34 (2)	20 (5)
	21			65 (7)	457 (14)		42 (2)	58 (2)	**7.9 (0.6)**	**32 (2)**	143 (5)	**359 (18)**	18 (2)	28 (1)	37 (3)	17 (4)
	24	III		57 (3)	436 (35)		39 (4)	61 (4)	**9.7 (0.2)**	**37 (1)**	163 (7)	353 (33)	19 (2)	24 (2)	**33 (3)**	24 (5)
	48			**59 (6)**	380 (18)		35 (3)	65 (3)	**10.1 (0.7)**	**39 (3)**	160 (10)	360 (21)	**16 (1)**	**23 (2)**	**43 (2)**	**18 (3)**
FU	2.5	I	**38 (8)**	**121 (16)**	512 (39)	**21 (5)**	39 (4)	40 (3)	5.8 (0.7)	21 (2)	109 (9)	311 (16)	20 (2)	**32 (3)**	**36 (1)**	**12 (3)**
	5		**39 (11)**	**134 (23)**	565 (31)	**18 (4)**	35 (5)	47 (1)	4.6 (0.9)	20 (1)	104 (4)	285 (18)	11 (3)	30 (2)	32 (3)	27 (8)
	15	II		78 (3)	545 (19)		43 (2)	57 (2)	9.1 (0.9)	33 (2)	162 (9)	392 (23)	19 (1)	27 (2)	33 (1)	21 (3)
	21			**91 (9)**	516 (73)		42 (2)	58 (2)	10.3 (0.4)	38 (1)	150 (2)	439 (20)	15 (2)	25 (3)	34 (3)	26 (7)
	24	III		**72 (4)**	408 (41)		38 (4)	62 (4)	9.8 (0.8)	39 (3)	160 (13)	400 (41)	**14 (2)**	26 (3)	40 (1)	20 (5)
	48			78 (9)	434 (23)		33 (2)	67 (2)	13.0 (0.9)	47 (2)	**185 (12)**	404 (30)	10 (1)	**24 (1)**	48 (1)	**18 (2)**

[a]Standard deviations are indicated in parentheses. [b]In bold and bold underlined, significantly ($p < 0.05$) higher and lower values than MS ones, respectively. Φ denotes the three phases of imbibition (see Figure 1). The values associated with the radicle emergence at the end of phase II (21 h of imbibition) appear on a grey background.

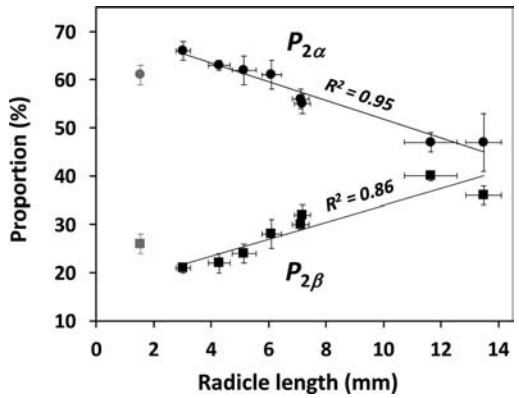

Figure 4. Evolution of T_2 relaxation proportions $P_{2\alpha}$ (circle symbol) and $P_{2\beta}$ (square symbol) determined at the frozen state (−20 °C) during the phase III of germination (refer to Table 1) as a function of radicle length of *M. truncatula* seeds for all germination media (MS, oryzalin and fusicoccin). The straight lines result from linear regression of data (excluding the shortest value of radicle length, identified by gray symbols), with the correlation coefficient R^2 mentioned for each regression.

emergence and thereafter, differentiation between the two growth modulators was clearly displayed in the freeze−thawed samples. The fusicoccin-treated seeds had systematically higher T_2 values from 21 to 48 h and higher T_{1l} values compared with oryzalin-treated seeds. In this third phase, the only significant differences in proportions were observed at 24 and 48 h for P_{2i} and P_{2k} with lower and higher values, respectively, for fusicoccin-treated seeds. Along phase III, the frozen seeds treated with fusicoccin also differed significantly from seeds treated with oryzalin by lower $P_{2\alpha}$ and greater $P_{2\beta}$ proportions at 24 and 48 h, shorter $T_{1\nu}$ and $T_{1\mu}$ at 21 and 48 h, and greater $P_{1\mu}$ and lower $P_{1\nu}$ at 24 h.

Free Sugars and Galactooligosaccharides. Along with water uptake, the composition in free sugars (glucose, fructose, sucrose) and oligosaccharides (α-galactoside: raffinose, stachyose) participating in water fluxes during cell development was determined in the germinating seed (Figure 7).

Evolution of Free Carbohydrate Contents in Seeds Germinating on MS Medium. Glucose was the major free sugar, and its content increased early on until 5 h of imbibition, then plateaued up to 21 h and rose again until 38 h of imbibition (Figure 7A). Fructose, which was a minor sugar at the beginning of germination, increased a little in content until 5 h, steeply from 15 to 24 h, and continued to increase until 48 h of imbibition, albeit at a slower rate (Figure 7B). Sucrose showed an evolution of content close to that of glucose until radicle protrusion, but with proportions divided by a factor of about 2 (Figure 7C). Between 24 and 38 h, sucrose concentration increased ∼3-fold and markedly decreased between 38 and 48 h imbibition, reaching a value close to zero.

As expected, stachyose was the major α-galactoside in *M. truncatula* seed.[43] Its content decreased particularly after 15 h of imbibition to reach a constant, low content after 24 h of imbibition (Figure 7E). The very low raffinose content displayed behavior very similar to that of the stachyose content until radicle protrusion, but a steep decrease was observed at 48 h of imbibition (Figure 7F).

Total free sugars (Figure 7D) increased slightly until 15 h of imbibition and then about three times as fast before stabilizing after 38 h of imbibition.

Effect of Oryzalin and Fusicoccin Treatments on Free Sugars and α-Galactosides Concentrations. The fate of free sugar and oligosaccharides in germinating oryzaline- and fusicocin-treated seeds was significantly different from that of seeds germinating on MS medium. Compared with MS-imbibed seeds and fusicoccin-treated seeds, oryzalin-treated seeds exhibited systematically a deficiency of free sugars after 2.5 h of

DOI: 10.1021/jf505515n
J. Agric. Food Chem. 2015, 63, 1698−1710

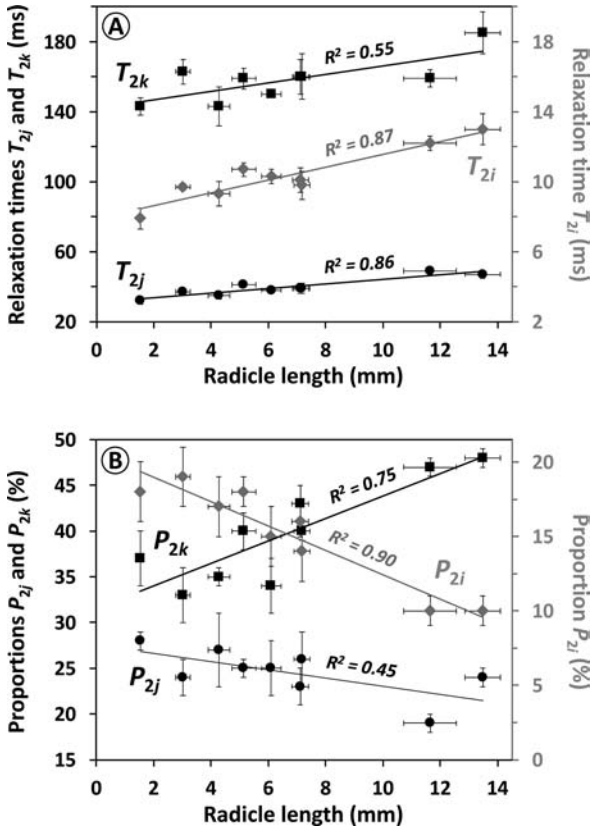

Figure 5. Evolution of (A) relaxation time components T_{2i}, T_{2j}, and T_{2k} and (B) their associated proportions P_{2i}, P_{2j}, and P_{2k} determined for freeze−thawed *M. truncatula* seeds (refer to Table 2) as a function of radicle length for all germination media (MS, oryzalin, and fusicoccin). The components *i*, *j*, and *k* are identified by the symbols ◆, ●, and ■, respectively. The straight lines result from linear regression of data, with the correlation coefficient R^2 mentioned for each regression.

imbibition. Subsequently, free sugars in oryzalin-treated seeds displayed an evolution similar to that observed in MS-imbibed seeds but with lower concentrations, except for a higher sucrose content at 48 h of imbibition. Regarding the fusicoccin effect, all free sugar contents were significantly higher than those of the oryzalin effect at 2.5 h of imbibition. Thereafter, the first marked significant differences in sugar contents appeared at 21 h of imbibition, with higher glucose and fructose concentrations compared with MS and oryzalin treatment. After 21 h, this highest glucose content steeply decreased to reach significantly lower values after 38 and 48 h of imbibition. At this last time, unlike what was observed at 2.5 h, the oryzalin treatment induced higher free sugar contents than the fusicoccin one, except for fructose.

Concerning the α-galactosides, the stachyose content was significantly lower after 15 h and higher after 24 h of imbibition in the presence of the two growth modulators compared with MS medium. After 48 h, the stachyose and raffinose contents were significantly higher with oryzalin treatment than with fusicoccin treatment.

■ DISCUSSION

The present study showed that NMR relaxometry allowed changes in seed chemistry and microstructure during the different phases of germination to be revealed. Variations in both T_1 and T_2 relaxation times and proportions displayed different dynamics of water diffusion and exchanges among *M. truncatula* seed tissues components (cell membranes, cell wall polysaccharide assemblies, vacuole, inclusion bodies, organelles, intercellular spaces, solutes, etc.) all along germination. These changes were observed within the three phases of germination and were likely associated with specific water diffusion events observed in other seeds by MRI.[4−8,21] They were also probably related to microstructural changes associated with the recovery of the metabolic processes of protein and α-galactosides as well as with endosperm cell wall galactomannan swelling and degradation after radicle protrusion. Evolutions of T_1 and T_2 relaxation times and proportions resulted from the combination of (i) higher water mobility associated with water uptake and macromolecular disassembly (cell wall, reserve protein bodies), (ii) lower water mobility due to interactions with the generated mobile solutes and newly synthesized macromolecules, and (iii) water exchange between the different cellular components and tissue compartments. Lowering temperature reduces the water self-diffusion coefficient and slows the exchange of water molecules among the various compartments. This changes the water relaxation time distribution into the slow exchange regime so that some compartments are potentially more easily resolved. The existence of multiple unfrozen water fractions at freezing temperatures can be attributed to mainly three effects: (i) the freezing point depression due to small solutes; (ii) the freezing point depression due to macromolecules, membranes, and other hydrophilic ultrastructure; and (iii) the effects of viscosity.[44,45] For example, changes in the distribution of water proton transverse relaxation times were used to monitor the subcellular compartmentation of water during freezing of apple, carrot, and tomato tissues.[46−48] This is possible because ice, which has short proton relaxation times of a few microseconds, is not detected on the millisecond time scales of the NMR pulse sequences classically used for the T_1 and T_2 measurements. However, it should be noted that information on some water compartments or environments will be partly lost as a result of the ice's forming.

The complexity of the overlapping events occurring during imbibition with the different seed tissue components makes it difficult to identify distinctive water relaxometric features as probes of cellular events, such as cell elongation or division in the whole seed. It also should be noted that the compartmental analysis is complicated because no direct relationship can be simply established between the relaxation time components T_{1n} and T_{2n}. Nevertheless, some specific periods of seed imbibition displayed particular water relaxation characteristics within the 0−48 h seed imbibition period, which can be associated with some noteworthy physiological and morphological events, as discussed in the two following sections.

Seed Imbibition Kinetics, Free Carbohydrates Evolution, and Water Dynamics in Seeds Germinating on MS Medium. The first specific period of imbibition is within the first half of phase I of germination. Between 0 and 2.5 h, changes in relaxation times and proportions were observed for both T_1 and T_2 components. The significant amount of water absorbed after 1 h of imbibition resulted in a 44% w/w water content (initially 9% w/w), while the proportion of unfreezable water was two times larger than in dry seeds (Figure 2) as a result of the hydration of matrixes, such as the cell walls and reserve biopolymers. The new markedly longest T_{1z} and T_{2d} components observed for fresh seeds (Figure 3A,B) reflect this rapid seed rehydration. These components correspond to new water species, with the highest mobility likely distributed in the first hydrated seed tissue during the early imbibition stage, such as the seed coat and endosperm. The freeze−thawing process induced a

DOI: 10.1021/jf505515n
J. Agric. Food Chem. 2015, 63, 1698−1710

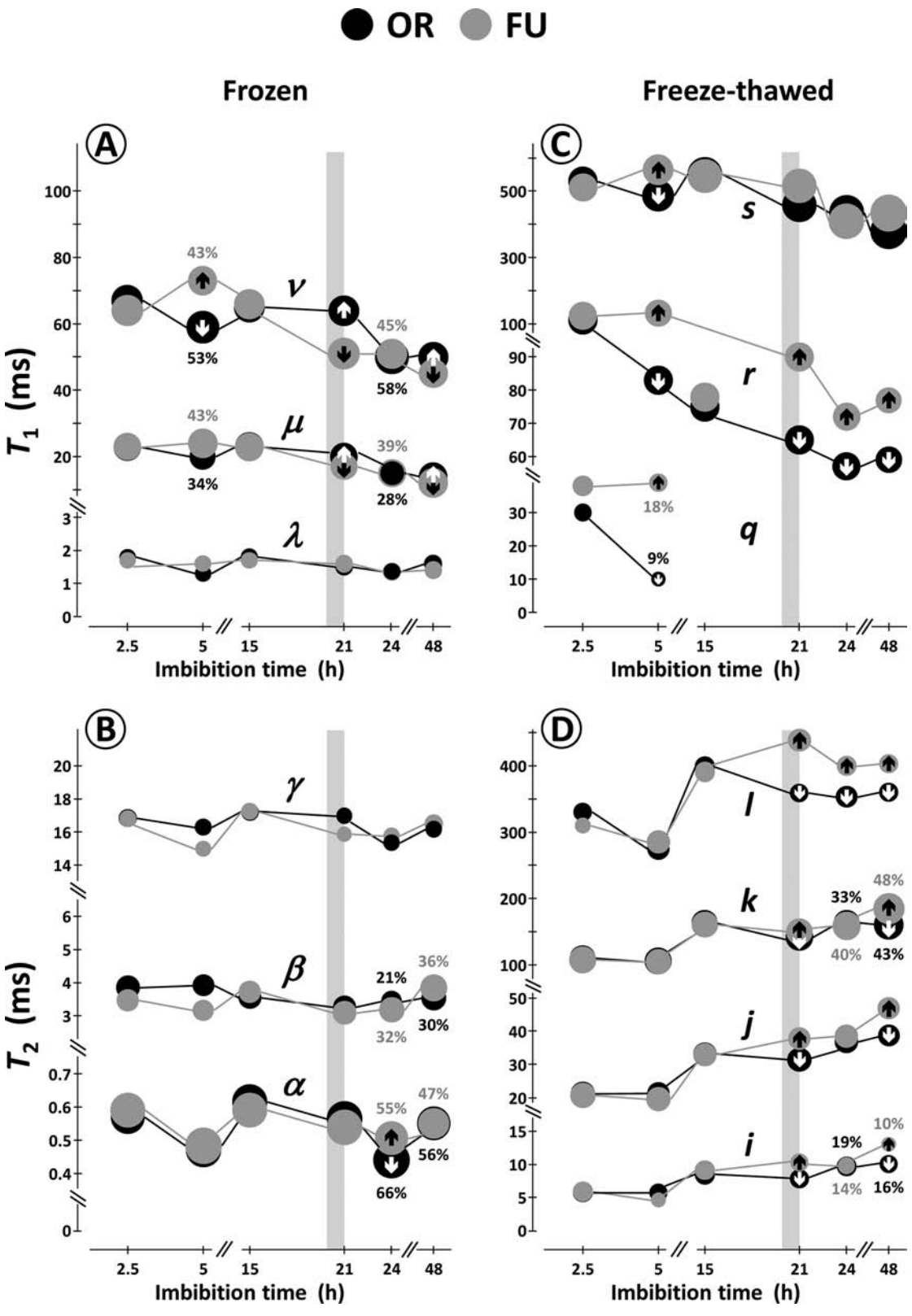

Figure 6. T_1 (A,C) and T_2 (B,D) components of germinating *M. truncatula* seeds supplemented with oryzalin (OR, black circles) and fusicoccin (FU, gray circles) modulators registered at −20 °C (A,B) and 20 °C after thawing (C,D) for the different imbibition times. In order not to overload the figure, standard errors on relaxation times and proportions, reported in Tables 1 and 2, have been omitted. The letters (α, β, γ, λ, μ, υ at −20 °C, and *a*, *b*, *c*, *d*; *q*, *r*, *s* at 20 °C) refer to the different relaxation time components (see Table 1 and 2). When significantly different ($p < 0.05$), proportions of relaxation time components are mentioned. The up/down arrows into circles indicated significantly ($p < 0.05$) higher/lower relaxation time values between OR (white arrow) and FU (black arrow) media. The shaded area corresponds to radicle emergence period. For each relaxation time component, the line is a guide to the eye.

DOI: 10.1021/jf505515n
J. Agric. Food Chem. 2015, 63, 1698−1710

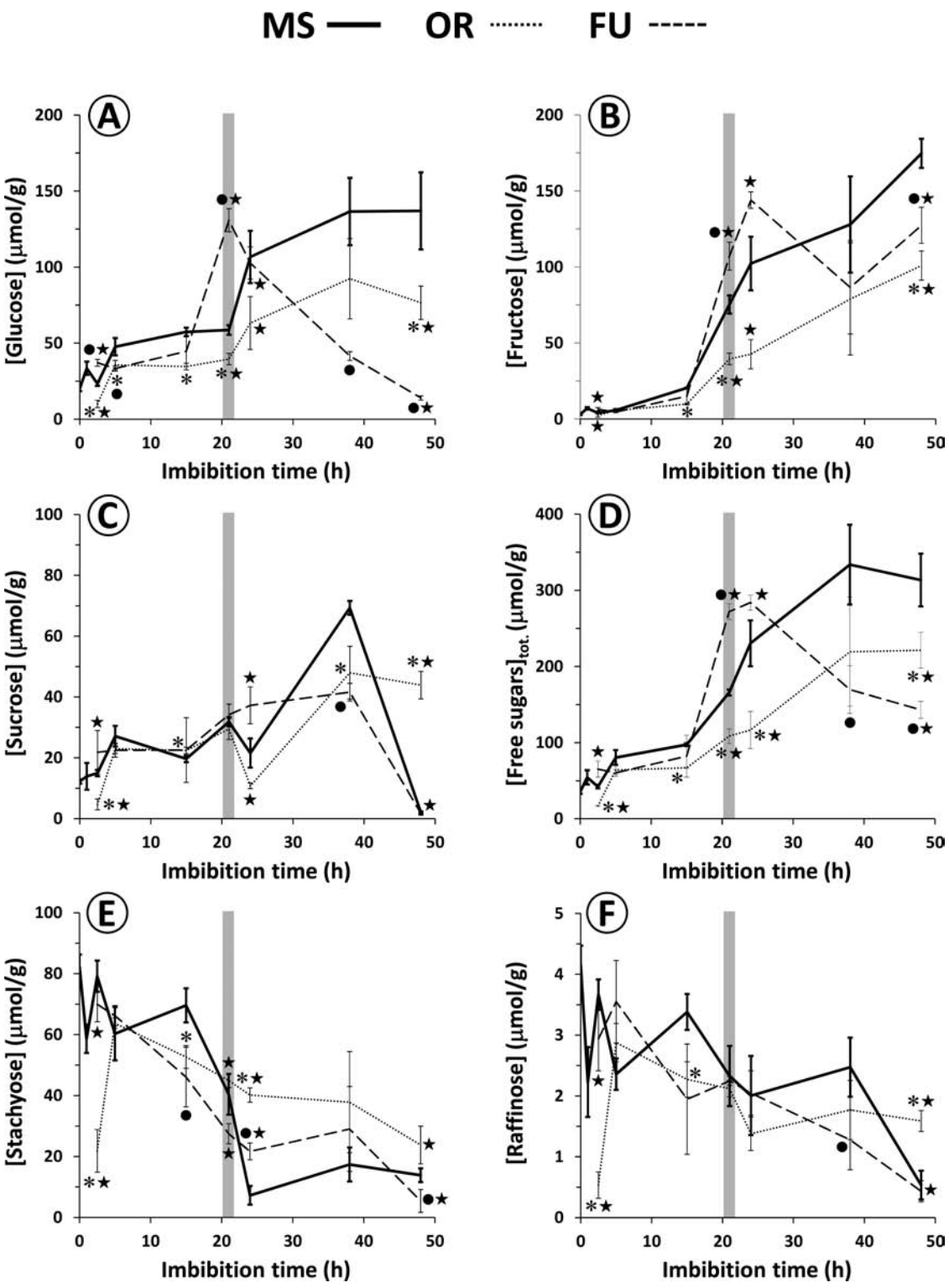

Figure 7. Free sugars (glucose (A), fructose (B), and sucrose (C)), total free sugars (D) and oligosaccharides (stachyose, E; and raffinose, F) concentration (in μmol/g) evolution of the germinating *M. truncatula* seeds on MS medium (solid line) and supplemented by oryzalin (OR, dotted line) or fusicoccin (FU, dashed line). Bar: standard deviation on three repetitions from a pool of five biological repetitions. Significant difference ($p < 0.05$) between OR and FU media with MS medium are indicated by symbols * and ●, respectively. The symbol ★ indicates significant difference between OR and FU media. The shaded area corresponds to the radicle emergence period.

drastic change in these two new components, shortening the T_{1z} component from 950 to 350 ms for T_{1s}, and leading to a new T_{2j} component of ~14 ms, instead of 850 ms for the new T_{2a}, but with a similar proportion for P_{2j} (39%) compared with P_{2a} (43%).

These results reflect an early "structural reorganization" due to solute and macromolecular rehydration. The freezing process causes ice crystal formation with a partial breakdown of cellular structures. The subsequent thawing modifies the concentration of solutes as a result of the redistribution of vacuolar, cytoplasmic,

DOI: 10.1021/jf505515n
J. Agric. Food Chem. 2015, 63, 1698−1710

and apoplastic fluids that probably led to local increases in viscosity, resulting in the short T_{2j} and T_{1s} values. The marked increases in the proportion $P_{2\alpha}$ from 29% to 50% of the shortest $T_{2\alpha}$ component in the frozen state (Figure 3F) can be attributed more specifically to the rehydration of macromolecules, such as reserve proteins and cell wall biopolymers. Compared with 1 h of imbibition, this last phenomenon was still observed after 2.5 h of imbibition but less marked. The water content reached approximately 64% w/w while the unfreezable water content (about 14% w/w; Figure 2) and the concentration of free sugars (Figure 7) remain unchanged. In addition, the marked decrease in P_{1z} from 43% to 28% (the latter being the lowest P_{1z} value observed during the 48 h imbibition period studied), the marked decrease in P_{2d} with a concomitant decrease in P_{2l} for the freeze−thawed seeds, and the marked increases in P_{1x} (from 13% to 31%) and P_{2a} (from 21% to 31%) observed for fresh seeds (Figure 3A,B) revealed a new mobilization and relatively large redistribution of water in seed tissues at 2.5 h of imbibition. This is likely related to the gradual resumption of energy metabolism.[1] This is corroborated by the significant increase in glucose and sucrose concentrations at the end of phase I (Figure 7) and an overall decrease in water mobility at 5 h of imbibition, irrespective of the thermal treatment of seeds (Figure 3).

The second noteworthy period of imbibition was during phase II within the 5−15 h time period. The overall increase in water mobility observed for fresh and freeze−thawed seeds (see, for example, the very marked increase in T_{2d} and P_{2d} values in fresh seeds; Figure 3B) following the moderate water uptake of about 5% w/w and a relative stability of carbohydrate concentrations, may be associated with the embryonic axis development and the concomitant clustering of cortical parenchyma cells in spindle-shaped form all along the embryo axes.[34] This was also accompanied by a higher water diffusivity inside or between the various seed tissues/compartments, as demonstrated by the significant increase in the three T_1 component values in fresh seeds (Figure 3A) and the permanent loss of the shortest T_{1q} component of lowest proportion ($P_{1q} \approx 10\%$ at 5 h imbibition) in freeze−thawed seeds (Figure 3C).

During the third period, between 15 h and the end of phase II (21 h imbibition), which corresponds to the emergence of the radicle (Figure 1), fructose and sucrose concentrations increased while that of the α-galactosides decreased (Figure 7). A similar peak in fructose and glucose was reported in the same germination phase of *Medicago sativa*, along with that of amino acids, such as proline, known to be part of the osmoregulators.[49,50] For fresh seeds, this third time period was characterized by a drastic decrease in the longest relaxation times, T_{1z} and T_{2d}, as well as their proportions P_{1z} and P_{2d}, with a concomitant increase in the proportions of P_{1y}, P_{2c}, and P_{2b} of the intermediate relaxation time components T_{1y}, T_{2c}, and T_{2b} (Figure 3A,B). These changes occurred while modifications of the cell wall polysaccharide chemistry related to cellulose-rich primary wall synthesis were observed along with an increase in embryonic axis size in the seed.[34] These changes were also likely related to water interactions with reallocated carbohydrates to cell wall polysaccharide and to increase osmolyte concentrations in vacuoles. The latter is particularly important for driving water into the cell for turgor pressure maintenance and build-up as cells in the embryonic axis elongate. Also remarkable was the very high similarity in the four T_{2n}−P_{2n} values between fresh and freeze−thawed seeds ($a \equiv i$; $b \equiv j$; $c \equiv k$; $d \equiv l$) at 21 h of imbibition (Figure 3B,D, respectively). Indeed, there is no controversy that the freezing−thawing process causes extensive damages in the cell structure, such as cell wall breakdown, damages which also depend on the cooling velocity.[51] Even if moderated by the cryoprotectant effect of some solutes, such as sugars and amino acids, freeze−thawing induces a morphological destructuring of tissue, leading to a redistribution of water to some extent. Despite this, the present results display that the $T_{2n} - P_{2n}$ values remained unchanged after the freezing−thawing process compared with fresh seeds, which means that each T_2−P_2 pair is more likely associated with a specific "class" of water interaction/environment, regardless of any link with tissue compartmentation. Thus, the concept very widely and usually used for the interpretation of the multicomponent behavior of NMR transverse relaxation in biological tissue that relates each T_2 component to a particular water compartment, such as vacuole (longest T_2 component), cytoplasm, or extracellular space (intermediate T_2 components) or cell wall (shortest T_2 component), proves to be most probably inappropriate or at least too simplistic.

To our knowledge, our results are the first experimental results that clearly demonstrate that no simple direct relationship exists between T_2 components and morphological compartments in biological tissue. The drastic decrease between 15 and 21 h of imbibition of the more mobile water proportion P_{2d} in fresh seeds from 44% to 20% (Figure 3B), water component usually associated with vacuolar water, supports this view. Indeed, a 2-fold decrease in the water content in vacuoles is unrealistic. In fact, the 24% reduction in P_{2d} proved to be mainly balanced by the 11% increase in both P_{2b} and P_{2c}, which means that these two components would also be partly present in the vacuole, reflecting, for example, the increase in sugar concentrations in vacuoles, as mentioned above. It should also be noted that the two T_1 components observed for the freeze−thawed seeds, instead of three for the fresh ones, show evidence of the destructuring effect of freezing, which promotes water exchange and diffusion phenomena and, contrary to T_2, allows discriminating between the two different temperature treatments of seeds and, thus, proved to be a valuable and complementary parameter for water dynamics characterization.

The last time period was during phase III, which consists of radicle elongation. Between 21 and 24 h, a slight increase in the unfreezable water content was observed for the first time from the beginning of seed imbibition (Figure 2). This could partly reflect a cell wall biosynthesis enhancement due to the activation of cell division in embryo axis, as revealed by the overexpression of the mitotic gene Cyclin B-1,2 and a peak activity of gene encoding cellulose synthase responsible for the synthesis of cell wall constituents at about 24 h after seed imbibition.[34] The significant increase in glucose and fructose concentrations (Figure 7A,B) could also contribute to this phenomenon. After 48 h of imbibition, fresh seeds displayed a marked increase in overall T_1 and T_2 relaxation time components and in proportions P_{1z} and P_{2d} of the longest ones (Figure 3A and 3B). Furthermore, during the 21−48 h imbibition period, the evolution of each of the three T_{2b}, T_{2c}, and T_{2d} relaxation times revealed an excellent linear positive correlation ($R^2 \approx 1$) with the radicle length (not shown). Along with the water uptake of ∼16%, this correlation could reflect the increase in the cell mean size from about 6 to 200 μm in the cortical parenchyma of the elongating radicle and, thereby, the development of large vacuoles during the protrusion-elongation phase, III.[34] In the frozen state, the significant decrease in the shortest T_2 proportion ($P_{2\alpha}$) from 62% to 49% and the concomitant increase in the intermediate one ($P_{2\beta}$) observed at 48 h (Figure 3F) likely reflected the cell wall loosening, as evidenced, at the same imbibition time, by the

DOI: 10.1021/jf505515n
J. Agric. Food Chem. 2015, 63, 1698−1710

highest expression of cell wall reshuffling enzymes and proteins, such as α-expansins involved in the cell wall expansion.[34] This wall loosening mechanism would promote turgor-driven polymer slippage by disrupting noncovalent binding between wall polymers (e.g., hydrogen bonding of matrix polysaccharides to cellulose microfibrils).[52] The water fraction involved in the hydrogen bonding of this complex would also be affected by this mechanism, as suggested by the marked change of $P_{2\alpha}$ and $P_{2\beta}$ water proportions. The decrease in the two shortest T_2 proportions (P_{2i} and P_{2j}) concomitantly to the increase in the two longest ones (P_{2k} and P_{2l}) observed at 48 h for freeze−thawed seeds (Figure 3D), as well as the increase in the longest T_1 proportion P_{1s} (Figure 3C), could also be related to this cell architecture weakening more specifically localized in the radicle.

Growth Modulator Effects on Free Sugars Evolution and Water Dynamics. Changes in the water status resulting from typical drugs affecting plant development, such as oryzalin and fusicoccin, were assessed by relaxometry on frozen and freeze−thawed seeds. Oryzalin, by blocking microtubule polymerization, inhibits cell division and alters cell elongation as a result of impaired cellulose deposition.[40,53] It was expected to alter water dynamics with respect to the MS-imbibed seeds because of a blockage of cell elongation prior to radicle protrusion and cell division in the developing hypocotyl. Fusicoccin, by promoting seed germination and increasing cell enlargement, was expected to modify the embryonic axis elongation stage and growth of the emerged radicle.[38,39]

The effect of the two drugs on the exact time of radicle protrusion was not determined in this study because we knew that it was likely to be slightly advanced with fusicoccin and very little affected by oryzalin compared with MS medium.[34,39] However, radicle elongation was observed in both drug treatments as well as for the MS medium from 21 h of imbibition. Fusicoccin accelerated the early elongation rate on the emergence of the radicle, leading to a significant increase in the radicle length. The opposite situation was observed with oryzalin, leading to a markedly shorter radicle (Figure 1). Despite minor variations in the rate of radicle elongation among the three germination media, the mechanisms involved in this elongation would not be very different. The two drugs modified α-galactosides and free sugar concentrations during seed germination and radicle growth (Figure 7). In the MS medium, α-galactosides were consumed early during seed imbibition and were partly transformed into free fructose and glucose. Of interest was a marked increase in the fructose content at radicle emergence, whereas the glucose content increase occurred after radicle emergence (Figure 7A,B). Fructose and glucose may contribute to turgor regulation, but the different kinetics in concentration changes of these two sugars may reflect different rates of use as a source of energy or as starting building blocks of cell wall polysaccharides. This is particularly emphasized with the fusicoccin-treated seeds, in which axis growth was faster. Glucose content peaked first after 21 h imbibition with radicle protrusion; maximum fructose content was observed after 24 h. Then glucose content particularly declined with active elongation of the radicle. In comparison with the MS medium, oryzalin-treated seeds displayed a parallel shift in the evolution of the total sugar content (Figure 7D), with significantly lower values along the imbibition, testifying for a perturbed seed metabolism. The latter may be delayed, as observed by the significantly higher sucrose content observed after 48 h of germination compared with MS and fusicoccin (Figure 7C).

Regarding T_1 and T_2 relaxation time components, fusicoccin and oryzalin affected water dynamics in both frozen and freeze−thawed samples (see Tables 1 and 2, respectively). The main significant differences between the two drugs occurred at 5 h and during the germinating phase III (Figure 6). At 5 h of imbibition, the overall longest T_1 relaxation times observed for fusicoccin-treated seeds compared with MS and oryzalin ones, could be related to the stimulation of osmotic efficiencies and transcellular water flux by the drug, thus promoting water exchange and diffusion phenomena.[38] Oryzalin affected the water dynamics, but at a later stage. The earliest significant differences were after 21 h of imbibition, indicating a possible influence of the drug on tubulin polymerization required for radicle cell elongation and, later on, for cell division for hypocotyl growth.

The cytoskeleton plays an important role in mitosis and in guiding cellulose deposition in expanding cells; both phenomena could contribute to reducing the radicle length after germination.[53] During the phase of radicle elongation (21−48 h imbibition period), the water dynamics associated with each of the two growth modulator media were quite well differentiated (Figure 6). In addition, relationships between relaxometric parameters and radicle length could be identified, regardless of the germination media. In the frozen state, proportions $P_{2\beta}$ and $P_{2\gamma}$ correlated well with radicle length (Figure 4). Regarding the cell wall loosening mechanism occurring during the radicle elongation, this supports the previous assumption of a significant contribution of water fractions closely associated with cell wall biopolymers to the cell elongation process. For freeze−thawed seeds, fairly good correlations between transverse relaxation parameters ($T_{2i,j,k}$; $P_{2i,j,k}$) and radicle length were also demonstrated (Figure 5). The increase in the three T_2 relaxation time values and the relative increase in P_{2k} likely reflected the weakening of the radicle cell wall and the increase in cell size during the period of radicle elongation. This set of linear relationships, determined without germination medium consideration, points out that growth modulators (oryzalin and fusicoccin) would not significantly affect the molecular composition after radicle protrusion.

In conclusion, comparing NMR relaxometric characteristics of water in fresh, frozen, and freeze−thawed germinating *M. truncatula* seeds allowed us to distinguish developmental phases and to detect further specific events occurring within them related to organ and tissue microstructural developments. It also allowed detection of the effects of growth modulators (oryzalin and fusicoccin) on cell development. The sensitivity of low-field NMR relaxometry in detecting physiological events makes this technique promising for characterizing seed quality and the impact of abiotic and biotic stresses on germination. With regard to the interpretation of the multicomponent relaxation, the similarity of T_2 relaxation results obtained during the radicle emergence period between fresh and freeze−thawed seeds clearly demonstrated the necessity for a reinterpretation of the classical analysis linking relaxations to cell structures in biological systems. It is proposed that the different T_2 components be preferentially assigned to specific "classes" of water interaction/environment rather than to individual tissue compartments, such as vacuole, extra-cellular space, or cell wall.

AUTHOR INFORMATION

Corresponding Authors

*Phone: 33 (0)2 40 67 50 63. Fax: 33 (0)2 40 67 50 84. E-mail: Marc.Lahaye@nantes.inra.fr.

*Phone: 33 (0)2 40 67 50 50. Fax: 33 (0)2 40 67 52 29. E-mail: Loic.Foucat@nantes.inra.fr.

DOI: 10.1021/jf505515n
J. Agric. Food Chem. 2015, 63, 1698−1710

Funding

This work and salary (X.F.) were supported in part by the Region Pays de la Loire Research Contract QUALISEM.

Notes

The authors declare no competing financial interest.

■ ACKNOWLEDGMENTS

NMR analyses were performed within the BIBS platform (INRA, Centre Angers-Nantes, http://www.bibs.inra.fr).

■ REFERENCES

(1) Nonogaki, H.; Bassel, G. W.; Bewley, J. D. Germination—Still a mystery. *Plant Sci.* **2010**, *179*, 574−581.

(2) Rajjou, L.; Duval, M.; Gallardo, K.; Catusse, J.; Bally, J.; Job, C.; Job, D. Seed germination and vigor. *Annu. Rev. Plant Biol.* **2012**, *63*, 507−533.

(3) Foucat, L.; Chavagnat, A.; Renou, J. P. Nuclear-magnetic-resonance imaging and X-radiography as possible techniques to study seed-germination. *Sci. Hortic.* **1993**, *55*, 323−331.

(4) Manz, B.; Muller, K.; Kucera, B.; Volke, F.; Leubner-Metzger, G. Water uptake and distribution in germinating tobacco seeds investigated in vivo by nuclear magnetic resonance imaging. *Plant Physiol.* **2005**, *138*, 1538−1551.

(5) Rathjen, J. R.; Strounina, E. V.; Mares, D. J. Water movement into dormant and non-dormant wheat (*Triticum aestivum* L.) grains. *J. Exp. Bot.* **2009**, *60*, 1619−1631.

(6) Terskikh, V. V.; Feurtado, J. A.; Ren, C. W.; Abrams, S. R.; Kermode, A. R. Water uptake and oil distribution during imbibition of seeds of western white pine (*Pinus monticola* Dougl. ex D. Don) monitored in vivo using magnetic resonance imaging. *Planta* **2005**, *221*, 17−27.

(7) Pietrzak, L. N.; Fregeau-Reid, J.; Chatson, B.; Blackwell, B. Observations on water distribution in soybean seed during hydration processes using nuclear magnetic resonance imaging. *Can. J. Plant Sci.* **2002**, *82*, 513−519.

(8) Garnczarska, M.; Zalewski, T.; Kempka, M. Changes in water status and water distribution in maturing lupin seeds studied by MR imaging and NMR spectroscopy. *J. Exp. Bot.* **2007**, *58*, 3961−3969.

(9) Sliwinska, E.; Bassel, G. W.; Bewley, J. D. Germination of *Arabidopsis thaliana* seeds is not completed as a result of elongation of the radicle but of the adjacent transition zone and lower hypocotyl. *J. Exp. Bot.* **2009**, *60*, 3587−3594.

(10) Weitbrecht, K.; Muller, K.; Leubner-Metzger, G. First off the mark: early seed germination. *J. Exp. Bot.* **2011**, *62*, 3289−3309.

(11) Linkies, A.; Leubner-Metzger, G. Beyond gibberellins and abscisic acid: How ethylene and jasmonates control seed germination. *Plant Cell Rep.* **2012**, *31*, 253−270.

(12) Schopfer, P. Biomechanics of plant growth. *Am. J. Bot.* **2006**, *93*, 1415−1425.

(13) Terskikh, V.; Müller, K.; Kermode, A. R.; Leubner-Metzger, G. In vivo ^{1}H-NMR microimaging during seed imbibition, germination, and early growth. *Methods Mol. Biol.* **2011**, *773*, 319−327.

(14) Hills, B. P.; Clark, C. J. Quality assessment of horticultural products by NMR. *Annu. Rev. NMR Spectrosc.* **2003**, *50*, 75−120.

(15) Hansen, C. L.; Thybo, A. K.; Bertram, H. C.; Viereck, N.; van den Erg, F.; Engelsen, S. B. Determination of dry matter content in potato tubers by Low-Field Nuclear Magnetic Resonance (LF-NMR). *J. Agric. Food Chem.* **2010**, *58*, 10300−10304.

(16) Belton, P. S.; Colquhoun, I. J. NMR and FTIR studies of structure and function in food biopolymers. *Abstr. Pap. Am. Chem. Soc.* **1990**, *200*, 208−AGFD.

(17) Lenk, R.; Degliagosti, R.; Greppin, H. Studies of oat seeds germination by NMR. *Biol. Plant.* **1991**, *33*, 501−504.

(18) Miedziejko, E. M. Impact of chemical stimuli and temperature on water transport and mobility in germinating rape seeds by pulsed ^{1}H NMR spectroscopy. *Magn. Reson. Chem.* **1997**, *35*, S61−S68.

(19) Pouliquen, D.; Gross, D.; Lehmann, V.; Ducournau, S.; Demilly, D.; Lechappe, J. Study of water and oil bodies in seeds by nuclear magnetic resonance. *C. R. Acad. Sci. III Vie/Life Sci.* **1997**, *320*, 131−138.

(20) Pedersen, H. T.; Munck, L.; Engelsen, S. B. Low-field ^{1}H nuclear magnetic resonance and chemometrics combined for simultaneous determination of water, oil, and protein contents in oilseeds. *J. Am. Oil Chem. Soc.* **2000**, *77*, 1069−1076.

(21) Garnczarska, M.; Zalewski, T.; Kempka, M. Water uptake and distribution in germinating lupine seeds studied by magnetic resonance imaging and NMR spectroscopy. *Physiol. Plantarum* **2007**, *130*, 23−32.

(22) Sarkar, B. K.; Yang, W. Y.; Wu, Z.; Tang, H. R.; Ding, S. W. Variations of water uptake, lipid consumption, and dynamics during the germination of sesamum indicum seed: A nuclear magnetic resonance spectroscopic investigation. *J. Agric. Food Chem.* **2009**, *57*, 8213−8219.

(23) Krishnan, P.; Singh, R.; Verma, A. P. S.; Joshi, D. K.; Singh, S. Changes in seed water status as characterized by NMR in developing soybean seed grown under moisture stress conditions. *Biochem. Biophys. Res. Com* **2014**, *444*, 485−490.

(24) Rocculi, P.; Sacchetti, G.; Venturi, L.; Cremonini, M.; Rosa, M. D.; Pittia, P. Role of water state and mobility on the antiplasticization of green and roasted coffee beans. *J. Agric. Food Chem.* **2011**, *59*, 8265−8271.

(25) Hills, B. P.; Takacs, S. F.; Belton, P. S. A new interpretation of proton NMR relaxation-time measurements of water in food. *Food Chem.* **1990**, *37*, 95−111.

(26) Snaar, J. E. M.; Van As, H. Probing water compartments and membrane permeability in plant cells by ^{1}H NMR relaxation measurements. *Biophys. J.* **1992**, *63*, 1654−1658.

(27) Snaar, J. E. M.; Vanas, H. A method for the simultaneous measurement of NMR spin-lattice and spin spin relaxation-times in compartmentalized systems. *J. Magn. Reson.* **1992**, *99*, 139−148.

(28) Tang, H.-R.; Godward, J.; Hills, B. The distribution of water in native starch granules—A multinuclear NMR study. *Carbohydr. Polym.* **2000**, *43*, 375−387.

(29) Overloop, K.; van Gerven, L. Freezing phenomena in adsorbed water as studied by NMR. *J. Magn. Reson.* **1993**, *A 101*, 179−187.

(30) Volke, F.; Pampel, A.; Haensler, M.; Ullmann, G. Proton MAS NMR of a protein in a frozen aqueous solution. *Chem. Phys. Lett.* **1996**, *262*, 374−378.

(31) Belton, P. S. NMR and mobility of water in polysaccharide gels. *Int. J. Biol. Macromol.* **1997**, *21*, 81−88.

(32) Glevarec, G.; Bouton, S.; Jaspard, E.; Riou, M. T.; Cliquet, J. B.; Suzuki, A.; Limami, A. M. Respective roles of the glutamine synthetase/glutamate synthase cycle and glutamate dehydrogenase in ammonium and amino acid metabolism during germination and post-germinative growth in the model legume *Medicago truncatula*. *Planta* **2004**, *219*, 286−297.

(33) Gallardo, K.; Lesignor, C.; Darmency, M.; Burstin, J.; Thompson, R.; Rochat, C.; Boutin, J. P.; Kuster, H.; Buitink, J.; Leprince, O.; Limami, A.; Gusak, M. A. Seed biology of *Medicago truncatula*. In *Medicago truncatula handbook* [Online]; Mathesius, U., Journet, E. P., Summer, L. W., Eds.; The Samuel Roberts Noble Fundation: Ardmore, OK, 2006; http://www.noble.org/MedicagoHandbook.

(34) Gimeno-Gilles, C.; Lelievre, E.; Viau, L.; Malik-Ghulam, M.; Ricoult, C.; Niebel, A.; Leduc, N.; Limami, A. M. ABA-mediated inhibition of germination is related to the inhibition of genes encoding cell-wall biosynthetic and architecture: modifying enzymes and structural proteins in *Medicago truncatula* embryo axis. *Mol. Plant* **2009**, *2*, 108−119.

(35) Reid, J. S. G.; Bewley, J. D. Dual role for the endosperm and its galactomannan reserves in the germinative physiology of fenugreek (*Trigonella-Foenum-Graecum* L.), an endospermic leguminous seed. *Planta* **1979**, *147*, 145−150.

(36) Buckeridge, M. S. Seed cell wall storage polysaccharides: Models to understand cell wall biosynthesis and degradation. *Plant Physiol.* **2010**, *154*, 1017−1023.

(37) Kaschani, F.; van der Hoorn, R. Small molecule approaches in plants. *Curr. Opin. Chem. Biol.* **2007**, *11*, 88−98.

DOI: 10.1021/jf505515n
J. Agric. Food Chem. 2015, 63, 1698−1710

(38) Marre, E. Fusicoccin: A tool in plant physiology. *Annu. Rev. Plant Physiol.* **1979**, *30*, 273−288.
(39) Antipova, O. V.; Bartova, L. M.; Kalashnikova, T. S.; Obroucheva, N. V.; Voblikova, V. D.; Muromtsev, G. S. Fusicoccin-induced cell elongation and endogenous fusicoccin-like ligands in germinating seeds. *Plant Physiol. Biochem.* **2003**, *41*, 157−164.
(40) Morejohn, L. C.; Bureau, T. E.; Molebajer, J.; Bajer, A. S.; Fosket, D. E. Oryzalin, a dinitroaniline herbicide, binds to plant tubulin and inhibits microtubule polymerization *in vitro*. *Planta* **1987**, *172*, 252−264.
(41) R Core Team R: A language and environment for statistical computing. In *R Foundation for Statistical Computing*; Vienna, Austria, 2014; http://www.R-project.org.
(42) Overloop, K.; van Gerven, L. NMR relaxation in adsorbed water. *J. Magn. Reson.* **1992**, *100*, 303−315.
(43) Djemel, N.; Guedon, D.; Lechevalier, A.; Salon, C.; Miquel, M.; Prosperi, J. M.; Rochat, C.; Boutin, J. P. Development and composition of the seeds of nine genotypes of the *Medicago truncatula* species complex. *Plant Physiol. Biochem.* **2005**, *43*, 557−566.
(44) Wolfe, J.; Bryant, G.; Koster, K. L. What is 'unfreezable water', how unfreezable is it and how much is there? *Cryoletters* **2002**, *23*, 157−166.
(45) Cameron, I. L.; Haskin, C. L.; Fullerton, G. D. Multiple unfrozen water fractions in biological tissues: freezing point and size. *Water* **2013**, *5*, 45−56.
(46) Hills, B. P.; Remigereau, B. NMR studies of changes in subcellular water compartmentation in parenchyma apple tissue during drying and freezing. *Int. J. Food Sci. Technol.* **1997**, *32*, 51−61.
(47) Hills, B. P.; Nott, K. P. NMR studies of water compartmentation in carrot parenchyma tissue during drying and freezing. *Appl. Magn. Reson.* **1999**, *17*, 521−535.
(48) Foucat, L.; Lahaye, M. A subzero ^{1}H NMR relaxation investigation of water dynamics in tomato pericarp. *Food Chem.* **2014**, *158*, 278−282.
(49) Lai, F.-M.; Lecouteux, C. G.; McKersie, B. D. Germination of alfalfa (*Medicago sativa* L.) seeds and desiccated somatic embryos: I. Mobilization of storage reserves. *J. Plant Physiol.* **1995**, *145*, 507−513.
(50) Morgan, J. M. Osmoregulation and water stress in higher plants. *Annu. Rev. Plant Physiol.* **1984**, *35*, 299−319.
(51) Mazur, P. Freezing of living cells: mechanisms and implications. *Am. J. Physiol. - Cell Physiol.* **1984**, *247*, C125−C142.
(52) Cosgrove, D. J. Loosening of plant cell walls by expansins. *Nature* **2000**, *407*, 321−326.
(53) Taylor, N. G. Cellulose biosynthesis and deposition in higher plants. *New Phytologist* **2008**, *178*, 239−252.

DOI: 10.1021/jf505515n
J. Agric. Food Chem. 2015, 63, 1698−1710

bioinformatics analyses, assay optimization, characterization, and in-house validation were conducted by the MBG Unit of the IHCP with the samples provided by IRRI. The characterization and validation of the two assays were performed in accordance with the European Network of GMO Laboratories (ENGL) minimum performance requirements (MPR) for analytical methods of GMO testing,[14] the requirements of the Codex Alimentarius for methods for detection, identification and quantification of specific DNA sequences,[25] and taking into account International Union of Pure and Applied Chemistry (IUPAC) harmonized guidelines for single-laboratory validation of methods of analysis.[26]

MATERIALS AND METHODS

Bioinformatics Analyses. Bioinformatics analyses were conducted on the JRC Central Core DNA Sequence Information System (CCSIS)[27] using PLD gene sequence (GenBank accession number NM_001064552.1) and sequence data for event Golden Rice 2-R (GR2-R) provided by IRRI for the two PLD-GR taxon-specific assays (Set1 and Set2) and the GR2 event-specific assays (LB-01 and RB-BS), respectively. Similarity searches were performed with BLASTN 2.2.15:[28] both primer sequences and the corresponding amplicon were used as query to scan the CCSIS DNA set, the plant sequence data section of the EMBL database, the NCBI nucleotide sequence and the rice TIGR databases, the vector sequences from synthetic (syn) division of GenBank, the NCBI patent nucleotide sequence, and the NCBI UniVec databases (web addresses available in the Supporting Information).

Genomic DNA and Plant Materials. Frozen leaves of non-GM rice (*Oryza sativa* ssp. Japonica, cv. Kaybonnet) and GM rice (homozygous for GR2-R, GR2-E, GR2-G, GR2-L, GR2-T, or GR2-W GR2 transformation events, cv. Kaybonnet), and genomic DNA extracted from 131 non-GM rice varieties (complete list available in Table S1, Supporting Information) were provided by IRRI. DNA from sorghum (*Sorghum vulgare*), barley (*Hordeum vulgare*), wheat (*Triticum durum*), triticale (*x Triticosecale*), and rye (*Secale cereale*) was extracted from ground seeds or leaves at the European Union Reference Laboratory for GM Food and Feed (EU-RL GMFF). Genomic DNA from non-GM soybean (*Glycine max*), rapeseed (*Brassica napus*), cotton (*Gossypium hirsutum*), sugar beet (*Beta vulgaris*), potato (*Solanum tuberosum*), and from the GM events listed in "Genomic DNA and plant materials", Supporting Information, was prepared by the EU-RL GMFF.

Genomic DNA Extraction and Evaluation of Quality and Quantity. Barley, rice, rye, sorghum, triticale, and wheat genomic DNA was extracted with either a CTAB DNA extraction method (modified from ISO 21571[29]) or a phenol-chloroform method optimized for rice leaves (modified from Sambrook and colleagues[30]). All extracted DNAs were tested for integrity using a 1% (w/v) agarose gel electrophoresis and for purity by assessing the presence of PCR inhibitors as described by Zel and colleagues[31] and the absence of contamination with the GR2-R event. DNA concentration was determined fluorimetrically with the Quant-iT PicoGreen dsDNA Assay Kit (Molecular Probes, Eugene, U.S.) with a five-point standard curve ranging from 1 to 500 ng/mL with a Biorad (Hercules, U.S.) VersaFluor fluorometer. Only pure, noninhibited high molecular weight DNA was used.

Sample Preparation. Samples for optimization and in-house testing of the taxon- and event-specific assays were prepared diluting DNAs in 0.1 × TE. Samples for the relative quantification were prepared in haploid genome equivalents (hge) ratio by mixing GM (GR2-R event) and non-GM (cv. Kaybonnet) rice DNA. Standard curve samples were prepared by serial dilution; test samples were prepared independently. Genome sizes taken into account for the calculation of hge contents are listed in "Genome Sizes", Supporting Information.

Specificity. For the taxon-specific assay (Set1 and Set2), all of the species mentioned in the section Genomic DNA and Plant Materials (except carnation) were tested with 200 ng DNA/reaction; reactions were performed in triplicate, and the resulting Cqs were averaged. Rice DNA was included as positive control at 100 ng/reaction, with six replicates. For the event-specific assay (RB-BS set), the events listed in "Genomic DNA and Plant Materials", Supporting Information, were tested, as well as non-GM DNA from the same species tested with the taxon-specific assay, with a DNA amount corresponding to 200 000 hge/reaction, up to a maximum of 200 ng of DNA. Reactions were performed in triplicate, and the resulting Cqs averaged. The DNA amount used for each event/species and the GM material used are reported in "Specificity", Supporting Information. DNAs used for the tests were previously checked for the absence of inhibition as described in ref 31 with a suitable taxon-specific assay.

Stability of the Taxon-Specific Assay. The variability of the Cqs obtained with the PLD-GR taxon-specific assay (Set1) with a fixed DNA concentration was evaluated on 131 rice varieties, selected by IRRI as representative of global genetic diversity, and the Kaybonnet variety. The variability between plates was maintained as low as possible by performing all qPCR experiments on the same day and the same instrument; the same baseline and threshold were used for the analysis of the results of all plates. The list of the varieties tested, subspecies they belong to, and the obtained Cq are available in Table S1, Supporting Information. The genomic DNA of each variety was diluted to 25 ng/reaction, corresponding to 50 000 hge; reactions were performed in triplicate, and the resulting Cqs were averaged.

Dynamic Range and LOQ. A set of standard curve and test samples was prepared for the PLD-GR (Set1) and one for the GR2 (RB-BS set) assay, with non-GM and GR2-R DNA, respectively. Table S2, Supporting Information, reports the hge and DNA content of the standard curve and the test samples. Each standard curve sample was analyzed in three plates in triplicate, for a total of nine replicates, and each test sample was measured in three plates with eight replicates, for a total of 24 replicates. The hge content of the test samples was estimated by interpolation from the standard curve constructed with the standard curve samples. The limit of quantification (LOQ) of the two assays was evaluated concurrently.

LOD. The limit of detection (LOD) of the two assays was first assessed with 10 replicates over a range of 3−50 hge/reaction, on the samples described in Table S3, Supporting Information. The 0.1, 0.5, and 1 hge samples were included in the test to verify the correctness of the dilution, by evaluating the number of negative replicates obtained. Samples D1−D9 were prepared by serial dilution of non-GM rice DNA or GR2-R GM DNA for the taxon- and event-specific assays, respectively; the 0.5 hge sample was prepared and assessed only for the event-specific assay. To reach the 95% level of confidence, on the basis of the pilot test, two hge levels were selected for each assay, which were then tested, together with the 0.1 and 1 hge samples, with 60 replicates. For the PLD-GR taxon-specific assay, the 4.5 and 3 hge levels were selected, for the GR2 event-specific assay, the 6 and 4 hge levels. The LOD was set at the lowest concentration yielding at least 59 positive results.[32,33]

Robustness. The robustness of the PLD-GR (Set1) and the GR2 (RB-BS set) assays was tested by introducing variations in the volume of reaction mix per reaction (21 μL or 19 μL instead of 20 μL), the concentration of Mastermix (±20%), the concentration of primers or probe (±30%), the annealing temperature (±1 °C), and the qPCR equipment: Roche (Basel, Switzerland) LightCycler (LC) 480, Stratagene (La Jolla, CA) Mx3005P, Applied Biosystems (ABI, Waltham, U.S.) 7500. RSD_r and bias were evaluated on quantification of three test samples chosen to cover the full dynamic range of the GR2 assay (from 40 to 200 000 hge) and almost all that of the PLD-GR assay (from 30 to 200 000 hge). Test samples were quantified in repeatability conditions, with 3 replicates over one run for each condition. Standard curve and test samples were prepared with non-GM DNA for the taxon-specific assay and with GM (GR2-R) DNA for the event-specific assay (Table S4, Supporting Information).

Relative Quantification. Three test samples with a GM % ranging from 0.1% to 4.5% were prepared on the basis of their hge content and quantified with two qPCR runs and 6 replicates for each GM-level on each plate, with the PLD-GR (Set2) and the GR2 (RB-BS set) assays,

DOI: 10.1021/jf505516y
J. Agric. Food Chem. 2015, 63, 1711−1721

Table 1. Position, Amplicon Size, Target, and Sequence Information for the Four Primers/Probe Sets Tested in This Study[a]

assay	sequence (5′−3′)	target	amplicon size (bp)	position (bp)
GR2 (LB-01)	For- CCGAGCTGCGAGAAGGAGTA	GR2-R event, left border - plant, DNA junction	120	518−637
	Rev-CGTTTCCCGCCTTCAGTTTA			
	Probe-CGACCTGCAGAAACCCACCACCA			
GR2 (RB-BS)	For-TGGCCGTATCCGCAATGTG	GR2-R event, right border - plant, DNA junction	121	9541−9660
	Rev-GCTGCGCCTCTAACCAGGTAT			
	Probe-TCGATATGATTCCTTCATCGAGCGAGC			
PLD-GR (Set1)	For-GGCAAGAACAACACCATTGACA	*Oryza sativa* PLD α 2 gene sequence (GenBank NM_001064552.1)	124	Exon 2 (1635−1758)
	Rev-CGGCTTTCCATGCAAATGA			
	Probe-ATTCGCCGCGCCAAGAACTTCA			
PLD-GR (Set2)	For-GGCAGCTCATTTGCATGGA	*Oryza sativa* PLD α 2 gene sequence (GenBank NM_001064552.1)	121	Exon 2 (1734−1854)
	Rev-CAAAACGCTCACCAGCTTCA			
	Probe-ACATTGAGGCGTTGCATCTGATTCCC			

[a]bp, base pairs.

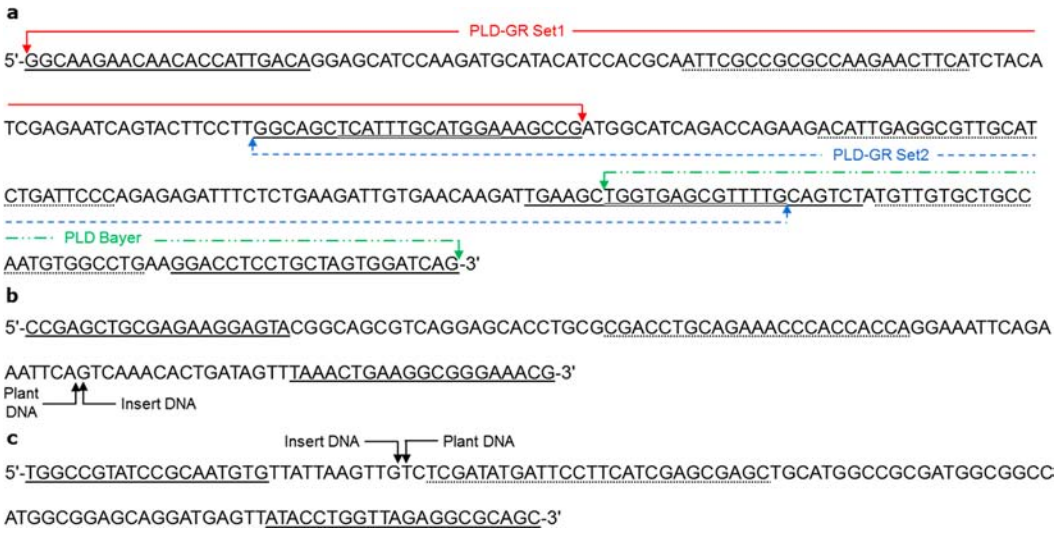

Figure 1. Amplicon sequence of PLD taxon-specific assays and GR2 event-specific assays. (a) PLD-GR Set1 and Set2, and PLD taxon-specific assay developed by Bayer;[22] (b) GR2 LB-01 primers/probe set; (c) GR2 RB-BS set. PLG-GR Set1 and Set2 overlap of 25 bp at their 5′ and 3′ ends, respectively; PLD-GR Set2 and PLD from Bayer overlap of 14 bp at their 5′ and 3′ ends, respectively; GR2 LB-01 set covers the 3′ plant-to-insert DNA junction; GR2 RB-BS set covers the 5′ insert-to-plant junction. Primer sequences are underlined with a single line, or a double line if two primers overlap, probe sequences are underlined with a dotted line; the junction between plant and transgenic insert DNA is indicated with arrows in GR2 amplicons; PLD-GR Set1 amplicon is indicated with a solid, red line, PLD-GR Set2 amplicon with a blue, broken line, and PLD amplicon developed by Bayer with a green broken and dotted line.

with a five-point standard curve with a GM % content ranging from 5% to 0.07%. The GR2 hge and PLD hge content of the standard curve and test samples were included in the dynamic range of the two assays. Hge and DNA content, dilution factor (standard curve only), and GM % of the standard curve and test samples are reported in Table S5, Supporting Information.

PCR Primers and Probes. Primers and TaqMan probes sequences were designed by IRRI using Primer Express Software (Life Technologies, Carlsbad, CA) and selected by the EU-RL GMFF on the basis of bioinformatics analyses. Primers were also tested against known plant genomes using the ePCR prediction tool.[34] The selected TaqMan probes are labeled with 6-carboxyfluorescein (FAM) fluorophore at 5′ and with tetramethylrhodamine (TAMRA) quencher at 3′. The sequence, annealing position of the primers and probes, and length of the obtained amplicons are reported in Table 1. Primers were purchased from Eurofins MWG operon (Ebersberg, Germany) and probes from ABI UK (Warrington, United Kingdom). The primers/probe concentration for PLD-GR taxon-specific assay and for GR2 event-specific assay was optimized by testing different primers/probe concentrations on a serial 4-fold dilution of DNA starting from 200 ng of non-GM DNA/reaction to 0.78 ng/reaction for the taxon-specific assay and from 100 to 0.39 ng of GM (GR2-R event) DNA/reaction for the event-specific assay. An optimal primer concentration was first selected, keeping the probe at 150 nM and testing the primers from 150 to 450 nM by 100 nM increases; probe concentrations tested ranged from 100 to 250 nM by 50 nM increases, with primers at 350 nM. The selection criteria were: profile and level of fluorescence of the amplification curves at different DNA concentrations, presence/absence of inhibition, and slope of the dilution. The final selection was 300 nM primers and 150 nM probe for the two primers/probe pairs tested for each of the two assays.

Real-Time PCR. The optimized qPCR reaction mixture for all four primers/probe sets tested contained the following reagents: 1x TaqMan universal master mix (ABI), 300 nM primer forward, 300 nM primer reverse, 150 nM probe, 5 μL of DNA sample, and nuclease free water (Promega, Madison, WI) up to a volume of 25 μL/reaction. All qPCR runs, except where specified for the robustness test, were performed with ABI 7900 platform (Life Technologies, Carlsbad, CA) with the following thermal profile: 50 °C for 2 min; 95 °C, 10 min; 45 cycles of 95 °C, 15 s and 60 °C, 60 s; fluorescence data were acquired at the end of each cycle.

DOI: 10.1021/jf505516y
J. Agric. Food Chem. 2015, 63, 1711−1721

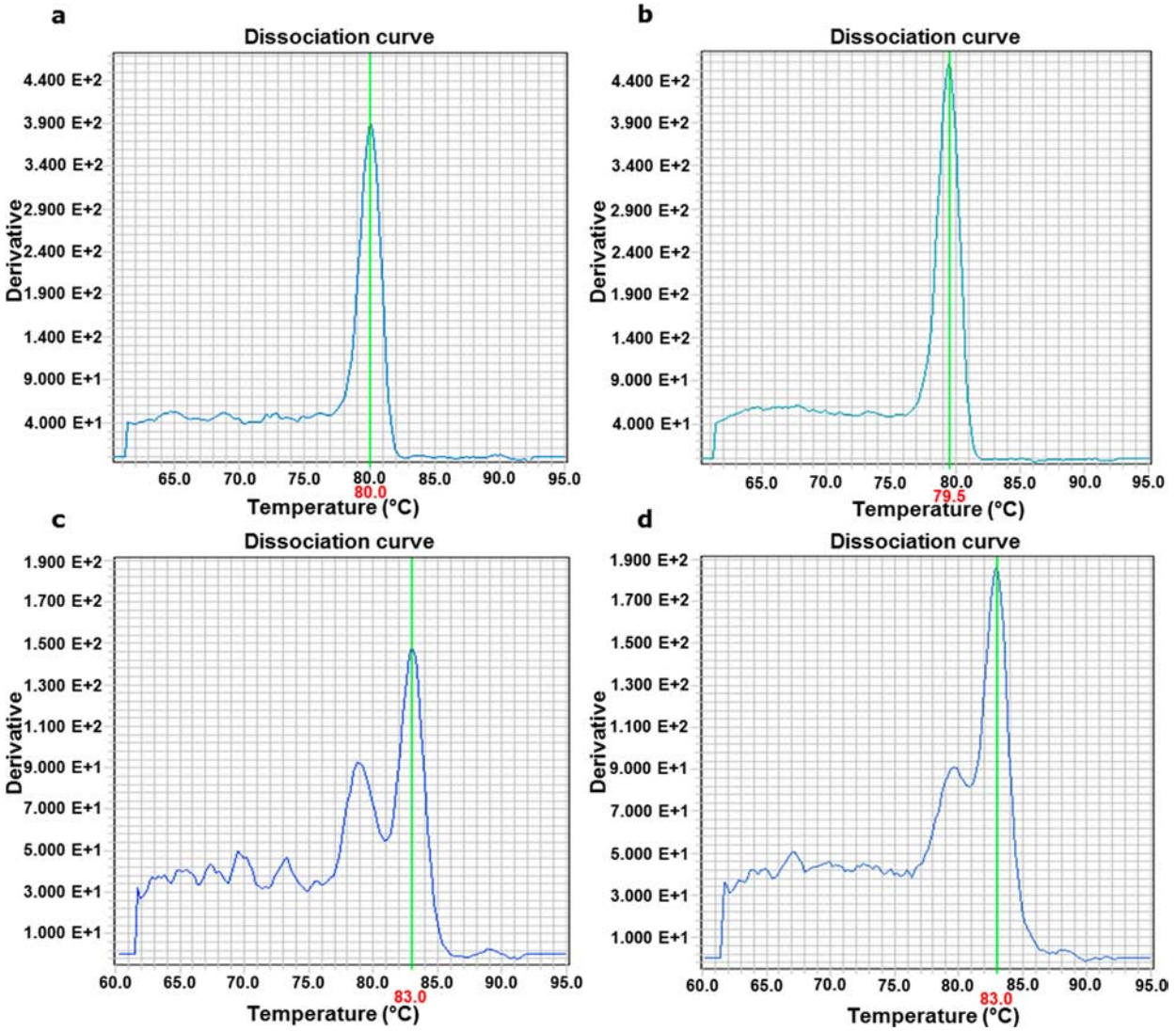

Figure 2. Melting curve profile of (a) PLD-GR taxon-specific assay, Set1; (b) PLD-GR taxon-specific assay, Set2; (c) GR2 event-specific assay, LB-01 set; and (d) GR2 event-specific assay, RB-BS set. A single peak is present in PLD-GR Set1 and Set2 assays melting profile; a weaker peak (lower melting temperature, putative primer dimers) and a stronger peak (higher melting temperature, specific amplification) are present in the GR2 LB-01 and RB-BS assays melting profile, the weaker peak being more evident in the LB-01 assay melting profile.

Melting curve analysis, Agilent microfluidic chip assay, sequencing, and digital PCR methods are described in the Supporting Information.

Data Analysis. Standard curves were generated by plotting the Cq values measured for the calibration points against the logarithm of the DNA hge content and by fitting a linear regression line into these data. The hge content of the test samples was then estimated by interpolation from the standard curve. Experiments performed on ABI 7900 qPCR equipment were analyzed with the SDS 2.4 software (Life Technologies, Carlsbad, CA); the baseline was set manually three cycles before the cycle number at which the threshold line crosses the first amplification curve; the threshold was set manually in the area where the amplification profiles appeared linear and there was no fork effect between replicates of the same sample. MIQE guidelines were taken into consideration when applicable to the present work.[35] Robust mean calculation and cluster analysis are described in the Supporting Information.

Performance Criteria. Performance parameters of the PLD-GR and GR2 assays were evaluated in accordance with ENGL MPR.[14] Specificity, dynamic range, accuracy, PCR efficiency, linearity, LOQ, LOD, and robustness were evaluated, as well as copy number and stability of the PLD-GR taxon-specific assay. Accuracy was evaluated on the basis of two parameters: trueness and precision. Trueness was expressed as mean percent bias (difference between the mean value of test results and the accepted reference value divided by the latter). Precision was expressed as relative repeatability standard deviation (RSD_r) in percent relative to the accepted reference value. Amplification efficiency was calculated from the slope of the standard curve using the formula: efficiency = $((10^{(-1/\text{slope})}) - 1) \times 100$. Linearity was expressed as coefficient of determination of the standard curve obtained by linear regression analysis. The criteria set for each of these parameters are discussed throughout the text.

RESULTS

Bioinformatics Analyses. The two sets of primers and probes for the PLD-GR taxon-specific assay (see Table 1 for primers and probes sequence and location) produced alignments only with exon 2 of the PLD α2 gene in *Oryza sativa* and with sequences from *Oryza glaberrima*, African rice (data not shown). Set1 and Set2 PCR amplicons overlap for 25 bp and Set2 overlaps for 14 bp with the amplicon of the PLD assay developed by Bayer (Figure 1a).[22] The two sets of primers and probes for the event-specific assay produced alignments with no other sequence than the GR2-R event. The LB-01 set is

DOI: 10.1021/jf505516y
J. Agric. Food Chem. 2015, 63, 1711−1721

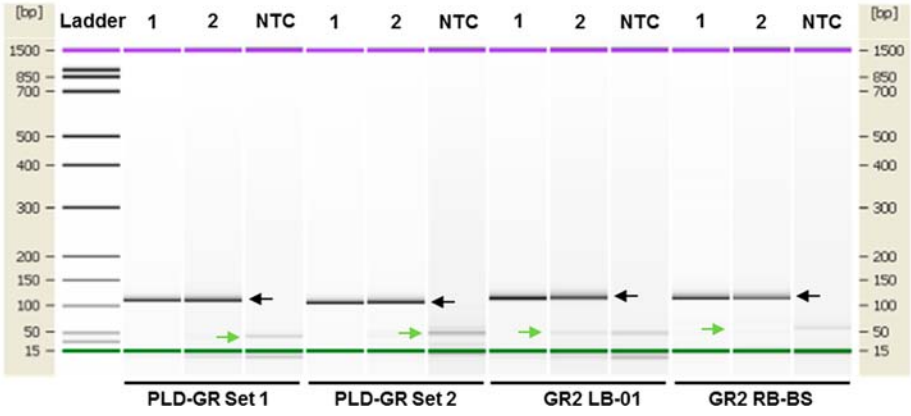

Figure 3. Virtual gel representation of capillary electrophoresis of the amplification products of PLD-GR taxon-specific assay Set1 and Set2, and GR2 event-specific assay LB-01 and RB-BS sets. PLD-GR Set1 and Set2 assays show one specific amplification product (black arrow, pointing left) for the two template DNA concentrations loaded (1, 40 000 hge; 2, 156 hge), and a lower band of putative primer dimers (green arrow, pointing right) only in the no template control (NTC). GR2 LB-01 and RB-BS sets show one specific amplification product for the two template DNA concentrations loaded and primer dimers in the no template control and with a weak (LB-01 set) and very weak band (RB-BS set) also in the amplification with lower template DNA concentration. bp, base pairs.

designed across the 5′ plant−insert DNA junction, the RB-BS set across the 3′ insert−plant DNA junction (Figure 1b,c).

Optimization and Characterization of the PLD-GR and GR2 Assays. We optimized and characterized the PLD-GR taxon-specific and the GR2-R event-specific qPCR assays independently. We defined the optimal concentration of primers and probes as described in the Materials and Methods, which resulted to be 300 nM primers and 150 nM probe for all sets. We characterized the PCR products of the four primers/probe sets with melting curve analysis, capillary electrophoresis, and amplicon sequencing. The melting temperature of the PLD-GR assay ranged, depending on the amount of DNA in reaction, from 79.7 to 80.3 °C with an average of 80.0 °C for Set1 and from 79.2 to 79.9 °C with an average of 79.5 °C for Set2; the profiles of the dissociation curves were indicative of specific amplification (Figure 2a,b). Capillary electrophoresis showed the presence of a single band of the expected size for both sets, on a clean background (Figure 3). The sequences generated on both strands of PLD-GR Set1 and Set2 amplicons showed 100% identity with PLD α2 gene, further confirming the specificity of the amplification. For the GR2 assay, the melting temperature ranged from 82.5 to 83.0 °C with an average of 82.8 °C for the LB-01 set and from 82.5 to 83.0 °C with an average of 82.9 °C for RB-BS primer set. The melting profiles of the two sets were indicative of specific amplification, although they showed peaks consistent with the formation of putative primer-dimers, more evident for the LB-01 set (Figure 2c,d). Capillary electrophoresis showed the presence of a single band of the expected size for both sets, and smaller bands barely visible, with a size consistent with primer-dimers (Figure 3). The sequences obtained for GR2 LB-01 and RB-BS amplicons showed 100% identity with the sequence of the GR2 event provided by IRRI. Because both melting curve analysis and capillary electrophoresis indicated that the formation of primer dimers was less evident for GR2 RB-BS primer set as compared to LB-01 primer set, we chose the RB-BS set for further analyses.

Specificity. We tested the specificity of the PLD-GR and GR2 assays experimentally, verifying their amplification with genomic DNA from other species and/or events. PLD-GR Set1 assay amplified only rice DNA, while PLD-GR Set2 produced unspecific amplification, with high Cqs, with DNA from barley, wheat, and rye (Table S6, Supporting Information). We thus selected Set1 primers and probe for further analyses, and discarded Set2. We tested the specificity of the GR2 assay on the same species listed for the PLD-GR assay and on DNA from all of the GM events, which were authorized or in the course of authorization in the EU at the moment of testing, plus all GR2 transformation events, rice events LL62 and LL601, and carnation event IFD-25958. We did not observe any unspecific amplification. A detailed list of the DNAs and the DNA amount tested is reported in the Materials and Methods and as Supporting Information, and the list of the species and events tested with the obtained Cqs is available in Table S7, Supporting Information.

Copy Number and Stability of the PLD-GR Taxon-Specific Assay. We performed the digital PCR experiment as described in the Supporting Information, and obtained a mean ratio between event-specific and taxon-specific amplification of 1.033, which, given that the 95% confidence interval of the mean spans around one, is not significantly different from the expected ratio of one (Table 2). We thus confirmed that the PLD-GR amplicon is present in single copy in the haploid genome of the transformed variety.

Table 2. Results of Digital PCR Analysis Conducted with the GR2 and PLD-GR Assays on GM DNA, 100% GM for GR2 Event

mean ratio (GR2/PLD-GR)	1.033
standard deviation	0.106
RSD$_r$, %	10.230
standard error of the mean	0.027
upper 95% CI of the mean	1.090
lower 95% CI of the mean	0.977

We then assessed the stability of the PLD-GR assay as described in the Materials and Methods. The results of the test are presented in Figure 4, where the Cq value obtained for each variety (Kaybonnet plus 131 varieties) is plotted, together with the overall mean, median, and robust mean (i.e., a mean whose estimate is less influenced by potential outliers in the data), and ±0.5 Cq intervals. According to ENGL MPR,[14] the range of

DOI: 10.1021/jf505516y
J. Agric. Food Chem. 2015, 63, 1711−1721

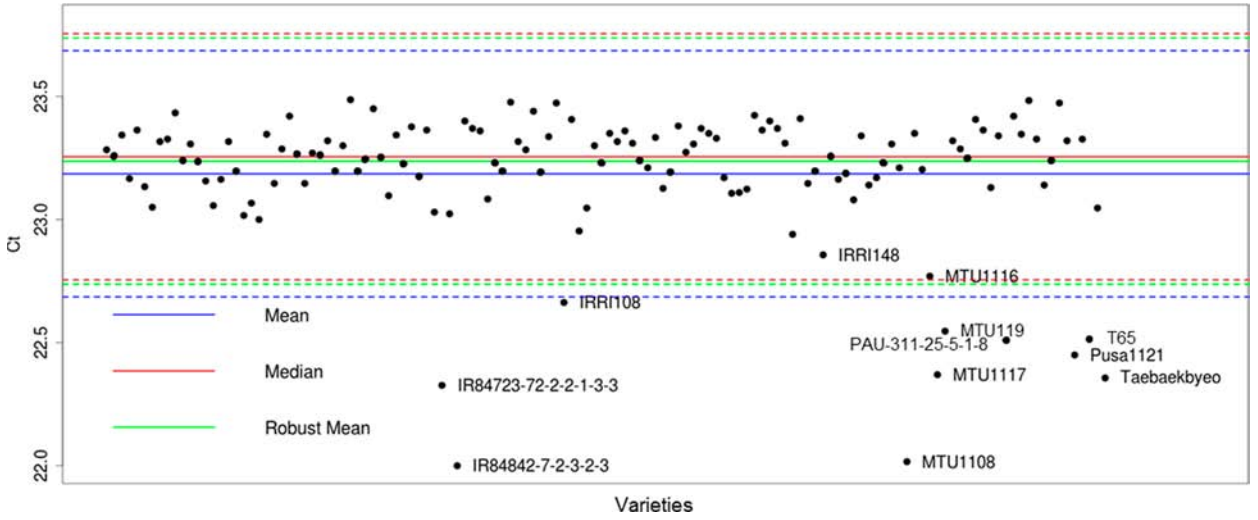

Figure 4. Results of the stability test for PLD-GR taxon-specific assay (Set1). The average Cq value obtained for each variety is plotted along the *x* axis; the mean of all measured Cq values (blue line), the median (red line), and the robust mean (green line) are represented; broken lines represent the mean (blue), median (red), and robust mean (green) plus or minus 0.5 Cq. Most varieties (122 out of 132) are distributed within ±0.5 Cq from the mean/median/robust mean. Twelve varieties, labeled with a text string, were identified as a cluster distinct from the other varieties.

Table 3. Results of the Quantification of the Test Samples for the Determination of the Dynamic Range and LOQ of PLD-GR Taxon-Specific Assay and GR2 Event-Specific Assay

PLD-GR				GR2			
expected hge/reaction	measured mean	RSD_r %	bias %	expected hge/reaction	measured mean	RSD_r %	bias %
200 000	170 507	4.2	−14.7	200 000	213 864	10.1	6.9
20 000	20 650	6.5	3.3	20 000	20 647	11.7	3.2
2000	2043	8.8	2.2	2000	1939	8.7	−3.0
200	170	10.4	−14.8	200	184	12.4	−8.0
60	63	17.4	5.4	60	54	21.0	−9.5
50	42	19.8	−15.1	50	49	13.5	−1.6
40	46	16.7	15.5	40	37	20.0	−8.6
30	37	17.8	22.2	30	31	**33.8**	2.9

Table 4. Standard Curve Parameters Obtained in the Experiment for the Determination of the Dynamic Range and LOQ of PLD-GR Taxon-Specific Assay and GR2 Event-Specific Assay

PLD-GR				GR2			
plate	slope	PCR efficiency	linearity	plate	slope	PCR efficiency	linearity
A	−3.59	89.8	0.996	A	−3.50	93.0	0.998
B	−3.55	91.2	0.998	B	−3.55	91.2	0.998
C	−3.56	91.1	0.997	C	−3.56	91.1	0.999
mean	−3.57	90.7	0.997	mean	−3.54	91.8	0.998

variability of Cq values within the taxon should not exceed 1 Cq. As shown in Figure 4, most varieties (120 out 132) were comprised between 22.94 and 23.49 Cq with a maximum distance of 0.55 Cq (unlabeled varieties). To identify possible outlying varieties, we performed cluster analysis, a technique that aims at discovering groups of objects with similar characteristics in a set of data, and we labeled with a text string the varieties that were identified as a distinct cluster. Some of the labeled varieties were however comprised in the mean ±0.5 Cq interval (IRRI148 and MTU1116) or at least in an interval of 1 Cq from the variety with the highest Cq value (IRRI108, MTU1119, T65, and PAU-311-25-5-1-3). Only six varieties (Pusa1121, MTU1117, Taebaekbyeo, IR84723-72-2-2-1-3-3, MTU1108, and IR84842-7-2-3-2-3) were outside that 1-Cq interval. The Cq we measured for those varieties was lower than the accepted range, thus excluding the possibility that sequence variability in the region amplified by the PLD-GR assay would lead to lower PCR efficiency, and thus to a higher Cq value.

Dynamic Range of the Two Assays. We assessed the dynamic range of the two assays as reported in the Materials and Methods. Table 3 reports the hge content, RSD_r, and bias measured for each test sample, for the PLD-GR and the GR2 assays. For the PLD-GR taxon-specific assay, the RSD_r was acceptable between 200 000 and 30 hge per reaction, for the GR2 event-specific assay between 200 000 and 40 hge. Bias was below 25% for all test samples for both the PLD-GR and the GR2 assays. On the basis of these values of RSD_r and bias, and in accordance with ENGL MPR,[14] which establishes that the RSD_r and bias should be below 25% over the whole dynamic range, we defined the dynamic range of the PLD-GR taxon-specific assay to be between 30 and 200 000 hge and between

DOI: 10.1021/jf505516y
J. Agric. Food Chem. 2015, 63, 1711−1721

Table 5. Results of the Quantification of the Test Samples for the Determination of the Robustness of the PLD-GR Taxon-Specific Assay

	200 000 hge/reaction			2000 hge/reaction			40 hge/reaction		
condition	estimated hge	RSD_r %	bias %	estimated hge	RSD_r %	bias %	estimated hge	RSD_r %	bias %
21 μL of reaction mix	209 046	4.0	4.5	2363	2.2	18.2	41	13.5	1.6
19 μL of reaction mix	180 696	5.4	−9.7	2074	5.7	3.7	32	9.0	−19.7
+20% Mastermix	211 853	2.2	5.9	2202	4.8	10.1	34	8.0	−13.8
−20% Mastermix	190 496	2.0	−4.8	2018	6.0	0.90	31	7.2	−23.4
+30% primers	178 343	24.7	−10.8	2230	5.4	11.5	45	15.8	12.9
−30% primers	182 927	5.3	−8.5	1972	6.0	−1.4	32	9.1	−21.2
+30% probe	187 402	3.0	−6.3	1862	3.3	−6.9	43	22.3	8.2
−30% probe	187 864	0.55	−6.1	2074	2.4	3.7	43	13.9	6.3
+1 °C annealing *T*	188 213	7.8	−5.9	1981	5.4	−0.9	45	3.9	12.7
−1 °C annealing *T*	207 456	2.3	3.7	1877	3.1	−6.2	32	9.7	−19.4
Cycler B (Roche)	176 620	1.7	−11.7	2101	2.7	5.1	34	20.3	−15.5
Cycler C (Stratagene)	233 789	6.2	16.9	2025	4.1	1.3	33	16.9	−16.6
Cycler D (ABI 7500)	181 524	2.8	−9.2	1931	3.9	−3.5	45	6.8	11.7

Table 6. Results of the Quantification of the Test Samples for the Determination of the Robustness of the GR2 Event-Specific Assay

	200 000 hge/reaction			2000 hge/reaction			40 hge/reaction		
condition	estimated hge	RSD_r %	bias %	estimated hge	RSD_r %	bias %	estimated hge	RSD_r %	bias %
21 μL of reaction mix	193 669	2.9	−3.2	1799	4.7	−10.1	30	13.0	−24.4
19 μL of reaction mix	196 258	5.1	−1.9	1956	7.3	−2.2	35	6.3	−11.5
+20% Mastermix	195 887	3.9	−2.1	1696	3.3	−15.2	30	7.2	−23.8
−20% Mastermix	183 955	8.6	−8.0	1570	3.1	−21.5	32	20.6	−20.5
+30% primers	190 938	6.6	−4.5	1844	3.5	−7.8	44	8.7	11.0
−30% primers	196 258	5.1	−1.9	1956	7.3	−2.2	35	6.3	−11.5
+30% probe	187 233	5.5	−6.4	1716	12.2	−14.2	35	8.0	−13.7
−30% probe	209 074	1.4	4.5	1649	0.66	−17.6	31	11.4	−21.4
+1 °C annealing *T*	190 313	3.6	−4.8	1690	11.1	−15.5	30	16.2	−24.9
−1 °C annealing *T*	183 526	3.1	−8.2	1663	3.4	−16.8	37	13.9	−7.4
Cycler B (Roche)	196 018	2.6	−2.0	1871	0.39	−6.5	29	4.2	**-27.9**
Cycler C (Stratagene)	201 041	2.5	0.52	2053	8.3	2.6	39	21.1	−2.2
Cycler D (ABI 7500)	187 506	2.3	−6.2	1976	1.1	−1.2	38	11.6	−5.3

40 and 200 000 hge for GR2 event-specific assay. As reported in Table 4, for the PLD-GR assay and the GR2 assay, slope values were below −3.6; the average PCR efficiency was above 90% and the average R^2 coefficient was above 0.99. These values are within the limits established by ENGL MPR.[14]

LOQ and LOD. According to ENGL MPR,[14] the LOQ of a method should be equal to or below the lowest amount or concentration included in the dynamic range. In this study, we assessed the LOQ together with the dynamic range of the method, and it consequently corresponds to the lowest test sample included in the dynamic range. For the PLD-GR assay, we thus established the LOQ at 30 hge per reaction, with a RSD_r of 17.8% and a bias of 22.2%; for the GR2 assay at 40 hge per reaction, with a RSD_r of 20.0% and a bias of −8.6% (Table 3).

The LOD of a method should be below 25 hge with a level of confidence of 95%, ensuring less than or equal to 5% false negative results.[14] The results of the test are reported in Table S8, Supporting Information: the LOD was at 4.5 hge/reaction for the PLD-GR assay and at 4 hge for the GR2 assay. The 1 hge level had 36.7% and 33.3% negative results, respectively, for the PLD-GR and the GR2 assay, in line with the value of 36% that is expected taking into account the probability of distribution of the target DNA in the 60 replicates.[36]

Robustness. Robustness was evaluated as described in the Materials and Methods. The results of the quantification for the determination of the robustness are illustrated in Table 5 for the PLD-GR assay and in Table 6 for the GR2 assay. The measured RSD_r was below 25% for the three test samples with all of the conditions tested for both the PLD-GR and the GR2 assays, in line with ENGL MPR;[14] bias was within ±25% for all of the conditions and test samples for the PLD-GR assay, while for the GR2 assay there was only one value of bias below −25% for the test sample at the LOQ, with Roche LC 480 qPCR instrument. We also evaluated the efficiency and linearity of the two assays, and the results are reported in Table 7. The values of slope and linearity were within the ENGL MPR[14] for both assays; the PCR efficiency was above 90% for both assays with all conditions, with the exception of the experiments performed with the GR2 assay with a concentration of primers 30% lower and on ABI 7500, for which the efficiency was 89.5% and 89.9%, respectively.

Relative Quantification. The results of the relative quantification are reported in Table 8: for the three test samples, the measured RSD_r ranged from 9.9% to 13.1%, and bias ranged from −6.2% to 5.3%. Both parameters are below 25%. The slope, PCR efficiency, and linearity of the standard curves for the two runs and their average over the two runs are

DOI: 10.1021/jf505516y
J. Agric. Food Chem. 2015, 63, 1711−1721

Table 7. Standard Curve Parameters Obtained with the Experiment for the Determination of the Robustness of PLD-GR Taxon-Specific Assay and GR2 Event-Specific Assay

	PLD-GR			GR2		
condition	slope	PCR efficiency	linearity	slope	PCR efficiency	linearity
21 μL of reaction mix	−3.46	94.4	0.998	−3.53	91.9	0.999
19 μL of reaction mix	−3.48	93.6	0.999	−3.55	91.1	0.998
+20% Mastermix	−3.44	95.4	0.998	−3.47	94.3	0.998
−20% Mastermix	−3.39	97.1	0.999	−3.53	92.1	0.998
+30% primers	−3.45	95.1	0.998	−3.57	90.5	0.999
−30% primers	−3.44	95.3	0.998	−3.60	**89.5**	0.997
+30% probe	−3.39	97.3	0.999	−3.53	91.9	0.998
−30% probe	−3.44	95.2	0.998	−3.50	93.1	0.998
+1 °C annealing *T*	−3.44	95.1	0.998	−3.51	92.7	0.998
−1 °C annealing *T*	−3.40	97.0	0.998	−3.58	90.2	0.998
Cycler B (Roche)	−3.44	95.2	0.998	−3.55	91.3	0.999
Cycler C (Stratagene)	−3.33	99.5	0.998	−3.53	92.0	1.000
Cycler D (ABI 7500)	−3.40	96.9	1.000	−3.59	**89.9**	0.999

Table 8. Relative Quantification Test Results

expected GM %	measured GM %	RSD_r %	bias %
4.5	4.74	9.9	5.3
0.9	0.90	13.1	0.4
0.1	0.09	10.4	−6.2

reported in Table 9. All parameters are within ENGL MPR[14] for both assays.

Table 9. Standard Curve Parameters Obtained for PLD-GR Taxon-Specific Assay and GR2 Event-Specific Assay in the Relative Quantification Experiment

	PLD-GR taxon-specific assay			GR2 event-specific assay		
	slope	PCR efficiency	R^2	slope	PCR efficiency	R^2
run A	−3.27	102.10	0.999	−3.48	93.77	0.997
run B	−3.45	95.02	0.997	−3.46	94.42	0.998
average	−3.36	98.56	0.998	−3.47	94.10	0.997

DISCUSSION

In this study, we describe the development, optimization, and in-house validation of the two TaqMan qPCR assays that compose the method for the event-specific detection and quantification of GR2 with a new rice taxon-specific assay, PLD-GR. The GR2 event-specific assay amplifies a 121-bp fragment across the 3′ junction between transgenic insert and plant DNA; the new PLD-GR taxon-specific assay amplifies a 124-bp fragment of rice PLD gene. These two assays were validated independently, on hge basis, and their performance was evaluated following European guidelines[14] and taking into consideration IUPAC harmonized guidelines for single-laboratory validation of methods of analysis.[26] All performance criteria adopted in this study satisfy the requirements of the Codex Alimentarius for methods for detection, identification, and quantification of specific DNA sequences.[25]

According to the principle of modularity, different parts of an analytical procedure, for example, DNA extraction and qPCR, can be evaluated and validated independently, provided that specific performance requirements are satisfied for each module.[37−39] In this study, we developed and validated only the qPCR module, independently of the DNA extraction method, in line with the principle of modularity. This approach is also supported by a study that compared the results of 53 collaborative trials for the validation of qPCR methods and indicated that the standard deviation introduced by the DNA extraction step with respect to GM quantification is negligible when compared to the one introduced by the qPCR step.[40] Furthermore, we considered the taxon- and the event-specific assays that constitute the GR2 qPCR method as independent modules, as already discussed in Kagkli et al.[39] This strategy is advantageous because it offers increased flexibility and potentially lowers the cost of method testing and validation, allowing, for example, the use of the same taxon-specific assay in combination with different event-specific assays, without the need to revalidate the combination of assays. A GMO testing laboratory could select the best combination of taxon- and event-specific assays, depending on the availability of PCR reagents or of verified and implemented taxon-specific assays. When a detection method for a new GMO event would have to be developed, the taxon-specific assay would not need to be developed and/or validated a second time. This approach also allows a wider freedom in the GM percentages that can be tested, which are instead limited to the validated dynamic range when the qPCR method is treated as a single module, and on whether to use a delta Cq method or a two-standard curves method. The results of the relative quantification experiment performed with the GR2 method confirmed that the two assays can be used in combination to quantify GR2 relative content, with acceptable levels of trueness and precision (Table 8).

For the PLD-GR taxon-specific assay, bioinformatics analyses with PLD-GR primer sets and amplicons evidenced that perfect alignments were produced only with rice and African rice sequences. Our bioinformatics analyses showed that also the primers for the PLD assay from Bayer, the SPS, and the gos9 assays[17−22] may potentially amplify sequences from African rice, suggesting that sequence variability between rice and African rice is low, which restricts the possibilities to design primers specific for one of the two species. The production of African rice is however limited, and the color of the African rice grain normally ranges from red to brown, easy to distinguish from rice by eye inspection. The specificity of amplification of the selected event- and taxon-specific assays was confirmed by melting curve analysis, capillary electrophoresis, and amplicon sequencing. The specificity of the GR2 and PLD-GR assays was also verified against the DNA of a number of other species, representative of the most important GM crops and a selection of cereals and grasses; the GR2 assay was additionally tested on DNA from 53 GM events and from five independent GR2 transformation events. The GR2 and PLD-GR assays did not show unspecific amplifications with the species tested. The PLD-GR taxon-specific assay was designed taking into consideration the polymorphisms reported for the region.[41,42] We demonstrated that the newly developed PLD-GR taxon-specific assay is present in single copy in the rice genome of the Kaybonnet variety and that its amplification stability is good

DOI: 10.1021/jf505516y
J. Agric. Food Chem. 2015, 63, 1711−1721

across the 132 rice varieties tested, belonging to both the indica and the japonica subspecies. The Cq values obtained with DNA from 120 out of 132 varieties were within a range of 0.55 Cq, and only six varieties were outside a range of 1 Cq calculated from the variety with the highest measured Cq value (Table 2, Figure 4, and Table S1, Supporting Information). All of the outlying varieties showed a lower Cq, suggesting either the presence of a second amplicon for the PLD-GR assay or an incorrect quantification of the DNA that was added to the reaction. Both hypotheses were investigated, by sequencing the amplification products of these varieties, and by requantifying their DNA with Picogreen and spettrophotometric methods. However, we did not identify a second amplification product (which seems to exclude the hypothesis of the presence of a second PLD-GR amplicon) and did not obtain significantly different quantification results. We will further investigate these results, but given that the test on the stability of the PLD-GR assay did not indicate the presence of sequence polymorphisms in the primers/probe region negatively influencing the efficiency of amplification, and that less than 5% of the varieties tested were outside the established Cq range, the PLD-GR taxon-specific assay can be classified as having good performance in terms of stability.

We established that the dynamic range of the GR2 event-specific assay is between 200 000 and 40 hge, with the LOQ at 40 hge and the LOD at 4 hge, and the dynamic range of the PLD-GR taxon-specific assay is between 200 000 and 30 hge, with the LOQ at 30 hge and the LOD at 4.5 hge (Table 3 and Table S8, Supporting Information). These numbers are in line with the criteria set in the ENGL MPR document.[14] The RSD_r was generally higher at the lower end of the dynamic range for both assays, a trend common to most calibration systems;[43] the linearity of the standard curves for the event- and taxon-specific assays was in line with that measured for most calibration systems, while PCR efficiency was slightly below the average when compared to data from the EU Database of Reference Methods for GMO Analysis.[44] It has to be taken into consideration, however, that the data available on the EU Database of Reference Methods for GMO Analysis are the results of full validation experiments, while we presented the results of the in-house validation of the two assays.

We optimized the GR2 and the PLD-GR assays on ABI 7900HT qPCR equipment, chosen for being one of the most common qPCR equipment in GMO testing laboratories, and tested the robustness of the two assays on three other common qPCR instruments: Roche LC 480, Stratagene Mx3005P, and ABI 7500. The results of the quantification of three test samples distributed over the whole dynamic range showed that the two assays can be transferred to other qPCR equipment without losing their accuracy; only the sample at the LOQ reported a bias of −27.9% with Roche LC 480 for the GR2 event-specific assay (Tables 5 and 6). It was already observed that deviations from the expected performance occurred at low GM contents with some qPCR methods when Roche LC 480 was employed;[45] in this case, the deviation was small and only at the lower limit of the dynamic range of the assay. However, particular care should be taken when using this platform to perform the GR2 assay. The certification of GMO testing laboratories under ISO 17025[46] requires that validated methods be verified in-house before being implemented for routine analysis; we suggest performing this verification on all of the different qPCR platforms on which the method is planned to be used. The slope, efficiency, and linearity of the standard curves generated with the two assays on the three qPCR instruments were within the performance requirements,[14] with the only exception of the PCR efficiency of the GR2 assay on ABI7500, which was very near to 90%. This small deviation did not influence the quantification results, which showed a RSD_r between 1.1% and 11.6% and bias between −6.2% and −1.2%. We tested the robustness of the two assays also with deliberate and small changes to the reaction conditions and the quantification remained reliable, although as a general trend bias was higher for the samples with lower hge content, especially for the GR2 assay (Tables 5 and 6). It has to be taken into consideration that we tested the GR2 assay at its LOQ; it is thus more likely that changes to the reaction mix or the PCR program have a higher influence at the lower extreme of the dynamic range. The slope, efficiency, and linearity of the standard curves of the two assays were within the performance requirements[14] with the exception of the PCR efficiency of the GR2 assay with 30% lower primer concentration, for which a small decrease in efficiency led to a quantification that was still acceptable, with a RSD_r comprised between 5.1% and 7.3% and a bias between −11.5% and −1.9%. The two assays can thus be considered robust against small deviations from the protocol.

GR2 is intended for cultivation and consumption in developing countries that use rice as a staple crop, with the objective of fighting vitamin A deficiency, and at present its commercialization is not foreseen outside those countries. The humanitarian license that regulates its use and distribution establishes that only national sales of the product are allowed.[1,2,47−49] It cannot however be excluded that this rice will enter the EU, either as a contamination in food imports or as fortified food. In this view, the development of a qPCR detection method for GR2 is important to ensure the traceability of this GM event. The applicability range of the qPCR GR2 detection method that we developed is wide in terms of haploid genome equivalents that can be detected, also as a result of the choice of treating the event and taxon-specific assays that compose the method as independent modules. The method can thus be applied in different regions of the world, notwithstanding the diverse provisions set for the unintended presence of GMOs.[50]

■ ASSOCIATED CONTENT

Supporting Information

List of rice varieties and GR2 transformation events provided by IRRI for this study (Table S1); description of the samples for the determination of the dynamic range, LOQ, LOD, and robustness of the two assays and for the relative quantification test (Tables S2−S5); results of the specificity test for PLD-GR and GR2 assays (Tables S6 and S7); and results of the LOD for the two assays (Table S8). This material is available free of charge via the Internet at http://pubs.acs.org.

■ AUTHOR INFORMATION

Corresponding Author

*E-mail: marco.mazzara@ec.europa.eu.

Author Contributions

[§]These authors contributed equally.

Funding

We acknowledge funding for this project from the European Commission (budget lines BGUE-B2012-10.020100-C1-JRC A7001050016 and BGUE-B2013-10.020100-C1-JRC A7001050016), the Bill and Melinda Gates Foundation, the

DOI: 10.1021/jf505516y
J. Agric. Food Chem. 2015, 63, 1711−1721

United States Agency for International Development (USAID), and the Rockefeller Foundation.

Notes

The authors declare no competing financial interest.

■ ACKNOWLEDGMENTS

We thank Gerard Barry for his supervision of the Golden Rice Project at IRRI, and Parminder Virk for his participation in the project.

■ ABBREVIATIONS USED

ABI, Applied Biosystems; CCSIS, Central Core DNA Sequence Information System; ENGL, European Network of GMO Laboratories; EU-RL GMFF, European Union Reference Laboratory for Genetically Modified Food and Feed; FAM, 6-carboxyfluorescein; GMO, genetically modified organism; GR2, Golden Rice 2; hge, haploid genome equivalents; IHCP, Institute for Health and Consumer Protection; IRRI, International Rice Research Institute; IUPAC, International Union of Pure and Applied Chemistry; JRC, Joint Research Centre; LC, LightCycler; LOD, limit of detection; LOQ, limit of quantification; MBG, Molecular Biology and Genomics; MPR, minimum performance requirements; PLD, Phospholipase D; ppi-PPF, ppi phosphofructokinase; qPCR, quantitative real-time polymerase chain reaction; RSD_r, relative repeatability standard deviation; SPS, sucrose phosphate synthase; TAMRA, tetramethylrhodamine

■ REFERENCES

(1) Ye, X.; Al-Babili, S.; Klöti, A.; Zhang, J.; Lucca, P.; Beyer, P.; Potrykus, I. Engineering the provitamin A (beta-carotene) biosynthetic pathway into (carotenoid-free) rice endosperm. *Science* **2000**, *287*, 303−305.

(2) Beyer, P.; Al-Babili, S.; Ye, X.; Lucca, P.; Schaub, P.; Welsch, R.; Potrykus, I. Golden Rice: introducing the beta-carotene biosynthesis pathway into rice endosperm by genetic engineering to defeat vitamin A deficiency. *J. Nutr.* **2002**, *132*, 506S−510S.

(3) Paine, J. A.; Shipton, C. A.; Chaggar, S.; Howells, R. M.; Kennedy, M. J.; Vernon, G.; Wright, S. Y.; Hinchliffe, E.; Adams, J. L.; Silverstone, A. L.; Drake, R. Improving the nutritional value of Golden Rice through increased pro-vitamin A content. *Nat. Biotechnol.* **2005**, *23*, 482−487.

(4) Rodríguez-Lázaro, D.; Lombard, B.; Smith, H.; Rzezutka, A.; D'Agostino, M.; Helmuth, R.; Schroeter, A.; Malorny, B.; Miko, A.; Guerra, B.; Davison, J.; Kobilinsky, A.; Hernández, M.; Bertheau, Y.; Cook, N. Trends in analytical methodology in food safety and quality: monitoring microorganisms and genetically modified organisms. *Trends Food Sci. Technol.* **2007**, *18*, 306−319.

(5) Elenis, D. S.; Kalogianni, D. P.; Glynou, K.; Ioannou, P. C.; Christopoulos, T. K. Advances in molecular techniques for the detection and quantification of genetically modified organisms. *Anal. Bioanal. Chem.* **2008**, *392*, 347−354.

(6) European Union Reference Laboratory for GM Food and Feed. Status of dossiers (http://gmo-crl.jrc.ec.europa.eu/StatusOfDossiers.aspx) (November 29, 2014).

(7) European Union Reference Laboratory for GM Food and Feed. Emergencies/Unauthorised (http://gmo-crl.jrc.ec.europa.eu/emergunauth.html) (November 29, 2014).

(8) Kluga, L.; Folloni, S.; Kagkli, D. M.; Bogni, A.; Foti, N.; Savini, C.; Mazzara, M.; Van den Eede, G.; Van den Bulcke, M. Combinatory SYBR Green real-time PCR screening approach for tracing materials derived from genetically modified rice. *Food Anal. Methods* **2013**, *6*, 361−369.

(9) Querci, M.; Foti, N.; Bogni, A.; Kluga, L.; Broll, H.; Van den Eede, G. Real-time PCR based ready-to-use multi-target analytical system for GMO detection. *Food Anal. Methods* **2009**, *2*, 325−336.

(10) Leimanis, S.; Hamels, S.; Florence, N. F.; Mbella, G. M.; Sneyers, M.; Hochegger, R.; Broll, H.; Roth, L.; Dallmann, K.; Micsinai, A.; La Paz, J. L.; Pla, M.; Brünen-Nieweler, C.; Papazova, N.; Taverniers, I.; Hess, N.; Kirschneit, B.; Bertheau, Y.; Audeon, C.; Laval, V.; Busch, U.; Pecoraro, S.; Neumann, K.; Rösel, S.; van Dijk, J.; Kok, E.; Bellocchi, G.; Foti, N.; Mazzara, M.; Moens, W.; Remacle, J.; Van Den Eede, G. Validation of the performance of a GMO multiplex screening assay based on microarray detection. *Eur. Food Res. Technol.* **2008**, *227*, 1621−1632.

(11) Holst-Jensen, A.; Bertheau, Y.; de Loose, M.; Grohmann, L.; Hamels, S.; Hougs, L.; Morisset, D.; Pecoraro, S.; Pla, M.; Van den Bulcke, M.; Wulff, D. Detecting un-authorized genetically modified organisms (GMOs) and derived materials. *Biotechnol. Adv.* **2012**, *30*, 1318−1335.

(12) Hernandez, M.; Duplan, M. N.; Berthier, G.; Vaitilingom, M.; Hauser, W.; Freyer, R.; Pla, M.; Bertheau, Y. Development and comparison of four real-time polymerase chain reaction systems for specific detection and quantification of *Zea mays* L. *J. Agric. Food Chem.* **2004**, *52*, 4632−4637.

(13) Papazova, N.; Zhang, D.; Gruden, K.; Vojvoda, J.; Yang, L.; Buh Gasparic, M.; Blejec, A.; Fouilloux, S.; De Loose, M.; Taverniers, I. Evaluation of the reliability of maize reference assays for GMO quantification. *Anal. Bioanal. Chem.* **2010**, *396*, 2189−2201.

(14) European Network of GMO Laboratories. Definition of minimum performance requirements for analytical methods of GMO testing (http://gmo-crl.jrc.ec.europa.eu/doc/Min_Perf_Requirements_Analytical_methods.pdf), 2008 (November 29, 2014).

(15) Chaouachi, M.; Giancola, S.; Romaniuk, M.; Laval, V.; Bertheau, Y.; Brunel, D. A strategy for designing multi-taxa specific reference gene systems. Example of application−ppi Phosphofructokinase (ppi-PPF) used for the detection and quantification of three taxa: maize (*Zea mays*), cotton (*Gossypium hirsutum*) and rice (*Oryza sativa*). *J. Agric. Food Chem.* **2007**, *55*, 8003−8010.

(16) Jeong, S. C.; Pack, I. S.; Cho, E. Y.; Youk, E. S.; Park, S.; Yoon, W. K.; Kim, C. G.; Choi, Y. D.; Kim, J. K.; Kim, H. M. Molecular analysis and quantitative detection of a transgenic rice line expressing a bifunctional fusion TPSP. *Food Control* **2007**, *18*, 1434−1442.

(17) Hernández, M.; Esteve, T.; Pla, M. Real-time polymerase chain reaction based assays for quantitative detection of barley, rice, sunflower, and wheat. *J. Agric. Food Chem.* **2005**, *53*, 7003−7009.

(18) Mäde, D.; Degner, C.; Grohmann, L. Detection of genetically modified rice: a construct-specific real-time PCR method based on DNA sequences from transgenic Bt rice. *Eur. Food Res. Technol.* **2006**, *224*, 271−278.

(19) Grohmann, L.; Mäde, D. Detection of genetically modified rice: collaborative validation study of a construct-specific real-time PCR method for detection of transgenic Bt rice. *Eur. Food Res. Technol.* **2009**, *228*, 497−500.

(20) Ding, J.; Jia, J.; Yang, L.; Wen, H.; Zhang, C.; Liu, W.; Zhang, D. Validation of a rice specific gene, sucrose phosphate synthase, used as the endogenous reference gene for qualitative and real-time quantitative PCR detection of transgenes. *J. Agric. Food Chem.* **2004**, *52*, 3372−3377.

(21) Jiang, L.; Yang, L.; Zhang, H.; Guo, J.; Mazzara, M.; Van, E. G.; Zhang, D. International collaborative study of the endogenous reference gene, sucrose phosphate synthase (SPS), used for qualitative and quantitative analysis of genetically modified rice. *J. Agric. Food Chem.* **2009**, *57*, 3525−3532.

(22) Mazzara, M.; Grazioli, E.; Savini, C. Event-specific method for the quantitation of rice line LLRICE62 using real-time PCR (http://gmo-crl.jrc.ec.europa.eu/summaries/LLRICE62_val_report.pdf), 2006 (November 29, 2014).

(23) Zhang, L.; Cao, Y.; Liu, X.; Wu, G.; Wu, Y.; Lu, C. In-depth analysis of the endogenous reference genes used in the quantitative PCR detection systems for rice. *Eur. Food Res. Technol.* **2012**, *234*, 981−993.

(24) Wang, C.; Jiang, L.; Rao, J.; Liu, Y.; Yang, L.; Zhang, D. Evaluation of four genes in rice for their suitability as endogenous

DOI: 10.1021/jf505516y
J. Agric. Food Chem. 2015, 63, 1711−1721

reference standards in quantitative PCR. *J. Agric. Food Chem.* **2010**, *58*, 11543−11547.
(25) Codex Committee on Methods of Analysis and Sampling. Guidelines on performance criteria and validation of methods for detection, identification and quantification of specific DNA sequences and specific proteins in foods, 2010; CAC/GL 74-2010.
(26) Thompson, M.; Ellison, S. L. R.; Wood, R. Harmonized guidelines for single-laboratory validation of methods of analysis (IUPAC Technical Report). *Pure Appl. Chem.* **2002**, *74*, 835−855.
(27) Patak, A. CCSIS specialist EMBnet node: AGM2011 report. *EMBnet.journal* **2011**, *17*, 13−14.
(28) Altschul, S. F.; Madden, T. L.; Schäffer, A. A.; Zhang, J.; Zhang, Z.; Miller, W.; Lipman, D. J. Gapped BLAST and PSI-BLAST: a new generation of protein database search programs. *Nucleic Acids Res.* **1997**, *25*, 3389−3402.
(29) International Standard (ISO) 21571:2005. *Foodstuffs − Methods of Analysis for the Detection of Genetically Modified Organisms and Derived Products − Nucleic Acid Extraction*; International Organization for Standardization: Geneva, 2005.
(30) Sambrook, J.; Fritsch, E. F.; Maniatis, T. *Molecular Cloning: A Laboratory Manual*, 2nd ed.; Cold Spring Harbor Laboratory Press: Cold Spring Harbor, New York, 1989; Vol. *3*, pp E3−E4.
(31) Žel, J.; Mazzara, M.; Savini, C.; Cordeil, S.; Camloh, M.; Štebih, D.; Cankar, K.; Gruden, K.; Morisset, D.; Van den Eede, G. Method validation and quality management in the flexible scope of accreditation: an example of laboratories testing for genetically modified organisms. *Food Anal. Methods* **2008**, *1*, 61−72.
(32) Cochran, W. G. *Sampling Techniques*, 3rd ed.; John Wiley and Sons: New York, 1977.
(33) Zar, J. *Biostatistical Analysis*, 4th ed.; Prentice Hall, Upper Saddle River, NJ, 1999.
(34) Rotmistrovsky, K.; Jang, W.; Schuler, G. D. A web server for performing electronic PCR. *Nucleic Acids Res.* **2004**, *32*, W108−W112.
(35) Bustin, S. A.; Benes, V.; Garson, J. A.; Hellemans, J.; Huggett, J.; Kubista, M.; Mueller, R.; Nolan, T.; Pfaffl, M. W.; Shipley, G. L.; Vandesompele, J.; Wittwer, C. T. The MIQE guidelines: minimum information for publication of quantitative real-time PCR experiments. *Clin. Chem.* **2009**, *55*, 611−622.
(36) NMKL. *Measurement Uncertainty in Quantitative Microbiological Examination of Foods. No. 8*, 4th ed.; 2008.
(37) Holst-Jensen, A.; Berdal, K. G. The modular analytical procedure and validation approach and the units of measurement for genetically modified materials in foods and feeds. *J. AOAC Int.* **2004**, *87*, 927−936.
(38) Bellocchi, G.; De Giacomo, M.; Foti, N.; Mazzara, M.; Palmaccio, E.; Savini, C.; Di Domenicantonio, C.; Onori, R.; Van den Eede, G. Testing the interaction between analytical modules: an example with Roundup Ready soybean line GTS 40-3-2. *BMC Biotechnol.* **2010**, *10*, 55.
(39) Kagkli, D. M.; Weber, T. P.; Van den Bulcke, M.; Folloni, S.; Tozzoli, R.; Morabito, S.; Ermolli, M.; Gribaldo, L.; Van den Eede, G. Application of the modular approach to an in-house validation study of real-time PCR methods for the detection and serogroup determination of verocytotoxigenic *Escherichia coli*. *Appl. Environ. Microbiol.* **2011**, *77*, 6954−6963.
(40) Kodama, T.; Kurosawa, Y.; Kitta, K.; Naito, S. Tendency for interlaboratory precision in the GMO analysis method based on real-time PCR. *J. AOAC Int.* **2010**, *93*, 734−749.
(41) McNally, K. L.; Childs, K. L.; Bohnert, R.; Davidson, R. M.; Zhao, K.; Ulat, V. J.; Zeller, G.; Clark, R. M.; Hoen, D. R.; Bureau, T. E.; Stokowski, R.; Ballinger, D. G.; Frazer, K. A.; Cox, D. R.; Padhukasahasram, B.; Bustamante, C. D.; Weigel, D.; Mackill, D. J.; Bruskiewich, R. M.; Rätsch, G.; Buell, C. R.; Leung, H.; Leach, J. E. Genomewide SNP variation reveals relationships among landraces and modern varieties of rice. *Proc. Natl. Acad. Sci. U.S.A.* **2009**, *106*, 12273−12278.
(42) Zhao, K.; Tung, C. W.; Eizenga, G. C.; Wright, M. H.; Ali, M. L.; Price, A. H.; Norton, G. J.; qul Islam, M. R.; Reynolds, A.; Mezey, J.; McClung, A. M.; Bustamante, C. D.; McCouch, S. R. Genome-wide association mapping reveals a rich genetic architecture of complex traits in *Oryza sativa*. *Nat. Commun.* **2011**, *2*, 467.
(43) Kodama, T.; Kurosawa, Y.; Kitta, K.; Naito, S. Tendency for interlaboratory precision in the GMO analysis method based on real-time PCR. *J. AOAC Int.* **2010**, *93*, 734−749.
(44) EU Database of Reference Methods for GMO Analysis (http://gmo-crl.jrc.ec.europa.eu/gmomethods/) (November 29, 2014).
(45) Luque-Perez, E.; Mazzara, M.; Weber, T. P.; Foti, N.; Grazioli, E.; Munaro, B.; Pinski, G.; Bellocchi, G.; Van den Eede, G.; Savini, C. Testing the robustness of validated methods for quantitative detection of GMOs across qPCR instruments. *Food Anal. Methods* **2013**, *6*, 343−360.
(46) International Standard (ISO) ISO/IEC 17025:2005. *General Requirements for the Competence of Testing and Calibration Laboratories*; International Organization for Standardization: Geneva, 2005.
(47) Kryder, D.; Kowalski, S. P.; Krattiger, A. F. *The Intellectual and Technical Property Components of pro-Vitamin A Rice (Golden Rice): A Preliminary Freedom-to-Operate Review*; ISAAA Briefs No. 20; ISAAA: Ithaca, NY, 2000.
(48) Golden Rice Humanitarian Board. Golden Rice Project (www.goldenrice.org) (29 November, 2014).
(49) Mayer, J. E. Delivering golden rice to developing countries. *J. AOAC Int.* **2007**, *90*, 1445−1449.
(50) Zhang, D.; Guo, J. The development and standardization of testing methods for genetically modified organisms and their derived products. *J. Integr. Plant Biol.* **2011**, *53*, 539−551.

DOI: 10.1021/jf505516y
J. Agric. Food Chem. 2015, 63, 1711−1721

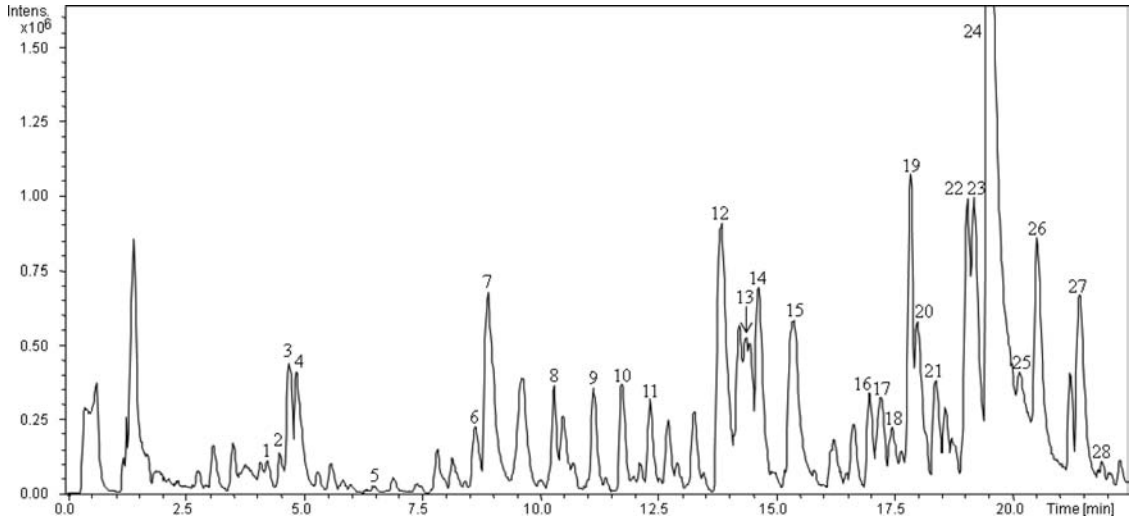

Figure 1. Base peak chromatogram (BPC) of 'Arbequina' olive leaf extract in December, obtained by HPLC-DAD-TOF-MS. See Table 1 for identification numbers.

some phenolic compounds in olive leaves, or the influence of factors such as water deficit, genetic factor, or seasonal period.[21−25]

In a previous work,[26] our group reported the phenolic composition of 'Sikitita' ('Chiquitita' in the U.S.), a newly bred olive cultivar.[27] In the present work, an exhaustive number of phenolic compounds and cultivars were considered with the main aim of providing further insights into the evolution of olive leaves phenolic compounds in different olive cultivars during their growth and the olive ripening period under the Andalusian climate. We also highlight the optimal sampling time to use olive leaves as a source of bioactive compounds.

MATERIALS AND METHODS

Chemicals and Reagents. Methanol, the reagent used for extracting the phenolic compounds from the olive-leaf samples, was purchased from Panreac (Barcelona, Spain), and HPLC-grade acetonitrile was purchased from Labscan (Dublin, Ireland). The acetic acid used was of analytical grade (assayed at >99.5%) and was purchased from Fluka (Switzerland). Water was purified using a Milli-Q system (Millipore, Bedford, MA). Standard compounds such as hydroxytyrosol, tyrosol, luteolin, and apigenin were purchased from Sigma-Aldrich (St. Louis, MO), and oleuropein was from Extrasynthèse (Lyon, France). The stock solutions containing these analytes were prepared in methanol. All chemicals were of analytical reagent grade and used as received. All of the solutions were stored in a dark flask at −20 °C until use.

Samples. Olive leaves (*Olea europaea* L.) from cultivars 'Arbequina', 'Arbosana', 'Changlot Real', 'Koroneiki', 'Picual', and 'Sikitita' were used in this study. These cultivars were selected as some of the most widely used in new orchards currently in Spain, highly productive, well adapted to modern olive growing techniques, and initially originated in different areas: 'Arbequina' and 'Arbosana' from Catalonia (Spain), 'Changlot Real' from Valencia (Spain), 'Picual' from Andalusia (Spain), 'Koroneiki' (Greece), and 'Sikitita', a new Spanish cultivar from cross-breeding between 'Arbequina' and 'Picual'. All cultivars were grown under the same agronomic and environmental conditions in the same olive orchards located at "IFAPA, Centro Alameda del Obispo" in Córdoba, Spain (37°51′36.5″ N 4°47′53.7″ W). Samples were processed at four times: mid-June (fruit-set), mid-August, mid-October, and mid-December (fruit-ripening) in 2012. Adult leaves were collected from three individuals of each cultivar, in 5 year old trees of these cultivars planted at 7 × 5 m spacing and trained as single-trunk vase. Standard cultural practices were followed, with minimal pruning to allow early bearing and irrigation by in-line drips with 2000 m^3/ha per year to avoid water stress of plants. All of the leaves collected from the same tree were pooled in a unique sample, immediately transferred to the laboratory, and dried outdoors. Finally, samples were stored at −80 °C until needed.

Extraction of Phenolic Compounds from Olive Leaves. Sample extraction was performed as described previously by Talhaoui et al.[26] Briefly, dry leaves (0.5 g) were crushed and extracted via Ultra-Turrax IKA T18 basic using 30 mL of MeOH/H_2O (80/20). After solvent evaporation, the extracts were reconstituted with 2 mL of MeOH/H_2O (50/50). Three replicates of each sample were processed.

Determination of Phenolic Compounds by HPLC-DAD-TOF-MS. Phenolic compounds were separated by a Poroshell 120 EC-C18 analytical column (4.6 × 100 mm, 2.7 μm) from Agilent Technologies, on an Agilent 1200 series rapid resolution liquid chromatograph (Agilent Technologies, CA). The gradient eluent, at a flow rate of 0.8 mL/min, was achieved using the method previously described by Talhaoui et al.[26] The column temperature was maintained at 25 °C, and the injection volume was 2.5 μL.

The HPLC system with diode-array detection was coupled to a micrOTOF (Bruker Daltonics, Bremen, Germany), an orthogonal-accelerated TOF mass spectrometer, using an electrospray interface (model G1607A from Agilent Technologies, Palo Alto, CA). The effluent from the HPLC column was split using a T-type phase separator before being introduced into the mass spectrometer (split ratio = 1:3). Analysis parameters were set using a negative-ion mode with spectra acquired over a mass range from m/z 50 to 1000. The optimum values of the ESI−MS parameters were: capillary voltage, +4.5 kV; drying gas temperature, 190 °C; drying gas flow, 9.0 L/min; and nebulizing gas pressure, 2 bar. The accurate mass data on the molecular ions were processed through the newest Data Analysis 4.0 software (Bruker Daltonics, Bremen, Germany), which provided a list of possible elemental formulas via the Smart Formula Editor. The Smart Formula Editor uses a CHNO algorithm, which provides standard functionalities such as minimum/maximum elemental range, electron configuration, and ring-plus double-bond equivalents, as well as a sophisticated comparison of the theoretical with the measured isotope pattern (Sigma Value) for increased confidence in the suggested molecular formula. Peak areas of phenolic compounds were integrated using Bruker Compass Target Analysis 1.2 software for compound screening (Bruker Daltonics, Bremen, Germany). All phenolic compounds showed good levels for quantification in the various samples on each date of sampling. Five standard calibration graphs were prepared for quantification of the phenolic compounds in the olive leaves using five commercial standards (oleuropein, hydroxytyrosol, tyrosol, apigenin, and luteolin).

DOI: 10.1021/jf5058205
J. Agric. Food Chem. 2015, 63, 1722−1729

Table 1. Phenolic Compounds Identified in Olive Leaves Extract by HPLC-DAD-TOF-MS, Including Retention Time, m/z, Discrimination Group, Means of All Cultivars and Total (mg/g of Dry Olive Leaves), and Standard Deviations (in Parentheses)[a]

	name	m/z	RT (min)	group	June	August	October	December
1	oleoside	389	4.27	4	0.023(0.012)	0.007(0.003)	0.026(0.005)	0.039(0.012)
2	hydroxytyrosol-hexose isomer a	315	4.54	3	0.490(0.534)	0.126(0.070)	0.120(0.074)	0.518(0.260)
3	hydroxytyrosol-hexose isomer b	315	4.75	3	1.121(0.423)	0.179(0.046)	0.362(0.185)	1.284(0.401)
4	secologanoside isomer a	389	4.89	4	0.430(0.164)	0.153(0.051)	0.389(0.136)	0.574(0.191)
5	tyrosol glucoside	299	6.54	3	0.461(0.473)	0.041(0.022)	0.138(0.106)	1.083(0.689)
6	elenolic acid glucoside isomer a	403	8.65	5	0.838(1.303)	0.080(0.077)	0.124(0.126)	0.062(0.038)
7	secologanoside isomer b	389	8.93	4	0.784(0.272)	0.163(0.064)	0.300(0.128)	0.478(0.138)
8	elenolic acid glucoside isomer b	403	10.30	5	0.065(0.037)	0.045(0.030)	0.068(0.025)	0.097(0.059)
9	oleuropein aglycon	377	11.14	1	0.183(0.176)	0.050(0.033)	0.080(0.053)	0.167(0.102)
10	luteolin-diglucoside	609	11.73	2	0.170(0.163)	0.150(0.065)	0.194(0.086)	0.175(0.071)
11	elenolic acid glucoside isomer c	403	12.33	5	0.110(0.098)	0.050(0.027)	0.152(0.099)	0.250(0.160)
12	demethyloleuropein	525	13.83	1	1.230(0.866)	0.354(0.091)	0.282(0.170)	0.345(0.215)
13	rutin	609	14.40	2	0.967(0.656)	0.205(0.171)	0.314(0.283)	0.267(0.157)
14	luteolin rutinoside	593	14.62	2	0.458(0.384)	0.271(0.181)	0.298(0.189)	0.300(0.135)
15	luteolin glucoside isomer a	447	15.32	2	0.872(0.567)	0.376(0.142)	0.729(0.259)	0.973(0.315)
16	apigenin rutinoside	577	16.96	2	0.081(0.065)	0.074(0.059)	0.084(0.031)	0.111(0.087)
17	oleuropein diglucoside isomer a	701	17.23	1	0.075(0.045)	0.090(0.031)	0.089(0.031)	0.132(0.056)
18	oleuropein diglucoside isomer b	701	17.48	1	0.210(0.162)	0.156(0.078)	0.129(0.066)	0.232(0.092)
19	oleuropein diglucoside isomer c	701	17.81	1	0.422(0.267)	0.294(0.101)	0.326(0.114)	0.521(0.140)
20	luteolin glucoside isomer b	447	17.95	2	0.581(0.473)	0.291(0.158)	0.526(0.174)	0.678(0.168
21	chrysoeriol-7-*O*-glucoside	461	18.36	2	0.090(0.078)	0.057(0.033)	0.108(0.060)	0.089(0.041)
22	2″-methoxyoleuropein isomer a	569	19.02	1	0.391(0.285)	0.187(0.052)	0.244(0.120)	0.079(0.123)
23	2″-methoxyoleuropein isomer b	569	19.17	1	0.615(0.479)	0.300(0.174)	0.524(0.181)	0.160(0.186)
24	oleuropein isomer a	539	19.52	1	33.142(11.806)	9.868(2.373)	26.966(4.693)	42.493(15.897)
25	oleuropein isomer b	539	20.12	1	0.594(0.246)	0.120(0.054)	0.316(0.150)	0.847(0.450)
26	oleuropein/oleuroside	539	20.51	1	1.340(0.751)	0.396(0.158)	0.884(0.340)	2.007(0.778)
27	ligstroside	523	21.37	1	0.599(0.243)	0.159(0.056)	0.432(0.142)	0.829(0.450)
28	luteolin	285	21.86	2	0.026(0.015)	0.023(0.015)	0.020(0.008)	0.020(0.015)
	total				53.73(8.16)	14.27(3.09)	34.23(5.37)	54.81(19.03)

[a]Group 1 (secoiridoid); group 2 (flavonoids); group 3 (simple phenols); group 4 (oleosides); group 5 (elenolic acids).

Statistical Analysis. All assays were run in triplicate. Values of different results were expressed as the means mg/g olive leaves. Results were tested for statistical significance by one-way ANOVA. Significant statistical differences among treatments ($p < 0.001$) were assessed by Tukey's honest significant-difference multiple comparisons. Statistica 8.0 software (2001, StatSoft, Tulsa, OK) was used for statistical determinations. Principal components analysis (PCA) was elaborated using the MatLab function "princomp ()" version R 2012a.

RESULTS AND DISCUSSION

Identification and Quantification of Phenolic Compounds. Samples of phenolic extracts from olive leaves picked at different times were analyzed by HPLC with UV−vis and MS detection. The identification of phenolic compounds from samples was carried out as previously reported by Talhaoui et al.[26] The compounds were identified by interpreting their mass spectra determined via TOF-MS and taking into account the data reported in the literature. All of these results were complemented with the UV spectra provided by DAD, which gave additional information about the family of compounds, in terms of the absorbance bands. However, quantification was performed using MS data. Twenty-eight compounds were detected in all of the samples and for all sampling times, except for 'Arbosana' in which tyrosol glucoside was only detected in December (Table a, Supporting Information). No qualitative differences in phenolic compounds were detected between leaves from the six different olive cultivars. Figure 1 shows the base peak chromatogram of 'Arbequina' cultivar in December as a representative example. The calibration plots indicated good correlations between peak areas and analyte concentrations, and regression coefficients were higher than 0.990 in all cases. Sensitivity (RSD, %), linearity (r^2), calibration ranges, calibration curves, and limits of detection and quantification are reported (Table b, Supporting Information). The limit of quantification (LOQ) was determined as a signal-to-noise ratio of 10:1, and the limit of detection (LOD) was determined as a signal-to-noise ratio of 3:1. LOD was found to be within the range 0.53−27.63 μg/L, while LOQ was within 1.76−92.10 μg/L. Intraday and interday precisions were developed to assess the repeatability of the method. An olive leaf extract was injected six times on the same day (intraday precision, $n = 6$) for 3 consecutive days (interday precision, $n = 18$). The intraday repeatability of the peak area, expressed by the RSD, was 1.03%, whereas the interday repeatability was 3.6%. Oleuropein and other secoiridoids were quantified with the calibration curve for oleuropein; hydroxytyrosol-hexose isomers were quantified with the calibration curve for hydroxytyrosol; tyrosol glucoside was quantified with the calibration curve for tyrosol; apigenin rutinoside was quantified with the calibration curve for apigenin and luteolin; and luteolin-diglucoside and the other flavonoids were quantified with the calibration curve for luteolin. All phenolic compound contents are reported as mg of compound/g dry olive leaves (Tables a, c, d, e, f, g, Supporting Information).

DOI: 10.1021/jf5058205
J. Agric. Food Chem. 2015, 63, 1722−1729

Table 2. Mean Values (mg/g of Dry Olive Leaves) for the Phenolic Groups Studied in the Four Sampling Times[a]

	cultivar	June	August	October	December
group 1: secoiridoids	'Arbequina'	44.22 a,b	44.22 c	44.22 d	44.22 c
	'Arbosana'	49.40 a,b	15.32 a	27.55 d,c	29.81 c
	'Changlot Real'	43.26 b	13.62 b	29.95 b,c	73.26 a
	'Koroneiki'	53.48 a	12.30 b	36.99 a	32.62 d
	'Picual'	45.93 a,b	12.59 b	32.78 a,b	70.69 a
	'Sikitita'	44.62 a,b	8.16 d	30.21 b,c	43.29 b
group 2: flavonoids	'Arbequina'	2.71 c	0.96 c	2.46 c	2.46 c
	'Arbosana'	5.30 b	2.00 a	3.10 b	3.20 a,b
	'Changlot Real'	0.65 e	1.68 b	1.82 d	2.95 b
	'Koroneiki'	6.11 a	1.74 b	3.57 a	1.72 e
	'Picual'	2.40 c	1.55 b	1.74 d	3.32 a
	'Sikitita'	1.90 d	0.76 c	0.96 e	2.03 d
group 3: simple phenols	'Arbequina'	1.27 e	0.43 a	0.96 a	2.13 d
	'Arbosana'	1.79 c	0.43 a	0.37 e	1.15 e
	'Changlot Real'	1.32 e	0.17 d	0.36 e	3.36 b
	'Koroneiki'	3.50 a	0.33 c	0.86 b	3.96 a
	'Picual'	1.53 d	0.35 b,c	0.70 c	2.87 c
	'Sikitita'	2.50 b	0.37 b	0.48 d	3.85 a
group 4: oleosides	'Arbequina'	1.42 b	0.22 d	0.72 c,d	0.93 b
	'Arbosana'	1.05 d	0.32 b	0.79 b,c	0.72 c
	'Changlot Real'	1.21 c,d	0.34 b	0.63 d	1.48 a
	'Koroneiki'	1.77 a	0.39 a	0.99 a	0.91 b
	'Picual'	1.33 b,c	0.40 a	0.87 a,b	1.50 a
	'Sikitita'	1.40 b	0.27 c	0.30 e	1.01 b
group 5: elenolic acids	'Arbequina'	0.30 c	0.13 c	0.29 c	0.17 e
	'Arbosana'	0.95 a	0.33 a	0.49 a	0.28 d
	'Changlot Real'	0.27 c	0.18 b	0.32 c	0.61 b
	'Koroneiki'	0.46 b	0.20 b	0.43 b	0.34 c
	'Picual'	0.22 c,d	0.20 b	0.40 b	0.68 a
	'Sikitita'	0.13 d	0.05 d	0.14 d	0.37 c

[a]Different letters indicate significant differences among cultivar by sampling time and phenolic group ($P < 0.001$).

Chemometric Approach. Because of the large amounts of data obtained, it was indispensable to adapt the appropriate statistical method so that it could facilitate discrimination between cultivars and/or sampling times. Hence, the data on the concentrations determined for the 28 compounds were grouped into five groups (Table 1): secoiridoids, group 1 (oleuropein aglycon, demethyloleuropein, three isomers of oleuropein diglucoside, two isomers of 2″-methoxyoleuropein, two isomers of oleuropein, oleuropein/oleuroside, and ligstroside); flavonoids, group 2 (luteolin diglucoside, luteolin rutinoside, apigenin rutinoside, two isomers of luteolin glucoside, luteolin, chrysoeriol-7-*O*-glucoside, and rutin); simple phenols, group 3 (hydroxytyrosol-hexose and isomer, and tyrosol glucoside); oleosides, group 4 (oleoside, secologanoside isomers a and b); and elenolic acids, group 5 (elenolic acid glucoside isomers a, b, and c). Subsequently, the statistical analysis was applied to a data set consisting of a matrix of 288 rows (one for each analysis) and 5 columns (one for each compound group).

Comparison of Total Phenolic Compounds among Sampling Times. The total concentration of phenolic compounds in the samples collected in June and December presented the highest mean concentrations, while those collected in August presented the minimum values. This general trend was also observed for most of the individual phenolic compounds (Table 1). The total concentration means of phenolic compounds for the six cultivars are in agreement with those reported for every single cultivar, except for 'Koroneiki' and 'Arbosana' cultivar samples, in which the variation in phenolic compound content did not show any significant difference from October to December (Tables a, c, d, e, f, g, Supporting Information). Considering the standard deviation (SD), there was little variability between cultivars in August and October. To evaluate whether the differences between sampling times were statistically significant or not, a matched Student's *t*-test was performed between the total concentrations from each pair of seasons. Highly significant differences were obtained for all seasonal pair comparisons ($p < 0.001$), except when comparing June and December ($p = 0.70$). In fact, the phenolic compound content of olive leaves is in general greatly influenced by the time of collection.[28] Indeed, studies carried out on different cultivars and in different seasons by Hashemi et al.[25] reported that the concentration of oleuropein, the major component of olive leaves, was significantly higher in the cold season than in the warm season. The same results have been confirmed by other authors, such as Brahmi et al.[22] for total *o*-diphenols and total flavonoids. Mert et al.[24] studied the annual variation in the quantity of oleuropein in the leaves of the 'Gemlik' cultivar and demonstrated the same pattern observed in the present study. Changes in oleuropein levels in different flower and fruit developmental stages have also been reported previously. Thus, Malik and Bradford[29] found a sharp decrease in oleuropein level during the transition from vegetative to flower buds, followed by a rapid increase at the initial stages of fruit development and again a sharp decrease with fruit maturity.

DOI: 10.1021/jf5058205
J. Agric. Food Chem. 2015, 63, 1722−1729

Seasonal Variability of Phenolic Compound Groups. To analyze the seasonal variability in the phenolic content in olive leaves, total concentrations for each compound group were averaged for all samples (individuals and replicas) for each sampling time and cultivar. Considering the general mean of each phenolic compound group for all cultivars per sampling time (Table 2), an evident reduction in concentrations was observed in August with respect to June. From August on, the concentrations gradually increased until December. In fact, the mean secoiridoids concentration decreased from 46.82 mg/g dry olive leaves in June to 11.97 mg/g dry olive leaves in August, before starting to increase up to a maximum value in December, 47.81 mg/g dry olive leaves. Regarding flavonoids, mean values decreased from 3.18 mg/g dry olive leaves in June to 1.45 mg/g dry olive leaves in August, but returned to increasing in December, reaching 2.61 mg/g dry olive leaves.

The mean concentrations of the simple phenols, oleosides, and elenolic acids groups decreased from 1.98, 1.36, and 0.39 mg/g dry olive leaves (June) to 0.35, 0.32, and 0.18 mg/g dry olive l leaves (August), respectively, while in December their concentrations reached 2.89, 1.09, and 0.41 mg/g dry olive leaves, respectively. The increase in elenolic acids content observed from August is likely the result of some oleuropein degradation that is accentuated in autumn.[30] The same behavior was observed in all cultivars for the five groups, although some exceptions were noted, especially between concentrations in October and December (Table 2). In fact, the concentration of the flavonoids group for 'Changlot Real' increased from June to December. The concentration of the flavonoids group for the 'Koroneiki' cultivar was decreased by one-half in December from its value in October. The concentration of the oleosides group showed a small decrease, by 8.2% and 8.9%, from October to December for the 'Koroneiki' and 'Arbosana' cultivars, respectively. Finally, the concentrations in the elenolic acids group decreased from October to December for the 'Koroneiki' and 'Arbequina' cultivars, displaying decreases of 20.8% and 42.6%, respectively. The large increase observed in winter in all phenolic groups probably occurred as a consequence of olive tree reaction to the low temperatures (Figure a, Supporting Information).

Comparison of Phenolic Compounds Groups among Cultivars. It is noteworthy that the concentration of each phenolic group was greatly dependent on the cultivar. In fact, the sum of squares (SS) distribution between sources of variation (cultivar and experimental error) showed a great influence of the cultivar on all sampling dates. Indeed, cultivar was responsible for 76%−99% of the variation in all groups. This result supports other studies reporting that genetic factors have a significant impact in the content of oleuropein in olive leaves.[21,31] Significant differences in phenolic compound composition have also been observed in the oils of different olive breeding selections.[32] In June, the 'Koroneiki' cultivar showed the highest concentrations of phenolic compounds for all cultivars and for all groups except the elenolic acid group, for which 'Arbosana' presented by far the highest concentration (Table 2). In August, the 'Arbosana' cultivar presented the highest values for secoiridoids, flavonoids, simple phenols (with 'Arbequina'), and elenolic acids, while 'Koroneiki' and 'Picual' showed the highest concentrations for oleosides. In October, the highest values for secoiridoids, oleosides, and flavonoids were registered for the 'Koroneiki' cultivar, whereas the highest value for simple phenols was registered for the 'Arbequina' cultivar. 'Arbosana' showed the highest concentration of elenolic acids. In contrast, the 'Sikitita' cultivar presented the lowest concentrations of flavonoids, oleosides, and elenolic acids in October. Except for simple phenols, the 'Picual' cultivar was the richest in terms of secoiridoids, oleosides, flavonoids, and elenolic acids among the studied samples in December. In addition, 'Changlot Real' also showed a high value of secoiridoids at that sampling time, with 73.25 mg/g dry olive leaves, insignificantly different from the 'Picual' cultivar with 70.69 mg/g dry olive leaves (Table 2). Previous studies have reported that oleuropein concentration in the 'Picual' cultivar decreases significantly in fruits while increasing in leaves during olive ripening.[33] Many studies also stipulate that antioxidant capacity, assumed to be almost entirely due to phenolic compounds, is greatly dependent on the severity of the stress as well as the species and developmental stage.[34] Hence, differences observed are probably associated with each cultivar's resistance or tolerance to environmental conditions for each season and the plants' need for protection against external pathogenic agents, which are according to the genetic endowment.

Principal Component Analysis (PCA) of the Phenolic Content. Even though the seasonal tendency was similar for all compounds groups and cultivars, the plots in Table 1 also show differences among cultivars or among compound groups. To study these differences, a principal component analysis (PCA) was applied to the data set containing the concentrations of the five previously described compound groups, including all 288 samples. Before applying the PCA, the data were preprocessed by applying a 10-base logarithm to the concentrations and mean and variance normalization. The logarithmic scaling puts the emphasis on relative variations in concentration (i.e., a change from 1 to 1.5 is more important than a change from 100 to 100.5), and the normalization equalizes the different components of the data vector. The PCA analysis was performed using the MatLab function "princomp()". Tables 3 and 4 show the variances of the principal components, the cumulative variance expressed as a percentage, and the coefficients providing the principal components as a function of the original components. As can be seen, the first and second principal components describe 88.4% of the data variability.

Table 3. Variances of Principal Components

	component				
	PC1	PC2	PC3	PC4	PC5
variance	3.63	0.79	0.31	0.19	0.08
cumulative variance (%)	72.61	88.44	94.63	89.41	100.00

According to the coefficients, principal components 1 and 2 can be computed from the normalized concentrations for different groups of compounds according to the following equations:

$$PC1 = -0.4899*C_{G1} - 0.3985*C_{G2} - 0.4333*C_{G3} - 0.4874*C_{G4} - 0.4194*C_{G5}$$

$$PC2 = 0.2266*C_{G1} - 0.5929*C_{G2} + 0.5101*C_{G3} + 0.2530*C_{G4} - 0.5224*C_{G5}$$

Under these equations, the first principal component is a weighted average of the normalized concentration for each group, where all of the original components contribute with a

DOI: 10.1021/jf5058205
J. Agric. Food Chem. 2015, 63, 1722−1729

Table 4. Coefficients of the Principal Components

	PC1	PC2	PC3	PC4	PC5
concentration group 1	−0.4899	0.2266	−0.2894	0.3299	0.7184
concentration group 2	−0.3985	−0.5929	0.6784	0.0710	0.1560
concentration group 3	−0.4333	0.5101	0.2705	−0.6914	−0.0299
concentration group 4	−0.4874	0.2530	0.0276	0.5309	−0.6449
concentration group 5	−0.4194	−0.5224	−0.6181	−0.3554	−0.2070

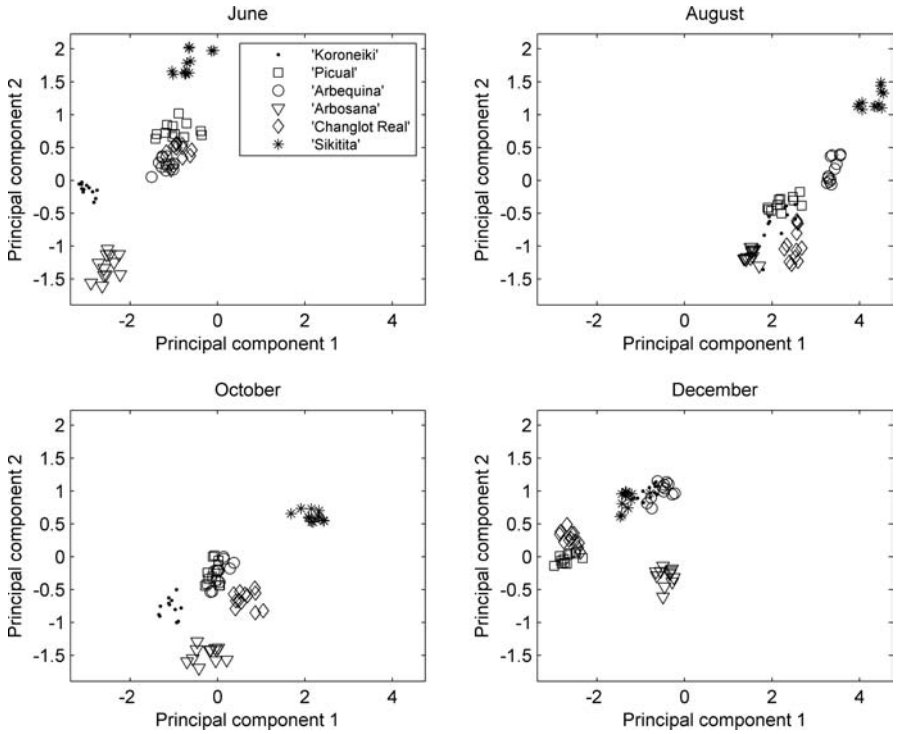

Figure 2. Scatter plots of the first and second principal components for sampling time.

negative coefficient to the first PC (and, therefore, a decrease in this principal component represents a global increase in the phenolic content of the sample). On the other hand, the second principal component is clearly dominated by the concentration of group 2 (although again with a negative coefficient; i.e., a decrease in PC2 can be roughly interpreted as an increase in the concentration of compounds in group 5).

Figures 2 and 3 represent scatter plots of the first and second principal components. To allow a detailed analysis of the PCA study, the scatter plots have been separated by seasons (Figure 2) and cultivars (Figure 3). As can be seen, different cultivars can be separated in the scatter plots: the separation becomes difficult only between 'Picual' and 'Arbequina' in October, with 'Koroneiki' in August and December, and between 'Picual' and 'Changlot Real' in December. This separation reveals a strong dependence of the phenolic profile's seasonal pattern on the cultivar. This dependence has already been described in the paragraph above.

Figure 3 reveals a strong dependence of the phenolic profile on the season, because the points corresponding to each season are clearly separable in each plot. In general, all of the cultivars showed global reductions in their phenolic contents in August (principal component 1 reaches its highest value at this sampling time for all cultivars). The largest increase in phenolic content (lowest value of PC1) was reached in June or December, depending on the cultivar. The plots in Figure 3 evidence again the differences in the seasonal changes associated with each cultivar. According to these results, it can be concluded that the principal component analysis enables separation of the phenolic profile in olive leaves for different seasons and cultivars. This separation capacity is notable because PCA does not aim to discriminate among classes but to represent the maximum variability in the data with the minimum number of components, and reveal changes in the phenolic profile associated with the season (or seasonal changes in the environment) and with the cultivar.

In summary, olive leaves from different cultivars grown in the same orchard under the same environmental conditions and collected at different times showed marked differences in individual and total phenolic compound content. Despite these differences observed among cultivars, all of them showed a similar trend during ripening. The differences among seasons and cultivars should be taken into account for understanding the availability of phenolic compounds in each cultivar and the importance of seasonal changes in the context of the plants' biochemistry. On the other hand, knowledge of the phenolic profile for each season and cultivar is useful when the olive leaves are considered as a source of specific phenolic compounds, because the availability of each compound depends on both the season and the cultivar. To our knowledge, the present study reports the seasonal variability of a large number of phenolic compounds for the first time. At the studied sampling times, June and December seem to be the best periods to use olive leaves as a source of phenolic

DOI: 10.1021/jf5058205
J. Agric. Food Chem. 2015, 63, 1722−1729

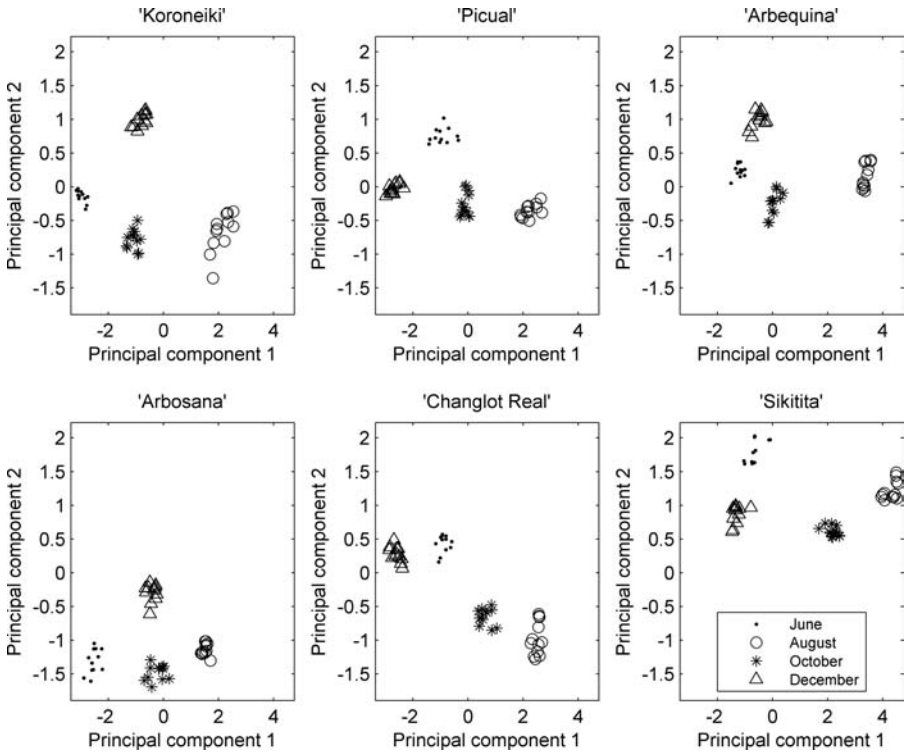

Figure 3. Scatter plots of the first and second principal components for cultivar.

compounds as both of them present similar concentrations of phenolic compounds. In practice, the results shown in December could be rewarding as it coincides with the fruit harvesting period in Andalusia (Spain), the region where the study was performed, during which 432 984 tons of olive leaves is produced annually.[16] In this period, olive leaves could be valorized efficiently as olive byproducts.

■ ASSOCIATED CONTENT

Supporting Information

Quantification of the identified phenolic compounds in olive leaves of the six cultivars, the analytical parameters of the method proposed, and the climatic data during the sampling time. This material is available free of charge via the Internet at http://pubs.acs.org.

■ AUTHOR INFORMATION

Corresponding Author

*Tel.: +34-958-637206. Fax: +34-958-637083. E-mail: anagomez@ugr.es.

Funding

This research was financially supported by the Spanish Ministry of Education and Science (AGL2011-29857-C03-02), the Andalusian Regional Government Council of Innovation and Science (P09-CTS-4564, P10-FQM-6563, and P11-CTS-7625), the International Olive Oil Council (IOOC) scholarship (ref: T1 6-Doct 1/12), and a postdoctoral contract to Juan de la Cierva JCI-2012-12566.

Notes

The authors declare no competing financial interest.

■ REFERENCES

(1) Latouche, G.; Bellow, S.; Poutaraud, A.; Meyer, S.; Cerovic, Z. G. Influence of constitutive phenolic compounds on the response of grapevine (*Vitis vinifera* L.) leaves to infection by Plasmopara viticola. *Planta* **2013**, *237*, 351−61.

(2) Bennett, B.; Richard, N.; Wallsgrove, R. M. Secondary metabolites in plant defence mechanisms. *New Phytol.* **1994**, *127*, 617−633.

(3) Gómez-Caravaca, A. M.; Verardo, V.; Segura-Carretero, A.; Fernández-Gutiérrez, A.; Caboni, M. F. Phenolic compounds and saponins in plants grown under different irrigation regimes. In *Stress and Polyphenols in Plants*; Watson, R., Ed.; Academic Press: New York, 2013; pp 37−48.

(4) Ben Abdallah, S.; Rabhi, M.; Harbaoui, F.; Zar-kalai, F.; Lachâal, M.; Karray-Bouraoui, N. Distribution of phenolic compounds and antioxidant activity between young and old leaves of *Carthamus tinctorius* L. and their induction by salt stress. *Acta Physiol. Plant.* **2012**, *35*, 1161−1169.

(5) Yordanov, I.; Velikova, V.; Tsonev, T. Plant responses to drought and stress tolerance. *Bulg. J. Plant Physiol.* **2003**, 187−206.

(6) Palese, A. M.; Nuzzo, V.; Favati, F.; Pietrafesa, A.; Celano, G.; Xiloyannis, C. Effects of water deficit on the vegetative response, yield and oil quality of olive trees (*Olea europaea* L., cv Coratina) grown under intensive cultivation. *Sci. Hortic. (Amsterdam, Neth.)* **2010**, *125*, 222−229.

(7) Lattanzio, V. Bioactive polyphenols: Their role in quality and storability of fruit and vegetables. *J. Appl. Bot.* **2003**, *77*, 128−146.

(8) Kliebenstein, D. J. Plant defense compounds: systems approaches to metabolic analysis. *Annu. Rev. Phytopathol.* **2012**, *50*, 155−73.

(9) Seigler, D. S. *Plant Secondary Metabolism*; Kluwer Academic Publishers: Boston, MA, 1998; p 711.

(10) Ghanbari, R.; Anwar, F.; Alkharfy, K. M.; Gilani, A.-H.; Saari, N. Valuable nutrients and functional bioactives in different parts of olive (*Olea europaea* L.)-A review. *Int. J. Mol. Sci.* **2012**, *13*, 3291−3340.

(11) Sofo, A.; Manfreda, S.; Fiorentino, M.; Dichio, B.; Xiloyannis, C. The olive tree: a paradigm for drought tolerance in Mediterranean climates. *Hydrol. Earth Syst. Sci.* **2008**, *12*, 293−301.

(12) Bacelar, E. A.; Santos, D. L.; Moutinho-Pereira, J. M.; Lopes, J. I.; Gonçalves, B. C.; Ferreira, T. C.; Correia, C. M. Physiological behaviour, oxidative damage and antioxidative protection of olive trees grown under different irrigation regimes. *Plant Soil* **2007**, *292*, 1−12.

DOI: 10.1021/jf5058205
J. Agric. Food Chem. 2015, 63, 1722−1729

(13) Del Río, J. A.; Báidez, A. G.; Botía, J. M.; Ortuño, A. Enhancement of phenolic compounds in olive plants (*Olea europaea* L.) and their influence on resistance against Phytophthora sp. *Food Chem.* **2003**, *83*, 75−78.
(14) El Aabidine, A. Z.; Baissac, Y.; Moukhli, A.; Jay-Allemand, C.; Khadari, B.; El Modafar, C. Resistance of Olive Tree to *Spilocaea oleagina* is Mediated by the Synthesis of Phenolic Compounds. *Int. J. Agric. Biol.* **2010**, *12*, 61−67.
(15) Báidez, A. G.; Gómez, P.; Del Río, J. A.; Ortuño, A. Dysfunctionality of the xylem in *Olea europaea* L. Plants associated with the infection process by *Verticillium dahliae* Kleb. Role of phenolic compounds in plant defense mechanism. *J. Agric. Food Chem.* **2007**, *55*, 3373−3377.
(16) López, J. A. C.; Heras, T. P.; Gordillo, T. M. Potencial energético de los subproductos de la industria olivarera en Andalucía. *Secretaría General Del Medio Rural Y la Producción Ecolgóica Junta de Andalucia*, 2010; pp 1−68.
(17) Molina-Alcaide, E.; Yáñez-Ruiz, D. R. Potential use of olive by-products in ruminant feeding: A review. *Anim. Feed Sci. Technol.* **2008**, *147*, 247−264.
(18) D'Andria, R.; Di Salle, A.; Petillo, O.; Sorrentino, G.; Peluso, G. Nutraceutical, cosmetic, health products derived from olive: Present and future of the Mediterannean olive sector. *Options Méditerranéennes, A* **2013**, *106*, 153−161.
(19) Susalit, E.; Agus, N.; Effendi, I.; Tjandrawinata, R. R.; Nofiarny, D.; Perrinjaquet-Moccetti, T.; Verbruggen, M. Olive (*Olea europaea*) leaf extract effective in patients with stage-1 hypertension: comparison with Captopril. *Phytomedicine* **2011**, *18*, 251−258.
(20) Sada, A. Olive leaf. *Alt. Med. Rev. Vol.* **2009**, *14*, 62−66.
(21) Ortega-García, F.; Peragón, J. Phenol metabolism in the leaves of the olive tree (*Olea europaea* L.) cv. Picual, Verdial, Arbequina, and Frantoio during ripening. *J. Agric. Food Chem.* **2010**, *58*, 12440−12448.
(22) Brahmi, F.; Mechri, B.; Dhibi, M.; Hammami, M. Variations in phenolic compounds and antiradical scavenging activity of *Olea europaea* leaves and fruits extracts collected in two different seasons. *Ind. Crops Prod.* **2013**, *49*, 256−264.
(23) Petridis, A.; Therios, I.; Samouris, G.; Koundouras, S.; Giannakoula, A. Effect of water deficit on leaf phenolic composition, gas exchange, oxidative damage and antioxidant activity of four Greek olive (*Olea europaea* L.) cultivars. *Plant Physiol. Biochem.* **2012**, *60*, 1−11.
(24) Mert, C.; Barut, E.; Ipek, A. Quantitative seasonal changes in the leaf phenolic content related to the alternate-bearing patterns of olive (*Olea europaea* L. cv. Gemlik). *J. Agric. Sci. Technol.* **2013**, *15*, 995−1006.
(25) Hashemi, P.; Delfan, B.; Ghiasvand, A. R.; Alborzi, M.; Raeisi, F. A study of the effects of cultivation variety, collection time, and climate on the amount of oleuropein in olive leaves. *Acta Chromatogr.* **2010**, *22*, 133−140.
(26) Talhaoui, N.; Gómez-Caravaca, A. M.; León, L.; De la Rosa, R.; Segura-Carretero, A.; Fernández-Gutiérrez, A. Determination of phenolic compounds of 'Sikitita' olive leaves by HPLC-DAD-TOF-MS. Comparison with its parents 'Arbequina' and 'Picual' olive leaves. *LWT—Food Sci. Technol.* **2014**, *58*, 28−34.
(27) Rallo, L.; Barranco, D.; De la Rosa, R.; León, L. Chiquitita olive. *HortScience* **2008**, *43*, 529−531.
(28) Papoti, V. T.; Tsimidou, M. Z. Impact of sampling parameters on the radical scavenging potential of olive (*Olea europaea* L.) leaves. *J. Agric. Food Chem.* **2009**, *57*, 3470−3477.
(29) Malik, N. S. A.; Bradford, J. M. Changes in oleuropein levels during differentiation and development of floral buds in "Arbequina" olives. *Sci. Hortic. (Amsterdam, Neth.)* **2006**, *110*, 274−278.
(30) Amiot, M. J.; Fleuriet, A.; Macheix, J. J. Importance and evolution of phenolic compounds in olive during growth and maturation. *J. Agric. Food Chem.* **1986**, *34*, 823−826.
(31) Ranalli, A.; Contento, S.; Lucera, L.; Di Febo, M.; Marchegiani, D.; Di Fonzo, V. Factors affecting the contents of iridoid oleuropein in olive leaves (*Olea europaea* L.). *J. Agric. Food Chem.* **2006**, *54*, 434−440.
(32) El Riachy, M.; Priego-Capote, F.; Rallo, L.; Luque-de Castro, M. D.; León, L. Phenolic composition of virgin olive oils from cross breeding segregating populations. *Eur. J. Lipid Sci. Technol.* **2012**, *114*, 542−551.
(33) Ortega-García, F.; Blanco, S.; Peinado, M. A.; Peragón, J. Polyphenol oxidase and its relationship with oleuropein concentration in fruits and leaves of olive (*Olea europaea*) cv. 'Picual' trees during fruit ripening. *Tree Physiol.* **2008**, *28*, 45−54.
(34) Chaves, M. M.; Maroco, J. P.; Pereira, J. S. Understanding plant responses to drought—from genes to the whole plant. *Funct. Plant Biol.* **2003**, *30*, 239−264.

DOI: 10.1021/jf5058205
J. Agric. Food Chem. 2015, 63, 1722−1729

MATERIALS AND METHODS

Reagents and Antibodies. 6-Shogaol (6-SH) and 6-gingerol (6-GL) were purchased from Sigma Chemical Co. (St. Louis, MO, USA). *Recombinant human* (*rh*) CCL2 protein was obtained from R&D Systems (Minneapolis, MN, USA).

Cell Culture. Human breast cancer MDA-MB-231, lung cancer A549, mouse mammary tumor 4T1, and Lewis lung carcinoma (LLC) cells were purchased from American Type Culture Collection (ATCC) (Manassas, VA, USA). The MDA-MB-231 cells were cultured in Leibovitz's L-15 medium supplemented with 10% fetal bovine serum (FBS), penicillin, and streptomycin in a CO_2-free incubator. The A549, 4T1, and LLC cells were cultured in F-12K medium (Kaighn's modification of Ham's F-12 medium) or RPMI1640 and DMEM containing 10% FBS in a 5% CO_2 incubator. For the conditioned medium (CM) collection, the MDA-MB-231 and A549 cells (1×10^6) were seeded in a 10 cm dish and the supernatants collected, filtered (0.22 mm), and defined as MDA-CM and A549-CM.

Isolation of $CD14^+$ Monocytes and Differentiation of Monocyte-Derived DCs (mdDCs). Monocytes were purified from peripheral blood mononuclear cells (PBMCs) obtained from healthy consenting donors. Mononuclear cells were isolated from the blood by the Ficoll–Hypaque gradient (GE Healthcare Bio-Sciences, Little Chalfont, UK). $CD14^+$ monocytes were purified using $CD14^+$ monoclonal antibody-conjugated magnetic beads (MACS MicroBeads, Miltenyi Biotec), according to the manufacturer's protocol. Monocyte-derived DCs (mdDCs) were generated by culturing $CD14^+$ monocytes in RPMI 1640 medium containing 10% FBS (Invitrogen, Carlsbad, CA, USA) and 20 ng/mL GM-CSF and 10 ng/mL IL-4 (R&D Systems) with or without 6-SH (1 or 10 μM) for 5 days. The medium was replaced with fresh medium containing GM-CSF and IL-4 on day 3. The hospital's Institutional Review Board approved the study, and all of the patients provided informed consent in accordance with the Declaration of Helsinki. A549 and MDA-MB-231 tumor-associated mdDCs (A549-TADCs) and MDA-MB-231-TADCs were generated by culturing $CD14^+$ monocytes in RPMI 1640 medium containing FBS, GM-CSF, and IL-4 presenting in A549-CM (20%) and MDA-MB-231-CM (20%) with or without 6-SH (1 or 10 μM) for 5 days. After washing, the supernatants were collected, frozen, stored at −80 °C, and thawed singly for the study.

Measurement of Secreted Factors. Supernatants from mdDCs, A549-TADC, MDA-TADCs, 6-shogaol-treated mdDC, and TADC were collected. $CD11c^+F4/80^-$ cells were isolated from mice and cultured in RPMI 1640 medium. After 24 h, the supernatants were harvested. CXCL1, CCL2, and CCL4 levels were quantified using human and mouse MILLIPLEX MAP kits.

Quantitative Real-Time PCR (qRT-PCR). Isolation of RNA was performed using the TRIzol reagent (Invitrogen). cDNA was prepared using an oligo (dT) primer and reverse transcriptase (Takara, Shiga, Japan) following standard protocols. Real-time PCR was performed using SYBR Green on the ABI *StepOnePlus* real-time PCR instrument (Applied Biosystems, Foster City, CA, USA). Each PCR reaction mixture contained 100 nM of each primer, 5 μL of 2× SYBR Green PCR Master Mix (Applied Biosystems, Foster City, CA, USA), 2.5 μL of cDNA, and RNase-free water for a total volume of 10 μL. The PCR reaction was conducted with a denaturation step at 95 °C for 10 min, and then for 40 cycles at 95 °C for 15 s and 60 °C for 1 min. All of the PCRs were performed in triplicate and normalized to internal control glyceraldehyde-3-phosphate dehydrogenase (GAPDH) mRNA. The relative expression is presented using the $2^{-\triangle\triangle CT}$ method.

Tumor Spheroid Formation. A549 and MDA-MB-231 cells were labeled with PKH67 (Sigma-Aldrich) following the manufacturer's procedures. The cells were seeded in ultralow-attachment wells with or without 6-shogaol preset conditioned media (20%) of mdDCs or TADCs for tumor sphere formation. On day 10, the tumor spheres were assessed by fluorescence microscopy or dissociated into single cells for ALDHFLOR analysis.

Flow Cytometry Analysis. Aldehyde dehydrogenases (ALDH) activity was assessed using an ALDHFLOR kit (Stem Cell Tech-

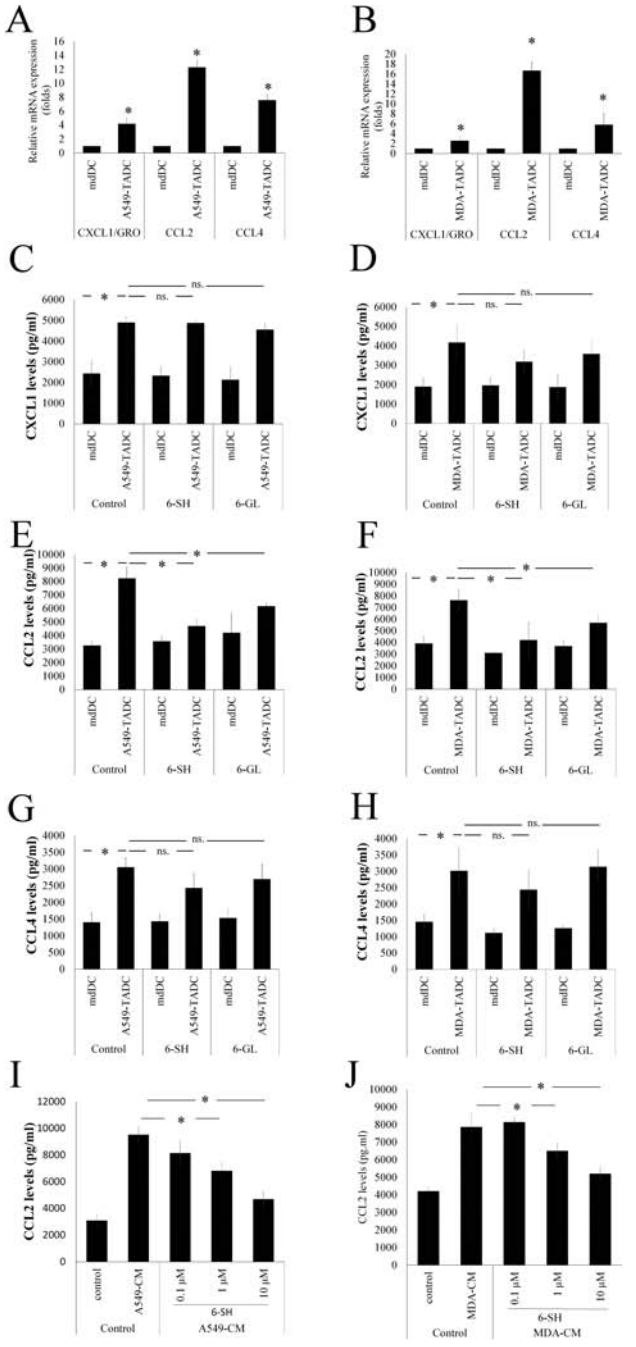

Figure 1. 6-Shogaol and 6-gingerol decreased the expression of CCL2 in TADC: Up-regulation of inflammatory chemokines in (A) A549- and (B) MDA-MB-231-derived TADC, as determined by qRT-PCR. The active components of ginger failed to inhibit the up-regulation of CXCL1 in both (C) A549- and (D) MDA-MB-231-derived TADCs. 6-Shogaol (10 μM) and 6-gingerol (10 μM) decreased the expression of CCL2 in (E) A549- and (F) MDA-MB-231-derived TADCs. 6-Shogaol (10 μM) and 6-gingerol (10 μM) did not affect the stimulatory effect of (G) A549 and (H) MDA-MB-231 cells on CCL4 expression of TADCs. 6-Shogaol decreased the expression of CCL2 in (I) A549 and (J) MDA-MB-231-derived TADCs in a dose-dependent manner. The expression of mRNA and protein was assessed by qRT-PCR and MILLIPLEX MAP kits. All results are representative of at least three independent experiments. The results are reported as the mean ± SD; (*) $p < 0.05$.

DOI: 10.1021/jf504934m
J. Agric. Food Chem. 2015, 63, 1730−1738

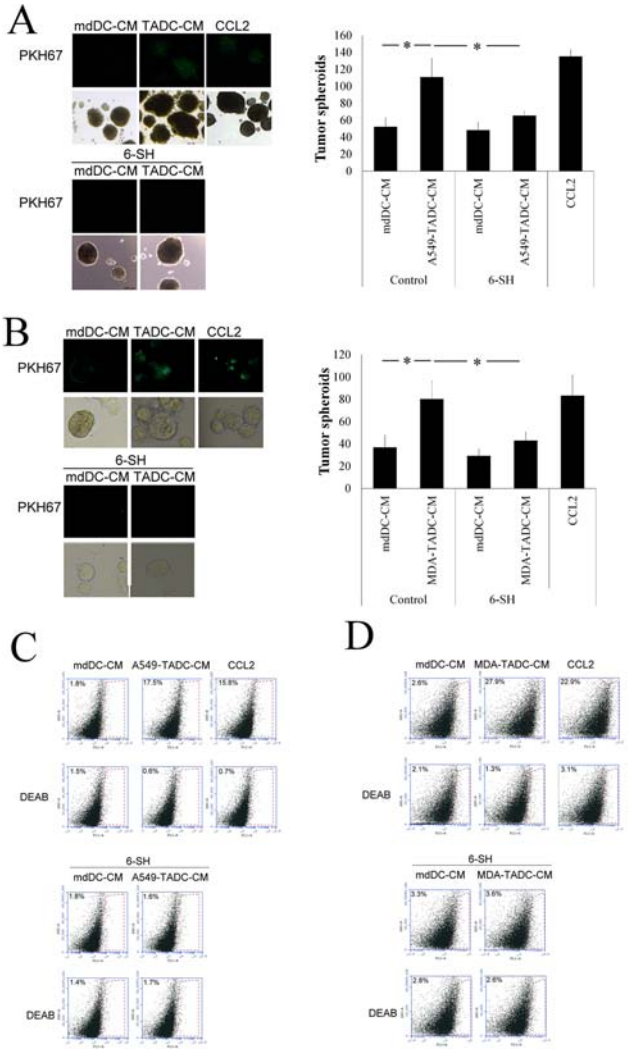

Figure 2. 6-Shogaol decreased TADC-mediated cancer tumorigenesis. 6-Shogaol (10 μM) reduced the stimulatory effect of TADCs on tumor spheroid formation of (A) A549 and (B) MDA-MB-231. 6-Shogaol (10 μM) decreased the up-regulation of TADCs on ALDH activity (C) A549 and (D) MDA-MB-231 tumor spheroids. mdDCs and TADCs (A549-TADCs and MDA-TADCs) were derived by culturing $CD14^+$ monocytes in RPMI 1640 medium containing GM-CSF and IL-4 with or without A549-CM or MDA-CM (20%) for 5 days. 6-Shogaol-treated mdDCs and TADCs were generated by using the same procedure but contained 6-shogaol (10 μM). The supernatants of various DCs were collected. A549 and MDA-MB-231 cells were treated with CMs (20%) of mdDCs, TADCs, 6-shogaol-treated mdDCs, or TADCs in ultralow-attachment wells for 10 days. The tumor spheroids were stained by PHK67 and counted by fluorescence microscope, and ALDH activity was determined by ALDHEFLUOR kit. All results are representative of at least three independent experiments. The results are reported as the mean ± SD; (*) $p < 0.05$.

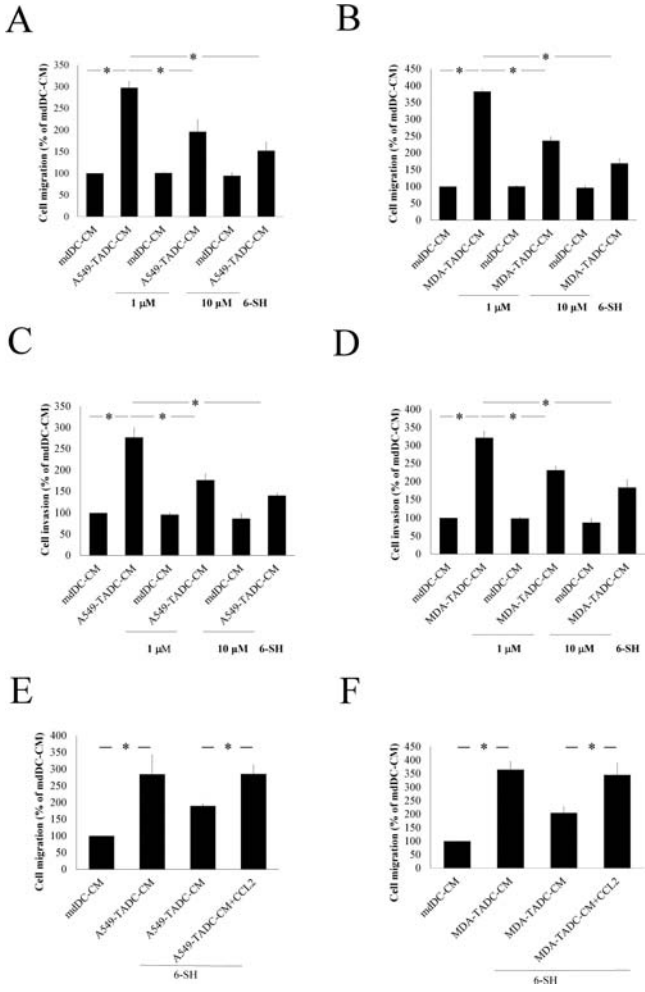

Figure 3. 6-Shogaol decreased TADC-mediated cancer progression. 6-Shogaol (1 and 10 μM) decreased the stimulatory effect of TADCs on migration of (A) A549 and (B) MDA-MB-231. 6-Shogaol reduced the enhanced effect of TADCs on the invasion of (C) A549 and (D) MDA-MB-231 cells. The addition of CCL2 reversed the inhibitory effect of 6-shogaol on TADC-mediated cell migration in (E) A549 and (F) MDA-MB-231 cells. mdDCs and TADCs (A549-TADCs and MDA-TADCs) were derived by culturing $CD14^+$ monocytes in RPMI 1640 medium containing GM-CSF and IL-4 with or without A549-CM or MDA-CM (20%) for 5 days. 6-Shogaol-treated mdDCs and TADCs were generated by using the same procedure but contained 6-shogaol (1 or 10 μM). A549 and MDA-MB-231 cells were seeded into the top transwell insert, and the various CMs of mdDCs, TADCs, 6-shogaol-treated mdDCs, or TADCs were added to the bottom cells as chemoattractant for 24 h (for migration) or 48 h (for invasion). The invasive and migration abilities of the A549 and MDA-MB-231 cells were quantified by CyQUANT GR dye. All results are representative of at least three independent experiments. The results are reported as the mean ± SD; (*) $p < 0.05$.

nologies, Vancouver, BC, Canada). Briefly, cells were incubated in Aldefluor assay buffer containing ALDH substrate (1 μmol l^{-1} per 1×10^6cells), with or without diethylaminobenzaldehyde (DEAB), a specific ALDH inhibitor. After incubation at 37 °C for 30 min, the cells were centrifuged and resuspended in cold Aldefluor buffer. ALDH activity was determined by an Acuri C6 flow cytometer (Becton Dickinson Immuno-cytometry Systems). The cells isolated from the lungs and mammary tumors of mice were stained by antibodies against mouse CD11b labeled by FITC (BD Biosciences, San Jose, CA, USA) and F4/80 labeled by allophycocyanin (APC) (Biolegend). The expression of each molecule was analyzed using an Acuri C6 flow cytometer (BD Biosciences).

Cell Migration and Invasion Analysis. A quantitative migration and invasion assay was conducted using the QCM 24-well Cell Migration Assay and Invasion System (Millipore Corp., Billerica, MA, USA). Briefly, 3×10^4 A549 or MDA-MB-231 cells were seeded into the top chamber, and CMs of mdDC, TADC, 6-shogaol-treated mdDC, and TADC were added to the bottom wells as chemoattractant for 24 h (for migration) or 48 h (for invasion). At the end of treatment, the cells were poststained with CyQuant GR dye in cell lysis buffer for 15 min at room temperature. Fluorescence

DOI: 10.1021/jf504934m
J. Agric. Food Chem. 2015, 63, 1730−1738

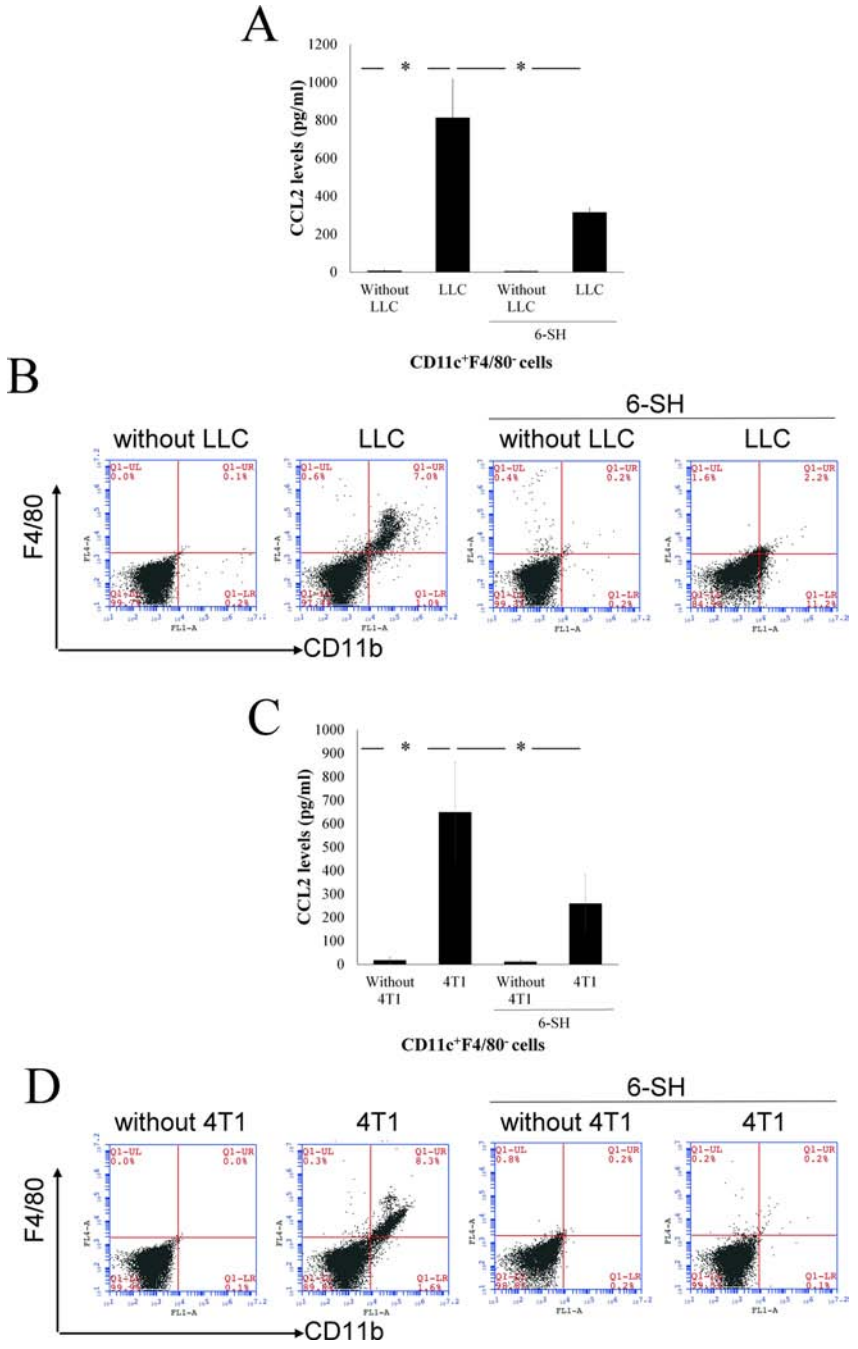

Figure 4. 6-Shogaol reduced CCL2-mediated immunosuppression in vivo. 6-Shogaol decreased the (A) CCL2 expression of CCL2 of TADCs and (B) TAM infiltration in LLC-transplanted mice. 6-Shogaol decreased the (C) CCL2 expression of TADCs and (D) TAM infiltration in 4T1-transplanted mice. 4T1 cells were implanted into mammary fat pads of BALB/c mice, and LLC cells were implanted into C57BL mice via tail vein injection. The mice were then randomly divided into two groups: the 6-shogaol-treated group was given ip daily with 6-shogaol (dose = 30 mg/kg of body weight), whereas the control group was given an equal volume of normal saline. Tumor-bearing mice were sacrificed 14 days after transplantation. TADC ($CD11c^+$, $F4/80^-$) and TAM ($CD11b^+$) cells were isolated from lungs (LLC) and mammary tumors (4T1). The subgroups of immune cells were determined by staining of surface markers and by flow cytometry analysis. All results are representative of at least three independent experiments. The results are reported as the mean ± SD; (*) $p < 0.05$.

of the migratory or invaded cells was read using a fluorescence plate reader at excitation and emission wavelengths of 485 and 540 nm, respectively.

Immunoblot Analysis. $CD14^+$ monocytes (4×10^6) were pretreated with 6-shogaol for 1 h and the A549- or MDA-MB-231-CMs were added for 30 min. Total cell extracts were prepared in RIPA lysis buffer (Millipore). Equivalent amounts of protein were resolved by the SDS-PAGE and transferred to PVDF membranes. After the membranes were blocked in Tris-buffer saline containing 0.05% Tween 20 (TBST) and 5% nonfat powdered milk, they were incubated with primary antibodies against p-STAT3, STAT3, and GAPDH (Cell Signaling Technology) at 4 °C overnight. After three washings with TBST, the membranes were incubated with horseradish peroxidase-labeled secondary antibody for 1 h and then rewashed. Detection was performed using an enhanced chemiluminescence blotting detection system (Millipore).

Chromatin Immunoprecipitation (ChIP). ChIP was conducted according to the protocol of the Pierce Agarose ChIP kit (Pierce, Thermo Scientific, Rockford, IL, USA). Immunoprecipitation was

DOI: 10.1021/jf504934m
J. Agric. Food Chem. 2015, 63, 1730−1738

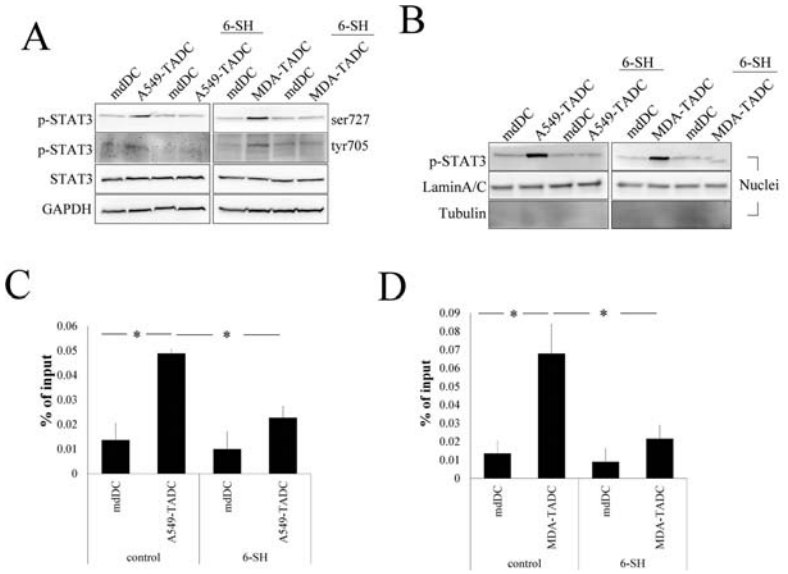

Figure 5. Effect of 6-shogaol on STAT3 activation in TADCs. 6-Shogaol (10 μM) decreased the phosphorylation of STAT3 in (A) A549-TADCs and MDA-MB-231-TADCs. (B) 6-Shogaol (10 μM) inhibited active STAT3 in the nuclear fraction in A549- and MDA-MB-231-TADCs. It also reduced the DNA binding of STAT3 on the promoter of CCL2 in (C) A549- and (D) MDA-MB-231-TADCs. $CD14^+$ monocytes were pretreated with 6-shogaol (10 μM) for 1 h, and then A549 or MDA-MB-231-CM was added for 30 min. The phosphorylation of STAT3 was assessed by immunoblot. STAT3 activity was assessed by ChIP analysis. All results are representative of at least three independent experiments. The results are reported as the mean ± SD; (*) $p < 0.05$.

conducted using anti-STAT3 transcription factors (Cell Signaling Technology) or by normal rabbit IgG (Cell Signaling Technology) as the negative control. Input DNA and immunoprecipitated DNA were analyzed by quantitative PCR. Primer sequences were obtained from Qiagen (GPH1005667(−)01A).

Lung Metastasis of Lung and Breast Cancer in Vivo. Male C57BL and female BALB/c mice (5−6 weeks old) from the National Science Council Animal Center (Taipei, Taiwan) were maintained in pathogen-free conditions. 4T1 cells (2×10^6) were implanted into mammary fat pads of BALB/c mice and LLC cells were implanted into C57BL mice via tail vein injection. The mice were then randomly divided into two groups: the 6-shogaol-treated group was given a daily intraperitoneal injection (ip) of 0.2 mL of 6-shogaol (dose = 30 mg/kg of body weight), whereas the control group was given an equal volume of normal saline. Tumor-bearing mice were sacrificed 14−21 days after transplantation. Lung (LLC-bearing mice) and mammary tumors (4T1-bearing mice) were collected and minced. Single-cell suspensions were obtained after enzymatic digestion (1 mg/mL collagenase A; Roche Diagnostics) and 100 IU/mL type I DNase (Sigma-Aldrich) for 2 h at 37 °C and 5% CO_2 in RPMI 1640 medium. A single-cell suspension was filtered through a 70 μm nylon mesh (BD Biosciences), and cells were washed twice by PBS. $CD11c^+$ and $CD11b^+$ cells were purified using anti-CD11c or CD11b monoclonal antibody-conjugated magnetic beads (MACS MicroBeads, Miltenyi Biotec). $F4/80^+$ cells were depleted from $CD11c^+$ cells by using $F4/80^+$ antibody−biotin beads (Miltenyi Biotec). Alternatively, the lungs were removed and the metastatic tumor nodules counted. All animal experiments were performed according to a protocol approved by the Institutional Animal Care and Use Committee of Kaohsiung Medical University Hospital.

Statistical Analysis. Data are expressed as the mean ± SD. Statistical analyses between control and experimental groups were analyzed by an unpaired Student's t test. Multiple comparisons were evaluated by a one-way ANOVA, and differences in the mean values among groups were conducted by a Fischer post hoc analysis. p values <0.05 were considered to be statistically significant.

RESULTS

Lung Cancer- and Breast Cancer-Derived TADCs Secrete High Levels of CCL2, Which Are Decreased by 6-Shogaol and 6-Gingerol. Previous studies and data show that lung cancer A549 and breast cancer MDA-MB-231 cells increase the expression of some inflammatory chemokines in TADCs.[6] This study therefore assessed whether the active components of ginger, 6-shogaol (6-SH) and 6-gingerol (6-GL), could decrease the expression of these cytokines/chemokines in TADCs. The qRT-PCR data demonstrated that A549- and MDA-MB-231-CMs (MDA-CM) increased levels of CXCL1 (chemokine (C-X-C motif) ligand 1), CCL2, and CCL4 (chemokine (C-C motif) ligand 4) mRNA transcripts in TADC, when compared to mdDCs (Figure 1A,B). As determined by ELISA, the CMs of lung and breast cancers increased the expressions of CXCL1, CCL2, and CCL4 in protein levels in TADCs (Figure 1C−H). 6-Shogaol decreased the production of CCL2 in TADCs in protein levels (Figure 1E,F). The inhibitory effect of 6-shogaol on CCL2 secretion in TADCs was greater than that of 6-gingerol. In addition, 6-shogaol decreased the expression of CCL2 in TADCs in a dose-dependent manner ranging from 0.1 to 10 μM (Figure 1I,J). Neither 6-shogaol nor 6-gingerol prevented the stimulative effect of cancers on the expression of CXCL1 and CCL4 in TADCs (Figure 1C,D,F,G). To eliminate the possibility of cytokines being reduced due to altered cell viability, we assessed the effect of 6-shogaol and 6-gingerol (0.1−10 μM) on the cell viability of TADCs. The data show that 6-shogaol and 6-gingerol do not affect the viability of TADCs (data not shown).

6-Shogaol Decreases the Effect of TADC-Derived CCL2 on the Formation of Tumor Spheroids, Migration, and Invasion. Because CCL2 has been reported to increase cancer-stem cell like property and enhance cancer progression,[20] this study assessed the effect of 6-shogaol on the bioactivities of TADC-derived CCL2. The stem cell-like phenotype is determined by tumor spheroid formation and aldehyde dehydrogenase (ALDH) activity. A549- and MDA-MB-231-TADC-CM increased tumor spheroid formation in A549 and MDA-MB-231 cell lines, respectively (Figure 2A,B). However, TADCs lost their inductive effect on tumor spheroid formation if they were generated in the presence of 6-shogaol

DOI: 10.1021/jf504934m
J. Agric. Food Chem. 2015, 63, 1730−1738

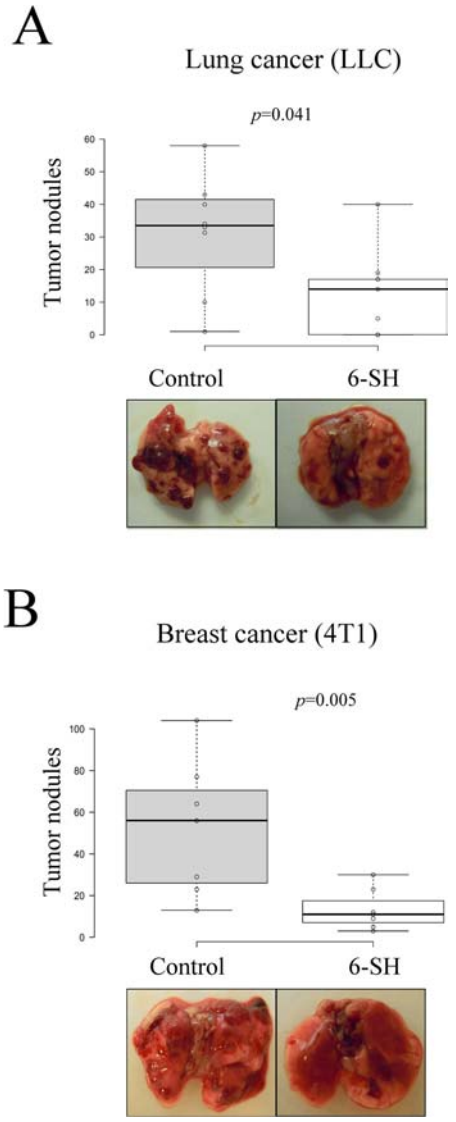

Figure 6. 6-Shogaol decreased cancer metastasis in vivo. 6-Shogaol decreased the metastasis of (A) LLC and (B) 4T1 in mice. 4T1 cells were implanted into mammary fat pads of BALB/c mice, and LLC cells were implanted into C57BL mice via tail vein injection. The mice were then randomly divided into two groups: the 6-shogaol-treated group was given ip daily 6-shogaol (dose = 30 mg/kg of body weight), whereas the control group was given an equal volume of normal saline. Tumor-bearing mice were sacrificed 14 (for LLC) or 21 (for 4T1) days after transplantation. Their lungs were removed and the metastatic tumor nodules counted. Each value is the mean ± SD of three determinations. (*) Significant difference between the two test groups, as analyzed by Student's *t* test ($p < 0.05$).

(Figure 2A,B). The PKH^{high} cells undergo fewer divisions during sphere formation, which implies they possess a stem cell phenotype, in contrast to high proliferation nonstem PKH^{low} cells. The ratio of PKH^{high} cells increased in tumor spheroids cultured in TADC-CMs when compared to those cultured in mdDC-CMs. 6-Shogaol treatment decreased the ratio of PKH^{high} cell population in tumor spheroids, revealing 6-shogaol reduces the stem cell characteristics in both lung and breast cancers (Figure 2A,B). Moreover, the activity of ALDH, a stem cell marker, was enhanced in tumor spheroids cultured in TADC-CMs when compared to those cultured in mdDC-CMs. However, the ALDH activity of tumor spheroids was reduced when the TADCs were generated in the presence of 6-shogaol (Figure 2C,D). We next assessed the effect of 6-shogaol on TADC-mediated cancer progression. A549- and MDA-MB-231-TADC-CM increased A549 and MDA-MB-231 cell migration, respectively. However, TADCs lost their inductive effect on cancer migration if they were generated in the presence of 6-shogaol (Figure 3A,B). Similarly, A549- and MDA-MB-231-TADC-CM increased cell invasion in A549 and MDA-MB-231 cells, but not if the TADC-CMs were derived in the presence of 6-shogaol (Figure 3C,D). In contrast, the addition of rhCCL2 reduced the inhibitory effect of 6-shogaol on TADC-mediated A549 and MDA-MB-231 cell migration (Figure 3E,F).

6-Shogaol Improves CCL2-Mediated Immunosurveillance in Lung and Breast Cancers in Vivo. Because CCL2 increases immunosuppressive response by decreasing macrophage infiltration in mice with cancer,[20] this study assessed if 6-shogaol could alter immunosurveillance in mice. LLCs were transplanted into mice by tail vein injection. The mice were sacrificed after 14 days, and TADC ($CD11c^+F4/80^-$) cells from metastatic tumor nodules in the lungs were isolated and examined. CCL2 expression in TADCs ($CD11c^+/F4/80^-$) of the lungs of mice with LLC transplantation was higher than the dendritic cells isolated from the lungs of normal mice. Administration of 6-shogaol decreased CCL2 levels in TADCs of the lungs of mice with LLC transplantation (Figure 4A). 6-Shogaol treatment also decreased tumor-associated macrophage (TAM) ($CD11b^+F4/80^+$) infiltration when compared to vehicle-treated mice with LLC transplantation (Figure 4B). To assess the effect of 6-shogaol on immunosurveillance in breast cancer in vivo, 4T1 was implanted in the mammary fat pads of mice. On day 14 post-tumor implantation, TAM and TADCs were isolated from both mammary tissue and lungs with metastatic 4T1 tumors. 4T1 breast cancer cells also had increased CCL2 expression in TADCs when compared to dendritic cells isolated from normal mammaries. This CCL2 up-regulation was inhibited by 6-shogaol administration (Figure 4C). Similarly, TAM infiltration also decreased in 6-shogaol-treated mice (Figure 4D).

6-Shogaol Decreases CCL2 Expression by Inhibiting STAT3 Activation in TADCs. Because STAT3 was reported to bind to and activate the promoter of *CCL2*,[20] this study assessed if 6-shoagol could decrease the activation of STAT3. The CMs of lung cancer A549 and breast cancer MDA-MB-231 cells increased the phosphorylation of STAT3 in TADCs more than in mdDCs (Figure 5A). The CMs of lung and breast cancers also enhanced the nuclear translocation of activated STAT3 (Figure 5B). These effects, including STAT3 activation and nuclear translocation, were inhibited by 6-shogaol in TADCs. ChIP analysis further revealed that CMs of A549 and MDA-MB-231 cancer increased the binding of STAT3 on the promoter of CCL2 gene, but this was inhibited by 6-shogaol treatment (Figure 5C,D).

6-Shaogol Decreases Metastasis in Lung and Breast Cancers in Vivo. To assess the activity of 6-shogaol on the metastasis of lung and breast cancers, LLC (by tail vein injection) and 4T1 (by mammary fad pad implantation) were transplanted into mice, which were sacrificed after 14 and 21 days, respectively. The tumors in the lungs of mice were collected and counted. 6-Shogaol treatment decreased the number of LLC tumor nodules in mice (Figure 6A). Similarly, 6-shogaol also reduced the lung metastasis of breast cancer 4T1 in mice (Figure 6B).

DOI: 10.1021/jf504934m
J. Agric. Food Chem. 2015, 63, 1730−1738

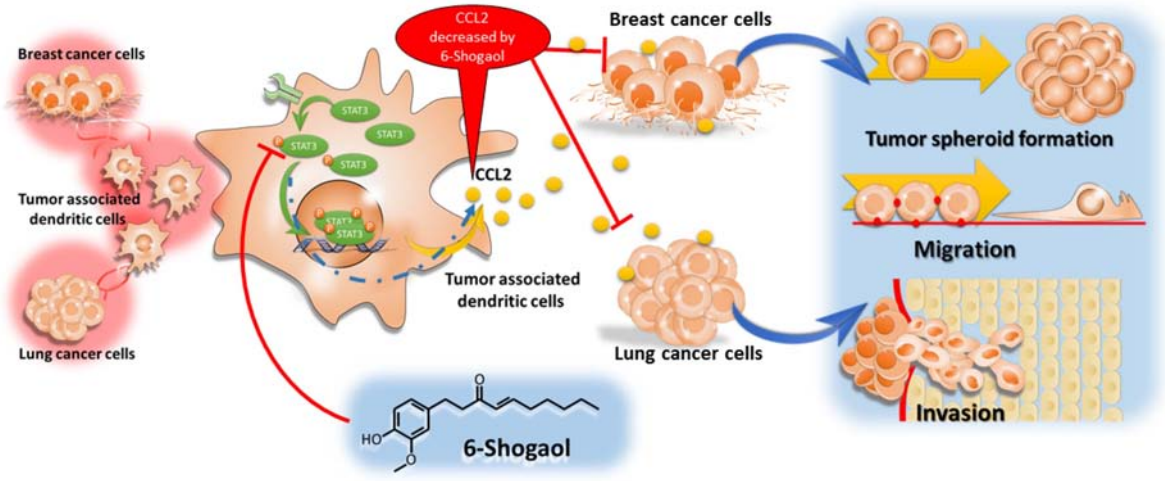

Figure 7. Scheme of proposed 6-shogaol impairment of cancer development and lung metastasis by inhibiting the secretion of CCL2 in tumor-associated dendritic cells.

DISCUSSION

Tumor microenvironment is characterized by a stroma of hematopoietic precursors, inflammatory immune cells, dysregulated vessel endothelial cells, and proteolytic enzymes.[21,22] TADCs have been shown to lose their antigen-presenting function and also to promote cancer progression by modulating multiple components in the cancer niche, thereby creating a permissive and supportive microenvironment for tumor survival, proliferation, and spread.[7,23,24] This study has two novel findings. It is the first study to demonstrate that TADCs facilitate lung and breast cancer metastasis in vitro and in vivo by secreting inflammatory mediator CCL2. It is also the first study to demonstrate that 6-shogaol decreases cancer development and progression by inhibiting the production of TADC-derived CCL2 (Figure 7).

CCL2 has been implicated in cancer progression and metastasis. Serum CCL2 levels are significantly correlated to the cancer stage and have been shown to have significant prognostic value for relapse-free survival.[25−27] CCL2 appears to play a dual role in regulating tumor immunosurveillance and in sustaining the development and advancement of established malignancy. CCL2 has also been implicated in directly affecting cancers by switching the cancer stem cell-like phenotype and by enhancing cancer cell survival, growth, angiogenesis, migration, and metastasis.[28,29] It has also been reported to indirectly facilitate carcinogenesis and metastasis by altering the host's immune response, including the accumulation of suppressive immune cells TAM, MDSCs, and regulatory DC and T cells.[20,30−32] CCL2 expression is modulated in the interaction between tumor and niche cells, including fibroblasts and adipocytes.[20,30]

This study demonstrates that cancer cells stimulate TADCs to express high levels of CCL2, which in turn increase tumorigenesis by increasing cancer stem cell-like properties. TADC-derived CCL2 also increases cancer migration and invasion, key characteristics of metastatic cancer. However, these enhancing effects of TADCs on cancer development are prevented by 6-shogaol treatment in vitro and in vivo. 6-Shogaol administration decreases immunosuppressive TAM infiltration in cancer, suggesting that 6-shogaol may restore the host's immune system.

Accumulating evidence supports a role for the STAT3 pathway in the establishment of the inflammatory microenvironment. Constitutively activated STAT3 can drive various pro-tumorigenic and inflammatory mediator expressions in cancer cells per se, as well as in niche cells.[20,33,34] Breast cancer stimulates fibroblasts to express high levels of CCL2 via a STAT3-dependent mechanism, resulting in increased tumorigenesis. In contrast, inhibition of STAT3 in DCs enhances its ability to prime T cells that have elevated IFNγ production,[35] suggesting that STAT3 is a potential target for developing a strategy that restores the host's immunity against tumors.

The results of this study reveal that cancer increases the activation and DNA binding activity of STAT3, which in turn enhances the expression of CCL2 in TADCs. 6-Shogaol decreases the cancer-induced activation of STAT3, subsequently reducing CCL2 levels in TADCs. According to the studies presented here, 6-shogaol may have a novel mechanism for inhibiting STAT3 activation in TADCs, resulting in decreased pro-tumorigenesis and inflammatory mediators in cancer niches.

In summary, this study provides novel insights for understanding the paracrine interaction initiated by cancer cells to induce CCL2 production by TADCs. TADC-derived CCL2 promotes cancer progression by regulating cancer stem cell-like properties, migration/invasion, and immunosuppressive immune cell infiltration. 6-Shogaol has also been demonstrated to inhibit the effect of TADCs on cancer tumorigenesis and progression by decreasing CCL2 production. 6-Shoagol also reduces the accumulation of immunosuppressive cells, suggesting that 6-shogaol may serve as a future therapeutic agent for efficiently blocking the cancer−DC interaction to overcome immune dysregulation and cancer progression.

AUTHOR INFORMATION

Corresponding Author

*(P.-L.K.) Mail: Institute of Clinical Medicine, College of Medicine, Kaohsiung Medical University, No. 100 Shih-Chuan First Road, Kaohsiung 807, Taiwan. E-mail: kuopolin@seed.net.tw. Phone: +886-7-312-1101, ext 2512 #33. Fax: +886-7-321-0701.

Funding

This study was supported by grants from the National Science Council of Taiwan (NSC 101-2628-B-037-001-MY3, NSC 101-2320-B-037-043-MY3, NSC 102-2628-B-037-002-MY3, NSC 102-2632-B-037-001-MY3, and NSC 102-2314-B-037-035-MY3), the Ministry of Science and Technology (MOST 103-2320-B-037-006-MY3 and MOST 103-2314-B-037-052), the

DOI: 10.1021/jf504934m
J. Agric. Food Chem. 2015, 63, 1730−1738

Excellence for Cancer Research Center Grant, the Ministry of Health and Welfare, Executive Yuan, Taipei, Taiwan (MOHW 103-TD-B-111-05), the Kaohsiung Medical University "Aim for the Top 500 Universities Grant" KMU-DT103008, and the Kaohsiung Medical University "Aim for the Top Universities Grants" KMU-TP103A19 and KMU-TP103A20.

Notes

The authors declare no competing financial interest.

■ ACKNOWLEDGMENTS

We thank the Center for Resources, Research, and Development of Kaohsiung Medical University for its support with the instrumentation.

■ REFERENCES

(1) Swann, J. B.; Smyth, M. J. Immune surveillance of tumors. *J. Clin. Invest.* **2007**, *117*, 1137−1146.

(2) Pinzon-Charry, A.; Maxwell, T.; López, J. A. Dendritic cell dysfunction in cancer: a mechanism for immunosuppression. *Immunol. Cell Biol.* **2005**, *83*, 451−461.

(3) Pyfferoen, L.; Mestdagh, P.; Vergote, K.; De Cabooter, N.; Vandesompele, J.; Lambrecht, B. N.; Vermaelen, K. Y. Lung tumours reprogram pulmonary dendritic cell immunogenicity at the microRNA level. *Int. J. Cancer* **2014**, DOI: 10.1002/ijc.28945.

(4) Obermajer, N.; Muthuswamy, R.; Lesnock, J.; Edwards, R. P.; Kalinski, P. Positive feedback between PGE2 and COX2 redirects the differentiation of human dendritic cells toward stable myeloid-derived suppressor cells. *Blood* **2011**, *118*, 5498−5505.

(5) Zhou, Z.; Li, W.; Song, Y.; Wang, L.; Zhang, K.; Yang, J.; Zhang, W.; Su, H.; Zhang, Y. Growth differentiation factor-15 suppresses maturation and function of dendritic cells and inhibits tumor-specific immune response. *PLoS One* **2013**, *8*, No. e78618.

(6) Kuo, P. L.; Huang, M. S.; Hung, J. Y.; Chou, S. H.; Chiang, S. Y.; Huang, Y. F.; Yang, C. J.; Tsai, M. J.; Chang, W. A.; Hsu, Y. L. Synergistic effect of lung tumor-associated dendritic cell-derived HB-EGF and CXCL5 on cancer progression. *Int. J. Cancer* **2014**, *135*, 96−108.

(7) Kuo, C. H.; Chen, K. F.; Chou, S. H.; Huang, Y. F.; Wu, C. Y.; Cheng, D. E.; Chen, Y. W.; Yang, C. J.; Hung, J. Y.; Huang, M. S. Lung tumor-associated dendritic cell-derived resistin promoted cancer progression by increasing Wolf-Hirschhorn syndrome candidate 1/Twist pathway. *Carcinogenesis* **2013**, *34*, 2600−2609.

(8) Hansen, M. T.; Forst, B.; Cremers, N.; Quagliata, L.; Ambartsumian, N.; Grum-Schwensen, B.; Klingelhöfer, J.; Abdul-Al, A.; Herrmann, P.; Osterland, M.; Stein, U.; Nielsen, G. H.; Scherer, P. E.; Lukanidin, E.; Sleeman, J. P.; Grigorian, M. A link between inflammation and metastasis: serum amyloid A1 and A3 induce metastasis, and are targets of metastasis-inducing S100A4. *Oncogene* **2014**, DOI: 10.1038/onc.2013.568.

(9) Slattery, M. L.; John, E. M.; Torres-Mejia, G.; Lundgreen, A.; Herrick, J. S.; Baumgartner, K. B.; Hines, L. M.; Stern, M. C.; Wolff, R. K. Genetic variation in genes involved in hormones,inflammation and energetic factors and breast cancer risk in an admixed population. *Carcinogenesis* **2012**, *33*, 1512−1521.

(10) Kurihara, T.; Bravo, R. Cloning and functional expression of mCCR2, a murine receptor for the C-C chemokines JE and FIC. *J. Biol. Chem.* **1996**, *271*, 11603−11607.

(11) Chen, K.; Liu, M.; Liu, Y.; Wang, C.; Yoshimura, T.; Gong, W.; Le, Y.; Tessarollo, L.; Wang, J. M. Signal relay by CC chemokine receptor 2 (CCR2) and formylpeptide receptor 2 (Fpr2) in the recruitment of monocyte-derived dendritic cells in allergic airway inflammation. *J. Biol. Chem.* **2013**, *288*, 16262−16273.

(12) Ueno, T.; Toi, M.; Saji, H.; Muta, M.; Bando, H.; Kuroi, K.; Koike, M.; Inadera, H.; Matsushima, K. Significance of macrophage chemoattractant protein-1 in macrophage recruitment, angiogenesis, and survival in human breast cancer. *Clin. Cancer Res.* **2000**, *6*, 3282−3289.

(13) Rahuman, A. A.; Gopalakrishnan, G.; Venkatesan, P.; Geetha, K.; Bagavan, A. Mosquito larvicidal activity of isolated compounds from the rhizome of *Zingiber officinale*. *Phytother. Res.* **2008**, *22*, 1035−1039.

(14) Weng, C. J.; Chou, C. P.; Ho, C. T.; Yen, G. C. Molecular mechanism inhibiting human hepatocarcinoma cell invasion by 6-shogaol and 6-gingerol. *Mol. Nutr. Food Res.* **2012**, *56*, 1304−1314.

(15) Weng, C. J.; Wu, C. F.; Huang, H. W.; Ho, C. T.; Yen, G. C. Anti-invasion effects of 6-shogaol and 6-gingerol, two active components in ginger, on human hepatocarcinoma cells. *Mol. Nutr. Food Res.* **2010**, *54*, 1618−1627.

(16) Shieh, P. C.; Chen, Y. O.; Kuo, D. H.; Chen, F. A.; Tsai, M. L.; Chang, I. S.; Wu, H.; Sang, S.; Ho, C. T.; Pan, M. H. Induction of apoptosis by [8]-shogaol via reactive oxygen species generation, glutathione depletion, and caspase activation in human leukemia cells. *J. Agric. Food Chem.* **2010**, *58*, 3847−3854.

(17) Sang, S.; Hong, J.; Wu, H.; Liu, J.; Yang, C. S.; Pan, M. H.; Badmaev, V.; Ho, C. T. Increased growth inhibitory effects on human cancer cells and anti-inflammatory potency of shogaols from *Zingiber officinale* relative to gingerols. *J. Agric. Food Chem.* **2009**, *57*, 10645−10650.

(18) Pan, M. H.; Hsieh, M. C.; Hsu, P. C.; Ho, S. Y.; Lai, C. S.; Wu, H.; Sang, S.; Ho, C. T. 6-Shogaol suppressed lipopolysaccharide-induced up-expression of iNOS and COX-2 in murine macrophages. *Mol. Nutr. Food Res.* **2008**, *52*, 1467−1477.

(19) Pan, M. H.; Hsieh, M. C.; Kuo, J. M.; Lai, C. S.; Wu, H.; Sang, S.; Ho, C. T. 6-Shogaol induces apoptosis in human colorectal carcinoma cells via ROS production, caspase activation, and GADD 153 expression. *Mol. Nutr. Food Res.* **2008**, *52*, 527−537.

(20) Tsuyada, A.; Chow, A.; Wu, J.; Somlo, G.; Chu, P.; Loera, S.; Luu, T.; Li, A. X.; Wu, X.; Ye, W.; Chen, S.; Zhou, W.; Yu, Y.; Wang, Y. Z.; Ren, X.; Li, H.; Scherle, P.; Kuroki, Y.; Wang, S. E. CCL2 mediates cross-talk between cancer cells and stromal fibroblasts that regulates breast cancer stem cells. *Cancer Res.* **2012**, *72*, 2768−2779.

(21) Xiang, T.; Long, H.; He, L.; Han, X.; Lin, K.; Liang, Z.; Zhuo, W.; Xie, R.; Zhu, B. Interleukin-17 produced by tumor microenvironment promotes self-renewal of CD133(+) cancer stem-like cells in ovarian cancer. *Oncogene* **2013**, DOI: 10.1038/onc.2013.537.

(22) Louie, E.; Chen, X. F.; Coomes, A.; Ji, K.; Tsirka, S.; Chen, E. I. Neurotrophin-3 modulates breast cancer cells and the microenvironment to promote the growth of breast cancer brain metastasis. *Oncogene* **2013**, *32*, 4064−4077.

(23) Watkins, S. K.; Zhu, Z.; Riboldi, E.; Shafer-Weaver, K. A.; Stagliano, K. E.; Sklavos, M. M.; Ambs, S.; Yagita, H.; Hurwitz, A. A. FOXO3 programs tumor-associated DCs to become tolerogenic in human and murine prostate cancer. *J. Clin. Invest.* **2011**, *121*, 1361−1372.

(24) Gottfried, E.; Kunz-Schughart, L. A.; Ebner, S.; Mueller-Klieser, W.; Hoves, S.; Andreesen, R.; Mackensen, A.; Kreutz, M. Tumor-derived lactic acid modulates dendritic cell activation and antigen expression. *Blood* **2006**, *107*, 2013−2021.

(25) Wu, J.; Liu, X.; Wang, Y. Predictive value of preoperative serum CCL2, CCL18, and VEGF for the patients with gastric cancer. *BMC Clin. Pathol.* **2013**, *13*, 15.

(26) Steiner, J. L.; Murphy, E. A. Importance of chemokine (CC-motif) ligand 2 in breast cancer. *Int. J. Biol. Markers* **2012**, *27*, e179−e185.

(27) Zhang, X. W.; Qin, X.; Qin, C. Y.; Yin, Y. L.; Chen, Y.; Zhu, H. L. Expression of monocyte chemoattractant protein-1 and CC chemokine receptor 2 in non-small cell lung cancer and its significance. *Cancer Immunol. Immunother.* **2013**, *62*, 563−570.

(28) Li, X.; Xu, Q.; Wu, Y.; Li, J.; Tang, D.; Han, L.; Fan, Q. A CCL2/ROS autoregulation loop is critical for cancer-associated fibroblasts-enhanced tumor growth of oral squamous cell carcinoma. *Carcinogenesis* **2014**, *35*, 1362−1370.

(29) Lin, T. H.; Liu, H. H.; Tsai, T. H.; Chen, C. C.; Hsieh, T. F.; Lee, S. S.; Lee, Y. J.; Chen, W. C.; Tang, C. H. CCL2 increases $\alpha v\beta 3$ integrin expression and subsequently promotes prostate cancer migration. *Biochim. Biophys. Acta* **2013**, *1830*, 4917−4927.

(30) Arendt, L. M.; McCready, J.; Keller, P. J.; Baker, D. D.; Naber, S. P.; Seewaldt, V.; Kuperwasser, C. Obesity promotes breast cancer by CCL2-mediated macrophage recruitment and angiogenesis. *Cancer Res.* **2013**, *73*, 6080−6093.
(31) van Deventer, H. W.; Palmieri, D. A.; Wu, Q. P.; McCook, E. C.; Serody, J. S. Circulating fibrocytes prepare the lung for cancer metastasis by recruiting Ly-6C+ monocytes via CCL2. *J. Immunol.* **2013**, *190*, 4861−4867.
(32) Kudo-Saito, C.; Shirako, H.; Ohike, M.; Tsukamoto, N.; Kawakami, Y. CCL2 is critical for immunosuppression to promote cancer metastasis. *Clin. Exp. Metastasis* **2013**, *30*, 393−405.
(33) Fukuda, A.; Wang, S. C.; Morris, J. P., 4th; Folias, A. E.; Liou, A.; Kim, G. E.; Akira, S.; Boucher, K. M.; Firpo, M. A.; Mulvihill, S. J.; Hebrok, M. Stat3 and MMP7 contribute to pancreatic ductal adenocarcinoma initiation and progression. *Cancer Cell* **2011**, *19*, 441−455.
(34) Vasquez-Dunddel, D.; Pan, F.; Zeng, Q.; Gorbounov, M.; Albesiano, E.; Fu, J.; Blosser, R. L.; Tam, A. J.; Bruno, T.; Zhang, H.; Pardoll, D.; Kim, Y. STAT3 regulates arginase-I inmyeloid-derived suppressor cells from cancer patients. *J. Clin. Invest.* **2013**, *123*, 1580−1589.
(35) Sanseverino, I.; Purificato, C.; Varano, B.; Conti, L.; Gessani, S.; Gauzzi, M. C. STAT3-silenced human dendritic cells have an enhanced ability to prime IFNγ production by both $\alpha\beta$ and $\gamma\delta$ T lymphocytes. *Immunobiology* **2014**, *219*, 503−511.

DOI: 10.1021/jf504934m
J. Agric. Food Chem. 2015, 63, 1730−1738

Scheme 1. Synthesis of F3-A

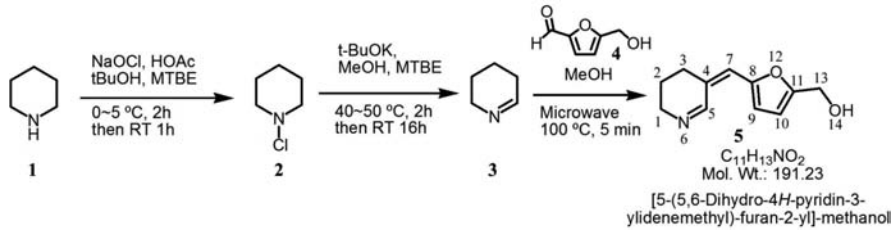

MATERIALS AND METHODS

Preparation and Separation of [5-(5,6-Dihydro-4*H*-pyridin-3-ylidenemethyl)furan-2-yl]methanol (F3-A). We repeated our original MR protocol to recover F3-A from a heated aqueous Glc-Lys MR mixture.[4] Briefly, D-glucose (0.8 mol/L) was mixed with L-lysine monohydrochlide (0.8 mol/L) in 100 mL of ddH_2O and adjusted to pH 7. The mixtures were autoclaved (Laboratory VMP, Cliton, NJ) at 121 °C for 60 min in screw-capped glass bottles and then rapidly chilled on ice and centrifuged at 3400×*g*. In a preliminary experiment to increase the yield of F3-A on extraction, MR mixtures were adjusted to pH 2, 6, and 12, respectively, and then extracted with chloroform. We found that F3-A was recovered in the chloroform fraction at a higher amount when the pH was adjusted to 12. Therefore, in the following experiment, the supernatant was adjusted to pH 12 using sodium hydroxide, followed by extraction with chloroform, three times using a 2:1 (v/v) ratio. Pooled chloroform fractions were collected and evaporated under reduced pressure using a rotary evaporator. The concentrated sample (around 1 g) was redissolved in 10 mL of dichloromethane (DCM) and loaded onto a glass column (3 × 25 cm) packed with 50 g of silica gel (32−63 μm, 230−400 mesh, Selecto Scientific, Georgia). The column was sequentially eluted with 200 mL of DCM, 90% DCM/10% MeOH, 80% DCM/20% MeOH, 70% DCM/30% MeOH, and 60% DCM/40% MeOH, respectively, using flash chromatography. Eluents (20 mL/per tube) were collected, and the presence of F3-A in the eluent was detected using both analytical thin layer chromatography (TLC) and HPLC. TLC was performed using aluminum plates precoated with silica gel 60F-254 (EMD Millipore Corporation, Billerica, MA). Plates were developed in DCM:MeOH (8:2, v/v) mixture and air-dried. F3-A with a retention factor (Rf) of 0.53 on the plate was visualized using a $KMnO_4$ staining solution, followed by air drying. The eluent containing F3-A collected from the silica column was combined and evaporated under vacuum. The concentrated crude extract was reloaded onto a newly prepared silica gel column and eluted with 100 mL of dichloromethane, 200 mL of 90% DCM/10% MeOH, 300 mL of 80% DCM/20% MeOH, and 100 mL of 70% DCM/30% MeOH, respectively. TLC analysis identified tube 19 containing F3-A which was used for NMR and high-resolution mass spectrometry analysis. This fraction was named F3-AC19. Purity of F3-A in the F3-AC19 fraction was greater than 95%, as determined by NMR.

Synthesis of [5-(5,6-Dihydro-4*H*-pyridin-3-ylidenemethyl)-furan-2-yl]methanol (F3-A). Scheme 1 shows the procedures to synthesize intermediate compounds and F3-A.

*N-Chloropiperidine (**2**).* In a 500 mL, 3-neck round-bottom flask was added methyl *tert*-butyl ether (MTBE, 160 mL), piperidine (5 mL, 50 mmol), and *t*-BuOH (2.4 mL, 25 mmol). The solution was cooled to 0 °C in an ice/water bath. Bleach (active ingredient NaOCl, nominal 5% active chlorine, 0.5 M, 110 mL) and acetic acid (3.2 mL, diluted with 3.2 mL of water) were added simultaneously from two dropping funnels, at a rate that maintained internal temperature below 10 °C. The mixture was stirred at 0 °C for 1 h, and the organic phase was separated leaving the aqueous phase which was extracted with MTBE (100 mL). The combined organic fractions were dried with Na_2SO_4 and filtered. This solution was used in the next step without isolation or purification.

*1,2-Dehydropiperidine (**3**).* To the above filtrate kept at 0 °C in an ice/water bath was added solid *t*-BuOK (11.2 g, 100 mmol) in one batch, followed by MeOH (80 mL, in 10−20 mL portions). The mixture was heated in a warm water bath (∼50 °C) for 2 h and then cooled in an ice/water bath overnight. The mixture was diluted with water to dissolve solids, and the aqueous layer was then extracted twice with MTBE (100 mL). The combined organic phases were dried with Na_2SO_4 and concentrated by rotary evaporation to yield an oily, pale yellow residue, 1,2-dehydropiperidine (dHP, **3**, ∼4 g). This crude material was stored in a −20 °C freezer and used in the next step without further purification.

*[5-(5,6-Dihydro-4H-pyridin-3-ylidenemethyl)-furan-2-yl]-methanol (**5**).* HMF (**4**, 160 mg, 1.3 mmol) was dissolved in MeOH (500 μL) in a BioTage 0.5−2 mL microwave vial, and dHP (**3**, 300 mg, 3.6 mmol) was added. The vessel was sealed and irradiated using microwave set at 100 °C for 5 min. In a separate reaction, HMF (**4**, 260 mg, 2.1 mmol) and dHP (**3**, 500 mg, 6.0 mmol) were reacted in the same manner. The two runs were combined and purified by dry-loading flash chromatography on a SiliCycle SiliaSep-HP 12 g cartridge performed on a BioTae Isolera instrument using a 2−20% MeOH/DCM linear gradient as the eluent. Fractions with significant 370 nm absorption were pooled and concentrated to thick oil, which solidified upon standing. Trituration in MTBE (∼2 mL) gave a crystalline powder that was filtered and washed with MTBE (total ∼10 mL in 3 portions). Drying on high vacuum at room temperature gave F3-A (**5**) as light brown powder, 186 mg (yield 29.2%). The synthesized F3-A was named F3-AS. ^{1}H NMR (500 MHz, DMSO) δ: 7.92 (s, 1 H), 6.62 (d, J = 3.3 Hz, 1 H), 6.53 (s, 1 H), 6.43 (d, J = 3.3 Hz, 1 H), 5.31 (s, 1 H), 4.42 (s, 2 H), 3.54 (td, J = 5.6, 1.8 Hz, 2 H), 3.33 (s, 4 H), 2.66 (td, J = 6.8, 1.9 Hz, 2 H), 1.74−1.49 (m, 2 H) ppm. ^{13}C NMR (126 MHz, DMSO) δ: 161.85, 156.97, 150.97, 128.29, 122.29, 114.23, 109.47, 55.77, 48.67, 24.28, 20.78 ppm.

Determination of Optimal Reaction Conditions for F3-A Production Using Taguchi Orthogonal Design. A four-factor /four-level (L16 (4^4)) Taguchi orthogonal array (Table 1) was chosen

Table 1. Taguchi Orthogonal Array and F3-A and HMF Yield[a]

exp. no.	S:AA ratio	pH	T (°C)	t (min)	F3-A (μg/g)	HMF (μg/g)
1	0.5:1	5	70	30	ND[b]	ND
2	0.5:1	6	80	60	ND	ND
3	0.5:1	7	90	90	0.3 ± 0.0	3.1 ± 1.8
4	0.5:1	8	100	120	ND	ND
5	1:1	5	80	90	ND	ND
6	1:1	6	70	120	ND	ND
7	1:1	7	100	30	ND	0.7 ± 0.2
8	1:1	8	90	60	0.9 ± 0.3	8.5 ± 2.3
9	2:1	5	90	120	5.7 ± 2.5	9.1 ± 3.9
10	2:1	6	100	90	11.1 ± 3.3	4.9 ± 1.6
11	2:1	7	70	60	ND	0.4 ± 0.1
12	2:1	8	80	30	ND	ND
13	3:1	5	100	60	0.7 ± 0.3	2.5 ± 0.9
14	3:1	6	90	30	ND	0.1 ± 0.0
15	3:1	7	80	120	0.9 ± 0.2	4.1 ± 0.8
16	3:1	8	70	90	ND	1.8 ± 0.5

[a]S:AA ratio, sugar:amino acid ratio; T, temperature (°C); t, heating time (min). [b]ND, not detectable.

DOI: 10.1021/jf505579m
J. Agric. Food Chem. 2015, 63, 1739−1746

to investigate the effects of four different reaction conditions including sugar:amino acid ratio, pH, heating temperature, and heating time on the yield of F3-A in a Glc-Lys MR mixture. The experiments were performed in triplicate over three concessive days. Glucose was mixed with L-lysine (0.8 mol/L) at sugar to amino acid ratios (mole ratio) of 0.5:1, 1:1, 2:1, or 3:1 in ddH_2O, and pH was adjusted to 5, 6, 7, or 8, respectively, using concentrated HCl. The mixtures (100 mL) were put in capped glass bottles and heated in an oven (Blue M electronic company, Blue Island, IL) at 70, 80, 90, or 100 °C, for 30, 60, 90, or 120 min time periods, respectively, after which they were rapidly chilled on ice. An aliquot (15 mL) of sample was stored at −20 °C for further analysis, and the remainder was freeze-dried.

Effects of Reactants and Concentration and Heating Time on the Yield of F3-A. According to the optimal conditions from Taguchi design, glucose was mixed with L-lysine at sugar to amino acid (S:AA) mole ratios of 0.2:0.1, 0.4:0.2, 0.8:0.4, or 1.6:0.8 in distilled deionized water, and the pH was adjusted to 6 using 1 N HCl. The mixtures were heated at 100 °C for 1.5, 3, 6, 9, 12, and 24 h, respectively, in an oven (Blue M electronic company, Blue Island, IL) and then rapidly chilled on ice. The yield of F3-A was measured using HPLC, and F3-AS was used as standard. To determine if specific sugars produced relatively greater F3-A, we also compared yield derived from fructose, glucose, sucrose, and lactose (1.6 mol/L), respectively, mixed with lysine (0.8 mol/L) at an adjusted pH 6. The mixtures were heated at 100 °C for 4 h, and the yield of F3-A was measured using HPLC.

HPLC Analysis. F3-A was detected by analytical reverse phase HPLC using an Agilent 1100 LC system (Agilent, Santa Clara, CA) equipped with a Zorbax SB-C18 column (4.6 × 150 mm, 3.5 μm, Agilent, U.S.A.) and monitored with a diode array detector (DAD) at 370 and 385 nm. A linear gradient comprised of 5−20% MeOH/0.2% formic acid delivered at a flow rate of 1 mL/min for 6 min was used to separate the sample components. The column temperature was set at 30 °C.

FTIR and UV−Vis Spectrophotometry Analysis. F3-AC19 and F3-AS were dissolved in methanol, and Fourier transform infrared spectroscopy (FTIR) spectrum on both samples was measured by PerkinElmer Spectrum 100 FTIR spectrometer with a horizontal attenuated total reflectance (HATR) sampling accessory. For ultraviolet−visible (UV−vis) spectrophotometry, F3-AC19 and F3-AS were dissolved in MeOH or 0.002% formic acid/ddH_2O at a concentration of 0.02 mg/mL, respectively. UV-vis spectrum 200−700 nm was recorded using a spectrophotometer (Multiskan Ascent, Thermo-Labsystems, Finland).

HRMS. High-resolution mass spectrometry (HRMS) of F3-AC19 was conducted using a Bruker maXis Impact Ultra-High Resolution tandem time-of-flight (UHR-Qq-TOF) mass spectrometer, and the data was acquired using Compass 1.5 software. The MS condition was set as follows: ionization mode, positive electrospray ionization (+ESI), gas temperature, 180 °C; gas flow, 8 L/min, nebulizer, 2 bar; capillary voltage: 3800 V; mass scanning range, 50−1500 Da. For MS/MS, nitrogen was used as the collision gas, collision energy was 35 eV, and sodium formate was the accurate mass calibrant.

NMR. ^1H and ^{13}C NMR spectra were recorded with a Bruker Avance III 600 MHz spectrometer using a QNP Cryoprobe. NMR data processing was performed with Topspin3.1 software The spectra were referenced to the corresponding solvent signals.[12]

Cell Culture. Caco-2 cells (HTB-37, ATCC) were cultured in complete Minimum Essential Medium (MEM) containing Earle's salts and supplemented with 10% FBS (Invitrogen, Canada) and 100 units/mL of penicillin and 100 μg/mL of streptomycin (Sigma, St. Louis, MO). Cells were incubated at 37 °C under a 5% CO_2 atm. The medium was changed every 2−3 days. Caco-2 cells were subcultured weekly.

NO Inhibitory Activity in Caco-2 Cell. NO in Caco-2 cells was measured using the conditions reported by Chen and Kitts (2008).[11] Caco-2 cells seeded on 96-well plates (Sarstedt, Nümbrecht, Germany) at a density of 10^5 cells/cm^2 in complete MEM (100 μL) were cultured for 3 weeks. The fully differentiated Caco-2 cells were supplied with fresh MEM without FBS and incubated with, or without, experimental samples for 1 h followed by a treatment of inducer which consisted of 8000 U/mL IFN-γ + 0.1 μg/mL PMA for 48 h. NO levels in the culture medium were determined using the Griess reagent (50 μL of 1% sulfanilamide in 5% phosphoric acid and 50 μL of 0.1% *N*-(1-naphthyl)ethylenediamine dihydrochloride) after reducing nitrate to nitrite with nitrate reductase (Sigma, St. Louis, MO). The color change was measured by a spectrophotometer (Multiskan Ascent, ThermoLabsystems, Finland) at 540 nm. Nitrite and nitrate levels were determined using sodium nitrate as the standard. Percent inhibition was calculated using the following equation

$$(NO_{st} - NO_{sample})/(NO_{st} - NO_{blank}) \times 100\%$$

where NO_{st} is the NO concentration of the cell supernatant incubated with inducer; NO_{blank} is the NO concentration of the cell supernatant without samples and inducer; NO_{sample} is the NO concentration of cells incubated with samples and inducer.

Cell Viability. The cell viability was tested using MTT (3-(4,5-dimethylthiazol-2-yl)-2,5-diphenyltetrazolium bromide, Sigma, St. Louis, MO) assay described by Chen and Kitts.[4] After cells were treated with sample and inducer, they were then incubated with 0.5 mg/mL MTT in complete MEM for 4 h, followed by an overnight incubation with 10% sodium dodecyl sulfate (SDS). Absorbance was read at 570 nm using a spectrophotometer (Multiskan Ascent, Thermo Labsystems, Helsinki, Finland).

RESULTS AND DISCUSSION

Effects of Reaction Conditions and Type of Reactants on the Yield of F3-A. In order to increase the yield of F3-A, two steps were performed to optimize the reaction conditions. First, a Taguchi design was used to determine the sugar to amino acid ratio, pH, temperature, and heating time. Previously, we have used Taguchi design to successfully optimize the inducers for NO production in differentiated Caco-2 cells[11] and to define the coculture conditions for Caco-2 and HT29-MTX cells.[13] Herein, a four-factor/four-level

Table 2. Yield (μg/g) of F3-A in Glc-Lys with Different Concentration and Heating Time[a]

	S:AA[b](mol/L: mol/L)			
time (h)	0.2:0.1	0.4:0.2	0.8:0.4	1.6:0.8
1.5	ND$^{A\alpha}$	ND$^{A\alpha}$	ND$^{A\alpha}$	9 ± 0$^{A\beta}$
3	2 ± 1$^{A\alpha}$	6 ± 0$^{A\alpha}$	50 ± 8$^{A\alpha}$	392 ± 90$^{A\beta}$
6	5 ± 1$^{A\alpha}$	25 ± 5$^{A\alpha}$	147 ± 7$^{A\alpha}$	4560 ± 602$^{A\beta}$
9	28 ± 4$^{B\alpha}$	80 ± 5$^{B\alpha}$	527 ± 49$^{B\alpha}$	9682 ± 395$^{D\beta}$
12	43 ± 8$^{C\alpha}$	226 ± 33$^{C\alpha}$	3558 ± 369$^{B\beta}$	11115 ± 484$^{E\gamma}$
24	96 ± 1$^{D\alpha}$	389 ± 19$^{D\alpha}$	11807 ± 154$^{C\beta}$	6789 ± 672$^{C\beta}$

[a]All samples were adjusted to pH 6 and heated at 100 °C. Superscripts with different letters (A−E) denote significantly different ($P < 0.05$) in the same column. Superscripts ($\alpha\beta\gamma$) with different letters denotes significantly different ($P < 0.05$) in the same row. [b]S:AA ratio, sugar:amino acid ratio.

Table 3. Effects of Type of Sugar on the Yield (μg/g) of F3-A[a]

models	yield (μg/g)[b]
Lac-Lys	104 ± 7^B
Suc-Lys	32 ± 1^A
Fru-Lys	363 ± 1^C
Glu-Lys	2286 ± 26^D

[a]Sugar (1.6 mol/L) and lysine (0.8 mol/L) mixtures were adjusted to pH 6 and heated at 100 °C for 4 h. [b]Superscripts (A−D) with different letters denotes significantly different ($P < 0.05$) in the same column.

DOI: 10.1021/jf505579m
J. Agric. Food Chem. 2015, 63, 1739−1746

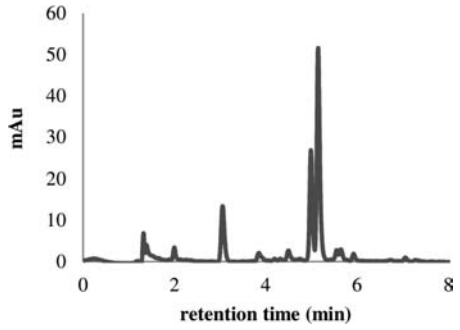

Figure 1. HPLC profile of Glc-Lys heated mixture monitored at 370 nm.

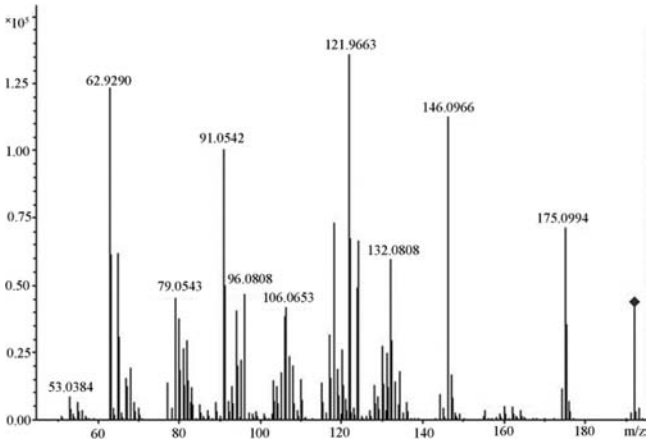

Figure 2. HRMS spectrum of F3-A.

Table 4. NMR Data of F3-A

position	δ_c	δ_H (m, J in Hz)
1	48.72	3.65 (2H, t, J = 5.94)
2	20.84	1.77 (2H, m)
3	24.61	2.75 (2H, t, J = 6.61)
4	128.45	
5	163.35	7.90 (1H, s)
7	124.23	6.46 (1H, d, J = 2.08)
8	151.78	
9	114.61	6.54 (1H, d, J = 3.36)
10	110.20	6.44 (1H, d, J = 3.42)
11	156.35	
13	57.23	4.66 (2H, s)
14		4.01 (1H, s)

(L16) Taguchi design (Table 1) which includes 16 experiments in the orthogonal array was used to investigate the effects of four levels of the four reaction conditions (control factors) including S:AA ratio, pH, temperature, and heating time on F3-A production in glucose and lysine aqueous mixtures. Within the multiple conditions tested, F3-A concentration ranged from undetectable amounts to 11.1 ± 3.3 (μg/g) (Table 1). From the ANOVA table, the relative impact of the different factors tested to affect production of F3-A followed in descending order: sugar:amino acid (S:AA) ratio < temperature (T) < heating time (t) < pH. The optimal conditions for producing F3-A were determined to be S:AA ratio = 2:1, T = 100 °C, t = 90 min, pH = 6. The production of F3-A precursor, HMF, was also measured. The amount of HMF was positively significantly (P = 0.023) correlated with the yield of F3-A.

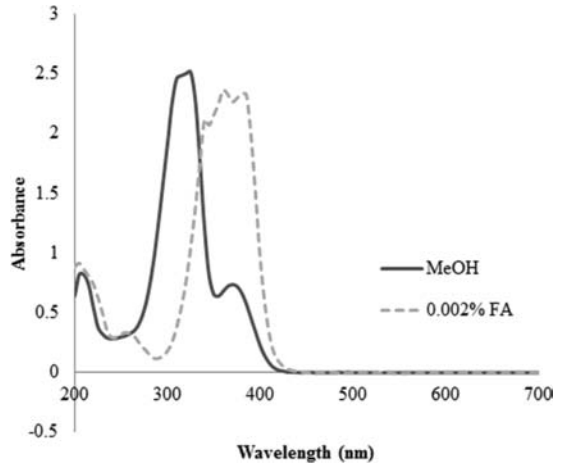

Figure 3. UV−vis spectrum of F3-A in MeOH and 0.002% formic acid at a concentration of 0.02 mg/mL.

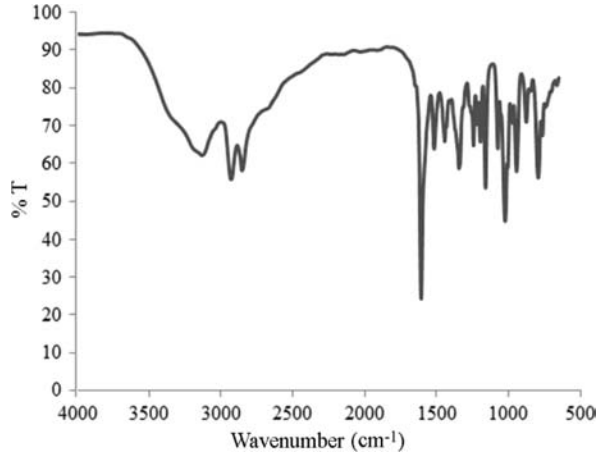

Figure 4. FTIR spectrum of F3-A.

Since the yield of F3-A was still low using conditions obtained from Taguchi design, in the second step, we held constant temperature, pH, and reactant ratio conditions that were obtained from the Taguchi design and varied the reactant concentration and the heating time, using a factorial design. The yield of F3-A from Glc-Lys mixture decreased as the reactant concentration was lowered, when keeping the molar ratio the same (Table 2). In general, more F3-A was produced when heating time was increased to 24 h. One exception existed when the sugar:amino acid ratio of 1.6:0.8 (mol/L: mol/L) was used; however, we attribute this to the gel like precipitates that were formed when reactants at these concentrations were heated for 24 h. Therefore, the optimal conditions used are Glc:Lys ratio set at 1.6:0.8 (mol/L: mol/L) and a heating duration of 12 h. The yield of F3-A increased more than 1000-fold when the Glu-Lys mixture (1.6:0.8, mol/L: mol/L) was heated for 12 h, compared to shorter heating times (e.g., 1.5 h).

In order to show the effects of various sugar types on the yield of F3-A, we conducted F3-A recovery experiments using fructose, glucose, lactose, and sucrose, respectively. Hence, hexoses or disaccharides comprised of hexose, known to generate HMF during heating and involving MR or caramelizing, were found to be necessary precursors to produce F3-A. Monosaccharides had a significantly (P < 0.05) greater affinity to produce F3-A compared to disaccharides containing hexose

DOI: 10.1021/jf505579m
J. Agric. Food Chem. 2015, 63, 1739−1746

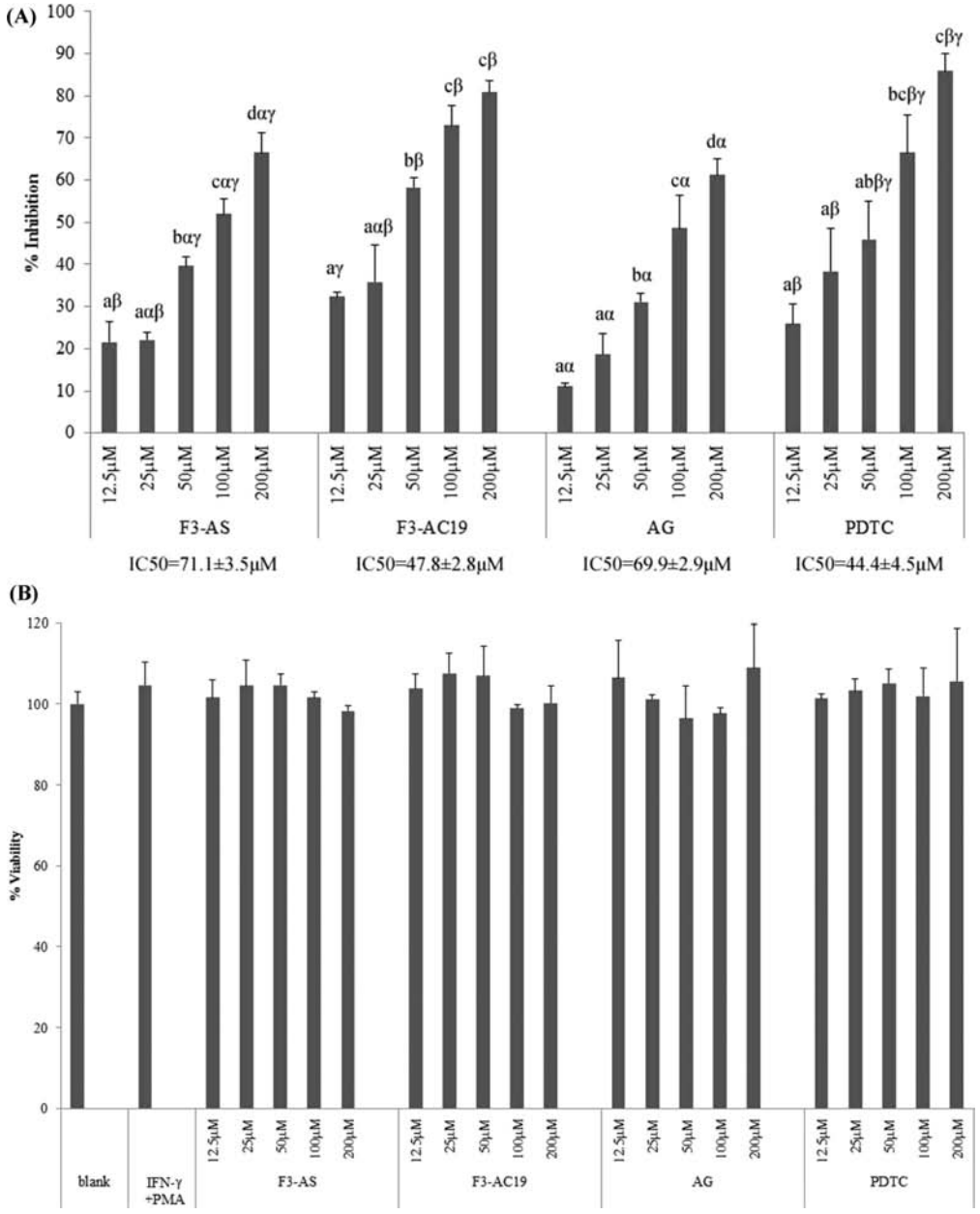

Figure 5. NO inhibitory (A) and cell viability (B) effects of F3-AS, F3-AC19, AG, and PDTC on Caco-2 cells. F3-AS: synthetic F3-A; F3-AC19: isolated F3-A from Glu-Lys MR mixture.

(Table 3). Nonenzymatic browning of aldohexoses in the presence of lysine has been reported to occur faster than that of ketohexoses in similar heat-processed, aqueous model systems.[14−16] This would explain the relatively higher production of F3-A from the glucose than the fructose MR model. Sucrose itself is a nonreducing sugar; hence, without hydrolysis there should not be a Maillard sugar−amino acid interaction. The fact that we detected a trace amount of F3-A from sucrose, compared to lactose, a reducing disaccharide, indicates sucrose hydrolyzed to glucose and fructose at 100 °C under pH 6. Results of Buera et al. (1987)[17] confirm this with their report that 10% hydrolysis of sucrose occurred when heated at 55 °C at pH 6 and produced yellow-brownish products. Alternatively, degradation of sucrose occurring with caramelizing will also result in HMF formation.[18] However, Lee and Nagy (1990)[19] showed that the rate of HMF formation in fructose is much faster than in sucrose followed by glucose when sugars were heated 50 °C under pH 3.5. The presence of amino acid increased HMF formation rate for glucose but not sucrose. Our results indicated that the production of F3-A precursor, HMF, is faster in glucose and lysine MR models than that of fructose and sucrose in our experimental conditions, the ultimate outcome being a higher F3-A production from glucose models.

Proposed Reaction Route for Synthesis of F3-A. We found that the chemical synthesis of F3-A favored acidic conditions and that both the alpha and epsilon amino groups of lysine were involved in the reaction.[20] A possible route for F3-A production in Glc-Lys can therefore be related to the production of HMF and reaction with compound **3**, 1,2-dehydropiperidine.[21] HMF is formed via various pathways, including the aldo−keto isomerization of aldohexose, followed by the dehydration of furanose tautomers,[22] decomposition from 3-deoxyhexosone produced by MR or by carameliza-

DOI: 10.1021/jf505579m
J. Agric. Food Chem. 2015, 63, 1739−1746

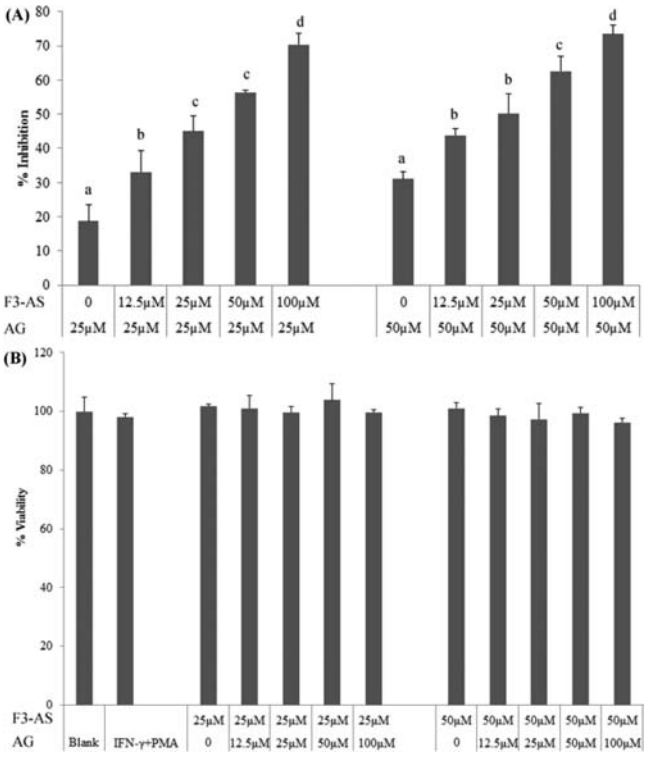

Figure 6. NO inhibitory and cell viability effects of AG supplement with F3-AS in Caco-2 cell. F3-AS: synthetic F3-A.

tion,[18,23] or methylglyoxal recombination with glyceraldehyde.[24] Under acidic conditions, glucose is isomerized to fructose through Lobry de Bruyn–Alberda van Ekenstein transformation, followed by three dehydration steps to produce HMF.[25] First, the furanose ring at C5 loses one H_2O molecule to form fructofuranosyl oxocation; this is followed by enolization to the enol of 2,5-anhydro-D-mannose after loss of a proton. Second, the second H_2O molecule is released to form a double bond in the furan ring. An additional H_2O molecule is lost to form HMF.[26] At pH 7, or acidic conditions, the Amadori product in Glc-Lys MR mixture undergoes 1,2-enolization to produce HMF.[27] L-Lysine also undergoes Strecker degradation during MR to produce 5-aminopentanal which can be cyclized to 1,2-dehydropiperidine. HMF and 1,2-dehydropiperidine undergo aldo condensation and dehydration to form F3-A.[21]

Chemical Properties and Chemical Structure of [5-(5,6-Dihydro-4*H*-pyridin-3-ylidenemethyl)-furan-2-yl]-methanol. The HPLC profile of Glc-Lys heated mixture is shown in Figure 1. The retention time of F3-A was 5.15 min. The accurate mass data for F3-A (Figure 2) gave a signal that corresponded to the protonated form of the compound at m/z 192.1021 Da with major fragments including m/z 175.0994, 146.0966, 121.9663, 91.0542, and 62.9290 Da. Most of the error values are within ±5 ppm except for a few fragment ions, thus confirming a formula $C_{11}H_{13}NO_2$. The unusual large number of fragment ions and the presence of multiple signals in one nominal mass such as m/z 123.0676 and 123.0441 are evidence of the m/z 192.1021 ion undergoing complex rearrangements in the fragmentation processes.

Small amounts of F3-AC19 were dissolved in CD_3OD; ^1H, ^{13}C, COSY, ^{13}C-APT, HSQC, and HMBC-NMR experiments were performed. The NMR data along with the molecular formula ($C_{11}H_{13}NO_2$) derived from the MS results were input in CMC-se software (version 2.0.10) for possible chemical structures which were ranked based on observed correlations and chemical shift predictions. The chemical shift and ^1H and ^{13}C NMR spectrum are shown in Table 4. After manual verification, F3-AC19 was identified as [5-(5,6-dihydro-4*H*-pyridin-3-ylidenemethyl)-furan-2-yl]methanol. The compound has a root-mean-square (rms) deviation of 4.6 ppm, indicating a good match between both proposed and actual chemical structures. This compound was also synthesized as described previously, and the ^1H and ^{13}C spectra were compared with the isolated compounds. The results confirmed that F3-AS and F3-AC19 had the same structure.

F3-A is easily soluble in MeOH and acidic ddH_2O. When dissolved in MeOH, F3-A gave two major absorbance peaks at 315 and 370 nm, with maximum absorbance peak occurring at 315 nm (Figure 3). Under acidic condition, the maximum absorbance (λ_{max}) of F3-A shifted to a higher wavelength (370 nm). This result indicated that protonation increased the solubility of F3-A in H_2O and therefore might have also caused the rearrangement of double bond resulting in the red shift of λ_{max}. In previous work, Totsuka et. al[28] and Miller et. al[20] identified F3-A from HMF-Lys and Glc-Lys MR models, respectively. The physiochemical properties, FTIR (Figure 4), MS, and NMR data of separated and synthesized compounds were identical in our experiments and similar to previous work.

NO Inhibitory Effects in Caco-2 Cells. The NO inhibitory effects of separated F3-AC19 and synthesized F3-AS were tested using Caco-2 cells. A NO inhibitor AG and a NF-κB inhibitor PDTC were chosen to compare the NO inhibitory effect with our samples. F3-AC19 and F3-AS both produced a dose dependent inhibition of NO production in Caco-2 cells (Figure 5 A) with an IC50 = 47.8 ± 2.8 and 71.1 ± 3.5 μmol/L, respectively. The cell viabilities of all treatments were comparable to the untreated cells (Figure 5 B). The IC50 of F3-AC19 was significantly ($P < 0.05$) lower than that of F3-AS, indicating that the isolated F3-AC19 had higher NO inhibitory affinity than the synthesized sample. We attribute this result to the possible trace amounts of other MRPs in F3-AC19 that could contribute to a higher NO inhibitory capacity. F3-A can exist at both Z and E configurations; thus, in aqueous conditions the isomers interconvert. It is possible that one of the configurations has a relatively higher activity than the other, and the production and separation process for F3-AC19 from Glc-Lys MR model possible tended to produce the isomer with a characteristically higher NO inhibitory activity. Of particular importance was the observation that the IC50 of F3-AS was similar to that of AG and that the IC50 of F3-AC19 was also equivalent to that of PDTC. AG is a selective iNOS inhibitor that prevents NO and iNOS synthesis in IFN-γ + PMA induced Caco-2 cells.[11] PDTC, a NF-κB inhibitor, prevents NF-κB activation, thus inhibiting both NO and iNOS in activated Caco-2 cells.[29] The results described herein indicate that F3-A has a similar NO inhibitory capacity to that of the iNOS and NF-κB inhibitors in inflamed Caco-2 cells. When the synthetic F3-A was coincubated with AG, it showed an additive NO inhibitory effect in Caco-2 cells (Figure 6), thereby further indicating that F3-A could be useful to increase activity of known anti-inflammation drugs.

Previous studies from our laboratory have reported that a fraction (F3) composed of small molecular weight components derived from a Glc-Lys MR mixture was effective at inhibiting inflammatory reactions in Caco-2 cells induced by IFN-γ and PMA cocktail.[5,6] Anti-inflammatory activity of F-3 was shown

DOI: 10.1021/jf505579m
J. Agric. Food Chem. 2015, 63, 1739−1746

to be mediated through iNOS inhibition and down regulation of genes in NF-κB signaling;[5] these activities correspond to NO inhibition. This study has elucidated the structure of the bioactive component present in F3, being [5-(5,6-dihydro-4*H*-pyridin-3-ylidenemethyl)-furan-2-yl]methanol, which was active at inhibiting NO in inflamed Caco-2 cells. We also found that process variables that influenced the yield of F3-A from a heated aqueous Glc-Lys reaction were lower pH and higher reactant concentration. Moreover, MR models comprised of aldohexose produce a higher amount of F3-A compared to ketohexose and disaccharides. The relative anti-inflammatory potency of F3-A corresponded to similar activity observed with AG, a selective iNOS inhibitor, and also PDTC, a Nf-κB inhibitor, both of which are involved in iNOS and NO inhibition.

AUTHOR INFORMATION

Corresponding Author

*Tel.: 1-604-822-5560. Fax: 1-604-822-5143. E-mail: david.kitts@ubc.ca.

Funding

This work was supported by a NSERC-discovery grant to D.D.K.

Notes

The authors declare no competing financial interest.

ABBREVIATIONS USED

AG, aminoguanidine; APT, attached proton test; COSY, correlation spectroscopy; COX-2, cyclooxygenase-2; DAD, diode array detector; DCM, dichloromethane; dHP, 1,2-dehydropiperidine; ESI, electrospray ionization; FTIR, Fourier transform infrared spectroscopy; Glc, glucose; HATR, horizontal attenuated total reflectance; HMBC, heteronuclear multiple bond correlation; HMF, 5-hydroxymethyl-2-furfural; HMFA, 5-hydroxymethyl-2-furoic acid; HPLC, high-perform-anc liquid chromatography; HRMS, high-resolution mass spectrometry; HSQC, heteronuclear single quantum coherence; IBD, inflammatory bowel diseases; IFN-γ, interferon-γ; iNOS, inducible nitric oxide synthase; Lys, lysine; 3-MCP, 3-methyl-1,2-cyclopentanedione; MEM, minimum essential medium; MR, Maillard reaction; MRPs, Maillard reaction products; MTBE, methyl *tert*-butyl ether; MTT, 3-(4,5-dimethylthiazol-2-yl)-2,5-diphenyltetrazolium bromide; Nf-κB, nuclear factor-kappa B; NMR, nuclear magnetic resonance; NO, nitric oxide; PDTC, pyrrolidine dithiocarbamate; PMA, phorbol 12-myristate 13-acetate; rms, root-mean-square; RT, room temperature; SDS, sodium dodecyl sulfate; S:AA, sugar:amino acid; TLC, thin layer chromatography; UHR-Qq-TOF, ultrahigh-resolution tandem time-of-flight; UV−vis, ultraviolet−visible

REFERENCES

(1) Tuohy, K. M.; Hinton, D. J. S.; Davies, S. J.; Crabbe, M. J. C.; Gibson, G. R.; Ames, J. M. Metabolism of Maillard reaction products by the human gut microbiota—Implications for health. *Mol. Nutr. Food Res.* **2006**, *50*, 847−857.

(2) Chung, J. H.; Choi, S. Y.; Kim, J. Y.; Kim, D. H.; Lee, J. W.; Choi, J. S.; Chung, H. Y. 3-Methyl-1,2-cyclopentanedione down-regulates age-related NF-kappa B signaling cascade. *J. Agric. Food Chem.* **2007**, *55*, 6787−6792.

(3) Jin, P.; Kim, J. A.; Choi, D. Y.; Lee, Y. J.; Jung, H. S.; Hong, J. T. Anti-inflammatory and anti-amyloidogenic effects of a small molecule, 2,4-bis(*p*-hydroxyphenyl)-2-butenal in Tg2576 Alzheimer's disease mice model. *J. Neuroinflammation* **2013**, *10*, 2.

(4) Chen, X. M.; Kitts, D. D. Antioxidant and anti-inflammatory activities of Maillard reaction products isolated from sugar−amino acid model systems. *J. Agric. Food Chem.* **2011**, *59*, 11294−11303.

(5) Chen, X. M.; Kitts, D. D. Characterization of antioxidant and anti-inflammatory activities of bioactive fractions recovered from a glucose−lysine Maillard reaction model system. *Mol. Cell. Biochem.* **2012**, *364*, 147−157.

(6) Kitts, D. D.; Chen, X. M.; Jing, H. Demonstration of antioxidant and anti-inflammatory bioactivities from sugar−amino acid Maillard reaction products. *J. Agric. Food Chem.* **2012**, *60*, 6718−6727.

(7) Alican, I.; Kubes, P. A critical role for nitric oxide in intestinal barrier function and dysfunction. *Am. J. Physiol.: Gastrointest. Liver Physiol.* **1996**, *270*, G225−G237.

(8) Marion, R.; Coeffier, M.; Leplingard, A.; Favennec, L.; Ducrotte, P.; Dechelotte, P. Cytokine-stimulated nitric oxide production and inducible NO-synthase mRNA level in human intestinal cells: Lack of modulation by glutamine. *Clin. Nutr.* **2003**, *22*, 523−528.

(9) Romier, B.; Van De Walle, J.; During, A.; Larondelle, Y.; Schneider, Y. J. Modulation of signalling nuclear factor−kappa B activation pathway by polyphenols in human intestinal Caco-2 cells. *Br. J. Nutr.* **2008**, *100*, 542−551.

(10) Cirillo, C.; Sarnelli, G.; Esposito, G.; Grosso, M.; Petruzzelli, R.; Izzo, P.; Cali, G.; D'Armiento, F. P.; Rocco, A.; Nardone, G.; Iuvone, T.; Steardo, L.; Cuomo, R. Increased mucosal nitric oxide production in ulcerative colitis is mediated in part by the enteroglial-derived S100B protein. *Neurogastroenterol. Motil.* **2009**, *21*, 1209−e112.

(11) Chen, X. M.; Kitts, D. D. Determining conditions for nitric oxide synthesis in Caco-2 cells using Taguchi and factorial experimental designs. *Anal. Biochem.* **2008**, *381*, 185−192.

(12) Gottlieb, H. E.; Kotlyar, V.; Nudelman, A. NMR chemical shifts of common laboratory solvents as trace impurities. *J. Org. Chem.* **1997**, *62*, 7512−7515.

(13) Chen, X. M.; Elisia, I.; Kitts, D. D. Defining conditions for the co-culture of Caco-2 and HT29-MTX cells using Taguchi design. *J. Pharmacol. Toxicol. Methods* **2010**, *61*, 334−342.

(14) Baxter, J. H. Free amino-acid stability in reducing sugar systems. *J. Food Sci.* **1995**, *60*, 405−408.

(15) Hayashi, T.; Namiki, M. Role of sugar fragmentation in an early stage browning of amino−carbonyl reaction of sugar with amino-acid. *Agric. Biol. Chem.* **1986**, *50*, 1965−1970.

(16) Jing, H.; Kitts, D. D. Comparison of the antioxidative and cytotoxic properties of glucose−lysine and fructose−lysine Maillard reaction products. *Food Res. Int.* **2000**, *33*, 509−516.

(17) Buera, M. D.; Chirife, J.; Resnik, S. L.; Wetzler, G. Nonenzymatic browning in liquid model systems of high water activity—Kinetics of color changes due to Maillard reaction between different single sugars and glycine and comparison with caramelization browning. *J. Food Sci.* **1987**, *52*, 1063−1067.

(18) Kroh, L. W. Caramelisation in food and beverages. *Food Chem.* **1994**, *51*, 373−379.

(19) Lee, H. S.; Nagy, S. Relative reactivities of sugars in the formation of 5-hydroxymethylfurfural in sugar−catalyst model systems. *J. Food Process. Preserv.* **1990**, *14*, 171−178.

(20) Miller, R.; Olsson, K.; Pernemalm, P. A. Formation of aromatic-compounds from carbohydrates. 9. Reaction of D-glucose and L-lysine in slightly acidic, aqueous-solution. *Acta Chem. Scand., Ser. B* **1984**, *38*, 689−694.

(21) Miller, R. Synthesis and stereochemistry of (*E*)-5-(3,4,5,6-tetrahydropyrid-3-ylidenemethyl)-2-furanmethanol, a product of the reaction between D-glucose and L-lysine. *Acta Chem. Scand., Ser. B* **1987**, *41*, 208−209.

(22) Mednick, M. L. Acid-base-catalyzed conversion of aldohexose into 5-(hydroxymethyl)-2-furfural. *J. Org. Chem.* **1962**, *27*, 398−&.

(23) Richards, E. L. Non-enzymic browning—Reaction between D-glucose and glycine in the dry state. *Biochem. J.* **1956**, *64*, 639−644.

DOI: 10.1021/jf505579m
J. Agric. Food Chem. 2015, 63, 1739−1746

(24) Cammerer, B.; Wedzicha, B. L.; Kroh, L. W. Nonenzymatic browning reactions of retro-aldol degradation products of carbohydrates. *Eur. Food Res. Technol.* **1999**, *209*, 261−265.
(25) Kowalski, S.; Lukasiewicz, M.; Duda-Chodak, A.; Ziec, G. 5-Hydroxymethyl-2-furfural (HMF) heat-induced formation, occurrence in food and biotransformation—A Review. *Polym. J. Food Nutr. Sci.* **2013**, *63*, 207−225.
(26) Locas, C. P.; Yaylayan, V. A. Origin and mechanistic pathways of formation of the parent furan—A food toxicant. *J. Agric. Food Chem.* **2004**, *52*, 6830−6836.
(27) Martins, S. I. F. S.; Jongen, W. M. F.; van Boekel, M. A. J. S. A review of Maillard reaction in food and implications to kinetic modelling. *Trends Food Sci. Technol.* **2000**, *11*, 364−373.
(28) Totsuka, H.; Tokuzen, K.; Ono, H.; Murata, M. A novel yellow compound and furpipate derivatives formed from furfural or 5-hydroxymethylfurfural in the presence of lysine. *Food Sci. Technol. Res.* **2009**, *15*, 45−50.
(29) Cavicchi, M.; Whittle, B. J. R. Regulation of induction of nitric oxide synthase and the inhibitory actions of dexamethasone in the human intestinal epithelial cell line, Caco-2: Influence of cell differentiation. *Br. J. Pharmacol.* **1999**, *128*, 705−715.

DOI: 10.1021/jf505579m
J. Agric. Food Chem. 2015, 63, 1739−1746

have been reported since GSH was first quantified in grapes in 1989.[25] This may be because the food sample matrix is too complicated and needs laborious pretreatment procedures. Moreover, due to the easy autoxidation of GSH during the pretreatment, especially the centrifugal process, accurate measurement of GSH is arduous. Therefore, a simple and effective method for GSH detection in food samples is highly desirable.

It should be noted that a new type of graphitic carbon nitride quantum dot (g-CNQD) fluorescent materials have recently attracted significant research attention with promising biosensing application. The g-CNQDs emerge as a novel fluorescent probe for biological and environment detection with unique physicochemical properties, such as bright fluorescence, water solubility, biocompatibility, and nontoxicity.[26] As an ideal fluorescent probe, its fluorescence could be completely and specifically quenched by Hg^{2+} and reversed by GSH. On the basis of this phenomenon, the g-CNQDs have been utilized in this work to detect GSH in foods. Their preparation is according to a low-temperature solid-phase process with sodium citrate and urea as the precursors, which was energy-saving and environmentally friendly.[27]

Herein, a selective and rapid fluorescence probe via a "switch-on" strategy for GSH sensing in foods is demonstrated. The sensing system set out by quenching the fluorescence from g-CNQDs by Hg^{2+} through electron transfer. Interestingly, the quenching effect could be reversed by coordination of Hg^{2+} to GSH, thereby switching on the fluorescence of the chemosensor. Furthermore, the chemical response of g-CNQDs is specific toward GSH, relative to other different biomolecules or electrolytes. Furthermore, the g-CNQDs–Hg^{2+} probe was also successfully applied for the quantification and comparison of GSH level in various food samples.

EXPERIMENTAL PROCEDURES

Materials. Trisodium citrate, urea, and $HgCl_2$ were purchased from Tianjin Guangfu Chemical Reagents Co. Ltd. (Tianjin, China). NaCl, KCl, $MgCl_2$, and vitamin C were acquired from Sinopharm Chemical Reagent Co. Ltd. (Shanghai, China). All amino acids were bought from Shenggong Biological Engineering Co. Ltd. (Shanghai, China). All chemicals were of analytical reagent grade and used without further purification. The ultrapure water used throughout the experiments was purified through a 18202 V AXL water purification system (Asura Technology Development Co. Ltd., Chongqing, China).

Apparatus and Characterization. A TU-1901 double-beam UV–vis spectrophotometer (Purkine General Instrument Co. Ltd., Beijing, China) was used to record absorption spectra and measure absorbance. Fluorescent emission spectra were recorded on an RF-5301PC spectrofluorometer (Shimadzu, Kyoto, Japan). A Hitachi-600 transmission electron microscope (TEM, Hitachi, Kyoto, Japan) was used for measuring the morphology and size of g-CNQDs. The sample for TEM characterization was prepared by placing a drop of colloidal solution on a carbon-coated copper grid and dried at room temperature. FT-IR spectra were performed on a Nicolet Nexus 670 Fourier transform infrared spectrometer (Nicolet Instrument Co., Madison, WI, USA) using KBr pellets, scanning from 4000 to 400 cm^{-1} at room temperature.

Preparation of g-CNQDs. The process was according to the previously reported procedure with a little modification.[27] In typical synthesis, 0.081 g (0.28 mmol) of sodium citrate and 0.101 g (1.68 mmol) of urea were mixed in an agate mortar and ground into fine powder. The mixture was then transferred to a poly(tetrafluoroethylene) (Teflon)-lined autoclave and heated at 180 °C for 1 h. After the reaction was finished, the autoclave was naturally cooled to ambient temperature. The final yellowish product was dispersed in 5 mL of ultrapure water and centrifuged at 12000 rpm for 5 min. The supernatant was extracted by removing the precipitation and subsequently dialyzing against ultrapure water through a dialysis membrane (3 kDa) for 24 h. The as-synthesized g-CNQDs were stored at 4 °C for further detection and characterization.

Sample Pretreatment. The food samples were prepared according to a previous paper with a little modification.[15] All of the food samples were purchased in the local market in Lanzhou, China. First, all of the samples were cleaned with tap water and ultrapure water. Then, they were naturally dried in air and accurately weighed, followed by homogenization in a commercial blender. After centrifugation in a refrigerated centrifuge (to prevent oxidation caused by the high temperature produced by the centrifuge) at 3000 rpm for 15 min, the supernatant was filtered through a 0.45 μm pore size filter membrane and diluted to appropriate concentration in the detection range with ultrapure water. The final juices of tomatoes, cherry tomatoes, purple grapes, white grapes, spinach, and cucumber were diluted to 10, 20, 10, 1, 1, and 1 times, respectively. All of the samples were stored in a refrigerator at 4 °C for use.

Quantification of GSH in Food Samples. The GSH level in food samples was determined according to the following steps: (a) A 3.3 μM Hg^{2+} solution was incubated with 60 μL of g-CNQDs in 2.5 mL of 0.2 M phosphate buffer solution (PBS, NaH_2PO_4–Na_2HPO_4, pH 8.0) for 5 min so that the probe could be formed. (b) Five hundred microliters of sample solution was then added and mixed thoroughly. The resulting solution was maintained at room temperature for 5 min to hold the reaction completely. Finally, the spectra were recorded under excitation at 400 nm, and the slit widths were set at 5/5 nm. The recovery rate was calculated according to the following equation:

$$\text{recovery} = (c_{\text{measured}} - c_{\text{initial}})/c_{\text{added}}$$

RESULTS AND DISCUSSION

Characterization. As shown in Figure 1, the remarkable optical properties of the as-obtained g-CNQDs were confirmed

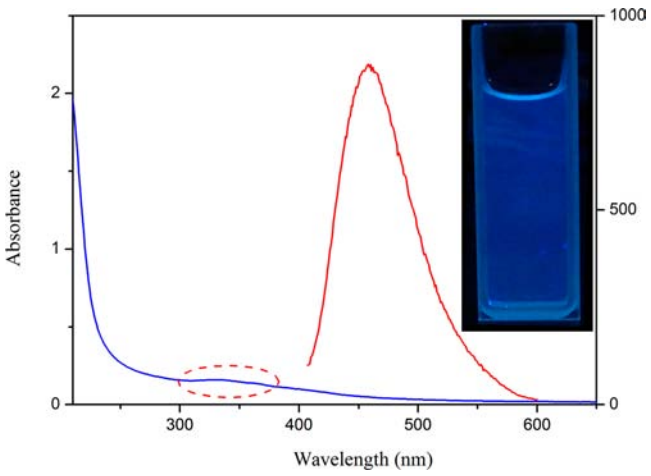

Figure 1. UV–vis absorption (blue line) and fluorescence emission (red line) spectra of the g-CNQDs. (Inset) Photograph of g-CNQD dispersion under UV light (365 nm).

by UV–vis absorption and fluorescent (FL) spectra of the aqueous dispersion. The UV–vis spectrum exhibited a characteristic absorption peak at 340 nm. The narrow and symmetrical fluorescence peak at 460 nm, resulted from their narrow size distribution, was observed when the aqueous solution was excited at 400 nm. The digital picture of the aqueous dispersions further showed that the obtained g-CNQDs are water-soluble and exhibit strong blue fluorescence under 365 nm UV light. The morphology and microstructure were identified by the typical TEM image of the prepared g-CNQDs solution. As shown in Figure 2, g-CNQDs are regular in shape and monodisperse, and their size is about 2.1–4.5 nm with an average diameter of 3.5 nm.

DOI: 10.1021/jf505759z
J. Agric. Food Chem. 2015, 63, 1747–1755

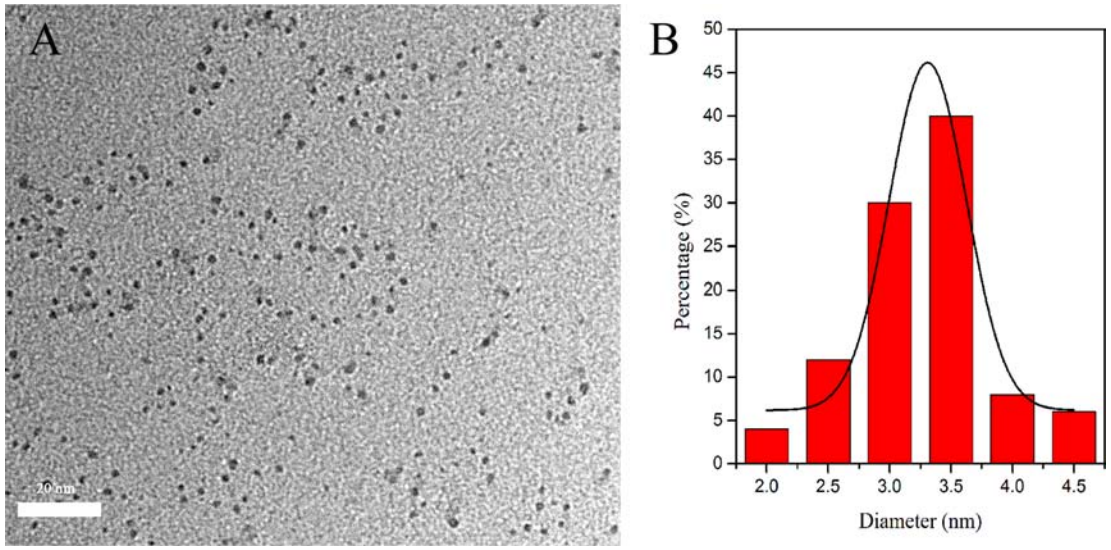

Figure 2. TEM image of g-CNQDs (A) and the corresponding size distribution histogram (B).

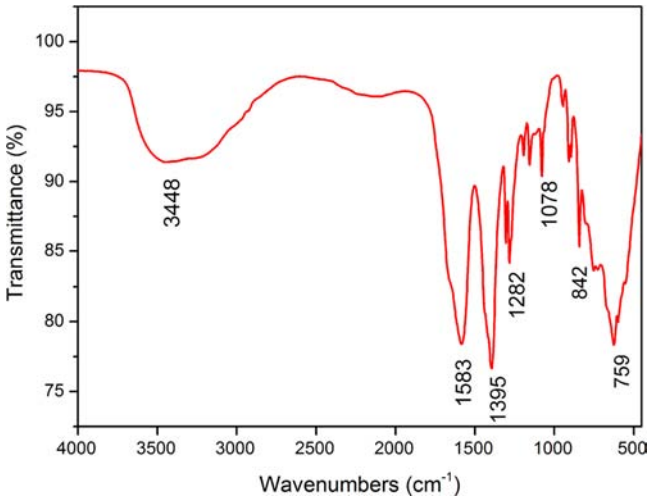

Figure 3. FT-IR spectrum of g-CNQDs.

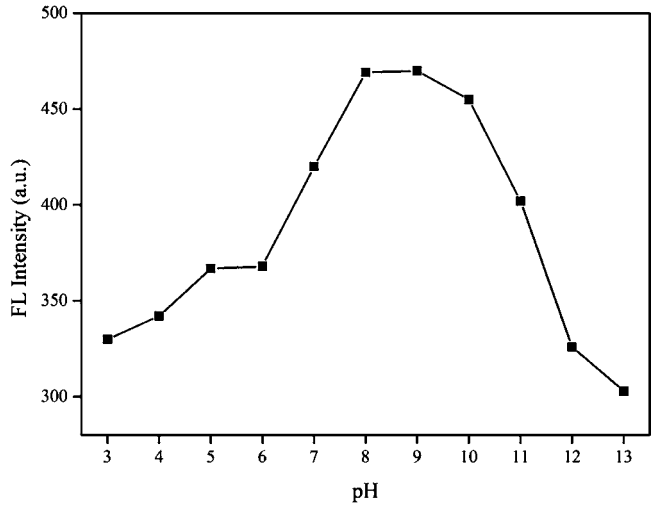

Figure 4. Fluorescence intensity of g-CNQDs at different pH values.

At least 50 particles were selected at random to characterize the size distribution of g-CNQDs. The FT-IR spectrum (Figure 3) was used to confirm the surface chemistry of the as-prepared g-CNQDs. The characteristic absorption broad bands at about 3100−3600 cm^{-1} corresponded to the stretching vibrations of O−H and N−H. The sharp peak at 1395 cm^{-1} was from the bending vibration of C−NH, and the peak at about 1000−1300 cm^{-1} was related to the C−OH stretching vibration.[28] The high intensity of the peak at 1583 cm^{-1} was ascribed to the asymmetric stretching vibrations of the carboxylate anions.[29] These abundant hydrophilic groups presented on the surface significantly improved the water solubility and stability of g-CNQDs. From the characterization results, we could confirm that the synthesized g-CNQDs with high performance were basically identified with that from the literature.[27]

The FL intensity of g-CNQDs at different pH values is presented in Figure 4, and as can be seen the FL intensity of the g-CNQDs was pH dependent. They have extremely poor stability and could be severely quenched in too acidic and alkaline solution due to the destruction of the surface groups. Such a phenomenon was in agreement with those of carbon nanoparticles modified with hydroxyl and carboxylic.[30,31] It is worthwhile mentioning that these pH-sensitive g-CNQDs have great potential for monitoring pH changes.

Design Principle and Mechanism Study of Chemosensor for GSH. As depicted in Scheme 1, the original fluorescence of g-CNQDs was quenched after the addition of Hg^{2+}. Upon the addition of GSH, Hg^{2+} was strongly captured by GSH and released from the surface of g-CNQDs. In other words, the structure of the g-CNQDs−Hg^{2+} probe was decomposed, and the fluorescence intensity of g-CNQDs was restored remarkably as the GSH concentration increased.

Quenching Mechanism. We, not unexpectedly, found that the FL intensity of g-CNQDs gradually decreased upon the successive addition of Hg^{2+}. The measurement of zeta potential indicated that the g-CNQDs are negatively surface charged.[27] On the basis of this result, we deduced that there perhaps existed an electrostatic interaction between the negative groups (carboxyl and hydroxyl groups) of g-CNQDs and Hg^{2+}. The capture of the nanomaterials with oxygen-containing groups to Hg^{2+} was specific.[29,32] Furthermore, electron transfer occurred between g-CNQDs and Hg^{2+}.[29,31,33] Both electrostatic interaction and electron transfer could lead to the decrease of g-CNQDs emission, but the latter effect may play a leading role.

DOI: 10.1021/jf505759z
J. Agric. Food Chem. 2015, 63, 1747−1755

Scheme 1. Schematic Illustration of the Principle of the g-CNQDs−Hg^{2+} System Based Chemosensor for GSH

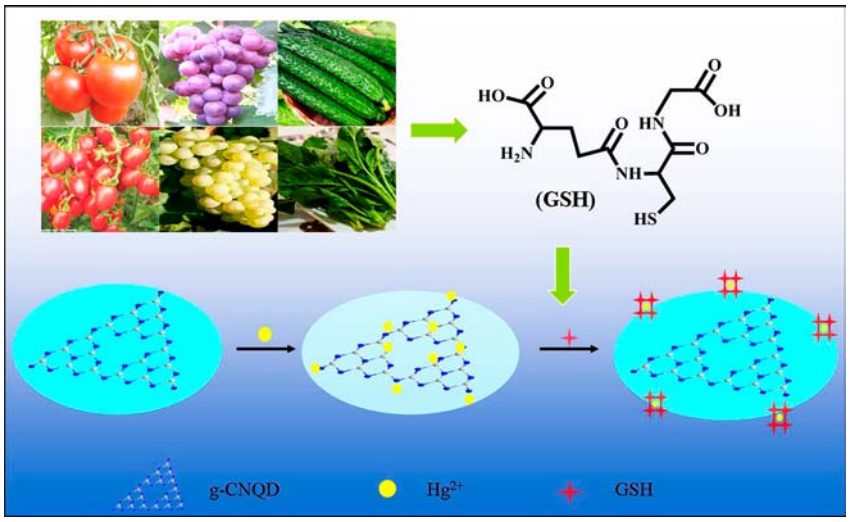

Restoration Mechanism. Evidently, a recovery of g-CNQDs was observed immediately upon addition of GSH to the g-CNQDs−Hg^{2+} system. At this stage, the fluorescence probe was switched to the "on" state. Negligible changes of the pure g-CNQD emission were observed after treatment with excess GSH (Figure 5). This illustrated that the enhancement in FL intensity of g-CNQDs should be ascribed to the interaction between GSH and Hg^{2+}, which is consistent with previous studies.[34,35] As we know, the Hg^{2+} cation, as a thiophilic metal ion, has a particular binding preference to GSH.[34] GSH has specific steric structure with several potential coordinating sites: sulfhydryl, amino group, and carboxyls.[36] Therefore, Hg^{2+} can be easily released from the surface of g-CNQDs after the addition of GSH, which leads to the dissociation of the g-CNQDs−Hg^{2+} probe. As mentioned above, we established the "switch-on" fluorescence sensor for sensitive, selective, and rapid determination of glutathione.

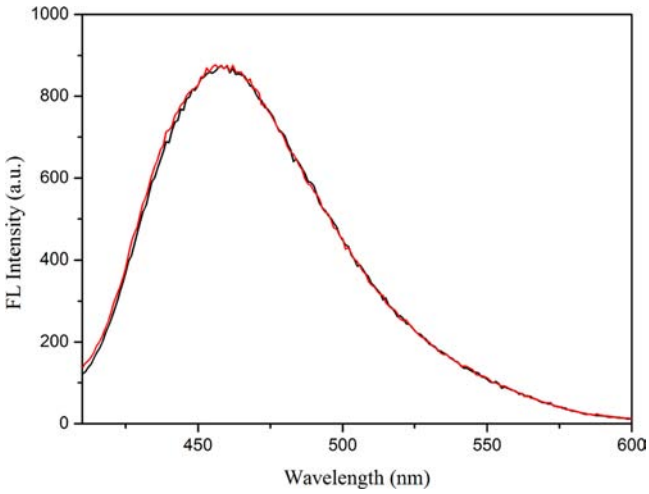

Figure 5. Fluorescence emission spectra of 60 μL of g-CNQDs (black line) solution and 60 μL of g-CNQDs solution with 100 μM GSH (red line). All experiments were conducted in 0.2 M PBS buffer and incubated for 5 min.

Optimization of Experimental Conditions. To further improve the detection sensitivity of the system, we systematically optimized the relative conditions and found that the Hg^{2+} concentration and the pH of the buffer solution remarkably influenced the assay sensitivity. Besides, the reaction time also has a certain effect.

Figure 6A displays the fluorescence restoration changes with increasing Hg^{2+} concentration. We noted that less Hg^{2+} cannot quench the fluorescence thoroughly and thus cause an inapparent FL restoration. However, an excess amount of Hg^{2+} leads to GSH binding with free Hg^{2+} in solution instead of Hg^{2+} on the surface of g-CNQDs, which resulted in poor sensitivity. From the above, we selected 3.3 μM as the optimum Hg^{2+} concentration.

The effect of pH on the assay performance was studied over a pH range from 5.0 to 10.0 with a universal PBS buffer (Figure 6B). On the one hand, the material had strong FL intensity and was stable in the range of pH 8.0−10.0 (Figure 4). On the other hand, $[Hg(GSH)_n]^{(2-3n)-}$ (n = 2 or 3) complexes, the dominant formations, have higher stability in alkaline solutions than in acidic solution.[37] Taking the two factors into account, pH 8.0 is recommended as the optimal pH value for further detection.

In addition to the Hg^{2+} concentration and pH, the kinetics of both the quenching and restoration processes were measured to optimize the required incubation times (Figure 6C,D). The test was performed with the optimized and typical assay protocol in 0.2 M PBS buffer (pH 8.0) with 3.3 μM Hg^{2+}. As demonstrated in Figure 6, the two procedures both leveled off after ∼5 min with the extension of incubation time, revealing the equilibrium of the two kinetic behaviors. Hence, considering the efficiency, an incubation time of 5 min was selected for both the two processes to achieve the rapid and sensitive determination of GSH in the subsequent experiments.

Analytical Performance for GSH Sensing. *Sensitivity.* The sensitivity of the sensing strategy was investigated by adding different concentrations of GSH into a 0.2 M PBS solution (pH 8.0), containing the same amount of g-CNQDs and 3.3 μM Hg^{2+}. The restoration rate was very fast within 5 min to reach the plateau. As indicated in Figure 7A, the enhancement of fluorescence intensity was closely relevant to the concentration of GSH. The inset image shows the linear plot of the logarithm of $\Delta F/F_0$ against the concentration of GSH over a range of 0.16−16 μM, where ΔF is the difference between F and F_0, corresponding to the fluorescence intensity after and before the

DOI: 10.1021/jf505759z
J. Agric. Food Chem. 2015, 63, 1747−1755

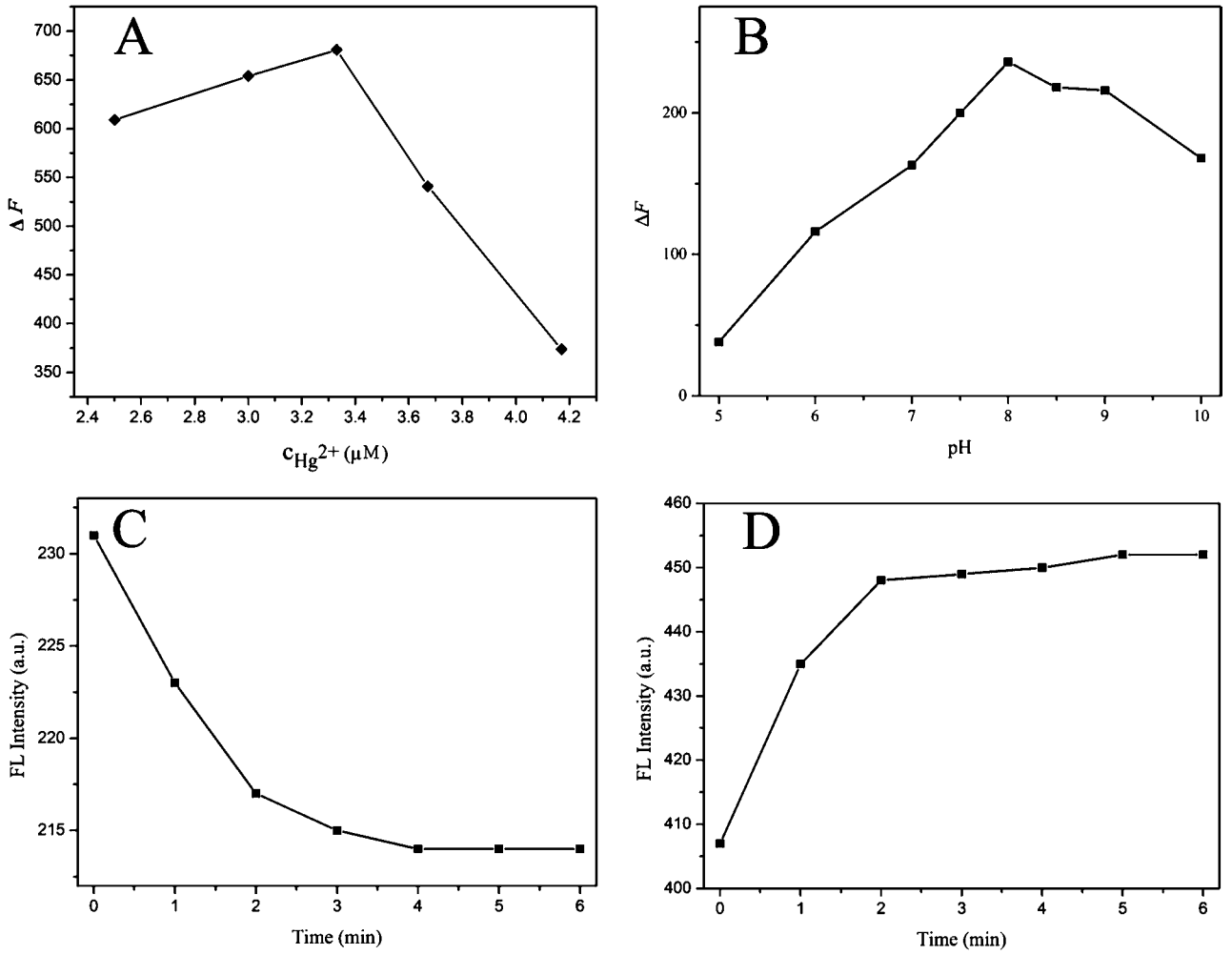

Figure 6. Effects of (A) concentration of Hg^{2+} and (B) pH of buffer solution on fluorescence restoration. $\Delta F = F - F_0$, where F and F_0 are the fluorescence intensities of g-CNQDs-Hg^{2+} in the presence and absence of GSH. (C, D) Relationship between fluorescence intensity and incubation time of quenching and restoration, respectively. Experimental conditions: 0.2 M PBS buffer, 8.3 μM GSH.

Table 1. Comparison of Different Methods for GSH Sensing

probe	analytical methods	linear range	LOD	note	ref
g-C_3N_4–MnO_2	fluorescence	200–500 μM	0.2 μM	low sensitivity, special equipment, sophisticated technique	23
CdTe–Hg(II)	fluorescence	0.6–20.0 μM	0.1 μM	low selectivity, low sensitivity	34
AuNCs–Hg(II)	fluorescence	0–250 nM	9.4 nM	low selectivity, costly material	35
CdSe–ZnS QDs–MV^{2+}	fluorescence	5–250 μM	0.6 μM	low sensitivity, complicated operation, time-consuming	39
Fe_3O_4–ABTS–H_2O_2	colorimetry	3.0–30 μM	not given	time consuming	40
g-CNQDs–Hg^{2+}	fluorescence	0.16–16.0 μM	37 nM	high selectivity, sensitivity, fast, cost-effective	this work

Table 2. Comparison of the Analytical Performances of Different Concentration of Hg^{2+} for GSH Sensing (n = 3)

Hg^{2+} concn (μM)	linear range (μM)	regression eq[a]	LOD (nM)	R^2	RSD (n = 3, %)
1.6	0.33–5.0	$\log y = -1.318 + 0.157x$	54	0.9558	0.7–2.0
3.3	0.16–16.0	$\log y = -1.058 + 0.0995x$	37	0.9807	1.9–3.1
5.0	6.66–20.0	$\log y = -1.348 + 0.0788x$	178	0.9840	1.4–3.2

[a] y is $\Delta F/F_0$, where ΔF is the difference between F and F_0 (corresponding to the fluorescence intensity in the presence and absence of GSH, respectively); x is the concentration of GSH.

addition of GSH. The curve followed the standard regression equation $\log(\Delta F/F_0) = -1.058 + 0.0995[\text{GSH}]$ ($R^2 = 0.9807$). On the basis of three parallel determinations (n = 3), the repeatability ranged from 0.19 to 0.31% (expressed as the relative standard deviation, RSD), demonstrating the excellent reliability of this fluorescence chemosensor. Under the optimal conditions, the detection limit (LOD) was estimated to be 37 nM on the basis of the generalized 3σ method, which is comparable to or even better than the previous reports for GSH sensing (see Table 1).

The appropriate concentration of Hg^{2+} should be crucial to achieve a good analytical performance for the switch-on fluorescent sensing of GSH. To illustrate this, the other two

DOI: 10.1021/jf505759z
J. Agric. Food Chem. 2015, 63, 1747–1755

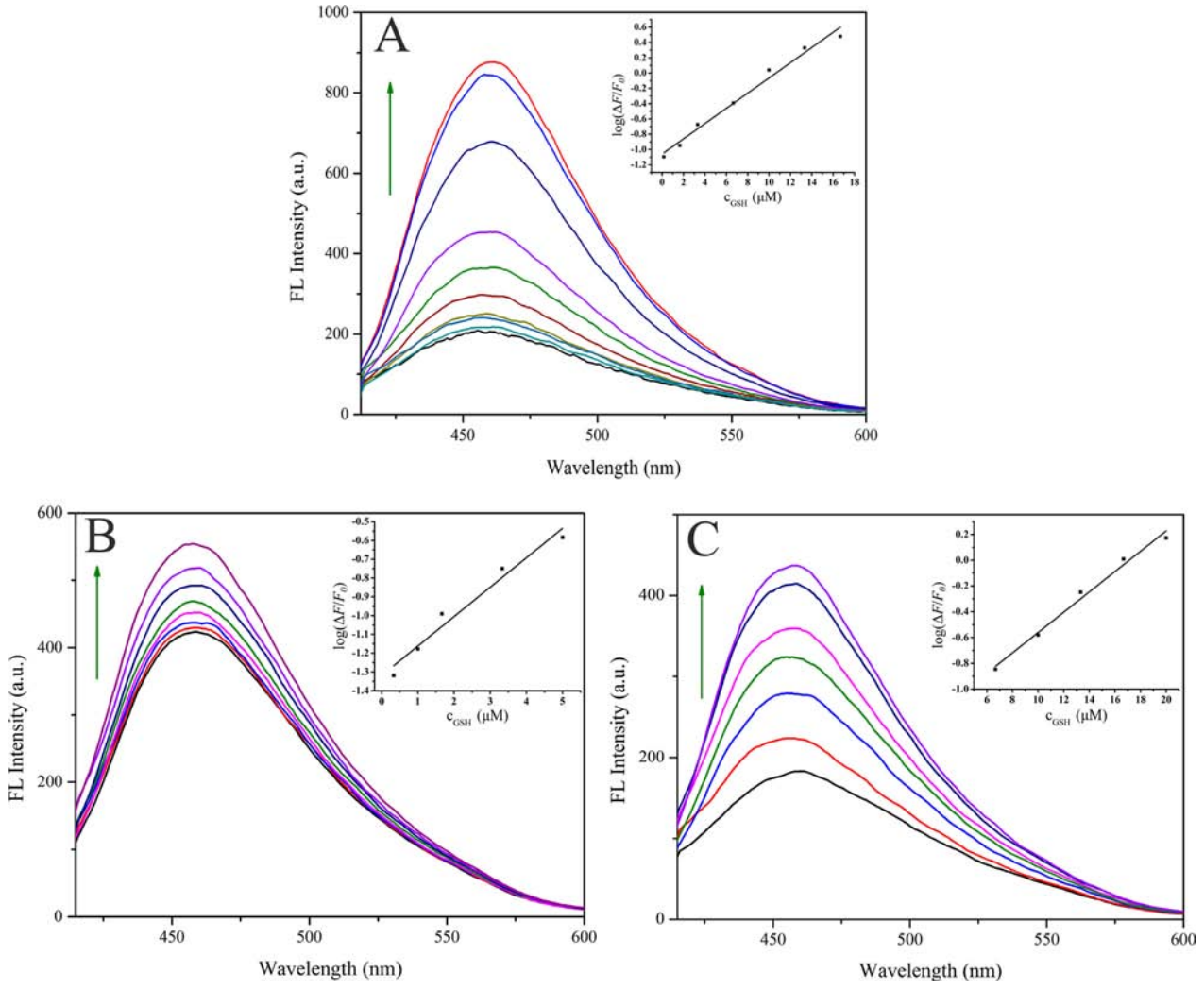

Figure 7. Fluorescence emission spectra of g-CNQDs with increasing concentration of GSH in the presence of 3.3 μM Hg^{2+} (A), 1.6 μM Hg^{2+} (B), and 5.0 μM Hg^{2+} (C). (Inset) Relationship between $\log(\Delta F/F_0)$ and concentration of GSH. The fluorescence emission intensity at 460 nm was measured with an excitation of 400 nm.

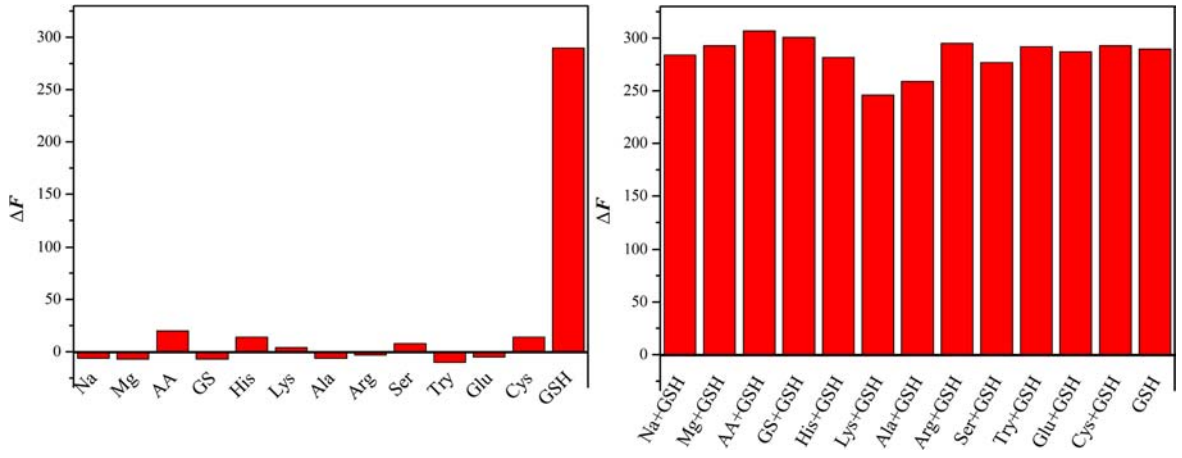

Figure 8. (A) Fluorescence emission intensity of g-CNQDs–Hg^{2+} to 0.5 mM GSH and 12 other analytes (10-fold concentration of GSH). (B) Fluorescence emission intensity of g-CNQDs–Hg^{2+} to GSH and 12 other analytes (0.5 mM) in the presence of GSH (0.5 mM).

concentrations of Hg^{2+} (1.6 and 5.0 μM, respectively) were added to the above system, replacing 3.3 μM Hg^{2+}. In Figure 7B,C, there were similar changes in the fluorescence intensity of the chemosensor with the increase of Hg^{2+} concentration as in Figure 7A. The calculated regression equation, correlation coefficient (R^2), LOD, and RSD are listed in Table 2. Obviously, 3.3 μM Hg^{2+} was optimum in terms of the wider linear range, higher sensitivity, and better repeatability.

DOI: 10.1021/jf505759z
J. Agric. Food Chem. 2015, 63, 1747–1755

Table 1 presented the characteristics of different sensors to detect GSH proposed in recent years, including quantum dots, nanocluster, Fe_3O_4, and carbon-based materials. No doubt, our proposed method is a highly sensitive and selective method for the detection of GSH. Although the detection limits of several reported sensors are better than ours, they need special equipment, a sophisticated technique, and complicated operations. Besides the simplicity in operation and inexpensive detection cost, the response speed of our switch-on chemosensor is much faster than that of most of the reported sensors.

Selectivity. To evaluate the selectivity of the present assay strategy, we have studied the effect of foreign substances. The potential interferences in fruits and vegetables consisted of a number of amino acids and mineral substances, especially vitamin C (AA), glucose (GS), and metal ions, such as Na^+ and K^+.

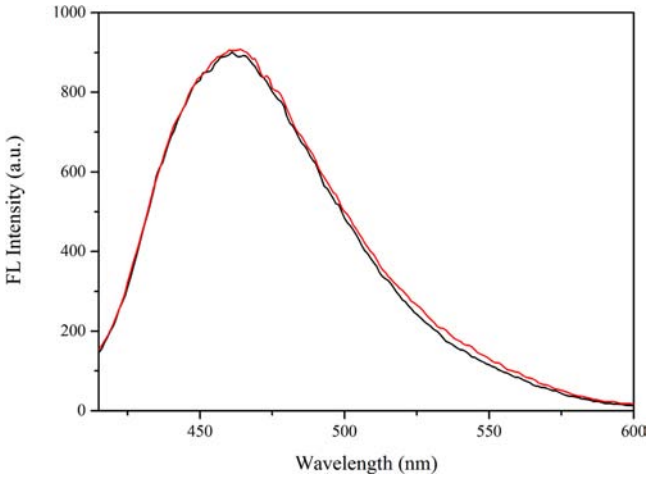

Figure 9. Fluorescence emission spectra of 60 μL of g-CNQDs solution (black line) and 60 μL of g-CNQDs solution with 500 μL of cucumber sample (red line). All experiments were conducted in 0.2 M PBS buffer and incubated for 5 min.

As the experimental data show in Figure 8A, under the same conditions, GSH showed a drastic enhancement of the fluorescence intensity against all other analytes at a 10-fold concentration of GSH, demonstrating that this detection system presented an excellent selectivity. Anti-interference experiments were also carried out to study the selectivity of the sensing toward GSH (Figure 8B). The recovery caused by the mixture of GSH (0.5 mM) with the other analytes (0.5 mM) was similar to that caused solely by GSH.

We have found that Cys has little effect on the recovery of the "switch-on" probe in the detection range, although it is well-known that the structure of Cys is similar to that of GSH. We inferred the following reasons: There exist abundant functional groups (carboxyl and hydroxyl) decorated on the surface of g-CNQDs. As a consequence, Hg^{2+} was tightly captured by g-CNQDs and required a very strong external force to remove. Considering the enormous differences in coordination ability between GSH and Cys due to the multidentate anchor along with the particular steric structure existing in GSH,[36] we deduced that Hg^{2+} can bind GSH preferably. Such results fully reflected the outstanding selectivity and specificity of the sensor platform.

Application in Food Samples. To examine the practical application of the proposed chemosensor, the detection of GSH concentration in various kinds of food was explored. Prior to the sample analysis, cucumber extract was selected as the model sample and used to investigate the effect of sample matrix on GSH sensing. A seen from Figure 9, FL emission spectra of g-CNQDs had no obvious change after the addition of a certain amount of cucumber extract. This was similar in other foods, pointing out no influence from sample matrix. Furthermore, we conducted the recovery test by spiking a series of different known concentration of GSH to ensure the accuracy of the sample test. As the results summarized in Table 3 show, the average recoveries of GSH in tomatoes, cherry tomatoes, purple grapes, white purples, cucumbers, and spinach were found to be in the ranges of 98.3−100.9, 96.5−99.7, 97.1−101.8, 99.5−114.3,

Table 3. Recovery Test of GSH in Various Food Samples

sample	initial amount (mg/100 g)	added amount (μM)	recovery (%)	av recovery (%)	RSD (n = 3, %)
tomato	6.24	3.33	98.6−102.4	100.9	2.0
		6.66	98.4−99.7	98.8	0.7
		10.0	97.4−99.2	98.3	0.9
cherry tomato	5.61	2.00	96.5−103.1	99.7	3.3
		4.00	94.7−100.0	96.5	3.2
		6.00	95.4−99.4	97.6	2.1
purple grape	1.89	1.00	98.5−102.0	101.8	3.2
		3.00	95.8−104.5	101.2	4.4
		5.00	94.3−100.5	97.1	3.0
white grape	1.00	2.50	108.0−120.0	114.3	5.3
		5.00	103.0−105.8	104.2	1.4
		10.0	99.4−99.6	99.5	0.6
cucumber	1.17	2.50	103.6−107.2	105.1	1.8
		5.00	95.4−97.1	96.1	0.9
		10.0	94.9−96.8	96.0	1.0
spinach	2.77	1.00	105.1−115.0	111.0	4.7
		3.00	99.4−107.2	105.0	4.6
		5.00	103.8−105.3	104.5	0.7

DOI: 10.1021/jf505759z
J. Agric. Food Chem. 2015, 63, 1747−1755

96.0−105.1, and 104.5−111.0%, respectively. These results indicated that the restoration of fluorescence was entirely generated by GSH in the food samples.

The amounts of GSH in tomatoes, cherry tomatoes, purple grapes, white purples, cucumbers, and spinach determined by the proposed chemosensor are 6.24, 5.61, 1.89, 1.00, 1.17, and 2.77 mg/100 g, respectively. The detection results of GSH in tomatoes and grapes are respectively consistent with the result achieved from the book (7.0 mg/100 g)[38] and literature (1.89 mg/100 g),[25] which strongly proved the feasibility and reliability of our method. From the analytical results mentioned above, tomatoes and cherry tomatoes are two kinds of food rich in GSH. Therefore, they are excellent food sources for GSH supplements and benefit human health.

In summary, we have successfully developed a "switch-on" fluorescence chemosensor for glutathione detection in food samples. This method, based on the fluorescence recovery of the g-CNQDs−Hg^{2+} probe in the presence of glutathione, displayed several appealing properties, including low cost, quick response, high sensitivity, excellent selectivity, label-free measurement, and switch-on fluorescence response. We believe that such a fluorescence sensor not only would be suitable for GSH assay in food samples but also shows great potential in cell imaging and biological investigation.

AUTHOR INFORMATION

Corresponding Author

*(H.C.) E-mail: hlchen@lzu.edu.cn. Phone: 86-931-8912763. Fax: 86-931-8912582.

Funding

This work was financially supported by the National Nature Science Foundation of China (No. 21475053).

Notes

The authors declare no competing financial interest.

REFERENCES

(1) Yin, J.; Kwon, Y.; Kim, D.; Lee, D.; Kim, G.; Hu, Y.; Ryu, J.-H.; Yoon, J. Cyanine-based fluorescent probe for highly selective detection of glutathione in cell cultures and live mouse tissues. *J. Am. Chem. Soc.* **2014**, *136*, 5351−5358.

(2) Sies, H. Glutathione and its role in cellular functions. *Free Radical Biol. Med.* **1999**, *27*, 916−921.

(3) Chauhan, A.; Chauhan, V. Oxidative stress in autism. *Pathophysiology* **2006**, *13*, 171−181.

(4) Estrela, J. M.; Ortega, A.; Obrador, E. Glutathione in cancer biology and therapy. *Crit. Rev. Clin. Lab. Sci.* **2006**, *43*, 143−181.

(5) Herzenberg, L. A.; DeRosa, S. C.; Dubs, J. G.; Roederer, M.; Anderson, M. T.; Ela, S. W.; Deresinski, S. C.; Herzenberg, L. A. Glutathione deficiency is associated with impaired survival in HIV disease. *Proc. Natl. Acad. Sci. U.S.A.* **1997**, *94*, 1967−1972.

(6) Samiec, P. S.; Drews-Botsch, C.; Flagg, E. W.; Kurtz, J. C.; Sternberg, P.; Reed, R. L.; Jones, D. P. Glutathione in human plasma: decline in association with aging, age-related macular degeneration, and diabetes. *Free Radical Biol. Med.* **1998**, *24*, 699−704.

(7) Townsend, D. M.; Tew, K. D.; Tapiero, H. The importance of glutathione in human disease. *Biomed. Pharmacother.* **2003**, *57*, 145−155.

(8) Yuan, Y.; Zhang, J.; Wang, M. J.; Mei, B.; Guan, Y. F.; Liang, G. L. Detection of glutathione in vitro and in cells by the controlled self-assembly of nanorings. *Anal. Chem.* **2013**, *85*, 1280−1284.

(9) Hofer, T.; Jørgensen, T. Ø.; Olsen, R. L. Comparison of food antioxidants and iron chelators in two cellular free radical assays: strong protection by luteolin. *J. Agric. Food Chem.* **2014**, *62*, 8402−8410.

(10) Hagen, T. M.; Wierzbicka, G. T.; Sillau, A. H.; Bowman, B. B.; Jones, D. P. Bioavailability of dietary glutathione: effect on plasma concentration. *Am. J. Physiol.* **1990**, *259*, G524−G529.

(11) Bayram, B.; Rimbach, G.; Frank, J.; Esatbeyoglu, T. Rapid method for glutathione quantitation using high-performance liquid chromatography with coulometric electrochemical detection. *J. Agric. Food Chem.* **2014**, *62*, 402−408.

(12) du Toit, W. J.; Lisjak, K.; Stander, M.; Prevoo, D. Using LC-MSMS to assess glutathione levels in South African white grape juices and wines made with different levels of oxygen. *J. Agric. Food Chem.* **2007**, *55*, 2765−2769.

(13) Janeš, L.; Lisjak, K.; Vanzo, A. Determination of glutathione content in grape juice and wine by high-performance liquid chromatography with fluorescence detection. *Anal. Chim. Acta* **2010**, *674*, 239−242.

(14) Saetre, R.; Rabenstein, D. L. Determination of cysteine and glutathione in fruit by high-performance liquid chromatography. *J. Agric. Food Chem.* **1978**, *26*, 982−983.

(15) Yan, N.; Zhu, Z. F.; Ding, N.; Zhou, L.; Dong, Y. L.; Chen, X. G. In-line preconcentration of oxidized and reduced glutathione in capillary zone electrophoresis using transient isotachophoresis under strong counter-electroosmotic flow. *J. Chromatogr., A* **2009**, *1216*, 8665−8670.

(16) Lavigne, V.; Pons, A.; Dubourdieu, D. Assay of glutathione in must and wines using capillary electrophoresis and laser-induced fluorescence detection: changes in concentration in dry white wines during alcoholic fermentation and aging. *J. Chromatogr., A* **2007**, *1139*, 130−135.

(17) Wang, Y.; Lu, J.; Tang, L. H.; Chang, H. X.; Li, J. H. Graphene oxide amplified electrogenerated chemiluminescence of quantum dots and its selective sensing for glutathione from thiol-containing compounds. *Anal. Chem.* **2009**, *81*, 9710−9715.

(18) Pacsial-Ong, E. J.; McCarley, R. L.; Wang, W. H.; Strongin, R. M. Electrochemical detection of glutathione using redox indicators. *Anal. Chem.* **2006**, *78*, 7577−7581.

(19) Safavi, A.; Maleki, N.; Farjami, E.; Mahyari, F. A. Simultaneous electrochemical determination of glutathione and glutathione disulfide at a nanoscale copper hydroxide composite carbon ionic liquid electrode. *Anal. Chem.* **2009**, *81*, 7538−7543.

(20) Huang, G. G.; Han, X. X.; Hossain, M. K.; Ozaki, Y. Development of a heat-induced surface-enhanced Raman scattering sensing method for rapid detection of glutathione in aqueous solutions. *Anal. Chem.* **2009**, *81*, 5881−5888.

(21) Sudeep, P. K.; Joseph, S. T. S.; Thomas, K. G. Selective detection of cysteine and glutathione using gold nanorods. *J. Am. Chem. Soc.* **2005**, *127*, 6516−6517.

(22) Tian, D. H.; Qian, Z. S.; Xia, Y. S.; Zhu, C. Q. Gold nanocluster-based fluorescent probes for near-infrared and turn-on sensing of glutathione in living cells. *Langmuir* **2012**, *28*, 3945−3951.

(23) Zhang, X. L.; Zheng, C.; Guo, S. S.; Li, J.; Yang, H. H.; Chen, G. N. Turn-on fluorescence sensor for intracellular imaging of glutathione using g-C_3N_4 nanosheet-MnO_2 sandwich nanocomposite. *Anal. Chem.* **2014**, *86*, 3426−3434.

(24) Kubalczyk, P.; Bald, E. Analysis of orange juice for total cysteine and glutathione content by CZE with UV-absorption detection. *Electrophoresis* **2009**, *30*, 2280−2283.

(25) Cheynier, V.; Souquet, J. M.; Moutounet, M. Glutathione content and glutathione to hydroxycinnamic acid ratio in *Vitis vinifera* grapes and musts. *Am. J. Enol. Vitic.* **1989**, *40*, 320−324.

(26) Cheng, C. M.; Huang, Y.; Tian, X. Q.; Zheng, B. Z.; Li, Y.; Yuan, H. Y.; Xiao, D.; Xie, S. P.; Choi, M. M. F. Electrogenerated chemiluminescence behavior of graphite-like carbon nitride and its application in selective sensing Cu^{2+}. *Anal. Chem.* **2012**, *84*, 4754−4759.

(27) Zhou, J.; Yang, Y.; Zhang, C. Y. A low-temperature solid-phase method to synthesize highly fluorescent carbon nitride dots with tunable emission. *Chem. Commun.* **2013**, *49*, 8605−8607.

(28) Zhang, H. J.; Chen, Y. L.; Liang, M. J.; Xu, L. F.; Qi, S. D.; Chen, H. L.; Chen, X. G. Solid-phase synthesis of highly fluorescent nitrogen-doped carbon dots for sensitive and selective probing ferric ions in living cells. *Anal. Chem.* **2014**, *86*, 9846−9852.

DOI: 10.1021/jf505759z
J. Agric. Food Chem. 2015, 63, 1747−1755

(29) Guo, Y. M.; Wang, Z.; Shao, H. W.; Jiang, X. Y. Hydrothermal synthesis of highly fluorescent carbon nanoparticles from sodium citrate and their use for the detection of mercury ions. *Carbon* **2013**, *52*, 583−589.
(30) Liu, H. P.; Ye, T.; Mao, C. D. Fluorescent carbon nanoparticles derived from candle soot. *Angew. Chem., Int. Ed.* **2007**, *46*, 6473−6475.
(31) Lu, W. B.; Qin, X. Y.; Liu, S.; Chang, G. H.; Zhang, Y. W.; Luo, Y. L.; Asiri, A. M.; Al-Youbi, A. O.; Sun, X. P. Economical, green synthesis of fluorescent carbon nanoparticles and their use as probes for sensitive and selective detection of mercury(II) ions. *Anal. Chem.* **2012**, *84*, 5351−5357.
(32) Zhou, L.; Lin, Y. H.; Huang, Z. Z.; Ren, J. S.; Qu, X. G. Carbon nanodots as fluorescence probes for rapid, sensitive, and label-free detection of Hg^{2+} and biothiols in complex matrices. *Chem. Commun.* **2012**, *48*, 1147−1149.
(33) Barman, S.; Sadhukhan, M. Facile bulk production of highly blue fluorescent graphitic carbon nitride quantum dots and their application as highly selective and sensitive sensors for the detection of mercuric and iodide ions in aqueous media. *J. Mater. Chem.* **2012**, *22*, 21832−21837.
(34) Han, B. Y.; Yuan, J. P.; Wang, E. K. Sensitive and selective sensor for biothiols in the cell based on the recovered fluorescence of the CdTe quantum dots-Hg(II) system. *Anal. Chem.* **2009**, *81*, 5569−5573.
(35) Park, K. S.; Kim, M. I.; Woo, M.-A.; Park, H. G. A label-free method for detecting biological thiols based on blocking of Hg^{2+}-quenching of fluorescent gold nanoclusters. *Biosens. Bioelectron.* **2013**, *45*, 65−69.
(36) Shi, Y. P.; Pan, Y.; Zhang, H.; Zhang, Z. M.; Li, M. J.; Yi, C. Q.; Yang, M. S. A dual-mode nanosensor based on carbon quantum dots and gold nanoparticles for discriminative detection of glutathione in human plasma. *Biosens. Bioelectron.* **2014**, *56*, 39−45.
(37) Mah, V.; Jalilehvand, F. Mercury(II) complex formation with glutathione in alkaline aqueous solution. *JBIC, J. Biol. Inorg. Chem.* **2008**, *13*, 541−553.
(38) Fang, Y. Free radicals and nutrition. *Theory and Application of Free Radical Biology*; Fang, Y., Zheng, R., Eds.; Science Press: Beijing, China, 2002; pp 665−666.
(39) Liu, J. F.; Bao, C. Y.; Zhong, X. H.; Zhao, C. C.; Zhu, L. Y. Highly selective detection of glutathione using a quantum-dot-based off-on fluorescent probe. *Chem. Commun.* **2010**, *46*, 2971−2973.
(40) Ma, Y. H.; Zhang, Z. Y.; Ren, C. L.; Liu, G. Y.; Chen, X. G. A novel colorimetric determination of reduced glutathione in A549 cells based on Fe_3O_4 magnetic nanoparticles as peroxidase mimetics. *Analyst* **2012**, *137*, 485−489.

DOI: 10.1021/jf505759z
J. Agric. Food Chem. 2015, 63, 1747−1755

Table 1. Identification of Phenolic Compounds in Commercial Aqueous *Q. saponaria* Molina Wood Extracts

compd no.	retention time (min)	compd identity	HPLC−UV/Vis abs. max. (nm)	HPLC−ESI[(−) and (+)]-MS experiment (m/z)	HPLC−ESI-MS^n experiment (m/z)
1	7.1	unknown	280	$[M - H]^-$: 271	[271]: 253(100), 181(50), 191(49), 235(23),, 109(14) 123(12)
2	11.4	(+)-piscidic acid[a]	275	$[M - H]^-$: 255	[255]: 165(100), 193(24), 166(11), 209(10), 177(7), 149(6), 93(2)
					[255 → 165]: 107(100), 135(59), 58(38), 147(36), 137(29), 119(15), 93(10)
					[255 → 193]: 149(100), 165(30), 93(26), 99(13), 150(9), 147(8)
					[255 → 209]: 165(100)
				$[M + Na]^+$: 279	[279]: 189(100), 217(47), 149(42)
3	16.3	vanillic acid 4-hexoside	253/291	$[M - H]^-$: 329	[329]: 167(100)
					[329 → 167]: 152(100), 123(81), 108(21)
4	18.4	vanillic acid 4-hexosylpentoside	254/292	$[M - H]^-$: 461	[461]: 167(100), 152(21), 153(8), 329(8)
					[329 → 167]: 152(100), 123(50)
5	19.4	syringic acid 4-*O*-*β*-D-glucopyranoside (glucosyringic acid)[a]	262/292sh	$[M - H]^-$: 359	[359]: 197(100), 182(12), 123(2), 167(1), 153(1)
					[359 → 197]: 182(100), 153(21), 138(11), 167(2), 123(1)
6	20.7	catechin hexoside	280	$[M - H]^-$: 451	[451]: 289(100), 245(10)
					[451 → 289]: 245(100), 205(40), 179(38), 125(36), 247(20), 231(18), 203(15), 161(7), 137(9), 175(5)
7	21.0	syringic acid hexosylpentoside	263/293sh	$[M - H]^-$: 491	[491]: 197(100), 182(31), 167(10), 447(7), 198(5), 359(4)
					[491 → 197]: 182(100), 153(17), 138(7)
8	21.5	catechin hexosyl derivative	280	$[M - H]^-$: 739	[739]: 587(100), 407(76), 559(39), 451(37), 567(28), 289(18), 613(17), 577(15), 533(13), 560(11), 408(8), 425(2)
9	21.7	*p*-coumaric acid derivative	281/315	$[M - H]^-$: 1007	[1007]: 779(100), 925(83), 861(19), 633(13), 453(2)
					[1007 → 779]: 633(100), 259(41), 471(38)
10	22.0	*p*-coumaric acid derivative	285/316	$[M - H]^-$: 1007	[1007]: 779(100), 925(85), 861(17), 633(9)
					[1007 → 779]: 633(100), 615(13), 487(1)
11	22.1	vanillic acid	261/293	$[M - H]^-$: 167	[167]: 152(100), 123(70), 108(29)
12	24.1	syringic acid	275	$[M - H]^-$: 197	[197]: 153(100), 182(82), 138(56)
13	25.2	unknown	303	$[M - H]^-$: 175	[175]: 131(100)
14	25.8	vanillic acid derivative	261/292	$[M - H]^-$: 611	[611]: 443(100)
					[611 → 443]: 167(100)
15	26.1	unknown	262/285	$[M - H]^-$: 189	[189]: 171(100)
16	26.4	*p*-coumaric acid	298/310	$[M - H]^-$: 163	[163]: 119 (100)
17	27.7	ferulic acid	295sh/325	$[M - H]^-$: 193	[193]: 178 (100), 149(68), 134(24)
18	28.2	unknown	273/275	$[M - H]^-$: 467	[467]: 205(100), 163(61), 247(46), 143(36), 171(25), 449(14), 131(11), 145(7)
19	28.5	*p*-coumaric acid derivative	314	$[M - H]^-$: 1057	[1057]: 911(100), 912(41), 925(23), 765(7), 893(7), 926(6), 913(6), 779(4), 633(1)
					[1057 → 911]: 765(100), 766(74), 337(42), 732(27), 509(18)
					[1057 → 633]: 341(100), 487(72)
20	28.7	*p*-coumaric acid derivative	314	$[M - H]^-$: 925	[925]: 779(100), 780(29), 633(18), 761(3)
					[925 → 779]: 633(100)
					[925 → 633]: 341(100), 487(63), 471(61), 231(19)
21	28.9	unknown	303	$[M - H]^-$: 313	[313]: 165(100), 221(53), 218(39), 278(38), 269(32)
22	29.6	*p*-coumaric acid derivative	314	$[M - H]^-$: 925	[925]: 779(100), 780(28), 633(23), 615(5), 634(5), 761(3), 599(3)
23	30.9	*p*-coumaric acid derivative	314	$[M - H]^-$: 1057	[1057]: 911(100), 912(36), 925(8), 779(7), 765(7), 633(3)
24	31.3	*p*-coumaric acid derivative	314	$[M - H]^-$: 925	[925]: 779(100), 780(21), 633(11), 761(6)
25	31.6	*p*-coumaric acid derivative	313	$[M - H]^-$: 925	na
26	32.2	*p*-coumaric acid derivative	313	na	na
27	32.6	unknown	304	$[M - H]^-$: 623	[623]: 315(100), 300(21), 271(15), 316(14), 255(12)
28	33.0	unknown	304	$[M - H]^-$: 1217	[1217]: 1071(100), 1072(50), 925(17), 926(10), 779(3)
29	33.5	unknown	304	$[M - H]^-$: 1071	[1071]: 925(100), 926(33), 779(27), 780(6), 633(3)
30	33.7	*p*-coumaric acid derivative	313	na	na
31	35.5	*p*-coumaric acid derivative	313	na	na

[a]Identity confirmed by NMR spectroscopy, polarimetry (piscidic acid only), and GC−MS (glucosyringic acid only).

(batch 1) and no. 1718-0211-PSD-06 ORG (batch 2)) and one batch of "Andean QDP ultra" (no. 310-709-02-PSD-03) contained at least 60% (w/w) *Quillaja* saponins. In addition, 0.47 ± 0.02% sodium benzoate was added by the manufacturer to Andean QDP ultra.

DOI: 10.1021/jf506277p
J. Agric. Food Chem. 2015, 63, 1756−1762

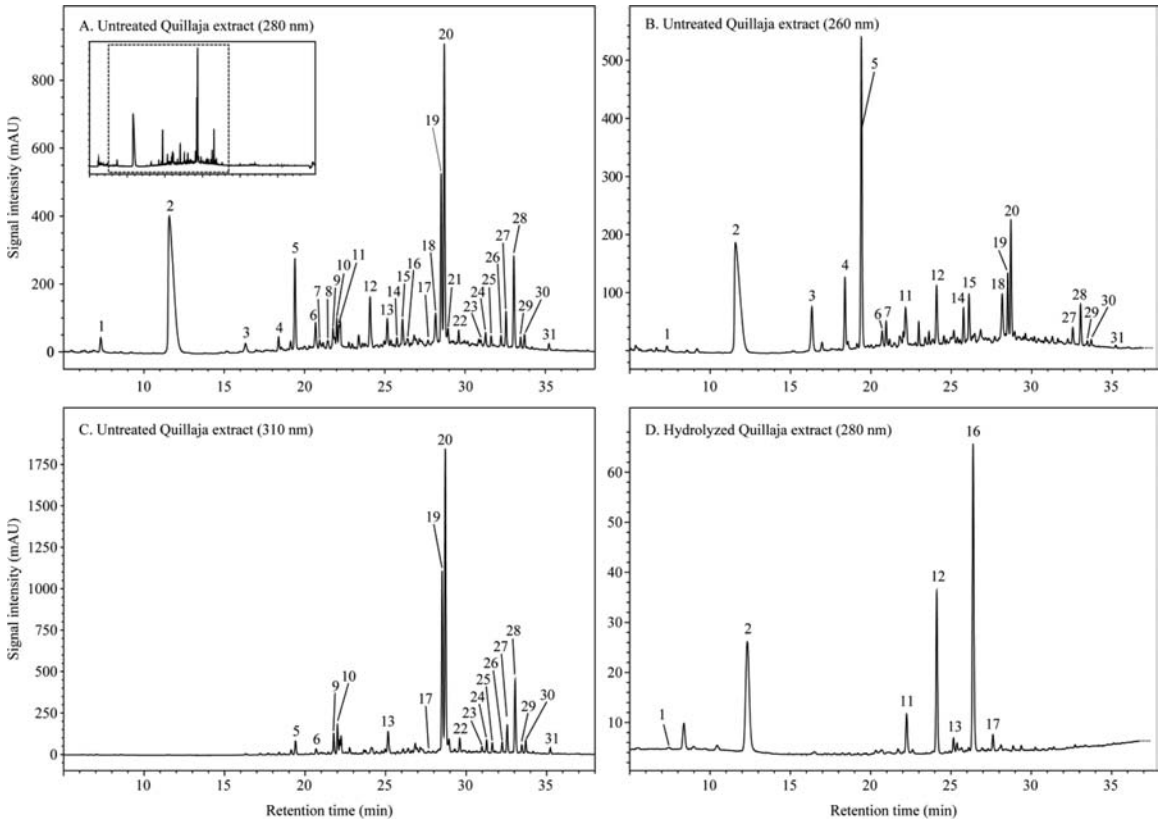

Figure 1. HPLC separation of phenolic compounds in aqueous *Q. saponaria* wood extracts (untreated) monitored at 280 nm (A), 260 nm (B), and 310 nm (C) and in an acid-hydrolyzed extract (D) at 280 nm.

Ultrapure water was used throughout the study (Milli-Q system, Millipore, France).

HPLC-PDA–ESI/MS^n Analyses. Dry commercial *Quillaja* powders and the liquid *Quillaja* preparation were dissolved and diluted in 1% (v/v) aqueous formic acid, respectively. All samples were membrane filtered (0.45 μm) prior to HPLC separation. HPLC-PDA analyses were performed on an 1100 series HPLC system (Agilent, Waldbronn, Germany) equipped with a 250 × 4.6 mm i.d., 5 μm particle size, 100 Å pore size, Kinetex C_{18} column fitted with a 4.0 × 2.0 mm i.d. guard column of the same material (Phenomenex, Torrance, Canada). The column was operated at 35 °C. The mobile phase consisted of 1% (v/v) formic acid in water (solvent A) and 1% (v/v) formic acid in methanol (solvent B), using the following gradient program: 5% B isocratic (10 min), 5–100% B (40 min), 100% B isocratic (5 min), 100–5% B (1 min), 5% B isocratic (4 min). The total run time was 60 min at a flow rate of 1.0 mL/min. Injection volumes of 10 and 20 μL were used. Phenolic compounds were monitored at 260, 280, 310, and 370 nm, and additional UV/vis spectra were acquired in the range of 200–600 nm, employing a model G1315A photodiode array (PDA) detector (Agilent).

For HPLC–ESI-MS^n analyses, the HPLC system described above was serially interfaced with a Bruker (Bremen, Germany) Esquire 3000+ ion trap mass spectrometer via an electrospray ionization (ESI) source operated in both positive and negative modes. Ion mass spectra of the column eluate were recorded in the range m/z 100–1400 at a scan speed of 13 000 m/z/s. Nitrogen was used as a drying gas at a flow rate of 11.0 L/min and as a nebulizing gas at a pressure of 60.0 psi. The nebulizer temperature was set at 365 °C. Helium was used as a collision gas for collision-induced dissociation (CID) at a pressure of 4.0×10^{-6} mbar.

Individual compounds were quantitated using linear calibration curves of authentic reference compounds (ferulic acid, *p*-coumaric acid, syringic acid, and vanillic acid). Derivatives of these phenolic acids were quantitated according to the calibration of the free compound using molecular weight correction factors. For quantitation of (+)-piscidic acid, the compound isolated from *Quillaja* extract was used. Quantitation experiments were performed in duplicate.

Preparative Isolation of Major *Quillaja* Extract Compounds. Four fractions containing major phenolic components as identified by HPLC-PDA–MS^n were isolated from the *Quillaja* extract Andean QDP ultra organic by preparative HPLC. The *Quillaja* extract was dissolved in water/methanol (90/10, v/v) containing 0.1% formic acid for the isolation of compounds **2** and **5** (Table 1 for peak assignment). For isolation of compounds **19** and **20**, the extract was adjusted to pH 2 with formic acid. After membrane filtration (0.45 μm), phenolic compounds were separated with an Ultimate 3000 preparative HPLC system equipped with two solvent delivery modules, a diode array detector (DAD-3000), and an automatic fraction collector (AFC-3000). Separation of compounds **2** and **5** was performed with a 150 × 21.0 mm i.d., 5 μm particle size, 175 Å pore size, Hypersil Gold silica column (Thermo Fisher Scientific, Waltham, MA). The mobile phase consisted of 0.1% (v/v) formic acid in water (solvent A) and 0.1% formic acid in methanol (solvent B) using a multistep gradient as follows: 10% B isocratic (10 min), 10–40% B (5 min), 40–100% B (0.5 min), 100% B isocratic (4.5 min), 100–10% B (1 min), 10% B isocratic (9 min). The total run time was 30 min at a constant flow rate of 15 mL/min. Using this method, the retention times of compounds **2** and **5** were 8.8 and 14.2 min, respectively. Monitoring and peak detection were performed at 256 nm.

Isolation of compounds **19** and **20** was performed with a preparative 250 × 21.1 mm i.d., 5 μm particle size, 125 Å pore size, Phenomenex Aqua C_{18} reversed-phase column. The mobile phase consisted of water (solvent A) and methanol (solvent B), which were both acidified to pH 2 with formic acid. The following gradient was used: 20% B isocratic (10 min), 20–40% B (18 min), 40% B isocratic (20 min), 40–100% B (2 min), 100% B isocratic (8 min), 100–20% B (2 min), 20% B isocratic (10 min). The total run time was 70 min at a constant flow rate of 8 mL/min. Using this method, the retention times of compounds **19** and **20** were 40.2 and 41.0 min, respectively. Monitoring and compound detection were performed at 310 nm.

DOI: 10.1021/jf506277p
J. Agric. Food Chem. 2015, 63, 1756–1762

Aliquots of 1000 μL of the *Quillaja* Andean QDP ultra organic extract were injected for each preparative HPLC run. The collected fractions were evaporated to dryness at 40 °C under reduced pressure (T_{max} = 40 °C), freeze-dried, and stored at −20 °C until further use. Compound purity was checked by HPLC-PDA−MS^n as described above.

Acidic Hydrolysis of Extracts and Individual Compounds. The *Quillaja* Andean QDP ultra organic extract, *p*-coumaric acid, and the isolated fractions containing compounds **2**, **5**, **19**, and **20** were dissolved in aqueous 4 N HCl, heated to ∼85 °C for 20−120 min, and subsequently neutralized with aqueous NaOH. Hydrolyzed samples were membrane filtered (0.45 μm) and analyzed with HPLC-PDA−MS^n as described above.

Determination of the Absolute Configuration of Compound 2 and Absolute Sugar Conformation of Compound 5. Specific rotation values for compound **2** were measured with a PerkinElmer model 341 polarimeter (PerkinElmer, Waltham, MA). Compound **5** (ca. 1 mg) was heated with aqueous 2 M TFA at 85 °C for 2 h. The reaction mixture was evaporated at 45 °C in vacuo, dissolved in pyridine (0.2 mL), and treated with L-cysteine methyl ester hydrochloride in pyridine (12 mg in 0.1 mL) at 65 °C for 1.5 h. Subsequent trimethylsilylation was carried out with the above-mentioned silylation mixture (0.3 mL) at 65 °C for 1 h. The reaction mixture was partitioned between hexane and H_2O (0.3 mL each), and the hexane layer was analyzed by GC−MS (column, 30 m × 0.25 mm i.d., d_f = 0.25 μm, HP-5 ms Agilent J&W; column temperature, 100 °C for 1 min, 15 °C/min to 200 °C, hold for 1.33 min, 2.5 °C/min to 240 °C, 15 °C/min to 300 °C, hold for 5 min; carrier gas, helium). The sugar derivative was identified as D-glucose with the retention time of 20.15 min, being identical to the respective retention time of derivatized authentic D-glucose. Under the same conditions, the L-glucose derivative revealed a retention time of 20.61 min.

NMR Spectroscopy. ^1H and ^{13}C NMR spectra of isolated compounds **2** and **5** were recorded on a Varian Unity Inova 500 MHz spectrometer (Darmstadt, Germany). Compound **2** was dissolved in MeOH-d_4 and compound **5** in D_2O. The ^1H and ^{13}C chemical shifts were referenced to residual solvent signals at δ_H 3.35 and δ_C 49.0 for methanol as well as δ_H 4.70 for deuterated water relative to TMS. Adiabatic 2D broad-band and band-selective gHSQC and gHMBC as well as gDQFCOSY spectra were recorded using CHEMPACK 4.0 pulse sequences (implemented in Varian Vnmrj 2.1B software). Coupling constants, *J*, were directly taken from the spectra and are not averaged.

Piscidic Acid, 2. ^1H NMR (CD_3OD, 500 MHz): δ 3.03 (1H, d, *J* = 13.8 Hz, 4-Ha), 3.18 (1H, d, *J* = 14.4 Hz, 4-Hb), 4.55 (1H, s, 2-H), 6.69 (2H, d-like, *J* = 8.8 Hz, 3′-H, 5′-H), 7.11 (2H, d-like, *J* = 8.8 Hz, 2′-H, 6′-H). ^{13}C NMR (CD_3OD, 125 MHz): δ 174.6 (C-1), 76.4 (C-2), 81.4 (C-3), 42.0 (C-4), 175.9 (C-5), 128.0 (C-1′), 132.5 (C-2′, C-6′), 115.7 (C-3′, C-5′), 157.2 (C-4′). NMR data of compound **2** were in agreement with previously published data for piscidic acid.[8]

Syringic Acid 4-O-β-D-Glucopyranoside (Glucosyringic Acid), 5. ^1H NMR (D_2O, 500 MHz): δ 3.29 (1H, ddd, *J* = 2.3, 5.3, 9.7 Hz, 5′-H), 3.42 (1H, t-like, *J* = 9.5 Hz, 4′-H), 3.48 (1H, t-like, 3′-H), 3.51 (1H, ov, 2′-H), 3.63 (1H, dd, *J* = 5.2, 12.5 Hz, 6′-Hb), 3.74 (1H, dd, *J* = 2.4, 12.6 Hz, 6′-Ha), 3.84 (6H, s, 8-H, 9-H, $-OCH_3$), 5.08 (1H, d, *J* = 7.4 Hz, 1′-H), 7.33 (2H, s, 2-H, 6-H). ^{13}C NMR (D_2O, 125 MHz): δ 127.2 (C-1), 107.5 (C-2, C-6), 152.2 (C-3, C-5), 137.6 (C-4), 170.1 (C-7, O−C═O), 56.3 (C-8,C-9, $-OCH_3$), 102.6 (C-1′), 73.6 (C-2′), 75.6 (C-3′), 69.3 (C-4′), 76.3 (C-5′), 60.4 (C-6′). This compound was previously reported by Wolfram et al.[9] and Liu et al.[10]

RESULTS AND DISCUSSION

Characterization of Phenolic Compounds. Typical chromatograms of an aqueous saponin-rich *Q. saponaria* extract are illustrated in parts A (280 nm), B (260 nm), and C (310 nm) of Figure 1. Acidic sample hydrolysis led to a simplified chromatogram shown in Figure 1D (280 nm). In both untreated and hydrolyzed extracts, vanillic acid (**11**), syringic acid (**12**), *p*-coumaric acid (**16**), and ferulic acid (**17**) were identified by comparison of their retention times, UV/vis spectra, and mass spectra to those of authentic reference substances (Figure 2). Furthermore, compounds **1** and **2** were

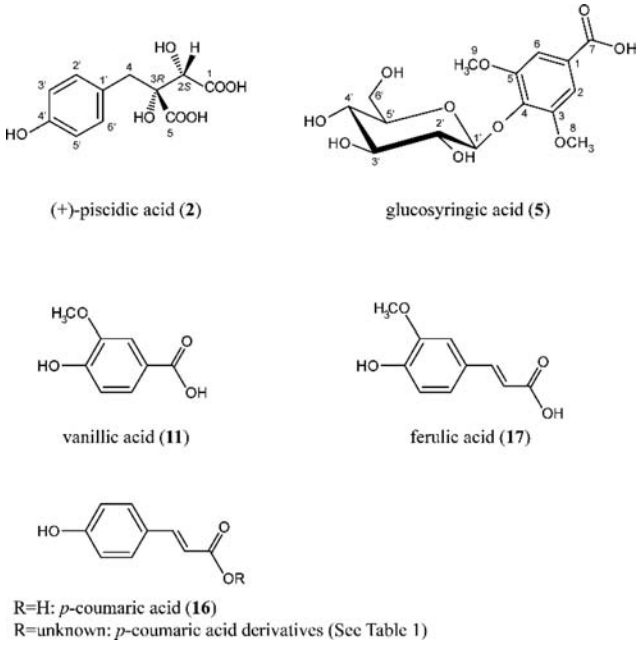

Figure 2. Major phenolic compounds in aqueous *Q. saponaria* wood extracts.

present in both untreated and hydrolyzed extracts. The minor compound **1** remained unidentified in our study. Compound **2** eluted at 11.4 min and represented the major phenolic component in all extracts, showing a UV absorption maximum at 275 nm. In negative ionization mass spectrometry, it produced a quasi-molecular ion, $[M - H]^-$, at *m/z* 255, while a corresponding sodium adduct ion, $[M + Na]^+$, at *m/z* 279 was produced in positive ionization mode (Table 1). The latter ion $[M + Na]^+$ at *m/z* 279 produced a dominant fragment, $[M + Na - 90]^+$, at *m/z* 189 after CID, possibly representing the simultaneous loss of two carboxyl groups. Fragmentation of the analogous negative quasi-molecular ion $[M - H]^-$ at *m/z* 255 yielded a strong signal, $[M - H - 90]^-$, at *m/z* 165. The predominant MS^3 fragments of this daughter ion at *m/z* 165 were observed at *m/z* 147, 135, and 107, indicating the loss of water, a CH_2O group, and a $C_2H_2O_2$ group, respectively. The presumably corresponding ion of the latter $C_2H_2O_2$ group was detected at *m/z* 58 at high signal intensity (Table 1). After isolation by preparative HPLC, NMR spectroscopic data allowed the identification of compound **2** as piscidic acid. Since a rotational value of $[\alpha]_D^{25}$ +41.0° (*c* 5.4, H_2O) was determined in good agreement with previously described data for (+)-piscidic acid ($[\alpha]_D^{24}$ +40.5° and $[\alpha]_D^{23}$ +42.5°),[11] compound **2** was unambiguously identified as (2*S*,3*R*)-(+)-piscidic acid (Figure 2), which was previously found in *Piscidia erythrina* L. (Jamaican dogwood).[12,13]

Compounds **3** and **4** exhibited highly similar UV absorption spectra and identical dominant MS^2 daughter ions at *m/z* 167, derived from parent ions at *m/z* 329 and 461, respectively. Moreover, MS^3 spectra of these ions at *m/z* 167 yielded similar major fragments at *m/z* 152, 123, and 108, being characteristic for the elimination of a methyl moiety, decarboxylation, and a combination of both losses, respectively. In agreement with

DOI: 10.1021/jf506277p
J. Agric. Food Chem. 2015, 63, 1756−1762

Table 2. Quantification of Phenolic Compounds in Aqueous Extracts of Wood from *Q. saponaria* Molina (mg/g of DM)

				Andean QDP ultra organic	
compd no.	compd identity	Andean Q ultra	Andean QDP ultra	batch 1	batch 2
2	(+)-piscidic acid	23.60 ± 0.05	22.09 ± 0.12	33.99 ± 0.15	32.75 ± 0.31
3	vanillic acid 4-hexoside	0.27 ± 0.00	0.23 ± 0.00	0.29 ± 0.01	0.29 ± 0.00
4	vanillic acid 4-hexosylpentoside	0.10 ± 0.00	0.17 ± 0.00	0.45 ± 0.00	0.42 ± 0.01
5	glucosyringic acid	0.47 ± 0.00	0.41 ± 0.00	0.81 ± 0.01	0.78 ± 0.00
9	*p*-coumaric acid derivative	0.24 ± 0.00	0.25 ± 0.00	0.46 ± 0.00	0.35 ± 0.01
10	*p*-coumaric acid derivative	0.29 ± 0.00	0.37 ± 0.00	0.26 ± 0.00	0.27 ± 0.03
11	vanillic acid	tr[a]	0.06 ± 0.05	0.05 ± 0.00	0.04 ± 0.00
12	syringic acid	0.29 ± 0.00	0.21 ± 0.01	0.29 ± 0.01	0.26 ± 0.00
14	vanillic acid derivative	0.17 ± 0.00	0.22 ± 0.01	0.39 ± 0.01	0.38 ± 0.01
19	*p*-coumaric acid derivative	0.55 ± 0.00	1.30 ± 0.01	3.33 ± 0.01	2.78 ± 0.01
20	*p*-coumaric acid derivative	1.12 ± 0.00	2.46 ± 0.01	5.21 ± 0.05	4.17 ± 0.01
total polyphenols (mg/g of DM)		27.10	27.78	45.52	42.49

[a]The abbreviation "tr" means nonquantitated traces.

Fischer et al.[14] and data obtained by an authentic vanillic acid standard, both compounds were identified as vanillic acid derivatives. Compound **3** yielded the fragment $[M - H - 162]^-$ at m/z 167 after elimination of a putative hexose moiety from the molecular ion at m/z 329. The quasi-molecular ion of compound **4** at m/z 461 exhibited a loss of 294 Da, possibly representing a hexose−pentose moiety. Their UV absorption spectrum showed high similarity to that of vanillic acid (**11**). While esterification of vanillic acid with hexoses was reported to cause a bathochromic shift, the absorption bands remain mostly unaltered after glycosylation of the hydroxyl group.[14,15] Therefore, compounds **3** and **4** were tentatively identified as vanillic acid 4-hexoside and 4-hexosylpentoside, respectively. Compound **14** was also tentatively identified as a vanillic acid derivative, eluting at 25.8 min and exhibiting a characteristic UV absorption spectrum and a dominant CID fragment at m/z 167 (Table 1).

By analogy to compounds **3** and **4**, the quasi-molecular ions $[M - H]^-$ of compounds **5** (m/z 359) and **7** (m/z 491) showed identical losses of 162 and 294 Da, although both yielded a strong MS^2 signal at m/z 197. MS^3 spectra of the daughter ion at m/z 197 yielded characteristic fragments at m/z 182, 167, and 153, which allowed the tentative assignment of compounds **5** and **7** to syringic acid derivatives. After isolation of compound **5** by preparative HPLC, acidic hydrolysis resulted in the appearance of free syringic acid, supporting the tentative identification. In agreement, NMR spectroscopy allowed the complete elucidation of compound **5** as syringic acid 4-*O*-*β*-D-glucopyranoside (glucosyringic acid) (Figure 2). The absolute configuration of the sugar moiety of compound 5 was determined to be D-glucose by GC−MS. Since UV absorption and mass spectra indicated a high structural similarity of compounds **5** and **7**, except for the above-described difference in primary mass loss of 294 Da, compound **7** was tentatively assigned to be a yet uncharacterized syringic acid hexosylpentoside.

Compound **6** showed a UV absorption maximum at 280 nm and a quasi-molecular ion at m/z 451, which produced a strong signal, $[M - H - 162]^-$, at m/z 289 due to the putative loss of a hexose moiety after CID. Since the MS^3 fragmentation pattern of this daughter ion at m/z 289 was highly similar to the fragmentation pattern of an analytical (+)-catechin standard, compound **6** was tentatively identified as catechin hexoside. Compound **8** revealed a UV absorption spectrum similar to that of compound **6** and a quasi-molecular ion, $[M - H]^-$, at m/z 739. The main daughter ions obtained at m/z 587, 407, and 559 could not be specified, while the daughter ions at m/z 451 and 289 indicate a possible structural similarity to compound **6**, a catechin hexoside. Therefore, compound **8** was tentatively identified as a catechin hexosyl derivative.

A total of 11 different compounds (**9**, **10**, **19**, **20**, **22**−**26**, **30**, **31**) were assigned to *p*-coumaric acid derivatives. All of them showed a UV absorption spectrum highly similar to a *p*-coumaric acid standard, while ESI(−)-MS analyses yielded signals at uncommonly high m/z values. Compounds **20**, **22**, **24**, and **25** exhibited a quasi-molecular ion, $[M - H]^-$, at m/z 925, while $[M - H]^-$, ions at m/z 1007 were observed for compounds **9** and **10** and at m/z 1057 for compounds **19** and **23**. Irrespective of their parent ion, common fragment ions were observed at m/z 925, 779, and 633 for all of the above-mentioned compounds. Compounds **19** and **20** were isolated by preparative HPLC and subjected to acidic hydrolysis, yielding free *p*-coumaric acid (Figure 2) as identified by comparing the retention times and UV and mass spectra to those of an authentic standard. In agreement, the neutral loss of 164 Da (*p*-coumaric acid) to yield daughter ions $[M - H - 164]^-$ at m/z 893 and 761 for compound **19** and **20**, respectively, was observed during ESI(−) experiments (Table 1). Therefore, the above-mentioned compounds were assigned to yet uncharacterized *p*-coumaric acid derivatives (Table 1). Further investigations for their detailed characterization by NMR spectroscopy are ongoing.

Compounds **28** and **29** revealed quasi-molecular ions at m/z 1217 and 1071, respectively. Their fragmentation pattern yielded daughter ions at m/z 925, 779, and 633, highly similar to those of the above-described *p*-coumaric acid derivatives (e.g., compounds **19** and **20**). However, their UV absorption maximum was different (ca. 304 nm) as compared to that of *p*-coumaric acid and its derivatives (ca. 314 nm). Several other unknown compounds displaying analogous absorption spectra were found (compounds **13**, **21**, and **27**−**29**). While compounds **21**, **27**, **28**, and **29** disappeared after acidic hydrolysis, compound **13** was still retained in the hydrolyzed extract. Thus, compound **13** may represent a basic structural element of the above-mentioned compounds. In agreement, the quasi-molecular ion of compound **13** was detected at m/z 175, whereas compounds **21**, **27**, **28**, and **29** produced signals at higher m/z 313, 623, 1217, and 1071, respectively. The quasi-

DOI: 10.1021/jf506277p
J. Agric. Food Chem. 2015, 63, 1756−1762

molecular ion of compound **13**, $[M - H]^-$, at m/z 175 produced a single detectable fragment at m/z 131, indicating the elimination of CO_2 and, hence, the presence of a carboxyl function. However, we were unable to identify compound **13** and its tentative derivatives, compounds **21** and **27**−**29** (Table 1).

Quantification of Phenolic Compounds. The identified (+)-piscidic acid represented the major phenolic compound (75−87% of all phenolic compounds) in all *Quillaja* extracts, ranging from 22.09 ± 0.12 to 33.99 ± 0.15 mg/g of DM (Table 2). Although quantitative reports about the natural occurrence of piscidic acid are scarce, dried *Cimicifuga* rhizomes were reported to contain from 0.28 to 4.47 mg of piscidic acid/g of DM previously.[16]

Compounds **3**−**5**, **9**−**12**, and **14** were minor phenolic compounds at levels below 3 mg/g of DM (7% of the total identified phenolic compounds). The *p*-coumaric acid derivative contents (compounds **19** and **20**) ranged between 1.67 mg/g of DM (6.2%) and 8.54 mg/g of DM (18.8%) as shown in Table 2. Generally, all four *Quillaja* extract batches showed similar portions of their polyphenolics. However, both Andean QDP ultra organic batches revealed slightly higher total polyphenol concentrations (42.5 and 45.5 mg/g of DM, respectively) when compared to the batches of Andean QDP ultra and Andean Q ultra (27.8 and 27.1 mg/g of DM, respectively). Previously, the total phenolic content of a less purified *Q. saponaria* bark extract (20% sapogenins) has been assessed by the highly unspecific Folin−Ciocalteu assay to contain 72.14 mg of total phenolics/g of DM.[17]

Since the extracts investigated are frequently used for emulsification in commercial applications, we sought to compare the phenolic contents of *Quillaja* wood extracts with those of other polyphenol-rich emulsifiers. For instance, Rombouts and Thibault[18,19] reported a polyphenol content of 1−2% (DM) in the alcohol-insoluble residue (AIR) obtained from sugar beet pulp, containing feruloyl groups covalently linked to the pectin molecule. Cashew tree gum exudate, representing a natural emulsifier, has been found to contain less than 0.5% (DM) phenols.[20] Consequently, *Quillaja* extracts contain substantially higher levels of total phenolic compounds (up to 4.6%, w/w) than sugar beet pectin and cashew gum exudate.

Since a number of characteristic phenolic acids were present in *Quillaja* wood extracts, their occurrence might be useful for the detection of *Quillaja* extracts in foods, cosmetics, and pharmaceutical formulations. In particular, the high content of 2.2−3.4% (w/w, DM) piscidic acid in the dried extracts is highly characteristic. Due to its monohydroxylated benzene moiety, piscidic acid is most likely susceptible to enzymatic oxidation. Monophenol oxidases (tyrosinase, EC 1.14.18.1) from plants and microorganisms efficiently catalyze the hydroxylation of monohydroxy phenolics to *o*-dihydroxy phenolics. The latter are rapidly oxidized to *o*-quinones by *o*-diphenol:oxygen oxidoreductases (EC 1.10.3.2), which then nonenzymatically polymerize to yield commonly undesired brown or black melanins.[21,22] Oxidases originating from other starting materials should be completely inactivated to prevent undesired browning during *Quillaja* processing. However, (+)-piscidic acid was previously shown to effectively complex Fe^{3+} in pigeon pea root exudates[23] and, therefore, may also be capable of inactivating phenol oxidases by sequestering the copper cation cofactor of these enzymes. Besides enzymatic oxidation, autoxidation of *Quillaja* polyphenols might contribute to discoloration. The presence of catalysts such as excessive metal ions beyond the complexing capacity of piscidic acid as well as excessive oxygen and heat exposure might further accelerate the autoxidation of polyphenols.[24,25]

In addition, polyphenolic compounds with high affinity for iron ions were previously shown to exert an antimicrobial activity.[26] Besides their high content in saponins, the iron-sequestering piscidic acid may therefore represent a further antimicrobial and hemolytic agent of *Quillaja* extracts.[27,28]

In summary, the qualitative and quantitative characterization of phenolic compounds in different commercially available saponin-rich *Q. saponaria* extracts revealed a unique profile of polyphenols that might be applicable for their authentication. Furthermore, the high levels of polyphenols observed in the extracts might exert desired antioxidant properties but, at the same time, cause undesired browning reactions within the food matrix.

AUTHOR INFORMATION

Corresponding Author

*Phone +49 711 459 22995. Fax: +49 711 459 24110. E-mail: ralf.schweiggert@uni-hohenheim.de.

Notes

The authors declare no competing financial interest.

ACKNOWLEDGMENTS

We acknowledge Pera Ingredients GmbH (Springe-Eldagsen, Germany) for generously providing *Q. saponaria* extract samples.

REFERENCES

(1) Marciani, D. J., Triterpene saponin analogs having adjuvant and immunostimulatory activity. Patent US 5977081 A, 1999.

(2) van Setten, D. C.; van de Werken, G. Molecular structures of saponins from *Quillaja saponaria* Molina. In *Saponins Used in Traditional and Modern Medicine*; Waller, G. R., Yamasaki, K., Eds.; Advances in Experimental Medicine and Biology, Vol. *404*; Springer: New York, 1996; pp 185−193.

(3) San Martín, R.; Briones, R. Industrial uses and sustainable supply of *Quillaja saponaria* (Rosaceae) saponins. *Econ. Bot.* **1999**, *53*, 302−311.

(4) San Martín, R.; Briones, R. Quality control of commercial quillaja (*Quillaja saponaria* Molina) extracts by reverse phase HPLC. *Sci. Food Agric.* **2000**, *80*, 2063−2068.

(5) Kähkönen, M. P.; Hopia, A. I.; Vuorela, H. J.; Rauha, J.-P.; Pihlaja, K.; Kujala, T. S.; Heinonen, M. Antioxidant activity of plant extracts containing phenolic compounds. *J. Agric. Food Chem.* **1999**, *47*, 3954−3962.

(6) Rice-Evans, C. A.; Miller, N. J.; Paganga, G. Structure-antioxidant activity relationships of flavonoids and phenolic acids. *Free Radical Biol. Med.* **1996**, *20*, 933−956.

(7) Walther, R. U.; Padilla, L.; González, J.; Otero, R. *Quillaja saponaria* wood extract: Refined processing and forestry management guarantee sustainability and ecological benefits. *Compend. Detergency—Suppl. Household Pers. Care Today* **2011**, 20−22.

(8) Takahira, M.; Kusano, A.; Shibano, M.; Kusano, G.; Miyase, T. Piscidic acid and fukiic acid esters from *Cimicifuga simplex*. *Phytochemistry* **1998**, *49*, 2115−2119.

(9) Wolfram, K.; Schmidt, J.; Wray, V.; Milkowski, C.; Schliemann, W.; Strack, D. Profiling of phenylpropanoids in transgenic low-sinapine oilseed rape (*Brassica napus*). *Phytochemistry* **2010**, *71*, 1076−1084.

(10) Liu, J. X.; Di, D. L.; Shi, Y. P. Diversity of chemical constituents from *Saxifraga montana* H. *J. Chin. Chem. Soc.* **2008**, *55*, 863−870.

DOI: 10.1021/jf506277p
J. Agric. Food Chem. 2015, 63, 1756−1762

(11) Toshima, H.; Saito, M.; Yoshihara, T. Total syntheses of all four stereoisomers of piscidic acid *via* catalytic asymmetric dihydroxylation of (*Z*)- and (*E*)-trisubstituted olefins. *Biosci., Biotechnol., Biochem.* **1999**, *63*, 1934−1941.
(12) Culbreth, D. M. *A Manual of Materia Medica and Pharmacology*; Health Research Books: Pomeroy, WA, 1996.
(13) Bridge, W.; Coleman, F.; Robertson, A. Constituents of "Cortex *Piscidiae erythrinae*." Part I. The structure of piscidic acid. *J. Chem. Soc.* **1948**, 257−260.
(14) Fischer, U. A.; Carle, R.; Kammerer, D. R. Identification and quantification of phenolic compounds from pomegranate (*Punica granatum* L.) peel, mesocarp, aril and differently produced juices by HPLC-DAD-ESI/MS^n. *Food Chem.* **2011**, *127*, 807−821.
(15) Vanholme, R.; Storme, V.; Vanholme, B.; Sundin, L.; Christensen, J. H.; Goeminne, G.; Halpin, C.; Rohde, A.; Morreel, K.; Boerjan, W. A systems biology view of responses to lignin biosynthesis perturbations in *Arabidopsis*. *Plant Cell* **2012**, *24*, 3506−3529.
(16) Takahira, M.; Yanagi, M.; Kusano, A.; Shibano, M.; Baba, K.; Kusano, G.; Sakurai, N.; Nagai, M. Phenolic constituents of *Cimicifuga* species rhizomes. *Nat. Med.* **1998**, *52*, 330−338.
(17) Nasri, S.; Luciano, G.; Vasta, V.; Aouadi, D.; Priolo, A.; Makkar, H. P. S.; Ben Salem, H. Effect of *Quillaja saponaria* dietary administration on colour, oxidative stability and volatile profile of muscle longissimus dorsi of Barbarine lamb. *Meat Sci.* **2012**, *92*, 582−586.
(18) Rombouts, F. M.; Thibault, J.-F. Enzymic and chemical degradation and the fine structure of pectins from sugar-beet pulp. *Carbohydr. Res.* **1986**, *154*, 189−203.
(19) Rombouts, F. M.; Thibault, J.-F. Feruloylated pectic substances from sugar-beet pulp. *Carbohydr. Res.* **1986**, *154*, 177−187.
(20) Marques, M. R.; Xavier-Filho, J. Enzymatic and inhibitory activities of cashew tree gum exudate. *Phytochemistry* **1991**, *30*, 1431−1433.
(21) Mayer, A. M. Polyphenol oxidases in plants and fungi: Going places? A review. *Phytochemistry* **2006**, *67*, 2318−2331.
(22) Martinez, M. V.; Whitaker, J. R. The biochemistry and control of enzymatic browning. *Trends Food Sci. Technol.* **1995**, *6*, 195−200.
(23) Ae, N.; Arihara, J.; Okada, K.; Yoshihara, T.; Johansen, C. Phosphorus uptake by pigeon pea and its role in cropping systems of the Indian subcontinent. *Science* **1990**, *248*, 477−480.
(24) Nkhili, E.; Loonis, M.; Mihai, S.; El Hajji, H.; Dangles, O. Reactivity of food phenols with iron and copper ions: Binding, dioxygen activation and oxidation mechanisms. *Food Funct.* **2014**, *5*, 1186−1202.
(25) Talcott, S. T.; Howard, L. R. Phenolic autoxidation is responsible for color degradation in processed carrot puree. *J. Agric. Food Chem.* **1999**, *47*, 2109−2115.
(26) Engels, C.; Schieber, A.; Gänzle, M. G. Inhibitory spectra and modes of antimicrobial action of gallotannins from mango kernels (*Mangifera indica* L.). *Appl. Environ. Microbiol.* **2011**, *77*, 2215−2223.
(27) Hassan, S.; Byrd, J.; Cartwright, A.; Bailey, C. Hemolytic and antimicrobial activities differ among saponin-rich extracts from guar, quillaja, yucca, and soybean. *Appl. Biochem. Biotechnol.* **2010**, *162*, 1008−1017.
(28) Wallace, R. J. Antimicrobial properties of plant secondary metabolites. *Proc. Nutr. Soc.* **2004**, *63*, 621−629.

DOI: 10.1021/jf506277p
J. Agric. Food Chem. 2015, 63, 1756−1762

Table 1. Compositional Yield and Crystallinity Index of the Control and Treated *E. grandis* Fibers

	carbohydrate[a] content (%)								
sample	Ara	Gal	Glc	Man	Xyl	AIL[b]	ASL	yield (%)	CrI (%)
F_1	0.21	1.47	48.74	0.77	16.06	28.68	1.21	100	37.29
F_2	0.04	0.68	50.97	0.71	11.23	33.63	0.83	67.2	41.92
F_3	0.08	0.91	47.96	0.64	14.47	29.33	0.94	97.5	38.79
F_4	ND[c]	0.52	50.22	0.71	14.94	31.41	0.32	62.8	41.28

[a]Ara, arabinose; Gal, galactose; Glc, glucose; Man, mannose; Xyl, xylose. [b]AIL, acid insoluble lignin; ASL, acid soluble lignin; O, other components; CrI, Crystallinity Index. [c]ND, not detected.

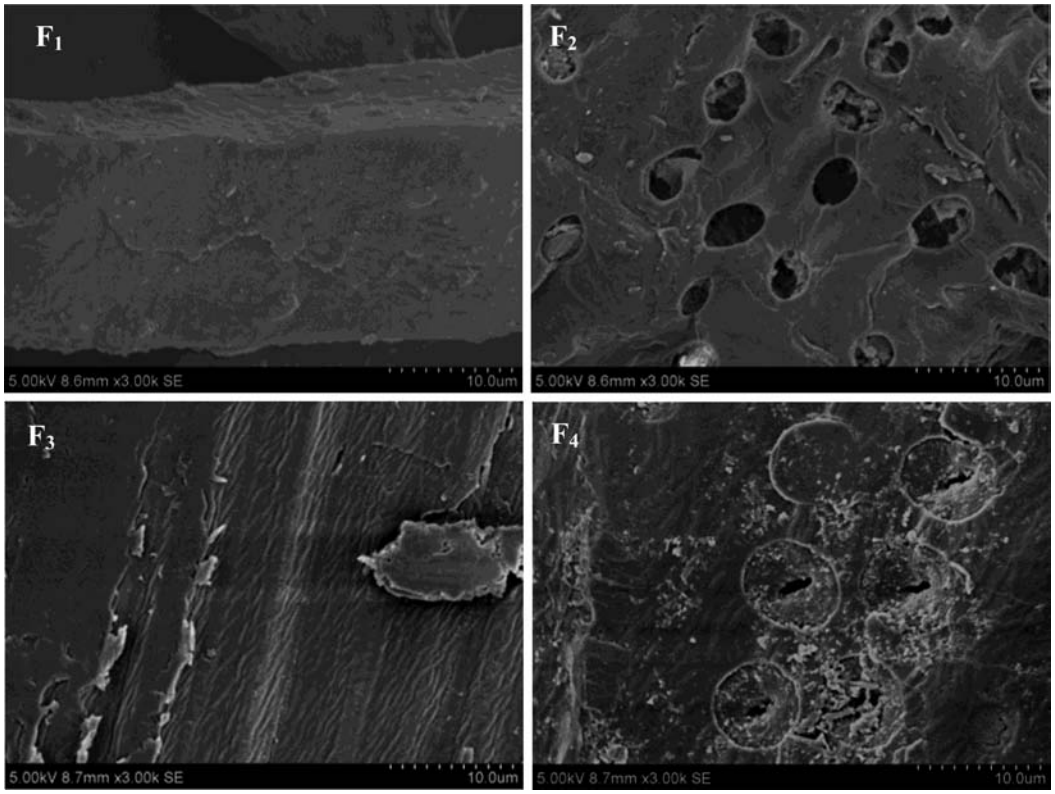

Figure 1. SEM micrographs of the control and treated fibers: control fibers (F_1), hot-compressed water treated fibers (F_2), laccase mediator treated fibers (F_3), and integrated treated fibers (F_4).

being extensively planted in Southern China. The fibers without bark were collected in this study. A fungal laccase (phenoloxidases, EC 1.10.3.2) originated from *Aspergillus oryzae* was purchased from Hubei Yuancheng Pharmaceutical Co., Ltd., China. One unit of laccase activity was defined as the amount of enzyme that oxidized 1 μmol of 2,2′-azinobis-3-ethylbenzthiazoline-6-sulfonate (ABTS)/min, under standard conditions of pH 4.0 and temperature 30 °C, respectively. The cellulolytic enzyme was Celluclast 1.5 L (Novozymes, filter paper activity, 100 FPU/g), containing hemicellulase activities. All chemicals used as received were of analytical or reagent grade.

Treatment of the Fibers. The *E. grandis* fibers were extracted with toluene/ethanol (2:1, v/v) in a Soxhlet apparatus for 6 h. The extracted fibers without exposure to any other processes were regarded as the control fibers (F_1). For the HCW treatment, 25 g of extracted fibers (dry weight, dw) was soaked in 750 mL of deionized water in a stainless-steel reactor with a magnetic stirrer. This reactor was sealed with a steel cover and autoclaved at 170 °C for 1 h. After the HCW treatment, the mixtures were cooled to about 30 °C, and then the treated fibers were filtered with a Buchner funnel. The treated fibers were washed repeatedly with deionized water until the filtrate was neutral and then dried for 24 h at 40 °C in a drying oven. The resulting dry samples were named hot-compressed water treated fibers (F_2). For the laccase-mediated treatment, the extracted fibers were treated with laccase in an aqueous suspension at 5% consistency with a dosage of 24 U/g fiber (dw) and with ABTS 1.5% (dw, w/w) at the saturated air bubbling atmosphere. They were held at approximately 25 °C and pH 4.0 for 2 h. After the laccase-mediated treatment, the mixtures were filtered, and the treated fibers were dried at 40 °C for 24 h. These samples were considered as the laccase-mediated fibers (F_3). Integrated fibers (F_4) were obtained by the same HCW treatment used to prepare the F_2 samples followed by the same laccase-mediated treatment used to prepare the F_3 samples. It should be mentioned that all the treatments were carried out in duplicate.

Isolation of MWL. Milled wood lignin (MWL) was prepared from the fibers according to the method of Björkman.[19] Approximately 15 g of fibers were milled (5 h) in a Fritsch planetary ball mill (Germany) according to previous literature.[20] The ball-milled sample was extracted with dioxane/water solution (96:4, v/v) for 24 h. The mixture was filtered, and then the filtrate was concentrated to ca. 30 mL. The dissolved lignin was isolated by precipitating the concentrated liquor into 10 volumes of acidified water (pH 2.0) adjusted by 6 M HCl. The precipitated MWL was obtained by first centrifugation, then washed with the same acidified water, and finally freeze-dried. The four fiber samples (F_1, F_2, F_3, and F_4) underwent the same processes, and the four resulting lignin samples were titled as L_1, L_2, L_3, and L_4, respectively.

Preparation of EHL. Enzymatic hydrolysis lignin (EHL) was isolated as described by Wen et al.[20] The ball-milled sample (0.3 g)

DOI: 10.1021/jf506042s
J. Agric. Food Chem. 2015, 63, 1763−1772

was subjected to enzymatic hydrolysis (100 FPU cellulase/g substrate) at 2% solid loading with 50 mM NaOAc buffer (pH 4.8). The mixed slurry was incubated in a rotary shaker (150 rpm) at 50 °C for 48 h. After the enzymatic hydrolysis treatment, the residue (named as EHL) was obtained by centrifugation and thoroughly washed with 70 °C water, and then freeze-dried. No further purification was conducted to preserve all structural features of the isolated EHL. The four fiber samples (F_1, F_2, F_3, and F_4) underwent the same processes, and the four resulting lignin samples were named EHL_1, EHL_2, EHL_3, and ELL_4, respectively. The freeze-dried sample (30 mg) was suspended in DMSO-d_6 (0.5 mL), and the mixture was ultrasonically processed at 45 °C for 5 h to complete dissolution.

Characterization of the Fibers. The composition of the four fiber samples was determined by the National Renewable Energy Laboratory (NREL) protocol using a two-step acid hydrolysis method.[21] FT-IR spectra of the fibers were collected in the range of 4000 to 700 cm^{-1} at 4 cm^{-1} resolution and 128 scans per sample.[20] Scanning electron microscopy images were carried out with a Hitachi S-3400N II (Hitachi, Tokyo, Japan) instrument at 15 kV. For each sample, five different surface areas on average were imaged on each single piece by the functionalized SEM tip. Ten sample pieces were imaged by different amplification factors, and 150 recognition images were randomly selected for the analysis. The crystallinity index of fiber samples was measured using an XRD-6000 instrument (Shimadzu, Japan) with a C_u K_α radiation source (λ = 0.154 nm) at 40 kV and 30 mA. Samples were scanned from 5° to 40° (2θ) at a speed of 2° /min.

Characterization of the Lignins. The carbohydrate moieties associated with the four lignin samples were determined by hydrolysis with dilute sulfuric acid according to a previous report.[22] The weight-average (M_w) and number-average (M_n) molecular weights of the acetylated lignin preparations were determined by GPC with an ultraviolet detector (UV) at 280 nm. The column used was a 300 mm × 7.5 mm i.d., 10 μm, PL-gel 10 μm mixed-B, with a 50 mm × 7.5 mm i.d. guard column of the same material (Agilent Technologies, Scotland, UK). For the quantitative ^{13}C NMR experiments, 140 mg of lignin was dissolved in 0.5 mL of DMSO-d_6, and 20 μL of chromium(III) acetylacetonate (0.01 M) was added as a relaxation agent to reduce the relaxation delay. For the quantitative 2D-HSQC spectra, approximately 90 mg of lignin was dissolved in 0.5 mL of DMSO-d_6. Functional groups of the lignin samples were determined by ^{31}P NMR spectra according to previous publications.[20,24] The detailed NMR analysis operation conditions have been given previously.[20,23,24]

RESULTS AND DISCUSSION

Chemical Composition of the Fibers. It should be mentioned that the OH groups in hemicelluloses and cellulose are mainly attributed to the hygroscopicity and dimensional changes of fiberboard. From the perspective of fiberboard performance standards, it is desired to simultaneously minimize the water-absorbing capacity and maximize the strength of the product as much as possible. A feasible solution for this challenge is to remove the hemicelluloses but keep the cellulose. In the present study, HCW treatment at a lower temperature of 170 °C for 1 h was performed to partially remove hemicelluloses and boost the fiberboard performance. The selection of the operational parameters employed in this work was based on our previous research and other published work.[25,26] The elevation of pretreatment temperature from 110 to 170 °C for 1 h and 170 to 230 °C for 0.5 h resulted a notable increase of the degradation and solubilization of hemicelluloses. However, the dissolving rate of the hemicelluloses tended to be slightly in the range of 170 to 230 °C for 0.5 h.[25] The similar fractionation of hemicelluloses could be achieved in the experiments performed under the mildest conditions assayed (175 °C, 1 h) according to the report of Romaní etc.[26] In addition, considering the energy consumption and the cost, the experimental condition of 170 °C for 1 h was chosen.

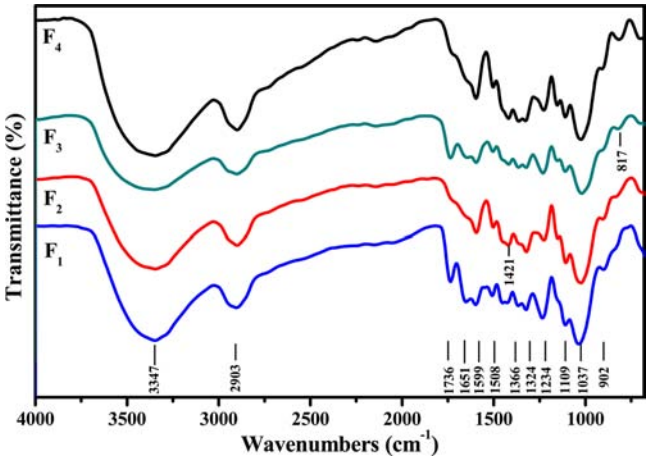

Figure 2. FT-IR spectra of the control and treated fibers.

As shown in Table 1, the yield of F_3 (97.5%) was relatively very high, whereas, the yields of F_2 (67.2%) and F_4 (62.8%) were decreased greatly due to the HCW treatments. The content of arabinose, galactose, mannose, and xylose, which are representative of hemicellulosic fractions, was significantly affected by the HCW treatment. A reduction of their total contents from 18.51% in the control fiber (F_1) to 12.66% in the HCW fiber (F_2) was observed. In particular, xylose presented a maximal decrease of 30.00%. It has been reported that the HCW treatment can cause a significant reduction of the proportion of hemicelluloses.[27] However, the content of glucose, the main constituent of cellulose, was relatively stable in this study, possibly explained by the less intensive HCW treatment conditions used. Furthermore, the lignin content slightly increased in all of the treated samples. This result could be explained by the fact that the hemicellulose content was reduced and the relative content of lignin was increased proportionally. The CrI of F_3 increased just 1.50% compared to that of the control sample, and F_1 was inferior to that of F_2 (4.63%). It was assumed that the increase of CrI could be ascribed to the partial removal of the amorphous portion, mainly hemicelluloses and to some extent of lignin. These results indicated that the HCW and laccase-mediated treatments could enhance the mechanical properties of fiber by increasing the CrI.

Surface Morphology of the Fibers. Scanning electron microscope images of the fibers revealed a rather conspicuous structure on the surface of the fibers (Figure 1). F_1 was observed to be relatively smooth, exhibiting a homogeneous surface that was covered by a thin layer of noncellulosic material. This smooth layer was probably due to the melted lignin spread on the surface of the fiber. It was logical to suppose that the lignin of the middle lamella was plasticized at a high temperature above its glass-transition-point during the thermo-mechanical pulping process and then spread over the nearby fiber surfaces. When the temperature cooled down, a surface coating was likely formed.[28] Fernando et al.[29] also reported a crust on the surface of the unbleached TMP fibers. However, it was obviously observed that the cellulose microfibril aggregates and granules on the surface of F_3 showed a rough and wrinkled mark. Simultaneously, it could be noticed that a large number of holes, which would enhance the accessibility of the enzyme, were present on the surface of F_2

DOI: 10.1021/jf506042s
J. Agric. Food Chem. 2015, 63, 1763−1772

Table 2. Yield and Carbohydrate Contents of the Four MWL Samples

	yield (%)			carbohydrate[a] content (%)				
sample	with sugars[b]	without sugars	total sugar content (%)	Rha	Ara	Gal	Glc	Xyl
L_1	9.8	9.5	3.11	0.17	0.02	0.78	1.29	0.85
L_2	11.3	11.1	1.12	0.06	0.30	0.51	0.25	ND[c]
L_3	9.4	9.2	1.78	0.09	0.18	0.47	0.62	0.42
L_4	11.9	11.8	1.01	0.03	0.63	0.22	0.13	ND

[a]Rha, rhamnose; Ara, arabinose; Gal, galactose; Glc, glucose; Xyl, xylose. [b]On the basis of the dry mass of Klason lignin (%, w/w). [c]ND, not detected.

Table 3. Weight-Average (M_w) and Number-Average (M_n) Molecular Weights and Polydispersity (M_w/M_n) of the Four MWL Samples

	lignin sample			
	L_1	L_2	L_3	L_4
M_w	4790	4340	4370	4030
M_n	2930	2590	2670	2200
M_w/M_n	1.64	1.68	1.64	1.83

and F_4 but not in the other two samples. The phenomenon could be ascribed to the hydronium ion (H_3O^+) initially causing depolymerization of xylose and cleavage of the acetyl group. At a high temperature, H_3O^+ is originated from water autoionization, causing hydrolysis and deacetylation of hemicelluloses. Meanwhile, H_3O^+ is reproduced from the released acetic acid with the further degradation of hemicelluloses. Since the abundance of side groups and the less uniform structure of the hemicelluloses would be easily solubilized and hydrolyzed

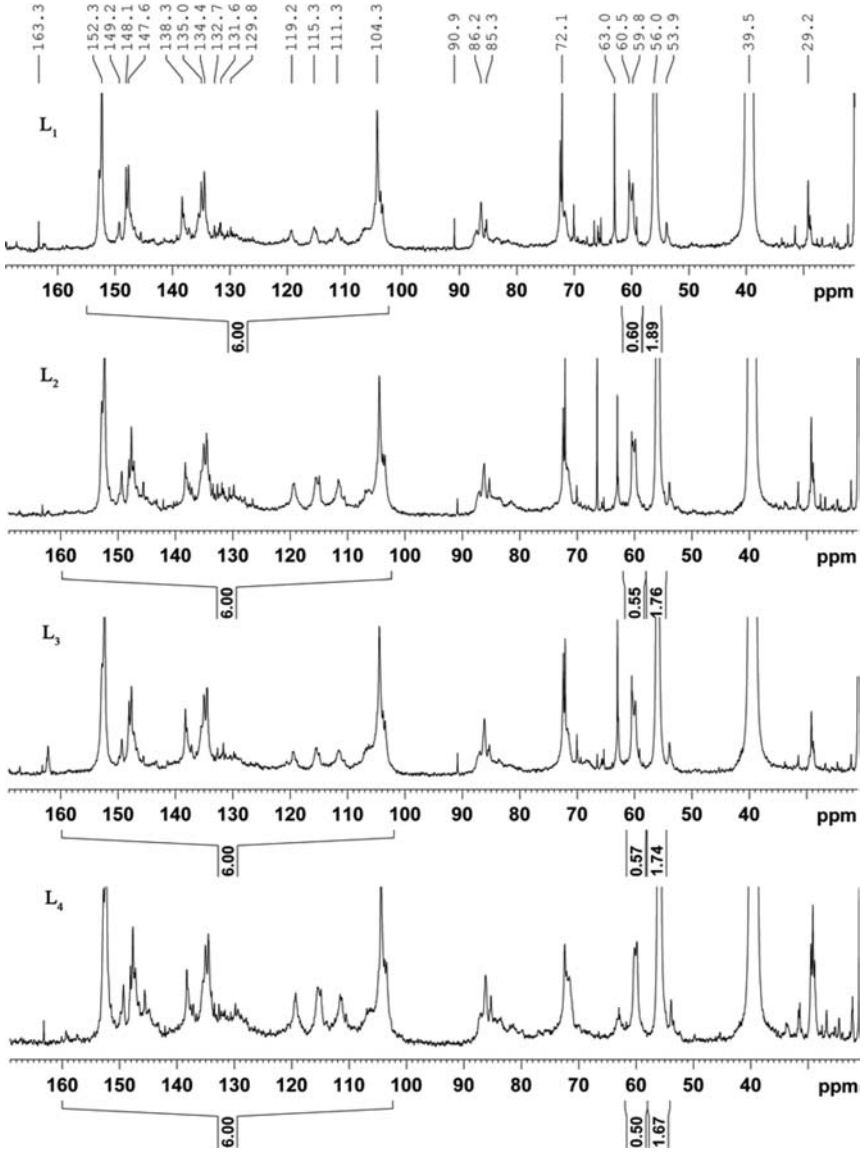

Figure 3. Quantitative ^{31}C NMR spectra of the four MWL samples.

DOI: 10.1021/jf506042s
J. Agric. Food Chem. 2015, 63, 1763−1772

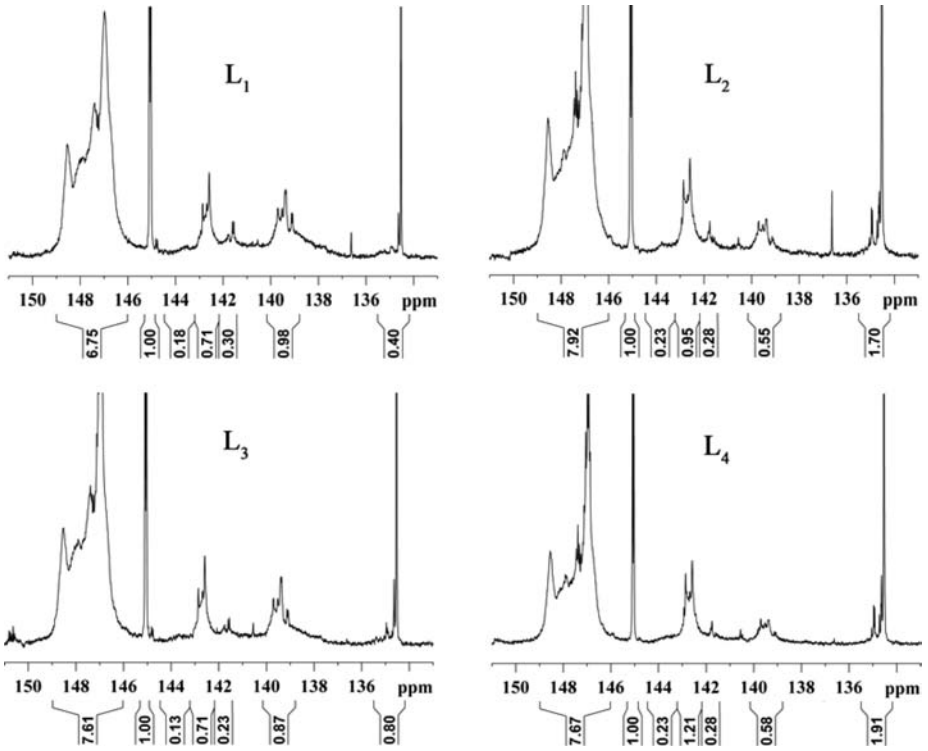

Figure 4. Quantitative ^{31}P NMR spectra of the four MWL samples.

Table 4. Functional Groups of the Four MWL Lignins As Determined by the Quantitative ^{31}P-NMR Method (mmol per g)

		syringyl OH		guaiacyl OH			
lignin	aliphtic OH	C[a]	NC[a]	C	NC	carboxylic group	total phenolic OH
L_1	3.66	0.10	0.38	0.16	0.53	0.22	1.17
L_2	4.29	0.12	0.51	0.15	0.30	0.92	1.08
L_3	4.12	0.07	0.38	0.12	0.47	0.43	1.04
L_4	4.15	0.12	0.66	0.15	0.31	1.03	1.24

[a]Abbreviations: C, condensed; NC, noncondensed.

in water,[16,17,30,31] the formation of holes may have been promoted. The "granular" materials on the surface of F_4 after the integrated treatment were due to the deposition of lignin, which was in line with previous reports.[32,33] Through the analysis of the SEM and AFM images, Kristensen et al.[34] reported that the hydrothermal pretreatment could induce the formation and migration of spherical lignin deposits onto the surface of fibers. The incremental content of deposited lignin on the surface of the fibers increased the effect of the laccase-mediated treatment.

FT-IR Analysis of the Fibers. Figure 2 shows the FT-IR spectra of the four fiber samples with the bands assigned according to previous literature results.[4,6,35] The O−H stretching vibration in OH groups was observed as a wide absorption band at 3347 cm^{-1}, and the band at 2903 cm^{-1} was attributed to the C−H asymmetric vibrations in methyl and methylene groups. The signals at 1599, 1508, and 1421 cm^{-1} were originated from the aromatic skeletal vibrations and C−H deformation. The symmetric stretching of C−O−C presented at 1037 cm^{-1} was due to the presence of cellulose and hemicelluloses. Some different absorption peaks were clearly distinguished in the four FT-IR spectra. An evident signal at 1736 cm^{-1} could be found in the spectra of F_1 and F_3, which was originated from the carbonyl stretching in unconjugated ketone, carbonyl, and ester groups.[22] The intensity of this signal was decreased in the spectra of F_2 and F_4. The same trend was observed regarding the intensity of the band at 1651 cm^{-1} (carbonyl stretching in conjugated ketones). As mentioned above, the hydronium ions (H_3O^+) could cause depolymerization of hemicelluloses and cleavage of the acetyl group, which could decrease the content of carbonyl groups. Furthermore, the deposition of lignin on the surface of the fibers, which contains minor amounts of carbonyl groups as compared to hemicelluloses, may reduce the signals of carbonyl groups.

Yield and Carbohydrate Content in the Isolated MWL Samples. The yields and carbohydrate contents of the isolated MWL samples are given in Table 2. The yield of L_1, L_2, L_3, and L_4 was 9.8%, 11.3%, 9.4%, and 11.9%, respectively. MWL could act as a representative of native lignin,[36,37] but its yield is limited and extensively relies upon milling time and the nature of the lignocellulosic materials.[38] Although all MWL samples obtained have been purified, some carbohydrates still associated with the MWL samples. As shown in Table 2, glucose and galactose were the primary sugars, while the amounts of arabinose, rhamnose and xylose were slight. However, the glucose content decreased to 0.25% and 0.62% after HCW and laccase-mediated processes, respectively. Furthermore, xylose disappeared in L_2 and L_4, suggesting that most of the xylose that was attached to lignin was removed after the HCW treatment. This observation indicated that the HCW treatment was an effective method to remove hemicelluloses.

Molecular Weight Distributions of the Four MWL Samples. As can be seen from Table 3, the molecular weights of these four MWL samples ranged from 4030 to 4790 g/mol. As compared to the M_w of L_1, the other three lignin samples exhibited a decreasing tendency. Specifically, the M_w of L_4 after

DOI: 10.1021/jf506042s
J. Agric. Food Chem. 2015, 63, 1763−1772

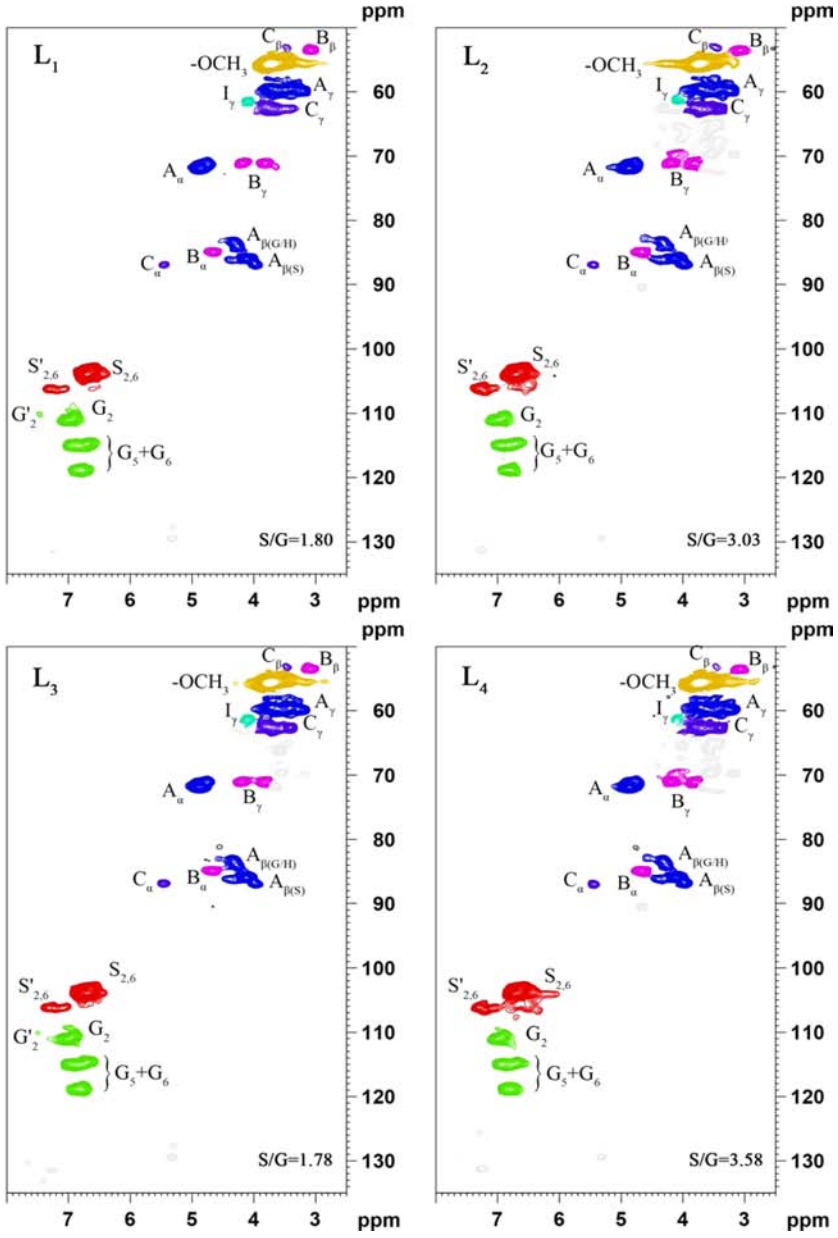

Figure 5. 2D-HSQC NMR spectra of the four MWL samples.

the integrated treatment was 4030 g/mol. The results revealed that the integrated treatment reduced the molecular weight of L_4, which was related to the depolymerization of lignin.[39] The difference in the carbohydrates contents could also be explained for this phenomenon.[23,36] In addition, the four lignin samples presented a relatively low polydispersity (M_w/M_n < 2). Furthermore, after a relatively short incubation with the laccase mediator, more activated sites and stable lignin fragments were obtained. Cleavage of linkages was the main reaction, and as a result, phenolic monomers were formed.[40]

Quantitative ^{13}C NMR Spectra of the Four MWL Samples. The quantitative ^{13}C NMR spectra of the four MWL samples are presented in Figure 3. The amount of specific substructures was calculated based on an aromatic ring (Ar).[23,24] The detailed assignments of the signals in the spectra have been given in previous literature.[24] The spectra of the MWL samples were similar to each other with the exception of several peaks. The low carbohydrate contents were verified by the diminished signals between 90 and 102 ppm, which was also confirmed by the aforementioned sugar analysis, and suggested that the lignin-carbohydrate complex linkages were partly cleaved after the treatments. The peak at 163.2 ppm originated from carboxyl groups was visible in L_1 and L_3, whereas its intensity was decreased in L_2 and L_4 due to the HCW treatment. The aryl ether bond (β-O-4′, δ 61.3−58.0) and the methoxy group (OMe, δ 58.0−54.0) regions were applied to calculate the quantitative information on the structural features. The value of OMe was decreased from 1.89/Ar in L_1 to 1.76/Ar (L_2) after HCW treatment and to 1.74/Ar (L_3) after laccase-mediator treatment, which was mainly as a result of the demethoxylation reactions that occurred in the G and/or S units. The content of β-O-4′ substructures was reduced after the treatments, and there was an especially marked decline from 0.60 to 0.50/Ar after the integrated treatment. It has been demonstrated that the predominant reactions in lignin were fragmentation rather

DOI: 10.1021/jf506042s
J. Agric. Food Chem. 2015, 63, 1763−1772

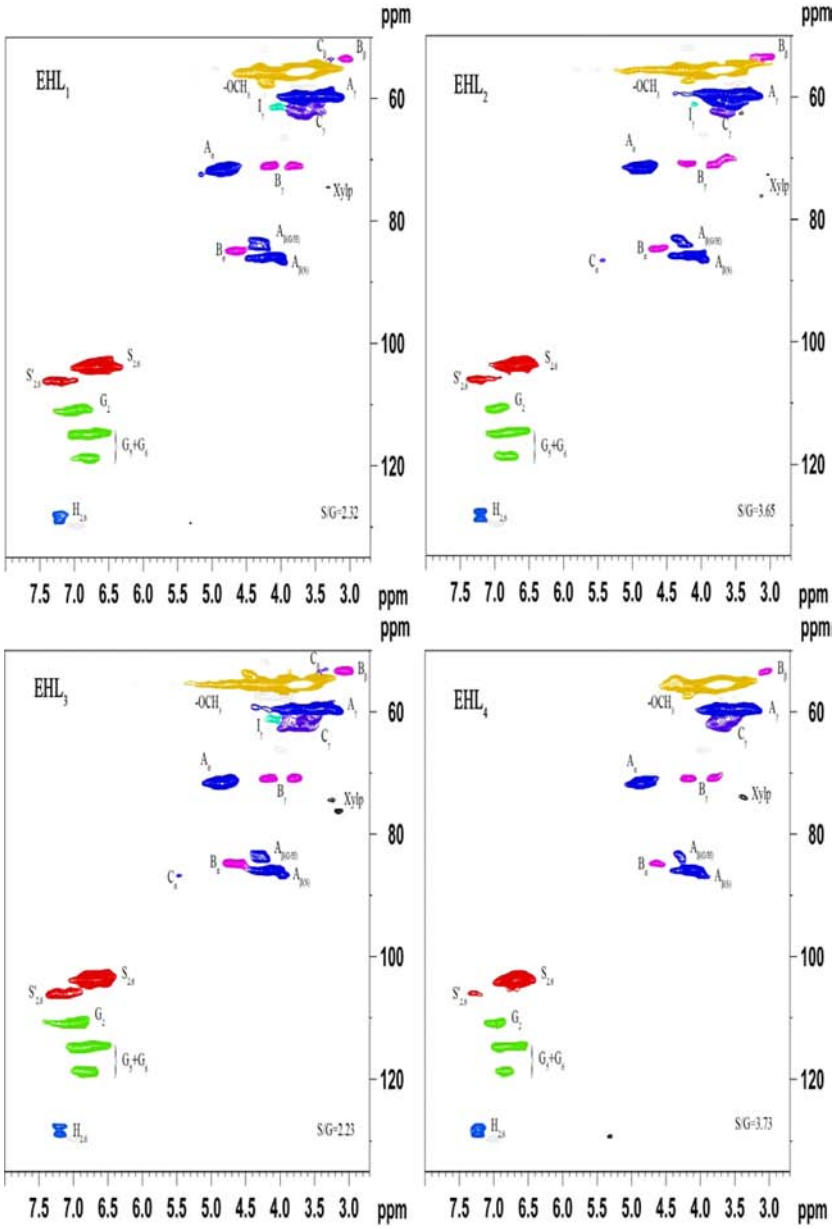

Figure 6. 2D-HSQC NMR spectra of the four EHL samples.

than polymerization. This fact was also confirmed by 2D NMR integration results.

Quantitative ^{31}P NMR Spectra of the Four MWL Samples. The reactivity of lignin is mainly defined by the OH groups, especially by the free phenolic OH groups.[41] ^{31}P NMR spectroscopy is an ideal technique for quantitating the major OH groups in lignin, such as aliphatic OH, condensed and uncondensed phenolic OH, and carboxylic acids groups.[23,42] The ^{31}P NMR spectra of L_1 to L_4 are shown in Figure 4, and the contents of different OH groups are given in Table 4. The amounts of noncondensed syringyl OH were calculated to be 0.38, 0.51, 0.38, and 0.66 mmol/g for L_1, L_2, L_3, and L_4, respectively. These results suggested that the HCW treatment could induce an augmentation of the noncondensed syringyl OH, revealing the split of *β*-*O*-4′ linkages. The content of noncondensed guaiacyl OH was gradually decreased after the HCW and laccase-mediator treatments; however, there was no obvious difference of the condensed guaiacyl OH content among these samples. This implied that parts of the guaiacyl-type lignin units were degraded and possibly released into the hydrolysate.[43] The amount of carboxylic groups in L_2, L_3, and L_4 were elevated, up to 0.92, 0.43, and 1.03 mmol/g, respectively, as compared to L_1 (0.22 mmol/g). This increment was likely attributable to the oxidation of lignin side chains during the HCW and laccase mediator treatments.[5]

2D-HSQC NMR Spectra of the Four MWL Samples. The four MWL samples were investigated by 2D-HSQC NMR techniques to reveal their detailed structures. The corresponding spectra are exhibited in Figure 5, and the main substructures are described in Figure 7. As shown in Figure 5, the prominent correlations observed in the side-chain region (δ_C/δ_H 50−90/2.5−6.0) of all of the four spectra were the *β*-*O*-4′ ether linkages (substructure A). Specifically, the correlations at δ_C/δ_H 71.7/4.85, δ_C/δ_H 83.4−85.9/4.10−4.30, and δ_C/δ_H 59.8/3.39−3.69 belong to the C_α-H_α, C_β-H_β, and C_γ-H_γ linkages of the *β*-*O*-4′ ether substructures, respectively. *β*-*β*′ (resinol, B) and *β*-5′

DOI: 10.1021/jf506042s
J. Agric. Food Chem. 2015, 63, 1763−1772

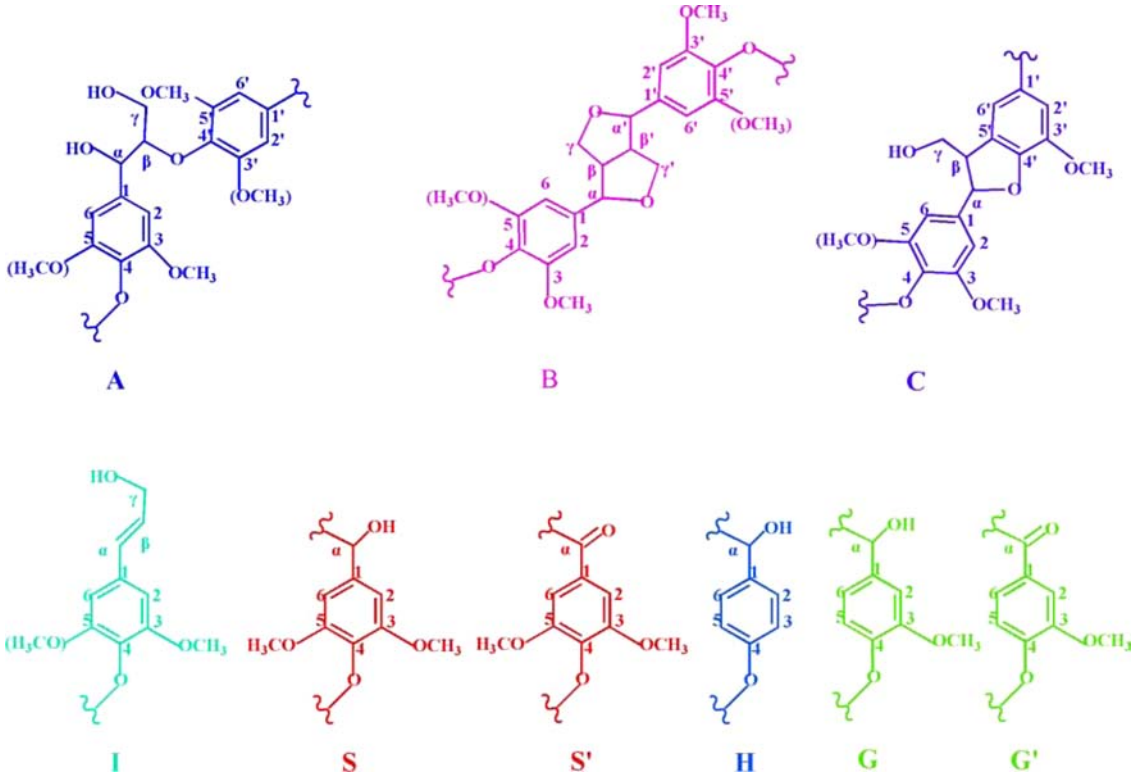

Figure 7. Main classical substructures, involving different side-chain linkages and aromatic units identified by 2D-NMR of MWL: (A) *β*-*O*-4′ aryl ether linkages with a free −OH at the *γ*-carbon; (B) resinol substructures formed by *β*-*β*′, *α*-*O*-*γ*′, and *γ*-*O*-*α*′ linkages; (C) phenylcoumaran substructures formed by *β*-5′ and *α*-*O*-4′ linkages; (I) *p*-hydroxycinnamyl alcohol end groups; (S) syringyl units; (S′) oxidized syringyl units with a C_α-ketone; (G) guaiacyl units; (G′) oxidized guaiacyl units with a C_α-ketone; (H) *p*-hydroxyphenyl units.

Table 5. Quantitation of the Four MWL and EHL Samples by the 2D-HSQC NMR Method

sample	*β*-*O*-4′[a]	*β*-*β*′	*β*-5′	S/G[b]
L_1	47.6	13.6	2.9	1.80
L_2	50.3	14.6	1.9	3.03
L_3	46.7	14.3	3.8	1.78
L_4	46.0	14.3	2.7	3.58
EHL_1	52.41	11.29	ND[c]	2.32
EHL_2	57.19	10.60	0.91	3.65
EHL_3	49.46	10.12	0.68	2.23
EHL_4	46.93	8.64	ND	3.73

[a]Results expressed per 100 Ar based on quantitative 2D-HSQC spectra. [b]S/G ratio obtained by the equation: S/G ratio = $0.5IS_{2,6}/IG_2$. [c]ND, not detected.

(phenylcoumaran, C) linkages could also be observed. Strong signals for resinol substructures B were detected at δ_C/δ_H 84.9/4.66 (C_α-H_α) and δ_C/δ_H 53.5/3.07 (C_β-H_β). The correlations located at δ_C/δ_H 71.0/3.80 and δ_C/δ_H 70.9/4.18 were ascribed to their *γ*-position. Phenylcoumaran substructures C presented relatively low levels, as shown by the correlations at δ_C/δ_H 86.97/5.46, 53.3/3.46, and 62.5/3.72 corresponding to C_α-H_α, C_β-H_β, and C_γ-H_γ, respectively.

In the aromatic region (δ_C/δ_H 100−135/5.5−8.5), the predominant correlations of S and G units could be observed in all of the spectra. The $C_{2,6}$-$H_{2,6}$ correlation for the normal S-type lignin units was found as a prominent signal at δ_C/δ_H 104.2/6.69, whereas the corresponding correlation in C_α-oxidized S′ units was shifted to δ_C/δ_H 106.3/7.21. The C_2−H_2, C_5−H_5, and C_6−H_6 correlations for the G units were identified at δ_C/δ_H 111.2/6.99, 114.5/6.82, and 118.8/6.79, respectively. The correlation for the C_2−H_2 in oxidized *α*-ketone G′ units (δ_C/δ_H 110.1/7.47) was only detected in the spectra of L_1 and L_3. Moreover, some condensed lignin structures could also be detected at $S_{2/6}$, especially for L_2 and L_4, but the formed mechanism was still not revealed.[44]

The absolute percentages of lignin substructures in the four MWL samples are listed in Table 5. The primary substructures were estimated to be *β*-*O*-4′ aryl ether linkages, ranging from 46.0% to 50.3%. The secondary substructures were detected to be *β*−*β*′ linkages (13.6−14.6%). The *β*-5′ linkages was present in lower proportions (1.9−3.8%). It could be found that the percentage of the *β*-*O*-4′ aryl ether linkages (A) decreased to 46.0% in L_4. Three different reactions have been considered to take place with the lignin polymers during the incubation period with the laccase mediator: (i) oxidation; (ii) partial polymerization with perhaps concomitant degradation and possible repolymerization; and (iii) cleavage of lignin carbohydrate bonds.[3,5,6,9,11] According to the present data, it could be concluded that a preferential degradation of lignin occurred after incubation with the laccase mediator. As can be seen form Table 5, the S/G ratio of L_1 was calculated to be 1.80. However, for L_2 isolated from HCW treated fibers and L_4 isolated from the integrated treated fibers the S/G ratio was estimated to be 3.03 and 3.58, respectively. The increased S/G ratios of L_2 and L_4 further confirmed the preferential degradation or removal of the G-type lignin in the treated fibers during hydrothermal pretreatment.[45] The correlations of the G′ units (oxidized G units with a C*α*-ketone) disappeared in the corresponding spectra of L_2 and L_4, which could only be seen at lower contour levels. In addition, the S/G ratio in L_3

DOI: 10.1021/jf506042s
J. Agric. Food Chem. 2015, 63, 1763−1772

(1.78) isolated from the laccase-mediator-treated fiber exhibited a slight reduction, which was also in line with the previous literature.[46]

2D-HSQC NMR Spectra of the Four EHL Samples. To further verify the structural transformations of lignin in the fibers, the EHL samples were isolated to make a comparison with the MWL samples. Undoubtedly, almost all lignin fractions in the materials could be obtained as EHL samples, which were more representative than the MWL samples. To preserve all structural features of the isolated EHL, no further purification was conducted. As shown in Figure 6, the four EHL samples exhibited clearly distinguishable spectra, which were similar to those of the corresponding MWL samples. The primary structural features of lignin, including S, G, and H units as well as various interunit linkages, such as β-*O*-4′, β-β′, and β-5′ linkages, can be clearly identified in the 2D-HSQC spectrum of EHL.

In the side chain region, however, the correlations at δ_C/δ_H 86.7/5.43, which originated from the C_α-H_α of the phenylcoumaran C (β-5′) substructures, could only be found in the spectra of EHL_1 and EHL_3, but still be observed at lower contour levels in the other two samples. In the aromatic region, the cross-signals from S, G, and H units could be clearly identified. The C_2−H_2 correlations in the G′ units (δ_C/δ_H 110.1/7.47) disappeared in all of the EHL samples. Whereas, the $C_{2,6}$-$H_{2,6}$ correlations from H units were clearly observed at δ_C/δ_H 127.8−128.7/7.23, which disappeared in all of the MWL samples. This phenomenon could be ascribed to MWL including a higher proportion of middle lamella material, containing few H units, and the enzymatic treatment removing most of the carbohydrates, preserving the inner H units.

The absolute percentages of β-*O*-4′, β-β′, and β-5′ linkages as well as S/G ratios of EHL samples are also listed in Table 5. Obviously, the contents of β-*O*-4′ linkages and the S/G ratios presented similar features to the corresponding MWL samples. The downtrend of the content of β-β′ linkages was observed after the hot-compressed water, laccase-mediator system, and integrated treatments. However, the content of β-5′ was very low, not even detected in the EHL_1 and EHL_4 samples. In general, the MWL and EHL samples display great similarity and either could be considered as a good representative of native lignin.

AUTHOR INFORMATION

Corresponding Author

*Tel: +86-10-62336903. Fax: +86-10-62336903. E-mail: ytq581234@bjfu.edu.cn.

Funding

We are grateful for the financial support of this research from the National Natural Science Foundation of China (31400296, 31430092, and 31110103902) and Beijing Municipal Commission of Education (20131002201).

Notes

The authors declare no competing financial interest.

REFERENCES

(1) Hüttermann, A.; Mai, C.; Kharazipour, A. Modification of lignin for the production of new compounded materials. *Appl. Microbiol. Biotechnol.* **2001**, *55*, 387−394.

(2) Liu, C.; Zhang, Y.; Wang, S.; Meng, Y.; Hosseinaei, O. Micromechanical properties of the interphase in cellulose nanofiber-reinforced phenol formaldehyde bondlines. *BioResources* **2014**, *9*, 5529−5541.

(3) Euring, M.; Trojanowski, J.; Horstmann, M.; Kharazipour, A. Studies of enzymatic oxidation of TMP-fibers and lignin model compounds by a Laccase-Mediator-System using different ^{14}C and ^{13}C techniques. *Wood Sci. Technol.* **2012**, *46*, 699−708.

(4) Nasir, M.; Gupta, A.; Beg, M. D. H.; Chua, G. K. Laccase application in medium density fibreboard to prepare a bio-composite. *RSC Adv.* **2014**, *4*, 11520−11527.

(5) Euring, M.; Trojanowski, J.; Kharazipour, A. Laccase-mediator catalazed modification of wood fibers: studies on the reaction mechanism and making of medium-density fiberboard. *Forest Prod. J.* **2013**, *63*, 54−60.

(6) Nasir, M.; Gupta, A.; Beg, M. D. H.; Chua, G. K.; Kumar, A. Fabrication of medium density fibreboard from enzyme treated rubber wood (*Hevea brasiliensis*) fibre and modified organosolv lignin. *Int. J. Adhes. Adhes.* **2013**, *44*, 99−104.

(7) Euring, M.; Ruhl, M.; Ritter, N.; Kues, U.; Kharazipour, A. Laccase mediator systems for eco-frendly production of medium-density fiberboard (MDF) on a pilot scale: Physicoochemical analysis of the reaction mechanism. *J. Biotechnol.* **2011**, *6* (s1), 1253−1261.

(8) Shiraishi, T.; Sannami, Y.; Kamitakahara, H.; Takano, T. Comparison of a series of laccase mediators in the electro-oxidation reaction of nonphenolic lignin model compounds. *Electrochim. Acta* **2013**, *106*, 440−446.

(9) West, M. A.; Hickson, A. C.; Mattinen, M. L.; Lloyd-Jones, G. Evaluating lignins as enzyme subatrates: insight and methodological recommendations from a study of laccase-catalyzed lignin polymerization. *BioResources* **2014**, *9*, 2782−2796.

(10) Widsten, P.; Kandelbauer, A. Adhesion improvement of lignocellulosic products by enzymatic pre-treatment. *Biotechnol. Adv.* **2008**, *26*, 379−386.

(11) Felby, C.; Thygesen, L. G.; Sanadi, A.; Barsberg, S. Native lignin for bonding of fiber board-evaluation of bonding mechanisms in boards made from laccase-treated fibers of beech (*Fagus sylvatica*). *Ind. Crop. Prod.* **2004**, *20*, 181−189.

(12) Alvarez, C.; Rojano, B.; Almaza, O.; Rojas, O. J.; Ganan, P. Self-bonding boards from plantain fiber bundles after enzymatic treatment: adhesion improvement of lignocellulosic products by enzymatic pre-treatment. *J. Polym. Environ.* **2011**, *19*, 182−188.

(13) Hu, F.; Jung, S.; Ragauskas, A. Impact of pseudolignin versus dilute acid-pretreated lignin on enzymatic hydrolysis of cellulose. *ACS Sustainable Chem. Eng.* **2012**, *1*, 62−65.

(14) Liu, J.; Hu, H. R.; Xu, J. F.; Wen, Y. B. Optimizing enzymatic pretreatment of recycled fiber to improve its draining ability using response surface methodology. *BioResources* **2012**, *7*, 2121−2140.

(15) Runge, T.; Wipperfurth, P.; Zhang, C. H. Improving biomass combustion quality using a liquid hotwater treatment. *Biofuels* **2013**, *4*, 73−83.

(16) Ma, X. J.; Yang, X. F.; Zheng, X.; Lin, L.; Chen, L. H.; Huang, L. L.; Cao, S. L. Degradation and dissolution of hemicelluloses during bamboo hydrothermal pretreatment. *Bioresour. Technol.* **2014**, *161*, 215−220.

(17) Xu, J.; Thomsen, M. H.; Thomsen, A. B. Feasibility of hydrothermal pretreatment on Maize Silage for bioethanol production. *Appl. Biochem. Biotechnol.* **2010**, *162*, 33−42.

(18) Solala, L.; Antikainen, T.; Reza, M.; Johansson, L. S.; Hughes, M.; Vuorinen, T. Spruce fiber properties after high-temperature thermomechanical pulping (HT-TMP). *Holzforschung* **2014**, *68*, 195−201.

(19) Björkman, A. Isolation of lignin from finely divided wood with neutral solvents. *Nature* **1954**, *174*, 1057−1058.

(20) Wen, J. L.; Xue, B. L.; Xu, F.; Sun, R. C. Unveiling the structural heterogeneity of bamboo lignin by in situ HSQC NMR technique. *Bioenerg. Res.* **2012**, *5*, 886−903.

(21) Sluiter, A.; Hames, B.; Ruiz, R.; Scarlata, C.; Sluiter, J.; Templeton, D.; Crocker, D. *Laboratory Analytical Procedure (LAP): Determination of Structural Carbohydrates and Lignin in Biomass*; Technical Report: NREL/TP-510-42618. National Renewable Energy Laboratory: Golden, CO, 2008.

DOI: 10.1021/jf506042s
J. Agric. Food Chem. 2015, 63, 1763−1772

(22) Yuan, T. Q.; Xu, F.; He, J.; Sun, R. C. Structural and physicochemical characterization of hemicelluloses from ultrasound-assisted extractions of partially delignified fast-growing poplar wood through organic solvent and alkaline solutions. *Biotechnol. Adv.* **2010**, *28*, 583−593.
(23) Yuan, T. Q.; Sun, S. N.; Xu, F.; Sun, R. C. Characterization of lignin structures and lignin−carbohydrate complex (LCC) linkages by quantitative ^{13}C and 2D HSQC NMR spectroscopy. *J. Agric. Food Chem.* **2011**, *59*, 10604−10614.
(24) Wen, J. L.; Sun, S. L.; Yuan, T. Q.; Xu, F.; Sun, R. C. Structural elucidation of lignin polymers of *Eucalyptus* chips during organosolv pretreatment and extended delignification. *J. Agric. Food Chem.* **2013**, *61*, 11067−11075.
(25) Sun, S. L.; Wen, J. L.; Ma, M. G.; Sun, R. C. Structural elucidation of sorghum lignins from an integrated biorefinery process based on hydrothermal and alkaline treatments. *J. Agric. Food Chem.* **2014**, *62*, 8120−8128.
(26) Romaní, A.; Garrote, G.; López, F.; Parajó, J. C. *Eucalyptus globulus* wood fractionation by autohydrolysis and organosolv delignification. *Bioresour. Technol.* **2011**, *102*, 5896−5904.
(27) López-Linares, J. C.; Romero, I.; Cara, C.; Ruiz, E.; Castro, E.; Moya, M. Experimental study on ethanol production from hydrothermal pretreated rapeseed straw by simultaneous saccharification and fermentation. *J. Chem. Technol. Biotechnol.* **2014**, *89*, 104−110.
(28) Heinemann, S.; Wang, S. X.; Peltonen, J.; Kleen, M. Characterization of fiber wall surface structure of chemically modified TMP fibers from Norway spruce. *Nord. Pulp. Pap. Res. J.* **2011**, *26*, 21−30.
(29) Fermando, D.; Muhic, D.; Engstrand, P.; Daniel, G. Fundamental understanding of pulp property development under different thermo-mechanical pulp refining condition as observed by a new Simons' staining method and SEM observation of the ultrastructure of surfaces. *Holzforschung* **2011**, *65*, 777−786.
(30) Dogaris, I.; Karapati, S.; Mamma, D.; Kalogeris, E.; Kekos, D. Hydrothermal processing and enzymatic hydrolysis of sorghum bagasse for fermentable carbohydrates production. *Bioresour. Technol.* **2009**, *100*, 6543−6549.
(31) Kim, T. H.; Lee, Y. Y. Fractionation of corn stover by hot-water and aqueous ammonia treatment. *Bioresour. Technol.* **2006**, *97*, 224−232.
(32) Ruiz, H. A.; Rodríguez-Jasso, R. M.; Fernandes, B. D.; Vicente, A. A.; Teixeira, J. A. Hydrothermal processing, as an alternative for upgrading agriculture residues and marine biomass according to the biorefinery concept: A review. *Renewable Sustainable Energy Rev.* **2013**, *21*, 35−51.
(33) Zhang, M. M.; Chen, G. J.; Kumar, R.; Xu, B. Q. Mapping out the strutural changes of natural and pretreated plant cell wall surfaces by atomic force microscopy single molecular recognition imaging. *Biotechnol. Biofuels.* **2013**, *6*, 147.
(34) Kristensen, J. B.; Thygesen, L. G.; Felby, C.; Jørgensen, H.; Elder, T. Cell-wall structural changes in wheat straw pretreated for bioethnol production. *Biotechnol. Biofuels.* **2008**, *1*, 5.
(35) Wang, S. H.; Liu, J. L.; Li, F.; Dai, J. M.; Jia, H. S.; Xu, B. S. Study on converting cotton pulp fiber into carbonaceous microspheres. *Fiber Polym.* **2014**, *15*, 286−290.
(36) Yuan, T. Q.; Sun, S. N.; Xu, F.; Sun, R. C. Structural characterization of lignin from triploid of *Populus tomentosa* Carr. *J. Agric. Food Chem.* **2011**, *59*, 6605−6615.
(37) Wen, J. L.; Xue, B. L.; Xu, F.; Sun, R. C.; Pinkertc, A. Unmasking the structural features and property of lignin from bamboo. *Ind. Crops Prod.* **2013**, *42*, 332−343.
(38) Rencoret, J.; Marques, G.; Gutiérrez, A.; Nieto, L.; Santoe, J. L.; Jiménez-Barbero, J.; Martínez, A. T.; del Río, J. C. HSQC-NMR analysis of lignin in woody (*Eucalyptus globulus* and *Picea abies*) and non-woody (*Agave sisalana*) ball-milled plant materials at the gel state. *Holzforschung* **2009**, *63*, 691−698.
(39) Yelle, D. J.; Kaparaju, P.; Hunt, C. G.; Hirth, K.; Kim, H.; Ralph, J.; Felby, C. Two-dimensional NMR evidence for cleavage of lignin and xylan substituents in wheat straw through hydrothermal pretreatment and enzymatic hydrolysis. *Bioenergy Res.* **2013**, *6*, 211−221.
(40) Trajano, H. L.; Engle, N. L.; Foston, M.; Ragauskas, A. J.; Tschaplinski, T. J.; Wyman, C. E. The fate of lignin during hydrothermal pretreatment. *Biotechnol. Biofuels* **2013**, *6*, 110.
(41) Akim, L. G.; Argyropoulos, D. S.; Jouanin, L.; Leplé, J.-C.; Pilate, G.; Pollet, B.; Lapierre, C. Quantitative ^{31}P NMR spectroscopy of lignins from transgenic poplars. *Holzforschung* **2001**, *55*, 386−390.
(42) Argyropoulos, D. S. ^{31}P NMR in wood chemistry: A review of recent progress. *Res. Chem. Intermed.* **1995**, *21*, 373−395.
(43) Nicolas, B.; Roland, E.-H.; Mounir, C.; Mathieu, P.; Stéphane, D.; Philippe, G. Investigation of the chemical modifications of beech wood lignin during heat treatment. *Polym. Degrad. Stab.* **2010**, *95*, 1721−1726.
(44) Torr, K. M.; Love, K. T.; Cetinkol, Ö. P.; Donaldson, L. A.; George, A.; Holmes, B. M.; Simmons, B. A. The impact of ionic liquid pretreatment on the chemistry and enzymatic digestibility of *Pinus radiata* compression wood. *Green Chem.* **2012**, *14*, 778−787.
(45) Xiao, L. P.; Shi, Z. J.; Xu, F.; Sun, R. C. Characterization of lignins isolated with alkaline ethanol from the hydrothermal pretreated *Tamarix ramosissima*. *Bioenerg. Res.* **2013**, *6*, 519−532.
(46) Ibarra, D.; Chavez, M. I.; Rencoret, J.; del Río, J. C.; Gutierrez, A.; Romero, J.; Camarero, S.; Martínez, M. J.; Jiménez-Barbero, J.; Martinez, A. T. Structural modification of eucalypt pulp lignin in a totally chlorine-free bleaching sequence including a laccase-mediator stage. *Holzforschung* **2007**, *61*, 634−646.

DOI: 10.1021/jf506042s
J. Agric. Food Chem. 2015, 63, 1763−1772

containing 12% dry matter. Then the concentrated microalgae were lyophilized to yield dry flakes containing 95−97% dry matter. The dry algae samples were stored at −26 °C and processed within 3 days.

Chemicals and Reagents. FAME mix standards (GLC 566) was purchased from Nu-Chek (Elysian, MN, USA). Cholesterol (≥99% GC), 5α-cholestane (≥97% GC), and hexadecane (99%) used in the determination of GC response factors were purchased from Sigma-Aldrich (St. Louis, MO, USA). Other analytical grade solvents (isopropanol, chloroform, and methanol) were purchased from Fisher Scientific (Fair Lawn, NJ, USA).

Proximate Analysis of Microalgae Biomass. Dry matter content was determined by weight difference after oven-drying at 110 °C for 5 h. Lipid content was determined gravimetrically after solvent extractions as described below, and protein content was determined by using the Dumas nitrogen combustion method with an ElementarVario MAXCN analyzer (Elementar Analysensysteme GmbH, Hanau, Germany) and a nitrogen-to-protein conversion factor of 4.36.[19] Ash content was determined by heating the dry algae samples at 550 °C for 5 h and then weighing the residual ash (AOAC Official Method 923.03). All of the algae samples were washed with DI water to remove growth media before drying/dewatering prior to ash determination.

Microalga Lipid Extraction. Dry algae sample (20 g) was first extracted with isopropanol (300 mL) for 1 h with continuous stirring (300 rpm) to deactivate hydrolytic enzymes that might be present. After isopropanol extract was recovered by filtration, the residual wet solids were mixed with chloroform/methanol (300 mL, 2:1, v/v) and then homogenized using an Ultra-Turrax T25 homogenizer (Ika Works, Wilmington, NC, USA) at 10,000 rpm for 3 min, followed by a 2 h continuous stirring at 300 rpm and then a sequential extraction with chloroform/methanol at ratios of 2:1, 1:1, and 1:2 (v/v). Each extraction used 300 mL of solvent, a 300 rpm stirring rate, and a duration of 1 h. The extracts from isopropanol and chloroform/methanol extractions were combined, and the solvent was removed by rotary evaporation at 45 °C. The crude lipid was subjected to the modified Folch wash[20] twice using a mixed solvent of chloroform, methanol, and water in a ratio of 8:4:3. The lipids obtained from the chloroform phase were filtered through a PTFE filter disk (0.45 μm) and then dried by rotary evaporation at 45 °C and vacuum oven at 23 °C for 12 h. The quantity of extracted lipids was determined gravimetrically. Four replicates of extractions were performed to determine lipid content. Then the lipids of each alga were combined and dissolved in a small amount of chloroform and stored at −26 °C until further analysis.

Fractionation of Neutral Lipid, FFA, and Polar Lipid by TLC. Algae total lipids (30−40 mg) dissolved in chloroform were applied on a preparative TLC plate (silica gel G, 500 μm, Analtech, Newark, DE, USA), and the plate was developed in a mixed solvent of hexane/diethyl ether/acetic acid (70:30:1, by vol). The separation was visualized under ultraviolet light after spraying with 0.1% (w/v) 2′,7′-dichlorofluorescein in methanol. The bands of TAG and FFA were scraped off the plate and extracted four times with 10 mL of chloroform/methanol (2:1). The bands of other lipid components (including polar lipids, sterols, and chlorophyll derivatives) that were located below the FFA band, referred to as the polar lipid fraction, were extracted twice with 10 mL of chloroform/methanol (2:1) and then twice with 10 mL of chloroform/methanol/water (5:5:1). The solvent of combined extracts of each fraction was removed by rotary evaporation at 45 °C. Residual water was removed with a small amount of isopropanol by rotary evaporation. The recovered lipids were converted to FAME in the presence of 1 mg of nonadecanoic acid (internal standard) and analyzed by GC following the procedure described below. Because only fatty acids' GC peaks were quantified, sterols and chlorophyll derivatives in the polar lipid fraction did not interfere with FAME quantification. The weight percentage of FAME was converted to TAG and FFA equivalents using the factors given in AOCS Official Method Ce 1i-07. Three replicates of total lipids from each alga were fractionated by TLC. Because polar lipids of the examined algae contained a variety of molecular species, which varied by the type of algae, estimation of polar lipid content based on GC-FAME result would be inaccurate if converting it to one type of polar lipid. Instead, the weight percentage of glycolipids and phospholipids obtained from LC-MS quantification was used in the calculation.

Fatty Acid Composition. The fatty acid composition of the total lipids and those of neutral and polar lipid fractions were determined by GC analysis of FAME. The lipids (10−20 mg) were methylated with 2% sulfuric acid in methanol (3 mL) by incubation at 65 °C for 18 h with occasional shaking. The resulting FAME were extracted with 3 mL of hexane and washed with 10 mL of water. The hexane extract (1 μL) was injected into an Agilent 7890 GC (Santa Clara, CA, USA) equipped with a DBWAXtre capillary column (30 m × 0.25 mm × 0.25 μm; Agilent, Santa Clara, CA). Helium was used as a carrier gas with a flow rate of 1 mL/min. The split ratio was 50:1. The temperature of the injector and FID detector was 260 °C. GC oven temperature was programmed from 100 °C (1 min) to 240 °C (15 min) at a rate of 4 °C/min. GC peaks were identified by the mixed FAME standard (GLC 566) and confirmed by GC-MS. The relative percentage of fatty acids was reported on the basis of the peak area without using correction factors. Three replicates of FAME samples were prepared from each alga.

The GC-MS system for the identification of fatty acids in each microalga included an Agilent 6890 GC and a Waters GCT time-of-flight mass spectrometer (Milford, MA, USA) operated in electron ionization (+) mode at 70 eV. Data were acquired with accurate mass precision (7000 resolution fwhm). The MS scanned from 45 to 650 Da each 0.5 s. Data were processed with MassLynx 4.0 (Waters Inc.) and compared with MS libraries Wiley 7th edition (2000) and NIST 2011. GC column specification, oven temperature program, injector temperature, carrier gas flow rate, and split ratio were the same as those used for fatty acid composition analysis.

Unsaponifiable Matters (USP). The percentage of USP in the total algae lipids was determined according to AOCS Official Method Ca 6b-53. Briefly, 2 g of total lipids was saponified with 95% ethanol and 50% KOH, and then the USP was extracted multiple times with diethyl ether. Total USP was determined by the weight of the ether extract after solvent removal and expressed as the weight percent of total lipids. The profile of USP was determined by GC-FID and GC-MS. For GC-FID analysis, USP dissolved in chloroform (3 mg/mL) was injected into an Agilent 7890 GC equipped with SAC-5 fused silica capillary column (30 m × 0.25 mm × 0.25 μm; Supelco, Bellefonte, PA, USA). The split ratio of GC injector was 50:1. The temperature of the injector and FID detector was 300 °C. GC oven temperature was programmed from 200 °C (1 min) to 300 °C (19 min hold) at a rate of 10 °C/min. The percentage of USP that were GC quantifiable was determined by using an internal standard, 5α-chloestane. GC response factors of hydrocarbons and sterols relative to 5α-chloestane were determined to be 0.862 for hexadecane and 0.775 for cholesterol, according to AOCS Official Method Ce 1j-07, and these factors were used in the calculations. Two replicates of microalgae total lipids were saponified.

The USP of *Chlamy*, *Chlorella*, *Nanno*, and *Scene* were fractionated on a silica gel TLC using a solvent system of hexane/diethyl ether/acetic acid (60:40:1, by vol). Six TLC fractions were collected from each microalga on the basis of their polarity or the position on the plates. Both the total USP and TLC fractionated USP of four green microalgae and the total USP of *Schizo* were then analyzed by GC-MS. The GC-MS unit for USP analysis was the same as that used for fatty acid analysis. GC column specification, oven temperature program, injector temperature, carrier gas flow rate, and split ratio in GC-MS were the same as those used for GC-FID analysis of USP.

Profiling of Polar Lipid (Glycolipids and Phospholipids) by TLC and ESI-MS/MS. A preliminary qualification of polar lipids was performed using normal phase TLC. First, the total lipids was applied on a normal phase SPE column (silica, 2000 mg, Alltech Extract-Clean column; Grace, Columbia, MD, USA), and then the cartridge was sequentially washed with 20 column volumes of hexane/diethyl ether (4:1), acetone, chloroform/methanol (1:1), and chloroform/methanol/water (5:5:1). The first fraction (hexane/diethyl ether) contained exclusively nonpolar lipids and was discarded. Other SPE fractions were applied on an analytical TLC plate (silica gel GHL, 250 μm;

DOI: 10.1021/jf5050603
J. Agric. Food Chem. 2015, 63, 1773−1787

Table 1. Microalgae Biomass Composition on a Dry Weight Basis[a]

	Chlamy	*Chlorella*	*Nanno*	*Scene*	*Schizo*
lipid	24.2 (0.1)	17.9 (3.3)	25.0 (0.4)	10.5 (0.4)	56.7 (0.8)
protein[b]	34.2 (0.3)	28.2 (1.4)	32.2 (0.1)	24.6 (0.3)	12.4 (0.3)
ash	6.1 (0.2)	10.5 (0.3)	5.5 (0.3)	29.5 (0.3)	5.6 (0.1)
carbohydrates[c]	35.5	43.4	37.3	35.4	25.3

[a]Values in parentheses are standard deviations of three replicates. [b]Nitrogen-to-protein conversion factor of 4.36 is used (Gerde et al.[19]). [c]Carbohydrate content is calculated by subtracting lipid, protein, and ash contents from 100%.

Table 2. Microalgae Lipid Class Composition (Weight Percent)[a]

	Chlamy	*Chlorella*	*Nanno*	*Scene*	*Schizo*
neutral lipids	51.3	57.2	14.5	31.5	78.2
TAG	24.5 (2.2)	26.6 (2.8)	8.6 (1.5)	4.1 (0.8)	77.5 (6.4)
FFA	26.8 (2.3)	30.6 (2.1)	5.9 (0.6)	27.4 (1.3)	0.7 (0.6)
polar lipids[b]	9.7 (0.3)	0.7 (0.0)	24.6 (0.4)	0.7 (0.1)	0.9 (0.2)
USP[c]	13.1 (0.1)	13.2 (0.4)	14.6 (0.4)	18.7 (0.6)	1.9 (0.0)
chlorophyllides[c]	16.8	14.6	5.8	14.3	
others[d]	9.1	14.3	40.5	34.8	19.1

[a]Values in parentheses are standard deviations of three replicates for TAG and FFA and differences of two replicates for USP and polar lipids. [b]Polar lipids in this table are glycolipids and phospholipids quantified by HPLC-MS. [c]The wt % of phytol chain of chlorophylls is included in USP (unsaponifiable matters). Chlorophyllide (nonphytol moiety of chlorophylls) is calculated on the basis of the assumption that all of the chlorophyll pigments had the same molecular structure as chlorophyll *a*. [d]"Others" represents the differences between 100 and the known components.

Analtech, Newark, DE, USA). The developing solvent system was methyl acetate/isopropanol/chloroform/methanol/0.25% aqueous KCl (25:25:25:10:4, v/v), which was based on a published method[21] with a minor modification of the ratio of aqueous KCl. Glycolipid standards MGDG, DGDG, and steryl glucoside (purchased from Matreya, Pleasant Gap, PA, USA), SQDG (purchased from Larodan, Sweden), phospholipid standards PC, PE, PG, and PI (purchased from Avanti, Alabaster, AL, USA), and soy lecithin (Fisher Scientific) were used in the comparison with microalgae lipid components. The spraying agent of 70% orcinol in sulfuric acid was used for the identification of glycolipids and steryl glucoside, and molybdenum blue was used for phospholipids.[20]

Polar lipid (i.e., glycolipids and phospholipids) analysis by LC-MS was performed by Kansas Lipidomics Research Center Analytical Laboratory (Manhattan, KS, USA). ESI-MS/MS analysis and quantification were conducted as described previously.[22] Microalgae lipid samples (total lipid extract) were introduced by continuous infusion into the electrospray ionization source on a triple-quadrupole MS/MS (API 4000; Applied Biosystems, Foster City, CA, USA). Lipid species were detected using sequential precursor and neutral loss scans. Lipids in each class were quantified in comparison with the two internal standards of that class using a correction curve determined between standards. The compositional data are presented as nanomoles (per weight) or weight percent of the total lipids analyzed. Two replicates of unfractionated total lipids of each microalga were analyzed.

Analysis of Chlorophyll Derivatives by TLC and LC/APCI-MS. The TLC fractionated polar lipid fraction of green microalgae were dissolved in iso-octane/toluene/acetone/methanol (5:5:1:1)[7] to a concentration of 1 mg/mL, and 2 μL was injected to an Agilent HPLC system equipped with the 1200 series Agilent binary pump system. A guard column (2.0 × 23 mm, s-0.5 μm; YMC, Allentown, PA, USA) and a YMC PVA-SIL column (150 mm × 2 mm, s-0.5 μm, 12 nm; YMC) were used in all separation experiments. The column temperature was maintained at 35 °C. The flow rate was 0.5 mL/min. The solvent composition and gradient program were modified on the basis of previous studies.[7,23,24] The solvent system consisted of isopropanol/hexane (2:98, by vol, with 0.1% of stoichiometric triethylamine/formic acid, solvent A1), isopropanol/acetonitrile/chloroform/acetic acid (84:8:8:0.025, by vol, solvent B1), and chloroform/isopropanol/methanol (39:21:40, by vol, solvent A2). The gradient elution program was as follows: 0−2.5 min, 100% A1; 2.5−40 min, 0−100% B1. After 40 min, the column was flushed with A2 (0−100%) for 15 min and reconditioned with A1 for 15 min. Mass spectrometry analysis was performed using the Agilent 6540 Accurate-Mass Q-TOF mass spectrometer with MassHunter Qualitative Analysis software for data acquisition and processing. The atmospheric pressure chemical ionization (APCI) source was set to operate in negative ion mode with a vaporizer temperature of 250 °C. Resolution was 40,000 fwhm, and mass accuracy was better than 2 ppm across the mass range. The instrument was tuned and calibrated with an Agilent tune mix prior to all LC-MS experiments.

Melting and Crystallization Temperatures of Microalgae Lipids and Their Methyl and Isopropyl Esters. The methyl and isopropyl esters of microalgae lipids were obtained by sulfuric acid (2%) catalyzed alcoholysis. The reaction conditions and purification procedure were the same as those used in FAME preparation described above. The melting and crystallization properties of lipid samples were determined by using a differential scanning calorimeter (Diamond DSC; PerkinElmer, Norwalk, CT, USA) equipped with an Intracooling II system. A sample of 3−5 mg was weighed in an aluminum pan (PerkinElmer) and sealed. Indium and *n*-decane were used as calibration standards. The temperature program started with a 1 min hold at 25 °C, followed by a rapid heating (40 °C/min) to 80 °C and a 5 min hold at 80 °C. Then the sample was cooled to −40 °C at a rate of 10 °C/min. After a 15 min hold at −40 °C, the sample was heated to 80 °C at a rate of 5 °C/min. The crystallization onset and completion of melting were recorded during the cooling and the last heating steps, respectively. Two replicates from each alga were measured.

Statistical Analysis. The number of replicates of each analysis was described above. Standard deviations were given for the mean values obtained with three or more replicates. Differences between two values were also given when there were only two replicates.

RESULTS AND DISCUSSION

Proximate Composition. Of the examined microalgae in this study, *Chlamy* (taxonomic class: Chlorophyceae), *Chlorella* (taxonomic class: Trebouxiophyceae), and *Scene* (taxonomic class: Chlorophyceae) are freshwater green algae; *Nanno* (taxonomic class: Eustigmatophyceae) is a saltwater green alga; and *Schizo* (taxonomic class: Thraustochytriaceae) is a saltwater heterotrophic alga.[25,26] Microalgae biomass composition is given in Table 1. *Scene* and *Schizo* had the lowest (11%)

DOI: 10.1021/jf5050603
J. Agric. Food Chem. 2015, 63, 1773−1787

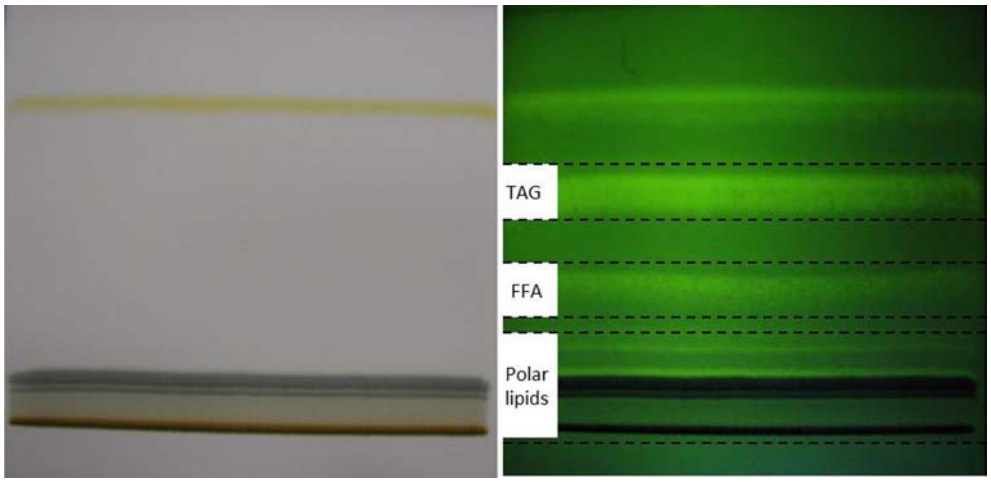

Figure 1. Separation of neutral and polar lipids of *Nanno*. The images on the left and right were taken before and after the fluorescence spray. The dashed lines illustrate how the fractions/silica strips were taken. The developing solvent was hexane/diethyl ether/acetic acid (70:30:1, by vol).

and highest lipid contents (57%), respectively. *Chlamy*, *Chlorella*, and *Nanno* had lipid contents in the range of 18−25%, similar to that of common oilseeds, such as soybeans. Their lipid contents were not unusual as compared to the literature.[3,5,7,25] *Scene* had an exceptionally high level of ash content (30%), followed by the 11% of *Chlorella*. The other three species contained 5−6% ash. Green microalgae contained higher protein contents (25−34%) than *Schizo* (12% proteins). Protein contents of *Chlamy*, *Chlorella*, and *Scene* were generally lower than the values summarized by Becker.[27] It is noted that protein content was not only affected by the growth conditions but also varied with the determination method.[19]

Microalgae Lipid Class Composition. *Nanno* contained the least amount of neutral lipids (15%) but the greatest amount of polar lipids (25%) among the green microalgae (Table 2). Because sterols and hydrocarbons are discussed separately, neutral lipids in this paper are defined as the simple acyl lipids, which include TAG and FFA. *Schizo* was mainly composed of TAG (78%) with <1% of polar lipids. All of the green microalgae had appreciable amounts of chlorophylls (6−17%) and USP (13−19%). *Chlamy* and *Chlorella* had similar lipid class compositions in terms of neutral lipids (51−57%), USP (13%), and chlorophylls (15−17%). Freshwater species were found to contain 27−31% FFA in this study, which more likely resulted from lipid degradation during storage and processing[28] rather than the algae responding to the change of or detrimental growth condition.[29] The relative ratio of TAG/FFA/polar lipids varied by algae species.[2,6] Even for the same species, the compositions of fatty acids and complex lipids in algae heavily fluctuate depending on growth conditions such as light, temperature, nitrogen level, salt stress and the growth stages at which they are harvested.[30,31] Detailed reviews on lipid metabolism in response to various growth factors were given by Harwood and Jones[2] and Guschina and Harwood.[3] For the above reasons, a compositional comparison of fatty acids and complex lipids of the microalgae examined with literature values is not given here. "Others" in Table 2 might include, but is not limited to, the acyl chains of sterol esters, carotenoids, and other polar lipids, such as diacylglycerol trimethylhomoserine ether (DGTS), which were reported as a major component in green algae, and chlorosulfolipids, which were found in freshwater species.[2] The polar lipid composition was very complex as seen by TLC. The lipid components with high polarity covered nearly the entire lower half of the TLC plate. The TLC images of separation of neutral and polar lipids of *Nanno* are given in Figures 1 and 2.

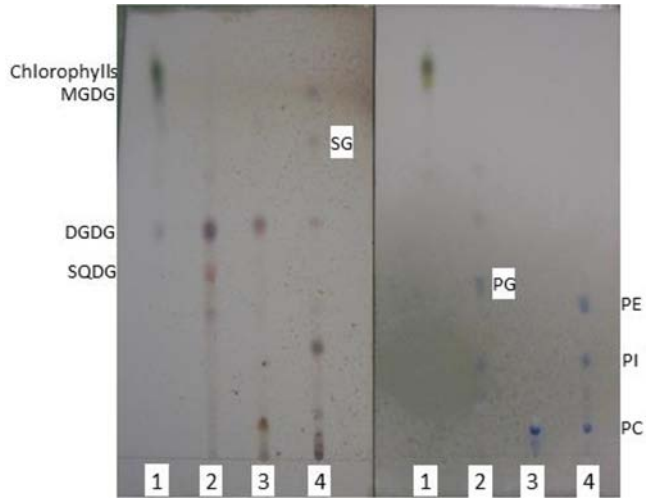

Figure 2. TLC separation of polar lipids of *Nanno*. The plates on the left and right were sprayed with 70% orcinol in sulfuric acid and molybdenum blue, respectively. The samples on the two plates were the same, which were the fractions collected after SPE separation of *Nanno* total lipids. Lanes: 1, acetone fraction; 2, chloroform/methanol (1:1) fraction; 3, chloroform/methanol/water (5:5:1) fraction; 4, soy lecithin. The developing solvent was methyl acetate/isopropanol/chloroform/methanol/0.25% aqueous KCl (25:25:25:10:4, by vol).

FAME Composition of Total Lipids, TAG, FFA, and Polar Lipids. Table 3 presents the FAME composition of unfractionated total lipids of five microalgae, as well as those in their TAG, FFA, and polar lipid fractions separated by normal phase TLC. Table 4 summarizes the distribution of saturated (SFA), monounsaturated (MUFA), and polyunsaturated fatty acids (PUFA) of five microalgae as well as their n-3 fatty acid contents.

Major fatty acids in *Chlamy* were C16:0 (27%), C16:4 (6%), C18:1*c* (16%), C18:2 (16%), and C18:3 (10%), representing 75% of total fatty acids. Although there were some differences in the proportion of individual fatty acids when TAG, FFA, and polar lipid fractions were compared with the total lipids of

DOI: 10.1021/jf5050603
J. Agric. Food Chem. 2015, 63, 1773−1787

Table 3. FAME Composition (relative weight percent) of Unfractionated Total Lipids, TAG, FFA, and Polar Lipids[a]

	Chlamy				*Chlorella*				*Nanno*			
	total lipids	TAG	FFA	polar lipids	total lipids	TAG	FFA	polar lipids	total lipids	TAG	FFA	polar lipids
C8:0									0.3 (0.0)			
C10:0									0.1 (0.0)			0.1
C12:0									0.3 (0.0)	0.8	0.6	0.2
C14:0	1.4 (0.5)	0.3	0.2	5.6	1.3 (0.1)	0.3	0.1	0.2	6.0 (0.2)	5.9	5.4	6.2
C14:1	0.6 (0.2)				0.2 (0.0)				0.2 (0.0)			
C15:0br[b]						0.1	0.1	0.1	0.5 (0.1)			
C15:0									0.3 (0.0)	0.3		0.6
C16:0	26.7 (0.3)	29.2	28.5	25.8	20.0 (0.8)	22.8	21.4	23.7	19.4 (0.1)	18.9	7.6	21.7
C16:1 isomer	4.7 (0.2)	3.5	5.7	3.8	4.0 (0.1)	3.7	3.5	3.5	1.3 (0.6)		0.8	2.8
C16:1	0.2 (0.0)	0.1	0.2		0.4 (0.0)	0.3	0.4	1.5	24.3 (0.1)	25.7	18.7	24.7
C16:2	4.1 (0.1)	3.0	5.1	3.5	6.0 (0.0)	4.2	7.1	6.3	0.3 (0.1)	0.2	0.1	0.3
C16:3	1.9 (0.4)	0.9	0.8	1.1	12.5 (0.5)	9.8	12.2	12.2	1.1 (0.2)			0.9
C16:4	5.6 (0.4)	4.3	5.4	6.8								
C17:0	2.4 (0.1)	0.5	2.8	3	0.2 (0.0)	0.4	0.3	0.8	0.2 (0.1)	0.2	0.1	0.3
C17:1					0.2 (0.0)	0.1	0.2		0.7 (0.1)	0.6	0.5	0.8
C18:0	2.8 (0.1)	4.0	2.7	3.8	1.2 (0.0)	2.4	0.6	5.3	0.4 (0.1)	1.7	0.5	0.6
C18:1*c*	16.3 (0.7)	21.9	14.8	13.4	9.2 (0.3)	12.2	7.8	8.4	3.2 (0.0)	1.9	1.9	3.7
C18:1*t*	2.6 (0.1)	3.2	2.1	2.8	0.9 (0.0)	0.9	0.9	2.6	0.3 (0.0)	0.4	0.4	0.3
C18:2	16.4 (0.0)	15.1	18.1	12.3	22.6 (0.0)	26.5	21.8	17.8	3.8 (0.0)	1.3	2.8	2.4
C18:3γ	4.1 (0.0)	5.2	3.5	3.5					0.5 (0.0)			
C18:3	10.3 (0.3)	7.7	10.4	10.6	21.0 (0.8)	15.7	23.4	18.0				
C18:4												
C20:0	0.3 (0.3)	0.5	0.2	0.5	0.2 (0.0)	0.3	0.1					
C20:1	0.4 (0.0)	0.7	0.2	0.5								
C20:3n-6									0.4 (0.0)	0.6	0.4	0.3
C20:4									6.1 (0.1)	6.8	9.0	5.8
C20:5									30.1 (0.3)	34.4	51.1	28.0
C22:0					0.1 (0.1)	0.1						
C22:5												
C22:6												
C24:0					0.2 (0.1)	0.1	0.1					

	Scene				*Schizo*			
	total lipids	TAG	FFA	polar lipids	total lipids	TAG	FFA	polar lipids
C8:0								
C10:0								
C12:0					0.1 (0.0)	0.1		0.1
C14:0	1.9 (0.6)	1.3	0.5	1.3	4.4 (0.2)	5	4.9	3.6
C14:1	0.3 (0.0)							
C15:0br[b]	1.2 (0.3)	0.6	0.1	0.0				
C15:0	0.3 (0.0)		0.2		1.3 (0.1)	1.5	0.7	1.1
C16:0	31.1 (0.0)	15.8	39.5	15.2	60.1 (1.5)	66.2	71.7	67.2
C16:1 isomer	1.7 (0.1)	0.7	1.3	0.0				
C16:1	0.8 (0.0)	1.1	0.6	1.1	0.1 (0.0)	0.1		0.3
C16:2	0.8 (0.0)	0.7	0.9	0.7				
C16:3	2.4 (0.3)	0.4	1.6	2.6	0.1 (0.0)	0.1		0.4
C16:4	5.5 (0.0)	1.6	6.2	3.5				
C17:0	0.3 (0.0)		0.4	0.5	0.5 (0.0)	0.6	0.7	0.6
C17:1	0.2 (0.0)	1.3	0.1					
C18:0	1.6 (0.0)	2.8	2.0	2.7	1.5 (0.1)	1.8	6.9	2.3
C18:1*c*	10.5 (0.1)	16	10.3	15.5				0.1
C18:1*t*	2.4 (0.1)	2.8	2.0	2.7			0.2	0.1
C18:2	11.1 (0.0)	17.4	10.7	16.9				
C18:3γ	1.5 (0.0)				0.1 (0.0)			
C18:3	21 (0.2)	33.2	20.5	32.4	0.1 (0.0)			0.2
C18:4	4.4 (0.0)	3.5	2.5	3.4	0.1 (0.0)	0.1		
C20:0					0.1 (0.0)	0.1	2.1	0.1
C20:1	0.4 (0.0)	0.5	0.3		0.1 (0.0)			
C20:3n-6					0.1 (0.0)			
C20:4					0.4 (0.0)	0.3		0.1

DOI: 10.1021/jf5050603
J. Agric. Food Chem. 2015, 63, 1773−1787

Table 3. continued

	Scene				*Schizo*			
	total lipids	TAG	FFA	polar lipids	total lipids	TAG	FFA	polar lipids
C20:5					0.5 (0.0)	0.3		0.6
C22:0	0.2 (0.2)	0.2	0.1	0.5	0.1 (0.0)	0.1		
C22:5					5.1 (0.2)	4.2	3	3.9
C22:6					25.6 (1.6)	19.4	9.7	19.3
C24:0	0.6 (0.0)		0.2	0.0				

[a]Values in parentheses are standard deviations of three replicates. Standard deviations of other fractions are generally <1% and are not presented. [b]"br" stands for "branched".

Table 4. Distribution of Saturated, Monounsaturated, and Polyunsaturated Fatty Acids, and n-3 Fatty Acids Content (Weight Percent) of Unfractionated Total Lipids

fatty acid	*Chlamy*	*Chlorella*	*Nanno*	*Scene*	*Schizo*
saturated (SFA)	33.6	23.2	27.5	37.2	68.1
monounsaturated (MUFA)	24.8	14.9	30.0	16.3	0.1
polyunsaturated (PUFA)	42.4	62.1	42.3	46.7	32.1
n-3	12.2	33.5	37.3	23.4	31.8

Chlamy, the general distributions of saturated versus unsaturated fatty acids and MUFA versus PUFA were the same. The polar lipid fraction contained slightly higher levels of C14:0 and C16:4, but reduced levels of C18:1*c* and C18:2, which was opposite to the TAG fraction. Fatty acid distribution in the FFA fraction was similar to that in total lipids.

Chlorella was rich in C16:0 (20%), C16:3 (13%), C18:1*c* (9%), C18:2 (23%), and C18:3 (21%), which accounted for 86% of the total. *Chlorella* contained the highest amount of PUFA and total unsaturated fatty acids. *Chlorella*'s TAG, FFA, and polar lipid fraction had similar fatty acid compositions.

Nanno was rich in C14:0 (6%), C16:0 (19%), C16:1 (24%), C20:4 (6%), and C20:5 (30%), totaling 85%. *Nanno* also contained the highest amount of n-3 fatty acids, at about 37%. There was a reduced level of C18 fatty acids in *Nanno*. Compared to the total lipids, the FFA fraction contained less C16:0 and C16:1, but had more than half of its fatty acids as C20:5. *Nanno*'s polar lipid and TAG fractions had fatty acid distributiond similar to its total lipids.

Scene was rich in C16:0 (31%), C16:4 (6%), C18:1*c* (11%), C18:2 (11%), and C18:3 (21%), accounting for 80% of the total. The unusual n-3 fatty acid C18:4 was present in *Scene* at 4% level. Studies have shown that C18:4 was as effective as marine oil derived long-chain n-3 fatty acids in providing the health benefits in humans relating to cardiovascular disease.[32] *Scene* had the highest amount of SFA among the four green microalgae. The FFA fraction of *Scene* had fatty acids similar to the total lipids. The TAG and polar lipids had lower levels of C16:0 and C16:4 and higher levels of C18 fatty acids.

Schizo has a narrow distribution of fatty acids, with 68% SFA and 32% PUFA. The main fatty acids were C14:0 (4%), C16:0 (60%), C22:5 (5%), and C22:6 (26%). The unique fatty acid distribution of *Schizo* made this species an ideal substrate for the production of functional lipids because its relatively simple fatty acid composition would facilitate the fractionation or purification of long-chain PUFA. The TAG, FFA, and polar lipid fractions all had high proportions of C16:0 and low levels of C22:5 and C22:6, which suggests that long-chain PUFA might have been oxidized during the TLC fractionation, or some of them might be present in other lipid classes that were not identified. The ability of efficient accumulation of DHA and DPA has made *Schizo* a commercial interest for producing purified long-chain n-3 PUFA as a nutritional ingredient in foods.[33]

The similarity of fatty acid composition of FFA to that of total lipids for most species suggests that these FFAs were released from lipid degradation as mentioned earlier. There are

Table 5. Glycolipids and Phospholipids Composition (Weight Percent) of Unfractionated Total Lipids by LC-MS[a]

	Chlamy	*Chlorella*	*Nanno*	*Scene*	*Schizo*
total glycolipids	9.02	0.43	11.99	0.35	0.07
DGDG	4.28 (0.34)	0.34 (0.03)	9.09 (0.53)	0.13 (0.01)	0.02 (0.01)
MGDG	4.29 (0.15)	0.08 (0.00)	1.71 (0.12)	0.19 (0.06)	0.05 (0.09)
SQDG	0.46 (0.1)	0.01 (0.01)	1.19 (0.04)	0.03 (0.01)	0
total phospholipids	0.64	0.28	12.59	0.34	0.80
PG	0.22 (0.01)	0.13 (0.00)	2.89 (0.12)	0.11 (0.04)	0.11 (0.01)
LPG	0.02 (0.01)	0.00 (0.01)	0.29 (0.00)	0.03 (0.02)	0.05 (0.01)
LPC	0	0	1.05 (0.02)	0.01 (0.00)	0
LPE	0	0	0.13 (0.01)	0	0
PC	0.01 (0.01)	0.06 (0.00)	5.10 (0.14)	0.12 (0.00)	0.55 (0.04)
PE	0.01 (0.00)	0	0.34 (0.02)	0.02 (0.00)	0
PI	0.36 (0.03)	0.07 (0.00)	2.77 (0.05)	0.04 (0.01)	0.06 (0.00)
PS	0.01 (0.00)	0.01 (0.00)	0	0.00 (0.01)	0.01 (0.01)
PA	0.01 (0.00)	0	0.01 (0.00)	0.01 (0.00)	0
total polar lipids	9.66	0.71	24.58	0.69	0.87

[a]Values in parentheses are the differences of two replicates.

DOI: 10.1021/jf5050603
J. Agric. Food Chem. 2015, 63, 1773−1787

Table 6. Molecular Species of Glycolipids and Phospholipids (Nanomoles per Milligram of Total Lipids)[a]

lipid molecular species (total acyl carbons:total double bonds)	mass	*Chlamy*	*Chlorella*	*Nanno*	*Scene*	*Schizo*
DGDG (34:6)	926.6	1.12	1.09	0.29	0.05	0.01
DGDG (34:5)	928.6	4.36	0.79	23.59	0.08	0.03
DGDG (34:4)	930.6	7.40	0.45	0.24	0.17	0.00
DGDG (34:3)	932.6	8.73	0.27	1.77	0.47	0.01
DGDG (34:2)	934.6	6.20	0.15	1.68	0.13	0.00
DGDG (34:1)	936.6	15.00	0.46	0.80	0.12	0.03
DGDG (36:6)	954.6	1.14	0.19	24.52	0.10	0.01
DGDG (36:5)	956.6	0.81	0.12	41.77	0.14	0.00
DGDG (36:4)	958.6	0.52	0.06	0.00	0.04	0.00
DGDG (36:3)	960.6	0.26	0.01	0.23	0.03	0.04
DGDG (36:1)	964.7	0.09	0.01	0.05	0.03	0.08
DGDG (38:6)	982.6	0.00	0.00	0.57	0.01	0.00
DGDG (38:5)	984.6	0.01	0.00	0.13	0.00	0.00
DGDG (38:3)	988.7	0.00	0.00	0.13	0.01	0.00
total DGDG		45.64	3.60	95.77	1.38	0.21
MGDG (34:6)	764.5	9.45	0.31	0.13	0.21	0.04
MGDG (34:5)	766.5	14.03	0.37	11.58	0.19	0.00
MGDG (34:4)	768.5	11.29	0.12	0.00	0.32	0.01
MGDG (34:3)	770.5	8.54	0.06	0.22	0.68	0.00
MGDG (34:2)	772.6	6.14	0.02	0.23	0.10	0.00
MGDG (34:1)	774.6	4.11	0.02	0.06	0.12	0.00
MGDG (36:6)	792.5	0.58	0.04	1.65	0.04	0.02
MGDG (36:5)	794.5	0.64	0.01	6.59	0.07	0.00
MGDG (36:4)	796.6	0.39	0.01	0.05	0.06	0.00
MGDG (36:3)	798.6	0.37	0.00	0.06	0.03	0.00
MGDG (36:1)	802.6	0.08	0.03	0.58	0.13	0.08
MGDG (38:6)	820.6	0.01	0.04	0.47	0.20	0.34
MGDG (38:5)	822.6	0.00	0.03	0.17	0.02	0.11
MGDG (38:4)	824.6	0.02	0.00	0.03	0.11	0.05
MGDG (38:3)	826.6	0.00	0.00	0.13	0.09	0.00
total MGDG		55.65	1.06	21.95	2.37	0.65
SQDG (32:2)	789.5	0.01	0.00	0.65	0.00	0.00
SQDG (32:1)	791.5	0.07	0.00	13.84	0.01	0.00
SQDG (32:0)	793.5	4.46	0.08	0.26	0.23	0.01
SQDG (34:3)	815.5	0.39	0.01	0.03	0.02	0.00
SQDG (34:2)	817.5	0.33	0.00	0.09	0.05	0.00
SQDG (34:1)	819.5	0.42	0.00	0.11	0.03	0.00
total SQDG		5.68	0.09	14.98	0.34	0.01
PG (32:1)	738.5	0.09	0.12	5.87	0.07	0.00
PG (32:0)	740.5	0.74	0.39	0.28	0.13	1.33
PG (34:4)	760.5	0.13	0.20	0.03	0.28	0.00
PG (34:3)	762.5	0.34	0.30	0.15	0.08	0.01
PG (34:2)	764.5	0.44	0.43	0.27	0.10	0.00
PG (34:1)	766.5	0.82	0.24	0.27	0.20	0.01
PG (36:6)	784.5	0.25	0.00	25.03	0.14	0.00
PG (36:5)	786.5	0.00	0.00	5.04	0.00	0.00
PG (36:4)	788.5	0.00	0.00	0.17	0.02	0.00
PG (36:2)	792.5	0.01	0.03	0.06	0.23	0.00
PG (36:1)	794.6	0.00	0.00	0.00	0.10	0.02
total PG		2.82	1.71	37.17	1.35	1.37
LPG(16:1)	500.3	0.10	0.01	4.13	0.15	0.05
LPG(16:0)	502.3	0.25	0.05	1.46	0.14	1.00
LPG(18:1)	528.3	0.07	0.01	0.12	0.33	0.01
total LPG		0.42	0.07	5.71	0.62	1.06
LPC (16:1)	494.3	0.00	0.00	10.03	0.02	0.00
LPC (16:0)	496.3	0.00	0.01	1.61	0.05	0.08

DOI: 10.1021/jf5050603
J. Agric. Food Chem. 2015, 63, 1773−1787

Table 6. continued

lipid molecular species (total acyl carbons:total double bonds)	mass	*Chlamy*	*Chlorella*	*Nanno*	*Scene*	*Schizo*
LPC (18:3)	518.3	0.00	0.01	0.95	0.00	0.00
LPC (18:2)	520.3	0.00	0.00	5.16	0.01	0.00
LPC (18:1)	522.3	0.00	0.01	3.08	0.03	0.00
total LPC		0.00	0.03	20.83	0.11	0.08
LPE (16:1)	452.3	0.00	0.00	1.80	0.02	0.00
LPE (16:0)	454.3	0.01	0.01	0.29	0.01	0.03
LPE (18:2)	478.3	0.00	0.00	0.33	0.01	0.00
LPE (18:1)	480.3	0.00	0.00	0.34	0.01	0.00
total LPE		0.01	0.01	2.76	0.05	0.03
PC (32:0)	734.6	0.00	0.00	0.43	0.04	0.06
PC (34:4)	754.5	0.00	0.08	3.54	0.02	0.01
PC (34:3)	756.5	0.02	0.16	13.92	0.08	0.01
PC (34:2)	758.6	0.06	0.12	14.52	0.13	0.01
PC (34:1)	760.6	0.04	0.04	3.37	0.22	0.01
PC (36:6)	778.5	0.01	0.05	6.75	0.02	0.09
PC (36:5)	780.5	0.01	0.06	7.39	0.02	0.05
PC (36:4)	782.6	0.01	0.10	4.18	0.08	0.02
PC (36:3)	784.6	0.01	0.06	3.61	0.09	0.01
PC (36:2)	786.6	0.02	0.05	1.19	0.57	0.01
PC (36:1)	788.6	0.01	0.01	0.42	0.13	0.02
PC (38:6)	806.6	0.00	0.01	3.65	0.04	5.13
PC (38:5)	808.6	0.00	0.01	1.48	0.03	1.07
PC (38:4)	810.6	0.00	0.01	0.19	0.02	0.01
PC (38:3)	812.6	0.00	0.01	0.29	0.01	0.01
PC (38:2)	814.6	0.00	0.03	0.77	0.03	0.01
PC (40:5)	836.6	0.00	0.00	0.18	0.00	0.03
PC (40:4)	838.6	0.00	0.00	0.07	0.00	0.24
total PC		0.19	0.80	65.95	1.53	6.80
PE (32:3)	686.5	0.00	0.00	0.12	0.00	0.00
PE (32:2)	688.5	0.00	0.00	1.46	0.02	0.00
PE (32:1)	690.5	0.02	0.00	0.31	0.02	0.00
PE (34:4)	712.5	0.00	0.00	0.10	0.00	0.00
PE (34:3)	714.5	0.00	0.00	0.16	0.00	0.00
PE (34:2)	716.5	0.03	0.02	0.15	0.02	0.00
PE (36:6)	736.5	0.00	0.00	0.48	0.01	0.00
PE (36:5)	738.5	0.00	0.00	0.65	0.00	0.00
PE (36:4)	740.5	0.00	0.00	0.17	0.01	0.00
PE (38:6)	764.5	0.00	0.00	0.53	0.00	0.03
PE (38:5)	766.5	0.00	0.00	0.27	0.01	0.01
total PE		0.05	0.02	4.40	0.09	0.04
PI(32:3)	822.5	0.00	0.03	0.13	0.01	0.00
PI (32:2)	824.5	0.00	0.05	3.25	0.02	0.01
PI (32:1)	826.5	0.01	0.02	20.45	0.09	0.03
PI (32:0)	828.5	0.12	0.01	0.27	0.12	0.62
PI (34:4)	848.5	0.02	0.03	0.17	0.00	0.00
PI (34:3)	850.5	0.16	0.11	0.61	0.02	0.01
PI (34:2)	852.5	0.40	0.23	3.21	0.04	0.01
PI (34:1)	854.5	3.08	0.08	3.57	0.06	0.01
PI (36:6)	872.5	0.02	0.01	0.58	0.00	0.02
PI (36:5)	874.5	0.01	0.02	0.75	0.01	0.03
PI (36:4)	876.5	0.04	0.05	0.12	0.02	0.02
PI (36:1)	882.6	0.20	0.10	0.01	0.02	0.02
total PI		4.06	0.74	33.12	0.41	0.78

[a]Values are the averages of two replicates. The difference of two replicates is not included. Lipid molecular species that had concentrations below 0.1 nmol/mg are not included.

DOI: 10.1021/jf5050603
J. Agric. Food Chem. 2015, 63, 1773−1787

Table 7. Composition (Weight Percent) of Unsaponifiable Matters[a]

	Chlamy	*Chlorella*	*Nanno*	*Scene*	*Schizo*
GC quantifiable of total USP	76.5 (1.0)	68.3 (0.3)	47.7 (1.6)	79.9 (4.1)	36.8 (1.2)
of GC quantifiable USP					
hydrocarbons	0.4 (0.0)	3.7 (0.6)	12.9 (0.3)	20.9 (0.4)	0.5 (0.0)
phytol	83.2 (0.4)	80.1 (1.6)	41.1 (0.3)	47.3 (6.8)	0
sterols	13.7 (1.4)	7.8 (4.6)	34.9 (0.2)	22.9 (0.1)	90.0 (0.3)
others	2.7	8.4	11.1	8.9	9.8

[a]Values in parentheses are the differences of two replicates.

a few discrepancies; that is, fatty acids of the three fractions do not account for that in total lipid extracts. This suggests the presence of other acyl lipids, most likely in the "others" fraction in Table 2, that have contributed significantly to the total lipid fatty acid composition.

As reviewed by Harwood and Jones,[2] freshwater algae typically contain fatty acids similar to those of plants, but with a relatively high proportion of C16 fatty acids and a reduced level of C18 unsaturated fatty acids. Among the photosynthetic species examined, freshwater microalgae *Chlamy*, *Chlorella*, and *Scene* had low levels (<1%) of long-chain fatty acids that have more than 20 carbons, but an appreciable quantity (9−19%) of 16-carbon polyunsaturated fatty acids, which were not usually found in plant oils. The two saltwater microalgae, *Nanno* and *Schizo*, had much higher levels of PUFA of C20 (37%) and C22 (31%), respectively, than those found in fish oil, egg yolk, or other available sources. They are good sources of specialty oil. Small quantities of branched-chain fatty acids were found in *Chlorella*, *Nanno*, and *Scene*, in agreement with previous findings for *Chlorella* and *Scenedesmus* species.[34] All of the algae examined contained significant amounts of n-3 fatty acids (12−37%). In particular, *Chlorella*, *Nanno*, and *Schizo* had one-third of their fatty acids as n-3 fatty acids.

Polar Lipids (Glycolipids and Phospholipids) Composition by LC-MS and TLC. MGDG, DGDG, SQDG, and PG are the major components of chloroplast lipids in microalgae.[2,35] They function as membrane structural lipids and signaling molecules in the cells. These four classes of polar lipids represented 96, 79, 61, and 67% of the total polar lipids of the green microalgae *Chlamy*, *Chlorella*, *Nanno*, and *Scene*, respectively, as quantified by LC-MS (Table 5). TLC analysis confirmed the presence of MGDG, DGDG, SQDG, PC, PE, PI, and PG in the green microalgae by comparison with commercial standards and the literature.[20] The decrease of the ratio of water in the developing solvent from 9 (as used in the literature[20]) to 4 enabled the TLC separation of PG and SQDG and moved PE further below PG. An example of the separation of polar lipids of *Nanno* is given in Figure 2. Steryl glucoside, which was previously found in *Nanno*,[5] was not detected in the present work as examined by the TLC method.

Nanno contained the greatest amount of total polar lipids, 3 times more than that of *Chlamy*, the second ranked. It has been reported that phospholipids are generally present at minor quantities in microalgae,[6] as observed for *Chlamy* in this study. However, the two saltwater species, *Nanno* and *Schizo*, had more phospholipids than glycolipids. *Chlorella* and *Scene* had roughly the same amount of phospholipids as glycolipids. Unlike other species containing one or two types of major phospholipids, *Nanno* contained significant amounts of PC, PG, PI, and LPC. The high level of phospholipids in *Nanno* was suggested to relate to EPA biosynthesis.[3] The proportion of individual glycolipid varied with species. DGDG was dominant in *Nanno*. In addition, *Nanno* contained the highest level of SQDG (12%) among the microalgae examined. The ratio of MGDG to DGDG in *Chlamy* was close to 1, and SQDG represent only 5% of polar lipids in *Chlamy*. *Schizo* had a very low level of polar lipids, which were mainly phospholipids. The MS spectra of the polar lipids of *Nanno*, as an example, are given in the Appendix I (Supporting Information).

Glycolipids have been shown to have various biological properties including antiviral, antitumor, anti-inflammatory, and immune-suppressive activities.[36] Some of the biological properties of MDGD and DGDG might be dependent on the structure of sugar and acyl moieties.[37] Table 6 reports the molecular species of glycolipids and phospholipids determined by LC-MS. On the basis of the fatty acid composition in Table 3, we could reasonably infer the major acyl groups of each individual polar lipid. For *Nanno*, the dominant SQDG isoform (32:1) is composed mainly of the 16:1/16:0 diacyl group, in agreement with the result of He et al.[8] The principal MGDG isoform (34:5) mainly contains the 14:0/20:5 diacyl group. A minor MGDG isoform (36:5) contains the 16:0/20:5 diacyl group. DGDG is rich in 16:0/20:5, 16:1/20:5, and 14:0/20:5 fatty acids. The major PG isoform (36:6) mainly comprises 16:1/20:5. Two minor PG isoforms contain 16:1/16:0 and 16:0/20:5. The principal LPG, PE, and LPE contain the 16:1 acyl group. LPC mainly comprises 16:1 and 18:2 (minor) acyl groups. The major PC isoforms, 34:3 and 34:2, mainly comprise the 16:1/18:2 and 16:1/18:1 or 16:0/18:2 diacyl groups. The dominant PI isoform (32:1) is composed mainly of the 16:1/16:0 diacyl group.

For *Chlamy*, the major SQDG contains 16:0 fatty acid. The major DGDG and MGDG isoforms have 34 carbons and 1−6 double bonds distributed in two acyl groups, which covers all of the C16 and C18 major fatty acids in *Chlamy* total lipids.

The principal isoform (38:6) of PC, which is the most abundant polar lipid of *Schizo*, is composed of the 16:0/22:6 diacyl group, in agreement with the previous study.[38]

The acyl groups of polar lipids in *Chlorella* and *Scene* are not separately discussed here. In general, SQDG, LPG, PE, LPE, LPC, PC, and PI prefer SFA and MUFA, whereas MGDG, DGDG, and PG prefer PUFA, confirming previous results.[3,6,8]

Unsaponifiable Matters. *Scene* had the highest level of USP (19% of total lipids), followed by *Nanno* (15%), *Chlorella* and *Chlamy* (13% for both), and *Schizo* (2%) (Table 2). These values differed from the literature data to different extents.[5,9] The composition of USP was determined by GC-MS. Table 7 shows that a significant portion of USP was not GC quantifiable (with a SAC-5 column). GC-quantifiable USP of freshwater microalgae *Chlamy*, *Chlorella*, and *Scene* accounted for 68−80% of their total USP, much higher than the 37−48% of saltwater microalgae *Nanno* and *Schizo*. Wang and Wang[5] reported up to 70 and 30% of GC-unquantifiable USP in *Nanno* and *Schizo*, respectively. The GC-unquantifiable USP were nonvolatiles

DOI: 10.1021/jf5050603
J. Agric. Food Chem. 2015, 63, 1773−1787

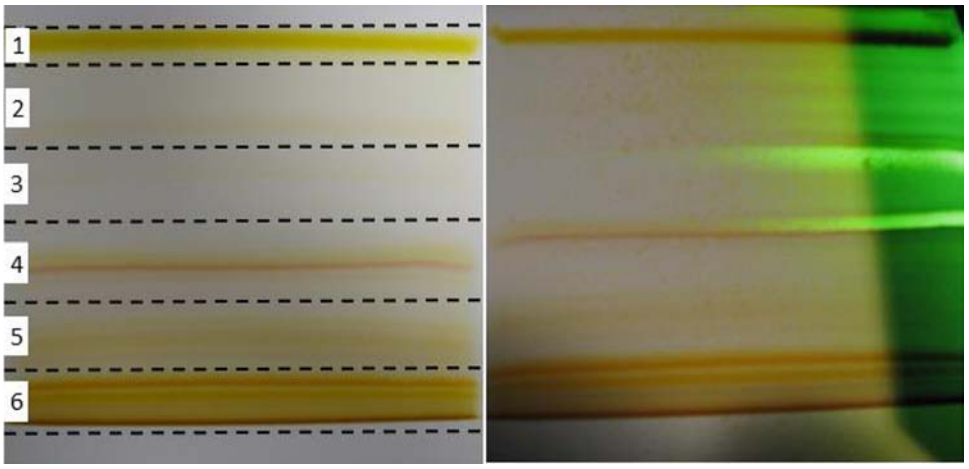

Figure 3. Preparative TLC image of unsaponifiables of *Nanno*. The image on the left was taken before fluorescence spray was applied. The dashed lines illustrate how the six fractions were taken. The image on the right was visualized under UV light after the right half of the plate was sprayed with fluorescence indicator. The developing solvent was hexane/diethyl ether/acetic acid (60:40:1, by vol).

under our GC conditions, present mainly in TLC fractions 5 and 6 (Figure 3), and had color from orange to red. They showed peaks upon HPLC normal phase elution (data not shown). Many of these unidentified USP were likely carotenoids. Carotenoids such as β-carotene and xanthophylls are commonly found in microalgae, as they are not only utilized in photosynthesis but also function as antioxidants.[7,9] The USP of *Scenedesmus quadricauda*, for example, contained 6% carotenoids and 0.5% β-carotene.[9] We did not further characterize these compounds, so the HPLC chromatograms are not included.

TLC fractionation of USP provided information on the relative polarity of the various compounds, which further assisted in structure identification. The preparative TLC separation of *Nanno* USP as illustrated in Figure 3 demonstrates the complexity of microalgae USP. A comparison of the USP of five examined microalgae is shown in the analytical TLC image of Figure 4.

The major USP components of green microalgae were hydrocarbons (TLC fraction 1, Figure 3), phytol (TLC fractions 2 and 3), and sterols (TLC fraction 4), in agreement with the findings of Paoletti et al.[9] Phytol is a diterpene alcohol and is the hydrocarbon tail of chlorophylls. The presence of phytol is attributed to the degradation of chlorophyll during saponification of the total lipids.[10] The level of phytol in the USP can be used as a quantitative indicator of the pigment. *Chlamy* and *Chlorella* contained the highest amount of phytol, representing 80−83% of their GC quantifiable USP, 2-fold higher than those of *Nanno* and *Scene*, which had phytol contents ranging from 40 to 50% (Table 7). *Scene* had the greatest amount of hydrocarbons (21%), whereas *Chlamy* and *Schizo* contained nearly no hydrocarbons. Sterols of the examined green microalgae accounted for 8−35% of total GC quantifiable USP. *Schizo* had a very different USP composition in that 90% of its GC-quantifiable USP was sterols despite the total USP of *Schizo* accounting for only 2% of its total lipids. In all of the species examined, higher amounts of sterols than hydrocarbons were found, in agreement with Paoletti et al.[9]

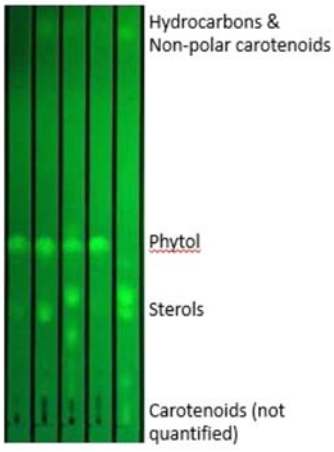

Figure 4. Analytical TLC image of unsaponifiables of microalgae. Lanes (from left to right): *Chlamy*, *Scene*, *Nanno*, *Chlorella*, and *Schizo*. The developing solvent was hexane/diethyl ether/acetic acid (60:40:1, by vol).

Table 8 presents the markedly different distribution pattern of hydrocarbons in these microalgae. Squalene was detected in all of the algae except for *Nanno* and was the only hydrocarbon found in *Schizo*, consistent with the previous result.[5]

Chlamy was mainly composed of odd-chain monounsaturated hydrocarbons, that is, 82% heptadecene and 18% nonadecene.

Chlorella had 88% of heptadecane and 13% of squalene. This differs from the previous result on a saltwater *Chlorella*, which had a wide range of hydrocarbons from C14 to C30 including branched-chain species.[7] However, two earlier papers showed that C17 alkane and alkene were the major components in *Chlorella* sp., albeit they were of different strains.

The major components in *Scene* were pentacosene (63%), heptadecane (6%), $C_{25}H_{48}$ (22%), and $C_{27}H_{54}$ (6%). The abundance of C25 hydrocarbons and the presence of a small amount of C_{27} alkene in *Scene* were also observed in previous studies except for the discrepancy on the level of unsaturation.[9,39]

Nanno had a variety of hydrocarbons from C14 to C30 including both saturated and unsaturated and even- and odd-chain species. The most abundant hydrocarbons in *Nanno* were heptadecane (8%), $C_{25}H_{48}$ (14%), hexacosene (7%), $C_{27}H_{52}$ (20%), and $C_{30}H_{44}$ (18%). Because *Nanno* had 35% sterols (mainly cholesterol) but no squalene, it is reasonable to consider the presence of certain types of biological precursor of

DOI: 10.1021/jf5050603
J. Agric. Food Chem. 2015, 63, 1773−1787

Table 8. Composition (Relative Weight Percent) of Hydrocarbons of the Five Microalgae[a]

RT[b] (min)	hydrocarbon[c]	formula	*Chlamy*	*Chlorella*	*Nanno*	*Scene*	*Schizo*
2.0	tetradecane	$C_{14}H_{30}$			tr[d]		
2.7	hexadecane	$C_{16}H_{34}$			0.8 (0.0)		
3.1	8(3)-heptadecene	$C_{17}H_{34}$	81.8 (1.5)		2.7 (0.2)		
3.1	heptadecane	$C_{17}H_{36}$		87.5 (1.3)	8.1 (0.2)	5.7 (0.6)	
3.6	9-octadecene	$C_{18}H_{36}$			tr		
3.7	octadecane	$C_{18}H_{38}$			3.3 (0.1)		
4.2	5-nonadecene	$C_{19}H_{38}$	18.1 (1.5)		2.6 (1.4)		
4.3	nonadecane	$C_{19}H_{40}$			3.9 (0.0)		
5.7	9-henicosene	$C_{21}H_{42}$			0.7 (0.1)		
5.7	henicosane	$C_{21}H_{44}$			0.9 (0.2)		
7.2	*	$C_{23}H_{46}$			2.1 (0.0)		
8.7	12-pentacosene	$C_{25}H_{50}$			3.5 (0.0)	63.0 (0.3)	
9.0	*	$C_{25}H_{48}$			14.0 (0.3)	21.5 (0.2)	
9.5	1-hexacosene	$C_{26}H_{52}$			6.8 (0.3)	1.7 (0.0)	
10.0	*	$C_{27}H_{52}$			19.8 (0.3)	2.0 (0.0)	
10.2	*	$C_{27}H_{54}$			6.0 (0.2)	5.5 (0.0)	
10.3	*	$C_{27}H_{50}$			5.4 (0.2)		
10.8	*	$C_{27}H_{54}$			2.0 (0.1)		
11.2	squalene	$C_{30}H_{50}$	tr	12.7 (1.0)		0.60	100
11.5	*	$C_{30}H_{44}$			17.5 (0.0)		

[a]Values in parentheses are the differences of two replicates. The double bond position of unsaturated hydrocarbons is not confirmed. [b]RT, retention time. [c]Structures of compounds marked with an asterisk (*) are not completely resolved so that only their chemical formulas are given. [d]tr, trace

Table 9. Composition (Relative Weight Percent) of Sterols of the Green Microalgae[a]

RT[b](min)	compound[c]	MW or formula	*Chlamy*	*Chlorella*	*Nanno*	*Scene*	*Schizo*
12.6	n/a	376[d]	1.4 (0.1)	2.7 (0.6)			
13.5	n/a	390[d]	1.2 (0.1)				
14.0	cholesterol	$C_{27}H_{46}O$	2.7 (0.1)	tr[e]	83.5 (0.1)	tr	70.8
14.6	anthraergostatetraenol	$C_{28}H_{42}O$		4.5 (0.1)			
14.7	lathosterol	$C_{27}H_{46}O$					8.3
15.1	ergosterol	$C_{28}H_{44}O$	38.1 (2.4)	65.5 (7.0)			
15.1	cholesta-3,5-dien-7-one	$C_{27}H_{42}O$					1.6
15.2	5,6-dihydroergosterol	$C_{28}H_{46}O$	5.3 (0.4)				
15.9	ergosta-5,24(28)-dien-3β-ol, or ergosta-5,8-dien-3β-ol	$C_{28}H_{46}O$		7.2 (6.7)			3.7
16.1	γ-ergostenol	$C_{28}H_{48}O$	11.9 (1.5)	15.2 (0.2)		27.9 (0.0)	
	Δ7-stigmasterol	$C_{29}H_{48}O$	24.6 (1.3)				1.8
16.5	chondrillasterol	$C_{29}H_{48}O$	5.3 (0.5)			68.1 (0.0)	7.1
16.5	fucosterol	$C_{29}H_{48}O$			7.0 (0.0)		
16.6	isofucosterol	$C_{29}H_{48}O$			9.5 (0.1)		
17.4	stigmasta-7,16-dien-3β-ol	$C_{29}H_{48}O$					3.6
17.4	Δ7-chondrilla-stenol	$C_{29}H_{50}O$	2.7 (0.1)			4.1 (0.0)	
17.6	n/a	$C_{30}H_{50}O$					2.3
17.8	9,19-cyclolanost-24-en-3β-ol	$C_{30}H_{50}O$	6.7 (1.1)	5.0 (0.0)			0.9

[a]Values in parentheses following means are the differences of two replicates. We did not have enough *Schizo* samples to do the second replicate of saponification. [b]RT, retention time. [c]The mass spectra of compounds marked with "n/a did not match those given by MS NIST library, so that only their formula or MW is given. The sterol compounds are listed in the order of their GC retention time on the SAC-5 column. [d]Mass pattern similar to anthraergostatetraenol. [e]tr, trace.

sterols that have structures similar to squalene. This compound could be $C_{30}H_{44}$, which accounted for 18% of hydrocarbons in *Nanno* as shown in Table 8.

Sterol distribution in microalgae greatly varies with the microalgae classes, genera, and species.[40] The occurrence of sterols in these microalgae in relation to their evolutionary history and growth conditions has been extensively discussed in the literature cited.[40] Sterols are essential components of the membranes of eukaryotic organisms, having various biological functions.[40] Beneficial health effects of phytosterol have been reported.[41] A recent study has shown that sterol extract from *Schizochytrium* sp. had cholesterol-lowering activity.[42] The great diversity of sterol distribution in microalgae has long been recognized,[10,11,40] as observed in the present study. As shown in Table 9, saltwater microalgae *Nanno* and *Schizo* were rich in cholesterol, whereas freshwater microalgae *Chlamy*, *Chlorella*, and *Scene* were mainly composed of C28−C30 phytosterols, in agreement with previous reviews.[12,40] Both cholesterol and phytosterols were found in the species examined. Ergosterol (ergosta-5,7,22-trien-3β-ol) was the major sterol in *Chlamy* and *Chlorella*. *Chlamy*, *Chlorella*, and *Scene* contained 12−28% of γ-ergostenol (5α-ergost-7-en-3β-ol). Additionally, *Chlamy* contained 25% of Δ7-stigmasterol (stigmasta-5,7,22-trien-3β-ol), 5% of chondrillasterol (5α-stigmasta-7,22-dien-3β-ol), 3% of

DOI: 10.1021/jf5050603
J. Agric. Food Chem. 2015, 63, 1773−1787

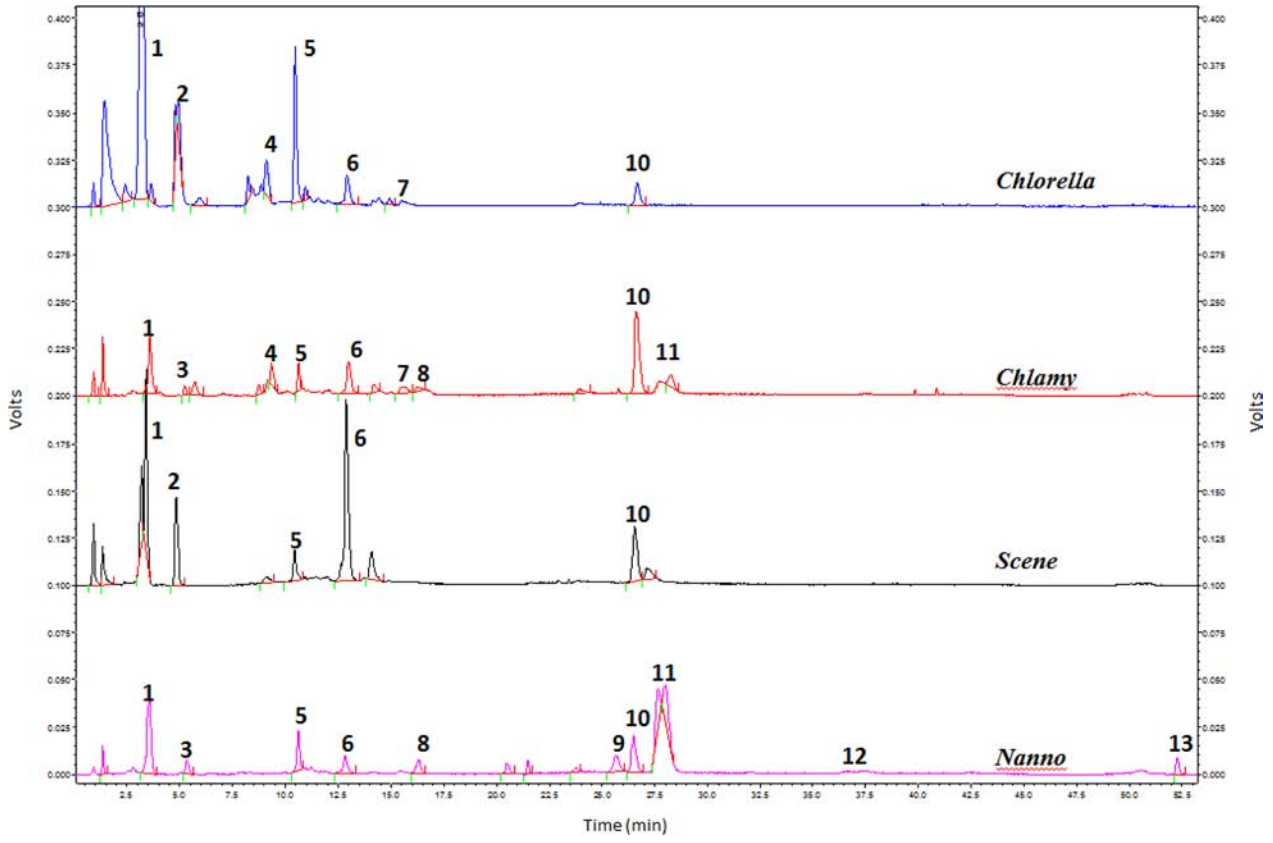

Figure 5. HPLC normal phase separation of polar lipid fractions of four green microalgae (qualitative). Peaks: 1, pheophytin *a*; 2, pheophytin *b*; 3, hydroxypheophytin *a*; 4, hydroxypheophytin *b*; 5, unidentified; 6, chlorophyllide *b*; 7, hydroxychlorophyllide *b*; 8, MGDG; 9, PG; 10, DGDG; 11, SQDG; 12, PI; 13, PC.

each of cholesterol and Δ7-chondrillastenol (stigmast-7-en-3-ol, (3*β*,5*α*,24S)-), and 5% of 5,6-dihydroergosterol (ergosta-7,22-dien-3*β*-ol), which is generally in agreement with the results of Paoletti et al.[10] on five Chlorophyceae. The characteristics of predominant chondrillasterol (68%) and *γ*-ergostenol (28%) of *Scene* in the present work are consistent with those found in *S. obliquus* examined by Patterson.[11] The principal sterols of *Chlorella* were ergosterol (66%) and *γ*-ergostenol (15%), differing from previous results showing the predominance of C29 sterols.[11−14,40] However, Rzama et al.[15] also found that ergosterol was the principal sterol in *C. vulgaris*. *Nanno* contained 84% of cholesterol as its major sterol, with the remaining being fucosterol and its isomer. Fucosterol was identified as the dominant sterol of brown algae,[11] but it was also found in some green algae in a small amount.[40] The other saltwater microalga, *Schizo*, had a more diverse distribution of sterols when compared to *Nanno*. Besides the dominant cholesterol (71%), *Schizo* contained a few C29 phytosterols as minor components. Although the relative percentages of sterols in *Schizo* differed from the reported values, the types of sterols were generally similar to those in the literature.[42]

Other GC-quantifiable USP in Table 7 included compounds having intermediate polarity (TLC fraction 2, Figure 3), such as 6,10,14-trimethyl-2-pentadecanone, which was found in *Chlamy*, *Nanno*, and *Scene* in small quantities, and some unidentified substances. A trace amount of *α*-tocopherolquinone was detected in the USP of *Nanno*. It is a membrane-bound quinone and previously found in blue-green algae.[43] Straight-chain alcohols as reported by Paoletti et al.[10] were not detected. Fatty amides were previously found in freshwater green algae.[44] In the present work, *m*/*z* 59 and 72 were observed in *Chlamy*'s USP (TLC fraction 5, Figure 3), which are the characteristic amide peaks resulting from McLaffery rearrangement of *γ*-cleavage,[45] indicating the presence of a trace of fatty amide in *Chlamy*.

Chlorophylls and Related Metabolites. Chlorophylls are the principal pigments involved in photosynthesis. They are natural food coloring agents and valuable bioactive compounds showing antimutagenic activity and other health benefits.[46,47] Green microalgae contain a great amount of chlorophyll and its metabolites for photosynthesis, suggesting a potential opportunity for value-added coproduct if an effective extraction and fractionation method is developed.[48] In addition, the separation of chlorophylls from the acyl lipids of microalgae also will improve the quality of the produced biodiesel.[49]

Pheophytins and chlorophyllides are derived from chlorophylls after loss of the central Mg atom and the phytol chain, respectively. They are both essential metabolites in chlorophyll biosynthesis and breakdown. The large amount of phytol that was detected in GC-MS analysis of USP suggested that chlorophylls were present in these green microalgae at a significant level. LC/APCI revealed the presence of the following degradation products of chlorophylls: pheophytin *a* [(*m*/*z* 870 ([M − H]$^-$)], pheophytin *b* [(*m*/*z* 884 ([M − H]$^-$)], hydroxypheophytin *a* [(*m*/*z* 886 ([M − H]$^-$)], hydroxypheophytin *b* [(*m*/*z* 900 ([M − H]$^-$)], chlorophyllide *b* [(*m*/*z* 627 ([M − H]$^-$)], and hydroxychlorophyllide *b* [(*m*/*z* 643 ([M − H]$^-$)] (Figure 5). The *m*/*z* values of the molecular ions found from the LC/APCI agreed with the reported values.[50,51] The detection of these compounds suggested that

DOI: 10.1021/jf5050603
J. Agric. Food Chem. 2015, 63, 1773−1787

Table 10. Temperature of Completion of Melting and Onset of Crystallization of Microalga Total Lipids and Their Methyl and Isopropyl Esters[a]

	methyl ester		isopropyl ester		total lipids	
	melting (°C)	crystallization (°C)	melting (°C)	crystallization (°C)	melting (°C)	crystallization (°C)
Chlamy	14.1	−1.0	−5.0	−12.5	48.0	10.0
Chlorella	10.8	−3.8	−4.1	−14.8	30.1	1.5
Nanno	5.4	−4.0	−10.3	−14.0	66.7	47.1
Scene	38.4	31.0	32.5	25.5	57.2	38.9
Schizo	26.2	17.5	13.2	1.8	53.8	25.9

[a]Values are the means of duplicate samples. All differences between the two replicates of melting temperature are <1 °C, and all differences between the duplicates of crystallization are <3 °C.

both chlorophyll *a* and chlorophyll *b* were present in these green microalgae. Peak 5 in Figure 5 was not identified. It had the same retention time as chlorophyll *a* [(m/z 928 ([M + Cl]$^-$)], but an m/z of 902. Quantification of these individual pigments was not carried out. Further structural confirmation with MS/MS is needed. None of chlorophylls or its metabolites were found in *Schizo*.

DSC Melting and Crystallization Temperatures of the Total Lipids of Microalgae and Their Methyl and Isopropyl Esters. Knowledge of the melting and crystallization behavior of microalgae lipids is useful in determining their suitable applications. Table 10 shows that melting points of total lipids of the microalgae examined ranged from 30 to 67 °C, with the highest melting temperature from *Nanno*. The high melting temperatures are caused by the saturated acyl lipids as well as the high melting components in USP such as sterols. When used as biodiesel, total lipids would be converted to methyl (or isopropyl) esters. Monoesters of fatty acids have lower melting and crystallization temperatures than triacylglycerides, phospholipids, and glycolipids. Methyl and isopropyl esters of the microalgae had much reduced melting temperatures compared to their total lipids. The greatest reduction was found in *Nanno*, with the lowest melting point of 5 °C. The current melting temperatures of the esters of these algae would not be satisfactory in biofuel application. The presence of sterols, chlorophyll, and other substances that are soluble in organic solvent would act as crystallization initiators, adversely affecting the quality of the fuels. Appropriate fractionation technology has to be developed to remove these high-melting components. The melting and crystallization behavior of microalgae lipids also have an impact on how they are utilized in food and functional health products.

In summary, lipid characterizations of five microalgae including freshwater and saltwater types are presented. A combination of instrumental analyses was used to obtain the complete lipid profile. All of the examined microalgae are good sources of n-3 fatty acids. *Nanno* and *Chlamy* contained significant amounts of bioactive glycolipids. Freshwater microalgae are rich in phytosterols, whereas saltwater species are rich in cholesterol. The compositional information and methodology presented in this paper are valuable references for future study on algae strain selection and algae cultivation optimization, as well as for the production of value-added coproducts from microalgae.

■ ASSOCIATED CONTENT

Supporting Information

Appendix I. This material is available free of charge via the Internet at http://pubs.acs.org.

■ AUTHOR INFORMATION

Corresponding Author

*(T.W.) Mail: 2312 Food Sciences Building, Iowa State University, Ames, IA 50011, USA. Phone: (515) 294-5448. Fax: (515) 294-8181. E-mail: tongwang@iastate.edu.

Present Address

§(J.A.G.) Departamento de Producción Vegetal, Facultad de Ciencias Agrarias, Universidad Nacional de Rosario/CONICET, Zavalla, Santa Fe, S2125ZAA, Argentina.

Notes

The authors declare no competing financial interest.

■ ACKNOWLEDGMENTS

Dr. Zhiyou Wen and his research group assisted in producing several algae as described under Materials and Methods. LC-MS analysis work was performed at Kansas Lipidomics Research Center.

■ ABBREVIATIONS USED

Chlamy	*Chlamydomonas reinhardtii*
Chl	chlorophyll
Chld	chlorophyllide
Chlorella	*Chlorella vulgaria*
DGDG	digalactosyldiacylglycerol
DGTS	diacylglycerol trimethylhomoserine ether
FFA	free fatty acid
LPC	lysophosphatidylcholine
LPE	lysophosphatidylethanolamine
LPG	lysophosphatidylglycerol
LPI	lysophosphatidylinositol
MGDG	monogalactosyldiacylglycerol
MUFA	monounsaturated fatty acid
Nanno	*Nannochloropsis* sp.
PA	phosphatidic acid
PC	phosphatidylcholine
PE	phosphatidylethanolamine
PG	phosphatidylglycerol
PI	phosphatidylinositol
PS	phosphatidylserine
PUFA	polyunsaturated fatty acid
SFA	saturated fatty acid
Scene	*Scenedesmus* sp.
Schizo	*Schizochytrium limacinum* SR-21
SG	steryl glucoside
SQDG	sulfoquinovosyl diacylglycerol
TAG	triacylglycerols
USP	unsaponifiable matters
TLC	thin layer chromatography

DOI: 10.1021/jf5050603
J. Agric. Food Chem. 2015, 63, 1773−1787

REFERENCES

(1) Andersen, R. A. Diversity of eukaryotic algae. *Biodivers. Conserv.* **1992**, *1*, 267−292.
(2) Harwood, J. L.; Jones, A. L. Lipid metabolism in algae. *Adv. Bot. Res.* **1989**, *16*, 1−53.
(3) Guschina, I. A.; Harwood, J. L. Lipids and lipid metabolism in eukaryotic algae. *Prog. Lipid Res.* **2006**, *45*, 160−186.
(4) Ethier, S.; Woisard, K.; Vaughan, D.; Wen, Z. Continuous culture of the microalgae *Schizochytrium limacinum* on biodiesel derived crude glycerol for producing docosahexaenoic acid. *Bioresour. Technol.* **2011**, *102*, 88−93.
(5) Wang, G.; Wang, T. Characterization of lipid components in two microalgae for biofuel application. *J. Am. Oil Chem. Soc.* **2012**, *89*, 135−143.
(6) Alonso, D. L.; Belarbi, E. H.; Rodríguez-Ruiz, J.; Segura, C. I.; Giménez, A. Acyl lipids of three microalgae. *Phytochemistry* **1998**, *47*, 1473−1481.
(7) Jones, J.; Manning, S.; Montoya, M.; Keller, K.; Poenie, M. Extraction of algal lipids and their analysis by HPLC and mass spectrometry. *J. Am. Oil Chem. Soc.* **2012**, *89*, 1371−1381.
(8) He, H.; Rodgers, R. P.; Marshall, A. G.; Hsu, C. S. Algae polar lipids characterized by online liquid chromatography coupled with hybrid linear quadrupole ion trap/fourier transform ion cyclotron resonance mass spectrometry. *Energy Fuels* **2011**, *25*, 4770−4775.
(9) Paoletti, C.; Pushparaj, B.; Florenzano, G.; Capella, P.; Lercker, G. Unsaponifiable matter of green and blue-green algal lipids as a factor of biochemical differentiation of their biomasses: I. Total unsaponifiable and hydrocarbon fraction. *Lipids* **1976**, *11*, 259−265.
(10) Paoletti, C.; Pushparaj, B.; Florenzano, G.; Capella, P.; Lercker, G. Unsaponifiable matter of green and blue-green algal lipids as a factor of biochemical differentiation of their biomasses: II. Terpenic alcohol and sterol fractions. *Lipids* **1976**, *11*, 266−271.
(11) Patterson, G. W. The distribution of sterols in algae. *Lipids* **1971**, *6*, 120−127.
(12) Patterson, G. W. Sterols of algae. In *Physiology and Biochemistry of Sterols*; Patterson, G. W., Krauss, R. W., Eds.; AOCS Press: Champaign, IL, USA, 1991; pp 118−157.
(13) Volkman, J. K.; Barrett, S. M.; Dunstan, G. A.; Jeffrey, S. W. Sterol biomarkers for microalgae from the green algal class Prasinophyceae. *Org. Geochem.* **1994**, *21*, 1211−1218.
(14) Kodner, R. B.; Pearson, A.; Summons, R. E.; Knoll, A. H. Sterols in red and green algae: quantification, phylogeny, and relevance for the interpretation of geologic steranes. *Geobiology* **2008**, *6*, 411−420.
(15) Rzama, A.; Dufourc, E. J.; Arreguy, B. Sterols from green and blue-green algae grown on reused waste water. *Phytochemistry* **1994**, *37*, 1625−1628.
(16) Gross, M.; Henry, W.; Michael, C.; Wen, Z. Development of a rotating algal biofilm growth system for attached microalgae growth with in-situ biomass harvest. *Bioresour. Technol.* **2013**, *150*, 195−201.
(17) Vance, P.; Spalding, M. Growth, photosynthesis, and gene expression in *Chlamydomonas* over a range of CO_2 concentrations and CO_2/O_2 ratios: CO_2 regulates multiple acclimation states. *Can. J. Bot.* **2005**, *83*, 796−809.
(18) Gerde, J. A.; Yao, L.; Lio, J. Y.; Wen, Z.; Wang, T. Microalgae flocculation: impact of flocculant type, algae species and cell concentration. *Algal Res.* **2014**, *3*, 30−35.
(19) Gerde, J. A.; Yao, L.; Jung, S.; Lamsal, B.; Johnson, L. A.; Wang, T. Optimizing protein isolation from defatted and non-defatted *Nannochloropsis* microalgae biomass. *Algal Res.* **2013**, *2*, 145−153.
(20) Christie, W. W.; Han, X. *Lipid Analysis: Isolation, Separation, Identification and Lipidomic Analysis*, 4th ed.; The Oily Press: Bridgewater, UK, 2010; pp 63−103.
(21) Henderson, R. J.; Tocher, D. R. Thin-layer chromatography. In *Lipid Analysis. A Practical Approach*; Hamilton, R. J., Hamilton, S., Eds.; IRL Press: Oxford, UK, 1993; pp 65−111.
(22) Brügger, B.; Erben, G.; Sandhoff, R.; Wieland, F. T.; Lehmann, W. D. Quantitative analysis of biological membrane lipids at the low picomole level by nano-electrospray ionization tandem mass spectrometry. *Proc. Natl. Acad. Sci. U.S.A.* **1997**, *94*, 2339−2344.
(23) Christie, W. W.; Gill, S.; Nordbäck, J.; Itabashi, Y.; Sanda, S.; Slabas, A. R. New procedures for rapid screening of leaf lipid components from *Arabidopsis*. *Phytochem. Anal.* **1998**, *9*, 53−57.
(24) Deschamps, F. S.; Chaminade, P.; Ferrier, D.; Baillet, A. Assessment of the retention properties of poly(vinyl alcohol) stationary phase for lipid class profiling in liquid chromatography. *J. Chromatogr., A* **2001**, *928*, 127−137.
(25) Ryckebosch, E.; Muylaert, K.; Foubert, I. Optimization of an analytical procedure for extraction of lipids from microalgae. *J. Am. Oil Chem. Soc.* **2011**, *89*, 189−198.
(26) Guiry, M. D.; Guiry, G. M. 2014. AlgaeBase, World-wide electronic publication, National University of Ireland, Galway; http://www.algaebase.org (accessed May 16, 2014).
(27) Becker, E. W. Micro-algae as a source of protein. *Biotechnol. Adv.* **2007**, *25*, 207−210.
(28) Chen, L.; Liu, T.; Zhang, W.; Chen, X.; Wang, J. Biodiesel production from algae oil high in free fatty acids by two-step catalytic conversion. *Bioresour. Technol.* **2012**, *111*, 208−214.
(29) Widjaja, A.; Chien, C.-C.; Ju, Y.-H. Study of increasing lipid production from fresh water microalgae *Chlorella vulgaris*. *J. Taiwan Inst. Chem. Eng.* **2009**, *40*, 13−20.
(30) Olofsson, M.; Lamela, T.; Nilsson, E.; Bergé, J. P.; del Pino, V.; Uronen, P.; Legrand, C. Seasonal variation of lipids and fatty acids of the microalgae *Nannochloropsis oculata* grown in outdoor large-scale photobioreactors. *Energies* **2012**, *5*, 1577−1592.
(31) Bigogno, C.; Khozin-Goldberg, I.; Boussiba, S.; Vonshak, A.; Cohen, Z. Lipid and fatty acid composition of the green oleaginous alga *Parietochloris incise*, the richest plant source of arachidonic acid. *Phytochemistry* **2002**, *60*, 497−503.
(32) Surette, M. E. Dietary omega-3 PUFA and health: stearidonic acid-containing seed oils as effective and sustainable alternatives to traditional marine oils. *Mol. Nutr. Food Res.* **2013**, *57*, 748−759.
(33) Martek Biosciences Corp. Application for the authorization of DHA and EPA-rich algal oil from *Schizochytrium* sp.; available at http://multimedia.food.gov.uk/multimedia/pdfs/dhaoapplicdossier.pdf (accessed May 7, 2014).
(34) Rezanka, T.; Jokoun, J.; Slavicek, J.; Podojic, M. Determination of fatty acids in algae by capillary gas chromatography-mass spectrometry. *J. Chromatogr.* **1983**, *268*, 71−78.
(35) Hölzl, G.; Dörmann, P. Structure and function of glycoglycerolipids in plants and bacteria. *Prog. Lipid Res.* **2007**, *46*, 225−243.
(36) Christensen, L. P. Galactolipids as potential health promoting compounds in vegetable foods. *Recent Pat. Food Nutr. Agric.* **2009**, *1*, 50−58.
(37) Kinjo, Y.; Illarionov, P.; Vela, J. L.; Pei, B.; Girardi, E.; Li, X.; Li, Y.; Imamura, M.; Kaneko, Y.; Okawara, A.; Miyazaki, Y.; Gómez-Velasco, A.; Rogers, P.; Dahesh, S.; Uchiyama, S.; Khurana, A.; Kawahara, K.; Yesilkaya, H.; Andrew, P. W.; Wong, C. H.; Kawakami, K.; Nizet, V.; Besra, G. S.; Tsuji, M.; Zajonc, D. M.; Kronenberg, M. Invariant natural killer T cells recognize glycolipids from pathogenic Gram-positive bacteria. *Nat. Immunol.* **2011**, *12*, 966−974.
(38) Yaguchi, T.; Tanaka, S.; Yokochi, T.; Nakahara, T.; Higashihara, T. Production of high yield of docosahexaenoic acid by *Schizochytrium* sp. strain SR21. *J. Am. Oil Chem. Soc.* **1997**, *74*, 1431−1434.
(39) Gelpi, E.; Schneider, H.; Mann, J.; Oró, J. Hydrocarbons of geochemical significance in microscopic algae. *Phytochemistry* **1970**, *9*, 603−612.
(40) Volkman, J. K. Sterols in microorganisms. *Appl. Microbiol. Biotechnol.* **2003**, *60*, 495−506.
(41) Kritchevsky, D.; Chen, S. C. Phytosterols − health benefits and potential concerns: a review. *Nutr. Res. (N.Y.)* **2005**, *25*, 413−428.
(42) Chen, J.; Jiao, R.; Jiang, Y.; Bi, Y.; Chen, Z.-Y. Algal sterols are as effective as β-sitosterol in reducing plasma cholesterol concentration. *J. Agric. Food Chem.* **2014**, *62*, 675−681.
(43) Carr, N. G.; Exell, G.; Flynn, V.; Hallaway, M.; Talukdar, S. Minor quinone of some myxophyceae. *Arch. Biochem. Biophys.* **1967**, *120*, 503−507.

DOI: 10.1021/jf5050603
J. Agric. Food Chem. 2015, 63, 1773−1787

(44) Dembitsky, V. M.; Shkrob, I.; Rozentsvet, O. A. Fatty acid amides from freshwater green alga *Rhizoclonium hieroglyphicum*. *Phytochemistry* **2000**, *54*, 965−967.
(45) Levinson, W. E.; Kuo, T. M.; Knothe, G. Characterization of fatty amides produced by lipase-catalyzed amidation of multi-hydroxylated fatty acids. *Bioresour. Technol.* **2008**, *99*, 2706−2709.
(46) Pangestutu, R.; Kim, S.-K. Biological activities and health benefit effects of natural pigments derived from marine algae. *J. Funct. Food* **2011**, *3*, 255−266.
(47) Simonich, M. T.; Egner, P. A.; Roebuck, B. D.; Orner, G. A.; Jubert, C.; Pereira, C.; Groopman, J. D.; Kensler, T. W.; Dashwood, R. H.; Williams, D. E.; Bailey, G. S. Natural chlorophyll inhibits aflatoxin B1-induced multi-organ carcinogenesis in the rat. *Carcinogenesis* **2007**, *28*, 1294−1302.
(48) Hosikian, A.; Lim, S.; Halim, R.; Danquah, M. K. Chlorophyll extraction from microalgae: a review on the process engineering aspects. *Int. J. Chem. Eng.* **2010**, article ID 391632.
(49) U.S. Department of Energy. National Algal Biofuels Technology Roadmap (TechnologyRoadmap); http://energy.gov/sites/prod/files/2014/03/f14/algal_biofuels_roadmap.pdf (accessed Oct 9, 2014).
(50) Van Breemen, R. B.; Canjura, F. L.; Schwartz, S. J. Identification of chlorophyll derivatives by mass spectrometry. *J. Agric. Food Chem.* **1991**, *39*, 1452−1456.
(51) Kao, T. H.; Chen, C. J.; Chen, B. H. An improved high performance liquid chromatography−photodiode array detection−atmospheric pressure chemical ionization−mass spectrometry method for determination of chlorophylls and their derivatives in freeze-dried and hot-air-dried *Rhinacanthus nasutus* (L.) Kurz. *Talanta* **2011**, *86*, 349−355.

DOI: 10.1021/jf5050603
J. Agric. Food Chem. 2015, 63, 1773−1787

fragment identical to nucleotides 192−414 of *Ara h 2.01*.[10] Upon transcription, a 222 bp hairpin is formed by the sense and antisense fragments. The same construct also targets *Ara h 6* because *Ara h 2* and *Ara h 6* share 63% sequence identity overall[11] and 81% identity across the region used for the inverted repeat.[10] The RNAi construct was delivered by particle bombardment to 9 month old embryogenic clusters developed from mature zygotic embryos of peanut cultivar Georgia Green.

Testing Stability of Seed Allergen Content Across Three Transgenic Generations. In the field study, to test the stability of seed allergen content by silencing of *Ara h 2* and *Ara h 6* genes, seeds for T_4 and T_5 transgenic generations were raised in the greenhouse starting with bulked seeds of the T_2 generation. Transgenic generations T_3, T_4, and T_5 were grown in the field at the University of Georgia, Tifton Campus, from June 2010 to Oct 2010. There were four replications of T_3, T_4, and T_5 generations and three replications of non-transgenic segregants (similar to "Georgia Green") as controls. Each plot was 1.95 × 0.9 m in dimension, leaving 0.6 m between plots. A total of 66 seeds were sown in each plot, 33 in each of two rows at 16.2 plants/m (5 seeds/ft). Seeds were coated with Vitavax fungicide before sowing. Non-transgenic plants bordered the entire experimental area. The field test was conducted under notification (USDA-APHIS-BRS number 10-116-101n).

Testing Effects of Sulfur on Seed Allergen Content in Transgenic Lines Grown in the Greenhouse. To test the effect of sulfur on seed allergen content in the T_3 generation, seeds were planted in polyethylene containers 90 × 60 × 20 cm in dimension filled with a mixture of sand, vermiculite, and perlite in the ratio of 2:1:1. Each container had three transgenic and three non-transgenic plants. The planting mixture was irrigated with deionized water before planting. The nutrient solution for irrigation was prepared in deionized water with constant concentrations of macro- and micronutrients, except for sulfur (Table 1). Three concentrations of sulfur (S) were

Table 1. Composition of Nutrient Solution

chemical	molarity (mM)
KNO_3	1
$Ca(NO_3)$	4
NaH_2PO_4	1
$MnCl_2$	0.025
$ZnSO_4{\cdot}7H_2O$	0.006
$CuSO_4{\cdot}5H_2O$	0.006
H_3BO_3	0.1
Na_2MoO_4	0.001
$CoCl_2{\cdot}6H_2O$	0.1 μM
FeEDTA	0.02
$MgSO_4{\cdot}7H_2O$	
low S	0.012
medium S	0.3
high S	3.0
$MgCl_2{\cdot}6H_2O$	
low S	2.97
medium S	2.7
high S	0

provided as $MgSO_4$ at 3 mM (high S), 0.3 mM (medium S), and 0.012 mM (low S). The concentration of Mg was kept constant with $MgCl_2$ at 2.97 mM (in low S solution), 2.7 mM (in medium S solution), and 0 mM (in high S solution). The pH of the solution was adjusted to 5.8. There were five replications for each S treatment concentration (0.012, 0.3, and 3 mM). The plants were watered on alternate days with nutrient solution at 500 mL per plant. The potting medium was flushed with deionized water after every three applications of nutrient solution to prevent salt accumulation in the root zone.

Protein Extraction. In the study, to test stability across three transgenic generations, 15 seeds were pooled separately from three replications of T_3, T_4, and T_5 transgenic generations and non-transgenic control. To study the effect of sulfur on seed allergen expression, seeds were selected from each plant for protein extraction. Two seeds per plant were selected from low S treatment (0.012 mM) and pooled to obtain six seeds for each transgenic and non-transgenic genotype per replication. For medium (0.3 mM) and high (3 mM) S treatments, five seeds per plant were selected and pooled to obtain 15 seeds for each transgenic and non-transgenic genotype per replication. Thus, there were five pooled replicates from each sulfur treatment. Homogeneity of seed maturity within treatments was maintained by choosing the most mature seeds of nearly uniform size. A standard curve for quantitative westerns was derived using protein extracted from 15 seeds of field grown "Georgia Green". Seeds were weighed; testas were removed; and cotyledons were ground in liquid nitrogen. The seed powder was defatted with hexane at 1:35 (w/v) for 4 h, keeping the sample on ice. Defatted and air-dried seed powder was passed through a 30 mesh sieve. Seed protein was extracted using Tris-buffered saline (TBS, 150 mM NaCl and 50 mM Tris) at pH 7.4, containing ethylenediaminetetraacetic acid (EDTA)-free protease inhibitor (Roche Diagnostics, Indianapolis, IN). The defatted and air-dried peanut flour was mixed with ice-cold TBS in the ratio of 1:10 (w/v) and mixed overnight at 4 °C.[20] The mixture was centrifuged at 16060*g* for 15 min at 4 °C, and crude protein extract (CPE) was collected, aliquoted, and stored at −80 °C. Quantification of protein in the crude protein extract was performed using the Pierce bicinchoninic acid protein assay kit (Thermo Scientific, Rockford, IL) according to the protocol of the manufacturer.

Quantitative Western Blots. Seed protein was denatured at 95 °C for 5 min, resolved by running on 15% polyacrylamide gels for 1.5 h, and blotted onto Amersham Hybond-P polyvinylidene fluoride (PVDF) membrane (GE Healthcare, Piscataway, NJ) by electro-transfer at 100 V for 1 h. The PVDF membrane was dried at 37 °C overnight. To test for equal loading of proteins, the membrane was stained with SYPRO Ruby (Invitrogen, Grand Island, NY) as per the protocol of the manufacturer. Briefly, proteins on the PVDF membrane were fixed with a solution containing 10% methanol and 5% acetic acid, washed with deionized water 4 times for 5 min each, stained with SYPRO Ruby, and washed. Fluorescence detection and imaging were performed with a STORM molecular imager (Amersham Biosciences, Piscataway, NJ) at 450 nm excitation/520 nm emission. For western blotting, the membranes were blocked with 5% non-fat dry milk in Tris-buffered saline and Tween 20 (TBST) for 1 h, followed by incubation with anti-Ara h 1 (1:5000), anti-Ara h 2 (1:8000), anti-Ara h 3 (1:5000), or anti-Ara h 6 (1:5000) primary antibodies custom manufactured by Sigma Immunosys (Woodlands, TX). Subsequent to three washes with TBST, the membranes were reacted with alkaline phosphatase (AP)-labeled rabbit anti-chicken/turkey secondary antibody (Invitrogen) at 1:10 000 for $^1/_2$ h. Signal detection was performed with enhanced chemifluorescence (ECF) substrate (GE Healthcare, Piscataway, NJ) treatment for 5 min. Fluorescence was detected with a STORM molecular imager (Amersham Biosciences) at 450 nm excitation/520 nm emission.

Quantification of Allergens in Seed Protein Extract. The standard curve for allergen quantification was derived from "Georgia Green" protein at concentrations of 20, 10, 5, and 2.5 μg obtained by loading 5 μL per well of protein at 4, 2, 1, and 0.5 μg/μL, respectively. For Ara h 1 and Ara h 3 quantification, 5 μg of total protein of test samples was loaded. For Ara h 2 and Ara h 6 quantification, 20 μg of total protein of test samples was loaded. The volume of each band was quantified with Image Quant software after background correction by the object average method. Allergen band volume calculated for test samples was normalized with that of "Georgia Green".

Because allergens are quantified relative to "Georgia Green" total protein concentration, the concentration of individual allergens will be proportional to the total protein concentration. The mean allergen concentration was compared by Tukey's t test at $p \leq 0.05$ using SAS software.[21]

Carbon−Nitrogen−Sulfur (CNS) Analysis. In the sulfur study, CNS analysis was conducted on the same seed samples used for quantitative westerns. Replicate seed samples, four each from low, medium, and high sulfur treatments, were used. Analysis was

DOI: 10.1021/jf504892f
J. Agric. Food Chem. 2015, 63, 1788−1797

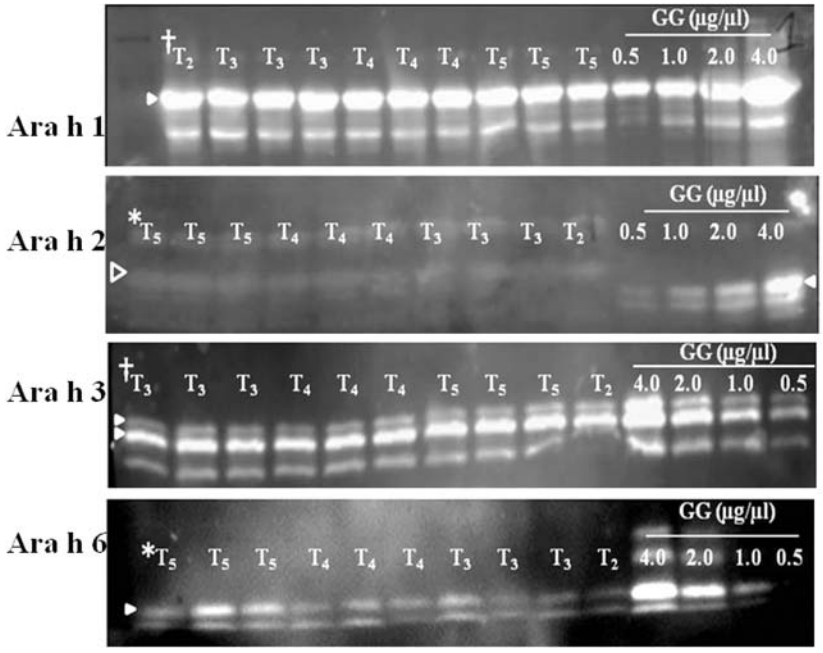

Figure 1. Western blot for allergen quantification in transgenic generations T_3, T_4, and T_5. A total of 5 μL of Tg and "Georgia Green" (GG) protein were loaded for SDS−PAGE. Western blotting was performed using a 1:5000 dilution of anti-Ara h 1, anti-Ara h 3, and anti-Ara h 6 and 1:8000 dilution of anti-Ara h 2 primary antibodies, followed by AP-labeled secondary antibody in 1:10 000 dilution. Signal detection of allergens was performed with ECF substrate with a STORM molecular imager at 450 nm excitation/520 nm emission. Allergen band selected for quantification was indicated by filled triangles. A standard curve was developed using the GG protein concentration and corresponding allergen band volume. The band volume for each allergen was calculated using Image Quant software. The control for protein loading in the Ara h 2 blot was performed with primary Ara h 3. A non-filled arrow in Ara h 2 blot corresponds to Ara h 3 detected with primary Ara h 3 antibody at 0.2:5000 dilution. (†) Transgenic (Tg) protein samples at 1 μg/μL. (∗) Transgenic protein samples at 4 μg/μL.

Table 2. Amount of "Georgia Green" Total Protein Equivalent Relative to Allergen Band Intensity in 1 μg/μL Total Protein from Transgenic Generations T_3, T_4, and T_5 and Non-transgenic (NTg) Null Segregants Grown in the Field

	"Georgia Green" protein equivalent corresponding to allergen band intensity (μg/μL)			
generation	Ara h 1[a,b]	Ara h 3[a,b]	Ara h 2[a,c]	Ara h 6[a,c]
T_3	1.451 ± 0.105 a[d]	1.697 ± 0.240 a	0 b	0.220 ± 0.057 b
T_4	1.204 ± 0.214 a	1.672 ± 0.102 a	0 b	0.218 ± 0.042 b
T_5	1.290 ± 0.126 a	1.664 ± 0.225 a	0 b	0.316 ± 0.075 b
NTg	1.158 ± 0.619 a	1.232 ± 0.404 a	0.954 ± 0.059 a	1.148 ± 0.095 a
observed p value	0.73	0.17	<0.0001	<0.0001

[a]Band volume calculated for each allergen in total protein, by quantitative western blotting, was normalized with "Georgia Green" protein concentration used to develop a standard curve. Each value represents the average ± standard deviation from two technical replications of each of three biological replicates. Means were analyzed by Tukey's t test at $p \leq 0.05$. [b]Loaded 5 μL of protein at 1000 ng/μL. [c]Loaded 5 μL of protein at 4000 ng/μL. [d]Values within a column represented by the same letter are not significantly different.

performed with the dry combustion method in a Leco CNS 2000 analyzer at the Laboratory for Environmental Analysis, University of Georgia, Athens, GA. Carbon and sulfur were detected as CO_2 and SO_2, respectively, by infrared absorption measurement. Nitrogen was determined by thermal conductivity.

Amino Acid Analysis. Free and total amino acid analysis was conducted with one pooled seed sample each, from low-, medium- and high-sulfur plants of transgenic and non-transgenic genotypes. Seed samples (0.05 g each) were pooled from four pooled replicates (same as the replicates used for quantitative western blots) from each sulfur treatment. Amino acid analysis was conducted at the Molecular Structure Facility, University of California, Davis, Davis, CA. Briefly, for total amino acid detection, approximately 10 mg of seed meal was dissolved in 1 N HCl and heated to 56 °C for 15 min. The mixture was defatted with CH_2Cl_2 (2-chloromethane), and the supernatant was collected, dried, and hydrolyzed with 6 N HCl at 110 °C for 24 h. NorLeu dilution buffer was added, and samples were analyzed on a L-8800 Hitachi instrument. For analysis of cysteine and methionine, performic acid oxidation was performed prior to acid hydrolysis. For free amino acid determination, approximately 10 mg of seed meal was dissolved in 1 N HCl and heated to 56 °C for 10 min, proteins were precipitated with 10% sulfosalicylic acid, and supernatant was collected, dried, dissolved in AE-cysteine buffer and analyzed on a L-8800 Hitachi instrument.

RESULTS AND DISCUSSION

Germination, Extractable Seed Protein, and Allergen Expression in T_3, T_4, and T_5 Generations. The germination percentage of T_3, T_4, and T_5 generations and the non-transgenic control varied from 82.95 to 93.2%, although no statistically significant variation was observed ($p \leq 0.05$). The percentage of the total seed extractable protein varied from 6.09 to 10.4%, and no significant difference was detected among three transgenic and non-transgenic generations. Protein extraction efficiency differs with buffer, meal/buffer ratio,[22] and pH of buffer.[23] Peanut seed protein ranged from 20.7 to

DOI: 10.1021/jf504892f
J. Agric. Food Chem. 2015, 63, 1788−1797

28.1% in analysis of 64 peanut genotypes[24] and was reported as 21% in a comparative study of edible seed nuts.[25] Both of these studies measured protein by applying a conversion factor to total nitrogen content. In our study, only soluble protein was assayed, hence the variation from expected protein content per unit mass of defatted meal observed in this study.

No statistically significant difference was seen between "Georgia Green" and null segregants in quantitative western blots for Ara h 1, Ara h 2, Ara h 3, and Ara h 6 levels (results not shown). As shown by quantitative western blot (Figure 1 and Table 2), Ara h 1 and Ara h 3 levels in T_3, T_4, and T_5 generations were not significantly different from those of non-transgenics, although transgenics consistently showed numerically higher Ara h 1 and Ara h 3 than the null segregant. No signal for Ara h 2 proteins was detectable in RNAi lines, which was significantly different ($p \leq 0.0001$) from the non-transgenics. The concentration of Ara h 6 in all three transgenic generations was also significantly lower than in the null segregant ($p \leq 0.0001$).

The present study shows that inheritance and expression of the transgene are stable in T_3, T_4, and T_5 generations for both Ara h 2 and Ara h 6 under field conditions. This is in agreement with stable integration and inheritance of transgenes across multiple generations in other transgenic plants.[26,27] Because the transgene silencing of Ara h 2 was found to be stable across four generations (this study and the study by Chu et al.[10]), it is possible that the integration event may be near matrix attachment or hypomethylated chromosomal regions,[27] although this could only be determined with further molecular evidence.

Collateral changes in seed proteins were seen in soybean[28,29] and *Phaseolus vulgaris*,[30−32] where lines deficient in one seed protein showed an increase in other proteins and enzymes. The lack of a significant quantitative change in Ara h 1 and Ara h 3 probably would result in only minor changes in allergenicity because of these proteins. Mass spectrometry analysis of proteins from the same line did show a significant increase in 13-lipoxygenase and 11S Ahy-3 (Ara h 3-related) proteins.[19] This variation in detection efficiency is due to the sensitivity and ability of mass spectrometry to differentiate products of multiple gene families. In this study, a band was observed in transgenics alone when Ara h 3 primary antibody was used at dilution of 0.2:5000 with 4 μg/μL total protein (Ara h 2 in Figure 1). This band was not detectable with 1 μg/μL total protein used for Ara h 3 quantification in this study. A higher but statistically insignificant level of Ara h 3 in transgenics observed in this study could be attributed to differential detection of Ara h 3 isoforms by western blotting under the conditions employed in this study. Thus, the data from quantitative western blots of major allergens should be combined with more global proteomics platforms to develop a more comprehensive profile of differences between transgenic and non-transgenic lines.

An effect of the environment on silencing was not observed in this study, because both greenhouse-raised plants (T_3) and field-grown plants showed stable expression of the transgene. Environmental effects on transgene expression have been observed between field and greenhouse-grown *Gladiolus*,[33] in *Chrysanthemum* grown under different temperatures,[34] and in *Nicotiana* exposed to different light intensities.[35]

Of the four major allergens analyzed in this study, Ara h 1 and Ara h 2 constitute approximately 12−16 and 5.9−9.3% of the total seed protein, respectively.[12,13] Because there was no statistically significant difference in the extractable seed protein of field-grown transgenic compared to non-transgenic lines across generations, decreasing Ara h 2 and Ara h 6 proteins in seeds must be tempered by compensation with multiple proteins, including slight increases in Ara h 1 and Ara h 3.

Plant Morphology in the T_3 Generation under Varying Soil Sulfur Levels. Plants that received low sulfur nutrition (0.012 mM) showed clear symptoms of sulfur deficiency, including extensive yellowing, reduced vegetative growth, reduced seed number, and reduced seed weight, when compared to the plants grown under medium (0.3 mM) and high (3.0 mM) sulfur nutrition (Figures 2 and 3). Sulfur is an essential macronutrient for plants and impacts CO_2 assimilation, Rubisco enzyme activity, and photosynthesis.[36,37] Sulfur participates in several redox reactions and is essential for synthesis of amino acids methionine and cysteine, several proteins, co-enzymes, and iron−sulfur clusters. An adequate soil sulfur concentration is essential for nitrogen fixation.[38] Sulfur deficiency is associated with chlorosis, growth retardation, and reduced yield.[39,40] Reproductive growth was more affected than vegetative growth by sulfur deficiency in wheat.[40] Poor growth, reduced seed weight, and low yield under low sulfur were observed in this study and in other crops.[41−43]

Figure 2. Peanut plants 3 months after planting in two different soil sulfur levels.

Figure 3. Seed samples used for protein extraction and quantification of relative amounts of peanut allergens. For low S, two seeds were collected per plant from three plants per replication and pooled to obtain six seeds per replication of transgenic/non-transgenic seeds. For medium and high S, five seeds were collected per plant from three plants per replication and pooled to obtain 15 seeds per replication of transgenic/non-transgenic seeds.

Relative Concentrations of Allergens Ara h 1, Ara h 2, Ara h 3, and Ara h 6 in Peanut Transgenic Line B11.1.1 under Different Soil Sulfur Levels. Total extractable seed protein in greenhouse-grown seeds showed significant variation

DOI: 10.1021/jf504892f
J. Agric. Food Chem. 2015, 63, 1788−1797

Table 3. Extractable Seed Protein in T_3 Generation Transgenic (Tg) and Non-transgenic (NTg) Plants Grown in the Greenhouse under Three Soil Sulfur Levels

		total protein[a] (%)	observed F	observed p	F critical
sulfur (S)	0.012 mM	4.35 ± 0.84 b[b]	5.35	0.01	$F(2, 24) = 3.40$
	0.3 mM	4.66 ± 0.80 ab			
	3.0 mM	5.47 ± 1.05 a			
genotype	Tg	5.27 ± 0.93 a	9.13	0.005	$F(1, 24) = 4.25$
	NTg	4.39 ± 0.88 b			

[a]Seed protein was extracted from six pooled seeds of low S and 15 pooled seeds of medium and high S from each of the five replications and quantified by a bicinchoninic acid assay. Total protein values represent the average ± standard deviation from two technical replications of each of the five biological replicates. [b]Means were compared by Tukey's t test, and values with the same letter within a row (S and genotype) are not statistically significant at $p \leq 0.05$.

between transgenic plants (5.27%) and non-transgenic plants (4.39%) and between low S (4.35%) and high S (5.47%) treatments (Table 3). Contrary to results from field-grown seeds, there was a significantly higher percentage of extractable protein in transgenic versus non-transgenic plants, suggesting a possible environmental effect.

As tested by two-way ANOVA, relative levels of Ara h 1 in non-transgenic and T_3 generation transgenic seeds were not influenced by genotype or sulfur nutrition. Sulfur nutrition did influence seed Ara h 3 levels [$F(2, 18) = 3.55$; $p < 0.0001$)], but no effect of genotype or genotype × sulfur interaction was observed. The relative Ara h 3 protein concentration in seeds of plants grown under low sulfur status was reduced 9−10-fold compared to plants grown with medium- or high-sulfur nutrition (Figure 4). Effects of genotype [$F(2, 18) = 3.55$; $p < 0.0001$)], sulfur [$F(1, 18) = 4.41$; $p < 0.0001$)], and genotype × sulfur interaction [$F(2, 18) = 3.55$; $p < 0.0001$)] were significant for seed Ara h 2 and Ara h 6 levels. No Ara h 2 signal was detected in Ara h 2-silenced peanut at any sulfur level by quantitative western blot experiments (Figure 4). Quantitative westerns detected Ara h 6 in transgenics grown under medium- and high-sulfur nutrition but at significantly lower amounts than in non-transgenics (Figure 4). Non-transgenic plants grown under low-sulfur nutrition showed significantly lower concentrations of Ara h 2 and Ara h 6 proteins, lowered by ∼6 and ∼22 times, respectively, than those grown at medium- and high-sulfur levels.

The levels of Ara h 1 in low-, medium-, and high-sulfur treatments among transgenic and non-transgenic plants showed no significant variation, as might be expected for a protein that is not sulfur-rich. On the other hand, low levels of sulfur caused an approximately 10-fold reduction in Ara h 3 compared to high-sulfur levels. Ara h 3 belongs to the glycinin family of proteins. Glycinins comprise major 11S storage proteins in soybeans.[44] Increased legumin (glycinin) mRNA levels and higher legumin mRNA stability have been reported under high S conditions in pea.[45,46] Transcription and transcript stability were not tested in the current study. Ara h 3, like soy glycinin, has acidic and basic subunits covalently linked by disulfide bonds. C88 of the acidic subunit (residues 1−325) and C338 of the basic subunit (residues 326−510) of Ara h 3 are linked by disulfide bonds, as shown by sodium dodecyl sulfate−polyacrylamide gel electrophoresis (SDS−PAGE) and mass spectrometry analysis.[47,48] Disulfide bonding in glycinin is important for stabilizing protein conformation.[49] Low sulfur levels in soil were found to reduce the cysteine and methionine contents in barley[41] and *Arabidopsis*.[50] A similar reduction of the cysteine content (Table 4) in seeds of peanut under low-sulfur nutrition was observed, thus lowering the concentration of glycinin Ara h 3, which has also conserved cysteine residues in acidic and basic polypeptides.

Lines silenced for Ara h 2 showed no chemifluorescence signal for Ara h 2 proteins in seeds from the T_3 generation at any sulfur level. These results confirm the stability of RNAi silencing in the T_3 generation and that variation in S nutrition does not alter the stability of transgene expression, even though significant interaction was seen between the sulfur level and genotype. The level of Ara h 2 reduction is consistent with other studies for detection of Ara h 2 proteins in seeds from the T_2 generation.[10] Statistically significant low levels of Ara h 6 detected in transgenics at medium and high S levels compared to non-transgenics also showed stability of transgene expression to added S. At low S, the available S was insufficient for the synthesis of Ara h 6 in the transgenic lines because no chemifluorescent signal was detected. The low level of Ara h 6 in transgenic peanut at medium and high sulfur levels should be the consequence of efficient post-transcriptional mRNA degradation through RNAi, which probably is unaffected by sulfur nutrition.

Free and Total Amino Acids. Because developing seeds can modulate the amino acid and protein composition based on nutrient availability,[51] the amino acid profile of the plants grown at different sulfur levels was tested. The proportion of each amino acid in the free and total amino acid pool under various S treatments (Tables 4 and 5) and total and free amino acids per unit seed mass (Table 6) was determined to assess any differences in amino acid profile among treatments. These unreplicated data are helpful only in deriving the trend in amino acid profile changes under different S levels in genotypes tested. Accordingly, in the present study, the highest total amino acid content was shown by low-S treatment. Wide variation was seen between low S and the two higher S levels for all amino acids. Under low S, the majority of amino acids was found in low proportions, except for six, namely, histidine, arginine, asparagine, ornithine, hydroxyproline, and glutamine. Among these six, histidine, ornithine, hydroxyproline, and glutamine were measurable only under low-S conditions. At low S, both free and total arginine levels were higher than in medium- and high-S treatments. Arginine represented 68% of the free amino acid pool and ∼18% of the total amino acid pool. Under higher S levels, it represented ∼5−9 and ∼7−9% of free and total amino acid pools, respectively. Except for arginine and asparagine, total amino acids (Table 4) did not vary much, for most amino acids, between S levels compared to the variation seen for free amino acids (Table 5). Arginine levels also were higher in non-transgenics under medium and high S levels. Cysteine and methionine levels were higher under

DOI: 10.1021/jf504892f
J. Agric. Food Chem. 2015, 63, 1788−1797

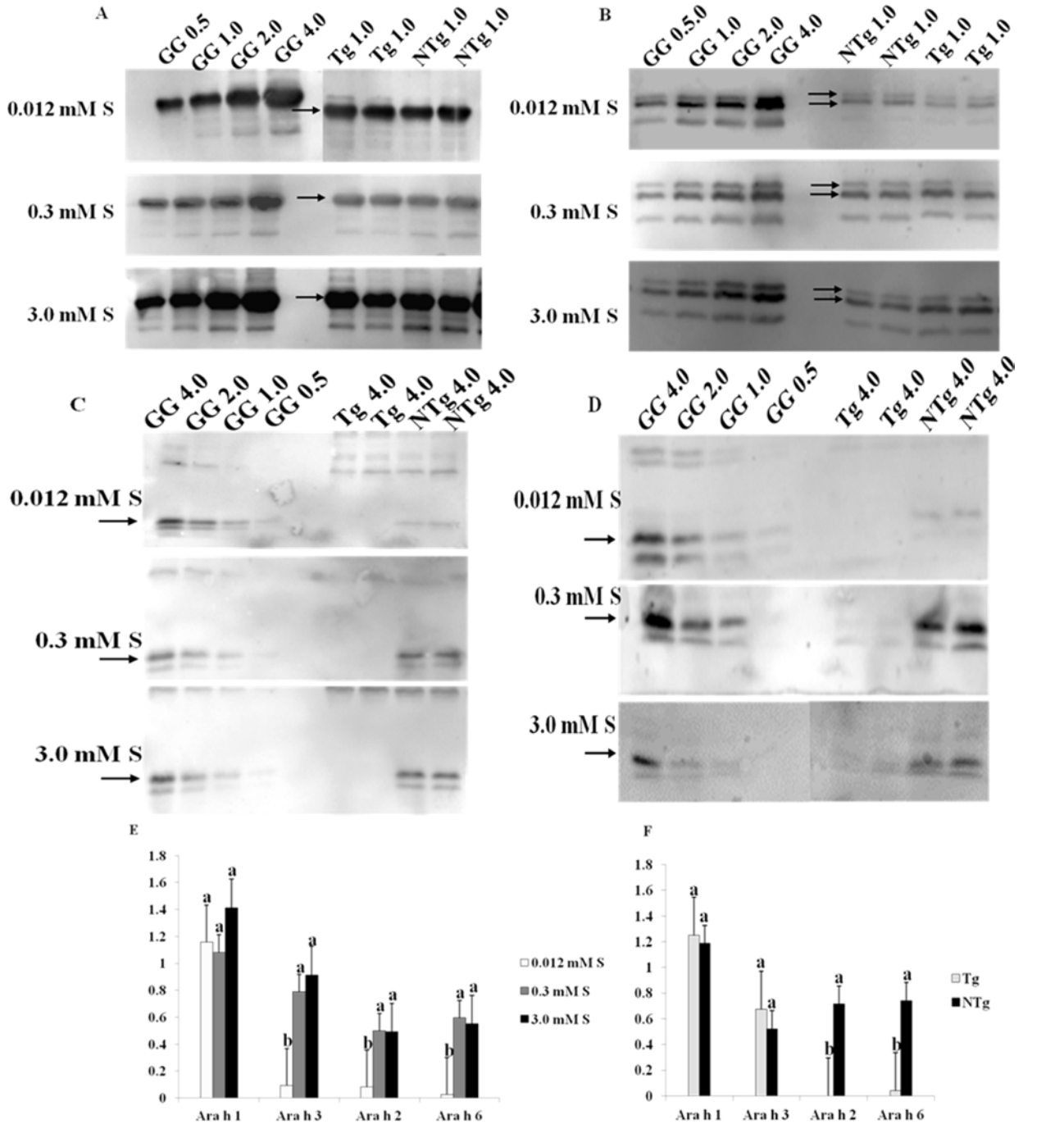

Figure 4. Western blot of allergens in T_3 generation transgenic (Tg) and non-transgenic (NTg) plants grown under three soil sulfur levels. A total of 5 μL of Tg, NTg, and "Georgia Green" (GG) protein was loaded for SDS−PAGE. Numbers corresponding to Tg, NTg, and GG indicate protein concentration in μg/μL. Western blotting was performed using (A) 1:5000 dilution of anti-Ara h 1 primary antibody, (B) 1:5000 dilution of anti-Ara h 3 primary antibody, (C) 1:8000 dilution of anti-Ara h 2 primary antibody, and (D) 1:5000 dilution of anti-Ara h 6 primary antibody, followed by AP-labeled secondary antibody in 1:10 000 dilution. Signal detection of allergen was performed using ECF substrate with STORM molecular imager at 450 nm excitation/520 nm emission. The allergen band selected for quantification is indicated by arrows in western blot images. The standard curve was developed using the GG protein concentration and corresponding allergen band volume. The band volume was calculated using Image Quant software. For Ara h1 and Ara h 3, band volume in 1 μg/μL of total protein was calculated. For Ara h 2 and Ara h 6, band volume in 4 μg/μL of total protein was calculated. (E) Effect of three soil sulfur levels on the allergen content. (F) Effect of genotype (Tg or NTg) on the allergen content. For panels E and F, error bars correspond to standard error, means were compared by Tukey's *t* test, and values with the same letter in bars for an allergen are not statistically significant at $p \leq 0.05$.

medium- and high-S treatments as well as higher in non-transgenics compared to transgenics under these two levels.

Abiotic stress[52−54] and unbalanced nitrogen metabolism[55−57] lead to accumulation of nitrogen-containing compounds, and members of the serine−arginine-rich protein family are found to be induced during abiotic stress.[58] This might explain the increased arginine and other amino acids in the free and total amino acid pools under low-S conditions, which can also lead

DOI: 10.1021/jf504892f
J. Agric. Food Chem. 2015, 63, 1788−1797

Table 4. Percentage of Total Amino Acids in Seeds of T_3 Generation Transgenics (Tg) and Non-transgenic (NTg) Plants Grown in the Greenhouse under Three Soil Sulfur Levels

amino acid	L-Tg[a]	L-NTg[a]	M-Tg[a]	M-NTg[a]	H-Tg[a]	H-NTg[a]
asparagine/aspartic acid	13.5	13.1	10.3	11.8	10.7	12.0
threonine	2.5	2.5	3.1	2.6	3.0	2.7
serine	4.9	5.2	6.0	6.0	5.8	6.1
glutamine/glutamic acid	14.4	14.9	15.2	18.7	15.9	18.2
glycine	12.3	12.8	20.0	14.0	18.7	12.9
alanine	5.0	5.0	5.4	4.9	5.6	5.1
valine	3.6	3.6	4.1	3.7	4.2	4.1
isoleucine	2.8	2.8	2.8	2.8	2.9	3.0
leucine	5.0	5.2	5.2	6.1	5.4	6.3
tyrosine	2.8	3.0	2.9	2.7	2.8	2.9
phenylalanine	3.3	3.5	3.7	3.3	3.8	3.6
lysine	3.8	3.6	4.9	3.8	4.3	3.7
histidine	2.2	2.1	2.2	2.0	2.2	2.0
arginine	18.9	17.4	7.7	9.5	7.9	9.5
proline	4.4	4.5	4.2	4.5	4.5	4.6
cysteic acid	0.7	0.7	1.7	2.6	1.6	2.3
methionine sulfone	0.0	0.0	0.6	1.1	0.6	1.1

[a]Percentage of each amino acid calculated on the basis of amino acids (nanomoles) in 50 μL of final volume analyzed on a L-8800 Hitachi analyzer, in a single analysis of four pooled samples for each treatment. L, low S (0.012 mM); M, medium S (0.30 mM); and H, high S (3.0 mM).

Table 5. Percentage of Free Amino Acids in Seeds of T_3 Generation Transgenics (Tg) and Non-transgenic (NTg) Plants Grown in the Greenhouse under Three Soil Sulfur Levels

amino acid	L-Tg[a]	L-NTg[a]	M-Tg[a]	M-NTg[a]	H-Tg[a]	H-NTg[a]
aspartic acid	0.2	0.2	9.2	12.7	8.7	11.8
threonine	0.4	0.3	1.3	1.2	1.4	1.1
serine	0.5	0.5	1.5	1.4	1.4	1.4
glutamic acid	5.5	6.4	38.8	36.6	35.5	30.4
glycine	0.8	0.7	7.4	6.7	6.4	6.0
alanine	1.6	1.6	7.1	6.7	6.1	6.9
valine	0.3	0.3	2.1	2.1	2.1	2.4
isoleucine	0.1	0.1	0.7	0.7	0.7	0.7
leucine	0.1	0.1	0.9	0.9	0.9	1.1
tyrosine	0.1	0.1	0.7	0.6	0.7	0.9
phenylalanine	0.3	0.5	4.6	3.5	6.7	3.2
lysine	2.7	2.4	1.8	1.6	1.8	1.8
histidine	1.6	1.2				
arginine	68.4	68.2	6.0	4.7	9.1	8.7
proline	0.8	0.6	3.5	4.0	2.9	4.2
asparagine	14.5	13.7	6.4	10.0	6.3	14.6
ornithine	0.7	0.8				
hydroxyproline	0.2	0.2				
citrulline	0.4	0.6	8.0	6.6	9.2	4.7
glutamine	0.9	1.5				

[a]Percentage of each amino acid calculated on the basis of free amino acids (nanomoles) in 50 μL of final volume analyzed on a L-8800 Hitachi analyzer, in a single analysis of four pooled samples. L, low S (0.012 mM); M, medium S (0.30 mM); and H, high S (3.0 mM).

Table 6. Total (TAA) and Free (FAA) Amino Acids Per Unit Mass of Defatted Seed Meal in T_3 Generation Transgenics (Tg) and Non-transgenic (NTg) Plants Grown in the Greenhouse under Three Soil Sulfur Levels

sulfur (mM)	genotype	TAA[a] (nmol/mg)	FAA[a] (nmol/mg)
0.012	Tg	1644.5	269.2
	NTg	1833.7	237.16
0.3	Tg	836.3	23.43
	NTg	1275.9	25.7
3.0	Tg	1006.2	22.46
	NTg	1552.1	25.55

[a]TAA and FAA per unit mass of defatted seed mass represent single measurements of four pooled samples, analyzed with a L-8800 Hitachi analyzer.

to a high nitrogen content, as seen in this study. Free amino acids are critical for the roasted flavor of peanut. Free amino acids react with the sugars in seed to produce organic compounds, which impart the typical roasted peanut flavor through the Maillard reaction.[59,60] Typical roasted flavor is attributed by glutamic acid, glutamine, asparagine, phenylalanine, aspartic acid, and histidine. Free arginine, tyrosine, lysine, and threonine are responsible for the atypical flavors.[60,61] Arginine, although beneficial to human health in multiple ways,[62] can be detrimental at high concentrations with regard to peanut-roasting quality. Hence, sulfur nutrition is important for maintaining the quality of peanut because low S levels showed higher arginine, irrespective of the plant genotype. Low levels of cysteine and methionine, in the total amino acid pool, in transgenics is due to the silencing of sulfur-rich Ara h 2 and Ara h 6 in these lines.

Seed CNS Content. The percentage of carbon in dry defatted meal varied from 49% in low-S treatment to 56% in high-S treatment (Table 7). Seed carbon was influenced by sulfur (p = 0.000 12); however, no significant variation in seed carbon was seen between transgenic and non-transgenic plants, and no genotype × sulfur effect was observed. Both genotype (p < 0.0001) and soil sulfur (p = 0.0002) levels showed significant effects on seed nitrogen in two-way ANOVA, although no effect of interaction was observed. Seed nitrogen content was significantly higher in the low-S treatment (8.62%), and no significant difference was shown between medium (7.13%) and high (6.92%) sulfur. Significant variation was observed between transgenic and non-transgenic plants in seed nitrogen content, with non-transgenics having higher nitrogen (8.31%) than transgenics (6.80%). Seed sulfur was influenced by sulfur nutrition (p < 0.0001) and genotype (p = 0.000 15),

DOI: 10.1021/jf504892f
J. Agric. Food Chem. 2015, 63, 1788−1797

Table 7. Seed CNS in T_3 Generation Transgenics (Tg) and Non-transgenics (NTg) Grown in the Greenhouse under Three Soil Sulfur Levels

		carbon (%)[a]	nitrogen (%)[a]	sulfur (%)[a]	N/S
sulfur (S)	0.012 mM	49.89 ± 1.35 b[b]	8.62 ± 0.08 a	0.18 ± 0.03 b	49.67 ± 6.36 a
	0.3 mM	53.52 ± 3.96 a	7.13 ± 1.35 b	0.26 ± 0.07 a	28.07 ± 4.40 b
	3.0 mM	56.54 ± 1.28 a	6.92 ± 0.90 b	0.27 ± 0.04 a	25.68 ± 2.39 b
observed F		15.36	13.92	17.57	66.32
observed p		0.00012	0.0002	5.86×10^{-5}	4.96×10^{-9}
F critical (2, 18) = 3.55					
genotype	Tg	52.79 ± 3.94 a	6.80 ± 1.12 b	0.20 ± 0.04 b	35.90 ± 12.39 a
	NTg	53.84 ± 3.49 a	8.31 ± 0.92 a	0.27 ± 0.07 a	33.04 ± 11.73 a
observed F		1.128	28.05	22.82	2.32
observed p		0.302	4.91×10^{-5}	0.00015	0.144
F critical (1, 18) = 4.41					

[a]CNS values represent averages of four biological replicates analyzed using 0.2 g of defatted and lyophilized seed meal in a Leco CNS analyzer. [b]Means were compared by Tukey's t test, and values with the same letter in columns within a row (S, genotype, and S × genotype) are not significantly different at $p \leq 0.05$.

and no genotype × sulfur interaction was observed. The sulfur content in seeds ranged from 0.18 to 0.27% in the three S nutrient regimes. Non-transgenic plants grown under three S treatments showed significantly higher seed S content (0.27%) than transgenics (0.2%). The seed N/S ratio was influenced by sulfur alone ($p < 0.0001$). Nitrogen/sulfur ratios varied from 25.68 in high-S conditions to 49.67 in low-S conditions. The N/S ratio was higher in low-S treatment, and no difference was seen between transgenic and non-transgenic plants (Table 7)

Seeds from lupin plants carrying the sunflower seed albumin transgene showed higher total S and S amino acids than non-transgenic plants.[63] In the current study, transgenic peanuts showed significantly low seed S, a result expected to be contrary to that of lupins, given the difference between overexpressing and silencing S-rich proteins. Under abiotic stress, nitrogen-containing compounds accumulate, with the most common being amino acids, such as arginine, proline, amides (glutamine and asparagine), citrulline, and ornithine, which are formed as products of detoxification of excess ammonium produced under stress.[52−54] In barley grown under low sulfur, a high proportion of aspartic acid and asparagine and low levels of methionine and cysteine were found.[41] The difference in the percentage of N between transgenic and non-transgenic plants can possibly be due to the differences in the amino acid content in the two genotypes, with the non-transgenic controls having a high total amino acid content compared to transgenics (Table 6). Low S and high nitrogen contents of seeds resulted in high and unfavorable N/S ratios under S deficiency and varied significantly from plants under medium- and high-S nutrition. This is in accordance with reports where higher seed and plant S was seen with higher S nutrition in both high and low N levels.[64,65] Carbon, nitrogen, and sulfur contents in seeds result from interactions between carbon, nitrogen, and sulfur metabolic pathways. Sulfur is a component of chloroplast Fe−S cluster proteins, and low S concentrations lead to reduced chlorophyll, Rubisco level, photosynthesis, and CO_2 fixation in rice and barley.[37,52] A low seed carbon content in seeds of low-S treatment in this study may be a consequence of the reduced growth and photosynthesis under S deficiency. Also, when S is limited, activity of the nitrate reductase enzyme is reduced, leading to reduced nitrogen assimilation,[66,67] because the enzymatic activity of nitrate reductase depends upon S−Mo biochemistry.[68] Nitrogenase activity and nitrogen fixation in roots of white clover were also reduced under S deficiency[55] because S is an essential component of the Fe−Mo cofactor of the nitrogenase protein.[56] The unbalanced nitrogen metabolism results in accumulation of nitrogen compounds, especially nitrogen-rich amino acids.[55,57] Reduced S also impairs synthesis of sulfolipids and *S*-adenosyl methionine, required for photosynthesis. Thus, S limitation leads to reduced metabolism by its influence on photosynthesis and the carbon assimilation pathway.[57]

In summary, the stability of allergen gene silencing by RNAi was tested in the present study. Concentrations of Ara h 1, Ara h 2, Ara h 3, and Ara h 6 were analyzed relative to "Georgia Green" by quantitative western blotting. Silencing of Ara h 2 and partial silencing of Ara h 6 were stably inherited across three generations. Also, relative levels of Ara h 1 and Ara h 3 were slightly but not significantly higher in transgenics compared to non-transgenics. Soil sulfur had no effect on levels of completely silenced Ara h 2 and partially silenced Ara h 6, although high-sulfur nutrition increases Ara h 2 and Ara h 6 as well as cysteine and methionine in non-transgenic peanuts. Western blotting should be coupled with more sensitive proteomics techniques to develop a detailed protein profile of transgenic peanut line B11.1.1 across generations and under different environmental conditions. This transgenic line can also serve as a good experimental material for deducing the sulfur assimilation and metabolism pathways in perturbed and non-perturbed systems.

AUTHOR INFORMATION

Corresponding Author

*Telephone: 229-386-3902. Fax: 229-386-7371. E-mail: pozias@uga.edu.

Funding

This work was supported by The Peanut Foundation, The National Peanut Board, and The Agriculture and Food Research Initiative Competitive Grant 2010-85117-20550 of the USDA National Institute of Food and Agriculture.

Notes

The authors declare no competing financial interest.

REFERENCES

(1) Pandey, M. K.; Monyo, E.; Ozias-Akins, P.; Liang, X. Q.; Guimaraes, P.; Nigam, S. N.; Upadhyaya, H. D.; Janila, P.; Zhang, X. Y.; Guo, B. Z.; Cook, D. R.; Bertioli, D. J.; Michelmore, R.; Varshney,

DOI: 10.1021/jf504892f
J. Agric. Food Chem. 2015, 63, 1788−1797

R. K. Advances in *Arachis* genomics for peanut improvement. *Biotechnol. Adv.* **2012**, *30*, 639−651.
(2) Yocum, M. W.; Khan, D. A. Assessment of patients who have experienced anaphylaxis—A 3-year survey. *Mayo Clin. Proc.* **1994**, *69*, 16−23.
(3) Sampson, H. A. Update on food allergy. *J. Allergy Clin. Immunol.* **2004**, *113*, 805−819.
(4) Scurlock, A. M.; Burks, A. W. Peanut allergenicity. *Ann. Allergy Asthma Immunol.* **2004**, *93*, S12−S18.
(5) Burks, W.; Sampson, H. A.; Bannon, G. Peanut allergens. *Allergy* **1998**, *53*, 725−730.
(6) Flinterman, A. E.; van Hoffen, E.; Jager, C. F. D.; Koppelman, S.; Pasmans, S. G.; Hoekstra, M. O.; Bruijnzeel-Koomen, C. A.; Knulst, A. C.; Knol, E. F. Children with peanut allergy recognize predominantly Ara h 2 and Ara h 6, which remains stable over time. *Clin. Exp. Allergy* **2007**, *37*, 1221−1228.
(7) www.allergen.org.
(8) Kang, I. H.; Gallo, M.; Tillman, B. L. Distribution of allergen composition in peanut (*Arachis hypogaea* L.) and wild progenitor (*Arachis*) species. *Crop Sci.* **2007**, *47*, 997−1003.
(9) Krause, S.; Latendorf, T.; Schmidt, H.; Darcan-Nicolaisen, Y.; Reese, G.; Petersen, A.; Janssen, O.; Becker, W. M. Peanut varieties with reduced Ara h 1 content indicating no reduced allergenicity. *Mol. Nutr. Food Res.* **2010**, *54*, 381−387.
(10) Chu, Y.; Faustinelli, P.; Laura Ramos, M.; Hajduch, M.; Stevenson, S.; Thelen, J. J.; Maleki, S. J.; Cheng, H.; Ozias-Akins, P. Reduction of IgE binding and nonpromotion of *Aspergillus flavus* fungal growth by simultaneously silencing Ara h 2 and Ara h 6 in peanut. *J. Agric. Food Chem.* **2008**, *56*, 11225−11233.
(11) Ramos, M. L.; Fleming, G.; Chu, Y.; Akiyama, Y.; Gallo, M.; Ozias-Akins, P. Chromosomal and phylogenetic context for conglutin genes in *Arachis* based on genomic sequence. *Mol. Genet. Genomics* **2006**, *275*, 578−592.
(12) Koppelman, S. J.; Vlooswijk, R. A. A.; Knippels, L. M. J.; Hessing, M.; Knol, E. F.; Van Reijsen, F. C.; Bruijnzeel-Koomen, C. A. F. M. Quantification of major peanut allergens Ara h 1 and Ara h 2 in the peanut varieties Runner, Spanish, Virginia, and Valencia, bred in different parts of the world. *Allergy* **2001**, *56*, 132−137.
(13) Stanley, J. S.; King, N.; Burks, A. W.; Huang, S. K.; Sampson, H.; Cockrell, G.; Helm, R. M.; West, C. M.; Bannon, G. A. Identification and mutational analysis of the immunodominant IgE binding epitopes of the major peanut allergen Ara h 2. *Arch. Biochem. Biophys.* **1997**, *342*, 244−253.
(14) Chatel, J. M.; Bernard, H.; Orson, F. M. Isolation and characterization of two complete Ara h 2 isoforms cDNA. *Int. Arch. Allergy Immunol.* **2003**, *131*, 14−18.
(15) Kulis, M.; Chen, X.; Lew, J.; Wang, Q.; Patel, O. P.; Zhuang, Y.; Murray, K. S.; Duncan, M. W.; Porterfield, H. S.; Burks, A. W.; Dreskin, S. C. The 2S albumin allergens of *Arachis hypogaea*, Ara h 2 and Ara h 6, are the major elicitors of anaphylaxis and can effectively desensitize peanut-allergic mice. *Clin. Exp. Allergy* **2012**, *42*, 326−336.
(16) Randall, P. J.; Thomson, J. A.; Schroeder, H. E. Cotyledonary storage proteins in *Pisum sativum*. 4. Effects of sulfur, phosphorus, potassium and magnesium deficiencies. *Aust. J. Plant Physiol.* **1979**, *6*, 11−24.
(17) Gayler, K. R.; Sykes, G. E. Effects of nutritional stress on the storage proteins of soybeans. *Plant Physiol.* **1985**, *78*, 582−585.
(18) Sexton, P. J.; Paek, N. C.; Shibles, R. M. Effects of nitrogen source and timing of sulfur deficiency on seed yield and expression of 11S and 7S seed storage proteins of soybean. *Field Crops Res.* **1998**, *59*, 1−8.
(19) Stevenson, S. E.; Chu, Y.; Ozias-Akins, P.; Thelen, J. J. Validation of gel-free, label-free quantitative proteomics approaches: Applications for seed allergen profiling. *J. Proteomics* **2009**, *72*, 555−566.
(20) Porterfield, H. S.; Murray, K. S.; Schlichting, D. G.; Chen, X.; Hansen, K. C.; Duncan, M. W.; Dreskin, S. C. Effector activity of peanut allergens: A critical role for Ara h 2, Ara h 6, and their variants. *Clin. Exp. Allergy* **2009**, *39*, 1099−1108.
(21) SAS Institute, Inc. *Administering SAS Enterprise Guide 4.2*; SAS Institute, Inc.: Cary, NC, 2009.
(22) Basha, S. M.; Cherry, J. P. Composition, solubility, and gel electrophoretic properties of proteins isolated from Florunner (*Arachis hypogaea* L.) peanut seeds. *J. Agric. Food Chem.* **1976**, *24*, 359−365.
(23) Poms, R. E.; Capelletti, C.; Anklam, E. Effect of roasting history and buffer composition on peanut protein extraction efficiency. *Mol. Nutr. Food Res.* **2004**, *48*, 459−464.
(24) Dwivedi, S. L.; Jambunathan, R.; Nigam, S. N.; Raghunath, K.; Shankar, K. R.; Nagabhushanam, G. V. S. Relationship of seed mass to oil and protein contents in peanut *Arachis hypogaea* L. *Peanut Sci.* **1990**, *17*, 48−52.
(25) Venkatachalam, M.; Sathe, S. K. Chemical composition of selected edible nut seeds. *J. Agric. Food Chem.* **2006**, *54*, 4705−4714.
(26) Chawla, R.; Ariza-Nieto, M.; Wilson, A. J.; Moore, S. K.; Srivastava, V. Transgene expression produced by biolistic-mediated, site-specific gene integration is consistently inherited by the subsequent generations. *Plant Biotechnol. J.* **2006**, *4*, 209−218.
(27) Kohli, A.; Miro, B.; Twyman, R. M. Transgene integration, expression and stability in plants: Strategies for improvements. In *Transgenic Crop Plants. Principles and Development*; Kole, C., Michler, C. H., Abbott, A. G., Hall, T. C., Eds.; Springer: Heidelberg, Germany, 2010; Vol. *1*, pp 201−237.
(28) Ogawa, T.; Tayama, E.; Kitamura, K.; Kaizuma, N. Genetic improvement of seed storage proteins using three variant alleles of 7s globulin subunits in soybean (*Glycine max* L.). *Jpn. J. Breed.* **1989**, *39*, 137−147.
(29) Takahashi, M.; Uematsu, Y.; Kashiwaba, K.; Yagasaki, K.; Hajika, M.; Matsunaga, R.; Komatsu, K.; Ishimoto, M. Accumulation of high levels of free amino acids in soybean seeds through integration of mutations conferring seed protein deficiency. *Planta* **2003**, *217*, 577−586.
(30) Hartweck, L. M.; Osborn, T. C. Altering protein composition by genetically removing phaseolin from common bean seeds containing arcelin or phytohemagglutinin. *Theor. Appl. Genet.* **1997**, *95*, 1012−1017.
(31) Liao, D. Q.; Pajak, A.; Karcz, S. R.; Chapman, B. P.; Sharpe, A. G.; Austin, R. S.; Datla, R.; Dhaubhadel, S.; Marsolais, F. Transcripts of sulphur metabolic genes are co-ordinately regulated in developing seeds of common bean lacking phaseolin and major lectins. *J. Exp. Bot.* **2012**, *63*, 6283−6295.
(32) Marsolais, F.; Pajak, A.; Yin, F. Q.; Taylor, M.; Gabriel, M.; Merino, D. M.; Ma, V.; Kameka, A.; Vijayan, P.; Pham, H.; Huang, S. Z.; Rivoal, J.; Bett, K.; Hernandez-Sebastia, C.; Liu, Q. A.; Bertrand, A.; Chapman, R. Proteomic analysis of common bean seed with storage protein deficiency reveals up-regulation of sulfur-rich proteins and starch and raffinose metabolic enzymes, and down-regulation of the secretory pathway. *J. Proteomics* **2010**, *73*, 1587−1600.
(33) Kamo, K. Transgene expression for *Gladiolus* plants grown outdoors and in the greenhouse. *Sci. Hortic.* **2008**, *117*, 275−280.
(34) Shinoyama, H.; Sano, T.; Saito, M.; Ezura, H.; Aida, R.; Nomura, Y.; Kamada, H. Induction of male sterility in transgenic chrysanthemums (*Chrysanthemum morifolium* Ramat.) by expression of a mutated ethylene receptor gene, *Cm-ETR1/H69A*, and the stability of this sterility at varying growth temperatures. *Mol. Breed.* **2012**, *29*, 285−295.
(35) Kotakis, C.; Vrettos, N.; Kotsis, D.; Tsagris, M.; Kotzabasis, K.; Kalantidis, K. Light intensity affects RNA silencing of a transgene in *Nicotiana benthamiana* plants. *BMC Plant Biol.* **2010**, *10*, 220.
(36) Gilbert, S. M.; Clarkson, D. T.; Cambridge, M.; Lambers, H.; Hawkesford, M. J. SO_4^{2-} deprivation has an early effect on the content of ribulose-1,5-bisphosphate carboxylase/oxygenase and photosynthesis in young leaves of wheat. *Plant Physiol.* **1997**, *115*, 1231−1239.
(37) Lunde, C.; Zygadlo, A.; Simonsen, H. T.; Nielsen, P. L.; Blennow, A.; Haldrup, A. Sulfur starvation in rice: The effect on photosynthesis, carbohydrate metabolism, and oxidative stress protective pathways. *Physiol. Plant.* **2008**, *134*, 508−521.
(38) Scherer, H. W.; Pacyna, S.; Spoth, K. R.; Schulz, M. Low levels of ferredoxin, ATP and leghemoglobin contribute to limited N_2

DOI: 10.1021/jf504892f
J. Agric. Food Chem. 2015, 63, 1788−1797

fixation of peas (*Pisum sativum* L.) and alfalfa (*Medicago sativa* L.) under S deficiency conditions. *Biol. Fertil. Soils* **2008**, *44*, 909−916.
(39) Nikiforova, V. J.; Gakiere, B.; Kempa, S.; Adamik, M.; Willmitzer, L.; Hesse, H.; Hoefgen, R. Towards dissecting nutrient metabolism in plants: a systems biology case study on sulphur metabolism. *J. Exp. Bot.* **2004**, *55*, 1861−1870.
(40) Zhao, F. J.; Hawkesford, M. J.; McGrath, S. P. Sulphur assimilation and effects on yield and quality of wheat. *J. Cereal Sci.* **1999**, *30*, 1−17.
(41) Shewry, P. R.; Franklin, J.; Parmar, S.; Smith, S. J.; Miflin, B. J. The effects of sulfur starvation on the amino acid and protein compositions of barley grain. *J. Cereal Sci.* **1983**, *1*, 21−31.
(42) Yin, X. H.; Gwathmey, O.; Main, C.; Johnson, A. Effects of sulfur application rates and foliar zinc fertilization on cotton lint yields and quality. *Agron. J.* **2011**, *103*, 1794−1803.
(43) Cazzato, E.; Laudadio, V.; Stellacci, A. M.; Ceci, E.; Tufarelli, V. Influence of sulphur application on protein quality, fatty acid composition and nitrogen fixation of white lupin (*Lupinus albus* L.). *Eur. Food Res. Technol.* **2012**, *235*, 963−969.
(44) Beilinson, V.; Chen, Z.; Shoemaker, R. C.; Fischer, R. L.; Goldberg, R. B.; Nielsen, N. C. Genomic organization of glycinin genes in soybean. *Theor. Appl. Genet.* **2002**, *104*, 1132−1140.
(45) Beach, L. R.; Spencer, D.; Randall, P. J.; Higgins, T. J. V. Transcriptional and post-transcriptional regulation of storage protein gene-expression in sulfur-deficient pea seeds. *Nucleic Acids Res.* **1985**, *13*, 999−1013.
(46) Evans, I. M.; Gatehouse, J. A.; Boulter, D. Regulation of storage protein synthesis in pea (*Pisum sativum* L.) cotyledons under conditions of sulfur deficiency. *Biochem. J.* **1985**, *232*, 261−265.
(47) Koppelman, S. J.; Knol, E. F.; Vlooswijk, R. A. A.; Wensing, M.; Knulst, A. C.; Hefle, S. L.; Gruppen, H.; Piersma, S. Peanut allergen Ara h 3: Isolation from peanuts and biochemical characterization. *Allergy* **2003**, *58*, 1133−1151.
(48) Piersma, S. R.; Gaspari, M.; Hefle, S. L.; Koppelman, S. J. Proteolytic processing of the peanut allergen Ara h 3. *Mol. Nutr. Food Res.* **2005**, *49*, 744−755.
(49) Hoshi, Y.; Yamauchi, F. Determination of sulfhydryl and disulfide contents of soybean-11s globulin and their change by lyophilization. *Agric. Biol. Chem.* **1983**, *47*, 2435−2440.
(50) Nikiforova, V. J.; Bielecka, M.; Gakiere, B.; Krueger, S.; Rinder, J.; Kempa, S.; Morcuende, R.; Scheible, W. R.; Hesse, H.; Hoefgen, R. Effect of sulfur availability on the integrity of amino acid biosynthesis in plants. *Amino Acids* **2006**, *30*, 173−183.
(51) Tabe, L.; Hagan, N.; Higgins, T. J. V. Plasticity of seed protein composition in response to nitrogen and sulfur availability. *Curr. Opin. Plant Biol.* **2002**, *5*, 212−217.
(52) Karmoker, J. L.; Clarkson, D. T.; Saker, L. R.; Rooney, J. M.; Purves, J. V. Sulfate deprivation depresses the transport of nitrogen to the xylem and the hydraulic conductivity of barley (*Hordeum vulgare* L.) roots. *Planta* **1991**, *185*, 269−278.
(53) Rabe, E. Stress physiology—The functional significance of the accumulation of nitrogen-containing compounds. *J. Hortic. Sci.* **1990**, *65*, 231−243.
(54) Rai, V. K. Role of amino acids in plant responses to stresses. *Biol. Plant.* **2002**, *45*, 481−487.
(55) Varin, S.; Cliquet, J. B.; Personeni, E.; Avice, J. C.; Lemauviel-Lavenant, S. How does sulphur availability modify N acquisition of white clover (*Trifolium repens* L.)? *J. Exp. Bot.* **2010**, *61*, 225−234.
(56) Chan, M. K.; Kim, J. S.; Rees, D. C. The nitrogenase feMo-cofactor and P-cluster pair: 2.2 Å resolution structures. *Science* **1993**, *260*, 792−794.
(57) Hoefgen, R.; Nikiforova, V. J. Metabolomics integrated with transcriptomics: Assessing systems response to sulfur-deficiency stress. *Physiol. Plant.* **2008**, *132*, 190−198.
(58) Duque, P. A role for SR proteins in plant stress responses. *Plant Signaling Behav.* **2011**, *6*, 49−54.
(59) Basha, S. M.; Young, C. T. Changes in the polypeptide composition of peanut (*Arachis hypogaea* L.) seed during oil roasting. *J. Agric. Food Chem.* **1985**, *33*, 350−354.
(60) Mason, M. E.; Johnson, B.; Hamming, M. C. Volatile components of roasted peanuts. Major monocarbonyls and some noncarbonyl components. *J. Agric. Food Chem.* **1967**, *15*, 66−73.
(61) Newell, J. A.; Mason, M. E.; Matlock, R. S. Precursors of typical and atypical roasted peanut flavor. *J. Agric. Food Chem.* **1967**, *15*, 767.
(62) Wu, G. Y.; Bazer, F. W.; Davis, T. A.; Kim, S. W.; Li, P.; Rhoads, J. M.; Satterfield, M. C.; Smith, S. B.; Spencer, T. E.; Yin, Y. L. Arginine metabolism and nutrition in growth, health and disease. *Amino Acids* **2009**, *37*, 153−168.
(63) Tabe, L. M.; Droux, M. Limits to sulfur accumulation in transgenic lupin seeds expressing a foreign sulfur-rich protein. *Plant Physiol.* **2002**, *128*, 1137−1148.
(64) Chiaiese, P.; Ohkama-Ohtsu, N.; Molvig, L.; Godfree, R.; Dove, H.; Hocart, C.; Fujiwara, T.; Higgins, T. J. V.; Tabe, L. M. Sulphur and nitrogen nutrition influence the response of chickpea seeds to an added, transgenic sink for organic sulphur. *J. Exp. Bot.* **2004**, *55*, 1889−1901.
(65) Sexton, P. J.; Naeve, S. L.; Paek, N. C.; Shibles, R. Sulfur availability, cotyledon nitrogen: Sulfur ratio, and relative abundance of seed storage proteins of soybean. *Crop Sci.* **1998**, *38*, 983−986.
(66) Jamal, A.; Fazli, I. S.; Ahmad, S.; Kim, K. T.; Oh, D. G.; Abdin, M. Z. Effect of sulfur on nitrate reductase and ATP sulfurylase activities in groundnut (*Arachis hypogea* L.). *J. Plant Biol.* **2006**, *49*, 513−517.
(67) Ruiz, J. M.; Rivero, R. M.; Romero, L. Regulation of nitrogen assimilation by sulfur in bean. *J. Plant Nutr.* **2005**, *28*, 1163−1174.
(68) Cerqueira, N.; Gonzalez, P. J.; Brondino, C. D.; Romao, M. J.; Romao, C. C.; Moura, I.; Moura, J. J. G. The effect of the sixth sulfur ligand in the catalytic mechanism of periplasmic nitrate reductase. *J. Comput. Chem.* **2009**, *30*, 2466−2484.

DOI: 10.1021/jf504892f
J. Agric. Food Chem. 2015, 63, 1788−1797

element content may have an adverse effect on human health; for example, accumulation of aluminum (Al) in tea infusion is associated with Alzheimer's disease.[19] Therefore, analytical methods for analyzing such samples must discriminate between different elements to properly assess the quality and safety of such preparations. Furthermore, the element determination of the entire plant is not adequate for risk assessment, and further attempts are made to determine the element composition of matured wild hawthorn fruit tea.[20]

The collection and analysis of medicinal herb components, especially those that are associated with human health and disease, provide data for food composition databases.[21] The aim of this study is a detailed metal characterization of hawthorn organs and tea preparations, including essential and toxic elements. Furthermore, the optimum decoction time for the diffusion of minerals into water was determined.

MATERIALS AND METHODS

Chemicals. For the experimental work, nitric acid (p.a.) and a multielement standard element analyzer (ICP Multielement Standard IV) from Merck (Darmstadt, Germany) were used. The standard reference material of strawberry leaves (LGC7162) was purchased from LGC Standards (Middlesex, UK). All glassware was cleaned with nitric acid prior to use. Ultrapure water produced in-house was used for all dilutions and blanks.

Samples. Fresh wild hawthorn whole fruits, leaves, and flowers were collected from hawthorn trees growing in Slunj, Croatia (N, 45.07°; E, 15.36°; A, 280 m) in 2011; leaves and flowers were sampled in spring, when the plant was in full blossom, and fruits in autumn, after reaching ripeness. All samples were dried at room temperature in paper bags and stored in a dry and dark room at ambient temperature in plastic bottles prior to analysis. The samples were then homogenized in a metal-free mortar.

Sample Preparation. The plant organs were digested using a microwave-assisted system, as commonly used for this kind of sample.[22]

For the microwave-assisted digestion of the samples, MWS-2 Microwave System Speedware from Berghof Laborprodukte GmbH (Eningen, Germany) was used, and the digestion procedure was conducted in three temperature steps (1, 110 °C/15 min; 2, 170 °C/15 min; and 3, 140 °C/15 min). Approximately 0.1−0.25 g (weighed to the nearest 0.1 mg) of the samples (leaves, flowers, and berries) was weighed into a Teflon reaction vessel (in duplicate). Different digestion mixtures were tested: I, 5 mL of HNO_3 (50:50 v/v); II, 5 mL of HNO_3 (25:75 v/v); and III, 5 mL of HNO_3 (25:75 v/v) + 2 mL of H_2O_2 (1 mol/L). The resulting clear solutions of the digestion procedure were then brought up to 10.0 mL with ultrapure water.

For the infusions, dried plant parts (approximately 2 g, weighed to the nearest 0.1 mg) were added to 98 mL of boiling water for different time periods (1, 5, 10, and 20 min). The infusions were then filtered with Whatman no. 541 filter paper.

If necessary, dilution of samples with diluted nitric acid was performed prior to elemental analysis.

ICP-AES Measurements. Mineral content of the digests and infusions was determined with a Prodigy High Dispersive ICP-AES spectrometer from Teledyne Leeman (Hudson, NH, USA) working in a simultaneous mode applying the instrumental conditions listed in Table 1.

All samples (infusions and blank solutions) were measured in triplicate. The quantitative determinations were carried out by external calibration using multielement standard solutions in the concentration range from 0.05 to the expected maximum concentration (5−20 mg/L) of the elements of interest. A multielement standard stock solution (1000 mg/L) was used for the preparation of standard solutions in 1% w/w HNO_3. Blank solutions were prepared in the same media.

The emission lines selected for the determination of the elements (wavelength in nm) were Al, 308.215; Ba, 455.403; Ca, 396.847; Cd, 214.441; Co, 228.615; Cr, 206.149; Cu, 224.700; Fe, 238.204; K, 766.491; Mg, 280.271; Mn, 257.610; Na, 589.592; Ni, 231.604; Pb, 220.353; Sr, 407.771; and Zn, 213.856.

Table 1. ICP-AES Operating Conditions

instrument	Prodigy High Dispersive ICP
spectrometer	high-resolution Echelle polychromator
	large-format programmable array detector (L-PAD)
RF generator	40 MHz "free-running"
output power	1.1 kW
argon flow	coolant: 18 L min^{-1}
	auxiliary: 0.8 L min^{-1}
	nebulizer: 1 L min^{-1}
peristaltic pump	1.0 mL min^{-1}
nebulizer	pneumatic (glass concentric)
spray chamber	glass cyclonic
plasma viewing	axial
replicates for each analysis run	3
sample uptake delay	30 s

ICP-MS. Elemental analysis was carried out on an Element 2 ICP-SFMS from Thermo Fisher (Bremen, Germany) equipped with the self-aspirating PFA microflow nebulizer (ESI) operated at a flow of 100 mL/min, a PC^3 cyclonic quartz chamber (ESI) operated at 4 °C, a quartz injector pipe and torch (Thermo Fisher), aluminum sampler, and skimmer cone (Thermo Fisher). The following operating conditions were applied: RF power of 1300 W and plasma gas flow of 16 L/min; sample gas and auxiliary gas flows were set to 1.06 L/min and 0.86 L/min, respectively.

The isotopes analyzed were, at low resolution, ^{7}Li, ^{82}Se, ^{88}Sr, ^{111}Cd, ^{208}Pb; at medium resolution, ^{52}Cr, ^{55} Mn, ^{56}Fe, ^{59}Co, ^{60}Ni, ^{65}Cu, ^{66}Zn, and ^{98} Mo; and at high resolution, ^{75}As.

^{115}Indium (1.1 μg/L) was used as internal standard at all resolutions. Nominal mass resolution values of the Element 2 ICP-SFMS for low resolution (LR), medium resolution (MR), and high resolution (HR) are 350, 4500, and 10000, respectively.

Optimization and Characterization of the Analytical Method. The trueness of the method for plant organs was determined by analyzing a standard reference material of strawberry leaves (LGC7162) using HNO_3 (50:50 v/v) for digestion. Recoveries of analytes from infusions were determined by spiking: Aqueous multielement standard solutions were added to a set of infusions at three concentration levels (1.0, 3.0, and 5.0 mg/L). All spiked samples were prepared and measured in triplicate.

To check the overall repeatability of the instruments, selected samples were analyzed after calibration on two different days. The precision was evaluated by measuring the solutions of all sample types five times and is presented as relative standard deviations (RSD).

The sensitivity of the method with respect to each metal was evaluated using the resultant slope of the calibration curves.

The limits of detection were calculated according to the method of Boumans using 3σ.[23] All standard deviations are based on measurements in triplicate.

Statistics. The variability of a food composition data point is best determined by looking at the standard deviation (SD).[21] Each sample is digested in triplicate and each digest measured three times. The resulting SD for each data point is thus based on nine results. The RSD values (RSD = SD/mean) are furthermore calculated for better comparison of data.

RESULTS AND DISCUSSION

Analytical Method. The limits of detection (LOD) for the digested flowers and leaves were below 2 μg/g for all analytes for ICP-AES and below 0.5 μg/g for ICP-MS.

The recoveries determined with the standard reference material of strawberry leaves (LGC7162) range from 94 to 129% for the digested plant material, from 92 to 115% for the

DOI: 10.1021/jf504474t
J. Agric. Food Chem. 2015, 63, 1798−1802

Table 2. Elemental Composition (in μg/g Dry Matter) of Hawthorn Flowers, Leaves, Berries, and Seeds (Mean Values; %RSD Values in the Range from 2 to 8%)

element	berries	leaves	flowers	seeds
Al	917	29.4	13.1	551
As	0.012	nd[a]	0.020	0.042
Ba	4.17	4.84	9.50	1.40
Ca	3722	1369	1327	4002
Cd	0.045	0.121	0.069	0.085
Co	0.058	0.161	<LOD	0.096
Cr	1.31	0.148	<LOD	1.42
Cu	0.550	7.35	1.75	0.73
Fe	2.40	37.4	8.32	1.33
K	4223	4099	4986	5089
Li	0.51	nd	0.34	0.081
Mg	987	1045	1715	1165
Mn	1.88	12.6	13.3	0.803
Mo	0.097	nd	0.121	0.172
Na	6.34	238	108	3.47
Ni	0.067	0.574	0.267	0.10
Pb	0.027	1.59	2.06	0.11
Sr	0.406	1.14	2.42	0.19
Zn	1.12	17.6	30.7	1.23

[a]nd, not determined.

infusions by ICP-AES, and from 89 to 109%, except for Zn (115%), for ICP-MS.

The sensitivity of the method was evaluated using the resultant slopes of the respective calibration curves. The correlation coefficients for calibration curves were all >0.9995.

The precision (expressed as %RSD) ranged from 0.02 to 1.5%. Within-day repeatability was found to be <2.3%.

The obtained figures of merit of both analytical methods are in the range for the determination of micro- and macroelements in biological samples.

The analytical parameters recovery, precision, and LOD for digest obtained for the three different acid mixtures applied were compared by applying a paired *t* test. Because only statistically insignificant differences were found ($p > 0.05$), mixture I (HNO_3 7 mol/L) was used for further experiments.

Elemental Analysis. Elemental compositions of hawthorn flowers, leaves, berries, and seeds are listed in Table 2 as mean values. For better clarity of results, the single standard deviations are not included in the table. For all samples and analytes, the %RSD values were in the range from 2 to 8%. Selenium was below the LOD (0.002 μg/g) in all samples.

Berries. Concentrations of macroelements in berries are given in μg/g dry matter: 4223 K; 3722 Ca; 987 Mg; 917 Al; 6.34 Na. In comparison to our results, Ozcan et al. found only 33 μg/g Al in berries, but higher concentrations of K (13531 μg/g), Mg (1502 μg/g), and Na (312 μg/g) and a similar concentration of Ca (3046 μg/g).[20]

Furthermore, in hawthorn berries, As, Ba, Cd, Co, Cr, Cu, Fe, Mn, Mo, Li, Ni, Pb, Sr, and Zn were found. Except for Cr (1.31 vs 1.1 μg/g) and Ni (1.89 vs 1.1 μg/g), lower concentrations were determined than reported by Ozcan, that is, Fe 2.4 vs 33 μg/g, Li 0.51 vs 1.62 μg/g, Pb (0.027 vs 0.71 μg/g), and Se (<LOD vs 0.56 μg/g).[20]

Hawthorn fruits collected in a polluted area in Transylvania contain much higher amounts of Cd, Cu, and Zn,[24] namely, 1.8, 6, and 60 μg/g, respectively.

Leaves. Only rare literature on white hawthorn leaves is currently available. Cd, Cu, and Zn contents in hawthorn leaves from a polluted area in Transylvania were found to be 1.9, 4.5, and 90 μg/g, respectively.[14] Except for Cu, these values are much higher than our results.

Leaves of other plants grown in nonpolluted areas are given below for comparison.

Leaves of poplar analyzed in Portugal were found to have the following concentrations: 2−3 μg/g for Pb, 0.1−0.2 μg/g for Cd, and 4−5 μg/g for Cu.[25] These values are similar to those determined in the present study, namely, 1.5−2 μg/g, 0.12−0.14 μg/g, and 6−7.5 μg/g for Pb, Cd, and Cu, respectively. Peppermint leaves, however, were found to contain 2.41 μg/g Pb, 0.09 μg/g Cd, and 12 μg/g Cu.[16]

With regard to the other elements determined, it was found that white hawthorn leaves contain lower amounts of metals than mint leaves:[16] Ba, 5−9 μg/g in comparison to 31 μg/g; Cr, 0.15−0.17 vs 0.94 μg/g; Mn, 9−13 vs 188 μg/g; Ni, 0.17−0.57 vs 2.99 μg/g; Sr, 1.2−1.7 vs 2.4 μg/g; and Zn, 15−18 vs 51 μg/g. Only Co is present in both leaves in the same order of magnitude, 0.13−0.16 vs 0.10 μg/g.

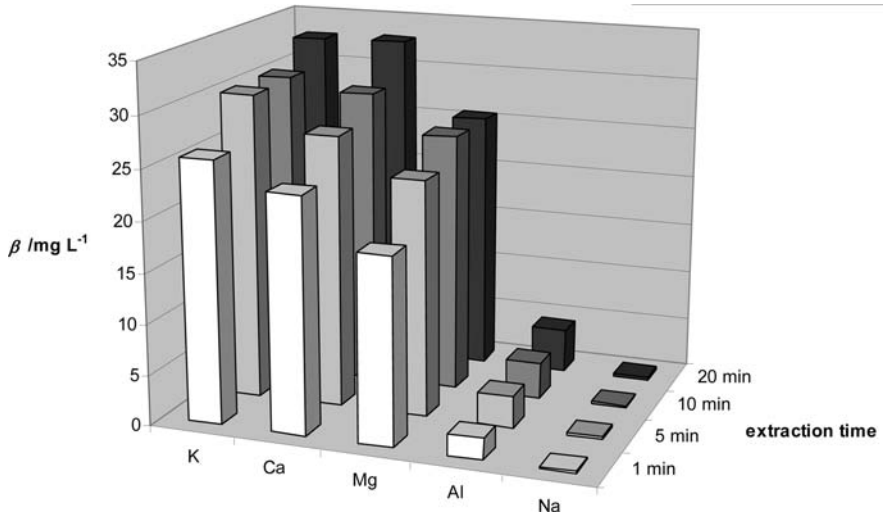

Figure 1. Concentrations of major elements in infusions after different extraction times.

DOI: 10.1021/jf504474t
J. Agric. Food Chem. 2015, 63, 1798−1802

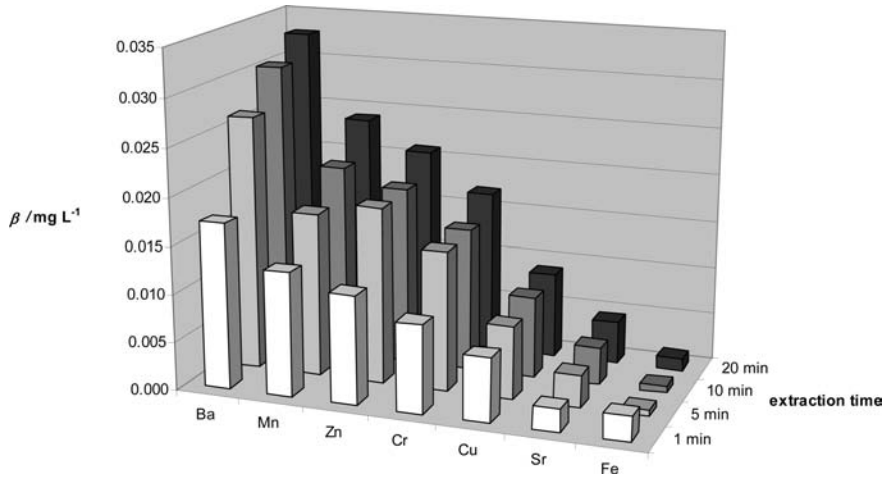

Figure 2. Concentrations of minor elements in infusions after different extraction times.

Table 3. Extraction Yields (%) for Selected Elements in Hawthorn Infusions Prepared from Leaves and Flowers Compared with the Literature (Zengin at al.)[28]

Element	leaves	flowers	plant (2.5 g/50 mL) [28]
Ba	1.9	3.8	----
Ca	1.2	2.3	11
Cd	1.9	2.8	14
Co	8.8	7.7	20
Cr	3.8	1.6	7.5
Cu	4.7	6.6	27
Fe	0.41	0.6	1.5
K	10	11.5	55
Mg	3.6	9.5	24
Mn	2.3	3.8	21
Mo	6.6	7.1	----
Na	9.2	8.9	23
Ni	7.9	6.1	44
Sr	2.7	2.5	----
Zn	10	9.7	37

Flowers. Trace elements in the flowers of white hawthorn were characterized by Goji and Dinulica,[24] but they analyzed samples harvested in a polluted area. Cd level in flowers were reported as 2.2 μg/g, Cu as 11 μg/g, and Zn as 90 μg/g. The flowers of the remote area in Croatia were found to contain only 0.069, 1.75, and 30 μg/g Cd, Cu, and Zn, respectively. By comparison of the data for hawthorn flowers with those for chamomile, it can be seen that the trace elements Al, Cd, Pb, and Zn were in similar concentration ranges. Higher values were found for Fe and Mn, but lower values for Cu, Cr, and Ni. The amounts of major elements (Ca, K, Mg, and Na) were found to be higher in hawthorn flowers. These elements mainly depend on the soil composition. Furthermore, each plant tends to accumulate various metals in different amounts. Chamomile is stated as an accumulator for only Ca, K, and Na.[26]

Seeds. Literature regarding the elemental composition of white hawthorn seeds is not available. The seeds of the berries analyzed show a similar pattern as the berries themselves for both major and minor elements, but differ from the values for the flowers and leaves (refer to Table 2).

Comparison of Different Organs. The major element K is present in berries, leaves, seeds, and flowers at approximately the same level. Mg is similar in berries, seeds, and leaves, but almost double the concentration is present in the flowers. Ca is mainly accumulated in berries and seeds, approximately 3 times higher than in leaves and flowers. Na shows a different pattern: this element is mainly present in leaves, followed by flowers (half concentration) and much less in berries and seeds. Al is present in berries and seeds at a relatively high level (mg/g) in comparison with leaves and flowers (μg/g). With regard to the microelements, it was found that Fe, Cd, Cu, and Ni are mostly accumulated in leaves, followed by flowers, then by seeds and berries. Mn is present in leaves and flowers at the same concentrations, whereas in the berries and seeds only about 10% of that amount is found. The Zn concentration is 10 times higher in leaves than in the berries and seeds, but only half of the level found in flowers. Cr is mainly present in berries and seeds. Ba is found with the same content in berries and leaves and double amount in flowers; seeds contain the lowest level. Co could be detected only in leaves, seeds, and berries, the latter having an even lower concentration. Amounts of Sr and Pb increase from berries and seeds to leaves and flowers.

Infusions. To obtain the optimum decoction time, periods from 5 to 30 min were examined, and 10 min was found to be adequate to prepare a good-quality tea beverage regarding element extraction. The element concentrations in the infusions did not significantly change after 5 min of extraction time. Already >90% of the maximum extracted concentration is reached after 5 min; thus, this period is considered to be the minimum recommended decoction time. The elemental

DOI: 10.1021/jf504474t
J. Agric. Food Chem. 2015, 63, 1798−1802

distributions of the infusions prepared from leaves and flowers are depicted in the Figures 1 and 2.

Hawthorn infusions are described also by Ozcan and co-workers,[27] but prepared from another species, *Crataegus orientalis*, instead of the *C. monogyna* used in this study. Except for Mn and Al, all metal concentrations found are lower than previously reported.

For all elements detected in the infusions, the extraction yield was calculated. Zengin et al.[28] used more plant material for the preparation of the teas (as compared to 2 g/100 mL used in this work), resulting in higher extraction yields, as shown in Table 3. Elemental analyses of different hawthorn organs is a valuable approach to study the nutritional value of trace elements or their potential harmful effects. Hawthorn berries and their derived infusions are a good dietary source of essential metals especially regarding K, Ca, Mg, Na, Ba, Mn, Zn, Cr, Cu, Sr, and Fe. The majority of metals were found to be extracted after a decoction time of only 5 min. The hawthorn infusions contained high amounts of K, Ca, Mg, and Na at concentration levels of mg/L, whereas Ba, Mn, Zn, Cr, Cu, Sr, and Fe are present at μg/L. The toxic elements Cd and Pb were not found in the final infusions, only in the berries in very low concentrations, and do not cause any risk to humans when consumed at such levels. The organs of white hawthorn show different elemental distribution, justifying its use as a valuable medicinal plant for the heart and cardiovascular system.

AUTHOR INFORMATION

Corresponding Author

*(I.J.C.) Phone: +385 4606 199. Fax: +385 4606 181. E-mail: ijuranovic@chem.pmf.hr.

Notes

The authors declare no competing financial interest.

REFERENCES

(1) Stankov Jovanović, V. P.; Ilić, M. D.; Marković, M. S.; Mitić, V. D.; Nikolić Mandić, S. D.; Stojanović, G. S. Wild fire impact on copper, zinc, lead and cadmium distribution in soil and relation with abundance in selected plants of Lamiaceae family from Vidlic Mountain (Serbia). *Chemosphere* **2011**, *84*, 1584−1591.

(2) Karak, T.; Bhagat, R. M. Trace elements in tea leaves, made tea and tea infusion: a review. *Food Res. Int.* **2010**, *43*, 2234−2252.

(3) deMan, J. M. *Principles of Food Chemistry*; Aspen Publishers: Gaithersburg, MD, USA, 1999.

(4) Kosalec, I.; Cvek, J.; Tomić, S. Contaminants of medicinal herbs and herbal products. *Arh. Hig. Rada Toksikol.* **2009**, *60*, 485−501.

(5) Burlingame, B.; Pineiro, M. The essential balance: risks and benefits in food safety and quality. *J. Agric. Food Chem.* **2007**, *20*, 139−146.

(6) Arpadjan, S.; Celik, G.; Taskesen, S.; Gucer, S. Arsenic, cadmium and lead in medicianl herbs and their fractionation. *Food Chem. Toxicol.* **2008**, *46*, 2871−2875.

(7) Divrikli, U.; Horzum, N.; Soylak, M.; Elci, L. Trace heavy metal contents of some spices and herbal plants from western Anatolia, Turkey. *Int. J. Food Sci. Technol.* **2006**, *41*, 712−716.

(8) Juranović Cindrić, I.; Zeiner, M.; Glamuzina, E.; Stingeder, G. Elemental characterisation of the medical herbs *Salvia officinalis* L. and *Teucrium montanum* L. grown in Croatia. *Microchem. J.* **2013**, *107*, 185−189.

(9) Baughman, K. L.; Bradley, D. J. Hawthorn extract: is it time to turn over a new leaf? *Am. J. Med.* **2003**, *114*, 700 −701.

(10) Holubarsch, C. J. F.; Colucci, W. S.; Meinertz, T.; Gaus, W.; Tendera, M. The efficacy and safety of *Crataegus* extract WSR 1442 in patients with heart failure: the SPICE trial. *Eur. J. Heart Fail.* **2008**, *10*, 1255−1263.

(11) Kirakosyan, A.; Seymour, E.; Kaufman, P. B.; Warber, S.; Bolling, S.; Chang, S. C. Antioxidant capacity of polyphenolic extracts from leaves of *Crataegus laevigata* and *Crataegus monogyna* (hawthorn) subjected to drought and cold stress. *J. Agric. Food Chem.* **2003**, *51*, 3973−3976.

(12) Mikulic-Petkovsek, M.; Slatnar, A.; Stampar, F.; Veberic, R. HPLC−MSn identification and quantification of flavonol glycosides in 28 wild and cultivated berry species. *Food Chem.* **2012**, *135*, 2138−2146.

(13) Basgel, S. S.; Erdemoglu, B. Determination of mineral and trace elements in some medicinal herbs and their infusions consumed in Turkey. *Sci. Total Environ.* **2006**, *359*, 82−89.

(14) Gallaher, R. N.; Gallaher, K.; Marshall, A. J.; Marshall, A. C. Mineral analysis of ten types of commercially available tea. *J. Food Compos. Anal.* **2006**, *19*, S53−S57.

(15) Fernandez, P. L.; Pablos, F.; Martin, M. J.; Gonzalez, A. G. Multi-element analysis of tea beverages by inductively coupled plasma atomic emission spectrometry. *Food Chem.* **2002**, *76*, 483−489.

(16) Łozak, A.; Sołtyk, K.; Ostapczuk, P.; Fijałek, Z. Determination of selected trace elements in herbs and their infusions. *Sci. Total Environ.* **2002**, *289*, 33−40.

(17) Fung, K. F.; Zhang, Z. Q.; Wong, J. W. C.; Wong, M. H. Aluminium and fluoride concentrations of three tea varieties growing at Lantua Island, Hong Kong. *Environ. Geochem. Health* **2003**, *25*, 219−232.

(18) Dambiec, M.; Polechońska, L.; Klink, A. Levels of essential and non-essential elements in black teas commercialized in Poland and their transfer to tea infusion. *J. Agric. Food Chem.* **2013**, *31*, 62−66.

(19) Koch, K. R.; Pougnet, M. A.; de Villiers, S.; Monteagudo, F. Increased urinary excretion of Al after drinking tea. *Nature* **1988**, *333*, 122.

(20) Ozcan, M. M.; Hacıseferoğulları, H.; Marakoğlu, T.; Arslan, D. Hawthorn (*Crataegus* spp.) fruit: some physical and chemical properties. *J. Food Eng.* **2005**, *69*, 409−413.

(21) Pennington, J. A. T. Applications of food composition data: data sources and considerations for use. *J. Agric. Food Chem.* **2008**, *21*, S3−S12.

(22) Soylak, M.; Tuzen, M.; Souza, A. S.; Korn, M. d. G. A.; Ferreira, S. L. C. Optimization of microwave assisted digestion procedure for the determination of zinc, copper and nickel in tea samples employing flame atomic absorption spectrometry. *J. Hazard. Mater.* **2007**, *149*, 264−268.

(23) Boumans, P. W. J. M. Basic concepts and characteristics of ICP-AES. In *Inductively Coupled Plasma Emission Spectroscopy. Part I. Methodology, Instrumentation, and Performance*; Boumans, P. W. J. M., Ed.; Wiley: New York, 1987.

(24) Goji, G.; Dinulica, F. Distribution of some heavy metals in different hawthorn organs. *Bull. Transilv. Univ. Brasov, Ser. B* **2011**, *4* (53), 47−52.

(25) Silva, N. A. F.; Lopes, M. I.; Leitao, R. A. E; Silva, H. F. A.; Matos, M. J. Simultaneous monitoring of toxic metals on white poplar (*Populus*) by SWASV. *J. Bras. Chem. Soc.* **2005**, *16*, 1275−1282.

(26) Kovačik, J.; Gruz, J.; Klejdus, B.; Štork, F.; Hedbavny, J. Accumulation of metals and selected nutritional parameters in the field-grown chamomile anthodia. *Food Chem.* **2012**, *131*, 55−62.

(27) Ozcan, M. M.; Unver, A.; Ucar, T.; Arslan, D. Mineral content of some herbs and herbal teas by infusion and decoction. *Food Chem.* **2008**, *106*, 1120−1127.

(28) Zengin, M.; Ozcan, M. M.; Cetin, U.; Gezgin, S. Mineral contents of some aromatic plants, their growth soils and infusions. *J. Sci. Food Agric.* **2008**, *88*, 581−589.

DOI: 10.1021/jf504474t
J. Agric. Food Chem. 2015, 63, 1798−1802

ACN composition in nasturtium flowers is very limited; only Garzón and Wrolstad[16] have reported the main ACN composition of orange flowers. Furthermore, there is no information on their non-ACN phenolic composition. The aim of this study was to evaluate the potential use of nasturtium flowers as a nutraceutical and pharmaceutical ingredient by outlining the ACNs and non-ACN phenolics profile in the petals of three different varieties, namely, red, orange, and yellow. Their total phenolics content (TPC), antioxidant activity, and antimicrobial activities were also assessed.

MATERIALS AND METHODS

Reagents. For the high-performance liquid chromatography (HPLC) work, cyanidin-3-glucoside (cy-3-glu) and pelargonidin-3-sophoroside (pg-3-soph) were purchased from Extrasynthese (Lyon, France), cyn-3-soph was from Polyphenols (Sandnes, Norway), and 5-caffeoylquinic acid (5-CQA) was from Sigma-Aldrich Chemie GmbH (Steinheim, Germany). The Folin−Ciocalteau reagent was purchased from MP Biomedicals, LLC (Illkirch, France). For the antioxidant studies, gallic acid, fluorescein sodium salt, and 2,2′-azobis(2-methylpropionamidine) dihydrochloride (AAPH) were obtained from Sigma-Aldrich (St. Louis, MO, USA); Trolox (6-hydroxy-2,5,7,8-tetramethylchroman-2-carboxylic acid) was obtained from Acros Organics (Morris Plains, NJ, USA); and both sodium phosphate monobasic and sodium phosphate dibasic were purchased from Fisher Scientific (Fair Lawn, NJ, USA). For the antimicrobial studies, trypticase soy agar was purchased from Becton, Dickinson and Co. (Sparks, MD, USA). Various HPLC grade organic solvents for extractions and subsequent analyses were purchased from Fisher Scientific (Pittsburgh, PA, USA).

Plant Material. Petals of orange nasturtium flowers were collected from open fields around different locations in Bogotá, Colombia, in June of 2013, whereas petals of red and yellow flowers were collected from gardens in Geneva, NY, USA, during the summer of 2013. All petals were lyophilized and stored at −80 °C until analyzed.

Polyphenolic Extraction. For the extraction and isolation of ACNs and other polyphenolics, the freeze-dried plant material was milled. The powder (0.5 g) was placed in a centrifuge tube and mixed with 1:1 (w/v) 70% aqueous acetone under a nitrogen atmosphere. The tube was capped, and ultrasound-assisted extraction at a fixed frequency of 50 kHz was performed for 10 min in a chilled water bath (B-2200R-1; Branson, Shelton, CT, USA). The sample was centrifuged for 20 min at 4 °C at 3000*g* using an Eppendorf 5810 R centrifuge (Hamburg, Germany) to pellet the solids. The acetone extract was then transferred to a separate vial, and five successive re-extractions were performed on the pellet as described. The pooled extracts were partitioned with chloroform (1:2 acetone/chloroform, v/v) under nitrogen atmosphere. After centrifugation, the aqueous portion containing the ACNs and non-ACN phenolics was recovered and separated from the residual acetone in a Buchi rotoevaporator set at 40 °C and resolubilized in water. Extracts were stored under nitrogen at −80 °C until needed.

Determination of Monomeric Anthocyanin Content, and Total Phenolics. The extracted monomeric ACN pigment content was determined by the pH differential method.[17] Absorbencies were read at 490 and 700 nm for orange flowers and at 510 and 700 nm for red flowers. For comparison purposes, pigment content was calculated as cy-3-glu equivalents using an extinction coefficient (ε) of 26900 L cm^{-1} mol^{-1} and a molar mass of 449.2 g mol^{-1}. Measurements were performed in triplicate with standard deviations reported about the means.

Total phenolics content was determined as gallic acid equivalents (GAE)/100 g FW.[18] A 20 μL sample aliquot of extract or gallic acid standard (50−500 mg/L) was mixed with 1.58 mL of water followed by 100 μL of Folin−Ciocalteau's reagent. After vortexing and incubating at room temperature for 8 min, 300 μL of a 20% (w/v) aqueous sodium carbonate solution was added. Samples were vortexed and held at room temperature for 2 h. The absorbance of the blue solution was recorded at 765 nm on a Shimadzu UV−visible spectrophotometer, model UV 160 U (Kyoto, Japan), using 1 cm disposable cells. All measurements were performed in triplicate.

Acid Hydrolysis of Flavonols and Cleanup via Solid-Phase Extraction (SPE). Confirmative determination of non-ACN aglycones (kaempferol or luteolin) was achieved following a modification of the protocol described by Durst and Wrolstad[19] for acid hydrolysis of ACNs. Approximately 1 mg of the pigment was mixed with 15 mL of 2 M HCl in a screw-cap test tube. The mix was flushed with nitrogen, capped, hydrolyzed for 45 min at 100 °C, and subsequently cooled in an ice bath. The hydrolyzed extract containing the polyphenolics was cleaned using a 20 mL capacity high-load C-18 cartridge (Alltech Association, Inc., Deerfield, IL, USA). After methanolic conditioning and sample loading, the column was washed with water to remove sugars, acids, and other water-soluble compounds. The methanolic eluent containing the aglycones was subsequently evaporated using the Buchi rotoevaporator at 40 °C. The extract was freeze-dried until HPLC- photodiode array (PDA) analysis.

HPLC-PDA Analysis. All processed and freeze-dried extracts were reconstituted in 1 mL of 20% aqueous MeOH (v/v) and passed through a 0.2 μm nylon filter. For ACN, non-ACN phenolics, and aglycones, an Agilent 1260 Infinity series HPLC (Agilent Technologies, Santa Clara, CA, USA) was used. The equipment consisted of a G1322A inline degassing unit, a G1312B binary pump, a G1329B autosampler, a G1316A thermostated column compartment, a G4212B diode array detector fitted with a 10 mm path, and a 1 μL volume Max-Light cartridge flow cell. The instrument was controlled using an Agilent Chemstation software version B.04.02, service pack 1 with the spectral software module. Chromatographic separations were performed on a C_{18} Kinetex column (4.6 mm × 100 mm, 100 Å pore size, 2.6 μm particle size; Phenomenex, Torrance, CA, USA). The mobile phase composition for all analyses was (A) H_2O/H_3PO_4 (99.5:0.5) and (B) $ACN/H_2O/H_3PO_4$ (50:49.5:0.5). Chromatographic conditions for phenolic separations were as described previously.[20] ACNs were monitored at 520 nm, whereas non-ACN phenolics were monitored at 320 and 360 nm for hydroxycinammic acids (HCAs) and flavonols, respectively.

HPLC-Electrospray Ionization Quadrupole Time-of-Flight Mass Spectrometry. Initial reconstitution of the freeze-dried extracts followed similar protocols as described above. Separation of phenolic compounds was conducted under the following conditions: Detection was performed using a quadrupole/time-of-flight mass spectrometer (QTof Premier, Micromass Limited, Manchester, UK) equipped with an electrospray ionization (ESI) source operated in both positive and negative modes of polarity.

ESI conditions included a capillary voltage of 3.2 kV for positive mode, 2.8 kV for negative, a cone voltage of 35 V, ion guide at 1 V, source temperature of 100 °C, and nitrogen desolvation gas temperature of 400 °C flowing at 600 L/h. During experiments employing collisionally induced dissociation (CID), argon was held at a pressure of 3.0×10^{-3} mbar. To screen for potential parent/daughter ion relationships, both positive and negative ESI mode quadrupole time-of-flight mass spectrometry (QTOF-MS^e) runs were conducted.

For QTOF-MS^e experiments two functions were involved, one performed at low collision energy (LE) (5 eV) and the second at high collision energy (HE) to induce fragmentation (25 eV). Coincident retention times for a given pair of ions (one from LE, another from HE), where in HE the lower mass ion is enhanced and the higher mass ion is reduced, imply a parent/daughter MS/MS relationship. High-energy spectra for each of the ions in Table 3 with reported fragment ions are provided in the Supporting Information. The accurate masses of the parent and daughter ions combined with the ultraviolet−visible (UV−vis) spectra, retention times, and a comparison of these properties with those of available authentic standards and with those reported in the literature[16,21−23] lead to the tentative identifications of phenolics investigated in this study.

Quantification of Anthocyanins and Non-anthocyanin Phenolics. In addition to calculation of monomeric ACN concentration by the pH differential method, ACN quantification was based on peak areas extracted from HPLC-PDA monitored at 520

DOI: 10.1021/jf503366c
J. Agric. Food Chem. 2015, 63, 1803−1811

Table 1. Anthocyanin Composition of Nasturtium Flowers (*Tropaeolum majus*)[a]

anthocyanin[b]	mg Cy-3-glu/100 g DW			mg Cy-3-glu/100 g FW		
	yellow	orange	red	yellow	orange	red
dp-3-dihexoside[c]	95.1 ± 80.7[A]	35.9 ± 17.2[A]	591.6 ± 53.1[B]	12.4 ± 10.5[a]	4.3 ± 2.1[a]	76.9 ± 6.9[b]
cy-3-soph[c]	24.8 ± 18.3[A]	10 ± 8.7[A]	76.0 ± 6.2[B]	3.2 ± 2.4[a]	1.2 ± 1.0[a]	9.9 ± 0.8[b]
pg-3-soph[c]	125.7 ± 86.2[A]	439.6 ± 231.5[A]	212.7 ± 65.2[A]	16.3 ± 11.2[a]	52.7 ± 27.8[a]	27.7 ± 8.5[a]
total ACN[c]	245.5 ± 167.3[A]	485.4 ± 237.6[AB]	880.3 ± 18.3[B]	31.9 ± 21.7[a]	58.2 ± 28.5[a]	114.5 ± 2.3[b]
total monomeric ACN[d]	ND[e]	873.5 ± 342.8[A]	1292.2 ± 56.3[A]	ND	108 ± 37.2[a]	168.0 ± 7.3[a]

[a]Results are expressed as mean ± SD (n = 3). Values in rows with different letters are significantly different at the 95% confidence level. [b]Individual compounds presented as percentage of total peak area monitored at 520 nm. dp, delphinidin; cy, cyanidin; pg, pelargonidin; soph, sophoroside. [c]Calculated by HPLC-PDA. [d]Calculated by pH differential. [e]ND, nondetectable.

nm and external calibration curves. For comparison purposes, cy-3-glu was used as a standard. Quantification of total and individual flavonoids was based on peak areas extracted from HPLC-PDA monitored at 360 nm using external calibration curves of quercetin, kaempferol, and myricentin, whereas quantification of quinic acid esters was based on the peak area at 320 nm by external calibration curves of 5-CQA. Levels of all flavonoid derivatives were calculated using the calibration curve of the respective free flavonoids. All samples were analyzed in triplicate, and for comparison purposes, values are expressed as mg/100 g DW and mg/100 g FW.

Determination of Antioxidant Activity. The automated ORAC assay was conducted using 96-well microplates according to the method described by Prior et al.[24] with modifications. An aliquot (25 μL) of a petal extract or a trolox standard was mixed with 150 μL of 4 nM fluorescein in a 75 mM NaH_2PO_4 buffer at pH 7.4. Following 30 min of incubation at 37 °C, 25 μL of AAPH was added to each well and the fluorescence was recorded 485/528 nm (emission/excitation) once a minute for 3 h using a Synergy HT fluorescence microplate reader (Biotek Instruments, Winooski, VT, USA). The calibration curves consisted of various concentrations of Trolox (0−100 μM) made up in a phosphate buffer. Results were calculated on the basis of differences in areas under the fluorescence decay curve between the blank, samples, and standards. Final ORAC values were expressed as μmol of Trolox equivalents (TE)/100g DW and μmol of TE/100 g FW.

Antibacterial Activity. The antibacterial activity of the extracts against foodborne pathogenic strains including *Salmonella enterica*, serovar Hartford, *Escherichia coli* ATCC 43895, *Listeria monocytogenes* 104025, *Staphylococcus aureus* 9144, and *Bacillus cereus* F 4550 was determined using the spot-on-lawn assay.[25] A 50 μL aliquot of an overnight culture of the respective strain was inoculated in 7 mL of liquid TSB agar media (0.7% agar) and poured onto plates containing a TSA agar base. After the agar in the plates solidified, 20 μL of each extract was spotted onto this lawn, and plates were incubated overnight at 37 °C for 24 h. After incubation, the inhibition zones were evaluated.

Statistical Analyses. Quantitative data are presented as mean values with the respective standard deviation. Significant (P < 0.05) differences among means were identified using the least significant difference (LSD) multiple-range test after a multifactor analysis of variance (ANOVA). All analyses were performed with Statgraphics plus, version 2.1.

RESULTS AND DISCUSSION

Anthocyanin and Total Phenolics Content. The means of total ACN as determined by the pH differential method were 108.8 ± 37.2 and 168.0 ± 7.3 mg cy-3-glu/100 g FW in orange and red flowers, respectively (Table 1). These averages are comparable to the range of 70.3−201.0 mg cy-3-glu/100 g FW and the mean of 137 mg cy-3-glu/100 g FW for 21 blackberry samples taken from different origins as reported by Chiang and Wrolstad.[26]

The high SD for the average value in the orange flowers may be due to the varied geographic sampling site as the samples were collected from different locations across Bogotá, Colombia. Conversely, the yellow and red samples were collected in localized small gardens in the city of Geneva, NY, USA. This variability is expected as it has been reported that plant phenolics vary in response to environmental factors such as light intensity and nutrient availability.[27]

The TPC in red flowers was 908.7 ± 284.6 mg GAE/100 g FW, equivalent to the TPC in orange flowers (687.7 ± 161.3 mg GAE/100 g FW) and significantly higher than that one in yellow flowers (538.4 ± 6.5 mg GAE/100 g FW) (p < 0.01). The lower TPC content of yellow flowers is driven by the low content of ACNs.

The three samples showed TPC values comparable to tropical fruits with known elevated phenolic concentrations. Vasco et al.[28] tested 17 fruits from Ecuador, and Rufino et al.[29] studied 18 tropical fruits from Brazil. According to their classification, fruits with a TPC > 500 mg GAE/100 g FW are considered high.

According to Vasco's classification, at 1010 mg GAE/100 g FW, banana passion fruit (*Passiflora mollissima* L.) displayed the highest TPC. Likewise, Rufino et al. found that camu-camu (*Myrciaria dubia*) and acerola (*Malpighiae marginata*) had 1176 and 1063 mg GAE/100 g FW, respectively. Therefore, these fruits were placed at the top of the analyzed fruits as excellent sources of polyphenols.

Anthocyanin and Non-anthocyanin Polyphenolic Composition. Petals from red, orange, and yellow flowers shared similar ACN profiles (Figure 1). Delphinidin-3-dihexoside (dp-3-dihesoxide), cy-3-soph, and pg-3-soph were detected in each sample.

The results from the HPLC-ESI-QTOF-MS[e] analysis of ACNs are shown in Table 2. Delphinidin-3-dihexoside with parent ions at m/z 627.158, $[M + H]^+$, and m/z 625.146, $[M - H]^-$, resulted in HE delphinidin aglycone ion signals at m/z 303.051, $[M + H - X]^+$, and m/z 301.033, $[M - H - X]^-$, arising from a 324 amu loss, suggesting a dihexoside moiety. Accordingly, this compound was labeled delphinidin-3-dihexoside (dp-3-dihexoside). Cyanidin-3-soph was characterized by molecular ions at m/z 609.15, $[M - H]^-$, and m/z 611.162, $[M + H]^+$, with the resultant HE daughter ions at m/z 285.037 and 287.058, corresponding to the cyanidin aglycone. Identification of pg-3-soph was determined via molecular ions at m/z 595.168, $[M + H]^+$, and m/z 593.157, $[M - H]^-$, and aglycone ion signals at m/z 271.063, $[M + H - X]^+$, and m/z 269.042, $[M - H - X]^-$. These last two ACNs were also confirmed on the basis of congruence of retention time and UV−vis properties with authentic cy-3-soph and pg-3-soph standards. These findings confirm previous investigations on the ACN composition of orange nasturtium flowers (Garzón and

DOI: 10.1021/jf503366c
J. Agric. Food Chem. 2015, 63, 1803−1811

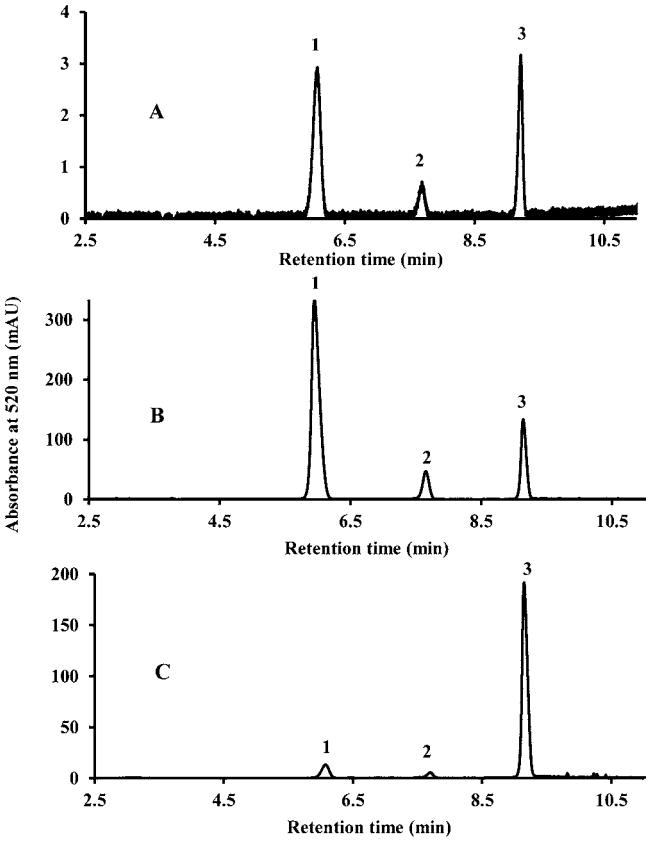

Figure 1. HPLC-PDA profile of anthocyanins in nasturtium flowers (*Tropaeolum majus*) detected at 512 nm: (A) yellow flowers; (B) orange flowers; (C) red flowers. Peaks: 1, delphinidin-3-dihexoside; 2, cyanidin-3-sophoroside; 3, pelargonidin-3-sophoroside.

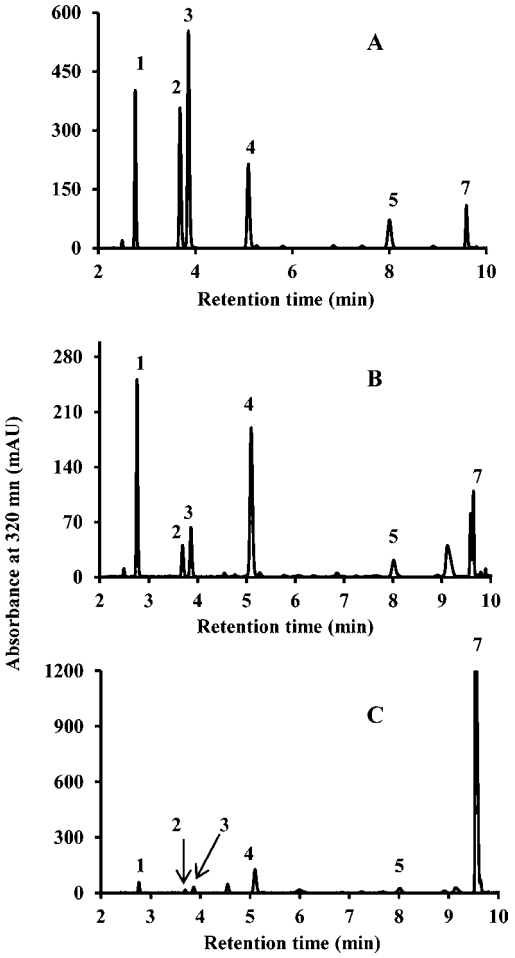

Figure 2. HPLC-PDA profile of hydroxycinnamic acids in nasturtium flowers (*Tropaeolum majus*) detected at 320 nm: (A) yellow flowers; (B) orange flowers; (C) red flowers. Peaks: 1, 3-caffeoylquinic acid (neochlorogenic acid); 2, *cis*-3-*p*-coumaroylquinic acid; 3, *trans*-3-*p*-coumaroylquinic acid; 4, 5-caffeoylquinic acid (chlorogenic acid); 5, *cis*-5-*p*-coumaroylquinic acid; 7, *trans*-5-*p*-coumaroylquinic acid.

Wrolstad[16]) and provide the first report of the ACN profile of red and yellow flowers.

The HPLC-PDA profile of non-ACN phenolics in flowers of *T. majus* is shown in Figure 2, whereas the HPLC-ESI-QTOF-MS^e results from the analysis of these compounds are shown in Table 3. Non-anthocyanin phenolics included HCAs and flavonols. Six HCAs belonging to chlorogenic acid family (esters of *trans*-cinnamic acids and quinic acid) were found. The first and fourth eluting compounds with λ_{max} 323 and 322 nm, respectively, and a difference in t_R of 1.56 min yielded molecular ions $[M - H]^-$ at m/z 353.087 and $[M - H + Na]^+$ and at m/z 375.069 with an HE fragment at m/z 191.053 identical to the 5-CQA standard. The fragment at m/z 191.053 corresponds to the loss of hydrogen from quinic acid typical of chlorogenic acids and their derivatives in tandem mass spectrum extracted ion chromatogram (EIC).[22] Because the order of elution between neochlorogenic acid (3-CQA) and chlorogenic acid (5-CQA) has been established in reverse-phase chromatography,[21] peaks 1 and 4 were identified as 3-CQA and 5-CQA, respectively.

Peaks 2, 3, 5, and 7 produced parent ions at m/z 337.092, $[M-H]^-$, which fragmented in HE daughter ions at m/z 163.037 ($[p$-coumaric acid-$H]^-$) and m/z 191.053 ($[$quinic acid-$H]^-$). On the basis of the strong signal at m/z 163.037, peaks 2 and 3 were tentatively labeled as *cis*-3-*p*-coumaroyl quinic acid (CoQA) and *trans*-3-*p*-CoQA, respectively.[21] In contrast, based on the prominent signal at m/z 191.053 and the later elution of compounds **5** and **7**,[21] they were labeled as *cis*-5-*p*-CoQA and *trans*-5-*p*-CoQA.[21]

Figure 3 is the HPLC-PDA profile of flavonols in nasturtium flowers. Myricetin conjugates (peaks 6, 8, and 10) with t_R = 7.16, 7.75, and 7.96 min, respectively, exhibited UV−vis absorption maxima at 354−356 nm. Compound **6** provided molecular ions at m/z 641.138, $[M - H]^-$, and m/z 665.135, $[M + H + Na^+]^+$. The HE fragment $[M - H - X]^-$ at m/z 317.03 was produced after cleavage of a dihexoside (324 amu)

Table 2. HPLC-ESI-QTOF-MS^e Analysis of Anthocyanins Present in Nasturtium Flowers (*Tropaeolum majus*)

peak	t_R (min)	λ_{max} (nm)	LE MS^e$[M - H]^-$$m/z$	HE MS^e$[M - H]^-$$m/z$	LE MS^e$[M + H]^+$$m/z$	HE MS^e$[M + H]^+$$m/z$	tentative peak assignment
1	5.75	524	625.146	300.026, 301.033	627.158	303.051	delphinidin-3-dihexoside
2	7.37	515	609.15	284.031, 285.037	611.162	287.058	cyanidin-3-sophoroside
3	9.14	503	593.157	268.036, 269.042	595.168	271.063	pelargonidin-3-sophoroside

DOI: 10.1021/jf503366c
J. Agric. Food Chem. 2015, 63, 1803−1811

Table 3. HPLC-ESI-QTOF-MS^e Analysis of Non-anthocyanin Phenolics Present in Nasturtium Flowers (*Tropaeolum majus*)

peak	t_R (min)	λ_{max} (nm)	LE MS^e[M − H]$^-$ *m/z*	HE MS^e[M − H]$^-$ *m/z*	LE MS^e[M + H]$^+$ *m/z*	HE MS^e[M + H]$^+$ *m/z*	tentative peak assignment
1	4.0	323	353.087, 375.069	191.053, 179.030	ND	ND	3-caffeoylquinic acid (neochlorogenic acid)
2	4.73	315	337.092, 359.073	163.037, 191.053	ND	ND	*cis*-3-*p*-coumaroylquinic acid
3	4.93	308	337.092, 359.073	163.037,191.053	ND	ND	*trans*-3-*p*-coumaroylquinic acid
4	5.56	322	353.087, 375.069	191.053, 179.030	ND	ND	5-caffeoylquinic acid (chlorogenic acid)
5	5.57	320	337.092, 359.073	163.037, 191.053	ND	ND	*cis*-5-*p*-coumaroylquinic acid
6	7.16	354	641.138	316.015, 317.03	665.135	319.047	myricetin dihexoside
7	7.44	320	337.092, 359.073	163.037, 191.053	ND	ND	*trans*-5-*p*-coumaroylquinic acid
8	7.75	356	683.15	316.015, 317.03	ND	319.047	myricetin acetyl dihexoside
9	7.77	356	625.145	300.026, 301.032	649.141	303.053	quercetin dihexoside
10	7.96	356	479.083	316.015, 317.03	503	319.047	myricetin hexoside
11	8.41	345	609.151	284.032, 285.039	633.145, 611.165	287.058	kaempferol dihexoside
12	9.05	344	651.157	284.032, 285.039	ND	303.059	kaempferol acetyl dihexoside
13	9.44	350	505.099	300.026, 301.033	ND	303.053	quercetin acetyl hexoside
14	9.71	344	447.092	284.032, 285.039	471.091	287.057	kaempferol hexoside
15	10.41	350	489.105	284.032, 285.039	ND	287.057	kaempferol acetyl hexoside

moiety from the corresponding myricetin aglycon. As such, this peak was tentatively identified as myricetin dihesoxide. Peak 8, with a loss of 366 amu from a molecular ion at *m/z* 683.15, [M − H]$^-$, agrees with the loss of an acetyl-dihexoside moiety. Peak 10 yielded a molecular ion at *m/z* 479.083 in the negative ESI mode and a HE fragment at *m/z* 317.03. The loss of 162 amu from the aglycon revealed the cleavage of a hexose moiety.

Quercetin derivatives (peaks 9 and 13) showed UV−vis absorption maxima at 356 and 350 nm, respectively. Peak 9 with t_R = 7.77 and parent ions at *m/z* 625.144, [M − H]$^-$, and *m/z* 649.14, [M + H − X + Na$^+$]$^+$, had a typical HE fragment at *m/z* 301.033, [M − H − X]$^-$, and was identified as a quercetin dihexoside on the basis of the loss of a dihexoside moiety (324 amu). Peak 13 with t_R = 9.44 had a molecular ion at *m/z* 505.099 in the negative ESI mode and an HE fragment 301.033. The loss of 204 amu equates to the loss of an acetyl hexoside moiety.

For compounds **11**, **12**, **14**, and **15**, a λ_{max} between 344 and 350 nm was observed. The molar mass of kaempferol and luteolin is the same; therefore, they will yield the same parent ion mass fragmentation pattern in MS. Furthermore, whereas these two compounds, under certain conditions and columns, have been known to commonly coelute,[30] they did not under the conditions employed for this study. Therefore, acid hydrolysis is important when distinguishing between these two compounds. As such, this work unequivocally identified each of these compounds as kaempferol derivatives. From a bioactive prospective, it is essential to differentiate between these two flavonoids because their differential bioactivity may be attributed to their ability to react with reactive oxygen species and their interaction with membrane lipid bilayers. Tsuchiya[31] indicated that in the structure−membrane interactivity, 3-hydroxylation of the C ring and 5,7-dihydroxylation of the A ring provide flavonoids with the greatest ability to interact with membranes and protect them. Therefore, kaempferol would have a better protective effect on the lipid bilayer than luteolin.

The HE fragmentation of peak 11 led to the kaempferol aglycone at *m/z* 285.039 in a negative mode and *m/z* 287.05 in the positive mode. The loss of 32 amu is assumed to be from the cleavage of a dihexoside. A sodium adduct at *m/z* 633.145 was seen in the positive ESI mode. Peak 12 with t_R = 9.05 had [M − H]$^-$ at *m/z* 651.157 with a fragment at *m/z* 285.039

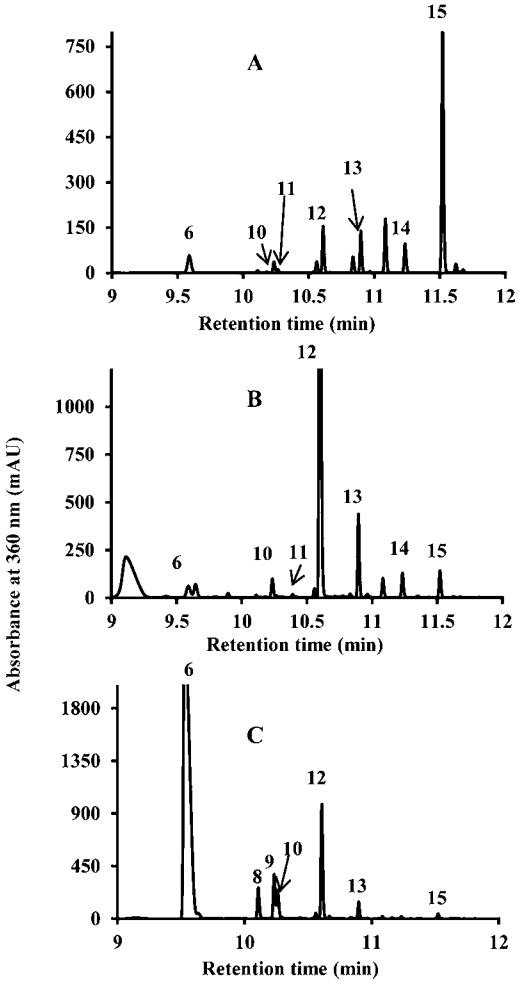

Figure 3. HPLC-PDA profile of flavonoids in nasturtium flowers (*Tropaeolum majus*) detected at 360 nm: (A) yellow flowers; (B) orange flowers; (C) red flowers. Peaks: 6, myricetin dihexoside; 8, myricetin acetyl dihexoside; 9, quercetin dihexoside; 10, myricetin hexoside; 11, kaempferol dihexoside; 12, kaempferol acetyl dihexoside; 13, quercetin acetyl hexoside; 14, kaempferol hexoside; 15, kaempferol acetyl hexoside.

DOI: 10.1021/jf503366c
J. Agric. Food Chem. 2015, 63, 1803−1811

Table 4. Content of Non-anthocyanin Phenolics in Nasturtium Flowers (*Tropaeolum majus*)[a]

	content (mg/100 g DW)			content (mg/100 g FW)		
phenolic compound	yellow	orange	red	yellow	orange	red
hydroxycinnamic acids			**Chlorogenic Acid Equivalents**			
neochlorogenic acid	283.2 ± 14.5^{A}	181.6 ± 12.7^{B}	36.4 ± 6.2^{C}	36.8 ± 1.^{a}	21.8 ± 1.5^{b}	4.7 ± 0.8^{c}
cis-3-*p*-CoQA	405.3 ± 51.6^{A}	60.1 ± 41.3^{B}	9.9 ± 6.3^{B}	52.7 ± 6.7^{a}	7.2 ± 5.0^{b}	1.3 ± 0.8^{b}
cis-5-*p*-CoQA	639.2 ± 56^{A}	105.8 ± 76^{B}	35.4 ± 6.4^{B}	83.1 ± 7.3^{a}	12.7 ± 9.1^{a}	4.6 ± 0.8^{b}
chlorogenic acid	246.6 ± 36.2^{A}	233.0 ± 41.6^{AB}	138 ± 38.3^{B}	32.1 ± 4.7^{a}	28.0 ± 5.0^{a}	17.9 ± 5.0^{b}
trans-5-*p*-CoQA	141.3 ± 11.0^{A}	49.0 ± 15.1^{B}	36.8 ± 10.0^{B}	18.4 ± 1.4^{a}	5.9 ± 1.8^{b}	4.8 ± 1.3^{b}
p-coumaroylquinic isomer 4	96.9 ± 6.6^{A}	46.8 ± 8.7^{B}	ND^{b}	12.6 ± 0.9^{a}	5.6 ± 1.1^{b}	ND
total	1718.8 ± 110.1^{A}	550.6 ± 74.9^{B}	256.5 ± 54.4^{C}	235.6 ± 8.1^{a}	81.2 ± 13.9^{b}	33.3 ± 7.1^{c}
flavonols			**Myricetin Equivalents**			
myricetin dihexoside	0.8 ± 0.1^{A}	0.64 ± 0.13^{A}	2264.8 ± 9.3^{B}	ND	ND	294.4 ± 1.2
myricetin acetyl dihexoside	2.3 ± 0.7^{A}	4.7 ± 3.0^{A}	74.7 ± 8.7^{B}	0.3 ± 0.1^{a}	0.6 ± 0.4^{a}	9.7 ± 1.1^{b}
myricetin hexoside	3.1 ± 1.6^{A}	4.4 ± 1.7^{A}	84.5 ± 0.3^{B}	0.4 ± 0.2^{a}	0.5 ± 0.2^{a}	11.0 ± 0.0^{b}
total	6.0 ± 2.5^{A}	9.7 ± 4.7^{A}	2424.0 ± 18.3^{B}	0.8 ± 0.3^{a}	1.2 ± 0.6^{a}	315.1 ± 2.4^{b}
			Quercentin Equivalents			
quercetin dihexoside	8.2 ± 2.0^{A}	50.1 ± 9.6^{B}	117.4 ± 13.1^{C}	1.1 ± 0.3^{a}	6.0 ± 1.2^{b}	15.3 ± 1.7^{c}
quercetin acetyl hexoside	34.6 ± 16.2^{A}	30.4 ± 24.9^{A}	6.2 ± 2.3^{A}	4.5 ± 2.1^{a}	3.7 ± 3.0^{a}	0.8 ± 0.3^{a}
total	42.8 ± 18.2^{A}	80.5 ± 27.5^{AB}	123.6 ± 15.6^{B}	5.6 ± 2.4^{a}	9.7 ± 3.3^{ab}	16.1 ± 2.0^{b}
			Kaempferol Equivalents			
kaempferol dihexoside	36.9 ± 10.9^{A}	1198.9 ± 479.8^{B}	267.7 ± 77.7^{A}	4.8 ± 1.4^{a}	143.9 ± 57.6^{b}	34.8 ± 10.1^{a}
kaempferol acetyl dihexoside	31.8 ± 6.7^{A}	121.2 ± 17.7^{B}	30.7 ± 0.71^{A}	4.1 ± 0.1^{a}	14.5 ± 2.1^{b}	4.0 ± 0.1^{a}
kaempferol hexoside	15.8 ± 8.2^{A}	38.4 ± 17.7^{B}	5.3 ± 1.3^{A}	2.1 ± 1.1^{a}	4.6 ± 2.1^{b}	0.7 ± 0.2^{ab}
kaempferol acetyl hexoside	143.1 ± 50.6^{A}	33.5 ± 23.4^{B}	10.8 ± 2.0^{B}	18.6 ± 6.6^{a}	4.0 ± 2.8^{b}	1.4 ± 0.3^{b}
total	227.6 ± 58.5^{A}	1392.0 ± 480.3^{B}	314.4 ± 81.7^{A}	29.6 ± 7.6^{a}	167.0 ± 57.6^{b}	40.9 ± 10.6^{a}

[a]Results are expressed as the mean ± SD (n = 3). Values in rows with different letters are significantly different at the 95% confidence level. [b]ND, nondetectable.

(acetyl-dihexoside moiety, 366 amu) and was identified as kaempferol acetyl dihexoside. Peak 14 had ions at m/z 447.092, $[M - H]^-$, and m/z 471.091, $[M + H + Na]^+$, which is consistent with kaempferol hexoside.

Compound **15** was tentatively assigned as kaempferol acetyl hexoside on the basis of its molecular ion ($[M - H]^-$) at m/z 489.105 as it showed a mass difference of 42 amu in relation to its nonacylated analogue kaempferol hexoside (peak 14).

The non-ACN phenolic composition of petals from nasturtium flowers is comparable with the composition of *T. majus* seeds. In 2013, Bazylko et al.[23] reported the presence of 3-*p*-CoQA, 4-CoQA, 5-CoQA, 3-CQA, 3-CQA, and 5-CQA in 60 aqueous ethanol extracts. With regard to the flavonoid composition, the authors found quercetin and kaempferol derivatives, but not myricetin conjugates. Seeds also contained a methoxyquercetin derivative, isoquercetin, and astragalin.

Quantification of Anthocyanins and Non-anthocyanin Polyphenolics by HPLC. Despite the similarity in constituent ACNs among petals with different colors, there were variations in total ACN concentration and amount of each pigment. A significant difference ($p < 0.05$) in the amount of ACNs as influenced by color was found. The highest amount of pigment was found in red flowers (114.5 ± 2.3 mg cy-3-glu/100 g FW), followed by orange flowers (58.2 ± 28.5 mg cy-3-glu/100 g FW) and yellow flowers (31.9 ± 21.7 mg cy-3-glu/100 g FW).

Whereas the value of ACN content as determined by HPLC was lower than the value determined by the pH differential method, similar results have been observed by other authors. Pacheco-Palencia et al.[32] found that the concentration of açai (*Euterpe oleracea*) ACNs quantified by spectrophotometry was 2.6 times higher than values for total anthocyanins determined by HPLC. The authors attributed these results to the presence of ACN polymers that influence color as well as copigmentation reactions that involve the formation of weak complexes between anthocyanin glycosides and other noncolored components such as phenolic acids, flavonoids, and flavonol derivatives. This results in a hyperchromic response that may result in an overestimation of total anthocyanins in spectrophotometric assays.

Orange flowers showed an abundance of pg-3-soph (52.7 ± 27.8 mg cy-3-glu equiv/100 g FW) and low concentrations of dp-3-dihesoxide and cy-3-soph. Conversely, red flowers presented high values of dp-3-dihesoxide (76.9.6 ± 6.9 mg cy-3-glu equiv/100 g FW) and pg-3-soph (27.7 ± 8.5 mg cy-3-glu equiv/100 g FW), whereas yellow flowers showed small concentration of each ACN with similar concentrations of pg-3-soph and dp-3-dihesoxide.

The concentrations of phenolic compounds in the extracts from petals with different colors as determined by peak area in the HPLC-PDA chromatogram are shown in Table 4. The highest level of flavonols was found in red flowers, with myricetin derivatives being the dominant flavonoids (315.1 ± 2.4 mg myricetin equiv/100 g FW or 2424.0 ± 18.3 mg myricetin equiv/100 g DW) followed by kaempferol derivatives (40.9 ± 10.6 mg kaempferol equiv/100 g FW or 314.4 ± 81.7 mg kaempferol equiv/100 g DW) and quercetin derivatives (16.1 ± 2.0 mg quercetin equiv/100 g FW or 123.6 ± 15.6 mg quercetin equiv/100 g DW). The quercetin content in red flowers is comparable with the amount present in food and medicinal plants with a very high concentration of this

DOI: 10.1021/jf503366c
J. Agric. Food Chem. 2015, 63, 1803−1811

compound. White onion (*Allium cepa*) contains 113.0 ± 6.0 mg quercetin equiv/100 g DW, *Ginkgo biloba* leaf has 136.0 ± 6.0 mg quercetin equiv/100 g DW, and *Calendula officinalis* flower has 112.0 ± 6.0 mg quercetin equiv/100 g DW.[30] On the other hand, the primary source of quercetin in the American diet (onions, tea, and apples) is either much lower or comparable to that of nasturtium flowers of any color.[31,33]

Quercetin has been shown to be an excellent antioxidant with anti-inflammatory, antiproliferative, and gene expression changing capacities in vitro.[34] In addition, antioxidative and anti-inflammatory effects have also been demonstrated in vivo, especially in people with hypertension and sarcoidosis.[34] This high antioxidant activity is attributed to its *o*-dihydroxy structure on the B ring and a −OH group at position 3, which results in the ability of quercetin to transfer a hydrogen atom to radicals.[35]

Kaempferol derivatives were the main flavonoids in orange flowers (167.0 ± 57.6 mg kaempferol equiv/100 g FW or 1,392.0 ± 480.3 mg kaempferol equiv/100 g DW). The second most abundant group of compounds in these petals were members of the chlorogenic acid family (81.2 ± 13.9 mg chlorogenic acid equiv/100 g FW or 550.6 ± 74.9 mg chlorogenic acid equiv/100 g DW), followed by small amounts of quercetin derivatives (9.7 ± 3.3 mg quercetin equiv/100 g FW or 80.5 ± 27.5 mg quercetin equiv/100 g DW) and myricetin conjugates (1.2 ± 0.6 mg myricetin equiv/100 g FW or 9.7 ± 4.7 mg myricetin equiv/100 g DW). Among 20 plant materials, *Rosa damascene* flower showed the highest kaempferol content (1480.0 ± 35.0 mg kaempferol equiv/100 g DW),[30] comparable to the kaempferol content in orange flowers. The high flavonoid content of this flower seems to be the primary reason for its protective effects on the cardiovascular system.[36]

Although kaempferol has only one OH group, accounting for a lower antioxidant activity than quercetin, epidemiologically, in vitro and in vivo studies show a positive association between the consumption of kaempferol and their glycosides, and subsequent pharmacological activities, including anti-inflammatory, antimicrobial, anticancer, cardioprotective, neuroprotective, antidiabetic, antiallergic, and antiasthmatic activities.[37] Several studies have explained that the presence of a double bond at C2−C3 in conjugation with an oxo group at C4 and the presence of hydroxyl groups or an acylated structure at C3, C5, and C4′ are the primary structural impetus for the antioxidant activity of kaempferol.[37] It has been estimated that the human dietary average intake of this polyphenol is approximately 10 mg/day.[38] Therefore, 10 g of fresh orange flowers would supply this intake.

Myricetin has been reported as a bioactive flavonoid during in vivo trials. Administration of aqueous and ethanolic extracts of myricetin glycosides from *Myrtus communis* L. showed significant antihyperglycemic, anti-inflammatory, and antinociceptive effects in albino mice as compared with control groups and reference drugs.[39] Similarly, the methanolic extract of *Cotinus coggygria* showed medicinal potential as an antigenotoxic and antihepatotoxic natural agent in albino Wistar rats. Because myricetin is the main flavonoid of this plant, the authors hypothesized that this compound could be responsible for the observed bioactivity and free radical scavenging activity.[40]

In contrast, the most representative polyphenolic compounds present in yellow flowers were hydroxycinammates. The total concentration of isomers of CQA and *p*-CoQA in this sample (235.6 ± 8.1 mg chlorogenic acid equiv/100 g FW) was significantly higher ($p < 0.05$) than the concentration in red and orange flowers. Conversely, as compared to yellow flowers, the amount of myricetin and quercetin conjugates was significantly higher ($p < 0.05$) in red petals, whereas the concentration of kaempferol conjugates was significantly higher ($p < 0.05$) in orange petals.

It has been reported that chlorogenic acid has antioxidant, anticarcinogenic, anti-inflamatory, and cholesterol-lowering activities[41] as well as protective properties against degenerative age-related diseases in animals.[42] Coffee is considered the main source of chlorogenic acids in the human diet; it is estimated that a 200 mL cup delivers 200 mg of total chlorogenic acids.[43] Thus, 100 g of fresh yellow petals would provide an amount of chlorogenic acid comparable to a 200 mL cup of coffee.

Generally, total phenolics, including ACNs and non-ACN polyphenols, were much lower in yellow flowers as compared with orange and red flowers. Mato et al.[44] stated that in edible flowers, an increased content of ACNs is correlated with high levels of total flavonoids. Terahara and Yamaguchi[45] explained that there is a common pathway of synthesis of flavonoids and ACNs; pale flowers lack enzymes such as flavanone 3-hydroxylase, dihydroflavonol 4-reductase,[44] and/or anthocyanidin synthase.[46]

Antioxidant Activity. The ORAC radical-scavenging activity of the red flowers (18719 ± 696 μmol TE/100 g FW) was significantly higher ($p < 0.05$) than those of the orange flowers (11790 ± 1570 μmol TE/100 g FW) and yellow flowers (7111 ± 3545 μmol TE/100 g FW).

ORAC values reflect the capacity of the cumulative extracted antioxidants present to donate a proton to the AAPH radical. When components with an important antioxidant capacity are present in high concentrations, the ORAC value is driven by these high-performing compounds. Furthermore, synergistic effects among components with high antioxidant properties have been found.[47] Red flowers exhibited the highest TPC and ACN concentrations as well as the highest antioxidant activity. This can be explained by the high concentration and specific chemical structure of phenolic compounds present in red flower extracts. It has been shown that cyanidin, delphinidin, and quercetin derivatives have a high radical-scavenging activity and an antioxidant capacity comparable to the activities of the well-known antioxidants α-tocopherol and Trolox.[48]

The extracts from *T. majus* petals did not exhibit any antimicrobial activity against any of the tested microorganisms. In a previous study,[23] the authors observed no effect of nasturtium seed extracts on *S. aureus* ATCC 9341 or *E. coli* ATCC 25922. The authors hypothesized that the low content of benzyl isothiocyante (a compound with antimicrobial activity and breakdown product of glucotropaeloin) in the extract was responsible for the lack of antimicrobial activity.

In conclusion, this comparative study revealed the profile of phenolic compounds in *T. majus* petals of different colors. Their antioxidant activity was also evaluated, and the results showed that they appear to be good sources of natural antioxidants that can be used as food additives or dietary antioxidants once their bioavailability and mechanism of action have been evaluated.

■ ASSOCIATED CONTENT

Supporting Information

QTOF-ESI-MS[e] for fragment ions in HE for non-anthocyanin phenolics present in nasturtium flowers (*Tropaeolum majus*); labels in each figure correspond to peak numbers as reported in

DOI: 10.1021/jf503366c
J. Agric. Food Chem. 2015, 63, 1803−1811

Table 3. This material is available free of charge via the Internet at http://pubs.acs.org.

AUTHOR INFORMATION

Corresponding Author

*(G.A.G.) Phone: 571 316 5000, ext. 14457. Fax: 571 3165220. E-mail: agarzonmo@unal.edu.co.

Notes

The authors declare no competing financial interest.

ACKNOWLEDGMENTS

We thank Tom Gibson (Cornell University) for technical assistance.

REFERENCES

(1) Mlcek, J.; Rop, O. Fresh edible flowers of ornamental plants – a new source of nutraceutical foods. *Trends Food Sci. Technol.* **2011**, *22*, 561–569.

(2) Pratt, D. E. Natural antioxidants from plant material. *ACS Symp. Ser.* **1992**, *No. 507*, 54–71.

(3) Kelley, K. M.; Behe, B. K.; Biernbaum, J. A.; Poff, K. L. Consumer ratings of edible flower quality, mix and color. *HortTechnology* **2001**, *11*, 644–647.

(4) Grzeszczuk, M.; Kawecka, A.; Jadczak, D. Nasturcja większa *Tropaeolum majus* L. *Panacea* **2010**, *31*, 20–21 (in Polish).

(5) Lorenzi, H.; Matos, F. J. A. *Plantas Medicinais no Brasil: Nativas e Exóticas*; Instituto Plantarum de Studos da Flora: São Paulo, Brazil, 2002.

(6) Ferreira, R. B. G.; Vieira, M. C.; Zárete, N. A. H. Análise de crescimento de *Tropaeolum majus* 'Jewel' em funcão de espaçamentos entre plantas. *Rev. Bras. Plantas Med.* **2004**, *7*, 57–66.

(7) Ferro D. Legislação de Fitoterapia. In *Fitoterapia: Conceitos Clínicos*; Atheneu: São Paulo, Brazil, 2006; pp 83–114.

(8) Bown, D. *Encyclopedia of Herbs and Their Uses*; Pharmaceutical Products Press: DK Publishing: New York, 1995; pp 105–109.

(9) Santo, A. P. E.; Martins, I. S. S.; Tomy, S. C.; Ferro, V. O. Efeito anticoagulante *in vitro* do extrato hidroetanolico de folhas e flores édulas de *Tropaeolum majus* L (Tropaeolaceae) sobreo plasma humano. *Lat. Am. J. Pharm.* **2007**, *26*, 732–736.

(10) Gasparotto Junior, A.; Gasparotto, F. M.; Botelho Lourenço, E. L.; Crestani, S.; Alves Stefanello, M. E.; Salvador, M. J.; Da Silva-Santos, J. E.; Andrade Marques, M. C.; Leite Kassuyab, C. A. Antihypertensive effects of isoquercitrin and extracts from *Tropaeolum majus* L.: evidence for the inhibition of angiotensin converting enzyme. *J. Ethnopharmacol.* **2011**, *2*, 363–372.

(11) Gasparotto Junior, A.; Gasparotto, F. M.; Boffo, M. A.; Botelho Lourenço, E. L.; Alves Stefanello, M. E.; Salvador, M. J.; Da Silva-Santos, J. E.; Andrade Marques, M. C.; Leite Kassuyab, C. A. Diuretic and potassium-sparing effect of isoquercitrin – an active flavonoid of *Tropaeolum majus* L. *J. Ethnopharmacol.* **2011**, *2*, 210–215.

(12) Goos, K. H.; Albrecht, U.; Schneider, B. Efficacy and safety profile of an herbal drug containing nasturtium herb and horseradish root in acute sinusitis, acute bronchitis and acute urinary tract infection in comparison with other treatments in the daily practice/results of a prospective cohort study. *Arzneimittelforschung* **2006**, *56*, 249–257.

(13) Koriem, K. M.; Arbid, M. S.; El-Gendy, N. F. The protective role of *Tropaeolum majus* on blood and liver toxicity induced by diethyl maleate in rats. *Toxicol. Mech. Methods* **2010**, *20*, 579–586.

(14) Schreiner, M.; Krumbein, A.; Mewis, A.; Ulrichs, C.; Huyskens-Keil, S. Short-term and moderate UV-B radiation effects on secondary plant metabolism in different organs of nasturtium (*Tropaeolum majus* L.). *Innovative Food Sci. Emerging Technol.* **2009**, *10*, 93–96.

(15) Gasparotto, A., Jr.; Boffo, M. A.; Lourençoa, E. L.; Stefanello, M. E.; Kassuya, C. A.; Marques, M. C. Natriuretic and diuretic effects of *Tropaeolum majus* (Tropaeolaceae) in rats. *J. Ethnopharmacol.* **2009**, *3*, 517–522.

(16) Garzón, G. A.; Wrolstad, R. E. Major anthocyanins and antioxidant activity of nasturtium flowers (*Tropaeolum majus*). *Food Chem.* **2009**, *114*, 44–49.

(17) Giusti, M. M.; Wrolstad, R. E. Characterization and measurement of anthocyanins by UV–visible spectroscopy. In *Handbook of Food Analytical Chemistry*; Wiley: Hoboken, NJ, USA, 2001; Vol. 2, pp 19–31.

(18) Waterhouse, L. Determination of total phenolics. In *Handbook of Food Analytical Chemistry*; Wiley: Hoboken, NJ, USA, 2001; Vol. 2, pp 463–470.

(19) Durst, R., Wrolstad, R. E. Separation and characterization of anthocyanins by HPLC. In *Handbook of Food Analytical Chemistry*; Wiley: Hoboken, NJ, USA, 2001; Vol. 2, pp 33–45.

(20) Manns, D. C.; Mansfield, A. K. A core–shell column approach to a comprehensive high-performance liquid chromatography phenolic analysis of *Vitis vinifera* L. and interspecific hybrid grape juices, wines, and other matrices following either solid phase extraction or direct injection. *J. Chromatogr., A* **2012**, *1251*, 111–121.

(21) Clifford, M. N.; Johnston, K. L.; Knight, S.; Kuhnert, N. Hierarchical scheme for LC-MS^n identification of chlorogenic acids. *J. Agric. Food Chem.* **2003**, *51*, 2900–2911.

(22) Jaiswal, R.; Karaköse, S.; Rühmann, S.; Goldner, K.; Neumüller, M.; Treutter, D.; Kuhnert, N. Identification of phenolic compounds in plum fruits (*Prunus salicina* L. and *Prunus domestica* L.) by high-performance liquid chromatography/tandem mass spectrometry and characterization of varieties by quantitative phenolic fingerprints. *J. Agric. Food Chem.* **2013**, *49*, 12020–12031.

(23) Bazylko, A.; Granica, S.; Filipek, A.; Piwowarski, J.; Stefańska, J.; Osińska, E.; Kiss, A. K. Comparison of antioxidant, anti-inflammatory, antimicrobial activity and chemical composition of aqueous and hydroethanolic extracts of the herb of *Tropaeolum majus* L. *Ind. Crops Prod.* **2013**, *50*, 88–94.

(24) Prior, R. L.; Hoang, H.; Gu, L.; Wu, X.; Bacchiocca, M.; Howard, L.; Hampsch-Woodill, M.; Huang, D.; Ou, B.; Jacob, R. Assays for hydrophilic and lipophilic antioxidant capacity oxygen radical absorbance capacity (ORACFL) of plasma and other biological and food samples. *J. Agric. Food Chem.* **2003**, *51*, 3273–3279.

(25) Mayr-Harting, A.; Hedges, A. J.; Berkeley, R. C. W. Methods for studying bacteriocins. *Methods Microbiol.* **1972**, *7A*, 315–422.

(26) Chiang, H.; Wrolstad, R. E. Anthocyanin pigment composition of blackberries. *J. Food Sci.* **2005**, *70*, 750–3841.

(27) Herms, D. A.; Mattson, W. J. The dilemma of plants: to grow or defend. *Q. Rev. Biol.* **1992**, *67*, 283–335.

(28) Vasco, C.; Ruales, J.; Kamal-Eldin, A. Total phenolic compounds and antioxidant capacities of major fruits from Ecuador. *Food Chem.* **2008**, *4*, 816–823.

(29) Rufino, M.; Alves, R. E.; De Brito, E. S.; Pérez-Jiménez, J.; Saura-Calixto, F.; Mancini-Filho, J. Bioactive compounds and antioxidant capacities of 18 non-traditional tropical fruits from Brazil. *Food Chem.* **2010**, *121*, 996–1002.

(30) Haghi, G. A.; Hatami, A. Simultaneous quantification of flavonoids and phenolic acids in plant materials by a newly developed isocratic high-performance liquid chromatography approach. *J. Agric. Food Chem.* **2010**, *58*, 10812–10816.

(31) Tsuchiya, H. Structure-dependent membrane interaction of flavonoids associated with their bioactivity. *Food Chem.* **2010**, *120*, 1089–1096.

(32) Pacheco-Palencia, L. A.; Palo, H.; Talcott, S. T. Phytochemical, antioxidant and pigment stability of açai (*Euterpe oleracea* Mart.) as affected by clarification, ascorbic acid fortification and storage. *Food Res. Int.* **2007**, *40*, 620–628.

(33) Sampson, L.; Rimm, E.; Hollman, P. C. E.; De Vries, J. H. M.; Katan, M. Flavonol and flavone intakes in US health professionals. *J. Am. Diet. Assoc.* **2002**, 1414–1420.

(34) Boots, A. W.; Haenen, G.; Bast, A. Health effects of quercetin: from antioxidant to nutraceutical. *Eur. J. Pharmacol.* **2008**, *585*, 325–337.

DOI: 10.1021/jf503366c
J. Agric. Food Chem. 2015, 63, 1803–1811

(35) Rice Evans, C. A.; Miller, N.; Paganga, G. Structure-antioxidant activity relationships of flavonoids and phenolic acids. *Free Radical Biol. Med.* **1996**, *20*, 933−956.
(36) Kwon, E.-K.; Lee, D.-W.; Lee, H.; Kim, D.-O.; Baek, N. I.; Kim, Y.-O.; Kim, H.-Y. Flavonoids from the buds of *Rosa damascena* inhibit the activity of 3-hydroxy-3-methylglutaryl-coenzyme a reductase and angiotensin I-converting enzyme. *J. Agric. Food Chem.* **2010**, *58*, 882−886.
(37) Oszmiański, J.; Kolniak-Ostek, J.; Wojdyło, A. Characterization and content of flavonol derivatives of *Allium ursinum* L. plant. *J. Agric. Food Chem.* **2013**, *61*, 176−184.
(38) De Vries, J. H.; Janssen, P. L.; Hollman, P. C.; Van Staveren, W. A.; Katan, M. B. Consumption of quercetin and kaempferol in free living subjects eating a variety of diets. *Cancer Lett.* **1997**, *19*, 141−144.
(39) Mahmoud, I.; Nassar, M. I.; Aboutabl, E. A.; Ahmed, R. F.; El-Khrisy, E. A.; Ibrahim, K. M.; Amany, A.; Sleem, A. A. Secondary metabolites and bioactivity of *Myrtus communis*. *Pharmacognosy Res.* **2010**, *2*, 325−329.
(40) Matić, S.; Stanić, S.; Bogojević, D.; Vidaković, M.; Grdović, N.; Dinić, S.; Solujić, S.; Milan Mladenović, M.; Stanković, N.; Mihailović, M. Methanol extract from the stem of *Cotinus coggygria* Scop., and its major bioactive phytochemical constituent myricetin modulate pyrogallol-induced DNA damage and liver injury. *Mutat. Res. Genet. Toxicol. Environ. Mutagen* **2013**, *755*, 81−89.
(41) Parveen, I.; Threadgill, M.; Hauck, B.; Donnison, I.; Winters, A. Isolation, identification and quantitation of hydroxycinnamic acid conjugates, potential platform chemicals, in the leaves and stems of *Miscanthus* × *giganteus* using LC−ESI-MS^n. *Phytochemistry* **2011**, *72*, 2376−2384.
(42) Niggeweg, R.; Michael, A. J.; Martin, C. Engineering plants with increased levels of the antioxidant chlorogenic acid. *Nat. Biotechnol.* **2004**, *22*, 746−754.
(43) Febi, M. F.; Jaiswal, R.; Kuhnert, N. Investigating the chemical changes of chlorogenic acids during coffee brewing: conjugate addition of water to the olefinic moiety of chlorogenic acids and their quinides. *J. Agric. Food Chem.* **2012**, *60*, 12105−12115.
(44) Mato, M.; Onazaki, T.; Ozeki, Y.; Higeta, D.; Itoh, Y.; Yoshimoto, Y. Flavonoid biosynthesis in white flowered Sim carnations (*Dianthus caryophyllus*). *Sci. Hortic.* **2000**, *84*, 333−347.
(45) Terahara, N.; Yamaguchi, M. ^{1}H NMR spectral analysis of malylated anthocyanins from dianthus. *Phytochemistry* **1986**, *25*, 2906−2907.
(46) Mato, M.; Onazaki, T.; Ozeki, Y.; Higeta, D.; Itoh, Y.; Hisamatsu, T. Flavonoid biosynthesis in pink flowered cultivars derived from William Sim carnation (*Dianthus caryophylus*). *Jpn. Soc. Hortic. Sci.* **2001**, *70*, 315−319.
(47) Bentayeb, K.; Vera, P.; Rubio, C.; Nerín, C. The additive properties of oxygen radical absorbance capacity (ORAC) assay: the case of essential oils. *Food Chem.* **2014**, *148*, 204−208.
(48) Kahkönen, M. P.; Heinonen, M. Antioxidant activity of anthocyanins and their aglycons. *J. Agric. Food Chem.* **2003**, *51*, 628−633.

DOI: 10.1021/jf503366c
J. Agric. Food Chem. 2015, 63, 1803−1811

updating the body of lipid oxidation knowledge in low-moisture foods in an attempt to better understand oxidation mechanisms that can be instrumental in developing new antioxidant technologies. Ultimately, this work has broad and long-lasting implications on the development of stable foods that substitute heart-healthy polyunsaturated oils for saturated fats.

MATERIALS AND METHODS

Materials. Baking soda (Arm & Hammer; Princeton, NJ), iodized table salt (Morton; Chicago, IL), all-purpose flour (Gold Medal, original; Minneapolis, MN), traditional saltine crackers (Savoritz; Batavia, IL), and whole-wheat saltine crackers (Nabisco; East Hanover, NJ) were purchased from local (Amherst, MA) grocery stores. Interesterified soybean oil #762420 (henceforth referred to as ISO) was provided by Archer Daniels Midland Company (Decatur, IL) and selected for its recommended use in cracker applications. Dry goods were stored in closeable freezer bags; ISO was kept frozen (−20 °C) until use. The nonpolar dye Bodipy 493/503 ("Bodipy") was purchased from Invitrogen (Carlsbad, CA). The fluorescent probes Nile Red and Rhodamine B and all other chemicals were purchased from Sigma-Aldrich (St. Louis, MO). All solutions were prepared using double distilled water.

General Sample Manufacture and Preparation. Crackers were prepared by traditional baking methods and ingredients (Table 1).

Table 1. Ingredient Composition

ingredient	mass (g)	percentage (w/w)
flour	62.50	50.6
DI water	39.00	31.6
interesterified soybean oil	10.00	8.1
salt	1.50	1.2
baking soda	0.58	0.5
flour for sprinkling on surface	10.00	8.1
total	123.58	100

Sifted flour, baking soda, and salt were mixed together and then added to the ISO (∼1 min; speed 2 on a Kitchen Aid mixer, model #KSM95; Mississauga, Ontario) until an agglomerated powder formed. After exchanging the mixer's standard beater for a dough hook, water was added (speed 2; ∼1 min) to form dough. This dough was briefly kneaded by hand until all flour was visibly incorporated. A measured amount of additional flour was sprinkled on the surface of a baking mat to prevent sticking and was incorporated into the dough by kneading. The dough was flattened by twice by passing it through a pasta roller (Kitchen Aid KPSA attachment; thickness setting 2; Mississauga Ontario) to simulate industrial sheeting. The dough was then cut with a pizza cutter along the horizontal and vertical axes to form 2.5 cm × 2.5 cm crackers. The crackers were baked on an ungreased cookie sheet at 163 °C for 21 min in an electric oven (General Electric model JB350DFWW; Fairfield, CT). After baking, crackers were coarsely crumbled using a mortar and pestle, and 0.5 g was placed into acid-washed, 10-ml glass GC vials (Supelco Analytical; Bellefonte, PA), closed with aluminum caps containing PTFE/silicone septa (Supelco Analytical; Bellefonte, PA), and stored at 55 °C in the dark for 25−45 d depending upon lag phase. Treatments were produced in duplicate, and three samples were tested per treatment batch.

Addition of Confocal Dyes to Samples. Nile Red alone was added to some treatments, while a combination of Bodipy and Rhodamine B was added to other treatments. A stock solution of Nile Red was prepared at 0.5% (w/w) in ethanol, and 1 mL of this solution was mixed with the lipid (10 g) until even dispersal of colored dye was visually observed (∼20 s). Bodipy and Rhodamine B were added based on Matalanis and McClements.[13] Specifically, Bodipy (1.0 mg) was dissolved in 1 mL ethanol, and this entire amount was mixed with the lipid in the same manner as Nile Red. In contrast, 0.3 mg of Rhodamine B was dissolved in the double distilled water added directly to the dough when the dough hook was attached. One milliliter ethanol was added to control treatments to mimic the dye addition.

Addition of Iron. The iron content of the control dough was determined by Covance (Madison, WI) using inductively coupled plasma emission spectrometry. Crackers were then made with 1.0, 1.5, 2.0, 5.0, and 10 times the endogenous iron in the dough. Specifically, reduced elemental iron (product #R140100; 300 mesh) from Watkins (West Haven, CT) was mixed with the dry ingredients before adding liquids to make the dough as detailed above; this is the most common form of iron used to fortify most all-purpose flours.

Addition of FFA and Chelating Agents. Oleic acid was mixed directly into the lipid (∼20 s at mixer speed 1) before the addition of dry ingredients at concentrations of 0, 0.2, 0.4, 1.0, 2.0, or 3.0% of the total lipid. The chelating agents desferrioxamine (DFO), citric acid (CA), and ethylenediaminetetraacetic acid (EDTA) were dissolved in pH-adjusted solutions (pH 7.0) and added to the dough at a final molar mass of 0.2 mmol, which is equivalent to the maximum concentration of EDTA allowed in any food product (500 ppm in canned strawberry pie filling, CFR 21 [172.135]). They were added with the water when making the dough.

Basic Analyses. Cracker pH was determined by crushing crackers from each batch treatment and homogenizing the crackers with 10 parts distilled water to form a slurry. The pH of the slurry was measured during constant stirring using a Denver Instrument UB-10 pH meter ultraBASIC (Denver Instruments). Measurements were conducted in quadruplicate and averaged. Water activity on experimental and commercial crackers was determined at 24−25 °C using a Decagon Devices AquaLab Series 3 water activity meter (Pullman, WA) according to the manufacturer's instruction.[14] Measurements from each treatment batch were conducted in quadruplicate and averaged. Water content was determined using an A&D MX-50 digital moisture balance (Elk Grove, IL) according to the manufacturer's instructions.[15]

Measurement of Lipid Oxidation. Lipid hydroperoxides were measured in triplicate using a modified version of the International Dairy Federation method as described by Shantha and Decker.[16] Cracker samples (0.1 g) were pulverized using mortar and pestle and added to a mixture of chloroform and methanol (5 mL; 2:1 v/v), vortexed briefly, and centrifuged (3400*g*) for 10 min to extract the hydroperoxide fraction. This extract (200 μL) was mixed with 16.7 μL of a 50/50 solution (ferrous sulfate dissolved in double distilled water + barium chloride dissolved in 0.4 N HCl) and 16.7 μL of ammonium thiocyanate dissolved in water. The final mixture was vortexed, covered to prevent evaporation, and incubated for 20 min. Absorbance was measured at 500 nm on a Genesys 20 spectrophotometer (ThermoSpectronic; Waltham, MA). The concentration of hydroperoxides was calculated from a cumene hydroperoxide standard curve.

Headspace hexanal was measured in triplicate with a GC-2014 Shimadzu gas chromatograph equipped with an AOC-5000 autosampler (Shimadzu; Kyoto, Japan) based on the method by Panya et al.[17] A 50/30 μm divinylbenzene/carboxen/polydimethylsiloxane (DVB/Carboxen/PDMS) stable flex solid phase microextraction (SPME) fiber (Supelco, Bellefonte, PA) was inserted through the vial septum and exposed to the sample headspace for 10 min at 55 °C. The volatiles on the SPME fiber were desorbed at 250 °C for 3 min in the GC detector at a split ratio of 1:7. The chromatographic separation of volatile aldehydes was performed on a fused-silica capillary column (30 m × 0.32 mm inner diameter (i.d.) × 1 μm) coated with 100% poly(dimethylsiloxane) (Equity-1, Supelco). The temperatures of the oven, injector, and flame ionization detector were 65, 250, and 250 °C, respectively. Sample run time was 6 min. Peak integration was calculated using Shimadzu EZstart (version 7.4). Concentrations were calculated by using a standard curve made from cracker crush spiked with known hexanal concentrations (hexanal was diluted in methanol).

Imaging by Microscopy. A Nikon Confocal Microscope (C1 Digital Eclipse, Tokyo, Japan) with a PL FLUOTAR ELWD 20.0 × 0.45 objective lens was used to capture the confocal images. An air-cooled argon ion laser (Model 376 IMA1010 BOS; Melles Griot;

DOI: 10.1021/jf5048018
J. Agric. Food Chem. 2015, 63, 1812−1818

Carlsbad, CA) was used to excite Nile Red at 488 nm in the lipid phase, and emission spectra were collected at 515 ± 30 nm. Crackers containing both Bodipy (lipid soluble) and Rhodamine B (protein specific) were imaged sequentially, and the resulting images were overlaid. Bodipy was excited at 488 nm, and emission spectra were collected at 515 ± 30 nm; Rhodamine B was excited at 543 nm with a Melles Griot helium−neon laser (Model 05-381 LGP-193; Carlsbad, CA), and emission spectra were collected at 605 ± 75 nm. Bodipy was used instead of Nile Red in the experiments with Rhodamine B because the broad emission spectrum of Nile Red (525−605 nm) overlaps with that of Rhodamine B and prevented images from being overlaid. Detector pinhole size was always 150 μm. All resulting images consisted of 512 × 512 pixels, with a pixel size of 414 nm, and a pixel dwell time of 10.40 μs. Confocal microscopy images were analyzed using EZ-CS1 (version 3.8) software (Nikon; Melville, NY), while optical images taken on the same microscope were analyzed using NIS-Elements (version 3.0) software (Nikon, Melville, NY).

Statistical Analysis. Oxidation lag phases were defined as the first datum point that was significantly greater than the time-zero value with all subsequent data points also being significantly greater than the time-zero value. In all cases, comparisons of the means were performed using analysis of variance (General Linear Model with Tukey's Honestly Significant Difference test as a post hoc test for multiple comparisons). A significance level of $p < 0.05$ was defined as being statistically different. All calculations were performed using XLSTAT statistical software (version 2006.3, Addinsoft, New York, NY).

RESULTS AND DISCUSSION

Composition and Microstructure. The model crackers had a moisture content of 3.2% w/w and a water activity of 0.17. The water activity of commercial regular and whole wheat saltine crackers were both 0.22. The pH of the model crackers was 8.7 and did not vary significantly with the addition of chelators, confocal dyes, or oleic acid at any of the tested concentrations.

The ISO was selected based on its use in commercial manufacture of baked goods, making the model system a good representation of products currently available to consumers. According to the supplier's analysis, the ISO was comprised primarily of 10.9% (w/w) palmitic acid, 31.1% stearic acid, 13.8% oleic acid, 35.1% linoleic acid, and 4.9% linolenic acid. Saturated fatty acids accounted for 43.0% of the lipid, and 1.2% of the unsaturated fatty acids were present in the *trans* form. This composition meant the model system contained significant amounts of omega-6 fatty acids, which ensured that hexanal would be a major secondary lipid oxidation product in the later experiments.

Bodipy and Rhodamine dyes were added to view the lipid and protein fractions, respectively, under confocal microscopy. Starch granules were identified based on their size[18] and shape, nonabsorption of protein and lipid-specific confocal dyes, and ability to be stained with Lugol's iodine solution (visualized using the basic light microscopy function of the Nikon microscope; data not shown). Air bubbles were identified based on size and the absence of dye stain.

Samples were removed during each stage of cracker development, including after the lipid was mixed with dye; after water was added to the dry ingredient-lipid mixture to form the dough ball; after the final 10 g flour was incorporated but before the dough was sheeted through rollers; and after dough sheeting. Images of the lipid alone showed that the solid ISO was able to entrap air during mixing (Figure 1a) as would be expected from the solid fat fraction. Figure 1b shows images of the initial dough. At this point, lipid can be observed surrounding the starch granules and the protein shows a

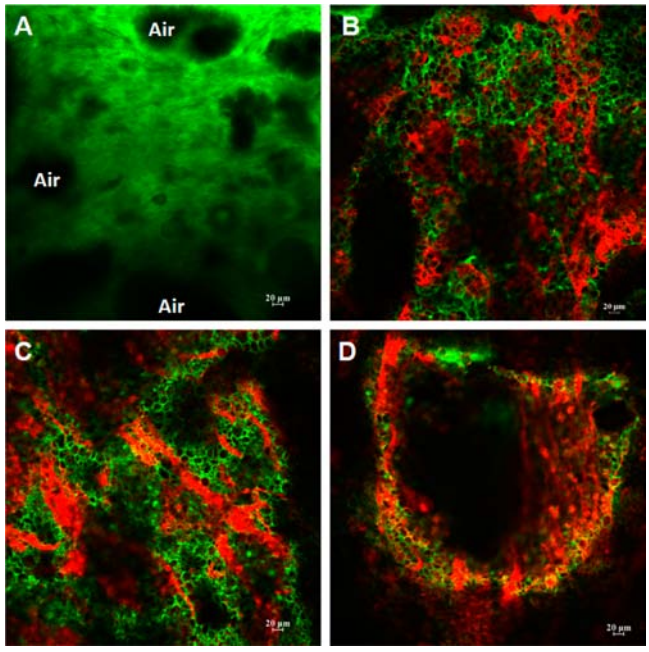

Figure 1. Confocal microscopy fluorescence of Bodipy 493/503 (green; lipid) and Rhodamine B (red; protein) in (A) the interesterified soybean oil; (B) dough before kneading; (C) kneading by hand and (D) after sheeting through pasta roller. All images taken before baking. Scale bar: 20 μm.

striated pattern typical of gluten formation. With the exception of slightly more striation due to gluten development, few changes are observed after kneading the final 10 g flour into the dough ball and sheeting the dough through the pasta roller (Figure 1c and d). Slade and Levine[19] and Kweon et al.[20] recently found that the low-sugar environment of crackers fosters gluten development during mixing and sheeting. Many of the structures developed during dough formation remain in the final, baked product (Figure 2).

It is important to understand the composition and microstructure of the crackers for several reasons. First, we wanted to understand how lipids were distributed in the cracker to see if lipid distribution was similar to other foods such as meats or emulsions. This information could provide clues on which lipids might be most susceptible to oxidation (e.g., high oxygen exposure); which prooxidants might easily access the lipids (e.g., aqueous phase metals that have an interface with the lipids as in emulsions); and how other components in the cracker associate with the lipids; and thus might influence oxidation reactions (e.g., the encapsulation of lipids with proteins. Alternatively air is quite hydrophobic, meaning that there could have been a tendency for lipid to partition to the air interface). However, the large number of examined confocal images (such as Figure 2) showed that the lipid was evenly distributed throughout the cracker and not highly associated with the air bubbles. The final water content of the crackers was low, and the confocal images confirmed that the crackers did not contain large water droplet that could be a site for lipid oxidation, especially via the metal-promoted reactions seen in emulsions.[21] The protein in the cracker formed striated bands that did not surround the lipid, with the latter more typical of meat or oil-in-water emulsions. This indicated that the protein would not provide a physical barrier on the surface of the lipid that might have influenced lipid oxidation. Finally, lipids

DOI: 10.1021/jf5048018
J. Agric. Food Chem. 2015, 63, 1812−1818

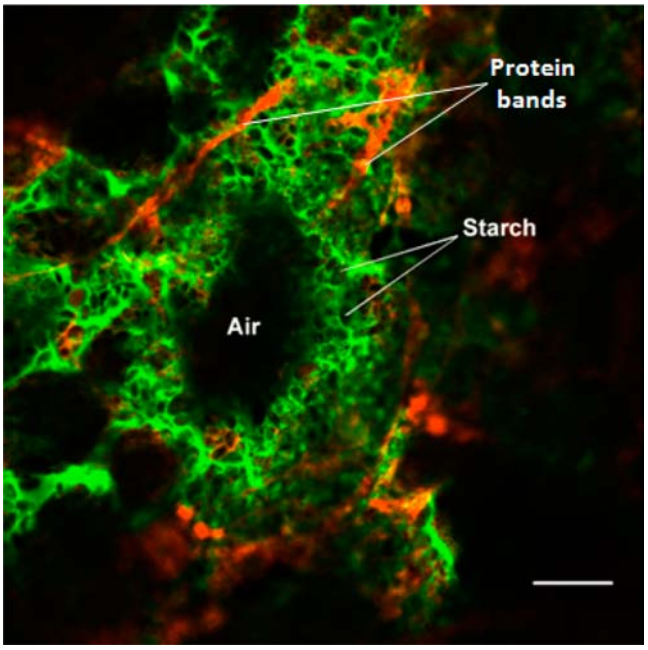

Figure 2. Confocal microscopy fluorescence of Bodipy 493/503 (green; lipid) and Rhodamine B (red; protein) in control crackers after baking. Scale bar: 50 μm.

produced a continuous phase that surrounded the starch granules, which is the opposite microstructure of most spray-dried powders where biopolymers (polysaccharides, proteins, gums) surround lipids, a structure that has been shown to reduce lipid oxidation rates.[22−24] Overall, protein−starch−lipid, lipid−air, protein−lipid, and starch−lipid interfaces were all observed within the cracker; that contrasts with other foods such as bulk oils with association colloids, oil-in-water emulsions, water-in-oil emulsions, and meat products that have only lipid−water interfaces, which are important sites for lipid oxidation.[21,25,26] This suggests that strategies to slow lipid oxidation in crackers might differ greatly from those strategies used with lipid dispersion oils.

Lipid Oxidation in Crackers. Primary (hydroperoxide) and secondary (hexanal) lipid oxidation products were both measured in the crackers during storage at 55 °C. Interestingly, the lag phases for these two measurements differed by approximately 23 d, and this trend was consistently seen in all experiments (Figures 3−6). In control crackers, the lipid hydroperoxide lag phase was 7 d. It is logical that hydroperoxides could exhibit a shorter lag phase since they are formed first and their breakdown produces secondary products. The difference in lag phases is likely due to greater lipid hydroperoxide stability in the low-moisture cracker environment than in bulk oils, meats, or emulsions where lipid hydroperoxides and hexanal lag phases differ by only a few days.[27,28] Hydroperoxides may have a longer life in crackers than in bulk oils, meats, or emulsions because the prooxidants (e.g., transition metals) that decompose lipid hydroperoxides are not readily diffusible in the low-moisture environment and so cannot readily interact with hydroperoxides. No secondary oxidation products can form if the hydroperoxides do not decompose. Hence, we needed to better understand the effects of iron in the system.

The most abundant ingredient in crackers is all-purpose white flour fortified with iron. Iron in the crackers is potentially

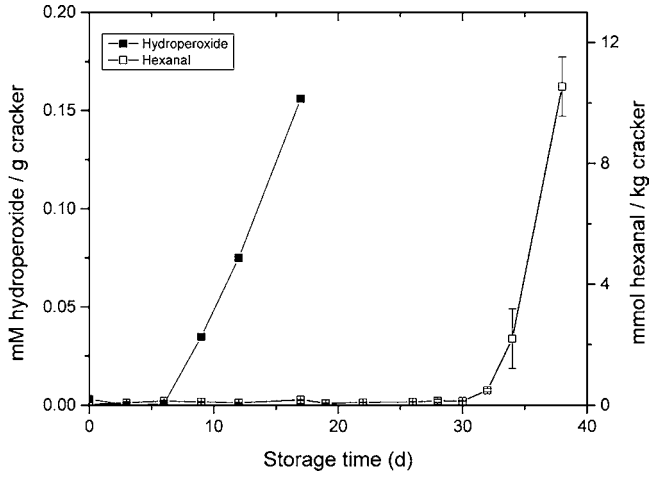

Figure 3. Lipid hydroperoxides and hexanal in control crackers stored at 55 °C in the dark. Standard error bars are smaller than data points in some instances.

an important prooxidant since it can decompose hydrogen peroxides and lipid hydroperoxides into free radicals through a redox cycling pathway.[11] Although iron can be detrimental from a shelf-stability standpoint, its fortification into flours is beneficial to consumer health by minimizing iron-based anemia in the population, which is why researchers are trying to genetically modify cereal grains to contain more iron.[29] Even traditionally bred, nonfortified wheat contains transition metals, which means presence of prooxidant iron will always be a challenge. Processing equipment containing iron or copper could also contaminate the dough with metal. Furthermore, most products are manufactured with tap water, another potential source of iron.[30] Thus, iron could contribute to the oxidation of low-moisture foods, although its role is not well understood.

To better understand the role of iron on the oxidative stability of the model cracker systems, increasing amounts of iron were added to the cracker dough. The cracker dough was found to contain 0.004% iron, which matches the USDA's reported value of 0.0046% iron in enriched, bleached, all-purpose flour.[31] Increasing the iron concentration up to 10-fold had no significant effect on either the hydroperoxides or hexanal lag phases (Figure 4).

To further determine the prooxidant effect of transition metals, metal chelators were added to the crackers. The chelator solutions (and the water for the control treatment) were pH-adjusted to 7.0. In addition, the cracker pH was 8.7, meaning that all chelators would be above their pK_a and thus would be charged and capable of binding metals. All chelator treatments exhibited the same lipid hydroperoxide (~7 d) lag phase (Figure 5a). Control crackers, DFO, EDTA, and CA treatments had similar hexanal lag phases (31 d), again supporting the hypothesis that iron is not an important prooxidant in the crackers. While EDTA did decrease the rate of hexanal formation after the lag phase, this is not important to the shelf life of a food because, at this point, the product is rancid.

The iron addition and chelator studies suggest that metals are not very active in the cracker system. A study using flour fortified with ferrous sulfate (0−75 ppm), EDTA, and folic acid to make naan flatbread showed that iron fortification significantly affected color, texture, flexibility, and chewability

DOI: 10.1021/jf5048018
J. Agric. Food Chem. 2015, 63, 1812−1818

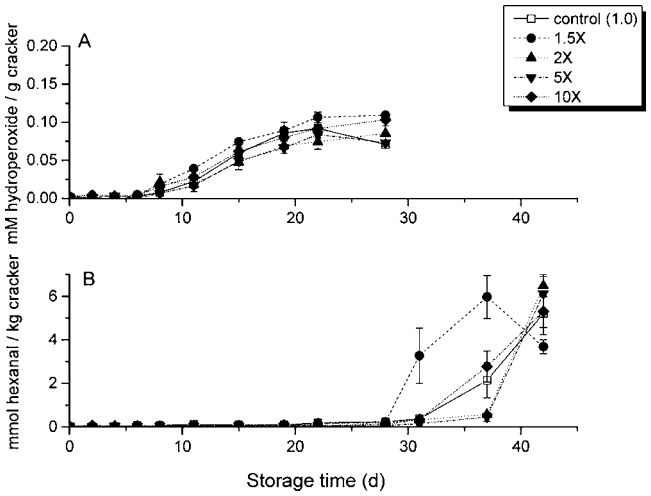

Figure 4. (A) Lipid hydroperoxides and (B) headspace hexanal in crackers made with 1, 1.5, 2.0, 5.0, and 10 times the amount of reduced iron found in the control cracker dough (0.004% iron) and stored in the dark at 55 °C. Standard error bars are smaller than data points in some instances.

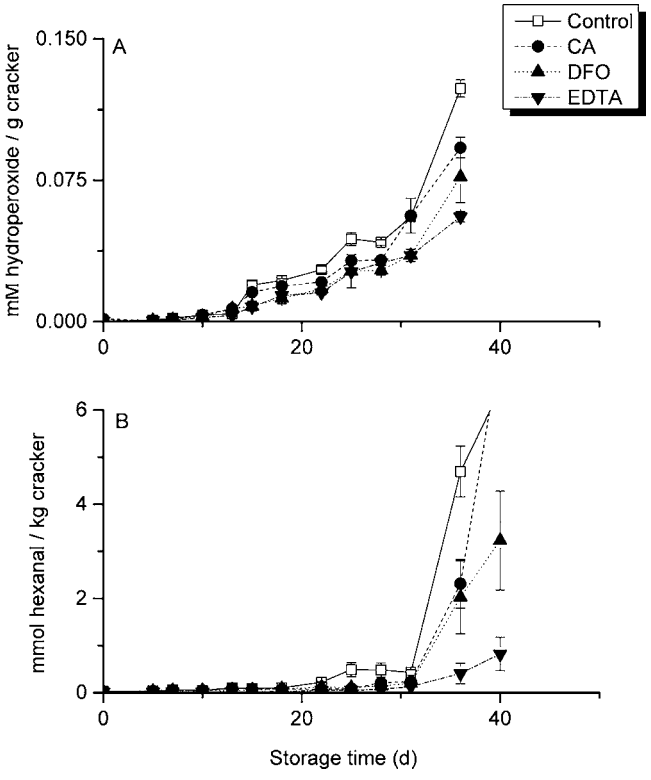

Figure 5. (A) Lipid hydroperoxides and (B) headspace hexanal in crackers made with citric acid (CA), desferrioxamine (DFO), and ethylenediaminetetraacetic acid (EDTA) and stored in the dark at 55 °C. Standard error bars are smaller than data points in some instances.

but not taste or flavor.[32] These latter two sensory attributes are most closely related to oxidative rancidity, suggesting that iron had little impact on lipid oxidation. In contrast, chelators, especially EDTA and DFO, can be very effective antioxidants in oil-in-water and water-in-oil emulsions, increasing secondary lag phases at least 4- and 3-fold, respectively.[33,34] The cracker's low water content and water activity likely limited iron diffusibility. This could explain why additional iron was not strongly prooxidative and why chelators were weaker antioxidants than seen in other foods. Of course, bulk oils also have a low water activity, but they do contain a fluid mobile phase unlike crackers and other low-moisture foods. In addition, iron could be a stronger prooxidant in bulk oils due to the presence of reverse micelles that can concentrate metals and serve as reaction centers.[21,26] The results in crackers suggest that iron fortification of low-moisture foods is an effective nutritional strategy since the iron in these products has minimal impact on product shelf life.

FFA are considered prooxidants because they can locate at water−lipid interfaces, and their negative charged is thought to attract positively charged iron to the reaction site.[35−37] In the case of crackers, both the flour and lipid are potential sources of FFA since enriched, bleached, all-purpose flour has been shown to contain free fatty acids.[31] Oleic acid was used in this study because it is a predominant fatty acid in soybean oil; it is liquid at room temperature and thus easy to distribute into the dough; and its monounsaturated and thus more oxidatively stable than polyunsaturated fatty acids, making it less likely to promote oxidation on its own. Figure 6 shows that the control, 0.2, 0.4,

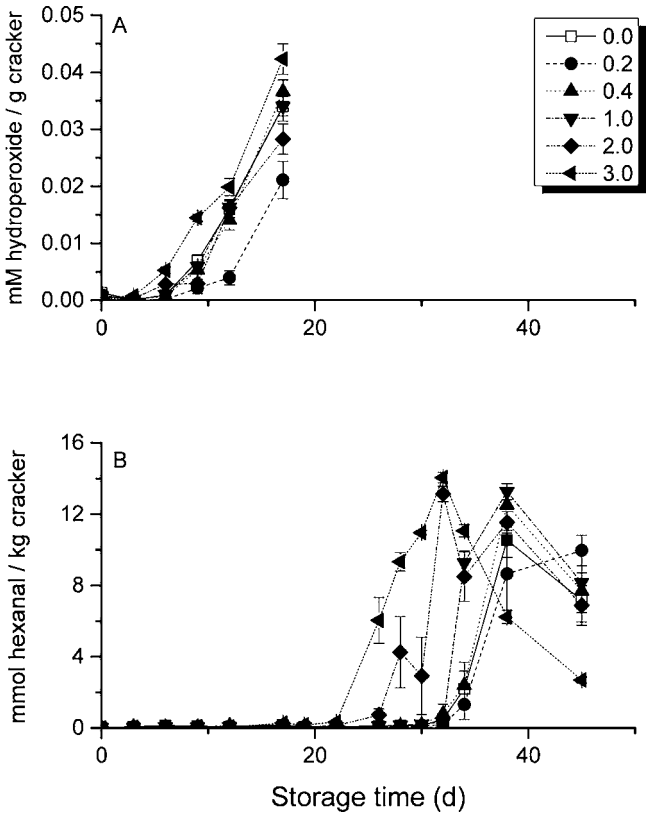

Figure 6. (A) Lipid hydroperoxides and (B) headspace hexanal in crackers made with 0−3% added oleic acid on a lipid basis and stored in the dark at 55 °C. Standard error bars are smaller than data points in some instances.

and 1.0% oleic acid in the lipids exhibited statistically similar lipid hydroperoxide (~6 d) and hexanal (~32 d) lag phases. In contrast, treatments with 2.0 and 3.0% oleic acid in the lipids exhibited significantly shorter lag phases at 3 d for hydroperoxides and ~22 d for hexanal. Crackers in general, however, are more stable to the prooxidant effects of FFA than bulk oil and emulsion systems. For instance, addition of oleic acid at concentrations as low as 0.25% decreased the lag phase of lipid

DOI: 10.1021/jf5048018
J. Agric. Food Chem. 2015, 63, 1812−1818

hydroperoxide and hexanal formation by over 30% in soybean-based oil-in-water emulsions.[38] Likewise, both saturated and unsaturated FFA were shown to accelerate lipid oxidation in walnut-based water-in-oil emulsions at concentrations as low as 0.05% oleic acid and 0.5% lauric, palmitic, or stearic acid, decreasing the oxidation lag phase by 15% and over 30%, repectively.[39] The prooxidant effect of FFA in emulsions and bulk oils is thought to be due to their ability to increase the prooxidant activity of metals and decompose lipid hydroperoxides. The shorter lipid hydroperoxide and hexanal lag phases of the cracker treatments containing 2.0 and 3.0% FFA suggests that, at great enough concentrations, the FFA may help solubilize metal, thereby increasing its accessibility to the lipid (Figure 6). This could also help explain why the FFAs had a greater effect on hexanal formation than hydroperoxide since the increased reactivity of iron would accelerate lipid hydroperoxide decomposition, which in turn would form hexanal.

The research in this study presented a systematic investigation of some of the factors influencing lipid oxidation in low-moisture foods. Ultimately, it was found that low-moisture foods differ in numerous ways from bulk oils and emulsions. From a microstructure standpoint, it was observed that lipid formed a continuous phase around the starch granules versus being dispersed as lipid droplets. The lag phases between lipid hydroperoxides and hexanal differed markedly—on the order of at least 20 d—whereas these lag phases tend to be similar in most other food systems. The lack of strong prooxidant activity of added iron and FFA, in addition to the low antioxidant activity of chelators, also suggested that transition metals are not a major prooxidant in the low-moisture crackers compared to meats, oil-in-water emulsions, and bulk oils. The limited diffusion of metals in the low-moisture system likely explains why they are not strong prooxidants even though the cracker had metal levels that would be strongly prooxidative in other food systems. This research suggests that free radical scavengers could be the best option for stabilizing lipids in low-moisture crackers.

AUTHOR INFORMATION

Corresponding Author

*Tel.: +1 (413) 545 2276. Fax: +1 (413) 545 1262. E-mail: edecker@foodsci.umass.edu.

Funding

This work was supported by a United States Department of Agriculture National Institute of Food and Agriculture (USDA NIFA) National Needs grant.

Notes

The authors declare no competing financial interest.

ABBREVIATIONS

DFO, desferrioxamine; EDTA, ethylenediaminetetraacetic acid; FFA, free fatty acid(s); ISO, interesterfied soybean oil

REFERENCES

(1) Labuza, T. P.; Tannenbaum, S. R.; Karel, M. Water content and stability of low-moisture and intermediate-moisture foods. *Food Technol.* **1970**, *24*, 543−544 546−548, 550..

(2) National Cancer Institute. Top food sources of saturated fat among U.S. population, 2005−2006 NHANES. 2010, http://appliedresearch.cancer.gov/diet/foodsources/sat_fat/sf.html, (accessed Nov. 2013).

(3) National Cancer Institute. Mean intake of solid fats and percentage contribution (kcal) of various foods among U.S. children and adolescents, by age, NHANES 2003−04. 2010. http://appliedresearch.cancer.gov/diet/foodsources/solid_fats/table2a.html (accessed Nov. 2013).

(4) Holman, R. T.; Elmer, O. C. The rates of oxidation of unsaturated fatty acids and esters. *J. Am. Oil Chem. Soc.* **1947**, *24*, 127−129.

(5) Buttery, R. G.; Hendel, C. E.; Boggs, M. M. Off-flavors in potato products. Autoxidation of potato granules. *J. Agric. Food Chem.* **1961**, *9*, 245−252.

(6) Labuza, T. P.; McNally, L.; Gallagher, D.; Hawkes, J.; Hurtado, F. Stability of intermediate moisture foods. 1. Lipid oxidation. *J. Food Sci.* **1972**, *37*, 154−159.

(7) Chou, H.; Acott, K. M.; Labuza, T. P. Sorption hysteresis and chemical reactivity: Lipid oxidation. *J. Food Sci.* **1973**, *38*, 316−319.

(8) Harnkarnsujarit, N.; Charoenrein, S.; Roos, Y. H. Porosity and water activity effects on stability of crystalline β-carotene in freeze-dried solids. *J. Food Sci.* **2012**, *77*, E313−E320.

(9) Lavelli, V.; Kerr, W.; Sri Harsha, P. S. C. Phytochemical stability in dried tomato pulp and peel as affected by moisture properties. *J. Agric. Food Chem.* **2013**, *61*, 700−707.

(10) Sacchetti, G.; Neri, L.; Laghi, L.; Capozzi, F.; Mastrocola, D.; Pittia, P. Multidisciplinary approach to study the effect of water status and mobility on the activity of peroxidase in solutions. *Food Chem.* **2014**, *144*, 36−43.

(11) McClements, D. J.; Decker, E. A. Lipids. In *Fennema's Food Chemistry*, 4th ed.; Damodaran, S., Parkin, K. L., and Fennema, O. R., Eds.; CRC Press/Taylor & Francis: Boca Raton, 2008; pp 155−216.

(12) Barden, L.; Decker, E. A. Lipid oxidation in low-moisture food: A review. *Crit. Rev. Food Sci. Nutr.* **2013**, DOI: 10.1080/10408398.2013.848833.

(13) Matalanis, A.; McClements, D. J. Impact of encapsulation within hydrogel microspheres on lipid digestion: An in vitro study. *Food Biophys.* **2012**, *7*, 145−154.

(14) Decagon Devices, Inc. AquaLab water activity meter operator's manual, v6; 2009. http://manuals.decagon.com/Manuals/Discontinued/10607_AquaLab%20Series%203%20and%203TE_Web.pdf (accessed April 2011).

(15) A&D Weighing. Moisture Analyzer MX-50/MF-50 Users' Handbook, v2.20; 2003. http://www.scalenet.com/pdf/moisture-balance.pdf (accessed April 2011).

(16) Shantha, N. C.; Decker, E. A. Rapid, sensitive, iron-based spectrophotometric methods for determination of peroxide values of food lipids. *J. Am. Oil Chem. Soc. Int.* **1994**, *77*, 421−424.

(17) Panya, A.; Laguerre, M.; Bayrasy, C.; Lecomte, J.; Villeneuve, P.; McClements, D. J.; Decker, E. A. An investigation of the versatile antioxidant mechanisms of action of rosmarinate alkyl esters in oil-in-water emulsions. *J. Agric. Food Chem.* **2012**, *60*, 2692−2700.

(18) Wilson, J. D.; Bechtel, D. B.; Todd, T. C.; Seib, P. A. Measurement of wheat starch granule size distribution using image analysis and laser diffraction technology. *Cereal Chem.* **2006**, *83*, 259−268.

(19) Slade, L.; Levine, H. Structure−function relationships of cookie and cracker ingredients. In *The Science of Cookie and Cracker Production*; Faridi, H., Ed.; Chapman & Hall: New York, 1994; pp 24−141.

(20) Kweon, M.; Slade, L.; Levine, H.; Gannon, D. Cookie-versus cracker-baking—What's the difference? Flour functionality requirements explored by SRC and alveography. *Crit. Rev. Food Sci. Nutr.* **2014**, *54*, 115−138.

(21) Chaiyasit, W.; Stanley, C. B.; Strey, H. H.; McClements, D. J.; Decker, E. A. Impact of surface active compounds on iron catalyzed oxidation of methyl linolenate in AOT−water−hexadecane systems. *Food Biophys.* **2007**, *2*, 57−66.

(22) Anandaraman, S.; Reineccius, G. A. Stability of encapsulated orange peel oil. *Food Technol.* **1986**, *40*, 88−93.

(23) Kagami, Y.; Sugimura, S.; Fujishima, N.; Matsuda, K.; Kometani, T.; Matsumura, Y. Oxidative stability, structure, and physical

DOI: 10.1021/jf5048018
J. Agric. Food Chem. 2015, 63, 1812−1818

characteristics of microcapsules formed by spray drying of fish oil with protein and dextrin wall materials. *J. Food Sci.* **2003**, *68*, 2248−2255.
(24) Jimenez, M.; Garcia, H. S.; Beristain, C. I. Spray-dried encapsulation of conjugated linoleic acid (CLA) with polymeric matrices. *J. Sci. Food Agric.* **2006**, *86*, 2431−2437.
(25) Chaiyasit, W.; Elias, R. J.; McClements, D. J.; Decker, E. A. Role of physical structures in bulk oils on lipid oxidation. *Crit. Rev. Food Sci. Nutr.* **2007**, *47*, 299−317.
(26) Chen, B.; Han, A.; McClements, D. J.; Decker, E. A. Physical structures in soybean oil and their impact on lipid oxidation. *J. Agric. Food Chem.* **2010**, *58*, 11993−11999.
(27) Frankel, E.; Huang, S.; Prior, E.; Aeschbach, R. Evaluation of antioxidant activity of rosemary extracts, carnosol, and carnosic acid in bulk vegetable oils and fish oil and their emulsions. *J. Sci. Food Agric.* **1996**, *72*, 201−208.
(28) Pignoli, G.; Bou, R.; Rodriguez-Estrada, M. T.; Decker, E. A. Suitability of saturated aldehydes as lipid oxidation markers in washed turkey meat. *Meat Sci.* **2009**, *83*, 412−416.
(29) McKevith, B. Briefing paper: Nutritional aspects of cereals. *Nutr. Bull.* **2004**, *29*, 111−142.
(30) Taylor, A. J. Effect of water quality on lipid oxidation. *Food Sci. Technol. Today* **1987**, *1*, 158−159.
(31) USDA (United States Department of Agriculture) Agricultural Research Service National Agricultural Library. Basic Report: 20081, wheat flour, white, all-purpose, enriched, bleached; 2011. http://ndb.nal.usda.gov (accessed Jan. 2014).
(32) Alam, S. *Int. J. Food Sci. Nutr.* **2007**, *58*, 54−62.
(33) Mancuso, J. R.; McClements, D. J.; Decker, E. A. The effects of surfactant type, pH, and chelators on the oxidation of salmon oil-in-water emulsions. *J. Ag. Food Chem.* **1999**, *47*, 4112−4116.
(34) Chen, B.; Panya, A.; McClements, D. J.; Decker, E. A. New insights into the role of iron in the promotion of lipid oxidation in bulk oils containing reverse micelles. *J. Agric. Food Chem.* **2012**, *60*, 3524−3532.
(35) Miyashita, K.; Takagi, T. Study on the oxidative rate and prooxidant activity of free fatty acids. *J. Am. Oil Chem. Soc.* **1986**, *63*, 1380−1384.
(36) Waraho, T.; Cardenia, V.; Rodriguez-Estrada, M. T.; Mcclements, D. J.; Decker, E. A. Prooxidant mechanisms of free fatty acids in stripped soybean oil-in-water emulsions. *J. Ag. Food Chem.* **2009**, *57*, 7112−7117.
(37) Gomes, T.; Caponio, F.; Bruno, G.; Summo, C.; Paradiso, V. M. Effects of monoacylglycerols on the oxidative stability of olive oil. *J. Sci. Food Agric.* **2010**, *90*, 2228−2232.
(38) Waraho, T.; McClements, D. J.; Decker, E. A. Impact of free fatty acid concentration and structure on lipid oxidation in oil-in-water emulsions. *Food Chem.* **2011**, *129*, 854−859.
(39) Yi, J.; Zhu, Z.; Dong, W.; McClements, D. J.; Decker, E. A. Influence of free fatty acids on oxidative stability in water-in-walnut oil emulsions. *Eur. J. Lipid Sci. Technol.* **2013**, *115*, 1013−1020.

DOI: 10.1021/jf5048018
J. Agric. Food Chem. 2015, 63, 1812−1818

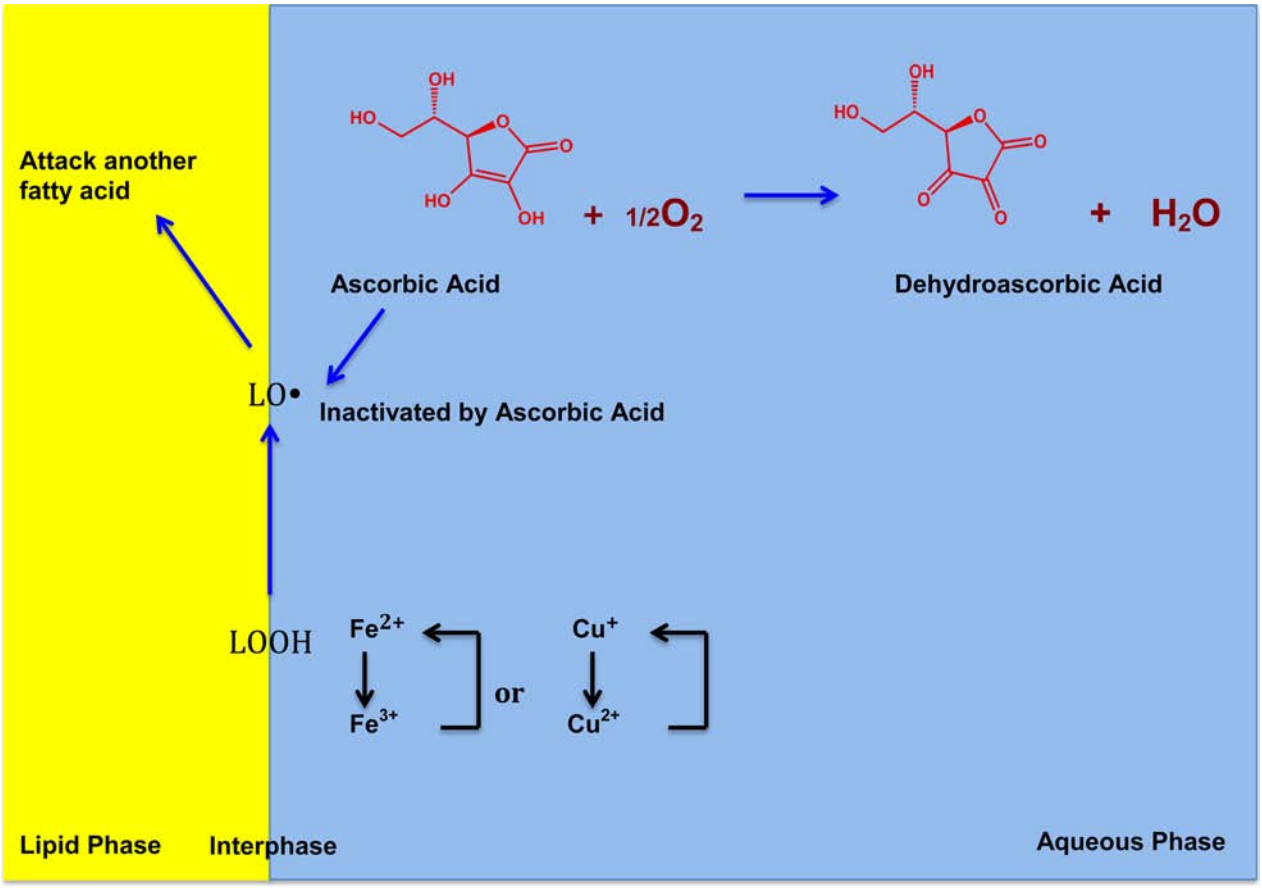

Figure 1. Potential reaction schemes for AA in an emulsion system.

lipid oxidation in food systems. These studies are important because AA can act as both an antioxidant and a prooxidant.

Oil-in-water (O/W) emulsions, such as salad dressing, beverages, and mayonnaise, are very susceptible to oxidative deterioration[24] and represent a food where AA could be added immediately prior to packaging to reduce oxygen concentrations. Therefore, the aim of this study was to investigate the conditions of oxygen reduction by AA in both a buffer system and O/W emulsions. Factors, such as AA concentrations, temperature, and presence of metals, were tested to determine optimum conditions for oxygen reduction. The ability of AA to both decrease oxygen concentrations and inhibit lipid oxidation was determined in O/W emulsions by determining lipid hydroperoxides and headspace hexanal.

MATERIALS AND METHODS

Chemicals and Materials. Soybean oil was purchased from a local grocer (Amherst, MA). Medium-chain triacylglycerols (MCTs, Miglyol) were obtained from Sasol North America, Inc. (Houston, TX). The fluorescent dye tris(4,7-diphenyl-1,10-phenanthroline) ruthenium(II) bis(hexafluorophosphate) complex was purchased from Santa Cruz Biotechnology, Inc. (Santa Cruz, CA). AA was purchased from Sigma-Aldrich (St. Louis, MO). All other reagents were of analytical or chromatographic grade.

Emulsion Preparation. The current study used two types of O/W emulsions. First, O/W emulsions were prepared using 1.0 wt % MCT in a 10 mM sodium acetate/imidazole buffer solution (pH 3.0 and 7) to produce emulsions that did not have oxidizable fatty acids. Tween 20 was used as an emulsifier at a 1:10 emulsifier/oil ratio. MCT, Tween 20, and sodium acetate/imidazole were added to a beaker, and a coarse emulsion was made by blending with a hand-held homogenizer (M133/1281-0, Biospec Products, Inc., Bartlesville, OK) for 2 min. The coarse emulsion was then homogenized with a microfluidizer (Microfluidics, Newton, MA) at a pressure of 9 kbar for three passes. The MCT O/W emulsion system was used for headspace oxygen analysis, and AA was added to the O/W emulsions at a final concentration ranging from 0.01 to 200 mM.

To represent a more realistic food matrix with oxidizable fatty acids, O/W emulsions were prepared using 1.0 wt % commercial soybean oil in 10 mM sodium acetate/imidazole (pH 4.0). Tween 20 was used as an emulsifier at a 1:10 emulsifier/oil ratio. Emulsion preparation was carried out as previously mentioned. The soybean oil O/W system was used to determine lipid oxidation products, and AA was added to the O/W emulsions at a final concentration ranging from 2.5 to 20 mM.

Measurement of the Particle Size of Emulsion. The sizes of the emulsion droplets were measured by dynamic light scattering (Zetasizer Nano-ZS, model ZEN3600, Malvern Instruments, Worchester, U.K.). Results were expressed as the *Z*-average mean diameter. Samples were diluted 50 times with the same buffer as the emulsion, mixed, and immediately measured by transferring the samples into 3 mL plastic cuvettes to determine the size. Measurements were performed on three replicates for each sample at room temperature. The emulsion droplet size averaged 174.1 ± 0.55 nm, and there was no significant change in the droplet size of each emulsion over the course of study (data not shown). In addition, there was no visual observation of creaming during storage in all treatments.

Headspace and Dissolved Oxygen (DO) Analysis. To measure headspace oxygen, the MCT O/W emulsion was first mixed with AA solution (final concentration of 0.01−200 mM) and the final emulsion (5 mL) was transferred to 10 mL of gas chromatography (GC) vials, sealed with (tetrafluoroethylene) butyl rubber septa, and then stored at 10, 20, 32, 37, and 45 °C in the dark. Headspace oxygen was determined using a headspace O_2/CO_2 anaylzer (Benchtop 902D Dualtark, U.S.A.).

DOI: 10.1021/jf5053942
J. Agric. Food Chem. 2015, 63, 1819−1824

The fluorescent dye, tris(4,7-diphenyl-1,10-phenanthroline) ruthenium(II) bis(hexafluorophosphate) complex, was used to determine DO in the buffer and O/W emulsion system using a $\lambda_{excitation}$ = 455 nm and a $\lambda_{emission}$ = 615 nm. Fluorescence intensity of the dye increased with a decrease in the oxygen concentration. A stock dye solution was prepared by dissolving 1 mg of the dye in 1 mL of methanol. This stock solution was then added to buffer and soybean oil O/W emulsions to achieve a final dye concentration of 50 μg/g in oil.[25] The samples were mixed with AA (0.01−200 mM final concentration in the solution), and the final samples (2 mL) were transferred to 10 mL GC vials, sealed with (tetrafluoroethylene) butyl rubber septa, and stored at 55 °C in the dark. Three vials of each treatment were sampled at each day of analysis. Standard fluorescence was used in the buffer model. Front-face fluorescence was used to measure DO in the O/W emulsion using steady-state measurements recorded with a PTI spectrofluorometer (PTI, London, Ontario, Canada). Spectral bandwidth for both excitation and emission slits was 2.0 nm; integration time was 30 s; and wavelength increment was 2.5 nm. Quantification of DO was calculated according the Stern−Volmer equation.[26]

Effect of Transition Metals on AA Degradation in Buffer. The ability of transition metals (e.g., copper and iron) to impact the ability of AA to reduce the DO concentration was determined in an acetic acid/imidazole buffer system (10 mM, pH 3). $FeSO_4$ and CuCl solutions were added to the buffer (final concentration of 2.5 or 10 μM) followed by the addition of AA (75 mM final concentration). The final solution (7 mL) was transferred to 10 mL GC vials, sealed with (tetrafluoroethylene) butyl rubber septa, and stored at 32 °C in the dark. Three vials of each treatment were analyzed for DO at each sampling time. Results were expressed as mean values ± standard deviation.

Determination of AA Degradation. Quantification of AA was determined directly in the buffer system or in the aqueous phase of the emulsion. The aqueous phase of the emulsified system was obtained by centrifuging at 38518*g* (17 000 rpm) for 1 h at 4 °C using a Fiberlite F40L-8 × 100 rotor with a high-speed centrifuge (Thermo Scientific WX Ultra 80, Asheville, NC). After the centrifugation, the lower aqueous phase was carefully removed using a syringe.

AA was analyzed according the method described by Acar et al., with minor modifications.[27] Briefly, 2,6-dichlorofenolindophenol (approximately 15 mg) was dissolved in double-distilled water until the absorbance was 0.800 ± 0.020 at 520 nm. Samples were diluted (1:100) with oxalic acid solution (0.04%, w/v) and mixed with the 2,6-dichlorofenolindophenol solution (1:100). The subsequent reaction results in non-oxidized AA reducing the indicator dye to a colorless compound. The absorbance was detected at 520 nm after vortexing for 10 s using an ultraviolet−visible (UV−vis) spectrophotometer (Genesys 20, Thermo Spectronic). AA concentrations were calculated from a standard curve prepared with reagent-grade AA. Results were expressed as mean values ± standard deviation.

Measurements of Lipid Oxidation Products. Lipid hydroperoxides and hexanal were measured as primary and secondary lipid oxidation products, respectively. Lipid hydroperoxide formation in emulsion samples was determined according to the method by Shantha and Decker.[28] Emulsion samples (0.3 mL) were mixed with 1.5 mL of isooctane/2-propanol solution (3:1, v/v) and vortexed (10 s, 3 times). The mixed solution was centrifuged at 3400*g* for 10 min (Centrific Centrifuge, Thermo Fisher Scientific, Inc., Fairlawn, NJ). The upper organic layer (200 μL) was mixed with 2.8 mL of methanol/butanol solution (2:1, v/v), followed by the addition of 15 μL of 3.94 M ammonium thiocyanate and 15 μL of Fe^{2+} solution. The Fe^{2+} solution was prepared freshly from the supernatant of a mixture of equal amounts of 0.132 M $BaCl_2$ in 0.4 M HCl and 0.144 M $FeSO_4$. The solution was vortexed and held 20 min at room temperature, and the absorbance was measured at 510 nm in a UV−vis spectrophotometer (Genesys 20, Thermo Fisher Scientific, Inc., Waltham, MA). Hydroperoxide concentrations were determined using a standard curve prepared from cumene hydroperoxide.

Headspace hexanal was measured according to the method described by Panya et al.[29] using a gas chromatograph (model GC-2014, Shimadzu Co., Tokyo, Japan) equipped with a solid-phase microextraction (SPME) auto injector (model AOC-5000, Shimadzu Co., Tokyo, Japan). Emulsions (1 mL) in 10 mL glass vials capped with aluminum caps with polytetrafluoroethylene (PTFE)/silicone septa were heated at 55 °C for 10 min in the autosampler heating sampler heating block before measurement. A 50/3 μm divinylbenzene (DVB)/carboxen/polydimethylsiloxane (PDMS) stable flex (SPME) fiber (Supelco Co., Bellefonte, PA) was then inserted into the vial headspace for 2 min to absorb volatiles. The fiber was transferred to the GC injector port (250 °C) for 3 min. The injection port was operated in split mode, and the split ratio was set at 1:7. Volatiles were separated on a fused-silica capillary Equity-1 Supelco column (30 × 0.32 mm inner diameter × μm) coated with 100% PDMS at 65 °C for 10 min. A flame ionization detector was used at a temperature of 250 °C. Hexanal concentrations were determined from peak areas using a standard curve made from authentic hexanal. Each measurement was performed in triplicate, and results were expressed as mean values ± standard deviation.

Statistical Analysis. All data result were analyzed by analysis of variance (ANOVA) using SPSS 20 (SPSS, Inc., Chicago, IL). The differences between mean values were compared using Duncan's multiple-range test with a level of significance of $p \leq 0.05$.

RESULTS AND DISCUSSION

Headspace Oxygen Analysis. Headspace oxygen concentrations in MCT O/W emulsions (pH 3 and 7) were only slightly decreased (<1%; data not shown) in the absence and presence of AA (0.01−200 mM), regardless of incubation temperature (10, 20, 32, 37, and 45 °C). In this closed O/W emulsion system, AA is located in aqueous phase and headspace oxygen exists above the emulsion. The AA and headspace oxygen reaction can be only occur at the limited surface area that exist between the emulsion and the headspace gas. Therefore, to obtain a decrease in headspace oxygen, DO concentrations would first have to be reduced and then headspace oxygen would have to diffuse into the emulsion. This observation is consistent with a previous report that showed headspace oxygen depletion by ascorbate occurred slowly.[30,31] While a small decrease in headspace oxygen may not seem significant, other reports suggested that reducing headspace oxygen by even a small percentage can lead to increased protection against lipid oxidation.[30,31] This is likely due to the fact that a large decrease in DO is needed to obtain a small decrease in headspace oxygen. Because of the lack of sensitivity of headspace oxygen, all further studies were performed using DO.

Effect of Transition Metals on AA Degradation and DO Concentrations. Copper and iron are common transition metals in food systems. These metals pose a serious threat to the oxidative stability of foods because they can accelerate lipid oxidation reactions.[2,31] However, transition metals have also been suggested to increase the ability of AA to decrease DO, meaning that they could allow AA to rapidly create an anaerobic environment in a food system.[32] Thus, it is important to determine the effect of metals on both AA degradation and DO depletion. Decreasing DO was determined in the buffer system, containing Fe^{2+} and Cu^{+} ions (2.5 and 10 μM) at pH 3 (Figure 2). The DO concentration in the presence of AA alone (75 mM) decreased quickly until day 10 as concentrations approached 0. Iron and copper only increased DO depletion rates, by 10.6−16.4% from day 1 to 7, with little difference in DO depletion occurring as a function of the metal concentration. These percentages are calculated in comparison to the control. By day 10, there was no statistical difference in DO among all samples.

DOI: 10.1021/jf5053942
J. Agric. Food Chem. 2015, 63, 1819−1824

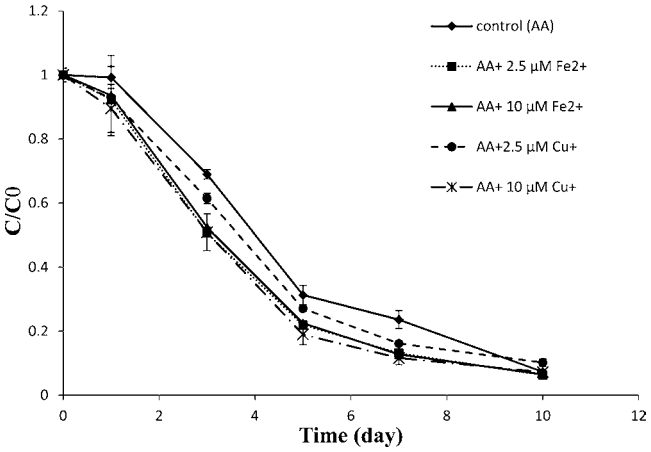

Figure 2. Reduction of dissolved O_2 by 75 mM AA in the presence and absence of Fe^{2+} and Cu^{+} (2.5 or 10 μM) in an acetic acid/imidazole buffer system (pH 3) during the storage at 32 °C. Data points and error bars represent means (n = 3) ± standard deviations.

Degradation of AA in the presence or absence of Fe^{2+} and Cu^{+} results is shown Figure 3. Both metals increased AA

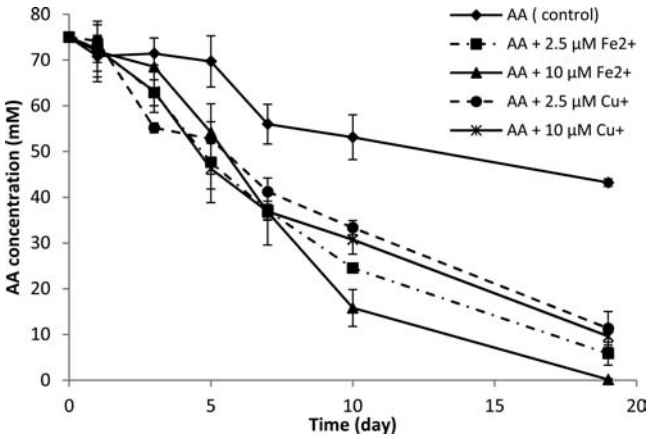

Figure 3. Degradation of AA by 75 mM AA in the presence and absence of Fe^{2+} and Cu^{+} (2.5 or 10 μM) in an acetic acid/imidazole buffer system (pH 3) during the storage at 32 °C. Data points and error bars represent means (n = 3) ± standard deviations.

degradation reactions compared to the control. After day 10, degradation of ascorbate was greatest in the presence of 10 μM iron. AA degradation rates were similar for both copper concentrations. Degradation of AA continued after day 10, even though DO was almost completely removed from the buffer (Figure 2). Previous studies suggested that anaerobic degradation of AA occurs at a much slower rate than the aerobic AA degradation at pH 2;[32] this condition was observed in the present study, because the rate of AA degradation was much higher in an aerobic environment than under an anaerobic environment. Copper has been reported by others[30] to degrade AA more rapidly than iron at pH 7. Lack of differences between iron and copper in this study could be due to the lower pH (3.0).

Effect of AA on DO and Lipid Oxidation in an O/W Emulsion. The ability of AA to both scavenge oxidation and inhibit lipid oxidation was determined in an O/W emulsion containing AA at varying concentrations to produce emulsions with reduced oxidation as well as low or high residual AA concentrations after DO depletion was complete. Lipid oxidation was monitored with lipid hydroperoxide and headspace hexanal in a soybean O/W emulsion at 55 °C. Degradation of AA and decreases in DO were also determined to evaluate the impact of AA and oxygen concentration on lipid oxidation kinetics.

Decreasing DO concentrations are shown at Figure 4, and degradation of AA results are shown at Figure 5. We again

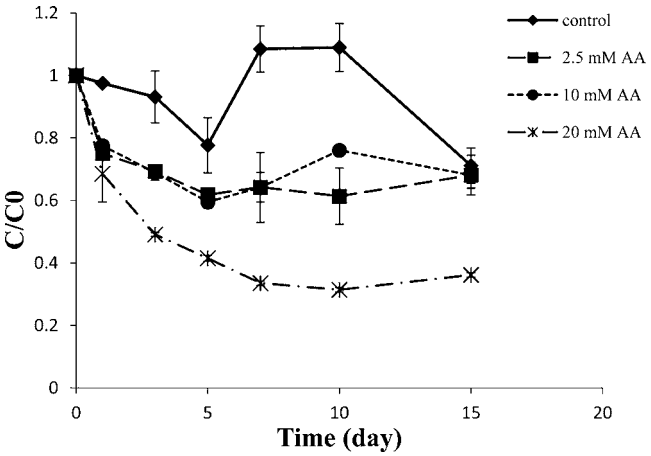

Figure 4. Reduction of dissolved O_2 in 1% soybean oil/Tween 20 emulsions (pH 4.0) at 55 °C in the presence of different concentrations of AA (2.5−20 mM). Data points and error bars represent means (n = 3) ± standard deviations.

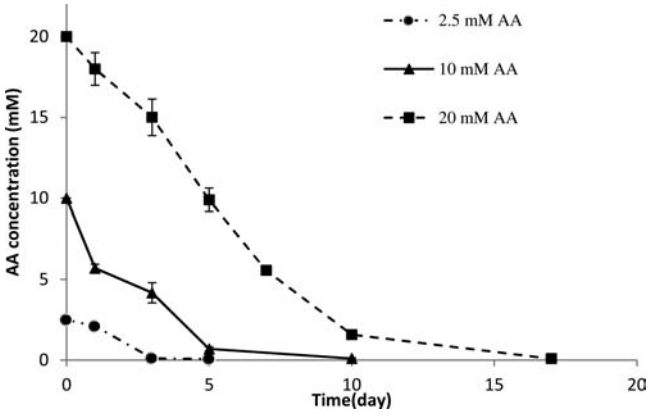

Figure 5. Degradation of AA in 1% soybean oil/Tween 20 emulsions (pH 4.0) at 55 °C in the presence of different concentrations of AA (2.5−20 mM). Data points and error bars represent means (n = 3) ± standard deviations.

attempted to increase the rate of DO removal with iron, but this was not effective (data not shown), which is similar to our observations in the buffer system. Both 2.5 and 10 mM AA decreased DO 32.0% after 5 days of storage, with no further decreases afterward. Decreasing the DO rate in the O/W emulsion system containing 20 mM AA was greatest with a maximal DO reduction of 64.0% after 10 days of storage. Samples with 2.5 and 10 mM exhibited a slight increase in DO after AA was depleted. This is likely due to diffusion of oxygen into the emulsion from the headspace and because there was no AA remaining to consume the oxygen. The lowest concentrations of AA were observed in the presence of 2.5, 10, and 20 mM AA after 3, 5, and 17 days, respectively. This was similar to

DOI: 10.1021/jf5053942
J. Agric. Food Chem. 2015, 63, 1819−1824

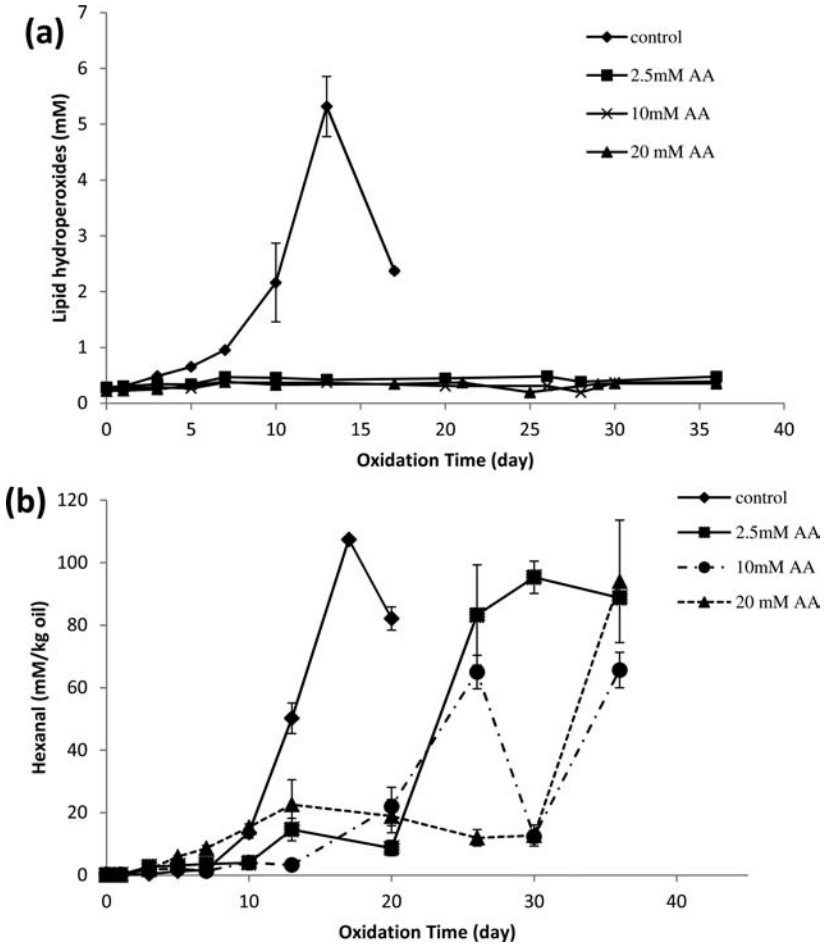

Figure 6. (a) Lipid hydroperoxide and (b) hexanal in 1% soybean oil/Tween 20 emulsions (pH 4.0) at 55 °C in the presence of different concentrations of AA. Data points and error bars represent means (n = 3) ± standard deviations.

the time to reach the lowest DO concentrations, suggesting that, once AA was consumed, no further reduction in DO was observed. Degradation of AA in an O/W emulsion system was faster than that in a buffer system (Figure 3). This could be due to AA degradation from both interactions with oxygen as well as free radicals generated by oxidizing lipids. DO depletion was also less than the buffer system (Figure 2), which can be explained by the more rapid loss of AA, which would result in lower amounts of AA being available for oxygen scavenging.

The formation of lipid hydroperoxides did not increase for any of the samples with AA (Figure 6a). This could be due to AA causing redox cycling of metals, making the metals more reactive. The reduced metals could then decompose hydroperoxides into secondary oxidation products, such as hexanal, faster than their formation, thus preventing their accumulation. A lack of hydroperoxide accumulation with the formation of secondary aldehydes has also been observed in sodium dodecyl sulfate-stabilized O/W emulsion at pH 3.0, where iron was added as a prooxidant.[33] The lack of hydroperoxide accumulation with the formation of secondary aldehydes has also been observed in a Tween-20-stabilized O/W emulsion at pH 3.0.[34] The lag phase for hydroperoxide formation in the control was 3 days, while the lag phase for hexanal formation was 7 days. It is not uncommon for aldehyde formation to occur later than hydroperoxide formation because the aldehydes are formed from the decomposition of the hydroperoxides.[35] The lag phase for hexanal formation was similar for 2.5 and 10 mM AA (20 days). This is somewhat surprising because residual AA in the emulsions with 10 mM AA was higher than samples with 2.5 mM AA during the first 5 days of storage. However, both 2.5 and 10 mM AA produced similar levels of DO reduction, suggesting that the observed inhibition could be due to the reduction of oxygen levels more than the ability of AA to scavenge free radicals. AA at 20 mM resulted in a hexanal lag phase of 26 days, which is only 1.3-fold longer than the 2.5 and 10 mM AA samples (Figure 6b). One might have expected that 20 mM AA would have been a more effective antioxidant because residual AA was observed in the emulsions for a much longer period of time and oxygen reduction was almost double that of the 2.5 and 10 mM samples. It could be possible that the unexpectedly low activity of 20 mM AA could be due to the ability of AA to act also as an prooxidant by reducing transition metals, and this prooxidant activity would decrease the effectiveness of its free radical scavenging and oxygen reduction.

In conclusion, AA can act as an edible oxygen scavenger, but its ability to reduce oxygen concentrations is less in O/W emulsions than a simple buffer system, which is likely to be due to the consumption of AA by both oxygen and free radicals in the emulsion system. At 2.5 and 10 mM AA, the ability of AA to inhibit hexanal formation was similar, which suggested that the antioxidant activity of AA was primarily due to its ability to decrease DO. The ability of 20 mM AA to inhibit lipid oxidation was better than 2.5 and 10 mM AA, but the improved

DOI: 10.1021/jf5053942
J. Agric. Food Chem. 2015, 63, 1819−1824

activity was only 1.3-fold greater, even though the concentrations of AA were much higher and DO reduction was much greater than the lower AA concentrations. These data suggested that the dual prooxidant and antioxidant role of AA could be decreasing its ability to increase oxidative stability. Overall, AA could be used to inhibit lipid oxidation in foods because of its dual ability to decrease DO and scavenge free radicals. However, these antioxidative properties could be diminished by the prooxidative activity of AA, and thus, the activity of AA could possibly be improved by metal chelators, which would bind metals and decrease the prooxidant activity of AA.

AUTHOR INFORMATION

Corresponding Author

*Telephone: +1-413-835-1723. Fax: +1-413-545-1262. E-mail: sibeluluata@foodsci.umass.edu.

Funding

The authors thank the Turkish Government for providing financial support for Sibel Uluata. The authors also acknowledge the TUBITAK 2219-A Program for providing funding for Sibel Uluata.

Notes

The authors declare no competing financial interest.

ABBREVIATIONS USED

AA, ascorbic acid; DO, dissolved oxygen; MCT, medium-chain triacylglycerol

REFERENCES

(1) Reische, D. W.; Lillard, D. A.; Eitenmiller, R. R. Antioxidants. In *Food Lipids*, 3rd ed.; Akoh, C., Min, D. B., Eds.; CRS Press: London, U.K., 2008; pp 413−422.

(2) Halliwell, B.; Gutteridge, J. M. Role of free radicals and catalytic metal ions in human disease: An overview. *Methods Enzymol.* **1990**, *186*, 1861−1885.

(3) Davey, M. W.; Montagu, M. V.; Inzé, D.; Sanmartin, M.; Kanellis, A.; Smirnoff, N.; Benzie, I. J.; Strain, J. J.; Favell, D.; Fletcher, J. Plant L-ascorbic acid: Chemistry, function, metabolism, bioavailability and effects of processing. *J. Sci. Food Agric.* **2000**, *80*, 825−860.

(4) Eitenmiller, R. R.; Landen, W. O., Jr. Vitamins. In *Analyzing Food for Nutrition Labeling and Hazardous Contaminants*; Jeon, I. J., Ikins, W. G., Eds.; Marcel Dekker: New York, 1995; p 195.

(5) Johnson, L. E. Food technology of the antioxidant nutrients. *Crit. Rev. Food Sci. Nutr.* **1995**, *35*, 149.

(6) Schuler, P. Natural antioxidants exploited commercially. In *Food Antioxidants*; Hudson, B. J. F., Eds.; Elsevier Applied Science: New York, 1990; p 99.

(7) Liao, M. L.; Seib, P. A. Chemistry of L-ascorbic acid related to foods. *Food Chem.* **1998**, 289−312.

(8) Charles, D. J. Natural antioxidants. *Antioxidant Properties of Spices, Herbs and Other Sources*; Springer: New York, 2013; p 59.

(9) Chaiyasit, W.; Elias, R. J.; McClements, D. J.; Decker, E. A. Role of physical structures in bulk oils on lipid oxidation. *Crit. Rev. Food Sci. Nutr.* **2007**, *47*, 299−317.

(10) Kolakowska, A.; Sikorski, Z. E. The role of lipids in food quality, *Chemical and Functional Properties of Food Lipids*; CRC Press: Boca Raton, FL, 2003; pp 1−8.

(11) Niki, E. Action of ascorbic acid as a scavenger of active and stable oxygen radicals. *Am. J. Clin. Nutr.* **1991**, *54*, 1119S−1124S.

(12) Nawar, W. W. Antioxidants. In *Food Chemistry*; Fennema, O. R., Eds.; Marcel Dekker: New York, 1996; p 199.

(13) Cort, W. M. Antioxidant properties of ascorbic acid in foods. In *Ascorbic Acid: Chemistry, Metabolism, and Uses*; Seib, P. A., Tolbert, B. M., Eds.; American Chemical Society (ACS): Washington, D.C., 1982; Advances in Chemistry, Vol. *200*, Chapter 22, pp 532−584.

(14) Alamed, J.; Chaiyasit, W.; McClements, D. J.; Decker, E. A. Relationships between free radical scavenging and antioxidant activity in foods. *J. Agric. Food Chem.* **2009**, *57*, 2969−76.

(15) Cort, W. M. Antioxidant activity of tocopherols, ascorbyl palmitate, and ascorbic acid and their mode of action. *J. Am. Oil Chem. Soc.* **1974**, 321−325.

(16) Sun, Y.; Wang, W.; Chen, H.; Li, C. Autoxidation of unsaturated lipids in food emulsion. *Crit. Rev. Food Sci. Nutr.* **2011**, *51*, 453−466.

(17) Erickson, M. C. Lipid oxidation of muscle foods. In *Food Lipids*, 2rd ed.; Akoh, C., Min, D. B., Eds.; Marcel Dekker: New York, 2002; p 381.

(18) McClements, D. J.; Decker, E. A. Lipids. In *Fennema's Food Chemistry*; Damodaran, S., Parkin, K., Fennema, O., Eds.; CRC Press: Boca Raton, FL, 2008; pp 155−216.

(19) Cruz, R. S.; Camilloto, G. P.; Dos Santos Pires, A. C. Oxygen scavengers: An approach on food preservation. In *Structure and Function of Engineering*; Eissa, A. A., Ed.; InTech: New York, 2012; pp 21−40.

(20) Cruz, R. S.; Soares, N. F. F.; Andrade, N. J. Efficiency of oxygen: Absorbing sachets in different relative humidities and temperatures. *Cienc. Agrotecnol.* **2007**, *31*, 1800−1804.

(21) Tian, F.; Decker, E. A.; Goddard, J. M. Controlling lipid oxidation of food by active packaging technologies. *Rev. Food Funct.* **2013**, *4*, 669−680.

(22) Charles, F.; Sanchez, J.; Gontard, N. Absorption kinetics of oxygen and carbon dioxide scavengers as part of active modified atmosphere packaging. *J. Food Eng.* **2006**, *72*, 1−7.

(23) Byun, Y.; Darby, D.; Cooksey, K.; Dawson, P.; Whiteside, S. Development of oxygen scavenging system containing a natural free radical scavenger and a transition metal. *Food Chem.* **2011**, *124*, 615−619.

(24) Waraho, T.; McClements, D. J.; Decker, E. A. Mechanisms of lipid oxidation in food dispersions. *Rev. Trends Food Sci. Technol.* **2011**, *22*, 3−13.

(25) Tikekar, R. V.; Johnson, A.; Nitin, N. Real-time measurement of oxygen transport across an oil−water emulsion interface. *J. Food Eng.* **2011**, *103*, 14−20.

(26) Watkins, A. N.; Wenner, B. R.; Jordan, J. D.; Xu, W. Y.; Demas, J. N.; Bright, F. V. Portable, low-cost, solid-state luminescence-based O_2 sensor. *Appl. Spectrosc.* **1998**, *52* (5), 750−754.

(27) Acar, J.; Alper, N.; Gökmen, V. *Fruit and Vegetable Quality Control Laboratory Manual Technology*; Hacettepe University Engineering Press: Ankara, Turkey, 1997; pp 57−66.

(28) Shantha, N.; Decker, E. A. Rapid, sensitive, iron-based spectrophotometric methods for determination of peroxide values of food lipids. *J.—Assoc. Off. Anal. Chem.* **1994**, *77*, 412−424.

(29) Panya, A.; Laguerre, M.; Lecomte, J.; Villeneuve, P.; Weiss, J.; McClements, D. J.; Decker, E. A. Effects of chitosan and rosmarinate esters on the physical and oxidative stability of liposomes. *J. Agric. Food Chem.* **2010**, *58* (9), 5679−5684.

(30) Graf, E. Cooper(II) ascorbate: A novel food preservation system. *J. Agric. Food Chem.* **1994**, *42*, 1616−1619.

(31) Andersson, K.; Lingnert, H. Influence of oxygen and copper concentration. On lipid oxidation in rapeseed oil. *J. Am. Oil Chem. Soc.* **1998**, *75* (8), 1041−1046.

(32) Hulein, F. E.; Coggiola, I. M.; Sidhu, G. S.; Kennett, B. H. The anaerobic decomposition of ascorbic acid in the pH range of foods and in more acid solution. *J. Sci. Food Agric.* **1971**, *22*, 540−542.

(33) Mei, L.; McClements, D. J.; Wu, J.; Decker, E. A. Iron-catalyzed lipid oxidation in emulsion as affected by surfactant, pH and NaCl. *Food Chem.* **1998**, *61*, 307−312.

(34) Mancuso, J. R.; McClements, D. J.; Wu, J.; Decker, E. A. The effect of surfactant type, pH and chelators on the oxidation of salmon oil-in-water emulsion. *J. Agric. Food Chem.* **1999**, *47*, 4112−4116.

(35) Waraho, T.; Cardenia, V.; Nishino, Y.; Seneviratne, K. N.; Rodriguez-Estrada, M. T.; McClements, D. J.; Decker, E. A. Antioxidant effects of mono- and diacylglycerols in non-stripped and stripped soybean oil-in-water emulsions. *Food Res. Int.* **2012**, *48*, 353−358.

DOI: 10.1021/jf5053942
J. Agric. Food Chem. 2015, 63, 1819−1824

in over- or underestimation of gluten.[24] The gluten quantitation by ELISA can be further affected by thermal[25−27] and nonthermal[28−30] food processing conditions.

Since most ELISA methods use gliadin as a calibration standard, the calculated gluten content would be derived from the measured gliadin.[31,32] However, such quantitation may not give an accurate measure for other prolamins (secalin and hordein) and glutelins. Prolamins and glutelins differ in their proportions and molecular properties in wheat, rye and barley.[33,34] This will influence the availability of gluten epitopes, affecting antigen−antibody interaction in immunoassays and causing variability in gluten quantitation. Moreover, hydrolysis of gluten proteins may reduce the number of available epitopes leading to underestimation of gluten content. Hence, it is important to assess the contribution of prolamin and glutelin fractions and their hydrolysates to facilitate accurate gluten quantitation. So far, there is limited information available on the analysis of prolamins from rye and barley.[30] Furthermore, the quantitation of glutelin fractions from wheat, rye and barley is not well studied. The aim of this study was to assess the relative recovery of prolamin and glutelin fractions and their pepsin-trypsin (PT)-digests based on the gluten quantitation by various commercial ELISA kits.

MATERIALS AND METHODS

Materials. Pure grains of wheat, rye, barley, oats and corn were obtained from the Grain Inspection, Packers & Stockyards Administration (GIPSA), U.S. Department of Agriculture (USDA). Commercial gliadin (S1), wheat gluten (S2), casein (S3), pepsin and trypsin were from Sigma (St. Louis, MO). The sandwich ELISA kits used were RIDASCREEN Gliadin (R7001; R-Biopharm AG, Darmstadt, Germany), Wheat protein ELISA kit (gliadin) (181 GD; Morinaga Institute of Biological Science, Inc., Yokohama, Japan) and AgraQuant Gluten G12 (COKAL0200; Romer Labs UK Ltd., Cheshire, UK), whereas the competitive ELISA kits included RIDASCREEN Gliadin competitive (R7021; R-Biopharm AG, Darmstadt, Germany) and GlutenTox ELISA Competitive (KT-4758; Biomedal, Spain). BenchMark prestained protein ladder was purchased from Invitrogen (Grand Island, NY).

Methods. *Isolation of Gluten.* The grains of wheat, rye, barley, oats and corn were ground to flour and then independently subjected to Osborne fractionation as described by Tatham et al. (2000)[17] with minor modifications. Briefly, 100 g flour was suspended in 1000 mL 0.5 M NaCl and magnetically stirred for 1 h at room temperature (RT), followed by centrifugation at 5,000g for 10 min at 20 °C. The extraction was repeated again with the pellet by suspending in 0.5 M NaCl and the two supernatants (containing albumins and globulins) were pooled before dialyzing against distilled water for a total of 48 h with at least 6 water changes using an 8 kDa cutoff dialysis membrane. The globulins were separated by centrifuging at 10,000g for 15 min at 4 °C. Thereafter, all centrifugation steps were carried out at 5,000g for 10 min at 20 °C. The residual flour from NaCl extraction was washed with water for 10 min at RT followed by centrifugation. The washed residual flour was then resuspended twice in 1000 mL 70% ethanol (for oats, 50% ethanol) and magnetically stirred for 1 h at RT, followed by centrifugation. The pooled supernatant containing prolamins was precipitated overnight at 4 °C with 2 volumes of 1.5 M NaCl, centrifuged, resuspended the pellet in 100 mL 70% ethanol (for oats, 50% ethanol) and dialyzed against 0.1 M acetic acid for 48 h with at least 6 changes of 0.1 M acetic acid. Glutelins were finally extracted by resuspending the residual flour from ethanol extraction twice in 1000 mL 50% propan-1-ol containing 1% acetic acid and 2% β- mercaptoethanol for 1 h at RT, followed by centrifugation. The pooled supernatant was precipitated overnight at 4 °C with 2 volumes of 1.5 M NaCl, centrifuged, resuspended the pellet in 100 mL 50% propan-1-ol containing 1% acetic acid and 2% β- mercaptoethanol, followed by dialysis against 0.1 M acetic acid for 48 h with at least 6 changes of 0.1 M acetic acid. All the fractions were lyophilized and stored at −20 °C until further use. The protein content of all lyophilized fractions was analyzed by micro-Kjeldahl method (Micro-Analysis, Inc. Wilmington, DE) using the conversion factor of 5.83.

Pepsin-Trypsin (PT)-Digestion. Approximately 250 mg protein was dissolved in 2.5 mL pepsin solution (2 mg/mL prepared in 0.2 N HCl), followed by addition of 2.5 mL 0.2 N HCl. The enzyme to protein ratio was 1:50 (w/w). The tubes were incubated at 37 °C for 2 h in shaking water bath. The peptic digest was then adjusted to pH 7.4 with 2 M NaOH, followed by addition of 50 μL trypsin solution (100 mg/mL prepared in distilled water) to have an enzyme to protein ratio of 1:50 (w/w). The tubes were mixed and incubated at 37 °C for 4 h in shaking water bath. Thereafter, the tubes were transferred to a boiling water bath and incubated for 30 min to inactivate the enzymes. Appropriate controls (S1, Sigma gliadin; S2, Sigma gluten; S3, Sigma casein) were also used. Ten milligram aliquots of PT-digest were lyophilized and stored at −20 °C until further use.

Sodium Dodecyl Sulfate-Polyacrylamide Gel Electrophoresis (SDS-PAGE) and Western Blotting. Protein samples were boiled in 1x SDS-PAGE Laemmli sample buffer (Biorad, Hercules, CA) for 10 min, and suitable aliquots were loaded on large 1.5 mm thick 10−20% SDS-PAGE Tris-Glycine gel (Jule, Inc., Milford, CT). The gels were run at 50 mA current per gel for 1.5 h, and then reduced to 30 mA per gel until the dye reached the bottom edge of the gel. The gels were stained overnight with 0.25% w/v Coomassie Brilliant Blue R containing 50% v/v methanol and 10% v/v acetic acid. The gels were destained once with 50% v/v methanol containing 10% v/v acetic acid (destain buffer), followed by destaining buffer diluted with distilled water (∼1:1 v/v) until the background was clear.

For the Western blot analysis, the polypeptides were separated on 10−20% SDS-PAGE Tris-Glycine gels (Invitrogen, Grand Island, NY) by running at 100 V until the dye reached the bottom edge. The separated polypeptides were transferred to a polyvinylidene fluoride (PVDF) membrane at 0.4A current for 1.5−2 h at 8 °C. The transferred proteins were visualized by Ponceau S stain. The membrane was washed with Tris buffered saline containing 0.05% Tween 20 (TBS-T) to remove the stain and then blocked for 1 h at RT with 5% nonfat dried milk in TBS-T. The membrane was briefly washed with TBS-T and incubated with anti-gluten antibodies conjugated to horseradish peroxidase (HRP) overnight at 4 °C. The membrane was then washed thrice for 15 min each with TBS-T. The reactive bands on the membrane were developed on X-ray film using ECL substrate (Pierce).

Estimation of Gluten by Enzyme-Linked Immunosorbent Assay (ELISA). Both undigested and PT-digested prolamins and glutelins were quantified using sandwich and competitive ELISA kits as per the manufacturers' instructions. Briefly, lyophilized gluten fractions were dissolved in the extraction buffers of respective kits, and were used as stock solutions to prepare dilutions of appropriate protein content (10−100 ng/mL), based on calculated protein amounts analyzed by micro-Kjeldhal method. Appropriate controls (Sigma gliadin, S1; Sigma gluten, S2; Sigma casein, S3) were also used. The ELISA plates were read using a SpectraMax M5 microplate reader (Molecular Devices, Sunnyvale, CA). A four parameter standard curve was plotted using the SoftMax Pro 5.4 software, and was used to calculate the measured gluten/wheat protein. Further, the recovery was represented as a percent ratio of the measured gluten to the actual protein assayed. For all ELISAs, two samples of each protein fraction were analyzed in duplicate (n = 4), and the data were presented as mean ± standard error (SE).

RESULTS

Gluten Fractions and Their PT-Digests. The protein content of lyophilized prolamin and glutelin fractions from wheat, rye and barley were estimated by the micro-Kjeldahl method. Lower protein content was observed in oat (prolamin, 33% and glutelin, 59%) and corn (prolamin, 42% and glutelin, 64%) fractions as compared to wheat (prolamin, 68% and glutelin, 82%), rye (prolamin, 52% and glutelin, 71%) and

DOI: 10.1021/jf505716p
J. Agric. Food Chem. 2015, 63, 1825−1832

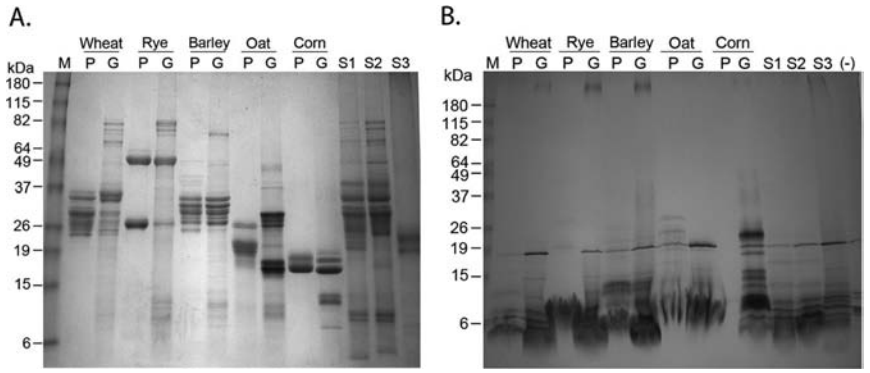

Figure 1. Coomassie stained SDS-PAGE gels of prolamin and glutelin fractions. Intact (A) and PT-digested (B) protein fractions. Protein load was 20 μg/lane for undigested and 50 μg/lane for PT-digested fractions. P, prolamin; G, glutelin; S1, gliadin; S2, gluten; S3, casein; M, MW marker; (−), pepsin-trypsin only.

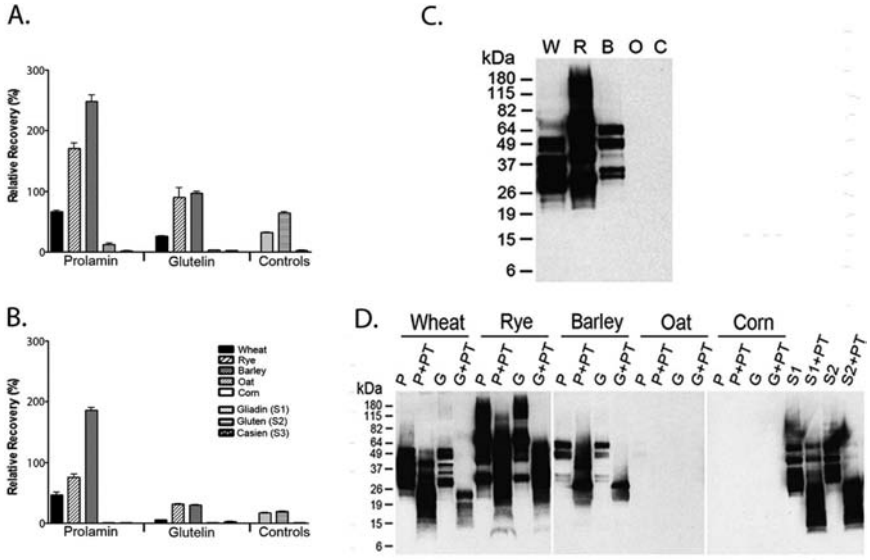

Figure 2. Analysis of gluten fractions and their PT-digests using the R-Biopharm sandwich ELISA kit and its antibodies. Recoveries of intact gluten fractions (A) and their PT-digests (B) in ELISA. Western blot analysis of flour proteins (C) and their gluten fractions (D) using the R-Biopharm kit antibodies. For ELISA, 25 ng/mL of sample extract was used, except that 100 ng/mL of PT-digests were used when the measured value was less than LOQ. W, wheat; R, rye; B, barley; O, oat; C, corn; P, prolamin; G, glutelin; PT, pepsin-trypsin.

barley (prolamin, 62% and glutelin, 71%). All experiments in this study were carried out based on the micro-Kjeldahl estimated protein contents. The yield of prolamin and glutelin proteins per 100 g of flour was 1.44 and 2.66 g (wheat), 0.61 and 0.81 g (rye), 1.41 and 1.7 g (barley), 0.79 and 2.78 g (oat), and 0.55 and 1.27 g (corn), respectively.

The purity and protein composition of the prolamin and glutelin fractions of different grains were analyzed on a 10−20% SDS-PAGE gel (Figure 1A). Gluten fractions of wheat, rye, barley and oats consisted of polypeptides in the expected molecular weight range in agreement with the previous reports.[2,17,35,36] Upon treating with pepsin and trypsin (PT), the gluten fractions from all grains were digested predominantly to low molecular weight polypeptides (<15 kDa) (Figure 1B). The corn prolamin exhibited poor solubility after PT-digestion. Aggregates were observed in the PT-digested glutelin fractions from wheat, rye and barley (Figure 1B).

ELISA

Three sandwich and two competitive ELISA kits employing anti-gluten antibodies (monoclonal or polyclonal) were used to measure the percent gluten recovery from various gluten fractions and their hydrolysates.

Sandwich ELISA. In general, the S1 and S2 controls behaved similar to wheat gluten fractions, as they are isolated from wheat. The average measured value for S3 and all oat and corn protein fractions used to calculate the percent gluten recovery was found to be lower than the limit of quantitation (LOQ) of the respective sandwich ELISA. The LOQs are 5 ppm gluten (R-Biopharm), 0.3 ppm wheat protein (Morinaga) and 4 ppm gluten (Romer Labs). Barley flour protein showed lower immunoreactivity than wheat and rye in Western blot. However, a high gluten recovery was observed with barley prolamin by ELISA. More detailed results on immunoreactivity of different grain protein fractions are described below.

With the R-Biopharm kit, the wheat gluten fractions showed a lower gluten recovery as compared to recoveries from rye and barley. The percent gluten recovery of prolamin and glutelin ranged from 65.8 (wheat) to 248.3 (barley) and 25.4 (wheat) to 97.0 (barley), respectively (Figure 2A). However, upon PT-digestion, the recovery was further reduced as compared to the undigested proteins, and it was 46.5 (wheat) to 185.8 (barley)

DOI: 10.1021/jf505716p
J. Agric. Food Chem. 2015, 63, 1825−1832

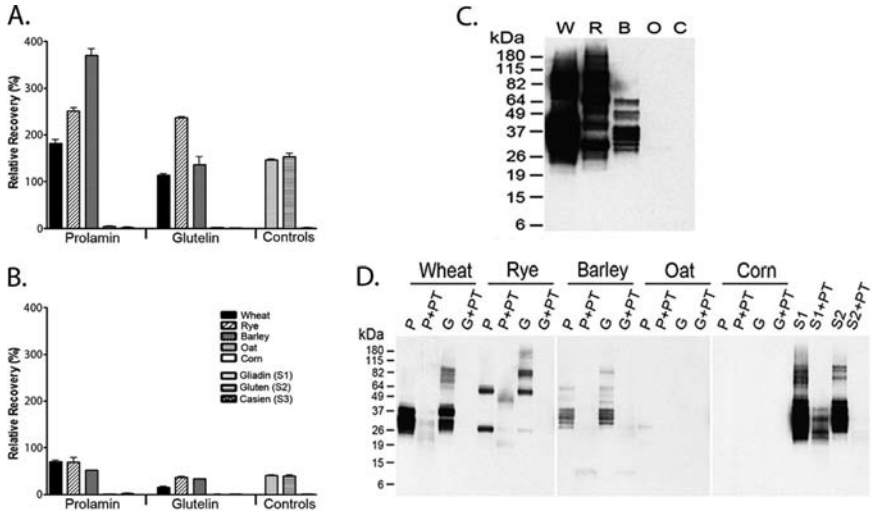

Figure 3. Analysis of gluten fractions and their PT-digests using the Morinaga sandwich ELISA kit and its antibodies. Recoveries of intact gluten fractions (A) and their PT-digests (B) in ELISA. Western blot analysis of flour proteins (C) and their gluten fractions (D) using the Morinaga kit antibodies. For ELISA, 10 ng/mL of sample extract was used, except that 40 ng/mL of PT-digested sample was used when the measured value was less than LOQ. W, wheat; R, rye; B, barley; O, oat; C, corn; P, prolamin; G, glutelin; PT, pepsin-trypsin.

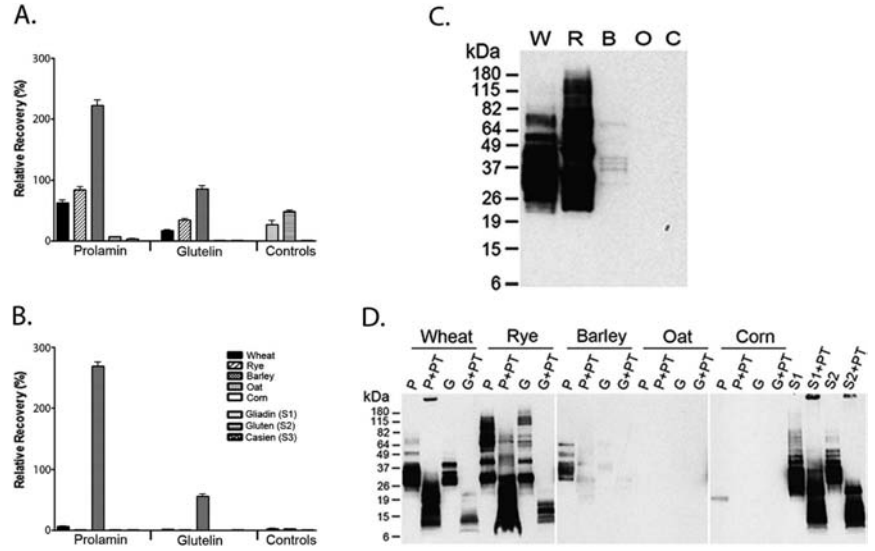

Figure 4. Analysis of gluten fractions and their PT-digests using the Romer Labs sandwich ELISA kit and its antibodies. Recoveries of intact gluten fractions (A) and their PT-digests (B) in ELISA. Western blot analysis of flour proteins (C) and their gluten fractions (D) using the Romer Labs kit antibodies. For ELISA, 50 ng/mL of sample was used, except that 100 ng/mL of PT-digested sample was used when the measured value was less than LOQ. W, wheat; R, rye; B, barley; O, oat; C, corn; P, prolamin; G, glutelin; PT, pepsin-trypsin.

for prolamin, and 4.9 (wheat) to 31.0 (rye) for glutelin (Figure 2B). The rye glutelin behaved similar to barley glutelin in both the undigested and digested samples. Interestingly, the recovery of S2 control (64.0%) behaved similar to that of wheat prolamin (65.8%), whereas a lower recovery was observed for the S1 control (31.5%). The average measured gluten level from 100 ng/mL PT-digests of wheat glutelin was lower than the LOQ. Since oat and corn flour proteins did not show any immunoreactivity with the R5-antibody (Figure 2C), it was likely that their fractions would not react in ELISA (Figure 2A and 2B) and Western analyses (Figure 2D).

With the Morinaga kit, the barley prolamin (369.4%) showed higher gluten recovery as compared to the prolamin of wheat (181.9%) and rye (251.3), while rye glutelin (237.1%) showed higher recovery as compared to the corresponding fractions in wheat (113.3%) and barley (135.9%) (Figure 3A). Among the PT-digested gluten fractions, gluten recovery was higher from the prolamin fractions as compared to their respective glutelin fractions (Figure 3B). Both S1 and S2 showed similar gluten recoveries, which were reduced upon PT-digestion. Oat and corn proteins did not react with Morinaga kit antibodies (Figure 3C). While the prolamin and glutelin fractions from wheat, rye and barley showed reactivity to Morinaga antibodies, their corresponding PT-digests had poor immunoreactivity (Figure 3D).

With the Romer Labs kit, gluten recovery was higher from the barley fractions as compared to those of wheat and rye. The percent recovery of prolamin ranged from 62.4 (wheat) to 222.5 (barley), while the glutelin ranged from 16.6 (wheat) to 84.9 (barley) (Figure 4A). The recoveries were substantially reduced upon PT-digestion for all fractions, except for barley (Figure 4B). Surprisingly, upon PT-digestion, the percent

DOI: 10.1021/jf505716p
J. Agric. Food Chem. 2015, 63, 1825−1832

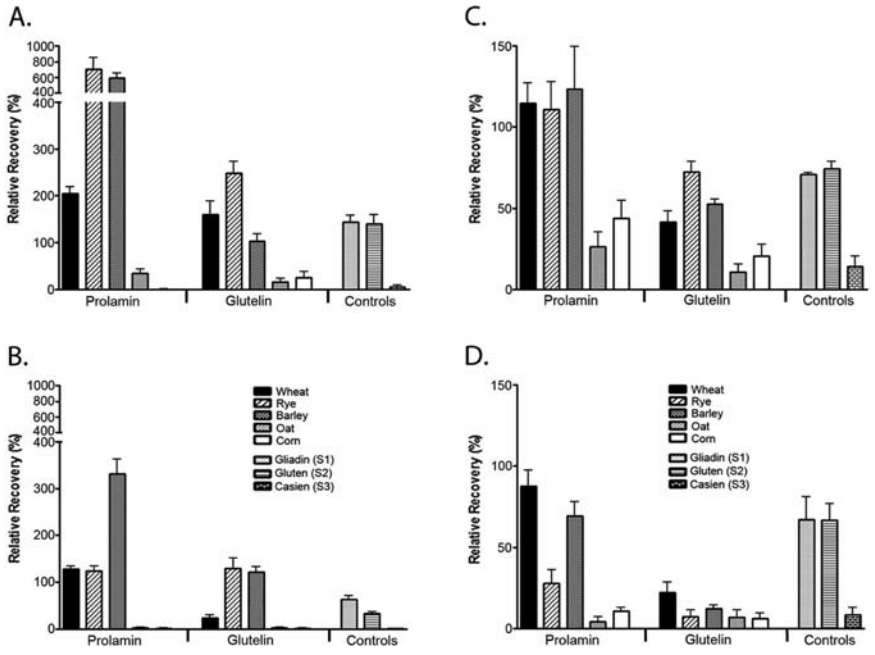

Figure 5. Analysis of gluten fractions and their PT-digests by competitive ELISA. Recoveries of intact gluten fractions (A and C) and their PT-digests (B and D) using the R-Biopharm (A and B) and the Biomedal Diagnostics (C and D) competitive ELISA kit. For ELISA, 25 ng/mL of sample was used, except that 100 ng/mL of PT-digested sample was used when the measured value was less than LOQ.

gluten recovery of barley prolamin (268.8) increased as compared to the undigested protein (222.5). The average measured gluten levels for 100 ng/mL of PT-digests of rye prolamin, wheat and rye glutelins, S1 and S2 were below the LOQ. The Romer Labs G12 antibodies did not show reactivity to oat and corn proteins (Figure 4C). Also, barley proteins showed poor immunoreactivity to G12 antibodies as compared to that of wheat and rye, as reported earlier.[37] The prolamin and glutelin fractions, including their PT-digests, from wheat and rye showed reactivity to G12 antibodies in Western blot, but only the prolamin fraction of barley was immunoreactive (Figure 4D).

Competitive ELISA. As observed with the sandwich format, the average measured gluten levels for S3 and all oat and corn protein fractions were lower than the LOQ of the respective competitive ELISA. The LOQ for the R-Biopharm R5-based competitive kit is 10 ppm gluten and the LOQ for the Biomedal G12-based competitive kit is 15 ppm gluten.

With the R-Biopharm competitive kit, the percent gluten recovery of prolamins ranged from 203.8 (wheat) to 703.5 (rye) and that of glutelins ranged from 102.6 (barley) to 247.4 (rye) (Figure 5A). As seen with the R5-based sandwich ELISA, the gluten recoveries from the rye and barley prolamins were higher than that of the wheat prolamin, even though the gluten recoveries were different between the two ELISA formats. Depending on the grain source of prolamin, the gluten recovery was at least 2 to 4 times higher with the competitive ELISA as compared to the sandwich ELISA (Figure 5A vs Figure 2A). The percent gluten recoveries of PT-digested prolamins were more than one hundred percent, ranging from 124.0 (rye) to 331.5 (barley), although recoveries were lower than those of the undigested prolamins (Figure 5B). The PT-digested glutelins showed percent gluten recoveries in the range of 23.0 (wheat) to 129.4 (rye). Reduced recoveries were observed for the PT-digests of S1 (2.3-fold) and S2 (4.2-fold) as compared to their respective undigested proteins.

The Biomedal competitive kit had similar gluten recoveries for wheat, rye and barley prolamins (110.9 to 123.5%). Even though the oat and corn prolamin fractions showed 26 and 44% recoveries, respectively, the measured value for the 25 ng/mL protein sample used in ELISA was below the LOQ. Among glutelins, only rye (72.2% recovery) had a measured value above the LOQ at 25 ng/mL of protein sample used in ELISA (Figure 5C). Similar recoveries were observed between S1 (70.6%) and S2 (74.2%). The PT-digested gluten fractions yielded lower recoveries when compared to the undigested proteins. Among the PT-digested prolamins, rye (27.8%) showed a significantly lower recovery as compared to wheat (87.7%) and barley (69.1%) (Figure 5D). The measured gluten level of the 100 ng/mL PT-digested protein sample was just above the LOQ when using the wheat glutelin fraction, while the gluten content of the rye and barley glutelin fractions were below the LOQ. The gluten recovery of S1 and S2 was not significantly reduced following the PT-digestion.

DISCUSSION

Gluten not only serves as a protein source but also imparts functional properties in many foods. Gluten is used in foods as either an intact protein or hydrolysate. We isolated prolamin and glutelin fractions from different grains and analyzed them by SDS-PAGE under reducing conditions (Figure 1A). Even though the polypeptide patterns of prolamins and glutelins on SDS-PAGE are different among wheat, rye and barley, all these proteins are linked to causing CD in genetically susceptible individuals. Gluten hydrolysis in the gastrointestinal tract is carried out by acid and digestive enzymes, such as pepsin and trypsin. Incomplete hydrolysis of gluten by PT-digestion, as observed in Figure 1B, allows the release of gluten peptides (<15 kDa), which can cause CD.

Gluten-free labeled foods are available as safe food choices for CD patients. Accurate gluten estimation (intact or hydrolyzed) in such foods is essential to comply with the

DOI: 10.1021/jf505716p
J. Agric. Food Chem. 2015, 63, 1825−1832

thresholds set for gluten-free labeling. ELISA offers rapid and sensitive quantitation of gluten, and many commercial kits are available in both sandwich and competitive formats. But, it is challenging to accurately quantitate gluten from different grains using ELISA because of differences in antibody affinity and calibration standards. For example, an ELISA kit that uses wheat prolamin as a calibration standard may not accurately estimate gluten from rye and barley, if the detection antibody does not have equal affinity for gluten from different grain sources. This may be circumvented by the use of grain-specific gluten calibration standards in ELISA, if the grain source of gluten contamination in food is known. Furthermore, the measurement of prolamin to quantitate gluten using a common multiplication factor of 2 may not accurately determine gluten content if prolamin and glutelin are not present in equal proportions.[34] Hence, it is important to assess the extent of immunoreactivity imparted by prolamin and glutelin fractions from wheat, rye and barley to facilitate gluten quantitation.

Both monoclonal (R-Biopharm and Romer Labs) and polyclonal (Morinaga) antibodies are used in ELISA for gluten quantitation. Monoclonal antibodies recognize one epitope, whereas polyclonal antibodies recognize many epitopes on a single protein. Among the different ELISA kits used in this study, variable results were observed in the recovery of both prolamin and glutelin fractions. Moreover, the glutelin fractions showed lower gluten recovery compared to their respective prolamin fractions from wheat, rye and barley. This could possibly be due to the reduced number of epitopes recognized in the glutelin fractions. The Morinaga polyclonal antibodies recognize many epitopes in gluten. Since there may be common amino acid sequences between prolamins and glutelins, the polyclonal antibodies aid in obtaining better recovery of glutelins compared to monoclonal antibodies (Figure 3A vs 2A and 4A). R-Biopharm (sandwich and competitive) ELISA uses the R5-monoclonal antibody, which was produced against secalin and recognizes amino acid sequences QQPFP, LQPFP, QQQFP and QLPFP as epitopes in wheat, rye and barley.[38] Hence, it is expected that the R5 antibody would react strongly to rye, and less so toward wheat and barley (Figure 2C). An NCBI database search of the four epitopes recognized by R5 antibody in the gluten sequences showed their presence in higher number in rye and barley, as compared to wheat. Among the gluten proteins (GenBank accession no. in parentheses following the protein type), one of the high affinity R5 epitopes (QQPFP) was repeated 33 times in rye [14 times each in ω- (ACQ83628.1) and γ-75k- (ABY71029.1), and 5 times in γ-40k- secalin (AEW46837.1)]; 20 times in barley [13 times in C- (AAA92333.1), 4 times in B- (AAZ76368.1) and 3 times in γ-1- hordein (AAA32955.1)]; and 8 times in wheat [5 times in γ- (AAA34272.1), 2 times in ω- (AAT01617.1) and once in α-gliadin (AFX69628.1)]. The repetitive epitopes could enhance antibody binding, resulting in the overestimation of rye and barley in the R5-based ELISA using gliadin as a calibration standard.

The G12 monoclonal antibody (used in the Romer Labs and Biomedal ELISA kits) was raised against the immunotoxic 33-mer peptide of α-2 gliadin, and it recognizes amino acid sequences QPQLPY, QPQLPF, QPQLPL and QPQQPY as epitopes in the reducing order of affinity.[39] The high affinity G12 epitope (QPQLPY), in the above-mentioned GenBank sequences, was found only in α-gliadin (repeated thrice). However, QPQLPF occurred once in wheat (γ-gliadin), twice in rye (one each in γ-40k- and ω-secalin) and once in barley (C hordein). Further, QPQQPY was present 3 times in γ-75k secalin and once in C hordein. It is interesting to see that despite having a lower number of epitopes, the gluten content of barley was overestimated when compared to that of wheat and rye (Figure 4A). A similar high sensitivity of the G12 antibody toward barley gluten has been reported earlier.[39] This suggests that there may be other factors involved in the overestimation of barley that would need further investigation.

Our observations show that the recovery of gluten in most PT-digested prolamin and glutelin fractions was reduced drastically as compared to the recoveries of their respective intact proteins in the sandwich ELISA. Competitive ELISA is more suitable for hydrolyzed proteins because it requires only one epitope, as compared to the sandwich format that would require at least two epitopes for target analyte detection. The competitive format may be useful for gluten estimation in fermented foods, such as beer and malt extracts.[30,40] We observed higher recoveries of intact gluten fractions as compared to their respective PT-digests with both competitive ELISA kits used in this study (Figure 5). Furthermore, acceptable gluten recoveries were obtained with PT-digested prolamins, with the exception of barley prolamin (high recovery) in the R5-based (Figure 5B) and rye prolamin (low recovery) in the G12-based (Figure 5D) competitive ELISAs. However, the suitability of a competitive format for intact proteins may be dependent upon the calibration standards used in the assay. For example, gluten peptide fragments used as calibration standards may undergo nonspecific cleavage of some epitopes, causing inaccurate estimations of intact gluten. Moreover, the gluten recovery may vary among fermented foods since various hydrolytic enzymes (for example, from plant seed germination, or of microbial or fungal origin) can hydrolyze gluten differentially and generate a set of gluten peptides that are different from those used as the ELISA calibration standards.

In summary, high variability in gluten quantitation by ELISA was observed depending upon the grain source, gluten protein and its level of hydrolysis. Based on the ELISA kit used for gluten quantitation, some intact prolamins and glutelins were overestimated. In particular, the recovery of barley prolamin was higher than that of wheat and rye prolamins by the sandwich ELISA. Even when the same antibodies (R5 or G12) were used, we observed different gluten recoveries between corresponding sandwich and competitive formats. This could be due to the differences in their assay conditions and calibration standards. Other non-immuno-based methods such as mass spectrometry,[41,42] polymerase chain reaction[43] and high pressure liquid chromatography[44] can be used to complement ELISA for a robust gluten analysis. Moreover, the availability of standard reference material may help to achieve consistency in gluten quantitation among different analytical methods. Thus, it is important to understand the effect of grain source (wheat, rye and barley), gluten protein (prolamin and glutelin), food ingredients (e.g., hydrolyzed gluten) and food processing methods (e.g., fermentation) in selecting a suitable ELISA for accurate gluten estimation.

AUTHOR INFORMATION

Corresponding Author

*Phone: 240-402-3284, fax: 301-210-4769, E-mail: Prasad.Rallabhandi@fda.hhs.gov.

Author Contributions

†P.R. and G.M.S. contributed equally to this study.

DOI: 10.1021/jf505716p
J. Agric. Food Chem. 2015, 63, 1825−1832

Funding

This work was supported by a U.S. FDA Office of Women's Health (OWH) grant (to Prasad Rallabhandi).

Notes

The authors declare no competing financial interest.

■ ACKNOWLEDGMENTS

The authors would like to thank Dr. Marianne Solomotis, Center for Food Safety and Applied Nutrition, FDA, for critical reading of this manuscript.

■ REFERENCES

(1) Diaz-Amigo, C.; Yeung, J. M. In *Pathogens and Toxins in Foods:Challenges and Interventions*; Sofos, V. K. J. J. N., Ed.; ASM Press: Washington, DC, 2010; pp 286−300.

(2) Wieser, H. Chemistry of gluten proteins. *Food Microbiology* **2007**, *24*, 115−119.

(3) Fasano, A. Systemic autoimmune disorders in celiac disease. *Curr. Opin. Gastroenterol.* **2006**, *22*, 674−679.

(4) Rallabhandi, P. Gluten and celiac disease—an immunological perspective. *J. AOAC Int.* **2012**, *95*, 349−355.

(5) Fasano, A.; Berti, I.; Gerarduzzi, T.; Not, T.; Colletti, R. B.; Drago, S.; Elitsur, Y.; Green, P. H.; Guandalini, S.; Hill, I. D.; Pietzak, M.; Ventura, A.; Thorpe, M.; Kryszak, D.; Fornaroli, F.; Wasserman, S. S.; Murray, J. A.; Horvath, K. Prevalence of celiac disease in at-risk and not-at-risk groups in the United States: a large multicenter study. *Arch. Int. Med.* **2003**, *163*, 286−292.

(6) Briani, C.; Samaroo, D.; Alaedini, A. Celiac disease: from gluten to autoimmunity. *Autoimmun. Rev.* **2008**, *7*, 644−650.

(7) Sapone, A.; Lammers, K. M.; Casolaro, V.; Cammarota, M.; Giuliano, M. T.; De Rosa, M.; Stefanile, R.; Mazzarella, G.; Tolone, C.; Russo, M. I.; Esposito, P.; Ferraraccio, F.; Carteni, M.; Riegler, G.; de Magistris, L.; Fasano, A. Divergence of gut permeability and mucosal immune gene expression in two gluten-associated conditions: celiac disease and gluten sensitivity. *BMC Med.* **2011**, *9*, 23.

(8) Simonato, B.; De Lazzari, F.; Pasini, G.; Polato, F.; Giannattasio, M.; Gemignani, C.; Peruffo, A. D.; Santucci, B.; Plebani, M.; Curioni, A. IgE binding to soluble and insoluble wheat flour proteins in atopic and non-atopic patients suffering from gastrointestinal symptoms after wheat ingestion. *Clin. Exp. Allergy: J. Br. Soc. Allergy Clin. Immunol.* **2001**, *31*, 1771−1778.

(9) Zarkadas, M.; Cranney, A.; Case, S.; Molloy, M.; Switzer, C.; Graham, I. D.; Butzner, J. D.; Rashid, M.; Warren, R. E.; Burrows, V. The impact of a gluten-free diet on adults with coeliac disease: results of a national survey. *J. Human Nutrition Dietetics: Official J. Br. Dietetic Assoc.* **2006**, *19*, 41−49.

(10) Pulido, O. M.; Gillespie, Z.; Zarkadas, M.; Dubois, S.; Vavasour, E.; Rashid, M.; Switzer, C.; Godefroy, S. B. Introduction of oats in the diet of individuals with celiac disease: a systematic review. *Adv. Food Nutr. Res.* **2009**, *57*, 235−285.

(11) Sey, M. S.; Parfitt, J.; Gregor, J. Prospective study of clinical and histological safety of pure and uncontaminated Canadian oats in the management of celiac disease. *JPEN, J. Parenter. Enteral Nutr.* **2011**, *35*, 459−464.

(12) Comino, I.; Real, A.; de Lorenzo, L.; Cornell, H.; Lopez-Casado, M. A.; Barro, F.; Lorite, P.; Torres, M. I.; Cebolla, A.; Sousa, C. Diversity in oat potential immunogenicity: basis for the selection of oat varieties with no toxicity in coeliac disease. *Gut* **2011**, *60*, 915−922.

(13) Silano, M.; Pozo, E. P.; Uberti, F.; Manferdelli, S.; Del Pinto, T.; Felli, C.; Budelli, A.; Vincentini, O.; Restani, P. Diversity of oat varieties in eliciting the early inflammatory events in celiac disease. *Eur. J. Nutr.* **2014**, *53*, 1177−1186.

(14) Silano, M.; Di Benedetto, R.; Maialetti, F.; De Vincenzi, A.; Calcaterra, R.; Cornell, H. J.; De Vincenzi, M. Avenins from different cultivars of oats elicit response by coeliac peripheral lymphocytes. *Scand. J. Gastroenterol.* **2007**, *42*, 1302−1305.

(15) Gendel, S. M.; Zhu, J. Analysis of U.S. Food and Drug Administration food allergen recalls after implementation of the food allergen labeling and consumer protection act. *J. Food Prot.* **2013**, *76*, 1933−1938.

(16) Osborne, T. B. *The vegetable proteins*, 2nd ed.; Longmans Green: London, U.K., 1924.

(17) Tatham, A. S.; Gilbert, S. M.; Fido, R. J.; Shewry, P. R. Extraction, separation, and purification of wheat gluten proteins and related proteins of barley, rye, and oats. *Methods Mol. Med.* **2000**, *41*, 55−73.

(18) Shewry, P. R.; Tatham, A. S.; Forde, J.; Kreis, M.; Miflin, B. J. The Classification and Nomenclature of Wheat Gluten Proteins—a Reassessment. *J. Cereal Sci.* **1986**, *4*, 97−106.

(19) Shan, L.; Molberg, O.; Parrot, I.; Hausch, F.; Filiz, F.; Gray, G. M.; Sollid, L. M.; Khosla, C. Structural basis for gluten intolerance in celiac sprue. *Science* **2002**, *297*, 2275−2279.

(20) Howdle, P. D. Gliadin, glutenin or both? The search for the Holy Grail in coeliac disease. *Eur. J. Gastroenterol. Hepatol.* **2006**, *18*, 703−706.

(21) Vader, W.; Kooy, Y.; Van Veelen, P.; De Ru, A.; Harris, D.; Benckhuijsen, W.; Pena, S.; Mearin, L.; Drijfhout, J. W.; Koning, F. The gluten response in children with celiac disease is directed toward multiple gliadin and glutenin peptides. *Gastroenterology* **2002**, *122*, 1729−1737.

(22) Ellis, H. J.; Lozano-Sanchez, P.; Bermudo Redondo, C.; Suligoj, T.; Biagi, F.; Bianchi, P. I.; Corazza, G. R.; De Silvestri, A.; Bravi, E.; Katakis, I.; O'Sullivan, C. K.; Ciclitira, P. J. Antibodies to wheat high-molecular-weight glutenin subunits in patients with celiac disease. *Int. Archives Allergy Immunol.* **2012**, *159*, 428−434.

(23) Dewar, D. H.; Amato, M.; Ellis, H. J.; Pollock, E. L.; Gonzalez-Cinca, N.; Wieser, H.; Ciclitira, P. J. The toxicity of high molecular weight glutenin subunits of wheat to patients with coeliac disease. *Eur. J. Gastroenterol. Hepatol.* **2006**, *18*, 483−491.

(24) Diaz-Amigo, C.; Popping, B. Accuracy of ELISA detection methods for gluten and reference materials: a realistic assessment. *J. Agric. Food Chem.* **2013**, *61*, 5681−5688.

(25) Sharma, G. M.; Khuda, S. E.; Pereira, M.; Slate, A.; Jackson, L. S.; Pardo, C.; Williams, K. M.; Whitaker, T. B. Development of an incurred cornbread model for gluten detection by immunoassays. *J. Agric. Food Chem.* **2013**, *61*, 12146−12154.

(26) Bugyi, Z.; Torok, K.; Hajas, L.; Adonyi, Z.; Popping, B.; Tomoskozi, S. Comparative study of commercially available gluten ELISA kits using an incurred reference material. *Qual. Assur. Saf. Crop* **2013**, *5*, 79−87.

(27) Gomaa, A.; Boye, J. I. Impact of thermal processing time and cookie size on the detection of casein, egg, gluten and soy allergens in food. *Food Res. Int.* **2013**, *52*, 483−489.

(28) Colgrave, M. L.; Goswami, H.; Blundell, M.; Howitt, C. A.; Tanner, G. J. Using mass spectrometry to detect hydrolysed gluten in beer that is responsible for false negatives by ELISA. *J. Chromatogr., A* **2014**, *1370*, 105−114.

(29) Kanerva, P.; Brinck, O.; Sontag-Strohm, T.; Salovaara, H.; Loponen, J. Deamidation of gluten proteins and peptides decreases the antibody affinity in gluten analysis assays. *J. Cereal Sci.* **2011**, *53*, 335−339.

(30) Gessendorfer, B.; Koehler, P.; Wieser, H. Preparation and characterization of enzymatically hydrolyzed prolamins from wheat, rye, and barley as references for the immunochemical quantitation of partially hydrolyzed gluten. *Anal. Bioanal. Chem.* **2009**, *395*, 1721−1728.

(31) Immer, U.; Haas-Lauterbach, S. Gliadin as a measure of gluten in foods containing wheat, rye, and barley-enzyme immunoassay method based on a specific monoclonal antibody to the potentially celiac toxic amino acid prolamin sequences: collaborative study. *J. AOAC Int.* **2012**, *95*, 1118−1124.

(32) Mendez, E.; Vela, C.; Immer, U.; Janssen, F. W. Report of a collaborative trial to investigate the performance of the R5 enzyme linked immunoassay to determine gliadin in gluten-free food. *Eur. J. Gastroenterol. Hepatol.* **2005**, *17*, 1053−1063.

DOI: 10.1021/jf505716p
J. Agric. Food Chem. 2015, 63, 1825−1832

(33) Sharma, G. M.; Rallabhandi, P. The Effects of Processing on Gluten from Wheat, Rye and Barley and its Detection in Foods. In *Processing and Impact on Active Components in Food*; Preedy, V., Ed.; Elsevier Publications: United Kingdom, 2015; Vol. *36*, pp 295−300.
(34) Wieser, H.; Koehler, P. Is the calculation of the gluten content by multiplying the prolamin content by a factor of 2 valid? *Eur. Food Res. Technol.* **2009**, *229*, 9−13.
(35) Gellrich, C.; Schieberle, P.; Weiser, H. Biochemical characterization and quantification of the storage protein (secalin) types in rye flour. *Cereal Chem.* **2003**, *80*, 102−109.
(36) Salplachta, J.; Bobalova, J. MALDI-TOF mass spectrometry of hordeins: rapid approach for identification of malting barley varieties. *J. Mass Spectrom.* **2009**, *44*, 1287−1292.
(37) Moron, B.; Cebolla, A.; Manyani, H.; Alvarez-Maqueda, M.; Megias, M.; Thomas Mdel, C.; Lopez, M. C.; Sousa, C. Sensitive detection of cereal fractions that are toxic to celiac disease patients by using monoclonal antibodies to a main immunogenic wheat peptide. *Am. J. Clin. Nutr.* **2008**, *87*, 405−414.
(38) Kahlenberg, F.; Sanchez, D.; Lachmann, I.; Tuckova, L.; Tlaskalova, H.; Mendez, E.; Mothes, T. Monoclonal antibody R5 for detection of putatively coeliac-toxic gliadin peptides (vol 222, pg 78, 2006). *Eur. Food Res. Technol.* **2006**, *222*, 743−743.
(39) Moron, B.; Bethune, M. T.; Comino, I.; Manyani, H.; Ferragud, M.; Lopez, M. C.; Cebolla, A.; Khosla, C.; Sousa, C. Toward the assessment of food toxicity for celiac patients: characterization of monoclonal antibodies to a main immunogenic gluten peptide. *PloS One* **2008**, *3*, e2294.
(40) Dostalek, P.; Hochel, I.; Mendez, E.; Hernando, A.; Gabrovska, D. Immunochemical determination of gluten in malts and beers. *Food Additives Contaminants* **2006**, *23*, 1074−1078.
(41) Fiedler, K. L.; McGrath, S. C.; Callahan, J. H.; Ross, M. M. Characterization of grain-specific peptide markers for the detection of gluten by mass spectrometry. *J. Agric. Food Chem.* **2014**, *62*, 5835−5844.
(42) Sealey-Voyksner, J. A.; Khosla, C.; Voyksner, R. D.; Jorgenson, J. W. Novel aspects of quantitation of immunogenic wheat gluten peptides by liquid chromatography-mass spectrometry/mass spectrometry. *J. Chromatogr., A* **2010**, *1217*, 4167−4183.
(43) Mujico, J. R.; Lombardia, M.; Mena, M. C.; Mendez, E.; Albar, J. P. A highly sensitive real-time PCR system for quantification of wheat contamination in gluten-free food for celiac patients. *Food Chem.* **2011**, *128*, 795−801.
(44) Koenig, A.; Konitzer, K.; Wieser, H.; Koehler, P. Classification of spelt cultivars based on differences in storage protein compositions from wheat. *Food Chem.* **2015**, *168*, 176−182.

DOI: 10.1021/jf505716p
J. Agric. Food Chem. 2015, 63, 1825−1832

MATERIALS AND METHODS

Plant Material and Extract Preparation. Sample provenance and voucher codes (CHR (Christchurch) kept at the Landcare Herbarium, Lincoln, others at Plant & Food Research, Dunedin) are shown in Table 1. The *L. oleraceum* plants for tasting and postharvest treatment experiments were originally sourced from a near-shore rock stack near Te Akau (Waikato) with the plants supplied by Forest Flora Plants, Ngaruawahia, and a second line purchased (Sept 2, 2010) from Taupo Native Nursery. They were cultivated in an unheated greenhouse with the controlled release fertilizer Osmocote Plus (Scotts Europe BV, Heerlen, The Netherlands). The fertilizer nutrient content included NPK (17:1.6:8.7), 0.6 Mg + trace elements (0.01 B, 0.25 Cu, 0.2 Fe, 0.03 Mn, 0.01 Mo, 0.01 Zn) + 9.0% organic resin coating based on vegetable oils. It was applied to the surface of the pots (5 g/pot) on Sept 2 and Nov 18, 2010. After the first harvest (Nov 18, 2010) the plants were moved to a shade house (80% shaded) until the second harvest (Feb 25, 2011). Te Akau rock stack material (sample 12) was harvested on Nov 15, 2009. The Landcare Research collection (samples 1, 2, 5−11, and 13−15) was harvested on Nov 16, 2009. *Lepidium banksii* samples 3 and 4 (Table 1) were harvested on April 3, 2014. Frozen leaves from the harvested plants were freeze-dried and ground to a powder using a mortar and pestle prior to analyses. Whole leafy lateral shoots of the *L. oleraceum* plants for tasting and postharvest treatment experiments were harvested using a pair of hand pruning clippers and then dried for 48 h either in a forced air cabinet drier at 45 or 75 °C or in a Virtis 12 sl (Gardiner, NY) freeze-drying unit. The dried herb material was ground to a powder using a ZM100 Retsch ultracentrifugal mill (Haan, Germany) screened to 0.75 or 0.20 mm and stored frozen (−20 °C) prior to analyses.

Table 1. New Zealand *Lepidium* Collections[a]

species (ID no.)	voucher code	provenance
L. aegrum (1)	CHR 609821[b]	Island Bay rock stack, Banks Peninsula, South Island
L. banksii (2)	CHR 616805[b,c]	Moutere inlet, Nelson, South Island
L. banksii (3)	140403-01	Waimea inlet, Nelson, South Island
L. banksii (4)	140403-02[d]	Motueka, Nelson, South Island
L. castellanum (5)	CHR 609796[b]	Raoul Island, Kermadec Islands
L. crassum (6)	CHR 609822[b]	Orore Point, Herbert, Otago, South Island
L. crassum (7)	CHR 609814[b]	Wharekakahu Island, Otago Peninsula, South Island
L. juvencum (8)	CHR 609803[b]	Long Beach, Purakanui, Otago, South Island
L. oblitum (9)	CHR 609815[b]	Robin Bush, Mangere Island, Chatham Islands
L. oblitum (10)	CHR 609813[b]	Back Landing, Mangere Island, Chatham Islands
L. oblitum (11)	CHR 609817[b]	Top Plateau, Mangere Island, Chatham Islands
L. oleraceum (12)	091115-01[e,f]	Te Akau rock stack, Waikato, North Island
L. oleraceum (13)	CHR 609818[b]	Ngtutura Point, Port Waikato, North Island
L. panniforme (14)	CHR 609812[b]	Front landing, Mangere Island, Chatham Islands
L. panniforme (15)	CHR 609826[b]	Hut Track, Mangere Island, Chatham Islands

[a]See de Lange et al.[8] for taxonomic authorities. [b]Cultivated at Landcare Lincoln. [c]Bulk leaves from 16 plants. [d]Cultivated at the Department of Conservation, Nelson. [e]Cultivated at Plant & Food Research, Lincoln. [f]Source of material for flavor assessment.

Glucosinolates by LC−MS. A subsample of freeze-dried leaf powder (200 mg) was weighed into a 15 mL tube, extracted with boiling H_2O (10 mL), and placed in a simmering H_2O bath for 10 min (cf. blanching[18]). We found a negligible difference in *Lepidium* glucosinolates by this method compared to using heated MeOH. Extracts were then centrifuged at 20817*g* for 10 min, and the supernatant was diluted to a final volume of 25 mL with H_2O. An aliquot was filtered (0.22 μm) into glass vials for LC−MS analysis. The LC−MS system consisted of a Thermo Electron Corp. (San Jose, CA) Finnigan Surveyor MS pump, Finnigan MicroAS autosampler, and Finnigan Surveyor PDA detector and a ThermaSphere TS-130 column heater (Phenomenex, Torrance, CA). A 2 μL aliquot of each prepared extract was separated with a mobile phase consisting of 0.1% formic acid in H_2O (A) and 0.1% formic acid in MeCN (B) by reversed-phase chromatography. The column used was a 150 × 3 mm i.d., 3 μm, 80 Å, Luna C18(2) with a 4 × 2 mm i.d., 10 μm, guard column of the same material (Phenomenex), maintained at 30 °C with a flow rate of 200 μL/min. A gradient was applied: 0−3 min, 98% A; 15 min, 85% A; 20 min, 60% A; 25 min, 50% A; 30−33 min, 2% A; followed by a return to the starting condition over 5 min. The eluent was scanned by PDA (190−390 nm) and LTQ 2D linear ion-trap API-MS (Thermo-Finnigan, San Jose, CA) with electrospray ionization (ESI) in the negative mode. Data were acquired for precursor masses from m/z 250 to m/z 1000 with Pulsed Q collision-induced dissociation (PQD) fragmentation at 40 arbitrary units. PQD fragmentation at MS^2 allowed collection of lower m/z data (<1/3 of the precursor), thus m/z 96 and m/z 97 ions (sulfate fragments) indicating glucosinolates as used by Mellon et al.[19] Data were processed with the aid of Xcalibur 2.05 software (Thermo Electron Corp.). The concentration of the glucosinolates was calculated relative to an external standard of sinigrin, **3**, 99% (Sigma-Aldrich, St. Louis, MO).

Gluconapin, 1, Content of the Flavor Evaluation Samples by LC−MS. A subsample (30−40 mg) of the cultivated *L. oleraceum* plants was extracted and analyzed as above, with the following changes: A standard of **1**, 87% (PhytoLab, Vestenbergsgreuth, Germany), stock solution (100 μg/mL) was diluted with H_2O to give external standards ranging from 0.1 to 20 μg/mL. Using the HPLC systems described above, the following solvent gradient was applied: 0−2 min, 75% A; 6−8 min, 5% A; 8.5−11 min, 75% A. The flow rate was stepped from 200 to 400 μL/min between 8.5 and 10.9 min. Data were acquired by selective ion monitoring (SRM) based on **1** with precursor isolation of m/z 372, and an applied collision energy (CE) of 35 (arbitrary units), measuring the area response for product ions of m/z 259, 275, and 195 at t_R = 6.70 min.

Isolation of Gluconapin, 1. Freeze-dried ground *L. oleraceum* (500 mg) was extracted in 70% MeOH (5 mL) by shaking overnight. The dried extract (103 mg) was applied in H_2O to an IST Isolute (Hengoed, Mid-Glamorgan, U.K.) prepacked C18 column (500 mg) eluting with 0−100% MeCN in H_2O followed by EtOAc. **1** eluted with 20% MeCN and was identified by comparison of the ^1H NMR spectrum (D_2O, 400 MHz) with published data.[20]

Reaction of Gluconapin, 1, and Myrosinase. Endogenous *L. oleraceum* myrosinase activity was shown to hydrolyze the glucosinolate completely by mixing freeze-dried material, as used for the quantification procedure, with H_2O at room temperature (18 °C) and at 37 °C for 2 h with periodic mixing.

HS-SPME-GC−MS Analysis of Isothiocyanates. Ground dried *L. oleraceum* leaf (10 mg) was weighed into a 20 mL SPME autosampler vial, which was closed until analysis. Before analysis a 20 μL internal standard solution consisting of 5 μL of allyl isothiocyanate, **4**, 95% (Sigma-Aldrich), in 50 mL of H_2O and pH 4 0.1 M citrate buffer (0.5 mL) were added. The sample was equilibrated at 35 °C for 1 min, followed by head space absorption onto a preconditioned 65 μm PDMS−DVB SPME fiber (Supelco, Bellefonte, PA), with agitation throughout. Analyses were performed on an Agilent 7890A gas chromatograph with a CTC Analytics PAL system autosampler and an Agilent 5975C inert XL MSD with triple axis detector (under the control of Enhanced ChemStation software). A 30 m J&W HP-5 ms column with a 0.25 mm i.d. and 0.25 μm film was used for analyses. The SPME fiber was desorbed for 1 min into the injector (splitless, 260 °C), with a purge flow of 50 mL/min. The carrier gas was H_2 at 1.7 mL/min. The oven was held at 40 °C for 4 min and then heated to 120 °C at 10 °C/min. The MS transfer line was at 300 °C, the MS source at 230 °C, and the MS quadrupole at 150 °C. Peaks were

DOI: 10.1021/jf505859u
J. Agric. Food Chem. 2015, 63, 1833−1838

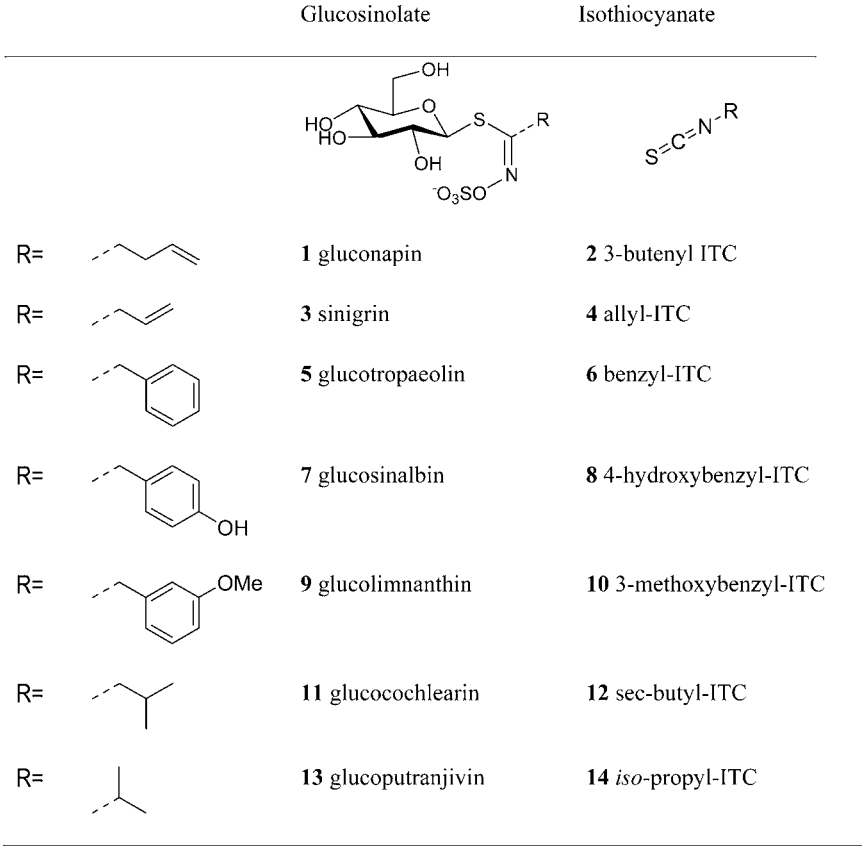

Figure 1. Compound structures

detected as total ion current, monitoring from m/z 35 to m/z 300 and identified by comparison with the NIST MS library and retention indices. 3-Butenyl isothiocyanate, **2**, was quantitated relative to the **4** internal standard peak, expressed as "relative units" based on TIC area and corrected for sample mass.

Free Isothiocyanate by GC−MS. Ground *L. oleraceum* plant material (100 mg) was extracted with EtOAc (0.5 mL) containing allyl isothiocyanate, **4** (216 μg/mL), as the internal standard. The solution was mixed thoroughly and then kept for 2 h, followed by a second mixing and filtering through a 0.45 μm PTFE filter before analysis. Analysis was by GC−MS using the method above but with direct 1 μL injection. A calibration curve was made using **4**.

Informal Sensory Evaluation. The samples assessed in this study were obtained from two harvests of the cultivated *L. oleraceum*. Water activity measurements were taken for food safety consideration, and all samples were less than 0.7a_w. Plant & Food Research staff experienced in food evaluation, but not considered trained descriptive sensory panelists, informally evaluated the color, flavor, and texture of the samples. Samples from the first harvest date were evaluated by three assessors, and samples from the second harvest date were evaluated by six assessors. *Lepidium* leaf material was tasted undiluted in a powdered form, and samples were blinded with a three-digit code for the evaluations. Assessors tasted each sample and recorded the flavors, aromas, and textures that they perceived. All comments were then tabulated and discussed as a group.

RESULTS AND DISCUSSION

Freeze-dried ground leaves of cultivated *L. oleraceum* plants (Table 1) were extracted with boiling water (to inactivate myrosinase) and analyzed for glucosinolates by LC−MS. The glucosinolate peaks were identified by characteristic m/z 96 and 97 sulfate fragments.[19] The predominant glucosinolate had an $[M - H]^-$ ion at m/z 372, suggesting a C_4H_7 side chain. By far the most common glucosinolate with this structure is gluconapin, **1**[10] (see Figure 1 for the structures of the compounds). Partial purification by reversed-phase chromatography gave a fraction dominated by glucosinolate signals in its ^{1}H NMR spectrum, matching the published data for **1**.[20] A commercial reference sample of **1** was purchased, and its LC retention and MS fragmentation were also matched.

Gluconapin, **1**, is widely distributed, but only one report from a *Lepidium* species was listed in a 2001 review,[10] at a low concentration in seeds of *Lepidium subulatum* from Spain.[21] However, there are more recent reports, for example, from perennial pepperweed, *Lepidium latifolium*, at highly variable concentrations up to 0.05 mg/g fresh weight.[22] We found concentrations of **1** in *L. oleraceum* leaves of 7−22 mg/g dry matter (DM), which is in the high range compared to reported concentrations in other Brassicaceae, e.g., 0.25−9.09 mg/g DM (assuming 90% H_2O) in Brussels sprouts, a *Brassica oleracea* cultivar.[23]

The flavor chemistry of Brassicaceae is complicated: the dynamic release of isothiocyanates and other compounds by myrosinase activity during processing and consumption gives pungency at pain receptors,[24] plus volatile aroma compounds reaching olfactory receptors. For example, the main pungent component of wasabi is allyl isothiocyanate, **4**, but the fresh green aroma is due to ω-(methylthio)alkyl isothiocyanates.[25] Endogenous myrosinase activity in *L. oleraceum* was shown to hydrolyze gluconapin, **1**, completely by mixing ground freeze-dried leaves with water. As expected, the predominant volatile product was 3-butenyl isothiocyanate (3BITC), **2**, but no free **2** was detected from an EtOAc extraction of dry leaf material.

3-BITC, **2**, is pungent,[25] but we could not find any quantitative comparisons of isothiocyanate pungency (i.e., no

DOI: 10.1021/jf505859u
J. Agric. Food Chem. 2015, 63, 1833−1838

Table 2. Gluconapin, 3BITC, and Flavor in *L. oleraceum* Powders from Different Treatments

harvest	drying temp (°C)	grinding size (mm)	gluconapin (LC−MS) [mg/g, mean[c] (SD, *n*)]	3-BITC (HS-SPME/GC−MS) [relative units, mean[c](SD, *n*)]	flavor comments
1[a]	0 (FD)	0.20	7.9 (−, 2)	8.7 (−, 2)	grassy, bitter, slight wasabi
1	0 (FD)	0.75	7.7 (−, 2)	7.0 (−, 2)	grassy, slight wasabi
1	45	0.20	15.5 (−, 1)	9.8 (−, 2)	grassy, slight wasabi flavor/heat
1	45	0.75	14.8 (−, 1)	17.4 (−, 2)	grassy, slight wasabi flavor/heat
1	75	0.20	11.7 (−, 1)	2.3 (−, 2)	grassy, no wasabi flavor
1	75	0.75	11.9 (−, 1)	3.5 (−, 2)	grassy, no wasabi flavor
2[b]	45	0.20	20.1 (1.2, 4)	158 (65, 6)	grassy, slight wasabi flavor/heat
2	45	0.75	20.1 (1.3, 4)	156 (42, 5)	sweet, bitter, grassy, slight wasabi flavor
2	75	0.20	19.4 (−, 2)	7.4 (−, 2)	grassy, bitter, no wasabi flavor/heat
2	75	0.75	19.6 (−, 2)	13.1 (−, 2)	grassy, green, no wasabi flavor/heat

[a]November 2010, n = 3 informal assessors. [b]February 2011, n = 6 informal assessors. [c]Average, when n = 2.

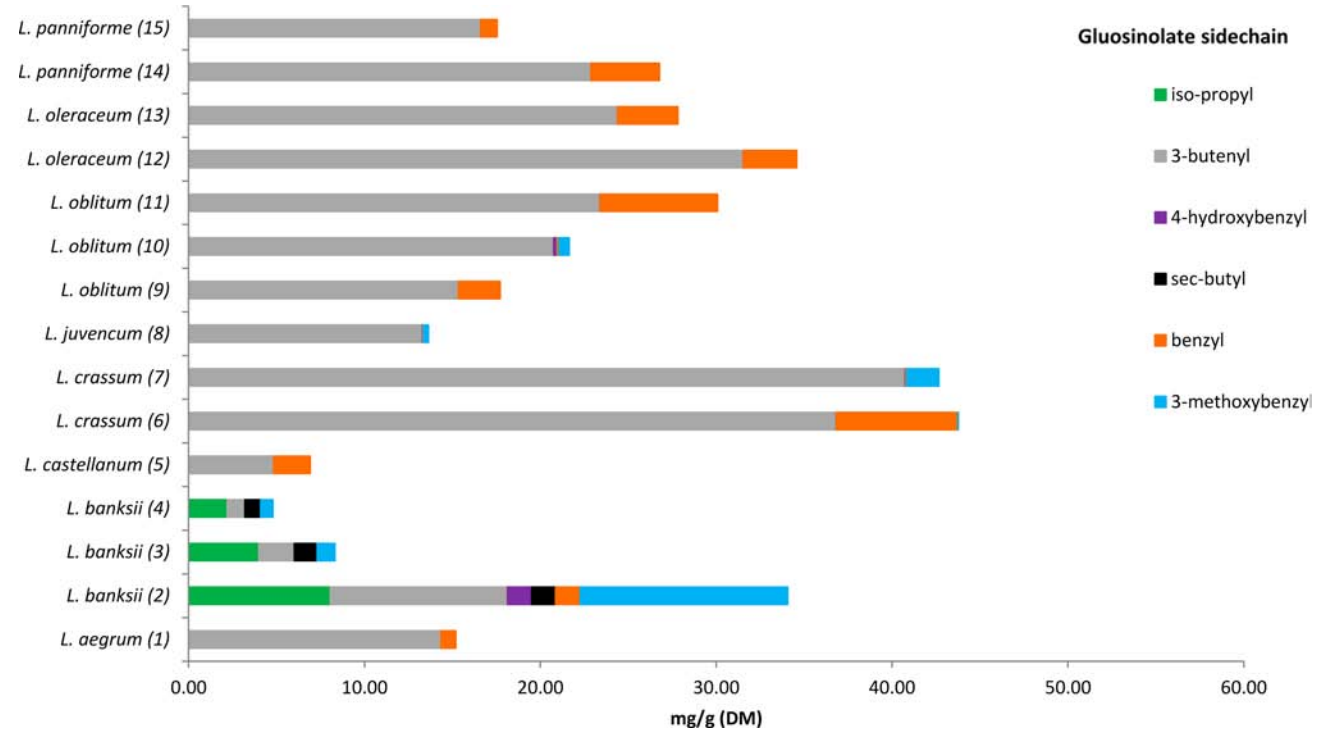

Figure 2. Glucosinolate concentrations in the leaves of New Zealand *Lepidium* species.

analogy of the Scoville scale used for pungent capsaicinoids[26]). Buttery et al.[26] studied the aroma impacts of isothiocyanates by sniffing the headspace above water solutions and found the odor threshold of **2** to be 380 ppb. This was practically the same as the odor threshold of allyl isothiocyanate (375 ppb), whereas other isothiocyanates had much more potent aromas; e.g., the ω-(methylthio)butyl isothiocyanate odor threshold was 3.4 ppb.[27] Therefore, minor glucosinolates in *Lepidium* may be important for aroma, although no other glucosinolates were detected in this *L. oleraceum* sample.

Various conditions inactivate myrosinase in different Brassicaceae.[25,28,29] To understand the parameters for *L. oleraceum*, different postharvest treatments were used to prepare dry leaf powders as potential flavor products. These were tasted and analyzed for gluconapin, **1**, and we also used an HS-SPME-GC−MS method to check the myrosinase activity by release of 3BITC, **2**. HS-SPME-GC has been used to analyze isothiocyanates from various Brassicaceae, e.g., mustard,[30] but we could not find any reports of using HS-SPME to monitor isothiocyanate release by immediate myrosinase action. Dried leaf powder was mixed with buffer solution at 35 °C for 1 min with agitation (cf. chewing) and then exposed to the SPME fiber for 10 s (cf. retro-nasal aroma sniffing[31]).

L. oleraceum leaves were dried at 0 (freeze-dried), 45, or 75 °C and ground to pass through 0.75 or 0.2 mm sieves. Samples from the higher temperature treatment were brown-green, while all other samples remained green. Chemical analyses and informal tasting results for this harvest 1 are presented in Table 2. All the samples had the grassy, green flavor that is typical of the fresh plant. Low amounts of wasabi-like pungency flavor were detected in nau leaf powders air-dried at 45 °C or freeze-dried, but not in samples dried at 75 °C. These flavor differences were not explained by differences in the concentrations of gluconapin, **1**. There were significant differences in the concentrations of **1** between drying treatments ($p < 0.001$, ANOVA), but the concentrations in the nonpungent 75 °C samples were higher than in the pungent freeze-dried samples (Table 1). The difference is in the myrosinase activity, shown by the nonpungent 75 °C samples releasing significantly ($p < 0.001$) lower amounts of

DOI: 10.1021/jf505859u
J. Agric. Food Chem. 2015, 63, 1833−1838

isothiocyanate **2** than the pungent freeze-dried and 45 °C samples (Table 1). There was also a significant ($p < 0.001$) effect of grinding size on release of **2** in this experiment, with the larger particles retaining more myrosinase activity (Table 2). However, this particle size effect was only seen for the 75 °C dried material in harvest 2 (Table 2).

We analyzed samples from a second harvest to check these results, but without the freeze-drying treatment, since this would be expensive commercially and gave lower concentrations of gluconapin, **1**, and 3BITC, **2**. The overall concentration of **1** was significantly ($p < 0.001$) higher in the nau leaves from this second harvest (Table 2). This was presumably due to seasonal variation, as has been reported for glucosinolates in various *Brassica*.[29] The overall release of **2** was also significantly ($p < 0.001$) higher from the nau leaves of this second harvest (Table 2) and disproportionately higher (about 10 times) than the rise in glucosinolate concentrations (about 1.3 times) (Table 2). Since the postharvest treatments were as similar as we could make them, this could be due to an increase in myrosinase concentration and/or activity and/or stability. This second experiment confirmed the highly significant ($p < 0.001$) difference in release of **2** between drying at 45 and at 75 °C, reflected by the lack of pungent wasabi-like flavor in the higher temperature samples (Table 2). A range of thermal stabilities have been reported for myrosinase from *Brassica*, from "up to 30 °C" to "up to 90 °C".[29]

These experiments showed that the pungent wasabi-like flavor of nau leaf powders is due to release of 3BITC, **2**, in the consumer's mouth due to the action of plant myrosinase, since there is no free **2** in leaf powders and no pungency if myrosinase is heat deactivated. Wasabi is generally used freshly grated to get the best flavor, but dried wasabi powders have been tested. These lost pungency on storage, but this could be slowed by readdition of L-ascorbic acid to preserve myrosinase activity.[25]

For this study we collected samples of nau as *L. oleraceum* sensu lato[7,32] from its geographic range across New Zealand: North Island, South Island, and off-shore islands (Table 1). We also collected *L. banksii* Kirk, which has long been recognized as a distinct species and called coastal peppercress.[7,32] However, the taxonomic revision published[8] during our work elevated most of these collections to distinct species, as shown in Table 1. Freeze-dried ground leaves from the full range of samples were analyzed for glucosinolates by LC−MS of boiling water extracts and for isothiocyanates, released by endogenous myrosinase, by HS-SPME-GC−MS.

The concentrations of glucosinolates in the leaves of eight New Zealand *Lepidium* species are shown in Figure 2. The major glucosinolate in seven of these species, all *L. oleraceum* sensu lato, was gluconapin, **1**, with benzyl glucosinolate, **5**, glucotropaeolin, the next most common component. Compound **5** has been reported from many other *Lepidium* species,[10] and the corresponding isothiocyanate, **6**, has a "chemical, pungent" odor with a threshold similar to that of 3BITC, **2**.[33] All three samples of *L. banksii* had a very distinct glucosinolate profile (Figure 2) and stood out as having a high proportion of isopropyl glucosinolate, **13**, plus *sec*-butyl glucosinolate, **11**, which were not detected in any of the other *Lepidium* species. 3-Methoxybenzyl glucosinolate, **9**, was also found in *L. banksii* and some of the other *Lepidium* species (Figure 2) and has been reported along with glucosinolates **5** and **7** as important components of *Lepidium meyenii*,[34,35] a South American tuber crop known as maca. Therefore, *L. banksii*, which is already being cultivated to save it from extinction,[7] could provide an alternative flavor crop. Further investigation on the chemical variability of New Zealand *Lepidium* species, especially using the rapid HS-SPME-GC−MS technique, could add to the studies of genetic variation under way using DNA markers.[17]

■ ASSOCIATED CONTENT

Supporting Information

Table S1 listing the glucosinolate/isothiocyanate identifications in *Lepidium*. This material is available free of charge via the Internet at http://pubs.acs.org.

■ AUTHOR INFORMATION

Corresponding Author

*Phone: +64 3 479 8966. E-mail: john.vanklink@plantandfood.co.nz.

Funding

This work was supported by the New Zealand Foundation for Research, Science and Technology (now the Ministry of Business, Innovation and Employment) via Contract C02X0601.

Notes

The authors declare no competing financial interest.

■ ACKNOWLEDGMENTS

We thank P. Heenan (Landcare Research, Lincoln) and R. Gaskell (Department of Conservation, Nelson) for supplying samples and taxonomic identifications and I. Ho, L. Huffman, C. Massarotto, C. Redman, and V. Corrigan (Plant & Food Research, Palmerston North) for sensory evaluation.

■ REFERENCES

(1) Radulovic, N.; Zlatkovic, B.; Skropeta, D.; Palic, R. Chemotaxonomy of the peppergrass *Lepidium coronopus* (L.) Al-Shehbaz (syn. *Coronopus squamatus*) based on its volatile glucosinolate autolysis products. *Biochem. Syst. Ecol.* **2008**, *36*, 807−811.

(2) Mummenhoff, K.; Linder, P.; Friesen, N.; Bowman, J. L.; Lee, J. Y.; Franzke, A. Molecular evidence for bicontinental hybridogenous genomic constitution in *Lepidium* sensu stricto (Brassicaceae) species from Australia and New Zealand. *Am. J. Bot.* **2004**, *91*, 254−261.

(3) Riley, M. *Maori Healing and Herbal*; Viking Sevenseas N.Z. Ltd.: Paraparaumu, New Zealand, 1994.

(4) McDonald, C.; McArtney, L.; Innes, H. *Medicines of the Maori*; Collins: Auckland, New Zealand, 1975.

(5) Cook, J. *Captain Cook's Journal. First Voyage*; Elliot Stock, 62 Paternoster Row; see Project Gutenberg, London, 1893. http://www.gutenberg.org/files/8106/8106-h/8106-h.htm (accessed Nov 28, 2014).

(6) de Lange, P. J.; Norton, D. A. To what New Zealand plant does the vernacular "scurvy grass" refer? *N. Z. J. Bot.* **1996**, *34*, 417−420.

(7) de Lange, P. J.; Heenan, P. B.; Norton, D.; Rolfe, J.; Sawyer, J. *Threatened Plants of New Zealand*; Canterbury University Press: Christchurch, New Zealand, 2010.

(8) de Lange, P.; Heenan, P.; Houliston, G.; Rolfe, J.; Mitchell, A. New *Lepidium* (Brassicaceae) from New Zealand. *PhytoKeys* **2013**, *24*, 1−147.

(9) Clarke, D. B. Glucosinolates, structures and analysis in food. *Anal. Methods* **2010**, *2*, 310−325.

(10) Fahey, J. W.; Zalcmann, A. T.; Talalay, P. The chemical diversity and distribution of glucosinolates and isothiocyanates among plants. *Phytochemistry* **2001**, *56*, 5−51.

(11) Jang, M.; Hong, E.; Kim, G.-H. Evaluation of antibacterial activity of 3-butenyl, 4-pentenyl, 2-phenylethyl, and benzyl isothiocyanate in *Brassica* vegetables. *J. Food Sci.* **2010**, *75*, M412−M416.

DOI: 10.1021/jf505859u
J. Agric. Food Chem. 2015, 63, 1833−1838

(12) McNaughton, S. A.; Marks, G. C. Development of a food composition databse for the estimation of dietary intakes of glucosinolates, the biologically active constitiuents of cruciferous vegetables. *Br. J. Nutr.* **2003**, *90*, 687−697.
(13) Agerbirk, N.; Olsen, C. E. Glucosinolate structures in evolution. *Phytochemistry* **2012**, *77*, 16−45.
(14) Hanschen, F. S.; Lamy, E.; Schreiner, M.; Rohn, S. Reactivity and stability of glucosinolates and their breakdown products in foods. *Angew. Chem., Int. Ed.* **2014**, *53*, 11430−11450.
(15) Gould, K. S.; Thodey, K.; Philpott, M.; Ferguson, L. R. Antioxidant activities of extracts from traditional Maori food plants. *N. Z. J. Bot.* **2006**, *44*, 1−4.
(16) Sansom, C. E.; Heenan, P. B.; Perry, N. B.; Smallfield, B. M.; van Klink, J. W. Chemosystematic analysis of volatiles from New Zealand and Australian *Gingidia* species. *Chem. Biodiversity* **2013**, *10*, 2226−2234.
(17) Robin, E.; Houliston, G. J.; Heenan, P. B. Genetic and morphological variation of two rare species of *Lepidium* (Brassicaceae) on Mangere Island, Chatham Islands, and implications for their conservation management. *Folia Geobot.* **2014**, *49*, 209−221.
(18) Oerlemans, K.; Barrett, D. M.; Suades, C. B.; Verkerk, R.; Dekker, M. Thermal degradation of glucosinolates in red cabbage. *Food Chem.* **2006**, *95*, 19−29.
(19) Mellon, F. A.; Bennett, R. N.; Holst, B.; Williamson, G. Intact glucosinolate analysis in plant extracts by programmed cone voltage electrospray LC/MS: Performance and comparison with LC/MS/MS methods. *Anal. Biochem.* **2002**, *306*, 83−91.
(20) Prestera, T.; Fahey, J. W.; Holtzclaw, W. D.; Abeygunawardana, C.; Kachinski, J. L.; Talalay, P. Comprehensive chromatographic and spectroscopic methods for the separation and identification of intact glucosinolates. *Anal. Biochem.* **1996**, *239*, 168−179.
(21) Daxenbichler, M. E.; Spencer, G. F.; Carlson, D. G.; Rose, G. B.; Brinker, A. M.; Powell, R. G. Glucosinolate composition of seeds from 297 species of wild plants. *Phytochemistry* **1991**, *30*, 2623−2638.
(22) Kaur, T.; Hussain, K.; Koul, S.; Vishwakarma, R.; Vyas, D. Evaluation of nutritional and antioxidant status of *Lepidium latifolium* Linn.: A novel phytofood from Ladakh. *PLoS One* **2013**, *8*, e69112.
(23) Sones, K.; Heaney, R. K.; Fenwick, G. R. An estimate of the mean daily intake of glucosinolates from cruciferous vegetables in the UK. *J. Sci. Food Agric.* **1984**, *35*, 712−720.
(24) Hinman, A.; Chuang, H. H.; Bautista, D. M.; Julius, D. TRP channel activation by reversible covalent modification. *Proc. Natl. Acad. Sci. U.S.A.* **2006**, *103*, 19564−19568.
(25) Depree, J. A.; Howard, T. M.; Savage, G. P. Flavour and pharmaceutical properties of the volatile sulphur compounds of Wasabi (*Wasabia japonica*). *Food Res. Int.* **1998**, *31*, 329−337.
(26) Weaver, K. M.; Luker, R. G.; Neale, M. E. Rapid quality control procedure for the determination of Scoville heat units and the detection of chillies in black pepper, via high-performance liquid chromatography. *J. Chromatogr.* **1986**, *367*, 438−442.
(27) Buttery, R. G.; Guadagni, D. G.; Ling, L. C.; Seifert, R. M.; Lipton, W. Additional volatile components of cabbage, broccoli, and cauliflower. *J. Agric. Food Chem.* **1976**, *24*, 829−832.
(28) Jones, R. B.; Faragher, J. D.; Winkler, S. A review of the influence of postharvest treatments on quality and glucosinolate content in broccoli (*Brassica oleraceae* var *italica*) heads. *Postharvest Biol. Technol.* **2006**, *41*, 1−8.
(29) Dal Pra, V.; Jardim, N. S.; Dolwitsch, C. B.; Mazutti, M. A.; Viana, C.; Bohrer, D.; Nascimento, P. C.; Machado de Carvalho, L.; Barreto da Silva, M.; Amaro de Carvalho, C.; Barcellos da Rosa, M. A review of influence of environment and process parameters on glucosinolate-myrosinase system from *Brassica*. *J. Appl. Pharm. Sci.* **2013**, *3*, 121−128.
(30) Zhang, D.; Tang, J.; Ding, X. Analysis of volatile components during potherb mustard (*Brassica juncea*, Coss.) pickle fermentation using SPME−GC-MS. *LWT—-Food Sci. Technol.* **2007**, *40*, 439−447.
(31) Civille, G. V.; Oftedal, K. N. Sensory evaluation techniques—Make "good for you" taste "good". *Physiol. Behav.* **2012**, *107*, 598−605.
(32) Allan, H. H. *Flora of New Zealand. Indigenous Tracheophyta. Psilopsida, Lycopsida, Filicopsida, Gymnospermae, Dicotyledones*; DSIR: Wellington, New Zealand, 1961; Vol. *I*.
(33) Masuda, H.; Harada, Y.; Tanaka, K.; Nakajima, M.; Tabeta, H. Characteristic odorants of wasabi (*Wasabia japonica* Matum), Japanese horseradish, in comparison with those of horseradish (*Armoracia rusticana*). *ACS Symp. Ser.* **1996**, *637*, 67−78.
(34) Piacente, S.; Carbone, V.; Plaza, A.; Zampelli, A.; Pizza, C. Investigation of the tuber constituents of maca (*Lepidium meyenii* Walp.). *J. Agric. Food Chem.* **2002**, *50*, 5621−5625.
(35) Yabar, E.; Pedreschi, R.; Chirinos, R.; Campos, D. Glucosinolate content and myrosinase activity evolution in three maca (*Lepidium meyenii* Walp.) ecotypes during preharvest, harvest and postharvest drying. *Food Chem.* **2011**, *127*, 1576−1583.

DOI: 10.1021/jf505859u
J. Agric. Food Chem. 2015, 63, 1833−1838

elimination of a fatty acid to form a cyclic acyloxonium cation reactive intermediate, followed with a nucleophilic substitution with a chlorine anion to form 3-MCPD diesters.[15] However, no direct evidence was provided to support the hypothesis. Whether TAG could be the precursor for 3-MCPD monoester formation also remained unknown.

The present study aimed to investigate whether TAG may serve as precursors for 3-MCPD di- and monoesters and to explore possible chemical mechanisms for their formation. TAG and selected chlorine-containing compounds were reacted under a high-temperature and low-moisture condition for 3-MCPD ester formation. An electron spin resonance (ESR) spectrometer was utilized to detect free radicals, whereas Fourier transform infrared spectroscopy (FT-IR) was used to examine the possible involvement of carbonyl group(s). The results from this study may serve as the scientific foundation for reducing the level of 3-MCPD esters in refined edible oils and other food products.

MATERIALS AND METHODS

Materials. Tristearoylglycerol (TSG) and lindane were purchased from J&K Scientific (Beijing, China). Sodium acetate (MS grade), iron chloride, DMPO, ferric sulfate, and ferrous sulfate were purchased from Sigma-Aldrich (St. Louis, MO, USA). Hexadecane and iron dichloride were purchased from Aladdin Reagent (Shanghai, China). Sodium hydroxide, toluene, sodium chloride, potassium chloride, copper chloride, zinc chloride, and concentrated HCl were bought from Ambrosia Pharmaceuticals (Shanghai, China). High-purity nitrogen (99.999%) was purchased from Ruili Chemical Gas Co., Ltd. (Shanghai, China). 2-Propanol and methanol (LC-MS grade) were obtained from Merck (Darmstadt, Germany). GHP membrane (0.2 μm) was purchased from Pall Corp. (New York, NY, USA). The refined palm oil was a gift from the Yihai Kerry/Wilmar Biotechnology Research and Development Center (Shanghai, China).

Model Reaction between TSG and Selected Chlorine-Containing Compounds. For the reaction between solid chloride agents and TSG, 2 mg of NaCl, KCl, $FeCl_2$, $CuCl_2$, $ZnCl_2$, $FeCl_3$, or lindane was added into 10 mL of 0.5 mg/mL TSG solution in hexadecane, respectively, according to a previous study.[14] HCl gas was prepared by heating concentrated HCl, followed by drying through 98% H_2SO_4, and introduced into 10 mL of a 0.5 mg/mL TSG solution. To examine whether Fe^{2+} or Fe^{3+} could catalyze the formation of 3-MCPD esters, 2 mg of $FeSO_4$ or $Fe_2(SO_4)_3$ was added into the mixture of 2 mg of KCl, $CuCl_2$, or lindane and 10 mL of 0.5 mg/mL TSG solution, respectively. Each reaction was refluxed with stirring for 20 min under ambient temperature or 120 or 240 °C, respectively. The nonpolar reaction system was low in moisture content. After cooling to ambient temperature, the mixture was diluted to 1/100 (v/v) with methanol, filtered through a GHP 0.2 μm membrane, and subjected to UPLC-Q-TOF-MS analysis (Waters Xevo G_2 Q-TOF-MS, Milford, MA, USA).[14]

ESR Determination of Radical Signals. To determine whether free radical was generated in the formation of 3-MCPD esters from TSG at different temperatures, TSG solution, TSG solution containing DMPO, TSG solution containing DMPO and $FeCl_3$, and TSG solution containing DMPO, KCl and $Fe_2(SO_4)_3$ were kept at ambient temperature or 60, 80, or 120 °C, respectively, for 20 min and measured on a Bruker EMX-8/2.7C spectrometer equipped with a variable-temperature system (Bruker Optics, Karlsruhe, Germany) in a 0.1 mL quartz tube for their ESR signals.[14] The concentration of TSG solution was 0.5 mg/mL in toluene. The final DMPO concentration was 20 mmol/L in the reaction mixture, whereas the concentration of $FeCl_3$ or $Fe_2(SO_4)_3$ was 0.2 mg/mL. The ESR conditions were the same as described before.[14]

FT-IR Measurements. TSG was directly applied onto the attenuated total reflectance (ATR) crystal and scanned immediately at 25 °C and then heated to 120 °C and scanned immediately.[14] FT-IR spectra were recorded on a Spectrum 100 FT-IR spectrometer (PerkinElmer, Waltham, MA, USA) equipped with a pressure application device, combined with a deuterated triglycine sulfate (DTGS) detector and a single bounce diamond temperature controller.

Effect of Chelating Agent. Two milligrams of $FeCl_3$ was added into 5 mL of 0.5 mg/mL TSG solution, followed by ultrasonic oscillation for 30 min after the addition of a series of different amount of EDTA-2Na (1.2, 2.3, 4.6, 9.2, and 23.0 mg). The control reaction contained no EDTA-2Na. The reaction was carried out at 120 °C for 20 min with continuous stirring. When the mixtures were cooled to ambient temperature, they were diluted with 50-fold of methanol/2-propanol (1:1, v/v) and examined by UPLC-Q-TOF MS after filtration.[14]

The experiment was also conducted using refined palm oil under a high-temperature and low-moisture condition. $FeCl_3$ (400 mg) was added into 80 g of refined palm oil and mixed well, then 0, 0.938, or 4.655 g of EDTA-2Na was added, respectively, for the control reaction and low and high levels of EDTA-2Na. The mixture was kept at 240 °C for 1 h with a nitrogen flow rate of 2 L/min at a pressure of about 5 mbar. After the reaction, inlet N_2 was stopped, and vacuum was released when the temperature was below 100 °C. The mixture was diluted with 2-propanol, filtered through a GHP 0.2 μm membrane, and analyzed by UPLC-Q-TOF MS.

Q-TOF MS Examination of DMPO Radical Adducts. TSG solutions (0.5 mg/mL in toluene) with $Fe_2(SO_4)_3$ and DMPO were heated to 120 °C and kept for 20 min. The final concentrations of $Fe_2(SO_4)_3$ and DMPO in the TSG solutions were 0.2 mg/mL and 20 mmol/L, respectively. After cooling to ambient temperature, the TSG solution was further diluted with methanol for 100-fold and injected directly into the Q-TOF mass spectrometer for analysis according to a method described previously.[14] Briefly, an ESI positive mode was selected with lockspray as an internal standard; capillary voltage for positive ion mode was 3.0 kV; sampling cone voltage was 30.0 kV; source temperature was 120 °C with a desolvation temperature at 450 °C; cone gas flow and desolvation gas flow were 50 and 800 L/h, respectively; scan range was m/z 50−1000 Da; scan time was 0.1 s. Data were collected and analyzed using Masslynx 4.1 software, and all peak areas were determined using the total ion counts in the extracted ion chromatogram.

Statistical Analysis. Data were expressed as the mean ± standard deviation (SD) for each experiment. Differences between means were determined by the analysis of one-way ANOVA and Tukey's test, using SPSS software (SPSS for Windows, version rel. 16.0, SPSS Inc., Chicago, IL, USA). Statistical significance was declared at $P < 0.05$.

RESULTS AND DISCUSSION

Potential of Forming 3-MCPD Esters from TSG. NaCl, KCl, $FeCl_2$, $CuCl_2$, $ZnCl_2$, $FeCl_3$, and dry HCl gas were examined as the inorganic chlorine donors, whereas lindane was selected as an organic chloride-containing compound to react with TSG because they were able to react with *sn*-1,2-stearoylglycerol (DSG) to form 3-MCPD fatty acid diester.[14] UPLC-Q-TOF-MS analysis of the reaction products showed that only $FeCl_2$ and $FeCl_3$ at 120 and 240 °C and HCl gas at 240 °C formed 3-MCPD diesters. It was reported that NaCl, KCl, $FeCl_2$, $CuCl_2$, $ZnCl_2$, $FeCl_3$, HCl gas, and lindane were able to react with DSG at 240 °C to form 3-MCPD diester.[14] It was also reported that only HCl gas, $FeCl_2$, and $FeCl_3$ were able to react with DSG and form detectable amounts of 3-MCPD diester at 120 °C.[14] Taken together, these results suggested that TSG might be less active in reacting with chlorine-containing compounds to form 3-MCPD diesters compared to DSG. Also, $FeCl_2$ and $FeCl_3$ might have greater reactivity with TAG/TSG and DAG/DSG than HCl gas and other inorganic and organic chlorine compounds to generate 3-MCPD esters.

In addition, 3-MCPD fatty acid monoester was also generated in the reaction of $FeCl_3$ and TSG at both 120 and

DOI: 10.1021/jf5061216
J. Agric. Food Chem. 2015, 63, 1839−1848

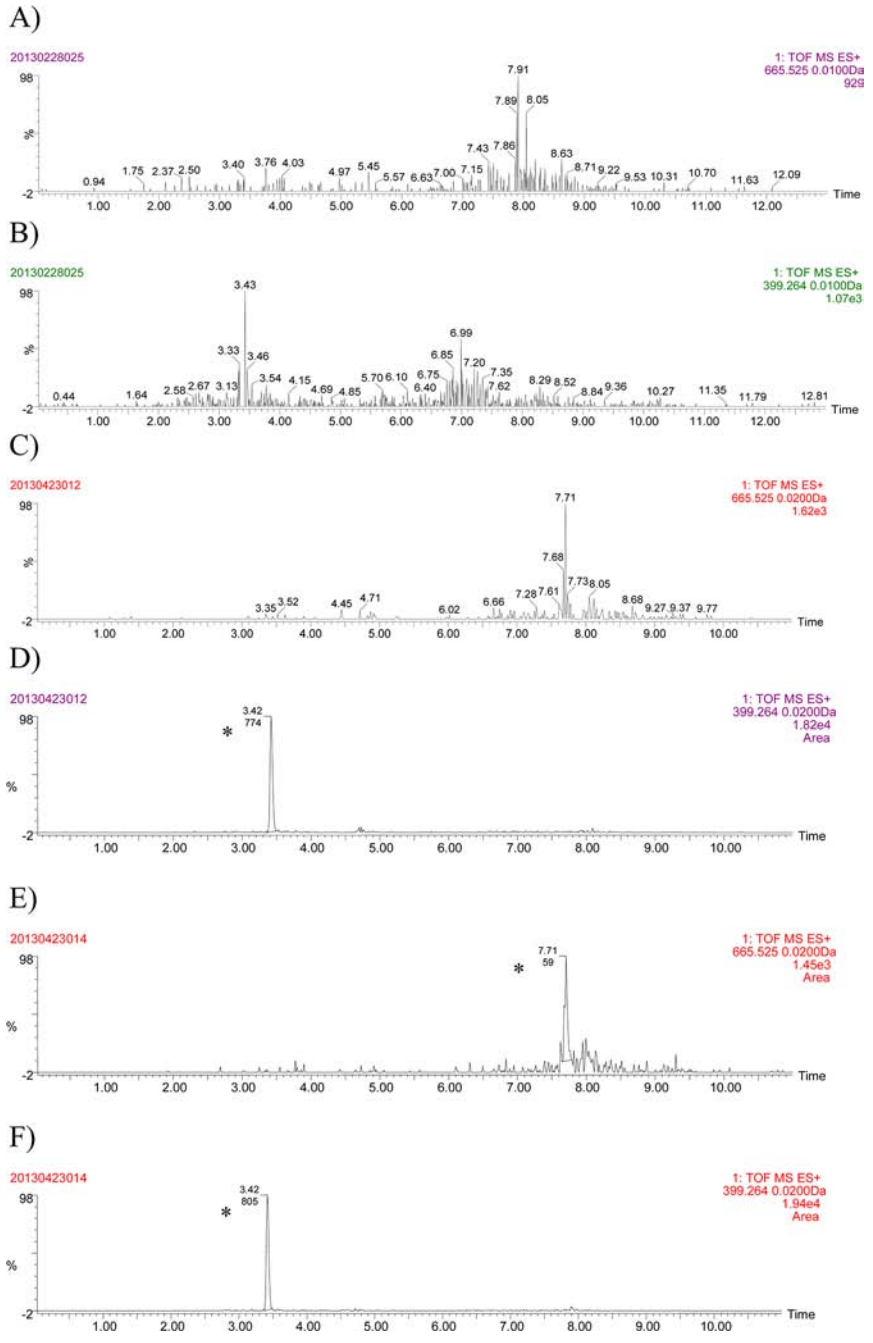

Figure 1. UPLC-QTOF MS extracted-ion chromatograms for the reaction products of TSG and lindane. The extracted ions were for 3-MCPD (A) diester ion, (B) monoester, (C) diester with $Fe_2(SO_4)_3$, (D) monoester with $Fe_2(SO_4)_3$, (E) diester with $FeSO_4$, and (F) monoester with $FeSO_4$. The concentration was 0.5 mg/mL for TSG and the reaction temperature was 120 °C. The concentration was 0.2 mg/mL for $Fe_2(SO_4)_3$ and $FeSO_4$. ∗ indicates the peak area for a 3-MCPD di- or monoester ion.

240 °C, suggesting that TSG or other TAGs might also serve as precursors for 3-MCPD fatty acid monoester formation under the same high-temperature and low-moisture condition. Interestingly, no detectable amount of 3-MCPD monoester was formed in the reactions of DSG with all of the tested chlorine-containing compounds in an earlier study.[14] To our knowledge, this was the first time that TAG was found to form 3-MCPD monoester under a high-temperature and low-moisture condition. The fact that only $FeCl_2$ or $FeCl_3$ could react with TAG to form 3-MCPD esters under a high-temperature and low-moisture condition, similar to that during oil deodorization, also raised the question of whether Fe^{3+} or Fe^{2+} could play a role in 3-MCPD ester formation.

Possible Role of Fe^{3+} or Fe^{2+} in 3-MCPD Ester Formation. To examine the possible role of Fe^{3+} or Fe^{2+} in the formation of 3-MCPD fatty acid esters from TAG, $Fe_2(SO_4)_3$ and $FeSO_4$ were tested as the Fe^{3+} and Fe^{2+} donors, respectively. TSG was reacted with both inorganic chlorides including KCl and $CuCl_2$ and an organic chlorine compound lindane in the presence of Fe^{3+} or Fe^{2+} at room temperature and 120 and 240 °C, respectively. Figure 1 reports the 3-MCPD ester formation in the reaction mixture of TSG and lindane at 120 °C. No detectable amount of either 3-MCPD

DOI: 10.1021/jf5061216
J. Agric. Food Chem. 2015, 63, 1839−1848

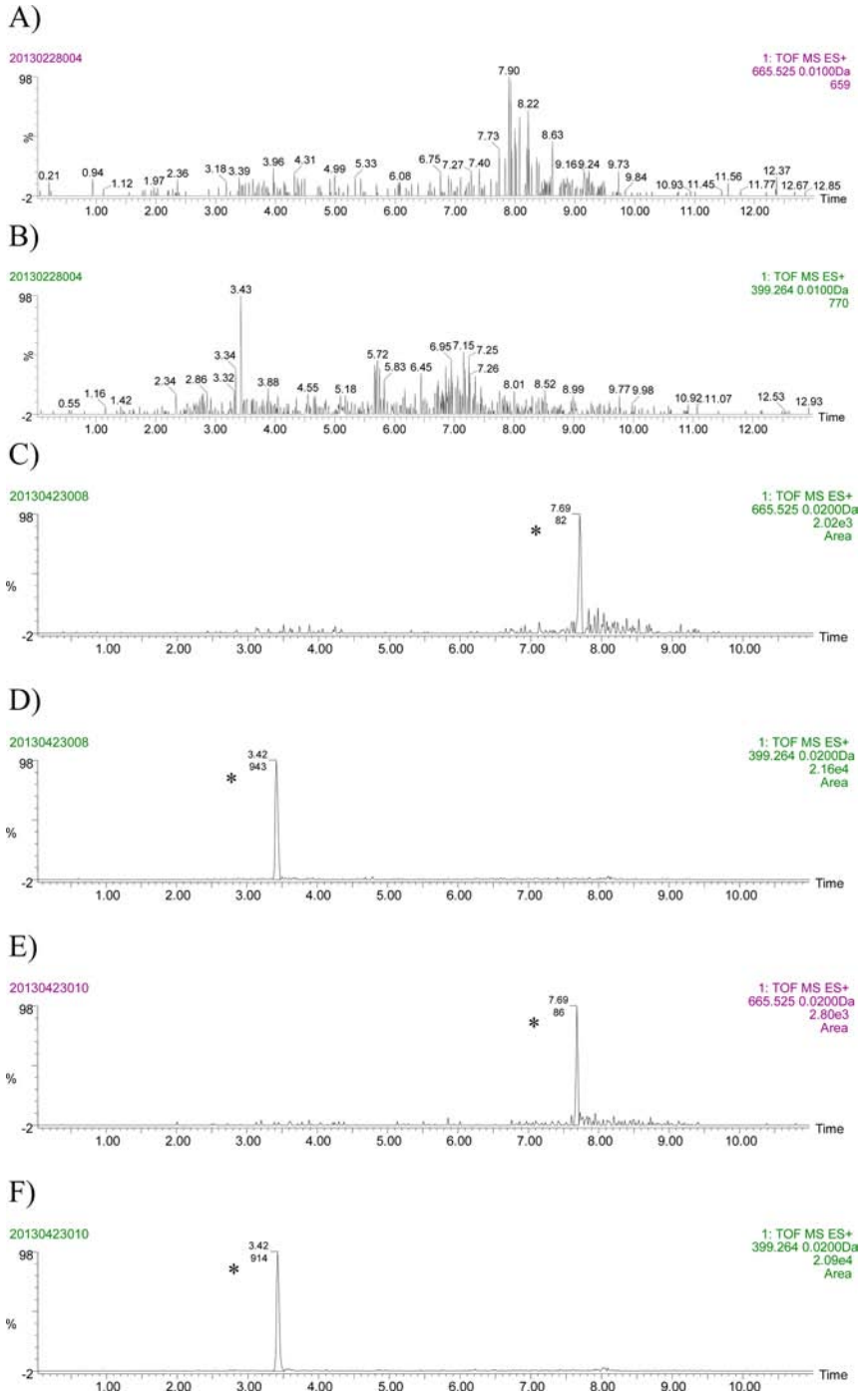

Figure 2. UPLC-QTOF MS extracted-ion chromatograms for the reaction products of TSG and KCl. The extracted ions were for 3-MCPD (A) diester ion, (B) monoester, (C) diester with $Fe_2(SO_4)_3$, (D) monoester with $Fe_2(SO_4)_3$, (E) diester with $FeSO_4$, and (F) monoester with $FeSO_4$. The concentration was 0.5 mg/mL for TSG and the reaction temperature was 120 °C. The concentration was 0.2 mg/mL for $Fe_2(SO_4)_3$ and $FeSO_4$. ∗ indicates the peak area for a 3-MCPD di- or monoester ion.

diester (Figure 1A) or monoester (Figure 1B) was observed under the experimental conditions. Significant amounts of 3-MCPD diesters at the retention time of 7.71 min with an m/z value of 665.5248 (calculated as 665.5252) were detected with the presence of $Fe_2(SO_4)_3$ or $FeSO_4$ (Figure 1, panels C and E, respectively), with significant levels of the monoester at 3.45 min with m/z 399.2640 (calculated as 399.2642) (Figure 1D,F). The structures of the 3-MCPD fatty acid mono- and diesters were confirmed with high-resolution MS analysis (data not shown). The possible catalytic effect of Fe^{3+} or Fe^{2+} in 3-MCPD ester formation was also confirmed with an inorganic chlorine compound KCl (Figure 2). No 3-MCPD esters were detected in the reaction mixture of TSG and KCl (Figure 2A,B), whereas significant contents of 3-MCPD diester at 7.69 min and monoester at 3.42 min were detected when $Fe_2(SO_4)_3$ was added (Figure 2C,D) or $FeSO_4$ was added in the reaction (Figure 2E,F). Furthermore, no difference in catalytic activity was observed between $Fe_2(SO_4)_3$ and $FeSO_4$. Interestingly, the ratio of 3-MCPD monoester to diester was approximately 10:1 when TSG reacted with KCl in the presence of $Fe_2(SO_4)_3$ or

DOI: 10.1021/jf5061216
J. Agric. Food Chem. 2015, 63, 1839−1848

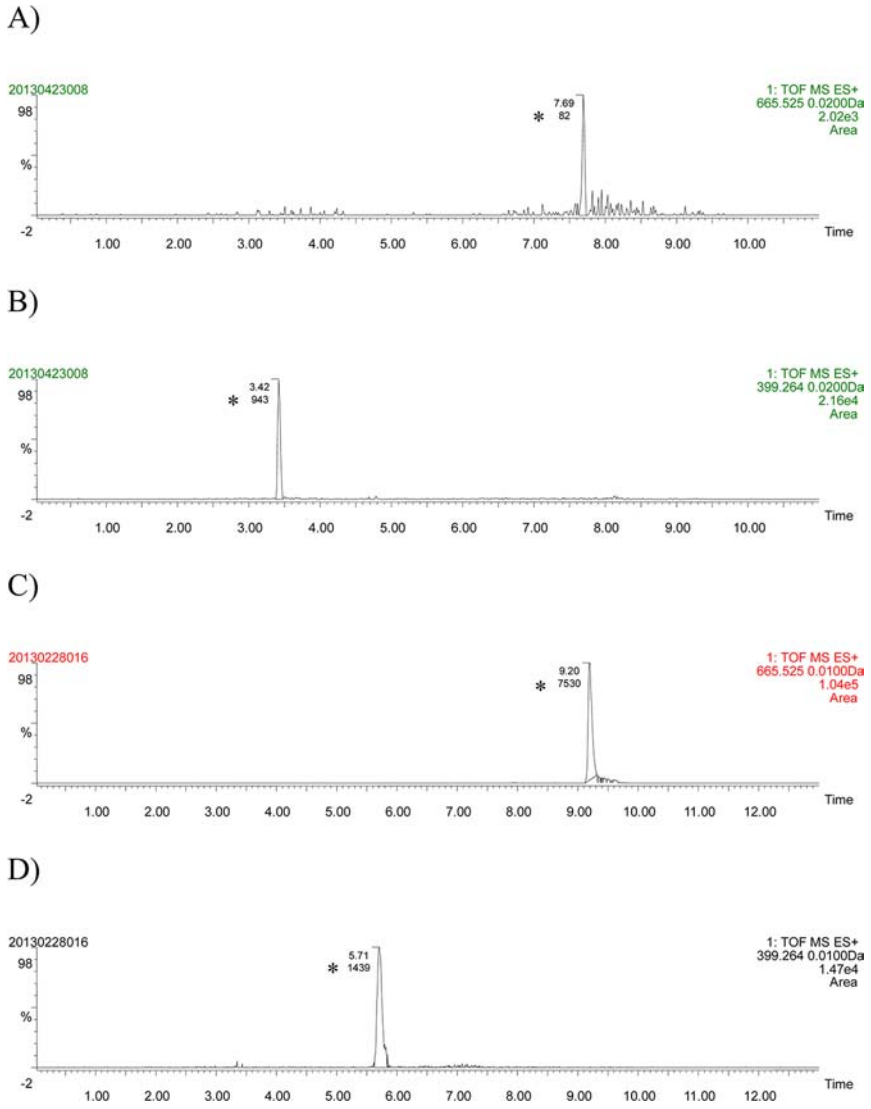

Figure 3. UPLC-QTOF MS extracted-ion chromatograms for the reaction products of TSG and different chlorine sources: (A) 3-MCPD diester ion with KCl and $Fe_2(SO_4)_3$; (B) 3-MCPD monoester ion with KCl and $Fe_2(SO_4)_3$; (C) 3-MCPD diester ion with $FeCl_3$; (D) monoester ion with $FeCl_3$. The retention times of both diester and monoester are different between injections because the UPLC columns were different. The concentration was 0.5 mg/mL for TSG the and reaction temperature was 120 °C. The concentration was 0.2 mg/mL for $Fe_2(SO_4)_3$ and $FeSO_4$. * indicates the peak area for a 3-MCPD di- or monoester ion.

$FeSO_4$ (Figure 2D−F, respectively), whereas the ratio was 1:10 when TSG reacted with $FeCl_3$ (Figure 3). The results suggested that both Fe^{3+} and Fe^{2+} were able to catalyze the formation of 3-MCPD fatty acid di- and monoesters from TAG and might favor the formation of 3-MCPD monoesters under a high-temperature and low-moisture condition, indicating their important role in forming 3-MCPD esters during the oil deodorization process. The results also suggested that the overall amount and profile of 3-MCPD esters also depended on the type of chlorine sources. This was the first report about the possible catalytic effect of Fe^{3+} or Fe^{2+} in 3-MCPD ester formation from TAG, suggesting a possible approach to mitigate 3-MCPD esters in refined oils through reducing the Fe availability. This was also the first report that chlorine source ($FeCl_3$ vs KCl with $Fe_2(SO_4)_3$ or $FeSO_4$) may alter the final 3-MCPD ester profile.

In addition, the two facts that 3-MCPD esters were formed through the reaction of lindane and TSG in the presence of Fe^{3+} or Fe^{2+} and that lindane is an organic chlorine compound also suggested a possible free radical mediated mechanism for 3-MCPD ester formation from TAG. It was interesting why or how Fe^{3+} or Fe^{2+} was able to facilitate the 3-MCPD ester formation under a low-moisture and high-temperature condition.

Electron Spin Resonance Examination of Possible Free Radicals. ESR examination was performed to examine and confirm the presence of free radicals under the experimental conditions, because our previous study showed a free radical mediated mechanism for 3-MCPD fatty acid diester formation from diacylglycerol.[14] As shown in Figure 4A, heating TSG with DMPO, a spin trapping agent, at 60 °C for 20 min did not result in any detectable level of free radicals, whereas significant ESR signal was detected in TSG with DMPO kept at 120 °C for 20 min (Figure 4B), indicating the generation of free radicals due to the thermal treatment. To test the role of Fe^{3+}, the mixture of TSG and DMPO with $Fe_2(SO_4)_3$ or $FeCl_3$ was heated for 20 min under the same conditions and examined for possible ESR signals. Weak ESR

DOI: 10.1021/jf5061216
J. Agric. Food Chem. 2015, 63, 1839−1848

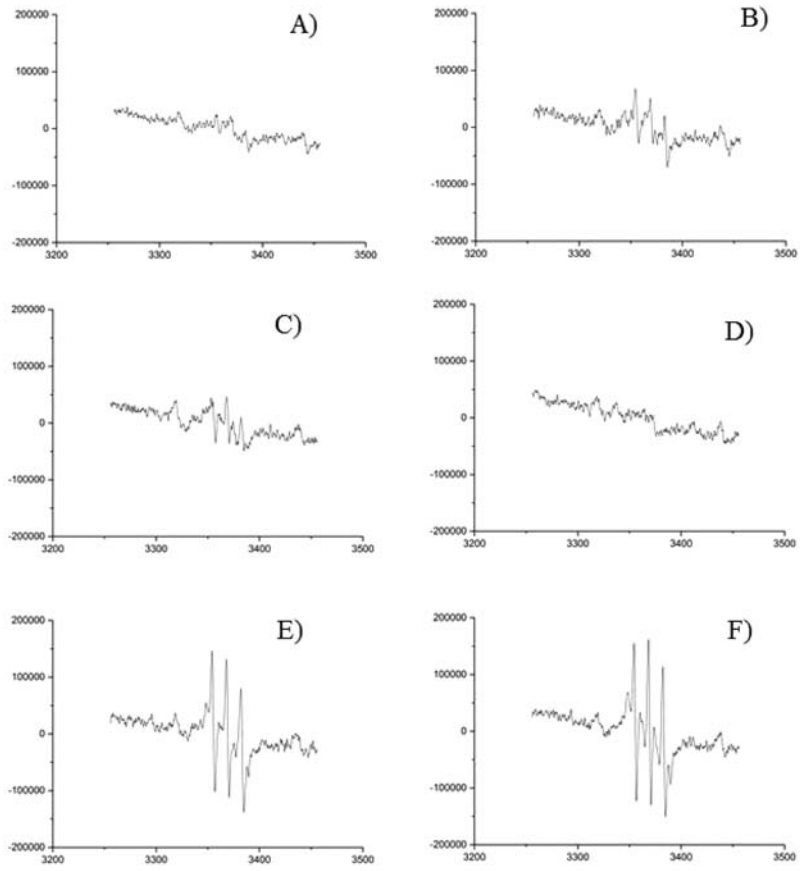

Figure 4. ESR examination of TSG mixtures. The TSG reaction mixtures were kept at (A) 60 °C without Fe, (B) 120 °C without Fe, (C) 60 °C with $FeCl_3$, (D) 120 °C with $FeCl_3$, (E) 60 °C with $Fe_2(SO_4)_3$, and (F) 120 °C with $Fe_2(SO_4)_3$. All TSG reaction mixtures contained 0.5 mg/mL TSG and 20 mmol/L DMPO, as well as different chlorine compounds. The concentration was 0.2 mg/mL for $FeCl_3$ and $Fe_2(SO_4)_3$. All reactions were carried out for 20 min in toluene at the temperature before ESR analysis.

signal was observed when the mixture of $FeCl_3$, TSG, and DMPO was heated at 25 °C (Supporting Information, Figure S1) and 60 °C (Figure 4C), but no significant ESR signal was detected in the mixture kept at 80 °C (Figure S1) and 120 °C (Figure 4D). Interestingly, the mixture of $Fe_2(SO_4)_3$, TSG, and DMPO kept at 60 °C (Figure 4E), 80 °C (Figure S2), and 120 °C (Figure 4F) had significant levels of ESR signals. These results suggested that $Fe_2(SO_4)_3$ might promote radical generation at a high-temperature and low-moisture condition and consequently stimulate 3-MCPD ester formation from TSG or other TAGs when a chlorine source is also available. The absence of ESR signals in the mixture of TSG, DMPO, and $FeCl_3$ at a relatively higher temperature might be explained by the availability of chlorine in $FeCl_3$, which immediately reacted with the radical intermediate(s) to form the 3-MCPD ester final product(s) under the experimental conditions. The catalytic activity of Fe^{3+} or Fe^{2+} in generating free radicals might depend on their electronic structures and electron availability. The weaker ESR signals detected in the $FeCl_3$ and TSG reactions might also be partially explained by the lesser electron availability of $FeCl_3$ compared to that of $Fe_2(SO_4)_3$.

Effect of Chelating Agent. To further examine the role of Fe^{3+} or Fe^{2+} in forming 3-MCPD esters, a chelating agent, EDTA-2Na, was selected and investigated for its possible influence on 3-MCPD ester formation in the presence of Fe^{3+}. Figure 5A shows that EDTA-2Na at a molar ratio to $FeCl_3$ of 1:1 or greater significantly decreased 3-MCPD diester formation from TSG in a dose-dependent manner, but had little effect on the monoester amount (data not shown).

The effect of EDTA on 3-MCPD ester formation was also investigated using refined palm oil. As shown in Figure 5B, the addition of EDTA in the reaction mixture was able to suppress the formation of 1-palmitoyl, 1-oleoyl, and 1-linoleoyl 3-MCPD esters in a dose-dependent matter. The levels of other 3-MCPD esters were not estimated as their levels were low in the reaction mixture and could not be accurately quantified. The result further confirmed the catalytic role of Fe^{3+} or Fe^{2+} in forming 3-MCPD fatty acid esters from TAG under a high-temperature and low-moisture condition and suggested that chelating agents might suppress 3-MCPD fatty acid formation from TAG through reducing Fe^{2+} or Fe^{3+} availability.

Taken together, the data in Figure 5 indicate that the oil composition might alter the 3-MCPD ester formation and modulate the catalytic effect of Fe^{3+} or Fe^{2+}, suggesting that 3-MCPD ester formation during oil refining could be very complicated and warrant additional research. This finding was partially supported by the earlier observation that the oil composition or type of oil might alter the generation of 3-MCPD esters.[19]

FT-IR Determination of TSG at 25 and 120 °C. To further examine the proposed free radical mechanism(s) for 3-MCPD di- and monoester formation, TSG kept at 25 and 120 °C was measured for FT-IT spectra. As shown in Figure 6A, because the carbonyl ester groups at C-1 and C-3 positions have the same chemical environment, TSG exhibited two

DOI: 10.1021/jf5061216
J. Agric. Food Chem. 2015, 63, 1839−1848

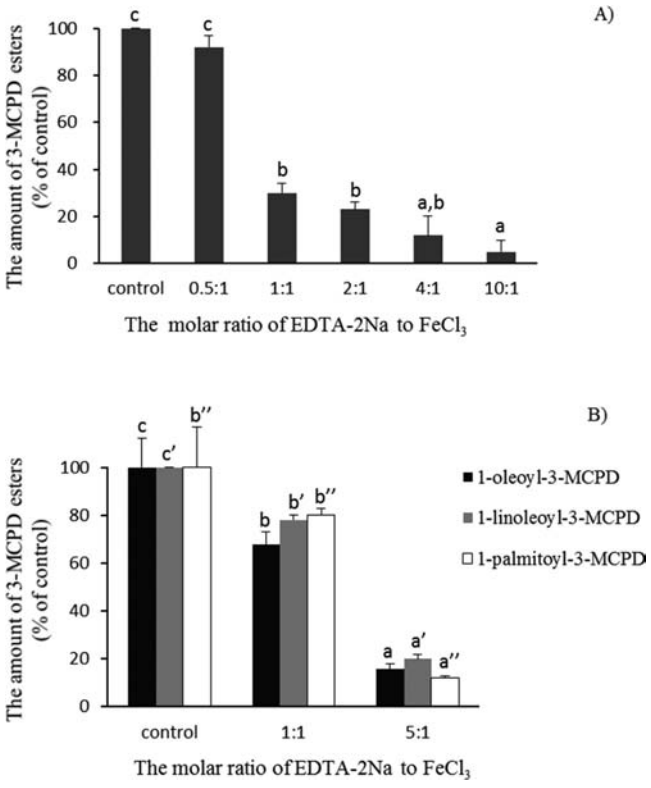

Figure 5. Effect of EDTA on 3-MCPD ester formation: (A) 3-MCPD diester formation from TSG; (B) formation of the three 3-MCPD monoesters from a refined palm oil. The relative amounts of 3-MCPD esters are reported. Different letters (a–c) in panel A reflect significant differences in the relative amount of 3-MCPD diester in TSG ($P < 0.05$), whereas different letters (a–c, a′–c′, and a″–c″) in panel B represent significant difference in relative amount of 1-oleoyl, 1-linoleoyl, and 1-palmitoyl 3-MCPD esters in the palm oil, respectively ($P < 0.05$).

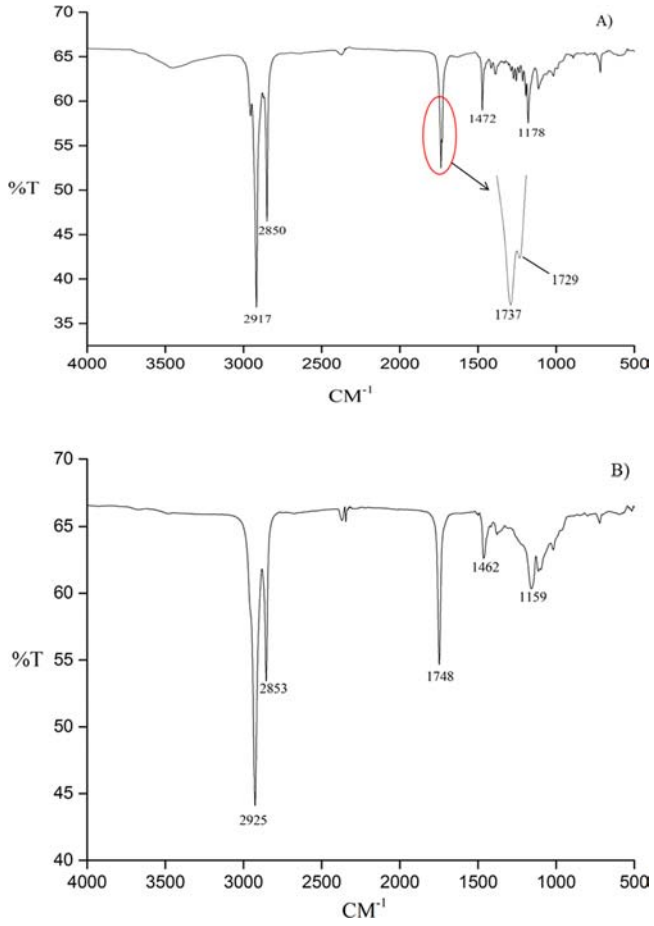

Figure 6. FT-IR spectra of TSG kept at (A) 25 °C and (B) 120 °C.

carbonyl absorbance bands at 25 °C, one centered at 1737 cm^{-1} and the other centered at 1729 cm^{-1}. However, when heated to 120 °C, only one carbonyl absorbance band centered at 1748 cm^{-1} was detected, reflecting a hypochromic shift of the carbonyl group (Figure 6B). The results indicated the involvement of the carbonyl ester group at the C-2 position or two of the three carbonyl groups at a high temperature in forming 3-MCPD esters.[14]

Proposed Mechanism for 3-MCPD Ester Formation from TAG. On the basis of the data, a new mechanism was proposed for 3-MCPD ester formation from a triacylglycerol under a high-temperature and low-moisture condition. As shown in Figure 7, the reaction might be initiated by the formation of a carbon-centered radical (**I**) by eliminating a RCOO$^{\bullet}$ from C-1 or C-3 of TSG (TAG) in step a due to the thermal treatment and/or the catalytic effect(s) of Fe^{3+} or Fe^{2+}. The carbon-centered radical was not stable and might immediately attack the ester carbonyl group located at the C-2 and form a cyclic acyloxonium free radical (**II**, CAFR) through step b or form a epoxide ring free radical (**III**, ERFR) through step c. CAFR and ERFR could be relatively stable because of the dislocation of the unpaired electron among multiple atoms within the ring structures. CAFR could either react with a chlorine radical or extract a chlorine radical from a chlorine-containing compound, such as HCl, Cl_2, NaCl, KCl, $FeCl_2$, $FeCl_3$, $CuCl_2$, or $ZnCl_2$, to form 3-MCPD diesters through step d or e, respectively, whereas EAFR could undergo a similar reaction to form 3-MCPD monoesters (Figure 7). The proposed mechanism(s) could explain the formation of both 3-MCPD fatty acid diesters and monoesters under a high-temperature and low-moisture condition, such as that during the deodorization procedure in the oil-refining process. The mechanism(s) could also explain the copresence of 3-MCPD and glycidol fatty acid esters in the refined edible oils.[20]

It was reported that both Fe^{2+} and Fe^{3+} were associated with free radical generation[21] and lipid peroxidation.[22] Fe^{2+} and Fe^{3+} may serve as a detrimental catalyst in 3-MCPD and glycidol fatty acid ester formation through promoting radical generation and forming complexes with the radical intermediates to enhance their stability. These might be explained by their special electron structures. For instance, Fe^{2+} and Fe^{3+} have been proposed to form iron–oxygen complexes such as preferred ion (Fe^{2+}–O_2 or Fe^{3+}–O_2) or ferryl ion (FeO^{2+}) to facilitate lipid peroxidation.[22]

To further examine the proposed radical mechanism(s), TSG was heated with $Fe_2(SO_4)_3$ and DMPO to 120 °C for 20 min, and the reaction mixtures were examined using Q-TOF MS. However, neither the intermediate free radical–DMPO adducts nor other possible product ions of the intermediates were detected.

Possible Role of Thermal Treatment on 3-MCPD Ester Formation. The effect of thermal treatment degree on 3-MCPD ester formation was also investigated by reacting TSG with $FeCl_3$ at 120 and 240 °C, and the concentrations of products were semiquantified on the basis of the peak areas of

DOI: 10.1021/jf5061216
J. Agric. Food Chem. 2015, 63, 1839–1848

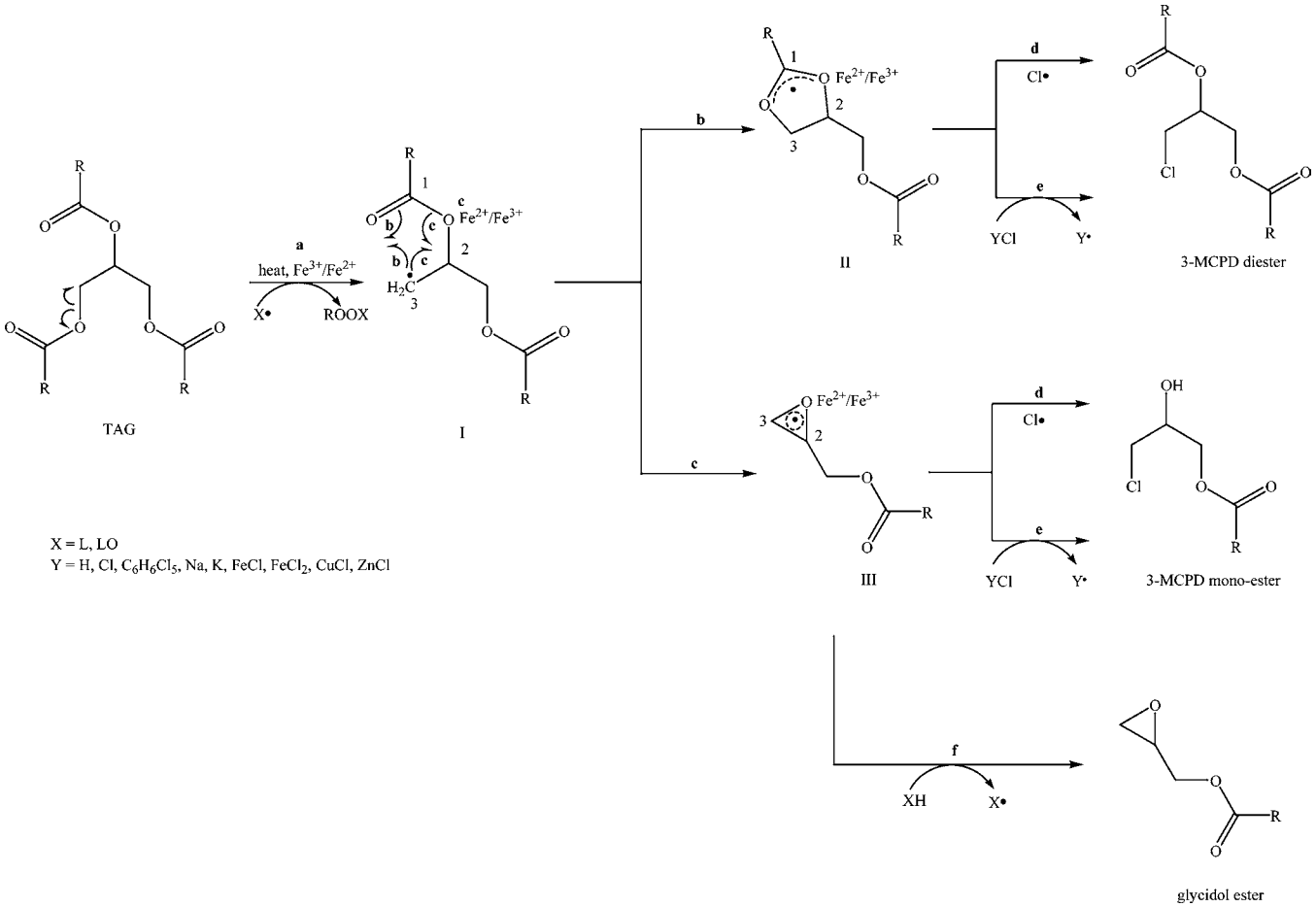

Figure 7. Proposed chemical mechanisms for 3-MCPD ester formation from triacylglycerol (TAG).

their extracted ion chromatogram. At 120 °C, the total ion count for 3-MCPD di- and monoesters was 8969 and was 5588 when the reaction was carried out at 240 °C, suggesting that a higher degree of thermal treatment might result in a lower overall 3-MCPD ester amount in the oil products (Figure 8). The finding was further confirmed with the reactions of TSG and KCl in the presence of either Fe^{3+} or Fe^{2+}. Compared to the reactions carried out at 240 °C, greater levels of total 3-MCPD esters were detected at 120 °C, regardless of the form of Fe (Supporting Information, Figures S3 and S4). This finding was in contrast to the observation by Svejkovská and others that MCPD ester concentration was proportional to the reaction temperature,[23] but supported an earlier observation that 3-MCPD esters undergo thermal degradation with the rate proportional to the thermal treatment degree.[24]

In addition, the ratio of 3-MCPD diester to monoester was more than 5:1 at 120 °C, whereas the ratio became about 1.3 when reacted at 240 °C (Figure 8), suggesting the possible influence of thermal treatment degree on the ratio of 3-MCPD di- and monoesters. Also noted was that TSG with KCl and Fe^{3+} also resulted in an ion count of 943 for 3-MCPD monoester and 82 for diester at 120 °C, respectively, whereas the reaction generated an ion count of 788 for 3-MCPD monoester without detectable diester (Supporting Information, Figure S3). For the reaction of TSG with KCl and Fe^{3+}, the ratios between diester and monoester were 1:10.6 and 1:14.5 at 120 and 240 °C, respectively (Figure S4). These data suggested the thermal degradation of 3-MCPD esters might include both dechlorination and deacylation, and deacylation may be more preferred under the experimental conditions. This finding was in contrast to the conclusion by Ermacora and Hrncirik that dechlorination was preferred over deacylation for 3-MCPD dipalmitate and dilaurate.[24] The degradation experiment was conducted with the residues of two 3-MCPD diesters in a temperature-controlled oven and kept at 180, 240, and 260 °C for 20 min. The conclusion was based on the analysis of 3-MCPD diesters and their degradation products. In the present study, the overall amounts for 3-MCPD di- and monoesters from TSG reacting with a chlorine compound were the results of both formation and degradation reactions. Taken together, these data suggested a possibility to reduce final 3-MCPD ester concentration in the refined oils through an extended thermal treatment degree. It needs to be pointed out that the thermal treatment may promote lipid oxidation and other chemical changes in the edible oil products through reducing their 3-MCPD ester contents.

In summary, the possible mechanisms behind the formation of 3-MCPD mono- and diesters from triglycerides might involve either a cyclic acyloxonium or a glycidol ester radical intermediate under a high-temperature and low-moisture condition. This study also reported that glycidol esters might be a coproduct from TAG during 3-MCPD ester formation under the experimental conditions. In addition, Fe^{2+} and Fe^{3+} might catalyze both 3-MCPD and glycidol esters' formation from TAG. These results suggested that reducing the availability of Fe^{2+} and Fe^{3+} through controlling ingredients,

DOI: 10.1021/jf5061216
J. Agric. Food Chem. 2015, 63, 1839−1848

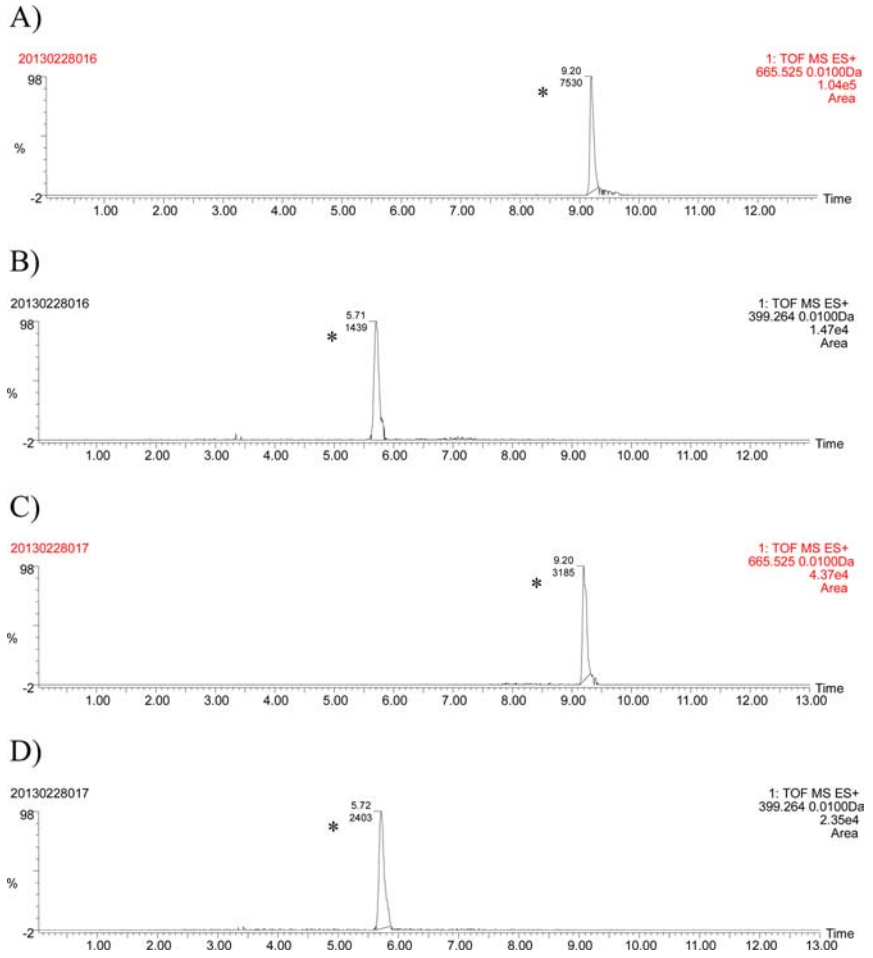

Figure 8. UPLC-QTOF MS extracted-ion chromatograms for the reaction products of TSG and $FeCl_3$. The reactions were carried out for 20 min at 120 or 240 °C. The extracted ions were for 3-MCPD (A) diester ion at 120 °C, (B) monoester ion at 120 °C, (C) diester ion at 120 °C, and (D) monoester ion at 120 °C. The concentration was 0.5 mg/mL for TSG, and the concentration was 0.2 mg/mL for $FeCl_3$. ∗ indicates the peak area for a 3-MCPD di- or monoester ion.

equipment, and containers and processing agents including water, using chelating agents in selected processing steps, as well as improvement of the thermal processing degree may lead to reduced levels of 3-MCPD esters and related toxicants such as glycidol esters in the refined edible oils and food products.

■ ASSOCIATED CONTENT

Ⓢ Supporting Information

Figures S1−S4. This material is available free of charge via the Internet at http://pubs.acs.org.

■ AUTHOR INFORMATION

Corresponding Author

*(L.Y.) Phone: (301) 405-0761. Fax: (301) 314-3313. E-mail: lyu5@umd.edu.

Author Contributions

⊥These authors made equal contributions to the manuscript.

Funding

This research was supported by a special fund for Argo-scientific Research in the Public Interest (Grant 201203069), two grants from the National High Technology Research and Development Program of China (Grants 2013AA102202 and 2013AA102207), a grant from the Wilmar (Shanghai) Biotechnology Research and Development Center Co., Ltd., and grants from SJTU 985-III disciplines platform and talent funds (Grants TS0414115001 and TS0320215001).

Notes

The authors declare no competing financial interest.

■ ACKNOWLEDGMENTS

We thank Yihai Kerry/Wilmar (Shanghai) Biotechnology Research and Development Center for providing refined palm oil and Dr. Hai Zhang for his editorial assistance and scientific comments during manuscript revision.

■ ABBREVIATIONS USED

3-MCPD, 3-monochloro-1,2-propanediol; TAG, triacylglycerol; ESR, electron spin resonance; DMPO, 5,5-dimethylpyrroline-*N*-oxide; Q-TOF MS, quadrupole−time-of-flight mass spectrometer; DAG, diacylglycerol; MAG, monoacylglycerol; FT-IR, Fourier transform infrared

■ REFERENCES

(1) Velisek, J.; Davidek, J.; Kubelka, V.; Janicek, G.; Svobodova, Z.; Simicova, Z. New chlorine-containing organic compounds in protein hydrolysates. *J. Agric. Food Chem.* **1980**, *28*, 1142−1144.

(2) Liu, M.; Gao, B.; Qin, F.; Wu, P.; Shi, H.; Luo, W.; Ma, A.; Jiang, Y.; Xu, X.; Yu, L. Acute oral toxicity of 3-MCPD mono- and di-

DOI: 10.1021/jf5061216
J. Agric. Food Chem. 2015, 63, 1839−1848

palmitic esters in Swiss mice and their cytotoxicity in NRK-52E rat kidney cells. *Food Chem. Toxicol.* **2012**, *50*, 3785−3791.
(3) Hamlet, C. G.; Sadd, P. A.; Gray, D. A. Chloropropanols and their esters in baked cereal products. In *Abstracts, 224th National Meeting of the American Chemical Society*; ACS: Washington, DC, USA, 2004.
(4) Hamlet, C. G.; Asuncion, L.; Velisek, J.; Dolezal, M.; Zelinkova, Z.; Crews, C. Formation and occurrence of esters of 3-chloropropane-1,2-diol (3-CPD) in foods: what we know and what we assume. *Eur. J. Lipid Sci. Technol.* **2011**, *113*, 279−303.
(5) Pudel, F.; Benecke, P.; Fehling, P.; Freudenstein, A.; Matthaeus, B.; Schwaf, A. On the necessity of edible oil refining and possible sources of 3-MCPD and glycidyl esters. *Eur. J. Lipid Sci. Technol.* **2011**, *113*, 368−373.
(6) Svejkovska, B.; Novotny, O.; Divinova, V.; Reblova, Z.; Dolezal, M.; Velisek, J. Esters of 3-chloropropane-1,2-diol in foodstuffs. *Czech J. Food Sci.* **2004**, *22*, 190−196.
(7) Zelinkova, Z.; Svejkovska, B.; Velisek, J.; Dolezal, M. Fatty acid esters of 3-chloropropane-1,2-diol in edible oils. *Food Addit. Contam.* **2006**, *23*, 1290−1298.
(8) Zelinková, Z.; Doležal, M.; Velíšek, J. Occurrence of 3-chloropropane-1,2-diol fatty acid esters in infant and baby foods. *Eur. Food Res. Technol.* **2009**, *228*, 571−578.
(9) Zelinkova, Z.; Novotny, O.; Schurek, J.; Velisek, J.; Hajslova, J.; Dolezal, M. Occurrence of 3-MCPD fatty acid esters in human breast milk. *Food Addit. Contam.* **2008**, *25*, 669−676.
(10) Weisshaar, R. 3-MCPD-esters in edible fats and oils − a new and worldwide problem. *Eur. J. Lipid Sci. Technol.* **2008**, *110*, 671−672.
(11) Franke, K.; Strijowski, U.; Fleck, G.; Pudel, F. Influence of chemical refining process and oil type on bound 3-chloro-1,2-propanediol contents in palm oil and rapeseed oil. *LWT−Food Sci. Technol.* **2009**, *42*, 1751−1754.
(12) Rahn, A. K. K.; Yaylayan, V. A. Monitoring cyclic acyloxonium ion formation in palmitin systems using infrared spectroscopy and isotope labelling technique. *Eur. J. Lipid Sci. Technol.* **2011**, *113*, 330−334.
(13) Rahn, A. K. K.; Yaylayan, V. A. What do we know about the molecular mechanism of 3-MCPD ester formation? *Eur. J. Lipid Sci. Technol.* **2011**, *113*, 323−329.
(14) Zhang, X.; Gao, B.; Qin, F.; Shi, H.; Jiang, Y.; Xu, X.; Yu, L. Free radical mediated formation of 3-monochloropropanediol (3-MCPD) fatty acid diesters. *J. Agric. Food Chem.* **2013**, *61*, 2548−2555.
(15) Destaillats, F.; Craft, B. D.; Sandoz, L.; Nagy, K. Formation mechanisms of monochloropropanediol (MCPD) fatty acid diesters in refined palm (*Elaeis guineensis*) oil and related fractions. *Food Addit. Contam.* **2012**, *29*, 29−37.
(16) Collier, P. D.; Cromie, D. D. O.; Davies, A. P. Mechanism of formation of chloropropanols present in protein hydrolysates. *J. Am. Oil Chem. Soc.* **1991**, *68*, 785−790.
(17) Velíšek, J.; Doležal, M.; Crews, C.; Dvořák, T. Optical isomers of chloropropanediols: mechanisms of their formation and decomposition in protein hydrolysates. *Czech J. Food Sci.* **2002**, *20*, 161−170.
(18) Sonnet, P. E. A short highly regio- and stereoselective synthesis of triacylglycerols. *Chem. Phys. Lipids* **1991**, *58*, 35−39.
(19) Ermacora, A.; Hrncirik, K. Influence of oil composition on the formation of fatty acid esters of 2-chloropropane-1, 3-diol (2-MCPD) and 3-chloropropane-1, 2-diol (3-MCPD) under conditions simulating oil refining. *Food Chem.* **2014**, *161*, 383−389.
(20) Weißhaar, R.; Perz, R. Fatty acid esters of glycidol in refined fats and oils. *Eur. J. Lipid Sci. Technol.* **2010**, *112*, 158−165.
(21) Welch, K. D.; Davis, T. Z.; Aust, S. D. Iron autoxidation and free radical generation: effects of buffers, ligands, and chelators. *Arch. Biochem. Biophys.* **2002**, *397*, 360−369.
(22) Schafer, F. Q.; Qian, S. Y.; Buettner, G. R. Iron and free radical oxidations in cell membranes. *Cell. Mol. Biol.* **2000**, *46*, 657−662.
(23) Svejkovska, B.; Dolezal, M.; Velisek, J. Formation and decomposition of 3-chloropropane-1,2-diol esters in models simulating processed foods. *Czech J. Food Sci.* **2006**, *24*, 172−179.
(24) Ermacora, A.; Hrncirik, K. Study on the thermal degradation of 3-MCPD esters in model systems simulating deodorization of vegetable oils. *Food Chem.* **2014**, *150*, 158−163.

DOI: 10.1021/jf5061216
J. Agric. Food Chem. 2015, 63, 1839−1848

extraction buffers,[9,11] food matrices,[10,12] and processing methods,[11,13−15] and the outcomes of these studies confirm that a wide variation in the recovery of peanut proteins exists among different kits.

Moreover, the reference material used to prepare the kit standards is not always known and is not standardized between ELISA kits, which is another source of variability between different kits. The National Institute of Standards and Technology (NIST) has developed a standard reference material (SRM) for peanut (2387), a peanut butter. However, a comparison of commercial peanut ELISA kits for their sensitivity of detection of peanut from SRM 2387 peanut butter is yet to be accomplished. Furthermore, although all peanut ELISA kits detect peanut proteins, no study has compared the specificity of recognition of individual peanut allergens by the antisera used in these kits.

Several peanut proteins have been identified as being major allergens including the seed storage proteins, Ara h 1, Ara h 2, Ara h 3, and Ara h 6. Both Ara h 1 and Ara h 3 belong to the cupin superfamily of proteins. Ara h 1 is a 7S vicilin-type protein, while Ara h 3 is an 11S legumin-type protein. Ara h 2 and Ara h 6 are both 2S albumins that show close homology to each other.[16,17] Although Ara h 1 and Ara h 3 are the more abundant peanut proteins, several studies have proven that Ara h 2 and Ara h 6 bind more strongly with IgE from peanut allergic patients and release mediators more efficiently from basophils, which confirm that these are also more potent allergens in in vitro systems[18−21] and in vivo.[20,22,23] Moreover, it has been observed that both Ara h 2 and Ara h 6 are recognized more strongly and more frequently than Ara h 1 and Ara h 3 by peanut allergic children with almost all of them showing IgE reactivity to these two allergens.[24] Other peanut allergens have been identified,[25,26] but their clinical significance remains to be firmly established.

Therefore, in the current study, we used the reference peanut butter SRM 2387 from NIST to compare the performance of six commercial peanut ELISA kits, and we applied purified peanut allergens Ara h 1, Ara h 2, Ara h 3, and Ara h 6 to assess the specificity of these ELISA kits.

MATERIALS AND METHODS

Reference Material and Peanut Allergens. SRM 2387 peanut butter was purchased from NIST. The purified peanut allergens Ara h 1, Ara h 2, Ara h 3, and Ara h 6 were obtained from lyophilized stock preparations made as described earlier.[19,20,22]

Peanut ELISA Test Kits. Six commercial ELISA test kits were used in this study: Veratox for peanut allergen from Neogen, Lansing, MI, USA; BioKits peanut assay kit from Neogen, Lansing, MI, USA; AgraQuant peanut assay from Romer Laboratories UK Ltd.; RIDASCREEN fast peanut from R-Biopharm, Germany; Peanut protein ELISA kit from Morinaga Institute of Biological Science, Inc. Japan; and Peanut residue from ELISA Systems Pty Ltd. Australia.

Preparation of Reference Material and Peanut Allergens. *Reference Material.* An initial stock sample containing 50 000 ppm (mg/kg) peanut butter was prepared both as a suspension and an extract. Grinding or homogenization of the sample as instructed in the kit inserts was not required since SRM 2387 is of a creamy consistency. The suspension was prepared by mixing 1 g of SRM 2387 peanut butter with 20 mL of sample extraction buffer of each respective ELISA kit and vortexing to obtain a uniform suspension of 50 000 ppm peanut butter in extraction buffer. For the extract, 1 g of peanut butter was mixed with 20 mL of preheated (at RT with the Morinaga kit) extraction buffer and extracted at RT (Morinaga, BioKits) or at 60 °C (Veratox, Romer, R-Biopharm and ELISA Systems) for 10 min (R-Biopharm) or 15 min (Veratox, BioKits, Romer, Morinaga and ELISA Systems). Following extraction, samples were centrifuged at 3000 *g* for 15 min at 25 °C, and the resulting supernatant containing 50 000 ppm peanut butter was obtained. Any extraction additives supplied by the kit manufacturers (i.e., Veratox) were added to the initial extract but not to the initial suspension. A series of dilutions ranging from 10−500 ppm were prepared with both the initial suspension and extract for all six kits. Each of the initial stocks and the series of dilutions were prepared in duplicate. Protein extraction from each of these dilutions was carried out as per manufacturers' instructions for each kit. Following protein extraction, an aliquot of the extract was transferred to a 1.5 mL Eppendorf tube and centrifuged at 14 000 rpm for 5 min with the resulting supernatant used for subsequent testing by ELISA.

Peanut Allergens. With each purified allergen, 1.5 mg was dissolved in either 1 mL of phosphate buffered saline (PBS), pH 7.4 containing 20 mM phosphate, 150 mM NaCl (Ara h 1 and Ara h 2), or distilled water (Ara h 3 and Ara h 6). Absorbance was measured at 280 nm (Thermo Scientific NanoDrop 2000c Wilmington, Delaware, USA), and the protein concentration (mg/mL) was determined by dividing the absorbance value by the absorbance coefficient for each allergen as can be found in the Uniprot database using ProtParam (0.657, 0.59, 0.77, and 0.21 for Ara h 1, Ara h 2, Ara h 3, and Ara h 6, respectively). Subsequently, the final protein concentration of each allergen was adjusted to 1 mg/mL by adding an appropriate volume of the primary dissolving fluid. Sample aliquots were put into screw-top Corning cryogenic tubes, frozen by snap-freezing in liquid nitrogen, and stored at −80 °C until further use. Prior to testing by ELISA, further dilutions of the 1 mg/mL allergens were prepared in each kits' extraction buffer. On the basis of the sensitivity of the test kit and reactivity of the allergen, dilutions ranging from 0.001−100 μg/mL were prepared for each allergen. The extraction and dilution procedure outlined in each kit was followed for extraction of proteins from each of the prepared dilutions. An aliquot of the extracted sample was centrifuged at 14 000 rpm for 5 min, and the resulting supernatant was used for subsequent testing by ELISA.

ELISA Test Procedure. ELISA was performed in duplicate for each sample according to the instructions supplied by each kit manufacturer. Where appropriate, extracted sample dilutions of the SRM 2387 peanut butter were further diluted in extraction buffer prior to testing by ELISA in order for the sample to be within the range of the kits' quantification. The purified allergens were tested directly by ELISA without any further dilutions other than dilutions specified by the kit manufacturers (BioKits and Morinaga test kits). The absorbance of the samples as well as the kit standards was measured at the wavelength specified by each kit using a microtiter plate reader (BioTek Instruments Inc. USA). To allow for uniform comparison between test kits, the concentration of kit standards of each kit were converted to μg/mL peanut protein. For the SRM 2387 peanut butter, the peanut concentration in each sample dilution was interpolated from the standard curve using the software supplied by the kit manufacturers (Veratox, Romer Laboratories and R-Biopharm) or the GraphPad Prism 4 software (BioKits, Morinaga and ELISA Systems). By taking into account any dilutions and conversion factors, the total peanut protein recovered (in ppm) was calculated as a percentage relative to expected recovery for each dilution and test kit.

SDS-PAGE Analysis. The SRM 2387 peanut butter and the purified allergens Ara h 1, Ara h 2, Ara h 3, and Ara h 6 were analyzed under reducing conditions (β-mercapotoethanol) using Mini-Protean TGX Precast 4−20% gradient gels (Biorad, Veenendaal, The Netherlands). For the purified allergens, 5 ug per lane was loaded. For the SRM 2387 peanut butter, an amount of protein was loaded (20 μg) such that the multiple bands of the allergens could be visualized. Gels were run for 90 min at 120 V and stained with Coomassie Brilliant Blue R-250 (Sigma-Aldrich, Germany). Molecular weight (MW) markers were Precision Plus Protein (all blue standard, 10−250 kDa, Bio-Rad).

Statistical Analysis. SRM 2387 peanut butter samples and dilutions were prepared in duplicate and each dilution analyzed in duplicate ELISA wells. Tests on peanut allergens were repeated twice, and for each trial, all concentrations were tested in duplicate by ELISA.

DOI: 10.1021/jf504741t
J. Agric. Food Chem. 2015, 63, 1849−1855

Table 1. Comparison of Assay Characteristics and Sensitivity of the Kit Standards in the Detection of Peanut Proteins for Six Commercially Available Peanut ELISA Kits

ELISA kit	sample extraction ratio (w/v)	sample dilution (1/fold)	conversion weight to protein (1/fold)	total dilution	range of quantification: total peanut in unextracted product (ppm)	range of quantification: peanut protein in the ELISA well (μg/mL)
Veratox (Neogen)	1/25	none	1/4	100	2.5−25	0.025−0.25
BioKits (Neogen)	1/10	1/10	1/4	400	1−20	0.0025−0.05
AgraQuant (Romer Laboratories)	1/20	none	1/4	80	1−40	0.0125−0.50
Ridascreen (R-Biopharm)	1/20	none	1/10	200	2.5−20	0.0125−0.1
Peanut Protein (Morinaga)	1/20	1/20	1/4	1600	1.25−80	0.00078−0.05
Peanut Residue (ELISA Systems)	1/10	none	1/4	40	4−60	0.1−1.5

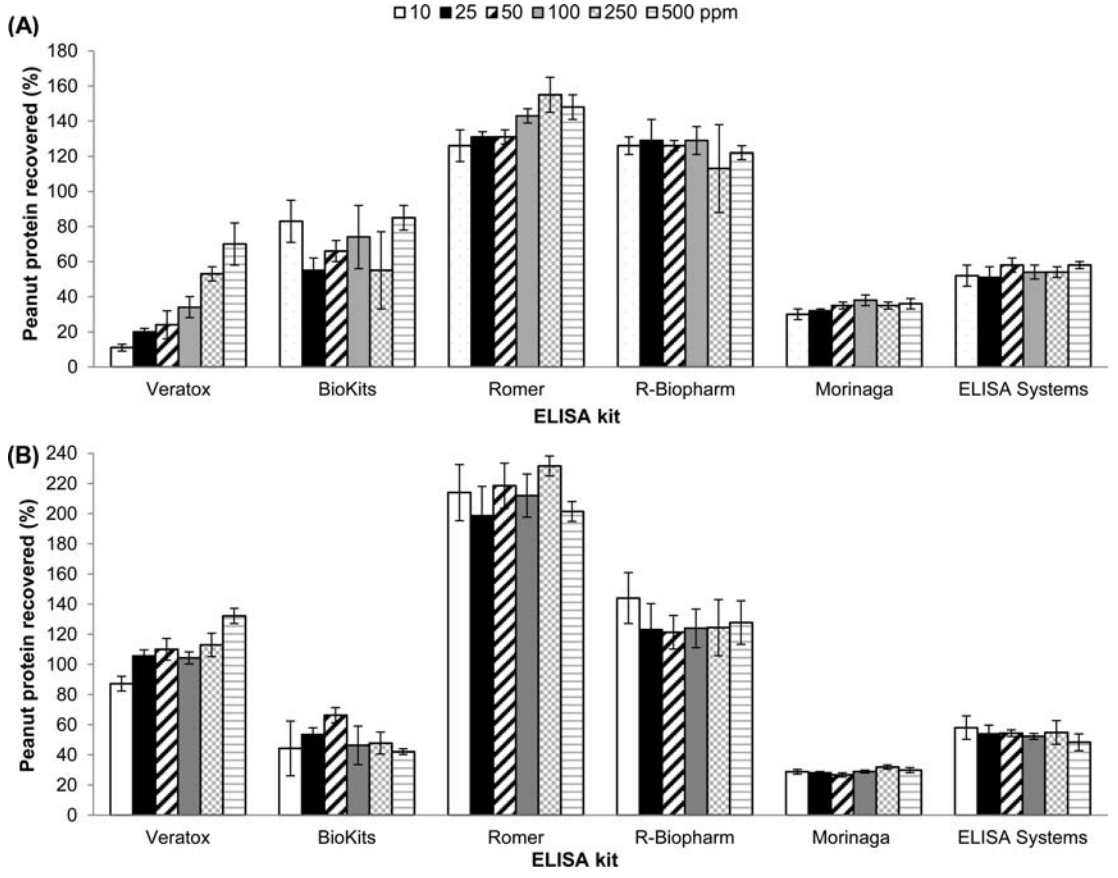

Figure 1. Comparison of percentage peanut protein recovered from an initial suspension (A) and extract (B) of SRM 2387 peanut butter by six different commercial peanut ELISA kits at sample concentrations ranging from 10−500 ppm. Protein extraction for each sample concentration was performed twice, and each extract was analyzed in duplicate by ELISA. Data are expressed as mean ± standard deviation (n = 4).

All statistical analyses were performed using the SAS 9.2 software package. Fisher's protected least significant difference (LSD) test and matched pairs t test were used to determine statistical significance, and the level of significance was set at $p \leq 0.05$.

RESULTS

Comparison of the Sensitivity of the ELISA Kits. The six peanut ELISA test kits used in this study differed from one to another in detection range, detection limit, unit of quantification as well as on the sample to extraction buffer ratio and the dilutions used. In four of the kits, results are expressed as ppm of total peanut (Veratox, BioKits, Romer and R-Biopharm). In the ELISA Systems test kit, results are expressed in ppm peanut protein, while in the Morinaga assay, the results are given in ng/mL of peanut protein. To allow for a comparison of the sensitivity between different kits, we calculated the range of quantification of each of the test kit standards in μg peanut protein/mL (Table 1). Since peanut kernels contain ~25% protein,[27] we used a conversion factor of 0.25 to calculate for peanut protein from total peanut for five of the test kits. For the R-Biopharm kit, a conversion ratio of 0.1 was used since the kit manufacturer states that a peanut raw material containing 10% protein was used for the preparation of their standards. As can be seen from Table 1, the six ELISAs were different in sensitivity. In particular, the sensitivity of one of them (Peanut Residue from ELISA Systems) seemed to be

DOI: 10.1021/jf504741t
J. Agric. Food Chem. 2015, 63, 1849−1855

about 10-fold lower than that of the other kits. By applying different dilutions, as specified in the kit, this ELISA also reached a sensitivity range (relative to the unextracted food products) similar to that of the other kits, that is, 4−60 ppm.

Efficacy of Recovery of Peanut Protein from Peanut Butter. The percentage of peanut protein recovered from both the peanut butter suspension and extract at sample dilutions ranging from 10−500 ppm was widely variable with the different kits as displayed in Figure 1. Of the six ELISA kits compared, the highest percentages of recovery of peanut proteins were obtained with the Romer and R-Biopharm kits with both methods of sample preparation. With the Veratox and Romer kits, a higher percentage of peanut was recovered when the sample was prepared as an extract rather than a suspension ($p < 0.05$). However, recovery was comparable with both methods of sample preparation with the BioKits, R-Biopharm, and ELISA Systems kits ($p > 0.05$). Recovery of peanut differed widely within the same test kit at different sample dilutions especially with the Veratox kit (11−70%) and to a lesser extent with the BioKits kit (55−85%) when the initial sample was prepared as a suspension. This effect of sample concentration on peanut recovery was not evident with the remaining test kits with either method of sample preparation.

Recognition of Individual Peanut Allergens by ELISA. The polypeptide profiles obtained with the individual peanut proteins (Ara h 1, Ara h 2, Ara h 3, and Ara h 6) and SRM 2387 peanut butter are shown in Figure 2. The gel profile and

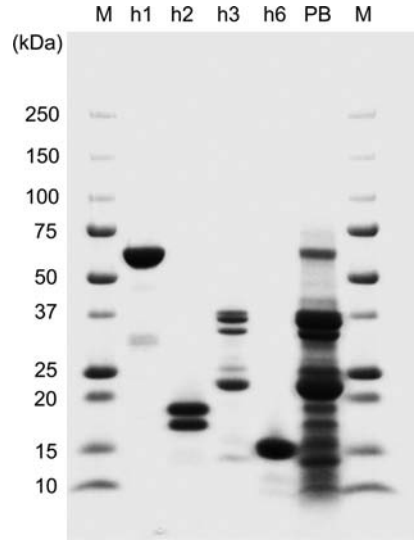

Figure 2. SDS-PAGE analysis of purified peanut allergens and SRM 2387 peanut butter under reducing conditions. M, molecular weight marker (indicated in kDa in left margin); h 1, Ara h 1; h2, Ara h 2; h3, Ara h 3; h6, Ara h 6; PB, SRM 2387 peanut butter from NIST. The protein load in each lane was 5 μg for the purified proteins and 20 μg for SRM 2387 peanut butter.

molecular sizes of the allergens Ara h 1 (63 kDa), Ara h 2 (17−20 kDa doublet), Ara h 3 (a series of polypeptides ranging from 14−45 kDa), and Ara h 6 (15 kDa) are in line with previously published findings.[20,22] Furthermore, the gel profile confirms the purity of allergens and that none of the allergens contain other allergen types except perhaps as minor contaminants. The protein profile of SRM 2387 peanut butter indicates that Ara h 3 is the most abundant protein and that the other three allergens are also present but in lower amounts.

When the specificity and sensitivity of recognition of purified peanut allergens, Ara h 1, Ara h 2, Ara h 3, and Ara h 6, at concentrations ranging from 0.001−100 μg/mL by the six commercial peanut ELISA test kits were compared, five of the kits were most sensitive in the recognition of Ara h 3, while their reactivity for the other allergens was substantially lower (Figure 3). Initially, each allergen was screened against each of the test kits in order to identify the range of sensitivity for each allergen−test kit combination. On the basis of this preliminary data, the range of dilutions tested was adjusted accordingly to span the range from nonreactivity to maximum reactivity. In four of these five kits (the exception being ELISA Systems), Ara h 3 was more reactive than the respective kit standards provided by each kit. The Morinaga kit was significantly different from the other five kits in that Ara h 3 was the least recognized allergen by this kit. Moreover, while the other five kits were least sensitive in the recognition of Ara h 2 and Ara h 6, the Morinaga kit showed the highest sensitivity of recognition for these two allergens. Thus, the Morinaga kit stands out from the other five kits in being the most sensitive in detecting Ara h 2 and Ara h 6, the two allergens that were least recognized by the other kits.

Except for Morinaga, in the other five kits, Ara h 1 was the second most reactive allergen, and in all five, reactivity of this allergen was less than the kit standard. However, the reactivity of Ara h 1 did show differences between these kits (Figure 3), most notably that the reactivity between Ara h 3 and Ara h 1 was approximately two-fold for the ELISA Systems kit, while it was about 300-fold in the Romer kit.

When Ara h 2 was considered, the signal was found to increase at very low allergen concentrations (0.003−0.03 μg/mL) but then level off at a low plateau with the R-Biopharm and ELISA Systems kits. This observation of being recognized at low concentrations and at the same time showing very low reactivity could most probably be due to having a low concentration of highly reactive antibodies against Ara h 2. However, with the Veratox and especially the Morinaga kits, the signal of Ara h 2 continued to increase with increasing concentrations of the allergen. In contrast, for both the BioKits and Romer kits, the signal remained at a low plateau for the entire range of concentrations where Ara h 2 seemed to show a low binding affinity for the antibodies.

Most of the kits reacted at higher concentrations of Ara h 6 ($\geq$ 0.03 μg/mL), although Veratox did show some reactivity at 0.01 μg/mL. The exception was the Morinaga kit where the kit reacted to the allergen at a concentration as low as 0.001 μg/mL. At the same time, other than for the Romer and Veratox kits where reactivity plateaus off, in all of the other kits, reactivity of Ara h 6 showed an increase with increasing allergen concentrations. However, compared to the reactivity of Ara h 3, reactivity of Ara h 6 was about 1000−10 000-fold lower in the R-Biopharm, BioKits, and Romer kits. Moreover, in comparison to the other kits, the kit from Romer Laboratories was found to be the least sensitive in the detection of Ara h 1, Ara h 2, and Ara h 6.

Some variations in kit specificity occurred among the kits. The Veratox, Romer, and Morinaga kit manufacturers do not indicate that their peanut ELISAs are targeted against specific peanut proteins/allergens. For the BioKits ELISA, it is stated that this kit specifically detects the peanut allergen, Ara h 1. Both the R-Biopharm and the ELISA Systems kits specify that

DOI: 10.1021/jf504741t
J. Agric. Food Chem. 2015, 63, 1849−1855

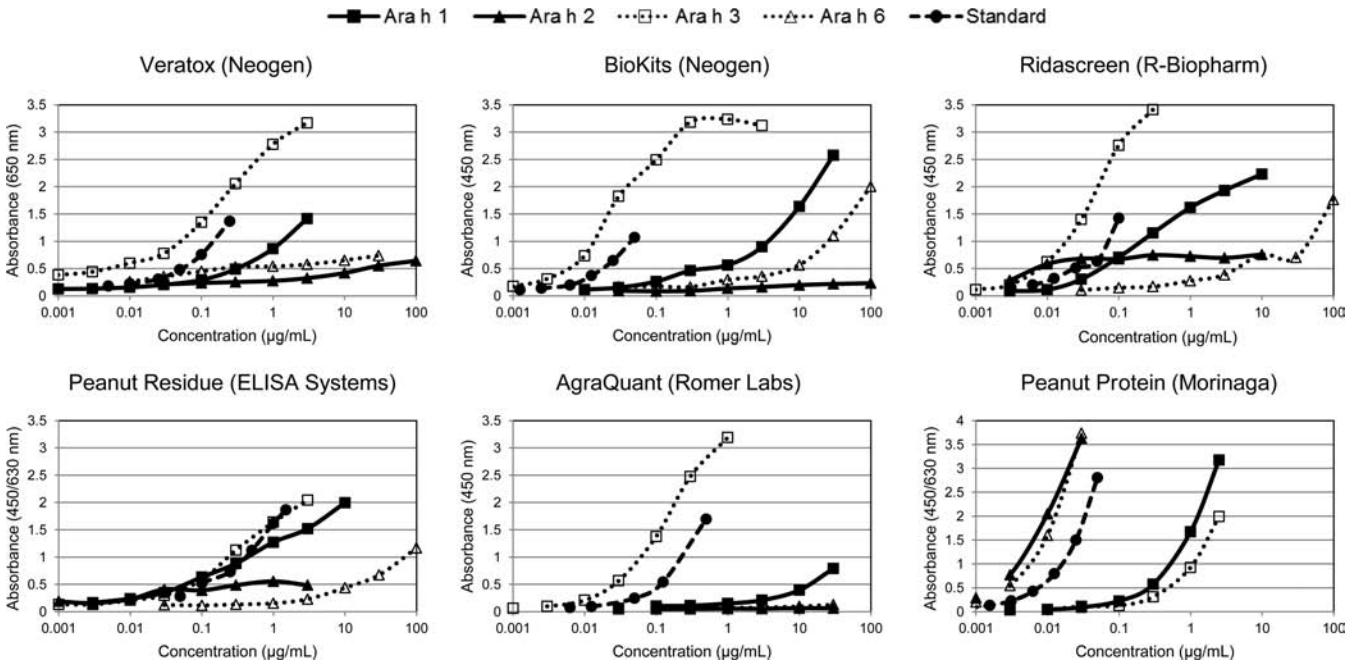

Figure 3. Recognition of the peanut allergens Ara h 1, Ara h 2, Ara h 3, and Ara h 6 by six ELISA kits at sample (peanut allergen) concentrations ranging from 0.001−100 μg/mL. The *x*-axis in logarithmic scale indicates sample concentration in the ELISA well. Standard refers to the calibration standards included in each respective ELISA kit.

their antibodies target peanut proteins including the allergens Ara h 1 and Ara h 2. As this study indicates, although these three kits do show reactivity against the specified allergens, they are most sensitive in the detection of Ara h 3. Importantly, the quantification of individual allergens within the same kit as well as between kits is not easy due to several reasons. First, other than the BioKits and R-Biopharm kits, in which the standards are calibrated with SRM 2387 peanut butter, none of the other kits specify the source or type of peanut used in the preparation of the kit standards, and as such this may vary between kits. Second, the reactivity curves of the individual allergens are not completely parallel with the standard curve or with each other.

DISCUSSION

Several ELISA kits for the detection and quantification of peanut residues in food products are commercially available. In this study, we compared the recovery of standard peanut butter (NIST SRM 2387) with six commercial sandwich ELISA kits and tested their ability to recognize individual peanut allergens.

All six test kits gave reasonably good recoveries with SRM 2387 peanut butter even though percentage recoveries varied widely between test kits. Given the differences in extraction buffers and the likely differences in the sources of peanut used to raise antibodies, which would translate into differences in the amount of protein extracted and differences in the antigens recognized by the antibodies, respectively, this is not unduly surprising. Overall, a low recovery of peanut was observed with the Morinaga kit with both methods of sample preparation (Figure 1). The kit manufacturers of Morinaga indicate that their kit gives 100% reactivity with dry peanuts and 60.3% reactivity with roasted peanuts. Since roasted peanuts are used in the manufacture of SRM 2387 peanut butter, this could at least partially explain the low recovery observed with the Morinaga kit. Poms et al.[11] suggest that antibodies raised against raw peanuts would have a lower affinity to heat-treated antigens, although none of the manufacturers of the six kits provide information about the sources of peanut used to raise antibodies.

Two kits, namely BioKits and R-Biopharm, indicate that their standards have been calibrated with SRM 2387 peanut butter. The high recovery observed with the R-Biopharm kit could be largely because it has already been standardized using SRM 2387 peanut butter. Nevertheless, as demonstrated by this study, the method of preparation of the peanut extracts influences the protein content in the extract. Thus, use of the same source to prepare the standard material does not necessarily guarantee uniform recoveries (compare BioKits vs R-Biopharm in Figure 1).

The underestimation of protein content in heat-treated peanut samples by ELISA is well documented.[13−15,28] Since the SRM 2387 peanut butter is heat-treated, the underestimation of peanut content from this peanut butter with some of the kits is supported by those previous observations. Accordingly, the kit manufacturers have optimized extraction procedures used with their kits, provided instructions intended to optimize extraction, and in some cases included an extraction additive to increase the recovery. Indeed, these steps are helpful for some of the kits (Figure 1).

The Morinaga kit differs significantly from the rest in containing the reducing agent, β-mercaptoethanol (2%), in its extraction buffer. This same manufacturer has developed a similar ELISA to detect egg albumin where they use an extraction buffer containing both a surfactant (SDS) and a reducing agent (β-mercaptoethanol), and the antibodies are also raised against denatured proteins.[29] Such an ELISA has the advantage of detecting denatured proteins in heat-processed samples as the reducing agent helps to redissolve aggregated proteins as was shown for an ELISA for soy earlier.[30]

In contrast to the Morinaga kit, the other five kits were highly sensitive in the recognition of Ara h 3 but recognized Ara h 2 and Ara h 6 only at high protein concentrations or at sensitivities about 1000-fold lower than that for Ara h 3. Both

DOI: 10.1021/jf504741t
J. Agric. Food Chem. 2015, 63, 1849−1855

Ara h 2 and Ara h 6 are 2S albumins containing up to five disulfide bonds, which makes them resistant to heat and digestive enzymes.[31] Moreover, Ara h 2 and Ara h 6 have been identified as being major peanut allergens that also share homologous regions.[18−20,24,32] However, a study on immune responses to peanut allergens has shown that upon oral exposure, Ara h 1 and Ara h 3 induce a comparatively higher IgG response, while Ara h 2 and Ara h 6 induce much lower responses.[33] Thus, this study confirms that Ara h 1 and Ara h 3 would be better immunogens for raising an IgG antibody response than Ara h 2 and Ara h 6. Accordingly, this would support our observation that five of the kits showed the highest recognition for Ara h 3 followed by Ara h 1, while recognition of Ara h 2 and Ara h 6 was much lower. Additionally, of the total protein content of peanut kernels, Ara h 3 is the most abundant and Ara h 1content is about 12−16%, while both Ara h 2 and Ara h 6 are present in approximately the same concentration, 6−9%.[20,34,35] Although none of the kit manufacturers provide information regarding the peanut extract/type used in the production of antibodies, the relative content of each allergen in peanut kernels could also contribute to the significantly lower sensitivity of recognition of Ara h 2 and Ara h 6 by five of the test kits.

Another reason that antibodies against both Ara h 2 and Ara h 6 seem under-represented in five out of the six kits may lie in the stable core structure of both Ara h 2 and Ara h 6. Processing of these two allergens by antigen presenting cells (APCs) in the laboratory animals used to raise antibodies would be less efficient. Thus, immunization to produce antibodies would lead to a response against other proteins, particularly Ara h 3. Reduction of the disulfide bonds of these two allergens will denature Ara h 2[36] as well as Ara h 6,[37] which would perhaps make these allergens more susceptible for processing by APC and consequently into better immunogens. Thus, the approach used with the Morinaga kit, that is, under conditions that reduce the disulfide bonds, would indeed increase detection of Ara h 2 and Ara h 6 especially since the antibodies are also produced against reduced peanut proteins.

The Veratox ELISA has been shown to have a low sensitivity in the detection of both Ara h 1 and Ara h 2.[38] Compared to a sensitivity of 30 ng/mL for a monoclonal antibody-based ELISA that specifically targets Ara h 1, Veratox showed a sensitivity of only 2−4 μg/mL for Ara h 1. This observation is in agreement with that of the present study where the Veratox ELISA is primarily specific for the detection of Ara h 3.

Additionally, the peptide profile of SRM 2387 peanut butter in Figure 2 shows that although all four allergens are represented, Ara h 3 appears the most intense, while Ara h 1 is much lower in intensity. Several previous studies have shown that heating/roasting of peanuts results in a decrease in Ara h 1 levels[28,39,40] presumably owing to a loss of solubility. The loss of Ara h 1 due to heating/roasting would be a disadvantage with a kit that was oriented to the specific detection of Ara h 1. However, the five test kits that predominantly recognized Ara h 3 showed a high recovery of peanut from SRM 2387 peanut butter. In contrast, the Morinaga kit, with a low reactivity to Ara h 3, showed low recovery of peanut protein from peanut butter in the present study.

Therefore, five of the commercial kits show the highest reactivity to the most abundant peanut protein, Ara h 3, a protein that also happens to be an excellent immunogen. In contrast, the Morinaga kit shows the highest reactivity to the more potent and therefore more relevant peanut allergens, Ara h 2 and Ara h 6. Given that Ara h 2 and Ara h 6 are less susceptible to denaturation and aggregation than other peanut proteins, these allergens may be better targets than Ara h 1 or Ara h 3 for quantification of peanut in processed food.

In conclusion, the present study proved that SRM 2387 peanut butter is recognized by all six commercial ELISA kits, but recovery was not uniform across different kits or at different sample concentrations. With regard to purified allergens, regardless of what is specified by some of the commercial kit manufacturers, five of the kits were most sensitive in the detection of Ara h 3, the most abundant protein in peanut kernels. The Morinaga kit was unique in that it showed the highest sensitivity in the detection of Ara h 2 and Ara h 6, the most relevant allergens in terms of allergenicity. Thus, while the detection of peanut residues in processed food products can likely be accomplished with any of these kits, comparable results should not be expected when analyzing the same sample across more than one kit. Surprisingly, this marked difference in specificity does not preclude kits recognizing heat labile proteins from quantifying peanut in peanut butter.

AUTHOR INFORMATION

Corresponding Author

*Phone: 402-472-3070. Fax: 402-472-5306. E-mail: jbaumert2@unl.edu.

Funding

This project was partially supported by the Agriculture and Food Research Initiative Competitive Grant No. 2011−67017−20080 from the USDA National Institute of Food and Agriculture. Additional support was obtained from funding for the Food Allergy Research and Resource Program, a food industry-funded consortium of more than 80 member companies, and the Agricultural Research Division of the University of Nebraska-Lincoln.

Notes

The authors declare no competing financial interest.

REFERENCES

(1) Taylor, S. L.; Baumert, J. L. Food allergies and intolerances. In *Present Knowledge in Nutrition*, 10th ed.; Erdman Jr, J. W., MacDonald, I. A., Zeisel, S. H., Eds.; John Wiley & Sons: Washington DC, 2012; pp 1222−1235.

(2) Sicherer, S. H.; Sampson, H. A. Food allergy. *J. Allergy Clin. Immunol.* **2010**, *125*, S116−S125.

(3) Gupta, R. S.; Springston, E. E.; Warrier, M. R.; Smith, B.; Kumar, R.; Pongracic, J.; Holl, J. H. The prevalence, severity, and distribution of childhood food allergy in the United States. *Pediatrics* **2011**, *128*, e9−e17.

(4) Sicherer, S. H.; Sampson, H. A. Peanut allergy: Emerging concepts and approaches for an apparent epidemic. *J. Allergy Clin. Immunol.* **2007**, *120*, 491−503.

(5) Sicherer, S. H.; Sampson, H. A. Food allergy: Epidemiology, pathogenesis, diagnosis, and treatment. *J. Allergy Clin. Immunol.* **2014**, *133* (2), 291−307.

(6) Furlong, T. J.; DeSimone, J.; Sicherer, S. H. Peanut and tree nut allergic reactions in restaurants and other food establishments. *J. Allergy Clin. Immunol.* **2001**, *108*, 867−870.

(7) Poms, R.; Klein, C.; Anklam, E. Methods for allergen analysis in food: A review. *Food Addit. Contam.* **2004**, *21*, 1−31.

(8) Schubert-Ullrich, P.; Rudolf, J.; Ansari, P.; Galler, B.; Führer, M.; Molinelli, A.; Baumgartner, S. Commercialized rapid immunoanalytical tests for determination of allergenic food proteins: An overview. *Anal. Bioanal. Chem.* **2009**, *395*, 69−81.

DOI: 10.1021/jf504741t
J. Agric. Food Chem. 2015, 63, 1849−1855

(9) Zeleny, R.; Schimmel, H. Towards comparability of ELISA results for peanut proteins in food: A feasibility study. *Food Chem.* **2010**, *123*, 1343−1351.
(10) Poms, R. E.; Agazzi, M. E.; Bau, A.; Brohee, M.; Capelletti, C.; Nørgaard, J. V.; Anklam, E. Interlaboratory validation study of five commercial ELISA test kits for the determination of peanut proteins in biscuits and dark chocolate. *Food Addit. Contam.* **2005**, *22* (2), 104−112.
(11) Poms, R. E.; Capelletti, C.; Anklam, E. Effect of roasting history and buffer composition on peanut protein extraction efficiency. *Mol. Nutr. Food Res.* **2004**, *48*, 459−464.
(12) Hurst, W. J.; Krout, E. R.; Burks, W. R. A comparison of commercially available peanut ELISA test kits on the analysis of samples of dark and milk chocolate. *J. Immunoassay Immunochem.* **2002**, *23* (4), 451−459.
(13) Fu, T.; Maks, N. Impact of thermal processing on ELISA detection of peanut allergens. *J. Agric. Food Chem.* **2013**, *61*, 5649−5658.
(14) Scaravelli, E.; Brohée, M.; Marchelli, R.; van Hengel, A. J. The effect of heat treatment on the detection of peanut allergens as determined by ELISA and real-time PCR. *Anal. Bioanal. Chem.* **2009**, *395*, 127−137.
(15) Koch, P.; Schäppi, G. F.; Poms, R. E.; Wüthrich, B.; Anklam, E.; Battaglia, R. Comparison of commercially available ELISA kits with human sera-based detection methods for peanut allergens in foods. *Food Addit. Contam.* **2003**, *20* (9), 797−803.
(16) Breiteneder, H.; Radauer, C. A classification of plant food allergens. *J. Allergy Clin. Immunol.* **2004**, *113*, 821−830.
(17) Lehmann, K.; Schweimer, K.; Reese, G.; Randow, S.; Suhr, M.; Becker, W.; Vieths, S.; Rösch, P. Structure and stability of 2S albumin-type peanut allergens: Implications for the severity of peanut allergic reactions. *Biochem. J.* **2006**, *395*, 463−472.
(18) Porterfield, H. S.; Murray, K. S.; Schlichting, D. G.; Chen, X.; Hansen, K. C.; Duncan, M. W.; Dreskin, S. C. Effector activity of peanut allergens: A critical role for Ara h 2, Ara h 6, and their variants. *Clin. Exp. Allergy* **2009**, *39*, 1099−1108.
(19) de Jong, E. C.; van Zijverden, M.; Spanhaak, S.; Koppelman, S. J.; Pellegrom, H.; Penninks, A. H. Identification and partial characterization of multiple major allergens in peanut proteins. *Clin. Exp. Allergy* **1998**, *28*, 743−751.
(20) Koppelman, S. J.; de Jong, G. A.; Laaper-Ertmann, M.; Peeters, K. A. B. M.; Knulst, A. C.; Hefle, S. L.; Knol, E. F. Purification and immunoglobulin E-binding properties of peanut allergen Ara h 6: Evidence for cross-reactivity with Ara h 2. *Clin. Exp. Allergy* **2005**, *35*, 490−497.
(21) Palmer, G. W.; Dibbern, D. A., Jr.; Burks, A. W.; Bannon, G. A.; Bock, S. A.; Porterfield, H. S.; McDermott, R. A.; Dreskin, S. C. Comparative potency of Ara h 1 and Ara h 2 in immunochemical and functional assays of allergenicity. *Clin. Immunol.* **2005**, *115*, 302−312.
(22) Koppelman, S. J.; Knol, E. F.; Vlooswijk, R. A. A.; Wensing, M.; Knulst, A. C.; Hefle, S. L.; Gruppen, H.; Piersma, S. Peanut allergen Ara h 3: Isolation from peanuts and biochemical characterization. *Allergy* **2003**, *58*, 1144−1151.
(23) Peeters, K. A. B. M.; Koppelman, S. J.; Hoffen, E. V.; Tas, C. W. H. V. D.; Jager, C. F. D. H.; Penninks, A. H.; Hefle, S. L.; Bruijnzeel-Koomen, C. A. F. M.; Knol, E. F.; Knulst, A. C. Does skin prick test reactivity to purified allergens correlate with clinical severity of peanut allergy? *Clin. Exp. Allergy* **2007**, *37*, 108−115.
(24) Flinterman, A. E.; van Hoffen, E.; den Hartog Jager, C. F.; Koppelman, S. J.; Pasmans, S. G.; Hoekstra, M. O.; Bruijnzeel-Koomen, C. A.; Knulst, A. C.; Knol, E. F. Children with peanut allergy recognize predominantly Ara h 2 and Ara h 6, which remains stable over time. *Clin. Exp. Allergy* **2007**, *37*, 1221−1228.
(25) Pons, L.; Chery, C.; Romano, A.; Namour, F.; Artesani, M. C.; Guéant, J. L. The 18 kDa peanut oleosin is a candidate allergen for IgE-mediated reactions to peanuts. *Allergy* **2002**, *57* (s72), 88−93.
(26) Schmidt, H.; Krause, S.; Gelhaus, C.; Petersen, A.; Janssen, O.; Becker, W. M. Detection and structural characterization of natural Ara h 7, the third peanut allergen of the 2S albumin family. *J. Proteome Res.* **2010**, *9* (7), 3701−3709.
(27) Oerise, N. L.; Lau, H. A.; Ritchey, S. J.; Murphy, E. W. Yield, proximate composition, and mineral element content of three cultivars of raw and roasted peanuts. *J. Food Sci.* **1974**, *39* (2), 264−266.
(28) Holzhauser, T.; Vieths, S. Indirect competitive ELISA for determination of traces of peanut (*Arachis hypogea* L.) protein in complex food matrices. *J. Agric. Food Chem.* **1999**, *47* (2), 603−611.
(29) Watanabe, Y.; Aburatani, K.; Mizumura, T.; Sakai, M.; Muraoka, S.; Mamegosi, S.; Honjoh, T. Novel ELISA for the detection of raw and processed egg using extraction buffer containing a surfactant and a reducing agent. *J. Immunol. Methods* **2005**, *300*, 115−123.
(30) Morishita, N.; Kamjya, K.; Matsumoto, T.; Sakai, S.; Teshima, R.; Urisu, A.; Moriyama, T.; Ogawa, T.; Akiyama, H.; Morimatsu, F. Reliable enzyme-linked immunosorbent assay for the determination of soybean proteins in processed foods. *J. Agric. Food Chem.* **2008**, *56* (16), 6818−6824.
(31) Sen, M.; Kopper, R.; Pons, L.; Abraham, E. C.; Burks, A. W.; Bannon, G. A. Protein structure plays a critical role in peanut allergen stability and may determine immunodominant IgE-biding epitopes. *J. Immunol.* **2002**, *169*, 882−887.
(32) Koppelman, S. J.; Wensing, M.; Ertmann, M.; Knulst, A. C.; Knol, E. F. Relevance of Ara h 1, Ara h 2, and Ara h 3 in peanut-allergic patients, as determined by immunoglobulin E Western blotting, basophil-histamine release, and intracutaneous testing: Ara h 2 is the most important peanut allergen. *Clin. Exp. Allergy* **2004**, *34*, 583−590.
(33) van Wijk, F.; Hartgring, S.; Koppelman, S. J.; Pieters, R.; Knippels, L. M. Mixed antibody and T cell responses to peanut and the peanut allergens Ara h 1, Ara h 2, Ara h 3, and Ara h 6 in an oral sensitization model. *Clin. Exp. Allergy* **2004**, *34*, 1422−1428.
(34) Koppelman, S. J.; Vlooswijk, R. A. A.; Knippels, L. M. J.; Hessing, M.; Knol, E. F.; van Reijsen, F. C.; Bruijnzeel-Koomen, C. A. F. M. Quantification of major peanut allergens Ara h 1 and Ara h 2 in the peanut varieties Runner, Spanish, Virginia, and Valencia bred in different parts of the world. *Allergy* **2001**, *56*, 132−137.
(35) Nogueira, M. C. L.; McDonald, R.; Westphal, C.; Maleki, S. J.; Yeung, J. M. Can commercial peanut assay kits detect peanut allergens? *J. AOAC Int.* **2004**, *87*, 1480−1484.
(36) Starkl, P.; Felix, F.; Krishnamurthy, D.; Stremnitzer, C.; Roth-Walter, F.; Prickett, S. R.; Voskamp, A. L.; Willensdorfer, A.; Szalai, K.; Weichselbaumer, M.; O'Hehir, R. E.; Jensen-Jarolim, E. An unfolded variant of the major peanut allergen Ara h 2 with decreased anaphylactic potential. *Clin. Exp. Allergy* **2012**, *42* (12), 1801−1812.
(37) Apostolovic, D.; Luykx, D.; Warmenhoven, H.; Verbart, D.; Stanic-Vucinic, D.; de Jong, G. A.; Velickovic, T. C.; Koppelman, S. J. Reduction and alkylation of peanut allergen isoforms Ara h 2 and Ara h 6; characterization of intermediate and end products. *Biochim. Biophys. Acta* **2013**, *1834*, 2832−2842.
(38) Pomés, A.; Helm, R. M.; Bannon, G. A.; Burks, A. W.; Tsay, A.; Chapman, M. D. Monitoring peanut allergen in food products by measuring Ara h 1. *J. Allergy Clin. Immunol.* **2003**, *111*, 640−645.
(39) Maleki, S. J.; Chung, S. Y.; Champagne, E. T.; Raufman, J. P. The effects of roasting on the allergenic properties of peanut proteins. *J. Allergy Clin. Immunol.* **2000**, *106* (4), 763−768.
(40) Schmitt, D. A.; Nesbit, J. B.; Hurlburt, B. K.; Cheng, H.; Maleki, S. J. Processing can alter the properties of peanut extract preparations. *J. Agric. Food Chem.* **2010**, *58*, 1138−1143.

DOI: 10.1021/jf504741t
J. Agric. Food Chem. 2015, 63, 1849−1855

Sangon Biological Engineering Technology and Services Co. (Shanghai, China), and the Beijing Solarbio Science & Technology Co. (Beijing, China).

Fish Maintenance and Toxicity Testing. In this study, adult male (mean weight: 0.33 ± 0. 01 g, mean length: 2.48 ± 0.02 cm) and female (mean weight: 0.27 ± 0. 01 g, mean length: 2.47 ± 0.03 cm) zebrafish (*Danio rerio*) were purchased from the Qixin tropical fish aquarium (Taian, Shandong, China). Fish were separated by sex and acclimatized for 2 weeks prior to the experiments. The fish were then divided into separate groups of 100 males and females and were housed in 12 L fish tanks. Fish were maintained according to Du et al.[18] with the following parameters: a 12:12 h light/dark cycle, a temperature of 26 ± 1 °C, oxygen saturation greater than 70%, and pH 7.4 to 8.1. The fish were fed twice a day with commercial dry flakes. Feeding ceased 24 h before the fish were tested to avoid interference from fecal matter during the assays. The stability of imidacloprid in water has been reported,[19−21] and a semistatic exposure system was used. Half of the fish water was changed every 2 days to maintain the concentration of imidacloprid, and uneaten food and feces were cleared away from the fish water in a timely manner using a siphon. In this study, all males and females were exposed to the same treatment concentrations of imidacloprid (0, 0.3, 1.25, and 5 mg/L). The fish were sampled in triplicate at days 7, 14, 21, and 28 and used to determine the levels of SOD, CAT, ROS, MDA, and DNA damage.

Enzyme Extraction and Measurement of Protein Content. Enzymes were extracted from the zebrafish livers using the method described by Shao et al. with slight modifications,[22] and the enzyme protein concentrations were determined using the method described by Bradford.[23]

Measurement of Enzyme Activities (SOD, CAT, and GST), ROS Production, and MDA Content. SOD, CAT, and GST activities were measured according to the methods described by Song et al.,[24] Xu et al.,[25] and Habig et al.,[26] respectively. The ROS production and MDA content were determined according to the methods described by Zhang et al.[27] Six fish (including three females and three males) from each treatment were sampled to detect protein concentration, enzymatic activity and MDA content. Ten fish (female/male = 1:1) were selected to test ROS levels. Three repeat experiments were completed.

Measurement of DNA Damage. DNA damage was evaluated by single-cell gel electrophoresis (SCGE). The cell suspensions of livers were obtained from four fish (including two females and two males) according to the noninvasive approach described by Diekmann et al.[28] The livers dissected from the anesthetized zebrafish were rinsed and processed in a tube containing 0.1 M PBS (0.14 M NaCl, 2.68 mM KCl, 0.01 M Na_2HPO_4, and 1.76 mM KH_2PO_4, pH 7.4) (1 mL). Liver suspensions were then filtered through 74 μm sieve, and the interstitial fluid obtained was centrifuged at 180*g* for 10 min at 4 °C. Afterward, the supernatant was decanted, and the precipitation was resuspended using 0.1 M PBS prior to the comet assay. The SCGE assay was performed according to Shao et al.[22] Finally, Olive Tail Moment (OTM) was used to determine the extent of DNA damage caused by imidacloprid to zebrafish. OTM is the distance between the center of the head and the center of the tail, and the percent of tail DNA was used to evaluate the extent of DNA damage.[29]

Statistics. Each treatment was conducted in triplicate, and the means and standard errors were considered in the calculation. SPSS 18.0 was used to analyze biochemical responses by a bifactorial analysis of variance (ANOVA) according to the concentration, the time of exposure, and their interaction. A posthoc test using a least significant difference (LSD) calculation at $p < 0.05$ preceded bifactorial ANOVA results. One-way ANOVA analyses ($p < 0.05$) were conducted to evaluate the significant effects of all data among the treatments at the same sample times. Final results were expressed as the mean ± SD (standard deviation).

RESULTS

Effects of Imidacloprid on ROS Levels in Zebrafish (*Danio rerio*). The ROS levels in zebrafish exposed to imidacloprid is depicted in Figure 1.

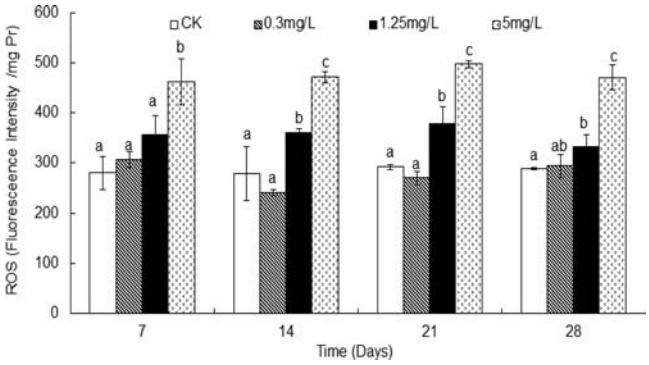

Figure 1. Effect of imidacloprid on ROS levels in the zebrafish liver (Pr = protein). Data represent means ± standard deviation ($n = 3$). Different labels above bars indicate significant differences at $p < 0.05$ between treatments.

Compared with the controls, no significant difference in ROS levels was detected in zebrafish exposed to 0.3 mg/L imidacloprid throughout the exposure period (7, 14, 21, and 28 days). However, the ROS levels of the high-concentration imidacloprid (1.25 and 5 mg/L) in fish were higher than those of the controls at days 14, 21, and 28. A higher ROS value compared with controls was also detected in fish treated with 5 mg/L imidacloprid during the entire exposure period.

SOD Activities. Changes in zebrafish SOD activities during imidacloprid exposure are described in Figure 2.

As shown in Figure 2, only the first week of exposure showed dose-dependent changes in SOD activity. Noticeably, there was

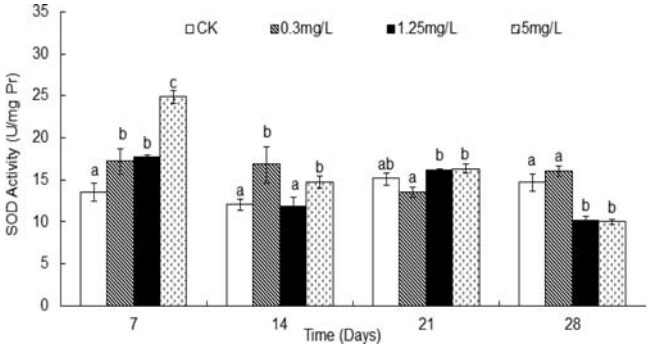

Figure 2. Effect of imidacloprid on SOD activity in the zebrafish liver (Pr = protein). Data represent means ± standard deviation ($n = 3$). Different labels above bars indicate significant differences at $p < 0.05$ between treatments.

DOI: 10.1021/jf504895h
J. Agric. Food Chem. 2015, 63, 1856−1862

a significant increase in SOD activity on day 14 in all treatment groups except the 1.25 mg/L group. At 21 days, no statistically significant differences in SOD activities between any exposure concentration and the control were observed. On the 28th day, SOD activities in the low concentration (0.3 mg/L) treatment group were the same as those in the control group. In addition, there was a significant decrease in SOD activity in the 1.25 and 5 mg/L treatment groups at day 28, which suggests inhibition of the SOD enzyme.

CAT Activities. The effects of imidacloprid on CAT activity in zebrafish are illustrated in Figure 3.

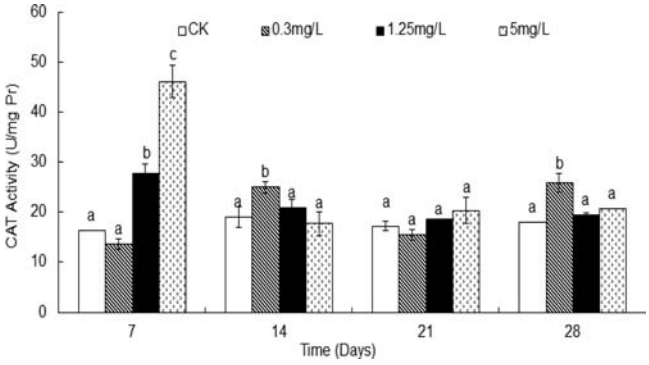

Figure 3. Effect of imidacloprid on CAT activity in the zebrafish liver (Pr = protein). Data represent means ± standard deviation (n = 3). Different labels above bars indicate significant differences at $p < 0.05$ between treatments.

Significant differences in CAT activity between the imidacloprid-exposed fish and the controls were observed only in the first week of exposure. After this time point, no differences were observed among the treatment groups except the 0.3 mg/L treatment group on days 14 and 28. Obvious increases in CAT activities in the 0.3 mg/L treatment group compared with controls were detected at days 14 and 28. No significant difference among the treatment groups was observed at day 21. In this case, no inhibition of CAT was observed at any time point.

GST Activities. The results of GST activities are depicted in Figure 4.

As indicated in Figure 4, on day 7, GST activities in zebrafish were not significantly different between any treatment group and the control group. A significant increase in GST activity relative to the control group could be observed on day 21. However, there were no difference among treatments (except in the 1.25 mg/L treatment group) compared with the control on day 14. GST activity was slightly higher in zebrafish exposed to imidacloprid (1.25 mg/L) than in controls. A dose-dependent decrease in GST activity was observed in all treatment groups at day 28.

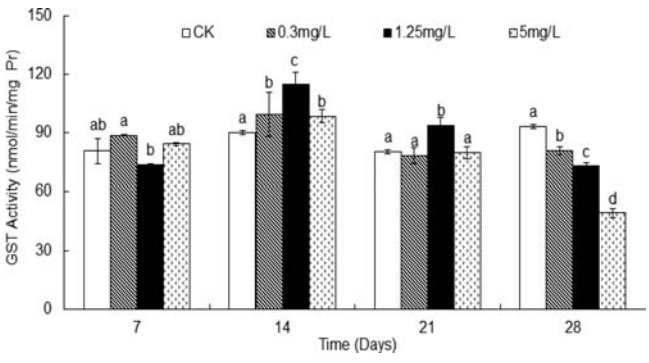

Figure 4. Effect of imidacloprid on GST activity in the zebrafish liver (Pr = protein). Data represent means ± standard deviation (n = 3). Different labels above bars indicate significant differences at $p < 0.05$ between treatments.

MDA Content. In this assay, the zebrafish MDA content was used to evaluate the level of lipid peroxidation caused by imidacloprid, and the results are illustrated in Figure 5.

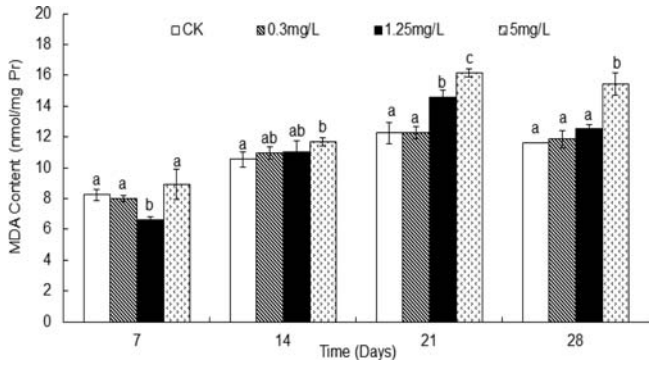

Figure 5. Effect of imidacloprid on MDA content in the zebrafish liver (Pr = protein). Data represent means ± standard deviation (n = 3). Different labels above bars indicate significant differences at $p < 0.05$ between treatments.

The MDA contents in zebrafish treated with different concentrations of imidacloprid were not significantly different at day 7, except in the 1.25 mg/L treatment group. Similarly, no obvious increase was found in the low concentration (0.3 and 1.25 mg/L) groups on days 14 and 28, when there was a significant difference in the highest treatment (5 mg/L) group compared with the control. On day 21, MDA production increased only in the highest concentration treatment (1.25 and 5 mg/L) groups compared with controls, whereas no significant difference was observed in the low concentration treatment (0.3 mg/L) group compared with control.

DNA Damage. The OTMs in zebrafish treated with different doses of imidacloprid are shown in Figure 6.

All of the OTMs obtained from the imidacloprid-exposed fish were significantly different from the control, which indicated that imidacloprid caused dose-dependent DNA

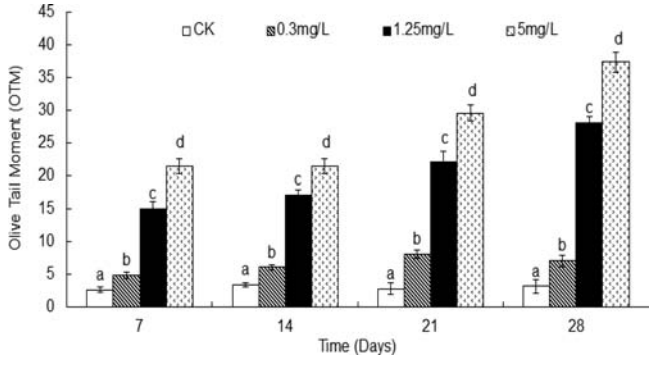

Figure 6. Effect of imidacloprid on DNA damage in the zebrafish liver. Data represent means ± standard deviation (n = 3). Different labels above bars indicate significant differences at $p < 0.05$ between treatments.

DOI: 10.1021/jf504895h
J. Agric. Food Chem. 2015, 63, 1856−1862

Table 1. ANOVA Results for the Biochemical Responses of Zebrafish Exposed to Imidacloprid on Days 7, 14, 21, and 28

	dose			time			dose* time		
biomarkers	df	*F*	*p*	df	*F*	*p*	df	*F*	*p*
SOD activity	3	20.78	0.000*	3	72.54	0.000*	9	33.14	0.000*
CAT activity	3	58.49	0.000*	3	54.04	0.000*	9	75.17	0.000*
GST activity	3	10.48	0.000*	3	57.49	0.000*	9	16.81	0.000*
ROS level	3	127.49	0.000*	3	1.06	0.385	9	1.31	0.280
MDA content	3	53.55	0.000*	3	290.93	0.000*	9	10.71	0.000*
DNA damage	3	25716.93	0.000*	3	2809.04	0.000*	9	799.44	0.000*

*Indicates a significant effect of imidacloprid concentration, time of exposure and their interaction on biochemical responses ($p < 0.05$).

damage in zebrafish. In the same treatment group, the OTM values in zebrafish increased distinctly with the extended exposure duration, and the level of DNA damage in zebrafish was also dependent upon the exposure time, which showed a time−effect relationship.

Bifactorial ANOVA Results of Biochemical Responses. A significant interaction between imidacloprid concentration and exposure time was found for all biomarkers assessed, except the ROS level (Table 1), which indicated that changes in these biomarkers in zebrafish livers were due to the combined effects of dose and exposure time. In addition, imidacloprid concentration had a significant effect on all biomarkers tested, and exposure time had an important influence on all biomarkers except ROS. Followed by bifactorial ANOVA (Table 2), the post hoc test results showed that changes in exposure dose or time could significantly affect the biomarker levels compared with controls.

Table 2. Results of Post-hoc Test by LSD after Bi-factorial ANOVA for Biochemical Responses of Zebrafish Exposed to Imidacloprid on Days 7, 14, 21, and 28

	dose (mg/L)				time (days)			
biomarkers	0	0.3	1.25	5	7	14	21	28
SOD activity	a	b	a	b	a	b	c	d
CAT activity	a	b	c	d	a	b	c	b
GST activity	a	a	a	b	a	b	a	c
ROS level	a	a	b	c	a	a	a	a
MDA content	a	ab	b	c	a	b	c	d
DNA damage	a	b	c	d	a	b	c	d

Different letters indicate significant differences at $p < 0.05$ between different dosages and exposure time.

The results of CAT activity and DNA damage were significantly different in each imidacloprid concentration treatment group. SOD activity, MDA content, and DNA damage were significantly different at each time point. These results were also reflected in the one-way ANOVA results that indicated the significant differences among various imidacloprid concentrations at the same exposure time.

DISCUSSION

Effects of Imidacloprid on ROS Levels. Many studies have demonstrated that intracellular oxidative stress is triggered due to excess ROS, which can be induced by toxicants, and that this excess is the main cause of cell damage.[30] In this assay, the ROS levels increased in a dose-dependent manner throughout the trial period. This may be because the antioxidant systems in zebrafish liver cannot completely remove excess ROS from the body, and thus, the dynamic equilibrium between ROS levels and the antioxidant defense system is destroyed, eventually leading to oxidative stress. Though the ROS levels of zebrafish exposed to 0.3 mg/L of imidacloprid remained stable, there was no significant difference between these fish and the controls. These results showed that a low concentration (0.3 mg/L) of imidacloprid was insufficient to cause significant changes in ROS content.

Effects of Imidacloprid on SOD Activities. SOD activity increased at different concentrations of imidacloprid during the early exposure period (7 and 14 days). On the basis of the study by Liu et al.,[31] we inferred that an increase in oxygen free radical production occurred in zebrafish under light stress. Consequently, excessive ROS may have induced the synthesis of more SOD or increased its activity to protect against oxidative stress. Increased SOD activity in organisms indicated that ROS levels were still in the range in which SOD could resist the oxidative stress. As the exposure time increased (21 and 28 days), SOD activity decreased to or below the levels detected in the control groups. This may be because the increased oxygen free radicals in zebrafish rendered SOD inactive by oxidation. Previous research demonstrated that SOD activity was activated under mild adverse stress and declined under more intense stress.[22] Our results confirm those findings. The inhibition of SOD activity can be explained by the metabolism of imidacloprid over time, which may have reduced the toxicant concentrations during prolonged exposure, and the adverse effects exerted on SOD synthesis and its activity were induced by excess ROS. These results show that the toxic effect of imidacloprid on SOD activity is much more obvious at higher concentrations.

Effects of Imidacloprid on CAT Activities. In this assay, CAT activities in zebrafish exposed to different imidacloprid concentrations increased during the first week of exposure and then decreased to control levels at later time points. A study by Olga et al.[32] showed that ROS levels were increased in crustaceans following imidacloprid treatment but then gradually decreased, which is in agreement with our results. Imidacloprid can induce CAT synthesis in zebrafish in response to scavenging H_2O_2 into H_2O and O_2 to maintain free radical balance. On day 7, the CAT activity in zebrafish exposed to a low imidacloprid concentration (0.3 mg/L) remained near the control level. At 14 days, both SOD activity and CAT activity were elevated, and CAT activity was significantly higher than SOD activity, which may be because the CAT was required to remove H_2O_2 generated by the oxidated environment and SOD catalysis. At the end of the exposure period (28 days), CAT activity was elevated, whereas SOD activity declined to control levels and was even inhibited. This illustrated that the CAT enzyme was needed to eliminate the excess H_2O_2 to maintain the balance of H_2O_2 in the cell. The CAT activities and SOD activities in zebrafish exposed to medium high (1.25 mg/L) and

DOI: 10.1021/jf504895h
J. Agric. Food Chem. 2015, 63, 1856−1862

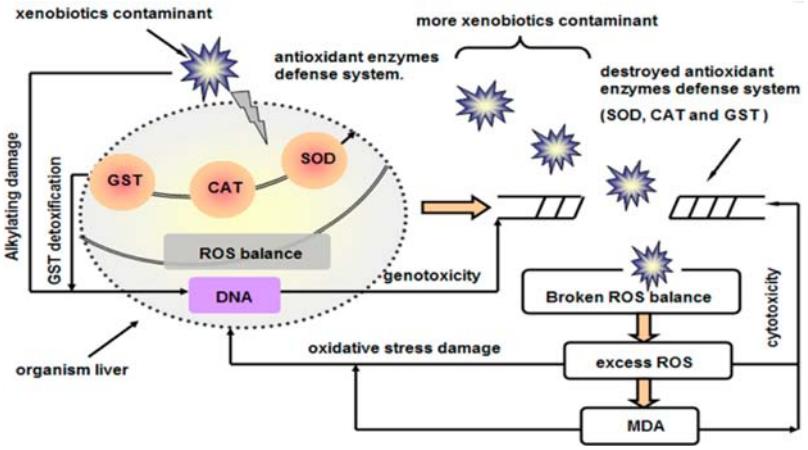

Figure 7. Relationship between each indicator. The connection among SOD, CAT, GST activities, ROS level, MDA content, and DNA damage in liver tissue.

high concentrations (5 mg/L) of imidacloprid treatments exhibited similar trends, in which both enzyme levels increased at first and then declined. CAT activity returned to control levels, whereas SOD activity was suppressed during the late exposure time point (28 days). This demonstrated that SOD was more sensitive than CAT to the same level of oxidative stress. These results show that during mild oxidative stress, SOD is activated earlier than CAT.

Effects of Imidacloprid on GST Activities. Glutathione S-transferase (GST) is a phase II biotransformation enzyme that can detoxify ROS.[33] In our study, the GST levels did not significantly change during early exposure (7 days). A possible reason for this phenomenon might be that the converted products of the phase I enzyme failed to reach adequate levels to activate GST. In addition, ROS levels might not have been sufficiently high to elevate GST activity. The GST activities in zebrafish exposed to all concentrations of imidacloprid were slightly activated by day 14 and were then suppressed by 28 days of exposure. When GST detoxifies ROS, its own activity can be impacted by exogenous substances. A study by Svensson et al.[34] showed that the sulfhydryl of microsomal GST's 49th cysteine could specifically combine with hydrogen peroxide (alkylating agent, etc.), thus enhancing GST activity. Therefore, in this assay, GST activity was possibly elevated because imidacloprid induced detoxification through the combination of intracellular GSH and harmful metabolites, such as membranous peroxide and DNA oxidative degradation products. Excess ROS induced by imidacloprid and imidacloprid itself could also have activated GST. At 28 days, the GST activity of every imidacloprid-exposed treatment group was inhibited. According to Egaas et al.,[35] this decline in enzymatic activity seems to be connected to excessive consumption of GSH as substrate and the change in GST composition triggered by many intermediate metabolites. Another correlative factor is the possible competitive inhibition between GST and its substrate (such as CDNB). Our research results have shown variations in GST activity in imidacloprid-exposed zebrafish, which is similar to previously reported studies.[22,36]

Effects of Imidacloprid on MDA Content. The free radical intermediate and the final breakdown products of lipid peroxidation, such as MDA, may severely damage cell membranes. Therefore, the measurement of MDA content can indirectly reflect the degree of lipid peroxidation. At present, many researchers have used MDA as a biomarker to detect the environmental effect of pollutants (such as polycyclic musk and textile wastewater) to earthworms or zebrafish, and some valuable results have been reported.[37,38] In our study, the MDA content in zebrafish treated with imidacloprid showed no significant differences from controls on days 7 and 14 but increased significantly afterward in the highest treatment groups. A possible reason for this observation is connected to ROS content and GST activity. For instance, the ROS content in zebrafish increased at 1.25 and 5 mg/L imidacloprid concentrations of imidacloprid. By 7 days, the GST activities of all imidacloprid-exposed zebrafish remained near the control levels and then increased after 14 days. The lack of significant variations in MDA content may have occurred because the ROS increase induced by these relatively low concentrations of imidacloprid was inadequate to initiate the lipid peroxidation that can be inhibited by GST detoxification. Certainly, the GSH-Px and other enzymes that are briefly discussed in our study may accelerate the catabolism of MDA. At prolonged exposure times, the MDA content in fish exposed to high concentrations (5 mg/L) of imidacloprid increased gradually. This can be interpreted as a reduction or inhibition of GST activity to increase the degree of lipid peroxidation, leading to the increase of MDA content ultimately. Because lower ROS levels and relatively lower levels of GST activity were induced by lower concentrations of imidacloprid, excessive accumulation of MDA was avoided. Moreover, the unchanged MDA content indicates that low doses of imidacloprid do not cause obvious lipid peroxidation damage to zebrafish, which further explains that MDA has no obvious indicative function during low concentrations of imidacloprid stress.

DNA Damage in Zebrafish. The single-cell gel electrophoresis assay (comet assay) is widely used to detect the genotoxicity of environmental pollutants to assess the DNA damage. The results showed that imidacloprid caused dose-dependent DNA damage to zebrafish livers. Additionally, a time−response relationship was observed under the same exposure conditions. Some studies have reported the dose−effect relationship between pollutants and DNA damage in organisms.[24,39,40] Pollutants that contain alkyl radicals can cause alkylation of DNA, thus inducing DNA damage. The reaction product of free radicals not only causes damage to base exchange (DNA−protein cross-linking and DNA chain rupture) but may lead to lipid peroxidation and generate lipid superoxide free radicals and alkyl radicals. This may further

DOI: 10.1021/jf504895h
J. Agric. Food Chem. 2015, 63, 1856−1862

intensify DNA damage or even change gene expression. The significant induction of GST activity could protect against DNA damage indirectly by inhibiting lipid peroxidation. In our assay, the ROS levels were increased and persisted as the imidacloprid concentration and exposure time increased; however, the MDA content at higher concentrations of imidacloprid increased during the later stages of exposure, and DNA damage also increased during the entire exposure to imidacloprid, which is in accordance with the study of Cooke et al.[41] Therefore, we infer that the accumulation of MDA is correlated with the production of ROS and the induction of DNA damage. During the exposure period, although GST activity increased slightly at day 14, the DNA damage could not be fully repaired. Additionally, the variations in ROS levels and MDA content were not in line with that of the DNA damage. It is possible that DNA damage could also be affected by other biochemical processes. The DNA damage observed in zebrafish livers may originate from the combined accumulation of reactive oxygen species and lipid peroxidation products, cell apoptosis, and the direct effects of imidacloprid. Compared with other indicators, DNA damage detected by comet assay was more sensitive and stable in our study.

Association Analysis Concerning the Results of Each Indicator. The production and elimination of ROS in the liver tissue was in a dynamic equilibrium under normal physiological conditions (Figure 7).

As shown in Figure 7, when exogenous pollutants enter the body, they induce organisms to generate ROS in abundance, and the antioxidant enzymes (SOD, CAT, and GST) are activated to scavenge the excess ROS to minimize the adverse effects caused by exogenous pollutants. With internal pollutant levels increasing over time during continuous exposure, the excess ROS generated cannot be scavenged entirely, and the ROS balance is broken thus causing cytotoxicity. This is reflected in a reduced, or even inhibited, activity of the detoxification system (e.g., SOD, CAT, and GST enzymes).[42] Additionally, the accumulation of ROS can induce lipid peroxidation and may lead to accumulation of the end-product MDA. Moreover, MDA is cytotoxic and can exert an adverse effect on the performance and synthesis of antioxidant enzymes. Furthermore, MDA and excess ROS may result in DNA strand breakage and base swaps, which can lead to DNA damage in liver tissue. Damaged DNA, as a result of alkylation or oxidative stress, can also inhibit the synthesis of detoxifying enzymes (genotoxicity). Moreover, GST can not only eliminate ROS, but it can also detoxify the liver tissue that has been directly damaged by exogenous pollutants.[43] Thus, detoxification by GST plays a significant role in protecting cells from DNA damage.

Our results indicated that very high concentrations of imidacloprid induced a marked increase in ROS levels in the zebrafish liver, and the activities of SOD, CAT, and GST were elevated to scavenge excess ROS. When excess production of ROS reached a certain level beyond the typical function of the antioxidant system, a decrease in antioxidant enzymes activity was induced. As time progressed, ROS attacked cell membranes leading to an increase in MDA, which caused DNA damage and was scavenged by the increased GST activity. After an analysis of these results, the protective capability of GST against DNA damage was not obvious. The DNA damage induced by imidacloprid increased with exposure concentrations and time, whereas GST activity in zebrafish livers decreased, even to the point of inhibition.

AUTHOR INFORMATION

Corresponding Authors

*E-mail: wjh@sdau.edu.cn. Phone:+86 538 8249789. Fax: +86 538 8242549.

*E-mail: lushzhu@vip.163.com.

Author Contributions

§W.G. and S.Y. contributed equally to this work.

Funding

The present study was supported by Grants from the National Natural Science Foundation of China (Nos. 21377075, 21277083, 41071164, and 41001152), the Specialized Research Fund for the Doctoral Program of Higher Education (20113702110007), and Natural Science Foundation of Shandong (ZR2013DQ007).

Notes

The authors declare no competing financial interest.

ACKNOWLEDGMENTS

We gratefully acknowledge Dr. Frederick Ernst (University of California, Riverside) for his helpful suggestions and review of the manuscript.

ABBREVIATIONS USED

CAT, catalase; SOD, superoxide dismutase; ROS, reactive oxygen species; GST, glutathione-S-transferase; MDA, malondialdehyde; SCGE, single-cell gel electrophoresis

REFERENCES

(1) Schippers, N.; Schwack, W. Photochemistry of Imidacloprid in Model Systems. *J. Agric. Food Chem.* **2008**, *56*, 8023−8029.

(2) Ding, F.; Peng, W.; Diao, J. X.; Zhang, L.; Sun, Y. Characteristics and Essences upon Conjugation of Imidacloprid with Two Model Proteins. *J. Agric. Food Chem.* **2013**, *61*, 4497−4505.

(3) Tomizawa, M.; Casida, J. E. Neonicotinoid insecticide toxicology: mechanisms of selective action. *Annu. Rev. Pharmacol. Toxicol.* **2005**, *45*, 247−268.

(4) Ford, K. A.; Gulevich, A. G.; Swenson, T. L.; Casida, J. E. Neonicotinoid Insecticides: Oxidative Stress in Planta and Metallo-oxidase Inhibition. *J. Agric. Food Chem.* **2011**, *59*, 4860−4867.

(5) Jeschke, P.; Nauen, R.; Schindled, M.; Elbert, A. Overview of the statusand global strategy for neonicotinoids. *J. Agric. Food. Chem.* **2011**, *59*, 2897−2908.

(6) Felsot, A. S.; Cone, W.; Yu, J.; Ruppert, J. R. Distribution of imidacloprid in soil following subsurface drip chemigation. *Bull. Environ. Contam. Toxicol.* **1998**, *60*, 363−370.

(7) Gonzales-Pradas, E.; Fernandez-Perez, M.; Villafranca-Sanchez, M.; Flore-Cespedes, F. Mobility of imidacloprid from alginate-bentonite controlled- release formulations in greenhouse soils. *Pestic. Sci.* **1999**, *55*, 1109−1115.

(8) Tišler, T.; Jemec, A.; Mozetic, B.; Jemec, A.; Mozetic, B.; Trebse, P. Hazard identification of imidacloprid to aquatic environment. *Chemosphere* **2009**, *76*, 907−914.

(9) Van Dijk, T. C.; Van Staalduinen, M. A.; Van der Sluijs, J. P. Macro-invertebrate decline in surface water polluted with imidacloprid. *PLoS One* **2013**, *8*, e62374.

(10) Kreuger, J.; Graaf, S.; Patring, J.; Adieslsson, S. Pesticides in surface water in areas with open ground and greenhouse horticultural crops in Sweden 2008. http://pub.epsilon.slu.se/5413/1/kreuger_j_et_al_101014.pdf (accessed September 20, 2014).

(11) Van Dijk, T. C. Effects of neonicotinoid pesticide pollution of Dutch surface water on non-target species abundance. http://beyondpesticides.org/pollinators/Nicotinoid%20Pollution%20of%20Dutch%20Surface%20Waters.pdf (accessed September 10, 2014).

DOI: 10.1021/jf504895h
J. Agric. Food Chem. 2015, 63, 1856−1862

(12) Lamers, M.; Anyusheva, M.; La, N.; Nguten, V.; Streck, T. Pesticide pollution in surface- and groundwater by paddy rice cultivation: a case study from Northern Vietnam. *Clean: Soil, Air, Water* **2011**, *39*, 356−361.
(13) Valavanidis, A.; Vlahogianni, T.; Dassenakis, M.; Scoullos, M. Molecular biomarkers of oxidative stress in aquatic organisms in relation to toxic environmental pollutants. *Ecotoxicol. Environ. Saf.* **2006**, *64*, 178−189.
(14) Sun, R. L.; Zhou, Q. X.; Sun, F. H.; Jin, C. X. Antioxidative defense and proline/phytochelatin accumulation in a newly discovered Cd-hyperaccumulator, *Solanum nigrum* L. *Environ. Exp. Bot.* **2007**, *60*, 468−476.
(15) Kilili, K. G.; Atamassova, N.; Vardanyan, A.; Clatot, N.; Al-Subarea, K.; Kanellopoulos, P. N.; Makris, A. M.; Kampranis, S. C. Differential roles of tau class glutathione S-transferases in oxidative stress. *J. Biol. Chem.* **2004**, *279*, 24540−24551.
(16) Suzuki, Y. J.; Ford, G. D. Redox regulation of signal transduction in cardiac and smooth muscle. *J. Mol. Cell Cardiol.* **1999**, *31*, 345−353.
(17) Singh, N. P.; McCoy, M. T.; Tice, R. R.; Schneider, E. L. A simple technique for quantitation of low levels of DNA damage in individual cells. *Exp. Cell Res.* **1988**, *175*, 184−191.
(18) Du, Z. K.; Zhu, L. S.; Dong, M.; Wang, J. H.; Wang, J.; Xie, H.; Zhu, S. Y. Effects of the ionic liquid [Omim]PF_6 on antioxidant enzyme systems, ROS and DNA damage in zebrafish (*Danio rerio*). *Aquat. Toxicol.* **2012**, *124*−*125*, 91−93.
(19) Overmyer, J. P.; Mason, B. N.; Armbrust, K. L. Acute toxicity of imidacloprid and fipronil to a nontarget aquatic insect, *Simulium vittatum* Zetterstedt cytospecies IS-7. *Bull. Environ. Contam. Toxicol.* **2005**, *74*, 872−879.
(20) Tišler, T.; Jemec, A.; Mozetič, B.; Trebše, P. Hazard identification of imidacloprid to aquatic environment. *Chemosphere* **2009**, *76*, 907−914.
(21) Pandey, G.; Dorrian, S. J.; Russell, R. J.; et al. Biotransformation of the neonicotinoid insecticides imidacloprid and thiamethoxam by Pseudomonas sp.1G. *Biochem. Biophys. Res. Commun.* **2009**, *380* (3), 710−714.
(22) Shao, B.; Zhu, L. S.; Dong, M.; Wang, J.; Wang, J. H.; Xie, H.; Zhang, Q. M.; Du, Z. Q.; Zhu, S. Y. DNA damage and oxidative stress induced by endosulfan exposure in zebrafish (*Danio rerio*). *Ecotoxicology* **2012**, *21*, 1533−1540.
(23) Bradford, M. M. A rapid and sensitive method for the quantization of microgram quantities of protein utilizing the principle of protein-dye binding. *Anal. Biochem.* **1976**, *72*, 248−254.
(24) Song, Y.; Zhu, L. S.; Wang, J.; Wang, J. H.; Liu, W.; Xie, H. DNA damage and effects on antioxidative enzymes in earthworm (*Eisenia foetida*) induced by atrazine. *Soil Biol. Biochem.* **2009**, *41*, 905−909.
(25) Xu, J. B.; Yuan, X. F.; Lang, P. Z. Determination of catalase activity and catalase inhibition by ultraviolet spectrophotometry. *Environ. Chem.* **1997**, *16*, 73−76.
(26) Habig, W.; Pabst, M. J.; Jacoby, W. B. Glutathione-S-transferase: the first step in mercapturic acid formation. *J. Biol. Chem.* **1974**, *249*, 1730−1739.
(27) Zhang, Q. M.; Zhu, L. S.; Wang, J.; Xie, H.; Wang, J. H.; Han, Y. N.; Yang, J. H. Oxidative stress and lipid peroxidation in the earthworm Eisenia fetida induced by low doses of fomesafen. *Environ. Sci. Pollut. Res.* **2013**, *20*, 201−208.
(28) Diekmann, M.; Hultsch, V.; Nagel, R. On the relevance of genotoxicity for fish populations I: effects of a model genotoxicant on zebrafish (*Danio rerio*) in a complete life-cycle test. *Aquat. Toxicol.* **2004**, *68*, 13−26.
(29) Wang, M. H.; Wang, D. Z.; Lin, L.; Hong, H. S. Protein profiles in zebrafish (Danio rerio) brains exposed to chronic microcystin-LR. *Chemosphere* **2010**, *81*, 716−724.
(30) Banaee, M. Physiological dysfunction in fish after insecticides exposure. In *Agricultural and biological sciences insecticides, development of safer and more effective technologies*; Trdan, S., Ed.; InTech: Croatia, **2013**; pp 103−143.
(31) Liu, Y.; Zhou, Q. X.; Xie, X. J.; Lin, D. S.; Dong, L. X. Oxidative stress and DNA damage in the earthworm Eisenia fetida induced by toluene, ethylbenzene and xylene. *Ecotoxicology* **2010**, *19*, 1551−1559.
(32) Olga, M.; Roberta, S. K.; Elsa, F.; Polonca, T. Comparative toxicity of imidacloprid and its transformation product 6-chloronicotinic acid to non-target aquatic organisms: Microalgae Desmodesmus subspicatus and amphipod Gammarus fossarum. *Pestic. Biochem. Physiol.* **2012**, *104*, 178−186.
(33) Wu, Y. Q.; Wang, C. G.; Wang, Y.; Zhao, Y.; Chen, Y. X.; Zuo, Z. H. Antioxidant responses to benzo [a] pyrene, tributyltin and their mixture in the spleen of Sebasticus marmoratu. *J. Environ. Sci.* **2007**, *19*, 1129−1135 (in Chinese).
(34) Svensson, R.; Rinaldi, R.; Swedmark, S.; Morgenstern, R. Reactivity of cysteine-49 and its influence on the activation of microsomal glutathione transferase 1: evidence for subunit interaction. *Biochemistry* **2000**, *39*, 15144−15149.
(35) Egaas, E.; Sandvik, M.; Fjeld, E.; Kallqvist, T.; Goksoyr, A.; Svensen, A. Some effects of the fungicide propiconazole on cytochrome P450 and glutathione S-transferase in brown trout (*Salmo trutta*). *Comp. Biochem. Physiol., Part C: Pharmacol., Toxicol. Endocrinol.* **1999**, *l22*, 337−344.
(36) Wang, Y. C.; Chaung, R. H.; Tung, L. C. Comparison of the cytotoxicity induced by different exposure to sodium arsenite in two fish cell lines. *Aquat.Toxicol.* **2004**, *69*, 67−79.
(37) Chen, C.; Zhou, Q.; Liu, S.; Xiu, Z. Acute toxicity, biochemical and gene expression responses of the earthworm Eisenia fetida exposed to polycyclic musks. *Chemosphere* **2011**, *83*, 1147−1154.
(38) Zhang, W. J.; Liu, W.; Zhang, J.; Zhao, H. M.; Zhang, Y. B.; Quan, X.; Jin, Y. Characterisation of acute toxicity, genotoxicity and oxidative stress posed by textile effluent on zebrafish. *J. Environ. Sci.* **2012**, *24*, 2019−2027 (in Chinese).
(39) Song, Y.; Zhu, L. S.; Xie, H.; Wang, J.; Wang, J. H.; Liu, W.; Dong, X. L. Effects of atrazine on DNA damage and antioxidative enzymes in Vicia faba. *Environ. Toxicol. Chem.* **2009b**, *28*, 1059−1062.
(40) Seitz, N.; Bottcher, M.; Keiter, S.; Kosmehl, T.; Manz, W.; Hollert, H.; Braunbeck, T. A novel statistical approach for the evaluation of comet assay data. *Mutat. Res.* **2008**, *652*, 38−45.
(41) Cooke, M. S.; Evans, M. D.; Dizdaroglu, M.; Lunec, J. Oxidative DNA damage: mechanisms, mutation, and disease. *FASEB J.* **2003**, *17*, 1195−1214.
(42) Brendler-Schwaab, S.; Hartmann, A.; Pfuhler, S.; Speit, G. The in vivocomet assay: use and status in genotoxicity testing. *Mutagenesis* **2005**, *20*, 245−254.
(43) Choi, C. Y.; An, K. W.; An, M. I. Molecular characterization and mRNA expression of glutathione peroxidase and glutathione S-transferase duringosmotic stress in olive flounder (*Paralichthys olivaceus*). *Comp. Biochem. Physiol., Part A: Mol. Integr. Physiol.* **2008**, *149*, 330−337.

DOI: 10.1021/jf504895h
J. Agric. Food Chem. 2015, 63, 1856−1862

postharvest storage. The chemical profiles of broccoli microgreens were monitored for different growth periods and different shelf time after harvest. The goal of this study was to identify the differences in the chemical profiles for each experimental factor different group of samples and to further validate the findings quantitatively.

MATERIALS AND METHODS

Chemicals. Formic acid and high-performance liquid chromatography (HPLC)-grade methanol and acetonitrile were purchased from VWR International, Inc. (Clarksburg, MD). HPLC-grade water was prepared from distilled water using a Milli-Q system (Millipore Lab., Bedford, MA, USA). (−) Sinigrin hydrate (≥99.0%), sulfatase (from *Helix pomatia*), imidazole, and Sephadex A-25 chloride form were purchased from Sigma−Aldrich (St. Louis, MO, USA). Glucoerucin potassium salt, glucoiberin potassium salt, and glucoraphanin potassium salt were purchased from Chromadex (Irvine, CA, USA).

Plant Materials and Sample Preparation for Metabolomic Study. Broccoli microgreens were grown in a growth chamber (25 °C) as previously described.[15] Hydroponic "Sure seeds" were then spread evenly over the damp pad. The trays were kept in a growth chamber at 25 °C. During the first four days, the trays were covered, and the seeds were germinated in the dark. For the next six days, the seedlings were exposed to light with the light intensity of 42 μmol s^{-1} m^{-2} for 12 h/12 h (light/dark). The seedlings were sprayed once a day with H_2O (pH 5.6) only or 10 mM $CaCl_2$. Each treatment of microgreens has three trays as triplicate. Three trays of the microgreens were collected at the fourth day after sowing from each treatment group and labeled as "Preharvest Day 4". All of the rest of the microgreens, including hypocotyl and cotyledons, were harvested on 10 days after sowing (labeled as "Harvest Day") by cutting near the bottom of each hypocotyl with a pair of sterilized scissors. Harvested broccoli microgreens (0.01 kg each) were packaged in sealed bags (0.1 m × 0.1 m) prepared with polyethylene films of 16.6 pmol s^{-1} m^{-2} Pa^{-1} oxygen transmission rate (OTR). The film OTR was determined by the film manufacturer (Packaging Concept Inc., Salinas, CA, USA). Packaged microgreens were stored at 5 °C and collected on 4, 7, and 14 d postharvest and labeled as "Postharvest Day 4", "Postharvest Day 7", and "Postharvest Day 14", respectively.

All samples were lyophilized and then ground. Powdered samples (300 mg) were extracted with 5.00 mL of methanol−water (60:40, v/v) using sonication for 60 min at room temperature and then centrifuged at 1000*g* for 15 min (IEC Clinical Centrifuge, Damon/IEC Division, Needham, MA, USA). The supernatant was filtered through a 17 mm (0.45 μm) PVDF syringe filter (VWR Scientific, Seattle, WA, USA), and 10 μL of the extract was used for each HPLC injection.

Extration and Desulfation of GLs. The extraction of GLs was performed following the ISO9167-1 method with slight modification. A 200 mg amount of broccoli microgreen powder was weighed into screw-top graduated glass tubes and extracted with 5 mL of methanol, and then, the liquid level was marked . The tube was heated at 70 °C for 20 min using a water heating bath and then centrifuged at 5000 rpm for 10 min. After waiting for the tube to cool down, methanol was added to bring the liquid level back to the mark. A 200 μL amount of 5 mM 2-propenyl-glucosinolate (sinigrin) was added to the tube as an internal standard. A 1 mL volume of the extract was transferred to a prepared Sephadex A-25 column without disturbing the resin surface, and draining was allowed. Then, two 1 mL portions of sodium acetate buffer (pH = 4) was added, and the buffer was allowed to drain after each addition. Purified sulphatase (100 μL) was added to the column, and desulphation was done overnight (12 h) at room temperature. The resultant desulfo-GLs were eluted with two washes of 500 μL of water prior to separation by ultra-high-performance liquid chromatography with mass spectrometry (UHPLC-HRMS) analysis.

UHPLC-PDA-ESI/HRMS/MS^n Conditions for Metabolomic Study. The UHPLC-HRMS system used consisted of an LTQ Orbitrap XL mass spectrometer with an Accela 1250 binary pump, a PAL HTC Accela TMO autosampler, a PDA detector (ThermoFisher Scientific, San Jose, CA, USA), and a G1316A column compartment (Agilent, Palo Alto, CA, USA). Separation was carried out on a Hypersil Gold AQ RP-C_{18} UHPLC column (200 mm × 2.1 mm i.d., 1.9 μm, ThermoFisher Scientific) with an UltraShield precolumn filter (Analytical Scientific Instruments, Richmond, CA, USA) at a flow rate of 0.3 mL/min. The mobile phase consisted of a combination of solution A (0.1% formic acid in water, v/v) and solution B (0.1% formic acid in acetonitrile, v/v). The linear gradient was from 4% to 20% B (v/v) at 40 min, to 35% B at 60 min, to 100% B at 61 min, and held at 100% B to 65 min. The MS parameters were optimized using a standard solution of sinigrin (100 ng/mL) infused with mobile phase at a flow rate 0.3 mL/min. The optimized conditions were set as follows: sheath gas at 70 (arbitrary units), aux and sweep gas at 15 (arbitrary units), spray voltage at 4.8 kV, capillary temp at 270 °C, capillary voltage at 15 V, and tube lens at 70 V. The mass range was from 100 to 1500 amu with a resolution of 15 000, FTMS AGC target at 2×10^5, FT-MS/MS AGC target at 1×10^5, isolation width of 1.5 amu, and max ion injection time of 500 ms. The most intense ion was selected for the data-dependent scan to offer their MS^2 to MS^5product ions, respectively, with the normalization collision energy at 35%.

Qualitative and Quantitative Analysis of GLs. GLs were determined using a UHPLC-HRMS method that simultaneously separates intact GLs and other phenolics. The separated intact GLs, hydroxycinnamic acids (chlorogenic acid derivatives and sinapic acid derivatives), and flavonols were identified following their $MS^2 \sim MS^4$ fragmentations, UV−visible spectra, and the order of elution previously described for similar acquisition conditions.

The PDA signal at 229 nm was used to quantify the desulfo-GLs.The type and amount of desulfo-GLs in microgreen broccoli were calculated using known concentrations of standard sinigrin and recommended relative response factors.[25] The major GL compounds were quantified by integration of the peak areas using Xcalibur 2.1.

LC-MS Data Pretreatment and Handling. Acquired UHPLC-HRMS raw files were converted into mzXML format using Proteowizard 3.0. 3569 (http://proteowizard.sourceforge.net/), and then XCMS[26] was employed for peak detection, noise filtering, and peak alignment. A two-dimensional data matrix was generated from XCMS including variable index (paired m/z−retention time), sample names (observations), and peak intensities. Multivariate analysis was performed on the output table from XCMS using Sigma 13 (Umetrics, Umeå, Sweden), where principal component analysis (PCA) was performed to visualize group clustering, trends, or outliers among the observations, and then, supervised orthogonal projection to latent structural discriminate analysis (OPLS-DA) was performed. Pareto scaling was used for data normalization before multivariate data analysis (MVDA). PC1 and PC2 scores were used for the PCA models as these principal components seemed to reflect the main variation and separation in data. The score plot of PCA was used to observe clustering and trends among all samples. The loadings plot of the first two principle components was applied to evaluate the variables causing the separation between the groups. The structures of the marker compounds were annotated by searching free databases of Scripps Metlin (http://metlin.scripps.edu/) using exact mass and MS/MS spectra and structures. Available standards were used for the confirmation of the identity of the compounds.

RESULTS AND DISCUSSION

Profiling of the Major Compounds in Broccoli Microgreens. GLs and hydroxycinnamic acid derivatives are two major groups of compounds found in microgreen broccoli, which were reported in the matured broccoli.[27,28] In our previous study of other brassica microgreens,[9] it was found that hydroxycinnamic acid derivatives have good response under negative ionization mode. GLs are hydrophilic compounds with a sulfonate moiety in structure, which occur in nature as the anionic form. The most diagnostic ions were observed at m/z 259 and 275 in MS^2 or MS^3 spectra, produced by intraring rearrangement. This typical fragmentation can be used for fast characterization of GLs.[29−31] An UHPLC-MS profiling method

DOI: 10.1021/jf504710r
J. Agric. Food Chem. 2015, 63, 1863−1868

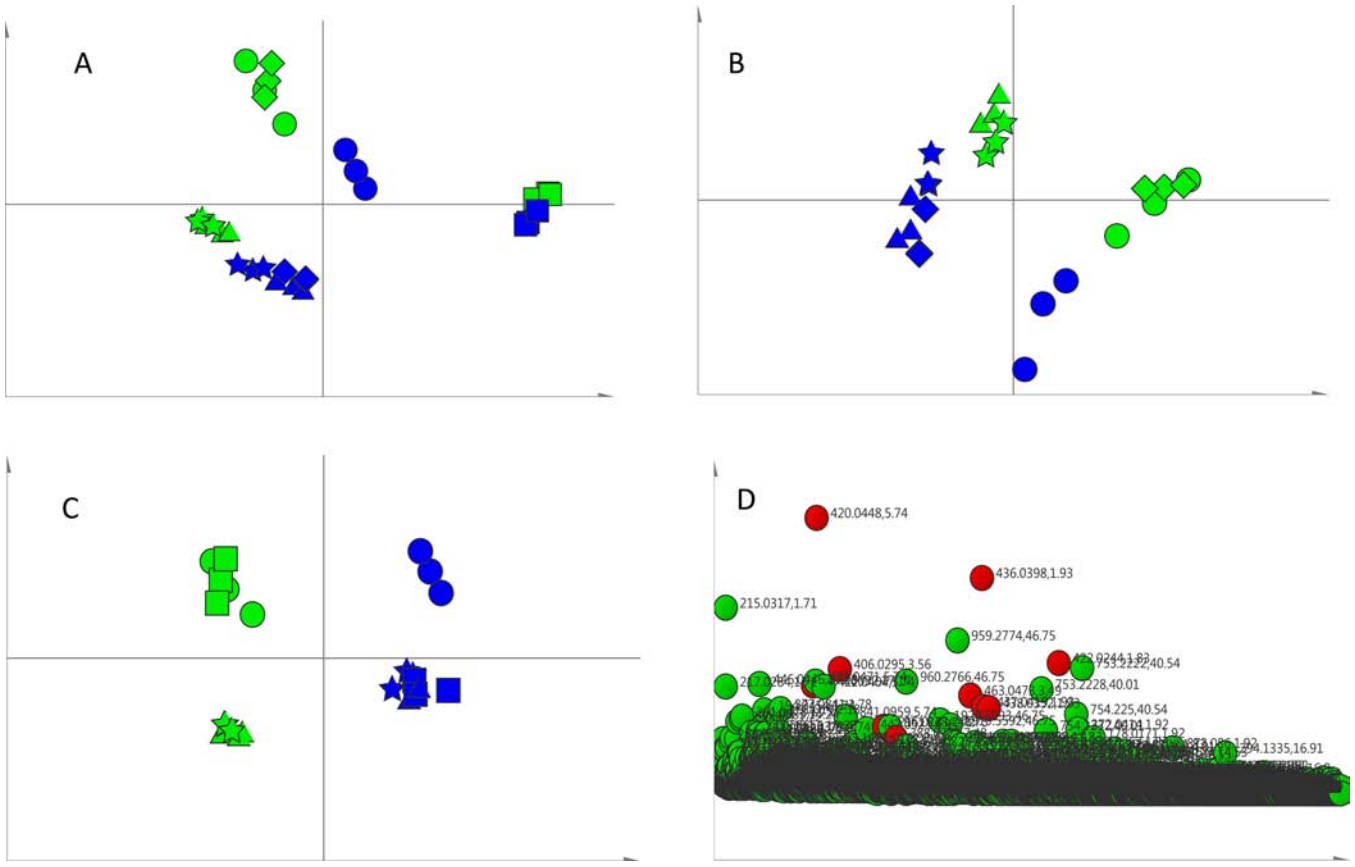

Figure 1. (A) PCA score plot on all samples; (B) PCA plots on postharvest samples; (C) OPLS-DA score plot on postharvest samples; (blue) $CaCl_2$ treated, (green) H_2O treated, (■) Preharvest Day 4, (▲) Harvest Day, (★) Postharvest Day 4, (♦) Postharvest Day 7, (●) Postharvest Day 14. (D) VIP plot of all the ion features (each red dot represents individual GL).

under negative ionization mode with a data-dependent scan was developed for a comprehensive study of the GLs and other phenolic components, and it leads to the identification of 15 GLs, 3 acylated flavonolglucosides, 1 flavan 3-ol, 6 hydroxycinnamic acid derivatives, and 2 sugars in broccoli microgreens.

A total of 15 GLs including 11 aliphatic GLs and 4 indolic GLs were identified (Figure S1, Supporting Information). The major ones were glucoerucin (ERN), glucoraphanin (RPN), glucoiberin (IBN), glucoiberverin (IVN), 4-hydroxyglucobrassicin (OHGBRN), gluconasturtiin (GSN), pentyl glucosinolates (PGN), hexyl glucosinolate (HXG), glucobrassicin (GBRN), and 4-methoxyglucobrassicin (MGBRN). Six hydroxyl cinnamoyl derivatives, including 1,2-disinapoylgentiobiose, 1,2-bis-*O*-sinapoyl-*β*-D-glucoside, 1,2,2′-trisinapoylgentiobioside, 2-feruloyl-1,2′-disinapoylgentiobiose 1-*O*-sinapoylglucose, and their isomers were identified by comparing the HRMS data with the previous reports for broccoli or other brassica vegetables.[32−34] Other compounds such as catechin, acylated-kaemperol glycosides,[35] and sugars were also found. Detailed accurate mass and mass fragmentation information can be found in Table S1 (Supporting Information).

Metabolomic Analysis of Different Stages of Microgreen Samples between $CaCl_2$ Treated and Control Groups. As shown in Figure S1 (Supporting Information), it would be very difficult to find the differences by visual examination of the chromatograms between the $CaCl_2$ treated microgreens and the control (H_2O) group. A metabolomic approach was employed for characterization of the chemical difference between the groups. The original UHPLC-HRMS raw data led to 5107 ion features from 30 samples. The PCA based on the relative intensities of these ion features revealed the effects of $CaCl_2$ treatment after pareto scaling (Figure 1A). The first two components accounted for 79.4% of the total variance. It showed no significant difference between the $CaCl_2$ group and the control group (H_2O) on the fourth day after sowing. They are grouped closely on the right of the PCA scoreplot. Another PCA was performed with postharvest samples only, as shown in Figure 1B. They are separated into two groups according to the postharvest times. The samples from harvest day (Day 0) and postharvest day 4 are clustered closely against the postharvest day 7 and day 14 groups on PC1, and the $CaCl_2$ treated samples are separated with H_2O treated samples on PC2. It suggested that the sampling time is another import factor for chemical composition of the samples. In order to define the effects on the $CaCl_2$ treatment and to minimize other factors, a supervised OPLS-DA statistical model was utilized to focus on the discrimination of the $CaCl_2$ treatment and H_2O spray only. The OPLS-DA approach has been widely used in metabolomic studies on botanical materials with different growth conditions, species, locations, harvest times, and so forth.[36−41] The OPLS-DA model resulted in one predictive and one orthogonal (1 + 1) component with the cross-validated predictive ability $Q^2(Y)$ 98.2% and the total explained variance ($R2(X)$) 58.0% (Figure 1C). In addition, a permutation test (n = 100) was carried out to evaluate the overfitting of the model. The discriminatory ion features were picked out by a variable importance projection (VIP) plot. The ion features with larger VIP values (more than 4) were

DOI: 10.1021/jf504710r
J. Agric. Food Chem. 2015, 63, 1863−1868

considered more relevant for sample classification in this study, as shown in Figure 1D. After filtering out the ion features for adduct ions, isotope ions, and fragment ions, 12 constituents including 9 GLs, 2 sinapinic acid derivatives, and a hexose were considered as major marker compounds responsible for the group classification, as shown in Table 1. For example, ion feature (m/z 420.0448, t_R = 5.74 min) has a calculated elemental composition of $C_{12}H_{23}NO_9S_3$ (3.4 ppm). The diagnostic ions at m/z 259 and 275 were observed in the MS^2 spectrum. It was identified as glucoerucin, a compound previously reported in broccoli.[42−44] Using the same approach, we conclude that the marker GL compounds are ERN, RPN, IBN, IVN, GBRN, neoglucobrassicin (NGBRN), OHGBRN, HXG, and PGN.

Table 1. Discriminatory Metabolites Responsible for the Group Classification between the $CaCl_2$ and H_2O Treated Groups

ion feature (m/z, t_R)	VIP value	formula	possible identification
420.0448, 5.74	20.63	$C_{11}H_{20}O_{10}NS_3$	glucoerucin
436.0398, 1.93	16.16	$C_{12}H_{22}O_{10}NS_3$	glucoraphanin
215.0317, 1.71	13.84	$C_6H_{12}O_6Cl$	hexose
959.2774, 46.75	11.49	$C_{45}H_{51}O_{23}$	1,2,2′-trisinapoylgentiobioside
422.0244, 1.83	9.75	$C_{11}H_{20}O_{10}NS_3$	glucoiberin
406.0295, 3.56	9.26	$C_{11}H_{20}NO_9S_3$	glucoiberverin
477.0632, 17.17	8.05	$C_{17}H_{21}O_{10}N_2S_2$	neoglucobrassicin
753.2228, 40.01	7.77	$C_{34}H_{41}O_{19}$	1,2-disinapoylgentiobiose
463.0473, 3.49	7.37	$C_{16}H_{19}N_2O_{10}S_2$	4-hydroxyglucobrassicin
402.0883, 14.24	5.57	$C_{13}H_{24}NO_9S_2$	hexyl glucosinolate
447.0523, 6.90	4.85	$C_{16}H_{19}N_2O_9S_2$	glucobrassicin
388.0727, 7.48	4.18	$C_{12}H_{23}NO_9S_2$	pentyl glucosinolate

Verification of the Marker GLs by Targeted GL Analysis. The metabolomic approach suggested that the major marker compounds, which changed significantly by $CaCl_2$ treatment, were GLs. However, the comparison of marker compounds is based on peak area of the marker compounds. In order to confirm the findings from the nontargeted metabolomic approach, the targeted analysis of GLs in microgreen broccoli was carried out according to the guidelines established in ISO 9167-1.[45] ISO 9167-1 specifies the method for the determination of GL content in rapeseed by quantifying the desulfo derivatives, using HPLC after sulfatase hydrolysis and anion ion-exchange concentration.

Because of the lack of reference standards, the desulfo-GLs are confirmed using HRMS. The product ion at m/z 195.03 ($C_6H_{11}O_5S^-$) that represents the thioglucose group was used for fast identification of desulfo-GLs. Figure S2 (Supporting Information) shows the typical chromatogram for GL determination using the ISO method, and a total of 10 different GLs was identified together with the internal standard

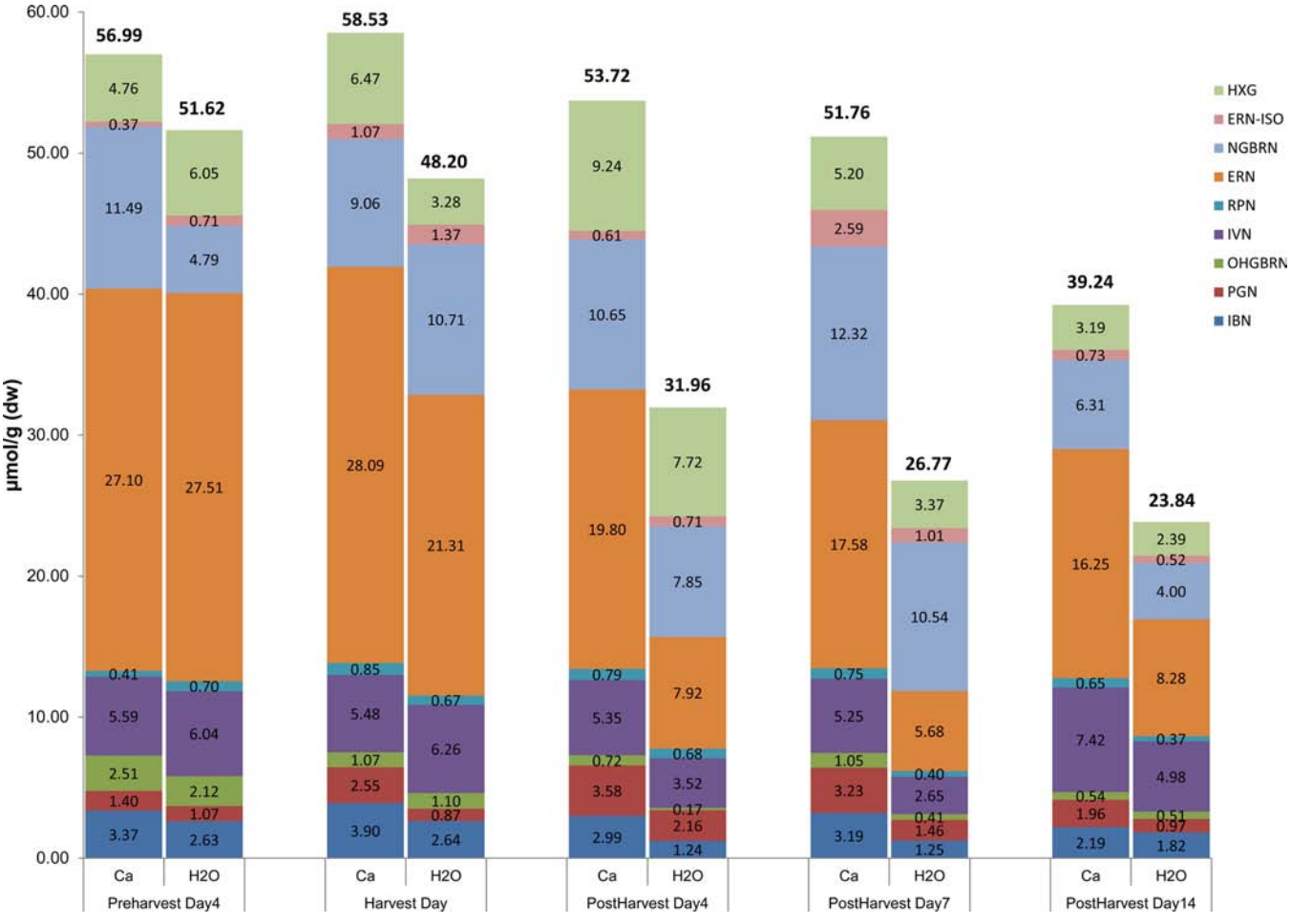

Figure 2. GL content in $CaCl_2$ (Ca) treated and control (H_2O) groups on different days.

DOI: 10.1021/jf504710r
J. Agric. Food Chem. 2015, 63, 1863−1868

sinigrin. They were desulfo-IBN, desulfo-IVN, desulfo-RPN, desulfo-ERN, desulfo-PGN, desulfo-HXG, desulfo-OHGBRN, and desulfo-NGBRN. The desulfo forms of two indolic marker GLs, GBRN and MGBRN, detected in the HPLC-HRMS profiling were not found using the ISO method. It may be due to that UV detection is much less sensitive compared to MS detection. The most abundant GLs are ERN followed by NGBRN and IVN. The GL profile in microgreen broccoli is different from that of broccoli sprouts but shows comparable total GL content.[46−48]

In comparison with the metabolomic approaches, the results show that aliphatic and indole GLs increase significantly after harvest but not for the preharvest samples in $CaCl_2$ treated samples. As shown in Figure 2, the highest GL concentration was observed at preharvest samples for both $CaCl_2$ and H_2O treated samples. The total GLs are 56.99 μmol/g dry weight (dw) and 51.62 μmol/g dw detected in the $CaCl_2$ treated and the control sample in the preharvest samples, respectively. After harvest, both the $CaCl_2$ treated and the control group showed decreasing of total GLs. For the $CaCl_2$ treated samples, the total GLs decreased to 39.24 μmol/g (by 33.0%) at day 14, while the GL samples in the control samples dropped to 23.84 μmol/g (by 50.5%). At each time point after harvest, the $CaCl_2$ treated samples showed an elevated level of total GLs together with the higher individual GLs such as ERN, IBN, RPN, IVN, OHGBRN, HXG, NGBRN, and PGN.

Accumulating evidence indicates that GL biosynthesis in plants can be upregulated by environmental stress signals and pathogen attacks.[3,4] Calcium has been shown to be an important secondary messenger in the relay of developmental, environmental, and hormonal signals that regulate plant growth and development as well as responses to biotic and abiotic stresses.[49−51] It has been reported the overexpression of a calcium/calmodulin-binding IQD1 leads to the expression of multiple genes with roles in GL metabolism.[52]Knockout of another calcium/calmodulin regulated transcription factor AtSR1/CaMTA3 resulted in the decreased GL levels and plant defense against insect herbivory.[53] Previously, we observed that calcium treatment retarded the broccoli microgreen decay during storage and extended shelf life.[15] This could be contributed, at least partially, by the increased GL levels thereby enhancing the microgreen stress tolerance and defense.

■ ASSOCIATED CONTENT

Supporting Information

Typical HPLC chromatograms and the identification of the major compounds in broccoli microgreen (Figure S1 and Table S1); the extracted base peak (m/z 195) chromatogram of desulfo-GLs (Figure S2). This material is available free of charge via the Internet at http://pubs.acs.org.

■ AUTHOR INFORMATION

Corresponding Author

*Phone: (301) 504-8144; fax: (301) 504-8314; e-mail: pei.chen@ars.usda.gov.

Funding

This research is supported by the Agricultural Research Service of the U.S. Department of Agriculture, an Interagency Agreement with the Office of Dietary Supplements at the National Institutes of Health.

Notes

The authors declare no competing financial interest.

■ REFERENCES

(1) Bjorkman, M.; Klingen, I.; Birch, A. N. E.; Bones, A. M.; Bruce, T. J. A.; Johansen, T. J.; Meadow, R.; Molmann, J.; Seljasen, R.; Smart, L. E.; Stewart, D. Phytochemicals of Brassicaceae in plant protection and human health − Influences of climate, environment and agronomic practice. *Phytochemistry* **2011**, *72*, 538−556.

(2) Fahey, J. W.; Zhang, Y. S.; Talalay, P. Broccoli sprouts: An exceptionally rich source of inducers of enzymes that protect against chemical carcinogens. *Proc. Natl. Acad. Sci. U.S.A.* **1997**, *94*, 10367−10372.

(3) Martinez-Ballesta, M. D.; Moreno, D. A.; Carvajal, M. The physiological importance of glucosinolates on plant response to abiotic stress in Brassica. *Int. J. Mol. Sci.* **2013**, *14*, 11607−11625.

(4) Baenas, N.; Garcia-Viguera, C.; Moreno, D. A. Biotic elicitors effectively increase the glucosinolates content in *Brassicaceae* sprouts. *J. Agric. Food Chem.* **2014**, *62*, 1881−1889.

(5) Das, S.; Tyagi, A. K.; Kaur, H. Cancer modulation by glucosinolates: A review. *Curr. Sci. India* **2000**, *79*, 1665−1671.

(6) Hayes, J. D.; Kelleher, M. O.; Eggleston, I. M. The cancer chemopreventive actions of phytochemicals derived from glucosinolates. *Eur. J. Nutr.* **2008**, *47*, 73−88.

(7) Sarikamis, G. Glucosinolates in crucifers and their potential effects against cancer: Review. *Can. J. Plant. Sci.* **2009**, *89*, 953−959.

(8) Xiao, Z.; Lester, G. E.; Luo, Y.; Xie, Z. K.; Yu, L. L.; Wang, Q. Effect of light exposure on sensorial quality, concentrations of bioactive compounds and antioxidant capacity of radish microgreens during low temperature storage. *Food Chem.* **2014**, *151*, 472−479.

(9) Sun, J.; Xiao, Z.; Lin, L. Z.; Lester, G. E.; Wang, Q.; Harnly, J. M.; Chen, P. Profiling polyphenols in five *Brassica* species microgreens by UHPLC-PDA-ESI/HRMS^n. *J. Agric. Food Chem.* **2013**, *61*, 10960−10970.

(10) Xiao, Z.; Lester, G. E.; Luo, Y.; Wang, Q. Assessment of vitamin and carotenoid concentrations of emerging food products: Edible microgreens. *J. Agric. Food Chem.* **2012**, *60*, 7644−7651.

(11) Chandra, D.; Kim, J. G.; Kim, Y. P. Changes in microbial population and quality of microgreens treated with different sanitizers and packaging films. *Hortic., Environ. Biotechnol.* **2012**, *53*, 32−40.

(12) Kou, L. P.; Luo, Y. G.; Yang, T. B.; Xiao, Z. L.; Turner, E. R.; Lester, G. E.; Wang, Q.; Camp, M. J. Postharvest biology, quality and shelf life of buckwheat microgreens. *LWT−Food Sci. Technol.* **2013**, *51*, 73−78.

(13) Hussain, P. R.; Meena, R. S.; Dar, M. A.; Wani, A. M. Effect of post-harvest calcium chloride dip treatment and gamma irradiation on storage quality and shelf-life extension of Red delicious apple. *J. Food Sci. Techol.* **2012**, *49*, 415−426.

(14) Conway, W. S.; Sams, C. E.; Wang, C. Y.; Abbott, J. A. Additive effects of postharvest calcium and heat-treatment on reducing decay and maintaining quality in apples. *J. Am. Soc. Hortic. Sci.* **1994**, *119*, 49−53.

(15) Kou, L. P.; Yang, T. B.; Luo, Y. G.; Liu, X. J.; Huang, L. H.; Codling, E. Pre-harvest calcium application increases biomass and delays senescence of broccoli microgreens. *Postharvest Biol. Technol.* **2014**, *87*, 70−78.

(16) Whitfield, P. D.; German, A. J.; Noble, P. J. Metabolomics: An emerging post-genomic tool for nutrition. *Br. J. Nutr.* **2004**, *92*, 549−555.

(17) Koulman, A.; Volmer, D. A. Perspectives for metabolomics in human nutrition: An overview. *Nutr. Bull.* **2008**, *33*, 324−330.

(18) Nielsen, K. L.; Hartvigsen, M. L.; Hedemann, M. S.; Laerke, H. N.; Hermansen, K.; Bach Knudsen, K. E. Similar metabolic responses in pigs and humans to breads with different contents and compositions of dietary fibers: a metabolomics study. *Am. J. Clin. Nutr.* **2014**, *99*, 941−949.

(19) Park, S. Y.; Park, W. T.; Park, Y. C.; Ju, J. I.; Park, S. U.; Kim, J. K. Metabolomics for the quality assessment of *Lycium chinense* fruits. *Biosci., Biotechnol., Biochem.* **2012**, *76*, 2188−2194.

(20) Fujimura, Y.; Kurihara, K.; Ida, M.; Kosaka, R.; Miura, D.; Wariishi, H.; Maeda-Yamamoto, M.; Nesumi, A.; Saito, T.; Kanda, T.;

DOI: 10.1021/jf504710r
J. Agric. Food Chem. 2015, 63, 1863−1868

Yamada, K.; Tachibana, H. Metabolomics-driven nutraceutical evaluation of diverse green tea cultivars. *PLoS One* **2011**, *6*, e23426.
(21) Jumhawan, U.; Putri, S. P.; Yusianto; Marwani, E.; Bamba, T.; Fukusaki, E. Selection of discriminant markers for authentication of Asian palm civet coffee (Kopi Luwak): A metabolomics approach. *J. Agric. Food Chem.* **2013**, *61*, 7994−8001.
(22) Cuthbertson, D.; Andrews, P. K.; Reganold, J. P.; Davies, N. M.; Lange, B. M. Utility of metabolomics toward assessing the metabolic basis of quality traits in apple fruit with an emphasis on antioxidants. *J. Agric. Food Chem.* **2012**, *60*, 8552−8560.
(23) Moco, S.; Martin, F. P.; Rezzi, S. Metabolomics view on gut microbiome modulation by polyphenol-rich foods. *J. Proteome Res.* **2012**, *11*, 4781−90.
(24) Jones, D. P.; Park, Y.; Ziegler, T. R. Nutritional metabolomics: Progress in addressing complexity in diet and health. *Annu. Rev. Nutr.* **2012**, *32*, 183−202.
(25) Gorissen, A.; Kraut, N. U.; de Visser, R.; de Vries, M.; Roelofsen, H.; Vonk, R. J. No de novo sulforaphane biosynthesis in broccoli seedlings. *Food Chem.* **2011**, *127*, 192−196.
(26) Tautenhahn, R.; Patti, G. J.; Rinehart, D.; Siuzdak, G. XCMS Online: A web-based platform to process untargeted metabolomic data. *Anal. Chem.* **2012**, *84*, 5035−5039.
(27) Tian, Q.; Rosselot, R. A.; Schwartz, S. J. Quantitative determination of intact glucosinolates in broccoli, broccoli sprouts, Brussels sprouts, and cauliflower by high-performance liquid chromatography-electrospray ionization-tandem mass spectrometry. *Anal. Biochem.* **2005**, *343*, 93−99.
(28) Maldini, M.; Baima, S.; Morelli, G.; Scaccini, C.; Natella, F. A liquid chromatography-mass spectrometry approach to study "glucosinoloma" in broccoli sprouts. *J. Mass Spectrom.* **2012**, *47*, 1198−1206.
(29) Cataldi, T. R.; Lelario, F.; Orlando, D.; Bufo, S. A. Collision-induced dissociation of the A + 2 isotope ion facilitates glucosinolates structure elucidation by electrospray ionization-tandem mass spectrometry with a linear quadrupole ion trap. *Anal. Chem.* **2010**, *82*, 5686−5696.
(30) Rochfort, S. J.; Trenerry, V. C.; Imsic, M.; Panozzo, J.; Jones, R. Class targeted metabolomics: ESI ion trap screening methods for glucosinolates based on MS^n fragmentation. *Phytochemistry* **2008**, *69*, 1671−1679.
(31) Fabre, N.; Poinsot, V.; Debrauwer, L.; Vigor, C.; Tulliez, J.; Fouraste, I.; Moulis, C. Characterisation of glucosinolates using electrospray ion trap and electrospray quadrupole time-of-flight mass spectrometry. *Phytochem. Anal.* **2007**, *18*, 306−319.
(32) Luthria, D. L.; Lin, L. Z.; Robbins, R. J.; Finley, J. W.; Banuelos, G. S.; Harnly, J. M. Discriminating between cultivars and treatments of broccoli using mass spectral fingerprinting and analysis of variance-principal component analysis. *J. Agric. Food Chem.* **2008**, *56*, 9819−9827.
(33) Lin, L. Z.; Sun, J. H.; Chen, P.; Harnly, J. UHPLC-PDA-ESI/HRMS/MS^n analysis of anthocyanins, flavonol glycosides, and hydroxycinnamic acid derivatives in red mustard greens (*Brassica juncea* Coss variety). *J. Agric. Food Chem.* **2011**, *59*, 12059−12072.
(34) Lin, L. Z.; Harnly, J. M. Phenolic component profiles of mustard greens, yu choy, and 15 other *Brassica* vegetables. *J. Agric. Food Chem.* **2010**, *58*, 6850−6857.
(35) Vallejo, F.; Tomas-Barberan, F. A.; Ferreres, F. Characterisation of flavonols in broccoli (*Brassica oleracea* L. var. *italica*) by liquid chromatography−UV diode-array detection−electrospray ionisation mass spectrometry. *J. Chromatogr. A* **2004**, *1054*, 181−193.
(36) Mao, Q.; Bai, M.; Xu, J. D.; Kong, M.; Zhu, L. Y.; Zhu, H.; Wang, Q.; Li, S. L. Discrimination of leaves of *Panax ginseng* and *P. quinquefolius* by ultra high performance liquid chromatography quadrupole/time-of-flight mass spectrometry based metabolomics approach. *J. Pharm. Biomed. Anal.* **2014**, *97*, 129−140.
(37) Sun, J.; Chen, P. Differentiation of *Panax quinquefolius* grown in the USA and China using LC/MS-based chromatographic finger-printing and chemometric approaches. *Anal. Bioanal. Chem.* **2011**, *399*, 1877−1889.
(38) Zhang, H. M.; Li, S. L.; Zhang, H.; Wang, Y.; Zhao, Z. L.; Chen, S. L.; Xu, H. X. Holistic quality evaluation of commercial white and red ginseng using a UPLC-QTOF-MS/MS-based metabolomics approach. *J. Pharm. Biomed. Anal.* **2012**, *62*, 258−273.
(39) Ku, K. M.; Choi, J. N.; Kim, J.; Kim, J. K.; Yoo, L. G.; Lee, S. J.; Hong, Y. S.; Lee, C. H. Metabolomics analysis reveals the compositional differences of shade grown tea (*Camellia sinensis* L.). *J. Agric. Food Chem.* **2010**, *58*, 418−426.
(40) Choi, J. N.; Kim, J.; Lee, M. Y.; Park, D. K.; Hong, Y. S.; Lee, C. H. Metabolomics revealed novel isoflavones and optimal cultivation time of *Cordyceps militaris* fermentation. *J. Agric. Food Chem.* **2010**, *58*, 4258−4267.
(41) Consonni, R.; Cagliani, L. R.; Stocchero, M.; Porretta, S. Triple concentrated tomato paste: Discrimination between Italian and Chinese products. *J. Agric. Food Chem.* **2009**, *57*, 4506−4513.
(42) Troyer, J. K.; Stephenson, K. K.; Fahey, J. W. Analysis of glucosinolates from broccoli and other cruciferous vegetables by hydrophilic interaction liquid chromatography. *J. Chromatogr. A* **2001**, *919*, 299−304.
(43) Vallejo, F.; Garcia-Viguera, C.; Tomas-Barberan, F. A. Changes in broccoli (*Brassica oleracea* L. var. *italica*) health-promoting compounds with inflorescence development. *J. Agric. Food Chem.* **2003**, *51*, 3776−3782.
(44) Schreiner, M.; Peters, P.; Krumbein, A. Changes of glucosinolates in mixed fresh-cut broccoli and cauliflower florets in modified atmosphere packaging. *J. Food Sci.* **2007**, *72*, S585−S589.
(45) International Organization for Standardization (ISO). ISO 9167-1:1992. Rapeseed — Determination of glucosinolates content — Part 1: Method using high-performance liquid chromatography; ISO: Geneva, Switzerland, 1992; http://www.iso.org/iso/catalogue_detail.htm?csnumber=16763.
(46) Song, L.; Morrison, J. J.; Botting, N. P.; Thornalley, P. J. Analysis of glucosinolates, isothiocyanates, and amine degradation products in vegetable extracts and blood plasma by LC-MS/MS. *Anal. Biochem.* **2005**, *347*, 234−243.
(47) Vallejo, F.; Tomas-Barberan, F. A.; Garcia-Viguera, C. Glucosinolates and vitamin C content in edible parts of broccoli florets after domestic cooking. *Eur. Food Res. Technol.* **2002**, *215*, 310−316.
(48) Hansen, M.; Møller, P.; Sørensen, H.; Cantwell de Trejo, M. Glucosinolates in broccoli stored under controlled-atmosphere. *J. Am. Soc. Hortic. Sci.* **1995**, *120*, 1069−1074.
(49) DeFalco, T. A.; Bender, K. W.; Snedden, W. A. Breaking the code: Ca^{2+} sensors in plant signalling. *Biochem. J.* **2010**, *425*, 27−40.
(50) Poovaiah, B. W.; Du, L. Q.; Wang, H. Z.; Yang, T. B. Recent advances in calcium/calmodulin-mediated signaling with an emphasis on plant-microbe interactions. *Plant Physiol.* **2013**, *163*, 531−542.
(51) Reddy, A. S. N.; Ali, G. S.; Celesnik, H.; Day, I. S. Coping with stresses: Roles of calcium- and calcium/calmodulin-regulated gene expression. *Plant Cell* **2011**, *23*, 2010−2032.
(52) Levy, M.; Wang, Q. M.; Kaspi, R.; Parrella, M. P.; Abel, S. Arabidopsis IQD1, a novel calmodulin-binding nuclear protein, stimulates glucosinolate accumulation and plant defense. *Plant J.* **2005**, *43*, 79−96.
(53) Laluk, K.; Prasad, K. V. S. K.; Savchenko, T.; Celesnik, H.; Dehesh, K.; Levy, M.; Mitchell-Olds, T.; Reddy, A. S. N. The calmodulin-binding transcription factor SIGNAL RESPONSIVE1 is a novel regulator of glucosinolate metabolism and herbivory tolerance in Arabidopsis. *Plant Cell Physiol.* **2012**, *53*, 2008−2015.

DOI: 10.1021/jf504710r
J. Agric. Food Chem. 2015, 63, 1863−1868

trometry (MS)-based proteomic techniques have been developed. Among them, two-dimensional electrophoresis (2-DE) and label-free liquid chromatography (LC)-MS/MS shotgun analysis are mostly applied.[12] In 2-DE, separated proteins are detected by staining and isolated from the gel, followed by matrix-assisted laser desorption/ionization mass spectrometry (MALDI-MS) or surface-enhanced laser desorption/ionization mass spectrometry (SELDI-MS).[13] Shotgun proteomics performs the mass spectrometry in data-dependent acquisition mode. In this mode, peptide fragmentation is guided by the abundance of detectable precursor ions. The specific detected peptide ions are further selected for collision induced dissociation (CID) and fragment ion (MS2) spectra. The recorded information is then searched against protein sequence database to deduce the peptide sequences and corresponding proteins.[14] Compared with 2-DE, shotgun proteomics shows higher sensitivity, protein throughput, quantitative accuracy, proteome coverage, and reproducibility.[15]

Although several studies have been performed to investigate the effect of high-fat diet on hepatic proteomics, rats or mice were chosen instead of hamsters.[16−19] Hamsters are considered a better model for the study of metabolic diseases because they respond consistently to dietary modulation and show close similarity to the human lipoprotein profile compared to other rodents.[20] The aim of this study was to explore the differences in hepatic protein expression between hamsters fed control diet and high-fat diet by shotgun proteomic analysis. We hypothesized that a set of differentially expressed proteins will be identified as molecular markers for elucidating the pathological mechanism of high-fat diet.

MATERIALS AND METHODS

Antibodies. Antiaconitate hydratase, antixanthine dehydrogenase, and antiannexin 5 were purchase from Epitomics (Burlingame, CA). Antiadenosine kinase was obtained from Novus (Littleton, CO). Anti-HADHA (trifunctional enzyme subunit α, mitochondria) and antiannexin 3 were purchased from Proteintech Group (Chicago, IL). Goat antirabbit peroxidase-conjugated antibody was purchased from Jackson ImmunoResearch (West Grove, PA).

Animals and Diets. Male eight-week-old Syrian hamsters purchased from National Laboratory Animal Breeding and Research Center (Taipei, Taiwan) were maintained at 22 ± 2 °C and 12-h light/dark cycle. After 1 week of acclimation, animals were randomly assigned to the control group or the high-fat diet group (n = 7). The diets and water were provided *ad libitum*. Feed intake and body weights were measured daily and once a week, respectively. The ingredients of the control diet are (g/kg) corn starch, 452; sucrose, 200; casein, 200; soybean oil, 50; AIN-76 mineral mix, 35; AIN-76 vitamin mix, 10; methylated cellulose, 50; DL-methionine, 3. In the high-fat diet, 170 g of lard and 2 g of cholesterol per kilogram were supplemented to replace part of the corn starch. At the end of 8 weeks, all animals were sacrificed. Bloods and livers were collected for biochemical and proteomic analysis (Supporting Information Figure 1). This protocol was approved by Shih Chien University Animal Care and Use Committee.

Determination of Serum Lipids, Uric Acid, AST, and ALT. Serum TG, total cholesterol (TC), and HDL-cholesterol (HDL-C) were determined by using commercial kits (Fortree Diagnostics, Antrim, U.K.). Serum uric acid (UA), aspartate aminotransferase (AST), and alanine aminotransferase (ALT) were also quantified by the kits (Randox, Antrim, U.K.).

Determination of Liver Lipids. Liver lipids were measured according to the method of Folch et al. with modification.[21] In brief, the livers were homogenized with Folch reagent (chloroform/methanol = 2:1, v/v) at the ratio of 20:1. The homogenates were centrifuged at 936g for 10 min. Equal volumes of supernatant and triton-100 (Sigma, St. Louis, MO) were mixed and left in the fume hood to remove organic solvent before the contents of lipids were measured by commercial kits (Randox, Antrim, U.K.).

Liver Histoloty. Liver tissues were fixed in 10% buffered formalin overnight, embedded in paraffin, sectioned at 5 μm thickness, and stained with hematoxylin and eosin (H&E). The slides were examined with histopathological findings recorded by a veterinary pathologist who was blinded to the treatments.

SDS-PAGE and In-Gel Digestion. Total proteins of each sample (50 μg) were fractionated by SDS-PAGE (dodecyl sulfate polyacrylamide gel electrophoresis), and the gel was stained with Coomassie Brilliant Blue G-250 (Bio-Rad, Hercules, CA). The proteins in each lane were separated and sliced into 10 fractions based on molecular weight, followed by destaining in a solution of 25 mM NH_4HCO_3 and 50% (v/v) acetonitrile (1:1). After drying in a Speed-Vac (Thermo Election, Waltham, MA), all the gel slices were incubated with 25 mM NH_4HCO_3 and 1% β-mercaptoethanol in the dark for 20 min to reduce the disulfide bonds, followed by the incubation with solution consists of 5% 4-vinylpyridine in 25 mM NH_4HCO_3 and 50% acetonitrile (1:1) for 20 min for alkylation of the cysteine residues. Subsequently, the slices were dried in the Speed-Vac for 20 min. The in-gel digestion by the action of modified trypsin (Promega, Mannheim, Germany) in 25 mM NH_4HCO_3 (1%, w/v) was performed at 37 °C overnight. The digested peptides were removed from the gel, washed by 25 mM NH_4HCO_3 for 10 min, dried by Speed-Vac, and then kept at −20 °C until further analysis. The peptides were resuspended in 0.1% formic acid immediately prior to subsequent analysis.[22]

Mass Spectrometric Analysis. The tryptic peptides were analyzed by a nanoflow high-performance liquid chromatography system (Agilent Technologies 1200 series, Waldbronn, Germany) coupled to an LTQ-Orbitrap Discovery hybrid mass spectrometer with a nanoelectrospray ionization source (Thermo Electron, Waltham, MA). An analytical column (100 × 0.075 mm, 3.5 μm, Angilent C18) was operated at a flow rate of 0.5 μL/min in conjunction with a gradient elution solvent system using solvent A (0.1% formic acid in water) and solvent B (0.1% formic acid in acetonitrile). The course of gradient elution was programmed as a 30 min linear gradient of 5% to 35% solvent followed by 95% solvent B for a duration of 10 min. After each full scan at the m/z range 200−2000, a data-dependent acquired MS/MS scan for precursor ions was selected on the basis of conventional MS spectra performed at high resolution (M/DM, 60000 full width half-maximum). From each spectrum, the precise mass value and the charge state of the precursor ions were obtained. Following MS_1, the fragment ions were generated on the basic of collision-induced dissociation (CID) spectrum.[23]

Database Search. The spectra generated from nano-LC/MS/MS were analyzed by Xcalibur 2.0 SRI software (Thermo Electron, Waltham, MA). The TurboSequest algorithm was used to identify the peptide sequences against the hamster database in Universal Proteins Resource knowledgebase (UniProt; http://www.unipro.org/).[24] The peptides were filtered by Xcorr versus charge state with a significance level of 0.05. Xcorr was used for a match with 1.9 for singly charged ions, 2.2 for doubly charged ions, and 3.75 for triply charged ions. The proteins were identified as hepatic proteins when more than two peptides from a single protein met the Xcorr score. The mass spectra of candidate biomarkers were analyzed by our in-house post-translational modification (PTM) finder programs PTM-Miner and PTM-Q for identification of PTM peptide sequence, site of PTM, and quantification. Fix modification on the cysteine residues (carboxyamidomethylation, 57 Da), variable modification on the methionine residues (methionine, 16 Da), fragment mass tolerance at 1 Da, and peptide mass tolerance at 1.5 Da were not considered as specific PTM. The fragmented ions obtained were labeled as b, y, y-NH_3, and b-H_2O ions.[22,25]

Ingenuity Pathways Analysis. Accession numbers of proteins expressed differently in high-fat group were uploaded as an Excel file into the Ingenuity Pathway Analysis (IPA) software (http://www.igenuity.com). The proteins were grouped by known relationships into "functional analysis" and "canonical pathway analysis" of a network.

DOI: 10.1021/jf506118j
J. Agric. Food Chem. 2015, 63, 1869−1881

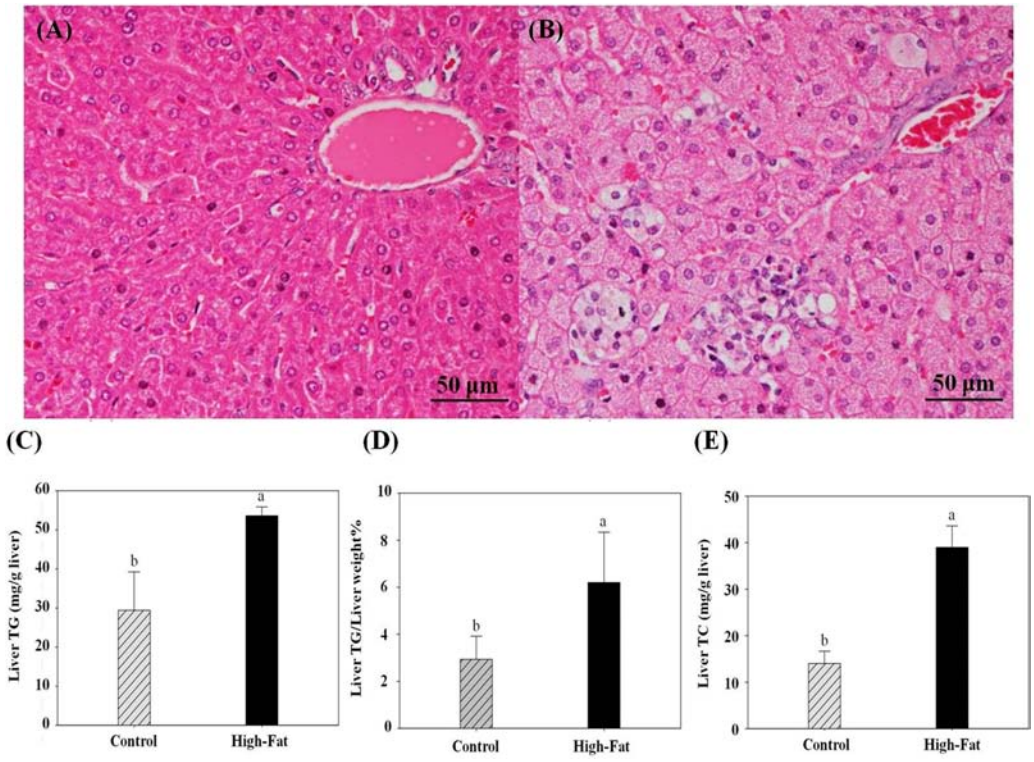

Figure 1. H&E stain of liver tissues from (A) control and (B) high-fat groups (400×). Panels C, D, and E show liver TG, relative weight of TG in liver (%), and liver TC, respectively. Hamsters were sacrificed after 8 weeks of feeding on the control diet or the high-fat diet. TG, triglyceride; TC, total cholesterol. Groups with the same letter are not significantly different (α = 0.05).

The significance of association between proteins and functional/canonical pathways was computed by Fisher's exact text (α = 0.05). IPA calculates a *p*-score as $-\log_{10}(p\text{-value})$ to rank networks. A score of 3 or higher indicates that the proteins are not clustered in a pathway by random chance at the confidence level of 99.99% or higher.[21,26]

Western Blotting. Livers were thawed on ice and homogenized in 25 mM Tris-HCl, pH 7.5, containing 250 mM sucrose and 1 mM ethylene-diaminetetra-acetic acid (10%, w/v). The homogenate was centrifuged at 105 000*g* for 30 min. After centrifugation, the supernatant was collected for analysis and its protein content was determined by Dc Protein Assay Kit (Bio-Rad, Hercules, CA). An equal amount of proteins from each sample was separated by SDS-PAGE before being transferred to polyvinylidene fluoride (PVDF) membranes (PerkinElmer, Waltham, MA). The membranes were blocked with 5% nonfat dry milk in Tris-buffered saline containing Tween (TBST) (20 mM Tris-HCl, pH 8.3, 137 mM NaCl, and 0.1% Tween-20) for 1 h before being sequentially incubated with primary antibody overnight in a cold room and horseradish peroxidase-conjugated secondary antibody for 1 h at room temperature. Immunoreactive proteins were detected using an enhanced chem-iluminescence kit (ECL, PerkinElmer, Waltham, MA), and the film was analyzed by ImageQuant software (Molecular Dynamics, Sunnyvale, CA). For stripping and reprobing, the membrane was incubated with stripping buffer (0.2 M glycine, 3.5 mM SDS, 0.1% Tween-20, pH 2.2) at room temperature for 10 min. After the buffer was discarded, the membrane was incubated with fresh stripping buffer for another 10 min followed by two 10 min washes by PBS buffer and two 5 min washes by TBST buffer. After striping, the blocking and probing were performed as mentioned above.[22]

Statistical Analysis. Statistical analysis was performed using the Statistical Analysis System (SAS Institute, Cary, NC). The *t*-test was used to determine significant difference among control group and high-fat group (α = 0.05).

RESULTS AND DISCUSSION

Hepatic proteomics is an important parameter for the studies of metabolic diseases. The animal model and the diet both have significant influences on the results of proteomic analysis. In most of the hepatic proteomic studies, rats or mice were chosen as models.[16−19] However, hamsters that show closer similarity to human lipid metabolism compared to rats/mice were used as the model in this present study. Hamsters and other rodents respond differently to dietary fats. Similar to humans, hamsters were hyper-responsive to the dietary cholesterol whereas rats were hypo-responsive.[27] Moreover, the effect of dietary cholesterol on lipoprotein profile in hamsters is similar to that of humans.[28] It is clear that hamsters could be a better model to study the physiological effect of dietary fats.

In addition to the difference in animal model, the composition of diet in current study is different from those in other proteomic studies. In this study, 17% lard and 0.2% cholesterol were supplemented to the diet (42.27% of calories from fats) to induce hyperlipidemia and accumulation of lipids in liver. In Zhang et al.'s proteomic study, 60% fructose was used to induce fatty liver in hamsters.[29] In a rat proteomic study, 2% cholesterol, 7% lard, and 10% yolk powder were used to formula a high-fat diet.[16] Luo et al. used a commercial 60% fat diet to study changes in hepatic protein abundance in mice.[18] Baiges et al. used bacon, sweets, biscuits with foie gras, cheese, muffins, carrots, and milk with sugar to formulate a cafeteria high-fat diet.[17] Different diet formulas lead to different results in proteomic analysis. The diet of this current study closely lines up with the Western pattern diet, which typically contains high amounts of saturated fat and sugar.

In our present study, we used label-free nano-LC/MS/MS (shotgun proteomics), a high-throughput proteomic tool, to

DOI: 10.1021/jf506118j
J. Agric. Food Chem. 2015, 63, 1869−1881

Table 1. Proteins Expressed Differentially in the High-Fat Group

	protein name	protein ID	control (mean ± SE)	HF[a] (mean ± SE)	fold[b]	t-test p-value[c]
1	14−3−3 protein γ	G3HA25	0 ± 0	2.32 ± 0.69	100	0.0156
2	14−3−3 protein γ	G3IPD7	0 ± 0	1.23 ± 0.44	100	0.0310
3	annexin A3	G3IEB1	0 ± 0	2.25 ± 0.59	100	0.0084
4	elongation factor 1-β	G3HDL6	0 ± 0	1.1 ± 0.39	100	0.0296
5	endoplasmic reticulum resident protein 29	G3H284	0 ± 0	1.05 ± 0.42	100	0.0465
6	fibrinogen A-α-chain (fragment)	Q08283	0 ± 0	0.69 ± 0.23	100	0.0247
7	histone H1.5-like protein	A0A061IB71	0 ± 0	1.12 ± 0.38	100	0.0270
8	selenium-binding protein 1	G3H302	0 ± 0	0.68 ± 0.23	100	0.0249
9	succinyl-CoA ligase [GDP-forming] subunit β, mitochondrial	G3GS40	0 ± 0	1.68 ± 0.58	100	0.0272
10	titin	G3HAC6	0 ± 0	1.29 ± 0.29	100	0.0046
11	valyl-tRNA synthetase	G3HZE9	0 ± 0	1.03 ± 0.37	100	0.0309
12	annexin	A0A061IML2	0.18 ± 0.18	2.58 ± 0.38	14.58	0.0012
13	annexin A5	G3I5A4	0.18 ± 0.18	2.58 ± 0.38	14.58	0.0012
14	40S ribosomal protein S3a	G3HKG8	0.24 ± 0.24	2.9 ± 1.01	12.22	0.0428
15	3-hydroxyanthranilate 3,4-dioxygenase	G3GV35	0.35 ± 0.2	1.75 ± 0.51	4.93	0.0446
16	glutamine synthetase	G3HG36	1.19 ± 0.4	5.5 ± 1.21	4.63	0.0147
17	epoxide hydrolase 1	G3I0X4	0.61 ± 0.36	2 ± 0.27	3.27	0.0215
18	xanthine dehydrogenase/oxidase	G3I4G1	0.47 ± 0.27	1.52 ± 0.23	3.21	0.0264
19	xanthine dehydrogenase/oxidase-like protein	A0A061HWK7	0.47 ± 0.27	1.52 ± 0.23	3.21	0.0264
20	xanthine dehydrogenase/oxidase-like protein	A0A061I0 × 3	0.47 ± 0.27	1.52 ± 0.23	3.21	0.02648
21	xanthine dehydrogenase/oxidase-like protein	A0A061I342	0.47 ± 0.27	1.52 ± 0.23	3.21	0.02648
22	calnexin	Q920L9	0.37 ± 0.21	1.04 ± 0.09	2.83	0.0274
23	F-actin-capping protein subunit β-like protein	A0A061IH36	0.55 ± 0.18	1.34 ± 0.15	2.46	0.0152
24	F-actin-capping protein subunit β-like protein	A0A061II46	0.55 ± 0.18	1.34 ± 0.15	2.46	0.0152
25	major vault protein	A0A061IB55	5.08 ± 0.59	10.04 ± 1.52	1.98	0.0228
26	major vault protein	G3I4I9	5.08 ± 0.59	10.04 ± 1.52	1.98	0.0228
27	thiomorpholine-carboxylate dehydrogenase	A0A061IGJ9	2.63 ± 0.25	4.77 ± 0.65	1.82	0.0220
28	α-actinin-1	G3H1K9	3.33 ± 0.67	5.91 ± 0.46	1.78	0.0194
29	alanine−tRNA ligase, cytoplasmic	Q8CFX8	3.06 ± 0.26	5.22 ± 0.41	1.7	0.0042
30	adenylate kinase 2, mitochondrial	G3IPK9	1.98 ± 0.21	3.2 ± 0.32	1.62	0.0185
31	endoplasmin	G3HQM6	7.51 ± 0.94	12.01 ± 1.57	1.6	0.0490
32	adenylate kinase 2, mitochondrial	G3H928	3.82 ± 0.45	5.96 ± 0.69	1.56	0.0414
33	glutathione S-transferase	P70686	24.1 ± 1.66	36.63 ± 2.78	1.52	0.0082
34	aldehyde dehydrogenase, mitochondrial	P81178	13.2 ± 0.56	11.28 ± 0.15	−1.17	0.0163
35	carbamoyl-phosphate synthase [ammonia], mitochondrial	G3H4W9	143.45 ± 2.59	106.09 ± 8.47	−1.35	0.0055
36	aspartate aminotransferase	A0A061IAK8	7.59 ± 0.72	5.6 ± 0.23	−1.36	0.0395
37	apoptosis-inducing factor 1	A0A061HYH9	3.63 ± 0.46	2.21 ± 0.27	−1.64	0.0369
38	apoptosis-inducing factor 1	A0A061HZ30	3.63 ± 0.46	2.21 ± 0.27	−1.64	0.0369
39	apoptosis-inducing factor 1	G3H3X1	3.63 ± 0.46	2.21 ± 0.27	−1.64	0.0369
40	trifunctional enzyme subunit α, mitochondrial	G3GXQ3	11.24 ± 1.06	6.48 ± 0.68	−1.73	0.0092
41	stress-70 protein, mitochondrial	O35501	7.45 ± 0.79	4.17 ± 0.31	−1.79	0.0085
42	acetyl-CoA acetyltransferase, cytosolic	G3HGP4	4.24 ± 0.4	2.3 ± 0.17	−1.84	0.0040
43	sarcosine dehydrogenase, mitochondrial	G3IG06	4.6 ± 0.69	2.49 ± 0.29	−1.85	0.0304
44	fatty acid synthase	G3GXD7	33.26 ± 3.94	17.39 ± 2.47	−1.91	0.0142
45	aconitate hydratase, mitochondrial	G3II47	5.85 ± 0.64	3.04 ± 0.79	−1.92	0.0323
46	short/branched chain specific acyl-CoA dehydrogenase, mitochondrial	G3I5V3	3.64 ± 0.43	1.79 ± 0.45	−2.03	0.0249
47	plectin (fragment)	Q9JI55	20.74 ± 3.93	9.83 ± 1.81	−2.11	0.0452
48	ubiquitin	G3I129	17.11 ± 0.98	7.86 ± 1.46	−2.18	0.0019
49	arginase	E7CXR7	10.35 ± 1.16	4.57 ± 1.06	−2.27	0.0104
50	ubiquitin	G3GVL0	16.99 ± 0.64	7.42 ± 1.16	−2.29	0.0003
51	ornithine carbamoyltransferase, mitochondrial (fragment)	G3GSF7	2.76 ± 0.25	1.19 ± 0.03	−2.32	0.0007
52	polyubiquitin	P62976	62.31 ± 2.47	26.18 ± 4.25	−2.38	0.0003
53	cytochrome P450 2D27	Q9QYG6	1.53 ± 0.15	0.63 ± 0.21	−2.41	0.0141
54	3-hydroxyhexobarbital dehydrogenase 1/3-α, 17-β-hydroxysteroid dehydrogenase	Q8K4V1	2.68 ± 0.48	1.11 ± 0.38	−2.43	0.0420
55	transketolase	G3GUU5	6.02 ± 0.58	2.46 ± 0.46	−2.45	0.0029
56	ubiquitin/ribosomal protein CEP52 fusion protein	Q792I7	8.86 ± 0.32	3.5 ± 0.83	−2.53	0.0009
57	polyubiquitin	O35080	62.48 ± 2.28	24.11 ± 4.37	−2.59	0.0002
58	methylmalonyl-CoA mutase	A0A061ILK7	6.01 ± 0.54	2.24 ± 0.58	−2.68	0.0030
59	methylmalonyl-CoA mutase, mitochondrial	G3I6B2	6.01 ± 0.54	2.24 ± 0.58	−2.68	0.0030

DOI: 10.1021/jf506118j
J. Agric. Food Chem. 2015, 63, 1869−1881

Table 1. continued

	protein name	protein ID	control (mean ± SE)	HF[a] (mean ± SE)	fold[b]	t-test p-value[c]
60	abhydrolase domain-containing protein 14B	G3H894	2.03 ± 0.13	0.75 ± 0.44	−2.72	0.0317
61	tubulin β-2C chain	G3IG44	4.88 ± 0.56	1.69 ± 0.32	−2.88	0.0025
62	succinyl-CoA ligase [GDP-forming] subunit α, mitochondrial	G3HQ05	3.45 ± 0.23	1.17 ± 0.48	−2.96	0.0051
63	cytochrome P450 2D20	Q9QYG5	5.59 ± 0.32	1.86 ± 1.05	−3.01	0.0144
64	argininosuccinate lyase	G3IDU6	2.47 ± 0.32	0.82 ± 0.47	−3.01	0.0284
65	argininosuccinate lyase isoform 1	A0A061I991	2.47 ± 0.32	0.82 ± 0.47	−3.01	0.0284
66	acidic leucine-rich nuclear phosphoprotein 32 family member A	G3H8Q4	1.73 ± 0.28	0.54 ± 0.31	−3.22	0.0299
67	3 β-hydroxysteroid dehydrogenase/δ 5→4-isomerase type 2	Q64421	1.96 ± 0.38	0.6 ± 0.35	−3.26	0.0393
68	arginase	A0A061IMD3	3.36 ± 0.4	0.97 ± 0.36	−3.46	0.0042
69	peptidyl-prolyl *cis*−*trans* isomerase	G3H533	2.58 ± 0.19	0.72 ± 0.72	−3.56	0.0477
70	argininosuccinate synthase	G3IMU3	2.4 ± 0.28	0.65 ± 0.42	−3.7	0.0130
71	glyceraldehyde-3-phosphate dehydrogenase	G3GZ97	4 ± 0.33	1.08 ± 1.08	−3.72	0.0406
72	phosphatidylethanolamine-binding protein 1	G3GU60	3.27 ± 0.2	0.87 ± 0.87	−3.76	0.0358
73	histone H2A	G3HDT6	4.19 ± 0.38	1.04 ± 0.75	−4.01	0.00958
74	histone H3	G3H2T7	6.26 ± 0.76	1.49 ± 1.25	−4.2	0.0173
75	histone H2A type 1	G3HPV6	7.02 ± 0.75	1.66 ± 1.66	−4.22	0.0262
76	glutathione peroxidase	G3H8G0	4.17 ± 0.29	0.94 ± 0.94	−4.43	0.0168
77	aspartate aminotransferase	G3GZZ0	1.65 ± 0.13	0.37 ± 0.37	−4.44	0.0177
78	vacuolar protein sorting-associated protein 35	A0A061IC10	0.99 ± 0.12	0.22 ± 0.22	−4.56	0.0202
79	ATP synthase subunit δ (fragment)	A0A061IBF1	1.04 ± 0.05	0.22 ± 0.22	−4.81	0.0098
80	histone H4	G3HPV7	6.28 ± 0.53	1.3 ± 1.3	−4.83	0.0122
81	dynamin-like 120 kDa protein, mitochondrial	G3HWY6	1.05 ± 0.17	0.22 ± 0.22	−4.86	0.0237
82	nucleophosmin	G3IBF1	1.18 ± 0.29	0.23 ± 0.23	−5.1	0.0441
83	T-complex protein 1 subunit β	G3HZ42	1.27 ± 0.24	0.25 ± 0.25	−5.12	0.0256
84	ATP synthase subunit d, mitochondrial	G3GTF9	1.59 ± 0.3	0.29 ± 0.29	−5.5	0.0212
85	adenosine kinase	P55262	1.28 ± 0.17	0.23 ± 0.23	−5.56	0.0106
86	adenosine kinase	G3GWQ3	1.28 ± 0.17	0.23 ± 0.23	−5.56	0.0106
87	hemoglobin subunit α	P01945	24.46 ± 2.77	4.28 ± 3.8	−5.72	0.0051
88	histone H3.1t	G3HHM2	8.87 ± 1.2	1.45 ± 1.45	−6.13	0.0075
89	cytochrome b5	P70116	3.62 ± 0.26	0.58 ± 0.58	−6.26	0.0030
90	α-1,4 glucan phosphorylase	G3H6Z4	1.36 ± 0.3	0.22 ± 0.22	−6.27	0.0222
91	40S ribosomal protein SA	G3HQX0	1.47 ± 0.29	0.23 ± 0.23	−6.37	0.0152
92	phosphoenolpyruvate carboxykinase, cytosolic [GTP]	G3HBK8	1.61 ± 0.18	0.25 ± 0.25	−6.45	0.0043
93	peptidyl-prolyl *cis*−*trans* isomerase A	P14851	5.91 ± 0.18	0.87 ± 0.87	−6.81	0.0012
94	histone H2A	G3HDS3	5.09 ± 0.85	0.72 ± 0.72	−7.03	0.0079
95	amine oxidase [flavin-containing] B	G3I526	1.37 ± 0.28	0.19 ± 0.19	−7.3	0.0123
96	UDP-glucuronosyltransferase 1−7C	G3IET7	1.41 ± 0.19	0.19 ± 0.19	−7.53	0.0038
97	3 β-hydroxysteroid dehydrogenase type 3	O35296	0.96 ± 0.37	0 ± 0	−100	0.0413
98	3-hydroxyisobutyryl-CoA hydrolase, mitochondrial	G3IHA0	1.03 ± 0.35	0 ± 0	−100	0.0262
99	40S ribosomal protein S11	G3I004	1.06 ± 0.21	0 ± 0	−100	0.0022
100	40S ribosomal protein S14	P62265	2.2 ± 0.25	0 ± 0	−100	0.0001
101	40S ribosomal protein S17	P63274	1.41 ± 0.25	0 ± 0	−100	0.0012
102	aldo-keto reductase family 1 member C13	P82809	1.27 ± 0.43	0 ± 0	−100	0.0254
103	ankyrin-1 (fragment)	G3HHI1	1.26 ± 0.49	0 ± 0	−100	0.0406
104	ATP-dependent RNA helicase DDX3X	A0A061HXV1	0.79 ± 0.27	0 ± 0	−100	0.0257
105	ATP-dependent RNA helicase DDX3X	A0A061HYF2	0.79 ± 0.27	0 ± 0	−100	0.0257
106	cytochrome *b*-c1 complex subunit 9	G3HP15	0.67 ± 0.23	0 ± 0	−100	0.0256
107	cytochrome P-450	Q9QZ50	2.03 ± 0.3	0 ± 0	−100	0.0005
108	cytochrome P450 2C25	Q08078	1.52 ± 0.46	0 ± 0	−100	0.0157
109	cytochrome P450 2C27	P33264	1.71 ± 0.24	0 ± 0	−100	0.0003
110	cytochrome P450 2D20	G3I0E9	2.98 ± 1.01	0 ± 0	−100	0.0256
111	dihydropyrimidinase	G3HVF7	0.87 ± 0.29	0 ± 0	−100	0.0254
112	eukaryotic translation initiation factor 4H	G3HLP4	0.67 ± 0.23	0 ± 0	−100	0.0256
113	ferritin heavy chain	P29389	2.39 ± 0.27	0 ± 0	−100	0.0001
114	glutaredoxin-1	G3H756	0.55 ± 0.18	0 ± 0	−100	0.0243
115	heterogeneous nuclear ribonucleoprotein U	G3H7M8	0.93 ± 0.32	0 ± 0	−100	0.0271
116	histone H2B	A0A061IP52	6.48 ± 2.37	0 ± 0	−100	0.0338
117	histone H2B	G3H2T4	6.48 ± 2.37	0 ± 0	−100	0.0338
118	histone H2B	G3H2U0	6.48 ± 2.37	0 ± 0	−100	0.0338
119	histone H2B	G3HDU3	6.48 ± 2.37	0 ± 0	−100	0.0338

DOI: 10.1021/jf506118j
J. Agric. Food Chem. 2015, 63, 1869−1881

Table 1. continued

	protein name	protein ID	control (mean ± SE)	HF[a] (mean ± SE)	fold[b]	t-test p-value[c]
120	histone H2B	G3HPV1	6.48 ± 2.37	0 ± 0	−100	0.0338
121	histone H2B	G3INX0	6.48 ± 2.37	0 ± 0	−100	0.0338
122	isovaleryl-CoA dehydrogenase, mitochondrial	G3ICJ8	2.26 ± 0.52	0 ± 0	−100	0.0048
123	methionine-R-sulfoxide reductase B2, mitochondrial	G3H5C7	0.73 ± 0.24	0 ± 0	−100	0.0242
124	methylcrotonoyl-CoA carboxylase subunit α	A0A061IQ54	0.55 ± 0.18	0 ± 0	−100	0.0243
125	methylcrotonoyl-CoA carboxylase subunit α, mitochondrial	G3I7H8	0.55 ± 0.18	0 ± 0	−100	0.0243
126	phosphoserine aminotransferase	G3IKH9	1.22 ± 0.11	0 ± 0	−100	0.0001
127	protein disulfide-isomerase A3	G3H0U6	7.28 ± 0.48	0 ± 0	−100	0.0001
128	putative 2-oxoglutarate dehydrogenase E1 component DHKTD1, mitochondrial	G3GVP3	1.1 ± 0.15	0 ± 0	−100	0.0003
129	RNA helicase	Q8K5D5	0.79 ± 0.27	0 ± 0	−100	0.0257
130	splicing factor, proline-and glutamine-rich	G3H9U3	0.75 ± 0.25	0 ± 0	−100	0.0243
131	talin-2-like protein	A0A061I0N6	3.32 ± 0.43	0 ± 0	−100	0.0002
132	talin-2-like protein	A0A061I1X9	3.32 ± 0.43	0 ± 0	−100	0.0002
133	talin-2-like protein	A0A061I7B4	2.23 ± 0.79	0 ± 0	−100	0.0296
134	tubulin β-4 chain	G3HCL2	3.59 ± 0.57	0 ± 0	−100	0.0007
135	urocanate hydratase	G3GRZ9	0.68 ± 0.25	0 ± 0	−100	0.0331

[a]High-fat group. [b]High-fat group/control group. [c]Significant level =0.05.

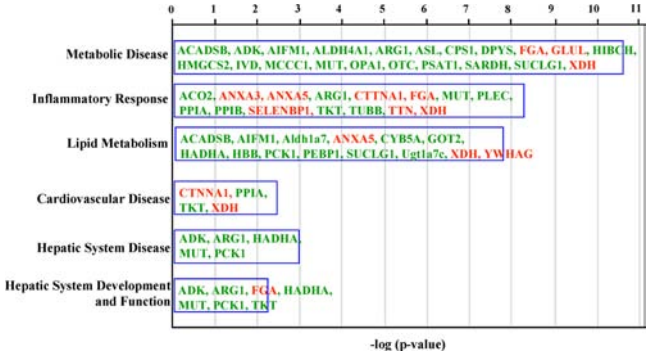

Figure 2. Proteins that were altered by the high-fat diet challenge and involved in metabolic diseases. Proteins marked green were down-regulated by the high-fat diet while those marked red were up-regulated. The full names of proteins are listed in Supporting Information Table 2. IPA computes a p score as $-\log_{10}(p\text{-value})$. A score of 3 or higher indicates that the proteins are not clustered in a pathway by random chance at the confidence level of 99.99% or higher.

perform the quantification of protein instead of two-dimensional electrophoresis (2-DE) as described in most studies.[16,29,30] Compared with 2-DE, label-free LC/MS/MS keeps the cost down and works more efficiently, allowing us to compare the expression of whole proteomics at a time. In addition to the changes in protein abundance, we also investigated the PTM of ANXA3, ANXA5, and XDH, three proteins that expressed differentially by the challenge of high-fat diet.

Body Weight and Organ Weight. Compared to control group, animals in high-fat group had lower daily feed intake; however, their weight gain, organ weight, and relative organ weight were higher than those of control group (Supporting Information Table 1).

Serum Lipids, AST, and ALT in Animals. Hamsters in the high-fat diet group had significantly ($p < 0.05$) higher serum TC and HDL-C (Supporting Information Figure 2). The level of serum TG was also higher in the high-fat group (Supporting Information Figure 2A), but not statistically significant ($p > 0.05$). The ratio of HDL-C to TC (Supporting Information Figure 2D) was lower in the high-fat group ($p > 0.05$). The activities of serum AST and ALT (Supporting Information Figure 2E and F), two clinical markers of liver damage, were significantly higher in animals maintained on the high-fat diet ($p < 0.05$).

Liver Lipids and Histopathology. Figure 1A shows the liver tissue of an animal in the control group while Figure 1B shows the liver tissue of an animal in the high-fat group. Microscopically, the liver from high-fat group revealed diffuse hepatocellular swelling with intracytoplasmic accumulation of lipid droplets (microvesicular steatosis). There were also multifocal, well-delineated ballooned hepatocytes in the periportal area. Some ballooned hepatocytes had pyknotic nuclei concurrent with varying degrees of neutrophils and lymphocytes infiltration.

Animals of high-fat group had significantly ($p < 0.05$) more hepatic TG and TC accumulation than those of control group (Figure 1C and E). Moreover, the average percentage of TG accumulated in the livers of high-fat group is higher than 5% (Figure 1D), which meets the clinical definition of fatty liver.[31]

Proteomic Analysis. Hepatic proteins were separated by electrophoresis and digested by trypsin before being analyzed by tandem mass spectrometry. The spectra generated were analyzed by TurboSequest to identify the peptide sequences against hamster database in UniProt. The results of analysis were scored using Xcorr. The proteins were regarded as hepatic proteins if more than two peptides from a single protein met the threshold of Xcorr score. On the basis of this criterion, 1191 proteins in liver were identified and 135 of them were altered by the challenge of high-fat diet (names of proteins and normalized spectrum counts of each protein were listed in Supporting Information Table 2). Table 1 shows the protein name, accession number, molecular function, and fold of change (high-fat/control) of all 135 proteins. Among these 135 proteins, 33 were up-regulated with the high-fat diet. The FDR (false discovery rate) of this analysis is 2.36%, higher than the minimal requirement of 5%. For some proteins that were not detected, it may result from their low abundance or the methodology of TurboSequest algorithm. By TurboSequest's specific algorithm, a protein will be ignored if it shares common sequences with other proteins that possess unique a peptide.

DOI: 10.1021/jf506118j
J. Agric. Food Chem. 2015, 63, 1869−1881

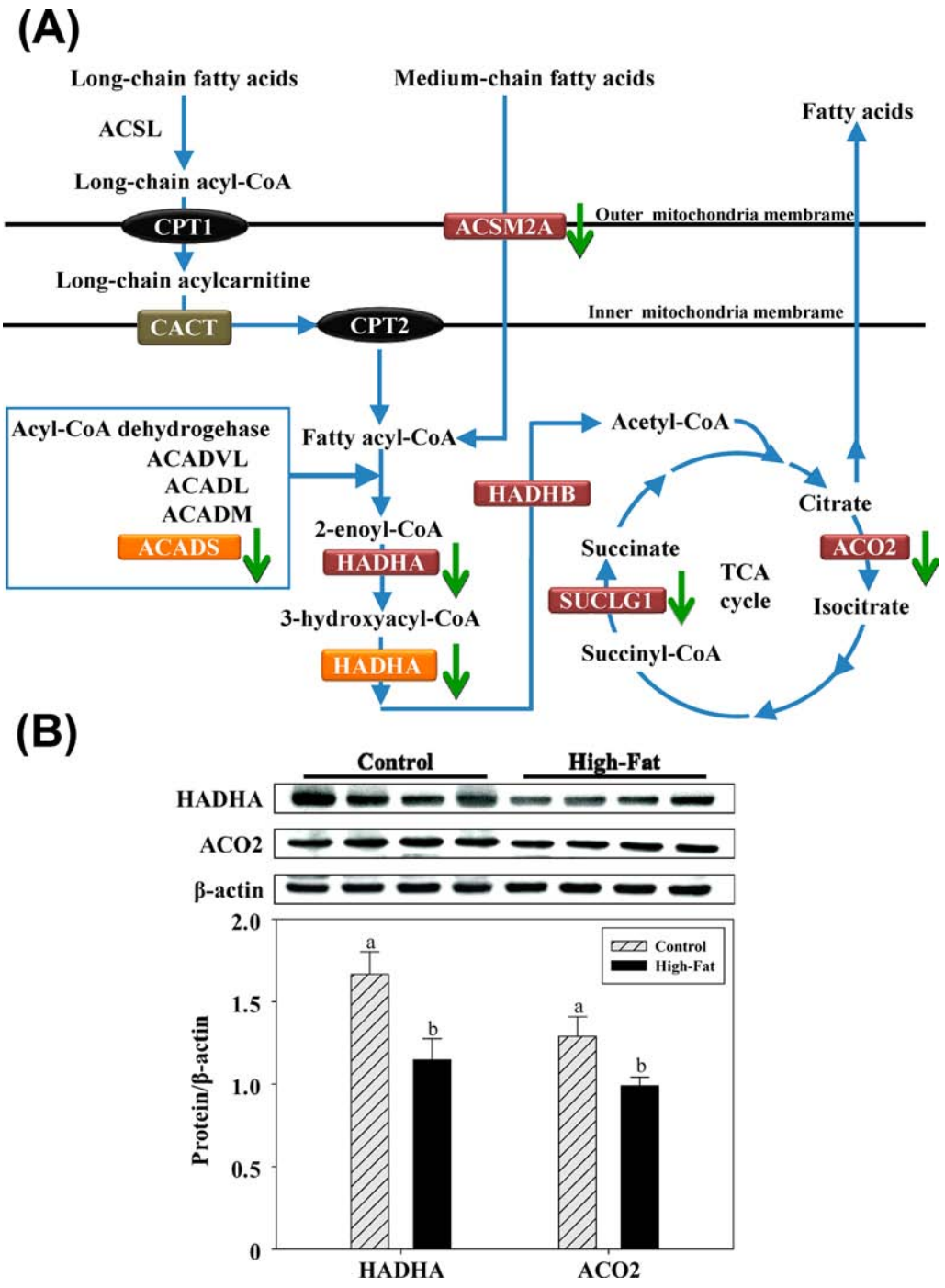

Figure 3. (A) Pathway of β-oxidation and TCA cycle. (B) Expression of HADHA and ACO2. Values are means of three replicated experiments. Groups with the same letter are not significantly different ($\alpha = 0.05$). Green arrows indicate down-regulation of proteins. ACSL, long-chain acyl-CoA synthase (ACSM refers to medium-chain acyl-CoA synthase); CPT, carnitine palmitoyltransferase; CACT, carnitine-acylcarnitine translocase; ACADS short-chain acyl-CoA dehydrogenase (VL, L, and M refer to very long-chain, long-chain, and medium-chain, respectively); HADHA, α-unit of mitochondrial trifunctional protein, containing the activities of enoyl-CoA hydratase and 3-hydroxyacyl-CoA dehydrogenase actvities; HADHB, β-unit of mitochondrial trifunctional protein, containing the activity of 3-ketoacyl-CoA thiolase. ACO2, aconitate hydratase 2; SUCLG, succinyl-CoA ligase.

Ingenuity Pathways Analysis. The proteins with altered expression were assessed through IPA. IPA calculates a p score as $-\log_{10}(p\text{-value})$ to rank networks. A score of 3 or higher indicates that the proteins are not clustered in a pathway by random chance at the confidence level of 99.99% or higher. Because high-fat diet significantly contributes to the etiology of metabolic diseases, proteins grouped into the related interactions by IPA are shown in Figure 2 (the full names of proteins are listed in Supporting Information Table 3). Proteins marked green were down-regulated by the high-fat diet, while those marked red were up-regulated. For proteins involved in metabolic diseases, 18 were down-regulated and 3 were up-regulated. For those that play a role in inflammatory response, 8 were down-regulated and 7 were up-regulated. With regard to

DOI: 10.1021/jf506118j
J. Agric. Food Chem. 2015, 63, 1869−1881

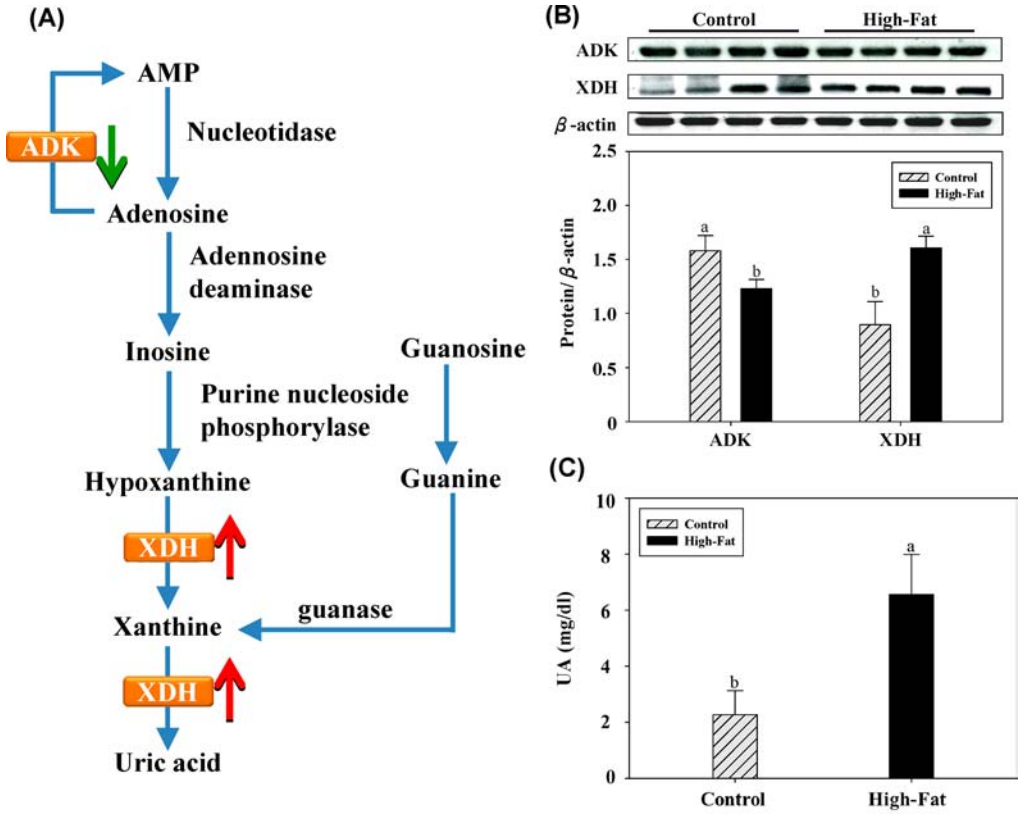

Figure 4. (A) Pathway of uric acid synthesis. (B) Expression of ADK and XDH. (C) Serum concentration of uric acid. Values are means of three replicated experiments. Groups with the same letter are not significantly different (α = 0.05). Green arrows indicate down-regulation of proteins and red arrows indicate up-regulation of proteins. ADK, adenosine kinase; XDH, xanthine dehydrogenase; UA, uric acid.

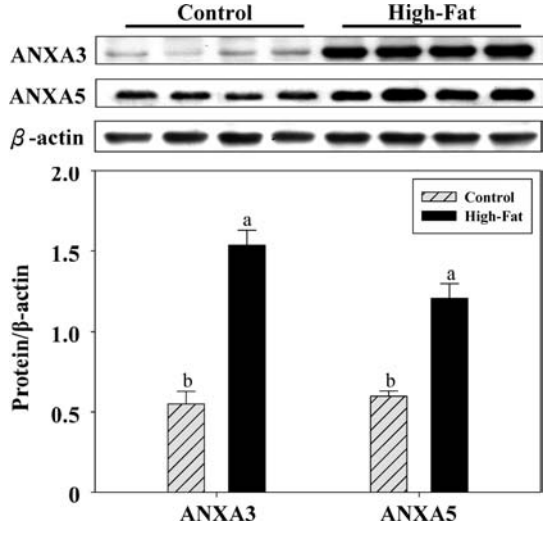

Figure 5. Expression of ANXA3 and ANXA5. Values are means of three replicated experiments. Groups with the same letter are not significantly different (α = 0.05). ANX, annexin.

lipid metabolism, 11 proteins were down-regulated and 3 were up-regulated. For proteins related to the development of cardiovascular disease, 2 were up-regulated and 2 were down-regulated. In the pathways involved in hepatic functions and diseases, 6 were down-regulated and 1 was up-regulated. Further Western blotting analysis was carried out to confirm the expression of some proteins mentioned above.

Expression of Enzymes Involved in Fatty Acid β-Oxidation. Mitochondrial β-oxidation is the main route for metabolism of fatty acids.[32] Prior to the translocation into mitochondria for β-oxidation, free long-chain fatty acids (LCFAs) must be activated by acyl-CoA synthetase long-chain (ACSL) (Figure 3A). After being activated to the CoA derivative, LCFAs translocate into a mitochondrion via the carnitine transacylation pathway, but medium-chain fatty acids can enter mitochondria without the carnitine shuttle. ACSs are classified as short-chain ACS (ACSS), medium-chain (ACSM), and ACSL according to their specificities for fatty acids of varying length.[33] Proteomic analysis shows that the expression of ACSM2A (medium-chain acyl-CoA synthetase family member 2A) was down-regulated by the high-fat diet (Table 1). Attenuated expression of ACSM2A decreased the opportunity for medium-chain fatty acids being transported into mitochondria for β-oxidation.

The first reaction within mitochondrial matrix is the acyl-CoA dehydrogenation catalyzed by acyl-CoA dehydrogenase (ACAD) (Figure 3A). Nine members were identified in the ACAD family, including the four members that are involved in β-oxidation: short, medium, long, and very long chain acyl-CoA dehydrogenase (ACADS, ACADM, ACADL, and ACADVL, respectively).[34] Following dehydrogenation, enoyl-CoA hydratase catalyzes the formation of 3-hydroxyacyl-CoA, which is further followed by the formation of 3-ketoacyl-CoA. Finally, acetyl-CoA is generated through a thiolysis reaction. The last three steps of reactions are catalyzed by mitochondrial trifunctional protein (MTP), which is composed of an α-unit (HADHA) and a β-unit (HADHB). HADHA contains long-chain enoyl-CoA hydratase and 3-hydroxyacyl-CoA dehydro-

DOI: 10.1021/jf506118j
J. Agric. Food Chem. 2015, 63, 1869−1881

Table 2. Post-translational Modifications of ANXA3, ANXA5, and XDH

protein	PTM	site	modified peptides	position[a]	obs. m/z[b]	calc. m/z[c]	dM[d]
ANXA3[e]	Hex-HexNac[g]	Thr (154)	ALL**T**$_{\#}$LADGRRDESLK	151−165	675.008	675.024	−0.016
	levuglandinyl-lysine lactam aduct[g]	Lys (93)	DDLKGDLSGHFEHIMVALVTAPALFDAK#	66−93	1114.919	1114.914	0.005
	n-octanoate[g]	Thr (303)	HYGYSLHSAIQSD**T**$_{\#}$SGDYRLVLLK	290−313	950.498	950.500	−0.002
ANXA5	NeuAc-Hex-Hex-HexNAc-Hex-HexNAc-Hex	Ser (116)	GAGTNEKVLTEIIAS#R	102−117	948.809	948.812	−0.003
	4-hydroxy-2-nonenal[g]	Lys (63)	TLFG**K**$_{\#}$DLLDDLK	59−70	505.946	505.959	−0.013
	4-hydroxynonenal[g]	Lys (301)	KNFATSLYSMI**K**$_{\#}$GDTSGDYK	290−309	794.743	794.733	0.01
	NE-(carboxymethyl)lysine[g]	Lys (76)	TLFGKDLLDDLKSELTG**K**$_{\#}$	59−76	684.361	684.367	−0.006
	carboxylation[g]	Glu (107)	GAGTN**E**$_{\#}$KVLTEIIASR	102−117	851.948	851.951	−0.003
	oxoalanine[g]	Ser (44)	GLGTDEESILTLLT**S**$_{\#}$R	30−45	851.948	851.946	0.002
XDH[f]	carboxylation	Glu (231)	FEG**E**$_{\#}$RVTWIQASTLGELLDIKAQHPDAK	228−255	1066.216	1066.213	0.003
	4-oxo-2-nonenal	Lys (890)	SIMERALFHMDNAY**K**$_{\#}$	876−890	654.665	654.657	0.008
	dihydroxylation	Lys (270)	AQHPDAKLVVGNTEIGIEM*KF**K**$_{\#}$	249−270	825.096	825.094	0.002
	S-farnesyl cysteine[g]	Cys (112)	SHGSQ**C**$_{\#}$GFCTPGIVM*SM*YTLLR	107−128	910.447	910.446	0.001
	methylation[g]	His (884)	ALF**H**$_{\#}$MDNAY**K**$_{\#}$IPNI**R**$_{\#}$	881−895	923.009	922.993	0.016
		Lys (890)					
		Arg (895)					
	monoglutamyl[g]	Glu (960)	LE$_{\#}$VFNLPR	959−966	558.824	558.805	0.019

[a]Site of modified peptide. [b]Obs.: observed m/z of the modified peptides. [c]Calc.: calculated m/z of the modified peptides. [d]The difference between obs. and calc. [e]ANX: annexin. [f]XDH: xanthine dehydrogenase. [g]Presence in high-fat group.

genase actvities, whereas HADHB contains the 3-ketoacyl-CoA thiolase activity.[35]

Proteomic analysis shows that the expression of ACADS and HADHA was down-regulated by the high-fat diet challenge (Table 1 and Figure 3B). Down-regulation of ACAD and HADHA would limit the capacity of mitochondria to oxidize fatty acids, leading to hepatic steatosis. Mice deficient in short-chain ACAD (ACADS) develop a fatty liver upon dietary fat challenge.[36] Medium-chain acyl-CoA dehydrogenase (ACADM) is the most common inherited disorder of mitochondrial β-oxidation in humans. Mice deficient in ACADM also develop a fatty liver.[37] MTP consists of four α and four β subunits that catalyze the final three steps of long-chain fatty acid β-oxidation. Newborn mice with MTP α subunit (HADHA) null allele ($Mtpa^{-}/^{-}$) revealed rapid development of hepatic steatosis after birth and significant necrosis of cardiac myocytes later.[35] In the aging heterozygous $Mtpa^{+}/^{-}$ mice, significantly higher hepatic triglyceride content and serum ALT activity were measured compared with the $Mtpa^{+}/^{+}$ littermates.[38] Rats with a high-fat diet induced hepatic steatosis had reduced level of enoyl-coenzyme A hydratase. Down-regulation of enoyl-coenzyme A hydratase in mice significantly exacerbated high-fat diet induced hepatic steatosis.[16]

In this study, decreased expression of ACSM2A, ACADS, and HADHA in the high-fat group (Table 1 and Figure 3B) may attenuate the oxidation of fatty acids, increasing the availability of fatty acids for synthesis of TG. This finding may explain the development of fatty liver as observed in the high-fat group.

Expression of Enzymes Involved in TCA Cycle. Acetyl-CoA enters TCA cycle by condensing with oxaloacetate to form citrate (Figure 3A). The citrate is then converted to isocitrate through the action of aconitate hydratase (ACO, also named as aconitase). Isocitrate undergoes dehydrogenation and decarboxylation to form α-ketoglutarate. Ketoglutarate is further decarboxylated to form succinyl-CoA. To continue the cycle, succinyl-CoA is converted to succinate by the action of succinyl-CoA ligase (also called succinate synthetase or succinate thiokinase). Succinate is further metabolized to fumurate, followed by the formation of malate. Malate is then converted to oxaloacetate through dehydrogenation reaction.[39]

Proteomic analysis showed the ACO was down-regulated by high-fat diet (Table 1 and Figure 3B). Mammals express two isoforms of ACO, ACO1 (soluble), and ACO2 (mitochondrial). Cui et al. found a significant decrease of ACO2 expression in splenic lymphocytes of mice that were fed a high-fat diet for 10 weeks.[40] Loss of ACO activity limits TCA cycle activity, which will favor the translocation of citrate from mitochondria to cytosol to undergo fatty acid synthesis.[41]

Proteomic analysis showed that SUCLG1 was also down-regulated by high-fat diet (Table 1). SUCLG converts succinyl-CoA to succinate and free coenzyme A, and converts adenosine diphosphate (ADP) to adenosine triphosphate (ATP) or guanosine diphosphate (GDP) to guanosine triphosphate (GTP). SUCLG is composed of two subunits, and the α-subunit is encoded by *SUCLG1* gene with specificity for GDP. Liver biopsy of subjects with SUCLG1 deficiency showed both micro- and macrosteatosis.[42]

Expression of Enzymes Involved in Uric Acid Synthesis. Uric acid is the final breakdown product of purine metabolism. In the metabolism of purine nucleotide, adenosine is first deaminated to inosine in the reaction catalyzed by deaminase or phosphorylated to AMP by the action of adenosine kinase (ADK) (Figure 4A).[43] Catalyzed by purine nucleotide phosphorylase, inosine and guanosine are converted to hypoxanthine and guanine, respectively. Hypoxanthine and guanine next form xanthine in reactions catalyzed by xanthine dehydrogenase (XDH) and guanase, respectively. Xanthine is then oxidized to uric acid by the second reaction catalyzed by XDH.[44]

In the present study, the high-fat diet down-regulated ADK but up-regulated XDH (Table 1 and Figure 4B). ADK is highly expressed in liver. It is essential for maintaining normal level of adenine nucleotides and S-adenosylmethionine-dependent transmethylation process.[43] A decreased level of ADK decreases the recycle of adenosine to AMP, leading to more adenosine available for the biosynthesis of uric acid and reduced level of

DOI: 10.1021/jf506118j
J. Agric. Food Chem. 2015, 63, 1869−1881

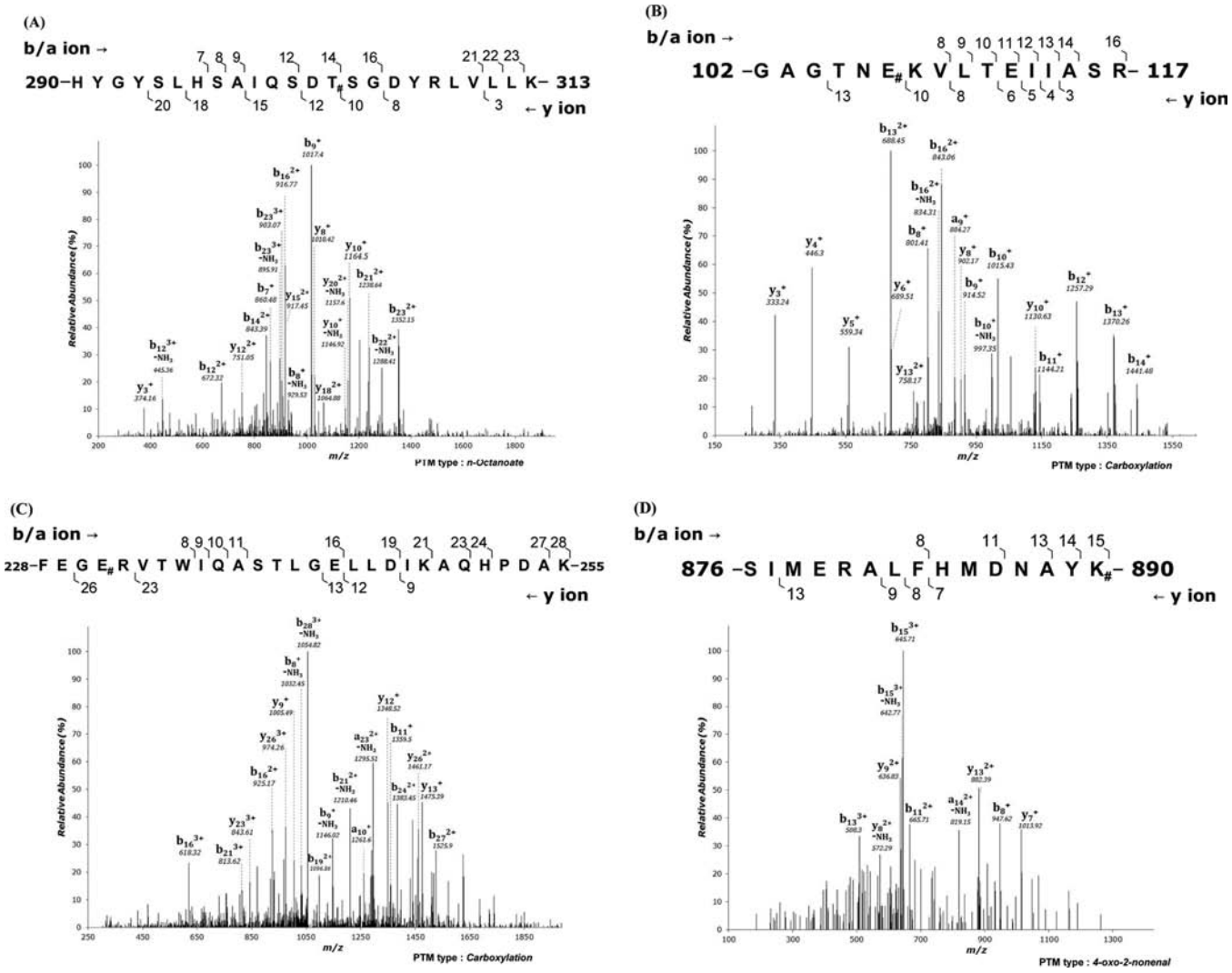

Figure 6. (A) Tandom mass spectrum of the *n*-octanoate peptide with the sequence 290-HYGYSLHSAIQSDT#SGDYRLVLLK-313 on ANXA3. (B) Tandom mass spectrum of the carboxylation peptide with the sequence 102-GAGTNEKVLTEIIAS#R-117 on ANXA5. (C) Tandom mass spectrum of the carboxylation peptide with the sequence 228-FEGE#RVTWIQASTLGELLDIKAQHPDAK-255 on XDH. (D) Tandom mass spectrum of the 4-oxo-2-nonenal peptide with the sequence 876-SIMERALFHMDNAYK#-890 on XDH. ANX, annexin; XDH, xanthine dehydrogena.

adenine nucleotides. Because the metabolic rate in liver mitochondria is proportional to the level of adenine nucleotides, a decreased amount of adenine nucleotides in the liver would lead to an impairment of mitochondrial function. Newborns with $Adk^{-/-}$ displayed microvesicular hepatic steatosis and died within 14 days with fatty livers.[44]

Xanthine oxidoreductase, a member of molybdoenzyme family, has two interconvertible forms, xanthine dehydroenase (XDH) and xanthine oxidase (XO). Both XDH and XO catalyze the conversion of hypoxanthine to xanthine and xanthine to uric acid.[45] Under physiological conditions, the enzyme is primarily present as XDH. Up-regulated expression of XDH by the challenge of a high-fat diet in the current study (Figure 4B) promoted the formation of uric acid, as indicated by the increased serum concentration of uric acid in animals of high-fat group (Figure 4C). Because high uric acid levels may cause frequent attacks of gout, it is reasonable to infer that high-fat diet is associated with etiology of gout.

Expression of Annexin A3 and Annexin A5. In this present study, proteomic analysis indicated that the challenge of a high-fat diet up-regulated both annexin A3 (ANXA3) and annexin A5 (ANXA5) (Table 1 and Figure 5). ANXs are a family of Ca^{2+}-regulated membrane- and phospholipid-binding proteins that have been implicated in many cellular processes including inflammation, apoptosis, proliferation, and differentiation.[46] Annexin A3 is a novel angiogenic factor that induces vascular endothelial growth factor (VEGF) production through the hypoxia-inducible factor-1 (HIF-1) pathway.[47] Poloxamer P-407 hyperlipidemia mouse is a nondiet-induced and genetically unaltered model of atherosclerosis. Kuzman et al. detected an up-regulation of annexin A3 in this mouse model.[48] By using an experimental model of tumor necrosis factor-α (TNF-α)-mediated inflammation, Pitroda et al. reported increased expression of ANXA3 in four types of human cancer and several human diseases associated with chronic inflammation.[49]

ANXA5 is associated with the development and progression of breast cancer, prostate cancer, cervical cancer, colorectal adenocarcinoma, gastric cancer, pancreatic adenocarcinoma, sarcoma, bladder cancer, and glioma. ANXA5 is considered as a predictive marker for tumor development and a therapeutic target for early diagnosis and treatment of tumors.[50] In the

DOI: 10.1021/jf506118j
J. Agric. Food Chem. 2015, 63, 1869–1881

present study, up-regulation of ANXA3 and ANXA5 implies an inflammatory and procarcinogenic status induced by high-fat diet.

Expression of Enzymes Involved in Urea Synthesis. The urea cycle is the major pathway for detoxification of ammonia in mammals. In the present study, proteomic analysis showed that several enzymes involved in urea synthesis were down-regulated by high-fat diet, including carbamoyl-phosphate synthetase 1 (CPS1), ornithine transcarbamoylase (OTC), argininosuccinate synthetase (ASS), argininosuccinate lyase (ASL), and arginase 1 (ARG1) (Table 1 and Supporting Information Figure 3).

CPS1 and OTC are mitochondrial enzymes catalyzing the first and second steps of the urea cycle, respectively. The expression of both enzymes is higher in hepatocytes than in other tissues.[51] Deficiency and reduced activity of CPS1/OTC cause hyperammonaemia.[52,53] ASS catalyzes the reversible condensation of citrulline with aspartate to form argininosuccinate. Argininosuccinate is then split into arginine and funarate in a reaction catalyzed by ASL. ASS is a highly conserved enzymes expressed in various tissues. Decreased expression of ASS attenuates the metabolism of ammonia and formation of argininosuccinate, resulting in abnormally higher concentration of ammonia and citrulline in the blood.[54] Patients with ASL deficiency were detected with increased blood ammonia.[55] ARG is the final enzyme of the urea cycle, catalyzing the metabolism of arginine to urea and ornithine. ARG1 knockout mice exhibited severe symptoms of hyperammonemia and hepatocyte abnormalities.[56,57]

Post-translational Modification of ANXA and XDH. PTMs are site specific amino acid side chain alterations taking place after translation of mRNA into a protein. It affects the folding, conformation, and functions of proteins. More than 300 different types of PTMs have been characterized to date, including carboxylation, methylation, phosphorylation, glycosylation, carboxylation, ubiquitination, prenylation, and sulphation. PTMs lead to higher structural and functional protein diversity, playing significant roles in physiological process and disease progression.[58,59] Identification of PTM on ANXA3, ANXA5, and XDH were carried out by our in-house PTM finder programs PTM-Miner and PTM-Q. The identified peptides and corresponding modified sites are listed in Table 2.

Four representative spectra for ANXA3, ANXA5, and XDH are shown in Figure 6. Figure 6A is the fragment ion spectrum for the modified peptide 290-HYGYSLH-SAIQSD**T**$_{\#}$SGDYRLVLLK-313 of ANXA3. The spacing of b and y ions was used to decipher the sequence of modified peptide. The novel *n*-octanoate site was detected based on the unmodified b14 ion and the mass shift of 126.10 Da for the y12 ion on modified peptide. The matched peaks were labeled according to the Biemann nomenclature. Figure 6B shows the fragment ion spectrum for the modified peptide 102-GAGTN**E**$_{\#}$KVLTEIIASR-117 of ANXA5. The novel carboxylation site was detected based on the unmodified y10 ion and the mass shift of 43.99 Da for the b8 ion on modified peptide. Figure 6C is the fragment ion spectrum for the modified peptide 228-FEG**E**$_{\#}$RVTWIQASTLGELLDIKAQHPDAK-255 of XDH. The novel carboxylation site was detected based on the unmodified y23 ion and the mass shift of 43.99 Da for the b8 ion on modified peptide. Figure 6D shows the fragment ion spectrum for the modified peptide 876- SIMERALFHMD-NAY**K**$_{\#}$-890 of XDH. The novel 4-oxo-2-nonenal site was detected based on the unmodified b14 ion and the mass shift of 136.09 Da for the y7 ion on modified peptide.

Proteomics is a powerful tool in monitoring the changes of protein profile induced by dietary manipulation. The findings of this study show that the challenge of a high-fat diet for 8 weeks impairs β-oxidation and ammonia metabolism; moreover, the high-fat diet up-regulates expression of inflammatory markers and synthesis of uric acid.

■ ASSOCIATED CONTENT

Ⓢ Supporting Information

Supporting tables and figures. This material is available free of charge via the Internet at http://pubs.acs.org.

■ AUTHOR INFORMATION

Corresponding Author

*E-mail: drkuo@mail.usc.edu.tw. Tel: 886-2-25381111-6214.

Funding

This study was supported by National Scientific Council, Taiwan (NSC 101-2313-B-158-001) and Shih Chien University (USC-101-05-02001).

Notes

The authors declare no competing financial interest.

■ REFERENCES

(1) Eckel, R. H.; Grudy, G. M.; Zimmet, P. Z. The metabolic syndrome. *Lancet* **2005**, *365*, 1415−1428.

(2) Matteoni, C. A.; Younossi, Z. M.; ramlich, T.; Boparai, N.; Liu, Y. C.; Mccullough, A. J. Nonalcoholic fatty liver disease: A spectrum of clinical and pathological severity. *Gastroenterology* **1999**, *116*, 1413−1419.

(3) Angulo, P.; Lindor, K. D. Treatment of nonalcoholic steatohepatitis. *Best Pract. Res. Clin. Gastroenterol.* **2002**, *16*, 797−810.

(4) Memon, R. A.; Feingold, K. R.; Moser, A. H.; Fuller, J.; Grundeld, C. Regulation of fatty acid transport protein and fatty acid translocase mRNA levels by endotoxin and cytokines. *Am. J. Physiol.* **1998**, *274*, E210−E217.

(5) Ryedn, M.; Dicker, A.; van Harmelen, V.; Hauner, H.; Brunnberg, M.; Perbeck, L.; Lonnqvist, F.; Arner, P. Mapping of early signaling events in tumor necrosis factor-α-mediated lipolysis in human fat cells. *J. Biol. Chem.* **2002**, *277*, 1085−1091.

(6) Bradbury, M. W.; Berk, P. D. Lipid metabolism in hepatic steatosis. *Clin. Liver Dis.* **2004**, *8*, 639−671.

(7) Dentin, R.; Girard, J.; Postic, C. Carbohydrate responsive element binding protein (ChREBP) and sterol regulatory element binding protein-1c (SREBP-1c): Two key regulators of glucose metabolism and lipid synthesis in liver. *Biochimie* **2005**, *87*, 81−86.

(8) Anderson, N. L.; Anderson, N. G. Proteome and proteomics: New technologies, new concepts, and new words. *Electrophoresis* **1998**, *19*, 1853−1861.

(9) Morand, J. P.; Macri, J.; Adeli, K. Proteomics profiling of hepatic endoplasmic reticulum-associated proteins in an animal model of insulin resistance and metabolic dyslipidemia. *J. Biol. Chem.* **2005**, *280*, 17626−17633.

(10) Meneses-Lorente, G.; Watt, A.; Salim, K.; Gaskell, S. J.; Muniappa, N.; Lawrence, J.; Guest, P. C. Identification of early proteomic markers for hepatic steatosis. *Chem. Res. Toxicol.* **2006**, *19*, 986−989.

(11) Santamaria, E.; Muñoz, J.; Fernández-Irigoyen, J.; Prieto, J.; Corrales, F. J. Toward the discovery of new biomarkers of hepatocellular carcinoma by proteomics. *Liver Int.* **2007**, *27*, 163−173.

(12) Walther, T. C.; Mann, M. Mass spectrometry-based proteomics in cell biology. *J. Cell Biol.* **2010**, *190*, 491−500.

(13) Aldred, S.; Grant, M. M.; Griffiths, H. R. The use of proteomics for the assessment of clinical samples in research. *Clin. Biochem.* **2004**, *37*, 93−952.

DOI: 10.1021/jf506118j
J. Agric. Food Chem. 2015, 63, 1869−1881

(14) Marcotte, E. M. How do shotgun proteomics algorithms identify proteins? *Nat. Biotechnol.* **2007**, *25*, 755−757.
(15) Abdallah, C.; Dumas-Gaudot, E.; Renaut, J.; Slergeant, K. Gel-based and gel-free quantitative proteomics approaches at a glance. *Int. J. Plant Genomics* **2012**, *2012*, No. 494572.
(16) Zhang, X.; Yang, J.; Guo, Y.; Yu, C.; Xu, C.; Xu, L.; Wu, S.; Sun, W.; Wei, H.; Gao, X.; Zhu, Y.; Qian, X.; Jiang, Y.; Li, Y.; He, F. Functional proteomic analysis of nonalcoholic fatty liver disease in rat models: Enoyl-coenzyme A hydratase down-regulation exacerbates hepatic steatosis. *Hepatology* **2010**, *51*, 1190−1199.
(17) Baiges, I.; Palmfeldt, J.; Bladé, C.; Gregersen, N.; Arola, L. Lipogenesis is decreased by grape seed proanthocyanidins according to liver proteomics of rats fed a high fat diet. *Mol. Cell. Proteomics* **2010**, *9*, 1499−1513.
(18) Luo, M.; Mengos, A. E.; Stubblefield, T. M.; Mandarino, L. J. High fat diet-induced changes in hepatic protein abundance in mice. *J. Proteomics Bioinform.* **2012**, *5*, 60−66.
(19) Bertram, H. C.; Larsen, L. B.; Chen, X.; Jeppesen, P. B. Impact of high-fat and high-carbohydrate diets on liver metabolism studied in a rat model with a systems biology approach. *J. Agric. Food Chem.* **2012**, *60*, 676−684.
(20) Bhathena, J.; Kulamarva, A.; Martoni, C.; Urbanska, A. M.; Malhotra, M.; Paul, A.; Prakash, S. Diet-induced metabolic hamster model of nonalcoholic fatty liver disease. *Diabetes Metab. Syndr. Obes. Target Ther.* **2011**, *4*, 195−203.
(21) Folch, J.; Lees, M.; Sloane Stanley, G. H. A simple method for the isolation and purification of total lipids from animal tissues. *J. Biol. Chem.* **1957**, *226*, 497−509.
(22) Liao, C. C.; Chen, Y. W.; Jeng, T. L.; Li, C. R.; Kuo, C. F. Consumption of purple sweet potato affects post-translational modification of plasma proteins in hamsters. *J. Agric. Food Chem.* **2013**, *61*, 12450−12458.
(23) Rajkumar, R.; Karthikeyan, K.; Archunan, G.; Huang, P. H.; Chen, Y. W.; Ng, W. V.; Liao, C. C. Using mass spectrometry to detect buffalo salivary odorant-binding protein and its post-translational modifications. *Rapid Commun. Mass Spectrom.* **2010**, *24*, 3248−54.
(24) Lundgren, D. H.; Han, D. K.; Eng, J. K. Protein identification using TurboSEQUEST. *Curr. Protoc. Bioinformatics* **2005**, *10*, 13.3.1−13.3.13.
(25) Piersma, S. R.; Fiedler, U.; Span, S.; Lingnau, A.; Pham, T. V.; Hoffmann, S.; Kubbutat, M. H.; Jiménez, C. R. Workflow comparison for label-free, quantitative secretome proteomics for cancer biomarker discovery: Method evaluation, differential analysis, and verification in serum. *J. Proteome Res.* **2010**, *9*, 1913−1922.
(26) Uen, Y.-H.; Lin, K.-Y.; Sun, D.-P.; Liao, C.-C.; Hsieh, M.-S.; Huang, Y.-K.; Chen, Y.-W.; Huang, P.-H.; Chen, W.-J.; Tai, C.-C.; Lee, K.-W.; Chen, Y.-C.; Lin, C.-Y. Comparative proteomics, network analysis, and post-translational modification identification reveal differential profiles of plasma Con A-bound glycoprotein biomarkers in gastric cancer. *J. Proteomics* **2013**, *83*, 197−213.
(27) Stein, O.; Thiery, J.; Stein, Y. Is there a genetic basis for resistance to atherosclerosis. *Atherosclerosis* **2002**, *160*, 1−10.
(28) Zhang, Z.; Wang, H.; Jiao, R.; Peng, C.; Wong, Y. M.; Yeung, V. S. Y.; Huang, Y.; Chen, Z.-Y. Choosing hamsters but not rats as a model for studying plasma cholesterol-lowering activity of functional foods. *Mol. Nutr. Food Res.* **2009**, *53*, 921−930.
(29) Zhang, L.; Perdomo, G.; Kim, D. H.; Qu, S.; Ringquist, S.; Trucco, M.; Dong, H. Proteomic analysis of fructose-induced fatty liver in hamsters. *Metabolism* **2008**, *57*, 1115−1124.
(30) Li, Lin.; Lu, D.-Z.; Li, Y.-M.; Zhang, X.-Q.; Zhou, X.-X.; Jin, X. Proteomic analysis of liver mitochondria from rats with nonalcoholic steatohepatitis. *World J. Gastroenterol.* **2014**, *20*, 4778−4786.
(31) Hernaez, R.; Lazo, M.; Bonekamp, S.; Kamel, I.; Brancati, F. L.; Guallar, E.; Clark, J. M. Diagnostic accuracy and reliability of ultrasonography for the detection of fatty liver: A meta-analysis. *Hepatology* **2011**, *54*, 1082−1090.
(32) Reddy, J. K. Nonalcoholic steatosis and steatohepatitis. III. Peroxisomal β-oxidation, PPAR α, and steatohepatitis. *Am. J. Physiol. Gastrointest. Liver Physiol.* **2001**, *281*, G1333−G1339.
(33) Watkins, P. Fatty acid activation. *Prog. Lipid Res.* **1997**, *36*, 55−83.
(34) Kim, J.-J.; Miura, R. Acyl-CoA dehydrogenases and acyl-CoA oxidases, structural basis for mechanistic similarities and differences. *Eur. J. Biochem.* **2004**, *271*, 483−493.
(35) Ibdah, J. A.; Paul, H.; Zhao, Y.; Binford, S.; Salleng, K.; Cline, M.; Matern, D.; Bennett, M. J.; Rinaldo, P.; Strauss, A. W. Lack of mitochondrial trifunctional protein in mice causes neonatal hypoglycemia and sudden death. *J. Clin. Invest.* **2001**, *107*, 1403−1409.
(36) Wood, P. A.; Amendt, B. A.; Rhead, W. J.; Millington, D. S.; Inoue, F.; Armstrong, D. Short-chain acyl-coenzyme A dehydrogenase deficiency in mice. *Pediatr. Res.* **1989**, *25*, 38−43.
(37) Tolwani, R. J.; Hamm, D. A.; Tian, L.; Sharer, J. D.; Vockley, J.; Rinaldo, P.; Matern, D.; Schoeb, T. R.; Wood, P. A. Medium-chain acyl-CoA dehydrogenase deficiency in gene-targeted mice. *PloS Genet.* **2005**, *1*, 205−212.
(38) Ibdah, J. A.; Perlegas, P.; Zhao, E.; Angdisen, J.; Borgerink, H.; Shadoan, M. K.; Wagner, J. D.; Matern, D.; Rinaldo, P.; Cline, J. M. Mice heterozygous for a defect in mitochondrial trifunctional protein develop hepatic steatosis and insulin resistance. *Gastroenterology* **2005**, *128*, 1381−1390.
(39) Krebs, H. A. Rate control of the tricarboxylic acid cycle. *Adv. Enzyme Regul.* **1970**, *8*, 335−353.
(40) Cui, J.; Xiao, Y.; Shi, Y.-H.; Le, G. W.; Miao, X. Y. Comparative proteome analysis of splenic lymphocytes in long-term high-fat diet and dietary supplement with lipoic acid mice. *Cell. Immunol.* **2010**, *264*, 156−162.
(41) Hanson, R. W.; Ballard, F. J. The relative significance of acetate and glucose as precursors for lipid synthesis in liver and adipose tissue from ruminants. *Biochem. J.* **1967**, *105*, 529−536.
(42) Van Hove, J. L. K.; Saenz, M. S.; Thomas, J. A.; Gallaghe, R.; Lovell, M. A.; Fenton, L. Z.; Shanske, S.; Myers, S. M.; Wanders, R. J. A.; Ruiter, J.; Turkenburg, M.; Waterham, H. R. Succinyl-CoA ligase deficiency: A mitochondrial hepatoencephalomyopathy. *Pediatr. Res.* **2010**, *68*, 159−164.
(43) Bjursell, M. K.; Blom, H. J.; Cayuela, J. A.; Engvall, M. L.; Lesko, N.; Balasubramaniam, S.; Brandberg, G.; Halldin, M.; Falkenberg, M.; Jakobs, C.; Smith, D.; Struys, E.; Döbeln, U.; Gustafsson, C. M.; Lundeberg, J.; Wedell, A. Adenosine kinase deficiency disrupts the methionine cycle and causes hypermethioninemia, encephalopathy, and abnormal liver function. *Am. J. Hum. Genet.* **2011**, *89*, 507−511.
(44) Boison, D.; Scheurer, L.; Zumsteg, V.; Rülicke, T.; Litynski, P.; Fowler, B.; Brandner, S.; Mohler, H. Neonatal hepatic steatosis by disruption of the adenosine kinase gene. *Proc. Natl. Acad. Sci., U.S.A.* **2002**, *99*, 6985−6990.
(45) Hille, R.; Nishino, T. Xanthine oxidase and xanthine dehydrogenase. *FASEB J.* **1995**, *9*, 995−1003.
(46) Gerke, V.; Moss, S. E. Annexins: From structure to function. *Physiol. Rev.* **2002**, *82*, 331−371.
(47) Park, J. E.; Lee, D. H.; Lee, J. A.; Park, S. G.; Kim, N.-S.; Park, B.-C.; Cho, S. Annexin A3 is a potential angiogenic mediator. *Biochem. Biophys. Res. Commun.* **2005**, *337*, 1283−1287.
(48) Kuaman, D.; Tacer, K. F.; Cerne, M.; Rezen, T.; Acimovic, J.; Cegovnik, U.; Kocjan, D.; Urleb, U.; Rozman, D. Modulation of hepatic transcriptome in the poloxamer P-407 hyperlipidemia mouse model. *Acta Chim. Stov.* **2009**, *56*, 262−269.
(49) Pitroda, S. P.; Zhou, T.; Sweis, R. F.; Filippo, M.; Labay, E.; Beckett, M. A.; Mauceri, H. J.; Liang, H.; Darga, T. E.; Perakis, S.; Khan, S. A.; Sutton, H. G.; Zhang, W.; Khodarev, N. N.; Garcia, J. G. N.; Weichselbaum, R. R. Tumor endothelial inflammation predicts clinical outcome in diverse human cancers. *PloS One* **2012**, *7*, e46104.
(50) Peng, B.; Guo, C.; Guan, H.; Liu, S.; Sun, M.-Z. Annexin A5 as a potential marker in tumors. *Clin. Chim. Acta* **2014**, *427*, 42−48.
(51) Ryall, J.; Nguyen, M.; Bendayan, M.; Shore, G. C. Expression of nuclear genes encoding the urea cycle enzymes, carbamoyl-phosphate synthetase I and ornithine carbamoyl transferase, in rat liver and intestinal mucosa. *Eur. J. Biochem.* **1985**, *152*, 287−292.

DOI: 10.1021/jf506118j
J. Agric. Food Chem. 2015, 63, 1869−1881

(52) Nakamura, K.; Kido, J.; Mitsubuchi, H.; Endo, F. Diagnosis and treatment of urea cycle disorders in Japan. *Pediatr. Int.* **2014**, *56*, 506−509.
(53) Ihara, K.; Miyako, K.; Ishimura, M.; Kuromaru, R.; Wang, H. Y.; Yasuda, K.; Hara, T. A case of hyperinsulinism/hyperammonaemia syndrome with reduced carbamoyl-phosphate synthetase-1 activity in liver: A pitfall in enzymatic diagnosis for hyperammonaemia. *J. Inherit. Metab. Dis.* **2005**, *28*, 681−687.
(54) Husson, A.; Brasse-Lagnel, C.; Fairand, A.; Renouf, S.; Lavoinne, A. Argininosuccinate synthetase from the urea cycle to the citruline−NO cycle. *Eur. J. Biochem.* **2003**, *270*, 1887−1899.
(55) Ficicioglu, C.; Mandell, R.; Shih, V. E. Argininosuccinate lyase deficiency: Long term outcome of 13 patients detected by newborn screening. *Mol. Genet. Metab.* **2009**, *98*, 273−277.
(56) Iyer, R. K.; Jenkinson, C. P.; Vockley, J. G.; Kern, R. M.; Grody, W. W.; Cederbaum, S. D. The human arginases and arginase deficiency. *J. Inherit. Metab. Dis.* **1998**, *1* (suppl. 21), 86−100.
(57) Iyer, R. K.; Yoo, P. K.; Kern, R. M.; Rozengurt, N.; Tsoa, R.; O'Brien, W. E.; Yu, H.; Grody, W. W.; Cederbaum, S. D. Mouse model for human arginase deficiency. *Mol. Cell. Biol.* **2002**, *22*, 4491−4498.
(58) Witze, E. S.; Old, W. M.; Resing, K. A.; Ahn, N. G. Mapping protein post-translational modifications with mass spectrometry. *Nat. Methods* **2007**, *4*, 798−806.
(59) van Kasteren, S. I.; Kramer, H. B.; Jensen, H. H.; Campbell, S. J.; Kirkpatrick, J.; Oldham, N. J.; Anthony, D. C.; Davis, B. G. Expanding the diversity of chemical protein modification allows post-translational mimicry. *Nature* **2007**, *446*, 1105−1109.

DOI: 10.1021/jf506118j
J. Agric. Food Chem. 2015, 63, 1869−1881

JOURNAL OF AGRICULTURAL AND FOOD CHEMISTRY

Addition/Correction

pubs.acs.org/JAFC

Correction to Supplementation of a High-Fat Diet with Chlorogenic Acid Is Associated with Insulin Resistance and Hepatic Lipid Accumulation in Mice

Aidilla Mubarak, Jonathan M. Hodgson, Michael J. Considine, Kevin D. Croft, and Vance B. Matthews*

J. Agric. Food Chem. **2013**, *61* (18), 4371−4378. DOI: 10.1021/jf400920x

Funding for the original paper was listed in error; the author wishes to retract any mention of funding support for the study reported.

Published: February 9, 2015

ACS Publications © 2015 American Chemical Society

DOI: 10.1021/acs.jafc.5b00621
J. Agric. Food Chem. 2015, 63, 1882−1882

Table 1. Content of Conjugated Fatty Acid in Food Sources

isomer	food source	concentration	comments	ref
CLA (mainly *cis*-9,*trans*-11)	ruminant meats	0.27−0.56%	U.S. foods	3
		0.11−1.20%	German foods	5
	dairy products	0.17−0.7%	U.S. foods	3
		0.34−0.80%	U.S. foods	6
		0.4−1.7%	German foods	5
		0.53−2.59%	Italian dairy products	7
		0.4−0.84%	Brazilian dairy products	8
		0.19−0.73%	U.K. cheese	9
		0.09−0.37%	U.K. non-cheese dairy products	9
		0.29−0.60%	U.K. meat products	9
		0.516−0.986%	Italian and French commercial cheeses	10
		0.128−0.976%	cow's, sheep's, and goat's milk yogurts from Greece	11
		approx 0.5−7 mg/g cheese	Canadian cheeses	12
		0.432−1.021%	cheeses from Italian	13
		nondetected to 0.933%	Spanish plain fermented milks	14
	plant oils	0.01−0.70%	U.S. foods	3
		nondetected	German foods	5
	seafood	0.03−0.06%	U.S. foods	3
	fish	0.01−0.09%	German foods	5
punicic acid	pomegranate seed	5.277−73.55%	Israel	15
		76.1%	China	16
		82.99%	Japan	17
	trichosanthes seed	32.27%	China	18
α-eleostearic acid	tung seed	67.69%	Japan	17
	bitter gourd seed	56.24%	Japan	17
		54.1%	China	16
		50.1−60.0%	India	19
	snake gourd seed	48.48%	Japan	17
		47.7%	India	19

Alternative splicing and differential promoter usage results in two isoforms of PPAR γ, PPAR γ1 and PPAR γ2, differing for the additional 28 amino acids in the N terminus present in PPAR γ2 and not in PPAR γ1.[24,25] PPAR γ1 is expressed generally in multiple tissues, including the lower intestine, macrophages, and white adipose tissue (WAT), whereas PPAR γ2 expression is almost exclusively restricted to WAT.[21] PPAR γ is a master regulator of adipogenesis as well as a potent modulator of insulin sensitivity, lipogenesis, and adipocyte survival and function.[26−28] Moreover, PPAR γ has been considered as a molecular target for cancer chemoprevention[29−31] and has been shown to be involved also in the regulation of genes contributing to hypertension and atherosclerosis.[32]

PPAR γ could exert pleiotropic effects by ligand-dependent transactivation of specific genes. Following ligand binding, the conformation of PPAR γ is changed and then causes the release of histone deacetylase corepressors, thus enabling PPAR γ to heterodimerize with RXR. RNA polymerase II and coactivators with histone acetyl transferase activity are then recruited to this complex, which binds to PPREs in the promoter region of the respective target genes, leading to chromatin remodeling and ultimately to increased transcription. On the other hand, PPAR γ can also down-regulate the expression of its target genes by interfering with other proteins and transcription factors such as nuclear factor kappa B (NF-κB) and activator protein-1 (AP-1) through a transrepression mechanism.[31,33] In addition to their transactivating and transrepressional activity, the PPAR family also exerts nongenomic actions, which are too rapid to involve gene expression modulation.[34]

The transcriptional activity of PPAR γ could be mediated by agonist and antagonist. Fatty acids and prostanoids, as the endogenous ligands for PPAR γ, can bind and activate PPAR γ.[35,36] However, they are weak agonists compared to the strong synthetic thiazolidinedione agonists with robust insulin-sensitizing activities.[37] The transcriptional activity of PPAR γ is also regulated by post-translational modifications including phosphorylation, sumoylation, and ubiquitination, providing additional possibilities for fine-tuning.[34]

MODULATION OF PPAR γ BY CLA IN OBESITY

The prevalence of obesity and its associated comorbidities has grown to epidemic proportions worldwide. Thus, developing safe and effective therapeutic approaches against these widespread and debilitating diseases is important and timely.[38] Since Park et al. (1997) demonstrated that CLA modulated body fat in mice, interest in CLA as a weight loss treatment has increased.[39] The antiobesity activity of CLA has been extensively studied, and multiple animal studies and some human studies have confirmed that supplementation with a CLA mixture (i.e., equal concentrations of the *trans*-10,*cis*-12 CLA and *cis*-9,*trans*-11 CLA isomers) or the *trans*-10,*cis*-12 CLA isomer alone decreases body fat mass.[4,40] Of the two major isomers of CLA, the *trans*-10,*cis*-12 CLA isomer is specifically responsible for the antiobesity effects[41−44] and mechanisms involved in its impact on energy metabolism, adipogenesis, inflammation, lipid

DOI: 10.1021/jf505050c
J. Agric. Food Chem. 2015, 63, 1883−1895

metabolism, and apoptosis.[43] In the present review, the regulation of adipogenesis, lipogenesis, and inflammation through modulation of PPAR γ by *trans*-10,*cis*-12 CLA (Figures 1 and 2) is discussed.

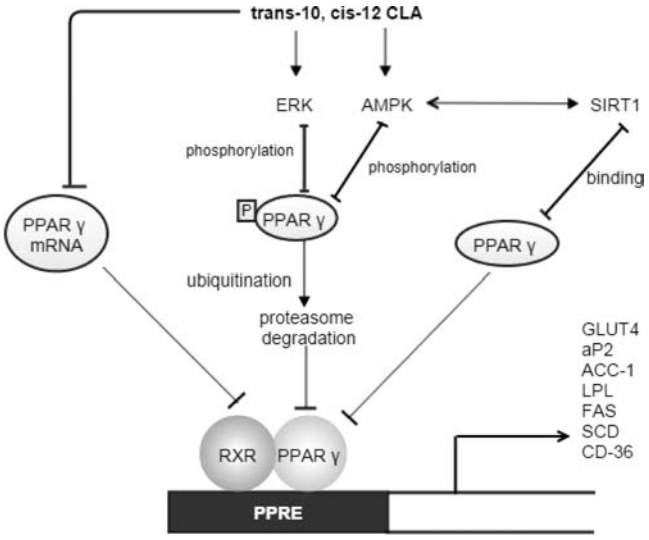

Figure 1. Proposed mechanism of action of CLA in adipogenesis and lipogenesis by modulation of PPAR γ. *trans*-10,*cis*-12 CLA reduced adipogenesis and lipogenesis by (1) regulating the expression PPAR γ and its target genes and (2) modulating the transactivating activity of PPAR γ, thereby reducing the expression of PPAR γ target genes. Ligand-dependent PPAR γ transactivating activity is antagonized by *trans*-10,*cis*-12 CLA, possibly via PPAR γ phosphorylation by ERK and AMPK. There is cross-regulation between SIRT1, AMPK, and PPAR γ. The transactivating activity of PPAR γ is attenuated by SIRT1 via binding directly or indirectly to PPAR γ. SIRT1 and AMPK activity are stimulated by one another and repressed by PPAR γ via a nontranscriptional mechanism.

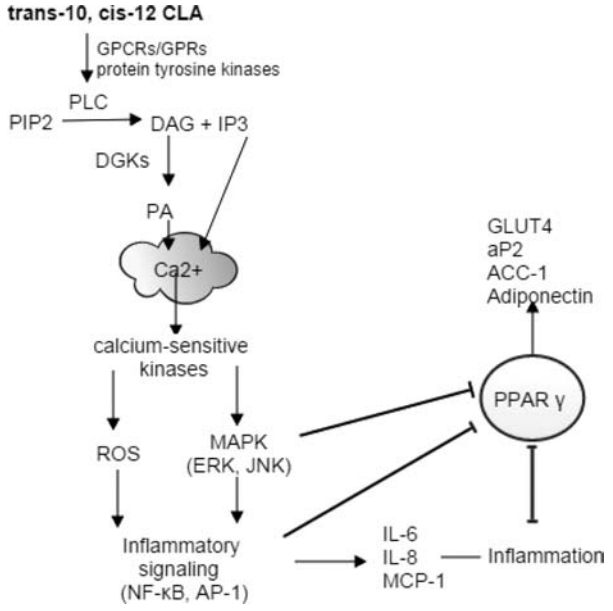

Figure 2. Proposed mechanism of action of CLA-mediated inflammation by modulation of PPAR γ. The *trans*-10,*cis*-12 CLA activates the specific cell surface receptors, including G protein coupled receptor, G protein receptor, or protein tyrosine kinases, and consequently stimulates the translocation of PLC to the plasma membrane, thereby generating DAG and IP3 from PIP2. DGKs convert DAG into PA and, together with IP3, stimulate calcium release from ER. Increased intracellular calcium accumulation activates calcium-sensitive kinases, such as CaMKII, which promotes ROS production and MAPK activation. MAPK subsequently activates inflammatory signaling, NF-κB, and AP-1. These inflammatory signals lead to a rise of secretion of inflammatory proteins, such as IL-6, IL-8, and MCP-1 and antagonize PPAR γ abundance and activity, thereby suppressing the expression of PPAR γ target genes and lipogenesis.

Regulation of Adipogenesis and Lipogenesis through PPAR γ by CLA. PPAR γ was originally described as a factor induced during adipocyte differentiation and function as a master regulator of adipocyte differentiation and metabolism.[26,45−47] Adipogenesis has been studied extensively in vitro, in particular using the murine 3T3-L1 preadipocyte cell line.[28,48−50] The regulation of adipogenesis through PPAR γ by CLA also has been investigated by using the 3T3-L1 preadipocyte cell line. CLA suppresses preadipocyte differentiation in animal[51−56] and human preadipocytes[57,58] by attenuating the expression and activity of adipogenic transcription factors such as PPAR γ and CAAT/enhancer binding protein α (C/EBP α).

PPAR γ is best known for its role in regulating adipogenic and lipogenic pathways[59] and is also crucial for controlling gene networks involved in lipid metabolism and glucose homeostasis, including adipocyte fatty acid binding protein (aP2),[60] insulin-dependent glucose transporter 4 (GLUT4),[61] lipoprotein lipase (LPL),[62] and the fatty acid translocase (CD-36/FAT).[63] *trans*-10,*cis*-12 CLA has been shown to reduce triglyceride (TG) accumulation in adipocyte cell culture models[42,52,53,64] and in the mouse[65] by attenuating the expression and activity of PPAR γ and its target genes such as LPL, acetyl-CoA carboxylase (ACC), fatty acid synthase (FAS), and stearoyl-CoA desaturase (SCD).

CLA and the Expression of PPAR γ and Its Target Genes. The expression of PPAR γ was decreased after *trans*-10,*cis*-12 CLA supplementation in rodents.[66−69] The expression and activity of PPAR γ and PPAR γ target genes and lipid content were also decreased substantially after *trans*-10,*cis*-12 CLA treatment in mature in vitro differentiated primary human adipocytes[51,70] or in mature 3T3-L1 adipocytes.[57] On the other hand, direct effects of CLA isomers on the PPAR γ expression were investigated by using a luciferase reporter assay system in a number of studies. These studies found that the *cis*-9,*trans*-11 CLA isomer was a PPAR γ agonist, whereas the *trans*-10,*cis*-12 CLA isomer appeared to be a partial antagonist or weak agonist.[58,64,71,72] However, Brown et al. showed that treatment with either *cis*-9,*trans*-11 CLA or *trans*-10,*cis*-12 CLA led to a slight decrease in luciferase activity by using 3T3-L1 cells transiently transfected with a luciferase reporter construct containing a PPRE, suggesting that these two isomers may antagonize PPAR γ activity in adipocytes.[58] There is no clear consensus regarding the activation or antagonism of PPAR γ by *trans*-10,*cis*-12 CLA, indicating that the way in which *trans*-10,*cis*-12 CLA affects PPAR γ expression is still unclear.

The inhibitory effect in PPAR γ-induced gene expression could be due to reduced PPAR γ expression or post-translational inhibition of PPAR γ activity per se.[43] Reduced PPAR γ activity could inhibit the expression of PPAR γ because PPAR γ directly or indirectly induces its own expression. Therefore, it is difficult to determine the levels at which inhibition occurs.[43]

CLA and the Activity of PPAR γ. PPAR γ activity can be modulated directly and indirectly at different levels (Figure 1). Several mechanisms are involved in the regulation of PPAR γ activity by supplementation with *trans*-10,*cis*-12 CLA. Phosphorylation, which can be mediated by the mitogen-activated protein

DOI: 10.1021/jf505050c
J. Agric. Food Chem. 2015, 63, 1883−1895

kinase (MAPK) pathway,[73,74] is the most investigated post-translational regulatory mechanism of PPAR γ.[21] The Ser82 in PPAR γ1 and Ser112 in PPAR γ2 in the mouse and the corresponding serines 84 and 114 in the human PPAR γ isoforms have been described to be phosphorylated by all MAPKs (extracellular signal-related kinase, ERK; cJun-NH2-terminal kinase, JNK, and p38), resulting in the inhibition of both ligand-dependent and -independent transactivation activity of the receptor.[21,34] Phosphorylation of PPAR γ may decrease its activity via ubiquitination and proteasome degradation.[75] Kennedy et al. demonstrated that 24 h of treatment with *trans*-10,*cis*-12 CLA increased PPAR γ phosphorylation and ERK 1/2 phosphorylation without significantly decreasing its protein levels, suggesting that the down-regulation of PPAR γ target genes is due to decreased transactivating activity in primary cultures of human adipocytes.[70] These suggested that *trans*-10,*cis*-12 CLA antagonizes ligand-dependent PPAR γ transactivating activity, possibly via PPAR γ phosphorylation by ERK.[70] A similar inhibitory effect on PPAR γ transactivating activity has been found for AMP-activated protein kinase (AMPK) via the phosphorylation of specific sites of PPAR γ.[76] AMPK was directly or indirectly responsible for the increased phosphorylation at Ser112 of PPAR γ in *trans*-10,*cis*-12 CLA treated adipocytes.[77]

The activity of PPAR γ could also be modulated by sirtuin 1 (SIRT1). SIRT1, a histone/protein deacetylase, is particularly involved in regulating cell energy metabolism, cell stress, and cell fate.[78] SIRT1 could directly bind directly or indirectly to PPAR γ to repress PPAR γ transactivating activity, inhibit adipogenesis, and promote fat loss in adipocytes.[79] After treatment with *trans*-10,*cis*-12 CLA, cross-regulation between SIRT1, AMPK, and PPAR γ occurred in 3T3-L1 adipocytes.[77] SIRT1 stimulated AMPK activity and attenuated PPAR γ activity, whereas AMPK stimulated SIRT1 activity and attenuated PPAR γ activity in *trans*-10,*cis*-12 CLA treated 3T3-L1 adipocytes. That PPAR γ has a repressive effect on the activities of AMPK and SIRT1, which is consistent with the opposing roles of PPAR γ in stimulating lipid biosynthesis and the catabolic energy-generating roles of AMPK and SIRT1.[51,80] PPAR γ achieved these inhibitory effects via a nontranscriptional mechanism because PPAR γ affected the activity levels of SIRT1 and AMPK without changing the total amounts of these proteins in the response to *trans*-10,*cis*-12 CLA. Besides the well-known transactivating and transrepressional activity of PPAR γ, these results suggested an emerging role for PPAR γ in regulating nongenomic processes.[34,81]

Regulation of Obesity-Related Inflammation through PPAR γ by CLA. *CLA and Obesity-Related Inflammation.* To date there is no clear consensus regarding anti-inflammatory effects of CLA. It is likely that the effects of CLA on inflammation of adipose tissue are isomer-dependent. *cis*-9,*trans*-11 CLA reduces adipose tissue inflammation in ob/ob mice,[82] whereas *trans*-10,*cis*-12 CLA reduces adiposity without improving or worsening insulin resistance and adipose tissue inflammation in hamsters and mice.[67,83]

Obesity is characterized by a chronic low-grade inflammation, primarily due to an imbalance between production/secretion of pro-inflammatory cytokines versus anti-inflammatory cytokines.[84] Adipose tissue is not simply an energy reservoir, thermal regulator, or protective padding for important organs but also a metabolically active endocrine organ.[85] Adipose tissue has the ability to produce a number of pro-inflammatory adipokines including tumor necrosis factor-alpha (TNF-α), interleukin-1 beta (IL-1β), interleukin-2 (IL-2), interleukin-6 (IL-6), interleukin-8 (IL-8), monocyte chemoattractant protein-1 (MCP-1), plasminogen activator inhibitor-1 (PAI-1), and resistin.[86,87] Adipose tissue can also produce anti-inflammatory cytokines such as adiponectin and interleukin-10 (IL-10).[87] These pro-inflammatory adipokines produced by adipose tissue can cause insulin resistance, thereby suppressing lipid synthesis and increasing lipolysis in adipocytes.[43]

The expression of PPAR γ and its target genes could be directly down-regulated by *trans*-10,*cis*-12 CLA supplementation. In contrast, PPAR γ and its target genes also could be indirectly inhibited by cytokines induced by *trans*-10,*cis*-12 CLA.[62,84−86] ERK[57] and NF-κB[67,88] in adipocytes could be activated by *trans*-10,*cis*-12 CLA supplementation and, consequently, these signaling pathways increased the expression or secretion of cytokines, for example, IL-6 and IL-8[57,67,68,70,88] and TNF-α and IL-1β,[89] which are known to antagonize PPAR γ target gene expression and insulin sensitivity.[69,90−92]

trans-10,*cis*-12 CLA supplementation increased PGF 2α secretion in human adipocytes in vitro.[93] *trans*-10,*cis*-12 CLA treatment also increased the levels of inflammatory prostaglandins (PGs) and C-reactive protein in humans in vivo.[94] Supplementation with an oil mixture with *trans*-10,*cis*-12 CLA (5.5 g/day for 16 weeks) exhibited higher levels of C-reactive protein in serum and 8-iso-PGF 2α in urine of healthy postmenopausal women, compared with *cis*-9,*trans*-11 CLA.[94] Inflammatory PGs such as PGF 2α have been reported to block adipogenesis through activation of MAPK, resulting in inhibitory phosphorylation of PPAR γ in 3T3-L1 preadipocytes.[95] PGF 2α has also been demonstrated to inhibit adipogenesis through normoxic activation of the hypoxia-inducible factor-1 (HIF-1) signaling pathway during 3T3-L1 preadipocyte differentiation under normal oxygen conditions.[96] HIF-1 decreases the expression of PPAR γ and C/EBP α via the increased expression of the DEC1 transcriptional repressor.[97] In addition, PGF 2α could inhibit adipogenesis by activating pro-inflammatory transcription factors that can antagonize PPAR γ.[43]

CLA and Inflammatory Signaling Cascade. The inflammatory signaling cascade is also involved in CLA-reduced adiposity (Figure 2). *trans*-10,*cis*-12 CLA mediated suppression of adipogenesis and lipogenesis and adipocyte delipidation were dependent on inflammatory signaling[57,88,98] and linked to endoplasmic reticulum (ER) release of calcium and increased intracellular calcium ($[Ca^{2+}]$ i) accumulation.[99] Up-regulation of inflammatory pathways by *trans*-10,*cis*-12 CLA increased the activities of NF-κB, AP-1, and MAPK,[57,88,98] which led to inhibition of PPAR γ abundance and activity,[58,70,100] reduction of glucose and fatty acid uptake, and de novo lipogenesis.[42,57,58] The molecular mechanisms by which NF-κB inhibits PPAR γ activity are not completely understood. However, unlike suppression of the PPAR γ transactivating activity by MAPK-induced growth factor signaling through phosphorylation of PPAR γ, NF-κB blocked PPAR γ binding to DNA by forming a complex with PPAR γ and its AF-1-specific coactivator PGC-2 in the bone marrow stromal cell line ST2.[90]

Up to now, the upstream signals activated by *trans*-10,*cis*-12 CLA that initiate this inflammatory signaling cascade were investigated by a number of studies.[99,101−103] One possible upstream mediator of *trans*-10,*cis*-12 CLA induced inflammation is $[Ca^{2+}]$ i, which is a vital second messenger for the activation of proteins involved in adipocyte proliferation, differentiation, and metabolism.[101] *trans*-10,*cis*-12 CLA increased $[Ca^{2+}]$ i levels, leading to the production of reactive oxygen species (ROS), NF-κB, JNK, ERK1/2, and, ultimately, the induction of inflammatory

DOI: 10.1021/jf505050c
J. Agric. Food Chem. 2015, 63, 1883−1895

Table 2. Effect of Conjugated Fatty Acids on Inflammatory Bowel Disease[a]

isomer (purity)	model	dose and duration	effects	ref
CLA				
CLA mixture (*cis*-9,*trans*-11/*trans*-9,*cis*-11, 12.36%; *trans*-11,*trans*-10,*cis*-12/*cis*-10,*trans*-12, 13.30%; *trans*-9,*trans*-11, 13.32%; other CLA isomers, 12.99%)	(1) pigs challenged with *Brachyspira hyodysenteria* (2) pigs immunized with proteinase-digested *Brachyspira hyodysenteria* bacteria	1.33 wt % diet, 72 days	↓ enlargement of the colonic mucosa ↓ mucosal damage	124
50:50 mixture of *cis*-9,*trans*-11 and *trans*-10,*cis*-12 CLA isomers	early weaned pigs with DSS-induced colitis	2.21 wt % diet, 42 days	↓ onset of IBD ↓ colitis severe ↓ growth suppression	117
50:50 mixture of *cis*-9,*trans*-11 and *trans*-10,*cis*-12 CLA isomers	(1) C57BL/6J mice with DSS-induced colitis (2) C57BL/6J mice with $CD4^+CD45RB^{hi}$ transfer colitis	1 wt % diet, 42 days	↓ disease activity ↓ tissue damage ↓ colitis	116
50:50 mixture of *cis*-9,*trans*-11 and *trans*-10,*cis*-12 CLA isomers	female BALB/c mice with DSS-induced colitis	100 mg/kg/day, 7 days	↓ colon shortening ↓ disease activity index	127
50:50 mixture of *cis*-9,*trans*-11, and *trans*-10,*cis*-12 CLA isomers	C57BL/6 mice treated with azoxymethane and then challenged with 2% DSS	1 wt % diet, 42 days	↓ disease activity ↓ colitis ↓ adenocarcinoma formation	125
(1) 50:50 mixture of *cis*-9,*trans*-11, *trans*-10,*cis*-12 CLA isomers	C57BL6 mice with DSS induced-colitis	1 wt % diet, 24 days	↓ disease activity ↓ colitis	126
(2) VSL#3		0.0072 g VSL#3, 24 days	↓ colonic bacterial diversity ↓ macrophage accumulation	
50:50 mixture of *cis*-9,*trans*-11, and *trans*-10,*cis*-12 CLA isomers (capsules, 77.7%)	patients with mild to moderate Crohn's disease	6 g/day CLA, 12 weeks	↓ disease activity ↑ quality of life of patients	128
CLNA				
PUA-enriched PSO (ND)	male Wistar rats with TNBS-induced colitis	2 wt % diet, 10 days	↓ ulceration status and tissue damage	106
pure PUA	male Wistar rats with TNBS-induced colitis	400 μg/day, 10 days	↓ ulceration status and tissue damage	106
PUA-enriched PSO (71%)	IL-10−/− model mice with spontaneous pan-enteritis	1 wt % diet, 42 days	↓ lymphoplasmacytic infiltration ↓ enlargement of the colonic mucosa	155
PUA-enriched PSO (71%)	C57BL/6J mice with DSS-induced colitis	1 wt % diet, 42 days	↓ experimental IBD	155
PUA-enriched PSO (ND)	neonatal Sprague−Dawley rats with induced NEC	1.5 wt % diet, 96 h	↓ incidence of NEC from 61 to 26% ↓ necrotizing colitis severity	156
α-ESA-enriched BGO (ND)	C57BL/6J mice with DSS-induced colitis	not mentioned, 42 days	↓ disease activity ↓ IBD-related disease phenotypes	160

[a]PSO, pomegranate seed oil; BGO, bitter melon seed oil; PUA, punicic acid; α-ESA, α-eleostearic acid; IBD, inflammatory bowel disease; NEC, necrotizing enterocolitis; ND, not determined. Δ change; ↓ decrease.

genes and PGs and insulin resistance in human adipocytes.[99] Possible upstream signals of *trans*-10,*cis*-12 CLA mediated increased $[Ca^{2+}]$ i and inflammation included phospholipase C (PLC)[102] and diacylglycerol kinases (DGKs).[103] PLC, as an upstream enzyme that produces diacylglycerol (DAG), a substrate for DGK, and inositol-3-phosphate (IP3), an inducer of calcium release from the ER, was found to play an important role in *trans*-10,*cis*-12 CLA mediated activation of $[Ca^{2+}]$ i accumulation, inflammatory signaling, delipidation, and insulin resistance in human primary adipocytes.[102] DGKs are a family of kinases that phosphorylate DAG, resulting in the conversion of DAG into phosphatidic acid (PA). DAG and PA acted as second messengers that activated an array of target proteins, resulting in significant changes in cellular signaling.[104] DGKs, particularly DGK η, may also be involved in the regulation of *trans*-10,*cis*-12 CLA mediated inflammatory signaling, insulin resistance, and delipidation in primary human adipocytes.[103] On the basis of the studies by Shen et al. and Martinez et al., the mechanism of CLA-mediated inflammation and PPAR γ activity could be proposed (Figure 2).[102,103] *trans*-10,*cis*-12 CLA may activate the specific cell surface receptors, including G protein coupled receptor, G protein receptor, or protein tyrosine kinases, and consequently stimulate the translocation of PLC to the plasma membrane, thereby generating DAG and IP3 from PIP2. DGKs convert DAG into PA and, together with IP3, stimulate calcium release from ER. Increased intracellular calcium accumulation activates calcium-sensitive kinases, such as CaMKII, which promotes ROS production and MAPK activation. MAPK subsequently activates inflammatory signaling, NF-κB and AP-1. These inflammatory signals lead to a rise of secretion of inflammatory proteins, such as

DOI: 10.1021/jf505050c
J. Agric. Food Chem. 2015, 63, 1883−1895

IL-6, IL-8, and MCP-1, and antagonizes PPAR γ abundance and activity, thereby suppressing insulin-stimulated glucose uptake and lipogenesis.[102,103]

MODULATION OF PPAR γ BY CLA IN IBD

Inflammatory disorders including IBD, rheumatoid arthritis, atherosclerosis, metabolic syndrome, and ischemia/reperfusion injury are recognized as a major health problemd worldwide.[105] One common characteristic of these diseases is excessive production of pro-inflammatory mediators such as TNF-α, GM-CSF, IL-1, IL-6, IL-8, leukotriene B4, and PAF; the presence of highly activated inflammatory cells such as neutrophils, monocytes, and macrophages; and excessive production of ROS.[106] IBD is characterized by inflammation of the gastrointestinal tract and the most common IBD including ulcerative colitis and Crohn's disease and some atypical forms such as collagenous colitis and intractable colitis. Conventional therapies for IBD patients are represented by salicylates, steroids, immunosuppressants, and anti-TNF-α drugs. However, conventional therapies showed variable response rates and potential side effects. IBD patients tend not to adhere to conventional pharmacological therapy, mainly due to the fear of long-term side effects.[107] Thus, exploring novel therapeutic and preventive approaches for IBD is important and increasingly interesting.[108,109]

PPARs are the receptors for endogenous lipid molecules representing promising new targets for the treatment and prevention of inflammatory disorders such as IBD. The colon is a major tissue that expresses PPAR γ in epithelial cells and, to a lesser degree, in macrophages and lymphocytes. PPAR γ plays a role in the regulation of intestinal inflammation. Animal studies suggested that PPAR γ ligands have beneficial effects in different models of experimental colitis, with possible implications in the therapy of IBD.[109] Synthetic PPAR γ ligands such as troglitazone and rosiglitazone, have been proven effective in rodent models of IBD,[110,111] and their therapeutic efficacy is being tested in IBD clinical trials.[112,113] However, the universal application of rosiglitazone or rosiglitazone for the management and treatment of IBD is unlikely due to the reported serious side effects such as weight gain, increased bone fracture, fluid retention, and heart failure.[114] Interestingly, the use of dietary supplements such as CLA, CLNA, and probiotics (VSL#3) has proved beneficial on animal models of intestinal inflammation through the activation of PPAR γ.[115]

CLA has potent immunomodulatory effects in a wide range of inflammatory-based disorders including IBD,[116,117] atherosclerosis,[118,119] and diabetes.[120,121] The potent immunomodulatory effect of CLA is exhibited in an isomer-specific manner. Evidence suggested that *cis*-9,*trans*-11 CLA is responsible for the anti-inflammatory effect attributed to CLA, whereas *trans*-10,*cis*-12 CLA appears to be responsible for antiadipogenic effects.[122] The anti-inflammatory potential of *cis*-9,*trans*-11 CLA has been demonstrated in animal models of IBD and human study. For animal studies of IBD, two main standardized methods are used to produce an experimental animal model of IBD: (1) oral administration of dextran sulfate sodium (DSS) in drinking water; (2) intracolonic administration of trinitrobenzenesulfonic acid (TNBS).[123] A number of studies showed that CLA ameliorates experimental IBD in mice and pigs (Table 2).[116,117,124−127] CLA also was shown to ameliorate the IBD in humans. In this open-label study, oral CLA administration (6 g/day, 50:50 mixture of the *cis*-9,*trans*-11,*trans*-10,*cis*-12 CLA isomers) was well tolerated and suppressed the ability of peripheral blood T cells to produce pro-inflammatory cytokines, decreased disease onset, and increased the quality of life of patients with mild to moderate Crohn's disease.[128]

The protective effect of CLA against IBD could be mediated though PPAR γ activation.[116,124] Dietary CLA supplementation suppressed colonic inflammation and up-regulated colonic PPAR γ expression in pigs with bacterial-induced colitis.[124] Activation of colonic PPAR γ by CLA mediated protection from experimental IBD in mice with a targeted deletion of PPAR γ in immune and epithelial cells.[116] Furthermore, dietary CLA ameliorated disease activity, decreased colitis, and prevented adenocarcinoma formation in the PPAR γ-expressing floxed mice but not in the tissue-specific PPAR γ-null mice, suggesting that CLA ameliorates colitis and prevents tumor formation in part through a PPAR γ-dependent mechanism.[125] Indeed, besides induction of PPAR γ in vivo, other studies confirmed the increase of PPAR γ expression and activity in adipocytes,[129] skeletal muscle,[130] and macrophages[131,132] with CLA or CLA-rich diets. In contrast to the reduction in PPAR γ expression by *trans*-10,*cis*-12 CLA, treatment with *cis*-9,*trans*-11 CLA or mixtures of *cis*-9,*trans*-11 CLA and *trans*10,*cis*-12 CLA activated the expression of PPAR γ. This may be due to cell-type specificity of the response to CLA or isomer specificity because the *trans*-10,*cis*-12 CLA was able to reduce PPAR γ expression in adipocytes, but the *cis*-9,*trans*-11 CLA failed to show the same suppressive effect on PPAR γ activity.[133]

Trefoil peptides (TFF) were found to be involved into CLA-mediated DSS-induced colitis.[127] TFFs are small protease-resistant proteins characterized by a conserved cysteine-rich domain and comprise the gastric peptide (TFF1), the spasmolytic peptide (TFF2), and the intestinal trefoil factor (TFF3).[134] TFFs could be involved in IBD pathogenesis, and they could be a potential treatment option.[135] The colonic levels of TFF3 was increased after dietary supplementation of CLA-enriched diet, and the activation of TFF3 by CLA is mediated by PPAR γ, suggesting that the DSS-induced injury in mice is ameliorated by CLA through the colonic activation of PPAR γ, which in turn will increase the levels of TFF3.[127]

Interestingly, VSL#3 probiotic bacteria produce CLA locally in the gut and were shown to suppress colitis by targeting macrophage PPAR γ.[126] VSL#3 is a multistrain, high-potency probiotic preparation composed of four strains of lactobacilli (*Lactobacillus casei*, *Lactobacillus plantarum*, *Lactobacillus bulgaricus*, and *Lactobacillus acidophilus*), three strains of bifidobacteria (*Bifidobacterium longum*, *Bifidobacterium breve*, and *Bifidobacterium infantis*), and *Streptococcus thermophilus*. VSL#3 has been demonstrated to ameliorate colitis,[126] prevent colitis-associated colorectal cancer in animal models of colitis,[136,137] and induce remission in patients with ulcerative colitis.[138,139] VSL#3 treatment could produce *cis*-9,*trans*-11 CLA in vivo,[126,140] and a high concentration of *cis*-9,*trans*-11 CLA was found only in the mouse colon, but without systemic distribution in blood.[126] The loss of PPAR γ in myeloid cells abrogated the protective effect of VSL#3 and CLA in mice with DSS colitis, suggesting that PPAR γ possibly plays a vital role in VSL#3 and CLA amelioration of the colitis in mice. VSL#3 could suppress intestinal inflammation by altering colonic microbial diversity and enhancing microbial CLA production locally that in turn activates PPAR γ.[126] The CLA-producing probiotics may offer an alternative approach to conventional therapy in IBD by altering the intestinal microflora and enhancing CLA concentration; further exploration of the role of these bacteria in preventing human IBD is encouraged.

DOI: 10.1021/jf505050c
J. Agric. Food Chem. 2015, 63, 1883−1895

Table 3. Effect of the Conjugated Linolenic Acid on Obesity[a]

isomer (purity)	model	dose and duration	effects	ref
conjugated linolenic acid mixtures (49.1%)	male Sprague−Dawley rats	1.0 wt % diet, 4 weeks	↓ perirenal and epididymal adipose tissue weight	141
PUA-enriched PSO (ND)	male OLETF obese rats	1.0 wt % diet, 2 weeks	↓ omental white adipose tissue weight (27%) no Δ abdominal white adipose tissue	142
PUA-enriched PSO (approximately 80%)	male ICR CD-1 mice	0.5 wt % diet, 4 weeks	↓ perirenal and epididymal adipose tissue weight	143
genetically modified rapeseed oil containing PUA (2.5%)	male ICR CD-1 mice	0.25 wt % diet, 4 weeks	↓ perirenal and epididymal adipose tissue weight	143
PUA-enriched PSO (64.79%)	male CD-1 mice with high-fat feeding	61.79 mg/day PSO, 14 weeks	↓ body weight ↓ weight gain	144
PUA-enriched PSO (ND)	male C57BL/6J mice with diet-induced obesity	1% PSO wt diet, 12 weeks	↓ body weight ↓ body fat mass	145
α-ESA-enriched BGO (50%)	male C57BL/6J mice with diet-induced obesity	7.5 wt % diet, 5 weeks	↓ 21% body fat	146
α-ESA-enriched BGO (50%)	male C57BL/6J mice with diet-induced obesity	2.5, 5, and 7.5 wt % diet, 11 weeks	↓ 32, 35, and 65% of body fat	147
PUA-enriched PSO (70%) or α-ESA-enriched tung seed oil (70%)	male Golden Syrian hamsters	1.22−1.27 wt % diet, 6 weeks	no Δ body weight	148
α-ESA-enriched BGO (54.1%) or PUA-enriched PSO (76.1%)	male ICR mice	1 wt % diet, 6 weeks	no Δ body weight no Δ perirenal or epididymal adipose tissues	149
PUA-enriched PSO (ND)	male Wistar rats fed an obesogenic diet	0.5 wt % diet, 6 weeks	no Δ body weight no Δ white adipose tissue or interscapular brown adipose tissue weights	150

[a]PSO, pomegranate seed oil; BGO, bitter melon seed oil; PUA, punicic acid; α-ESA, α-eleostearic acid; ND, not determined; change; ↓ decrease.

MODULATION OF PPAR γ BY CLNA IN OBESITY

The effect of CLNA isomers on body weight showed inconsistent outcomes in animal obesity models (Table 3). CLNA mixtures prepared by alkaline isomerization reduced perirenal adipose tissue weight to a larger extent when compared with linoleic acid, CLA, and α-linolenic acid in Sprague−Dawley rats.[141] A PUA-enriched pomegranate seed oil (PSO) dietary supplement also reduced omental WAT weights, but not abdominal WAT weights in obese and hyperlipidemic OLETF rats.[142] Supplementation with PSO or genetically modified rapeseed oil containing PUA decreased the weight of perirenal adipose tissue in ICR CD1 mice in a dose-dependent manner.[143] Dietary supplementation with 61.79 mg/day of PSO significantly lowered the body weight and weight gain in mice with high-fat feeding, compared with the control.[144] In another study, dietary supplementation with 1% of PSO ameliorated high-fat diet induced obesity and insulin resistance in mice, independent of changes in food intake or energy expenditure.[145] Supplementation with α-ESA enriched bitter gourd seed oil (BGO) was shown to be more potent than soybean oil in attenuating high-fat diet induced body fat deposition in mice.[146,147]

In contrast, dietary supplementation with 1.22−1.27 or 1% of CLNA (α-ESA or PUA) for 6 weeks did not significantly change the body weight of hamsters or mice, respectively.[148,149] A recent paper also showed that dietary supplementation of 0.5% of PUA did not lead to decreased fat accumulation in adipose tissue, liver, or skeletal muscle when rats were fed an obesogenic diet.[150]

The potential mechanism by which CLNA isomers exert the antiobesity effect is not clear. Because *cis*-9,*trans*-11 CLA has no antiadiposity activity,[2,43] the antiadiposity potential of PUA and α-ESA cannot be attributed to CLA derived from α-ESA in vivo, because PUA and α-ESA are proved to be metabolized into *cis*-9,*trans*-11 CLA, rather than *trans*-10,*cis*-12 CLA.[151,152] PUA, α-ESA, and *trans*-10,*cis*-12 CLA might share a common metabolic or signaling pathway, leading to a qualitatively similar outcome in the WAT.[147] Similarly to *trans*-10,*cis*-12 CLA, CLNAs might exert their antiadiposity effect by induction of the expression or secretion of cytokines and inhibition of adipogenesis and preadipocyte differentiation through the regulation of PPAR γ.[141,146,153,154] BGO and CLNA mixtures were shown to elevate the TNF-α level in C57BL/6J mice with diet-induced obesity and Sprague−Dawley rats,[141,146] respectively, which are known to antagonize PPAR γ target gene expression.[90] PSO was also shown to inhibit the adipogenesis and differentiation and decrease the protein level of PPAR γ in 3T3-L1 preadipocytes.[153] Moreover, sustained activation of the ERK/MAPK signaling pathway, accompanied by PPAR γ phosphorylation, caused by α-ESA in the 3T3-L1 cell differentiation model might not only contribute to apoptosis but also have an inhibitory effect on adipogenesis.[154]

MODULATION OF PPAR γ BY CLNA IN IBD

PUA and IBD. Several in vivo studies assessed the anti-inflammatory effects of PSO and PUA on IBD intestinal inflammation and the model of necrotizing enterocolitis (NEC) (Table 2). Oral administration of pure PUA (400 μg/day) or 0.5 mL/day of PUA-enriched PSO for 10 days before TNBS injection in a colitis rat model ameliorated ulceration status and tissue damage, limiting neutrophil activation and lipid peroxidation.[106] Supplementation with 1% of dietary PUA ameliorated spontaneous pan-enteritis in an IL-10$^{-/-}$ mouse model of IBD for 42 days and in mice with experimental IBD during a 7 day challenge with DSS.[155] PSO has also been shown to be effective in a model of NEC. Oral administration with 1.5% of PSO decreased the incidence of NEC from 61 to 26% and the severity of necrotizing colitis, protecting the epithelial barrier and preserving the intestinal integrity in a neonatal model of NEC rats.[156] These results suggested that PUA- or PUA-enriched PSO could ameliorate intestinal inflammation and damage.

The underlying mechanisms by which PUA ameliorates experimental IBD are incompletely understood. Similarly to *cis*-9,*trans*-11 CLA, PUA was suggested as a potential PPAR γ agonist.[155,157,158] PUA was shown to robustly bind and activate PPAR γ, therefore increasing PPAR γ-responsive gene expression and ameliorating diabetes and gut inflammation.[159] PUA ameliorated spontaneous pan-enteritis in IL-10$^{-/-}$ mice and

DOI: 10.1021/jf505050c
J. Agric. Food Chem. 2015, 63, 1883−1895

DSS colitis, up-regulated Foxp3 expression in T-cells, and suppressed TNF-α, but the loss of functional PPAR γ or δ impaired these anti-inflammatory effects. The deletion of PPAR γ in macrophages completely abrogated the amelioration effect of PUA on experimental colitis, whereas the deletion of PPAR δ or intestinal epithelial cell-specific PPAR γ decreased its anti-inflammatory efficacy. These results strongly suggested that PUA ameliorates experimental IBD by regulating macrophage and T-cell function through PPAR γ- and δ-dependent mechanisms.[155]

α-ESA and IBD. α-ESA was also identified as a natural PPAR γ agonist by using complementary computational and experimental methods and found to be effective in ameliorating disease-associated phenotypes in mice with DSS colitis.[160] Activation of PPAR γ by α-ESA could play an important role in amelioration of DSS-induced IBD. The anti-inflammatory actions of α-ESA may be both PPAR γ-dependent and -independent responses that ameliorated disease activity and intestinal lesions in mice with DSS colitis.[160]

Targeting PPAR γ represents a promising avenue for developing novel prophylactic and therapeutic interventions for IBD[161,162] and obesity.[163] Due to the side effects of full thiazolidinedione agonists of PPAR γ, there is a demand for naturally occurring PPAR γ modulators from edible items with minimum adverse effect and high tolerance to the human body.[164] *trans*-10,*cis*-12 CLA has demonstrated antiobesity effects through regulation of expression and activity of PPAR γ, which is involved in reducing adipogenesis and lipogenesis and increasing inflammation. CLA (*cis*-9,*trans*-11 CLA or mixtures of *cis*-9,*trans*-11 and *trans*-10,*cis*-12 CLA) was also effective in ameliorating the experimental IBD though activation of PPAR γ. However, the safety of CLA is still of utmost concern and has been evaluated in numerous animal studies and human clinical trials.[4] A minority of studies have reported ambiguous or deleterious effects of CLA supplementation with regard to liver functions, milk fat depression, insulin resistance, and oxidative markers.[94,165−167] Although the safety of Clarinol and Tonalin TG 80, two oils with approximately 80% of the CLA 50:50 mixture of *cis*-9,*trans*-11 and *trans*-10,*cis*-12 isomers, has been established for the proposed uses and daily doses (3.75 g of Clarinol and 4.5 g of Tonalin TG 80 corresponding to approximately 3 and 3.5 g of CLA, respectively) for up to 6 months by the EFSA Panel on Dietetic Products, Nutrition and Allergies. However, the safety of CLA consumption for periods >6 months has not been established under the proposed conditions of use.[168] These observations must be carefully considered, and further investigation is necessary before the widespread use of CLA as a functional food component.

PUA and α-ESA, which were identified as natural agonists of PPAR γ, have proven beneficial effect on animal models of intestinal inflammation. PUA and α-ESA also exerted an antiadiposity effect through regulation of PPAR γ. Acute toxicological studies have demonstrated that PUA is safe in rats.[169] Therefore, these plant-derived natural products are safer and may open the possibility to be used as functional foods and nutraceuticals. However, the exact mechanism by which PUA and α-ESA exert their physiological roles and human intervention studies are necessary to determine their beneficial effects on individuals with obesity or IBD.

In summary, CLA (*cis*-9,*trans*-11 CLA and *trans*-10,*cis*-12 CLA) and CLNA (PUA and α-ESA) play an important role in modulating the expression or activity of PPAR γ and that could in turn be employed as complementary treatment for obesity and IBD. Available evidence suggested that *trans*-10, *cis*-12 CLA reduces adipogenesis and lipogenesis in adipocytes and rodents by (1) regulating the expression PPAR and PPAR γ target genes and (2) modulating the transactivating activity of PPAR γ. Ligand-dependent PPAR γ transactivating activity is antagonized by *trans*-10,*cis*-12 CLA, possibly via PPAR γ phosphorylation by ERK and AMPK. The transactivating activity of PPAR γ could also be modulated by SIRT1 via binding directly or indirectly to PPAR γ in adipocyte. In addition, up-regulation of inflammatory signaling pathways by *trans*-10,*cis*-12 CLA increases the expression or secretion of cytokines and the activity of NF-κB, AP-1, and MAPK, which lead to inhibition of PPAR γ abundance and activity. Besides their antiobesity effect, CLAs also ameliorate experimental IBD through activation of PPAR γ. PUA and α-ESA are identified as natural agonists of PPAR γ and exert beneficial effects on animal models of intestinal inflammation through the activation of PPAR γ. In addition, PUA and α-ESA might exert their antiadiposity effect by induction of cytokine and inhibition of adipogenesis and preadipocyte differentiation through regulation of PPAR γ.

Some issues remain to be resolved before CLAs and CLNAs can be recommended to humans with confidence to improve health and quality of life, particularly regarding mechanisms and safety concerns. More well-controlled clinical trials with defined subject characteristics, study duration, and doses and preparations on the safety and physiological effects are urgently needed. Moreover, further studies are necessary to identify the diversified molecular signaling pathways and the crosstalk among these signaling pathways mediated by CLAs and CLNAs to provide valuable information on the efficacy, specificity, and potential side effects of CLAs and CLNAs.

AUTHOR INFORMATION

Corresponding Author

*(D.L.) Mail: Department of Food Science and Nutrition, Zhejiang University, 866 Yuhangtang Road, Hangzhou 310058, China. Phone: 86-571-8898 2024. Fax: 86-571-8898 2024. E-mail: duoli@zju.edu.cn.

Funding

The manuscript reports one of the studies funded by the Natural Science Foundation of Zhejiang Province (LY14C200004 and LY12C20007); G.Y. is the principal investigator.

Notes

The authors declare no competing financial interest.

ABBREVIATIONS USED

AMPK	AMP-activated protein kinase
ACC	acetyl-CoA carboxylase
AP-1	activator protein-1
aP2	adipocyte fatty acid binding protein
BGO	nitter gourd seed oil
CD-36/FAT	fatty acid translocase
C/EBP α	CAAT/enhancer binding protein α
CFA	conjugated fatty acid
CLA	conjugated linoleic acid
CLNA	conjugated linolenic acid
DAG	diacylglycerol
DGK	diacylglycerol kinases
DSS	dextran sulfate sodium
ER	endoplasmic reticulum
ERK	extracellular signal-related kinase
α-ESA	α-eleostearic acid
FAS	fatty acid synthase

DOI: 10.1021/jf505050c
J. Agric. Food Chem. 2015, 63, 1883−1895

GLUT4	insulin-dependent glucose transporter 4
HIF-1	hypoxia-inducible factor-1
IBD	inflammatory bowel disease
IL-1β	interleukin-1 beta
IL-2	interleukin-2
IL-6	interleukin-6
IL-8	interleukin-8
IL-10	interleukin-10
IP3	inositol-3-phosphate
JNK	cJun-NH_2-terminal kinase
MAPK	mitogen-activated protein kinase
MCP-1	monocyte chemoattractant protein-1
NEC	necrotizing enterocolitis
NF-κB	nuclear factor kappa B
PUA	punicic acid
PA	phosphatidic acid
PAI-1	plasminogen activator inhibitor-1
PLC	phospholipase C
PGs	prostaglandins
PPRE	PPAR-responsive regulatory element
PPAR	peroxisome proliferator-activated receptor
PSO	pomegranate seed oil
ROS	reactive oxygen species
SCD	stearoyl-CoA desaturase
SIRT1	sirtuin 1
TNF-α	tumor necrosis factor-α
TFF	trefoil peptides
TFF1	gastric peptide
TFF2	spasmolytic peptide
TFF3	intestinal trefoil factor
TG	triglyceride
TNBS	trinitrobenzenesulfonic acid
$[Ca^{2+}]$ i	intracellular calcium

REFERENCES

(1) Yuan, G. F.; Chen, X. E.; Li, D. Conjugated linolenic acids and their bioactivities: a review. *Food Funct.* **2014**, *5*, 1360−1368.

(2) Bhattacharya, A.; Banu, J.; Rahman, M.; Causey, J.; Fernandes, G. Biological effects of conjugated linoleic acids in health and disease. *J. Nutr. Biochem.* **2006**, *17*, 789−810.

(3) Chin, S. F.; Liu, W.; Storkson, J. M.; Ha, Y. L.; Pariza, M. W. Dietary sources of conjugated dienoic isomers of linoleic acid, a newly recognized class of anticarcinogens. *J. Food Compos. Anal.* **1992**, *5*, 185−197.

(4) Dilzer, A.; Park, Y. Implication of conjugated linoleic acid (CLA) in human health. *Crit. Rev. Food Sci.* **2012**, *52*, 488−513.

(5) Fritsche, J.; Steinhart, H. Amounts of conjugated linoleic acid (CLA) in German foods and evaluation of daily intake. *Z. Lebensm. Unters. Forsch. A* **1998**, *206*, 77−82.

(6) Lin, H.; Boylston, T. D.; Chang, M. J.; Luedecke, L. O.; Shultz, T. D. Survey of the conjugated linoleic acid contents of dairy products. *J. Dairy Sci.* **1995**, *78*, 2358−2365.

(7) Prandini, A.; Sigolo, S.; Tansini, G.; Brogna, N.; Piva, G. Different level of conjugated linoleic acid (CLA) in dairy products from Italy. *J. Food Compos. Anal.* **2007**, *20*, 472−479.

(8) Nunes, J. C.; Torres, A. G. Fatty acid and CLA composition of Brazilian dairy products, and contribution to daily intake of CLA. *J. Food Compos. Anal.* **2010**, *23*, 782−789.

(9) Mushtaq, S.; Mangiapane, E. H.; Hunter, K. A. Estimation of *cis*-9, *trans*-11 conjugated linoleic acid content in UK foods and assessment of dietary intake in a cohort of healthy adults. *Br. J. Nutr.* **2010**, *103*, 1366−1374.

(10) Prandini, A.; Sigolo, S.; Piva, G. A comparative study of fatty acid composition and CLA concentration in commercial cheeses. *J. Food Compos. Anal.* **2011**, *24*, 55−61.

(11) Serafeimidou, A.; Zlatanos, S.; Laskaridis, K.; Sagredos, A. Chemical characteristics, fatty acid composition and conjugated linoleic acid (CLA) content of traditional Greek yogurts. *Food Chem.* **2012**, *134*, 1839−1846.

(12) Prema, D.; Pilfold, J. L.; Krauchi, J.; Church, J. S.; Donkor, K. K.; Cinel, B. Rapid determination of total conjugated linoleic acid content in select Canadian cheeses by H-1 NMR spectroscopy. *J. Agric. Food Chem.* **2013**, *61*, 9915−9921.

(13) Cicognini, F. M.; Rossi, F.; Sigolo, S.; Gallo, A.; Prandini, A. Conjugated linoleic acid isomer (*cis*9,*trans*11 and *trans*10,*cis*12) content in cheeses from Italian large-scale retail trade. *Int. Dairy J.* **2014**, *34*, 180−183.

(14) Trigueros, L.; Sendra, E. Fatty acid and conjugated linoleic acid (CLA) content in fermented milks as assessed by direct methylation. *LWT−Food Sci. Technol.* **2015**, *60*, 315−319.

(15) Kaufman, M.; Wiesman, Z. Pomegranate oil analysis with emphasis on MALDI-TOF/MS triacylglycerol fingerprinting. *J. Agric. Food Chem.* **2007**, *55*, 10405−10413.

(16) Yuan, G. F.; Sinclair, A. J.; Sun, H. Y.; Li, D. Fatty acid composition in tissues of mice fed diets containing conjugated linolenic acid and conjugated linoleic acid. *J. Food Lipids* **2009**, *16*, 148−163.

(17) Takagi, T.; Itabashi, Y. Occurrence of mixtures of geometrical-isomers of conjugated octadecatrienoic acids in some seed oils − analysis by open-tubular gas-liquid-chromatography. *Lipids* **1981**, *16*, 546−551.

(18) Yuan, G. F.; Yuan, J. Q.; Li, D. Punicic acid from *Trichosanthes kirilowii* seed oil is rapidly metabolized to conjugated linoleic acid in rats. *J. Med. Food* **2009**, *12*, 416−422.

(19) Devi, P. S. TLC as a tool for quantitative isolation of conjugated trienoic FA. *J. Am. Oil Chem. Soc.* **2003**, *80*, 315−318.

(20) Evans, R. M.; Barish, G. D.; Wang, Y. X. PPARs and the complex journey to obesity. *Nat. Med.* **2004**, *10*, 355−361.

(21) van Beekum, O.; Fleskens, V.; Kalkhoven, E. Posttranslational modifications of PPAR-gamma: fine-tuning the metabolic master regulator. *Obesity* **2009**, *17*, 213−219.

(22) Wang, L.; Waltenberger, B.; Pferschy-Wenzig, E. M.; Blunder, M.; Liu, X.; Malainer, C.; Blazevic, T.; Schwaiger, S.; Rollinger, J. M.; Heiss, E. H.; Schuster, D.; Kopp, B.; Bauer, R.; Stuppner, H.; Dirsch, V. M.; Atanasov, A. G. Natural product agonists of peroxisome proliferator-activated receptor gamma (PPAR-γ): a review. *Biochem. Pharmacol.* **2014**, *92*, 73−89.

(23) Straus, D. S.; Glass, C. K. Anti-inflammatory actions of PPAR ligands: new insights on cellular and molecular mechanisms. *Trends Immunol.* **2007**, *28*, 551−558.

(24) Lehrke, M.; Lazar, M. A. The many faces of PPAR gamma. *Cell* **2005**, *123*, 993−999.

(25) Knouff, C.; Auwerx, J. Peroxisome proliferator-activated receptor-gamma calls for activation in moderation: lessons from genetics and pharmacology. *Endocr. Rev.* **2004**, *25*, 899−918.

(26) Tontonoz, P.; Spiegelman, B. M. Fat and beyond: the diverse biology of PPAR gamma. *Annu. Rev. Biochem.* **2008**, *77*, 289−312.

(27) Siersbaek, R.; Nielsen, R.; Mandrup, S. PPAR gamma in adipocyte differentiation and metabolism − novel insights from genome-wide studies. *FEBS Lett.* **2010**, *584*, 3242−3249.

(28) Tang, Q. Q.; Lane, M. D. Adipogenesis: from stem cell to adipocyte. *Annu. Rev. Biochem.* **2012**, *81*, 715−736.

(29) Suh, N.; Wang, Y. P.; Williams, C. R.; Risingsong, R.; Gilmer, T.; Willson, T. M.; Sporn, M. B. A new ligand for the peroxisome proliferator-activated receptor-gamma (PPAR-γ), GW7845, inhibits rat mammary carcinogenesis. *Cancer Res.* **1999**, *59*, 5671−5673.

(30) Brown, P. H.; Lippman, S. M. Chemoprevention of breast cancer. *Breast. Cancer Res. Treat.* **2000**, *62*, 1−17.

(31) Peters, J. M.; Shah, Y. M.; Gonzalez, F. J. The role of peroxisome proliferator-activated receptors in carcinogenesis and chemoprevention. *Nat. Rev. Can.* **2012**, *12*, 181−195.

(32) Gurnell, M. 'Striking the right balance' in targeting ppar gamma in the metabolic syndrome: novel insights from human genetic studies. *PPAR Res.* **2007**, No. 083593.

(33) Chung, S. W.; Kang, B. Y.; Kim, S. H.; Pak, Y. K.; Cho, D.; Trinchieri, G.; Kim, T. S. Oxidized low density lipoprotein inhibits

DOI: 10.1021/jf505050c
J. Agric. Food Chem. 2015, 63, 1883−1895

interleukin-12 production in lipopolysaccharide-activated mouse macrophages via direct interactions between peroxisome proliferator-activated receptor-γ and nuclear factor-κB. *J. Biol. Chem.* **2000**, *275*, 32681−32687.
(34) Luconi, M.; Cantini, G.; Serio, M. Peroxisome proliferator-activated receptor gamma (PPARγ): is the genomic activity the only answer? *Steroids* **2010**, *75*, 585−594.
(35) Dussault, I.; Forman, B. M. Prostaglandins and fatty acids regulate transcriptional signaling via the peroxisome proliferator activated receptor nuclear receptors. *Prostaglandins Other Lipid Med.* **2000**, *62*, 1−13.
(36) Kliewer, S. A.; Sundseth, S. S.; Jones, S. A.; Brown, P. J.; Wisely, G. B.; Koble, C. S.; Devchand, P.; Wahli, W.; Willson, T. M.; Lenhard, J. M.; Lehmann, J. M. Fatty acids and eicosanoids regulate gene expression through direct interactions with peroxisome proliferator-activated receptors alpha and gamma. *Proc. Natl. Acad. Sci. U.S.A.* **1997**, *94*, 4318−4323.
(37) Kung, J.; Henry, R. R. Thiazolidinedione safety. *Expert Opin. Drug Saf.* **2012**, *11*, 565−579.
(38) Bassaganya-Riera, J.; Guri, A. J.; Hontecillas, R. Treatment of obesity-related complications with novel classes of naturally occurring PPAR agonists. *J. Obes.* **2011**, No. 897894.
(39) Park, Y.; Albright, K. J.; Liu, W.; Storkson, J. M.; Cook, M. E.; Pariza, M. W. Effect of conjugated linoleic acid on body composition in mice. *Lipids* **1997**, *32*, 853−858.
(40) Kim, J. H.; Pan, J. H.; Park, H. G.; Yoon, H. G.; Kwon, O. J.; Kim, T. W.; Shin, D. H.; Kim, Y. J. Functional comparison of esterified and free forms of conjugated linoleic acid in high-fat-diet-induced obese C57BL/6J mice. *J. Agric. Food Chem.* **2010**, *58*, 11441−11447.
(41) Park, Y.; Storkson, J. M.; Albright, K. J.; Liu, W.; Pariza, M. W. Evidence that the *trans*-10,*cis*-12 isomer of conjugated linoleic acid induces body composition changes in mice. *Lipids* **1999**, *34*, 235−241.
(42) Brown, J. M.; Halvorsen, Y. D.; Lea-Currie, Y. R.; Geigerman, C.; McIntosh, M. *trans*-10, *cis*-12, but not *cis*-9, *trans*-11, conjugated linoleic acid attenuates lipogenesis in primary cultures of stromal vascular cells from human adipose tissue. *J. Nutr.* **2001**, *131*, 2316−2321.
(43) Kennedy, A.; Martinez, K.; Schmidt, S.; Mandrup, S.; LaPoint, K.; McIntosh, M. Antiobesity mechanisms of action of conjugated linoleic acid. *J. Nutr. Biochem.* **2010**, *21*, 171−179.
(44) Martorell, P.; Llopis, S.; Gonzalez, N.; Monton, F.; Ortiz, P.; Genoves, S.; Ramon, D. *Caenorhabditis elegans* as a model to study the effectiveness and metabolic targets of dietary supplements used for obesity treatment: the specific case of a conjugated linoleic acid mixture (Tonalin). *J. Agric. Food Chem.* **2012**, *60*, 11071−11079.
(45) Tontonoz, P.; Hu, E.; Spiegelman, B. M. Stimulation of adipogenesis in fibroblasts by PPAR gamma 2, a lipid-activated transcription factor. *Cell* **1994**, *79*, 1147−1156.
(46) Brun, R. P.; Tontonoz, P.; Forman, B. M.; Ellis, R.; Chen, J.; Evans, R. M.; Spiegelman, B. M. Differential activation of adipogenesis by multiple PPAR isoforms. *Gene Dev.* **1996**, *10*, 974−984.
(47) Barak, Y.; Nelson, M. C.; Ong, E. S.; Jones, Y. Z.; Ruiz-Lozano, P.; Chien, K. R.; Koder, A.; Evans, R. M. PPAR gamma is required for placental, cardiac, and adipose tissue development. *Mol. Cell* **1999**, *4*, 585−595.
(48) Siersbaek, R.; Nielsen, R.; Mandrup, S. Transcriptional networks and chromatin remodeling controlling adipogenesis. *Trends Endocrinol. Metab.* **2012**, *23*, 56−64.
(49) Lefterova, M. I.; Lazar, M. A. New developments in adipogenesis. *Trends Endocrinol. Metab.* **2009**, *20*, 107−114.
(50) Rosen, E. D.; Spiegelman, B. M. What we talk about when we talk about fat. *Cell* **2014**, *156*, 20−44.
(51) Miller, J. R.; Siripurkpong, P.; Hawes, J.; Majdalawieh, A.; Ro, H. S.; McLeod, R. S. The *trans*-10, *cis*-12 isomer of conjugated linoleic acid decreases adiponectin assembly by PPARgamma-dependent and PPARgamma-independent mechanisms. *J. Lipid Res.* **2008**, *49*, 550−562.
(52) Evans, M.; Geigerman, C.; Cook, J.; Curtis, L.; Kuebler, B.; McIntosh, M. Conjugated linoleic acid suppresses triglyceride accumulation and induces apoptosis in 3T3-L1 preadipocytes. *Lipids* **2000**, *35*, 899−910.
(53) Brodie, A. E.; Manning, V. A.; Ferguson, K. R.; Jewell, D. E.; Hu, C. Y. Conjugated linoleic acid inhibits differentiation of pre- and post-confluent 3T3-L1 preadipocytes but inhibits cell proliferation only in preconfluent cells. *J. Nutr.* **1999**, *129*, 602−606.
(54) Satory, D. L.; Smith, S. B. Conjugated linoleic acid inhibits proliferation but stimulates lipid filling of murine 3T3-L1 preadipocytes. *J. Nutr.* **1999**, *129*, 92−97.
(55) Choi, Y.; Kim, Y. C.; Han, Y. B.; Park, Y.; Pariza, M. W.; Ntambi, J. M. The *trans*-10,*cis*-12 isomer of conjugated linoleic acid downregulates stearoyl-CoA desaturase 1 gene expression in 3T3-L1 adipocytes. *J. Nutr.* **2000**, *130*, 1920−1924.
(56) Kang, K.; Liu, W.; Albright, K. J.; Park, Y.; Pariza, M. W. *Trans*-10,*cis*-12 CLA inhibits differentiation of 3T3-L1 adipocytes and decreases PPAR gamma expression. *Biochem. Biophys. Res. Commun.* **2003**, *303*, 795−799.
(57) Brown, J. M.; Boysen, M. S.; Chung, S.; Fabiyi, O.; Morrison, R. F.; Mandrup, S.; McIntosh, M. K. Conjugated linoleic acid induces human adipocyte delipidation: autocrine/paracrine regulation of MEK/ERK signaling by adipocytokines. *J. Biol. Chem.* **2004**, *279*, 26735−26747.
(58) Brown, J. M.; Boysen, M. S.; Jensen, S. S.; Morrison, R. F.; Storkson, J.; Lea-Currie, R.; Pariza, M.; Mandrup, S.; McIntosh, M. K. Isomer-specific regulation of metabolism and PPAR gamma signaling by CLA in human preadipocytes. *J. Lipid Res.* **2003**, *44*, 1287−1300.
(59) Ahmadian, M.; Suh, J. M.; Hah, N.; Liddle, C.; Atkins, A. R.; Downes, M.; Evans, R. M. PPAR gamma signaling and metabolism: the good, the bad and the future. *Nat. Med.* **2013**, *19*, 557−566.
(60) Tontonoz, P.; Hu, E.; Graves, R. A.; Budavari, A. I.; Spiegelman, B. M. PPAR gamma 2: tissue-specific regulator of an adipocyte enhancer. *Gene Dev.* **1994**, *8*, 1224−1234.
(61) Wu, Z. D.; Xie, Y. H.; Morrison, R. F.; Bucher, N. L. R.; Farmer, S. R. PPAR gamma induces the insulin-dependent glucose transporter GLUT4 in the absence of C/EBP alpha during the conversion of 3T3 fibroblasts into adipocytes. *J. Clin. Invest.* **1998**, *101*, 22−32.
(62) Schoonjans, K.; PeinadoOnsurbe, J.; Lefebvre, A. M.; Heyman, R. A.; Briggs, M.; Deeb, S.; Staels, B.; Auwerx, J. PPAR alpha and PPAR gamma activators direct a distinct tissue-specific transcriptional response via a PPRE in the lipoprotein lipase gene. *EMBO J.* **1996**, *15*, 5336−5348.
(63) Sato, O.; Kuriki, C.; Fukui, Y.; Motojima, K. Dual promoter structure of mouse and human fatty acid translocase/CD36 genes and unique transcriptional activation by peroxisome proliferator-activated receptor alpha and gamma ligands. *J. Biol. Chem.* **2002**, *277*, 15703−15711.
(64) Granlund, L.; Juvet, L. K.; Pedersen, J. I.; Nebb, H. I. *trans*10, *cis*12-conjugated linoleic acid prevents triacylglycerol accumulation in adipocytes by acting as a PPAR gamma modulator. *J. Lipid Res.* **2003**, *44*, 1441−1452.
(65) Navarro, V.; Fernandez-Quintela, A.; Churruca, I.; Portillo, M. P. The body fat-lowering effect of conjugated linoleic acid: a comparison between animal and human studies. *J. Physiol. Biochem.* **2006**, *62*, 137−147.
(66) Shen, W.; Chuang, C. C.; Martinez, K.; Reid, T.; Brown, J. M.; Xi, L.; Hixson, L.; Hopkins, R.; Starnes, J.; McIntosh, M. Conjugated linoleic acid reduces adiposity and increases markers of browning and inflammation in white adipose tissue of mice. *J. Lipid Res.* **2013**, *54*, 909−922.
(67) Poirier, H.; Shapiro, J. S.; Kim, R. J.; Lazar, M. A. Nutritional supplementation with *trans*-10, *cis*-12-conjugated linoleic acid induces inflammation of white adipose tissue. *Diabetes* **2006**, *55*, 1634−1641.
(68) LaRosa, P. C.; Miner, J.; Xia, Y.; Zhou, Y.; Kachman, S.; Fromm, M. E. *trans*-10, *cis*-12 conjugated linoleic acid causes inflammation and delipidation of white adipose tissue in mice: a microarray and histological analysis. *Physiol. Genomics* **2006**, *27*, 282−294.
(69) Liu, L. F.; Purushotham, A.; Wendel, A. A.; Belury, M. A. Combined effects of rosiglitazone and conjugated linoleic acid on

DOI: 10.1021/jf505050c
J. Agric. Food Chem. 2015, 63, 1883−1895

adiposity, insulin sensitivity, and hepatic steatosis in high-fat-fed mice. *Am. J. Physiol. Gastrointest. Liver Physiol.* **2007**, *292*, G1671−1682.
(70) Kennedy, A.; Chung, S.; LaPoint, K.; Fabiyi, O.; McIntosh, M. K. *trans*-10, *cis*-12 conjugated linoleic acid antagonizes ligand-dependent PPAR gamma activity in primary cultures of human adipocytes. *J. Nutr.* **2008**, *138*, 455−461.
(71) Clement, L.; Poirier, H.; Niot, I.; Bocher, V.; Guerre-Millo, M.; Krief, S.; Staels, B.; Besnard, P. Dietary *trans*-10,*cis*-12 conjugated linoleic acid induces hyperinsulinemia and fatty liver in the mouse. *J. Lipid Res.* **2002**, *43*, 1400−1409.
(72) Belury, M. A.; Moya-Camarena, S. Y.; Lu, M.; Shi, L. L.; Leesnitzer, L. M.; Blanchard, S. G. Conjugated linoleic acid is an activator and ligand for peroxisome proliferator-activated receptor-gamma (PPAR γ). *Nutr. Res. (N.Y.)* **2002**, *22*, 817−824.
(73) Hu, E.; Kim, J. B.; Sarraf, P.; Spiegelman, B. M. Inhibition of adipogenesis through MAP kinase-mediated phosphorylation of PPARgamma. *Science* **1996**, *274*, 2100−2103.
(74) Camp, H. S.; Tafuri, S. R.; Leff, T. c-Jun N-terminal kinase phosphorylates peroxisome proliferator-activated receptor-gamma1 and negatively regulates its transcriptional activity. *Endocrinology* **1999**, *140*, 392−397.
(75) Floyd, Z. E.; Stephens, J. M. Interferon-gamma-mediated activation and ubiquitin-proteasome-dependent degradation of PPARgamma in adipocytes. *J. Biol. Chem.* **2002**, *277*, 4062−4068.
(76) Leff, T. AMP-activated protein kinase regulates gene expression by direct phosphorylation of nuclear proteins. *Biochem. Soc. Trans.* **2003**, *31*, 224−227.
(77) Jiang, S.; Wang, W.; Miner, J.; Fromm, M. Cross regulation of sirtuin 1, AMPK, and PPARgamma in conjugated linoleic acid treated adipocytes. *PLoS One* **2012**, *7*, No. e48874.
(78) Finkel, T.; Deng, C. X.; Mostoslavsky, R. Recent progress in the biology and physiology of sirtuins. *Nature* **2009**, *460*, 587−591.
(79) Picard, F.; Kurtev, M.; Chung, N. J.; Topark-Ngarm, A.; Senawong, T.; de Oliveira, R. M.; Leid, M.; McBurney, M. W.; Guarente, L. Sirt1 promotes fat mobilization in white adipocytes by repressing PPAR-gamma. *Nature* **2004**, *429*, 771−776.
(80) Ruderman, N. B.; Xu, X. J.; Nelson, L.; Cacicedo, J. M.; Saha, A. K.; Lan, F.; Ido, Y. AMPK and SIRT1: a long-standing partnership? *Am. J. Physiol. Endocrinol. Metab.* **2010**, *298*, E751−760.
(81) Burgermeister, E.; Seger, R. MAPK kinases as nucleo-cytoplasmic shuttles for PPARgamma. *Cell Cycle* **2007**, *6*, 1539−1548.
(82) Moloney, F.; Toomey, S.; Noone, E.; Nugent, A.; Allan, B.; Loscher, C. E.; Roche, H. M. Antidiabetic effects of *cis*-9, *trans*-11-conjugated linoleic acid may be mediated via anti-inflammatory effects in white adipose tissue. *Diabetes* **2007**, *56*, 574−582.
(83) Simon, E.; Macarulla, M. T.; Churruca, I.; Fernandez-Quintela, A.; Portillo, M. P. *trans*-10,*cis*-12 Conjugated linoleic acid prevents adiposity but not insulin resistance induced by an atherogenic diet in hamsters. *J. Nutr. Biochem.* **2006**, *17*, 126−131.
(84) Hotamisligil, G. S. Inflammation and metabolic disorders. *Nature* **2006**, *444*, 860−867.
(85) Siriwardhana, N.; Kalupahana, N. S.; Cekanova, M.; LeMieux, M.; Greer, B.; Moustaid-Moussa, N. Modulation of adipose tissue inflammation by bioactive food compounds. *J. Nutr. Biochem.* **2013**, *24*, 613−623.
(86) Kershaw, E. E.; Flier, J. S. Adipose tissue as an endocrine organ. *J. Clin. Endocrinol. Metab.* **2004**, *89*, 2548−2556.
(87) Ouchi, N.; Parker, J. L.; Lugus, J. J.; Walsh, K. Adipokines in inflammation and metabolic disease. *Nat. Rev. Immunol.* **2011**, *11*, 85−97.
(88) Chung, S.; Brown, J. M.; Provo, J. N.; Hopkins, R.; McIntosh, M. K. Conjugated linoleic acid promotes human adipocyte insulin resistance through NFkappaB-dependent cytokine production. *J. Biol. Chem.* **2005**, *280*, 38445−38456.
(89) Lagathu, C.; Yvan-Charvet, L.; Bastard, J. P.; Maachi, M.; Quignard-Boulange, A.; Capeau, J.; Caron, M. Long-term treatment with interleukin-1beta induces insulin resistance in murine and human adipocytes. *Diabetologia* **2006**, *49*, 2162−2173.
(90) Suzawa, M.; Takada, I.; Yanagisawa, J.; Ohtake, F.; Ogawa, S.; Yamauchi, T.; Kadowaki, T.; Takeuchi, Y.; Shibuya, H.; Gotoh, Y.; Matsumoto, K.; Kato, S. Cytokines suppress adipogenesis and PPAR-gamma function through the TAK1/TAB1/NIK cascade. *Nat. Cell Biol.* **2003**, *5*, 224−230.
(91) Purushotham, A.; Wendel, A. A.; Liu, L. F.; Belury, M. A. Maintenance of adiponectin attenuates insulin resistance induced by dietary conjugated linoleic acid in mice. *J. Lipid Res.* **2007**, *48*, 444−452.
(92) Adams, M.; Reginato, M. J.; Shao, D.; Lazar, M. A.; Chatterjee, V. K. Transcriptional activation by peroxisome proliferator-activated receptor gamma is inhibited by phosphorylation at a consensus mitogen-activated protein kinase site. *J. Biol. Chem.* **1997**, *272*, 5128−5132.
(93) Kennedy, A.; Overman, A.; LaPoint, K.; Hopkins, R.; West, T.; Chuang, C. C.; Martinez, K.; Bell, D.; McIntosh, M. Conjugated linoleic acid-mediated inflammation and insulin resistance in human adipocytes are attenuated by resveratrol. *J. Lipid Res.* **2009**, *50*, 225−232.
(94) Tholstrup, T.; Raff, M.; Straarup, E. M.; Lund, P.; Basu, S.; Bruun, J. M. An oil mixture with *trans*-10, *cis*-12 conjugated linoleic acid increases markers of inflammation and *in vivo* lipid peroxidation compared with *cis*-9, *trans*-11 conjugated linoleic acid in postmenopausal women. *J. Nutr.* **2008**, *138*, 1445−1451.
(95) Reginato, M. J.; Krakow, S. L.; Bailey, S. T.; Lazar, M. K. Prostaglandins promote and block adipogenesis through opposing effects on peroxisome proliferator-activated receptor gamma. *J. Biol. Chem.* **1998**, *273*, 1855−1858.
(96) Liu, L.; Clipstone, N. A. Prostaglandin F2 alpha induces the normoxic activation of the hypoxia-inducible factor-1 transcription factor in differentiating 3T3-L1 preadipocytes: potential role in the regulation of adipogenesis. *J. Cell Biochem.* **2008**, *105*, 89−98.
(97) Liu, L.; Clipstone, N. A. Prostaglandin F2 alpha inhibits adipocyte differentiation via a G alpha q-calcium-calcineurin-dependent signaling pathway. *J. Cell Biochem.* **2007**, *100*, 161−173.
(98) Martinez, K.; Kennedy, A.; West, T.; Milatovic, D.; Aschner, M.; McIntosh, M. *trans*-10,*cis*-12-conjugated linoleic acid instigates inflammation in human adipocytes compared with preadipocytes. *J. Biol. Chem.* **2010**, *285*, 17701−17712.
(99) Kennedy, A.; Martinez, K.; Chung, S.; LaPoint, K.; Hopkins, R.; Schmidt, S. F.; Andersen, K.; Mandrup, S.; McIntosh, M. Inflammation and insulin resistance induced by *trans*-10, *cis*-12 conjugated linoleic acid depend on intracellular calcium levels in primary cultures of human adipocytes. *J. Lipid Res.* **2010**, *51*, 1906−1917.
(100) Obsen, T.; Faergeman, N. J.; Chung, S.; Martinez, K.; Gobern, S.; Loreau, O.; Wabitsch, M.; Mandrup, S.; McIntosh, M. *trans*-10, *cis*-12 conjugated linoleic acid decreases *de novo* lipid synthesis in human adipocytes. *J. Nutr. Biochem.* **2012**, *23*, 580−590.
(101) Zemel, M. B. Nutritional and endocrine modulation of intracellular calcium: implications in obesity, insulin resistance and hypertension. *Mol. Cell. Biochem.* **1998**, *188*, 129−136.
(102) Shen, W.; Martinez, K.; Chuang, C. C.; McIntosh, M. The phospholipase C inhibitor U73122 attenuates *trans*-10, *cis*-12 conjugated linoleic acid-mediated inflammatory signaling and insulin resistance in human adipocytes. *J. Nutr.* **2013**, *143*, 584−590.
(103) Martinez, K.; Shyamasundar, S.; Kennedy, A.; Chuang, C. C.; Marsh, A.; Kincaid, J.; Reid, T.; McIntosh, M. Diacylglycerol kinase inhibitor R59022 attenuates conjugated linoleic acid-mediated inflammation in human adipocytes. *J. Lipid Res.* **2013**, *54*, 662−670.
(104) Sakane, F.; Imai, S.; Kai, M.; Yasuda, S.; Kanoh, H. Diacylglycerol kinases: why so many of them? *Biochim. Biophys. Acta* **2007**, *1771*, 793−806.
(105) Nathan, C. Points of control in inflammation. *Nature* **2002**, *420*, 846−852.
(106) Boussetta, T.; Raad, H.; Letteron, P.; Gougerot-Pocidalo, M. A.; Marie, J. C.; Driss, F.; El-Benna, J. Punicic acid a conjugated linolenic acid inhibits TNFalpha-induced neutrophil hyperactivation and protects from experimental colon inflammation in rats. *PLoS One* **2009**, *4*, No. e6458.
(107) Gilardi, D.; Fiorino, G.; Genua, M.; Allocca, M.; Danese, S. Complementary and alternative medicine in inflammatory bowel

DOI: 10.1021/jf505050c
J. Agric. Food Chem. 2015, 63, 1883−1895

diseases: what is the future in the field of herbal medicine? *Expert Rev. Gastroenterol.* **2014**, *8*, 835−846.
(108) Rahimi, R.; Nikfar, S.; Abdollahi, M. Induction of clinical response and remission of inflammatory bowel disease by use of herbal medicines: a meta-analysis. *World J. Gastroenterol.* **2013**, *19*, 5738−5749.
(109) Annese, V.; Rogai, F.; Settesoldi, A.; Bagnoli, S. PPAR gamma in inflammatory bowel disease. *PPAR Res.* **2012**, No. 620839.
(110) Su, C. G.; Wen, X. M.; Bailey, S. T.; Jiang, W.; Rangwala, S. M.; Keilbaugh, S. A.; Flanigan, A.; Murthy, S.; Lazar, M. A.; Wu, G. D. A novel therapy for colitis utilizing PPAR-gamma ligands to inhibit the epithelial inflammatory response. *J. Clin. Invest.* **1999**, *104*, 383−389.
(111) Ramakers, J. D.; Verstege, M. I.; Thuijls, G.; Te Velde, A. A.; Mensink, R. P.; Plat, J. The PPARgamma agonist rosiglitazone impairs colonic inflammation in mice with experimental colitis. *J. Clin. Immunol.* **2007**, *27*, 275−283.
(112) Lewis, J. D.; Lichtenstein, G. R.; Deren, J. J.; Sands, B. E.; Hanauer, S. B.; Katz, J. A.; Lashner, B.; Present, D. H.; Chuai, S.; Ellenbergr, J. H.; Nessel, L.; Wu, G. D.; Colitis, R. U. Rosiglitazone for active ulcerative colitis: a randomized placebo-controlled trial. *Gastroenterology* **2008**, *134*, 688−695.
(113) Pedersen, G.; Brynskov, J. Topical rosiglitazone treatment improves ulcerative colitis by restoring peroxisome proliferator-activated receptor-gamma activity. *Am. J. Gastroenterol.* **2010**, *105*, 1595−1603.
(114) Nesto, R. W.; Bell, D.; Bonow, R. O.; Fonseca, V.; Grundy, S. M.; Horton, E. S.; Le Winter, M.; Porte, D.; Semenkovich, C. F.; Smith, S.; Young, L. H.; Kahn, R. Thiazolidinedione use, fluid retention, and congestive heart failure. *Diabetes Care* **2004**, *27*, 256−263.
(115) Marion-Letellier, R.; Dechelotte, P.; Iacucci, M.; Ghosh, S. Dietary modulation of peroxisome proliferator-activated receptor gamma. *Gut* **2009**, *58*, 586−593.
(116) Bassaganya-Riera, J.; Reynolds, K.; Martino-Catt, S.; Cui, Y.; Hennighausen, L.; Gonzalez, F.; Rohrer, J.; Benninghoff, A. U.; Hontecillas, R. Activation of PPAR gamma and delta by conjugated linoleic acid mediates protection from experimental inflammatory bowel disease. *Gastroenterology* **2004**, *127*, 777−791.
(117) Bassaganya-Riera, J.; Hontecillas, R. CLA and n-3 PUFA differentially modulate clinical activity and colonic PPAR-responsive gene expression in a pig model of experimental IBD. *Clin. Nutr.* **2006**, *25*, 454−465.
(118) Lee, J. H.; Cho, K. H.; Lee, K. T.; Kim, M. R. Antiatherogenic effects of structured lipid containing conjugated linoleic acid in C57BL/6J mice. *J. Agric. Food Chem.* **2005**, *53*, 7295−7301.
(119) Toomey, S.; Harhen, B.; Roche, H. M.; Fitzgerald, D.; Belton, O. Profound resolution of early atherosclerosis with conjugated linoleic acid. *Atherosclerosis* **2006**, *187*, 40−49.
(120) Inoue, N.; Nagao, K.; Wang, Y. M.; Noguchi, H.; Shirouchi, B.; Yanagita, T. Dietary conjugated linoleic acid lowered tumor necrosis factor-alpha content and altered expression of genes related to lipid metabolism and insulin sensitivity in the skeletal muscle of Zucker rats. *J. Agric. Food Chem.* **2006**, *54*, 7935−7939.
(121) Qin, H.; Liu, Y.; Lu, N.; Li, Y.; Sun, C. H. *cis*-9,*trans*-11-Conjugated linoleic acid activates AMP-activated protein kinase in attenuation of insulin resistance in c2c12 myotubes. *J. Agric. Food Chem.* **2009**, *57*, 4452−4458.
(122) Reynolds, C. M.; Roche, H. M. Conjugated linoleic acid and inflammatory cell signalling. *Prostag. Leukotr. Ess.* **2010**, *82*, 199−204.
(123) Colombo, E.; Sangiovanni, E.; Dell'agli, M. A review on the anti-inflammatory activity of pomegranate in the gastrointestinal tract. *Evidence-Based Complement. Altern. Med.* **2013**, No. 247145.
(124) Hontecillas, R.; Wannemeulher, M. J.; Zimmerman, D. R.; Hutto, D. L.; Wilson, J. H.; Ahn, D. U.; Bassaganya-Riera, J. Nutritional regulation of porcine bacterial-induced colitis by conjugated linoleic acid. *J. Nutr.* **2002**, *132*, 2019−2027.
(125) Evans, N. P.; Misyak, S. A.; Schmelz, E. M.; Guri, A. J.; Hontecillas, R.; Bassaganya-Riera, J. Conjugated linoleic acid ameliorates inflammation-induced colorectal cancer in mice through activation of PPAR gamma. *J. Nutr.* **2010**, *140*, 515−521.
(126) Bassaganya-Riera, J.; Viladomiu, M.; Pedragosa, M.; De Simone, C.; Carbo, A.; Shaykhutdinov, R.; Jobin, C.; Arthur, J. C.; Corl, B. A.; Vogel, H.; Storr, M.; Hontecillas, R. Probiotic bacteria produce conjugated linoleic acid locally in the gut that targets macrophage PPAR gamma to suppress colitis. *PLoS One* **2012**, *7*, No. e31238.
(127) Borniquel, S.; Jadert, C.; Lundberg, J. O. Dietary conjugated linoleic acid activates PPARgamma and the intestinal trefoil factor in SW480 cells and mice with dextran sulfate sodium-induced colitis. *J. Nutr.* **2012**, *142*, 2135−2140.
(128) Bassaganya-Riera, J.; Hontecillas, R.; Horne, W. T.; Sandridge, M.; Herfarth, H. H.; Bloomfeld, R.; Isaacs, K. L. Conjugated linoleic acid modulates immune responses in patients with mild to moderately active Crohn's disease. *Clin. Nutr.* **2012**, *31*, 721−727.
(129) McNeel, R. L.; Smith, E. O.; Mersmann, H. J. Isomers of conjugated linoleic acid modulate human preadipocyte differentiation. *In Vitro Cell Dev. Biol. Anim.* **2003**, *39*, 375−382.
(130) Meadus, W. J.; MacInnis, R.; Dugan, M. E. Prolonged dietary treatment with conjugated linoleic acid stimulates porcine muscle peroxisome proliferator activated receptor gamma and glutamine-fructose aminotransferase gene expression in vivo. *J. Mol. Endocrinol.* **2002**, *28*, 79−86.
(131) Yu, Y.; Correll, P. H.; Vanden Heuvel, J. P. Conjugated linoleic acid decreases production of pro-inflammatory products in macrophages: evidence for a PPAR gamma-dependent mechanism. *Biochim. Biophys. Acta* **2002**, *1581*, 89−99.
(132) Stachowska, E.; Kijowski, J.; Dziedziejko, V.; Siennicka, A.; Chlubek, D. Conjugated linoleic acid regulates phosphorylation of PPAR gamma by modulation of ERK 1/2 and p38 signaling in human macrophages/fatty acid-laden macrophages. *J. Agric. Food Chem.* **2011**, *59*, 11846−11852.
(133) Bassaganya-Riera, J.; Hontecillas, R. Dietary conjugated linoleic acid and n-3 polyunsaturated fatty acids in inflammatory bowel disease. *Curr. Opin. Clin. Nutr. Metab. Care* **2010**, *13*, 569−573.
(134) Taupin, D.; Podolsky, D. K. Trefoil factors: initiators of mucosal healing. *Nat. Rev. Mol. Cell Biol.* **2003**, *4*, 721−732.
(135) Aamann, L.; Vestergaard, E. M.; Gronbaek, H. Trefoil factors in inflammatory bowel disease. *World J. Gastroenterol.* **2014**, *20*, 3223−3230.
(136) Bassaganya-Riera, J.; Viladomiu, M.; Pedragosa, M.; De Simone, C.; Hontecillas, R. Immunoregulatory mechanisms underlying prevention of colitis-associated colorectal cancer by probiotic bacteria. *PLoS One* **2012**, *7*, No. e34676.
(137) Appleyard, C. B.; Cruz, M. L.; Isidro, A. A.; Arthur, J. C.; Jobin, C.; De Simone, C. Pretreatment with the probiotic VSL#3 delays transition from inflammation to dysplasia in a rat model of colitis-associated cancer. *Am. J. Physiol. Gastrointest. Liver Physiol.* **2011**, *301*, G1004−G1013.
(138) Huynh, H. Q.; deBruyn, J.; Guan, L. L.; Diaz, H.; Li, M. J.; Girgis, S.; Turner, J.; Fedorak, R.; Madsen, K. Probiotic preparation VSL#3 induces remission in children with mild to moderate acute ulcerative colitis: a pilot study. *Inflamm. Bowel Dis.* **2009**, *15*, 760−768.
(139) Sood, A.; Midha, V.; Makharia, G. K.; Ahuja, V.; Singal, D.; Goswami, P.; Tandon, R. K. The probiotic preparation, VSL#3 induces remission in patients with mild-to-moderately active ulcerative colitis. *Clin. Gastroenterol. Hepatol.* **2009**, *7*, 1202−1209.
(140) Ewaschuk, J. B.; Walker, J. W.; Diaz, H.; Madsen, K. L. Bioproduction of conjugated linoleic acid by probiotic bacteria occurs *in vitro* and *in vivo* in mice. *J. Nutr.* **2006**, *136*, 1483−1487.
(141) Koba, K.; Akahoshi, A.; Yamasaki, M.; Tanaka, K.; Yamada, K.; Iwata, T.; Kamegai, T.; Tsutsumi, K.; Sugano, M. Dietary conjugated linolenic acid in relation to CLA differently modifies body fat mass and serum and liver lipid levels in rats. *Lipids* **2002**, *37*, 343−350.
(142) Arao, K.; Wang, Y. M.; Inoue, N.; Hirata, J.; Cha, J. Y.; Nagao, K.; Yanagita, T. Dietary effect of pomegranate seed oil rich in 9*cis*, 11*trans*, 13*cis* conjugated linolenic acid on lipid metabolism in obese, hyperlipidemic OLETF rats. *Lipids Health Dis.* **2004**, *3*, 24.
(143) Koba, K.; Imamura, J.; Akashoshi, A.; Kohno-Murase, J.; Nishizono, S.; Iwabuchi, M.; Tanaka, K.; Sugano, M. Genetically modified rapeseed oil containing *cis*-9,*trans*-11,*cis*-13-octadecatrienoic

DOI: 10.1021/jf505050c
J. Agric. Food Chem. 2015, 63, 1883−1895

acid affects body fat mass and lipid metabolism in mice. *J. Agric. Food Chem.* **2007**, *55*, 3741−3748.
(144) McFarlin, B. K.; Strohacker, K. A.; Kueht, M. L. Pomegranate seed oil consumption during a period of high-fat feeding reduces weight gain and reduces type 2 diabetes risk in CD-1 mice. *Br. J. Nutr.* **2009**, *102*, 54−59.
(145) Vroegrijk, I. O.; van Diepen, J. A.; van den Berg, S.; Westbroek, I.; Keizer, H.; Gambelli, L.; Hontecillas, R.; Bassaganya-Riera, J.; Zondag, G. C.; Romijn, J. A.; Havekes, L. M.; Voshol, P. J. Pomegranate seed oil, a rich source of punicic acid, prevents diet-induced obesity and insulin resistance in mice. *Food Chem. Toxicol.* **2011**, *49*, 1426−1430.
(146) Chen, P. H.; Chen, G. C.; Yang, M. F.; Hsieh, C. H.; Chuang, S. H.; Yang, H. L.; Kuo, Y. H.; Chyuan, J. H.; Chao, P. M. Bitter melon seed oil-attenuated body fat accumulation in diet-induced obese mice is associated with cAMP-dependent protein kinase activation and cell death in white adipose tissue. *J. Nutr.* **2012**, *142*, 1197−1204.
(147) Hsieh, C. H.; Chen, G. C.; Chen, P. H.; Wu, T. F.; Chao, P. M. Altered white adipose tissue protein profile in C57BL/6J mice displaying delipidative, inflammatory, and browning characteristics after bitter melon seed oil treatment. *PLoS One* **2013**, *8*, No. e72917.
(148) Yang, L.; Leung, K. Y.; Cao, Y.; Huang, Y.; Ratnayake, W. M.; Chen, Z. Y. Alpha-linolenic acid but not conjugated linolenic acid is hypocholesterolaemic in hamsters. *Br. J. Nutr.* **2005**, *93*, 433−438.
(149) Yuan, G.; Sun, H.; Sinclair, A. J.; Li, D. Effects of conjugated linolenic acid and conjugated linoleic acid on lipid metabolism in mice. *Eur. J. Lipid Sci. Technol.* **2009**, *111*, 537−545.
(150) Miranda, J.; Aguirre, L.; Fernandez-Quintela, A.; Macarulla, M. T.; Martinez-Castano, M. G.; Ayo, J.; Bilbao, E.; Portillo, M. P. Effects of pomegranate seed oil on glucose and lipid metabolism-related organs in rats fed an obesogenic diet. *J. Agric. Food Chem.* **2013**, *61*, 5089−5096.
(151) Tsuzuki, T.; Tokuyama, Y.; Igarashi, M.; Nakagawa, K.; Ohsaki, Y.; Komai, M.; Miyazawa, T. Alpha-eleostearic acid (9Z11E13E-18:3) is quickly converted to conjugated linoleic acid (9Z11E-18:2) in rats. *J. Nutr.* **2004**, *134*, 2634−2639.
(152) Yuan, G. F.; Sinclair, A. J.; Zhou, C. Q.; Li, D. α-Eleostearic acid is more effectively metabolized into conjugated linoleic acid than punicic acid in mice. *J. Sci. Food Agric.* **2009**, *89*, 1006−1011.
(153) Lai, C. S.; Tsai, M. L.; Badmaev, V.; Jimenez, M.; Ho, C. T.; Pan, M. H. Xanthigen suppresses preadipocyte differentiation and adipogenesis through down-regulation of PPAR gamma and C/EBPs and modulation of SIRT-1, AMPK, and FoxO pathways. *J. Agric. Food Chem.* **2012**, *60*, 1094−1101.
(154) Chou, Y. C.; Su, H. M.; Lai, T. W.; Chyuan, J. H.; Chao, P. M. *cis*-9, *trans*-11, *trans*-13-conjugated linolenic acid induces apoptosis and sustained ERK phosphorylation in 3T3-L1 preadipocytes. *Nutrition* **2012**, *28*, 803−811.
(155) Bassaganya-Riera, J.; DiGuardo, M.; Climent, M.; Vives, C.; Carbo, A.; Jouni, Z. E.; Einerhand, A. W.; O'Shea, M.; Hontecillas, R. Activation of PPARgamma and delta by dietary punicic acid ameliorates intestinal inflammation in mice. *Br. J. Nutr.* **2011**, *106*, 878−886.
(156) Coursodon-Boyiddle, C. F.; Snarrenberg, C. L.; Adkins-Rieck, C. K.; Bassaganya-Riera, J.; Hontecillas, R.; Lawrence, P.; Brenna, J. T.; Jouni, Z. E.; Dvorak, B. Pomegranate seed oil reduces intestinal damage in a rat model of necrotizing enterocolitis. *Am. J. Physiol. Gastrointestinal Liver Physiol.* **2012**, *303*, G744−G751.
(157) Hontecillas, R.; O'Shea, M.; Einerhand, A.; Diguardo, M.; Bassaganya-Riera, J. Activation of PPAR gamma and alpha by punicic acid ameliorates glucose tolerance and suppresses obesity-related inflammation. *J. Am. Coll. Nutr.* **2009**, *28*, 184−195.
(158) Anusree, S. S.; Priyanka, A.; Nisha, V. M.; Das, A. A.; Raghu, K. G. An *in vitro* study reveals the nutraceutical potential of punicic acid relevant to diabetes via enhanced GLUT4 expression and adiponectin secretion. *Food Funct.* **2014**, *5*, 2590−2601.
(159) Viladomiu, M.; Hontecillas, R.; Yuan, L. J.; Lu, P. Y.; Bassaganya-Riera, J. Nutritional protective mechanisms against gut inflammation. *J. Nutr. Biochem.* **2013**, *24*, 929−939.
(160) Lewis, S. N.; Brannan, L.; Guri, A. J.; Lu, P.; Hontecillas, R.; Bassaganya-Riera, J.; Bevan, D. R. Dietary alpha-eleostearic acid ameliorates experimental inflammatory bowel disease in mice by activating peroxisome proliferator-activated receptor-gamma. *PLoS One* **2011**, *6*, No. e24031.
(161) Dubuquoy, L.; Rousseaux, C.; Thuru, X.; Peyrin-Biroulet, L.; Romano, O.; Chavatte, P.; Chamaillard, M.; Desreumaux, P. PPARγ as a new therapeutic target in inflammatory bowel diseases. *Gut* **2006**, *55*, 1341−1349.
(162) Bertin, B.; Dubuquoy, L.; Colombel, J. F.; Desreumaux, P. PPAR-gamma in ulcerative colitis: a novel target for intervention. *Curr. Drug Targets* **2013**, *14*, 1501−1507.
(163) Tasdelen, I. *Modulation of the Adipogenic Master Regulator PPARγ*; Utrecht University: Amsterdam, The Netherlands, 2014.
(164) Penumetcha, M.; Santanam, N. Nutraceuticals as ligands of PPAR gamma. *PPAR Res.* **2012**, No. 858352.
(165) Ramos, R.; Mascarenhas, J.; Duarte, P.; Vicente, C.; Casteleiro, C. Conjugated linoleic acid-induced toxic hepatitis: first case report. *Dig. Dis. Sci.* **2009**, *54*, 1141−1143.
(166) Masters, N.; McGuire, M. A.; Beerman, K. A.; Dasgupta, N.; McGuire, M. K. Maternal supplementation with CLA decreases milk fat in humans. *Lipids* **2002**, *37*, 133−138.
(167) Riserus, U.; Basu, S.; Jovinge, S.; Fredrikson, G. N.; Arnlov, J.; Vessby, B. Supplementation with conjugated linoleic acid causes isomer-dependent oxidative stress and elevated C-reactive protein − a potential link to fatty acid-induced insulin resistance. *Circulation* **2002**, *106*, 1925−1929.
(168) EFSA Panel on Dietetic Products, N. a. A. N.. Scientific Opinion − Statement on the safety of the "conjugated linoleic acid (CLA)-rich oils" Clarinol® and Tonalin TG 80 as novel food ingredients. *EFSA J.* **2012**, *10*, 2700.
(169) Meerts, I. A. T. M.; Verspeek-Rip, C. M.; Buskens, C. A. F.; Keizer, H. G.; Bassaganya-Riera, J.; Jouni, Z. E.; van Huygevoort, A. H. B. M.; van Otterdijk, F. M.; van de Waart, E. J. Toxicological evaluation of pomegranate seed oil. *Food Chem. Toxicol.* **2009**, *47*, 1085−1092.

DOI: 10.1021/jf505050c
J. Agric. Food Chem. 2015, 63, 1883−1895

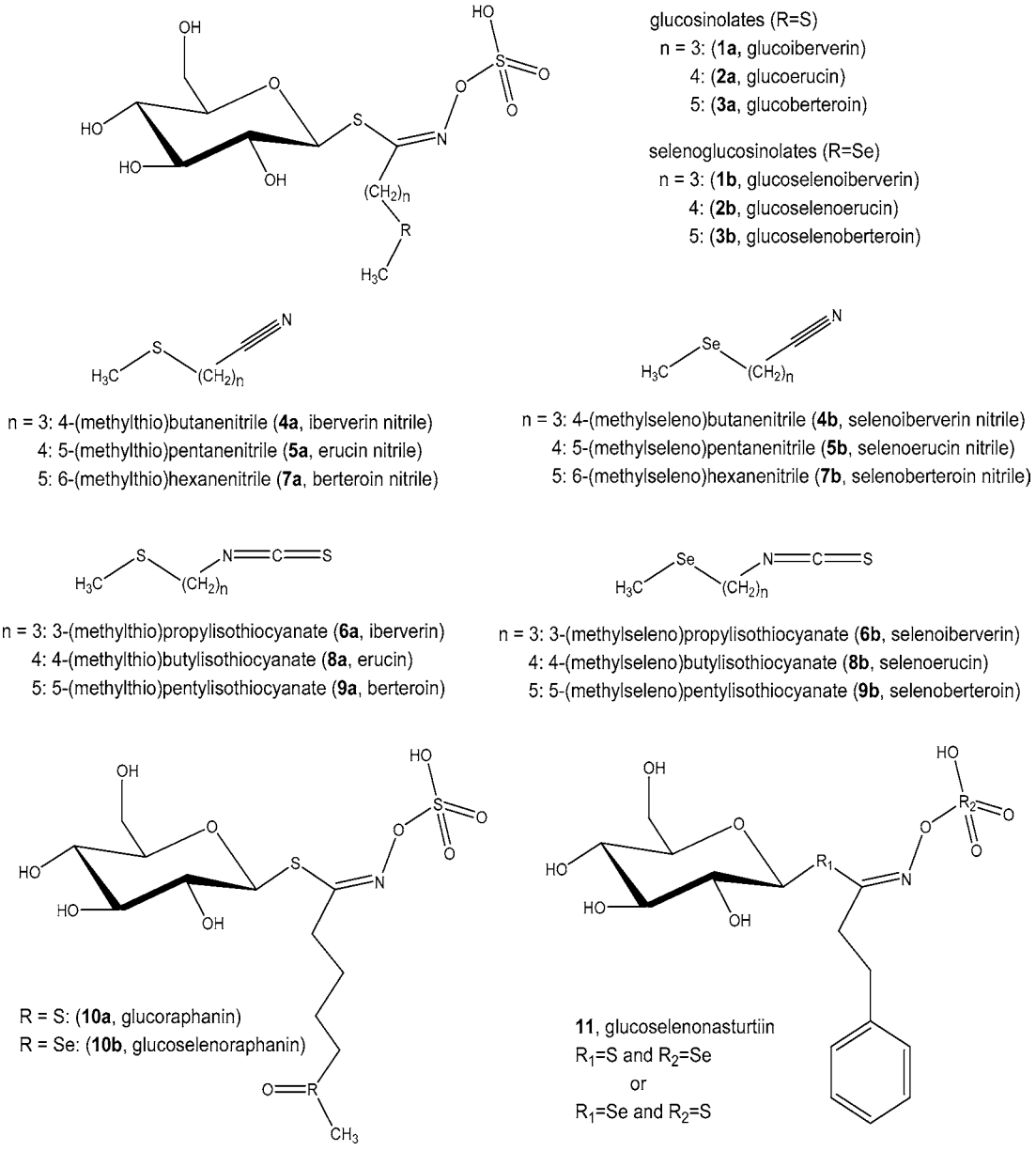

Figure 1. Structures of the glucosinolates and their modified aglycons (myrosinase enzyme hydrolysis products).

the only selenoamino acid incorporated into animal selenoproteins under direct genetic control. Selenoproteins are important in the control of cellular redox balance.[15] Additionally, the Brassicaceae contain the Se-specific enzyme selenocysteine methyltransferase, which catalyzes methylation of SeCys to methyl selenocysteine (3-(methylseleno)-L-alanine) and the downstream production of γ-glutamylselenomethyl selenocysteine (γ-glutamyl-3-(methylseleno)-L-alanine). Both of these modified amino acids have reported anticancer properties in mammals, the latter compound not directly so but as methyl selenocysteine to which it hydrolyzes in the intestinal tract.[14] At the cellular level it is proposed that the active cancer chemopreventative agent is actually methylselenol, which arises from the β-lyase hydrolysis of methyl selenocysteine.[14] The Brassicaceae are therefore of increasing interest for health benefits associated with their production of S-containing glucosinolates and selenoamino acids.

Recently, we reported several new Se-containing glucosinolates, and their aglycons, in the florets of broccoli and cauliflower and the tap roots of forage rape plants treated with sodium selenate fertilizer.[16] The selenoglucosinolates were of the methylseleno class (MeSe-GSLs), most likely derived from SeMet, and their downstream metabolites were methylseleno nitriles and isothiocyanates. In these experiments, the incorporation of Se into MeSe-GSLs, in the different tissues, appeared poorly correlated with the amounts of GSLs present. For example, forage rape tap roots had much higher concentrations of MeS-aglycons than the broccoli and cauliflower florets, yet the forage rape tap roots did not have correspondingly higher concentrations of the MeSe-aglycons.[16] Furthermore, broccoli is reported to have its highest total and aliphatic GSL concentrations in the florets,[17,18] but the highest concentrations of the major MeS-GSL glucoerucin[16,19] were found in the tap roots.[18] If incorporation of Se into glucoerucin is as efficient in the tap roots as it is in the florets, then the broccoli tap roots might produce higher concentrations of MeSe-GSLs.

DOI: 10.1021/jf505963c
J. Agric. Food Chem. 2015, 63, 1896−1905

Other workers have synthesized a number of isoselenocyanates: selenosulforaphane and several alkyl and phenylalkyl isoselenocyanates.[20,21] These synthetic compounds were reported as more bioeffective than their S analogues at reducing the incidence and progression of carcinogenesis. However, in these synthetic organoselenides the Se atom would have been located in the glucose moiety (e.g., compound **11**, R_1 = Se) of the parent GSL, in contrast with the methylseleno compounds found in planta, where the Se atom has been found only in the position derived from methionine.[16]

We were therefore interested in investigating which *Brassica* plant tissues had the highest concentrations of GSL compounds capable of incorporating Se, whether they also had the highest concentrations of the newly discovered methylseleno compounds, and also whether Se-GSLs with the Se incorporated into the thioglucose group could also be produced in *Brassica*.

MATERIALS AND METHODS

Plant Growth and Harvesting. The two broccoli (*B. oleracea* L. var. *italica*) cultivars chosen were a high-GSL-producing cultivar ('Booster', hereafter referred to as high-GSL broccoli) and a moderate- to low-GSL-producing cultivar ('Triathlon', hereafter referred to as low-GSL broccoli). Cauliflower (*B. oleracea* L. var. *botrytis* cv. 'Liberty') and forage rape (*B. napus* cv. 'Maxima') were also selected. Plants were grown from seed in separate 8 L bags of potting mix in a glass house at Plant & Food Research, Palmerston North, New Zealand. Plants were watered once daily via watering spikes for 1 min. Selenium feeding was commenced for broccoli and cauliflower following the emergence of immature floret material from the meristem and for forage rape once the plants had a well-established stem (ca. 16 cm from the soil to the top of the meristem) and approximately 10 fully expanded leaves. Plants were fed via the soil with 20 mL of 5.0 mM sodium selenate twice weekly, for 4 weeks, after watering. This Se application is equivalent to ca. 15 kg/ha, which is considerably higher than the 3−76 g/ha applied to agricultural and forage crops.[11] Broccoli produced at this high rate of Se application contained at least 500-fold more Se than control samples[22] but suffered no adverse effects upon its growth. Following the Se feeding, the leaves, stems, and lower stem/tap root (3−4 cm long) were harvested from all of the plants, after four months of growth, as well as mature floret tissue from the broccoli and cauliflower plants. For the forage rape roots, the outer fibrous ring was removed and only the inner pith was sampled. All material was immediately frozen in liquid nitrogen before storage at −80 °C until extraction.

Extraction of Glucosinolates for LC−MS Analysis. Triplicate extractions were performed on the tissue from selenized and duplicate extractions from control (nonselenized) plants, with each replicate comprising tissue from a separate plant. In the case of the leaves, for each replicate the two most recently expanded leaves were harvested from each of two separate plants (four leaves per replicate). For each replicate frozen tissue (2−10 g FW) was accurately weighed, ground with dry ice to a powder in a coffee grinder, and poured into boiling 70% ethanol (10 volumes (v/w)), which was refluxed for 5 min to inactivate the myrosinase.[8] Samples were cooled to 5 °C and concentrated in vacuo at 40 °C to volumes of ca. 5 mL. Pigments were removed from the concentrates by washing with an equal volume of dichloromethane (2× for the leaf and floret extracts), and solids were removed by centrifugation at 1000*g* for 1 min in a Hema-C centrifuge (Jouan, Saint Herblain, France). A cold (ice−water) acidic (0.5% AcOH) methanol extraction of GSLs was also performed on the high-GSL broccoli florets, based upon the method of Hsu et al.[23] The extracts were colorless, so pigment removal was not necessary. The amounts of glucoselenoraphanin in two replicates were compared with those in two parallel hot ethanolic extracts.

Extraction of Glucosinolate Hydrolysis Products (Modified Aglycons) for GC−MS Analysis. The same number of replicates was used as above for the glucosinolate extractions. For each replicate 3−5 g FW was accurately weighed and ground with dry ice to a powder in a coffee grinder. The sample was combined with 2 volumes (v/w) of prechilled diethyl ether on ice in a Schott bottle, which was sealed and left at 1 °C for a week with daily mixing before the solid material was frozen at −20 °C and the solvent poured off. The solvent extracts were dried ($MgSO_4$) and their volumes reduced to ca. 1.5 mL under a gentle stream of nitrogen.

LC−MS Analysis of Glucosinolates. Separations were performed on an Ultimate 3000 rapid separation liquid chromatograph (Dionex, Germering, Germany) with a micrOTOF-Q II mass spectrometer (Bruker Daltonics, Bremen, Germany) fitted with an electrospray source operating in negative mode. Sample injections (1 μL) were made onto a 50 mm × 2.1 mm i.d., 1.8 μm, Zorbax SB-C18 (Agilent) analytical column maintained at 50 °C and with a flow of 400 μL/min. Solvent A was H_2O/MeOH (10:90, v/v), and solvent B was HCO_2H/H_2O (0.5:99.5, v/v). The solvent ramp was 1:99 (solvent A:solvent B) from injection to 0.5 min, followed by a linear gradient to 30:70 (0.5−8 min), to 75:25 (8−13 min), and to 100:0 (13−15 min) and holding at 100:0 (15−17 min). The micrOTOF-Q II source parameters were as follows: 200 °C; drying N_2 flow, 8 L/min; nebulizer N_2, 4 bar (400 kPa); end plate offset, −500 V; capillary voltage, +3500 V; mass range, 100−1500 Da; 2 scans/s. Postacquisition internal mass calibration used sodium formate clusters with the sodium formate delivered by a syringe pump at the start of each analysis. MS data were processed by Compass DataAnalysis (Bruker Daltonics). The external standard used for quantitation (using $[M - H]^-$ current peak areas) was glucoerucin, **2a** ([4-(methylthio)butyl]glucosinolate) (Cfm Oskar Tropitzsch, Marktredwitz, Germany). The external standard and the plant extracts were spiked with an internal standard, epicatechin (Sigma-Aldrich, Auckland, New Zealand), to enable correction for sample volumes and for changes in LC−MS system responses. Identification of the S- and Se-GSLs by high-resolution LC−MS/MS has been described previously.[16]

Total Elemental Se Present as GSLs in the Plant Tissues. The total concentration of elemental Se present as MeSe-GSLs in each plant part was calculated by summing the concentrations of elemental Se in each of the individual MeSe-GSLs, using the molecular weight of the GSLs and the percentage of that MW that was constituted by elemental Se.

GC−MS Analysis of Glucosinolate Hydrolysis Products (Modified Aglycons). Separations were performed on an Agilent 6890N gas chromatograph coupled to a Waters GCT time-of-flight (ToF) mass spectrometer with an EI energy of 70 eV and a scan time of 0.4 s. Splitless injections of 1 μL over 30 s were made at 220 °C onto a 20 m × 0.18 mm i.d. × 0.18 μm film, Stabilwax (Restek, Bellefonte, PA) capillary column with a He flow of 0.9 mL/min. The oven temperature program was 1 min at 35 °C, 3 °C/min to 100 °C, and 7 °C/min to 240 °C, which was held for 5 min. Compounds were quantitated (using M^+ peak areas) against the synthetic[16] external standard selenoerucin nitrile, **5b**, $CH_3SeC_4H_8CN$, at concentrations of 0.02, 0.08, and 0.5 μL/L, to provide a response calibration curve. To keep the concentrations of compounds in the solvent extracts in the linear range of the MS detector, samples were injected neat and at 10- and 50-fold dilutions. All external standards and plant extracts were spiked with an internal standard (pentadecafluorooctanol) (Pierce Chemicals, Rockford, IL) to enable correction for extract sample volumes and changes in GC−MS system responses.

GC−MS Data. 6-(Methylseleno)hexanenitrile, $CH_3SeC_5H_{10}CN$ (Figure 1). RI (Wax) 2109. HR-ToF-EIMS: *m/z* 191.0194 (−1.9 mDa), $[M]^+$. ToF-EIMS (Figure 2): *m/z* (fragment) (rel intens) 193 ($[M]^+$, Se^{82}) (9),191 ($[M]^+$, Se^{80}) (55), 189 ($[M]^+$, Se^{78}) (27), 187 ($[M]^+$, Se^{76}) (11), 123 $[CH_3SeC_2H_4]^+$ (9), 109 $[CH_3SeCH_2]^+$ (30), 96 $[C_5H_{10}CN]^+$ (100) and $[CH_3SeH]^+$ (minor), 94 $[CH_2Se]^+$ (25), 69 $[C_4H_7N]^+$ (70), 55 $[C_3H_5N]^+$ (89), 41 $[C_2H_3N]^+$ (39).

LC−MS Data. Glucoselenoraphanin, $C_{12}H_{22}NO_{10}S_2Se$, $[M - H]^-$, *m/z* 483.9856 (+0.6 mDa). MS/MS: $C_6H_{11}O_5S^-$, *m/z* 195.0281 (−4.6 mDa); $C_6H_{11}O_6SO_3^-$, *m/z* 259.0104 (−2 mDa), $C_6H_{11}O_5SSO_3^-$, *m/z* 274.9882 (−1.3 mDa); $C_{11}H_{18}NO_9S_2^-$, *m/z* 372.0424 (+0.1 mDa).

Statistical Treatment. Error values are standard errors of the mean (SEM), calculated using the Microsoft Excel 2007 "standard deviation" function and dividing the value obtained by the square root

DOI: 10.1021/jf505963c
J. Agric. Food Chem. 2015, 63, 1896−1905

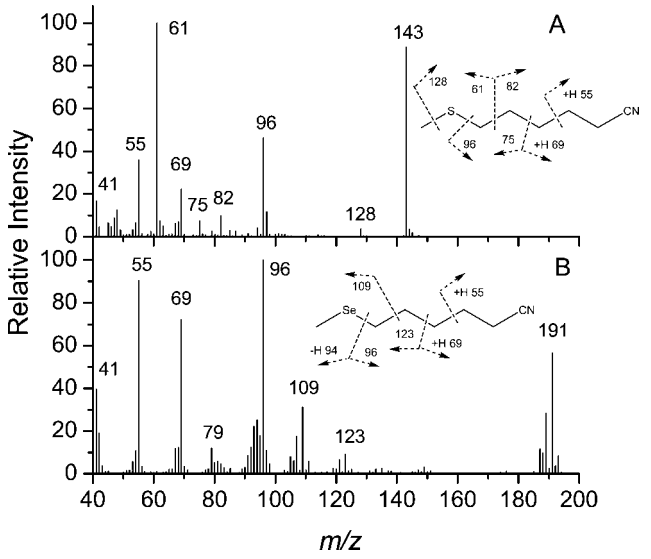

Figure 2. Comparison between the mass spectra (EI, 70 eV) of (A) 6-(methylthio)hexanenitrile (berteroin nitrile, **7a**) and (B) its Se analogue 6-(methylseleno)hexanenitrile (selenoberteroin nitrile, **7b**), the latter compound being newly reported.

of the number of replicates. Statistical differences between sample means were analyzed using Student's *t* test.

RESULTS AND DISCUSSION

New Se-Containing Metabolites. This study targeted the methylthio-containing family of glucosinolates (MeS-GSLs) and their aglycons, which represent about 10% of the total glucosinolate content of the *Brassica* investigated and are the glucosinolates known to assimilate Se.[16] In addition to nine previously discovered organoselenides, **1b**–**9b** (Figure 1),[16] we have identified three new Se-containing metabolites. Glucoselenoraphanin, **10b**, was identified in high-GSL broccoli florets, and a Se-containing isomer of gluconasturtiin, **11** ((2-phenylethyl)glucosinolate), was tentatively identified in forage rape tap roots. These compounds are the Se analogues of the most abundant GSLs in these tissues. In addition, selenoberteroin nitrile, **7b** (6-(methylseleno)hexanenitrile), was tentatively identified in the tap roots and stem of forage rape.

New Compound Identification. Glucoselenoraphanin, **10b**, was identified from its pseudomolecular ion $C_{12}H_{22}NO_{10}S_2Se$, $[M - H]^-$, with a distinctive Se isotope pattern. It eluted 0.6 min after glucoraphanin and 4.1 min before glucoselenoerucin, **2b**, on the reversed phase LC column. **10b** constituted less than 0.08% of the glucoraphanin and 1.3% of the **2b** present in broccoli florets. Several diagnostic MS/MS daughter ions were obtained for glucoselenoraphanin by fragmentation of the pseudomolecular ion:[24] the thioglucose group $C_6H_{11}O_5S^-$, which precluded the attachment of the Se atom to glucose; the glucose sulfate ion $C_6H_{11}O_6SO_3^-$, from rearrangement and neutral loss of $CH_3Se(O)C_4H_8N{=}C{=}S$; $C_6H_{11}O_5SSO_3^-$, from rearrangement and neutral loss of $CH_3Se(O)C_4H_8N{=}C{=}O$; $C_{11}H_{18}NO_9S_2$, from neutral loss of CH_3SeOH. These fragments all indicated that the Se was located neither in the thioglucose nor in the sulfate moieties but was present as a selenoxide derived from SeMet as observed for the other major selenoglucosinolates discussed here.

Glucoraphanin, the parent GSL of sulforaphane, is the most abundant S-containing GSL in broccoli[8] and seriously overloaded the detector of the mass spectrometer for the broccoli florets we analyzed. Despite these very high levels of glucoraphanin, we did not identify its selenoxide analogue **10b** in any of the selenized *Brassica* in our previous study in which a low-GSL broccoli was selenized.[16] Selenoxides are generally considered to be thermally unstable;[25] hence, it was surprising to identify glucoselenoraphanin. Thermal instability may however explain the extremely low levels of selenization (<0.08%) observed for this particular glucosinolate. Given that the glucosinolates were extracted in boiling 70% ethanol, the concentration of glucoselenoraphanin in the broccoli may be higher than we have measured. Another possibility is that it accumulates due to autoxidation of glucoselenoerucin in the sample during cold storage prior to analysis.

The glucoraphanin aglycons sulforaphane ($CH_3S(O)$-C_4H_8NCS) and sulforaphane nitrile ($CH_3S(O)C_4H_8CN$) are well-known in *Brassica*,[26,27] but were not identified in this study as these compounds eluted after the 45 min run time used on the polar GC column employed here. Considerable amounts of both compounds were identified in samples run on a less polar (DB-5) GC column (data not shown), but their selenoxide analogues were not detected as expected due to their thermal instability.

Given the interest in sulforaphane as a compound associated with inhibition of carcinogenesis and the potential importance of its Se analogue, we investigated the effect of cold acidic methanolic versus hot ethanolic extractions of GSLs from high-glucoraphanin broccoli tissues to determine if there exist significant concentrations of glucoselenoraphanin, **10b**, and thus possibly selenosulforaphane, in selenized *Brassica*. The two replicate cold acidic methanol extracts contained concentrations of glucoraphanin similar to those in the hot ethanolic extracts. However, only one of the cold methanolic extracts contained detectable glucoselenoraphanin, which occurred at about 20% of the concentrations found in the two hot ethanolic extracts. Selenoxides are used as mild oxidizing agents, the reaction generally taking place under mildly acidic conditions.[28] Therefore, extraction with acidic methanol was counterproductive, possibility having resulted in the reduction of the glucoselenoraphanin to glucoselenoerucin. There was also approximately 14-fold more glucoselenoerucin in the hot-extracted samples than in the cold acidic extracts, whereas there was only 25% more glucoerucin in the hot-extracted samples. Clearly there is a problem with the acidic extraction of the selenoglucosinolates, and the question of whether there exist substantial quantities of glucoselenoraphanin and selenosulforaphane in selenized broccoli remains to be answered.

Glucoselenonasturtiin, **11**, $C_{15}H_{20}NO_9SSe$, $[M - H]^-$, was the other glucosinolate identified, with a distinctive Se isotope pattern, eluting 0.5 min after gluconasturtiin. The site of selenization remains unknown as the samples were too dilute for LC–MS/MS analysis. This Se-GSL constituted less than 0.04% of the total gluconasturtiin and was a very minor contributor to the Se-GSL content of the forage rape.

We did not unambiguously detect any GSLs, or their aglycons, containing the Se atom in the isothiocyanate moiety, as produced in synthetic selenosulforaphane and alkyl and phenylalkyl isoselenocyanate compounds.[20,21] There have been other reports of the incorporation of trace amounts of Se into *Brassica* glucosinolates and their aglycons. Radioactive selenosinigrin was identified in the sinigrin (2-propenylglucosinolate) fraction isolated from horseradish (*Armoracia lapathidolia)* leaves treated with radioactive $Na_2{}^{75}SeO_4$.[29] Similarly, selenized gluconasturtiin was identified in the hairy

DOI: 10.1021/jf505963c
J. Agric. Food Chem. 2015, 63, 1896–1905

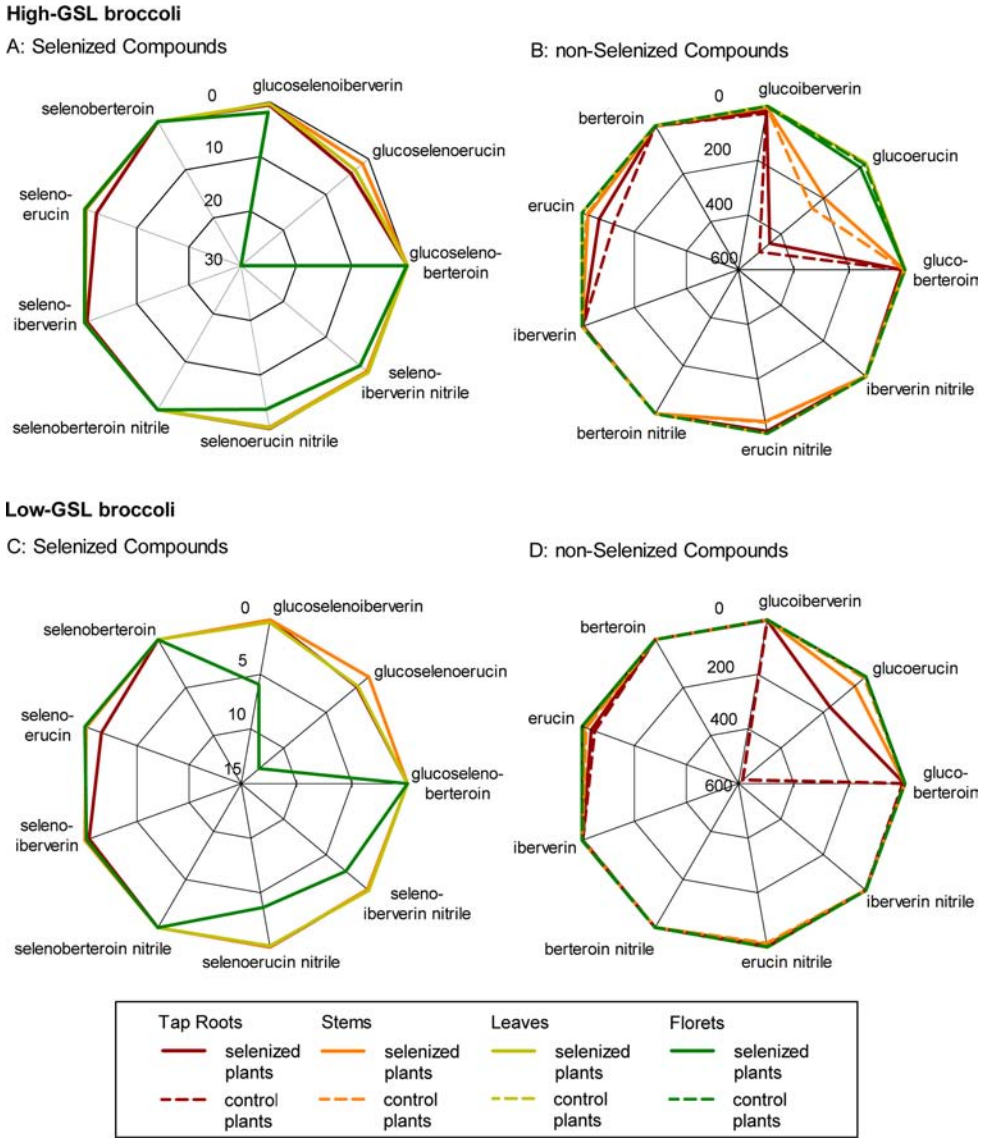

Figure 3. Glucosinolates and their nitrile and isothiocyanate hydrolysis products (modified aglycons) in the tap roots, stems, leaves, and florets of broccoli fertilized with 5 mM sodium selenate. (A) Selenized compounds in high-GSL broccoli: concentrations (mg/kg FW) of glucoselenoiberverin, glucoselenoerucin, and glucoselenoberteroin and their modified aglycons. (B) Nonselenized compounds in high-GSL broccoli: effect of Se fertilization on the concentrations (mg/kg FW) of glucoiberverin, glucoerucin, and glucoberteroin and their aglycons. (C) Selenized compounds in low-GSL broccoli: concentrations (mg/kg FW) of glucoselenoiberverin, glucoselenoerucin, and glucoselenoberteroin and their modified aglycons. (D) Nonselenized compounds in low-GSL broccoli: effect of Se fertilization on the concentrations (mg/kg FW) of glucoiberverin, glucoerucin, and glucoberteroin and their aglycons. Quantitation of the GSLs was by LC−MS as glucoerucin equivalents, and that of the modified aglycons was by GC−MS as erucin nitrile equivalents. Values are the average of three samples for selenized plants and two samples for the control plants, each replicate from a separate plant.

root cultures of *Nasturtium officinale* treated with a growth medium containing inorganic Se.[30] In neither case was it determined whether the Se was in the thioglucose or the sulfate group. A confident determination of the location of selenization in a glucosinolate was made in *Stanleya pinnata* plants grown hydroponically with Na_2SeO_3. The researchers identified 3-butenyl isoselenocyanate, but with a very low level of Se incorporation.[31] Even though similar concentrations of S and Se were applied, the Se aglycon was at less than 0.05% of the concentration of its S analogue. This is similar to the very low incorporation of Se into gluconasturtiin and glucoraphanin reported here and suggests that biosynthesis via SeMet provides the only efficient route for incorporation of Se into *Brassica* glucosinolates.

Selenoberteroin nitrile has not been reported in the literature, and our identification was based upon its order of elution in the gas chromatograph (after berteroin nitrile) and its mass spectrum shown in Figure 2, along with that of berteroin nitrile, **7a**. Berteroin nitrile has been reported in broccoli and cauliflower[32] and in forage rape roots[10,33] and buds.[34] We have previously identified both glucoberteroin and glucoselenoberteroin in broccoli and forage rape.[16]

Methyl thiocyanate and methyl selenocyanate were also identified in broccoli and cauliflower leaves and florets,[16] and methyl thiocyanate was identified in the leaves of forage rape (data not shown). We could not identify a parent GSL for these compounds nor find a literature reference for the occurrence of such a GSL. These two compounds may result from the

DOI: 10.1021/jf505963c
J. Agric. Food Chem. 2015, 63, 1896−1905

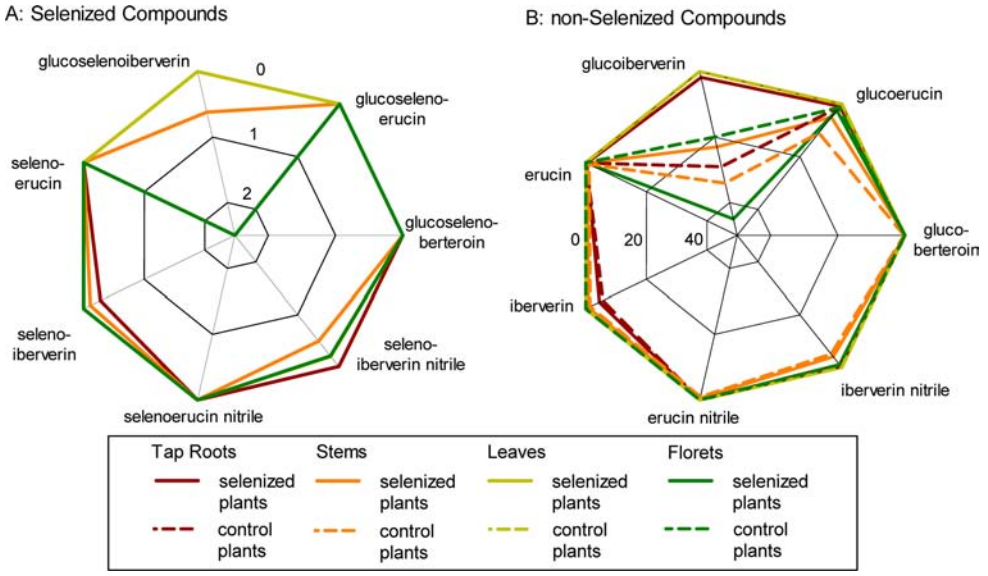

Figure 4. Glucosinolates and their nitrile and isothiocyanate hydrolysis products (modified aglycons) in the tap roots, stems, leaves, and florets of cauliflower fertilized with 5 mM sodium selenate. (A) Selenized compounds: concentrations (mg/kg FW) of glucoselenoiberverin, glucoselenoerucin, and glucoselenoberteroin and their modified aglycons. (B) Nonselenized compounds: effect of Se fertilization on the concentrations (mg/kg FW) of glucoiberverin, glucoerucin, and glucoberteroin and their modified aglycons. Quantitation of the GSLs was by LC−MS as glucoerucin equivalents, and that of the modified aglycons was by GC−MS as erucin nitrile equivalents. Values are the average of three samples for selenized plants and two samples for the control plants, each replicate from a separate plant.

methylation of thiocyanate and selenocyanate ions by a thiol methyltransferase (TMT).[35]

MeSe-GSL Concentrations in Broccoli. A high-GSL-producing cultivar ('Booster') and a moderate- to low-GSL-producing cultivar ('Triathlon') were chosen to examine the effect of Se fertilization on GSL production and to determine if high Se incorporation was peculiar to high-GSL-producing cultivars. In the high-GSL broccoli the concentrations of selenizable GSLs in the tap roots were 70 and 2200 times higher than in the florets and leaves, respectively (Figure 3B). The low-GSL cultivar had no detectable selenizable GSLs in the florets. Despite this, the florets had the highest MeSe-GSL concentrations, the predominant compound being glucoselenoerucin, **2b** (Figure 3A,C). The leaves and florets of the low-GSL broccoli also contained glucoselenoiberverin, **1b**, as a significant proportion of the MeSe-GSL content, which was not the case in high-GSL broccoli, possibly because when the latter was selenized, it showed a very large increase in its glucoerucin concentrations. In both cultivars, MeSe-GSL concentrations in the tap roots, leaves, and stems were about 10% of those in the florets (Figure 3A,C). Glucoselenoerucin and glucoerucin, **2a**, were the main MeSe- and MeS-containing compounds in all tissues (Figure 3A,D).

The MeS-GSLs of the stems and tap roots were around 1% selenized, the florets were 50% and 97% selenized (high-GSL and low-GSL broccoli, respectively), and the leaves were around 70% selenized. Thus, even though the concentrations of selenizable GSLs were low in the leaves, the measured MeSe-GSL concentrations were similar to those in the roots and stems. Treatment of these plants with Se did not commence until the florets started to emerge from the meristem, when the plant was diverting resources to the development of floret and leaf tissue. This may explain the greater accumulation of MeSe-GSLs in the growing florets and leaves than in the stems and tap roots. In accord with this result, sulfur fertilization of broccoli gave consistently higher assimilation and incorporation of S into GSLs in the florets and leaves compared to the roots.[17] This selective accumulation of MeSe-GSLs into the florets could be used to most economically produce high-Se broccoli.

Differential Alteration of the Total Concentrations of MeS-GSLs in Broccoli by Selenization. In selenized high-GSL broccoli, the total concentrations of the MeS/Se-GSLs were slightly, but not significantly, lower in the roots and stems but significantly higher in the leaves (20-fold) and florets (8-fold) than in the control plants, due to the presence of glucoselenoerucin and higher concentrations of glucoerucin (Figure 3A,B). In a study of floret GSL concentrations, Se fertilization caused an average 36% reduction in total GSL concentrations, which was mostly due to lower glucoraphanin levels, which we did not examine.[19] Robbins et al.[36] reported that very high levels of Se fertilizers reduced the concentrations of the aliphatic but not the indole GSLs. Kim and Juvik[37] reported that different broccoli cultivars displayed different responses to Se fertilization, with one of the five cultivars studied showing a small nonsignificant increased aliphatic GSL accumulation while the other four cultivars showed decreases.

MeSe-GSL Concentrations in Cauliflower. The highest concentrations of cauliflower MeSe-GSLs were in the florets (Figure 4A), but Se incorporation was much lower than in broccoli. MeSe-GSLs in the cauliflower florets totaled 2.5 mg/kg FW compared with 32.4 and 18.8 mg/kg FW, respectively, in the high- and low-GSL broccoli. While the major MeSe-GSL in broccoli was glucoselenoerucin, **2b**, the single MeSe-GSL in cauliflower florets and stems was glucoselenoiberverin, **1b**. Its sulfur analogue glucoiberverin, **1a**, is the major cauliflower MeS-GSL, which predominated in all tissues apart from the leaves in which GSLs were not detected.[8,9]

The cauliflower stems had more MeS-GSLs than low-GSL broccoli and less than the high-GSL broccoli stems, but with similarly low Se incorporation. MeSe-GSLs were not found in cauliflower tap roots whose MeS-GSL concentrations were

DOI: 10.1021/jf505963c
J. Agric. Food Chem. 2015, 63, 1896−1905

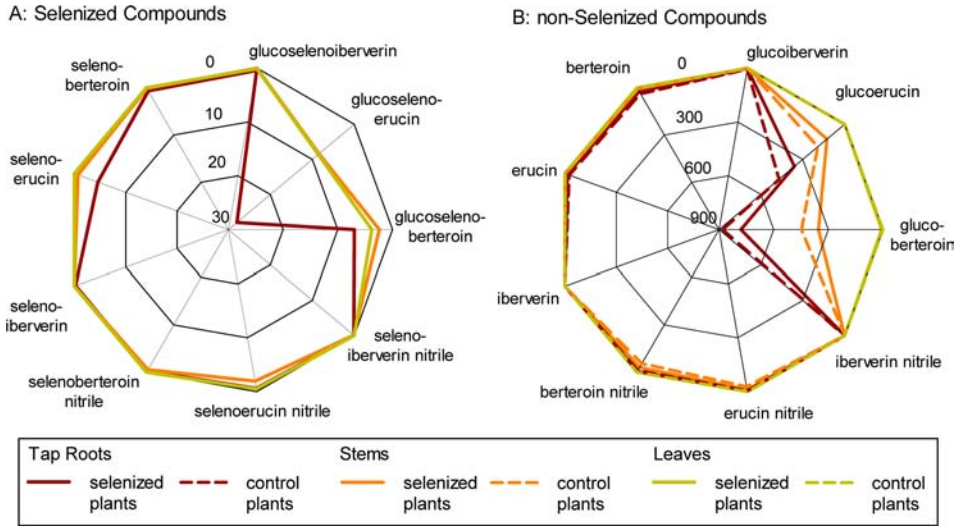

Figure 5. Glucosinolates and their nitrile and isothiocyanate hydrolysis products (modified aglycons) in the tap roots, stems, and leaves of forage rape fertilized with 5 mM sodium selenate. (A) Selenized compounds: concentrations (mg/kg FW) of glucoselenoiberverin, glucoselenoerucin, and glucoselenoberteroin and their modified aglycons. (B) Nonselenized compounds: effect of Se fertilization on the concentrations (mg/kg FW) of glucoiberverin, glucoerucin, and glucoberteroin and their modified aglycons. Quantitation of the GSLs was by LC−MS as glucoerucin equivalents, and that of the modified aglycons was by GC−MS as erucin nitrile equivalents. Values are the average of three samples for selenized plants and two samples for the control plants, each replicate from a separate plant.

similar to those in the stems and florets (Figure 4A) and at a mere 5% of the concentrations found in the broccoli tap roots. We did not detect Se analogues of the cauliflower GSLs glucoerucin and glucoberteroin (Figure 4B). The major cauliflower GSL is the indolic glucobrassicin in contrast to glucoraphanin in broccoli.[8,9]

Differential Alteration of the Total Concentrations of MeS-GSLs in Cauliflower by Selenization. In the selenized cauliflower both the tap roots ($P < 0.08$) and stems had lower concentrations of MeS-GSLs than the control plants, while the florets had higher, but not significantly so, concentrations of MeS-GSLs (Figure 4B). Most of this increase was due to glucoiberverin, although the variance in these data was high.

MeSe-GSL Concentrations in Forage Rape. Selenium incorporation into the forage rape tap root GSLs was low (3%, Figure 5, part A vs part B) as seen previously,[16] but 3 times higher than in the broccoli. Also, the total concentration of MeS-GSLs (1360 mg/kg FW) in the forage rape tap roots was 2 times that measured in broccoli and 40-fold higher than in cauliflower tap roots. Therefore, the forage rape tap roots had MeSe-GSL concentrations similar to those in the broccoli florets, with the major compound in both cases being glucoselenoerucin. The major GSL in forage rape tap roots is gluconasturtiin, **11**, which has been measured at 1900 mg/kg FW,[10] and which only incorporated trace amounts of Se.

The concentrations of MeS-GSLs and MeSe-GSLs in the forage rape stems and leaves were both higher than found in the other *Brassica*, so overall, forage rape plants had higher total concentrations of MeSe-GSLs than the other *Brassica* studied, despite not having the floret structure which contained most of the MeSe-GSLs in broccoli and cauliflower. The summed concentrations of all MeSe-GSLs, in all tissues studied, were 59.1 mg/kg (forage rape), 42.1 mg/kg (high-GSL broccoli), 21.7 mg/kg (low-GSL broccoli), and 3.1 mg/kg (cauliflower).

Glucoberteroin, **3a**, was the most abundant MeS-GSL in forage rape at 2 times the concentration of glucoerucin, **2a** (Figure 5B). The reverse was observed for the MeSe-GSLs with glucoselenoerucin at up to 4 times the concentration of glucoselenoberteroin (Figure 5A), indicating a differential incorporation of Se. Glucoiberverin and glucoselenoiberverin were both present as minor GSLs. The three GSLs glucoberteroin, glucoerucin, and glucoiberverin have previously been reported as the main MeS-GSLs in the roots of other forage rape cultivars.[10,38]

Modified Aglycons from Hydrolysis of the GSLs. A new selenium-containing aglycon, selenoberteroin nitrile, **7b** (6-(methylseleno)hexanenitrile) (Figure 1), in forage rape is reported for the first time (Figure 2). Se aglycons were present in extracts of all tissues of the Se-fed plants, though varying considerably in numbers of compounds and concentration (Figures 3−5). They loosely reflected the presence and concentration of the parent MeSe-GSL, but there were occurrences of MeSe aglycons without their MeSe-GSL precursors being detected and vice versa, viz., the aglycons selenoiberverin and selenoerucin in low-GSL broccoli without either of their GSL parents and glucoselenoberteroin in high-GSL broccoli florets without any of its aglycons. Similarly, in cauliflower the presence of the Se aglycons in all plant parts infers the presence of their corresponding Se-GSLs even though we did not identify them in the tap roots or leaves. Conversion of GSLs to the modified aglycons is influenced considerably by the conditions operating during tissue disruption.[27,39,40] We have not attempted to optimize this conversion, but breakdown of the MeSe-GSLs into the MeSe aglycons appears to occur at an efficiency similar to the formation of MeS aglycons.

The aglycon organosulfides identified here have previously been reported from broccoli florets,[32,41] although most interest has been in sulforaphane and sulforaphane nitrile because of the putative anticancer properties of the former[26,42] and possibly because it is the main aglycon from broccoli.[26] Comparisons between the amounts of particular aglycons, such as sulforaphane, have been conducted from different parts of broccoli plants,[43,44] but we have not been able to find reports that discuss the range of compounds from the different tissues. We recently identified the MeSe aglycons from broccoli

DOI: 10.1021/jf505963c
J. Agric. Food Chem. 2015, 63, 1896−1905

florets,[16] these tissues being of interest because they are the most consumed parts of these plants. The current study is the first we are aware of in which the distribution of MeS- and MeSe-GSL aglycons produced from different parts of broccoli plants has been examined.

All the cauliflower MeS aglycons reported in the present study (Figure 4B) are well-known.[32,41,45,46] However, as with broccoli, there is little information reporting the range of aglycons from different parts of cauliflower plants. In steam distillates of cauliflower florets and leaves, the summed nitrile and isothiocyanate concentration was higher in the florets,[46] as we observed. The MeS aglycons reported by these workers were iberverin, iberverin nitrile, erucin, and erucin nitrile. We have not been able to find other reports of MeS aglycons from plant parts of cauliflower and no reports of MeSe aglycons, apart from our previous paper.[16]

The complement of nitrile and isothiocyanate MeSe aglycons identified in extracts from forage rape tap roots (Figure 5A) reflected the presence of all three MeSe-GSLs in this tissue. Previously, we reported aglycons from forage rape tap roots, but not from the stems or leaves.[16] Erucin, erucin nitrile, berteroin, and berteroin nitrile have been reported by other workers from the tap roots, but not from the leaves and stems of forage rape.[10] We also identified iberverin and iberverin nitrile from the tap roots and iberverin nitrile, erucin nitrile, berteroin nitrile, erucin, and berteroin from the stems and leaves: these compounds have not previously been reported from forage rape.

Differential Alteration of the Concentrations of GSL Hydrolysis Products by Selenization. The total concentrations of modified aglycons in plant parts of some *Brassica* responded to selenization similarly to those of their GSLs. There were significantly higher summed concentrations of nitriles and isothiocyanates in the broccoli leaves (28-fold) and florets (7-fold), while there was a reduction, but not significantly, in their concentrations in the broccoli tap roots (ca. 40%) and in forage rape tap roots (35%) and stems (40%). The other plant parts did not display notable changes in the concentrations of these compounds as a result of selenization. While high-Se broccoli florets contain more MeS/Se aglycons, the reverse is reported for sulforaphane. In very high Se broccoli florets, Robbins et al.[36] measured lower concentrations of glucoraphanin and concentrations of sulforaphane reduced to 20% of those in the control plants. As a consequence, the biological activity of such broccoli with respect to sulforaphane may be reduced. In a study on the effect of selenized broccoli extracts upon mouse hepatoma cells, the selenized broccoli inhibited oxidative DNA damage, but the concomitant low sulforaphane concentrations reduced the ability of the broccoli extract to induce phase II detoxification proteins, which also exhibit antioxidant activity.[47] In broccoli with total selenium concentrations at edible levels, these complications may not arise. In a recent study glucoraphanin and sulforaphane concentrations were not adversely affected under more modest Se fertilization regimes which produce edible broccoli.[48]

Use of Selenized *Brassica* in Biological Experiments. Table 1 estimates the amounts of elemental Se present as Se-GSLs in each plant tissue. Cauliflower and broccoli had the highest concentrations of GSL-derived Se in their florets, between 4- and 10-fold higher than in their other tissues. For forage rape, the tap roots had the highest concentration of GSL-derived Se, at around 3-fold higher than in its other tissues. Therefore, the forage rape roots and the broccoli florets would be the best sources for Se-GSLs. A 100 g portion of selenized high-GSL broccoli floret, produced in this experiment, would however contain 550 μg (5.5 ppm) of elemental Se as Se-GSLs. This amount of selenium is above both the recommended minimum and recommended maximum daily Se intake levels of 55−90 and 400 μg/d, respectively.[49,50] Selenium is present in *Brassica* in several other chemical forms, and Finley et al., who used a similar fertilization regime for broccoli, measured a total elemental Se concentration of 500 μg/g DW. A 100 g (FW) portion would contain approximately 5 mg of elemental Se.[22] For biological testing, extracts of this plant material could be used to ensure suitable levels of MeSe-GSLs and of Se, particularly if they are shown to be beneficial to human health. Alternately, florets of broccoli grown with low-Se fertilization, to produce total Se at levels safe for human consumption, also contain smaller amounts of glucoselenoerucin and glucoselenoiberverin and some of their selenium isothiocyanate and selenium nitrile products.[48] The precise concentrations of glucoselenoraphanin and selenosulforaphane in these *Brassica* remain uncertain, and further work is required to develop "gentle" extraction methods for their quantitation. Discovery of these Se-GSLs, together with knowledge of their capacity to produce Se-containing nitriles and isothiocyanates, and of their distribution in planta, provides new opportunities for investigating how consumption of *Brassica* vegetables may impact human health.

Table 1. Concentrations of Elemental Se Present as Se-GSLs in the Plant Parts of Broccoli, Cauliflower, and Forage Rape (mg/kg FW)[a]

plant part	high-GSL broccoli Se	low-GSL broccoli Se	cauliflower Se	forage rape Se
florets	5.5 (0.8)	3.3 (1.2)	0.44 (−)	
leaves	0.58 (0.41)	0.26 (0.24)		2.2 (1.2)
stems	0.84 (0.35)		0.11 (−)	1.8 (0.98)
roots	0.79 (0.2)	0.24 (0.03)		6.0 (2.5)

[a]Values for each tissue are the sums of the elemental Se present in each of the selenized glucosinolates and were calculated from the concentration and molecular weight of each Se-GSL. Values in parentheses are the standard errors of the means.

■ ASSOCIATED CONTENT

Ⓢ Supporting Information

Table S1 giving information on the identification of the ions used for quantitation of the compounds discussed herein and Tables S2−S9 giving the concentrations of selenized and nonselenized glucosinolates and their modified aglycons in the three *Brassica* samples. This material is available free of charge via the Internet at http://pubs.acs.org.

■ AUTHOR INFORMATION

Corresponding Author

*Phone: +64 6 9537679. Fax: +64 6 3517050. E-mail: adam.matich@plantandfood.co.nz.

Notes

The authors declare no competing financial interest.

■ ACKNOWLEDGMENTS

We thank Julie Ryan (Plant & Food Research (PFR), Palmerston North, New Zealand) for maintaining the plants in the greenhouse and Martin Hunt (PFR) for assistance with the mass spectrometry.

DOI: 10.1021/jf505963c
J. Agric. Food Chem. 2015, 63, 1896−1905

ABBREVIATIONS USED

GSL, glucosinolate; MeSe-GSL, (methylseleno)glucosinolate; MeS-GSL, (methylthio)glucosinolate; SeMet, selenomethionine

REFERENCES

(1) Verkerk, R.; Schreiner, M.; Krumbein, A.; Ciska, E.; Holst, B.; Rowland, I.; De Schrijver, R.; Hansen, M.; Gerh, C.; Mithen, R.; Dekker, M. Review: Glucosinolates in Brassica vegetables: The influence of the food supply chain on intake, bioavailability and human health. *Mol. Nutr. Food Res.* **2009**, *53*, S219−S265.

(2) Sonderby, I. E.; Geu-Flores, F.; Halkier, B. A. Biosynthesis of glucosinolates—Gene discovery and beyond. *Trends Plant Sci.* **2010**, *15*, 283−290.

(3) Rask, L.; Andréasson, E.; Ekbom, B.; Eriksson, S.; Pontoppidan, B.; Meijer, J. Myrosinase: Gene family evolution and herbivore defense in Brassicaceae. In *Plant Molecular Evolution*; Doyle, J., Gaut, B., Eds.; Springer: Dordrecht, The Netherlands, 2000; pp 93−113.

(4) Halkier, B. A.; Gershenzon, J. Biology and biochemistry of glucosinolates. *Annu. Rev. Plant Biol.* **2006**, *57*, 303−333.

(5) Bruce, T. J. A. Glucosinolates in oilseed rape: Secondary metabolites that influence interactions with herbivores and their natural enemies. *Ann. Appl. Biol.* **2014**, *164*, 348−353.

(6) Hayes, J. D.; Kelleher, M. O.; Eggleston, I. M. The cancer chemopreventive actions of phytochemicals derived from glucosinolates. *Eur. J. Nutr.* **2008**, *47* (Suppl. 2), 73−88.

(7) Rosa, E. A. S.; Rodrigues, P. M. F. The effect of light and temperature on glucosinolate concentration in the leaves and roots of cabbage seedlings. *J. Sci. Food Agric.* **1998**, *78*, 208−212.

(8) Tian, Q.; Rosselot, R. A.; Schwartz, S. J. Quantitative determination of intact glucosinolates in broccoli, broccoli sprouts, Brussels sprouts, and cauliflower by high-performance liquid chromatography-electrospray ionization-tandem mass spectrometry. *Anal. Biochem.* **2005**, *343*, 93−99.

(9) Nilsson, J.; Olsson, K.; Engqvist, G.; Ekvall, J.; Olsson, M.; Nyman, M.; Åkesson, B. Variation in the content of glucosinolates, hydroxycinnamic acids, carotenoids, total antioxidant capacity and low-molecular-weight carbohydrates in *Brassica* vegetables. *J. Sci. Food Agric.* **2006**, *86*, 528−538.

(10) Brown, P. D.; Morra, M. J. Hydrolysis products of glucosinolates in *Brassica napus* tissues as inhibitors of seed germination. *Plant Soil* **1996**, *181*, 307−316.

(11) Broadley, M. R.; White, P. J.; Bryson, R. J.; Meacham, M. C.; Bowen, H. C.; Johnson, S. E.; Hawkesford, M. J.; McGrath, S. P.; Zhao, F.-J.; Breward, N.; Harriman, M.; Tucker, M. Biofortification of UK food crops with selenium. *Proc. Nutr. Soc.* **2006**, *65*, 169−181.

(12) Rayman, M. P. Food-chain selenium and human health: Emphasis on intake. *Br. J. Nutr.* **2008**, *100*, 254−268.

(13) Fairweather-Tait, S. J.; Bao, Y.; Broadley, M. R.; Collings, R.; Ford, D.; Hesketh, J. E.; Hurst, R. Selenium in human health and disease: Comprehensive invited review. *Antioxid. Redox Signaling* **2011**, *14*, 1337−1383.

(14) Whanger, P. D. Selenium and its relationship to cancer: An update. *Br. J. Nutr.* **2004**, *91*, 11−28.

(15) Raman, A. V.; Berry, M. J. Selenoproteins in cellular redox regulation and signaling. In *Oxidative Stress in Vertebrates and Invertebrates*; John Wiley & Sons, Inc.: Hoboken, NJ, 2011; pp 195−208.

(16) Matich, A. J.; McKenzie, M. J.; Lill, R. E.; Brummell, D. A.; McGhie, T. K.; Chen, R. K. Y.; Rowan, D. D. Selenoglucosinolates and their metabolites produced in *Brassica* spp. fertilised with sodium selenate. *Phytochemistry* **2012**, *75*, 140−152.

(17) Omirou, M. D.; Papadopoulou, K. K.; Papastylianou, I.; Constantinou, M.; Karpouzas, D. G.; Asimakopoulos, I.; Ehaliotis, C. Impact of nitrogen and sulfur fertilization on the composition of glucosinolates in relation to sulfur assimilation in different plant organs of broccoli. *J. Agric. Food Chem.* **2009**, *57*, 9408−9417.

(18) Sun, B.; Xu, Y.; Xu, T.; Yuan, G.; Guo, R.; Wang, B.; Wang, Q. Variation of bioactive compounds and nutrients among different organs of broccoli (*Brassica oleracea* var. *italica* Planck). *Acta Hortic. Sin.* **2010**, *37*, 59−64.

(19) Avila, F. W.; Faquin, V.; Yang, Y.; Ramos, S. W.; Guilherme, L. R. G.; Thannhauser, T. W.; Li, L. Assessment of the anticancer compounds Se-methylselenocysteine and glucosinolates in Se-biofortified broccoli (*Brassica oleracea* L. var. *italica*) sprouts and florets. *J. Agric. Food Chem.* **2013**, *61*, 6216−6223.

(20) Emmert, S. W.; Desai, D.; Amin, S.; Richie, J. P. Enhanced Nrf2-dependent induction of glutathione in mouse embryonic fibroblasts by isoselenocyanate analog of sulforaphane. *Bioorg. Med. Chem. Lett.* **2010**, *20*, 2675−2679.

(21) Sharma, A. K.; Sharma, A.; Desai, D.; Madhunapantula, S. V.; Huh, S. J.; Robertson, G. P.; Amin, S. Synthesis and anticancer activity comparison of phenylalkyl isoselenocyanates with corresponding naturally occurring and synthetic isothiocyanates. *J. Med. Chem.* **2008**, *51*, 7820−7826.

(22) Finley, J. W.; Davis, C. D.; Feng, Y. Selenium from high selenium broccoli protects rats from colon cancer. *J. Nutr.* **2000**, *130*, 2384−2389.

(23) Hsu, F.-C.; Wirtz, M.; Heppel, S. C.; Bogs, J.; KrÄMer, U. T. E.; Khan, M. S.; Bub, A.; Hell, R.; Rausch, T. Generation of Se-fortified broccoli as functional food: Impact of Se fertilization on S metabolism. *Plant, Cell Environ.* **2011**, *34*, 192−207.

(24) Cataldi, T. R. I.; Lelario, F.; Orlando, D.; Bufo, S. A. Collision-induced dissociation of the A + 2 isotope ion facilitates glucosinolates structure elucidation by electrospray ionization-tandem mass spectrometry with a linear quadrupole ion trap. *Anal. Chem.* **2010**, *82*, 5686−5696.

(25) Sharpless, K. B.; Lauer, R. F. Mild procedure for the conversion of epoxides to allylic alcohols. First organoselenium reagent. *J. Am. Chem. Soc.* **1973**, *95*, 2697−2699.

(26) Munday, R.; Munday, C. M. Induction of phase II detoxification enzymes in rats by plant-derived isothiocyanates: Comparison of allyl isothiocyanate with sulforaphane and related compounds. *J. Agric. Food Chem.* **2004**, *52*, 1867−1871.

(27) Matusheski, N. V.; Juvik, J. A.; Jeffery, E. H. Heating decreases epithiospecifier protein activity and increases sulforaphane formation in broccoli. *Phytochemistry* **2004**, *65*, 1273−1281.

(28) Reich, H. J. Organoselenium oxidations. In *Oxidation in Organic Chemistry*; Trahanovsky, W., Ed.; Academic Press: New York, 1978; Vol. 5-C, Part 3, pp 13−15.

(29) Stewart, J. M.; Nigam, S. N.; McConnell, W. B. Metabolism of $Na_2{}^{75}SeO_4$ in horseradish: Formation of selenosinigrin. *Can. J. Biochem.* **1974**, *52*, 144−145.

(30) Wielanek, M.; Bergier, K.; Andrzejewska, R.; Sklodowska, M. Incorporation of inorganic selenium into seleno-glucosinolates in hairy root cultures of *Nasturtium officinale* R.Br. *Biol. Lett. (Poznan, Pol.)* **2005**, *42*, 222−223.

(31) Bertelsen, F.; Gissel-Nielsen, G.; Kjaer, A.; Skrydstrup, T. Selenoglucosinolates in nature: Fact or myth? *Phytochemistry* **1988**, *27*, 3743−3749.

(32) Di Cesare, L. F.; Vitale, R.; Acciarri, N.; Branca, F. The characteristic volatile composition of some horticultural cultivars of broccoli, cauliflower and cabbage grown in Italy. *Ind. Aliment. (Pinerolo, Italy)* **2001**, *40*, 508−512.

(33) Gardiner, J. B.; Morra, M. J.; Eberlein, C. V.; Brown, P. D.; Borek, V. Allelochemicals released in soil following incorporation of rapeseed (*Brassica napus*) green manures. *J. Agric. Food Chem.* **1999**, *47*, 3837−3842.

(34) Tollsten, L.; Bergström, G. Headspace volatiles of whole plants and macerated plant parts of *Brassica* and *Sinapis*. *Phytochemistry* **1988**, *27*, 2073−2077.

(35) Attieh, J.; Djiana, R.; Koonjul, P.; Étienne, C.; Sparace, S.; Saini, H. Cloning and functional expression of two plant thiol methyltransferases: A new class of enzymes involved in the biosynthesis of sulfur volatiles. *Plant Mol. Biol.* **2002**, *50*, 511−521.

DOI: 10.1021/jf505963c
J. Agric. Food Chem. 2015, 63, 1896−1905

(36) Robbins, R. J.; Keck, A.-S.; Banuelos, G.; Finley, J. W. Cultivation conditions and selenium fertilization alter the phenolic profile, glucosinolate, and sulforaphane content of broccoli. *J. Med. Food* **2005**, *8*, 204−214.
(37) Kim, H. S.; Juvik, J. A. Effect of selenium fertilization and methyl jasmonate treatment on glucosinolate accumulation in broccoli florets. *J. Am. Soc. Hortic. Sci.* **2011**, *136*, 239−246.
(38) Birch, A. N. E.; Griffiths, D. W.; Hopkins, R. J.; Macfarlane Smith, W. H.; McKinlay, R. G. Glucosinolate responses of swede, kale, forage and oilseed rape to root damage by turnip root fly (*Delia floralis*) larvae. *J. Sci. Food Agric.* **1992**, *60*, 1−9.
(39) Charron, C. S.; Saxton, A. M.; Sams, C. E. Relationship of climate and genotype to seasonal variation in the glucosinolate−myrosinase system. II. Myrosinase activity in ten cultivars of *Brassica oleracea* grown in fall and spring seasons. *J. Sci. Food Agric.* **2005**, *85*, 682−690.
(40) Keck, A.-S.; Finley, J. W. Cruciferous vegetables: Cancer protective mechanisms of glucosinolate hydrolysis products and selenium. *Integr. Cancer Ther.* **2004**, *3*, 5−12.
(41) Buttery, B. G.; Guadagni, D. C.; Ling, L. C.; Seifert, R. M.; Lipton, W. Additional volatile components of cabbage, broccoli and cauliflower. *J. Agric. Food Chem.* **1976**, *24*, 829−832.
(42) Zhang, Y.; Talalay, P.; Cho, C.-G.; Posner, G. H. A major inducer of anticarcinogenic protective enzymes from broccoli: Isolation and elucidation of structure. *Proc. Natl. Acad. Sci. U.S.A.* **1992**, *89*, 2399−2403.
(43) Campas-Baypoli, O. N.; Bueno-Solano, C.; Martínez-Ibarra, D. M.; Camacho-Gil, F.; Villa-Lerma, A. G.; Rodríguez-Núñez, J. R.; López-Cervantes, J.; Sánchez-Machado, D. I. Contenido de sulforafano (1-isotiocianato-4-(metilsulfinil)-butano) en vegetales crucíferos. *Arch. Latinoam. Nutr.* **2009**, *59*, 95−100.
(44) Azizi Naser, S.; Amiri-Besheli, B.; Sharifi-Mehr, S. The isolation and determination of sulforaphane from broccoli tissues by reverse phase-high performance liquid chromatography. *J. Chin. Chem. Soc.* **2011**, *58*, 906−910.
(45) Di Cesare, L. F.; Vitale, R.; Ferrari, V. Volatile compounds composition of different cauliflower cultivars obtained by genetic improvement of the "Verde di Macerata" ecotype. *Ind. Aliment. (Pinerolo, Italy)* **2002**, *41*, 562−567.
(46) Valette, L.; Fernandez, X.; Poulain, S.; Loiseau, A. M.; Lizzani-Cuvelier, L.; Levieil, R.; Restier, L. Volatile constituents from Romanesco cauliflower. *Food Chem.* **2003**, *80*, 353−358.
(47) Keck, A.-S.; Finley, J. W. Aqueous extracts of selenium-fertilized broccoli increase selenoprotein activity and inhibit DNA single-strand breaks, but decrease the activity of quinone reductase in Hepa 1c1c7 cells. *Food Chem. Toxicol.* **2006**, *44*, 695−703.
(48) Bentley-Hewitt, K. L.; Chen, R.; Lill, R.; Hedderley, D.; Herath, T. D.; Matich, A.; McKenzie, M. Consumption of selenium-enriched broccoli increases cytokine production in human peripheral blood mononuclear cells stimulated *ex vivo*, a preliminary human intervention study. *Mol. Nutr. Food Res.* **2014**, *58*, 2350−2357.
(49) Duffield, A. J.; Thomson, C. D.; Hill, K. E.; Williams, S. An estimation of selenium requirements for New Zealanders. *Am. J. Clin. Nutr.* **1999**, *70*, 896−903.
(50) U.S. National Institutes of Health. Health risks from excessive selenium. http://ods.od.nih.gov/factsheets/Selenium-HealthProfessional/#h8 (accessed Jan 20, 2015).

DOI: 10.1021/jf505963c
J. Agric. Food Chem. 2015, 63, 1896−1905

Scheme 1. General Synthetic Route of Compounds 2-Aryl-6-chloro-3,4-dihydroisoquinolin-2-ium Bromides[a]

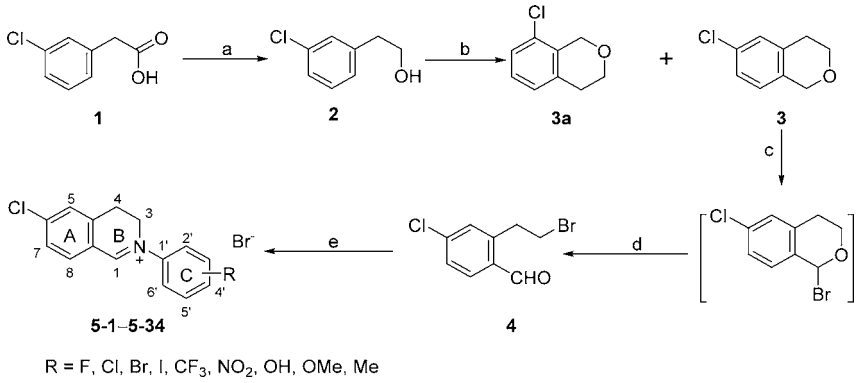

[a]Reagents and conditions: (a) $NaBH_4$, I_2, dry THF, overnight; (b) HCHO, TFA, 0 °C to r.t.; (c) Br_2, CCl_4, reflux; (d) 40% HBr, reflux; (e) Ar-NH_2, dioxane.

MATERIALS AND METHODS

Chemicals. Azoxystrobin, a commercial fungicide, was purchased from Jiangsu Frey Agrochemical Co. Ltd. (Jiangsu, China). Sanguinarine iodide (>98%) and chelerythrine iodide (>99%) were obtained in our laboratory by isolation from the whole plant of *M. microcarpa* (Maxim) Fedde. Dimethyl sulfoxide (DMSO) and the starting material, 2-(3-chlorophenyl)acetic acid, were purchased from J&K Chemical Ltd. (Beijing, China). Other reagents and solvents were obtained locally and of analytical grade or purified according to standard methods before use. The water used was redistilled and ion-free.

Fungi. The plant pathogenic fungi, *Alternaria alternate* (*A. alternate*), *Curvularia lunata* (*C. lunata*), and *Valsa mali* (*V. mali*), were provided by the Center of Pesticide Research, Northwest A&F University, China. These fungi were grown on PDA plates at 28 °C and maintained at 4 °C with periodic subculturing.

Instruments. Melting points were determined on a digital melting-point apparatus and uncorrected. Infrared spectra (IR) were recorded on a Bruker TENSOR 27 spectrometer with KBr disks. Ultraviolet spectra (UV) were obtained using a Thermo Scientific Evolution 300 UV−vis spectrophotometer. Nuclear magnetic resonance spectra (NMR) were performed on a Bruker Avance III 500 MHz instrument. Chemical shifts (δ values) and coupling constants (J values) were given in ppm and Hz, respectively. High resolution mass spectra (HR-MS) were carried out with a Micromass Auto Spec-3000 instrument. Low resolution mass spectra (LR-MS) were carried out with a Thermo Fisher LCQ Fleet instrument.

Synthesis. The synthetic route of target compounds **5-1** to **5-34** was outlined in Scheme 1 using 2-(3-chlorophenyl)acetic acid as a starting material.

*Synthesis of 2-(3-chlorophenyl)ethan-1-ol (**2**).* $NaBH_4$ (21.7 g, 0.57 mol) was added portion-wise in 30 min to a solution of 2-(3-chlorophenyl) acetic acid (**1**, 49.0 g, 0.29 mol) in 300 mL dried THF under ice bath, and then a solution of iodine (72.9 g, 0.29 mol) in 100 mL dried THF was dropwise added into the mixture over a period of 3 h with stirring. The reaction solution was stirred at room temperature for several hours until the reaction was completed according to TLC analysis. The solution was evaporated under reduced pressure. To the residue was added 100 mL saturated brine, extracted with ethyl acetate (3 × 100 mL), sequentially washed with saturated solution of Na_2SO_3 (3 × 60 mL) and saturated saline solution (2 × 60 mL), and finally dried over anhydrous $MgSO_4$. After filtration, the solution was evaporated under vacuum to yield 2-(3-chlorophenyl) ethan-1-ol (**2**) as colorless oil (44.5 g, yield 99%). The crude intermediate **2** was directly used in the following step. ^{1}H NMR (500 MHz, $CDCl_3$) δ: 7.16 (3H, d-like, J = 7.2 Hz), 7.04 (1H, d, J = 6.7 Hz), 3.67 (2H, t, J = 6.8 Hz), 3.26(1H, s), 2.73 (2H, t, J = 6.8 Hz); ^{13}C NMR (125 MHz, $CDCl_3$) δ: 140.9, 134.2, 129.8, 129.1, 127.3, 126.5, 63.0, 38.7.

*Synthesis of 6-chloroisochromane (**3**).* Paraformaldehyde (10.2 g, 0.34 mol) and trifluoroacetic acid (30 mL) were added into a round flask, and vigorously stirred at 50 °C for 30 min to provide a clear solution, and then cooled to 0 °C. To the resulting solution was added 2-(3-chlorophenyl) ethan-1-ol (**2**, 44.5 g, 0.28 mol) and stirred for 1 h at 0 °C and then for 2 h at room temperature. Trifluoroacetic acid was removed under vacuum. To the residue was added 60 mL ice−water, extracted with diethyl ether (3 × 70 mL), washed with water (1 × 40 mL), aqueous saturated $NaHCO_3$ (3 × 40 mL) and saturated saline solution (1 × 40 mL), finally dried over anhydrous $MgSO_4$. After filtration, the solution was evaporated under vacuum. The residue was purified by column chromatography on silica gel eluting with petroleum ether−ethyl acetate (V:V = 150:1) to afford 6-chloroisochromane (**3**) as colorless oil (22.5 g, yield 47%)and 8-chloroisochromane (**3a**) as colorless oil (23.1 g, yield 48%). **3**: ^{1}H NMR (500 MHz, $CDCl_3$) δ: 7.12(2H, d-like, J = 8.6 Hz), 6.90(1H, d, J = 8.0 Hz), 4.72(2H, s), 3.94(2H, t, J = 5.7 Hz), 2.82(2H, t, J = 5.7 Hz); ^{13}C NMR (125 MHz, $CDCl_3$) δ: 135.2, 133.3, 129.6, 128.8, 126.2, 125.8, 67.6, 65.0, 28.2. **3a**: ^{1}H NMR (500 MHz, $CDCl_3$) δ: 7.17 (1H, d, J = 7.8 Hz), 7.10 (1H, t, J = 7.8 Hz), 7.02 (1H, d, J = 7.8 Hz), 4.76 (2H, s), 3.92 (2H, t, J = 5.6 Hz), 2.84 (2H, t, J = 5.6 Hz); ^{13}C NMR (125 MHz, $CDCl_3$) δ: 135.8, 132.6, 131.0, 127.3, 127.2, 126.8, 66.3, 64.8, 28.3.

*Synthesis of 2-(2-bromoethyl)-4-chlorobenzaldehyde (**4**).* Bromine (21.3 g, 0.13 mol) was added slowly to an ice-cooled solution of 6-chloroisochromane (**3**, 22.5 g, 0.13 mol) in carbon tetrachloride (50 mL) in 10 min with stirring. After the exothermic reaction subsided, the mixture was refluxed for 2 h to obtain a pale yellow solution. The solvent was evaporated under vacuum. To the residue was added aqueous hydrobromic acid (40%, 32.4 g) and was refluxed for 20 min. The solution was extracted with diethyl ether (3 × 40 mL). The combined organic phase was washed with water (2 × 30 mL), aqueous saturated $NaHCO_3$ (2 × 30 mL) and dried over anhydrous $MgSO_4$. After filtration, the solution was evaporated under vacuum to yield orange oil. The obtained crude product was chromatographed on silica gel eluting with petroleum ether−ethyl acetate (V:V = 50:1) to afford 2-(2-bromoethyl)-4-chloro benzaldehyde (**4**) as brown liquid (24.4 g, yield 74%). ^{1}H NMR (500 MHz, $CDCl_3$) δ: 10.10 (1H, s), 7.76 (1H, d, J = 8.2 Hz), 7.45 (1H, dd, J = 8.2, 2.0 Hz), 7.34 (1H, d, J = 2.0 Hz), 3.60 (2H, t, J = 6.5 Hz), 3.54 (2H, t, J = 6.5 Hz); ^{13}C NMR (125 MHz, $CDCl_3$) δ: 191.6, 142.4, 140.1, 135.6, 132.4, 132.2, 128.0, 35.8, 32.2.

*Synthesis of compounds **5-1** to **5-34**.* According to our previously reported method,[8] compounds **5-1** to **5-34** were prepared through the direct condensation of 2-(2-bromo ethyl)-4-chlorobenzaldehyde (**4**) with aniline or substituted aromatic amine. General procedure was as follows. Compound **4** (350 mg, 1.4 mmol) was slowly added to a solution of aniline or substituted aniline (1.4 mmol) in 1,4-dioxane (6 mL) under stirring. The resulting solution was stirred overnight at room temperature to yield colored precipitate. The solid was collected by filtration and repeatedly washed with a small volume of diethyl ether and recrystallized in a mixed solution of methanol and 1,4-dioxane to provide the desired compounds (**5-1** to **5-34**).

*6-Chloro-2-phenyl-3,4-dihydroisoquinolin-2-ium bromide (**5-1**).* Yield, 72%; yellow powder; mp 167.4−168.3 °C; IR, υ_{max} (KBr) cm^{-1}:

DOI: 10.1021/jf505609z
J. Agric. Food Chem. 2015, 63, 1906−1914

1638 (s, C═N); UV λ_{max} (lg ε) (MeOH) 323 (4.08) nm; ^{1}H NMR (500 MHz, CD_3OD) δ: 9.56 (1H, s, H-1), 8.06 (1H, d, J = 8.2 Hz, H-8), 7.87 (2H, d-like, J = 6.6 Hz), 7.70−7.68 (5H, m), 4.68 (2H, t, J = 8.0 Hz, H-3), 3.55 (2H, t, J = 8.0 Hz, H-4); ^{13}C NMR (125 MHz, CD_3OD) δ: 166.3 (C-1), 145.0 (C-1′), 143.0, 139.1, 136.1, 131.1, 130.1 (C-2′,6′), 129.9, 128.7, 128.5, 122.3 (C-3′,5′), 51.0 (C-3), 25.0 (C-4); HR-MS [M - Br]$^+$: Calcd for $C_{15}H_{13}ClN^+$, 242.0731, found 242.0740; Negative ESI-MS m/z: 78.7 [$^{79}Br^-$], 80.7 [$^{81}Br^-$].

*6-Chloro-2-(4-fluorophenyl)-3,4-dihydroisoquinolin-2-ium bromide (**5-2**).* Yield: 80%; yellow powder; mp 233.2−234.1 °C; IR, υ_{max} (KBr) cm^{-1}: 1634 (s, C═N); UV λ_{max} (lg ε) (MeOH) 324 (4.11) nm; ^{1}H NMR (500 MHz, CD_3OD) δ: 9.55 (1H, s, H-1), 8.04 (1H, d, J = 8.1 Hz, H-8), 7.93 (2H, q-like), 7.71−7.68 (2H, m), 7.46 (2H, t, J = 8.4 Hz), 4.65 (2H, t, J = 7.6 Hz, H-3), 3.54 (2H, t, J = 7.6 Hz, H-4); ^{13}C NMR (125 MHz, CD_3OD) δ: 166.5 (C-1), 163.8 (d, J = 251.4 Hz, C-4′), 145.0 (C-1′), 139.3, 139.0, 136.2, 128.7, 128.5, 125.0 (d, J = 9.2 Hz, C-2′,6′), 124.0, 116.9 (d, J = 24.0 Hz, C-3′,5′), 51.3 (C-3), 25.0 (C-4); HR-MS [M - Br]$^+$: Calcd for $C_{15}H_{12}ClFN^+$, 260.0637, found 260.0640; Negative ESI-MS m/z: 78.7 [$^{79}Br^-$], 80.7 [$^{81}Br^-$].

*6-Chloro-2-(3-fluorophenyl)-3,4-dihydroisoquinolin-2-ium bromide (**5-3**).* Yield: 77%; yellow powder; mp 174.4−174.8 °C; IR, υ_{max} (KBr) cm^{-1}: 1629 (s, C═N); UV λ_{max} (lg ε) (MeOH) 322 (3.90) nm; ^{1}H NMR (500 MHz, CD_3OD) δ: 9.59 (1H, s, H-1), 8.05 (1H, d, J = 8.1 Hz, H-8), 7.76−7.69(5H, m), 7.47 (1H, t, J = 7.6 Hz), 4.66 (2H, t, J = 8.0 Hz, H-3), 3.54 (2H, t, J = 8.0 Hz, H-4); ^{13}C NMR (125 MHz, CD_3OD) δ: 167.2 (C-1), 162.9 (d, J = 249.0 Hz, C-3′), 145.3 (C-1′), 144.1, 139.3, 136.4, 131.9 (d, J = 8.8 Hz, C-5′), 128.8, 128.6, 124.0, 118.5, 117.9 (d, J = 22.6 Hz, C-2′), 110.3 (d, J = 27.1 Hz, C-4′), 51.0 (C-3), 25.0 (C-4); HR-MS [M - Br]$^+$: Calcd for $C_{15}H_{12}ClFN^+$, 260.0637, found 260.0634; Negative ESI-MS m/z: 78.8 [$^{79}Br^-$], 80.7 [$^{81}Br^-$].

*6-Chloro-2-(2-fluorophenyl)-3,4-dihydroisoquinolin-2-ium bromide (**5-4**).* Yield: 78%; pale yellow powder; mp 177.2−177.5 °C; IR, υ_{max} (KBr) cm^{-1}: 1632 (s, C═N); UV λ_{max} (lg ε) (MeOH) 318 (3.88) nm; ^{1}H NMR (500 MHz, CD_3OD) δ: 9.57 (1H, s, H-1), 8.05 (1H, d, J = 8.2 Hz, H-8), 7.91 (1H, t, J = 7.8 Hz), 7.77−7.70 (3H, m), 7.57−7.51 (2H, m), 4.60 (2H, t, J = 7.9 Hz, H-3), 3.55 (2H, t, J = 7.9 Hz, H-4); ^{13}C NMR (125 MHz, CD_3OD) δ: 170.0 (C-1), 155.0 (d, J = 253.6 Hz, C-2′), 145.8 (C-1′), 139.5, 136.5, 133.3, 130.6, 128.9, 128.8, 125.8 (d, J = 4.4 Hz, C-4′), 125.7, 123.8, 117.3 (d, J = 19.2 Hz, C-3′), 52.0 (C-3), 25.0 (C-4); HR-MS [M - Br]$^+$: Calcd for $C_{15}H_{12}ClFN^+$, 260.0637, found 260.0636; Negative ESI-MS m/z: 78.7 [$^{79}Br^-$], 80.8 [$^{81}Br^-$].

*6-Chloro-2-(4-chlorophenyl)-3,4-dihydroisoquinolin-2-ium bromide (**5-5**).* Yield: 77%; yellow powder; mp 210.3−210.9 °C; IR, υ_{max} (KBr) cm^{-1}: 1630 (s, C═N); UV λ_{max} (lg ε) (MeOH) 328 (4.08) nm; ^{1}H NMR (500 MHz, CD_3OD) δ: 9.58 (1H, s, H-1),8.06 (1H, d, J = 8.2 Hz, H-8), 7.89 (2H, d, J = 8.7 Hz, H-2′,6′), 7.72 (2H, d, J = 8.7 Hz, H-3′,5′), 7.71 (1H, s, H-5), 7.69 (1H, d, J = 8.2 Hz, H-7), 4.66 (2H, t, J = 7.9 Hz,H-3), 3.55 (2H, t, J = 7.9 Hz, H-4); ^{13}C NMR (125 MHz, CD_3OD) δ: 166.7(C-1), 145.2 (C-1′), 141.5, 139.2, 136.9, 136.3, 130.1 (C-2′,6′), 130.0, 128.8, 128.6, 124.1 (C-3′,5′), 51.0 (C-3), 25.0 (C-4); HR-MS [M - Br]$^+$: Calcd for $C_{15}H_{12}Cl_2N^+$, 276.0341, found 276.0338; Negative ESI-MS m/z: 78.7 [$^{79}Br^-$], 80.7 [$^{81}Br^-$].

*6-Chloro-2-(3-chlorophenyl)-3,4-dihydroisoquinolin-2-ium bromide (**5-6**).* Yield: 80%; orange powder; mp 168.6−169.2 °C; IR, υ_{max} (KBr) cm^{-1}: 1618 (s, C═N); UV λ_{max}(lg ε) (MeOH) 320 (4.00) nm; ^{1}H NMR (500 MHz, CD_3OD) δ: 9.59 (1H, s, H-1), 8.04 (1H, d, J = 8.2 Hz, H-8), 7.99 (1H, s, H-2′), 7.82 (1H, d, J = 7.4 Hz), 7.71−7.68 (4H, m), 4.65 (2H, t, J = 7.9 Hz,H-3), 3.54 (2H, t, J = 7.9 Hz, H-4); ^{13}C NMR (125 MHz, CD_3OD) δ: 167.3 (C-1), 145.5 (C-1′), 143.9, 139.3, 136.4, 135.5, 131.4, 131.1, 128.8, 128.6, 124.0, 122.8, 120.9, 51.0 (C-3), 25.0 (C-4); HR-MS [M - Br]$^+$: Calcd for $C_{15}H_{12}Cl_2N^+$, 276.0341, found 276.0338; Negative ESI-MS m/z: 78.7 [$^{79}Br^-$], 80.7 [$^{81}Br^-$].

*6-Chloro-2-(2-chlorophenyl)-3,4-dihydroisoquinolin-2-ium bromide (**5-7**).* Yield: 74%; yellow powder; mp 182.8−183.6 °C; IR, υ_{max} (KBr) cm^{-1}: 1631 (s, C═N); UV λ_{max} (lg ε) (MeOH) 311 (4.08) nm; ^{1}H NMR (500 MHz, CD_3OD) δ: 9.56 (1H, s, H-1), 8.06 (1H, d, J = 8.2 Hz, H-8), 7.94 (1H, dd, J = 7.8,1.5 Hz), 7.82 (1H, dd, J = 8.0,1.4 Hz), 7.75 (1H, s, H-5), 7.74−7.66 (3H, m), 4.43 (2H, t, J = 8.1 Hz, H-3), 3.51 (2H, t, J = 8.1 Hz, H-4); ^{13}C NMR (125 MHz, CD_3OD) δ: 170.8 (C-1), 146.0 (C-1′), 140.3, 139.5, 136.6, 132.7, 131.1, 129.0, 128.9 (2 × C), 128.1, 126.8, 123.6, 52.1 (C-3), 25.1 (C-4); HR-MS [M - Br]$^+$: Calcd for $C_{15}H_{12}Cl_2N^+$, 276.0341, found 276.0336; Negative ESI-MS m/z: 78.7 [$^{79}Br^-$], 80.7 [$^{81}Br^-$].

*2-(4-Bromophenyl)-6-chloro-3,4-dihydroisoquinolin-2-ium bromide (**5-8**).* Yield: 76%; yellow powder; mp 211.9−212.4 °C; IR, υ_{max} (KBr) cm^{-1}: 1621 (s, C═N); UV λ_{max} (lg ε) (MeOH) 331 (4.00) nm; ^{1}H NMR (500 MHz, CD_3OD) δ: 9.58 (1H, s, H-1), 8.05 (1H, d, J = 8.2 Hz, H-8), 7.88 (2H, d, J = 8.8 Hz, H-2′,6′), 7.80 (2H, d, J = 8.8 Hz, H-3′,5′), 7.71 (1H, s, H-5), 7.69 (1H, d, J = 8.2 Hz, H-7), 4.65 (2H, t, J = 8.0 Hz, H-3), 3.54 (2H, t, J = 8.0 Hz, H-4); ^{13}C NMR (125 MHz, CD_3OD) δ: 166.7 (C-1), 145.2 (C-1′), 142.0, 139.2, 136.3, 133.2 (C-2′,6′), 128.8, 128.6, 124.9, 124.2 (C-3′,5′), 124.1, 50.9 (C-3), 25.0 (C-4); HR-MS [M - Br]$^+$: Calcd for $C_{15}H_{12}BrClN^+$, 319.9836, found 319.9832; Negative ESI-MS m/z: 78.7 [$^{79}Br^-$], 80.7 [$^{81}Br^-$].

*2-(3-Bromophenyl)-6-chloro-3,4-dihydroisoquinolin-2-ium bromide (**5-9**).* Yield: 75%; orange powder; mp 175.7−176.6 °C; IR, υ_{max} (KBr) cm^{-1}: 1617 (s, C═N); UV λ_{max} (lg ε) (MeOH) 320 (4.10) nm; ^{1}H NMR (500 MHz, CD_3OD) δ: 9.59 (1H, s, H-1), 8.13 (1H, s, H-2′), 8.04 (1H, d, J = 8.1 Hz, H-8), 7.86 (2H, t, J = 7.2 Hz), 7.71 (1H, s, H-5), 7.70 (1H, d, J = 8.6 Hz), 7.63 (1H, t, J = 8.1 Hz), 4.65 (2H, t, J = 7.9 Hz, H-3), 3.53 (2H, t, J = 7.9 Hz, H-4); ^{13}C NMR (125 MHz, CD_3OD) δ: 167.3 (C-1), 145.4 (C-1′), 144.0, 139.3, 136.4, 134.1, 131.6, 128.8, 128.6, 125.7, 124.0, 123.1, 121.4, 51.0(C-3), 24.9(C-4); HR-MS [M - Br]$^+$: Calcd for $C_{15}H_{12}BrClN^+$, 319.9836, found 319.9824; Negative ESI-MS m/z: 78.7 [$^{79}Br^-$], 80.7 [$^{81}Br^-$].

*2-(2-Bromophenyl)-6-chloro-3,4-dihydroisoquinolin-2-ium bromide (**5-10**).* Yield: 72%; yellow powder; mp 186.4−187.2 °C; IR, υ_{max} (KBr) cm^{-1}: 1630 (s, C═N); UV λ_{max} (lg ε) (MeOH) 311 (4.08) nm; ^{1}H NMR (500 MHz, CD_3OD) δ: 9.56 (1H, s, H-1), 8.05 (1H, d, J = 8.2 Hz, H-8), 7.98 (1H, dd, J = 8.1,1.3 Hz), 7.92 (1H, dd, J = 7.9,1.5 Hz), 7.76 (1H, s, H-5), 7.71 (2H, td, J = 11.6,1.3 Hz), 7.63 (1H, td, J = 11.6,1.3 Hz), 4.53 (2H, t, J = 8.0 Hz, H-3), 3.62 (2H, t, J = 8.0 Hz, H-4); ^{13}C NMR (125 MHz, CD_3OD) δ: 170.8 (C-1), 146.1 (C-1′), 141.9, 139.4, 136.6, 134.2, 132.8, 129.5, 129.0 (2 × C), 126.8, 123.5, 117.3, 52.2 (C-3), 25.1 (C-4); HR-MS [M - Br]$^+$: Calcd for $C_{15}H_{12}BrClN^+$, 319.9836, found 319.9833; Negative ESI-MS m/z: 78.7 [$^{79}Br^-$], 80.7 [$^{81}Br^-$].

*6-Chloro-2-(4-iodophenyl)-3,4-dihydroisoquinolin-2-ium bromide (**5-11**).* Yield: 75%; yellow powder; mp 230.0−230.6 °C; IR, υ_{max} (KBr) cm^{-1}: 1627 (s, C═N); UV λ_{max} (lg ε) (MeOH) 342 (4.07) nm; ^{1}H NMR (500 MHz, CD_3OD) δ: 9.56 (1H, s, H-1), 8.07 (2H, d, J = 8.3 Hz, H-2′,6′), 8.03 (1H, d, J = 8.1 Hz, H-8), 7.71−7.68 (2H, m), 7.62 (2H, d, J = 8.3 Hz, H-3′,5′), 4.64 (2H, t, J = 7.8 Hz, H-3), 3.52 (2H, t, J = 7.8 Hz, H-4); ^{13}C NMR (125 MHz, CD_3OD) δ: 166.6 (C-1), 145.3 (C-1′), 142.6, 139.3 (C-2′,6′), 139.1, 136.2, 128.8, 128.6, 124.3, 123.9 (C-3′,5′), 96.7 (C-4′), 50.8 (C-3), 24.9 (C-4); HR-MS [M - Br]$^+$: Calcd for $C_{15}H_{12}ClIN^+$, 367.9697, found 367.9690 Negative ESI-MS m/z: 78.7 [$^{79}Br^-$], 80.7 [$^{81}Br^-$].

*6-Chloro-2-(3-iodophenyl)-3,4-dihydroisoquinolin-2-ium bromide (**5-12**).* Yield: 67%; yellow powder; mp 177.1−177.5 °C; IR, υ_{max} (KBr) cm^{-1}: 1620 (s, C═N); UV λ_{max} (lg ε) (MeOH) 319 (4.07) nm; ^{1}H NMR (500 MHz, CD_3OD) δ: 9.57 (1H, s, H-1), 8.28 (1H, s, H-2′), 8.05 (2H, t, J = 7.8 Hz), 7.88 (1H, d, J = 8.3 Hz, H-8), 7.71 (1H, s, H-5), 7.69 (1H, d, J = 8.3 Hz, H-7), 7.47 (1H, t, J = 8.1 Hz), 4.63 (2H, t, J = 7.9 Hz, H-3), 3.53 (2H, t, J = 7.9 Hz, H-4); ^{13}C NMR (125 MHz, CD_3OD) δ: 167.1 (C-1), 145.3 (C-1′), 143.8, 140.2, 139.2, 136.4, 131.4, 131.3, 128.8, 128.6, 124.0, 121.8, 94.1 (C-3′), 51.0 (C-3), 25.0 (C-4); HR-MS [M - Br]$^+$: Calcd for $C_{15}H_{12}ClIN^+$, 367.9697, found 367.9693; Negative ESI-MS m/z: 78.8 [$^{79}Br^-$], 80.7 [$^{81}Br^-$].

*6-Chloro-2-(2-iodophenyl)-3,4-dihydroisoquinolin-2-ium bromide (**5-13**).* Yield: 76%; yellow powder; mp 176.9−177.3 °C; IR, υ_{max} (KBr) cm^{-1}: 1639 (s, C═N); UV λ_{max} (lg ε) (MeOH) 310 (3.98) nm; ^{1}H NMR (500 MHz, CD_3OD) δ: 9.53 (1H, s, H-1), 8.19 (1H, d, J = 7.8 Hz, H-6′), 8.05 (1H, d, J = 8.1 Hz, H-8), 7.85 (1H, d, J = 7.7 Hz), 7.76−7.70 (3H, m), 7.45 (1H, t, J = 7.5 Hz), 4.50 (2H, br s, H-3), 3.67 (2H, br s, H-4); ^{13}C NMR(125 MHz, CD_3OD) δ: 170.8 (C-1), 146.1 (C-1′), 145.5, 140.6, 139.3, 138.8, 136.5, 132.5, 130.2, 129.0, 125.9, 123.5, 92.3 (C-2′), 52.4 (C-3), 25.3 (C-4); HR-MS [M - Br]$^+$: Calcd for $C_{15}H_{12}ClIN^+$, 367.9697, found 367.9696; Negative ESI-MS m/z: 78.7 [$^{79}Br^-$], 80.7 [$^{81}Br^-$].

DOI: 10.1021/jf505609z
J. Agric. Food Chem. 2015, 63, 1906−1914

*6-Chloro-2-(2-fluoro-4-iodophenyl)-3,4-dihydroisoquinolin-2-ium bromide (**5-14**).* Yield: 58%; orange powder; mp 220.9−221.4 °C; IR, υ_{max} (KBr) cm^{-1}: 1626 (s, C═N); UV λ_{max} (lg ε) (MeOH) 329 (3.79) nm; ^{1}H NMR (500 MHz, DMSO-d_6) δ: 9.76 (1H, s, H-1), 8.12 (1H, d, J = 10.1 Hz, H-3′), 8.08 (1H, d, J = 8.3 Hz, H-8), 7.93 (1H, d, J = 8.3 Hz, H-7), 7.79−7.74 (3H, m), 4.49 (2H, t, J = 7.7 Hz, H-3), 3.42 (2H, t, J = 7.7 Hz, H-4); ^{13}C NMR (125 MHz, DMSO-d_6) δ: 170.1 (C-1), 154.5 (d, J = 258.3 Hz, C-2′), 144.1 (C-1′), 140.2, 137.1, 135.1, 130.7 (d, J = 10.9 Hz, C-3′), 129.1, 128.4, 126.6, 126.5, 124.8, 99.3 (C-4′), 51.8 (C-3), 25.2 (C-4); HR-MS [M - Br]$^+$: Calcd for $C_{15}H_{11}ClFIN^+$, 385.9603, found 385.9600; Negative ESI-MS m/z: 78.7 [$^{79}Br^-$], 80.7 [$^{81}Br^-$].

*6-Chloro-2-(3,5-dichlorophenyl)-3,4-dihydroisoquinolin-2-ium bromide (**5-15**).* Yield: 76%; yellow powder; mp 182.5−183.4 °C; IR, υ_{max} (KBr) cm^{-1}: 1621(s, C═N); UV λ_{max} (lg ε) (MeOH) 263 (4.16), 309 (3.72) nm; ^{1}H NMR (500 MHz, DMSO-d_6) δ: 9.83 (1H, s, H-1), 8.14(2H, s), 8.06 (1H, d, J = 8.1 Hz, H-8), 7.98 (1H, s), 7.78 (1H, s), 7.74 (1H, d, J = 8.1 Hz, H-7), 4.57 (2H, t, J = 7.6 Hz, H-3), 3.43 (2H, t, J = 7.6 Hz, H-4); ^{13}C NMR (125 MHz, DMSO-d_6) δ: 168.2 (C-1), 144.8 (C-1′), 143.9, 140.0, 137.1, 135.4, 130.8, 129.1, 129.0, 124.8, 122.9, 50.9(C-3), 25.2(C-4); HR-MS [M - Br]$^+$: Calcd for $C_{15}H_{11}Cl_3N^+$, 309.9952, found 309.9947; Negative ESI-MS m/z: 78.7 [$^{79}Br^-$], 80.7 [$^{81}Br^-$].

*2-(4-Bromo-2-fluorophenyl)-6-chloro-3,4-dihydroisoquinolin-2-ium bromide (**5-16**).* Yield: 73%; yellow powder; mp 184.1−184.5 °C; IR, υ_{max} (KBr) cm^{-1}: 1624 (s, C═N); UV λ_{max} (lg ε) (MeOH) 254 (3.97), 323(3.97) nm; ^{1}H NMR (500 MHz, CD_3OD) δ: 9.58 (1H, s, H-1), 8.06 (1H, d, J = 8.2 Hz, H-8), 7.89−7.83 (2H, m), 7.72−7.70 (3H, m), 4.58 (2H, t, J = 7.9 Hz, H-3), 3.54 (2H, t, J = 7.9 Hz, H-4); ^{13}C NMR (125 MHz, CD_3OD) δ: 170.2 (C-1), 154.9 (d, J = 257.8 Hz, C-2′), 146.0 (C-1′), 139.6, 136.6, 129.8, 129.1 (d, J = 3.7 Hz, C-4′), 128.9, 128.8, 127.1, 123.9, 120.9 (d, J = 22.4 Hz, C-3′), 51.9 (C-3), 25.0 (C-4); HR-MS [M - Br]$^+$: Calcd for $C_{15}H_{11}BrClFN^+$, 337.9742, found 337.9730; Negative ESI-MS m/z: 78.7 [$^{79}Br^-$], 80.7 [$^{81}Br^-$].

*6-Chloro-2-(2,4-dichlorophenyl)-3,4-dihydroisoquinolin-2-ium bromide (**5-17**).* Yield: 66%; yellow powder; mp 187.6−187.9 °C; IR, υ_{max} (KBr) cm^{-1}: 1631 (s, C═N); UV λ_{max} (lg ε) (MeOH) 258 (3.64), 313 (3.94) nm; ^{1}H NMR (500 MHz, CD_3OD) δ: 9.57 (1H, s, H-1), 8.05 (1H, d, J = 8.2 Hz, H-8), 7.95 (2H, d-like, J = 9.4 Hz), 7.75 (1H, s), 7.73−7.70 (2H, m), 4.53 (2H, t, J = 7.8 Hz, H-3), 3.52 (2H, t, J = 7.8 Hz, H-4); ^{13}C NMR (125 MHz, CD_3OD) δ: 171.2 (C-1), 146.3 (C-1′), 139.6, 138.9, 137.8, 136.7, 130.8, 129.4, 129.1, 129.0, 128.9, 128.0, 123.6, 52.0 (C-3), 25.1 (C-4); HR-MS [M - Br]$^+$: Calcd for $C_{15}H_{11}Cl_3N^+$, 309.9952, found 309.9948; Negative ESI-MS m/z: 78.7 [$^{79}Br^-$], 80.7 [$^{81}Br^-$].

*6-Chloro-2-(2,4-dibromophenyl)-3,4-dihydroisoquinolin-2-ium bromide (**5-18**).* Yield: 70%; yellow powder; mp 219.8−220.6 °C; IR, υ_{max} (KBr) cm^{-1}: 1628 (s, C═N); UV λ_{max} (lg ε) (MeOH) 260 (3.86), 312 (4.15) nm; ^{1}H NMR (500 MHz, CD_3OD) δ: 9.57 (1H, s, H-1), 8.22 (1H, d, J = 2.0 Hz, H-3′), 8.06 (1H, d, J = 8.2 Hz, H-8), 7.90 (1H, dd, J = 8.5,2.0 Hz, H-5′), 7.86 (1H, d, J = 8.5 Hz, H-6′), 7.75 (1H, s, H-5), 7.72 (1H, dd, J = 8.2,1.9 Hz, H-7), 4.52 (2H, t, J = 7.9 Hz, H-3), 3.61 (2H, t, J = 7.9 Hz, H-4); ^{13}C NMR (125 MHz, CD_3OD) δ: 171.1 (C-1), 146.3 (C-1′), 141.0, 139.5, 136.7, 136.5, 132.7, 129.0, 128.1, 125.6, 123.5, 118.6 (2 × C), 52.1 (C-3), 25.1 (C-4); HR-MS [M - Br]$^+$: Calcd for $C_{15}H_{11}Br_2ClN^+$, 397.8941, found 397.8923; Negative ESI-MS m/z: 78.7 [$^{79}Br^-$], 80.7 [$^{81}Br^-$].

*6-Chloro-2-(2,6-difluorophenyl)-3,4-dihydroisoquinolin-2-ium bromide (**5-19**).* Yield: 58%; yellow powder; mp 195.6−196.0 °C; IR, υ_{max} (KBr) cm^{-1}: 1629 (s, C═N); UV λ_{max} (lg ε) (MeOH) 319 (3.89) nm; ^{1}H NMR (500 MHz, CD_3OD) δ: 9.62 (1H, s, H-1), 8.07 (1H, d, J = 8.2 Hz, H-8), 7.79−7.72 (3H, m), 7.44 (2H, t, J = 8.5 Hz), 4.57(2H, t, J = 7.9 Hz, H-3), 3.56(2H, t, J = 7.9 Hz, H-4); ^{13}C NMR (125 MHz, CD_3OD) δ: 156.0 (d, J = 255.2 Hz, C-2′,6′), 146.7 (C-1′), 140.0, 136.9, 133.3, 129.1, 129.0, 123.7, 119.8, 113.0 (dd, J = 19.3,3.5 Hz, C-3′,5′), 52.1 (C-3), 25.1 (C-4); HR-MS [M - Br]$^+$: Calcd for $C_{15}H_{11}ClF_2N^+$, 278.0543, found 278.0539; Negative ESI-MS m/z: 78.7 [$^{79}Br^-$], 80.7 [$^{81}Br^-$].

*6-Chloro-2-(4-methoxyphenyl)-3,4-dihydroisoquinolin-2-ium bromide (**5-20**).* Yield: 74%; yellow powder; mp 173.8−174.4 °C; IR, υ_{max} (KBr) cm^{-1}: 1624 (s, C═N); UV λ_{max} (lg ε) (MeOH) 294 (3.80), 364 (3.95) nm; ^{1}H NMR (500 MHz, CD_3OD) δ: 9.45 (1H, s, H-1), 8.02 (1H, d, J = 8.2 Hz, H-8), 7.81 (2H, d-like, J = 9.1 Hz, H-2′,6′), 7.68−7.65 (2H, m), 7.21 (2H, d-like, J = 9.1 Hz, H-3′,5′), 4.64 (2H, t, J = 8.0 Hz, H-3), 3.93 (3H, s, -OC$\underline{H}_3$), 3.52 (2H, t, J = 8.0 Hz, H-4); ^{13}C NMR (125 MHz, CD_3OD) δ:164.5 (C-1), 161.9 (C-4′), 144.5 (C-1′), 138.8, 135.8, 135.7, 128.7, 128.4, 124.2, 123.8 (C-2′,6′), 115.0 (C-3′,5′), 55.1 (-O$\underline{C}H_3$), 51.1 (C-3), 25.0 (C-4); HR-MS [M - Br]$^+$: Calcd for $C_{16}H_{15}ClNO^+$, 272.0837, found 272.0835; Negative ESI-MS m/z: 78.7 [$^{79}Br^-$], 80.7 [$^{81}Br^-$].

*6-Chloro-2-(3-methoxyphenyl)-3,4-dihydroisoquinolin-2-ium bromide (**5-21**).* Yield: 81%; brown powder; mp 154.7−155.6 °C; IR, υ_{max} (KBr) cm^{-1}: 1636 (s, C═N); UV λ_{max} (lg ε) (MeOH) 318 (3.93) nm; ^{1}H NMR (500 MHz, CD_3OD) δ: 9.56 (1H, s, H-1), 8.07 (1H, d, J = 8.2 Hz, H-8), 7.70 (1H, s, H-5), 7.67 (1H, dd, J = 8.2,1.8 Hz), 7.59 (1H, t, J = 8.2 Hz), 7.47 (1H, t-like, J = 2.2 Hz), 7.41 (1H, dd, J = 8.0,1.8 Hz), 7.24 (1H, dd, J = 8.4,2.2 Hz), 4.67 (2H, t, J = 8.0 Hz, H-3), 3.95 (3H, s, -OC$\underline{H}_3$), 3.54 (2H, t, J = 8.0 Hz, H-4); ^{13}C NMR (125 MHz, CD_3OD) δ: 166.3 (C-1), 161.0 (C-3′), 144.9 (C-1′), 144.1, 139.2, 136.2, 130.9, 128.7, 128.5, 124.1, 117.0, 114.1, 108.0, 55.2 (-O$\underline{C}H_3$), 51.1 (C-3), 25.0(C-4); HR-MS [M - Br]$^+$: Calcd for $C_{16}H_{15}ClNO^+$, 272.0837, found 272.0831; Negative ESI-MS m/z: 78.7 [$^{79}Br^-$], 80.7 [$^{81}Br^-$].

*6-Chloro-2-(2-methoxyphenyl)-3,4-dihydroisoquinolin-2-ium bromide (**5-22**).* Yield: 81%; yellow powder; mp 172.3−172.8 °C; IR, υ_{max} (KBr) cm^{-1}: 1632 (s, C═N); UV λ_{max} (lg ε) (MeOH) 308 (4.14) nm; ^{1}H NMR (500 MHz, CD_3OD) δ: 9.41 (1H, s, H-1), 8.03 (1H, d, J = 8.2 Hz, H-8), 7.75−7.65 (4H, m), 7.39 (1H, d, J = 8.4 Hz), 7.23 (1H, td, J = 7.7,1.0 Hz), 4.50 (2H, t, J = 7.9 Hz, H-3), 4.04 (3H, s, -OC$\underline{H}_3$), 3.54 (2H, t, J = 7.9 Hz, H-4); ^{13}C NMR (125 MHz, CD_3OD) δ: 168.8 (C-1), 152.4 (C-2′), 145.1 (C-1′), 139.4, 136.0, 132.8, 131.6, 128.7, 128.6, 125.3, 123.9, 121.2, 112.9, 55.7 (-O$\underline{C}H_3$), 51.9 (C-3), 25.2 (C-4); HR-MS [M - Br]$^+$: Calcd for $C_{16}H_{15}ClNO^+$, 272.0837, found 272.0831; Negative ESI-MS m/z: 78.7 [$^{79}Br^-$], 80.7 [$^{81}Br^-$].

*6-Chloro-2-(4-(trifluoromethyl)phenyl)-3,4-dihydroisoquinolin-2-ium bromide (**5-23**).* Yield: 68%; yellow powder; mp 166.3−167.0 °C; IR, υ_{max} (KBr) cm^{-1}: 1633 (s, C═N); UV λ_{max} (lg ε) (MeOH) 266 (4.03), 320 (3.78) nm; ^{1}H NMR (500 MHz, CD_3OD) δ: 9.69 (1H, s, H-1), 8.11 (3H, brs), 8.03 (2H, d, J = 8.5 Hz), 7.72 (1H, s, H-5), 7.70 (1H, d, J = 8.3 Hz), 4.71 (2H, t, J = 7.9 Hz, H-3), 3.58 (2H, t, J = 7.9 Hz, H-4); ^{13}C NMR (125 MHz, CD_3OD) δ: 167.7 (C-1), 145.7 (C-1′), 139.4 (C-2′,6′), 136.6, 130.5, 128.8, 128.6, 127.2 (q, J = 3.8 Hz, C-3′,5′), 125.7, 124.1, 123.5, 123.4 (q, J = 271.8 Hz, -$\underline{C}F_3$), 51.0 (C-3), 25.0 (C-4); HR-MS [M - Br]$^+$: Calcd for $C_{16}H_{12}ClF_3N^+$, 310.0605, found 310.0596; Negative ESI-MS m/z: 78.7 [$^{79}Br^-$], 80.7 [$^{81}Br^-$].

*6-Chloro-2-(3-(trifluoromethyl)phenyl)-3,4-dihydroisoquinolin-2-ium bromide (**5-24**).* Yield: 72%; yellow powder; mp 193.2−193.7 °C; IR, υ_{max} (KBr) cm^{-1}: 1642 (s, C═N); UV λ_{max} (lg ε) (MeOH) 317 (4.16) nm; ^{1}H NMR (500 MHz, CD_3OD) δ: 9.67 (1H, s, H-1), 8.28 (1H, s, H-2′), 8.17 (1H, d, J = 7.8 Hz), 8.07 (1H, d, J = 8.2 Hz, H-8), 8.02 (1H, d, J = 7.8 Hz), 7.94 (1H, t, J = 8.0 Hz), 7.72 (1H, s, H-5), 7.70 (1H, d, J = 8.2 Hz, H-7), 4.71 (2H, t, J = 8.0 Hz, H-3), 3.57 (2H, t, J = 8.0 Hz, H-4); ^{13}C NMR (125 MHz, CD_3OD) δ: 167.8 (C-1), 145.5 (C-1′), 143.5, 139.3, 136.5, 132.2 (q, J = 33.5 Hz, C-3′), 131.2, 128.8, 128.6, 127.6, 126.4, 124.0, 123.3 (d, J = 271.8 Hz, -$\underline{C}F_3$), 119.9, 51.1 (C-3), 25.0 (C-4); HR-MS [M - Br]$^+$: Calcd for $C_{16}H_{12}ClF_3N^+$, 310.0605, found 310.0599; Negative ESI-MS m/z: 78.7 [$^{79}Br^-$], 80.7 [$^{81}Br^-$].

*6-Chloro-2-(2-(trifluoromethyl)phenyl)-3,4-dihydroisoquinolin-2-ium bromide (**5-25**).* Yield: 63%; yellow powder; mp 200.4−200.9 °C; IR, υ_{max} (KBr) cm^{-1}: 1636 (s, C═N); UV λ_{max} (lg ε) (MeOH) 310 (4.01) nm; ^{1}H NMR (500 MHz, CD_3OD) δ: 9.66 (1H, s, H-1), 8.10−8.00 (4H, m), 7.94 (1H, t, J = 7.5 Hz), 7.76 (1H, s, H-5), 7.73 (1H, dd, J = 8.2,1.7 Hz), 4.67 (1H, s, H-3a), 4.48 (1H, s, H-3b), 3.58 (2H, brs, H-4); ^{13}C NMR (125 MHz, CD_3OD) δ: 171.3 (C-1), 146.6 (C-1′), 139.7, 139.3, 136.8, 134.7, 132.0, 129.1, 127.9 (q, J = 4.9 Hz, C-3′), 127.2, 124.3 (q, J = 31.8 Hz, C-2′), 123.3, 122.9 (q, J = 274.0 Hz, -$\underline{C}F_3$), 53.3 (C-3), 24.9 (C-4); HR-MS [M - Br]$^+$: Calcd for $C_{16}H_{12}ClF_3N^+$, 310.0605, found 310.0598 Negative ESI-MS m/z: 78.8 [$^{79}Br^-$], 80.7 [$^{81}Br^-$].

*6-Chloro-2-(4-hydroxyphenyl)-3,4-dihydroisoquinolin-2-ium bromide (**5-26**).* Yield: 71%; brown powder; mp 228.2−229.1 °C; IR, υ_{max} (KBr) cm^{-1}: 1636 (s, C═N); UV λ_{max} (lg ε) (MeOH) 293 (3.77), 369

DOI: 10.1021/jf505609z
J. Agric. Food Chem. 2015, 63, 1906−1914

(3.90) nm; ^{1}H NMR (500 MHz, CD_3OD) δ: 9.50 (1H, s, H-1), 8.07 (1H, d, J = 8.2 Hz, H-8), 7.77−7.74 (4H, m), 7.11 (2H, d-like, J = 9.0 Hz), 4.65 (2H, t, J = 8.0 Hz, H-3), 3.54 (2H, t, J = 8.0 Hz. H-4); ^{13}C NMR (125 MHz, CD_3OD) δ: 164.1 (C-1), 160.3 (C-4′), 143.8 (C-1′), 139.0, 135.9, 134.9, 128.7, 128.6, 124.6, 124.2 (C-2′,6′), 116.4 (C-3′,5′), 51.0 (C-3), 25.1 (C-4); HR-MS $[M - Br]^+$: Calcd for $C_{15}H_{13}ClNO^+$, 258.0680, found 258.0678; Negative ESI-MS m/z: 78.7 [$^{79}Br^-$], 80.7 [$^{81}Br^-$].

*6-Chloro-2-(3-hydroxyphenyl)-3,4-dihydroisoquinolin-2-ium bromide (**5-27**).* Yield: 83%; brown powder; mp 171.5−172.4 °C; IR, υ_{max} (KBr) cm^{-1}: 1629 (s, C═N); UV λ_{max} (lg ε) (MeOH) 317 (3.91) nm; ^{1}H NMR (500 MHz, CD_3OD) δ: 9.49 (1H, s, H-1), 8.05 (1H, d, J = 8.2 Hz, H-8), 7.68 (1H, s, H-5), 7.66 (1H, d, J = 8.3 Hz), 7.48 (1H, t, J = 8.2 Hz), 7.28 (1H, d-like, J = 8.0 Hz), 7.24 (1H, t, J = 2.0 Hz), 7.08 (1H, dd, J = 8.2,1.9 Hz), 4.63 (2H, t, J = 8.0 Hz, H-3), 3.52 (2H, t, J = 8.0 Hz, H-4); ^{13}C NMR (125 MHz, CD_3OD) δ: 165.9 (C-1), 159.0 (C-3′), 144.8 (C-1′), 144.1, 139.1, 136.1, 130.9, 128.7, 128.5, 124.1, 118.0, 112.8, 109.1, 51.0 (C-3), 25.0 (C-4); HR-MS $[M - Br]^+$: Calcd for $C_{15}H_{13}ClNO^+$, 258.0680, found 258.0675; Negative ESI-MS m/z: 78.7 [$^{79}Br^-$], 80.7 [$^{81}Br^-$].

*6-Chloro-2-(2-hydroxyphenyl)-3,4-dihydroisoquinolin-2-ium bromide (**5-28**).* Yield: 72%; yellow powder; mp 202.1−202.8 °C; IR, υ_{max} (KBr) cm^{-1}: 1632 (s, C═N); UV λ_{max} (lg ε) (MeOH) 307 (4.03) nm; ^{1}H NMR (500 MHz, CD_3OD) δ: 9.40 (1H, s, H-1), 8.03 (1H, d, J = 8.2 Hz, H-8), 7.70 (1H, s, H-5), 7.67 (2H, dq, J = 8.1,1.6 Hz), 7.50 (1H, td, J = 8.4,1.6 Hz), 7.16 (1H, dd, J = 8.3,1.0 Hz), 7.10 (1H, td, J = 7.7,1.0 Hz), 4.53 (2H, t, J = 7.9 Hz, H-3), 3.52 (2H, t, J = 7.9 Hz, H-4); ^{13}C NMR (125 MHz, CD_3OD) δ: 168.2 (C-1), 150.6 (C-2′), 144.9 (C-1′), 139.3, 135.8, 132.4, 130.5, 128.7, 128.6, 125.1, 123.9, 120.2, 116.9, 51.6 (C-3), 25.1 (C-4); HR-MS $[M - Br]^+$: Calcd for $C_{15}H_{13}ClNO^+$, 258.0680, found 258.0678; Negative ESI-MS m/z: 78.7 [$^{79}Br^-$], 80.7 [$^{81}Br^-$].

*6-Chloro-2-(4-nitrophenyl)-3,4-dihydroisoquinolin-2-ium bromide (**5-29**).* Yield: 66%; yellow powder; mp 175.8−176.4 °C; IR, υ_{max} (KBr) cm^{-1}: 1626 (s, C═N); UV λ_{max} (lg ε) (MeOH) 369 (4.24) nm; ^{1}H NMR (500 MHz, DMSO-d_6) δ: 9.92 (1H, s, H-1), 8.54 (2H, brs), 8.19 (2H, brs), 8.13 (1H, brs), 7.77 (2H, d-like, J = 18.8 Hz), 4.64 (2H, brs, H-3), 3.46 (2H, brs, H-4); ^{13}C NMR (125 MHz, DMSO-d_6) δ: 167.7 (C-1), 148.1 (C-4′), 147.0 (C-1′), 143.4, 139.5, 136.6, 128.4 (C-2′,6′), 125.1 (3 × C), 124.4 (C-3′,5′), 51.3 (C-3), 24.6 (C-4); HR-MS $[M - Br]^+$: Calcd for $C_{15}H_{12}ClN_2O_2^+$, 287.0582, found 287.0577; Negative ESI-MS m/z: 78.7 [$^{79}Br^-$], 80.7 [$^{81}Br^-$].

*6-Chloro-2-(3-nitrophenyl)-3,4-dihydroisoquinolin-2-ium bromide (**5-30**).* Yield: 68%; yellow powder; mp 170.5−171.3 °C; IR, υ_{max} (KBr) cm^{-1}: 1639 (s, C═N); UV λ_{max} (lg ε) (MeOH) 255 (4.29), 320 (3.84) nm; ^{1}H NMR (500 MHz, CD_3OD) δ: 9.75 (1H, s, H-1), 8.81 (1H, s, H-2′), 8.53 (1H, d, J = 7.5 Hz), 8.33 (1H, d, J = 7.1 Hz), 8.10 (1H, d, J = 8.2 Hz, H-8), 7.98 (1H, t, J = 8.2 Hz), 7.73 (1H, s, H-5), 7.70 (1H, d, J = 8.2 Hz, H-7), 4.74 (2H, brs, H-3), 3.60 (2H, t, J = 7.9 Hz, H-4); ^{13}C NMR (125 MHz, CD_3OD) δ: 168.2 (C-1), 148.9 (C-3′), 145.7 (C-1′), 143.6, 139.5, 136.7, 131.4, 128.8, 128.7 (2 × C), 125.3, 124.1, 118.2, 51.1 (C-3), 25.1 (C-4); HR-MS $[M - Br]^+$: Calcd for $C_{15}H_{12}ClN_2O_2^+$, 287.0582, found 287.0577; Negative ESI-MS m/z: 78.7 [$^{79}Br^-$], 80.7 [$^{81}Br^-$].

*6-Chloro-2-(2-nitrophenyl)-3,4-dihydroisoquinolin-2-ium bromide (**5-31**).* Yield: 62%; yellow powder; mp 122.5−123.6 °C; IR, υ_{max} (KBr) cm^{-1}: 1633 (s, C═N); UV λ_{max} (lg ε) (MeOH) 310 (3.96), 426 (3.54) nm; ^{1}H NMR (500 MHz, CD_3OD) δ: 9.57 (1H, s, H-1), 8.55 (1H, d, J = 7.9 Hz), 8.10−8.08 (2H, m), 8.03 (1H, d, J = 8.2 Hz, H-8), 8.02−7.98 (1H, m), 7.75 (1H, s, H-5), 7.71 (1H, dd, J = 8.2,1.8 Hz, H-7), 4.61 (2H, t, J = 7.9 Hz, H-3), 3.64 (2H, t, J = 7.9 Hz, H-4); ^{13}C NMR (125 MHz, CD_3OD) δ: 170.0 (C-1), 146.1 (C-1′), 142.4, 139.4, 136.7, 136.1, 135.8, 132.8, 129.0, 128.9, 128.2, 126.8, 123.5, 53.0 (C-3), 25.3 (C-4); HR-MS $[M - Br]^+$: Calcd for $C_{15}H_{12}ClN_2O_2^+$, 287.0582, found 287.0577; Negative ESI-MS m/z: 78.7 [$^{79}Br^-$], 80.7 [$^{81}Br^-$].

*6-Chloro-2-(p-tolyl)-3,4-dihydroisoquinolin-2-ium bromide (**5-32**).* Yield: 79%; yellow powder; mp 159.6−160.3 °C; IR, υ_{max} (KBr) cm^{-1}: 1623 (s, C═N); UV λ_{max} (lg ε) (MeOH) 233 (3.90), 337 (4.03) nm; ^{1}H NMR (500 MHz, CD_3OD) δ: 9.50 (1H, s, H-1), 8.04 (1H, d, J = 8.2 Hz, H-8), 7.74 (2H, d, J = 8.3 Hz, H-2′,6′), 7.69 (1H, s, H-5), 7.67 (1H, dd, J = 8.2,1.8 Hz, H-7), 7.52 (1H, d, J = 8.3 Hz, H-3′,5′), 4.65 (2H, t, J = 8.0 Hz, H-3), 3.53 (2H, t, J = 8.0 Hz, H-4), 2.49 (3H, s, -C$\underline{H}_3$); ^{13}C NMR (125 MHz, CD_3OD) δ: 165.5 (C-1), 144.8 (C-1′), 142.1, 140.6, 139.0, 135.9, 130.5 (C-2′,6′), 128.7, 128.5, 124.1, 122.0 (C-3′,5′), 51.0 (C-3), 25.0 (C-4), 19.8 (-$\underline{C}H_3$); HR-MS $[M - Br]^+$: Calcd for $C_{16}H_{15}ClN^+$, 256.0888, found 256.0885; Negative ESI-MS m/z: 78.7 [$^{79}Br^-$], 80.7 [$^{81}Br^-$].

*6-Chloro-2-(m-tolyl)-3,4-dihydroisoquinolin-2-ium bromide (**5-33**).* Yield: 70%; brown powder; mp 164.7−165.4 °C; IR, υ_{max} (KBr) cm^{-1}: 1634 (s, C═N); UV λ_{max}(lg ε) (MeOH) 230 (3.91), 325 (4.06) nm; ^{1}H NMR (500 MHz, CD_3OD) δ: 9.55 (1H, s, H-1), 8.07 (1H, d, J = 8.2 Hz, H-8), 7.73 (1H, s, H-2′), 7.70 (1H, s, H-5), 7.67 (2H, dd, J = 8.2, 2.0 Hz), 7.58 (1H, t, J = 7.9 Hz), 7.51 (1H, d, J = 7.6 Hz), 4.67 (2H, t, J = 8.0 Hz, H-3), 3.55 (2H, t, J = 8.0 Hz, H-4), 2.52 (3H, s, -C$\underline{H}_3$); ^{13}C NMR (125 MHz, CD_3OD) δ: 166.0 (C-1), 144.8 (C-1′), 143.0, 140.9, 139.1, 136.1, 131.8, 129.8, 128.7, 128.5, 124.1, 122.7, 119.3, 51.0 (C-3), 25.0 (C-4), 20.0 (-$\underline{C}H_3$); HR-MS $[M - Br]^+$: Calcd for $C_{16}H_{15}ClN^+$, 256.0888, found 256.0886; Negative ESI-MS m/z: 78.7 [$^{79}Br^-$], 80.7 [$^{81}Br^-$].

*6-Chloro-2-(o-tolyl)-3,4-dihydroisoquinolin-2-ium bromide (**5-34**).* Yield: 69%; yellow powder; mp 191.7−192.3 °C; IR, υ_{max} (KBr) cm^{-1}: 1634 (s, C═N); UV λ_{max} (lg ε) (MeOH) 227 (3.97), 308 (4.08) nm; ^{1}H NMR (500 MHz, CD_3OD) δ: 9.44 (1H, s, H-1), 8.06 (1H, d, J = 8.2 Hz, H-8), 7.73 (1H, s, H-5), 7.70 (2H, dd, J = 8.3,1.9 Hz), 7.61−7.56 (2H, m), 7.51 (1H, td, J = 7.8,1.8 Hz), 4.51 (2H, t, J = 8.0 Hz, H-3), 3.59 (2H, t, J = 8.0 Hz, H-4), 2.52 (3H, s, -C$\underline{H}_3$); ^{13}C NMR (125 MHz, CD_3OD) δ: 169.1 (C-1), 145.2 (C-1′), 142.5, 139.2, 136.2, 132.1, 132.0, 131.1, 128.8 (2 × C), 127.6, 124.6, 123.8, 52.0 (C-3), 25.1 (C-4), 16.3 (-$\underline{C}H_3$); HR-MS $[M - Br]^+$: Calcd for $C_{16}H_{15}ClN^+$, 256.0888, found 256.0886; Negative ESI-MS m/z: 78.7 [$^{79}Br^-$], 80.7 [$^{81}Br^-$].

Antifungal Assay. The antifungal activities *in vitro* of all the synthetic compounds against three plant pathogenic fungi (*A. alternate*, *C. lunata* and *V. mali*) were assayed by the mycelium linear growth rate method as previously reported.[5,8,9,11] The test fungi maintained on potato dextrose agar (PDA) medium slants were subcultured for 48 h in Petri dishes prior to testing and used for inoculation of fungal strains on PDA plates.

The tested compound was completely dissolved in 0.5 mL of DMSO and then added to 9.5 mL of sterile water. The resulting solution was added to 90 mL of melted PDA agar at 50 °C and, after quickly and completely mixing, poured into a Petri dish in a laminar flow chamber. The final concentration of the test compound in the culture medium was 50 or 25 μg/mL for the activity screening test, and the final concentration of DMSO was 0.5%, which was proven to have no significant effect on the growth of tested fungi. Azoxystrobin (50 or 25 μg/mL) in the culture medium containing 0.5% DMSO (v/v) and 0.5% DMSO in culture medium were used as a positive control and a blank control, respectively. When the medium in the plate was partially solidified, a 5 mm thick and 4 mm diameter disc of fungus cut from beforehand subcultured Petri dishes was placed at the center of the semisolid medium. The dishes were kept in an incubator at 28 °C for 72 h. Each experiment was carried out in triplicate. The diameters (in mm) of inhibition zones were measured with a caliper in three different directions, and the growth inhibition rates were calculated according to the following formula and expressed as means ± S.D.

$$\text{Inhibition rate } (\%) = [(d_c - d_0) - (d_s - d_0)]/(d_c - d_0) \times 100$$

where d_0 is the diameter of the fungus cut, d_c is the diameter of a fungal colony in the blank test, and d_s is the diameter of a fungal colony in the compound-treated test.

Based on the results of *in vitro* antifungal activity, the more active compounds were selected to determine their median effective concentration (EC_{50}) according to the same method described above. The stock solution was mixed with the autoclaved PDA medium to prepare a set of mediums containing 70, 50, 35, 25, 12.5, 6.25, and 3.125 μg/mL of the tested compound. Similarly, 0.5% DMSO in culture medium was used as a blank control. Each test was performed in triplicate. EC_{50} values and their confidence intervals at 95% probability (95% CI) were calculated by using PRISM software ver. 5.0 (GraphPad Software Inc., San Diego, CA, USA).

DOI: 10.1021/jf505609z
J. Agric. Food Chem. 2015, 63, 1906−1914

Table 1. Substitution Patterns of Compounds 5-1 to 5-34 and Their Preliminary Antifungal Activity

Compounds		Average inhibition rate ± SD (%) (n = 3)					
		A. alternate		*C. lunata*		*V. mali*	
No.	R	50 μg/mL	25 μg/mL	50 μg/mL	25 μg/mL	50 μg/mL	25 μg/mL
5-1	H	66.7 ± 0.0	49.8 ± 1.1	97.1 ± 0.0	84.6 ± 0.8	60.5 ± 0.0	43.6 ± 1.3
5-2	4′-F	78.2 ± 0.2	62.7 ± 0.3	95.2 ± 0.7	87.3 ± 0.9	67.1 ± 0.0	53.6 ± 0.4
5-3	3′-F	67.9 ± 0.8	51.3 ± 0.5	83.7 ± 0.1	68.8 ± 0.2	56.6 ± 1.8	41.3 ± 0.4
5-4	2′-F	79.3 ± 0.2	67.5 ± 0.3	89.3 ± 0.7	80.3 ± 0.7	72.1 ± 0.6	57.0 ± 0.3
5-5	4′-Cl	70.6 ± 0.0	53.9 ± 1.7	84.6 ± 0.8	73.7 ± 0.0	57.8 ± 0.7	38.7 ± 0.4
5-6	3′-Cl	66.7 ± 0.0	54.5 ± 0.0	84.1 ± 0.2	60.4 ± 0.7	59.8 ± 1.0	47.6 ± 0.6
5-7	2′-Cl	68.5 ± 0.8	54.2 ± 1.2	79.1 ± 0.7	65.4 ± 1.3	72.1 ± 0.9	57.8 ± 1.0
5-8	4′-Br	68.2 ± 0.0	55.6 ± 0.9	84.6 ± 0.0	66.3 ± 0.0	55.5 ± 0.3	37.9 ± 0.8
5-9	3′-Br	65.7 ± 0.8	51.5 ± 0.0	81.2 ± 0.7	65.4 ± 0.0	55.0 ± 0.0	37.1 ± 1.2
5-10	2′-Br	67.2 ± 0.8	51.0 ± 0.8	76.9 ± 0.0	62.8 ± 0.0	65.6 ± 0.7	46.8 ± 1.6
5-11	4′-I	62.2 ± 0.8	47.1 ± 0.0	82.0 ± 0.8	63.7 ± 0.7	41.0 ± 1.0	35.9 ± 1.0
5-12	3′-I	57.1 ± 0.0	44.0 ± 1.0	71.4 ± 0.0	55.2 ± 0.8	57.7 ± 0.9	48.8 ± 0.6
5-13	2′-I	64.7 ± 0.0	52.9 ± 0.0	74.6 ± 0.7	57.9 ± 1.3	67.5 ± 1.5	51.3 ± 0.0
5-14	2′-F-4′-I	64.7 ± 0.0	52.9 ± 0.0	71.6 ± 0.0	61.3 ± 1.6	55.1 ± 0.9	48.4 ± 0.4
5-15	3′,5′-diCl	50.0 ± 0.0	42.9 ± 0.0	65.7 ± 0.0	57.1 ± 0.0	71.4 ± 0.0	55.2 ± 1.6
5-16	2′-F-4′-Br	70.6 ± 0.0	58.8 ± 0.0	74.3 ± 1.3	65.3 ± 0.8	52.0 ± 0.7	46.4 ± 0.6
5-17	2′,4′-diCl	61.8 ± 0.0	49.0 ± 0.8	68.9 ± 0.8	54.4 ± 1.5	68.0 ± 1.3	51.3 ± 0.0
5-18	2′,4′-diBr	51.5 ± 0.0	45.7 ± 0.5	61.8 ± 0.5	49.1 ± 0.8	53.9 ± 0.6	48.8 ± 1.0
5-19	2′,6′-diF	53.1 ± 0.0	37.5 ± 0.0	71.6 ± 0.2	56.9 ± 1.0	48.5 ± 0.4	38.2 ± 0.5
5-20	4′-OMe	61.1 ± 0.9	43.2 ± 0.9	79.1 ± 0.8	65.4 ± 0.7	63.3 ± 0.9	41.9 ± 1.0
5-21	3′-OMe	31.3 ± 0.0	18.8 ± 0.0	43.5 ± 1.1	31.3 ± 0.2	26.0 ± 1.4	19.4 ± 0.6
5-22	2′-OMe	66.7 ± 0.0	48.4 ± 1.6	91.8 ± 0.7	78.2 ± 0.6	78.5 ± 1.4	51.1 ± 0.4
5-23	4′-CF_3	68.1 ± 0.8	54.4 ± 1.5	80.6 ± 0.8	68.0 ± 0.8	55.5 ± 0.6	49.3 ± 0.7
5-24	3′-CF_3	61.8 ± 0.0	49.5 ± 0.8	78.8 ± 0.2	65.6 ± 0.3	52.0 ± 1.4	41.8 ± 0.4
5-25	2′-CF_3	63.8 ± 1.1	51.1 ± 0.5	72.5 ± 1.3	61.4 ± 0.3	70.8 ± 0.9	55.8 ± 0.6
5-26	4′−OH	50.3 ± 1.2	32.8 ± 1.6	68.6 ± 0.4	47.8 ± 0.4	68.1 ± 0.5	48.9 ± 0.4
5-27	3′−OH	26.2 ± 1.1	11.8 ± 0.8	26.7 ± 0.9	5.3 ± 1.3	13.5 ± 0.7	5.6 ± 0.7
5-28	2′−OH	58.8 ± 0.8	37.0 ± 0.9	67.4 ± 0.9	51.1 ± 0.4	71.5 ± 0.5	39.2 ± 1.7
5-29	4′-NO_2	56.7 ± 1.3	45.2 ± 1.1	57.6 ± 1.0	49.1 ± 0.4	51.2 ± 1.5	39.7 ± 1.3
5-30	3′-NO_2	64.7 ± 0.0	52.0 ± 0.8	79.0 ± 0.0	68.0 ± 0.8	62.8 ± 0.5	48.7 ± 0.0
5-31	2′-NO_2	34.8 ± 0.8	21.8 ± 0.8	17.3 ± 0.1	7.1 ± 0.7	30.3 ± 0.7	15.4 ± 1.3
5-32	4′-Me	62.0 ± 0.8	45.2 ± 0.5	82.1 ± 0.0	79.4 ± 0.8	57.5 ± 1.2	38.9 ± 0.7
5-33	3′-Me	61.5 ± 0.4	40.6 ± 1.1	82.0 ± 0.8	63.2 ± 0.0	42.0 ± 0.6	24.4 ± 1.3
5-34	2′-Me	61.6 ± 0.3	51.2 ± 0.4	92.4 ± 0.7	80.3 ± 0.4	97.1 ± 0.0	95.2 ± 0.0
Sanguinarine		47.7 ± 1.2		58.7 ± 1.5		69.1 ± 0.7	
Chelerythrine		50.3 ± 1.8		48.7 ± 1.3		57.1 ± 0.9	
Azoxystrobin		55.7 ± 0.9	52.6 ± 0.9	44.2 ± 0.6	35.6 ± 0.5	51.6 ± 0.3	48.4 ± 0.3

RESULTS AND DISCUSSION

Chemistry. The synthetic route of compounds **5-1** to **5-34** was outlined in Scheme 1, and their substitution patterns are listed in Table 1. Commercially available 2-(3-chlorophenyl)-acetic acid (**1**) as a starting material was reduced with $NaBH_4$ in anhydrous THF in the presence of an equimolar amount of iodine to obtain **2** in 99% yield. Compound **2** reacted with paraformaldehyde in trifluoroacetic acid to obtain 6-chloroisochromane (**3**) and a byproduct 8-chloroisochromane (**3a**) in 95% yield in an approximately equimolar ratio, similar to the results reported elsewhere.[12,13] The mixture of **3** and **3a** was subjected to column chromatography over silica gel to yield the desired compound **3**. 2-(2-Bromoethyl)-4-chlorobenzaldehyde (**4**) as a key intermediate was obtained in 74% by α-bromination of 6-chloroisochromane (**3**) followed by the treatment with aqueous hydrobromic acid. Compound **4** reacted with various primary aromatic amines in 1,4-dioxane to obtain the desired 2-aryl-3,4-dihydroisoquinolin-2-ium bromides (**5-1** to **5-34**).

The structures of the synthesized compounds were confirmed by spectroscopic analysis including UV, IR, HR-MS, ^{1}H NMR and ^{13}C NMR. Due to the structural similarity, all compounds **5-1** to **5-34** showed similar spectroscopic characteristics. Each of them showed a wavelength of maximum absorption in the range of 227 to 426 nm in UV spectra due to the presence of the conjugated system, a strong absorption (C═N$^+$) in the range of 1617 to 1642 cm^{-1} in IR spectra, a characteristic ion peak at m/z [M − Br]$^+$ in positive ESI-HR-MS spectra, and the ion peaks at m/z [^{79}Br$^-$] and [^{81}Br$^-$] in negative ESI-MS spectra. In ^{1}H and ^{13}C NMR spectra, all the compounds revealed one singlet signal in the range of δ_H 9.40 to 9.92 ppm due to the proton of HC═N$^+$ and one signal in the range of δ_C 164.1 to 171.2 ppm due to C-1.

Antifungal Activity. According to the mycelium linear growth rate method reported by us, the antifungal activities *in vitro* of compounds **5-1** to **5-34** were screened against three plant pathogenic fungi (*A. alternate*, *C. lunata*, and *V. Mali*) at 50 and 25 μg/mL. The results listed in Table 1 showed all the compounds displayed the activity in varying degrees against each of the test fungi. For each fungus, at the test concentration of 25

DOI: 10.1021/jf505609z
J. Agric. Food Chem. 2015, 63, 1906−1914

Table 2. Antifungal Activities of Compounds 2-Aryl-6-chloro-3,4-dihydroisoquinolin-2-ium Bromides

Compounds		EC_{50} (95% CI[a])		
No.	R	*A. alternate*	*C. lunata*	*V. mali*
5-1	H	≈ 25[b]	6.6 (6.2−7.0)	25−50[b]
5-2	4′-F	15.9 (15.6−16.2)	4.6 (4.5−4.9)	24.8 (24.4−25.3)
5-3	3′-F	23.3 (22.6−24.0)	9.9 (9.4−10.5)	25−50[b]
5-4	2′-F	10.3 (10.0−10.6)	4.7 (4.5−4.9)	18.0 (17.5−18.6)
5-5	4′-Cl	19.8 (19.2−20.4)	8.4 (8.0−8.8)	25−50[b]
5-6	3′-Cl	19.4 (18.7−20.0)	12.9 (12.3−13.7)	25−50[b]
5-7	2′-Cl	20.3 (19.3-21.2)	8.8 (8.3−9.3)	18.0 (17.4−18.5)
5-8	4′-Br	18.6 (18.0−19.3)	11.0 (10.5−11.5)	25−50[b]
5-9	3′-Br	23.5 (23.2−23.9)	10.3 (9.7−10.9)	25−50[b]
5-10	2′-Br	24.9 (24.1−25.7)	13.6 (13.2−14.1)	25−50[b]
5-11	4′-I	25−50[b]	12.3 (11.8−12.7)	>50[b]
5-12	3′-I	25−50[b]	17.4 (16.6−18.1)	25−50[b]
5-13	2′-I	22.0 (21.3−22.6)	15.6 (14.9−16.5)	24.7 (24.0−25.3)
5-14	2′-F-4′-I	20.3 (19.9−20.8)	12.2 (11.8−12.6)	25−50[b]
5-15	3′,5′-diCl	≈ 50[b]	14.9 (14.2−15.6)	20.1 (19.4−20.8)
5-16	2′-F-4′-Br	15.0 (14.4−15.6)	8.5 (8.2−8.9)	25−50[b]
5-17	2′,4′-diCl	≈ 25[b]	18.9 (18.4−19.5)	24.8 (23.8−25.8)
5-18	2′,4′-diBr	25−50[b]	≈ 25[b]	25−50[b]
5-19	2′,6′-diF	25−50[b]	18.0 (17.4−18.6)	≈ 50[b]
5-20	4′-OMe	25−50[b]	12.4 (12.0−12.9)	25−50[b]
5-21	3′-OMe	>50[b]	>50[b]	>50[b]
5-22	2′-OMe	≈ 25[b]	8.4 (8.2−8.6)	23.9 (23.4−24.3)
5-23	4′-CF_3	19.0 (18.3−19.8)	7.9 (7.5−8.2)	25−50[b]
5-24	3′-CF_3	≈ 25[b]	10.8 (10.5−11.1)	25−50[b]
5-25	2′-CF_3	24.7 (23.7−25.7)	14.6 (13.9−15.2)	20.5 (19.9−21.2)
5-26	4′-OH	≈ 50[b]	25−50[b]	≈ 25[b]
5-27	3′-OH	>50[b]	>50[b]	>50[b]
5-28	2′-OH	25−50[b]	24.8 (24.3−25.2)	25−50[b]
5-29	4′-NO_2	25−50[b]	≈ 25[b]	≈ 50[b]
5-30	3′-NO_2	23.6 (23.0−24.3)	9.1 (8.8−9.4)	≈ 25[b]
5-31	2′-NO_2	>50[b]	>50[b]	>50[b]
5-32	4′-Me	25−50[b]	7.6 (7.4−7.9)	25−50[b]
5-33	3′-Me	25−50[b]	14.3 (13.8−14.8)	>50[b]
5-34	2′-Me	24.2 (23.3−25.1)	5.8 (5.6−6.1)	3.9 (3.8−4.0)
Sanguinarine		53.0 (28.2−99.7)	35.6 (23.4−54.1)	25.6 (17.2−38.1)
Chelerythrine		49.5 (21.5−113.9)	15.7 (6.1−40.7)	39.7 (16.2−97.4)
Azoxystrobin		12.8 (11.8−13.8)	71.9 (67.6−76.4)	37.2 (34.7−40.0)

[a]95% CI, confidence intervals at 95% probability. [b]Estimated values based on the results shown in Table 1.

or 50 μg/mL, part or most of the synthesized compounds were more active than their natural model compounds, sanguinarine and chelerythrine, and the positive control azoxystrobin. Especially for *C. lunata*, almost all the compounds except **5-21**, **5-27**, and **5-31** showed higher activity at 25 or 50 μg/mL than azoxystrobin, with inhibition rates of 44.2% at 50 μg/mL and 35.6% at 25 μg/mL. For all the synthesized compounds, 88% of all the test items at 50 μg/mL (90/102) and 52% at 25 μg/mL (53/102) revealed good to excellent activity with inhibition rates of 50% to 97.1%. In general, these compounds showed higher activity on *C. lunata* followed by *A. alternate* and *V. mali*.

In order to further explore the antifungal potential and structure−activity relationship, the compounds with inhibition rates >50% at 25 μg/mL were further examined to determine their median effective concentrations (EC_{50}) against three strains of fungi. The results are shown in Table 2.

From Table 2, it was clearly seen that all of the 28 tested compounds showed excellent activity, with EC_{50} values of 4.6−24.8 μg/mL against *C. lunata*, much higher than the positive control azoxystrobin (EC_{50} = 71.9 μg/mL) and the reference compound sanguinarine (EC_{50} = 35.6 μg/mL); EC_{50} values of 12 out of 28 were below 10.0 μg/mL. For *A. alternate*, all 16 tested compounds showed good activity, with EC_{50} values of 10.3−24.9 μg/mL, and **5-4** showed the highest activity, with an EC_{50} value of 10.3 μg/mL, superior to azoxystrobin (EC_{50} = 12.8 μg/mL), sanguinarine (EC_{50} = 53.0 μg/mL), and chelerythrine (EC_{50} = 49.5 μg/mL). Regarding *V. mali*, all of the 9 tested compounds showed higher activity, with EC_{50} values of 3.9−24.8 μg/mL, than azoxystrobin (EC_{50} = 37.2 μg/mL), sanguinarine (EC_{50} = 25.6 μg/mL), and chelerythrine (EC_{50} = 39.7 μg/mL). The above results indicated that the susceptibility order of three strains of fungi to these compounds was *C. lunata* > *A. alternate* > *V. mali*, which was in agreement with the screening results in Table 1.

From comparison of the EC_{50} values of various compounds in Table 2, in conjunction with the inhibition rates at 25 μg/mL in Table 1, it was concluded that the type and position of substituents on the C-ring had significant effects on the activity (Figure 2). The general trend is that the presence of 2′-F, 4′-F, or 2′-CH_3 always leads to an increase of the activity against all three

DOI: 10.1021/jf505609z
J. Agric. Food Chem. 2015, 63, 1906−1914

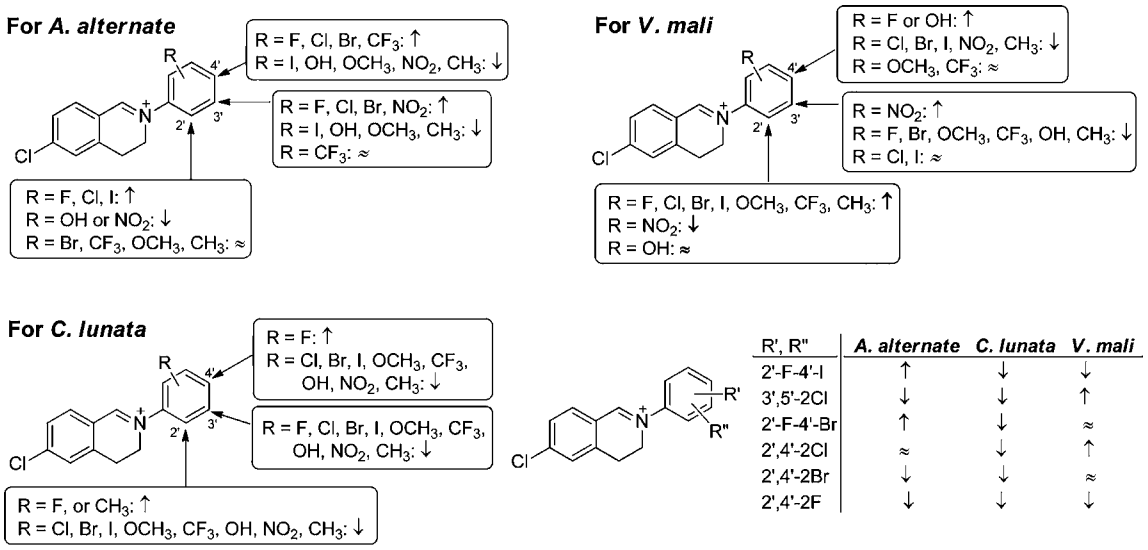

R', R"	A. alternate	C. lunata	V. mali
2'-F-4'-I	↑	↓	↓
3',5'-2Cl	↓	↓	↑
2'-F-4'-Br	↑	↓	≈
2',4'-2Cl	≈	↓	↑
2',4'-2Br	↓	↓	≈
2',4'-2F	↓	↓	↓

Figure 2. Structure−activity relationship of compounds **5-2** to **5-34**.

test fungi compared with compound **5-1** (R = H), whereas the effects of other substituents on the activity depend on their positions and the species of the fungi. For *A. alternate*, the presence of a monohalogen atom (F, Cl, Br, I) (**5-2** to **5-13**) or a trifluoromethyl group (**5-23** to **5-25**) at the 2′, 3′, or 4′ position improves the activity in most cases, whereas the introduction of a methoxy group (**5-20** to **5-22**), a hydroxy group (**5-26** to **5-28**), a methyl group (**5-32** to **5-34**), or a nitro group (**5-29** to **5-31**) generally decreases the activity; as to *C. lunata*, although most of the compounds showed higher activity than the reference azoxystrobin, only 4′-F, 2′-F, and 2′-CH_3 substituted compounds (**5-2**, **5-4**, and **5-34**) showed higher activity than **5-1** (R = H), indicating that the presence of the various substituents on the C-ring generally led to reduction of the activity against *C. lunata*. A similar case was observed for *V. mali*, where only the minority of the compounds were slightly more active than **5-1**, showing that the introduction of substituents to the C-ring was of less importance for enhancement of the activity against *V. mali*. The structure−activity relationships above are different from the case of 2-aryl-3,4-dihydroisoquinolin-2-ium bromides[8] and 2-aryl-6,7-methylenedioxy-3,4-dihydroisoquinolin-2-ium bromides[9] reported by us. For 2-aryl-3,4-dihydroisoquinolin-2-ium bromides, the presence of halogen atoms (F, Cl, Br, or I) or CF_3 groups at any site in the C-ring as well as 4′-OH remarkably enhances the activity against *A. alternate*, *C. lunata*, and *V. mali*, whereas the introduction of CH_3 or OCH_3 to the 2′-, 3′-, or 4′-site as well as 2′-OH leads to a decrease of activity.[8] Similar cases were observed for 2-aryl-6,7-methylenedioxy-3,4-dihydroisoquinolin-2-ium bromides.[9]

The noteworthy compounds were fluorinated (**5-2** to **5-4**), methyl-substituted (**5-32** to **5-34**), and nitro-substituted (**5-29** to **5-31**) isomers. Among all the synthesized compounds, **5-2** and **5-4** not only showed the top three activities on almost all of the three tested fungi, but also were more active than **5-1** for all the fungi. This result suggested that the presence of 2′-F and 4′-F was beneficial to the improvement of the activity. Compound **5-34** (2′-CH_3) showed the highest activity (EC_{50} = 3.9 μg/mL) against *V. mali*, the third highest activity (EC_{50} = 5.8 μg/mL) against *C. lunata* among all the synthesized compounds. This result indicated that the introduction of 2′-CH_3 could significantly improve the activity against both *C. lunata* and *V. mali* but have less influence on the activity against *A. alternate*. This case was completely different from the results observed for 2-aryl-3,4-dihydroisoquinolin-2-ium bromides[8] and 2-aryl-6,7-methylenedioxy-3,4-dihydroisoquinolin-2-ium bromides,[9] where the presence of 2′-, 3′-, or 4′-CH_3 lead to a decrease of the activities. For nitro-substituted compounds, the presence of 2′-NO_2 (**5-31**) caused reduction of the activities against all three fungi, and the presence of 3′-NO_2 (**5-30**) could lead to an increase of the activities against *A. alternate* and *V. mali*, similar to that observed for 2-aryl-3,4-dihydroisoquinolin-2-ium bromides[8] and 2-aryl-6,7-methylenedioxy-3,4-dihydroisoquinolin-2-ium bromides.[9] However, 4′-NO_2 in three series of the compounds has different effects on the activity. For **5-29**, the introduction of 4′-NO_2 led to a decrease of the activities against all three fungi, whereas for 2-(4-nitrophenyl)-3,4-dihydroisoquinolin-2-ium bromides and 2-(4-nitrophenyl)-6,7-methylenedioxy-3,4-dihydroisoquinolin-2-ium bromides, the presence of 4′-NO_2 could increase the activities against both *A. alternate* and *V. mali*. The above results obviously showed that there was an interaction effect between substituents on the A-ring and the C-ring, and the activity of compounds depended on the combined effect of substituents on the A-ring and the C-ring. This observation proved to be useful for the design of new 2-aryl-3,4-dihydroisoquinolin-2-iums with more potent antifungal activity.

Additionally, compared with compounds **5-2** to **5-13**, with one halogen atom on the C-ring, compounds **5-14** to **5-19**, containing two halogen atoms on the C-ring, did not improve the activities in most cases. This result indicated, to a certain degree, that the increase of halogen atom number on the C-ring made no contribution to the improvement of activity.

Our previous research proved that the iminium moiety (C═N^+) in sanguinarine and chelerythrine was a key structural moiety for their antimicrobial, acaricidal, and anticancer activity.[5−7,14] A similar case was also observed in 2-aryl-3,4-dihydroisoquinolin-2-ium compounds on the basis of the fact that reduction of the iminium moiety (C═N^+) led to loss of the activity (unpublished). The facts above suggested that the bioactivity of 3,4-dihydroisoquinolin-2-ium compounds should be related with the electron density of their iminium moiety. Our

DOI: 10.1021/jf505609z
J. Agric. Food Chem. 2015, 63, 1906−1914

previous research on 2-aryl-3,4-dihydroisoquinolin-2-ium compounds showed that the introduction of electron-withdrawing groups such as halogen atoms or CF_3 and NO_2 groups to C-ring could significantly increase the antifungal activity, indicating that the low electron density of the iminium moiety was a benefit to the improvement of the activity. However, for the present compounds (**5-2** to **5-34**), the electron density of the iminium moiety not only depends on the substituent in the C-ring but also on the chlorine atom in the A-ring. Therefore, the activity of **5-2** to **5-34** depends on the combined electron effect of substituents in the A-ring and the C-ring. This is the reason that **5-2** to **5-34** showed different SAR from 2-aryl-3,4-dihydroisoquinolin-2-ium bromides and 2-aryl-6,7-methylenedioxy-3,4-dihydroisoquinolin-2-ium bromides.

In conclusion, we reported the synthesis of a new series of 2-aryl-6-chloro-3,4-dihydroisoquinolin-2-ium bromides and the evaluation of their antifungal activity *in vitro* against three plant pathogenic fungi. All the synthesized compounds showed the obvious growth inhibition activity against all the tested fungi, and most of them were more active than azoxystrobin. Among all the tested compounds, **5-2** and **5-4** showed higher activity against all the tested fungi, with EC_{50} values of 4.6−24.8 μg/mL, and **5-34** showed the highest activity against *V. mali* with an EC_{50} value of 3.9 μg/mL and the third highest activity against *C. lunata* with an EC_{50} value of 5.8 μg/mL. Some of the compounds, especially **5-2**, **5-4**, **5-7**, **5-13**, **5-25**, and **5-34**, were of great potential to be developed as new antifungal agents for plant protection. SAR analysis showed that the C-ring was a highly sensitive structural moiety to the activity and the type as well as position of substituents on C-ring could make significant effects on the activity. In most cases, the introduction of monohalogen atom to the C-ring could enhance the activity, whereas the presence of −OH, -OMe, $-NO_2$ or $-CF_3$ caused decrease or slight increase of the activity. The presence of 2′-Me could significantly enhance the activities, especially on *C. lunata* and *V. mali*, but 3′- or 4′-Me caused decrease of the activities. Thus, the present results were of great importance for the design, synthesis and development of novel isoquinoline antifungal agents. Further research was necessary on the more extensive structural modification, the determination of an antifungal spectrum and the *in vivo* activity of these compounds.

■ ASSOCIATED CONTENT

Supporting Information

UV, IR, ^{1}H NMR, ^{13}C NMR, and HRMS spectra for the target compounds. This material is available free of charge via the Internet at http://pubs.acs.org.

■ AUTHOR INFORMATION

Corresponding Authors

*Tel./Fax: +86-29-87092226; E-mail: zhoulechem@nwsuaf.edu.cn (L. Zhou).

*Tel./Fax: +86-29-87092226; E-mail: miaofangmf@163.com (F. Miao).

Funding

This project was financially supported by the National Natural Science Foundation of China (Nos. 31172365, 31101469). This study was also supported by New Century Excellent Talents by Ministry of Education of China (NCET-12-0475) and the Fund of Youth Science and Technology Stars by Shaanxi Province (2012KJXX-16).

Notes

The authors declare no competing financial interest.

■ REFERENCES

(1) Brase, S.; Encinas, A.; Keck, J.; Nising, C. F. Chemistry and biology of mycotoxins and relatedfungal metabolites. *Chem. Rev.* **2009**, *109*, 3903−3990.

(2) Savary, S.; Teng, P. S.; Willocquet, L.; Nutter, F. W., Jr. Quantification and modeling of croplosses: A review of purposes. *Annu. Rev. Phytopathol.* **2006**, *44*, 89−112.

(3) Delp, C. J. Coping with resistance to plant disease control agents. *Plant Dis.* **1980**, *64*, 652−658.

(4) Wedge, D. E.; Camper, N. D. Biologically active natural products. In *Agrochemicals and Pharmaceuticals*; Cutler, H. G., Cutler, S. J., Eds.; CRC Press: Boca Raton, FL, USA, 2000; pp 1−15.

(5) Yang, X. J.; Miao, F.; Yao, Y.; Cao, F. J.; Yang, R.; Ma, Y. N.; Qin, B. F.; Zhou, L. In vitro antifungal activity of sanguinarine and chelerythrine derivatives against phytopathogenic fungi. *Molecules* **2012**, *17*, 13026−13035.

(6) Miao, F.; Yang, X. J.; Zhou, L.; Hu, H. J.; Zheng, F.; Ding, X. D.; Sun, D. M.; Zhou, C. D.; Sun, W. Structural modification of sanguinarine and chelerythrine and their antibacterial activity. *Nat. Prod. Res.* **2011**, *25*, 863−875.

(7) Miao, F.; Yang, X. J.; Ma, Y. N.; Zheng, F.; Song, X. P.; Zhou, L. Structural modification of sanguinarine and chelerythrine and their in vitro acaricidal activity against *Psoroptes cuniculi*. *Chem. Pharm. Bull.* **2012**, *60*, 1508−1513.

(8) Hou, Z.; Yang, R.; Zhang, C.; Zhu, L. F.; Miao, F.; Yang, X. J.; Zhou, L. 2-(Substituted phenyl)-3,4-dihydroisoquinolin-2-iums as novel antifungal lead compounds: biological evaluation and structure-activity relationships. *Molecules* **2013**, *18*, 10413−10424.

(9) Yang, X. J.; Yao, Y.; Qin, Y. Y.; Hou, Z.; Yang, R.; Miao, F.; Zhou, L. Synthesis and in vitro antifungal activities of new 2-aryl-6,7-methylenedioxy-3,4-dihydroisoquinolin-2-ium bromides. *Chem. Pharm. Bull.* **2013**, *61*, 731−739.

(10) Zhang, B. Y.; Zheng, Z. L.; Miao, F.; Yang, X. J.; Ma, X. H.; Zhou, L. Effects of 2-aryl-3,4-dihydroisoquinolin-2-iums on seed germination and seedling growth. *J. Northwest A&F University (Nat. Sci. Ed.).* **2013**, *42*, 169−174.

(11) Miao, F.; Yang, R.; Chen, D. D.; Wang, Y.; Qin, B. F.; Yang, X. J.; Zhou, L. Isolation, identification and antimicrobial activities of two secondary metabolites of *Talaromyces verruculosus*. *Molecules* **2012**, *17*, 14091−14098.

(12) Favor, D. A.; Johnson, D. S.; Powers, J. J.; Li, T. S.; Madabattula, R. Synthesis of chromanyl and dihydrobenzofuranyl piperazines. *Tetrahedron Lett.* **2007**, *48*, 3039−3041.

(13) Reisman, S. E.; Doyle, A. G.; Jacobsen, E. N. Enantioselective thiourea-catalyzed additions to oxocarbenium ions. *J. Am. Chem. Soc.* **2008**, *130*, 7198−7199.

(14) Cao, F. J.; Yang, R.; Lv, C.; Ma, Q.; Lei, M.; Geng, H. L.; Zhou, L. Pseudocyanides of sanguinarine and chelerythrine and their series of structurally simple analogues as new anticancer lead compounds: cytotoxic activity, structure-activity relationship and apoptosis induction. *Eur. J. Pharm. Sci.* **2015**, *67*, 45−54.

DOI: 10.1021/jf505609z
J. Agric. Food Chem. 2015, 63, 1906−1914

phy−mass spectrometry (MDGC-MS) techniques, novel VSCs were synthesized and characterized. In addition, aroma extract dilution analysis (AEDA) by gas chromatography−olfactometry (GC-O) was applied to assign flavor dilution (FD) factors to the odor-active compounds in the lemon extract.

MATERIALS AND METHODS

Materials. Conventional Lisbon lemons (SK Choice grade, large size) were ordered from Saticoy Lemon Associates and Sunkist Growers in Oxnard, CA, USA. Upon arrival, the lemons were worked up immediately. A microplane zester (OXO, Chambersburg, PA, USA) was used to zest the peel.

Chemicals. The following reagents were purchased from Sigma-Aldrich (St. Louis, MO, USA): dichloromethane (DCM), methanol (MeOH), hexane, anhydrous magnesium sulfate ($MgSO_4$), 1,5-dibromopentane, 1,3-dibromopropane, Li_2CuCl_4, 2-pentylmagnesium bromide−diethyl ether solution, and 2-propionylthiophene. The following compounds were purchased from the FCH Group (Ukraine): 3-methylundecanal and 3-methyldodecanal. Finally, the following Grignard reagents were purchased from Novel Chemical Solutions (Crete, NE, USA): 2-hexylmagnesium bromide−THF solution, 2-heptylmagnesium bromide−THF solution, 2-octylmagnesium bromide−THF solution, 2-nonylmagnesium bromide−THF solution, 2-decylmagnesium bromide−THF solution, and 2-undecylmagnesium bromide−THF solution.

Synthesis of 6-Methylnonanal 136. The synthesis of **136** involved a four-step pathway (Figure 1) and is described in detail as an example of the 6-methyl and 4-methylalkyl aldehydes synthesized in this study.

*1-Bromo-6-methylnonane (**3a**).* Under N_2, a 1 L, four-necked flask, equipped with a mechanical stirrer, was charged with 1,5-dibromopentane (**1a**; 5.1 g, 25 mmol), THF (50 mL), and Li_2CuCl_4 (2.5 mL, 250 mmol) in 0.1 M THF and cooled to 0 °C. A 2-pentylmagnesium bromide−diethyl ether solution (**2a**; 100 mL, 25 mmol) was added to the reaction and stirred for 45 min at 0 °C under argon. The mixture was allowed to reach ambient temperature and quenched with water (200 mL) and 1 M HCl (25 mmol). The aqueous layer was extracted with hexane (3 × 100 mL), and the combined organic phases were washed with a 5% solution of $NaHCO_3$ (100 mL) and brine (100 mL). The organic phase was dried over $MgSO_4$, and **3a** was concentrated under partial vacuum to remove the solvent and used as-is in the next step.

*6-Methylnonyl Acetate (**4a**).* A 250 mL, four-necked flask was charged with the crude mixture of **3a** (16.0 g, 61 mmol) and DMF (50 mL). To this mixture was added sodium acetate (9.9 g, 120 mmol) in excess, and the reaction was run for 10 h at 100 °C. The reaction mixture was allowed to reach ambient temperature, followed by the addition of water (300 mL). The mixture was then extracted with hexane (3 × 100 mL), and the combined organic fractions were washed with water (2 × 100 mL) and brine (100 mL) and dried over $MgSO_4$. The solvent was evaporated under reduced pressure to produce **4a** and used as-is in the next step.

*6-Methylnonanol (**5a**).* A 1 L, four-necked flask was charged with the crude mixture of **4a** (10.0 g, 41 mmol), along with MeOH (200 mL) and a catalytic amount of K_2CO_3 (1.0 g, 7 mmol) and run for 5 h at ambient temperature. The MeOH was evaporated off and hexane (100 mL) and water (100 mL) were added to the residue. The phases were allowed to separate, and the organic phase was washed with water (50 mL) and brine (50 mL), dried over $MgSO_4$, and evaporated. The raw product mixture was purified by column chromatography (silica; hexane/ethyl acetate) giving **5a** (2.0 g) as a clear oil.

*6-Methylnonanal **136**.* A 1 L, four-necked flask was charged with **5a** (2.0 g, 10 mmol), KBr (0.1 g, 1 mmol), $NaHCO_3$ (1.7 g, 20 mmol), and DCM (150 mL). 2,2,6,6-Tetramethyl-1-oxylpiperidine (TEMPO; 16 mg, 100 mmol) was added to the flask, followed by water (5 mL), and allowed to cool to 0 °C. A 15% solution of NaClO (8.9 g, 13 mmol, d = 1.2) was added dropwise at 5 °C and stirred for 1 h at 10 °C. A 5 g solution of L-ascorbic acid (30% in water) was added and heated to reflux for 2 h. After cooling, the phases were allowed to separate, and the organic phase was washed with water (100 mL) and brine (100 mL) and dried over $MgSO_4$. After filtration and concentration, **136** (0.4 g, 20%) was obtained by column chromatography (silica; ethyl acetate/hexanes). The total yield based on the four-step synthesis beginning with **1a** was 10%. ^{1}H NMR ($CDCl_3$, 500 MHz): δ 9.76 (t, J = 1.9 Hz, 1H), 2.42 (td, J = 7.4 Hz, 1.9 Hz, 2H), 1.56−1.67 (m, 2H), 1.21−1.42 (m, 7H), 1.04−1.17 (m, 2H), 0.88 (t, J = 7.3 Hz, 3H), 0.84 (d, J = 6.6 Hz, 3H). EI-MS: 156 (0, M^+), 95 (100), 43 (78), 71 (63), 70 (60), 69 (60), 41 (54), 57 (49), 55 (47), 96 (42), 84 (38).

The synthesis of 6-methyldecanal **215** followed a similar procedure but instead used a 2-hexylmagnesium bromide−THF solution as the Grignard reagent. The 4-methylalkyl aldehydes were prepared in a similar fashion except using 1,3-dibromopropane instead of 1,5-dibromopentane, along with the associated Grignard reagent.

*6-Methyldecanal **215**:* yield (14%); ^{1}H NMR ($CDCl_3$, 400 MHz) δ 9.77 (t, J = 1.9 Hz, 1H), 2.39−2.48 (m, 2H), 1.53−1.74 (m, 2H), 1.19−1.40 (m, 9H), 1.06−1.16 (m, 2H), 0.88 (t, J = 6.8 Hz, 3H), 0.84 (d, J = 6.5 Hz, 3H)' EI-MS 170 (0, M^+), 43 (100), 95 (84), 69 (67), 41 (67), 57 (66), 85 (61), 84 (59), 55 (46), 96 (44), 29 (39).

*4-Methyloctanal **86**:* yield (25%); ^{1}H NMR ($CDCl_3$, 400 MHz) δ 9.77 (t, J = 1.9 Hz, 1H), 2.35−2.49 (m, 2H), 1.55−1.72 (m, 1H), 1.36−1.49 (m, 2H), 1.19−1.34 (m, 5H), 1.04−1.19 (m, 1H), 0.89 (t, J = 6.6 Hz, 3H), 0.88 (d, J = 6.4 Hz, 3H); EI-MS 142 (0, M^+), 56 (100), 57 (56), 43 (49), 70 (44), 41 (43), 29 (36), 85 (33), 55 (27), 27 (22).

*4-Methylnonanal **140**:* yield (20%); ^{1}H NMR ($CDCl_3$, 500 MHz) δ 9.77 (t, J = 1.9 Hz, 1H), 2.30−2.48 (m, 2H), 1.57−1.73 (m, 1H), 1.35−1.50 (m, 2H), 1.21−1.34 (m, 7H), 1.04−1.20 (m, 1H), 0.89 (t, J = 6.6 Hz, 3H), 0.88 (d, J = 6.4 Hz, 3H); EI-MS 156 (0, M^+), 57 (100), 56 (83), 41 (47), 55 (33), 43 (31), 29 (23), 85 (20), 69 (19), 84 (17) 112 (16).

*4-Methyldecanal **217**:* yield (20%); ^{1}H NMR ($CDCl_3$, 400 MHz) δ 9.77 (t, J = 1.9 Hz, 1H), 2.35−2.48 (m, 2H), 1.55−1.71 (m, 1H), 1.35−1.50 (m, 2H), 1.22−1.34 (m, 9H), 1.04−1.20 (m, 1H), 0.89 (t, J = 6.6 Hz, 3H), 0.88 (d, J = 6.4 Hz, 3H); EI-MS 170 (0, M^+), 56 (100), 57 (97), 41 (53), 43 (52), 69 (43), 29 (43), 55 (43), 71 (43), 85 (34), 82 (28).

*4-Methylundecanal **274**:* yield (18%); ^{1}H NMR ($CDCl_3$, 500 MHz) δ 9.77 (t, J = 1.9 Hz, 1H), 2.32−2.50 (m, 2H), 1.56−1.76 (m, 1H), 1.38−1.56 (m, 2H), 1.22−1.33 (m, 11H), 1.03−1.20 (m, 1H), 0.89 (t, J = 6.6 Hz, 3H), 0.88 (d, J = 6.4 Hz, 3H); EI-MS 184 (0, M^+), 56 (100), 57 (87), 85 (56), 43 (55), 41 (53), 69 (49), 29 (46), 55 (45), 71 (39), 82 (39).

*4-Methyldodecanal **321**:* yield (20%); ^{1}H NMR ($CDCl_3$, 500 MHz) δ 9.77 (t, J = 1.9 Hz, 1H), 2.32−2.50 (m, 2H), 1.56−1.76 (m, 1H), 1.38−1.56 (m, 2H), 1.22−1.33 (m, 13H), 1.03−1.20 (m, 1H), 0.89 (t, J = 6.6 Hz, 3H), 0.88 (d, J = 6.4 Hz, 3H); EI-MS 198 (0, M^+), 56 (100), 57 (98), 41 (57), 43 (56), 85 (50), 55 (49), 69 (44), 82 (37), 29 (31), 81 (28).

*4-Methyltridecanal **370**:* yield (15%); ^{1}H NMR ($CDCl_3$, 400 MHz) δ 9.77 (t, J = 1.9 Hz, 1H), 2.35−2.48 (m, 2H), 1.56−1.76 (m, 1H), 1.38−1.48 (m, 2H), 1.21−1.33 (m, 15H), 1.04−1.20 (m, 1H), 0.89 (t, J = 6.6 Hz, 3H), 0.88 (d, J = 6.4 Hz, 3H); EI-MS 212 (0, M^+), 57 (100), 56 (87), 85 (58), 43 (47), 55 (47), 41 (45), 82 (44), 69 (43), 95 (31), 81 (31).

Synthesis of 3-Mercapto-3,7-dimethyl-6-octenyl Acetate 378. The multistep synthesis of **378** is shown in Figure 4.

*S-(3,7-Dimethyl-1-oxooct-6-en-3-yl)ethanethioate (**2b**).* Under N_2, a 1 L, four-necked flask was charged with citral (**1b**; 50.0 g, 330 mmol) and piperidine (2.8 g, 30 mmol). Thioacetic acid (37.5 g, 490 mmol) was added dropwise to the mixture and heated to 60 °C for 3 h. The mixture was then cooled to room temperature, and methyl *tert*-butyl ether (MTBE; 200 mL) was added followed by a wash with brine (100 mL), a 5% solution of $NaHCO_3$ (100 mL), and brine (100 mL) successively. The solvent was removed under vacuum, and the crude of **2b** (10.0 g) was used as-is for the next step.

*3-Mercapto-3,7-dimethyl-6-octenyl Acetate **378**.* Under N_2, a 1 L, four-necked flask was charged with $NaBH_4$ (2.5 g, 66 mmol), which was dissolved in ethanol (40 mL) and water (10 mL). The temperature of the reaction was lowered to 0 °C, and **2b** (10.0 g,

DOI: 10.1021/jf505177r
J. Agric. Food Chem. 2015, 63, 1915−1931

44 mmol) was added dropwise to the reaction flask, keeping the temperature below 10 °C. After addition, the reaction mixture was stirred at room temperature for 30 min. The mixture was then poured into a 10% solution of NH_4Cl (100 mL), transferred to a separatory funnel, and extracted with MTBE (200 mL). The organic layer was washed with brine (2 × 100 mL). The solvent was removed under vacuum, and **378** (8.2 g, 81%) was obtained by column chromatography (silica; ethyl acetate/hexanes): ^{1}H NMR ($CDCl_3$, 400 MHz) δ 5.00−5.14 (m, 1H), 4.21−4.30 (m, 2H), 2.07−2.15 (m, 2H), 2.04 (s, 3H), 1.92−1.96 (m, 2H), 1.68 (s, 3H), 1.62 (s, 3H), 1.56−1.70 (m, 3H), 1.38 (s, 3H); EI-MS 230 (3, M^+), 121 (100), 69 (31), 93 (20), 109 (15), 136 (13), 81 (13), 101 (13), 122 (12), 67 (10), 43 (9).

Synthesis of 2-(5-Isopropyl-2-methyltetrahydrothiophen-2-yl)ethanol 304 and 307. The multistep synthesis of **304** and **307** is shown in Figure 4, where intermediate **2b** was synthesized in a similar fashion as above and was used as-is for the next step.

*3-Mercapto-3,7-dimethyl-6-octenol (**3b**).* Under N_2, a 1 L, four-necked flask was charged with $LiAlH_4$ (3.3 g, 88 mmol), which was dissolved in THF (200 mL) at room temperature. The temperature of the reaction mixture was then lowered to 0 °C, and **2b** (20.0 g, 88 mmol) was added dropwise to the reaction flask, maintaining the temperature below 10 °C. After filtration and concentration, the crude of **3b** (15.0 g) was used as-is for the next step.

*2-(5-Isopropyl-2-methyltetrahydrothiophen-2-yl)ethanol **304** and **307**.* Crude **3b** (15.0 g, 80 mmol) was dissolved in THF (200 mL), refluxed for 1 h, and poured into a 10% solution of NH_4Cl (200 mL). The mixture was then transferred to a separatory funnel and extracted with MTBE (400 mL). The organic layer was washed with brine (2 × 100 mL), and the solvent was removed under vacuum. **304** and **307** (8.3 g, 50%) were obtained by vacuum distillation (bp 130 °C/1.0 mmHg): ^{1}H NMR ($CDCl_3$, 500 MHz) δ 3.72−3.86 (m, 2H), 3.24−3.32 (m, 1H), 2.59 (br, 1H), 1.56−2.18 (m, 7H), 1.41 (s, ∼50% of 3H), 1.38 (s, ∼50% of 3H), 0.92−0.98 (m, 6H); EI-MS 188 (20, M^+), 101 (100), 69 (42), 93 (41), 41 (27), 81 (21), 143 (21), 55 (20), 99 (16), 145 (15), 67 (13).

Synthesis of 2-(5-Isopropyl-2-methyltetrahydrothiophen-2-yl)ethyl Acetate 373 and 375. Compounds **304** and **307** (0.6 g, 3 mmol) were added to DCM (5 mL) at room temperature. The reaction mixture was cooled to 0 °C, and triethylamine (0.5 g, 5 mmol) and acetyl chloride (0.3 g, 4 mmol) were added as shown in Figure 4. After 1 h, 1 M HCl (5 mL) was added, and the reaction was extracted with DCM (2 × 5 mL), washed with water (10 mL) and brine (10 mL), and dried over $MgSO_4$. The solvent was removed under vacuum, and **373** and **375** (0.5 g, 90%) were obtained by column chromatography (silica; hexanes/ethyl acetate): ^{1}H NMR ($CDCl_3$, 500 MHz) δ 4.12−4.33 (m, 2H), 3.17−3.36 (m, 1H), 2.07−2.20 (m, 1H), 2.04 (s, 3H), 1.64−2.03 (m, 6H), 1.42 (s, ∼50% of 3H), 1.40 (s, ∼50% of 3H), 0.91−0.98 (m, 6H); EI-MS 230 (22, M^+), 93 (100), 43 (84), 127 (83), 69 (66), 41 (39), 99 (36), 81 (34), 143 (30), 55 (26), 67 (23).

Synthesis of 2-(2-Methyltetrahydrothiophen-2-yl)ethyl Acetate 281. The multistep synthesis of **281** is shown in Figure 5.

*Methyl 2-(2-Methyltetrahydrothiophen-2-yl)acetate (**2c**).* 2-(2-Methyltetrahydrothiophen-2-yl)acetic acid (**1c**; 5.1 g, 32 mmol), synthesized according to the procedure described by Bunce et al.,[25] was dissolved in MeOH (100 mL). *p*-Toluenesulfonic acid monohydrate (0.6 g, 3 mmol) was added, and the mixture was refluxed for 3 h. The solvent was removed under vacuum, and ethyl acetate (100 mL) was added to the residue. The organic layer was washed with a 5% solution of $NaHCO_3$ (100 mL) and brine (100 mL) and then dried over $MgSO_4$. After filtration and concentration, the crude of **2c** (5.0 g) was obtained and used as-is in the next step.

*2-(2-Methyltetrahydrothiophen-2-yl)ethanol (**3c**).* $LiAlH_4$ (1.1 g, 29 mmol) was dissolved in THF (100 mL). Under N_2, a solution of **2c** (5.0 g, 29 mmol) in THF (40 mL) was added dropwise to the reaction flask. After addition, the mixture was allowed to stir for an additional 2 h at room temperature. The mixture was then added to a 10% solution of NH_4Cl (200 mL) and extracted with ether (200 mL). The organic layer was washed with brine (100 mL) and dried over $MgSO_4$. After filtration and concentration, **3c** (3.8 g, 81%) was obtained by column chromatography (silica; ethyl acetate/hexanes).

*2-(2-Methyltetrahydrothiophen-2-yl)ethyl Acetate **281**.* **3c** (3.8 g, 26 mmol) and triethylamine (3.2 g, 32 mmol) were dissolved in DCM (100 mL) and cooled to 0 °C. With stirring, a solution of acetyl chloride (2.5 g, 32 mmol) in DCM (20 mL) was added dropwise to the reaction flask. After addition, the reaction was stirred for an additional 2 h at room temperature. The mixture was transferred to a separatory funnel and washed with a 10% solution of NH_4Cl (100 mL), a 5% solution of $NaHCO_3$ (100 mL), and brine (100 mL) and then dried over $MgSO_4$. After filtration and concentration, **281** (3.4 g, 70%) was obtained by column chromatography (silica; ethyl acetate/hexanes): ^{1}H NMR ($CDCl_3$, 400 MHz) δ 4.17−4.29 (m, 2H), 2.88−3.01 (m, 2H), 1.98−2.12 (m, 4H), 2.05 (s, 3H), 1.73−1.89 (m, 2H), 1.42 (s, 3H); EI-MS 188 (17, M^+), 101 (100), 43 (27), 113 (25), 67 (12), 81 (9), 59 (9), 41 (7), 102 (7), 79 (6), 100 (6).

Synthesis of 2-[5-(1-Hydroxy-1-methylethyl)-2-methyltetrahydrothiophen-2-yl]ethyl Acetate 401 and 406. This five-step synthesis is shown in Figure 6.

*6,7-Epoxyneral **246**.* Citral (**1d**, 100.0 g, 660 mmol) was dissolved in DCM (400 mL) and cooled to 0 °C. With stirring, a solution of *m*-chloroperbenzoic acid (136.0 g, 790 mmol) in DCM (200 mL) was added dropwise to the reaction flask. After addition, the reaction mixture was stirred for an additional 2 h at 0 °C. The organic layer was washed with a 5% solution of $NaHCO_3$ (2 × 100 mL) and brine (2 × 100 mL) and then dried over $MgSO_4$. After filtration and concentration, the crude of **246** (111.0 g) was obtained and used as-is for the next step.

*S-[1-(3,3-Dimethyloxiran-2-yl)-3-methyl-5-oxopentan-3-yl]-ethanethioate (**2d**).* **246** (111.0 g, 660 mmol), thioacetic acid (60.0 g, 790 mmol), and piperidine (5.6 g, 70 mmol) were mixed and heated at 60 °C for 6 h under N_2. The reaction mixture was dissolved in ether (500 mL) and washed with a 5% solution of $NaHCO_3$ (100 mL) and brine (100 mL) and then dried over $MgSO_4$. After filtration and concentration, the crude of **2d** (160.0 g) was obtained and used as-is in the next step.

*2-[5-(2-Hydroxypropan-2-yl)-2-methyltetrahydrothiophen-2-yl]-acetaldehyde (**3d**).* **2d** (17.5 g, 70 mmol) was dissolved in THF (200 mL) and cooled to 0 °C. With stirring, a solution of NaOH (2.9 g, 70 mmol) in water (10 mL) was added dropwise to the reaction flask and allowed to stir for an additional 10 min at 0 °C. The mixture was added to ethyl acetate (200 mL), transferred to a separatory funnel, washed with a 10% solution of NH_4Cl (100 mL) and brine (100 mL), and then dried over $MgSO_4$. After filtration and concentration, **3d** (10.2 g, 70%) was obtained by column chromatography (silica; ethyl acetate/hexanes).

*2-[5-(2-Hydroxypropan-2-yl)-5-methyltetrahydrothiophen-2-yl]-ethanol (**4d**).* $NaBH_4$ (3.0 g, 80 mmol) was dissolved in ethanol (60 mL) and water (40 mL). The mixture was cooled to 0 °C. With stirring, the solution of **3d** (16.0 g, 90 mmol) in ethanol (20 mL) was added dropwise to the reaction flask. After addition, the reaction mixture was stirred for an additional 30 min at 0 °C. The mixture was then added to ethyl acetate (200 mL), transferred to a separatory funnel, washed with a 10% solution of NH_4Cl (100 mL) and brine (100 mL), and dried over $MgSO_4$. After filtration and concentration, **4d** (10.7 g, 66%) was obtained by column chromatography (silica; ethyl acetate/hexanes).

*2-[5-(1-Hydroxy-1-methylethyl)-2-methyltetrahydrothiophen-2-yl]ethyl Acetate **401** and **406**.* **4d** (3.0 g, 15 mmol) and triethylamine (1.5 g, 15 mmol) were dissolved in DCM (100 mL), and the mixture was cooled to 0 °C. With stirring, a solution of acetyl chloride (1.2 g, 15 mmol) in DCM (10 mL) was added dropwise to the reaction flask and stirred for an additional 10 min at 0 °C. The mixture was then transferred to a separatory funnel, washed with a 10% solution of NH_4Cl (100 mL), a 5% solution of $NaHCO_3$ (100 mL), and brine (100 mL), and dried over $MgSO_4$. After filtration and concentration, **401** and **406** (3.4 g, 94%) were obtained by column chromatography (silica; ethyl acetate/hexanes): ^{1}H NMR ($CDCl_3$, 500 MHz) δ 4.15−4.32 (m, 2H), 3.63−3.72 (m, 1H), 2.49 (br s, 1H), 1.98−2.12 (m, 7H), 1.79−1.96 (m, 2H), 1.41−1.44 (m, 3H), 1.18−1.24 (m, 6H); EI-

DOI: 10.1021/jf505177r
J. Agric. Food Chem. 2015, 63, 1915−1931

MS 246 (1, M^+), 101 (100), 43 (82), 59 (35), 100 (28), 99 (25), 69 (22), 93 (16), 41 (16), 113 (14), 128 (13).

Synthesis of 2-(5-Isopropylidene-2-methyltetrahydrothiophen-2-yl)ethyl Acetate 395. Compounds **401** and **406** (7.9 g, 32 mmol) were mixed with *p*-toluenesulfonic acid monohydrate (1.2 g, 6 mmol) in toluene (100 mL) and refluxed for 30 min (Figure 6). The mixture was then transferred to a separatory funnel, washed with a 5% solution of $NaHCO_3$ (100 mL) and brine (100 mL), and dried over $MgSO_4$. After filtration and concentration, **395** (4.1 g, 56%) was obtained by column chromatography (silica; ethyl acetate/hexanes): ^{1}H NMR ($CDCl_3$, 400 MHz) δ 4.17−4.30 (m, 2H), 2.61−2.71 (m, 2H), 2.06 (s, 3H), 1.85−2.10 (m, 4H), 1.64−1.74 (m, 6H), 1.45 (s, 3H); EI-MS 228 (74, M^+), 43 (100), 141 (68), 85 (47), 41 (45), 67 (44), 59 (32), 79 (31), 99 (30), 125 (27), 107 (26).

The mass spectra for each of the synthesized VSCs and branched aliphatic aldehydes are detailed in the Supporting Information.

CAS Registry Numbers for identified compounds: 2-(5-Isopropyl-2-methyltetrahydrothiophen-2-yl)ethanol **304** and **307**, 1612888-42-2.

Extraction of Lemon Peel. The peels from 100 lemons were zested over a microplane grater and collected in 1 L jars. The peel (2.0 kg) was steeped in DCM (600 mL) for 24 h in a refrigerator (4 °C). The solvent extract was passed through filter paper, dried over $MgSO_4$, and concentrated using a Zymark Turbovap (Biotage, Uppsala, Sweden) to 100 mL. It was then further reduced under a stream of N_2 to obtain a 25 mL concentrated extract.

Fractionation of Lemon Peel Extract. The peel extract (5.0 g) was diluted in hexane (5.0 g). The diluted extract was fractionated using a Biotage Isolera Prime, which was equipped with a 40 × 150 mm FLASH 40+M silica cartridge (Biotage). The first solvent gradient started with hexane/DCM at a ratio of 100:0. When the ratio reached 0:100, a second gradient of DCM/MeOH began at 100:0 and increased to 0:100. The flow rate was continuous at 25 mL/min, and the collection mode was set to "collect all". A total of 105 fractions were collected. On the basis of GC and GC-MS analyses from a selection of the individual fractions, the fractions were combined chronologically in groups of 10. The resulting 11 fractions were each concentrated using a Zymark Turbovap to 15 mL and further reduced under a stream of N_2 to 1 mL.

Supercritical Fluid Extraction. A Spe-ed Supercritical Fluid Extraction Prime (Applied Separations, Allentown, PA, USA) instrument was used to extract the lemon peel oil. The chiller was turned on 12 h prior to extraction, and the system lines were prepressurized by liquid CO_2 1 h before the extraction. Freshly zested lemon peels (20.0 g) were packed into a 50 mL high-pressure cell. The dead volume in the cell was filled with glass beads and then capped with PTFE frits before the ends were secured with threaded steel end-caps. After the sample cell had been connected to the unit, the cell temperature was set to 40 °C and prepressurized with CO_2. The compressed air was set to 120 psi, and the sample was pressurized with compressed air after the prepressurization process. The flow valve was opened to the metering valve, which then slowly opened to the recovery vial (placed in a dry ice/acetonitrile trap at −50 °C). The metering valve was opened enough to maintain a sample cell flow of approximately 1−2 L/min. Once stable flows were established, the peel was extracted for 45 min.

Gas Chromatography. The peel extract and its fractions were analyzed on apolar and polar phases using an Agilent 7890A GC (Santa Clara, CA, USA). The apolar capillary column had dimensions of 50 m × 320 μm × 0.52 mm (Restek RTX-1 F&F), and the polar capillary column was 50 m × 320 μm × 0.5 mm (Varian CP-Wax 58 FFAP CB column). Samples were introduced to the GC using an autosampler at a volume of 1 μL with a split ratio of 5:1. For the apolar column, the hydrogen carrier gas flow rate was held constant at 2 mL/min, and the temperature program started at an initial temperature of 40 °C and then increased at 2 °C/min to 310 °C with a 10 min hold at 310 °C. The temperature program for the polar column had the same initial temperature and 2 °C/min ramp, but the final temperature reached only 250 °C with a 10 min hold at 250 °C. The GC was calibrated using a homologous series of C1−C18 ethyl esters to generate index values for the observed peaks. The index values were calculated on the basis of previous work by van den Dool and Kratz,[26] which takes into account the GC oven temperature program and non-alkane-based calibrants, specifically ethyl esters. Although this is an industry standard, it is commonly expected to report Kovats retention indices (RI), which are based on a calibration with a homologous series of *n*-alkanes. A linear relationship between the ethyl ester values and Kovats RI is found when the measured values for the homologous series of the ethyl esters are plotted versus the Kovats values. On the basis of this relationship, linear equations were derived for both polar and apolar phases, which allowed for the calculated Kovats values reported herein.

Gas Chromatography−Olfactometry. The peel extract and its fractions were analyzed on the same apolar column described above using an Agilent 6890A GC. All samples were introduced to the GC inlet using an autosampler at 1 μL with a split ratio of 5:1. For all samples, the following parameters remained constant. The hydrogen carrier gas flow rate was 2 mL/min, and the temperature program started at an initial oven temperature of 40 °C, then increased at 6 °C/min to 80 °C, at 4 °C/min to 150 °C, at 2 °C/min to 200 °C, and finally at 10 °C/min to 310 °C with a 5 min hold. In addition, two olfactory detection ports (ODP, Gerstel, Inc., Linthicum, MD, USA) were equipped on the GC. The effluent was split 4:4:1 (ODP:ODP:FID), and the ODP transfer lines were heated to 225 °C. Olfactory comments were recorded using Dragon Naturally Speaking, Speech Recognition Software 12.0 (Nuance Communications, Inc., Burlington, MA, USA) in conjunction with the ODP software. The GC was calibrated using a homologous series of C1−C18 ethyl esters to generate index values for the observed peaks and then converted to Kovats values using the aforementioned equation.

Aroma Extract Dilution Analysis. To obtain dilutions of the original extract, the lemon peel extract was diluted stepwise, 3-fold, with DCM (1:3 by volume).[27] Two experienced assessors simultaneously conducted GC-O on these dilutions until no odorant could be detected. Each odorant was therefore assigned a FD factor that represented the last dilution in which the odorant was detected.

Gas Chromatography−Chemiluminescence. The peel extract and its fractions were analyzed on an Agilent 6890 GC equipped with an Antek 7090 sulfur/nitrogen chemiluminescence detector (PAC, Houston, TX, USA; CLSD) in the sulfur detection mode. All samples were introduced to the GC inlet using an autosampler, at a volume of 1 μL in the splitless mode. The apolar, 50 m × 320 μm × 0.52 μm, column (Restek RTX-1 F&F) was split two ways to two detectors. The hydrogen carrier gas flow rate was 2 mL/min, and the temperature program had an initial oven temperature of 40 °C, then increased at 2 °C/min to 270 °C with a 10 min hold at 270 °C. The FID and CLSD were calibrated using a homologous series of C1−C18 ethyl esters to generate index values for the observed peaks and then converted to Kovats values.

Gas Chromatography−Mass Spectrometry. The chromatographic conditions were the same as described for the GC analyses. All data were acquired using a Waters GCT-Premier orthogonal acceleration time-of-flight mass spectrometer (Milford, MA, USA) in electron ionization (EI) mode. The ion source was operated at 150 °C with an electron energy of 70 eV and a trap current of 50 μA. The temperature of the transfer line was 250 °C. Spectra were acquired between 27 and 400 Da in a time of 0.05 s and a delay of 0.01 s (approximately 20 spectra/s). Exact mass spectra were obtained using a single-point lock mass (m/z 218.9856 from perfluorotri-*n*-butylamine) infused into the ion source continuously during the run. Mass spectral library identification was achieved using in-house and commercial libraries, including Wiley 8 and NIST. Standard relative retention data were used for confirmation, which was obtained by calibrating the instrument with a homologous series of ethyl esters.

An Agilent 6890 GC, coupled to a Waters Quattro Micro triple-quadrupole mass spectrometer, was used to develop a method operating in the multiple reaction monitoring (MRM) mode. The instrument was equipped with a Varian CP-Wax 58 FFAP CB column (50 m × 320 μm × 0.20 μm) and a Varian VF-1 ms column (50 m × 320 μm × 0.40 μm). The oven ramp was set to an initial temperature

DOI: 10.1021/jf505177r
J. Agric. Food Chem. 2015, 63, 1915−1931

of 75 °C with an increase of 3 °C/min to 240 °C. The collision energy was set to 10 eV, and the following transitions were monitored as the major mass intensities from the spectrum: m/z 110.0 to 95.0 and 95.0 to 67.0 were monitored for 6-methylnonanal **136**; m/z 188.0 to 101.0 and 145.0 to 101.0 were monitored for 2-(5-isopropyl-2-methyltetrahydrothiophen-2-yl)-ethanol **304** and **307**.

Multidimensional Gas Chromatography−Mass Spectrometry. A Shimadzu GCMS-QP2010 system (Shimadzu Corp., Kyoto, Japan), which consisted of two GC2010 GCs, was equipped with a Deans switch transfer device, an MS-QP2010 quadrupole mass spectrometer, and an AOC-20i autosampler. The first GC, where the initial split/splitless injections take place, contained the apolar, 50 m × 320 μm × 0.50 μm, column (Restek RTX-1 F&F), a transfer line to a FID, and a transfer line to the Deans switch. An advanced pressure control (APC) system is utilized to supply carrier gas at constant pressure, in this case helium, to the Deans switch. The Deans switch serves as a means to transfer effluent from the first GC to the second GC, which is equipped with an orthogonal column phase to achieve advanced second-dimensional separation. The instrument parameters were as follows: the 300 °C inlet was held at a constant pressure of 220 kPa, and samples were introduced to the inlet using an autosampler at 1 μL with a 10:1 split ratio. The first-dimension oven temperature program started at an initial temperature of 40 °C and then increased at 2 °C/min to 310 °C. The transfer line between the two GCs was 150 °C, and the APC, operating in the constant pressure mode, was held at 180 kPa. The second GC was equipped with a Sol−Gel Wax polar, 60 m × 320 μm × 0.25 μm, column (SGE Analytical Services). The oven was set to an initial temperature of 30 °C and increased at a rate of 4 °C/min to 260 °C. The end of the second column was inserted into the mass spectrometer source, which was operated under EI conditions. The source temperature was 200 °C, with the interface temperature at 230 °C. The mass scan range was set to scan from m/z 33 to 250 with a scan speed of 800 u/s, and the EI energy was set to 70 eV.

Nuclear Magnetic Resonance. NMR spectra were recorded at 26.8 °C in deuterated chloroform (containing 0.05% v/v tetramethylsilane) on a Bruker Avance III 400 MHz or a Bruker Avance 500 MHz spectrometer (Billerica, MA, USA), with 5 mm BBO probes. ^{1}H chemical shifts are expressed as parts per million (ppm) with residual chloroform (δ 7.26) or tetramethylsilane (δ 0.00) as references and are reported as chemical shift (δH), relative integral, and multiplicity (s, singlet; br, broad; d, doublet; t, triplet; higher multiplicities as, e.g., dd, doublet of doublets; m, multiplet), and coupling constants (J) are reported in hertz.

RESULTS AND DISCUSSION

Aroma-Active Compounds in Lemon Peel Extract. Peel oil can be obtained commercially by cold-pressed or distillation techniques, as well as in the laboratory by hand-pressing or grating. For the grated peel, different organic solvents are available to preferentially extract the volatile constituents from the grated peel. The Lisbon lemon peels in this research were zested and extracted with DCM, an organic solvent with a high extraction capacity and affinity for a wide range of volatile constituents. Using paper blotters, the aroma of the lemon peel extract was described as bright, aldehydic, and citrus-like with subtle sulfurous notes. Identifying and characterizing the odor-active compounds in lemon oil has been completed in the past.[28,29] To the best of our knowledge, this was the first attempt to perform AEDA and assign FD factors to the aroma-active compounds from laboratory-extracted lemon peel oil.

In the lemon extract, 27 odor-active regions were detected by GC-O with FD factors of at least 3 (Table 1). Four of the odor-active areas with the highest dilution factors included limonene **80**, linalool **106**, neral **202**, and geranial **216**. The fifth area with an equally high dilution factor had a "sulfurous, skunk-like" aroma. At this particular area, no peak appeared by FID or CLSD runs. The concentration at which this presumed VSC was found in the lemon extract must therefore be below the limit of detection for the sulfur chemiluminescence detector, which is 0.1 ppm of sulfur. With knowledge of the RI from the odor from two orthogonal columns by GC-O, prenyl mercaptan was proposed as the source of the odor. This compound has been identified as a highly odorous compound in other natural products, including beer,[30] coffee,[31] wine,[32] durian,[33] and most recently virgin olive oil,[34] but never in citrus fruits. This compound was subsequently spiked into the lemon extract at a concentration high enough to produce a signal on the GC. The RI and odor descriptors from the two GC-O runs on orthogonal columns of this spiked extract matched that of the original extract. Although there is no GC-MS evidence to support this claim, prenyl mercaptan, which can be formed from cysteine via free radical mechanisms,[35] appears to be found in the lemon peel extract in the parts per billion or parts per trillion range and significantly contributes to the aroma of the extract.

Relative flavor activity (RFA), which is a measure of the log of the FD factor divided by the weight percent of the compound, can be a valuable calculation to understand which

Table 1. Aroma-Active Compounds in California Lemon Peel Extract

RI (apol)	odor description[a]	odorant[b]	FD factor (3^n)
773	green, apple	(*Z*)-3-hexenal	9
813	sulfurous, skunk-like	prenyl mercaptan[c]	243
839	green, grass	(*Z*)-3-hexenol	3
932	pine, green	α-pinene	9
983	aldehydic, orange	octanal	27
988	orange, zest, citrus	myrcene	81
1017	minty, eucalyptus	1,8-cineole	27
1040	citrusy, lemon zest	limonene	243
1060	like lemon juice	γ-terpinene	27
1066	plastic	*p*-cresol	9
1090	floral, sweet	linalool	243
1136	floral, waxy, herbal	citronellal	27
1156	green, peely, citrus	8-methylnonanal	3
1162	floral, fresh	4-terpinenol	3
1174	floral, metallic, citrus	α-terpineol	3
1188	aldehydic, soapy	decanal	9
1215	floral, citrus	nerol + citronellol	9
1219	fresh, peely, sweet	neral	243
1241	floral, rose	geraniol	9
1247	lemony, sweet	geranial	243
1257	green, woody, cucumber	8-methyldecanal	27
1286	woody, eugenol-like	2-methoxy-4-vinylphenol	27
1347	citrus, soapy	neryl acetate	27
1360	woody, pencil shavings	unknown	27
1365	citrus, soapy	geranyl acetate	9
1504	lemony, citrus	β-bisabolene	3
1562	sulfury	3-mercapto-3,7-dimethyl-6-octenyl acetate	9

[a]Odor perceived at the end of the ODP. [b]Identified by matching odor quality of odorant to the mass spectrum and RI on an apolar column. [c]Coincidence of RI and odors on two capillary columns (apolar and polar) with that of pure reference standard.

DOI: 10.1021/jf505177r
J. Agric. Food Chem. 2015, 63, 1915−1931

Table 2. Volatile Compounds Identified in the Extraction and Fractionation of Lisbon Lemon Peels (*Citrus limon* L. Burm. f. cv. Lisbon)

no.[a]	compound	%[b]	RI (apol)[c]	RI (pol)[d]	ID[e]
1	sulfur dioxide	tr	441		1
2	acetaldehyde	tr	476	534	1
3	acetic acid	tr	565	1232	1
4	ethyl acetate	tr	593	634	1
5	valeraldehyde	tr (7)	664	722	1
6	acetoin	tr	669	1077	1
7	propionic acid	tr (10)	693	1310	1
8	ethyl propionate	tr (7)	694	734	1
9	heptane	tr	696	700	1
10	2-methylbutanol	tr (10)	724	1001	1
11	butan-2-yl acetate	tr (8)	740	769	1
12	isoamyl alcohol	tr	747	1003	1
13	1-methyl-1,3-cyclohexadiene	tr	752	727	1
14	isobutyl acetate	tr (7)	754	796	1
15	3-hexanone	tr (6−10)	762	852	1
16	2-hexanone	tr (6−10)	765	859	1
17	(*Z*)-3-hexenal	tr (7)	773	935	1
18	hexanal	0.02	778	877	1
19	3-hexanol	tr (6−10)	785	983	1
20	2-hexanol	tr (7−11)	788	1022	1
21	butyl acetate	tr (6−8)	798	868	1
22	furfural	tr (8)	801	1240	1
23	octane	tr	801	800	1
24	(*E*)-2-hexenal	0.01	826	1021	1
25	(*Z*)-3-hexenol	0.02	839	1177	1
26	1,3,3-trimethylcyclohexene	tr (8)	841	752	1
27	2-methylenehexanal	tr (6)	842	965	1
28	(*E*)-2-hexenol	tr	850	1193	1
29	hexanol	0.01	853	1141	1
30	2-methylbutyl acetate	tr(7)	862	920	1
31	methional	tr (6)	865	1237	1
32	2-heptanone	tr (6−8)	868	974	1
33	γ-butyrolactone	tr (8)	874	1392	1
34	heptanal	tr	881	949	1
35	nonane	tr	902	899	1
36	methyl hexanoate	tr (7)	912	985	1
37	tricyclene	0.01	919	814	1
38	α-thujene	0.36	924	817	1
39	benzaldehyde	tr	928	1300	1
40	α-pinene	1.56	932	835	1
41	2-ethylhexanal	tr (6)	935	990	1
42	α-fenchene	0.01	938	866	1
43	2-methylheptanal	tr (6, 7)	943	1009	1
44	camphene	0.05	943	873	1
45	6-methylheptanal	tr (6, 7)	945	1048	1
46	4-octanone	tr (7)	952	1024	1
47	heptanol	tr	960	1242	1
48	2,3-octanedione	tr (6)	960	1121	1
49	2,2,6-trimethyl-6-vinyltetrahydropyran	tr (6)	962	924	1
50	4-methylpentyl acetate	tr (7)	962	1002	1
51	hexanoic acid	tr	965	1616	1
52	6-methyl-5-hepten-2-one	tr	969	1131	1
53	(*Z*)-5-octenal	tr (7)	971	1136	1
54	phenol	tr	971	1758	1
55	sabinene	0.44	973	928	1
56	2-amylfuran	tr (6, 7)	974	1037	1
57	β-pinene	14.52	977	925	1
58	2,3-dehydro-1,8-cineole	tr (9, 10)	978	973	1
59	octanal	0.04	983	1082	1
60	myrcene	1.44	988	962	1

DOI: 10.1021/jf505177r
J. Agric. Food Chem. 2015, 63, 1915−1931

Table 2. continued

no.[a]	compound	%[b]	RI (apol)[c]	RI (pol)[d]	ID[e]
61	2-methyl-5-isopropenyl-2-vinyltetrahydrofuran (isomer 1)	tr (9, 10)	991	1010	1
62	(*Z*)-3-hexenyl acetate	tr	994	1111	1
63	2-methyl-5-isopropenyl-2-vinyltetrahydrofuran (isomer 2)	tr (7−10)	995	1043	1
64	hexyl acetate	tr (7)	998	1072	1
65	*α*-phellandrene	0.04	999	973	1
66	3-carene	tr (4)	1004	953	1
67	benzyl alcohol	tr	1008	1630	1
68	*α*-terpinene	0.06	1011	983	1
69	2-methyl-(*E*)-2-heptenal	tr (7, 8)	1014	1164	1
70	*γ*-hexalactone	tr	1014	1477	1
71	*p*-cymene	0.33	1015	1071	1
72	*p*-menth-1-ene	tr(9)	1015	944	1
73	1,8-cineole	tr (6−11)	1017	1012	1
74	*β*-phellandrene	tr (3−7)	1019	1013	1
75	2-ethylhexanol	tr	1022	1277	1
76	acetophenone	tr (6−8)	1034	1430	1
77	3-methylbenzaldehyde	tr (6)	1036	1393	1
78	(*E*)-2-octenal	tr (8)	1036	1226	1
79	2,5,5-trimethyl-2-cyclohexenone	tr (8)	1037	1243	1
80	limonene	63.74	1040	1002	1
81	(*Z*)-*β*-ocimene	0.05	1041	1035	1
82	melonal	tr	1043	1149	1
83	dihydrotagetone	tr (3)	1044	1105	1
84	2-methyloctanal	tr (6)	1045	1115	1
85	(*E*)-*β*-ocimene	0.06	1045	1050	1
86	4-methyloctanal	tr (6, 7)	1046	1144	2
87	(*Z*)-5-octenol	tr	1053	1401	1
88	6-methyloctanal	tr (6, 7)	1054	1167	1
89	*γ*-terpinene	9.89	1060	1049	1
90	octanol	0.03	1063	1354	1
91	linalool oxide furan (isomer 1)	tr	1064	1232	1
92	(*E*)-sabinene hydrate	0.08	1065	1265	1
93	*p*-cresol	tr (9)	1066	1836	1
94	4-methylhexyl acetate	tr (7)	1068		1
95	2-nonanone	tr(6)	1070	1184	1
96	fenchone	tr	1072	1192	1
97	linalool oxide furan (isomer 2)	tr (10)	1072	1258	1
98	(*Z*)-4-nonenal	tr (6)	1075	1237	1
99	2,3-myrcene epoxide	tr (8)	1076	1209	1
100	*p*-*α*-dimethylstyrene	tr	1077	1233	1
101	terpinolene	0.42	1083	1084	1
102	rose furan	tr	1085	1194	1
103	(*Z*)-sabinene hydrate	0.06	1086	1332	1
104	nonanal	0.11	1088	1190	1
105	unidentified	tr	1090		1
106	linalool	0.17	1090	1334	1
107	heptyl acetate	tr	1092	1174	1
108	(*Z*)-rose oxide	tr (8)	1093	1155	1
109	perillene	tr	1094	1212	1
110	*p*-mentha-1,3,8-triene	tr (2−5)	1099	1209	1
111	undecane	tr	1103	1097	1
112	(*Z*)-*p*-mentha-2,8-dien-1-ol	tr	1105	1409	1
113	(*E*)-4,8-dimethyl-1,3,7-nonatriene	tr	1107	1111	1
114	(*Z*)-*p*-menth-2-en-1-ol	tr	1109	1358	1
115	pinanol (isomer 1)	tr	1110	1339	1
116	2-methyl-(*E*)-2-octenal	tr (7, 8)	1112	1261	1
117	campholenic aldehyde	tr	1112	1270	1
118	methyl octanoate	tr	1114	1193	1
119	octyl formate	tr (6)	1114	1231	1
120	3,5,5-trimethyl-2-cyclohexene-1,4-dione	tr	1115	1472	1
121	melonol	tr	1116	1440	1

DOI: 10.1021/jf505177r
J. Agric. Food Chem. 2015, 63, 1915−1931

Table 2. continued

no.[a]	compound	%[b]	RI (apol)[c]	RI (pol)[d]	ID[e]
122	(*E*)-*p*-mentha-2,8-dien-1-ol	tr	1118	1450	1
123	(*Z*)-limonene-1,2-oxide	tr	1119	1243	1
124	4-acetyl-1-methyl-1-cyclohexene	tr (8)	1120	1349	1
125	camphor	0.01	1120	1299	1
126	alloocimene	tr (2)	1121	1184	1
127	pinanol (isomer 2)	tr (10)	1121	1389	1
128	(*E*)-*p*-menth-2-en-1-ol	tr	1125	1424	1
129	isopulegol (isomer 1)	tr (6−10)	1128	1350	1
130	4,8-terpinolene epoxide	tr	1132	1256	1
131	(*E*)-limonene-1,2-oxide	tr (7, 8)	1135	1253	1
132	citronellal	0.09	1136	1270	1
133	isopulegol (isomer 2)	tr (6−9)	1140	1362	1
134	(*E*)-2-nonenal	tr (7, 8)	1140	1331	1
135	pinocarvone	tr	1142	1374	1
136	6-methylnonanal	tr (6)	1143	1246	2[f]
137	*δ*-terpineol	tr (10)	1144	1471	1
138	7-methyl-3-methylen-6-octenal	0.01	1145	1306	1
139	2-methylnonanal	tr	1147	1213	1
140	4-methylnonanal	tr	1151	1254	2
141	4-methylacetophenone	tr (9)	1152	1537	1
142	rosefuran epoxide	tr (8)	1152	1382	1
143	8-methylnonanal	tr	1156	1254	1
144	pinocamphone	tr	1157	1305	1
145	3,7-dimethyl-(*E*)-3,6-octadienal	tr (9)	1158	1362	1
146	(*E*)-2-nonenol	tr	1158	1500	1
147	borneol	tr	1159	1481	1
148	3,7-dimethyl-(*Z*)-3,6-octadienal	tr (7−9)	1160	1335	1
149	nonanol	0.01	1160	1452	1
150	4-limonenol	0.01	1161	1480	1
151	4-terpinenol	0.08	1162	1385	1
152	2-propionylthiophene	tr (7)	1163	1627	2
153	*p*-cymen-8-ol	tr	1165	1627	1
154	myrtenal	tr (7, 8)	1166	1402	1
155	dill ether	tr	1167	1308	1
156	octanoic acid	tr	1169	1820	1
157	4,7-dimethyl-3-bicyclo[3.2.1]octen-6-one	tr	1170		1
158	(*Z*)-4-decenal	tr (6, 7)	1170	1338	1
159	2-decanone	tr (6−8)	1171	1295	1
160	(*E*,*Z*)-2,4-nonadienal	tr (7, 8)	1171	1445	1
161	methylchavicol	tr (6)	1173	1446	1
162	*α*-terpineol	0.32	1174	1475	1
163	butyl hexanoate	tr (7)	1176	1218	1
164	(*E*)-dihydrocarvone	tr	1176	1385	1
165	3,4-dimethylphenol	tr (8, 9)	1177	1959	1
166	3-octenyl acetate	tr (7)	1177		1
167	methyl salicylate	tr (7)	1177	1555	1
168	3-decanone	tr (7)	1178	1263	1
169	hexyl butyrate	tr (7)	1179	1217	1
170	(*E*)-1,2-dihydroperillaldehyde	tr (7, 8)	1179	1396	1
171	myrtenol	tr	1180	1619	1
172	5-limonenol	tr (7)	1183		1
173	8,9-limonene epoxide (isomer 1)	tr	1183	1314	1
174	propyl heptanoate	tr (8)	1183	1223	1
175	safranal	tr (7)	1183	1438	1
176	ethyl octanoate	tr (7)	1184	1234	1
177	8,9-limonene epoxide (isomer 2)	tr	1184	1324	1
178	(*Z*)-piperitol	tr	1185	1466	1
179	decanal	0.07	1188	1291	1
180	1-dodecene	tr (1)	1192	1051	1
181	(*Z*)-5-octenyl acetate	tr	1193	1327	1
182	*p*-menth-1-en-9-al (isomer 1)	tr	1197	1414	1

DOI: 10.1021/jf505177r
J. Agric. Food Chem. 2015, 63, 1915−1931

Table 2. continued

no.[a]	compound	%[b]	RI (apol)[c]	RI (pol)[d]	ID[e]
183	*p*-menth-1-en-9-al (isomer 2)	tr	1198	1417	1
184	(*E*)-carveol	tr (10)	1198	1611	1
185	octyl acetate	0.01	1199	1278	1
186	(*E*)-piperitol	tr	1201	1524	1
187	2,3-epoxygeranial (isomer 1)	tr	1202		1
188	2-hydroxy-1,8-cineole	tr (10)	1202		1
189	dodecane	tr (1)	1203	1199	1
190	methyl nonanoate	tr	1203	1294	1
191	2,3-epoxygeranial (isomer 2)	0.01	1204		1
192	(*Z*)-*p*-mentha-1(7),8-dien-2-ol	tr (8)	1204	1634	1
193	(*E*)-*p*-mentha-1(7),8-dien-2-ol	tr	1207	1644	1
194	2-methyl-6-methylen-2,7-octadienal	tr	1208		1
195	ascaridole	tr (8)	1210	1489	1
196	cuminaldehyde	tr (7)	1211	1545	1
197	4-vinylphenol	tr	1213	2106	1
198	citronellol	0.05	1214	1545	1
199	nerol	0.21	1215	1574	1
200	carvone	tr (8, 9)	1216	1510	1
201	2-methyl-(*E*)-2-nonenal	tr	1218	1358	1
202	neral	0.60	1219	1460	1
203	4-methylnonanol	tr(10)	1220	1515	1
204	carvotanacetone	tr	1223	1455	1
205	anisaldehyde	tr	1225	1786	1
206	hexyl 2-methylbutyrate	tr (6)	1226	1229	1
207	piperitone	0.01	1227	1503	1
208	unidentified	tr	1233		1
209	isogeraniol	tr	1233	1565	1
210	isopiperitenone	tr	1237	1597	1
211	melonyl acetate	tr (7)	1237	1349	1
212	piperitone epoxide	tr (8)	1237	1495	1
213	geraniol	0.34	1241	1619	1
214	(*E*)-2-decenal	tr	1244	1427	1
215	6-methyldecanal	tr (6)	1245	1341	2
216	geranial	0.92	1247	1509	1
217	4-methyldecanal	tr	1248	1344	2
218	perilla aldehyde	0.03	1249	1552	1
219	2-methyldecanal	tr (6)	1250	1311	1
220	8-methyldecanal	tr (6, 7)	1257	1374	1
221	(*E*)-2-decenol	tr	1257	1596	1
222	indole	tr	1258	2171	1
223	decanol	0.01	1261	1551	1
224	(*Z*)-1,2-dihydroperilla alcohol	tr	1263	1675	1
225	*p*-mentha-1,4-dien-7-al	tr	1265	1584	1
226	3-undecanone	tr(5,6)	1266	1260	1
227	(*E*)-1,2-dihydroperilla alcohol	tr	1267	1698	1
228	nonanoic acid	0.02	1269	1928	1
229	2-undecanone	tr (5, 6)	1270	1395	1
230	bornyl acetate	0.01	1272	1381	1
231	(*E*,*Z*)-2,4-decadienal	tr (8)	1272	1536	1
232	10-limonenol	0.01	1275	1755	1
233	perilla alcohol	tr	1277	1767	1
234	thymol	0.01	1279	1938	1
235	ascaridole epoxide	tr	1281	1634	1
236	*p*-menth-1-en-9-ol (isomer 1)	tr	1282	1723	1
237	*p*-menth-1-en-9-ol (isomer 2)	tr	1282	1727	1
238	carvacrol	0.02	1283	1963	1
239	(*E*,*E*)-2,4-decadienal	tr	1284	1584	1
240	2-methoxy-4-vinylphenol	tr	1286	1946	1
241	2,4,7-decatrienal	tr (8)	1289	1592	1
242	undecanal	0.04	1289	1397	1
243	1-tridecene	tr (1)	1291	1151	1

DOI: 10.1021/jf505177r
J. Agric. Food Chem. 2015, 63, 1915−1931

Table 2. continued

no.[a]	compound	%[b]	RI (apol)[c]	RI (pol)[d]	ID[e]
244	nonyl acetate	0.01	1298	1380	1
245	methyl nerate	tr (7−9)	1300	1426	1
246	6,7-epoxyneral	tr (8)	1301	1726	1
247	tridecane	0.01	1304	1300	1
248	myrtenyl acetate	tr	1306	1476	1
249	methyl geranate	0.01	1307	1488	1
250	methyl decanoate	tr (6)	1308	1396	1
251	*p*-menthane-3,8-diol	tr	1309	1859	1
252	citronellic acid	tr	1311	1991	1
253	neric acid	tr	1314	2077	1
254	limonen-4-yl hydroperoxide	tr (9)	1317		1
255	(*E*)-carvyl acetate	tr	1318	1523	1
256	piperitenone	tr (8, 9)	1319	1696	1
257	limonen-1,2-diol	tr	1321	2034	1
258	linalyl propionate	tr (7)	1328	1409	1
259	δ-elemene (isomer 1)	tr (2−4)	1330	1275	1
260	γ-nonalactone	tr (6)	1330	1788	1
261	*p*-menth-1-en-3-yl acetate	tr (7)	1331		1
262	δ-elemene (isomer 2)	0.01	1333	1277	1
263	6,7-epoxygeranial	tr (8)	1335	1790	1
264	geranic acid	tr (9, 10)	1336	2099	1
265	citronellyl acetate	0.05	1338	1455	1
266	eugenol	tr (8)	1338	1925	1
267	α-cubebene	tr (1)	1344	1259	1
268	3-methylundecanal	tr (6)	1344	1429	2
269	2-methylundecanal	tr (6)	1345	1415	1
270	(*E*)-2-undecenal	tr (6−8)	1345	1542	1
271	(*Z*)-carvyl acetate	tr (6)	1346	1555	1
272	neryl acetate	0.60	1347	1517	1
273	decanoic acid	tr	1351	2019	1
274	4-methylundecanal	tr	1353	1445	2
275	vanillin	tr (10)	1358	2250	1
276	α-terpinyl acetate	0.01	1360	1479	1
277	(*Z*)-5-dodecenal	tr (6, 7)	1363	1529	1
278	undecanol	tr	1363	1659	1
279	(*Z*)-3-hexenyl hexanoate	tr (6)	1365	1447	1
280	geranyl acetate	0.58	1365	1541	1
281	2-(2-methyltetrahydrothiophen-2-yl)ethyl acetate	tr(8)	1365	1674	2
282	hexyl hexanoate	tr (6)	1369	1413	1
283	α-copaene	tr	1372	1291	1
284	4-dodecanone	tr (6)	1372		1
285	2-dodecanone	tr (5−7)	1374	1495	1
286	(*E*)-2-hexenyl hexanoate	tr (6)	1376	1460	1
287	6-dodecanone	tr (6)	1377		1
288	8-hydroxycarvone	tr	1380	2104	1
289	ethyl decanoate	tr	1382	1434	1
290	methyleugenol	tr (7, 8)	1384	1789	1
291	(*Z*)-6-dodecenal	tr (7)	1386		1
292	β-elemene	0.01	1388	1390	1
293	methyl *n*-methylanthranilate	tr (6, 7)	1388	1832	1
294	1-tetradecene	tr (1)	1390	1244	1
295	dodecanal	0.01	1390	1506	1
296	decyl acetate	0.01	1391	1484	1
297	limonen-10-yl acetate	0.01	1392	1634	1
298	nonyl propionate	tr (7)	1392	1435	1
299	cuminyl acetate	tr (7)	1396	1732	1
300	*p*-menth-1-en-9-yl acetate	tr	1399	1614	1
301	4-methyl-5-(3-methylbut-2-en-1-yl)-furan-2(5*H*)-one	tr	1402	1998	1
302	tetradecane	0.02	1404	1401	1
303	methyl undecanoate	tr (6)	1409	1499	1
304	2-(5-isopropyl-2-methyltetrahydrothiophen-2-yl)ethanol (isomer 1)	tr (8)	1410	1929	2[f]

DOI: 10.1021/jf505177r
J. Agric. Food Chem. 2015, 63, 1915−1931

Table 2. continued

no.[a]	compound	%[b]	RI (apol)[c]	RI (pol)[d]	ID[e]
305	(*Z*)-α-bergamotene	0.03	1410		1
306	α-santalene	tr (1)	1413	1370	1
307	2-(5-isopropyl-2-methyltetrahydrothiophen-2-yl)-ethanol (isomer 2)	tr (8)	1414	1930	2[f]
308	β-caryophyllene	0.26	1414	1382	1
309	perilla acetate	tr	1418	1681	1
310	citronellyl propionate	tr	1420	1521	1
311	2-methyl-(*E*)-2-undecenal	tr	1427	1569	1
312	(*E*,*Z*)-2,6-dodecadienal	tr	1433	1670	1
313	geranyl acetone	tr (7,8)	1434	1641	1
314	(*E*)-α-bergamotene	0.42	1434	1382	1
315	undecanoic acid	tr (10)	1441	2121	1
316	epi-β-santalene	0.01	1443	1415	1
317	3-methyldodecanal	tr (6, 7)	1443	1537	2
318	(*E*)-2-dodecenal	tr	1444	1640	1
319	α-humulene	0.02	1446	1460	1
320	2-methyldodecanal	tr (6)	1447	1518	1
321	4-methyldodecanal	tr (6)	1449	1546	2
322	(*E*)-β-farnesene	0.02	1450	1465	1
323	neryl propionate	0.02	1452	1581	1
324	β-santalene	0.02	1454	1429	1
325	geranyl propionate	tr	1455	1610	1
326	β-ionone-2,3-epoxide	tr	1461	1753	1
327	5-hexyl-4-methyldihydro-2(3*H*)-furanone	tr	1464	1867	1
328	γ-muurolene	tr (8)	1465	1486	1
329	β-ionone	tr	1469	1706	1
330	γ-curcumene	tr (1−3)	1470	1468	1
331	*ar*-curcumene	0.01	1472	1562	1
332	3-tridecanone	tr (5, 7)	1472	1563	1
333	1-pentadecene	tr	1474	1356	1
334	unidentified	0.02	1476		1
335	limonen-10-yl propionate	tr	1479	1734	1
336	2-tridecanone	0.01	1481	1593	1
337	γ-elemene	tr (2)	1484		1
338	valencene	0.09	1484	1505	1
339	α-selinene	tr (1)	1487	1513	1
340	(*Z*)-α-bisabolene	0.07	1487	434	1
341	decyl propionate	tr	1488	1542	1
342	bicyclogermacrene	0.05	1489	1514	1
343	myristicin	tr (7)	1489	2016	1
344	(*E*,*E*)-α-farnesene	tr (3)	1489	1543	1
345	ethyl undecanoate	tr	1490	1534	1
346	dihydroactinidiolide	tr	1493	2037	1
347	pentadecane	0.06	1494	1501	1
348	sesquicineole	tr (8)	1495	1538	1
349	α-muurolene	tr	1496	1541	1
350	undecyl acetate	tr (7)	1496	1574	1
351	methyl dodecanoate	tr(6)	1498	1600	1
352	γ-cadinene	tr (8)	1500	1549	1
353	β-bisabolene	0.68	1504	1519	1
354	calamenene	tr (5,8)	1504	1601	1
355	tridecanal	tr	1506	1616	1
356	γ-bisabolene (isomer 1)	0.01	1508		1
357	δ-cadinene	tr (1−9)	1510	1541	1
358	perilla propionate	tr (7)	1510		1
359	(*Z*)-9-dodecen-12-olide	tr	1511	1772	1
360	cubebol	0.01	1514		1
361	cadina-1,4-diene	tr (8)	1519		1
362	γ-bisabolene (isomer 2)	tr(1−3)	1520		1
363	7-epi-α-selinene	tr	1523	1560	1
364	2,6-dimethoxy-4-vinylphenol	0.01	1531	2289	1
365	(*E*)-α-bisabolene	0.01	1534	1564	1

DOI: 10.1021/jf505177r
J. Agric. Food Chem. 2015, 63, 1915−1931

Table 2. continued

no.[a]	compound	%[b]	RI (apol)[c]	RI (pol)[d]	ID[e]
366	hexyl benzoate	tr (6)	1537	1847	1
367	γ-undecalactone	tr (8)	1538	2005	1
368	neryl butyrate	tr (7)	1539	1648	1
369	2-methyltridecanal	tr (6)	1540	1621	1
370	4-methyltridecanal	tr (6)	1543	1649	2
371	dodecanoic acid	tr (9, 10)	1543	2232	1
372	(*E*)-2-tridecenal	tr (7)	1545	1753	1
373	2-(5-isopropyl-2-methyltetrahydrothiophen-2-yl)-ethyl acetate (isomer 1)	tr (7, 8)	1547	1822	2
374	(*E*)-nerolidol	tr	1549	1821	1
375	2-(5-isopropyl-2-methyltetrahydrothiophen-2-yl)-ethyl acetate (isomer 2)	tr (7, 8)	1553	1841	2
376	4-tetradecenal (isomer 1)	tr (6, 7)	1559		1
377	endo-1-bourbonanol	0.02	1559	2111	1
378	3-mercapto-3,7-dimethyl-6-octenyl acetate	tr	1562	1884	2
379	spathulenol	tr	1563	1889	1
380	4-tetradecenal (isomer 2)	tr (6)	1564		1
381	(*Z*)-3-hexenyl octanoate	tr	1565	1652	1
382	β-caryophyllene oxide	tr	1566	1734	1
383	hexyl octanoate	tr	1568	1605	1
384	5-dodecenyl acetate	tr (7)	1570		1
385	5-heptyl-4-methyldihydro-2(3*H*)-furanone	tr (8)	1572	1976	1
386	sesquisabinene hydrate	tr	1575		1
387	2-tetradecanone	tr (7)	1578	1704	1
388	unidentified	0.01	1578		1
389	ethyl dodecanoate	tr	1582	1634	1
390	1-hexadecene	tr (1)	1588	1434	1
391	tetradecanal	0.02	1593	1708	1
392	syringaldehyde	tr (10)	1594	2584	1
393	dodecyl acetate	tr	1598	1683	1
394	hexadecane	tr (1)	1600	1599	1
395	2-(5-isopropylidene-2-methyltetrahydrothiophen-2-yl)ethyl acetate	tr(7,8)	1601	2004	2
396	isopropyl dodecanoate	tr (6)	1614	1627	1
397	τ-cadinol	tr (8)	1617	1936	1
398	2-methyl-(*E*)-2-tridecenal	tr (7)	1620		1
399	α-cadinol	tr (10)	1621	1942	1
400	β-eudesmol	tr (11)	1625	1870	1
401	2-[5-(1-hydroxy-1-methylethyl)-2-methyltetrahydrothiophen-2-yl]-ethyl acetate (isomer 1)	tr (7, 8)	1630	2237	2
402	α-eudesmol	tr (11)	1631	1964	1
403	2-isopropenyl-8,8a-dimethyloctahydro-4a(2*H*)-naphthol	tr (7)	1632	1943	1
404	hydroxy-β-santalene	tr (7−9)	1634		1
405	campherenol	0.05	1635	2020	1
406	2-[5-(1-hydroxy-1-methylethyl)-2-methyltetrahydrothiophen-2-yl]ethyl acetate (isomer 2)	tr (7)	1635	2265	2
407	(*E*)-2-tetradecenal	tr (7)	1645	1858	1
408	intermedeol	0.02	1648	1968	1
409	β-bisabolol	0.01	1651	1920	1
410	hexyl nonanoate	tr (6)	1663	1704	1
411	α-bisabolol	0.04	1666	1980	1
412	β-sinensal	tr (7)	1666	1984	1
413	nootkatol	tr	1671	2188	1
414	2-pentadecanone	tr (7)	1680	1807	1
415	(*E*,*Z*)-farnesal	tr (8)	1683	1994	1
416	pentadecanal	0.01	1696	1814	1
417	methyl tetradecanoate	tr (6)	1697	1804	1
418	oplopanone	tr (8)	1697	2258	1
419	(*E*,*E*)-farnesal	tr	1712	2044	1
420	neryl hexanoate	tr (6)	1713	1829	1
421	α-sinensal	tr (7)	1718	2088	1
422	geranyl hexanoate	tr (6)	1729	1874	1
423	tetradecanoic acid	tr (9, 10)	1734	2429	1
424	β-bisabolenal	tr	1744		1
425	(*Z*)-3-hexenyl decanoate	tr (6)	1744	1834	1
426	methyl γ-tridecalactone	tr (9)	1746		1

DOI: 10.1021/jf505177r
J. Agric. Food Chem. 2015, 63, 1915−1931

Table 2. continued

no.[a]	compound	%[b]	RI (apol)[c]	RI (pol)[d]	ID[e]
427	octyl octanoate	tr (6)	1748	1800	1
428	nootkatone	0.01	1763	2235	1
429	(*Z*)-9-hexadecenal	tr (6)	1767	1924	1
430	ethyl tetradecanoate	tr	1776	1834	1
431	6-isopropenyl-4,8a-dimethyl-4a,5,6,7,8,8a-hexahydro-2(1*H*)-naphthalenone	tr (9)	1793	2210	1
432	hexadecanal	0.02	1797	1914	1
433	methyl pentadecanoate	tr (6)	1798	1907	1
434	(*E*,*E*)-farnesyl acetate	tr(7)	1813	2039	1
435	methyl γ-tetradecalactone	tr (9)	1856		1
436	heptadecanal	tr (6)	1895	2014	1
437	methyl hexadecanoate	tr (6)	1906	1995	1
438	citropten	0.12	1911	2751	1
439	hexadecanoic acid	0.02	1926	2745	1
440	(*Z*)-9-octadecenal	tr (6)	1964	2129	1
441	(*E*)-9-octadecenal	tr (6)	1969	2129	1
442	octadecanal	tr (6)	1994	2114	1
443	methyl linoleate	tr (6, 7)	2041	2253	1
444	methyl linolenate	tr (6, 7)	2043	2320	1
445	methyl oleate	tr (6, 7)	2044	2195	1
total adjusted PPT of named components		100.00			

[a]Compounds detected by order of elution on an apolar column. [b]Relative percentage determined by FID on an apolar column with response factor adjustment; tr, trace compounds in the extract below 0.00% or identified in the fractions (1−11). [c]RI on an apolar column. [d]RI on polar column. [e](1) Tentative identification based on RI and/or EI mass spectral comparison with in-house, NIST, and/or Wiley libraries; (2) identification based on RI and EI mass spectral comparison with synthesized standards. [f]Required MRM to confirm presence on polar column.

flavor components contribute to the aroma of a sample.[36,37] These values are not shown in Table 1 mainly because of the difficulty of calculating this value when compounds do not have a measured weight percentage. For example, prenyl mercaptan and 3-mercapto-3,7-dimethyl-6-octenyl acetate **378** did not have measured weight percentages by GC, but would have two of the highest RFA values due to its FD factor and extremely low concentration, which is quite remarkable and unique for lemons. A similar conclusion could be made for 8-methylnonanal **143** (green, peely, citrus) and 8-methyldecanal **220** (green, woody, cucumber), which were found at trace levels in the fractions and possess low odor thresholds.[38]

Composition of Volatile Compounds in the Lemon Peel Extract. Due to the complexity of natural product extracts, fractionation has become a primary technique to circumvent peak coelution and identify lower concentration compounds by selectively separating compound classes using gradient elution. Specifically for lemons, fractionation on both the juice[39] and the peel[10] has led to novel findings. To separate and enhance the trace volatiles from the complex volatile lemon peel matrix and to assist with properly linking GC-O data, the peel extract in this study was fractionated into its different chemical classes. Furthermore, monodimensional analysis has its limitations in citrus extracts as terpenes and sesquiterpenes interfere with lower concentration potentially odor-active components. Therefore, MDGC-MS was utilized for the analysis of the peel extract and its fractions. Unresolved peaks on the primary column were heart-cut onto a secondary (orthogonal) column using the Deans switch.[40] A summary of the volatile compounds in the peel extract and fractions is listed in Table 2 in order of elution on an apolar column. Known compounds were identified using RI from apolar and polar columns, coupled with mass spectral data. Several unknown compounds were postulated, synthesized, and confirmed in the lemon extract by comparing the RI of two orthogonal column phases and mass spectral data. The major components of the peel extract included limonene (63.7%), β-pinene (14.5%), and γ-terpinene (9.9%). The composition of the major chemical classes in the peel extract represented 94.8% hydrocarbons, 2.0% aldehydes, 1.6% alcohols, and 1.3% esters.

Aldehydes are known to play a key role in the aroma of citrus fruits, especially lemons. The medium-polarity fractions from the lemon extract comprised a series of 2-methyl, 3-methyl, 4-methyl, 6-methyl, and 8-methyl branched aliphatic aldehydes, many of which were synthesized and confirmed for the first time in lemons, citrus fruits, or any other botanical species. Only the branched aldehydes 4-methylnonanal **140** and 4-methylundecanal **274** have been previously identified in lemons.[10] It should be noted that 6-methylnonanal **136** required MRM for confirmation in one of the lemon fractions, where the transitions of m/z 110.0 to 95.0 and 95.0 to 67.0 were monitored for the fraction, the standard solution of **136**, and the fraction spiked with the standard. The synthesis scheme for **136** is shown in Figure 1. A similar mechanism was used for the synthesis of 6-methyldecanal **215** and the series of 4-methyl branched aliphatic aldehydes.

Identification of Volatile Sulfur Compounds. As each of the fractions was analyzed, it was increasingly evident that there were several unknown VSCs present. Formed through biochemical and enzymatic pathways,[41] as well as thermal processing,[42] VSCs are rarely reported in citrus research literature. The Lisbon lemons were purchased in early spring, the main harvest season for this lemon variety in the state of California. An elemental specific analysis for VSCs in the peel extract was carried out using a GC coupled to a CLSD in the sulfur mode only. Supercritical fluid extraction (SFE) of the peel was used to compare and validate the chromatographic results from the CLSD trace of the lemon peel DCM extract. Figure 2 shows the chromatograms obtained for both extraction techniques. Because the two chromatograms mirrored one another, the peel extract that was steeped in DCM was chosen for further research due to the large amount of extract, an

DOI: 10.1021/jf505177r
J. Agric. Food Chem. 2015, 63, 1915−1931

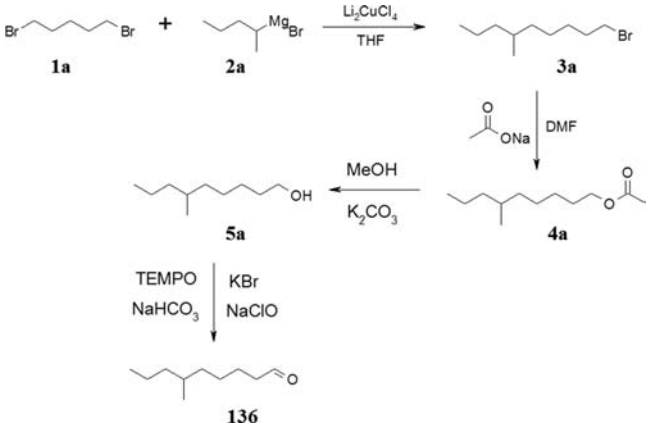

Figure 1. Synthesis of 6-methylnonanal **136**.

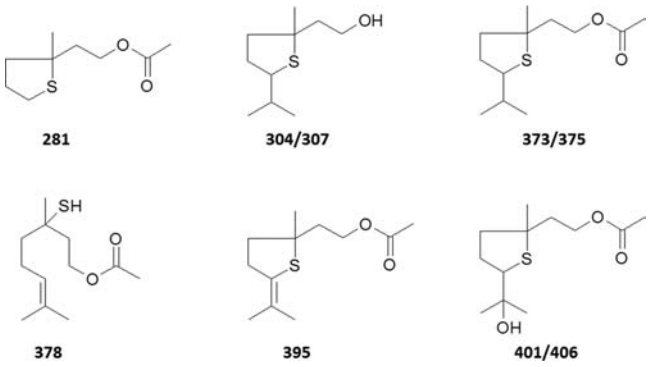

Figure 3. Chemical structures of synthesized VSCs.

important factor when multiple analytical techniques are used. Three well-known sulfur compounds were identified in the fractions: sulfur dioxide **1**, 2-propionylthiophene **152**, and methional **31**. First identified in black tea,[43] **152** is new to lemons and has been described in reaction mechanisms involving ascorbic acid and cysteine.[44] The medium-polarity fractions led to the identification of **31**, which is also new to lemons.

There were several novel VSCs identified in the peel extract (Figure 3), including one VSC that was present at a high enough concentration in the extract to produce a mass spectral signal. On the basis of the fragmentation pattern and accurate mass measurements of that peak, the structure was postulated as 3-mercapto-3,7-dimethyl-6-octenyl acetate **378**. This structure was synthesized (Figure 4) and confirmed by NMR. During the sodium borohydride reduction to produce **378**, it should be noted that a clean acetyl moiety migration occurred, as careful analysis of the crude did not yield the intermediate (**4b**). The RI on two orthogonal columns and the mass spectrum for the synthesized structure supported the presence of this compound in the peel extract. Even though the synthesized structure is highly unstable, **378** produced the strongest signal on the CLSD, as shown in Figure 2, and is considered stabilized by the antioxidants and tocopherols in the matrix of the peel extract. This was confirmed experimentally as

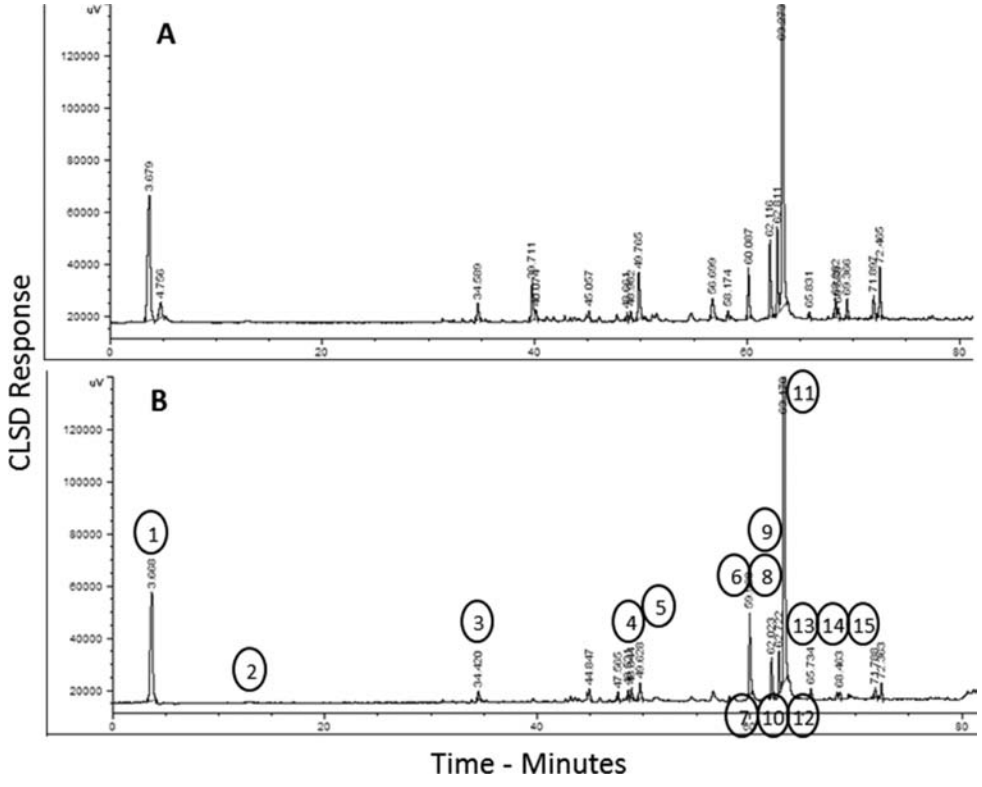

Figure 2. Comparison of the CLSD chromatograms by SFE (A) and DCM extraction (B). Peak identification from the DCM extraction (B) is as follows: (1) sulfur dioxide **1**; (2) methional **31**; (3) 2-propionylthiophene **152**; (4) 2-(2-methyltetrahydrothiophen-2-yl)ethyl acetate **281**; (5) 2-(5-isopropyl-2-methyltetrahydrothiophen-2-yl)ethanol **304** and **307**; (6) 2-(5-isopropyl-2-methyltetrahydrothiophen-2-yl)ethyl acetate (isomer 1) **373**; (7) 2-(5-isopropyl-2-methyltetrahydrothiophen-2-yl)ethyl acetate (isomer 2) **375**; (8) 3-mercapto-3,7-dimethyl-6-octenyl acetate **378**; (9) 2-(5-isopropylidene-2-methyltetrahydrothiophen-2-yl)ethyl acetate **395**; (10) 2-[5-(1-hydroxy-1-methylethyl)-2-methyltetrahydrothiophen-2-yl]ethyl acetate (isomer 1) **401**; (11) 2-[5-(1-hydroxy-1-methylethyl)-2-methyltetrahydrothiophen-2-yl]ethyl acetate (isomer 2) **406**.

DOI: 10.1021/jf505177r
J. Agric. Food Chem. 2015, 63, 1915−1931

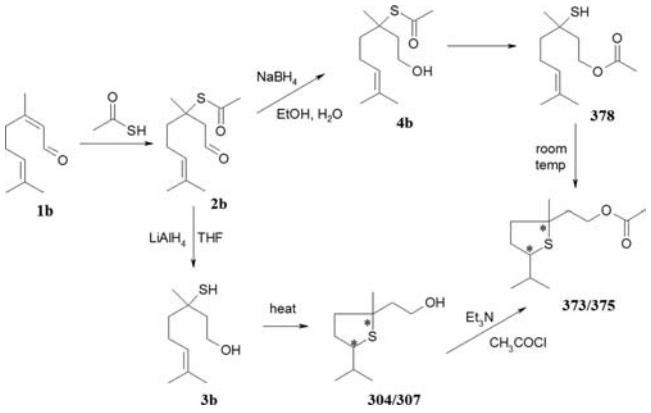

Figure 4. Synthesis of 2-(5-isopropyl-2-methyltetrahydrothiophen-2-yl)-ethanol **304** and **307**, 3-mercapto-3,7-dimethyl-6-octenyl acetate **378**, and 2-(5-isopropyl-2-methyltetrahydrothiophen-2-yl)-ethyl acetate **373** and **375**. The asterisks in the final product of both lemon VSCs indicate there are a set of unresolved chiral centers from the diastereomeric mixtures.

the addition of tocopherols at the end of the synthesis of **378** produces a stable material in a shelf-life study (data not shown). The biochemical or enzymatic mechanism by which this VSC forms is still under investigation. There is evidence that the amino acids cysteine and methionine, the precursors from which VSCs could form, are present in lemons.[45−48] In addition, hydrogen sulfide has been quantitated in the headspace of fresh lemon juice.[23] It was postulated that **378** could form from the reaction of hydrogen sulfide and neryl acetate, which tends to comprise a larger percentage of the volatile constituents in lemons compared to other citrus fruits.

To identify the other peaks on the CLSD chromatogram, the fractions were studied in-depth by GC-MS and MDGC-MS. Two unknown peaks in two of the polar fractions appeared to be isomers of each other with the same molecular weight and elemental formula as **378**. With NMR and mass spectral data from the synthesis and instability of **378** (Figure 4), there was a clear understanding that these two unknown isomers were 2-(5-isopropyl-2-methyltetrahydrothiophen-2-yl)ethyl acetate **373** and **375**. The thiol group from **378** readily attacks the double bond and undergoes internal cyclization to form **373** and **375**. This internal cyclization occurs rapidly, as **378** is unstable even at cooler temperatures.

Also in the polar fractions were what appeared to be two unknown isomeric VSCs that produced a clear signal on a polar column. After further investigation from data on the mass intensities and the elemental composition, the structure was proposed as 2-(5-isopropyl-2-methyltetrahydrothiophen-2-yl)-ethanol **304** and **307** and synthesized (Figure 4). Using a Waters Quattro Micro triple-quadrupole MS, a method operating in the MRM mode was developed to identify this compound in the lemon extract using the synthesized structure. The collision energy was set to 10 eV, and the transitions, *m*/*z* 188.0 to 101.0 and 145.0 to 101.0, were monitored as the major mass intensities from the spectrum of **304** and **307** for the fraction, a standard solution of **304** and **307**, and the fraction spiked with the standard. Similar to the formation of **373** and **375**, it was proposed that **304** and **307** could form in the lemon peel from the internal cyclization from 3-mercapto-3,7-dimethyl-6-octenol (the reaction of hydrogen sulfide and nerol; not observed) or from the hydrolysis of the corresponding esters **373** and **375** in acidic conditions.

Interestingly, there was another sulfur peak with the same molecular weight and similar mass spectral fragmentation as **304** and **307** that eluted earlier on both columns (see mass spectral data in the Supporting Information). From the analysis of the elemental composition, this sulfur peak had a different molecular formula and double bond equivalency. The postulated structure, 2-(2-methyltetrahydrothiophen-2-yl)ethyl acetate **281**, was synthesized as shown in Figure 5 and

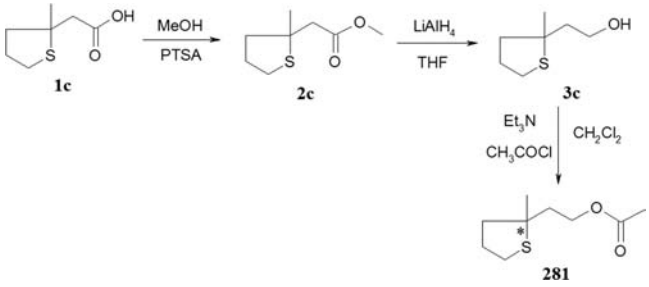

Figure 5. Synthesis of 2-(2-methyltetrahydrothiophen-2-yl)ethyl acetate **281**. The asterisk in the final product of **281** indicates there is an unresolved chiral center from the enantiomeric mixture.

confirmed as matching RI and mass spectral data for the peak in the lemon extract. The mechanism of formation for **281** is very difficult to understand, as the earlier mentioned VSCs can partly be explained through the internal cyclization of the citral-like backbone, but **281** appears to have derived through another pathway.

The final VSCs identified in the polar fractions included 2-[5-(1-hydroxy-1-methylethyl)-2-methyltetrahydrothiophen-2-yl]-ethyl acetate **401** and **406** and 2-(5-isopropylidene-2-methyltetrahydrothiophen-2-yl)ethyl acetate **395**. Similar to **304** and **307**, the synthesis of these compounds involved an internal cyclization step, but, unlike **304** and **307**, which used citral as the starting material, 6,7-epoxyneral **246** was chosen as the starting material to generate the final tertiary alcohol for **401** and **406** (Figure 6). In the lemon peel, however, the mechanism of formation is unknown for these compounds, although it appears as if **395** could form from the dehydration of **401** and **406**.

As shown in Figures 4−6, the lemon VSCs are a mixture of diastereomers. Unfortunately, the authors cannot comment on

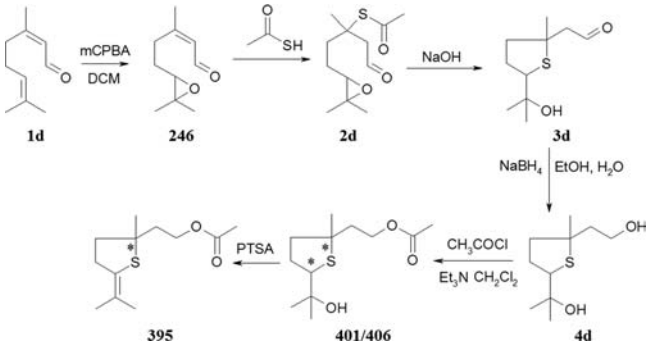

Figure 6. Synthesis of 2-(5-isopropylidene-2-methyltetrahydrothiophen-2-yl)ethyl acetate **395** and 2-[5-(1-hydroxy-1-methylethyl)-2-methyltetrahydrothiophen-2-yl]ethyl acetate **401** and **406**. The asterisks in the final product of both lemon VSCs indicate there are a set of unresolved chiral centers from the diastereomeric mixtures.

DOI: 10.1021/jf505177r
J. Agric. Food Chem. 2015, 63, 1915−1931

Table 3. Orthonasal and Retronasal Evaluations of Novel VSCs

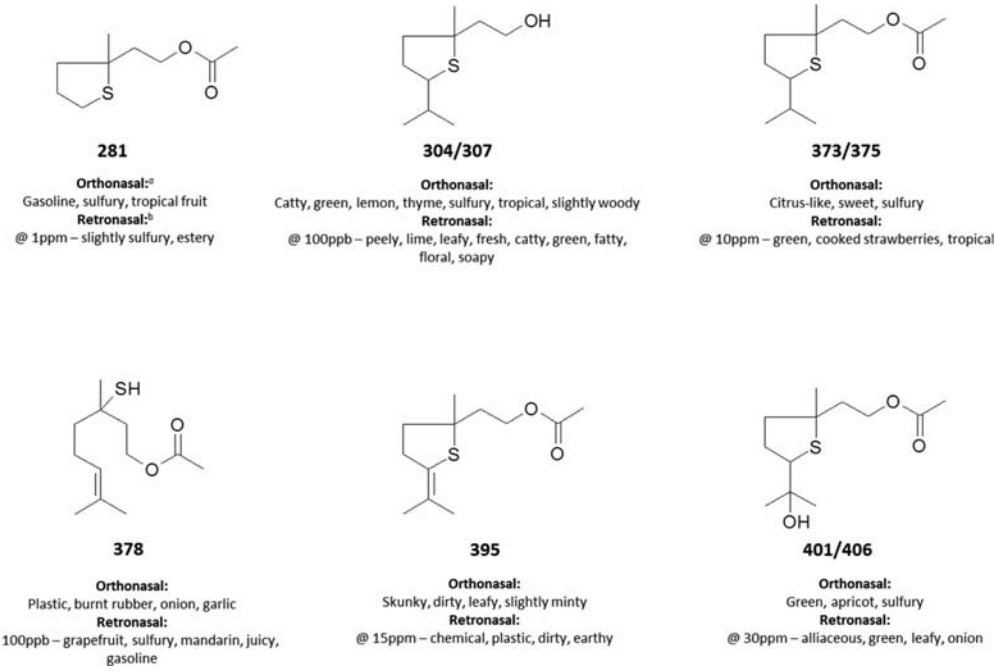

[a]Orthonasal evaluations were conducted using paper blotters at a 0.1% solution in ethanol. [b]Retronasal evaluations were conducted at various concentrations in water.

the identity or quantity for each of the chiral compounds as it was outside the scope of this work.

Organoleptic Evaluation of Synthesized VSCs. The novel VSCs were synthesized to not only confirm their presence in lemons but to gain a better understanding of the orthonasal and retronasal properties of each compound. The orthonasal evaluations were completed on paper blotters, and the retronasal evaluations were completed in water (Table 3).

■ ASSOCIATED CONTENT

Ⓢ Supporting Information

Additional chemical structures and mass spectra. This material is available free of charge via the Internet at http://pubs.acs.org.

■ AUTHOR INFORMATION

Corresponding Author

*(R.J.C.) Phone: (732) 335-2668. Fax: (732) 335-2591. E-mail: robert.cannon@iff.com.

Notes

The authors declare no competing financial interest.

■ ACKNOWLEDGMENTS

We are grateful for the following members of the IFF team who assisted in all aspects of this research: Susan Joseph, Stephen Toth, Sharon Brown, Dennis Swijter, Danielle Dinallo, Ubaideen Hassan, Jerry Kowalczyk, Mauricio Poulsen, Kurt Nordman, Kelly Carroll, Dennis Kujawski, Jung-A Kim, and Cynthia Vuich. We are also thankful for Dr. Russell Rouseff's recommendation for analyzing lemons as a potential source for VSCs.

■ ABBREVIATIONS USED

AEDA, aroma extract dilution analysis; CLSD, chemiluminescence detector; DCM, dichloromethane; FD, flavor dilution; GC, gas chromatography; GC-MS, gas chromatography–mass spectrometry; GC-O, gas chromatography–olfactometry; MDGC-MS, multidimensional gas chromatography–mass spectrometry; MRM, multiple reaction monitoring; ODP, olfactory detection port; RI, retention index; RFA, relative flavor activity; SFE, supercritical fluid extraction; VSC, volatile sulfur compound

■ REFERENCES

(1) Poore, H. D. Analyses and composition of California lemon and orange oils. *Technol. Bull.* **1932**, *241*, 1–30.

(2) Bernhard, R. Analysis and composition of oil of lemon by gas-liquid chromatography. *J. Chromatogr.* **1960**, *3*, 471–476.

(3) Ikeda, R. M.; Rolle, L. A.; Vannier, S. H.; Stanley, W. L. Isolation and identification of aldehydes in cold-pressed lemon oil. *J. Agric. Food Chem.* **1962**, *10* (2), 98–102.

(4) Moshonas, M. G.; Shaw, P. E.; Veldhuis, M. K. Analysis of volatile constituents from Meyer lemon oil. *J. Agric. Food Chem.* **1972**, *20* (4), 751–752.

(5) Chamblee, T. S.; Clark, B. C., Jr.; Brewster, G. B.; Radford, T.; Iacobucci, G. A. Quantitative analysis of the volatile constituents of lemon peel oil. Effects of silica gel chromatography on the composition of its hydrocarbon and oxygenate fractions. *J. Agric. Food Chem.* **1991**, *39*, 162–169.

(6) Dellacassa, E.; Lorenzo, D.; Moyna, P.; Verzera, A.; Mondello, L.; Dugo, P. Uruguayan essential oils. Part VI. Composition of lemon oil. *Flavour Fragrance J.* **1997**, *12*, 247–255.

(7) Verzera, A.; Russo, C.; La Rosa, G.; Bonaccorsi, I.; Cotroneo, A. Influence of cultivar on lemon oil composition. *J. Essent. Oil Res.* **2001**, *13*, 343–347.

(8) Lota, M.; de Serra, D.; Tomi, F.; Jacquemond, C.; Casanova, J. Volatile components of peel and leaf oils of lemon and lime species. *J. Agric. Food Chem.* **2002**, *50*, 796–805.

(9) Dugo, P.; Ragonese, C.; Russo, M.; Sciarrone, D.; Santi, L.; Cotroneo, A.; Mondello, L. Sicilian lemon oil: composition of volatile and oxygen heterocyclic fractions and enantiomeric distribution of volatile components. *J. Sep. Sci.* **2010**, *33*, 3374–3385.

DOI: 10.1021/jf505177r
J. Agric. Food Chem. 2015, 63, 1915–1931

(10) Naef, R.; Jaquier, A. New aldehydes and related alcohols in fresh lemon peel extract (*Citrus limon* L.). *Flavour Fragrance J.* **2006**, *21*, 768−771.
(11) Fischer, A.; Grab, W.; Schieberle, P. Characterisation of the most odour-active compounds in a peel oil extract from Pontianak oranges (*Citrus nobilis* var. Lour. *microcarpa* Hassk.). *Eur. Food Res. Technol.* **2008**, *227*, 735−744.
(12) Delort, E.; Jacquier, A. Novel terpenyl esters from Australian finger lime (*Citrus australasica*) peel extract. *Flavour Fragrance J.* **2009**, *24*, 123−132.
(13) Buettner, A.; Schieberle, P. Characterization of the most odor-active volatiles in fresh, hand-squeezed juice of grapefruit (*Citrus paradise* Macfayden). *J. Agric. Food Chem.* **1999**, *47*, 5189−5193.
(14) Buettner, A.; Schieberle, P. Stable isotope dilution assays for the quantification of odor-active thiols in hand-squeezed grapefruit juices (*Citrus paradise* Macfayden). In *Frontiers of Flavor Science*, 9; Schieberle, P., Engel, K.-H., Eds.; Deutsche Forschungsanstalt für Lebensmittelchemie: Freising, Germany, 2000; pp 132−134.
(15) Lin, J.; Rouseff, R. L. Characterization of aroma-impact compounds in cold-pressed grapefruit oil using time-intensity gc-olfactometry and gc-ms. *Flavour Fragrance J.* **2001**, *16*, 457−463.
(16) Shaw, P. E.; Ammons, J. M.; Braman, R. S. Volatile sulfur compounds in fresh orange and grapefruit juices: identification, quantitation, and possible importance to juice flavor. *J. Agric. Food Chem.* **1980**, *28*, 778−781.
(17) Demole, E.; Enggist, P.; Ohloff, G. 1-*p*-Menthene-8-thiol: a powerful flavor impact constituent of grapefruit juice (*Citrus paradise* Macfayden). *Helv. Chim. Acta* **1982**, *65*, 1785−1794.
(18) Hinterholzer, A.; Schieberle, P. Identification of the most odour-active volatiles in fresh, hand-extracted juice of Valencia late oranges by odour dilution techniques. *Flavour Fragrance J.* **1998**, *13*, 49−55.
(19) Rouseff, R. L.; Perez-Cacho, P.; Jabalpurwala, F. Historical review of citrus flavor research during the past 100 years. *J. Agric. Food Chem.* **2009**, *57*, 8115−8124.
(20) Naef, R.; Velluz, A.; Meyer, A. P. Volatile constituents of blood and blond orange juices: a comparison. *J. Essent. Oil Res.* **1996**, *8*, 587−595.
(21) Starkenmann, C.; Niclass, Y.; Escher, S. Volatile organic sulfur-containing constituents in *Poncirus trifoliata* (L.) Raf. (Rutaceae). *J. Agric. Food Chem.* **2007**, *55*, 4511−4517.
(22) Naef, R.; Velluz, A. Volatile constituents in extracts of mandarin and tangerine peel. *J. Essent. Oil Res.* **2001**, *13* (3), 154−157.
(23) Shaw, P. E.; Wilson, C. W. Volatile sulfides in headspace gases of fresh and processed citrus juices. *J. Agric. Food Chem.* **1982**, *30*, 685−688.
(24) Allegrone, G.; Belliardo, F.; Cabella, P. Comparison of volatile concentrations in hand-squeezed juices of four different lemon varieties. *J. Agric. Food Chem.* **2006**, *54*, 1844−1848.
(25) Bunce, R. A.; Peeples, C. J.; Jones, P. B. Tandem S_N2-Michael reactions for the preparation of simple five- and six-membered-ring nitrogen and sulfur heterocycles. *J. Org. Chem.* **1992**, *57*, 1727−1733.
(26) Van den Dool, H.; Kratz, P. D. A generalization of the retention index system including linear temperature programmed gas-liquid partition chromatography. *J. Chromatogr.* **1963**, *11*, 463−471.
(27) Schieberle, P. New developments in methods for analysis of volatile flavor compounds and their precursors. In *Characterization of Food: Emerging Methods*; Gaonkar, A. G., Ed.; Elsevier Science: Amsterdam, The Netherlands, 1995; pp 403−431.
(28) Drawert, F.; Christoph, N. Significance of the sniffing-technique for the determination of odour thresholds and detection of aroma impacts of trace volatiles. In *Analysis of Volatiles*; Schreier, P., Ed.; de Gruyter: Berlin, Germany, 1984; pp 269−291.
(29) Schieberle, P.; Grosch, W. Identification of potent flavor compounds formed in an aqueous lemon oil/citric acid emulsion. *J. Agric. Food Chem.* **1988**, *36*, 797−800.
(30) Kuroiwa, Y.; Naoki, H. Composition of sunstruck flavor substance of beer. *Agric. Biol. Chem.* **1961**, *25*, 257−258.
(31) Holscher, W.; Vitzthum, O. G.; Steinhart, H. Prenyl alcohol − source for odorants in roasted coffee. *J. Agric. Food Chem.* **1992**, *40*, 655−658.
(32) Bailly, S.; Jerkovic, V.; Marchand-Brynaert, J.; Collin, S. Aroma extraction dilution analysis of Sauternes wines. Key role of polyfunctional thiols. *J. Agric. Food Chem.* **2006**, *54*, 7227−7234.
(33) Li, J.; Schieberle, P.; Steinhaus, M. Characterization of the major odor-active compounds in Thai durian (*Durio zibethinus* L. 'Monthong') by aroma extract dilution analysis and headspace gas chromatography-olfactometry. *J. Agric. Food Chem.* **2012**, *60*, 11253−11262.
(34) Vichi, S.; Cortes-Francisco, N.; Romero, A.; Caixach, J. Determination of volatile thiols in virgin olive oil by derivatisation and LC-HRMS, and relation with sensory attributes. *Food Chem.* **2014**, *149*, 313−318.
(35) Kuroiwa, Y.; Hashimoto, N. Composition of sunstruck flavor substance and mechanism of its evolution. *Proc. Am. Soc. Brew. Chem.* **1961**, 28−36.
(36) Song, H. S.; Sawamura, M.; Ito, T.; Ido, A.; Ukeda, H. Quantitative determination and characteristic flavor of daidai (*Citrus aurantium* L. var. *cyathifera* Y. Tanaka) peel oil. *Flavour Fragrance J.* **2000**, *15*, 323−328.
(37) Choi, H.; Kondo, Y.; Sawamura, M. Characterization of the odor-active volatiles in *Citrus* Hyuganatsu (*Citrus tamurana* Hort. ex Tanaka). *J. Agric. Food Chem.* **2001**, *49*, 2404−2408.
(38) Miyazawa, N.; Tomita, N.; Kurobayashi, Y.; Nakanishi, A.; Ohkubo, Y.; Maeda, T.; Fujita, A. Novel character impact compounds in yuzu (*Citrus junos* Sieb. ex Tanaka) peel oil. *J. Agric. Food Chem.* **2009**, *57*, 1990−1996.
(39) Mussinan, C. J.; Mookherjee, B. D.; Malcolm, G. I. Isolation and identification of the volatile constituents of fresh lemon juice. In *Essential Oils*; Mookherjee, B. D., Mussinan, C. J., Eds.; Allured Publishing: Wheaton, IL, USA, 1981; pp 199−228.
(40) Mondello, L.; Catalfamo, M.; Dugo, G. Multidimensional tandem capillary gas chromatography system for the analysis of real complex samples. Part I: Development of a fully automated tandem gas chromatography system. *J. Chromatogr. Sci.* **1998**, *36*, 201−209.
(41) Starkenmann, C.; Troccaz, M.; Howell, K. The role of cysteine and cysteine-S conjugates as odour precursors in the flavor and fragrance industry. *Flavour Fragrance J.* **2008**, *23*, 369−381.
(42) Perez-Cacho, P.; Mahattanatawee, K.; Smoot, J. M.; Rouseff, R. Identification of sulfur volatiles in canned orange juices lacking orange flavor. *J. Agric. Food Chem.* **2007**, *55*, 5761−5767.
(43) Mick, W.; Schreier, P. Additional volatiles of black tea aroma. *J. Agric. Food Chem.* **1984**, *32*, 924−929.
(44) Liu, Y.; Yu, A. Effect of reaction temperature and time on aroma compounds generation from Maillard reaction of ascorbic acid and cysteine. *Shipin Keji* **2011**, *36*, 262−267.
(45) Miller, J. M.; Rockland, L. B. Determination of cysteine and glutathione in citrus juices by filter paper chromatography. *Arch. Biochem. Biophys.* **1952**, *40*, 416−423.
(46) Lifshitz, A.; Stepak, Y. Detection of adulteration of fruit juice. I. Characterization of Israel lemon juice. *J. AOAC* **1971**, *54* (6), 1262−1265.
(47) Vandercock, C. E.; Price, R. L. The application of amino acid composition to the characterization of citrus juice. *J. Food Sci.* **1972**, *37* (3), 384−386.
(48) Ortiz, J. M.; Garcia-Lidon, A.; Tadeo, J. L.; De Cordova, F.; Martin, B.; Estelles, A. Comparative study of physical and chemical characteristics of four lemon cultivars. *J. Hortic. Sci.* **1986**, *61* (2), 277−281.

DOI: 10.1021/jf505177r
J. Agric. Food Chem. 2015, 63, 1915−1931

biotransformations in vivo. We report here the synthesis of a series of deuterium-labeled standards and the use of these as internal standards in GC-MS to compare the evolution of several guaiane derivatives during in vitro aerial oxidation of α-guaiene (**1**) and α-bulnesene (**5**) over time at ambient temperature and on a submilligram scale.

MATERIALS AND METHODS

Chemicals. Acetic anhydride (≥98%, ACS reagent grade), pyridinium dichlorochromate (PDC), *tert*-butyl hydroperoxide (5−6 M in decane), selenium dioxide (SeO_2), cerium chloride heptahydrate ($CeCl_3{\cdot}7H_2O$), sodium borohydride ($NaBH_4$), lithium aluminum deuteride ($LiAlD_4$), deuterium oxide (D_2O), d_6-ethanol, triethylamine (Et_3N), palladium acetate ($Pd(OAc)_2$), 4-dimethylamino pyridine (DMAP), sodium sulfite (Na_2SO_3), and anhydrous magnesium sulfate were purchased from Sigma-Aldrich. Deuterated benzene (C_6D_6) and deuterated chloroform ($CDCl_3$) were purchased from Cambridge Isotope Laboratories, Inc. (Tewksbury, MA, USA). Anhydrous aluminum trichloride ($AlCl_3$), silver nitrate ($AgNO_3$), AR-grade hexanes, methanol, ethyl acetate, acetonitrile, tetrahydrofuran, toluene, and HPLC-grade dichloromethane were purchased from Merck. Sodium ethoxide solid was prepared freshly by dissolving sodium metal in absolute ethanol under N_2 followed by solvent removal and drying in vacuo. Guaiac wood essential oil (steam distilled from Bulnesia sarmientoi, Paraguay) was purchased from the Australian Botanical Products Co. as viscous oil.

General Experimental Procedures. All reagents were purchased from commercial sources and used directly unless otherwise stated. Solvents for synthesis were purified according to known procedures wherever needed.[12] NMR data were recorded on Varian-Inova 500/600 MHz spectrometers. $CDCl_3$ and C_6D_6 were used as solvents for NMR experiments. All ^1H and ^{13}C NMR spectra were calibrated utilizing residual ^1H and ^{13}C signals of deuterated solvents set at 7.26 and 77.0 ppm for $CDCl_3$ and 7.16 and 128.06 ppm for C_6D_6, respectively. GC-MS quantitative analysis was performed with an Agilent 6890 GC- 5973N MSD equipped with a DB-Wax capillary column (30 m × 250 μm I.D. × 0.25 μm film thickness, Agilent technologies). GC-MS analysis was performed with the following acquisition parameters: oven temperature was initially set at 100 °C and increased to 200 °C at 8 °C/min and then to 240 °C at 20 °C/min and held at 240 °C for a further 3 min; injection was in splitless mode with a purge flow of 6 mL/min in 0.05 min; front inlet temperature was set at 240 °C with a pressure of 12.92 psi; injection volume was 2 μL, and gas flow rate was 1.2 mL/min; MSD was in selective ion monitoring (SIM) mode. The ions 204 (for **1**, **5**), 220 (for **2a**, **2b**, **6a**, **6b**), 211 (for **10**, **15**), 218 (for **3**, **7**), 225 (for **11a, 11b**, **16**), and 223 (for **9**, **14**) were selected as quantifiers. Qualifier ions selected for the corresponding quantifiers were 105, 147, and 161 for **1**, 105, 163, and 205 for **2a** and **2b**, 105, 147, and 203 for **3**, 107, 147, and 161 for **4**, 147, 163, and 204 for **6a** and **6b**, 147, 161, and 203 for **7**, 108, 165, and 208 for **9**, 108, 165, and 196 for **10**, 108, 165, and 208 for **11a** and **11b**, 111, 163, and 208 for **14**, 112, 150, 166 for **15**, and 111, 165, 208 for **16**. The dwell times for all selected ions were set at 100 ms, gain factor was 1 and EI 70 eV, transfer line temperature was 240 °C, MS source was at 230 °C, and MS quadrupler was at 150 °C. Whatman grade 1 filter paper was the support medium for oxidation of **1** and **5**. Silica column chromatography (SCC) was performed using either LC60A 40−63 μm silica (Grace Davison) or Silica gel 60 (0.015−0.040 mm, Merck). TLC was conducted with TLC silica gel 60 F_{254} plates (Merck KGaA) using standard vanillin stain for visualization. Silver nitrate impregnated silica (SNIS) was prepared according to the literature.[13] Rotundone (**3**) and the rotund-2-ols (**2a**/**b**) were prepared as described previously.[3,5]

Synthesis of Deuterium-Labeled Standards for GC-MS. *d_5-Rotundone (**9**).* **9** was prepared as described previously with slight modification.[14] Rotundone (**3**) (180 mg, 0.83 mmol) was dissolved in a 1 M solution of NaOEt in d_6-ethanol (1 mL) in a vial (4 mL), which was capped under N_2 and left at room temperature overnight (ca. 20 h). Brine (2 mL) was added, and the resulting mixture was extracted with Et_2O (4 × 5 mL). The combined ether layers were concentrated, dried over anhydrous $MgSO_4$, and filtered, and the filtrate was concentrated in vacuo. The residue was purified with silica (15−40 μm) column chromatography (Et_2O/hexanes, 8%), affording **9** (75 mg, 42%) as a pale yellow oil. Spectroscopic data of **9** including NMR and MS was in accord with those reported in the literature.[14]

*d_7-α-Guaiene (**10**).* $LiAlD_4$ (42 mg, 1 mmol) was suspended in dry ether (1 mL) at room temperature under N_2. To the above solution was added dropwise a solution of anhydrous $AlCl_3$ (159 mg, 1.19 mmol) in dry ether (1 mL) with stirring. After 10 min, a premixed solution of d_5-rotundone **9** (32.1 mg, 0.14 mmol) in dry ether (0.5 mL) and anhydrous $AlCl_3$ (133.5 mg, 1 mmol) in dry ether (0.5 mL) was added dropwise. After stirring for 1 h, the reaction mixture was chilled in an ice bath before being quenched by slow addition of D_2O (2 mL) followed by 6 N H_2SO_4 (2 mL). The resulting mixture was extracted with ether (3 × 20 mL), and the combined ether layers were washed with brine (10 mL), dried over anhydrous $MgSO_4$, and filtered. The filtrate was concentrated in vacuo, and the residue was purified by SNIS chromatography (hexanes) to yield **10** (27.2 mg, 88%). ^1H NMR (600 MHz, $CDCl_3$) δ 4.68 (br s, 1H, H_{12a}), 4.62 (dq, 1H, J = 2.4, 1.5 Hz, H_{12b}), 2.34 (m, 1H, H_{10}), 2.11 (m, 1H, H_7), 1.72 (s, 3H, H_{13}), 1.71−1.67 (m, 3H, $H_{8a,\ 8b,\ 9a}$), 1.59 (m, 1H, H_{9b}), 1.01 (d, 3H, J = 6.6 Hz, H_{15}), 0.92 (s, 3H, H_{14}); ^{13}C NMR (150 MHz, $CDCl_3$) δ 152.4 (C_{11}), 140.5 (C_1), 138.5 (C_5), 107.9 (C_{12}), 46.4 (C_7), 33.8 (C_9), 33.7 (C_{10}), 31.0 (C_8), 20.4 (C_{13}), 19.7 (C_{14}), 18.6 (C_{15}). See Supporting Information for the mass spectra of **10** and other deuterium-labeled compounds.

*d_5-2R-Rotundol (**11a**) and d_5-2S-rotundol (**11b**).* **11a** and **11b** were synthesized from d_5-rotundone using the same protocol as described for preparing d_0-rotundols (**2a**/**b**)[5] except that d_5-rotundone (**5**, 40 mg, 0.18 mmol), $CeCl_3{\cdot}7H_2O$ (70 mg, 0.19 mmol), MeOH (5 mL), and $NaBH_4$ (10 mg, 0.27 mmol) were used. d_5-2*R*-Rotundol (**11a**, 23 mg, 65%, based on 87% conversion) and d_5-2*S*-rotundol (**11b**, 4 mg, 11% based on 87% conversion) were obtained as a white solid and a colorless liquid, respectively, with d_5-rotundone (5 mg, 13%) recovered after purification by silica (15−40 μm) column chromatography (Et_2O/hexanes, 8%−12%). **11a**: ^1H NMR (600 MHz, C_6D_6) δ 4.79 (dq, 1H, J = 1.8, 1.5 Hz, H_{12a}), 4.73 (dq, 1H, J = 2.0, 1.4 Hz, H_{12b}), 4.38 (s, 1H, H_2), 2.50 (qdd, 1H, J = 7.2, 4.2, 3.6 Hz, H_{10}), 1.95 (m, 1H, H_7), 1.84 (dddd, 1H, J = 13.8, 12.0, 11.4, 2.4 Hz, H_{8a}), 1.73 (dddd, 1H, J = 13.8, 6.0, 2.7, 2.3 Hz, H_{8b}), 1.65 (s, 3H, H_{13}), 1.60 (dddd, 1H, J = 13.8, 6.0, 4.2, 2.4 Hz, H_{9a}), 1.56 (m, 1H, H_{9b}), 1.21 (d, 3H, J = 7.2 Hz, H_{15}), 0.96 (s, 3H, H_{14}); ^{13}C NMR (150 MHz, C_6D_6) δ 151.7 (C_{11}), 144.1 (C_1), 142.4 (C_5), 108.3 (C_{12}), 80.5 (C_2), 46.5 (C_7), 33.6 (C_9), 31.7 (C_{10}), 31.1 (C_8), 20.7 (C_{14}), 20.0 (C_{13}), 18.2 (C_{15}); EI-MS m/z (rel. intensity) 225 ($[M]^+$, 30), 206 (14), 191 (15), 179 (19), 167 (100), 148 (26), 135 (21), 121 (36), 108 (42), 95 (45), 81 (30), 67 (24), 55 (21). **11b**: ^1H NMR (600 MHz, C_6D_6) δ 4.80 (br s, 1H, H_{12a}), 4.74 (dq, 1H, J = 2.4, 1.8 Hz, H_{12b}), 4.57 (br s, 1H, H_2), 2.65 (qdd, 1H, J = 7.2, 4.2, 3.6 Hz, H_{10}), 2.14 (m, 1H, H_7), 1.75−1.71 (m, 2H, $H_{8a,\ 8b}$), 1.70−1.69 (m, 1H, H_{9a}), 1.64 (s, 3H, H_{13}), 1.61 (m, 1H, H_{9b}), 1.01 (d, 3H, J = 7.2 Hz, H_{15}), 0.83 (s, 3H, H_{14}); ^{13}C NMR (150 MHz, C_6D_6) δ 152.2 (C_{11}), 144.5 (C_5), 143.2 (C_1), 109.0 (C_{12}), 79.0 (C_2), 47.1 (C_7), 34.8 (C_9), 31.7 (C_8), 30.8 (C_{10}), 20.8 (C_{13}), 20.6 (C_{14}), 18.4 (C_{15}).

Forty Seven Percent α-Bulnesene Hydrocarbons. The guaiacwood oil mother liquor containing ca. 47% α-bulnesol (**12**) was obtained after repeated recrystallization of guaiol with MeCN and used for the synthesis of bulnesene-enriched hydrocarbons employing acylation followed by pyrolysis as described for the synthesis of **1**.[15] To the guaiacwood oil mother liquor (33 g) was added acetic anhydride (100 mL) and DMAP (330 mg). The resulting mixture was heated under reflux at 150 °C under N_2 for 6 h. After being cooled to room temperature, the reaction products were extracted with hexanes (4 × 200 mL) and the combined hexane layers washed with substantial water, and brine and dried over anhydrous $MgSO_4$. The hexane extract was filtered through filter paper, and solvent removal gave a crude product (40 g) containing 47% bulnesyl acetate (**13**, GC-MS). Crude bulnesyl acetate (23 g) was heated to ∼220 °C under N_2 for 3.5 h, while the acetic acid generated was condensed and collected in a

DOI: 10.1021/jf505537s
J. Agric. Food Chem. 2015, 63, 1932−1938

receiving flask. The reaction was terminated and its temperature lowered to room temperature when no more acetic acid was being generated. To this reaction mixture was added hexanes (100 mL) and silica (ca. 30 g). The resulting suspension was filtered through a bed of silica (ca. 100 g) and further eluted with hexanes (3 × 100 mL). The combined filtrates were concentrated in vacuo to afford the bulnesene-rich hydrocarbons (47% by GC-MS, 15.6 g, 90% from **12**). Pure α-bulnesene (**5**) was obtained as a colorless oil after repeated SNIS chromatography (hexanes) of the 47% bulnesene hydrocarbon mixture. α-Bulnesene (**5**): ^{1}H NMR (600 MHz, $CDCl_3$) δ 4.66 (br s, 1H, H_{12a}), 4.64 (dq, 1H, *J* = 2.0, 1.5 Hz, H_{12b}), 2.47 (dd, 1H, *J* = 12.0, 7.2 Hz, H_5), 2.33 (m, 1H, H_{2a}), 2.23−2.15 (m, 2H, $H_{9a,\ 2b}$), 2.13−2.08 (m, 2H, $H_{4,\ 7}$), 2.01 (br dd, 1H, *J* = 15.0, 7.2 Hz, H_{9b}), 1.73−1.69 (m, 1H, H_{8a}), 1.71 (br s, 3H, H_{13}), 1.67 (br s, 3H, H_{15}), 1.65 (m, 1H, H_{3a}), 1.62 (m, 1H, H_{6a}), 1.35 (dq, 1H, *J* = 12.0, 7.8 Hz, H_{3b}), 1.26 (dddd, 1H, *J* = 13.2, 11.4, 11.4, 1.5 Hz, H_{8b}), 1.03 (ddd, 1H, *J* = 12.6, 12.0, 12.0 Hz, H_{6b}), 0.90 (d, 3H, *J* = 7.2 Hz, H_{14}); ^{13}C NMR (150 MHz, $CDCl_3$) δ 152.4 (C_{11}), 142.0 (C_1), 128.8 (C_{10}), 108.0 (C_{12}), 50.8 (C_7), 46.8 (C_5), 38.8 (C_4), 34.6 (C_9), 33.1 (C_3), 32.6 (C_6), 31.7 (C_8), 30.4 (C_2), 22.2 (C_{15}), 20.9 (C_{13}), 15.4 (C_{14}). EI-MS *m*/*z* (rel. intensity): 204 ([M]$^+$, 27), 189 (55), 161 (18), 147 (36), 133 (35), 119 (35), 107 (100), 93 (86), 79 (55), 67 (28), 55 (28). ^{1}H NMR data are consistent with that reported in the literature.[16]

*2S-Bulnesol (**6b**).* SeO_2 (1.38 g, 0.5 equiv, 12.5 mmol) was suspended in CH_2Cl_2 (100 mL) under N_2, and the suspension was cooled down to 0 °C. To the stirred suspension at 0 °C was added dropwise a solution of TBHP (5−6 M in decane, 10 mL, 50−60 mmol) in CH_2Cl_2 (15 mL) followed by a solution of α-bulnesene (47% by GC-MS, 5.1 g, 25 mmol) in CH_2Cl_2 (10 mL). After stirring at 0 °C for 3.5 h, the reaction was quenched with saturated aq Na_2SO_3 (50 mL). The resulting mixture was allowed to stir for an additional 0.5 h before being extracted with CH_2Cl_2 (3 × 100 mL), and the combined organic layers were further washed with brine, dried over anhydrous $MgSO_4$, and filtered. The filtrate was concentrated in vacuo, and the residue was purified by SCC (Et_2O/hexanes, from 4% to 12%) to furnish **6b** (1.54 g, 57%) as a white solid. Spectroscopic data was in agreement with those reported in the literature.[17]

*α-Bulnesone (**7**).* α-Bulnesone was synthesized by oxidation of **6b** using palladium-catalyzed oxidation with molecular oxygen.[18] To a stirred solution of **6b** (660 mg, 3 mmol) in THF/toluene (15%, 30 mL) was added $Pd(OAc)_2$ (20.2 mg, 90 μmol) and Et_3N (20 μL, 0.14 mmol). The solution was stirred under an O_2 atmosphere at 45 °C after being evacuated and refilled with O_2 three times. The oxidation was terminated after 52 h by filtration of the reaction mixture through a silica plug (ca. 10 g), which was further rinsed with Et_2O (3 × 20 mL). The combined filtrates were concentrated in vacuo, and the residue was purified by SCC (Et_2O/hexanes, from 4% to 16%) to yield **7** (347 mg, 53%) as a colorless oil. Spectroscopic data of **7** was in agreement with those reported in the literature.[19]

*d_5-Bulnesone (**14**).* Ketone **7** (326 mg, 1.5 mmol) was dissolved in a 1 M solution of NaOEt (102 mg, 1.5 mmol) in d_6-ethanol (1.5 mL), and the resulting mixture was left at room temperature overnight. After ca. 24 h brine was added (5 mL), the aqueous solution was extracted with Et_2O (3 × 15 mL), and the organic layers were combined, dried over anhydrous $MgSO_4$, and filtered. The filtrate was concentrated in vacuo and purified by SCC (Et_2O/hexanes, 8%) to give **14** (293 mg, 88%) as a colorless oil. ^{1}H NMR (600 MHz, $CDCl_3$) δ 4.68 (br s, 2H, $H_{12a,b}$), 2.86 (dd, 1H, *J* = 12.0, 7.2 Hz, H_5), 2.30 (m, 0.6H, H_{9a}), 2.28 (q, 1H, *J* = 7.2 Hz, H_4), 2.25 (ddd, 0.9H, *J* = 14.4, 9.6, 7.8 Hz, H_{9b}), 2.21−2.18 (m, 1H, H_7), 1.80 (m, 1H, H_{8a}), 1.74 (dd, 1H, *J* = 13.2, 3.6 Hz, H_{6a}), 1.70 (br s, 3H, H_{13}), 1.33 (m, 1H, H_{8b}), 1.22 (m, 1H, H_{6b}), 0.94 (d, 3H, *J* = 7.2 Hz, H_{14}); ^{13}C NMR (150 MHz, $CDCl_3$) δ 207.2 (C_2), 154.9 (C_1), 150.8 (C_{11}), 137.0 (C_{10}), 108.8 (C_{12}), 49.3 (C_7), 44.6 (C_5), 36.6 (C_9), 32.5 (C_6), 31.6 (C_4), 29.8 (C_8), 20.9 (C_{13}), 16.0 (C_{14}).

*d_7-α-Bulnesene (**15**).* d_7-Bulnesene was synthesized using the same procedure as that for d_7-α-guaiene except that $LiAlD_4$ (48 mg, 1.12 mmol), anhydrous $AlCl_3$ (159 mg 1.19 mmol), and the mixture of d_5-bulnesone (80 mg, 0.36 mmol) and $AlCl_3$ (133.5 mg, 1 mmol) were utilized. The crude reaction products were purified by repeated SNIS chromatography to yield d_7-bulnesene (33 mg, 44%) as a colorless oil. **15**: ^{1}H NMR (600 MHz, $CDCl_3$) δ 4.66 (br s, 1H, H_{2a}), 4.64 (br s, 1H, H_{12a}), 2.45 (dd, 1H, *J* = 12.0, 7.2 Hz, H_5), 2.19 (br dd, 0.6H, *J* = 15.0, 11.4 Hz, H_{9a}), 2.11−2.06 (m, 2H, $H_{4,\ 7}$), 2.01 (m, 0.9H, H_{9b}), 1.71 (br s, 3H, H_{13}), 1.70 (m, 1H, H_{8a}), 1.62 (ddd, 1H, *J* = 13.2, 1.8, 1.5 Hz, H_{6a}), 1.26 (m, 1H, H_{8b}), 1.03 (ddd, 1H, *J* = 13.2, 12.0, 10.8 Hz, H_{6b}), 0.90 (d, 3H, *J* = 7.2 Hz, H_{14}); ^{13}C NMR (150 MHz, $CDCl_3$) δ 152.4 (C_{11}), 141.9 (C_1), 128.8 (C_{10}), 108.0 (C_{12}), 50.8 (C_7), 46.1 (C_5), 38.7 (C_4), 34.4 (C_9), 32.7 (C_6), 31.8 (C_8), 20.9 (C_{13}), 15.4 (C_{14}).

*2R-Bulnesol (**6a**).* Compound **6a** was synthesized employing Luche reduction as used for the synthesis of 2*R*-rotundol (**4a**)[5] except that α-bulnesone (**7**, 14 mg, 64 μmol), MeOH (3 mL), $CeCl_3{\cdot}7H_2O$ (13 mg, 35 μmol), and $NaBH_4$ (9 mg, 243 μmol) were used, and the reaction was conducted at 0 °C. Purification of the reaction mixture by SCC (Et_2O/hexanes, 10%) yielded 2*R*-bulnesol (6.8 mg, 48%) as a colorless oil. ^{1}H NMR (500 MHz, C_6D_6) δ 4.81 (dq, 1H, *J* = 3.0, 0.8 Hz, H_{12a}), 4.78 (dq, 1H, *J* = 2.0, 1.5 Hz, H_{12b}), 4.53 (dd, 1H, *J* = 6.5, 4.5 Hz, H_2), 2.35 (br dd, 1H, *J* = 12.0, 7.5 Hz, H_5), 2.12 (br dd, 1H, *J* = 15.0, 11.5 Hz, H_{9a}), 2.02 (dddd, 1H, *J* = 12.0, 10.5, 3.0, 2.0 Hz, H_7), 1.94 (qd, 1H, *J* = 7.0, 6.5 Hz, H_4), 1.91 (ddd, 1H, *J* = 15.0, 7.0, 1.5 Hz, H_{9b}), 1.81 (dd, 1H, *J* = 13.0, 6.5 Hz, H_{3a}), 1.79 (ddd, 3H, *J* = 1.5, 1.0, 0.5 Hz, H_{15}), 1.75 (m, 1H, H_{6a}), 1.71 (m, 1H, H_{8a}), 1.68 (dd, 3H, *J* = 1.5, 0.8 Hz, H_{13}), 1.46 (dddd, 1H, *J* = 13.0, 6.5, 4.5, 0.5 Hz, H_{3b}), 1.28 (dddd, 1H, *J* = 13.5, 11.5, 10.5, 1.5 Hz, H_{8b}), 1.22 (ddd, 1H, *J* = 13.0, 12.0, 12.0 Hz, H_{6b}), 1.02 (d, 3H, *J* = 7.0 Hz, H_{14}); ^{13}C NMR (125 MHz, C_6D_6) δ 151.9 (C_{11}), 145.3 (C_1), 135.5 (C_{10}), 108.8 (C_{12}), 74.0 (C_2), 51.3 (C_7), 46.6 (C_5), 43.5 (C_3), 36.3 (C_4), 35.7 (C_9), 34.0 (C_6), 32.1 (C_8), 22.1 (C_{15}), 21.0 (C_{13}), 17.0 (C_{14}). EI-MS *m*/*z* (rel. intensity): 220 ([M]$^+$, 23), 205 (16), 187 (21), 177 (13), 163 (42), 138 (28), 119 (47), 108 (100), 95 (64), 79 (42), 67 (37), 55 (38). ^{13}C NMR data was in agreement with those reported.[4]

*d_5-2R-Bulnesol (**16**).* d_5-Bulnesone was synthesized using the same procedure as that for 2*R*-bulnesol except that d_5-bulnesone (16.7 mg, 75 μmol), $CeCl_3{\cdot}7H_2O$ (16 mg, 43 μmol), and $NaBH_4$ (8 mg, 216 μmol) were used. Purification of the reaction products by SCC (Et_2O/hexanes, 10%) gave d_5-2*R*-bulnesol (10.2 mg, 61%) as a colorless oil. ^{1}H NMR (500 MHz, C_6D_6) δ 4.81 (dq, 1H, *J* = 3.0, 0.8 Hz, H_{12a}), 4.78 (dq, 1H, *J* = 2.0, 1.5 Hz, H_{12b}), 4.52 (s, 1H, H_2), 2.35 (br dd, 1H, *J* = 12.0, 7.5 Hz, H_5), 2.12 (br dd, 0.6H, *J* = 15.0, 11.5 Hz, H_{9a}), 2.02 (dddd, 1H, *J* = 12.0, 10.5, 3.0, 2.0 Hz, H_7), 1.94 (dq, 1H, *J* = 7.5, 7.0 Hz, H_4), 1.91 (m, 0.9H, H_{9b}), 1.75 (m, 1H, H_{6a}), 1.71 (m, 1H, H_{8a}), 1.68 (dd, 3H, *J* = 1.5, 0.8 Hz, H_{13}), 1.28 (m, 1H, H_{8b}), 1.22 (ddd, 1H, *J* = 13.0, 12.0, 12.0 Hz, H_{6b}), 1.02 (d, 3H, *J* = 7.0 Hz, H_{14}); ^{13}C NMR (125 MHz, C_6D_6) δ 151.9 (C_{11}), 108.8 (C_{12}), 73.9 (C_2), 51.2 (C_7), 46.5 (C_5), 43.5 (C_3), 36.3 (C_4), 35.7 (C_9), 34.0 (C_6), 32.1 (C_8), 21.0 (C_{13}), 17.0 (C_{14}).

Preparation and Validation of Calibration Curves. Stock standard solutions in EtOAc were prepared from more concentrated solutions of synthetic standards as follows: Solution A contained **1** (160 μg/mL) and **2a**, **2b**, and **3** (each 80 μg/mL); solution B contained **5**, **6a**, **6b**, and **7** (each 160 μg/mL); solution C contained **9** and **10** (each 80 μg/mL), **11a** (32 μg/mL), and **11b** (128 μg/mL); solution D contained **14**, **15**, and **16** (each 80 μg/mL). Solution A was diluted with EtOAc to a scale of eight concentration levels and each spiked with an equal volume (250 μL) of diluted solution **C** (1:10 dilution) to make up the final concentrations of 0, 0.625, 1.25, 2.5, 5.0, 10.0, 20.0, and 40.0 μg/mL for **2a**, **2b**, and **3** and 0, 1.25, 2.5, 5.0, 10.0, 20.0, 40.0, and 80.0 μg/mL for **1** with corresponding labeled IS at 4.0 μg/mL for **9** and **10**, 1.6 μg/mL for **11a**, and 6.4 μg/mL for **11b**. In a similar fashion, solution B was diluted with EtOAc to a scale of eight concentration levels and each spiked with an equal volume (250 μL) of diluted solution D (1:10 dilution) to make up final concentrations of 0, 1.25, 2.5, 5.0, 10.0, 20.0, 40.0, and 80.0 μg/mL for **5**, **6a**, **6b**, and **7** with corresponding labeled IS at 4.0 μg/mL for **14**, **15** and **16**. The above concentrations of analytes were prepared in duplicate and analyzed by the GC-MS method outlined in the General Experimental Procedures. For generating the calibration curves, the ratios of response areas of selected ions at their corresponding retention times at each concentration [204/211 (**1**/**10**), 220/225 (**2a**/**11a**), 220/225 (**2b**/

DOI: 10.1021/jf505537s
J. Agric. Food Chem. 2015, 63, 1932−1938

11a), 218/223 (**3a**/**9**), 204/211 (**5**/**15**), 220/225 (**6a**/**16**), 220/225 (**6b**/**16**), and 218/223 (**7**/**14**)] were plotted against the ratios of concentrations of analytes versus those of labeled IS [c(**1**/**8**), c(**2a**/**11a**), c(**2b**/**11b**), c(**3**/**9**), c(**5**/**15**), c(**6a**/**16**), c(**6b**/**16**), c(**7**/**14**)]. Samples for quantitative analysis were each spiked with deuterium-labeled IS mixed solutions C or D to make up the final concentrations as those of IS in the preparation of the calibration curves. The concentrations of analytes in the samples were calculated based on calibration equations listed in Table S1, Supporting Information. The method was verified by linearity, relative standard deviation of quantitative analysis, limit of detection (LOD), and limit of quantitation (LOQ). LOD and LOQ are defined as the concentration giving a signal-to-noise (S/N) ratio of 3:1 and 10:1, respectively (Table S1, Supporting Information).

*Oxidation of α-Guaiene (**1**) and α-Bulnesene (**5**).* An α-guaiene solution (ca. 92 mg/mL) was prepared by dissolving **1** (ca. 92 mg) with EtOAc to a total volume of 1.0 mL. An aliquot (5 μL) of the above solution was added to a 1 cm^2 filter paper each in an empty vial (SAMCO specimen tubes 50 × 19 mm). The vials were left uncapped to allow contact with air at room temperature, and the changes of concentrations of **1**, **2a**, **2b**, and **3** at different time points were quantitated for duplicate samples at each time point by SIDA with GC-MS. For determining analyte concentrations, EtOAc (1 mL) was added to each sample vial. An aliquot of the analyte solution (80 μL) was diluted with EtOAc and spiked with solution of labeled IS mixture to make up a total volume of 0.5 mL of solution containing 4 μg/mL labeled IS with a dilution factor of 6.25 for analytes. This solution was analyzed by GC-MS using the parameters described in the General Experimental Procedures, and concentrations of analytes were obtained based on the calibration curves generated above. α-Bulnesene solution was prepared by dissolving α-bulnesene-enriched essential oil containing no **6a**, **6b**, or **7** (ca. 80% bulnesene by GC-MS, 150 mg) in EtOAc (1 mL). Oxidation of α-bulnesene (**5**) and determination of analytes were performed using the same procedure as that described for α-guaiene (**1**).

RESULTS AND DISCUSSION

Synthesis of Deuterium-Labeled Internal Standards (IS). On the basis of the readily synthesized d_5-rotundone (**9**), d_5-rotund-2-ols (**11a**/**b**) could be easily prepared by Luche reduction of **9**. Employing the stronger reducing reagent AlD_3 generated in situ by $LiAlD_4$ and anhydrous $AlCl_3$ realized the reduction of the enone carbonyl to furnish desired **10** in an excellent 88% yield, Figure 2. Our initial attempts to access

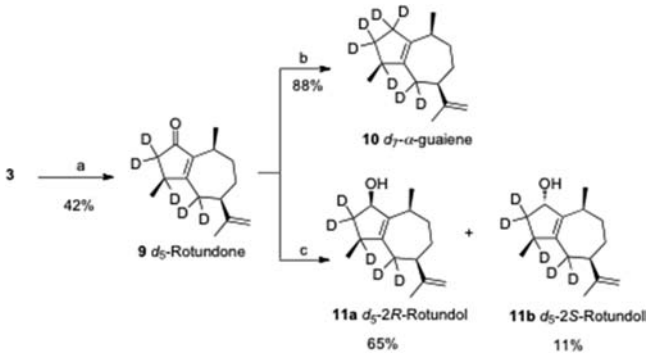

Figure 2. Synthesis of d_7-α-guaiene (**10**) and d_5-rotund-2-ols (**11a**/**b**).

deuterated α-bulnesene **15** via simple isomerization of d_7-α-guaiene **10** under various group VIII metal-catalyzed (e.g., $PdCl_2$, $Pd(OAc)_2$, $RhCl_3$), strongly acidic or basic conditions proved to be ineffective. Therefore, our focus was shifted onto constructing a carbonyl moiety at C2 within α-bulnesene **5** itself to enable initial deuterium exchange followed by removal of the carbonyl moiety by reduction to allow for the preparation of d_7-α-bulnesene (**15**), Figure 3. Direct attempts

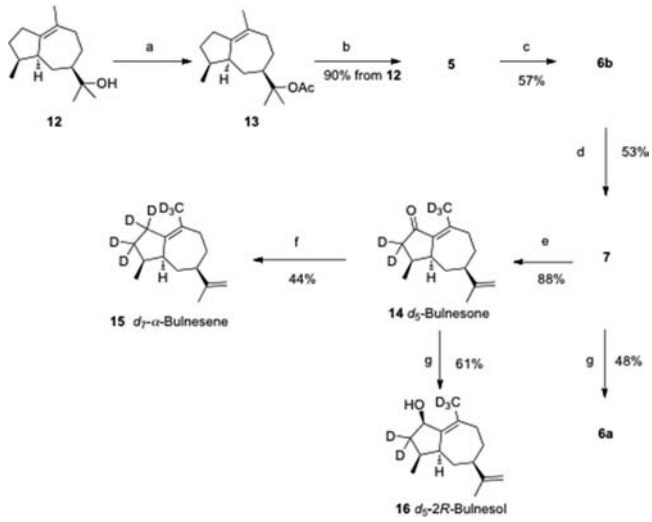

Figure 3. Synthesis of d_5-bulnesone (**14**), d_7-α-bulnesene (**15**), and d_5-2-bulnesols (**16**).

at allylic oxidation of **5** into α-bulnesone (**7**) in a single step exploiting chromium- and cobalt-based oxidants coupled with TBHP were unsuccessful, but allylic oxidation of **5** with SeO_2 and TBHP furnished 2*S*-bulnesol (**6b**) in a moderate 57% yield. Palladium-catalyzed oxidation of **6b** afforded ketone **7** again in moderate yield, which was subjected to deuterium exchange under basic conditions to furnish the desired d_5-bulnesone (**14**) in an excellent yield of 88%. d_5-2*R*-Bulnesol (**16**) and d_7-α-bulnesene (**15**) were successfully synthesized by reduction of **14** in similar fashions as those utilized for the synthesis of the d_5-rotund-2-ols (**11a**/**b**) and d_7-α-guaiene (**10**). Deuterium incorporation by hydrogen exchange is an equilibrium and will always yield a mixture of deuterium-labeled compounds with various degrees of deuterium incorporation at different sites of the substrates depending on the ease of exchange of the hydrogen atoms. For example, deuterium exchange of α-bulnesone **7** was found to be incomplete after the exchange equilibrium was reached, with a very small percentage of α-bulnesone **7** still existing in the labeled d_5-bulnesone **14** mixture. Consequently, this undeuterated analogue was carried through to the d_5-2*R*-bulnesol (**16**) after direct Luche reduction with $NaBH_4$. The nomenclature used here for the deuterium standards **9**, **10**, **11a**/**b**, **14**, **15**, and **16** and their structures are depicted in Figures 2 and 3 and represent the number of exchangeable hydrogens that are mainly substituted with deuterium. A low incorporation of deuterium onto C_9 was apparent for **14**−**16**. The determined deuterium incorporation percentages for all the synthetic standards are presented in Table 1. Approximately 0.6% of **14** and **16** had no deuterium incorporation when equilibrium of exchange had been reached, but the d_0 ions from spiked IS were negligible compared to those for the analytes during GC-MS. The various standard solutions for analysis were prepared at room temperature, stored under N_2, and kept in a freezer before and after each usage but allowed to attain ambient temperature immediately before usage. These standard solutions were found to be stable during handling and under the analysis conditions. Importantly, no autoxidation of the solutions was evident during use.

DOI: 10.1021/jf505537s
J. Agric. Food Chem. 2015, 63, 1932−1938

Table 1. Percentage of Deuterium Incorporation of Deuterium-Labeled IS[a]

IS's	d_0	d_1	d_2	d_3	d_4	d_5	d_6	d_7	d_8	d_9
9	nd	1.1%	5.6%	21.3%	39.5%	28.6%	2.4%	1.6%	nd	nd
10	nd	nd	0.6%	4.4%	14.3%	28.0%	29.4%	16.3%	5.1%	2.1%
11a	nd	0.4%	9.5%	23.2%	35.3%	27.6%	2.8%	1.3%	nd	nd
11b	nd	nd	4.8%	23.3%	38.0%	29.3%	2.2%	1.9%	0.5%	nd
14	0.6%	4.1%	13.4%	25.3%	28.7%	19.7%	7.2%	1.0%	nd	nd
15	nd	nd	nd	3.5%	12.1%	25.0%	30.2%	21%	7.6%	0.8%
16	0.7%	4.2%	13.4%	24.6%	28.7%	20.0%	7.4%	1.0%	nd	nd

[a]Signals arising from the ^{13}C signals of the parent ions have been excluded. nd: not detected.

Evolution of Sesquiterpene Products under Aerial Oxidation Conditions. Employing these deuterium-labeled analogues in GC-MS we were able to monitor the rate of degradation of α-guaiene **1** and α-bulnesene **5** when exposed to air at ambient temperature. To better mimic the oxidation of **1** and **5** on dry herbs and plant materials we used cellulose filter paper as the supporting medium by coating **1** (ca. 380 μg) and **5** (ca. 600 μg) onto filter paper (1 cm^2), respectively. Aerial oxidation of both **1** and **5** produced the corresponding C2 alcohols and ketones, suggesting that oxidation of **5** could follow a similar oxidative pathway to that of **1** via the generation and decomposition of the C2 hydroperoxide epimers as recently described.[3,5]

As shown in Figure 4, some 99% of the α-guaiene **1** was consumed within 48 h. By contrast, the α-bulnesene **5** reacted

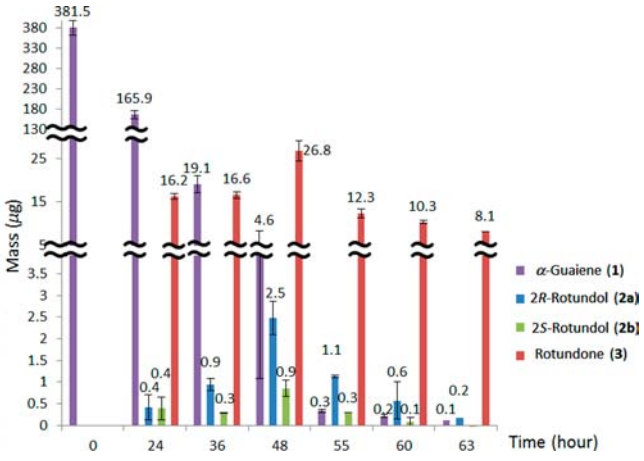

Figure 4. Formation of products from the aerial oxidation of α-guaiene (**1**).

more slowly with 80% remaining after this period. Only a very small quantity of α-bulnesene **5** (ca. 2 μg) was lost over the first 24 h, suggesting that evaporation was not significant under these conditions and indicating that the loss of α-guaiene **1** was due to facile chemical reactions rather than evaporation, based on their similar physical properties. The accelerated degradation of **1** and **5** after the first 24 h can be ascribed to a buildup of reactive radical species following initiation of the autoxidation reactions.

Previously,[3,5] we showed that aerial oxidation of α-guaiene, either in solution or when adsorbed onto filter paper, produced a complex array of products, observable by GC-MS, that could be isolated by column chromatography on deacidified silica or by multi-layer coil counter-current chromatography and identified by spectroscopic methods and X-ray crystallography. These included rotundone **3** (as a major product), the rotundols **2a**/**2b**, and the hydroperoxide **4b**. This last compound decomposed to **3** and **2b** on GC. Therefore, while **3** and **2a**/**2b** are undoubtably genuine autoxidation products of α-guaiene, the peaks observed in the GC could be augmented by decomposition products of hydroperoxides present in the reaction mixture during analysis. Thus, the concentration values for **3**, **2a**/**2b**, **7**, and **6a**/**6b** shown in Figures 4 and 5 could be greater than actually present in the reaction mixtures.

The amount of rotundone measured by GC-MS reached a peak of 26.8 μg (6.6% yield) at the 48 h time point, but this then decreased to 8.1 μg (2% yield) as the reaction progressed further. These figures accord with a previous yield of rotundone (5%) isolated by column chromatography after the reaction was conducted in a similar way but on gram scale and at higher temperature.[5] We had earlier monitored the effect of temperature on the progress of α-guaiene autoxidation by comparing the ratio of α-guaiene:rotundone, showing that this ratio increased faster at higher temperature.[3] The data in Figure 4 indicates that this ratio was due to a rapid degradation of α-guaiene rather than a continuing formation of rotundone. The possibility of rotundone being further oxidized in the reaction mixture was supported by the isolation of oxidized forms of rotundone during the earlier study. In pure form, rotundone **3** is relatively stable to air with only 26% being lost after contact with pure oxygen over 46 days. This suggests that the formation of oxidized forms of **3** will only take place over a short time period when in the presence of a pool of reactive oxygen species or other radical intermediates generated from more reactive substrates such as α-guaiene.

The generation of the products **6a**/**6b** and **7** from autoxidation of α-bulnesene **5** was significantly slower than **2a**/**2b** and **3** from α-guaiene, with the measured amount of the former products reaching a maximum after 108 h. The overall pattern of autoxidation of **5** resembles that of **1** but at a lower overall reaction rate. Interestingly, the formation of the rotund-2-ols (**2a**/**b**) and bulnes-2-ols (**6a**/**b**) over time displayed discrepant stereochemical preferences with the formation of the rotund-2-ols favoring the β-orientation (**2a**) over α-(**2b**) and the bulnes-2-ols favoring the formation of the opposite α-orientation (**6b**) over β-(**6a**).The formation ratio of **2a** vs **2b** was ca. 1:1 in 24 h, increased to ca. 3:1 at 36 h through 48 h, and further rose to ca. 4:1 and 6:1 at 55 and 60 h, respectively, whereas that of **6a** vs **6b** stayed at approximately 1:3. Consequently, it appears that the 2*S*-rotundol **2b** undergoes further oxidation into rotundone **3** in a much more facile fashion when compared to its 2*R*-counterpart **2a** under the specific oxidative conditions outlined herein.

This study has demonstrated that, in a similar fashion to the formation of rotundone (**3**) from α-guaiene (**1**), α-bulnesene (**5**) will generate the aroma compounds 2*R*/2*S*-bulnesol (**6a**

DOI: 10.1021/jf505537s
J. Agric. Food Chem. 2015, 63, 1932−1938

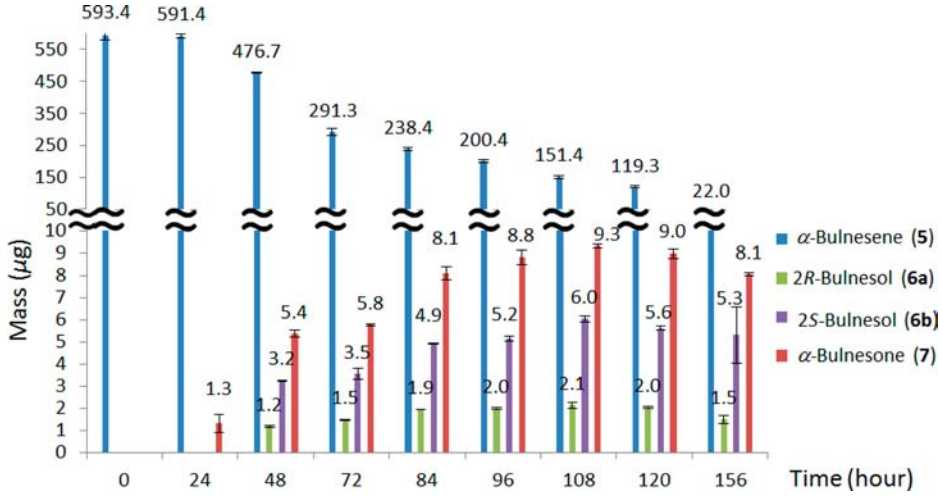

Figure 5. Formation of products from the aerial oxidation of α-bulnesene (**5**).

and **6b**) under simple aerial oxidation condition but that the latter process is much slower than the former. Furthermore, it was found that the formation of 2*R*/2*S*-rotundols (**2a** and **2b**) and 2*R*/2*S*-bulnesols (**6a** and **6b**) displayed stereochemical preferences, which is undoubtedly related to (a) the initial stereochemical preference for formation of the C2-hydroperoxide intermediates from the C2 requisite free radicals followed by decomposition into the observed C2-alcohols with retention of stereochemistry[5] and (b) the unequal consumption of these C2-alcohols by downstream oxidative processes. This study also provides further evidence on how various oxygenated sesquiterpenes may be formed from their precursor hydrocarbons under simple aerial oxidative conditions, shows that for some substrates such transformations can be rapid, even under ambient conditions, and may have implications on the storage and processing of herbs and spices originating from plant materials that contain these sesquiterpene hydrocarbons. Finally, the deuterium-labeled analogues prepared herein may be used to develop more sensitive quantitative analysis methods for the analysis of more complex plant-based matrices.

■ ASSOCIATED CONTENT

Supporting Information

Mass spectra of deuterium-labeled internal standards **9**, **10**, **11a/b**, and **14**−**16**; calibration curves for quantitative analysis of analytes **1**, **2**, **3a/b**, **5**, **6a/b**, and **7**. This material is available free of charge via the Internet at http://pubs.acs.org.

■ AUTHOR INFORMATION

Corresponding Author

*Phone: +61-8-8313-7239. Fax: +61-8-8313-4711. E-mail: dennis.taylor@adelaide.edu.au.

Funding

This project was supported by the School of Agriculture, Food and Wine, The University of Adelaide, as well as by Australia's grape growers and winemakers through their investment body, the Australian Grape and Wine Authority (AGWA), formally known as the Grape and Wine Research and Development Corporation (GWRDC), with matching funds from the Australian Government. A.C.H is indebted to the University of Adelaide and the China Scholarship Council for a joint Ph.D. scholarship.

Notes

The authors declare no competing financial interest.

■ ABBREVIATIONS AND NOMENCLATURE

TBHP, *tert*-butyl hydroperoxide; SNIS, silver nitrite impregnated silica; SCC, silica column chromatography; LOQ, limit of quantitation; LOD, limit of detection

■ REFERENCES

(1) Ansari, H.; Curtis, A. Sesquiterpenes in the perfumery industry. *J. Soc. Cosmet. Chem.* **1974**, *25*, 203−231.

(2) Wood, C.; Siebert, T.; Parker, M.; Capone, D.; Elsey, G.; Pollnitz, A.; Eggers, M.; Meier, M.; Vössing, T.; Widder, S. From wine to pepper: rotundone, an obscure sesquiterpene, is a potent spicy aroma compound. *J. Agric. Food Chem.* **2008**, *56* (10), 3738−3744.

(3) Huang, A.-C.; Burrett, S.; Sefton, M.; Taylor, D. Production of the Pepper Aroma Compound, (−)-Rotundone, by Aerial Oxidation of α-Guaiene. *J. Agric. Food Chem.* **2014**, *62* (44), 10809−10815.

(4) Schilling, B.; Granier, T.; Locher, E. Preparation of 1-hydroxyoctahydroazulenes as fragrances. WO2012001018A1, 2012.

(5) Huang, A.-C.; Sefton, M.; Sumby, C.; Tiekink, E. T. R.; Taylor, D. Mechanistic Studies on the Autoxidation of a-Guaiene: The Structural Diversity of the Sesquiterpenoid Downstream Products. *J. Nat. Prod.* **2014**, DOI: 10.1021/np500819f.

(6) Kumeta, Y.; Ito, M. Characterization of δ-guaiene synthases from cultured cells of Aquilaria, responsible for the formation of the sesquiterpenes in agarwood. *Plant Physiol.* **2010**, *154* (4), 1998−2007.

(7) Kapadia, V. H.; Naik, V. G.; Wadia, M. S.; Dev, S. Sesquiterpenoids from the essential oil of cyperus rotundus. *Tetrahedron Lett.* **1967**, *8* (47), 4661−4667.

(8) Liu, X. C.; Zhou, L.; Liu, Z. L., Identification of Insecticidal Constituents from the Essential Oil of Valeriana jatamansi Jones against Liposcelis bostrychophila Badonnel. *J. Chem.* **2013**, *2013*.

(9) Prakash, O.; Joshi, S.; Shukla, A. K.; Pant, A. K. Sesquiterpenoid Rich Essential Oil from the Leaves of Pogostemon patchouli Pellet Grown Organically Under Tarai Conditions. *J. Essent. Oil Bear. Plants* **2007**, *10* (2), 157−161.

(10) Winck, C. R.; Cardoso, C. A.; Jeller, A. H.; Ré-Poppi, N.; Coelho, R. M.; Schleder, E. J. D. Identification of the volatile compounds of leaf oil of Anacardium humile (Anacardiaceae). *J. Essent. Oil Res.* **2010**, *22* (1), 11−12.

(11) Verma, R. S.; Verma, R. K.; Padalia, R. C.; Chauhan, A.; Singh, A.; Singh, H. P. Chemical Diversity in the Essential Oil of Indian Valerian (Valeriana jatamansiJones). *Chem. Biodiversity* **2011**, *8* (10), 1921−1929.

(12) Armarego, W. L. F.; Chai, C. L. L. *Purification of Laboratory Chemicals*, 5th ed.; Elsevier Inc.: New York, 2003.

DOI: 10.1021/jf505537s
J. Agric. Food Chem. 2015, 63, 1932−1938

(13) Gupta, A. S.; Dev, S. Chromatography of organic compounds. I. Thin-layer chromatography of olefins. *J. Chromatogr.* **1963**, *12* (2), 189−95.
(14) Siebert, T.; Wood, C.; Elsey, G.; Pollnitz, A. Determination of rotundone, the pepper aroma impact compound, in grapes and wine. *J. Agric. Food Chem.* **2008**, *56* (10), 3745−3748.
(15) Huang, A.-C.; Sumby, C.; Tiekink, E. R. T.; Taylor, D. Synthesis of Guaia-4(5)-en-11-ol, Guaia-5(6)-en-11-ol, Aciphyllene, 1-epi-Melicodenone C and E and other Guaiane-type Sesquiterpenoids via the Diastereoselective Epoxidation of Guaiol. *J. Nat. Prod.* **2014**, *77* (11), 2522−2536.
(16) Faraldos, J. A.; Wu, S.; Chappell, J.; Coates, R. M. doubly deuterium-labeled patchouli alcohol from cyclization of singly labeled [2-$^2H_1$] farnesyl diphosphate catalyzed by recombinant patchoulol synthase. *J. Am. Chem. Soc.* **2010**, *132*, 2998−3008.
(17) Ishihara, M.; Tsuneya, T.; Shiga, M.; Uneyama, K. Three sesquiterpenes from agarwood. *Phytochemistry* **1991**, *30* (2), 563−6.
(18) Batt, F.; Bourcet, E.; Kassab, Y.; Fache, F. Selective aerobic oxidation of allylic alcohols to carbonyl compounds using catalytic $Pd(OAc)_2$. High intramolecular selectivity. *Synlett* **2007**, 1869−1872.
(19) Ishihara, M.; Masatsugu, Y.; Uneyama, K. Preparation of (−)-guaia-1(10),11-dien-15,2-olide and (−)-2α-hydroxyguaia-1(10),11-dien-15-oic acid, fragrant sesquiterpenes in agarwood (Aquilaria agallocha Roxb.). *Tetrahedron* **1992**, *48* (47), 10265−10276.

DOI: 10.1021/jf505537s
J. Agric. Food Chem. 2015, 63, 1932−1938

durian wines; and (3) to establish the relationship between samples, sensory attributes, and aroma compounds using multivariate analysis of PLSR. A better understanding of these points will be helpful for improving the characteristic aroma of durian wine by adjusting fermentation parameters or compensating for typical aroma compounds after alcoholic fermentation.

MATERIALS AND METHODS

Yeast Strains. Five different commercial yeast (*Saccharomyces cerevisiae*) strains were used in this research. Strains GRE (Y1), Lalvin RC212 (Y3), and Lalvin D254 (Y4) were supplied by Lallemand (France). The result showed that strain GRE was capable of producing high amounts of volatile esters, whereas strains RC212 and D254 showed excellent capability in the production of alcohol compounds.[9] Two strains were isolated from Sichuan province, China, named CGMCC2.23 (Y2) and CGMCC2.4 (Y5), and preserved in the Northeast Institute of Science.

Chemicals. Acetaldehyde, methanethiol, ethanethiol, dimethyl sulfide, 1-propanol, 2,3-butanedione, propane-1-thiol, ethyl acetate, 2-butenal, acetic acid, 1-butanol, 2-pentanone, dimethyl disulfide, methyl propanoate, (*Z*)-2-but-2-ene-1-thiol, methyl butanoate, 3-methylbutanol, 2-methylbutanol, 2-octanol (internal standard), 2-methyl-2-butenal, ethyl 2-methylpropanoate, butanoic acid, 2,3-butanediol, ethyl butanoate, propyl propanoate, butyl acetate, 3-methylbut-2-ene-1-thiol, 2-methyl-2-pentenal, methyl ethyl disulfide, ethyl 2-butenoate, ethyl thiolacetate, ethyl 2-methylbutanoate, ethyl 3-methylbutanoate, diethyl disulfide, propyl 2-methylbutanoate, 3-methylbutyl propanoate, 3-methylthio-1-propanol, ethyl hexanoate, propyl 2-methyl-2-butenoic acid, ethyl 2-hexenoate, propyl hexanoate, ethyl heptanoate, dipropyl disulfide, ethyl 2-methylhexanoate, methyl octanoate, 3,5-dimethyl-1,2,4-trithiolane, diethyl trisulfide, and ethyl octanoate were purchased from Sigma-Aldrich (St. Louis, MO, USA). All of them were analytical reagents.

Durian Musts. Fresh durian fruits (*Durio zibethinus* L.) cultivar 'Monthong' originating in Malaysia were purchased from Wal-Mart Stores in Shanghai. Only fully ripened fruits without any split on the husk were selected for the study. Five kilograms of durian fruits was washed in clean water to remove plant residue. Next, the pulp was extracted manually by mechanical pressure. Seeds and pulp residue were separated from the juice by centrifugation (RCF = 11000, 12 min, 18 °C).

Then, the musts were pasteurized for 30 min at 65 °C, cooled, and poured into 10 L bottles. The initial values of musts were as follows: total sugars, 163 g/L; pH, 6.3. The fruit musts were mixed with a sucrose solution to adjust the total sugars to 210 g/L. The pH was adjusted to 3.5 with 1 mol/L DL-malic acid. Sulfur dioxide, in the form of potassium pyrosulfite, was added into the musts to maintain the concentration of 50 mg/L free SO_2 to inhibit bacterial growth. All experiments were carried out in triplicate.

Durian Wine Production. The fermentation temperature for durian wine production was approximately 20 °C, and no stirring was performed during any stage of the fermentation. Yeast strains were grown in YPG medium (1% yeast extracts, 2% peptone, and 2% glucose). With a platinum loop, yeasts were inoculated into tubes containing 200 mL of YPG broth at 20 °C until the cell density reached approximately 10^7 cells/mL. The cells were counted, and an equal amount of cells per strain was resuspended in the same medium for the fermentation. Each vat was then inoculated with 10 mL of prepared suspension to obtain the final cell density of 10^6 cells/mL. Four liters of durian musts was utilized for durian wine production. All vinifications were carried out in a 10 L bioreactor at 20 °C. Fermentation was monitored through measuring viable cells and total reducing sugars. The fermentation was considered to be ended when the sugar content was below 1 g/L. After fermentation, fermented durian musts were transferred to the 10 L bottles and stored at 5 °C for biomass sedimentation. After 24 h, the durian wines were transferred to new bottles without aeration. After 10 days, wines were then filtered with cellulose filters and stored at 5 °C in sealed glass bottles to avoid oxygen entrance.

Standard Chemical Analysis. The official methods of the Office Internationale de Vigne et Vin (OIV)[10] were employed for the conventional determinations, such as pH, ethanol content, total acidity, free SO_2, and total reducing sugar. To analyze glycerol, the Boehringer-Mannheim (Germany) test kit was used. Yeast growth was followed spectrophotometrically (Shimadzu, Kyoto, Japan) by absorbance at 600 nm. Viable cells were determined by plating and counting of colonies on YPG agar.

SBSE Adsorption of Aroma Compounds. Each wine sample (5 mL) was placed in a 20 mL vial, in which 20 μL of internal standard solution (2-octanol, 50 mg/L in the ethanolic solution) was added. A stir bar (Twister) coated with polydimethylsiloxane (PDMS) phase (1 cm length, 0.5 mm thickness, Gerstel Inc., Baltimore, MD, USA) was used to extract the aroma compounds from the sample. The Twister bar was constantly stirred for 50 min at a speed of 600 rpm and 40 °C for extraction temperature. After sampling, the Twister bar was rinsed with distilled water, dried with a Kimwipe tissue paper, and placed into the sample holder of the thermal desorption unit (TDU) (Gerstel, Inc.).

The analyses were performed using a TDU sampler (Gerstel, Inc.) mounted on an Agilent GC-MS system (7890-5975, Agilent Technologies, Santa Clara, CA, USA). The analytes were thermally desorbed at the TDU in splitless mode, ramping from 45 to 240 °C at a rate of 5 °C/min, and held at the final temperature for 5 min. The desorbed analytes were cryofocused (−80 °C) in a programmed temperature vaporizing (PTV) injector (CIS 4, Gerstel, Inc.) with liquid nitrogen. After desorption, the PTV was heated from −80 to 240 °C at a rate of 10 °C/s and held at 240 °C for 5 min. The solvent vent injection mode was employed.

GC-MS Identification of Aroma Compounds. The analyses were performed using a Hewlett-Packard 7890 GC with a 5975 mass selective detector (MSD) (Agilent Technologies) instrument operating under electron ionization (EI) mode (70 eV, ion source temperature 230 °C) with the quadrupole in a scanning mode (scan range was m/z 30−450 at a scan rate of 1 scan/s). Separation of compounds was achieved on Innowax-Wax (60 m × 0.25 mm i.d. × 0.25 μm film thickness, Agilent Technologies) and DB-5 (60 m × 0.25 mm i.d. × 0.25 μm film thickness, Agilent Technologies). Helium (purity = 99.999%) was used as a carrier with a constant flow velocity of 1 mL/min. The quadrupole mass filter was at 150 °C. The transfer line temperature was operated at 250 °C. The oven temperature was held at 35 °C for 3 min, then ramped to 60 °C at the rate of 2 °C/min, and ramped at the rate of 6 °C/min to 240 °C for the last 5 min. The volatile compounds were identified by comparing retention indices and retention times with those obtained for authentic standards, or those of literature data, or with mass spectra in the Wiley and NIST11 libraries. The RIs were determined via sample injection with a homologous series of alkanes (C5−C30) (Sigma-Aldrich, St. Louis, MO, USA).

GC-MS Quantitation of Aroma Compounds. To obtain a matrix similar to that of durian wine, model wine was prepared containing 15.0 g/L malic acid, 0.5 g/L lactic acid, 2.0 g/L citric acid, 10.0 g/L fructose, 8.0 g/L glucose, and 12% of ethanol in Milli-Q deionized water. The pH was adjusted to 4.0. Quantitation of the major aroma compounds was carried out by standard curves obtained by each compound from six different concentrations in ethanol. The levels of the aroma compounds were normalized by 2-octanol equivalents. The ethanolic solution of internal standard 2-octanol (20 μL of 50 mg/L) was introduced to the 5 mL of model wine in a 20 mL vial and then extracted by SBSE, as was performed for the durian wines.

The standard curves were shown in the research, where y represented the peak area ratio (peak area of volatile standard/peak area of internal standard) and x represented the concentration ratio (concentration of volatile standard/concentration of internal standard). The calibration curves were obtained from Chemstation software (Agilent Technologies Inc.) and used for calculation of volatiles in juices and durian wines.

DOI: 10.1021/jf505666y
J. Agric. Food Chem. 2015, 63, 1939−1947

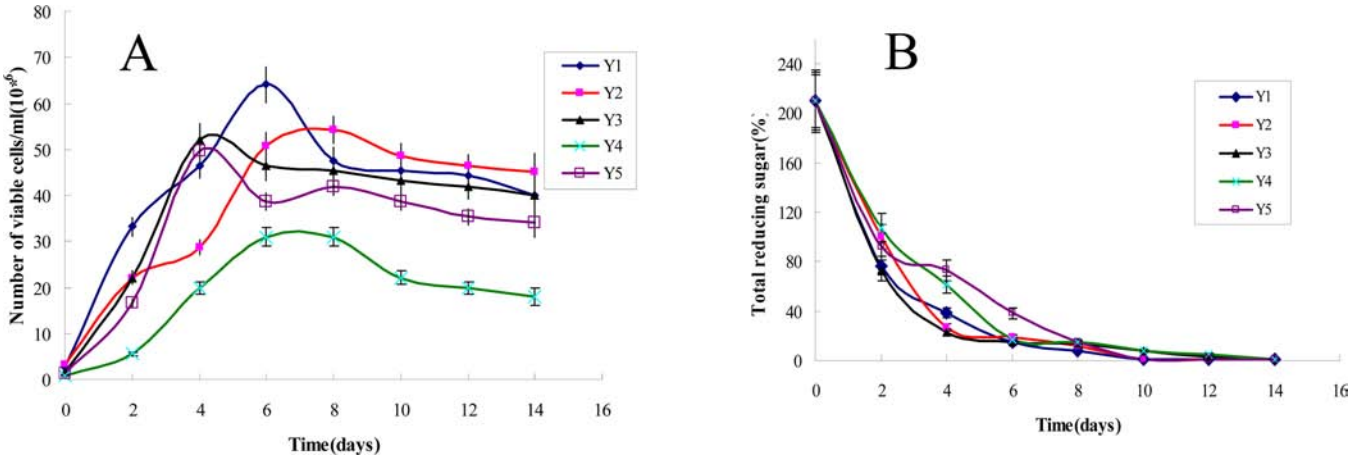

Figure 1. Evolution of yeasts (A) (as viable cell counts) and total reducing sugar (B) in durian wine during fermentation.

Table 1. Means (n = 3) of General Parameters of Wines Fermented by Five Different Yeast Strains[a]

	Y1	Y2	Y3	Y4	Y5
pH	3.95 ± 0.01ab	4.08 ± 0.01a	3.87 ± 0.02b	4.01 ± 0.01ab	3.89 ± 0.01b
ethanol content (% vol)	11.2 ± 0.1a	11.3 ± 0.2a	11.4 ± 0.1a	11.5 ± 0.2a	11.6 ± 0.1a
total acidity (g/L)	6.2 ± 0.1a	5.9 ± 0.2ab	5.4 ± 0.2b	5.7 ± 0.1ab	5.8 ± 0.1ab
free SO_2 (mg/L)	14.2 ± 0.3b	17.5 ± 0.2b	13.8 ± 0.4b	17.3 ± 0.3a	17.8 ± 0.2a
glycerol (g/L)	1.4 ± 0.1b	1.5 ± 0.2a	1.6 ± 0.2a	1.3 ± 0.1c	1.1 ± 0.3d
reducing sugar (g/L)	0.64 ± 0.04c	0.76 ± 0.08b	0.81 ± 0.11ab	0.91 ± 0.12a	0.82 ± 0.09ab

[a]Values with different letters (a–d) in the same row are significantly different according to the Duncan test ($p < 0.05$).

Gas Chromatography–PFPD. A HP-5890 series II GC from Agilent equipped with a 5380 PFPD detector from OI Analytical (College Station, TX, USA) was used in the sulfur mode. Separation of compounds was achieved on Innowax-Wax (60 m × 0.25 mm i.d. × 0.25 μm film thickness, Agilent Technologies) and DB-5 (60 m × 0.25 mm i.d. × 0.25 μm film thickness, Agilent Technologies) columns. The oven temperature was held at 35 °C for 3 min, then ramped to 60 °C at the rate of 2 °C/min, and ramped at the rate of 6 °C/min to 240 °C for the last 5 min. GC was operated in a constant flow mode (1 mL/min) with helium as the carrier gas. The PFPD detector was set at 250 °C, and the PMT voltage was set at 500 V. The sulfur-containing compounds were confirmed by comparison with authentic standards on both columns and RI value matching. The quantitation method was identical to the GC-MS analysis as described in the above section. The samples were run in triplicate.

Sensory Analysis. A quantitative descriptive sensory analysis was applied for evaluating five fruit wine samples using a 18 cm line scale by a well-trained panel consisting of 20 members (10 females and 10 males, ages 20–30 years). Before the quantitative descriptive analysis, 30 mL of fruit wine was put in a 100 mL volume white china cup covered with a plastic Petri dish and was served to a panelist in a laboratory at a room temperature (25 °C). Twenty judges had discussed aroma compositions of samples through three preliminary sessions (each needs 3 h), until everyone agreed to use them as the attributes. Then, the quantitative descriptive analysis was executed using five sensory attributes ("fruity", "sulfur", "sweety", "off-flavor", and "harmony") for all five samples that were randomly divided into two sessions. In every session, samples were randomly presented for every member to avert causing a so-called order effect. All of the samples were evaluated in triplicate.

Odor Activity Values (OAV). The contribution of each odor to the overall fruit wine aroma was evaluated by the OAV, which was measured as the ratio of the concentration of each compound to its detection threshold. The threshold values were taken from information available in the references (shown in Table 3).

Statistical Analysis. The chemical data and quantitative descriptive sensory analysis were submitted to variance analysis (ANOVA). Duncan's multiple-comparison tests were applied to determine significant differences between the samples and sensory attributes. All of the analyses was carried out employing XLSTAT ver. 7.5 (Addinsoft, New York, NY, USA).

Partial least-squares regression (PLSR) was employed to explore the correlations between samples, aroma compounds, and sensory attributes using Unscrambler version 9.7 (CAMO ASA, Oslo, Norway). All variables were centered and standardized (1/SD) so as to make each variable have a unit variance and zero mean before applying PLS analyses to finally obtain the unbiased contribution of each variable to the criterion. All PLSR models were validated using full cross-validation.

RESULTS AND DISCUSSION

Microvinifications. The five *S. cerevisiae* (Y1, Y2, Y3, Y4, and Y5) commercial fruit wine yeast strains showed growth indication when incubated at 20 °C (Figure 1). Fermentation parameters were calculated for these strains. Among the five strains, the growth rate of strain Y1 was higher than that of the other strains, and the cell density reached 6.4 × 10^7 cells/mL on day 6 of growth (Figure 1A). Then the viability decreased, and viability loss was measured at 25.8% after day 8 in culture Y1. Strains Y3 and Y5 presented a cell density increase in the first 4 days of incubation and reached their maximum cell densities of 5.1 × 10^7 and 4.9 × 10^7 cells/mL,respectively;thereafter, the cell densities remained almost constant at 1 × 10^7 cells/mL. Strain Y4 had a 2 day adaptation period (lag phase) and then started to grow at a slower rate than the other strains. Although strain Y4 showed delayed growth, it remained a strain with a rapid growth rate overall.

The sugar values in five *S. cerevisiae* strains displayed similar patterns of rapid initial reduction (Figure 1B). Strains Y1, Y2, and Y5 showed a gradual reduction in sugar value over the 10 day fermentation period and reached a stable sugar level around 1.1–1.2 g/L, indicating that almost all of the sugars were consumed and that the fermentation process was considered to

DOI: 10.1021/jf505666y
J. Agric. Food Chem. 2015, 63, 1939–1947

Table 2. Average Values (Mean ± Standard Deviation) (Milligrams per Liter) and Identification of Volatile Compounds Detected in Durian Juices and Wines Fermented by Five Different Yeast Strains

		RI[a]			juices		Y1		Y2		Y3		Y4		Y5	
code[b]	compound	DB-5	Innowax	identification[c]	av[d]	SD[e]	av	SD	av	SD	av	SD	av	SD	av	SD
1	acetaldehyde	<500	714	MS, RI, Sta	2.700	0.351	24.250	1.455	17.891	1.073	19.126	2.525	13.199	1.184	7.681	0.538
2	methanethiol	500	700	PFPD, RI, Sta	0.006	0.001	nd[f]		nd		nd		nd		nd	
3	ethanethiol	508	722	PFPD, RI, Sta	0.003	0.000	nd		nd		nd		nd		nd	
4	dimethyl sulfide	521	716	PFPD, RI, Sta	1.688	0.101	0.261	0.029	0.822	0.090	0.705	0.048	0.411	0.046	0.599	0.055
5	1-propanol	540	1045	MS, RI, Sta	81.019	5.671	49.122	4.519	33.290	3.063	33.233	3.549	22.559	2.407	49.039	5.885
6	2,3-butanedione	602	970	MS, RI, Sta	1.502	0.180	1.149	0.138	0.914	0.110	0.867	0.090	0.473	0.041	0.677	0.088
7	propane-1-thiol	607	861	PFPD, RI, Sta	0.003	0.000	nd		nd		nd		nd		nd	
8	ethyl acetate	608	907	MS, RI, Sta	14.212	1.307	39.626	3.447	13.264	1.154	23.603	2.672	12.640	1.990	10.726	1.051
9	2-butenal	632	1047	MS, RI, Sta	nd		0.032	0.003	0.017	0.002	nd		nd		nd	
10	acetic acid	642	1451	MS, RI, Sta	2.396	0.312	0.477	0.042	0.211	0.018	0.265	0.028	0.186	0.018	0.211	0.019
11	1-butanol	680	1160	MS, RI, Sta	nd		nd		nd		0.020	0.002	0.021	0.002	0.020	0.002
12	2-pentanone	688	983	MS, RI, Sta	5.501	0.539	8.686	0.715	6.299	0.518	5.545	0.479	3.816	0.377	3.566	0.225
13	dimethyl disulfide	710	1071	PFPD, RI, Sta	1.551	0.135	0.337	0.021	1.323	0.083	1.103	0.104	0.387	0.034	0.644	0.072
14	methyl propanoate	721	920	MS, RI, Sta	13.902	1.283	110.439	12.369	79.579	8.913	53.122	4.678	78.388	4.642	12.621	1.300
15	(*Z*)-2-but-2-ene-1-thiol	722	965	PFPD, RI, Sta	0.033	0.003	nd		nd		nd		nd		nd	
16	methyl butanoate	728	1036	MS, RI, Sta	0.371	0.023	1.747	0.140	1.768	0.141	0.879	0.093	0.637	0.058	0.154	0.011
17	3-methylbutanol	746	1252	MS, RI, Sta	30.734	3.442	1.628	0.121	15.612	1.160	4.862	0.481	10.598	0.704	2.445	0.204
18	2-methylbutanol	749	1210	MS, RI, Sta	7.597	0.782	2.035	0.170	4.632	0.386	4.231	0.301	5.872	0.388	4.431	0.369
19	2-methyl-2-butenal	756	1102	MS, RI, Sta	10.584	0.847	6.795	0.565	nd		6.879	0.424	nd		14.952	1.256
20	ethyl 2-methylpropanoate	762	955	MS, RI, Sta	0.873	0.065	2.510	0.301	1.158	0.101	3.697	0.274	1.697	0.102	2.116	0.285
21	butanoic acid	784	1619	MS, RI, Sta	2.147	0.179	0.167	0.013	0.161	0.016	0.197	0.015	0.190	0.013	0.390	0.042
22	2,3-butanediol	800	1581	MS, RI, Sta	42.078	3.501	23.513	1.411	15.448	1.347	15.961	2.107	34.602	4.152	3.254	0.266
23	ethyl butanoate	807	1042	MS, RI, Sta	7.452	0.596	30.764	2.153	12.188	1.125	17.060	1.759	9.834	1.082	4.888	0.551
24	propyl propanoate	812	1160	MS, RI, Sta	nd		10.003	1.200	7.582	0.624	8.190	0.953	2.309	0.212	2.286	0.288
25	butyl acetate	817	1075	MS, RI, Sta	4.754	0.333	19.400	2.134	20.725	1.306	20.066	2.322	9.257	1.111	22.037	1.808
26	3-methylbut-2-ene-1-thiol	819	1096	PFPD, RI, Sta	0.008	0.001	0.002	0.000	0.001	0.000	0.002	0.000	0.001	0.000	nd	
27	2-methyl-2-pentenal	830	1108	MS, RI, Sta	1.552	0.171	6.857	0.823	1.811	0.186	nd		nd		1.329	0.140
28	methyl ethyl disulfide	838	1120	PFPD, RI, Sta	2.856	0.263	1.996	0.260	12.241	0.979	8.877	0.730	4.156	0.407	6.800	0.603
29	ethyl 2-butenoate	846	1245	MS, RI, Sta	nd		nd		8.947	0.665	nd		13.721	1.197	3.395	0.277
30	ethyl thiolacetate	846	1086	PFPD, RI, Sta	0.023	0.003	0.003	0.000	0.006	0.000	0.004	0.000	0.003	0.000	0.003	0.000
31	ethyl 2-methylbutanoate	856	1118	MS, RI, Sta	2.921	0.254	34.361	2.996	18.549	1.543	21.967	1.329	14.573	1.199	9.234	1.107
32	ethyl 3-methylbutanoate	929	1115	MS, RI, Sta	0.383	0.037	9.805	0.905	nd		4.498	0.499	nd		7.065	0.779
33	diethyl disulfide	942	1195	PFPD, RI, Sta	0.457	0.040	0.060	0.005	0.300	0.036	0.237	0.025	0.080	0.009	0.179	0.013
34	propyl 2-methylbutanoate	947	1164	MS, RI, Sta	nd		nd		39.265	4.319	nd		12.032	1.239	nd	
35	3-methylbutyl propanoate	954	1165	MS, RI, Sta	nd		2.667	0.299	1.609	0.148	2.103	0.167	1.598	0.128	1.355	0.101
36	3-methylthio-1-propanol	989	1723	PFPD, RI, Sta	0.032	0.002	0.061	0.006	0.068	0.008	0.071	0.006	0.040	0.003	0.030	0.002
37	ethyl hexanoate	1001	1182	MS, RI, Sta	3.765	0.422	49.802	3.984	30.363	3.947	45.501	3.634	15.225	1.270	10.179	1.323
38	propyl 2-methyl-2-butenoic acid	1046	1194	MS, RI, Sta	nd		4.518	0.336	2.228	0.194	6.655	0.579	0.667	0.056	1.512	0.132
39	ethyl 2-hexenoate	1067	1343	MS, RI, Sta	0.305	0.024	10.110	0.843	3.837	0.376	7.976	0.782	0.812	0.109	4.863	0.477
40	propyl hexanoate	1078	1445	MS, RI, Sta	nd		6.804	0.566	7.038	0.614	2.757	0.240	3.355	0.358	5.551	0.484
41	ethyl heptanoate	1102	1329	MS, RI, Sta	1.355	0.113	6.237	0.748	9.203	0.849	4.523	0.417	2.366	0.194	6.632	0.612

J. Agric. Food Chem. 2015, 63, 1939−1947

DOI: 10.1021/jf505666y

Table 2. continued

code[b]	compound	RI[a]		identification[c]	juices		Y1		Y2		Y3		Y4		Y5	
		DB-5	Innowax		av[d]	SD[e]	av	SD	av	SD	av	SD	av	SD	av	SD
42	dipropyl disulfide	1112	1787	PFPD, RI, Sta	0.009	0.001	0.004	0.000	0.005	0.000	nd		0.006	0.001	nd	
43	ethyl 2-methylhexanoate	1114	1367	MS, RI, Sta	nd		2.884	0.251	2.091	0.132	nd		0.865	0.109	2.117	0.133
44	methyl octanoate	1120	1401	MS, RI, Sta	0.002	0.000	nd		0.628	0.070	0.656	0.074	1.419	0.116	0.495	0.055
45	3,5-dimethyl-1,2,4-trithiolane	1133	1640	PFPD, RI, Sta	0.040	0.004	0.470	0.041	1.643	0.169	1.456	0.150	0.940	0.102	1.315	0.135
46	diethyl trisulfide	1136	1515	PFPD, RI, Sta	0.093	0.009	0.041	0.004	0.051	0.004	0.054	0.004	0.027	0.003	0.021	0.002
47	ethyl octanoate	1180	1442	MS, RI, Sta	3.001	0.262	51.497	4.238	37.347	2.775	40.623	3.018	35.052	3.106	15.134	1.124

[a]Retention indices of compounds on DB-5 and Innowax columns. [b]Code for the volatile compounds detected in the juices and fermented wines. [c]Method of identification: MS, mass spectrum comparison using Wiley library; RI, retention index in agreement with literature value; Sta, confirmed by authentic standards. [d]av, average. [e]SD, standard deviation. [f]nd, not detected.

have ended. Both strains Y3 and Y4 showed a similar behavior; that is, a 14 day fermentation period was noted.

Different strains of *S. cerevisiae* showed significantly different growth rates and different abilities in metabolizing sugars as a result of their biochemical mechanisms and metabolic activity during alcoholic fermentation. Furthermore, it had been suggested that differences in the genes of *S. cerevisiae* strains play a central role in explaining the diversity of aroma profiles produced by each different strain.[11] Therefore, the choice of the proper yeast strain could be critical for the development of the desired flavor and aroma of such fruit wines.

Table 1 presents the values of each major parameter (mean ± standard deviation, $n = 3$) of durian wines fermented with the five yeast strains. The statistical analysis demonstrated that the yeast strains showed significant differences in the values of important parameters, such as the values of pH, total acidity, reducing sugar, free SO_2, and glycerol. The alcohol content of the fruit wines varied a little between 11.2 and 11.5% (v/v): the highest content was measured in a fruit wine fermented with strain Y5 and the lowest content in that produced by strain Y1. However, on the basis of Duncan's multiple-comparison tests, the fruit wines fermented with those two strains showed no significant difference in alcohol content. The highest concentration (17.8 mg/L) of free SO_2 was found in the Y5-derived fruit wine, and the lowest concentration (13.8 mg/L) was detected in the Y3-derived fruit wine. As shown in Table 1, the fruit wine fermented with strain Y1 presented the lowest concentration of reducing sugars of 0.64 g/L. The results indicated that strain Y1 possessed the highest capability to ferment reducing sugar.

Strain Y3 was an efficient producer of glycerol (1.6 g/L), which was produced from dihydroxyacetone phosphate in the initial fermentation stage. In this stage, the excessive NADH generated during biomass formation would be converted into NAD^+ by the yeast cells.[12] Besides ethanol and carbon dioxide, glycerol was quantitatively the most important fermentation product, and it was considered to contribute positively to the sensory quality of fruit wine.[12,13]

Identification of Volatile Compounds in Durian Juices and Wines. SBSE with GC-MS and GC-PFPD was applied for the first time in the analysis of the aroma fraction of durian juices and wines. The main parameters that were known to influence the methodology were investigated, such as extraction time, extraction temperature, and sample volume. According to the results obtained (data not shown), optimized SBSE experimental conditions were established, that is, 50 min of extraction time, 40 °C extraction temperature, and a sample volume of 5 mL.

In the present work, 38 and 43 aroma compounds in durian juices and wines were analyzed by GC-MS and GC-PFPD with the aid of SBSE, respectively. The aroma compounds with higher concentration detected in the juice included alcohols (1-propanol, 2,3-butanediol, and 3-methylbutanol), esters (ethyl acetate and methyl propanoate), and sulfur-containing compounds (dimethyl sulfide, dimethyl disulfide, methyl ethyl disulfide, and diethyl disulfide). Compared with the juice, the content of compounds such as ethyl octanoate, ethyl 2-hexenonate, ethyl hexanoate, and ethyl 2-methylbutanoate predominated in durian wines.

Among the aroma compounds present in fruit wine, only a subset was sensorily detectable. Thus, to evaluate the influence of compounds on the formation of aroma characteristics of durian wines, the selection of specific compounds from GC

DOI: 10.1021/jf505666y
J. Agric. Food Chem. 2015, 63, 1939−1947

Table 3. OAVs (>1) for the Main Volatile Compounds in Durian Juices and Wines Fermented by Five Different Yeast Strains

code	compound	Oth (mg/L)	ID[a]	juices	Y1	Y2	Y3	Y4	Y5	descripors
C1	dimethyl sulfide	0.027	18	62.520	9.680	30.440	26.120	15.240	22.200	cooked cabbage, onion, corn
C2	2,3-butanedione	0.1	26	15.018	11.488	9.140	8.665	4.734	6.767	creamy, sweety, caramel, butter scotch
C3	ethyl acetate	5	26	2.842	7.925	2.653	4.721	2.528	2.145	fruity, buttery, orange
C4	dimethyl disulfide	0.03	26	51.705	11.220	44.086	36.759	12.895	21.478	cooked cabbage, onion
C5	methyl propanoate	8.5	27, 28	1.636	12.993	9.362	6.250	9.222	1.485	fruity odor reminiscent of rum
C6	methyl butanoate	0.1	27, 28	3.715	17.466	17.679	8.790	6.371	1.542	apple-like odor
C7	3-methylbutanol	30	27, 28	1.024	0.054	0.520	0.162	0.353	0.082	herbaceous and cacao
C8	ethyl 2-methylpropanoate	0.2	26	4.367	12.549	5.792	18.486	8.484	10.578	strawberry, fruity, sweet
C9	ethyl butanoate	1	26	7.452	30.764	12.188	17.060	9.834	4.888	fruity, papaya, butter, sweetish, apple, perfumed
C10	propyl propanoate	0.23	26		43.490	32.965	35.611	10.038	9.940	complex fruity odor reminiscent of apple banana
C11	methyl ethyl disulfide	0.062	7	46.068	32.198	197.434	143.174	67.029	109.679	cooked cabbage, sulfur,onion
C12	ethyl 2-methylbutanoate	0.2	26	14.603	171.807	92.744	109.837	72.865	46.171	sweet caramel, grape
C13	diethyl disulfide	0.0043	18	106.192	14.011	69.811	55.062	18.682	41.543	sulfury, roasty, cabbage-like odor
C14	3-methylbutyl propanoate	0.23	27, 28		11.598	6.995	9.145	6.946	5.892	pineapple-apricot-like odor
C15	ethyl hexanoate	2.3	26	1.637	21.653	13.201	19.783	6.620	4.426	fruity, green apple
C16	ethyl octanoate	2	27, 28	1.500	25.749	18.673	20.311	17.526	7.567	sulfury, heavy, cocoa odor

[a]Code representing the reference number.

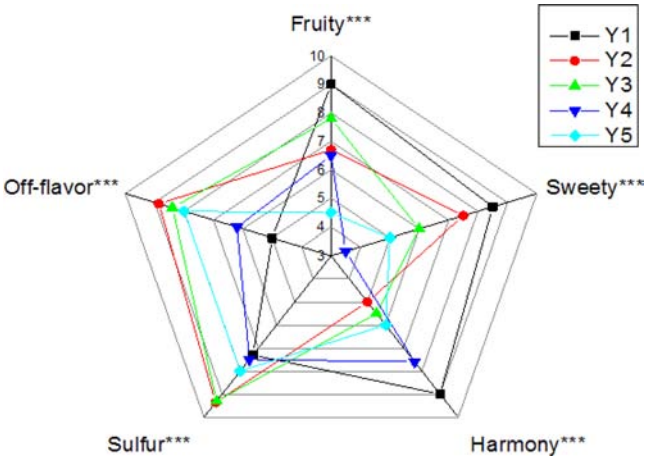

Figure 2. Quantitative descriptive analysis of durian wines produced by five yeast strains of *Saccharomyces cerevisiae*. In sensorial parameters indicated by (***) a difference among some trials is verified for $p < 0.001$.

analysis to represent the attributes in samples might be useful. As reported by previous literature,[14] the low concentrations of several fermentative aroma compounds could not actually reflect the influence on the perceived aroma intensity in samples due to their low detection thresholds. This phenomenon was particularly evident in tropical fruits. Therefore, the OAV was usually used to provide a rough evaluation of the real contribution of each aroma compound to the global aroma.[15] Compounds with OAVs > 1 were commonly at the perception level and considered important aroma compounds contributing to fruit wine aroma.[16]

According to OAVs (Table 3), only 11 and 15 aroma compounds were analyzed with the OAVs > 1 in juice or durian wines: dimethyl sulfide, 2,3-butanedione, ethyl acetate, dimethyl disulfide, ethyl propanoate, methyl butanoate, 3-methylbutanol, ethyl 2-methylpropanoate, ethyl butanoate, propyl propanoate, methyl ethyl disulfide, ethyl 2-methylbutanoate, diethyl disulfide, 3-methylbutyl propanoate, ethyl hexanoate, 3,5-dimethyl-1,2,4-trithiolane, and ethyl octanoate. Among these compounds, 2,3-butanedione, 3-methylbutanol, dimethyl sulfide, dimethyl disulfide, methyl ethyl disulfide, ethyl 2-methylbutanoate, ethyl butanoate, and ethyl octanoate were major contributors to aroma of juices and wines.

3-Methylbutanol, which was responsible for vinous, herbaceous, and cacao aromas, is formed during fermentation by deamination and decarboxylation reactions from isoleucine.[17] Compared to five durian wines, the concentration (30.734 mg/L) of this compound only slightly surpassed the odor threshold (30 mg/L) in durian juice. In other words, this compound decreased with the progress of fermentation. Obviously, the conclusion was in contradiction with other literature.[17] The reason might be that 3-methylbutanol was consumed by the esterification reaction. Correspondingly, the concentration of ethyl 3-methylbutanoate increased during the fermentation process.

Ester compounds were responsible for the fruity aroma in fruit juice and wines; in particular, those compounds were correlated with the freshness and fruitiness of new wines.[13] These compounds in fruit wines were mainly synthesized from their corresponding precursors by enzymatic ethanolysis with the aid of acyl-CoA during yeast fermentation. Their concentrations were influenced by many parameters, such as yeast strain, fermentation temperature, degree of aeration, and sugar content.[18]

On the one hand, propyl propanoate, ethyl 2-butenoate, ethyl 2-methylhexanoate, 3-methylbutyl propanoate, propyl 2-methyl-2-butenoic acid, ethyl 2-methylhexanoate, and propyl hexanote were detected only in the fermented wines. The phenomenon demonstrated that the function of yeasts in the production of aroma was to synthesize yeast-derived aroma compounds during fermentation. On the other hand, as shown

DOI: 10.1021/jf505666y
J. Agric. Food Chem. 2015, 63, 1939−1947

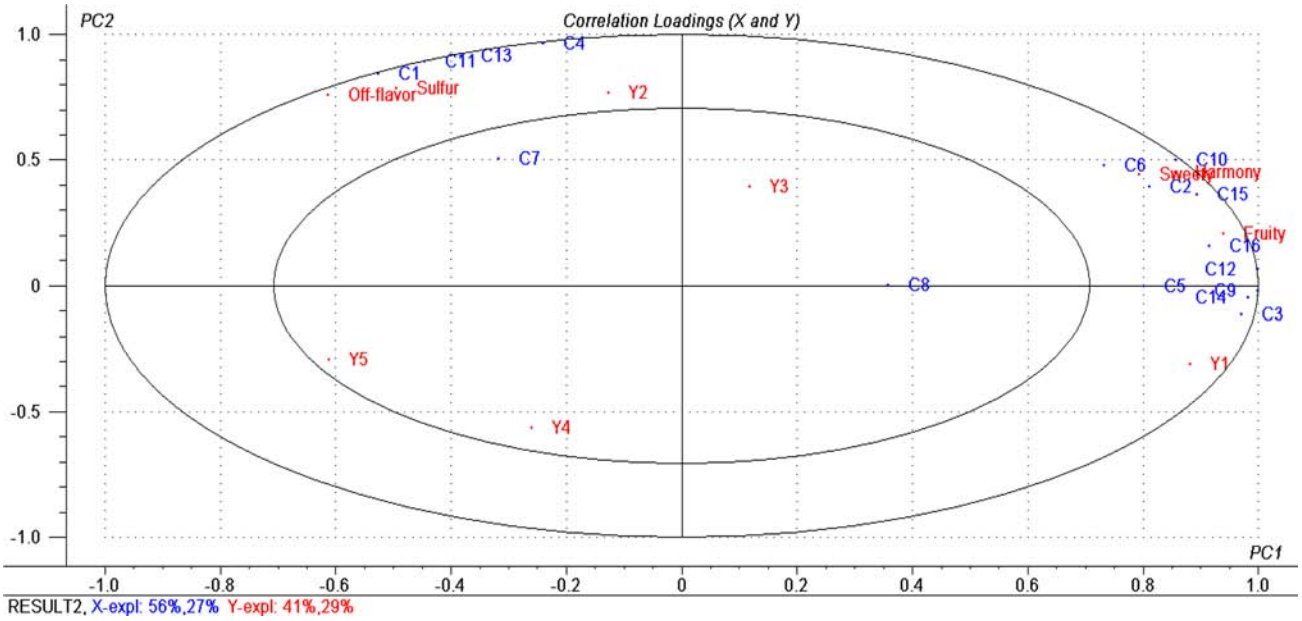

Figure 3. Overview of the variation found in the mean data from partial least-squares regression (PLSR) correlation loading plot for five samples. The model was derived from aroma compounds (OAV > 1) as the *X*-matrix and samples and sensory variables as the *Y*-matrix. The concentric circles represent R^2 = 0.5 and 1.0, respectively.

in Table 3, ethyl 2-methylbutanoate presented the highest value of OAVs, which ranged from 14.603 to 171.807 in juice and five durian wines. As a result, this compound contributed to the juices and wines with banana and pear aroma.[17] Another important ester compound was ethyl octanoate, which was far above its threshold in durian wines, indicating that this compound was a significant contributor to fruity aroma of durian wines. Ethyl octanoate showed its highest OAV (25.749) in Y1-derived durian wine. From the above-mentioned, major aroma compounds such as ethyl 2-methylbutanoate and ethyl octanoate were synthesized during the fermentation process. Moreover, strain Y1 led to durian wines with the highest OAVs of ester compounds, suggesting that Y1 strain possessed a relatively higher ability for ester synthesis.

Five sulfur-containing aroma compounds were identified across the range of durian wines analyzed, including dimethyl sulfide, dimethyl disulfide, methyl ethyl disulfide, diethyl disulfide, and 3,5-dimethyl-1,2,4-trithiolane. Most of those compounds (dimethyl sulfide, dimethyl disulfide, and diethyl disulfide) decreased rapidly with the progress of fermentation. The reduction of sulfur-containing compounds varied with fermentations, where strain Y1 had the slowest reduction followed by strains Y4 and Y5. The result was according with the findings of literature, which showed that most sulfur-containing compounds might be consumed or degraded to other compounds during the fermentation.[19]

Despite the fact that some sulfur aroma compounds were present in only low relative concentrations, as in the case of dimethyl sulfide and diethyl disulfide in this study, these compounds contributed a strong onion-like odor to the fruit wines due to their extremely low thresholds, 0.027 and 0.0043 μg/L, respectively. The sulfur aroma compounds found in this study might serve as character-impact compounds in durian that contributed to its sulfur note.[7,20] Dimethyl sulfide was considered as a beneficial compound in low concentrations. The formation of dimethyl sulfide in juice and wine existed not only from its fruit and fruit wine maturation but also during fermentation, which had also variously been linked to cysteine, cystine, or glutathione metabolism in yeast.[18]

What is worth mentioning was that 3,5-dimethyl-1,2,4-trithiolane seemed to make a significant contribution to the durian wine, but it was likely an artificial compound formed during the desorption process with the method of SBSE.[21−23] Thus, the compound 3,5-dimethyl-1,2,4-trithiolane had been excluded as an aroma-active compound in the juices and wines.

From Table 2, methanethiol, ethanethiol, propanethiol, and (2*Z*)-but-2-ene-1-thiol were present only in juices. Although the concentrations of these compounds were relatively low, the contribution to the aroma of the juice might be great due to the low threshold. The result was consistent with the findings of the literature,[19] which showed that these sulfur-containing compounds presented a significant contribution to durian juice aroma. The reason that these compounds were absent from fermented durian wines might be the result of strong volatilization or utilization by the yeast strains.

Although sulfur compounds were character-impact compounds for durian fruit, these compounds were usually perceived as offensive due to the unpleasant aroma.[7,18] On the one hand, it is well-known that the quality and value of fruit wines was strongly related to the characteristic aroma profile developed during fermentation process, which contributed to the strengthening of its characteristic organoleptic aroma. On the other hand, there is no doubt that the off-flavor compounds should be controlled in the fermentation process. Therefore, the balance between characteristic aroma and off-flavor attribute was the key to durian fermentation.

Sensory Analysis. Sensory analysis was performed by the evaluation of the organoleptic qualities of durian wines fermented by the different *S. cerevisiae* strains, using five descriptors including "fruity", "sulfur", "sweety", "off-flavor", and "harmony" for their aromas. ANOVA was used to distinguish different durian wines by their sensory evaluation scores. The statistical analysis demonstrated that samples fermented by yeast strains showed significant differences in

DOI: 10.1021/jf505666y
J. Agric. Food Chem. 2015, 63, 1939−1947

all attributes, which indicated that these fruit wines had different aroma intensities ($p < 0.001$).

Although judges exhibited significant subjectivity in their use of "fruity", "sulfur", "sweety", "off-flavor", and "harmony" as attribute descriptors, this result was inevitable in such a quantitative descriptive analysis. The reason might be because the judges expressed their perceptions against different scoring criteria, due to their differences in age, background, and olfactory sensitivity. From the research, no significant interaction between judge and replication was found, indicating that all of the judges were reproducible with regard to the scoring of all attributes in triplicate. Similarly, there was no significant interaction between sample and replication (in any attribute).

However, according to the statistical analysis, the interaction between sample and judge showed significant differences for the "fruity" ($p < 0.01$), "sulfur" ($p < 0.001$), "off-flavor" ($p < 0.01$), "sweety" ($p < 0.01$), and "harmony" ($p < 0.001$) attributes. This result suggested that the judges were scoring samples not consistent with each attribute.

Sensory analysis highlighted that some descriptors were statistically influenced by yeast starters (Figure 2). The durian wines fermented by strains Y1 and Y3 were accompanied by fruity notes more than in other strains. This phenomenon indicated that strains Y1 and Y3 yielded the highest content of compounds able to influence the fruity aroma of the corresponding fruit wine. It is common knowledge that the "fruity" attribute was the fundamental part of the overall perception of the aroma of durian wine. Therefore, the "fruity" attribute was an important symbol of fruit wine quality. The durian wines fermented by strains Y1 and Y2 were mostly associated with a greater "sweety" attribute than wines produced by other strains. The fruit wines fermented by strains Y2 and Y3 were rated as having the highest values of sulfur aroma, whereas durian wine produced by strain Y1 presented low sensorial scores for sulfur aroma. Traditionally, this sulfur aroma was typically associated with a negative sensory contribution to fruit wine (5).[7] However, the "sulfur" attribute remained the characteristic aroma of tropical fruit, which could obviously be distinguished from other fruits by this specific property. In addition, a similar behavior was observed for the "off-flavor" attribute in five fruit wines. The reason might be that sulfur-containing aroma compounds were typically perceived as offensive, they had very low detection thresholds, and they generally conferred a negative sensory contribution to fruit wine.[5,7,18] The result was consistent with findings of the literature,[24] which showed that the sulfur-containing aroma compounds were the main source of "off-flavor" attributes in fruit wines. The highest score under the "harmony" attribute was found in fruit wine produced by strain Y1, whereas the lowest score was found in that produced by strain Y5. Interestingly, by comparing the sensory analysis of "harmony" and "off-flavor" attributes, we found that these two attributes presented completely opposite scores when evaluated by our judges.

Relationship between Samples, Aroma Compounds, and Sensory Attributes. PLSR was used to process the mean data accumulated from sensory evaluation by the judges, aroma compounds (OAVs > 1), and samples. The *X*-matrix was designated as representing the aroma compounds of fruit wines; the *Y*-matrix was designated as representing the sensory variables and fruit wine samples. The derived PLSR model included two significant PCs explaining 83% of the cross-validated variance (Figure 3). The result demonstrated that the optimal number of components in the PLSR model presented was determined as two principal components (PC2): the issue of PC2 versus PC3 results was not presented here, as no additional information was gained by its examination.

The estimated regression coefficients from the jack-knife uncertainty test showed that all of the aroma compounds, except 3-methylbutanol (C7) and ethyl 3-methylpropanoate (C8), were significant for one or more of the five samples and five significant sensory descriptors. Five of the sensory attributes were placed between the inner and outer ellipses, $R^2 = 0.5$ and 1.0, respectively. The result indicated that they were well explained by the PLSR model.

From Figure 3, samples appeared to be divided into three groups according to strain. Among these samples, the fruit wine fermented by strain Y1 was located on the positive region of PC1 and the negative region of PC2. The fruit wines produced by strains Y4 and Y5, which were located on the negative region of PC1 and PC2, were clearly differentiated from samples fermented by other strains. The wines fermented by strains Y2 and Y3 lay in upper part of PC2.

The first PC was mainly defined by the aroma descriptors showing a contrast between "fruity", "harmony", and "sweety" attributes on the positive dimension and "sulfur" and "off-flavor" attributes on the negative dimension. The fruit wines produced by strains Y4 and Y5 were negatively correlated to all of the sensory variables and all aroma compounds even though they showed a certain aroma profile in the judges' evaluations thereof. This phenomenon might have been caused by sensory evaluation error, or it might be that those fruit wines could not possess characteristic, or distinguishing, aromas marking them apart from other fruit wines.

As compared with other wines, fruit wine fermented by strain Y1 was highly correlated with the sensory attributes of "fruity", "harmony", and "sweety". This was related to aroma compounds such as 2,3-butanedione (C2), ethyl acetate (C3), ethyl propanoate (C5), methyl butanoate (C6), ethyl butanoate (C9), ethyl 2-methylbutanoate (C12), and ethyl octanoate (C16). This phenomenon indicated that strain Y1 should have a higher ethyl acetate yield ability. Some aroma compounds are directly derived from chemical components of the musts, whereas many fruit-derived compounds were released or modified by the action of aroma-active yeast, and a further substantial portion of fruit wine aroma substances resulted from the metabolic activities of these fruit wine microbes.[2,25] Therefore, the selection of yeasts was central to the development of fruit wine aroma.

In contrast, "sulfur" and "off-flavor" attributes were strongly correlated with each other and showed high loadings in the opposite direction from other attributes. These attributes, which were pronounced in fruit wines fermented by strains Y2 and Y3, were strongly connected with the following compounds: dimethyl sulfide (C1), dimthyl disulfide (C4), methyl ethyl disulfide (C11), and diethyl disulfide (C13).

AUTHOR INFORMATION

Corresponding Author

*(Z.X.) Mail: School of Perfume and Aroma Technology, Shanghai Institute of Technology, 100 Haiquan Road, Shanghai 200233, People's Republic of China. Phone: 0086-021-60873424. Fax: 0086-021-54487207. E-mail: flavorsit@163.com.

DOI: 10.1021/jf505666y
J. Agric. Food Chem. 2015, 63, 1939−1947

Funding

This research was funded by the Natural Science Foundation of Shanghai Institute of Technology (Grant YYY-11607), the National Natural Science Foundation of China (Grants 21476140 and 21306114), and the "Twelfth Five Year" National Science and Technology Support Program Topic (Grant 2011BAD23B01).

Notes

The authors declare no competing financial interest.

■ ABBREVIATIONS USED

GC-MS, gas chromatography−mass spectrometry; PFPD, pulsed flame photometric detection; SBSE, stir bar sorptive extraction; OAV, odor activity value; PLSR, partial least-squares regression; PDMS, polydimethylsiloxane; TDU, thermal desorption unit; PTV, programmed temperature vaporizing

■ REFERENCES

(1) Saberi, S.; Cliff, M. A.; Van, H. J. J. Impact of mixed *S. cerevisiae* strains on the production of volatiles and estimated sensory profiles of Chardonnay wines. *Food Res. Int.* **2012**, *48*, 725−735.

(2) Câmara, J. S.; Alves, M. A.; Marques, J. C. Multivariate analysis for the classification and differentiation of Madeira wines according to main grape varieties. *Talanta* **2006**, *68*, 1512−1521.

(3) Swiegers, J.; Francis, I.; Herderich, M.; Pretorius, I. Meeting consumer expectations through management in vineyard and winery. *Wine Ind. J. (Aust. N. Z.)* **2006**, *21*, 34−42.

(4) Weenen, H.; Koolhaas, W. E.; Apriyantono, A. Sulfur-containing volatiles of durian fruits (*Durio zibethinus* Murr.). *J. Agric. Food Chem.* **1996**, *44*, 3291−3293.

(5) Norjana, I.; Noor Aziah, A. Quality attributes of durian (*Durio zibethinus* Murr) juice after pectinase enzyme treatment. *Food Res. Int. J.* **2011**, *18*, 1117−1122.

(6) Li, J.-X.; Schieberle, P.; Steinhaus, M. Characterization of the major odor-active compounds in Thai durian (*Durio zibethinus* L. 'Monthong') by aroma extract dilution analysis and headspace gas chromatography−olfactometry. *J. Agric. Food Chem.* **2012**, *60*, 11253−11262.

(7) Voon, Y. Y.; Abdul Hamid, N. S.; Rusul, G.; Osman, A.; Quek, S. Characterisation of Malaysian durian (*Durio zibethinus* Murr.) cultivars: relationship of physicochemical and flavor properties with sensory properties. *Food Chem.* **2007**, *103*, 1217−1227.

(8) Lee, P.-R.; Toh, M.; Yu, B.; Curran, P.; Liu, S.-Q. Manipulation of volatile compound transformation in durian wine by nitrogen supplementation. *Int. J. Food Sci. Technol.* **2013**, *48*, 650−662.

(9) Sun, S. Y.; Jiang, W. G.; Zhao, Y. P. Evaluation of different *Saccharomyces cerevisiae* strains on the profile of volatile compounds and polyphenols in cherry wines. *Food Chem.* **2011**, *127*, 547−555.

(10) *Compendium of International Methods of Wine and Must Analysis*; OIV: Paris, France, 2009.

(11) Birch, A. N.; Petersen, M. A.; Arneborg, N.; Hansen, Å. S. Influence of commercial baker's yeasts on bread aroma profiles. *Food Res. Int.* **2013**, *52*, 160−166.

(12) Pretorius, I. S. Tailoring wine yeast for the new millennium: novel approaches to the ancient art of winemaking. *Yeast* **2000**, *16*, 675−729.

(13) Torrens, J.; Urpí, P.; Riu-Aumatell, M.; Vichi, S.; López-Tamames, E.; Buxaderas, S. Different commercial yeast strains affecting the volatile and sensory profile of cava base wine. *Int. J. Food Microbiol.* **2008**, *124*, 48−57.

(14) Lambrechts, M.; Pretorius, I. Yeast and its importance to wine aroma − a review. *S. Afr. J. Enol. Vitic.* **2000**, *21*, 97−129.

(15) Guth, H. Quantitation and sensory studies of character impact odorants of different white wine varieties. *J. Agric. Food Chem.* **1997**, *45*, 3027−3032.

(16) Molina, A. M.; Guadalupe, V.; Varela, C.; Swiegers, J. H.; Pretorius, I. S.; Agosin, E. Differential synthesis of fermentative aroma compounds of two related commercial wine yeast strains. *Food Chem.* **2009**, *117*, 189−195.

(17) Sun, S. Y.; Che, C. Y.; Sun, T. F.; Lv, Z. Z.; He, S. X.; Gu, H. N.; Shen, W. J.; Chi, d. C.; Gao, Y. Evaluation of sequential inoculation of *Saccharomyces cerevisiae* and *Oenococcus oeni* strains on the chemical and aromatic profiles of cherry wines. *Food Chem.* **2013**, *138*, 2233−2241.

(18) Swiegers, J. H.; Pretorius, I. S. Yeast modulation of wine flavor. *Adv. Appl. Microbiol.* **2005**, *57*, 131−175.

(19) Lee, P.-R.; Saputra, A.; Yu, B.; Curran, P.; Liu, S.-Q. Biotransformation of durian pulp by mono- and mixed-cultures of *Saccharomyces cerevisiae* and *Williopsis saturnus*. *LWT−Food Sci. Technol.* **2012**, *46*, 84−90.

(20) Dantes, P. T. G.; Maninang, J. S.; Elepaño, A. R.; Gemma, H. In *Analysis of Aroma Volatile Profile of Philippine Durian Pulp (Durio zibethinus Rumph. ex Murray) using Headspace Solid Phase Micro-extraction (HS-SPME) Coupled with GC-MS*, 13th ASEAN Food Conference, Singapore; September 9−11, 2013.

(21) Granvogl, M.; Christlbauer, M.; Schieberle, P. Quantitation of the intense aroma compound 3-mercapto-2-methylpentan-1-ol in raw and processed onions (*Allium cepa*) of different origins and in other *Allium* varieties using a stable isotope dilution assay. *J. Agric. Food Chem.* **2004**, *52*, 2797−2802.

(22) Wu, C. M.; Wang, Z. Volatile compounds in fresh and processed shiitake mushrooms (*Lentinus edodes* Sing.). *Food Sci. Technol. Res.* **2000**, *6*, 166−170.

(23) Granvogl, M.; Schieberle, P. Facts and 'artefacts' in the flavour chemistry of onions. *Dev. Food Sci.* **2006**, *43*, 359−362.

(24) Mestres, M.; Busto, O.; Guasch, J. Analysis of organic sulfur compounds in wine aroma. *J. Chromatogr. A* **2000**, *881*, 569−581.

(25) Ferreira, V.; López, R.; Cacho, J. F. Quantitative determination of the odorants of young red wines from different grape varieties. *J. Sci. Food Agric.* **2000**, *80*, 1659−1667.

(26) Giri, A.; Osako, K.; Okamoto, A.; Ohshima, T. Olfactometric characterization of aroma active compounds in fermented fish paste in comparison with fish sauce, fermented soy paste and sauce products. *Food Res. Int.* **2010**, *43*, 1027−1040.

(27) Näf, R.; Velluz, A. Sulfur compounds and some uncommon esters in durian (*Durio zibethinus* Murr.). *Flavour Fragrance J.* **1996**, *11*, 295−303.

(28) van Gemert, L. J. *Complilations of Odour Threshold Values in Air, Water and Other Media*; Van Setten Kwadraat: Houten, The Netherlands, 2003.

DOI: 10.1021/jf505666y
J. Agric. Food Chem. 2015, 63, 1939−1947

commercial Cognac by application of the AEDA and to identify the most odor-active compounds. Aroma compounds with the highest flavor dilution (FD) factors should be quantitated using stable isotope dilution assays, their OAVs (ratio of concentration to odor threshold) should be calculated on the basis of their odor thresholds in water/ethanol, and the results should finally be confirmed by means of an aroma recombinate. In addition, an AEDA was applied on a German brandy to find differences in the key odorants, which may be useful to distinguish Cognac from brandies.

MATERIALS AND METHODS

Cognac. According to the label, the commercial Cognac investigated (Hennessy) was labeled VS and had been stored in Limousin oak barrels for two years. This selection was not done for advertising purpose, nor does it imply any research contract with the manufacturer, but was done on the basis of a hedonic preference test performed by a group of 16 trained panelists (average age = 30 years; 60% women). The grape variety used for the production of the Cognac was Ugni Blanc, and the product was manufactured according to the regulation of the AOC Cognac. Several batches of the same production of the Cognac year were bought in a German supermarket. The German brandy (Mariacron) was selected because it showed the clearest difference in the overall aroma when compared to the Cognac.

Reference Odorants. These were obtained from the following commercial sources: 4-Allyl-2-methoxyphenol, α-damascenone, 1,1-diethoxyethane, ethyl acetate, ethyl hexanoate, 4-ethyl-2-methoxyphenol, ethyl 3-methylbutanoate, ethyl octanoate, 4-ethylphenol, ethyl 2-phenylacetate, 3-hydroxy-4,5-dimethyl-2(5*H*)-furanone, 2-isopropyl-3-methoxypyrazine, methylpropanal, 3-methylbutanal, 3-methylbutanol, 3-methylbutyl acetate, (*E*)-2-nonenal, phenylacetaldehyde, 2-phenylacetic acid, (3*S*,4*S*)-*cis*- and (3*S*,4*R*)-*trans*-whiskey lactone, ethyl butanoate, ethyl methylpropanoate, ethyl pentanoate, ethyl propanoate, methylpropanol, (*E*)-2-nonanal, ethyl (*S*)-2-methylbutanoate, ethyl decanoate, octanoic acid, acetic acid, 2-methylbutanoic acid, 3-methylbutanoic acid, 2,3-butanedione, (*Z*)-3-hexenol, ethyl 2-hydroxy-3-methylbutanoate, and 2-phenylethanol were from Sigma-Aldrich Chemie (Taufkirchen, Germany). Acetaldehyde, ethanol, 4-hydroxy-3-methoxybenzaldehyde, and 2-methoxyphenol were from Merck (Darmstadt, Germany), and 4-hydroxy-2,5-dimethyl-3(2*H*)-furanone was from SAFC (Hamburg, Germany). Cyclohexanoyl acetate was supplied by Lancaster (Griesheim, Germany); 1-hexanol by Fluka (Buchs, Switzerland), 4-vinyl-2-methoxyphenol from Alfa Aesar (Karlsruhe, Germany), and hexanoic acid from Acros Organics (Geel, Belgium). (*E*)-β-Damascenone was a gift from Symrise (Holzminden, Germany).

Isotopically Labeled Internal Standards. Most of the isotopically labeled internal standards were synthesized as listed in a previous study:[11] In addition, [$^2H_2$]-methylpropanol,[12] [$^2H_2$]-(*Z*)-3-hexenol,[13] [$^2H_2$]-butanoic acid,[14] [$^2H_5$]-ethyl pentanoate,[15] [$^2H_3$]-hexanoic acid,[16] [$^{13}C_2$]-3-hydroxy-4,5-dimethyl-2(5*H*)-furanone,[17] [$^2H_2$]-3-methylbutanoic acid,[18] [$^2H_2$]-octanoic acid,[19] and [$^{13}C_2$]-phenylacetaldehyde[20] were synthesized as previously reported. [$^{13}C_2$]-Phenylacetic acid was bought from Merck.

Isolation of the Volatiles. For volatile isolation, the spirit (25 mL) was diluted with brine and extracted with diethyl ether (3 × 50 mL), and the combined extracts were washed three times with brine (25 mL). Nonvolatile compounds were separated by high-vacuum distillation using the SAFE distillation;[21] the distillate was washed with brine (3 × 25 mL) and concentrated to ∼100 μL using a Vigreux column (60 cm × 1 cm i.d.) followed by microdistillation.[22] The distillate was separated into a fraction containing the neutral/basic volatiles (NBF) and the acidic volatiles (AF) by treatment with an aqueous sodium bicarbonate solution as previously described.[22]

Fractionation of the Neutral/Basic Volatiles by Column Chromatography. The neutral/basic fraction was concentrated to ∼1 mL and was applied onto a water-cooled glass column (30 cm × 1 cm) filled with silica 60 (30 g) in *n*-pentane. Using six *n*-pentane/diethyl ether mixtures (v/v) of increasing polarity (100 mL each; fraction A, 100:0; fraction B, 95:5; fraction C, 90:10; fraction D, 80:20; fraction E, 50:50; fraction F, diethyl ether), the compounds were separated and each fraction was concentrated to ∼1 mL as described above. These fractions were used to relocate the odor-active compounds for identification by GC-MS.

Gas Chromatography−Flame Ionization Detector (GC-FID) and Gas Chromatography−Olfactometry (GC-O). The analyses were performed by means of a gas chromatograph type 8000 (Fisons Instruments, Mainz, Germany) equipped with the following capillaries: DB-5 (30 m × 0.25 mm i.d.; 0.25 μm film thickness) (Varian, Palo Alto, CA, USA) and DB-FFAP (30 m × 0.32 mm i.d.; 0.25 μm film thickness) (J&W Scientific, Folsom, CA, USA). For GC-O, the end of the capillary was connected to a deactivated Y-shaped glass splitter dividing the effluent into two equal parts, which were transferred via two deactivated but uncoated fused silica capillaries (50 cm × 0.25 mm) to a sniffing port and an FID, respectively. The sniffing port was held at 180 °C, whereas the temperature of the FID was at 240 °C; nitrogen was used as the makeup gas. Sample injection (0.5 μL) was done at 40 °C, and after 2 min, the temperature were raised at 6 °C/min to 230 °C and held for 10 min. All aroma-active areas annotated by three panelists were marked in the chromatogram, and the odor qualities were described. For the original extracts, sniffing time was ∼15 min; that is, the entire chromatogram were sniffed 0−15, 15−30, and 30−45 min. Linear retention indices (RI) of the compounds were calculated from the retention times of a series of *n*-alkanes C-8−C-24.

Aroma Extract Dilution Analysis. The distillate was stepwise diluted with diethyl ether to obtain the dilutions 1:1, 1:2, 1:4, 1:8, 1:16, etc., and finally 1:2048 of the original extract.[22] Each odorant was, thus, assigned an FD factor representing the final dilution in which the odorant could be detected. Sniffing was continued until no odorant was detectable by GC-O. Odor qualities were assigned on the basis of a flavor language previously developed in our group.[23] The AEDA was performed in parallel by at least three panelists, and the results were averaged.

Gas Chromatography−Mass Spectrometry (GC-MS). Mass spectra were recorded by means of a gas chromatograph 5890 series II (Hewlett-Packard, Waldbronn, Germany) connected to an MAT 95 S sector field mass spectrometer (Finnigan, Bremen, Germany). Mass spectra in the electron ionization mode (MS-EI) were recorded at 70 eV, and mass spectra in the chemical ionization mode (MS-CI) were measured at 115 eV with isobutane as the reactant gas.

Quantitation by Stable Isotope Dilution Assays in Combination with Two-Dimensional High-Resolution Gas Chromatography (TDGC-MS). The labeled internal standards (2−10 μg; depending on the amounts of the respective analyte estimated in a preliminary trial) dissolved in diethyl ether (0.5 mL) were added to aliquots of the spirit. After the addition of brine (50 mL) and diethyl ether (50 mL), the solution was stirred for 1 h. The combined extracts were dried over anhydrous sodium sulfate and concentrated to ∼100 mL at 37 °C using a Vigreux column (50 cm × 1 cm i.d.). The nonvolatile material was removed by SAFE distillation at 40 °C, and the distillate was concentrated to 100 μL by means of microdistillation.[22]

For TDGC-MS a gas chromatograph Trace 2000 (ThermoQuest, Mainz, Germany) coupled via a moving column stream switching system (ThermoQuest, Mainz, Germany) to a gas chromatograph CP 3800 (Varian, Darmstadt, Germany) was used. In the first dimension, the separation of the distillate was achieved on the FFAP column. First, the retention time of the analyte under investigation was determined by means of reference substances. Then, at the respective elution time, the effluent was quantitatively transferred into a cold trap (−80 °C) and, after the cooling was turned off, the trapped material was transferred onto the DB-5 column in the second oven. The effluent was finally monitored using an ITD Saturn 2000 ion trap mass spectrometer (Varian, Darmstadt, Germany). Mass spectra in the chemical ionization mode (MS-CI) were generated at 70 eV using methanol as reagent gas. The peak areas of the selected ions of the labeled standard and the analyte were separately determined in the mass chromatogram by using either the molecular ions or selected

DOI: 10.1021/jf506307x
J. Agric. Food Chem. 2015, 63, 1948−1956

fragments given in Table 1. Concentrations were calculated and corrected using response factors obtained by measuring defined mixtures of the respective labeled and the unlabeled compound.[20]

Table 1. Selected Ions (m/z) ($M^+ + 1$; MS-CI) of Analytes and Isotopically Labeled Standards (ILS) Used in the Stable Isotope Dilution Assays

compound	analyte (m/z)	isotope label	ILS (m/z)	MS response factor
1,1-diethoxyethane	73	$^{13}C_2$	75	0.94
acetic acid	61	$^{2}H_3$	64	1.03
ethyl propanoate	103	$^{2}H_3$	105	1.01
ethyl butanoate	117	$^{2}H_3$	120	0.97
ethyl pentanoate	131	$^{2}H_5$	136	0.86
ethyl hexanoate	145	$^{2}H_3$	148	0.99
ethyl octanoate	173	$^{2}H_3$	176	0.90
ethyl decanoate	201	$^{2}H_5$	206	1.02
ethyl methylpropanoate	117	$^{2}H_3$	120	1.00
ethyl (*S*)-2-methylbutanoate	131	$^{2}H_5$	136	1.00
ethyl 3-methylbutanoate	131	$^{2}H_3$	134	0.95
(*S*)-ethyl 2-hydroxy-3-methylbutanoate	147	$^{2}H_5$	152	0.93
cyclohexanoyl acetate	157	$^{2}H_3$	160	1.03
hexanol	103	$^{2}H_4$	107	0.89
(*Z*)-3-hexen-1-ol	83	$^{2}H_5$	88	0.99
(*E*)-β-damascenone	191	$^{2}H_{4-6}$	195−197	1.01
3-methylbutanol	71	$^{2}H_2$	73	1.00
(*S*)-2-methylbutanol	71	$^{2}H_2$	73	1.00
methylpropanol	57	$^{2}H_7$	64	0.99
methylpropanal	73	$^{2}H_7$	80	0.98
3-methylbutanal	87	$^{2}H_2$	89	1.02
2,3-butanedione	87	$^{13}C_4$	91	0.89
(*E*)-2-nonenal	141	$^{2}H_2$	143	0.98
2-phenylethanol	105	$^{13}C_2$	107	1.05
3-methylbutyl acetate	148	$^{2}H_2$	150	0.98
(3*S*,4*S*)-*cis*-whiskey lactone	157	$^{2}H_2$	159	1.00
4-hydroxy-3-methoxybenzaldehyde	153	$^{2}H_3$	156	0.94
4-allyl-2-methoxyphenol	165	$^{2}H_3$	168	0.92
2-methoxyphenol	125	$^{2}H_2$	127	0.99
4-ethyl-2-methoxyphenol	153	$^{2}H_2$	155	1.05
3-hydroxy-4,5-dimethyl-2-furanone	129	$^{2}H_2$	131	0.98

Quantitation of Ethanol. Ethanol was determined on the basis of density by weighing exactly 20 mL of a steam distillate of Cognac.

Separation of (*S*)-2- and (*R*)-2- and -3-Methylbutanol. Due to coelution on the DB-FFAP column, the separation of the three methylbutanols was achieved on a chiral BGB 174 E column (30 m × 0.25 mm i.d., 0.25 μm film thickness) (BGB Analytic, Anwill, Switzerland) by means of TD-HRGC/MS with the DB-FFAP column in the first and the BGB 174 E column in the second dimension.

Determination of Odor Thresholds. First, the purity of the reference odorants was checked by GC-O. For the determination of the odor thresholds, a defined amount of the purified aroma compound in ethanol (10 μL) was then pipetted into a Teflon vessel containing 25 mL of ethanol/water (6:4, v/v). After stepwise dilution (1:1, v/v), the samples were judged by 16 trained assessors. Triangular tests were performed using 25 mL of water/ethanol (6:4, v/v) as the control, and the odorants were presented in Teflon vessels (45 mL) with lid in decreasing concentrations. The assessors were recruited from the German Research Center for Food Chemistry, and sensory evaluations were performed in a sensory panel room at 21 ± 1 °C. Odor thresholds were calculated according to the method of § 64 LFGB, methods 00.90-7 and 00.90-9.[24]

Descriptive Profile Tests. The panelists were asked to rate the odor intensity of the aroma attributes of Cognac from 0 to 3 (0, not perceivable; 1, weak; 2, significant; and 3, strong) using a seven-point scale of 0, 0.5, 1, 1.5, up to 3.0. Eight suprathreshold aqueous solutions (25 mL in Teflon vessels) of 3-methylbutanol (malty), (*E*)-β-damascenone (cooked apple-like), ethyl 3-methylbutanoate (fruity), 2-phenylethanol (flowery), 4-hydroxy-3-methoxybenzaldehyde (vanilla-like), phenylacetic acid (honey-like), 2-methoxy-4-vinylphenol (clove-like), and (3*S*,4*S*)-*cis*-whiskey lactone (coconut-like) were used for the weekly training of the sensory panel. For the evaluation of the Cognac aroma, the panelists had to evaluate the intensities of the eight odor qualities represented by solutions of the reference aroma compounds on a seven-point intensity scale. The results of the aroma profile analysis were displayed in a spider web diagram.

For the aroma recombinate, a mixture consisting of 34 reference key odorants in the concentrations determined in the Cognac and showing OAVs ≥ 1 was dissolved in water/ethanol (6:4, v/v), and the pH was adjusted to 3.9 with aqueous H_2SO_4 (1 mol/L) (recombinate A). For the second aroma recombinate (recombinate B) aliquots of the same 34 compounds were added to an odorless Cognac matrix. To obtain this matrix, a Cognac sample (100 mL) was sequentially extracted with diethyl ether and distilled using the SAFE apparatus. The residue obtained was treated with water followed by *n*-pentane and finally freeze-dried until odorless. An aliquot of the residue, representing 100 mL of Cognac, was dissolved in water/ethanol (6:4, v/v) and was added to 100 mL of the recombinate. An overall aroma profile of both recombinates was determined in the same way as described above for Cognac. Separately, the similarity of the overall aromas of the Cognac and the Cognac recombinates were compared. The similarity was ranked using a seven-point scale from 0 (no similarity) to 3 (100% identical).

RESULTS AND DISCUSSION

In a first experiment, a sensory panel was asked to perform an aroma profile analysis of the Cognac. On the basis of eight odor qualities agreed to in a preliminary session, the panel evaluated fruity, malty, and baked-apple like attributes as the important odor qualities, followed by clove- and honey-like impressions (Figure 1). To assess the odorants responsible for these aroma

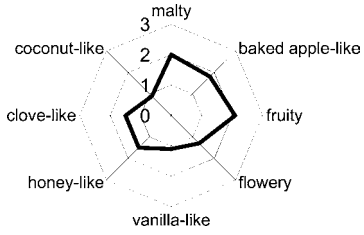

Figure 1. Aroma profile analysis of the Cognac Hennessy.

qualities, first, the most appropriate solvent for volatile extraction was selected from pentane/diethyl ether (1:1, v/v), dichloromethane, and diethyl ether. The diethyl ether extract exhibited the most similar aroma compared to the original Cognac when a drop of the extract was evaluated on a strip of filter paper, and thus this solvent was used for further analyses.

Identification of Odor-Active Compounds. A distillate of 25 mL of Cognac prepared by extraction/SAFE distillation was subjected to GC-O after concentration. A total of 39 odor-active areas could be detected in the FD factor range of 8−2048. Among them, the cooked-apple-like odor, which was smelled at position **26** (Figure 2) showed the highest FD factor followed by a fruity (**5**) and a malty (**12**) odor. Further

DOI: 10.1021/jf506307x
J. Agric. Food Chem. 2015, 63, 1948−1956

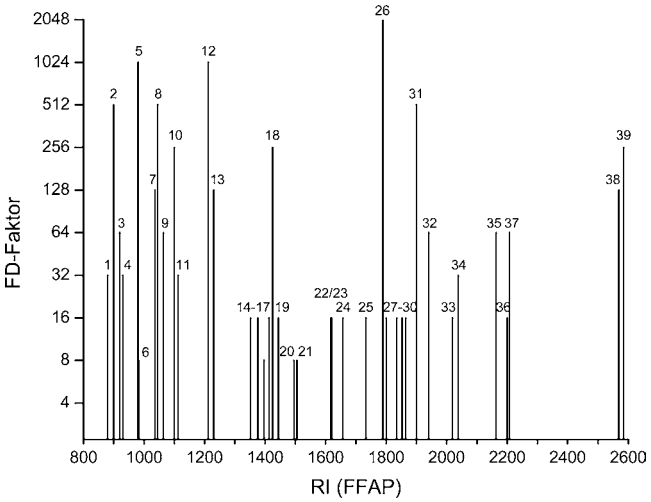

Figure 2. Flavor dilution (FD) chromatogram obtained by application of the aroma extract dilution analysis on a distillate of the volatiles isolated from the Cognac.

compounds with fruity notes (**2**, **8**, and **18**) showed somewhat lower FD factors. In addition, a flowery-smelling odorant (**31**), the malty smelling odorant (**10**), and the vanilla-like smelling odorant (**39**) showed quite high FD factors of 256.

To identify the compounds responsible for these odors, first, the retention indices of the odor-active areas were compared to an in-house database, suggesting potential structures for each odorant. To confirm these, the compounds present in the neutral/basic volatiles fraction were separated on silica gel. This procedure was necessary to avoid coelution of trace odorants with volatiles present in high amounts in the extract. The odor-active areas were then relocated in the respective fractions by GC-O, and mass spectra in the electron impact mode (MS-EI) and the chemical ionization mode (MS-CI) were recorded.

Compound **26** with the highest FD factor was, thus, identified as (*E*)-*β*-damascenone (Figure 3). Compound **12** with the second highest FD factor consisted of two compounds, (*S*)-2-methylbutanol (ee > 99%) and 3-methylbutanol, both of which could be separated on a chiral BGB E 174 column. The

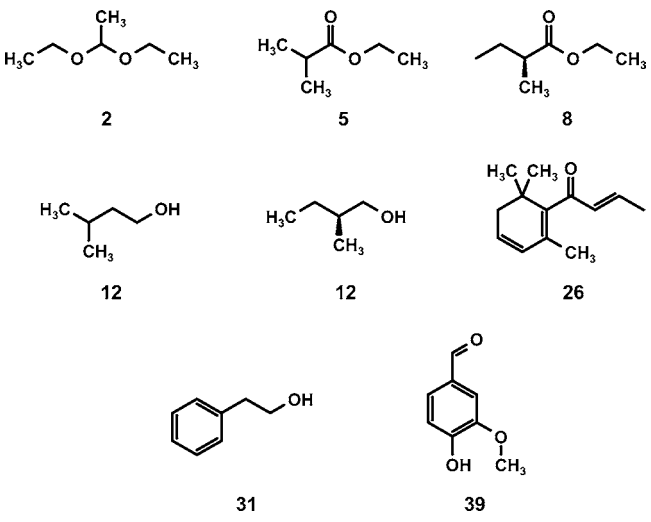

Figure 3. Structures of the most odor active compounds identified in Cognac. The alcohol isomers (12) could not be separated on the GC stationary phase used in GC−O.

ratio was determined to be 84% 3-methylbutanol and 16% (*S*)-2-methylbutanol. The fruity odors (**2**, **5**, and **8**) were evoked by diethoxyethane, ethyl methylpropanoate, and ethyl (*S*)-2-methylbutanoate. The flowery smell (**31**) was caused by 2-phenylethanol, and the vanilla-like odor was attributed to vanillin (**39**). The results of the further identification experiments are summarized in Table 2. Besides phenylacetic acid (**38**) with an FD factor of 128, other odor-active acids were detected, hexanoic acid (**28**), acetic acid (**19**), butanoic acid (**23**), and 2- and 3-methylbutanoic acid (**24**), all with an FD factor of 16.

Compounds with clove-like and phenolic aroma constituents were 4-allyl-2-methoxyphenol (**35**) with an FD factor of 64, and 2-methoxyphenol (**29**), 4-ethyl-2-methoxyphenol (**33**), and 2-methoxy-4-vinylphenol (**36**), all with FD factors of 16 (Table 2). Compounds **30** and **32** with a coconut-like odor were identified as (3*S*,4*S*)-*cis*- and (3*S*,4*R*)-*trans*-whiskey lactone.

α-Damascone (**25**) was another norisoprenoid eliciting a cooked apple-like smell. This odorant and also cyclohexanoyl acetate (**16**), 2-isopropyl-3-methoxypyrazine (**17**), 2-isobutyl-3-methoxypyrazine (**20**), (*E*)-2-nonenal (**21**), 2-methoxy-4-vinylphenol (**36**), 3-hydroxy-4,5-dimethyl-2-(5*H*)-furanone (**37**), and phenylacetic acid (**38**) were detected for the first time in a Cognac or brandy, respectively.

Quantitation by Stable Isotope Dilution Assays. The AEDA is an appropriate method to find odorants potentially contributing to the overall aroma of foods. However, this method does not permit conclusions on the influence of the food matrix, for example, on odorant binding, or on the interactions of odorants at the receptor level when matching the overall odor impression of a given food. For this reason the odor activity values were calculated as a next step.[7] For this purpose, the 37 aroma compounds that had shown the highest FD factors (Table 2) were quantitated using stable isotope dilution assays. In addition, ethyl pentanoate was quantitated, because it was found to be an important marker to differentiate brandies from Cognac samples.

The results of the quantitative measurements (Table 3) revealed ethanol (316 g/L) and 3-methylbutanol (1044 mg/L) as compounds with the highest concentrations, followed by methylpropanol, acetic acid (126 mg/L), 2-methylbutanol (107 mg/L), acetaldehyde (52 mg/L), hexanol (41 mg/L), 1,1-diethoxyethane (16.7 mg/L), and hexanoic acid (12.4 mg/L). Most odorants were, however, present in low amounts between 170 and 0.5 μg/L (Table 3).

Aroma compounds showing the lowest concentrations were (*E*)-2-nonenal (9.0 μg/L), 3-hydroxy-4,5-dimethyl-2(5*H*)-furanone (5.7 μg/L), cyclohexanoyl acetate (6.0 μg/L), ethyl pentanoate (3 μg/L), and 2-isobutyl-3-methoxypyrazine (0.5 μg/L).

Odor activity values (ratio of concentration to odor threshold) are a valuable tool to correlate quantitative data with the volatility of a compound from the respective matrix,[6] but it is necessary that the thresholds of single components are determined in a matrix as close as possible to the food itself. Thus, for Cognac the odor thresholds were determined in water/ethanol (6:4, v/v) as previously reported in a study on whiskey aroma.[11] To indicate the importance of the matrix, Table 4 shows a comparison of odor thresholds for selected odorants in water and in water/ethanol (6:4, v/v). With the exception of phenylacetic acid, all odorants showed higher odor thresholds in water, with (*E*)-*β*-damascenone, 3-methylbutanol,

DOI: 10.1021/jf506307x
J. Agric. Food Chem. 2015, 63, 1948−1956

Table 2. Most Aroma-Active Compounds (FD ≥ 8) Detected in a Distillate of Volatiles Prepared from Hennessy Cognac

no.[b]	odorant[c]	odor quality[d]	fract[e]	RI[a] on FFAP	RI[a] on DB-5	FD factor[f]	earlier reported as volatile compound in brandies
1	methylpropanal[g]	malty	C	880	<600	32	8, 10
2	1,1-diethoxyethane	fruity	B	900	725	512	3, 8, 10
3	ethyl acetate	fruity	B	920	<600	64	3, 8, 10
4	3-methylbutanal	malty	C	930	650	32	8
5	ethyl 2-methypropanoate	fruity	B	980	763	1024	3, 10
6	2,3-butanedione	butter-like	C	983	<600	8	10
7	ethyl butanoate	fruity	B	1036	803	128	3, 10
8	ethyl 2-methylbutanoate	fruity	B	1045	865	512	3, 10
9	ethyl 3-methylbutanoate	fruity	B	1064	858	64	3, 8, 10
10	2-methylpropanol	malty	D	1100	637	256	3, 8, 10
11	3-methylbutyl acetate	fruity	B	1113	888	32	8, 10
12	2- and 3-methylbutanol	malty	D	1213	742	1024	3, 8, 10
13	ethyl hexanoate	fruity	B	1230	1005	128	3, 8, 10
14	hexanol	green	D	1352	880	16	3, 8, 10
15	(*Z*)-3-hexen-1-ol	green	D	1376	873	16	3, 8, 10
16	cyclohexyl acetate	aromatic, fruity	C	1396	1131	8	
17	2-isopropyl-3-methoxypyrazine	earthy	C	1413	1091	16	
18	ethyl octanoate	fruity	B	1424	1200	256	3, 8
19	acetic acid	vinegar	AF	1444	680	16	8
20	2-isobutyl-3-methoxypyrazine	earthy	D	1495	1167	8	
21	(*E*)-2-nonenal	green	C	1505		8	
22	ethyl decanoate	flowery	B	1618	1405	16	3, 10
23	butanoic acid	sweaty	AF	1620		16	8
24	2- and 3-methylbutanoic acid	sweaty	AF	1657		16	8
25	α-damascone	cooked apple-like	C	1733	1392	16	
26	(*E*)-β-damascenone	cooked apple-like	C	1789	1392	2048	3, 8, 10
27	2-phenylethyl acetate	fruity	B	1800	1259	16	8
28	hexanoic acid	sweaty	AF	1835		16	8
29	2-methoxyphenol	phenolic	D	1853	1096	16	8
30	(3*S*,4*R*)-*trans*-whiskey lactone	coconut-like	D	1865	1290	16	3, 10
31	2-phenylethanol	flowery	D	1900	1123	512	3, 8, 10
32	(3*S*,4*S*)-*cis*-whiskey lactone	coconut-like	D	1941	1331	64	3
33	4-ethyl-2-methoxyphenol	phenolic, clove-like	D	2019	1282	16	9, 10
34	4-hydroxy-2,5-dimethyl-3(2*H*)-furanone	caramel-like	AF	2038	1053	32	9
35	4-allyl-2-methoxyphenol	clove-like	D	2163	1322	64	9, 10
36	2-methoxy-4-vinylphenol	clove-like	D	2200	1315	16	
37	3-hydroxy-4,5-dimethyl-2(5*H*)-furanone[g]	seasoning-like	D	2207	1111	64	
38	phenylacetic acid	honey-like	AF	2569	1267	128	
39	4-hydroxy-3-methoxybenzaldehyde	vanilla-like	AF	2585	1409	256	8, 9

[a]Retention index. [b]Odorants were consecutively numbered according to their elution order from the FFAP column. [c]Odorants were identified by comparing them with reference compounds on the basis of the following criteria: (i) retention indices on the FFAP and DB-5 capillary columns, (ii) mass spectra obtained by MS-EI and MS-CI; and (iii) odor quality and odor threshold determined by GC-O. [d]Odor quality as perceived at the sniffing port during GC-O. [e]Column chromatography fractions A–F and AF (acid fraction) in which the odorant was detected. [f]FD factor, flavor dilution factor. [g]An unequivocal mass spectrum could not be obtained. The identification is based on the resting criteria detailed in footnote *b*.

and methylpropanol showing the largest difference between both media.

Using the odor thresholds in water/ethanol, the OAVs for 34 Cognac odorants were calculated (Table 5). The highest OAV was obtained for ethanol (12690) and confirmed the dominating aroma contribution of ethanol in spirits as recently found also for whiskey[11] or pear brandy.[25] The concentrations of all 34 aroma compounds clearly exceeded their thresholds in water/ethanol, and among them (*E*)-β-damascenone, due to its low odor threshold of 0.14 μg/L, had the second highest OAV. Quite high OAVs were also calculated for the fruity-smelling odorants ethyl (*S*)-2-methylbutanoate (195), ethyl methylpropanoate (120), ethyl 3-methylbutanoate (100), ethyl hexanoate (97), ethyl butanoate (69), and ethyl octanoate (61). Ethyl butanoate and ethyl hexanoate have also previously been suggested by Webb et al.[26] as important aroma compounds in Cognac.

To confirm the contribution of the 34 key aroma compounds to the overall aroma of the Cognac, an aroma recombinate was prepared containing reference chemicals of all odorants that had shown OAVs ≥ 1 in water/ethanol (6:4, v/v) in the concentrations measured in Cognac (Table 3). First, a recombinate in water/ethanol (6:4, v/v) was evaluated by the sensory panel. As shown in Figure 4A, in particular the flowery and fruity quality was somewhat weaker than determined for Cognac (Figure 4B), and the overall similarity was only rated 2.2 on scale from 0 to 3.

DOI: 10.1021/jf506307x
J. Agric. Food Chem. 2015, 63, 1948–1956

Table 3. Concentrations of 34 Potent Odorants in the Hennessy Cognac

odorant	concn[a] (μg/L)
ethanol	316000000
3-methylbutanol	1043835
methylpropanol	526644
acetic acid	126275
2-methylbutanol	107267
acetaldehyde	51700
hexanol	41046
1,1-diethoxyethane	16700
hexanoic acid	12415
ethyl octanoate	9022
2-phenylethanol	8206
methylpropanal	5020
ethyl hexanoate	2892
(*Z*)-3-hexenol	1180
3-methylbutyl acetate	730
ethyl butanoate	657
ethyl methylpropanoate	541
4-hydroxy-3-methoxybenzaldehyde	532
(*E*)-β-damascenone	330
3-methylbutanal	205
(3*S*,4*S*)-*cis*-whiskey lactone	220
2-phenylethyl acetate	202
2,3-butanedione	200
(3*S*,4*R*)-*trans*-whiskey lactone	192
ethyl 3-methylbutanoate	160
ethyl 2-hydroxy-3-methylbutanoate	106
2-methoxyphenol	96
4-vinyl-2-methoxyphenol	48
ethyl 2-methylbutanoate	43
4-ethyl-2-methoxyphenol	43
phenylacetic acid	23
(*E*)-2-nonenal	9.0
cyclohexanoyl acetate	6.0
3-hydroxy-4,5-dimethyl-2(5*H*)-furanone	5.7

[a]Data are mean values of triplicates.

Table 4. Comparison of Odor Thresholds of Selected Odorants in Water and in Water/Ethanol (6:4, v/v)

	odor threshold (μg/L) in		
compound	water	water/ethanol	ratio of water/ethanol to water
(*E*)-β-damascenone[a]	0.0007	0.14	200
methylpropanol	1000	100690	101
(*Z*)-3-hexenol	30	1257	42
acetic acid	22000	75521	3
hexanoic acid	1500	7563	5
3-methylbutanol[a]	250	56100	224
phenylacetic acid[a]	1000	9.2	9×10^{-3}
ethyl butanoate[a]	0.1	9	90
ethyl hexanoate[a]	0.5	30	60
2,3-butanedione[a]	0.03	2.8	93
ethyl (*S*)-2-methylbutanoate[a]	0.01	0.22	22

[a]Odor thresholds recently determined.[11]

If all aroma compounds were identified and quantitated, it can be assumed that nonvolatile compounds may interact with the odorants in Cognac, thus influencing the overall aroma perception. This was also recently proven for red wine.[27] Thus, to evaluate the influence of the nonvolatile fraction from Cognac, deodorized, nonvolatile material was isolated from Cognac, then added to the recombinate, and again a descriptive profile analysis against the original Cognac was performed. Now, the aroma profile of the recombinate (Figure 4C) was nearly identical with the aroma profile of the Cognac (Figure 4B), and in the similarity test this recombinate received 2.6 of 3.0 points.

Nordström[28] suggested the formation of ethyl esters from lower fatty acids during fermentation with *Saccharomyces cerevisiae*, and ethyl esters have been described as the largest group among the volatile compounds in Cognac.[2] Our study corroborated that ethyl esters make an important contribution to the aroma of Cognac, because high OAVs were calculated for ethyl (*S*)-2-methylbutanoate, ethyl methylpropanoate, ethyl 3-methylbutanoate, and ethyl hexanoate. The concentrations

Table 5. Orthonasal Detection Odor Thresholds in Water/Ethanol and Odor Activity Values (OAVs) of 34 Odorants in Cognac

compound	odor threshold (μg/L) in water/ethanol (6:4, v/v)	OAV[a]
ethanol[b]	24900	12690
(*E*)-β-damascenone[c]	0.14	2357
methylpropanal[c]	5.9	850
ethyl (*S*)-2-methylbutanoate[c]	0.22	195
ethyl methylpropanoate[c]	4.5	120
ethyl 3-methylbutanoate[c]	1.6	100
ethyl hexanoate[c]	29.7	97
3-methylbutanal[c]	2.8	73
2,3-butanedione[c]	2.8	71
ethyl butanoate[c]	9.5	69
ethyl octanoate[c]	147.0	61
4-hydroxy-3-methoxybenzaldehyde[c]	22.0	24
1,1-diethoxyethane[c]	719.0	23
3-methylbutanol[c]	56100.0	19
(*E*)-2-nonenal[c]	0.6	15
2-methoxyphenol[c]	9.2	10
4-vinyl-2-methoxyphenol[c]	7.1	7
4-ethyl-2-methoxyphenol[c]	6.9	6
methylpropanol	100691.0	5
1-hexanol	8000.0	5
ethyl 2-hydroxy-3-methylbutanoate[c]	30.5	4
cyclohexanoyl acetate	1.6	4
3-methyl-1-butylacetate[c]	245.0	3
phenylacetic acid	9.2	3
2-phenylethanol[c]	2600.0	3
(3*S*,4*S*)-*cis*-whiskey lactone[c]	67.0	3
acetaldehyde	19200.0	3
hexanoic acid	7563.0	2
3-hydroxy-4,5-dimethyl-2(5*H*)-furanone	24.2	2
2-phenylethyl acetate	108.0	2
acetic acid	75521.0	2
ethyl pentanoate	3.0	1
(*Z*)-3-hexenol	1257.0	1
2-methylbutanol[c]	211800.0	1

[a]The odor activity value for ethanol was calculated by dividing its concentration by its odor threshold in water. [b]The odor threshold was measured in water. [c]Odor thresholds previously reported.[11]

DOI: 10.1021/jf506307x
J. Agric. Food Chem. 2015, 63, 1948−1956

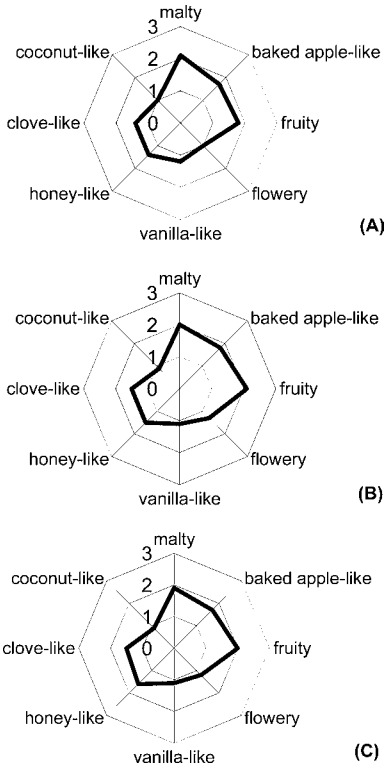

Figure 4. Aroma profile analysis of (A) the aroma recombinate in water/ethanol (6:4, v/v), (B) the Cognac, and (C) the aroma recombinate with a nonvolatile matrix prepared from Cognac added.

measured in the Cognac for ethyl 2-methylbutanoate, ethyl 3-methylbutanoate, and ethyl hexanoate were in good agreement with data reported earlier by Schreier et al.[3]

Janacova et al.[9] suggested methylpropanol, 2-methylbutanol, and 3-methylbutanol to be important in the aroma of Slovac brandies, and Webb et al.[26] also quantitated 3-methylbutanol, 2-methylbutanol and methylpropanol in Cognac with quite similar values as found here (3-methylbutanol, 1650−2190 mg/L; 2-methylbutanol, 330−430 mg/L; and 2-methylpropanol, 910−1100 mg/L). These alcohols have long been known as amino acid metabolites of yeast by the Ehrlich mechanism and have been detected in many fermented foods. They were also recently shown by us to be key odorants in whiskey,[11] Williams Christ brandy,[25] or wheat beer, respectively.[29]

Guichard et al.[30] quantitated whiskey lactones in different brandies. From the four possible stereoisomers they only found the (3*S*,4*S*)-*cis*-whiskey lactone and the (3*S*,4*R*)-*trans*-whiskey lactone, which is also in agreement with the result found here. Mosandl and Kustermann[31] reported that both enantiomers were mainly present in American white oak (*Quercus alba*). Maga[32] and Guymon and Crowell[33] investigated brandies aged in American and French oak barrels and found both whiskey lactone isomers in quite high concentrations in brandies aged in American oak, but in lower concentrations in French oak aged brandies. The Cognac used in this study was stored in French oak barrels, and, thus, the concentrations of these whiskey lactones were rather low, thus supporting the literature results.

In the present study a total of eight aroma compounds were detected for the first time in the volatile fraction of Cognac, namely, 2-methoxy-4-vinylphenol, phenylacetic acid, (*E*)-2-nonenal, 3-hydroxy-4,5,-dimethyl-2(5*H*)-furanone, ethyl cyclohexanoyl acetate, 2-isopropyl-3-methoxypyrazine, 2-isobutyl-3-methoxypyrazine, and α-damascone (Table 2). Among them, in particular, 2-methoxy-4-vinylphenol, phenylacetic acid, and (*E*)-2-nonenal showed quite high odor activity values.

Compared to wine[34] and other spirits,[25] the concentration of (*E*)-β-damascenone was quite high in the Cognac. Therefore, the odorant was quantitated in further Cognacs from different manufacturers, and interestingly the concentrations were quite high in all spirits, ranging from 108 to 330 μg/L (Table 6). By contrast, the norisoprenoid was much lower in seven German brandies (3−31 μg/L) as well as in Spanish (8−12 μg/L) and two French brandies (30−40 μg/L).

Table 6. Concentrations of (*E*)-β-Damascenone (DC) and Ethyl Pentanoate (EP) in Different Commercial Brandies and Cognacs

	concn (μg/L) of		
product	DC	EP	ratio DC/EP
Cognacs			
Hennessy VSOP	330	3	110
Hennessy special	199	7	28
Remy Martin VSOP	305	9	34
Courvoisier VSOP	169	10	17
Landy VSOP	150	13	12
Camus VSOP	150	9	17
Otard VSOP	324	13	25
Comte Joseph	127	5	25
Jean Pierre Delator	108	9	12
Lephard VSOP	128	10	13
Lephard VS	144	8	18
Eduard	123	8	15
brandies			
Mariacron (Germany)	16	320	0.05
Chantré (Germany)	31	108	0.29
Tisserad (Germany)	11	175	0.06
No Name (Germany)	24	167	0.14
Scharlachberg (Germany)	12	68	0.18
Goldkrone (Germany)	3	201	0.05
Senatsrat (Germany)	9	289	0.03
Lepanto (Spain)	8	121	0.07
Carlos I (Spain)	12	129	0.09
Napoleon (France)	30	113	0.27
Dujardin Imperial (France)	40	151	0.26

Odorants in a German Brandy. For a first comparison of the key odorants in a German brandy, the AEDA was applied on a distillate from the German brandy Mariacron. The data revealed distinct differences, but in particular ethyl pentanoate was higher in the German brandy (Table 7). The quantitation of this ester in the 12 Cognacs and the 7 German brandies revealed clear differences in their concentrations (Table 6). The same was true for two Spanish and two French brandies. Whereas only 3−13 μg/L of the ester was present in the 12 Cognacs analyzed, 68−320 μg/L of the odorant was present in the 7 German brandies (Table 6).

By calculating the ratio of the β-damascenone concentration to that of ethyl pentanoate, the German and Spanish brandies could easily be differentiated from the Cognacs. Even two French brandies (Dujardin and Napoleon) could easily be differentiated on the basis of these data, suggesting the pair (*E*)-β-damascenone/ethyl pentanoate as a possible indicator for the differentiation of Cognac from other brandies.

DOI: 10.1021/jf506307x
J. Agric. Food Chem. 2015, 63, 1948−1956

Table 7. Comparison of the Most Odor-Active (FD ≥ 32) Volatile Constituents in Aroma Extracts of the German Brandy Mariacron (GB) and the Cognac Hennessy (C) on the Basis of Flavor Dilution (FD) Factors

odorant[a]	odor quality[b]	FD factor in C	FD factor in GB
methylpropanal	malty	32	16
1,1-diethoxyethane	fruity	512	512
ethyl acetate	glue-like	64	64
3-methylbutanal	malty	32	16
ethyl 2-methylpropanoate	fruity	1024	128
ethyl butanoate	fruity	128	64
(*S*)-ethyl 2-methylbutanoate	fruity	512	128
ethyl 3-methylbutanoate	fruity	64	32
2-methylpropanol	malty	256	256
3-methyl-1-butylacetate	banana-like	32	16
ethyl pentanoate	fruity	1	32
2- and 3-methylbutanol	malty	1024	1024
ethyl hexanoate	fruity	128	64
ethyl octanoate	fruity	256	32
(*E*)-*β*-damascenone	cooked apple-like	2048	256
2-phenylethanol	flowery	512	256
cis-whiskey lactone	coconut-like	64	<8
4-hydroxy-2,5-dimethyl-3(2*H*)-furanone	caramel-like	32	8
4-allyl-2-methoxyphenol	clove-like	64	16
3-hydroxy-4,5-dimethyl-2(5*H*)-furanone	seasoning-like	64	32
phenyl acetic acid	honey-like	128	64
4-hydroxy-3-methoxybenzaldehyde	vanilla-like	256	512

[a]The odorant was identified by comparing it with the reference compound on the basis of the following criteria: (i) retention indices on the capillary; (ii) mass spectra obtained by MS-EI and MS-CI; and (iii) odor quality and odor threshold determined by GC-O. [b]Odor quality perceived at the sniffing port.

Compared to data reported on the key odorants in other spirits, the results showed that the differences in the overall aromas of most distilled spirits aged in oak barrels are obviously caused by differences in the concentrations of odor-active constituents rather than by specific compounds present in the overall set of key odorants. This is, however, not a general rule, because for some spirits, such as pear brandy,[25] so-called specialists[7] among the key aroma compounds, such as ethyl decadienoate, can be the cause for overall differences in the aroma profile. Further studies will be undertaken to examine the influence of single processing steps as sources of the key aroma compounds in brandies by means of systematic studies on intermediates of the manufacturing process.

AUTHOR INFORMATION

Corresponding Author

*(P.S.) Phone: +49 8161 71 2932. Fax: +49 8161 71 2970. E-mail: Peter.Schieberle@ch.tum.de.

Notes

The authors declare no competing financial interest.

REFERENCES

(1) Reinhard, C. Gas-chromatographic study of wine, distilled wine and brandy. *Wein-Wiss.* **1968**, *23*, 475−486.

(2) Postel, W.; Adam, L. Gas-chromatographic characterisation of brandy, Cognac and Armagnac II. Concentrations of volatile contents. *Branntweinwirtschaft* **1980**, *2*, 154−164.

(3) Schreier, P.; Drawert, F.; Schmid, M. Composition of neutral volatile constituents in grape brandies. *J. Agric. Food Chem.* **1979**, *27*, 365−372.

(4) Ledauphin, J.; Milbeau, C.; Barillier, D.; Hennequin, D. Differences in the volatile compositions of French labeled brandies (Armagnac, Calvados, Cognac and Mirabelle) using GC-MS and PLS-DA. *J. Agric. Food Chem.* **2004**, *52*, 5124−5134.

(5) De Rijke, D.; Heide, R. Flavor compounds in rum, cognac and whisky. In *Flavor of Distilled Beverages: Origin and Development*; Piggott, J. R., Ed.; Ellis Horwood: Chichester, UK, 1983; pp 192−202.

(6) Schieberle, P.; Hofmann, T. Mapping the combinatorial code of food flavors by means of molecular sensory science approach. In *Chemical and Functional Properties of Food Components Series. Food Flavors. Chemical, Sensory and Technological Properties*; Jelen, H., Ed.; CRC Press: Boca Raton, FL, USA, 2012; ISBN 978-1-4398-1491-8, pp 413−438.

(7) Dunkel, A.; Steinhaus, M.; Kotthoff, M.; Nowak, B.; Krautwurst, D.; Schieberle, P.; Hofmann, T. Nature's chemical signatures in human olfaction: a foodborne perspective for future biotechnology. *Angew. Chem. Int. Ed.* **2014**, 7124−7143.

(8) Ferrari, G.; Lablanquie, O.; Cantagrel, R.; Ledauphin, J.; Payot, T.; Fournier, N.; Guichard, E. Determination of key odorant compounds in freshly distilled Cognac using GC/O, GC/MS and sensory evaluation. *J. Agric. Food Chem.* **2004**, *52*, 5670−5676.

(9) Janacova, A.; Sadecka, J.; Kohajdova, Z.; Spanik, J. The identification of aroma-active compounds in Slovak brandies using GC-sniffing, GC/MS and sensory evaluation. *Chromatographia* **2008**, *67*, 113−121.

(10) Zhao, Y.; Xu, J.; Fan, W.; Jiang, W. Characterization of aroma compounds of four brandies by aroma extract dilution analysis. *Am. J. Enol. Vitic.* **2009**, *60*, 269−276.

(11) Poisson, L.; Schieberle, P. Characterization of the key aroma compounds in an American Bourbon whisky by quantitative measurements, aroma recombination and omission studies. *J. Agric. Food Chem.* **2008**, *56*, 5820−5826.

(12) Schieberle, P. Primary odorants of pale lager beer. Differences to other beers and changes during storage. *Z. Lebensm. Unters. Forsch.* **1991**, *193*, 403−431.

(13) Guth, H.; Grosch, W. Determination of soya-bean oil: quantification of primary flavor compounds using a stable isotope dilution assay. *Lebensm. Wiss. Technol.* **1990**, *23*, 513−522.

(14) Kirchhoff, E.; Schieberle, P. Quantitation of odor-active compounds in rye flour and rye sourdough using stable isotope dilution assays. *J. Agric. Food Chem.* **2002**, *50*, 5378−5385.

(15) Komarek, D. *Key Odorants in Beer − Influence of Storage on the Flavor Stability*. Ph.D. thesis, Technical University of Munich, 2001.

(16) Jagella, T.; Grosch, W. Flavour and off-flavour compounds of black and white pepper (*Piper nigrum* L.). III. Desirable and undesirable odorants of white pepper. *Eur. Food Res. Technol.* **1999**, *209*, 27−31.

(17) Blank, I.; Schieberle, P. Analysis of the seasoning-like flavour substances of a commercial lovage extract (*Levisticum officinale* Koch.). *Flavour Fragrance J.* **1993**, *8*, 191−195.

(18) Guth, H.; Grosch, W. Identification of the character impact odorants of stewed beef juice by instrumental analysis and sensory studies. *J. Agric. Food Chem.* **1994**, *42*, 2862−2866.

(19) Czerny, M.; Schieberle, P. Influence of the polyethylene packaging on the absorption of odor-active compounds from UHT-milk. *Eur. Food Res. Technol.* **2007**, *225*, 215−223.

(20) Schuh, C.; Schieberle, P. Characterization of the key aroma compounds in the beverage preared from Darjeeling black tea: quantitative differences between tea leaves. *J. Agric. Food Chem.* **2006**, *54*, 916−924.

(21) Engel, W.; Bahr, W.; Schieberle, P. Solvent assisted flavour evaporation − a new and versatile technique for the careful and direct isolation of aroma compounds from complex food matrices. *Eur. Food Res. Technol.* **1999**, *209*, 237−241.

DOI: 10.1021/jf506307x
J. Agric. Food Chem. 2015, 63, 1948−1956

(22) Hinterholzer, A.; Schieberle, P. Identification of the most odor-active volatiles in fresh, hand-extracted juice of Valencia late oranges by odor dilution techniques. *Flavor Fragrance J.* **1998**, *13*, 49−55.
(23) Czerny, M.; Christlbauer, M.; Christlbauer, M.; Fischer, A.; Granvogel, M.; Hammer, M.; Hartl, C.; Hernandez, N. M.; Schieberle, P. Re-investigation on odor thresholds of key food aroma compounds and development of an aroma language based on odor qualities of defined aqueous odorant solutions. *Eur. Food Res. Technol.* **2008**, *228*, 265−273.
(24) Bundesamt für Verbraucherschutz und Lebensmittelsicherheit BLV. *Sensorische Prüfverfahren: Dreiecksprüfung (00.90-7). Amtliche Sammlung von Untersuchungsverfahren nach § 64 LFGB*; Beuth Verlag: Berlin, Germany, 2005.
(25) Willner, B.; Granvogl, M.; Schieberle, P. Characterization of the key aroma compounds in Bartlett pear brandies by means of the sensomics concept. *J. Agric. Food Chem.* **2013**, *61*, 9583−9593.
(26) Webb, A.; Kepner, R. E.; Ikeda, R. M. Composition of a typical grape brandy fusel oil. *Anal. Chem.* **1952**, *24*, 1944−1949.
(27) Frank, S.; Wollmann, N.; Schieberle, P.; Hofmann, T. Reconstitution of the flavor signature of Dornfelder red wine on the basis of the natural concentrations of its key aroma and taste compounds. *J. Agric. Food Chem.* **2011**, *59*, 8866−8874.
(28) Nordström, K. Formation of esters from acids by brewer's yeast, II. Formation from lower fatty acids. *J. Inst. Brew.* **1963**, *70*, 42−55.
(29) Langos, D.; Granvogl, M.; Schieberle, P. Characterization of the key aroma compounds in two Bavarian wheat beers by means of the Sensomics approach. *J. Agric. Food Chem.* **2013**, *61*, 11303−11311.
(30) Guichard, E.; Fournier, N.; Masson, G.; Puech, J.-L. Stereoisomers of β-methyl-γ-octalactone. I. Quantitation in brandies as a function of wood origin and treatment of the barrels. *Am. J. Enol. Vitic.* **1995**, *46*, 419−423.
(31) Mosandl, A.; Kustermann, A. Stereoisomeric flavor compounds. XXX. HRGC analysis of chiral γ-lactones from beverages and fruit preparations. *Z. Lebensm. Unters. Forsch.* **1989**, *189*, 212−215.
(32) Maga, J. *Formation and Extraction of cis- and trans-β-Methyl-γ-octalactone from Quercus alba in Distilled Beverage Flavor: Recent Developments*; Piggott, J. R., Paterson, A., Eds.; Ellis Horwood: Chichester, UK, 1989; pp 171−176.
(33) Guymon, J. F.; Crowell, E. A. GC-separated brandy components derived from French and American oaks. *Am. J. Enol. Vitic.* **1977**, *23*, 113−120.
(34) Kotseridis, Y.; Baumes, R.; Skouroumounis, G. Quantitative determination of free and hydrolytically liberated β-damascenon in red grapes and wines using a stable isotope dilution assay. *J. Chromatogr., A* **1999**, *849*, 245−254.

DOI: 10.1021/jf506307x
J. Agric. Food Chem. 2015, 63, 1948−1956

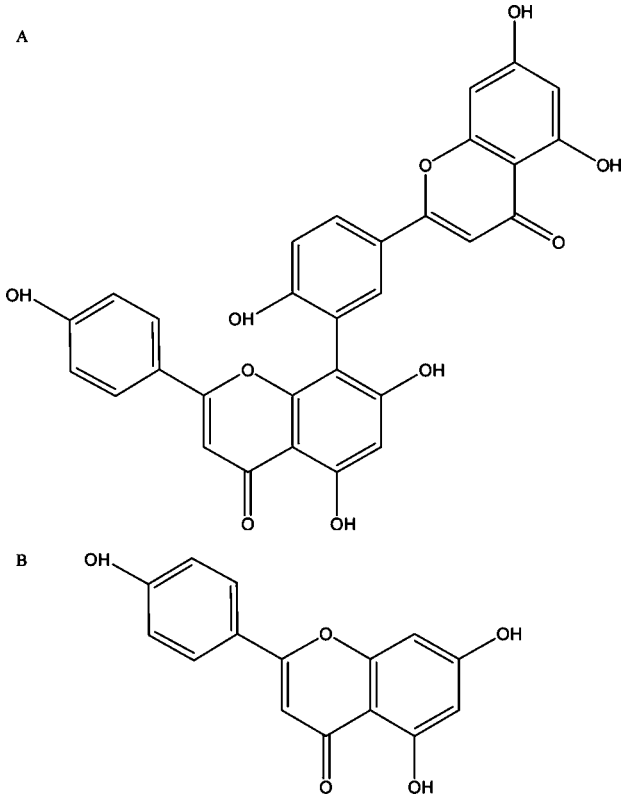

Figure 1. Chemical structure of amentoflavone AMF (A) and the internal standard (B).

inhibitors of cytochrome (CYP) 2C9, CYP 3A4, and especially CYP 1A2/1A1,[14−16] the other flavones present in the herbal extracts used in these studies could potentially alter the metabolism and disposition of AMF. On the other hand, because of simultaneous quantitation of multiple free and total biflavone components, including AMF, in rat plasma and human urine, respectively, the short cycle time and limit of detection were sacrificed for sufficient separation and accurate quantification of multicomponents in both methods. To improve understanding of the bioactivity and role of AMF beyond that provided by previous pharmacodynamics studies,[17,18] we developed a new specific, sensitive, and rapid liquid chromatography−tandem mass spectrometry (LC−MS/MS) method to detect the total content of AMF following β-glucuronidase/sulfatase hydrolysis. The present method had the advantages of a shorter detection time and lower limit of detection than the two published methods.[7,8] We used this method to generate a full pharmacokinetic profile for AMF in rats by administering a single dose by various routes, and then fully analyzing the conjugate metabolites of AMF, including its glucuronide/sulfate forms. Further, the pharmacokinetic differences between AMF administered to rats via alternative routes and the bioavailability of the compound were investigated. The resulting data are very useful for developing an improved understanding of the pharmacological profile of AMF in vivo, which will be beneficial for preclinical research and clinical use of AMF.

MATERIALS AND METHODS

Chemicals. AMF (98.0%) and apiolin (internal standard, 99.0%) were obtained from the National Institute for the Control of Pharmaceutical and Biological Products (Beijing, China). Methanol (HPLC grade) was purchased from Sigma-Aldrich (St. Louis, MO). β-Glucuronidase (type H-1 from *Helix pomatia*, which contained 300 units of β-glucuronidase and 15.3 units of sulfatase/mg), was purchased from Sigma-Aldrich. Formic acid was purchased from J.T. Baker. Wahaha deionized water (Hangzhou, China) was used throughout the study. Ethyl acetate and other chemicals were of analytical grade and obtained from Beijing Chemical Co. (Beijing, China).

Animal Treatment and Pharmacokinetic Analysis. Male Sprague−Dawley (SD) rats (190−210 g) were supplied by Beijing Vital River Laboratories Animal Technology Co. Ltd. All the experimental protocols were approved by the Animal Ethics Committee of Beijing Institute of Pharmacology and Toxicology (No. 11400700031602). Fifteen SD rats were randomly divided into three groups and were fasted overnight with free access to water prior to AMF administration. Animals in the first group received a single 10 mg/kg intravenous (iv) dose of AMF via the tail vein. Animals in the second group received a single 10 mg/kg intraperitoneal (ip) dose of AMF suspended in 0.1% Tween 80. Animals in the third group received a single 300 mg/kg dose of AMF suspended in 1% Tween 80 by oral gavage (po).

Blood samples were obtained via retro-orbital puncture with a glass capillary at 0, 0.033, 0.083, 0.167, 0.25, 0.5, 1, 2, 4, 6, 9, 12, and 24 h after iv and ip administration and at 0, 0.017, 0.5, 0.75, 1, 1.5, 2, 2.5, 3, 4, 6, 8, 12, and 24 h after po administration. The blood samples were collected into heparinized plastic tubes, and the plasma was separated by centrifugation at 4000 rpm at 4 °C for 10 min. The resulting plasma samples were stored frozen (−30 °C) until analyzed.

LC−MS/MS Method. The LC method employed a Thermo Syncronis C18 column (2.1 mm × 50 mm, 5 μm) equipped with an online filter and maintained at room temperature. Using a Finnigan Surveyor HPLC system, peaks were separated using a mobile phase of methanol, water, and formic acid (70:30:0.1, v/v/v) at a flow rate of 0.2 mL/min. The injection volume was 5 μL, and the run time was 3 min. A triple-stage quadrupole mass spectrometer (TSQ Quantum Discovery, ThermoElectron, San Jose, CA) equipped with an electrospray ionization (ESI) source was used for AMF detection. Xcalibur version 1.4 software (Thermo-Fisher, USA) controlled the HPLC system, mass spectrometer, and autosampler, and data analyses were completed using LCQuan software (Thermo Finnigan, USA). The mass spectrometer was operated in the negative ion detection mode, and quantification was performed using selected reaction monitoring (SRM) of the transitions of m/z 537.1 → m/z 374.9 for AMF (Figure 2A) and of m/z 269.2 → m/z 224.9 for apiolin (as an internal standard, Figure 2B) with a scan time of 0.1 s per transition. The optimum ion source parameters were as follows: ESI source temperature, 300 °C; spray voltage, 3500 V; sheath gas pressure, 43 psi; auxiliary gas pressure, 20 psi.

Standard and Quality Control (QC) Sample Preparation. Stock solutions of AMF and the internal standard were prepared individually by dissolving 10 mg of AMF or 20 mg of apiolin in 100 mL of methanol. Ten working standard solutions containing 9.3, 18.6, 37.2, 93.0, 186, 465, 930, 1860, 4650, and 9300 nmol/L of AMF were prepared by serial dilution of the stock solution using appropriate volumes of methanol. A working solution of the internal standard was prepared by diluting the stock solution with ethyl acetate by a factor of 1000 to a final concentration of 700 nmol/L. All stock solutions were stored at 4 °C, and all working solutions were freshly prepared each week. Plasma calibration standards were prepared by spiking 45 μL of fresh rat plasma with 5 μL of the appropriate working solution to achieve AMF concentrations of 0.93, 1.86, 3.72, 9.30, 18.6, 46.5, 93, 186, 465, and 930 nmol/L. QC samples containing three concentrations of AMF (low, 2.79 nmol/L; medium, 37.2 nmol/L; and high, 744 nmol/L) were prepared similarly.

Sample Preparation. The utilization of a mixture of β-glucuronidase/sulfatase to hydrolyze glucuronidated/sulfated conjugates has been successfully applied for the quantification of drugs in plasma.[19−23] In brief, prior to the determination of the total AMF (including free AMF plus its conjugated metabolites), plasma samples were treated with β-glucuronidase/sulfatase (type H-1) in vitro,

DOI: 10.1021/jf5019615
J. Agric. Food Chem. 2015, 63, 1957−1966

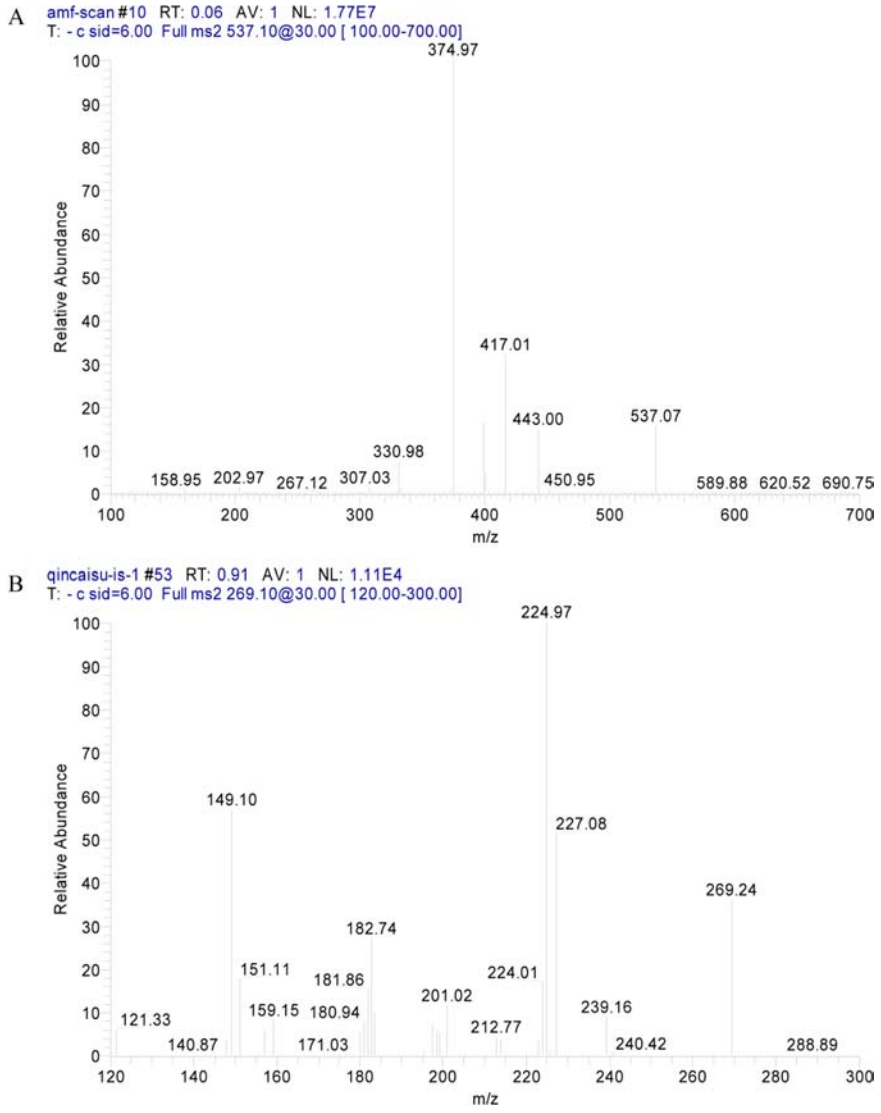

Figure 2. Product ion mass spectra of deprotonated molecules of amentoflavone (AMF, A) and the internal standard (B).

whereas no enzyme treatment was used before determination of free AMF. However, extensive efforts were made to optimize the conditions used in this first enzymatic step prior to liquid−liquid extraction (Supporting Information). Based on these results, we established the following optimal enzymolysis conditions: For enzymolysis, 50 μL plasma samples were mixed with 50 μL of β-glucuronidase/sulfatase solution in 0.1 M acetate buffer, pH 5 (500/16.6 units/mL for samples from rats dosed po and 5,000/166 units/mL for samples from rats dosed iv and ip), and 10 μL of ascorbic acid (200 mg/mL), followed by incubation at 37 °C for 12 h under anaerobic conditions in the dark with gentle shaking. After hydrolysis, the plasma was partitioned using 1 mL of ethyl acetate containing 700 nmol/L of the internal standard. The mixture was vortexed for 3 min and centrifuged at 4000*g* for 10 min at 4 °C. The ethyl acetate layer was then evaporated to dryness under N_2 gas and reconstituted with 50 μL of methanol. For determination of free AMF, 50 μL plasma samples were processed in the same manner, except that no enzyme was included in the 0.1 M acetate buffer.

To prepare calibrator samples, 45 μL of plasma was mixed with 5 μL of the appropriate AMF working solution. The mixture was added to 50 μL of 0.1 M acetate buffer (pH 5) and processed in the same way as the other samples.

Method Validation. The method was validated for selectivity, linearity, precision, accuracy, recovery, matrix effect, and stability. The validation assays were carried out in accordance with currently accepted U.S. Food and Drug Administration (FDA) guidelines for use in industry.[24]

Specificity. The specificity of the LC−MS/MS method was investigated by comparing blank rat plasma from six different rats with the corresponding rat plasma samples spiked with AMF at the lower limit of quantification (LLOQ, 0.93 nmol/L). This enabled evaluation of the influences of endogenous substances in rat plasma on AMF quantification.

Recovery and Matrix Effect. The extraction recovery of AMF from rat plasma was determined at the LLOQ (0.93 nmol/L) and at 2.79, 37.2, and 744 nmol/L for QC samples. Extraction recovery was defined as the ratio of the analyte peak area from extracted QC plasma to the mean peak area from extracted blank plasma spiked with AMF. Matrix effects were quantified as the ratio of the analyte peak area from an extracted plasma blank spiked with AMF to the mean peak area observed during analysis of the standard AMF solution, at the same concentration, prepared in methanol.

Linearity and LLOQ. Calibration curves were calculated by linear regression analysis of the peak area ratio of AMF to internal standard plotted against the normalized concentration of AMF, with a weighting factor of $1/x^2$. Curve fits were not forced to intersect the origin. The LLOQ of the assay was defined as the lowest concentration of AMF detected with precision and accuracy lower than 20% (n = 6).

Precision and Accuracy. QC samples were processed (n = 6) at the LLOQ and at 2.79, 37.2, and 744 nmol/L in rat plasma for each run

DOI: 10.1021/jf5019615
J. Agric. Food Chem. 2015, 63, 1957−1966

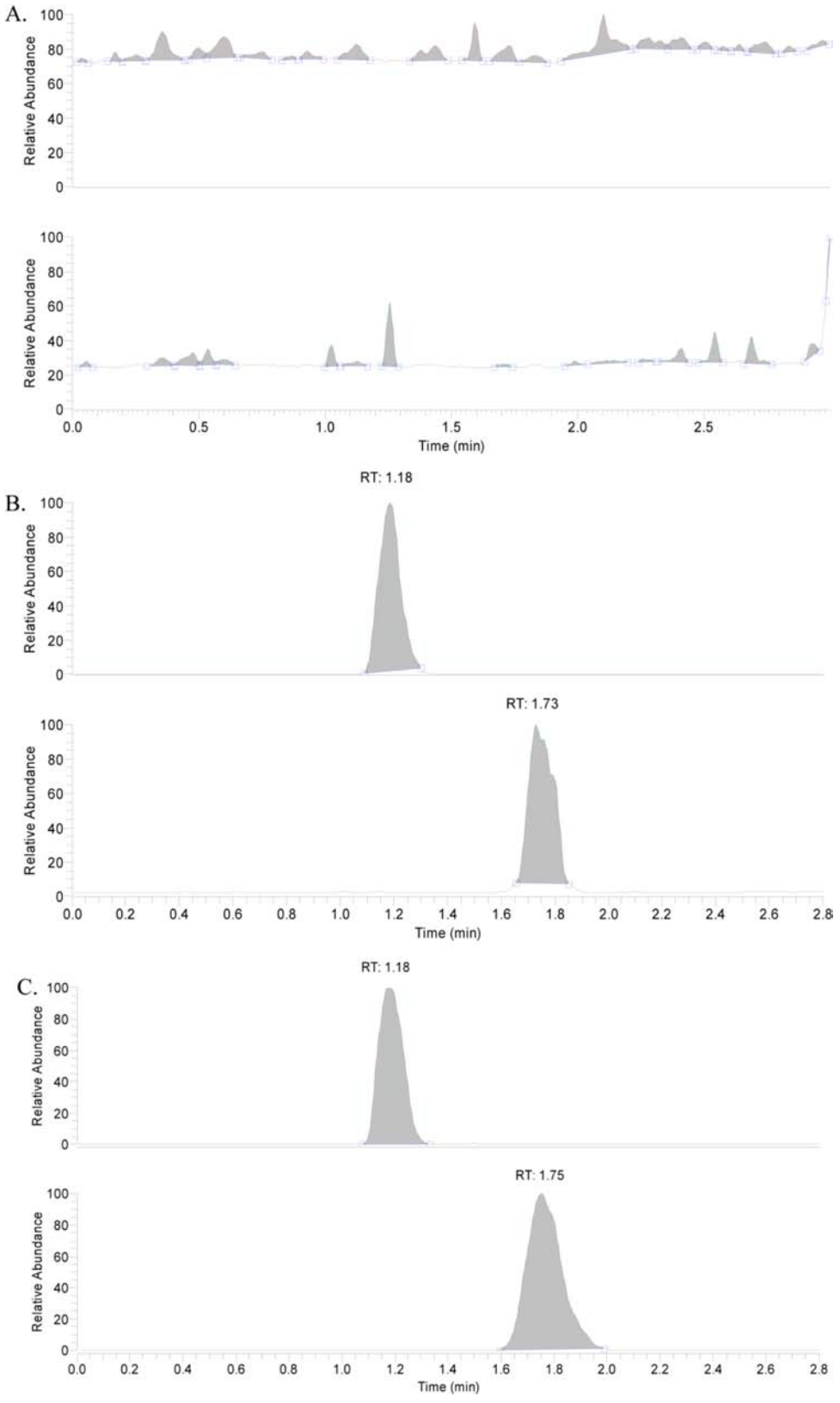

Figure 3. Representative selected reaction monitoring (SRM) chromatograms of amentoflavone (AMF, I) and internal standard (II) in rat plasma: (A) blank plasma sample; (B) blank plasma sample spiked with AMF at the lowest limit of quantification (0.93 nmol/L) and the internal standard (700 nmol/L); (C) plasma sample obtained from a rat 3 h after oral administration of AMF, when the concentration of AMF was found to be 0.16 nmol/mL.

over 3 days. The concentrations in the QC and the unknown samples were calculated from the equation of the calibration curve. Accuracy was measured by the deviation or bias (%) of the mean calculated concentration from the actual concentration. Precision was defined as

DOI: 10.1021/jf5019615
J. Agric. Food Chem. 2015, 63, 1957−1966

the coefficient of variation (CV, %). Precision and accuracy were determined within each day for the LLOQ and three concentrations of QCs, with six replicates and one calibration set prepared each day. Precision and accuracy between different days were evaluated for each QC concentration and for the LLOQ using 18 replicates obtained over three different days.

Stability and Dilution. The stability of AMF in rat plasma at the LLOQ and at the three QC concentrations was determined at room temperature (24 °C for 6 h), after three freeze−thaw cycles (−30 °C to room temperature), at the storage temperature (14 days at −30 °C), and in the autosampler at 4 °C. Five aliquots were analyzed for each condition, and the stability was calculated according to a published procedure.[25] The analyte was considered stable when the accuracy bias was within ±15% of the nominal concentration. Notably, some samples obtained from animals receiving iv AMF were observed to have AMF levels exceeding the highest concentration of the calibration curve. Therefore, to accurately evaluate the precision and accuracy for these samples, 25- and 5-fold more concentrated QC samples were diluted into blank matrix and analyzed in the same way as the other samples.[26] For these samples, accuracy was within ±15% and precision was ≤20%.

Carry-Over. To evaluate carry-over between samples, a blank sample was tested immediately after testing an AMF standard at the upper limit of quantitation (ULOQ).[27]

Data Evaluation and Statistics. The concentrations of the conjugate metabolites of AMF in plasma were calculated by comparing samples treated with β-glucuronidase/sulfatase to samples with no enzyme treatment, as follows:

$$\text{glucuronidated + sulfated AMF} = \text{AMF after β-glucuronidase/sulfatase treatment} - \text{free AMF} \quad (1)$$

The pharmacokinetic parameters were calculated using the Drugs and Statistics 2.0 software program (DAS 2.0, Shanghai, China), assuming a noncompartmental model. The area under the plasma concentration−time curve (AUC) was calculated using the trapezoidal method; the maximum plasma concentration (C_{max}) and the time to reach the maximum plasma concentration (t_{max}) were obtained by visual inspection of the experimental data; the terminal half-life ($t_{1/2}$) was calculated as 0.693/k, with k defined as the slope of the terminal regression line. The bioavailability (F) of AMF after ip and po administration was calculated using the following equation:

$$F = \frac{\text{po, ip AUC}_{0-t}}{\text{iv AUC}_{0-t}} \times \frac{\text{iv dose}}{\text{po, ip dose}} \quad (2)$$

where AUC_{0-t} represents the AUC from time 0 to the last time point.

The results were analyzed using Student's t-test to detect significant differences between the AMF and AMF conjugate pharmacokinetic data. Comparisons with $p < 0.05$ were considered to be significantly different. All results were expressed as the mean ± standard deviation (SD) for all replicates.

RESULTS

Method Development. A new LC−MS/MS method was optimized for the determination of plasma concentrations of AMF and its metabolites. We found that AMF could be measured in the positive- or negative-ion mode, but the mass response of AMF under positive mode was not sensitive enough to enable quantitative pharmacokinetic analysis. The most abundant molecular ion for AMF was $[M - H]^-$ (m/z 537.1). This was chosen for fragmentation analysis, and MS optimization was then performed by automatic tuning of the instrument to detect the product ion m/z 374.9. The fragment ion (m/z 224.9) of the internal standard (m/z 269.2) was obtained in a similar way. The product ion spectra of AMF (m/z 374.9) and the internal standard (m/z 224.9) are shown in Figure 2.

We found that changing the methanol:water ratio from 90:10 to 50:50 (v/v) improved the MS response area and peak symmetry and also reduced the run time for the target ions. For chromatographic separation, we found that a mobile phase of 70% methanol at a flow rate of 0.2 mL/min gave an ideal retention time of less than 3 min, which enabled rapid analysis of multiple samples. We also observed that, compared to lower percentages, 70% methanol enhanced the peak signal, most likely by enhancing ionization. Like most biflavonoids, AMF contains a carboxylic acid group, making the pH of the solvent critical for mass response. When 0.1% formic acid was included in the mobile phase, the peaks of both AMF and the internal standard were symmetrical and sharp.

The sample preparation method was also optimized to ensure reproducibility, minimal matrix effects, and a low cost. Apiolin was chosen as the internal standard because it has similar chemical structure, physicochemical properties, and mass spectrometric behavior to those of AMF. A single-step liquid−liquid extraction procedure was used to enrich and clean the target compound from plasma. Although several organic solvents, including ethyl acetate, acetonitrile, methanol, and diethyl ether, were investigated as extraction solvents, ethyl acetate produced the highest recovery and cleanest samples.

Method Validation. *Selectivity.* The SRM chromatograms of blank rat plasma, blank plasma spiked with AMF at the LLOQ (0.93 nmol/L) and with the internal standard (700 nmol/L), and plasma samples obtained 3 h after po administration of 300 mg/kg AMF are shown in Figure 3. No endogenous interference was observed in the chromatograms of control blank rat plasma ($n = 6$) over the period when AMF and the internal standard eluted, indicating that the analysis was highly selective.

Linearity and Sensitivity. The LLOQ for this method was 0.93 nmol/L for AMF in rat plasma. The standard curve was obtained by plotting the ratio of AMF to internal standard peak area versus the concentration of AMF added (0.93−930 nmol/L). Linear regression to $1/x^2$ yielded a correlation coefficient ≥0.9955, and the slope of each regression line was reproducible, with a relative standard deviation of <2% (Table 1). Calibration standards showed good precision (% CV between 4.9% and 11%) and accuracy (% bias between −8.2% and 6.7%) over the range of 0.93−930 nmol/L (Table 2).

Accuracy and Precision. The intra- and interassay accuracy (% bias) and precision (% CV) of the assay at the LLOQ and for three QCs at concentrations of 0.93−744 nmol/L are summarized in Table 3. The values for intra- and interday QC accuracy ranged from −5.55% to −1.25% and from −0.38% to −4.57%, respectively. The accuracy at the LLOQ was within

Table 1. Linearity for Amentoflavone (AMF)[a]

assay no.	slope	intercept	correlation coeff
1	0.0503	0.1864	0.9963
2	0.0518	0.2588	0.9977
3	0.0504	0.2073	0.9981
4	0.0558	0.0587	0.9995
5	0.0544	0.1628	0.9990
6	0.0525	0.1339	0.9991

[a]Regression to $1/x^2$.

DOI: 10.1021/jf5019615
J. Agric. Food Chem. 2015, 63, 1957−1966

Table 2. Standard Curve Accuracy and Precision for Amentoflavone (AMF; n = 6)

	nominal concn (nmol/L)									
param	0.93	1.86	3.72	9.30	18.6	46.5	93.0	186	465	930
n	6	6	6	6	6	6	6	6	6	6
mean	0.97	1.80	3.42	9.51	19.1	46.5	95.9	199	455	877
% CV	11.01	12.14	11.73	8.37	9.50	10.13	8.45	6.22	4.92	6.00
% bias	3.27	−2.88	−8.17	2.33	3.43	0.12	3.23	6.67	−2.14	−5.55

Table 3. Precision (% CV), Accuracy, Recovery, and Matrix Effect (ME) (%) in Rat Plasma

	concn added (nmol/L)	mean concn (nmol/L)	CV (%)	bias (%)	recovery	ME
intraassay (n = 6)	0.93 (LLOQ-QC)	0.91	7.05	−1.83	92.0	90.7
	2.79 (low-QC)	2.75	11.6	−1.25	88.4	100.9
	37.2 (mid-QC)	35.1	5.17	−5.55	98.6	98.6
	744 (high-QC)	703.9	5.83	−5.31	89.7	103.7
interassay (3 days, n = 18)	0.93 (LLOQ-QC)	0.91	7.53	−2.82		
	2.79 (low-QC)	2.75	10.10	−1.32		
	37.2 (mid-QC)	37.0	7.79	−0.38		
	744 (high-QC)	709.4	5.66	−4.57		

Table 4. Stability of Different Concentrations of Amentoflavone (AMF) in Rat Plasma under Different Storage Conditions (n = 5)

storage condtns	concn added (nmol/L)	mean concn (nmol/L)	CV (%)	bias (%)
short-term (6 h at 24 °C)	0.93	0.89	8.64	−3.61
	2.79	2.79	8.32	2.58
	37.2	39.3	6.56	5.86
	744	711.8	4.72	−4.24
long-term (14 days at −30 °C)	0.93	0.84	8.32	−10.07
	2.79	2.75	12.31	−2.27
	37.2	35.11	5.39	−5.53
	744	704.2	4.94	−5.27
three freeze−thaw cycles	0.93	0.91	7.36	−1.18
	2.79	2.81	10.02	0.85
	37.2	39.01	6.39	4.96
	744	718.8	3.56	−3.3
autosampler for 24 h (4 °C)	0.93	0.95	6.27	1.37
	2.79	2.69	6.24	−3.10
	37.2	39.1	6.69	5.21
	744	711.2	4.98	−4.32

3%, with a CV of <8%. The intra- and interday precision ranged from 5.17% to 11.6% and 5.66% to 10.1%, respectively. The accuracy and precision for AMF were within ±15% for all QCs and ±20% at the LLOQ. These parameters indicated that the LC−MS/MS assay provided accurate and precise detection of AMF over the 0.93−930 nmol/L range, and that detection could be extended to higher concentrations.

Extraction Efficiency and Matrix Effects. The AMF extraction efficiency from rat plasma was determined at the LLOQ and at three QC concentrations: 2.79, 37.2, and 744 nmol/L. Extraction efficiency ranged from 88% to 98% (Table 3), and it was consistent, precise, and reproducible. Analysis of the matrix effect of AMF at the LLOQ and at the three QC concentrations (n = 6; Table 3) indicated that there was no significant matrix effect on AMF extraction from rat plasma.

Stability and Dilution. The stability of AMF in rat plasma at the LLOQ and at the three QC concentrations was investigated under a variety of storage and processing conditions that simulated sample handling during the entire protocol (Table 4). These results indicated that AMF was stable over three freeze−thaw cycles, at room temperature for 24 h, in the autosampler for 24 h at 4 °C, and frozen at −30 °C for 15 days. In addition, we evaluated the CV and accuracy after dilution in rat plasma, since some of the early pharmacokinetic samples required dilution due to having concentrations above the ULOQ. We found that the precision and accuracy were unaffected by 25- or 5-fold dilution.

Carry-Over. To ensure that there was no carry-over between samples, we washed the syringe and injection port multiple times with 50% methanol between samples, and we also directly confirmed that no carry-over was observed using a plasma blank sample.

Pharmacokinetic Application. Although AMF has previously been administered iv, ip, or po in studies evaluating its efficacy,[17,18,28] detailed pharmacokinetic analyses of AMF have not been reported. We used our sensitive and specific LC−MS/MS method to evaluate AMF pharmacokinetics in rats after a single po, iv, or ip dose (Figure 4). The pharmacokinetic parameters of the conjugated and free forms of AMF are listed in Tables 5 and 6.

After iv dosing, AMF and its conjugates showed biexponential clearance kinetics (Figure 4A), with the

DOI: 10.1021/jf5019615
J. Agric. Food Chem. 2015, 63, 1957−1966

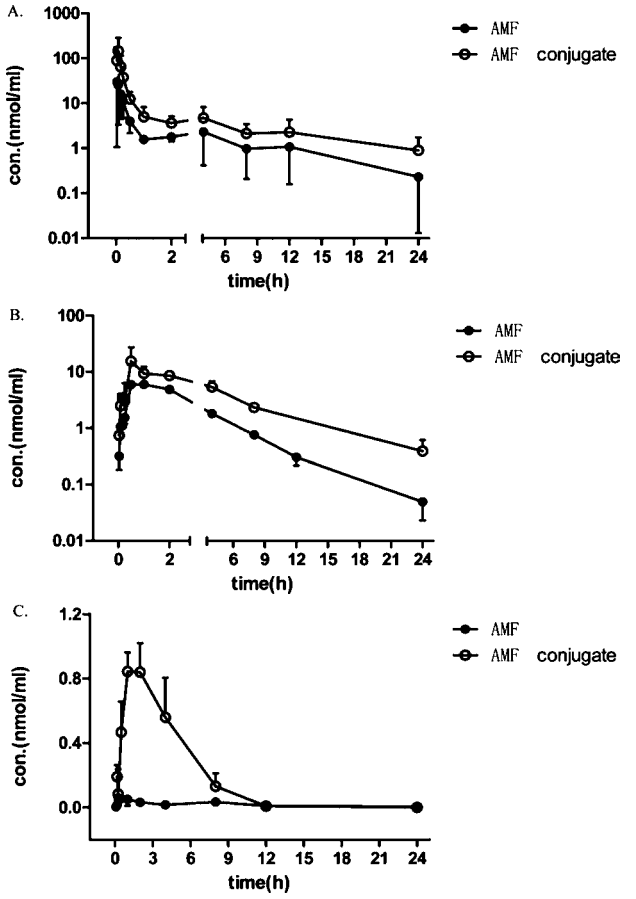

Figure 4. The pharmacokinetic profiles of amentoflavone (AMF) and its conjugates. Plasma concentration of AMF and its conjugates are shown after administration of (A) 10 mg/kg intravenous (iv) AMF, (B) 10 mg/kg intraperitoneal (ip) AMF, and (C) 300 mg/kg oral (po) AMF (mean ± standard deviation, n = 5).

conjugates present at higher concentrations throughout. Based on the AUC, 26.8% of the total AMF detected was nonconjugated, and 73.2% was conjugated (Table 6). Moreover, in plasma samples treated with the glucuronidase/sulfatase enzymes in vitro, the measured plasma AMF concentrations increased by ~2.0 to 5.6-fold, consistent with the measured ratio between conjugated and nonconjugated forms. Based on noncompartmental modeling of the data, both species had essentially the same (p >0.05) mean residence time (MRT_{0-t}), $t_{1/2}$, and t_{max} (Table 5). These data collectively suggested that AMF was rapidly conjugated (glucuronidated and/or sulfated) in the bloodstream, which may explain its rapid clearance time and high volume of distribution.

After a 300 mg/kg po dose, a low level of the free form of AMF was detected in the bloodstream throughout the analysis period (Figure 4C and Table 5). In contrast, higher concentrations of the AMF conjugates were detected, representing 90.7% of the total AMF, based on the AUC_{0-t} (Table 6). Comparison of the AUC_{0-t} values following po and iv doses indicated that the absolute oral bioavailability of total AMF was low (~0.13% ± 0.04%).

The pharmacokinetic profile and bioavailability were further assessed following ip administration of 10 mg/kg (Figure 4B and Table 5). The ratio of conjugate to the free form of AMF after ip dosing was similar to the ratio observed following iv administration, indicating that rapid conjugation still occurred

Table 5. Pharmacokinetic Parameters of Amentoflavone (AMF) and Its Conjugates after Intravenous (Iv), Intraperitoneal (Ip), or Oral (Po) Administration to Rats (n = 5)

dose		t_{max} (h)	C_{max} (nmol/mL)	$AUC_{(0-t)}$ (nmol/mL h)	$AUC_{(0\to\infty)}$ (nmol/mL h)	$MRT_{(0-24h)}$ (h)	$t_{1/2}$ (h)	V_Z (L/kg)	CL (mL/h/kg)	bioavailability (%)
iv 10 mg/kg	AMF	0.11 ± 0.02	31.2 ± 27.0	33.0 ± 11.9	35.2 ± 13.9	5.39 ± 3.33	5.88 ± 1.78	2.53 ± 0.65	320 ± 139	
	AMF conjugates	0.11 ± 0.05	149 ± 134	87.4 ± 11.9	98.5 ± 22.9	5.29 ± 3.90	7.17 ± 2.64	1.03 ± 0.23	105 ± 25.0	
	total (AMF + conjugates)	0.12 ± 0.03	175 ± 156	121 ± 23.8	133 ± 36.3	5.30 ± 3.74	6.48 ± 2.26	0.69 ± 0.13	79.1 ± 22.3	
ip 10 mg/kg	AMF	0.83 ± 0.29	6.26 ± 0.33	25.5 ± 1.08	25.7 ± 0.82	4.01 ± 0.38	3.42 ± 1.45			77.4 ± 28.0
	AMF conjugates	1.0 ± 0.87	17.2 ± 9.18	64.2 ± 5.03	67.1 ± 6.40	4.97 ± 1.08	4.86 ± 0.88			73.5 ± 19.7
	total (AMF + conjugates)	1.1 ± 0.83	23.2 ± 9.77	80.6 ± 2.72	82.7 ± 2.13	4.26 ± 0.29	3.78 ± 1.61			66.9 ± 13.4
po 300 mg/kg	AMF	0.33 ± 0.14	0.06 ± 0.03	0.41 ± 0.08	0.49 ± 0.12	7.91 ± 1.17	11.3 ± 3.61			0.04 ± 0.01
	AMF conjugates	1.33 ± 0.58	0.94 ± 0.09	4.31 ± 1.22	4.39 ± 1.15	3.14 ± 0.67	1.66 ± 0.17			0.16 ± 0.03
	total (AMF + conjugates)	1.35 ± 0.67	1.00 ± 0.09	4.58 ± 1.23	4.69 ± 1.17	3.27 ± 0.67	1.84 ± 0.14			0.13 ± 0.04

DOI: 10.1021/jf5019615
J. Agric. Food Chem. 2015, 63, 1957−1966

Table 6. Ratios of AUC_{0-t} of Free AMF and Its Conjugates to the Total AUC_{0-t} of AMF after Iv, Ip, or Po Administration to Rats ($n = 5$)[a]

param	10 mg/kg iv	10 mg/kg ip	300 mg/kg po
free AMF (%)[b]	26.8 ± 4.65	29.8 ± 3.27	9.33 ± 4.11
AMF conjugates (%)[c]	73.2 ± 6.29	70.2 ± 5.18	90.7 ± 8.32

[a]All values are mean ± SD. The data shown represent the ratios of the areas under the plasma concentration−time curves (AUC) for free and conjugated AMF to total AMF following intravenous (iv), intraperitoneal (ip), or oral (po) administration, respectively. [b]AMF (%) = 100 × (AUC_{0-t} of free AMF)/(AUC_{0-t} of free AMF + AUC_{0-t} of AMF conjugates). [c]AMF conjugates (%) =100 × (AUC_{0-t} of AMF conjugates)/(AUC_{0-t} of free AMF + AUC_{0-t} of AMF conjugates).

after ip dosing. The bioavailability of total AMF was higher for the 10 mg/kg ip dose (66.9%) than it was following the 300 mg/kg po dose. Similar to iv injection, free AMF and AMF conjugates showed similar time courses, with no significant differences in t_{max} and $t_{1/2}$ observed between AMF and AMF conjugates ($p > 0.05$).

DISCUSSION

Herein, we report the development and validation of a method for the accurate determination of plasma concentrations of the free and conjugate metabolized forms of AMF, an important bioactive biflavonoid derived from various herbal sources. Since no authentic standards exist for the glucuronide or sulfate metabolites of AMF, the method included in vitro treatment with β-glucuronidase/sulfatase, liquid−liquid extraction, centrifugation, and analysis by LC−MS/MS. Compared with the previously reported methods,[7,8] the present assay showed excellent performance in terms of sensitivity (increased by about 4-fold) and throughput (3 min per sample versus 6−10 min per sample). Using this method, we could accurately detect both the conjugated and nonconjugated forms of AMF. The high sensitivity and accuracy, as well as the rapid sample analysis, make this method suitable for routine evaluation of AMF pharmacokinetics. We used the method to compare pharmacokinetic behavior following administration by three different routes and to study the bioavailability of AMF in rats.

Although encouraging efficacy data has been reported for AMF in rats,[17,18] there have been no careful analyses of the drug metabolism and pharmacokinetic (DMPK) properties of AMF. Previous analyses of related compounds demonstrated that the biflavonoid glycoside moiety can undergo extensive biotransformation in vivo,[29,31] and that the glucuronide and sulfate conjugates are actually the predominant forms found in the bloodstream, urine, and bile. Hence, it is reasonable to assume that the conjugates are the bioactive forms.[30] Our preliminary investigations of the biotransformation of AMF after po dosing in rats revealed that glucuronide, sulfate, and sulfate/glucuronide conjugates predominated over the parent compound in the urine and feces, and an in situ perfused rat intestine−liver model also confirmed this result (unpublished data). Thus, like other biflavonoids, the conjugated form of AMF is most likely to be the bioactive form.

The dose of AMF used in this study was based on previously reported levels, as well as on our recent pharmacodynamics studies of efficacy. We have previously observed that AMF (20, 10, and 5 mg/kg iv and ip, and 300 mg/kg po) protected from the sperm damage induced by microwave radiation in rats (unpublished data). There are at least two published papers that have reported pharmacological effects of AMF at doses similar to those employed in the present study. Sakthivel et al.[18] reported that AMF (10 mg/kg, ip and iv) protected against acetic acid induced ulcerative colitis. Kim et al.[17] reported that AMF showed anti-inflammatory and analgesic activities when it was administered po at 100 mg/kg. As oral administration is more convenient than injection, we characterized the pharmacokinetics fates of free AMF and its conjugates in rats after po administration.

These results of the present study also suggested that AMF metabolism occurred very rapidly in rats. Several pathways for flavonoids have been previously described;[32,33] glucuronidation and sulfation are well-known mechanisms for increasing the polarity of compounds to aid detoxification.[34] Spencer et al.[35] and Piskula[33] proposed that the first conjugation step for dietary biflavonoids is glucuronidation in the intestinal mucosa. After entering the bloodstream as the glucuronidated form, sulfation occurs in the liver or kidneys. Our finding that oral dosing led to higher levels of conjugation than ip or iv dosing was consistent with this model, and this suggested that glucuronidation and sulfation are critical to biflavonoid metabolism and absorption. Our results also suggested that the activity reported for unmodified AMF in vitro may not fully explain its activity in vivo. Future characterization of the in vitro activity of AMF conjugates could help to clarify this.

Our study also confirmed that AMF showed very low bioavailability after oral dosing. Although the reasons for this are not entirely clear, it is generally thought that large, highly polar molecules are not absorbed efficiently following oral administration.[36,37] Consistent with this hypothesis, the apical transporter multidrug resistance-associated protein 2 (MRP2) can efflux some flavonoids, resulting in a dramatically reduced uptake.[9] At any rate, oral administration is clearly not the preferred route for AMF delivery. It is expected that further investigation of AMF DMPK using our method, combined with a better understanding of the antioxidant properties of the AMF conjugates, will help to advance the potential application of this important phenolic antioxidant constituent of a number of medicinal herbs. In addition, we are working on a pharmaceutical formula that may improve the absorption of AMF.

In this study, we report the development and validation of a reliable, rapid, and accurate LC−MS/MS method to quantify AMF and its conjugate metabolites in rat plasma. We used the method to evaluate the pharmacokinetics of AMF following its iv, ip, and po administration to rats. The resulting data have improved understanding of the DMPK properties of AMF and provided guidelines for further evaluation and development of AMF as a bioactive antioxidant.

ASSOCIATED CONTENT

Supporting Information

Figure depicting time course of AMF release by β-glucuronidase/sulfatase at different concentrations in plasma samples obtained from rats after iv, ip, and po administration. This material is available free of charge via the Internet at http://pubs.acs.org.

AUTHOR INFORMATION

Corresponding Authors

*(Z.Z.) Tel/fax: +86 10 66931632. E-mail: zqzhang55@126.com; antisense@163.com.

DOI: 10.1021/jf5019615
J. Agric. Food Chem. 2015, 63, 1957−1966

*(S.W.) Tel/fax: +86 10 66932211. E-mail: sqwang@nic.bmi.ac.cn.

Funding

This work was supported by two grants from the National Natural Science Foundation of China (No. 81172981, No. 81001469 and No. 81373472) and the National Science and Technology Major Projects for Major New Drugs Innovation and Development of China (2012ZX09301003-001-007).

Notes

The authors declare no competing financial interest.

REFERENCES

(1) Kim, H. K.; Son, K. H.; Chang, H. W.; Kang, S. S.; Kim, H. P. Amentoflavone, a plant biflavone: a new potential anti-inflammatory agent. *Arch. Pharm. Res.* **1998**, *21*, 406−410.

(2) Woo, E. R.; Lee, J. Y.; Cho, I. J.; Kim, S. G.; Kang, K. W. Amentoflavone inhibits the induction of nitric oxide synthase by inhibiting NF-kappaB activation in macrophages. *Pharmacol. Res.* **2005**, *51*, 539−546.

(3) Banerjee, T.; Valacchi, G.; Ziboh, V. A.; van der Vliet, A. Inhibition of TNFalpha-induced cyclooxygenase-2 expression by amentoflavone through suppression of NF-kappaB activation in A549 cells. *Mol. Cell. Biochem.* **2002**, *238*, 105−110.

(4) Simmen, U.; Higelin, J.; Berger-Buter, K.; Schaffner, W.; Lundstrom, K. Neurochemical studies with St. John's wort *in vitro*. *Pharmacopsychiatry* **2001**, *34* (Suppl. 1), S137−142.

(5) Rager, I.; Roos, G.; Schmidt, P. C.; Kovar, K. A. Rapid quantification of constituents in St. John's wort extracts by NIR spectroscopy. *J. Pharm. Biomed. Anal.* **2002**, *28*, 439−446.

(6) Tatsis, E. C.; Boeren, S.; Exarchou, V.; Troganis, A. N.; Vervoort, J.; Gerothanassis, I. P. Identification of the major constituents of Hypericum perforatum by LC/SPE/NMR and/or LC/MS. *Phytochemistry* **2007**, *68*, 383−393.

(7) Michler, H.; Laakmann, G.; Wagner, H. Development of an LC-MS method for simultaneous quantitation of amentoflavone and biapigenin, the minor and major biflavones from Hypericum perforatum L., in human plasma and its application to real blood. *Phytochem. Anal.* **2011**, *22*, 42−50.

(8) Wang, X.; Zhao, X.; Gu, L.; Lv, C.; He, B.; Liu, Z.; Hou, P.; Bi, K.; Chen, X. Simultaneous determination of five free and total flavonoids in rat plasma by ultra HPLC-MS/MS and its application to a comparative pharmacokinetic study in normal and hyperlipidemic rats. *J. Chromatogr. B: Anal. Technol. Biomed. Life Sci.* **2014**, *953−954*, 1−10.

(9) Walgren, R. A.; Lin, J. T.; Kinne, R. K.; Walle, T. Cellular uptake of dietary flavonoid quercetin 4′-beta-glucoside by sodium-dependent glucose transporter SGLT1. *J. Pharmacol. Exp. Ther.* **2000**, *294*, 837−843.

(10) Wolffram, S.; Block, M.; Ader, P. Quercetin-3-glucoside is transported by the glucose carrier SGLT1 across the brush border membrane of rat small intestine. *J. Nutr.* **2002**, *132*, 630−635.

(11) Walgren, R. A.; Lin, J. T.; Kinne, R. K.; Walle, T. Cellular uptake of dietary flavonoid quercetin 4′-beta-glucoside by sodium-dependent glucose transporter SGLT1. *J. Pharmacol. Exp. Ther.* **2000**, *294*, 837−843.

(12) Vaidyanathan, J. B.; Walle, T. Cellular uptake and efflux of the tea flavonoid (−)epicatechin-3-gallate in the human intestinal cell line Caco-2. *J. Pharmacol. Exp. Ther.* **2003**, *307*, 745−752.

(13) Walle, T.; Walle, U. K. The beta-D-glucoside and sodium-dependent glucose transporter 1 (SGLT1)-inhibitor phloridzin is transported by both SGLT1 and multidrug resistance-associated proteins 1/2. *Drug Metab. Dispos.* **2003**, *31*, 1288−1291.

(14) Tsyrlov, I. B.; Mikhailenko, V. M.; Gelboin, H. V. Isozyme- and species-specific susceptibility of cDNA-expressed CYP1A P-450s to different flavonoids. *Biochim. Biophys. Acta* **1994**, *1205*, 325−335.

(15) Lee, H.; Yeom, H.; Kim, Y. G.; Yoon, C. N.; Jin, C.; Choi, J. S.; Kim, B. R.; Kim, D. H. Structure-related inhibition of human hepatic caffeine N3-demethylation by naturally occurring flavonoids. *Biochem. Pharmacol.* **1998**, *55*, 1369−1375.

(16) Zhai, S.; Dai, R.; Friedman, F. K.; Vestal, R. E. Comparative inhibition of human cytochromes P450 1A1 and 1A2 by flavonoids. *Drug Metab. Dispos.* **1998**, *26*, 989−992.

(17) Kim, H. K.; Son, K. H.; Chang, H. W.; Kang, S. S.; Kim, H. P. Amentoflavone, a plant biflavone: a new potential anti-inflammatory agent. *Arch. Pharm. Res.* **1998**, *21*, 406−410.

(18) Sakthivel, K. M.; Guruvayoorappan, C. Amentoflavone inhibits iNOS, COX-2 expression and modulates cytokine profile, NF-kappaB signal transduction pathways in rats with ulcerative colitis. *Int. Immunopharmacol.* **2013**, *17*, 907−916.

(19) Azorin-Ortuno, M.; Yanez-Gascon, M. J.; Pallares, F. J.; Vallejo, F.; Larrosa, M.; Garcia-Conesa, M. T.; Tomas-Barberan, F.; Espin, J. C. Pharmacokinetic study of trans-resveratrol in adult pigs. *J. Agric. Food. Chem.* **2010**, *58*, 11165−11171.

(20) Azuma, K.; Ippoushi, K.; Nakayama, M.; Ito, H.; Higashio, H.; Terao, J. Absorption of chlorogenic acid and caffeic acid in rats after oral administration. *J. Agric. Food. Chem.* **2000**, *48*, 5496−5500.

(21) Jan, K. C.; Ho, C. T.; Hwang, L. S. Bioavailability and tissue distribution of sesamol in rat. *J. Agric. Food. Chem.* **2008**, *56*, 7032−7037.

(22) Konishi, Y.; Hitomi, Y.; Yoshida, M.; Yoshioka, E. Pharmacokinetic study of caffeic and rosmarinic acids in rats after oral administration. *J. Agric. Food. Chem.* **2005**, *53*, 4740−4746.

(23) Zhao, G.; Zou, L.; Wang, Z.; Hu, H.; Hu, Y.; Peng, L. Pharmacokinetic profile of total quercetin after single oral dose of tartary buckwheat extracts in rats. *J. Agric. Food. Chem.* **2011**, *59*, 4435−4441.

(24) Center for Drug Evaluation and Research of the U.S. Department of Healthand Human Services Food and Drug Administration, Guidance for indus-try: Bioanalytical method validation, 2001. http://www.fda.gov/Drugs/GuidanceComplianceRegulatoryInformation/Guidances/ucm064964.htm (accessed 10.12.12).

(25) Timm, U.; Wall, M.; Dell, D. A new approach for dealing with the stability of drugs in biological fluids. *J. Pharm. Sci.* **1985**, *74*, 972−977.

(26) Amoako, A. A.; Marczylo, T. H.; Lam, P. M.; Willets, J. M.; Derry, A.; Elson, J.; Konje, J. C. Quantitative analysis of anandamide and related acylethanolamides in human seminal plasma by ultra performance liquid chromatography tandem mass spectrometry. *J. Chromatogr. B: Anal. Technol. Biomed. Life Sci.* **2010**, *878*, 3231−3237.

(27) Ghassabian, S.; Moosavi, S. M.; Valero, Y. G.; Shekar, K.; Fraser, J. F.; Smith, M. T. High-throughput assay for simultaneous quantification of the plasma concentrations of morphine, fentanyl, midazolam and their major metabolites using automated SPE coupled to LC-MS/MS. *J. Chromatogr. B: Anal. Technol. Biomed. Life Sci.* **2012**, *903*, 126−133.

(28) Guruvayoorappan, C.; Kuttan, G. Amentoflavone inhibits experimental tumor metastasis through a regulatory mechanism involving MMP-2, MMP-9, prolyl hydroxylase, lysyl oxidase, VEGF, ERK-1, ERK-2, STAT-1, NM23 and cytokines in lung tissues of C57BL/6 mice. *Immunopharmacol. Immunotoxicol.* **2008**, *30*, 711−727.

(29) Hollman, P. C.; de Vries, J. H.; van Leeuwen, S. D.; Mengelers, M. J.; Katan, M. B. Absorption of dietary quercetin glycosides and quercetin in healthy ileostomy volunteers. *Am. J. Clin. Nutr.* **1995**, *62*, 1276−1282.

(30) Akao, T.; Kawabata, K.; Yanagisawa, E.; Ishihara, K.; Mizuhara, Y.; Wakui, Y.; Sakashita, Y.; Kobashi, K. Baicalin, the predominant flavone glucuronide of scutellariae radix, is absorbed from the rat gastrointestinal tract as the aglycone and restored to its original form. *J. Pharm. Pharmacol.* **2000**, *52*, 1563−1568.

(31) Williamson, G.; Day, A. J.; Plumb, G. W.; Couteau, D. Human metabolic pathways of dietary flavonoids and cinnamates. *Biochem. Soc. Trans.* **2000**, *28*, 16−22.

(32) Osorio, E.; Londono, J.; Bastida, J. Low-density lipoprotein (LDL)-antioxidant biflavonoids from Garcinia madruno. *Molecules* **2013**, *18*, 6092−6100.

DOI: 10.1021/jf5019615
J. Agric. Food Chem. 2015, 63, 1957−1966

(33) Piskula, M. K.; Terao, J. Accumulation of (−)-epicatechin metabolites in rat plasma after oral administration and distribution of conjugation enzymes in rat tissues. *J. Nutr.* **1998**, *128*, 1172−1178.
(34) Rondini, L.; Peyrat-Maillard, M. N.; Marsset-Baglieri, A.; Berset, C. Sulfated ferulic acid is the main *in vivo* metabolite found after short-term ingestion of free ferulic acid in rats. *J. Agric. Food. Chem.* **2002**, *50*, 3037−3041.
(35) Spencer, J. P.; Chowrimootoo, G.; Choudhury, R.; Debnam, E. S.; Srai, S. K.; Rice-Evans, C. The small intestine can both absorb and glucuronidate luminal flavonoids. *FEBS Lett.* **1999**, *458*, 224−230.
(36) Griffiths, L. A.; Barrow, A. Metabolism of flavonoid compounds in germ-free rats. *Biochem. J.* **1972**, *130*, 1161−1162.
(37) Bokkenheuser, V. D.; Shackleton, C. H.; Winter, J. Hydrolysis of dietary flavonoid glycosides by strains of intestinal Bacteroides from humans. *Biochem. J.* **1987**, *248*, 953−956.

DOI: 10.1021/jf5019615
J. Agric. Food Chem. 2015, 63, 1957−1966

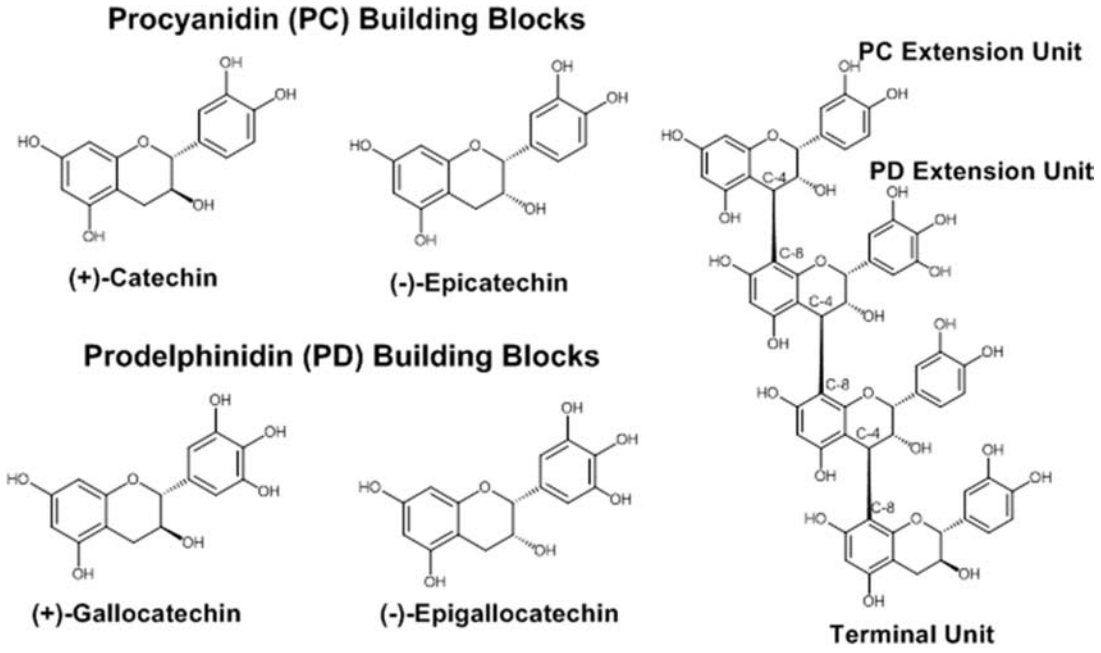

Figure 1. Structures of common flavan-3-ol monomeric subunits found in condensed tannins (left) and a condensed tannin tetramer (right) showing C4−C8 (B-type) linkages, PC and PD extension units, and a terminal unit.

monomeric flavan-3-ol adducts. In this method, extension units are converted into stable C-4 thio ethers, whereas terminal units of the polymers are liberated as intact flavan-3-ol monomers. HPLC analysis of the mixtures obtained from these depolymerization studies allows qualitative and quantitative assessment of CT composition in terms of ratios of PC/PD and *cis*/*trans* subunits and overall mDP. It can thus be used to calculate the purity of isolated CT samples on the basis of the total flavan-3-ol yield. Currently, thiolysis represents one of the most useful techniques available for the analysis of CT composition.

One-dimensional (1D) NMR spectroscopic studies have been used previously to determine the compositional aspects of isolated condensed tannin samples by either solution state ^{13}C NMR spectroscopy[18−27] or cross-polarization magic angle spinning (CPMAS) solid state ^{13}C NMR spectroscopy.[28−31] Solution state ^{13}C NMR spectroscopy has been utilized for the determination of PC/PD[18−20,22−27] and *cis*/*trans* ratios,[18,19,22,24−27] estimations of mDP,[18−20,22,24,26,27] and the identification of C4−C6 and C4−C8 linkages.[20,21] These NMR techniques, however, suffer from broad and often unresolved signals, long acquisition times, and low signal-to-noise ratios, which hamper an accurate assessment of CT composition. Solid phase studies of CT-containing plant material have been conducted using ^{13}C CPMAS NMR techniques.[28−31] Although this technique provides good signal-to-noise ratios, signals in the spectra are still broad and frequently overlap with non-CT signals. In addition, ^{13}C CPMAS requires the use of highly specialized equipment.

By contrast, common two-dimensional (2D) NMR techniques have not been extensively explored for assessing the composition of either purified CTs or CTs present in whole plant materials.[32] Here we report the use of ^{1}H−^{13}C HSQC NMR spectroscopy as a means to determine PC/PD and *cis*/*trans* ratios of isolated CT samples.

MATERIALS AND METHODS

General Procedure for the Purification and Characterization of Condensed Tannins. Condensed tannins were purified from dried and milled plant material and analyzed for CT composition and purity as previously described.[15,16] Briefly, dried plant material was milled (typically using a cyclone mill) containing a 1 or 0.5 mm screen, and the resulting ground material was extracted with 7:3 acetone/water (3 × 10 mL/g of dried material) and filtered. The combined filtrates were concentrated on a rotary evaporator (<40 °C) to remove acetone, and the resulting aqueous layer was extracted with a half volume of dichloromethane (2 times) and was freeze-dried. The freeze-dried residue was purified in one of two ways. The first method involved dissolving the freeze-dried residue in water and applying the resulting mixture to the top of a Sephadex LH-20 column prepacked in water. The column was eluted with water, removing a majority of the carbohydrates present. Column elution was continued with 3:7 acetone/water (providing sample fraction 1) followed by elution of the column with 1:1 acetone/water to give sample fraction 2, which typically contained CTs of highest purity. Alternatively, the dried extraction residue is adsorbed onto Sephadex LH-20 as a 1:1 methanol/water solution to provide a mixture with the consistency of wet sand. This material is then placed in a Buchner funnel and consecutively rinsed with methanol/water (1:1) followed by a series of acetone/water mixtures (1:1, 7:3, 9:1) with each rinsing conducted three times with 5 mL of solvent per gram of Sephadex LH-20. The three rinse filtrates for each solvent were pooled, concentrated on a rotary evaporator (<40 °C) to remove the volatile solvent, and freeze-dried. In both purification methods, the freeze-dried samples were analyzed by ^{1}H−^{13}C HSQC NMR spectroscopy to assess relative purity and/or thiolysis to provide a numerical purity.

NMR Spectroscopy. ^{1}H, ^{13}C, and ^{1}H−^{13}C HSQC NMR spectra were recorded at 27 °C on a BrukerBiospin DMX-500 (^{1}H 500.13 MHz, ^{13}C 125.76 MHz) instrument equipped with TopSpin 2.1 software and a cryogenically cooled 5 mm TXI ^{1}H/^{13}C/^{15}N gradient probe in inverse geometry. Spectra were recorded in DMSO-d_6/pyridine-d_5 (4:1) mixtures and were referenced to the residual signals of DMSO-d_6 (2.49 ppm for ^{1}H and 39.5 ppm for ^{13}C spectra). ^{13}C NMR spectra were obtained using 5000 scans (acquisition time of 4 h and 30 min each). For ^{1}H−^{13}C HSQC experiments, spectra were obtained using 128 scans (acquisition time of 18 h 30 min each) obtained using the standard Bruker pulse program (hsqcegtpsi) with

DOI: 10.1021/jf504743b
J. Agric. Food Chem. 2015, 63, 1967−1973

Table 1. Comparison of Data from Thiolysis and $^{1}H-^{13}C$ HSQC NMR Determinations for 22 Condensed Tannin (CT) Samples[a]

CT sample	plant species	CT content (thiolysis) (%)*	SD	% PC (thiolysis)	SD	% PC (NMR)	SD	% *cis* (thiolysis)	SD	% *cis* (NMR)	SD
1	*Lespedeza cuneata*	96.3	0.08	5.9	0.06	4.9	0.06	79.2	0.26	73.2	1.19
2	*Lotus corniculatus*	92.5	0.03	54.0	0.62	55.6	1.17	93.3	0.58	86.8	0.59
3	*Lotus corniculatus*	78.1	0.40	68.0	0.35	70.9	0.19	87.5	0.15	88.7	1.17
4	*Lotus corniculatus*	75.3	0.01	57.1	0.12	60.8	0.32	91.3	0.13	87.0	1.58
5	*Lotus pedunculatus*	108.0	0.01	16.0	0.07	14.6	0.80	81.7	0.22	69.3	1.63
6	*Lotus pedunculatus*	91.3	0.35	25.9	0.29	23.7	0.28	78.7	0.23	75.4	1.22
7	*Lotus pedunculatus*	85.8	0.01	17.5	0.06	17.5	0.50	79.5	0.05	71.7	0.45
8	*Lotus pedunculatus*	80.3	0.41	28.1	0.17	29.0	1.02	74.4	0.15	71.0	1.79
9	*Onobrychis viciifolia*	102.2	8.13	37.3	0.29	39.1	3.23	82.9	0.27	84.4	5.05
10	*Onobrychis viciifolia*	93.7	4.55	19.2	0.06	19.1	0.28	83.3	0.21	77.9	1.96
11	*Onobrychis viciifolia*	82.4	1.10	51.7	0.32	56.7	0.62	83.5	0.10	79.7	0.90
12	*Onobrychis viciifolia*	44.3	0.17	57.3	0.07	59.0	1.45	68.7	0.00	64.9	1.10
13	*Securigera varia*	56.6	$n = 1$	18.2	$n = 1$	22.5	0.17	89.7	$n = 1$	87.6	0.56
14	*Sorghum bicolor*	58.8	0.02	100.0	0.00	100.0	0.00	85.5	0.09	87.1	2.60
15	*Theobroma cacao*	63.8	$n = 1$	100.0	$n = 1$	100.0	nd	93.4	$n = 1$	100.0	nd
16	*Theobroma cacao*	49.0	0.01	100.0	0.0	100.0	0.00	90.1	0.12	88.7	2.06
17	*Tilia* sp.	92.7	0.04	98.5	0.05	99.2	0.19	95.5	0.09	91.2	0.15
18	*Tilia* sp.	61.1	0.47	98.1	0.14	99.2	0.47	89.4	0.11	89.1	0.73
19	*Trifolium repens*	120.6	0.01	0.8	0.00	0.0	nd	69.3	0.07	61.1	1.01
20	*Trifolium repens*	111.4	4.80	1.3	0.00	0.0	nd	58.9	1.27	56.3	0.75
21	*Trifolium repens*	106.6	5.08	0.9	0.04	0.0	nd	58.3	0.24	50.6	1.22
22	*Trifolium repens*	97.6	0.01	1.1	0.04	0.0	nd	69.8	0.02	56.1	1.60

[a]% purity refers to g tannins/100 g fraction; % PD = 100 − % PC; % *trans* = 100 − % *cis*. nd, not detected.

the following parameters: acquisition, TD 1024 (F2), 320 (F1); SW, 10.0 ppm (F2), 160 ppm (F1); O1, 2500.65 Hz; O2, 11,318.20 Hz; D1 = 1.50 s; CNST2 = 145; acquisition time, F2 channel, 102.55 ms; F1 channel, 7.9511 ms; processing, SI = 1024 (F2, F1), WDW = QSINE, LB = 1.00 Hz (F2), 0.30 Hz (F1); PH_mod = pk; baseline correction ABSG = 5 (F2, F1), BCFW = 1.00 ppm, BC_mod = quad (F2), no (F1); linear prediction = no (F2), LPfr (F1). Samples sizes used for these spectra ranged from 10 to 15 mg providing NMR sample solutions with concentrations of 20−30 mg/mL.

Calculating Procyanidin/Prodelphinidin (PC/PD) and *cis*/*trans*-Flavan-3-ol Ratios. The percentage of PCs in the CT sample was calculated using eq 1

$$\%PC = PC\text{-}6'/[(PD\text{-}2'6'/2) + PC\text{-}6'] \times 100 \quad (1)$$

where PC-6′ is the integration of the contour for the H/C-6′cross-peak of the PC units and PD-2′6′ is the integration of the contour for the H/C-2′,6′ cross-peak of the PD units. The PD-2′6′ value is divided by 2 to account for the signal arising from two sets of correlated nuclei. The percentage of *cis* isomers present in the CT sample was calculated through integration of the respective H/C-4 *cis*- and *trans*-flavan-3-ol cross-peak contours centered around $^{1}H/^{13}C$ chemical shifts of 4.5−4.8/36.0 and 4.4−4.65/37.5 ppm, respectively, and used in eq 2:

$$\%cis\text{-flavan-3-ols} = cis\text{-flavan-3-ols}/[cis\text{-flavan-3-ols} + trans\text{-flavan-3-ols}] \times 100 \quad (2)$$

Integrations of cross-peaks were performed in triplicate, and the values were averaged. Integration of the peaks was performed using Topspin 2.1 software.

RESULTS AND DISCUSSION

We have recently shown that $^{1}H-^{13}C$ HSQC NMR spectroscopy can be a useful tool when assessing the presence of CT in forages and detection of CT left in residues after HCl−butanol treatment,[16] demonstrating the power of 2D NMR techniques. The current study included examining the $^{1}H-^{13}C$ HSQC NMR spectra of 22 purified CT samples prepared from 9 different plant species. The CT samples had PC/PD ratios ranging from 0/100 to 99/1, *cis*/*trans* ratios ranging from 58/42 to 95/5, and a CT content of 44−∼100% as determined by thiolysis (Table 1). As an example, the $^{1}H-^{13}C$ HSQC NMR spectrum of CT purified from *Lotus pedunculatus* (big trefoil, sample 6, Table 1) is given in Figure 2A along with cross-peak assignments. The absence of significant cross-peak NMR signals from non-CT organic compounds in this spectrum also confirms a high degree of purity of this sample.

Determination of PC/PD Ratios. Quantification of signals arising from polymeric materials by $^{1}H-^{13}C$ HSQC NMR spectroscopy is often hampered by nuclei having differing *T1* and *T2* relaxation times and differences in coupling constants and resonance offset effects.[33] The presence of these effects results in skewing of cross-peak signal contour volumes and thus typically limits the utility of these contours for quantifying structural information. Usually these effects require special spectroscopic treatments and alterations in NMR acquisition parameters, such as changes in pulse sequences or increased relaxation delays, before reliable quantification can be made.[34−36]

DOI: 10.1021/jf504743b
J. Agric. Food Chem. 2015, 63, 1967−1973

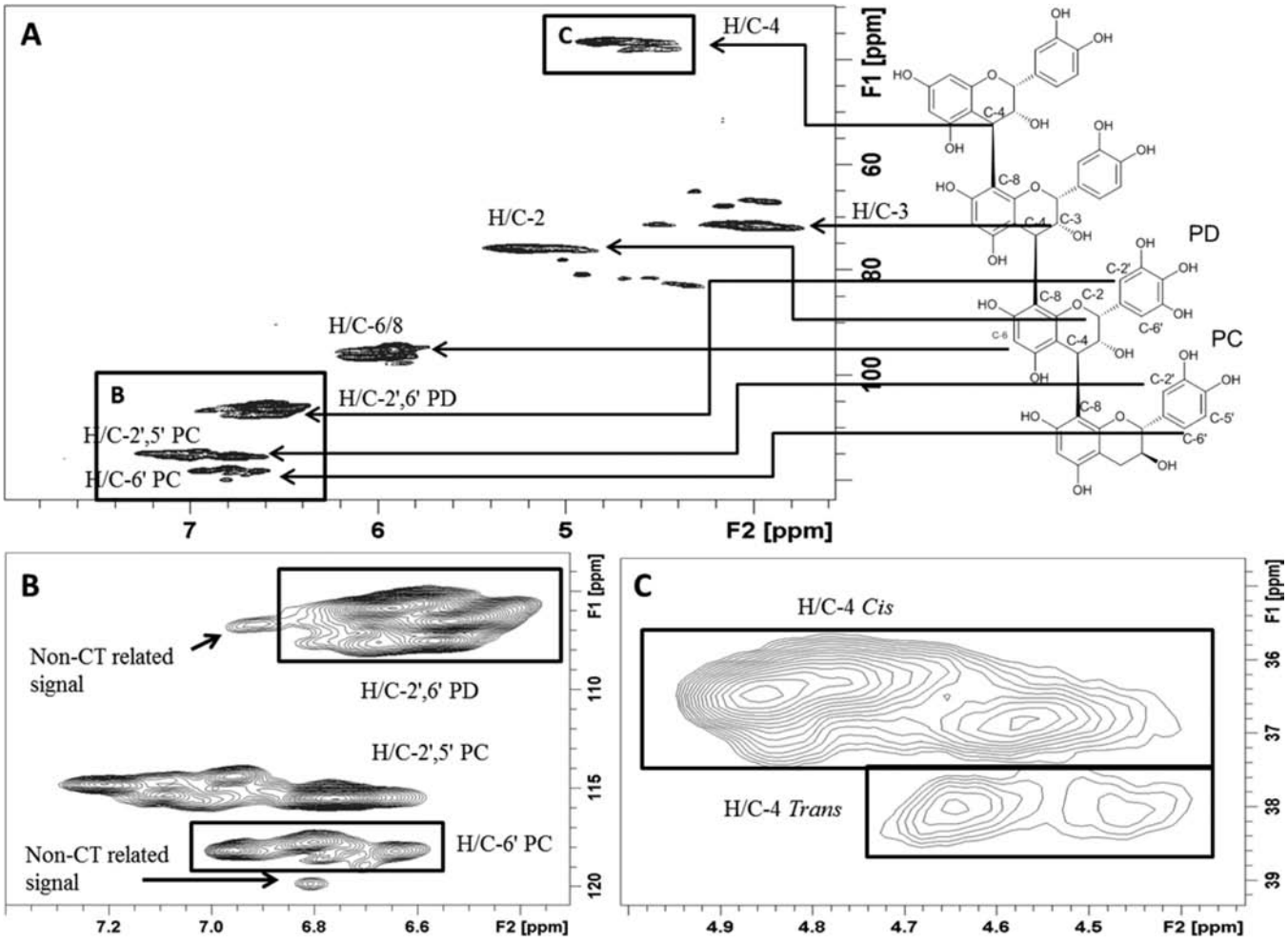

Figure 2. (A) Signal assignments for the $^{1}H-^{13}C$ HSQC NMR spectrum (500/125 MHz, DMSO-d_6/pyridine-d_5, 4:1) of purified condensed tannin sample (Table 1, sample 6) from *Lotus pedunculatus* (big trefoil) leaves. (B) B-Ring aromatic region cross-peak signals including H/C-2′,6′ PD signal and the H/C-2′,5′ and 6′ signals from procyanidin units. (C) H/C-4 *cis*- and *trans*-flavan-3-ol cross-peak signals. Contours were integrated as indicated by boxes. Non-tannin-related signals arising from impurities are noted and are not included in the integration.

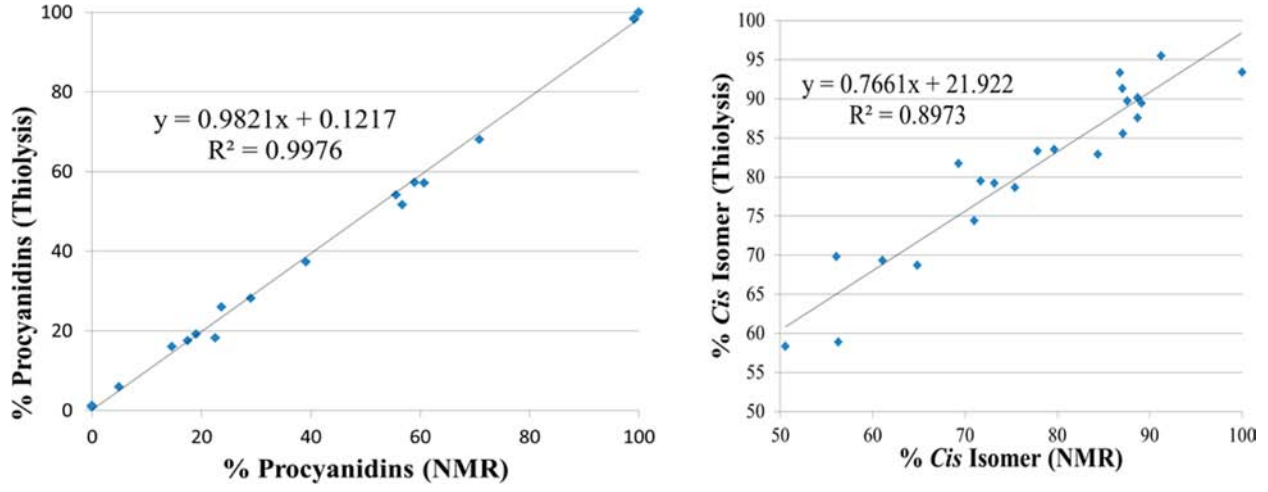

Figure 3. Proportion of procyanidin subunits (left) and *cis* subunits (right) *cis* subunits in 22 isolated condensed tannin samples as determined by thiolysis versus $^{1}H-^{13}C$ HSQC NMR.

In the $^{1}H-^{13}C$ HSQC NMR spectra of these samples, a combination of the nuclei *T1* and *T2* relaxation and resonance offset effects can be observed for most cross-peak signals. The results of these effects lead to cross-peak contours in the spectra the volumes of which are not proportional to the corresponding nuclei ratios. As a prime example, integration of the contours for signals arising from H/C-2′,5′ of PC units versus those from H/C-6′ of PC units would normally provide a ratio of 2:1 if

DOI: 10.1021/jf504743b
J. Agric. Food Chem. 2015, 63, 1967−1973

Table 2. Comparison of Duplicate NMR Data with Thiolysis Data Obtained from Condensed Tannin (CT) Samples[a]

CT sample	% PC (thiolysis)	SD	% PC (NMR)	SD	% *cis* (thiolysis)	SD	% *cis* (NMR)	SD
3	68.0	0.35	70.0	0.49	87.5	0.15	88.6	1.32
3			71.1	0.50			88.6	0.68
4	57.1	0.12	60.4	0.41	91.3	0.13	89.8	0.53
4			59.7	0.53			91.1	0.50
6	26.0	0.29	24.4	0.35	78.7	0.23	75.4	1.02
6			23.7	0.17			75.1	0.99
7	17.5	0.06	17.5	0.50	79.5	0.05	71.6	0.45
7			18.6	0.47			71.8	2.20
11	51.7	0.32	56.9	0.42	83.5	0.10	79.5	1.20
11			55.5	0.13			80.9	0.68

[a]% PC = percentage of procyanidins in CT sample; % *cis* = percentage of *cis*-flavan-3-ols in CT sample. Percentages for prodelphinidins (PD) and *trans*-flavanols are not shown as % PD = 100 − % PC and % *trans* = 100 − % *cis*.

none of the above-mentioned effects were observed (Figure 2B). However, the integration ratios of H/C-2′,5′ versus H/C-6′ cross-peak contours in PC containing samples from this study showed wide variability with a range from 2.37:1 to 3.86:1 (n = 17, av = 3.15, SD ±0.48). Most of the signals in the ^{1}H−^{13}C HSQC NMR spectra of these purified CT samples followed this trend. A comparison of integration values obtained from the cross-peak contours could not be directly correlated with theoretical relative intensities of the nuclei giving rise to the signal. Similarly, in an attempt to assess the mDP of these samples, integration of the terminal methylene unit versus any of the other CT cross-peak signals in the spectra also led to no obvious correlation with the thiolysis data of this study. It is worth noting that even integrations of the C-4 methylene units of the flavan-3-ol monomers catechin, epicatechin, and epigallocatechin under identical conditions only integrate, on average, to 72% of other signals present in the ^{1}H−^{13}C HSQC NMR spectrum.

However, integration ratios of H/C-6′ cross-peak signals from PC units and the H/C-2′,6′ cross-peak signal from PD units did show an extremely strong and unbiased relationship with PC/PD estimates from thiolysis determinations (Figure 3). Thus, this is the first time that ^{1}H−^{13}C HSQC NMR data from purified CT samples have been corroborated with data from an alternative method (thiolysis) to quantify compositional characteristics of CTs. Separate NMR analyses conducted on a limited set of other purified CT samples at the University of Reading confirmed this method as providing reliable PC/PD ratios.

It is not clear how all of the parameters controlling contour intensities are interrelated: Do the nuclei involved impart the same or similar *T1* and *T2* relaxation times, coupling constants, and resonance offset effects, allowing for accurate comparison of the two contours, or is this simply a coincidence of cancellation of the effects? Answers to these questions remain to be determined.

To test for variability in sample-to-sample preparation and data acquisition, we prepared duplicate NMR solutions from the same CT samples and obtained NMR spectra of these preparations on different days. These results are given in Table 2. As shown, there is excellent reproducibility of the method between these duplicate runs. In all, these experiments prove that this is a robust method for the estimation of PC/PD ratios in purified CT samples.

Determination of *cis*/*trans*-Flavan-3-ol Ratios. To assess *cis*- and *trans*-flavan-3-ol ratios (i.e., ratio of epicatechin and epigallocatechin versus catechin and gallocatechin) in these samples, we focused on the H/C-4 cross-peak signal (Figure 2C). It has been reported[32] that this signal is segregated into two cross-peaks with ^{1}H/^{13}C chemical shifts of ∼4.5−4.8/36.0 and ∼4.4−4.65/37.5 ppm for the *cis*- and *trans*-flavan-3-ol subunits, respectively. The integration of cross-peak signals in ^{1}H−^{13}C HSQC NMR spectra of the same nuclei with the same connectivity in nearly identical electronic environments should be straightforward as they should possess similar, if not identical, *T1* and *T2* relaxation times and pose little or no differences in coupling constants and resonance offset effects. Thus, we should be able to use the data obtained from these ^{1}H−^{13}C HSQC NMR spectra to directly measure this structural element of isolated CTs. The percentage of *cis* isomers present in the CT sample was calculated through integration of the respective H/C-4 *cis* and *trans* cross-peak contours (Figure 2C). Integration ratios from these contours provided strongly related but biased estimates of *cis*/*trans* ratios relative to thiolysis (Figure 3). A literature search revealed that this segregation of the *cis* and *trans* signals of flavan-3-ol moieties is most likely not absolute, and this could provide an explanation for the bias in *cis*/*trans* estimates relative to thiolysis. NMR spectroscopic data from epicatechin (*cis*) oligomers report ^{13}C chemical shift in the range of 37.5 ppm, overlapping into the previously designated "*trans*" signal region.[37,38] The lack of signal segregation is more pronounced in structures containing C4−C6 interflavanyl linkages.[38,39] Thus, overlapping of signals from *cis*- and *trans*-flavan-3-ol subunits is the most likely contributing factor for slightly larger discrepancies between the thiolysis/NMR correlations for *cis*/*trans*-flavan-3-ol subunit assessments and may also be responsible for the biased regression fit (Figure 3).

Precautions. The first issue here, as with most analytical techniques, is to obtain a spectrum with strong signal-to-noise ratio before the integration of data is attempted. If sample size is limited, extended acquisition times need to be considered. When using this technique on samples of low purity, it is imperative that the user be able to recognize any non-CT impurity signals present and avoid incorporating them into the integration values. For PC/PD ratio evaluations, we have found that the signals indicated in Figure 2B are the most common impurity signals which may interfere in obtaining reliable results. These signals most likely arise from trace amounts of non-CT polyphenols present in the sample. For the assessment of *cis*/*trans* ratios, the problem of integration of non-CT impurities does not seem to be an issue. The H/C-4 cross-peak signals appear, even in spectra of whole plant material, in an area void of other non-CT signals. The major issue in the *cis*/

DOI: 10.1021/jf504743b
J. Agric. Food Chem. 2015, 63, 1967−1973

trans ratio assessment is the resolution of the two signals. In some cases these signals are not well resolved (Figure 2C), and care needs to be taken in selecting the integration areas.

In conclusion, the method developed now permits analytical assessment, via 2D $^{1}H-^{13}C$ HSQC NMR spectroscopy, of two specific chemical properties of purified CT samples: PC/PD and *cis*/*trans* ratios. The purified CT samples examined encompass the entire range of procyanidin/prodelphinidin ratios from 0/100 to 99/1 and a substantial range of *cis*/*trans*-flavan-3-ol ratios from 58:42 to 95.5:4.5. The observations outlined here also provide validation of thiolysis data for analysis of CT composition. In contrast to thiolysis, NMR spectroscopy represents a nondestructive analytical tool, which can be important when sample quantities are limited. Thiolysis requires ca. 4 mg for a single determination, whereas NMR analysis requires only 10 mg for an 18 h acquisition time using the described instrumentation. No additional straightforward correlations were found upon examination of other cross-peak signals in these $^{1}H-^{13}C$ HSQC NMR spectra. Additional spectroscopic examination of these samples is warranted to investigate whether other significant structural information can be obtained using quantitative $^{1}H-^{13}C$ HSQC NMR data[34−36] or alternative NMR techniques.

AUTHOR INFORMATION

Corresponding Author

*(W.E.Z.) E-mail: wayne.zeller@ars.usda.gov. Phone: (608) 890-0071. Fax: (608) 890-0076.

Funding

This work was funded in part by a USDA-ARS specific cooperative agreement no. 58-3655-0-155F with the University of Reading, UK, and was supported by a European Union Marie Curie Initial Training Network (PITN-GA-2011-289377, "LegumePlus"). Mention of trade names or commercial products in this paper is solely for the purpose of providing specific information and does not imply recommendation or endorsement by the U.S. Department of Agriculture.

Notes

The authors declare no competing financial interest.

ACKNOWLEDGMENTS

We acknowledge the technical of assistance of Abert Vang, Jane Marita for assistance with NMR experiments, Scott Kronberg for lespedeza pellets, and Heike Hofstetter for valuable discussions.

ABBREVIATIONS USED

$^{1}H-^{13}C$ HSQC, proton−carbon-13 heteronuclear single-quantum coherence; NMR, nuclear magnetic resonance; PC, procyanidin; PD, prodelphinidin; *cis*, 2,3-*cis*; *trans*, 2,3-*trans*; CT, condensed tannins; mDP, mean degree of polymerization; ^{13}C, carbon-13; CPMAS, cross-polarization magic angle spinning; 1D, one-dimensional; 2D, two-dimensional; 5K, five thousand; DMSO-d_6, perdeuterated dimethyl sulfoxide

REFERENCES

(1) Hagerman, A. E. *Tannin Handbook*; Miami University: Oxford, OH, USA, 2002; available at http://www.users.muohio.edu/hagermae/.

(2) Schofield, P.; Mbugua, D. M.; Pell, A. N. Analysis of condensed tannins: a review. *Anim. Feed Sci. Technol.* **2001**, *91*, 21−40.

(3) Min, B. R.; Barry, T. N.; Attwood, G. T.; McNabb, W. C. The effect of condensed tannins on the nutrition and health of ruminants fed fresh temperate forages: a review. *Anim. Feed Sci. Technol.* **2003**, *106*, 3−19.

(4) Waghorn, G. C.; Douglas, G. B.; Niezen, J. H.; McNabb, W. C.; Foote, A. G. Forages with condensed tannins − their management and nutritive value for ruminants. *Proc. N. Z. Grassl. Assoc.* **1998**, *60*, 89−98.

(5) Barry, T. N.; McNabb, W. C. The implications of condensed tannins on the nutritive value of temperate forages fed to ruminants. *Br. J. Nutr.* **1999**, *81*, 263−272.

(6) Albrecht, K. A.; Muck, R. E. Proteolysis in ensiled forage legumes that vary in tannin concentration. *Crop Sci.* **1991**, *31*, 464−469.

(7) Coblentz, W. K.; Grabber, J. H. *In situ* protein degradation of alfalfa and birdsfoot trefoil hays and silages as influenced by condensed tannin concentration. *J. Dairy Sci.* **2013**, *96*, 3120−3137.

(8) McMahon, L. R.; McAllister, T. A.; Berg, B. P.; Majak, W.; Acharya, S. N.; Popp, J. D.; Coulman, B. E.; Wang, Y.; Cheng, K.-J. A review of the effects of forage condensed tannins on ruminal fermentation and bloat in grazing cattle. *Can. J. Plant Sci.* **2000**, *80*, 469−485.

(9) Hoste, H.; Jackson, F.; Athanasiadou, S.; Thamsborg, S. M.; Hoskin, S. O. The effects of tannin-rich plants on parasitic nematodes in ruminants. *Trends Parasitol.* **2006**, *22*, 253−261.

(10) Patra, A. K.; Saxena, J. A new perspective on the use of plant secondary metabolites to inhibit methanogenesis in the rumen. *Phytochemistry* **2010**, *71*, 1198−1222.

(11) Pellikaan, W. F.; Stringano, E.; Leenaars, J.; Bongers, D. J. G. M.; van Laar-van Schuppen, S.; Plant, J.; Mueller-Harvey, I. Evaluating effects of tannins on extent and rate of in vitro gas and CH_4 production using an automated pressure evaluation system (APES). *Anim. Feed Sci. Technol.* **2011**, *166−167*, 377−390.

(12) Hümmer, W.; Schreier, P. Analysis of proanthocyanidins. *Mol. Nutr. Food Res.* **2008**, *52*, 1381−1398.

(13) Santos-Buelga, C.; Scalbert, A. Proanthocyanidins and tannin-like compounds − nature, occurrence, dietary intake and effects on nutrition and health. *J. Sci. Food Agric.* **2000**, *80*, 1094−1117.

(14) Patra, A. K.; Saxena, J. Exploitation of dietary tannins to improve rumen metabolism and ruminant nutrition. *J. Sci. Food Agric.* **2011**, *91*, 24−37.

(15) Gea, A.; Stringano, E.; Brown, R. H.; Mueller-Harvey, I. *In situ* analysis and structural elucidation of sainfoin (*Onobrychis viciifolia*) tannins for high-throughput germplasm screening. *J. Agric. Food Chem.* **2011**, *59*, 495−503.

(16) Grabber, J. H.; Zeller, W. E.; Mueller-Harvey, I. Acetone enhances the direct analysis of procyanidin- and prodelphinidin-based condensed tannins in *Lotus* species by the butanol−HCl−iron assay. *J. Agric. Food Chem.* **2013**, *61*, 2669−2678.

(17) Stringano, E.; Hayot Carbonero, C.; Smith, L. M. J.; Brown, R. H.; Mueller-Harvey, I. Proanthocyanidin diversity in the EU 'HealthyHay' sainfoin (*Onobrychis viciifolia*) germplasm collection. *Phytochemistry* **2012**, *77*, 197−208.

(18) Czochanska, Z.; Foo, L. Y.; Newman, R. H.; Porter, L. J.; Thomas, W. A. Direct proof of a homogeneous polyflavan-3-ol structure for polymeric proanthocyanidins. *J. Chem. Soc., Chem. Comm.* **1979**, 375−377.

(19) Czochanska, Z.; Foo, L. Y.; Newman, R. H.; Porter, L. J. Polymeric proanthocyanidins. Stereochemistry, structural units, and molecular weight. *J. Chem. Soc., Perkin Trans. 1* **1980**, 2278−2286.

(20) Pizzi, A.; Stephanou, A. A comparative ^{13}C NMR study of polyflavonoid tannin extracts for phenolic polycondensates. *J. Appl. Polym. Sci.* **1993**, *50*, 2105−2113.

(21) Newman, R. H.; Porter, L. J.; Foo, L. Y.; Johns, S. R.; Willing, R. I. High-resolution ^{13}C NMR studies of proanthocyanidin polymers (condensed tannins). *Magn. Reson. Chem.* **1987**, *25*, 118−124.

(22) Foo, L. Y.; Lu, Y.; Molan, A. L.; Woodfield, D. R.; McNabb, W. C. The phenols and prodelphinidins of white clover flowers. *Phytochemistry* **2000**, *54*, 539−548.

DOI: 10.1021/jf504743b
J. Agric. Food Chem. 2015, 63, 1967−1973

(23) Ossipova, S.; Ossipov, V.; Haukioja, E.; Loponen, J.; Pihlaja, K. Proanthocyanidins of mountain birch leaves: quantification and properties. *Phytochem. Anal.* **2001**, *12*, 128−133.
(24) Kraus, T. E. C.; Yu, Z.; Preston, C. M.; Dahlgren, R. A.; Zasoski, R. J. Linking chemical reactivity and protein precipitation to structural characteristics of foliar tannins. *J. Chem. Ecol.* **2003**, *29*, 703−730.
(25) Qa'dan, F.; Nahrstedt, A.; Schmidt, M.; Mansoor, K. Polyphenols from *Ginkgo biloba*. *Sci. Pharm.* **2010**, *78*, 897−907.
(26) Zhang, L.-L.; Lin, Y.-M.; Zhou, H.-C.; Wei, S.-D.; Chen, J.-H. Condensed tannins from mangrove species *Kandelia candel* and *Rhizophora mangle* and their antioxidant activity. *Molecules* **2010**, *15*, 420−431.
(27) Chai, W.-M.; Shi, Y.; Feng, H.-L.; Qiu, L.; Zhou, H.-C.; Deng, Z.-W.; Yan, C.-L.; Chen, Q.-X. NMR, HPLC-ESI-MS, and MALDI-TOF MS analysis of condensed tannins from *Delonix regia* (Bojer ex Hook.) Raf. and their bioactivities. *J. Agric. Food Chem.* **2012**, *60*, 5013−5022.
(28) Hoong, Y. B.; Pizzi, A.; Tahir, P. Md.; Pasch, H. Characterization of *Acacia mangium* polyflavonoid tannins by MALDI-TOF mass spectrometry and CP-MAS ^{13}C NMR. *Eur. Polym. J.* **2010**, *46*, 1268−1277.
(29) Reid, D. G.; Bonnet, S. L.; Kemp, G.; Van der Westhuizen, J. H. Analysis of commercial proanthocyanidins. Part 4: Solid state ^{13}C NMR as a tool for in situ analysis of proanthocyanidin tannins, in heartwood and bark of quebracho and acacia, and related species. *Phytochemistry* **2013**, *94*, 243−248.
(30) Romer, F. H.; Underwood, A. P.; Senekal, N. D.; Bonnet, S. L.; Duer, M. J.; Reid, D. G.; Van der Westhuizen, J. H. Tannin fingerprinting in vegetable tanned leather by solid state NMR spectroscopy and comparison with leathers tanned by other processes. *Molecules* **2011**, *16*, 1240−1252.
(31) Lorenz, K.; Preston, C. M. Characterization of high-tannin fractions from humus by carbon-13 cross-polarization and magic-angle spinning nuclear magnetic resonance. *J. Environ. Qual.* **2002**, *31*, 431−436.
(32) Zhang, L.; Gellerstedt, G. 2D Heteronuclear ($^{1}H-^{13}C$) single quantum correlation (HSQC) NMR analysis of norway spruce bark components. In *Characterization of Lignocellulosic Materials*, 1st ed.; Hu, T. Q., Ed.; Blackwell Publishing: Oxford, UK, 2008; Vol. 1, pp 3−16.
(33) Zhang, L.; Gellerstedt, G. Quantitative 2D HSQC NMR determination of polymer structures by selecting suitable internal standard references. *Magn. Reson. Chem.* **2007**, *45*, 37−45.
(34) Sette, M.; Lange, H.; Crestini, C. Quantitative HSQC analyses of lignin: a practical comparison. *Comput. Struct. Biotechnol. J.* **2013**, *6*, No. e201303016.
(35) Hu, K.; Westler, W. M.; Markley, J. L. Simultaneous quantification and identification of individuals chemicals in metabolite mixtures by two-dimensional extrapolated time-zero $^{1}H-^{13}C$ HSQC ($HSQC_0$). *J. Am. Chem. Soc.* **2011**, *133*, 1662−1665.
(36) Heikkinen, S.; Toikka, M. M.; Karhunen, P. T.; Kilpeläinen, I. A. Quantitative 2D HSQC (Q-HSQC) via suppression of *J*-dependence of polarization transfer in NMR spectroscopy: application to wood lignin. *J. Am. Chem. Soc.* **2003**, *125*, 4362−4367.
(37) Shoji, T.; Mutsuga, M.; Nakamura, T.; Kanda, T.; Akiyama, H.; Goda, Y. Isolation and structural elucidation of some procyanidins from apple by low-temperature nuclear magnetic resonance. *J. Agric. Food Chem.* **2003**, *51*, 3806−3813.
(38) Nakashima, S.; Oda, C.; Masuda, S.; Tagashira, M.; Kanda, T. Isolation and structure elucidation of tetrameric procyanidins from unripe apples (*Malus pumila* cv. Fuji) by NMR spectroscopy. *Phytochemistry* **2012**, *83*, 144−152.
(39) Cui, C.-B.; Tezuka, Y.; Yamashita, H.; Kikuchi, T.; Nakano, H.; Tamaoki, T.; Park, J.-H. Constituents of a fern, *Davallia mariesii* Moore. V. Isolation and structures of davallin, a new tetrameric proanthocyanidin, and two new phenolic glycosides. *Chem. Pharm. Bull.* **1993**, *41*, 1491−1497.

DOI: 10.1021/jf504743b
J. Agric. Food Chem. 2015, 63, 1967−1973

Table 1. Collection Sites of Potatoes and Carrots and Related Isotopic Compositions of Methoxyl Groups, Meteoric Water, and Isotope Fractionation

site/code	geographical location	altitude (m)	$\delta^2H_{OCH_3}$ (‰)	$\delta^2H_{tissue\ water}$ (‰)	$\varepsilon_{m/w}$ [b]
		Carrots			
Pamplona, Spain/C4	42°49′N, 01°38′W	427	−213.0 ± 0.9	−40.0 ± 3.0[a]	−180
Narbonne, France/C6	43°11′N, 03°00′E	13	−208.2 ± 0.6	−37.0 ± 5.0[a]	−178
Avignon, France/C8	43°57′N, 04°49′E	23	−213.5 ± 0.5	−37.0 ± 6.0[a]	−183
Mainz, Germany/C9	49°58′N, 08°21′E	90	−217.8 ± 2.1	−54.0 ± 3.0[a]	−173
Dettelbach, Germany/C11	49°47′N, 10°10′E	193	−233.4 ± 0.6	−53.7 ± 1.0	−190
Hamburg, Germany/C12	53°30′N, 10°09′E	5	−254.0 ± 0.6	−54.4 ± 1.0	−211
Tomaszów Lubelski, Poland/C13	50°27′N, 23°25′E	273	−241.1 ± 1.4	−68.4 ± 1.0	−185
Umeå, Sweden/C14	63°49′N, 20°15′E	9	−262.1 ± 1.0	−75.0 ± 1.0	−202
Mainz, Germany/C16	49°58′N, 08°21′E	90	−203.7 ± 1.4	−41.2 ± 1.0	−169
Umeå, Sweden/C17	63°49′N, 20°15′E	9	−233.5 ± 2.0	−80.2 ± 1.0	−167
Belfast, Northern Ireland/C18	54°35′N, 05°56′W	22	−214.2 ± 2.2	−38.4 ± 1.0	−183
	mean isotope fractionation ε				−184 ± 13
		Potatoes			
La Linea de la Concepciòn, Spain/P1	36°09′N, 05°20′W	9	−208.2 ± 2.8	−49.1 ± 1.0	−167
Murcia, Spain/P2	37°58′N, 01°07′W	49	−210.6 ± 1.5	−40.6 ± 1.0	−177
Valencia, Spain/P3	39°29′N, 00°20′W	5	−218.9 ± 4.0	−54.0 ± 1.0	−174
Pamplona, Spain/P4	42°49′N, 01°38′W	427	−177.0 ± 4.2	−33.4 ± 1.0	−149
Narbonne, France/P6	42°41′N, 02°53′E	37	−172.9 ± 1.3	−33.0 ± 1.0	−145
Villeneuve, France/P7	43°53′N, 05°51′E	480	−192.2 ± 2.8	−64.8 ± 1.0	−136
Noirmoutier, France/P8	46°59′N, 02°15′W	3	−201.8 ± 4.9	−52.0 ± 1.0	−158
Sicily, Italy/P10	37°00′N, 14°00′E	nn	−200.0 ± 1.7	−37.0 ± 1.0	−169
Mainz, Germany/P11	49°57′N, 08°22′E	85	−190.4 ± 2.0	−54 ± 3.0[a]	−144
Albertshofen, Germany/P12	49°46′N, 10°09′E	193	−202.5 ± 2.2	−54.3 ± 1.0	−157
Gleschendorf, Germany/P13	54°01′N, 10°39′E	23	−203.9 ± 1.9	−52.3 ± 1.0	−160
Tomaszów Lubelski, Poland/P14	50°27′N, 23°25′E	273	−195.6 ± 7.2	−55.7 ± 1.0	−148
Umeå, Sweden/P15	63°49′N, 20°15′E	9	−246.6 ± 0.8	−92.0 ± 1.0	−170
	mean isotope fractionation ε				−158 ± 13

[a]Determination of $\delta^2H_{tissue\ water}$ was not possible. Values calculated using OIPC (cf. Hydrogen Isotope Fractionation and Correlation between Tissue Water and Plant Matter Methoxyl Groups). [b]Isotope fractionation was calculated according to eq 3.

application, the following questions should be investigated by suitable experiments. (1) How does the δ^2H value of methoxyl groups correlate with the original plant tissue water, and does the value remain unchanged and constant during the evaporative processes? (2) How do the δ^2H and the $\delta^{18}O$ values of plant tissue water behave and correlate during the evaporative processes? (3) How do the δ^2H and the $\delta^{18}O$ values of tissue water correlate to the loss of water from biomass as measured by weight loss? (4) What is the potential of the methodology for the practical assessment of freshness of fruits and vegetables?

These questions will be investigated in a model experiment by measuring the δ^2H values of methoxyl groups, the δ^2H and the $\delta^{18}O$ values of tissue water, and the weight loss under controlled conditions from apples, carrots, and potatoes.

EXPERIMENTAL PROCEDURES

Chemicals. Hydriodic acid (puriss. p.a., 55−60%, not stabilized) and methyl iodide (99.5%) were purchased from Sigma-Aldrich (Seelze, Germany, and Gillingham, U.K., respectively).

Fruit and Vegetable Samples. Apples (*Malus domestica* var. Jonagold, 31 apples from a single tree) were harvested on September 29, 2009, at a local farm in Germany (geographic position, 49°57′34″N, 08°12′50″E; altitude, 190 m). Carrots (40 carrots per set) were provided from three different locations. One sample set, purchased at the local market in Mainz on August 17, 2010, had been grown nearby (geographic position, 49°58′17″N, 8°21′17″E; altitude, 86 m). The two other carrot sample sets were obtained from Umeå, Sweden (63°49′N, 20°15′E), and Belfast, Northern Ireland (54°35′N, 5°56′W). After being harvested, both sample sets were stored under controlled conditions at 4 °C and processed within 2 days.

Three apples and carrots were selected to represent a sample (to be analyzed after different storage time periods). The samples were stored at 22 °C and a relative humidity of 55%. Water loss relative to the fresh weight was calculated from the difference between the initial weight and that after storage before squeezing. Every 4 and 7 days, samples of carrots and apples, respectively, were processed by being squeezed in a commercial juice extractor; tissue water was collected and the residual organic matter lyophilized. Both samples were stored at −20 °C until stable isotope ratio analysis was conducted.

Moreover, during a sample campaign from Gibraltar, Spain, to Mainz, Germany, in May 2009 at different locations, several carrot and potato samples were collected along a south−north gradient covering a latitude range of ∼14° (36°−50°N) (see Table 1). These samples were stored at 4 °C and analyzed in the same manner described above.

Isotope Ratio Analysis of Samples. *Sample Preparation and Instrumentation for the ^2H Analysis of Methoxyl Groups.* Hydrogen isotope signatures of the methoxyl groups from fruit and vegetable matter were measured as CH_3I released upon treatment of the lyophilized samples with HI by the procedure of Greule et al.[12] HI (0.5 mL, 55−60%) was added to the sample (150−300 mg) in a crimp glass vial (1.5 mL). The vials were sealed with crimp caps containing PTFE-lined butyl rubber septa (thickness of 0.9 mm) and incubated for 30 min at 130 °C. After being heated, the samples were allowed to equilibrate at room temperature (22 ± 0.5 °C, air-conditioned room) for at least 30 min before an aliquot of the headspace (10−90 μL) was collected and directly injected into the analytical system.

The δ^2H values (see below) of CH_3I released from methoxyl groups in the samples ($\delta^2H_{OCH_3}$) were measured using an HP 6890N gas chromatograph (Agilent, Santa Clara, CA) equipped with an

DOI: 10.1021/jf505192p
J. Agric. Food Chem. 2015, 63, 1974−1981

autosampler (A200S, CTC Analytics, Zwingen, Switzerland), coupled to a Delta^{PLUS}XL isotope ratio mass spectrometer (ThermoQuest Finnigan, Bremen, Germany) via a thermo conversion reactor [ceramic tube (Al_2O_3), length of 320 mm, 0.5 mm inside diameter, reactor temperature of 1450 °C] and a GC Combustion III Interface (ThermoQuest Finnigan). The gas chromatograph (GC) was fit with a HP-5MS capillary column (Agilent) (30 m × 0.25 mm inside diameter; d_f = 0.5 μm), and the following conditions were employed: split injection (4:1), initial oven temperature of 30 °C for 3.8 min, ramp at 30 °C/min to 100 °C. Helium was used as the carrier gas at a constant flow of 0.6 mL/min.

A tank of high-purity hydrogen (hydrogen 5.0, Linde, Höllriegelskreuth, Germany) with a known δ^2H value of −295‰ (V-SMOW) was used as the working reference gas. The H_3^+ factor, determined daily during the measurement period, was in the range of 4.1−4.4. Samples were analyzed five times (n = 5), and the average standard deviations of the Gas chromatography-high temperature conversion-isotope ratio mass spectrometry (GC-HTC-IRMS) measurements were in the range of 0.3−4.2‰. All $\delta^2H_{OCH_3}$ values were mathematically corrected by adjustment for an offset derived from the difference between the nominal and measured δ^2H values of a single CH_3I working standard relative to V-SMOW. The δ^2H value of CH_3I was calibrated against international reference substances [IA-R002 ($\delta^2H_{V\text{-}SMOW}$ = −111.2‰), IAEA-CH-7 ($\delta^2H_{V\text{-}SMOW}$ = −100.3‰), and NBS-22 ($\delta^2H_{V\text{-}SMOW}$ = −118.5‰)] using an offline EA-IRMS (elemental analyzer-isotopic ratio mass spectrometer, Iso-Analytical Ltd., Sandbach, U.K.). The calibrated δ^2H value versus V-SMOW for CH_3I was −179.0 ± 2.9‰ (n = 15; 1σ). The standard was measured after every fifth sample injection.

As this procedure represents solely a one-point calibration, it has to be pointed out that the δ^2H data might be affected by an additional error ("scale compression"). Unfortunately, CH_3I working standards with distinct isotopic signatures spanning the full range of measured δ^2H values were not available for this study to eliminate or minimize such an error. The authors are very aware that traceability and therefore international comparability of stable isotope abundance measurements ideally require a two-scale anchor calibration with accepted isotope abundance values as recommended by the IUPAC guidelines.[14,15]

δ^2H and δ^{18}O Analysis of Tissue Water. Stable isotope analysis of tissue water was conducted at Isolab (Laboratorium für Stabile Isotope, isolab GmbH, Schweitenkirchen, Germany). In brief, samples of tissue water were homogenized, and the liquid was separated from solids by centrifugation. This liquid was subsequently used to measure δ^2H (after distillation) and δ^{18}O (after equilibration and dual inlet measurement) values of tissue water. A homemade equilibration unit coupled to a dual-inlet IRMS (Thermo MAT 250) was employed for oxygen isotope analysis and an equilibration unit based on platinum-catalyzed hydrogen exchange between water and hydrogen gas for hydrogen isotope analysis. The reliability of the isotopic analyses was checked by measuring in-house reference water of a known isotopic content (δ^{18}O, −10.3‰; δ^2H, −72‰) regularly in each sample batch. The reference water had been calibrated versus V-SMOW and V-SLAP international standard waters. To prevent microbial degradation of the dissolved organic compounds (CO_2 formation) during oxygen isotope analysis by equilibration, sodium azide was added to the samples before they were placed into the equilibration vessels.

Definition of δ Values and Calculation of Isotope Fractionation ε. Throughout this paper, the "delta" (δ) notation, the relative difference of the isotope ratio of a material to that of a standard V-SMOW (Vienna Standard Mean Ocean Water), is used. Values of δ^2H and δ^{18}O relative to that for V-SMOW are defined by the following equations:

$$\delta^2H = ({}^2H/{}^1H)_{sample}/({}^2H/{}^1H)_{standard} - 1 \quad (1)$$

$$\delta^{18}O = ({}^{18}O/{}^{16}O)_{sample}/({}^{18}O/{}^{16}O)_{standard} - 1 \quad (2)$$

However, for practical reasons, we use δ values in ‰, and as our method has originally been developed and is still preferably applied for geochemical questions, definitions for ε and Δ are as usual in this discipline.[8,16] Therefore, the hydrogen isotope fractionation between plant tissue water (index w) and methoxyl groups (index m) during the synthesis of biomass, the "isotope enrichment", is (R is here the isotope ratio)

$$\begin{aligned}\varepsilon_{m/w} &= R_m/R_w - 1\\ &= ({}^2H/{}^1H)_m/({}^2H/{}^1H)_w - 1\\ &= (\delta^2H_m + 1)/(\delta^2H_w + 1) - 1\end{aligned} \quad (3)$$

The authors are aware that this is an approximation and would like to refer to the studies of Coplen et al. and Schmidt et al. for further reading.[14,17] Throughout the paper, we use the short form $\varepsilon_{m/w}$ for $\varepsilon_{methoxyl/water}$.

RESULTS AND DISCUSSION

Hydrogen Isotope Fractionation and Correlation between Tissue Water and Plant Matter Methoxyl Groups. In our initial experiments, we determined the hydrogen isotope fractionation between tissue water and methoxyl groups of fresh potatoes and carrots, collected in different geographic locations in Europe (cf. Fruit and Vegetable Samples).

For some samples (carrot samples C4−C9), it was not possible to analyze the δ^2H values of tissue water as the amount of juice obtained was not sufficient to allow isotope analysis. For these samples, δ^2H values of tissue water were calculated using the Online Isotope Precipitation Calculator [OIPC (http://www.waterisotopes.org/)], employing the IAEA database and interpolation algorithms.[18−20] For this approach, we made the simplification and/or assumption that the δ^2H values of the water taken up by the potatoes and carrots were similar to that of the annual precipitation at the sampling site.

The mean isotope fractionations between tissue water and methoxyl groups ($\varepsilon_{m/w}$) were −184 ± 13‰ and −158 ± 13‰ for the carrots and potatoes, respectively (Table 1). This shows the necessity of determining the isotope fractionation for each species of fruit and vegetable separately. The slopes of the linear regressions for data of both potatoes and carrots are close to 1 with coefficients of determination (R^2) close to 0.6 (Figure 1a; for carrots, R^2 = 0.59, n = 11, and p < 0.006; for potatoes, R^2 = 0.56, n = 13, and p < 0.003). Furthermore, the mean isotope fractionation $\varepsilon_{m/w}$ of the potato samples is in excellent agreement with data previously been reported by Keppler et al. ($\varepsilon_{m/w}$ = −161 ± 11‰).[21] Via combination of the latter data with this data set (Table 1 and Figure 1b), R^2 increases to ∼0.85 (R^2 = 0.85, n = 30, and p < 0.001), highlighting the importance of larger data sets.

Relationship between δ^2H and δ^{18}O in Tissue Water of Fruits and Vegetables. The δ^2H and δ^{18}O values of meteoric water show a linear correlation, well-known as the "meteoric water line" (MWL) roughly expressed by the equation $\delta^2H = 8 \times \delta^{18}O + 10$.[22] Because of transpiration, tissue water in plants becomes enriched in δ^2H and δ^{18}O relative to source water.[23] This isotope enrichment is transferred to fruits and vegetables[24] but shows, as compared to MWL, a relative larger enrichment of ^{18}O and then of ^{2}H, which might be due to the relative mass difference of the water isotopologues that is twice as large for oxygen [$H_2{}^{18}O$ (mass of 20) − $H_2{}^{16}O$ (mass of 18) = 2] as it is for hydrogen [^{2}HHO (mass of 19) − H_2O (mass of 18) = 1]. More probably, however, different diffusion constants of the stomata lead to the observed difference in the enrichments of ^{18}O and ^{2}H. Thus, the slope of the resulting relationship

DOI: 10.1021/jf505192p
J. Agric. Food Chem. 2015, 63, 1974−1981

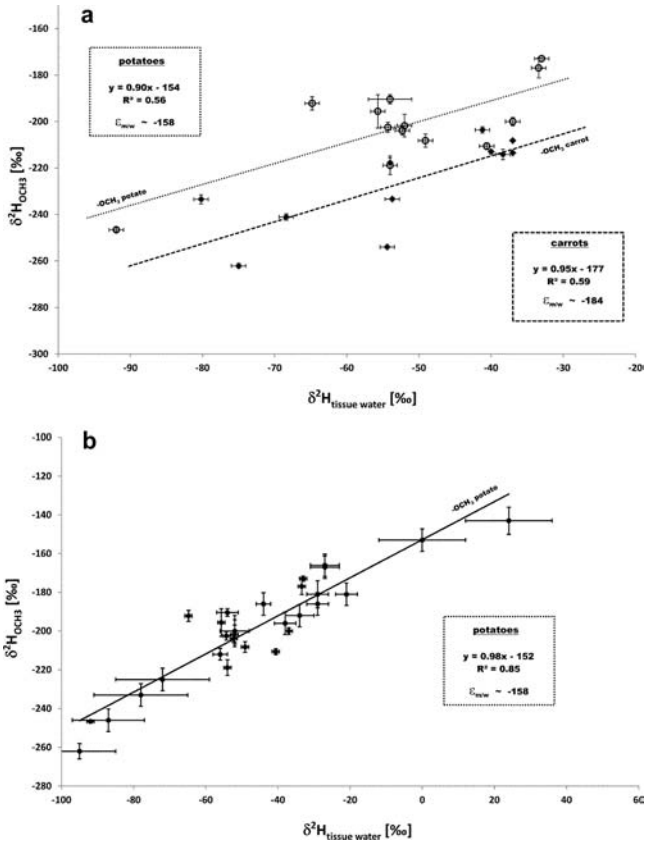

Figure 1. (a) Relationship between δ^2H values of tissue water and organic matter methoxyl groups of potatoes (○) and carrots (■) harvested at different geographic locations. Error bars indicate (i) for methoxyl groups the standard deviation of mean values (n = 4) and (ii) for δ^2H values of tissue water the confidence intervals calculated by the Online Isotope Precipitation Calculator (OIPC). (b) Relationship between δ^2H values of tissue water and organic matter methoxyl groups of potatoes harvested at different geographic locations. Combination of the current data set and that from a previous study.[10] Error bars indicate (i) for methoxyl groups the standard deviation of mean values (n = 4) and (ii) for δ^2H values of tissue water the confidence intervals calculated by the OIPC.

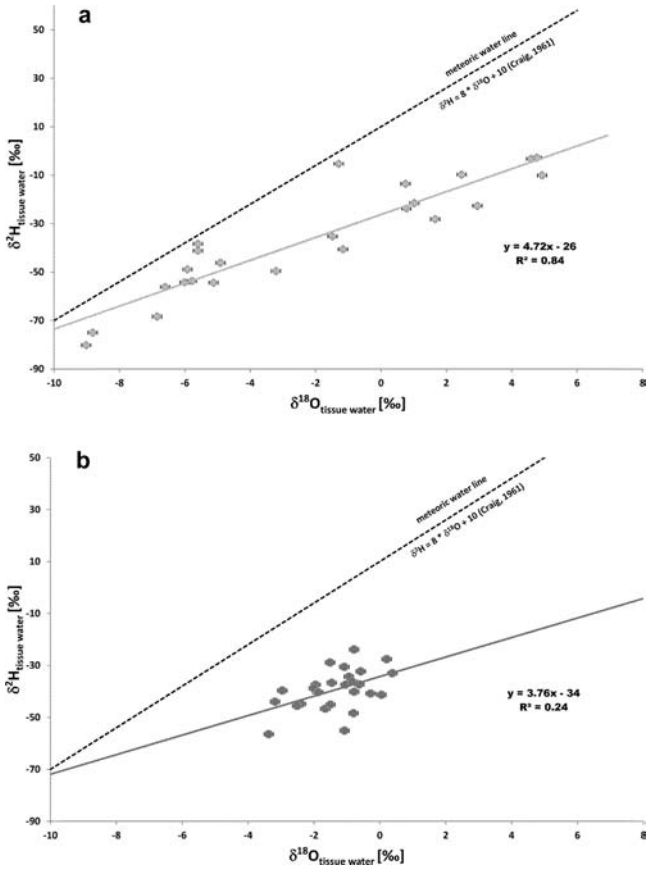

Figure 2. Relationship between δ^2H and δ^{18}O values in tissue water of (a) carrots and (b) apples. In analogy to the meteoric water line, we refer to the relationship as the "fruit water line". Error bars show the precision of sample measurement.

between δ^2H and δ^{18}O in tissue water that we define as the "fruit water line" is lower than the meteoric water line: in the literature, slopes of 2−4 can be found.[24−27] Although the "fruit water line" must be determined individually for each of the different fruits and vegetables, once it has been established the isotopic signatures of ^{2}H and ^{18}O of tissue water can be deduced from one another. Nevertheless, we cannot completely rule out the possibility that storage conditions might have an influence on the relationship between δ^2H and δ^{18}O in tissue water ($\delta^{18}O_{tw}$ and δ^2H_{tw}) and thus on the slope of the "fruit water line". This possibility should be further considered and investigated in the future.

Here, we determined δ^2H and δ^{18}O values of the "fruit water line" of carrots and apples. The slopes of the linear regressions for data of both carrots and apples are significantly lower than the MWL {4.72 and 3.76, respectively [panels a (carrots) and b (apples) of Figure 2]} and in good agreement with literature data (*Lupinus angustifolius*, 3.1;[26] grapes, 3.9[24]). The carrot samples showed an R^2 (R^2 = 0.84, n = 24, and p < 0.001) considerably higher than that of the apple samples (R^2 = 0.24, n = 27, and p < 0.01).

Relationship among δ^{18}O and δ^2H of Tissue Water, δ^2H of Methoxyl Groups, and Storage Time. A main factor to be controlled during the storage of fruit and vegetable is the loss of water by evaporation. The degree of water loss depends on storage time, temperature, and humidity. In this study, the controlled conditions were 22 °C and a relative humidity of 55%. Details of sample storage and measurement of the δ^{18}O and δ^2H values of tissue water of carrots and apples and the respective δ^2H values of the methoxyl groups during storage are described in the Experimental Section.

Our results (Figure 3) show that with storage time and water loss both $\delta^{18}O_{tw}$ and δ^2H_{tw} of the residual tissue water become more positive, because of the preferred loss of the lighter isotopes during transpiration. As described in the previous section, $\delta^{18}O_{tw}$ correlates significantly better with water loss than δ^2H_{tw}, for both carrots (R^2 = 0.90 ↔ 0.49) and apples (R^2 = 0.92 ↔ 0.18). No significant change in the δ^2H values of the methoxyl groups ($\delta^2H_{OCH_3}$) was observed for the same samples during storage for up to 20 and 69 days for carrots and apples, respectively (Figure 4). Thus, methoxyl groups of fruit and vegetable can be considered a plant archive that records the δ^2H values of the plant tissue water before harvest.

The results further prove that the hydrogen atoms remain fixed to the nonpolar C−H bond of the methoxyl groups and do not exchange with water once they are bound, and hence, their isotope value remains stable. At this point, it is important to note that this is not the case for the CO−H bond of carbohydrates. These results would indicate that most reliable

DOI: 10.1021/jf505192p
J. Agric. Food Chem. 2015, 63, 1974−1981

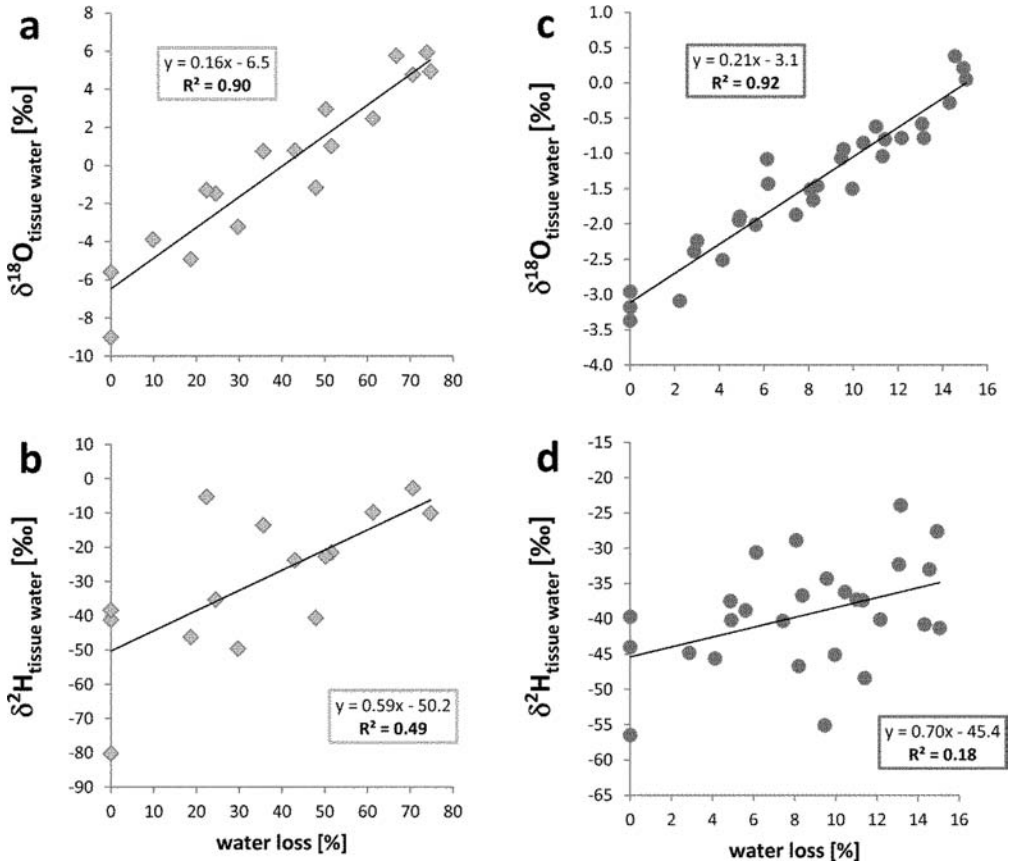

Figure 3. Relationship between water loss (%) and stable isotope values of tissue water from carrots [(a) δ^{18}O and (b) δ^{2}H] and apples [(c) δ^{18}O and (d) δ^{2}H].

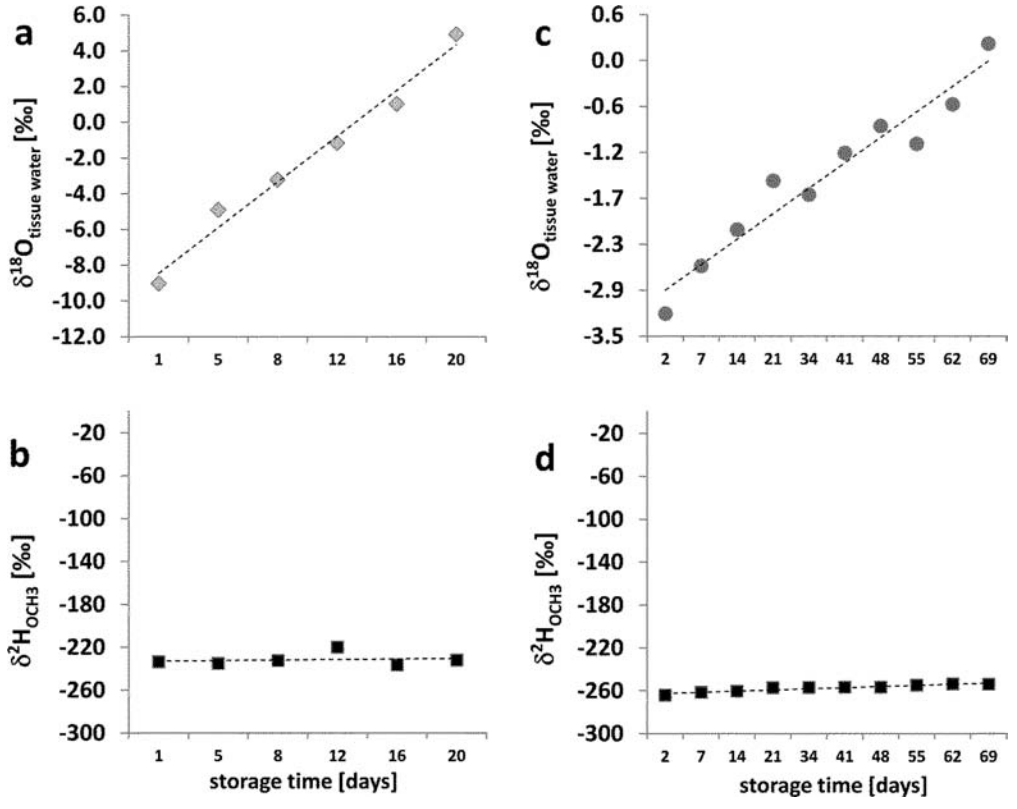

Figure 4. δ^{2}H signatures of methoxyl groups {stable parameter [(a) carrots and (c) apples]} and δ^{18}O signatures of tissue water (changing parameter) during storage time [(b) carrots and (d) apples].

DOI: 10.1021/jf505192p
J. Agric. Food Chem. 2015, 63, 1974−1981

and promising use for the reconstruction of the tissue water loss would be a combination of $\delta^2H_{OCH_3}$ and $\delta^{18}O_{tw}$. In the subsequent sections, we will demonstrate in detail how this can practicably be undertaken.

Application of the Method for the Determination of the Initial $\delta^2H/\delta^{18}O$ Ratios of Tissue Water from the δ^2H Values of Methoxyl Groups. The complete isotopic signature of tissue water of plant tissue prior to harvest can be deduced from the δ^2H values of its methoxyl groups. The δ^2H value can be calculated from the correlation between the isotope signatures of methoxyl groups and tissue water (Figure 1a,b), and the $\delta^{18}O$ value from the "fruit water line" that is derived from δ^2H and $\delta^{18}O$ values of tissue water (eq 5 and Figure 2a,b). Because water loss is best reconstructed from $\delta^2H_{OCH_3}$ and $\delta^{18}O_{tw}$ in the first step, it is necessary to calculate the initial δ^2H value of tissue water (δ^2H_{twi}) using the respective food specific constant isotope fractionation between the δ^2H values of tissue water and methoxyl groups (eq 4).

$$\delta^2H_{twi} = \delta^2H_{OCH_3} - \text{isotope fractionation } \varepsilon_{m/w} \quad (4)$$

Then the next step is to determine the initial $\delta^{18}O$ value of tissue water ($\delta^{18}O_{twi}$) from the "fruit water line", the relationship between $\delta^{18}O$ and δ^2H values in fruits and vegetables (eq 5).

$$\delta^{18}O_{twi} = (\delta^2H_{twi} - \text{axis intercept}_{\text{"fruit water line"}}) / \text{slope}_{\text{"fruit water line"}} \quad (5)$$

As an example, this procedure is graphically illustrated in Figure 5.

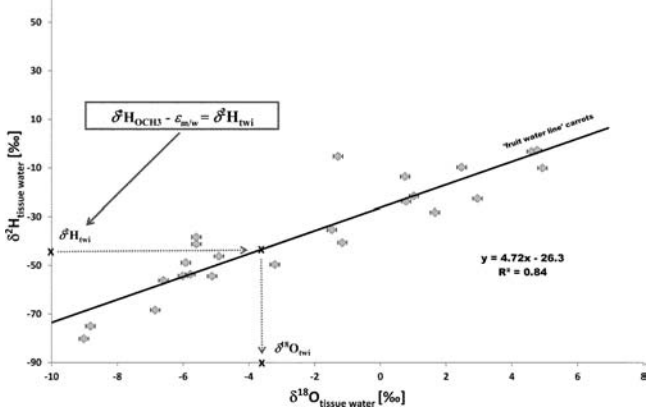

Figure 5. Calculation of the initial $\delta^{18}O$ value of tissue water from the δ^2H value of tissue water and the corresponding "fruit water line".

Deduction of Relative Water Loss from $\delta^{18}O$ of Tissue Water and δ^2H of Methoxyl Groups. Two further steps are necessary to calculate the relative water loss of fruits and vegetables during storage. First, we need to calculate the oxygen isotope discrimination $\Delta^{i18}O_{twm/twi}$ ("delta over baseline, DOB") or "isotopic difference" between the $\delta^{18}O$ value of tissue water measured at an unknown stage of storage time ($\delta^{18}O_{twm}$) and the initial value of the water present during biosynthesis ($\delta^{18}O_{twi}$) as obtained from the δ^2H value of the corresponding methoxyl group (cf. eq 5) and its correlation to the $\delta^{18}O$ value:

$$\Delta^{i18}O_{twm/twi} = (\delta^{18}O_{twm} - \delta^{18}O_{twi})/(1 + \delta^{18}O_{twi})$$

or, as

$$\delta^{18}O_{twi} << 1$$

$$\Delta^{i18}O_{twm/twi} = \delta^{18}O_{twm} - \delta^{18}O_{twi} \quad (6)$$

Finally, when $\Delta^{i18}O_{twm/twi}$ is divided by the slope of the food specific linear regression, this will yield the percentage water loss (eq 7):

$$\%\text{water loss} = \Delta^{i18}O_{twm/twi}/\text{slope} \quad (7)$$

A graphic illustration of the last step is shown in Figure 6. Via application of the procedure described above, the correlation

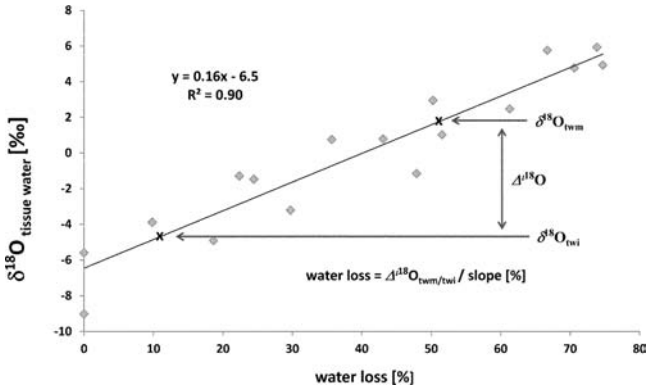

Figure 6. Calculation of water loss (%) using the calculated initial $\delta^{18}O$ value of tissue water (cf. Figure 5) and the measured $\delta^{18}O$ value of tissue water.

line of Figure 3a, and the equations given above, the relative water loss from an actual sample (carrot; measured values, $\delta^2H_{OCH_3} = -236.4 \pm 2.4‰$, $\delta^{18}O_{twm} = 1.02 \pm 0.14‰$, and $\varepsilon_{m/w} = -184‰$) after storage for 16 days at 22 °C and a relative humidity of 55% was found to be 40.8 ± 11.8%. The error was calculated using a Gaussian error propagation including uncertainties of $\delta^{18}O$ and δ^2H measurements, the regression equation of the relationship between δ^2H of tissue water and methoxyl groups [isotope fractionation (cf. Figure 1)], and the regression equation of the carrot "fruit water line" (cf. Figure 2a). The rather high error can most likely be explained by the small data sets on which the linear regressions have been calculated. Nevertheless, because our intention was to demonstrate the principle of this new method, we did not place too much emphasis on minimizing the uncertainties at this stage because we were aware that it was well beyond the capabilities of one study to provide such an extensive data set.

For comparison, the gravimetrically measured water loss for the same sample was found to be 46.6%, which is in reasonable agreement with the water loss determined by this new approach (40.8 ± 11.8%).

Conclusion. Postharvest alterations of plant tissue water, as water loss during storage or illegal tap water addition, decrease the quality of plant products. The aim of this study was therefore to investigate an easy and reliable method for the detection of such changes.

As shown in this study and previous studies, methoxyl groups of organic samples are very easily converted to CH_3I. From this investigation, the δ^2H value of the latter compound was found to be a stable and reliable biomarker for the isotope characteristics of plant tissue water prior to harvest. The

DOI: 10.1021/jf505192p
J. Agric. Food Chem. 2015, 63, 1974−1981

model experiments conducted with apples, carrots, and potatoes under controlled storage conditions revealed that water loss during storage was accompanied by an enhancement of the δ^2H and δ^{18}O values of tissue water. The correlations of these values were distinct for the individual plants and differed from the MWL. δ^{18}O values were better correlated to water loss, as measured by weight, than δ^2H values.

Therefore, for assessment of postharvest tissue water loss of fruits and vegetables, we suggest that a procedure should be based on the determination of the δ^2H values of the methyl groups of the organic matter and the δ^{18}O value of the actual tissue water. The extension of this procedure to the practical control of fruit or vegetable freshness would require investigation of samples stored under normal commercial conditions. For this, we would envisage that the range of isotopic data from such samples would be wider than those found in the model experiment, and therefore, calibration with several isotope standards covering this expanded range would be necessary. Moreover, as we would also expect the isotopic shifts under commercial storage conditions to be smaller than those observed in this study, it would be necessary to undertake considerably more development and refinement of the current protocol.

AUTHOR INFORMATION

Corresponding Author

*Telephone: +49 6221-545228. Fax: +49 6221-545503. E-mail: markus.greule@geow.uni-heidelberg.de.

Funding

F.K. and M.G. were supported by the German Science Foundation (KE 884/6-1 and KE 884/8-1).

Notes

The authors declare no competing financial interest.

ACKNOWLEDGMENTS

We thank Daniela Polag, Jennifer Rinne, Evelyne Kasparek, and Ilka Hermes for technical assistance. We are grateful to Colin McRoberts und Jürgen Schleucher for providing carrot samples from Northern Ireland and Sweden, respectively. We thank John Hamilton for comments on an earlier version of the manuscript.

REFERENCES

(1) Augusti, A.; Schleucher, J. The Ins and Outs of Stable Isotopes in Plants. *New Phytol.* **2007**, *174*, 473−475.

(2) Sternberg, L. d. S. L. O. Oxygen and Hydrogen Isotope Ratios in Plant Cellulose: Mechanisms and Applications. In *Stable Isotopes in Ecological Research*; Rundel, P., Ehleringer, J. R., Nagy, K., Eds.; Springer-Verlag: New York, 1989; Vol. *68*, pp 124−141.

(3) Sternberg, L. d. S. L. O. Oxygen Stable Isotope Ratios of Tree-Ring Cellulose: The Next Phase of Understanding. *New Phytol.* **2009**, *181*, 553−562.

(4) Sternberg, L.; Pinzon, M. C.; Anderson, W. T.; Jahren, A. H. Variation in Oxygen Isotope Fractionation during Cellulose Synthesis: Intramolecular and Biosynthetic Effects. *Plant, Cell Environ.* **2006**, *29*, 1881−1889.

(5) Sternberg, L.; Ellsworth, P. F. V. Divergent Biochemical Fractionation, Not Convergent Temperature, Explains Cellulose Oxygen Isotope Enrichment Across Latitudes. *PLoS One* **2011**, *6*, No. e28040.

(6) Jamin, E.; Guérin, R.; Rétif, M.; Lees, M.; Martin, G. J. Improved Detection of Added Water in Orange Juice by Simultaneous Determination of the Oxygen-18/Oxygen-16 Isotope Ratios of Water and Ethanol Derived from Sugars. *J. Agric. Food Chem.* **2003**, *51*, 5202−5206.

(7) Perini, M.; Camin, F. δ^{18}O of Ethanol in Wine and Spirits for Authentication Purposes. *J. Food Sci.* **2013**, *78*, C839−C844.

(8) Sachse, D.; Billault, I.; Bowen, G. J.; Chikaraishi, Y.; Dawson, T. E.; Feakins, S. J.; Freeman, K. H.; Magill, C. R.; McInerney, F. A.; van der Meer, M. T. J.; et al. Molecular Paleohydrology: Interpreting the Hydrogen-Isotopic Composition of Lipid Biomarkers from Photosynthesizing Organisms. *Annu. Rev. Earth Planet. Sci.* **2012**, *40*, 221−249.

(9) Keppler, F.; Harper, D. B.; Kalin, R. M.; Meier-Augenstein, W.; Farmer, N.; Davis, S.; Schmidt, H.-L.; Brown, D. M.; Hamilton, J. T. G. Stable Hydrogen Isotope Ratios of Lignin Methoxyl Groups as a Paleoclimate Proxy and Constraint of the Geographical Origin of Wood. *New Phytol.* **2007**, *176*, 600−609.

(10) Keppler, F.; Hamilton, J. T. G.; McRoberts, W. C.; Vigano, I.; Brass, M.; Röckmann, T. Methoxyl Groups of Plant Pectin as a Precursor of Atmospheric Methane: Evidence from Deuterium Labelling Studies. *New Phytol.* **2008**, *178*, 808−814.

(11) Greule, M.; Tumino, L. D.; Kronewald, T.; Hener, U.; Schleucher, J.; Mosandl, A.; Keppler, F. Improved Rapid Authentication of Vanillin Using δ^{13}C and δ^2H Values. *Eur. Food Res. Technol.* **2010**, *231*, 933−941.

(12) Greule, M.; Mosandl, A.; Hamilton, J. T. G.; Keppler, F. A Rapid and Precise Method for Determination of D/H Ratios of Plant Methoxyl Groups. *Rapid Commun. Mass Spectrom.* **2008**, *22*, 3983−3988.

(13) Greule, M.; Mosandl, A.; Hamilton, J. T. G.; Keppler, F. A Simple Rapid Method to Precisely Determine ^{13}C/^{12}C Ratios of Plant Methoxyl Groups. *Rapid Commun. Mass Spectrom.* **2009**, *23*, 1710−1714.

(14) Coplen, T. B. Guidelines and Recommended Terms for Expression of Stable-Isotope-Ratio and Gas-Ratio Measurement Results. *Rapid Commun. Mass Spectrom.* **2011**, *25*, 2538−2560.

(15) Meier-Augenstein, W.; Hobson, K. A.; Wassenaar, L. I. Critique: Measuring Hydrogen Stable Isotope Abundance of Proteins to Infer Origins of Wildlife, Food and People. *Bioanalysis* **2013**, *5*, 751−767.

(16) Hayes, J. M. Fractionation of Carbon and Hydrogen Isotopes in Biosynthetic Processes. *Rev. Mineral. Geochem.* **2001**, *43*, 225−277.

(17) Schmidt, H.-L.; Robins, R. R.; Werner, R. A. Multi-Factorial *in Vivo* Stable Isotope Fractionation: Causes, Correlations, Consequences and Applications. *Isot. Environ. Health Stud.* **2015**, DOI: 10.1080/10256016.2015.1014355.

(18) Bowen, G. J.; Wilkinson, B. Spatial Distribution of δ^{18}O in Meteoric Precipitation. *Geology* **2002**, *30*, 315.

(19) Bowen, G. J. Interpolating the Isotopic Composition of Modern Meteoric Precipitation. *Water Resour. Res.* **2003**, *39*, 1−13.

(20) Bowen, G. J.; Wassenaar, L. I.; Hobson, K. A. Global Application of Stable Hydrogen and Oxygen Isotopes to Wildlife Forensics. *Oecologia* **2005**, *143*, 337−348.

(21) Keppler, F.; Hamilton, J. T. G. Tracing the Geographical Origin of Early Potato Tubers Using Stable Hydrogen Isotope Ratios of Methoxyl Groups. *Isot. Environ. Health Stud.* **2008**, *44*, 337−347.

(22) Craig, H. Isotopic Variations in Meteoric Waters. *Science* **1961**, *133*, 1702−1703.

(23) Allison, G. B.; Gat, J. R.; Leaney, F. W. J. The Relationship between Deuterium and Oxygen-18 Delta Values in Leaf Water. *Chem. Geol.* **1985**, *58*, 145−156.

(24) Dunbar, J.; Wilson, A. T. Oxygen and Hydrogen Isotopes in Fruit and Vegetable Juices. *Plant Physiol.* **1983**, *72*, 725−727.

(25) Leaney, F. W.; Osmond, C. B.; Allison, G. B.; Ziegler, H. Hydrogen-Isotope Composition of Leaf Water in C3 and C4 Plants: Its Relationship to the Hydrogen-Isotope Composition of Dry Matter. *Planta* **1985**, *164*, 215−220.

(26) Cernusak, L. A.; Pate, J. S.; Farquhar, G. D. Diurnal Variation in the Stable Isotope Composition of Water and Dry Matter in Fruiting *Lupinus angustifolius* under Field Conditions. *Plant, Cell Environ.* **2002**, *25*, 893−907.

DOI: 10.1021/jf505192p
J. Agric. Food Chem. 2015, 63, 1974−1981

(27) Nissenbaum, A.; Lifshitz, A.; Stepek, Y. Detection of Citrus Fruits Adulteration Using the Distribution of Natural Isotopes. *Lebensm.-Wiss. Technol. (1968-2004)* **1974**, *7*, 152−154.

DOI: 10.1021/jf505192p
J. Agric. Food Chem. 2015, 63, 1974−1981

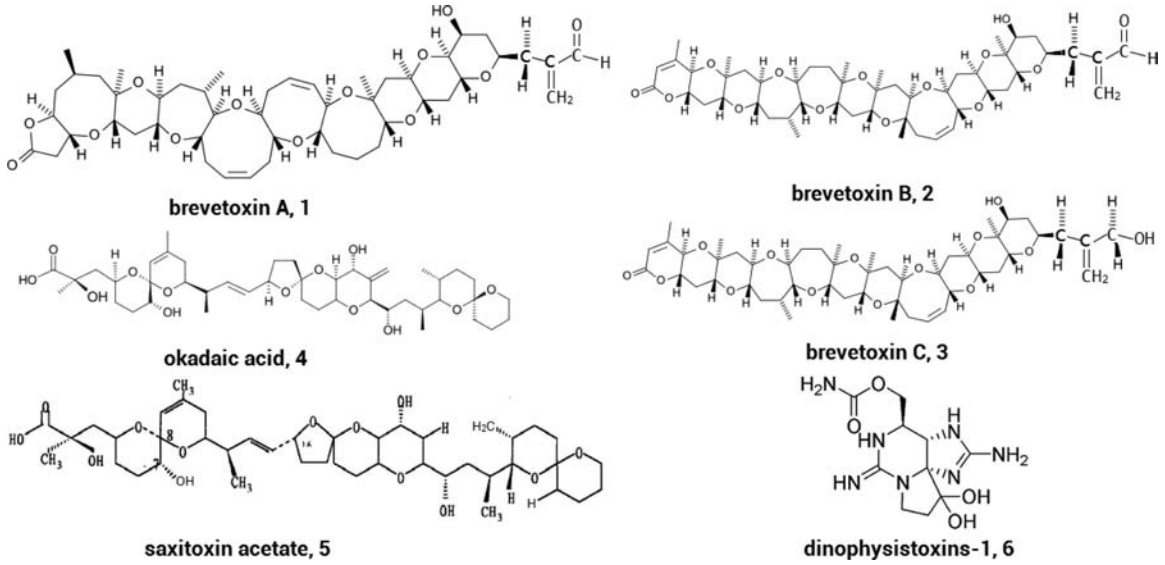

Figure 1. Chemical structures of different marine toxins: brevetoxin A, **1**; brevetoxin B, **2**; brevetoxin C, **3**; okadaic acid, **4**; saxitoxin acetate, **5**; dinophysistoxin-1, **6**.

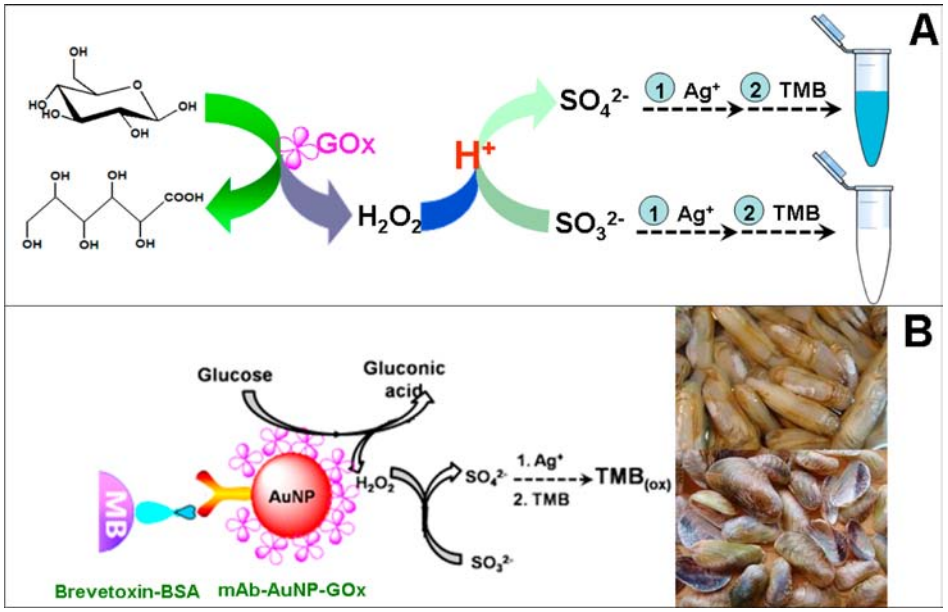

Figure 2. Schematic illustration of (A) GOx-mediated sulfite-to-sulfate chemical conversion for color development of the Ag(I)−TMB system and (B) Ag(I)−TMB-based colorimetric immunoassay by coupling with enzyme-controlled sulfite-to-sulfate chemical conversion.

MATERIALS AND METHODS

Safety. To avoid possible exposure and potential contamination, all tools and items in contact with marine toxins should be put into a 10 wt % bleach solution for 2−3 h before they are discarded because marine toxins are powerful hepatotoxins and carcinogens. Pure marine toxin standards were handled in a hood with great caution.

Materials and Reagent. Monoclonal mouse anti-brevetoxin antibody (mAb) and brevetoxin B−bovine serum albumin (brevetoxin−BSA) conjugate were gifted from the College of Chemistry of Soochow University (Suzhou, China). The standards including brevetoxins A, B, and C, **1**, **2**, and **3**, okadaic acid, **4**, saxitoxin acetate, **5**, and dinophysistoxin-1, **6** (Figure 1), were purchased from Express Technology Co., Ltd. (Beijing, China). GOx and $HAuCl_4{\cdot}4H_2O$ were purchased from Sigma-Aldrich (Shanghai, China). Silver nitrate ($AgNO_3$), TMB, and BSA were purchased from Sinopharm Chemical Reagent Co., Ltd. (Shanghai, China). Sodium sulfite (Na_2SO_3) and sodium sulfate (Na_2SO_4) were obtained from Fuchen Chemicals (Tianjin, China). The brevetoxin B ELISA kit was obtained from Abraxis LLC (Warminster, PA, USA). All other reagents were used as received without further purification. All water used was of Milli-Q ultrapure grade (Merck Millipore, Darmstadt, Germany). Different buffer solutions including pH 9.6 carbonate buffer, pH 7.0 phosphate-buffered saline (PBS, 0.5 mM), and pH 7.4 PBS were purchased from Sigma-Aldrich (Shanghai, China).

Food Samples and Extraction Procedure. A *Musculista senhousia* matrix (5.0 g, ground blank) was first milled with a small food mixer and then extracted with aqueous dimethyl sulfoxide (20 mL, 50%, w/v). After slight stirring for 60 min, the suspension was filtered with a nylon mesh (100 nm), no. 1 filter, and a GF/B filter (Whatman, Dassel, Germany) in turn. The extract color was a slight opalescent yellow. Finally, the solution for the calibration curve was prepared by spiking brevetoxin B standards into the diluted extract with various volumes.

Preparation of Brevetoxin−BSA-Conjugated Magnetic Bead and mAb/GOx-Labeled Gold Nanoparticle. Bevetoxin−BSA-

DOI: 10.1021/acs.jafc.5b00425
J. Agric. Food Chem. 2015, 63, 1982−1989

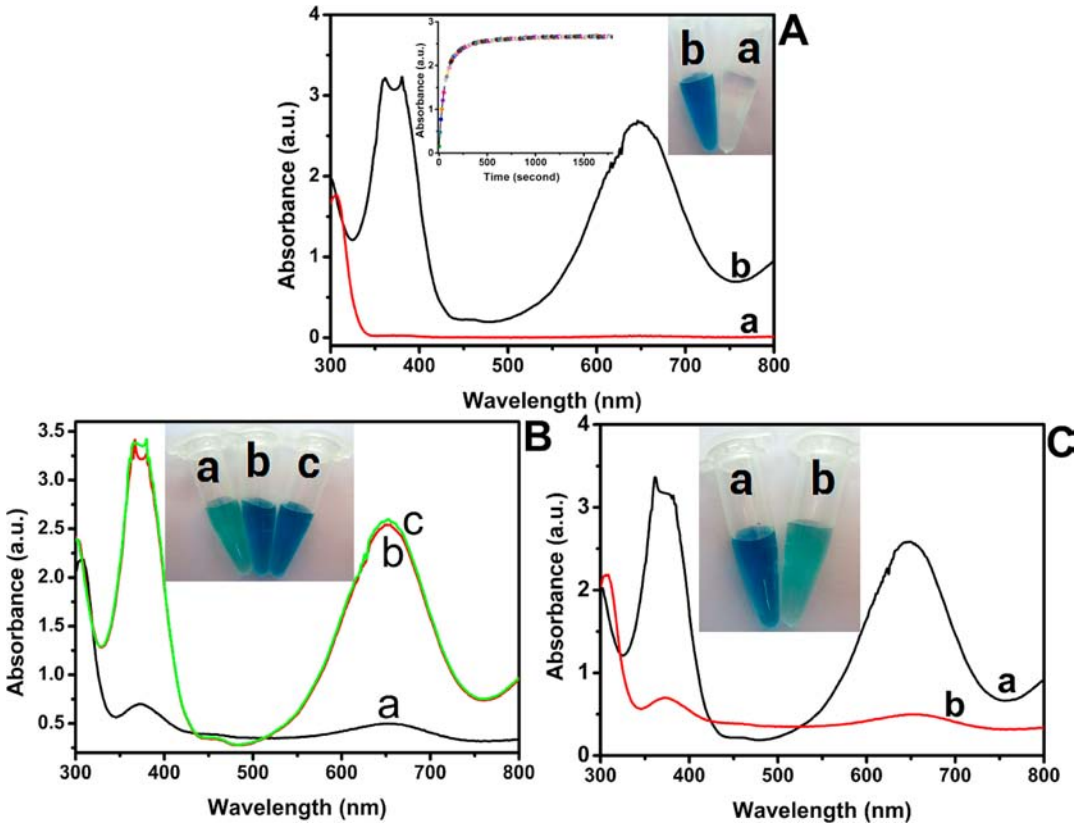

Figure 3. UV−vis absorption spectra of (A) (a) 1.0 mM TMB and (b) 1.0 mM TMB + 2.0 mM Ag(I); (B) (a) 2.0 mM sulfite + 2.0 mM Ag(I) + 1.0 mM TMB, (b) 2.0 mM sulfate + 2.0 mM Ag(I) + 1.0 mM TMB, and (c) 2.0 mM Ag(I) + 1.0 mM TMB; and (C) (a) 1.0 mM H_2O_2 + 1.0 mM sulfite + 2.0 mM Ag(I) + 1.0 mM TMB and (b) 0 mM H_2O_2 + 1.0 mM sulfite +2.0 mM Ag(I) + 1.0 mM TMB. (Insets) Corresponding photographs.

conjugated magnetic bead was prepared similarly to our previous study.[27] Briefly, 3-aminopropyltriethoxysilane (30 μL, 98 wt %) was initially added into 1.0 mL of anhydrous ethanol containing 50 mg of magnetic beads (~100 nm) (Chemical GmbH, Berlin, Germany) for reaction for 6 h at room temperature under gentle shaking on a shaker. Following that, the aminated magnetic beads, collected by an external magnet, were suspended in 1.0 mL of 15 wt % glutaraldehyde and reacted for another 6 h. Afterward, the precipitate obtained by magnetic separation was placed into brevetoxin−BSA carbonate buffer (1.0 mL, 100 μg/mL, pH 9.6) and incubated for 6 h under the same conditions. Finally, the as-prepared brevetoxin−BSA-conjugated magnetic beads (brevetoxin−magnetic bead) were magnetically separated and stored in 1.0 mL of pH 7.4 PBS containing 1.0 wt % BSA and 0.1 wt % sodium azide for further use.

Gold nanoparticle (AuNP, ~16 nm) was synthesized and functionalized with mAb/GOx according to our previous work.[27] One microliter of 1.0 mg/mL mAb and 10 μL of 1.0 mg/mL GOx were simultaneously added into 1.0 mL of 0.24 μM gold colloids (pH 9.0). The resulting mixture was incubated for 12 h at 4 °C with slight shaking. Following that, the pellet (i.e., mAb−AuNP−GOx) obtained by centrifugation (14000 rpm, 20 min, 4 °C) was suspended in 1.0 mL of pH 7.4 PBS containing 1.0 wt % BSA and 0.1 wt % sodium azide.

Monitoring of GOx Activity Based on Sulfite-to-Sulfate Conversion with Ag(I)−TMB System. Figure 2A displays the detection principle of GOx activity based on sulfite-to-sulfate conversion with the Ag(I)−TMB system. The assay was carried out as follows: (i) 10 μL of GOx with different concentrations (from 0 to 500 μg/mL) was added into 50 μL of 0.5 mM PBS (pH 7.0) containing 4.0 mM glucose and incubated for 30 min at 37 °C; (ii) 20 μL of 2.0 mM nitric acid and 50 μL of 1.0 mM sodium sulfite were injected into the resulting solution and reacted for 2 min at room temperature; (iii) 50 μL of 2.0 mM silver nitrate was added into the mixture and reacted for 1 min at room temperature; and (iv) 100 μL of 1.0 mM TMB substrate solution (ethanol/buffer, 1:9, v/v) in pH 4.0 citrate acid−disodium hydrogen phosphate buffer was added and incubated for 30 min at room temperature. The resultant mixture was monitored on an SH-1000 microplate reader (Corona Electric Co., Ltd., Japan), and the absorbance was recorded at 652 nm.

Colorimetric Immunoassay toward Brevetoxin B Based on Enzyme-Controlled Sulfite-to-Sulfate Chemical Conversion with the Ag(I)−TMB System. Figure 2B gives the monitoring process of colorimetric immunoassay toward target brevetoxin B based on enzyme-controlled sulfite-to-sulfate chemical conversion with the Ag(I)−TMB system. Initially, 25 μL of brevetoxin B standard/sample and 50 μL of GOx−AuNP−mAb suspension ($C_{[Au]} \approx 0.24$ μM) were added in sequence to 25 μL of brevetoxin−magnetic bead suspension (6.0 mg/mL) in a 200 μL PCR tube and incubated for 60 min at 37 °C with gentle shaking. After that, the resulting suspension was collected by using an external cylindrical magnet, 10 mm in diameter and 10 mm in depth, to produce an inhomogeneous magnetic density, 0.2 T at the surface (Shanghai Da Xue Electromagnetic Devices Co., Ltd., China), and washed with the washing buffer. Fifty microliters of 4.0 mM glucose (pH 7.0, PBS) was added to the precipitate and incubated for 30 min at 37 °C. Following that, 20 μL of 2.0 mM nitric acid, 50 μL of 1.0 mM sodium sulfite, and 50 μL of 2.0 mM silver nitrate were injected into the mixture in turn as before. Finally, 100 μL of 1.0 mM TMB substrate solution was added and incubated for 30 min for color development. Meanwhile, the absorbance was registered and recorded at 652 nm on a plate reader.

RESULTS AND DISCUSSION

Design Strategy of Ag(I)−TMB System Based on Sulfite-to-Sulfate Chemical Conversion. To develop a user-friendly and sensitive colorimetric immunoassay, a stable and highly efficient color progression would be advantageous.

DOI: 10.1021/acs.jafc.5b00425
J. Agric. Food Chem. 2015, 63, 1982−1989

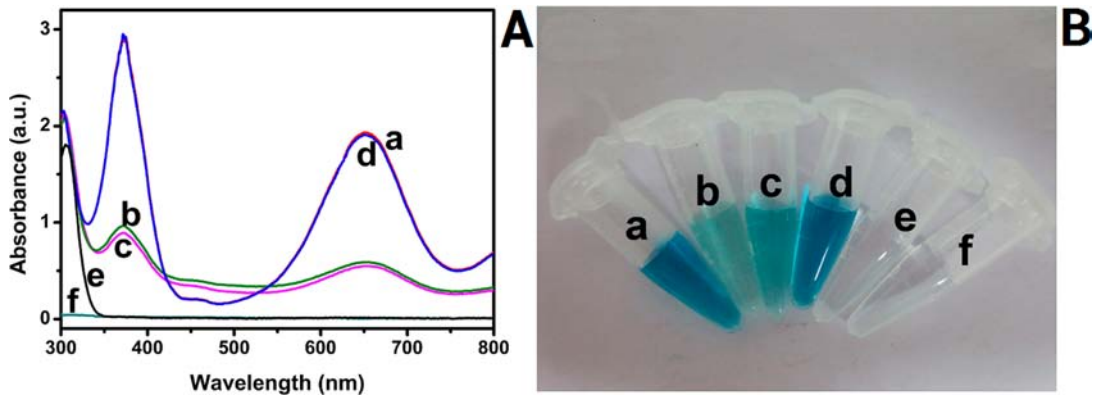

Figure 4. (A) UV−vis absorption spectra of (a) glucose + GOx + sulfite + silver(I) + TMB, (b) glucose + sulfite + silver(I) + TMB, (c) GOx + sulfite + silver(I) + TMB, (d) glucose + GOx + silver(I) + TMB, (e) glucose + GOx + sulfite + silver(I), and (f) glucose + GOx + sulfite + TMB, respectively; (B) corresponding photographs.

Typically, the peroxidase-based H_2O_2−TMB system has been widely used for ELISA development. However, most systems involve low sensitivity or poor visible color and thus are unfavorable for routine use. Recent papers have shown that TMB could be used as a selective and sensitive indicator for in situ quantification of Ag(I).[30,31] Addition of TMB into an Ag(I) aqueous solution could give rise to the oxidized form of TMB and Ag(0), thereby inducing a blue color and a strong characteristic absorption peak centered at 652 nm. As is well-known, silver sulfite is insoluble in water, whereas silver sulfate is slightly soluble. However, the sulfite can be oxidized to sulfate through hydrogen peroxide under acidic condition.[32] Thus, the sulfite can be used as an inhibitor of silver ion to control and tailor the color development of TMB at the visualization stage upon hydrogen peroxide introduction. Typically, hydrogen peroxide can be generated by glucose oxidase in the catalytic oxidation of β-D-glucose. In this case, H_2O_2-controlled chemical conversion of sulfite to sulfate can be utilized for quantitative monitoring of GOx activity in the presence of glucose. Figure 3A shows the UV−vis adsorption spectra of TMB solution in the absence and presence of 2.0 mM Ag(I). No characteristic absorption peak from 800 to 300 nm was observed at pure TMB solution (curve a). In contrast, two strong absorption peaks were simultaneously achieved after interaction of 1.0 mM TMB with 2.0 mM Ag(I) (curve b), which was ascribed to the oxidation of TMB by Ag(I). Moreover, the colorless TMB solution (Figure 3A, photograph a) exhibited an obvious blue color change in the presence of Ag(I) (Figure 3A, photograph b). Furthermore, we also investigated the dynamic response curve (absorbance vs reaction time) between TMB and Ag(I) (Figure 3A, left inset). The absorbance intensity rapidly increased with the increasing reaction time and tended to level off after 5 min. To ensure adequate reaction between Ag(I) and TMB, 30 min was used for the color development in this work. These results revealed that Ag(I) could oxidize TMB to the oxidized TMB to trigger a blue color and an absorption peak at 652 nm.

The second concern in our design was whether the sulfite-to-sulfate conversion could induce the progression of the Ag(I)−TMB system. To determine this point, sulfite and sulfate alone (2.0 mM) were added into the Ag(I)−TMB system, respectively. Ag(I) was initially incubated with sulfite/sulfate for 30 min at room temperature, and then TMB was added into the resulting solution. The resulting mixture was monitored using UV−vis absorption spectroscopy (Figure 3B). As seen from curve b, introduction of sulfate into the system did not appreciably change the characteristic peak or absorbance in comparison with the Ag(I)−TMB system alone (curve c). When the sulfite was added into the Ag(I)−TMB system, significantly, the absorbance largely decreased (curve a). This was attributed to the fact that the added sulfite initially reacted with Ag(I) to form the insoluble silver sulfite (Ag_2SO_3) and hindered the interaction of Ag(I) with TMB. The results revealed that the sulfite could hinder the progression of the Ag(I)−TMB system, whereas the sulfate had almost no effect on the colorimetric assay of the system. Therefore, the chemical conversion of sulfite to sulfate could trigger the continuance of the Ag(I)−TMB system with the colored product in the presence of sulfite.

The third important question arises as to whether hydrogen peroxide (H_2O_2) could cause the chemical conversion between sulfite and sulfate to complement the Ag(I)−TMB system. To demonstrate this, 50 μL of 1.0 mM sodium sulfite, 50 μL of 2.0 mM silver nitrate, and 100 μL of 1.0 mM TMB were added into acidic solution containing 1.0 mM H_2O_2 in turn. As shown from curve a in Figure 3C, the characteristic absorption peaks were almost the same as that of the Ag(I)−TMB system alone (Figure 3A, curve b). When 50 μL of 2.0 mM silver nitrate and 100 μL of 1.0 mM TMB were injected in sequence into 50 μL of 1.0 mM sodium sulfite, however, almost no absorption peaks were observed (Figure 3C, curve b). Meanwhile, the resulting mixture changed from blue to colorless (Figure 3C, insets). On the basis of the results in Figure 3, we deduced that the added H_2O_2 could convert the sulfite into the sulfate and relieve the inhibition effect of sulfite toward Ag(I), thereby resulting in increasing absorbance and colorimetric progression. Usually, H_2O_2 can be produced through glucose oxidase through the catalytic oxidation of glucose in the presence of oxygen. Therefore, the designed system could be utilized for monitoring the activity of GOx.

Control Tests for Ag(I)−TMB System with Sulfite-to-Sulfate Conversion. To further investigate that the Ag(I)−TMB system could be realized by GOx-triggered production of H_2O_2 accompanying the chemical conversion between sulfite and sulfate, several control tests were carried out under different conditions (Figure 4). As indicated from curve a, two strong absorption peaks at 652 and 372 nm appeared when glucose, sulfite, Ag(I), and TMB were added into GOx solution in sequence. Moreover, the absorbance at 652 nm increased with increasing GOx concentration. The reason might be most

DOI: 10.1021/acs.jafc.5b00425
J. Agric. Food Chem. 2015, 63, 1982−1989

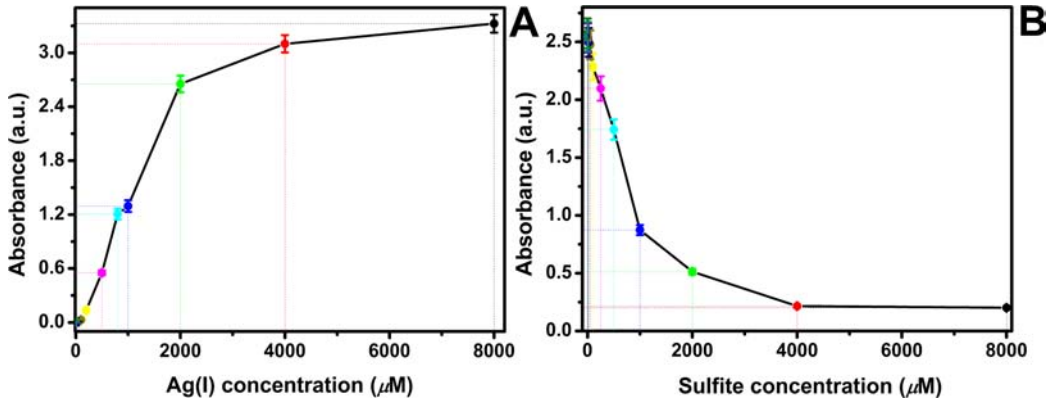

Figure 5. Effects of (A) silver(I) concentration and (B) sulfite concentration on the absorbance of the Ag(I)−TMB system by coupling with the sulfite-to-sulfate chemical conversion (1.0 mM TMB used in the case).

likely a consequence of the fact that Ag(I) could be released through the oxidizing reaction of enzymatic product toward sulfite to oxidize TMB into $TMB_{(ox)}$. When GOx (curve b) or glucose (curve c) was absent from the system, however, the absorbance greatly decreased and the color became light blue (Figure 4B, tubes b and c). The results indicated that glucose or GOx alone did not eliminate the inhibition effect of sulfite toward the Ag(I)−TMB system. However, the inhibition effect of the Ag(I)−TMB system could be relieved by sulfite regardless of the presence of glucose and GOx (Figure 4A, curve d, and Figure 4B, tube d). For comparison, we also monitored the effect of Ag(I) and TMB toward the designed system. As seen from curves e and f (Figure 4A), no absorption peak was achieved in the absence of Ag(I) or TMB even if glucose/GOx/sulfite simultaneously existed in the system. Furthermore, the resultant solution was colorless (Figure 4B, tubes e and f). These results further revealed that (i) the visible color mainly originated from the interaction between Ag(I) and TMB; (ii) sulfite could hinder the interaction of Ag(I) with TMB; (iii) H_2O_2 could oxidize sulfite to sulfate, which could not hinder the interaction between Ag(I) and TMB; and (iv) the colorimetric assay could be controlled by changing the GOx level. Such a cascade reaction could be used for monitoring enzymatic activity, which could be employed for colorimetric immunoassay development based on the change in the visible color by conjugating GOx with detection antibody.

Optimization of Assay Conditions. To achieve a good colorimetric immunoassay with high sensitivity for subsequent work, one important precondition was that the Ag(I)−TMB system should be highly efficient toward the sulfite-to-sulfate chemical conversion in the presence of low-concentration GOx. Actually, the system mainly consisted of three steps: (i) the added glucose was oxidized to gluconic acid and H_2O_2 by GOx; (ii) the produced H_2O_2 catalytically oxidized sulfite to sulfate under the acidic condition; and (iii) the generated sulfate triggered the colored product relative to the Ag(I)−TMB system. During this process, the sulfite (SO_3^{2-}) was used as an inhibitor of Ag(I) to hinder the color development of TMB owing to the formation of insoluble silver sulfite, which could be eliminated through the sulfate (SO_4^{2-}). To adequately complement the catalytic efficiency of GOx, the concentrations of sulfite, Ag(I), and TMB should be optimized. First, we investigated the effect of Ag(I) on the Ag(I)−TMB system. In this case, 1.0 mM TMB was used for color development on the basis of our previous work.[27] As shown in Figure 5A, the absorbance initially rapidly increased with increasing Ag(I) concentration and then tended to slow after 2.0 mM. To decrease the background signal and avoid excessive Ag(I), 2.0 mM Ag(I) was used for development of the colorimetric assay.

Normally, the free Ag(I) in the solution can trigger TMB to promote the change in the absorbance and color development. However, the colorimetric assay can be hindered in the presence of sulfite. By using 1.0 mM TMB and 2 mM Ag(I), we also investigated the effect of sulfite concentration on the colorimetric assay. As seen from Figure 5B, the absorbance decreased with the increase in sulfite concentration and reached a minimum value at 4.0 mM. However, we found that the absorbance (i.e., the slope for the plots) changed very quickly within the low-concentration range of 0−1.0 mM, suggesting that a slight decrease in the sulfite level induced a big increase in the absorbance. Considering the subsequent reaction between sulfite and H_2O_2 with high sensitivity, the high-concentration sulfite should not be preferable. Therefore, 1.0 mM sulfite was chosen as the inhibitor of Ag(I) to hinder color development in this work.

Monitoring for the Ag(I)−TMB System toward H_2O_2 and GOx. As is well-known, H_2O_2 can oxidize sulfite to sulfate under acidic conditions. To achieve a high sensitivity for development of the subsequent colorimetric immunoassay, the determination of low-concentration H_2O_2 with the system would be valuable. For this purpose, the Ag(I)−TMB system was utilized for the detection of H_2O_2 by using sulfite as the inhibitor. Experimental results indicated that the Ag(I)−TMB system could be used for monitoring of H_2O_2 concentration with a wide linear range (10 μM−1.0 mM) and a low detection limit (2.5 μM). The linear regression equation could be fitted to $y = 0.0016 \times C_{[H2O2]} + 0.8218$ (μM, $R^2 = 0.9976$). Furthermore, we also investigated the Ag(I)−TMB system for the detection of GOx by using glucose as the enzymatic substrate. H_2O_2 was obtained through GOx by the catalytic oxidation of glucose. The absorbance linearly increased with increasing GOx concentration within the range of 0.5−20 μg/mL. A detection limit of 0.1 μg/mL GOx could be achieved at the $3s_{blank}$ criterion. The linear regression equation could be fitted to $y = 0.0531 \times C_{[GOx]} + 0.7354$ (μg/mL, $R^2 = 0.9982$). Such a low detection limit provided a precondition for the development of a high-sensitivity colorimetric immunoassay.

Analytical Performance of the Ag(I)−TMB-Based Colorimetric Immunoassay. Figure 2 shows the fabrication process of the colorimetric immunoassay for the detection of brevetoxin B, used as a model, based on the Ag(I)−TMB system accompanying enzyme-triggered sulfite-to-sulfate chem-

DOI: 10.1021/acs.jafc.5b00425
J. Agric. Food Chem. 2015, 63, 1982−1989

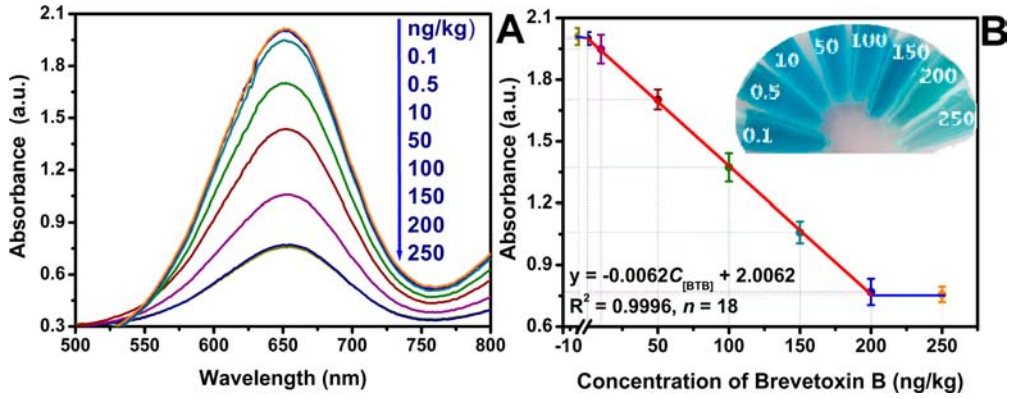

Figure 6. (A) Absorbance intensity; (B) calibration plots of Ag(I)−TMB-based colorimetric immunoassay by coupling with enzyme-mediated sulfite-to-sulfate chemical conversion toward different concentrations of BTB standards. (Inset) Corresponding photographs.

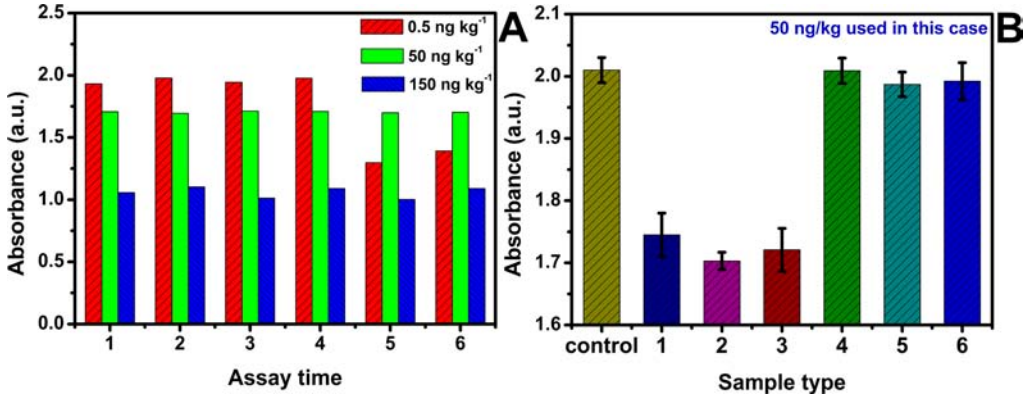

Figure 7. (A) Reproducibility; (B) specificity of the Ag(I)−TMB-based colorimetric immunoassay by coupling with enzyme-mediated sulfite-to-sulfate chemical conversion.

ical conversion. The assay was carried out on brevetoxin−magnetic bead by using mAb−AuNP−GOx as the detection antibody with a competitive-type immunoassay format. Brevetoxin−magnetic beads were prepared by covalent conjugation of brevetoxin−BSA onto the aminated magnetic bead with glutaraldehyde, whereas mAb−AuNP−GOx was synthesized on the basis of the interaction between gold nanoparticles and proteins. In the presence of target brevetoxin B, the analyte competed with the immobilized brevetoxin−BSA on magnetic beads for the labeled anti-brevetoxin B antibody on the AuNP. Accompanying the immunocomplex, the GOx catalyzed glucose into gluconic acid and H_2O_2, and the produced H_2O_2 could oxidize sulfite to sulfate under acidic condition, which could make Ag(I) oxidize TMB to TMB_{ox}, thus resulting in the change of the absorbance. As shown from Figure 6A, the absorbance decreased with increasing brevetoxin B concentration in the sample. A good linear dependence between the absorbance (au) and brevetoxin B level (ng/kg) could be acquired in the dynamic range from 0.5 to 200 ng/kg. The linear regression equation could be fitted to $y = -0.0062 \times C_{[\text{brevetoxin B}]} + 2.0062$ (ng/kg, $R^2 = 0.9996$, $n = 18$). The detection limit (LOD) was estimated to be 0.1 ng/kg (ppt) at the $3s_{blank}$ criterion, whereas the limit of quantification (LOQ) was calculated to be 0.3 ng/kg according to our previous method[29] (Figure 6B). To further clarify the merits of Ag(I)−TMB-based colorimetric immunoassay, the obtained LOD was compared with commercialized brevetoxin ELISA kits obtained from Abraxis LLC (LOD = 50 ng/kg) and other detection schemes (e.g., capillary electrophoresis-based immunoassay = 100 ng/kg,[33] competitive ELISA = 25 mg/kg,[34] LC-MS/MS = 12 μg/kg,[35] immunodipstick assay = 100 ng/kg,[36] glucometer-based immunoassay = 10 ng/kg).[37] Due to the legal limit of brevetoxin (≤80 μg of toxin per 100 g of shellfish tissue),[38,39] the Ag(I)−TMB-based colorimetric immunoassay could completely meet the requirement of brevetoxin B monitoring in seafood.

Next, we investigated the reproducibility and precision of the as-prepared brevetoxin−magnetic bead and mAb−AuNP−GOx by monitoring three brevetoxin B concentrations including 0.5, 50, and 150 ng/kg, respectively. Each sample concentration was determined six times. As seen from Figure 7A, the relative standard deviations (RSD) were 9.8, 6.9, and 7.5% ($n = 6$) for the above-mentioned target brevetoxin B, respectively. Therefore, the reproducibility and precision of the Ag(I)−TMB-based colorimetric immunoassay were acceptable.

Furthermore, the specificity and selectivity of the Ag(I)−TMB-based colorimetric immunoassay were also studied by spiking brevetoxin A, **1** (50 ng/kg), brevetoxin B, **2** (50 ng/kg), brevetoxin C, **3** (50 ng/kg), okadaic acid, **4** (50 ng/kg), saxitoxin acetate, **5** (50 ng/kg), and dinophysistoxin-1, **6** (50 ng/kg), into blank *M. senhousia* matrix. As shown in Figure 7B, the as-prepared brevetoxin−magnetic bead and mAb−AuNP−GOx displayed high cross-reactivity toward brevetoxins A and C, whereas no false compliant results were achieved for okadaic acid, saxitoxin acetate, and dinophysistoxin-1. The reason might be the fact that brevetoxins A and C had chemical structures similar to that of brevetoxin B.

DOI: 10.1021/acs.jafc.5b00425
J. Agric. Food Chem. 2015, 63, 1982−1989

Monitoring of *M. senhousia* Samples. The feasibility of applying the as-prepared brevetoxin−magnetic bead and mAb−AuNP−GOx to evaluate brevetoxin levels in a complex matrix was monitored. Initially, we spiked brevetoxin B standards at random concentrations into *M. senhousia* homogenate, followed by centrifugation and extraction. Finally, these samples were assayed by the Ag(I)−TMB-based colorimetric immunoassay and the commercialized Abraxis brevetoxin B ELISA kit, respectively. The content of brevetoxin B in these samples obtained by Ag(I)−TMB-based colorimetric immunoassay was calculated according to the above-fitted regression equation ($y = -0.0062 \times C_{[\text{brevetoxin B}]} + 2.0062$). The results are listed in Table 1. As seen from this table, all RSD values were <13%.

Table 1. Results Obtained by the Ag(I)−TMB-Based Colorimetric Immunoassay and Commercial Abraxis BTB ELISA Kit for Spiked *Musculista senhousia* Samples

no.	Ag(I)−TMB-based immunoassay[a] (ng/kg)	BTB ELISA kit[a] (ng/kg)	RSD[b] (%)
1	62.4	68.4	6.5
2	190	171	7.2
3	12.3	nd[c]	nd
4	365	397	5.9
5	244	215	8.8
6	98.3	113	9.7
7	146	165	8.6
8	1.14	nd	nd
9	187	172	6.1
10	456	479	3.4
11	278	255	6.2
12	65.5	74.4	9.0

[a]Each sample was determined in triplicate, and the high-concentration BTB sample was assayed with an appropriate dilution. The linear regression equation for these usable mean data between two methods are as follows: $y = 1.024x - 3.2806$ ($R^2 = 0.9754$, $n = 30$; x axis, by Ag(I)−TMB-based colorimetric immunoassay; y axis, by BTB ELISA kit. [b]RSD for each sample was calculated according to the mean values obtained by two methods, and the statistical analysis method was described in our previous work.[40] [c]Not detected because the minimum concentration of BTB detectable by ELISA kit is 50 ng/kg.

Moreover, the slope and intercept of the regression equation between two methods ($y = 1.024x - 3.2806$) were close to ideal, 1 and 0, respectively, indicating these two methods had a good correlation for the determination of brevetoxin B in real samples.

In the present work, we for the first time systematically demonstrate the unconventional application of enzyme-triggered sulfite-to-sulfate chemical conversion in the colorimetric immunoassay through coupling with the Ag(I)−TMB system. During the signal transduction cascade, the inhibition effect of sulfite toward Ag(I) could be efficiently weakened by enzyme-catalyzed product (H_2O_2), thereby resulting in the development of the visible color and the change in the absorbance. Compared with traditional enzyme-based colorimetric immunoassays, our design should be feasible, sensitive, and specific. The system was capable of continuously carrying out all steps in ∼2.5 h for one sample, including incubation, washing, enzymatic reaction, and measurement. Although the system mainly focuses on target brevetoxin B, it can be easily extended to determine other small molecular biotoxins or low-abundant proteins. Importantly, the nanoparticle-based colorimetric immunoassay does not require sophisticated instrumentations and is well-suited for high-throughput biomedical sensing and application for other areas.

AUTHOR INFORMATION

Corresponding Author

*(D.T.) Phone: +86-591-2286 6125. Fax: +86-591-2286 6135. E-mail: dianping.tang@fzu.edu.cn.

Funding

This work was financially supported by the National Natural Science Foundation of China (41176079 and 21475025), the National Science Foundation of Fujian Province (2014J07001), and the Program for Changjiang Scholars and Innovative Research Team in University (IRT1116).

Notes

The authors declare no competing financial interest.

REFERENCES

(1) Khare, S.; Ratsimandresey, R.; de Almeida, L.; Cuda, C.; Rellick, S.; Misharin, A.; Wallin, M.; Gangopadhyay, A.; Forte, E.; Gottwein, E.; Perlman, H.; Reed, J.; Greaves, D.; Dorfleutner, A.; Stehlik, C. The PYRIN domain-only protein POP3 inhibits ALR inflammasomes and regulates responses to infection with DNA viruses. *Nat. Immunol.* **2014**, *15*, 343−353.

(2) Akhavan-Tafti, H.; Binger, D.; Blackwood, J.; Chen, Y.; Creager, R.; de Silva, R.; Eickholt, R.; Gaibor, J.; Handley, R.; Kapsner, K.; Lopac, S.; Mazelis, M.; McLernon, T.; Mendoza, J.; Odegaard, B.; Reddy, S.; Salvati, M.; Schoenfelner, B.; Shapir, N.; Shelly, K.; Todtleben, J.; Wang, G.; Xie, W. A homogeneous chemiluminescent immunoassay method. *J. Am. Chem. Soc.* **2013**, *135*, 4191−4194.

(3) Elizabeth Welch, M.; Ritzert, N.; Chen, H.; Smith, N.; Tague, M.; Xu, Y.; Baird, B.; Abruna, H.; Ober, C. Quantification of the surface diffusion of tripodal binding motifs on graphene using scanning electrochemical microscopy. *J. Am. Chem. Soc.* **2014**, *136*, 1879−1883.

(4) Hu, R.; Zhang, X.; Zhao, Z.; Zhu, G.; Chen, T.; Fu, T.; Tan, W. DNA nanoflowers for multiplexed cellular imaging and traceable targeted drug delivery. *Angew. Chem., Int. Ed.* **2014**, *53*, 5821−5826.

(5) Hu, J.; Wang, T.; Kim, J.; Shannon, C.; Easley, C. Quantitation of femtomolar protein levels via direct readout with the electrochemical proximity assay. *J. Am. Chem. Soc.* **2012**, *134*, 7066−7072.

(6) Zheng, T.; Zhang, Q.; Feng, S.; Zhu, J.; Wang, Q.; Wang, H. Robust nonenzymatic hybrid nanoelectrocatalysts for signal amplification toward ultrasensitive electrochemical cytosensing. *J. Am. Chem. Soc.* **2014**, *136*, 2288−2291.

(7) Wang, R.; Zhu, G.; Mei, L.; Xie, Y.; Ma, H.; Ye, M.; Qing, F.; Tan, W. Automated modular synthesis of aptamer−drug conjugates for targeted drug delivery. *J. Am. Chem. Soc.* **2014**, *136*, 2731−2734.

(8) Zhu, G.; Zheng, J.; Song, E.; Donovan, M.; Zhang, K.; Liu, C.; Tan, W. Self-assembled, aptamer-tethered DNA nanotrains for targeted transport of molecular drugs in cancer theranostics. *Proc. Natl. Acad. Sci. U.S.A.* **2013**, *110*, 7998−8003.

(9) Gao, Z.; Xu, M.; Hou, L.; Chen, G.; Tang, D. Magnetic bead-based reverse colorimetric immunoassay strategy for sensing biomolecules. *Anal. Chem.* **2013**, *85*, 6945−6952.

(10) Kim, M.; Ye, Y.; Woo, M.; Lee, J.; Park, H. A highly efficient colorimetric immunoassay using a nanocomposite entrapping magnetic and platinum nanoparticles in ordered mesoporous carbon. *Adv. Healthcare Mater.* **2014**, *3*, 36−41.

(11) Gao, Z.; Hou, L.; Xu, M.; Tang, D. Enhanced colorimetric immunoassay accompanying with enzyme cascade amplification strategy for ultrasensitive detection of low-abundance protein. *Sci. Rep.* **2014**, *4*, 3966.

(12) Wang, F.; Wang, L.; Chen, X.; Yoon, J. Recent progress in the development of fluorometric and colorimetric chemosensors for detection of cyanide ions. *Chem. Soc. Rev.* **2014**, *43*, 4312−4324.

(13) Zhou, Y.; Zhang, J.; Yoon, J. Fluorescence and colorimetric chemosensors for fluoride-ion detection. *Chem. Rev.* **2014**, *114*, 5511−5571.

DOI: 10.1021/acs.jafc.5b00425
J. Agric. Food Chem. 2015, 63, 1982−1989

(14) Zhang, X.; Yin, J.; Yoon, J. Recent advances in development of chiral fluorescent and colorimetric sensors. *Chem. Rev.* **2014**, *114*, 4918−4959.
(15) Chang, C.; Chen, C.; Lee, C.; Chen, C.; Lin, C. Colorimetric detection of human chorionic gonadotropin using catalytic gold nanoparticles and a peptide aptamer. *Chem. Commun.* **2014**, *50*, 14443−14446.
(16) Wen, J.; Zhou, S.; Chen, J. Colorimetric detection of *Shewanella oneidensis* based on immunomagnetic capture and bacterial intrinsic peroxidase activity. *Sci. Rep.* **2014**, *4*, 5191.
(17) Zhou, C.; Zhao, J.; Pand, D.; Zhang, Z. Enzyme-induced metallization as a signal amplification strategy for highly sensitive colorimetric detection of avian influenza virus particles. *Anal. Chem.* **2014**, *86*, 2752−2759.
(18) Le Goff, G.; Blum, L.; Marquette, C. Enhanced colorimetric detection on porous microarrays using in situ substrate production. *Anal. Chem.* **2011**, *83*, 3610−3615.
(19) Su, X.; Huey, F.; Lieu, X.; Gao, Z. Enzyme-based colorimetric detection of nucleic acids using peptide nucleic acid-immobilized microwell plates. *Anal. Chem.* **2007**, *79*, 7192−7197.
(20) Gao, Z.; Deng, K.; Wang, X.; Miro, M.; Tang, D. A high-resolution colorimetric assay for rapid visual readout of phosphatase activity based on gold/silver core/shell nanorod. *ACS Appl. Mater. Interface* **2014**, *6*, 18243−18250.
(21) Ni, P.; Sun, Y.; Dai, H.; Hu, J.; Jiang, S.; Wang, Y.; Li, Z. Highly sensitive and selective colorimetric detection of glutathione based on Ag[I] ion-3,3′,5,5′-tetramethylbenzidine (TMB). *Biosens. Bioelectron.* **2015**, *63*, 47−52.
(22) Hu, J.; Dong, Y.; Zhang, H.; Chen, X.; Chen, X.; Zhang, H.; Chen, H. Naked eye detection of benzoyl peroxide in wheat flour using 3,3′,5,5′-tetramethylbenzidine as a chromogenic agent. *RSC Adv.* **2013**, *3*, 26307−26312.
(23) Wang, X.; Yang, Y.; Li, L.; Sun, M.; Yin, H.; Qin, W. A polymeric liquid membrane electrode responsive to 3,3′,5,5′-tetramethylbenzidine oxidation for sensitive peroxidase/peroxidase mimetic-based potentiometric biosensing. *Anal. Chem.* **2014**, *86*, 4416−4422.
(24) Gao, L.; Wu, J.; Gao, D. Enzyme-controlled self-assembly and transformation of nanostructures in a tetramethylbenzidine/horseradish peroxidase/H_2O_2 system. *ACS Nano* **2011**, *5*, 6736−6742.
(25) Zhang, B.; Tang, D.; Goryacheva, I.; Niessner, R.; Knopp, D. Anodic stripping voltammetric immunoassay for ultrasensitive detection of low-abundance-proteins using quantum dots-aggregated hollow microspheres. *Chem.−Eur. J.* **2013**, *19*, 2496−2503.
(26) Wild, D. *The Immunoassay Handbook*, 3rd ed.; Elsevier: Amsterdam, The Netherlands, 2005; p 194.
(27) Lai, W.; Tang, D.; Zhuang, J.; Chen, G.; Yang, H. Magnetic bead-based enzyme-chromogenic substrate system for ultrasensitive colorimetric immunoassay accompanying cascade reaction for enzymatic fomation of squaric acid-iron(III) chelate. *Anal. Chem.* **2014**, *86*, 5061−5068.
(28) González-Fuenzalida, R.; Moliner-Martínez, Y.; González-Béjar, M.; Molons-Legua, C.; Verdú-Andres, J.; Pérez-Prieto, J.; Campins-Falcó, P. In situ colorimetric quantification of silver cations in the presence of silver nanoparticles. *Anal. Chem.* **2013**, *85*, 10013−10016.
(29) Zhang, B.; Hou, L.; Tang, D.; Liu, B.; Li, J.; Chen, G. Simultaneous multiplexed stripping voltammetric monitoring of marine toxins in seafood based on distinguishable metal nanocluster-labeled molecular tags. *J. Agric. Food Chem.* **2012**, *60*, 8974−8982.
(30) Liu, S.; Tian, J.; Wang, L.; Su, X. Highly sensitive and selective colorimetric detection of Ag(I) ion using 3,3′,5,5′-tetramethylbenzidine (TMB) as an indicator. *Sens. Actuators B* **2012**, *165*, 44−47.
(31) Ni, P.; Sun, Y.; Dai, H.; Hu, J.; Jiang, S.; Wang, Y.; Li, Z. Highly sensitive and selective colorimetric detection of glutathione based on Ag[I] ion−3,3′,5,5′-tetramethylbenzidine (TMB). *Biosens. Bioelectron.* **2015**, *63*, 47−52.
(32) Hanazaki, I.; Ishibashi, N.; Mori, H.; Tanimoto, Y. Bifurcation structure in the hydrogen peroxide-sulfite system. *J. Phys. Chem. A* **2000**, *104*, 7695−7699.
(33) Zhang, X.; Zhang, Z. Capillary electrophoresis-based immunoassay for the determination of brevetoxin-B in shellfish using electrochemical detection. *J. Chromatogr. Sci.* **2013**, *51*, 107−111.
(34) Narr, J.; Bourdelais, A.; Tomas, C.; Kubanek, J.; Whitney, P.; Flewelling, L.; Steidinger, K.; Lancaster, J.; Baden, D. New fish-killing alga in coastal Delaware produces neurotoxins. *Environ. Health Perspect.* **2002**, *110*, 179−185.
(35) McNabb, P.; Selwood, A.; Van Ginkel, R.; Boundy, M.; Holland, P. Determination of brevetoxins in shellfish by LC/MS/MS: single-laboratory validation. *J. AOAC Int.* **2012**, *95*, 1097−1105.
(36) Zhang, K.; Wu, J.; Li, Y.; Wu, Y.; Huang, T.; Tang, D. Hollow nanogold microsphere-signalized lateral flow immunodipstick for the sensitive determination of the neurotoxin brevetoxin B. *Microchim. Acta* **2014**, *181*, 1147−1454.
(37) Gao, Z.; Tang, D.; Xu, M.; Chen, G.; Yang, H. Nanoparticle-based pseudo hapten for target-responsive cargo release for magnetic mesoporous silica nanocontainer. *Chem. Commun.* **2014**, *50*, 6256−6258.
(38) Hunt, D.; Tufts, N. Monitoring programs and epidemiology. In *Toxic Dinoflagellate Blooms*; Taylor, D., Seliger, H., Eds.; Elsevier Press: New York, 1979; pp 489−492.
(39) Trainer, V.; Baden, D. An enzyme immunoassay for the detection of Florida red tide brevetoxins. *Toxicon* **1991**, *29*, 1387−1394.
(40) Tang, D.; Zhong, Z.; Niessner, R.; Knopp, D. *Analyst* **2009**, *134*, 1554−1560.

DOI: 10.1021/acs.jafc.5b00425
J. Agric. Food Chem. 2015, 63, 1982−1989

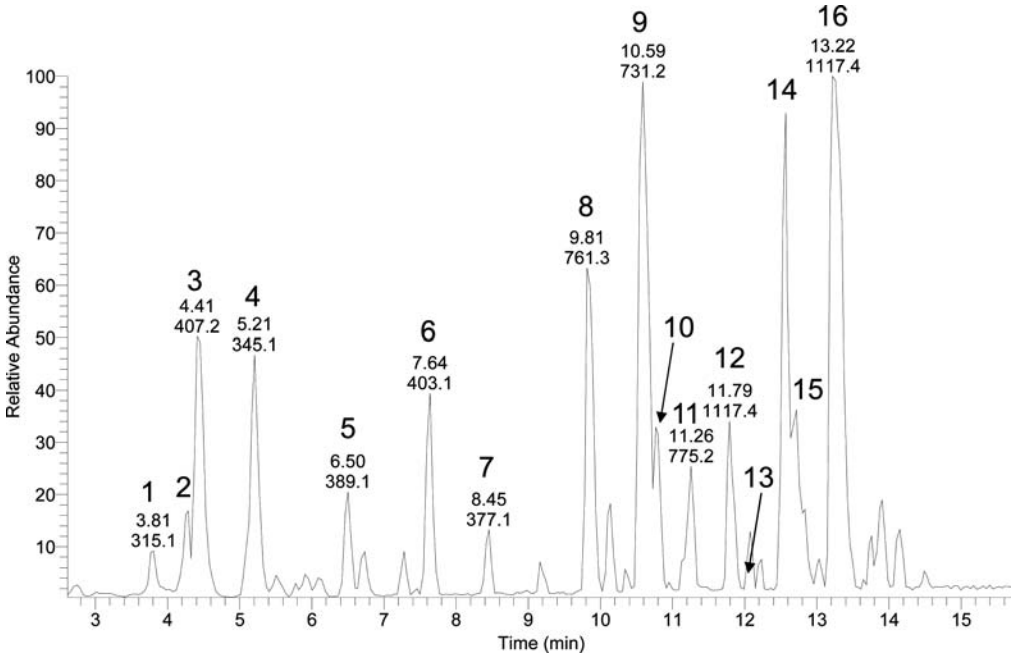

Figure 1. Negative ion chromatogram from LC−MS/MS analysis of an 80% aqueous methanol extract of Chemlali olive stones.

were purchased from Fisher Scientific (U.K.). Double distilled water used in the LC mobile phases was produced in-house. DPPH (2, 2-Diphenyl-1-picrylhydrazyl), 2,6-di*tert*-butyl-4-hydroxy-boxylic acid (BHT), 2,2′-azinobis (3-ethylbenzothiazoline-6-sulfonate) (ABTS), and 6-hydroxy-2,5,7,8-tetramethylchroman-2-carboxylic acid (Trolox), were purchased from Sigma-Aldrich (Chemie Gmbh, Steinhein, Germany). Several phenolic standards were used for quantification purposes, namely hydroxytyrosol, tyrosol, nuezhenide, and oleuropein were supplied by Sigma-Aldrich (Chemie Gmbh, Steinhein, Germany).

Sample Preparation and Extraction. *Olea europaea* L. fruits (Chemlali cultivar) were obtained from in olive orchard in Sfax, Tunisia. Samples were collected in February 2012, when the black olives mature. Fruit (1000 g) were sampled randomly from the trees, olive stones (300 g) were prepared from fresh olives. The pulps were removed and the stones brushed. The stones were then abundantly rinsed by distilled water three times and dried at ambient temperature. After that the stones were crashed using a stainless steel hammer. The powder obtained was stored at −20 °C until analysis. Voucher material (ABM 2012) has been deposited at the laboratory.

Sample Extraction. The powder obtained (200 g) was extracted according to the method of Bouaziz et al.[4] An aqueous 80% methanol extract was made by adding 250 mL to 100 g of powder. This was left to stand under agitation for 24 h at 4 °C in the dark. Subsequently, the solution was filtered using GF/F filter paper and washed with 100 mL hexane, to remove oil. The extract was concentrated by evaporation to dryness at 40 °C and the residue obtained was stored in glass vials at 0 °C in the dark until LC−MS analysis. This extract was given the reference code BI-21470. The sample was rehydrated with 80% aqueous methanol and a 1 mL aliquot was placed in an LC−MS vial and 5 μL were injected onto the LC−MS.

LC−MS Analysis. LC−MS analyses were performed as described by Kite et al.,[21] on a Thermo Scientific System consisting of an Accela U-HPLC unit with a photodiode array detector and an LTQ Orbitrap XL mass spectrometer fitted with an electrospray source. Chromatography was performed on 5 μL sample injections onto a 150 × 3 mm^2 i.d., 3 um, Luna C18(2) column (Phenomenex) using a 400 μL/min linear mobile phase gradient of methanol/water/acetonitrile +1% formic acid changing from 0:90:10 to 90:0:10 over 20 min followed by an isocratic phase for 5 min and then a column wash phase and equilibrium of column for 3 min before the next injection. The ESI source of the mass spectrometer was operated in both positive and negative modes under the recommended manufacturers' conditions for the mobile phase parameters. The orbitrap mass analyzer was set to scan in range m/z 200−2000 at 30 000 resolutions in negative polarity, while the linear ion-trap analyzer performed MS^n analyses on the most abundant ions in both polarities using an ion isolation window of ±2 m/z and relative collision energy of 35%.

High-Performance Liquid Chromatography (HPLC). Quantification of individual phenolic compounds was carried out by HPLC analysis. It was performed on a Shimadzu apparatus composed of an LC-10ATvp pump and an SPD-10Avp detector. The columns used to analyze monomeric phenols were, respectively, a C-18 (4.6 × 250 mm^2) Shim-pack VP-ODS and a C-8 (4.6 × 250 mm^2) Shim-pack CLC. The temperature was maintained at 40 °C. The mobile phase was 0.2% acetic acid (pH 3.1) in water (A)/methanol (B) at a flow rate of 1.5 mL/min. The total running time was 55 min, and the gradient changed as follows: 95% A/5% B for 2 min, 75% A/25% B in 8 min, 60% A/40% B in 10 min, 50% A/50% B in 10 min, and 0% A/100% B in 10 min, maintained for 5 min, returned to initial conditions in 10 min; the total running time was 55 min.

Determination of Antioxidant Activity. *DPPH Radical Scavenging Assay.* The capacity to scavenge the free radical 2, 2-diphenyl-1-picrylhydrazyl (DPPH) was monitored according to the method described by Bouaziz et al.[4] The extract solution (0.25 mL) was mixed with 0.5 mL of methanolic solution containing DPPH radicals (6×10^{-6} M). The mixture was shaken vigorously and left to stand for 30 min at room temperature in the dark (until stable absorbance values were obtained). The reduction of the DPPH-radical was measured by continuous monitoring of the absorption decrease at 517 nm. DPPH scavenging effect was calculated as the percentage of DPPH discoloration using the following equation: % scavenging effect = $[(A_{DPPH} - A_E)/A_{DPPH}] \times 100$, where A_E is the absorbance of the solution when the sample extract is added at a particular level, and A_{DPPH} is the absorbance of the DPPH solution. The extract concentration providing 50% inhibition (IC_{50}) was calculated from the graph of scavenging effect percentage against extract concentration in the solution.

ABTS Assay. The free-radical scavenging capacity was measured using the ABTS decoloration method described by Re et al.[22] with some modifications. Briefly, ABTS was dissolved in water to get a 7 mM concentration. ABTS radical ($ABTS^{\cdot+}$) was produced by reacting this stock solution with a 2.45 mM $K_2S_2O_8$ solution and allowing the mixture to stand in the dark at room temperature for 12 to 16 h before use. The $ABTS^{\cdot+}$ solution was diluted with methanol to an absorbance

DOI: 10.1021/acs.jafc.5b00353
J. Agric. Food Chem. 2015, 63, 1990−1995

Table 1. Assignment of Chromatographic Peaks Observed From Negative Ion LC−MS Analysis of Chemlali Olive Stonnes Extract (Numbered in Figure 1)[a]

no.	compound assignment	retention time (min)	molecular formula	major ion (m/z)	ion species	error in formula assignment (ppm)
1	2-(dihydroxyphenyl)ethanol hexoside	3.77	$C_{14}H_{20}O_8$	315.1083	$[M-H]^-$	−0.6
2	2-(hydroxyphenyl)ethanol dihexoside	4.29	$C_{20}H_{30}O_{12}$	507.1716	$[M+HCOO]^-$	−0.7
3	(not assigned)	4.41	$C_{17}H_{28}O_{11}$	407.1554	$[M-H]^-$	−1.3
4	2-(hydroxyphenyl)ethanol hexoside	5.21	$C_{14}H_{20}O_7$	345.1187	$[M+HCOO]^-$	−1.3
5	oleoside	6.50	$C_{16}H_{22}O_{11}$	389.1087	$[M-H]^-$	−0.7
6	oleoside 11-methyl ester	7.64	$C_{17}H_{24}O_{11}$	403.1244	$[M-H]^-$	−0.5
7	(not assigned)	8.45	$C_{16}H_{26}O_{10}$	377.1450	$[M-H]^-$	−0.8
8	methoxy derivative of nuezhenide (isomer 1)	9.85	$C_{32}H_{44}O_{18}$	761.2500	$[M+HCOO]^-$	−1.3
9	nuezhenide	10.59	$C_{31}H_{42}O_{17}$	731.2389	$[M+HCOO]^-$	−2.0
10	methoxy derivative of nuezhenide (isomer 2)	10.77	$C_{32}H_{44}O_{18}$	761.2493	$[M+HCOO]^-$	0.9
11	oleoside-11-methyloleoside	11.25	$C_{33}H_{44}O_{21}$	775.2295	$[M-H]^-$	−1.0
12	nuezhenide-11-methyloleoside (isomer 1)	11.79	$C_{48}H_{64}O_{27}$	1117.3582	$[M+HCOO]^-$	−3.1
13	oleuropein	12.03	$C_{25}H_{32}O_{13}$	539.1768	$[M-H]^-$	−0.4
14	(not assigned)	12.57	$C_{34}H_{46}O_{21}$	789.2443	$[M-H]^-$	−2.0
15	(not assigned)	12.67	$C_{25}H_{28}O_{13}$	535.1453	$[M-H]^-$	−1.0
16	nuezhenide-11-methyloleoside (isomer 2)	13.32	$C_{48}H_{64}O_{27}$	1117.3582	$[M+HCOO]^-$	−3.1

[a]See text for assignment criteria.

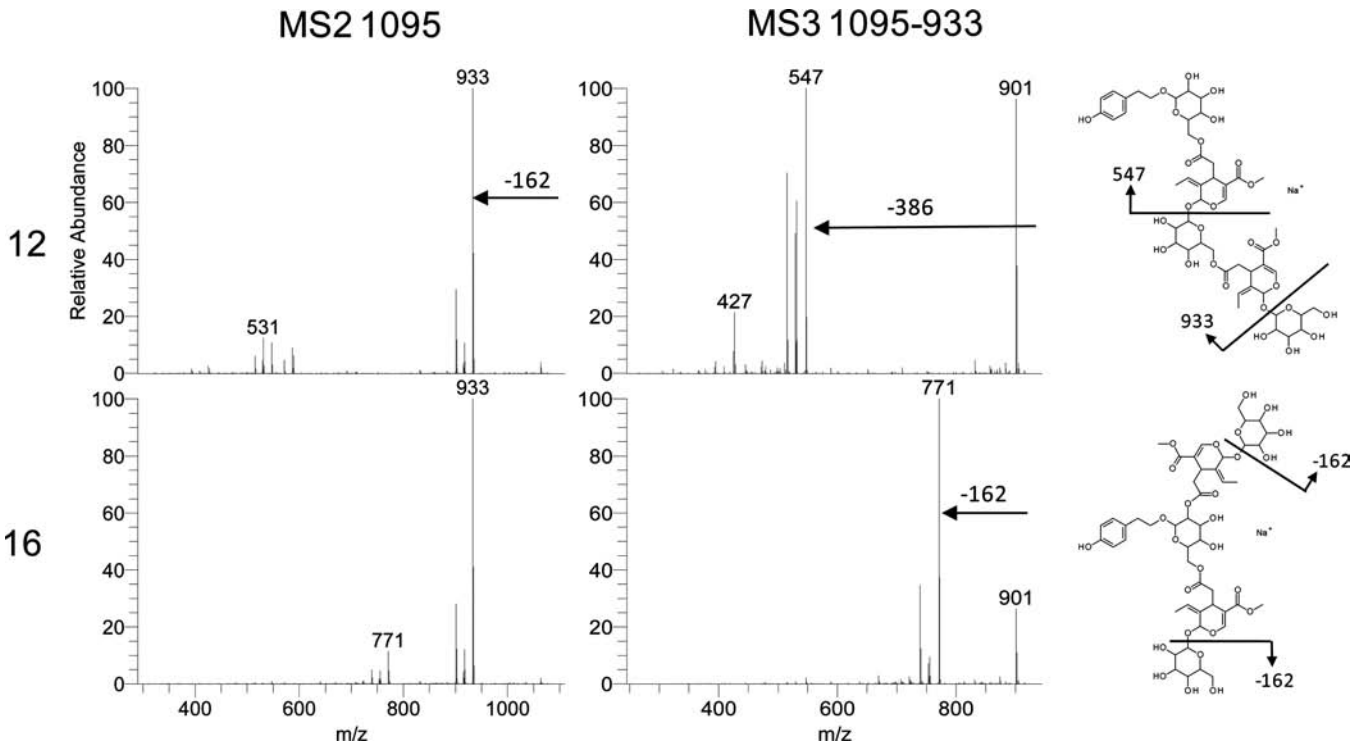

Figure 2. MS^n spectra of the sodiated molecules (m/z 1095) of compounds **12** and **16** rationalised against two possible condensation products of nuezhenide and 11-methyloleoside.

of 0.70 ± 0.02 at 730 nm. After the addition of 100 μL of sample, methanol as a blank, or Trolox standard to 2.9 mL of diluted $ABTS^{\cdot+}$ solution, absorbance readings were taken after 6 min. Methanolic solutions of known concentrations of Trolox were used for calibration. This standard curve was linear between 0.2 and 0.8 mM of Trolox (y = 0.6792x). The results were expressed in Trolox equivalent antioxidant capacity (TEAC; mM).

RESULTS AND DISCUSSION

Compound Assignment by LC−MS. LC−MS analysis of an aqueous 80% methanol extract (BI-21470) of the stone of *Olea europea* Chemali revealed the presence of numerous compounds, of which 12 of the main components were given tentative assignments (Figure 1; Table 1).

Compounds **9** and **16** produced the largest chromatographic peaks, both with photodiode array detection and negative ion mass spectrometry. Compound **9** generated a formate adduct, the formula of which was in accordance with the formate adduct of nuezhenide reported as the predominant phenol in olive stones.[12] The assignment of **9** to nuezhenide was supported by serial MS (m/z 731 → 685) that generated

DOI: 10.1021/acs.jafc.5b00353
J. Agric. Food Chem. 2015, 63, 1990−1995

fragments corresponding to the deprotonated molecules of the two subunits of nuezhenide, namely oleoside 11-methyl ester (at *m/z* 403) and 2-(4-hyroxyphenyl)ethanol 1-*O*-glucoside (= tyrosol 1-*O*-glucoside, salidroside, at *m/z* 299), and the spectrum matches that shown for nuezhenide by Silva et al.[18]

Compound **16**, of which an isomer was also present (**12**), generated a formate adduct (at *m/z* 1117) and its accurate mass suggested a formula that was greater than **9** by $C_{17}H_{22}O_{10}$, equivalent to the dehydrated residue of oleoside 11-methyl ester (386 Da). Therefore, **12** and **16** are possibly nuezhenide (**9**) with an additional oleoside 11-methyl ester moiety, as also concluded by Silva et al.[18] and as in oleonuezhenide and *iso*-oleonuezhenide reported from species of *Ligustrum*.[23,24] As also found by Silva et al.,[18] support of these assignments was difficult to obtain from the serial MS of the formate adducts of **12** or **16** (as neither generated high abundance ions), but in positive mode, sodiated **12** and **16** (at *m/z* 1095) lost 162 Da (hexosyl) upon MS2 to give a fragment at *m/z* 933 which upon MS^3 analysis lost a further 162 Da (hexosyl) in **16** and 386 Da in **12** (Figure 2). These data are in accordance with **16** being a condensation product of nuezhenide and oleoside 11-methyl ester with two terminal glucose moieties (as in oleonuezhenide) and **12** being a condensation product with one terminal glucose moiety (as in *iso*-oleonuezhenide). The subunits of nuezhenide (**9**), namely tyrosol 1-*O*-glucoside and oleoside 11-methyl ester, also occurred separately in the extract as accurate mass data assigned the corresponding formulas to **4** and **6**, respectively. Accordingly, **6** showed loss of 180 Da (glucose) from the deprotonated molecule while **4** showed loss of 120 Da (dehydrated tyrosol). Although the positions of glycosylation and hydroxylation of **4** cannot be determined, it seems most likely that **4** is tyrosol 1-*O*-glucoside (salidroside), given that this isomer occurs as the subunit of nuezhenide and salidroside is reported from olives.

Oleoside was assigned to peak **5**, eluting before its 11-methyl ester (**6**). This is the first report of oleoside from olive stones. No oleoside analogue of nuezhenide (**9**) could be detected, but a component (**11**) was present with a molecular formula suggesting it was a condensation product of oleoside and oleoside 11-methyl ester. The deprotonated molecule of **11** (at *m/z* 775) showed losses of 404 (oleoside 11-methyl ester) and 372 (dehydrated oleoside).

The molecular formulas of two isomers, **8** and **10**, suggested they could be methoxy derivatives of nuezhenide. The MS2 spectrum of deprotonated **10** showed a fragment at *m/z* 329, 30 Da greater than the tyrosol-1-*O*-glucosyl fragment in **9** suggesting the methoxy group was located on the phenylethanoid glycoside moiety. In the MS2 spectrum of **8**, the corresponding fragment was at *m/z* 315, but the deprotonated molecule did show direct losses of 168 Da (i.e., 30 greater than tyrosol) and 162 (hexosyl); the latter data again suggesting the methoxy group was located on the phenylethanoid glycoside moiety.

Only one very minor peak gave the deprotonated ion expected for oleuropein (**13**), a major phenolic component of olive oil.[25] Two other minor components were phenylethanoid glycosides, **1** and **2**. Compound **1** contained one more oxygen atom than **4** and the deprotonated molecule lost 162 (hexosyl) upon MS^2, so **1** is likely to be hydroxytyrosol glucoside. Three isomers of hydroxytyrosol glucoside have been reported in species of *Olea*.[26−28] Bianco et al.[29] found hydroxytyrosol-4′-*O*-glucoside to be the most abundant isomer in olive pulp, while other authors have identified hydroxytyrosol-1-*O*-glucoside in olive pulp.[28,29] The MS^2 spectrum of deprotonated **1** showed great similarity to that reported by De Nino et al.,[30] indicating that **1** was most likely hydroxytyrosol-1-*O*-glucoside.

Deprotonated **2** showed the loss of 162 Da (hexosyl) or 138 Da (tyrosol) and is likely to be a hexoside of **1** (i.e., a dihexoside of tyrosol) (Figure 3). This compound was identified for the first time in olive stones.

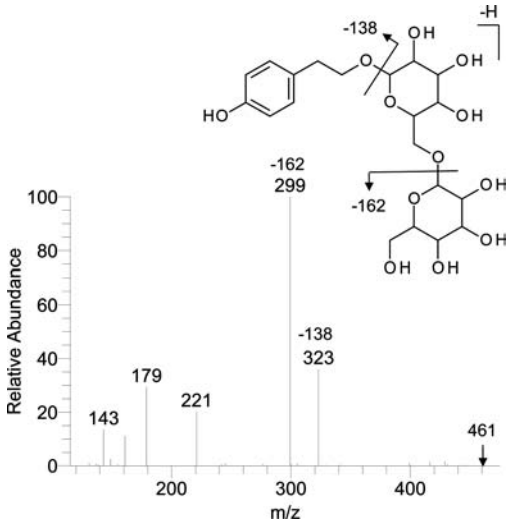

Figure 3. MS^3 (507 → 461) spectrum of the formate adduct of **2** (equivalent to the MS^2 spectrum of deprotonated **2**) rationalized against a possible structure.

Quantification of Phenolic Compunds. Six phenolic compounds were quantified in stones *Olea. europea* L. cv. Chemlali, such as hydroxytyrosol, tyrosol, nuezhenide, methoxy derivative of nuezhenide, nuezhenide-11-methyloleoside, and oleuropein as shown in Figure 4. The changes in the contents of the quantified phenolics in olives stones showed that nuezhenide presented the highest concentration (325.78 mg/100 g). This result is similar to the data previously reported by Servilli et al.[17] The second major compounds were methoxy derivative of nuezhenide and nuezhenide-11-methyloleoside which were quantified as nuezhenide equivalent given a concentration at 132.46 mg/100 g and 82.91 mg/100 g, respectively. Other minor phenolic compounds were detected, such as hydroxytyrosol (5.57 mg/100 g), tyrosol (9.81 mg/100 g), and oleuropein (5.21 mg/100 g).

Antioxidant Activity. Antioxidants have recently become a topic of increasing interest to health and food science researchers or medical experts. The antioxidant activities of the olives stones extract were measured (DPPH and ABTS) and compared to that of commercial synthetic antioxidants such as BHT (IC_{50} = 8.32 μg/mL, TEAC = 1.35 mM), are shown in Table 2. The lowest IC_{50} values indicated the highest free radical scavenging activity of the sample. Consequently, the olive stone extract showed a strong antioxidant activity and was the most effective with IC_{50} value 13.84 μg/mL and TEAC value 0.43 mM. This high antioxidant activity of the olive stone extract was attributed to its richness in phenolic content, especially in nuezhenide (325.78 mg/100g), methoxy derivative of nuezhenide (132.46), and nuezhenide-11-methyloleoside (82.91). In a previous study,[4] we compared the effect of phenolic compounds in preventing of radical scavenging. It is generally assumed that the ability to act as a hydrogen donor

DOI: 10.1021/acs.jafc.5b00353
J. Agric. Food Chem. 2015, 63, 1990−1995

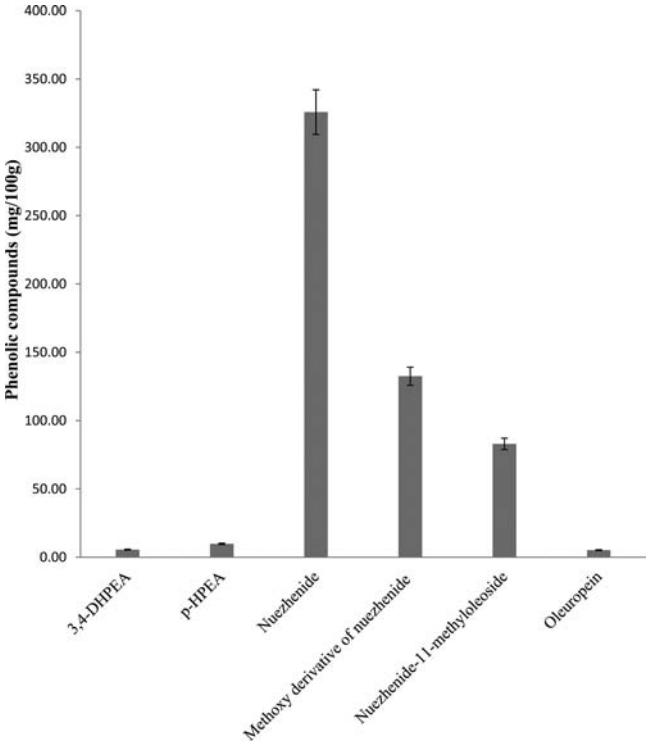

Figure 4. Composition of the phenolic compounds obtained from stones of Chemlali cultivar expressed in mg/100 g.

Table 2. Radical-Scavenging and ABTS Activities of Olives Stones Extract Compared to Those of BHT

	IC50 (μg/mL) (DPPH assay)	TEAC (mM) (ABTS assay)
olives stones	13.84 ± 0.26	0.436 ± 0.003
BHT	8.32 ± 0.05	1.35 ± 0.08

and the inhibition of oxidation are enhanced by increasing the number of hydroxyl groups in the phenol. The solubility and partitioning behavior of the phenols will also influence their reactive activity.[31,32]

In conclusion, a comprehensive knowledge of the phenolic composition of olive stones is fundamental to better understand the biochemical pathways in which they are involved and, ultimately, to shed more light on the physiology of olive trees.

To our knowledge, this is the first report on the characterization of secoiridoids based on oleoside detected in olive stones from the Chemlali cultivar. It showed that nuezhenide, methoxy derivative of nuezhenide, and nuezhenide-11-methyloleoside are the most abundant phenolic compounds in the Chemlali olive stone extract and may explain the high antioxidant activity of this extract. Therefore, this is of great interest for promoting the olive culture and better exploitation of olive fruits stones.

AUTHOR INFORMATION

Corresponding Author

*Tel: +216 98 667 581. Fax: +216 74 674 364. E-mail: mohamed.bouaziz@fsg.rnu.tn (M.B.).

Funding

The authors would like to thank the Ministry of Higher Education and Scientific Research of Tunisia (Contrat programme LR14ES08), for their support of this research work.

Notes

The authors declare no competing financial interest.

REFERENCES

(1) Khlif, M.; Ayadi, M.; Grati-Kammoun, N.; Arous, M. N.; Rekik, H.; Hamdi, M. T.; Rekik-Fakhfakh, B. Identifying Chemlali olive variety in its traditional area. *Acta Hortic.* **2002**, *586*, 117−120.

(2) Gargouri, B.; Ammar, S.; Zribi, A.; Ben Mansour, A.; Bouaziz, M. Effect of growing region on quality characteristics and phenolic compounds of chemlali extra-virgin olive oils. *Acta Physiol. Plant* **2013**, *35*, 2801−2812.

(3) Ammar, S.; Zribi, A.; Ben-Mansour, A.; Ayadi, M.; Abdelhedi, R.; Bouaziz, M. Effect of Processing Systems on the Quality and Stability of Chemlali Olive Oils. *J. Oleo Sci.* **2014**, *63*, 311−323.

(4) Obied, H. K.; Bedgood, D. R.; Prenzler, P. D.; Robards, K. Chemical screening of olive biophenol extracts by hyphenated liquid chromatography. *Anal. Chim. Acta* **2007**, *603*, 176−189.

(5) Bouaziz, M.; Grayer, R. J.; Simmonds, M. S. J.; Damak, M.; Sayadi, S. Identification and Antioxidant Potential of Flavonoids and Low Molecular Weight Phenols in Olive Cultivar Chemlali Growing in Tunisia. *J. Agric. Food Chem.* **2005**, *53*, 236−241.

(6) Landete, J. M.; Curiel, J. A.; Rodriguez, H.; Rivas, B. L.; Munoz, R. Study of the inhibitory activity of phenolic compounds found in olive products and their degradation by *Lactobacillus plantarum* strains. *Food Chem.* **2008**, *107*, 320−326.

(7) Servili, M.; Montedoro, G. Contribution of phenolic compounds in virgin olive oil quality. *J. Eur. Lipid. Sci. Technol.* **2002**, *104*, 602−613.

(8) Najar-Souissi, S.; Ouedereni, A.; Ratel, A. Adsorption of dyes onto activated carbon prepared from olive stones. *J. Environ. Sci. China* **2005**, *17*, 998−1003.

(9) Budinova, T.; Petrov, N.; Razvigorova, M.; Parra, J.; Galiatsatou, P. Removal of arsenic (III) from aqueous solution by activated carbons prepared from solvent extracted olive pulp and olive stones. *Ind. Eng. Chem. Res.* **2006**, *45*, 1896−1901.

(10) Montane, D.; Salvado, J.; Torras, C.; Farriol, X. High-temperature dilute acid hydrolysis of olive stone for furfural production. *Biomass. Bioenerg.* **2001**, *22*, 295−304.

(11) Siracusa, G.; La Rosa, A. D.; Siracusa, V.; Trovato, M. Eco compatible use of olive huso as filler in thermoplastic composites. *J. Polym. Environ.* **2001**, *9*, 157−161.

(12) Rodríguez, G.; Lama, A.; Rodríguez, R.; Jiménez, A.; Guillén, R.; Fernández-Bolaños, J. Olive stones an attractive source of bioactive and valuable compounds. *Biores. Technol.* **2008**, *99*, 5261−5269.

(13) Carraro, L.; Trocino, A.; Xiccato, G. Dietary supplementation with olive stone meal in growing rabbits. *Ital. J. Anim. Sci.* **2005**, *4*, 88−90.

(14) Tejeda-Ricardez, J.; Vaca-Garcia, C.; Borredon, M. E. Design of a batch solvolytic liquefaction reactor for the vaporization of residues from the agricultural foodstuff. *Chem. Eng. Res.* **2003**, *81*, 1066−1070.

(15) Tserki, V.; Matzinos, P.; Kokkou, S.; Panayiotou, C. Novel biodegradable composites based on treated lignocellulosic waste flour as filler. Part I. Surface chemical modification and caracterisation of waste flour. *Compos. Part A* **2005**, *36*, 965−974.

(16) Maestro-Durán, R.; Cabello, L. R.; Gutiérrez, R. V.; Roncero, V. A. Glucósidos fenólicos amargos de las semillas del olivo (*Olea europaea*). *Grasas y Aceites.* **1994**, *45*, 332−335.

(17) Servili, M.; Baldioli, M.; Selvagini, R.; Macchioni, A.; Montedoro, G. Phenolic compounds of olive fruit: one and two-dimensional nuclear magnetic resonance characterization of nüzhenide and its distribution in the constitutive parts of fruit. *J. Agric. Food. Chem.* **1999**, *47*, 12−18.

(18) Silva, S.; Gomes, L.; Leitão, F.; Bronze, M.; Coelho, A. V.; Villas-Boas, L. Secoiridoids in olive seed: characterization of nüzhenide and 11-methyl oleosides by liquid chromatography with diode array and mass spectrometry. *Grasas y Aceites.* **2010**, *61*, 157−164.

(19) Ryan, D.; Prenzler, P. D.; Lavee, S.; Antolovich, M.; Robards, K. Quantitative changes in phenolic content during physiological

DOI: 10.1021/acs.jafc.5b00353
J. Agric. Food Chem. 2015, 63, 1990−1995

development of the olive (*Olea europaea*) cultivar Hardy's Mammoth. *J. Agric. Food Chem.* **2003**, *51*, 2532−2538.
(20) Ryan, D.; Robards, K.; Prenzler, P.; Jardine, D.; Herlt, T.; Antolovich, M. Liquid chromatography with electrospray ionisation mass spectrometric detection of phenolic compounds from *Olea europaea*. *J. Chromatogr.. A* **1999**, *855*, 529−537.
(21) Kite, G. C.; Stoneham, C. A.; Veitch, N. C. Flavonol tetraglycosides and other constituents from leaves of *Styphnolobium japonicum* (Leguminosae) and related taxa. *Phytochemistry* **2007**, *68*, 1407−1416.
(22) Re, R.; Pellegrini, N.; Proteggente, A.; Pannalla, A.; Yang, M.; Rice-Evans, C. Antioxidant activity applying an improved ABTS radical cation decolorization assay. *Free Radical Biol. Med.* **1999**, *26*, 1231−37.
(23) Fukuyama, Y.; Koshino, K.; Hasegawa, T.; Yamada, T.; Nakagawa, K. New secoiridoid glucosides from *Ligustrum japonicum*. *Planta Med.* **1987**, *53*, 427−431.
(24) Fu, G.; Ip, F. C.; Pang, H.; Ip, N. Y. New secoiridoid glucosides from *Ligustrum lucidum* induce ERK and CREB phosphorylation in cultured cortical neurons. *Planta Med.* **2010**, *76*, 998−1003.
(25) Haris-Omar, S. Oleuropein in Olive and its Pharmacological Effects. *Sci. Pharm.* **2010**, *78*, 133−154.
(26) Yermakov, A. I.; Arasimov, V. V.; Yarosh, N. P. *Methods of Biochemical Analysis of Plants*; Agropromizdat: Leningrad, 1987; pp 122−142.
(27) Mateo, R.; Espartero, J. L.; Trujillo, M.; Rios, J. J.; Leon-Camacho, M.; Alcudia, F. Determination of phenols, flavones and lignans in virgin olive oils by solid-phase extraction and high-performance liquid chromatography with diode array ultraviolet detection. *J. Agric. Food. Chem.* **2001**, *49*, 2185−2192.
(28) Abian, J.; Oosterkamp, A. J.; Gelpi, E. Comparison of conventional, narrow bore and capillary liquid chromatography/mass spectrometry for electrospray ionization mass spectrometry: Practical considerations. *J. Mass. Spect.* **1999**, *34*, 244−254.
(29) Bianco, A.; Mazzei, R. A.; Melchioni, C.; Romeo, G.; Scarpati, M. L.; Soriero, A. Micro components of olive oil−III Glucosides of 2(3,4-dihydroxy-phenyl) ethanol. *Food Chem.* **1998**, *63*, 461−464.
(30) De Nino, A.; Mazzotti, F.; Morrone, S. P.; Perri, E.; Raffaelli, A.; Sindona, G. Characterization of Cassanese olive cultivar through the identification of new trace components by ionspray tandem mass spectrometry. *J. Mass Spectrom.* **1999**, *34*, 10−16.
(31) Moure, A.; Cruz, J. M.; Franco, D.; Dominguez, J. M.; Sineiro, J.; Dominguez, H.; Munez, M. J.; Parajo, J. C. Natural antioxidants from residual sources. *Food Chem.* **2001**, *72*, 145−171.
(32) Rice-Evans, C. A.; Miller, N. J.; Paganga, G. Structure antioxidant activity relationships of flavonoids and phenolic acids. *Free Radical Biol. Med.* **1996**, *20*, 933−956.

DOI: 10.1021/acs.jafc.5b00353
J. Agric. Food Chem. 2015, 63, 1990−1995

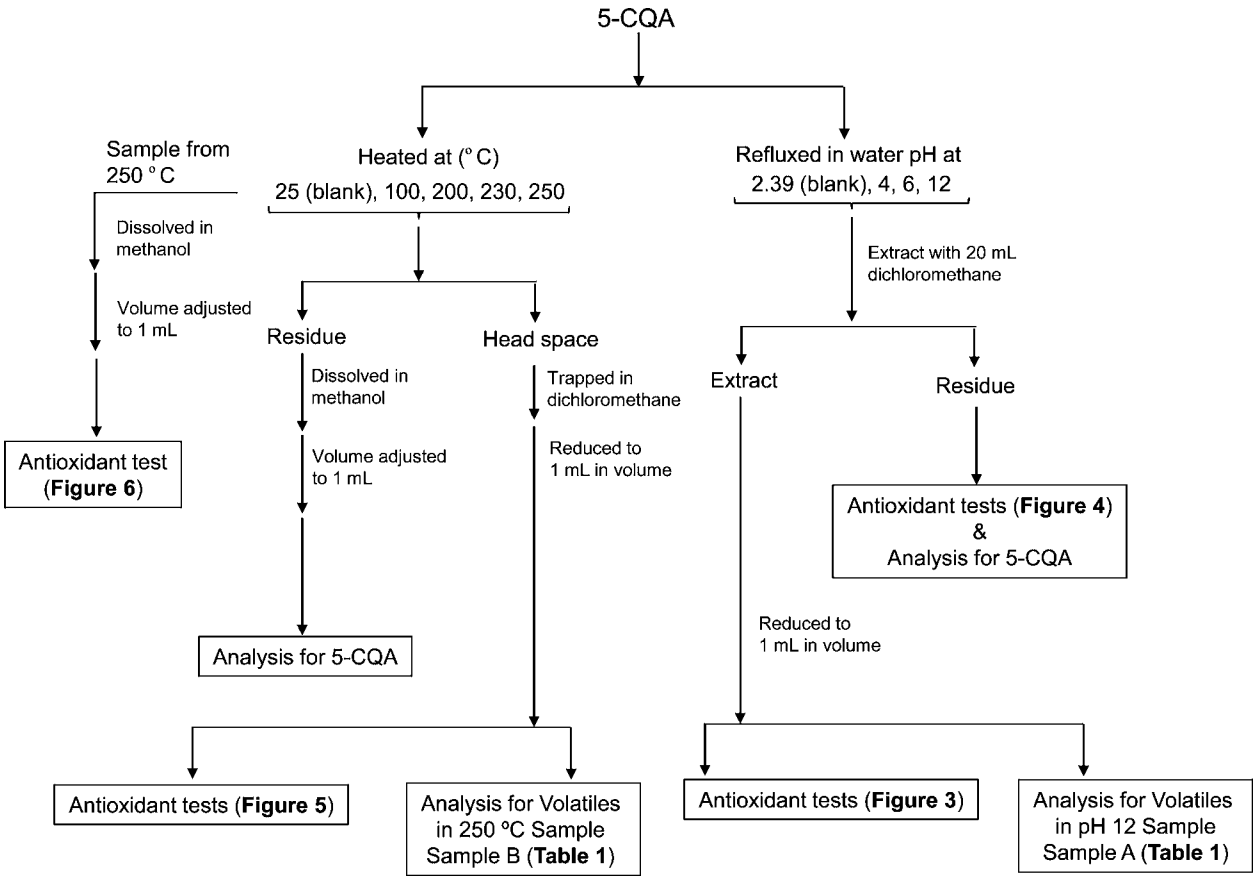

Figure 1. Experimental processes of sample preparations from 5-CQA.

(Sunbeam Products Inc., Boca Raton, FL, USA). Brewed coffee samples were cooled to room temperature in an ice bath. The pH of each brewed coffee sample was measured using a Corning 430 pH meter (Corning Inc., Corning, NY, USA). Because the color of the brewed coffee was too dark to measure the UV absorbance, the coffee samples were then diluted to 1/500, 1/1000, and 1/10000 with deionized water for the 1,1-diphenyl-2-picrylhydrazyl (DPPH) assay. The samples were also diluted to 1/10, 1/100, and 1/1000 with deionized water for the malonaldehyde−gas chromatography (MA-GC) assay. This was done to provide samples comparable to those used for the DPPH assay. Antioxidant assays were performed using 100 μL of each of the diluted samples.

Sample Preparation of Dichloromethane Extracts from Brewed Coffee for Antioxidant Assays. Brewed coffee VIa prepared above (500 mL) was extracted for 6 h with 150 mL of dichloromethane using a liquid−liquid continuous extractor at room temperature. After the extract was dried over anhydrous sodium sulfate, it was condensed to exactly 4 mL in volume by rotary evaporator, followed by purging with a purified nitrogen stream. The extracted sample was stored at 5 °C until analysis for volatile chemicals.

Preparation of 5-CQA Degradation Samples for Antioxidant Activities and Analysis. Two degradation methods were used to prepare 5-CQA degradation samples. The entire experimental processes are shown in Figure 1.

Degradation of 5-CQA in Aqueous Solution. An aqueous solution containing 5-CQA (mg/mL) was refluxed for 2 h in a 250 mL round-bottomed flask. The pH of the solution was adjusted to 4, 6, or 12 with 1 N sodium hydroxide solution. The pH of the original solution was 2.39 (blank sample). After the solution was cooled to room temperature, it was extracted for 3 h with 50 mL of dichloromethane using a liquid−liquid continuous extractor. The extract was dried over anhydrous sodium sulfate and then condensed to 1 mL in volume. The extract obtained from the sample refluxed at pH 12 was analyzed by GC, and the total volatiles were calculated to be 8.5 mg. The concentration of each chemical identified was calculated using a previously reported equation.[16] Residual aqueous solutions and dichloromethane extracts were stored at 5 °C for analysis and antioxidant assays.

Thermal Degradation of 5-CQA. Thermal degradation of 5-CQA and collection of products were conducted using a previously reported apparatus and method.[17] Briefly, the surfaces of 4 mm diameter glass beads were coated with 5-CQA (1 g) in a glass tube (250 mm × 40 mm i.d.). The sample tube was heated at 100, 200, 230, or 250 °C for 30 min while being purged with an air stream at 500 mL/min. The volatile degradation compounds were trapped in 200 mL of dichloromethane in an impinger (200 mm × 40 mm i.d.) cooled with ice-cooled brine water (−20 °C). After the dichloromethane solution was dried over anhydrous sodium sulfate, it was condensed to 1 mL in volume using a rotary flash evaporator followed by purging with a purified nitrogen stream. The samples were stored at 5 °C for analysis and antioxidant assays.

5-CQA (1 g) was heated at 250 °C for 30 min using the apparatus described above without purging with an air stream, then the heated sample was removed with 20 mL of methanol. The methanol solution was reduced to dryness by purging with a purified nitrogen stream. Approximately 800 mg of viscous brown liquid was obtained and stored at 5 °C until used for antioxidant assays and residual 5-CQA analysis by HPLC.

Determination of Antioxidant Activities of Samples. The antioxidant activities of the coffee samples were examined by two different assays, the DPPH assay and the MA-GC assay. Antioxidant activity was calculated using a previously reported method.[18]

The DPPH assay was conducted according to a previously reported method.[19] Briefly, a mixture containing a test sample (500 μL/mL) and 300 mM DPPH (500 μL) was incubated at room temperature for 30 min, and then the absorbance at 517 nm was measured using a Hewlett-Packard 8452A diode array spectrophotometer (Hewlett-Packard Co., Palo Alto, CA, USA). Butylated hydroxytoluene

DOI: 10.1021/jf5060563
J. Agric. Food Chem. 2015, 63, 1996−2005

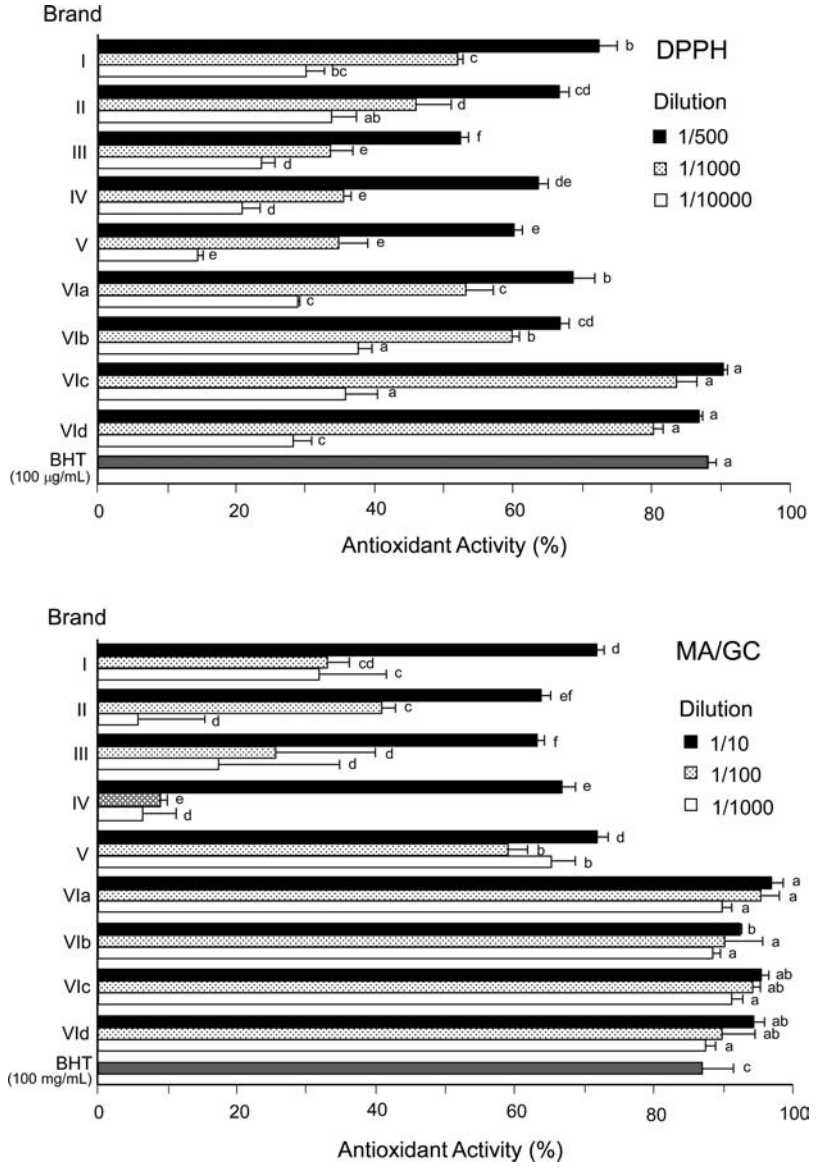

Figure 2. Results of antioxidant assays on six commercial coffee brands. Values are means ± SD (n = 3).

(BHT; 100 μg/mL) was used as a standard antioxidant to validate the assay.

The MA-GC assay was also performed according to a previously reported method.[17] Briefly, a test sample was added to an assay solution (5 mL) containing cod liver oil (10 μL) in a 20 mL test tube. After incubation of the sample at 37 °C for 18 h, the MA formed was analyzed as the 1-methylpyrazole derivative, using an Agilent Technologies 6890N GC equipped with a 30 m × 0.25 mm i.d. (d_f = 0.25 μm) DB-WAX fused-silica capillary column (Agilent Technologies Inc., Santa Clara, CA, USA) and a nitrogen−phosphorus detector. The GC oven temperature was programmed to increase from 70 to 120 °C at 4 °C/min. The injector and detector temperatures were 260 and 280 °C, respectively. The helium carrier gas flow rate was 1.4 mL/min. BHT (100 μg/mL) was used as a standard antioxidant and to validate the assay.

Analysis of Chemicals in Samples from 5-CQA Degradation Experiments. Chemicals in the 5-CQA samples were analyzed using gas chromatography (GC) and GC−mass spectrometry (GC-MS) for dichloromethane extracts (samples A and B) and liquid chromatography (LC)−MS for 5-CQA in the residual aqueous solution (refer to Figure 1). The experimental processes followed previously reported methods.[20] Briefly, the dichloromethane extracts from degradation samples were analyzed using an Agilent model 6890 GC equipped with a 60 m × 0.25 mm i.d. (d_f = 0.25 μm) DB-WAX bonded-phase fused-silica capillary column (J&W Scientific, Folsom, CA, USA) and a flame ionization detector (FID). The linear velocity of the helium carrier gas was 30 cm/s at a split ratio of 20:1. The injector and detector temperatures were 250 °C. The oven temperature was programmed to increase from 40 to 200 °C at 2 °C/min. The mass spectrum of each GC peak was obtained with an Agilent model 6890 GC interfaced to an Agilent 5971A mass selective detector (Foster City, CA, USA) at an MS ionization voltage of 70 eV. The GC conditions were the same as the ones used for GC-FID. Volatile chemicals were identified by comparison of the Kovats GC retention index I and the MS fragmentation pattern of each chemical with those of the authentic chemical. The identities of the chemicals were also confirmed using the National Institute of Standards MS library (AMDIS software, version 2.1).

Analysis of 5-CQA remaining in the residual aqueous samples from the experiments of 5-CQA degradation in an aqueous solution was performed according to a previously reported method.[7] An Agilent 1100 model HPLC system equipped with a Zorbax Eclipse XDB C-18 column (5 μm, 150 mm × 4.6 mm) and a multiple-wavelength detector was used. Mobile phases A and B were 10 mM citric acid and methanol, respectively. Identification of 5-CQA was confirmed

DOI: 10.1021/jf5060563
J. Agric. Food Chem. 2015, 63, 1996−2005

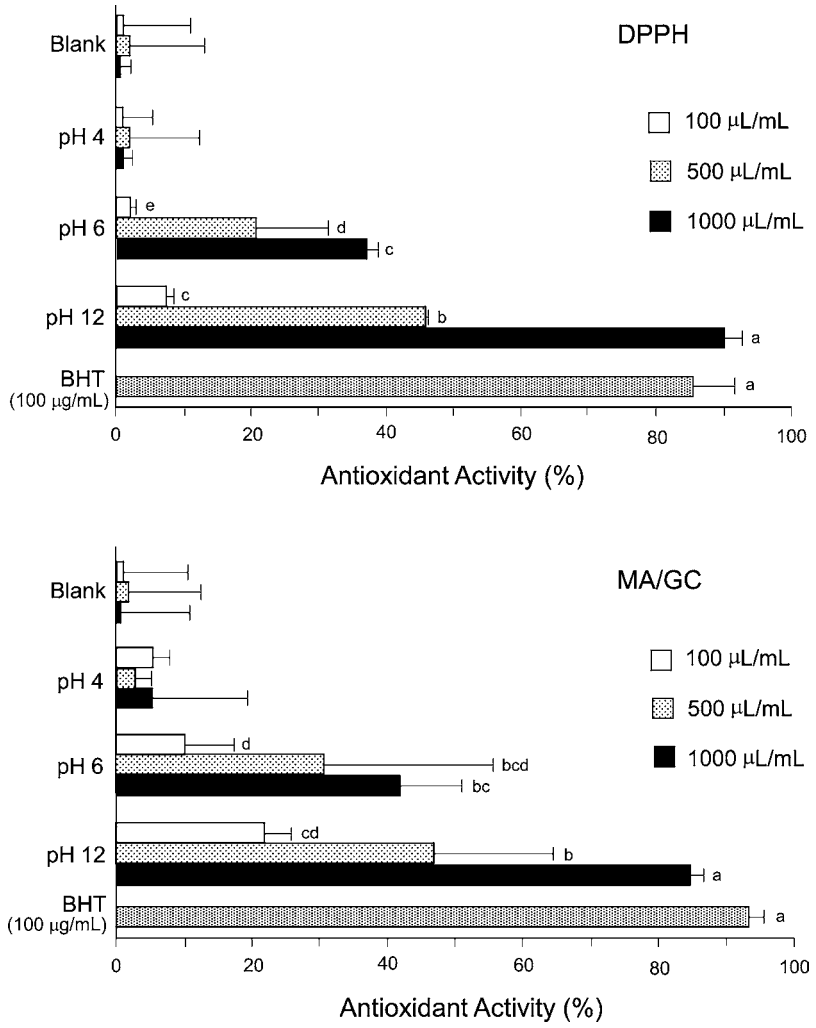

Figure 3. Results of antioxidant assays on dichloromethane extracts of the samples from 5-CQA refluxed in pH 4, 6, or 12 aqueous solution. Values are means ± SD (n = 3).

by an Agilent 1100 LC interfaced to an Applied Biosystems API 2000 MS/MS.

Statistical Analysis. Results were expressed as the mean ± standard deviation (n = 3). The values of antioxidant activities obtained in the present study were treated with an ANOVA analysis based on the SAS system, and the level of significance was determined using Duncan's multiple-range test at α = 0.05. Each experiment was repeated three times.

RESULTS AND DISCUSSION

Antioxidant Activity of Commercial Coffees Tested by DPPH and MA-GC Assays. The DPPH assay may be the most commonly and widely used in food and plant components because it is relatively simple. One of the drawbacks of this method is that the spectrophotometric absorption is interfered with by other components if a sample is dark in color, as in the case of coffee. Therefore, it is not possible to use this assay to examine the antioxidant activity of brewed coffee samples without diluting the samples. The MA-GC assay, on the other hand, is applicable to a dark-colored samples such as brewed coffee because it monitors the amount of MA by GC.

We previously reported that the total content of CQAs in commercial brands of coffee ranged from 5.26 ± 0.09 to 17.10 ± 0.34 mg/g.[7] The amount of 5-CQA was the greatest of the nine CQA isomers found, ranging from 2.13 to 7.06 mg/g in ground roasted coffee beans. 5-CQA comprised nearly 40% of the total CQAs in roasted coffee beans. It has also been reported that the lower the level of CQAs, the less acidic (higher pH) the resultant brewed coffees was.[21] In the present study, the pH of brewed coffee samples was 5.15 in brand I, 4.78 in brand II, 5.01 in brand III, 5.11 in brand IV, 5.06 in brand V, 5.49 in brand VIa, 5.57 in brand VIb, 5.64 in brand VIc, and 5.63 in brand VId. Therefore, 5-CQA was chosen to investigate the possible formation of antioxidants from degradation of chlorogenic acids in coffee during processing.

Figure 2 shows the results of the antioxidant assays on six commercial coffee brands. Values are means ± SD (n = 3). The antioxidant activity of BHT (standard antioxidant) was 88.05 ± 1.18% by the DPPH assay and 86.87 ± 4.38% by the MA-GC assay at the level of 100 μg/mL, indicating that these two antioxidant assays are valid in the present study. All brewed coffee samples exhibited dose-dependent antioxidant activity except for brand V in the MA-GC assay. The antioxidant activity of the brewed coffee samples ranged from 52.19 ± 1.18% (brand III) to 90.24 ± 0.67% (brand VIc) by DPPH assay and from 63.13 ± 1.01% (brand III) to 96.80 ± 1.68% (brand VIa) by MA-GC assay at the highest levels tested (1/500 dilution for the DPPH assay and 1/10 assay for the MA-GC assay). Generally, brand VI showed the most

DOI: 10.1021/jf5060563
J. Agric. Food Chem. 2015, 63, 1996−2005

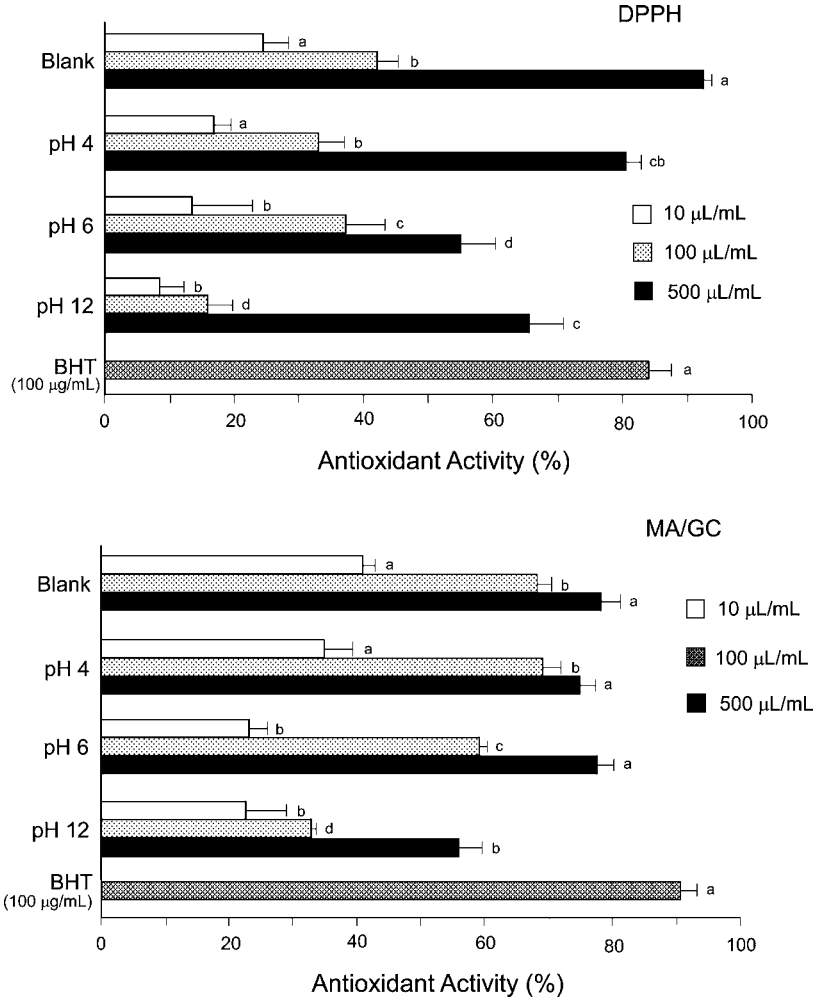

Figure 4. Results of antioxidant assays on residual aqueous solution samples from 5-CQA refluxed in pH 4, 6, or 12 aqueous solution. Values are means ± SD (n = 3).

potent antioxidant activity of the six brands tested in the present study at all levels. The average activity of the four brand VI products was 78.02% by DPPH assay and 94.66% by MA-GC assay.

Degradation Studies on 5-CQA. In this experiment, samples were prepared to simulate brewing processes and roasting processes. Figure 3 shows the results of the antioxidant assays on the dichloromethane extracts of the samples from 5-CQA refluxed in pH 4, 6, or 12 aqueous solution. A standard antioxidant, BHT, exhibited activities of 85.67 ± 6.58 and 93.35 ± 2.27% in DPPH and MA-GC assays, respectively, indicating that these assays are valid in the present study. Similar results were obtained from the two assays. The control samples did not show any appreciable antioxidant activity in either assay, suggesting that 5-CQA does not degrade or produce sufficient volatile antioxidants at the relatively acidic condition of pH 3.4. In fact, LC-MS analysis revealed only 8.46% of 5-CQA was degraded by reflux at this pH. On the other hand, 49.92% degradation was observed at pH 4, 63.59% degradation at pH 6, and 99.99% degradation at pH 12. The degradation of 5-CQA is obviously correlated with the antioxidant activity of the samples obtained from reflux. A dichloromethane extract from the 5-CQA solution refluxed at pH 12 exhibited potent antioxidant activities at the level of 1000 μL/mL (90.44 ± 2.48% in the DPPH assay and 84. 89 ± 1.35% in the MA-GC assay). These results suggest that some CQAs degrade into potent volatile antioxidants during the brewing process.

The extracts from 5-CQA refluxed at pH 6 exhibited moderate antioxidant activity at the level of 1000 μL/mL (37.99 ± 1.61 and 41.84 ± 9.21% in DPPH and MA-GC assays, respectively). Therefore, the commercial brewed coffees with a pH near 6 (brand VI) may produce volatile antioxidants during brewing and, consequently, have higher antioxidant activity than those with a pH near 5 because neither the samples from the control nor those with a pH of 4 showed appreciable antioxidant activity. These results suggest that chlorogenic acids degrade into some volatile antioxidants during brewing.

Figure 4 shows the results of the antioxidant assays on the residual aqueous solutions from the reflux experiments. The antioxidant activities of BHT at a level of 100 μg/mL were 84.01 ± 3/31 and 90.31 ± 2.61% in the DPPH and MA-GC assays, respectively, indicating that these assays are valid in the present study. All samples exhibited moderate (40−50%) or potent (>70%) dose-dependent antioxidant activities. The antioxidant activities at the highest levels (500 μL/mL) tested ranged from 54.78 ± 5.33% (pH 6 sample) to 92.10 ± 1.10% (blank) in the DPPH assay and from 55.70 ± 3.54% (pH 12 sample) to 78.03 ± 2.98% (blank) in the MA-GC assay. The low antioxidant activity of the samples with a high pH may be because the volatile antioxidants formed from 5-CQA were removed with the extraction.

DOI: 10.1021/jf5060563
J. Agric. Food Chem. 2015, 63, 1996−2005

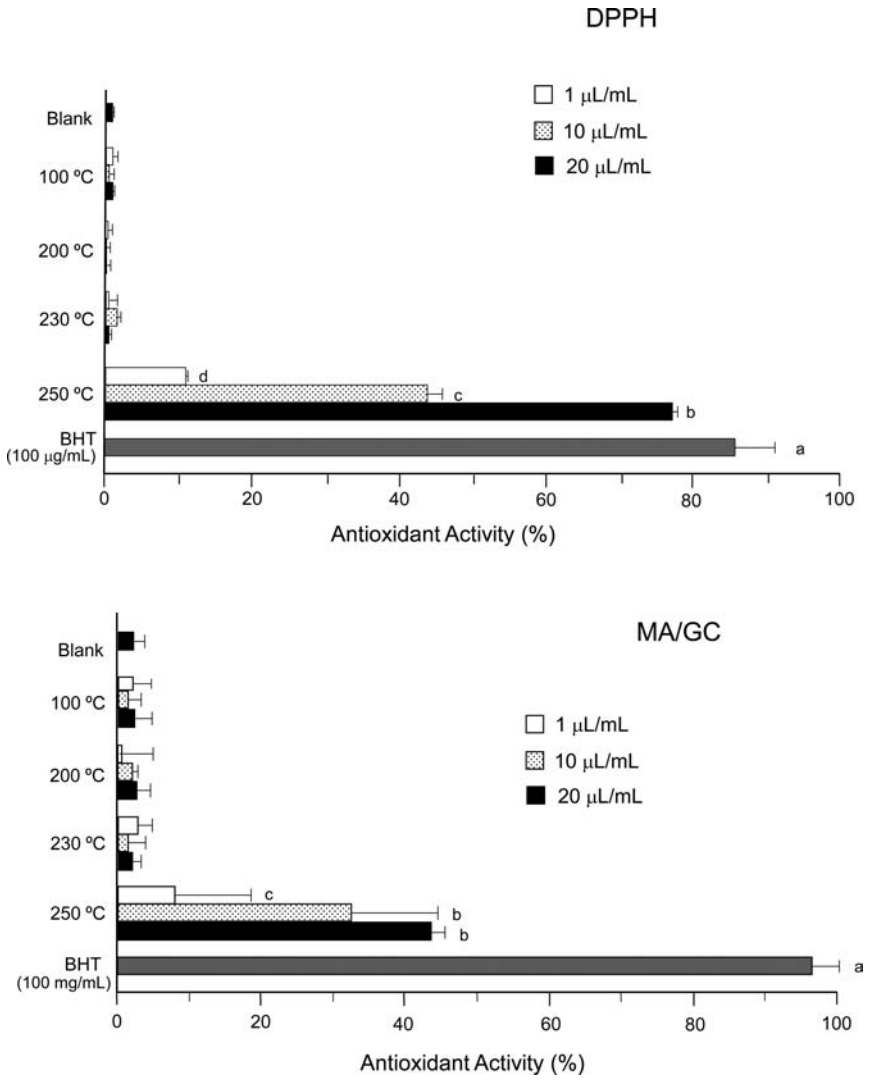

Figure 5. Results of antioxidant assays on the headspace samples trapped in dichloromethane from the thermal degradation of 5-CQA experiments at various temperatures. Values are means ± SD (n = 3).

Figure 5 shows the results of the antioxidant assays on the headspace samples trapped in dichloromethane from the experiments on the thermal degradation of 5-CQA. The antioxidant activities of BHT were 85.74 ± 5.42 and 96.32 ± 3.68% in the DPPH and MA-GC assays, respectively, indicating that these assays were valid in the present study. The samples from 5-CQA heated at 100, 200, and 230 °C for 30 min did not show any appreciable antioxidant activity in either the DPPH or MA-GC assay. On the other hand, when 5-CQA was heated at 250 °C, obvious formation of antioxidants was observed: 7.708 ± 0.72 and 43.46 ± 2.58% at the level of 20 μL/mL in the DPPH and MA-GC assays, respectively. The samples heated at 250 °C exhibited clear dose-dependent activity. Our previous study demonstrated that the amount of total CQAs decreases with increased roasting temperature.[14] In this study, we reported that roasting green coffee beans at 230 °C for 12 min (light roasting) decreased the total CQAs from 69.09 ± 2.36 to 32.09 ± 0.75 mg/g and decreased 5-CQA from 50.70 ± 1.61 to 15.11 ± 0.35 mg/g, whereas when they were heated at 250 °C for 21 min (French roasting), the total for CQAs was 0.34 ± 0.003 mg/g and that for 5-CQA was 0.16 ± 0.01 mg/g. These results indicate that CQAs, including 5-CQA, degrade under generally used roasting conditions, particularly in French roasts, and consequently increase antioxidant activity.

Figure 6 shows the results of the antioxidant tests on samples from unheated 5-CQA and from 5-CQA heated at 250 °C. BHT exhibited 93.25 ± 1.26 and 89.33 ± 3.77% at the level of 100 μg/mL in the DPPH and MA-GC assays, respectively, indicating that these assays are valid in this experiment. 5-CQA showed moderate antioxidant activities at the level of 100 μg/mL in both assays (44.41 ± 0.27%). The antioxidant activities of 5-CQA exhibited clear dose dependence and ranged from 5.18 ± 0.82% (1 μg/mL) to 50.69 ± 0.27% (20 μg/mL) in the DPPH assay and from 1.36 ± 0.54 to 44.41 ± 0.27% in the MA-GC assay. On the other hand, the sample from the heated 5-CQA exhibited potent antioxidant activities at 10 μg/mL (79.12 ± 2.49% in the DPPH assay and 70.88 ± 7.97% in the MA-GC assay). The same sample showed moderate antioxidant activities at 1 μg/mL (31.32 ± 1.10% in the DPPH assay and 43.96 ± 5.79% in the MA-GC assay), whereas 5-CQA did not show any appreciable antioxidant activity at the same level (5.18 ± 0.82% in the DPPH assay and 1.36 ± 0.54% in the MA-GC assay). These results clearly indicate that degradation of 5-CQA produced additional antioxidants. HPLC analysis of a

DOI: 10.1021/jf5060563
J. Agric. Food Chem. 2015, 63, 1996−2005

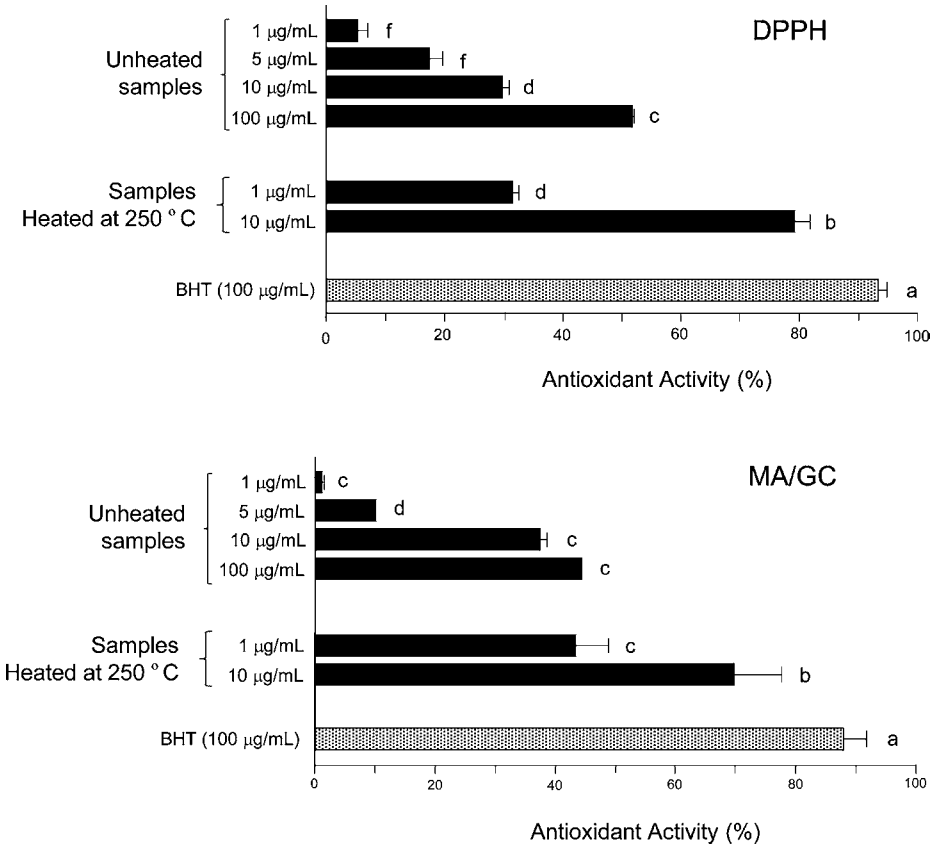

Figure 6. Results of antioxidant tests on samples from 5-CQA heated at 250 °C and untreated 5-CQA. Values are means ± SD (n = 3).

methanol solution of this sample confirmed that approximately 70% of 5-CAQ degraded into other chemicals.

Table 1 shows the compounds identified in the dichloromethane samples (refer to Figure 1). The amount of each compound identified was calculated according to a previously reported method.[20] Among the 29 compounds positively identified in sample A, acetone was found in the greatest amount (3060.0 μg/g), followed by 4-vinylphenol (1783.3 μg/g), benzoic acid (1269.1 μg/g), hexadecanoic acid (748 μg/g), octadecanoic acid (183.6 μg/g), 2-methoxy-4-vinylphenol (159.0 μg/g), and pyrocatechol (147.9 μg/g). All of these chemicals have been found in coffee except 4-vinylphenol.[22] It is interesting to note that 4-vinylphenol may have antioxidant activity, but it has not been reported in coffee. Only eight volatile compounds were isolated and identified in sample B. Pyrocatechol was found in the greatest concentration (2809.3 μg/g), followed by phenol (1275.0 μg/g), 2,5-dimethylfuran (259.3 μg/g), 2-methylcyclohexanone (107.1 μg/g), and 2-methoxy-4-vinylphenol (46.4 μg/g). All of these chemicals were reported in coffee except 2-methylcyclohexanone.[22] The compositional differences between the samples are due to the different preparation methods; sample A was prepared by direct extraction, whereas sample B was prepared from the headspace. Therefore, direct comparison of these samples is not appropriate. Three possible phenolic antioxidants (2-methoxy-4-vinylphenol, 4-vinylphenol, and pyrocatechol) were formed in relatively high concentrations in both samples A and B. Therefore, the antioxidant activity of these three phenolic chemicals identified in the present study along with caffeic acid and 4-ethylcatechol was examined. Caffeic acid and 4-ethylcatechol were examined because they were reported as chlorogenic degradation products in our previous study.[20] Figure 7 shows the proposed formation pathways of possible antioxidants formed from the caffeic acid that was formed from 5-CQA upon hydrolysis.[20]

Figure 8 shows the antioxidant activities of the major chemicals found in the samples obtained from the 5-CQA degradation experiments. BHT showed antioxidant activities (82.38 ± 0.49% in the DPPH assay and 85.23 ± 1.42% in the MA-GC assay) at a level of 100 μg/mL, indicating that the assays used in these experiments were valid. All chemicals tested exhibited dose-dependent antioxidant activity. Among them, 2-methoxy-4-vinylphenol showed the strongest antioxidant activities (98.63 ± 0.01% in the DPPH assay and 98.63 ± 2.18 in the MA-GC assay) at a level of 20 μg/mL. On the other hand, pyrocatechol had the most potent antioxidant activity (71.66 ± 0.01% in the DPPH assay and 76.57 ± 3.00% in the MA-GC assay) at a level of 10 μg/mL. All 5-CQA degradation products exhibited higher antioxidant activities than those of 5-CQA at all levels tested.

4-Vinylphenol, which has not been reported in coffee but was found in a sample from 5-CQA refluxed at pH 12 in relatively high concentration (1783.3 μg/g), exhibited antioxidant activity comparable to that of a standard antioxidant, BHT, with dose dependence. The antioxidant activity in 4-vinylphenol was 65.9 ± 0.81% in the DPPH assay and 85.23 ± 1.42% in the MA-GC assay at the level of 20 μg/mL. These results suggest that 4-vinylphenol forms from chlorogenic acids during brewing under low acidic conditions. The other chemicals formed in large quantities in this sample—acetone (3060.0 μg/mg) and benzoic acid (1269.1 μg/g)—did not show any appreciable antioxidant activity at the levels tested (1, 10, and 20 μg/mL).

DOI: 10.1021/jf5060563
J. Agric. Food Chem. 2015, 63, 1996−2005

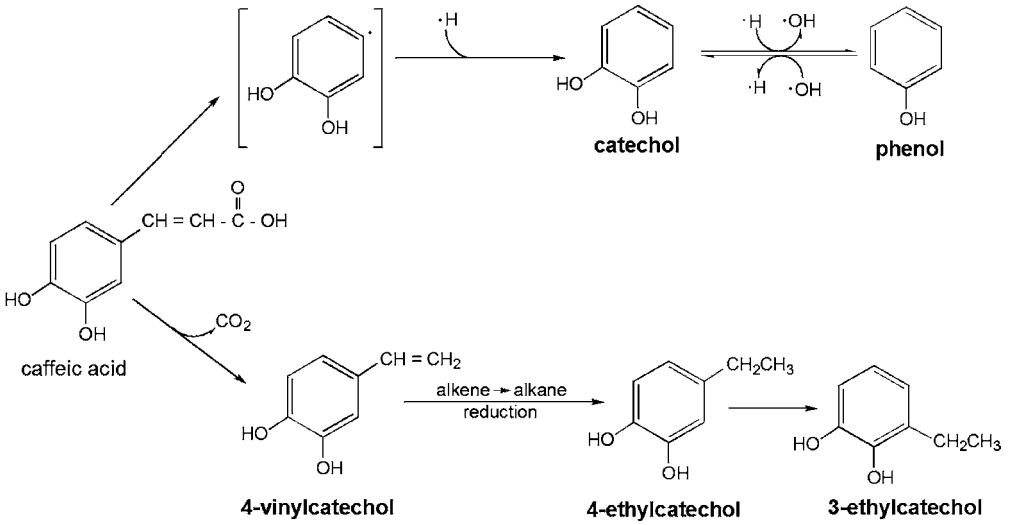

Figure 7. Proposed formation pathways of possible antioxidants formed from caffeic acid.

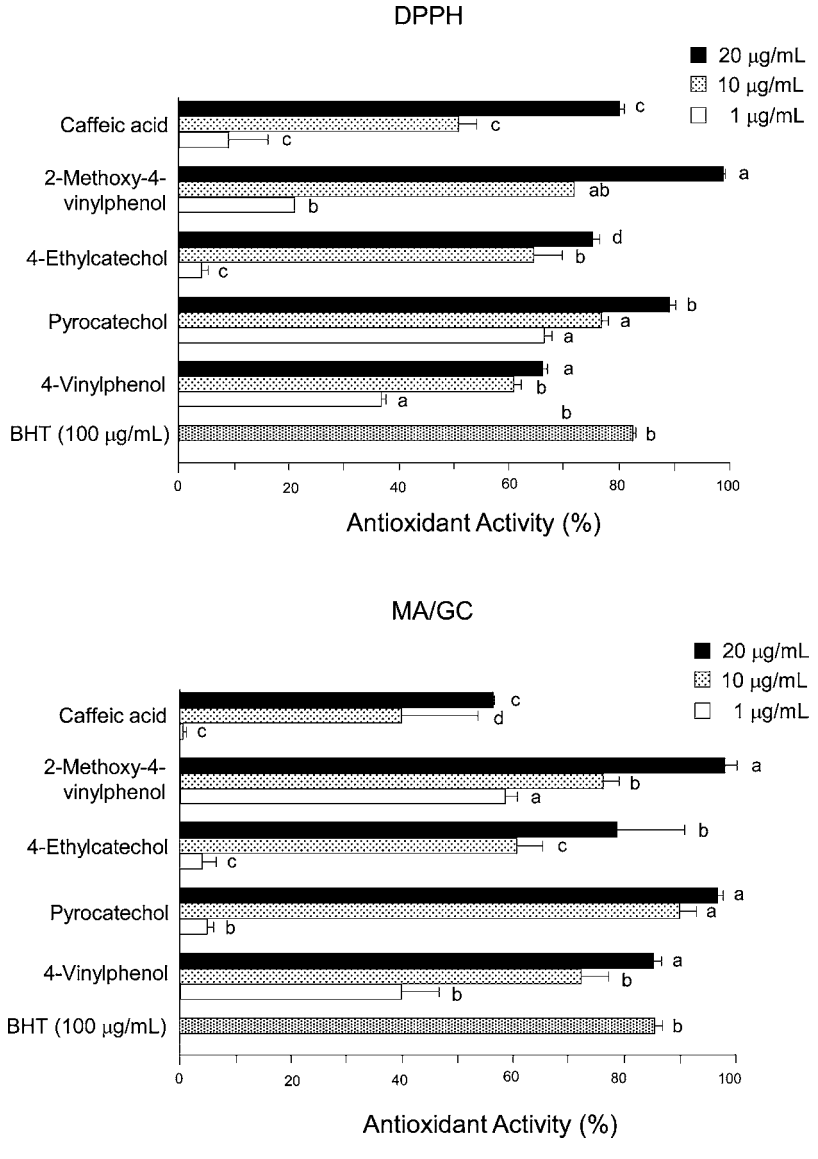

Figure 8. Antioxidant activity of major chemicals found in the samples obtained from 5-CQA degradation experiments. Values are means ± SD (n = 3).

DOI: 10.1021/jf5060563
J. Agric. Food Chem. 2015, 63, 1996−2005

Table 1. Compounds Identified in a Dichloromethane Extract from 5-CQA Refluxed in Aqueous Solution at pH 12 (Sample A) and in a Dichloromethane Trap from the Headspace of Heated 5-CQA at 250 °C (Sample B)

compound	I^a	amount (μg/g) in sample A	amount (μg/g) in sample B
alkyl hydrocarbons, alcohols, acids, aldehydes, and ketones			
acetone	898	3060.0	–[b]
3-methyl-2-butanone	926	57.8	–
2-methyl-2-butanol	1013	33.2	–
2-methyl-3-buten-2-ol	1036	4.3	–
3-penten-2-one	1117	7.7	–
2-methyl-1-buten-3-ol	1165	54.4	–
(*E*)-2-methyl-2-butenol	1316	8.5	–
2,3-dimethyl-2-cyclopenten-1-one	1597	7.7	–
2,6,10,14-tetramethylpentadecane	1674	25.5	–
2-methylcyclohexanone	1775	–	107.1
octadecane	1800	11.9	–
2-hydroxy-3-methyl-2-cyclopenten-1-one	1860	–	29.8
hexanoic acid	1871	–	15.3
dodecanol	1965	13.6	–
3,4-cyclohexanedione	1975	20.4	–
benzoic acid	1478	1269.1	–
hexadecanoic acid	2811	748.0	–
octadecanoic acid	2845	183.6	–
heterocyclic compounds			
2,5-dimethylfuran	943	–	259.3
5-methyl-2-(1-hydroxypropyl)furan	1697	15.3	–
N-methyl-2-pyrrolidone	1680	3.4	–
(*S*)-(+)-dihydro-5-(hydroxypropyl)-2(3*H*)-furanone	2467	24.7	–
(*S*)-(−)-β-hydroxy-γ-butyrolactone	2583	40.0	–
aromatic compounds			
1,3-benzodioxole	1530	–	12.8
2-phenyl-2-propanol	1752	7.7	–
benzyl alcohol	1866	4.3	–
phenylethyl alcohol	1903	12.8	–
phenol	1997	12.8	1275.0
2-methoxy-4-vinylphenol	2181	159.0	46.4
4-methoxybenzyl alcohol (anise alcohol)	2269	74.8	–
2,4-di-*tert*-butylphenol	2305	122.4	–
4-vinylphenol	2379	1783.3	–
3-(2-hydroxyphenyl)-2-propenoic acid*	2405	68.0	–
pyrocatechol	2683	147.9	2809.3

[a]Kovats index on DB-WAX. [b]Amount <0.01 μg/g or not detected.

Also, 2,5-dimethylfuran (259.3 mg/g) and phenol (1275.0 mg/g) formed from 5-CQA heated at 250 °C in relatively high levels but, at the levels tested, did not show any appreciable antioxidant activity as other chemicals did. However, phenol exhibited moderate antioxidant activity (49.54 ± 4.21%) at an extremely high level (10 mg/mL) in the DPPH assay. A previous study demonstrated that unsubstituted furan inhibited hexanal oxidation by 80% at a 500 mg/mL level over 40 days,[23] suggesting that 2,5-dimethylfuran contributed to the antioxidant activity of a sample from heated 5-CQA.

The present study demonstrates that chlorogenic acids present in green coffee beans produce potent antioxidants under heat treatment, suggesting that the roasting conditions for coffee beans play an important role in the formation of antioxidants and the acidic condition of the brewed coffee.

AUTHOR INFORMATION

Corresponding Author

*(T.S.) Phone: (530) 752-4523. Fax: (530) 752-3393. E-mail: tshibamoto@ucdavis.edu.

Present Addresses

†(M.K.) Department of Anti-Aging Vessel, School of Internal Medicine, National Defense Medical College, 3-2 Namiki, Tokorozawa-shi, Saitama-ken 359-8513, Japan.

‡(J.-K.M.) Department of Plant Life and Environmental Sciences, Hankyong National University, Ansung, Republic of Korea.

§(H.W.J.) Korea Food Research Institute, 1201-62 Anyangpangyoro, Bundanggu, Seongnamsi, Gyeonggido 463-756, Republic of Korea.

Funding

This work was financially supported in part by the Strategic Young Researcher Overseas Visits Program for Accelerating Brain Circulation, Japan Society for the Promotion of Science.

Notes

The authors declare no competing financial interest.

ABBREVIATIONS USED

BHT, butylated hydroxytoluene; CQA, chlorogenic acid; DPPH, 1,1-diphenyl-2-picrylhydrazyl; FID, flame ionization detector; HPLC, high-performance liquid chromatography; LC-MS, liquid chromatography−mass spectrometry; MA-GC, malonaldehyde−gas chromatography

REFERENCES

(1) Butt, M. S.; Sultan, M. T. Coffee and its consumption: benefits and risks. *Crit. Rev. Food Sci. Nutr.* **2011**, *51*, 363−373.

(2) Singhara, A.; Macku, C.; Shibamoto, T. Antioxidative activity of brewed coffee extracts. In *Functional Foods for Disease Prevention II: Medicinal Plants and Other Foods*; ACS Symposium Series 701; American Chemical Society: Washington, DC, USA, 1998; pp 101−109.

(3) Cano-Marguina, A.; Tarin, J. J.; Cano, A. The impact of coffee on health. *Maturitas* **2013**, *75*, 7−21.

(4) Mandair, D. S.; Rossi, R. E.; Pericleous, M.; Whvand, T.; Caplin, M. The impact of diet and nutrition in the prevention and progression of hepatocellular carcinoma. *Expert. Rev. Gastroenterol Hepatol.* **2014**, *8*, 369−383.

(5) Kempf, K.; Martin, S. Coffee and diabetes. *Med. Klin.* **2010**, *105*, 910−915.

(6) Vitaglione, P.; Fogliano, V.; Pellegrini, N. Coffee, colon function and colorectal cancer. *Food Funct.* **2012**, *3*, 916−922.

(7) Fujioka, K.; Shibamoto, T. Quantitation of volatiles and nonvolatile acids in an extract from coffee beverages: correlation with antioxidant activity. *J. Agric. Food Chem.* **2006**, *54*, 6054−6058.

(8) Fang, Y. Z.; Yang, S.; Wu, G. Free radicals, antioxidants, and nutrition. *Nutrition* **2002**, *18*, 872−879.

(9) Benzie, I. F.; Choi, S. W. Antioxidants in food: content, measurement, significance, action, cautions, caveats, and research needs. *Adv. Food Nutr. Res.* **2014**, *71*, 1−53.

(10) Lee, D. R.; Lee, J.; Rota, M.; Lee, J.; Ahn, H. S.; Parki, S. M.; Shin, D. Coffee consumption and risk of fractures: a systematic review and dose-response meta-analysis. *Bone* **2014**, *63*, 20−28.

(11) Gülçin, I. Antioxidant activity of food constituents: an overview. *Arch. Toxicol.* **2012**, *86*, 345−391.

(12) Wang, Y.; Ho, C. T. Polyphenolic chemistry of tea and coffee: a century of progress. *J. Agric. Food Chem.* **2009**, *57*, 8109−8114.

DOI: 10.1021/jf5060563
J. Agric. Food Chem. 2015, 63, 1996−2005

(13) Upadhyay, R.; Mohan Rao, L. J. An outlook on chlorogenic acids-occurrence, chemistry, technology, and biological activities. *Crit. Rev. Food Sci. Nutr.* **2013**, *53*, 968−984.
(14) Moon, J.-K.; Yoo, H. S.; Shibamoto, T. Role of roasting conditions in the level of chlorogenic acid content in coffee beans: correlation with coffee acidity. *J. Agric. Food Chem.* **2009**, *57*, 5365−5369.
(15) Nicoli, M. C.; Anese, M.; Manzocco, L.; Lerici, C. R. Antioxidant properties of coffee brews in relation to the roasting degree. *Lebensm.-Wiss. -Technol.* **1997**, *30*, 292−297.
(16) Umano, K.; Hagi, Y.; Nakahara, K.; Shoji, A.; Shibamoto, T. Volatile chemicals identified in extracts from leaves of Japanese mugwort (*Artemisia princeps* Pamp.). *J. Agric. Food Chem.* **2000**, *48*, 3463−3469.
(17) Moon, J.-K.; Shibamoto, T. Antioxidant assays for plant and food components. *J. Agric. Food Chem.* **2009**, *57*, 1655−1666.
(18) Nam, S.; Jang, H.-W.; Shibamoto, T. Antioxidant activities of extract from teas prepared from medicinal plants, *Morus alba* L., *Camellia sinensis* L., and *Cudrania tricuspidata*, and their volatile components. *J. Agric. Food Chem.* **2012**, *60*, 9097−9105.
(19) Kamiyama, M.; Horiuchi, M.; Umano, K.; Kondo, K.; Otsuka, Y.; Shibamoto, T. Antioxidant/anti-inflammatory activities and chemical composition of extracts from the mushroom *Trametes versicolor*. *Int. J. Nutr. Food Sci.* **2013**, *2*, 85−91.
(20) Moon, J. K.; Shibamoto, T. Formation of volatile chemicals from thermal degradation of less-volatile coffee components: quinic acid, caffeic acid, and chlorogenic acid. *J. Agric. Food Chem.* **2010**, *58*, 5465−5470.
(21) Fujioka, K.; Shibamoto, T. Chlorogenic acid and caffeine contents in various commercial brewed coffees. *Food Chem.* **2008**, *106*, 217−231.
(22) Flament, I.; Bessiere-Thomas, Y. *Coffee Flavor Chemistry*; Wiley: New York, 2002.
(23) Yanagimoto, K.; Lee, K.-G.; Ochi, H.; Shibamoto, T. Antioxidative activity of heterocyclic compounds found in coffee volatiles produced by Maillard reaction. *J. Agric. Food Chem.* **2002**, *50*, 5480−5484.

DOI: 10.1021/jf5060563
J. Agric. Food Chem. 2015, 63, 1996−2005

Table 1. Validation of Applied Correction Factors from Reference in Relation to Increased Analyte Concentration Ranges

	Dobberstein and Bunzel[7]			current study	
	range tested (μg/mL)	correlation coefficient	correction factor	range tested (μg/mL)	correlation coefficient
8-8(aryltetralin)-DFA	2.5−12.5	0.9975	4.350	6.0−60.0	0.9934
8-8-DFA	2.5−12.5	0.9893	1.936	*a*	*a*
8-8(tetrahydrofuran)-DFA	2.5−12.5	0.9931	6.040	*a*	*a*
8-5-DFA	6.0−30.0	0.9984	1.509	6.0−60.0	0.9964
5-5-DFA	6.0−30.0	0.9980	1.514	14.0−140.0	0.9974
8-8(aryltetralin),8-*O*-4-TriFA	6.0−30.0	0.9864	3.591	*a*	*a*
8-*O*-4-DFA	6.0−30.0	0.9997	0.845	10.0−100.0	0.9950
8-5(benzofuran)-DFA	6.0−30.0	0.9997	4.597	11.0−110.0	0.9965
5,5,8-*O*-4-TriFA	2.5−12.5	0.9839	2.089	5.0−50.0	0.9958
5,5(methylated)-DFA	6.0−30.0	0.9981	1.000	6.0−60.0	0.9971
8-*O*-4,8-*O*-4-TriFA	1.0−5.0	0.9979	*b*	*a*	*a*
8,5(decarboxylated)-DFA	2.5−12.5	0.9992	1.341	6.0−60.0	0.9839

[a]Not determined as concentration range did not exceed that of Dobberstein and Bunzel.[7] [b]Not determined due to lack of standard compound.

unprocessed corn grain samples were analyzed by reversed phase high-performance chromatography (RP-HPLC) with ultraviolet (UV) detection for the identification of 12 different cell wall-bound DFAs and TriFAs.

MATERIALS AND METHODS

Materials and Instrumentation. Standard compounds of 8-8(aryltetralin)-DFA, 8-8-DFA, 5-5-DFA, 8-*O*-4-DFA, 8-5-(benzofuran)-DFA, 8-5-DFA, 8-5(decarboxylated)-DFA, 5-5/8-*O*-4-TriFA, 8-8(aryltetralin)/8-*O*-4-TriFA, 8-*O*-4/8-*O*-4-TriFA were isolated as described by Jilek and Bunzel[8] and Bunzel et al.[13] The 5-5(methylated)-DFA (monomethylated 5-5-dehydrodiferulic acid) as internal standard[8] was kindly provided by Prof. Dr. John Ralph, University of Wisconsin, Madison, WI, USA.

An analytical phenyl-hexyl HPLC column (250 × 4.6 mm, 5 μm particle size) was purchased from Phenomenex (Germany). RP-HPLC was carried out with the following instrumentation for DFA and TriFA analysis: LC-20AT pumps, CTO-20AC column oven, SPD-M20A photodiode array detector (PDA), SIL-20AC autosampler, DGU-20A degasser, and CBM-20A communication bus module from Shimadzu, Japan. All solvents used were of HPLC grade, and water was distilled and deionized.

Sample Materials. A total of 63 DDGS samples were collected from 24 ethanol plants in the United States and European Union (EU), covering the following three parent grain origins: corn (*Z. mays*), wheat (*T. aestivum*), and a mix of cereals grains [wheat (*T. aestivum*), barley (*H. vulgare* L.), rye (*S. cereale*)], and triticale (a hybrid of wheat and rye). In addition, 11 unprocessed corn grain (*Z. mays*) samples were also collected. All samples have previously been characterized for contents of common constituents and NSP profiles in our laboratory.[2]

A total of 47 corn DDGS samples were collected from 21 different ethanol plants in the United States; 11 DDGS samples along with 11 unprocessed corn grain samples were sampled over 11 months with 1 sample every month from a plant in Nevada (P1); 5 samples were sampled over 1.5 months from a plant in Minnesota (P2); 5 samples were sampled over 20 days from another plant in Minnesota (P3); 5 samples were sampled over 20 days from a plant in Wisconsin (P4); 5 samples were sampled over 8 days from a plant in Iowa (P5); and 16 samples were supplied by a DDGS supplier in Iowa, representing samples from 7 plants in Minnesota, 4 plants in Iowa, 2 plants in Nevada, and 1 plant each in Illinois, Indiana, and Kentucky.

A total of 11 wheat DDGS samples were collected from 2 different ethanol plants in the EU, with 6 samples from a plant in the United Kingdom sampled over a period of approximately 3 months and 5 samples from a plant in France sampled over 20 days.

Finally, 5 DDGS samples of a mixed cereal grains were sampled over 20 days from a plant in Sweden. The parent grains used in the production of the mixed DDGS were wheat, triticale, barley, and rye; however, their individual proportions are unknown.

All 63 DDGS samples and 11 unprocessed corn grain samples were milled (0.5 mm) prior to analysis using a centrifugal mill (Retsch ZM200).

Pretreatment, Alkaline Hydrolysis, and Extraction of Phenolic Acids. Samples of 50, 175, or 200 mg were weighed out for corn DDGS, corn, and wheat and mixed-cereal DDGS, respectively. All samples were washed twice with 10 mL of 80% (v/v) ethanol and twice with 10 mL of acetone followed by centrifugation and removal of supernatant between and after extractions. The residues were dried under a fume hood. Saponification (5 mL of 2 mol/L NaOH) of the residues was carried out under nitrogen, protected from light, and under continuous stirring for 18 h, following a procedure described by Dobberstein and Bunzel.[7] Following acidification with 0.95 mL of concentrated HCl, 25 μg of 5-5(methylated)-DFA was added as internal standard for the quantification of DFAs and TriFAs. Extraction was carried out three times with 4 mL of diethyl ether. The diethyl ether extracts were dried under nitrogen and redissolved in 500 μL of THF/water (50:50 (v/v)) using ultra sonication and used directly for the determination of DFAs and TriFAs.

Phenyl-Hexyl RP-HPLC-PDA Analysis of DFAs and TriFAs. The procedure basically followed a protocol described by Dobberstein and Bunzel.[7] DFAs and TriFAs were analyzed using a Luna phenyl-hexyl column (250 mm × 4.6 mm i.d., 5 μm particle size, plus 3 mm × 4.6 mm i.d. guard column) and a ternary gradient made up of 1 mM aqueous trifluoroacetic acid (TFA), acetonitrile (ACN), and methanol (MeOH) at the flow rate of 1.0 mL/min. The sample (20 μL) was injected, and the separation was performed at 45 °C, with chromatograms monitored at 280 nm. The following gradients were used: eluent A, 1 mM aqueous TFA; eluent B, ACN/1 mM aqueous TFA [90:10 (v/v)]; eluent C, MeOH/1 mM aqueous TFA [90:10 (v/v)]. Separation of DFAs and TriFAs was carried out with initially 85% A, 15% B, and 0% C, linear over 15 min to 82% A, 18% B, and 0% C; linear over 5 min to 80% A, 20% B, and 0% C; linear over 5 min to 72% A, 25% B, and 3% C; linear over 5 min to 70% A, 25% B, and 5% C; linear over 10 min to 65% A, 30% B, and 5% C; held for 5 min; and linear over 10 min to 55% A, 45% B, and 5% C, following a rinsing and an equilibration step.

Identification of 8-8(Tetrahydrofuran)-DFA in DDGS Samples. Because no purified standard was available for the 8-8-(tetrahydrofuran)-DFA, the presence of this particular dimer was validated by its relative retention time and UV spectrum characteristics, as described by Dobberstein and Bunzel.[7] Furthermore, the elution order for the 8-8(tetrahydrofuran)-DFA was validated by screening for its mass (m/z 403 [M^{-1}]) using liquid chromatography−mass spectrometry, basically as described by Jilek and Bunzel.[8] Finally, gas chromatography−mass spectrometry of a silylated extract was exemplarily applied to validate the presence of the 8-8-(tetrahydrofur-

DOI: 10.1021/jf505150g
J. Agric. Food Chem. 2015, 63, 2006−2012

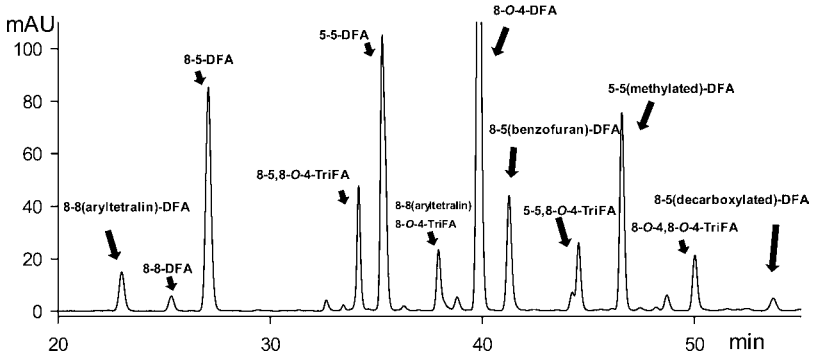

Figure 1. Separation of ferulic acid dehydrodimers and dehydrotrimers by using RP-HPLC/UV with detection at 280 nm.

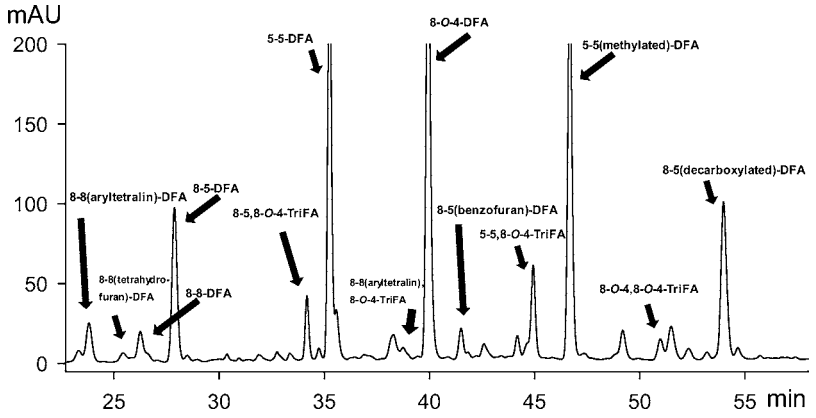

Figure 2. Separation of ferulic acid dehydrodimers and dehydrotrimer in corn DDGS with detection at 280 nm.

Table 2. Composition of Ferulic Acid Dehydrodimers and Dehydrotrimers in DDGS of Various Origins

	corn DDGS			wheat DDGS			mixed DDGS		
	mean[a]	range[b]	SD	mean[c]	range[d]	SD	mean[e]	range[f]	SD
∑DFA (μg/g DM)	3310g	(2811−4825)	308	621h	(543−698)	3	556h	(476−664)	69
∑8-8-DFA (% DFA)	20g	(16−23)	1	30h	(26−34)	3	32h	(30−34)	2
∑8-5-DFA (% DFA)	35g	(32−40)	2	31h	(25−36)	4	32gh	(31−33)	1
5-5 (% DFA)	27g	(25−28)	1	21h	(21−22)	1	19i	(18−20)	1
8-*O*-4 (% DFA)	18g	(17−20)	1	18g	(16−20)	2	18g	(17−18)	0
∑TriFA (μg/g DM)	440g	(332−651)	52	77h	(65−97)	6	70h	(57−88)	11
5-5,8-O-4 (%TriFA)	69g	(56−80)	5	78g	(75−82)	2	72g	(69−74)	2
8-8,8-O-4 (%TriFA)	31g	(20−44)	5	22g	(18−25)	2	28g	(26−31)	2

[a]Average of means from 21 plants. Means in the same row that do not share a letter (g, h, i)are significantly different at $P < 0.05$. [b]$N = 47$. [c]Average of means from 2 plants. [d]$N = 11$. [e]Mean from 1 plant. [f]$N = 5$.

an)-DFA based on the mass spectral characteristics described by Schatz et al.[14]

Calculations and Statistical Analysis. The contents of DFAs and TriFAs were calculated relative to the area of the internal standard by using the correction factors reported by Dobberstein and Bunzel[7] (Table 1).

A one-way ANOVA was applied for comparison among means followed by Tukey's pairwise comparison with overall significance level at $P = 0.05$, using Minitab 16 (Minitab Inc.). The compositional data were analyzed by principal component analysis (PCA) with evenly spread seven-fold partial cross-validation after mean centering, and unit variance scaling, using Evince 2.5.5 software (UmBio AB), was performed as previously discussed.[15] PCA was used to detect correlations of DFAs and TriFAs with previously reported data on composition of common nutrients and NSPs from Pedersen et al.[2]

RESULTS

Detection of Ferulic Acid Dehydrodimers and Dehydrotrimers and Validation of Correction Factors. A chromatogram of the standard compounds of the DFAs and TriFAs monitored at 280 nm is shown in Figure 1, indicating an acceptable separation of eight dimers and four trimers. The 8-8(tetrahydrofuran)-DFA was not incorporated into the standard mix (see also Identification of 8-8(Tetrahydrofuran)-DFA in DDGS Samples) because a purified standard compound was not available. Because the concentration range of DFAs and TriFAs in the samples exceeded the ranges validated by Dobberstein and Bunzel,[7] increased concentration ranges of DFA and TriFA standards were analyzed for linear responses and are presented in Table 1. The linearity was validated by inspecting plots of the area on the *y*-axis versus analyte concentration on the *x*-axis, with observed correlation factors

DOI: 10.1021/jf505150g
J. Agric. Food Chem. 2015, 63, 2006−2012

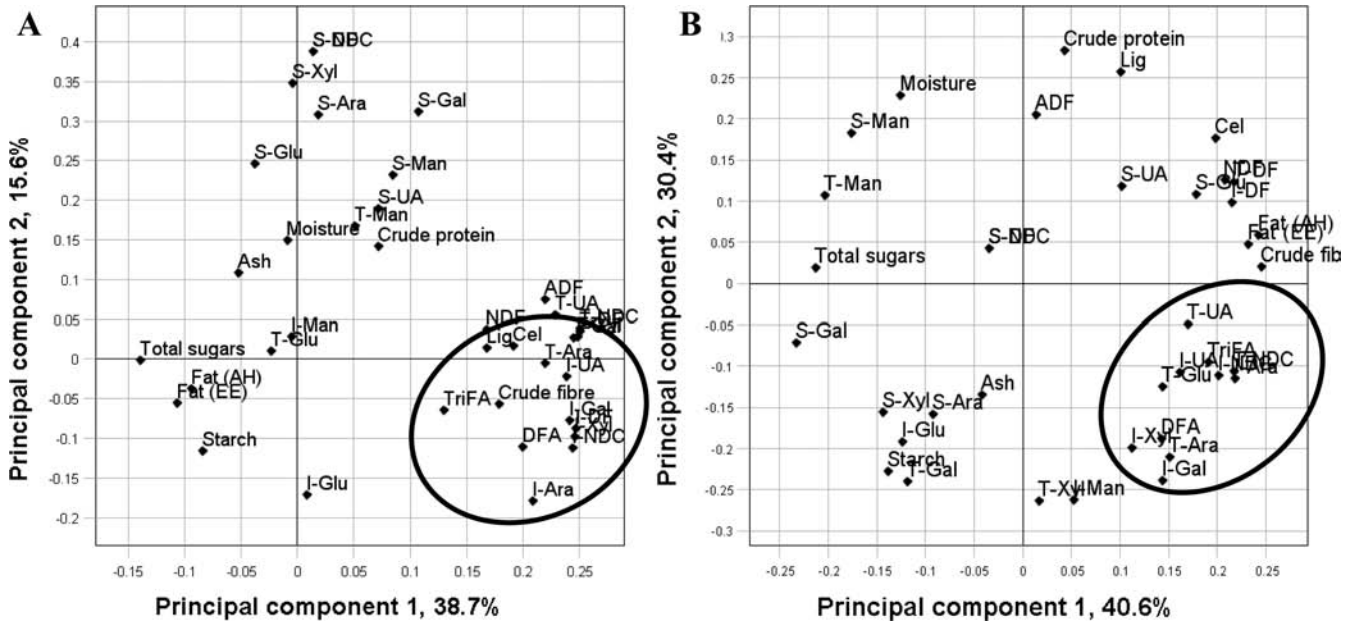

Figure 3. Loading plot of principal component analysis of corn DDGS (A) and wheat and mixed-cereal DDGS (B) constructed by combining DFA and TriFA profiles with additional compositional data from Pedersen et al. as model variables. ADF, acid detergent fiber; AH, acid hydrolysis; Ara, arabinose; Cel, cellulose; DF, dietary fiber; DFA, ferulic acid dehydrodimer; EE, ether extract; Gal, galactose; Glu, NCP-glucose; I, insoluble; Lig, Klason lignin; Man, mannose; NDC, nondigestible carbohydrates; NDF, neutral detergent fiber; S, soluble; T, total; TriFA, ferulic acid dehydrotrimer; Xyl, xylose.

ranging from 0.9839 to 0.9974 for the eight DFAs and TriFAs tested. Visual inspection of the graphs indicated a minor tendency toward curve flattening for the highest concentrations of the 8-5(decarboxylated)-DFA, which may lead to a slight underestimation of this particular dimer. Inspection of the graphs for the remaining DFAs and TriFAs indicated a consistent linear response between area and concentration of analyte measured in the samples.

Variation in Ferulic Acid Dehydrodimer and Dehydrotrimer Profiles in DDGS of Various Origins. A typical chromatogram of the analysis of alkaline extractable DFAs and TriFAs in DDGS is presented in Figure 2, demonstrating the suitability of this chromatographic method for DDGS samples. The results of the DFA and TriFA compositional analysis of the DDGS are listed in Table 2. The eight DFAs and the two TriFAs used to quantify the total content of DFA and TriFA were identified in all three DDGS origins. The dentity of these dimers and trimers was verified by comparison of relative retention times and comparison of the UV spectra with those of the isolated standard compounds. In addition, the 8-*O*-4/8-*O*-4-TriFA and the 8-5/8-*O*-4-TriFA were also identified by comparison to isolated standard compounds. However, because the amounts of these trimers were not sufficient for an appropriate validation, these TriFAs were not quantitated. Corn DDGS contained 5.3 and 5.9 times the content of total alkaline extractable DFAs than in wheat DDGS ($P < 0.001$) and mixed DDGS ($P < 0.001$), respectively. Similarly, the observed contents of total alkaline extractable TriFAs were 5.7 and 6.3 times greater in corn DDGS than in wheat DDGS ($P < 0.001$) and mixed-cereal DDGS ($P < 0.001$), respectively.

For corn DDGS the ∑8-5-DFA coupled dimers comprised the greatest proportion of the total DFA content, whereas for wheat and mixed-cereal DDGS the ∑8-8-DFA and ∑8-5-DFA coupled dimers contributed equally to the total DFA content. In corn DDGS the proportion of the 5-5-DFA was higher than in wheat ($P < 0.001$) and mixed-cereal DDGS ($P < 0.001$). Furthermore, corn DDGS contained a greater proportion for the ∑8-5-DFA coupled dimers than in wheat DDGS ($P = 0.024$). On the other hand, wheat and mixed-cereal DDGS contained a greater proportion of total DFA for the ∑8-8-DFA coupled dimers compared with corn DDGS ($P < 0.001$). No difference between the different DDGS origins was observed in contribution of the 8-*O*-4-DFA ($P = 0.481$) to the total DFA contents.

Independent of DDGS origin, higher amounts of 5-5,8-*O*-4-TriFA than 8-8,8-*O*-4-TriFA were observed. Both the 5-5,8-*O*-4-TriFA and 8-8,8-*O*-4-TriFA proportions were overall significantly different among the three DDGS origins ($P = 0.029$); however, the difference was not strong enough to be significant for pairwise comparisons among origins ($P \geq 0.09$).

The PCA loading plot illustrated with which compositional fractions of the DDGS (for DDGS composition see also Pedersen et al.[2]) the DFA and TriFA shared the highest correlation, presented for corn DDGS (Figure 3A) and wheat and mixed-cereal DDGS (Figure 3B). Both corn DDGS and wheat and mixed-cereal DDGS showed correlation of the total DFAs to the contents of insoluble xylose, insoluble uronic acids, and insoluble galactose. In addition, corn DDGS DFAs correlated to insoluble arabinose, insoluble dietary fiber, and crude fiber, whereas wheat and mixed-cereal DDGS further correlated to the total arabinose content. The TriFAs in corn DDGS correlated to Klason lignin, cellulose, neutral detergent fiber, and crude fiber, whereas the TriFAs in wheat and mixed-cereal DDGS correlated to total and insoluble uronic acids, insoluble arabinose, total and insoluble nondigestible carbohydrates, and cellulose (for principal component 1).

Analyses of corn DDGS samples from five different ethanol plants (P1, $N = 11$; P2, $N = 5$; P3, $N = 5$; P4, $N = 5$; P5, $N = 5$) revealed a greater content of total DFAs for P1 (4030 μg/g DM, $P < 0.001$) compared with P2 (3371 μg/g DM), P3 (3317

DOI: 10.1021/jf505150g
J. Agric. Food Chem. 2015, 63, 2006−2012

Table 3. Composition of Ferulic Acid Dehydrodimers (DFA) and Dehydrotrimers (TriFA) in Corn and Corresponding DDGS

	corn (N = 11)			DDGS (N = 11)			
	mean[a]	range	SD	mean	range	SD	ratio[b]
∑DFA (μg/g DM)	1135b	(976−1419)	140	4030c	(3594−4828)	366	3.6
∑8-8-DFA (% DFA)	18b	(17−19)	1	18b	(17−18)	1	
∑8-5-DFA (% DFA)	37b	(36−38)	1	38b	(36−40)	1	
5-5 (% DFA)	27b	(26−28)	1	26c	(25−27)	0	
8-*O*-4 (% DFA)	18b	(17−18)	0	18[c]	(18−19)	0	
∑TriFA (μg/g DM)	137b	(107−158)	17	504c	(388−651)	83	3.7
5-5,8-O-4 (%TriFA)	70b	(63−76)	4	71b	(62−74)	4	
8-8,8-O-4 (%TriFA)	30b	(24−37)	4	29b	(24−38)	4	

[a]Means in the same row that do not share a letter (b, c) are significantly different at $P < 0.05$. [b]Average corn-to-corn DDGS ratio.

μg/g DM), P4 (3292 μg/g DM), and P5 (3509 μg/g DM). However, the contents of total TriFAs were not different among the ethanol plants with an overall range of 426−504 μg/g DM (P = 0.12). The coefficient of variation (CV) ranged from 0.04 to 0.09 among the plants for the content of total DFAs with highest CVs for P1, whereas CVs of 0.01−0.02 was observed for the total TriFA contents among the ethanol plants.

Variation in Ferulic Acid Dehydrodimer and Dehydrotrimer Profile between Corn and Corresponding DDGS. The DFA and TriFA profiles of corn and corresponding DDGS, sampled simultaneously from the ethanol plant (P1) over a period of 11 months, are presented in Table 3. DDGS had a 3.6-fold increase in total DFA contents along with a 3.7-fold increase in total TriFA contents compared with corn. No difference in the proportions of ∑8-8-DFA (P = 0.773) and ∑8-5-DFA (P = 0.290) of total DFA and of 5-5,8-*O*-4-TriFA (P = 0.719) and 8-8,8-*O*-4-TriFA (P = 0.719) of total TriFAs was observed between corn and corresponding DDGS (Table 3).

DISCUSSION

Saponification with 2 mol/L NaOH at room temperature cleaves ester linkages. Thus, DFAs and TriFAs ester-linked to polymeric cell wall components were analyzed in this study. The applied chromatographic methodology allowed for separation and quantification of eight DFAs and two TriFAs, along with the identification of two additional TriFAs. Validation of the extended analyte concentration ranges (if compared to Dobberstein and Bunzel[7]) indicated that the 8-5(decarboxylated)-DFA might be slightly underestimated compared to the other DFAs. Because the 8-5-DFA, the 8-5(benzofuran)-DFA, and the 8-5(decarboxylated)-DFA presumably have the same precursor in vivo, the results of the 8-5-DFAs were reported as the sum of 8-5-coupled dimers.[6,8] Also, the contents of the 8-8-DFAs were reported as the sum of the 8-8-coupled dimers according to Dobberstein and Bunzel,[7] although it is likely that these three 8-8-DFAs occur as individual DFAs in vivo.[6]

Because only starch is removed during the fermentation process, the nutrient composition of DDGS is expected to partially reflect the composition of the parent grain.[2,16] The higher content of total DFAs and TriFAs observed in corn DDGS compared to wheat DDGS is in line with previous reports of the DFA and TriFA contents in corn and wheat insoluble fiber[7,17,18] and whole grain flours.[8] Also, the observed dominating proportion of the ∑8-5-DFAs (35% of total DFA) in corn DDGS is well in line with previous reports of 39%[8] and 42%[7] in corn, just as the proportion of the 8-*O*-4-DFA (18% of total) in corn DDGS is consistent with previous reports of 18%[8] and 17%[7] in corn. For corn DDGS the proportions of 5-5-DFA (27% of total) and the ∑8-8-DFAs (20% of total) were slightly different from previous reports on corn ranging from 18 to 19% and from 21 to 26% of total DFAs, respectively. For wheat DDGS the observed proportion of the ∑8-5-DFAs (31% of total) was lower than the previous reports of 49%[8] and 44%.[7] On the other hand, the observed proportions of the ∑8-8-DFAs (30% of total) and the 8-*O*-4-DFA (18% of total) in wheat DDGS were roughly comparable to previous reports ranging between 24 and 25% and between 15 and 16%, respectively.[7,8]

The 5-5,8-*O*-4-TriFA was the dominating TriFA in corn DDGS, just as reported for the parent grain.[7,8] Despite being dominant, the proportion of the 5-5,8-*O*-4-TriFA reported here is overestimated because a recent study quantitated five TriFAs in corn,[8] whereas only two were used for quantification in this study. As shown in Figure 2, at least two other trimers were identified in corn DDGS. The same consideration needs to be done for wheat DDGS, as the same study of Jilek and Bunzel[8] indicates an equal proportions of both the 5-5,8-*O*-4-TriFA and the 8-*O*-4,8-*O*-4-TriFA in wheat.

Arabinoxylan consists of a D-xylose backbone joined by β-1,4-linkages substituted with L-arabinose residues along the xylose chain. The arabinose substitution occurs randomly, allowing other substitutes such as D-glucuronic acid, acetyl groups, galactose, and feruloylated arabinose residues to be attached to the xylan backbone.[19] Evidence that DFAs are indeed attached to arabinoxylans has been reported for the 5-5-DFA by use of carbohydrases and mild acidic hydrolysis followed by structural characterization in bamboo and corn bran[20,21] and for the 8-*O*-4-DFA and 8-8-DFA from corn bran insoluble fiber.[22,23] The use of PCA multivariate data analysis based on the combination of DFA and TriFA profiles with compositional data previously reported[2] indicated a clear correlation between DFAs and TriFAs in the DDGS and the content of insoluble arabinoxylan (sum of anhydrous arabinose and xylose), uronic acids, insoluble galactose, and cellulose. In addition to pointing out that DFAs are attached to arabinoxylan as mentioned above, these results logically indicate a similar association for the TriFAs. The observed correlation of DFAs to insoluble galactose is in line with previous studies describing highly complex feruloylated heteroxylan side chains containing up to two galactose residues from corn bran.[24,25] The observed greater content of DFAs in DDGS from P1 is likely related to the higher content of insoluble arabinoxylan in DDGS from P1 than from P2−P5, as reported by Pedersen et al.[2]

The simultaneous sampling of both corn grains and corresponding DDGS over 11 months allowed for investigating

DOI: 10.1021/jf505150g
J. Agric. Food Chem. 2015, 63, 2006−2012

the potential changes in DFA and TriFA profiles after the fermentation and drying process. Although corn grains and DDGS were sampled simultaneously, it should be noted that due to practical challenges the samples did not originate from the same fermentation batch. Furthermore, it should be noted that the results may not be the same for all ethanol plants, emphasized by the variation in DFAs and TriFAs content from the 21 corn DDGS ethanol plants. The 3.6- and 3.7-fold increases in DFA and TriFA contents, respectively, in DDGS are in accordance with the 3.4-fold average increase in nutrients from the same set of samples reported by Pedersen et al.[2] and with previous studies reporting a similar nutrient increase in DDGS compared with the parent grain.[26,27]

Overall, the analysis of corn and DDGS indicated that the individual composition of DFAs and TriFAs is conserved, indicating that DFAs and TriFAs are basically not modified during ethanol fermentation and subsequent drying of DDGS. Previous characterization of NSP profiles of the samples led to the hypothesis that only arabinoxylan from corn endosperm, which comprises only a minor fraction of the total arabinoxylan, was modified during DDGS production.[2] Considering the latter and the fact that corn endosperm arabinoxylan contains markedly less feruloylated cross-linkages compared to corn bran heteroxylan,[28−30] the observed conservation of the DFA and TriFA patterns in corn DDGS is well in line. Because the major fraction of feruloylated arabinoxylan remains unmodified, the remaining arabinoxylan in DDGS is probably more complex than in the parent grain because the readily degradable arabinoxylan was modified during processing.

Large differences in enzymatic degradability were reported for corn- and wheat-based substrates,[31] with a markedly greater degradation potential for wheat than for corn. Furthermore, with regard to enzymatic degradation, corn DDGS[26] and especially corn bran have been described as recalcitrant substrates due to the highly complex structure of the arabinoxylan.[32−34] Especially the DFA and TriFA cross-links are suspected to play a major role in hindering the enzymatic degradation of cereal cell walls.[9−12] Thus, the results from this study on DFA and TriFA contents may indicate a generally higher potential for enzymatic degradation of wheat DDGS compared to corn DDGS. As a consequence of the difference in cell wall complexity, differences in digestibility, microbial fermentation, and resistance to fiber degrading enzymes may be observed when feeding either wheat DDGS or corn DDGS.

The use of DDGS in swine feed has been limited due to a reputation of having variable nutrient composition and protein quality, potentially high content of mycotoxins, and high fiber content. The high fiber content in DDGS is associated with nutritional challenges and negative effect on nutrient digestibility when fed in high quantities. To overcome the negative effects associated with high fiber content, studies have been performed to investigate the effects of adding fiber degrading enzymes to animal diets containing DDGS.[35−37] However, the results are inconclusive.

The results presented in this study may indicate that fiber-degrading enzymes applied for the degradation of DDGS need to be targeted toward highly complex substrates, especially when applied to diets high in corn DDGS.

In conclusion, the current study demonstrated a large variation in the content of DFAs and TriFAs between DDGS of three different origins. Corn DDGS contained 5.3 and 5.7 times greater content of total DFAs and TriFAs, respectively, compared with wheat DDGS. The contents of total DFA and TriFA correlated to the content of insoluble arabinoxylan, uronic acids, insoluble galactose, and cellulose in DDGS. A similar proportional profile of the individual DFAs and TriFAs was observed in both corn and corresponding DDGS, indicating that ferulic acid cross-links in the corn cell wall are presumably not modified during fermentation and DDGS processing. The results presented herein may add to the overall understanding and implication of compositional differences between DDGS sources in relation to animal nutrition and enzyme digestibility.

AUTHOR INFORMATION

Corresponding Author

*(M.B.P.) Phone: +45 8943 5327. E-mail: madsb.pedersen@anis.au.dk.

Funding

This project was partially supported by The Danish Ministry of Science, Innovation and Higher Education.

Notes

The authors declare no competing financial interest.

ACKNOWLEDGMENTS

The following people are acknowledged for their assistance in collecting DDGS samples from different bioethanol plants: M. Chow, D. Ko, A. Riley, D. Ward, G. Jones, C. Miller-Fosmore, and E. Seward.

ABBREVIATIONS USED

ACN, acetonitrile; CV, coefficient of variation; DDGS, distillers' dried grains with solubles; DFA, ferulic acid dehydrodimer; DM, dry matter; HPLC, high-performance liquid chromatography; MeOH, methanol; NSP, nonstarch polysaccharides; PCA, principal component analysis; PDA, photodiode array detector; RP-HPLC, reversed phase HPLC; TriFA, ferulic acid dehydrotrimer; TFA, trifluoroacetic acid; UV, ultraviolet

REFERENCES

(1) Stein, H. H.; Shurson, G. C. Board-invited review: the use and application of distillers dried grains with solubles in swine diets. *J. Anim. Sci.* **2009**, *87*, 1292−303.

(2) Pedersen, M. B.; Dalsgaard, S.; Knudsen, K. E. B.; Yu, S.; Lærke, H. N. Compositional profile and variation of distillers dried grains with solubles from various origins with focus on non-starch polysaccharides. *Anim. Feed Sci. Technol.* **2014**, *197*, 130−141.

(3) Ralph, J.; Grabber, J. H.; Hatfield, R. D. Lignin-ferulate cross-links in grasses: active incorporation of ferulate polysaccharide esters into ryegrass lignins. *Carbohydr. Res.* **1995**, *275*, 167−178.

(4) Bunzel, M.; Ralph, J.; Lu, F.; Hatfield, R. D.; Steinhart, H. Lignins and ferulate-coniferyl alcohol cross-coupling products in cereal grains. *J. Agric. Food Chem.* **2004**, *52*, 6496−6502.

(5) Piber, M.; Koehler, P. Identification of dehydro-ferulic acid-tyrosine in rye and wheat: evidence for a covalent cross-link between arabinoxylans and proteins. *J. Agric. Food Chem.* **2005**, *53*, 5276−5284.

(6) Bunzel, M. Chemistry and occurrence of hydroxycinnamate oligomers. *Phytochem. Rev.* **2010**, *9*, 47−64.

(7) Dobberstein, D.; Bunzel, M. Separation and detection of cell wall-bound ferulic acid dehydrodimers and dehydrotrimers in cereals and other plant materials by reversed phase high-performance liquid chromatography with ultraviolet detection. *J. Agric. Food Chem.* **2010**, *58*, 8927−8935.

(8) Jilek, M. L.; Bunzel, M. Dehydrotriferulic and dehydrodiferulic acid profiles of cereal and pseudocereal flours. *Cereal Chem. J.* **2013**, *90*, 507−514.

DOI: 10.1021/jf505150g
J. Agric. Food Chem. 2015, 63, 2006−2012

(9) Bily, A. C.; Reid, L. M.; Taylor, J. H.; Johnston, D.; Malouin, C.; Burt, A. J.; Bakan, B.; Regnault-Roger, C.; Pauls, K. P.; Arnason, J. T.; Philogène, B. J. R. Dehydrodimers of ferulic acid in maize grain pericarp and aleurone: resistance factors to *Fusarium graminearum*. *Phytopathology* **2003**, *93*, 712−719.
(10) Santiago, R.; Reid, L. M.; Arnason, J. T.; Zhu, X.; Martinez, N.; Malvar, R. A. Phenolics in maize genotypes differing in susceptibility to gibberella stalk rot (*Fusarium graminearum* Schwabe). *J. Agric. Food Chem.* **2007**, *55*, 5186−5193.
(11) Grabber, J. H.; Hatfield, R. D.; Ralph, J. Diferulate cross-links impede the enzymatic degradation of non-lignified maize walls. *J. Sci. Food Agric.* **1998**, *77*, 193−200.
(12) Grabber, J. H.; Ralph, J.; Hatfield, R. D. Ferulate cross-links limit the enzymatic degradation of synthetically lignified primary walls of maize. *J. Agric. Food Chem.* **1998**, *46*, 2609−2614.
(13) Bunzel, M.; Funk, C.; Steinhart, H. Semipreparative isolation of dehydrodiferulic and dehydrotriferulic acids as standard substances from maize bran. *J. Sep. Sci.* **2004**, *27*, 1080−1086.
(14) Schatz, P. F.; Ralph, J.; Lu, F.; Guzei, I. A.; Bunzel, M. Synthesis and identification of 2,5-bis-(4-hydroxy-3-methoxyphenyl)-tetrahydrofuran-3,4-dicarboxylic acid, an unanticipated ferulate 8-8-coupling product acylating cereal plant cell walls. *Org. Biomol. Chem.* **2006**, *4*, 2801−2806.
(15) Shewry, P. R.; Hawkesford, M. J.; Piironen, V.; Lampi, A.-M.; Gebruers, K.; Boros, D.; Andersson, A. A. M.; Åman, P.; Rakszegi, M.; Bedo, Z.; Ward, J. L. Natural variation in grain composition of wheat and related cereals. *J. Agric. Food Chem.* **2013**, *61*, 8295−8303.
(16) Widyaratne, G. P.; Zijlstra, R. T. Nutritional value of wheat and corn distiller's dried grain with solubles: digestibility and digestible contents of energy, amino acids and phosphorus, nutrient excretion and growth performance of grower-finisher pigs. *Can. J. Anim. Sci.* **2007**, *87*, 103−114.
(17) Renger, A.; Steinhart, H. Ferulic acid dehydrodimers as structural elements in cereal dietary fibre. *Eur. Food Res. Technol.* **2000**, *211*, 422−428.
(18) Bunzel, M.; Ralph, J.; Marita, J. M.; Hatfield, R. D.; Steinhart, H. Diferulates as structural components in soluble and insoluble cereal dietary fibre. *J. Sci. Food Agric.* **2001**, *81*, 653−660.
(19) Izydorczyk, M. S.; Biliaderis, C. G. Cereal arabinoxylans: advances in structure and physicochemical properties. *Carbohydr. Polym.* **1995**, *28*, 33−48.
(20) Ishii, T. Isolation and characterization of a diferuloyl arabinoxylan hexasaccharide from bamboo shoot cell-walls. *Carbohydr. Res.* **1991**, *219*, 15−22.
(21) Saulnier, L.; Crépeau, M.-J.; Lahaye, M.; Thibault, J.-F.; Garcia-Conesa, M. T.; Kroon, P. A.; Williamson, G. Isolation and structural determination of two 5,5′-diferuloyl oligosaccharides indicate that maize heteroxylans are covalently cross-linked by oxidatively coupled ferulates. *Carbohydr. Res.* **1999**, *320*, 82−92.
(22) Allerdings, E.; Ralph, J.; Schatz, P. F.; Gniechwitz, D.; Steinhart, H.; Bunzel, M. Isolation and structural identification of diarabinosyl 8-O-4-dehydrodiferulate from maize bran insoluble fibre. *Phytochemistry* **2005**, *66*, 113−124.
(23) Bunzel, M.; Allerdings, E.; Ralph, J.; Steinhart, H. Cross-linking of arabinoxylans via 8-8-coupled diferulates as demonstrated by isolation and identification of diarabinosyl 8-8(cyclic)-dehydrodiferulate from maize bran. *J. Cereal Sci.* **2008**, *47*, 29−40.
(24) Allerdings, E.; Ralph, J.; Steinhart, H.; Bunzel, M. Isolation and structural identification of complex feruloylated heteroxylan side-chains from maize bran. *Phytochemistry* **2006**, *67*, 1276−1286.
(25) Saulnier, L.; Vigouroux, J.; Thibault, J.-F. Isolation and partial characterization of feruloylated oligosaccharides from maize bran. *Carbohydr. Res.* **1995**, *272*, 241−253.
(26) de Vries, S.; Pustjens, A. M.; Kabel, M. A.; Salazar-Villanea, S.; Hendriks, W. H.; Gerrits, W. J. J. Processing technologies and cell wall degrading enzymes to improve nutritional value of dried distillers grain with solubles for animal feed: an in vitro digestion study. *J. Agric. Food Chem.* **2013**, *61*, 8821−8828.
(27) Urriola, P. E.; Shurson, G. C.; Stein, H. H. Digestibility of dietary fiber in distillers coproducts fed to growing pigs. *J. Anim. Sci.* **2010**, *88*, 2373−2381.
(28) Bunzel, M.; Ralph, J.; Brüning, P.; Steinhart, H. Structural identification of dehydrotriferulic and dehydrotetraferulic acids isolated from insoluble maize bran fiber. *J. Agric. Food Chem.* **2006**, *54*, 6409−6418.
(29) Gallardo, C.; Jiménez, L.; García-Conesa, M. T. Hydroxycinnamic acid composition and in vitro antioxidant activity of selected grain fractions. *Food Chem.* **2006**, *99*, 455−463.
(30) Saulnier, L.; Thibault, J.-F. Ferulic acid and diferulic acids as components of sugar-beet pectins and maize bran heteroxylans. *J. Sci. Food Agric.* **1999**, *79*, 396−402.
(31) Rose, D.; Inglett, G. A method for the determination of soluble arabinoxylan released from insoluble substrates by xylanases. *Food Anal. Methods* **2011**, *4*, 66−72.
(32) Agger, J.; Vikso-Nielsen, A.; Meyer, A. S. Enzymatic xylose release from pretreated corn bran arabinoxylan: differential effects of deacetylation and deferuloylation on insoluble and soluble substrate fractions. *J. Agric. Food Chem.* **2010**, *58*, 6141−6148.
(33) Faulds, C. B.; Kroon, P. A.; Saulnier, L.; Thibault, J.-F.; Williamson, G. Release of ferulic acid from maize bran and derived oligosaccharides by *Aspergillus niger* esterases. *Carbohydr. Polym.* **1995**, *27*, 187−190.
(34) Saulnier, L.; Marot, C.; Elgorriaga, M.; Bonnin, E.; Thibault, J. F. Thermal and enzymatic treatments for the release of free ferulic acid from maize bran. *Carbohydr. Polym.* **2001**, *45*, 269−275.
(35) Anderson, P. V.; Kerr, B. J.; Weber, T. E.; Ziemer, C. J.; Shurson, G. C. Determination and prediction of digestible and metabolizable energy from chemical analysis of corn coproducts fed to finishing pigs. *J. Anim. Sci.* **2012**, *90*, 1242−1254.
(36) Pedersen, C.; Boersma, M. G.; Stein, H. H. Digestibility of energy and phosphorus in ten samples of distillers dried grains with solubles fed to growing pigs. *J. Anim. Sci.* **2007**, *85*, 1168−1176.
(37) Stein, H. H.; Gibson, M. L.; Pedersen, C.; Boersma, M. G. Amino acid and energy digestibility in ten samples of distillers dried grain with solubles fed to growing pigs. *J. Anim. Sci.* **2006**, *84*, 853−860.

DOI: 10.1021/jf505150g
J. Agric. Food Chem. 2015, 63, 2006−2012

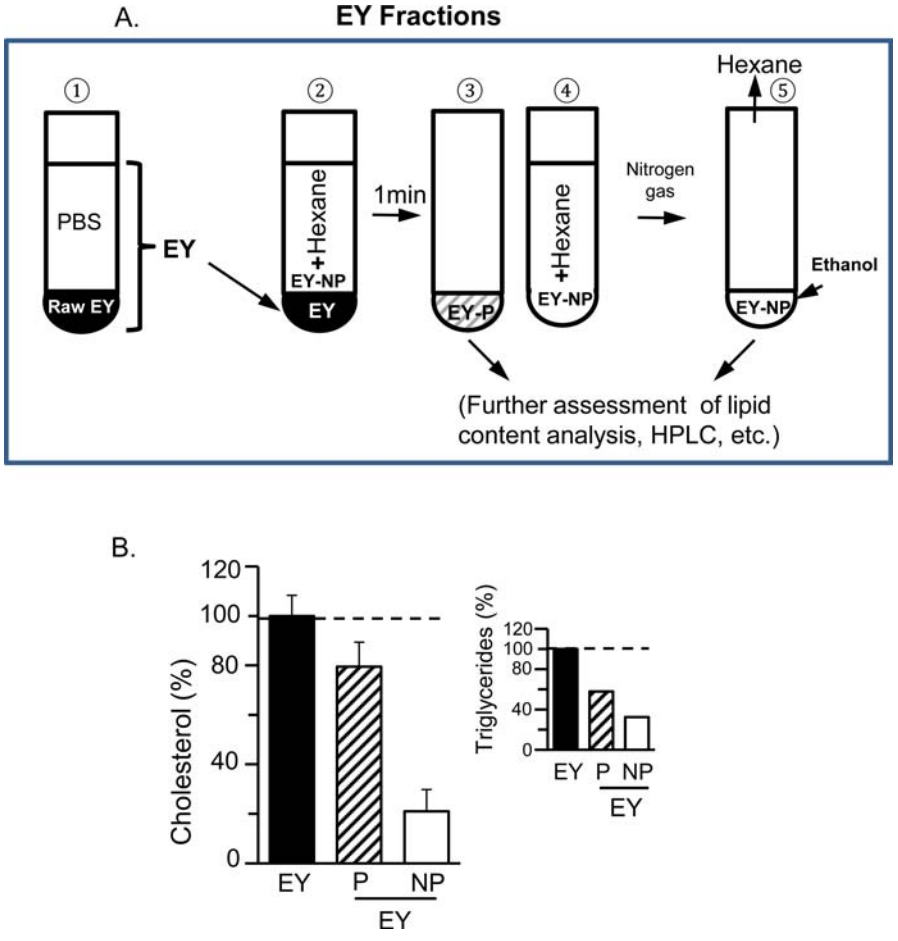

Figure 1. Delipidation of EY with hexane extraction moderately reduces its cholesterol and triglyceride content. (A) Schematic of EY extraction procedure. EY (~15 mL) was diluted with PBS to obtain 50 mL of whole EY solution (no. 1 tube). Then 1 mL of EY (black area in no. 2 tube) was extracted with hexane in a 10 mL glass tube. The remaining 1 mL fraction was termed polar "EY-P" (hatched area in no. 3 tube). Hexane phase was collected to another glass tube (no. 4 tube), evaporated by nitrogen gas, and then reconstituted in 1 mL of ethanol. This phase was termed nonpolar "EY-NP" (white area in no. 5 tube). For analysis of fatty acids and vitamins, EY-P fraction was additionally extracted as described in methods. (B) Cholesterol content in EY (black bars), EY-P (hatched bars), and EY-NP (white bars) fractions was measured in EY. Here and throughout study, we used EY obtained from different suppliers. Data (n = 5, mean ± SD) are shown as percent of esterified and nonesterified cholesterol in EY fractions (100%, dashed line). (B, low insert) Triglyceride content is shown as % of EY content (100%, n = 3, dashed line).

production and other mechanisms.[21−23] Vitamin E and polyphenols have been shown to inhibit NF-κB activation by disabling signaling cascades, counteracting ROS production as antioxidants, and through activation of redox-active transcription factors, e.g., nuclear factor (erythroid-derived 2)-like 2 (NRF2).[22]

Many dietary products have complex bioactive macro- and micronutrient composition. Recent research highlighted the anti-inflammatory[24] and pain-reducing[25] properties of egg yolk (EY). These effects have been attributed to specific lipid-soluble extracts[25] and water-soluble proteins.[24] EY contains an unique combination of vitamins A, D, E, carotenoids such as lutein and zeaxanthin, and phospholipids that can potentially diminish inflammation and oxidative stress.[26] However, the EY also contains cholesterol and fatty acids that can contribute to pro-inflammatory pathways.[27] The role of EY composition on the regulation of NF-κB has not been investigated. In this paper, we show that partial delipidation of the EY without changes to the EY's carotenoid/vitamin content, is sufficient to markedly reduce the activation of NF-κB and its target cytokines.

MATERIALS AND METHODS

Reagents and Supplies. We purchased reagents for cell culture from Invitrogen (Carlsbad, CA). Other reagents were acquired from Sigma-Aldrich (St. Louis, MO) unless otherwise indicated. Vectors were purchased: Cignal Lenti NFκB Reporter (GFP) Kit from SABiociences/Qiagen (Valencia, CA), mCherry constitutive expression vector from Genecopoeia (Rockville, MD). We bought four types of regular eggs from Sauder's egg (EY1), Kroger medium egg (EY2), Kroger large egg (EY3), and EggLand's Best egg (EY4). Cholesterol was purchased from MP Biomedicals (Santa Ana, CA).

EY Extraction. First, 15 mL of whole EY was diluted in 35 mL of phosphate buffered saline (PBS) (1:3.33, v/v). This solution was termed "EY". Hexane (4 mL) was added to 1 mL of EY and inverted vigorously by hand for 1 min. The hexane phase was removed and dried under nitrogen and then resuspended in 1 mL ethanol. The hexane extract of the EY was termed "Nonpolar, (EY-NP)" and the remaining phase was "Polar, (EY-P)" (Figure 1A). These EY, EY-NP, and EY-P extracts were used for cholesterol/cholesteryl ester quantification, triglyceride quantification, gas chromatography, high performance liquid chromatography (HPLC), and cell stimulation.

Cell Culture Studies. *Nfkb*-RE/GFP cell line was derived from murine 3T3-L1 preadipocyte clone stably transfected with lentiviral *Nfkb*-RE GFP reporter construct and control mCherry overexpression construct as described.[28] The *Nfkb*-RE/GFP cell line derivation

DOI: 10.1021/jf5056584
J. Agric. Food Chem. 2015, 63, 2013−2025

procedure and its characterization in the presence of pro- and anti-inflammatory mediators was described before.[28] *Nfkb*-RE/GFP cells were cultured in standard culture medium (high glucose DMEM containing 10% CS and 1% penicillin−streptomycin). Similar to the parent 3T3-L1 cell line, *Nfkb*-RE/GFP preadipocytes were capable of differentiation.[28] Differentiation was induced (day 0) in confluent preadipocytes using differentiation media I (DMI) containing 3-isobutyl-1-methylxanthine (0.5 mM), dexamethasone (1 μM), insulin (1.7 μM), 10% fetal bovine serum (FBS), and 1% penicillin−streptomycin in DMEM. Differentiation media II (DMII) contained 10% FBS, insulin (1.7 μM), and 1% penicillin−streptomycin in DMEM. Every 48 h post adipogenesis induction, cell media was replaced with DMII using standard protocol.[29] Prior to measuring fluorescence, cells were washed twice with PBS and lysed with an appropriate volume (i.e., 120 μL/well for 24-well plate, 150 μL/P60 dish) of RIPA buffer (Boston BioProducts, Ashland, MA) containing complete protease inhibitors (Roche Diagnostics Corporation, Indianapolis, IN). Cells were incubated on ice for 15 min, and then the plate was scratched using a tip to lyse residual cells. Cell lysate (80 μL/well) was transferred to a black 96-well plate (Fisher Scientific Company, Hanover, IL) to measure fluorescence at wavelengths Ex/Em 485/528 for GFP and then, at Ex/Em 587/640 for mCherry using Synergy H1 hybrid multimode microplate reader (BioTek, Winooski, VT). *Nfkb*-RE activation was calculated as ratio of GFP to mCherry control fluorescence (GFP/mCherry), or GFP/protein if mCherry fluorescence was below the detection limit. 3T3-L1 preadipocytes were cultured and differentiated under the same conditions as *Nfkb*-RE/GFP preadipocytes.

mRNA Analyses. The quantitative analysis of mRNA was performed using the nCounter mouse inflammation expression V2 Panel Kit (NanoString Technologies, Seattle, WA). NanoString's nCounter technology is based on direct detection of target molecules using color-coded molecular barcodes, providing a digital simultaneous quantification of the number of target molecules.[29] All data was normalized to six housekeeping genes quantified in the same samples. Total mRNA (100 ng in 5 μL) was hybridized overnight with nCounter Reporter (20 μL) probes in hybridization buffer and in excess of nCounter Capture probes (5 μL) at 65 °C for 16−20 h. The hybridization mixture containing target/probe complexes was allowed to bind to magnetic beads containing complementary sequences on the capture probe. After each target found a probe pair, excess probes were washed followed by a sequential binding to sequences on the reporter probe. Biotinylated capture probe-bound samples were immobilized and recovered on a streptavidin-coated cartridge. The abundance of specific target molecules was then quantified using the nCounter digital analyzer. Individual fluorescent barcodes and target molecules present in each sample were recorded with a CCD camera by performing a high-density scan (600 fields of view). Images were processed internally into a digital format and were normalized using the NanoString nSolver software analysis tool. Counts were normalized for all target RNAs in all samples based on the positive control RNA to account for differences in hybridization efficiency and posthybridization processing, including purification and immobilization of complexes. The average was normalized by background counts for each sample obtained from the average of the eight negative control counts. Subsequently, a normalization of mRNA content was performed based on six internal reference housekeeping genes *Cltc*, *Gapdh*, *Gusb*, *Hprt1*, *Pgk1*, and *Tubb* using nSolver Software (NanoString Technologies, Seattle, WA).

Protein Assay of Cell Lysates. The protein content was measured using a BCA kit (Thermo Fisher Scientific, Rockford, IL). The absorbance (562 nm) was measured using the Synergy H1 hybrid multimode microplate reader.

Lipid Content Analysis of EY Fractions. The EY, EY-P, and EY-NP fractions were prepared by hexane extract procedure as described above. To enable enzymatic reaction, EY-NP fraction was resuspended in 200 μL of chloroform and 300 μL of cholesterol assay buffer (from the Cholesterol Quantitation Kit) instead of 1 mL of ethanol. The suspension was mixed well by tapping and then sonicated to evaporate chloroform. Then 10 μL of EY-NP from this stock (in 300 μL cholesterol assay buffer) was diluted with DI water (to 33 μL) to achieve an original concentration in 1 mL EY. All EY fractions were then diluted in cholesterol assay buffer according to manufacturer's instruction and L-Type Triglyceride M Kit (Wako Diagnostics, Richmond, VA) was performed. The absorbance (650 nm) was measured using the Synergy H1 hybrid multimode microplate reader.

Cholesterol Enzymatic Kit (Wako Diagnostics) was performed according to the manufacturer's description. The absorbance (600 nm) was measured using the Synergy H1 hybrid multimode microplate reader.

For the cholesterol ester analysis, the EY and EY-NP fractions were prepared by hexane extract procedure as described above; however, EY-NP fraction was resuspended in 200 μL of cholesterol assay buffer (NP). Then 0.3 μL of EY, 0.5 μL of EY-P, and 10 μL of EY-NP were diluted with cholesterol assay buffer (total volume 50 μL). The cholesterol Quantification Kit was performed according to the manufacturer's description. The absorbance (570 nm) was measured using the Synergy H1 hybrid multimode microplate reader.

Fatty Acid Analysis. Total lipids were extracted from all EY fractions with 2:1 (v/v) chloroform:methanol and washed with 0.88% KCl.[30] Fatty acid methyl esters were prepared using 5% hydrochloric acid in methanol at 76 °C.[31] Analysis of fatty acid methyl esters was completed by gas chromatography with columns and conditions as previously described.[32] Retention times were compared to standards (Matreya, LLC, Pleasant Gap, PA, Supelco, Bellefonte, PA, and Nu-Check Prep Inc., Elysian, MN) and fatty acids were reported as percent of total identified fatty acids.

HPLC−Tandem Mass Spectrometry Analysis (HPLC/MS/MS). Prior to analysis, EY-P fractions were further extracted using hexane/ethanol/acetone/toluene (10:6:7:7, v/v/v/v, termed HEAT).[33] The EY-NP extracts and HEAT-extracted EY-P fractions were injected on a YMC C30 column (4.6 mm × 150 mm, 5um, Waters Corp.) and separated with a gradient solution 1 (80/18/2 MeOH/water/2% ammonium acetate) and solution 2 (78/20/2 MtBE/MeOH/2% ammonium acetate at 1.8 mL/min and 40 °C. Diode array spectra were collected with an Agilent 1260 diode-array detector with 60 mm path length flow cell (Agilent Technologies). Eluent was introduced to a QTrap 5500 (ABSciex, Concord, Canada) mass spectrometer via an atmospheric pressure chemical ionization (APCI) probe operated in positive ion mode. Multiple reaction monitoring (MRM) MS/MS transitions were used to detect vitamins and carotenoids. Lutein/zeaxanthin and retinol were quantified based on external standards.

Statistical Analysis. Data was shown as mean ± SD based on 3−4 independent experiments. Statistical comparison of groups was examined by both Student's *t* test and Mann−Whitney U test. Correlation analysis was performed using Pearson test. $P < 0.05$ was considered statistically significant.

RESULTS

Hexane Extraction Procedure Moderately Reduces Cholesterol and Triglycerides in EY Content. EY contains many lipophilic compounds that can potentially promote and suppress inflammation.[26,27] To assess how lipophilic compounds influence properties of whole EY, we performed a hexane extraction procedure on the EY (Figure 1A) and characterized the composition of the nonpolar (EY-NP) and polar (EY-P) fractions. To account for variability related to egg production, we performed experiments using EY obtained from four different suppliers. Due to the high level of amphipathic phospholipids in EY, the hexane extraction removed approximately 20% of total cholesterol from EY (100%) (Figure 1B). EY contained 65% free cholesterol (43% in EY-P and 22% in EY-NP fractions) and 35% cholesteryl ester (27% in EY-P and 8% in EY-NP fractions). Hexane extraction also removed 30% of triglycerides that were found in the EY (100%) (Figure 1B, insert). Thus, the majority of cholesterol was retained in the

DOI: 10.1021/jf5056584
J. Agric. Food Chem. 2015, 63, 2013−2025

EY-P fraction, while the EY-NP fraction contained only 20−30% of cholesterol and triglycerides content from the EY.

EY-P and EY-NP Fractions Have Similar Composition of Major Fatty Acids. Next we compared the composition of fatty acids in the EY, EY-P, and EY-NP fractions after their hydrolysis from complex lipids. The major fatty acids in all fractions were saturated palmitic (16:0), monounsaturated oleic (18:1), and polyunsaturated omega 6 linoleic (18:2) acids that comprised approximately 27%, 37%, and 19% of all fatty acids, in the EY, EY-P, or EY-NP fractions (Figure 2A−C). We found significant, but minor differences between different fractions (less than 2% compared to total fatty acid content) in the less abundant saturated (18:0, 14:0, 20:0), monounsaturated (16:1n7), and polyunsaturated (22:5n3) fatty acids. In the EY-P fraction, 22:5n3 was less than in EY (Figure 2D), while the content of saturated (18:0, 14:0) and monounsatured (16:1n7) fatty acids was greater in EY-P compared to EY-NP fractions. Overall, the relative composition of fatty acids was similar among the EY, EY-P, and EY-NP fractions.

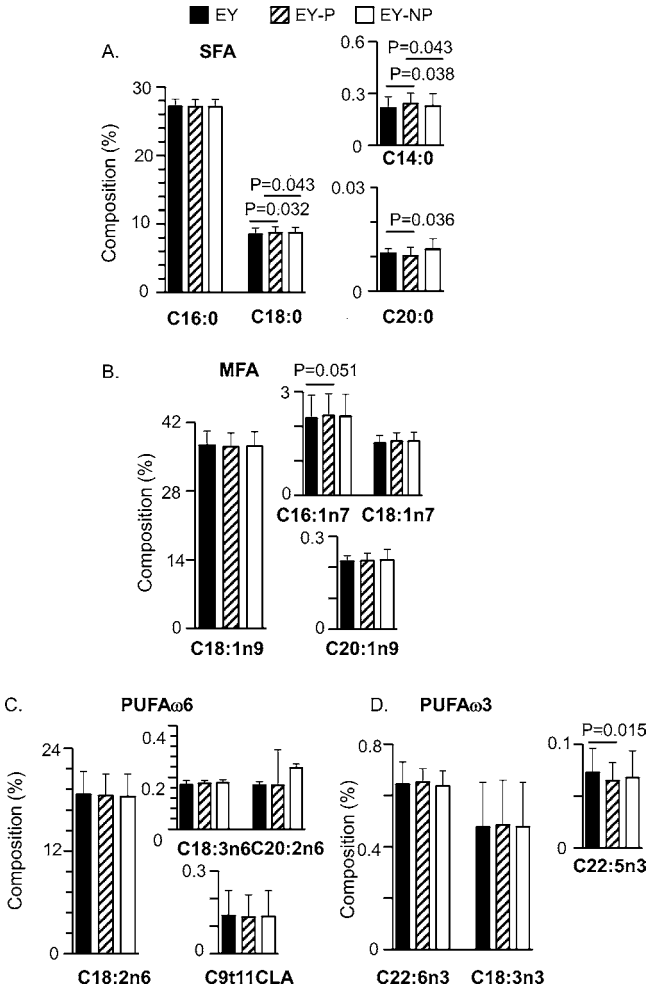

Figure 2. Low variability in fatty acid composition across EY fractions from different suppliers. Fatty acid composition was measured in EY (black bars), EY-P (hatched bars), and EY-NP (white bars) fractions (n = 4). Data are shown as mean ± SD % of distribution in whole FA in each fraction. P values were determined using Mann−Whitney U test. (A) Saturated fatty acids: C16:0, palmitic acid; C18:0, stearic acid. (A, upper insert) C14:0, myristic acid. (A, lower insert) C20:0, arachidic acid. (B) Monounsaturated fatty acids: vaccenic acid; C18:1n9, (B, upper insert) C16:1n7, palmitoleic acid; C18:1n7, oleic acid. (B, lower insert) C20:1n9, cetoleic acid. (C) Polyunsaturated ω6 fatty acids: C18:2n6, linoleic acid. (C, upper insert) C18:3n6, gamma linoleic acid; C20:2n6, eicosadienoic acid. (C, lower insert) Conjugated linoleic acid, C9t11CLA. (D) Polyunsaturated ω3 fatty acids: C22:6n3, docosahexaenoic acid; C18:3n3, alpha linolenic acid; (D, upper insert) C22:5n3, docosapentaenoic acid.

Lipophilic Vitamins and Carotenoids Were Retained Exclusively in EY-P Fraction. Simultaneous determination of vitamins E (α-tocopherol), D (D3), A (retinol and retinyl esters), and carotenoids (free and esterified lutein and zeaxanthin esters) was performed using HPLC/MS/MS. Carotenoids and retinol were quantified based on external standards. No detectable levels of lipophilic vitamins and carotenoids were found in the EY-NP fraction (Figure 3). All lipid soluble vitamins and carotenoids were found in the EY-P fraction, probably due to their interaction with phospholipids. The amounts of lutein and zeaxanthin were the most variable (∼25%) among the EY-P fractions from different EY suppliers (Figure 3A). The variability of retinol content in EY was less than 6% (Figure 3B). Vitamins E and D3 were not quantified but were detected in the EY-P fractions from all suppliers (Figure 3C). Thus, the EY-P fraction contained all lipophilic vitamins and carotenoids from the EY.

In summary: The EY-NP fraction contained 20−30% of cholesterol and triglycerides compared to EY (100%). The EY-P fraction contained 70−80% of cholesterol and triglycerides and all of the lipophilic vitamins and carotenoids seen in EY (100%).

EY-P Fraction Inhibits NF-κB Pathway in Adipocytes. *1. EY-P Fraction Inhibits the Activation of NF-κB and Its Target Genes in Adipocytes.* To assess whether similar composition of the EY and EY-P fractions exerted comparable activation of NF-κB, we performed reporter assays in the 3T3-L1-*Nfκb*-RE preadipocyte cell line. This reporter cell line was previously validated using both pro-inflammatory agents and anti-inflammatory antioxidants.[28] We compared *Nfκb*-RE activation in adipocytes stimulated with the EY, EY-P, and EY-NP fractions. Although both the EY and EY-P fractions contained carotenoids and vitamins, *Nfκb*-RE activation was suppressed only in adipocytes stimulated with the EY-P fractions. Compared to *Nfκb*-RE activation in nontreated adipocytes, stimulation with EY increased *Nfκb*-RE activation to 126%. In contrast, the EY-P fraction from the same EYs reduced *Nfκb*-RE activation (40%) compared to control adipocytes (Figure 4A). The suppression of *Nfκb*-RE activation by the EY-P fraction was seen in eggs from different suppliers. The variability of response to the EY, EY-P, and EY-NP fractions from EY obtained from different suppliers reached 33%, 20%, and 30%, respectively (data not shown). The suppression of *Nfκb*-RE activation by EY-P fraction occurs in a concentration-dependent manner (Figure 4B).

The inhibitory effect EY-P fraction on NF-κB target genes was further examined in the classical preadipocyte 3T3-L1 cell line. We stimulated differentiated 3T3-L1 preadipocytes with the EY, EY-P, and EY-NP. Then we simultaneously quantified expression of multiple genes in these cells. First, we analyzed the expression of classical NF-κB target genes such as MCP1 (CCL2). MCP1 was the most abundantly expressed cytokine in 3T3-L1 adipocytes followed by MCP3 (CCL7) and MCP2 (CCL8) (Figure 4C). In spite of differences in basal expression, all *Mcp* genes were markedly suppressed by the EY-P fraction. EY-P inhibited expression of *Mcp1* by 59% (Figure 4D), *Mcp2* by 61% (Figure 4E), and *Mcp3* by 49% (Figure 4F) compared

DOI: 10.1021/jf5056584
J. Agric. Food Chem. 2015, 63, 2013−2025

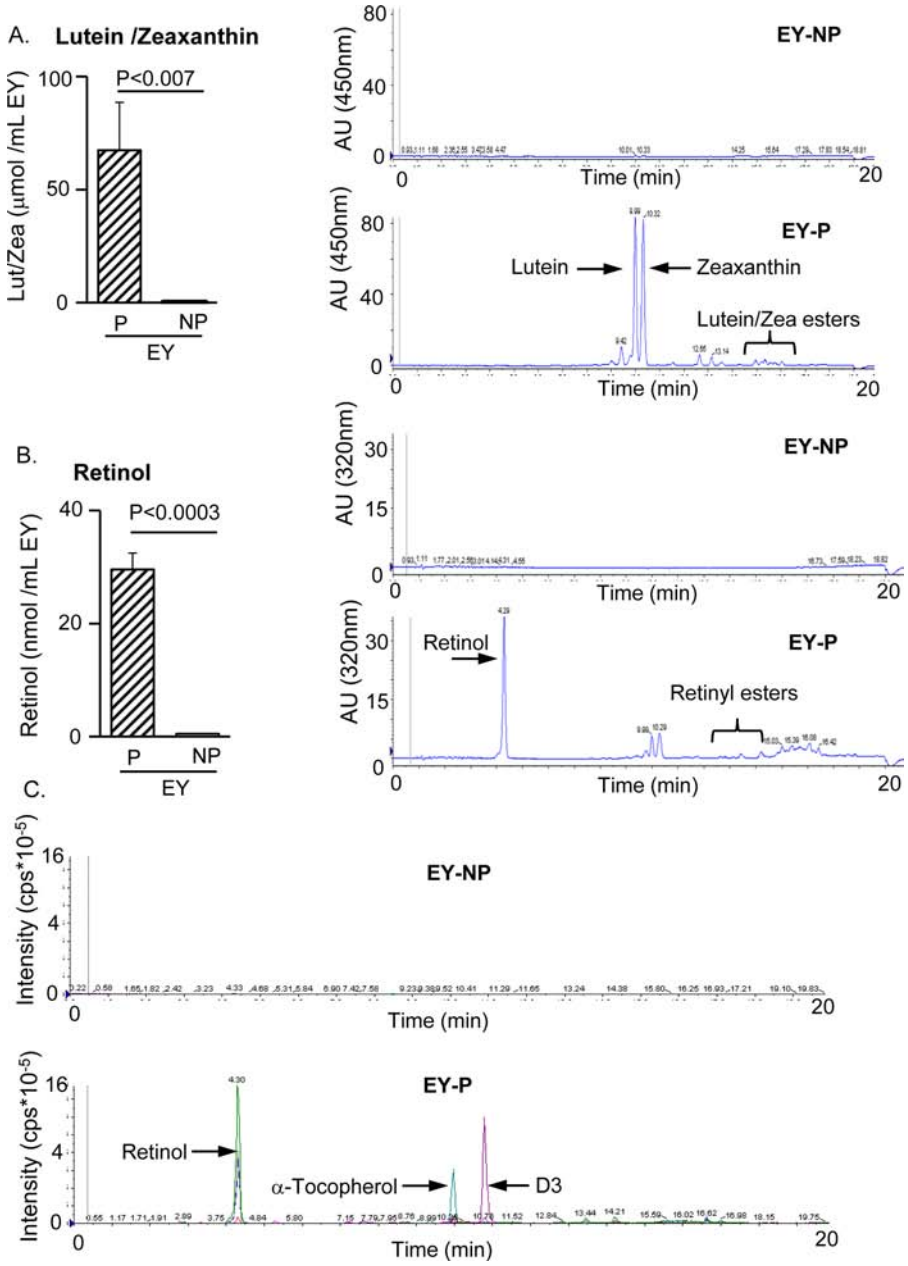

Figure 3. Vitamin and carotenoids are present in EY-P and absent in EY-NP fractions after hexane extraction. Same EY fractions (n = 4) that were examined for fatty acid composition (Figure 2) were analyzed for vitamin and carotenoids content using HPLC/MS/MS. (A) Concentrations of lutein/zeaxanthin in EY-P and EY-NP fractions. Inserts show one representative chromatogram for EY-NP (upper) and EY-P (lower) fractions. (B) Concentrations of retinol in EY-P and EY-NP fractions. Inserts show one representative chromatogram for EY-NP (upper) and EY-P (lower) fractions. (C) Representative chromatograms of EY-NP (upper insert) and EY-P (lower insert) fractions showed absence vitamins A, E, and D in EY-NP fraction.

to nonstimulated adipocytes. The EY and EY-NP fractions did not significantly influence expression of these genes.

We also explored the specificity of cytokine production in response to the EY fractions. All INFs (*Infa1*, 7 ± 3; *Infb1*, 51 ± 6; *Infg*, 7 ± 3 AU) were expressed at low levels in 3T3-L1 adipocytes. The EY fractions did not significantly influence expression of all *Infs* (data not shown). *Cxcl5* and *Cxcl1* cytokines are coregulated by NF-κB and STAT1 transcription factors,[3,14] whereas mitogene-inducible gene (Mig), interferon gamma-induced protein 10 (Ip10), and Rantes are coregulated by NF-κB, STAT1, and IRF transcription factors[11,34−37] (Figure 5A). Stimulation of 3T3-L1 adipocytes with the EY-P fraction markedly decreased expression of *Cxcl5* (Figure 5B) and *Cxcl1* (Figure 5C) to 9% and 22%, respectively, compared to nontreated control adipocytes. In contrast, all EY, EY-P and EY-NP fractions lead to a modest (less than 40%) reduction in expression of *Ip10* (Figure 5D), *Mig* (data not shown), or *Rantes* (Figure 5E) compared to the control. The reduction of *Ip10* and *Mig* expression was only significant in adipocytes stimulated with the EY-P fraction and *Rantes* only with the EY fraction compared to control adipocytes. None of the EY fractions significantly influenced the expression of other *Ccl* cytokines, *Tnfa*, and *Il6* (data not shown). Given that the EY-P fraction led to the most potent (10-fold) reduction in the expression of *Cxcl5*, which was known to be regulated by both STAT1 and NF-κB,[3,14,38] we also analyzed the expression of

DOI: 10.1021/jf5056584
J. Agric. Food Chem. 2015, 63, 2013−2025

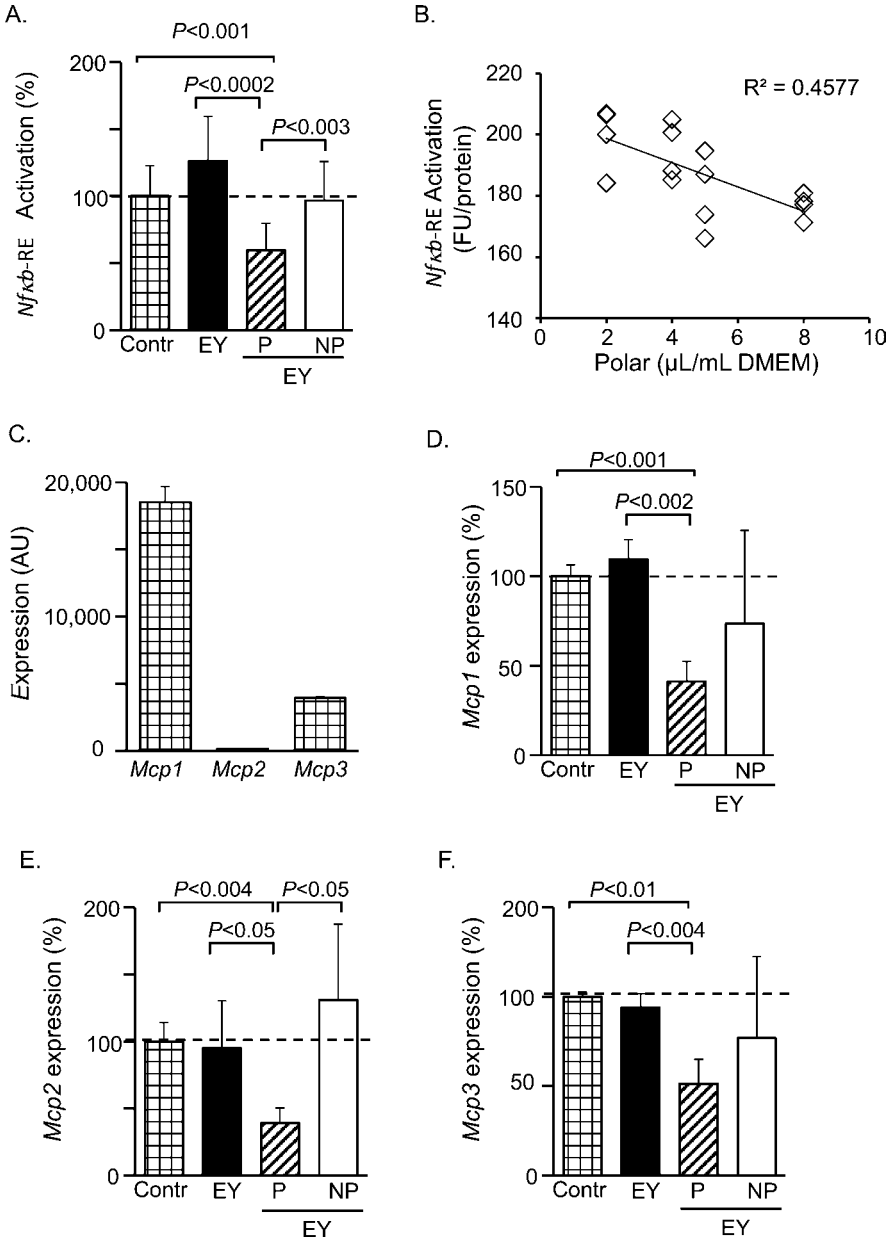

Figure 4. EY-P fractions inhibit NF-κB activity in *Nfκb*-RE/GFP and 3T3-L1 adipocytes. (A) *Nfκb*-RE/GFP preadipocytes were differentiated after 3 days and stimulated with identical concentrations of EY (black bar), EY-P (hatched bar), and EY-NP (white bar) EY fractions (5 μL EY fraction/mL DMII) for 24 h. Control, *Nfκb*-RE/GFP cells were maintained in DMII (Contr, gridded bar). Data is shown as mean ± SD, $n = 12$ for Control and EY or $n = 11$ for EY-P and EY-NP treated cells. The fluorescence/protein ratio was obtained from total cell lysates in RIPA buffer. Data are shown as a % of control fluorescence/protein ratio (100%, dashed line). (B) *Nfκb*-RE/GFP preadipocytes were differentiated for 3 days and stimulated with 2, 4, 5, and 8 μL EY-P/mL DMII. Data are shown as mean ± SD of fluorescence/protein ratio ($n = 4$). Correlation was examined by Pearson test, groups were compared using Mann−Whitney U test. (C) 3T3-L1 preadipocytes were differentiated for 4 days. The expression of *Mcp* gene family was measured using the nCounter data analysis system from NanoString Technologies. *Mcp* expression in 3T3-L1 adipocytes are shown as mean ± SD ($n = 3$). (D−F) 3T3-L1 preadipocytes were differentiated for 3 days and stimulated with EY (black bar), EY-P (hatched bar), and EY-NP (white bar) fractions (5 μL EY fraction/mL DMII) for 24 h. The expression of *Mcp1*, *Mcp2*, and *Mcp3* was shown as % of expression compared to in control adipocytes (gridded bar, 100%, dashed line) (mean ± SD, $n = 3$). Significance was examined using Mann−Whitney U test.

Stat1. We found a 10-fold reduction of *Stat1* expression in the presence of EY-P in adipocytes (Figure 5F). Thus, in spite of similar content of lipophilic vitamins in the EY-P and EY fractions, EY-P inhibited the activation of *Nfκb*-RE and expression of NF-κB target genes and *Stat1*, whereas EY and EY-NP exerted a similar level of NF-κB activation as nontreated adipocytes. The expression of genes that regulated apoptosis, such as *Bcl2l1* and *Fasl*, was not different in control compared to treated cells (Data are not shown).

2. Inhibition of NF-κB Activation by EY-P Fraction Is Associated with Selective Regulation of Tlr Receptors and Their Inhibitor Proteins. Among nine *Tlr* receptors, *Tlr2* was the most abundantly expressed receptor in 3T3-L1 adipocytes followed by *Tlr3* and *Tlr4* (Figure 6A). *Tlr2* expression was similar in nontreated adipocytes and adipocytes treated with EY-NP fraction (Figure 6B). EY moderately reduced expression of *Tlr2* (to 75%), whereas the EY-P fraction decreased *Tlr2* expression to 31% compared to control adipocytes. The

DOI: 10.1021/jf5056584
J. Agric. Food Chem. 2015, 63, 2013−2025

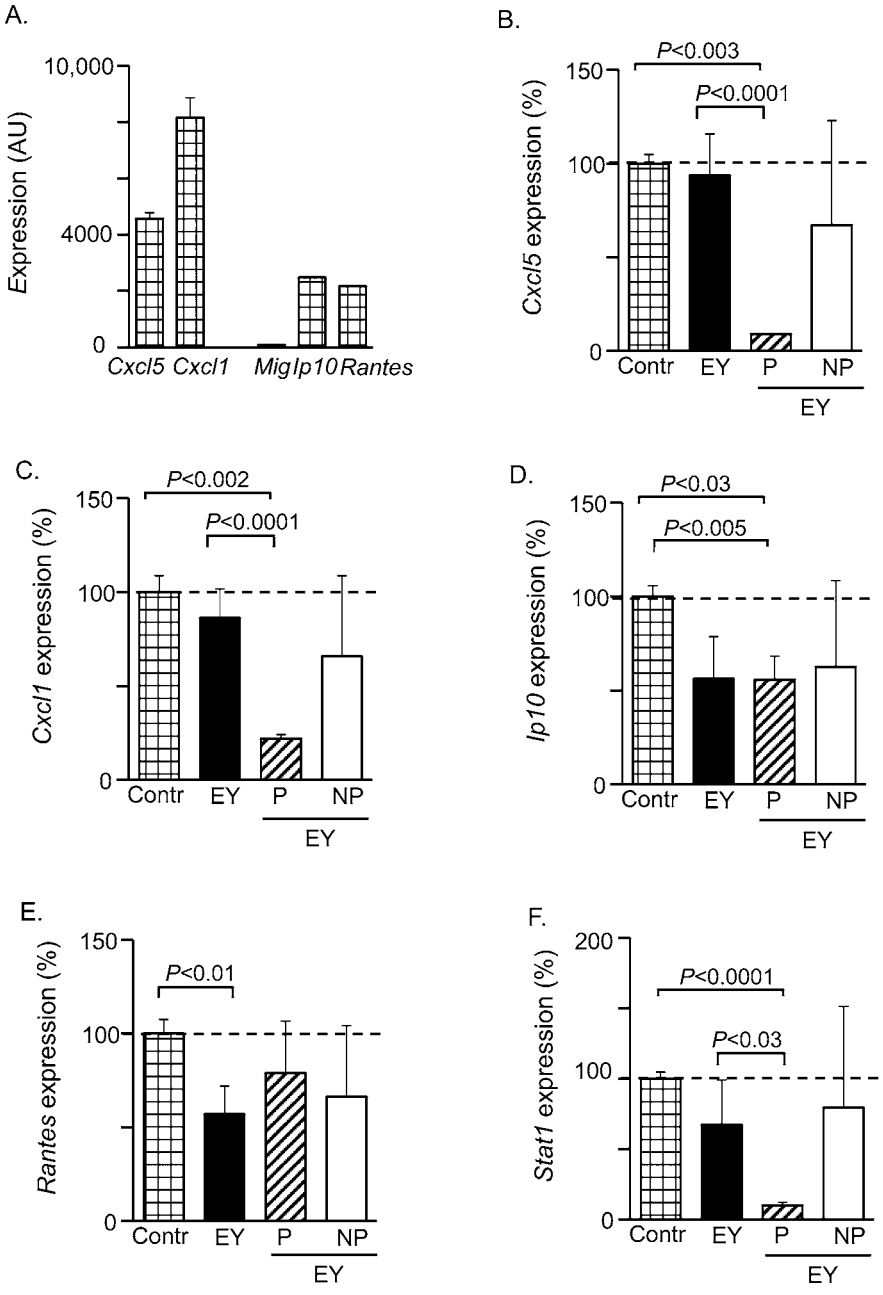

Figure 5. EY-P fractions suppress expression of NF-κB-regulated downstream genes in 3T3-L1 adipocytes. (A) The relative expression of *Cxcl5*, *Cxcl1*, *Mig*, *Ip10*, *Rantes*, and *Stat1* was measured by the nCounter data analysis system from NanoString Technologies using same samples that were described in Figure 4C. (B–F) Expression of *Cxcl5*, *Cxcl1*, *Mig*, *Ip10*, *Rantes*, and *Stat1* genes in same 3T3-L1 adipocytes described in Figure 4D–F.

expression of two other major, *Tlr3* and *Tlr4* receptors was not significantly affected by the treatment with any EY fractions (Figure 6C, D). However, the EY-P fraction significantly increased the expression of *Ly96* (to 224%) compared to control adipocytes (Figure 6E). The interaction of Ly96 with TLR4 prevents ligand binding to this receptor and the activation of NF-κB. The expression of an inhibitory adaptor protein, Tollip, was also increaed (to 145%) in EY-P fraction compared to control adipocytes. (Figure 6F). Therefore, decreased activation of NF-κB was associated with inhibited expression of *Tlr* either via direct inhibition of expression of *Tlr2* or indirectly via up-regulation of the expression of inhibitory *Ly96* and *Tollip* by the EY-P but not the EY-NP and EY fractions.

3. Dissimilar Regulation of Expression by EY-NP and EY-P Fractions Influence Proteins with Potential Binding Sites for Both SREBP and NFκB. To obtain a clue for specific regulation of *Tlr* and inhibitory *Ly96* and *Tollip* by the EY-P, but not the EY and EY-NP fractions, we analyzed the putative SREBP binding sites. This transcription factor has been established as a sensor of cholesterol/phospholipid ratio on the membranes or as factor activated by signaling cascades (e.g., insulin).[39] We found three potential high score SREBP binding sites in *Tlr2* (score 92–93) and two SREBP binding sites in *Tollip* (score 86) and one in *Ly96* (score 88). *Tlr2* and *Ly96* could be potentially regulated by NF-κB because they also contained five and two potential NF-κB binding sites, respectively. *Stat1* contains two SREBP and nine NF-κB binding sites. To examine the putative contribution of SREBP to dissimilar responses

DOI: 10.1021/jf5056584
J. Agric. Food Chem. 2015, 63, 2013–2025

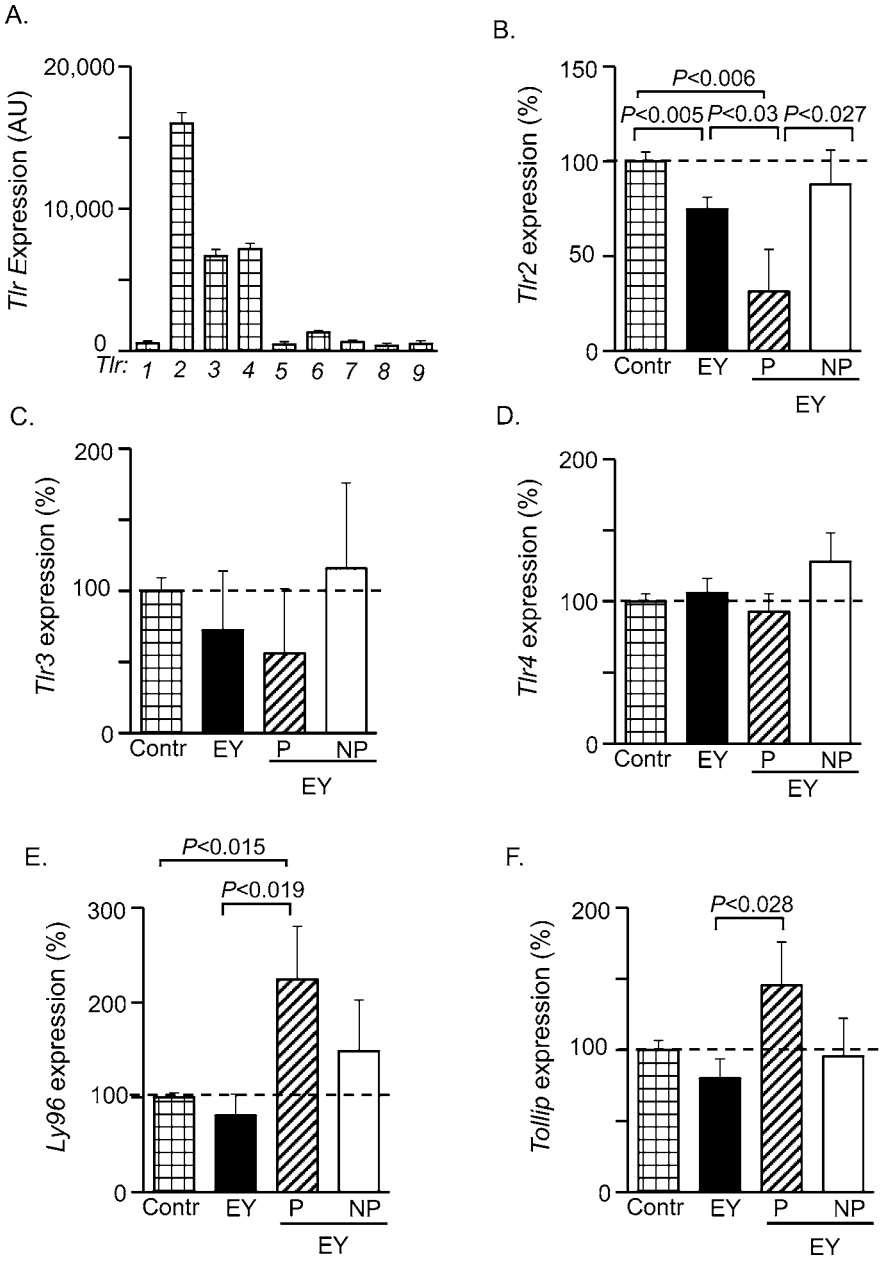

Figure 6. EY-P fractions inhibit expression of specific Toll-like (Tlr) receptors. (A) The relative expression of *Tlr1−9* was measured by NanoString using same samples that were described in Figure 4C. (B−D) Expression of *Tlr2*, *Tlr3*, and *Tlr4* genes as well as Ly96 (E) and Tollip in same 3T3-L1 adipocytes described in Figure 4D−F.

among the EY, EY-P, and EY-NP fractions, we examined the effect of SREBP inhibitor, fatostatin,[40] on NF-κB activation in *Nfkb*-RE/GFP preadipocyte cell line. Fatostatin significantly inhibited *Nfκb*-RE activation by 52% compared to the activation induced by the EY-NP fraction (Figure 7A). Thus, SREBP partially contributed to the activation of *Nfκb*-RE associated with the EY-NP fraction. Next we stimulated of *Nfkb*-RE/GFP preadipocytes with water-soluble cholesterol during differentiation. Cholesterol-induced concentration-dependent NF-κB activation reached 170% plateau compared to nonstimulated adipocytes (Figure 7B). Stimulations of *Nfkb*-RE/GFP preadipocytes with *all-trans* retinol (Figure 7C), lutein (Figure 7D), and α-tocopherol (Figure 7E) had the opposite effect. However, the significant concentration-dependent inhibition of NF-κB occurred only in the presence of *all-trans* retinol and lutein. Each of these compounds suppressed 30% of NF-κB activation compared to nonstimulated adipocytes.

DISCUSSION

Our data demonstrates that EY contains a mixture of compounds that can effectively suppress the key inflammatory transcription pathway of NF-κB in vitro; however, these effects were blunted in the presence of nonpolar cholesterol and TG. EY-P compounds efficiently inhibited:

(1) initiation of receptor-mediated signaling that leads to the activation of NF-κB pathway,
(2) binding of transcriptional complex to regulatory DNA sequences, and
(3) expression of target cytokines.

DOI: 10.1021/jf5056584
J. Agric. Food Chem. 2015, 63, 2013−2025

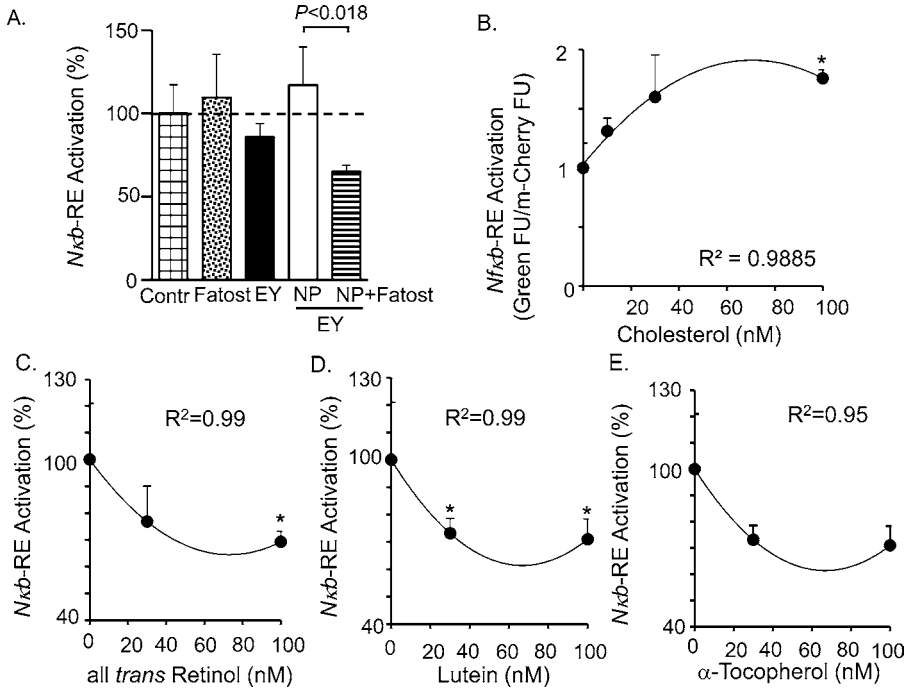

Figure 7. Fatostatin, retinol, and lutein suppressed EY-NP-induced NF-κB activation in *Nfκb*-RE/GFP adipocytes. (A) Control *Nfκb*-RE/GFP preadipocytes were differentiated for 4 days (Contr, gird bar). *Nfκb*-RE/GFP preadipocytes were differentiated for 3 days and stimulated for 24 h with 20 nM fatostatin (Fatost, dotted bars), EY (black bar), EY-NP (white bar), and EY-NP with fatostatin (20 nM, EY-NP+Fatost, bar with horizontal lines). Data are shown as % of control (100%, dashed line). Data (mean ± SD, n = 3) are shown as % of expression compared to in control adipocytes. *P*, Mann−Whitney U test. Different concentrations of cholesterol (B), *all-trans* retinol (C), lutein (D) and α-tocopherol (E) were added during the induction of *Nfκb*-RE/GFP preadipocyte differentiation and were replaced every 48 h. Differentiation continued for 5 days. Data are shown as GFP/mCherry ratio (n = 3). Correlation was examined by Pearson test. Groups were compared using Mann−Whitney U test. An asterisk indicates significant difference between control and cholesterol stimulated adipocytes.

The receptors regulating NF-κB in adipocytes exhibit a specific pattern. 3T3-L1 adipocytes expressed predominantly three *Tlr*s: *Tlr2* > *Tlr3* = *Tlr4*. EY-P fraction suppressed expression of *Tlr2*, whereas the expression of the seven other *Tlr*s remained unchanged. The inhibition of other TLRs was mediated via inhibitory adaptor protein, Tollip, and TLR4 inhibitor, Ly96. Polar lipids in the EY-P fraction induced expression of these inhibitory proteins. These changes in TLRs were associated with inhibition of NF-κB activation and the expression of NF-κB-dependent genes by EY-P compounds. Unexpectedly, EY supported NF-κB activation even though the EY and EY-P fractions shared similar content of vitamins, carotenoids, and fatty acids. Partial removal of nonpolar cholesterol and TG from the EY was required to reveal its inhibitory effects on the NF-κB pathway. Although these studies were performed in adipocytes, EY fractions expect to exert similar effects in other cells that are under NF-κB and SREBP transcriptional control such as mucosal epithelial cells exposed to EY-containing products such as mayonnaise. In other pathophysiological situations in vivo, EY can potentially have beneficial effects without delipidation.[41,42]

The inhibition of *Nfκb*-RE activation together with the suppressed expression of NF-κB-regulated cytokines and TLR2 receptor suggests that EY-P may exert anti-inflammatory properties. The association of anti-inflammatory properties with EY-P, but not EY fractions, appears to be independent of the variation in EY composition as the effects were seen using regular quality eggs from four different suppliers. The highest variability in composition was associated with the cholesterol content in the EY-NP fraction and lutein and zeaxanthin content in the EY-P fraction; however, all EY-P fractions inhibited expression of genes in the NF-κB cascade after partial delipidation. Although numerous studies showed that NF-κB pathways are regulated by fatty acids,[12] in our study similar fatty acid composition among the EY fractions suggest their unlikely role in dissimilar NF-κB activation. The mechanism by which cholesterol regulates NF-κB remains unclear. In macrophages, cholesterol mobilization to lipid rafts contributes to the activation of TLR.[43] Activation of NF-κB via TLR4 is blocked by mevinolin, suggesting that the activation of TLR4 may require binding of cholesterol or its metabolic precursors.[44] Decades of studies with statins, inhibitors of cholesterol synthesis, showed that anti-inflammatory effects of these pharmaceuticals depend on inhibition of NF-κB in a variety of tissues.[45−47] The regulation of cholesterol metabolism and fatty acid synthesis is controlled by a SREBP family of transcription factors. In adipocytes, SREBP is activated by insulin/JNK pathways[39] and glucose/JAK/STAT pathways,[48] which regulate differentiation, glycolytic pathways, fatty acid synthesis, and lipid droplet formation in adipocytes.[49] In our studies, all proteins participating in NF-κB activation cascade, TLR2, Tollip, and Ly96, had putative binding sites for SREBP. Given that detailed analysis of promoters was beyond the scope of our first study, we accessed the global impact of SREBP in the regulation of NF-κB by EY-NP fraction using its specific inhibitor fatostatin.[40] *Nfκb*-RE activation was significantly reduced by fatostatin compared to nontreated adipocytes, whereas cholesterol induced *Nfκb*-RE activation in a concentration-dependent manner. However, effects of fatostatin was less pronounced than that achieved by EY-P compounds.

DOI: 10.1021/jf5056584
J. Agric. Food Chem. 2015, 63, 2013−2025

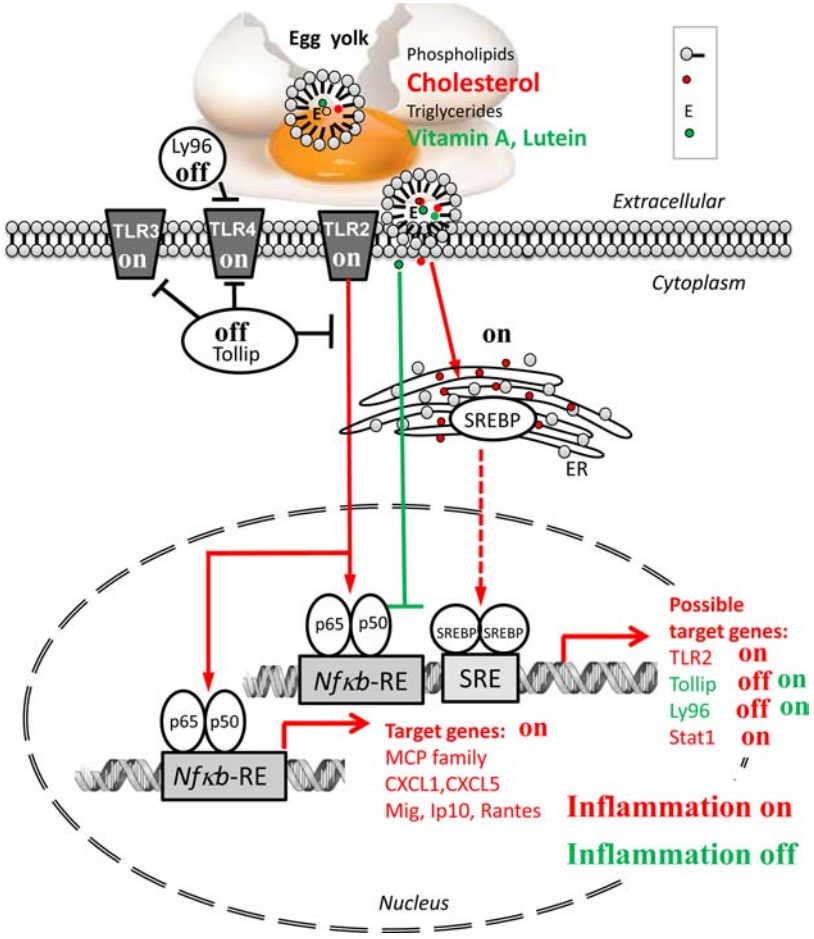

Figure 8. Hypothetical mechanism for EY-P-suppressed NF-κB activation in adipocytes. The major TLR on adipocytes are TLR2, TLR3, and TLR4. The inhibition of TLRs was mediated via inhibitory adaptor protein Tollip, while Ly96 inhibited TLR4 activation. TLR activation induces signaling cascade leading to translocation of NF-κB complex, for example, p50/p65 into nucleus and activation of activation of NF-κB-dependent genes (*MCP* family, *CXC* family, *Mig*, *Ip10*, *Rantes*, etc.). Cholesterol to phospholipid ratio in the endoplasmic reticulum (ER) membranes control activation of SREBP transcription factor, which coregulate genes involved in NF-κB activation (*Tlr2*, *Tollip*, *Ly96*, *Stat1*, etc.). EY and EY-NP fractions activate NF-κB through SREBP-dependent pathways and could be inhibited by SREBP inhibitor fatostatin. Partial delipidation EY (such as EY-P fraction, which is not shown in the schematics) alters phospholipid to cholesterol ratio and might prevent SREBP activation, resulted in the suppression of TLR2 and elevated expression of Tollip and Ly96 inhibitory proteins in adipocytes. Thus, partially delipidated EY-P fraction leads to the inhibition of NF-κB activation and its downstream inflammatory targets.

Vitamin A and lutein inhibited *Nfκb*-RE activation at low concentrations and could be potentially accounted for the inhibition mediated by EY-P fraction. Thus, partial delipidation of EY may lead first to the disruption of SREBP-dependent genes involved in NF-κB activation and then enable lutein and retinol to exert their potential anti-inflammatory effects (Figure 8).

A remaining question is why only partial delipidation was needed to improve the inhibition of NF-κB by the EY-P fraction? Although specific studies are needed to answer this question, a possible explanation can be found in the relationship between membrane composition and activation of SREBP. Recent studies showed that SREBP activation could be triggered by reduced phospholipid concentrations in the membranes.[50] After partial delipidation, the EY-P fraction has an increased ratio of phospholipid to cholesterol, which, possibly, prevents SREBP activation. The decrease in ratio of cholesterol to phospholipid could also improve the delivery of lipophilic vitamins and carotenoids to adipocytes.

Our study also revealed that partial delipidation of EY can influence inflammation via STAT1. This transcription factor is a critical mediator of interferon-mediated inflammation[51] and promotes a variety of diseases, including hepatitis[3] and type 1 diabetes in experimental animal models.[4] *Stat1* controls apoptosis in pancreatic β cells[52] via transcription of *Cxcl1* and *Cxcl2*. These cytokines promote neutrophil migration into pancreatic islets.[14] Insulin resistance in patients with obesity and hepatitis[3] were attributed to another STAT1-regulated cytokine, CXCL5. CXCL1 and CXCL5 are also NF-κB target genes.[14,38] The deficient NF-κB activation and *Stat1* in our studies markedly diminished expression of *Cxcl1* and *Cxcl5* expression (by 80% and 90% decrease in the presence of EY-P compared to control). It is unlikely that INF was the major regulator of *Stat1* in adipocytes because the expression of all *Inf* was very low in adipocytes and was not regulated by EY fractions (data not shown). Accordingly, the expression of INFγ-regulated *Ip10* and *Rantes* was only moderately regulated by EY fractions (Figure 5). Recent studies showed that CXCL5 could be another mechanism that leads to the activation activation of STAT1 in adipocytes.[53] Suppression of NF-κB activation and CXCL5 expression by EY-P fraction can also result in deficient *Stat1* expression. Regardless of these

DOI: 10.1021/jf5056584
J. Agric. Food Chem. 2015, 63, 2013−2025

speculative mechanisms, the results of our study suggest that regular EY contains compounds that can selectively regulate expression of inflammatory cytokines through two major transcriptional pathways, NF-κB and STAT1. Identification of these compounds and/or their mixtures can help to develop novel therapeutics and functional foods, which can potentially improve the treatment of metabolic diseases. Our data helps to recognize the pivotal role of lipophilic compounds in EY that can sensitize inflammatory pathways and disable anti-inflammatory effects of *all-trans* retinol and lutein associated with the EY-P fraction. We propose partial delipidation of EY as an efficient solution to improve beneficial effects of EY.

AUTHOR INFORMATION

Corresponding Author

*Phone: 614 292 5034. Fax: 614 292 8880. E-mail: ziouzenkova.1@osu.edu.

Funding

This research was supported by award no. 20020728 from American Egg Board and award no. 10040042 from Novo Nordisk Pharmaceuticals as well as by the Food Innovation Center, Office for International Affairs and Center for Advanced Functional Foods Research and Entrepreneurship at OSU, and Daskal Foundation (O.Z., Q.S., C. L., L.X.). The project described was supported by award no. R21OD017244 (O.Z.) and UL1RR025755 (OSUCCC) from the National Center for Research Resources, funded by the Office of the Director, National Institutes of Health (OD) and supported by the NIH Roadmap for Medical Research.

Notes

The authors declare no competing financial interest.

ACKNOWLEDGMENTS

We express our gratitude to Dr. Paolo Fadda at the Nucleic Acid Shared Resource at The Ohio State University (OSU) for excellent technical and intellectual support and Dr. Kirsteen Maclean at NanoString Technologies for her help with data analysis. HPLC-MS/MS analyses were conducted by the Nutrient & Phytochemical Analytic Shared Resource (OSU Comprehensive Cancer Center). The content is solely the responsibility of the authors and does not necessarily represent the official views of the National Center for Research Resources or the National Institutes of Health.

ABBREVIATIONS USED

APCI-MS, atmospheric pressure chemical ionization-mass spectrometry; CCL, CC chemokine ligands; CXC, chemokines; GFP, green fluorescent protein; Cxcl1, chemokine (C-X-C motif) ligand 1, alias GRO1, GROα, KC, NAP-3; Cxcl5, chemokine (C-X-C motif) ligand 1, alias ENA78; EY, egg yolk; EY-P, egg yolk polar fraction; EY-NP, egg yolk nonpolar fraction; HPLC, high-performance liquid chromatography; Ip10, interferon γ-induced protein 10; IRF, interferon; Ly96, lymphocyte antigen 96; MCP1, monocyte chemotactic protein-1; Mig, mitogene-inducible gene; NF-κB, nuclear factor κ B; *Nfkb*-RE, nuclear factor κB response element; NRF2, nuclear factor erythroid 2 related factor; PPARγ, peroxisome proliferator-activated receptor γ; PUFA, polyunsaturated fatty acid; RAR, retinoic acid receptor; ROS, reactive oxygen species; SREBP, sterol regulatory binding protein; STAT, signal transducers and activators of transcription family; TLR, Toll-like receptors; Tollip, toll interacting protein; VDR, vitamin D receptor

REFERENCES

(1) Baker, R. G.; Hayden, M. S.; Ghosh, S. NF-kappaB, inflammation, and metabolic disease. *Cell Metab.* **2011**, *13*, 11−22.

(2) Alison, M. R.; Nicholson, L. J.; Lin, W. R. Chronic inflammation and hepatocellular carcinoma. *Recent Results Cancer Res.* **2011**, *185*, 135−148.

(3) Jaruga, B.; Hong, F.; Kim, W. H.; Gao, B. IFN-gamma/STAT1 acts as a proinflammatory signal in T cell-mediated hepatitis via induction of multiple chemokines and adhesion molecules: a critical role of IRF-1. *Am. J. Physiol.: Gastrointest. Liver Physiol.* **2004**, *287*, G1044−G1052.

(4) Kim, S.; Kim, H. S.; Chung, K. W.; Oh, S. H.; Yun, J. W.; Im, S. H.; Lee, M. K.; Kim, K. W.; Lee, M. S. Essential role for signal transducer and activator of transcription-1 in pancreatic beta-cell death and autoimmune type 1 diabetes of nonobese diabetic mice. *Diabetes* **2007**, *56*, 2561−2568.

(5) Chavey, C.; Lazennec, G.; Lagarrigue, S.; Clape, C.; Iankova, I.; Teyssier, J.; Annicotte, J. S.; Schmidt, J.; Mataki, C.; Yamamoto, H.; Sanches, R.; Guma, A.; Stich, V.; Vitkova, M.; Jardin-Watelet, B.; Renard, E.; Strieter, R.; Tuthill, A.; Hotamisligil, G. S.; Vidal-Puig, A.; Zorzano, A.; Langin, D.; Fajas, L. CXC ligand 5 is an adipose-tissue derived factor that links obesity to insulin resistance. *Cell Metab.* **2009**, *9*, 339−349.

(6) Berg, A. H.; Lin, Y.; Lisanti, M. P.; Scherer, P. E. Adipocyte differentiation induces dynamic changes in NF-kappaB expression and activity. *Am. J. Physiol.: Endocrinol. Metab.* **2004**, *287*, E1178−E1188.

(7) Shaw, O. M.; Pool, B.; Dalbeth, N.; Harper, J. L. The effect of diet-induced obesity on the inflammatory phenotype of non-adipose-resident macrophages in an in vivo model of gout. *Rheumatology (Oxford, U. K.)* **2014**, *53*, 1901−1905.

(8) Nov, O.; Shapiro, H.; Ovadia, H.; Tarnovscki, T.; Dvir, I.; Shemesh, E.; Kovsan, J.; Shelef, I.; Carmi, Y.; Voronov, E.; Apte, R. N.; Lewis, E.; Haim, Y.; Konrad, D.; Bashan, N.; Rudich, A. Interleukin-1beta regulates fat-liver crosstalk in obesity by auto-paracrine modulation of adipose tissue inflammation and expandability. *PLoS One* **2013**, *8*, e53626.

(9) Ridker, P. M. Moving beyond JUPITER: will inhibiting inflammation reduce vascular event rates? *Curr. Atheroscler. Rep.* **2013**, *15*, 295.

(10) Jialal, I.; Kaur, H.; Devaraj, S. Toll-like receptor status in obesity and metabolic syndrome: a translational perspective. *J. Clin Endocrinol. Metab.* **2014**, *99*, 39−48.

(11) Majumder, S.; Zhou, L. Z.; Chaturvedi, P.; Babcock, G.; Aras, S.; Ransohoff, R. M. p48/STAT-1alpha-containing complexes play a predominant role in induction of IFN-gamma-inducible protein, 10 kDa (IP-10) by IFN-gamma alone or in synergy with TNF-alpha. *J. Immunol.* **1998**, *161*, 4736−4744.

(12) Jin, C.; Flavell, R. A. Innate sensors of pathogen and stress: linking inflammation to obesity. *J. Allergy Clin. Immunol.* **2013**, *132*, 287−294.

(13) Yan, X.; Zhu, M. J.; Xu, W.; Tong, J. F.; Ford, S. P.; Nathanielsz, P. W.; Du, M. Up-regulation of Toll-like receptor 4/nuclear factor-kappaB signaling is associated with enhanced adipogenesis and insulin resistance in fetal skeletal muscle of obese sheep at late gestation. *Endocrinology* **2010**, *151*, 380−387.

(14) Burke, S. J.; Lu, D.; Sparer, T. E.; Masi, T.; Goff, M. R.; Karlstad, M. D.; Collier, J. J. NF-kappaB and STAT1 control CXCL1 and CXCL2 gene transcription. *Am. J. Physiol.: Endocrinol. Metab.* **2014**, *306*, E131−E149.

(15) Taniguchi, T.; Ogasawara, K.; Takaoka, A.; Tanaka, N. IRF family of transcription factors as regulators of host defense. *Annu. Rev. Immunol.* **2001**, *19*, 623−655.

(16) Brasier, A. R. The NF-kappaB regulatory network. *Cardiovasc. Toxicol.* **2006**, *6*, 111−130.

DOI: 10.1021/jf5056584
J. Agric. Food Chem. 2015, 63, 2013−2025

(17) Thach, C. T.; Finkelstein, J. N. Cationic nanoparticles disrupt cellular signaling in a cholesterol dependent manner. *Toxicol. In Vitro* **2013**, *27*, 1277−1286.
(18) D'Amore, S.; Vacca, M.; Graziano, G.; D'Orazio, A.; Cariello, M.; Martelli, N.; Di Tullio, G.; Salvia, R.; Grandaliano, G.; Belfiore, A.; Pellegrini, F.; Palasciano, G.; Moschetta, A. Nuclear receptors expression chart in peripheral blood mononuclear cells identifies patients with Metabolic Syndrome. *Biochim. Biophys. Acta* **2013**, *1832*, 2289−2301.
(19) Siriwardhana, N.; Kalupahana, N. S.; Cekanova, M.; LeMieux, M.; Greer, B.; Moustaid-Moussa, N. Modulation of adipose tissue inflammation by bioactive food compounds. *J. Nutr. Biochem.* **2013**, *24*, 613−623.
(20) Ziouzenkova, O.; Perrey, S.; Asatryan, L.; Hwang, J.; MacNaul, K. L.; M?ller, D. E.; Rader, D. J.; Sevanian, A.; Zechner, R.; Hoefler, G.; Plutzky, J. Lipolysis of triglyceride-rich lipoproteins generates PPAR ligands: evidence for an antiinflammatory role for lipoprotein lipase. *Proc. Natl. Acad. Sci. U. S. A.* **2003**, *100*, 2730−2735.
(21) Chinetti, G.; Fruchart, J. C.; Staels, B. Peroxisome proliferator-activated receptors (PPARs): nuclear receptors at the crossroads between lipid metabolism and inflammation. *Inflamm. Res.* **2000**, *49*, 497−505.
(22) Glauert, H. P. Vitamin E and NF-kappaB activation: a review. *Vitam. Horm.* **2007**, *76*, 135−153.
(23) Carlsen, H.; Alexander, G.; Austenaa, L. M.; Ebihara, K.; Blomhoff, R. Molecular imaging of the transcription factor NF-kappaB, a primary regulator of stress response. *Mutat. Res.* **2004**, *551*, 199−211.
(24) Ma, J.; Wang, H.; Wang, Y.; Zhang, S. Endotoxin-neutralizing activity of hen egg phosvitin. *Mol. Immunol.* **2013**, *53*, 355−362.
(25) Mahmoudi, M.; Ebrahimzadeh, M. A.; Pourmorad, F.; Rezaie, N.; Mahmoudi, M. A. Anti-inflammatory and analgesic effects of egg yolk: a comparison between organic and machine made. *Eur. Rev. Med. Pharmacol. Sci.* **2013**, *17*, 472−476.
(26) Anderson, K. E. Comparison of fatty acid, cholesterol, vitamin A and E composition, and trans fats in eggs from brown and white egg strains that were molted or nonmolted. *Poult. Sci.* **2013**, *92*, 3259−3265.
(27) Golzar Adabi, S. H.; Ahbab, M.; Fani, A. R.; Hajbabaei, A.; Ceylan, N.; Cooper, R. G. Egg yolk fatty acid profile of avian species—influence on human nutrition. *J. Anim. Physiol. Anim. Nutr.* **2013**, *97*, 27−38.
(28) Shen, Q.; Chitchumroonchokchai, C.; Thomas, J. L.; Gushchina, L. V.; Disilvestro, D.; Failla, M. L.; Ziouzenkova, O. Adipocyte reporter assays: application for identification of anti-inflammatory and antioxidant properties of mangosteen xanthones. *Mol. Nutr. Food Res.* **2014**, *58*, 239−247.
(29) Yasmeen, R.; Reichert, B.; Deiuliis, J.; Yang, F.; Lynch, A.; Meyers, J.; Sharlach, M.; Shin, S.; Volz, K. S.; Green, K. B.; Lee, K.; Alder, H.; Duester, G.; Zechner, R.; Rajagopalan, S.; Ziouzenkova, O. Autocrine function of aldehyde dehydrogenase 1 as a determinant of diet- and sex-specific differences in visceral adiposity. *Diabetes* **2013**, *62*, 124−136.
(30) Folch, J.; Lees, M.; Sloane Stanley, G. H. A simple method for the isolation and purification of total lipides from animal tissues. *J. Biol. Chem.* **1957**, *226*, 497−509.
(31) Stoffel, W.; Chu, F.; Ahrens, E. H. Analysis of Long-Chain Fatty Acids by Gas−Liquid Chromatography. *Anal. Chem.* **1959**, *31*, 307−308.
(32) Belury, M. A.; Kempa-Steczko, A. Conjugated linoleic acid modulates hepatic lipid composition in mice. *Lipids* **1997**, *32*, 199−204.
(33) Kopec, R. E.; Schweiggert, R. M.; Riedl, K. M.; Carle, R.; Schwartz, S. J. Comparison of high-performance liquid chromatography/tandem mass spectrometry and high-performance liquid chromatography/photo-diode array detection for the quantitation of carotenoids, retinyl esters, alpha-tocopherol and phylloquinone in chylomicron-rich fractions of human plasma. *Rapid Commun. Mass Spectrom.* **2013**, *27*, 1393−1402.
(34) Krinninger, P.; Brunner, C.; Ruiz, P. A.; Schneider, E.; Marx, N.; Foryst-Ludwig, A.; Kintscher, U.; Haller, D.; Laumen, H.; Hauner, H. Role of the adipocyte-specific NF-kappaB activity in the regulation of IP-10 and T cell migration. *Am. J. Physiol.: Endocrinol. Metab.* **2011**, *300*, E304−E311.
(35) Moriuchi, H.; Moriuchi, M.; Fauci, A. S. Nuclear factor-kappa B potently up-regulates the promoter activity of RANTES, a chemokine that blocks HIV infection. *J. Immunol* **1997**, *158*, 3483−3491.
(36) Matsuzaki, S.; Ishizuka, T.; Hisada, T.; Aoki, H.; Komachi, M.; Ichimonji, I.; Utsugi, M.; Ono, A.; Koga, Y.; Dobashi, K.; Kurose, H.; Tomura, H.; Mori, M.; Okajima, F. Lysophosphatidic acid inhibits CC chemokine ligand 5/RANTES production by blocking IRF-1-mediated gene transcription in human bronchial epithelial cells. *J. Immunol.* **2010**, *185*, 4863−4872.
(37) Ohmori, Y.; Schreiber, R. D.; Hamilton, T. A. Synergy between interferon-gamma and tumor necrosis factor-alpha in transcriptional activation is mediated by cooperation between signal transducer and activator of transcription 1 and nuclear factor kappaB. *J. Biol. Chem.* **1997**, *272*, 14899−14907.
(38) Sun, H.; Chung, W. C.; Ryu, S. H.; Ju, Z.; Tran, H. T.; Kim, E.; Kurie, J. M.; Koo, J. S. Cyclic AMP-responsive element binding protein- and nuclear factor-kappaB-regulated CXC chemokine gene expression in lung carcinogenesis. *Cancer Prev. Res.* **2008**, *1*, 316−328.
(39) Ito, M.; Nagasawa, M.; Omae, N.; Tsunoda, M.; Ishiyama, J.; Ide, T.; Akasaka, Y.; Murakami, K. A novel JNK2/SREBP-1c pathway involved in insulin-induced fatty acid synthesis in human adipocytes. *J. Lipid Res.* **2013**, *54*, 1531−1540.
(40) Kamisuki, S.; Mao, Q.; Abu-Elheiga, L.; Gu, Z.; Kugimiya, A.; Kwon, Y.; Shinohara, T.; Kawazoe, Y.; Sato, S.; Asakura, K.; Choo, H. Y.; Sakai, J.; Wakil, S. J.; Uesugi, M. A small molecule that blocks fat synthesis by inhibiting the activation of SREBP. *Chem. Biol.* **2009**, *16*, 882−892.
(41) Pearce, K. L.; Clifton, P. M.; Noakes, M. Egg consumption as part of an energy-restricted high-protein diet improves blood lipid and blood glucose profiles in individuals with type 2 diabetes. *Br. J. Nutr.* **2011**, *105*, 584−592.
(42) Goodrow, E. F.; Wilson, T. A.; Houde, S. C.; Vishwanathan, R.; Scollin, P. A.; Handelman, G.; Nicolosi, R. J. Consumption of one egg per day increases serum lutein and zeaxanthin concentrations in older adults without altering serum lipid and lipoprotein cholesterol concentrations. *J. Nutr.* **2006**, *136*, 2519−2524.
(43) Zhu, X.; Owen, J. S.; Wilson, M. D.; Li, H.; Griffiths, G. L.; Thomas, M. J.; Hiltbold, E. M.; Fessler, M. B.; Parks, J. S. Macrophage ABCA1 reduces MyD88-dependent Toll-like receptor trafficking to lipid rafts by reduction of lipid raft cholesterol. *J. Lipid Res.* **2010**, *51*, 3196−3206.
(44) Law, R. E.; Stimmel, J. B.; Damore, M. A.; Carter, C.; Clarke, S.; Wall, R. Lipopolysaccharide-induced NF-kappa B activation in mouse 70Z/3 pre-B lymphocytes is inhibited by mevinolin and 5′-methylthioadenosine: roles of protein isoprenylation and carboxyl methylation reactions. *Mol. Cell. Biol.* **1992**, *12*, 103−111.
(45) Guijarro, C.; Kim, Y.; Schoonover, C. M.; Massy, Z. A.; O'Donnell, M. P.; Kasiske, B. L.; Keane, W. F.; Kashtan, C. E. Lovastatin inhibits lipopolysaccharide-induced NF-kappaB activation in human mesangial cells. *Nephrol., Dial., Transplant.* **1996**, *11*, 990−996.
(46) van der Meij, E.; Koning, G. G.; Vriens, P. W.; Peeters, M. F.; Meijer, C. A.; Kortekaas, K. E.; Dalman, R. L.; van Bockel, J. H.; Hanemaaijer, R.; Kooistra, T.; Kleemann, R.; Lindeman, J. H. A clinical evaluation of statin pleiotropy: statins selectively and dose-dependently reduce vascular inflammation. *PLoS One* **2013**, *8*, e53882.
(47) Malik, S.; Sharma, A. K.; Bharti, S.; Nepal, S.; Bhatia, J.; Nag, T. C.; Narang, R.; Arya, D. S. In vivo cardioprotection by pitavastatin from ischemic-reperfusion injury through suppression of IKK/NF-kappaB and upregulation of pAkt-e-NOS. *J. Cardiovasc. Pharmacol.* **2011**, *58*, 199−206.
(48) Guillet-Deniau, I.; Pichard, A. L.; Kone, A.; Esnous, C.; Nieruchalski, M.; Girard, J.; Prip-Buus, C. Glucose induces de novo lipogenesis in rat muscle satellite cells through a sterol-regulatory-

DOI: 10.1021/jf5056584
J. Agric. Food Chem. 2015, 63, 2013−2025

element-binding-protein-1c-dependent pathway. *J. Cell Sci.* **2004**, *117*, 1937−1944.
(49) Kim, J. B.; Sarraf, P.; Wright, M.; Yao, K. M.; Mueller, E.; Solanes, G.; Lowell, B. B.; Spiegelman, B. M. Nutritional and insulin regulation of fatty acid synthetase and leptin gene expression through ADD1/SREBP1. *J. Clin. Invest.* **1998**, *101*, 1−9.
(50) Walker, A. K.; Jacobs, R. L.; Watts, J. L.; Rottiers, V.; Jiang, K.; Finnegan, D. M.; Shioda, T.; Hansen, M.; Yang, F.; Niebergall, L. J.; Vance, D. E.; Tzoneva, M.; Hart, A. C.; Naar, A. M. A conserved SREBP-1/phosphatidylcholine feedback circuit regulates lipogenesis in metazoans. *Cell* **2011**, *147*, 840−852.
(51) Darnell, J. E., Jr.; Kerr, I. M.; Stark, G. R. Jak-STAT pathways and transcriptional activation in response to IFNs and other extracellular signaling proteins. *Science* **1994**, *264*, 1415−1421.
(52) Moore, F.; Naamane, N.; Colli, M. L.; Bouckenooghe, T.; Ortis, F.; Gurzov, E. N.; Igoillo-Esteve, M.; Mathieu, C.; Bontempi, G.; Thykjaer, T.; Orntoft, T. F.; Eizirik, D. L. STAT1 is a master regulator of pancreatic {beta}-cell apoptosis and islet inflammation. *J. Biol. Chem.* **2011**, *286*, 929−941.
(53) Zhang, H.; Yang, R.; Wang, Z.; Lin, G.; Lue, T. F.; Lin, C. S. Adipose tissue-derived stem cells secrete CXCL5 cytokine with neurotrophic effects on cavernous nerve regeneration. *J. Sex. Med.* **2011**, *8*, 437−446.

DOI: 10.1021/jf5056584
J. Agric. Food Chem. 2015, 63, 2013−2025

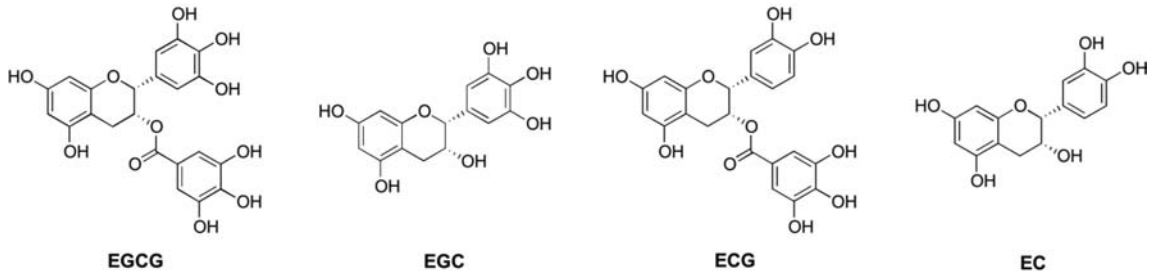

Figure 1. Structures of (+)-epigallocatechin-3-gallate (EGCG), (+)-epigallocatechin (EGC), (+)-epicatechin-3-gallate (ECG), and (+)-epicatechin (EC).

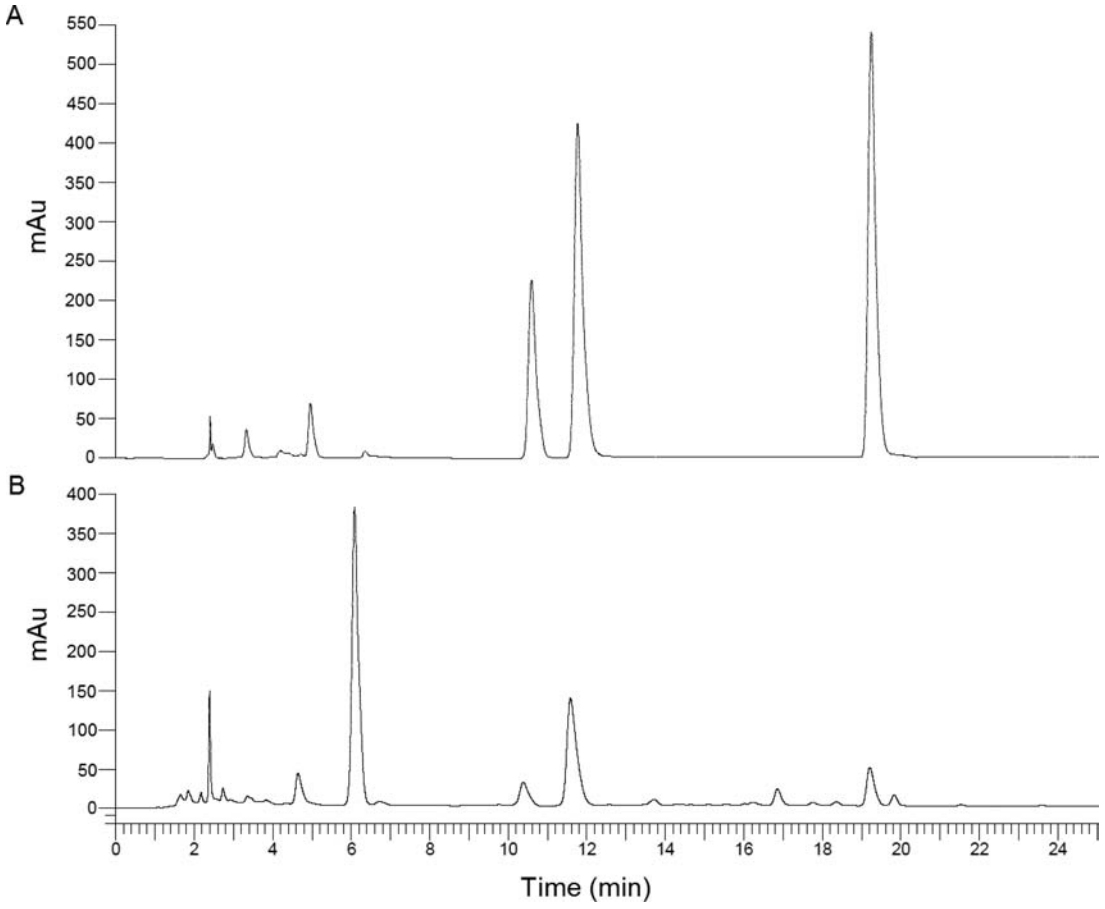

Figure 2. Representative HPLC chromatograms of (A) standards mixture and (B) white tea extract.

Analysis of Total Polyphenol Content (TPC). The TPC of tea extract was determined using the Folin−Ciocalteu method.[17,18] Results were expressed as milligrams of gallic acid equivalents per grams of leaves (GAE mg/g).

HPLC Analysis of Catechins Content. Catechins in white tea extract were identified and quantitated using a modified HPLC method.[19] A 20 μL aliquot of the standard (EGCG, ECG, EGC, and EC) solutions and sample extract was injected and analyzed two times using a Flexar HPLC (PerkinElmer Inc., Waltham, MA). The column used was a 250 mm × 4.6 mm i.d., 5 μm, Restek ultra C18 (Restek Corporation, Bellefonte, PA), with an elution flow rate of 1.5 mL/min, and a linear solvent gradient of A−B [(A, 10 mM KH_2PO_4 (pH 4.0); B, CH_3CN/H_2O (65%/35%)], as follows: 0 min, 20% B; 5 min, 20% B; 15 min, 30% B; 40 min, 60% B. The absorbance was measured at 280 nm. TotalChrome software program was used for data acquisition and processing. The catechins content of the white tea extract was expressed as a percentage by mass on a sample dry matter basis.

Nanoparticle Formulations. The white tea extract was encapsulated into polymeric NPs by using a nanoprecipitation method. Polycaprolactone (PCL) was dissolved in 3 mL of acetonitrile and added dropwise, under magnetic stirring (700 rpm), into a solution containing F-127 (0.5% w/v), alginate (0.1%, 0.5%, and 1.0% w/v), white tea extract, and water (2:2:1:5 v/v), to give a final polymer concentration of 6.0 mg/mL. The resulting colloidal suspension was evaporated under stirring (500 rpm) at room temperature for 1 h to remove the organic solvent. NPs were centrifuged at 10 000 rpm for 5 min and washed three times with water to remove the unencapsulated extract. A part of the NPs dispersion was lyophilized, and collected for other experiments.

Nanoparticle Characterization. *Scanning Electron Microscopy (SEM) Analysis.* Morphological examination of NPs was performed by analysis with a model 962 scanning electron microscope (Carl Zeiss Inc., Jena, Germany). A drop of the NPs aqueous suspension was placed on an aluminum stub and dried under a vacuum for 12 h. The

DOI: 10.1021/jf505850q
J. Agric. Food Chem. 2015, 63, 2026−2032

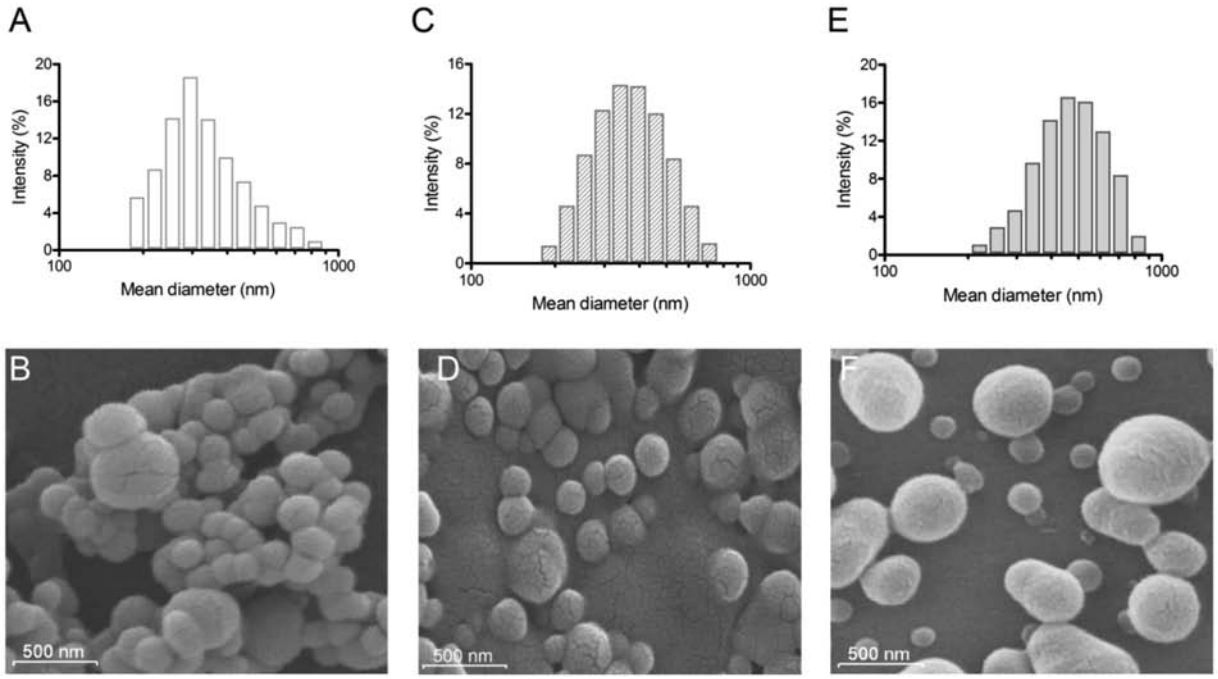

Figure 3. Particle size distributions and SEM images of white tea extract-loaded NPs prepared by using (A, B) 0.1%, (C, D) 0.5%, and (E, F) 1.0% of alginate (% w/v), respectively.

samples were analyzed at 20 kV acceleration voltage after gold sputtering, under an argon atmosphere.

Measurement of Particle Size (PS) and Polydispersity Index (PI). PS and PI were measured by using photon correlation spectroscopy with a Zetasizer Nano ZS (Malvern Instruments, Worcestershire, UK) at 25 °C, and a scattering angle of 90° after dilution of samples with Milli-Q water. Each sample was measured in triplicate.

Encapsulation Efficiency (EE%). The extract encapsulation capacity of NPs was evaluated in terms of both TPC and catechins content.

An aliquot of 1.0 mg of freeze-dried NPs was dissolved in 100 μL of acetonitrile and added to 100 μL of water. After centrifugation (10 000 rpm, 10 min), the supernatant was analyzed by using the Folin−Ciocalteu assay and the HPLC method previously reported. The EE% was calculated as the ratio between the amount of TPC and catechins encapsulated in NPs and their weight in the extract used for NPs preparation.

Fourier Transform Infrared Spectroscopy (FT-IR). The chemical composition of the white tea extract, PCL, alginate, tea extract-loaded NPs, tea extract/PCL, and tea extract/alginate blends was analyzed by FT-IR spectroscopic measurements by using a Bruker Vertex 70v spectrophotometer (Bruker Optik, Ettlingen, Germany) at a resolution of 4 cm^{-1} in KBr pellets, in the range 400−4000 cm^{-1}.

Release Kinetics of Polyphenols. A known amount of NPs (10 mg) suspended in 400 μL of distilled water or unencapsulated white tea extract (200 μL) was placed into dialysis bags and suspended in 20 mL of 0.1 M HCl (pH 1.2) for 2 h followed by PBS buffer solution (pH 7.4, 20 mL) for 5 h, to simulate gastric and intestinal fluids, respectively (37 ± 0.5 °C, 400 rpm). At defined time intervals, 1.0 mL of the supernatant was withdrawn and replaced with an equal volume of fresh medium to maintain a constant volume. The cumulative amount of TPC released was analyzed by using the Folin−Ciocalteu assay and expressed as % with respect to TPC into NPs.

Determination of Antioxidant Activity by the Scavenging of the Stable Radical DPPH•. The antioxidant activity by the scavenging of the stable free radical, DPPH•, was determined according to the methods previously reported.[20] The experiments were carried out on various concentrations of unencapsulated white tea extract (0.25−25 μg/mL) and white tea extract-loaded NPs (25−300 μg/mL).

Stability Studies. The stability of encapsulated white tea extract was evaluated by monitoring TPC and catechin contents during storage. Tea extract-loaded NPs (3.0 mg) in aqueous suspension (200 μL) and white tea extract were stored, under static conditions, at different temperatures (25 and 40 °C) for 30 days. Before analysis, the NPs were freeze-dried and then dissolved in 200 μL of acetonitrile.

The TPC and catechin content of NPs and white tea extract samples were then analyzed by using the Folin−Ciocalteu assay and HPLC method, respectively, as reported above.

Statistical Analysis. All data were expressed as the mean ± SD of three replications of the experiment. Statistical analysis was performed by one-way analysis of variance (ANOVA) and Student's t test. Significant difference was considered at $p < 0.05$.

RESULTS AND DISCUSSION

Preparation and Characterization of White Tea Extract. Tea leaves were extracted using water as solvent, chosen because of its high yield rate, low cost, safety, and accessibility in comparison with the organic solvents. The other extraction parameters (temperature, time, and the ratio of water-to-tea) were selected on the basis of their impact on the extraction process efficiency, previously investigated for the green tea.[21]

An average of 291.33 ± 6.11 mg of the extract was collected from 1.0 g of dry white tea leaves. In agreement with literature data,[22] TPC of tea extract, determined by Folin−Ciocalteu reagent assay, resulted in 87.29 ± 0.48 GAE mg/g, corresponding to 29.96 ± 0.63% of dry extract.

The major catechins in white tea extract were identified by a comparison of their retention times with those of standards at UV absorption spectra of 280 nm. Figure 2A and B shows the representative chromatogram of a standard mixture and white tea extract, respectively. As illustrated, the retention times for the studied catechins, EGC, EC, EGCG, and ECG, were 4.3, 10.5, 11.8, and 19.3 min, respectively. Moreover, the peak detected at 6.1 min in tea extract (Figure 2B) corresponds to caffeine.

DOI: 10.1021/jf505850q
J. Agric. Food Chem. 2015, 63, 2026−2032

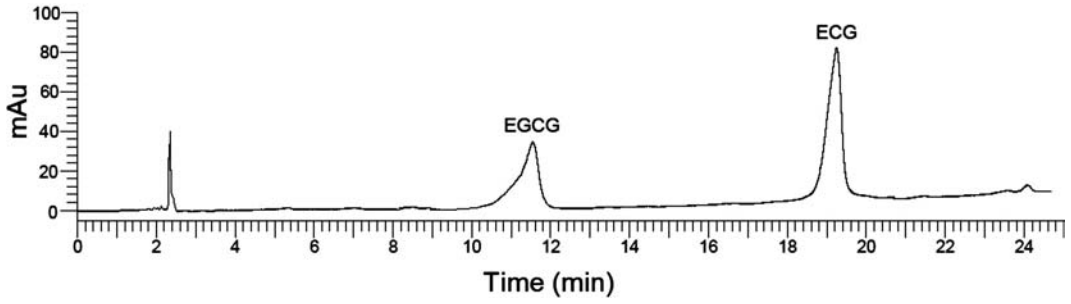

Figure 4. HPLC chromatogram of white tea extract-loaded NPs.

As expected, the tea extract was rich in catechins, predominantly in EGCG (31.31 ± 2.54 of mg/g dry white tea leaves), followed by ECG (6.87 ± 0.56 mg/g), EGC (2.70 ± 0.12 mg/g), and EC (1.46 ± 0.39 mg/g).

Formulation and Characterization of White Tea Extract-Loaded NPs. In this study, white tea extract was encapsulated into polymeric NPs by a nanoprecipitation technique using PCL and alginate as carrier materials. Among biodegradable polymers, PCL alone or in combination with many other polymers shows an excellent biocompatibility and great permeability, which make it a suitable candidate for controlled drug delivery.[23,24] In our previous studies, docetaxel-loaded NPs composed of block copolymers of poly(D,L-lactide-*co*-caprolactone) and poly(L-lactide-*co*-caprolactone-*co*-glycolide)[25] and resveratrol-loaded NPs based on PCL and poly-D,L-lactide-*co*-glycolic acid)−poly(ethylene glycol) blend were successfully prepared and explored for prostate cancer treatment.[26] However, the naturally occurring biopolymer alginate has been employed for the production of a broad spectrum of drug delivery micro- and nanosystems.[27,28] To optimize the NPs formulation conditions, different amounts of alginate (0.1%, 0.5%, and 1.0% w/v) were initially employed. Results demonstrated that the composition of NPs strongly influenced the size and distribution of NPs. In particular, as displayed in Figure 3, NPs obtained with alginate at lower concentration (0.1% w/v) are characterized by a mean particle size of about 300 nm with a wide distribution (PDI 0.397 ± 0.27) (Figure 3A and B). Conversely, by increasing the alginate concentration to 1.0% w/v, NPs showed a larger particle size distribution (560.80 ± 17.77 nm), probably due to the high viscosity of alginate solution that promoted a larger particle precipitation with a tendency to separate (Figure 3E and F). The optimal alginate concentration was found to be 0.5% w/v that produced NPs with spherical shape, a mean diameter of 380.80 ± 37.97 nm, and a unimodal distribution (PDI 0.15 ± 0.06) (Figure 3C and D). With regard to particle size and colloidal stability, these NPs were selected for the subsequent studies.

The TPC encapsulation efficiency, calculated by the Folin−Ciocalteu assay, was established as 24.07 ± 1.26%, corresponding to 24.24 ± 1.60 GAE μg/mg of NPs. However, the HPLC chromatograms of extract encapsulated into NPs revealed the presence only of the most abundant catechins EGCG and ECG (Figure 4). The amount of EGCG and ECG detected corresponds to encapsulation efficiency values of 30.62 ± 0.89% and 32.60 ± 5.39%, respectively. Additionally, the complete disappearance of the caffeine peak was observed in the chromatogram. We hypothesize that, during the encapsulation process, the caffeine can establish strong interactions with acidic groups of alginate in solution, contributing to a reduced incorporation into the polymer matrix and can be removed later during washing or freeze-drying steps.

The chemical interactions after encapsulation of tea extract into NPs were investigated by FT-IR spectroscopy, and the results are reported in Figure 5. According to the literature,[26,29]

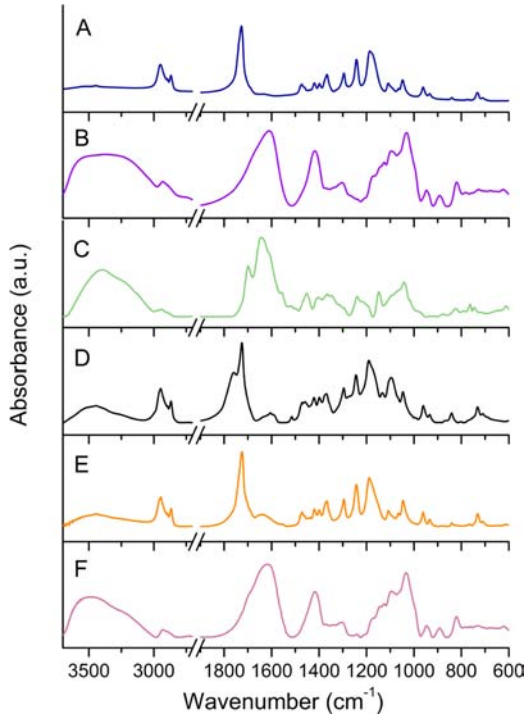

Figure 5. FTIR spectra of (A) pure PCL, (B) pure alginate, (C) white tea extract, (D) white tea extract-loaded NPs, (E) tea extract/PCL blend, and (F) tea extract/alginate blend.

for PCL, the bands at 2950−2865 cm^{-1} were assigned to CH_2 stretching. The peak at 1725 cm^{-1} represented C═O ester stretching, while peaks at 1293, 1240, and 1190 cm^{-1} corresponded to C−O and C−C, C−O−C, and O−C−O stretching, respectively. Sodium alginate showed a broad band at 3650−3000 cm^{-1} due to O−H stretching, the bands at 1620 and 1418 cm^{-1} were assigned to asymmetric and symmetric stretching peaks of carboxylate salt groups, respectively, and the bands around 1030 cm^{-1} were attributed to C−O−C stretching.[30] Most of the absorptions of white tea extract are well consistent with the data reported in the literature.[31] The broad band between 3650 and 3000 cm^{-1} was consistent with O−H stretching and with N−H stretching in primary and secondary amines, and amides. The bands between 2940 and 2860 cm^{-1} were assigned to C−H stretching of aliphatic

DOI: 10.1021/jf505850q
J. Agric. Food Chem. 2015, 63, 2026−2032

groups. The band at 1700 cm^{-1} represented the C═O vibrations. The strong band at 1640 cm^{-1} was due to the C═C vibration of aromatic structures, C═O stretching of primary amide, and carboxylic acids. Another broad band was noted between 1450 and 1360 cm^{-1} arising from the O−H, and C−O vibration stretching. The band at 1250 cm^{-1} is generally linked to C−H stretch and O−H deformation of carboxyl groups, and to the N−H of amide II.[32] The presence of the extract in NPs was confirmed by the broad band between 3650 and 3000 cm^{-1}, and the band at 1600 cm^{-1}, while the shifted peak at 1760 cm^{-1} indicated both the intermolecular and the hydrogen-bonding interactions between polymers and white tea extract. Meanwhile, the FTIR spectra of tea extract/PCL and tea extract/alginate in physical mixtures did not shown any significant shift, suggesting that the mentioned chemical interactions were most favored during the nanoprecipitation process.

Release Kinetics of Polyphenols. To assess the potential of prepared NPs for oral administration, we performed the in vitro release test at pH 1.2 for 2 h followed by pH 7.4 for 5 h, to reproduce the gastric and intestinal fluids, respectively.

As shown in Figure 6, in the case of free tea extract a rapid and complete dissolution of polyphenols within the first 2 h at

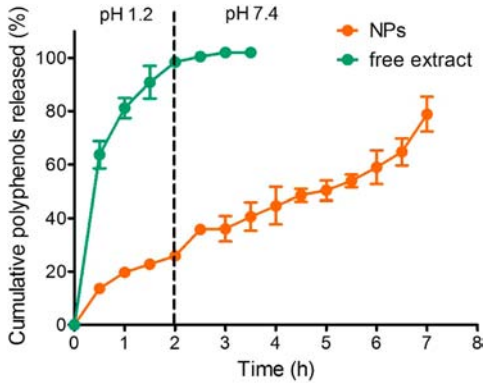

Figure 6. In vitro release profiles of polyphenols (TPC) from free white tea extract and from tea extract-loaded NPs in 0.1 M HCl (pH 1.2) for 2 h, followed by PBS (pH 7.4) for 5 h. Data are means ± SD, $n = 3$.

acidic pH was observed. In contrast, the tea extract-loaded NPs exhibited a controlled release in both tested conditions. In particular, NPs released about 20% of the encapsulated polyphenols in simulated gastric medium, and about 80% content within the subsequent 5 h at pH 7.4. This finding could be related to the low permeability of the water in the hydrophobic matrix of the NPs, due to the presence of PCL, and to the interaction of polyphenols−polymers that makes difficult the polyphenols' dissolution in water, thus retarding the release.[33] In addition, the presence of alginate promotes the formation of a gelatinous layer following the hydration, which can act as a polyphenols diffusion barrier.[34]

To assess the kinetics of polyphenols release from NPs, the in vitro release data were fitted to established mathematical models (zero-order $[Q = k_0 t]$, first order $[\ln\{100 - Q\} = \ln Q_0 - k_1 t]$, Higuchi $[Q = k_H t^{1/2}]$). Additionally, to better understand the release mechanism, the data were fitted to the Korsmeyer−Peppas exponential model $M_t/M_\infty = ktn$, where M_t/M_∞ is the fraction of polyphenols released after time t, k is a kinetic constant, and n is the release exponent that characterizes the different release mechanism.[35,36]

The correlation values (R^2) were used as an indicator of the best fitting of the models considered for loaded-NPs at different pH values. Comparison of the correlation coefficients identified the Higuchi model as that with the best fit of data at acidic pH (0.9918), while at pH 7.4 the release profile was consistent with zero-order kinetics (0.9840) (data not shown).

In simulated gastric conditions, the value of $n \leq 0.5$ revealed that the polyphenols' release follows a classical Fickian diffusion-controlled mechanism, which is assumed to be facilitated by the swelling of alginate, whereas for values $0.5 < n < 1$ found at pH 7.4, it is an indicator of both phenomena (drug diffusion in the hydrated matrix and polymer relaxation), which usually describes anomalous transport.[37]

DPPH• Inhibition. The polyphenolic composition of tea and especially the amount of catechins have aroused great interest because of their ability to scavenge free radicals, thereby inhibiting oxidative stress that is believed to be involved in several diseases.[38,39]

Free radical scavenging activities of unencapsulated white tea extract as a function of concentration are shown in Figure 7A.

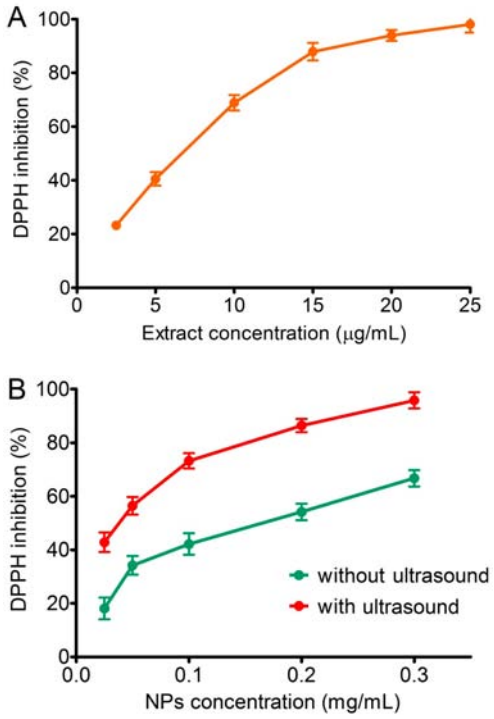

Figure 7. Comparison of DPPH• inhibition percentage of white tea extract (a) and tea extract-loaded NPs (b) at different concentrations, with and without ultrasound treatment. Data are means ± SD, $n = 3$.

The results indicated that the antioxidant activity of tea extract is concentration-dependent. This DPPH• inhibition percentage reached its maximum (98.07 ± 3.02%) at a concentration of 25 μg/mL white tea extract, with an IC_{50} value of 7.30 ± 0.27 μg/mL.

To prove the retention of antioxidant activity of tea extract after encapsulation, the DPPH• inhibition test was performed at different concentrations of tea extract-loaded NPs. As depicted in Figure 7B (without the ultrasound), only 60% of DPPH• inhibition was observed at higher concentration (0.3 mg/mL), with an IC_{50} value of 0.190 ± 0.16 mg/mL, probably

DOI: 10.1021/jf505850q
J. Agric. Food Chem. 2015, 63, 2026−2032

due to the slow release of loaded polyphenols. Because only the free polyphenols are able to show the activity toward DPPH•, to facilitate their release from NPs the test was then performed by incubation of the samples in an ultrasonic bath. As shown, a significant increase ($p < 0.05$) of DPPH• inhibition percentage at all tested concentrations was obtained, with an IC_{50} of 0.043 mg/mL, indicating that white tea extract maintained a good free radical scavenging activity after encapsulation into NPs.

Stability Studies. Several studies reported that polyphenols are subject to degradation by many environmental conditions, and temperature represents the dominant factor.[40,41] The catechin degradation involves different reactions (i.e., epimerization, oxidation, polymerization, etc.), and it was associated with a loss of catechins, mainly of EGCG, which appears to be susceptible to degradation during storage.[42,43]

In this study, the TPC and catechin retention of tea extract-loaded NPs and unencapsulated tea extract, stored at different temperature (25 and 40 °C), was monitored over 30 days. The results show that, overall, the polyphenols content was strongly influenced by the storage temperature (data not shown). The exposure of tea extract at 25 °C produced about 65% of TPC retention that significantly decreased to 43.7 ± 3.2% for the samples stored at 40 °C. However, the encapsulation of tea extract into NPs largely prevented its degradation with respect to free white tea extract, providing a TPC loss of 12.6% and 24% of the initial content with increasing storage temperature.

These results were also confirmed by HPLC analyses that revealed a significant reduction of EGCG concentration in the free white tea extract in comparison to the encapsulated extract (data not shown). The catechin content of loaded NPs, measured at 25 and 40 °C, was 1.3- and 1.7-fold higher than that in the free tea extract, respectively.

In summary, in this study the formulation of white tea extract into novel polymeric NPs for nutraceutical applications has been investigated. The results clearly demonstrated the effectiveness of the nanoencapsulation to control the white tea extract release in gastrointestinal fluids and to preserve the antioxidant activity of the polyphenols. Moreover, the encapsulation of the white tea extract into NPs significantly increased stability, thus preventing the losses of TPC and catechins over 30 days of storage. The application of this nanotechnology could offer interesting perspectives for the potential use of white tea extract as innovative nutraceuticals.

AUTHOR INFORMATION

Corresponding Author

*Tel.: +39 079998616. Fax: +39 079229559. E-mail: vsanna@uniss.it.

Funding

We gratefully acknowledge the Regione Autonoma della Sardegna for financial support of Grant CRP 25920, awarded to M.S. within the frame of "Legge regionale n. 7/2007 - Annualità 2010".

Notes

The authors declare no competing financial interest.

ACKNOWLEDGMENTS

We thank the Erboristeria Ghinato (Sassari, Italy) for providing white tea (Pai Mu Tan) leaves.

REFERENCES

(1) Gadkaria, P. V.; Balaraman, M. Catechins: Sources, extraction and encapsulation: A review. *Food Bioprod. Process.* **2013**, in press, http://dx.doi.org/10.1016/j.fbp.2013.12.004.

(2) Galland, L. Functional foods: health effects and clinical applications. *Encyclopedia of Human Nutrition*, 2nd ed.; John Wiley: London, UK, 2005; pp 360−366.

(3) Leclercq, S.; Harlander, K. R.; Reineccius, G. A. Formation and characterization of microcapsules by complex coacervation with liquid or solid aroma cores. *Flavour Fragrance J.* **2009**, *24*, 17−24.

(4) Sanna, V.; Siddiqui, I. A.; Sechi, M.; Mukhtar, H. Nanoformulation of natural products for prevention and therapy of prostate cancer. *Cancer Lett.* **2013**, *334*, 142−151.

(5) Dehkharghanian, M.; Salmieri, S.; Lacroix, M.; Vijayalakshmi, M. A. Antioxidant properties of green tea polyphenols encapsulated in caseinate beads. *Dairy Sci. Technol.* **2009**, *89*, 485−499.

(6) Dube, A.; Nicolazzo, J. A.; Larson, I. Chitosan nanoparticles enhance the intestinal absorption of the green tea catechins (+)-catechin and (−)-epigallocatechin gallate. *Eur. J. Pharm. Sci.* **2010**, *2*, 219−225.

(7) Wang, H.; Provan, G.; Helliwell, K. The functional benefits of flavonoids: the case of tea. In *Phytochemical Functional Foods*, 1st ed.; Johnson, I., Williamson, G., Eds.; Woodhead Publishing: UK, 2003; pp 128−159.

(8) Sanna, V.; Pintus, G.; Roggio, A. M.; Punzoni, S.; Posadino, A. M.; Arca, A.; Marceddu, S.; Bandiera, P.; Uzzau, S.; Sechi, M. Targeted biocompatibile nanoparticles for the delivery of (−)-epigallocatechin 3-gallate to prostate cancer cells. *J. Med. Chem.* **2011**, *54*, 1321−1332.

(9) Siddiqui, I. A.; Adhami, V. M.; Bharali, D. J.; Hafeez, B. B.; Asim, M.; Khwaja, S. I.; Ahmad, N.; Cui, H.; Mousa, S. A.; Mukhtar, H. Introducing nanochemoprevention as a novel approach for cancer control: Proof of principle with green tea polyphenol epigallocatechin-3-gallate. *Cancer Res.* **2009**, *69*, 1712−1716.

(10) Shutava, T. G.; Balkundi, S. S.; Lvov, Y. M. (−)-Epigallocatechin gallate/gelatin layer-by-layer assembled films and microcapsules. *J. Colloid Interface Sci.* **2009**, *330*, 276−283.

(11) Li, Z.; Ha, J.; Zou, T.; Gu, L. Fabrication of coated bovine serum albumin (BSA)-epigallocatechin gallate (EGCG) nanoparticles and their transport across monolayers of human intestinal epithelial Caco-2 cells. *Food Funct.* **2014**, *5*, 1278−1285.

(12) Haidong, L.; Fang, Y.; Zhihong, T.; Changle, R. Study on preparation of β-cyclodextrin encapsulation tea extract. *Int. J. Biol. Macromol.* **2011**, *49*, 561−566.

(13) Sosa, M. V.; Rodríguez-Rojo, S.; Mattea, F.; Cismondi, M.; Cocero, M. J. Green tea encapsulation by means of high pressure antisolvent coprecipitation. *J. Supercrit. Fluids* **2011**, *56*, 304−311.

(14) Dias, T. R.; Tomás, G.; Teixeira, N. F.; Alves, M. G.; Oliveira, P. F.; Silva, B. M. White tea (Camellia sinensis (L.)): antioxidant properties and beneficial health effects. *Int. J. Food Sci. Nutr. Diet.* **2013**, *2*, 1−15.

(15) Dias, T. R.; Alves, M. G.; Tomás, G. D.; Socorro, S.; Silva, B. M.; Oliveira, P. F. White tea as a promising antioxidant medium additive for sperm storage at room temperature: a comparative study with green tea. *J. Agric. Food Chem.* **2014**, *62*, 608−617.

(16) Azman, N. A.; Peiró, S.; Fajarí, L.; Julià, L.; Almajano, M. P. Radical scavenging of white tea and its flavonoid constituents by electron paramagnetic resonance (EPR) spectroscopy. *J. Agric. Food Chem.* **2014**, *62*, 5743−5748.

(17) Ainsworth, E. A.; Gillespie, K. M. Estimation of total phenolic content and other oxidation substrates in plant tissues using Folin-Ciocalteu reagent. *Nat. Protoc.* **2007**, *2*, 875−877.

(18) Stratil, P.; Klejdus, B.; Kuban, V. Determination of total content of phenolic compounds and their antioxidant activity in vegetables evaluation of spectrophotometric methods. *J. Agric. Food Chem.* **2006**, *54*, 607−616.

(19) Huang, W. Y.; Lin, Y. R.; Ho, R. F.; Liu, H. Y.; Lin, Y. S. Effects of water solutions on extracting green tea leaves. *Sci. World J.* **2013**, Article ID 368350.

DOI: 10.1021/jf505850q
J. Agric. Food Chem. 2015, 63, 2026−2032

(20) Gülçin, I. Antioxidant properties of resveratrol: A structure–activity insight. *Innovative Food Sci. Emerging Technol.* **2010**, *11*, 210–218.
(21) Vuong, Q. V.; Golding, J. B.; Stathopoulos, C. E.; Nguyen, M. H.; Roach, P. D. Optimizing conditions for the extraction of catechins from green tea using hot water. *J. Sep. Sci.* **2011**, *34*, 3099–3106.
(22) Harbowy, M. E.; Balentine, D. A. Tea chemistry. *Crit. Rev. Plant Sci.* **1997**, *16*, 415–480.
(23) Dash, T. K.; Konkimalla, V. B. Poly-ε-caprolactone based formulations for drug delivery and tissue engineering: A review. *J. Controlled Release* **2012**, *158*, 15–33.
(24) Sinha, V. R.; Bansal, K.; Kaushik, R.; Kumria, R.; Trehan, A. Poly-caprolactone microspheres and nanospheres: an overview. *Int. J. Pharm.* **2004**, *278*, 1–23.
(25) Sanna, V.; Roggio, A. M.; Posadino, A. M.; Cossu, A.; Marceddu, S.; Mariani, A.; Alzari, V.; Uzzau, S.; Pintus, G.; Sechi, M. Novel docetaxel-loaded nanoparticles based on poly(lactide-co-caprolactone) and poly(lactide-co-glycolide-co-caprolactone) for prostate cancer treatment: formulation, characterization, and cytotoxicity studies. *Nanoscale Res. Lett.* **2011**, *6*, 260.
(26) Sanna, V.; Siddiqui, I. A.; Sechi, M.; Mukhtar, H. Resveratrol-loaded nanoparticles based on poly(epsilon-caprolactone) and poly-(D,L-lactic-co-glycolic acid)-poly(ethylene glycol) blend for prostate cancer treatment. *Mol. Pharmaceutics* **2013**, *10*, 3871–3781.
(27) Goh, C. H.; Heng, P. W. S.; Chan, L. W. Alginates as a useful natural polymer for microencapsulation and therapeutic applications. *Carbohydr. Polym.* **2012**, *88*, 1–12.
(28) Durante, M.; Lenucci, M. S.; Laddomada, B.; Mita, G.; Caretto, S. Effects of sodium alginate bead encapsulation on the storage stability of durum wheat (*Triticum durum* Desf.) bran oil extracted by supercritical CO2. *J. Agric. Food Chem.* **2012**, *60*, 10689–10695.
(29) Elzein, T.; Nasser-Eddine, M.; Delaite, C.; Bistac, S.; Dumas, P. FTIR study of polycaprolactone chain organization at interfaces. *J. Colloid Interface Sci.* **2004**, *273*, 381–387.
(30) Sartori, C.; Finch, D. S.; Ralph, B. Determination of the cation content of alginate thin films by FTIR spectroscopy. *Polymer* **1997**, *38*, 43–51.
(31) Lin, D.; Pan, B.; Zhu, L.; Xing, B. Characterization and phenanthrene sorption of tea leaf powders. *J. Agric. Food Chem.* **2007**, *55*, 5718–24.
(32) Szymczycha-Madeja, A.; Welna, M.; Zyrnicki, W. Multi-element analysis, bioavailability and fractionation of herbal tea products. *J. Braz. Chem. Soc.* **2013**, *24*, 777–787.
(33) Munin, A.; Edwards-Lévy, F. Encapsulation of natural polyphenolic compounds; a review. *Pharmaceutics* **2011**, *3*, 793–829.
(34) Jain, D.; Bar-Shalom, D. Alginate drug delivery systems: application in context of pharmaceutical and biomedical research. *Drug Dev. Ind. Pharm.* **2014**, 1–9.
(35) Mehta, A. K.; Yadav, K. S.; Sawant, K. K. Nimodipine loaded PLGA nanoparticles: formulation optimization using factorial design, characterization and *in vitro* evaluation. *Curr. Drug Delivery* **2007**, *4*, 185–193.
(36) Sanna, V.; Roggio, A. M.; Siliani, S.; Piccinini, M.; Marceddu, S.; Mariani, A.; Sechi, M. Development of novel cationic chitosan- and anionic alginate-coated poly(D,L-lactide-co-glycolide) nanoparticles for controlled release and light protection of resveratrol. *Int. J. Nanomed.* **2012**, *7*, 5501–5516.
(37) Costa, P.; Sousa Lobo, J. M. Modeling and comparison of dissolution profiles. *Eur. J. Pharm. Sci.* **2001**, *13*, 123–133.
(38) Chan, E. W.; Soh, E. Y.; Tie, P. P.; Law, Y. P. Antioxidant and antibacterial properties of green, black, and herbal teas of *Camellia sinensis*. *Pharmacogn. Res.* **2011**, *3*, 266–272.
(39) Khurana, S.; Venkataraman, K.; Hollingsworth, A.; Piche, M.; Tai, T. C. Polyphenols: benefits to the cardiovascular system in health and in aging. *Nutrients* **2013**, *5*, 3779–3827.
(40) Sanna, V.; Roggio, A. M.; Pala, N.; Marceddu, S.; Lubinu, G.; Mariani, A.; Sechi, M. Effect of chitosan concentration on PLGA microcapsules for controlled release and stability of resveratrol. *Int. J. Biol. Macromol.* **2015**, *72*, 531–536.
(41) Li, N.; Taylor, L. S.; Mauer, L. J. Degradation kinetics of catechins in green tea powder: effects of temperature and relative humidity. *J. Agric. Food Chem.* **2011**, *59*, 6082–6090.
(42) Wang, R.; Zhou, W.; Jiang, X. Reaction kinetics of degradation and epimerization of epigallocatechin gallate (EGCG) in aqueous system over a wide temperature range. *J. Agric. Food Chem.* **2008**, *56*, 2694–2701.
(43) Wang, R.; Zhou, W.; Wen, R. A. H. Kinetic study of the thermal stability of tea catechins in aqueous systems using a microwave reactor. *J. Agric. Food Chem.* **2006**, *54*, 5924–5932.

DOI: 10.1021/jf505850q
J. Agric. Food Chem. 2015, 63, 2026–2032

or functional food supplement in China commonly used for its antidepressant, anti-inflammatory, antibacterial, antithrombotic, hepatoprotective, and choleretic effects.[23−26] Genipin is also a natural water-soluble bifunctional cross-linking reagent, which reacts with amines in proteins spontaneously, thus producing a semiinterpenetrating protein network within the developed hydrogel system.[27] Recently, stable casein microgels were developed from the covalent cross-linking of casein micelles with genipin, which showed resistance to dissociating agents.[28]

Herein the effects of genipin cross-linking of the interfacial casein layer on the colloid structure behavior induced by pH and the lipase lipolysis profile of the nanoemulsions were investigated. The casein-stabilized nanoemulsions were prepared through high pressure homogenization. The physicochemical properties of the genipin cross-linked nanoemulsions under different reaction conditions, including particle size, polydispersity index (PDI), surface charge, and morphology, as well as their variation under different gastrointestinal (GI) pH environments, were characterized by dynamic light scattering (DLS), zeta potential measurement, and TEM. The effects of different amounts of bile salt extract (BE), genipin/casein mass ratio, and cross-linking time on the lipolysis of lipid droplets were systematically investigated through measuring the completeness of lipolysis. It has been previously reported that there was little difference in the rate and extent of in vitro lipid digestion in emulsions stabilized by unheated and heated β-lactoglobulin, indicating that disulfide cross-linking of the interfacial protein did not influence the lipolysis of the emulsions.[29] The results presented here show a different trend.

MATERIALS AND METHODS

Materials. Extra virgin olive oil obtained from Agrioil SpA (Italy) was selected as the oil phase. According to the composition table provided by the manufacturer, the lipid content was 91.6 g/100 mL, which contained 13 g of saturated fatty acid. There was no protein, cholesterol, carbohydrate, or metal elements in the oil. Bovine casein of technical grade (C7078), BE (porcine, B8631), lipase from porcine pancreas (activity ≥2.0 USP units/mg, Type II, L3126), and NaOH were purchased from Sigma Co. (St. Louis, MO). Genipin (purity >98%) was purchased from Linchuan Zhixin Biotechnology Co., Ltd. (Jiangxi, China). All other chemicals were of analytical grade.

Preparation of Nanoemulsions. Aqueous solutions of casein protein with a concentration of 0.5%, 1%, and 2% (w/w) were prepared by dispersing the dried powders in pH 7.0 buffer (10 mM PBS) at room temperature and adjusting the pH to be around pH 8.0 until the protein was fully hydrated. Then the pH of the casein solution was adjusted back to pH 7.0 and mixed overnight to enhance hydration of the protein prior to homogenization. Extra virgin olive oil with a final concentration of 10% (w/w) in the emulsion was used as core material. The oil (40 mL) and aqueous (360 mL) phases were premixed with a high speed homogenizer (Ultra-Turrax T25 IKA Works Inc., Wilmington, NC) equipped with a S25 N18 G rotor operated at 24 000 rpm for 1 min at room temperature. The coarse emulsion (400 mL) was finely dispersed with a high pressure homogenizer (High Pressure Homogenization, NS1001 L2K, Niro Soavi, Italy) with pressures of 90 MPa for five passes.

Cross-Linking the Casein Emulsified Nanoemulsions with Genipin. For preparation of genipin cross-linked casein-stabilized nanoemulsions with a casein concentration of 20 mg/mL, different amounts of genipin with concentrations of 4, 8, and 16 mg/mL were added to the nanoemulsion droplet suspension, forming different final genipin/casein mass ratios of 0, 1:20, 1:10, and 1:5, with a reaction time of 24 h at 37 °C. For the nanoemulsion with a casein concentration of 10 mg/mL, the genipin concentrations were 2, 4, and 8 mg/mL. In addition, the reaction mixture was incubated at 37 °C for different times of 0, 6, 12, and 24 h, with a genipin/casein mass ratio of 1:10.

Nanoemulsion Stability and Structure Behavior in Simulated GI pH Environments. Equal amounts of the casein-emulsified nanoemulsion and the genipin cross-linked casein-emulsified nanoemulsion were first diluted 50 times in pH 1.2 (0.1 N HCl), pH 6.0 (10 mM PBS), and pH 7.0 (10 mM PBS) solutions for 2 h, respectively, simulating the pH environments of the GI tract. The size distribution, surface charge, and morphology of the nanoparticles at these distinct pH conditions were characterized by DLS, zeta potential measurement, and TEM.

Characterization of the Nanoemulsions. The measurement of particle size, polydispersity index (PDI), and zeta potential of the casein-emulsified nanoemulsion and the genipin cross-linked casein-emulsified nanoemulsion were performed on a Zetasizer Nano-ZS (Malvern Instruments) on the basis of DLS techniques. To avoid multiple scattering effects, emulsions were first diluted 50 times with deionized water (or simulated GI solution) and stirred continuously before measurement to ensure that the samples were homogeneous. All measurements were made in triplicate at 25 ± 1 °C.

The morphology of the casein-emulsified nanoemulsion and the one cross-linked with genipin was characterized by a high-performance digital imaging TEM machine (JEOL H-7650, Hitachi High-Technologies Corp.). One drop of the suspension was stained with 2% (w/v) phosphotungstic acid, placed on a copper grid, and allowed to evaporate in air. Once evaporated, the samples were placed in the TEM machine for imaging. The accelerating voltage used was 100 kV, and the images were taken on a Gatan electron energy loss spectrometry system using a 6 eV energy slit.

In Vitro Intestinal Lipid Digestion Model. The extent of in vitro intestinal digestion of casein-emulsified nanoemulsions and their counterparts cross-linked by genipin was determined using the pH-Stat method.[6,30,31] To evaluate the effect of BE on in vitro intestinal digestion, nanoemulsion systems were incubated with BE solution with different concentrations to obtain samples with different BE/casein mass ratios. To evaluate the influence of cross-linking degree on the extent of in vitro intestinal digestion, genipin cross-linked nanoemulsions with different genipin/casein mass ratios and different cross-linking times were applied as the digestion samples. The basic procedure for the in vitro intestinal digestion: (i) A 10.0 mL amount of nanoemulsion sample (with or without genipin cross-linking) was placed in a glass beaker and incubated in a water bath at 37 °C for 10 min, and then the system was adjusted to pH 7 using HCl or NaOH solutions. (ii) A 10.0 mL amount of BE solution with different concentrations, 1.0 mL of $CaCl_2$ solution, and 1.0 mL of NaCl solution were added to the sample under continuous stirring, and the system was adjusted back to pH 7 if required. (iii) A 1.0 mL amount of freshly prepared lipase solution was added to above mixture. The lipase solution was the supernatant obtained through centrifuging (4000 rpm for 5 min in 4 °C) the lipase powder dispersion (60 mg/mL in pH 7 phosphate buffer), which was incubated in 37 °C for 10 min before application. (iv) Immediately after step iii, the pH of the mixture under digestion was monitored with a Thomas Scientific pH meter (Model 8025) and maintained at pH 7.0 by titrating the free fatty acid released from lipolysis with an appropriate volume of 0.1 M NaOH until the pH value remained unchanged for 5 min. The final ionic concentration of the digestion medium before titration was 20 mM $CaCl_2$ and 150 mM NaCl in 10 mM phosphate buffer. The final BE concentration of the digestion medium before titration was in the range of 1.14−9.09 mg/mL. The volume of NaOH solution added to the digested mixture was recorded, which represented the free fatty acid generated by lipolysis.

In the present study, a mouth or stomach stage in the in vitro digestion model was not included; however, the passage of nanoemulsions through these regions of the GI tract could influence the composition, size, and interfacial characteristics of lipid droplets. Hydrolysis of the interfacial casein protein after genipin cross-linking by proteases in the stomach and intestine is also possible. In future studies, it would be useful to use a more sophisticated in vitro

DOI: 10.1021/jf505724c
J. Agric. Food Chem. 2015, 63, 2033−2040

digestion model to examine the effects of these additional digestive stages on the nanoemulsion performance.

Statistical Analysis. Data were expressed as mean ± standard deviation (SD) of at least triplicates. The least significant difference (LSD) test and one-way analysis of variance (ANOVA) were used for multiple comparisons by SPSS 16.0. A difference was considered to be statistically significant if $p < 0.05$ and very significant if $p < 0.01$.

RESULTS AND DISCUSSION

Original Microstructure. Figure 1 shows the diameters of olive oil emulsion droplets stabilized with casein as a function of the total protein concentrations. The average droplet sizes of the casein-emulsified nanoemulsion with different protein concentrations were in a range from 206.7 ± 17.0 nm to 271.5 ± 23.1 nm with the surface charge around −55 mV (data not shown). The PDIs of the droplet suspension were less than 0.3, indicating that the nanoemulsion was homogeneously dispersed in the solution. Figure 1 shows that the droplet size decreased with the increase in casein concentration from 5 mg/mL to 20 mg/mL. Meanwhile, the PDI of the nanoemulsion suspension decreased sharply, which indicated that the homogeneity of the nanoemulsion suspension was enhanced at high casein concentration. At lower protein concentrations, less protein could be adsorbed at the oil−water interface; hence, less interfacial area was covered by the protein, leading to an increase in emulsion droplet size and suspension heterogeneity. At higher protein concentrations, the surface of the droplet was fully covered by the protein, making the nanoemulsion structure smaller. Due to electrostatic repulsion between the droplets, the particle size of the droplets remained constant with the increasing casein concentration.[32,33]

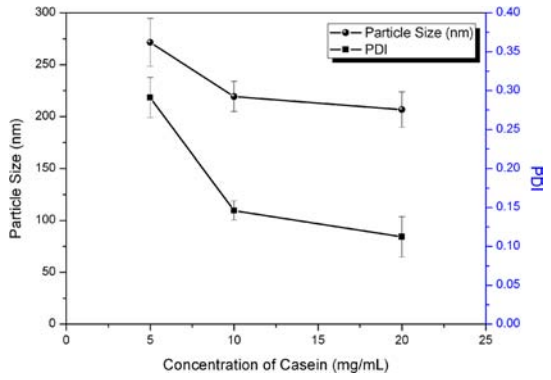

Figure 1. Average droplet size and PDI of the casein-emulsified nanoemulsion with different protein concentrations (5, 10, 20 mg/mL). Data were expressed as mean ± standard deviation (SD) of at least triplicates.

Genipin Cross-Linked Nanoemulsion Microstructure. Genipin covalently cross-linked the casein protein covering the surface of the olive oil nanoemulsion droplets spontaneously when genipin was added to the original suspension. The appearance of blue coloration in the reaction mixture was traditionally considered as rapid evidence that the cross-linking reaction was taking place.[27] The cross-linking reaction occurred by means of a complex mechanism.[34] A nucleophilic attack by the amino groups of casein protein on the olefinic carbon atom at C-3 in genipin occurred, followed by dihydropyran ring opening and attack by the secondary amino group on the newly formed aldehydo group. In the product, short chains of condensed genipin acted as cross-linking bridges. Figure 2 shows the droplet particle size and surface charge of the casein-emulsified nanoemulsion after cross-linking with genipin for 24 h as a function of different mass ratios between genipin and the protein (0, 1:20, 1:10, and 1:5). After cross-linking with genipin, the droplet size of the nanoemulsion with protein concentrations of either 10 or 20 mg/mL slightly increased compared with the nonmodified nanoemulsion (Figure 2A). This might be caused by the increased thickness of the interfacial protein layer due to the gelation of the casein adsorbed on the surface of oil droplet after intraparticle cross-linking, rather than interparticle association of the nanoemulsion droplets. It was reported previously that genipin could spontaneously cross-link casein to induce gelation of the protein.[28,35] The gelation rate increased significantly with the increase in genipin concentration and elevation of reaction temperature. Comparatively, no obvious changes in the droplet surface charge could be observed after cross-linking with genipin. The surface charge of casein-emulsified nanoemulsion droplets was in the range of −50 mV to −60 mV. Genipin cross-linked protein through its reaction with amino groups, with little impact on the carboxyl groups in the protein. Therefore, the surface charge of the nanoemulsion droplets was influenced little by genipin cross-linking.

Structure Stability of the Nanoemulsion and the Genipin Cross-Linked Nanoemulsion in Different Gastrointestinal pH Environments. Interfacial proteins impart emulsion stability by a combination of electrostatic and steric

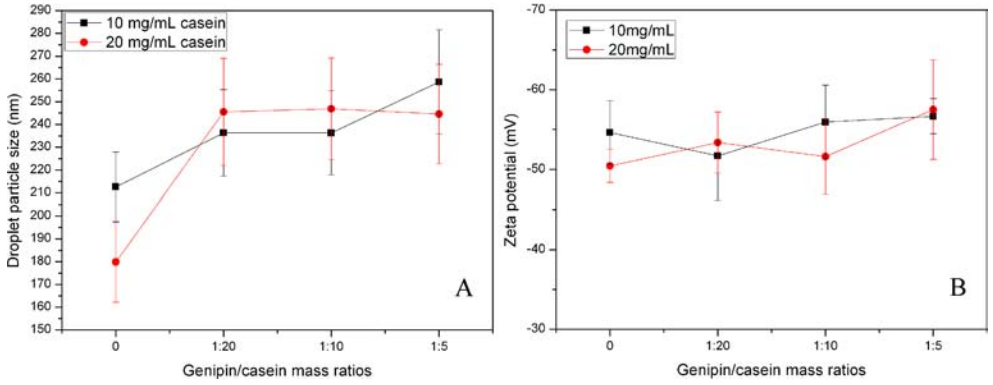

Figure 2. Droplet size (A) and surface charge (B) of the casein-emulsified nanoemulsion cross-linked with genipin under different genipin/casein mass ratios of 0, 1:20, 1:10, 1:5 (reaction at temperature of 37 °C for 24 h). Data were expressed as mean ± standard deviation (SD) of at least triplicates.

DOI: 10.1021/jf505724c
J. Agric. Food Chem. 2015, 63, 2033−2040

mechanisms.[32] The electrostatic effect of the emulsified protein on emulsion stability could be significantly influenced by the environmental pH conditions. Stability and structure behaviors of emulsions in the GI environment have received increasing attention because they impart not only the delivery profile of the nanoemulsion as drug or nutriceutical carriers but also the oil digestion rate and degree.[36,37] Figure 3A shows the droplet size of the casein-emulsified nanoemulsion with or without genipin cross-linking under simulated gastric acidic conditions. The droplet size of the nanoemulsion without genipin cross-linking increased significantly with prolonged incubation time under harsh gastric acidic conditions (pH 1.2). Similar phenomena were also reported in previous studies on the structure behaviors of protein-emulsified emulsions. Sarkar et al. found that β-lactoglobulin (β-lg)-stabilized emulsions underwent extensive droplet flocculation, with some coalescence, upon mixing with simulated gastric solution, which was primarily attributed to the acidic pH.[38] Golding et al. investigated the structure behavior of a protein-stabilized, negatively charged emulsion under simulated GI conditions and also found that incubation in a gastric pH environment resulted in emulsion flocculation.[9]

Interestingly, after cross-linking with genipin, the stability of casein protein-emulsified nanoemulsion was enhanced. Especially, with genipin/protein mass ratios of 1:10 and 1:5, the droplet size of the nanoemulsion was significantly ($p < 0.05$) or very significantly ($p < 0.01$) smaller than that of the non-cross-linked nanoemulsion at the same incubation time intervals. For the genipin cross-linked nanoemulsion with a genipin/protein mass ratio of 1:5, no changes in droplet size could be observed within the incubation time under the simulated gastric pH condition (pH 1.2). Under simulated intestinal pH environments, pH 6.0 for the duodenum and pH 7.0 for the proximal ileum, both the genipin cross-linked and non-cross-linked casein-emulsified nanoemulsions remained stable without changes in droplet size within the incubation time (Figure 3b,c).

Figure 4 shows the particle size distribution of the cross-linked nanoemulsion (genipin/protein mass ratio of 1:5) and the non-cross-linked nanoemulsion in a simulated gastric environment of pH 1.2 for 30 min. The droplet size distribution of the casein-emulsified nanoemulsion changed sharply (Figure 4a,b). Comparatively, no significant changes in the droplet size distribution of the genipin cross-linked nanoemulsions could be found under the same gastric pH condition for the same incubation time (Figure 4c,d). Similar phenomena were also found in a previous study where casein-stabilized emulsions enzymatically cross-linked by transglutaminase maintained colloid stability under gastric acidic conditions.[39] In the present study, the negative surface charge of the genipin cross-linked nanoemulsion droplets decreased in the same trend (data not shown) as that which occurred in the surface charge of the non-cross-linked nanoemulsion when it was incubated in the simulated gastric pH environment. Therefore, the significantly enhanced colloid stability of the genipin cross-linked nanoemulsion under strong acidic conditions might be mainly attributed to the amplified steric mechanics caused by gelation of the casein protein, rather than the electrostatic mechanics.

Morphology of the Nanoemulsions. TEM images of the nanoemulsion with stable structure were examined for the effects of genipin cross-linking on the morphology of the casein-emulsified nanoemulsion and its structure in a strong acidic environment. Figure 5 shows the morphology of the

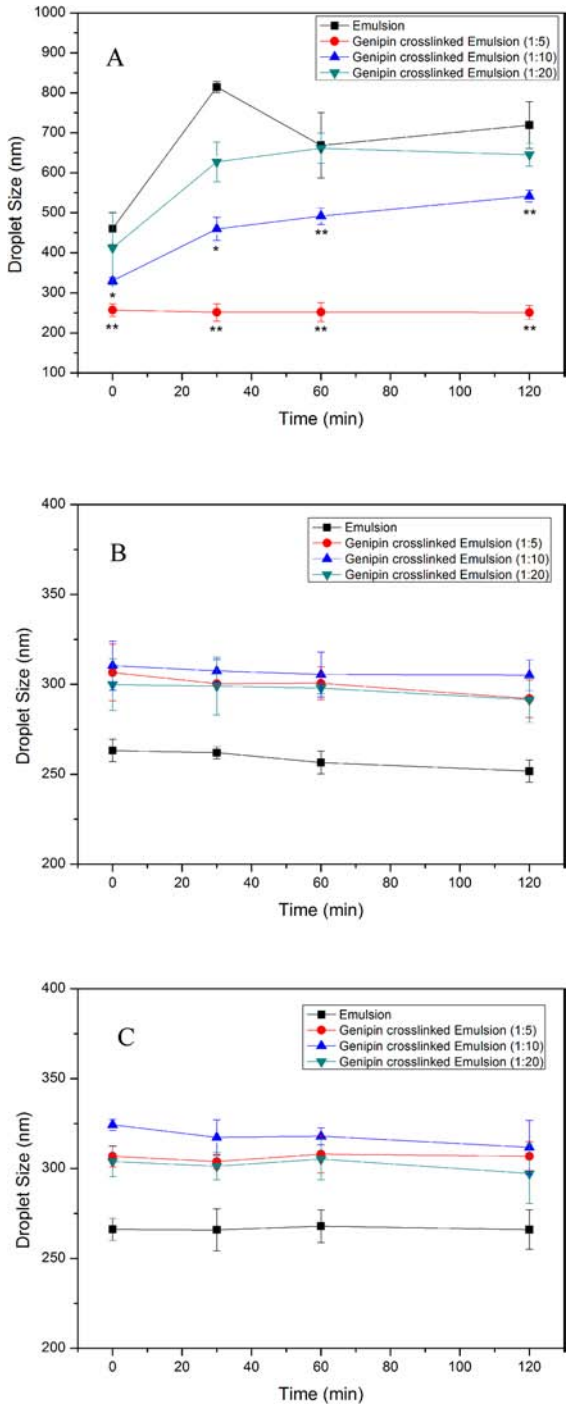

Figure 3. Droplet size of the casein (20 mg/mL)-emulsified nanoemulsion cross-linked with genipin with different genipin/casein mass ratios of 0, 1:20, 1:10, 1:5 under gastric pH (A, pH 1.2) and intestinal pH (B, pH 6.0; C, pH 7.0) conditions. The cross-linking reaction took place at a temperature of 37 °C for 24 h. Data were expressed as mean ± standard deviation (SD) of at least triplicates (*$p < 0.05$; **$p < 0.01$).

casein-emulsified nanoemulsion, genipin cross-linked casein-emulsified nanoemulsion (genipin/casein mass ratio of 1:5, reaction time of 24 h), and their counterparts under simulated gastric pH conditions (pH 1.2). The nanoemulsion droplets in Figure 5A−C were all homogeneously dispersed. No interparticle association of the nanoemulsion droplets could be observed after cross-linking the casein-emulsified nano-

DOI: 10.1021/jf505724c
J. Agric. Food Chem. 2015, 63, 2033−2040

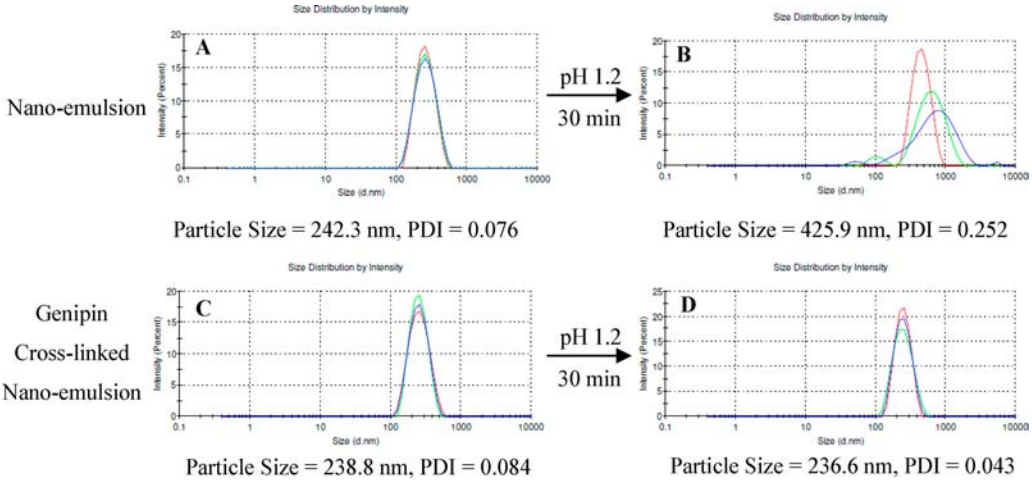

Figure 4. Droplet size distribution of the casein-emulsified nanoemulsions and their counterparts cross-linked with genipin with a genipin/casein mass ratio of 1:5 in a gastric environment (pH 1.2) for 30 min. (Casein concentration was 20 mg/mL, and the lines with different colors represented the three measurement results from the same sample.)

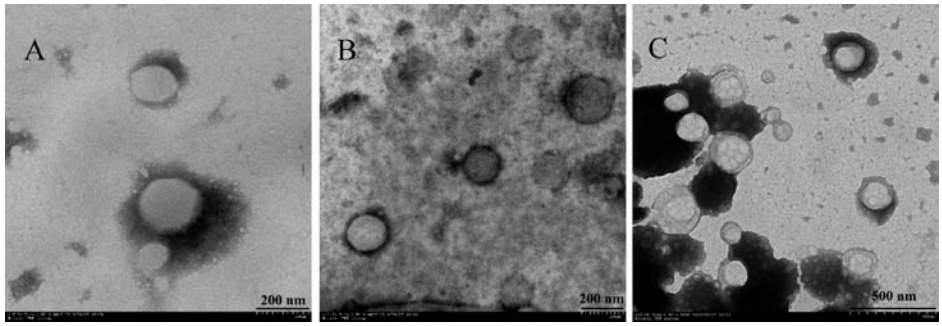

Figure 5. (A) TEM images of the casein-emulsified (20 mg/mL) nanoemulsion, (B) genipin cross-linked nanoemulsion with a genipin/casein mass ratio of 1:5 and reaction time of 24 h, and (C) the genipin cross-linked nanoemulsion incubated under simulated gastric pH conditions (pH 1.2) for 2 h.

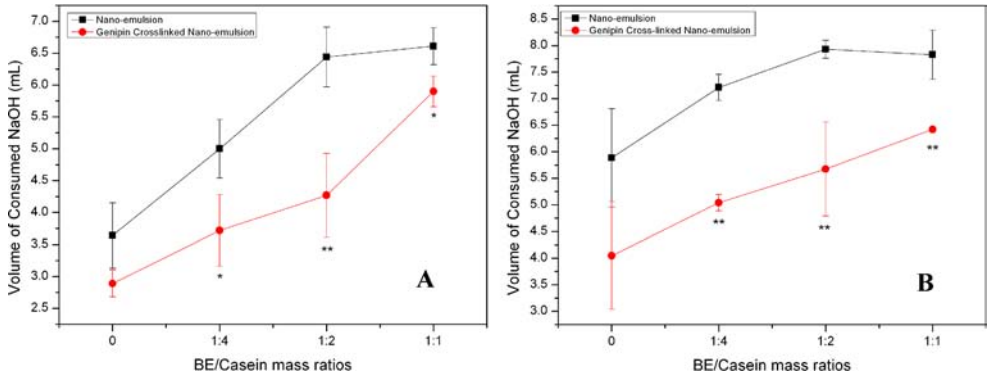

Figure 6. Extent of lipid digestion of the nanoemulsion and genipin cross-linked nanoemulsion stabilized with 10 mg/mL (A) and 20 mg/mL (B) casein protein under different BE/casein mass ratios. Data were expressed as mean ± standard deviation (SD) of at least triplicates. (The genipin cross-linking reaction took replace with genipin/casein mass ratio of 1:10 for 12 h. $*p < 0.05$; $**p < 0.01$.)

emulsion with genipin. The droplet size of the genipin cross-linked nanoemulsion was similar to that of the original one in the TEM images (Figure 5A,B). These results were consistent with those obtained from the DLS results (Figure 2A). Compared with the casein-emulsified nanoemulsion droplets in Figure 5A, the genipin cross-linked ones in Figure 5B showed more compact microstructure with clearer and defined contour. After incubation in the pH 1.2 solution for 2 h, the genipin cross-linked nanoemulsion droplets were still stable and dispersed homogeneously (Figure 5C). It was consistent with the result in Figure 3A. Interestingly, the nanoemulsion droplets showed "core−shell" structure with a phantomlike shell and clear core, which might be caused by the swelling of the surface protein gelation film under strong acidic conditions.

Effects of Different BE/Protein Mass Ratios on Lipid Digestion of the Nanoemulsions and Genipin Cross-Linked Nanoemulsions. Figure 6 shows the volume of NaOH (0.1 M) consumed to neutralize the released free fatty

DOI: 10.1021/jf505724c
J. Agric. Food Chem. 2015, 63, 2033−2040

acid during in vitro intestinal digestion of the nanoemulsion lipid droplets with different BE/protein mass ratios ranging from 0, 1:4, 1:2, to 1:1. The amount of consumed NaOH increased with the increase of BE amount added to the nanoemulsion system, indicating that lipolysis was enhanced. The increased amount of casein covering the surface of the lipid droplets might be replaced by the elevated amount of BE, leading to a larger proportion of the drop surface ready for adsorption of lipase.[6,10] Therefore, an increased amount of free fatty acid was released from intestinal digestion of the lipid droplets in the system. Interestingly, cross-linking of the casein (10 and 20 mg/mL)-stabilized nanoemulsions with genipin significantly ($p < 0.05$) or very significantly ($p < 0.01$) decreased the amount of consumed NaOH compared with their non-cross-linking counterparts at the same BE/protein mass ratio, which indicated that lipolysis of the lipid droplets was effectively delayed. It was reported that the steric resistance between the interfacial layer and the bile salt played an important role in the displacement of the casein protein on the surface of lipid droplets.[13] One strategy that was applied in previous studies to enhance the steric resistance for inhibiting the displacement by bile salts was to associate casein protein on the nanoemulsion droplet surface with polysaccharides, which could further inhibit the absorption of the lipase.[17−19] In the present study, cross-linking of the droplet surface casein protein with genipin also formed a stable steric film that might resist the interfacial displacement by the bile salts to control the lipid digestion process, as it could retard the next action of lipase.

Effects of Different Genipin/Protein Mass Ratios on the Lipid Digestion of the Genipin Cross-Linked Nanoemulsion. Figure 7 shows that the amount of NaOH consumed to neutralize the released free fatty acid during lipid hydrolysis decreased with the increase in genipin/protein mass ratio in lipid nanoemulsions stabilized with 10 and 20 mg/mL casein protein, which indicated that the amount of released free acid decreased with the increase in genipin/protein mass ratio. The free fatty acid released from the cross-linked nanoemulsion (protein concentration of 10 mg/mL at genpin/protein mass ratios of 1:10 and 1:5, and protein concentration of 20 mg/mL at genpin/protein mass ratios of 1:20, 1:10, and 1:5) was very significantly ($p < 0.01$) less than that of their non-cross-linking counterparts. It was reported in a recent study that casein microgels were formed through cross-linking casein micelles with genipin, which were resistant to the presence of dissociating agents, did not dissociate at the air−solution interface, and formed solidlike interfaces rather than a viscoelastic gel.[28] In the present study, it has been revealed in the DLS results (Figure 2) that the increased genipin/protein mass ratios increased the thickness of the interfacial casein protein layer. This could also be caused by the formation of casein microgels on the O/W interface, which enhanced its resistance against bile salt displacement. Further, the lipolysis of the nanoemulsion lipid droplets was inhibited by retarding the following action of lipase. Therefore, the intestinal digestion of lipid could be effectively decreased and controlled through modulating genipin cross-linking degrees. The lipid digestion extent of the nanoemulsion droplet emulsified with 20 mg/mL casein was higher than that of the nanoemulsion droplet emulsified with 10 mg/mL casein, which was mainly related to the decrease in droplet size with the increase in casein concentration. It was reported that the extent of lipid digestion increased with the decrease in mean droplet diameter, which was attributed to the increase in lipid surface area exposed to pancreatic lipase with decreasing droplet size.[40]

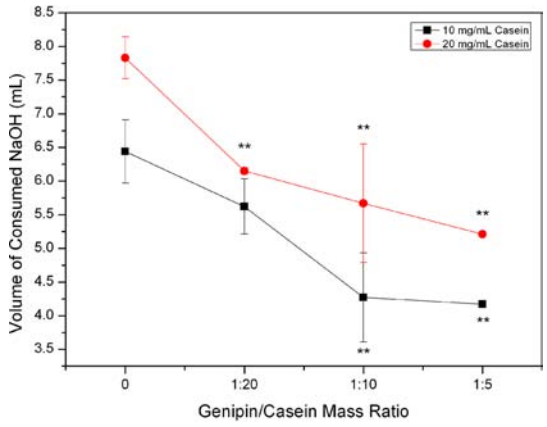

Figure 7. Extent of lipid digestion of the genipin cross-linked nanoemulsions stabilized with 10 and 20 mg/mL casein protein under different genipin/casein mass ratios. Data were expressed as mean ± standard deviation (SD) of at least triplicates. (The genipin cross-linking reaction took place for 12 h, and the BE/casein mass ratio was 1:2 for the in vitro intestinal digestion model. $^{**}p < 0.01$.)

Effects of Different Genipin Cross-Linking Time on the Lipid Digestion of the Genipin Cross-Linked Nanoemulsion. At the same genipin/protein mass ratio of 1:10, the cross-linking degree could also be adjusted through changing the cross-linking time. Figure 8 shows that the amount of NaOH consumed to neutralize the released fatty acid decreased with the increase in genipin cross-linking time during the 24 h testing. For the nanoemulsion droplets with a casein concentration of 10 mg/mL, intestinal digestion of the lipid droplets were very significantly ($p < 0.01$) decreased with the cross-linking times of 6, 12, and 24 h, compared with their counterpart digestion system with a cross-linking time of 0. The amounts of free fatty acid released from the digestion of the original nanoemulsion and the immediate mixture of the original nanoemulsion and genipin without cross-linking time were similar, indicating that the delay effect of genipin cross-

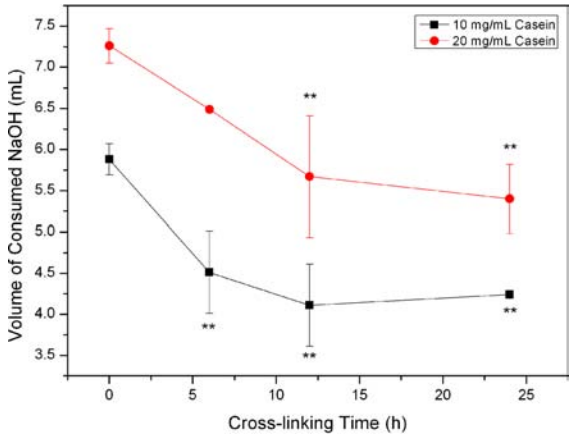

Figure 8. Extent of lipid digestion of the genipin cross-linked nanoemulsions stabilized with 10 and 20 mg/mL casein protein with different cross-linking times. Data were expressed as mean ± standard deviation (SD) of at least triplicates. (The genipin cross-linking reaction took place with a genipin/casein mass ratio of 1:10, and a BE/casein mass ratio was 1:2 for the in vitro digestion model. $^{**}p < 0.01$.)

DOI: 10.1021/jf505724c
J. Agric. Food Chem. 2015, 63, 2033−2040

linking on lipase digestion was mainly attributed to the casein layer's resistance against bile salt displacement rather than a direct influence on lipase activity. There was no significant difference between the lipid digestion extent of the genipin cross-linked nanoemulsion with cross-linking times of 12 and 24 h, which indicated that complete cross-linking of the droplet surface casein protein was achieved with a genipin cross-linking time of 12 h. In previous studies, it was found that the swelling rate of casein hydrogel cross-linked with genipin and the release rate of its loaded drug decreased with the increase in cross-linking degree, which meant that more compact net structure was formed with an enhanced genipin cross-linking degree.[35]

A green and effective method, cross-linking of the interfacial casein layer on the surface of nanoemulsion droplets with genipin, was successfully established to significantly enhance the stability of the nanoemulsions under GI pH conditions and delay the digestion of lipid in the droplets. The droplet size of the homogeneously dispersed (PDI < 0.3), casein-emulsified nanoemulsion was in the range of 206.7 ± 17.0 nm to 271.5 ± 23.1 nm, and its surface charge was around −55 mV. Droplet size and surface charge of the nanoemulsions decreased with the increase in protein concentration from 5 to 20 mg/mL. Genipin cross-linking slightly increased the nanoemulsion droplet size and did not change the surface charge. The stability of the nanoemulsion under a harsh gastric pH environment was enhanced significantly ($p < 0.05$) or very significantly ($p < 0.01$) with steady particle size after cross-linking with genipin under different genipin/casein mass ratios. The flocculation that normally occurred on the casein-emulsified nanoemulsion in a gastric environment was successfully prevented. Regular spherical droplets with a particle size of 200−300 nm were observed by TEM. The genipin cross-linked nanoemulsion droplets showed more compact microstructure with clear and defined contour. Incubated under gastric pH conditions, the genipin cross-linking nanoemulsion showed a "core−shell" structure that might be caused by the swelling of the surface protein film. Interestingly, the digestion extent of the lipid in the nanoemulsion droplets by lipase under simulated intestinal fluid conditions was delayed very significantly ($p < 0.01$) after cross-linking the interfacial casein layer with genipin, which was enhanced by the increase in genipin/casein mass ratio and cross-linking time. Further study of the detailed mechanism of the resistant effect of genipin cross-linked casein against bile salts displacement is in progress.

AUTHOR INFORMATION

Corresponding Authors

*Tel (+) 86-139-15983201; e-mail: hubing212002@njau.edu.cn.

*Tel/Fax (+) 86-25-84396791; e-mail: zengxx@njau.edu.cn.

Funding

This work was supported by The Natural Science Foundation of Jiangsu Province, China (BK2012367), Project Funded by the Priority Academic Program Development of Jiangsu Higher Education Institutions, Specialized Research Fund for the Doctoral Program of Higher Education of China (No. 20120097120001), and an Undergraduate Student Research Training (SRT) program from Nanjing Agricultural University (1418A07).

Notes

The authors declare no competing financial interest.

REFERENCES

(1) Foster, R.; Lunn, J. 40th Anniversary Briefing Paper: Food availability and our changing diet. *Nutr. Bull.* **2007**, *32*, 187−249.

(2) Singh, H. Aspects of milk-protein-stabilised emulsions. *Food Hydrocolloids* **2011**, *25*, 1938−1944.

(3) Armand, M.; Pasquier, B.; Andre, M.; Borel, P.; Senft, M.; Peyrot, J.; Salducci, J.; Portugal, H.; Jaussan, V.; Lairon, D. Digestion and absorption of 2 fat emulsions with different droplet sizes in the human digestive tract. *Am. J. Clin. Nutr.* **1999**, *70*, 1096−1099.

(4) Maljaars, P. W. J.; van der Wal, R. J. P.; Wiersma, T.; Peters, H. P. F.; Haddeman, E.; Masclee, A. A. M. The effect of lipid droplet size on satiety and peptide secretion is intestinal site-specific. *Clin. Nutr.* **2012**, *31*, 535−542.

(5) Singh, H.; Ye, A. Structural and biochemical factors affecting the digestion of protein-stabilized emulsions. *Curr. Opin. Colloid Interface Sci.* **2013**, *18*, 360−370.

(6) Mun, S.; Decker, E.; Park, Y.; Weiss, J.; McClements, D. J. Influence of interfacial composition on in vitro digestibility of emulsified lipids: Potential mechanism for chitosan's ability to inhibit fat digestion. *Food Biophys.* **2006**, *1*, 21−29.

(7) Singh, H.; Ye, A.; Horne, D. Structuring food emulsions in the gastrointestinal tract to modify lipid digestion. *Prog. Lipid Res.* **2009**, *48*, 92−100.

(8) Wilde, P. J.; Chu, B. S. Interfacial & colloidal aspects of lipid digestion. *Adv. Colloid Interface Sci.* **2011**, *165*, 14−22.

(9) Golding, M.; Wooster, T. J. The influence of emulsion structure and stability on lipid digestion. *Curr. Opin. Colloid Interface Sci.* **2010**, *15*, 90−101.

(10) Maldonado-Valderrama, J.; Woodward, N. C.; Gunning, A. P.; Ridout, M. J.; Husband, F. A.; Mackie, A. R.; Morris, V. J.; Wilde, P. J. Interfacial characterization of β-lactoglobulin networks: Displacement by biles salts. *Langmuir* **2008**, *24*, 6759−6767.

(11) Malone, M. E.; Appelqvist, I. A. M.; Norton, I. T. Oral behaviour of food hydrocolloids and emulsions. Part 2. Taste and aroma release. *Food Hydrocolloids* **2003**, *17*, 775−784.

(12) Maldonado-Valderrama, J.; Miller, R.; Fainerman, V. B.; Wilde, P. J.; Morris, V. J. Effect of gastric conditions on β-lactoglobulin interfacial networks: Influence of the oil phase on protein structure. *Langmuir* **2010**, *26*, 15901−15908.

(13) Euston, S. R.; Baird, W. G.; Campbell, L.; Kuhns, M. Competitive adsorption of dihydroxy and trihydroxy bile salts with whey protein and casein in oil-in-water emulsions. *Biomacromolecules* **2013**, *14*, 1850−1858.

(14) Yao, X. L.; Wang, N.; Fang, Y. P.; Phillips, G. O.; Jiang, F. T.; Hu, J. Z.; Lu, J.; Xu, Q.; Tian, D. Impact of surfactants on the lipase digestibility of gum arabic-stabilized O/W emulsions. *Food Hydrocolloids* **2013**, *33*, 393−401.

(15) Reis, P. M.; Raab, T. W.; Chuat, J. Y.; Leser, M. E.; Miller, R.; Watzke, H. J.; Holmberg, K. Influence of surfactants on lipase fat digestion in a model gastro-intestinal system. *Food Biophys.* **2008**, *3*, 370−381.

(16) Day, L.; Golding, M.; Xu, M.; Keogh, J.; Clifton, P.; Wooster, T. J. Tailoring the digestion of structured emulsions using mixed monoglyceride-caseinate interfaces. *Food Hydrocolloids* **2014**, *36*, 151−161.

(17) Wooster, T. J.; Day, L.; Xu, M.; Golding, M.; Oiseth, S.; Keogh, J.; Clifton, P. Impact of different biopolymer networks on the digestion of gastric structured emulsions. *Food Hydrocolloids* **2014**, *36*, 102−114.

(18) Li, Y.; McClements, D. J. Modulating lipid droplet intestinal lipolysis by electrostatic complexation with anionic polysaccharides: Influence of cosurfactants. *Food Hydrocolloids* **2014**, *35*, 367−374.

(19) Lesmes, U.; McClements, D. J. Controlling lipid digestibility: Response of lipid droplets coated by β-lactoglobulin-dextran Maillard conjugates to simulated gastrointestinal conditions. *Food Hydrocolloids* **2012**, *26*, 221−230.

(20) Sebastien, M. Bioaccessibility of nutrients and micronutrients from dispersed food systems: Impact of the multiscale bulk and interfacial structures. *Crit. Rev. Food Sci. Nutr.* **2013**, *53*, 76−108.

DOI: 10.1021/jf505724c
J. Agric. Food Chem. 2015, 63, 2033−2040

(21) Acosta, E. Bioavailability of nanoparticles in nutrient and nutraceutical delivery. *Curr. Opin. Colloid Interface Sci.* **2009**, *14*, 3−15.
(22) Gamboa, J. M.; Leong, K. W. In vitro and in vivo models for the study of oral delivery of nanoparticles. *Adv. Drug Delivery Rev.* **2013**, *65*, 800−810.
(23) Tian, J. S.; Shi, B. Y.; Xiang, H.; Gao, S.; Qin, X. M.; Du, G. H. ^{1}H-NMR-Based metabonomic studies on the anti-depressant effect of genipin in the chronic unpredictable mild stress rat model. *PLoS One* **2013**, *8*, e75721.
(24) Koo, H. J.; Lim, K. H.; Jung, H. J.; Park, E. H. Anti-inflammatory evaluation of gardenia extract, geniposide and genipin. *J. Ethnopharmacol.* **2006**, *103*, 496−500.
(25) He, Q.; Kong, X.; Wu, G.; Ren, P.; Tang, H.; Hao, F. H.; Huang, R. L.; Li, T. J.; Tan, B.; Li, P.; Tang, Z. R.; Yin, Y. L.; Wu, Y. N. Metabolomic analysis of the response of growing pigs to dietary L-arginine supplementation. *Amino Acids* **2009**, *37*, 199−208.
(26) Kim, B. C.; Kim, H. G.; Lee, S. A.; Lim, S.; Park, E. H.; Kim, S. J.; Lim, C. Genipin-induced apoptosis in hepatoma cells is mediated by reactive oxygen species/c-Jun NH2-terminal kinase-dependent activation of mitochondrial pathway. *J. Biochem. Pharmacol.* **2005**, *70*, 1398−1047.
(27) Muzzarelli, R. A. A. Genipin-crosslinked chitosan hydrogels as biomedical and pharmaceutical aids. *Carbohyd. Polym.* **2009**, *77*, 1−9.
(28) Silva, N. F. N.; Saint-Jalmes, A.; de Carvalho, A. F.; Gaucheron, F. Development of casein microgels from cross-linking of casein micelles by genipin. *Langmuir* **2014**, *30*, 10167−10175.
(29) Sandra, S.; Decker, E. A.; McClements, D. J. Effect of interfacial protein cross-linking on the in vitro digestibility of emulsified corn oil by pancreatic lipase. *J. Agric. Food Chem.* **2008**, *56*, 7488−7494.
(30) Hu, M.; Li, Y.; Decker, E. A.; McClements, D. J. Role of calcium and calcium binding agents on the lipase digestibility of emulsified lipids using an in vitro digestion model. *Food Hydrocolloids* **2010**, *24*, 719−725.
(31) Sarkar, A.; Goh, K. K. T.; Singh, H. Properties of oil-in-water emulsions stabilized by β-lactoglobulin in simulated gastric fluid as influenced by ionic strength and presence of mucin. *Food Hydrocolloids* **2010**, *24*, 534−541.
(32) Ye, A. Q.; Zhu, X. Q.; Singh, H. Oil-in-water emulsion system stabilized by protein-coated nanoemulsion droplets. *Langmuir* **2013**, *29*, 14403−14410.
(33) Dickinson, E. Milk protein interfacial layers and the relationship to emulsion stability and rheology. *Colloid Surf., B* **2001**, *20*, 197−210.
(34) Butler, M. F.; Ng, Y. F.; Pudney, P. D. A. Mechanism and kinetics of the crosslinking reaction between biopolymers containing primary amine groups and genipin. *J. Polym. Sci., Part A: Polym. Chem.* **2003**, *41*, 3941.
(35) Song, F.; Zhang, L.-M.; Yang, C.; Yan, L. Genipin-crosslinked casein hydrogels for controlled drug delivery. *Int. J. Pharm.* **2009**, *373*, 41−47.
(36) Lueamsaisuk, C.; Lentle, R. G.; MacGibbon, A. K. H.; Matia-Merino, L.; Golding, M. Factors influencing the dynamics of emulsion structure during neonatal gastric digestion in an in vitro model. *Food Hydrocolloids* **2014**, *36*, 162−172.
(37) Sarkar, A.; Horne, D. S.; Singh, H. Pancreatin-induced coalescence of oil-in-water emulsions in an in vitro duodenal model. *Int. Dairy J.* **2010**, *20*, 589−597.
(38) Sarkar, A.; Goh, K. K. T.; Singh, R. P.; Singh, H. Behaviour of an oil-in-water emulsion stabilized by beta-lactoglobulin in an in vitro gastric model. *Food Hydrocolloids* **2009**, *23*, 1563−1569.
(39) Macierzanka, A.; Bottger, F.; Rigby, N. M.; Lille, M.; Poutanen, K.; Mills, E. N. C.; Mackie, A. R. Enzymatically structured emulsions in simulated gastrointestinal environment: Impact on interfacial proteolysis and diffusion in intestinal mucus. *Langmuir* **2012**, *28*, 17349−17362.
(40) Salvia-Trujillo, L.; Qian, C.; Martin-Belloso, O.; McClements, D. J. Influence of particle size on lipid digestion and beta-carotene bioaccessibility in emulsions and nanoemulsions. *Food Chem.* **2013**, *141*, 1472−1480.

DOI: 10.1021/jf505724c
J. Agric. Food Chem. 2015, 63, 2033−2040

Table 1. Sample Code

substrate A		substrate B	
sample code	name	sample code	name
I1	initial step cycle 1	I1	initial step cycle 1
F1	final step cycle 1	F1	final step cycle 1
P1	pasteurized final step cycle 1	P1	pasteurized final step cycle 1
I2	initial step cycle 2	I2	initial step cycle 2
F2	final step cycle 2	F2	final step cycle 2
P2	pasteurized final step cycle 2	P2	pasteurized final step cycle 2
I3	initial step cycle 3	I3	initial step cycle 3
F3	final step cycle 3	F3	final step cycle 3
P3	pasteurized final step cycle 3	P3	pasteurized final step cycle 3
		I4	initial step cycle 4
		F4	final step cycle 4
		P4	pasteurized final step cycle 4

2. MATERIALS AND METHODS

2.1. Chemicals and Reagents. The standard compounds used were purchased from Fluka Sigma-Aldrich (St. Louis, MO, USA) [gallic acid, caffeic acid, p-coumaric acid, cinnamic acid, (−)-epicatechin, (+)-catechin, chlorogenic acid, ellagic acid, (−)-epicatechin gallate, kaempferol, kaempferol-3-*O*-*β*-D-glucuronide, kaempferol-3-glucoside, polydatin, penta-*O*-galloyl-*β*-D-glucose hydrate, apigenin, quinic acid, brevifolin, protocatechuic acid, isorhamnetin, (+)-taxifolin, eriodictyol, rutin, quercetin, homovanillic acid, and kaempferol glucuronide], Chromadex Inc. (USA) [procyanidin B1], and Extrasynthese [luteolin, (+)-aromadendrin, phloridzin, flavonomarein, and apigenin-7-*O*-glucoside]. DPPH, AAPH (2,2′-diazo-bis-amidine-propane-dihydrochloride), and Trolox (6-hydroxy-2,5,7,8-tetramethyl-chroman-2-carboxylic acid) were obtained from Sigma-Aldrich (St. Louis, MO, USA); acetonitrile, acetic acid, methanol, and formic acid (LC gradient) from Merck (Darmstadt, Germany), and methanol from Prolabo (Obregón, Mexico).

2.2. Samples. Two strawberry purée substrates (A and B) made with production surplus, grown in Huelva (Andalusia, Spain), were used as substrates of the fermentation process were analyzed and previously reported.[3] The principal cultivated varieties were Camarosa, Candonga, Festival, Ventana, Splendor, Honor, and Coral. They were provided by Hudisa Company (Lepe, Huelva, Spain). Substrate A corresponds to the 2011 harvest and B to the 2012 harvest. *Saccharomyces cerevisiae* (CET 13057 isolated from native strawberry yeast)[11] was used as a starter for the submerged fermentation process. The fermentation process was as follows: 3.6 L of strawberry purée was placed into the bioreactor and the conditions set (29 °C, 26.20 rad s^{-1}); the medium was saturated with oxygen only at the beginning of the fermentation process, before the inoculum was added [10% (w/v) glucose, 0.1% (w/v) $MgSO_4$, 0.2% (w/v) KH_2PO_4, 0.3% (w/v) $(NH_4)_2SO_4$, 0.4% (w/v) yeast extract, and 0.36% (w/v) bacteriological peptone]. At the moment when the inoculum was added, the initial samples were taken. The end of the fermentation process was established when the ferment reached alcoholic strengths of 3.02 and 1.8 for substrates A and B, respectively. The fermentation was carried out by batch, and a final sample was taken before the process continued with another fermentation cycle.

The pasteurization process consisted of heating the sample to 70−80 °C for 15 min and then rapidly cooling and freezing until analysis. Sample codes are shown in Table 1 and indicate: substrate named as A (more-concentrated purée) or B (less-concentrated purée); the cycles, referred to as 1, 2, 3, and 4; and finally the fermentation step I (initial), F (final), and P (pasteurized). Each cycle encompassed three analyzed samples.

Samples were analyzed in duplicate. In the case of substrate A, we studied four cycles, and with substrate B, three cycles. The fermented samples were supplied by the Department of Inorganic Chemistry and Chemical Engineering, Faculty of Science, University of Cordoba, Spain.

2.3. Sample Treatment. We followed a previously reported procedure[3,12] to extract nonanthocyanin polyphenol compounds from the samples.

2.4. Liquid Chromatography with Diode Array Detection (LC-DAD), Liquid Chromatography−Mass Spectrometry/Elec-

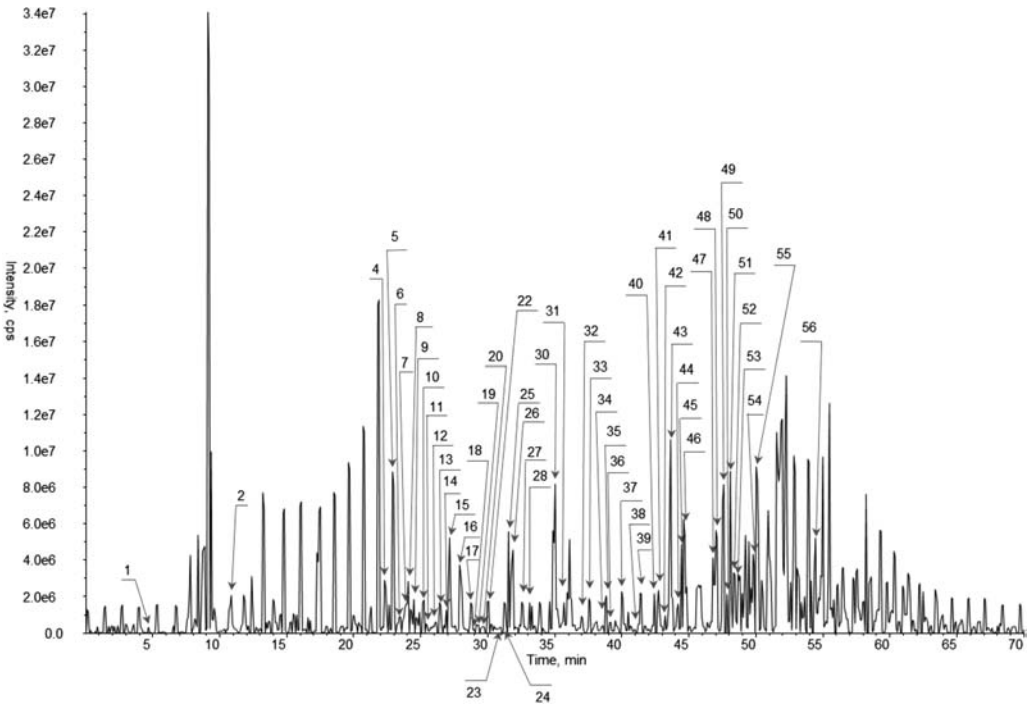

Figure 1. MS chromatogram of a final sample. The numbers represent the compounds shown in Table 2.

DOI: 10.1021/jf506076n
J. Agric. Food Chem. 2015, 63, 2041−2051

Table 2. Nonanthocyanin Phenolic Compounds in Alcoholic Fermentation Samples in negative ionization mode by QTRAP. Expected Mean, Retention Time (min), Molecular Weight, MS/MS Fragments, Identification and Reference. Peak Numbers Correspond to Mass Chromatogram (Figure 1)

peak N°	identification	MS t_R (min)	MW	$(M-H)^-$ (m/z)	MS/MS fragments	ref[a]
Hydroxybenzoics Acids and Derivatives						
1	gallic acid	4.78	170	169	125; 79	a
10	*p*-hydroxybenzoic acid	25.07	138	137	93; 65	a
16	protocatechuic acid 4-*O*-*β*-hexoside	28.8	316	315	152; 108	18
23	*p*-hydroxybenzoic-3-*O*-glucoside	30.72	300	299	137; 93	28
26	1-*O*-protocatechuyl-*β*-xylose	31.7	286	285	152; 108	32
Hydrolyzed Tannins						
4	HHDP-glucose	22.67	482	481	301; 275	25
13	monogalloyl glucose	26.00	332	331	313; 169; 151	25
20	bis-HHDP glucose	29.84	784	783	301; 481	16
25	HHDP-galloyl glucose	31.1	634	633	375; 301	16
28	Tris-galloyl-HHDP-hexose	33.28	952	951	907; 783; 605; 301	20
35	brevifolin carboxylic acid	38.9	292	291	248; 247; 203	22
37	galloyl-bis-HHDP-glucose	40.17	936	935	633;783; 301	16
39	agrimoniin	41.2	935	934	1085; 915; 897;783; 301	32
Ellagic Acid and Derivatives						
17	ellagic acid	29.71	302	301	284; 145	a
18	methyl ellagic acid pentoside	29.79	448	447	315; 331	20
38	ellagic acid deoxyhexoside	40.9	448	447	300; 257	17
46	ellagic acid rhamnoside	44.9	448	447	301; 285	20
52	dimethyl ellagic acid pentoside	47.9	462	461	300; 301; 145	20
56	ellagic acid pentoside	54.15	434	433	300	20
Flavanols						
5	(+)-catechin	23.02	290	289	245; 109	a
8	(−)-epicatechin	24.07	290	289	245; 109	a
19	(−)-epicatechin gallate	29.82	444	443	289; 169	a
Condensed Tannins						
9	procyanidin B1	24.4	578	577	288; 406	a
Hydroxycinnamic Acids						
2	ferulic acid glucuronide	10.78	370	369	193	30
3	dimer of caffeic acid-*O*-hexoside	13.07	684	683	341; 179	24
6	cinnamic acid	23.50	148	147	103; 77	a
7	cafeoylhexose	23.54	342	341	161; 179	27
11	*p*-coumaroyl hexose	25.66	326	325	187; 163; 145	17
12	caffeic acid	25.98	180	179	135; 107	a
14	ferulic acid hexose derivative	26.50	450	449	287; 269	28
15	galloylquinic acid	27.74	344	343	191; 169	25
22	*p*-coumaric acid	30.42	164	163	119; 93	a
24	ferulic acid	31.00	194	193	178; 134	a
29	(−)-chicoric acid	33.67	474	473	311; 149	a
41	ferulic acid hexoside	42.6	356	355	217; 193; 175; 160	25
53	5-hydroxyferuroyl hexose	48.1	372	371	281; 251; 221; 209; 165	25
54	sinapoyl glycoside	49.9	386	385	265; 223; 179	19
Flavonols						
27	luteolin-3′-xyloside	32.49	418	417	285; 241	
30	apigenin pentose	35.01	402	401	269; 161	32
31	luteolin-7-*O*-glucuronide	35.35		461	285; 241	21
40	apigenin-7-*O*-glucoside	42.3	432	431	270; 269; 311	a
42	quercetin-3-*O*-glucoside	43.7	464	463	300; 271; 255; 179; 151	28
43	isorhamnetin 3-*O*-glucoside	43.9	956	$[2M-H]^-$ 955	301; 477	26
44	quercetin	44.01	302	301	179; 151	a
45	kaempferol hexoside	44.5	448	447	284; 255; 227	20
47	kaempferol 3-glucuronide	46.8	462	461	285; 179; 161	32
48	isorhamnetin-*O*-glucuronide	47.17	492	491	315; 300; 271; 255; 113	25
49	kaempferol	47.25	286	285	117; 93	a
50	quercetin-3-(6′′acetyl glucoside)	47.5	506	505	463; 300; 271; 226; 179	32
51	kaempferol acetyl hexoside	47.82	490	489	327; 285; 284; 255	20
55	kaempferol coumaroyl glucoside	50.05	594	593	447; 284; 285	20

DOI: 10.1021/jf506076n
J. Agric. Food Chem. 2015, 63, 2041−2051

Table 2. continued

peak N°	identification	MS t_R (min)	MW	$(M-H)^-$ (m/z)	MS/MS fragments	ref[a]
Dihydroflavonols						
32	(+)-aromadendrin hexoside	37.17	450	449	431; 287; 269; 259; 243; 179	22
34	taxifolin-*O*-glucoside	38.5	466	465	285; 151	29
36	(+)-aromadendrin rhamnoside	39.95	434	433	287	35
Stilbenes						
21	*trans*-piceid	30.08	390	389	185; 227	a
Flavanones						
33	eriodyctiol-7-*O*-glucoside	37.65	450	449	287; 151; 135	26

[a]The letter a indicates that identification of the compound was confirmed by the authentic standard.

Table 3. Nonanthocyanin Phenolic Compounds in Alcoholic Fermentation Samples in negative ionization mode by ORBITRAP. Expected Mean Molecular Formula, Exact Mass, Mass Accuracy (ppm), MS/MS Fragments (%), Identification, and Reference[a]

identification	t_R (min)	molecular formula	exact mass $(M-H)^-$	MS/MS fragments	Δmass (ppm)	ref[a]
protocatechuic acid	1.92	$C_7H_6O_4$	153.0193	109.8292(84)	1.3902	a
citric acid isomer	2.77	$C_6H_8O_7$	191.0189	173.0081(2); 111.0074(100); 67.0174(1)	1.5281	32
dimer of caffeic acid-*O*-hexoside	13.07	$C_{30}H_{36}O_{18}$	683.1818	341.0872(100)	0.0406	24
(+)-taxifolin	21.04	$C_{15}H_{12}O_7$	303.0510	285.0406(100); 275.0562(10); 177.0184(26); 125.0231(72)	2.8118	a
(+)-aromadendrin	24.39	$C_{15}H_{12}O_6$	287.0562	259.0611(100); 243.0660(19); 125.0231(57)	4.1764	a
rutin	24.75	$C_{27}H_{30}O_{16}$	609.1465	300.0275(32); 301.0355(29); 151.0024(2)	1.6171	a
phloridzin	26.16	$C_{21}H_{24}O_{10}$	435.1294	273.0769(100); 167.0339(17); 125.0230(3)	0.9055	a
eriodictyol	27.64	$C_{15}H_{12}O_6$	287.0562	151.0025(100); 135.0439(32); 125.0231(6)	3.6448	a
homovanillic acid	28.03	$C_9H_{10}O_4$	181.0497	137.0232(66); 89.0230(64); 71.0124(82); 59.0124(100)	0.8981	a
protocatechuic acid 4-*O*-*β*-hexoside	28.8	$C_{13}H_{15}O_9$	315.0715	153.0191(100); 109.0295(9)	1.3131	18
quercetin	30.16	$C_{15}H_{10}O_7$	301.0352	178.9976(22); 151.0025(32)	3.0153	a
luteolin-3′-xyloside	32.49	$C_{20}H_{18}O_{10}$	417.0810	285.0612(100); 241.0715(32); 133.0296(4); 151.0402(22)	1.4360	
luteolin	32.83	$C_{15}H_{10}O_6$	285.0404	241.0503(1); 165.0181(3); 225.0550(1); 151.0024(1); 117.0330(1)	4.2938	a
apigenin	33.24	$C_{15}H_{10}O_5$	269.0455	225.0550(1); 151.0024(1); 117.0330(1)	4.4767	a
eriodyctiol-7-*O*-glucoside	37.65	$C_{21}H_{22}O_{11}$	449.1075	287.0558(100); 269.0452(39); 243.0662(1.50)	0.7903	26
(+)-taxifolin-*O*-glucoside	38.50	$C_{21}H_{22}O_{12}$	465.1025	285.0401(100); 303.0507(11); 151.0038(32.20)	0.5244	29
brevifolin carboxylic acid	38.90	$C_{13}H_8O_8$	291.0139	247.0246(100); 203.0357	1.0700	22
ferulic acid hexoside	42.62	$C_{16}H_{20}O_9$	355.1027	193.0507(100); 175.0403(69); 160.0168(8)	1.0239	25
isorhamnetin 3-*O*-glucoside	43.90	$C_{22}H_{22}O_{12}$	447.0558	301.0344(100); 315.0344(8); 151.0037(0.4)	0.0322	26

[a]The letter a indicates that identification of the compound was confirmed by the authentic standards.

trospray Ionization Tandem Mass Spectrometry (LC−MS/ESI−MS/MS), Multiple Reaction Monitoring (MRM) Analysis. *2.4.1. LC-DAD Analysis.* Chromatographic separation was performed using an LC Agilent Series 1100 system with a quaternary pump (Series 1100 G1311A), automatic injector (Series 1100 G1313A), and degasser (series 1100 G1379A). Detection took place using a UV−vis diode detector (Series 1100 G1379A) coupled to a Chemstation HP A.10.02 (HP/Agilent). The column used was a Merck LiChroCART 250−4 Superspher 100 RP-18 1.16056.0001. The method was a binary gradient and was the same as the one described and validated by Álvarez-Fernández et al.[3,12] Each sample was analyzed twice. Identification was achieved by matching the retention time and spectra of the peaks with the corresponding standards. Furthermore, samples were spiked with standards, where commercially available, to achieve complete identification. In accordance with the maximum absorbance of each compound, quantification was performed by external calibration at 280 nm, 320 nm, and 365 nm using the corresponding standards. Calibration curves were obtained by injecting standards diluted from five to eight different concentrations (R^2: 0.9949−0.9998). A duplicate was performed at each point of the calibration curve.

2.4.2. QTRAP Analysis. Mass analysis was performed using a PelkinElmer Series 200 HPLC system (Wellesley, USA) coupled to an Applied Biosystems QTRAP LC−MS/MS system (Foster City, USA) consisting of a hybrid triple quadrupole linear ion trap (QqQLIT) mass spectrometer equipped with an electrospray ion source. LC analyses were performed on a Merck LiChroCART 250−4 Superspher 100 RP-18 1.16056.0001 reversed-phase column. The flow rate was 400 μL min^{-1}. Chromatographic separation was performed using a binary gradient consisting of (A) water and (B) water/acetonitrile 20:80 (v/v). Both phases contained 0.1% formic acid (v/v). The elution gradient was the same as the one used in the LC-DAD analysis. The injection volume was 20 μL.

A MRM experiment was applied, where precursor ions and fragment ions were monitored at Q1 and Q3, respectively, using their corresponding standards.

For HPLC−ESI−MRM analyses, the mass spectrometer was set to the following optimized tune parameters: curtain gas 35 psi, ion spray voltage 4500 V, source temperature 350 °C, and source gas 60 psi. A dwell time was set at 50 ms for each transition.

2.4.3. High-Resolution Mass Spectrometry (HRMS). The experiments were performed using a Thermo Fisher Scientific (Bremen, Germany) LC system hybrid quadropole-orbitrap mass spectrometer (Q-OT-qIT). This benchtop UHPLC−MS/MS system combines quadropole precursor ion selection with high-resolution, accurate-mass spectrometer. Identification was performed according to mass spectra, exact mass, characteristic fragmentation, and retention time. Chromatographic separation was performed on a Phenomenex Luna

DOI: 10.1021/jf506076n
J. Agric. Food Chem. 2015, 63, 2041−2051

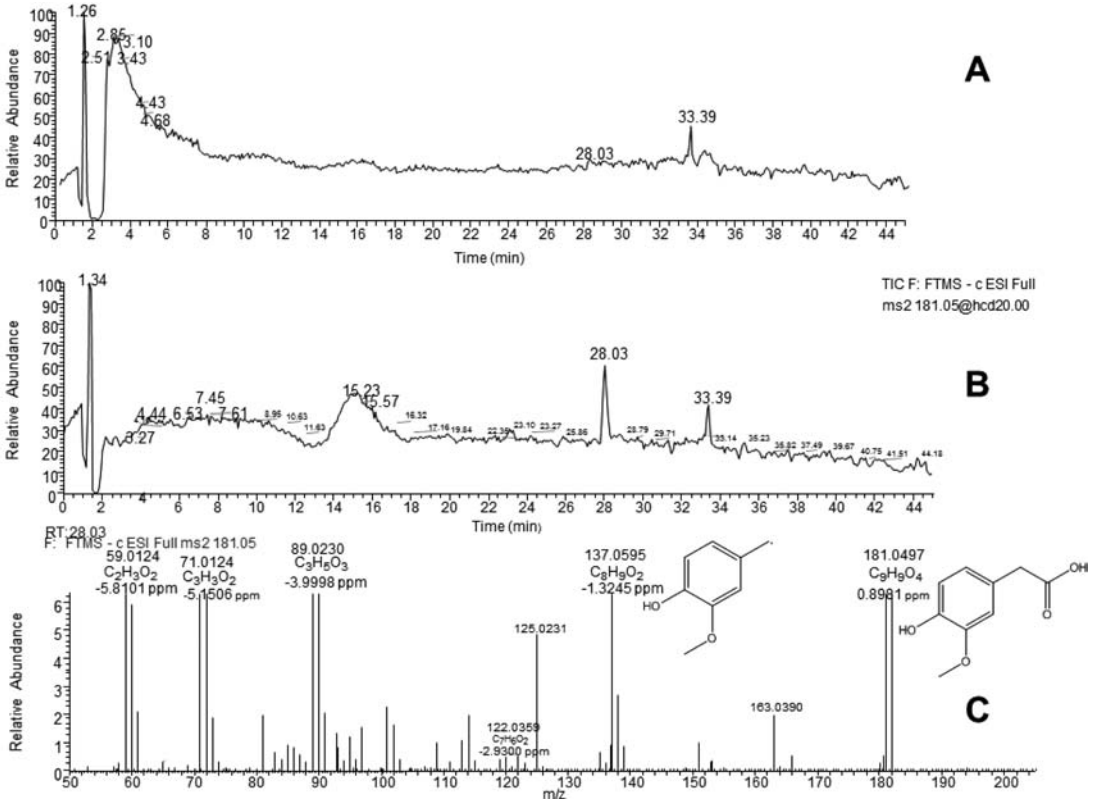

Figure 2. LC−MS/MS chromatogram of homovanillic acid. Panels A and B represent the TIC chromatogram of I and P steps of cycle three of substrate B, where the increase in signal is shown at 28.03 min after fermentation. Panel C represents the EPI chromatogram with the fragmentation pattern of a homovanillic acid isomer.

C18 (150 mm × 2.0 mm, 3 μm) column. The normalized collision energy of the high-collision-induced-dissociation (CID) cell was set at 20 eV. Twenty microliters of sample was injected, and the flow rate was 250 μL min^{-1}.

Identification in negative ionization mode using a binary gradient consisted of (A) water with 0.1% formic acid and (B) methanol with 0.1% formic acid 0.0−2.0 min 5% B, 2.0−40.0 min from 5−90% B, 40.0−42.0 min from 90−5% B, 42.0−45.0 5% B.

2.5. Antioxidant Activity. *2.5.1. ORAC Test.* The method used was as previously reported with the following modifications:[13] 100 μL of fluorescein (45 nM) and 50 μL of AAPH (15 mM) mixed with 50 μL of sample or Trolox. The reaction took place for a total time of 80 min. Fluorescence was assessed with a fluorometer (multidetector microplate Synergy HT, Biotek) with excitation, and emission wavelengths were 485 and 528 nm, respectively. Trolox was used as a calibration standard (0.5−9.5 μM). Fluorescein fluorescence readings were recorded every 5 min after addition of AAPH until they reached less than 5% of the initial reading. Results were calculated using the areas under the fluorescein decay curves between the blank and the sample and were expressed as micromols Trolox equivalents (TE) per gram of fresh weight. The reported values are the means of at least three experiments.

2.5.2. DPPH Method. Scavenging activity was also evaluated by DPPH using a slightly modified version of the literature method.[14] A 0.1 mL of sample in methanol (previously diluted 1:250) was added to 3.9 mL of DPPH methanolic solution (0.025 g L^{-1}) in a cuvette. Absorbance was recorded at 515 nm at the start time (when the sample was added) and 60 min later, when the reaction reached equilibrium. All measurements were the averages of at least three independent experiments, and methanol was used as the reference. To make the Trolox calibration curve, eight concentrations were used, which ranged from 0.9−0.12 mM. All values reported were recorded on a Hitachi UV-2800 spectrophotometer, thermostated with a Peltier system at 25 °C, and expressed as mmol of TE per kg of fresh weight.

2.6. Statistical Analysis. Statistical analyses were performed by means of Statistica software.[15] One-way analysis of variance (ANOVA) was used to test significant differences at the $p < 0.05$ level. Additionally, linear discriminant analysis (LDA) was tested to build a function to discriminate between the substrate (initial), fermented alcohol (final), and final pasteurized samples of all cycles and the two substrates A and B.

3. RESULTS AND DISCUSSION

3.1. Identification of Nonanthocyanin Phenolic Compounds. Sixty-six nonanthocyanin phenolic compounds and citric acid were identified in the strawberry purée and alcoholic-fermented samples. Figure 1 displays the LC−MS (QTrap) chromatogram, and Table 2 and 3 presents identification data. If standards were not available, identification was based on (I) retention time, (II) UV−vis spectra, (III) the deprotonated ion and mass spectra, (IV) accurate mass measurements, and (V) comparison with data reported in the literature.[16−34] When standards were available, identification was performed either by MRM or HRMS analysis.

As far as we know, 13 of these were identified for first time in strawberry and its derived alcoholic-fermented products: protocatechuic acid-4-*O*-β-hexoside (Peak 16), brevifolin carboxylic acid (Peak 35), ferulic acid glucuronide (Peak 2), dimer caffeic acid-*O*-hexoside (Peak 3), luteolin-3′-*O*-xyloside (Peak 27), isorhamnetin-3-*O*-glucoside (Peak 43), taxifolin-*O*-glucoside (Peak 34), (+)-aromadendrin rhamnoside (Peak 36), eriodictyol-7-*O*-glucoside (Peak 33), (+)-taxifolin, (+)-aromadendrin, eriodictyol, and homovanillic acid.

3.1.1. Hydroxybenzoic Acids and Derivatives. Peak 16 was tentatively identified as protocatechuic acid-4-*O*-β-hexoside. This compound exhibited a deprotonated [M-H]$^-$ ion at m/z

DOI: 10.1021/jf506076n
J. Agric. Food Chem. 2015, 63, 2041−2051

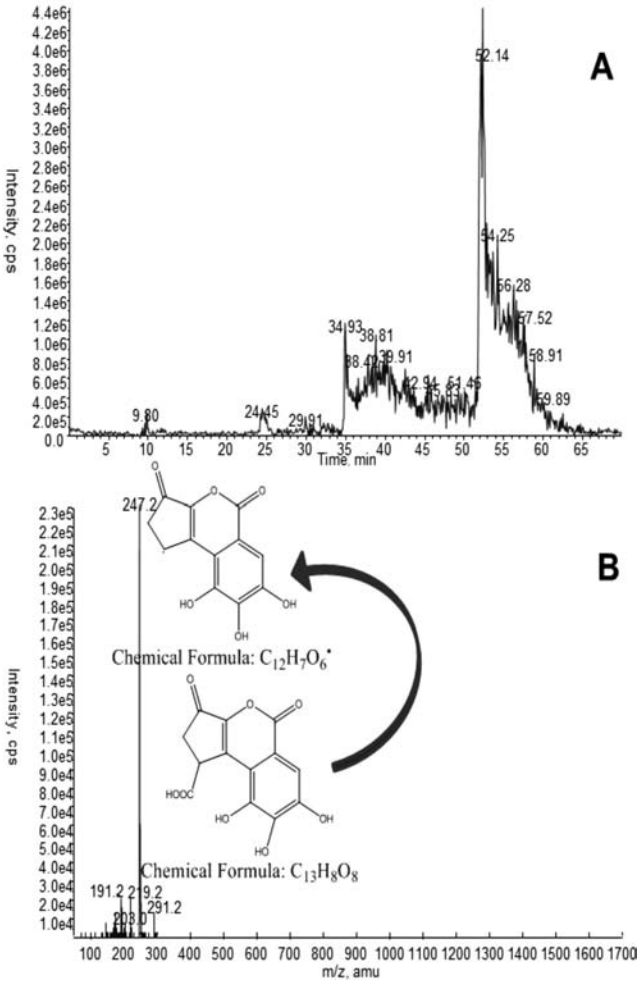

Figure 3. XIC and EPI chromatograms (A and B respectively) of brevifolin carboxylic acid and its fragmentation pattern.

315 and had MS/MS fragments at m/z 152 $[M\text{-}2H\text{-}162]^-$ (loss of glucose moiety) and 108 $[M\text{-}H\text{-}44]^-$ (loss of CO_2); it has been previously identified in artichoke.[18] Peak 26 was tentatively identified as 1-*O*-protocatechuic-*β*-xyloside. It presented a deprotonated ion at $[M\text{-}H]^-$ 285, and its fragmentation pattern was in accordance with the one reported in strawberry.[33] In our study, protocatechuic acid-4-*O*-*β*-hexoside was detected in strawberry (initial samples), in the alcoholic beverages (final sample) of both substrates, and in pasteurized samples of substrate A only.

3.1.2. Hydrolized Tannins. HHDP-Glucose (Peak 4) with pseudomolecular ion m/z 481 produced a fragment at m/z 301, which indicates the release of ellagic acid; this compound has been reported in strawberry before by Hanhineva et al.[25] Peak 28 had a pseudomolecular ion at m/z 951 and MS/MS fragmentation with m/z 907, 783, and 301. The fragmentation pattern and MW were in agreement with those reported before for Tris-galloyl-HHDP-hexose in *Fragaria vesca*.[20]

Peak 35 was tentatively identified as brevifolin carboxylic acid (Figure 3). This compound exhibited a deprotonated ion $[M\text{-}H]^-$ at m/z 291, and its fragmentation pattern had m/z 247, 203, which correspond to loss of carboxylic moieties. This compound was identified in all samples of substrate A. The results indicate the presence of this compound in strawberry and its alcoholic-fermented beverages. Brevifolin carboxylic acid has been reported before in pomegranate fruits,[22] but as far as we know, it has not yet been determined in strawberry.

3.1.3. Ellagic Acid and Derivatives. Peaks 18 and 52 were tentatively identified as methyl ellagic acid derivatives. Peak 18, with deprotonated $[M\text{-}H]^-$ ion 447 and fragmentation with MS/MS m/z 315, corresponds to the loss of pentoside residue, (132 Da), and m/z 301 resulted from the additional loss of a methyl group. This fragmentation pattern corresponds with methyl ellagic acid pentoside. Methyl ellagic derivatives have been reported before in strawberry.[32,20] The second peak, number 52, was tentatively identified as dimethyl ellagic acid pentoside with pseudomolecular ion $[M\text{-}H]^-$ 461, after loss of pentose moiety gave rise to m/z 315 and two fragments, m/z 300 and m/z 145, corresponding to ellagic acid. Many polyphenolic compounds occur naturally as metoxylated derivatives and exhibit a fragmentation pattern where loss of the methyl fragment from the pseudomolecular ion is common, which results in the production of the $[M\text{-}H\text{-}15]^-$ radical.[20]

3.1.4. Hydroxycinnamic Acids. Peak 2 was identified as ferulic acid glucuronide. This compound was detected only in the alcoholic fermented product (final samples of two substrates). It had a deprotonated $[M\text{-}H]^-$ ion 369 and exhibited a fragment with MS/MS m/z 193, which resulted from loss of a glucuronide moiety $[M\text{-}H\text{-}176]^-$. Peak 3 was tentatively identified as a dimer of caffeic acid-*O*-hexoside, described before in *Helichrysum obconicum*.[23] This compound had a pseudomolecular ion $[M\text{-}H]^-$ at 683 and a fragmentation pattern with two fragments, m/z 341 and 179, corresponding to caffeic acid hexoside and caffeic acid, respectively. This was detected only in substrate B, in the initial sample (strawberry) and alcoholic beverages (final samples).

3.1.5. Flavonols. Peak 27 was tentatively identified as luteolin-3′-xyloside with a deprotonated ion at m/z 417. After neutral loss of the sugar moiety $[M\text{-}H\text{-}132]^-$, it results in m/z 285 and 241 fragments, which are characteristic of luteolin aglycone. Peak 43 presented a pseudomolecular ion at m/z 955 and exhibited an MS/MS fragmentation pattern, which matched those attributed to isorhamnetin-3-*O*-glucoside in MassBank record PR040094[26] and ReSpect record PT204190.[31] It had a base peak, m/z 477, which gave rise to a fragment at m/z 301, characteristic of quercetin after cleavage of the molecule. This compound was present in all samples of the two substrates.

3.1.6. Dihydroflavonols. Peak 32 had an ion at 449 and was tentatively identified as (+)-aromadendrin hexoside, reported before in strawberry purée.[12] It presented a fragmentation pattern with base peak at m/z 431 $[M\text{-}H\text{-}18]^-$, which resulted from the dehydration process. Neutral loss of a hexose moiety $[M\text{-}H\text{-}162]^-$ gave rise to a fragment at m/z 287. The fragment at m/z 287 corresponded to (+)-aromadendrin aglycone.

Peak 36 was tentatively identified as (+)-aromadendrin rhamnoside in all samples of substrate A. This compound exhibited a deprotonated ion, $[M\text{-}H]^-$ 433, and presented a base peak at m/z 287, corresponding to (+)-aromadendrin aglycone and resulting from the loss of 146 Da, corresponding to dehydrated rhamnoside moiety. This compound has been described before in *Eucaliptus globulus*.[35]

Peak 34 was tentatively identified as taxifolin-*O*-glucoside in final and pasteurized samples of substrate A and initial and final samples of substrate B. It presented a pseudomolecular $[M\text{-}H]^-$ ion at 465 and MS/MS fragmentation with m/z 285, 151. The MW and fragmentation pattern were in accordance with those

DOI: 10.1021/jf506076n
J. Agric. Food Chem. 2015, 63, 2041−2051

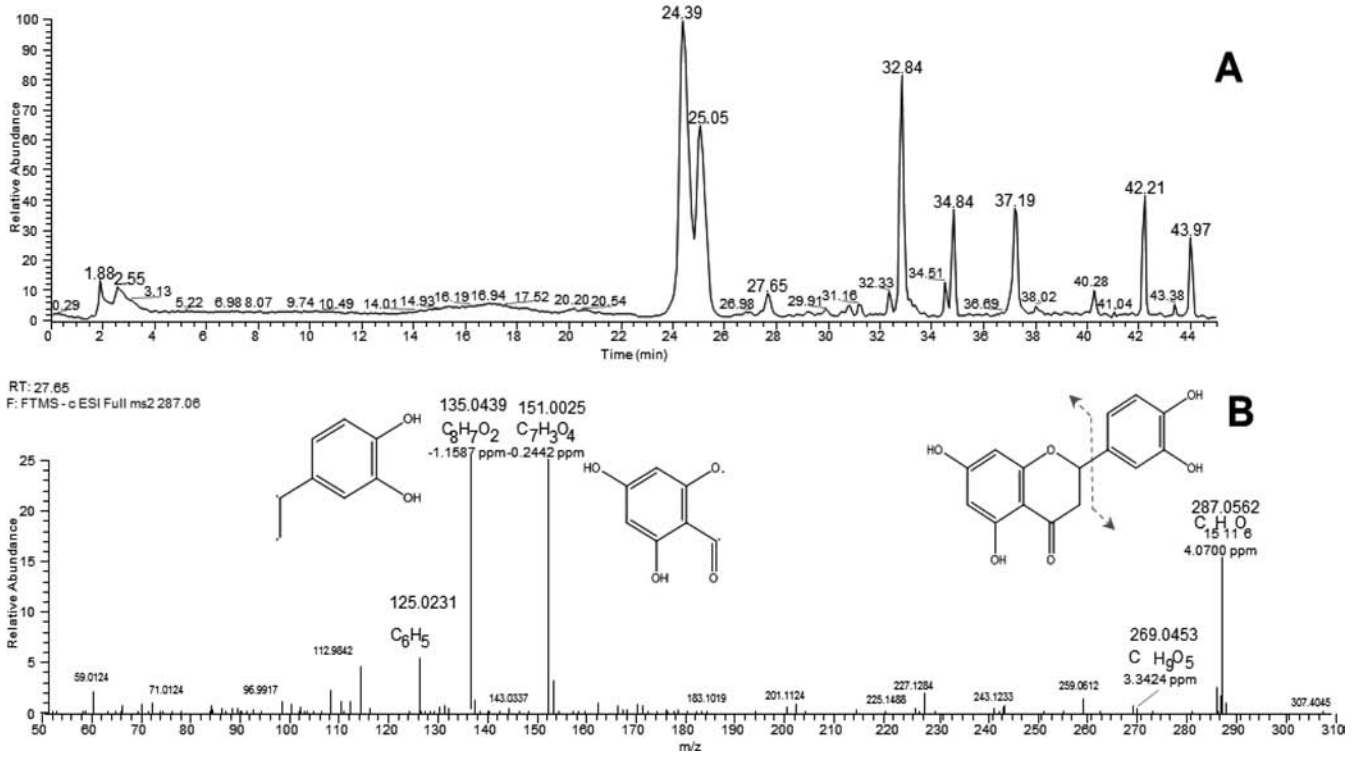

Figure 4. Mass chromatogram of eriodictyol at 25.65 min. (A) TIC chromatogram of a final sample, (B) EPI chromatogram with fragmentation.

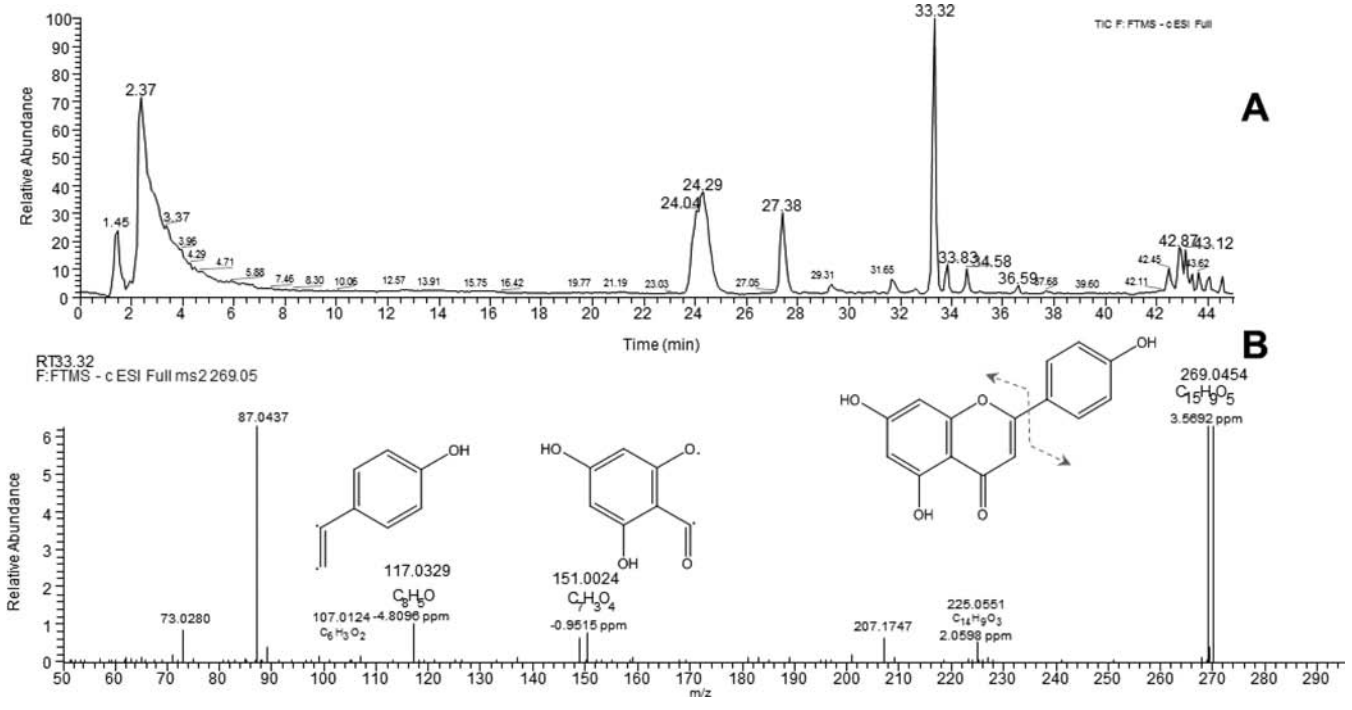

Figure 5. Mass chromatogram of apigenin. (A) TIC chromatogram and (B) EPI chromatogram with fragmentation pattern.

attributed to taxifolin-*O*-glucoside in grapes and red wine prepared from *Vitis vinifera*.[29]

3.1.7. Flavanones. Peak 33 was tentatively identified as eriodictyol-7-*O*-glucoside in all samples of substrate A and initial and final samples of substrate B. It exhibited a deprotonated $[M\text{-}H]^-$ ion at 449, which gave rise to m/z 287 $[M\text{-}H\text{-}162]^-$ by neutral loss, corresponding to sugar moiety (162 Da.). This ion corresponded to eriodictyol aglycone, and the presence of two fragments, m/z 151 and 135, characteristic of eriodictyol, confirmed this tentative identification.

3.1.8. Compounds Identified by HRMS. HRMS was used to confirm the identity of compounds with available standards (Figures 4 and 5). Eleven compounds were identified with standards by generating the molecular formula using accurate mass and matching with the isotopic pattern. The results are shown in Table 3. Three of these compounds, protocatechuic

DOI: 10.1021/jf506076n
J. Agric. Food Chem. 2015, 63, 2041−2051

Table 4. Contents of Nonanthocyanin Phenolic Compounds (mg kg fw^{-1}) in Alcoholic Fermentation Samples of Substrate A[a]

	Cycle 1			Cycle 2			Cycle 3		
Compounds	I	F	P	I	F	P	I	F	P
(-)-Epicatechin	3.30±0.29^{ab}	5.05±0.71^{a}	4.99±0.68^{b}	4.77±0.35	4.87±0.24	4.88±0.19	4.26±0.10^{a}	4.65±0.18^{a}	4.39±0.33
Eriodictyol-7-*O*-glucoside	1.16±0.12^{ab}	2.88±0.16^{ac}	2.63±0.08^{bc}	0.90±0.20^{ab}	1.17±0.07^{ac}	1.77±0.05^{bc}	0.90±0.00^{ab}	1.23±0.01^{ac}	0.98±0.02^{bc}
Caffeoyl hexose	1.81±0.01^{ab}	3.32±0.05^{ac}	3.53±0.03^{bc}	1.86±0.03^{ab}	2.99±0.02^{ac}	2.52±0.04^{bc}	1.86±0.00^{ab}	3.19±0.04^{ac}	2.98±0.13^{bc}
Ferulic acid derivative	1.26±0.05^{ab}	1.57±0.03^{ac}	1.68±0.03^{bc}	1.50±0.03	1.47±0.05^{c}	1.17±0.01^{c}	0.57±0.05^{ab}	1.44±0.05^{ac}	0.99±0.01^{bc}
Galloyl *bis*-HHDP-glucose	157.25±6.55^{ab}	95.29±1.94^{ac}	144.80±1.17^{bc}	165.44±4.52^{ab}	123.77±1.54^{ac}	127.15±0.52^{bc}	145.07±10.06^{b}	130.48±6.78^{b}	124.00±2.91
HHDP-glucose	2.85±0.44	2.37±0.20^{c}	3.13±0.18^{c}	4.64±0.67^{b}	5.52±1.65^{c}	3.29±0.25^{bc}	3.83±0.46^{a}	4.94±0.19^{ac}	4.02±0.21^{c}
Homovanillic acid	9.40±0.55^{ab}	11.11±0.33^{ac}	3.76±1.04^{bc}	12.81±1.48^{ab}	20.09±1.22^{ac}	3.058±0.39^{bc}	3.06±0.39^{ab}	10.30±0.20^{ac}	8.79±0.75^{bc}
Isorharmentin glucose	3.30±0.14^{a}	4.79±0.20^{ac}	3.48±0.21^{c}	3.80±0.13^{ab}	4.47±0.12^{a}	4.30±0.10^{b}	4.00±0.19^{ab}	5.49±0.16^{a}	3.38±0.42^{b}
Kaempferol glucuronide	2.52±0.18^{ab}	3.72±0.17^{a}	3.80±0.10^{b}	2.41±0.26^{b}	2.67±0.45	3.01±0.08^{b}	2.44±0.30^{a}	3.69±0.06^{a}	3.04±0.62
Luteolin-3′-xylose	2.87±0.05^{ab}	1.92±0.18^{a}	2.02±0.04^{b}	2.17±1.08	1.23±0.10	1.26±0.04	1.15±0.08	1.22±0.05^{c}	0.99±0.15^{c}
Methyl ellagic acid	1.23±0.13^{ab}	2.22±0.08^{ac}	2.78±0.05^{bc}	2.79±0.22^{a}	3.15±0.15^{ac}	2.86±0.08^{c}	1.33±0.07^{ab}	3.74±0.11^{ac}	3.19±0.31^{bc}
Monogalloyl glucose	5.97±2.12^{b}	7.98±0.74^{c}	9.24±0.17^{bc}	7.46±0.21^{a}	8.64±0.52^{ac}	7.58±0.22^{c}	6.05±0.07^{ab}	8.23±0.29^{ac}	7.19±0.36^{bc}
p-Coumaroyl hexoside	73.37±0.94^{ab}	77.17±2.13^{ac}	83.07±0.32^{bc}	82.80±2.64^{ab}	84.39±0.76^{a}	70.32±1.19^{b}	77.81±5.47	79.05±0.91	72.36±5.47
Phloridzin	1.54±0.07^{ab}	3.92±0.43^{a}	3.97±0.04^{b}	2.09±0.29^{b}	2.67±0.64	3.25±0.05^{b}	2.64.±0.22^{a}	4.22±0.03^{ac}	3.37±0.61^{c}
p-Hydroxybenzoic acid	1.51±0.41	1.34±0.12^{c}	1.71±0.04^{c}	0.87±0.43^{a}	3.61±0.68^{ac}	1.41±0.10^{c}	6.06±0.62^{b}	5.87±0.43^{c}	5.33±0.50^{bc}
Procyanidin B1	18.12±1.65^{b}	18.25±1.49^{c}	13.07±1.04^{bc}	17.85±1.47^{ab}	11.38±0.95^{ac}	13.08±0.98^{bc}	8.35±1.52^{ab}	4.31±0.97^{ac}	2.46±0.58^{bc}
Protocatechuic acid	0.34±0.16	0.76±0.35^{c}	0.27±0.09^{c}	0.20±0.08^{b}	0.27±0.11^{b}	nd	nd	6.12±0.25	6.34±0.81
Quercetin glucoside	1.00±0.07^{ab}	1.36±0.05^{ac}	0.50±0.09^{bc}	1.03±0.07^{ab}	1.17±0.08^{ac}	0.73±0.03^{bc}	0.75±0.03^{ab}	0.55±).05^{a}	0.58±0.11^{b}
Quercetin glucuronide	1.00±0.03^{ab}	1.21±0.09^{ac}	1.51±0.05^{bc}	1.57±0.21	1.62±0.16	1.50±0.02	1.52±0.10^{a}	0.99±0.02^{ac}	1.83±0.41^{c}

[a]Mean values and standard deviation. Superscript a indicates a significant difference ($p < 0.05$) between the initial samples (I) and final samples (F) of the same substrate. Superscript b indicates a significant difference ($p < 0.05$) between the initial samples (I) and pasteurized samples (P) of the same substrate. Superscript c indicates a significant difference ($p < 0.05$) between the pasteurized samples (P) and final samples (F) of the same substrate, by ANOVA statistical test. Samples were determined in duplicate. nd, no data.

acid, *p*-hydroxybenzoic acid, and homovanillic acid (Figure 2), were detected in I, F, and P samples and have been reported before as human colonic metabolites of phenolic compounds.[36] Furthermore, increased concentrations of protocatechuic acid and *p*-hydroxybenzoic acid have been reported before due to yeast fermentation in Bokbunja.[37]

3.2. Quantitation of Nonanthocyanin Phenolic Compounds in Alcoholic Fermented Beverages. Nonanthocyanin phenolic compounds were quantified by external calibration with standards, in accordance with the validated LC-DAD method reported.[3] Tables 4 and 5 show the concentrations of the phenolic compounds, with significant increases and decreases after the alcoholic fermentation process ($p < 0.05$). (+)-Catechin content stands out with concentrations ranging from 86.4−144.3 mg kg fw^{-1}, and along with (−)-epicatechin gallate, galloyl-bis-HHDP-glucose, and *p*-coumaroyl glucose, it represents 70% of the total quantified compounds for the two substrates (Supporting Information). The concentration of *p*-coumaroyl glucose and the contents of the others compound listed above are in accordance with the results of gluconic-fermented products reported.[12]

In accordance with the report on sweet wine by Figueredo-González et al.,[38] the condensed tannins detected in ours samples was mainly dimer, specifically procyanidin B1 and appear in concentrations ranged between 14.8 and 28.0 mg kg fw^{-1} on average in initial samples for substrates A and B, respectively.

The most abundant compound was galloyl bis-HHDP-glucose. This compound was described as a monomer unit of two of the most abundant ellagitannis in strawberry, agrimoniin and sanguiin H-6,[39] and decreased during the alcoholic fermentation process (25−59%) in most of the cycles and for both substrates.

The concentration of monogalloyl glucose underwent a significant increase, which ranged from 20−36%, as a consequence of fermentation.

Homovanillic acid showed significant increases, 3.2−3.6% on average, for the two substrates, respectively. Authors such as Jaganath et al.[40] and Dall'Asta et al.[36] attributed the increment of this compound to be a consequence of the transformation of quercetin, rutin, and other quercetin glycosides; they detected this compound as a metabolite derived from human colonic fermentation after application of a diet rich in natural polyphenols. In contrast, in this study, we detected a slight decrease or increase in rutin and quercetin glycosides.

Another compound considered to be a metabolite, produced as a consequence of human colonic fermentation, is *p*-hydroxybenzoic acid.[36,41] It followed a similar pattern to homovanillic acid and underwent a significant increment in the majority of cycles, in both substrates, in a range of increase of 1.28−2.41%. Additionally, Vinjanen et al.[42] reported an increase in the content of *p*-hydroxybenzoic acid in yeast fermentation of lingonberries (*Vaccinium vitis-idaea*). It is known that many compounds, such as anthocyanins and phenolics, are stored in fruits in glycosidically bound form, and fermentation-effect-produced glycosidases can release aglycones of these compounds.

The effects of the pasteurization process were slight and scarce, and when they happened tended to decrease concentrations, for example, in the cases of phloridzin and kaempferol derivatives. Their concentrations experienced reductions in all cycles in amounts ranging from 2−13% for the two substrates.

3.3. LDA Analysis. Quantitated phenolic compounds were used as variables for statistical analysis, and grouping variables were initial (I), final (F), and pasteurized (P) steps. First, ANOVA pinpointed the variables that underwent significant change after the fermentation or pasteurization process, as shown in Tables 4 and 5. Second, 19 variables presenting significant differences were selected for discriminant analysis. Standard stepwise analysis included the whole set of 19 variables in the model, which achieved 98.8% correct

DOI: 10.1021/jf506076n
J. Agric. Food Chem. 2015, 63, 2041−2051

Table 5. Contents of Nonanthocyanin Phenolic Compounds (mg kg fw^{-1}) in Alcoholic Fermentation Samples of Substrate B[a]

	Cycle 1			Cycle 2		
Compounds	I	F	P	I	F	P
(-)-Epicatechin	3.36±0.07^{ab}	1.81±0.63^{a}	nd	2.27±0.14^{b}	2.31±0.22^{c}	nd
Eriodictyol-7-*O*-glucoside	0.43±0.03^{ab}	0.54±0.07^{ac}	0.82±0.08^{bc}	0.90±0.08^{ab}	0.32±0.03^{a}	0.26±0.04^{b}
Caffeoyl hexose	1.92±0.02^{ab}	2.84±0.04^{ac}	2.61±0.04^{bc}	nd	3.38±0.13	3.30±0.34
Ferulic acid derivative	1.72±0.09^{b}	1.57±0.07^{c}	1.42±0.03^{bc}	1.56±0.04	1.68±0.11	1.61±0.24
Galloyl *bis*-HHDP-glucose	172.93±6.31^{b}	175.30±13.31^{c}	208.15±13.65^{bc}	156.51±2.96^{b}	134.04±12.29^{c}	103.03±1.06^{bc}
HHDP-glucose	9.44±0.30^{ab}	7.22±0.88^{ac}	2.35±0.55^{bc}	3.82±0.62^{ab}	8.47±0.60^{ac}	2.73±0.44^{bc}
Homovanillic acid	5.32±0.38^{ab}	23.73±3.20^{a}	20.25±0.69^{b}	3.39±0.27^{ab}	16.83±1.23^{ac}	13.26±1.04^{bc}
Isorharmentin glucose	3.28±0.05^{a}	4.33±0.41^{a}	4.50±0.34^{b}	2.16±0.08^{ab}	4.02±0.36^{ac}	2.70±0.19^{bc}
Kaempferol glucuronide	1.64±0.13	1.64±0.19	1.65±0.13	1.73±0.09	1.87±0.16	1.88±0.10
Luteolin-3′-xylose	2.16±0.20^{ab}	2.73±0.30^{a}	3.01±0.05^{b}	2.35±0.05^{ab}	0.85±0.02^{ac}	0.54±0.10^{bc}
Methyl ellagic acid	1.19±0.06^{b}	1.16±0.02^{c}	1.36±0.04^{bc}	1.14±0.02^{b}	1.17±0.10^{c}	0.99±0.05^{bc}
Monogalloyl glucose	4.68±0.57	4.26±0.48^{c}	4.11±0.11^{c}	4.45±0.27^{a}	5.59±0.41^{a}	5.54±0.09
p-Coumaroyl hexoside	82.17±1.05^{ab}	76.81±2.62^{ac}	70.96±1.26^{bc}	79.99±1.25^{a}	84.78±2.61^{a}	81.12±7.55
Phloridzin	0.32±0.02^{ab}	1.19±0.41^{a}	0.82±0.25^{b}	1.11±0.07^{ab}	0.41±0.04^{a}	0.36±0.11^{b}
p-Hydroxybenzoic acid	1.91±0.05^{ab}	3.45±0.82^{a}	3.73±0.43^{b}	1.65±0.21^{ab}	6.64±1.02^{ac}	4.51±0.89^{bc}
Procyanidin B1	38.36±6.95^{ab}	9.30±0.44^{a}	8.99±0.37^{b}	37.26±3.89^{ab}	19.02±0.82^{a}	19.75±1.82^{b}
Protocatechuic acid	2.24±0.53	2.77±0.56	2.36±0.34	1.90±0.33^{ab}	3.69±1.36^{a}	3.70±1.13^{b}
Quercetin glucoside	1.53±0.09^{b}	1.08±0.37^{c}	1.81±0.20^{bc}	1.54±0.05^{a}	1.80±0.13^{ac}	1.50±0.14^{c}
Quercetin glucuronide	1.19±0.06^{b}	1.32±0.13	1.40±0.04^{b}	1.16±0.02^{ab}	1.66±0.07^{ac}	1.29±0.03^{bc}

	Cycle 3			Cycle 4		
Compounds	I	F	P	I	F	P
(-)-Epicatechin	2.17±0.15^{ab}	1.64±0.13^{a}	1.73±0.04^{b}	4.95±0.36^{ab}	3.28±0.60^{a}	3.24±0.10^{b}
Eriodictyol-7-*O*-glucoside	0.29±0.05^{ab}	0.15±0.01^{ac}	0.10±0.01^{bc}	0.91±0.06^{ab}	0.55±0.02^{ac}	0.68±0.03^{bc}
Caffeoyl hexose	1.92±0.03^{ab}	2.15±0.02^{ac}	2.21±0.03^{bc}	1.85±0.01^{ab}	2.01±0.04^{ac}	2.07±0.01^{bc}
Ferulic acid derivative	1.19±0.11^{ab}	1.48±0.05^{a}	1.45±0.02^{b}	1.05±0.02^{b}	1.04±0.02^{c}	0.72±0.06^{bc}
Galloyl *bis*-HHDP-glucose	175.91±12.83^{ab}	151.27±7.99^{ac}	118.64±3.80^{bc}	85.01±5.75^{ab}	35.35±4.25^{a}	35.77±1.84^{b}
HHDP-glucose	2.11±0.52^{ab}	1.28±0.08^{a}	1.28±0.05^{b}	2.20±0.05^{b}	2.31±0.13^{c}	1.72±0.26^{bc}
Homovanillic acid	2.24±0.31^{ab}	6.30±0.08^{a}	6.14±0.29^{b}	4.55±0.13^{ab}	9.81±1.02^{a}	10.94±0.25^{b}
Isorharmentin glucose	3.51±0.33^{a}	4.63±0.19^{ac}	3.51±0.04^{c}	3.26±0.11^{ab}	3.75±0.24^{ac}	4.42±0.05^{bc}
Kaempferol glucuronide	1.87±0.33	2.15±0.14^{c}	1.75±0.11^{c}	3.85±0.11	3.82±0.11^{c}	3.50±0.17^{c}
Luteolin-3′-xylose	1.77±0.27^{b}	1.96±0.09^{c}	1.40±0.06^{bc}	0.30±0.02^{ab}	0.18±0.01^{ac}	0.10±0.04^{bc}
Methyl ellagic acid	1.13±0.11^{ab}	1.68±0.07^{ac}	1.55±0.03^{bc}	2.02±0.24	1.65±0.11	1.86±0.14
Monogalloyl glucose	4.77±0.51	5.68±0.20	5.92±0.02	3.13±0.11^{a}	2.79±0.23^{ac}	3.33±0.17^{c}
p-Coumaroyl hexoside	77.87±1.14^{ab}	68.87±2.63^{a}	69.93±0.53^{b}	53.63±2.64^{b}	53.29±2.68^{c}	47.74±1.53^{bc}
Phloridzin	0.15±0.02^{ab}	1.76±0.13^{a}	1.62±0.02^{b}	0.35±0.25^{ab}	0.93±0.03^{a}	0.93±0.10^{b}
p-Hydroxybenzoic acid	1.23±0.24^{ab}	2.24±0.18^{a}	2.27±0.12^{b}	1.14±0.15^{ab}	1.99±0.05^{ac}	2.85±0.22^{bc}
Procyanidin B1	24.99±1.44^{ab}	17.84±1.64^{a}	15.78±0.08^{b}	11.59±4.54^{ab}	6.60±0.16^{ac}	6.16±1.52^{bc}
Protocatechuic acid	1.01±0.30	1.92±0.15	0.78±0.08	0.72±0.05^{ab}	0.48±0.03^{ac}	0.63±0.06^{bc}
Quercetin glucoside	1.56±0.14^{b}	1.68±0.11	1.38±0.04^{b}	0.72±0.40	0.52±0.06^{c}	0.42±0.01^{c}
Quercetin glucuronide	1.51±0.11^{ab}	1.70±0.10^{a}	1.30±0.03^{c}	0.81±0.03^{b}	0.81±0.03^{c}	0.73±0.04^{bc}

[a]Mean values and standard deviation. Superscript a indicates a significant difference ($p < 0.05$) between the initial samples (I) and final samples (F) of the same substrate. Superscript b indicates a significant difference ($p < 0.05$) between the initial samples (I) and pasteurized samples (P) of the same substrate. Superscript c indicates a significant difference ($p < 0.05$) between the pasteurized samples (P) and final samples (F) of the same substrate, by ANOVA statistical test. Samples were determined in duplicate. nd, no data.

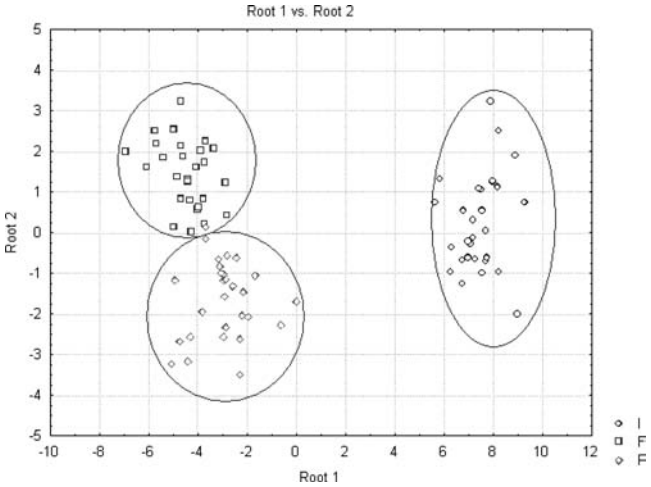

Figure 6. Scatterplot of canonical scores in discriminant analysis for two substrates and 19 variables with 98.8% of classification.

classification of samples. The only incorrectly classified sample was one pasteurized sample, classified as final. Figure 6 shows a scatterplot of the canonical roots obtained. As can be observed, F and P samples are closer than I (initial samples), which reflects the composition change produced by alcoholic fermentation.

3.4. Effect of Alcoholic Fermentation on Antioxidant Activity. Figure 7 displays the results of antioxidant activity determined by two methods, ORAC and DPPH, for the two substrates. The ORAC measurements revealed a significant decrease between initial and final samples for substrate B (17.6%). The same trend was observed between initial and pasteurized samples of the same substrate (15.2%). DPPH results show that only substrate A changed significantly and followed a similar trend to the ORAC data. A significant decrease was observed between initial and final samples (12.3%), and a decrease of and 13.9% between initial and pasteurized samples was observed. These results indicated that alcoholic fermentation caused antioxidant activity to decrease slightly; in contrast with reports on gluconic fermentation[12] and

DOI: 10.1021/jf506076n
J. Agric. Food Chem. 2015, 63, 2041−2051

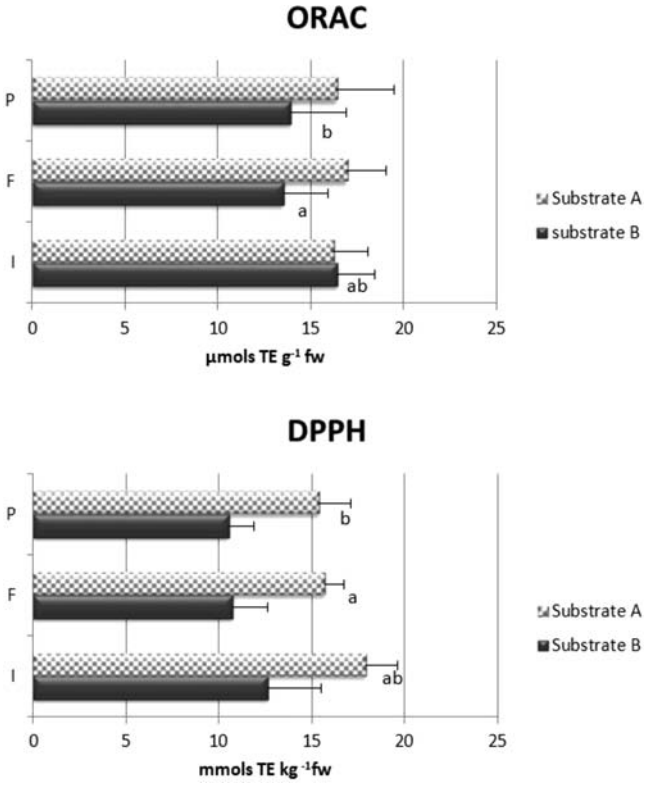

Figure 7. Bar representation of antioxidant activity by two methods, ORAC and DPPH, for the two substrates. Letters a, b, and c correspond to significant differences between I/F, I/P, and F/P samples, respectively.

alcoholic fermentation in mulberries,[43] no significant changes were detected. Apart from nonanthocyanin polyphenolic compounds, strawberry is a particularly rich source of anthocyanins,[44] which are outside the scope of this paper, which is focused on the identification of a large set of nonanthocyanin compounds. Indeed, the extracts for obtaining the nonanthocyanin fraction may present other compounds, which would account for a certain part of the antioxidant activity, which could also explain this average decrease.

3.5. Conclusions. Sixty-six compounds were identified by MS and HRMS. A total of 13 compounds was identified for the first time in strawberry and an alcoholic-fermented product: protocatechuic acid-4-*O*-*β*-hexoside, brevifolin carboxylic acid, ferulic acid glucuronide, dimer caffeic acid-*O*-hexoside, luteolin-3′-*O*-xyloside, isorhamnetin3-*O*-glucoside, taxifolin-*O*-glucoside, (+)-aromadendrin rhamnoside, eriodictyol-7-*O*-glucoside, (+)-taxifolin, (+)-aromadendrin, eriodictyol, and homovanillic acid.

LDA allows the correct classification of samples I, F, and P as alcoholic fermentation induces changes in phenolic composition, mainly related to the 19 compounds. Specifically, homovanillic acid and *p*-hydroxybenzoic acid increased significantly in almost every fermentation cycle.

■ ASSOCIATED CONTENT

Ⓢ Supporting Information

Contents of nonanthocyanin phenolic compounds that are not reported in this work for substrates A and B. This material is available free of charge via the Internet at http://pubs.acs.org.

■ AUTHOR INFORMATION

Corresponding Author

*Fax: +34954233765. E-mail: mcparrilla@us.es.

Notes

The authors declare no competing financial interest.

■ ACKNOWLEDGMENTS

The authors are very grateful to the Spanish Government for its financial assistance (Project MICINN AGL2010-22152-01 and AGL2010-2215-03). The authors also thank VPPI-US for the ABC current contract. We would also like to thank HUDISA Desarrollo Industrial S.A., in Lepe, Spain, for providing the strawberry pureé samples. We acknowledge the Biology and Mass Spectrometry services (CITIUS) of the University of Seville for the multidetector microplate reader and mass spectrometer instruments (Dr. M. Carballo-Álvarez, Dr. M.E. Soria-Díaz, R. Valderrama-Fernández).

■ REFERENCES

(1) Food and Agricultural Organization of the United Nations, FAOSTAT. *Faostat*, 2012. http://faostat3.fao.org/ (accessed October 2014).

(2) Mena, P.; Gironés-Vilaplana, A.; Martí, N.; García-Viguera, C. Pomegranate varietal wines: Phytochemical composition and quality parameters. *Food Chem.* **2012**, *133* (1), 108−115.

(3) Álvarez-Fernández, M. A.; Hornedo-Ortega, R.; Cerezo, A. B.; Troncoso, A. M.; García-Parrilla, M. C. Effects of the strawberry (*Fragaria x ananassa*) purée elaboration process on nonanthocyanin phenolic composition and antioxidant activity. *Food Chem.* **2014**, *164*, 104−112.

(4) Erlund, I.; Koli, R.; Alfthan, G.; Marniemi, J.; Puukka, P.; Mustonen, P.; Jula, A. Favorable effects of berry consumption on platelet function, blood pressure, and HDL cholesterol. *Am. J. Clin. Nutr.* **2008**, *87* (2), 323−331.

(5) Del Rio, D.; Borges, G.; Crozier, A. Berry flavonoids and phenolics: Bioavailability and evidence of protective effects. *Br. J. Nutr.* **2010**, *104* (Suppl. 3), S67−S90.

(6) Tresserra-Rimbau, A.; Medina-Remón, A.; Pérez-Jiménez, J.; Martínez-González, M. A.; Covas, M. I.; Corella, D.; Lamuela-Raventós, R. M. Dietary intake and major food sources of polyphenols in a Spanish population at high cardiovascular risk: The PREDIMED study. *Nutr., Metab. Cardiovasc. Dis.* **2013**, *23* (10), 953−959.

(7) Tresserra-Rimbau, A.; Rimm, E. B.; Medina-Remón, A.; Martínez-González, M. A.; de la Torre, R.; Corella, D.; Lamuela-Raventós, R. M. Inverse association between habitual polyphenol intake and incidence of cardiovascular events in the PREDIMED study. *Nutr., Metab. Cardiovasc. Dis.* **2014**, *24* (6), 639−647.

(8) Tresserra-Rimbau, A.; Rimm, E. B.; Medina-Remón, A.; Martínez-González, M. A.; López-Sabater, M. C.; Covas, M. I.; Lamuela-Raventós, R. M. Polyphenol intake and mortality risk: A re-analysis of the PREDIMED trial. *BMC Med.* **2014**, *12*, 77.

(9) Mozzi, F.; Ortiz, M. E.; Bleckwedel, J.; De Vuyst, L.; Pescuma, M. Metabolomics as a tool for the comprehensive understanding of fermented and functional foods with lactic acid bacteria. *Food Res. Int.* **2013**, *54* (1), 1152−1161.

(10) Oms-Oliu, G.; Odriozola-Serrano, I.; Martín-Belloso, O. Metabolomics for assessing safety and quality of plant-derived food. *Food Res. Int.* **2013**, *54* (1), 1172−1183.

(11) Hidalgo, C.; Torija, M. J.; Mas, A.; Mateo, E. Effect of inoculation on strawberry fermentation and acetification processes using native strains of yeast and acetic acid bacteria. *Food Microbiol.* **2013**, *34* (1), 88−94.

(12) Álvarez-Fernández, M. A.; Hornedo-Ortega, R.; Cerezo, A. B.; Troncoso, A. M.; García-Parrilla, M. C. Nonanthocyanin phenolic compounds and antioxidant activity of beverages obtained by gluconic

DOI: 10.1021/jf506076n
J. Agric. Food Chem. 2015, 63, 2041−2051

fermentation of strawberry. *Innovative Food Sci. Emerging Technol.* **2014**, *26*, 469−481.
(13) Ou, B.; Hampsch-Woodill, M.; Prior, R. L. Development and validation of an improved oxygen radical absorbance capacity assay using fluorescein as the fluorescent probe. *J. Agric. Food Chem.* **2001**, *49* (10), 4619−4626.
(14) Villaño, D.; Fernández-Pachón, M. S.; Moyá, M. L.; Troncoso, A. M.; García-Parrilla, M. C. Radical scavenging ability of polyphenolic compounds towards DPPH free radical. *Talanta* **2007**, *71*, 230−235.
(15) Statsoft, INC. *STATISTICA for Windows (Computer program manual)*; Tulsa, Staftsoft, Inc.: Tulsa, OK, 2001; pp74104−4442.
(16) Aaby, K.; Ekeberg, D.; Skrede, G. Characterization of phenolic compounds in strawberry (*Fragaria x ananassa*) fruits by different HPLC detectors and contribution of individual compounds to total antioxidant capacity. *J. Agric. Food Chem.* **2007**, *55* (11), 4395−4406.
(17) Aaby, K.; Mazur, S.; Nes, A.; Skrede, G. Phenolic compounds in strawberry (*Fragaria x ananassa* Duch.) fruits: Composition in 27 cultivars and changes during ripening. *Food Chem.* **2012**, *132* (1), 86−97.
(18) Abu-Reidah, I. M.; Arraez-Roman, D.; Segura-Carretero, A.; Fernandez-Gutierrez, A. Extensive characterisation of bioactive phenolic constituents from globe artichoke (*Cynara scolymus* L.) by HPLC-DAD−ESI−QTOF-MS. *Food Chem.* **2013**, *141* (3), 2269−2277.
(19) Chandrasekara, A.; Shahidi, F. Determination of antioxidant activity in free and hydrolyzed fractions of millet grains and characterization of their phenolic profiles by HPLC-DAD−ESI−MS. *J. Funct. Foods.* **2011**, *3* (3), 144−158.
(20) Del Bubba, M.; Checchini, L.; Chiuminatto, U.; Doumett, S.; Fibbi, D.; Giordani, E. Liquid chromatographic/electrospray ionization tandem mass spectrometric study of polyphenolic composition of four cultivars of *Fragaria vesca* L. berries and their comparative evaluation. *J. Mass Spectrom.* **2012**, *47* (9), 1207−1220.
(21) Ferreres, F.; Grosso, C.; Gil-Izquierdo, A.; Valentão, P.; Azevedo, C.; Andrade, P. B. HPLC-DAD−ESI/MS analysis of phenolic compounds for quality control of *Grindelia robusta* Nutt. and bioactivities. *J. Pharm. Biomed. Anal.* **2014**, *94*, 163−172.
(22) Fischer, U. A.; Carle, R.; Kammerer, D. R. Identification and quantification of phenolic compounds from pomegranate (*Punica granatum* L.) peel, mesocarp, aril, and differently produced juices by HPLC-DAD−ESI/MS. *Food Chem.* **2011**, *127* (2), 807−821.
(23) Gouveia, S. C.; Castilho, P. C. Analysis of phenolic compounds from different morphological parts of *Helichrysum devium* by liquid chromatography with on-line UV and electrospray ionization mass spectrometric detection. *Rapid Commun. Mass Spectrom.* **2009**, *23* (24), 3939−3953.
(24) Gouveia, S. C.; Castilho, P. C. Characterization of phenolic compounds in *Helichrysum melaleucum* by high-performance liquid chromatography with on-line ultraviolet and mass spectrometry detection. *Rapid Commun. Mass Spectrom.* **2010**, *24* (13), 1851−1868.
(25) Hanhineva, K.; Rogachev, I.; Kokko, H.; Mintz-Oron, S.; Venger, I.; Kärenlampi, S.; Aharoni, A. Nontargeted analysis of spatial metabolite composition in strawberry (*Fragaria x ananassa*) flowers. *Phytochemistry* **2008**, *69* (13), 2463−2481.
(26) Horai, H.; Arita, M.; Kanaya, S.; Nihei, Y.; Ikeda, T.; Suwa, K.; Nishioka, T. MassBank: A public repository for sharing mass spectral data for life sciences. *J. Mass Spectrom.* **2010**, *45* (7), 703−714.
(27) Määttä-Riihinen, K. R.; Kamal-Eldin, A.; Törrönen, A. R. Identification and quantification of phenolic compounds in berries of *Fragaria* and *Rubus* species (Family *Rosaceae*). *J. Agric. Food Chem.* **2004**, *52* (20), 6178−6187.
(28) Ornelas-Paz, J. J.; Yahia, E. M.; Ramírez-Bustamante, N.; Pérez-Martínez, J. D.; Escalante-Minakata, M. D. P.; Ibarra-Junquera, V.; Ochoa-Reyes, E. Physical attributes and chemical composition of organic strawberry fruit (*Fragaria x ananassa* Duch., cv. albion) at six stages of ripening. *Food Chem.* **2013**, *138* (1), 372−381.
(29) Püssa, T.; Floren, J.; Kuldkepp, P.; Raal, A. Survey of grapevine *Vitis vinifera* stem polyphenols by liquid chromatography-diode array detection−tandem mass spectrometry. *J. Agric. Food Chem.* **2006**, *54* (20), 7488−7494.
(30) Quirantes-Piné, R.; Herranz-López, M.; Funes, L.; Borrás-Linares, I.; Micol, V.; Segura-Carretero, A.; Fernández-Gutiérrez, A. Phenylpropanoids and their metabolites are the major compounds responsible for blood-cell protection against oxidative stress after administration of *Lippia citriodora* in rats. *Phytomedicine* **2013**, *20* (12), 1112−1118.
(31) Sawada, Y.; Nakabayashi, R.; Yamada, Y.; Suzuki, M.; Sato, M.; Sakata, A.; Akiyama, K.; Sakurai, T.; Matsuda, F.; Aoki, T.; Hirai, M. Y.; Saito, K. RIKEN tandem mass spectral database (ReSpect) for phytochemicals: A plant-specific MS/MS-based data resource and database. *Phytochemistry* **2012**, *82*, 38−45.
(32) Seeram, N. P.; Lee, R.; Scheuller, H. S.; Heber, D. Identification of phenolic compounds in strawberries by liquid chromatography electrospray ionization mass spectroscopy. *Food Chem.* **2006**, *97* (1), 1−11.
(33) Sun, J.; Liu, X.; Yang, T.; Slovin, J.; Chen, P. Profiling polyphenols of two diploid strawberry (*Fragaria vesca*) inbred lines using UHPLC−HRMS. *Food Chem.* **2014**, *146*, 289−298.
(34) Taamalli, A.; Iswaldi, I.; Arráez-Román, D.; Segura-Carretero, A.; Fernández-Gutiérrez, A.; Zarrouk, M. UPLC−QTOF/MS for a rapid characterisation of phenolic compounds from leaves of *Myrtus communis* L. *Phytochem. Anal.* **2014**, *25* (1), 89−96.
(35) Santos, S. A. O.; Freire, C. S. R.; Domingues, M. R. M.; Silvestre, A. J. D.; Neto, C. P. Characterization of phenolic components in polar extracts of *Eucalyptus globulus* Labill. bark by high-performance liquid chromatography−mass spectrometry. *J. Agric. Food Chem.* **2011**, *59* (17), 9386−9393.
(36) Dall'Asta, M.; Calani, L.; Tedeschi, M.; Jechiu, L.; Brighenti, F.; Del Rio, D. Identification of microbial metabolites derived from *in vitro* fecal fermentation of different polyphenolic food sources. *Nutrition* **2012**, *28* (2), 197−203.
(37) Ju, H. K.; Cho, E. J.; Jang, M. H.; Lee, Y. Y.; Hong, S. S.; Park, J. H.; Kwon, S. W. Characterization of increased phenolic compounds from fermented bokbunja (*Rubus coreanus* Miq.) and related antioxidant activity. *J. Pharm. Biomed. Anal.* **2009**, *49* (3), 820−827.
(38) Figueiredo-González, M.; Regueiro, J.; Cancho-Grande, B.; Simal-Gándara, J. Garnacha Tintorera-based sweet wines: Detailed phenolic composition by HPLC/DAD−ESI/MS analysis. *Food Chem.* **2014**, *143*, 282−292.
(39) Vrhovsek, U.; Guella, G.; Gasperotti, M.; Pojer, E.; Zancato, M.; Mattivi, F. Clarifying the identity of the main ellagitannin in the fruit of the strawberry, *Fragaria vesca* and *Fragaria ananassa* Duch. *J. Agric. Food Chem.* **2012**, *60* (10), 2507−2516.
(40) Jaganath, I. B.; Mullen, W.; Lean, M. E. J.; Edwards, C. A.; Crozier, A. In vitro catabolism of rutin by human fecal bacteria and the antioxidant capacity of its catabolites. *Free Radic. Biol. Med.* **2009**, *47* (8), 1180−1189.
(41) Serra, A.; Macià, A.; Romero, M.-P.; Reguant, J.; Ortega, N.; Motilva, M.-J. Metabolic pathways of the colonic metabolism of flavonoids (flavonols, flavones, and flavanones) and phenolic acids. *Food Chem.* **2012**, *130* (2), 383−393.
(42) Viljanen, K.; Heiniö, R.-L.; Juvonen, R.; Kössö, T.; Puupponen-Pimiä, R. Relation of sensory perception with chemical composition of bioprocessed lingonberry. *Food Chem.* **2014**, *157*, 148−156.
(43) Pérez-Gregorio, M.; Regueiro, J.; Alonso-González, E.; Pastrana-Castro, L.; Simal-Gándara, J. Influence of alcoholic fermentation process on antioxidant activity and phenolic levels from mulberries (*Morus nigra* L.). *LWT-Food Sci. Technol.* **2011**, *44* (8), 1793−1801.
(44) Cerezo, A. B; Cuevas, E.; Winterhalter, P.; Garcia-Parrilla, M. C.; Troncoso, A. M. Isolation, identification, and antioxidant activity of anthocyanin compounds in (*Camarosa*) strawberry. *Food Chem.* **2010**, *123* (3), 574−582.

DOI: 10.1021/jf506076n
J. Agric. Food Chem. 2015, 63, 2041−2051

and vegetables can be increased within the small intestine phase by coingesting them with lipids.[19−21] The bioaccessibility of curcumin can be increased in a similar manner using this approach.[4] This effect has been attributed to the ability of the lipid digestion products to form mixed micelles that solubilize and transport highly lipophilic components to the epithelium cells. An alternative strategy to improve the bioavailability of certain food components would be to incorporate efflux inhibitors, e.g., piperine (a constituent from black pepper) has been shown to act as an efflux inhibitor for curcumin.[22]

In the present study, we examined the possibility of developing excipient emulsions to increase the bioaccessibility of powdered curcumin. Crystalline forms of lipophilic bioactive agents usually have a much lower bioavailability than solubilized forms.[23] We therefore hypothesized that mixing powdered curcumin with an excipient emulsion would increase its bioaccessibility due to its ability to increase the solubility of curcumin in the intestinal fluids. The effect of incubation temperature and time on the transfer of curcumin into the excipient emulsion prior to ingestion was measured, as well as the bioaccessibility of curcumin after exposure to a simulated gastrointestinal tract (GIT). Two incubation temperatures (30 °C and 100 °C) were used to mimic conditions that curcumin might experience in food applications: (i) within ambient foods (such as salads); (ii) within cooked foods (such as curry sauces). The information obtained from this study may be useful for the design of excipient emulsions to increase the bioavailability and bioactivity of lipophilic nutraceuticals.

MATERIALS AND METHODS

Materials. Corn oil purchased from a local supermarket was used as an example of a digestible long chain triglyceride. The following chemicals were purchased from the Sigma Chemical Company (St. Louis, MO): curcumin (SLBH2403 V), mucin from porcine stomach (SLBH9969 V), pepsin from porcine gastric mucosa (SLBL1993 V), lipase from porcine pancreas pancreatin (SLBH6427 V), porcine bile extract (SLBK9078), Tween 80 (BCBG4438 V), and Nile Red (063 K3730 V). The supplier reported that the activity of the pepsin was around 250 units/mg, and the activity of the lipase was around 100−400 units/mg protein (using olive oil). All other chemicals were of analytical grade. Double distilled water was used to prepare all solutions and emulsions.

Excipient Emulsion Preparation. Initially, an aqueous phase was prepared by mixing 1% (w/w) Tween 80 with an aqueous buffer solution (10.0 mM phosphate-buffered saline (PBS), pH 6.5). Coarse oil-in-water emulsions were prepared by homogenizing 10% (w/w) corn oil with 90% (w/w) aqueous phase using a high-speed blender for 2 min (M133/1281-0, Biospec Products, Inc., ESGC, Switzerland). Fine emulsions were then obtained by passing the coarse emulsions through a microfluidizer (M110Y, Microfluidics, Newton, MA) with a 75 μm interaction chamber (F20Y) at an operational pressure of 9000 psi for five passes. The resulting excipient emulsions were stored in a refrigerator at 4 °C before use.

Preparation of Curcumin−Emulsion, Curcumin−Oil, and Curcumin−Buffer Mixtures. Curcumin (3 mg) was weighed into a beaker, and then excipient emulsion (10 mL) was added. The resulting mixtures were then incubated at either 30 °C or 100 °C for different times (ranging from 10 to 120 min for 30 °C and from 10 to 60 min for 100 °C). After incubation, selected samples were immediately placed in an ice−water bath and then used for the following experiments. In some experiments, the curcumin was mixed with bulk corn oil or with buffer (PBS) solution rather than an emulsion.

Curcumin Solubility in Mixtures. The solubility of curcumin in each mixture was measured spectrophotometrically based on the method of Ahmed, Li, McClements, and Xiao[4] with some modifications. Ten milliliters of mixture was collected and then centrifuged at 1750 rpm for 10 min at ambient temperature (CL10 centrifuge, Thermo, Scientific, Pittsburgh, PA) to remove non-dissolved (crystalline) curcumin. One milliliter of supernatant was then mixed with 5 mL of choloroform, vortexed, and centrifuged at 1750 rpm for 10 min at ambient temperature. The bottom layer containing the solubilized curcumin was collected, while the top layer was mixed with an additional 5 mL of chloroform and the same procedure was repeated. The two bottom chloroform layers were combined and diluted to an appreciate concentration to be analyzed by a UV−VIS spectrophotometer at 419 nm (Ultraspec 3000 pro, GE Health Sciences, Piscataway, NJ). A cuvette containing pure chloroform was used as a reference cell. The concentration of curcumin extracted from each mixture was calculated from a calibration curve of absorbance versus curcumin concentration in chloroform. The solubility of curcumin in each mixture was then calculated as the concentration of curcumin extracted from each mixture multiplied by the dilution factor.

Particle Characterization. The mean particle diameters (*Z*-average) and particle size distributions of the curcumin−emulsion mixtures after incubation at different temperatures were monitored using a dynamic light scattering instrument (Nano-ZS, Malvern Instruments Ltd., Worcestershire, UK). The electrical charge (ζ-potential) of the particles in these samples was measured using a microelectrophoresis instrument (Nano-ZS, Malvern Instruments Ltd.). Samples were diluted with buffer solution (10.0 mM PBS, pH 6.5) prior to measurements to avoid multiple scattering effects.

The mean particle diameter and particle size distribution of samples exposed to simulated gastrointestinal conditions was measured using static light scattering (Mastersizer 2000, Malvern Instruments Ltd.). Samples were diluted with appropriate buffer solutions (same pH as GIT phase) and stirred in the dispersion unit at a speed of 1200 rpm. The particle size is reported as the surface-weighted mean diameter (d_{32}).

Microstructural Analysis. The microstructure of samples was characterized using confocal scanning fluorescence microscopy (Nikon D-Eclipse C1 80i, Nikon, Melville, NY). Samples analyzed by confocal microscopy were dyed with Nile Red to highlight the location of the lipid phase. The Nile red was dissolved in absolute ethyl alcohol at a concentration (1 mg/mL). Then, before analysis, 2 mL emulsion samples were mixed with 0.1 mL of Nile Red solution (1 mg/mL ethanol) to dye the oil phase. All images were captured with a 10× eyepiece and a 60× objective lens (oil immersion). Changes in the properties of curcumin crystals in the mixtures were observed using a cross-polarized lens (C1 Digital Eclipse, Nikon, Tokyo, Japan).

Curcumin Oil-Solubility Characteristics. The temperature-dependence of the dissolution of crystalline curcumin into bulk corn oil was characterized by measuring the change in turbidity (600 nm) with temperature using a UV−visible spectrophotometer equipped with a temperature controller (Agilent Cary 200, Agilent, Santa Clara, CA). This method can be used to detect the presence of curcumin crystals in the oil phase and indirectly determine the solubility of curcumin in bulk corn oil. A weighed amount of curcumin (3 or 4 mg/mL) was dispersed in corn oil at ambient temperature, and then the mixture was heated from 25 to 100 °C and then cooled from 100 °C to 25 °C at a rate 1 °C/min with continuous stirring. In some experiments, the change in turbidity with time was measured at a fixed incubation temperature (30 °C or 100 °C) to determine the kinetics of isothermal dissolution.

Simulated Gastrointestinal Digestion. Powdered curcumin was mixed with excipient emulsion, corn oil, or buffer solution and then held at 30 °C for 30 min or 100 °C for 10 min. Each sample was passed through a three-step GIT model that consisted of mouth, gastric, and small intestine phases, which was slightly modified from the our previous study.[24]

Initial System. The initial systems were placed into a glass beaker in an incubator shaker at a rotation speed of 100 rpm for 15 min at 37 °C for preheating (Innova Incubator Shaker, Model 4080, New Brunswick Scientific, Edison, NJ). Three different initial systems were tested: (i) curcumin and excipient emulsion, (ii) curcumin, corn oil, and buffer

DOI: 10.1021/jf506149f
J. Agric. Food Chem. 2015, 63, 2052−2062

solution, or (iii) curcumin and buffer solution. The initial concentration of curcumin was the same in all systems, while the initial concentration of corn oil in systems i and ii were the same.

Mouth Phase. A simulated saliva fluid (SSF) containing 3 mg/mL mucin and various salts was prepared as described previously.[25] SSF was preheated to 37 °C and then mixed with the preheated curcumin mixture at a 1:1 mass ratio. The mixture was then adjusted to pH 6.8 and placed in an incubator shaker at 100 rpm and 37 °C for 10 min. This incubation time is longer than a food would normally spend in the mouth but was used to minimize sample-to-sample variations that might occur if very short times were used.

Stomach Phase. Simulated gastric fluid (SGF) was prepared by placing 2 g of NaCl and 7 mL of HCl into a container and then adding double distilled water to 1 L. The bolus sample from the mouth phase was then mixed with SGF containing 0.0032 g/mL pepsin preheated to 37 °C at a 1:1 mass ratio. The mixture was then adjusted to pH 2.5 and placed in a shaker at 100 rpm and 37 °C for 2 h to mimic stomach digestion. It should be noted that we did not include gastric lipase in the SGF because of the difficulty in obtaining a reliable and economically viable source of this digestive enzyme.[26] Gastric lipase typically promotes a limited amount of lipid digestion within the stomach phase and therefore its omission should only have a fairly modest impact on the gastrointestinal fate of the excipient emulsions.

Small Intestine Phase. Thirty milliliter chyme samples from the stomach phase were diluted with buffer solution (10 mM PBS, pH 6.5) to obtain a final corn oil concentration of 1.25%. The diluted chyme was then incubated in a water bath (37 °C) for 10 min, and then the solution was adjusted back to pH 7.0. Next, 3 mL of simulated intestinal fluid (containing 0.5 M $CaCl_2$ and 7.5 M NaCl) was added to 60 mL of digesta. Then, 7 mL bile extract, containing 375.0 mg of bile extract (pH 7.0, PBS), was added with stirring, and the pH was adjusted to 7.0. Finally, 5 mL of pancreatic suspension, containing 120 mg of lipase (pH 7.0, PBS), was added to the sample, and an automatic titration unit (Metrohm, USA Inc., Riverview, FL) was used to monitor the pH and control it to a fixed value (pH 7.0) by titrating 0.25 M NaOH solution into the reaction vessel for 2 h at 37 °C. The percentage of free fatty acids released in the sample was calculated from the number of moles of NaOH required to maintain neutral pH as described previously.[27] It should be noted that some of the free fatty acids may not be fully ionized at pH 7, and therefore the FFAs determined by the pH stat method are only the titrable ones.[28]

Curcumin Bioaccessibility. After in vitro digestion, 30 mL of raw digesta of each mixture was centrifuged (18000 rpm, Thermo Scientific, Waltham, MA) at 25 °C for 30 min. The clear supernatant was collected and assumed to be the "'micelle'" fraction in which the curcumin was solubilized. In some samples, a layer of nondigested oil was observed at the top of the samples, and it was removed from the micelle fraction. Aliquots of 5 mL of micelle fraction were mixed with 5 mL of chloroform, vortexed, and centrifuged at 1750 rpm for 10 min at ambient temperature. The bottom layer containing the solubilized curcumin was collected, while the top layer was mixed with an additional 5 mL of chloroform and the same procedure was repeated. The two collected chloroform layers were mixed together and then diluted to an appreciate concentration to be analyzed by a UV−vis spectrophotometer at 419 nm. The concentration of curcumin was calculated from the absorbance using a standard curve at a suitable dilution factor. The bioaccessibility of curcumin was calculated according to the following expression: BA% = 100 × c_M/c_D, where c_M and c_D are the curcumin concentrations in the mixed micelle phase and in the total digesta collected after the small intestine phase, respectively.

Statistical Analysis. All experiments were carried out on at least two freshly prepared samples. The results are expressed as means ± standard deviation (SD). Data was subjected to statistical analysis using SPSS software version 18.0. Differences were considered significant at $p < 0.05$.

RESULTS AND DISCUSSION

Effect of Incubation Temperature on Particle Characteristics. In this study, curcumin-containing samples were exposed to two different incubation temperatures to simulate different conditions that they might experience in food applications: (i) 30 °C for salads at ambient temperature; (ii) 100 °C for sauces at cooking temperatures. The mixture of curcumin and excipient emulsion was stirred to ensure homogeneity and then incubated at either 30 °C or 100 °C for different times. The mean particle diameter, particle size distribution, particle charge, and visual appearance of the different samples was then measured (Table 1, Figure 1a−c).

There were no appreciable changes in the characteristics of the droplets in the curcumin−emulsion mixtures during incubation at 30 °C for up to 120 min (Table 1 and Figure 1a). Indeed, there were no significant changes in the mean particle diameter, polydispersity index (PDI), or ζ-potential of the curcumin−emulsion mixtures when compared to the initial emulsions. The curcumin−emulsion systems were also stable to incubation at 100 °C from 10 to 30 min, with no significant changes in mean particle diameter, PDI, or ζ-potential. However, there was evidence of some droplet creaming in the curcumin−emulsion mixture after heating at 100 °C for 60 min (indicated by an arrow in Figure 1c). Moreover, there was a significant increase in the mean particle diameter and PDI for these emulsions (Figure 1b and Table 1). This effect may be due to droplet coalescence resulting from dehydration of the nonionic surfactant head groups at elevated temperatures.[29] There was no significant change in the magnitude of the electrical charge on the emulsion droplets when they were incubated at either 30 °C or 100 °C, which suggests that the interfacial composition remained relatively constant.

The microstructures of the curcumin−emulsion mixtures after heating at 30 °C and 100 °C for different times were recorded using confocal fluorescence microscopy (Figure 2a). There was little change in the microstructure of the mixed systems incubated at 30 °C for different times, confirming their high stability under these conditions. However, there was evidence of some larger oil droplets in the mixed systems after incubation at 100 °C for prolonged times, suggesting that some coalescence had occurred.

We also measured the amount of curcumin transferred into the excipient emulsions over time at different incubation temperatures. The amount of curcumin solubilized in the excipient emulsions depended on incubation temperature and time. There was a gradual increase in the amount of curcumin solubilized within the excipient emulsion for mixtures incubated at 30 °C (Table 1). On the other hand, there was a rapid increase in the amount of curcumin solubilized in the excipient emulsions during the first 10 min of incubation at 100 °C, followed by an appreciable decrease at longer incubation times. This decrease was attributed to the fact that droplet coalescence and oiling off occurred in the emulsions held at the higher temperature, which meant that some of the curcumin remained in the upper oil phase and was not therefore measured. Overall, the amount of curcumin solubilized within the excipient emulsions was considerable higher for the samples incubated at the higher holding temperatures. For example, the amount of curcumin solubilized in the emulsions was around 54 and 218 μg/mL after incubation for 60 min at 30 °C and 90 °C, respectively.

DOI: 10.1021/jf506149f
J. Agric. Food Chem. 2015, 63, 2052−2062

Table 1. Effect of Incubation Time and Temperature on the Mean Particle Diameter (Z-average), Polydispersity Index (PDI), ζ-Potential, and Curcumin Solubility of Mixtures of Curcumin and Excipient Emulsion[a]

		30 °C					100 °C				
	initial	10 min	20 min	30 min	60 min	120 min	10 min	20 min	30 min	60 min	
mean diameter (nm)	208 ± 9 [a]	205 ± 7 [a]	225 ± 21 [a]	213 ± 16 [a]	218 ± 19 [a]	208 ± 12 [a]	259 ± 25 [a]	267 ± 25 [a]	258 ± 18 [a]	984 ± 551 [b]	
PDI	0.20 ± 0.0 [a]	0.20 ± 0.01 [a]	0.26 ± 0.05 [a]	0.23 ± 0.06 [a]	0.23 ± 0.04 [a]	0.20 ± 0.03 [a]	0.27 ± 0.09 [a]	0.34 ± 0.08 [a]	0.28 ± 0.06 [a]	0.62 ± 0.3 [b]	
ζ-potential (mV)	−6.8 ± 1.2 [a]	−7.0 ± 3.7 [a]	−5.7 ± 1.8 [a]	−4.6 ± 0.9 [a]	−6.9 ± 4.2 [a]	−5.5 ± 1.0 [a]	−3.6 ± 1.0 [a]	−3.7 ± 0.7 [a]	−3.9 ± 0.6 [a]	−7.6 ± 2.7 [a]	
solubility (μg/mL)	ND	31 ± 10 [a]	36 ± 10 [ab]	49 ± 5 [bc]	54 ± 9 [c]	99 ± 10 [d]	274 ± 21 [f]	264 ± 30 [f]	266 ± 34 [f]	218 ± 66 [e]	

[a]Samples designated with different letters (a, b, c, d, e, f) were significantly different (Duncan, $p < 0.05$). The "initial" sample was the oil-in-water emulsion before adding curcumin and before incubation. ND = not determined.

The presence of curcumin crystals within the different mixtures after exposure to different incubation temperatures was observed using a crossed polarizer lens (Figure 2b). Some crystalline material was clearly observed in the curcumin−emulsion mixtures incubated at 30 °C from 10 to 120 min, which suggested that the curcumin crystals did not completely dissolve when held at this temperature in the presence of the excipient emulsion. Conversely, no crystals were observed in the curcumin−emulsion mixtures held at 100 °C at any incubation time, which indicated that curcumin crystals rapidly and completely dissolved within the emulsions at this elevated temperature. However, there was evidence of some large droplets in these samples after heating for prolonged times at 100 °C, again suggesting that droplet coalescence occurred.

Temperature Dependence of Curcumin Oil-Solubility. The dependence of the transfer of curcumin into the excipient emulsions on incubation temperature and time may be due to changes in its oil solubility with temperature.[30] We therefore used turbidity measurements to monitor the solubility of curcumin crystals in bulk corn oil at different temperatures. The principle of this method is that the turbidity of the curcumin−oil mixture is relatively high when curcumin crystals are present because they scatter light strongly, but it is relatively low when the crystals have melted or dissolved due to the decrease in light scattering.

The turbidity of curcumin in corn oil mixtures (3 mg/mL) decreased appreciably upon heating from 25 to 100 °C (Figure 3a) until it reached a value close to zero at 100 °C, indicating that the crystals had fully dissolved at this temperature. Upon cooling, the turbidity stayed low, suggesting that the curcumin remained dissolved within the oil. This may have occurred because curcumin was below its saturation temperature at the lower temperatures, or because of supersaturation/supercooling effects.[30] We therefore measured the change in turbidity with temperature for a curcumin−oil mixture containing a higher curcumin concentration (4 mg/mL). In this case, the turbidity still decreased appreciably with increasing temperature, but the final turbidity reached at high temperatures was considerably greater than that observed at the lower curcumin level. Indeed, the samples at the higher temperatures still appeared turbid, suggesting that not all of the curcumin crystals had dissolved. When this sample was cooled the turbidity remained relatively high and even increased slightly, which can be attributed to the fact that the solubility of curcumin decreases with decreasing temperature and the amount of curcumin present was above the saturation level. These results suggest that the solubility of curcumin in corn oil at ambient temperature was somewhere between 3 and 4 mg/mL, which is in agreement with the value of ≈3.2 ± 0.1 mg/mL reported previously.[4]

Information about the kinetics of curcumin dissolution at the two incubation temperatures was obtained by measuring changes in the turbidity of curcumin/oil mixtures (3 mg/mL) over time (Figure 3b). There was little change in the turbidity of the mixture held at 30 °C, suggesting that curcumin crystals only dissolved slowly at this temperature. On the other hand, the turbidity decreased rapidly in the mixture held at 100 °C, which indicated that the curcumin crystals rapidly dissolved in the corn oil at this elevated temperature. This knowledge may be important for developing effective processing operations for incorporating curcumin into food products.

Influence of Simulated Digestion on Particle Properties. In this section, we examined the influence of the excipient emulsions on the potential biological fate of curcumin using an

DOI: 10.1021/jf506149f
J. Agric. Food Chem. 2015, 63, 2052−2062

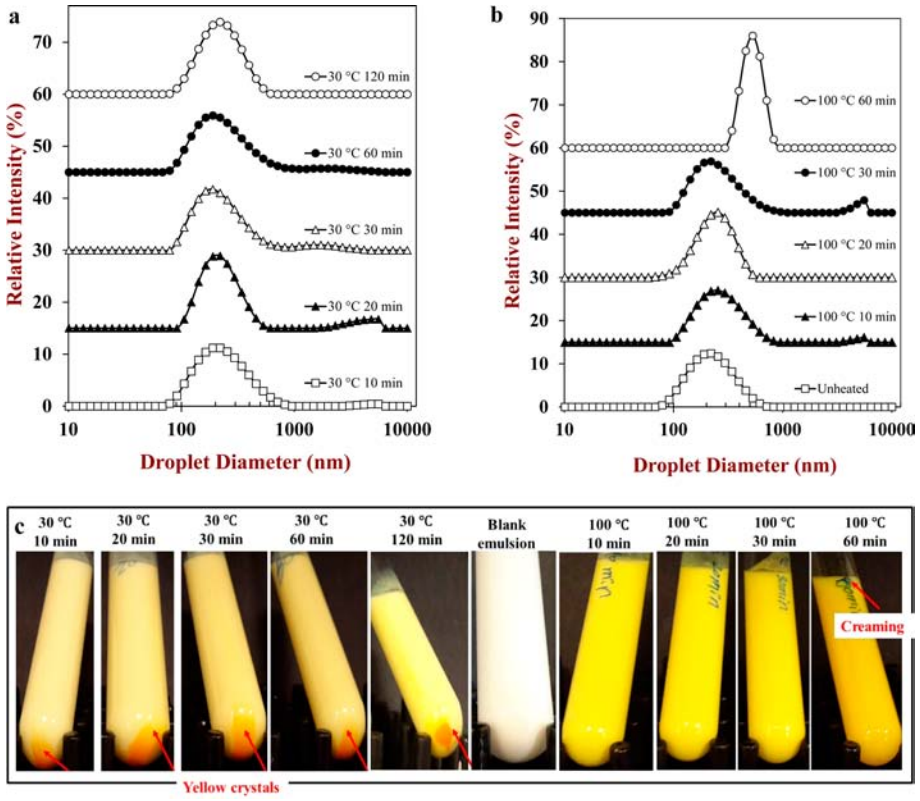

Figure 1. (a) Particle size distributions of mixtures of curcumin and excipient emulsion after incubation at 30 °C for different times. (b) Particle size distributions of mixtures of curcumin and excipient emulsion after incubation at 100 °C for different times. (c) Photographs of mixtures of curcumin and excipient emulsion after incubation at 30 and 100 °C. Note: yellow sediment (curcumin crystals) was observed at the bottom of the test tubes held at 30 °C, whereas a yellow oil layer was observed at the top of the test tubes after heating at 100 °C for 60 min (red arrows).

in vitro gastrointestinal tract (GIT) model that simulates the mouth, stomach, and small intestine phases. Curcumin−emulsion mixtures incubated at 30 °C for 30 min or at 100 °C for 10 min were selected for the GIT study to simulate ambient food applications (such as salad dressings) and cooking applications (such as curry sauces). These incubation times were selected because they led to excipient emulsions that were physically stable and that might simulate usage conditions. It should be noted that the amount of curcumin solubilized in the excipient emulsions at the higher temperature was not strongly dependent on incubation temperature. The results for the excipient emulsions were compared to curcumin−oil and curcumin−buffer mixtures that initially contained the same amount of curcumin. The particle size, microstructure, particle charge, and overall appearance of the different samples were then measured (Figures 4−6).

Particle Size and System Microstructure. The properties of the curcumin−emulsion mixture were evaluated at all stages of the GIT model, but the curcumin−oil mixture was only evaluated after incubation in the small intestine phase since reliable samples could not be obtained from the mouth or stomach phases. This was because the bulk oil tended to form a separate layer at the top of the mixtures, and therefore it was difficult to collect a representative sample. Similarly, the characteristics of the curcumin−buffer mixture were not determined in this series of experiments because it was difficult to collect reliable samples when there were only a few curcumin crystals present in a large volume of buffer solution.

In general, fairly similar trends were observed in the gastrointestinal behavior of curcumin−emulsion mixtures that had previously been incubated at either 30 °C or 100 °C, and so the results are discussed together. The mean particle diameter (d_{32}) determined by static light scattering remained relatively constant after exposure to the mouth and stomach phases but increased appreciably after exposure to the small intestine phase (Figure 4a). Examination of the full particle size distributions of these emulsions indicated that a large fraction of the droplets had fairly similar sizes to the initial emulsions after exposure to the mouth and stomach phases, which suggested that they were relatively stable to coalescence, presumably because they had a nonionic surfactant coating that was resistant to changes in pH, salt, and protease activity. Nevertheless, confocal microscopy images of the same samples indicated that extensive droplet flocculation occurred within the mouth and stomach phases (Figure 6), which may have been due to depletion or bridging flocculation promoted by mucin originating from the artificial saliva.[31] There appeared to be some dissociation of the flocs formed in the emulsions when they moved from the mouth to the stomach stage (Figure 6). This behavior is in agreement with previous studies[31] and may be caused by a number of factors including sample dilution, changes in solution composition, and/or mechanical agitation.[32,33]

The fact that the large particles observed in many of the samples by confocal microscopy were not observed by static light scattering suggests that the flocs dissociated upon dilution and stirring during sample preparation for the particle size analysis. This result highlights the importance of confirming light scattering measurements with microscopy measurements for this type of complex colloidal system.

DOI: 10.1021/jf506149f
J. Agric. Food Chem. 2015, 63, 2052−2062

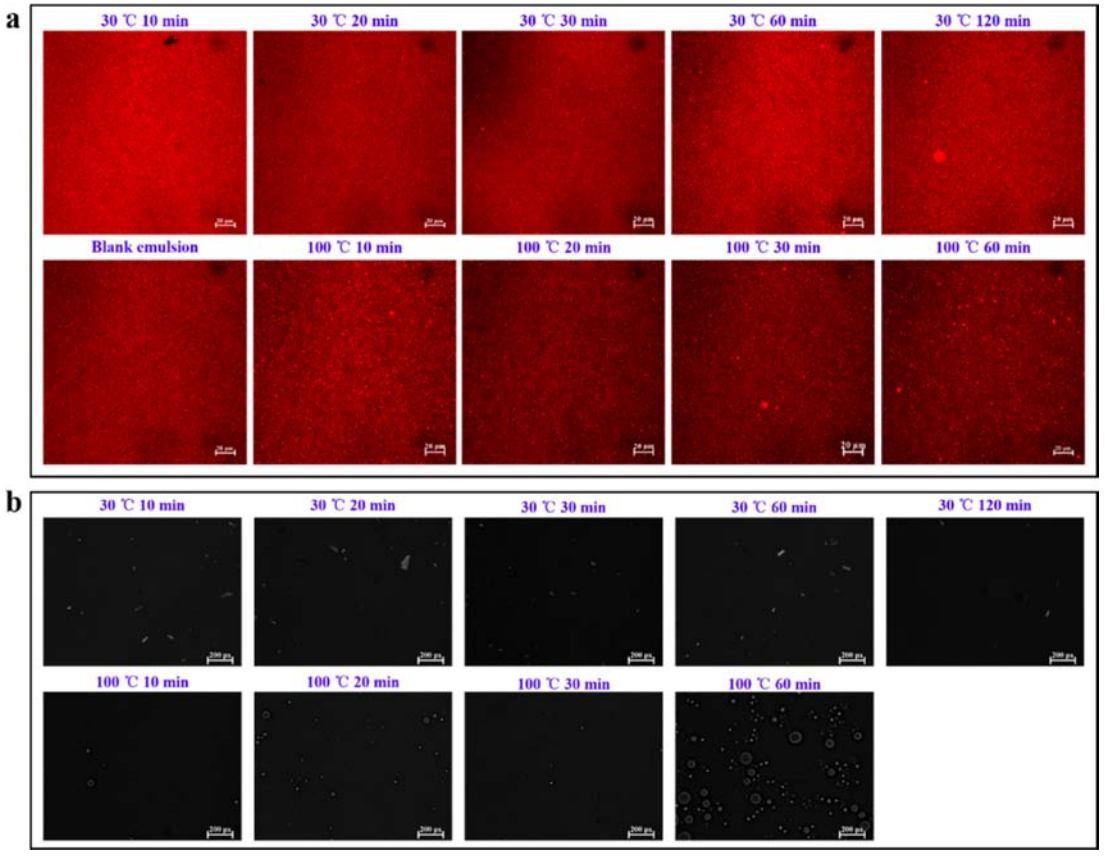

Figure 2. (a) Effect of temperature on microstructure of mixtures of curcumin and excipient emulsion. (b) Effect of temperature on polarized light microscopy of curcumin and excipient emulsion.

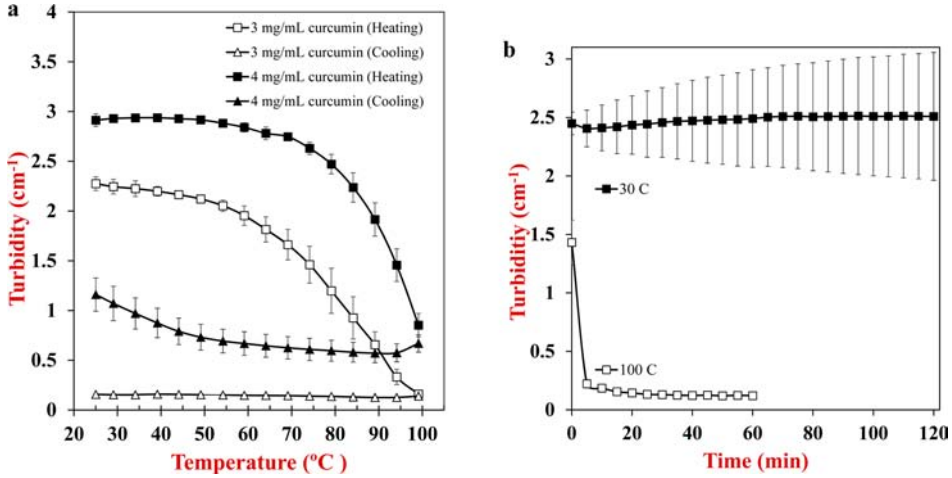

Figure 3. (a) Absorbance versus temperature profile of curcumin−corn oil mixtures (3 and 4 mg/mL). (b) Absorbance versus time profile of a curcumin−corn oil mixture (3 mg/mL) at different isothermal storage temperatures.

Light scattering measurements indicated that a population of relatively large particles was present in the curcumin−emulsion mixtures after exposure to the small intestine phase (Figure 5a and 5b), which was confirmed by confocal microcopy (Figure 6). It is difficult to identify the precise nature of these particles because the intestinal digesta may contain various types of colloidal species, including nondigested lipids, micelles, vesicles, liquid crystals, and insoluble matter (such as calcium soaps).

Light scattering (Figure 5) and confocal microscopy (Figure 6) indicated that there were much larger particles present in the curcumin−oil mixtures after exposure to the small intestine phase than in the curcumin−emulsion mixtures. A possible explanation for this effect is that the bulk corn oil was digested more slowly than the pre-emulsified corn oil (see later), and therefore there were some large nondigested lipid droplets present.

Electrical Characteristics. The electrical characteristics (ζ-potential) of the particles in emulsion−curcumin mixtures exposed to different incubation temperatures followed similar trends after passage through each stage of the simulated GIT (Figure 7), and so they will again be considered together. The particles in the initial curcumin−emulsion mixtures had

DOI: 10.1021/jf506149f
J. Agric. Food Chem. 2015, 63, 2052−2062

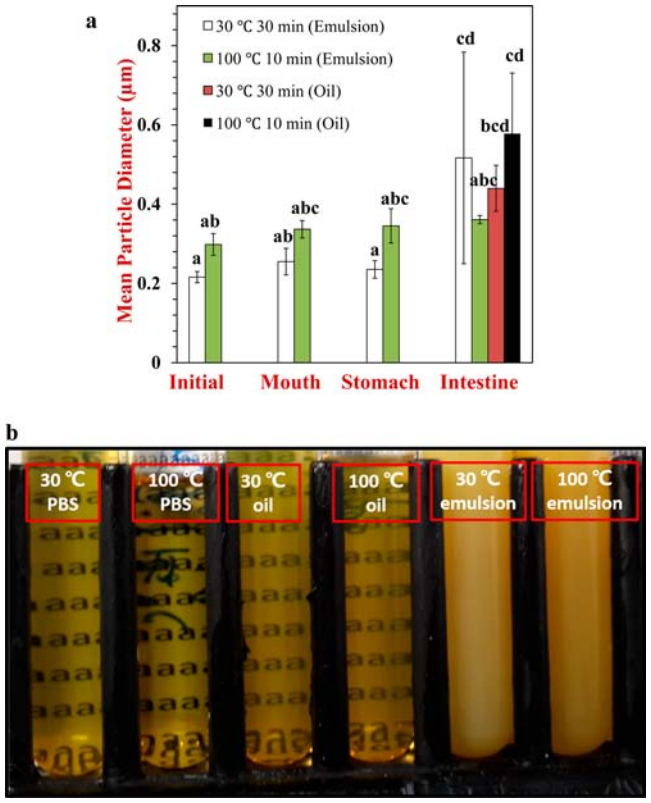

Figure 4. (a) Influence of simulated gastrointestinal conditions on the mean droplet diameter (d_{32}) of curcumin−emulsion and curcumin−oil mixtures after incubation at 30 °C for 30 min or at 100 °C for 10 min. Samples designated with different letters (a, b, c) were significantly different (Duncan, $p < 0.05$). (b) Image of micelle phase collected from curcumin−emulsion and curcumin−oil mixtures.

relatively low negative charges (≈−4 mV), which was due to the fact that a nonionic surfactant was used to coat the droplets. The particles became appreciably more negative after exposure to the mouth phase (≈−9 mV), which may have been due to association of anionic species (such as mucin) with the lipid droplet surfaces.[31] The particle charge became much less negative (≈−2 mV) after exposure to the stomach phase, which can be attributed to the relatively low pH and high ionic strength of the gastric fluids. Finally, the particle charge became highly negative (≈−47 mV) after exposure to the small intestinal fluids, which is probably due to the presence of various anionic constituents associated with this phase such as bile salts, phospholipids, and free fatty acids.[31] There were no significant differences between the electrical characteristics of the particles in the small intestine phase for the curcumin−emulsion and curcumin−oil mixtures at either incubation temperature. This effect can be attributed to the fact that the electrical characteristics were dominated by the presence of bile salts, phospholipids, and free fatty acids and were not strongly affected by sample microstructure.

Lipid Digestion. In this section, we used the pH stat method to determine the rate and extent of lipid digestion of curcumin−emulsion and curcumin−oil mixtures that had previously been incubated at either 30 °C or 100 °C. The volume of NaOH that had to be titrated into the samples to maintain a constant pH (7.0) was measured as a function of digestion time, and then the fraction of free fatty released from the mixture was calculated (Figure 8).

The initial incubation temperature (30 °C or 100 °C) had no effect on the rate and extent of lipid digestion for the curcumin−emulsion mixtures, which was probably due to the fact that the interfacial areas and compositions of the lipid droplets entering the small intestine phase were fairly similar (Figure 8). In these systems, there was a rapid increase in FFAs during the first 10 min, followed by a more gradual increase at longer times. Conversely, there was a much less steep increase in the FFAs released over time in the curcumin−oil mixtures for both incubation times (Figure 8). The origin of this effect can be attributed to the higher surface area of oil exposed to lipase for the emulsified corn oil than for the bulk corn oil. Indeed, the confocal microscopy images clearly highlighted that the fat droplets in the small intestine phase were much larger for the bulk oil than the emulsified oil (Figure 6). Additionally, the rate and extent of lipid digestion in the curcumin−oil mixture that had been incubated at 100 °C (56% FFAs released after 2 h) was higher than the one that had been incubated at

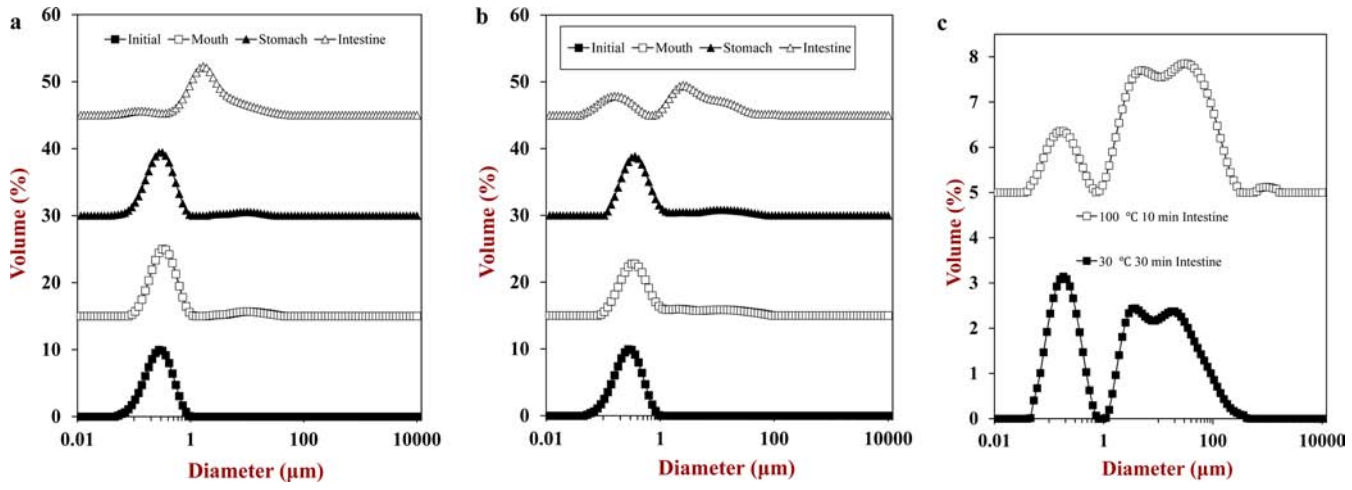

Figure 5. (a) Influence of simulated gastrointestinal conditions on the particle size distributions of curcumin−emulsion mixture after 30 min incubation at 30 °C. (b) Influence of simulated gastrointestinal conditions on the particle size distributions of curcumin−emulsion mixture after 10 min incubation at 100 °C. (c) Influence of simulated gastrointestinal conditions on the particle size distributions of curcumin−oil mixture in the small intestine (measurements could not be made in the initial, mouth, or stomach phases for this sample).

DOI: 10.1021/jf506149f
J. Agric. Food Chem. 2015, 63, 2052−2062

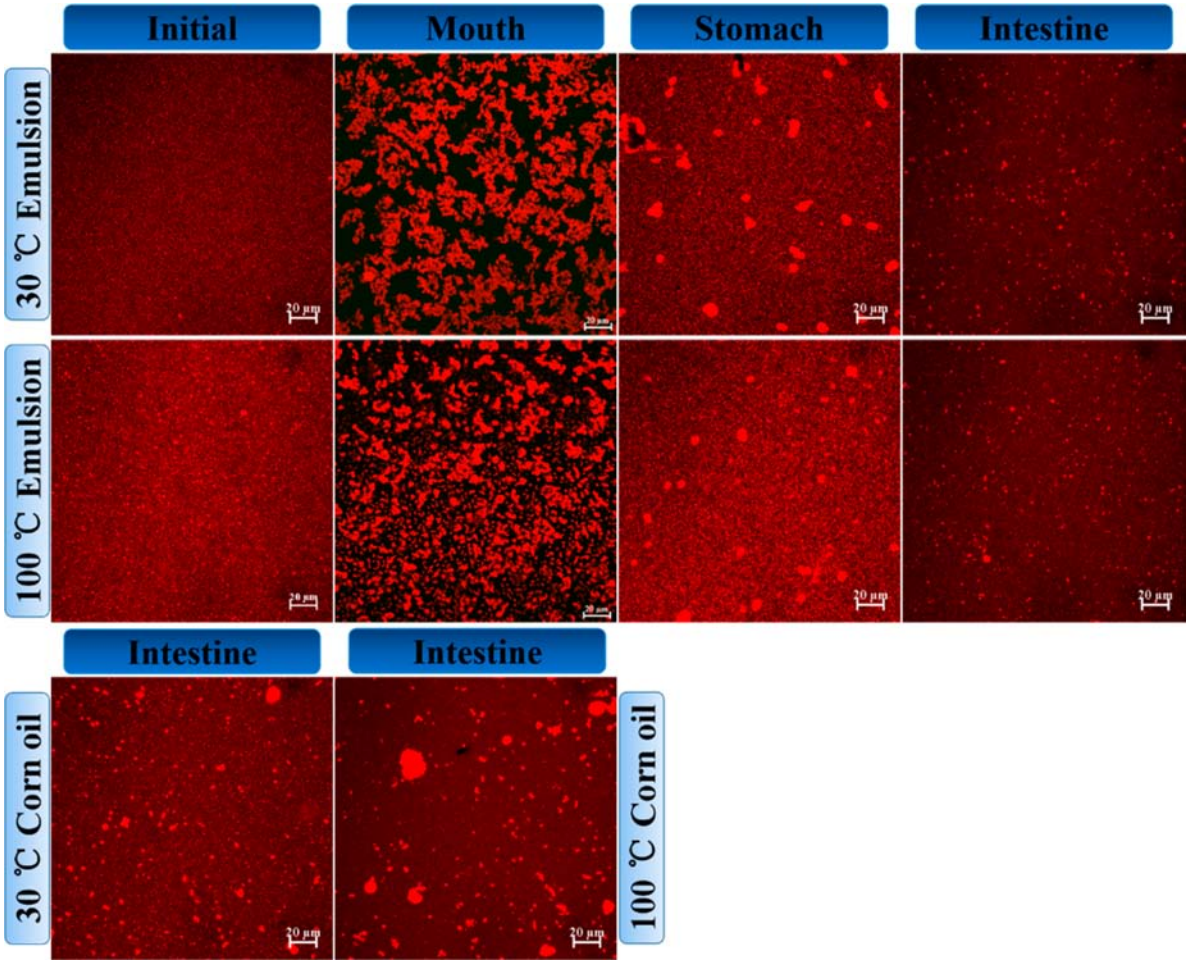

Figure 6. Influence of simulated gastrointestinal conditions on microstructure of curcumin−emulsion and curcumin−oil mixtures exposed to different incubation conditions (30 °C for 30 min or 100 °C for 10 min) determined by confocal fluorescence microscopy. The scale bars represent a length of 20 μm, and the red regions represent lipids.

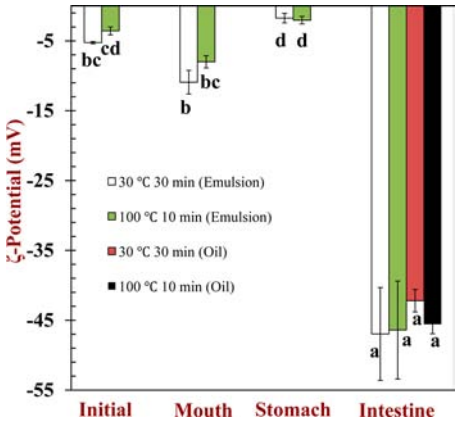

Figure 7. Influence of simulated gastrointestinal conditions on the particle charge of curcumin−emulsion and curcumin−oil mixtures exposed to different incubation conditions (30 °C for 30 min or 100 °C for 10 min). Samples designated with different letters (a, b, c) were significantly different (Duncan, $p < 0.05$).

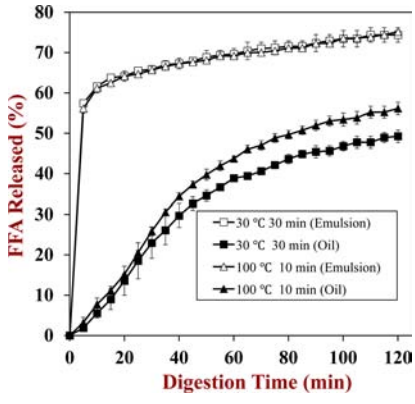

Figure 8. Influence of incubation temperature on the free fatty acids (FFA %) release profile for curcumin−emulsion and curcumin−oil mixtures exposed to different incubation conditions (30 °C for 30 min or 100 °C for 10 min).

30 °C (49% FFAs released after 2 h). The origin of this effect is unknown, but it may have been because the corn oil that had been incubated at the higher temperature was initially dispersed better in the water phase, i.e., formed smaller fat droplets (higher surface area).

Curcumin Solubilization and Mixed Micelle Properties. The characteristics of the particles in the mixed micelle phase formed after exposure of the samples to simulated small intestine conditions were measured, as well as the amount of curcumin solubilized within the mixed micelle phase (Table 2). It should be noted that the mixed micelle phase was collected by centrifugation, so that any large particles observed in the

DOI: 10.1021/jf506149f
J. Agric. Food Chem. 2015, 63, 2052−2062

Table 2. Influence of Incubation Temperature on the Curcumin Concentration, Particle Size, Polydispersity Index (PDI), and ζ-Potential of the Micelle Phase Isolated from Mixtures Containing Curcumin Dispersed in Emulsions, Corn Oil, or Buffer Solution[a]

	30 °C			100 °C		
	emulsion	oil	buffer	emulsion	oil	buffer
curcumin (μg/mL)	83.5 ± 19.5 [bc]	68.1 ± 6.8 [b]	12.7 ± 6.5 [a]	119.5 ± 23.8 [d]	95.2 ± 5.1 [c]	14.6 ± 1.0 [a]
mean diameter (nm)	194 ± 9 [b]	134 ± 7 [a]	ND	202 ± 9 [b]	146 ± 19 [a]	ND
PDI	0.47 ± 0.06 [c]	0.20 ± 0.06 [a]	ND	0.38 ± 0.01 [b]	0.21 ± 0.01 [a]	ND
ζ-potential (mV)	−56.6 ± 1.4 [a]	−44.4 ± 4.7 [b]	ND	−58.0 ± 0.2 [a]	−55.6 ± 1.0 [a]	ND

[a]Samples designated with different letters (a, b, c) were significantly different (Duncan, $p < 0.05$). ND = not determined.

small intestine digesta should have been removed. All of the mixed micelle samples contained highly negatively charged particles, which can be attributed to the fact that they consisted primarily of bile salts, phospholipids, and free fatty acids. The mean particle diameters in the micelle phase were around 100 to 200 nm, which suggests that they were probably vesicles since true micelles are much smaller than this (<10 nm). Surprisingly, the particles in the mixed micelle phase collected from digestion of the bulk oils were appreciably smaller than those collected from digestion of the emulsified oils (Table 2). There are a number of potential mechanisms that could account for this observation, such as differences in the rate and extent of lipid digestion, and the presence of nonionic surfactant in the emulsions. For both the curcumin−emulsion and curcumin−oil systems, there was no major difference between the size of the particles in samples that had been incubated at 30 °C or 100 °C.

The amount of curcumin present in the mixed micelle phase is a good indication of its bioaccessibility, i.e., the amount available for absorption. Overall, the concentration of curcumin measured in the mixed micelle phase was higher for the digested curcumin−emulsion mixtures that for the digested curcumin−oil mixtures (Table 2). This suggests that there was more efficient transfer of the curcumin into the mixed micelles for the emulsion than for the bulk oil. There are two major reasons for this phenomenon: (i) some of the bulk oil was not digested, and so some of the curcumin may have remained dissolved within this oil phase; (ii) more of the emulsified oil was digested, and so there will have been more mixed micelles available to solubilize the curcumin. The curcumin concentration in the mixed micelles obtained from digestion of the curcumin−emulsion mixture incubated at 100 °C was appreciably higher than that for the mixture incubated at 30 °C. This effect was probably due to the fact that a higher fraction of the crystalline curcumin was solubilized within the emulsion held at the higher incubation temperature. The amount of curcumin present within the mixed micelle phase resulting from digestion of the curcumin−oil mixture was also higher for the sample incubated at 100 °C than for the one incubated at 30 °C. This effect may again be due to the fact that a higher amount of curcumin was solubilized in the oil phase (rather than present as crystals) prior to digestion. In addition, there was a greater extent of lipid digestion in the bulk oil incubated at 100 °C, which may have resulted in greater curcumin release and solubilization.

Potential Mechanisms. The potential mechanisms responsible for the increase in bioaccessibility of curcumin by excipient emulsions are highlighted in Figure 9. Prior to ingestion, curcumin may be solubilized within the oil droplets when powdered curcumin is incubated with the emulsions. This may occur due to diffusion of curcumin molecules through the aqueous phase and occurs more rapidly for emulsifier oil than for bulk oil due to the higher surface area and shorter diffusion pathway. In addition, this process occurs more rapidly at higher temperatures due to the higher solubility of curcumin in the oil and water phases. After ingestion, curcumin may be solubilized within the mixed micelles resulting from digestion of the oil droplets. The transfer of curcumin into the mixed micelles may be more efficient for emulsified oil than for bulk oil due to the faster rate and greater extent of lipid digestion. Consequently, there are more mixed micelles available for the curcumin to the solubilized within.

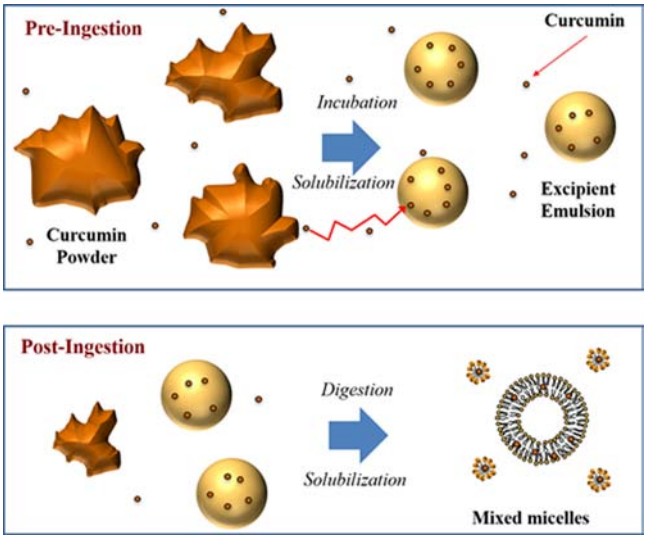

Figure 9. Schematic diagram of the preingestion and postingestion solubilization of curcumin in excipient emulsions. Prior to ingestion, curcumin may be solubilized in oil droplets when powdered curcumin is incubated with the emulsions. After ingestion, curcumin may be solubilized within the mixed micelles resulting from digestion of the oil droplets.

In summary, the present work has shown that excipient emulsions can be used to increase the bioaccessibility of powdered curcumin. We have shown that a greater amount of curcumin is transferred from the powder into the lipid droplets for curcumin−emulsion mixtures incubated at 100 °C than for those incubated at 30 °C. This effect was attributed to the fact that solubility of curcumin in the water and oil phases increases with increasing temperature, as well as the mass transport rate. It was shown that the curcumin concentration in the mixed micelle phase formed after exposure to a simulated gastrointestinal tract depended on the nature of the food matrix, decreasing in the following order: emulsified oil > bulk oil > buffer solution. This effect was attributed to the increased solubilization capacity of the small intestinal fluids when a

DOI: 10.1021/jf506149f
J. Agric. Food Chem. 2015, 63, 2052−2062

triglyceride oil is broken down into free fatty acids and monoglycerides that are incorporated into mixed micelles. In addition, the curcumin concentration in the mixed micelle phase was higher for curcumin−emulsion or curcumin−oil mixtures that had been incubated at 100 °C than for those that had been incubated at 30 °C, which was attributed to a greater solubilization of the curcumin into the oil phase prior to digestion. These results have important implications for designing food matrices to increase the oral bioavailability of lipophilic nutraceuticals and vitamins.

AUTHOR INFORMATION

Corresponding Authors

*Tel: + 86 791 88305872 × 8106. Fax: +86 791 88334509. E-mail: liuwei@ncu.edu.cn.

*Tel: (413) 545-1019. Fax: (413) 545-1262. E-mail: mcclements@foodsci.umass.edu.

Author Contributions

⊥These authors contributed equally to this manuscript.

Notes

The authors declare no competing financial interest.

ACKNOWLEDGMENTS

This material is based upon work supported by the Cooperative State Research, Extension, Education Service, United State Department of Agriculture, Massachusetts Agricultural Experiment Station (project no. 831) and by the United States Department of Agriculture, NRI Grants (2011-03539, 2013-03795, 2011-67021, and 2014-67021).

REFERENCES

(1) Syed, H. K.; Liew, K. B.; Loh, G. O. K.; Peh, K. K. Stability indicating HPLC−UV method for detection of curcumin in Curcuma longa extract and emulsion formulation. *Food Chem.* **2015**, *170*, 321−326.

(2) Prasad, S.; Gupta, S. C.; Tyagi, A. K.; Aggarwal, B. B. Curcumin, a component of golden spice: From bedside to bench and back. *Biotechnol. Adv.* **2014**, *32* (6), 1053−1064.

(3) Wilken, R.; Veena, M. S.; Wang, M. B.; Srivatsan, E. S. Curcumin: A review of anti-cancer properties and therapeutic activity in head and neck squamous cell carcinoma. *Mol. Cancer* **2011**, *10* (12), 1−19.

(4) Ahmed, K.; Li, Y.; McClements, D. J.; Xiao, H. Nanoemulsion- and emulsion-based delivery systems for curcumin: Encapsulation and release properties. *Food Chem.* **2012**, *132* (2), 799−807.

(5) Fu, S.; Shen, Z.; Ajlouni, S.; Ng, K.; Sanguansri, L.; Augustin, M. A. Interactions of buttermilk with curcuminoids. *Food Chem.* **2014**, *149* (0), 47−53.

(6) Patel, A. R.; Velikov, K. P. Colloidal delivery systems in foods: A general comparison with oral drug delivery. *LWT–Food Sci. Technol.* **2011**, *44* (9), 1958−1964.

(7) McClements, D. J. Advances in fabrication of emulsions with enhanced functionality using structural design principles. *Curr. Opin. Colloid Interface Sci.* **2012**, *17* (5), 235−245.

(8) Pan, K.; Luo, Y.; Gan, Y.; Baek, S. J.; Zhong, Q. pH-driven encapsulation of curcumin in self-assembled casein nanoparticles for enhanced dispersibility and bioactivity. *Soft Matter* **2014**, *10* (35), 6820−6830.

(9) Esmaili, M.; Ghaffari, S. M.; Moosavi-Movahedi, Z.; Atri, M. S.; Sharifizadeh, A.; Farhadi, M.; Yousefi, R.; Chobert, J.-M.; Haertlé, T.; Moosavi-Movahedi, A. A. Beta casein-micelle as a nano vehicle for solubility enhancement of curcumin; food industry application. *LWT–Food Sci. Technol.* **2011**, *44* (10), 2166−2172.

(10) Yu, H.; Huang, Q. Enhanced in vitro anti-cancer activity of curcumin encapsulated in hydrophobically modified starch. *Food Chem.* **2010**, *119* (2), 669−674.

(11) Margulis, K.; Magdassi, S.; Lee, H. S.; Macosko, C. W. Formation of curcumin nanoparticles by flash nanoprecipitation from emulsions. *J. Colloid Interface Sci.* **2014**, *434*, 65−70.

(12) Tapal, A.; Tiku, P. K. Complexation of curcumin with soy protein isolate and its implications on solubility and stability of curcumin. *Food Chem.* **2012**, *130* (4), 960−965.

(13) Maiti, K.; Mukherjee, K.; Gantait, A.; Saha, B. P.; Mukherjee, P. K. Curcumin−phospholipid complex: Preparation, therapeutic evaluation and pharmacokinetic study in rats. *Int. J. Pharm.* **2007**, *330* (1−2), 155−163.

(14) Zhao, Y.; Pan, Y.; Nitin, N.; Tikekar, R. V. Enhanced stability of curcumin in colloidosomes stabilized by silica aggregates. *LWT–Food Sci. Technol.* **2014**, *58* (2), 667−671.

(15) Niu, Y. M.; Ke, D.; Yang, Q. Q.; Wang, X. Y.; Chen, Z. Y.; An, X. Q.; Shen, W. G. Temperature-dependent stability and DPPH scavenging activity of liposomal curcumin at pH 7.0. *Food Chem.* **2012**, *135* (3), 1377−1382.

(16) Yu, H.; Shi, K.; Liu, D.; Huang, Q. Development of a food-grade organogel with high bioaccessibility and loading of curcuminoids. *Food Chem.* **2012**, *131* (1), 48−54.

(17) Tikekar, R. V.; Pan, Y.; Nitin, N. Fate of curcumin encapsulated in silica nanoparticle stabilized Pickering emulsion during storage and simulated digestion. *Food Res. Int.* **2013**, *51* (1), 370−377.

(18) McClements, D. J.; Xiao, H. Excipient foods: Designing food matrices that improve the oral bioavailability of pharmaceuticals and nutraceuticals. *Food Funct.* **2014**, *5* (7), 1320−1333.

(19) Failla, M. L.; Chitchumronchokchai, C.; Ferruzzi, M. G.; Goltz, S. R.; Campbell, W. W. Unsaturated fatty acids promote bioaccessibility and basolateral secretion of carotenoids and α-tocopherol by Caco-2 cells. *Food Funct.* **2014**, *5* (6), 1101−1112.

(20) Huo, T.; Ferruzzi, M. G.; Schwartz, S. J.; Failla, M. L. Impact of fatty acyl composition and quantity of triglycerides on bioaccessibility of dietary carotenoids. *J. Agric. Food Chem.* **2007**, *55* (22), 8950−8957.

(21) Colle, I. J. P.; Van Buggenhout, S.; Lemmens, L.; Van Loey, A. M.; Hendrickx, M. E. The type and quantity of lipids present during digestion influence the in vitro bioaccessibility of lycopene from raw tomato pulp. *Food Res. Int.* **2012**, *45* (1), 250−255.

(22) Dudhatra, G. B.; Mody, S. K.; Awale, M. M.; Patel, H. B.; Modi, C. M.; Kumar, A.; Kamani, D. R.; Chauhan, B. N. A Comprehensive review on pharmacotherapeutics of herbal bioenhancers. *Sci. World J.* **2012**, *2012*, 33.

(23) Williams, H. D.; Trevaskis, N. L.; Charman, S. A.; Shanker, R. M.; Charman, W. N.; Pouton, C. W.; Porter, C. J. H. Strategies to Address Low Drug Solubility in Discovery and Development. *Pharmacol. Rev.* **2013**, *65* (1), 315−499.

(24) Zhang, R.; Zhang, Z.; Zhang, H.; Decker, E. A.; McClements, D. J. Influence of emulsifier type on gastrointestinal fate of oil-in-water emulsions containing anionic dietary fiber (pectin). *Food Hydrocolloids* **2015**, *45* (0), 175−185.

(25) Mao, Y.; McClements, D. J. Influence of electrostatic heteroaggregation of lipid droplets on their stability and digestibility under simulated gastrointestinal conditions. *Food Funct.* **2012**, *3* (10), 1025−1034.

(26) Minekus, M.; Alminger, M.; Alvito, P.; Ballance, S.; Bohn, T.; Bourlieu, C.; Carriere, F.; Boutrou, R.; Corredig, M.; Dupont, D.; Dufour, C.; Egger, L.; Golding, M.; Karakaya, S.; Kirkhus, B.; Le Feunteun, S.; Lesmes, U.; Macierzanka, A.; Mackie, A.; Marze, S.; McClements, D. J.; Menard, O.; Recio, I.; Santos, C. N.; Singh, R. P.; Vegarud, G. E.; Wickham, M. S. J.; Weitschies, W.; Brodkorb, A. A standardised static in vitro digestion method suitable for food - an international consensus. *Food Funct.* **2014**, *5* (6), 1113−1124.

(27) Li, Y.; McClements, D. J. New mathematical model for interpreting pH-stat digestion profiles: Impact of lipid droplet characteristics on in vitro digestibility. *J. Agric. Food Chem.* **2010**, *58* (13), 8085−8092.

(28) Williams, H. D.; Sassene, P.; Kleberg, K.; Bakala-N'Goma, J. C.; Calderone, M.; Jannin, V.; Igonin, A.; Partheil, A.; Marchaud, D.; Jule, E.; Vertommen, J.; Maio, M.; Blundell, R.; Benameur, H.; Carriere, F.; Mullertz, A.; Porter, C. J. H.; Pouton, C. W. Toward the establishment

DOI: 10.1021/jf506149f
J. Agric. Food Chem. 2015, 63, 2052−2062

of standardized in vitro tests for lipid-based formulations, part 1: Method parameterization and comparison of in vitro digestion profiles across a range of representative formulations. *J. Pharm. Sci.* **2012**, *101* (9), 3360−3380.
(29) Saberi, A. H.; Fang, Y.; McClements, D. J. Effect of glycerol on formation, stability, and properties of vitamin-E enriched nanoemulsions produced using spontaneous emulsification. *J. Colloid Interface Sci.* **2013**, *411*, 105−113.
(30) McClements, D. J. Crystals and crystallization in oil-in-water emulsions: Implications for emulsion-based delivery systems. *Adv. Colloid Interface Sci.* **2012**, *174*, 1−30.
(31) Salvia-Trujillo, L.; Qian, C.; Martín-Belloso, O.; McClements, D. Influence of particle size on lipid digestion and *β*-carotene bioaccessibility in emulsions and nanoemulsions. *Food Chem.* **2013**, *141* (2), 1472−1480.
(32) Dickinson, E. Hydrocolloids at interfaces and the influence on the properties of dispersed systems. *Food Hydrocolloids* **2003**, *17* (1), 25−39.
(33) McClements, D. J. *Food emulsions: Principles, Practice, and Techniques*; CRC Press: Boca Raton, FL, 2005.

DOI: 10.1021/jf506149f
J. Agric. Food Chem. 2015, 63, 2052−2062

The experimental design was a randomized complete block with four replicate plots of each entry at each field site in the U.S. study and three replicate plots of each entry at each field site in the Brazil study. In the U.S. study, plots were four rows wide by 7.6 m long with 6 cm seed spacing and 76 cm row spacing. Each four row plot was separated from adjacent plots by two border rows of a commercially available nontransgenic soybean variety of similar maturity. In the Brazil study, plots were 10 rows wide by 10 m long with 10 cm seed spacing and 50 cm row spacing. In addition to DAS-81419-2 and the isoline, a total of five nontransgenic commercial varieties were used (DSR 75213-72, HiSOY 38C60, IL3503, Porter 75148, and Williams 82) in the U.S. study; three out of the five varieties were chosen at random and planted at each field site. In the Brazil study, the nontransgenic commercial variety CD 215 was planted at both field sites. Standard commercial agronomic practices (e.g., insect and weed control) were implemented at each field site (uniformly across the entire trial) to produce a commercially acceptable crop. Forage and seed samples were collected at the R3 (beginning pod) and R8 (full maturity) growth stages, respectively, and shipped to Covance Laboratories Inc. (Madison, Wisconsin) for compositional analysis. Samples were shipped frozen and were placed in freezer storage at the analytical laboratory where they remained until removal for preparation or analysis.

Compositional Analyses. At Covance Laboratories composition samples were cryogenically ground to a homogeneous state using a blender and liquid nitrogen prior to assay. Analytes in forage samples (9 total) included proximates (moisture, carbohydrates, ash, crude fat, and protein), fiber [acid detergent fiber (ADF) and neutral detergent fiber (NDF)], and minerals (calcium and phosphorus); seed analytes (80 total) included proximates (moisture, carbohydrates, ash, crude fat, and protein), fiber (ADF, NDF, crude fiber, and total dietary fiber), minerals (calcium, copper, iron, magnesium, manganese, phosphorus, potassium, selenium, sodium, and zinc), amino acids (alanine, arginine, aspartic acid, cystine, glutamic acid, glycine, histidine, isoleucine, leucine, lysine, methionine, phenylalanine, proline, serine, threonine, tryptophan, tyrosine, and valine), fatty acids (8:0 caprylic, 10:0 capric, 12:0 lauric, 14:0 myristic, 14:1 myristoleic, 15:0 pentadecanoic, 15:1 pentadecenoic, 16:0 palmitic, 16:1 palmitoleic, 17:0 heptadecanoic, 17:1 heptadecenoic, 18:0 stearic, 18:1 oleic, 18:2 linoleic, 18:3 linolenic, 18:3 γ-linolenic, 20:0 arachidic, 20:1 eicosenoic, 20:2 eicosadienoic, 20:3 eicosatrienoic, 20:4 arachidonic, and 22:0 behenic), vitamins [β-carotene, vitamin B_1 (thiamine hydrochloride), vitamin B_2 (riboflavin), vitamin B_3 (niacin), vitamin B_5 (pantothenic acid), vitamin B_6 (pyridoxine hydrochloride), vitamin B_9 (folic acid), vitamin C (ascorbic acid), tocopherols (α, β, γ, δ, total)], and bioactives (lectin, phytic acid, raffinose, stachyose, trypsin inhibitor, total daidzein equivalent, total genistein equivalent, and total glycitein equivalent). With the exception of crude fiber and selenium, samples were assayed using previously published methods.[23] Crude fiber was determined gravimetrically as the loss on ignition of dried residue remaining after digestion of the samples with 1.25% sulfuric acid and 1.25% sodium hydroxide solutions under specific conditions. Selenium samples were closed-vessel microwave digested with nitric acid (HNO_3) and water. After digestion, the solution was brought to a final volume with water. To normalize the organic contribution between samples and standards, a dilution was prepared for analysis that contained methanol. The selenium concentration was determined with Se^{78} using an inductively coupled plasma-mass spectrometer (ICP-MS) with a dynamic reaction cell (DRC) by comparing the counts generated by standard solutions.

Statistical Analysis. At Dow AgroSciences, analysis of variance (ANOVA) was conducted across field sites within the U.S. study and within the Brazil study using a mixed model where entry was considered a fixed effect and location, block within location, and location-by-entry were designated as random effects.[96] Paired contrasts were performed between DAS-81419-2 and the isoline using t tests, and a false-discovery rate adjustment was applied to the P-values to account for multiplicity.[97−99] Differences were considered significant at the 95% confidence level. Analytes were excluded from the statistical analysis if more than 50% of the results were less than the limit of

Table 1. Proximate, Fiber, and Mineral Composition of DAS-81419-2 Soybean Forage

	U.S. study					Brazil study				
analytical component[a]	P value[b]	isoline mean ± SE[c] min−max[d]	DAS-81419-2 mean ± SE[c] min−max[d]	reference variety range min−max[e]	P value[b]	isoline mean ± SE[c] min−max[d]	DAS-81419-2 mean ± SE[c] min−max[d]	reference variety range min−max[e]	literature range min−max[f]
ash	0.926	8.96 ± 0.31 7.01−16.9	8.99 ± 0.32 7.51−10.9	6.80−15.2	0.955	9.08 ± 0.72 7.63−10.6	8.88 ± 0.72 7.87−11.1	6.37−7.58	4.68−10.782
carbohydrates	0.693	68.2 ± 1.1 57.2−76.4	67.7 ± 1.1 60.3−75.7	50.1−75.6	0.700	64.6 ± 0.6 62.5−66.5	65.9 ± 0.6 64.7−66.8	69.7−71.5	59.8−80.18
crude protein	0.841	20.4 ± 0.8 13.9−29.8	20.6 ± 0.8 15.8−25.8	14.0−35.5	0.700	23.9 ± 0.6 21.7−25.5	22.7 ± 0.6 21.1−24.6	20.0−21.6	11.2−24.71
moisture	0.719	79.7 ± 0.8 75.8−84.3	79.4 ± 0.8 75.5−83.6	75.3−85.5	0.784	81.0 ± 0.8 80.4−81.6	81.8 ± 0.7 79.7−85.0	72.6−76.9	32.05−84.60
crude fat	0.607	2.49 ± 0.19 0.898−3.89	2.70 ± 0.20 0.857−4.32	0.685−5.32	0.955	2.6 ± 0.2 2.30−3.07	2.57 ± 0.25 1.40−3.71	1.78−2.84	1.01−9.87
ADF	0.611	34.7 ± 2.1 22.4−56.7	33.3 ± 2.1 22.2−45.4	19.4−63.3	0.960	25.1 ± 1.6 21.6-31.4	25.6 ± 1.6 19.7−31.3	24.9−29.8	22.72−59.03
NDF	0.609	41.6 ± 2.6 27.8−70.9	39.9 ± 2.6 27.2−59.3	25.2−82.0	0.955	31.3 ± 1.2 27.7−36.4	31.0 ± 1.2 27.5−34.0	31.2−35.8	19.61−73.05
calcium	0.616	1377 ± 64 940−1840	1401 ± 64 908−1740	874−2000	0.700	1134 ± 61 995−1380	1040 ± 61 950−1090	697−988	NR[g]
phosphorus	0.841	266 ± 7 206−327	268 ± 7 201−342	187−381	0.912	254 ± 16 211−296	262 ± 16 223−337	173−238	NR[g]

[a]Moisture = percent fresh weight; calcium and phosphorus = mg/100g dry weight; all others = percent dry weight. [b]P value (false discovery rate adjusted) for t test comparing DAS-81419-2 with isoline. [c]U.S. study: mean across 10 field sites with four replicates per site; Brazil study: mean across two field sites with three replicates per site. [d]Minimum (min) and maximum (max) represent values observed in single replicate plots. [e]U.S. study: reference variety range represents minimum (min) and maximum (max) values observed in single replicate plots across five commercially available nontransgenic soybean varieties with three varieties planted at each field site. Brazil study: reference variety range represents minimum (min) and maximum (max) values observed in single replicate plots of one commercially available nontransgenic soybean variety planted at both field sites. [f]See Materials and Methods section for reference citations. [g]NR = not reported.

DOI: 10.1021/jf505015y
J. Agric. Food Chem. 2015, 63, 2063−2073

Table 2. Proximate and Fiber Composition of DAS-81419-2 Soybean Seed

	U.S. study				Brazil study				
analytical component[a]	*P* value[b]	isoline mean ± SE[c] min–max[d]	DAS-81419-2 mean ± SE[c] min–max[d]	reference variety range min–max[e]	*P* value[b]	isoline mean ± SE[c] min–max[d]	DAS-81419-2 mean ± SE[c] min–max[d]	reference variety range min–max[e]	literature range min–max[f]
ash	0.233	5.06 ± 0.07 4.62–5.68	5.18 ± 0.07 4.57–6.05	3.79–6.79	0.786	5.35 ± 0.09 5.19–5.45	5.43 ± 0.09 5.14–5.60	4.84–5.15	3.885–6.994
carbohydrates	0.616	38.8 ± 0.7 33.6–41.2	39.0 ± 0.7 33.3–43.3	29.9–40.7	0.700	38.3 ± 2.9 33.7–44.2	32.9 ± 2.9 31.6–34.4	33.8–34.9	29.3–50.2
crude protein	0.662	37.9 ± 0.6 34.3–41.9	38.1 ± 0.6 32.9–42.8	36.5–46.0	0.972	39.9 ± 0.5 39.5–40.6	40.0 ± 0.5 38.9–41.5	38.5–40.4	32–48.4
moisture	0.196	12.3 ± 0.9 8.29–19.2	11.7 ± 0.9 7.56–17.9	7.94–22.7	0.700	36.0 ± 2.9 31.2–42.0	28.7 ± 2.9 25.7–30.6	14.9–18.6	4.7–34.4
crude fat	0.108	18.2 ± 0.5 15.4–21.5	17.7 ± 0.5 14.2–21.0	14.1–21.4	0.700	16.5 ± 2.6 11.1–21.1	21.7 ± 2.6 21.0–22.5	20.6–21.9	8.104–24.7
ADF	0.845	15.3 ± 0.7 10.6–22.8	15.2 ± 0.7 10.5–22.5	10.2–21.0	0.986	11.9 ± 0.9 9.03–15.7	11.9 ± 0.9 10.1–14.1	14.0–16.6	7.81–26.26
NDF	0.719	17.5 ± 0.8 11.7–24.2	17.7 ± 0.8 11.6–25.5	10.6–21.9	0.700	15.0 ± 0.8 12.8–17.6	14.4 ± 0.8 13.0–16.3	14.6–17.2	8.53–23.90
crude fiber	not measured				0.700	6.67 ± 0.99 5.28–8.21	7.72 ± 0.99 6.47–8.82	10.6–12.1	4.12–13.87
total dietary fiber	0.765	23.8 ± 0.9 17.6–29.1	24.0 ± 0.9 17.4–31.3	16.1–29.2	0.700	17.0 ± 0.4 16.4–17.4	17.6 ± 0.4 16.9–18.7	17.5–20.2	NR[g]

[a]Moisture = percent fresh weight; all others = percent dry weight. [b]*P* value (false discovery rate adjusted) for *t* test comparing DAS-81419-2 with isoline. [c]U.S. study: mean across 10 field sites with four replicates per site. Brazil study: mean across two field sites with three replicates per site. [d]Minimum (min) and maximum (max) represent values observed in single replicate plots. [e]U.S. study: reference variety range represents minimum (min) and maximum (max) values observed in single replicate plots across five commercially available nontransgenic soybean varieties with three varieties planted at each field site. Brazil study: reference variety range represents minimum (min) and maximum (max) values observed in single replicate plots of one commercially available nontransgenic soybean variety planted at both field sites. [f]See Materials and Methods section for reference citations. [g]NR = not reported.

Table 3. Mineral Composition of DAS-81419-2 Soybean Seed

	U.S. study				Brazil study				
analytical component[a]	*P* value[b]	isoline mean ± SE[c] min–max[d]	DAS-81419-2 mean ± SE[c] min–max[d]	reference variety range min–max[e]	*P* value[b]	isoline mean ± SE[c] min–max[d]	DAS-81419-2 mean ± SE[c] min–max[d]	reference variety range min–max[e]	literature range min–max[f]
calcium	0.476	270 ± 8 233–335	267 ± 8 205–328	181–308	0.700	332 ± 12 318–359	322 ± 12 304–341	264–350	116.55–510
copper	0.747	1.32 ± 0.06 0.922–1.64	1.33 ± 0.06 0.894–1.72	0.693–1.86	0.714	0.947 ± 0.140 0.765–1.13	0.911 ± 0.140 0.694–1.07	0.626–1.06	0.632–1.092
iron	0.693	9.56 ± 1.40 6.61–27.3	10.3 ± 1.4 6.21–42.9	6.33–151	0.700	20.1 ± 3.3 14.0–38.8	13.8 ± 3.3 11.4–14.7	6.34–13.5	3.734–10.954
magnesium	0.747	233 ± 4 204–256	232 ± 4 197–257	205–278	0.700	294 ± 8 281–314	267 ± 8 257–276	280–296	219.40–312.84
manganese	0.719	2.64 ± 0.09 2.13–3.09	2.67 ± 0.09 2.01–3.96	2.22–7.18	0.700	2.30 ± 0.27 1.84–2.71	2.48 ± 0.27 2.13–2.79	1.77–2.88	2.52–3.876
phosphorus	0.476	607 ± 14 536–704	619 ± 14 494–708	471–759	0.700	588 ± 29 539–655	620 ± 29 536–670	509–586	506.74–935.24
potassium	0.478	1799 ± 21 1660–1940	1819 ± 21 1490–1980	1650–2050	0.700	1858 ± 21 1790–1930	1977 ± 21 1910–2050	1760–1840	1868.01–2510
selenium	0.616	460 ± 187 <LOQ–2370	498 ± 187 <LOQ–2560	<LOQ–3060	NA[g]	NA[g] <LOQ	NA[g] <LOQ	<LOQ	NR[h]
sodium	NA	NA[g] <LOQ	NA[g] <LOQ	<LOQ–18.5	NA[g]	NA[g] <LOQ	NA[g] <LOQ	<LOQ	4.05–30
zinc	0.413	4.53 ± 0.15 3.66–5.73	4.63 ± 0.15 3.66–5.83	3.15–6.33	0.700	4.11 ± 0.14 3.72–4.48	4.40 ± 0.14 3.93–5.09	3.66–4.28	4.98–7.578

[a]Selenium = ppb dry weight; all others = mg/100 g dry weight. [b]*P* value (false discovery rate adjusted) for *t* test comparing DAS-81419-2 with isoline. [c]U.S. study: mean across ten field sites with four replicates per site. Brazil study: mean across two field sites with three replicates per site. [d]Minimum (min) and maximum (max) represent values observed in single replicate plots. [e]U.S. study: reference variety range represents minimum (min) and maximum (max) values observed in single replicate plots across five commercially available nontransgenic soybean varieties with three varieties planted at each field site. Brazil study: reference variety range represents minimum (min) and maximum (max) values observed in single replicate plots of one commercially available nontransgenic soybean variety planted at both field sites. [f]See Materials and Methods section for reference citations. [g]NA (not available) = analysis not performed; majority of data was <LOQ. [h]NR = not reported.

J. Agric. Food Chem. 2015, 63, 2063–2073
DOI: 10.1021/jf505015y

Table 4. Amino Acid Composition of DAS-81419-2 Soybean Seed

	U.S. study				Brazil study				
analytical component[a]	*P* value[b]	isoline mean ± SE[c] min−max[d]	DAS-81419-2 mean ± SE[c] min−max[d]	reference variety range min−max[e]	*P* value[b]	isoline mean ± SE[c] min−max[d]	DAS-81419-2 mean ± SE[c] min−max[d]	reference variety range min−max[e]	literature range min−max[f]
alanine	0.566	4.57 ± 0.03 4.31−4.76	4.59 ± 0.03 4.30−4.82	4.28−4.75	0.760	4.46 ± 0.03 4.39−4.57	4.49 ± 0.03 4.38−4.61	4.35−4.53	4.16−4.74
arginine	0.476	7.49 ± 0.05 7.04−7.79	7.44 ± 0.05 7.05−7.74	7.22−8.20	0.830	7.59 ± 0.05 7.47−7.68	7.57 ± 0.05 7.49−7.66	7.68−8.03	6.41−8.41
aspartic acid	0.476	11.5 ± 0.01 11.3−11.6	11.5 ± 0.01 11.3−11.8	9.99−11.74	0.700	11.5 ± 0.03 11.4−11.6	11.5 ± 0.03 11.4−11.5	11.4−11.6	11.37−12.68
cystine	0.609	1.61 ± 0.03 1.43−1.95	1.63 ± 0.03 1.45−1.86	1.24−1.79	0.700	1.46 ± 0.10 1.33−1.61	1.52 ± 0.10 1.42−1.62	1.23−1.48	1.02−1.87
glutamic acid	0.476	17.3 ± 0.11 16.3−18.0	17.2 ± 0.1 16.3−18.0	17.0−18.6	0.973	18.0 ± 0.1 17.7−18.3	18.0 ± 0.1 17.9−18.1	17.7−18.4	17.71−20.48
glycine	0.845	4.50 ± 0.20 4.34−4.67	4.50 ± 0.02 4.30−4.66	4.14−4.54	0.700	4.34 ± 0.01 4.31−4.40	4.31 ± 0.01 4.27−4.38	4.28−4.36	4.19−4.62
histidine	0.719	2.71 ± 0.02 2.58−2.82	2.70 ± 0.02 2.17−2.84	2.43−2.78	0.896	2.59 ± 0.01 2.55−2.64	2.60 ± 0.01 2.58−2.64	2.45−2.66	2.49−2.89
isoleucine	0.926	4.80 ± 0.02 4.65−4.96	4.80 ± 0.02 4.52−4.99	4.61−4.98	0.700	4.90 ± 0.02 4.82−5.00	4.83 ± 0.02 4.77−4.89	4.72−4.86	4.13−5.11
leucine	0.732	7.65 ± 0.01 7.51−7.83	7.64 ± 0.01 7.49−7.75	7.49−7.98	0.972	7.66 ± 0.02 7.60−7.70	7.67 ± 0.02 7.63−7.73	7.57−7.79	7.46−8.29
lysine	0.476	6.32 ± 0.08 5.90−7.51	6.44 ± 0.08 5.92−7.41	5.61−7.29	0.700	6.46 ± 0.03 6.40−6.63	6.40 ± 0.03 6.34−6.45	5.87−6.61	6.23−7.38
methionine	0.551	1.42 ± 0.01 1.31−1.61	1.44 ± 0.01 1.33−1.61	1.22−1.62	0.700	1.37 ± 0.02 1.33−1.41	1.35 ± 0.02 1.32−1.39	1.22−1.37	1.18−1.71
phenylalanine	0.108	5.15 ± 0.01 4.99−5.25	5.11 ± 0.01 4.92−5.22	4.88−5.37	0.760	5.23 ± 0.04 5.15−5.31	5.21 ± 0.04 5.15−5.25	5.24−5.46	4.91−5.44
proline	0.566	5.14 ± 0.04 4.86−5.97	5.20 ± 0.04 4.91−5.73	4.80−6.02	0.700	5.17 ± 0.04 5.12−5.27	5.24 ± 0.04 5.20−5.30	5.14−5.32	4.75−5.62
serine	0.670	5.13 ± 0.02 4.74−5.37	5.16 ± 0.02 4.85−5.38	4.81−5.53	0.700	5.02 ± 0.04 4.80−5.18	5.16 ± 0.04 5.10−5.22	4.73−5.14	3.25−6.04
threonine	0.616	4.19 ± 0.03 3.99−4.38	4.20 ± 0.03 3.96−4.44	3.86−4.25	0.760	4.03 ± 0.03 3.96−4.08	4.04 ± 0.03 4.00−4.09	3.94−4.05	3.15−4.24
tryptophan	0.747	1.52 ± 0.02 1.42−1.64	1.52 ± 0.02 1.40−1.65	1.27−1.69	0.714	1.38 ± 0.01 1.33−1.43	1.41 ± 0.01 1.37−1.44	1.33−1.38	0.95−1.49
tyrosine	0.638	3.97 ± 0.01 3.88−4.10	3.96 ± 0.01 3.83−4.06	3.82−4.16	0.786	3.94 ± 0.02 3.86−4.00	3.93 ± 0.02 3.89−4.00	3.99−4.07	2.62−3.72
valine	0.693	4.98 ± 0.02 4.74−5.22	4.96 ± 0.02 4.70−5.32	4.63−5.18	0.700	4.85 ± 0.02 4.79−4.91	4.78 ± 0.02 4.70−4.83	4.66−4.88	4.28−5.57

[a]Unit of measure = percent of total amino acids. [b]*P* value (false discovery rate adjusted) for *t* test comparing DAS-81419-2 with isoline. [c]U.S. study: mean across 10 field sites with four replicates per site. Brazil study: mean across two field sites with three replicates per site. [d]Minimum (min) and maximum (max) represent values observed in single replicate plots. [e]U.S. study: reference variety range represents minimum (min) and maximum (max) values observed in single replicate plots across five commercially available nontransgenic soybean varieties with three varieties planted at each field site. Brazil study: reference variety range represents minimum (min) and maximum (max) values observed in single replicate plots of one commercially available nontransgenic soybean variety planted at both field sites. [f]See Materials and Methods section for reference citations.

J. Agric. Food Chem. 2015, 63, 2063−2073

DOI: 10.1021/jf505015y

Table 5. Fatty Acid Composition of DAS-81419-2 Soybean Seed

	U.S. study				Brazil study				
analytical component[a]	*P* value[b]	isoline mean ± SE[c] min−max[d]	DAS-81419-2 mean ± SE[c] min−max[d]	reference variety range min−max[e]	*P* value[b]	isoline mean ± SE[c] min−max[d]	DAS-81419-2 mean ± SE[c] min−max[d]	reference variety range min−max[e]	literature range min−max[f]
8:0 caprylic	NA[g]	NA[g] <LOQ	NA[g] <LOQ	<LOQ	NA[g]	NA[g] <LOQ	NA[g] <LOQ	<LOQ	<LOQ–0.148
10:0 capric	NA[g]	NA[g] <LOQ	NA[g] <LOQ	<LOQ	NA[g]	NA[g] <LOQ	NA[g] <LOQ	<LOQ	<LOQ–0.27
12:0 lauric	NA[g]	NA[g] <LOQ	NA[g] <LOQ	<LOQ	NA[g]	NA[g] <LOQ	NA[g] <LOQ	<LOQ	<LOQ–0.132
14:0 myristic	NA[g]	NA[g] <LOQ[g]	NA[g] <LOQ[g]	<LOQ	0.700	0.0988 ± 0.0018 0.0930–0.103	0.103 ± 0.002 0.094–0.108	0.0724–0.0895	<LOQ–0.238
14:1 myristoleic	NA[g]	NA[g] <LOQ	NA[g] <LOQ	<LOQ	NA[g]	NA[g] <LOQ	NA[g] <LOQ	<LOQ	<LOQ–0.125
15:0 pentadecanoic	NA[g]	NA[g] <LOQ	NA[g] <LOQ	<LOQ	NA[g]	NA[g] <LOQ	NA[g] <LOQ	<LOQ	<LOQ
15:1 pentadecenoic	NA[g]	NA[g] <LOQ	NA[g] <LOQ	<LOQ	NA[g]	NA[g] <LOQ	NA[g] <LOQ	<LOQ	<LOQ
16:0 palmitic	<0.001[h]	11.1 ± 0.1 10.0–11.6	11.6 ± 0.1 10.9–12.3	9.12–11.5	0.749	13.0 ± 0.1 12.8–13.2	12.9 ± 0.1 12.6–13.1	11.3–12.2	1.40–15.77
16:1 palmitoleic	NA[g]	NA[g] <LOQ	NA[g] <LOQ–0.236	<LOQ[g]	0.700	0.108 ± 0.002 0.105–0.111	0.0915 ± 0.0017 0.0871–0.0961	0.111–0.131	<LOQ[g]–0.194
17:0 heptadecanoic	NA[g]	NA[g] <LOQ–0.127	NA[g] <LOQ–0.132	<LOQ[g]–0.133	0.896	0.103 ± 0.003 0.0955–0.111	0.102 ± 0.003 0.0972–0.106	0.0753–0.0877	<LOQ[g]–0.146
17:1 heptadecenoic	NA[g]	NA[g] <LOQ	NA[g] <LOQ	<LOQ	NA[g]	NA[g] <LOQ	NA[g] <LOQ	<LOQ	<LOQ–0.087
18:0 stearic	0.516	4.40 ± 0.12 3.67–5.27	4.46 ± 0.12 3.62–5.22	3.19–5.08	0.760	5.18 ± 0.11 4.85–5.46	5.07 ± 0.11 4.94–5.18	3.65–3.84	0.50–5.88
18:1 oleic	0.439	21.6 ± 0.4 19.6–25.2	21.2 ± 0.4 19.8–25.5	18.8–24.6	0.700	27.7 ± 1.1 26.0–30.4	22.1 ± 1.1 21.5–22.6	25.0–30.0	2.60–45.68
18:2 linoleic	0.476	54.1 ± 0.4 51.2–55.8	53.8 ± 0.4 50.5–55.7	53.6–57.5	0.700	47.5 ± 1.0 45.0–49.2	51.9 ± 1.0 51.5–52.4	47.3–50.7	7.58–58.8
18:3 linolenic	0.314	7.97 ± 0.15 6.91–8.76	8.17 ± 0.15 7.32–8.94	6.58–9.88	0.700	5.14 ± 0.26 4.54–5.64	6.56 ± 0.26 6.06–7.05	6.21–6.95	1.27–12.52
18:3 γ-linolenic	NA[g]	NA[g] <LOQ	NA[g] <LOQ	<LOQ	NA[g]	NA[g] <LOQ	NA[g] <LOQ	<LOQ	<LOQ
20:0 arachidic	0.413	0.319 ± 0.007 0.276–0.370	0.325 ± 0.007 0.282–0.372	0.254–0.383	0.700	0.453 ± 0.012 0.418–0.491	0.471 ± 0.012 0.450–0.484	0.396–0.409	0.038–0.57
20:1 eicosenoic	0.616	0.119 ± 0.019 <LOQ–0.189	0.105 ± 0.019 <LOQ–0.171	<LOQ[g]–0.191	0.700	0.223 ± 0.007 0.210–0.245	0.200 ± 0.006 0.184–0.214	0.205–0.220	0.024–0.35
20:2e icosadienoic	NA[g]	NA[g] <LOQ	NA[g] <LOQ	<LOQ	NA[g]	NA[g] <LOQ	NA[g] <LOQ	<LOQ	<LOQ–0.245
20:3 eicosatrienoic	NA[g]	NA[g] <LOQ	NA[g] <LOQ	<LOQ	NA[g]	NA[g] <LOQ	NA[g] <LOQ	<LOQ	<LOQ
20:4 arachidonic	NA[g]	NA[g] <LOQ	NA[g] <LOQ	<LOQ	NA[g]	NA[g] <LOQ	NA[g] <LOQ	<LOQ	<LOQ
22:0 behenic	0.476	0.317 ± 0.003 0.283–0.347	0.321 ± 0.003 0.263–0.345	0.281–0.390	0.986	0.466 ± 0.018 0.429–0.499	0.465 ± 0.018 0.438–0.490	0.517–0.534	0.043–0.65

[a]Percent of total fatty acids. [b]*P* value (false discovery rate adjusted) for *t* test comparing DAS-81419-2 with isoline. [c]U.S. study: mean across 10 field sites with four replicates per site. Brazil study: mean across two field sites with three replicates per site. [d]Minimum (min) and maximum (max) represent values observed in single replicate plots. [e]U.S. study: reference variety range represents minimum (min) and maximum (max) values observed in single replicate plots across five commercially available nontransgenic soybean varieties with three varieties planted at each field site. Brazil study: reference variety range represents minimum (min) and maximum (max) values observed in single replicate plots of one commercially available nontransgenic soybean variety planted at both field sites. [f]See Materials and Methods section for reference citations. [g]NA (not available) = analysis not performed: majority of data was <LOQ. [h]Statistically significant difference when compared with isoline ($P < 0.05$).

J. Agric. Food Chem. 2015, 63, 2063−2073

DOI: 10.1021/jf505015y

Table 6. Vitamin Composition of DAS-81419-2 Soybean Seed

	U.S. study				Brazil study				
analytical component[a]	*P* value[b]	isoline mean ± SE[c] min−max[d]	DAS-81419-2 mean ± SE[c] min−max[d]	reference variety range min−max[e]	*P* value[b]	isoline mean ± SE[c] min−max[d]	DAS-81419-2 mean ± SE[c] min−max[d]	reference variety range min−max[e]	literature range min−max[f]
α-tocopherol (vitamin E)	0.607	14.3 ± 1.3 8.56−29.3	13.6 ± 1.3 9.62−26.6	6.51−25.0	0.700	9.45 ± 0.91 6.98−11.5	12.5 ± 0.9 9.31−15.9	25.2−39.2	1.934−84.9
β-tocopherol	NA[g]	NA[c] <LOQ	NA[c] <LOQ	<LOQ	NA[c]	NA[c] <LOQ	NA[c] <LOQ	<LOQ	NR[g]
γ-tocopherol	0.616	168 ± 8 97−220	172 ± 8 118−219	77.5−204	0.700	39.4 ± 5.2 28.7−49.1	57.0 ± 5.2 36.7−77.9	176−215	NR[g]
δ-tocopherol	0.074	69.4 ± 2.7 41.3−83.1	74.7 ± 2.8 45.4−90.8	49.7−104	0.700	26.7 ± 2.1 22.7−33.5	31.6 ± 2.1 23.8−38.8	62.2−76.6	NR[g]
total tocopherols	0.476	252 ± 8 168−305	261 ± 8 205−301	160−304		not measured			NR[g]
β-carotene	NA	NA[c] <LOQ	NA[c] <LOQ	<LOQ−0.244		not measured			NR[g]
vitamin B_1 (thiamine hydrochloride)	0.662	3.51 ± 0.24 2.35−5.44	3.43 ± 0.24 2.20−5.16	1.82−4.60	0.700	5.69 ± 0.36 5.31−6.07	4.67 ± 0.36 4.08−5.78	3.95−5.40	1.01−2.54
vitamin B_2 (riboflavin)	0.476	3.40 ± 0.08 2.63−4.65	3.51 ± 0.08 2.58−4.64	2.42−5.00	0.700	4.98 ± 0.13 4.51−5.24	5.43 ± 0.13 5.05−5.89	4.53−5.70	1.90−3.21
vitamin B_3 (niacin)	0.413	25.0 ± 0.7 20.2−30.5	25.6 ± 0.7 20.3−32.1	20.7−29.0	0.700	34.3 ± 1.2 31.7−36.4	36.0 ± 1.2 34.3−37.9	18.4−23.0	NR[g]
vitamin B_5 (pantothenic acid)	0.074	14.8 ± 0.5 12.3−19.5	14.0 ± 0.5 11.8−16.8	8.97−18.0	0.700	14.8 ± 0.7 13.7−15.5	16.2 ± 0.72 14.7−18.3	14.4−16.7	NR[g]
vitamin B_6 (pyridoxine hydrochloride)	0.787	5.23 ± 0.11 4.42−6.43	5.18 ± 0.11 4.53−6.00	3.01−6.36	0.700	4.88 ± 0.19 4.71−5.04	4.31 ± 0.19 3.79−4.60	4.49−5.18	NR[g]
vitamin B_9 (folic acid)	0.732	4.21 ± 0.20 3.05−5.62	4.15 ± 0.20 2.75−5.51	2.94−5.59	0.700	5.08 ± 0.23 4.64−5.72	4.50 ± 0.23 4.16−5.06	4.02−4.42	2.386−4.709
vitamin C (ascorbic acid)	0.476	141 ± 13 75.2−231	133 ± 13 74.0−230	49.2−210	0.700	62.2 ± 9.0 48.0−98.8	46.9 ± 9.0 37.0−72.5	53.7−83.8	NR[g]

[a]mg/kg dry weight. [b]*P* value (false discovery rate adjusted) for *t* test comparing DAS-81419-2 with isoline. [c]U.S. study: mean across 10 field sites with four replicates per site. Brazil study: mean across two field sites with three replicates per site. [d]Minimum (min) and maximum (max) represent values observed in single replicate plots. [e]U.S. study: reference variety range represents minimum (min) and maximum (max) values observed in single replicate plots across five commercially available nontransgenic soybean varieties with three random varieties planted at each field site. Brazil study: reference variety range represents minimum (min) and maximum (max) values observed in single replicate plots of one commercially available nontransgenic soybean variety planted at both field sites. [f]See Materials and Methods section for reference citations. [g]NR = not reported.

J. Agric. Food Chem. 2015, 63, 2063−2073

DOI: 10.1021/jf505015y

Table 7. Antinutrient and Bioactive Composition of DAS-81419-2 Soybean Seed

	U.S. study				Brazil study				
analytical component[a]	P value[b]	isoline mean ± SE[c] min−max[d]	DAS-81419-2 mean ± SE[c] min−max[d]	reference variety range min−max[e]	P value[b]	isoline mean ± SE[c] min−max[d]	DAS-81419-2 mean ± SE[c] min−max[d]	reference variety range min−max[e]	literature range min−max[f]
lectin	0.638	30.8 ± 2.1 13.9−50.1	32.2 ± 2.1 12.4−52.6	7.89−45.2	0.760	9.11 ± 0.86 8.06−10.2	8.50 ± 0.86 6.19−9.98	2.63−6.23	37−323
phytic acid	0.662	1.22 ± 0.06 0.857−2.02	1.24 ± 0.06 0.911−1.52	0.752−1.71	0.972	1.40 ± 0.11 1.22−1.64	1.41 ± 0.11 1.11−1.61	0.998−1.27	0.41−2.68
raffinose	0.674	0.750 ± 0.038 0.505−1.02	0.766 ± 0.038 0.475−0.977	0.570−1.16	0.700	0.840 ± 0.044 0.816−0.903	1.07 ± 0.04 0.930−1.14	0.616−0.773	0.212−1.85
stachyose	0.747	3.68 ± 0.08 3.19−4.14	3.69 ± 0.08 3.15−4.29	3.01−5.28	0.955	3.50 ± 0.04 3.36−3.61	3.49 ± 0.04 3.37−3.54	3.44−3.78	1.21−6.65
total daidzein equivalent	0.609	950 ± 48 462−1200	932 ± 48 504−1190	585−1460	0.760	260 ± 18 207−310	272 ± 18 240−295	504−577	25−2453.5
total genistein equivalent	0.616	1296 ± 63 808−1680	1276 ± 63 922−1620	888−1950	0.760	450 ± 25 358−530	428 ± 25 370−477	614−705	28−2837.2
total glycitein equivalent	0.074	197 ± 6 156−266	180 ± 6 140−237	40.3−259	0.700	160 ± 4 154−171	206 ± 4 196−216	146−168	15.3−349.19
trypsin inhibitor	0.566	29.1 ± 1.2 22.2−46.5	30.2 ± 1.2 21.3−49.9	19.5−41.5	0.700	34.1 ± 4.1 29.3−40.0	38.5 ± 4.1 28.3−46.8	19.0−24.0	18.14−118.68

[a]Lectin = HU/mg protein dry weight; phytic acid, raffinose, and stachyose = % dry weight; isoflavones = μg/g dry weight; trypsin inhibitor = TIU/mg dry weight. [b]P value (false discovery rate adjusted) for t test comparing DAS-81419-2 with isoline. [c]U.S. study: mean across 10 field sites with four replicates per site. Brazil study: mean across two field sites with three replicates per site. [d]Minimum (min) and maximum (max) represent values observed in single replicate plots. [e]U.S. study: reference variety range represents minimum (min) and maximum (max) values observed in single replicate plots across

Figure 1. Site means for ADF and NDF in soybean forage. The shaded area represents the literature range and locations are represented by the following symbols: ○ = Richland, IA; × = Atlantic, IA; + = Carlyle, IL; Δ = Wyoming, IL; □ = Frankfort, IN;◇ = Fisk, MO; ● = La Plata, MO; ▲ = York, NE; ■ = Brunswick, NE; ◆ = Germansville, PA; # = Montividiu, Goiás; ∼ = Indianópolis, Minas Geráis. "Isoline" = near-isogenic nontransgenic line. Note that each nontransgenic commercial variety was included, on average, at only half of the field sites in the U.S. study, so the range of data for these entries is expected to be narrower than that of the isoline and DAS-81419-2 entries, which were present at all 10 sites.

quantitation (<LOQ); said analytes were excluded because data sets where most points are excluded or set to a given nominal value have substantially up-biased data or have improperly underestimated variability, respectively. No forage analytes were excluded, while seed analytes excluded from both the U.S. and Brazil studies were β-tocopherol, sodium, and the fatty acids 8:0 caprylic, 10:0 capric, 12:0 lauric, 14:1 myristoleic, 15:0 pentadecanoic, 15:1 pentadecenoic, 17:1 heptadecenoic, 18:3 γ-linolenic, 20:2 eicosadienoic, 20:3 eicosatrienoic, and 20:4 arachidonic. Additionally, β-carotene and the fatty acids 14:0 myristic, 16:1 palmitoleic, and 17:0 heptadecanoic were excluded from analysis of the U.S. data, and the mineral selenium was excluded from analysis of the Brazil data. The range of values observed in the nontransgenic commercial soybean varieties was included to put any statistically significant differences into context, and ranges for nontransgenic soybean in the literature were also compiled for further reference.[11,20,28,30,35,39,59,85,100−106]

RESULTS AND DISCUSSION

The composition of DAS-81419-2 soybean forage and seed was compared with that of the isoline at 10 field sites in the U.S.

DOI: 10.1021/jf505015y
J. Agric. Food Chem. 2015, 63, 2063−2073

and two field sites in Brazil. In addition to DAS-81419-2 and the isoline, the U.S. study included five commercially available nontransgenic soybean varieties, and the Brazil study included one commercially available nontransgenic soybean variety. Composition analytes evaluated in forage (9) included proximates, fiber, and minerals, while analytes evaluated in seed (80) included proximates, fiber, minerals, amino acids, fatty acids, vitamins, antinutrients, and bioactives. Of the 80 seed analytes, 18 were excluded from the statistical analysis of the U.S. and/or Brazil data sets because more than 50% of the results were <LOQ.

No statistically significant differences were detected between DAS-81419-2 and the isoline in both the U.S. and Brazil studies in all but one (16:0 palmitic acid) of the analytes included in the statistical analysis (Tables 1−7). Moreover, mean results for all analytes fell within the ranges observed in nontransgenic commercial reference varieties and/or the ranges of values for nontransgenic soybean in the literature. In the U.S. study only, a statistically significant difference was detected between the isoline and DAS-81419-2 soybean for 16:0 palmitic acid. Although statistically significant, the difference had no meaningful effect on nutritional value; the mean 16:0 palmitic acid content of DAS-81419-2 was only 4.5% higher than that of the isoline, and the entire range of values observed in DAS-81419-2 was encompassed by the range of values reported in the literature for nontransgenic soybean (Table 5). Furthermore, a difference for 16:0 palmitic acid was not observed in the Brazil study, where the DAS-81419-2 mean was actually slightly lower than the isoline.

While the composition of isoline and DAS-81419-2 soybean was similar both across and within field sites, results within each entry were highly variable across field sites; ADF and NDF in forage provide examples of this site to site variation (Figure 1). The lack of differences between the isoline and DAS-81419-2 coupled with the wide range of results across field sites in these studies indicates that environment has a substantial effect on crop composition and the effect of transgenesis is undetectable, as others have reported.[7,28,85,89,100,107−109]

CONCLUSIONS

On the basis of the absence of meaningful differences between the isoline and DAS-81419-2 soybean in studies that were conducted at multiple field sites in two countries, it is concluded that the composition of DAS-81419-2 soybean forage and seed is equivalent to that of nontransgenic soybean. The conclusion of this study is in concordance with 86 other published studies and over 100 regulatory submissions where compositional equivalence between the transgenic crop and nontransgenic crop was concluded.[7−92,110] Collectively, these results indicate that composition studies to detect unintended effects due to transgenesis with traits that are not expected to alter composition are of dubious value in assessing the safety of transgenic crops.

AUTHOR INFORMATION

Corresponding Author

*Phone: 317-337-3494. E-mail: BJFast@dow.com.

Notes

The authors declare the following competing financial interest(s): BF, AP, TJ, and RH are employed by Dow AgroSciences, which develops and markets transgenic seed. BP is employed by Covance Laboratories Inc., which was contracted by Dow AgroSciences to conduct the composition analytical portion of these studies..

ACKNOWLEDGMENTS

We thank Shane Andersen, David Bennett, Tim Boeker, Jay Deweese, Sue Dorsey, Eric Ehlers, Nathan Goldschmidt, Roger Johnson, Matthew Krause, Daniel Ramsdell, and Renan Gravena for conducting the field phase of these experiments and Michelle Anderson, Jason Dority, and Rebecca Hall for study coordination. We also thank Alyssa Brune, Kathryn Clayton, John Cuffe, Satish Guttikonda, Eric Kraus, Siva Kumpatla, Barry Schafer, and Laura Tagliani for reviewing a draft of this manuscript.

REFERENCES

(1) Aronson, A. I. Why *Bacillus thuringiensis* insecticidal toxins are so effective: unique features of their mode of action. *FEMS Microbiol. Lett.* **2001**, *195*, 1−8.

(2) Höfte, H.; Whiteley, H. R. Insecticidal Crystal Proteins of *Bacillus thuringiensis*. *Microbiol. Rev.* **1989**, *53*, 242−255.

(3) Schnepf, E.; Crickmore, N.; Van Rie, J.; Lereclus, D.; Baum, J.; Feitelson, J.; Zeigler, D. R.; Dean, D. H. *Bacillus thuringiensis* and its pesticidal crystal proteins. *Microbiol. Mol. Biol. Rev.* **1998**, *62*, 775−806.

(4) Dröge, W.; Broer, I.; Pühler, A. Transgenic plants containing the phosphinothricin-*N*-acetyltransferase gene metabolize the herbicide L-phosphinothricin (glufosinate) differently from untransformed plants. *Planta* **1992**, *187*, 142−151.

(5) Weber, N.; Halpin, C.; Hannah, L. C.; Jez, J. M.; Kough, J.; Parrott, W. Crop genome plasticity and its relevance to food and feed safety of genetically engineered breeding stacks. *Plant Physiol.* **2012**, *160*, 1842−1853.

(6) Schnell, J.; Steele, M.; Bean, J.; Neuspiel, M.; Girard, C.; Dormann, N.; Pearson, C.; Savoie, A.; Bourbonnière, L.; MacDonald, P. A comparative analysis of insertional effects in genetically engineered plants: considerations for pre-market assessments. *Transgenic Res.* **2014**, 1−17.

(7) Herman, R. A.; Phillips, A. M.; Lepping, M. D.; Fast, B. J.; Sabbatini, J. Compositional safety of event DAS-40278-9 (AAD-1) herbicide-tolerant maize. *GM Crops Food: Biotechnol. Agric.* **2010**, *1*, 294−311.

(8) Abdeen, A.; Schnell, J.; Miki, B. Transcriptome analysis reveals absence of unintended effects in drought-tolerant transgenic plants overexpressing the transcription factor ABF3. *BMC Genomics* **2010**, *11*, 69.

(9) Baker, J.; Hawkins, N.; Ward, J.; Lovegrove, A.; Napier, J.; Shewry, P.; Beale, M. A metabolomic study of substantial equivalence of field-grown genetically modified wheat. *Plant Biotechnol. J.* **2006**, *4*, 381−392.

(10) Berberich, S. A.; Ream, J. E.; Jackson, T. L.; Wood, R.; Stipanovic, R.; Harvey, P.; Patzer, S.; Fuchs, R. L. The composition of insect-protected cottonseed is equivalent to that of conventional cottonseed. *J. Agric. Food Chem.* **1996**, *44*, 365−371.

(11) Berman, K. H.; Harrigan, G. G.; Riordan, S. G.; Nemeth, M. A.; Hanson, C.; Smith, M.; Sorbet, R.; Zhu, E.; Ridley, W. P. Compositions of seed, forage, and processed fractions from insect-protected soybean MON 87701 are equivalent to those of conventional soybean. *J. Agric. Food Chem.* **2009**, *57*, 11360−11369.

(12) Catchpole, G.; Beckmann, M.; Enot, D.; Mondhe, M.; Zywicki, B.; Taylor, J.; Hardy, N.; Smith, A.; King, R.; Kell, D. Hierarchical metabolomics demonstrates substantial compositional similarity between genetically modified and conventional potato crops. *Proc. Natl. Acad. Sci. U. S. A.* **2005**, *102*, 14458−14462.

(13) Coll, A.; Nadal, A.; Collado, R.; Capellades, G.; Kubista, M.; Messeguer, J.; Pla, M. Natural variation explains most transcriptomic changes among maize plants of MON810 and comparable non-GM varieties subjected to two N-fertilization farming practices. *Plant Mol. Biol.* **2010**, *73*, 349−362.

(14) Drury, S. M.; Reynolds, T. L.; Ridley, W. P.; Bogdanova, N.; Riordan, S.; Nemeth, M. A.; Sorbet, R.; Trujillo, W. A.; Breeze, M. L. Composition of forage and grain from second-generation insect-

DOI: 10.1021/jf505015y
J. Agric. Food Chem. 2015, 63, 2063−2073

protected corn MON 89034 is equivalent to that of conventional corn (*Zea mays* L.). *J. Agric. Food Chem.* **2008**, *56*, 4623−4630.
(15) El-Khishin, D. A. A. H.; Amina; El Moghazy, G.; Metry, E. A. Assessment of genetically modified potato lines resistant to potato virus Y using compositional analysis and molecular markers. *Res. J. Agric. Biol. Sci.* **2009**, *5*, 261−271.
(16) Esposito, F.; Fogliano, V.; Cardi, T.; Carputo, D.; Filippone, E. Glycoalkaloid content and chemical composition of potatoes improved with nonconventional breeding approaches. *J. Agric. Food Chem.* **2002**, *50*, 1553−1561.
(17) George, C.; Ridley, W.; Obert, J. Composition of grain and forage from corn rootworm-protected corn event MON 863 is equivalent to that of conventional corn (*Zea mays* L.). *J. Agric. Food Chem.* **2004**, *52*, 4149−4158.
(18) Hamilton, K. A.; Pyla, P. D.; Breeze, M.; Olson, T.; Li, M. H.; Robinson, E.; Gallagher, S. P.; Sorbet, R.; Chen, Y. Bollgard II cotton: compositional analysis and feeding studies of cottonseed from insect-protected cotton (*Gossypium hirsutum* L.) producing the Cry1Ac and Cry2Ab2 proteins. *J. Agric. Food Chem.* **2004**, *52*, 6969−6976.
(19) Harrigan, G. G.; Ridley, W. P.; Miller, K. D.; Sorbet, R.; Riordan, S. G.; Nemeth, M. A.; Reeves, W.; Pestert, T. A. The forage and grain of MON 87460, a drought-tolerant corn hybrid, are compositionally equivalent to that of conventional corn. *J. Agric. Food Chem.* **2009**, *57*, 9754−9763.
(20) Harrigan, G. G.; Ridley, W. P.; Riordan, S. G.; Nemeth, M. A.; Sorbet, R.; Trujillo, W. A.; Breeze, M. L.; Schneider, R. W. Chemical composition of glyphosate-tolerant soybean 40-3-2 grown in Europe remains equivalent with that of conventional soybean (*Glycine max* L.). *J. Agric. Food Chem.* **2007**, *55*, 6160−6168.
(21) Herman, R.; Storer, N.; Phillips, A.; Prochaska, L.; Windels, P. Compositional assessment of event DAS-59122-7 maize using substantial equivalence. *Regul. Toxicol. Pharmacol.* **2007**, *47*, 37−47.
(22) Herman, R. A.; Phillips, A. M.; Collins, R. A.; Tagliani, L. A.; Claussen, F. A.; Graham, C. D.; Bickers, B. L.; Harris, T. A.; Prochaska, L. M. Compositional equivalency of Cry1F corn event TC6275 and conventional corn (*Zea mays* L.). *J. Agric. Food Chem.* **2004**, *52*, 2726−2734.
(23) Herman, R. A.; Phillips, A. M.; Lepping, M. D.; Sabbatini, J., Compositional safety of DAS-68416-4 (AAD-12) herbicide-tolerant soybean. *J. Nutr. Food Sci.* **2011**, *1:2*, DOI 10.4172/215-9600.1000103.
(24) Jiao, Z.; Deng, J.; Li, G.; Zhang, Z.; Cai, Z. Study on the compositional differences between transgenic and non-transgenic papaya (*Carica papaya* L.). *J. Food Compos. Anal.* **2010**, *23*, 640−647.
(25) Khalf, M.; Goulet, C.; Vorster, J.; Brunelle, F.; Anguenot, R.; Fliss, I.; Michaud, D. Tubers from potato lines expressing a tomato Kunitz protease inhibitor are substantially equivalent to parental and transigenic controls. *Plant Biotechnol. J.* **2010**, *8*, 155−169.
(26) Kim, J. K.; Chu, S. M.; Kim, S. J.; Lee, D. J.; Lee, S. Y.; Lim, S. H.; Ha, S.-H.; Kweon, S. J.; Cho, H. S. Variation of glucosinolates in vegetable crops of *Brassica rapa* L. ssp. pekinensis. *Food Chem.* **2010**, *119*, 423−428.
(27) Lin, C. H.; Lu, C. T.; Lin, H. T.; Pan, T. M. Safety assessment and detection method of genetically modified Chinese kale (*Brassica oleracea* cv. *alboglabra*). *J. Agric. Food Chem.* **2009**, *57*, 1876−1881.
(28) Lundry, D. R.; Ridley, W. P.; Meyer, J. J.; Riordan, S. G.; Nemeth, M. A.; Trujillo, W. A.; Breeze, M. L.; Sorbet, R. Composition of grain, forage, and processed fractions from second-generation glyphosate-tolerant soybean, MON 89788, is equivalent to that of conventional soybean (*Glycine max* L.). *J. Agric. Food Chem.* **2008**, *56*, 4611−4622.
(29) Malowicki, S. M. M.; Martin, R.; Qian, M. C. Comparison of sugar, acids, and volatile composition in raspberry bushy dwarf virus-resistant transgenic raspberries and the wild type 'Meeker' (*Rubus idaeus* L.). *J. Agric. Food Chem.* **2008**, *56*, 6648−6655.
(30) McCann, M. C.; Liu, K. S.; Trujillo, W. A.; Dobert, R. C. Glyphosate-tolerant soybeans remain compositionally equivalent to conventional soybeans (*Glycine max* L.) during three years of field testing. *J. Agric. Food Chem.* **2005**, *53*, 5331−5335.
(31) McCann, M. C.; Rogan, G. J.; Fitzpatrick, S.; Trujillo, W. A.; Sorbet, R.; Hartnell, G. F.; Riodan, S. G.; Nemeth, M. A. Glyphosate-tolerant alfalfa is compositionally equivalent to conventional alfalfa (*Medicago sativa* L.). *J. Agric. Food Chem.* **2006**, *54*, 7187−7192.
(32) McCann, M. C.; Trujillo, W. A.; Riordan, S. G.; Sorbet, R.; Bogdanova, N. N.; Sidhu, R. S. Comparison of the forage and grain composition from insect-protected and glyphosate-tolerant MON 88017 corn to conventional corn (*Zea mays* L.). *J. Agric. Food Chem.* **2007**, *55*, 4034−4042.
(33) Oberdoerfer, R.; Shillito, R.; de Beuckeleer, M.; Mitten, D. Rice (*Oryza sativa* L.) containing the bar gene is compositionally equivalent to the nontransgenic counterpart. *J. Agric. Food Chem.* **2005**, *53*, 1457−1465.
(34) Obert, J. C.; Ridley, W. P.; Schneider, R. W.; Riordan, S. G.; Nemeth, M. A.; Trujillo, W. A.; Breeze, M. L.; Sorbet, R.; Astwood, J. D. The composition of grain and forage from glyphosate tolerant wheat MON 71800 is equivalent to that of conventional wheat (*Triticum aestivum* L.). *J. Agric. Food Chem.* **2004**, *52*, 1375−1384.
(35) Padgette, S. R.; Taylor, N. B.; Nida, D. L.; Bailey, M. R.; MacDonald, J.; Holden, L. R.; Fuchs, R. L. The composition of glyphosate-tolerant soybean seeds is equivalent to that of conventional soybeans. *J. Nutr.* **1996**, *126*, 702−716.
(36) Poerschmann, J.; Rauschen, S.; Langer, U.; Augustin, J.; Górecki, T. Fatty acid patterns of genetically modified Cry3Bb1 expressing Bt-maize MON88017 and its near-isogenic line. *J. Agric. Food Chem.* **2008**, *57*, 127−132.
(37) Sidhu, R. S.; Hammond, B. G.; Fuchs, R. L.; Mutz, J.-N.; Holden, L. R.; George, B.; Olson, T. Glyphosate-tolerant corn: the composition and feeding value of grain from glyphosate-tolerant corn is equivalent to that of conventional corn (*Zea mays* L.). *J. Agric. Food Chem.* **2000**, *48*, 2305−2312.
(38) Tang, M. Z.; Huang, K. L.; Li, X.; Zhou, K.; He, X. Y.; Luo, Y. B. Absence of effect after introducing *Bacillus thuringiensis* gene on nutritional composition in cottonseed. *J. Food Sci.* **2006**, *71*, S38−S41.
(39) Taylor, N. B.; Fuchs, R. L.; MacDonald, J.; Shariff, A. R.; Padgette, S. R. Compositional analysis of glyphosate-tolerant soybeans treated with glyphosate. *J. Agric. Food Chem.* **1999**, *47*, 4469−4473.
(40) Venneria, E.; Fanasca, S.; Monastra, G.; Finotti, E.; Ambra, R.; Azzini, E.; Durazzo, A.; Foddai, M. S.; Maiani, G. Assessment of the nutritional values of genetically modified wheat, corn, and tomato crops. *J. Agric. Food Chem.* **2008**, *56*, 9206−9214.
(41) Wang, J.; Guo, L. Q.; Lin, J. F. Composition of transgenic *Volvariella volvacea* tolerant to cold stress is equivalent to that of conventional control. *J. Agric. Food Chem.* **2009**, *57*, 2392−2396.
(42) Xin, L.; Xiaoyun, H.; Yunbo, L.; Guoying, X.; Xianbin, J.; Kunlun, H. Comparative analysis of nutritional composition between herbicide-tolerant rice with bar gene and its non-transgenic counterpart. *J. Food Compos. Anal.* **2008**, *21*, 535−539.
(43) Zhu, J.; Patzoldt, W. L.; Shealy, R. T.; Vodkin, L. O.; Clough, S. J.; Tranel, P. J. Transcriptome response to glyphosate in sensitive and resistant soybean. *J. Agric. Food Chem.* **2008**, *56*, 6355−6363.
(44) Ridley, W. P.; Harrigan, G. G.; Breeze, M. L.; Nemeth, M. A.; Sidhu, R. S.; Glenn, K. C. Evaluation of compositional equivalence for multitrait biotechnology crops. *J. Agric. Food Chem.* **2011**, 5865−5876.
(45) Ridley, W. P.; Sidhu, R. S.; Pyla, P. D.; Nemeth, M. A.; Breeze, M. L.; Astwood, J. D. Comparison of the nutritional profile of glyphosate-tolerant corn event NK603 with that of conventional corn (*Zea mays* L.). *J. Agric. Food Chem.* **2002**, *50*, 7235−7243.
(46) Wang, Y.; Xu, W.; Zhao, W.; Hao, J.; Luo, Y.; Tang, X.; Zhang, Y.; Huang, K. Comparative analysis of the proteomic and nutritional composition of transgenic rice seeds with Cry1ab/ac genes and their non-transgenic counterparts. *J. Cereal Sci.* **2012**, *55*, 226−233.
(47) Frank, T.; Röhlig, R. M.; Davies, H. V.; Barros, E.; Engel, K.-H. Metabolite profiling of maize kernels—genetic modification versus environmental influence. *J. Agric. Food Chem.* **2012**, *60*, 3005−3012.
(48) Barros, E.; Lezar, S.; Anttonen, M. J.; Van Dijk, J. P.; Röhlig, R. M.; Kok, E. J.; Engel, K.-H. Comparison of two GM maize varieties with a near-isogenic non-GM variety using transcriptomics, proteomics and metabolomics. *Plant Biotechnol. J.* **2010**, *8*, 436−451.

DOI: 10.1021/jf505015y
J. Agric. Food Chem. 2015, 63, 2063−2073

(49) Baudo, M. M.; Lyons, R.; Powers, S.; Pastori, G. M.; Edwards, K. J.; Holdsworth, M. J.; Shewry, P. R. Transgenesis has less impact on the transcriptome of wheat grain than conventional breeding. *Plant Biotechnol. J.* **2006**, *4*, 369−380.
(50) Coll, A.; Nadal, A.; Collado, R.; Capellades, G.; Messeguer, J.; Melé, E.; Palaudelmàs, M.; Pla, M. Gene expression profiles of MON810 and comparable non-GM maize varieties cultured in the field are more similar than are those of conventional lines. *Transgenic Res.* **2009**, *18*, 801−808.
(51) Coll, A.; Nadal, A.; Palaudelmàs, M.; Messeguer, J.; Melé, E.; Puigdomènech, P.; Pla, M. Lack of repeatable differential expression patterns between MON810 and comparable commercial varieties of maize. *Plant Mol. Biol.* **2008**, *68*, 105−117.
(52) Harrigan, G. G.; Lundry, D.; Drury, S.; Berman, K.; Riordan, S. G.; Nemeth, M. A.; Ridley, W. P.; Glenn, K. C. Natural variation in crop composition and the impact of transgenesis. *Nature Biotechnol.* **2010**, *28*, 402−404.
(53) Lehesranta, S.; Davies, H.; Shepherd, L.; Nunan, N.; McNicol, J.; Auriola, S.; Koistinen, K.; Suomalainen, S.; Kokko, H.; Karenlampi, S. Comparison of tuber proteomes of potato varieties, landraces, and genetically modified lines. *Plant Physiol.* **2005**, *138*, 1690−1699.
(54) Park, H.; Lee, S.; Jeong, H.; Cho, S.; Chun, H.; Back, O.; Kim, D.; Lillehoj, H. The nutrient composition of the herbicide-tolerant green pepper is equivalent to that of the conventional green pepper. *Nutr. Res. (N. Y.)* **2006**, *26*, 546−548.
(55) Ricroch, A. E.; Berge, J. B.; Kuntz, M. Evaluation of genetically engineered crops using transcriptomic, proteomic and metabolomic profiling techniques. *Plant Physiol.* **2011**, *155*, 1752−1761.
(56) Kim, J.; Ryu, T.; Sohn, S.; Kim, J.; Chu, S.; Yu, C.; Baek, H. Metabolic fingerprinting study on the substantial equivalence of genetically modified (GM) chinese cabbage to non-GM cabbage. *J. Korean Soc. Appl. Biol. Chem.* **2009**, *52*, 186−192.
(57) Tripathi, S.; Suzuki, J. Y.; Carr, J. B.; McQuate, G. T.; Ferreira, S. A.; Manshardt, R. M.; Pitz, K. Y.; Wall, M. M.; Gonsalves, D. Nutritional composition of Rainbow papaya, the first commercialized transgenic fruit crop. *J. Food Compos. Anal.* **2011**, *24*, 140−147.
(58) Quemada, H.; Zarka, K.; Pett, W.; Bothma, G.; Felcher, K.; Mirendil, H.; Koch, M.; Brink, J.; Douches, D. Safety evaluations of the Cry1Ia1 protein found in the transgenic potato 'SpuntaG2'. *J. Am. Soc. Hortic. Sci.* **2010**, *135*, 325−332.
(59) Berman, K. H.; Harrigan, G. G.; Riordan, S. G.; Nemeth, M. A.; Hanson, C.; Smith, M.; Sorbet, R.; Zhu, E.; Ridley, W. P. Compositions of forage and seed from second-generation glyphosate-tolerant soybean MON 89788 and insect-protected soybean MON 87701 from Brazil are equivalent to those of conventional soybean (*Glycine max*). *J. Agric. Food Chem.* **2010**, *58*, 6270−6276.
(60) Zhou, J.; Harrigan, G. G.; Berman, K. H.; Webb, E. G.; Klusmeyer, T. H.; Nemeth, M. A. Stability in the composition equivalence of grain from insect-protected maize and seed from glyphosate-tolerant soybean to conventional counterparts over multiple seasons, locations, and breeding germplasms. *J. Agric. Food Chem.* **2011**, *59*, 8822−8828.
(61) Noteborn, H. P. J. M.; Bienenmann-Ploum, M. E.; van den Berg, J. H. J.; Alink, G. M.; Zolla, L.; Reynaerts, A.; Pensa, M.; Kuiper, H. A., Safety assessment of the *Bacillus thuringiensis* insecticidal crystal protein CRYIA(b) expressed in transgenic tomatoes. In *Genetically Modified Foods*; American Chemical Society: Washington, DC, 1995; Vol. *605*, pp 134−147.
(62) Qin, F.; Kang, L.; Guo, L.; Lin, J.; Song, J.; Zhao, Y. Composition of transgenic soybean seeds with higher γ-linolenic acid content is equivalent to that of conventional control. *J. Agric. Food Chem.* **2012**, *60*, 2200−2204.
(63) Kim, J.; Park, S.-Y.; Lee, S.; Lim, S.-H.; Kim, H.; Oh, S.-D.; Yeo, Y.; Cho, H.; Ha, S.-H. Unintended polar metabolite profiling of carotenoid-biofortified transgenic rice reveals substantial equivalence to its non-transgenic counterpart. *Plant Biotechnol. Rep.* **2012**, 19−26.
(64) Cheng, K.; Beaulieu, J.; Iquira, E.; Belzile, F.; Fortin, M.; Stromvik, M. Effect of transgenes on global gene expression in soybean is within the natural range of variation of conventional cultivars. *J. Agric. Food Chem.* **2008**, *56*, 3057−3067.
(65) Duke, S. O.; Rimando, A. M.; Pace, P. F.; Reddy, K. N.; Smeda, R. J. Isoflavone, glyphosate, and aminomethylphosphonic acid levels in seeds of glyphosate-treated, glyphosate-resistant soybean. *J. Agric. Food Chem.* **2002**, *51*, 340−344.
(66) Reuter, T.; Aulrich, K.; Berk, A.; Flachowsky, G. Investigations on genetically modified maize (Bt-maize) in pig nutrition: chemical composition and nutritional evaluation. *Arch. Tierernahrung* **2002**, *56*, 23−31.
(67) Beckles, D. M.; Tananuwong, K.; Shoemaker, C. F. Starch characteristics of transgenic wheat (*Triticum aestivum* L.) overexpressing the Dx5 high molecular weight glutenin subunit are substantially equivalent to those in nonmodified wheat. *J. Food Sci.* **2012**, *77*, C437−C442.
(68) Rogan, G. J.; Bookout, J. T.; Duncan, D. R.; Fuchs, R. L.; Lavrik, P. B.; Love, S. L.; Mueth, M.; Olson, T.; Owens, E. D.; Raymond, P. J.; Zalewski, J. Compositional analysis of tubers from insect and virus resistant potato plants. *J. Agric. Food Chem.* **2000**, *48*, 5936−5945.
(69) Roberts, M.; Minott, D. A.; Tennant, P. F.; Jackson, J. C. Assessment of compositional changes during ripening of transgenic papaya modified for protection against papaya ringspot virus. *J. Sci. Food Agric.* **2008**, *88*, 1911−1920.
(70) Park, S.-Y.; Lee, S.; Lee, J.-H.; Ko, H.-S.; Kweon, S.; Suh, S.-C.; Shin, K.-S.; Kim, J. Compositional comparative analysis between insect-resistant rice (*Oryza sativa* L.) with a synthetic *cry1Ac* gene and its non-transgenic counterpart. *Plant Biotechnol. Rep.* **2012**, *6*, 29−37.
(71) Nida, D. L.; Patzer, S.; Harvey, P.; Stipanovic, R.; Wood, R.; Fuchs, R. L. Glyphosate-tolerant cotton: the composition of the cottonseed is equivalent to that of conventional cottonseed. *J. Agric. Food Chem.* **1996**, *44*, 1967−1974.
(72) Cromwell, G. L.; Henry, B. J.; Scott, A. L.; Gerngross, M. F.; Dusek, D. L.; Fletcher, D. W. Glufosinate herbicide-tolerant (LibertyLink) rice vs. conventional rice in diets for growing-finishing swine. *J. Animal Sci.* **2005**, *83*, 1068−1074.
(73) Calsamiglia, S.; Hernandez, B.; Hartnell, G. F.; Phipps, R. Effects of corn silage derived from a genetically modified variety containing two transgenes on feed intake, milk production, and composition, and the absence of detectable transgenic deoxyribonucleic acid in milk in holstein dairy cows. *J. Dairy Sci.* **2007**, *90*, 4718−4723.
(74) Böhme, H.; Aulrich, K.; Daenicke, R.; Flachowsky, G. Genetically modified feeds in animal nutrition. 2nd communication: glufosinate tolerant sugar beets (roots and silage) and maize grains for ruminants and pigs. *Arch. Tierernahrung* **2001**, *54*, 197−207.
(75) Li, X.; Huang, K.; He, X.; Zhu, B.; Liang, Z.; Li, H.; Luo, Y. Comparison of nutritional quality between Chinese indica rice with sck and cry1Ac genes and its nontransgenic counterpart. *J. Food Sci.* **2007**, *72*, S420−S424.
(76) Choi, H.; Moon, J.-K.; Park, B.-S.; Park, H.-W.; Park, S.-Y.; Kim, T.-S.; Kim, D.-H.; Ryu, T.-H.; Kweon, S.-J.; Kim, J.-H. Comparative nutritional analysis for genetically modified rice, Iksan483 and Milyang204, and nontransgenic counterparts. *J. Korean Soc. Appl. Biol. Chem.* **2012**, *55*, 19−26.
(77) Chang, Y.; Zhao, C.; Zhu, Z.; Wu, Z.; Zhou, J.; Zhao, Y.; Lu, X.; Xu, G. Metabolic profiling based on LC/MS to evaluate unintended effects of transgenic rice with *cry1Ac* and *sck* genes. *Plant Mol. Biol.* **2012**, *78*, 477−487.
(78) Kim, J. K.; Park, S.-Y.; Ha, S.-H.; Lee, S. M.; Lim, S.-H.; Kim, H. J.; Ko, H.-S.; Oh, S.-D.; Park, J.-S.; Suh, S.-C. Compositional assessment of carotenoid-biofortified rice using substantial equivalence. *Afr. J. Biotechnol.* **2012**, *11*, 9330−9335.
(79) El Sanhoty, R.; Abd El-Rahman, A. A.; Bögl, K. W. Quality and safety evaluation of genetically modified potatoes Spunta with Cry V gene: compositional analysis, determination of some toxins, antinutrients compounds and feeding study in rats. *Food/Nahrung* **2004**, *48*, 13−18.
(80) Langkilde, S.; Schrøder, M.; Frank, T.; Shepherd, L. V. T.; Conner, S.; Davies, H. V.; Meyer, O.; Danier, J.; Rychlik, M.; Belknap, W. R.; McCue, K. F.; Engel, K.-H.; Stewart, D.; Knudsen, I.; Poulsen,

DOI: 10.1021/jf505015y
J. Agric. Food Chem. 2015, 63, 2063−2073

M. Compositional and toxicological analysis of a GM potato line with reduced α-solanine content—a 90-day feeding study in the Syrian Golden hamster. *Regul. Toxicol. Pharmacol.* **2012**, *64*, 177−185.
(81) Duke, S. O.; Lydon, J.; Koskinen, W. C.; Moorman, T. B.; Chaney, R. L.; Hammerschmidt, R. Glyphosate effects on plant mineral nutrition, crop rhizosphere microbiota, and plant disease in glyphosate-resistant crops. *J. Agric. Food Chem.* **2012**, *60*, 10375−10397.
(82) Bhandari, S.; Basnet, S.; Chung, K.; Ryu, K.-H.; Lee, Y.-S. Comparisons of nutritional and phytochemical property of genetically modified CMV-resistant red pepper and its parental cultivar. *Hortic., Environ. Biotechnol.* **2012**, *53*, 151−157.
(83) Corpillo, D.; Gardini, G.; Vaira, A. M.; Basso, M.; Aime, S.; Accotto, G. P.; Fasano, M. Proteomics as a tool to improve investigation of substantial equivalence in genetically modified organisms: The case of a virus-resistant tomato. *Proteomics* **2004**, *4*, 193−200.
(84) Shepherd, L.; McNicol, J.; Razzo, R.; Taylor, M.; Davies, H. Assessing the potential for unintended effects in genetically modified potatoes perturbed in metabolic and developmental processes. Targeted analysis of key nutrients and anti-nutrients. *Transgenic Res.* **2006**, *15*, 409−425.
(85) Berman, K. H.; Harrigan, G. G.; Nemeth, M. A.; Oliveira, W. S.; Berger, G. U.; Tagliaferro, F. S. Compositional equivalence of insect-protected glyphosate-tolerant soybean MON 87701 × MON 89788 to conventional soybean extends across different world regions and multiple growing seasons. *J. Agric. Food Chem.* **2011**, *59*, 11643−11651.
(86) Takagi, H.; Hirose, S.; Yasuda, H.; Takaiwa, F. Biochemical safety evaluation of transgenic rice seeds expressing T cell epitopes of Japanese cedar pollen allergens. *J. Agric. Food Chem.* **2006**, *54*, 9901−9905.
(87) Ricroch, A. E. Assessment of GE food safety using '-omics' techniques and long-term animal feeding studies. *New Biotechnol.* **2013**, *30*, 349−354.
(88) Gayen, D.; Sarkar, S. N.; Datta, S. K.; Datta, K. Comparative analysis of nutritional compositions of transgenic high iron rice with its non-transgenic counterpart. *Food Chem.* **2013**, *138*, 835−840.
(89) Lundry, D. R.; Burns, J. A.; Nemeth, M. A.; Riordan, S. G. Composition of Grain and Forage from Insect-Protected and Herbicide-Tolerant Corn, MON 89034 × TC1507 × MON 88017 × DAS-59122-7 (SmartStax) is Equivalent to That of Conventional Corn (*Zea mays* L). *J. Agric. Food Chem.* **2013**, *61*, 1991−1998.
(90) Herman, R. A.; Fast, B. J.; Johnson, T. Y.; Sabbatini, J.; Rudgers, G. W. Compositional Safety of Herbicide-Tolerant DAS-81910-7 Cotton. *J. Agric. Food Chem.* **2013**, *61*, 11683−11692.
(91) Lepping, M. D.; Herman, R. A.; Potts, B. L. Compositional Equivalence of DAS-44406-6 (AAD-12 + 2mEPSPS + PAT) Herbicide-Tolerant Soybean and Nontransgenic Soybean. *J. Agric. Food Chem.* **2013**, *61*, 11180−11190.
(92) Venkatesh, T.; Breeze, M. L.; Liu, K.; Harrigan, G. G.; Culler, A. H. Compositional Analysis of Grain and Forage from MON 87427, an Inducible Male Sterile and Tissue Selective Glyphosate-Tolerant Maize Product for Hybrid Seed Production. *J. Agric. Food Chem.* **2014**, *62*, 1964−1973.
(93) EFSA Panel on Genetically Modified Organisms (GMO), Guidance for Risk Assessment of Food and Feed from Genetically Modified Plants. *EFSA J.* **2011**, *9*, 2150−2186.
(94) Commission Implementing Regulation (EU) No 503/2013 on Applications for Authorisation of Genetically Modified Food and Feed in Accordance with Regulation (EC) No 1829/2003. *Official J. Eur Union* **2013**, *56*.
(95) *Application for Commodity Clearance of DAS-24236-5 × DAS-21023-5 (WideStrike) Cotton in the Republic of South Africa*; Dow AgroSciences LLC: Indianapolis, IN, 2013.
(96) *SAS/STAT 9.3 User's Guide*; SAS Institute Inc.: Cary, NC, 2011.
(97) Curran-Everett, D. Multiple comparisons: philosophies and illustrations. *Am. J. Physiol.: Regul., Integr. Compar. Physiol.* **2000**, *279*, R1−R8.
(98) Benjamini, Y.; Hochberg, Y. Controlling the false discovery rate—a practical and powerful approach to multiple testing. *J. R. Stat. Soc. Ser. B: Methodological* **1995**, *57*, 289−300.
(99) Colquhoun, D. An investigation of the false discovery rate and the misinterpretation of *p*-values. *R. Soc. Open Sci.* **2014**, *1*, 140216.
(100) Zhou, J.; Berman, K. H.; Breeze, M. L.; Nemeth, M. A.; Oliveira, W. S.; Braga, D. P. V.; Berger, G. U.; Harrigan, G. G. Compositional variability in conventional and glyphosate-tolerant soybean (*Glycine max* L.) varieties grown in different regions in Brazil. *J. Agric. Food Chem.* **2011**, *59*, 11652−11656.
(101) Bilyeu, K. D.; Zeng, P.; Coello, P.; Zhang, Z. J.; Krishnan, H. B.; Bailey, A.; Beuselinck, P. R.; Polacco, J. C. Quantitative Conversion of Phytate to Inorganic Phosphorus in Soybean Seeds Expressing a Bacterial Phytase. *Plant Physiol.* **2008**, *146*, 468−477.
(102) Hartwig, E. E.; Kilen, T. C. Yield and Composition of Soybean Seed from Parents with Different Protein, Similar Yield. *Crop Sci.* **1991**, *31*, 290−292.
(103) Iskander, F. Y. Maturation Stage and Mineral Content in Soybeans. *Food Chem.* **1987**, *24*, 29−35.
(104) Kakade, M. L.; Simons, N. R.; Liener, I. E.; Lambert, J. W. Biochemical and Nutritional Assessment of Different Varieties of Soybeans. *J. Agric. Food Chem.* **1972**, *20*, 87−90.
(105) *Environmental Health and Safety, Concensus Document on Compositional Considerations for New Varieties of Soybean: Key Food and Feed Nutrients and Anti-nutrients*; OECD: Paris, 2001; Vol. *15*, p 30.
(106) *International Life Sciences Institute Crop Composition Database*, version 4.2; International Life Sciences Institute: Washington, DC, 2011; www.cropcomposition.org.
(107) Herman, R. A.; Dunville, C. M.; Juberg, D. R.; Fletcher, D. W.; Cromwell, G. L. Performance of broiler chickens fed diets containing DAS-68416-4 soybean meal. *GM Crops* **2011**, *2*, 169−175.
(108) Harrigan, G. G.; Glenn, K. C.; Ridley, W. P. Assessing the natural variability in crop composition. *Regul. Toxicol. Pharmacol.* **2010**, *58*, S13−S20.
(109) Harrigan, G. G.; Culler, A. H.; Culler, M.; Breeze, M. L.; Berman, K. H.; Halls, S. C.; Harrison, J. M. Investigation of Biochemical Diversity in a Soybean Lineage Representing 35 Years of Breeding. *J. Agric. Food Chem.* **2013**, *61*, 6412−6422.
(110) Herman, R. A.; Price, W. D. Unintended Compositional Changes in Genetically Modified (GM) Crops: 20 Years of Research. *J. Agric. Food Chem.* **2013**, *61*, 11695−11701.

DOI: 10.1021/jf505015y
J. Agric. Food Chem. 2015, 63, 2063−2073

pigments, emulsifiers, and sweeteners a total of 18 types of food additives are permitted for use in specific foods, and the additives are prepared by extraction from natural sources or chemical synthesis, and the application and the amount of preservatives are regulated by Taiwan Food and Drug Administration (TFDA) "Standards for Specification, Scope, Application and Limitation of Food Additives List".[20] Items not included in the list are technically not permitted for use in processed foods.

In previous years, TFDA surveys of commercially available foods have found that illegal use of preservatives and addition of bleaching agents as food additives are very common in Taiwan.[21] It was also found that food additives and preservatives are added in amounts that exceed permissible limits for their use. Because the majority of the samples in the surveys of marketed foods by local government contained benzoic acid and sorbic acid, it is thus important to take a closer look at these two preservatives due to their popular use. These issues not only pose a risk to public health but also endanger the trade economy. Because of the growing concern regarding levels of preservatives in processed food exceeding their acceptable daily intake (ADI), preservative concentrations and estimated exposure of the population were subject to investigative examination. A survey of benzoic acid in foods in Finland identified fruit, berry juices, soft drinks, and semipreserved fish as the major sources of benzoic acid intake (40 mg/day, 13% of ADI),[22] and the 21st Australian TDS also estimated the dietary exposure to preservatives: benzoates and sorbates.[13]

The specific aims of this study include the following.

(1) To determine the concentrations of benzoic acid and sorbic acid in foods as consumed,
(2) To assess exposure and risk with regard to population groups of various ages,
(3) To identify which food pose the greatest exposure risk to consumers,
(4) To propose appropriate risk management options to protect consumers.

This study was deemed necessary, as dietary composition and intake patterns are distinctly different from Western countries where similar studies had been reported.

MATERIALS AND METHODS

Hazard Identification of Benzoic Acid. Repeated or prolonged exposure to benzoic acid can cause chronic health effects and damage to organs. Reproductive toxicity was observed in rats fed with benzoic acid at concentrations of 0.5 g/kg of body weight (BW)/day.[23] The use of benzoic acid with artificial food colors has also been linked to hyperactivity in children.[24] The Joint FAO/WHO Expert Committee on Food Additives (JECFA) has established an ADI of 0−5 mg/kg of BW/day for benzoic acid and benzoates. The no observed adverse effect level (NOAEL) was established at the highest experimental dose (500 mg/kg of BW/day) at which no adverse effects were observed based on long-term (lifetime) studies in rats. In establishing the ADI, a safety factor (SF) of 100 was applied to the NOAEL to take into account species differences and individual human variation.[25,26]

Hazard Identification of Sorbic Acid. Sorbic acid and potassium sorbate were practically nontoxic to rats and mice in acute oral toxicity studies.[27] They had a very low level of mammalian toxicity, even in chronic doses of up to 10% of the diet. They were found to be noncarcinogenic and nonmutagenic in vitro and in vivo.[28,29] However, oral toxicity studies showed that intake of sorbic acid may result in liver weight gain in 90 days.[30] The JECFA has established an ADI of 0−25 mg/kg of BW/day for sorbic acid and sorbates. The NOAEL was established at the highest experimental dose (2500 mg/kg of BW/day) at which no adverse effects were observed based on long-term (lifetime) studies in rats.[31] In establishing the ADI, a SF of 100 was applied to the dose level to take into account species differences and individual human variation.[32]

Core Food List for the Taiwan TDS. A large amount of food consumption data from the 2005−2008 Nutrition and Health Survey in Taiwan (NAHSIT) are available.[33] The sample population consisted of 6104 participants randomly selected from 48 counties. Information on dietary intake was collected by two nonconsecutive 24 h recalls in combination with a food frequency questionnaire. During the 24 h recall interviews, each respondent reported the quantity of all foods and beverages consumed during the preceding day. To construct the food list for the Taiwan TDS, 268431 raw data entries were first obtained from 6104 questionnaires and then consolidated into 11182 different food items which were grouped into 47 subcategories and 12 major categories on the basis of their nutrient content.[34,35] The number of food items selected from each subcategory for TDS was determined by the percentage of this subcategory in the total diet consumed. The second step involved determining which foods had the highest consumption rate (CR). The foods were ranked in the second step on the basis of percentage consumption, with 1% of the total diet being the cutoff rate. For example, the subcategory "rice and rice products" represented 10.4% of the amount of the total diet consumed daily; hence, the top 11 food items in this subcategory in descending order of CR were selected to represent this subcategory. In the third step, the amount of liquid food consumed was adjusted. The subcategories "ice and beverages" and "soup," where due to the large water content and relative uniformity of these food groups, the percentages of people consuming these groups (4.58 and 0.14%) instead of the percentages of amount consumed (29.80 and 10.72%) were used to keep the numbers of food items small. A total of 128 food items were selected from the 47 subcategories and 12 major categories to form a core list of food items to represent the total diet in Taiwan.

Food List for TDS of Preservatives. Not all food items contain preservatives. Only those containing high concentrations would have a significant contribution to health risk. Therefore, a food list specific to preservatives was constructed out of the core list of 128 items through the following adjustments: (1) Omitting from the core list the food items that were not likely to contain preservatives, such as fresh vegetables and fruits, (2) adding to the list the food items that were known to contain especially high levels of preservatives, including those known to frequently violate the preservative use regulations more than five times per year in the routine survey, and (3) adding to the list the food items that were legally permitted to contain preservatives. Thus, a preservative list of 97 food items from 47 subcategories and 12 major categories was established, which was not totally dependent upon levels of daily intake rate. These 97 items were used as the basis for purchasing food samples to be prepared for chemical analysis of food preservatives.

Purchasing of Food Samples and Preparation of Selected Foods. From this list of 97, one to three food products were selected for collection and preparation of samples for chemical analysis. A total of 239 food samples were obtained from 50 strategic sampling sites distributed among four cities and four counties in the northern, central, southern, and eastern parts of Taiwan. In each sampling site, food products were purchased from five wholesale stores, nine supermarkets, and 24 traditional wet markets. The purchased foods, food products, and food stuffs were combined, washed, cut, and cooked with flavoring agents according to standard recipes in the laboratory. For each item in the list of 97, at least eight products were purchased from the sampling sites, resulting in 2010 food products, which were used to prepare 239 food samples, including 46 cooked samples. These food samples were in turn used to prepare the 97 composite food samples for benzoic acid and sorbic acid analyses by mixing equal weights of food products collected from all sampling sites in two seasons. Each composite sample was homogenized and stored at −80 °C until analysis. All analyses were carried out from 2010 to 2011.

DOI: 10.1021/jf503987y
J. Agric. Food Chem. 2015, 63, 2074−2082

Table 1. Method Performance for Benzoic Acid and Sorbic Acid

analyte	matrix	LOQ (ppm)	recovery range (%)	RSD (%) (n = 5)	measurement uncertainty (ppm)	accreditation yes/no
benzoic acid	meat product	20	96.7 ± 1.90	1.76	250.0 ± 1.2	yes
sorbic acid	meat product	20	97.1 ± 1.07	1.26	250.0 ± 1.2	yes

Analysis of Preservatives. Analysis of food preservatives was conducted by first extracting benzoic acid and sorbic acid from 15 g of homogenized food matrix. Samples were extracted with 150 mL of 50% methanol by shaking for 30 min and then filtered. Deionized water was added to the filtrate to make up the volume to 250 mL, and the solution was filtered through a 0.45 μm membrane. The resulting extract was analyzed by high-performance liquid chromatography (HPLC) using a standard method (Chinese National Standards 10949-N6190). All chemicals used were of analytical reagent grade, and the solvents were of HPLC grade. HPLC was performed by the Hungkuang University Testing and Analysis Center for Food and Cosmetics. This center has been certified for microbial, chemical, and genetic analyses of foods and cosmetics under International Organization for Standardization (ISO) 17025 guidelines.[36] Chromatographic separation was performed using an Inertsil-ODS-2 (6 mm × 150 mm I.D.) analytical column, using methanol/acetonitrile/5 mM citric acid buffer (1:2:7, pH 4.0) as the mobile phase at a flow rate of 1 mL/min. A diode array detector was used for analyzing chromatographically separated analytes, and detection was carried out at a wavelength of 230 nm. This method simultaneously measures the concentrations of five food preservatives, namely, benzoic acid, sorbic acid, dehydroacetic acid, salicylic acid, and alkyl p-hydroxy benzoates at a limit of quantification (LOQ) of 0.02 g/kg. Thus, the detected concentration was labeled as "ND" (not detected) when it was lower than 0.02 g/kg. The analysis was performed in duplicate, using blank, control, and spiked samples for quality control. The target recovery rate was between 80 and 120%; however, in cases wherein the recovery rate was below 80% and above 120%, the samples were retested.

Estimation of Average Daily Dose (ADD) of Food Preservatives. The ADD of benzoic acid or sorbic acid was calculated on the basis of the daily food consumption rate (CR) and the concentration (C) of benzoic acid or sorbic acid in food. Thus, ADD of an analyte in the total diet from food item i for the specified age group j is calculated as follows:

$$\mathrm{ADD}_j = \sum_{i=1}^{n} \frac{C_i \times \mathrm{CR}_{ij}}{\mathrm{BW}_j} \quad (1)$$

where C_i is the concentration (mg/kg) of the analyte in food item i, CR_{ij} is the CR (g/person per day) of food item i by age group j, and BW_j is the average BW of age group j. The data for C in diet samples, BW of various age groups, and CRs were obtained from the NAHSIT. According to the recommendation of the WHO, when C is less than the LOD, the chemical is to be reported as nondetected (ND). When the ND rate is less than 60%, the data were replaced by $^1/_2$LOD, and C values below the LOQ but above the LOD were replaced by $^1/_2$LOQ. If the ND rate were over 60%, C values were assumed to be zero (ND).[37]

In this study, the exposure groups were classified according to sex (male and female) and age as in NAHSIT. A total of eight groups were classified by age and show the whole population. Eight groups included children of ages less than 1 year, 1−2 years, 3−6 years, 7−12 years, and 13−18 years; adults of ages 19−50 years and 51−65 years, and individuals above 66 years old. The CRs of the eight groups were estimated according to the 2005−2008 NAHSIT.[33]

In the NAHSIT have been given a unique coding for each food, each of the codes follow the nutritional content of different foods, food type, type of processing, and other related properties, to reclassification of all food into 230 food items. In the 47 subcategories (including 230 food items), the sum of the amount of 11182 available food intake records, we could get the total daily intake of all Taiwanese, and after conversion we could obtain the daily intake. The daily intake in the questionnaire was corrected by weighting to adjust the national daily intake data by the following steps: (1) The questionnaire weight was the total population in the layer/number of samples in the layer, (2) the individual food daily intake was multiplied by the questionnaire weight to obtain the national daily intake, and (3) national daily intake/number of the questionnaires in Taiwan and finally can get the food CR per person per day.

Distributions of CR and BW values were analyzed by Monte Carlo simulation techniques to obtain probabilistic parameters such as percentile values using the Crystal Ball software available from Decisioneering, Inc., Denver, Co., USA. Probabilistic distributions of CR were fitted to the 268431 raw data obtained from 6104 questionnaires. Distributions of the estimated BW of eight groups were fitted to the data obtained from 6104 participants. The selected log-normal distributions of CR and normal distributions of BW have optimal χ^2 fit and Kolmogorov−Smirnov (K−S) goodness-of-fit.

Hazard Index (HI, %ADI). The HI was calculated from the ADI and ADD according to the following equation:

$$\begin{aligned} \mathrm{HI}_j &= \sum_{i=1}^{n} \%\mathrm{ADI}_{ij} \\ &= \sum_{i=1}^{n} \frac{\mathrm{ADD}_{ij}}{\mathrm{ADI}_P} \times 100\% \\ &= \sum_{i=1}^{n} \frac{C_i \times \mathrm{CR}_{ij}}{\mathrm{BW}_j \times \mathrm{ADI}_P} \times 100\% \end{aligned} \quad (2)$$

where HI_j is the hazard index for age group j and ADI_p is the acceptable daily intake for chemical P. HI must be less than 100% to indicate that no harm would result from dietary exposure to the analyte in the lifetime of any consumer. ADI_P is generally accepted as an intrinsic property of the target chemical P. Toxicological and ADI data, as well as hazard characterization data for benzoic acid and sorbic acid, are collected from toxicological tests conducted on animals. ADI values of benzoic acid and sorbic acid used in this study were 5 mg/kg of BW/day and 25 mg/kg of BW/day,[31,39] respectively, as promulgated by the JECFA.

RESULTS AND DISCUSSION

Concentrations of Benzoic Acid and Sorbic Acid. Representative food samples, collected in the fall and winter of 2010 and in the spring and summer of 2011, were analyzed to determine the concentration of preservatives. The purchased food samples detection rates for benzoic acid and sorbic acid were approximately 30% and 22% respectively, of the total samples analyzed. The method performance for benzoic acid and sorbic acid show in Table 1. LOQ is 20 ppm and detected concentration lower than 20 ppm is labeled as "ND". In cases wherein the ND rate was greater than 60%, the concentration below the LOQ was assumed to be zero, and the concentrations of benzoic acid and sorbic acid were regarded as 0 mg/kg when calculating the daily intake.[35] LOD is 0.3 ppm considerably lower than that set by regulatory authorities in Taiwan. The analytical methods are in compliance with international standards for the analysis of food items in TDS requiring higher analytical sensitivities.[38]

Preservative concentrations in major categories show in Table 2. In the grains categories, 43 samples were analyzed. Frequency of detection is 44.2%, and mean concentration is 0.04 ppm in benzoic acid. Regulations pertaining to preservative use limit in Taiwan, the concentration of benzoic acid were 0.6 to 1.0 g/kg. In foods such as meats, sea urchins,

DOI: 10.1021/jf503987y
J. Agric. Food Chem. 2015, 63, 2074−2082

Table 2. Preservative Concentrations in Food Samples

major categories of food	preservative	no. of analysis performed	frequency of detection (%)	mean concentration ± SD (ppm)
(1) grains	benzoic acid	43	44.2	0.04 ± 0.07
	sorbic acid	43	34.9	0.04 ± 0.08
(2) oils	benzoic acid	4	25.0	0.02 ± 0.04
	sorbic acid	4	25.0	0.07 ± 0.14
(3) poultry and poultry products	benzoic acid	7	28.6	0.02 ± 0.03
	sorbic acid	7	14.3	0.02 ± 0.06
(4) meat and meat products	benzoic acid	17	35.3	0.06 ± 0.13
	sorbic acid	17	47.1	0.21 ± 0.35
(5) fish and aquatic products	benzoic acid	11	36.4	0.05 ± 0.08
	sorbic acid	11	45.5	0.09 ± 0.15
(6) other proteins	benzoic acid	43	62.8	0.2 ± 0.33
	sorbic acid	43	23.3	0.1 ± 0.29
(7) fruits (processed)	benzoic acid	6	16.7	0.06 ± 0.16
	sorbic acid	6	33.3	0.05 ± 0.08
(8) vegetables (processed)	benzoic acid	16	68.8	0.53 ± 0.94
	sorbic acid	16	31.3	0.05 ± 0.09
(9) dessert	benzoic acid	49	10.2	0.01 ± 0.02
	sorbic acid	49	14.3	0.04 ± 0.19
(10) alcoholic beverages	benzoic acid	2	0.0	
	sorbic acid	2	0.0	
(11) seasonings	benzoic acid	20	30.0	0.13 ± 0.28
	sorbic acid	20	10.0	0.01 ± 0.02
(12) others	benzoic acid	21	19.0	0.03 ± 0.08
	sorbic acid	21	14.3	0.05 ± 0.16

caviar, peanut butter, cheese, candied fruits, dried fruits, and dried radish containing no less than 25% moisture, cooked beans, miso, seaweed sauce, fermented bean curds, pastry, sauces, jam, juice, margarine, tomato sauce, chili sauce, thick candy syrup, and flavored syrup, the maximum permissible concentration is set at 1.0 g/kg. For foods such as mullet roe, dried fish, dried shellfish, beverages, pickles, dried bean curd, and salted vegetables, the maximum permissible concentration is set at 0.6 g/kg.

Sorbic acid regulations limit concentration added in food were 0.5 to 2.0 g/kg. For minced fish surimi products, meat products, urchins, caviar, peanut butter, soy sauce preserved vegetables, and dried radish containing no less than 25% moisture, pickled vegetables, dried bean curd products, cheeses: not more than 2.0 g/kg calculated as sorbic acid. For cooked beans, soy sauces, miso, dried mullet roe, dried fish, and shellfish products, seaweed pastes, soybean curd cheeses, syrup-preserved fruits, dried fruits, cakes, and cookies (including steamed Chinese-styled ones), jams, juices, butter, cream, margarine, ketchup, chili sauces, fruit syrups, flavored syrups, and other sauces: not more than 1.0 g/kg calculated as sorbic acid. For noncarbonated beverages and carbonated beverages, the maximum permissible concentration is set at 0.5 g/kg.

In our studies, the use of benzoic acid and sorbic acid as preservatives is permitted for only 34 food items in Taiwan. Of the 239 food samples from two sampling seasons that were analyzed for preservatives, there are 90 food samples that have little bearing on the 34 mentioned even though the use of benzoic acid and sorbic acid as preservatives is permitted for only 34 food items and 46 out of the these 90 food samples (51%) were found to contain these preservatives. In addition, we found that the concentrations of benzoic acid in some samples of dried tofu, packaged dried tofu, bean pastes, and dried pickled radish were above the regulation limit. These findings suggest that the preservatives are widely distributed among foods other than the regulated 34 food items, making it imperative to regularly monitor the food industry in Taiwan.

ADD of Benzoic Acid and Sorbic Acid. The ADD of food additives benzoic acid and sorbic acid in each item was estimated by measuring the concentration of the target chemical in the food sample. The results obtained by multiplying the concentration by the amount of food consumed are shown in Table 3. To estimate the ADD of a target chemical consumed by a sex-specific and age-specific population using the equation of ADD, data on the BW and the CR in 12 major categories of food were required. The exposure groups were classified according to eight age groups of ages under 1 year, 1−2 years, 3−6 years, 7−12 years, 13−18 years, 19−50 years, 51−65 years, and over 66 years were estimated according to the 2005−2008 NAHSIT.[33] The food list for the TDS, which was derived from the CR, contained 97

Table 3. ADD of Food Preservatives for Various Exposure Populations

	whole participators		participators (%) in 97 food items		benzoic acid				sorbic acid			
					50th ADD[a]		95th ADD		50th ADD		95th ADD	
age group	male	female	male	female	male	female	male	female	male	female	male	female
under 1 year	73	67	67.1	71.6	0.2	0.1	0.2	0.1	0.1	0.1	0.1	0.1
1−2 years	184	170	97.8	98.2	2.4	1.5	2.7	1.9	0.5	0.4	0.6	0.5
3−6 years	466	483	100.0	99.8	1.6	2.4	1.9	2.9	0.6	0.5	0.7	0.6
7−12 years	1170	1018	99.9	100.0	1.5	1.0	1.8	1.1	0.3	0.2	0.3	0.2
13−18 years	713	729	99.9	99.3	1.0	0.9	1.5	1.2	0.2	0.2	0.5	0.3
19−50 years	1062	1082	100.0	99.9	1.0	1.2	1.7	2.0	0.2	0.2	0.4	0.5
51−65 years	539	536	99.6	99.3	0.9	0.9	1.5	1.6	0.2	0.1	0.3	0.3
over 66 years	720	722	99.2	98.1	1.2	1.2	2.4	3.1	0.2	0.2	0.4	0.4
over 3 years	4670	4570	99.8	99.5	1.1	1.2	2.1	2.4	0.3	0.2	0.5	0.4

[a]ADD: average daily dose of food preservatives (mg/kg bw/day).

DOI: 10.1021/jf503987y
J. Agric. Food Chem. 2015, 63, 2074−2082

items selected to represent the total diet in Taiwan that may contain benzoic acid and sorbic acid. Items containing benzoic acid and sorbic acid that are consumed by the eight age populations were selected according to three selection criteria: (1) high relative CR, (2) historical high level of occurrence of the analytes, and (3) items for which the use of the analytes is permissible. The food items in the TDS list represented 83% of the weight (g) of the total diet of general consumers in Taiwan.

At the 50th percentile, males aged 1−2 years had the highest ADD of benzoic acid, with exposure level reaching 2.4 mg/kg of BW/day. In this group, the participators in 97 food items constituted 97.8% of a total of 184 people in the group, meaning that only four people did not take in these food items during the 24 h recall interviews. Females aged 3−6 years had the highest 95th percentile ADD of benzoic acid, with exposure level reaching 2.9 mg/kg of BW/day. The level of exposure to sorbic acid was 0.1 (under 1 year old group) to 0.7 (3−6 years old group) mg/kg of BW/day. Even at the 95th percentile, the exposure did not exceed 0.7 mg/kg of BW/day (3−6 years old group).

HI (%ADI) of Benzoic Acid and Sorbic Acid. The HI values of benzoic acid and sorbic acid were calculated as a percentage of respective ADI, 5 and 25 mg/kg of BW/day, using eq 2. The ratio of ADD to ADI, taken as %ADI (Figures 1 and 2), represents different exposure populations for benzoic and ascorbic acid. HI of benzoic acid and sorbic acid were calculated with the 50th percentile and 95th percentile of the different exposure populations.

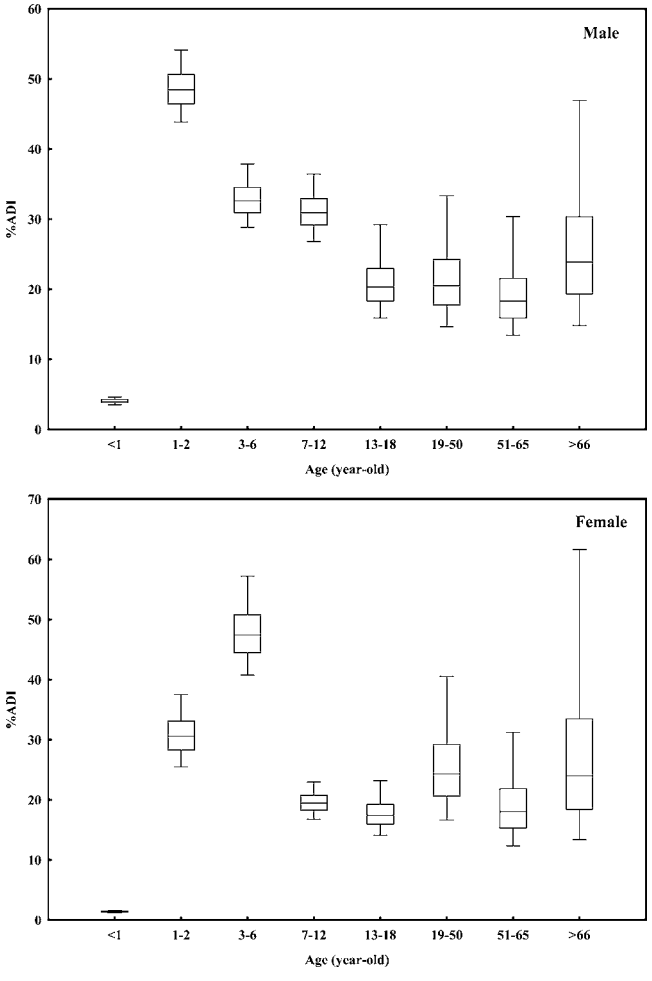

Figure 1. Food safety risk assessment hazard index (%ADI) of benzoic acid.

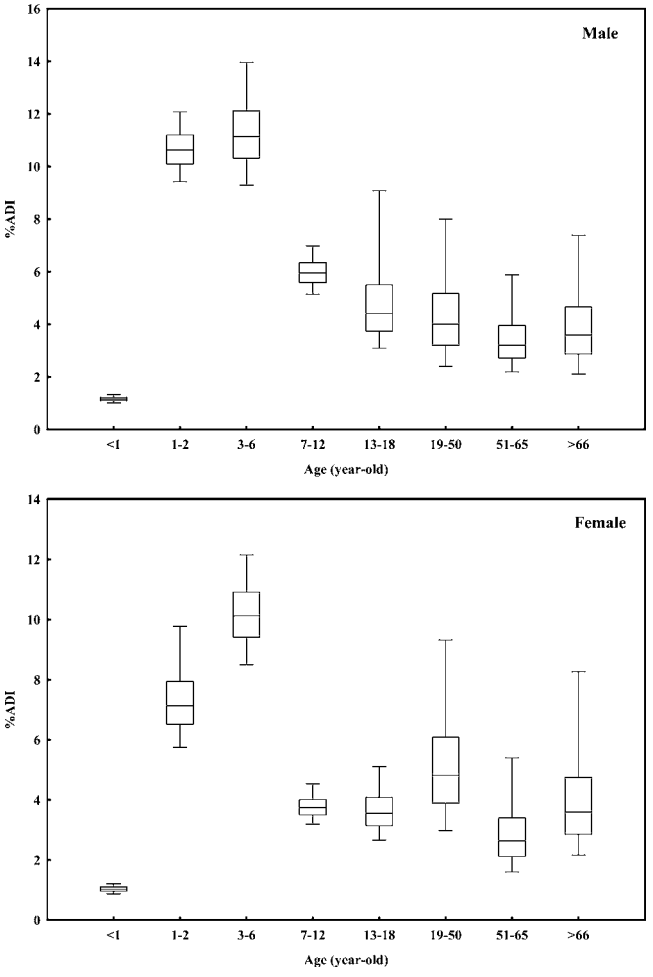

Figure 2. Food safety risk assessment hazard index (%ADI) of sorbic acid.

In Figure 1, the food safety risk assessment %ADI show males aged 1−2 years (48.5%) and females aged 3−6 years (47.4%) at the 50th percentile had the highest %ADI of benzoic acid, whereas males (11.2%) and females (10.1%) aged 3−6 years had the highest %ADI for sorbic acid at the 50th percentile shown in Figure 2. The values of HI for sorbic acid is generally lower than that for benzoic acid. HI of benzoic acid and sorbic acid are below the ADI. At the 95th percentile, the upper end of the intake distribution is still below the ADI; females over 66 years of age (61.7%) and males 3−6 years of age (14.0%) had the highest %ADI for benzoic acid and sorbic acid, respectively. These results indicate that there is a large margin of safety in the use of benzoic acid and sorbic acid as food preservatives in Taiwan.

In a study carried out in Belgium, the daily intake of benzoic acid in the male population exceeded the ADI (5 mg/kg of BW/day) at the 99th percentile, and the greatest contributor to the intake was soft drinks.[40] In our study, the ADD at the 99th percentile of men by all age groups did not exceed the ADI. In a study in Finland, fruit and berry juices, soft drinks, and semipreserved fish were identified as the major sources of benzoic acid intake, with the exposure level being 40 mg/day, or 13% ADI.[22] Comparing with the results of a 21st Australian

DOI: 10.1021/jf503987y
J. Agric. Food Chem. 2015, 63, 2074−2082

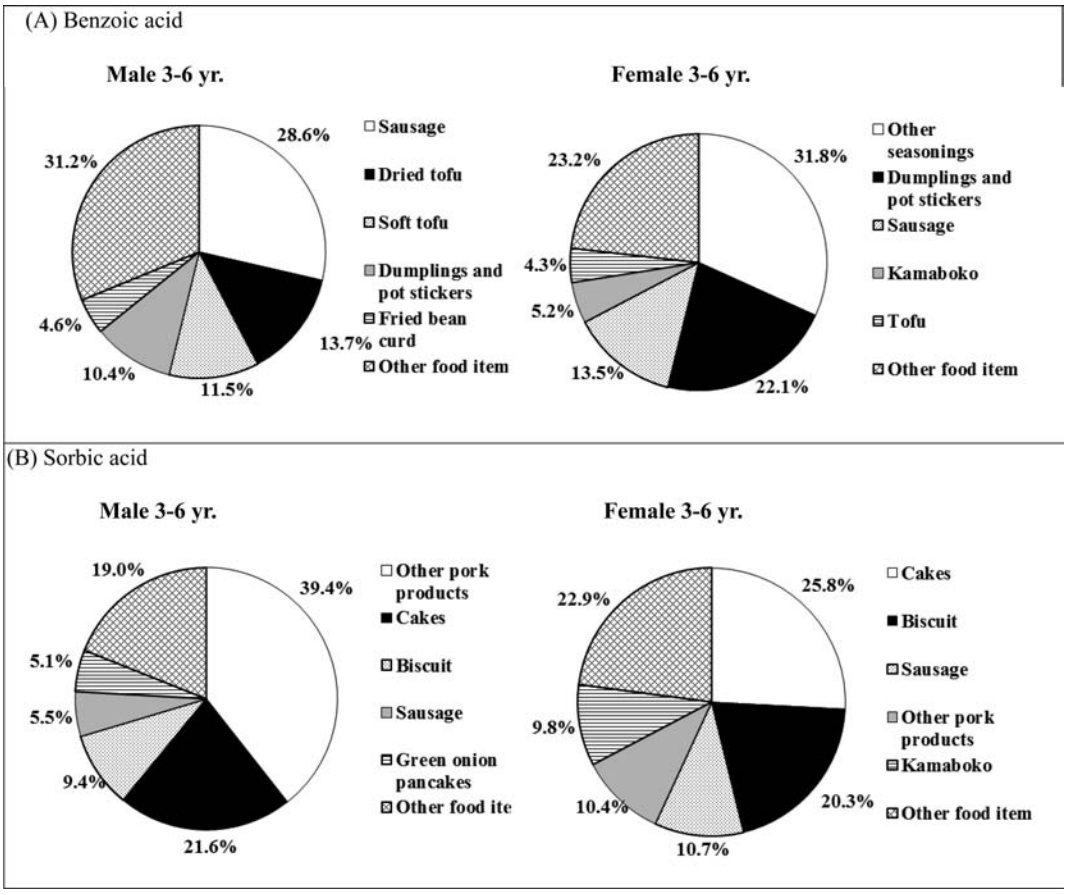

Figure 3. Exposure contributor of preservatives benzoic acid and sorbic acid for male and female aged 3−6 years old.

TDS,[13] the %ADI values for benzoic acid and sorbic acid of our study were slightly higher than those in Australia at 50th percentile, but lower at the 95th percentile. Although the eating habits in Taiwan are markedly different, the %ADI of benzoic acid and sorbic acid were nonetheless at very similar levels as in Australia. Although the results of the Australia study show that the mean estimated dietary exposure to benzoates was less than 50%ADI for all population groups assessed, the 95th percentile estimated dietary exposures to benzoates exceeded the ADI for young boys (approximately 140%) and young girls (approximately 120%) aged 2−5 years.[13] In the case of sorbates, the mean and 95th percentile estimated dietary exposure were less than or equal to 40%ADI for sorbates for all population groups assessed.

Our results indicate that the current exposure level to benzoic acid in foods in Taiwan is less than 60% of the ADI and hence not a hazard to public health. Combining the data for BW distribution and food CRs obtained in this study, we determined the HI for the Taiwanese population. The results indicate that in the 95th percentile, the exposure of the general population to benzoic acid is less than 60% of the ADI and hence not at a harmful level. Benzoic acid and sorbic acid are effective antimicrobials in acidic or slightly acidic foods. The temporary ADI was set at 5 mg/kg of BW by the European Scientific Committee on Food in 1994. The JECFA set an ADI of 5 mg/kg of BW in 1996, which was a confirmation of the evaluation in 1994. The 100-fold SF built into the ADI provides a significant margin of safety, which serves to reduce the likelihood of adverse effects on humans. As the %ADI is not over 100%, we assume that under the current exposure scenario, benzoic acid and sorbic acid pose no significant food safety risk in Taiwan. However, HIs even as high as 48.5%ADI (male 1−2 years group) at the 50th percentile, suggesting that regulatory actions must be implemented.[41]

HI (%ADI) Exposure Contributor for Benzoic Acid and Sorbic Acid. The intake of benzoic acid and sorbic acid through various food groups by various age groups is shown in Figures 3 and 4. According to the HI (%ADI) results, the 0−6 age sensitive population might have a higher risk of exposure to benzoic acid or sorbic acid. However, using adult food to estimate the infant (0−2 years old) dietary exposure would be an overestimation. Therefore, we focused on high-risk sensitive population aged 3−6 years and general population aged 19−50 years to explore further the exposure contributor of preservatives benzoic acid and sorbic acid (Figures 3 and 4). In 3−6 years population, the main HI contributors for benzoic acid were sausage (28.6%) for male and seasonings (31.8%) for female, respectively. The main HI contributors for sorbic acid were pork products (39.4%) for male and cakes (25.8%) for female, respectively. In the 19−50 years population, the main HI contributors for benzoic acid were dumplings and pot stickers (21.8%) for male and seasonings (34.5%) for female. The main HI contributors for sorbic acid were beef (29.5%) for male and cakes (23.7%) for female. Seasonings like tomato sauce, chili sauce, and soy sauce are added benzoic acid as a preservative to protect it from going bad. Dumpling and pot sticker skin were foods with high moisture that promotes growth of mold, yeast, and bacteria, whereas adding benzoic acid can inhibit them. Sorbic acid and its salts are used to protect cakes against mold spoilage and as inhibitors of

DOI: 10.1021/jf503987y
J. Agric. Food Chem. 2015, 63, 2074−2082

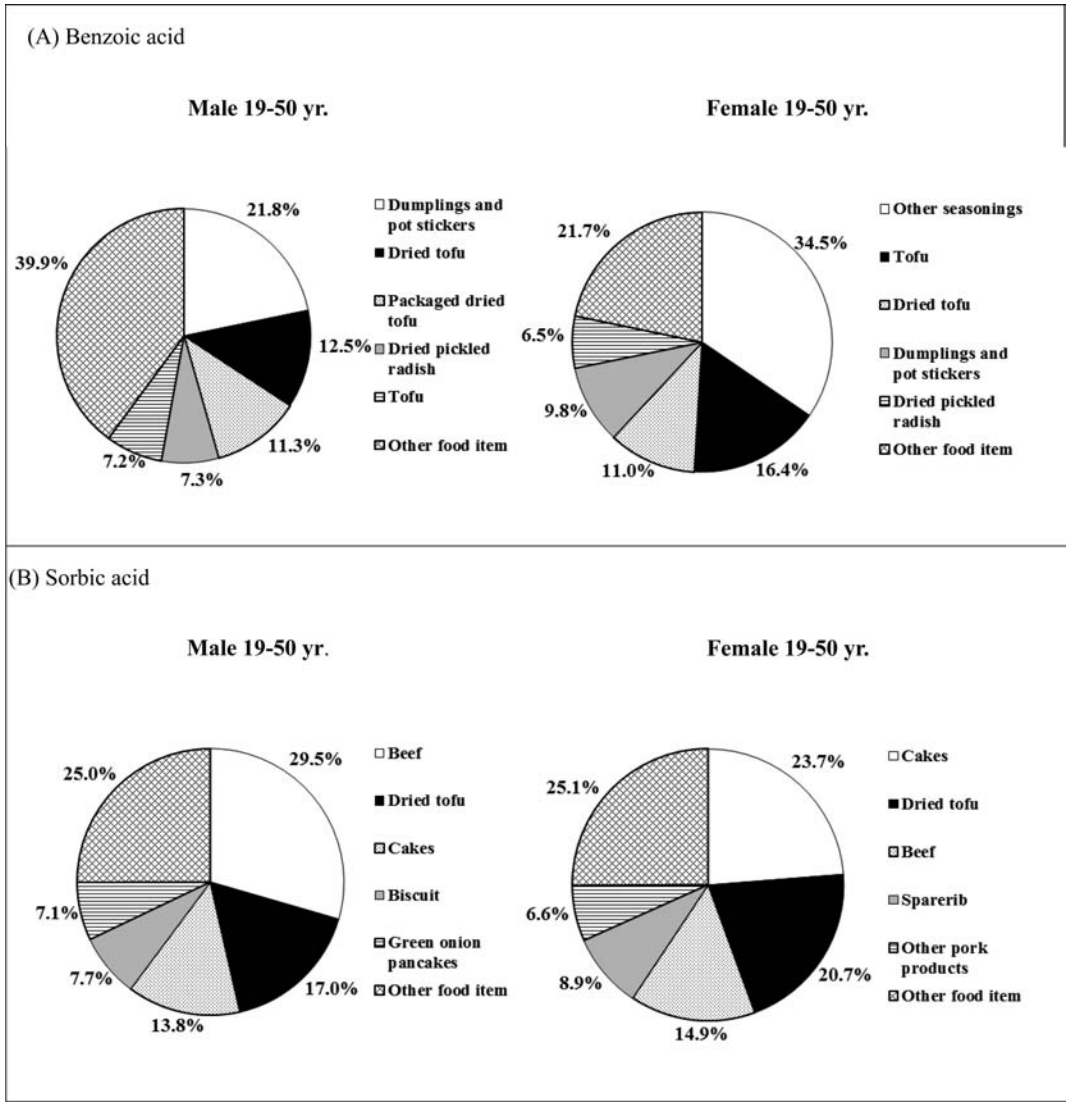

Figure 4. Exposure contributor of preservatives benzoic acid and sorbic acid for male and female aged 19−50 years old.

Clostridium botulinum in meat products in order to replace the use of nitrites, which produce carcinogenic nitrosamines.

In a study of dietary exposure to benzoic acid in secondary school students by Ma et al.,[15] the dietary exposures for average and high consumers of the school students from prepackaged beverages were 0.31 and 0.97 mg/kg BW per day, respectively. Both exposure levels were below the ADI established by JECFA. However, in the worst-case scenario where consumers had specific brand loyalty toward the fruit juice sample with the highest benzoic acid level detected in the study,[15] the general exposure in high consumers would exceed the ADI, leading to increased health risk.

In comparison, the major HI contributors for benzoic acid and sorbic acid in Australia were beverages (soft drinks) and fresh juices,[13] reflecting the vast difference in eating habits between the Orientals and the Caucasians. Likewise, in the Belgian study, the male group aged 15 years and older had a higher intake of benzoic acid than females due to a higher intake of soft drinks; their 99th percentile exposure exceed the ADI.[40] By conservative assessment of daily exposure, we found that seasoning, dumplings, and pot stickers were identified as the major sources of benzoic acid intake in Taiwan and hence require continuous monitoring.

Uncertainty Analysis. There are some methodological limitations and uncertainties in our study that need to be noted. First, Chinese foods are complex and dynamic, and it is very difficult to exactly match the food groups or items to be surveyed with the foods actually consumed. Second, foods analyzed in this survey were originally mapped to a wider range of foods described in the NAHSIT for a different research purpose, as the patterns of preservatives used in the mapped foods were assumed to be similar to the 97 food items analyzed, a kind of uncertainty inevitably was introduced. Third, it followed that the ADDs of preservatives were estimated with exposure factors associated with only these 97 items, introducing another kind of uncertainty. These uncertainties may cause underestimation. However, with our selection criteria, we believed that all the major sources of foodborne preservatives were covered. We also assessed the %ADI at the 95th percentile in order to avoid underestimation. In addition, the dietary exposures to benzoic acid and sorbic acid might have been overestimated in 1 year and 1−2 years because these groups are infants who consume mainly milk or baby food which are inherently different from adult food. Further studies will be conducted to examine this issue further. Finally, the one-day 24 h dietary recall records from the NAHSIT undoubtedly

DOI: 10.1021/jf503987y
J. Agric. Food Chem. 2015, 63, 2074−2082

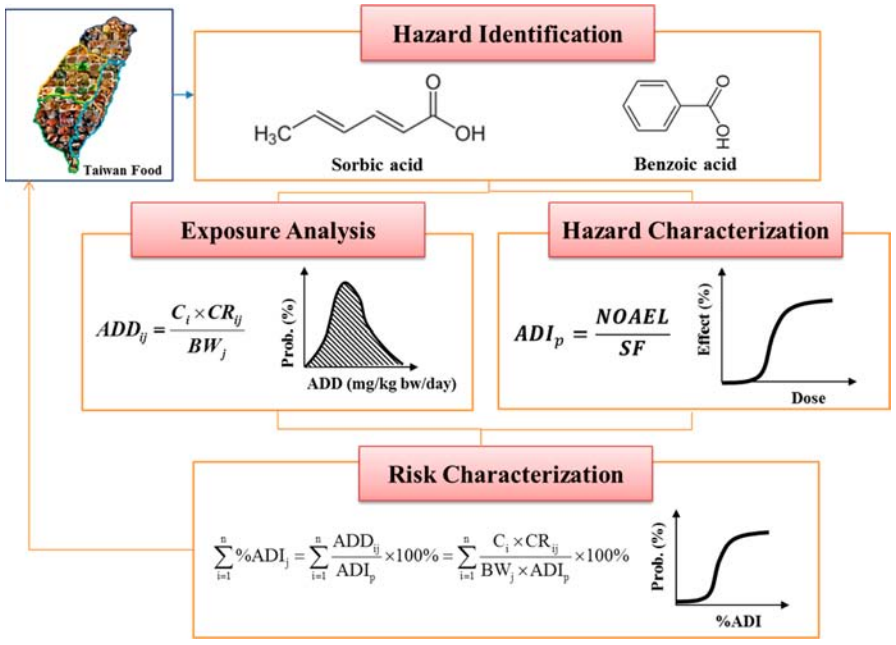

Figure 5. Flowchart of dietary exposure estimates for the food preservatives benzoic acid and sorbic acid in the total diet in Taiwan.

contained another kind of uncertainty due to individual differences in daily dietary practice. Our study therefore represents a preliminary attempt to construct a "market basket" for the total diet in Taiwan. To improve the accuracy of our estimates, future efforts are focused on minimizing the above-mentioned uncertainties and on validating the models and values of exposure factors in utilizing the data resources from NAHSIT, a major national research investment in Taiwan. In conclusion, the purpose of this study was to evaluate the HI (% ADI) of benzoic acid and sorbic acid through ingestion and thereby establish a model for total diet study on food additives in Taiwan by utilizing the existing data available from a national nutritional status survey, NAHSIT. The calculated 95th percentile ratios of ADD to ADI of benzoic acid and sorbic acid were less than 60%ADI, suggesting that the use of the two preservatives in food in Taiwan is within safe limits. This study provides a model for future work to address specific additives in specific foods as needed by food safety risk regulatory agencies.

In conclusion, this study demonstrated a dietary exposure estimates for the food preservatives benzoic acid and sorbic acid in the total diet in Taiwan (Figure 5). In hazard identification, related research in total diet study and the physical and chemical properties of preservatives benzoic acid and sorbic acid were collected. Then, in exposure analysis, ADD was estimated with Monte Carlo simulation. In hazard characterization, ADI, toxicological data (e.g., NOAEL) and SF of the preservatives from international institutions such as JECFA were analyzed. The dose−response profile was estimated according to the ADI by the JECFA. Lastly, in risk characterization, the probability distribution of the food safety risk was estimated and compared to ADI. In high-intake consumers, the highest HI of benzoic acid was 61.7%ADI for females aged over 66 years old. The highest HI of sorbic acid for male and female consumers aged 3−6 years old at the 95th percentile were 14.0%ADI and 12.2%ADI, respectively. These results indicate that the use of benzoic acid and sorbic acid as preservatives at the current level of use in the Taiwanese diet does not constitute a public health and safety concern, but the public is advised to maintain a varied and balanced diet so as to avoid excessive exposure of benzoic acid and sorbic acid from a small range of food items.

AUTHOR INFORMATION

Corresponding Author

*Phone: +886-4-2205-3366 ext 6508. Fax: +886-4-2207-0429. E-mail: lingmp@mail.cmu.edu.tw.

Funding

This TDS project was financed by the Taiwan Food and Drug Administration (TFDA), Department of Health (DOH), contract TFDA-TC-103.

Notes

The authors declare no competing financial interest.

ACKNOWLEDGMENTS

The data on related exposure factors, including BW and CR, were kindly provided by Dr. W. H. Pan, Principal Investigator of the National NAHSIT sponsored by the DOH (DOH94-FS-6-4). We thank our project manager at TFDA and the many food safety colleagues in Taiwan and TDS experts in China and elsewhere for their generous and professional help in completing this project. Without the help, we would not have been able to carry out this study. We would especially like to acknowledge the leadership and important contributions of coauthor DPHH, who has now honorably retired.

ABBREVIATIONS USED

ADD, average daily dose; ADI, acceptable daily intake; BW, body weight; C, concentration; CR, consumption rate; GEMS/Food, Global Environment Monitoring System—Food Contamination Monitoring and Assessment Program; HI, hazard index; HPLC, high-performance liquid chromatography; ISO, International Organization for Standardization; JECFA, Joint FAO/WHO Expert Committee on Food Additives; LOD, limit of detection; LOQ, limit of quantification; NAHSIT, Nutrition and Health Survey in Taiwan; ND, not detected; NOAEL, no observed adverse effect level; SF, safety factor; TDS, total diet

DOI: 10.1021/jf503987y
J. Agric. Food Chem. 2015, 63, 2074−2082

study; TFDA, Taiwan Food and Drug Administration; WR, weight ratio

REFERENCES

(1) Pennington, J. A. T.; Gunderson, E. L. History of the Food and Drug Adminstration's Total Diet Study—1961 to 1987. *J. AOAC Off. Anal. Chem.* **1987**, *70*, 772−782.

(2) *Codex Alimentarius Commission Procedural Manual*, 20th ed.; Joint FAO/WHO Food Standards Programme, WHO/FAO (World Health Organization/Food and Agriculture Organization): Rome, 2011; pp 112.

(3) EFSA (European Food Safety Authority). Joint Guidance of EFSA, FAO and WHO. Towards a harmonised Total Diet Study approach: a guidance document. *EFSA J.* **2011**, *9*(11), 2450.

(4) Moy, G. G. *Total Diet Studies*, 1st ed.; Springer: New York, 2011; pp 1−400.

(5) *State of the Art on Total Diet Studies Based on the Replies to the EFSA/FAO/WHO Questionnaire on National Total Diet Study Approaches*; Technical Report of EFSA, FAO and WHO; EFSA (European Food Safety Authority): Rome, 2011.

(6) Cunningham, W. C.; Anderson, D. L.; Baratta, E. J. Radionuclides in domestic and imported foods in the United States, 1987−1992. *J. AOAC Int.* **1994**, *77*, 1422−1427.

(7) Chen, H. L.; Su, H. J.; Hsu, J. F.; Liao, P. C.; Lee, C. C. High variation of PCDDs, PCDFs, and dioxin like PCBs ratio in cooked food from the first total diet survey in Taiwan. *Chemosphere* **2008**, *70*, 673−681.

(8) Li, X. W.; Gao, J. Q.; Chen, J. S. Chinese total diet study in 2000: the dietary mercuric intakes. *Wei Sheng Yan Jiu (J. Hyg. Res.)* **2006**, *3*, 323−325.

(9) Leblanc, J. C.; Tard, A.; Volatier, J. L.; Verger, P. Estimated dietary exposure to principal food mycotoxins from the first French Total Diet Study. *Food Addit. Contam.* **2005**, *22*, 652−672.

(10) Ministry of Agriculture and Forestry (MAF). *2009 New Zealand Total Diet Study: Agricultural Compound Residues, Selected Contaminant and Nutrient Elements*; Ministry of Agriculture and Forestry, Wellington, New Zealand, 2011.

(11) *The 22nd Australian Total Diet Study. A Total Diet Study of Five Trace Elements: Iodine, Selenium, Chromium, Molybdenum, And Nickel*; FSANZ (Food Standards Australia New Zealand): Canberra, Australia, Wellington, New Zealand, 2008.

(12) Tfouni, S. A.; Toledo, M. C. Estimates of the mean per capita daily intake of benzoic and sorbic acids in Brazil. *Food Addit. Contam.* **2002**, *19*, 647−654.

(13) *The 21st Australian Total Diet Study. A Total Diet Study of Sulphites, Benzoates and Sorbates*; FSANZ (Food Standards Australia New Zealand): Canberra, Australia, Wellington, New Zealand, 2005.

(14) Leth, T.; Christensen, T.; Larsen, I. K. Estimated intake of benzoic and sorbic acids in Denmark. *Food Addit. Contam.* **2010**, *27*, 783−792.

(15) Ma, K. M.; Chan, C. M.; Chung, S. W.; Ho, Y. Y.; Xiao, Y. Dietary exposure of secondary school students in Hong Kong to benzoic acid in prepackaged non-alcoholic beverages. *Food Addit. Contam.* **2009**, *26* (1), 12−6.

(16) Lino, C. M.; Pena, A. Occurrence of caffeine, saccharin, benzoic acid and sorbic acid in soft drinks and nectars in Portugal and subsequent exposure assessment. *Food Chem.* **2010**, *121*, 503−508.

(17) *GEMS Food Total Diet Studies: Report of the 3rd International Workshop on Total Diet Studies*; WHO (World Health Organization): Geneva. 2004.

(18) Suhr, K. I.; Nielsen, P. V. Effect of weak acid preservatives on growth of bakery product spoilage fungi at different water activities and pH values. *Int. J. Food Microbiol.* **2004**, *95*, 67−78.

(19) European Union. European Parliament and Council Directive No. 95/2/EC of 20 February 1995 on food additives other than colours and sweeteners. *Off. J. Eur. Union* **1995**, *61*, 1−40.

(20) *Standards for Specification, Scope, Application and Limitation of Food Additives List*; Taiwan Food and Drug Administration (TFDA), 2014; http://www.fda.gov.tw/EN/law.aspx (accessed May 19, 2014).

(21) *Annual Report of Food and Drug Research*; Taiwan Food and Drug Administration (TFDA), 2014; http://www.fda.gov.tw/TC/PublishResearch.aspx (accessed May 19, 2014).

(22) Pentilla, L.; Salminen, S.; Niemi, E. Estimates on the intake of food additives in Finland. *Z. Lebensm.-Unters. Forsch.* **1988**, *186*, 11−15.

(23) Kieckebusch, W.; Lang, K. The tolerability of benzoic acid in chronic feeding experiments. *Arzneimittelforschung* **1960**, *10*, 1001−1003.

(24) McCann, D.; Barrett, A.; Cooper, A.; Crumpler, D.; Dalen, L.; Grimshaw, K.; Kitchin, E.; Lok, K.; Porteous, L.; Prince, E.; Sonuga-Barke, E.; Warner, J. O.; Stevenson, J. Food additives and hyperactive behavior in 3-year-old and 8/9-year-old children in the community: a randomised, double-blinded, placebo-controlled trial. *Lancet* **2007**, *370*, 1560−1567.

(25) USEPA (U.S. Environmental Protection Agency). *Guidelines for Developmental Toxicity Risk Assessment*. Federal Register **1991**, *56*, 63798−63826.

(26) Renwick, A. G. Safety factors and establishment of acceptable daily intakes. *Food Addit Contam.* **1991**, *8*, 135−149.

(27) Sado, I. Synergistic toxicity of official permissible preservative food additives. *Nippon Eiseigaku Zasshi (Jpn. J. Hyg.)* **1973**, *28*, 463−476.

(28) Lang, K. The tolerability of sorbic acid. *Arzneimittelforschung* **1960**, *10*, 997−999.

(29) Walker, R. Toxicology of sorbic acid and sorbates. *Food Addit. Contam.* **1990**, *7* (5), 671−676.

(30) Deuel, H. J.; Alfin-slater, R.; Well, C. S.; Smyth, H. F. Sorbic acid as a fungistatic agent for foods. *Food Res.* **1954**, *19*, 1.

(31) JECFA (Joint FAO/WHO Expert Committee on Food Additives). *Evaluation of certain food additives and contaminants. Forty-Sixth Report of the Joint FAO/WHO Expert Committee on Food Additives*; WHO Technical Report Series No. 868; WHO: Geneva, 1996.

(32) WHO (World Health Organization). *Benzyl Acetate, Benzyl Alcohol, Benzaldehyde, Benzoic Acid and the Benzoate Salts, Forty Sixth Report of the Joint FAO/WHO Expert Committee on Food Additives*; WHO Technical Report Series No. 868; WHO: Geneva, 1997.

(33) Pan, W. H. *Nutrition and Health Survey in Taiwan 2004−2008*; Project Report, DOH94-FS-6-4; Food and Drug Administration, Department of Health, Taiwan, R.O.C., 2008.

(34) Egan, S. K.; Bolger, P. M.; Carrington, C. D. Update of US FDA's Total Diet Study food list and diets. *J. Exposure Sci. Environ. Epidemiol.* **2007**, *17* (6), 573−582.

(35) Egan, S. K.; Tao, S. S.; Pennington, J. A.; Bolger, P. M. US Food and Drug Administration's Total Diet Study: Intake of Nutritional and Toxic Elements 1991−96. *Food Addit. Contam.* **2002**, *19* (2), 103−125.

(36) *General Requirements for the Competence of Testing and Calibration Laboratories*; ISO 17025; ISO, 2005.

(37) *Principles and Methods for the Risk Assessment of Chemicals in Food: Chapter 6 Dietary Exposure Assessment of Chemicals in Food. Environmental Health Criteria*; *WHO (World Health Organization)* Geneva, 2009; Vol. *240*, Chapter 6, pp 19−21.

(38) *Pesticide Monitoring Program—FY 2008, Annual Report*; US FDA: Bethesda, MD, 2008.

(39) JECFA (Joint FAO/WHO Expert Committee on Food Additives). *Seventeenth Report of the Joint FAO/WHO Expert Committee on Food Additives*; WHO Technical Report Series No. 539. WHO: Geneva, 1973.

(40) Vandevijvere, S.; Andjelkovic, M.; De Wil, M.; Vinkx, C.; Huybrechts, I.; Van Loco, J.; Van Oyen, H.; Goeyens, L. Estimate of intake of benzoic acid in the Belgian adult population. *Food Addit. Contam.: Part A* **2009**, *26*, 958−968.

(41) *Procedural Manual. Codex Committee on Food Additives and Contaminants (CCFAC) Guidelines for Exposure Assessment of Contaminants and Toxins in Food or Food Groups*, 15th ed.; CAC (Codex Alimentarius Commission): Geneva, 2013.

DOI: 10.1021/jf503987y
J. Agric. Food Chem. 2015, 63, 2074−2082

dithiothreitol (DTT), phenyl-methanesulfonil fluoride (PMSF), potassium hydrogen carbonate, hydrogen peroxide, and superoxide dismutase (SOD) bovine (EC 1.15.1.1) were from Sigma-Aldrich (St. Louis, MO, USA). *ortho*-Phosphoric acid 85% was obtained from Panreac (Barcelona, Spain). Methanol and acetonitrile were obtained from Merck (Darmstadt, Germany). Sodium chloride, ethyl acetate, hydrochloric acid, and formic acid were from BDH Prolabo (Dublin, Ireland). Standards were obtained from Extrasynthese (Genay, France). Dulbecco's Modified Eagle Medium (DMEM) + GlutaMAX^{TM-I}, heat-inactivated fetal bovine serum (FBS), phosphate-buffered saline (PBS), nonessential amino acids (NEAA), Pen Strep solution (Penicillin 5000 units/mL and Streptomycin 5000 mg/mL), fungizone (250 μg/mL amphotericin B), human transferrin (4 mg/mL), and trypsin-EDTA were purchased from Gibco, Invitrogen (Invitrogen, Paisley, U.K.). Human epithelial colorectal adenocarcinoma (Caco-2) cell line was acquired from American Type Culture Collection (ATCC) (LGC Standards S.L.U., Barcelona, Spain). Water was deionized using a Milli-Q water purification system (Millipore, Bedford, MA, USA).

Samples. *E. plantagineum* bee pollen sample was provided by beekeepers in the Spanish Extremadura region in 2011. The botanical origin was assessed by Professor Paula B. Andrade (Laboratório de Farmacognosia, Faculdade de Farmácia da Universidade do Porto; voucher specimen EP-BP-032011). Bee pollen was stored protected from light under desiccating conditions to prevent alteration.

Extracts Preparation. Aliquots of 1 g of *E. plantagineum* bee pollen were accurately weighed, thoroughly mixed with 10 mL of methanol containing 0.5% HCl (v/v), sonicated for 1 h, and centrifuged at 4000 rpm for 10 min. The supernatant was decanted, and the residue was re-extracted by thoroughly mixing by vortexing for 2 min with 10 mL of methanol containing 0.5% HCl (v/v) and centrifuged at 4000 rpm for 10 min. The supernatants were pooled together, and the solvent was evaporated under reduced pressure at 30 °C. In order to obtain extracts enriched in phenolic compounds, a solid-phase extraction (SPE) procedure was performed using Chromabond C_{18} nonend-capped (NEC) columns (45 μm particle size, 60 Å pore size; 10 g sorbent mass/70 mL reservoir volume) from Macherey-Nagel (Düren, Germany). The residue was dissolved in 10 mL of water and applied to the SPE cartridge preconditioned with 20 mL of ethyl acetate, 20 mL of methanol, and 20 mL of water. The loaded cartridge was washed with 10 mL of water. A fraction containing noncolored phenolics was eluted with 100 mL of ethyl acetate (fraction I). A second fraction with anthocyanins (fraction II) was eluted with 40 mL of methanol. A combined extract was obtained by mixing ethyl acetate and methanol eluates (whole extract). The eluates were concentrated under reduced pressure, and the residues obtained were dissolved in 5 mL of methanol (final concentration of 200 mg/mL).

Acid Hydrolysis. A 1 mL amount of HCl 2 M was added to 2 mL of fraction II. The acid solution was heated at 100 °C for 30 min under reflux. The obtained anthocyanidins were recovered by SPE using a Chromabond C18 nonend-capped (NEC) column (45 μm particle size, 60 Å pore size; 1 g sorbent mass/6 mL reservoir volume) from Macherey-Nagel (Düren, Germany) previously conditioned with methanol and HCl, 2 M. Compounds were eluted with 20 mL of methanol. The solvent was evaporated under reduced pressure at 30 °C; the residue was dissolved in 2 mL of methanol, filtered through a 0.45 μm pore size filter, and injected for anthocyanidins identification.

HPLC-DAD Analysis. The extracts were analyzed on an analytical HPLC unit (Gilson) consisting of two pumps (321 model) and a Rheodyne injector (model 7125), connected to a diode array detector (Gilson 170 Diode Array detector). The HPLC was equipped with a Spherisorb ODS2 column (25.0 × 0.46 cm; 5 μm, particle diameter). Spectral data from all peaks were accumulated in the range 200−600 nm. The data were processed on a Unipoint Software system (Gilson Medical Electronics, Villiers le Bel, France). Peak purity was checked by the software contrast facilities.

Flavonols. The extracts were analyzed as described before.[4] Briefly, the mobile phase consisted of water−formic acid (1%) (A) and methanol (B). The following gradient was used: from 30% to 40% B (20 min), from 40% to 50% B (5 min), from 50% to 60% B (5 min), and from 60% to 80% B (2 min). The flow rate was 1 mL/min, and the injection volume was 20 μL. Phenolic compounds quantification was achieved by the absorbance recorded at 350 nm relative to external standards. Because standards of all identified kaempferol derivatives were not commercially available they were quantified as kaempferol-3-*O*-rutinoside, excepting kaempferol-3-*O*-glucoside, which was quantified as itself.

Anthocyanins. Colored phenolics were analyzed following a previously described method.[13] The mobile phase consisted of water/formic acid/acetonitrile (87:10:3, v/v/v; eluent A) and water/formic acid/acetonitrile (40:10:50, v/v/v; eluent B) using a gradient program as follows: from 10% to 25% B (10 min), from 25% to 31% B (5 min), from 31% to 40% B (5 min), from 40% to 50% B (10 min), from 50% to 100% B (10 min), and from 100% to 10% B (5 min). The flow rate was 0.8 mL/min, and the injection volume was 20 μL. Phenolic compounds in the extracts and in the hydrolyzed extracts were identified by comparing their retention times and UV−vis spectra with those of standards when commercially available and by comparison with the literature.[2] Quantification was performed at 500 nm. Delphinidin heterosides were quantified as delphinidin-3-*O*-glucoside; petunidin heterosides and malvidin-3-*O*-glucoside were quantified as malvidin-3-*O*-glucoside.

Caco-2 Culture Conditions and Treatments. Caco-2 cells were grown in DMEM+GlutaMAX^{TM-I} supplemented with 10% calf serum (FCS) heat-inactivated, 1% NEAA, 1% fungizone, 6 μg/mL transferrin, 1% penicillin, and 1% streptomycin, at 37 °C in 5% CO_2, until they reach 90% confluence. For cell treatments the culture medium was prepared without FCS. Cells were plated at 1.5×10^5 cells/mL using 200 μL/well of cell suspension in 96-well plates (viability assays), 1200 μL/well in 24-well plates (GSH, DCFA-DA), and 2.5 mL/well in 12-well plates (enzymes) and then incubated until they reached confluence.

Just before the assays, an aliquot of the extracts was evaporated under a nitrogen stream; the residue was dissolved in the same volume of culture medium without FCS and sterilized by filtration through a 0.22 mm size pore membrane. Five dilutions (1/2) were prepared, and cells were exposed for 24 h to the different concentrations of the extracts. In order to evaluate the antioxidant potential, cells were pre-exposed to the extracts for 24 h, then the extracts were removed, and cells were exposed to 150 μM *t*-BHP for 4 (DCFA-DA assay) or 6 h (other assays).

Viability Assays. The viability of cells was measured by the mitochondria-dependent reduction of MTT to formazan and by the release of the cytosolic enzyme lactate dehydrogenase (LDH) into culture medium by cells with disrupted cell membrane.

MTT Reduction. After cell treatment and removal of the culture medium, adherent cells were treated for 30 min with 0.5 mg/mL of MTT. The formazan crystals were then dissolved with DMSO and quantified by measuring the absorbance at 560 nm in a microplate reader (Multiskan ASCENT).[4,14] Results were expressed as percentage of control. Five independent experiments were performed in triplicate.

LDH Release. LDH was determined by adding pyruvate (124 μM) and NADH (154 μM) to the culture medium of treated cells and following the rate of oxidation of NADH at 340 nm during the conversion of pyruvate to lactate.[4,15] Results are expressed as percentage of control. Five independent experiments were performed in triplicate.

Reactive Species. The measurement of intracellular reactive species with DCFA-DA was performed using a previously described method,[16] with modifications. Cells were exposed to the extracts for 24 h, and the culture medium was removed. DCFA-DA (10 μM, dissolved in culture medium without phenol red) was added, and the cells were incubated with the probe for 30 min at 37 °C. The probe was removed, and *t*-BHP dissolved in culture medium without phenol red was added. Fluorescence (485 nm excitation, 528 nm emission) was read immediately and every 30 min, for 4 h, in a microplate spectrofluorimeter (Synergy HT, Bio-Tek Instruments Winooski, USA, operated by KC4 software). The plate was maintained at 37 °C between readings. Results are expressed as percent of control (without

DOI: 10.1021/jf505568h
J. Agric. Food Chem. 2015, 63, 2083−2091

t-BHP) and were normalized with the result at 0 min. Five independent assays were performed.

Glutathione. Total glutathione (GSHt) was measured by DTNB-glutathione reductase (GR) recycling assay, according to a previously described method.[17] Briefly, the culture medium was removed after cells treatment, and 250 μL of perchloric acid 5% was added to each well. Incubation was maintained for 10 min on ice in order to extract GSHt, and then the solution was collected and kept at −20 °C until analysis. A 250 μL amount of NaOH, 0.3 M, was added to the cells in each well to solubilize proteins for protein quantification.

GSHt was measured by following the increase of 5′-thio-2-nitrobenzoic acid (TNB) at 405 nm, resulting from the oxidation of GSH by DTNB (1.28 mM). The assay was performed after neutralizing perchloric acid with $KHCO_3$, 0.76 M, in the presence of GR (2.0 U/mL) and NADPH (0.21 mM), to recycle the glutathione disulfide GSSG increasing the detection limit. GSSG was measured after GSH derivatization by 2-vinilpyridine: 2-vinilpyridine (7.5 μL) was added to 150 μL of samples and mixed continuously in a shaker for 1 h at 4 °C. GSSG was then quantified as described above for GSHt. Five independent assays were performed.

Antioxidant Enzymes. The influence of the extracts on antioxidant enzymes activity was measured. After exposure to the extracts the culture medium was collected for extracellular SOD determination and the cells were lysed on ice for 30 min with 1% Triton X-100 in Tris-HCl 50 mM, pH = 8.0, containing 150 mM NaCl, 0.5 mM PMSF, and 1 mM DTT (for GPx analysis 0.5 mM of DTT was used). The lysates were centrifuged at 10 000 rpm for 10 min, at 4 °C, and the supernatants were collected for enzymatic and protein assays. Five independent assays were performed.

Glutathione Transferase (GST). GST activity was assayed according to a previously described method.[18] GSH (1 mM) was incubated at room temperature with 1-chloro-2,4-dinitrobenzene (CDNB, 1.5 mM), and the formation of the conjugate was monitored at 340 nm. GST activity was calculated by using an extinction coefficient of 9.6/mM/cm.

Glutathione Reductase (GR). GR activity was determined at room temperature, following the rate of oxidation of NADPH (0.5 mM) at 340 nm, during the reduction of GSSG (1.2 mM) to GSH.[19] GR activity was calculated by using an extinction coefficient of 6.22/mM/cm.

Glutathione Peroxidase (GPx). GPx activity was measured following a previously described method.[20] The activity was indirectly measured by a coupled assay of GSSG reduction under conditions in which GPx activity is rate limiting. The assay was performed at room temperature using *t*-BHP (150 μM) as substrate, GSH (1 mM) plus NADPH (0.15 mM), and GR (0.03 U/mL) to recycle the GSSG formed. The decrease of NADPH was measured at 340 nm. The enzyme activity was calculated by using an extinction coefficient of 6.22/mM/cm and expressed as mmol of NADPH oxidized/min/mg of protein.

Catalase. Catalase activity was measured at room temperature by monitoring the decomposition of H_2O_2 (10 mM) at 240 nm.[21] The enzyme activity was calculated by using an extinction coefficient of 39.4/M/cm.

Superoxide Dismutase (SOD). Extracellular SOD was assayed using a previously described method,[22] with modifications. A PMS (0.003 mM)−NADH (0.07 mM) system was used to generate superoxide radical ($O_2^{\bullet-}$). Subsequent reduction of NBT (0.03 mM) by $O_2^{\bullet-}$ was monitored at 560 nm. SOD activity was determined by interpolation of a calibration curve built under the same conditions with SOD bovine, with a concentration range of 0.025−0.25 U/mL.

In order to assess $O_2^{\bullet-}$ scavenging activity, an assay was performed incubating culture medium with the extracts but without cells and measuring NBT reduction as previously described. Four independent assays were performed. The results are expressed as percent of control and were compared with the ones obtained in the assay performed with cells.

Protein Quantification. Proteins were measured by the Bradford method using bovine serum albumin as reference.[23]

Statistical Analysis. Statistical analysis was performed using Graphpad Prism 6 Software (San Diego, CA, USA). Two Way ANOVA and Dunnets's test (LDH, MTT, DCFA-DA, and antioxidant enzymes) or Sidak's (GSHt, $O_2^{\bullet-}$), as posthoc test, were used to determine the statistical significance in comparison to control. Two-way ANOVA and Sidak's multiple comparisons test were used to compare between groups. Values of $p \leq 0.05$ were considered significant.

RESULTS AND DISCUSSION

Chemical Composition. The chemical composition of *E. plantagineum* bee pollen was determined after extraction of compounds with acidified methanol in order to recover both anthocyanins and noncolored phenolics. Anthocyanins are soluble in polar solvents but are instable in neutral or alkaline media, being usually extracted from plant materials with methanol containing an acid in small quantities to prevent alteration of acylated compounds.[24] The crude extract was fractioned by SPE using ethyl acetate (fraction I) and methanol (fraction II) as eluents. A whole extract was also characterized. Twelve phenolic compounds were identified, belonging to flavonols (seven compounds) and anthocyanins (five compounds).

Noncolored Phenolic Compounds. The identification of noncolored phenolics in fraction I, fraction II, and whole extract of *E. plantagineum* bee pollen was performed using the same chromatographic conditions of a previous study concerning a hydromethanolic extract of the same material.[4,5]

All of the determined noncolored phenolic compounds were derivatives of kaempferol (Figure 1A, Table 1). Fraction I (eluted with ethyl acetate) contained six compounds, while fraction II (collected with methanol, after ethyl acetate elution) and the whole extract contained all the identified compounds. Kaempferol-3-*O*-neohesperidoside was the major compound in all of the extracts, representing between 73.2% (Fraction I) and

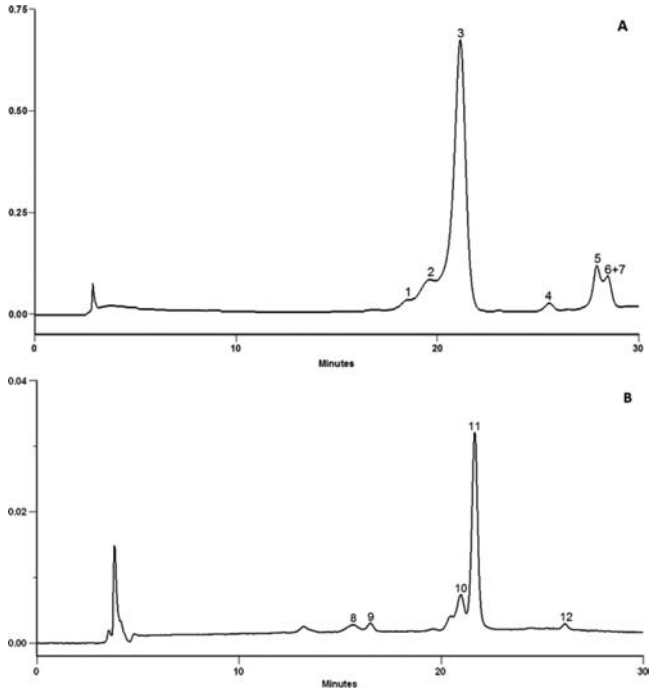

Figure 1. Phenolic profile of *E. plantagineum* bee pollen. (A) Noncolored phenolics (350 nm) from whole extract. (B) Anthocyanins (500 nm) from Fraction II. Peaks' identity as in Table 1

DOI: 10.1021/jf505568h
J. Agric. Food Chem. 2015, 63, 2083−2091

Table 1. Phenolic Compounds in *E. plantagineum* Bee Pollen Acidified Methanol Extract and Fractions (mg/kg of pollen)[a]

	compounds	fraction I	fraction II	whole
noncolored				
1	kaempferol-3-*O*-(4″-rhamnosyl)-neohesperidoside	[a]	148.27 ± 6.68[b]	146.07 ± 23.91[b]
2	kaempferol-3-*O*-sophoroside	658.49 ± 71.15[a]	87.34 ± 10.20[b]	635.68 ± 63.57[a]
3	kaempferol-3-*O*-neohesperidoside	4094.46 ± 49.52[a]	735.28 ± 19.08[b]	4890.54 ± 118.13[c]
4	kaempferol-3-*O*-neohesperidoside-7-*O*-rhamnoside	70.16 ± 0.35[a,b]	8.31 ± 0.55[a]	91.74 ± 1.64[b]
5	kaempferol-3-*O*-glucoside	395.47 ± 21.83[a]	10.82 ± 1.44[b]	402.17 ± 3.76[a]
6 + 7	kaempferol-3-*O*-rutinoside + kaempferol-3-*O*-(3″/4″-acetyl)-neohesperidoside	373.75 ± 8.53[a]	7.40 ± 0.65[b]	336.30 ± 14.58[a]
total		**5592.33 ± 151.38[a]**	**997.42 ± 31.93[b]**	**6502.50 ± 201.67[c]**
colored				
8	delphinidin-3-*O*-glucoside	[a]	1.21 ± 0.05[b]	1.03 ± 0.03[b]
9	delphinidin-3-*O*-rutinoside	[a]	0.95 ± 0.06[b]	0.88 ± 0.10[b]
10	petunidin-3-*O*-glucoside	[a]	5.41 ± 0.30[b]	5.88 ± 0.48[b]
11	petunidin-3-*O*-rutinoside	0.313 ± 0.003[a]	24.30 ± 0.17[b]	29.56 ± 0.58[c]
12	malvidin-3-*O*-rutinoside	[a]	0.68 ± 0.02[a,b]	0.92 ± 0.06[b]
total		**0.313 ± 0.003[a]**	**32.56 ± 0.60[b]**	**38.26 ± 1.26[c]**

[a]Values are expressed as mean ± standard deviation of three determinations. Different superscript letters in the same row mean statistically significant differences ($p < 0.05$ or higher).

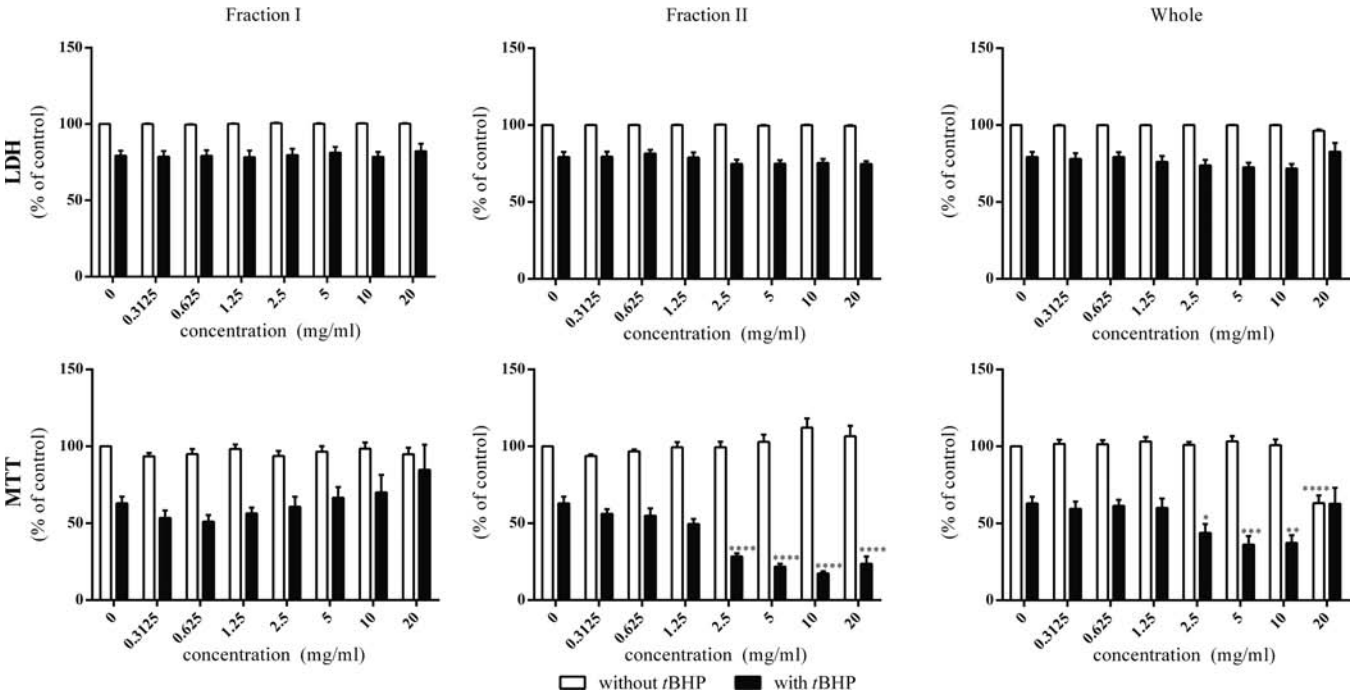

Figure 2. Viability of cells evaluated by LDH and MTT assays. Cells were treated with the extracts for 24 h or pretreated for 24 h with the extracts followed by 6 h treatment with 150 μM of *t*-BHP (without extract coincubation). Results are presented as mean ± standard error of the mean of five independent experiments performed in triplicate. *$p < 0.05$, **$p < 0.01$, ***$p < 0.001$, ****$p < 0.0001$ compared to the respective control (with or without *t*-BHP).

75.2% (whole extract) of the identified compounds. The total amount of flavonols was 5.6 times higher in fraction I than in fraction II, the amount in the whole extract approximately corresponding to the sum of flavonols present in both fractions (6.5 ± 2.0 g/kg) (Table 1). Fraction I contained higher relative amounts of compounds **2**, **5**, and **6 + 7** than fraction II, while compound **1** was absent. No statistical differences were found for the relative amounts of compounds **3** and **4** ($p > 0.05$).

Anthocyanins. As referred above, the dark blue color of *E. plantagineum* bee pollen was attributed to its anthocyanins.[2] Using SPE, a fraction containing almost all the anthocyanins present in the acidified methanolic extract was obtained (fraction II) by elution with methanol after eluting with ethyl acetate to remove some noncolored phenolic compounds.[13] The anthocyanins profile of fraction II can be seen in Figure 1B, being similar to the profile of the whole extract. In order to identify the compounds an acidic hydrolysis was performed and the obtained aglycones were identified by comparison with anthocyanidins standards. With the exceptions of delphinidin-3-*O*-glucoside and malvidin-3-*O*-glucoside, whose identity was confirmed with authentic standards, the complete identification of others heterosides present in the extracts was achieved taking into account what was described for this species[2] and further confirmed by our previous works with other matrices:[13] on using the same experimental conditions we obtained identical chromatograms in what concerns to order of elution and the

DOI: 10.1021/jf505568h
J. Agric. Food Chem. 2015, 63, 2083−2091

same UV spectra. Petunidin-3-*O*-rutinoside (compound **11**) was the major compound in fraction II and in the whole extract, this being the only anthocyanin found in fraction I (Table 1). This compound was quantified in the whole extract in higher quantity than its sum in fractions I and II. The total amount of identified anthocyanins corresponded to 0.313 mg/kg in fraction I, 32.6 mg/kg in fraction II, and 38.3 mg/kg in the whole extract, compound **11** representing 100.0%, 74.7%, and 77.3% of the total identified anthocyanins, respectively.

Cellular Viability. Before evaluating the antioxidant potential of the characterized extracts of *E. plantagineum* bee pollen its effects on the viability of Caco-2 cells under quiescent conditions were evaluated by LDH leakage and MTT reduction assays (Figure 2). No significant toxicity was observed in the concentration range from 0.31 to 20.0 mg/mL for fractions I and II. However, at the higher concentration tested, the whole extract caused a significant decrease in cellular viability, as assessed by the MTT assay ($p < 0.0001$, $n = 5$). This loss of cellular viability cannot be attributed to one class of phenolic compounds since neither fraction I (nearly free of anthocyanins) nor fraction II (containing 15% of total flavonols and anthocyanins) caused a significant loss in cell viability at this concentration. Rather the combined effects of anthocyanins with high amounts of flavonols may be responsible for the observed toxicity. Flavonoids can act as antioxidants in their reduced form, but when oxidized (to phenoxyl radicals or quinone/quinone methide intermediates), they can have pro-oxidant activities.[25] A pro-oxidant activity has been described for both classes of flavonoids present in *E. plantagineum* bee pollen. The flavonol compounds with a phenolic B ring like the kaempferol derivatives found in the extracts may act as pro-oxidants after oxidation by peroxidases/H_2O_2 to phenoxyl radicals, accompanied by GSH co-oxidation and oxygen activation, resulting in superoxide radical and H_2O_2 formation.[26] Also, a pro-oxidant effect of anthocyanidins in HL-60 cells was attributed to intracellular hydrogen peroxide production, triggering an apoptotic death program through oxidative stress.[27] This may explain why only in the MTT assay a significant loss of viability was observed.

As previously mentioned, oxidative stress can be induced in cells by *t*-BHP, which is metabolized by cytochrome P450, leading to the formation of toxic peroxyl and alkoxyl radicals that initiate lipid peroxidation, affect cell integrity, and form covalent bonds with cellular molecules, resulting in cell death.[9,28] The exposition of Caco-2 cells to 150 μM *t*-BHP for 6 h lead to a reduction of viability to 79.3 ± 3.2% of control in LDH leakage assay ($p < 0.0001$, $n = 5$) and 63.0 ± 0.3% in the MTT assay ($p < 0.001$; $n = 5$). The higher sensitivity of MTT in detecting *t*-BHP toxicity can be explained by the fact that its biotransformation by cytochrome P450 and GPx occurs mainly in the mitochondria.[10,12,27] The pretreatment of Caco-2 cells with the extracts did not prevent nor aggravate the toxicity of *t*-BHP as measured by the LDH leakage assay (Figure 2). However, the extracts containing anthocyanins (fraction II and the whole extract) significantly aggravated *t*-BHP toxicity as measured by the MTT assay, fraction II being more deleterious (Figure 2). When the cells were pretreated with this fraction a significant increase of cell death (compared to the control with *t*-BHP) was observed for extract concentrations higher than 1.25 mg/mL ($p < 0.0001$, $n = 5$), while with the whole extract the differences in cellular viability were only seen between 2.5 and 10 mg/mL ($p < 0.001$ or higher, $n = 5$). The additional cellular death, observed only in the MTT assay, may be a consequence of the depletion of cellular defenses of cells pre-exposed to anthocyanins, due to their ability to induce the production of reactive species.[27]

On the other hand, fraction I showed a tendency to protect Caco-2 cells from *t*-BHP-induced toxicity, directly dependent on its concentration, although the differences of cellular viability were not statistically significant (Figure 2). In cells pretreated with faction I at a concentration of 20 mg/mL the cellular viability measured by the MTT assay was increased to 84.7 ± 16.3% of control. Also, the pre-exposition to the whole extract at 20.0 mg/mL did not increase cellular death assessed by the MTT assay ($p > 0.05$, $n = 5$), which was nearly the same as in the cells exposed to *t*-BHP only, although at this concentration the whole extract induced cellular death by itself (Figure 2). It can be assumed that in insulted cells, the pre-exposition to flavonols may stimulate antioxidant defenses, which help to fight the subsequent oxidative stress induced by *t*-BHP. Probably, the pro-oxidant effects of anthocyanins do not prepare the cells for a subsequent insult, resulting in increased toxicity. As observed in the assay with the whole extract at 20 mg/mL, this toxicity can be counteracted by the defenses induced by flavonols, although they contribute to the overall oxidative stress observed in cells exposed to the extract.

The effects of *E. plantagineum* bee pollen in cellular viability greatly depend upon the cell line. In fact, a hydromethanolic extract of this material caused loss of macrophages viability at concentrations higher than 30 mg/mL,[4] but basophils showed decreased viability at 8 mg/mL.[7] Since macrophages are known to produce reactive species[29] and the gastrointestinal tract is constantly exposed to reactive oxygen, chlorine, and nitrogen species,[6] the sensitivity of the different cells lines can be explained by the oxidative stress induced by extract compounds and cellular ability to fight it.

Reactive Species. The levels of reactive species were measured by the DCFA-DA assay. The exposure of Caco-2 cells to 150 μM *t*-BHP lead to a significant increase of reactive species to 126.5 ± 1.4% of control after 30 min ($p < 0.0001$, $n = 5$), reaching a maximum of 133.7 ± 1.8% after 150 min and decreasing to 130.1 ± 2.9% after 240 min. Fraction I significantly decreased the levels of reactive species in a concentration- and time-dependent manner, this ability being reduced over time (Figure 3). The lower concentrations of fraction I and of the other extracts were more effective in reducing reactive species (Figure 3). For instance, pre-exposure to 1.25 mg/mL of fraction I reduced the level of reactive species induced by *t*-BHP to 111.6 ± 3.6% after 30 min ($p < 0.01$), but after 240 min the level of reactive species was 116.6 ± 4.2% ($p < 0.05$). On the other hand, the levels of reactive species were 122.4 ± 2.0% ($p > 0.05$) after 30 min and 137.7 ± 5.4% ($p > 0.05$) after 240 min, when the cells were pre-exposed to the extract at 20 mg/mL.

In cells pre-exposed to fraction II a more pronounced effect on the levels of reactive species induced by *t*-BHP was observed (Figure 3). All concentrations, excepting 20 mg/mL, lead to a significant decrease in the levels of reactive species during the 240 min evaluation ($p < 0.01$ or higher). It should be noted that the levels of reactive species were reduced to the levels attained in cells not exposed to *t*-BHP when the cells were pre-exposed to 1.25 mg/mL of fraction II (100.6 ± 4.5% after 30 min and 99.1 ± 3.8 after 240 min exposition to *t*-BHP). Although no statistical differences were seen for the concentration of 20 mg/mL, the levels of reactive species were lower than in cells not

DOI: 10.1021/jf505568h
J. Agric. Food Chem. 2015, 63, 2083−2091

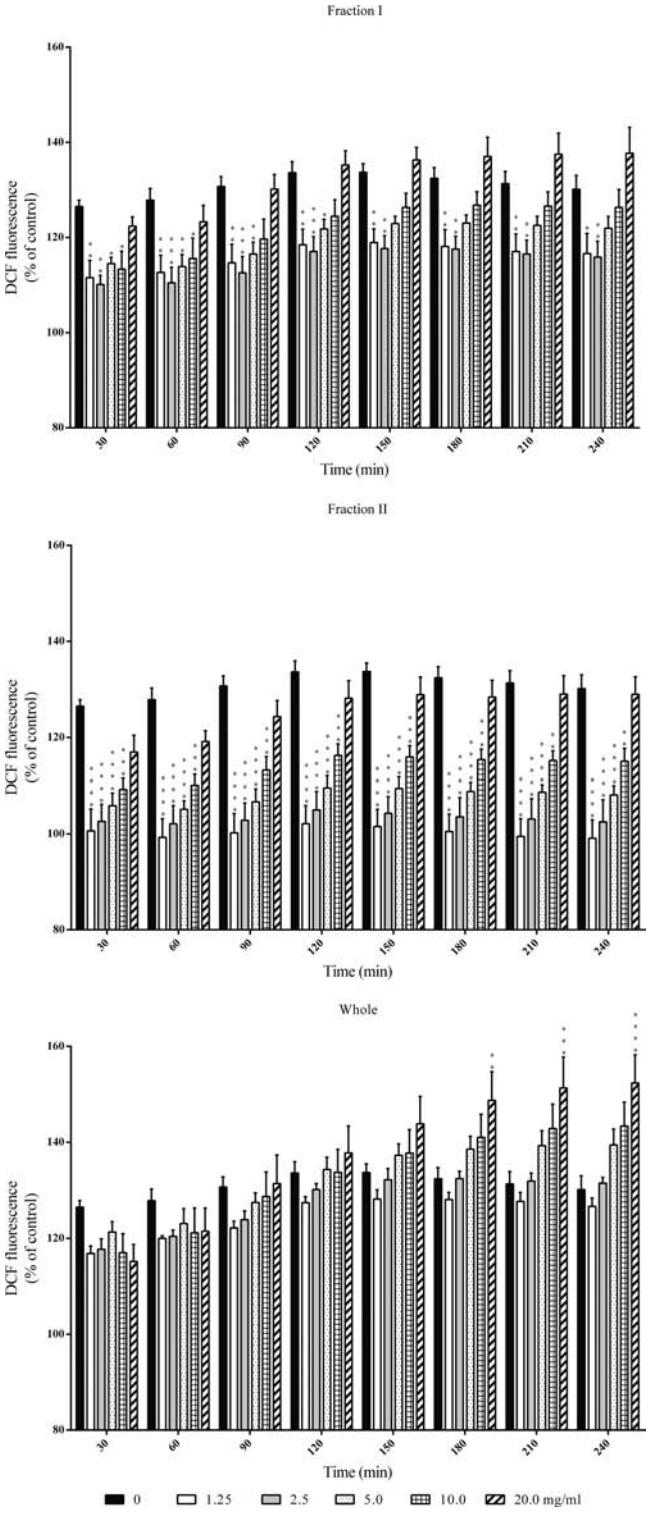

Figure 3. Time variation of reactive species in cells exposed to 150 μM *t*-BHP after pretreatment with the extracts for 24 h. Results are presented as mean ± standard error of the mean of five independent experiments. *p < 0.05, **p < 0.01, ***p < 0.001, ****p < 0.0001 compared to the control (with *t*-BHP).

pretreated with extract (116.9 ± 3.5 mg/mL after 30 min and 129.0 ± 3.7 mg/mL after 240 min).

Surprisingly, the whole extract, containing the compounds of both fractions, not only was unable to reduce the levels of reactive species induced by *t*-BHP but also further aggravated the oxidative stress after 180 min in cells pre-exposed to 20 mg/mL whole extract (Figure 3). At this concentration, the levels of reactive species reached 152.4 ± 5.9% after 240 min exposition to *t*-BHP (p < 0.0001). However, at the beginning of the measurements they were 115.2 ± 3.6% (p > 0.05), and for lower concentrations no statistical differences were seen (116.8 ± 1.5% after 30 min and 126.7 ± 1.7% after 240 min in cells pre-exposed to 1.25 mg/mL of whole extract). The whole extract was the one with higher variations in the levels of reactive species measured over time, this effect being detected earlier with higher concentrations. It showed a tendency to increase the levels of reactive species over time, with statistical differences being noticed, from the concentration of 2.5 mg/mL, while with the other extracts a significant increase was only seen at 20 mg/mL for fraction II and from 10 mg/mL for fraction I.

Although the levels of reactive species were measured without taking into account the viability of cells, a significant decrease in this parameter measured by the MTT assay was seen after 6 h exposure to *t*-BHP in cells pre-exposed to concentrations from 2.5 mg/mL of fraction II and from 2.5 to 10 mg/mL of the whole extract (Figure 2). Thus, the results may reflect the levels of reactive species in viable and inviable cells.

Fraction II, which showed the highest ability to aggravate the toxicity induced by *t*-BHP, was the one that reduced the levels of reactive species, measured with DCFH-DA, more pronouncedly (Figures 2 and 3). It is possible that reactive species produced during the pre-exposition to anthocyanins and other compounds present in fraction II have inactivated cytochrome P450, diminishing in this way the biotransformation of *t*-BHP and consequently the levels of reactive species. The inhibition of several cytochrome P450 isoforms activity by anthocyanins has already been described.[30,31] For instance, petunidin inhibited cytochrome P450 3A4 activity with an IC_{50} of 23 μM.[29] Flavonols (present in both fractions as well as in the whole extract) may also contribute to the inhibitory activity of these enzymes.[32] In cells pre-exposed to higher concentrations of fraction II cellular viability was adversely affected (as seen by the MTT assay) and the levels of reactive species induced by *t*-BHP were higher than in cells exposed to lower extract concentrations (Figures 2 and 3). It is possible that when cells with lower cytochrome P450 activity were exposed to *t*-BHP new radical species were generated by nonenzymatic reaction of *t*-BHP with iron, as demonstrated by Castilho and collaborators in an experiment using the iron chelator *o*-phenantroline with diminished toxicity of *t*-BHP.[33] This fact may also explain the increased toxicity observed with the whole extract, which can be due to the combined effects of anthocyanins and high amounts of flavonols in cytochrome P450 inhibition.

In addition to cytochrome P450 inhibition, the antioxidant ability of fractions I and II seen in this assay can be attributed to direct scavenging effect or metal chelating properties of the flavonoids absorbed by the cells previously to *t*-BHP exposure.[34,35]

Glutathione. The involvement of GSH in *t*-BHP detoxification is well known.[36] *t*-BHP acts as a substrate for cytosolic glutathione peroxidases, causing the oxidation of GSH to glutathione disulfide (GSSG). The activity of GR operating at the expense of NADPH and the release of GSSG into the extracellular medium maintains a steady state in intracellular levels of GSH.[37] In this work, the level of glutathione (reduced + oxidized; GSHt) was 22.88 ± 1.72 nmol/mg protein in

DOI: 10.1021/jf505568h
J. Agric. Food Chem. 2015, 63, 2083−2091

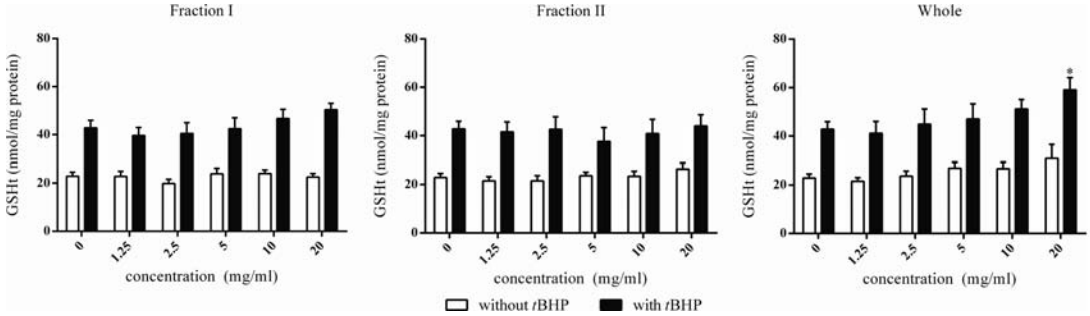

Figure 4. Glutathione levels in cells treated with the extracts for 24 h or pretreated for 24 h with the extracts followed by 6 h treatment with 150 μM of *t*-BHP (without extract coincubation). Results are presented as mean ± standard error of the mean of five independent experiments. *$p < 0.05$, compared to the respective control.

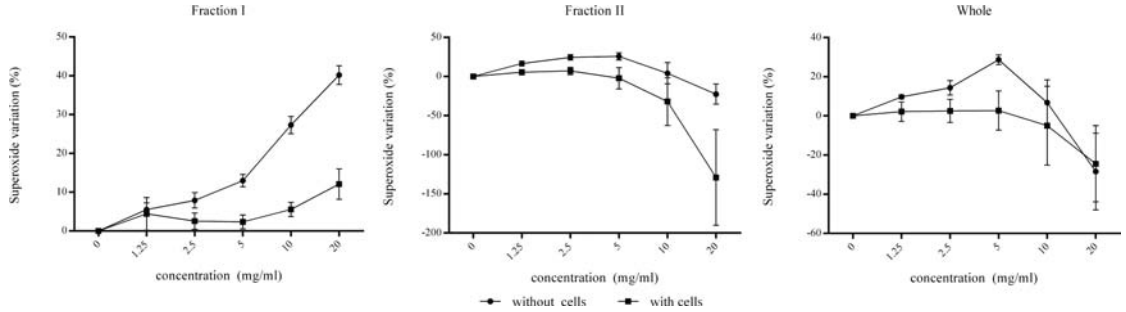

Figure 5. Effect of the extracts in superoxide levels. Superoxide was generated by the PMS/NADH system and monitored by the reduction of NBT in the presence of the extracts dissolved in culture medium and previously incubated for 24 h in a CO_2 incubator at 37 °C either with or without cells. Results are presented as mean ± standard error of the mean of four (without cells) or five (with cells) independent experiments.

quiescent cells and significantly increased to 42.84 ± 3.12 nmol/mg protein after 6 h exposure to 150 μM *t*-BHP ($p < 0.01$, $n = 5$). A further increase of GSHt levels was observed in cells previously exposed to 20 mg/mL of the whole extract ($p < 0.05$, $n = 5$) (Figure 4). It has been reported that the exposure of isolated hepatocytes to *t*-BHP leads to a rapid decrease of intracellular GSH levels.[9,38] However, similarly to the results found in this work, in Caco-2 cells an increase in GSH levels exposed to *t*-BHP has been observed.[39] The results may suggest an attempt of the cells to overcome the induced oxidative stress by increasing GSH, the main antioxidant involved in *t*-BHP detoxification.[38]

The increase of GSHt at the higher concentration of the whole extract (and less significantly at the higher concentration of fraction II and from 5 mg/mL of fraction I) may justify an inversion in the tendency of the extracts to aggravate the deleterious effects of *t*-BHP, although not accompanied by a significant reduction of the levels of reactive species seen with lower extract concentrations (Figures 2−4). The balance between antioxidant and pro-oxidant effects of the compounds present in the extracts may justify their dual behavior. It should be noted that the effects of flavonoids are not limited to antioxidant or pro-oxidant mechanisms, since these compounds can interfere with many cellular molecules and processes.[24,25]

In the assay conditions it was not possible to determine the intracellular levels of GSSG (below 0.38 nmol/mg protein). The low levels of GSSG (less than 1% of GSHt) can be explained by both its reduction to GSH by GR and its efflux from the cell.[37]

Antioxidant Enzymes. Since *t*-BHP detoxification involves its reduction by glutathione peroxidase (GPx) with concomitant oxidation of GSH to GSSG,[11] an attempt was made to quantify GPx and GR, the later being implicated in the recycling of GSSG back to GSH. In the assay conditions, the activity of GPx was below the detection limit of the method (<0.02 U/mg protein). GR activity in cells exposed to the extracts for 24 h was not statistically different from control (0.027 ± 0.001 U/mg protein) at the concentrations tested ($p > 0.05$; $n = 5$).

Mitochondrial GST may prevent lipid peroxidation in mitochondria by nonselenium glutathione-dependent peroxidase activity.[40] Because *t*-BHP is a known substrate for GST, the activity of this enzyme was determined, being of 0.101 ± 0.006 U/mg protein in control. GST activity in cells exposed to the extracts was not statistically different from the control ($p > 0.05$; $n = 5$). However, the noncolored phenolic extract showed a tendency to decrease GST activity, reaching 0.089 ± 0.006 U/mg protein at a concentration of 20 mg/mL fraction I.

Although *t*-BHP does not react with catalase,[11] the activity of this enzyme and of SOD was evaluated, due to their importance in the detoxification of H_2O_2 and superoxide that can be produced by a pro-oxidant effect of flavonoids, including flavonols and anthocyanins[26,27] and in the maintenance of the redox cellular status, in general. Catalase activity in control was 7.444 ± 1.012 U/mg protein. When the cells were exposed to *E. plantagineum* bee pollen extracts the enzyme activity varied between 5.998 ± 0.647 and 6.839 ± 0.829 U/mg protein. No statistical differences were seen for catalase activity ($p > 0.05$; $n = 5$).

The extracellular SOD is a copper−zinc isoform of SOD that contains a signal peptide that directs this isoform exclusively to extracellular spaces.[41] The activity of this enzyme in control was 0.100 ± 0.009 U/mg protein. Because the extracts exert a direct activity on superoxide, it was not possible to distinguish between the effects on SOD activity and the superoxide scavenging activity of the extracts. For this reason an assay was

DOI: 10.1021/jf505568h
J. Agric. Food Chem. 2015, 63, 2083−2091

performed using the extracts incubated in culture medium in the same conditions used to evaluate SOD activity but without cells. The results obtained for the variation of superoxide with or without the cells are presented in Figure 5. Fraction I demonstrated ability to decrease superoxide levels, but this ability was higher in the cell-free assay, indicating scavenging activity rather than induction of extracellular SOD. Significant differences from the control were observed from 2.5 mg/mL ($p < 0.01$; $n = 4$) in the cell-free assay and from 10 mg/mL ($p < 0.05$, $n = 5$) in the assay with cells. Comparing the two assays (with and without cells), they were significantly different from 5.0 mg/mL ($p < 0.0001$). This result can be explained by the inhibition of extracellular SOD, but it is possible that some compounds were absorbed or modified by the cells and were not available for superoxide scavenging. Considering fraction II and the whole extract, they exerted a slight scavenging activity (not statistically significant) for concentrations up to 5 mg/mL in the cell-free assay. This tendency was not observed in the assay with cells. At a concentration of 20 mg/mL a pro-oxidant effect was observed in both assays, although it was statistically significant only with fraction II in the assay with cells ($p < 0.001$).

The ability of fraction I to scavenge superoxide radicals may contribute to the tendency of this extract to protect Caco-2 cells from *t*-BHP-induced toxicity (Figures 2 and 5).

In conclusion, *E. plantagineum* bee pollen contains flavonoids that can interfere with many cellular processes. In Caco-2, a cell line that mimics the enterocytes of the small intestine, the oxidative stress induced by *t*-BHP was not efficiently counteracted by *E. plantagineum* bee pollen phenolic extracts, although the removal of anthocyanins from the extract not only ceased the pro-oxidant effects but also imparted a small protective effect. The cellular fate of *t*-BHP may explain the dual effect of the extracts: this short-chain analogue of lipid hydroperoxide is detoxified by GPx, but it can be bioactivated by cytochrome P450. Since a small increase in the levels of total glutathione was induced by the flavonols-rich extracts and flavonoids, in particular anthocyanins, are known inhibitors of cytochrome P450 enzymes, an antioxidant effect was expected. However, as in the presence of iron *t*-BHP can generate reactive species, which can be more deleterious than the ones generated by its biotransformation, the antioxidant potential of the compounds may be abrogated. The pro-oxidant effects seen with the extracts containing anthocyanins may also be explained by their ease in being themselves converted into radical species, although only the whole extract at the higher concentration tested significantly reduced the cellular viability.

Taking into account the obtained results, care should be taken in the consumption of high doses of *E. plantagineum* bee pollen. However, extracts with low recovery of anthocyanins prepared from this matrix can be protective in situations of oxidative stress.

AUTHOR INFORMATION

Corresponding Author

*Tel.: +351 220428654. Fax: +351 226093390. E-mail: pandrade@ff.up.pt.

Funding

The authors are grateful to the financial support from the European Union (FEDER funds through COMPETE) and National Funds (FCT, Fundação para a Ciência e Tecnologia) through project Pest-C/EQB/LA0006/2013 and from the European Union (FEDER funds) under the framework of QREN through Project NORTE-07-0124-FEDER-000069, to CYTED Programme (ref. 112RT0460) CORNUCOPIA Thematic Network, and to project AGL2011-23690 (CICYT). To all financing sources the authors are greatly indebted. F.F. is indebted to FCT for the grant (SFRH/BPD/98732/2013).

Notes

The authors declare no competing financial interest.

REFERENCES

(1) Chu, Q.; Tian, X.; Jiang, L.; Ye, J. Application of capillary electrophoresis to study phenolic profiles of honeybee-collected pollen. *J. Agric. Food Chem.* **2007**, *55*, 8864−886.

(2) Di Paola-Naranjo, R. D.; Sánchez-Sánchez, J.; González-Paramás, A. M.; Rivas-Gonzalo, J. C. Liquid chromatographic−mass spectrometric analysis of anthocyanin composition of dark blue bee pollen from *Echium plantagineum*. *J. Chromatogr. A* **2004**, *1054*, 205−210.

(3) Boppré, M.; Colegate, S. M.; Edgar, J. A. Pyrrolizidine alkaloids *of Echium vulgare* honey found in pure pollen. *J. Agric. Food Chem.* **2005**, *53*, 594−600.

(4) Moita, E.; Gil-Izquierdo, A.; Sousa, C.; Ferreres, F.; Silva, L. R.; Valentão, P.; Domínguez-Perles, R.; Baenas, N.; Andrade, P. B. Integrated analysis of COX-2 and iNOS derived inflammatory mediators in LPS-stimulated RAW macrophages pre-exposed to *Echium plantagineum* L. bee pollen extract. *PLoS One* **2013**, *8*, e59131.

(5) Ferreres, F.; Pereira, D. M.; Valentão, P.; Andrade, P. B. First report of non-coloured flavonoids in *Echium plantagineum* bee pollen: Differentiation of isomers by liquid chromatography/ion trap mass spectrometry. *Rapid Commun. Mass Spectrom.* **2010**, *24*, 801−806.

(6) Halliwell, B.; Rafter, J.; Jenner, A. Health promotion by flavonoids, tocopherols, tocotrienols, and other phenols: direct or indirect effects? Antioxidant or not? *Am. J. Clin. Nutr.* **2005**, *81*, 268S−2676S.

(7) Moita, E.; Sousa, C.; Andrade, P. B.; Fernandes, F.; Pinho, B. R.; Silva, L. R.; Valentão, P. Effects of *Echium plantagineum* L. bee pollen on basophil degranulation: Relationship with metabolic profile. *Molecules* **2014**, *19*, 10635−10649.

(8) Silva, R.; Carmo, H.; Dinis-Oliveira, R.; Cordeiro-da-Silva, A.; Lima, S. C.; Carvalho, F.; Bastos, M. L.; Remião, F. *In vitro* study of P-glycoprotein induction as an antidotal pathway to prevent cytotoxicity in Caco-2 cells. *Arch. Toxicol.* **2011**, *85*, 315−326.

(9) Valentão, P.; Carvalho, M.; Fernandes, E.; Carvalho, F.; Andrade, P. B.; Seabra, R. M.; Bastos, M. L. Protective activity of *Hypericum androsaemum* infusion against *tert*-butyl hydroperoxide-induced oxidative damage in isolated rat hepatocytes. *J. Ethnopharmacol.* **2004**, *92*, 79−84.

(10) Lötscher, H. R.; Winterhalter, K. H.; Carafoli, E.; Richter, C. Hydroperoxides can modulate the redox state of pyridine nucleotides and the calcium balance in rat liver mitochondria. *Proc. Natl. Acad. Sci. U.S.A.* **1979**, *76*, 4340−4344.

(11) Sies, H.; Gerstenecker, C. Oxidation in the NADP system and release of GSSG from hemoglobin-free perfused rat liver during peroxidatic oxidation of glutathione by hydroperoxides. *FEBS Lett.* **1972**, *27*, 171−175.

(12) Kennedy, C. H.; Church, D. F.; Winston, G. W.; Pryor, W. A. *tert*-Butyl hydroperoxide-induced radical production in rat liver mitochondria. *Free Radic. Biol. Med.* **1992**, *12*, 381−387.

(13) Dopico-García, M. S.; Fique, A.; Guerra, L.; Afonso, J. M.; Pereira, O.; Valentão, P.; Andrade, P. B.; Seabra, R. M. Principal components of phenolics to characterize red Vinho Verde grapes: Anthocyanins or non-coloured compounds? *Talanta* **2008**, *75*, 1190−1202.

(14) Hansen, M. B.; Nielson, S. E.; Berg, K. Re-examination and further development of a precise and rapid dye method for measuring cell growth: cell kill. *J. Immunol. Methods* **1989**, *119*, 203−210.

(15) Bergermeyer, H. U.; Bernt, E. UV-assay for lactate dehydrogenase with pyruvate and NADH. In *Methods of Enzymatic Analysis*; Bergermeyer, H. U., Ed.; Verlag Chemie GmbH: Weinheim, 1974.

DOI: 10.1021/jf505568h
J. Agric. Food Chem. 2015, 63, 2083−2091

(16) Taveira, M.; Sousa, C.; Valentão, P.; Ferreres, F.; Teixeira, J. P.; Andrade, P. B. Neuroprotective effect of steroidal alkaloids on glutamate-induced toxicity by preserving mitochondrial membrane potential and reducing oxidative *stress*. *J. Steroid Biochem. Mol. Biol.* **2014**, *140*, 106−115.
(17) Vandeputte, C.; Guizon, I.; Genestie-Denis, I.; Vannier, B.; Lorenzon, G. A microtiter plate assay for total glutathione and glutathione disulfide contents in cultured/isolated cells: performance study of a new miniaturized protocol. *Cell Biol. Toxicol.* **1994**, *10*, 415−421.
(18) Habig, W. H.; Pabst, M. J.; Jakoby, W. B. Glutathione S-transferases. The first enzymatic step in mercapturic acid formation. *J. Biol. Chem.* **1974**, *249*, 7130−7139.
(19) Remião, F.; Carmo, H.; Carvalho, F. D.; Bastos, M. L. Inhibition of glutathione reductase by isoproterenol oxidation products. *J. Enzyme Inhib.* **1999**, *15*, 47−61.
(20) Flohé, L.; Gunzler, W. A. Assays of glutathione peroxidase. *Methods Enzymol.* **1984**, *105*, 114−121.
(21) Aebi, H. Catalase *in vitro*. *Methods Enzymol.* **1984**, *105*, 121−126.
(22) Flohé, L.; Otting, F. Superoxide dismutase assays. *Methods Enzymol.* **1984**, *105*, 93−104.
(23) Bradford, M. M. A rapid and sensitive method for the quantitation of microgram quantities of protein utilizing the principle of protein-dye binding. *Anal. Biochem.* **1976**, *72*, 248−254.
(24) Bruneton, J. Pharmacognosie−Phytochimie. *Plantes médicinales*, 4th ed.; Éditions médicales internationales: Paris, 2009; Chapter 2.
(25) Galati, G.; O'Brien, P. J. Potential toxicity of flavonoids and other dietary phenolics: Significance for their chemopreventive and anticancer properties. *Free Radical Biol. Med.* **2004**, *37*, 287−303.
(26) Galati, G.; Sabzevari, O.; Wilson, J. X.; O'Brien, P. J. Prooxidant activity and cellular effects of the phenoxyl radicals of dietary flavonoids and other polyphenolics. *Toxicology* **2002**, *177*, 91−104.
(27) Hou, D. X.; Ose, T.; Lin, S.; Harazoro, K.; Imamura, I.; Kubo, M.; Uto, T.; Terahara, N.; Yoshimoto, M.; Fujii, M. Anthocyanidins induce apoptosis in human promyelocytic leukemia cells: Structure-activity relationship and mechanisms involved. *Int. J. Oncol.* **2003**, *23*, 705−712.
(28) Myers, C. R. Subcellular sites of xenobiotic-induced free radical generation. In *Free radical toxicology*; Wallace, K. B., Ed.; Taylor & Francis: Washington, DC, 1997; pp 30−31.
(29) Marletta, M. A.; Yoon, P. S.; Iyengar, R.; Leaf, C. D.; Wishnok, J. S. Macrophage oxidation of L-arginine to nitrite and nitrate: nitric oxide is an intermediate. *Biochemistry* **1988**, *27*, 8706−8711.
(30) Dreiseitel, A.; Schreier, P.; Oehme, A.; Locher, S.; Hajak, G.; Sand, P. G. Anthocyanins and their metabolites are weak inhibitors of cytochrome P450 3A4. *Mol. Nutr. Food Res.* **2008**, *52*, 1428−1433.
(31) Dreiseitel, A.; Schreier, P.; Oehme, A.; Locher, S.; Rogler, G.; Piberger, H.; Hajak, G.; Sand, P. G. Anthocyanins and anthocyanidins are poor inhibitors of CYP2D6. *Methods Find. Exp. Clin. Pharmacol.* **2009**, *31*, 3−9.
(32) Ubeda, A.; Esteve, M. L.; Alcaraz, M. J.; Cheeseman, K. H.; Slater, T. F. Effects of flavonoids on cytochrome P-450 from rat liver microsomes: Inhibition of enzyme activities and protection against peroxidative damage. *Phytother. Res.* **1995**, *9*, 416−420.
(33) Castilho, R. F.; Kowaltowski, A. J.; Meinicke, A. R.; Bechara, E. J. H.; Vercesi, A. E. Permeabilization of the inner mitochondrial membrane by Ca^{2+} ions is stimulated by *t*-butyl hydroperoxide and mediated by reactive oxygen species generated by mitochondria. *Free Radical Biol. Med.* **1995**, *18*, 479−486.
(34) Sawa, T.; Nakao, M.; Akaike, T.; Ono, K.; Maeda, H. Alkylperoxyl radical-scavenging activity of various flavonoids and other phenolic compounds: Implications for the anti-tumor-promoter effect of vegetables. *J. Agric. Food Chem.* **1999**, *47*, 397−402.
(35) Sestili, P.; Guidarelli, A.; Dacha, M.; Cantoni, O. Quercetin prevents DNA single strand breakage and cytotoxicity caused by *tert*-butylhydroperoxide: Free radical scavenging versus iron chelating mechanism. *Free Radical Biol. Med.* **1998**, *25*, 196−200.
(36) Jewell, S. A.; Di Monte, D.; Richelmi, P.; Bellomo, G.; Orrenius, S. *tert*-Butyl hydroperoxide-induced toxicity in isolated hepatocytes: contribution of thiol oxidation and lipid peroxidation. *J. Biochem. Toxicol.* **1986**, *1*, 13−22.
(37) Sies, H.; Wahlländer, A.; Waydhas, C.; Soboll, S.; Häberle, D. Functions of intracellular glutathione in hepatic hydroperoxide and drug metabolism and the role of extracellular glutathione. *Adv. Enzyme Regul.* **1980**, *18*, 303−320.
(38) Jewell, S. A.; Bellomo, G.; Thor, H.; Orrenius, S.; Smith, M. T. Bleb formation in hepatocytes during drug metabolism is caused by disturbances in thiol and calcium ion homeostasis. *Science* **1982**, *217*, 1257−1259.
(39) O'Sullivan, A. M.; O'Callaghan, Y. C.; O'Grady, M. N.; Queguineur, B.; Hanniffy, D.; Troy, D. J.; Kerry, J. P.; O'Brien, N. M. Assessment of the ability of seaweed extracts to protect against hydrogen peroxide and *tert*-butyl hydroperoxide induced cellular damage in Caco-2 cells. *Food Chem.* **2012**, *134*, 1137−1140.
(40) Liebler, D. C.; Reed, D. J. Free-radical defense and repair mechanisms. In *Free radical toxicology*; Wallace, K. B., Eds.; Taylor & Francis: Washington, DC, 1997; pp 154−155.
(41) Zelko, I. N.; Mariani, T. J.; Folz, R. J. Superoxide multigene family: a comparison of the CuZn-SOD (SOD 1), Mn-SOD (SOD 2) and EC-SOD (SOD 3) gene structures, evolution and expression. *Free Radical Biol. Med.* **2002**, *33*, 337−349.

DOI: 10.1021/jf505568h
J. Agric. Food Chem. 2015, 63, 2083−2091

Table 1. Serum Enzyme Activities and Exercise Tolerance from Goats Dosed with White Snakeroot and White Snakeroot Extracts and Residues[a]

	group (=material dosed)	day 1 (mean ± SD)	day 7 (mean ± SD)	day 9 (mean ± SD)	day 10 (mean ± SD)
alanine aminotransferase, ALT (U/L)	control	16 ± 3	36 ± 7	31 ± 7	13 ± 3
	ground white snakeroot	16 ± 3[a]	128 ± 171[b]*	199 ± 228[b]*	108 ± 119[b]*
	extracted plant residue	14 ± 3	36 ± 3	32 ± 7	15 ± 5
	hexane extract	18 ± 4	14 ± 7	14 ± 3	36 ± 5
	recombined extracts and residues	16 ± 2	14 ± 7	13 ± 1	36 ± 2
aspartate aminotransferase, AST (U/L)	control	60 ± 15	79 ± 19	76 ± 19	55 ± 13
	ground white snakeroot	65 ± 14[a]	145 ± 53[b]*	2611 ± 3867[bc]*	965 ± 1143[bc]*
	extracted plant residue	55 ± 5	90 ± 5	101 ± 10	73 ± 6
	hexane extract	55 ± 5	59 ± 30	59 ± 7	85 ± 10
	recombined extracts and residues	50 ± 8	58 ± 29	54 ± 5	96 ± 10
creatine kinase, CK (U/L)	control	152 ± 62	79 ± 20	68 ± 19	121 ± 31
	ground white snakeroot	160 ± 66[a]	3414 ± 6199[b]*	1536 ± 1892[b]*	2649 ± 2654[b]*
	extracted plant residue	128 ± 13	95 ± 14	112 ± 26	190 ± 62
	hexane extract	122 ± 21	115 ± 25	115 ± 16	178 ± 78
	recombined extracts and residues	105 ± 11	126 ± 48	121 ± 49	160 ± 54
goats that were exercise intolerant (unable to run 5 min)	control	0/4	0/4	0/4	0/4
	ground white snakeroot	0/4	2/4	3/4	2/3
	extracted plant residue	0/4	0/4	0/4	0/4
	hexane extract	0/3	0/3	0/3	0/3
	recombined extracts and residues	0/3	0/3	0/3	0/3

[a]Note: $n = 3$ on day 10 for the white snakeroot group because one goat was necropsied on day 9. Means that are significantly different ($p < 0.05$) from others within the same group are indicated with superscript letters. Means that are significantly different from other groups on the same day are indicated with an asterisk (*).

which Angora goats were exposed to white snakeroot and 53 of the goats died in Central Texas.[10] Dosing studies with the plant collected from that site in Texas resulted in acute death from hepatic necrosis with no myotoxic lesions and established an LD_{50} of 5 mg/kg of fresh white snakeroot.[10] Spanish goats have been shown to be a good model to study the toxicity of the benzofuran-containing plant, rayless goldenrod (*Isocoma pluriflora*),[11,12] which is thought to contain the same toxin as white snakeroot. Recent research in our laboratory has focused on identifying the toxic component of white snakeroot and demonstrating its toxicity in a live animal model.

The purpose of this study was 4-fold: First, to determine if white snakeroot that contained known concentrations of tremetone, **1**, 6-hydroxytremetone, **2**, and dehydrotremetone, **3**, was myotoxic in a goat model; second, to determine if a hexane extract of white snakeroot containing **1**, **2**, and **3**, adsorbed onto alfalfa at the same concentration as the white snakeroot plant material was toxic; third, to determine if the plant residue, following the hexane extraction of white snakeroot, that did not contain **1**, **2**, and **3**, was toxic; and fourth, to determine if the hexane extract recombined with the white snakeroot plant residue was toxic.

MATERIALS AND METHODS

Collection of Plant Material. The aerial parts of white snakeroot plants were collected from two locations near each other in Vermilion County, Illinois. The collection locations and GPS coordinates were: Interstate, 40°06.483′ N/87°40.866′ W, and Salt Fork, 40°05.536′ N/87°49.683′ W. The plants were collected in September while in early to full flower stages of growth. White snakeroot plants were identified by Dr. Stanley L. Welsh curator at the Stanley L. Welsh Herbarium at Brigham Young University, Provo, UT, and Dr. David S. Seigler, Professor, Department of Plant Biology, University of Illinois, Urbana−Champaign, Illinois. The current taxonomic classification for this plant is *Ageratina altissima* (L.) King & H. Rob. var. *altissima* as per the USDA, National Resources Conservation Service, Plant Database. Voucher specimens of white snakeroot, accession nos. 3555 and 3562 for the Salt Fork and the Interstate collections, respectively, were deposited in the Poisonous Plant Research Laboratory Herbarium, Logan, UT.

Preparation of Plant Material and Extracts. The white snakeroot from the Salt Fork and Interstate collections were air-dried at ambient temperature, mixed together in a ratio of approximately 0.40:0.60, and ground to pass through a 2.38 mm screen and mixed using a model 55 Mix-All, (Gehl Company, West Bend, WI).

Ground plant material (30 kg) was extensively extracted in 15 Soxhlet extractions of approximately 2 kg portions with *n*-hexane (50 h). The hexane extract from 8 of the extractions were concentrated to dryness by rotary evaporation, combined, and reconstituted to 4.0 L with dichloromethane and referred to as the hexane extract. The hexane extract was quantitatively adsorbed onto alfalfa (ratio of 1 mL hexane extract per 4 g alfalfa, which is equal to the hexane to plant ratio from which it was extracted) and allowed to dry overnight in a fume hood. The ground plant material extracted with *n*-hexane was recovered from the Soxhlet thimble, transferred to a paper bag, and dried in a fume hood for 24 h at ambient temperature to allow residual hexane to evaporate and is referred to as the extracted plant residue (=plant residue). The hexane extract and plant residue from seven Soxhlet extractions were quantitatively recombined and are referred to as the combined extract and residue (=extract+residue). The ground white snakeroot (=snakeroot), hexane extract, plant residue, and extract+residue, which were dosed to the snakeroot group, hexane extract group, plant residue group, and extract+residue

DOI: 10.1021/jf505614z
J. Agric. Food Chem. 2015, 63, 2092−2097

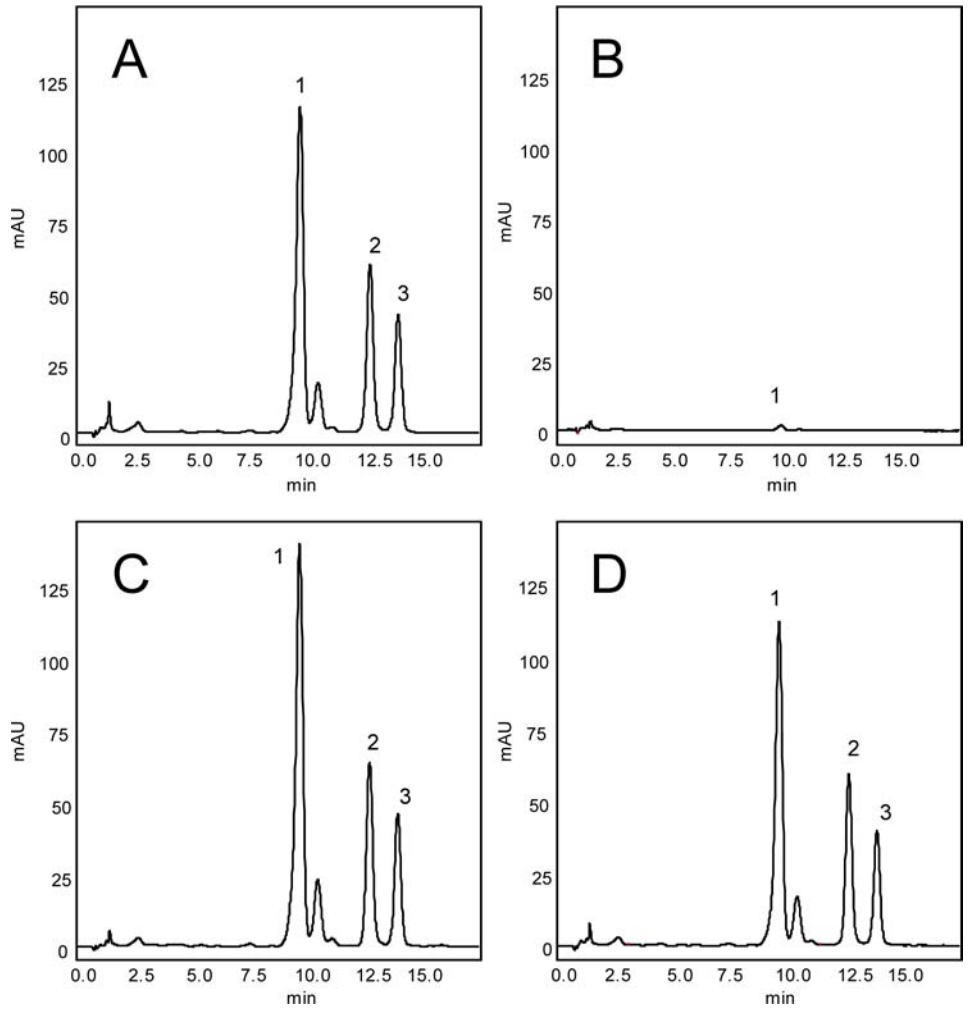

Figure 2. HPLC chromatograms from (A) white snakeroot plant material (white snakeroot); (B) white snakeroot plant material after extraction by hexane, (extracted plant residue); (C) white snakeroot hexane extract adsorbed onto alfalfa (hexane extract); (D) white snakeroot hexane extract adsorbed back onto extracted white snakeroot residue (combine extract and residue). Peak numbers refer to tremetone, **1**, 6-hydroxytremetone, **2**, and dehydrotremetone, **3**, whose chemical structures are shown in Figure 1.

group, respectively, were analyzed for the benzofurans. It was confirmed that the snakeroot, hexane extract, and extract +residue contained the same benzofuran compounds and at nearly equal concentrations. The plant residue contained only trace amounts of the benzofurans in the same dosed mass.

HPLC Analysis. The analysis of tremetone, **1**, 6-acetyl-7-methoxy-2,2-dimethylchromene, 6-hydroxytremetone, **2**, and dehydrotremetone, **3**, in snakeroot, hexane extract, plant residue, and extract+residue treatments was performed by HPLC as described previously.[2,13]

Dosing of Goats. Eighteen yearling Spanish goats in good body condition that weighed 29.1 ± 5.4 kg (mean ± SD) were selected from the same herd at the Poisonous Plant Research Laboratory. The goats were randomly divided into five groups with three or four animals per group (Table 1). The animals were trained to lead and to run for 5 min on a treadmill moving at 12 km/h on a 10% incline for 15 d before the start of the study. The day before the initial dosing, all animals were weighed, bled by jugular venipuncture, and exercised on a treadmill. The snakeroot, plant residue, hexane extract, and extract+residue groups were dosed with 1.67% body weight intraruminally via oral gavage, for 9 d. A negative control group was also dosed ground alfalfa hay via oral gavage at 1.67% of body weight. The dose was split and given twice per day at 9:00 AM and 9:00 PM. Throughout the duration of the study, the goats had access to water and long stem alfalfa hay *ad libitum*. One goat from the snakeroot group developed severe exercise intolerance, reluctance to move, and anorexia. The goat was euthanized on day 9. The rest of the goats were euthanized and necropsied during the morning of day 10.

Histological Analysis. At necropsy, samples of left lateral retroocular, tongue, masseter, superficial pectoral, triceps, intercostals, longissimus dorsi, semitendinosus, diaphragm, biceps femoris, biceps brachii, quadriceps femoris, gluteus medius, psoas major, adductor, and semimembranosus skeletal muscles were collected, attached to wooden tongue depressors, and fixed in 10% neutral buffered formalin. The heart was opened, cleaned with water, closely examined, fixed intact, and sectioned to examine portions of the right atrium, the right papillary muscle, the right ventricular free wall, the septum, the left atrium, the left papillary muscle, and the left ventricular free wall. Other tissues including brain, spinal cord, lung, liver, right and left kidneys, adrenal gland, urinary bladder, thyroid gland, mesenteric lymph node from the small intestine, esophagus, rumen omasum, abomasums, duodenum, pancreas, jejunum ileum, cecum, and colon were collected fixed, and prepared for

DOI: 10.1021/jf505614z
J. Agric. Food Chem. 2015, 63, 2092−2097

examination. Tissues were processed, sectioned, and stained using standard histologic techniques. Special stains of specific skeletal muscle, myocardium, and liver lesions included diastase-positive and diastase-resistant periodic acid-Schiff (PAS), Masson trichrome stain for collagen, and Congo red. Lesions were scored by distribution (percentage of tissue affected) and graded by the severity of lesion, (0 = none, 1 = minimal [loss of striation and hypereosinophilia], 2 = mild [sarcoplasmic clumping with myocyte swelling], 3 = moderate [sarcomere disruption with focal monocytic inflammation and mild nuclear proliferation], 4 = severe [extensive inflammation, regeneration with fibrosis]), by two pathologists who were "blinded" to the treatment groups. All animal work was done under veterinary supervision with the approval and supervision of the Utah State University Institutional Animal Care and Use Committee.

Exercise Tolerance. Goats were run on a treadmill (Horse Gym 2000 GmbH, Großsorheim, Germany) for 5 min to determine exercise tolerance. The treadmill was moving at 12 km/h on a 10% incline. If movement became labored and the goat was unable to keep pace before completion of the 5 min exercise period, as determined by an observer "blinded" to the treatment groups, then the treadmill was stopped and the animal was removed and considered to be exercise intolerant.

Serum Analyses. Serum biochemistries were analyzed as previously described.[12] Significant analytes that are reported herein include the activities of aspartate aminotransferase (AST), alanine aminotransferase (ALT), and creatine kinase (CK).

Statistical Analyses. Serum chemistry variables were analyzed using a mixed linear model approach (Proc Mixed in SAS 9.3). Serum variables were evaluated for normality, and all distributions were non-normal. Thus, a log transformation was performed before analysis; however, all means presented herein are untransformed values. The repeated measures model contained treatments, days and the day x treatment interaction, with animals as a random factor, and animals were nested within treatment groups. The appropriate covariance structure was determined using the lowest value of Akaike's information criteria (AIC) compared across models. Least square means were separated after a significant F test using the PDIFF option in SAS.

Subjective pathologic scores for each group were compared using an analysis of variance. Means that were significantly different were separated using Tukey's analysis ($p < 0.05$, SAS 9.3 Proc GLM).

RESULTS

The combined white snakeroot plant material from the Salt Fork and Interstate collections was analyzed by HPLC and found to contain 2.1 μg/mg, 0.72 μg/mg, 0.96 μg/mg, and 0.53 μg/mg of tremetone, **1**, 6-acetyl-7-methoxy-2,2-dimethylchromene, 6-hydroxytremetone, **2**, and dehydrotremetone, **3**, respectively. These compounds were quantitatively extracted into hexane when the white snakeroot plant material was Soxhlet extracted with hexane, evaporated and resolublized in dichloromethane and quantitatively reabsorbed on the same amount of ground alfalfa or plant residue and dosed as hexane extract and extract+residue, respectively. Dosed extracts were analyzed for benzofuran content after applying the extracts resuspended in dichloromethane to the alfalfa or plant residue and dried overnight. The chromatograms showing the benzofurans in each treatment are shown in Figure 2. The amounts of the hexane extract and the dosed extract+residue material contained tremetone, **1**, and total benzofurans at the same dosages (35.1 and 60 mg/kg body weight, respectively) as the dosed snakeroot. The dosed plant residue contained only trace amounts of tremetone and the other benzofurans.

On day 5, one goat from the snakeroot group developed clinical signs of poisoning and was unable to run on the treadmill for 5 min. The condition of the goat became more severe and it was euthanized on day 9. A second and third goat from the snakeroot group developed the same clinical signs and became exercise intolerant on days 6 and 9. None of the goats from the plant residue, hexane extract, or extract+residue groups exhibited clinical signs of poisoning or became exercise intolerant.

The mean ± SD of serum enzyme activities of AST, ALT, and CK for each of the dosed groups are shown in Table 1. There were significant ($p < 0.05$) treatment by day interactions for AST, ALT, and CK. There were significant increases in the serum activities of AST, ALT, and CK on day 7 in the snakeroot dosed goats. Serum CK activities of the snakeroot dosed goats that were poisoned increased to between 2285 and 17704 U/L within 1 day of becoming exercise intolerant. There were no significant changes in CK, AST, and ALT activities of control, hexane extract, plant residue, and extract+residue dosed groups during the 10 days of the study.

Occasionally, skeletal muscle from goats in the control, hexane extract, plant residue, and extract+residue groups had rare myofiber swelling and edema. These lesions were also seen histologically as focal myocyte degeneration and necrosis (Figure 3A). The degeneration was characterized by myocyte swelling with loss of striation and rarely individual myocyte necrosis with focal inflammation. These lesions were small and rare involving small clusters of myocytes suggesting they were background changes. All but one of the snakeroot dosed goats had severe skeletal muscle myodegeneration and necrosis. This was evident grossly as many of the muscles of both the appendicular and axial skeleton were swollen with pale streaking. Histologically, these lesions were characterized as extensive Zenker's necrosis with loss of striation, swelling, coagulation and clumping of sarcomere proteins, focally extensive inflammation and phagocytosis of myocyte debris and focal regeneration (Figure 3B). The lesions were most severe in many of the large appendicular muscles including the biceps brachii, biceps femoris, semitendinosus, semimembranosus, quadriceps femoris, and gluteus medius. Fewer skeletal muscles of the axial skeleton were also affected with smaller, less severe lesions in the psoas major, longissimus dorsi, and intercostal skeletal muscles.

The livers from all dosed animals, including the control goats, had mild centrilobular hepatocyte swelling with occasional vacuolation. The vacuoles were clear with prominent margins suggestive of lipid accumulation. No additional liver lesions were identified in any of the groups including the snakeroot dosed goats. No significant histologic lesions were identified in the other sampled tissues from goats in either the treated or control groups.

DISCUSSION

White snakeroot is a potent myotoxin in most livestock species. It has caused sporadic cases of poisoning in livestock and humans since the early 1800s. The results from this study demonstrate for the first time that white snakeroot is a potent myotoxin in goats that affects both appendicular and axial

DOI: 10.1021/jf505614z
J. Agric. Food Chem. 2015, 63, 2092−2097

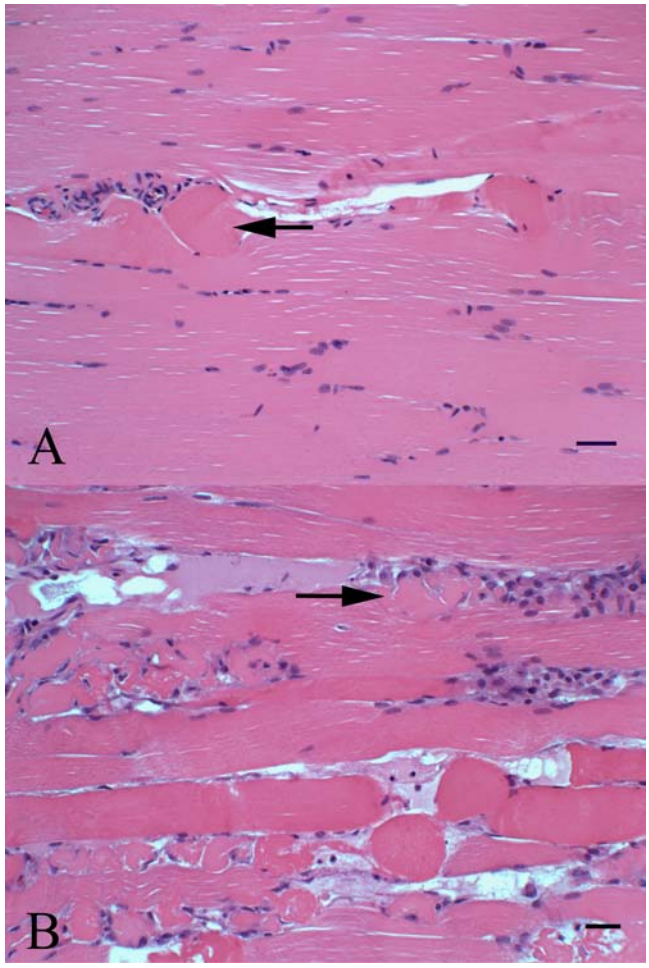

Figure 3. Photomicrograph of the skeletal muscle, quadriceps femoris from a goat from the (A) control group dosed with ground alfalfa; (B) white snakeroot dosed group that was treated with ground snakeroot, at 1.67% body weight for 9 d. Notice the rare myonecrosis and clumping of myocyte proteins (arrow) in part A. Such lesions never affected more than 1% of the myocytes in control animals. Also, notice the extensive myonecrosis, clumping of myocyte proteins (arrow) and focally extensive inflammation in Figure 3B. Such lesions were often severe and in some goats affected more than 60% of the myocytes. H&E, bar = 50 μm.

skeletal muscles in goats. The goats had severe skeletal muscle myodegeneration and necrosis and significant increases in serum activities (AST, ALT, and CK) of enzymes that can be used as indicators of muscle damage. The myotoxic lesions observed in this study are in contrast to the only reports of white snakeroot poisoning of goats in the literature,[10] in which a single fresh dose of white snakeroot from Texas was lethal to Angora goats within 24 to 48 h of dosing and was characterized by extensive para-acinar hepatic necrosis, and increases in serum LDH and SGOT (=AST) activities. The histological hepatic changes we observed appeared related mainly to increased lipid mobilization and metabolism. Similar hepatic changes in the control group suggest that it is not likely a toxic response but more likely associated with altered metabolism relating to the treatment (oral gavage and subsequent physiologic exercise). It may be that the chemical constituents of the white snakeroot from Texas are different from the white snakeroot from Illinois that was used in this study. The differences in the clinical disease produced by the two different populations of white snakeroot should be further investigated.

Previous dosing of goats with rayless goldenrod, which is thought to contain the same toxin as white snakeroot, caused lesions to develop mostly in the large appendicular muscles when orally gavaged at 2 and 3% body weight.[11] The rayless goldenrod dosed in that study contained tremetone, **1**, (0.53 μg/mg), dehydrotremetone, **3**, (1.34 μg/mg), and 3-oxyangeloyl-tremetone (2.39 μg/mg). The white snakeroot dosed in this study contained 2.1 μg/mg, 0.96 μg/mg, and 0.53 μg/mg of tremetone, **1**, 6-hydroxytremetone, **2**, and dehydrotremetone, **3**, respectively. The goats dosed with rayless goldenrod at 3% body weight received a total dose of 60 mg total benzofurans/kg body weight, which was the same dosage of total benzofurans administered to the snakeroot, hexane extract, and extract+residue dosed goats in this study even though they were orally gavaged with plant material at 1.67% body weight. The goats in the snakeroot, hexane extract, and extract+residue dosed groups in this study received nearly 3.3 times more tremetone than the goats dosed with rayless goldenrod at 2% of BW. If tremetone, **1**, is the sole toxin in white snakeroot and rayless goldenrod then the goats dosed with hexane extract and extract+residue should have poisoned similar to the goats dosed dried snakeroot.

Tremetol has been commonly accepted as the toxin in white snakeroot. In fact, as recently as 1985 it was referred to as the toxin in white snakeroot.[14] When tremetone, **1**, was dosed orally or by injection into breast muscle of cockerels for 7 days, no signs of poisoning or distress were observed.[9] Bowen and co-workers[9] concluded that tremetone, **1**, was not the toxin in white snakeroot. Results of cell culture cytotoxicity studies led to the proposal that microsomally activated tremetone, **1**, was responsible for the toxicity of the plant;[8] however, it still has not been demonstrated in any animal model. The hexane extract and the extract+residue groups in this study were gavaged with the same dosages of tremetone, **1**, 6-hydroxytremetone, **2**, and dehydrotremetone, **3**, as the snakeroot group. The hexane extract and extract+residue dosed groups did not develop clinical signs, exercise intolerance, serum enzyme changes, or histological lesions observed in the snakeroot dosed group. These results suggest that tremetone, **1**, and/or 6-hydroxytremetone, **2**, and dehydrotremetone, **3**, are not the singular toxin/toxins in white snakeroot. Consequently, there may be another compound or group of compounds that act either independently or synergistically with tremetone, **1**, or other benzofurans. The lack of toxicity observed in the extract+residue group further suggests that if another agent that acts singularly or synergistically with tremetone, **1**, and the other benzofurans is present in white snakeroot, this agent is modified and inactivated during the extraction-recombination process. However, since white snakeroot and rayless goldenrod both cause the same disease in livestock and both plants contain tremetone, **1**, and dehydrotremetone, **3**, it is possible that tremetone, **1**, (or a structurally related compound) is a marker for the active agent or that there is another compound that acts synergistically with one of the benzofurans.

In conclusion, the results from this study demonstrate for the first time that white snakeroot is a potent myotoxin in goats. The results also suggest that another compound besides tremetone, **1**, may have a significant role in producing trembles in livestock and milk sickness in humans.

DOI: 10.1021/jf505614z
J. Agric. Food Chem. 2015, 63, 2092−2097

■ ASSOCIATED CONTENT

Supporting Information

Histologic score of lesion severity and distribution in skeletal muscle of goats dosed with snakeroot, hexane extract, plant residue, and extract+residue. This material is available free of charge via the Internet at http://pubs.acs.org.

■ AUTHOR INFORMATION

Corresponding Author

*E-mail: zane.davis@ars.usda.gov. Tel: 435-752-2941. Fax: 435-753-5681.

Funding

This research was supported by USDA/ARS.

Notes

The authors declare no competing financial interest.

■ ACKNOWLEDGMENTS

The authors thank Katie Lott, Andrea Dolbear, and Ed Knoppel for their assistance with this research. We thank Dr. Stan Welsh of the Stan Welsh Herbarium and Dr. David Seigler of the University of Illinois at Urbana−Champaign for their assistance in identifying the plant material.

■ REFERENCES

(1) Kingsbury, J. M. *Poisonous Plants of the United States and Canada*; Prentice Hall: Englewood Cliffs, NJ, 1964.

(2) Lee, S. T.; Davis, T. Z.; Gardner, D. R.; Colgate, S. M.; Cook, D.; Green, B. T.; Meyerholtz, K. A.; Wilson, C. R.; Stegelmeier, B. L.; Evans, T. J. Tremetone and structurally related compounds in white snakeroot (*Ageratina altissima*): A plant associated with trembles and milk. *J. Agric. Food Chem.* **2010**, *58*, 8560−8565.

(3) Wolf, F. A.; Curtis, R. S.; Kaupp, B. F. A monograph on trembles or sickness and white snakeroot. *North Carolina Agric. Exp. Stn. Technol. Bull.* **1918**, 15.

(4) Couch, J. F. The toxic constituent of richweed or white snakeroot (*Eupatorium urticaefolium*). *J. Agric. Res.* **1927**, *35*, 547−576.

(5) Bonner, W. A.; DeGraw, J. I., Jr.; Bowen, D. M.; Shah, V. R. Toxic constituents of white snakeroot. *Tetrahedron Lett.* **1961**, *12*, 417−420.

(6) Bonner, W. A.; DeGraw, J. I., Jr. Ketones from "white snakeroot. *Eupatorium urticaefolium. Tetrahedron Lett.* **1962**, *18*, 1295−1309.

(7) Beier, R. C.; Norman, J. O.; Irvin, R. T.; Witzel, D. A. Microsomal activation of constituents of white snakeroot (*Eupatorium rugosum* Houtt) to form toxic products. *Am. J. Vet. Res.* **1987**, *48*, 583−585.

(8) Beier, R. C.; Norman, J. O.; Reagor, J. C.; Rees, M. S.; Mundy, B. P. Isolation of the major component in white snakeroot that is toxic after microsomal activation: Possible explanation of sporadic toxicity of white snakeroot plants and extracts. *Nat. Toxins* **1993**, *1*, 286−293.

(9) Bowen, D. M.; DeGraw, J. I., Jr.; Shah, V. R.; Bonner, W. A. The synthesis and pharmacological action of tremetone. *J. Med. Chem.* **1963**, *6*, 315−319.

(10) Beier, R. C.; Norman, J. O. The toxic factor in white snakeroot: Identity, analysis, and prevention. *Vet. Hum. Toxicol.* **1990**, *32*, 81−88.

(11) Stegelmeier, B. L.; Davis, T. Z.; Green, B. T.; Lee, S. T.; Hall, J. O. Experimental rayless goldenrod (*Isocoma pluriflora*) toxicosis in goats. *J. Vet. Diagn. Invest.* **2010**, *22*, 570−577.

(12) Davis, T. Z.; Green, B. T.; Stegelmeier, B. L.; Lee, S. T.; Welch, K. D.; Pfister, J. A. Physiological and serum biochemical changes associated with rayless goldenrod (*Isocoma pluriflora*) poisoning in goats. *Toxicon* **2013**, *76*, 247−254.

(13) Lee, S. T.; Davis, T. Z.; Gardner, D. R.; Stegelmeier, B. L.; Evans, T. J. A quantitative method for the measurement of three benzofuran ketones in rayless goldenrod (*Isocoma pluriflora*) and white snakeroot (*Ageratina altissima*) by HPLC. *J. Agric. Food Chem.* **2009**, *57*, 5639−5642.

(14) Niederhofer, R. E. The milk sickness. *J. Am. Med. Assoc.* **1985**, *254*, 2123−2125.

DOI: 10.1021/jf505614z
J. Agric. Food Chem. 2015, 63, 2092−2097

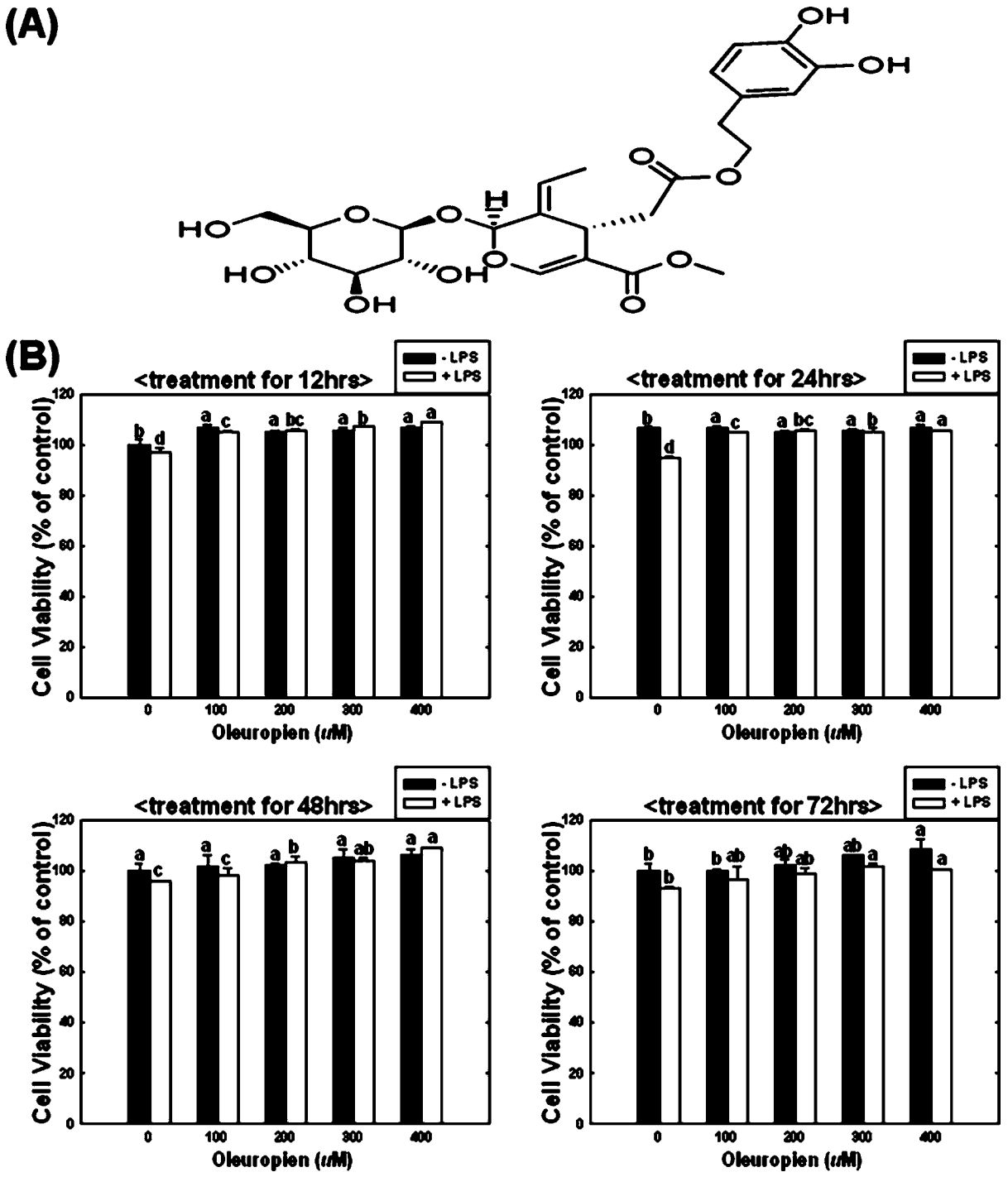

Figure 1. Chemical structure of oleuropein (A) and its effect on cell viability (B). RAW 264.7 cells (1 × 104/well) were treated with oleuropein (100−400 μg/mL) for 12, 24, 48, and 72 h. Cell viability was determined using the XTT assay (B). Data are presented as means with standard deviations of three replicates. Results were analyzed by ANOVA and Duncan's multiple range test ($p < 0.05$).

oleuropein on inflammatory responses and signaling in LPS-induced RAW 264.7 macrophages and a zebrafish model.

MATERIALS AND METHODS

Materials. Dulbecco's modified Eagle's medium (DMEM), fetal bovine serum (FBS), penicillin-streptomycin (P/S), and phosphate-buffered saline (PBS) were purchased from Gibco (Gaithersburg, MD). iNOS, COX-2, p65, p-IκB-α, IκB-α, p-ERK, ERK, p-p38, p38, p-JNK, JNK, and GAPDH monoclonal antibodies and secondary antibody were obtained from Cell Signaling Technology (Boston, MA). The enzyme immunoassay (EIA) kits for IL-1β and IL-6 were obtained from BioLegend (San Diego, CA). Maxime PT Premix KIT was purchased from iNtRON (Gyeonggi-do, Korea). iNOS, COX-2, IL-1β, IL-6, and GAPDH oligonucleotide primers were obtained from Bioneer (Seoul, Korea). Compound **2**, 3-bis(2-methoxy-4-nitro-5-sulfophenyl)-2*H*-tetrazolium-5-carbox-anilide (XTT), was purchased from WEL GENE (Daegu, Korea). Oleuropein (>98.0%), TRIzol reagent, diaminofluorophore 4-amino-5-methylanino-2,7-difluorofluoroescein diacetate (DAF-FM DA), Griess reagent, and lipopolysaccharide (LPS) (*Escherichia coli, serotype 0111:04*) were obtained from Sigma Chemical Co. (St. Louis, MO).

DOI: 10.1021/jf505894b
J. Agric. Food Chem. 2015, 63, 2098−2105

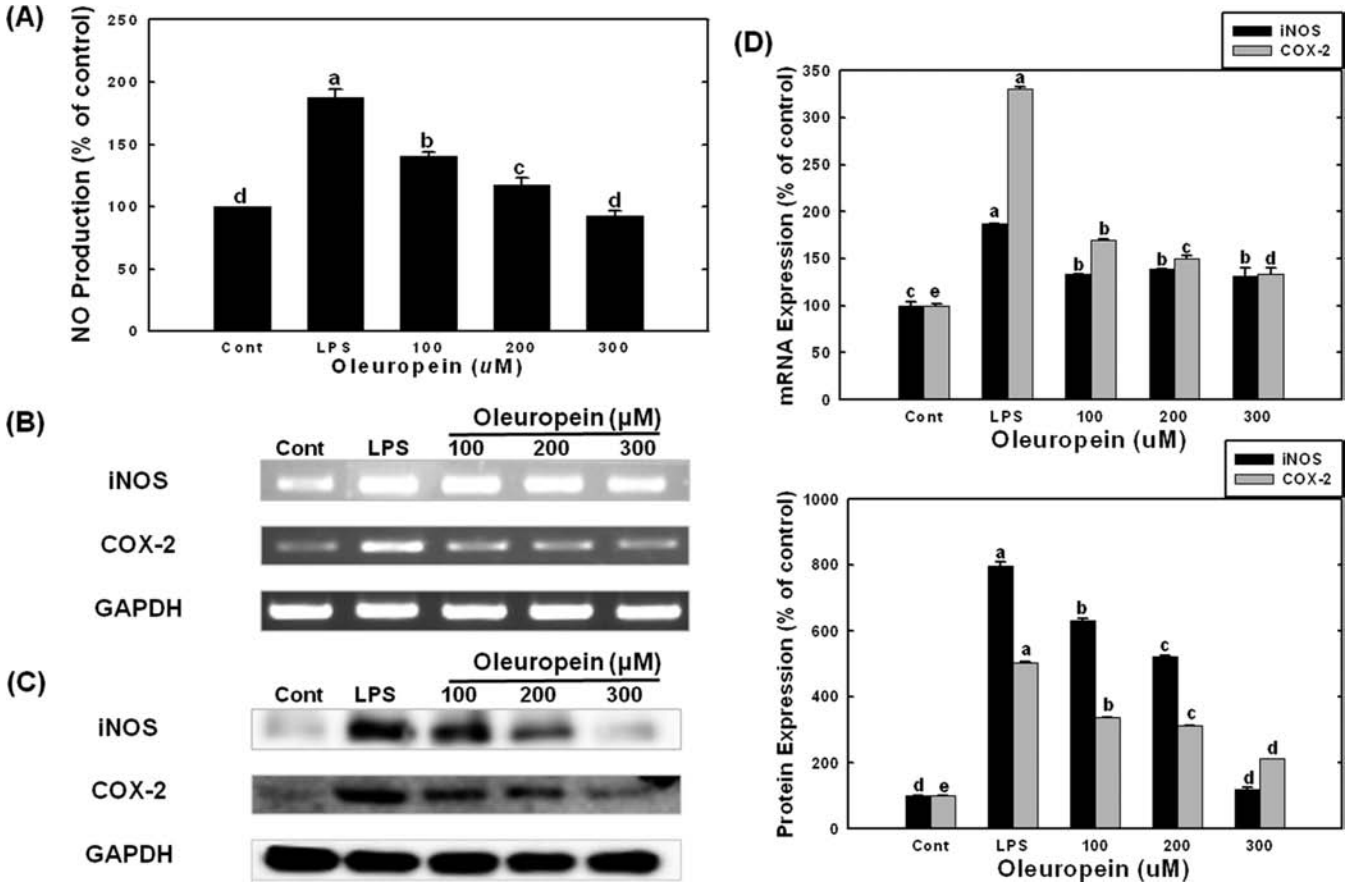

Figure 2. Inhibition by oleuropein of NO production and iNOS and COX-2 expression in LPS-stimulated RAW 264.7 cells. LPS-stimulated RAW 264.7 cells were treated with oleuropein (100, 200, or 300 μM) for 4 h, followed by oleuropein (100, 200, or 300 μM) and/or LPS for 24 h. Nitric oxide concentrations (A) in the culture media were determined by Griess assay. mRNA (B) and protein (C) levels were determined by RT-PCR and Western blot, respectively. The results were quantified using the ImageJ software (D). Data are presented as means with standard deviations of three replicates. Results were analyzed by ANOVA and Duncan's multiple range test ($p < 0.05$).

Cell Culture. RAW 264.7 macrophage cells (American Type Culture Collection, CL-173, and passage 5−7) were cultured in DMEM with 1.5 g/L sodium bicarbonate, 1% P/S, and 10% FBS at 37 °C and in a humidified chamber with a 5% CO_2 atmosphere. Cells were incubated with 100, 200, and 300 μM oleuropein, and then stimulated with LPS at 1 μg/mL for the indicated times.

XTT Assay. RAW 264.7 cells (~1×10^4 per well) were seeded in a 96-well plate and incubated in a CO_2 incubator at 37 °C for 12, 24, 48, and 72 h. Cells were treated with various concentrations (100−400 μg/mL) of oleuropein and incubated for 12, 24, 48, and 72 h, after which 2, 3-bis(2-methoxy-4-nitro-5-sulfophenyl)-2*H*-tetrazolium-5-carbox-anilide (XTT) was added to the culture medium. The cytotoxicity of oleuropein was determined on the basis of the absorbance at 450 and 690 nm measured using an ELISA plate reader.

Nitrite Determination in RAW 264.7. RAW 264.7 cells (~1×10^4 per well) were plated in 96-well plates, treated with various concentrations of oleuropein and then incubated with or without LPS (1 μg/mL) for 24 h. Nitrite levels, which reflect NO levels, in culture media were determined using the Griess reaction. Cell culture medium (100 μL) was mixed with 100 μL of Griess reagent and incubated at room temperature for 15 min. Absorbance was then measured at 540 nm using an ELISA reader. Nitrite levels in samples were determined using a standard sodium nitrite curve.

Enzyme-Linked Immunosorbent Assay (ELISA). RAW 264.7 cells were pretreated with various oleuropein concentrations for 1 h and then further stimulated with LPS (1 μg/mL) for 24 h. The supernatants were collected and stored at −80 °C until cytokine analysis. IL-1β and IL-6 levels in supernatants were determined using ELISA MAX Kits (BioLegend, San Diego, CA), according to the manufacturer's instructions.

RNA Isolation and Reverse Transcription Polymerase Chain Reaction. Total RNA was extracted using TRIzol (Invitrogen, Carlsbad, CA), and 1 μg of the total RNA was used to produce cDNA using an RT-PCR system. Amplification of the target genes was performed using specific oligonucleotide primers by PCR. The primers used were as follows: iNOS, forward (5′-CCCTTCCGAAGTTTCTGGCAGCAG-3′) and reverse (5′-GGCTGTCAGAGCCTCGTGGCTTTG-3′); COX-2, forward (5′-ATGCTCCTGCTTGAGTATGT-3′) and reverse (5′-CACTACATCCTGACCCACTT-3′); IL-6, forward (5′-CCATCTCTCCGTCTCTCACC-3′) and reverse (5′-AGACCGCTGCCTGTCTAAAA-3′); IL-1β, forward (5′-CAGGATGAGGACATGAGCACC-3′) and reverse (5′-CTCTGCACACTCAAACTCCAC-3′); GAPDH, forward (5′-AACTTTGGCATTGTGGAAGG-3′) and reverse (5′-ACACATTGGGGGTAGGAACA-3′). The PCR products were separated on 1.0% agarose gels, stained with ethidium bromide, and photographed. The expression levels were quantified by scanning using a gel documentation and analysis system (ImageJ, SAS).

Western Blot Analysis. RAW 264.7 cells were washed with PBS buffer, lysed with lysis buffer, and then centrifuged to remove cell debris. The total protein content of the supernatant was determined using the Bradford assay. Protein extracts (50 μg) were separated using SDS-PAGE and transferred to polyvinylidene fluoride membranes. The membranes were immunoblotted with primary antibodies specific for iNOS, COX-2, p65, p-IκB-α, IκB-α, p-ERK, ERK, p-p38, p38, p-JNK, JNK, and GAPDH overnight. Secondary antibodies conjugated to horseradish peroxidase (1:1000) were then applied for 1 h. The

DOI: 10.1021/jf505894b
J. Agric. Food Chem. 2015, 63, 2098−2105

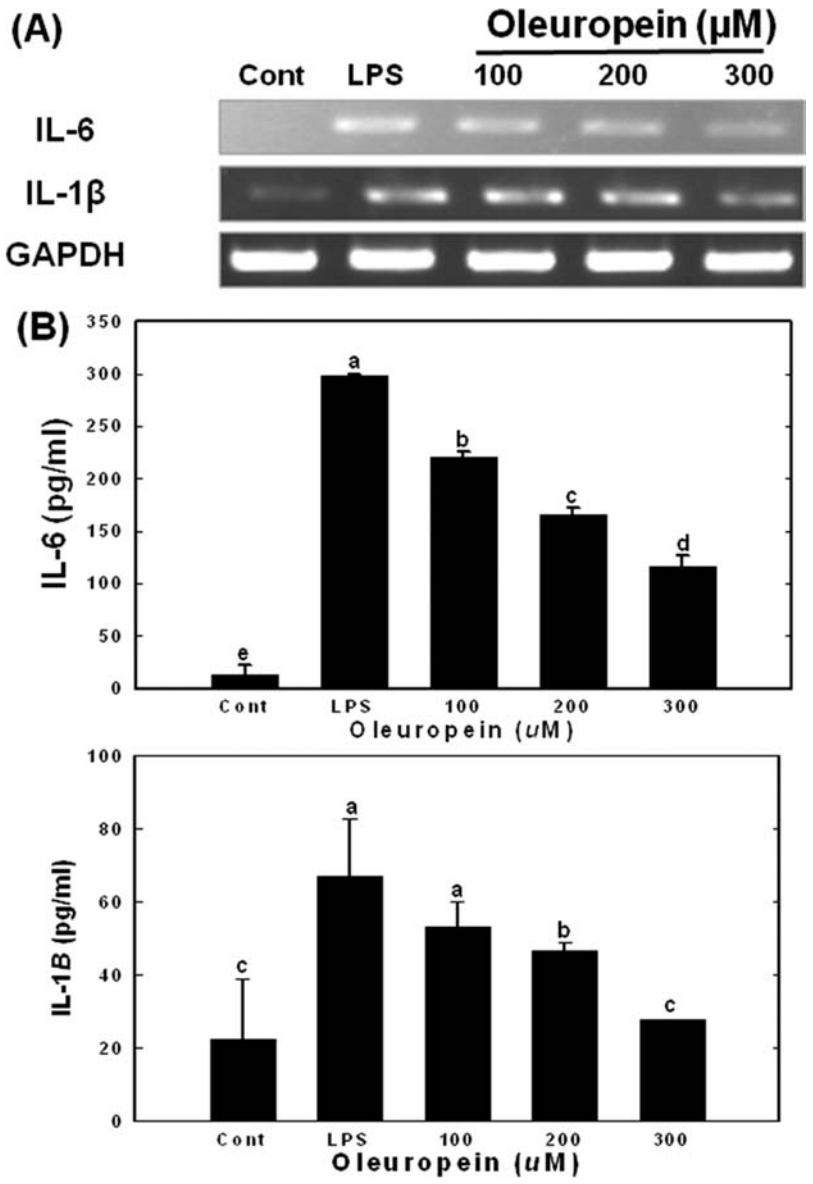

Figure 3. Effect of oleuropein on IL-6 and IL-1β mRNA and protein levels in LPS-stimulated RAW 264.7 cells. Cells were treated with oleuropein (100, 200, or 300 μM), followed by LPS. Cells were then incubated for a further 4 or 24 h. IL-6 and IL-1β mRNA levels were determined by RT-PCR and visualized on a gel. (A) Cytokine levels in culture media were determined using an enzyme immunoassay kit. (B) Data are presented as means with standard deviations of three replicates. Results were analyzed by ANOVA and Duncan's multiple range test ($p < 0.05$).

bands were visualized using enhanced chemiluminescence (ECL) and detected using the LAS imaging software (Fuji, New York, NY).

Nitrite Determination in Zebrafish. Synchronized zebrafish embryos were collected and rearranged using a pipet at 20 embryos/well in six-well plates containing 2 mL of egg water. After 7−9 h postfertilization (hpf), embryos were incubated with or without various concentrations of oleuropein for 1 h. Zebrafish were stimulated by LPS (5 μg/mL) for 24 h at 28.5 °C. The zebrafish embryos were then transferred into fresh embryo medium. NO levels in the inflammatory zebrafish model were measured using a fluorescent probe dye, diaminofluorophore 4-amino-5-methylanino-2,7-difluoro-fluoroescein diacetate (DAF-FM DA). Transformation of DAF-FM DA by NO generates highly fluorescent triazole derivatives. Following stimulation by LPS, the zebrafish larvae were transferred into 96-well plates and treated with DAF-FM DA solution (1 μM) for 1 h in the dark at 28.5 °C. After incubation, the zebrafish larvae were rinsed in fresh zebrafish embryo medium and anesthetized with tricaine methanesulfonate solution before observation. The fluorescence intensity of individual zebrafish larvae was quantified using an ECLIPSE E600 (Nikon, Tokyo, Japan).

Statistical Analysis. All experiments were performed in triplicate. The results were analyzed statistically using an analysis of variance (ANOVA) and Duncan's multiple range test. A p value < 0.05 was considered to indicate statistical significance (SAS Instititue, NC).

RESULTS AND DISCUSSION

Effect of Oleuropein on RAW 264.7 Cell Viability. There is the chemical structure of oleuropein in Figure 1A. Oleuropein was nontoxic to the RAW 264.7 cells at the indicated range of concentrations (Figure 1B) and also has no toxicity at serial time −12, 24, 48, and 72 h. No morphological changes in the cells were observed on the basis of microscopic analysis (data not shown). This result shows that oleuropein has no effect on cell apoptosis. Accordingly, all of the following experiments were performed using oleuropein concentrations of 100, 200, and 300 μM.

DOI: 10.1021/jf505894b
J. Agric. Food Chem. 2015, 63, 2098−2105

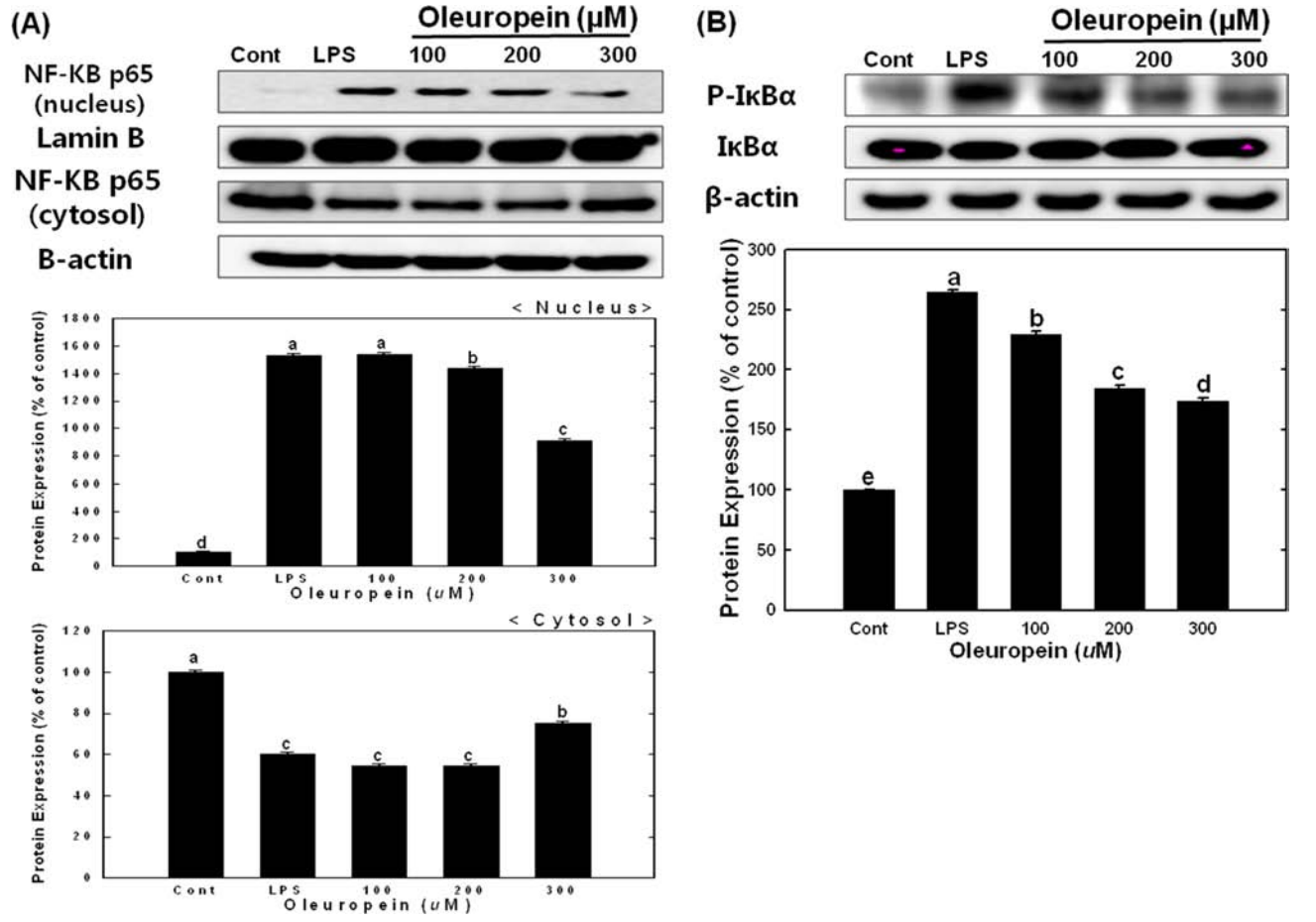

Figure 4. Effect of oleuropein on the phosphorylation of IκB-α and the nuclear translocation of NF-κB. Cells were pretreated with oleuropein (100, 200, or 300 μM) for 1 h and then with LPS (1 μg/mL) for 15 min. Protein levels were determined by Western blotting. NF-κb p65 levels in the cytosol and nucleus were quantified using the ImageJ software and normalized to Lamin B and β-actin, respectively. (A) The results were quantified using the ImageJ software and normalized to IκBα (B). Data are presented as means with standard deviations of three replicates. Results were analyzed by ANOVA and Duncan's multiple range test ($p < 0.05$).

Effect of Oleuropein on LPS-Induced NO Production and Expression of iNOS and COX-2. Overproduction of iNOS-mediated nitric oxide is a representative inflammatory reaction, and may be involved in other negative cellular physiologies such as mutagenesis, DNA damage, and the formation of *N*-nitrosoamine.[24−26] Cyclooxygenase-2 (COX-2), another inflammatory marker, is also associated with production of proinflammatory substances such as prostaglandins, and is upregulated during inflammation. In particular, COX-2-activated pathways, which are responsible for the conversion of arachidonic acid to prostaglandin and other eicosanoids, are of clinical importance as major targets for nonsteroid anti-inflammatory drugs such as aspirin, which is commonly used for inflammation and pain.[27] However, these drugs have several side effects such as gastrointestinal bleeding, swelling of skin tissue, and allergy. We examined the effect of oleuropein on LPS-induced NO production, a mediator of the inflammatory response. As shown in Figure 2A, the NO level in culture medium was reduced by oleuropein treatment in a dose-dependent manner. This decrease in NO production was due to the downregulation of iNOS, a major pro-inflammatory enzyme that produces NO, at the mRNA and protein levels (Figure 2B,C). In addition, COX-2 (also an inflammatory marker) mRNA and protein levels were decreased by oleuropein treatment in a dose-dependent manner (Figure 2B,C). Expression of iNOS and COX-2 in mRNA was reduced by 42% and 43%, respectively, and in protein levels was reduced by 72% and 45%, respectively, by 300 μM oleuropein (Figure 2D). Our data showed that oleuropein, an olive compound, decreased LPS-induced NO production dose-dependently by downregulating iNOS (Figure 2A,B), which is closely associated with the synthesis of NO and COX-2 expression. This result indicated that oleuropein could be a potential anti-inflammatory phytochemical. Recent studies identified various phytochemicals with anti-inflammatory effects. Resveratrol, EGCG, and tyrosol are also known to downregulate COX-2 and iNOS.[28−30]

Effect of Oleuropein on LPS-Induced IL-1β and IL-6 Release and Their mRNA Expressions. Inflammation generally involves the abnormal regulation of cytokines. Cytokines such as IL-6 and IL-1β are pro-inflammatory in vitro and in vivo.[31] Inflammation generally involves the abnormal regulation of cytokines. Cytokines such as IL-6 and IL-1β are pro-inflammatory in vitro and in vivo, and play important roles in the extent of inflammation and recruit other immune cells implicated in the pathogenesis of diverse inflammatory conditions, such as rheumatoid arthritis and septic shock.[32] We further examined the anti-inflammatory effect of oleuropein by assaying levels of pro-inflammatory cytokines. RT-PCR analysis showed that expression of IL-1β

DOI: 10.1021/jf505894b
J. Agric. Food Chem. 2015, 63, 2098−2105

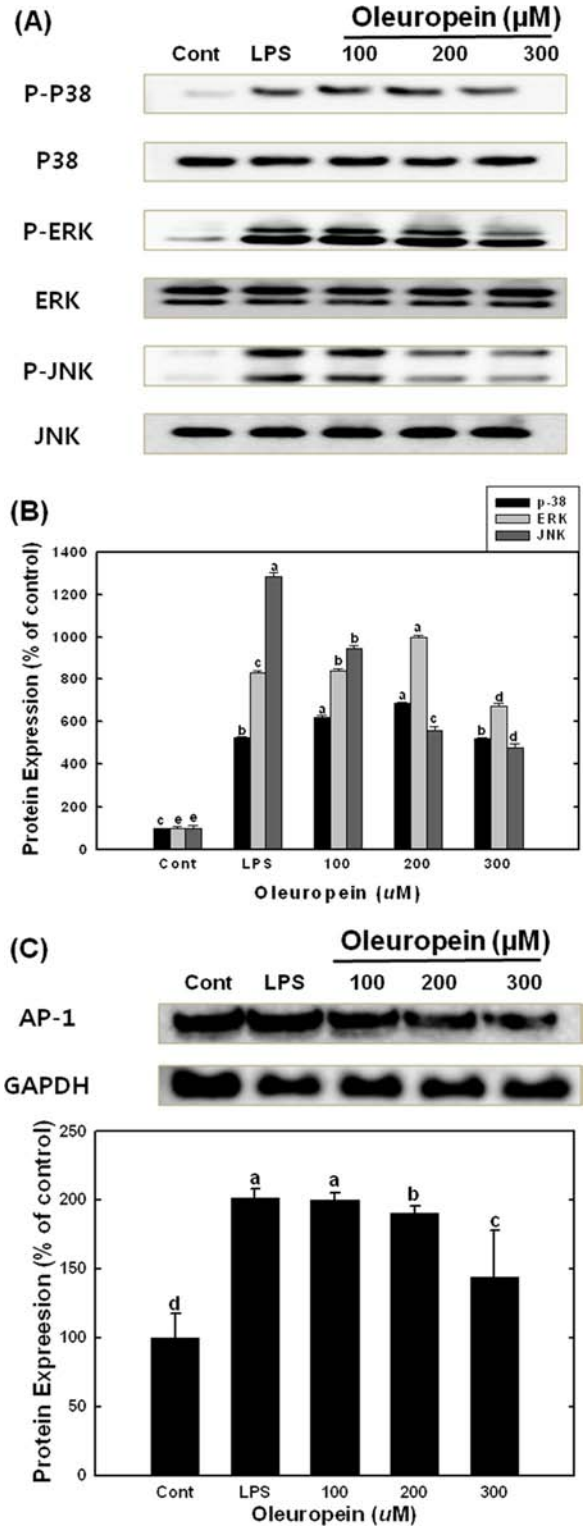

Figure 5. Inhibitory effect of oleuropein on LPS-induced activation of MAP kinases and AP-1 in RAW 264.7 cells. RAW 264.7 were pretreated with oleuropein (100, 200, or 300 μM) for 1 h and then with LPS (1 μg/mL) for 15 min. Total proteins (50 μg) were subjected to Western blotting (A and C). The protein levels were quantified using the ImageJ software, and those of the phosphorylated forms were normalized to total protein levels (B). The data of AP-1 were quantified using the ImageJ software and normalized to GAPDH (D). Data are presented as means with standard deviations of three replicates. Results were analyzed by ANOVA and Duncan's multiple range test ($p < 0.05$).

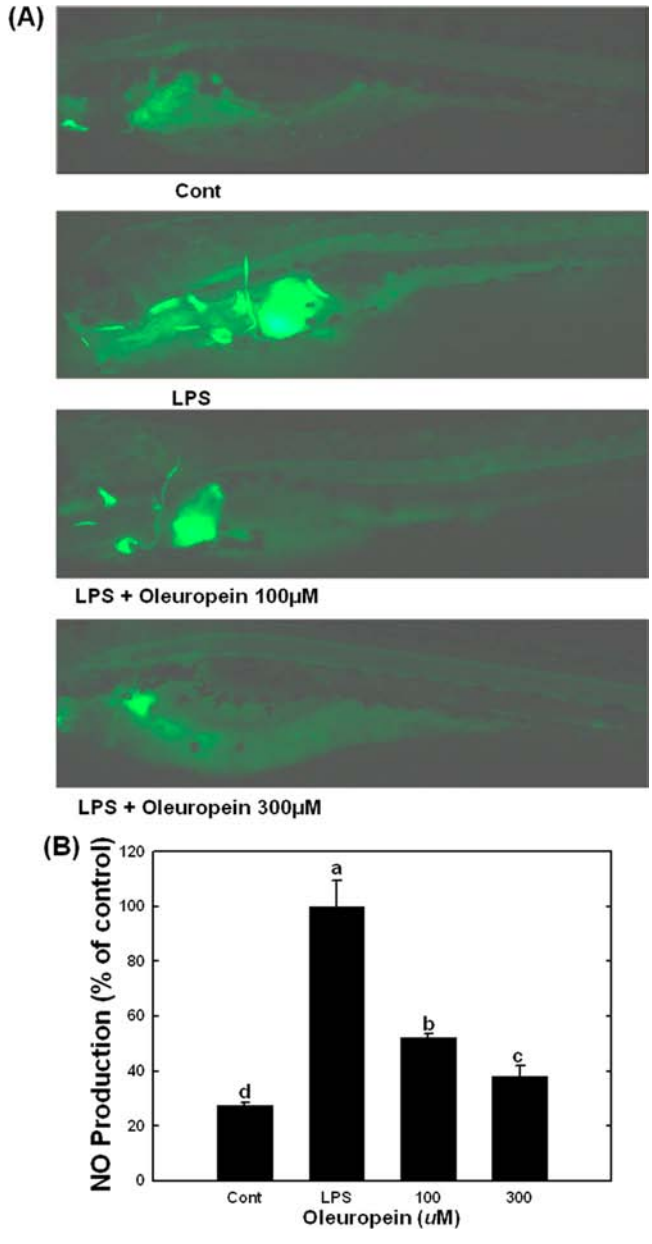

Figure 6. Effect of oleuropein on LPS-induced NO production in zebrafish embryo. Zebrafish embryos were pretreated with oleuropein for 1 h and then exposed to LPS (5 μg/mL) for 24 h (A). The NO level was measured after staining with DAF-FM-DA (A). The results were quantified using the ImageJ software. (B) Data are presented as means with standard deviations of three replicates. Results were analyzed by ANOVA and Duncan's multiple range test ($p < 0.05$).

and IL-6 (inflammatory cytokines) was reduced by oleuropein treatment (Figure 3A). Levels of these cytokines in culture medium were decreased by oleuropein treatment in a dose-dependent manner. IL-6 and IL-1β levels were decreased, respectively, compared with the LPS-induced group at 300 μM oleuropein (Figure 3B). In particular, IL-1β in the presence of 300 μM oleuropein was reduced to the level of the control (Figure 3B). Therefore, oleuropein suppressed the LPS-induced release of pro-inflammatory cytokines. Our results showed that LPS induced release of cytokines (Figure 3B) was effectively reduced by oleuropein treatment at the mRNA (Figure 3A). However, we did not explore whether other cytokines, such as TNF-α and IL-10, were also regulated by

DOI: 10.1021/jf505894b
J. Agric. Food Chem. 2015, 63, 2098−2105

oleuropein. Analysis of these cytokines would provide more information on the anti-inflammatory mechanism of oleuropein.

Effect of Oleuropein on LPS-Induced IκB Phosphorylation and NF-κB Translocation. Regulation of inflammatory cytokines and inflammatory responses is transcriptionally governed by NF-κb transcription factors. These transcription factors regulate inflammatory related genes in the nucleus, where they bind to the DNA of pro-inflammatory mediators to induce their transcription.[33,28] In addition, transcriptional activity of NF-κB is dependent on IκBα phosphorylation,[34] by which p65, a subunit of NF-κB, translocates into the nucleus to promote the expression of inflammatory genes including iNOS, COX-2, and cytokines such as IL-6 and IL-1β.[35,36] Our results showed that oleuropein-mediated inhibition of IκBα phosphorylation (Figure 4B) blocks the translocation of p65 from the cytosol to the nucleus (Figure 4A), suggesting that oleuropein exerts its anti-inflammatory effects by suppressing NK-κB, a major component of the TLR pathway. The nuclear NF-κB level increased significantly after LPS treatment compared with the normal control (Figure 4A). Oleuropein (300 μM) inhibited the translocation of p65, a subunit of NF-κB, into the nucleus by 40% compared with the LPS-induced control. However, lower concentrations of oleuropein exerted no significant effects on the translocation of p65 into the nucleus. Cytosolic NF-κB levels decreased with LPS treatment, but increased in the oleuropein-treated group (300 μM). This result was correlated with the nuclear NF-κB pattern, i.e., a reduction in the presence of oleuropein (300 μM) (Figure 4A). Translocation of NF-κB into the nucleus is associated with phosphorylation of IκB-α in the TLR4 pathway, a major inflammation pathway. Accordingly, we examined the phosphorylation of IκB-α, a mediator of NF-κB activation. Oleuropein inhibited IκB-α phosphorylation, suggesting that NF-κB translocation into the nucleus was inhibited by suppression of IκB-α phosphorylation (Figure 4B). Therefore, the inhibitory effect of oleuropein on LPS-induced inflammatory responses was due to the deactivation of NF-κb and IκB-α, major components in the TLR4 pathway.

Effect of Oleuropein on LPS-Induced Activation of Mitogen-Activated Protein (MAP) Kinase. MAP kinases are another signaling pathway that plays a critical role in inflammation through activation of NFκB.[17] This kinase family is composed of several subgroups, such as JNK, ERK, and p38. The activation of these kinase groups mediates various inflammatory responses in vitro and in vivo.[37−39] The inflammatory response can be activated through the MAP kinase pathway. Thus, we determined whether MAP kinase signaling is involved in oleuropein-mediated inhibition of LPS-induced inflammatory responses. MAP kinase plays a critical role in LPS-induced inflammation signaling at the transcriptional level. Since the MAP kinase pathway is phosphorylation-dependent, we examined the phosphorylation status of components of this pathway. Oleuropein significantly decreased LPS activated ERK and JNK by inhibiting their phosphorylation (Figure 5A). Phosphorylation of ERK and JNK induced by LPS was reduced by 20% and 62%, respectively, by 300 μM oleuropein (Figure 5B). However, phosphorylation of P38 induced by LPS, also a component of the MAP kinase pathway, was not decreased in the presence of oleuropein. Our data also showed that oleuropein decreased AP-1, downstream gene related with MAP kinase (Figure 5C). AP-1 is another inflammatory key gene by regulation NO.[18] Our results indicated that inhibition of ERK and JNK rather than p38 contributes to the anti-inflammatory effect of oleuropein in the LPS-induced inflammatory response. This result suggested that the anti-inflammatory effect of oleuropein might be due at least in part to the inhibition of ERK and JNK.

Effect of Oleuropein on LPS-Induced NO Production in Zebrafish Model. We used a zebrafish model to investigate the anti-inflammatory effect of oleuropein in vivo. Nitric oxide (NO) production in zebrafish was determined using a fluorescent probe dye. As shown in Figure 6A, the nitric oxide level in zebrafish was elevated after LPS treatment compared with the positive control. Therefore, LPS increased nitric oxide production in zebrafish, similar to that in RAW 264.7 cells. LPS-induced increases in NO production were significantly suppressed in the presence of oleuropein (Figure 6A). In particular, 300 μM oleuropein inhibited LPS-induced NO production in zebrafish by 62% compared with the LPS control group (Figure 6B). Our data showed that oleuropein effectively reduced LPS-induced NO production in zebrafish. This result was correlated with the in vitro cell culture data, suggesting that oleuropein exerts anti-inflammatory effects. To our knowledge, this is the first report of an anti-inflammatory effect of oleuropein in zebrafish. However, we did not explore the genetic regulation of inflammatory factors at the gene and protein levels. Thus, further studies on the inflammatory responses of zebrafish in the presence of oleuropein are required. Oleuropein is a relatively abundant phenolic compound in olive leaf compared with other components, such as tyrosol and hydroxytyrosol, which have been suggested to possess various biological activities; also, our data showed that oleuropein inhibited inflammatory responses in RAW 264.7 cells and zebrafish by suppressing NF-κB translocation and the MAP kinase pathway. Doses of oleuropein in the range 100−300 uM are very high so we think that concentrations were supraphysiological. Our study also provides information important for the development of anti-inflammatory agents containing oleuropein.

AUTHOR INFORMATION

Corresponding Author

*Phone: +82-31-725-8371. Fax: +82-31-725-8282. E-mail: bylee@cha.ac.kr.

Author Contributions

¶These authors contributed equally to this work.

Author Contributions

#Co-first author.

Notes

The authors declare no competing financial interest.

REFERENCES

(1) Sedef, N. E.; Sibel, K. Olive tree (Olea europaea) leaves: Potential beneficial effects on human health. *Nutr. Res. (N.Y.)* **2009**, *67*, 632−638.

(2) Hanbury, D. On the febrifuge properties of the olive (Olea europea, L.). *Pharmaceut. J. Provincial Trans. 1* **1854**, 353−354.

(3) Kontogianni, V. G.; Gerothanassis, I. P. Phenolic compounds and antioxidant activity of olive leaf extracts. *Nat. Prod. Res.* **2012**, *26*, 186−189.

(4) Riadh, D.; Shu, C.; Kazuichi, S. Oleuropein and hydroxytyrosol inhibit adipocyte differentiation in 3T3-L1 cells. *Life Sci.* **2011**, *89*, 708−716.

DOI: 10.1021/jf505894b
J. Agric. Food Chem. 2015, 63, 2098−2105

(5) Giuseppe, B.; Antonio, T.; Rossella, L. C.; Giuseppe, C.; Nicola, U.; Antonella, S. On the in-vitro antimicrobial of oleuropein and hydroxytyrosol. *J. Pharm. Phamacol.* **1999**, *51*, 971−974.
(6) Amer, A. B. Endogenous ligands of Toll-like receptors: implications for regulating inflammatory and immune responses. *Trends Immunol.* **2002**, *23*, 509−512.
(7) *Fundamentals of Inflammation 1*; Serhan, C. N., Ward, P. A., Gilroy, D. W., Eds.; Cambridge University Press: New York, 2010; p 111
(8) Lisa, M. C.; Zena, W. Inflammation and cancer. *Nature* **2002**, *420*, 860−867.
(9) Wellen, K. E.; Hotamisligil, G. S. Inflammation, stress, and diabetes. *J. Clin. Invest.* **2005**, *115*, 1111−1119.
(10) Bautista, L. E. Inflammation, endothelial dysfunction, and the risk of high blood pressure: Epidemiologic and biological evidence. *J. Hum. Hypertens.* **2003**, *17*, 223−230.
(11) Haiyan, X.; Glenn, T. B.; Qing, Y.; Guo, T.; Daseng, Y.; Chieh, J. C.; Jason, S.; Andrew, N.; Jeffrey, S. R.; Louis, A.; Tartaglia; Hong, C. Chronic inflammation in fat plays a crucial role in the development of obesity-related insulin resistance. *J. Clin. Invest.* **2003**, *112*, 1821−1830.
(12) Akira, S.; Uematsu, S.; Takeuchi, O. Pathogen recognition and innate immunity. *Cell* **2006**, *124*, 783−801.
(13) Brown, K. L.; Cosseau, C.; Gardy, J. L.; Hancock, R. E. Complexities of targeting innate immunity to treat infection. *Trends Immunol.* **2007**, *28*, 260−266.
(14) O'Neill, L. A. TLRs: Professor Mechnikov, sit on your hat. *Trends Immunol.* **2004**, *25*, 687−693.
(15) Keating, S. E.; Maloney, G. M.; Moran, E. M.; Bowie, A. G. IRAK-2 participates in multiple toll-like receptor signaling pathways to NFκB via activation of TRAF6 ubiquitination. *J. Biol. Chem.* **2007**, *282*, 33435−33443.
(16) Takaesu, G.; Ninomiya-Tsuji, J.; Kishida, S.; Li, X.; Stark, G. R.; Matsumoto, K. Interleukin-1 (IL-1) receptor-associated kinase leads to activation of TAK1 by inducing TAB2 translocation in the IL-1 signaling pathway. *Mol. Cell. Biol.* **2001**, *21*, 2475−2484.
(17) Berghe, W. V.; Plaisance, S.; Boone, E.; Bosscher, K. D.; Schmitz, M. L.; Fiers, W.; Haegeman, G. p38 and extracellular signal-regulated kinase mitogen-activated protein kinase pathways are required for nuclear factor-κB p65 transactivation mediated by tumor necrosis factor. *J. Biol. Chem.* **1998**, *273*, 3285−3290.
(18) Knethen, A. von.; Callsen, D.; Brüne, B. NF-κB and AP-1 Activation by Nitric Oxide Attenuated Apoptotic Cell Death in RAW 264.7 Macrophages. *Mol. Biol. Cell* **1998**, *10*, 361−372.
(19) Eisen, J. S. Zebrafish make a big splash. *Cell* **1996**, *87*, 969−977.
(20) Fishman, M. C. Zebrafish genetics: The enigma of arrival. *Proc. Nati. Acad. Sci. U.S.A.* **1999**, *96*, 10554−10556.
(21) Hertog, J. Chemical genetics: Drug screens in zebrafish. *Biosci. Rep.* **2005**, *25*, 289−297.
(22) Pichler, F. B.; Laurenson, S.; Williams, L. C.; Dodd, A.; Copp, B. R.; Love, D. R. Chemical discovery and global gene expression analysis in zebrafish. *Nat. Biotechnol.* **2003**, *21*, 879−883.
(23) Nikolaus, S. T.; Augustin, Z.; Leonard, I. Z. Fishing for lymphoid genes. *Trends Immunol.* **2001**, *22*, 302−307.
(24) Arroyo, P. L.; Hatch-Pigott, V.; Mower, H. F.; Cooney, R. V. Mutagenicity of nitric oxide and this inhibition by antioxidants. *Mutat. Res.* **1992**, *281*, 193−202.
(25) Miwa, M.; Stuehr, D. J.; Marletta, M. A.; Wishnok, J. S.; Tannenbaum, S. R. Nitrosation of amines by stimulated macrophage. *J. Carcinog.* **1987**, *8*, 955−958.
(26) Wink, D. A.; Kasprzak, K. S.; Maragos, C. M.; Elespuru, R. K.; Misra, M.; Dunams, T. M.; Cebula, T. A.; Koch, W. H.; Andrews, A. W.; Allen, J. S. DNA deaminating ability and genotoxicity of nitric oxide and its progenitors. *Science* **1991**, *254*, 1001−1003.
(27) Cryer, B.; Feldman, M. Cyclooxygenase-1 and cyclooxygenase-2 selectivity of widely used nonsteroidal anti-inflammatory drugs. *Am. J. Med.* **1998**, *104*, 413−421.
(28) Young-Joon, S.; Kyung-Soo, C.; Hyun-Ho, C.; Seong-Su, H.; Young-Sam, K.; Kwang-Kyun, P.; Sang-Sup, L. Molecular mechanisms underlying chemopreventive activities of anti-inflammatory phytochemicals: down-regulation of COX-2 and iNOS through suppression of NF-κB activation. *Mutat. Res.* **2001**, *480*−*481*, 243−268.
(29) Salahuddin, A.; Ayesha, R.; Absarul, H.; Matthew, L.; Victor, M. G.; Tariq, M. H. Green tea polyphenol epigallocatechin-3-gallate inhibits the IL-1β-induced activity and expression of cyclooxygenase-2 and nitric oxide synthase-2 in human chondrocytes. *Free Radicals Biol. Med.* **2002**, *33*, 1097−1106.
(30) Stefanoa, D. D.; Maiuria, M. C.; Simeona, V.; Grassiaa, G.; Sosciab, A.; Cinellib, M. P.; Carnuccioa, R. Lycopene, quercetin and tyrosol prevent macrophage activation induced by gliadin and IFN-γ. *Eur. J. Pharmacol.* **2007**, *566*, 192−199.
(31) Molloy, R. G.; Mannick, J. A.; Rodrick, M. L. Cytokines, sepsis and immunomodulation. *Br. J. Surg.* **1993**, *80*, 289−297.
(32) McInnes, I. B.; Schett, G. Cytokines in the pathogenesis of rheumatoid arthritis. *Nat. Rev. Immunol.* **2007**, *7*, 429−442.
(33) Lappas, M.; Permerzel, M.; Harry, H. G.; Gregory, E. R. Nuclear factor kappa B regulation of proinflammatory cytokines in human gestational tissues in vitro. *Biol. Reprod.* **2002**, *67*, 668−673.
(34) Young-Joon, S. Cancer chemoprevention with dietary phytochemicals. *Nat. Rev. Cancer* **2003**, *3*, 768−780.
(35) Dixit, V.; Mak, T. W. NF-κB signaling: Many Roads Lead to Madrid. *Cell* **2002**, *111*, 615−619.
(36) Tak, P. P.; Firestein, G. S. NF-kappaB: A key role in inflammatory diseases. *J. Clin. Invest.* **2001**, *107*, 7−11.
(37) Katrin, S.; Andreas, P. Inhibition of the MAP kinase ERK protects from lipopolysaccharide-induced lung injury. *Biochem. Phamacol.* **2009**, *77*, 1827−1834.
(38) Hambleton, J.; Weinstein, S. L.; Lem, L.; DeFranco, A. L. Activation of c-Jun N-terminal kinase in bacterial lipopolysaccharide-stimulated macrophages. *Proc. Nati. Acad. Sci. U.S.A.* **1996**, *93*, 2774−2778.
(39) Schnyder-Candrian, S.; Quesniaux, V. F. J.; Padova, F. D.; Maillet, I.; Noulin, N.; Couillin, I.; Moser, R.; Erard, F.; Vargaftig, B. B.; Ryffel, B.; Schnyder, B. Dual effects of p38 MAPK on TNF-dependent bronchoconstriction and TNF-independent neutrophil recruitment in lipopolysaccharide-induced acute respiratory distress syndrome. *J. Immunol.* **2005**, *175*, 262−269.

DOI: 10.1021/jf505894b
J. Agric. Food Chem. 2015, 63, 2098−2105

or branched chain. Several pathways for ester biosynthesis have been proposed, but conclusive evidence is lacking for some of the pathways. Precursors of straight-chain (SC) esters have been suggested to be formed from fatty acids by a combination of β-oxidation and lipoxygenase pathways,[11−13] and precursors of branched-chain (BC) esters have been suggested to be formed from the metabolic pathways associated with branched-chain amino acid (BCAA) formation[14−18] and via the recently proposed "citramalic acid pathway".[19] Identification of apple lines in the USDA Geneva *Malus* Germplasm Repository that differ markedly in the composition of their volatile profile should prove useful in the dissection of the various pathways of synthesis for ester precursors. Hypothetically, if the volatile profile data are of adequate quality and detail, statistical associations between classes of alcohols and/or esters should permit the selection of apple lines sufficiently divergent in their volatile profile to enable testing of proposed biochemical pathways.

The objective of this research was to investigate the diversity of volatile esters produced by ripe fruit from each line in the four-copy USDA Geneva *Malus* Core Collection and to use those data to investigate a hypothetical pathway implicated in the formation of odor-active esters. The information will serve to expand the GRIN system database and act as a resource for selection for volatile phenotype in breeding efforts.

MATERIALS AND METHODS

Plant Material. Apple fruit from 172 lines of the four-copy Geneva *Malus* Core Collection and an additional 12 Kazakhstan lines (all *M. sieversii*) were harvested on nine dates between August 24, 2005, and Oct 24, 2005, from the USDA Plant Genetic Resources Unit's *Malus* Germplasm Repository at Cornell University, Geneva, NY, USA. Several lines bore no fruit during the harvest season and so were omitted from the study. The 184 lines consisted of 39 taxa: 20 taxa were primary species (48 accessions), 8 were cultivated species (88 accessions), 9 were secondary species (12 accessions), 1 consisted of unidentified species (2 accessions), and 1 consisted of uncharacterized hybrid species (34 accessions). Harvest times were initially estimated on the basis of the GRIN harvest code, which classified lines relative to the timing for 'Delicious' maturation: (1) extreme early, >60 days before 'Delicious'; (2) very early, 50−60 days before 'Delicious'; (3) early, 30−50 days before 'Delicious'; (4) midearly, 20−30 days before 'Delicious'; (5) mid, 10 days before 'Delicious'; (6) midlate, same time as 'Delicious'; (7) late, 10 days later than 'Delicious'; (8) very late, 20−30 days later than 'Delicious'; (9) extremely late, >30 days later than 'Delicious'.

The harvested apples were packed and secured in a specialized corrugated cardboard box with polyurethane padding containing 7 cm diameter by 5 cm deep cylindrical cavities for individual apples to avoid bruising during shipping. The packed apples were shipped overnight to Michigan State University for evaluation. Samples for each of the 184 lines consisted of 3−50 fruits depending on fruit size and availability on the tree. On each occasion, fruit were held overnight in the laboratory to equilibrate to laboratory temperature (22 ± 1 °C) while covered with ventilated, black, 4 mil (0.1016 mm) thick plastic bags to avoid desiccation and responses to intermittent laboratory light before harvest maturity analysis. In addition to volatile profile, measurements included fresh weight, internal ethylene concentration (IEC), starch index, firmness, background color, and °Brix. Volatile compounds were analyzed after fruits were judged to be ripe according to IEC, starch index, °Brix, background color, and/or perceived intensity of aroma. If the fruit received were not yet ripening, they were re-sent at a later date or held for a short period to enable ripening to commence and re-evaluated.

Ten lines of apple fruit were also obtained from USDA Plant Genetic Resources Unit's *Malus* Germplasm Repository in the second season (2008) of the study based on ester composition determined during the first season. Lines were selected on the basis of their having high or low emission of esters derived from 2-methylbutan-1-ol or 2-methylbutanoate (2MB) relative to SC esters as described below. Handling was essentially the same as for the first year of the study except that the fruits were obtained on two separate dates: prior to the onset of the ethylene autocatalytic burst and after ripening was well advanced. Maturity and volatile analyses performed were the same as for the 184 lines in 2005. Additional analyses included the metabolites citramalic acid and the BCAAs isoleucine, leucine, and valine and the isoleucine precursor, threonine, as described subsequently. Four replicate fruits nearest the IEC median were used for volatile profile measurements, and two replicates (four fruits each) were used for metabolite analyses.

Measurement of IEC. The IEC was determined by withdrawing a 1 mL gas sample from the interior of the apples and subjecting the gas sample to GC (Carle series 400 AGC; Hach Co., Loveland, CO, USA) analysis as previously described.[20] Due to limitations on the interior gas space, the IEC could be accurately determined only on fruit with a mass >5 g. The ethylene detection limit was approximately 0.005 μL L^{-1}. The ethylene concentration was calculated relative to a certified standard (Matheson Gas Products Inc., Montgomeryville, PA, USA) containing 0.979 μL L^{-1} ethylene, 4.85% CO_2, and 1.95% O_2, balanced with N_2.

Measurement of Starch Index and °Brix. The starch index at harvest was determined by cutting fruit in half through the seed cavity along the plane perpendicular to the longitudinal axis. The cut flesh was dipped into an iodine solution containing 10 g of KI and 40 g of I_2 per 4 L of water. Color development was allowed to proceed for at least 1 min. Starch index (1−8) was determined by comparison to the Cornell Starch Chart.[21] °Brix was measured on a drop of juice expressed from the fruit cortex using a hand-held refractometer (Atago N1, Atago Co. Ltd., Tokyo, Japan).

Measurement of Firmness. Firmness was determined only on those lines with a fruit mass >20 g using a drill-stand-mounted Effegi penetrometer (FT-327; McCormick Fruit Tree Inc., Yakima, WA, USA) fitted with an 11 mm diameter probe. The penetrometer was calibrated at 53.4 N (12 lb) using a top-loading balance. Two skin disks (2−3 cm in diameter) and 3−5 mm of underlying cortex tissue were removed from opposite sides of each fruit. The penetrometer probe was pressed into the tissue of the cut surface to a depth of 8−9 mm in a single smooth motion requiring approximately 1 s. Data were recorded as pounds and converted to newtons by multiplying by 4.45 N/lb.

Measurement of Respiration. Respiration was measured as described by Sugimoto et al.,[19] using a 1 L Teflon chamber (Savillex Corp., Minnetonka, MN, USA) and a 20 min holding time at 20 °C. CO_2 concentration was measured on 0.1 mL gas samples withdrawn from a sampling port sealed with a Teflon-lined half-hole septum (Supelco Co., Bellefonte, PA, USA) using an insulin-type 0.5 mL plastic syringe. The gas sample was injected into an infrared gas analyzer (model 225-MK3; Analytical Development Co., Hoddesdon, UK) operated in a flow-through mode with N_2 as the carrier gas and a flow rate of 100 mL min^{-1}. The CO_2 concentration was calculated relative to the certified standard noted previously.

Measurement of Volatiles. For volatile measurement, a GC (HP-6890, Hewlett-Packard Co., Wilmington, DE, USA) was used in conjunction with a time-of-flight mass spectrometer (TOFMS) (Pegasus III, LECO Corp., St. Joseph, MI, USA). Fruit were placed in a 1-L Teflon container (Savillex Corp., Minnetonka, MN, USA) fitted with a gas-sampling port. The number of apples held in the container varied from 1 to 20 depending on the fruit size, and the analysis was performed on a minimum of 10 g of total fruit mass. Sampling ports were sealed with a Teflon-lined half-hole septum (Supelco Co., Bellefonte, PA, USA), and apples were incubated at 22 °C for 20 min. Headspace volatiles were sampled using a 1 cm long, solid-phase microextraction (SPME) fiber (65 μm PDMS-DVB, Supelco Co.) and a 3 min sorption period.[22] After sampling, the SPME fiber was immediately transferred to the GC for desorption and separation of volatiles. The injection port was operated in splitless mode and held isothermally at 230 °C; the desorption time was 2 min.

DOI: 10.1021/jf505523m
J. Agric. Food Chem. 2015, 63, 2106−2116

Desorbed volatiles were trapped on-column using a liquid nitrogen cryofocusing trap. Conditions of GC separation and TOFMS analysis were as previously described.[22] Identification of compounds was by comparison of the mass spectrum with authenticated reference standards and/or with spectra in the National Institute for Standard and Technology (NIST) mass spectrum library (version 05) when no standard was available. Volatile compound concentrations (nanomoles per liter) in the chamber headspace were quantified by calibration with a known concentration of an authenticated, high-purity, 72-component standard mixture of esters and alcohols as previously described.[22] Where no standard was available, quantization was by estimation of the instrument response factor based on the Kovats index for the compound of interest.[23]

Cluster Analysis for Volatiles. Hierarchical cluster analysis was performed on all of the esters detected in this study for all taxons using Cluster 3.0,[24] which was developed from the original program by Eisen et al.[25] and TreeView software.[25] The uncentered correlation and centroid linkage method was used.

Selection of Germplasm Lines for Metabolite Analysis. As noted above, *Malus* sp. lines from high and low 2MB/SC classes were selected for further characterization in season two. SC esters were defined as those having one, two, or four or more carbons arranged in a straight chain on both the alcohol and acid moieties of the ester. 2MB esters were those derived from 2-methylbutanoate or 2-methylbutan-1-ol and having either a branched or straight chain of any length for the complementary alcohol or acid moiety of the ester. The sum of the concentration (nanomoles per liter) of SC and 2MB esters were calculated for each of the 184 lines, and the ratio of 2MB/SC was determined. Selection of "high" and "low" 2MB/SC lines was based on the concentration of 2MB and SC ester concentrations in the chamber headspace and on the ratio of 2MB to SC esters. Selection required 2MB and SC ester emissions to exceed 3 nmol L^{-1}. In addition, high 2MB/SC lines had to have a 2MB/SC ester ratio >1, and low 2MB/SC esters had to have a ratio of <0.15. Fruit mass exceeded 85 g. Selected high 2MB/SC apple lines were 'Jonathan', 'PRI1312-6', 'PRI1176-1', 'Trent', and 'Nova Easygro', which had 2MB/SC ratios of 1.074, 1.180, 1.179, 1.679, and 1.958, respectively. Selected low 2MB/SC lines were 'Virginia Gold', 'Burgundy', 'PRI1850', 'Jonafree', and 'Cox's Orange Pippin', which had 2MB/SC ratios of 0.045, 0.073, 0.116, 0.103, and 0.119, respectively.

Apple lines identified as high and low 2MB/SC esters were shipped in the second season (2008) from the USDA *Malus* Germplasm Repository at the New York Agricultural Experiment Station in Geneva, NY, USA, to Michigan State University as previously described. Twenty fruits were acquired prior to the onset of ripening and after ripening had commenced. Ripening stage was determined on the basis of multiple indices of ripeness including IEC, °Brix, firmness, respiratory rate (CO_2 production), and starch index of the fruit, and the rate of ester synthesis (μmol kg^{-1} h^{-1}) was measured as previously described by Sugimoto et al.[19] IEC, °Brix, firmness, respiratory rate, and starch index averaged, respectively, 0.08 μL L^{-1}, 11.8%, 100.5 N, 27.7 mg kg^{-1} h^{-1}, and 2.0 for "unripe" fruit and 80.4 μL L^{-1}, 15.0%, 74.8 N, 43.6 mg kg^{-1} h^{-1}, and 6.9 for "ripe" fruit. The rates of volatile synthesis were used to calculate the 2MB/SC ratio, the ratio of the sum of 1-propanol- and propanoate-derived esters to SC esters (Prop/SC ratio), the ratio of the sum of 1-butanol- and butanoate-derived esters to SC esters (But/SC ratio), the ratio of the sum of 1-pentanol- and pentanoate-derived esters to SC esters (Pent/SC ratio), and the ratio of 2-methylbutan-1-ol to SC esters (2MBol/SC ratio).

Amino Acid Analysis. Apple tissue used for amino acid analyses was the epidermis and 2−3 mm of cortex removed with a manual rotary peeler (model 8, Goodell, Antrim, NH, USA). Upon collection, tissues were immediately frozen in liquid nitrogen and stored at −80 °C. There were two biological replicates, each consisting of pooled tissue samples from four fruits, and three technical replicates were analyzed per biological replicate. Approximately 5 g of the frozen apple tissue was ground into fine powder using a liquid N_2-cooled mortal and pestle. The ground tissue was divided into three technical replicates, each containing 0.5 g of tissue. The powdered tissue was transferred into 1 mL of preheated water, acetonitrile, and ethanol in 1:1:1 (v/v/v) ratio containing 10 μM deuterated methionine (Met-d_3) (Cambridge Isotope Laboratories Inc., Andover, MA, USA) as an internal standard, mixed vigorously, incubated at 70−80 °C for 5 min, and immediately transferred in ice. After centrifugation at 5000g_n for 10 min at 4 °C, the supernatant was filtered through a 0.22 μm filter (Millex GS, Millipore, Billerica, MA, USA). The cleared filtrate was diluted to one-fifth of its original concentration with water containing the internal standard and used for amino acid analysis.

The amino acids threonine, isoleucine, leucine, and valine (Sigma-Aldrich Corp., St. Louis, MO, USA) were dissolved in water containing 10 μM Met-d_3 to make individual stock solutions of 1 mM. A master mixture was created by mixing amino acids to a final concentration of 50 μM each. A series of six working standards ranging from 0.5 to 40 μM, each containing 10 μM Met-d_3, was prepared by serial dilutions from the 50 μM master mixture using water containing 10 μM Met-d_3. Amino acid samples were quantified by calibration curves obtained from the six working standards using linear regression, plotting amino acid concentration as a function of ratio of the amino acid peak area to the Met-d_3 peak area.

Amino acids were analyzed using a tandem mass spectrometer (Waters Quattro micro, Waters Inc., Milford, MA, USA) coupled to a high-pressure liquid chromatograph (LC-20AD HPLC, Shimadzu, Columbia, MD, USA) equipped with an autosampler (SIL-5000, Shimadzu). The 2.1 × 50 mm column was packed with a 2.7 μm diameter C18 stationary phase (Ascentis Express C18, Sigma-Aldrich) and held isothermally at 30 °C. Injection volume was 10 μL, and solvents used were 1 mM perfluoroheptanoic acid (mobile phase A) and acetonitrile (mobile phase B); the flow rate was held constant at 0.3 mL min^{-1}. The gradient program was as follows: 98% mobile phase A and 2% mobile phase B at start, 10% mobile phase B after 0.1 min, increasing to 25% mobile phase B at 0.5 min and held until 4 min, decreasing to 2% mobile phase B at 4.1 min for re-equilibration of the column. The total run time was 6 min. Mass spectra were acquired using electrospray ionization in positive ion mode (ESI+). The capillary voltage was 3.17 kV, the extractor voltage was 4 V, the rf lens was held at 0.3 V, the cone gas flow rate was 30 L h^{-1}, the desolvation gas flow rate was 400 L h^{-1}, the source temperature was 110 °C, and the desolvation temperature was 350 °C as described by Gu et al.[26] The data acquisition method was split into two functions, the first from 0 to 1.85 min and the second from 1.85 to 6.0 min. Ten multiple reaction monitoring (MRM) transitions were included in function 1 and 11 in function 2. Function number, collision energies, and masses of observed ions for each amino acid are were described by Sugimoto et al.[19] Data were collected and quantified with proprietary software (MassLynx 4.0 and QuanLynx; Waters).

Citramalic Acid Analysis. Approximately 5 g of frozen apple peel from each of the two four-fruit replicates was ground into fine powder using a liquid nitrogen cooled mortal and pestle. The ground tissue was divided into three technical replicates, each containing 0.5 g of tissue. The powdered tissue was transferred into 1 mL of preheated water, mixed vigorously, and incubated at 90−95 °C for 10 min. After centrifugation at 5000g_n for 5 min, the supernatant was filtered through a 0.22 μm filter (Millex GS, Millipore, Billerica, MA, USA), and the cleared filtrate diluted to one-tenth of its original concentration with water was used for analysis.

Citramalic acid (Sigma-Aldrich) was dissolved in water to make a stock solution of 1 mM. A master mixture (50 μM) was created for making standard dilutions. A series of five working standards ranging from 1 to 40 μM was prepared by serial dilutions from the 50 μM master mixture and used to create calibration curves.

Citramalic acid was analyzed using a mass spectrometer (Quattro Premier XE, Waters Corp., Milford, MA, USA) coupled to an ultraperformance liquid chromatograph (UPLC) (Acquity, Waters Corp.). The column (Thermo Betasil C18, 2.1 × 150 mm, 5 μm particles, Thermo Fisher Scientific Inc., Waltham, MA, USA) was held isothermally at 50 °C. The injection volume was 5 μL; solvents were 1 mM *N*,*N*-dimethylhexylammonium acetate (pH 7.7) in water (mobile phase A) and methanol (mobile phase B), and the flow rate was 0.4 mL min^{-1}. The gradient program was as follows: 80% mobile phase A and 20% mobile phase B at start, increasing to 75% mobile phase B

DOI: 10.1021/jf505523m
J. Agric. Food Chem. 2015, 63, 2106−2116

Table 1. Range of Values for Four Maturity Indices for 184 Lines of the Geneva *Malus* Core Collection and Kazakhstan Apple Lines (All *M. sieversii*)[a]

			maturity index			
fruit classification	mass (g)	no. of accessions	ethylene (μL L^{-1})	°Brix	starch index	firmness (N)
small	<2	35	nd	14−32	5−8	nd
small−medium	2−10	20	0.02−176.6	13−32	1−8	nd
medium	10−40	27	0.05−607.1	11−20.5	3−8	47.6−126.8
medium−large	40−100	25	0.19−761.1	11.5−19	2−8	49.4−138.0
large	>100	77	1.09−782.2	11−17.5	3−8	24.0−109.0

[a]Fruit were classified into five categories based on the mass, and the number of accessions that belong to the category is shown. Maturity indices include internal ethylene content, °Brix, starch index (1−8), and firmness. Fruit were harvested on nine dates between Aug 24, 2005, and Oct 24, 2005, from the USDA Plant Genetic Resources Unit's *Malus* Germplasm Repository at Cornell University, Geneva, NY, USA. Internal ethylene and firmness measurements were possible only on fruit with weights greater than 5 and 10 g, respectively. nd, not determined.

after 3 min, and decreasing to 20% mobile phase B at 4 min for re-equilibration of the column. The total run time was 5 min. Mass spectra were acquired using electrospray ionization in negative ion mode. The capillary voltage was set at 3.25 kV, the cone gas flow rate was 40 L h^{-1}, the desolvation gas flow rate was 600 L h^{-1}, the source temperature was 120 °C, and the desolvation temperature was 350 °C. Data were collected and quantified with proprietary software (MassLynx 4.0 and QuanLynx; Waters).

RESULTS AND DISCUSSION

Fruit Characteristics. Fruit mass ranged from 0.3 to 342.3 g (Table 1; Supporting Information, Table S1). For evaluating the relationship between fruit size and other variables, the apple lines were assigned one of five fruit size categories (small, small−medium, medium, medium−large, and large) for comparison. Lines of *M.* × *domestica* used for commercial fruit production were all in the large fruit category. The cube root of fruit weight was correlated with °Brix, internal ethylene, and firmness (data not shown). On average, smaller fruit tended to have a higher °Brix (R^2 = 0.76), lower ethylene (R^2 = 0.86), and higher firmness (R^2 = 0.98) than larger fruit (Table 1). The lower IEC in smaller fruit may, in part, be related to enhanced diffusion characteristics associated with smaller fruit size.[27] A number of the early-maturing varieties had relatively high IEC compared to late ones. IECs for very early to midearly maturing varieties (GRIN harvest codes 2−4) were 128 μL L^{-1} on average, whereas mid to very late maturing varieties (GRIN harvest codes 5−8) were 80 μL L^{-1}. This finding was similar to that from previous studies.[28,29] Harada et al.[30] suggested that the rates of ethylene production in apple are influenced by genotype of 1-aminocyclopropane-1-carboxylate synthase. However, this genotypic relationship was not supported in subsequent studies.[29,31]

High ethylene production did not correlate with low firmness (R^2 = 0.020) and late maturation (based on harvest code) and did not correlate with high firmness (R^2 = 0.005). In our study, medium-sized fruit had a higher firmness than larger fruit, averaging 98 N compared to 70 N for large fruit. De Salvador et al.[32] reported that smaller fruit had a higher firmness than larger fruit in 'Golden Delicious' and 'Red Chief' apples. Vincent[33] suggested that firmness is correlated with fruit density and is partially related to the amount of air space in the flesh. Goffinet et al.[34] reported that fruit size is positively correlated with cortex cell number. The cell density of members of the Geneva *Malus* collection is not known.

When multiple harvests were taken, starch index declined over time (data not shown), although starch degradation remained incomplete for several lines. About 5% of the lines evaluated emitted high levels of volatiles and copious amounts of ethylene even when the starch index was <5 (Supporting Information, Table S1). These lines were members of *M.* × *domestica*, *M.* × *hybrid*, and *M. sieversii* taxa. In some cases, fruit with a starch index of ≤5 became mealy, greasy, and obviously overripe while retaining significant levels of starch. Successful commercial cultivars typically exhibit overripe symptoms only after starch conversion is essentially complete.[35−37]

Ester Abundance and Diversity. Ester diversity tended to increase with increasing fruit weight (Figure 1) and was linearly correlated with the cube root of fruit weight (R^2 = 0.64). Large fruit averaged 46 different esters per variety compared to small fruit, which averaged 10 ester types per variety. A total of 67 different esters including three with unsaturated alkyl groups were detected in the 184 lines evaluated (Table 2). Free acids and formate esters were occasionally detected but not quantified. Alcohol- and acid-derived moieties of the esters tended to be unevenly distributed. For instance, pentyl alcohol-derived esters were abundant only in combination with acetate, but not with longer chain acid moieties. Ester abundance tended to be greatest for esters containing alkyl and alkanoate moieties composed of two, three, four, and six carbons or branched moieties derived from 2-methylbutan-1-ol or 2-methylbutanoate. Esters derived from 2-methylpropan-1-ol, 2-methylpropanoate, methanol, pentanoate, 1-heptanol, heptanoate, 1-octanol, and octanoate were generally in low abundance and less frequently detected. Esters containing unsaturated subgroups were relatively rare, and of these, only acetate esters were detected (Table 2; Supporting Information, Table S1). To our knowledge, unsaturated esters have not been previously detected in the emanations of whole apple fruit.

The three esters most frequently detected in apples of the core collection were butyl acetate (179 lines), hexyl acetate (168 lines), and hexyl 2-methylbutanoate (164 lines). For ester classes segregated by the alkanoate group, acetate esters were most often found in greatest abundance. The three most abundant acetates, in decreasing order, were ethyl acetate, butyl acetate, and 2-methylbutyl acetate. Two of these esters, butyl acetate and 2-methylbutyl acetate, together with hexyl acetate (the fourth most abundant acetate ester in this study) are considered to be primary contributors to apple aroma.[38] For esters classed by the alkyl moiety, ethyl esters tended to be the most abundant, although butyl and hexyl esters, which were slightly less abundant, were found more frequently. Ethyl esters are frequently detected in high amounts in fruits well advanced in their ripening.[7]

The saturated esters detected were consistent with the type and number of esters previously characterized.[4,40,41] In addition, we tentatively identified five esters not previously

DOI: 10.1021/jf505523m
J. Agric. Food Chem. 2015, 63, 2106−2116

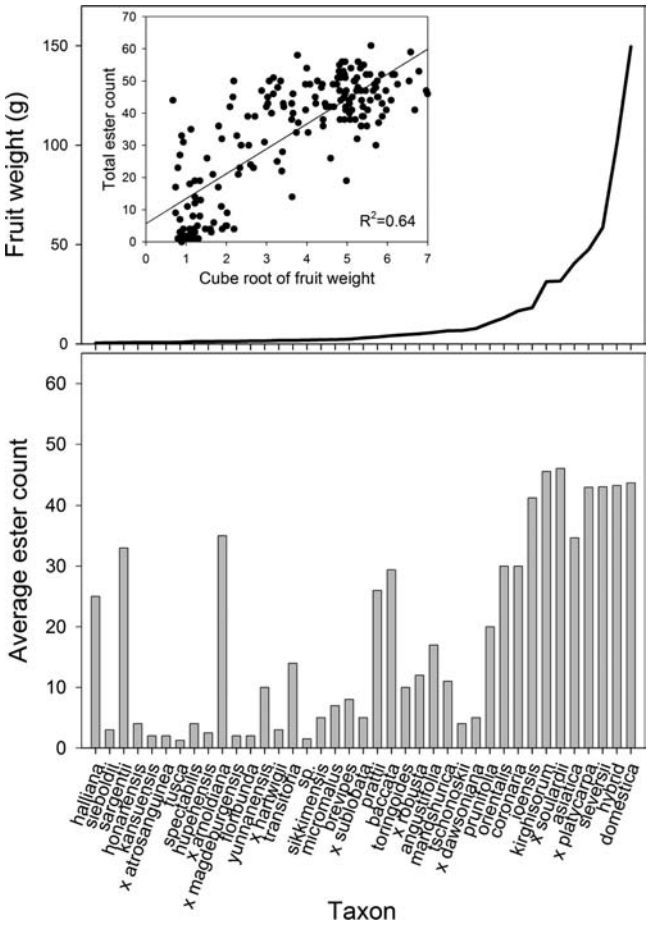

Figure 1. Ester count by taxon based on presence or absence of esters during ripening of the Geneva *Malus* four-copy core collection and the regression between ester count and the cube root of fruit weight. A total of 39 taxa including primary, cultivated, secondary, unidentified, and uncharacterized hybrid species[2] are listed in order by fruit weight ranging from small to large fruit. A total of 67 esters were detected, including 3 unsaturated esters.

reported: propyl 2-methylpropanote, 2-methylbutyl 2-methylpropanoate, heptyl butanoate, octyl 2-methylbutanoate, and methyl octanoate. Six esters (octyl butanoate, propyl pentanoate, pentyl pentanoate, propyl heptanoate, 2-methylpropyl octanoate, and pentyl octanoate) identified previously[4,39−41] were not detected in this study. The five previously unreported esters were found in several *M.* × *domestica* lines.

Cluster analysis of esters according to their alkyl and alkanoate groups across the 184 lines suggested that several classes of esters were more closely associated than others (Figure 2). Unsaturated esters did not cluster with any of the other ester types, which is suggestive of independent regulation. This is supported by what is known about the pathway of formation of the unsaturated C-6 aldehyde precursors,[42] which, as far as is known, would be exclusively via the lipoxygenase pathway.[43] Additionally, a seven-member alkanoate (acid) group (i.e., propanoate, 2-methylbutanoate, butanoate, 2-methylpropanoate, pentanoate, heptanoate, and hexanoate esters), clustered separately from a six-member alkyl ester group (i.e., propyl, 2-methylbutyl, butyl, 2-methylpropyl, pentyl, and hexyl esters). Interestingly, with the exception of heptyl esters, the members of these two clusters are acid and alcohol equivalents of the same carbon backbone. However, the separate clustering according to acid and alcohol precursors suggests differing metabolic regulation of corresponding acid and alcohol precursors for these ester classes. Ethyl and acetate esters clustered together, also, but this might reflect the very high quantity and frequency of ethyl acetate, which contains both ethyl and acetate moieties. Finally, methyl, heptyl, octyl, octanoate, and unsaturated esters clustered individually, suggesting distinct metabolic origins.

Within the alkanoate cluster, 2-methylbutanoate esters clustered with propanoate and butanoate esters. Similarly, Rowan et al.[44] also found a linkage between propanoate and 2-methylbutanoate esters in their evaluation of a diverse population of 240 breeding lines and suggested this and other cluster associations reveal underlying genetic linkages. 2-Methylbutanoate esters are derived from the pathway responsible for isoleucine formation.[16−19] Sugimoto et al.[19] proposed a novel entry point into the pathway for biosynthesis of isoleucine and 2-methylbutanoate (and 2-methylbutan-1-ol) esters by plants. The proposed pathway invoked the synthesis of citramalic acid from the α-keto acid pyruvate and acetyl-CoA in what they termed the "citramalic acid pathway". This pathway has been described in some bacteria and yeast[45−51] and has been implicated in the formation of acyl sugar esters in specialized organs in some Solanaceous plant species.[52] In *Saccharomyces cerevisiae*, the citramalic acid pathway has also been suggested to be present,[53] and citramalic acid synthase activity is evident in baker's yeast[54] and in *Saccharomyces carlsbergensis*.[55]

Sugimoto et al.[19] proposed the citramalic acid pathway would lead to the formation of α-ketobutyrate, elongating the carbon chain of pyruvate by one carbon. Data from bacteria, yeast, and plant studies suggest that α-ketobutyrate can be decarboxylated to yield propanoate and 1-propanol, which could be incorporated into esters. Furthermore, if the carbon backbone of α-ketobutyrate is further elongated by additional cycles of the three steps of the citramalic acid pathway, additional longer chain α-keto acids are formed.[52] For apple, this implies the pathway could also contribute to the formation of butyl, pentyl, and longer straight-chain esters (Figure 3).

Alcohols. Ester diversity is dependent on the diversity of the precursors apples synthesize, including alcohols.[56] In our study, alcohols differed between fruits of different size categories (Figure 4). Small fruit tended to produce methanol and unsaturated alcohols, whereas larger fruit tended to form BC alcohols and three- to six-carbon SC alcohols. The higher tendency of small apple lines to produce unsaturated six-carbon alcohols could be related to a higher peel/flesh ratio, which would mean a higher chloroplast content/flesh ratio. This is consistent with the observation that several LOX enzymes[57] and much of the fatty acid substrate[58] for the lipoxygenase pathway are mainly located in the chloroplasts/plastids.

All of the alcohols that we detected were similar to those reported previously.[4,7,39] In addition, the alcohols 2-butanol, 3-pentanol, 1-penten-3-ol, 2-methyl-2-propanol, and 2-penten-1-ol were also tentatively identified, but not quantified. The alcohols detected include some that have not been reported in apple fruit, but have been detected in other fruits, namely, 1-penten-3-ol and 2-methyl-2-propanol found in tangerine (*Citrus tangerina* Yu. Tanaka)[59] and 2-penten-1-ol found in yellow passion fruit (*Passiflora edulis* f. *flavicarpa*)[60] and kiwifruit (*Actinidia deliciosa* (A. Chev.) C.F. Liang et A.R. Ferguson).[61] On the other hand, 3-penten-2-ol, which has an apple-like

DOI: 10.1021/jf505523m
J. Agric. Food Chem. 2015, 63, 2106−2116

Table 2. Matrix of Detected Esters Organized by Acid and Alcohol Moieties for 184 Lines of the Four-Copy Geneva *Malus* Core Collection and Kazakhstan Apple Lines (All *M. sieversii*)[a]

	acid moiety								
alcohol moiety[b]	acetic	propanoic	2-Mpropanoic	butanoic	2-Mbutanoic	pentanoic	hexanoic	heptanoic	octanoic
methanol	187 (16)	21 (23)	1 (2)	214 (51)	132 (64)	1 (14)	19 (44)	nd (0)	<1 (12)
ethanol	6096 (74)	1570 (62)	70 (39)	2093 (79)	1227 (75)	35 (38)	377 (72)	4 (20)	50 (35)
1-propanol	1538 (67)	354 (66)	11 (49)	451 (77)	303 (74)	nd (0)	58 (70)	nd (0)	2 (26)
2-Mpropanol	259 (60)	25 (26)	1 (4)	35 (52)	14 (55)	nd (0)	4 (30)	nd (0)	nd (0)
1-butanol	3602 (97)	673 (77)	32 (65)	933 (83)	409 (82)	12 (62)	375 (80)	3 (34)	32 (53)
2-Mbutanol	2384 (84)	102 (61)	2 (21)	47 (73)	52 (64)	nd (0)	41 (65)	nd (0)	nd (0)
1-pentanol	504 (74)	110 (50)	2 (24)	32 (68)	27 (65)	nd (0)	12 (59)	nd (0)	nd (0)
1-hexanol	1809 (91)	264 (76)	18 (71)	277 (79)	1053 (89)	8 (53)	301 (77)	nd (0)	18 (14)
1-heptanol	10 (27)	nd (0)	nd (0)	1 (11)	2 (21)	nd (0)	nd (0)	nd (0)	nd (0)
1-octanol	3 (9)	nd (0)	nd (0)	nd (0)	1 (4)	nd (0)	nd (0)	nd (0)	nd (0)
2-hexen-1-ol	0.1 (1)	nd (0)	nd (0)	nd (0)	nd (0)	nd (0)	nd (0)	nd (0)	nd (0)
3-hexen-1-ol	1 (12)	nd (0)	nd (0)	nd (0)	nd (0)	nd (0)	nd (0)	nd (0)	nd (0)
5-hexen-1-ol	11 (40)	nd (0)	nd (0)	nd (0)	nd (0)	nd (0)	nd (0)	nd (0)	nd (0)

[a]Column and row headings refer, respectively, to the acid- and alcohol-derived subgroup of the ester (e.g., ethanol and acetic indicates the ester ethyl acetate). Nonparenthetical data are semiquantitative abundance data based on the sum of ester concentrations for all 184 lines (nmol L^{-1}). Data in parentheses indicate the percentage of the 184 lines producing that ester in detectable quantities. Details of ester complexity and abundance for individual lines can be found in the Supporting Information (Table S1). [b]2-Mpropanol, and 2-Mbutanol indicate 2-methylpropan-1-ol and 2-methylbutan-1-ol, respectively; 2-Mpropanoic and 2-Mbutanoic refer to 2-methylpropanoic and 2-methylbutanoic, respectively; nd, indicates not detected.

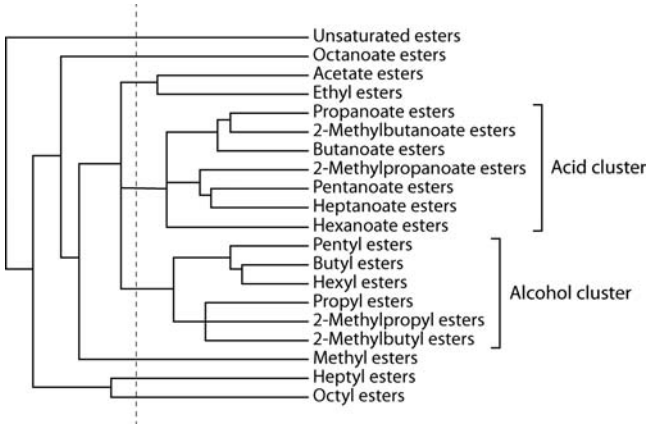

Figure 2. Cluster tree analysis of the esters classified according to alkyl (alcohol) and alkanoate (acid) groups across the four-copy core collection of the Geneva *Malus* Gerplasm Repository. Esters that comprise the alkyl or alkanoate classifications are found in Table 2. Vertical dashed line represents the threshold used for distinguishing clusters.

aroma and is found in 'Starkspur Golden' fruit,[62] was not detected.

Citramalic Acid and the Synthesis of Isoleucine and 2MB Esters. Of the 184 lines evaluated, 8 low and 11 high 2MB/SC lines were found. The lines having either high or low ratios for 2MB/SC esters did not associate with particular species or country of origin, suggesting that the capacity for differential synthesis of the 2MB and SC ester classes is quite ancient in *Malus*. For the 10 lines used for metabolite analysis, the 2MB/SC ratio for high 2MB/SC lines was, on average, 80-fold higher than for low 2MB/SC lines (Table 3). The low 2MB/SC ratios are similar in range to those previously reported for Italian cultivar 'Annurca', which produces primarily SC esters (96.8%) and little of the 2MB or other BC esters.[41] The extreme range in the ratios suggests that 2MB and SC esters are synthesized, at least in part, via differing pathways or are differentially regulated. As noted, ester formation is a function of precursor availability and the specificity of AAT,[63,64] and either of these options may be in play.

BC ester precursors have been proposed to be derived from BCAA degradation,[14,16,18,64] although this interpretation may be incomplete. Sugimoto et al.[19] noted that α-keto-β-methylvalerate, α-ketoisovalerate, and α-ketoisocaproate are precursors to isoleucine, valine, and leucine, respectively, and are also precursors to the BC alcohols and acids incorporated into esters. They found that isoleucine was not depleted, but rather accumulated during ripening in the 'Jonagold' apple, concomitant with the increase in 2MB ester production. They argued in this case an increase in the flux through the pathway, rather than isoleucine catabolism, was primarily responsible for the observed changes in 2MB esters during ripening.

In the current study, isoleucine levels did not differ between high and low 2MB/SC lines in unripe fruit (Table 3). However, upon ripening, isoleucine increased 4−30-fold for high 2MB/SC lines and declined slightly for low 2MB/SC lines. These data are therefore consistent with the suggestion that high 2MB ester production is linked to increased flux from α-ketobutyrate along both branches of the pathway to isoleucine and 2MB esters. Likely, there is an increase in the concentration of the key intermediate α-keto-β-methylvalerate as well, but this has not been determined in ripening apple to our knowledge. It should be noted that even the low 2MB/SC lines produced significant quantities of 2MB esters and that this production was accompanied by a decline in isoleucine of approximately 10 nmol g^{-1} on average. Thus, for some apple varieties, there does indeed appear to be a small depletion in the isoleucine pool. The decline in isoleucine in the low 2MB/SC lines might be sufficient to account for the amount of 2MB ester synthesized given that the rate of 2-methylbutan-1-ol emissions averaged 0.008 nmol g^{-1} h^{-1} and the 2MB ester production was >0.08 nmol g^{-1} h^{-1} for these fruits when ripe (Supporting Information, Table S2), such that in 5 days, a loss of approximately 11 nmol g^{-1} would accrue.

DOI: 10.1021/jf505523m
J. Agric. Food Chem. 2015, 63, 2106−2116

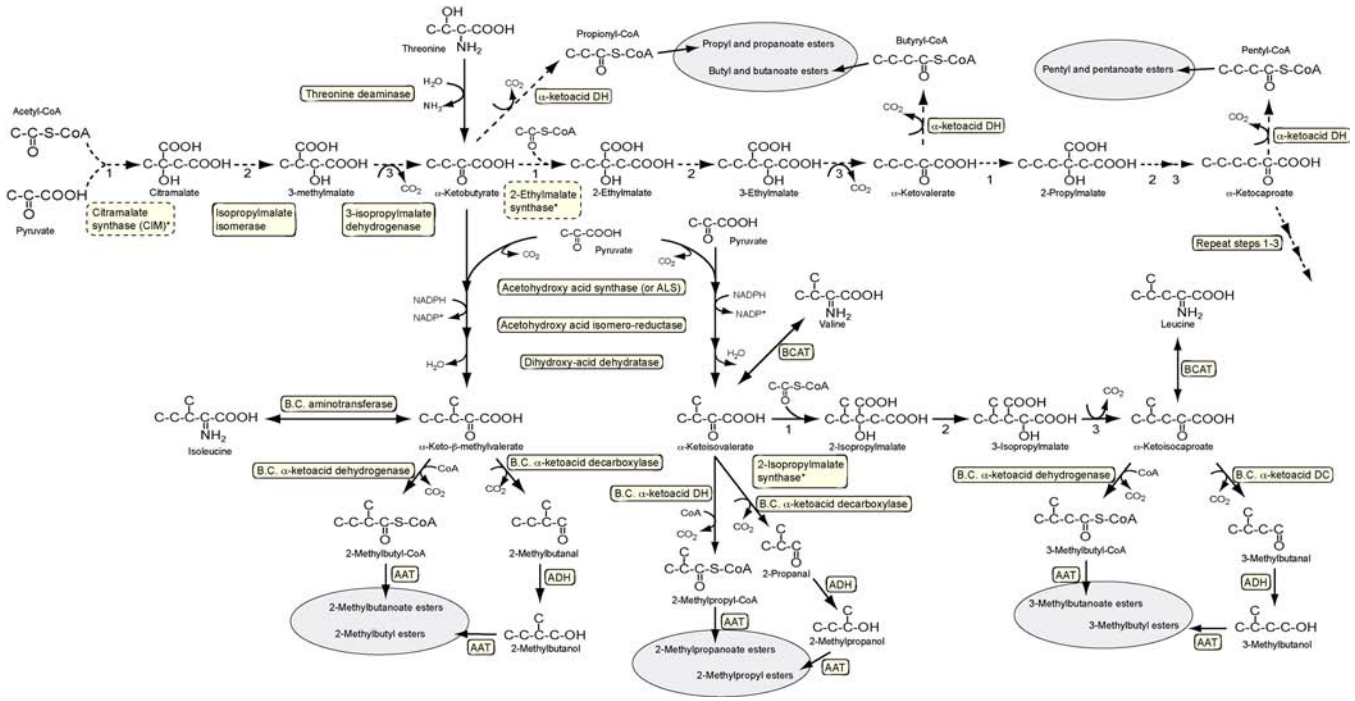

Figure 3. Putative (dashed lines) and demonstrated (solid lines) pathways and pathway elements involved in the biosynthesis of branched-chain amino acids, short, straight-chain fatty acids, and their related esters in plants as proposed by Sugimoto et al.[19] and Kroumova et al.[73] Threonine deaminase is feedback-inhibited by isoleucine, but stimulated by valine; acetohydroxy acid synthase [also known as acetolactate synthase (ALS)] is inhibited by valine and leucine; and 2-isopropylmalate synthase is inhibited by leucine. Hydrogens in carbon−hydrogen bonds are not shown. Reactions 2 and 3 in the putative pathway are considered to be catalyzed by isopropylmalate isomerase and 3-isopropylmalate dehydrogenase, respectively, per leucine biosynthesis.[52] The asterisk indicates similar reactions that may be catalyzed by the same or similar enzymes despite differing nomenclature (e.g., citramalate synthase, ethylmalate synthase, isopropylmalate synthase). BCAT, branched-chain amino transferase; DH, dehydrogenase; DC, decarboxylase; ADH, alcohol dehydrogenase; AAT, alcohol acyl-CoA transferase.

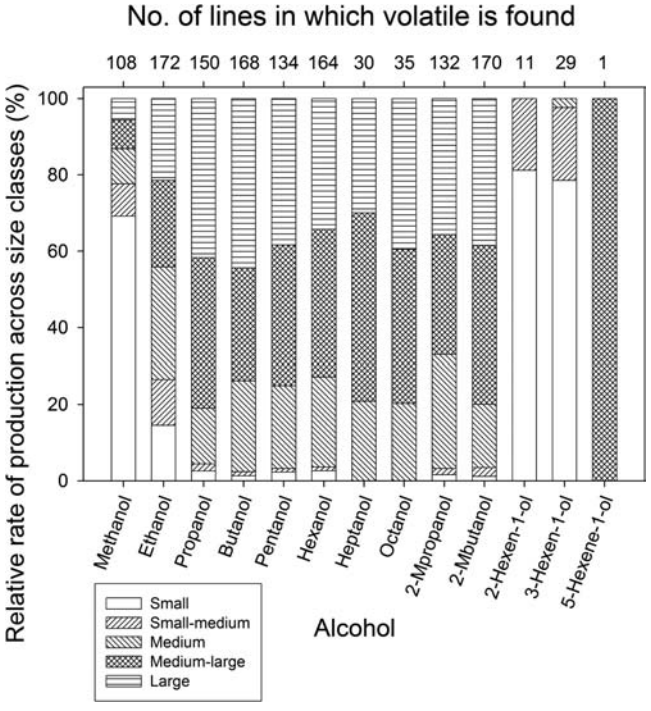

Figure 4. Relative rate of alcohol production across the Geneva *Malus* Core Collection and Kazakhstan apple (all *M. sieversii*) categorized by fruit weight ranging from small to large fruit. The numbers at the top indicate the number of lines in which the volatile is found.

In plants, isoleucine is synthesized from threonine via α-ketobutyrate.[65−68] In this study, the content of threonine was affected by stage of ripening and by 2MB/SC class (Table 3). The threonine content was similar for unripe fruit in low and high 2MB/SC lines, but declined with ripening only in low 2MB/SC lines. If threonine is required for the formation of isoleucine and 2MB esters, then one might expect a similar behavior for both lines as the production of 2MB esters increases with ripening. The approximate 50% reduction in threonine for low 2MB/SC lines upon ripening might suggest a facilitated conversion to α-ketobutyrate. A higher rate of α-ketobutyrate synthesis would be the expected result of lowered isoleucine levels, in that feedback inhibition of threonine deaminase by isoleucine would be lessened.[69,70] However, the lack of a similar reduction in threonine for the high 2MB/SC lines despite a many-fold higher flux in the formation of 2MB esters and accumulation in isoleucine suggests a different mechanism in the formation and/or regulation of this pathway in these lines. In high 2MB/SC lines, the greater rate of formation of 2MB esters was consistently associated with increased isoleucine content, which would not be anticipated in light of the aforementioned feedback inhibition of threonine deaminase by isoleucine. This paradox was also observed for 'Jonagold' apple fruit and led to the suggestion that a citramalic acid-dependent pathway may be functioning in some apple lines.[19]

In the citramalic acid pathway, acetyl-CoA and pyruvate are substrates for the formation of citramalic acid by citramalic acid synthase (CIM), which is a member of the 2-isopropylmalate synthase (IPMS) protein family (Figure 3). The subsequent

DOI: 10.1021/jf505523m
J. Agric. Food Chem. 2015, 63, 2106−2116

Table 3. Volatile Emission Ratios, Branched-Chain Amino Acids, and Citramalic Acid Content in 10 Select Lines of the Four-Copy USDA Geneva *Malus* Core Collection Having a High or Low Ratio of 2-Methylbutyl (2MB) Esters to Straight-Chain (SC) Esters[a]

apple line	ripeness	2MB/SC class	2MB/SC ratio	Prop/SC ratio	2MBol/SC ratio	THR (μmol/g)	LEU (μmol/g)	VAL (μmol/g)	ILE (μmol/g)	CIM (μmol/g)
Virginia Gold	unripe	low				0.099	0.021	0.011	0.020	0.007
	ripe	low	0.028	0.049	0.0038	0.068	0.010	0.004	0.013	0.013
Burgundy	unripe	low				0.185	0.011	0.031	0.012	0.003
	ripe	low	0.039	0.018	0.0107	0.089	0.014	0.016	0.012	0.009
PRI1850	unripe	low				0.294	0.011	0.033	0.010	0.012
	ripe	low	0.008	0.037	0.0023	0.201	0.011	0.016	0.009	0.016
Jonafree	unripe	low				0.260	0.038	0.058	0.048	0.006
	ripe	low	0.041	0.016	0.0153	0.139	0.015	0.017	0.014	0.011
Cox's Orange Pippin	unripe	low				0.276	0.018	0.037	0.023	0.003
	ripe	low	0.017	0.009	0.0035	0.065	0.024	0.023	0.011	0.009
Jonathan	unripe	high				0.200	0.027	0.026	0.036	0.009
	ripe	high	0.812	0.191	0.3425	0.117	0.033	0.016	0.411	0.891
PRI1312-6	unripe	high				0.297	0.028	0.035	0.042	0.006
	ripe	high	0.877	0.723	0.2284	0.183	0.058	0.050	0.605	1.013
PRI1176-1	unripe	high				0.203	0.027	0.027	0.121	0.083
	ripe	high	1.692	1.686	0.7062	0.183	0.044	0.043	0.494	1.283
Trent	unripe	high				0.202	0.023	0.030	0.090	0.049
	ripe	high	2.715	3.784	0.6851	0.133	0.039	0.036	0.431	0.996
Nova Easygro	unripe	high				0.176	0.018	0.034	0.034	0.007
	ripe	high	4.643	1.492	0.3316	0.271	0.066	0.073	0.916	0.837
factor			*p*	*p*	*p*	*p*	*p*	*p*	*p*	*p*
ripeness						<0.001	0.015	0.303	<0.001	<0.001
ripeness within "high"						0.057	<0.001	<0.001	<0.001	<0.001
ripeness within "low"						<0.001	0.331	<0.001	<0.001	0.810
2MB/SC class			<0.001	<0.001	<0.001	0.039	<0.001	<0.001	<0.001	<0.001
2MB/SC class within "unripe"						0.790	0.374	0.378	0.399	0.282
2MB/SC class within "ripe"						0.002	<0.001	<0.001	<0.001	<0.001

[a]2MB esters are represented by the sum of all esters derived from 2-methylbutanoate or 2-methylbutan-1-ol. SC esters are represented by the sum of all esters having 1, 2, or 4 or more carbons arranged in a straight chain on both the alcohol and acid moieties of the ester. Prop/SC ratio indicates the ratio of the sum of all esters derived from propanoate or 1-propanol to SC esters, and the 2MBol/SC ratio is the ratio of 2-methylbutan-1-ol to SC esters.

synthesis of α-ketobutyrate from citramalic acid would bypass threonine and thereby uncouple isoleucine formation from threonine metabolism and associated feedback mechanisms. If active, the citramalic acid pathway would yield increased isoleucine, 2-methylbutan-1-ol, and 2MB ester production concomitant with increased citramalic acid levels. Indeed, this is precisely what was observed in all five high 2MB/SC lines, but in none of the low 2MB/SC lines (Table 3). The extent of enhancement in citramalic acid ranged from approximately 20- to 100-fold in the high 2MB/SC lines. Hulme[71] also isolated citramalic acid from the peel of the mature apple fruit, and its concentration was shown to increase during ripening.[72] Hulme[71] proposed citramalic acid participated in the mitochondrial reactions of the TCA cycle, but no evidence has been forthcoming to support this hypothesis.

Kroumova and Wagner[52] inferred the existence of a fatty acid biosynthetic pathway involving one-carbon elongation from pyruvate through citramalic acid in the formation of sugar esters in some, but not all, members of the Solanaceae [e.g., tobacco (*Nicotiana tabacum*) and petunia (*Petunia* × *hybrida*)]. Kroumova et al.[73] and Kroumova and Wagner[52] noted that their proposed one-carbon elongation pathway for fatty acid biosynthesis would lead to the production of α-keto acids composed of chains of four, five, six, and seven carbons and longer. They noted that a series of straight- and branched-chain acids could be subsequently derived from this pathway via oxidative decarboxylation of the α-keto acids. In the proposed pathway, α-ketobutyrate would be expected to yield propanoic acid, which, in turn, would be activated by acyl acyl-CoA synthase to form propyl-CoA or reduced to form 1-propanol.[53,74−76] If the proposed pathway were preferentially active in the high 2MB/SC lines, then propyl and propanoate esters (Prop esters), butyl and butanoate esters (But esters), and pentyl and pentanoate esters (Pent esters) might also be expected to be elevated in these lines. This relationship was observed, in fact, with high 2MB/SC lines having a roughly 60-fold higher ratio of propyl and propanoate esters relative to SC esters (Prop/SC) than the low 2MB/SC lines (Table 3). Furthermore, there were elevated levels of synthesis of Prop, But, 2MB, and Pent esters and slightly lower synthesis rates of SC esters in the high 2MB/SC lines (Supporting Information, Table S2). Finally, it would be anticipated that enhanced

DOI: 10.1021/jf505523m
J. Agric. Food Chem. 2015, 63, 2106−2116

formation of 2-methylbutan-1-ol esters, which form the bulk of the 2MB esters, would be reflected in a larger pool of 2-methylbutan-1-ol. The ratio of 2-methylbutan-1-ol to SC esters (2MBol/SC) was on average 65-fold higher for the high 2MB/SC lines compared to the low 2MB/SC lines (Table 3), supporting this supposition and further supporting the suggestion that the elevated levels of citramalic acid may be linked with increased production of 2MB esters.

The two BCAAs leucine and valine were also affected by 2MB/SC class and by ripening. Valine, which is linked to the formation of esters derived from 2-methylpropan-1-ol and 2-methylpropanoate (2MP esters), declined approximately 50% during ripening in low 2MB/SC lines, but increased on average by approximately 40% in high 2MB/SC lines. This was true despite a decline in valine content for one line ('Jonathan'), with the end result that that valine levels averaged about 3-fold higher in ripe fruit of the high 2MB/SC lines compared to low 2MB/SC lines. Overall, 2MP ester production was quite low, averaging about $^{1}/_{20}$ that of 2MB esters. The rate of synthesis of 2MP esters (Supporting Information, Table S2) and the ratio of 2MP/SC esters (data not shown) were greater for high 2MB/SC ester lines compared to low 2MB/SC lines. This may suggest that the pathway for 2MP ester formation was influenced by regulatory changes associated with 2MB ester formation, which might be expected given that the pathways for 2MB and 2MP ester formation are quite similar.

Leucine levels were similar for unripe fruit in high and low 2MB/SC lines, increasing about 2-fold during ripening for the high 2MB/SC lines but remaining unchanged for the low 2-MB/SC lines. Interestingly, no esters derived from 3-methylbutan-1-ol or 3-methylbutanoate (3MB esters) were detected in any of the lines (Supporting Information, Table S1), which is in keeping with previously published analyses of apple esters.[5,77−79] The lack of 3MB esters may reflect substrate specificity limitations in AAT[80−87] or the enzymes responsible for BCAA dehydrogenase and decarboxylase reactions (Figure 3).

Collectively, the data demonstrate that the information on ester character for the four-copy core collection of the USDA Geneva *Malus* Germplasm Repository was useful in selecting appropriate apple lines for testing a pathway recently hypothesized to contribute to 2MB ester production. The data for 2MB, SC, Prop, But, and Pent ester synthesis, isoleucine and threonine levels, 2-methylbutan-1-ol production, and citramalic acid accumulation in this study all consistently support the hypothesis put forth by Sugimoto et al.[19] regarding the presence of the citramalic acid pathway in some apple lines. As yet, however, there has been no molecular characterization of the enzyme required for entry into the pathway, CIM, in any plant species to our knowledge.

The metabolite data related to 2MB ester formation suggest that the volatile profiles reported here for the members of the Geneva *Malus* collection may provide useful information in support of further physiological, biochemical, and molecular investigations. Likely, additional patterns could be identified for targeting biochemical pathways linked to ester synthesis. For instance, the ratio of esters derived from 1-hexanol to those derived from 1-butanol ranged from 0 to 10.8, and the ratio of 1-hexanol to 1-butanol ranged from 0 to 4.3, suggesting metabolite analysis might yield interesting new information regarding the formation of ester classes. Finally, our data have been supplied to the USDA GRIN system to expand on the phenotypic data available and are hoped to prove useful in breeding for flavor character in apple and, perhaps, other members of the Rosaceae family.

■ ASSOCIATED CONTENT

Ⓢ Supporting Information

Spreadsheet (Table S1) containing data related to maturity and the production of volatiles from all 184 lines of the USDA *Malus* Germplasm Repository in Geneva, NY, USA, and a table (Table S2) containing data summarizing the rates of synthesis of ester classes in the 10 high and low 2MB/SC lines. This information is intended to be shared and used by readers for the development of hypotheses related to the biochemistry of volatile formation, to identify lines with volatile characteristics that might be valuable as research material, and to identify plant material that might have utility in breeding for improved flavor characteristics. This material is available free of charge via the Internet at http://pubs.acs.org.

■ AUTHOR INFORMATION

Corresponding Author

*(R.B.) Phone: (517) 353-0303. Fax: (517) 353-0890. E-mail: beaudry@msu.edu.

Funding

We acknowledge financial support from the USDA-ARS Crop Germplasm Improvement Program and Michigan State University AgBioResearch.

Notes

The authors declare no competing financial interest.

■ ACKNOWLEDGMENTS

We gratefully acknowledge the technical assistance and advice of Dr. Daniel A. Jones, MSU, and William Srmak, USDA-ARS. We also acknowledge the technical and material support of the USDA *Malus* Germplasm Repository in Geneva, NY, USA.

■ REFERENCES

(1) Way, R. D.; Aldwinckle, H. S.; Lamb, R. C.; Rejman, A.; Sansavini, S.; Shen, T.; Watkins, R.; Westwood, M. N.; Yoshida, Y. Apples (*Malus*). *Acta Hortic.* **1991**, *290*, 3−46.

(2) Forsline, P. L.; Aldwinckle, H. S.; Dickson, E. E.; Luby, J. J.; Hokanson, S. C. Collection, maintenance, characterization, and utilization of wild apples of central Asia. *Hortic. Rev.* **2010**, *29*, 1−61.

(3) Janick, J.; Cummins, J. N.; Brown, S. K.; Hemmat, M. Apples. In *Fruit Breeding: Tree and Tropical Fruits*; Janick, J., Moor, J. N., Eds.; Wiley: New York, 1996; Vol. 1, pp 1−77.

(4) Paillard, N. M. M. The flavour of apples, pears and quinces. In *Food Flavours Part C. The Flavour of Fruits*; Morton, I. D., Macleod, A. J., Eds.; Elsevier: Amsterdam, The Netherlands, 1990; pp 1−41.

(5) Plotto, A.; McDaniel, M. R.; Mattheis, J. P. Characterization of changes in 'Gala' apple aroma during storage using OSME analysis, a gas chromatography-olfactometry technique. *J. Am. Soc. Hortic. Sci.* **2000**, *125*, 714−722.

(6) Guadagni, D. G.; Bomben, J. L.; Hudson, J. S. Factors influencing the development of aroma in apple peels. *J. Sci. Food Agric.* **1971**, *22*, 110−115.

(7) Mattheis, J. P.; Fellman, J. K.; Chen, P. M.; Patterson, M. E. Changes in headspace volatiles during physiological development of 'Bisbee Delicious' apple fruits. *J. Agric. Food Chem.* **1991**, *39*, 1902−1906.

(8) Mattheis, J. P.; Buchanan, D. A.; Fellman, J. K. Change in apple fruit volatiles after storage in atmospheres inducing anaerobic metabolism. *J. Agric. Food Chem.* **1991**, *39*, 1602−1605.

(9) Rudell, D. R.; Mattinson, D. S.; Mattheis, J. P.; Wyllie, S. G.; Fellman, J. K. Investigations of aroma volatile biosynthesis under anoxic conditions and in different tissues of 'Redchief Delicious' apple

DOI: 10.1021/jf505523m
J. Agric. Food Chem. 2015, 63, 2106−2116

fruit (*Malus domestica* Borkh.). *J. Agric. Food Chem.* **2002**, *50*, 2627−2632.
(10) Ueda, Y.; Ogata, K. Coenzyme A-dependent esterification of alcohols and acids in separated cells of banana pulp and its homogenate. *Nippon Shokuhin Kogyo Gakkaishi* **1977**, *24*, 624−630.
(11) Drawert, F. Biochemical formation of aroma components. In *Proceedings of the International Symposium on Aroma Research*; Maarse, H., Groenen, P. J., Eds.; Wageningen: Pudoc, 1975; pp 13−39.
(12) Sanz, C.; Olías, J. M.; Pérez, A. G. Aroma biochemistry of fruits and vegetables. In *Phytochemistry of Fruit and Vegetables*; Tomás-Barberán, F. A., Robins, R. J., Eds.; Oxford University Press: New York, 1997; pp 125−155.
(13) Yahia, E. M. Apple flavor. *Hortic. Rev.* **1994**, *16*, 197−234.
(14) Gonda, I.; Bar, E.; Portnoy, V.; Lev, S.; Burger, J.; Schaffer, A. A.; Tadmor, Y. A.; Gepstein, S.; Giovannoni, J. J.; Katzir, N.; Lewinsohn, E. Branched-chain and aromatic amino acid catabolism into aroma volatiles in *Cucumis melo* L. fruit. *J. Exp. Bot.* **2010**, *61*, 1111−1123.
(15) Pérez, A. G.; Olías, R.; Luaces, P.; Sanz, C. Biosynthesis of strawberry aroma compounds through amino acid metabolism. *J. Agric. Food Chem.* **2002**, *50*, 4037−4042.
(16) Rowan, D. D.; Lane, H. P.; Allen, J. M.; Fielder, S.; Hunt, M. B. Biosynthesis of 2-methylbutyl, 2-methyl-2-butenyl, and 2-methylbutanoate esters in Red Delicious and Granny Smith apples using deuterium-labeled substrates. *J. Agric. Food Chem.* **1996**, *44*, 3276−3285.
(17) Rowan, D. D.; Lane, H. P.; Hunt, M. B.; Allen, J. M. Metabolism of amino acids into aroma volatiles by five apple cultivars. *Acta Hortic.* **1998**, *464*, 490−490.
(18) Tressl, R.; Drawert, F. Biogenesis of banana volatiles. *J. Agric. Food Chem.* **1973**, *21*, 560−565.
(19) Sugimoto, N.; Jones, A. D.; Beaudry, R. M. Changes in free amino acid content in 'Jonagold' apple fruit as related to branched-chain ester production, ripening, and senescence. *J. Am. Soc. Hortic. Sci.* **2011**, *136*, 429−440.
(20) Mir, N. A.; Curell, E.; Khan, N.; Whitaker, M.; Beaudry, R. M. Harvest maturity, storage temperature, and 1-MCP application frequency alter firmness retention and chlorophyll fluorescence of 'Redchief Delicious' apples. *J. Am. Soc. Hortic. Sci.* **2001**, *126*, 618−624.
(21) Blanpied, G. D.; Silsby, K. *Predicting Harvest Date Windows for Apples*; Information Bulletin 221; Cornell University: Ithaca, NY, USA, 1992.
(22) Song, J.; Gardner, B. D.; Holland, J. F.; Beaudry, R. M. Rapid analysis of volatile flavor compounds in apple fruit using SPME and GC/time-of-flight mass spectrometry. *J. Agric. Food Chem.* **1997**, *45*, 1801−1807.
(23) Bartelt, R. J. Calibration of a commercial solid-phase microextraction device for measuring headspace concentrations of organic volatiles. *Anal. Chem.* **1997**, *69*, 364−372.
(24) de Hoon, M. J. L.; Imoto, S.; Nolan, J.; Miyano, S. Open source clustering software. *Bioinformatics* **2004**, *20*, 1453−1454.
(25) Eisen, M. B.; Spellman, P. T.; Brown, P. O.; Botstein, D. Cluster analysis and display of genome-wide expression patterns. *Proc. Natl. Acad. Sci. U.S.A.* **1998**, *95*, 14863−14868.
(26) Gu, L.; Jones, A. D.; Last, R. L. LC-MS/MS assay for protein amino acids and metabolically related compounds for large-scale screening of metabolic phenotypes. *Anal. Chem.* **2007**, *79*, 8067−8075.
(27) Ho, Q. T.; Verboven, P.; Verlinden, B. E.; Herremans, E.; Wevers, M.; Carmeliet, J.; Nicolaï, B. M. A three-dimensional multiscale model for gas exchange in fruit. *Plant Physiol.* **2012**, *155*, 1158−1168.
(28) Hansen, E. Quantitative study of ethylene production in apple varieties. *Plant Physiol.* **1945**, *20*, 631−635.
(29) Oraguzie, N. C.; Volz, R. K.; Whitworth, C. J.; Bassett, H. C. M.; Hall, A. J.; Gardiner, S. E. Influence of *Md-ACS1* allelotype and harvest season within an apple germplasm collection on fruit softening during cold air storage. *Postharvest Biol. Technol.* **2007**, *44*, 212−219.
(30) Harada, M.; Ueda, Y.; Iwata, T. Purification and some properties of alcohol acetyltransferase from banana fruit. *Plant Cell Physiol.* **1985**, *26*, 1067−1074.
(31) Sun, L.; Bukovac, M. J.; Forsline, P.; van Nocker, S. Natural variation in fruit abscission-related traits in apple (*Malus*). *Euphytica* **2009**, *165*, 55−67.
(32) De Salvador, F. R.; Fisichella, M.; Fontanari, M. Correlations between fruit size and fruit quality in apple trees with high and standard crop load levels. *J. Fruit Ornamental Plant Res.* **2006**, *14*, 113−122.
(33) Vincent, J. F. V. Relationship between density and stiffness of apple flesh. *J. Sci. Food Agric.* **1989**, *47*, 443−462.
(34) Goffinet, M. C.; Robinson, T. L.; Lakso, A. N. A comparison of 'Empire' apple fruit size and anatomy in unthinned and hand-thinned trees. *J. Hortic. Sci.* **1995**, *70*, 375−387.
(35) Beaudry, R.; Schwallier, P.; Lennington, M. Apple maturity prediction: an extension tool to aid fruit storage decisions. *HortTechnology* **1993**, *3*, 233−239.
(36) Brookfield, P.; Murphy, P.; Harker, R.; MacRae, E. Starch degradation and starch pattern indices; interpretation and relationship to maturity. *Postharvest Biol. Technol.* **1997**, *11*, 23−30.
(37) de Castro, E.; Biasi, W. V.; Mitcham, E. J. Quality of Pink Lady apples in relation to maturity at harvest, prestorage treatments, and controlled atmosphere during storage. *HortScience* **2007**, *42*, 605−610.
(38) Fellman, J. K.; Miller, T. W.; Mattinson, D. S.; Mattheis, J. P. Factors that influence biosynthesis of volatile flavor compounds in apple fruits. *HortScience* **2000**, *35*, 1026−1033.
(39) Dimick, P. S.; Hoskin, J. C. Review of apple flavor − state of the art. *Crit. Rev. Food Sci. Nutr.* **1983**, *18*, 387−409.
(40) Kakiuchi, N.; Moriguchi, S.; Fukuda, H.; Ichimura, N.; Kato, Y.; Banba, Y. Composition of volatile compounds of apple fruits in relation to cultivars. *J. Jpn. Soc. Hortic. Sci.* **1986**, *55*, 280−289.
(41) Lo Scalzo, R.; Testoni, A.; Genna, A. 'Annurca' apple fruit, a southern Italy apple cultivar: textural properties and aroma composition. *Food Chem.* **2001**, *73*, 333−343.
(42) Feussner, I.; Wasternack, C. The lipoxygenase pathway. *Annu. Rev. Plant Biol.* **2002**, *53*, 275−297.
(43) Contreras, C.; Beaudry, R. M. Lipoxygenase-associated apple volatiles and their relationship with aroma perception during ripening. *Postharvest Biol. Technol.* **2013**, *82*, 28−38.
(44) Rowan, D. D.; Hunt, M. B.; Alspach, P. A.; Whitworth, C. J.; Oraguzie, N. C. Heritability and genetic and phenotypic correlations of apple (*Malus* × *domestica*) fruit volatiles in a genetically diverse breeding population. *J. Agric. Food Chem.* **2009**, *57*, 7944−7952.
(45) Drevland, R. M.; Waheed, A.; Graham, D. E. Enzymology and evolution of the pyruvate pathway to 2-oxobutyrate in *Methanocaldococcus jannaschii*. *J. Bacteriol.* **2007**, *189*, 4391−4400.
(46) Gray, C. T.; Kornberg, H. L. Enzymic formation of citramalate from acetyl-coenzyme A and pyruvate in *Pseudomonas ovalis* Chester, catalysed by "pyruvate transacetase". *Biochim. Biophys. Acta* **1960**, *42*, 371−372.
(47) Hochuli, M.; Patzelt, H.; Oesterhelt, D.; Wuthrich, K.; Szyperski, T. Amino acid biosynthesis in the halophilic archaeon *Haloarcula hispanica*. *J. Bacteriol.* **1999**, *181*, 3226−3237.
(48) Risso, C.; Van Dien, S. J.; Orloff, A.; Lovley, D. R.; Coppi, M. V. Elucidation of an alternate isoleucine biosynthesis pathway in *Geobacter sulfurreducens*. *J. Bacteriol.* **2008**, *190*, 2266−2274.
(49) Howell, D. M.; Xu, H.; White, R. H. (*R*)-Citramalate synthase in *Methanogenic archaea*. *J. Bacteriol.* **1999**, *181*, 331−333.
(50) Westfall, H. N.; Charon, N. W.; Peterson, D. E. Multiple pathways for isoleucine biosynthesis in the spirochete *Leptospira*. *J. Bacteriol.* **1983**, *154*, 846−853.
(51) Xu, H.; Zhang, Y.; Guo, X.; Ren, S.; Staempfli, A. A.; Chiao, J.; Jiang, W.; Zhao, G. Isoleucine biosynthesis in *Leptospira interrogans* serotype lai strain 56601 proceeds via a threonine-independent pathway. *J. Bacteriol.* **2004**, *186*, 5400−5409.
(52) Kroumova, A. B.; Wagner, G. J. Different elongation pathways in the biosynthesis of acyl groups of trichome exudate sugar esters from various Solanaceous plants. *Planta* **2003**, *216*, 1013−1021.

DOI: 10.1021/jf505523m
J. Agric. Food Chem. 2015, 63, 2106−2116

(53) Vollbrecht, D. Three pathways of isoleucine biosynthesis in mutant strains of *Saccharomyces cerevisiae*. *Biochim. Biophys. Acta* **1974**, *362*, 382−389.
(54) Losada, M.; Cánovas, J. L.; Ruiz-Amil, M. Oxaloacetate, citramalate and glutamate formation from pyruvate in baker's yeast. *Biochem. Z.* **1964**, *340*, 60−74.
(55) Sai, T.; Aida, K.; Uemura, T. Studies on (−)-citramalic acid formation by respiration-deficient yeast mutants. V. Purification and some properties of citramalate condensing enzyme. *J. Gen. Appl. Microbiol.* **1969**, *15*, 345−363.
(56) Ueda, Y.; Tsuda, A.; Bai, J. H.; Fujishita, N.; Chachin, K. Characteristic pattern of aroma ester formation from banana, melon, and strawberry with reference to the substrate specificity of ester synthetase and alcohol contents in pulp. *J. Jpn. Soc. Food Sci. Technol.* **1992**, *39*, 183−187.
(57) Schwab, W.; Schiller, D.; Contreras, C.; Vogt, J.; Dunemann, F.; Defilippi, B.; Beaudry, R. A dual positional specific lipoxygenase functions in the generation of flavor compounds during climacteric ripening of apple. *Hortic. Res. (Nature)* **2015**, in press.
(58) Meigh, D. F.; Hulme, A. C. Fatty acid metabolism in the apple fruit during the respiration climacteric. *Phytochemistry* **1965**, *4*, 863−871.
(59) Miyazaki, T.; Plotto, A.; Goodner, K.; Gmitter, F. G., Jr. Distribution of aroma volatile compounds in tangerine hybrids and proposed inheritance. *J. Sci. Food Agric.* **2011**, *91*, 449−460.
(60) Werkhoff, P.; Güntert, M.; Krammer, G.; Sommer, H.; Kaulen, J. Vacuum headspace method in aroma research: flavor chemistry of yellow passion fruits. *J. Agric. Food Chem.* **1998**, *46*, 1076−1093.
(61) Takeoka, G. R.; Guntert, M.; Flath, R. A.; Wurz, R. E.; Jennings, W. Volatile constituents of kiwi fruit (*Actinidia chinensis* Planch.). *J. Agric. Food Chem.* **1986**, *34*, 576−578.
(62) Vanoli, M.; Visai, C.; Rizzolo, A. The influence of harvest date on the volatile composition of 'Starkspur Golden' apples. *Postharvest Biol. Technol.* **1995**, *6*, 225−234.
(63) Echeverría, G.; Graell, J.; López, M. L.; Lara, I. Volatile production, quality and aroma-related enzyme activities during maturation of 'Fuji' apples. *Postharvest Biol. Technol.* **2004**, *31*, 217−227.
(64) Wyllie, S. G.; Fellman, J. K. Formation of volatile branched chain esters in bananas (*Musa sapientum* L.). *J. Agric. Food Chem.* **2000**, *48*, 3493−3496.
(65) Azevedo, R. A.; Arruda, P.; Turner, W. L.; Lea, P. J. The biosynthesis and metabolism of the aspartate derived amino acids in higher plants. *Phytochemistry* **1997**, *46*, 395−419.
(66) Binder, S. Branched-chain amino acid metabolism in *Arabidopsis thaliana*. *Arabidopsis Book* **2010**, *8*, 1−14.
(67) Colau, D.; Negrutiu, I.; Van Montagu, M.; Hernalsteens, J. P. Complementation of a threonine dehydratase-deficient *Nicotiana plumbaginifolia* mutant after *Agrobacterium tumefaciens*-mediated transfer of the *Saccharomyces cerevisiae* ILV1 gene. *Mol. Cell. Biol.* **1987**, *7*, 2552−2557.
(68) Sidorov, V.; Menczel, L.; Maliga, P. Isoleucine-requiring *Nicotiana* plant deficient in threonine deaminase. *Nature* **1981**, *294*, 87−88.
(69) Eisenstein, E. Cloning, expression, purification, and characterization of biosynthetic threonine deaminase from *Escherichia coli*. *J. Biol. Chem.* **1991**, *266*, 5801−5807.
(70) Wessel, P. M.; Graciet, E.; Douce, R.; Dumas, R. Evidence for two distinct effector-binding sites in threonine deaminase by site-directed mutagenesis, kinetic, and binding experiments. *Biochemistry* **2000**, *39*, 15136−15143.
(71) Hulme, A. C. The isolation of L-citramalic acid from the peel of the apple fruit. *Biochim. Biophys. Acta* **1954**, *14*, 36−43.
(72) Hulme, A. C.; Wooltorton, L. S. C. Determination and isolation of the non-volatile acids of pome fruits and a study of acid changes in apples during storage. *J. Sci. Food Agric.* **1958**, *9*, 150−158.
(73) Kroumova, A. B.; Xie, Z.; Wagner, G. J. A pathway for the biosynthesis of straight and branched, odd- and even-length, medium-chain fatty acids in plants. *Proc. Natl. Acad. Sci. U.S.A.* **1994**, *91*, 11437−11441.
(74) Guymon, J. F.; Ingraham, J. L.; Crowell, E. A. The formation of *n*-propyl alcohol by *Saccharomyces cerevisiae*. *Arch. Biochem. Biophys.* **1961**, *95*, 163−168.
(75) Ingraham, J. L.; Guymon, J. F.; Crowell, E. A. The pathway of formation of *n*-butyl and *n*-amyl alcohols by a mutant strain of *Saccharomyces cerevisiae*. *Arch. Biochem. Biophys.* **1961**, *95*, 169−175.
(76) Atsumi, S.; Liao, J. C. Directed evolution of *Methanococcus jannaschii* citramalate synthase for biosynthesis of 1-propanol and 1-butanol by *Escherichia coli*. *Appl. Environ. Microbiol.* **2008**, *74*, 7802−7808.
(77) Ferenczi, A. *Patterns in the Volatile Profile for 'Redchief Delicious' Apple Fruit during Ripening and Senescence*; M.S. thesis, Department of Horticulture, Michigan State University, East Lansing, MI, USA, 2003.
(78) Mattheis, J. P.; Buchanan, D. A.; Fellman, J. K. Volatile compounds emitted by 'Gala' apples following dynamic atmosphere storage. *J. Am. Soc. Hortic. Sci.* **1998**, *123*, 426−432.
(79) Ortiz, A.; Echeverría, G.; Graell, J.; Lara, I. The emission of flavour-contributing volatile esters by 'Golden Reinders' apples is improved after mid-term storage by postharvest calcium treatment. *Postharvest Biol. Technol.* **2010**, *57*, 114−123.
(80) Aharoni, A.; Keizer, L. C.; Bouwmeester, H. J.; Sun, Z.; Alvarez-Huerta, M.; Verhoeven, H. A.; Blaas, J.; van Houwelingen, A. M.; De Vos, R. C.; van der Voet, H.; Jansen, R. C.; Guis, M.; Mol, J.; Davis, R. W.; Schena, M.; van Tunen, A. J.; O'Connell, A. P. Identification of the SAAT gene involved in strawberry flavor biogenesis by use of DNA microarrays. *Plant Cell* **2000**, *12*, 647−662.
(81) Balbontín, C.; Gaete-Eastman, C.; Fuentes, L.; Figueroa, C. R.; Herrera, R. L.; Manriquez, D.; Latché, A.; Pech, J. C.; Moya-León, M. A. *VpAAT1*, a gene encoding an alcohol acyltransferase, is involved in ester biosynthesis during ripening of mountain papaya fruit. *J. Agric. Food Chem.* **2010**, *58*, 5114−5121.
(82) El-Sharkawy, I.; Manríquez, D.; Flores, F. B.; Regad, F.; Bouzayen, M.; Latché, A.; Pech, J. C. Functional characterization of a melon alcohol acyl-transferase gene family involved in the biosynthesis of ester volatiles. Identification of the crucial role of a threonine residue for enzyme activity. *Plant Mol. Biol.* **2005**, *59*, 345−362.
(83) Harada, T.; Sunako, T.; Wakasa, Y.; Soejima, J.; Satoh, T.; Niizeki, M. An allele of the 1-aminocyclopropane-1-carboxylate synthase gene (*Md-ACS1*) accounts for the low level of ethylene production in climacteric fruits of some apple cultivars. *Theor. Appl. Genet.* **2000**, *101*, 742−746.
(84) Holland, D.; Larkov, O.; Bar-Ya'akov, I.; Bar, E.; Zax, A.; Brandeis, E.; Ravid, U.; Lewinsohn, E. Developmental and varietal differences in volatile ester formation and acetyl-CoA: alcohol acetyl transferase activities in apple (*Malus domestica* Borkh.) fruit. *J. Agric. Food Chem.* **2005**, *53*, 7198−7203.
(85) Olías, R.; Pérez, A. G.; Sanz, C. Catalytic properties of alcohol acyltransferase in different strawberry species and cultivars. *J. Agric. Food Chem.* **2002**, *50*, 4031−4036.
(86) Souleyre, E. J. F.; Greenwood, D. R.; Friel, E. N.; Karunairetnam, S.; Newcomb, R. D. An alcohol acyl transferase from apple (cv. Royal Gala), MpAAT1, produces esters involved in apple fruit flavor. *FEBS J.* **2005**, *272*, 3132−3144.
(87) Yahyaoui, F. E.; Wongs-Aree, C.; Latché, A.; Hackett, R.; Grierson, D.; Pech, J. C. Molecular and biochemical characteristics of a gene encoding an alcohol acyl-transferase involved in the generation of aroma volatile esters during melon ripening. *Eur. J. Biochem.* **2002**, *269*, 2359−2366.

DOI: 10.1021/jf505523m
J. Agric. Food Chem. 2015, 63, 2106−2116

JOURNAL OF AGRICULTURAL AND FOOD CHEMISTRY

Addition/Correction

pubs.acs.org/JAFC

Correction to UHPLC-MS/MS Determination of Ochratoxin A and Fumonisins in Coffee Using QuEChERS Extraction Combined with Mixed-Mode SPE Purification

Kristian Fog Nielsen, Archard Ferdinand Ngemela, Lene Bai Jensen, Lívia Soman de Medeiros, and Peter Have Rasmussen*

J. Agric. Food Chem. **2015**, *63* (3), 1029−1034. DOI: 10.1021/jf504254q

The LOQ and LOD values in Table 1 were in error in the ASAP publication of January 16, 2015, and in the issue publication of January 28, 2015. The values have been corrected as of February 13, 2015.

Published: February 13, 2015

ACS Publications © 2015 American Chemical Society

DOI: 10.1021/acs.jafc.5b00716
J. Agric. Food Chem. 2015, 63, 2117−2117

Table 1. Characteristics of the Insecticides Thiamethoxam and Chlorantraniliprole and Maximum Limit of Residues (MRL) Permitted for Rice Grains in Different Countries

parameters	thiamethoxam	chlorantraniliprole
chemical group[a]	neonicotinoid	anthranilicdiamide
molecular formula	$C_8H_{10}ClN_5O_3S$	$C_{18}H_{14}BrCl_2N_5O_2$
molecular Structure	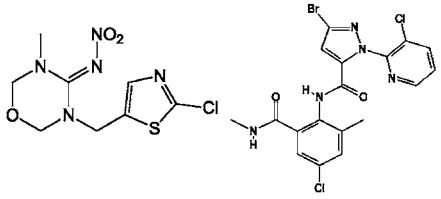	
molecular weight (g mol^{-1})	291.7	483.1
water solubility at 20°C (mg L^{-1})	4.1	0.8
log K_{ow}	-0.13	2.86
dissociation constant (pK_a) at 25°C	Not applicable	10.8
vapor pressure at 25°C (mPa)	6.6×10^{-6}	6.3×10^{-9}
henry's law constant at 25 °C (Pa m^{-3} mol^{-1})	4.7×10^{-10}	3.2×10^{-9}
maximum residue limits (MRL) permitted to rice grain (mg kg^{-1})		
codex alimentarius[b]	---*	0.02
United States[b]	0.02	0.15
European Union[b]	0.6	0.4
Brazil – ANVISA[c]	1.0	0.2
safety interval-ANVISA[c**]	21 days	15 days

[a]IUPAC agrochemical information.[16] [b]U.S. Department of Agriculture.[66] [c]ANVISA, Brazilian Health Surveillance Agency.[67] *Not registered for rice production. **Safety interval between application of the pesticide and harvesting of rice grains in Brazil.

in an uncontrolled release of calcium from internal stores in the sarcoplasmic reticulum,[21] causing impaired regulation of muscle contraction and leading to feeding cessation, lethargy, paralysis, and eventual death of target organisms.[22] Its use provides good lepidoptera control;[23,24] it is a systemic insecticide that tends to be translocated long distances ascendingly[3] in the plant and is recommended for and widely used in irrigated rice crops by foliar application.[11,12] The insecticide moves within the foliar tissue, where it is protected from leaching while remaining available to chewing insects in both top and bottom surfaces of the leaves. This transfoliar activity associated with its insecticide potential, resistance, and photodegradation are the bases for efficient protection in the tomato plant. It is noteworthy that this insecticide presents low toxicity to nontarget organisms such as mammals, birds, fishes, and others,[25,26] a good option for pest control with low environmental impact. The anthranilicdiamide class has no cross-resistance with other insecticide chemical groups[27] and is an efficient alternative in the insecticide rotation.[28]

In rice crops the increasing application of pesticides directly on the organ of the plant that is used for consumption and in association with the fact that rice does not receive intensive industrial processing, the analysis of residues of insecticides on the grain becomes essential as a way to ensure food safety, due to the fact that insecticide residues can persist until the harvest stage, resulting in the contamination of the rice grain.[29−31]

However, pesticides may also affect human life due to pesticide buildup throughout the food chain may lead to an ecologic phenomenon called biomagnification, which is the bioaccumulation of a pesticide through an ecological food chain by transfer of residues from the diet into body tissues. The tissue concentration increases at each trophic level in the food web when there is efficient uptake and slow elimination.[32] However, knowledge pertaining to the long-term effects of pesticides in human health is still very restricted,[33] but indicates that its effects may be associated with several health problems.[34−37] The literature presents several studies related to pesticide residues in food; however, there is little information on the use of insecticides in rice fields and its persistence in the grains. It is important to analyze pesticide residues not only on the rice grain itself but also on rice subproducts such as rice bran, which can be used in whole rice[38] and animal feed.[39,40] Overall, the results of these studies show variation in the presence of pesticide residues in rice grain, likely due to environmental factors that can interact and interfere with the persistence of pesticides. The literature presents several hypotheses regarding what may influence the persistence of pesticides in food, and many such reasons are not fully understood due to the characteristics of the active ingredients,[41,42] the moment of application,[43] solar radiation, temperature,[44] and the persistence of pesticides in plants.[45−47]

Thus, studies analyzing pesticide residues in rice grain are pertinent and provide a better understanding of if and how

DOI: 10.1021/jf5042504
J. Agric. Food Chem. 2015, 63, 2119−2126

Table 2. Pesticides Analyzed by UHPLC-MS/MS Using ESI and EI Ionization, Retention Time, and Cone and Collision Energy for Each Transition Monitored in the SRM Mode

pesticide	retention time (min)	ionization mode	precursor ion (m/z)	cone voltage (eV)	product ion (m/z)	collision energy (eV)
thiamethoxam	0.423	+	291.96	20	211.0;[a] 133.1[b]	12; 13
chlorantraniliprole	0.979	+	483.97	30	285.8;[a] 449.3[b]	14; 29

[a]Ion selected for quantification. [b]Ion selected for confirmation.

technologies used in commercial crops compromise grain quality. Another important issue may be related to the rate of pesticides applied to the aerial parts of plants; however, reports on the use of the recommended rate and double the recommended rate for the insecticide thiamethoxam have not been able to detect residues in polished rice grains.[46] However, it is important to analyze pesticide residues in rice as a whole because in a study with the insecticide thiamethoxam, the highest residue concentration was detected on the rice hull (62% of total detected), followed by rice bran (38% of total detected); no residues were detected on the polished rice grains.[48]

With regard to chlorantraniliprole in rice, residues were detected in polished rice grains varying with the applied rate [30 and 60 g active ingredient (ai) ha^{-1}]. The addition of a double rate of chlorantraniliprole presented the highest values of residues detected in polished rice grains, which was 85% higher than the recommended rate.[49]

The need for information regarding the persistence of pesticides in irrigated rice is relevant because of the nutritional and toxicological issues associated with rice consumption.[48] Therefore, it is necessary to study pesticide residues in rice grains to provide basic information for the use of thiamethoxam and chlorantraniliprole in pest management strategies for rice and grain quality.

The objective of this study was to analyze residues of the insecticides thiamethoxam and chlorantraniliprole in rice hull, bran, and polished grains when applied on the aerial part of the rice plants.

MATERIALS AND METHODS

The study was conducted in two stages; the first stage was conducted in the field and the second in the laboratory.

Experimental Procedures in the Field. The first phase of the experiment was conducted during the 2012 cropping season at Texas A&M Agrilife Research, David R. Wintermann Rice Research Station, near Eagle Lake, TX, USA. The rice was seeded on May 5, 2012, using the cultivar 'Presidio', with a seeding rate of 80 kg ha^{-1}. Each plot had seven rows spaced at 0.19 m from each other and measuring 4 m long. The management practices were conducted according to the technical recommendations for rice cultivation in Texas.[50]

Pesticide applications were performed at 5, 15, 25, and 35 days after flowering (DAF) using 1 and 2 times the recommended rate, that is, 30 g ai ha^{-1} of thiamethoxam and 30 g ai ha^{-1} of chlorantraniliprole (Table 1). Besides, two treatments using the insecticides recommended rate were applied sequentially at 5 and 25 DAF plus at 5, 25, and 35 DAF. Insecticide residues were analyzed in different sample fractions: rice hull, bran, and polished grains.

The applications were made with a CO_2 pressurized backpack sprayer calibrated to dispense a 205 L ha^{-1} spraying volume. The system was attached to a spray boom with three nozzles operating at 276 kPa. The experiment was conducted using a randomized complete block design with four replications.

For quantification of residues in grains, rice plants were harvested when the average moisture content in the grains reached 20%, based on Texas recommendations.[50] Rice harvest was performed 40 DAF from an area totaling 3.8 m^2 (4.0 × 0.95 m) in each plot. After grain harvest, a homogeneous sample of 2 kg was separated for each treatment. Subsequently, samples were cleaned and dried with forced air ventilation at 35 ± 2 °C until reaching an average moisture content of 13%. The samples were then stored at −20 °C during the 30 day period until extraction for pesticide residues.

Insecticide residues were analyzed using different fractions of rice samples including (1) rice hull, (2) rice bran, and (3) polished rice grains. These fractions were obtained by processing the samples in rice milling equipment (Zaccaria, model PAZ-1-DTA, Limeira, SP, Brazil).

Determination of the Pesticide Residues. The second stage of the study was conducted in the Department of Soil and Crop Sciences at Texas A&M University. Prior to chromatographic analysis, samples were extracted using an accelerated solvent extraction Dionex ASE 200 system (Dionex Co., Sunnyvalle, CA, USA), and afterward the samples were analyzed using ultrahigh-performance liquid chromatography–tandem mass spectrometry (UHPLC-MS/MS).

Sample Preparation for ASE. The sample preparation proceeded with 2 g of the matrix (rice hull, bran, or polished grains), 3 g of Chem tube hydromatrix (Agilent Technologies), and 2 g of Florisil (Acros Organics). Sample preparation was carried out in a 50 mL beaker, and the contents were mixed with a spatula to obtain a free-flowing powder. The cell size used was a 22 mL stainless steel cell, using two circular cellulose filters (size = 19.8 mm in diameter) at the low end of the cell. Fortification was done by adding appropriate volumes of solution to the samples, where they were equilibrated in the extraction in cells at room temperature for 10 min.

Optimization of ASE Conditions. Optimal extraction conditions demonstrating the highest chemical recoveries included were extraction temperatures of 75 °C for rice hull and 100 °C for rice bran and polished grains, pressure of 10.3 MPa, and solvent of acetonitrile (100%) determined from a previous experiment (unpublished data). The duration of static phase was 5 min, following 1 min of preheating and 5 min of equilibration. The solvent was collected in 60 mL vials with Teflon septa. Subsequently, each extraction cell containing the same sample went through another identical extraction cycle, and the solvent was collected in the same vial.

Optimization of Evaporation Conditions. The total extracted volume of 60 mL was transferred into 15 mL volumetric tubes 10 mL at a time for sample evaporation using a TurboVap LV Evaporator (Zymark Center, Hopkinton, MA, USA). Samples were evaporated at 45 °C to dryness using a gentle stream of nitrogen. Pesticides were resuspended in 2 mL of acetonitrile and shaken in a vortex mixer (Fisher Vortex Genie2, model G-560; Fisher Scientific, Bohemia, NY, USA) The samples were stored at 4 °C during the 2 h period to complete the preparation of all samples and begin analyses by chromatograph.

Chromatography Conditions. Analyses were performed using an UHPLC-MS/MS, model Acquity TQD (Waters Corp., Milford, MA, USA). Chromatographic separation was done with an ethylene-bridged hybrid (BEH) C_{18} column (50 × 2.1 mm; 1.7 μm) with controlled temperature of 30 °C and a 5 μL injection volume. Mobile phase was pumped from two solvent reservoirs consisting of 0.05% of formic acid in water (A) and acetonitrile (B) in an isocratic run (50 A/50 B) with a flow rate of 0.4 mL min^{-1}, and the estimated void time for this method is 0.3 min. The mass spectrometer was operated using electrospray ionization (ESI) in positive mode, capillary voltage at 2.2 kV, source and dissolution temperatures of 150 and 400 °C, and dissolution and cone gas flows of 800 and 50 L h^{-1}, respectively. Nitrogen (AOC, Bryan, TX, USA) was used as dissolution and cone gas and argon (AOC) as collision gas. The pesticides analyzed were

DOI: 10.1021/jf5042504
J. Agric. Food Chem. 2015, 63, 2119−2126

Table 3. Slope, Intercept, Determination Coefficient (r^2), Limits of Detection, and Limits of Quantification of Pesticides with the UHPLC-MS/MS Method

pesticide	slope	intercept	r^2	LOD (mg kg^{-1})	LOQ (mg kg^{-1})
thiamethoxam	5.2×10^{-3}	4.5×10^{-4}	0.998	0.00015	0.0005
chlorantraniliprole	3.9×10^{-3}	1.2×10^{-4}	0.996	0.00015	0.0005

confirmed using selected reaction monitoring (SRM) mode in which ionizations of the parent and one product were analyzed and monitored for each compound studied (Table 2).

Extraction Efficiency and Statistical Design. The efficiency of the extraction method was determined by sample fortification and analysis of quality control samples. Untreated rice samples were fortified to a concentration of 0.75 mg kg^{1}. The samples were then processed according to the extraction procedure previously described, and six repetitions of each sample were analyzed.

Limit of Detection (LOD) and Limit of Quantification (LOQ). The quantification was based on a seven-point calibration curve (0.0005, 0.001, 0.002, 0.01, 0.1, 0.5, and 1.0 mg kg^{-1}). A matrix effect was obtained by comparing each response generated from calibration standards, which were prepared in pure acetonitrile and in matrix extracts. ME (%) was calculated as follows: $(B/A) \times 100$, where B is a response of matrix-matched calibration standard and A is a slope of non-matrix-matched calibration standard. Matrix effect values between −20 and +20% are considered acceptable.[51]

LOD and LOQ were calculated according to the peak-to-peak noise method.[52] The baseline of the unfortified blank was magnified to obtain the instrument noise response and converted into a concentration estimate from the known concentration of the fortified extract. The LOD was estimated by multiplying the response of the method noise level by approximately 3 and then converting the total response into an estimated concentration. The LOQ was estimated by multiplying the response of method noise level by approximately 10 and then converting the total response into concentration.

Statistical Analysis. The experimental design was a completely randomized factorial arrangement with eight replications in laboratory. Data were subjected to analysis of variance, and means were compared using the Scott−Knott test ($p \leq 0.05$) using the SAS program (Statistical Analysis Systems, 9.2 software, SAS Institute Inc., Cary, NC, USA). The results plotted in the figure were determined by a 95% confidence interval.

RESULTS AND DISCUSSION

Recovery and Detection Limits. The standard calibration curves of thiamethoxam and chlorantraniliprole were constructed by plotting analyzed concentrations with the peak areas. Linearity of curves for each insecticide was achieved within the range from 5×10^{-4} to 1 mg kg^{-1} (Table 3). During the calibration step it was observed that thiamethoxam and chlorantraniliprole insecticides showed an increase or decrease effect in the detector response when the calibration solutions were prepared in matrix extracts or pure solvent. To assess the matrix effect of our extracts, the responses of calibration standard prepared in solvent and matrix extract were compared. In accordance with previously published works, soft matrix effects (suppression or enhancement of 0−20%) are negligible. Otherwise, if the pesticides suffer medium (suppression or enhancement of 20−50%) or strong (suppression or enhancement >50%) matrix effects, it is necessary to use certain calibration methods to overcome the influence of matrix. For hulls, grains, and bran extracts, thiamethoxam presented high suppression (−94, −34, and −88%, respectively). Moreover, for the same extracts chlorantraniliprole presented high suppression for hull (−75%) and bran (−59%). Otherwise, for grains the matrix effect for this pesticide was positive (31%). These results prove the importance of calculating the matrix effect.

The recovery study was conducted for hull, bran, and polished grains. Average recovery ranged from 89.6 to 109.7% with a relative standard deviation <0.05% (Figure 1).

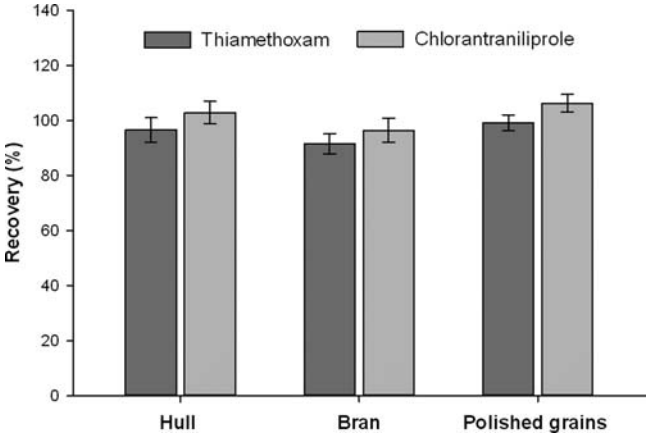

Figure 1. Recovery of thiamethoxam and chlorantraniliprole from rice hull, bran, and polished grains. Bars represent 95% confidence intervals.

Determination of Pesticide Residues in Rice Grains. Results showed thiamethoxam and chlorantraniliprole residues in rice hull, bran, and polished grains (Table 4).

Insecticide Thiamethoxam. For thiamethoxam, pesticide residues were quantified in rice hull for all analyzed treatments. The results showed that greater concentration of pesticides was observed for the sequential applications at 5, 25, and 35 DAF at the recommended rate (0.225 mg kg^{-1}); this result is 20% higher than the average of the other treatments. It is important to highlight that there was no difference regarding the recommended rate and the doubled rate.

The analysis carried out on the rice bran showed that for the insecticide thiamethoxam, the three-time sequential application using the recommended rate and the application at 35 DAF using the double rate resulted in the highest concentration of residues in rice bran. Treatments with applications at 5 and 15 DAF with the recommended rate and twice the rate had lower residues. This behavior may be related to the time between the applications of insecticides and the time of harvest, allowing the metabolism of these compounds,[41,46,53] which includes transformation of parent molecules into metabolites.[54]

Another hypothesis may be the hygroscopic behavior related to rice grains close to harvest,[55] which involves absorption and water loss to reach equilibrium with the relative moisture of the ambient air,[56] along with an increased rate of respiration of grain. This situation can facilitate penetration of insecticides into grain, associated with slow metabolism and translocation of assimilates in the rice plant.[57]

With respect to the analysis conducted in polished rice grains, residues of thiamethoxam insecticide were not detected for the applications using the recommended rate performed at 5 and 15 DAF. However, for all other treatments, residues were detected with the highest values for applications containing

DOI: 10.1021/jf5042504
J. Agric. Food Chem. 2015, 63, 2119−2126

Table 4. Thiamethoxam and Chlorantraniliprole Residues in Rice Hull, Bran, and Polished Grains[a]

rate (g ai ha^{-1})	application done DAF[b]	residue detected (mg kg^{-1}) hull	bran	polished grains
Thiamethoxam				
30	5	0.169 b	0.153 c	nd[c]
30	15	0.158 b	0.136 c	nd
30	25	0.195 b	0.192 b	0.0012 c
30	35	0.182 b	0.185 b	0.0022 b
30 + 30	5, 25	0.167 b	0.160 b	0.0027 b
30 + 30 + 30	5, 25, 35	0.225 a	0.244 a	0.0028 b
60	5	0.143 b	0.131 c	nd
60	15	0.187 b	0.153 c	<LOQ[d]
60	25	0.200 b	0.177 b	0.0040 a
60	35	0.204 b	0.230 a	0.0029 b
Chlorantraniliprole				
30	5	0.529 c	0.486 d	nd
30	15	0.519 c	0.510 d	0.0059 d
30	25	0.586 b	0.600 c	0.0069 c
30	35	0.531 bc	0.785 c	0.0090 c
30 + 30	5, 25	0.575 b	0.780 c	0.0074 c
30 + 30 + 30	5, 25, 35	0.707 a	1.100 a	0.0108 b
60	5	0.557 b	0.444 d	0.0015 d
60	15	0.568 b	0.657 c	0.0114 b
60	25	0.557 b	0.876 b	0.0121 a
60	35	0.601 b	1.125 a	0.0108 b

[a]Means followed by a different letter within a column are significantly different according to the Scott−Knott test ($p \leq 0.05$). Data from each insecticide were analyzed separately. [b]DAF, days after flowering. [c]nd, not detected. [d]<LOQ, below the limit of quantification of the analytical method applied.

twice the rate. Applications with double the recommended rate at 25 DAF resulted in greater concentrations of thiamethoxam residues when compared to sequential applications. This might be associated with a period of intense translocation of assimilates to the grain during rice grain filling.

In summary, the highest insecticide concentrations were observed in rice hull and rice bran, and the mean value detected in polished rice grains alone represents <1% of the total residue value detected on the sample (hull + bran + polished grain). Thus, the lipophilic composition of the hull and bran constituents may serve as a physical barrier to translocation of pesticides, lowering detected values in polished rice grains.[29] Similar tendencies in residue concentration were detected in rice hull, bran, and polished grains when several pesticides used in irrigated rice crops were studied, with results similar to the ones in this study when greater concentrations in hull and rice bran were detected.[48]

Experiments studying the dynamics and persistence of thiamethoxam from the chemical group of neonicotinoids did not show insecticide residues in polished rice grains.[46] Because of the relationship to dissipation and degradation of thiamethoxam in rice plants, about 40−60% of the initial residue dissipated 5 days after application, which after 15 days increased to 83−88%, regardless of the applied rate (33 or 66 g ai ha^{-1}). The calculated half-life values for thiamethoxam in rice plants were found to be 5.2 days for the 33 g ai ha^{-1} rate and 5.8 days for the double rate.[46]

Insecticide Chlorantraniliprole. Chlorantraniliprole residues were detected on the rice hull; it was noted that the applications using the recommended rate at 5−15 DAF resulted in lower pesticide concentrations. This demonstrated that applications made closer to rice flowering using the recommended rate, would favor dissipation or degradation of this insecticide. For other treatments, greater concentrations were quantified, especially for the treatment with three sequential applications that showed the highest value (0.707 mg kg^{-1}).

The literature presents several hypotheses that may influence the concentration of pesticide residues in the irrigated rice ecosystem. Many of the hypotheses are not fully understood because of the numerous factors involved. Some of the primary factors that can influence the persistence of pesticides are time of application, weather conditions, pesticide characteristics, and pesticide translocation within the plant.[58]

However, the adsorption or absorption of insecticides in rice grains, specifically in rice hulls, can be directly associated with the composition of the rice hull, which consists of >90% silica,[59] characterizing the rice hull polarity and contributing to the sequestration of pesticides in rice hull.

Chlorantraniliprole residues were detected on the rice bran, and the detected values are 22% higher than the value detected on the rice hull. The results showed that greater concentration of pesticides was observed for the sequential applications at 5, 25, and 35 DAF at recommended rates and for one application at 60 DAF with double the recommended rate.

These results may be related to the characteristics of the insecticide, highlighting that this insecticide presents greater lipophilic character; thus, distribution on these high lipid content matrices is reasonable.[48] This characteristic can be directly associated with increased quantification of residues in rice bran due to the fact that rice bran has a high lipid content.[60]

No residues for the 5 DAF applications with the recommended rate were detected on the polished rice grain. However, for all other treatments, residues were detected for chlorantraniliprole, with the highest values detected for applications containing double the recommended rate. Applications with double the recommended rate at 25 DAF resulted in greater concentrations of residues when compared to sequential applications. This might be associated with a period of intense translocation of assimilates to the grain during rice grain filling.

Chlorantraniliprole studies in rice plants demonstrated that there was a reduction of 98% of applied insecticide in 14 days after the application independent of the applied rate (30 or 60 g ai ha^{-1}).[49] In brown rice grains (processed grains with no polishing process), chlorantraniliprole residues were detected for the applications done at 21, 14, and 7 days before rice grain harvest for both of the applied rates. The highest values were detected for applications done 7 days before harvest (8 μg kg^{-1}, recommended rate; and 19 μg kg^{-1}, 2 times rate), showing that applications done near rice harvest had the highest residue concentration. In general, there were increases of 74 and 84% in residue concentrations for the applications made at 7 days before harvest in comparison to the application done 21 days before harvest, with the recommended rate and 2 times rate, respectively.[49]

Insecticide Residue Distribution. The distribution of residues throughout the rice grain is presented in Figure 2. The highest concentrations of thiamethoxam were observed in rice hulls, except for applications done at 35 DAF, for which the highest concentration was observed in rice bran.

DOI: 10.1021/jf5042504
J. Agric. Food Chem. 2015, 63, 2119−2126

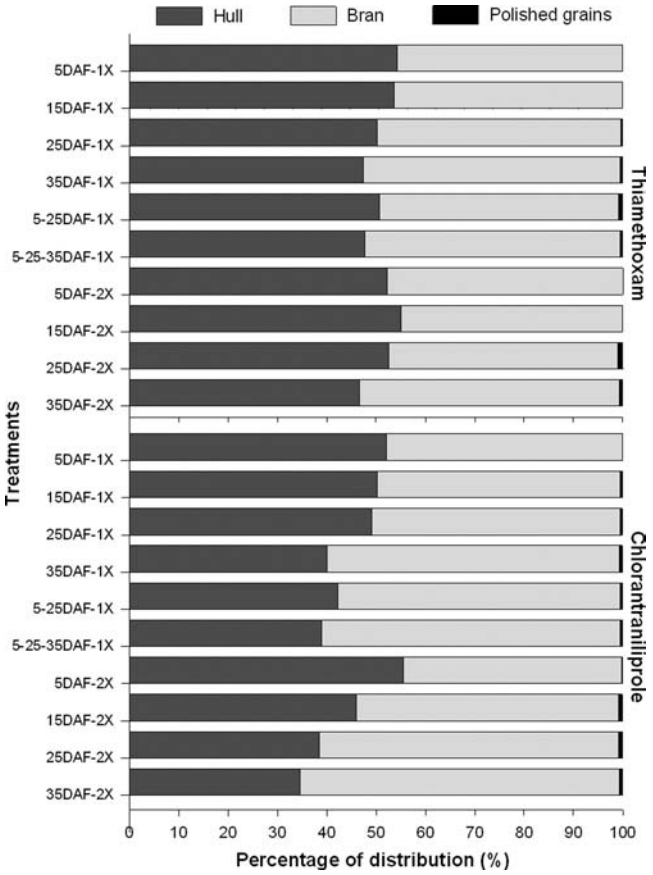

Figure 2. Percentage of thiamethoxam and chlorantraniliporle residues in rice hull, bran, and polished grains. Insecticides were applied at different timings after rice flowering using 1 and 2 times the recommended rate (30 g ai ha^{-1} recommended rate). DAF, days after flowering.

The highest concentrations in rice bran were found for the insecticide chlorantraniliprole, except for applications done at 5 DAF characterizing different behaviors between insecticides. A possible explanation could be that this pesticide is the most lipophilic compound; thus, its distribution on these high lipid content matrices is reasonable. The highest concentration of crude fat is in rice bran,[48] associated with higher concentrations of chlorantraniliprole. The rice hull and polished rice grains presented 96 and 97% less crude fat, respectively.[48]

The literature describes several factors that may influence how pesticide residues in plants may be affected by the time of application, application rate, weather conditions,[61] matrix chemical composition, pesticide lipophilicity, mode of action,[59] time of application, and weather conditions.[58] The correct pesticide residue distribution tendency on the rice grain is not clear; however, higher concentrations of pesticides have been detected on the rice hull and bran.[48]

For the rates applied in this study, the concentrations detected in polished rice grains were below the MRL set by Codex Alimentarius, the United States, the European Union, and the Brazilian Health Surveillance Agency (ANVISA). It is important to note that the MRLs are only for rice grain (Table 1).

It is important that management practices account for the limit of time between pesticide application and grain harvest. Overall, if the pesticides are applied according to good agricultural practices (GAP), MRLs are not exceeded; however, the misuse of these compounds is possible and may result in significant amounts of residues found in both food and the environment.[62,63] Corroborating this approach, there are no consolidated studies on concentrations of pesticide residues quantified in foods, especially those that exceed the maximum allowable limits for human consumption; the effects of accumulation of these compounds in humans are not yet known.[64,65]

In conclusion, the present study demonstrates that residues of thiamethoxam and chlorantraniliprole applied to rice were detected in hull, bran, and polished grains. Insecticide concentrations were higher in hull and bran, demonstrating the importance of evaluating the destination of a pesticide and its residues from the field to the final product.

AUTHOR INFORMATION

Corresponding Author

*(G.M.T.) Phone: (+55) 55-3220.8451. E-mail: gustavo.telo@yahoo.com.br.

Funding

We thank the Coordenação de Aperfeiçoamento de Pessoal de Nivel Superior (CAPES) for providing a doctorate sandwich scholarship to the first author and a postdoctoral scholarship to the fourth author. We acknowledge the Conselho Nacional de Desenvolvimento Científico e Tecnológico (CNPq) for the productivity and research scholarship of the third author.

Notes

The authors declare no competing financial interest.

ACKNOWLEDGMENTS

We thank the Department of Soil and Crop Sciences at Texas A&M University for the opportunity to work with the project.

REFERENCES

(1) Tsochatzis, E. D.; Tzimou-Tsitouridou, R.; Menkissoglu-Spiroudi, U.; Karpouzas, D. G.; Katsantonis, D. Laboratory and field dissipation of penoxsulam, tricyclazole and profoxydim in rice paddy systems. *Chemosphere* **2013**, *91* (7), 1049−1057.

(2) Lucía, P.; Fernández-Alba, A. R. Analytical methods for pesticide residues in rice. *TrAC−Trends Anal. Chem.* **2010**, *30* (2), 270−291.

(3) Jiang, L.; Zhu, L.; Ge, L.; Yang, G.; Wu, J. Rice grain damage by combination and sequence infestations by the rice leaffolder, *Cnaphalocrocis medinalis Guenee* (Lepidoptera: Pyralidae), and the white-backed rice planthopper, *Sogatella furcifera* horváth (Hemiptera: Delphacidae). *J. Integrative Agric.* **2014**, *13* (11), 2460−2470.

(4) Xu, J.; Jiang, L.; Wu, J. Changes in the survival rate and fecundity of the rice leaffolder, Cnaphalocrocis medinalis Guenée (Lepidoptera: Pyralidae), at different magnesium concentrations in hydroponic culture. *Crop Prot.* **2011**, *30* (7), 765−769.

(5) Ferreira, E.; Martins, J. F. S.; Rangel, P. H. N.; Cutrim, V. A. Resistência de arroz ao percevejo-do-colmo. *Pesqui Agropecu Bras.* **1986**, *21* (5), 565−569.

(6) Martins, J. F. S.; Botton, M.; Carbonari, J. J.; Quintela, E. D. Efficiency of *Metarhizium anisopliae* on rice stem bug *Tibraca limbativentris* (Heteroptera: Pentatomidae) control in flooded rice field. *Cienc. Rural* **2004**, *34* (6), 1681−1688.

(7) Ghahari, H.; Chérot, F.; Ostovan, H.; Sakenin, H. Heteroptera from rice fields and surrounding grasslands of northern Iran (Insecta), with special emphasis on predator species. *J. Entomol. Res. Soc.* **2008**, *10* (1), 13−25.

(8) Reay-Jones, F. P. F.; Way, M. O.; Reagan, T. E. Economic assessment of controlling stem borers (Lepidoptera: Crambidae) with insecticides in Texas rice. *Crop Prot.* **2007**, *26* (7), 963−970.

DOI: 10.1021/jf5042504
J. Agric. Food Chem. 2015, 63, 2119−2126

(9) Silva, D. R.; Ferreira, E.; Vieria, N. R. A. Evalution of upland rice losses caused by *Oebalus* spp. (hemíptera: pentatomidade). *Pesqui. Agropecu. Trop.* **2002**, *32* (1), 39−45.
(10) Tindall, K. V.; Williams, B. J.; Stout, M. J.; Geaghan, J. P.; Leonard, B. R.; Webster, E. P. Yield components and quality of rice in response to graminaceous weed density and rice stink bug populations. *Crop Prot.* **2005**, *24* (11), 991−998.
(11) Way, M. O.; McCauley, G. M.; Zhou, X. G.; Wilson, L. T. *2014 Texas Rice Production Guidelines*; Texas AgriLife Research Center at Beaumont, Texas AgriLife Extension and United States Department of Agriculture, Beaumont, TX, USA, 2014; 123 pp.
(12) Sociedade Sul-brasileira de Arroz Irrigado (SOSBAI). Arroz Irrigado: Recomendações Técnicas da Pesquisa para o Sul do Brasil; Bento Gonçalves, Rio Grande do Sul, Brazil, 2014; 189 pp.
(13) Hardke, J. T. *Arkansas Rice Production Handbook*; University of Arkansas Division of Agriculture: Little Rock, AR, USA, 2012.
(14) Muccio, A.; Fidente, P.; Barbini, D. A.; Dommarco, R.; Seccia, S.; Morrica, P. Application of solid-phase extraction and liquid chromatography-mass spectrometry to the determination of neonicotinoid pesticide residues in fruit and vegetables. *J. Chromatogr.* **2006**, *1108* (1), 1−6.
(15) Guzsvany, V. J.; Gaal, F. F.; Bjelica, L. J.; Okresz, S. N. Voltammetric determination of imidacloprid and thiamethoxam. *J. Serb. Chem. Soc.* **2005**, *70* (5), 735−743.
(16) Tomizawa, M.; Latli, B.; Casida, J. E. Structure and function of insect nicotinic acetylcholine receptors studied with nicotinoid insecticide affinity probes. *Abstr. Pap. Am. Chem. Soc.* **1999**, *214*, 271−292.
(17) International Union of Pure and Applied Chemistry (IUPAC). Pesticide properties database; available at http://sitem.herts.ac.uk/aeru/iupac/index.htm (accessed December 2014).
(18) Briggs, G. G.; Bromilow, R. H.; Evans, A. A. Relationships between lipophilicity and root uptake and translocation of non-ionised chemicals by barley. *Pestic. Sci.* **1982**, *13* (5), 495−504.
(19) Gao, C. F.; Ma, S. Z.; Shan, C. H.; Wu, S. F. Thiamethoxam resistance selected in the western flower thrips *Frankliniella occidentalis* (Thysanoptera: Thripidae): cross-resistance patterns, possible biochemical mechanisms and fitness costs analysis. *Pestic. Biochem. Physiol.* **2014**, *114*, 90−96.
(20) Cordova, D.; Benner, E. A.; Sacher, M. D.; Rauh, J. J.; Sopa, J. S.; Lahm, G. P.; Selby, T. P.; Stevenson, T. M.; Flexner, L.; Gutteridge, S.; Rhoades, D. F.; Wu, L.; Smith, R. M.; Tao, Y. Anthranilicdiamides: a new class of insecticides with a novel mode of action, ryanodine receptor activation. *Pestic. Biochem. Physiol.* **2006**, *84* (3), 196−214.
(21) Lahm, G. P.; Selby, T. P.; Freudenberger, J. H.; Stevenson, T. M.; Myers, B. J.; Seburyamo, G.; Smith, B. K.; Flexner, L.; Clark, C. E.; Cordova, D. Insecticidal anthranilic diamides: a new class of potent ryanodine receptor activators. *Bioorg. Med. Chem. Lett.* **2005**, *15* (22), 4898−4906.
(22) Cordova, D.; Benner, E. A.; Sacher, M. D.; Rauh, J. J.; Sopa, J. S.; Lahm, G. P.; Selby, T. P.; Stevenson, T. M.; Flexner, L.; Gutteridge, S.; Rhoades, D. F.; Wu, L.; Smith, R. M.; Tao, Y. Anthranilic diamides: a new class of insecticides with a novel mode of action, ryanodine receptor activation. *Pestic. Biochem. Physiol.* **2006**, *84* (3), 196−214.
(23) Muthusamy, R.; Vishnupriya, M.; Shivakumar, M. S. Biochemical mechanism of chlorantraniliprole resistance in *Spodoptera litura* (Fab) (Lepidoptera: Noctuidae). *J. Asia−Pac. Entomol.* **2014**, *17* (4), 865−869.
(24) Cameron, R. A.; Willians, C. J.; Portillo, H. E.; Marçon, P. C.; Teixeira, L. A. Systemic application of chlorantraniliprole to cabbage transplants for control of foliar-feeding lepidopteran pests. *Crop Prot.* **2015**, *67*, 13−19.
(25) Lahm, G. P.; Stevenson, T. M.; Selby, T. P.; Freudenberger, J. H.; Cordova, D.; Flexner, L.; Bellin, C. A.; Dubas, C. M.; Smith, B. K.; Hughes, K. A.; Hollingshaus, J. G.; Clark, C. E.; Benner, E. A. Rynaxypyr®: a new insecticidal anthranilic diamide that acts as a potent and selective ryanodine receptor activator. *Bioorg. Med. Chem. Lett.* **2007**, *17* (22), 6274−6279.
(26) Larson, J. L.; Redmond, C. T.; Potter, D. A. Comparative impact of an anthranilic diamide and other insecticidal chemistries on beneficial invertebrates and ecosystem services in turfgrass. *Pest Manag. Sci.* **2012**, *68* (5), 740−748.
(27) Cao, G.; Lu, Q.; Zhang, L.; Guo, F.; Liang, G.; Wu, K.; Wyckhuys, K. G. Toxicity of chlorantraniliprole to CryAc-susceptible and resistant strain of *Helicoverpa armigera*. *Pestic. Biochem. Physiol.* **2010**, *98*, 99−103.
(28) Sial, A. A.; Brunner, J. F.; Garczynski, S. F. Biochemical characterization of chlorantraniliprole and spinetoram resistance in laboratory-selected oblique banded leafroller, *Choristoneura rosaceana* (Harris) (Lepidoptera: Tortricidae). *Pestic. Biochem. Physiol.* **2011**, *99*, 274−279.
(29) Dors, G. C.; Primel, E. G.; Fagundes, C. A. A.; Mariot, C. H. P.; Badiale-Furlong, E. Distribution of pesticide residues in rice grain and in its coproducts. *J. Braz. Chem. Soc.* **2011**, *22* (10), 1921−1930.
(30) Jardim, A. N. O.; Caldas, E. D. Brazilian monitoring programs for pesticide residues in food and results from 2001 to 2010. *Food Control* **2012**, *25* (2), 607−616.
(31) Hou, X.; Han, M.; Dai, X.; Yang, X.; Yi, S. A multi-residue method for the determination of 124 pesticides in rice by modified QuEChERS extraction and gas chromatography-tandem mass spectrometry. *Food Chem.* **2013**, *138* (2−3), 1198−1205.
(32) Rand, G. M.; Petrocelli, S. R. *Fundamentals of Aquatic Toxicology*; Hemisphere: Washington, DC, USA, 1985; 1003 pp.
(33) Mostafalou, S.; Abdollahi, M. Pesticides and human chronic diseases: evidences, mechanisms and perspective. *Toxicol. Appl. Pharmacol.* **2013**, *268*, 157−177.
(34) Costa, L. G.; Giordano, G.; Guizzetti, M.; Vitalone, A. Neurotoxicity of pesticides: a brief review. *Front. Biosci.* **2008**, *13*, 1240−1249.
(35) Saadi, H. S.; Abdollahi, M. Is there a link between human infertilities and exposure to pesticides? *Int. J. Pharmacol.* **2012**, *8* (8), 708−710.
(36) Hernandez, A. F.; Parron, T.; Alarcon, R. Pesticides and asthma. *Curr. Opin. Allergy Clin. Immunol.* **2011**, *11* (2), 90−96.
(37) Alavanja, M. C.; Bonner, M. R. Occupational pesticide exposures and cancer risk: a review. *J. Toxicol. Environ. Health B: Crit. Rev.* **2012**, *15* (4), 238−263.
(38) Wu, F.; Chen, H.; Yang, N.; Wang, J.; Duan, X.; Jin, Z.; Xu, X. Effect of germination time on physicochemical properties of brown rice flour and starch from different rice cultivars. *J. Cereal Sci.* **2013**, *2*, 263−271.
(39) Atuahene, C. C.; Donkoh, A.; Ntim, I. Blend of oil palm slurry and rice bran as feed ingredient for broiler chickens. *Anim. Feed Sci. Technol.* **2000**, *83* (3−4), 185−193.
(40) Gadberry, M. S.; Beck, P. A.; Kellogg, D. W.; Gunter, S. A. Digestion characteristics and growth of steers fed a corn−grain based supplement compared to a de-oiled rice bran plus cottonseed supplement with or without extrusion processing. *Anim. Feed Sci. Technol.* **2005**, *118* (3−4), 267−277.
(41) Kanrar, B.; Ghosh, T.; Pramanik, S. K.; Dutta, S.; Bhattacharyya, A.; Dhuri, A. V. Degradation dynamic and persistence of imidacloprid in a rice ecosystem under west bengal climatic conditions. *Bull. Environ. Contam. Toxicol.* **2006**, *77* (5), 631−637.
(42) Komárek, M.; Cadková, E.; Chrastný, V.; Bordas, F.; Bollinger, J. Contamination of vineyard soils with fungicides: a review of environmental and toxicological aspects. *Environ. Int.* **2010**, *36* (1), 138−151.
(43) Navarro, S.; Vela, N.; Navarro, G. Fate of triazole fungicide residues during malting, mashing and boiling stages of beermaking. *Food Chem.* **2011**, *124* (1), 278−284.
(44) Peña, A.; Rodríguez-Liébana, J. A.; Mingorance, M. D. Persistence of two neonicotinoid insecticides in wastewater, and in aqueous solutions of surfactants and dissolved organic matter. *Chemosphere* **2011**, *84* (4), 464−470.
(45) Sundravadana, S.; Alice, D.; Kuttalam, S.; Samiyappan, R. Azoxystrobin activity on *Rhizoctonia solani* and its efficacy against rice sheath blight. *J. Plant Prot.* **2007**, *2* (2), 79−84.

DOI: 10.1021/jf5042504
J. Agric. Food Chem. 2015, 63, 2119−2126

(46) Barik, S. R.; Ganguly, P.; Kunda, S. K.; Kole, R. K.; Bhattacharyya, A. Persistence behaviour of thiamethoxam and λ-cyhalothrin in transplanted paddy. *Bull. Environ. Contam. Toxicol.* **2010**, *85* (4), 419−422.
(47) Macedo, W. R.; Araújo, D. K.; Castro, P. R. C. Unravelling the physiologic and metabolic action of thiamethoxam on rice plants. *Pest Biochem. Physiol.* **2013**, *107* (2), 244−249.
(48) Pareja, L.; Colazzo, M.; Pérez-Parada, A.; Besil, N.; Heinzen, H.; Böcking, B.; Cesio, V.; Fernández-Alba, A. R. Occurrence and distribution study of residues from pesticides applied under controlled conditions in the field during rice processing. *J. Agric. Food Chem.* **2012**, *60* (18), 4440−4448.
(49) Zhang, J. M.; Chai, W. G.; Wu, Y. L. Residues of chlorantraniliprole in rice field ecosystem. *Chemosphere* **2012**, *87* (2), 132−136.
(50) Way, M. O.; McCauley, G. M. *Texas Rice Production Guidelines*; Texas AgriLife Research, Texas AgriLife Extension, and U.S. Department of Agriculture: Beaumont, TX, USA, 2012; 90 pp.
(51) Economou, A.; Botitsi, H.; Antoniou, S.; Tsipi, D. Determination of multi-class pesticides in wines by solid-phase extraction and liquid chromatography-tandem mass spectrometry. *J. Chromatogr., A* **2009**, *1216* (31), 5856−5867.
(52) SANCO. European Commission Health and Consumer Protection Directorate-General. *Guidance Document on Analytical Quality Control and Validation Procedures for Pesticide Residues Analysis in Food and Feed*, 5th ed.; Document SANCO/12571/2013; Brussels, Belgium, 2013; 46 pp.
(53) Phong, T. K.; Nhung, D. T.; Yamazaki, K.; Takagi, K.; Watanabe, H. Behavior of sprayed tricyclazole in rice paddy lysimeters. *Chemosphere* **2009**, *74* (8), 1085−1089.
(54) Ahmed, F. E. Analyses of pesticides and their metabolites in foods and drinks. *TrAC−Trends Anal. Chem.* **2001**, *20* (11), 649−661.
(55) Marchezan, E. Effect of meteorological elements at the harvesting time on the percentage of head rice grains. *Cienc. Rural* **1995**, *25* (2), 191−195.
(56) Mohammed, A. R.; Tarpley, L. Effects of night 30 temperature, spikelet position and salicylic acid on yield and 31 yield-related parameters of rice (*Oryza sativa* L.) plants. *Eur. J. Agron.* **2010**, *33* (2), 117−123.
(57) Bethenod, O.; Le Corre, M.; Huber, L.; Sache, I. Modelling the impact of brown rust on wheat crop photosynthesis after flowering. *Agric. For. Meteorol.* **2005**, *131* (5), 41−53.
(58) Pfeil, R. Pesticide residues: pyrethroids. *Encycl. Food Saf.* **2014**, *3*, 31−34.
(59) Champagne, E. T.; Wood, D. F.; Juliano, B. O.; Bechtell, D. B. *The Rice Grain and Its Gross Composition. Rice Chemistry and Technology*, 3rd ed.; American Association of Cereal Chemists: St. Paul, MN, USA, 2004; pp 77−100.
(60) Lacerda, D. B. C. L.; Soares Junior, M. S.; Bassinello, P. Z.; Castro, M. V. L.; Silva-Lobo, V. L.; Campos, M. R. H.; Siqueira, B. S. Qualidade de farelos de arroz cru, extrusado e parboilizado. *Pesq. Agropec. Trop.* **2010**, *40* (4), 521−530.
(61) Juraske, R.; Castells, F.; Vijay, A.; Muñoz, P.; Antón, A. Uptake and persistence of pesticides in plants: measurements and model estimates for imidacloprid after foliar and soil application. *J. Hazard. Mater.* **2009**, *165* (1−3), 683−689.
(62) Thurman, E. M.; Ferrer, I.; Fernandez-Alba, A. R. Feasibility of LC/TOFMS and elemental database searching as a spectral library for pesticides in food. *Food Addit. Contam.* **2006**, *23*, 1169−1178.
(63) Jardim, I. C. S. F.; Andrade, J. A.; Queiroz, S. C. N. Pesticide residues in food: global environmental preoccupation. *Quim. Nova* **2009**, *32*, 996−1012.
(64) McDuffie, H. H.; Pahwa, P.; McLaughlin, J. R.; Spinelli, J. J.; Fincham, S.; Dosaman, J. A.; Robson, D.; Skinnider, L. F.; Choi, N. W. Non-Hodgkin's lymphoma and specific pesticide exposures in men: Cross-Canada study of pesticides and health. *Cancer Epidemiol. Biomarkers Prev.* **2001**, *10*, 155−1163.
(65) Frampton, G. K.; Dorne, J. L. C. M. The effects on terrestrial invertebrates of reducing pesticide inputs in arable crop edges: a meta-analysis. *J. Appl. Ecol.* **2007**, *44*, 362−373.
(66) U.S. Department of Agriculture. International Maximum Residue Level Database; www.mrldatabase.com (accessed December 2014).
(67) Brazilian Health Surveillance Agency (ANVISA). Monografia de Agrotóxicos; www.portal.anvisa.gov.br./wps/portal/anvisa/anvisa/home (accessed December 2014).

DOI: 10.1021/jf5042504
J. Agric. Food Chem. 2015, 63, 2119−2126

elucidate the role of plant volatile diversity in ecology of this particular insect−plant interaction. The findings on alternative host plant species and the identification of behaviorally active volatile blends in relation to the development of control methods for pea moth are discussed.

MATERIALS AND METHODS

Insects. *C. nigricana* were collected as larvae from infested pea pods in pea fields near Ås in eastern Norway (59°67′N, 10°77′E). The cocoons formed by the larvae were kept over winter in sand substrate under outdoor conditions, and in the spring they were transferred to a cold climate chamber (4 ± 2 °C, 60−70% relative humidity [RH], 0:24 h L:D) as previously stipulated.[19] Approximately 4 weeks before the start of the experiments, the boxes containing the larval cocoons were transferred to Plexiglas cages (30 × 30 × 30 cm) placed in a climate chamber under warmer conditions (18 ± 2 °C, 60−70% RH, 18:6 h L:D) for eclosion. Emerging adults were allowed to mate and had access to 10% honey water solution and water until the start of experiments. Antennal recordings and wind tunnel tests were performed using five- to seven-day-old mated females. Virgin females and males were not tested, because their behavioral response to host plant odor was found to be very low in a preliminary study.[12] After the experiments, the females were dissected to verify their mating status, and only data on mated females were used in the analyses. In oviposition experiments, one male and one female of the same age (five to seven days old) were used.

Plants. As host plants for *C. nigricana*, we used the grain pea, *P. sativum* "Faust", and three other Fabaceae species that are common in the experimental area (Ås in eastern Norway): the broad bean, *Vicia fabae* "Threefold White", the bush vetch, *Vicia sepium*, and the sweet pea, *Lathyrus odoratus* "Old Spice Mixed". An experimental field of *P. sativum* (0.5 ha, square base) was established near Ås on May 6, 2013. On the same day, all four host species were sown in pots (diameter 20 cm) in Plantejord commercial substrate (Plantasjen Norge AS, Kolbotn, Norway). The pots were buried in the ground, and the plants were cultivated under field conditions in experimental cages (1.5 × 1 × 1.5 m, gauze pore size 500 μm) in a location close to the experimental pea field. For oviposition experiments and collection of volatiles, the potted plants were transferred from the field to the laboratory immediately before use.

Plant Phenology and Pea Moth Flight Activity in the Field. The phenology of the potted plants of the four Fabaceae species and the pea plants grown in the experimental field were recorded twice a week according to the BBCH scale, which uses a code to identify the phenological stage of a plant.[20] The flight of *C. nigricana* was assessed in the experimental pea field using E8E10-12AC commercial pheromone monitoring traps (Trifolio-M GmbH, Lahnau, Germany) that were placed in each corner of the field 3 m in from the edge. The trapped moths were counted twice a week during the entire flight period of *C. nigricana*.

Oviposition and Larval Performance. To test *C. nigricana* regarding host plant acceptance (oviposition) and host suitability (larval performance), we performed no-choice experiments and studied egg laying and larval development on the four selected plant species. Cylindrical plant cages (diameter 48 cm, height 65 cm, gauze pore size 500 μm) were placed in a climate chamber under approximately natural conditions for oviposition (18 ± 2 °C, 60−70% RH, 18:6 h L:D), and potted plants from the field (two flowers/plant) were placed individually in separate cages. A male and a female pea moth were kept in each cage for 3 days, and six such moth pairs were tested on each of the four plant species (n = 6). During the experiment, the moths had access to 10% honey water solution and water. The eggs deposited on the plants were counted daily during the three-day period. The plants bearing eggs were subsequently returned to the field, where the pots were again buried in the ground, and the plants were cultivated under field conditions in the field cages until the pods were fully mature. Harvested pods from each plant were placed on a metal net (mesh size 1.2 cm) mounted over a plastic box (15 × 15 × 5 cm) filled with moist sand to enable the late instar (L5) *C. nigricana* larvae to leave their pods, drop to the sand, and spin cocoons to overwinter. The cocoons were counted 4 weeks after pod harvest. To ensure unrestricted development during diapause, the boxes containing the cocoons were stored in an open greenhouse under outdoor conditions but protected against rain until the beginning of February 2014. At that time, the sand was moistened, and the boxes with the larval cocoons were transferred to a climate chamber (18 ± 2 °C, 60−70% RH, 18:6 h L:D) to allow eclosion. Eclosed adults were counted and sexed daily.

Volatile Collection and Chemical Analysis. Volatile compounds were collected from plants at full flowering,[20] using cut plant material from the field. Possible qualitative differences in the volatile profile of this cut material compared to intact plants were accepted in the experimental setup, based on strong behavioral responses to such cut material exhibited by pea moths in a previous study.[12] Headspace collection and analyses of volatile compounds were made according to previously reported protocols.[12] Batches of five aerations of each plant species were conducted for identification and quantification on combined gas chromatography and mass spectrometry (GC-MS). Volatile compounds were identified using Deconvolution Reporting Software (DRS, ver. A.02.00) (Agilent Technologies, Santa Clara, CA), which combines automatic MS deconvolution and identification software (AMDIS version 2.62, NIST), a MS library (NIST05 database), and GC-MS software (ChemStation ver. D.03.00) (Agilent Technologies). The AMDIS database contained 1187 volatile compounds, 240 of which connected to Kovats retention indices.[21] To obtain comparable retention times for all samples, the retention time was locked and referenced according to the internal standard heptyl acetate at 10.75 min using the ChemStation retention time-locking program. Peaks that were present in the chromatogram but were not identified by the DRS were manually interpreted using the NIST05 database. To ensure reliable identification, a match factor of ≥70 was employed.[22] Identification of compounds was verified by comparing mass spectra and Kovats indices with those obtained for synthetic standards on the same column. Enantiomers of chiral compounds were not available. Relative amounts of identified compounds were calculated by dividing the peak area (using the area from the total ion chromatogram) by the area of the internal standard heptyl acetate. The compounds α-pinene, (*Z*)-3-hexenal, and (*E*)-4,8-dimethyl-1,3,7-nonatriene were provided by Yngve H. Stenstrøm (Norwegian University of Life Sciences, Ås, Norway); all other compounds were acquired as standards from Aldrich, Fluka, and Chiron AS.

Electrophysiology. Antennal recordings were made by coupled gas chromatography−electroantennogram detection (GC-EAD) using a HP 6890N GC connected to an electroantennogram apparatus (Syntech, Hilversum, The Netherlands). The column used was a 30 m × 0.25 mm i.d, 0.25 μm, J & W Scientific DB-Wax (Agilent Technologies). After injection of a sample, the temperature was held at 40 °C for 0.5 min, subsequently raised 8.0 °C/min to 160 °C and then 25.0 °C/min to 230 °C, and thereafter held constant at 230 °C for 4.0 min. The total running time was 22.30 min. The effluent from the GC column was split at a ratio of 1:1 between the flame ionization detector (FID) and a pair of *C. nigricana* antennae. Preparation of antennae and connection to EAD were performed according to a previously reported protocol.[12] The antennal signal and the FID signal were amplified and recorded simultaneously using Syntech software. On the basis of the results of the first wind tunnel experiment, volatile collections from *L. odoratus* were selected as the most attractive alternative host plant odor. GC-EAD was performed using the headspace extracts of flowering *L. odoratus* and antennae from mated females (n = 6), and a compound was considered active if four of the six replicates induced an antennal response. The responses were verified by GC-EAD recordings obtained using synthetic standards. The following 17 compounds in headspace extracts were found to induce antennal responses in pea moth females and were tested as synthetic standards, using 10 ng of each compound being delivered to the antennae (n = 6), as described elsewhere:[13] (*Z*)-β-ocimene and (*E*)-β-ocimene (90% pure, mix of isomers *Z*/*E* 1:8), hexan-1-ol (98%), (*E*)-2-hexen-1-ol (96%), (Z)-3-hexenal (98%), (*E*)-2-hexenal (98%), octanal (98%),

DOI: 10.1021/jf505934q
J. Agric. Food Chem. 2015, 63, 2127−2136

Table 1. Presence or Absence of Volatile Compounds in Headspace Extracts from Flowering Plants of the Four Fabaceae Host Species *P. sativum*, "Faust", *V. fabae*, "Threefold White", *V. sepium*, and *L. odoratus*, "Old Spice Mixed"

compound[a]	RT[b]	RI[c]	*P. sativum* $n = 5$	*V. fabae* $n = 5$	*V. sepium* $n = 5$	*L. odoratus* $n = 5$
α-pinene	4.24	1028	X	X		X
hexanal	5.14	1080	X	X	X	
sabinene	5.84	1120				X
(*Z*)-3-hexenal	6.14	1136	X	X	X	X
myrcene	6.66	1161				X
(*E*)-2-hexenal	7.57	1209	X	X	X	X
(*Z*)-β-ocimene	8.02	1232	X	X	X	X
(*E*)-β-ocimene	8.33	1247	X	X	X	X
hexyl acetate	8.77	1270	X	X	X	
octanal	9.05	1285	X	X	X	X
(*E*)-4,8-dimethyl-1,3,7-nonatriene	9.44	1304			X	X
(*Z*)-3-hexenyl acetate	9.57	1314	X	X	X	X
(*E*)-2-hexenyl acetate	9.91	1327	X		X	X
hexan-1-ol	10.32	1370	X	X	X	X
(*Z*)-3-hexen-1-ol	10.85	1376	X	X	X	X
nonanal	11.07	1387	X	X	X	X
(*E*)-2-hexen-1-ol	11.27	1398	X	X	X	X
1-octen-3-ol	12.12	1445	X		X	
2-ethylhexan-1-ol	12.89	1484	X	X	X	X
decanal	13.04	1492	X	X	X	X
benzaldehyde	13.16	1499				X
linalool	13.90	1540		X		X
1-octanol	14.12	1553			X	
β-caryophyllene	14.79	1593		X	X	X
phenylacetaldehyde	15.23	1617				X
(*Z*)-β-farnesene	15.60	1639				X
humulene	16.01	1664		X	X	
valencene	16.67	1704		X	X	
nerol acetate	16.90	1717				X
(*E*,*E*)-α-farnesene	17.34	1742		X	X	
methyl salicylate	17.45	1758	X		X	
citronellol	17.54	1758				X
β-sesquiphellandrene	17.63	1763				X
nerol	18.04	1789				X
dendrolasin	18.29	1805		X	X	
geraniol	18.77	1873				X

[a]Compounds present in a given sample are denoted with an X. Detection threshold ~0.2 μg/100 g plant material. All compounds except those indicated in bold text were verified by comparison of Kovats retention index and mass spectra with synthetic standards. [b]RT, retention time. [c]RI, Kovats retention index, DB-Wax.

(*Z*)-3-hexenyl acetate (98%), (*Z*)-3-hexen-1-ol (98%), nonanal (95%), (±)-sabinene (75%), myrcene (90%), (±)-linalool (97%), (±)-β-caryophyllene (80%), phenylacetaldehyde (90%), (±)-citronellol (95%), and nerol (97%).

Wind Tunnel. The wind tunnel used in this study had a flight section of 67 × 88 × 200 cm and has been described previously.[23] The air flow through the tunnel was 30 cm/s, and inside the tunnel the light intensity was approximately 1000 lx, the temperature ranged from 20 to 22 °C, and the RH was 60−70%. An ultrasonic sprayer equipped with a conical nozzle (Sono-Tek corporation, Milton, NY) and connected to a model 102 syringe pump (CMA Microdialysis AB, Solna, Sweden) was used to introduce the volatiles in the tunnel as described previously.[12,13] *C. nigricana* females were placed individually in glass tubes (12.5 × 2.6 cm) and transferred to the room housing the wind tunnel 3 h before the start of the experiments. All wind tunnel tests were conducted 5 to 1 h before the scotophase, corresponding approximately to the natural period of highest pea moth activity. The tubes containing the female moths were placed separately in the downwind end of the tunnel, 30 cm above the floor and at a distance of 160 cm from the odor source, and then the moths were set free and allowed to respond to the odor for 6 min. The flight behavior of the females was observed during that time, and landings were recorded. The order of the tested treatments was randomized each experimental day.

Wind Tunnel Experiment 1. To assess the attraction of *C. nigricana* females to olfactory cues of different Fabaceae species without visual cues, we investigated the upwind orientation of mated females toward headspace extracts. Volatile collections from *P. sativum*, *V. fabae*, *V. sepium*, and *L. odoratus* were tested. For each plant species, 50 mated females were tested in five batches of 8−12 individuals, and each batch was tested on different days, with a total of 40−60 moths tested on each experimental day. All but one of the tested females responded (flight activation) to the headspace extract within the 6 min exposure period. On the basis of the recorded landing responses in this experiment, the headspace extract of flowering *L. odoratus* was selected as the most attractive alternative host plant odor for use in further analyses.

Wind Tunnel Experiment 2. The 17 compounds from flowering *L. odoratus* inducing antennal responses in mated *C. nigricana* were selected for a second wind tunnel experiment. In this experiment, five different blends of the mentioned compounds (denoted stimuli II_{WT}−VI_{WT}) were tested using the quantities and ratios identified in

DOI: 10.1021/jf505934q
J. Agric. Food Chem. 2015, 63, 2127−2136

flowering sweet pea plants by GC-MS analysis (Figure 4). The headspace extract of flowering *L. odoratus* (stimulus I_{WT}) was used as a control for natural odor. To identify the volatiles involved in attraction of pea moths, the 17-compound sweet pea flower mimic (stimulus II_{WT}) was split into a ten-compound blend (stimulus III_{WT}) and a seven-compound blend (stimulus IV_{WT}). The ten-compound blend contained the common sweet pea flower volatiles that were also emitted from flowering pea plants and the other Fabaceae species, whereas the seven-compound blend contained the more specific sweet pea flower volatiles that were not released by *P. sativum* (Table 1). Since substantial attraction of *C. nigricana* to a blend of (*Z*)-*β*-ocimene, (*E*)-*β*-ocimene, hexan-1-ol, and (*E*)-2-hexen-1-ol had been observed in wind tunnel and field tests in a previous study,[13] we also combined these four compounds with the sweet-pea-specific seven-compound blend to yield an 11-compound blend (stimulus V_{WT}). Furthermore, due to the dominance of (*Z*)- and (*E*)-*β*-ocimene in pea and sweet pea flowers, shown by GC-MS analyses in the present study and other investigations,[12,24−26] and the importance of these compounds in pea moth attraction,[13] we combined (*Z*)-*β*-ocimene and (*E*)-*β*-ocimene with the sweet-pea-specific seven-compound blend to obtain a nine-compound blend (stimulus VI_{WT}). For each odor stimulus, 50 mated females were tested in five batches of 8−12 individuals, and each batch was tested on different days, using a total of 40−60 moths on each experimental day. All but three of the tested females exhibited flight activation in response to the synthetic blends within the 6 min test period.

Field Experiment. To confirm attraction of mated female moths to the synthetic blends, we conducted a trapping experiment in 2013 in the experimental pea field near Ås. This square field was surrounded by birch forest (*Betula* spp.), with wheat (*Triticum aestivum*) and grassland in the immediate vicinity. The peas were sown on May 6, the first flower buds appeared on June 18, and the flowering period started on June 27. (*Z*)- and (*E*)-*β*-Ocimene were only available as a mixture of isomers at a ratio of 1:8, which corresponds approximately to the natural release of these compounds from pea flowers (12.6:110.0 ng/h (*Z*:*E*))[12] and sweet pea flowers (11.5:100.0 ng/h; GC-MS analyses in the present study). Therefore, the *β*-ocimenes were used at a *Z*:*E* ratio of 1:8 in all blends in the field, whereas all other synthetic compounds were present at a 1:1 ratio (Figure 5). The total load of active ingredients in each dispenser was always 9 mg. The blends were diluted in mineral oil and pipetted on dispensers consisting of 1 cm Parotisroll, size 5 cotton wicks (Roeko, Langenau, Germany) inserted into 1.5 mL Easy-Fit polypropylene microtubes (Treff, Degersheim, Switzerland). The dispensers were mounted in cardboard delta traps equipped with sticky yellow bottoms (16.5 × 18 × 13 cm) (Silvandersson Sweden AB, Knäred, Sweden). In the field, the traps were installed on metal stands (height 1.2 m, diameter 0.8 cm) above the vegetation. When the first flower buds appeared on the pea plants, the traps were placed in the borders of the field (3 m from the edge) 5 m apart. Trapped moths were counted and sexed twice a week over a period of 5 weeks (10 trap inspections) from calendar week (CW) 25 (18 June) until the end of the pea moth flight period (CW 31). The mating status of the moths caught in the traps was not investigated. On the basis of the results of the wind tunnel experiments, four field stimuli (II_F, III_F, IV_F, and VI_F) and a blank control (pure mineral oil) were tested (Figure 5). Stimulus V was not tested in the field experiment, because stimuli V and VI had induced similar responses in wind tunnel experiment 2 (Figure 4) and a preliminary field test. As natural flower control (stimulus I_F), detached flowers of *L. odoratus* were inserted separately in 1.5 mL polypropylene microtubes filled with water, and these tubes were then mounted in cardboard delta traps in the same manner as the dispensers containing the synthetic blends. The microtubes were furnished with fresh flowers and water refills daily. For each treatment, four traps were installed in the experimental field, one on each side (n = 4). The dispensers were replaced after 2.5 weeks, because preliminary tests had shown that they retain their attraction capacity for that length of time.[13] In addition to the kairomone traps containing the female attractants, pheromone traps were used in the field as described above. Neither pest infestation nor crop damage was recorded in this experiment, because the objective was to test attraction of *C. nigricana* to synthetic volatile blends in a natural setting, not to evaluate pest management efficacy.

Statistical Analysis. The data on proportion of landings in the wind tunnel and total number of moths trapped in the field experiment were subjected to Levene's test to evaluate variance homogeneity and, if necessary, were subsequently normalized using arcsine square root or log transformation. Differences between treatments were assessed by analysis of variance (ANOVA). Due to the factorial design of the field experiment, the interaction effects were evaluated in addition to the effects of individual factors. If significant *F*-values were obtained, treatment means were compared using Tukey's test.[27] Data recorded as repeated measures over time were analyzed by repeated measures ANOVA, considering dates of evaluation as repeated parameters and using AUC (area under the curve) estimates.[28] If ANOVA showed significant differences between treatments, Tukey's test was used for multiple comparisons. Individual ANOVAs were performed to identify particular time intervals in which treatment effects differed. In all analyses, a significance level of α = 0.05 was selected using SAS 9.2 (SAS Institute Inc., Cary, NC).

RESULTS AND DISCUSSION

Selection of Attractive Alternative Host Plant Species. Several studies have shown that *C. nigricana* can use a number of pea-related herbaceous legumes as host plants, although *P. sativum* is the preferred host.[9−11] However, to our knowledge, no previous investigations have compared different Fabaceae species with regard to the attraction and oviposition responses they induce in pea moth females or their suitability for development of pea moth larvae. Therefore, we compared the phenology, and particularly the flowering period, of four Fabaceae species that can serve as host plants for *C. nigricana*, which showed that the wild-growing bush vetch *V. sepium* flowered much earlier than the other three tested species (Figure 1). The cultivated pea *P. sativum* and the broad bean *V. fabae* flowered at approximately the same time, and the sweet pea *L. odoratus* flowered later (Figure 1). Even though these four Fabaceae species had different flowering periods, they were all in bloom during the period of pea moth flight activity (Figure 1). In this study, we compared the phenologies of four host plant species, all sown on the same day. These species probably exhibit shifts in phenology as a function of abiotic or biotic parameters, such as sowing date, climatic conditions, or pest infestation. Nevertheless, a general concurrence of host plant flowering and pea moth flight activity can be assumed for

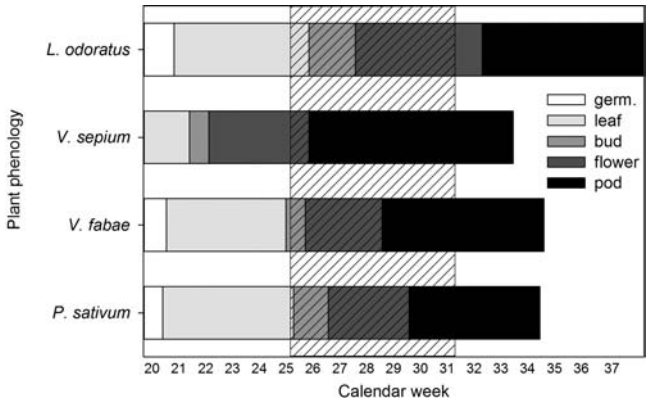

Figure 1. Phenology (germination, leaf, bud, flower, and pod stages) from sowing to harvest shown for the four tested host plant species *P. sativum*, "Faust", *V. fabae*, "Threefold White", *V. sepium*, and *L. odoratus*, "Old Spice Mixed". The diagonal shading indicates the period of pea moth flight activity in the experimental area.

DOI: 10.1021/jf505934q
J. Agric. Food Chem. 2015, 63, 2127−2136

the four species, as has previously been shown for *P. sativum*.[14,15,29−31] Such synchronization of the periods of host plant flowering and pea moth flight activity enables newly hatched larvae to penetrate emerging pods, in which they will have access to nutrition and be protected during development.

The wind tunnel experiments testing attraction of mated *C. nigricana* females to volatile collections of the four host species revealed significant differences (ANOVA: $F = 78.71_{3,16}$, $P < 0.001$) (Figure 2A). The landing response to headspace volatiles was markedly high for flowering *L. odoratus* (74%) and high for flowering *P. sativum* (56%) but was much lower for *V. sepium* (32%) and *V. fabae* (22%) (Figure 2A). There were also statistically significant differences in oviposition and larval performance on the four host species (ANOVA: $F_{eggs} = 21.48_{3,20}$, $F_{cocoons} = 15.79_{3,20}$, $F_{adults} = 33.00_{3,20}$, $P < 0.001$) (Figure 2B). Although mated females were more extensively attracted to *L. odoratus* than to *P. sativum* in the wind tunnel (Figure 2A), similar numbers of eggs were observed on both those host species in the oviposition experiments (9.7 and 10.5 eggs/plant, respectively) (Figure 2B). Moreover, for *L. odoratus* and *V. fabae*, there were similar numbers of eggs per plant (9.7 and 6.6) (Figure 2B) but higher upwind attraction of female moths to the former species than to the latter (Figure 2A). Also, there was similar attraction to *V. fabae* and *V. sepium* in the wind tunnel (Figure 2A), which did not correspond to the significantly lower number of eggs on *V. sepium* compared to *V. fabae* (0.8 versus 6.6) (Figure 2B). These discrepancies between attraction to a host plant odor (host location) and egg deposition on the plant (host acceptance) might be explained by specific behavioral decisions made during different steps of the host plant selection process.[32,33] However, both upwind orientation in the wind tunnel and oviposition in cage experiments showed that female moths preferred *P. sativum* and *L. odoratus* over *V. fabae* and *V. sepium*.

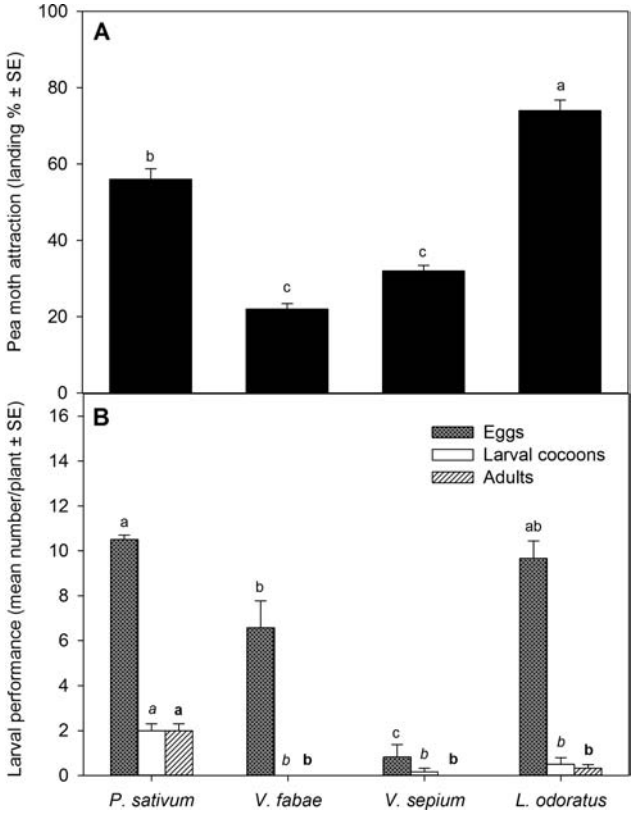

Figure 2. Attraction responses of mated *C. nigricana* females to headspace extracts from the four host plant species *P. sativum*, *V. fabae*, *V. sepium*, and *L. odoratus* recorded (A) in the wind tunnel, and (B) as oviposition and larval performance. The behavioral responses in the wind tunnel are presented as proportion (±SE) of female landings on the odor source ($n = 50$ for each plant species). Statistically significant differences are indicated by lower case letters (ANOVA, Tukey's test). Oviposition and larval performance are presented as mean number of eggs, larval cocoons, and emerging adults (±SE) on each plant ($n = 6$) of the four tested species. The four plant species were compared separately regarding phenological stages of *C. nigricana*: eggs (lower case letters), larval cocoons (lower case letters in italics), and adults (lower case letters in bold). Columns marked with the same letter indicate no statistically significant difference (ANOVA, Tukey's test).

Regarding larval performance on the four tested Fabaceae species, *P. sativum* appeared to be the most suitable host (Figure 2B). The highest mean numbers of cocoons and emerging adults per plant were found on *P. sativum* (both 2.0). By comparison, there were no or only low numbers of cocoons and adults on *L. odoratus* (0.5 cocoons, 0.3 adults), *V. sepium* (0.2 cocoons, 0 adults), and *V. fabae* (0 cocoons, 0 adults), indicating that those three species showed only limited or even no suitability as larval hosts (Figure 2B). For *P. sativum*, on average one larva survived on each developing pea pod, bearing in mind that the plants used in the experiments had two flowers each. The comparatively high number of eggs per pea plant and low survival of larvae (10.5 eggs compared to two cocoons and two emerging adults) might have been the result of the no-choice experimental design, which forced a female to lay her eggs on the only plant available. Consequently, the larvae might have cannibalized each other, because there were not enough seeds as a food source for all of them. An average infestation rate of one pea moth larva per pea pod has been observed in other studies.[14,15] Larger scale no-choice experiments (i.e., using more than one plant of the same species) and choice experiments using the four host species evaluated in the present study are needed to verify plant preferences. Also, a broader range of alternative host species should be tested to better elucidate the insect−plant interactions between the pea moth and Fabaceae species, as well as the underlying ecological mechanisms. However, the previously described high attractiveness and suitability of *P. sativum* for *C. nigricana*[10,11,14,15,29,30] were confirmed by the present study. In addition, the sweet pea *L. odoratus* was found to be highly attractive to *C. nigricana* females and moderately suitable for performance of larvae. The Mediterranean area and Asia Minor are the native habitat of wild pea and sweet pea, and there is evidence that both these species were originally short and bushy plants that had maroon-purple flowers and similar but stronger scents than they have today.[34,35] These similarities suggest coevolution of host plants and pest, which would explain why, like *P. sativum*, *L. odoratus* is highly attractive to *C. nigricana* as a host.

Identification of Volatiles Involved in Olfactory Host Recognition. We observed that the 17 compounds (*Z*)-*β*-ocimene, (*E*)-*β*-ocimene, hexan-1-ol, (*E*)-2-hexen-1-ol, (*Z*)-3-hexenal, (*E*)-2-hexenal, octanal, (*Z*)-3-hexenyl acetate, (*Z*)-3-hexen-1-ol, nonanal, sabinene, myrcene, linalool, *β*-caryophyllene, phenylacetaldehyde, citronellol, and nerol were released from flowering sweet pea plants and induced antennal responses in pea moth females (Table 1; Figure 3). We did not determine which enantiomers of the chiral compounds sabinene, linalool, *β*-caryophyllene, and citronellol were produced by the plants, and therefore it is unclear whether

DOI: 10.1021/jf505934q
J. Agric. Food Chem. 2015, 63, 2127−2136

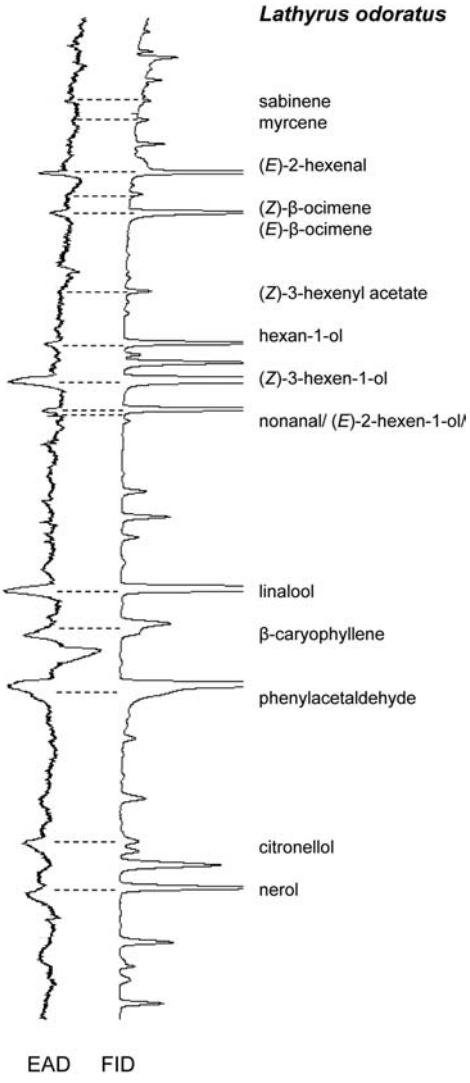

Figure 3. Example of simultaneously recorded GC-EAD analysis of volatiles from a flowering sweet pea plant (*L. odoratus*). The left trace represents the antennal responses (EAD) of a *C. nigricana* female, and the right trace shows the flame ionization detection responses (FID). (Z)-3-Hexenal and octanal were released from flowering sweet pea plants in small amounts (mean values 0.5 and 0.4 ng/h, respectively) and were not found in the headspace replicate used in the illustrated GC-EAD recording.

the correct enantiomers of those compounds were tested in subsequent experiments using synthetic standards. Notwithstanding, the behavioral responses recorded in further bioassays showed that the synthetics that were used were indeed active. (*Z*)-3-Hexenal and octanal were released in low and varying amounts (mean values 0.5 and 0.4 ng/h, respectively), and thus antennal responses to those two compounds were not recorded in all replicates (Figure 3). It can be mentioned that in previous studies,[12,13] (*Z*)-3-hexenal and octanal were found to be released from flowering *P. sativum* plants and elicit antennal responses in female *C. nigricana.* Figure 3 illustrates a typical example of antennal responses to sweet pea headspace extracts. Not all 17 compounds were found in all replicates (e.g., Figure 3, (*Z*)-3-hexenal and octanol are missing), and some compounds induced low antennal responses, such as sabinene, myrcene, and (*Z*)-3-hexenyl acetate. This highlights the natural variation in volatile emissions from *L. odoratus* plants and provides an indication of the plasticity necessary in odor detection by the moths.[3,5,18] Nonetheless, antennal responses to all 17 compounds were verified using synthetic standards, and therefore we included all 17 of the above-mentioned sweet pea volatiles in further behavioral assays. Odor profiles similar to those we recorded for flowering *L. odoratus* have been reported for other cultivars, including wild sweet pea, and showed (*E*)-*β*-ocimene and linalool as the predominant volatiles.[24−26,35] All 17 compounds we selected are ubiquitous volatiles in several plant species.[1,36] The ten compounds (*Z*)-*β*-ocimene, (*E*)-*β*-ocimene, hexan-1-ol, (*E*)-2-hexen-1-ol, (*Z*)-3-hexenal, (*E*)-2-hexenal, octanal, (*Z*)-3-hexenyl acetate, (*Z*)-3-hexen-1-ol, and nonanal were emitted by all four of the tested Fabaceae species (Table 1), whereas the other seven compounds (sabinene, myrcene, linalool, *β*-caryophyllene, phenylacetaldehyde, citronellol, and nerol) were released by flowering *L. odoratus* but not by flowering *P. sativum*.[12,24,25] Hence, *L. odoratus* headspace contained additional compounds that elicited antennal responses in female *C. nigricana* compared to those found in headspace extracts from all tested Fabaceae species. This finding suggests that *C. nigricana* has the physiological capacity to detect a broad range of compounds from the different host plants, as has previously been shown for the tortricid species *Lobesia botrana* and its two host plant species the wild-growing *Daphne gnidium* and the colonized *Vitis vinifera*.[18]

Behavioral Responses to Synthetic Blends in the Wind Tunnel and the Field. In the wind tunnel, the 17-compound synthetic mimic of flowering sweet pea (stimulus II_{WT}) caused marked attraction of mated *C. nigricana* females (66% landing) that was nearly as pronounced as that induced by the headspace extract of flowering *L. odoratus* (stimulus I_{WT}, 76% landing) (Figure 4). For the ten-compound blend containing the common volatiles of the flowering Fabaceae species (stimulus III_{WT}), the level of attraction was significantly lower (26% landing; $F = 30.98_{5,24}$, $P < 0.001$) when using natural quantities and the same ratios as found for *L. odoratus* (Figure 4). In a previous wind tunnel study,[12] testing of the same ten-compound blend, also in natural quantities but at ratios found for *P. sativum* "Avola", had resulted in 34% landing of *C. nigricana* females. Comparison of these responses in upwind orientation to the compounds found to be common to both hosts but released in species-specific ratios (i.e., 26% landing using the *L. odoratus*-specific ratio versus 34% landing using the *P. sativum*-specific ratio) suggests a certain plasticity in the host recognition behavior toward the ratio of behaviorally active volatiles.[3,5,18,37] However, attractiveness to females was substantially increased by combining sweet-pea-specific volatiles with the ten common volatiles (compare stimulus II_{WT} with stimuli III_{WT} and IV_{WT}) (Figure 4). Accordingly, the release of olfactory cues common to several host plant species cannot be the sole mechanism mediating host recognition in *C. nigricana.* No significant difference in attractiveness was found between the sweet-pea-specific seven-compound blend (stimulus IV_{WT}, 40% landing) and the ten-compound blend (stimulus III_{WT}, 26% landing; $F = 30.98_{5,24}$, $P = 0.069$) (Figure 4). However, combining stimulus IV_{WT} with either of two subsets of the ten common compounds (stimulus V_{WT} or VI_{WT}) resulted in increased attraction (64% and 62% landing, respectively; $F = 30.98_{5,24}$, $P < 0.001$) that was at nearly the same level as that elicited by the 17-compound sweet pea mimic (66% landing) and by the headspace of flowering *L. odoratus* (76% landing) (Figure 4). The importance of the

DOI: 10.1021/jf505934q
J. Agric. Food Chem. 2015, 63, 2127−2136

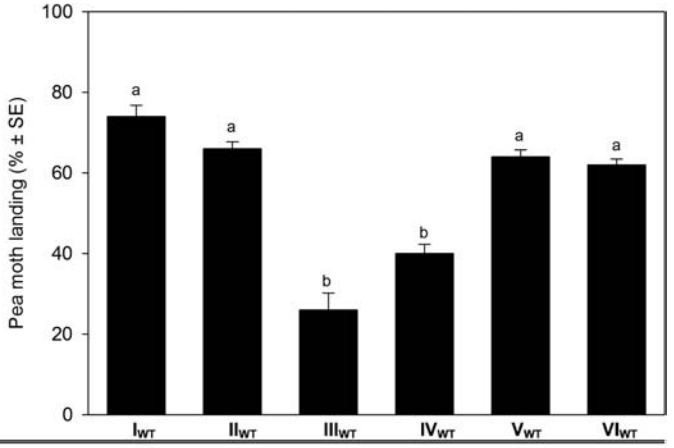

Odour stimulus		I_{WT}	II_{WT}	III_{WT}	IV_{WT}	V_{WT}	VI_{WT}
Headspace *L. odoratus*		•					
Compound	release rate (ng/h)						
(*Z*)-β-ocimene	11.5		•	•		•	•
(*E*)-β-ocimene	100.0		•	•		•	•
hexan-1-ol	18.5		•	•		•	
(*E*)-2-hexen-1-ol	17.6		•	•		•	
(*Z*)-3-hexenal	0.5		•	•			
(*E*)-2-hexenal	19.5		•	•			
octanal	0.4		•	•			
(*Z*)-3-hexenyl acetate	9.7		•	•			
(*Z*)-3-hexen-1-ol	200.0		•	•			
nonanal	1.2		•	•			
(±)-sabinene	4.4		•		•	•	•
myrcene	4.3		•		•	•	•
(±)-linalool	185.6		•		•	•	•
(±)-β-caryophyllene	14.1		•		•	•	•
phenylacetaldehyde	95.2		•		•	•	•
(±)-citronellol	5.1		•		•	•	•
nerol	40.6		•		•	•	•

*Synthetic standards of (*Z*)-β-ocimene (CAS 3338-55-4) and (*E*)-β-ocimene (CAS 3779-61-1) were used as a mixture of isomers.

Figure 4. Behavioral responses of mated *C. nigricana* females to headspace extracts of flowering *L. odoratus* (stimulus I_{WT}) and blends of synthetic sweet pea flower volatiles (stimuli II_{WT}–VI_{WT}) in the wind tunnel. The release rates of the synthetic compounds correspond to the natural release rates (ng/h) of volatiles from flowering sweet pea plants. The responses are presented as proportion (±SE) of female landings on the odor source (n = 50 for each stimulus). Statistically significant differences are indicated by lower case letters (ANOVA, Tukey's test).

volatiles from the two subsets (i.e., (*Z*)-*β*-ocimene, (*E*)-*β*-ocimene, hexan-1-ol, and (*E*)-2-hexen-1-ol) for host location by mated *C. nigricana* females and for insect attraction in general has been shown in previous investigations[13,36,38] and was verified in the present study. Overall, the current wind tunnel results indicated that, in addition to common host plant volatiles, more species-specific compounds influence host recognition.[4,5] Moreover, our results indicate additive effects between common and more specific host plant volatiles, provided they are presented in the context of the correct blend, which agrees with earlier investigations and the hypothesis of ratio-specific odor recognition.[3−5,13,18,39,40]

We performed field studies using traps to confirm the wind tunnel findings in a natural setting. The trap catches recorded demonstrate that our synthetic host volatile blends had a significant impact on the behavior of pea moths despite the presence of a complex background odor. Moths in the field were attracted to the traps even though we tested 1:1 ratios of the synthetic host volatiles, rather than ratios corresponding to the natural release from the host plant as we had used in the wind tunnel experiments. We accepted this flaw in our experimental set up, because the varying evaporation of the single synthetics makes it difficult to achieve constant ratios corresponding to natural plant volatile emissions over time in a field experiment. However, the behavioral significance of our synthetic host volatile blends was apparent in the presence of a complex background odor in the field, which together with the findings of the wind tunnel experiments supports the coincidence detection theory.[3,4,6−8]

Only single *C. nigricana* males were caught in the kairomone traps (stimuli II_F, III_F, and VI_F) (Figure 5), whereas large numbers of males were attracted to the pheromone traps (Figure 6A), which demonstrates the importance of the floral host plant volatiles for attraction of females. The tested Fabaceae volatiles were attractive only to pea moth females in the field experiment, which is in contrast to other studies of species such as *C. pomonella* showing that both sexes were attracted to host plant volatiles tested in the field.[16,41] Other investigators have reported that *C. nigricana* starts mating at the emergence site and not on the host plant, and mated females subsequently migrate toward their host plants, often over long distances,[12] whereas *C. pomonella* males and females locate their host plants and then mate directly on the plants.[41,42] These differences in mating behavior of the two *Cydia* species might explain the selectivity of pea moth females we observed in relation to host plant volatiles. Detailed studies of sex and mating status of the pea moth in relation to moth migration and attractiveness of plant volatiles in a natural setting would help clarify the overall host location behavior of *C. nigricana*.

In our study, the most extensive attraction of females (total mean catch 35 females/trap) was induced by natural odor of sweet pea flowers (stimulus I_F) followed by the 17-compound

DOI: 10.1021/jf505934q
J. Agric. Food Chem. 2015, 63, 2127−2136

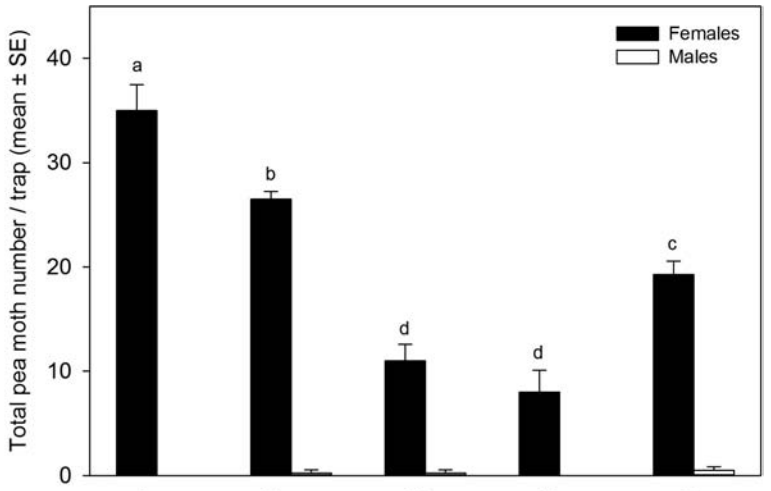

Odor stimulus		I_F	II_F	III_F	IV_F	VI_F
L. odoratus flower		•				
Compound	ratio					
(*Z*)-β-ocimene	0.22		•	•		•
(*E*)-β-ocimene	1.78		•	•		•
hexan-1-ol	1		•	•		
(*E*)-2-hexen-1-ol	1		•	•		
(*Z*)-3-hexenal	1		•	•		
(*E*)-2-hexenal	1		•	•		
octanal	1		•	•		
(*Z*)-3-hexenyl acetate	1		•	•		
(*Z*)-3-hexen-1-ol	1		•	•		
nonanal	1		•	•		
(±)-sabinene	1		•		•	•
myrcene	1		•		•	•
(±)-linalool	1		•		•	•
(±)-β-caryophyllene	1		•		•	•
phenylacetaldehyde	1		•		•	•
(±)-citronellol	1		•		•	•
nerol	1		•		•	•

Figure 5. Overall trap captures (mean number ± SE/trap) of *C. nigricana* males and females responding to a natural sweet pea flower control (stimulus I_F, detached flowers of *L. odoratus* mounted in delta traps; $n = 4$) and to blends of synthetic sweet pea flower volatiles (stimuli II_F, III_F, VI_F, and VI_F; each $n = 4$). The captures were recorded in an experimental pea field in eastern Norway as a cumulative value of 10 trap inspections over a period of 5 weeks. Differences between stimuli over the entire experimental period are indicated by lower case letters (ANOVA, Tukey's test).

synthetic sweet pea mimic (stimulus II_F, mean catch 26.5 females/trap) (Figure 5). As in the wind tunnel test, a significantly lower level of attraction ($F = 90.60_{4,15}$, $P < 0.001$) was observed in the field experiment for the ten-compound blend containing the common volatiles (stimulus III_F, 11 females/trap) and the sweet-pea-specific seven-compound blend (stimulus IV_F, 8 females/trap). Combining stimulus IV_F with (*Z*)- and (*E*)-*β*-ocimene (stimulus VI_F) significantly increased attraction ($F = 90.60_{4,15}$, $P < 0.001$), with an additive effect (19.25 females/trap) (Figure 5). However, in the field the attraction to stimulus VI_F was not as pronounced as that elicited by the 17-compound sweet pea mimic (stimulus VI_F versus II_F; $F = 90.60_{4,15}$, $P = 0.008$) (Figure 5) as observed in the wind tunnel (stimuli VI_{WT} and II_{WT}) (Figure 4). The influence of complexity of vegetation on arthropod orientation in a natural setting, i.e., the effects of plant species diversity and corresponding plant volatile diversity in the field on arthropod behavior, and the impact of background odor in this context have been discussed[6−8,41,43] and demonstrated for the pea moth and pea plants in a natural setting in a previous study.[13] In the present investigation, phenological stage-specific emission of volatiles from the pea crop[12] may also have affected orientation of *C. nigricana* females toward the synthetic lures that were used in the field (compare trap catches for CW 26/27 with those for CW 27/28 to CW 29/30) (Figure 6B). However, trap catches in the field can also be influenced by the size of the insect population, and there are often unexpected differences in trap catches when examining a small population (e.g., CW 26/27) (Figure 6B). Thus, an effect of pea phenological stage-specific volatile emissions on female attraction to synthetic odor cues is difficult to discern in the results of our field experiment. Nonetheless, those experimental findings might suggest that insect orientation in a natural environment is influenced not only by diversity of plant volatiles related to the diversity of plant species in the surroundings of a pea field but possibly also affected by other potential differences in volatile emissions associated with factors such as host plant phenology.[6,7,44] Considering the overall chemical complexity that exists in a natural setting, the following scenario is plausible: for a herbivorous insect that is a specialist on specific Fabaceae species, being able to perceive combinations of common and more species-specific host plant volatiles, as well as the ratios between those compounds, represents a reliable mechanism for locating the most suitable host plants.[2−5]

In insects in general, allelochemicals such as plant volatiles are fundamental signals for plant−insect interaction, and hence in some cases such chemicals can be used to control insect pests by modifying their behavior. For example, attractant host plant volatiles provide tools for monitoring the occurrence and reproductive status of females, which is an essential element in pest management. This is particularly important when dealing

DOI: 10.1021/jf505934q
J. Agric. Food Chem. 2015, 63, 2127−2136

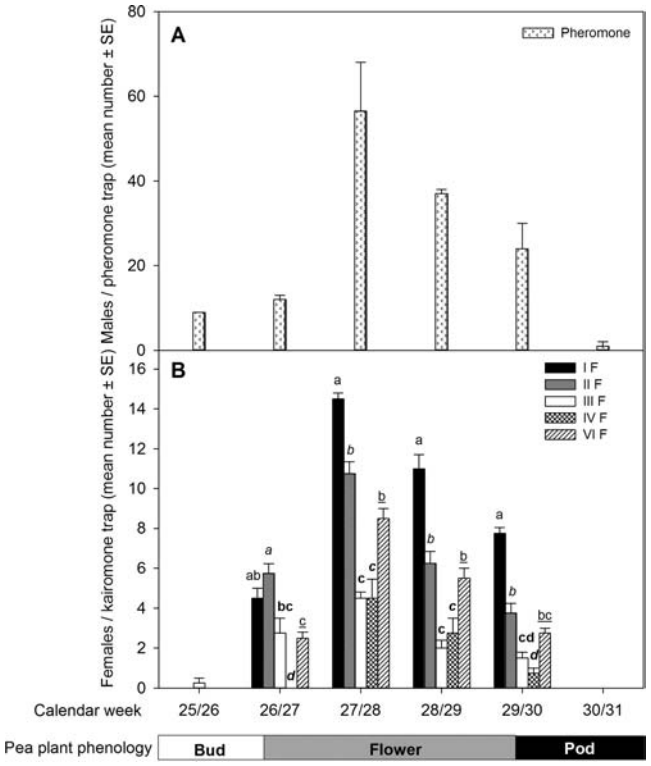

Figure 6. Weekly trap captures (mean number ± SE/trap) of *C. nigricana*: (A) males responding to sex pheromone (E8E10−12Ac), and (B) females responding to a natural sweet pea flower control (stimulus I_F, detached flowers of *L. odoratus*, mounted in delta traps, n = 4) and to blends of synthetic sweet pea flower volatiles (stimuli II_F, III_F, IV_F, and VI_F; each n = 4), shown together with the corresponding pea plant phenology. Observations were made in an experimental pea field in eastern Norway over a period of 5 weeks. Differences between stimuli for a particular (weekly) time interval are indicated by lower case letters (ANOVA, Tukey's test).

with pest species in which intraspecific communication is based on female-produced pheromones that attract only males, as is seen in the pea moth. Several methods aimed at controlling such pests have been developed by exploiting female attraction to volatile cues.[45−47] Flower volatiles are components of plant scents that are notably strong attractants for many different insects,[36,38] and synthetic floral attractants have been developed for several moth species.[48−50] Most such synthetics attracting female insects are based on volatiles that mimic a particular enticing host odor. An alternative approach is called "super-blending", which uses combinations of synthetic attractants that are not found in natural settings but represent various classes of volatile compounds regardless of the odor source (e.g., host or nonhost plants).[46,47] In the present study, a previously identified synthetic attractant for *C. nigricana* females[12,13] was improved by combining attractive flower volatiles from the main host plant *P. sativum* with those from an alternative host plant species, the sweet pea *L. odoratus*. In the long term, these results may serve as a basis for development of a kairomonal attractant that can be used to control *C. nigricana*. The efficiency of kairomones for pea moth control is being tested in an ongoing field study.

AUTHOR INFORMATION

Corresponding Author

*Tel: +47 92 01 13 07. Fax: +47 64 94 61 10. E-mail: gunda.thoeming@bioforsk.no.

Funding

This study was funded by Bioforsk, the Norwegian Institute for Agricultural and Environmental Research and DFG (Deutsche Forschungsgemeinschaft, TH 1453/2-1).

Notes

The authors declare no competing financial interest.

ACKNOWLEDGMENTS

We thank Armin Kratt at Trifolio-M GmbH (Lahnau, Germany) for providing pheromone-monitoring traps and pheromone, Yngve H. Stenstrøm for providing synthetic standards, and Yoshiko Shibata-Teufert and Karlheinz Teufert for translating literature in Japanese. Special thanks go to Geir K. Knudsen and Marco Tasin for valuable comments on the manuscript.

REFERENCES

(1) Knudsen, J. T.; Eriksson, R.; Gershenzon, J. Diversity and distribution of floral scent. *Bot. Rev.* **2006**, *72*, 1−120.

(2) Fraenkel, G. S. Raison d'être of secondary plant substances. *Science* **1959**, *129*, 1466−1470.

(3) Bruce, T. J. A.; Wadhams, L. J.; Woodcock, C. M. Insect host location: A volatile situation. *Trends Plant Sci.* **2005**, *10*, 269−274.

(4) Bruce, T. J. A.; Pickett, J. A. Perception of plant volatile blends by herbivorous insects − finding the right mix. *Phytochemistry* **2011**, *72*, 1605−1611.

(5) Visser, J. H. Host odour perception in phytophagous insects. *Annu. Rev. Entomol.* **1986**, *31*, 121−144.

(6) Randlkofer, B.; Obermaier, E.; Hilker, M.; Meiners, T. Vegetation complexity − the influence of plant species diversity and plant structures on plant chemical complexity and arthropods. *Basic Appl. Ecol.* **2010**, *11*, 383−395.

(7) Schroeder, R.; Hilker, M. The relevance of background odor in resource location by insect: A behavioural approach. *Bioscience* **2008**, *58*, 308−316.

(8) Webster, B.; Bruce, T.; Pickett, J.; Hardie, J. Volatile functioning as host cues in a blend become nonhost cues when presented alone to the black bean aphid. *Anim. Behav.* **2010**, *79*, 451−457.

(9) Hanson, A. J.; Webster, R. L. *The pea moth: Laspeyresia nigricana Steph.*; Bull. Wash. Agric. Exp. Stat. 327 (Bulletin, State College of Washington, Agricultural Experiment Station, no. 327), Pullman, WA, 1936.

(10) Wright, D. W.; Geering, Q. A. The biology and control of the pea moth *Laspeyresia nigricana* Steph. *Bull. Entomol. Res.* **1948**, *39*, 57−48.

(11) Sarwar, S. L. Untersuchungen zur Biologie und Bekämpfung des Erbsenwicklers, *Laspeyresia nigricana* Steph. Dissertation at Karl-Marx-Universität Leipzig, Germany, 1973.

(12) Thöming, G.; Norli, H. R.; Saucke, H.; Knudsen, G. K. Pea plant volatiles guide host location behaviour in the pea moth. *Arthropod-Plant Interact.* **2014**, *8*, 109−122.

(13) Thöming, G.; Knudsen, G. K. Attraction of pea moth *Cydia nigricana* to pea flower volatiles. *Phytochemistry* **2014**, *100*, 66−75.

(14) Nicolaisen, W. Der Erbsenwickler, *Grapholita* (*Cydia, Laspeyresia*) sp., sein Schaden und seine Bekämpfung unter Berücksichtigung der Anfälligkeit verschiedener Erbsensorten. *Kühn Archiv, Halle* **1928**, *19*, 196−256.

(15) Stenmark, A. Studies on the pea moth (*Laseyresia nigricana* Steph.) in central Sweden I and II. *Statens Växtskydanst.* **1971**, *15*, 1−47.

(16) Light, D. M.; Knight, A. L.; Henrick, C. A.; Rajapaska, D.; Lingren, B.; Dickens, J. C.; Reynolds, K. M.; Buttery, R. G.; Merrill, G.;

DOI: 10.1021/jf505934q
J. Agric. Food Chem. 2015, 63, 2127−2136

Roitman, J.; Campbell, B. C. A pear-derived kairomone with pheromonal potency that attracts male and female codling moth *Cydia pomonella* (L.). *Naturwissenschaften* **2001**, *88*, 333−338.
(17) Landolt, P. J.; Suckling, D. M.; Judd, G. J. R. Positive interaction of a feeding attractant and a host kairomone for trapping the codling moth, *Cydia pomonella* (L.). *J. Chem. Ecol.* **2007**, *33*, 2236−2244.
(18) Tasin, M.; Bäckmann, A.-C.; Anfora, G.; Carlin, S.; Ioriatti, C.; Witzgall, P. Attraction of female grapevine moth to common and specific olfactory cues from 2 host plants. *Chem. Senses* **2010**, *35*, 57−64.
(19) Thöming, G.; Saucke, H. Key factors affecting the spring emergence of pea moth (*Cydia nigricana*). *Bull. Entomol. Res.* **2011**, *101*, 127−133.
(20) Meier, U. *Growth stages of mono-and dicotyledonous plants*; Blackwell: Berlin, Germany, 1997.
(21) Kovats, E. Gas-chromatograpische Charakterisierung organischer Verbindungen. Teil 1: Retentionsindices aliphatischer Halogenide, Alkohole, Aldehyde und Ketone. *Helv. Chim. Acta* **1958**, *4*, 1915−1932.
(22) Stein, S. E. An integrated method for spectrum extraction and compound identification from gas chromatography/mass spectrometry data. *J. Am. Soc. Mass Spectrom.* **1999**, *10*, 770−781.
(23) Aak, A.; Knudsen, G. K.; Soleng, A. Wind tunnel behavioural response and field trapping of the blowfly *Calliphora vicina*. *Med. Vet. Entomol.* **2010**, *24*, 250−257.
(24) Porter, A. E. A.; Griffiths, D. W.; Robertson, G. W.; Sexton, R. Floral volatiles of sweet pea *Lathyrus odoratus*. *Phytochemistry* **1999**, *51*, 211−214.
(25) Inoue, T.; Kodama, T.; Nakanishi, H.; Tsuji, H.; Miura, Y.; Koike, Y.; Suzuki, S. Difference of floral volatiles among sweet pea (*Lathyrus odoratus*) cultivars. *J. Agric. Sci., Tokyo Univ. Agric.* **2002**, *46*, 241−249.
(26) Sexton, R.; Stopford, A. P.; Moodie, W. T.; Porter, A. E. A. Aroma production from cut sweet pea flowers (*Lathyrus odoratus*): The role of ethylene. *Physiol. Plant.* **2005**, *124*, 381−389.
(27) Sokal, R. R.; Rohlf, F. J. *Biometry: The principles and practice of statistics in biological research*; W. H. Freeman: New York, 1995.
(28) Zerbe, G. O. Randomization analysis of the completely randomized design extended to growth and response curves. *J. Am. Stat. Assoc.* **1979**, *74*, 215−221.
(29) Gould, H. J.; Legowski, T. J. Spray warnings for pea moth (*Laspeyresia nigricana*) based on its biology in the field. *Entomol. Exp. Appl.* **1964**, *7*, 131−138.
(30) Wright, D. W.; Geering, Q. A.; Dunn, J. A. Varietal differences in the susceptibility of peas to attack by the pea moth, *Laspeyresia nigricana* (Steph.). *Bull. Entomol. Res.* **1951**, *41*, 663−667.
(31) Thöming, G.; Pölitz, B.; Kühne, A.; Saucke, H. Risk assessment of pea moth *Cydia nigricana* infestation in organic green peas based on spatiotemporal distribution and phenology of the host plant. *Agric. Forest Entomol.* **2011**, *13*, 212−130.
(32) Renwick, J. A. A.; Chew, F. S. Oviposition behaviour in Lepitoptera. *Annu. Rev. Entomol.* **1994**, *39*, 377−400.
(33) Gripenberg, S.; Mayhew, P. J.; Parnell, M.; Roslin, T. A meta-analysis of preference-performance relationships in phytophagous insects. *Ecol. Lett.* **2010**, *13*, 383−393.
(34) Cuthbertson, W. *Sweet peas and antirrhinums (snapdragons)*, 2nd ed.; James Clarke & Co.: London, UK, 1919.
(35) Rice, G. *The sweet pea book*; Timber Press: Portland, OR, 2002.
(36) Dudareva, N.; Pichersky, E. *Biology of floral scent*; CRC Press, Taylor and Francis Group: Boca Raton, FL, 2006.
(37) Najar-Rodriguez, A. J.; Galizia, C. G.; Stierle, J.; Dorn, S. Behavioural and neurophysiological responses of an insect to changing ratios of constituents in host plant-derived volatile mixtures. *J. Exp. Biol.* **2010**, *213*, 3388−3397.
(38) Schiestl, F. P. The evolution of floral scents and insect chemical communication. *Ecol. Lett.* **2010**, *13*, 643−656.
(39) Guerin, P. M.; Sädler, E.; Buser, H. R. Identification of host plant attractants for carrot fly, *Psila rosae*. *J. Chem. Ecol.* **1983**, *9*, 843−861.
(40) Piñero, J. C.; Dorn, S. Synergism between aromatic compounds and green leaf volatiles derived from the host plant underlies female attraction in the oriental fruit moth. *Entomol. Exp. Appl.* **2007**, *125*, 185−194.
(41) Coracini, M.; Bengtsson, M.; Liblikas, I.; Witzgall, P. Attraction of codling moth males to apple volatiles. *Entomol. Exp. Appl.* **2004**, *110*, 1−10.
(42) Ansebo, L.; Coracini, M. D. A.; Bengtsson, M.; Liblikas, I.; Ramirez, M.; Borg-Karlson, A.-K.; Tasin, M.; Witzgall, P. Antennal and behavioural responses of codling moth Cydia pomonella to plant volatiles. *J. Appl. Entomol.* **2004**, *128*, 488−493.
(43) Knudsen, G. K.; Bengtsson, M.; Kobro, S.; Jaastad, G.; Hofsvang, T.; Witzgall, P. Discrepancy in laboratory and field attraction of apple fruit moth *Argyresthia conjugella* to host plant volatiles. *Physiol. Entomol.* **2008**, *33*, 1−6.
(44) Van Wijk, M.; de Bruijn, P. J. A.; Sabelis, M. W. Complex odor from plants under attack: Herbivore's enemies react to the whole, not its parts. *PLoS One* **2011**, *6*, e21742.
(45) French, B. W.; Chandler, L. D.; Riedell, W. E. Effectiveness of corn rootworm (Coleoptera: Chrysomelidae) areawide pest management in South Dakota. *J. Econ. Entomol.* **2007**, *100*, 1542−1554.
(46) Del Socorro, A. P.; Gregg, P. C.; Alter, D.; Moore, C. J. Development of a synthetic plant volatile-based attracticide for female noctuid moths. I. Potential sources of volatiles attractive to *Helicoverpa armigera* (Hübner) (Lepidoptera: Noctuidae). *Aust. J. Entomol.* **2010**, *49*, 10−20.
(47) Gregg, P. C.; del Socorro, A. P.; Henderson, G. S. Development of a synthetic plant volatile-based attracticide for female noctuid moths. II. Bioassays of synthetic plant volatles as attractants for adults of the cotton bollworm, *Helicoverpa armigera* (Hübner) (Lepidoptera: Noctuidae). *Aust. J. Entomol.* **2010**, *49*, 21−30.
(48) Landolt, P. J.; Adams, T.; Zack, R. S. Field response of alfalfa looper and cabbage looper moths (Lepidoptera: Noctuidae, Plusiinae) to single and binary blends of floral odorants. *Environ. Entomol.* **2006**, *35*, 276−281.
(49) Guédot, C.; Landolt, P. J.; Smithhisler, C. L. Odorants of the flowers of butterfly bush, *Buddleja davidii*, as possible attractants of pest species of moths. *Fla. Entomol.* **2008**, *91*, 576−582.
(50) Meagher, R. L.; Landoldt, P. J. Attractiveness of binary blends of floral odorant compounds to moths in Florida, USA. *Entomol. Exp. Appl.* **2008**, *128*, 323−329.

DOI: 10.1021/jf505934q
J. Agric. Food Chem. 2015, 63, 2127−2136

Cabernet Sauvignon, Durif, Mourvedre,[11] Schioppettino, and Vespolina, and in a white variety, Grüner Veltliner.[12] Schioppettino, Vespolina, and Grüner Veltliner are noted for their very "peppery" character and have correspondingly high concentrations of rotundone.[12] The concentration of rotundone in berries is extremely low at veraison but increases rapidly during ripening to reach maximal levels at harvest.[13] Studies of a range of varieties, including Shiraz, have shown that rotundone concentrations vary considerably between seasons and vineyard locations and even within vineyards, but as yet, there are no definitive data regarding the causal factors for this variation.[11−14]

In this paper, we describe the use of two different PGRs (Ethrel and NAA) to delay Shiraz berry ripening and how these treatments altered the profiles of a range of volatile flavor/aroma metabolites, the concentrations of rotundone and the sensorial properties of wine made from treated and control fruit.

MATERIALS AND METHODS

NAA and Ethrel Treatment of Field-Grown Shiraz Berries. *Vitis vinifera* L. cv Shiraz vines, on own roots, were grown on well-drained soil, with vertical shoot positioning trellising, at Hahndorf in the Adelaide Hills (−35°.02, 138°.84, elevation 400 m). Natural rainfall was supplemented by limited drip irrigation as required. Bunches were sprayed to runoff during the preveraison period with 50 mg/L NAA (Gibco BRL Life Technologies, Grand Island, NY) in 0.1% (v/v) Chemwet 1000 (Nufarm, Laverton North, VIC, Australia), (2-chloroethyl)phosphonic acid as Ethrel at 300 μL/L (Bayer Crop Science, East Hawthorn, VIC, Australia) in 0.1% (v/v) Chemwet 1000, or a 0.1% (v/v) Chemwet 1000 solution alone (control). Spray dates were as follows: for control and Ethrel, January 16, 2012 (8 days preveraison of control berries), and January 23, 2012 (1 day preveraison of control berries); for NAA treatment, January 23, 2012, and January 27, 2012 (3 days postveraison of control berries). Veraison was defined as the sample date previous to the first sample showing an increase in Brix value of more than two degrees per week. There was no precipitation during the 48 h period after each spray treatment. The trial was of a randomized triplicate design, and the sample size per replicate was 400 bunches (1200 bunches per treatment). Samples of 60 randomly harvested berries per replicate were taken throughout development (the sampling dates are indicated in Figure 2). Sampling was completed between 09:30 and 14:30 h. Berries were weighed, and total soluble solids (TSS) were measured for each of these replicates as described below. Anthocyanins were measured at two time points, February 14, 2012, and at harvest (which was different for each of the treatments), as described below. Minimum and maximum air temperatures (Figure S1 of the Supporting Information) for a site located near the vineyard (−35°.07, 138°.84) were obtained from the Australian Bureau of Meteorology (www.bom.gov.au).

Determination of Anthocyanin and Total Soluble Solid Levels. Frozen whole berries were ground to a powder using an IKA A11 basic analytical mill (IKA, Staufen, Germany). For the measurement of TSS (degrees Brix), 100 mg of berry powder was thawed on ice, the tissue was pelleted by centrifugation at 18000*g* for 5 min, and the supernatant was analyzed with an RFM710 digital refractometer (Bellingham Stanley, Tunbridge Wells, U.K.). For anthocyanin determination, 300 mg of a powdered sample was added to 1.5 mL of MeOH containing 1% (v/v) HCl. Anthocyanins were extracted at room temperature in the dark on a rotating mixer for 1 h. The tissue was pelleted by centrifugation at 18000*g* for 15 min and the supernatant retained. Depending on the developmental stage, the supernatant was diluted up to 20-fold with MeOH and 1% (v/v) HCl. Total anthocyanins were measured spectrophotometrically by reading the absorbance at 520 nm immediately following centrifugation. One-way ANOVA followed by Duncan's post hoc test was performed using IBM SPSS version 20 (IBM, Armonk, NY).

Small Scale Winemaking. Small scale winemaking was conducted by WIC Winemaking Services (Urrbrae, SA, Australia) using the following protocol. Control, Ethrel-treated, and NAA-treated fruit (20 kg for each of three replicates per treatment) were harvested at the times indicated in Figure 2. Harvested fruit was placed at 0 °C for 12 h, and the SO_2 concentrations were adjusted to 50 ppm during crushing and destemming. Yeast strain EC1118 (Lallemand, Edwardstown, SA, Australia) was added to a concentration of 200 ppm. The ferment was conducted on skins at 18−20 °C, and diammonium phosphate was added as required to a maximal concentration of 400 ppm. The cap was plunged 20 times twice daily. When the must reached 2°Baume, the must was pressed and then fermented to dryness, following which it was racked. SO_2 was added to a concentration of 60 ppm, and the wine was cold stabilized at 0 °C for 21 days. The wine was again racked, and SO_2 concentrations were adjusted to 80 ppm before being filtered and bottled with 30 × 60 Stelvin closures (Amcor, Hawthorn, VIC, Australia).

Sensory Analysis of Small Scale Wines. Detailed sensory profiles of all wines were generated by descriptive analysis (DA) conducted at the University of Adelaide sensory laboratory, which complies with international standards for the design of test rooms (ISO 8589:1988). The trained DA panel consisted of 12 members (eight female and four male, mean age of 36 years, ranging from 24 to 57) and underwent three 2 h training sessions, including evaluation of all wine samples before final assessment. The panel generated a standard list of vocabulary terms to profile the differences between the wines for appearance, aroma, palate, mouthfeel, and aftertaste. Reference standards (Table S2 of the Supporting Information) were developed to help clarify some of the aroma sensory attributes and ensure full agreement across assessors. The DA final assessment was conducted in triplicate in individual booths with panel members tasting up to 14 samples per day. Panelists received a sample volume of 30 mL served at 21 °C in 214 mL standardized tasting wine glasses (ISO 3591:1977). Each wine glass was covered with a watch glass to prevent headspace loss, and samples were poured immediately before being served to the assessor. Samples were blind-coded with random three-digit codes, and the order of sample assessment was randomized to account for first-order and carryover effects. Processed water crackers and water were consumed between samples to minimize carryover effects, and an interstimulus interval of at least 1 min was chosen as a suitable time between samples with a 5 min interval after flights of six wines. Panelists had access to and were encouraged to use all reference samples throughout final assessment. The experimental design was produced using the design generation package Design Express (Qi Statistics, Reading, U.K.). Attributes were rated on 0−15 line scales, with indented extreme end word anchors for each descriptive term. Data were recorded and stored using Fizz sensory data acquisition software (Biosystèmes, Couternon, France).

ANOVA was conducted to test the effects of Judge, Sample, Replicate, and all two-way interactions for each sensory attribute using a pseudomixed model with the Judge × Sample interaction as a denominator. IBM SPSS version 20 (IBM) was used for these analyses.

Nontargeted Headspace Volatile Analysis. SPME−GC−MS was used to analyze the volatile constituents of the wines produced from the control and treated fruit. Aliquots of the wines were analyzed at two different concentrations, 1:100 or 1:2 diluted with H_2O to a final volume of 10 mL. Three grams of NaCl was added to each SPME vial (20 mL) prior to sample addition.

The extraction and chromatographic conditions were identical to those described by Boss et al.[15] The identity of detected volatiles was determined by comparing mass spectra with those of authentic standards and spectral libraries. A laboratory-generated library (328 compounds) as well as the U.S. National Institute of Standards and Technology-11 (NIST-11) and the Wiley Registry 9th Edition mass spectral libraries were used for identification purposes. Compounds were considered positively identified after matching of both mass spectra and linear retention indices (LRI) with those of authentic samples. LRI was calculated from a compound's retention time relative to the retention of a series of *n*-alkanes (C_8−C_{26}). Other compounds

DOI: 10.1021/jf505491d
J. Agric. Food Chem. 2015, 63, 2137−2144

were tentatively identified on the basis of comparison with mass spectral libraries and published LRI, or comparisons with mass spectral libraries alone.

The components of the samples were quantified using Chemstation (Agilent, Forest Hill, VIC, Australia) relative to the relevant internal standard (d_{13}-hexanol, d_{11}-hexanoic acid, d_{16}-octanal, methyl nonanoate, or d_3-linalool) using the peak area of an extracted ion.

The effect of applying Ethrel and NAA to bunches on the concentration of volatiles in the headspace of the wines was analyzed by ANOVA using SPSS version 20 (IBM).

Synthesis of Rotundone and d_5-Rotundone. Guaiacwood essential oil was purchased from Auroma (Hallam, VIC, Australia). All reagents were purchased from commercial sources and used directly if no specific purification is mentioned.

The synthesis of rotundone (**4**) and d_5-rotundone (**5**) began with the synthesis of α-guaiene (**3**), which was prepared from guaiol (**1**) via acetylation and pyrolysis as described by Huang et al.[16] Rotundone (**4**) was then synthesized by one-step allylic oxidation of α-guaiene (**3**) by pyridinium dichromate (PDC) and *tert*-butyl hydroperoxide (TBHP) as described by Huang et al. (Figure 1).[17] d_5-Rotundone was synthesized by deuterium exchanged of rotundone with d_6-ethanol as described by Huang et al.[18]

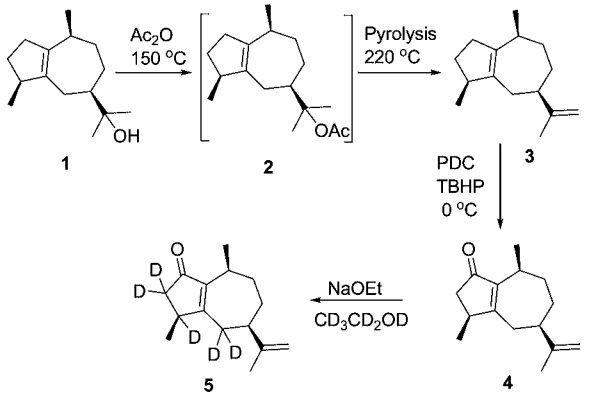

Figure 1. Synthesis of rotundone and d_5-rotundone from guaiol.

Rotundone Quantification. The method used for the extraction and analysis of rotundone was derived from ref 19. Styrene-divinylbenzene SPE cartridges (SDB-L, 500 mg/6 mL; Phenomenex, Lane Cove, NSW, Australia) were conditioned with a 10 mL *n*-pentane/ethyl acetate solvent (4:1), followed by 6 mL of methanol and then 6 mL of model wine (12% ethanol and 2 g/L potassium hydrogen tartrate, buffered to pH 3.2 with tartaric acid). A 100 mL aliquot of wine, containing 24 ng of d_5-rotundone in 100 μL of ethanol as an internal standard, was loaded onto the SPE cartridge. The cartridge was then washed with 10 mL of water followed by 2 mL of *n*-pentane and finally eluted with 10 mL of *n*-pentane/ethyl acetate solvent (9:1). This eluent was dried under a stream of N_2 and then redissolved in 1 mL of ethanol. The extract was added to a 20 mL amber SPME vial [Chromacol, Biolab (Aust) Ltd., Clayton, VIC, Australia] with 13 mL of aqueous tartrate buffer (2 g/L potassium hydrogen tartrate, buffered to pH 3.2 with tartaric acid) and analyzed by SPME−GC−MS.

SPME−GC−MS analysis was performed using an Agilent Technologies 7890A gas chromatograph coupled to a 5975C mass spectrometer with a MPS2 autosampler (Gerstel, Mülheim an der Ruhr, Germany). A polydimethylsiloxane/divinylbenzene 65 μm fiber (Supelco, Bellefonte, PA) was immersed in the sample for 60 min at 40 °C with agitation and then was desorbed in the inlet at 240 °C for 1 min in pulsed-splitless mode. A pressure pulse of 25.0 psi was applied for 30 s, and the flow was split with a total flow of 50 mL/min after 1 min. The fiber was cleaned for 4 min prior to extraction and also after desorption in a Gerstel fiber bake-out station at a temperature of 240 °C.

GC separation was performed on a 30 m ZB-Wax capillary column with an internal diameter of 0.25 mm and a film thickness of 0.25 μm (Phenomenex). Ultra High Purity Helium was used as a carrier gas with a constant flow rate of 1.0 mL/min. The oven temperature was initially held at 80 °C for 1 min and then increased to 220 °C at a rate of 3 °C/min, before being increased to 245 °C at a rate of 40 °C/min and then held at this final temperature for 10 min. The mass spectrometer transfer line was held at 250 °C. Selected ion monitoring (SIM) mode was used with ions at m/z 223 and 218 as the selected ions for quantification of d_5-rotundone and rotundone, respectively, and ions at m/z 147, 161, and 203 as the qualifying ions for rotundone and ions at m/z 147, 161, and 208 as the qualifying ions for d_5-rotundone (dwell time of 30 ms, electron impact of 70 eV). The analyses were performed in triplicate for each wine.

A Shiraz bag in box wine was selected for the preparation of the calibration curves as it was found to contain no rotundone by the preceding method. The wine was spiked in triplicate to give rotundone concentrations of 0, 1.2, 6, 12, 30, and 60 ng/L, and all samples were then analyzed as outlined above. The calibration was linear throughout the range with a correlation coefficient of 0.9996 and relative standard deviations of <5%. Using this method, the limit of detection for rotundone was 0.8 ng/L and the limit of quantification was 2.7 ng/L.

RESULTS

Both Ethrel and NAA Treatments Delay Shiraz Berry Ripening. The preveraison treatment of Shiraz berries with either Ethrel or NAA delayed the initiation of the phase of rapid increase in TSS and, by inference, sugar accumulation (Figure 2). After these differences in the onset of ripening, the rate of

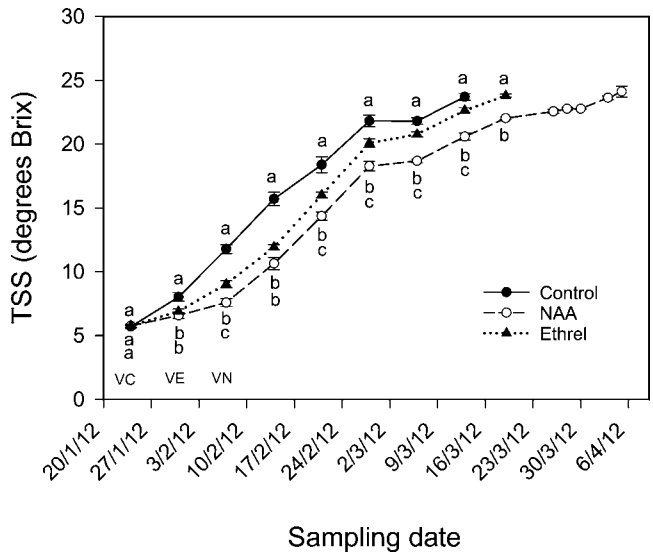

Figure 2. Effect of Ethrel and NAA treatments on total soluble solid (TSS) levels, measured as degrees Brix. All data represent means ± STERR (n = 3), and different letters denote significant differences between treatments at $p < 0.05$ using one-way ANOVA followed by Duncan's post hoc test. VC, VE, and VN indicate the time of veraison for control, Ethrel-treated, and NAA-treated fruit, respectively.

TSS increase was similar for all fruit, as can be seen from the similar slopes of the curves in Figure 2. At most of the time points after the first sampling, the TSS levels of all three treatments were significantly different ($p < 0.05$). The delay resulting from Ethrel treatment was less pronounced than that following NAA treatment. The fruit from all three treatments were harvested for winemaking at approximately the same mean TSS value [24.1°Brix for control, 24.0°Brix for Ethrel treatment, and 24.1°Brix for NAA treatment (ANOVA p =

DOI: 10.1021/jf505491d
J. Agric. Food Chem. 2015, 63, 2137−2144

0.961)]. The harvest of Ethrel- and NAA-treated fruit was delayed by 6 and 23 days, respectively. Despite the changes in ripening resulting from the treatments, the final mean berry weights for all three at harvest were similar [1.33 g/berry for control, 1.41 g/berry for Ethrel treatment, and 1.39 g/berry for NAA treatment (ANOVA $p = 0.583$)]. Anthocyanin accumulation was delayed by Ethrel and NAA treatments. Three weeks after veraison of the control fruit (February 14, 2012), control berries contained a significantly larger amount of anthocyanins than Ethrel- and NAA-treated fruit, which reflects the differences in soluble solid content. In contrast, the anthocyanin concentrations in berries of similar TSS levels (approximately 24°Brix) at harvest were not significantly different (Figure 3). There was also no significant difference

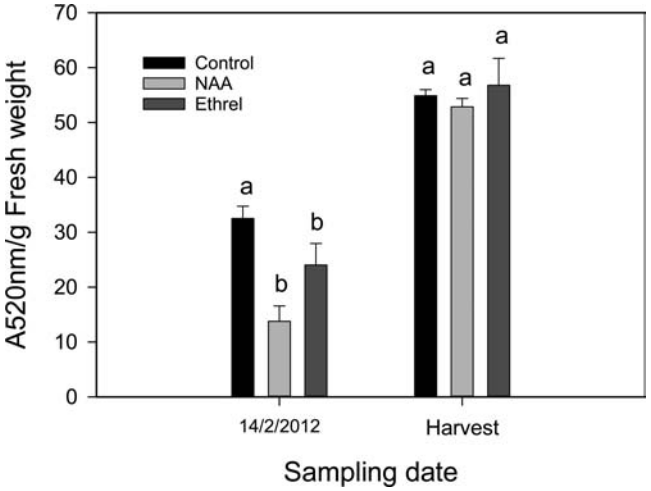

Figure 3. Effect of Ethrel and NAA treatments on anthocyanin accumulation (A_{520}). All data represent means ± STERR ($n = 3$), and different letters denote significant differences between treatments at $p < 0.05$ using one-way ANOVA followed by Duncan's post hoc test.

in titratable acidity at harvest [6.4 g/L for control, 6.7 g/L for NAA treatment, and 6.4 g/L for Ethrel treatment (ANOVA $p = 0.448$)]. From this, it appears that changes in both primary and secondary metabolism that occur during ripening were delayed by the preveraison application of Ethrel and, to a larger extent, NAA.

Wines were made from control, Ethrel-treated, and NAA-treated fruit for sensory and biochemical analysis. At the completion of winemaking, various basic measurements of the wine properties were taken. Small but statistically significant differences were observed in percent alcohol, acetic acid, pH, and titratable acidity (Table 1); these are unlikely to have an impact on the sensory properties of the wine.

Table 1. Measurements of Percent Alcohol, Acetic Acid, pH and T.A. of Wines at Bottling[a]

treatment	% alcohol (v/v)	acetic acid (g/L)	pH	T.A. (g/L of H^2T)
control	14.6 a	0.36 a	3.72 b	6.8 a
NAA	14.2 c	0.27 b	3.85 a	6.6 ab
Ethrel	14.4 b	0.30 b	3.80 a	6.3 b

[a]Values represent means ($n = 3$), and different letters denote significant differences between treatments at $p < 0.05$ using one-way ANOVA followed by Duncan's post hoc test.

Descriptive Sensory Analysis of the Wine. Twenty-four wine sensory attributes were scored across the wines using a trained panel. Two were attributes related to appearance, and eight were related to odor. Eleven were palate characteristics, and three measured wine mouthfeel properties. Of these, significant differences were identified between the wines for the two appearance attributes, four aroma attributes, three palate attributes, and one mouthfeel attribute (Table 2). Those

Table 2. Sensory Attributes Found To Be Significantly Different amongs the Wines through Descriptive Analysis[a]

attribute	control	ethrel-treated	NAA-treated	p value
color	7.59 b	6.03 c	9.06 a	0.001
transparency	8.50 b	5.61 c	9.70 a	<0.001
dark fruit aroma	8.05 b	6.91 c	9.40 a	0.003
red confection aroma	6.53 a	6.54 a	4.95 b	0.033
earthy/dusty aroma	1.84 b	2.63 ab	3.46 a	0.007
pepper aroma	2.99 b	2.63 b	6.01 a	0.003
red berry flavor	4.66 b	5.71 a	3.99 b	0.025
earthy/dusty flavor	2.18 b	2.97 ab	3.65 a	0.044
pepper flavor	4.41 b	4.58 b	7.59 a	<0.001
tannin quantity	8.89 a	8.00 ab	7.39 b	0.015

[a]Values represent means ($n = 3$), and different letters denote significant differences between treatments at $p < 0.05$ using one-way ANOVA followed by Duncan's post hoc test. The p value represents the "sample" effect (i.e., treatment) on the attribute.

attributes that were not significantly different because of the treatment of the fruit are listed in Table S3 of the Supporting Information. Wines produced from grapes treated with NAA were found to have more "color" and less "transparency" than those from the control and Ethrel-treated fruit (Table 2). Other sensory attributes more associated with the wines from the NAA-treated fruit included "dark fruit" and "pepper" aromas and "pepper" flavor on the palate (Table 2). It was also observed that scores for "red confection" odor and "red berry" flavor were significantly lower in the wine produced from NAA-treated grapes than in the wine from control and Ethrel-treated samples (Table 2). "Earthy/dusty" aroma and flavor were scored higher in the wines produced from the NAA treatment than in the control wines but were not significantly different from those of the wines from the Ethrel treatment (Table 2). In contrast, "tannin quantity" was found to be significantly lower in the wines from the NAA-treated fruit than in control wines but was not different from that of the wine from the Ethrel-treated bunches (Table 2). The Ethrel treatment also had a significant effect on wine attributes with significantly higher scores than the control and NAA wines for "red berry" flavor, but the lowest scores for wine "color", "transparency", and "dark fruit" aroma.

Analysis of Wine Volatiles. Significant differences were observed in the volatile profiles of the wines as determined using headspace SPME−GC−MS analysis. Of the 164 compounds quantified, eight were found in larger amounts in the headspace of the wines made from NAA-treated grapes compared to the control wines and 17 were more abundant in the control wines than in those made from the NAA-treated fruit (Table 3). No compounds were found in significantly greater concentrations in the wine from the Ethrel treatment compared with the other two treatments, but levels of two compounds (ethyl salicylate and hotrienol) were found to be lower in these wines than in wines from both the control and

DOI: 10.1021/jf505491d
J. Agric. Food Chem. 2015, 63, 2137−2144

Table 3. Volatile Compounds Found To Be Significantly Different in the Headspace of the Wines Produced from NAA-Treated, Ethrel-Treated, and Control Berries

compound	LRI[a]	compound ID[b]	control[c]	Ethrel	NAA
More Abundant in the Headspace of NAA-Treated Wines vs Control Wines					
α-calacorene	1901	B	0.039 b	0.062 b	0.184 a
cadalene	2215	B	0.014 b	0.014 b	0.033 a
3-ethoxy-1-propanol	1356	A	0.032 b	0.039 ab	0.051 a
ethenyl benzene	1241	A	3.445 b	3.906 b	4.912 a
methionol	1696	A	0.106 b	0.123 ab	0.135 a
ethyl salicylate	1794	B	0.004 b	0.002 c	0.005 a
phenylethyl butyrate	1946	A	0.013 b	0.013 b	0.016 a
1,1,6-trimethyl-1,2-dihydronaphthalene	1727	B	0.058 b	0.061 b	0.069 a
More Abundant in the Headspace of Control Wines vs NAA-Treated and/or Ethrel-Treated Wines					
(Z)-3-hexenyl acetate	1294	A	0.035 a	0.015 b	0.016 b
isoamyl isovalerate	1284	B	0.015 a	0.013 ab	0.007 b
hexyl acetate	1260	A	1.862 a	1.037 b	0.936 b
2-heptyl acetate	1252	B	0.016 a	0.006 b	0.009 ab
(Z)-3-hexen-1-ol	1365	A	0.268 a	0.197 b	0.154 c
ethyl (E)-2-hexenoate	1330	A	0.080 a	0.053 b	0.052 b
theaspirane A	1522	B	0.028 a	0.019 b	0.019 b
ethyl (Z)-3-hexenoate	1287	A	0.102 a	0.061 b	0.071 b
(E)-3-hexen-1-ol	1345	A	0.021 a	0.015 b	0.015 b
diethyl malate	2043	A	0.035 a	0.021 b	0.025 b
2-heptanol	1308	A	0.029 a	0.025 b	0.021 c
1-hexanol	1335	A	2.104 a	1.809 b	1.591 c
2-ethyl furoate	1605	A	0.049 a	0.044 a	0.037 b
1-penten-3-ol	1157	A	0.021 a	0.016 b	0.017 b
4-methyl-1-pentanol	1296	A	0.119 a	0.104 b	0.096 b
theaspirane B	1485	B	0.026 a	0.019 b	0.021 b
citronellyl acetate	1646	A	0.006 a	0.005 b	0.005 b
α-terpineol	1677	A	0.465 a	0.406 b	0.386 b
2-phenylethanol[d]	1910	A	0.305 a	0.253 b	0.264 ab
hotrienol	1591	B	0.006 a	0.005 b	0.006 a

[a]LRI (linear retention indices) calculated from retention of the compound relative to the retention of a series of *n*-alkanes (C_8–C_{26}). [b]Abbreviations: A, identity confirmed by matching mass spectra and LRI with that of authentic standards; B, tentative assignment based upon comparison with mass spectral libraries and published LRIs. [c]Values represent means ($n = 3$) of the areas under the peaks of a selected ion relative to the relevant internal standard. Different letters denote significant differences between treatments at $p < 0.05$ using one-way ANOVA followed by Duncan's post hoc test. [d]Compound quantified in the 1:100 dilution.

NAA-treated fruit (Table 3). However, the abundances of 18 compounds were lower in the wines produced from Ethrel-treated grapes than in those produced from control grapes (Table 3). The concentrations of 2-heptanol, 1-hexanol, and (Z)-3-hexen-1-ol were intermediate in the Ethrel treatment wines, being lowest after NAA treatment (Table 3).

Several compounds that are derived from the lipoxygenase pathway were present in lower abundances in the wines produced from NAA-treated grapes than in the control wines. These were 1-hexanol, (E)-3-hexen-1-ol, (Z)-3-hexen-1-ol, and the esters hexyl acetate, ethyl (Z)-3-hexenoate, ethyl (E)-2-hexenoate, and (Z)-3-hexenyl acetate, which have been shown to derive from C_6 alcohols and aldehydes produced by the lipoxygenase pathway.[20] Other lipid oxidation products with levels higher in control wines than in those produced from NAA-treated berries were 2-heptanol and 1-penten-3-ol. In general, the compounds that were significantly more abundant in the headspace of the control wines compared with those from the NAA treatment were less than 2-fold different, the exceptions being isoamyl isovalerate and (Z)-3-hexenyl acetate, with levels that were slightly more than 2-fold higher in the control wines than the NAA treatment wines.

Some aromatic compounds were more abundant in the wines from the NAA treatment than in the control wines. These were ethenyl benzene, ethyl salicylate, phenylethyl butyrate, and 1,1,6-trimethyl-1,2-dihydronaphthalene, the latter being derived from the degradation of carotenoids and the remainder from benzenoid metabolism. None of these compounds were more than 2-fold different in abundance between the wines.

The Concentration of Some Sesquiterpenes Is Elevated by NAA Treatment. Among the compounds found to be present at higher concentrations in the headspace of the wine from NAA-treated fruit were two sesquiterpenes tentatively identified as α-calacorene and cadalene. These volatile compounds were found in concentrations 4.7- and 2.4-fold higher, respectively, in the wines produced from the NAA-treated berries than in the control wines (Table 3). The compound responsible for pepper character in Shiraz wines has been identified as the sesquiterpene rotundone, which is sensorially active at very low concentrations.[11] Given that these two compounds had mass spectra typical of sesquiterpenes and that terpene synthase enzymes can make multiple products,[21] we decided to analyze the concentration of rotundone in the wines using a targeted analytical method. Rotundone could not be detected in the control wines, was present at low

DOI: 10.1021/jf505491d
J. Agric. Food Chem. 2015, 63, 2137–2144

concentrations (2 ± 0.4 ng/L) in the wine made from Ethrel-treated fruit, but was found at 14.5-fold higher concentrations (29 ± 1.6 ng/L) in the NAA treatment wines. The concentration found in the wine produced from NAA-treated fruit is above the odor threshold for rotundone, which was determined to be 16 ng/L in red wine, for those panelists sensitive to the compound.[11]

DISCUSSION

The results described above confirm previous studies showing that grape berry ripening and harvest can be delayed by the application of PGRs during the preveraison period of berry development. In this case, a considerable delay in harvest was achieved using NAA and a more modest delay when Ethrel was applied (Figure 2). On the basis of previous work,[3−6] Ethrel was applied earlier during berry development than NAA to achieve the desired, delaying effect. In a previous paper, it was shown that there is a likely explanation for the application of Ethrel (which releases ethylene) delaying ripening and harvest. It appears that ethylene can induce an increase in the level of biosynthesis and accumulation of the endogenous auxin indole-3-acetic acid (IAA) through the induction of putative IAA biosynthesis gene expression.[5] This increase in IAA concentration is a probable reason for the observed delay in ripening as the application of auxins has been shown to delay ripening.[8,9,22] NAA appears to be more efficacious than IAA in its ability to delay ripening. This may be due to it being a poor substrate for IAA-amino acid synthetases, the enzymes that inactivate IAA through conjugation,[2] thus increasing the longevity in the plant of any applied NAA. However, although it is less effective than NAA, it seems that an Ethrel-induced increase in IAA concentrations[5] could have occurred, and this was sufficient to delay the onset of ripening (Figure 2).

There were relatively few differences observed in the concentrations of headspace volatile compounds between the wines from control and NAA-treated grapes. Of the 164 compounds identified, only 25 were present in significantly different abundances (eight were higher in NAA wines, and 17 were higher in the control wines) (Table 3). In addition, the differences were mainly less than 2-fold. Four compounds, 2-heptanol, ethyl (*Z*)-3-hexenoate, ethyl (*E*)-2-hexenoate, and (*E*)-3-hexen-1-ol, have previously been found to be present at higher concentrations in control wine than in wine from ripening-delayed NAA-treated grapes, in Riesling, Shiraz, or both.[8,9] This indicates that NAA treatments affect the concentrations of some volatile compounds in a similar manner in different years and between different varieties. In contrast, levels of hexyl acetate and (*Z*)-3-hexenyl acetate, which were previously found to be at higher concentrations in wines made from NAA-treated Riesling grapes,[9] were higher in control wines in the current experiment (Table 3). Hexyl acetate was also at higher concentrations in NAA Shiraz wines compared to controls in a previous study.[8] These results indicate that NAA treatment and the subsequent delay in ripening significantly alter the abundances of relatively few of the measured volatile compounds. The changes in accumulation of some compounds in response to treatment with NAA seem to be consistent, but the concentrations of other compounds must be under more complex control as they vary independently.

Some compounds derived from the lipoxygenase pathway [1-hexanol, (*E*)-3-hexen-1-ol, (*Z*)-3-hexen-1-ol, and the esters hexyl acetate, ethyl (*Z*)-3-hexenoate, ethyl (*E*)-2-hexenoate, and (*Z*)-3-hexenyl acetate] were lower in the wines from NAA-treated fruit than in wines from control fruit (Table 3). The descriptors of all of these compounds are generally "green" for the alcohols and "green/fruity/apple" for the esters. However, green characters were not found to be significantly different among the wines. It is possible that these compounds are influencing the perception of "dark fruit" versus "red confection" in the wines; that is, larger amounts in the control wines make the fruit characteristics more "fresh" and "red" compared to those created by the smaller amounts in the wines from the NAA treatment where the fruit characters are described more as "cooked fruit" or "dark".

The increase in "pepper" aroma and flavor of the wine made from NAA-treated fruit was particularly noteworthy as it was observed during winemaking and was clearly distinguishable during the sensory testing (Table 2). The molecule responsible for "peppery" character in grapes has been identified as rotundone,[11] and its presence appears to be associated with the "pepper" aroma and flavor detected in the sensory analysis of the wines in this study. Although there were higher concentrations of rotundone in the wines made from Ethrel-treated grapes than in the control, the concentrations were not above the odor threshold in red wine,[11] and there was no significant difference in "pepper" character detected between the wines from control and Ethrel-treated grapes. The large increase in the level of rotundone in wine from NAA-treated grapes was detected sensorially (Table 3). Rotundone concentrations have been shown to vary considerably within a vineyard.[14] In the experiment described here, the sample replication in the field was maintained throughout winemaking, sensory analysis, and metabolite analysis, so the effects of any field variation can be tested by statistical analysis using ANOVA. While the effect of treatment on rotundone concentration was significant ($p = 0.002$), neither the effect of row ($p = 0.321$) nor the interaction of treatment and row ($p = 0.164$) was significant at the 0.05 level.

There are a number of possible explanations for the increased concentration of rotundone in wines from Ethrel-treated and, in particular, NAA-treated grapes. We have no evidence to indicate the mechanism involved in the increase in the concentration of rotundone, i.e., via an increased level of biosynthesis, a decreased level of catabolism, or a combination of both. As described above, it is feasible that auxins are the common factor in both NAA and Ethrel treatments because of the interaction of auxins and ethylene.[5,6] This may mean that there is a direct effect of auxins on rotundone metabolism that results in a sustained increase in its concentration and that the effect of NAA is greater than that for IAA because of the greater persistence of NAA in berries.

An alternative explanation is that the increased concentrations of rotundone, especially in wines made from NAA-treated grapes, were due to the delay in veraison. Certainly, the longer the delay in veraison, and therefore harvest, the greater the accumulation of rotundone. The increase in the level of rotundone could be caused by a lengthening of the period before veraison caused by the treatments. As rotundone appears to accumulate only after veraison,[13] an increase in the level of rotundone that was caused by a delay in ripening would have to result from an increase in the number of precursor molecules to rotundone during this period. The precursor for rotundone has been identified as α-guaiene, which can be converted to rotundone through oxidation.[17] Another possibility is that the delay in veraison means that ripening is occurring under different climatic conditions and that these conditions are more

DOI: 10.1021/jf505491d
J. Agric. Food Chem. 2015, 63, 2137−2144

favorable for rotundone accumulation. For example, some suggestions have been made that lower temperatures may result in increased pepper character (rotundone) accumulation.[10,13,14] There was no obvious change in the pattern of minimum and maximum temperatures during the period when rotundone accumulated (Figure S1 of the Supporting Information). Therefore, any effect of temperature on rotundone accumulation is quite subtle, or there are other factors that have a significant impact. One other parameter that differed between the control and NAA-treated fruit in particular was the length of time from veraison to harvest that was longer by approximately 8 days for NAA-treated fruit than for control fruit. As rotundone can be formed via the oxidation of α-guaiene,[17] it could be that the longer hang time of the NAA-treated fruit after harvest may have resulted in higher rotundone concentrations. Along with the increase in rotundone concentration, the concentrations of two other sesquiterpenes [α-calacorene and cadalene (Table 3)] were higher in wines from NAA-treated fruit, indicating that there may be a more general effect of the treatment on sesquiterpene metabolism.

Sensory analysis showed that although the wines from Ethrel-treated berries were quite similar to those from control berries there was a considerable difference between control and NAA wines as nine attributes were significantly different. The difference in rotundone concentrations can explain the differences observed in "pepper" aroma and flavor, but the other attributes are unlikely to be related to rotundone. Some of these differences could be related to changes in the levels of the volatile compounds measured (see above), but there may be other, undetected differences that influence aroma and flavor. Whatever the identity of the compounds, the difference in flavor and aroma is unlikely to be due to differences in sugar levels as there was no significant difference between the TSS values at harvest as determined by ANOVA.

In summary, both Ethrel and NAA treatments delayed the onset of berry ripening and harvest. NAA delayed ripening to a greater extent than Ethrel. Similarly, both treatments significantly altered wine volatile metabolite levels, but greater differences were induced by NAA treatment. NAA treatment, and to a lesser extent Ethrel treatment, also altered wine sensory character. Wines from NAA-treated fruit were notable for having higher scores for "pepper" aroma and flavor. Analysis by GC−MS showed that these wines had concentrations of rotundone above the sensory limit. The reason for an increased level of rotundone in the NAA wines is unknown but could arise from a direct effect of NAA on rotundone accumulation or be a result of the altered timing of the ripening phase affecting sesquiterpene metabolism.

■ ASSOCIATED CONTENT

Supporting Information

Graph of vineyard minimum and maximum air temperatures during the period of rotundone accumulation (Figure S1), composition of sensory reference standards used to define aroma (Table S2), and sensory attributes found to be not significantly different among the wines through descriptive analysis (Table S3). This material is available free of charge via the Internet at http://pubs.acs.org.

■ AUTHOR INFORMATION

Corresponding Author

*Telephone: +61 8 8303 8628. Fax: +61 8 8303 8601. E-mail: christopher.davies@csiro.au.

Funding

This project was supported by Australian grape growers and winemakers through their investment body, the Australian Grape and Wine Authority and CSIRO. CSIRO and the University of Adelaide are part of the Wine Innovation Cluster.

Notes

The authors declare no competing financial interest.

■ ACKNOWLEDGMENTS

We thank Australian Vintage Ltd. for assistance with these experiments.

■ ABBREVIATIONS USED

ANOVA, analysis of variance; DA, descriptive analysis; GC, gas chromatography; GC−MS, gas chromatography−mass spectrometry; IAA, indole-3-acetic acid; MS, mass spectrometry; NAA, 1-naphthaleneacetic acid; NMR, nuclear magnetic resonance; SIM, selected ion monitoring; SPME−GC−MS, solid phase microextraction−gas chromatography−mass spectrometry; TSS, total soluble solids

■ REFERENCES

(1) Böttcher, C.; Davies, C. Hormonal control of grape berry development and ripening. In *The Biochemistry of the Grape Berry*; Gerós, H., Chaves, M. M., Delrot, S., Eds.; Bentham Science: Sharjah, United Arab Emirates, 2012; pp 194−217.

(2) Böttcher, C.; Boss, P. K.; Davies, C. Acyl substrate preferences of an IAA-amido synthetase account for variations in grape (*Vitis vinifera* L.) berry ripening caused by different auxinic compounds indicating the importance of auxin conjugation in plant development. *J. Exp. Bot.* **2011**, *62*, 4267−4280.

(3) Hale, C. R.; Coombe, B. G.; Hawker, J. S. Effects of ethylene and 2-chloroethylphosphonic acid on the ripening of grapes. *Plant Physiol.* **1970**, *45*, 620−623.

(4) Coombe, B. G.; Hale, C. R. The hormone content of ripening grape berries and the effects of growth substance treatments. *Plant Physiol.* **1973**, *51*, 629−634.

(5) Böttcher, C.; Burbidge, C. A.; Boss, P. K.; Davies, C. Interactions between ethylene and auxin are crucial to the control of grape (*Vitis vinifera* L.) berry ripening. *BMC Plant Biol.* **2013**, *13*, 222.

(6) Böttcher, C.; Harvey, K. E.; Boss, P. K.; Davies, C. Ripening of grape berries can be advanced or delayed by reagents that either reduce or increase ethylene levels. *Funct. Plant Biol.* **2013**, *40*, 566−581.

(7) Webb, L. B.; Whetton, P. H.; Barlow, E. W. R. Observed trends in winegrape maturity in Australia. *Global Change Biology* **2011**, *17*, 2707−2719.

(8) Böttcher, C.; Harvey, K.; Forde, C. G.; Boss, P. K.; Davies, C. Auxin treatment of pre-veraison grape (*Vitis vinifera* L.) berries both delays ripening and increases the synchronicity of sugar accumulation. *Aust. J. Grape Wine Res.* **2011**, *17*, 1−8.

(9) Böttcher, C.; Boss, P. K.; Davies, C. Delaying Riesling grape berry ripening with a synthetic auxin affects malic acid metabolism and sugar accumulation, and alters wine sensory characters. *Funct. Plant Biol.* **2012**, *39*, 745−753.

(10) Iland, P.; Gago, P. *Australian Wine: Styles & tastes*; Patrick Iland Wine Promotions: Adelaide, Australia, 2002.

(11) Wood, C.; Siebert, T. E.; Parker, M.; Capone, D. L.; Elsey, G. M.; Pollnitz, A. P.; Eggers, M.; Meier, M.; Vössing, T.; Widder, S.; Krammer, G.; Sefton, M. A.; Herderich, M. J. From wine to pepper:

DOI: 10.1021/jf505491d
J. Agric. Food Chem. 2015, 63, 2137−2144

Rotundone, an obscure sesquiterpene, is a potent spicy aroma compound. *J. Agric. Food Chem.* **2008**, *56*, 3738−3744.
(12) Mattivi, F.; Caputi, L.; Carlin, S.; Lanza, T.; Minozzi, M.; Nanni, D.; Valenti, L.; Vrhovsek, U. Effective analysis of rotundone at below-threshold levels in red and white wines using solid-phase micro-extraction gas chromatography/tandem mass spectrometry. *Rapid Commun. Mass Spectrom.* **2011**, *25*, 483−488.
(13) Caputi, L.; Carlin, S.; Ghiglieno, I.; Stefanini, M.; Valenti, L.; Vrhovsek, U.; Mattivi, F. Relationship of changes in rotundone content during grape ripening and winemaking to manipulation of the 'peppery' character of wine. *J. Agric. Food Chem.* **2011**, *59*, 5565−5571.
(14) Scarlett, N. J.; Bramley, R. G. V.; Siebert, T. E. Within-vineyard variation in the 'pepper' compound rotundone is spatially structured and related to variation in the land underlying the vineyard. *Aust. J. Grape Wine Res.* **2014**, *20*, 214−222.
(15) Boss, P. K.; Böttcher, C.; Davies, C. Various influences of harvest date and fruit sugar content on different wine flavor and aroma compounds. *Am. J. Enol. Vitic.* **2014**, *65*, 341−353.
(16) Huang, A. C.; Sumby, C. J.; Tiekink, E. R. T.; Taylor, D. K. Synthesis of Guaia-4(5)-en-11-ol, Guaia-5(6)-en-11-ol, Aciphyllene, 1-*epi*-Melicodenones C and E, and other Guaiane-type Sesquiterpenoids via the Diastereoselective Expoxidation of Guaiol. *J. Nat. Prod.* **2014**, *77*, 2522−2536.
(17) Huang, A. C.; Burrett, S.; Sefton, M. A.; Taylor, D. K. Production of the Pepper Aroma Compound, (−)-Rotundone, by Aerial Oxidation of α-Guaiene. *J. Agric. Food Chem.* **2014**, *62*, 10809−10815.
(18) Huang, A.-C.; Sefton, M. A.; Taylor, D. K. Comparison of the Formation of Peppery and Woody Sesquiterpenes Derived from α-Guaiene and α-Bulnesene under Aerial Oxidative Conditions. *J. Agric. Food Chem.* **2015**, DOI: 10.1021/jf505537s.
(19) Siebert, T. E.; Wood, C.; Elsey, G. M.; Pollnitz, A. P. Determination of rotundone, the pepper aroma impact compound, in grapes and wine. *J. Agric. Food Chem.* **2008**, *56*, 3745−3748.
(20) Dennis, E. G.; Keyzers, R. A.; Kalua, C. M.; Maffei, S. M.; Nicholson, E. L.; Boss, P. K. Grape contribution to wine aroma: Production of hexyl acetate, octyl acetate, and benzyl acetate during yeast fermentation is dependent upon precursors in the must. *J. Agric. Food Chem.* **2012**, *60*, 2638−2646.
(21) Lücker, J.; Bowen, P.; Bohlmann, J. *Vitis vinifera* terpenoid cyclases: Functional identification of two sesquiterpene synthase cDNAs encoding (+)-valencene synthase and (−)-germacrene D synthase and expression of mono- and sesquiterpene synthases in grapevine flowers and berries. *Phytochemistry* **2004**, *65*, 2649−2659.
(22) Davies, C.; Boss, P. K.; Robinson, S. P. Treatment of grape berries, a nonclimacteric fruit with a synthetic auxin, retards ripening and alters the expression of developmentally regulated genes. *Plant Physiol.* **1997**, *115*, 1155−1161.

DOI: 10.1021/jf505491d
J. Agric. Food Chem. 2015, 63, 2137−2144

stable) o/w emulsions on the adhesion and spreading of fat on the tongue was previously reported.[6] It was found that o/w emulsions stabilized with little protein had a stronger adhesion on the tongue (i.e., more stable against rinsing with saliva) compared to o/w emulsions stabilized with a high concentration of protein. It was hypothesized that this was due to difference in stability of the interfacial layer of the emulsion against rupture and thus creating coalescence of the oil droplets.[6]

Although the mentioned studies have indicated relations between o/w emulsion properties, such as viscosity, emulsifier type and content, and oral coatings, the mechanisms on how different macronutrients influence the deposition and clearance of oral oil coatings and how they relate to after-feel perception are still not understood. The aims of this study are to investigate the influence of (i) protein type, (ii) protein content, and (iii) viscosity of o/w emulsions on the clearance of oral oil coatings and after-feel sensory perception. The deposition and clearance of oral oil coatings from the tongue surface was determined using in vivo fluorescence measurements. The after-feel perception was determined using progressive profiling. To study the influence of protein emulsifier type on oil coatings, o/w emulsions stabilized with proteins differing in flocculation behavior when mixed with saliva were prepared. Lysozyme which forms irreversible agglomerates upon mixing with saliva and Na-caseinate, which is hypothesized to form no agglomerates upon mixing with saliva were used.[13] To study the influence of protein content on clearance and after-feel sensory perception of oral oil coatings, three concentrations of protein were used (all in excess to stabilize the water/oil interface). We hypothesize that excess protein has a blending effect with saliva, resulting in faster clearance of oil deposits from the tongue surface. To study the influence of viscosity of o/w emulsions on the clearance and after-feel sensory perception of oral oil coatings, three o/w emulsions stabilized with Na-caseinate were thickened with varying concentrations of xanthan gum. Emulsions stabilized with Na-caseinate were chosen to study the influence of viscosity, independently from other factors, to rule out possible effects of emulsifier−saliva biopolymers. Xanthan gum was chosen as it is commonly used as a thickener in various food liquid foods.

MATERIALS AND METHODS

Materials. Sunflower oil (Perfekt, purchased from local retailer), Na-caseinate (Excellion sodium caseinate S, DMV International, The Netherlands, typical protein content: 91%), lysozyme hydrochloride (The Protein Company, Belgium, protein content: >99%), sucrose (AH basic, purchased from local retailer), xanthan gum (Keltrol Advanced Performance, CP Kelco, Denmark), curcumin (7% w/w curcumin dissolved in propylene glycol and polysorbate; L-WS; Sensient, The Netherlands), NaOH (Merck, Germany), and tap water were used. All ingredients were food grade. Pig's tongues were obtained from the VION Food Group (The Netherlands).

Preparation and Characterization of o/w Emulsions. Table 1 shows the composition of all the o/w emulsions. All o/w emulsions were prepared in a food-grade environment. The oil phase of the o/w emulsions consisted of sunflower oil (10% (w/w)). The aqueous phase of the o/w emulsions consisted of protein solution (concentrations see Table 1) with 8% (w/w) sucrose. The aqueous phase was prepared by first dissolving sucrose in tap water and later dissolving either Na-caseinate or lysozyme at room temperature. The aqueous phase with dissolved lysozyme was brought to a pH of 6.9 by addition of 1 M NaOH. Protein concentration in the aqueous phase varied (0.2, 3.0, and 5.8% (w/w)). The 0.2% (w/w) protein concentration was chosen, as the lowest concentration, as it allows to prepare stable emulsions with low concentrations of "free-protein" in the aqueous phase, i.e., protein that is not adsorbed into the oil droplets surface. The 3.0% (w/w) protein concentration was chosen as the middle concentration, as it is a protein concentration common in dairy drinks. The 5.8% (w/w) protein concentration was chosen as the highest concentration, as it creates emulsions with high concentration of "free-protein" in the aqueous phase and has an equal difference of protein concentration between the emulsion with 3.0% as the emulsion with 0.2%.

Table 1. Overview of o/w Emulsions[a]

o/w emulsion	protein (% w/w)	xanthan gum (% w/w)	$d_{3,2}$ ± stdev (μm)	η ± stdev at 63 s^{-1} (mPas)
Na-caseinate	0.2	0	2.04 ± 0.20	1.7 ± 0.01
	3.0	0	1.45 ± 0.08	5.0 ± 0.05
	5.8	0	1.46 ± 0.05	9.0 ± 0.07
lysozyme	0.2	0	1.16 ± 0.24	2.2 ± 0.05
	3.0	0	1.21 ± 0.28	2.3 ± 0.05
	5.8	0	1.35 ± 0.19	3.5 ± 0.13
Na-caseinate	3.0	0.05	1.28 ± 0.10	13.8 ± 0.15
	3.0	0.20		49.9 ± 1.50
	3.0	0.50		143 ± 7.28

[a]All o/w emulsions contained 10% (w/w) oil and 8% (w/w) sucrose. o/w emulsions differed in type and concentration of protein used as emulsifier and xanthan gum concentration. $d_{3,2}$, droplet size (averages of measurements of 3−4 batches) and viscosity at a shear rate of 63 s^{-1} are shown.

The aqueous phase was then prehomogenized with the oil phase (sunflower oil) using an Ultra Turrax (IKA RW 20 Digital) at 4000 min^{-1} for 3 min and homogenized with a two-stage homogenizer (Niro-Soavi SpA, NS1001L2K) at pressures between 250 and 350 bar. All o/w emulsions had a neutral pH. The o/w emulsions thickened with xanthan gum were prepared from an o/w stock emulsion and mixed at a ratio of 1:1 with preprepared aqueous xanthan gum solutions. Xanthan gum solutions were prepared by heating water to 70 °C and adding the xanthan gum under agitation. The xanthan gum thickened o/w emulsions contained 10% (w/w) oil, 3% (w/w) Na-caseinate, and 8% (w/w) sucrose in the aqueous phase and varying concentrations of xanthan gum (see Table 1).

Emulsions were stored after preparation in a refrigerator at 4 °C and used for further studies no later than 3 days after preparation. Curcumin was added to the emulsions as a hydrophobic fluorescent dye prior to the in vivo measurements. Then 1 μL of 7% curcumin per gram of o/w emulsions was added under magnetic stirring immediately before testing.

Particle size distribution was determined by light scattering (Malvern Instruments, Goffin Meyvis) using a refractive index for sunflower oil of 1.469. Particle size of the different o/w emulsions was measured for every batch made for the fluorescence measurements. Sample was added to the light scattering measurement device until the obscuration reached 10%. $d_{3,2}$ was obtained as a measure of oil droplet size and averaged over measurements of 3−4 batches.

For every emulsion, the number of oil droplets was estimated by calculating: $number\ of\ oil\ droplets\ (N) = ((volume\ of\ oil)/((4/3) \times \pi \times r^3))$, where r is radius of the oil droplet. By knowing the number of oil droplets in each emulsion, the surface area of the emulsion can be estimated by calculating: $surface\ area\ of\ emulsion = N \times 4 \times \pi \times r^2$. On the basis of previous studies, we can estimate the amount of protein needed to cover the surface area of the emulsions.[14] We estimate that for the o/w emulsions with lower protein concentrations (0.2% w/w), about 1 mg/m^2 (Na-caseinate) to 1.5 mg/m^2 (lysozyme) of protein is adsorbed onto the surface of the oil droplets. For the higher protein concentrations used in our study (>2.25% (w/w)), we estimate that about 3.2 mg/m^2 of protein (Na-caseinate and lysozyme) is adsorbed onto the surface of the oil droplets.[14] This corresponds to a minimum protein concentration absorbed on the oil droplet interface of 0.05% (w/w) for low and 0.15% (w/w) for high protein concentrations. Therefore, all protein concentrations used in our study to emulsify the

DOI: 10.1021/jf505653t
J. Agric. Food Chem. 2015, 63, 2145−2153

o/w emulsions are assumed to be higher than the minimum protein concentration required to cover the oil droplet surface (see Table 1). All o/w emulsions used contained an excess of protein as emulsifier.

Flow curves of all o/w emulsions were determined in duplicate at 20 °C at shear rates ranging from 0.01 to 1000 s^{-1} using a rheometer (Anton Paar GmbH, Physica MCR 301) with a double gap geometry. All samples displayed shear thinning behavior. The viscosities at a shear rate of 63 s^{-1} (closest value in the range of the reported in-mouth shear rate (50−100 s^{-1})[15,16]) were extracted from the flow curves and are reported in Table 1.

Light microscopy (Carl Zeiss, Axioskop 2 Plus) was used to characterize the structure of the o/w emulsions before and after mixing with human saliva at a magnification of 40×. Saliva was collected according to reported procedure.[13] Unstimulated saliva was collected for 30 min in the same morning as the experiments from one healthy subject. First the subject rinsed her mouth with water and then collected the saliva with closed lips and expectorated into ice-chilled beakers.[13] Mixtures between o/w emulsions and saliva were prepared at room temperature at a ratio of 1:1 as in previous reports.[17,18]

In Vivo Fluorescence Measurements to Determine Oil Fraction Deposited on Tongue Surface. *Fluorescence Measurements and Calibration Curves.* The method used in the present study has been previously described in detail.[5] Fluorescence measurements were made with a single point measurement (Fluorolog Instruments SA Inc., Jobin Yvon Spex) at an excitation wavelength of 440 nm, an emission wavelength of 495 nm, with a slit width of 0.95 mm and a measurement time of 0.1s. A fluorescence remote read fiber optic probe was used to measure on tongue surfaces (in vivo for determination of oil fraction, and ex vivo for calibration curves). A plastic ring (diameter 16.9 mm, height 5 mm) was attached to the end of the probe to ensure that the distance between the probe and the tongue surface remained constant. The probe was put perpendicularly to the tongue surface and with slight pressure to avoid deformation of the papillae and the coating. For all measurements, the background (fluorescence intensity of the tongue surface without o/w emulsion) was measured first. The background measured immediately before the measurement of the o/w emulsion was subtracted afterwards from the o/w emulsion measurement.

To convert the fluorescence intensity measured on the subject's tongue surface to the oil fraction deposited on the tongue surface, i.e., mass of oil per area of tongue (mg/cm^2), calibration lines were made following the procedure described previously.[5] Briefly, calibrations were made with pieces of the middle part of the pig's anterior tongue at 37.5 °C. Oil in water emulsions at room temperature were spread on the surface of the pig's tongue (2 cm × 2 cm), and fluorescence intensity was measured. For each measurement, a fresh piece of tongue was used.[5] As the protein type and content affects the fluorescence intensity of curcumin, calibrations (fluorescent intensities vs oil fraction on tongue surface) were made for each of the nine o/w emulsions. Calibration lines consisted of six data points, for targeted oil fractions of 0.10 mg/cm^2 ($V_{emulsion}$ = 4 μL), 0.20 mg/cm^2 ($V_{emulsion}$ = 8 μL), 0.50 mg/cm^2 ($V_{emulsion}$ = 20 μL), 0.63 mg/cm^2 ($V_{emulsion}$ = 25 μL), 0.88 mg/cm^2 ($V_{emulsion}$ = 35 μL), and 1.0 mg/cm^2 ($V_{emulsion}$ = 40 μL). All calibration measurements were performed in triplicate and are shown in the Supporting Information.

Presentation of o/w Emulsions. Oil in water emulsions were presented to the subjects at room temperature in three blocks. Each block consisted of two sessions of about 1 h, during which each o/w emulsion was presented in triplicate. The o/w emulsions were presented in randomized order over subjects per block. During the first block, the o/w emulsions stabilized with 0.2, 3.0, and 5.8% (w/w) Na-caseinate were assessed. During the second block, the o/w emulsions stabilized with 0.2, 3.0, and 5.8% (w/w) lysozyme were assessed. Finally, during the third block, the o/w emulsions stabilized with 3% Na-caseinate and thickened with 0.05, 0.2, and 0.5% (w/w) xanthan gum were assessed.

Determination of Oil Fraction Deposited on Tongue Surface. Twenty untrained subjects (7 men, 13 women, mean age 23.4 ± 3.2 years) assessed the nine o/w emulsions in triplicate. Only subjects without tongue piercings and braces participated in the study. Participants gave informed written consent and received a financial compensation for their participation.

Subjects were asked to ingest 20 mL of the o/w emulsions and let it flow freely in the mouth for 30 s. Then subjects expectorated the o/w emulsions and the fluorescence intensity was measured on the front and back part of the anterior tongue at 0, 15, 30, 45, 60, 90, 120, and 180 s after expectoration. Before presentation of the next o/w emulsion, subjects cleaned their tongue with a tongue scraper and crackers were provided together with warm water (40 °C) and room temperature water to rinse the oral cavity. A break of approximately 5 min was made between measurements.

Determination of After-Feel Perception of Oral Coatings. During the fluorescence measurements, subjects performed progressive sensory profiling of after-feel attributes fatty film, sweetness, and creaminess at 0, 30, 60, 90, 120, and 180 s after expectorating the o/w emulsions. The definition of attributes and evaluation protocol were explained to the subjects (Table 2). The three attributes for the progressive profiling were chosen, as they have been shown to relate to the after-feel perception of o/w emulsions after expectoration.[5,9,10] A continuous 100 mm visual analogue scale was used anchored with "little" and "very" at a distance of 5 mm from the ends.

Table 2. Overview of After-Feel Attributes Assessed during Progressive Profiling at Different Times Points after Expectorating (0, 30, 60, 90, 120, and 180 s) of o/w Emulsions with Definitions and Evaluation Protocol

sensory attribute	definition	evaluation protocol
fatty film	sensation of feeling a layer of oil covering the mouth	slide the tongue against the palate and lips and slide the lips against each other
sweetness	degree of sweetness that lingers in the mouth	evaluate the sweetness perceived after expectoration
creaminess	degree of creaminess perceived in the mouth	slide the tongue against the palate and evaluate degree of creaminess

Statistical Data Analysis. SPSS Statistics version 19 was used for the statistical analysis. Descriptive statistics were used to obtain the mean and standard error (SE). Outliers ($z > 2$) were removed from the data. Fluorescence intensity data was normalized with a square root transformation. The effect of position of probe (within subject factor; front and back), o/w emulsion (within subject factor; 0.2, 3.0, and 5.8% lysozyme; 0.2, 3.0, and 5.8% Na-caseinate; 0.05, 0.2, and 0.5% xanthan), time (within subject factor; 0, 15, 30, 45, 60, 90, 120, and 180 s after expectoration) and interactions on oil fraction deposited on the tongue were tested by repeated-measures ANOVA. For the sensory data, a repeated-measures ANOVA was used to investigate the effect of o/w emulsion (within subject factor; 0.2, 3.0, and 5.8% lysozyme; 0.2, 3.0, and 5.8% Na-caseinate; 0.05, 0.2, and 0.5% xanthan) and time (within subject factor: 0, 30, 60, 90, 120, and 180 s after expectoration) and interactions on "fatty film", "sweetness", and "creaminess" intensity. A significance level of $p < 0.05$ was chosen.

RESULTS

Influence of Protein Type and Content on Oil Deposition on Tongue. *Microstructure of o/w Emulsions Stabilized with Na-Caseinate and Lysozyme before and after Mixing with Saliva.* Figure 1 shows the microstructure of 10% (w/w) o/w emulsions stabilized with different concentrations of Na-caseinate and lysozyme before and after mixing with human saliva. The 0.2% Na-caseinate o/w emulsion showed separate oil droplets (i.e., no aggregation) before and after mixing with human saliva. The o/w emulsions stabilized with 3.0 and 5.8% w/w Na-caseinate showed aggregation of the emulsion droplets. The size of the aggregates of the 3.0 and 5.8% w/w Na-caseinate emulsions seemed to decrease slightly

DOI: 10.1021/jf505653t
J. Agric. Food Chem. 2015, 63, 2145−2153

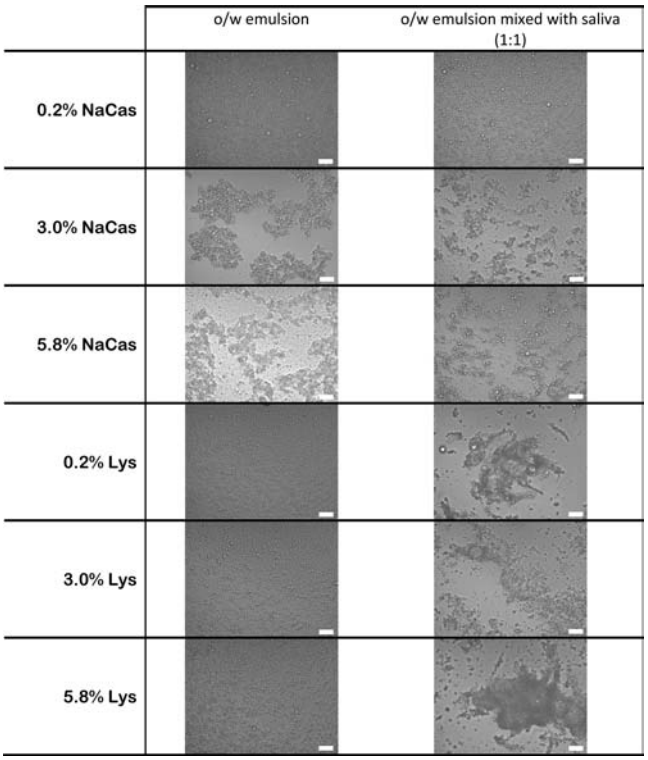

Figure 1. Light microscopy pictures. (left column) Images of 10% (w/w) o/w emulsions before mixing with human saliva and (right column) after mixing with human saliva at a ratio of o/w emulsion:saliva of 1:1. Scale bars represent 20 μm.

upon mixing with saliva. The o/w emulsions stabilized with Na-caseinate show no strong interaction with saliva because no considerable changes in the microstructure of the emulsions are observed comparing the microstructure before and after mixing with saliva. All lysozyme stabilized o/w emulsions (0.2, 3.0, and 5.8% (w/w) lysozyme) show individual, separate oil droplets before mixing with saliva. Oil in water emulsions stabilized with lysozyme revealed no flocculation at any of the lysozyme concentrations studied here. Upon mixing with saliva, agglomeration of lysozyme stabilized oil droplets was observed for all lysozyme concentrations.

Oil Deposition on Tongue Immediately after Expectoration of o/w Emulsions (t = 0 s). Figure 2 shows the oil fraction deposited on the tongue surface immediately after expectoration (t = 0 s) of the 10% (w/w) o/w emulsions stabilized with different concentrations of Na-caseinate and lysozyme at the front and back of the anterior tongue. Probe position had a significant main effect on oil fraction deposited on the tongue for emulsions stabilized by Na-caseinate as well as lysozyme (Na-caseinate, $F(1, 59) = 199$, $p < 0.001$; lysozyme, $F(1, 59) = 260$, $p < 0.001$). The oil fraction on the back part of the tongue was significantly higher than on the front part of the anterior tongue. No significant effect of Na-caseinate concentration on the oil fraction deposited on the tongue was found. With increasing lysozyme concentration, the oil fraction deposited on the tongue significantly decreased ($p < 0.05$).

Clearance of Oil Deposition on the Tongue after Expectoration. Time after expectoration had a significant main effect on oil fraction deposited on the tongue for o/w emulsions stabilized with Na-caseinate and lysozyme (Na-caseinate, $F(2.9, 176) = 412$, $p < 0.001$; lysozyme, $F(3.1, 184) = 207$, $p < 0.001$).

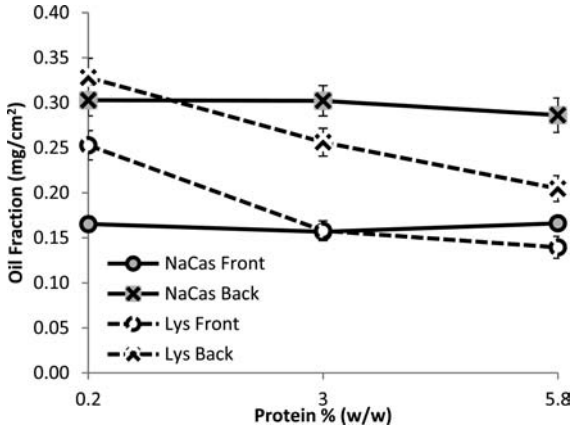

Figure 2. Oil fraction deposited on the front and back part of the anterior tongue immediately after expectoration (t = 0 s) as a function of protein concentration (% w/w) and type Na-caseinate (NaCas) and lysozyme (Lys). Each data point represents the average of n = 20 subjects and three replicates. Lines are drawn to guide the eye. Error bars represent standard error.

Figure 3 shows the clearance of oil deposited on the front (Figure 3A) and back part of the anterior tongue (Figure 3B) for 10% (w/w) o/w emulsions stabilized with different concentrations of Na-caseinate and lysozyme at different

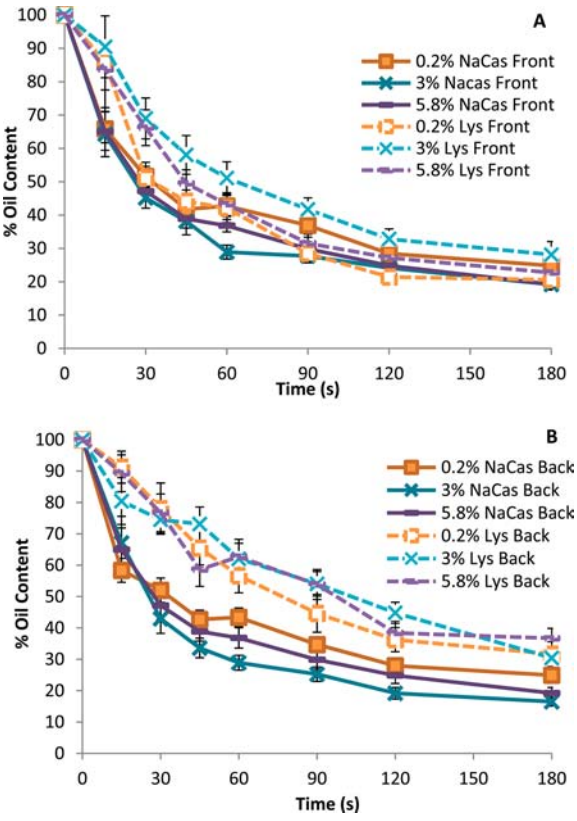

Figure 3. Relative oil content deposited on the front (A) and back (B) part of the anterior tongue for 10% (w/w) o/w emulsions stabilized with different concentrations of Na-caseinate (NaCas) and lysozyme (Lys) as a function of time. Each point represents the average of n = 20 subjects and three replicates. Lines are drawn to guide the eye. Error bars represent the standard error.

DOI: 10.1021/jf505653t
J. Agric. Food Chem. 2015, 63, 2145−2153

times after expectoration. Parts A and B of Figure 3 depict the relative oil content remaining on the tongue after expectoration, i.e., at time 0 s, the amount of oil on the tongue is 100% for all o/w emulsions. With increasing time, the relative oil content ($oil\ content(\%) = ((oil\ fraction_{t=x})/(oil\ fraction_{t=0s})) \times 100$ averaged over $n = 20$ subjects and three replicate measurements) decreases to lower percentages. Probe position had no influence on the oil clearance from o/w emulsions stabilized by Na-caseinate, showing no differences between the clearance rates of the oil deposited on the front vs back of the anterior part of tongue. In contrast, the probe position significantly affected the clearance rate of the o/w emulsion stabilized with 0.2% lysozyme from 30 s onward, and of the emulsion stabilized with 5.8% lysozyme from 60 s onward. For both cases, the oil deposited on the front part of the tongue was cleared faster, i.e., reached lower percentages of relative oil content after shorter time periods compared to the back part of the anterior tongue. The oil clearance from the o/w emulsion stabilized by 3% lysozyme was significantly different (front vs back) at time 90 s ($p = 0.06$) and 120s ($p = 0.03$).

Parts A and B of Figure 3 show that the oil deposited on the tongue of o/w emulsions stabilized with Na-caseinate had a faster clearance compared to o/w emulsions stabilized with lysozyme for both front and back parts of the tongue. These results were significant for the back part of the tongue from 30 s onward ($p < 0.05$). The o/w emulsions stabilized with lower concentrations of Na-caseinate (0.2% w/w) had a slower clearance of oil compared with the other two o/w emulsions stabilized with Na-caseinate (3.0 and 5.8% w/w). The concentration of lysozyme in the o/w emulsion did not affect the oil clearance from the tongue.

Influence of Protein Type and Content on After-Feel Perception of Oral Coatings. Figure 4 depicts the after-feel perception of 10% (w/w) o/w emulsions stabilized with different concentrations of Na-caseinate and lysozyme at different time points after expectorating the emulsions. Oil in water emulsions stabilized with Na-caseinate were perceived as significantly more intense for the after-feel attributes "fatty film", "sweetness", and "creaminess" ($p < 0.001$) than emulsions stabilized with lysozyme. The intensity of "fatty film" was significantly influenced by sample (i.e., 0.2, 3.0, and 5.8% lysozyme and 0.2, 3.0, and 5.8% Na-caseinate) [$F(2.6, 152) = 9.4$, $p < 0.001$], time [$F(2.6, 154) = 346$, $p < 0.001$] and sample × time [$F(8.2, 484) = 7.8$, $p < 0.001$]. Lysozyme concentration did not affect the perception of "fatty film" after-feel attributes of o/w emulsions stabilized with lysozyme. A trend was observed with higher concentration of Na-caseinate concentration, leading to higher "fatty film" after-feel perception. For the attribute "sweetness" the effects of sample (i.e., 0.2, 3.0, and 5.8% lysozyme and 0.2, 3.0, and 5.8% Na-caseinate) [$F(2.6, 157) = 21.5$], time [$F(2.1, 121) = 446$] and sample × time [$F(11.9, 702) = 7.8$] were significant at $p < 0.001$. The same was observed for the attribute "creaminess" (sample (i.e., 0.2, 3.0, and 5.8% lysozyme and 0.2, 3.0, and 5.8% Na-caseinate) [$F(3.6, 211) = 65.9$], time [$F(2.2, 127) = 464$, sample × time [$F(9.8, 577) = 13.5$]). The higher the concentration of Na-caseinate in the emulsion, the higher the perceived creaminess. No differences were found between the o/w emulsions stabilized with varying amounts of lysozyme.

Influence of Viscosity on Clearance of Oral Coatings. *Oil Deposition on Tongue Immediately after Expectoration (t = 0 s).* Figure 5 shows the oil fraction deposited on the front and back part of the anterior tongue immediately after

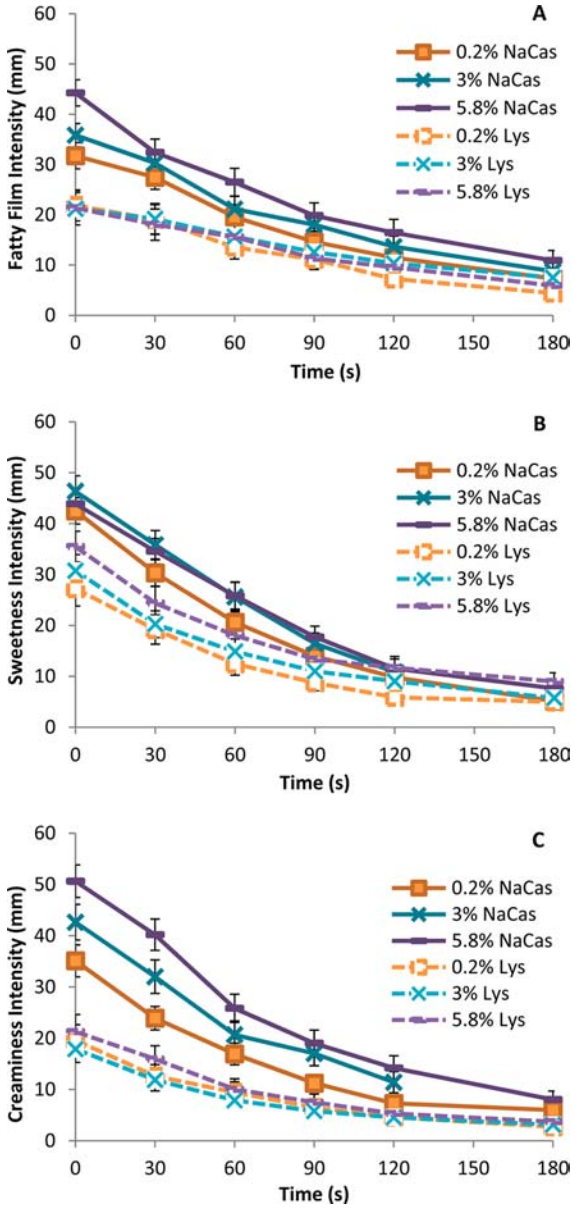

Figure 4. Intensity of after-feel attributes. Fatty film (A), sweetness (B), and creaminess (C) for 10% (w/w) emulsions differing in emulsifier type (Na-caseinate (NaCas) and lysozyme (Lys)) and content as a function of time after expectoration. Each point represents the average of $n = 20$ subjects and three replicates. Lines are drawn to guide the eye. Error bars represent the standard error.

expectoration ($t = 0$ s) of 10% (w/w) o/w emulsions stabilized with 3% (w/w) Na-caseinate differing in xanthan gum concentration. Sample (i.e., 0, 0.05, 0.2, and 0.5% xanthan gum) [$F(2.3, 133) = 137$, $p < 0.001$] and probe position [$F(1, 59) = 193$, $p < 0.001$] had a significant main effect on oil fraction deposited on the tongue for emulsions thickened with xanthan gum. Pairwise comparisons revealed no significant differences between o/w emulsions containing different concentrations of xanthan but only a significant difference between o/w emulsion without xanthan gum vs o/w emulsions with xanthan gum ($p < 0.001$). Immediately after expectoration of the o/w emulsions, the oil fraction deposited on the back part of the anterior tongue was significantly higher than on the front part of the tongue ($p < 0.001$). For both front and back part of the anterior tongue, the o/w emulsion with no xanthan

DOI: 10.1021/jf505653t
J. Agric. Food Chem. 2015, 63, 2145−2153

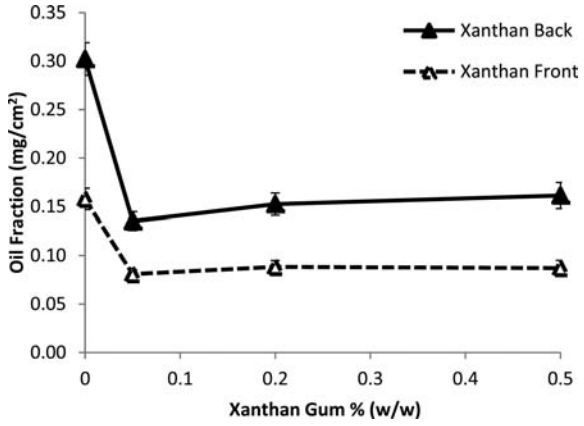

Figure 5. Oil fraction deposited on the front and back part of the anterior tongue immediately after expectoration (t = 0 s) as a function of concentration (% w/w) of xanthan gum in the 10% (w/w) o/w emulsions stabilized with 3% (w/w) Na-caseinate. Each point represents the average of n = 20 subjects and three replicates. Lines are drawn to guide the eye. Error bars represent the standard error.

gum had a significantly higher oil fraction deposited on the tongue than o/w emulsions containing xanthan ($p < 0.001$).

Clearance of Oil Deposited on the Tongue of o/w Emulsions Varying in Viscosity. Figure 6 depicts the relative oil content deposited on the front and back of the anterior tongue for the 10% (w/w) o/w emulsions stabilized with 3% (w/w) Na-caseinate thickened with different xanthan gum concentrations as a function of time. Time had a significant effect on oil fraction deposited on the tongue surface [$F(2.3, 136) = 525$, $p < 0.001$]. The oil clearance was not significantly different for o/w emulsions differing in concentration of xanthan gum ($p = 0.082$). Probe position had no significant effect on the values of relative oil content ($p = 0.155$).

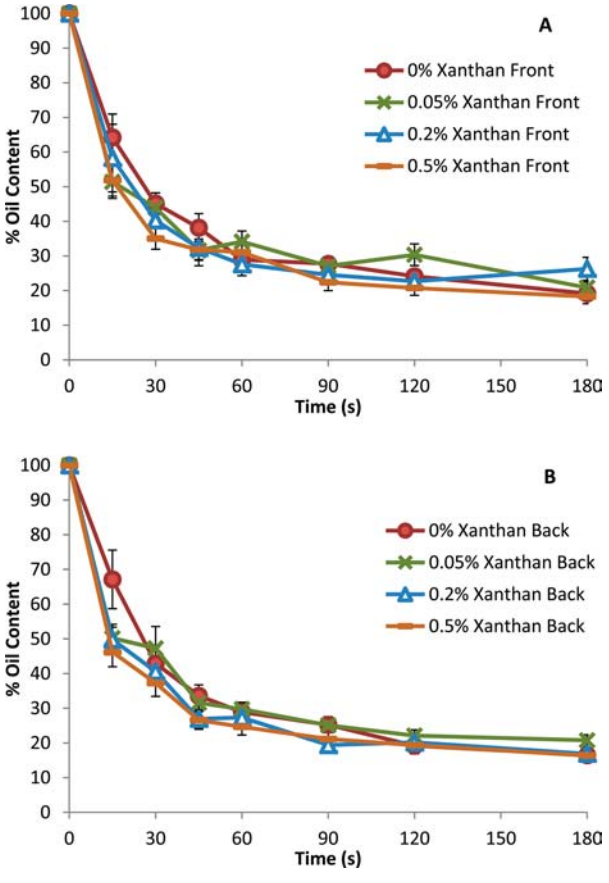

Figure 6. Relative oil content (%) deposited on the front (A) and back (B) part of the anterior tongue for the 10% (w/w) o/w emulsions stabilized with 3% w/w Na-caseinate differing in xanthan gum concentration as a function of time. Each point represents the average of n = 20 subjects and three replicates. Lines are drawn to guide the eye. Error bars represent the standard error.

Influence of Viscosity on After-Feel Perception of Oral Coatings. Figure 7 depicts the intensity of the after-feel attributes of the 10% (w/w) o/w emulsions stabilized with 3% (w/w) Na-caseinate thickened with different xanthan gum concentrations. For the attribute "fatty film", the effects of sample (i.e., 0, 0.05, 0.2, and 0.5% xanthan gum) [$F(2.1, 124) =$

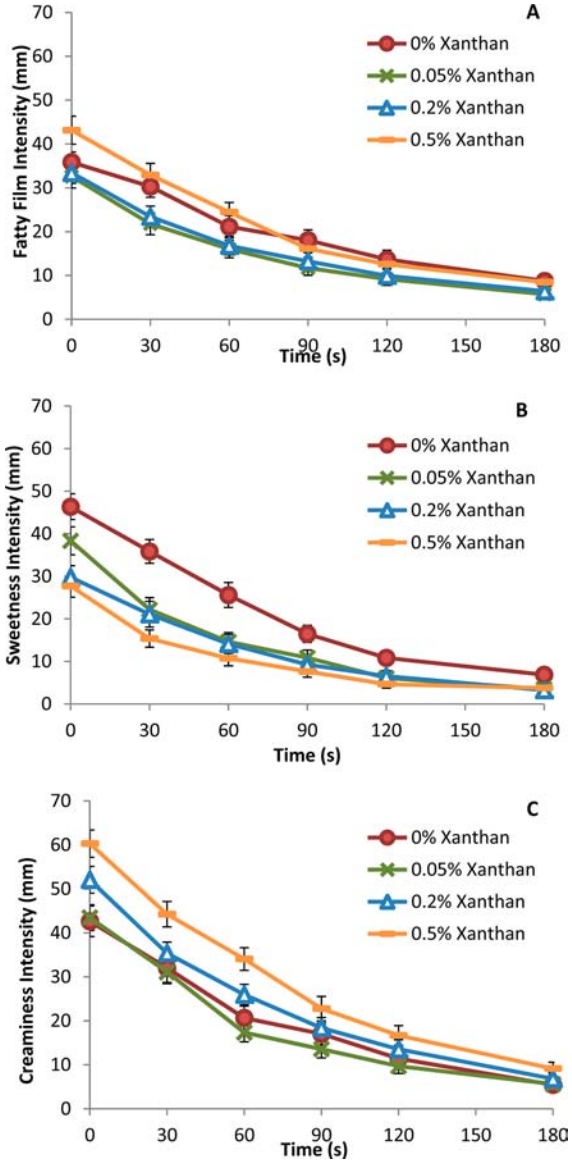

Figure 7. Intensity of the after-feel attributes Fatty film (A), sweetness (B), and creaminess (C) for o/w emulsions containing 10% (w/w) oil stabilized with 3% Na-caseinate differing in xanthan gum concentration as a function of time. Each point represents the average of n = 20 subjects and three replicates. Lines are drawn to guide the eye. Error bars represent the standard error.

DOI: 10.1021/jf505653t
J. Agric. Food Chem. 2015, 63, 2145−2153

13.45, $p < 0.001$], time [F(2.4, 140) = 387, $p < 0.001$], and sample × time [F(6.8, 398) = 3.3, $p < 0.05$] were significant. The emulsions with 0.5% xanthan and no xanthan were perceived significantly higher ($p < 0.05$) in "fatty film" intensity than the o/w emulsions thickened with 0.05 and 0.2% xanthan gum. The attribute "sweetness" was influenced by sample (i.e., 0, 0.05, 0.2, and 0.5% xanthan gum) [F(2.6, 153) = 38.1, $p < 0.001$], time [F(2.7, 161) = 382, $p < 0.001$], and sample × time [F(9.2, 543) = 7.0, $p < 0.001$]. The o/w emulsion with no xanthan was perceived as significantly sweeter ($p < 0.001$) than all other o/w emulsions. With increasing xanthan concentration, after-feel sweetness tended to decrease. The attribute "creaminess" was significantly influenced by sample (i.e., 0, 0.05, 0.2, and 0.5% xanthan gum) [F(2.6, 154) = 19.3 $p < 0.001$], time [F(2.5, 145) = 471, $p < 0.001$], and sample × time [F(8.2, 481) = 4.3, $p < 0.001$]. The o/w emulsion with 0.5% xanthan was perceived significantly creamier ($p < 0.05$) than all other o/w emulsions.

DISCUSSION

The aims of this study were to investigate the influence of (i) protein type, (ii) protein content, and (iii) viscosity of o/w emulsions on the oil fraction deposited on the tongue after expectoration of the samples and after-feel sensory perception.

The oil fraction deposited on the back part of the anterior tongue was by a factor of around 1.3−1.9 times higher compared with the oil fraction deposited on the front part of the anterior tongue for all o/w emulsion tested in this study. These results are in line with previous studies that showed that the coating deposition followed a similar spatial variation.[5,9] It has been suggested that the spatial variation in oil deposition on the tongue is due to differences in the morphology of the tongue and/or movement of the tongue while and after orally processing the samples.

Influence of Protein Type and Content on Clearance of Oral Oil Coatings. Light microscopy revealed the microstructure of the 10% (w/w) o/w emulsions stabilized with different concentrations of Na-caseinate and lysozyme before and after mixing with human saliva. All images were taken with o/w emulsions at neutral pH, at room temperature, and were mixed with the same batch of human saliva. The o/w emulsions stabilized with higher concentrations of Na-caseinate (3.0 and 5.8% w/w) showed aggregation likely due to depletion flocculation due to unadsorbed protein at high concentrations.[19] The flocculation properties of o/w emulsions stabilized with Na-caseinate were previously shown to be comparable to micelle induced depletion in surfactant-based systems.[19,20] As the unadsorbed protein concentration is increased, the flocculation is also expected to increase. This flocculation is weak and reversible.[19,20] The o/w emulsions stabilized with Na-caseinate showed very limited changes in the emulsion microstructure upon mixing with human saliva. No aggregation was observed upon mixing with human saliva for o/w emulsions stabilized by 0.2% Na-caseinate. This is in agreement with the hypothesis that negatively charged proteins result in negatively charged emulsion droplets, which do not interact with salivary biopolymers.[13]

The o/w emulsions stabilized with lysozyme showed no aggregation, even at higher concentrations (3.0 and 5.8% w/w). This is possibly due to the fact that lysozyme is a globular protein, and when in excess concentration to cover the oil droplets it can create multilayers of adsorbed protein around the emulsion droplet.[14] Lysozyme is known to form complexes with salivary proteins.[13] The complexes are formed by electrostatic interactions between the positively charged lysozyme and the negatively charged salivary biopolymers. The complex formation is responsible for the irreversible flocculation of the lysozyme emulsions.[13] Figure 1 shows that the lysozyme stabilized o/w emulsions (0.2, 3.0, and 5.8% lysozyme) used in this study formed large agglomerates upon mixing with saliva. In vivo fluorescence measurements showed that increasing the concentration of lysozyme led to smaller oil fractions deposited on the tongue immediately after expectoration of the o/w emulsion ($t = 0$ s, see Figure 2). It is possible that with higher concentrations of unadsorbed lysozyme more and larger agglomerates are formed upon mixing with saliva in the oral cavity. Previous studies found that starch granules were cleared faster from the tongue than xanthan gum.[11] They hypothesized that the larger starch granules might be too large to enter the voids between the papillae on the tongue and therefore were washed away easier.[11] As lysozyme forms aggregates, it is plausible that the aggregates were too large to enter the voids between the papillae during oral processing. When spitting out the o/w emulsions, it is likely that the formed complexes were spat out as well. On the other hand, there were no differences on oil fraction between the o/w emulsions stabilized with Na-caseinate. The depletion agglomerates of caseinate micelles are weak and reversible. It is likely that due to the constant stirring of the o/w emulsions prior to in mouth processing and to in mouth shear, these agglomerates were destroyed and thus did not have an effect on the oil deposition in mouth.

The oil coatings formed by lysozyme stabilized o/w emulsions had a slower oil clearance rate from the tongue than oil coatings formed by Na-caseinate stabilized o/w emulsions. Complex formation between salivary proteins and lysozyme can take place in the saliva fluid as well as with the mucous layer.[21] Complex formation with the mucous layer might slow down clearance. On the other hand, the coating formed by the Na-caseinate emulsions is likely to have no or very little binding with the mucous layer and as such, easier to be washed away by saliva and rubbing against palate.

No significant differences were found between the o/w emulsions stabilized with different concentrations of Na-caseinate. However, oil clearance tended to be slower at lower Na-caseinate concentrations. We hypothesized that excess protein has a blending effect with saliva, resulting in faster clearance of oil deposits from the tongue surface. The blending effect could be the underlying mechanism responsible for the observed trend. However, this effect depends on the behavior of the protein in mouth. In the case of the o/w emulsions stabilized with lysozyme, no trend was observed, indicating as dominant effect the behavior of the protein with saliva and to a lesser extent the concentration of protein in the emulsion.

The after-feel perception of lysozyme stabilized o/w emulsions was perceived as less intense compared to Na-caseinate stabilized o/w emulsions. As the clearance of the oil fraction deposited on the tongue for the o/w emulsions stabilized with lysozyme was slower than for o/w emulsions stabilized with Na-caseinate, the oil fraction deposited on tongue was larger at almost every measured time point (data not shown). It would be expected that the oil coatings left by the lysozyme stabilized o/w emulsions would be perceived as fattier and creamier because they effectively have more oil deposited on the tongue than Na-caseinate stabilized o/w

DOI: 10.1021/jf505653t
J. Agric. Food Chem. 2015, 63, 2145−2153

emulsions. It is known though that lysozyme provokes an astringent and dry sensation in the mouth,[8] which are sensations that are likely to reduce the intensity of the attributes "fatty film" and "creaminess". The flocculation of lysozyme stabilized o/w emulsions was found to have similarities to saliva flocculation observed by addition of tannins. The flocculation with proteins in saliva and mucous layer reduces the lubrication properties of saliva and increases friction in mouth, which leads to astringent and rough after-feel.[8] The after-feel sensations seem to be complex and not a sole function of the actual amount of oil deposited on the tongue.

Influence of Viscosity on Clearance of Oral Oil Coatings. A decrease in oil fraction deposited on the tongue immediately after expectoration of o/w emulsions when xanthan gum was present compared to o/w emulsions without xanthan was observed. This decrease was independent of xanthan concentration added to thicken the o/w emulsion. This suggests that the matrix created by xanthan is likely to capture the oil droplets and create a film which does not allow the oil droplets to enter the voids between the papillae and thus creating less oil deposition compared to emulsions without xanthan gum. Other studies have also shown that the addition of polysaccharides, such as guar gum, to emulsions reduces oil retention on the tongue surface.[8] Our results show that there is no significant difference in oil clearance dynamics depending on xanthan concentration. Furthermore, no influence on the fat clearance kinetics of different types of thickeners was found.[11]

It is interesting to note that "fatty film" perception was higher for o/w emulsions with the highest concentration of xanthan (0.5%). Physically, the oil deposition for both emulsions is very different with the emulsion with no xanthan having the highest oil fraction deposited on tongue. This suggests that xanthan gum might create a lubricating layer on the tongue, thereby decreasing the friction and increasing fatty after-feel. This lubrication effect is likely to dependent on the concentration of thickener. In accordance, "creaminess" was perceived as significantly higher for the 0.5% xanthan o/w emulsions compared to the o/w emulsions with lower concentrations of xanthan. All o/w emulsions with added xanthan were perceived as significantly less sweet compared with the 3% Na-caseinate stabilized o/w emulsion without xanthan. This was expected, as it is known that increasing viscosities in liquid foods can decrease taste perception.[22−24] Different explanations for taste suppression caused by thickeners were reported: kinetic and perceptual. Kinetic explanations suggest a reduction of the tastant release and diffusion rates in mouth due to the binding of tastants to the thickener or due to inhibition of the tastants transport due to the hydrocolloid chains.[25−27] Perceptual interactions were also demonstrated to contribute to the effect of taste perception due to texture differences caused by cross-modal interaction between tactile and taste signals.[28]

In conclusion, considerable differences were found in oil fraction deposited on the tongue and after-feel perception between o/w emulsions stabilized by Na-caseinate which do not aggregate under in mouth conditions and o/w emulsions stabilized by lysozyme which aggregate under in mouth conditions. The irreversible agglomeration of the o/w emulsions stabilized with lysozyme caused a slower oil clearance of the oral oil coating from the tongue compared to o/w emulsions stabilized with Na-caseinate. The increase of unadsorbed lysozyme in the o/w emulsion might have created larger agglomerates that were easier to expectorate, creating smaller depositions of oil immediately after expectoration than the Na-caseinate stabilized emulsions. The after-feel of o/w emulsions stabilized with Na-caseinate was perceived as creamier, fattier, and sweeter than the o/w emulsions stabilized with lysozyme. The addition of xanthan gum to Na-caseinate stabilized o/w emulsions decreased the deposition of oil on tongue although o/w emulsions with higher concentrations of xanthan had a similar or higher fatty and creamy after-feel perception than o/w emulsions without xanthan. We conclude that the after-feel perception of o/w emulsions is complex and that the physical deposited oil on the tongue contributes to it as well as factors such as the behavior of proteins in mouth and the presence of thickeners.

■ ASSOCIATED CONTENT

Ⓢ Supporting Information

The in vivo fluorescence results were translated into oil fraction by using calibration curves which relate fluorescence (relative fluorescence units (RFU)) to oil fraction (mass of oil per surface area of the tongue). Calibration lines for every sample measured by in vivo fluorescence in this study are included in the supporting information file. This material is available free of charge via the Internet at http://pubs.acs.org.

■ AUTHOR INFORMATION

Corresponding Author

*Phone: +31 317 481694. E-mail: markus.stieger@wur.nl.

Notes

The authors declare no competing financial interest.

■ ABBREVIATIONS USED

NaCas, Na-caseinate (sodium caseinate); Lys, lysozyme; xanthan, xanthan gum; o/w, oil in water

■ REFERENCES

(1) De Wijk, R. A.; Kapper, C.; Borsboom, P.; Prinz, J. F. Persistence of oral coatings of CMC and starch-based custard desserts. *Food Hydrocolloids* **2009**, *23*, 896−900.

(2) Ahn, N.; Frost, M. B.; Frandsen, L. W.; Dijksterhuis, G.; Martens, M. The effect of some beverages on the perception of succeeding basic tastes. *J. Sensory Sci.* **2002**, *17*, 571−581.

(3) Lynch, J.; Liu, Y. H.; Mela, D. J.; MacFie, H. J. H. A time−intensity study of the effect of oil mouthcoatings on taste perception. *Chem. Senses* **1993**, 121−129.

(4) Madrigal-Galan, B.; Heymann, H. Sensory effects of consuming cheese prior to evaluating red wine flavor. *Am J. Enol. Vitic.* **2006**, *57*, 12−22.

(5) Camacho, S.; van Riel, V.; de Graaf, C.; van de Velde, F.; Stieger, M. Physical and sensory characterizations of oral coatings of oil/water emulsions. *J. Agric. Food Chem.* **2014**, *62*, 5789−95.

(6) Dresselhuis, D. M.; Cohen Stuart, M. A.; van Aken, G. A.; Schipper, R. G.; de Hoog, E. H. A. Fat retention at the tongue and the role of saliva: adhesion and spreading of protein-poor versus protein-rich emulsions. *J. Colloid Interface Sci.* **2008**, *321*, 21−29.

(7) Ranc, H.; Elkhyat, A.; Servais, C.; Mac-Mary, S.; Launay, B.; Humbert, P. Friction coefficient and wettability of oral mucosa tissue: changes induced by a salivary layer. *Colloids Surf. A: Physicochem. Eng. Aspects* **2006**, *276*, 155−161.

(8) Vingerhoeds, M. H.; Silletti, E.; de Groot, J.; Schipper, R. G.; van Aken, G. A. Relating the effect of saliva-induced emulsion flocculation on rheological properties and retention on the tongue surface with sensory perception. *Food Hydrocolloids* **2009**, *23* (3), 773−785.

(9) Pivk, U.; Godinot, N.; Keller, C.; Antille, N.; Juillerat, M. A.; Raspor, P. Lipid deposition on the tongue after oral processing of

DOI: 10.1021/jf505653t
J. Agric. Food Chem. 2015, 63, 2145−2153

medium-chain triglycerides and impact on the perception of mouthfeel. *J. Agric. Food Chem.* **2008**, *56*, 1058−1064.
(10) van Aken, G. A.; Vingerhoeds, M. H.; de Wijk, R. A. Textural perception of liquid emulsions: role of oil content, oil viscosity and emulsion viscosity. *Food Hydrocolloids* **2011**, *25*, 789−796.
(11) De Jongh, H. H. J.; Janssen, A. M. Differential clearance kinetics of adhered layer constituents from the oral cavity as modulator for afterfeel of dressings: ATR FT-IR measurements of localized oral coatings. *J. Texture Stud.* **2007**, *38*, 70−86.
(12) Siletti, E.; Vitorino, R. M. P.; Schipper, R.; Amado, F. M. L.; Vingerhoeds, M. H. Identification of salivary proteins at oil−water interfaces stabilized by lysozyme and B-lactoglobulin. *Arch. Oral Biol.* **2010**, *55*, 268−278.
(13) Siletti, E.; Vingerhoeds, M. H.; Norde, W.; van Aken, G. A. The role of electrostatics in saliva-induced emulsion flocculation. *Food Hydrocolloids* **2007**, *21*, 596−606.
(14) Hunt, J. A.; Dalgleish, D. G. Adsorption behaviour of whey protein isolate and caseinate in soya oil-in-water emulsions. *Food Hydrocolloids* **1994**, *8*, 175−187.
(15) Wood, W. F. *Psychophysical Studies on the Consistency of Liquid Foodstuffs*; Society of Chemical Industry: London, U.K., 1968; Monograph Vol. *27*.
(16) Cook, D. J.; Hollowood, T. A.; Linforth, R. S. T.; Taylor, A. J. Oral shear stress predicts flavour perception in viscous solutions. *Chem. Senses* **2003**, *28*, 11−23.
(17) Vingerhoeds, M. H.; Blijdenstein, T. B. J.; Zoet, F. D.; van Aken, G. A. Emulsion flocculation induced by saliva and mucin. *Food Hydrocolloids* **2005**, *19*, 915−922.
(18) Silletti, E.; Vingerhoeds, M. H.; van Aken, G. A.; Norde, W. Rheological behavior of food emulsions mixed with saliva: effect of oil content, salivary protein content, and saliva type. *Food Biophys.* **2008**, *3*, 318−328.
(19) Dickinson, E.; Golding, M. Depletion flocculation of emulsions containing unadsorbed sodium caseinate. *Food Hydrocolloids* **1997**, *11*, 13−18.
(20) Dickinson, E.; Golding, M.; Povey, M. J. W. Creaming and Flocculation of Oil-in-Water Emulsions Containing Sodium Caseinate. *J. Colloid Interface Sci.* **1997**, *185*, 515−529.
(21) van Aken, G. A.; Vingerhoeds, M. H.; de Hoog, E. H. A. Food colloids under oral conditions. *Curr. Opin. Colloid Interface Sci.* **2007**, *12*, 251−262.
(22) Walker, S.; Prescott, J. The influence of solution viscosity and different viscosifying agents on apple juice flavor. *J. Sensory Stud.* **2000**, *15* (3), 285−307.
(23) Hollowood, T. A.; Linforth, R. S.; Taylor, A. J. The effect of viscosity on the perception of flavour. *Chem. Senses* **2002**, *27* (7), 583−591.
(24) Cook, D. J.; Linforth, R. S. T.; Taylor, A. J. Effects of hydrocolloid thickeners on the perception of savory flavors. *J. Agric. Food. Chem.* **2003**, *51* (10), 3067−3072.
(25) Ferry, A. L.; Hort, J.; Mitchell, J. R.; Cook, D. J.; Lagarrigue, S.; Pamies, B. V. Viscosity and flavour perception: why is starch different from hydrocolloids? *Food Hydrocolloids* **2006**, *20*, 855−862.
(26) Baines, Z.; Morris, E. Flavour/taste perception in thickened systems: the effect of guar gum above and below c*. *Food Hydrocolloids* **1987**, *3*, 197−295.
(27) Cook, D. J.; Hollowood, T. A.; Linforth, R. S. T.; Taylor, A. J. Correlating instrumental measurements of texture and flavour release with human perception. *Int. J. Food Sci. Technol.* **2005**, *40*, 631−641.
(28) Burseg, K. M. M.; Camacho, S.; Bult, J. H. F. Effects of Pulsation Rate and Viscosity on Pulsation-Induced Taste Enhancement: New Insights into Texture−Taste Interactions. *J. Agric. Food Chem.* **2011**, *59*, 5548−5553.

DOI: 10.1021/jf505653t
J. Agric. Food Chem. 2015, 63, 2145−2153

clusters.[25] MIL-101 has some advantages of large pore windows, mesoporous pores (2.9−3.4 nm), accessible coordinative unsaturated sites, and excellent chemical stability. These properties make it attractive in analytical applications, especially in chromatographic separation and sample pretreatment. MIL-101 has been explored as stationary phase for liquid chromatography.[26] In sample treatment, MIL-101 has been successfully used as sorbent to extract targets in aqueous samples.[27−29] Hasen et al. used MIL-101 to extract naproxen and clofibric acid from aqueous solution.[28] Hu et al. reported the application of MIL-101 packed microcolumn for the extraction of naproxen and its metabolite in urine samples.[29] The adsorption extraction with MIL-101 in nonpolar system is also attractive. In our previous work, MIL-101 was successfully used to clean up the extract of peanuts and a large mass of fat was separated.[3] Compared with conventional sorbents, MIL-101 shows better extraction efficiency in nonpolar solution. Thus, the MIL-101 could be potentially applied to the direct extraction of pesticides in vegetable oil and the sample preparation process can be effectively simplified and accelerated.

Herein, the dispersive microsolid-phase extraction (d-μ-SPE) based on MIL-101 was developed for extracting herbicides in vegetable oils. The herbicides were extracted directly with MIL-101 from diluted vegetable oils, and no further cleanup operation is needed. The fat remaining in sample solution was easily removed after centrifugation. The herbicides were separated and determined by HPLC. The operation is quick and simple, and the results are satisfactory.

MATERIAL AND METHODS

Chemicals. Fenuron, simeton, simazine, atraton, chlortoluron, secbumeton, and terbumeton were obtained from National Institute for the Control of Pharmaceutical and Biological Products (Beijing, China). Standard stock solutions for the herbicides (200 μg/mL) were prepared by dissolving 2.0 mg of the standard in 10.0 mL of acetonitrile. All of the stock standard solutions were stored in a refrigerator at 4 °C. Working and mixed working standard solutions were prepared by diluting stock standard solutions with acetonitrile. Chromatographic grade acetonitrile was purchased from Fisher Scientific Company (Pittsburgh, PA, USA). $Cr(NO_3)_3{\cdot}9H_2O$ (>99.0%) were purchased from XLong chemical Co., Ltd. (Guangdong, China). 1,4-Benzenedicarboxylic acid (H_2BDC, ≥98.5%) was purchased from Tianjin Guangfu Fine Chemical Research Institute (Tianjin, China). Hydrofluoric acid (HF, ≥40%) was purchased from Nanjing Chemical Reagent Co., Ltd. (Nanjing, China). Pure water was obtained with a Milli-Q water purification system (Millipore Co., USA). Primary secondary amine (PSA), C18, and graphitized carbon black (GCB) were purchased from Beijing Agela Technologies Inc. (Beijing, China). All of the other reagents (analytical-reagent grade) were purchased from Beijing Chemical Factory (Beijing, China).

Instruments. Chromatographic separation and determination of the herbicides were carried out on an Agilent 1100 series liquid chromatograph (Agilent Technologies Inc., USA) equipped with photodiode array detector (DAD) and quaternary gradient pump. Eclipse XDB-C18 column (3.5 μm, 4.6 mm × 150 mm, Agilent, USA) was used.

The KQ3200E ultrasonic cleaner was purchased from Kunshan Ultrasonic Instrument Co., Ltd. (Kunshan, China). The frequency and output power of the ultrasonic cleaner are 40 kHz and 150 W, respectively. An Allegra 64 R centrifuge was purchased from Beckman Coulter.

The X-ray diffraction (XRD) patterns were recorded on a Rigaku D/max-2550 diffractometer equipped with a graphite monochromator (Rigaku, Japan) and Cu Kα radiator (λ = 1.5418 Å). Transmission electron microscopic (TEM) characterization was performed on a Tecnai G2 F20 S-Twin (Philips, Holland). BET surface area was measured on an ASAP 2020 micropore physisorption analyzer (Micromeritics, Norcross, GA, USA) using nitrogen adsorption at 77 K. The synthesis and characterization of MIL-101 was consistent with our previous work.[3]

Sample Preparation. Vegetable oils were collected from local markets. Soybean oil (sample 1), corn oil (sample 2), sunflower oil (sample 3), and peanut oil (sample 4) were used. All samples were stored at room temperature.

Four fresh spiked samples containing triazine and phenylurea herbicides were prepared by adding the mixed working standard solution into the samples, shaking for 10 min, and standing for 1 h. The aged spiked sample of soybean oil was prepared by the method mentioned above except that the spiked soybean oil sample was kept in sealed bottle and stored for 1, 2, 3, and 4 weeks at 4 °C, respectively. In the "Analysis of Samples" section, four oil samples (sample 1−4) were used. The other experiments were performed with soybean oil sample (sample 1) only.

Extraction Procedure. *d-μ-SPE.* A 2 mL of vegetable oil sample was added into 25 mL centrifuge tube and diluted with 10 mL of *n*-hexane. Subsequently, 7 mg of MIL-101 was added into the tube and the ultrasonic extraction was carried out for 15 min. The mixture was centrifuged for 3 min at 8720*g*, and the supernatant was decanted. Then 0.5 mL of *n*-hexane was added into the tube and followed by the same procedure as mentioned above. The analytes were eluted from MIL-101 with 1.5 mL of methanol in an ultrasonic bath for 1 min. The mixture was centrifuged for 10 min at 8720*g*, and the supernatant was dried under nitrogen stream. The residue was dissolved in 200 μL of methanol. The resulting solution was filtered with 0.22 μm PTFE filter and referred to as analytical solution. Then 20 μL of the analytical solution was injected into the HPLC system.

QuEChERS Procedure. The quick, easy, cheap, effective, robust, and safe (QuEChERS) procedure was performed according to Sobhanzadeh et al.;[18] 2 mL of vegetable oil and 5 mL of water were added into a 25 mL centrifuge tube. Then, 7 mL of acetonitrile, 2.8 g of anhydrous magnesium sulfate, and 0.7 g of sodium chloride were added into the tube. The tube was vigorously shaken for 1 min. The mixture was centrifuged at 1395*g* for 1 min. The tube was horizontally stored in freezer at −20 °C for 2 h. Then the supernatant was transferred into a PTFE centrifuge tube containing 750 mg of anhydrous magnesium sulfate, 250 mg of PSA, 250 mg of C18 sorbent, and 250 mg of GCB. After shaking for 30 s, the mixture was centrifuged at 1395*g* for 1 min. The supernatant was evaporated to dryness and reconstituted in 200 μL of methanol. The resulting solution was filtered with 0.22 μm PTFE filter and referred to as analytical solution. Then 20 μL of the analytical solution was injected into the HPLC system.

HPLC Analysis. The HPLC analysis was conducted in gradient mode. Mobile phases A and B were water and acetonitrile, respectively. The gradient conditions are as follows: 0−8 min, 30−45% B; 8−10 min, 45% B; 10−15 min, 45−50% B; 15−19 min, 50−72% B. The column temperature was kept at 30 °C, and the flow rate of mobile phase was kept at 0.5 mL/min. Injection volume of analytical solution was 20 μL. The monitoring wavelengths were 244 nm for fenuron and chlortoluron and 222 nm for the other herbicides.

Statistics. The Student's *t*-test was applied to the evaluation of the reasonableness of the selected experimental parameters. The t is calculated from

$$t = \frac{x_1 - x_2}{S\sqrt{\frac{1}{n_1} + \frac{1}{n_2}}}$$

$$S = \frac{(n_1 - 1)S_1^2 + (n_2 - 1)S_2^2}{n_1 + n_2 - 2}$$

where x_1 and x_2 are the mean recoveries obtained under two experimental conditions, n_1 and n_2 are the sample sizes, s_1 and s_2 are the standard deviations, and $(n_1 + n_2 - 2)$ is degree of freedom.

RESULTS AND DISCUSSION

Optimization of d-μ-SPE. In the study, some experimental parameters that affect the extraction efficiency were investigated

DOI: 10.1021/jf505760y
J. Agric. Food Chem. 2015, 63, 2154−2161

and optimized. All optimization experiments were carried out by analyzing the spiked soybean oil sample in triplicate.

Effect of Volume Ratio of n-Hexane to Oil Sample. The dilution has a significant effect on the extraction efficiency. In this work, vegetable oil sample was diluted with *n*-hexane. The results are shown in Figure 1. The recoveries of herbicides

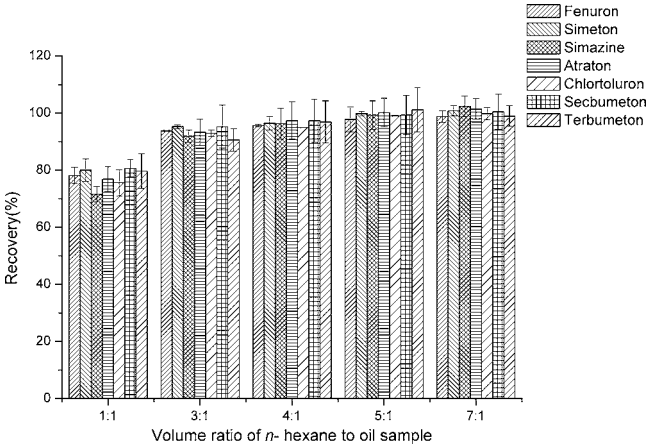

Figure 1. Effect of volume ratio of *n*-hexane to oil sample on recoveries of herbicides from soybean oil. Mass of MIL-101, 7 mg; extraction time, 15 min; centrifugation time, 3 min; eluting solvent, 1.5 mL of methanol; spiked concentration, 50 μg/L.

increase with the increase of the volume ratio of *n*-hexane to oil sample. The highest recoveries are obtained when the volume ratio is 5:1, and the recoveries change slightly with the further increase of the volume ratio. The reason could be that the viscosity of oil sample decreases with the increase of the volume of *n*-hexane, which is beneficial to the dispersion of sorbent and thus improvement of the extraction efficiency. In addition, the fat and other impurities are easily dissolved in nonpolar solvent (*n*-hexane). Consequently, the increase of *n*-hexane volume is beneficial to the removal of impurities. Therefore, the selected volume ratio of *n*-hexane to oil sample was 5:1.

Effect of Mass of MIL-101. The effect of mass of MIL-101 in the range of 0.5−12 mg on recoveries was investigated. The results shown in Figure 2 indicate that the recoveries of

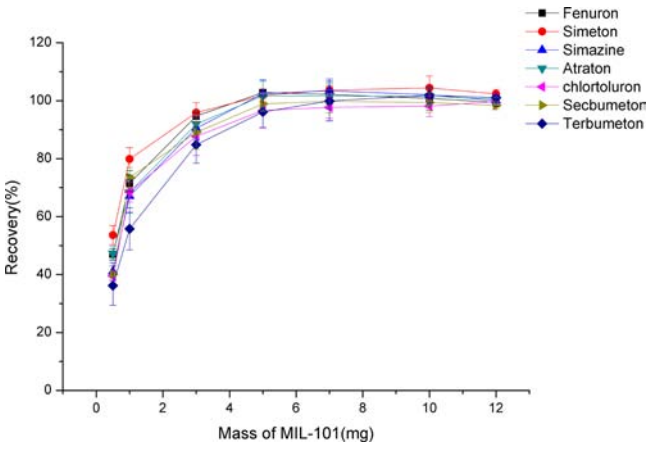

Figure 2. Effect of mass of MIL-101 on recoveries of herbicides from soybean oil. Volume ratio of *n*-hexane to oil sample, 5:1; extraction time, 15 min; centrifugation time, 3 min; eluting solvent, 1.5 mL of methanol; spiked concentration, 50 μg/L.

herbicides increase with the increase of mass of MIL-101 from 0.5 to 5 mg and change slightly when the mass of MIL-101 is more than 5 mg. To ensure sufficient extraction, 7 mg of MIL-101(Cr) was selected in the following experiments.

Effect of Extraction Time and Centrifugation Time. The effect of extraction time ranging from 1 to 30 min was investigated. The results are shown in Figure 3. The recoveries of

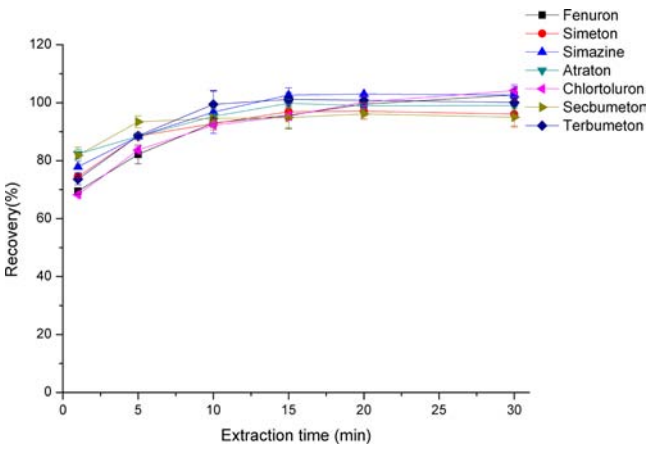

Figure 3. Effect of extraction time on recoveries of herbicides from soybean oil. Volume ratio of *n*-hexane to oil sample, 5:1; mass of MIL-101, 7 mg; centrifugation time, 3 min; eluting solvent, 1.5 mL of methanol; spiked concentration, 50 μg/L.

herbicides increase when extraction time increases from 1 to 15 min and change slightly with the further increase of extraction time. The recoveries increase rapidly within 10 min and increase slightly from 10 to 15 min. Therefore, the extraction time was selected as 15 min. The effect of centrifugation time was investigated in the range of 1−10 min. The effect of centrifugation time on the recoveries of herbicides is slight. The rapid separation of MIL-101 from sample solution may be due to the low density of sample solution. Therefore, 3 min was selected as centrifugation time.

Effect of Eluting Solvent and Elution Time. In this work, methanol and acetonitrile were used as eluting solvents in the volume range of 0.5−2 mL. The results shown in Figure 4 indicate that the recoveries of analytes increase with increasing

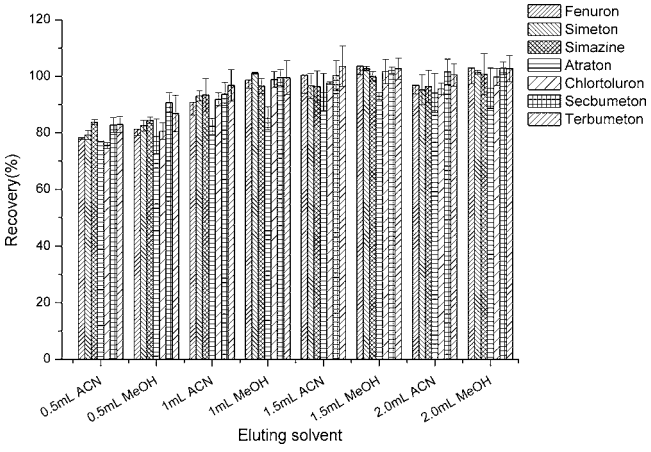

Figure 4. Effect of eluting solvent on recoveries of herbicides from soybean oil. Volume ratio of *n*-hexane to oil sample, 5:1; mass of MIL-101, 7 mg; extraction time, 15 min; centrifugation time, 3 min; spiked concentration, 50 μg/L.

DOI: 10.1021/jf505760y
J. Agric. Food Chem. 2015, 63, 2154−2161

Table 1. Calibration Lines, Linearity Ranges, and Detection Limits for Determination of Herbicides in Vegetable Oil Samples

analyte	calibration line	correlation coefficient	linearity range (μg/L)	LOD (μg/L)
fenuron	$y = (2.07 \pm 0.00411)x + (0.206 \pm 0.483)$	0.9999	3.90−250	1.04
simeton	$y = (3.36 \pm 0.0257)x + (1.81 \pm 3.02)$	0.9997	2.00−250	0.720
simazine	$y = (3.29 \pm 0.0149)x + (1.92 \pm 1.75)$	0.9999	2.00−250	0.609
atraton	$y = (3.30 \pm 0.0356)x + (2.75 \pm 4.19)$	0.9994	2.00−250	0.576
chlortoluron	$y = (2.08 \pm 0.0156)x + (2.66 \pm 1.84$	0.9997	3.90−250	0.974
secbumeton	$y = (3.06 \pm 0.0240)x + (0.723 \pm 2.83)$	0.9997	2.00−250	0.637
terbumeton	$y = (3.10 \pm 0.0202)x - (2.92 \pm 2.38)$	0.9998	2.00−250	0.585

Table 2. Recoveries of Herbicides from Soybean Oil Sample and Intra- and Interday Precision of the d-μ-SPE Method[a]

analytes	intraday precision	interday precision
fenuron	98.9 ± 4.28	100 ± 3.39
simeton	96.2 ± 2.65	101 ± 2.39
simazine	102 ± 1.63	101 ± 1.77
atraton	99.0 ± 1.33	99.4 ± 4.38
chlortoluron	99.4 ± 4.46	97.8 ± 1.72
secbumeton	95.8 ± 1.95	99.4 ± 3.02
terbumeton	101 ± 1.67	99.2 ± 2.23

[a]The values in the table are mean recovery ± standard deviation (%, $n = 5$).

the volume of eluting solvent and change slightly when the volume of eluting solvent is larger than 1.5 mL. The recoveries obtained with methanol are slightly higher than those obtained with acetonitrile. As methanol is cheaper than acetonitrile, 1.5 mL of methanol was selected as eluting solvent. The eluting of analytes was carried out in ultrasonic bath. The effect of elution time ranging from 0.5 to 5 min was studied. There is no significant change in recoveries with the increase of elution time. So, 1 min of elution time was selected.

Statistical Analysis. To evaluate the reasonableness of the selected experimental parameters, the Student's t test was applied and the t values were calculated (the detailed information was listed in Supporting Information, Table 1). The results indicate that the difference between the selected value and the near value of the experimental parameters are significant ($P < 0.01$). So the selected experimental parameters should be reasonable.

Evaluation of the Present Method. *Analytical Performance.* The calibration curves were constructed by plotting the peak areas measured versus the concentrations of analytes in the spiked oil samples. The linear regression equations and correlation coefficients are listed in Table 1. The limits of detection (LODs) were calculated based on the signal-to-noise (S/N) ratio of 3. The LODs for triazine and phenylurea herbicides range from 0.585 to 1.04 μg/L.

Repeatability was evaluated by determining target analytes in spiked oil samples at spiked concentration of 50 μg/L. The intraday precision was obtained by analyzing a sample five times during a working day. The interday precision was obtained by analyzing the same sample over five working days.

Table 3. Recoveries of Herbicides from Aged Soybean Oil Samples at Two Different Spiking Levels[a]

added (μg/L)	stored time (week)	fenuron	simeton	simazine	atraton	chlortoluron	secbumeton	terbutmeton
10.0	1	99.8 ± 3.57	99.9 ± 3.18	105 ± 3.05	102 ± 3.71	100 ± 0.314	99.9 ± 3.77	105 ± 2.28
	2	96.1 ± 0.973	97.8 ± 3.18	101 ± 0.407	97.6 ± 0.586	97.2 ± 3.14	95.1 ± 2.93	104 ± 2.51
	3	96.6 ± 6.16	99.5 ± 3.37	103 ± 0.813	99.2 ± 3.12	97.8 ± 0.941	94.2 ± 5.45	104 ± 3.19
	4	95.0 ± 2.60	95.6 ± 1.87	102 ± 1.42	99.7 ± 1.95	95.8 ± 2.51	93.2 ± 0.629	101 ± 1.82
100	1	100 ± 1.16	100 ± 0.445	104 ± 1.58	103 ± 2.00	101 ± 1.57	102 ± 1.31	107 ± 4.14
	2	96.9 ± 1.25	97.3 ± 2.47	101 ± 0.684	97.7 ± 0.306	98.2 ± 2.80	97.2 ± 5.92	104 ± 5.30
	3	98.7 ± 0.892	98.6 ± 2.41	100 ± 3.49	97.2 ± 3.03	98.8 ± 0.643	98.3 ± 4.03	104 ± 5.68
	4	95.9 ± 2.61	97.2 ± 0.465	99.5 ± 4.04	99.1 ± 1.67	96.7 ± 1.41	95.6 ± 0.645	102 ± 2.33

[a]The values in the table are mean recovery ± standard deviation (%, $n = 3$).

Table 4. Recoveries of Herbicides from Fresh Vegetable Oil Samples at Two Different Spiking Levels[a]

sample	added (μg/L)	fenuron	simeton	simazine	atraton	chlortoluron	secbumeton	terbumeton
1	10.0	101 ± 3.57	98.6 ± 5.05	99.2 ± 6.10	102 ± 2.73	97.8 ± 2.82	96.3 ± 4.19	102 ± 2.74
	100	102 ± 0.693	99.5 ± 2.26	99.7 ± 0.963	102 ± 2.59	98.3 ± 1.57	98.2 ± 4.09	99.1 ± 1.95
2	10.0	98.9 ± 7.46	92.5 ± 2.06	96.6 ± 1.22	100 ± 3.71	94.5 ± 5.02	95.9 ± 3.56	99.9 ± 2.74
	100	88.3 ± 1.09	94.0 ± 1.71	92.6 ± 3.69	97.7 ± 0.730	87.3 ± 3.76	90.9 ± 1.23	95.7 ± 2.17
3	10.0	103 ± 7.79	99.9 ± 3.93	93.4 ± 4.88	102 ± 1.17	95.4 ± 1.25	93.8 ± 4.40	103 ± 4.79
	100	98.2 ± 2.26	97.6 ± 0.587	97.2 ± 1.86	104 ± 1.21	96.2 ± 1.20	96.1 ± 1.75	97.7 ± 3.01
4	10.0	97.0 ± 1.62	102 ± 0.562	102 ± 3.66	95.6 ± 4.69	96.9 ± 1.57	93.8 ± 5.66	99.0 ± 5.47
	100	93.9 ± 3.96	91.9 ± 5.80	103 ± 4.84	99.3 ± 2.58	97.1 ± 6.19	93.4 ± 2.09	100 ± 6.06

[a]The values in the table are mean recovery ± standard deviation (%, $n = 3$).

DOI: 10.1021/jf505760y
J. Agric. Food Chem. 2015, 63, 2154−2161

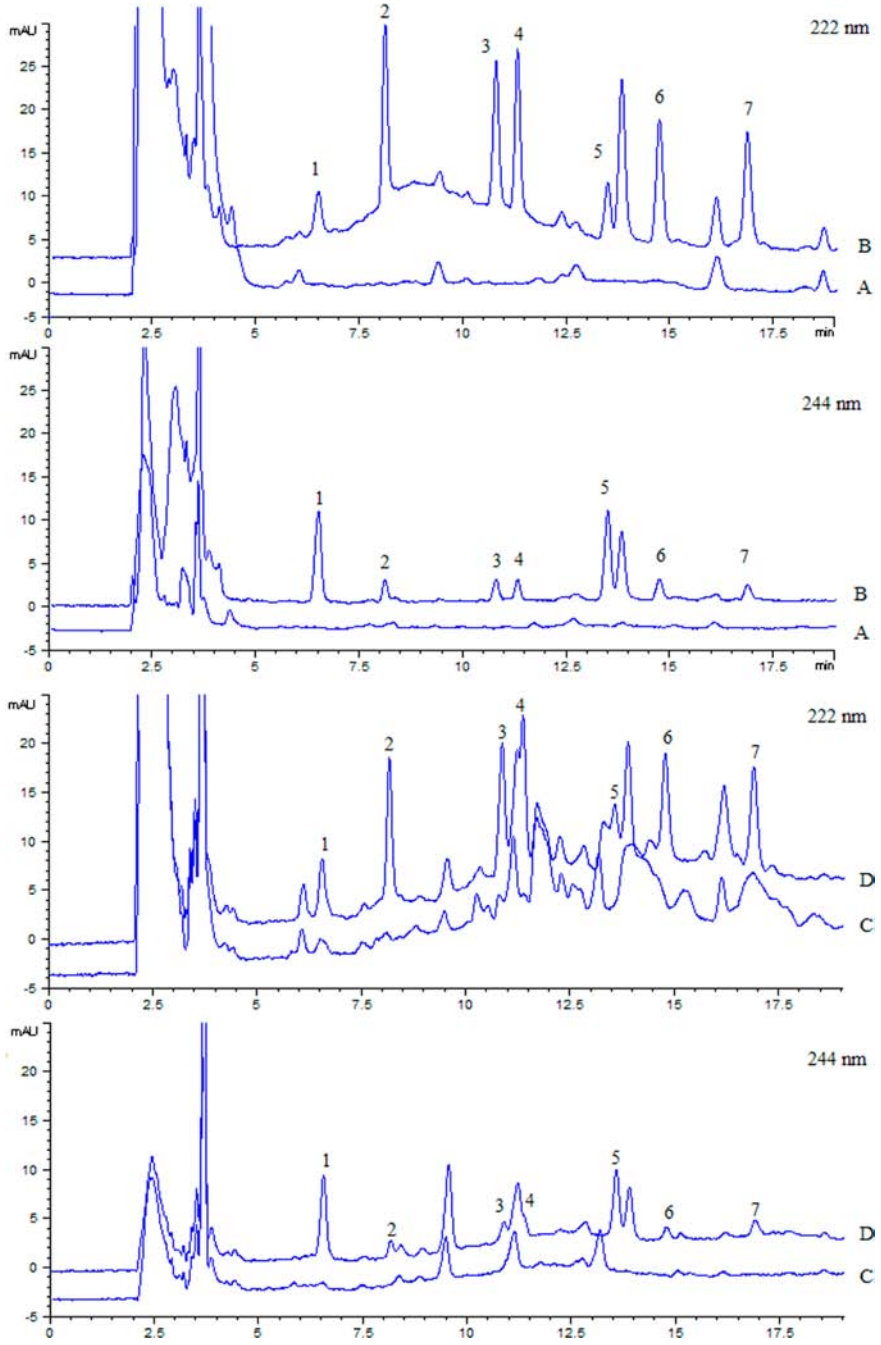

Figure 5. Chromatograms of extracts of soybean oil sample 1 (A) and spiked sample 1 (B) prepared by the d-μ-SPE method, and of soybean oil sample 1 (C) and spiked sample 1 (D) prepared by QuEChERS method. 1, fenuron; 2, simeton; 3, simazine; 4, atraton; 5, chlortoluron; 6, secbumeton; 7, terbumeton.

The results are listed in Table 2. The recoveries of intra- and interday range from 95.8 to 102%, with standard deviations ranging from 1.33 to 4.46%. The results indicate that the present method has good repeatability.

The long-term stability of the analytes in the sample was evaluated by analyzing one aged spiked sample of soybean oil. The recoveries of herbicides in aged spiked sample of soybean oil are listed in Table 3. It can be seen that the recoveries of herbicides range from 93.2 to 107%, with standard deviations ranging from 0.306 to 6.16%. It can be deduced that the herbicides in soybean oil are stable for at least 4 weeks.

Analysis of Samples. The target analytes were not found in vegetable oil samples. The practical applicability of the present method was evaluated by determining herbicides from four fresh spiked vegetable oils. The recoveries of herbicides in fresh spiked vegetable oil samples listed in Table 4 range from 87.3 to 104%, with standard deviations ranging from 0.562 to 7.79%. The results indicate that the present method provides satisfactory recoveries and acceptable precision at two concentration levels. The chromatograms of sample 1 and spiked sample 1 are shown in Figure 5.

Comparison with QuEChERS Method. For further evaluation, the present method was compared with QuEChERS method developed by Sobhanzadeh et al.[18] The chromatograms of the extracts obtained by QuEChERS method are shown in Figure 5. The resolutions of the peaks obtained by the present

DOI: 10.1021/jf505760y
J. Agric. Food Chem. 2015, 63, 2154−2161

method range from 2.04 to 24.6, and the selectivity ranges from 1.05 to 2.07. The resolutions of the peaks obtained by QuEChERS method range from 1.89 to 14.3, and the selectivity ranges from 1.04 to 1.42. In Figure 5, the chromatograms of the extracts obtained by QuEChERS method are much dirtier than those obtained by the present method. So the selectivity of the present method is higher than that of QuEChERS method. The high selectivity of the present method can be attributed to the reverse extraction way in which the analytes are adsorbed, while the fat and most of the interferents remain in sample solution. The large windows of MIL-101(Cr) make the introduction of the analytes into the cages easy.[3] The analytes were adsorbed on MIL-101 mainly by the coordination interaction between heteroatoms in analytes and the unsaturated metal sites, $\pi-\pi$ interaction between the analytes and terephthalic acid molecules of the framework, and the π-complexation between the π-electrons of analytes and Lewis acid sites in the pore of MIL-101. The analytes with log K_{ow} from 1.07 to 2.94 are relatively polar (the log K_{ow} was obtained from SciFinder scholar database). MOFs with open metal sites have great potential for enhancing adsorption of molecules with polarity.[30−32] The report by Huang and co-workers demonstrated that MIL-101 has high affinity to the volatile organic compounds containing heteroatom, especially the amines, and the surface of the MIL-101 is energetically heterogeneous.[31] Fu et al. also reported that the interaction between the open metal sites of MIL-101 and the polar analytes with electron-rich functional groups is very strong in nonpolar solvent.[32] The strong coordination interaction between the unsaturated metal sites of MIL-101 (electron acceptor) and the heteroatoms of analytes (electron donor) could have an important impact on the extraction process. Consequently, the herbicides in oil sample solution can be adsorbed effectively on MIL-101. Methanol, as a polar solvent, has strong dissolving ability toward analytes. Methanol, as a proton donor, could also chelate with the open metal sites of MIL-101 and weaken the interaction between MIL-101 and the analytes.[32] So the analytes can be easily eluted. The sensitivity of the method was evaluated by LODs. In Table 5, the LODs obtained by the present method are lower than those obtained by QuEChERS method. The accuracy was evaluated by the recovery of herbicides in spiked soybean oil samples. The results listed in Table 5 indicate that the two methods both provide acceptable accuracy. The comparison of the two methods on sample preparation process was also conducted and is shown in Table 5. Therefore, compared with QuEChERS method, the present method has some advantages in selectivity, sensitivity, sorbent and solvent consumption, operation procedure, and time consumption. So the present method is suitable to the extraction of herbicides in vegetable oils.

The present method was further compared with the reported methods for the determination of triazine and phenylurea herbicides in edible vegetable oils.[1,6,7,14,18−21,33−35] The results are shown in Table 5. The LODs obtained by the present method are lower than these obtained by most methods. The results indicate that the present method provides satisfactory sensitivity. In addition, compared with the other methods, the present method is quicker and simpler in terms of short extraction time and no additional cleanup step.

In the work, a d-μ-SPE method based on MIL-101 was developed for directly extracting triazine and phenylurea herbicides from diluted vegetable oils. A large mass of fat is easily separated. The experimental results indicated that the

Table 5. Comparison of the Present Method with Other Methods Reported in Literature

matrix	extraction	cleanup procedure	detection	recovery (%)	RSD (%)	LOD	ref
vegetable oil	d-μ-SPE: 7 mg MIL-101(Cr)		LC-DAD	93.4−102	2.83−6.68	0.585−1.04[a]	this work
vegetable oil	QuEChERS: 7 mL ACN[c]	low temperature fat precipitation (2 h) followed DSPE: 50 mg $MgSO_4$ + 250 mg PSA + 250 mg C18 + 250 mg GCB	LC-DAD	88.2−99.5	2.83−7.64	1.64−2.48	this work
rapeseed oil	LLE: 10 mL ACN containing 1% acetic acid	low temperature fat precipitation (12 h)	LC-MS/MS	47−80	3−5	not reported	1
virgin olive oil	LLE: 20 mL ACN	SPE: 500 mg ENVI-Carb cartridge	GC-NPD	69.5−73.3	4.9−15.8	6.4−7.5[b]	14
soybean oil	LLE: 10 mL ACN	low temperature fat precipitation (4 h) followed DSPE: 100 mg $MgSO_4$ + 500 mg Florisil	GC-MS	84−106	2−10	not reported	33
olive oil	QuEChERS: 10 mL ACN	DSPE: 750 mg $MgSO_4$ + 250 mg PSA + 250 mg C18 + 250 mg GCB	LC-MS/MS	not reported	<15	0.01−3.5[b]	34
palm oil	QuEChERS: 10 mL ACN	low temperature fat precipitation (2 h) + DSPE: 4 g $MgSO_4$ + 250 mg PSA + 250 mg C18 + 250 mg GCB	LC-TOF-MS	51.62−92.65	4.60−9.75	0.6−1.0[b]	18
olive oil	LLE: 10 mL ACN	GPC	GC-MS/MS	92−109	3−6	0.2−1.4[b]	6
olive oil	LLE: 35 mL ACN saturated with petroleum ether	MSPD: 2 g aminopropyl-bonded silica + 2 g florisil	LC/TOF-MS	81−111	2−4	1−5[b]	20
olive oil	LLE: 35 mL ACN saturated with petroleum ether	MSPD: 2 g aminopropyl-bonded silica + 2 g florisil	LC-MS/MS	83−104	5−10	0.2−2[b]	21
olive oil	LLE: 10 mL ACN	MSPD: 2 g PSA + 2 g Florisil/GCB	LC-TOF-MS	76.1−104.2	5.3−13.4	1.5−2.0[b]	7
palm oil	LLE: 10 mL ACN	low temperature fat precipitation (4 h) followed MSPD: 2 g PSA + 2 g GCB	LC-TOF-MS	76.1−107.4	4.3−13.4	1.5−5.0[b]	19
vegetable oil	DLLME: 90 μL [C_6mim][$FeCl_4$]	LLP: 1.5 mL water + 1.5 mL ethyl acetate	LC-UV	81.8−110.7	1.1−7.7	1.31−1.49[a]	35

[a]the unit of LOD is μg/L. [b]the unit of LOD is μg/kg. [c]ACN: acetonitrile.

DOI: 10.1021/jf505760y
J. Agric. Food Chem. 2015, 63, 2154−2161

present method has high selectivity, sensitivity, and accuracy. The present method is quick, simple, and effective, which shows great potential in the routine analysis of herbicides in vegetable oils. It would be an applicable method to extract contaminants in high-fat samples and also be a useful cleanup procedure for non- or low-fat samples by varying experimental parameters. The direct adsorption of analytes from oil samples is an attractive strategy to remove fat and improve method performance and MOFs are promising sorbents. It provides inspiration for the application of MOFs with unique structure and functions to the extraction of various contaminants in nonpolar system.

■ ASSOCIATED CONTENT

Supporting Information

Comparison of experimental parameters for dispersive micro-solid-phase extraction of herbicides from vegetable oil using the Student's *t* test. This material is available free of charge via the Internet at http://pubs.acs.org.

■ AUTHOR INFORMATION

Corresponding Author

*Phone: +86 431 85168399. Fax: +86 431 85112355. E-mail: analchem@jlu.edu.cn.

Funding

This work was supported by the National Natural Science Foundation of China (21207047).

Notes

The authors declare no competing financial interest.

■ REFERENCES

(1) Jiang, Y. P.; Li, Y. J.; Jiang, Y. T.; Li, J. G.; Pan, C. P. Determination of multiresidues in rapeseed, rapeseed oil, and rapeseed meal by acetonitrile extraction, low-temperature cleanup, and detection by liquid chromatography with tandem mass spectrometry. *J. Agric. Food Chem.* **2012**, *60*, 5089−5098.

(2) Wang, X. P.; Li, P. W.; Zhang, W.; Zhang, Q.; Ma, F.; Yu, L.; Wang, L. Screening for pesticide residues in oil seeds using solid-phase dispersion extraction and comprehensive two-dimensional gas chromatography time-of-flight mass spectrometr. *J. Sep. Sci.* **2012**, *35*, 1634−1643.

(3) Li, N.; Wang, Z. B.; Zhang, L. Y.; Nian, L.; Lei, L.; Yang, X.; Zhang, H. Q.; Yu, A. M. Liquid-phase extraction coupled with metal−organic frameworks-based dispersive solid phase extraction of herbicides in peanuts. *Talanta* **2014**, *128*, 345−353.

(4) Lentza-Rizos, C.; Avramides, E. J.; Cherasco, F. Low-temperature clean-up method for the determination of organophosphorus insecticides in olive oil. *J. Chromatogr., A* **2001**, *912*, 135−142.

(5) Hiskia, A. E.; Atmajidou, M. E.; Tsipi, D. F. Determination of organophosphorus pesticide residues in Greek virgin olive oil by capillary gas chromatography. *J. Agric. Food Chem.* **1998**, *46*, 570−574.

(6) Sánchez, A. G.; Martos, N. R.; Ballesteros, E. Multiresidue analysis of pesticides in olive oil by gel permeation chromatography followed by gas chromatography−tandem mass-spectrometric determination. *Anal. Chim. Acta* **2006**, *558*, 53−61.

(7) Sobhanzadeh, E.; Abu Bakar, N. K.; Bin Abas, M. R.; Nemati, K. An efficient extraction and clean-up procedure for pesticide determination in olive oil. *Eur. J. Lipid Sci. Technol.* **2011**, *113*, 862−869.

(8) Aramendía, M. A.; Borau, V.; Lafont, F.; Marinas, A.; Marinas, J. M.; Moreno, J. M.; Urbano, F. J. Determination of herbicide residues in olive oil by gas chromatography−tandem mass spectrometry. *Food Chem.* **2007**, *105*, 855−861.

(9) Fuentes, E.; Báez, M. E.; Díaz, J. Microwave-assisted extraction at atmospheric pressure coupled to different clean-up methods for the determination of organophosphorus pesticides in olive and avocado oil. *J. Chromatogr., A* **2009**, *1216*, 8859−8866.

(10) Díaz-Plaza, E. M.; Cortés, J. M.; Vázquez, A.; Villén, J. Automated determination of pesticide residues in olive oil by on-line reversed-phase liquid chromatography−gas chromatography using the through oven transfer adsorption desorption interface with electron-capture and nitrogen-phosphorus detectors operating simultaneously. *J. Chromatogr., A* **2007**, *1174*, 145−150.

(11) *EU Pesticides Database*; European Commission: Brussels; http://ec.europa.eu/sanco_pesticides/public/?event=homepage.

(12) Gilbert-López, B.; García-Reyes, J. F.; Molina-Díaz, A. Sample treatment and determination of pesticide residues in fatty vegetable matrices: a review. *Talanta* **2009**, *79*, 109−128.

(13) Zainudin, B. H.; Abu Bakar, N. K.; Muhamad, H. Determination of cypermethrin in palm oil matrices. *Eur. J. Lipid Sci. Technol.* **2009**, *111*, 1014−1019.

(14) Amvrazi, E. G.; Albanis, T. A. Multiresidue method for determination of 35 pesticides in virgin olive oil by using liquid−liquid extraction techniques coupled with solid-phase extraction clean up and gas chromatography with nitrogen phosphorus detection and electron capture detection. *J. Agric. Food Chem.* **2006**, *54*, 9642−9651.

(15) Li, L.; Xu, Y. J.; Pan, C. P.; Zhou, Z. Q.; Jiang, S. R.; Liu, F. M. Simplified pesticide multiresidue analysis of soybean oil by low-temperature cleanup and dispersive solid-phase extraction coupled with gas chromatography/mass spectrometry. *J. AOAC Int.* **2007**, *90*, 1387−1394.

(16) Li, L.; Zhang, H. Y.; Pan, C. P.; Zhou, Z. Q.; Jiang, S. R.; Liu, F. M. Multiresidue analytical method of pesticides in peanut oil using low-temperature cleanup and dispersive solid phase extraction byGC-MS. *J. Sep. Sci.* **2007**, *30*, 2097−2104.

(17) Moreno-González, D.; Huertas-Pérez, J. F.; García-Campaña, A. M.; Gámiz-Gracia, L. Determination of carbamates in edible vegetable oils by ultra-high performance liquid chromatography−tandem mass pectrometry using a new clean-up based on zirconia for QuEChERS methodology. *Talanta* **2014**, *128*, 299−304.

(18) Sobhanzadeh, E.; Abu Bakar, N. K.; Bin Abas, M. R.; Nemati, K. A simple and efficient multi-residue method based on QuEChERS for pesticides determination in palm oil by liquid chromatography time-of-flight mass spectrometry. *Environ. Monit. Assess.* **2012**, *184*, 5821−5828.

(19) Sobhanzadeh, E.; Abu Bakar, N. K.; Bin Abas, M. R.; Nemati, K. Low temperature followed by matrix solid-phase dispersion-sonication procedure for the determination of multiclass pesticides in palm oil using LC-TOF-MS. *J. Hazard. Mater.* **2011**, *186*, 1308−1313.

(20) Garcia-Reyes, J. F.; Ferrer, C.; Michael Thurman, E.; Fernandez-Alba, A. R.; Ferrer, I. Analysis of Herbicides in Olive Oil by Liquid Chromatography Time-of-Flight Mass Spectrometry. *J. Agric. Food Chem.* **2006**, *54*, 6493−6500.

(21) Ferrer, C.; Gomez, M. J.; Garcia-Reyes, J. F.; Ferrer, I.; Thurman, E. M.; Fernandez-Alba, A. R. Determination of pesticide residues in olives and olive oil by matrix solid-phase dispersion followed by gas chromatography/mass spectrometry and liquid chromatography/tandem mass spectrometry. *J. Chromatogr., A* **2005**, *1069*, 183−194.

(22) Barrek, S.; Paisse, O.; Grenier-Loustalot, M. F. Determination of residual pesticides in olive oil by GC-MS and HPLC-MS after extraction by size-exclusion chromatography. *Anal. Bioanal. Chem.* **2003**, *376*, 355−359.

(23) Li, J. D.; Liu, D. J.; Wu, T.; Zhao, W. T.; Zhou, Z. Q.; Wang, P. A simplified procedure for the determination of organochlorine pesticides and polychlorobiphenyls in edible vegetable oils. *Food Chem.* **2014**, *151*, 47−52.

(24) Bakas, I.; Ben Oujji, N.; Istamboulie, G.; Piletsky, S.; Piletska, E.; Ait-Addi, E.; Ait-Ichou, I.; Noguer, T.; Rouillon, R. Molecularly imprinted polymer cartridges coupled to high performance liquid chromatography (HPLC-UV) for simple and rapid analysis of fenthion in olive oil. *Talanta* **2014**, *125*, 313−318.

(25) Férey, G.; Mellot-Draznieks, C.; Serre, C.; Millange, F.; Dutour, J.; Surblé, S.; Margiolaki, I. A chromium terephthalate-based solid with

DOI: 10.1021/jf505760y
J. Agric. Food Chem. 2015, 63, 2154−2161

unusually large pore volumes and surface area. *Science* **2005**, *309*, 2040−2042.
(26) Yang, C. X.; Yan, X. P. Metal-organic framework MIL-101(Cr) for high-performance liquid chromatographic separation of substituted aromatics. *Anal. Chem.* **2011**, *83*, 7144−7150.
(27) Gu, Z. Y.; Yang, C. X.; Chang, N.; Yan, X. P. Metal−organic frameworks for analytical chemistry: from sample collection to chromatographic separation. *Acc. Chem. Res.* **2012**, *45*, 734−745.
(28) Hasan, Z.; Jeon, J.; Jhung, S. H. Adsorptive removal of naproxen and clofibric acid from water using metal−organic frameworks. *J. Hazard. Mater.* **2012**, *209− 210*, 151−157.
(29) Hu, Y. L.; Song, C. Y.; Liao, J.; Huang, Z. L.; Li, G. K. Water stable metal−organic framework packed microcolumn for online sorptive extraction and direct analysis of naproxen and its metabolite from urine sample. *J. Chromatogr., A* **2013**, *1294*, 17−24.
(30) Karra, J. R.; Walton, K. S. Effect of open metal sites on adsorption of polar and nonpolar molecules in metal−organic framework Cu-BTC. *Langmuir* **2008**, *24*, 8620−8626.
(31) Huang, C. Y.; Song, M.; Gu, Z. Y.; Wang, H. F.; Yan, X. P. Probing the adsorption characteristic of metal−organic framework MIL-101 for volatile organic compounds by quartz crystal microbalance. *Environ. Sci. Technol.* **2011**, *45*, 4490−4496.
(32) Fu, Y. Y.; Yang, C. X.; Yan, X. P. Control of the coordination status of the open metal sites in metal−organic frameworks for high performance separation of polar compounds. *Langmuir* **2012**, *28*, 6794−6802.
(33) Nguyen, T. D.; Lee, M. H.; Lee, G. H. Rapid determination of 95 pesticides in soybean oil using liquid−liquid extraction followed by centrifugation, freezing and dispersive solid phase extraction as cleanup steps and gas chromatography with mass spectrometric detection. *Microchem. J.* **2010**, *95*, 113−119.
(34) Hernando, M. D.; Ferrer, C.; Ulaszewska, M.; García-Reyes, J. F.; Molina-Díaz, A.; Fernández-Alba, A. R. Application of high-performance liquid chromatography−tandem mass spectrometry with a quadrupole/linear ion trap instrument for the analysis of pesticide residues in olive oil. *Anal. Bioanal. Chem.* **2007**, *389*, 1815−1831.
(35) Wang, Y.; Sun, Y.; Xu, B.; Li, X.; Jin, R.; Zhang, H.; Song, D. Magnetic ionic liquid-based dispersive liquid−liquid microextraction for the determination of triazine herbicides in vegetable oils by liquid chromatography. *J. Chromatogr., A* **2014**, *1373*, 9−16.

DOI: 10.1021/jf505760y
J. Agric. Food Chem. 2015, 63, 2154−2161

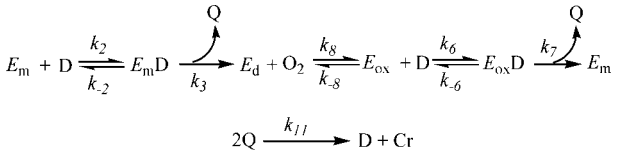

Figure 2. Action mechanism of tyrosinase on *o*-diphenols.

Considering the mechanism of action of the enzyme on monophenols and *o*-diphenols (Figures 1 and 2) and kinetic analysis of the two activities, the analytical expressions of the degrees of inhibition are obtained, and based on these, a test is proposed to differentiate a tyrosinase substrate other than L-tyrosine and L-dopa from an inhibitor of the enzyme. At the same time, the proper methodology is established to assay tyrosinase inhibition.

MATERIALS AND METHODS

Enzyme Source. Mushroom tyrosinase (3130 U/mg) was purchased from Sigma (Spain) and purified as previously described.[15] Protein content was determined by Bradford's method.[16]

Reagents. 4-*tert*-butylphenol (TBP), 4-*tert*-butylcatechol (TBC), L-dopa, L-tyrosine, sodium periodate, 3-methyl-2-benzothiazolinone hydrazone hydrochloride (MBTH), dimethylformamide (DMF), guaiacol, carvacrol, eugenol, isoeugenol, arbutin, benzoic acid, and cinnamic acid (see Figure 3) were purchased from Sigma. Stock solutions of substrates were prepared in 0.15 mM phosphoric acid to prevent auto-oxidation.

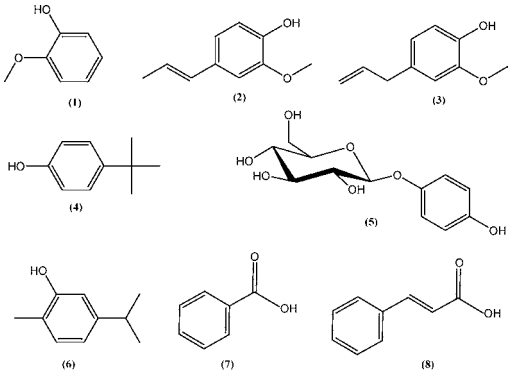

Figure 3. Chemical structures of the compounds studied. (1) Guaiacol, (2) isoeugenol, (3) eugenol, (4) 4-*tert*-butylphenol, (5) arbutin, (6) carvacrol, (7) benzoic acid, and (8) cinnamic acid.

Spectrophotometric Assays. Absorption spectra were recorded in a visible–ultraviolet PerkinElmer Lambda 35-spectrophotometer, online interfaced with a compatible PC 486DX microcomputer, with a 60 nm/s scanning speed controlled by the UV-Winlab software. The temperature was maintained at 25 °C using a Haake D16 circulating water bath with a heater/cooler and checked using a Cole–Palmer digital thermometer with a precision of 0.1 °C. Kinetic assays were also carried out with the above instruments by measuring the appearance of the products in the reaction medium. All the assays were carried out under saturating conditions of tyrosinase by molecular oxygen, 0.26 mM in the assay medium.[17] The activity on L-tyrosine and L-dopa was measured at 475 nm, which is the maximum absorption wavelength of dopachrome. The activity on TBC was followed at 410 nm.[18,19] The assays of activity in the presence of hydrogen peroxide were followed at wavelengths at which each generated product absorbed. All assays were made, unless otherwise stated, using 30 mM phosphate buffer pH 7.0.

Simulation Assays. The simulated progress curves were obtained by numerical solution of the nonlinear set of differential equations that describes the mechanisms corresponding to Figures 1, 2, 5, 6, 1SI, 4SI, and 2SI (see Supporting Information). The systems of differential equations were solved numerically for particular sets of values of the rate constants and of initial concentrations of the species involved in the reaction mechanism. The numerical integration used a fourth order Runge–Kutta method and the predictor-corrector Adams–Moulton algorithm, implemented on a PC-compatible computer program (WES).[20]

RESULTS AND DISCUSSION

Tyrosinase shows two enzymatic activities, the hydroxylation of L-tyrosine to L-dopa and the oxidation of the latter to *o*-dopaquinone. According to the mechanism shown in Figure 2, the formation and accumulation of dopachrome product is linear with time (data not shown). Figure 4 shows the tyrosinase activity on L-tyrosine: notice the apparition of a lag in the accumulation of dopachrome, curve a. At the same time, this lag decreased and was annulled when a certain amount of *o*-diphenol was added at the beginning of the reaction, curve b. The quantity of *o*-diphenol needed for the system to reach the steady state is given by $R = [D]_{ss}/[M]_{ss}$.[21] This equation establishes the quantity of *o*-diphenol [D] in the steady state $[D]_{ss}$ needed so that the monophenol concentration $[M]_{ss}$ reaches the steady state from $t = 0$. When more diphenol than needed was added to fulfill the relation R, a burst appeared at the beginning of the activity recording, curve c. In Figure 4, the inset shows the simulated progress curves a–c, obtained through numerical integration of the set of differential equations that describes the mechanism shown in Figure 1 (see Supporting Information).

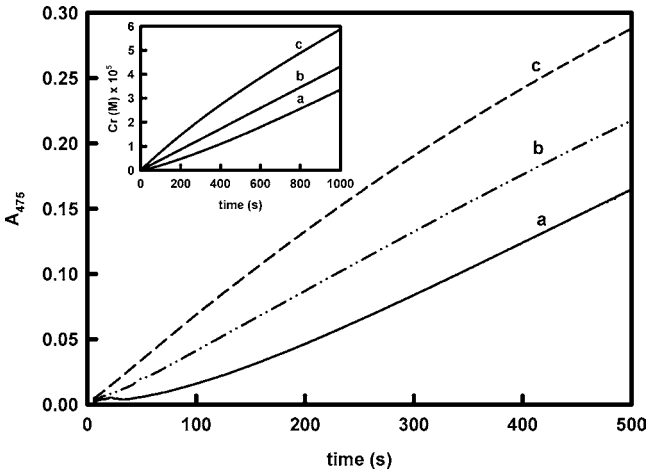

Figure 4. Relevance of the relation (R) between the *o*-diphenol, $[D]_{ss}$, and the monophenol, $[M]_{ss}$, in steady state ($R = [D]ss/[M]ss$). Dopachrome accumulation with time of using $[E]_0 = 8.0$ nM on L-tyrosine $[M]_0 = 0.25$ mM. (Curve a) L-dopa is not added at the beginning of the reaction $[D]_0 = 0$. (Curve b) L-dopa is added at the beginning of the reaction, $[D]_0 = 10.50$ μM, in order to fulfill the relation $R = 0.042$. (Curve c) More L-dopa than the required to fulfill the relation R is added, $[D]_0 = 28.75$ μM. (Inset) Simulated progress curves of the mechanism shown in Figure 1. The conditions were $[E]_0 = 22$ nM, $[E_{ox}]_0 = 0.3x[E]_0$, $[E_m]_0 = 0.7x[E]_0$, $[M]_0 = 0.25$ mM, (a) $[D]_0 = 0$, (b) $[D]_0 = 10.50$ μM, and (c) $[D]_0 = 28.75$ μM. The concentration of oxygen was 0.26 mM, and the rate constants were $k_1 = 2 \times 10^5$ M^{-1} s^{-1}, $k_{-1} = 10$ s^{-1}, $k_2 = 5 \times 10^6$ M^{-1} s^{-1}, $k_{-2} = 10$ s^{-1}, $k_3 = 900$ s^{-1}, $k_4 = 2 \times 10^4$ M^{-1} s^{-1}, $k_{-4} = 1$ s^{-1}, $k_5 = 5$ s^{-1}, $k_6 = 2.16 \times 10^5$ M^{-1} s^{-1}, $k_{-6} = 10$ s^{-1}, $k_7 = 108$ s^{-1}, $k_8 = 2.3 \times 10^8$ M^{-1} s^{-1}, $k_{-8} = 1.07 \times 10^3$ s^{-1}, and $k_{11} = 10$ s^{-1}.

DOI: 10.1021/jf5051816
J. Agric. Food Chem. 2015, 63, 2162–2171

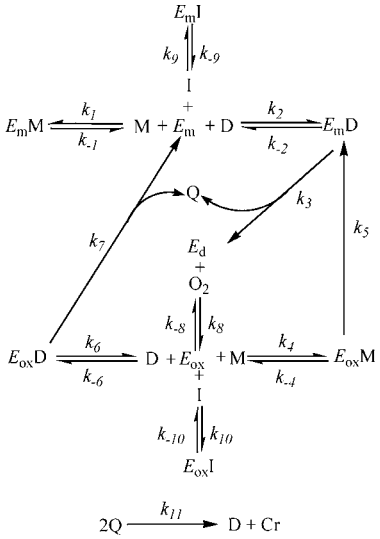

Figure 5. Action mechanism of tyrosinase on monophenols and *o*-diphenols in the presence of an inhibitor that binds to the enzymatic forms E_m and E_{ox}.

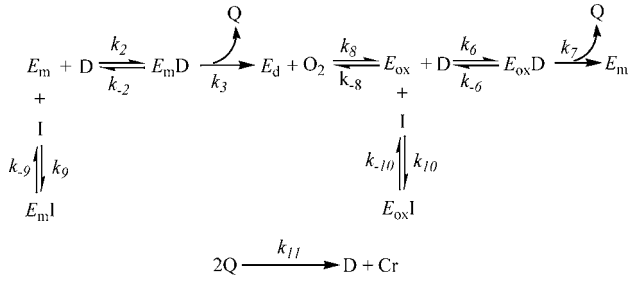

Figure 6. Action mechanism of tyrosinase on *o*-diphenols in the presence of an inhibitor that binds to the enzymatic forms E_m and E_{ox}.

The lag period observed at the beginning of the recording of the monophenolase activity of tyrosinase represents a substantial difficulty when making inhibitor assays.[22] It is essential to determine when the steady state is reached to measure the monophenolase activity. When an inhibitor is added to the reaction medium, the reaction rate of the enzyme decreases and so does the rate of accumulation of *o*-diphenol in the medium, and this means an increase in the lag period and the steady state is reached later, which therefore entails a longer measuring period. This has not usually been taken into account when studying the inhibition of the monophenolase activity, meaning that inexact values have been obtained for many studied inhibitors.[23−29]

We propose that to know whether the target molecules act as substrates or enzyme inhibitors, both the monophenolase and diphenolase activities must be studied. The monophenolase activity will be studied by adding the amount of *o*-diphenol necessary to avoid the lag period so that the steady state is reached from the beginning of the reaction.[22] In this case, the presence of an inhibitor in the medium will not involve an increase in the lag period, even though it will decrease the rate, so that the monophenolase activity can be measured from $t = 0$, both in the presence and absence of different concentrations of a target molecule.

In this work, we study two classic inhibitors of tyrosinase for comparative purposes (benzoic acid[30] and cinnamic acid) and investigate whether a group of target molecules (4-*tert*-

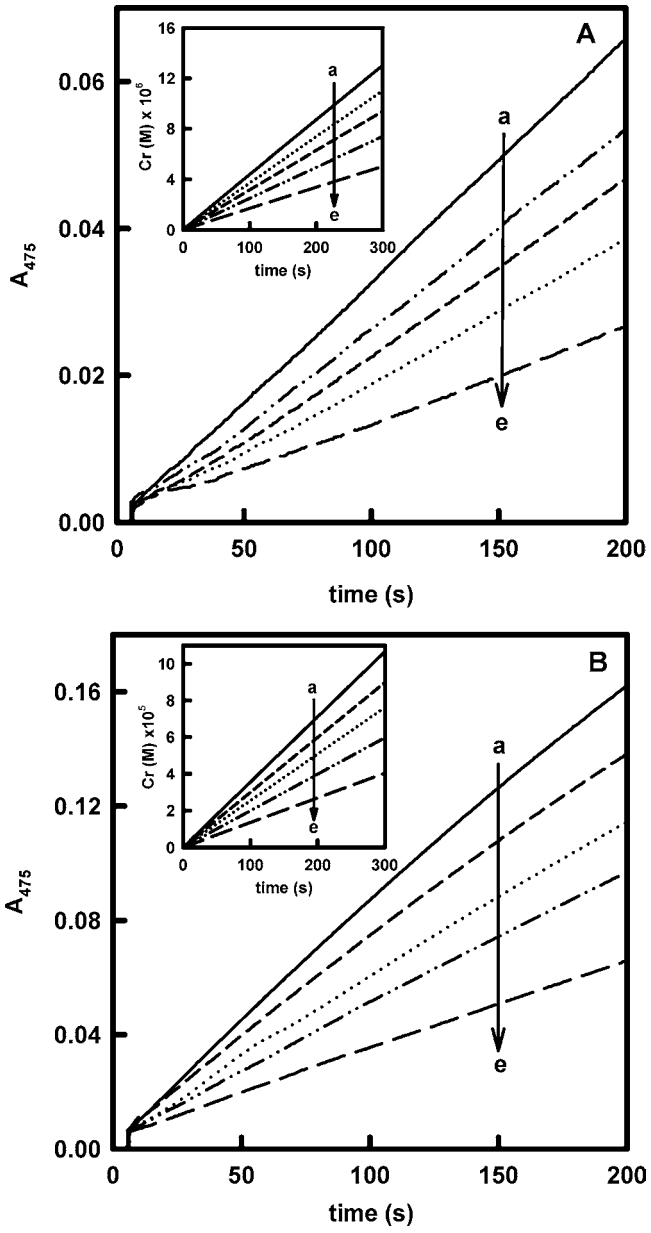

Figure 7. Action of benzoic acid on the diphenolase and monophenolase activities of tyrosinase. (A) Spectrophotometric recordings of the accumulation of dopachrome in the action of tyrosinase on L-tyrosine in the absence and presence of benzoic acid. The experimental conditions were $[M]_0 = 0.25$ mM, $[E]_0 = 7$ nM, $[D]_0 = 10.50$ μM, and the benzoic acid concentrations were (mM) (a) 0, (b) 0.15, (c) 0.35, (d) 0.70, and (e) 1.40. (A, inset) Simulated progress curves of the mechanism shown in Figure 5. The conditions were $[E]_0 = 22$ nM, $[E_{ox}]_0 = 0.3x[E]_0$, $[E_m]_0 = 0.7x[E]_0$, $[M]_0 = 0.25$ mM, and $[D]_0 = 10.50$ μM. The concentration of oxygen was 0.26 mM and the benzoic acid concentrations were the same as in part A. The rate constants were the same as in Figure 4 (inset) and $k_9 = 10^3$ M^{-1} s^{-1}, $k_{-9} = 4.1$ s^{-1}, $k_{10} = 10^4$ M^{-1} s^{-1}, and $k_{-10} = 4.1$ s^{-1}. (B) Records of the accumulation of dopachrome in the action of tyrosinase on L-dopa in the absence and presence of benzoic acid. The experimental conditions were $[D]_0 = 0.5$ mM, $[E]_0 = 5$ nM, and the benzoic acid concentrations were the same as in part A. (B, inset) Simulation of the mechanism shown in Figure 6. The conditions were $[E]_0 = 7.5$ nM, $[E_{ox}]_0 = 0.3x[E]_0$, $[E_m]_0 = 0.7x[E]_0$; $[D]_0 = 0.5$ mM. The concentration of oxygen was 0.26 mM and the concentrations of the inhibitor the same as in part B. The rate constants were the same as in part A (inset) and Figure 4 (inset).

DOI: 10.1021/jf5051816
J. Agric. Food Chem. 2015, 63, 2162−2171

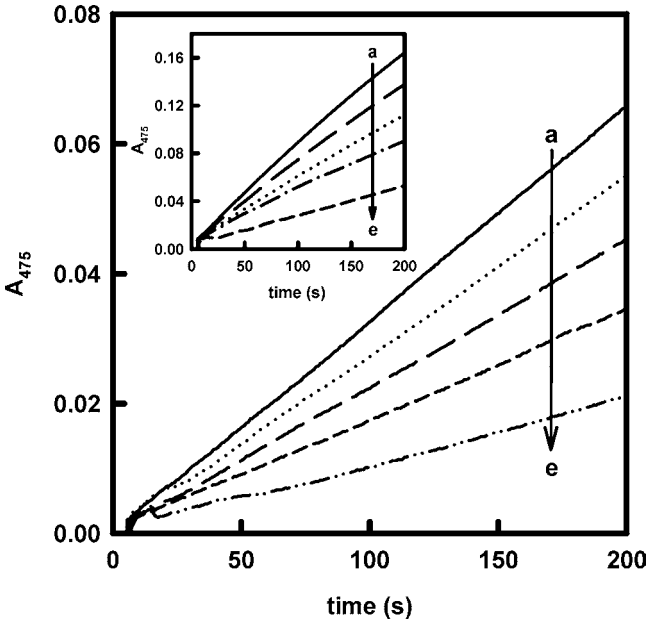

Figure 8. Action of cinnamic acid on the monophenolase and diphenolase activities of tyrosinase. Spectrophotometric recordings of the accumulation of dopachrome in the action of tyrosinase on L-tyrosine. The experimental conditions were $[M]_0$ = 0.25 mM, $[E]_0$ = 7 nM, and $[D]_0$ = 10.50 μM and the cinnamic acid concentrations were (mM) (a) 0, (b) 0.2, (c) 0.4, (d) 1.0, and (e) 2.0. (Inset) Spectrophotometric recordings of the accumulation of dopachrome in the action of tyrosinase on L-dopa in the presence of cinnamic acid. The experimental conditions were $[D]_0$ = 0.5 mM and $[E]_0$ = 5 nM. The cinnamic acid concentrations were the same as used in the monophenolase activity.

Table 1. Degree of Inhibition (i %) of the Monophenolase (i_M) and Diphenolase (i_D) Activities of Tyrosinase in the Presence of Different Concentrations of Two Competitive Inhibitors, Which Bind to the Enzymatic Forms E_m and E_{ox}

inhibitor	concn. (mM)	i_M	i_D
benzoic acid	0.15	17.92 ± 0.10	16.36 ± 0.03
	0.35	27.95 ± 0.12	29.35 ± 0.27
	0.70	42.15 ± 0.19	44.87 ± 0.12
	1.40	63.76 ± 0.45	62.90 ± 0.16
cinnamic acid	0.20	19.84 ± 0.08	19.44 ± 0.08
	0.40	33.31 ± 0.19	37.03 ± 0.10
	1.00	50.11 ± 0.28	47.61 ± 0.30
	2.00	70.06 ± 0.70	72.14 ± 0.93

butylphenol, eugenol, guaiacol, isoeugenol, carvacrol, and arbutin) act as tyrosinase substrates or inhibitors.

To determine whether a molecule of interest is a true substrate or an enzyme inhibitor, we must first ascertain if the enzyme reacts with the compound under study. In the case of target monophenols, this assay always shows no activity (data not shown), because monophenols, as described below, do not cause the chemical accumulation of *o*-diphenol in the medium.

Once this part of the test was completed, we determined the enzymatic activity on L-dopa in the presence and absence of a target molecule, measuring spectrophotometrically the accumulation of dopachrome at 475 nm. The concentration of L-dopa used was K_M^D. After this, measurements were made at different concentrations of the molecule of interest.

Table 2. Degree of Inhibition (i %) of the Monophenolase (i_M) and Diphenolase (i_D) Activities of Tyrosinase Obtained through Simulated Recordings by Numerical Integration of the Set of Differential Equations Corresponding to (a) the Mechanisms Shown in Figures 5 and 6, in Which Both Activities Are Shown in the Presence of Different Concentrations of an Inhibitor That Binds to the Enzymatic Species E_{ox} and E_m (Figure 7); (b) the Mechanisms Shown in Figures 1SI and 2SI Corresponding to the Tyrosinase Activity in the Presence of an Inhibitor That Binds to the Form E_{ox} in the Diphenolase Activity and E_{ox} and E_mM in the Monophenolase Activity (Figure 3SI)

inhibitor	concn. (mM)	i_M	i_D
(a) $i_M = i_D$	0.15	15.80	15.48
	0.35	28.54	27.98
	0.70	44.04	43.29
	1.40	62.18	61.37
(b) $i_M \neq i_D$	0.15	25.65	15.75
	0.35	42.11	28.46
	0.70	58.83	43.93
	1.40	74.88	62.09

Table 3. Degree of Inhibition (i %) of the Monophenolase (i_M) and Diphenolase (i_D) Activities of Tyrosinase in the Presence of Different Concentrations of Several Target Monophenols

target monophenol	concn. (mM)	i_M	i_D
guaiacol	4.0	63.78 ± 1.07	26.26 ± 0.10
	8.0	69.80 ± 0.90	39.35 ± 0.11
isoeugenol	0.9	46.46 ± 0.31	22.72 ± 0.07
	1.8	67.57 ± 0.92	40.96 ± 0.13
carvacrol	2.0	54.03 ± 0.63	14.15 ± 0.03
	4.8	70.05 ± 1.25	45.41 ± 0.17
TBP	0.1	64.80 ± 0.57	14.88 ± 0.03
	0.4	82.26 ± 1.76	33.52 ± 0.09
eugenol	0.9	37.76 ± 0.24	17.74 ± 0.04
	3.6	64.76 ± 0.49	58.74 ± 0.25
arbutin	0.3	33.02 ± 0.29	13.99 ± 0.04
	1.5	53.97 ± 0.76	27.59 ± 0.06

Similarly, the enzymatic activity on L-tyrosine was studied in the presence and absence of the target molecule, measuring the accumulation of dopachrome at 475 nm. The concentration of L-tyrosine used was K_M^M. Also, a concentration of L-dopa was added to fulfill $R = [D]_{ss}/[M]_{ss}$, reaching the steady state at t = 0.[31] After this, measurements were made at the same target molecule concentrations, as in the case of the diphenolase activity. To develop this kind of assay, it is not necessary to use concentrations of monophenol and *o*-diphenol similar to K_M, but the relations $[M]_0/K_M^M$ and $[D]_0/K_M^D$ must be the same.

Then, the degree of inhibition of the monophenolase (i_M) and diphenolase (i_D) activities were calculated and were compared. In cases where the inhibition degrees were the same ($i_M = i_D$), the molecule under study acted as an inhibitor. These mechanisms are described in Figures 5 and 6 and the results are shown in Table 2. The simulated progress curves obtained through numerical integration of the set of differential equations that describe the above mechanisms are shown in Figures 7A (inset) and 7B (inset). If the degree of inhibition differed ($i_M \neq i_D$), the molecule in question could either be an alternative substrate or an inhibitor (in which case it would

DOI: 10.1021/jf5051816
J. Agric. Food Chem. 2015, 63, 2162−2171

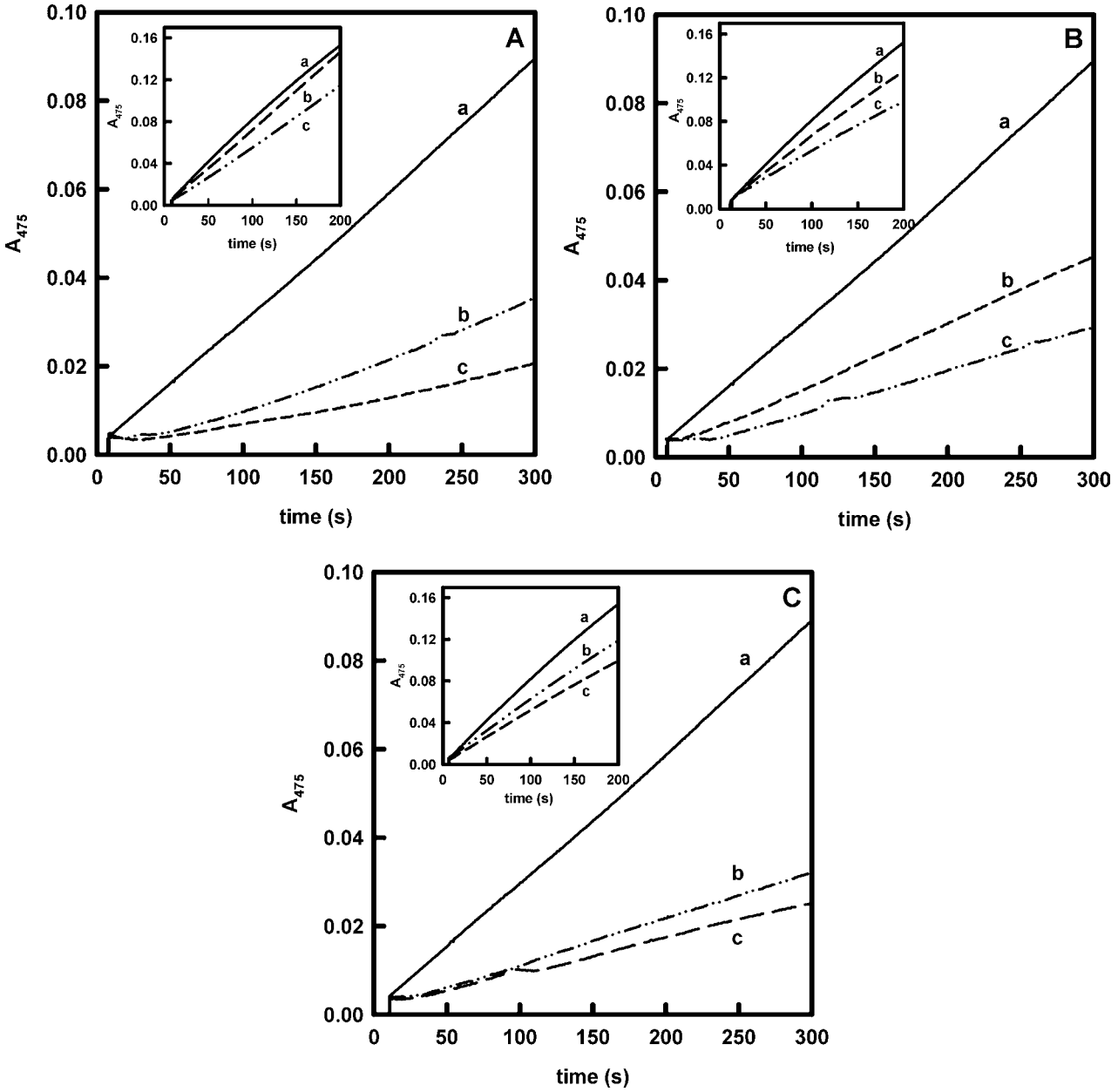

Figure 9. Action of the target molecules on the monophenolase and diphenolase activities of tyrosinase. (A) Action of TBP on the monophenolase activity on L-tyrosine. The experimental conditions were $[M]_0$ = 0.25 mM, $[E]_0$ = 7 nM, and $[D]_0$ = 10.50 μM. The concentrations of TBP were (mM) (a) 0, (b) 0.1, and (c) 0.4. (A, inset) Action of TBP on the diphenolase activity on L-dopa. The experimental conditions were $[D]_0$ = 0.5 mM and $[E]_0$ = 5 nM. The concentrations of TBP were the same as in part A. (B) Action of isoeugenol on the monophenolase activity of tyrosinase. The experimental conditions were the same as in part A, and the concentrations of isoeugenol were (mM) (a) 0, (b) 0.9, and (c) 1.8. (B, inset) Action of ioseugenol on the diphenolase activity of tyrosinase. The experimental conditions were the same as in part a, inset, and the concentrations of isoeugenol were the same as in part B. (C) Action of the guaiacol on the monophenolase activity of tyrosinase. The experimental conditions were the same as in parts A and B, and the concentrations of guaiacol were (mM) (a) 0, (b) 4, and (c) 8. (C, inset) Action of guaiacol on the diphenolase activity of tyrosinase. The experimental conditions were the same as in the insets of parts A and B, and the concentrations of guaiacol were the same as in part C.

bind to any of the enzymatic forms of the diphenolase mechanism, and to one of the E_mM or E_{ox}M complexes of the monophenolase mechanism). Possible mechanisms involved are shown in Figures 1SI and 2SI and the results in Table 2. In Figure 3SI, the simulated progress curves obtained through numerical integration of the set of differential equations that describe these mechanisms are shown. In this case ($i_M \neq i_D$), two types of additional assays had to be undertaken to confirm if the target molecules were alternative substrates or inhibitors (see below).

Figure 7A shows the recordings of the monophenolase activity of tyrosinase on L-tyrosine at different concentrations of benzoic acid, obtained by adding a given amount of *o*-diphenol from t = 0 ($[D] = [D]_{ss}$), so as to satisfy the relation $R = [D]_{ss}/[M]_{ss}$, and Figure 7B shows the diphenolase activity of tyrosinase on L-dopa at the same concentrations of benzoic acid. The insets in Figure 7, show the simulated progress curves

DOI: 10.1021/jf5051816
J. Agric. Food Chem. 2015, 63, 2162−2171

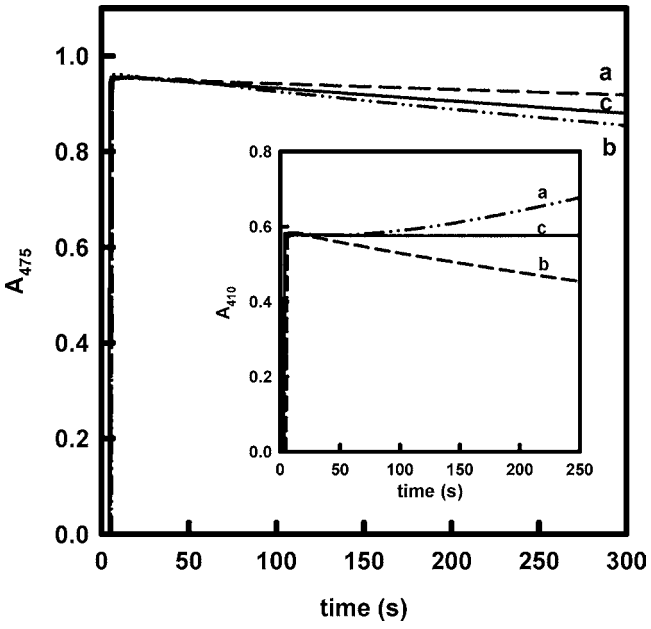

Figure 10. Possible reaction of the *o*-quinones of L-dopa or TBC with the phenols under study. L-Dopa 1 mM was oxidized with sodium periodate in default (0.53 mM), and then, the phenols were added (a) carvacrol 5.9 mM and (b) guaiacol 24 mM. The continuous recording (c) shows the stability of the dopachrome with time in the absence of the target molecules. (Inset) TBC 1.6 mM was oxidized with sodium periodate in default (0.53 mM), and then, the phenols were added (a) carvacrol 6.4 mM and (b) guaiacol 24.0 mM. The continuous recording (c) shows the stability of *o-tert*-butylquinone in the absence of the target molecules.

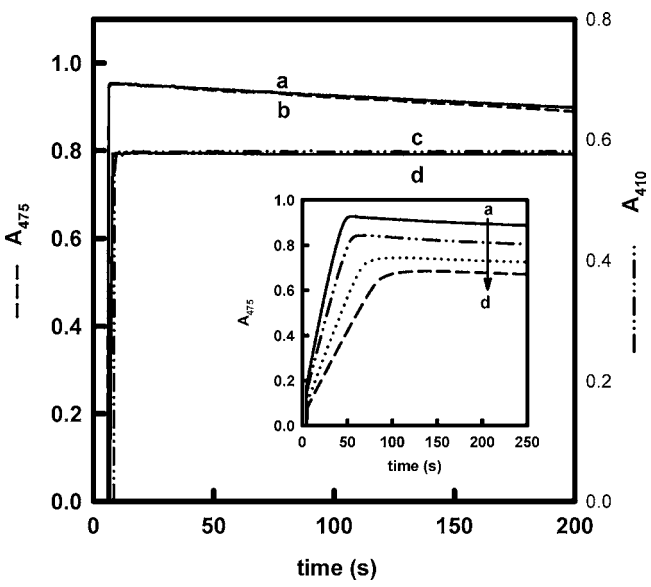

Figure 11. Stability of dopachrome and *o-tert*-butylquinone in the presence of arbutin. L-Dopa 1 mM was oxidized with sodium periodate in default (0.53 mM) and the stability of its *o*-quinone was recorded in the absence (a) and presence (b) of arbutin 18 mM. TBC was oxidized 1.6 mM with sodium periodate in default (0.53 mM) and the stability of the generated *o*-quinone was recorded in the absence (a) and presence (b) of arbutin 18 mM. (Inset) Increase in absorbance in the action of tyrosinase $[E]_0$ = 56 nM on L-dopa 1 mM, in the absence (a) and presence of arbutin (mM) (b) 0.6, (c) 3.0, and (d) 18.0, until all the oxygen was consumed.

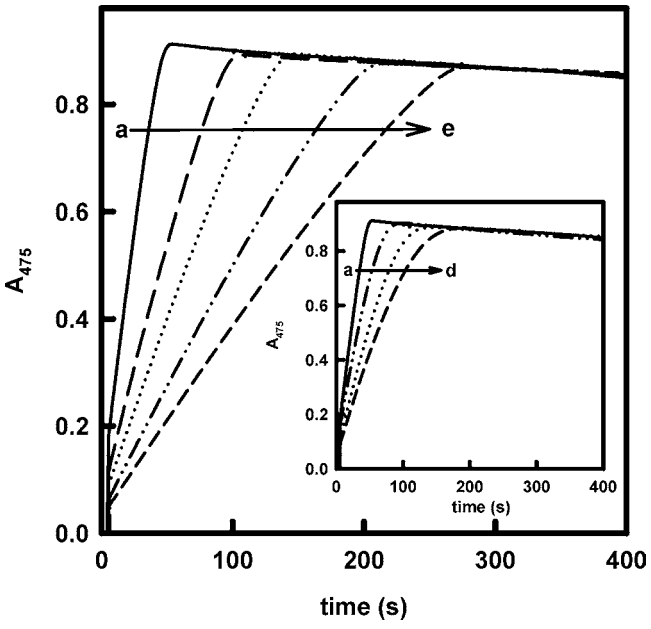

Figure 12. Oxidation of L-dopa through tyrosinase in the presence of different concentrations of benzoic acid until all the oxygen was consumed. The conditions were $[D]_0$ = 1 mM, $[E]_0$ = 56 nM, and the concentrations of benzoic acid were (mM) (a) 0, (b) 1.25, (c) 2.5, (d) 3.75, and (e) 5.0. (Inset) Oxidation of L-dopa by tyrosinase in the presence of cinnamic acid until all the oxygen was consumed. The experimental conditions were the same as in Figure 11, and the concentrations of cinnamic acid were (mM) (a) 0, (b) 0.6, (c) 1.2, and (d) 2.4.

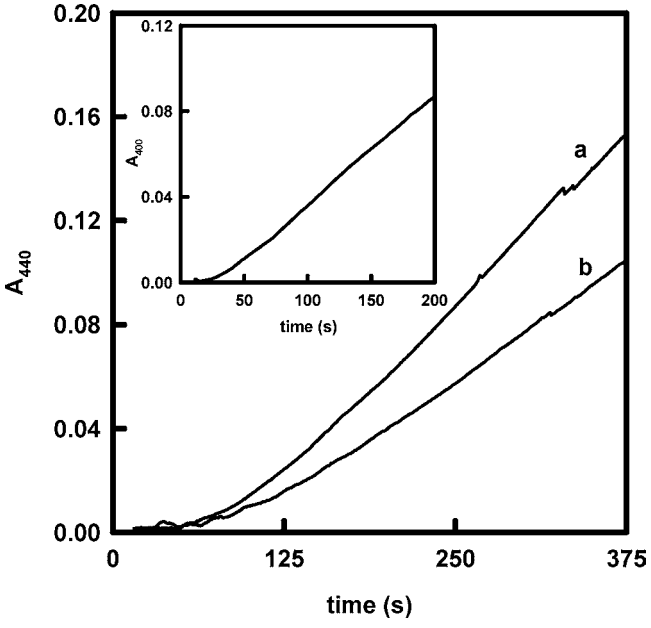

Figure 13. Action of tyrosinase on isoeugenol and eugenol in the presence of hydrogen peroxide (H_2O_2). Recordings of the variation of absorbance at 440 nm in the action on isoeugenol 1.75 mM (a) and eugenol 1.75 mM (b). The experimental conditions were: $[E]_0$ = 130 nM and H_2O_2 10 mM. (Inset) Action of the tyrosinase on TBP in the presence of H_2O_2. Recording of the variation of absorbance at 400 nm. The experimental conditions were: TBP 0.5 mM, $[E]_0$ = 3 nM, and H_2O_2 10 mM.

obtained through numerical integration of the sets of differential equations that describe the mechanisms of the

DOI: 10.1021/jf5051816
J. Agric. Food Chem. 2015, 63, 2162−2171

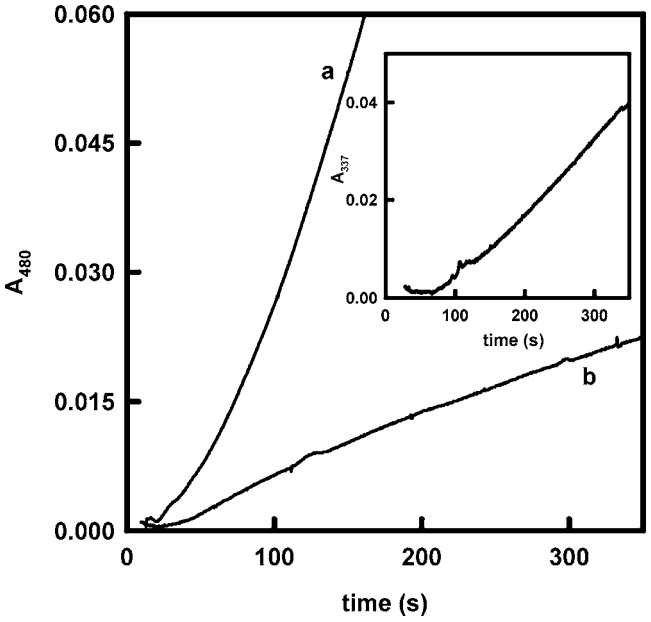

Figure 14. Action of tyrosinase on arbutin and carvacrol in the presence of hydrogen peroxide (H_2O_2). Variation of absorbance at 480 nm. The experimental conditions were (a) arbutin 5 mM, $[E]_0$ = 45 nM, and H_2O_2 5 mM and (b) carvacrol 1.4 mM, phosphate buffer 50 mM pH 7.0, $[E]_0$ = 0.16 μM, H_2O_2 0.05 mM, MBTH 4.5 mM, and DMF 2%. (Inset) Action of tyrosinase on guaiacol in the presence of H_2O_2. Variation of the absorbance at 337 nm. The experimental conditions were guaiacol 7.5 mM, $[E]_0$ = 85 nM, and H_2O_2 10 mM.

monophenolase and diphenolase activities of tyrosinase in the presence of a competitive inhibitor (Figures 5 and 6)[30] (see Supporting Information).

Figure 8 depicts the kinetic recordings of the inhibition of the monophenolase and diphenolase activities by cinnamic acid. From the results obtained, both experimental and simulated, of the inhibition of the monophenolase and diphenolase activities (Figures 7, 8, and 3SI), the degrees of inhibition were calculated and are shown in Tables 1 and 2.

Note that the degrees of inhibition in both activities are the same, both for the experimental and simulated cases (Tables 1 and 2a), which agrees with eqs 4A and 8A (see the Appendix).

Investigating whether a phenol showing varying degrees of inhibition of the monophenolase and diphenolase activities is a tyrosinase substrate or inhibitor.

In cases in which the degree of inhibition of both activities was ($i_M \neq i_D$), two types of additional steps were made to confirm whether these molecules were alternative substrates or inhibitors. Guaiacol, isoeugenol, carvacrol, TBP, eugenol, and arbutin[6,32−38] showed this kind of behavior ($i_M \neq i_D$). Results are shown in Table 3. The recordings obtained with some of these molecules (TBP, isoeugenol, and guaiacol) are shown in Figure 9A−C.

Step 1. Measurement of the formation of the product originated in the oxidation of an *o*-diphenol by tyrosinase until total consumption of oxygen. To do this, TBC and L-dopa were chosen: in the case of TBC, the *o*-quinone, *o-tert*-butylquinone, is very stable and in the case of L-dopa dopachrome is formed, which is relatively stable. This step takes into account the stoichiometry of the mechanism shown in Figure 2. For TBC $1O_2$:2 *o*-quinone and for L-dopa $1O_2$:1 dopachrome. When all the oxygen is consumed in the absence or presence of an inhibitor and, bearing in mind the stoichiometries, when measuring the accumulation of *o-tert*-butylquinone, with ε = 1100 M^{-1} cm^{-1}, or dopachrome, with ε = 3600 M^{-1} cm^{-1},[18,19] the absorbances are constant. Figure 5SI depicts the simulated progress curves obtained through numerical integration of the set of differential equations that describe the mechanism shown in Figure 1SI. It can be seen that if the target molecule is an inhibitor, the level of concentration of the final product is always the same. If the phenols of interest are substrates, the level of concentration of the product is lower because the target molecules consume oxygen. The simulations of the mechanism shown in Figure 4SI show this behavior (Figure 5SI, inset). From the experimental point of view, to ensure that the observed variation in absorbance was due to the different coefficients of absorptivity of the *o*-quinones from the target compound and not to the interaction of this compound with the *o*-quinones of the TBC or the L-dopa, prior to this assay, the stability of these *o*-quinones was assayed. To test this, TBC or L-dopa substrates were oxidized with sodium periodate in deficiency to generate *o-tert*-butylquinone and dopachrome, respectively. Immediately after, the target phenols were added and the reaction of the *o*-quinones was observed. In cases in which there was not any variation in absorbance with time, the oxygen consumption step could be used to help identify whether the compound under study is an inhibitor or an alternative substrate.

In the reaction of dopachrome or *o-tert*-butylquinone with carvacrol or guaiacol (Figure 10), the variation of absorbance with time was evident. It was therefore not advisable to develop the oxygen consumption assay with these molecules. However, when the arbutin was studied, the absorbance did not change with time (Figure 11), and so, in this case, the test could be run as described in Step 1 (Figure 11, inset). The arbutin was seen to act as an alternative substrate of tyrosinase, because total absorbance decreases as the arbutin concentration increases (Figure 11, inset).

When the experiment described in Step 1 was applied to true inhibitors benzoic acid and cinnamic acid, oxygen consumption followed the typical substrate-dependent stoichiometry (reaching the same absorbance value as in the absence of the inhibitor). The apparent constant decreased when the inhibitor concentration increased, with both L-dopa (Figure 12A and inset) and TBC (data not shown).

Step 2. Deviations of the absorbance, after carrying out the oxidation with sodium periodate, indicated an interaction of the target molecule with the *o*-quinones of TBC and L-dopa, and it would not be possible to carry out the Step 1 correctly. In these cases, we assayed the target phenol with enzyme and hydrogen peroxide. It is known that hydrogen peroxide changes met-tyrosinase, which is not active on monophenols, into oxy-tyrosinase, which is active. When the target phenols in the presence of tyrosinase and hydrogen peroxide were assayed, we observed a variation in absorbance in repeated scans. After testing that this variation was not due to an attack of the hydrogen peroxide on the molecules under study, we could conclude that they are alternative substrates. This Step 2 was applied to isoeugenol and eugenol (Figure 13, recordings a and b, respectively), TBP (Figure 13, inset), arbutin, and carvacrol (Figure 14 recording a and b, respectively) and guaiacol (Figure 14, inset), measuring the increase of absorbance of the generated *o*-quinones. Note how arbutin that fulfilled Step 1 of the test also fulfilled Step 2. These findings confirm that all the studied molecules are tyrosinase substrates.

DOI: 10.1021/jf5051816
J. Agric. Food Chem. 2015, 63, 2162−2171

In conclusion, an experimental design is proposed that allows us to establish whether a phenol of interest is an alternative substrate or inhibitor of tyrosinase. The spectrophotometric method consists of several stages. If the results of the degree of inhibition of the monophenolase and diphenolase activities in the presence of the target molecule are the same, it can be deduced that this compound is an inhibitor. However, if the degrees of inhibition of both activities are different, it is still necessary to undertake Steps 1 and 2 to confirm that the target molecule is really an alternative substrate or a tyrosinase inhibitor. Also, a methodology is proposed to study the effect of inhibitors on the monophenolase activity experimentally by adding the *o*-diphenol necessary to reach the steady state at $t = 0$.

APPENDIX

Analytical Expressions for the Degrees of Inhibition of the Diphenolase and Monophenolase Activities of Tyrosinase

The rate of formation of dopachrome in the action of tyrosinase on *o*-diphenols is

$$V_0^{D(Cr)} = \frac{V_{max}^{D(Cr)}[D]_0}{K_M^D + [D]_0} \quad (1A)$$

In the presence of an inhibitor that binds to the enzymatic forms E_m and E_{ox} (Figure 7), it is

$$V_{0(i)}^{D(Cr)} = \frac{V_{max}^{D(Cr)}[D]_0}{K_M^D\left(1 + \frac{k_6K_{10} + k_2K_9}{k_2K_9K_{10}}[I]_0\right) + [D]_0} \quad (2A)$$

The degree of inhibition is given by

$$i_D = \frac{K_M^D\left(1 + \frac{k_6K_{10} + k_2K_9}{k_2K_9K_{10}}[I]_0\right) - K_M^D}{K_M^D\left(1 + \frac{k_6K_{10} + k_2K_9}{k_2K_9K_{10}}[I]_0\right) + [D]_0}100 \quad (3A)$$

Working at $[D]_0 = K_M^D$ and considering that $k_2 \gg k_6$ gives

$$i_D = \frac{[I]_0}{2K_{10} + [I]_0}100 \quad (4A)$$

A similar equation to eq 4A can be obtained for the monophenolase activity:

$$V_0^{M(Cr)} = \frac{V_{max}^{M(Cr)}[M]_0}{K_M^M + [M]_0} \quad (5A)$$

In the presence of an inhibitor that binds to the enzymatic forms E_m and E_{ox} (Figure 6), the rate of formation of dopachrome is

$$V_{0(i)}^{M(Cr)} = \frac{V_{max}^{M(Cr)}[M]_0}{K_M^M\left(1 + \frac{k_6K_{10} + k_2K_9}{k_2K_9K_{10}}[I]_0\right) + [M]_0} \quad (6A)$$

The degree of inhibition is given by

$$i_M = \frac{K_M^M\left(1 + \frac{k_6K_{10} + k_2K_9}{k_2K_9K_{10}}[I]_0\right) - K_M^M}{K_M^M\left(1 + \frac{k_6K_{10} + k_2K_9}{k_2K_9K_{10}}[I]_0\right) + [M]_0} \quad (7A)$$

Working at $[M]_0 = K_M^M$ and considering that $k_2 \gg k_6$ gives

$$i_M = \frac{[I]_0}{2K_{10} + [I]_0}100 \quad (8A)$$

Thus, eqs 4A and 8A show that, in the presence of the same concentration of inhibitor and the concentration of substrate corresponding to its respective K_M, the degrees of inhibition of the monophenolase and diphenolase activities of tyrosinase are similar.

ASSOCIATED CONTENT

Supporting Information

Kinetic analysis of the proposed mechanisms and simulations of these mechanisms. This material is available free of charge via the Internet at http://pubs.acs.org.

AUTHOR INFORMATION

Corresponding Author

*Telephone: +34 868 884764. Fax: +34 868 883963. E-mail: canovasf@um.es.

Notes

The authors declare no competing financial interest.

ACKNOWLEDGMENTS

This work was partially supported by grants from several Spanish organizations: Projects SAF2013-48375-C2-1-R (MINECO, Madrid), UMU15452 and UMU17766 (University of Murcia, Murcia); V. Ortiz-Ruiz has a MEC-FPU fellowship (AP2010-4300).

ABBREVIATIONS USED

TBC, 4-*tert*-butylcatechol; $[TBC]_0$, initial concentration of 4-*tert*-butylcatechol; TBP, 4-*tert*-butylphenol; MBTH, 3-methyl-2-benzothiazolinone hydrazone hydrochloride; DMF, dimethylformamide; E_m, met-tyrosinase; E_d, deoxy-tyrosinase; E_{ox}, oxy-tyrosinase; E_mD, met-tyrosinase/L-dopa complex; $E_{ox}D$, oxy-tyrosinase/L-dopa complex; E_mM, met-tyrosinase/L-tyrosine complex; $E_{ox}M$, oxy-tyrosinase/L-tyrosine complex; E_mI, met-tyrosinase/inhibitor complex; $E_{ox}I$, oxy-tyrosinase/inhibitor complex; D, L-dopa; $[D]_0$, initial concentration of L-dopa; $[D]_{ss}$, L-dopa concentration in steady state; M, L-tyrosine; $[M]_0$, initial concentration of L-tyrosine; $[M]_{ss}$, L-tyrosine concentration in steady state; Q, *o*-quinone corresponding to L-dopa; [Q], instantaneous concentration of Q; Cr, dopachrome; [Cr], instantaneous concentration of dopachrome; I, inhibitor; $[I]_0$, initial concentration of inhibitor; $V_0^{D(Cr)}$, initial rate of tyrosinase acting on L-dopa (D), calculated by measuring Cr; $V_{max}^{D(Cr)}$, maximum rate of tyrosinase acting on L-dopa calculated by measuring Cr; $V_{0(i)}^{D(Cr)}$, initial rate of tyrosinase acting on L-dopa (D), calculated by measuring Cr in the presence of an inhibitor (I); $V_0^{M(Cr)}$, initial rate of tyrosinase acting on L-tyrosine (M), calculated by measuring Cr; $V_{max}^{M(Cr)}$, maximum rate of tyrosinase acting on L-tyrosine (M), calculating by measuring Cr; $V_{0(i)}^{M(Cr)}$, initial rate of tyrosinase acting on L-tyrosine (M), calculated by measuring Cr, in the presence of an inhibitor (I); i_D, degree of inhibition of the diphenolase activity; i_M, degree of inhibition of the monophenolase activity; *R*, ratio between $[D]_{ss}$ and $[M]_{ss}$, $R = [D]_{ss}/[M]_{ss} \approx [D]_{ss}/[M]_0$; k_i, rate constants; K_M^D, Michaelis constant for (D); K_M^M, Michaelis constant for (M); K_9, dissociation constant of the complex E_mI; K_{10}, dissociation constant of the complex $E_{ox}I$

DOI: 10.1021/jf5051816
J. Agric. Food Chem. 2015, 63, 2162−2171

REFERENCES

(1) Solomon, E. I.; Sundaram, U. M.; Machonkin, T. E. Multicopper oxidases and oxygenases. *Chem. Rev.* **1996**, *96*, 2563−2605.

(2) Sanchez-Ferrer, A.; Rodriguez-Lopez, J. N.; Garcia-Canovas, F.; Garcia-Carmona, F. Tyrosinase: A comprehensive review of its mechanism. *Biochim. Biophys. Acta* **1995**, *1247*, 1−11.

(3) Rodriguez-Lopez, J. N.; Fenoll, L. G.; Peñalver, M. J.; Garcia-Ruiz, P. A.; Varon, R.; Martinez-Ortiz, F.; Garcia-Canovas, F.; Tudela, J. Tyrosinase action on monophenols: Evidence for direct enzymatic release of *o*-diphenol. *Biochim. Biophys. Acta* **2001**, *1548*, 238−256.

(4) Rodriguez-Lopez, J. N.; Tudela, J.; Varon, R.; Garcia-Canovas, F. Kinetic study on the effect of pH on the melanin biosynthesis pathway. *Biochim. Biophys. Acta* **1991**, *1076*, 379−386.

(5) Garcia-Moreno, M.; Rodriguez-Lopez, J. N.; Martinez-Ortiz, F.; Tudela, J.; Varon, R.; Garcia-Canovas, F. Effect of pH on the oxidation pathway of dopamine catalyzed by tyrosinase. *Arch. Biochem. Biophys.* **1991**, *288*, 427−434.

(6) Garcia-Molina, M. M.; Muñoz-Muñoz, J. L.; Berna, J.; Rodriguez-Lopez, J. N.; Varon, R.; Garcia-Canovas, F. Hydrogen peroxide helps in the identification of monophenols as possible substrates of tyrosinase. *Biosci. Biotechnol. Biochem.* **2013**, *77*, 2383−2388.

(7) Garcia-Molina, M. M.; Muñoz-Muñoz, J. L.; Martinez-Ortiz, F.; Martinez, J. R.; Garcia-Ruiz, P. A.; Rodriguez-Lopez, J. N.; Garcia-Canovas, F. Tyrosinase-catalyzed hydroxylation of hydroquinone, a depigmenting agent, to hydroxyhydroquinone: A kinetic study. *Bioorg. Med. Chem.* **2014**, *22*, 3360−3369.

(8) Garcia-Molina, M. M.; Berna, J.; Muñoz-Muñoz, J. L.; Garcia-Ruiz, P. A.; Garcia-Moreno, M.; et al. Action of tyrosinase on hydroquinone in the presence of catalytic amounts of *o*-diphenol. A kinetic study. *React. Kinet., Mech. Catal.* **2014**, *112*, 305−320.

(9) Kashima, Y.; Miyazawa, M. Synthesis, antioxidant capacity, and structure−activity relationships of tri-O-methylnorbergenin analogues on tyrosinase inhibition. *Bioorg. Med. Chem. Lett.* **2013**, *23*, 6580−6584.

(10) Casañola-Martin, G. M.; Marrero-Ponce, Y.; Tareq Hassan Khan, M.; Torrens, F.; Perez-Gimenez, F.; Rescigno, A. Atom- and bond-based 2D TOMOCOMD-CARDD approach and ligand-based virtual screening for the drug discovery of new tyrosinase inhibitors. *J. Biomol. Screen.* **2008**, *13*, 1014−1024.

(11) Casañola-Martin, G. M.; Marrero-Ponce, Y.; Khan, M. T.; Khan, S. B.; Torrens, F.; Perez-Jimenez, F.; Rescigno, A.; Abad, C. Bond-based 2D quadratic fringerprints in QSAR studies: Virtual and in vitro tyrosinase inhibitory activity elucidation. *Chem. Biol. Drug. Des.* **2010**, *76*, 538−545.

(12) Casañola-Martin, G. M.; Le-Thi-Thu, H.; Marrero-Ponce, Y.; Castillo-Garit, J. A.; Torrens, F.; Rescigno, A.; Abad, C.; Khan, M. T. Tyrosinase enzyme: 1. An overview on a pharmacological target. *Curr. Top. Med. Chem.* **2014**, *14*, 1494−1501.

(13) Sun, W.; Wendt, M.; Klebe, G.; Rohm, K. H. On the interpretation of tyrosinase inhibition kinetics. *J. Enzyme Inhib. Med. Chem.* **2014**, *29*, 92−99.

(14) Le-Thi-Thu, H.; Casanola-Martin, G. M.; Marrero-Ponce, Y.; Rescigno, A.; Abad, C.; Khan, M. T. A rational workflow for sequential virtual screening of chemicals libraries on searching for new tyrosinase inhibitors. *Curr. Top. Med. Chem.* **2014**, *14*, 1473−1485.

(15) Rodriguez-Lopez, J. N.; Fenoll, L. G.; Garcia-Ruiz, P. A.; Varon, R.; Tudela, J.; Thorneley, R. N. F.; Garcia-Canovas, F. Stopped-flow and steady-state study of the diphenolase activity of mushroom tyrosinase. *Biochemistry* **2000**, *39*, 10497−10506.

(16) Bradford, M. M. A rapid and sensitive method for the quantitation of microgram quantities of protein utilizing the principle of protein-dye binding. *Anal. Biochem.* **1976**, *72*, 248−254.

(17) Fenoll, L. G.; Rodriguez-Lopez, J. N.; Garcia-Molina, F.; Garcia-Canovas, F.; Tudela, J. Michaelis constants of mushroom tyrosinase with respect to oxygen in the presence of monophenols and diphenols. *Int. J. Biochem. Cell Biol.* **2002**, *34*, 332−336.

(18) Garcia-Molina, F.; Muñoz, J. L.; Varon, R.; Rodriguez-Lopez, J. N.; Garcia-Canovas, F.; Tudela, J. A review on spectrophotometric methods for measuring the monophenolase and diphenolase activities of tyrosinase. *J. Agric. Food Chem.* **2007**, *55*, 9739−9749.

(19) Muñoz, J. L.; Garcia-Molina, F.; Varon, R.; Rodriguez-Lopez, J. N.; Garcia-Canovas, F.; Tudela, J. Calculating molar absorptivities for quinones: Application to the measurement of tyrosinase activity. *Anal. Biochem.* **2006**, *351*, 128−138.

(20) Garcia-Sevilla, F.; Garrido-del Solo, C.; Duggleby, R. G.; Garcia-Canovas, F.; Peyro, R.; Varon, R. Use of a Windows program for simulation of the progress curves of reactants and intermediates involved in enzyme-catalyzed reactions. *Biosystems* **2000**, *54*, 151−164.

(21) Ros, J. R.; Rodriguez-Lopez, J. N.; Garcia-Canovas, F. Tyrosinase: Kinetic analysis of the transient phase and the steady state. *Biochim. Biophys. Acta* **1994**, *1204*, 33−42.

(22) Garcia-Molina, F.; Muñoz, J. L.; Varon, R.; Rodriguez-Lopez, J. N.; Garcia-Canovas, F.; Tudela, J. An approximate analytical solution to the lag period of monophenolase activity of tyrosinase. *Int. J. Biochem. Cell Biol.* **2007**, *39*, 238−252.

(23) Chen, Q. X.; Ke, L. N.; Song, K. K.; Huang, H.; Liu, X. D. Inhibitory effects of hexylresorcinol and dodecylresorcinol on mushroom (*Agaricus bisporus*) tyrosinase. *Protein J.* **2004**, *23*, 135−141.

(24) Huang, X. H.; Chen, Q. X.; You, M. S.; Wang, Q.; Song, K. K.; Wang, J.; Sha, L.; Guan, X. Inhibitory effects of fluorobenzaldehydes on the activity of mushroom tyrosinase. *J. Enzyme Inhib. Med. Chem.* **2006**, *21*, 413−418.

(25) Baek, Y. S.; Ryu, Y. B.; Curtis-Long, M. J.; Ha, T. J.; Rengasamy, R.; Yang, M. S.; Park, K. H. Tyrosinase inhibitory effects of 1,3-diphenylpropanes from *Broussonetia kazinoki*. *Bioorg. Med. Chem.* **2009**, *17*, 35−41.

(26) Jeong, S. H.; Ryu, Y. B.; Curtis-Long, M. J.; Ryu, H. W.; Baek, Y. S.; Kang, J. E.; Lee, W. S.; Park, K. H. Tyrosinase inhibitory polyphenols from roots of morus ihou. *J. Agric. Food Chem.* **2009**, *57*, 1195−1203.

(27) Qiu, L.; Chen, Q. H.; Zhuang, J. X.; Zhong, X.; Zhou, J. J.; Guo, Y. J.; Chen, Q. X. Inhibitory effects of α-cyano-4-hydroxycinnamic acid on the activity of mushroom tyrosinase. *Food Chem.* **2009**, *112*, 609−613.

(28) Zhuang, J. X.; Li, W. G.; Qiu, L.; Zhong, X.; Zhou, J. J.; Chen, Q. X. Inhibitory effects of cefazolin and cefodizime on the activity of mushroom tyrosinase. *J. Enzyme Inhib. Med. Chem.* **2009**, *24*, 251−256.

(29) Lu, Y. H.; Chen, J.; Wei, D. Z.; Wang, Z. T.; Tao, X. Y. Tyrosinase inhibitory effect and inhibitory mechanism of tiliroside from raspberry. *J. Enzyme Inhib. Med. Chem.* **2009**, *24*, 1154−1160.

(30) Conrad, J. S.; Dawso, S. R.; Hubbard, E. R.; Meyers, T. E.; Stronthkamp, K. G. Inhibitor binding to the binuclear active site of tyrosinase: Temperature, pH, and solvent deuterium isotope effects. *Biochemistry* **1994**, *33*, 5739−5744.

(31) Rodriguez-Lopez, J. N.; Tudela, J.; Varon, R.; Garcia-Carmona, F.; Garcia-Canovas, F. Analysis of a kinetic model for melanin biosynthesis pathway. *J. Biol. Chem.* **1992**, *267*, 3801−3810.

(32) Parvez, S.; Kang, M.; Chung, H. S.; Cho, C.; Hong, M. C.; Shin, M. K.; Bae, H. Survey and mechanism of skin depigmenting and lightening agents. *Phytother. Res.* **2006**, *20*, 921−934.

(33) Hu, Z. M.; Zhou, Q.; Lei, T. C.; Ding, S. F.; Xu, S. Z. Effects of hydroquinone and its glucoside derivatives on melanogenesis and antioxidation: Biosafety as skin whitening agents. *J. Dermatol. Sci.* **2009**, *55*, 179−184.

(34) Maeda, K.; Fukuda, M. Arbutin: Mechanism of its depigmenting action in human melanocyte culture. *J. Pharmacol. Exp. Ther.* **1996**, *276*, 765−769.

(35) Hori, I.; Nihei, K.; Kubo, I. Structural criteria for depigmenting mechanism of arbutin. *Phytother. Res.* **2004**, *18*, 475−479.

(36) Satooka, H.; Kubo, I. Effects of thymol on mushroom tyrosinase-catalyzed melanin formation. *J. Agric. Food Chem.* **2011**, *59*, 8908−8914.

(37) Satooka, H.; Kubo, I. Effects of thymol on B16-F10 melanoma cells. *J. Agric. Food Chem.* **2012**, *60*, 2746−2752.

(38) Garcia-Molina, M. M.; Munoz-Munoz, J. L.; Garcia-Molina, F.; Garcia-Ruiz, P. A.; Garcia-Canovas, F. Action of tyrosinase on ortho-

DOI: 10.1021/jf5051816
J. Agric. Food Chem. 2015, 63, 2162−2171

substituted phenols: Possible influence on browning and melanogenesis. *J. Agric. Food Chem.* **2012**, *60*, 6447−6453.

DOI: 10.1021/jf5051816
J. Agric. Food Chem. 2015, 63, 2162−2171

be measured is bound between the capture antibody and the detection antibody.[17] By using a mouse mAb as a capture antibody and a rabbit polyclonal antibody (pAb) as the detected antibody, Chen et al. established a sandwich ELISA for detecting glycinin that showed high specificity for glycinin with a wider working range of 3−200 ng/mL and a limit of detection (LOD) of 1.63 ng/mL.[18]

Recently, as a developed technique based on ELISA method, immunochromatographic lateral flow test strips have been considered because they are inexpensive, rapid, portable, and extremely simple to operate. Immunochromatographic lateral flow test strips in the sandwich format have become a popular diagnostic tool for detecting high-molecular-mass analytes, such as viruses, bacteria, hormones, and parasite antigens.[19] However, these strips are not extensively used for the detection of food allergens, and there are no available lateral flow test strips for detecting glycinin. Therefore, in this study, we generated a pAb and a highly specific mAb against glycinin and developed a novel sandwich format lateral flow assay for the detection of glycinin in powdered milk.

MATERIALS AND METHODS

Materials and Apparatus. The following materials were used in this study: soybean β-conglycinin, agglutinin, trypsin inhibitor, peanut agglutinin (PNA), ovalbumin (OVA), casein, Freund's complete adjuvant (FCA), Freund's incomplete adjuvant (FIA), 3,3,5,5-tetramethylbenzidine (TMB), and mouse monoclonal antibody isotyping reagents, which were purchased from Sigma-Aldrich (St. Louis, MO, U.S.); PEG1500 was purchased from Roche (Mannheim, Germany); ELISA plates (96 wells) and other cell culture plastic wares were obtained from Costar (Cambridge, MA); goat antirabbit and goat antimouse IgG-horseradish peroxidase (HRP) were obtained from Abbkine (Redlands, CA); fetal bovine serum (FBS) was obtained from Hyclone (Logan, UT); Dulbecco's modified Eagle's medium (DMEM) was obtained from BRL-Gibco (Grand Island, NY); RPMI-1640, HAT, and HT medium were purchased from Invitrogen; nitrocellulose membrane, glass fiber, and absorbent pad were purchased from Millipore; and eight-week old female BALB/c mice and New Zealand White rabbits were obtained from the Laboratory Animal Center (Zhengzhou University, China) and were raised according to principles of the Henan Academy of Agricultural Sciences Animal Care and Use Committee. All other reagents and solvents were of analytical grade or higher.

The Model 450 Microplate Reader, electrophoresis cell vertical system, and semidry transfer cell used in this study were obtained from Bio-Rad (Richmond, CA). All water used was produced by a Milli-Q Academic Water Purification System (Millipore, Bedford, MA). The XYZ Biostrip Dispenser, CM 4000 Cutter, and TSR3000 membrane strip reader employed were purchased from Bio-Dot. The Multifuge X1R high-speed refrigerated centrifuge was purchased from Thermo Scientific (Osterode, Germany), and the FreeZone 2.5 Liter Benchtop Freeze-Dry System was purchased from LABCONCO (Kansas City, MO).

Glycinin Purification and Sample Protein Extraction. Soybeans and powdered milk were purchased at local supermarkets in Zhengzhou, China. Soybeans were ground to a fine powder and were passed through a 60 mesh sieve. The soybean powder was then defatted according to the method of Hei et al.[17] Soybean protein was then extracted by making a slurry with a 15-fold volume of water (adjusted to pH 9.0 with 2 N NaOH) under continuous agitation for 1 h, followed by centrifugation at 9000*g* for 30 min; the supernatant was then filtered through a 0.45 μm Millex GP filter (Millipore, Cork, Ireland). In accordance with a previous report,[20] 0.01 M $NaHSO_3$ was added to the soybean protein supernatant, and the pH was adjusted to 6.4 with 2 N HCl. The mixture was kept on ice overnight, and the precipitate was collected by refrigerated centrifugation at 6500*g* for 30 min at 4 °C. Crude extracts of glycinin were purified using Sepharose CL-6B (Sigma-Aldrich, St. Louis, MO), and the purified extracts were kept sealed after freeze-drying. The purity of the glycinin was estimated by high-performance liquid chromatography (HPLC) according to the method of García et al.[12] A Waters HPLC system (Milford, MA) equipped with a 600 Controller, In-Line Degasser AF, 2767 Sample Manager, and 2996 Photodiode Array Detector was used. The mobile phases employed were prepared with 0.1% (v/v) trifluoroacetic acid (TFA) in water (mobile phase A) and 0.1% (v/v) TFA in acetonitrile (ACN) (mobile phase B). Separation was performed with an reversed-phase (RP) perfusion column (POROS R2/H; 100 × 4.6 mm id) packed with cross-linked polystyrenedivinylbenzene beads (20 μm) from Perseptive Biosystems (Framingham, MA). The chromatographic method consisted of a linear binary gradient from 5 to 60% B over 5 min. The flow rate was 5 mL/min, the injection volume was 500 μL, and the detection was performed at 254 nm.

We procured commercially powdered milk without soybean included in the list of ingredients. Powdered milk was used in this study to evaluate glycinin recovery by the strip assay. The powdered milk was adulterated with different amounts of purified glycinin before being subjected to the defatting and protein extraction procedures described previously. The protein supernatants were analyzed either directly or following further dilution as required by the strip test.

Production of mAb against Glycinin. Three 8-week-old BALB/c female mice were immunized with purified glycinin. The first dose consisted of 50 μg of immunogen for subcutaneous injection as an emulsion of phosphate-buffered saline (PBS) and FCA. Three subsequent injections were administered at 3-week intervals with the same dosage of immunogen emulsified in FIA. Antisera samples were collected 4 weeks after the fourth immunization, and the samples were screened for antiglycinin activity by ELISA. The mouse with the highest antiglycinin activity received a fifth injection intraperitoneally. Three days later, the spleen of the injected mouse was removed for hybridoma production.

Hybridomas secreting antiglycinin antibodies were generated by standard methods.[21] Briefly, the spleen of the immunized mouse was removed, and the splenocytes were isolated and fused with NS0 cells using PEG1500. The fused cells were then distributed into 96-well culture plates in which mouse peritoneal macrophages were prepared on the day before fusion and were grown with the selective HAT medium. Ten days after fusion, the supernatants of hybridoma colonies were recovered and screened by indirect ELISA for the secretion of mAb binding to glycinin. Selected clones were subcloned by limiting dilution. Ascites fluids were produced in paraffin-primed BALB/c mice, and the mAb was then purified from the antiserum by ammonium sulfate precipitation. The subclass of the isotypes of the mAb was determined using mouse monoclonal antibody isotyping reagents. The measurement of monoclonal antibody affinity (Ka) was performed according to

DOI: 10.1021/jf5052128
J. Agric. Food Chem. 2015, 63, 2172−2178

the procedure described by Beatty et al.[22] The following formula was used to calculate Ka:

$$Ka = (n - 1)/2(n[Ab']t - [Ab]t)$$

$$n = [Ag]t/[Ag']t$$

where $[Ag]t$ and$[Ag']t$ represent two different concentrations of coating antigen and $[Ab]t$ and $[Ab']t$ represent the corresponding concentrations of mAb.

Indirect ELISA and Competitive Indirect ELISA. The antibody titer was monitored by indirect ELISA. Microplates were coated with 100 μL/well of purified glycinin (10 μg/mL) in 0.05 M carbonate-bicarbonate buffer (pH 9.6) and then were incubated at 37 °C for 2 h. After washing with PBST [PBS containing 0.05% Tween 20 (v/v), pH 7.4], the wells were blocked with 200 μL of 5% skim milk in PBST and then were incubated at 37 °C for 1 h. After another washing step, 100 μL/well of purified glycinin with 2-fold serially diluted antibody in blocking buffer was added and incubated for 15 min at 37 °C. Following the washing step, goat antimouse IgG-HRP conjugate (1:5000 in blocking buffer, 100 μL/well) was added and incubated for 30 min at 37 °C. The plates were washed again, and 100 μL/well of TMB in chromogen buffer was added; color development was terminated after 10 min with 2 mol/L H_2SO_4 (100 μL/well). The optical densities (ODs) were measured at 450 nm with a microplate reader. A competitive indirect ELISA was carried out to screen the antibody for antiglycinin activity. Microplates were coated as described previously, and 100 μL/well of glycinin serially diluted in PBS was then added with 100 μL/well of antibody and was incubated for 15 min at 37 °C. The following procedures were identical to those employed in indirect ELISA.

Sodium Dodecyl Sulfate-Polyacrylamide Gel Electrophoresis (SDS-PAGE) and Western Blot. The purified glycinin and isolated soybean protein were dissolved in PBS and were mixed with SDS sample buffer, and the samples were then loaded onto 5−12% polyacrylamide gradient gels. SDS-PAGE was performed at 90 V until the tracking dye migrated to the bottom edge of the gel. The gel was stained with 0.25% Coomassie Brilliant Blue R250.

The SDS-PAGE gels were transferred onto nitrocellulose membranes for 1.5 h at 15 V. The membranes were blocked with 5% skim milk in PBST at 4 °C overnight, and the membrane was incubated with antiglycinin mAb (1:5000) at room temperature for 1 h. After three PBST washes, the membrane was incubated with secondary antibodies (horseradish peroxidase-conjugated goat antimouse IgG 1:5000) at room temperature for 1 h, and 3-amino-9-ethylcarbozole (AEC) was used as a staining substrate.

Production of pAb against Glycinin. Two New Zealand White rabbits were used to produce pAb. Both rabbits were immunized subcutaneously with 200 μg of purified glycinin. The first subcutaneous injection was composed of an emulsion of PBS and FCA. Three subsequent injections were administered at 3-week intervals with the same dosage of immunogen emulsified in FIA. Four weeks after the fourth immunization, blood samples were collected directly from the heart and were screened for antiglycinin activity by ELISA. The antibody was purified from the antiserum by ammonium sulfate precipitation.

Preparation of Colloidal Gold-Labeled mAb. Colloidal gold with a mean diameter of 15 nm was produced by reduction of gold chloride with 1% sodium citrate (w/v), as described previously.[23] When preparing the colloidal gold-labeled mAb, the colloidal gold solution was adjusted to pH 9.0 with 0.2 mol/L sodium carbonate. The optimum ratio of mAb solution (1 mg/mL) to colloidal gold solution was determined according to a previous report.[24] Approximately 100 μL of mAb solution was added to 10 mL of the colloidal gold solution with constant stirring for 30 min. Then, 1 mL of 0.02 M sodium borate (pH 9.0) containing 10% bovine serum albumin (BSA) was added with stirring for 10 min to stabilize the conjugate. The colloidal gold-labeled antibody was washed three times with wash buffer (0.02 M sodium borate, pH 9.0; 1% BSA; and 0.1% sodium azide) by repeated centrifugation at 25 000*g* and 10 °C for 30 min. The precipitate was resuspended in 1 mL of wash buffer and was stored at 4 °C before use.

Fabrication of the Colloidal Gold Immunoassay Strip. The conjugation pad (7 mm × 300 mm) was prepared by dispensing a desired volume of colloidal gold-labeled mAb onto a glass fiber pad (Millipore) using an XYZ Biostrip Dispenser, followed by drying at 56 °C for 1 h before storage at 4 °C. Sample and absorbent pads were made from nonwoven material (Millipore). The sample pad (15 mm × 300 mm) was saturated with a buffer (pH 8.0) containing 20 mmol/L sodium borate, 2% (w/v) sucrose, 2% (w/v) BSA, and 0.1% (w/v) NaN_3, and the pad was then dried and stored as described previously. The nitrocellulose membrane (20 mm × 300 mm) was spotted using the same dispenser, with the optimal pAb and antimouse IgG antibodies applied in the test and control lines, leaving a 0.5 cm space between the two lines. After drying for 1 h at 40 °C, the membrane was blocked with 2% (w/v) BSA and then was dried, sealed, and stored under dry conditions. The absorbent pad was cut to dimensions of 20 mm × 300 mm. The sample pad, conjugate pad, blotted membrane, and absorption pad were assembled on a plastic backing support board (40 mm × 300 mm) sequentially with a 1−2 mm overlap. The master card was cut into 3 mm wide strips using a CM 4000 Cutter (Bio-Dot Irvine, CA, U.S.). The strips were then sealed in a plastic bag with desiccant gel and were stored at 4 °C.

Test Procedure and Principle. In the detection test, 100 μL of standard solution or sample extract is allowed to react with colloidal gold-labeled mAb. The mixture then moves upward on the nitrocellulose membrane chromatographically via capillary action. For a positive sample, glycinin binds to the mAb, forming a gold/antigen/antibody complex, which binds to pAb and forms a red color band in the test region. Higher amounts of glycinin in the sample result in a stronger test line color. The absence of this band suggests a negative result. To serve as a procedural control, a red band will always appear in the control region regardless of the presence of glycinin.

If both the test and control lines turn red, the sample is recorded as positive, indicating the presence of glycinin. If the control line but not the test line is colored, the sample is considered negative. If only the red test line appears, the strip is considered invalid, and the test should be repeated using a new strip.

Evaluation of the Lateral Flow Assay. The sensitivity of the test strips was determined by testing a series of diluted glycinin standard sample extracts in which various concentrations of purified glycinin, that is, 0, 50, 100, 200, 400, 800, 1600, 3200, 6400, and 12800 ng/mL, were used. Test lines were scanned with a Bio-Dot TSR3000 Membrane Strip Reader (BioDot, CA, U.S.). The assays were performed in triplicate using the test strip. The standard curve was constructed by

DOI: 10.1021/jf5052128
J. Agric. Food Chem. 2015, 63, 2172−2178

plotting the G/D × area (graph density × area) relative optical density (ROD) or G/peak-ROD values obtained from the standard samples against the logarithmic concentrations. The linearity of the analytes was assessed by the coefficient of determination (R^2), and the LOD was calculated from the regression equation.

To identify the specificity of the test strip, the soybean allergens (β-conglycinin, agglutinin, and trypsin inhibitor) and other food allergens (PNA, OVA, and casein) were tested at a concentration of 20 μg/mL.

To determine the accuracy of the test strip, powdered milk samples were spiked with purified glycinin at 3, 9, and 27 mg/kg; 100 g samples were defatted and mixed with 1500 mL water for protein extraction procedures and then were tested by the strip. The optical density of the test line was measured using the test strip reader, and sample values were calculated from the standard curve. Intra-assay precision was estimated using one batch of the test strips for replication analysis. For interassay precision, three batches of the test strips were used to detect the given samples. Precision was expressed as the coefficient of variation (CV, %).

RESULTS

Establishment of Hybridomas. The purity of glycinin was estimated to be 86.5% according to the HPLC analysis, which was sufficient for the immunization experiments. The BALB/c mouse immunized with purified glycinin with the highest titer (1:51 200) was selected for subsequent experiments for monoclonal antibody preparation.

Spleen cells from the mice immunized with glycinin were fused with NS0 myeloma cells, and the resulting hybridomas were selected in HAT medium. One or more growing hybridomas were observed in almost all wells after 7 days. The supernatants from each well were screened for antibodies against glycinin by direct ELISA using microtiter plates coated with glycinin. The cells from the wells showing the strongest response ($OD_{450\ nm}$ > 2.0) were tested again by competitive indirect ELISA for their ability to recognize free glycinin. Six selected hybridomas were screened and further cloned by limiting dilution. After culture and further screening, the most sensitive hybridomas (i.e., 2C3H5) were intraperitoneally injected into mice to produce ascites fluid, and the mAb was purified from the ascites fluid by ammonium sulfate precipitation.

Characterization of Antibody. The pAb from rabbit no. 2 was selected for further study because of its high titer of 1:1.024 × 10^6, which was the highest titer among the pAbs produced. The mAb 2C3H5 titer was 1:5.12 × 10^5, and the affinity constant (Ka) was 4.27 × 10^9 L/mol. The subtype of the mAb was identified as IgG1.

Western blot analysis was conducted to determine the polypeptide chains of glycinin that react with the mAb. Glycinin together with total soybean protein isolate was reacted with mAb 2C3H5. The results showed that there was a single band with a molecular weight of approximately 40 kDa, corresponding to the A3 acid polypeptide chain of glycinin (Figure 1A). The Western blot results indicated that the mAb reacted with the A3 acid polypeptide chain of glycinin specifically without cross-reaction with other polypeptide chains of glycinin or other soybean proteins.

Sensitivity of the Test Strip. The sensitivity of the test strip was determined by testing the series of diluted glycinin standard sample extracts. Test lines were scanned with a Bio-Dot TSR3000 Membrane Strip Reader. The G/D × area-ROD and G/peak-ROD values increased as the glycinin concentration in the samples increased, but they were saturated above 3200 ng/mL (Figure 2 and Table 1).

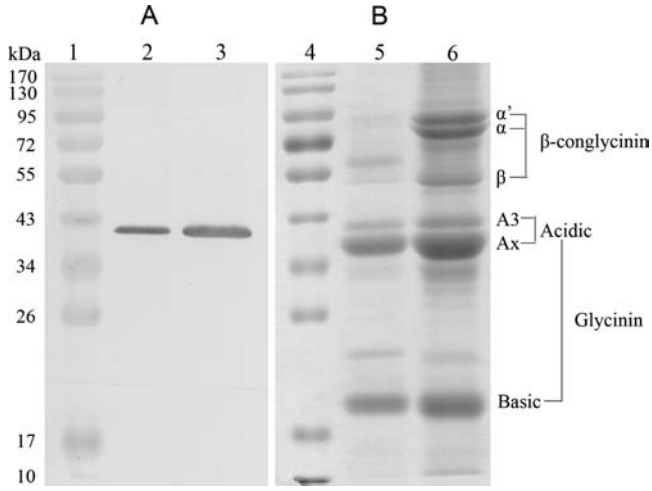

Figure 1. (A) Western blot analysis of mAb 2C3H5 with purified glycinin and soybean protein isolate. Lane 1, prestained protein marker; lane 2, purified glycinin; and lane 3, soybean protein isolate. (B) Protein profile of purified glycinin and isolated soybean protein determined by SDS-PAGE. Lane 4, prestained protein marker; lane 5, purified glycinin; and lane 6, isolated soybean protein. Subunits of β-conglycinin and polypeptide chains of glycinin are shown on the right (Ax indicates A1, A2, and A4).

The G/D × area and G/peak values of the ROD increased as the glycinin concentration in the samples increased. The concentration of standard glycinin and the G/D × area ROD produced a sigmoidal dose−response curve, which showed good linearity over the range of 50−3200 ng/mL. The standard curve was constructed by plotting the G/D × area-ROD percentage obtained from the standard samples against the logarithm concentrations (Figure 3). The LOD with the scanner was quantitatively defined as the amount of glycinin in the standard sample solution that caused a 10% increase in the G/D × area-ROD produced by the 0 ng/mL glycinin sample. Thus, a glycinin concentration of 46.1 ng/mL (equivalent to 0.69 mg/kg) was calculated to be the LOD for the test strip.

Specificity of the Test Strip. OVA, casein, PNA, soybean β-conglycinin, agglutinin, and trypsin inhibitor, each at a concentration of 20 μg/mL, were tested, and the color of the test line was the same as that of the negative control sample. The cross-reactivity results demonstrated that the test strip for glycinin was highly specific and showed negligible cross-reactivity with other food allergens (Figure 4).

Recovery of Glycinin in Powdered Milk Sample. To determine the accuracy of the test strips, powdered milk samples containing 3, 9, and 27 mg/kg of glycinin were tested. The test was performed in triplicate with a single batch of test strips. The optical density of the test line was measured using the test strip reader, and sample values were calculated from the standard curve. For intra-assay reproducibility, the recoveries ranged from 82.3 to 89.9%, with the highest coefficient of variation occurring at 5.29% (Table 2). For interassay reproducibility, three different batches of the test strips were used for triplicate measurements of the samples. Recoveries ranged from 80.5 to 87.7%, with the highest coefficient of variation occurring at 6.72%.

DOI: 10.1021/jf5052128
J. Agric. Food Chem. 2015, 63, 2172−2178

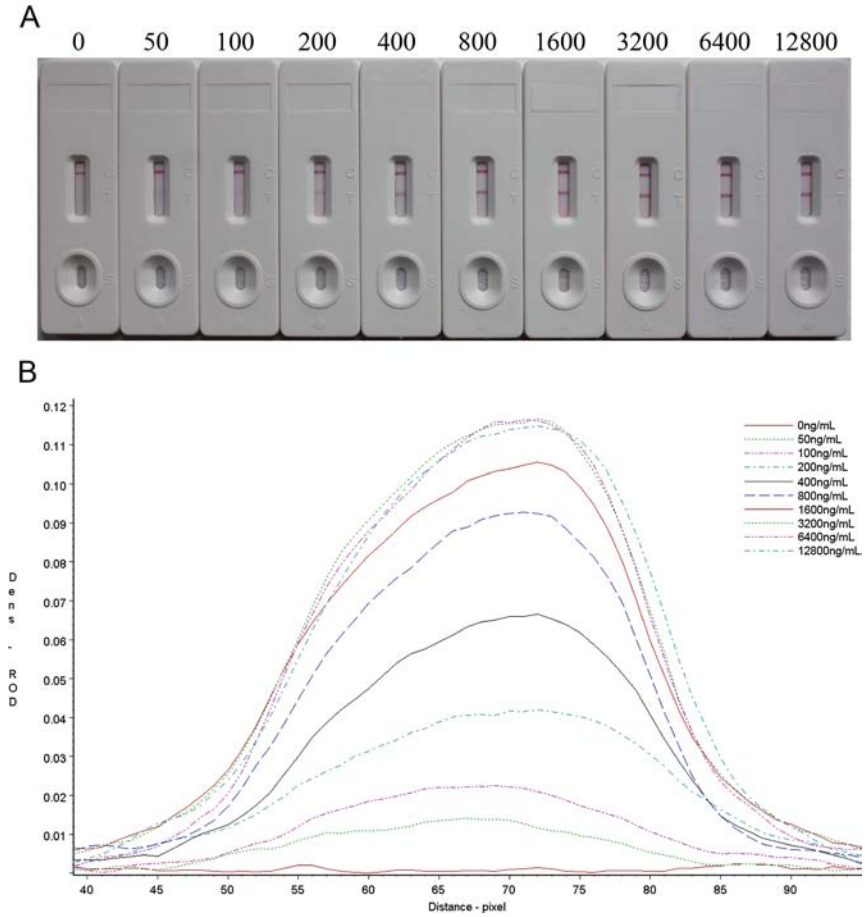

Figure 2. (A) Sample extracts added with glycinin standard solutions were tested using the test strips, and the test lines were identified with the naked eye. (B) Relative optical density (ROD) curves of the sample extracts. The extracts added with glycinin standard solutions at 0, 50, 100, 200, 400, 800, 1600, 3200, 6400, and 12 800 ng/mL were tested using the test strips. Test lines were scanned with a TSR3000 membrane strip reader.

Table 1. G/D × Area and G/Peak of the Relative Optical Density (ROD) of the Test Lines of the Sample Extracts Added with Glycinin Standard Solutions[a]

glycinin concentration (ng/mL)	G/D × area-ROD (pixel)	G/peak-ROD (pixel)
0	2.2518	0.0024
50	19.7731	0.0142
100	38.3656	0.0225
200	68.1175	0.042
400	93.8202	0.0666
800	128.8885	0.0927
1600	153.235	0.1055
3200	169.3604	0.1166
6400	169.0685	0.1163
12800	168.976	0.1147

[a]Sample extracts added to glycinin standard solutions were tested using the test strips, and the test lines were scanned with a TSR3000 Membrane Strip Reader. G/D × area-ROD: mean density value of the sampled line points multiplied by the area of the sampling window on the image. G/peak-ROD: peak value of the ROD points of the scanned line.

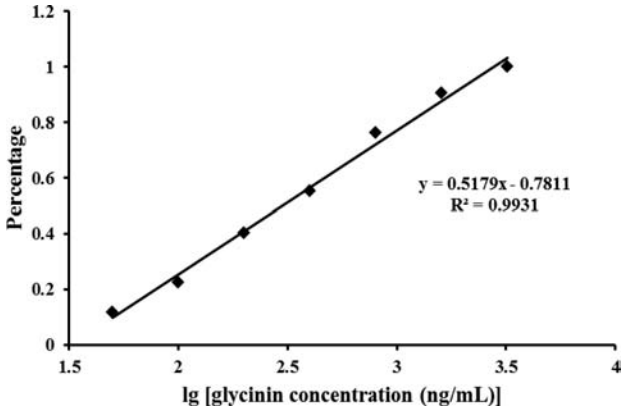

Figure 3. Standard curve for glycinin using test strip detection. The *x*-axis represents the logarithmic concentration. The *y*-axis represents the percentage of G/D × area-ROD of the standards divided by the G/D × area-ROD at saturation (3200 ng/mL). The linear regression correlation coefficient (R^2) is 0.9931.

DISCUSSION

Food allergies have become an important health problem in developed countries, affecting more than 1−2% of the population.[25] Undeclared allergens as contaminants in food products pose a major risk for sensitized persons. These issues are important because they could potentially have grave consequences for consumers and should be addressed by establishing reliable standards and methods for risk assessment.

Soybean allergy is of particular importance because soybeans are widely used in processed foods and therefore represent a particularly insidious source of hidden allergens.[26] To date,

DOI: 10.1021/jf5052128
J. Agric. Food Chem. 2015, 63, 2172−2178

Figure 4. Soybean β-conglycinin, agglutinin, trypsin inhibitor, PNA, OVA, and casein, each at a concentration of 20 μg/mL, were tested by test strip detection.

many ELISA methods have been developed for the detection of allergens using relatively inexpensive equipment and high-throughput screening. However, 2−3 h are required to perform such assays. In contrast, the immunochromatographic lateral flow test strip is a one-step assay that requires less professional personnel for the rapid identification of various analytes.

The key requirement for a successful immunochromatographic lateral flow test is the availability of antibodies with high specificity and the desired affinity.[27] In the present study, the monoclonal antibody prepared by the selected clone, 2C3H5, showed particularly high affinity for glycinin. The isotype of the mAb was identified as IgG1. The mAb 2C3H5 showed no cross-reactivity with other soybean allergens (soybean β-conglycinin, trypsin inhibitor, and agglutinin), resulting in a high specificity for glycinin.

Although some lateral flow assays designed for the determination of food allergens have been reported,[28−30] there has been no scientific report or sufficient validation of a lateral flow assay for detecting glycinin. In the present study, a novel immunochromatographic lateral flow test strip was developed using the sandwich format, which is applicable for target analytes with more than one epitope (high molecular mass analytes).[31] To evaluate the validity and reliability of the lateral flow test strip, sensitivity, specificity, and recovery studies were performed for the determination of glycinin in powdered milk. The results indicated that the lateral flow test strip was sensitive and reliable, and the lateral flow assay showed no reactivity toward other soybean allergens (β-conglycinin, agglutinin, and trypsin inhibitor) or other food allergens (PNA, OVA, and casein).

In conclusion, a high-affinity and specific mAb against glycinin was produced by immunizing mice with purified glycinin. Using the 2C3H5 mAb and rabbit pAb to develop the lateral flow test strip resulted in a highly sensitive test with an LOD of 0.69 mg/kg for glycinin, which is sufficient for the determination of glycinin in powdered milk. In addition, this lateral flow test strip can also be used to detect glycinin in other processed foods (e.g., cheese and sausage) when samples are appropriately extracted. Moreover, this effective method for detecting glycinin may be a valuable tool in identifying effective approaches for reducing the impact of glycinin.

AUTHOR INFORMATION

Corresponding Authors

*Tel: +86-029-87092486; e-mail: lizhixi@nwsuaf.edu.cn.
*Tel: +86-371-65723528; e-mail: huxf1972@126.com.

Funding

This research was supported by the Basic and Cutting-edge Project of Henan Province (132300413222) and the National Key Technology R&D Program of "12th Five-Year Plan" (2014BAD13B05).

Notes

The authors declare no competing financial interest.

REFERENCES

(1) Friedman, M.; Brandon, D. L. Nutritional and health benefits of soy proteins. *J. Agric. Food Chem.* **2001**, *49*, 1069−1086.
(2) Garcia, M. C.; Marina, M. L.; Laborda, F.; Torre, M. Chemical characterization of commercial soybean products. *Food Chem.* **1998**, *62*, 325−331.
(3) Sicherer, S. H.; Sampson, H. A. Food allergy. *J. Allergy Clin. Immunol.* **2010**, *125*, S116−S125.
(4) Savage, J. H.; Kaeding, A. J.; Matsui, E. C.; Wood, R. A. The natural history of soy allergy. *J. Allergy Clin. Immunol.* **2010**, *125*, 683−686.
(5) Wang, T.; Qin, G.; Sun, Z.; Zhao, Y. Advances of research on glycinin and β-conglycinin: a review of two major soybean allergenic proteins. *Crit. Rev. Food Sci.* **2014**, *54*, 850−862.
(6) European parliament and council directive 2007/68/EC of 27 November 2007 amending directive 2000/13/EC as regards certain food ingredients. *Off. J. Eur. Communities*, **2007**; pp L310/11.
(7) Murphy, P. A.; Resurreccion, A. P. Varietal and environmental differences in soybean glycinin and β-conglycinin content. *J. Agric. Food Chem.* **1984**, *32* (4), 911−915.
(8) Sun, P.; Li, D. F.; Li, Z. J.; Dong, B.; Wang, F. L. Effects of glycinin on IgE-mediated increase of mast cell numbers and histamine release in the small intestine. *J. Nutr. Biochem.* **2008**, *19*, 627−633.
(9) Liu, X.; Feng, J.; Xu, Z. R.; Wang, Y. Z.; Liu, J. X. Oral allergy syndrome and anaphylactic reactions in BALB/c mice caused by soybean glycinin and β-conglycinin. *Clin. Exp. Allergy* **2008**, *38*, 350−356.
(10) García, M. C.; Marina, M. L. Rapid detection of the addition of soybean proteins to cheese and other dairy products by reversed-phase perfusion chromatography. *Food Addit. Contam.* **2006**, *23*, 339−347.
(11) Castro, F.; Garcia, M. C.; Rodriguez, R.; Rodriguez, J.; Marina, M. L. Determination of soybean proteins in commercial heat-processed meat products prepared with chicken, beef or complex mixtures of meats from different species. *Food Chem.* **2007**, *100*, 468−476.

Table 2. Recovery and Intra- and Interassay Precision of the Test Strips for Glycinin-Spiked Powdered Milk Samples[a]

	intra-assay			interassay		
spiked glycinin (mg/kg)	mean ± SD (mg/kg)	mean recovery (%)	CV (%)	mean ± SD (mg/kg)	mean recovery (%)	CV (%)
3	2.47 ± 0.13	82.3	5.24	2.42 ± 0.16	80.5	6.72
9	7.59 ± 0.37	84.3	4.85	7.53 ± 0.48	83.6	6.38
27	24.26 ± 1.28	89.9	5.29	23.67 ± 1.55	87.7	6.56

[a]Intra-assay precision was estimated using one batch of the test strips (n = 6). For interassay precision, three batches of the test strips were used to test the samples. The recovery and coefficient of variation (CV, %) were calculated from triplicate assays in all cases.

DOI: 10.1021/jf5052128
J. Agric. Food Chem. 2015, 63, 2172−2178

(12) García, M. C.; Heras, J. M.; Marina, M. L. Simple and rapid characterization of soybean cultivars by perfusion reversed-phase HPLC: application to the estimation of the 11S and 7S globulin contents. *J. Sep. Sci.* **2007**, *30*, 475−482.
(13) Cucu, T.; Jacxsens, L.; De Meulenaer, B. Analysis to support allergen risk management: Which Way To Go? *J. Agric. Food Chem.* **2013**, *61*, 5624−5633.
(14) Brandon, D. L.; Friedman, M. Immunoassays of Soy Proteins. *J. Agric. Food Chem.* **2002**, *50* (22), 6635−6642.
(15) Tukur, H. M.; Lalles, J. P.; Plumb, G. W.; Mills, E. N. C.; Morgan, M. R. A.; Toullec, R. Investigation of the relationship between in vitro ELISA measures of immunoreactive soy globulins and in vivo effects of soy products. *J. Agric. Food Chem.* **1996**, *44* (8), 2155−2161.
(16) Ma, X.; Sun, P.; He, P.; Han, P.; Wang, J.; Qiao, S.; Li, D. Development of monoclonal antibodies and a competitive ELISA detection method for glycinin, an allergen in soybean. *Food Chem.* **2010**, *121*, 546−551.
(17) Hei, W.; Li, Z.; Ma, X.; He, P. Determination of beta-conglycinin in soybean and soybean products using a sandwich enzyme-linked immunosorbent assay. *Anal. Chim. Acta* **2012**, *734*, 62−68.
(18) Chen, J.; Wang, J.; Song, P.; Ma, X. Determination of glycinin in soybean and soybean products using a sandwich enzyme-linked immunosorbent assay. *Food Chem.* **2014**, *162*, 27−33.
(19) Qian, S. Z.; Bau, H. H. A mathematical model of lateral flow bioreactions applied to sandwich assays. *Anal. Biochem.* **2003**, *322*, 89−98.
(20) Nagano, T.; Hirotsuka, M.; Mori, H.; Kohyama, K.; Nishinari, K. Dynamic viscoelastic study on the gelation of 7S globulin from soybeans. *J. Agric. Food Chem.* **1992**, *40*, 941−944.
(21) Köhler, G.; Milstein, C. Continuous cultures of fused cells secreting antibody of predefined specificity. *Nature* **1975**, *256*, 495−497.
(22) Beatty, J. D.; Beatty, B. G.; Vlahos, W. G. Measurement of monoclonal antibody affinity by non-competitive enzyme immunoassay. *J. Immunol. Methods.* **1987**, *100*, 173−179.
(23) Song, C.; Liu, Q.; Zhi, A.; Yang, J.; Zhi, Y.; Li, Q.; Hu, X.; Deng, R.; Casas, J.; Tang, L. Development of a lateral flow colloidal gold immunoassay strip for the rapid detection of olaquindox residues. *J. Agric. Food Chem.* **2011**, *59*, 9319−9326.
(24) Zhang, G.; Wang, X.; Zhi, A.; Bao, Y.; Yang, Y.; Qu, M.; Luo, J.; Li, Q.; Guo, J.; Wang, Z.; Yang, J.; Xing, G.; Chai, S.; Shi, T.; Liu, Q. Development of a lateral flow immunoassay strip for screening of sulfamonomethoxine residues. *Food Addit. Contam.* **2008**, *25*, 413−423.
(25) Chafen, J.; Newberry, S. J.; Riedl, M. A.; Bravata, D. M.; Maglione, M.; Suttorp, M. J.; Sundaram, V.; Paige, N. M.; Towfigh, A.; Hulley, B. J.; Shekelle, P. G. Diagnosing and managing common food allergies: a systematic review. *JAMA, J. Am. Med. Assoc.* **2010**, *303*, 1848−1856.
(26) L'Hocine, L.; Boye, J. I. Allergenicity of soybean: new developments in identification of allergenic proteins, cross-reactivities and hypoallergenization technologies. *Crit. Rev. Food Sci.* **2007**, *47*, 127−143.
(27) Dzantiev, B. B.; Byzova, N. A.; Urusov, A. E.; Zherdev, A. V. Immunochromatographic methods in food analysis. *Trends Anal. Chem.* **2014**, *55*, 81−93.
(28) Koizumi, D.; Shirota, K.; Akita, R.; Oda, H.; Akiyama, H. Development and validation of a lateral flow assay for the detection of crustacean protein in processed foods. *Food Chem.* **2014**, *150*, 348−352.
(29) Richter, M.; Haas-Lauterbach, S.; Schmitt, K. Rapid lateral flow tests in a hazard analysis of critical control points-based approach for allergen monitoring. *Qual. Assur. Saf. Crops Food* **2010**, *2*, 165−172.
(30) Röder, M.; Vieths, S.; Holzhauser, T. Commercial lateral flow devices for rapid detection of peanut (Arachis hypogaea) and hazelnut (Corylus avellana) cross-contamination in the industrial production of cookies. *Anal. Bioanal. Chem.* **2009**, *395*, 103−109.
(31) Zhang, G. P.; Wang, X. N.; Yang, J. F.; Yang, Y. Y.; Xing, G. X.; Li, Q. M.; Zhao, D.; Chai, S. J.; Guo, J. Q. Development of an immunochromatographic lateral flow test strip for detection of β-adrenergic agonist clenbuterol residues. *J. Immunol. Methods* **2006**, *312*, 27−33.

DOI: 10.1021/jf5052128
J. Agric. Food Chem. 2015, 63, 2172−2178

Several studies have been carried out concerning the stability of olive oil under commercial and storage conditions using different types of packaging (see Table 1).[1,9−23] These studies conclude that the glass containers preserve the olive oils better than plastic bottles, because they provide greater protection against photo-oxidation and are impermeable to gases.[1−3] Other authors have concluded that the best container to package EVOO is the metal bottle, followed by the dark glass bottle.[10] From the revised works, only two papers have studied the effect of the Tetra-Brick package as a container to preserve the quality of EVOO.[1,20] Both studies concluded that the better package to preserve the EVOO is Tetra-Brick vs the metal container, at least during the time of study (6 and 9 months). It is important to take into account that these conclusions cannot be applied to any variety of EVOO, since different varieties have different behaviors under the same ambient conditions. As an example, it could be mentioned that Mendez et al.[1] did not show the variety used, while in the work of Samaniego-Sánchez et al.,[20] the variety used to carry out their study was *Picual*.

In this study, the stability of an EVOO from *Arbequina* olives over a long period of time (almost a year) according to container type and storage conditions is evaluated. This research was carried out by studying various quality-related parameters for olive oil.[24] To our knowledge, this is the first rigorous study assessing the stability of EVOO packaged in BB and in the more common package types (metal, glass, and PET) simulating household (Study 1) or supermarket storage of the oil (Study 2). And finally, as a second objective of this investigation, the results obtained with these physico-chemical analyses were for the first time compared with those for selected compounds present in the volatile fraction of EVOO as obtained in a single automatic analysis by headspace gas chromatography−ion mobility spectrometry (HS-GC-IMS).[25,26]

MATERIALS AND METHODS

Samples. Single-variety EVOO from *Arbequina* olives harvested in the 2012−2013 season was supplied by the firm *El Olivo Global* (Córdoba, Spain) and packaged in different types of containers that were all filled to the top in late January 2013 (month 0). The specific containers used were bag-in-box (BB, 5 L), metal bottle (M, 500 mL), dark glass bottle (DG, 500 mL), clear glass bottle (CG, 500 mL), and polyethylene bottle (PET, 500 mL). Notice that the different volume of BB with respect to the other types of containers is because a lower volume of commercial BB was not available. BB containers are usually used for packaging large amounts of olive oil. Although the initial volume of this container is 10 times higher than all others, it does not affect the comparison study, since BB prevents contact with air at all times, even after the package has been opened. A total of 30 different bottles (6 bottles of each one of the 5 types of containers) were filled for this study. All containers were exposed to alternating natural and fluorescent light to simulate supermarket storage conditions and household use of an olive oil package. The intensity of light was not controlled during the preservation of the samples. Also, all samples were stored at room temperature (approximately 23−25 °C) for 8 h each day over a period of 11 months. No temperature control was applied at any time during the rest of the day or at weekends. In addition, some samples were subjected to increased temperatures (above 30 °C) during the seventh month (August). In order to assess the effect of the container headspace and simulate typical domestic use of an olive oil bottle, a bottle of each container type was opened in February 2013 (month 1) and an amount of 50 g of oil withdrawn from each container at 2 month intervals (until December 2013) to create a substantial headspace. Once the sample was extracted of each container, the container was closed again and they were preserved, as mentioned above. This experiment was designated Study 1. Five bottles of each type of container were exposed to the experimental conditions of the study and a bottle of each container type was opened every 2 months and used to assess the stability of the oil on market shelves (Study 2). A schematic representation of the samples analyzed in this work is shown in Figure 1. All samples were filtered by gravity prior to analysis using filters of 85 g m^{-2} weight, 0.2 mm thickness, and 20−25 μm pore size supplied by FilterLab (Barcelona, Spain).

Reagents. The following chemicals were used in the physico-chemical analyses, all in analytical reagent grade except otherwise noted: acetic acid, chloroform, isooctane (spectrometric grade), and ethanol from JT Baker (Deventer, The Netherlands); sodium thiosulfate, potassium iodide, and potassium dichromate from Panreac (Barcelona, Spain); and soluble starch, diethyl ether, potassium hydroxide, and phenolphthalein from Sigma-Aldrich (St. Louis, MO, USA). All working-strength solutions used to assess oil quality were freshly prepared every 2 months.

The volatile compounds monitored, which had been identified by HS-GC-IMS in previous work,[27] were those possessing positive attributes or a rancid taste among those present or formed in EVOO, namely 2-penten-1-ol, hexyl acetate, 2-hexenal, 1-hexanol, 1-penten-3-one, 2-hexen-1-ol, hexanal, 2-heptenal, and 2-pentenal, all of which were purchased from Sigma-Aldrich and used to prepare stock solutions by dissolution in refined olive oil. All stock solutions were stored refrigerated at 4 °C prior to use.

Physico-chemical Analysis. Through EEC Regulation 2568/91[24] and EU Regulation 299/2013,[28] the International Olive Council and the European Community have defined the quality of olive oil in terms of physico-chemical parameters including free fatty acids, peroxide values and UV specific extinction coefficients (K_{232} and K_{270}).[24] These quality indices were evaluated in both oil batches at baseline and then at 2-month intervals. All parameters were determined at least in duplicate.

Direct Analysis of Volatile Compounds. Analyses for volatile compounds were carried out by HS-GC-IMS, using a FlavourSpec instrument from Gesellschaft für Analytische Sensorysteme mbH (G.A.S., Dortmund, Germany). For analysis, 1 g of sample was placed in a 20 mL vial that was then closed with magnetic caps. After 8 min incubation at 60 °C, 200 μL of sample headspace was automatically injected at 100 μL s^{-1} by means of a heated syringe at 80 °C inserted in a headspace autosampler from CTC Analytics (Zwingen, Switzerland) into the heated injector (80 °C) of the device. After injection, the carrier gas (N_2 from Abelló-Linde, Barcelona, Spain) was passed at 5 mL min^{-1} through the injector in order to drive the sample into the gas column, which was kept at 40 °C for timely separation. A 30 m long nonpolar gas chromatographic column from CS-Chromatographie Service GmbH (Dürem, Germany) packed with methyl, phenyl and vinyl silicone in a 94:5:1 proportion was used to separate the analytes. Then, the analytes were eluted in the isothermal mode and driven into the ionization chamber for ionization with a Tritium source (300 mBq < EURATOM allowed value) prior to spectrometric detection. The resulting ions were driven to the drift region via a shutter grid. The drift tube was 5 cm long and operated at a constant voltage of 400 V cm^{-1} and a temperature of 45 °C under a flow of N_2 (Abelló-Linde) at 250 mL min^{-1} as drift gas. Data were acquired in the positive ion mode. Each spectrum was the average of 32 scans obtained by using a grid pulse width of 100 μs, a repetition rate of 21 ms and a sampling frequency of 150 kHz. All samples were analyzed in triplicate. The procedure used to identify the volatile compounds by HS-GC-IMS is described in detail elsewhere.[27]

Data Analysis. Data were viewed and processed by using the software LAV v. 2.0.0 from G.A.S. One-way analysis of variance (ANOVA) using Tukey's test at the 5% significance level ($P \leq 0.05$) for all volatile compounds studied was done by using the software SPSS for Windows version 12.0 (SPSS, Inc., Chicago, USA) to identify variables exhibiting significant differences.

RESULTS AND DISCUSSION

The results obtained with classical analyses to assess the shelf life of EVOO under different storage conditions were compared

DOI: 10.1021/jf505415f
J. Agric. Food Chem. 2015, 63, 2179−2188

Table 1. State-of-the-Art about Studies of Stability of Olive Oil Samples

sample	type of package	storage conditions	storage time	study	conclusions	ref
four commercial samples of EVOO	clear PET bottles, PET bottle covered by A1 foil, glass bottle, tin and Tetra-brick	room temperature	6 mo.	influence of storage time on quality	Gradual loss of quality during storage, especially in plastic and glass bottles. The best containers for commercial packing of EVOO were tin and Tetra-brick.	(1)
EVOO (cv *Koroneiki*)	clear PET, clear PP, and clear glass bottles	22 °C with/without light incidence	12 mo.	effects of all three major packaging properties (oxygen permeability, light transmission rate, headspace volume) and storage temperature on the EVOO quality	The most appropriate material for olive oil packaging was glass, followed by PET and preferably a dark-colored container, stored in the dark, at temperatures less than or equal to 22ºC. Under such conditions the shelf life of extra virgin olive oil is 6 months.	(9)
EVOO (cvs *Picual*, *Hojiblanca*, and *Arbequina*)	0.5 mL dark and transparent glass bottles and tank	with/without headspace at 20 °C	12 mo.	evolution of the quality index of three EVOO varieties stored according to different packaging	The best packaging conditions for EVOO were deposits. *Arbequina* EVOO showed major changes throughout the storage period, while *Picual* EVOO was the most stable, and EVOO stored under nitrogen atmosphere could be packaged in glass bottles without appreciable quality changes.	(10)
EVOO (*Coratina* and *Oligliarola barese)*	clear and green glass bottles in light	light and dark, repeated opening of bottles and samplings	2 yrs	isomerization of 1,2-diacylglicerols to 1,3-diacyl-glycerols as a function of storage conditions	A significant increase in the 1,3-isomers took place during storage time, affected by the type of oil and the time.	(11)
EVOO	300 mL PET bottles	bottle with/ without oxygen scavenger (Amorsorb) in light and darkness at 20-22 °C	13 mo.	assessment the ability of active barrier PET bottles to preserve the quality of EVOO	The presence of a good oxygen scavenger dispersed in the PET bottles is useful to better preserve the original quality of EVOO.	(12)
EVVO (cvs *Bosana* and *Semidana*)	dark glass bottles	darkness at 20 °C with headspace	18 mo.	effect of extraction technology (traditional and with low oxidative stress technology) during storage	Free acidity, peroxide value, and K_{232} and K_{270} increased significantly during storage in both oils.	(13)
commercial Spanish EVOO	not reported	similar to conditions of market	12 mo.	stability of minor components with nutritional, antioxidant, and organoleptic properties	Higher market price is related to better quality and process control, giving a superior final product in terms of its content of minor components related to organoleptic properties.	(14)
seven samples of VOO (*Cornicabra*)	amber glass bottle	darkness at room temperature without headspace	21 mo.	evolution of major and minor components and oxidation indices	Quality indices PV, $K_{232,}$ and K_{270} increased linearly during the storage time studied. K_{232} was the first parameter that exceeded (8 weeks of storage) the established upper limit for EVOO.	(15)
EVOO (cv *Paragon)*	5 L containers	light and darkness at room temperature, and low temperature in the dark, with/ without headspace	12 mo.	how different storage conditions affect oil quality relative to that of fresh oil	EVOO stored at low temperature had characteristics similar to those of fresh olive oil, while oil stored in light conditions showed the largest departure from freshness. In the presence of oxygen, hexanal is a marker of storage in light conditions, free fatty acids in darkness, and acetic acid and pentanal at low temperatures. In the absence of oxygen, octane was the marker for storage in light conditions, whereas tyrosol and hexanol were markers for storage in the dark.	(16)

DOI: 10.1021/jf505415f
J. Agric. Food Chem. 2015, 63, 2179−2188

Table 1. continued

sample	type of package	storage conditions	storage time	study	conclusions	ref
four monovarietal Tunisian VOO (*Chemlali*, *Chétoui*, *El Hor*, and *Oueslati*)	not reported	accelerated oxidation conditions (50°C) in opened and closed bottles	8 mo.	changes in stability and antioxidant activity during long-term storage	A stronger and extended oxidation was observed in opened than in closed bottles throughout the storage period, with PV > 200 mequiv/kg.	(17)
EVOO (cv *Arbequina* and *Picual*)	glass flask	samples in closed flasks, irradiated with UV lamp	12 days	effects of UV radiation on the chemical and sensory characteristic of VOO	An abrupt decrease of the content in fatty acids and total phenols was observed during the irradiation time. Organic volatile compounds related to the rancid sensory attribute increased during the irradiation. *Arbequine* cv oil showed oxidation earlier than the *Picual* cv, which could be explained by the lower content in antioxidant in *Arbequine* against the *Picual*.	(18)
commercial EVOO (cv *Arbequina)*	amber glass bottle	darkness at ambient temperature	12 mo.	changes in lipid substrate in the phenolic fraction	An increase of oleic acid percentage was found in the fatty acid composition. Important losses of chlorophyll, carotenoids, and total phenol, secoiridoid derivatives, and 3,4-DHPEA-AC occur after the storage period. Lignans were the most stable phenolic compounds, and α-tocopheol disappeared after the storage period.	(19)
EVOO (cv *Picual*)	glass, PET, and Tetra-brick	stored at room (20 °C) and refrigerated (4 °C), darkness and no headspace	9 mo.	influence of factors affecting oxidation, such as time, storage temperature and the storage system, and their effect on EVOO quality	Storage of EVOO at low temperature offers a higher possibility for prolonged shelf life, in comparison to higher temperatures. The decrease of quality begins during the first month of storage. Oils placed in Tetra-brick were less altered than those packed in glass and plastic bottles.	(20)
EVOO (cv *Koroneiki*)	0.5 L tin containers	filtered and unfiltered oils, with/without nitrogen in the headspace; indoor conditions, 22 ± 5 °C; outdoor conditions, 0-20 °C (night-day) and 13-38 °C (night-day)	not reported	effects of olive oil storage indoors and outdoors	Increases in K_{232} and K_{270}, peroxides, total phenols and oxidative stability were very much reduced by inert headspace gas. Pattern of volatile compounds detected in olive oils stored indoors or outdoors showed subtle differences (3-pentenol, hexanal, and *trans*-2-hexenal).	(21)
EVOO (cv *Arbequina*)	transparent and amber glass bottles, PET, and tin containers	25 ± 1°C with and without illumination	6 mo.	effects of extraction system (pressure and centrifugation) and storage conditions (packaging material and illumination) on quality indices	Variations due to the extraction system were greater than those due to illumination conditions and package system. Glass and tin packages appear to be the most appropriate containers for maintaining the quality of olive oils, but this supposition is strongly dependent on the type of extraction.	(22)
EVOO (cv *Koroneiki)*	transparent glass and PVC bottle	stored at 28 °C, with different light intensities	10 mo.	effects of processing methods and commercial storage conditions (packing material and light intensities) on EVOO quality indexes	Oil exposed to daylight and artificial light attained maximum PV in the second or third month, while samples stored in darkness attained their maximum PV during the sixth month of storage. The rates of changes of PV, K_{232}, and K_{270} were affected similarly by the type of machinery, packing material, and light intensity. Samples packed in PVC showed higher PV than those packed in glass.	(23)

DOI: 10.1021/jf505415f
J. Agric. Food Chem. 2015, 63, 2179−2188

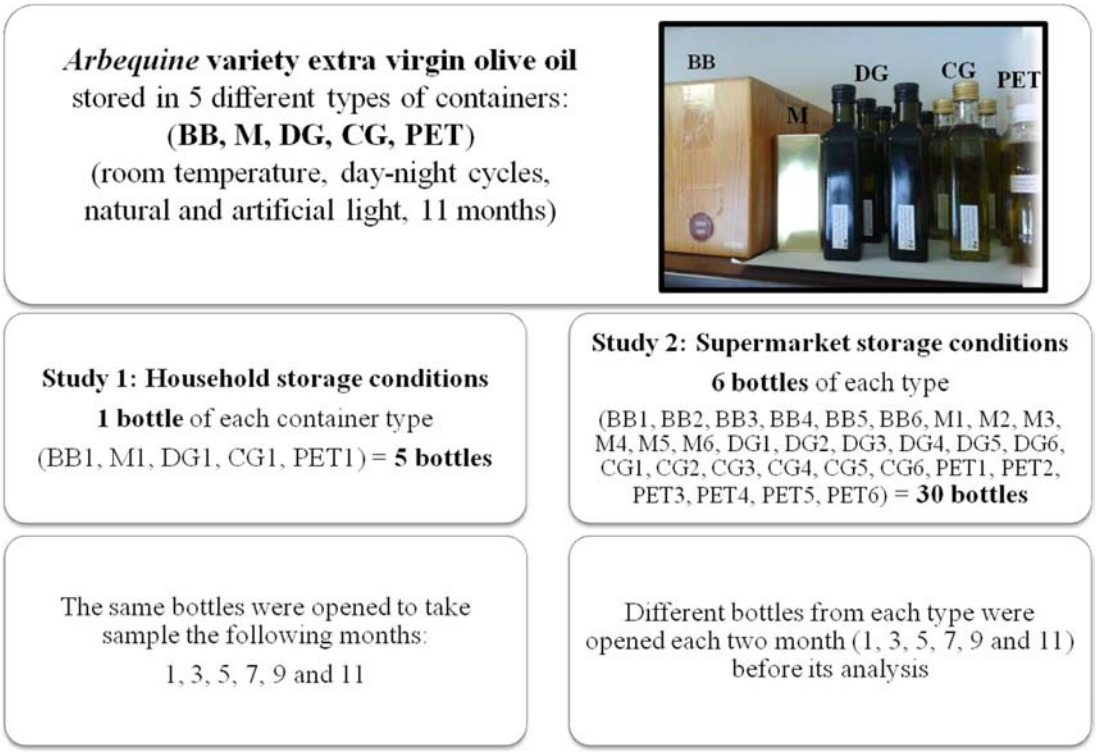

Figure 1. Schematic representation of the samples used in the shelf-life study.

with those obtained by HS-GC-IMS; this instrumental technique was used for the determination of some volatile compounds presented in olive oil samples. To this end, EVOO samples were stored in different types of packages and subjected to variable storage conditions in order to simulate household use (Study 1) and storage on supermarket shelves (Study 2).

Physico-chemical Analysis. Oil samples stored in different container types and conditions were subjected to baseline determinations of quality parameters including free acids, peroxide value and extinction coefficients (K_{232} and K_{270}). An increase in these parameters would indicate oxidation of the oil by effect of some storage condition or inappropriate processing of the oil. The initial values of all quality parameters (month 1) fell below the limits established by EU Regulation 1348/2013 for EVOO.[28] The results are discussed below.

Study 1: Simulation of Household Storage Conditions. Oil quality parameters were determined at 2 month intervals in order to assess the effect of the headspace created during consumption of EVOO samples in different types of containers. Acidity fell below the maximum acceptable levels established by the EEC regulations for EVOO (0.8% oleic acid) in all samples throughout the study. Also, storage for 11 months led to a slight increase in acidity in the five types of containers.

The initial peroxide values for the oils ranged from 10.4 to 15.8 mequiv of O_2/kg and were thus below the acceptable levels set by the EEC regulations (<20 mequiv of O_2/kg). As can be seen from Figure 2A, oxidation of the oil in DG, CG and PET after 5 months of storage was quite marked by effect of its high sensitivity to photo-oxidation; as a result, peroxide values exceeded the regulated limits for EVOO. In the containers where the oil was stored in the complete absence of light (viz., BB and M), the natural pigments in EVOO (chlorophylls) acted synergistically with phenolic antioxidants to inhibit auto-oxidation.[29] It should be borne in mind that when auto-oxidation starts it does not stop until all free radicals formed are inactivated.[30] Only the oil stored in BB retained EVOO grade at the end of the study period. On the other hand, as expected, the oil stored in PET exhibited the highest peroxide value as a result of the container material being the most permeable to oxygen and light,[1] and hence of its facilitating the formation and decomposition of hydroperoxides to volatile compounds responsible for the off-flavor of rancid oil.

The initial values of the coefficients K_{232} and K_{270} fell in the range 1.8−2.0 and 0.12−0.16, respectively, and hence below the legal limits for EVOO. Primary and secondary oxidation increased in the seventh month of storage (August, Figure 2B). Also, K_{232} exhibited a sharp increase in the containers exposed to high room temperatures that month; thereafter, however, K_{232} decreased gradually by effect of degradation into secondary products[23] in all samples except that stored in M. By contrast, K_{270} was not influenced by the high temperatures of August (see Figure 2C). At the end of the study, only the sample stored in BB had a K_{232} value below the acceptable limit for EVOO, and only those stored in BB, M, and DG had a K_{270} value under its limit. K_{270} peaked in the samples stored in transparent bottles.

Overall, the previous results are consistent with those of Pristouri et al.,[9] who found EVOO stored with a 200 mL headspace in clear PET bottles at 22 °C in the dark to lose its grade after 6 months. Based on our results, only the sample stored in BB retained its EVOO grade after 11 months. Therefore, BB was the best container type for storing EVOO under the influence of light and room temperature. Also, all traditional containers of commercial EVOO including glass and plastic bottles, which allow light to pass through, proved unsuitable for storing oil of this grade since, once the container was opened and the oil brought into contact with oxygen, the

DOI: 10.1021/jf505415f
J. Agric. Food Chem. 2015, 63, 2179−2188

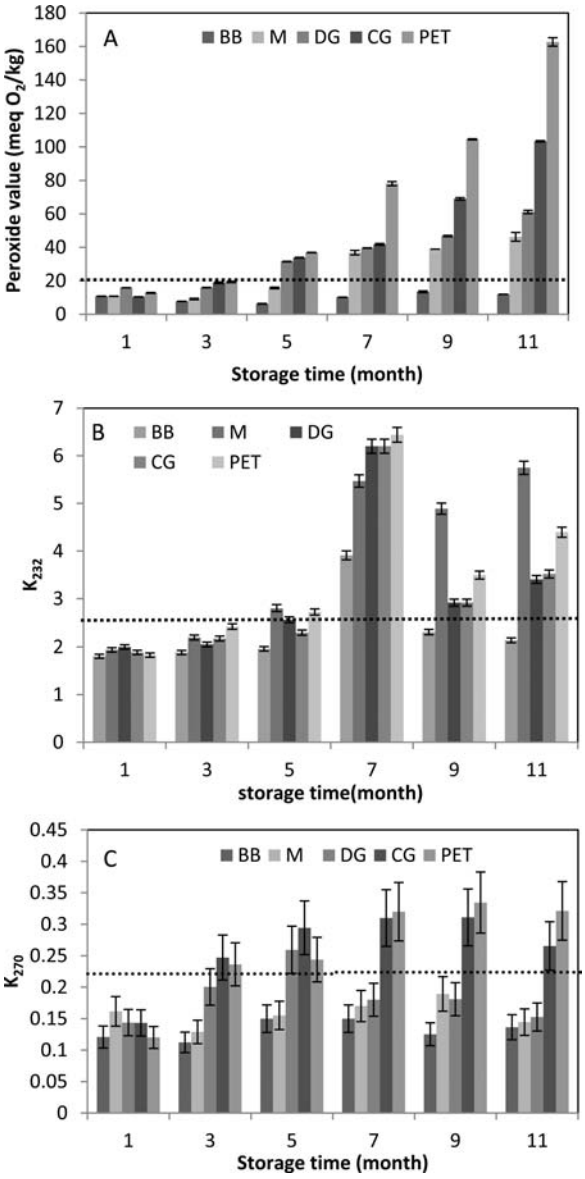

Figure 2. Variation of peroxide value (A), K_{232} (B), and K_{270} (C) in olive oil samples of the *Arbequine* variety held under household storage conditions in various types of containers. The dotted line sets the limit for EVOO grade according to ECC Regulation 2568/91.

oil degraded to an unacceptable extent after only 4 months. The sample stored in M, which is another typical container type for high-quality EVOO, lost its grade after 7 months (see Figure 2).

Study 2: Simulation of Supermarket Storage Conditions. In another experiment, we examined the variation of the target quality indices of EVOO from *Arbequina* olives over an 11-month period of storage in closed bottles under room temperature and light conditions in day/night cycles. The bottles were opened at 2-month intervals to withdraw oil samples for analysis. These conditions were intended to simulate storage of EVOO on a supermarket shelves. As expected, the oxidation rates were lower than those in the samples stored in containers with a headspace (Study 1).

Acidity increased slowly in all samples. The increase was somewhat greater in CG but all samples exhibited very similar values: 0.22−0.25% oleic acid. The peroxide value increased with storage time in all samples except that held in BB; also, only the oil stored in DG exceeded the acceptable limit for EVOO after 11 months—it should be noted, however, that this sample also exhibited the highest baseline peroxide value. The oil sample stored in PET exceeded only the accepted level for EVOO grade in the seventh and ninth months (see Figure 3A), possibly as a result of differences in surface area exposed to light and air between containers.

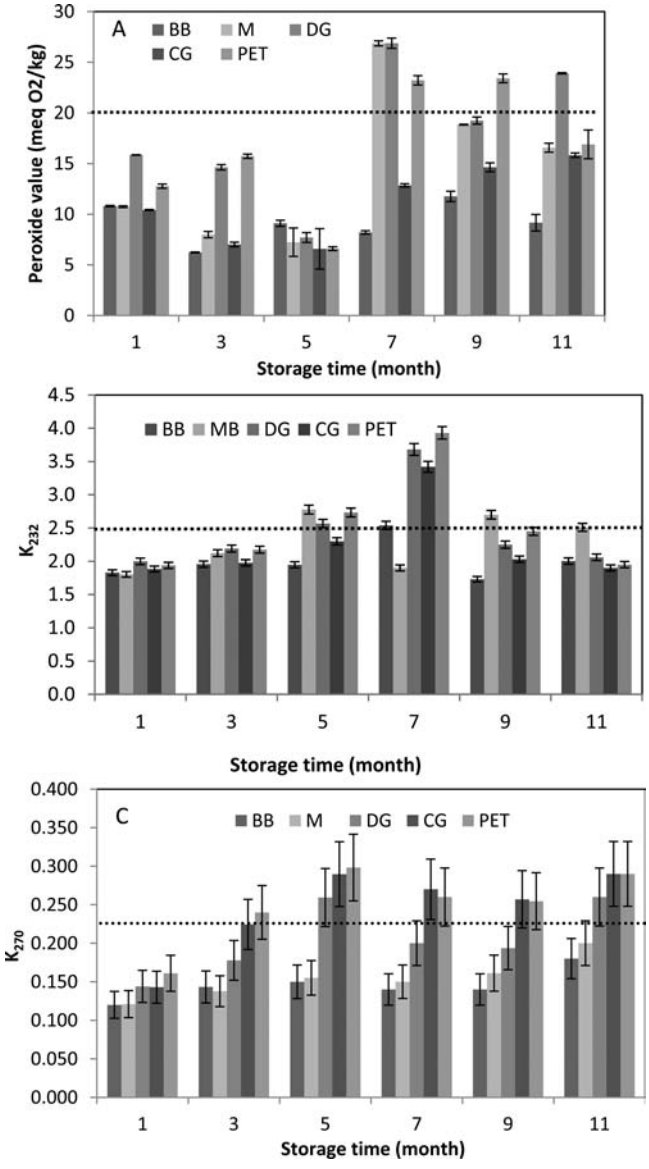

Figure 3. Variation of peroxide value (A), K_{232} (B), and K_{270} (C) in olive oil samples of the *Arbequine* variety held under supermarket storage conditions in various types of containers. The dotted line sets the limit for EVOO grade according to ECC Regulation 2568/91.

None the oil samples exceeded the K_{232} limits for EVOO grade ($\leq$2.5) at the end of the storage period (see Figure 3B). This parameter increased after 7 months but then decreased as in the samples stored with a headspace. These results are consistent with the low peroxide values obtained and hence with little primary oxidation. Also, they suggest that K_{232} was mainly influenced by the high temperatures reached in August owing to the absence of air conditioning in the storage room.

DOI: 10.1021/jf505415f
J. Agric. Food Chem. 2015, 63, 2179−2188

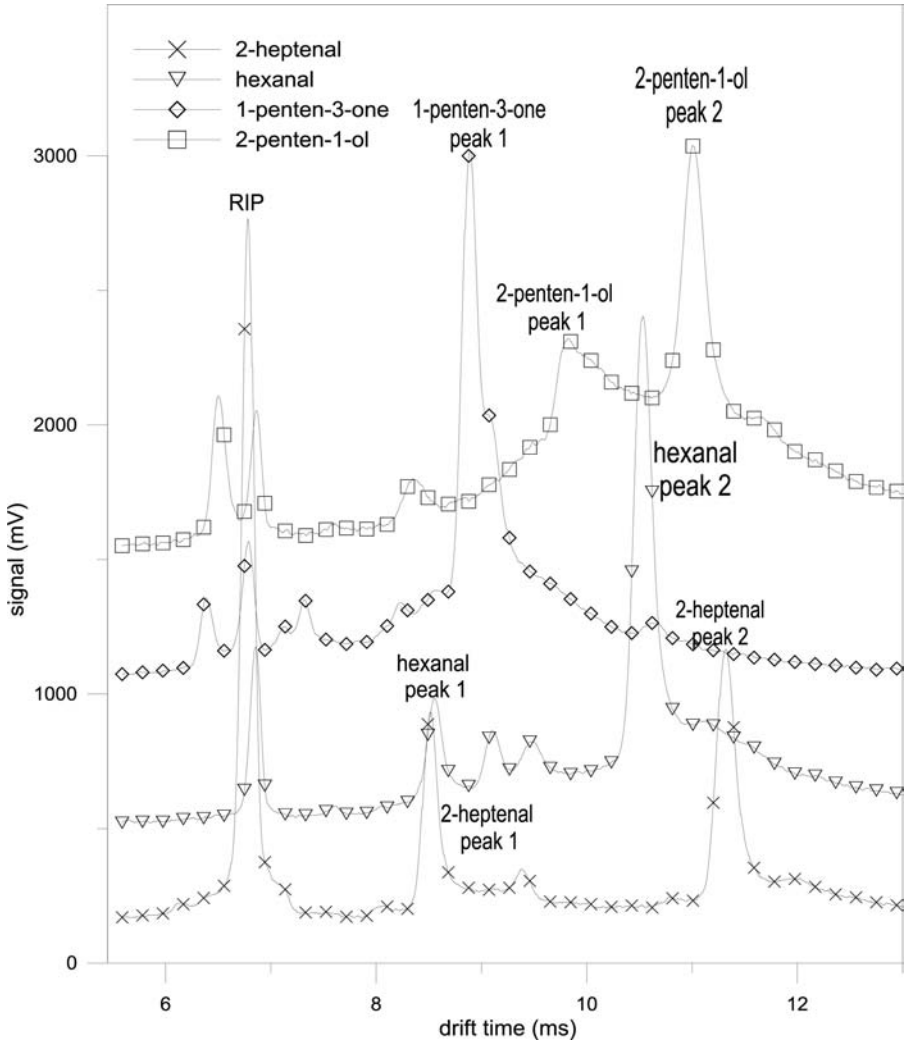

Figure 4. Ion mobility spectra from 2-heptenal, hexanal, 1-penten-3-one, and 2-penten-1-ol.

K_{270} behaved as expected (Figure 3C). Thus, the oil samples stored in CG, DG, and PET had K_{270} values above the accepted limit (0.22)—and suggestive of secondary oxidation—after 5 months that remained high through the end of the study. Consistent with previous results of Gutiérrez and Fernández,[31] K_{270} was the first quality index to exceed the legal limit for EVOO.

Based on the foregoing, the samples stored in BB and M retained EVOO grade for at least 11 months, whereas those held in the other types of containers lost it after only 5 months—as an exception, the DG samples seemingly remained intact for at least 9 months. The abnormal changes in some samples during the study can be ascribed to light and temperature having a different impact depending on the particular container.

Analysis of Volatile Compounds by HS-GC-IMS. HS-GC-IMS was used to determine the volatile fraction of the EVOO in order to evaluate the potential of this technique for assessing the shelf life of the oil. In this work, some major volatiles associated with positive and negative attributes of oil were determined at 1-month intervals in Study 1 and 2-month intervals in Study 2 to identify potential markers correlated with quality-related parameters for olive oil.

The aroma of olive oil has been attributed to aldehydes, alcohols, esters, hydrocarbons, and ketones among other compounds. The major volatiles in virgin olive oil are C6 and C5 compounds[16] that are enzymatically produced from polyunsaturated fatty acids via the so-called "lipoxygenase pathway". The main compounds with positive attributes examined in this study included 2-penten-1-ol, hexyl acetate, 2-hexenal, 1-hexanol, 1-penten-3-one, and 2-hexen-1-ol. Inappropriate storage of oil samples, however, can result in the production of volatiles conferring oil an off-flavor.[32,33] The volatile markers resulting from oxidation of virgin olive oil are mainly aldehydes. This led us to determine 2-pentenal, hexanal, 2-heptenal, and octanal, which are the main rancidity indicators according Solinas et al.[34]

Study 1: Simulation of Household Storage Conditions. As stated above, 5 bottles (one of each type) were opened in month 1 for analysis of the oil by HS-GC-IMS and the oil kept in its closed container for subsequent analysis on a monthly basis thereafter. The analytical results were subjected to ANOVA at the 0.05 significance level in order to identify those volatile compounds with a significant impact. Table S1 in the Supporting Information lists the mean values and standard deviations of the signal intensity for each compound as obtained by HS-GC-IMS. The compounds exhibiting significant differences in the ANOVA test were 2-heptenal, 2-penten-1-ol, hexanal, 1-penten-3-one, octanal, and 2-pentenal. Although 2-hexenal has been proposed as a marker of freshness

DOI: 10.1021/jf505415f
J. Agric. Food Chem. 2015, 63, 2179−2188

in EVOO,[4] the concentration of this compound failed to decrease with storage time in any container type here.

2-Heptenal has a typically rancid odor. This compound is present at increased concentrations in oxidized oil and is thus favored over hexanal or 2-pentenal as a marker for oil oxidation by some authors.[34] The ion mobility spectrum for 2-heptenal (Figure 4) exhibited two peaks, the first peak is known as protonated monomer and the second peak is a dimer ion with characteristics drift times. In some compounds (e.g., 1-penten-3-one), when the vapor concentration of the sample is high, only the dimer peak can be appreciated. As a general rule, it should be noted that the dimer ion is often formed with a decline in the intensity of the peak of the monomer ion and, the monomer peak can disappear from the spectrum or it cannot be distinguished from the background noise. Figure 5A shows the

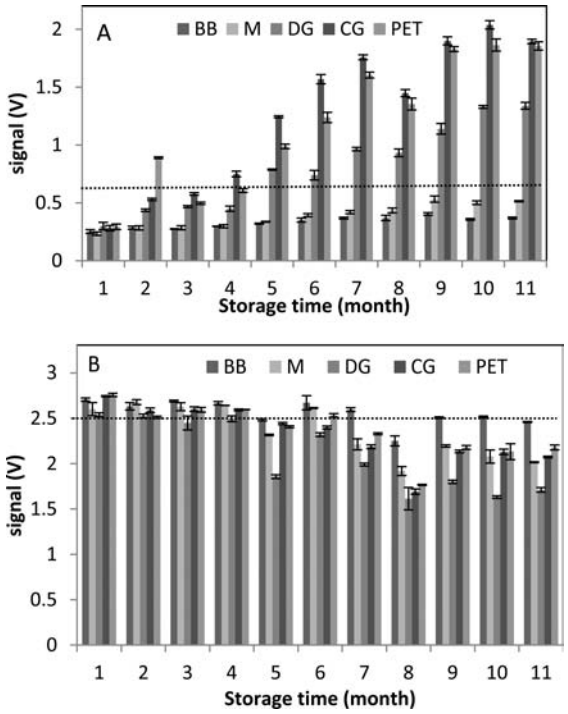

Figure 5. Variation of 2-heptenal (A) and 1-penten-3-one (B) in oils. Samples of the *Arbequine* variety held under household storage conditions in various types of containers.

temporal variation of the overall signal for 2-heptenal (peak 1, monomer ion + peak 2, dimer ion). The signal increased after the second month in the samples packaged in DG, CG, and PET, but particularly in those stored in the containers allowing light to pass through (viz., CG and PET). On the other hand, the signal for the oil stored in BB and M remained constant—as an exception, that for the sample stored in M increased slightly over the last 3 months. Formation of 2-heptenal was not altered by storage in BB because this package prevented contact of the oil with oxygen and also because the air chamber between the bag and the box isolated the oil from high temperatures. Based on the results, the increase in this compound was due to the effect of light mainly. The 2-heptenal concentration and the peroxide value were well correlated; in fact, as stated above, the formation and decomposition of hydroperoxides produces volatile compounds with rancid characteristics.

High-quality olive oil usually contains some hexanal, the concentration of which, however, can be increased by oxidative reactions. Hexanal is a product of the oxidation of linoleic acid occurring throughout the shelf life of olive oil. Like 2-heptenal, hexanal exhibited two IMS peaks (see Figure 4). The signal changed somewhat erratically. Thus, it initially increased for 5 months, and then leveled off for 3 months, and finally decreased through the rest of the study—particularly in PET. The changes in hexanal may be related to its contribution to oil flavor and off-flavor. A similar behavior was observed in 2-penten-1-ol.

1-Penten-3-one, which is present in quality olive oil, is responsible for green and spicy flavours in oil.[4] Figure 5B shows the temporal variation of this compound in EVOO stored in the different types of containers. As can be seen, its signal remained constant until the sixth month (July) in all samples and then decreased in all except that stored in BB. Also, the sample held in DG exhibited a more marked decrease in this compound than those stored in the other containers. The decrease may have resulted from the presence of oxygen in the containers and the high temperatures of month 7 (August).

2-Pentenal and octanal, which are also related to oil rancidity, exhibited significant differences in the ANOVA between samples, but no clear-cut variation in any container type.

The concentration of 2-heptenal was less markedly increased by storage in BB or M than in DG, CG or PET. The 1-penten-3-one content, were only preserved in the BB sample. The results for 2-heptenal (an aldehyde with negative connotations) and 1-penten-3-one (a ketone with favorable sensory attributes) confirm that the two can be used as markers for olive oil quality. A comparison between physico-chemical parameters and the intensity values of 1-penten-3-one and 2-heptenal compounds allowed establishing cutoff values. As peroxide values exceeded the regulated limits for EVOO after 5 months of storage, a cutoff value of 0.6 V for 2-heptenal and one of 2.5 V for 1-penten-3-one were established from the dotted lines of Figures 5A and 5B. Calibration curves for these compounds were run to find which values of concentration correspond to each intensity value corresponding to a concentration of 0.25 mg kg^{-1} for the aldehyde and 0.16 mg kg^{-1} for the ketone. Based on these cutoff values, the samples stored in containers allowing the passage of light lost their EVOO grade after 5 months and that stored in M after 7 months; also, the sample stored in BB retained its EVOO grade throughout. A similar conclusion can be drawn from the results of the physico-chemical analysis.

Study 2: Simulation of Supermarket Storage Conditions. As explained above, an aliquot from the sample stored in each type of container was withdrawn at 2-month intervals for analysis by HS-GC-IMS. The mean values and standard deviations of the IMS signal intensity for the target volatile compounds in each container, and the results of the ANOVA, are listed in Table S1 in the Supporting Information. The ANOVA revealed significant differences in 2-heptenal and 1-penten-3-one (i.e., the same compounds selected as markers from Study 1).

The signal for 2-heptenal (Figure 6A) increased in all containers except BB and M. In fact, all samples except that stored in BB exhibited an increase in this compound from the seventh month (August), probably as a result of the high prevailing temperatures and the little effect of this factor on the BB sample. Subsequently, the content of 2-heptenal decreased in all samples except those stored in CG and PET. The increase

DOI: 10.1021/jf505415f
J. Agric. Food Chem. 2015, 63, 2179−2188

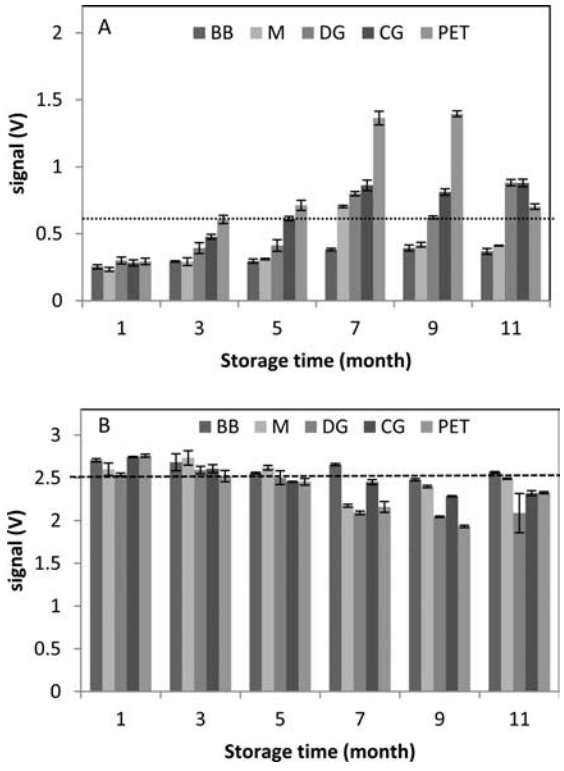

Figure 6. Variation of 2-heptenal (A) and 1-penten-3-one (B) in oils. Samples of the *Arbequine* variety held under supermarket storage conditions in various types of containers.

in 2-heptenal in the samples held in closed containers that were opened only once before analysis (Figure 6A) was less marked than that in the samples held under typical household storage conditions (Figure 5A). Therefore, the increased content of 2-heptenal was probably the main result of oxygen present in the bottles.

1-Penten-3-one (Figure 6B) decreased in all samples, but particularly in those allowing the passage of light: DG, CG, and PET. Also, all samples except those stored in BB and DG exhibited a sharp decline in this compound in the seventh month (August).

In conclusion, if a cutoff value of 0.6 V for 2-heptenal and one of 2.5 V for 1-penten-3-one are established from the dotted lines of Figure 6, panels A and B, then the only samples retaining EVOO grade at the end of the study were those stored in M and BB. On the other hand, the samples stored in completely transparent containers (CG and PET) lost their grade within 5 months, and that stored in DG within 7 months. The results obtained from the analysis of volatile compounds were similar to those of the physico-chemical analysis. Therefore, the HS-GC-IMS results for the studied volatile compounds confirm that 2-heptenal and 1-penten-3-one are two accurate markers of EVOO quality.

Advantages of HS-GC-IMS Method vs Others To Assess the Shelf Life of EVOO. Most existing methods for assessing shelf life in olive oil are classical methods (e.g., physico-chemical methods for determining quality-related parameters). These methods require large amounts of sample and solvents, and long processing times. The shelf life of EVOO has also been assessed by liquid (LC) or gas chromatography (GC). For example, fatty acids and diacylglycerols have been determined by GC with flame ionization detection[10,16] and antioxidants by LC.[25] Usually, these methods require dissolving the sample in an organic solvent or extracting the target compounds by using an effective method.[26]

HS-GC-IMS is also faster than physico-chemical analysis, and it uses less sample amount, does not needs solvents nor reagents, and is more environmentally friendly. The two methods provided similar results here. Thus, only the oil sample held in BB retained EVOO grade for at least 11 months under typical household storage conditions; by contrast, the sample held in M lost the extra grade after 7 months, and those stored in DG, CG, and PET after only 5 months. Among the samples stored under supermarket conditions, those held in BB and M retained their EVOO grade throughout; on the other hand, that stored in DG lost it after 7 months, and the others after 5 months, by effect of exposure to light and ambient temperature.

Based on the results of this study, and on previously reported data, the traditional containers for commercial EVOO (PET and glass) are unsuitable for storage on supermarket shelves. In fact, oil stored in these containers failed to retain its quality throughout its commercial lifetime in the presence of light. By contrast, oil stored in BB retained its EVOO grade throughout. Finally, it is important to mention that the variety used in this work (*Arbequine*) is more unstable than other varieties due to its low content of polyphenols.

■ ASSOCIATED CONTENT

Supporting Information

Additional table with the ANOVA results for significant differences in volatile compounds between container types. This material is available free of charge via the Internet at http://pubs.acs.org.

■ AUTHOR INFORMATION

Corresponding Author

*Phone and fax: +34 957 218616. E-mail: qa1meobj@uco.es.

Funding

This work was funded by DGI, Spanish Ministry of Economy and Competitiveness, within the framework of Project CTQ2011-23790.

Notes

The authors declare no competing financial interest.

■ ACKNOWLEDGMENTS

The authors would like to thank the firm El Olivo Global for kindly supplying the oil samples.

■ ABREVIATIONS USED

EVOO, extra virgin olive oil; HS, headspace; GC, gas chromatography; IMS, ion mobility spectrometry; BB, bag-in-box; M, metal; DG, dark glass; CG, clear glass; PET, polyethylene terephthalate; LC, liquid chromatography; EEC, Economic European Community; EU, European Union

■ REFERENCES

(1) Mendez, A. I.; Falque, A. Effect of storage time and container type on the quality of extra-virgin olive oil. *Food Chem.* **2007**, *18*, 521–529.

(2) Frankel, E. N. *Flavor chemistry of fats and oils*; AOCS: Champaign, IL, 1985.

DOI: 10.1021/jf505415f
J. Agric. Food Chem. 2015, 63, 2179–2188

(3) Ben-Hassine, K.; Taamalli, A.; Ferchichi, S.; Mlaouah, A.; Romano, E.; Flamini, G.; Lazzez, A.; Grati-Kamoun, N.; Perri, E.; Malouche, D.; Hammani, M. Physicochemical and sensory characteristics of virgin olive oils in relation to cultivar extraction system and storage conditions. *Food Res. Int.* **2013**, *54*, 1915−1925.
(4) Bendini, A.; Cerretani, L.; Salvador, M. D.; Fregapane, G.; Lercker, G. Stability of the sensory quality of VOO during storage: an overview. *It. J. Food Sci.* **2009**, *21*, 389−406.
(5) Kanavouras, A.; Hernandez-Muñoz, P.; Couteliers, F.; Selke, S. Oxidation-derived flavor compounds as quality indicators for packaged olive oil. *J. Am. Oil Chem. Soc.* **2004**, *81*, 251−257.
(6) Kiritsakis, A. K. *Olive Oil: from the Tree to the Table*, 2nd ed.; Food and Nutrition Press Inc.: Trumbull, CT, 1998.
(7) Kiritsakis, A. K.; Kanavouras, A. Chemical analysis, quality control and packaging issues of olive oil. *Eur. J. Lipid Sci. Technol.* **2002**, *104*, 628−638.
(8) Papachristou, C.; Badeka, A.; Chouliara, E.; Kondyli, E.; Koutis, L.; Kontominas, M. G. Evaluation of polyethylene terephthalate as a packaging material for premium quality whole pasteurized milk in Greece. Part II. Storage under fluorescent light. *Eur. Food Res. Technol.* **2006**, *224*, 237−247.
(9) Pristouri, G.; Badeka, A.; Kontominas, M. G. Effeect of packaging material headspace, oxygen and light transmission, temperature and storage time on quality characteristics of extra virgin olive oil. *Food Control.* **2010**, *21*, 412−418.
(10) Guil-Guerrero, J. L.; Urda-Romacho, J. Quality of extra virgin olive oil affected by several packaging variables. *Grasas Aceites* **2009**, *60*, 125−133.
(11) Caponio, F.; Paradiso, V. M.; Bilancia, M. T.; Summo, C.; Pasqualone, A. Diacylglycerol isomers in extra virgin olive oil: Effect of different storage conditions. *Food Chem.* **2013**, *140*, 772−774.
(12) Cecchi, T.; Passamonti, P.; Cecchi, P. Study of the quality of extra virgin olive oil stored in PET bottles with or without an oxygen scavenger. *Food Chem.* **2010**, *120*, 730−735.
(13) Fadda, C.; Del Caro, A.; Sanguinetti, A. M.; Urgeghe, P. P.; Vacca, V.; Arca, P. P.; Piga, A. Changes during storage of quality parameters and in vitro antioxidant activity of extra virgin monovarietal oils obtained with two extraction technologies. *Food Chem.* **2012**, *134*, 1542−1548.
(14) Fregapane, G.; Gomez-Rico, A.; Inarejos, A. M.; Salvador, M. D. Relevance of minor components stability in commercial olive oil quality during the market period. *Eur. J. Lipid Sci. Technol.* **2013**, *115*, 541−548.
(15) Gómez-Alonso, S.; Mancebo-Campos, V.; Salvador, M. D.; Fregapane, G. Evolution of major and minor components and oxidation indices of virgin olive oil during 21 months storage at room temperature. *Food Chem.* **2007**, *100*, 36−42.
(16) Kalua, C. M.; Bedgood, D. R.; Bishop, A. G.; Prenzler, P. D. Discrimination of storage conditions and freshness in virgin olive oil. *J. Agric. Food Chem.* **2006**, *54*, 7144−7151.
(17) Krichene, D.; Allalout, A.; Mancebo-Campos, V.; Salvador, M. D.; Zarrouk, M.; Fregapane, G. Stability of virgin olive oil and behaviour of its natural antioxidants under medium temperature accelerated storage conditions. *Food Chem.* **2010**, *121*, 171−177.
(18) Luna, G.; Morales, M. T.; Aparicio, R. Changes induced by UV radiation during virgin olive oil storage. *J. Agric. Food Chem.* **2006**, *54*, 4790−4794.
(19) Morelló, J. R.; Motilva, M. J.; Tovar, M. J.; Romero, M. P. Changes in commercial virgin olive oil (cv *Arbequina*) during storage, with special emphasis on the phenolic fraction. *Food Chem.* **2004**, *85*, 357−364.
(20) Samaniego-Sánchez, C.; Oliveras-López, M. J.; Quesada-Granados, J. J.; Villalón-Mir, M.; López-García Serrana, H. Alterations in picual extra virgin olive oils under different storage conditions. *Eur. J. Lipid Sci. Technol.* **2012**, *114*, 194−204.
(21) Stefanoudaki, E.; Willians, M.; Harwood, J. Changes in virgin olive oil characteristics during different storage conditions. *Eur. J. Lipid Sci. Technol.* **2010**, *112*, 906−914.
(22) Torres, M. M.; Maestri, D. M. Chemical composition of *Arbequina* virgin olive oil in relation to extraction and storage conditions. *J. Sci. Food Agric.* **2006**, *86*, 2311−2317.
(23) Veriaki, S.; Papadopoullou, P.; Kiritsakis, A. K. Effect of processing and commercial storage conditions on the extra virgin olive oil quality indexes. *Grasas Aceites* **2007**, *58*, 237−242.
(24) European Community. Commision Regulation No. 2568/91 on the characteristics of olive oil and olive residue oil and on the relevant methods of analysis. *Off. J. Eur. Commun.* **1991**, *L248*, 1−83.
(25) Garrido-Delgado, R.; Arce, L.; Valcárcel, M. Multicapillary column-ion mobility spectrometry: a potential screening system to differentiate virgin olive oils. *Anal. Bioanal. Chem.* **2012**, *402*, 489−498.
(26) Garrido-Delgado, R.; Mercader-Trejo, F.; Sielemann, S.; Bruyn, W.; Arce, L.; Valcárcel, M. Direct classification of olive oils by using two types of ion mobility spectrometers. *Anal. Chim. Acta* **2011**, *696*, 108−115.
(27) Garrido-Delgado, R.; Prieto-Dobao, M. M.; Arce, L.; Valcárcel, M. Determination of volatile compounds by GC-IMS to assign the quality of virgin olive oil. *Food Chem.* **2015**, submitted.
(28) European Community. Commission Implementing Regulation (EU) No. 1348/2013 of 16 December 2013 amending Regulation (EEC) No. 2568/91 on the characteristics of olive oil and olive-residue oil and on the relevant methods of analysis. *Off. J. Eur. Commun.* **2013**, *L90*, 31−67.
(29) Morales, M. T.; Przybylski, R. *Handbook of olive oil*, 2nd ed.; Springer: New York, 2013; Chapter 13.
(30) Kiritsakis, A. K. *El aceite de oliva*; Madrid Vicente Ediciones: Madrid, Spain, 1992.
(31) Gutiérrez, F.; Fernández, J. L. Determinant parameters and components in the storage of virgin olive oil. Prediction of storage time beyond which the oil is no longer of "extra" quality. *J. Agric. Food Chem.* **2002**, *50*, 571−577.
(32) Kiritsakis, A. K. Flavor components of olive oil—A review. *J. Am. Oil Chem. Soc.* **1998**, *75*, 673−681.
(33) Koprivnjak, O.; Procida, G.; Zelinotti, T. Changes in the volatile components of virgin olive oil during fruit storage in aqueous media. *Food Chem.* **2000**, *70*, 377−384.
(34) Solinas, M.; Marsilio, V.; Angerosa, F. Research of some flavour components of virgin olive oil in relation to olive varieties. *Riv. Ital. Sost. Grasse* **1987**, *64*, 475.

DOI: 10.1021/jf505415f
J. Agric. Food Chem. 2015, 63, 2179−2188

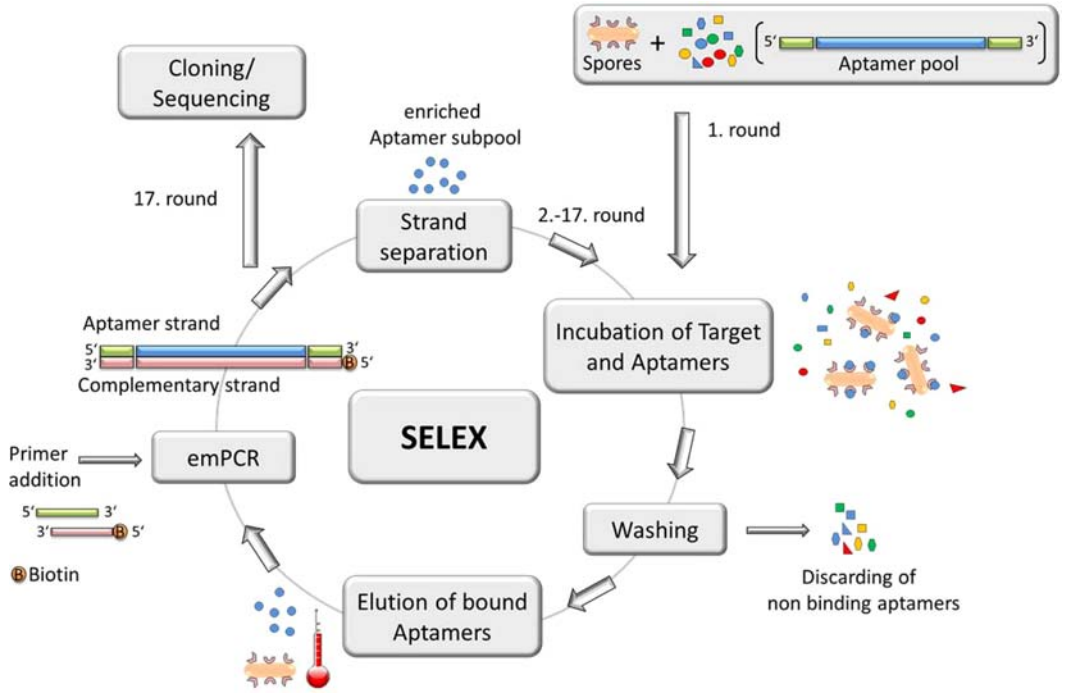

Figure 1. Schematic illustration of DNA aptamer selection for *Alicyclobacillus* spores by spore-SELEX in orange-juice-simulating buffer.

SELEX), and *Just-in-Time*-Selection (semiautomated two-step SELEX), but the field is still a part of current research, and further developments could be expected.[12,23,24]

Although aptamer amplification is established, common problems are (i) a preference for short DNA fragments during amplification and (ii) highly diverse aptamer pools which lead to undefined products by recombination of homologous template regions and formation of heteroduplexes.[25,26] Utilization of emulsion PCR (emPCR) provides significantly improved results, which are achieved by generating several different reaction compartments and a statistically ideal distribution of reaction compounds and templates.[27] To isolate single-stranded aptamers, the double-stranded nucleic acids have to be separated by utilization of a biotinylated reverse primer and streptavidin-coated magnetic beads.

In the present study, aptamers with an affinity to *Alicyclobacillus* spp. spores are selected in orange-juice-simulating buffer. The resulting aptamers are then used for selective trapping and enrichment of spores from orange juice, to supersede the classical time-consuming cultivation process. Hence, the aptamer-based trapping technique (e.g., magnetic separation) will help to accelerate the detection of these spores. The SELEX was verified by various techniques, including fluorescence-activated cell sorting (FACS), radioactive binding assays, and agarose gel electrophoresis (AGE). Aptamer characterization, including determination of dissociation constants (K_D values) and selectivity are performed by surface plasmon resonance (SPR) spectroscopy as well as fluorometric binding assay, flow cytometric binding assay, and fluorescence microscopy to validate the obtained results.

MATERIALS AND METHODS

Aptamer Selection. *Bacterial Strains.* For the spore-SELEX, *A. acidoterrestris* spores (DSM 2498, 10^8 cfu/mL; wild type, 10^8 cfu/mL) were received like all other spores from Lehrstuhl für Hygiene und Technologie der Milch, Tierärtzliche Fakultät, Ludwig-Maximilians-Universität (Munich, Germany), in paraformaldehyde (2%) and used as follows as SELEX targets: 1/1 v/v, final concentration 10^7 cfu/mL. The vegetative *Alicyclobacillus* cells used for counter selection during the first four SELEX rounds comprised ∼100 undefined wild *Alicyclobacillus* strains, obtained from Dr. B. Schütze, LADR GmbH (Geesthacht, Germany).

Aptamer Pool. The aptamer pool used for selection round one consists of the following sequence: 5′-CATCCGTCACACCTGCTC-$(N)_{40}$-GGTGTTGGCTCCCGTATC-3′ (Life Technologies GmbH, Darmstadt, Germany).

Aptamer Amplification and AGE. The emPCR was performed using the commercially available Micellula short DNA emulsion and purification kit (Roboklon GmbH, Berlin, Germany). The amplifications were carried out using biotinylated reverse primer for subsequent strand separation with the following sequences: 5′-CATCCGTC-ACACCTGCTC-3′ (forward primer, Life Technologies GmbH) and 5′-biotin-GATACGGGAGCCAACACC-3′ (reverse primer, Life Technologies GmbH). Aptamer amplification was carried out with 100 μL of aqueous phase in a 2 mL reaction tube as follows: 5 μL of DreamTaq-Polymerase (0.5 U/μL, Fisher Scientific GmbH, Schwerte, Germany), 10 μL of 10× DreamTaq buffer (Fisher Scientific GmbH), 8 μL of dNTPs (10 mM, Bioline GmbH, Luckenwalde, Germany), and 4 μL of each primer (100 μM, Life Technologies GmbH, Carlsbad, CA), and template was varied between 20 and 50 ng. After the aqueous phase was assembled, the oil-phase compounds were added to the reaction tube according to the manufacturer's protocol and mixed for 5 min at room temperature to create a homogeneous emulsion. Due to the volume of the reaction mixture, splitting into aliquots was necessary to perform a PCR under the following conditions: an initial denaturation step at 95 °C for 5 min, and subsequently 25 cycles of denaturation at 95 °C for 30 s, primer annealing at 56 °C for 30 s, and elongation at 72 °C for 30 s. Thereafter, a final elongation step at 72 °C for 5 min and finally a storage temperature of 4 °C followed. Afterward, the emulsion was broken according to the manufacturer's protocol, the oil phase was discarded, and the obtained emPCR products were purified using silica columns according to the protocol provided by the manufacturer. The emPCR products were analyzed by AGE.

Strand Separation. After the aptamer amplification, a strand separation step is mandatory to obtain again single-stranded DNA aptamers (subpool) for further selection rounds. Magnetic beads

DOI: 10.1021/jf505996m
J. Agric. Food Chem. 2015, 63, 2189−2197

(Dynabeads M-280 Streptavidin, Invitrogen Life Technologies GmbH, Carlsbad, CA) were incubated for 15 min under agitation with biotinylated emPCR products and the same volume of 2× binding-and-washing buffer (1 mM EDTA, 2 M NaCl, 10 mM Tris-HCl, pH 7.5). The supernatant was removed using a magnetic rack, and the beads were resuspended in 80 μL of ddH_2O before the tube was incubated 10 min at 95 °C for heat denaturation of double-stranded emPCR products. The heated supernatant was immediately centrifuged for 10 s at 10500*g*, and the tube was placed in a magnetic rack to agglomerate the magnetic beads at the bottom. The still-hot supernatant contained the desired aptamers, ready to be transferred into a new reaction tube.

General SELEX Protocol. To obtain aptamers with an affinity to *Alicyclobacillus* spores, the following SELEX protocol was used: 1 nmol of the corresponding aptamer pool (100 μM) was heated (5 min, 95 °C) in an orange-juice-simulating buffer (2 μM $CaCl_2$, 50 mM KCl, 2 μM $MgCl_2$, 40 mM Tris, pH 3.5), followed by immediately cooling (4 °C) to refold the aptamers and eliminate heteroduplexes. Afterward, a 20 μL aliquot of vegetative cells of *Alicyclobacillus* was added for counter selection. The mixture was incubated for 60 min at room temperature, followed by centrifugation (12 min at 10500*g*). The supernatant was refolded as described above and incubated for 60 min at room temperature with 20 μL of the SELEX target. Subsequently, the reaction mixture was centrifuged (12 min at 10500*g*), and the supernatant was removed. The resulting spore pellet was washed several times with 200 μL of 1× binding-and-washing buffer, centrifuged (12 min at 10500*g*), and resuspended in 35 μL of ddH_2O (Table 1). The obtained aptamer pool was heat eluted (5 min at 96 °C), and the hot supernatant was transferred to a new reaction tube. The obtained aptamers were amplified by emPCR followed by strand separation. For further SELEX rounds, 40 μL aliquots of each strand-separated aptamer pool (corresponding subpools) were used. A continuously rising stringency was achieved during the SELEX process by constantly increasing washing steps, decreasing target concentration and incubation times (Table 1). After 17 selection rounds, the final aptamer subpool was used for cloning and sequencing.

Table 1. Summary of SELEX Conditions To Increase Stringency during Selection Rounds

SELEX round	volume of spore mix (μL)	incubation time (min)	washing steps
1−4	20	60	1
5, 6	20	40	1
7	20	35	1
8	20	30	2
9	20	25	2
10	20	20	2
11	15	15	2
12, 13	15	15	3
14, 15	10	15	3
16, 17	10	10	3

Aptamer Cloning. The final aptamer subpool was ligated using a TOPO TA Cloning Kit (Life Technologies GmbH) and cloned into competent *Escherichia coli* cells XL1. Plasmid DNA was obtained and purified using the QIAprep Spin Miniprep Kit (Qiagen GmbH, Hilden, Germany). Ten aptamer candidates were sequenced by using the M13 universal primer (GATC-Biotech AG, Konstanz, Germany) (Table 2).

Determination of Aptamer Dissociation Constants (K_D) via SPR. *Spore Lysis.* Before immobilization of the target, the spores were fragmented using a TissueLyser (Qiagen GmbH). First, 40 μL of *Alicyclobacillus* spores (10^7 cfu/mL) and 250 mg of glass beads (0.5 mm diameter, Sigma-Aldrich-Chemie, Munich, Germany) were diluted with 360 μL of sodium acetate buffer (pH 5.0, Sierra Sensors GmbH, Hamburg, Germany), and the mixture was lysed twice (5 min, 30 Hz) at room temperature.

Sensor Chip Preparation. The resulting supernatant included the fragmented spores (10^6 cfu/mL) and was directly used for following immobilization and measurements using the SPR2 (Sierra Sensors GmbH). The HPA sensor chips (SPR-AS-HP, Sierra Sensors GmbH) are characterized by aliphatic hydrocarbon chains on the surface, and therefore highly hydrophobic interactions occur.[28,29] All SPR experiments were carried out at 25 °C with a flow rate of 25 μL/min using degassed orange-juice-simulating buffer containing 0.01% Tween 20. The HPA sensor chip was activated for 4 min by injecting a mixture (1/1 v/v) of isopropyl alcohol and sodium hydroxide (50 mM) on both channels. The chip was washed for 4 min by injecting the orange-juice-simulating buffer, and then the fragmented spores were injected for 8 min on channel 2. As a reference and to inhibit nonspecific interactions of injected aptamers with the chip surface, bovine serum albumin (BSA, 50 μg/mL, New England Biolabs GmbH, Frankfurt am Main, Germany) was immobilized by an injection for 8 min on both channels.

SPR Measurements. The K_D determinations were performed in orange-juice-simulating buffer as running buffer by injecting four different concentrations of pure aptamers (2.5, 5.0, 7.5, and 10.0 μM) for 6 min (Life Technologies GmbH). The obtained data were evaluated using AnalyserR2 (Sierra Sensors GmbH) and Scrubber (BioLogic Software Pty Ltd., Campbell, Australia) after subtraction of the reference signal from target signal. The sensor chip was regenerated by injecting regeneration buffer (100 mM hydrochloric acid) for 30 s after each aptamer injection. In addition, the orange-juice-simulating buffer was injected and used besides the BSA reference for a double-referenced calculation of dissociation constants.

Fluorescence Microscopy. To visualize the interactions between the spores and the aptamers, fluorescence microscopy was utilized. The visualization was carried out using a Cor2 fluorescence correlation spectroscope (Carl Zeiss AG, Oberkochen, Germany). Prior to the measurements, the aptamers were fluorescently labeled with Alexa488 by emPCR and strand separation using fluorescently labeled forward primer (5′-Alexa488-CATCCGTCACACCTGCTC-3′, Life Technologies GmbH) and biotinylated reverse primer. Subsequently, the aptamer concentration was determined using a Nanodrop ND-1000

Table 2. Sequences and SPR Estimated Dissociation Constants of Aptamers for *Alicyclobacillus* Spores

aptamer	aptamer sequence (5′−3′)	K_D (nM)
AliApt1	CATCCGTCACACCTGCTCCATCCGTCACACCTGCTCACGTCATCCGTCACACCTGCTCGGTGTTCGGTCCCGTATC	11.3
AliApt2	CATCCGTCACACCTGCTCCCATACCAGCCCCTGGTGTTGGCTCCCCGTATCACCGCTCGGTGTTCGGTCCCGTATC	32.8
AliApt3	CATCCGTCACACCTGCTCCAGCGTGCGTCGACCCCGGACCCTGTCAGCCCCCCTCGCGGGTGTTCGGTCCCGTATC	2.7
AliApt4	CATCCGTCACACCTGCTCCACCCGTCACACTGGTGTTGGCTCCCGTATCACCCGACTCGGTGTTCGGTCCCGTATC	37.6
AliApt5	CATCCGTCACACCTGCTCCCAGCGTGGCGTCGACCCGGACCCTGTCAGCCCCCTCGCGGGTGTTCGGTCCCGTATC	2.3
AliApt6	CATCCGTCACACCTGCTCCATCCGTCACACCTGCTCCCAGACCTGTCCTGCTCCCCTTGGTGTTCGGTCCCGTATC	33.0
AliApt7	CATCCGTCACACCTGCTCCCCACAACCGGTCCGGTGTTCGGTCCCCGTATCACGCCTCGGTGTTCGGTCCCGTATC	149.1
AliApt8	CATCCGTCACACCTGCTCCCCCCTGGTGCATGGGTGTTCGGTCCCGTATCACGCCTCGGTGTTCGGTCCCGTATC	34.4
AliApt9	CATCCGTCACACCTGCTCCACCCGTCACACCCATCCGTCACACCTGCTCCCCCCACTGGGTGTTCGGTCCCGTATC	16.0
AliApt10	CATCCGTCACACCTGCTCCCGTATCACCCCTCATCCGTCACACCCTGCTCCTACTGCGGGTGTTCGGTCCCGTATC	101.8

DOI: 10.1021/jf505996m
J. Agric. Food Chem. 2015, 63, 2189−2197

spectrometer (Thermo Fisher Scientific Oy, Vantaa, Finland) and set to 5 ng/μL. To 190 μL of orange-juice-simulating buffer was added 30 μL of a labeled mix of all obtained aptamers, and this was then incubated with 30 μL of *Alicyclobacillus* spores (10^7 cfu/mL) for 1 h at room temperature under light exclusion. The mixture was centrifuged (12 min at 10500*g*), and the supernatant was discarded to remove excess aptamers. The resulting spore pellet was washed once with 100 μL of 1× binding-and-washing buffer and centrifuged (12 min at 10500*g*) anew, and the pellet was solved in 100 μL of ddH_2O. The analysis was carried out under the following conditions: argon laser (5 mW) with 25% output and 3% transmission, 40× lens, and wavelength 488 nm, which corresponds to the absorption maximum of the used fluorophore Alexa488.

Determination of Aptamer Selectivity via SPR. The aptamer selectivity was investigated using SPR2 by measuring the affinity of the obtained aptamers to different *Bacillus* spores as well as *Clostridium* spores (Table 3). For the following measurements, high-capacity amine chips (SPR-AS-HCA, Sierra Sensors GmbH) were used.

Table 3. Different *Alicyclobacillus*, *Bacillus*, and *Clostridium* Spores Used for Determination of Aptamer Selectivity via SPR

Alicyclobacillus spores	
A. acidoterrestris (DSM 2498)	*A. acidocaldarius* (DSM 446)
A. acidoterrestris (DSM 3922)	*A. herbarius* (DSM 13609)
A. acidoterrestris (DSM 3929)	*A. acidiphilus* (DSM 14558)
A. acidoterrestris (DSM 3924)	*A. pomorum* (DSM 14955)
A. cycloheptanicus (DSM 4005)	*A. sacchari* (DSM 17974)
A. cycloheptanicus (DSM 4006)	*A. fastidiosus* (DSM 17978)
A. cycloheptanicus (DSM 4007)	34× undefined wild types
Bacillus spores	
B. subtilis (DSM 2109)	*B. weihenstepanensis* (wild type)
B. coagulans (ATCC 7050)	*B. thuringiensis* (ATCC 10792)
B. circulans (ATCC 9966)	*B. thuringiensis* (DSM 6029)
B. sphaericus (ATCC 245)	*B. licheniformis* (DSM 13)
4× *B. cereus* (wild types)	*Paenibacillus polymyxa* (ATCC 10401)
Clostridium spores	
2× *C. perfringens* (wild types)	

Sensor Chip Preparation. The sensor chips were activated for 4 min by injecting a mixture (1/1 v/v) of 100 mM *N*-hydroxysuccinimide (NHS, Sigma-Aldrich-Chemie) and 400 mM 1-ethyl-3-(3-(dimethylamino)propyl)carbodiimide (EDC, Applichem GmbH, Darmstadt, Germany) in PBS buffer. Afterward, a streptavidin solution (50 μg/mL, diluted in sodium acetate buffer, pH 5.0, Sierra Sensors GmbH) was immobilized by injecting for 6 min on both channels. Subsequently the sensor surface was blocked for 8 min by injecting ethanolamine (1 M, Sierra Sensors GmbH) on both channels. For the determination of selectivity, the aptamers were modified (5′-Biotin-TEG, Integrated DNA Technologies BVBA, Leuven, Belgium) and immobilized by injecting for approximately 8 min until a response signal of 200 RU (response unit) was obtained.

SPR Measurements. The aptamer selectivity was investigated in orange-juice-simulating buffer containing 0.01% Tween 20 as running buffer by injecting the spores listed in Table 3. The various spores were diluted to a concentration of 10^6 cfu/mL, fragmented as described above, and injected for 2 min. The sensor chip was regenerated by injecting regeneration buffer 2 (25 mM EDTA, 1% Tween 20, pH 12.0) for 30 s after each spore injection. In addition, the orange-juice-simulating buffer was injected for a referenced calculation of aptamer selectivity. The obtained data were evaluated as mentioned above.

RESULTS AND DISCUSSION

The occurrence of *Alicyclobacillus* spp. spores in juice is a major concern for fruit beverage industries due to the formation of an antiseptic and medicinal off-flavor by these microorganisms even after pasteurization. The endospores germinate under given conditions during the fruit juice production, especially in the course of the dilution of juice concentrates.[3] Prior to detection by various techniques, spores have to be enriched, typically by cultivation. Alternatives to the very time-consuming microbiological cultivation could be antibody-based or aptamer-based trapping and enrichment techniques. A prerequisite for aptamer applications is their selection using the so-called SELEX process.

Aptamer Selection. The specification of selection conditions, like buffer compositions and an increasing stringency during the selection process, is required to obtain aptamers with affinity to the target, i.e., the spores. The separation between aptamers with high affinity to spores, respectively vegetative cells, and aptamers with little or no affinity to spores, respectively vegetative cells, was achieved by centrifugation, which is common during cell- and spore-SELEX.[30,31] These particles accumulate by centrifugation due to the higher density of spores and vegetative cells and entrain the aptamers with an affinity for the corresponding target. In this work, defined *A. acidoterrestris* spores (DSM 2498, wild type, 1/1 v/v) were used as selection targets because these two strains seem to be representative for off-flavor production in fruit juices and are frequently abundant. To simulate the crucial conditions which influence aptamer secondary structures (ion composition: 2 μM Ca^{2+}, 50 mM K^+, 2 μM Mg^{2+}; pH 3.5), the used buffer compounds are, in terms of concentrations, as close as possible to orange juice. Especially the pH and the ionic bindings between cations and the DNA phosphate backbone have a huge impact on the secondary structure of aptamers and therefore on the binding properties.[32]

In addition, a continuously rising stringency during the SELEX process was achieved by constantly increasing washing steps, decreasing target concentration and incubation times (Table 1). Furthermore, a vegetative cell mix of ∼100 undefined *Alicyclcobacillus* spp. strains was used for a counter selection during selection rounds 1−4. The purpose of this approach was to generate aptamers selective to the spores of *Alicyclobacillus* spp., with little or no affinity to the vegetative cells. This strategy provides the opportunity to antagonize the enrichment of vegetative cells and therefore to inhibit false-positive results with the developed system.

The progress of aptamer selection was evaluated by various techniques to ensure the rising affinity toward the target during the SELEX process. After each SELEX round, the presence of aptamers was checked via agarose gel electrophoresis; furthermore, the increasing aptamer affinity was investigated via flow cytometric and radioactive binding assays (Supporting Information). After 17 SELEX rounds, the final aptamer subpool was ligated into plasmids, transferred into *E. coli* cells for isolation, and finally sequenced.

The 10 aptamers obtained with an affinity to *Alicyclobacillus* spores are listed in Table 2. Secondary structures are predicted using mfold V4.6 and shown for AliApt1, AliApt3, AliApt5, and AliApt9 in Figure 2.[33]

Aptamer Sequence Analysis. The secondary structure prediction was performed using mfold V4.6.[33] Taking into account the energy-minimization method, the secondary structure is calculated from a given primary structure, in which different characteristics of three-dimensional structures, such as hairpin structures, loops, or bubbles, are significant.[34] In addition, folding temperature and ion concentrations are

DOI: 10.1021/jf505996m
J. Agric. Food Chem. 2015, 63, 2189−2197

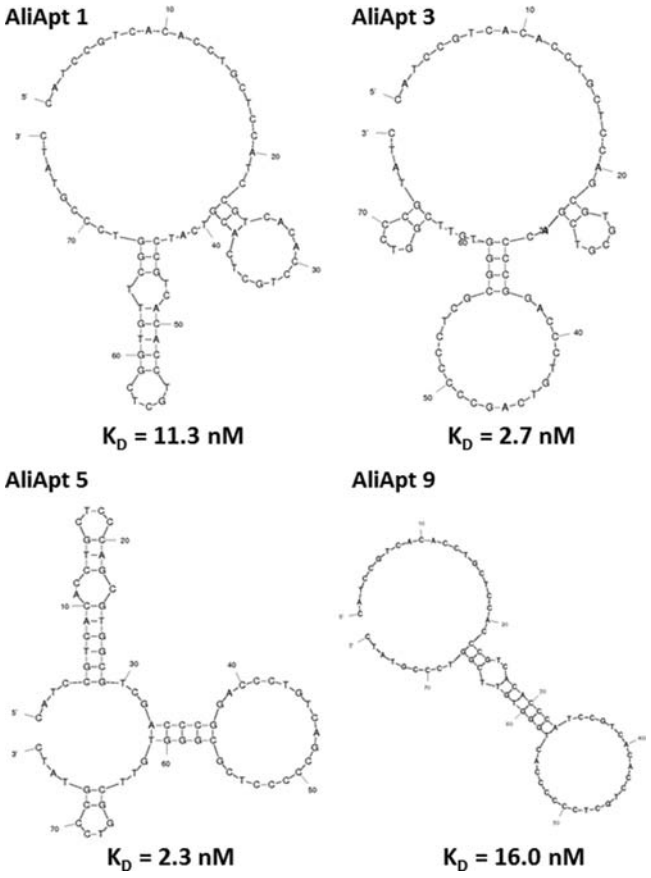

Figure 2. Secondary structural features with corresponding dissociation constants for AliApt1, AliApt3, AliApt5, and AliApt9, as predicted using mfold V4.6.

considered for calculation of the most energetically favorable secondary structure.[35] By comparison of the exemplary secondary structures (Figure 2), it could be noticed that homologous areas within similar structural features are observable. Furthermore, some characteristic structural features were unique in single secondary structures. The obtained aptamer sequences AliApt1−AliApt10 contain increasing numbers of cytosine repeats, which possibly form stable three-dimensional structures, called i-motifs.[36,37] These structural elements are very similar to guanosine quadruplexes and could be further investigated by NMR analysis. The high diversity of structural features led to the conclusion that the obtained aptamers presumably bind to various spore surface areas and not one defined spore coat. Further secondary aptamer structures are shown in the Supporting Information (Figure S3).

Determination of Aptamer Dissociation Constants (K_D) via SPR. To determine dissociation constants of the obtained aptamers to spores, several methods have been considered. For example, a flow system (quartz crystal microbalance, QCM) or immobilization-free techniques like microscale thermophoresis (MST) and isothermal titration calorimetry (ITC) have been previously used with cell lysates by Seidel et al. and Zhou et al., but suitable approaches for spores are not directly available.[38,39] Therefore, the well-established SPR technique was adapted to determine binding parameters of the obtained aptamers to the *Aliyclobacillus* spores.

In this context, we immobilized aptamers with different modifications on various sensor chip surfaces and injected spore suspensions without receiving evaluable data. It seems to be that the considerable differences in weights of the interacting partners and utilization of a flow system are responsible for steric hindrances and therefore non-evaluable data. Hence, like

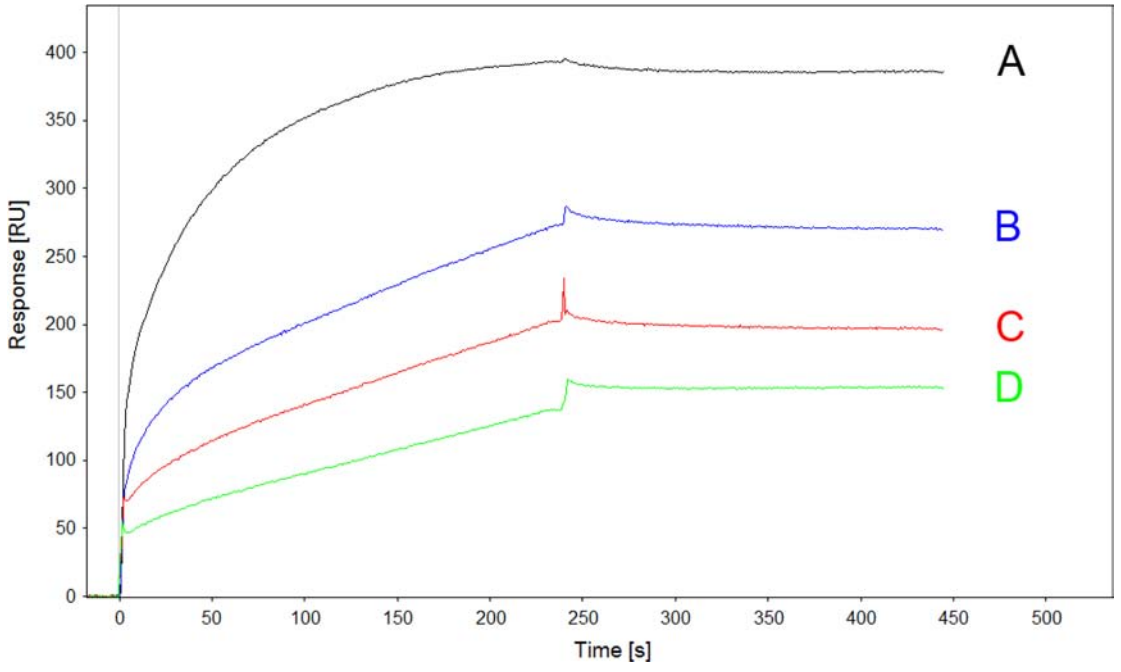

Figure 3. Overlay of AliApt3 sensorgrams with 360−840 pg immobilized spores fragments and several aptamer concentrations: (A) 10 μM, (B) 7.5 μM, (C) 5 μM, and (D) 2.5 μM. SPR measurements were carried out using orange-juice-simulating buffer (25 μL/min) to retain the secondary structures of aptamers. The double-referenced data are evaluated with AnalyserR2 (Sierra Sensors GmbH, Hamburg, Germany) and Scrubber (BioLogic Software Pty Ltd., Campbell, Australia).

DOI: 10.1021/jf505996m
J. Agric. Food Chem. 2015, 63, 2189−2197

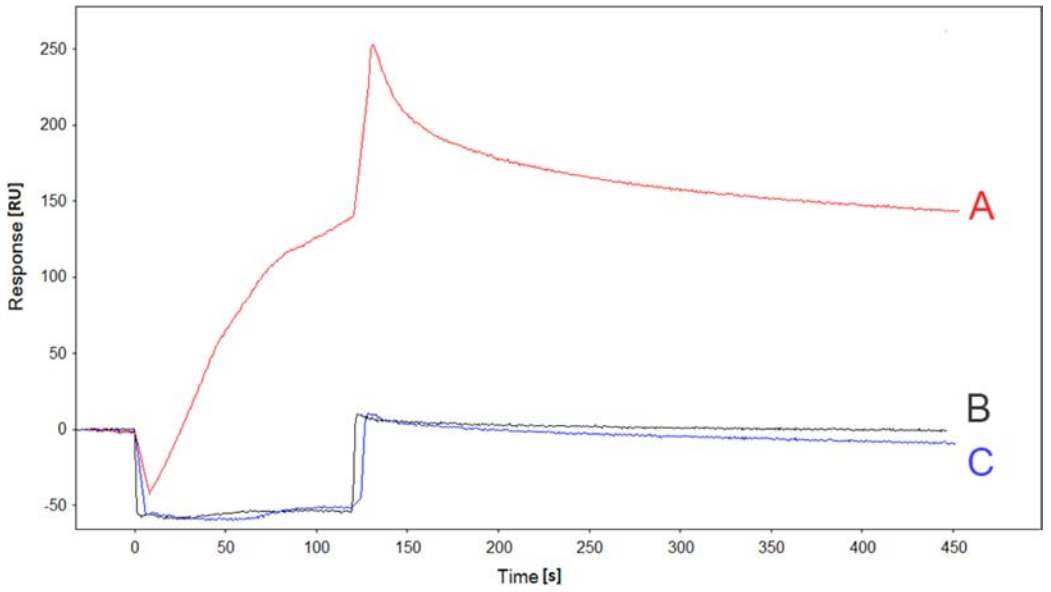

Figure 4. Exemplary SPR sensorgram overlay of spore lysate injections of (A) *A. acidoterrestris* as reference (DSM 2498, wild type, 10^7 cfu/mL), (B) *B. cereus* (wild type, 10^7 cfu/mL), and (C) *C. perfringens* (wild type, 10^7 cfu/mL), with immobilized streptavidin and 5′-biotin-TEG aptamer. SPR measurements were carried out using orange-juice-simulating buffer (25 μL/min) to retain the secondary structures of aptamers.

in the MST- and ITC-based techniques mentioned above, various methods using immobilized spores and spore lysates were investigated, whereby the utilization of a TissueLyser and glass beads enabled the preparation of an appropriate SPR sensor chip. In this context, the optimized parameters mentioned above (glass beads with several diameters, sodium acetate with different pH values, and the treatment time obviously) led to a suitable spores fragmentation degree for a subsequent immobilization on a sensor chip. In addition, several sensor chip surfaces (e.g., carboxylated dextran, carboxylated, aliphatic hydrocarbon chain) were examined, whereas the aliphatic hydrocarbon chains led to the most appropriate SPR sensorgrams with response signals of approximately 300−700 RU during immobilization. According to Karlsson one response unit corresponds roughly to 1 pg/mm^2 immobilized ligand on SPR sensor chips.[40] Considering the utilized sensor chip surface of 1.2 mm^2, a total weight of 360−840 pg of fragmented spores has been immobilized. Due to the high amount of immobilized ligands, it can be assumed that spore coat fragments have also been immobilized; therefore, the developed SPR immobilization method of spore lysate is applicable for determination of aptamer dissociation constants to *Alicyclobacillus* spores. The availability of spore coat fragments is a crucial prerequisite for SPR measurements due to the usage of whole spores during the SELEX process. It seems reasonable that the obtained aptamers possess an affinity to several coat compounds.

Furthermore, the developed surface regeneration procedure, including short contact times and minor chemical loads, is capable of being used for consecutive measurements without losses in response. Chip activity and stability were investigated by repeated injection of an aptamer (10 μM) and 50 subsequent regenerations (data not shown). The chip surface stability was decreased of approximately 10%, which is less than the recommended cutoff value of 20%.[41,42] In summary, the implemented spore immobilization procedure and regeneration fulfill the requirements of appropriate SPR measurements.

The aptamer dissociation constants were determined using orange-juice-simulating buffer to retain the secondary structures of aptamers and therefore the binding properties to the *Alicyclobacillus* spores under conditions which are comparable to those of orange juices. Here, the aptamers were injected on multiple SPR sensor chips for 6 min in rising concentrations (2.5, 5.0, 7.5, and 10.0 μM). To obtain double-referenced data, the RU signals of reference (BSA) and orange-juice-simulating buffer were subtracted. Examples of obtained sensorgram overlays of four different aptamer concentrations (2.5, 5, 7.5, and 10 μM) including the corresponding fits are shown in Figure 3. For calculation of dissociation constants, the obtained sensorgrams were fitted with a Langmuir 1:1 model, including a mass transport limitation factor, and separately calculated for each aptamer. Dixon's outliers were eliminated, and the averages of different SPR measurements were formed (Table 2). The obtained K_D values are in the low-nanomolar range (from 2.3 to 149.1 nM), which is quite comparable to those published for the aptamer for cells and proteins.[12,19,43]

Due to the mentioned SPR surface chip preparation using hydrophobic adsorption of spore lysates side effects like heterogeneous ligand sites, nonspecific binding, and charge-related attraction will influence binding kinetics of the injected aptamers. In contrast to a 1:1 interaction the obtained SPR sensorgrams for each aptamer injection reflect more a multivalent binding kinetic which explains the deviation of raw data and kinetic fits using a Langmuir 1:1 model including a mass transport limitation factor (Figure 3).

A binding model including all side effects of aptamer spore interactions on a heterogeneous surface, like a spore lysate, is currently not available, but use of a 1:1 model including a mass transport limitation factor seems to be a sufficient approach of the kinetic constants.

However, the obtained data, indicating a specific and concentration-dependent interaction of generated aptamers to the *Alicyclobacillus* spores, should be regarded with reservations based on the mentioned aspects. In addition, a fluorometric binding assay was performed by using fluorescently labeled

DOI: 10.1021/jf505996m
J. Agric. Food Chem. 2015, 63, 2189−2197

aptamers to confirm the assumed K_D values. Dissociation constants in a low-nanomolar range resulted from the fluorometric assay which supports the SPR measurements (data not shown).

Determination of Aptamer Selectivity via SPR. The determination of dissociation constants revealed four promising candidates with K_D values in the low-nanomolar range: AliApt1, AliApt3, AliApt5, and AliApt9 (Table 2). Selectivity is a crucial parameter for aptamer evaluation, as not only *Alicyclobacillus* spp. but also *Bacillus* spp. and *Clostridium* spp. occur as contaminants in fruit juice industry. Due to the high number of various endospores (Table 3) and the high price of SPR consumables, it was advantageous to develop a suitable aptamer immobilization method. In addition to the mentioned hindrances for SPR measurement of macromolecular analytes (e.g., flow system or/and different weights of interacting partners), the overall high densities of aptamers on sensor chip surfaces seem to be responsible for further steric hindrances and limitations toward evaluation of whole spore measurements. The utilization of biotin−streptavidin coupling and biotinylated aptamers with an appropriate spacer (triethylene glycol, TEG) enables SPR measurements of spore lysates by reducing the density and increasing the flexibility of the formed aptamer layer by concurrent reduction of target weight. This developed approach is completed by a suitable regeneration procedure, which was accomplished by regeneration buffer 2. In conclusion, the use of modified aptamers for immobilization and injection of spore lysate fulfills the requirements for the determination of aptamer selectivity via SPR.

To compare the obtained SPR data of different aptamers and various endospores, it was necessary to immobilize equal amounts of streptavidin and aptamers in terms of RU signals, respectively ligand densities, and inject similar spore concentrations. The spore suspensions were diluted to a concentration of 10^6 cfu/mL and lysed according to the above-mentioned protocol for fragmentation of *Alicyclobacillus* spp. in the context of sensor chip preparation. The lysate of *A. acidoterrestris* spores (DSM 2498, wild type), which were used as aptamer selection targets (1/1 v/v), was employed as reference and set as 100% aptamer affinity to the target to compare various species and strains (exemplary SPR sensorgram overlay in Figure 4).

The results of aptamer selectivity determination via SPR are stated in Table 4, where it can be seen that all four aptamers (AliApt 1, AliApt 3, AliApt 5, and AliApt 9) which have been immobilized show high affinities toward various *Alicyclobacillus* spp. and support the implemented K_D determinations. It should be noted that the four aptamers also possess a high affinity (76 to >100%) relative to SELEX target *Alicyclobacillus* spp. spores (DSM 2498 and a wild type) to two (AliApt 5 and AliApt 9), respectively three (AliApt 1 and AliApt 3), of the 12 different *Bacillus* spp. spores. In general, it seems that the investigated aptamers are more affine to spores of the genus *Alicyclobacillus* but also interact with several *Bacillus* and *Clostridium* spores (Table 4). The aptamer selectivity results gained via SPR were confirmed by fluorometric binding assay using fluorescently labeled aptamers (data not shown).

An explanation could be that the spore coats of *Alicyclobacillus*, *Bacillus*, and *Clostridium* are particularly similar, and therefore the selectivity of the generated aptamers is not sufficient enough to distinguish among the investigated genera. Due to the particularly high conformity in genome sequences of about 90% between *Alicyclobacillus* and *Bacillus*, it might be reasonable that the spore surfaces are highly similar, and therefore the generated aptamers possess an affinity to homologous spore surface proteins.[44,45] However, it is evident (Table 4) that the obtained aptamers are more affine to spores of *Alicyclobacillus* than to those of *Bacillus* and *Clostridium* and therefore usable for aptamer-based enrichment techniques. An extension toward a highly specific detection system could be achieved by combination with more specific molecular biological techniques, like real-time PCR or LAMP (loop-mediated isothermal amplification).[46]

Table 4. Summary of Aptamer Selectivity of Strains Given in Table 3[a]

	AliApt1	AliApt3	AliApt5	AliApt9
I	9 A	11 A	7 A	7 A
	3 B	3 B	2 B	1 B
	0 C	0 C	0 C	0 C
II	6 A	5 A	3 A	4 A
	0 B	0 B	0 B	1 B
	0 C	0 C	0 C	0 C
III	3 A	4 A	0 A	2 A
	0 B	1 B	0 B	0 B
	0 C	1 C	0 C	0 C
IV	14 A	13 A	10 A	1 A
	2 B	2 B	0 B	1 B
	1 C	1 C	0 C	0 C
V	11 A	11 A	9 A	7 A
	1 B	2 B	0 B	0 B
	1 C	0 C	0 C	0 C
VI	4 A	3 A	17 A	26 A
	7 B	5 B	11 B	11 B
	0 C	0 C	2 C	1 C
total	46 A	46 A	46 A	46 A
	13 B	13 B	13 B	13 B
	2 C	2 C	2 C	2 C

[a]In the first column, the code I−VI inidicates the percentage of the ΔRU value relative to the ΔRU value of the reference spore mix: I, >100%; II, 76−100%; III, 51−75%; IV, 26−50%; V, 0−25%; and VI, <0%. A = *Alicyclobacillus*, B = *Bacillus*, and C = *Clostridium*.

Visualization of Binding Interactions via Fluorescence Microscopy. Interactions between generated aptamers and *Alicyclobacillus* spores were visualized using a fluorescence microscope. In addition, the orange-juice-simulating buffer containing only *Alicyclobacillus* spores was considered as well and used as a reference to exclude the intrinsic fluorescence of spores. As shown in Figure 5, the spores exhibit a fluorescence signal after incubation with fluorescently labeled aptamers, while spores by itself show no fluorescence signal under the chosen conditions. Thereby it was possible to visualize the interactions between the generated aptamers and *Alicyclobacillus* spore coat via fluorescence microscopy.

During the presented work, aptamers with an affinity to *Alicyclobacillus* spores were selected by spore-SELEX. The aptamer selection process was carried out in orange-juice-simulating buffer to obtain aptamers which are able to bind the mentioned spores under real conditions. Furthermore, the process was verified by various techniques (flow cytometric binding assay, AGE, and radioactive binding assay). The aptamer sequences gained after 17 selection rounds were compared in terms of their secondary structures. For characterization (determination of dissociations constants and aptamer selectivity), several SPR assays were developed, immobilizing spore lysates and modified aptamers, and were

DOI: 10.1021/jf505996m
J. Agric. Food Chem. 2015, 63, 2189−2197

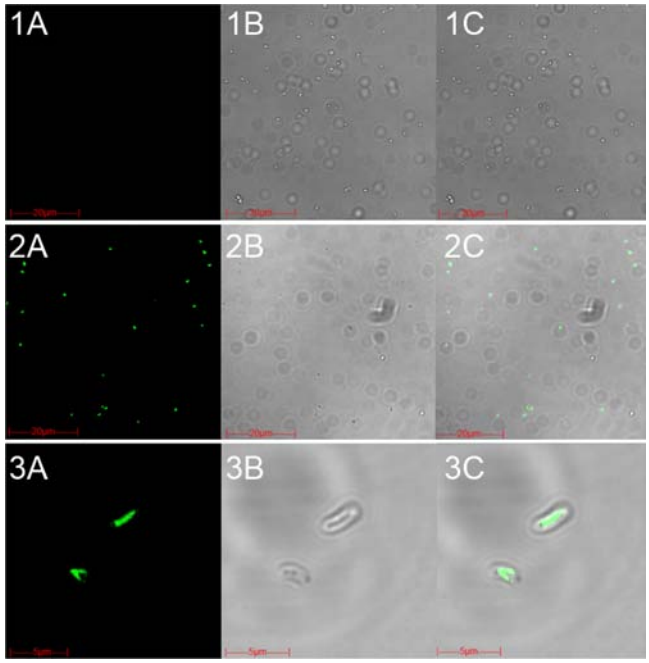

Figure 5. Fluorescence microscopy recordings of *A. acidoterrestris* spores in orange-juice-simulating buffer as blank sample (1A to 1C with 40× lens). Exemplary images of spores with prior incubation with a fluorescently labeled mix of obtained aptamers (2A to 2C with 40× lens; 3A to 3C with 100× lens). 1A to 3A show fluorescence images, 1B to 3B visual images, and 1C to 3C overlays of the fluorescence and visual images.

confirmed by fluorescence binding assays. Concerning K_D values and selectivity, suitable aptamers for corresponding enrichment techniques were obtained. Furthermore, the interactions between intact *Alicyclobacillus* spore coat and gained aptamer mix were visualized by fluorescence microscopy. To overcome microbiological plating methods, the gained aptamers could be integrated into aptamer-based techniques (e.g., magnetic separation) for the enrichment of *Alicyclobacillus* spores. Due to the lack of aptamer selectivity regarding differentiation of fruit-juice-related microbiological contaminants, the combination with further molecular biological techniques, like real-time PCR or LAMP, is necessary to increase sensitivity of the detection system.

In the future, the development and validation of an aptamer-based trapping and enrichment technique and the adaption to real orange juice samples will be integrated and compared to corresponding antibody-based systems. Furthermore, the development of different aptamer-based and rapid in-field applications, like lateral flow dipsticks/devices (LFDs), should be considered.[47] Also the replacement of antibodies in well-established techniques like enzyme-linked immunosorbent assay (ELISA) to develop a sensitive and easily applicable *Alicyclobacillus* spores detection system is conceivable.

■ ASSOCIATED CONTENT

Supporting Information

Procedures and results for radioactive binding assay and flow cytometric binding assay, predicted secondary structures of obtained aptamers AliApt1−AliApt10, and overlays of several AliApt injection sensorgrams. This material is available free of charge via the Internet at http://pubs.acs.org.

■ AUTHOR INFORMATION

Corresponding Author

*Tel.: +49-40-428384357. Fax: +49-40-428384342. E-mail: markus.fischer@chemie.uni-hamburg.de.

Funding

This research project was supported by the German Ministry of Economics and Technology (via AiF) and the FEI (Forschungskreis der Ernährungsindustrie e. V., Bonn, Germany). Project AiF 17245 N.

Notes

The authors declare no competing financial interest.

■ ACKNOWLEDGMENTS

The authors gratefully acknowledge Daniel Schwark for his help in various parts of the presented work, Dr. Burkhard Schütze (LADR GmbH, Geesthacht, Germany) for providing various *Alicyclobacillus* spp. strains (spores and vegetative cells), and the Institute of Biochemistry and Molecular Biology, University of Hamburg, for providing the technical equipment and their support in several fields. We also thank Sven Malik from Sierra Sensors GmbH, Hamburg, Germany, for the support with the SPR evaluations. Furthermore, we acknowledge our project partners Ludwig-Maximilians-Universität München, Lehrstuhl für Hygiene und Technologie der Milch (Oberschleißheim, Germany) and the Verband der Deutschen Fruchtsaft-Industrie e.V. (Bonn, Germany) for support.

■ REFERENCES

(1) Wang, Z.; Cai, R.; Yuan, Y.; Niu, C.; Hu, Z.; Yue, T. An immunomagnetic separation-real-time PCR system for the detection of Alicyclobacillus acidoterrestris in fruit products. *Int. J. Food. Microbiol.* **2014**, *175*, 30−35.

(2) Pettipher, G. L.; Osmundson, M. E.; Murphy, J. M. Methods for the detection and enumeration of Alicyclobacillus acidoterrestris and investigation of growth and production of taint in fruit juice and fruit juice-containing drinks. *Lett. Appl. Microbiol.* **1997**, *24*, 185−189.

(3) Steyn, C. E.; Cameron, M.; Witthuhn, R. C. Occurrence of Alicyclobacillus in the fruit processing environment—A review. *Int. J. Food Microbiol.* **2011**, *147*, 1−11.

(4) Chang, S. S.; Kang, D. H. Alicyclobacillus spp. in the fruit juice industry: history, characteristics, and current isolation/detection procedures. *Crit. Rev. Microbiol.* **2004**, *30*, 55−74.

(5) Smit, Y.; Cameron, M.; Venter, P.; Witthuhn, R. C. Alicyclobacillus spoilage and isolation—A review. *Food Microbiol.* **2011**, *28*, 331−349.

(6) Ulanowski, Z.; Ludlow, I. K. The Influence of the Cortex on Protoplast Dehydration in Bacterial-Spores Studied with Light-Scattering. *Curr. Microbiol.* **1993**, *26*, 31−35.

(7) Maldonado, M. C.; Belfiore, C.; Navarro, A. R. Temperature, soluble solids and pH effect on Alicyclobacillus acidoterrestris viability in lemon juice concentrate. *J. Ind. Microbiol. Biotechnol.* **2008**, *35*, 141−144.

(8) Danyluk, M. D.; Friedrich, L. M.; Jouquand, C.; Goodrich-Schneider, R.; Parish, M.; Rouseff, R. L. Prevalence, concentration, spoilage, and mitigation of Alicyclobacillus spp. in tropical and subtropical fruit juice concentrates. *Food Microbiol.* **2010**, 1−6.

(9) Lee, S. Y.; Dancer, G. I.; Chang, S. S.; Rhee, M. S.; Kang, D. H. Efficacy of chlorine dioxide gas against Alicyclobacillus acidoterrestris spores on apple surfaces. *Int. J. Food Microbiol.* **2006**, *108*, 364−368.

(10) Duan, N.; Wu, S.; Chen, X.; Huang, Y.; Xia, Y.; Ma, X.; Wang, Z. Selection and characterization of aptamers against Salmonella typhimurium using whole-bacterium Systemic Evolution of Ligands by Exponential Enrichment (SELEX). *J. Agric. Food Chem.* **2013**, *61*, 3229−3234.

DOI: 10.1021/jf505996m
J. Agric. Food Chem. 2015, 63, 2189−2197

(11) Padmavathy, B.; Patel, A.; Kumar, R. V.; Ali, B. M. J. Superparamagnetic Nanoparticles Based Immunomagnetic Separation-Multiplex Polymerase Chain Reaction Assay for Detection of Salmonella. *Sci. Adv. Mater.* **2012**, *4*, 114−120.
(12) Hünniger, T.; Wessels, H.; Fischer, C.; Paschke-Kratzin, A.; Fischer, M. Just in Time-Selection: A Rapid Semiautomated SELEX of DNA Aptamers Using Magnetic Separation and BEAMing. *Anal. Chem.* **2014**, *86*, 10940−10947.
(13) Tuerk, C.; Gold, L. Systematic evolution of ligands by exponential enrichment: RNA ligands to bacteriophage T4 DNA polymerase. *Science* **1990**, *249*, 505−510.
(14) Ellington, A. D.; Szostak, J. W. Selection in vitro of single-stranded DNA molecules that fold into specific ligand-binding structures. *Nature* **1992**, *355*, 850−852.
(15) Freeman, R.; Girsh, J.; Jou, A. F.; Ho, J. A.; Hug, T.; Dernedde, J.; Willner, I. Optical aptasensors for the analysis of the vascular endothelial growth factor (VEGF). *Anal. Chem.* **2012**, *84*, 6192−6198.
(16) Bruno, J. G.; Kiel, J. L. In vitro selection of DNA aptamers to anthrax spores with electrochemiluminescence detection. *Biosens. Bioelectron.* **1999**, *14*, 457−464.
(17) Zheng, D.; Zou, R.; Lou, X. Label-free fluorescent detection of ions, proteins, and small molecules using structure-switching aptamers, SYBR Gold, and exonuclease I. *Anal. Chem.* **2012**, *84*, 3554−3560.
(18) Kunii, T.; Ogura, S.; Mie, M.; Kobatake, E. Selection of DNA aptamers recognizing small cell lung cancer using living cell-SELEX. *Analyst* **2011**, *136*, 1310−1312.
(19) McKeague, M.; Giamberardino, A.; DeRosa, M. C. Advances in aptamer based biosensors for food safety. In *Environmental Biosensors*; Somerset, V., Ed.; InTech, 2011; DOI: 10.5772/22350.
(20) Avci-Adali, M.; Paul, A.; Wilhelm, N.; Ziemer, G.; Wendel, H. P. Upgrading SELEX technology by using lambda exonuclease digestion for single-stranded DNA generation. *Molecules* **2010**, *15*, 1−11.
(21) Glökler, J.; Schütze, T.; Konthur, Z. Automation in the High-throughput Selection of Random Combinatorial Libraries—Different Approaches for Select Applications. *Molecules* **2010**, *15*, 2478.
(22) Cox, J. C.; Rajendran, M.; Riedel, T.; Davidson, E. A.; Sooter, L. J.; Bayer, T. S.; Schmitz-Brown, M.; Ellington, A. D. Automated acquisition of aptamer sequences. *Comb. Chem. High Throughput Screen.* **2002**, *5*, 289−299.
(23) Mayer, G.; Ahmed, M. S.; Dolf, A.; Endl, E.; Knolle, P. A.; Famulok, M. Fluorescence-activated cell sorting for aptamer SELEX with cell mixtures. *Nat. Protoc.* **2010**, *5*, 1993−2004.
(24) Yang, J.; Bowser, M. T. Capillary electrophoresis-SELEX selection of catalytic DNA aptamers for a small-molecule porphyrin target. *Anal. Chem.* **2013**, *85*, 1525−1530.
(25) Williams, R.; Peisajovich, S. G.; Miller, O. J.; Magdassi, S.; Tawfik, D. S.; Griffiths, A. D. Amplification of complex gene libraries by emulsion PCR. *Nat. Methods* **2006**, *3*, 545−550.
(26) Shao, K.; Ding, W.; Wang, F.; Li, H.; Ma, D.; Wang, H. Emulsion PCR: a high efficient way of PCR amplification of random DNA libraries in aptamer selection. *PLoS One* **2011**, *6*, No. e24910.
(27) Schütze, T.; Rubelt, F.; Repkow, J.; Greiner, N.; Erdmann, V. A.; Lehrach, H.; Konthur, Z.; Glökler, J. A streamlined protocol for emulsion polymerase chain reaction and subsequent purification. *Anal. Biochem.* **2011**, *410*, 155−157.
(28) Cooper, M. A.; Try, A. C.; Carroll, J.; Ellar, D. J.; Williams, D. H. Surface plasmon resonance analysis at a supported lipid monolayer. *Biochim. Biophys. Acta* **1998**, *1373*, 101−111.
(29) Papo, N.; Shai, Y. Exploring peptide membrane interaction using surface plasmon resonance: Differentiation between pore formation versus membrane disruption by lytic peptides. *Biochemistry* **2003**, *42*, 458−466.
(30) Graham, J. C.; Zarbl, H. Use of cell-SELEX to generate DNA aptamers as molecular probes of HPV-associated cervical cancer cells. *PLoS One* **2012**, *7*, No. e36103.
(31) Meyer, C.; Hahn, U.; Rentmeister, A. Cell-specific aptamers as emerging therapeutics. *J. Nucleic Acids* **2011**, No. 904750.
(32) Girardot, M.; Gareil, P.; Varenne, A. Interaction study of a lysozyme-binding aptamer with mono- and divalent cations by ACE. *Electrophoresis* **2010**, *31*, 546−555.
(33) Zuker, M. Mfold web server for nucleic acid folding and hybridization prediction. *Nucleic Acids Res.* **2003**, *31*, 3406−3415.
(34) SantaLucia, J., Jr. A unified view of polymer, dumbbell, and oligonucleotide DNA nearest-neighbor thermodynamics. *Proc. Natl. Acad. Sci. U.S.A.* **1998**, *95*, 1460−1465.
(35) Peyret, N. Prediction of Nucleic Acid Hybridization: Parameters and Algorithmus. Ph.D. dissertation, Department of Chemistry, Wayne State University, Detroit, MI, 2000.
(36) Guittet, E.; Renciuk, D.; Leroy, J. L. Junctions between i-motif tetramers in supramolecular structures. *Nucleic Acids Res.* **2012**, *40*, 5162−5170.
(37) Leroy, J. L. The formation pathway of i-motif tetramers. *Nucleic Acids Res.* **2009**, *37*, 4127−4134.
(38) Seidel, S. A.; Dijkman, P. M.; Lea, W. A.; van den Bogaart, G.; Jerabek-Willemsen, M.; Lazic, A.; Joseph, J. S.; Srinivasan, P.; Baaske, P.; Simeonov, A.; Katritch, I.; Melo, F. A.; Ladbury, J. E.; Schreiber, G.; Watts, A.; Braun, D.; Duhr, S. Microscale thermophoresis quantifies biomolecular interactions under previously challenging conditions. *Methods* **2013**, *59*, 301−315.
(39) Zhou, X.; Kini, R. M.; Sivaraman, J. Application of isothermal titration calorimetry and column chromatography for identification of biomolecular targets. *Nat. Protoc.* **2011**, *6*, 158−165.
(40) Karlsson, R. SPR for molecular interaction analysis: a review of emerging application areas. *J. Mol. Recognit.* **2004**, *17*, 151−161.
(41) Skottrup, P.; Hearty, S.; Frokiaer, H.; Leonard, P.; Hejgaard, J.; O'Kennedy, R.; Nicolaisen, M.; Justesen, A. F. Detection of fungal spores using a generic surface plasmon resonance immunoassay. *Biosens. Bioelectron.* **2007**, *22*, 2724−2729.
(42) Wong, R. L.; Mytych, D.; Jacobs, S.; Bordens, R.; Swanson, S. J. Validation parameters for a novel biosensor assay which simultaneously measures serum concentrations of a humanized monoclonal antibody and detects induced antibodies. *J. Immunol. Methods* **1997**, *209*, 1−15.
(43) Shangguan, D.; Li, Y.; Tang, Z.; Cao, Z. C.; Chen, H. W.; Mallikaratchy, P.; Sefah, K.; Yang, C. J.; Tan, W. Aptamers evolved from live cells as effective molecular probes for cancer study. *Proc. Natl. Acad. Sci. U.S.A.* **2006**, *103*, 11838−11843.
(44) Wisotzkey, J. D.; Jurtshuk, P., Jr.; Fox, G. E.; Deinhard, G.; Poralla, K. Comparative sequence analyses on the 16S rRNA (rDNA) of Bacillus acidocaldarius, Bacillus acidoterrestris, and Bacillus cycloheptanicus and proposal for creation of a new genus, Alicyclobacillus gen. nov. *Int. J. Syst. Bacteriol.* **1992**, *42*, 263−269.
(45) Plomp, M.; Leighton, T. J.; Wheeler, K. E.; Malkin, A. J. Architecture and high-resolution structure of Bacillus thuringiensis and Bacillus cereus spore coat surfaces. *Langmuir* **2005**, *21*, 7892−7898.
(46) Chen, J.; Ma, X.; Yuan, Y.; Zhang, W. Sensitive and rapid detection of Alicyclobacillus acidoterrestris using loop-mediated isothermal amplification. *J. Sci. Food Agric.* **2011**, *91*, 1070−1074.
(47) Tombelli, S.; Minunni, M.; Mascini, M. Aptamers-based assays for diagnostics, environmental and food analysis. *Biomol. Eng.* **2007**, *24*, 191−200.

DOI: 10.1021/jf505996m
J. Agric. Food Chem. 2015, 63, 2189−2197

they also exist in *E. ulmoides* in a large amount. It seems that plant flavonoids also act as antihypertension agents.

In the course of our continuous investigation into the bioactive components from important edible and medicinal plants in the Qinba Mountains,[16,17] we have carried out a phytochemical study on the leaves of *E. ulmoides*, on both sEH and potential NF-κB inhibition for sustainable utilization of bioresources. In this study, we report here the isolation and structure identification of 27 metabolites from the leaves of *E. ulmoides* as well as their biological functions, including inhibitory effects on sEH and NF-κB activity. On the basis of the mechanism of action of sEH, the work could highlight the group of natural compounds in *E. ulmoides* that are responsible for its cardiovascular effects. Therefore, this research might be helpful to better understand the potential contribution of these compounds to the pharmacological activities of *E. ulmoides* leaves and to lay a significant basis for the development and utilization of it as food and drug.

MATERIALS AND METHODS

General Experimental Procedures. UV spectra were obtained using a Thermo Scientific Evolution 300 UV−vis Spectrophotometer. ^{1}H and ^{13}C NMR spectra were recorded on 400 and 500 MHz NMR instruments (Bruker Daltonics Inc., Bremen, Germany). Chemical shifts are reported using solvent residual peak as the internal standard. ESI-MS spectra were carried out on a Thermo Fisher LTQ Fleet instrument spectrometer (Thermo Fisher Scientific Inc., MA, U.S.). Column chromatography (CC) was carried out on silica gel (90−150 μm) (Qingdao Marine Chemical Inc., Qingdao, China), Sephadex LH-20 (40−70 μm) (Amersham Pharmacia Biotech AB, Uppsala, Sweden), and Lichroprep RP-18 gel (40−63 μm; Merck, Darmstadt, Germany). GF_{254} plates (Qingdao Marine Chemical Inc., Qingdao, China) were used for thin-layer chromatography (TLC). Preparative TLC (PTLC) was carried out on silica-gel 60 GF_{254} (Qingdao Marine Chemical, Ltd., Qingdao, China); semipreparative HPLC (Waters Corp., USA) was carried out by a Thermo BDS Hypersil column (250 × 4.6 mm and 250 × 10 mm, 5 μm) (Thermo Fisher Scientific Inc., MA, USA).

Reagents. 3-Phenyl-cyano(6-methoxy-2-naphthalenyl)methyl ester-2-oxiraneacetic acid (PHOME), 12-[[(tricyclo[3.3.1.13,7]dec-1-ylamino)carbonyl]amino]-dodecanoic acid (AUDA), and purified recombinant sEH were purchased from Cayman (Cayman, Michigan, USA). The other chemical reagents and standard compounds were purchased from Sigma-Aldrich (St. Louis, MO, USA). AB-8 macroporous resin was purchased from the Chemical Plant of Nankai University (Tianjin, China) and was cross-linked polystyrene copolymer. All chemicals used (methanol, chloroform, ethyl acetate, petroleum ether, *n*-butanol, etc.) were purchased from Kelong (Chengdu, China). HPLC methanol was purchased from Tedia, Inc. (Fairfield, USA). Ultrapure water was made in our lab.

Plant Materials. The green leaves of *E. ulmoides* were collected from Lveyang county, Shaanxi Province of China on August 25, 2012. The plant was taxonomically identified by one of authors (K.J.Z.). A voucher specimen (LXY-01234) has been deposited at the Herbarium of College of Life Sciences, Northwest A&F University, PR China.

Extraction, Isolation, and Purification. The dried and powdered leaves of *E. ulmoides* (1 kg) were extracted with 50% methanol. All the filtrates were combined and concentrated under reduced pressure to give a crude extract. The crude extract was suspended in water and then extracted 3 times with *n*-butanol to obtain an aqueous layer and an *n*-butanol layer. The aqueous fraction was subjected to silica-gel CC and eluted with $CHCl_3$-MeOH with increasing polarities (5:1, 5:2, 5:3, and 5:5) to give four fractions (frs. 1−4).

Fr. 1 was separated by Sephadex LH-20 (LH-20, MeOH) to obtain three fractions (frs. 1-1 to 1-3). Fr. 1-1 was purified by PTLC ($CHCl_3$-MeOH, 5:1), then HPLC (20% MeOH, flow rate = 2 mL/min, λ = 254 nm) to yield **10** (15 mg, t_R = 18.6 min). Fr. 1-2 was separated by CC on LH-20 (MeOH) and RP-18 (20% MeOH) to give **21** (10 mg), and fr. 1-3 was purified by silica-gel CC ($CHCl_3$-MeOH, 9:1) to give **22** (21 mg). Fr. 2 was subjected to AB-8 macroporous-resin CC and sequentially eluted with water, 15% MeOH, and MeOH to provide three fractions (frs. 2-1 to 2-3). Fr. 2-1 was separated by CC on LH-20 (MeOH), RP-18 CC (20% MeOH), and then silica gel with ($CHCl_3$-MeOH 20:1) to afford **19** (13 mg). Fr. 2-2 was separated by LH-20 CC (MeOH) to yield two fractions (frs. 2-2-1 and 2-2-2). Fr. 2-2-1 was purified by RP-18 CC (40% MeOH), and then by HPLC (32% MeOH, flow rate = 2 mL/min, λ = 254 nm) to afford **16** (45 mg). Fr. 2-2-2 was submitted to silica-gel CC and eluted with $CHCl_3$-MeOH with increasing polarities (9:1−5:1) to give four fractions (frs. 2-2-2-1 to 2-2-2-4). Fr. 2-2-2-1 was separated by RP-18 CC (20% MeOH) and then by HPLC (30% MeOH, flow rate = 2 mL/min, λ = 254 nm) to obtain **11** (32 mg, t_R = 18.9 min). Fr. 2-2-2-2 was subjected to RP-18 CC using 20% to 30% MeOH and then purified by HPLC (30% MeOH, flow rate = 2 mL/min, λ = 254 nm) to afford **27** (11 mg, t_R = 15.6 min) and **15** (20 mg, t_R = 21.3 min). Fr. 3 was loaded to an AB-8 column and successively eluted with water, 15% MeOH, and MeOH to yield three fractions (frs. 3-1 to 3-3). Purification of fr. 3-2 by LH-20 CC (MeOH) and silica-gel CC ($CHCl_3$-MeOH, 3:1) yielded **20** (60 mg), and purification of fr. 3-3 by LH-20 CC (MeOH) and HPLC (40% MeOH; flow rate = 2 mL/min, λ = 254 nm) afforded **4** (76 mg, t_R = 14.0 min) and **3** (18 mg, t_R = 22.0 min).

The *n*-butanol fraction was separated by CC over AB-8 macroporous resin with water and then increasing concentrations of MeOH to provide five fractions: frs. A through E. Fr. C, eluted with 50% MeOH, was separated by silica-gel CC using EtOAc-MeOH (20:1−5:1) as eluent to afford five subfractions (Fr. C-1 to 5). Fr. C-2 was separated by silica-gel CC ($CHCl_3$-MeOH, 5:1), sephadex LH-20 CC (MeOH), and then RP-18 CC (30% MeOH) to give **2** (18 mg). Purification of fr. C-3 by LH-20 CC (MeOH) followed by HPLC (35% MeOH, flow rate = 2 mL/min) provided **7** (26 mg, t_R = 18.5 min). Fr. C-4 was purified successively by LH-20 CC (MeOH), silica-gel CC ($CHCl_3$-MeOH, 10:1), and RP-18 CC to give **23** (10 mg). Fr. D, eluted with 75% MeOH, was subjected to silica-gel CC with EtOAc-MeOH (20:1−5:1) to afford four subfractions: frs. D-1 to 4. Fr. D-1 was submitted to silica-gel CC ($CHCl_3$-MeOH, 12:1) to obtain three subfractions: frs. D-1-1 to D-1-3. Purification of fr. D-1-1 by LH-20 CC (MeOH) and RP-18 CC (40% MeOH) to yielded **12** (86 mg). Fr. D-1-2 was fractionated by LH-20 CC (MeOH) and RP-18 CC (40% MeOH) to afford **1** (21 mg) and **18** (13 mg). Fractionation of Fr. D-1-3 by LH-20 CC (MeOH) gave five subfractions (frs. D-1-3-1 to D-1-3-5). Further purification of frs. D-1-3-2 and D-1-3-3 by RP-18 CC (30% MeOH) afforded **14** (50 mg) and **8** (8 mg), respectively, whereas purification of fr. D-1-3-5 by LH-20 CC (MeOH) produced **9** (10 mg). Fr. D-2 was separated by silica-gel CC ($CHCl_3$-MeOH, 10:1) and LH-20 CC (MeOH) to furnish **6** (16 mg). Fr. D-3 was fractionated by silica-gel CC ($CHCl_3$-MeOH, 20:1−10:1) to give three subfractions (frs. D-3-1 to D-3-3), and purification of frs. D-3-1 and D-3-2 by RP-18 CC (30% MeOH) and LH-20 CC (MeOH) afforded **17** (7 mg) and **13** (10 mg), respectively. Fr. E, eluted with 100% MeOH, was fractionated by silica-gel CC using EtOAc-MeOH (30:1−10:1) to afford four subfractions (frs. E-1 to 4). Purification of Fr. E-1 by silica-gel CC ($CHCl_3$-MeOH, 15:1), LH-20 CC (MeOH), and RP-18 CC (30% MeOH) gave **5** (10 mg). Fr. E-2 was separated by LH-20 CC (MeOH) and silica-gel CC ($CHCl_3$-MeOH, 20:1) to obtain **24** (11 mg). Fractionation of fr. E-3 by silica-gel CC ($CHCl_3$-MeOH, 15:1) afforded two subfractions (frs. E-3-1 and E-3-2). Fr. E-3-1 was further purified by LH-20 CC (MeOH) and then silica-gel CC ($CHCl_3$-MeOH, 10:1) to afford **25** (17 mg), whereas purification of fr. E-3-2 by LH-20 CC (MeOH) gave **26** (18 mg).

*2,5-Dimethoxy-3-glucopyranosyl cinnamic alcohol (**11**).* $C_{17}H_{24}O_9$, colorless solid; UV (MeOH) λ_{max} 229, 267 nm; ^{13}C NMR (125 MHz, DMSO-d_6) δ 152.7 (C1, C4), 104.5 (C2, C6), 133.9 (C3), 132.6 (C5), 128.4 (C7), 130.2 (C8), 61.4 (C9), 102.6 (C1′), 77.2 (C2′), 76.5 (C3′), 70.0 (C4′), 74.2 (C5′), 60.9 (C6′), 56.4 (2 × OCH_3); ^{1}H NMR (500 MHz, DMSO-d_6) δ 6.73 (2H, s, H2, H6), 6.47 (1H, d, J = 15.9 Hz, H7), 6.34 (1H, dt, J = 15.9, 5.0 Hz, H8), 4.11

DOI: 10.1021/acs.jafc.5b00055
J. Agric. Food Chem. 2015, 63, 2198−2205

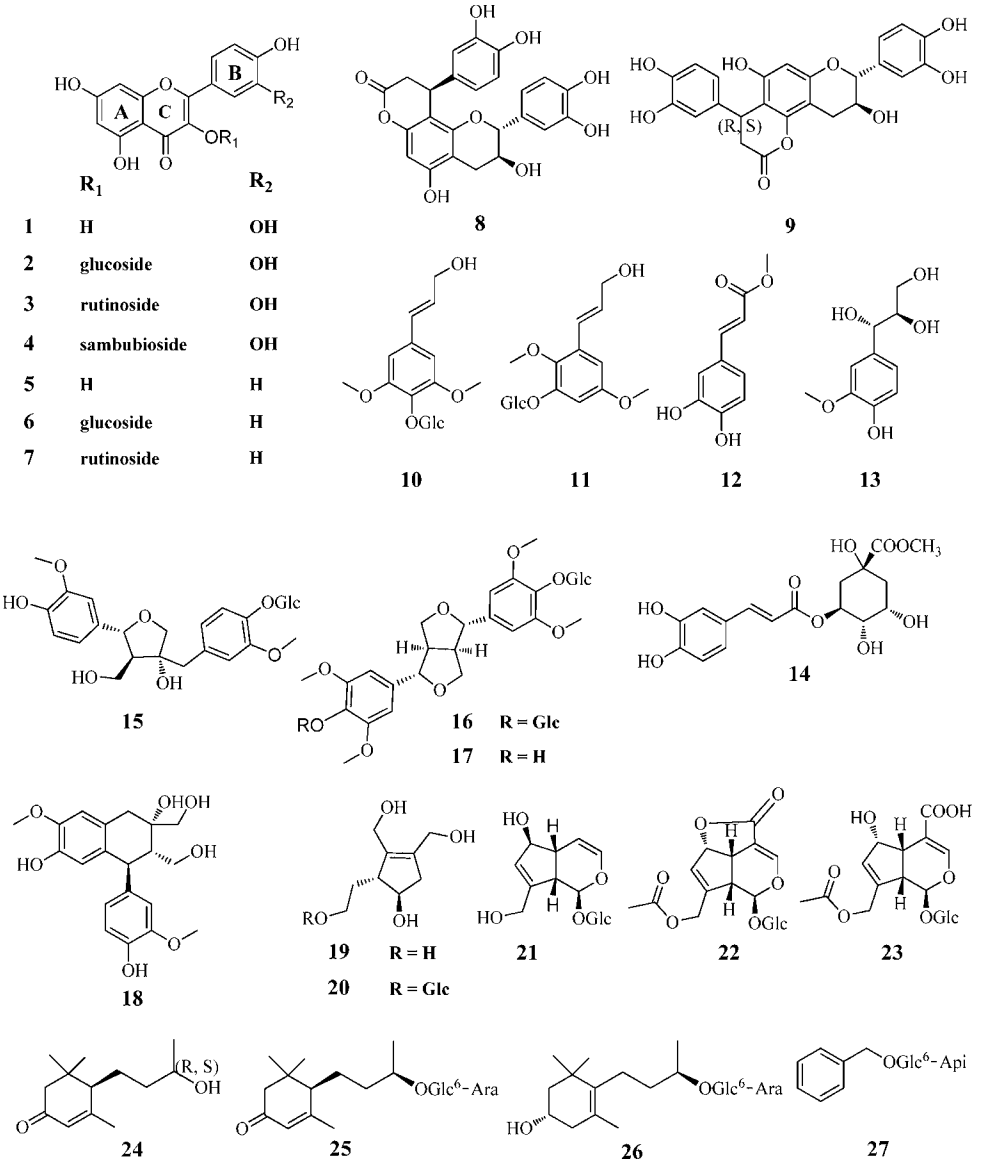

Figure 1. Structures of isolated compounds **1**−**27** from the leaves of *E. ulmoides* (Api, apiose; Ara, arabinosyl; Glc, glucosyl; Rut, rutinosyl).

(2H, m, H9), 4.91 (1H, d, J = 7.0 Hz, H1′), 3.04−3.60 (6H, m, H2′−H6′), 3.77 (6H, s, 2 × OCH_3); ESI-MS m/z 395.24 $[M + Na]^+$.

*Foliasalacioside E₂ (**26**).* $C_{24}H_{42}O_{11}$, amorphous solid; UV (MeOH) λ_{max} 206 nm; ^{13}C NMR (125 MHz, MeOH-d_4) δ 38.8 (C1), 49.5 (C2), 65.7 (C3), 42.9 (C4), 125.4 (C5), 138.4 (C6), 25.4 (C7), 39.0 (C8), 76.3 (C9), 19.8 (C10), 29.0 (C11), 30.4 (C12), 20.1 (C13), 102.2 (C1′), 75.1 (C2′), 78.1 (C3′), 71.8 (C4′), 76.9 (C5′), 69.7 (C6′), 105.2 (C1″), 72.4 (C2″), 74.2 (C3″), 69.4 (C4″), 66.6 (C5″); ^1H NMR (500 MHz, MeOH-d_4) δ 1.72 (1H, m, H2a), 1.41 (1H, dd, J = 11.6, 11.6 Hz, H2b), 3.87 (1H, m, H3), 2.20 (1H, m, H4a), 1.95 (1H, m, H4b), 2.24 (1H, m, H7a), 2.03 (1H, m, H7b), 1.59 (2H, m, H8a,b), 3.91 (1H, m, H9), 1.23 (3H, d, J = 6.1 Hz, H10), 1.07 (3H, s, H11), 1.09 (3H, s, H12), 1.68 (3H, s, H13), 4.37 (1H, d, J = 7.7 Hz, H1′), 4.38 (1H, d, J = 6.6 Hz, H1″); ESI-MS m/z 505.29 $[M - H]^-$.

*Icariside F₂ (**27**).* $C_{18}H_{26}O_{10}$, amorphous powder; UV (MeOH) λ_{max} 211 nm; ^{13}C NMR (125 MHz, MeOH-d_4) δ 139.0 (C1), 129.3 (C2), 129.3 (C3), 128.7 (C4), 129.3 (C5), 129.3 (C6), 71.8 (C7), 103.2 (C1′), 75.1 (C2′), 78.0 (C3′), 71.8 (C4′), 77.0 (C5′), 68.7 (C6′), 111.0 (C1″), 78.0 (C2″), 80.5 (C3″), 75.0 (C4″), 65.6 (C5″); ^1H NMR (500 MHz, MeOH-d_4) δ 7.28−7.70 (5H, m, H2, 3, 4, 5, 6), 4.69 (1H, d, J = 11.8 Hz, H7a), 4.93 (1H, d, J = 11.8 Hz, H7b), 4.37 (1H, d, J = 7.7 Hz, H1′), 5.09 (1H, d, J = 2.5 Hz, H1″); ESI-MS m/z 425.33 $[M + Na]^+$.

sEH Inhibitory Activity. sEH inhibitory activity was determined using a hydrolysis reaction of PHOME in the presence of sEH enzyme. Briefly, 130 μL of sEH (62.5 ng/mL) in 25 mM Bis-Tris buffer (including 0.1% bovine serum albumin, pH 7.0) and 20 μL of ligands diluted in MeOH were mixed in 96-well plate. A 50 μL aliquot of PHOME (40 μM) in buffer was added as substrate. After starting the sEH reaction at 37 °C, products were measured using a Geniosmicroplate reader (Tecan, Mannedorf, Switzerland) during an hour at excitation and emission wavelengths of 320 and 465 nm, respectively. sEH inhibitory activity for each sample was calculated as follows:

$$\text{sEH inhibitory activity (\%)} = 100 - [(S_{60} - S_0)/(C_{60} - C_0)] \times 100$$

where C_{60} and S_{60} were the fluorescence of control and inhibitor after 60 min, S_0 and C_0 is the fluorescence of control and inhibitor at zero min.

Cell Viability Assay. Cell viability was evaluated by Cell-Counting Kit (CCK)-8 methods. Briefly, CCK-8 was added to the cell culture medium for 1 h. The supernatant was removed, and formazan crystals

DOI: 10.1021/acs.jafc.5b00055
J. Agric. Food Chem. 2015, 63, 2198−2205

Table 1. sEH and NF-κB Inhibitory Activity of Compounds

compd[a]	sEH inhibition rate (%) at 100 μM[b]	sEH inhibitory activity IC_{50} (μM)[a,b]	kinetic mode (inhibition constant K_i, μM)	NF-κB inhibitory activity IC_{50} (μM)[b,c]
1	83.3 ± 0.2	22.5 ± 0.9	noncompetitive (18.2)	15.14 ± 2.29
2	69.9 ± 2.5	39.6 ± 1.4	NT	59.25 ± 2.90
3	68.7 ± 0.3	48.3 ± 1.7	NT	22.10 ± 2.49
4	62.6 ± 0.7	52.4 ± 1.5	NT	22.76 ± 2.20
5	80.7 ± 1.3	31.3 ± 2.6	noncompetitive (27.5)	20.52 ± 2.17
6	69.1 ± 2.2	49.8 ± 5.2	NT	35.08 ± 2.45
7	59.6 ± 5.9	61.9 ± 1.5	NT	>100
8	33.0 ± 6.9	NT	NT	18.45 ± 2.46
9	41.6 ± 4.1	NT	NT	15.23 ± 2.34
10	−5.5 ± 2.8	NT	NT	ND
11	−0.7 ± 9.7	NT	NT	>100
12	41.7 ± 0.7	NT	NT	24.68 ± 1.98
13	10.6 ± 12.2	NT	NT	59.44 ± 2.12
14	22.8 ± 0.3	NT	NT	92.6 ± 2.25
15	−0.3 ± 8.1	NT	NT	19.11 ± 2.14
16	−2.3 ± 2.9	NT	NT	34.23 ± 2.23
17	1.3 ± 0.4	NT	NT	ND
18	11.8 ± 1.0	NT	NT	70.28 ± 2.13
19	−12.1 ± 0.7	NT	NT	ND
20	−2.3 ± 2.9	NT	NT	16.88 ± 2.17
21	−4.5 ± 2.0	NT	NT	>100
22	8.4 ± 10.5	NT	NT	25.81 ± 2.33
23	6.9 ± 1.4	NT	NT	18.69 ± 2.18
24	2.1 ± 3.3	NT	NT	17.54 ± 2.11
25	−1.0 ± 9.6	NT	NT	22.26 ± 2.31
26	−0.6 ± 0.7	NT	NT	ND
27	−3.0 ± 7.6	NT	NT	16.25 ± 2.19
AUDA[d]	64.5 ± 2.5[e]	10.9 ± 1.2 nM		
apigenin[d]				1.64 ± 0.19

[a]All compounds were examined in a set of experiments three times. [b]Statistical significance was determined by one-way analysis of variance followed by Dunnett's multiple comparison test, $P < 0.05$ versus control. [c]Data were expressed as mean ± SD of at least three experiments carried out in triplicate. [d]Positive control. [e]At 25 nM.

were dissolved in dimethyl sulfoxide (DMSO). Absorbance was measured at 450 nm. The percentage of dead cells was determined relative to the control group.

All compounds were tested for cytotoxic activity against HepG2 cell lines. All cell lines were maintained in Dulbecco's modified Eagle's medium (DMEM) supplemented with 10% fetal bovine serum, 100 U/mL penicillin, and 100 mg/mL streptomycin at 37 °C with 5% CO_2. Each tested compound was dissolved with DMSO to obtain concentrations 0.1, 1, and 10 μM.

These were incubated with the cells for 72 h. The negative control received the same amount of DMSO (0.1% in the highest concentration). Doxorubicin (0.1−0.58 mg/mL) was used as a positive control. Cell viability was determined by reduction of the yellow dye 3-(4,5-dimethyl-2-thiazol)-2,5-diphenyl-2*H*-tetrazolium bromide (MTT) to a blue formazan product as described by Mosmann.[18]

NF-κB Inhibitory Activity Assay. Because NF-κB is essential for promoting inflammation-associated hepatic cancer, it is a potential target for prevention of hepatic cancer in chronic hepatic inflammatory diseases.[19] We examined the inhibitory effect of samples on NF-κB activated by TNF-α in hepatocellular carcinoma (HCC) cells such as HepG2 cells. The luciferase vector was first transfected into human hepatocarcinoma HepG2 cells. After a limited amount of time, the cells were lysed, and luciferin, the substrate of luciferase, was introduced into the cellular extract along with Mg^{2+} and an excess of ATP. Under these conditions, luciferase enzymes expressed by the reporter vector could catalyze the oxidative carboxylation of luciferin. Cells were seeded at 2×10^5 cells per well in 12-well plates and grown. After 24 h, cells were transfected with inducible NF-κB luciferase reporter and constitutively expressing Renilla reporter. After 24 h of transfection, the medium was changed to assay medium (Opti-MEM, 0.5% FBS, 0.1 mM NEAA, 1 mM sodium pyruvate, 100 units/mL penicillin, and 10 μg/mL streptomycin), and cells were pretreated for 1 h with vehicle (DMSO) and compounds, followed by 1 h of treatment with 10 ng/mL TNF-α for 20 h. Unstimulated cells were used as a negative control, and apigenin was used as a positive control. Dual luciferase assay was carried out 48 h after transfection, and promoter activity values are expressed as arbitrary units using a Renilla reporter for internal normalization.

Statistical Analysis. All data represent the mean ± SD of at least three independent experiments carried out in triplicate. Statistical significance is indicated as determined by one-way ANOVA followed by Dunnett's multiple comparison test, $P < 0.05$, using GraphPad Prism 6 (GraphPad Software Inc., San Diego, CA, USA).

RESULTS AND DISCUSSION

Extraction, Isolation, and Identification. *E. ulmoides* leaves were extracted with 50% methanol in water, and the crude methanol extract was fractionated into *n*-butanol and aqueous fractions by liquid−liquid separation. The *n*-butanol fraction was further subjected to column chromatography over AB-8 macroporous resin, silica gel, Sephadex LH-20, and finally semipreparative RP-HPLC to obtain 16 compounds: **1**, **2**, **5**−**9**, **12**−**14**, **17**, **18**, and **23**−**26**. Similarly, the water fraction was successively separated by multiple column chromatographies to yield 11 compounds: **3**, **4**, **10**, **11**, **15**, **16**, **19**−**22**, and **27** (Figure 1).

DOI: 10.1021/acs.jafc.5b00055
J. Agric. Food Chem. 2015, 63, 2198−2205

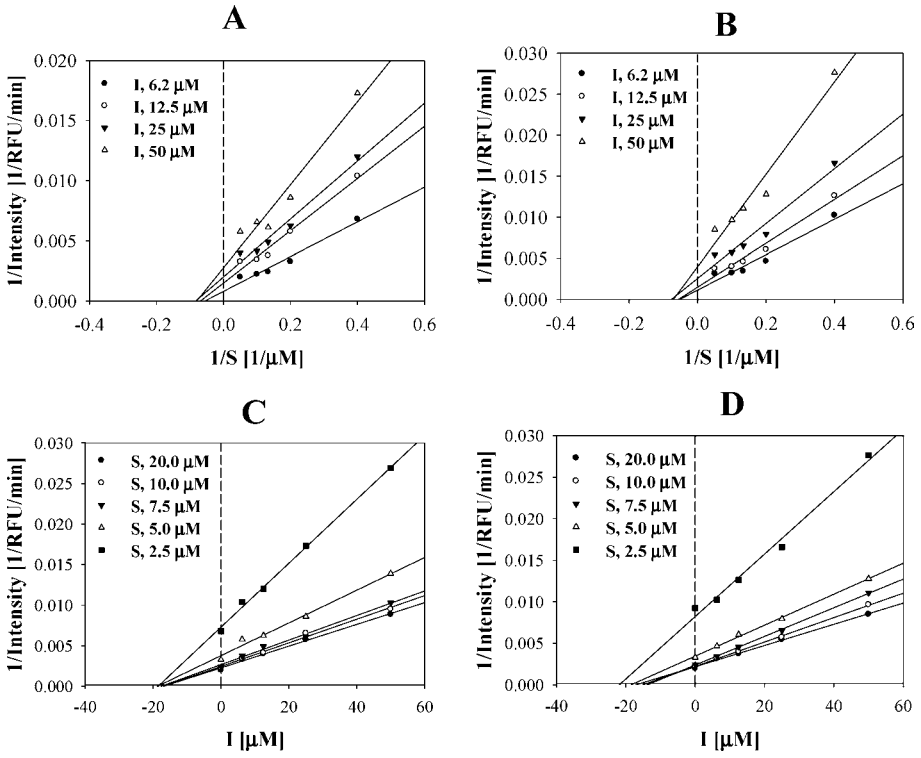

Figure 2. Study of binding mechanism between compounds **1** and **5** and sEH: (A and B) Lineweaver−Burk plots for the inhibition of compounds **1** and **5**, respectively, (C and D) Dixon plots for compound **1** and **5**, respectively. Data are the mean of three experiments carried out in triplicate and were determined by one-way analysis of variance followed by Dunnett's multiple comparison test, $P < 0.05$ versus control.

The structures of compounds **1**−**27** were characterized by ^{1}H and ^{13}C NMR, ESI-MS data, and comparison with published spectroscopic data. They were quercetin (**1**),[20] quercetin 3-glucoside (isoquercitrin, **2**), rutin (**3**),[21] quercetin 3-sambubioside (**4**),[22] kaempferol (**5**),[23] kaempferol 3-glucoside (astragalin, **6**),[21] kaempferol 3-rutinoside (**7**),[21] catechin-(7,8-bc)-4α-(3,4-dihydroxyphenyl)-dihydro-2(3H)-pyranone (**8**),[24,25] catechin-(5,6-bc)-4α,β-(3,4-dihydroxyphenyl)-dihydro-2(3H)-pyranone (**9**),[25] syringin (**10**),[26] 2,5-dimethoxy-3-glucopyranosyl cinnamic alcohol (**11**),[27] methyl caffeate (**12**),[28] erythro-guaiacylglycerol (**13**),[29] methyl chlorogenate (**14**),[30] sinenoside I (**15**),[31] liriodendrin (**16**),[32] syringaresinol 4′-O-glucopyranoside (**17**),[33] cyclo-olivil (**18**),[34] eucommiol (**19**),[35] eucommioside-I (**20**),[36] accubin (**21**),[37] asperuloside (**22**),[38] asperulosidic acid (**23**),[39] a mixture of blumenol C and 9-epi-blumenol C (**24**),[40] foliasalacioside B_1 (**25**),[41] foliasalacioside E_2 (**26**),[42] and icariside F_2 (**27**)[43] (Figure 1). Structure types of these compounds include flavonoids (**1**−**9**), phenylpropanoids (**10**−**14**), lignans (**15**−**18**), iridoids (**19**−**23**), and megastigmanes (**24**−**26**). Among these, compounds **11**, **26**, and **27** have been obtained from *E. ulmoides* for the first time.

Inhibitory Activity on sEH and Structure−Activity Relationships (SARs). sEH inhibitory activity of the isolated compounds (**1**−**27**) was evaluated using a fluorescent based on hydrolysis of the specific substrate PHOME in the presence of sEH enzyme. 12-(3-Adamantan-1-yl-ureido) dodecanoic acid (AUDA) was used as a positive control (50% inhibitory concentration, IC_{50} = 10.9 ± 1.2 nM). Compounds **1**−**27** were tested at 100 μM on sEH (Table 1). Isolated compounds **1**−**7** showed sEH inhibitory activity greater than 50% and were examined for further investigation at various concentrations for IC_{50}. IC_{50} was calculated using a dose-dependent response curve, as shown in Table 1. The results showed that compounds **1**−**7** displayed different inhibitory activity on sEH, with IC_{50} values of 22.5 ± 0.9−61.9 ± 1.5 μM. Among them, **1** and **5** showed strong inhibitory activity on sEH with IC_{50} values of 22.5 ± 0.9 and 31.3 ± 2.6 μM, respectively.

For the study of the binding mechanism between two compounds (**1** and **5**) and sEH, their activity was measured with different substrate and various inhibitor concentrations. As a result of this kinetic analysis, two compounds **1** and **5** were found to inhibit sEH activity in a noncompetitive manner because the different substrate concentrations resulted in a family of lines that did intersect on the x axis in a Lineweaver−Burk plot (Figure 2A,B) and on the negative x axis in Dixon plots (Figure 2C,D) with K_i values of 18.2 and 27.5 μM, respectively.

A structure−activity relationship (SAR) analysis of these tested compounds (**1**−**7**) is outlined as follows: (i) sEH inhibitory activity of flavonoid aglycones (**1** and **5**) is higher than that of their glycosides, e.g., **1** (IC_{50} = 22.5 ± 0.9 μM) vs **2**−**4** and **5** (IC_{50} = 31.3 ± 2.6 μM) vs **6** and **7**; (ii) for quercetin (**1**) or kaempferol (**5**), sEH inhibitory activity of monoglycosides is better than that of diglycosides, e.g., **2** (IC_{50} = 39.6 ± 1.4 μM) vs **4** (IC_{50} = 52.4 ± 1.5 μM) and **6** (IC_{50} = 49.8 ± 5.2 μM) vs **7**, indicating that an increase in the number of sugar at the C3 OH reduces their activity; (iii) the additional OH group at R_2 on the B ring of flavonoid aglycone enhances the activity, e.g., **1** > **5**; and (iv) the planar structures of the aglycones in the compounds tested seem to be essential because flavanonols **8** and **9**, bearing a nonconjugated moiety in the central C ring, had no activity. Taken together, it seems that the number of OH in the B ring of the tested compounds is able to increase sEH inhibitory activity, and the glycosylation of C3 OH is unfavorable to the activity. So far, the main inhibitors of sEH are urea and amides;[44] they were described as potent

DOI: 10.1021/acs.jafc.5b00055
J. Agric. Food Chem. 2015, 63, 2198−2205

and stable. However, their poor water-solubility and slow gastric absorption limit their use. In the future, good water-solubility, fast gastric absorption, and long duration of action would be the valuable direction to develop new sEH inhibitors. Flavonoids are less active than urea-based inhibitors, but their water-solubility, safety, and bioavailability are big advantages. In addition, wide distribution in natural resources give them great accessibility and promising prospects.

NF-κB Inhibition Activity in HepG2 cells. At a concentration of 10 μM, the MTT assay results indicated that compounds **1**−**27** showed little or no cytotoxic activities, suggesting that the leaves of this plant are safe (data not shown). Thus, all isolated compounds (**1**−**27**) were further tested for their ability to inhibit NF-κB by stimulation with TNF-α at various concentrations ranging from 0.1 to 10.0 μM, and IC_{50} values were calculated. As shown in Table 1, compounds **1**, **3**−**5**, **8**, **9**, **12**, **15**, **20**, **22**−**25**, and **27** showed marked NF-κB inhibitory activity, with IC_{50} values ranging from 15.14 ± 2.29 to 25.81 ± 2.33 μM, whereas compounds **6**, **16** both displayed weak inhibitory activities. Among the tested compounds, compounds **1**, **9**, **20**, and **27** turned out to be potent NF-κB inhibitors. Out of the flavonoid compounds (**1**−**9**), the best NF-κB inhibitors were compounds **1** and **9**, with similar IC_{50} data. In terms of the preliminary structure−activity relationship observations of **1**−**7**, glycosylation of the OH group at position C3 in quercetin (**1**) and kaempferol (**5**) caused a significant reducation of the NF-κB inhibitory effects (**1** vs **2** and **5** vs **7**), suggesting that the free C3 OH is important for enhanced activity (Table 1). In addition, although methyl caffeate (**12**) and methyl chlorogenate (**14**) both contained a caffeic acid moiety, **12**, bearing a small methyl group, was much more active than **14**, carrying a large bulky quinic acid group, in inhibiting potency. Because this is the only structural difference between the two compounds, it is very likely that this planar conformation is important for the binding of compound **12** to putative node proteins within the NF-κB signaling pathway.

Many plant flavonoids, such as quercetin (**1**), isoquercitrin (**2**), and kaempferol (**5**), found in many edible plants (e.g., tea, broccoli, and grapes), have been known as potential anti-inflammatory compounds through their inhibition of the expression of pro-inflammatory factors.[45−48] Quercetin (**1**) from lotus leaf (*Nelumbo nucifera*) has been shown to exhibit anti-inflammatory activities by inhibiting the JNK- and NF-κB-regulated pathways.[49] It has been reported that suppression of NF-kB by kaempferol (**5**) plays an important part in its anti-inflammatory activity.[48] Astragalin (**6**) has been reported to exert its anti-inflammatory effects, which are correlated with inhibition of TNF-α, interleukin-1 (IL-1), and interleukin-6 (IL-6) production, via inactivation of NF-κB.[50,51] Investigation of possible anti-inflammatory activity showed that isoquercitrin (**2**) may decrease the levels of prostaglandin E_2 produced by LPS-stimulated RAW264.7 cells.[52] Furthermore, methyl chlorogenate (**14**) is one of the main potent antioxidant components in the leaves of *Eriobotrya japonica*.[53] Compound **14** has been reported to be a potent suppressor of BHP-induced NF-κB activation in mouse liver, exhibiting its ability to downregulate NF-κB-dependent gene expression.[53] Jeong et al. have showed that accubin (**21**) suppressed the expression of TNF-α and IL-6 in Ag-stimulated rat basophilic leukemia (RBL)-2H3 mast cells. Because activator protein-1 binding activity was not affected, **21** was found to be a specific inhibitor of NF-κB activation in mast cells.[54] Moreover, recent studies revealed that flavonol glycosides such as isoquercitrin (**2**) and astragalin (**6**) with glycation inhibitory activity could be attributed to the antidiabetic action of *E. ulmoides* leaves.[21] However, in our experimental setup, flavonol glycoside (**2**), phenylpropanoids (**13** and **14**), lignan (**18**), and accubin (**21**) did not show discernible inhibitory effects on NF-κB in HepG2 cells with IC_{50} > 50 μM. Accordingly, flavonoids (except **2**) and iridoids (except **21**), megastigmanes, and **27** may be considered as the major anti-inflammatory components of the leaves of *E. ulmoides*. These results, in combination with our findings, further corroborate the anti-inflammatory effects of the compounds.

Crude extracts of *E. ulmoides* bark exhibit anti-inflammatory effects; thus, they may serve as a potential treatment for inflammatory diseases.[55,56] However, little is known about the anti-inflammatory actions of *E. ulmoides* leaves and its components. Recently, Luo et al.[57] identified two bioactive compounds, genipin and 4-(1,2-dimethoxyethyl)benzene-1,2-diol, from *E. ulmoides* leaves and showed that they had anti-inflammatory properties through inhibition of LPS-stimulated NO and TNF-α production. Methanolic extracts of *E. ulmoides* leaves were found to inhibit the growth of *Propionibacterium acnes*.[58] In addition, duzhong extracts also reduced the secretion of pro-inflammatory cytokines, such as TNF-α, IL-8, and IL-1β, in human monocytic THP-1 cells pretreated with heat-killed *P. acnes*.[58] To the best of our knowledge, this is the first report of sEH inhibitory and anti-inflammatory components in the leaves of *E. ulmoides*. In particluar, it has been believed that the anti-inflammatory properties of *E. ulmoides* should be ascribed to the combination of its various constituents and multiple targets, not limited solely to iridoids and/or flavonoids and a single target.

In conclusion, our findings demonstrate that the flavonoid components of the leaves of *E. ulmoides* are good sEH inhibitors (**1**, **5**) and that certain compounds (flavonoids **1** and **9**, iridoids **20** and **23**, megastigmane (**24**), and aromatic glycoside (**27**)) are potent inhibitors of the TNF-α-induced activation of NF-κB. Therefore, the fact that the extracts of *E. ulmoides* leaves are rich in phenolic compounds and iridoids might in part explain the use of this plant for the treatment of inflammatory or hypertensive conditions. This is the first report of the anti-inflammatory effects of components of *E. ulmoides* leaves by inhibiting both sEH and NF-κB. Additionally, the flavonoid components were at least revealed to be major components of the leaf agents with antihypertension activity through inhibition of sEH. Flavonoid, iridoid, and megastigmane components were verified as the key components responsible for NF-κB inhibition in our cell-based test system. This result is important for the development of *E. ulmoides* as an anti-inflammatory or antihypertensive functional food. Further studies should evaluate synergistic effects of the combination of these compounds in the treatment of inflammation or hypertension.

■ ASSOCIATED CONTENT

Supporting Information

^1H and ^{13}C NMR data of compounds **1**−**27**. This material is available free of charge via the Internet at http://pubs.acs.org.

■ AUTHOR INFORMATION

Corresponding Authors

*Y.H.K.: Tel.: +82-42-821-5933. Fax: +82-42-823-6566. E-mail: yhk@cnu.ac.kr.

DOI: 10.1021/acs.jafc.5b00055
J. Agric. Food Chem. 2015, 63, 2198−2205

*J.-M.G.: Tel.: +86-29-87092515. E-mail: jinminggao@nwsuaf.edu.cn.

Author Contributions

M.M.B. and W.S. contributed equally to this work.

Funding

This work was financially supported by the National Forestry Public Welfare Industry Research Project (201204603) and the Program of Science & Technology of Shaanxi Prevince (2013SF2-15) as well as by the Priority Research Center Program (2009-0093815) through the National Research Foundation of Korea (NRF), funded by the Ministry of Education, Science, and Technology, Republic of Korea.

Notes

The authors declare no competing financial interest.

REFERENCES

(1) Fitzpatrick, F. A.; Murphy, R. C. Cytochrome P-450 metabolism of arachidonic acid: formation and biological actions of "epoxygenase"-derived eicosanoids. *Pharmacol. Rev.* **1988**, *40*, 229−241.

(2) Campbell, W. B.; Gebremedhin, D.; Pratt, P. F.; Harder, D. R. Identification of epoxyeicosatrienoic acids as endothelium-derived hyperpolarizing factors. *Circ. Res.* **1996**, *78*, 415−423.

(3) Imig, J. D.; Hammock, B. D. Soluble epoxide hydrolase as a therapeutic target for cardiovascular diseases. *Nat. Rev. Drug Discovery* **2009**, *8*, 794−805.

(4) Tornatore, L.; Thotakura, A. K.; Bennett, J.; Moretti, M.; Franzoso, G. The nuclear factor kappa B signaling pathway: integrating metabolism with inflammation. *Trends Cell Biol.* **2012**, *22*, 557−566.

(5) Ghosh, S.; Hayden, M. S. New regulators of NF-κB in inflammation. *Nat. Rev. Immunol.* **2008**, *8*, 837−848.

(6) Wu, Z. H.; Miyamoto, S. Many faces of NF-κB signaling induced by genotoxic stress. *J. Mol. Med.* **2007**, *85*, 1187−1202.

(7) Rial, N. S.; Choi, K.; Nguyen, T.; Snyder, B.; Slepian, M. J. Nuclear factor kappa B (NF-κB): a novel cause for diabetes, coronaryartery disease and cancer initiation and promotion? *Med. Hypotheses* **2012**, *78*, 29−32.

(8) Luo, L. F.; Wu, W. H.; Zhou, Y. J.; Yan, J.; Yang, G. P.; Ouyang, D. S. Antihypertensive effect of *Eucommia ulmoides* Oliv. extracts in spontaneously hypertensive rats. *J. Ethnopharmacol.* **2010**, *129*, 238−243.

(9) Hung, M. Y.; Fu, T. Y.; Shih, P. H.; Lee, C. P.; Yen, G. C. Du-Zhong (*Eucommia ulmoides* Oliv.) leaves inhibits CCl_4-induced hepatic damage in rats. *Food Chem. Toxicol.* **2006**, *44*, 1424−1431.

(10) Li, Y.; Sato, T.; Metori, K.; Koike, K.; Che, Q. M.; Takahashi, S. The promoting effects of geniposidic acid and aucubin in *Eucommia ulmoides* Oliver leaves on collagen synthesis. *Biol. Pharm. Bull.* **1998**, *21*, 1306−1310.

(11) Ha, H.; Ho, J.; Shin, S.; Kim, H.; Koo, S.; Kim, I. H.; Kim, C. Effects of *Eucommiae* cortex on osteoblast-like cell proliferation and osteoclast inhibition. *Arch. Pharm. Res.* **2003**, *26*, 929−936.

(12) Hirata, T.; Kobayashi, T.; Wada, A.; Ueda, T.; Fujikawa, T.; Miyashita, H.; Ikeda, T.; Tsukamoto, S.; Nohara, T. Anti-obesity compounds in green leaves of *Eucommia ulmoides*. *Bioorg. Med. Chem. Lett.* **2011**, *21*, 1786−1791.

(13) Sih, C. J.; Ravikumar, P. R.; Huang, F. C.; Buckner, C.; Whitlock, H., Jr. Isolation and synthesis of pinoresinol diglucoside, a major antihypertensive principle of Tu-Chung (*Eucommia ulmoides* Oliver). *J. Am. Chem. Soc.* **1976**, *98*, 5412−5413.

(14) Deyama, T.; Nishibe, S.; Nakazawa, Y. Constituents and pharmacological effects of *Eucommia* and Siberian ginseng. *Acta Pharmacol. Sin.* **2001**, *22*, 1057−1070.

(15) Nishida, S.; Satoh, H. Comparative vasodilating actions among terpenoids and flavonoids contained in *Ginkgo biloba* extract. *Clin. Chim. Acta* **2004**, *339*, 129−133.

(16) Tang, J.-J.; Zhang, F.-Y.; Wang, D.-M.; Tian, J.-M.; Dong, S.; Gao, J.-M. Semisynthesis and antifeedant activity of new derivatives of a dihydro-β-agarofuran from *Parnassia wightiana*. *Int. J. Mol. Sci.* **2013**, *14*, 19484−19493.

(17) Liu, H. W.; Yu, X. Z.; Padula, D.; Pescitelli, G.; Lin, Z. W.; Wang, F.; Ding, K.; Lei, M.; Gao, J. M. Lignans from *Schisandra sphenathera* Rehd. et Wils. and semisynthetic schisantherin A analogues: Absolute configuration, and their estrogenic and anti-proliferative activity. *Eur. J. Med. Chem.* **2013**, *59*, 265−273.

(18) Mosmann, T. Rapid colorimetric assay for cellular growth and survival: application to proliferation and cytotoxicity assays. *J. Immunol. Methods* **1983**, *65*, 55−63.

(19) Li, W.; Sun, Y. N.; Yan, X. T.; Yang, S. Y.; Song, S. B.; Lee, Y. M.; Kim, Y. H. NF-κB inhibitory activity of sucrose fatty acid esters and related constituents from *Astragalus membranaceus*. *J. Agric. Food Chem.* **2013**, *61*, 7081−7088.

(20) Shen, C. C.; Chang, Y. S.; Ho, L. K. Nuclear-magnetic-resonance studies of 5,7-dihydroxyflavonoids. *Phytochemistry* **1993**, *34*, 843−845.

(21) Kim, H. Y.; Moon, B. H.; Lee, H. J.; Choi, D. H. Flavonol glycosides from the leaves of *Eucommia ulmoides* O. with glycation inhibitory activity. *J. Ethnopharmacol.* **2004**, *93*, 227−230.

(22) Hubner, G.; Wray, V.; Nahrstedt, A. Flavonol oligosaccharides from the seeds of *Aesculus hippocastanum*. *Planta Med.* **1999**, *65*, 636−642.

(23) Ding, H. Y.; Lin, H. C.; Teng, C. M.; Wu, Y. C. Phytochemical and pharmacological studies on Chinese *Paeonia* species. *J. Chin. Chem. Soc. (Taipei, Taiwan)* **2000**, *47*, 381−388.

(24) Foo, L. Y. Phenylpropanoid derivatives of catechin, epicatechin and phylloflavan from *Phyllocladus trichomanoides*. *Phytochemistry* **1987**, *26*, 2825−2830.

(25) Hsue-Fen, C.; Tanaka, T.; Nonaka, G.-I.; Fujioka, T.; Mihashi, K. Phenylpropanoid-substituted catechins from *Castanopsis hystrix* and structure revision of cinchonains. *Phytochemistry* **1993**, *33*, 183−187.

(26) Yang, M. C.; Lee, K. H.; Kim, K. H.; Choi, S. U.; Lee, K. R. Lignan and terpene constituents from the aerial parts of *Saussurea pulchella*. *Arch. Pharm. Res.* **2007**, *30*, 1067−1074.

(27) Ramsewak, R. S.; Nair, M. G.; DeWitt, D. L.; Mattson, W. G.; Zasada, J. Phenolic glycosides from *Dirca palustris*. *J. Nat. Prod.* **1999**, *62*, 1558−1561.

(28) He, Z. D.; Yang, C. R. Brandioside, a phenylpropanoid glycoside from *Brandisia hancei*. *Phytochemistry* **1991**, *30*, 701−702.

(29) Okuyama, E.; Fujimori, S.; Yamazaki, M.; Deyama, T. Pharmacologically active components of Viticis fructus (*Vitex rotundifolia*). II. The components having analgesic effects. *Chem. Pharm. Bull.* **1998**, *46*, 655−662.

(30) Deyama, T.; Ikawa, T.; Kitagawa, S.; Nishibe, S. The constituents of *Eucommia ulmoides* Oliv. V. Isolation of dihydroxydehydrodiconiferyl alcohol isomers and phenolic compounds. *Chem. Pharm. Bull.* **1987**, *35*, 1785−1789.

(31) Ouyang, M. A.; He, Z. D.; Wu, C. L. Anti-oxidative activity of glycosides from *Ligustrum sinense*. *Nat. Prod. Res.* **2003**, *17*, 381−387.

(32) Jolad, S. D.; Hoffmann, J. J.; Cole, J. R.; Tempesta, M. S.; Bates, R. B. Cytotoxic agent from *Penstemon deustus* (Scrophulariaceae): isolation and stereochemistry of liriodendrin, a symmetrically substituted furofuranoid lignan diglucoside. *J. Org. Chem.* **1980**, *45*, 1327−1329.

(33) Wang, C. Z.; Yu, D. Q. Lignan and acetylenic glycosides from *Aster auriculatus*. *Phytochemistry* **1998**, *48*, 711−717.

(34) Yue, Z. G.; Qin, H.; Li, Y. H.; Sun, Y.; Wang, Z. P.; Yang, T. H.; Liu, L.; Wang, M. C.; Feng, F.; Mei, Q. B. Chemical constituents of the root of *Jasminum giraldii*. *Molecules* **2013**, *18*, 4766−4775.

(35) Nakamura, T.; Nakazawa, Y.; Onizuka, S.; Tanaka, C.; Yahara, S.; Nohara, T. Studies on the constituents of *Eucommia ulmoides* iridoids from the leaves. *Nat. Med.* **1997**, *51*, 275−277.

(36) Bianco, A.; Bonini, C. C.; Iavarone, C.; Trogolo, C. Structure elucidation of eucommioside (2″-O-β-D-glucopyranosyleucommoil) from *Eucommia ulmoides*. *Phytochemistry* **1982**, *21*, 201−203.

(37) Bianco, A.; Passacantilli, P.; Nicoletti, M.; De Lima, R. A. Iridoids in equatorial and tropical flora. III. Isolation and partial

DOI: 10.1021/acs.jafc.5b00055
J. Agric. Food Chem. 2015, 63, 2198−2205

synthesis of 6-epiaucubin, a new glucosidic iridoid. *Tetrahedron* **1982**, *38*, 359−362.
(38) Suzuki, S.; Hisamichi, K.; Endo, K. NMR-studies and structural assignment of paederoside. *Heterocycles* **1993**, *35*, 895−900.
(39) Lee, T. G.; Kim, D. K. Iridoid compounds from the whole plant of *Galium verum* var. *asiaticum*. *Nat. Prod. Sci.* **2013**, *19*, 227−230.
(40) Matsunami, K.; Otsuka, H.; Takeda, Y. Structural revisions of blumenol C glucoside and byzantionoside B. *Chem. Pharm. Bull.* **2010**, *58*, 438−441.
(41) Nakamura, S.; Zhang, Y.; Pongpiriyadacha, Y.; Wang, T.; Matsuda, H.; Yoshikawa, M. Megastigmane glycosides from the leaves of *Salacia chinensis*. *Heterocycles* **2008**, *75*, 131−143.
(42) Zhang, Y.; Nakamura, S.; Pongpiriyadacha, Y.; Matsuda, H.; Yoshikawa, M. Absolute structures of new megastigmane glycosides, foliasalaciosides E_1, E_2, E_3, F, G, H, and I from the leaves of *Salacia chinensis*. *Chem. Pharm. Bull.* **2008**, *56*, 547−553.
(43) Miyase, T.; Ueno, A.; Takizawa, N.; Kobayashi, H.; Oguchi, H. Studies on the glycosides of *Epimedium grandiflorum* Morr. var. *thunbergianum* (Miq.) Nakai. III. *Chem. Pharm. Bull.* **1988**, *36*, 2475−2484.
(44) Morisseau, C.; Hammock, B. D. Epoxide hydrolases: mechanisms, inhibitor designs, and biological roles. *Annu. Rev. Pharmacol. Toxicol.* **2005**, *45*, 311−333.
(45) Zhou, H. P.; Lutterodt, H.; Cheng, Z. H.; Yu, L. L. Antiinflammatory and antiproliferative activities of trifolirhizin, a flavonoid from *Sophora flavescens* roots. *J. Agric. Food Chem.* **2009**, *57*, 4580−4585.
(46) Boots, A. W.; Haenen, G. R. M. M.; Bast, A. Health effects of quercetin: from antioxidant to nutraceutical. *Eur. J. Pharmacol.* **2008**, *585*, 325−337.
(47) Boots, A. W.; Drent, M.; de Boer, V. C. J.; Bast, A.; Haenen, G. R. M. M. Quercetin reduces markers of oxidative stress and inflammation in sarcoidosis. *Clin. Nutr.* **2011**, *30*, 506−512.
(48) Rajendran, P.; Rengarajan, T.; Nandakumar, N.; Palaniswami, R.; Nishigaki, Y.; Nishigaki, I. Kaempferol, a potential cytostatic and cure for inflammatory disorders. *Eur. J. Med. Chem.* **2014**, *86*, 103−112.
(49) Liu, S. H.; Lu, T. H.; Su, C. C.; Lay, I. S.; Lin, H. Y.; Fang, K. M.; Ho, T. J.; Chen, K. L.; Su, Y. C.; Chiang, W. C.; Chen, Y. W. Lotus leaf (*Nelumbo nucifera*) and its active constituents prevent inflammatory responses in macrophages via JNK/NF-κB signaling pathway. *Am. J. Chin. Med.* **2014**, *42*, 869−889.
(50) Kim, M. S.; Kim, S. H. Inhibitory effect of astragalin on expression of lipopolysaccharide-induced inflammatory mediators through NF-κB in macrophages. *Arch. Pharm. Res.* **2011**, *34*, 2101−2107.
(51) Soromou, L. W.; Chen, N.; Jiang, L.; Huo, M.; Wei, M.; Chu, X.; Millimouno, F. M.; Feng, H.; Sidime, Y.; Deng, X. Astragalin attenuates lipopolysaccharide-induced inflammatory responses by down-regulating NF-κB signaling pathway. *Biochem. Biophys. Res. Commun.* **2012**, *419*, 256−261.
(52) Hammer, K. D.; Hillwig, M. L.; Solco, A. K.; Dixon, P. M.; Delate, K.; Murphy, P. A.; Wurtele, E. S.; Birt, D. F. Inhibition of prostaglandin E2 production by anti-inflammatory *Hypericum perforatum* extracts and constituents in RAW264.7 mouse macrophage cells. *J. Agric. Food Chem.* **2007**, *55*, 7323−7331.
(53) Kwon, H. J.; Kang, M. J.; Kim, H. J.; Choi, J. S.; Paik, K. J.; Chung, H. Y. Inhibition of NF kappa B by methyl chlorogenate from *Eriobotrya japonica*. *Mol. Cells* **2000**, *10*, 241−246.
(54) Jeong, H. J.; Koo, H. N.; Na, H. J.; Kim, M. S.; Hong, S. H.; Eom, J. W.; Kim, K. S.; Shin, T. Y.; Kim, H. M. Inhibition of TNF-α and IL-6 production by aucubin through blockade of NF-κB activation in RBL-2H3 mast cells. *Cytokine* **2002**, *18*, 252−259.
(55) Kim, B. H.; Park, K. S.; Chang, I. M. Elucidation of anti-inflammatory potencies of *Eucommia ulmoides* Oliv. bark and *Plantago asiatica* seeds. *J. Med. Food* **2009**, *12*, 764−769.
(56) Kim, M. C.; Kim, D. S.; Kim, S. J.; Park, J.; Kim, H. L.; Kim, S. Y.; Ahn, K. S.; Jang, H. J.; Lee, S. G.; Lee, K. M.; Hong, S. H.; Um, J. Y. Eucommiae cortex inhibits TNF-α and IL-6 through the suppression of caspase-1 in lipopolysaccharide-stimulated mouse peritoneal macrophages. *Am. J. Chin. Med.* **2012**, *40*, 135−149.
(57) Luo, D.; Or, T. C.; Yang, C. L.; Lau, A. S. Anti-inflammatory activity of iridoid and catechol derivatives from *Eucommia ulmoides* Oliver. *ACS Chem. Neurosci.* **2014**, *5*, 855−866.
(58) Tsai, T. H.; Tsai, T. H.; Wu, W. H.; Tseng, J. T. P.; Tsai, P. J. *In vitro* antimicrobial and anti-inflammatory effects of herbs against *Propionibacterium acnes*. *Food Chem.* **2010**, *119*, 964−968.

DOI: 10.1021/acs.jafc.5b00055
J. Agric. Food Chem. 2015, 63, 2198−2205

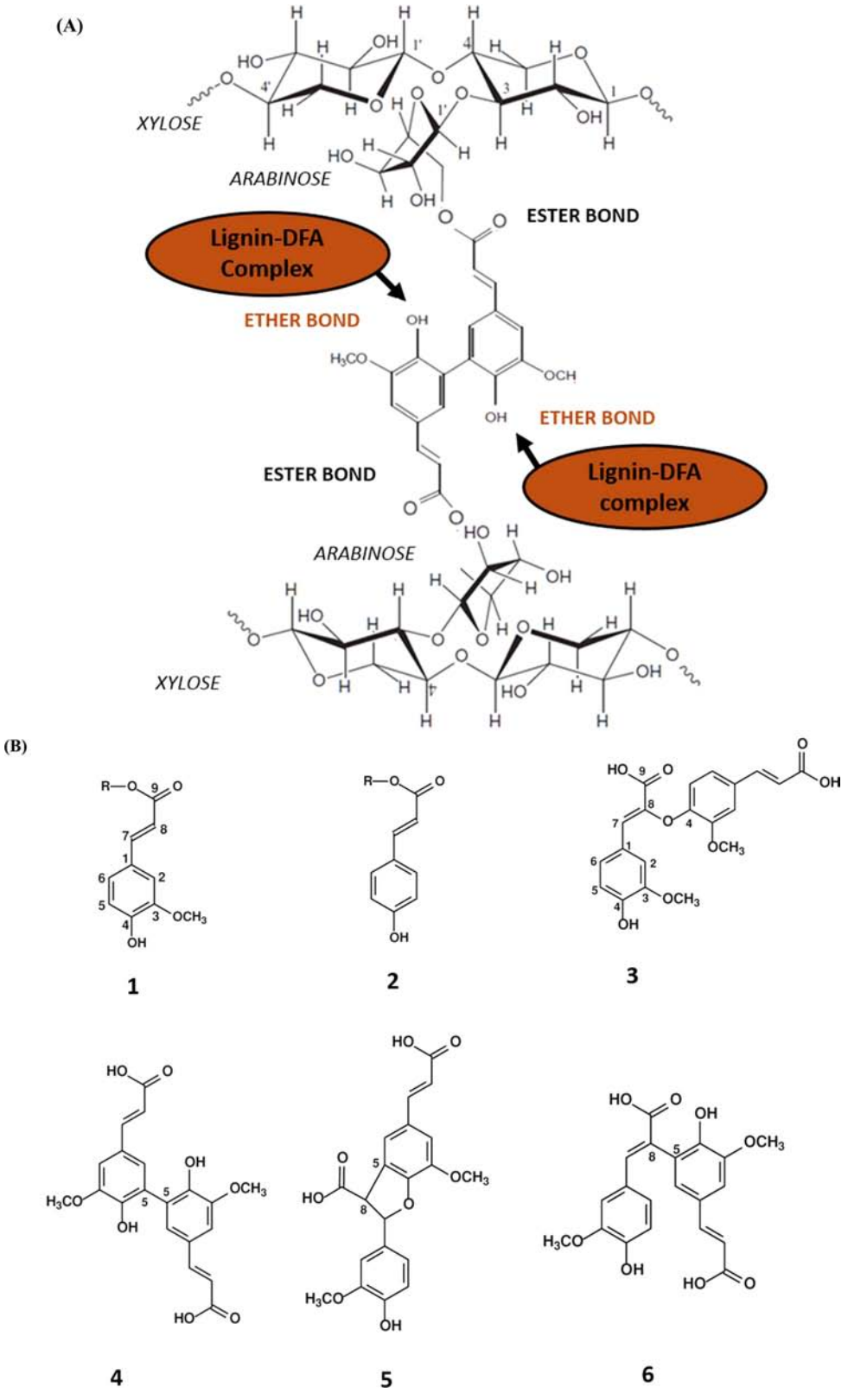

Figure 1. Dimerization of FA. (A) Cell-wall cross-linking between two arabinoxylan chains mediated by diferulate 5−5-DFA. The arrows indicate the hydroxyl groups where lignin monomers can be covalently linked via ether bonds.[23] (B) Structures of hydroxycinnamate monomers, FA (**1**) and *p*-coumaric acid (**2**), and DFA regioisomers quantified in the current study, 8−*O*−4-DFA (**3**), 5−5-DFA (**4**), 8−5-cyclic-DFA (**5**), and 8−5-non-cyclic-DFA (**6**).

(Figure 1A).[26] More than 50% of cell-wall-bound compound **1** can undergo dimerization via oxidative radical-coupling reactions catalyzed by phenoloxidases (H_2O_2-dependent peroxidases and/or O_2-dependent laccases), leading to the formation of 4−*O*−5, 5−5, 8−*O*−4, 8−5, and 8−8 linkages between the FA units (see Figure 1B for examples).[26−28] There

DOI: 10.1021/jf505341d
J. Agric. Food Chem. 2015, 63, 2206−2214

is strong evidence that this cross-linking between cell-wall polymers through ester-linked diferulates (DFAs) has an important role in maize resistance to corn borers.[29] Higher DFA deposition in diverse tissues and genotypic materials was found to be positively related with reduced corn borer damage.[30−33] Moreover, tall fescue transgenic plants with a modified level of cell-wall-esterified ferulates showed a reduction in cell-wall hydroxycinnamates and resulted in plants more susceptible to insect folivores, which imply a mechanical restriction to feeding or assimilation by these compounds.[34]

Most maize genotypes evaluated to date are limited to inbred lines with diverse genetic backgrounds and thereby maybe different defense mechanisms; therefore, experiments to provide direct evidence of the separate role of DFAs as a maize resistance mechanism against borers are needed. The genotypes developed in a previous selection program[35] maximize the differences in the DFA concentration in the main tissue that corn borer larvae use as feed and were used as model plant material to study the relationship between DFAs and corn borer resistance in maize. The objectives of the current work were (i) to field evaluate the severity of the damage in the DFA divergent maize populations under artificial corn borer infestations, (ii) to perform laboratory-feeding bioassays using the maize populations to evaluate the effects of plant endogenous DFA concentrations on larval growth, and (iii) to assess indirect effects of the selection program on the total amount of cell-wall material, mentioned as another pest-resistance-related trait.

MATERIALS AND METHODS

Chemicals. Methanol, high-performance liquid chromatography (HPLC)-grade methanol, acetone, acetonitrile, hydrochloric acid, ethyl acetate, and ethyl ether were purchased from Merck (Madrid, Spain). Sodium hydroxide and trifluoroacetic acid were purchased from Sigma-Aldrich Química (Madrid, Spain). Distilled water was purified with a Milli-Q system. Standards of FA and *p*-coumaric acid were purchased from Sigma-Aldrich Química (Madrid, Spain). DFA 5−5 was kindly provided by Dr. John T. Arnason, University of Ottawa, Ottawa, Ontario, Canada.

Field Evaluation Trials. Six maize populations were developed from a F_2 population derived from the inbred line cross CO125 and PB130. These two inbred lines were selected on the basis of their high (CO125) and low (PB130) DFA concentrations in stem pith tissue.[31] Divergent selection for total esterified DFA concentration (DFAT) in pith stalk tissues was conducted in the low (L) and high (H) directions for three generations to develop six populations (P1H, P2H, P3H, P1L, P2L, and P3L), following the procedure previously described by Barros-Rios et al.[35] Seed from P1L, P1H, P2L, P2H, P3H, and P3L was multiplied in a winter nursery in Chile (2009−2010) and evaluated in 2010 at two locations in Spain (Pontevedra, 42° 30′ N 8° 46′ W, and Zaragoza, 41° 44′ N, 0° 47′ W). The experimental design at both locations was a randomized complete block with three replicates. Plant density was approximately 60 000 plants ha^{-1}. Cultivation operations, fertilization, and weed control were carried out according to local practices and crop requirements. To accurately define the silking time of each genotype, plots were checked until 50% of plants were showing silks. At silking, 10 plants in each plot were artificially infested with the most abundant corn borer species at each location (MCB in Pontevedra and ECB in Zaragoza) by placing an egg mass between the shank of the main ear and the stem, as has been suggested by Butrón et al.[36] The rearing of MCB eggs and infestation methods followed standard procedures.[37] The eggs of ECB were purchased from the Research Centre of Poitou-Charentes (INRA, Luisignan, France). Plants were harvested at grain maturity. At harvest, the stem of infested plants was split longitudinally and the corn borer tunnel length was measured. Natural infestations by other borers in the studied area are low, and if any, these are not significant in comparison to the artificial infestations performed. Five non-infested plants were collected for DFA analysis 55 days after silking when internode elongation had ceased. The second and third elongated above-ground internodes from these plants were collected and frozen (−20 °C) for analysis. Each internode was dissected into pith and rind fractions, and subsequently, pith samples were lyophilized and ground through a 0.75 mm screen in a rotor mill.

Laboratory-Feeding Bioassays. Laboratory-reared MCB larvae were fed on pith stem tissues from the six maize populations evaluated. Single neonate larvae were initially weighed using a microbalance (Mettler-Toledo MT5) with ±1 μg accuracy and thereafter individually transferred to Petri dishes containing pith stem sections (±2 cm). Stem sections were obtained from four internodes below the main ear starting at silking time. A total of 60 larvae per population were used in the feeding experiments. Petri dishes were placed in a controlled environment room for 28 days at 26 °C with a photoperiod of 14:10 (L/D) h. Fresh pith stem tissues were replenished every 4 days to avoid tissue deterioration, and larval weight was recorded at 7, 14, 21, and 28 days.

Chemical Determinations. *Cell-Wall-Bound Phenolic Analyses.* Ester-bound ferulate (**1**), *p*-coumaric acid (**2**), and DFA extraction followed a procedure described by Santiago et al.,[28] with some minor modifications. Freeze-dried samples (500 mg) were extracted in 30 mL of 80% methanol and homogenized for 60 s with a Polytron mixer (Brinkman Instruments, Westbury, NY). Samples were extracted for 1 h in the dark and then centrifuged for 10 min at 1000*g*. Supernatant containing soluble phenolics was discarded, and the pellet with ester-bound phenolics was re-extracted twice with 20 mL of 80% methanol. The pellet was hydrolyzed with 20 mL of 2 N NaOH and shaken for 4 h in the dark under a nitrogen atmosphere. The hydrolysis reaction was stopped by adding 6 N HCl, and the pH was adjusted to 2.0. Samples were centrifuged as above, and the supernatant was collected. The pellet was washed twice with 10 mL of distilled water and centrifuged, and supernatants were combined, mixed, and extracted twice with ethyl acetate (50 and 35 mL each). The organic phase was dried using a Speed Vac for 6 h. The extracts were dissolved in 3 mL of HPLC-grade methanol and stored at −20 °C. All standards and samples were filtered through a 20 μm pore poly(tetrafluoroethylene) filter (Chromatographic Specialties, Brockville, Canada) before analysis.

HPLC analyses were performed on the basis of a previously described protocol,[31] with some minor modifications, using a 2690 Waters Separations Module (Waters, Milford, MA) equipped with a Waters 996 photodiode array detector and a Waters YMC ODSAM narrow-bore column (100 × 2 mm inner diameter, 3 μm particle size). Elution conditions with a mobile-phase system of acetonitrile (solvent A) and trifluoroacetic acid (0.05%) in water (pH 3.4) (solvent B) were as follows: initial conditions of 10:90 (A/B), changing to 30:70 in 3.5 min, then to 32:68 in 6.5 min, then to 100:0 in 4 min, and then to isocratic elution with 100:0 for 4.5 min, finally returning to the initial conditions in 3 min. The mobile-phase flow rate was 0.3 mL/min, and the total analysis time was 21.5 min. The sample injection volume was 4 μL, and the elution profiles were monitored online by ultraviolet (UV) absorbance at 325, 280, and 254 nm. Retention times were compared to those of freshly prepared standard solutions. Identities of FA dimers were confirmed by comparison to the authentic 5−5 standard or retention time and UV spectra previously published.[38] The DFAT concentration was calculated as the sum of three regioisomers of DFAs identified and quantified by this analytical procedure: 8−*O*−4-DFA (**3**), 5−5-DFA (**4**), and 8−5-DFA (**5** + **6**) (Figure 1B). The 8−5-DFA concentration was calculated as the sum of the 8−5-cyclic (or benzofuran)-DFA (**5**) and 8−5-non-cyclic (or open)-DFA (**6**) because the non-cyclic form is most likely formed during alkaline hydrolysis from the native cyclic form.[39]

Total Cell-Wall Content Analysis. The total amount of cell-wall material was isolated on the basis of a procedure previously described by Strack et al.,[40] with some minor modifications.[41] Pith samples (500 mg of dry matter) were homogenized in boiling ethanol (20 mL) and extracted for 15 min into an ultrasonic bath. After centrifugation (2700*g* for 10 min), the sediment was washed (stirring for 30 min)

DOI: 10.1021/jf505341d
J. Agric. Food Chem. 2015, 63, 2206−2214

with 20 mL of each of the following solvents in sequence: 30% methanol at 65 °C, methanol, acetone, ethyl acetate, and ethyl ether at room temperature, and dried at 60 °C to a constant weight.

Statistical Analysis. Combined analyses of variance over locations for cell-wall traits (compounds **1** and **2**, DFAT, and total amount of cell-wall material) and stem tunnel length were computed using the GLM procedure of SAS (version 6.12; SAS Institute, Inc., Cary, NC). The class variables were location, replication, and maize population. The analysis of variance for all traits was performed considering all factors as random effects, except populations. Means for the maize populations were compared using the Fisher protected least significant difference test (LSD; $p < 0.05$). In addition, the differences on larvae weight fed on the pith stem tissues obtained from the high and low DFAT populations (PHs and PLs, respectively) were compared using an orthogonal contrast.

To analyze the selection program efficiency, values of 3, 2, 1, −1, −2, and −3 were assigned to populations P3H, P2H, P1H, P1L, P2L, and P2L, respectively, and (1) simple linear regression analyses incorporating random effects in the model [environment and replication (environment)] were performed with the DFAT concentration as the dependent variable and population as the independent variable. Similar simple linear regression analyses were performed to determine (2) the relationships between tunnel length (dependent variable) and DFAT concentrations (independent variable), (3) the indirect response of selection for DFAs (DFAT as the independent variable) on hydroxycinnamate monomers and cell-wall concentration (dependent variables), and (4) the relationship between tunnel length (dependent variable) and hydroxycinnamate monomers and cell-wall concentration (independent variables). Variables included in the regression analyses were considered significant at the $p \leq 0.05$ level. All statistical analyses were performed using the SAS software package.[42]

RESULTS AND DISCUSSION

Response to Selection for Ester-Linked DFA Concentrations. For the cell-wall traits evaluated, the ferulate concentration (monomers and dimers with the exception of 5−5-DFA) differed significantly among the maize populations evaluated; the genotype × location interaction was not significant for any of the cell-wall traits evaluated (see Table S1 of the Supporting Information). After three generations of divergent selection, concentrations of compounds **3**, **5** + **6**, and DFAT, were 32, 23, and 31% higher in P3H than in P3L, respectively. Nevertheless, P2H had lower concentrations than expected for all DFAs evaluated. The reduction of DFAT in P2H was a "sawtooth" point in the selection program. Such "sawtooth" patterns have been previously observed for genetic gains in several agronomic traits during a selection program, usually associated with traits not 100% heritable.[43,44] The concentration of compound **1** was 25% higher in P3H than in P3L, and grouping of populations according to the LSD means that a comparison method followed a similar trend to that observed for DFAs (Table 1). Simple linear regression analysis equations showed significant and positive coefficients between compounds **3**, **5** + **6**, and DFAT concentrations and the maize populations (Figure 2A). After three generations of divergent selection, genetic gains were observed for compounds **3**, **5** + **6**, and DFAT (Figure 2A). Only the 8-coupled DFAs were significantly modified during the selection program. It appears that selection for the sum of all of the individual DFAs (DFAT) would be relatively efficient for 8-coupled DFA selection because these structures account for the largest proportion of the selection criteria (~80% of DFAT).

Mean comparisons and regression analyses showed that divergent selection was effective in altering the DFAT concentration in maize pith tissues and that it is possible to

Table 1. Mean ± Standard Error Comparisons for Damage Caused by Corn Borers (Stem Tunnel Length), Cell-Wall (CW) Ester-Linked Hydroxycinnamates, and Total Amount of CW Material among Six Maize Populations Developed for Divergent Total Ester-Linked DFAs ($N = 6$)[a]

		CW ester-linked hydroxycinnamates[b]						
population[c]	stem tunnel length[d] (cm)	**1** (g kg^{-1} of dry matter)	**2** (g kg^{-1} of dry matter)	**3** (g kg^{-1} of dry matter)	**4** (g kg^{-1} of dry matter)	**5** + **6** (g kg^{-1} of dry matter)	DFAT (g kg^{-1} of dry matter)	total CW (g kg^{-1} of dry matter)
P3H	22.6 ± 1.5 b	5.40 ± 0.20 a	10.91 ± 1.03 a	0.164 ± 0.007 a	0.119 ± 0.027 a	0.274 ± 0.010 a	0.557 ± 0.035 a	475 ± 24 a
P2H	33.9 ± 3.9 a	4.46 ± 0.19 bcd	12.36 ± 0.75 a	0.137 ± 0.007 b	0.081 ± 0.005 a	0.237 ± 0.008 ab	0.455 ± 0.007 bc	537 ± 9 a
P1H	25.8 ± 1.4 b	5.20 ± 0.31 ab	11.96 ± 0.86 a	0.169 ± 0.005 a	0.096 ± 0.005 a	0.261 ± 0.018 a	0.526 ± 0.005 a	499 ± 16 a
P1L	24.5 ± 3.7 b	4.75 ± 0.25 abc	10.13 ± 1.30 a	0.155 ± 0.008 a	0.097 ± 0.005 a	0.265 ± 0.010 a	0.516 ± 0.016 ab	571 ± 13 a
P2L	22.6 ± 2.1 b	3.97 ± 0.31 d	10.94 ± 0.61 a	0.121 ± 0.008 b	0.086 ± 0.009 a	0.212 ± 0.016 b	0.419 ± 0.019 c	517 ± 17 a
P3L	31.7 ± 3.6 a	4.32 ± 0.31 cd	11.21 ± 0.63 a	0.124 ± 0.008 b	0.079 ± 0.009 a	0.222 ± 0.017 b	0.424 ± 0.033 c	528 ± 10 a
LSD	5.7	0.74		0.017		0.038	0.066	

[a]Means in the same column not sharing a common letter are significantly different and determined by LSD ($p < 0.05$). [b]**1**, FA; **2**, *p*-coumaric acid; **3**, 8−O−4-DFA; **4**, 5−5-DFA; **5**, 8−5-cyclic-DFA; **6**, 8−5-non-cyclic-DFA; DFAT, total diferulates as the sum of all of the different DFA regioisomers quantified, equal to **3** + **4** + **5** + **6**; and total CW, total amount of cell-wall material. [c]Population = maize populations in the high (H) and low (L) direction of corn hybrid CO125 × PB130 divergently selected for DFAT. [d]Means for damage data measured as the stem tunnel length caused by the most abundant corn borer species at each location (MCB in Pontevedra and ECB in Zaragoza).

DOI: 10.1021/jf505341d
J. Agric. Food Chem. 2015, 63, 2206−2214

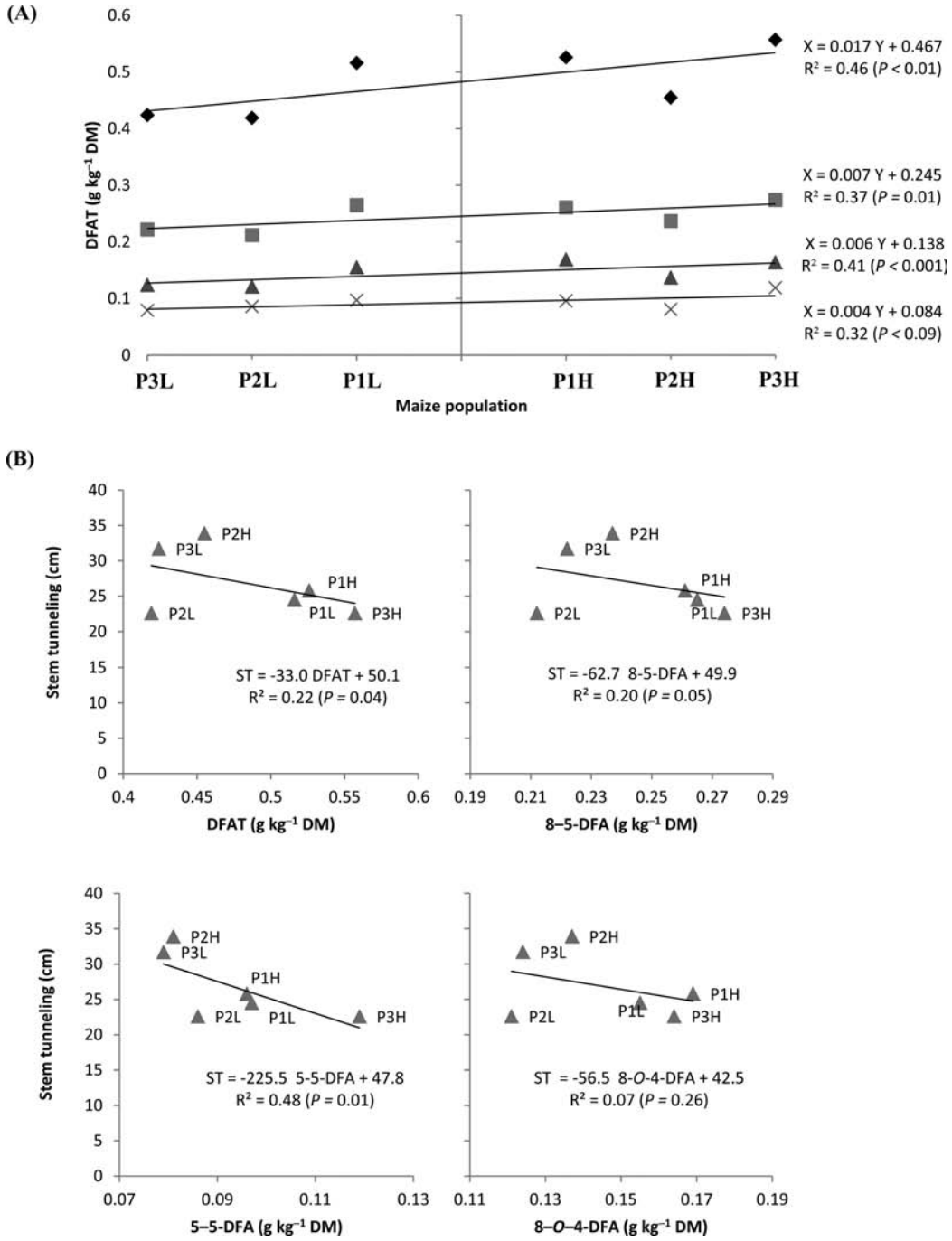

Figure 2. Response to selection for DFAs and DFA relationships with borer tunneling. Scatter plots and simple linear regression equations ($N = 36$) for (A) total and individual ester-linked DFA concentration as a function of maize populations developed, and (B) stem tunnel length (ST) caused by corn borers as a function of total and individual DFA concentration. To analyze the selection program efficiency, values of 3, 2, 1, −1, −2, and −3 were assigned to populations P3H, P2H, P1H, P1L, P2L, and P2L, respectively.

modulate the concentration of DFAs at 0.017 g kg^{-1} of dry matter per cycle of selection (Table 1 and Figure 2A).

After 3 cycles of divergent selection, P3H had 31% higher DFAT than P3L. Current analytical results agree with those previously observed after preceding evaluations of two generations of divergent selection, where P2H had 21% higher DFAT content than P2L,[33] indicating that the DFAT concentration is a heritable trait that can be modified through classical breeding techniques. An unexpected reduction of DFAs was observed in P2H in both current and preceding evaluations.[31] The ongoing selection program provides unique genotypes to study the effect of selection on other quantitative traits and to validate candidate genes potentially involved in FA dimerization. Additional cycles of selection will clarify if the DFAT concentration reaches a plateau in any direction of selection, which would indicate the existence of an upper or lower threshold DFAT concentration that compromises the plant development or viability.

DFAs as a Plant Resistance Mechanism against Pest and Diseases. The relationship between cell-wall cross-linking and insect resistance was initially suggested by Fry.[45] Since then, diverse studies have pointed out the role of cell-wall

DOI: 10.1021/jf505341d
J. Agric. Food Chem. 2015, 63, 2206−2214

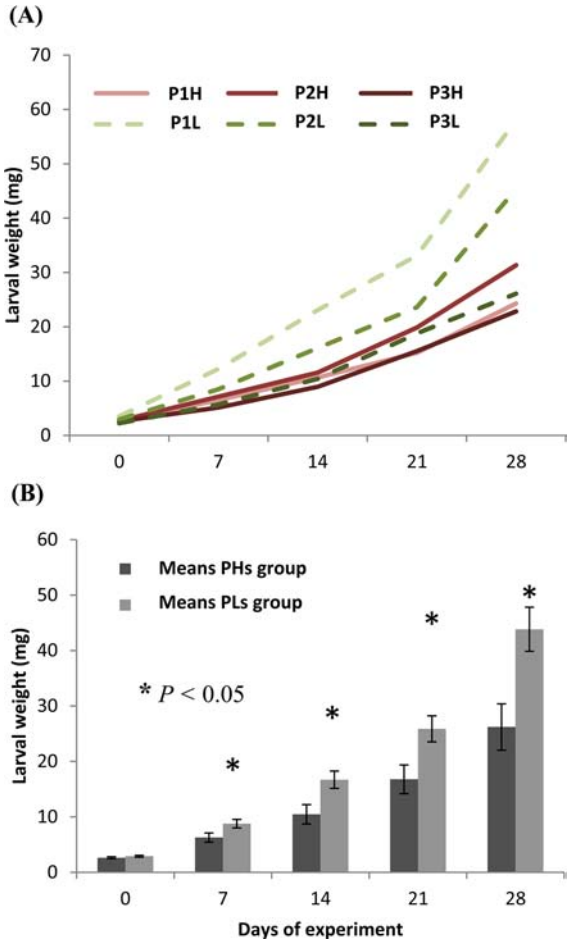

Figure 3. Laboratory-feeding bioassays with larvae fed on pith stem tissues from the six maize populations evaluated. (A) Weight (mg) of larvae fed on pith stem tissues from the six maize populations evaluated measured after 0, 7, 14, 21, and 28 days of experiment. (B) Orthogonal contrast for larval weight among high (P1H, P2H, and P3H) and low (P1L, P2L, and P3L) DFAT populations of corn hybrid CO125 × PB130 divergently selected for DFAT. Error bars are standard error of the means (N = 3). (∗) Probability level lower than 5%.

cross-linking through ferulates on resistance to stem borers in cotton (*Gossypium hirsutum*[46]) and armyworms in tall fescue (*Festuca arundinacea*[34]) as well as cereal beetles,[13] cereal aphids,[47,48] and cereal midges.[49,50] Cell-wall strengthening through FAs was also involved in the resistance to fungi, such as *Fusarium graminearum* and *Fusarium verticillioides* in maize,[51−53] *Clerotium rolfsii* in chickpea (*Cicer arietinum*[54]), and *Puccinia coronata* in smooth bromegrass (*Bromus inermis*[55]). The first study that observed negative correlations between the DFA concentration and damage caused by corn borer larvae was carried out by Bergvinson et al.[30] Subsequent experiments supported the relationship between DFAs and corn borer resistance in diverse and heterogeneous maize genotypes.[31,33,56,57]

Tissue toughness and hardness are two major mechanical defenses to herbivory of plants,[19,57] and several studies have shown a positive relationship between the DFA concentration and toughness of the tissues that corn borer larvae use as feed.[12,58] In the current trials under artificial infestation, the genotype × location interaction was not significant for the combined damage by both corn borer species as previously observed.[43] With the damage data combined across locations, borer stem tunneling was 29% lower in the P3H population than in P3L. The marked increase in tunnel length observed in P2H agreed with its unexpected low DFAT concentration (Table 1). The length of stem tunnels caused by corn borers showed a significant and negative regression coefficient with compounds **4**, **5** + **6**, and DFAT (Figure 2B). Similarly, Sampietro et al.[53] observed that compound **5** and DFAT were the best explanatory parameters for susceptibility to *F. verticillioides* in evaluations of 12 maize genotypes with different levels of resistance to this fungal pathogen.

Larvae weight obtained from laboratory-feeding bioassays showed significant differences between maize populations evaluated (Figure 3A). On the basis of significant orthogonal contrasts, larvae fed on PHs at 7, 14, 21, and 28 days had 29% (p = 0.03), 37% (p = 0.009), 35% (p = 0.01), and 40% (p = 0.003) lower weight, respectively, than larvae fed on PLs (Figure 3B). At these significant time points, P2H, which had an unexpected reduction of DFAs, showed a pattern closer to the maize populations with a low concentration of DFAs (panels A and B of Figure 3). In agreement with these results, significant negative correlations were found between the larvae weight and DFA concentration in the sheaths of six maize genotypes previously evaluated.[59] Furthermore, Buanafina and co-authors[46] showed that significantly reduced levels of these cell-wall ferulate monomers and dimers in tall fescue affected positively all measures of *Spodoptera frugiperda* (J. E. Smith) larval performance examined (pupal weight, duration of the larval stage, and growth rate).

Maize genotypes evaluated after the DFA selection program developed by our group showed, first, significant differences for the DFA concentration and, second, that these differences were significant and negatively correlated with the stem tunneling caused by corn borers. In addition, laboratory-feeding bioassays showed that corn borer larval performance was negatively associated with the level of DFAT in pith stem tissues that they were fed. From the point of view of resistance definitions, we demonstrate that DFAs have a role in plant resistance (as less tunnel length damage in the plant) and insect resistance (properly affecting borer development).

The concentration of compound **1** was the only cell-wall trait evaluated that showed significant differences among maize populations and significant and positive simple linear regression coefficients with the selection criterion (DFAs) (Table 1, Table S1 of the Supporting Informaton, and Figure 4A). As discussed above, the "sawtooth" pattern observed in P2H for DFA concentration might have also affected the deposition of FAs. The positive regression coefficient observed between ferulate monomers and dimers indicates that cell-wall ester-linked compound **1** was not significantly depleted by producing DFAs. These results agree with the hypothesis that a higher concentration of feruloylated arabinoxylan polymers present in the cell wall allows for compound **1** molecules to be placed in closer physical proximity, facilitating the ferulate dimerization reactions.[27]

The concentrations of compounds **1** and **2** and the total amount of cell-wall material were not significantly correlated with stem tunneling by corn borers (Figure 4B and Figure S1 of the Supporting Informaton). Most p-coumarate accretion occurs in tandem with lignification, making compound **2** accumulation a good indicator of lignin deposition.[60] Even though small amounts of compound **2** are esterified to arabinoxylans, most moieties are ester-linked to the γ position of the syringyl units of lignin.[38] Experimental observations

DOI: 10.1021/jf505341d
J. Agric. Food Chem. 2015, 63, 2206−2214

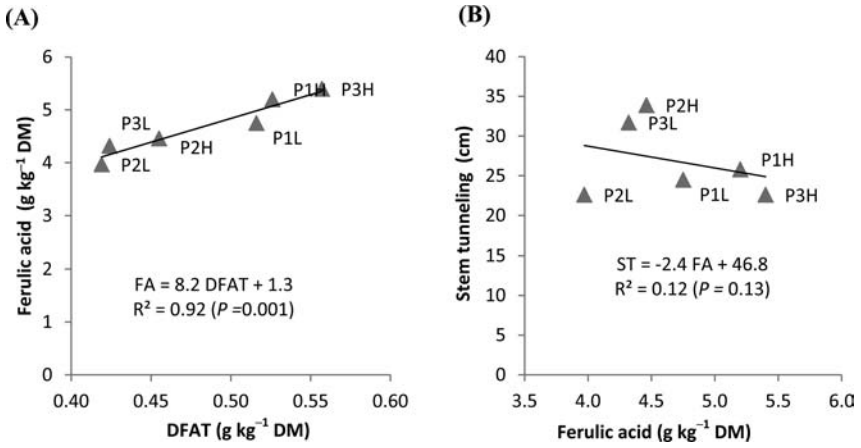

Figure 4. Relationships between FA, DFAs, and borer tunneling. Scatter plots and simple linear regression equations (N = 36) for (A) FA as a function of total ester-linked DFAs and (B) stem tunnel length (ST) by corn borers (in centimeters) as a function of FA (g kg^{-1} of dry matter).

suggest that substitution of sinapyl alcohol with compound **2** occurs prior to its incorporation into the lignin polymer and the presence of the ester linkage allows or facilitates the incorporation of sinapyl alcohol into the growing lignin polymer.[61,62] Maize populations evaluated in the current selection program showed no differences for the compound **2** concentration, and the regression analysis between compound **2** and DFAT showed non-significant regression coefficients (see Figure S1A of the Supporting Informaton). Current results agree with those previously observed after 2 cycles of divergent selection,[34] suggesting that compound **2** and, thereby, lignin deposition were not impaired during the selection program for DFAs. Conversely, some other approaches, such as the transgenic overexpression of a FA esterase gene (*faeA*) in tall fescue, significantly affect the concentration of other hydroxycinnamates, such as compound **2**.[46]

The total amount of cell-wall material has been considered a defense mechanism related with insect nutrition because elevated levels of indigestible cell-wall material increase the compactness of the diet to the point that insects are unable to ingest sufficient quantities of nutrients and water.[15,33,63] Additionally, the total amount of cell-wall material and cross-linking of cell-wall components through DFAs are physical barriers that herbivores must mechanically rupture through mastication to gain access to the cytoplasmic nutrients contained within feeding tissues.[57,46] Nevertheless, in the current evaluation, maize populations with the highest concentration of DFAs (P3Hs) were more resistant than P3Ls, despite having similar cell-wall contents (Table 1), suggesting that the stiffness conferred by DFAs rather than the total cell-wall content was critical for caterpillar deterrence.

As a summary, the results showed that the extent of cell-wall ester-linked DFA deposition in maize pith stem tissues can be genetically regulated through breeding. The concentration of FA monomers showed a significant and positive direct response to selection for DFAs; however, none of the cell-wall traits evaluated other than DFAs was significantly correlated with stem tunneling caused by corn borers. In addition, laboratory-feeding bioassays showed that corn borer larval performance was negatively associated with the level of DFAT in pith stem tissues that they were fed. These results suggest that cell-wall stiffness conferred by DFAs rather than the indigestibility of the cell-wall components is critical for corn borer larvae deterrence. Furthermore, this is the first report that demonstrates a direct relationship between DFA deposition in maize cell walls and corn borer resistance within the same genetic background, avoiding genotype-specific resistance mechanisms that may have biased the earlier works.

Overall, current results provide evidence to encourage further research to better understand the role of cell-wall cross-linking through ferulates as a common resistance mechanism against pests and diseases in grasses. Our results highlight the possibility of using conventional breeding to increase the concentration of DFAs and improve natural resistance in maize plants. Cross-linking of cell-wall polysaccharides through DFAs is a resistance factor that should be a candidate for inclusion as indirect selection criteria in Integrated Pest Management programs.

■ ASSOCIATED CONTENT

Supporting Information

Mean squares of main sources of variation from analysis of variance (Table S1) and relationships between DFAs and *p*-coumarate and cell-wall content and between *p*-coumarate and cell-wall content and borer tunneling (Figure S1). This material is available free of charge via the Internet at http://pubs.acs.org.

■ AUTHOR INFORMATION

Corresponding Author

*Telephone: +1-940-369-7235. E-mail: jaime.barros-rios@unt.edu.

Present Address

‡Jaime Barros-Rios: Department of Biological Sciences, University of North Texas, 1155 Union Circle #305220, Denton, Texas 76203, United States.

Funding

This research was supported by the National Plan for Research and Development of Spain (Project Codes AGL2006-13140, AGL2009-09611, and AGL2012-33415). Jaime Barros-Rios acknowledges a grant from the Ministry of Science and Innovation (Spain). Rogelio Santiago acknowledges a postdoctoral contract "Isidro Parga Pondal" financed by the Autonomous Government of Galicia (Spain) and the European Social Fund and "Ramón y Cajal" supported by the Ministry of Economy and Competitiveness of Spain and the Vigo University.

Notes

The authors declare no competing financial interest.

DOI: 10.1021/jf505341d
J. Agric. Food Chem. 2015, 63, 2206−2214

REFERENCES

(1) FAOSTAT. http://faostat.fao.org (accessed Oct 2012).

(2) Velasco, P.; Revilla, P.; Monetti, L.; Butrón, A.; Malvar, R. A. Corn borers (Lepidoptera: Noctuidae, Crambidae) in northwestern Spain: Population dynamics and distribution. *Maydica* **2007**, *52*, 195−203.

(3) Meissle, M.; Mouron, P.; Musa, T.; Bigler, F.; Pons, X.; Vasileiadis, V. P. Pests, pesticide use and alternative options in European maize production: Current status and future prospects. *J. Appl. Entomol.* **2010**, *134*, 357−375.

(4) Eizaguirre, M.; Fantinou, A. Abundance of *Sesamia nonagrioides* (Lef.) (Lepidoptera: Noctuidae) on the edges of the Mediterranean Basin. *J. Pest. Sci.* **2013**, *86*, 409−417.

(5) Vasileiadis, V. P.; Sattin, M.; Otto, S.; Veres, A.; Pálinkás, Z.; Ban, R.; Pons, X.; Kudsk, P.; van der Weide, R.; Czembor, E.; Mooneng, A. C.; Kissb, J. Crop protection in European maize-based cropping systems: Current practices and recommendations for innovative Integrated Pest Management. *Agric. Syst.* **2011**, *104*, 533−540.

(6) James, C. *Global Status of Commercialized Transgenic Crops: 2000*; ISAAA Publications: Ithaca, NY, 2000; ISAAA Briefs Number 21: Preview.

(7) Wesseler, J.; Scatasta, S.; Nillesen, E. The maximum incremental social tolerable irreversible costs (MISTICs) and other benefits and costs of introducing transgenic maize in the EU-15. *Pedobiologia* **2007**, *51*, 261−269.

(8) Anglade, B.; Gouesnard, A.; Boyat, A.; Panouillé, A. Effects of multitrait recurrent selection for ECB tolerance and for agronomic traits in FS12 maize synthetic. *Maydica* **1996**, *41*, 97−104.

(9) Hallauer, A. R.; Carena, M. J.; Miranda Filho, J. B. *Handbook of Plant Breeding: Quantitative Genetics in Maize Breeding*; Springer: Heidelberg, Germany, 2010.

(10) Collinge, D. B.; Jorgensen, H. J. L.; Lund, O. S.; Lyngkjar, M. F. Engineering pathogen resistance in crop plants: Current trends and future prospects. *Annu. Rev. Phytopathol.* **2010**, *48*, 269−291.

(11) Buendgen, M. R.; Coors, J. G.; Grombacher, A. W.; Russell, W. A. European corn borer resistance and cell wall composition of tree maize populations. *Crop Sci.* **1990**, *30*, 505−510.

(12) Bergvinson, D. J.; Arnason, J. T.; Hamilton, R. I. Phytochemical changes during recurrent selection for resistance to the European corn borer. *Crop Sci.* **1997**, *37*, 1567−1572.

(13) García-Lara, S.; Bergvinson, D.; Burt, A. J.; Ramputh, A. I.; Díaz-Pontones, D. M.; Arnason, J. T. The role of pericarp cell wall components in maize weevil resistance. *Crop Sci.* **2004**, *44*, 1546−1552.

(14) Malvar, R. A.; Butrón, A.; Ordás, B.; Santiago, R. Causes of natural resistance to stem borers in maize. In *Crop Protection Research Advances*; Williams, P. V., Ed.; Nova Science Publishers, Inc.: New York, 2008; pp 57−100.

(15) Hale, T. C.; Reinert, J. A.; White, R. H. Resistance of zoysiagrasses (*Zoysia* spp.) to fall armyworm (Lepidoptera: Noctuidae): I. Leaf tensile strength and cell wall components. *Int. Turfgrass Soc. Res. J.* **2009**, *11*, 639−648.

(16) Schoonhoven, L. M.; Jermey, T.; van Loon, J. J. A. *Insect-Plant Biology: From Physiology to Evolution*; Chapman & Hall: London, U.K., 1998.

(17) Reinert, J. A.; Engelke, M. C. Resistance in zoysiagrass, *Zoysia* spp., to the tropical sod webworm, *Herpetogramma phaeopteralis* Guenne. *Int. Turfgrass Soc. Res. J.* **2001**, *9*, 798−801.

(18) Choong, M. F. What makes a leaf tough and how this affects the pattern of *Castanopsis fissa* leaf consumption by caterpillars. *Funct. Ecol.* **1996**, *10*, 668−674.

(19) Clissold, F. J. The biomechanics of chewing and plant fracture: Mechanisms and implications. *Adv. Insect Physiol.* **2008**, *34*, 317−372.

(20) Dreyer, D. L.; Reese, J. C.; Kenneth, C. J. Aphid feeding deterrents in sorghum bioassay isolation and characterization. *J. Chem. Ecol.* **1981**, *7*, 273−284.

(21) Serratos, A.; Arnason, J. T.; Nozzolillo, C.; Lambert, J. D. H.; Philogène, B. J. R.; Fulcher, G.; Davidson, K.; Peacock, L.; Atkinson, J.; Morand, P. Factors contributing to resistance of exotic maize populations to maize weevil, *Sitophilus zeamais*. *J. Chem. Ecol.* **1987**, *13*, 751−762.

(22) Arnason, J. T.; Gale, J.; Conilh, B. B.; Sen, A.; Miller, S. S.; Philogène, B. J. R.; Lambert, J. D. H.; Fulcher, R. G.; Serratos, J. A.; Minh, J. A. Role of phenolics in resistance of maize grain to the stored grain insects, *Protstephanus trucantus* (Horn) and *Sitophilus zeamais* (Motsch). *J. Stored Prod. Res.* **1992**, *28*, 119−126.

(23) Hatfield, R. D.; Ralph, J. Modelling the feasibilty of intramolecular dehydro-diferulate formation in grass walls. *J. Sci. Food Agric.* **1999**, *79*, 425−427.

(24) Saulnier, L.; Thibault, J. F. Ferulic acid and diferulic acids as components of sugar-beet pectins and maize bran heteroxylans. *J. Sci. Food Agric.* **1999**, *79*, 396−402.

(25) Ishii, T.; Hiroi, T. Linkage of phenolic acids to cell-wall polysaccharides of bamboo shoot. *Carbohydr. Res.* **1990**, *206*, 297−310.

(26) Ralph, J.; Grabber, J. H.; Hatfield, R. D. Lignin-ferulate crosslinks in grasses: Active incorporation of ferulate polysaccharide esters into ryegrass lignins. *Carbohydr. Res.* **1995**, *275*, 167−178.

(27) Grabber, J. H.; Ralph, J.; Hatfield, R. D. Cross-linking of maize walls by ferulate dimerization and incorporation into lignin. *J. Agric. Food Chem.* **2000**, *48*, 6106−6113.

(28) Fry, S. C.; Willis, S. C.; Paterson, A. E. Intraprotoplasmic and wall-localised formation of arabinoxylan-bound diferulates and larger ferulate coupling-products in maize cell-suspension cultures. *Planta* **2000**, *211*, 679−692.

(29) Santiago, R.; Malvar, R. A. Role of dehydrodiferulates in maize resistance to pests and diseases. *Int. J. Mol. Sci.* **2010**, *11.2*, 691−703.

(30) Bergvinson, D. J.; Arnason, J. T.; Hamilton, R. I.; Mihm, J. A.; Jewell, D. C. Determining leaf toughness and its role in maize resistance to the European corn borer (Lepidoptera: Pyralidae). *J. Econ. Entomol.* **1994**, *87*, 1743−1748.

(31) Santiago, R.; Butrón, A.; Arnason, J. T.; Reid, L. M.; Souto, X. C.; Malvar, R. A. Putative role of pith cell wall phenylpropanoids in *Sesamia nonagrioides* (Lepidoptera: Noctuidae) resistance. *J. Agric. Food Chem.* **2006**, *54*, 2274−2279.

(32) Santiago, R.; Sandoya, G.; Butrón, A.; Barros, J.; Malvar, R. A. Changes in phenolic concentrations during recurrent selection for resistance to the Mediterranean corn borer (*Sesamia nonagrioides* Lef.). *J. Agric. Food Chem.* **2008**, *56*, 8017−8022.

(33) Barros-Rios, J.; Malvar, R. A.; Jung, H-J. G.; Santiago, R. Cell wall composition as a maize defense mechanism against corn borers. *Phytochemistry* **2011**, *72*, 365−371.

(34) de Buanafina, M. M. O.; Howard, W. F. Modification of esterified cell wall phenolics increases vulnerability of tall fescue to herbivory by fall armyworm. *Planta* **2012**, *236*, 513−523.

(35) Barros-Rios, J.; Malvar, R. A.; Jung, H.-J. G.; Bunzel, M.; Santiago, R. Divergent selection for ester-linked diferulates in maize pith stalk tissues. Effects on cell wall composition and degradability. *Phytochemistry* **2012**, *83*, 43−50.

(36) Butrón, A.; Malvar, R. A.; Velasco, P.; Vales, M. I.; Ordás, A. Combining abilities for maize stem antibiosis, yield loss, and yield under infestation and non infestation with pink stem borer. *Crop Sci.* **1999**, *39*, 691−696.

(37) Eizaguirre, M.; Albajes, R. Diapause induction in the stem corn borer, *Sesamia nonagrioides* (Lepidoptera: Noctuidae). *Entomol. Gen.* **1992**, *17*, 277−283.

(38) Waldron, K. W.; Parr, A. J.; Ng, A.; Ralph, J.; Williamson, G. Cell wall esterified phenolic dimers: identification and quantification by reversed phase highperformance liquid chromatography and diode array detection. *Phytochem. Anal.* **1996**, *7*, 305−312.

(39) Ralph, J.; Hatfield, R. D.; Quideau, S.; Helm, R. F.; Grabber, J. H.; Jung, H.-J. G. Pathway of *p*-coumaric acid incorporation into maize lignin as revealed by NMR. *J. Am. Chem. Soc.* **1994**, *116*, 9448−9456.

(40) Strack, D.; Heilemann, J.; Mömken, M.; Wray, V. Cell wall-conjugated phenolics from Coniferae leaves. *Phytochemistry* **1988**, *27*, 3517−3521.

DOI: 10.1021/jf505341d
J. Agric. Food Chem. 2015, 63, 2206−2214

(41) Weber, B.; Hoesch, L.; Rast, D. M. Protocatechualdehyde and other phenols as cell wall components of grapevine leaves. *Phytochemistry* **1995**, *40*, 433−437.
(42) SAS Institute, Inc. *The SAS System. SAS Online Doc HTML Format Version 8*; SAS Institute, Inc.: Cary, NC, 2007.
(43) Carena, M. J.; Hallauer, A. R. Response to inbred progeny recurrent selection in leaming and midland yellow dent populations. *Maydica* **2001**, *46*, 1−10.
(44) Sandoya, G.; Butrón, A.; Alvarez, A.; Ordás, A.; Malvar, R. A. Direct response of a maize synthetic to recurrent selection for resistance to stem borers. *Crop Sci.* **2008**, *48*, 113−118.
(45) Fry, S. C. Cross-linking of matrix polymers in the growing cell walls of angiosperms. *Annu. Rev. Plant Physiol.* **1986**, *37*, 165−186.
(46) Wang, Y.; Cai, Q. N.; Zhang, Q. W.; Han, Y. Effect of secondary substances from wheat on the growth and digestive physiology of cotton bollworm *Helicoverpa armigera* (Lepidoptera: Noctuidae). *Eur. J. Entomol.* **2006**, *103*, 255−258.
(47) Cabrera, H. M.; Munoz, O.; Zuniga, G. E.; Corcuera, L. J.; Argandona, V. H. Changes in ferulic acid and lipid content in aphid-infested barley. *Phytochemistry* **1995**, *39*, 1023−1026.
(48) Havlickova, H.; Cvikrova, M.; Eder, J. Phenolic acids in wheat cultivars in relation to plant suitability for and response to cereal aphids. *Pflanzenschutz* **1996**, *103*, 535−542.
(49) Ding, H.; Lamb, R. J.; Ames, N. Inducible production of phenolic acids in wheat and antibiotic resistance to *Sitodiplosis mosellana*. *J. Chem. Ecol.* **2000**, *26*, 969−985.
(50) Abdel-Aal, E. S. M.; Hucl, P.; Sosluski, F. W.; Graf, R.; Gillot, C.; Pietrzak, L. Screening spring wheat for midge resistance in relation to ferulic acid content. *J. Agric. Food Chem.* **1993**, *49*, 3559−3566.
(51) Bily, A. C.; Reid, L. M.; Taylor, J. H.; Johnston, D.; Malouin, C.; Burt, A. J.; Bakan, B.; Regnault-Roger, C.; Pauls, K. P.; Arnason, J. T.; Philogène, J. R. Dehydrodimers of ferulic acid in maize grain pericarp and aleurone: Resistance factors to *Fusarium graminearum*. *Phytopathology* **2003**, *93*, 712−719.
(52) Santiago, R.; Reid, L. M.; Arnason, J. T.; Zhu, X.; Martinez, N.; Malvar, R. A. Phenolics in maize genotypes differing in susceptibility to *Gibberella* stalk rot (*Fusarium graminearum* Schwabe). *J. Agric. Food Chem.* **2007**, *55*, 5186−5193.
(53) Sampietro, D. A.; Fauguel, C. M.; Vattuone, M. A.; Presello, D. A.; Catalán, C. A. N. Phenylpropanoids from maize pericarp: resistance factors to kernel infection and fumonisin accumulation by *Fusarium verticillioides*. *Eur. J. Plant Pathol.* **2012**, *135*, 105−113.
(54) Sarma, B. K.; Singh, U. P. Ferulic acid may prevent infection of *Cicer arietinum* by *Sclerotium rolfsii*. *World J. Microbiol. Biotechnol.* **2003**, *19*, 123−127.
(55) Delgado, N. J.; Casler, M. D.; Grau, C. R.; Jung, H. G. Reactions of smooth bromegrass clones with divergent lignin or etherified ferulic acid concentration to three fungal pathogens. *Crop Sci.* **2002**, *42*, 1824−1831.
(56) Bergvinson, D. J.; Hamilton, R. I.; Arnason, J. T. Leaf profile of maize resistance factors to European corn borer, *Ostrinia nubilalis*. *J. Chem. Ecol.* **1995**, *21*, 343−354.
(57) Lucas, P. W.; Turner, I. M.; Dominy, N. J.; Yamashita, N. Mechanical defences to herbivory. *Ann. Bot.* **2000**, *86*, 913−920.
(58) Santiago, R.; Souto, X. C.; Sotelo, J.; Butrón, A.; Malvar, R. A. Relationship between maize stem structural characteristics and resistance to pink stem borer (Lepidoptera: Noctuidae) attack. *J. Econ. Entomol.* **2003**, *96*, 1563−1570.
(59) Santiago, R.; Butrón, A.; Reid, L.; Arnason, J. T.; Sandoya, G.; Souto, X. C.; Malvar, R. A. Diferulate content of maize sheaths is associated with resistance to the Mediterranean Corn Borer *Sesamia nonagrioides* (Lepidoptera: Noctuidae). *J. Agric. Food Chem.* **2006**, *54*, 9140−9144.
(60) Morrison, T. A.; Jung, H. G.; Buxton, D. R.; Hatfield, R. D. Cell wall composition of maize internodes of varying maturity. *Crop Sci.* **1998**, *38*, 455−460.
(61) Lu, F.; Ralph, J. Detection and determination of *p*-coumaroylated units in lignins. *J. Agric. Food Chem.* **1999**, *47*, 1988−1992.
(62) Ralph, J.; Lundquist, K.; Brunow, G.; Lu, F.; Kim, H.; Schatz, P. F.; Marita, J. M.; Hatfield, R. D.; Ralph, S. A.; Christensen, J. H.; Boerjan, W. Lignins: Natural polymers from oxidative coupling of 4-hydroxyphenylpropanoids. *Phytochemistry* **2004**, *3*, 29−60.
(63) Bernays, E. A. Diet-induced head allometry among foliage-chewing insects and its importance for graminivores. *Science* **1986**, *231*, 495−497.

DOI: 10.1021/jf505341d
J. Agric. Food Chem. 2015, 63, 2206−2214

MATERIALS AND METHODS

Materials and Chemicals. Sephadex G-25, CM-Sepharose FF, phenyl-Sepharose HP, Superdex 75 16/60, preparative columns, and IEF calibration kit were purchased from GE Life sciences (Pittsburgh, PA, USA). Bovine fibrinogen and thrombin were purchased from the Tianjin Blood Institute (Tianjin, China). Human fibrinogen was purchased from Sigma Chemical Co. (St. Louis, MO, USA). Soybean trypsin inhibitor (SBTI), *N*-α-tosyl-L-phenylalanine chloromethyl ketone (TPCK), phenylmethanesulfonyl fluoride (PMSF), aprotinin, pepstatin, and low molecular weight SDS-PAGE Protein standard kit (ranging from 14.4 to 97.4 kDa) were purchased from Sangon (Shanghai, China).

Strain and Culture Conditions. *Cordyceps militaris* strain was stored on PDA slants. The mycelia were transferred from the slants to plate medium. The mycelia were inoculated aseptically into 250 mL shake flasks containing 50 mL of fermentation media composed of 2% sucrose and 5% soybean cake powder. Fermentation was carried out for 5 days at 23 °C, 180 rpm. The fermentation broth was centrifuged (10000 rpm, 10 min, 4 °C), and the supernatant was considered as the crude enzyme extract.

Enzyme Assay and Protein Determination. Fibrinolytic activity was determined by using the method of Astrup and Mullertz[22] with slight modifications. Fibrin plates were prepared as follows: fibrinogen (0.4%, w/v) dissolved in 5 mL of 100 mM barbital sodium−chlorhydric acid buffer, pH 7.8, was mixed with 5 mL of 0.5% (w/v) agarose solution along with 1 mL of thrombin solution (200 U/mL) and poured into Petri plates; after standing for 1 h at room temperature for clot formation, the plate was used to measure fibrinolytic activity. In brief, 10 μL of the enzyme solution was carefully placed on the fibrin plate and incubated at 37 °C for 6 h, and the diameter of the lytic circle was measured. The diameter was directly proportional to the potency of the fibrinolytic activity, and the unit of the enzyme activity was determined according to a calibration curve using urokinase as standard. The protein content was estimated by Lowry method[23] using bovine serum albumin as a standard. The carbohydrate content of the purified enzyme was quantified by anthrone colorimetric method using glucose as a standard.[24]

Purification of Fibrinolytic Enzyme. Crude sample was subjected to 0−20% saturation of $(NH_4)_2SO_4$ precipitation. The supernatant obtained by centrifugation (10000 rpm for 20 min at 4 °C) was buffer exchanged on a Sephadex G-25 column (1.6 cm × 50 cm) using 0.02 mol/L sodium phosphate buffer (pH 7.4). After buffer exchange, the enzyme solution was loaded onto a phenyl-Sepharose HP column (1.6 cm × 30 cm) which was earlier equilibrated with 0.02 mol/L sodium phosphate buffer (pH 7.4) containing 30% saturated $(NH_4)_2SO_4$. Bound proteins were eluted with a decreasing linear gradient of 30−0% $(NH_4)_2SO_4$ in 0.02 mol/L sodium phosphate buffer (pH 7.4). The active fractions were collected, buffer exchanged using 0.02 mol/L sodium phosphate buffer, pH 6.0, and loaded onto a cation exchange column CM-Sepharose FF (2.6 cm × 20 cm) which was previously equilibrated with the same buffer. Fractions exhibiting the most potent fibrinolytic activity were pooled and further purified on a Superdex 75 gel filtration column (1.6 cm × 60 cm) using 0.02 mol/L sodium phosphate buffer containing 0.3 mol/L NaCl (pH 6.0). Finally, the purified active fractions were pooled, lyophilized, and used for further characterization. All the purification steps were performed at 4 °C unless otherwise stated.

Determination of Molecular Weight and Isoelectric Point. The molecular weight of the purified enzyme was determined by SDS-PAGE (under reducing denaturing conditions) as described by Laemmli,[25] using a 12% polyacrylamide gel. Protein bands were visualized by staining the gel with Coomassie brilliant blue R-250. For calibration, an SDS-PAGE midrange molecular weight standard kit (Sangon Biotech, Shanghai, China) comprising rabbit phosphorylase B (97.4 kDa), bovine serum albumin (66.2 kDa), ovalbumin (42.7 kDa), bovine carbonic anhydrase (31.0 kDa), and chicken egg white lysozyme (14.4 kDa), was used.

The native molecular weight of the enzyme was determined by gel filtration chromatography using a Superdex 75 (1.6 cm × 60 cm) column in 20 mM phosphate buffer (pH 7.4) containing 300 mM NaCl. Gel filtration low molecular weight calibration kit comprising bovine serum albumin (67 kDa), ovalbumin (43 kDa), chymotrypsinogen A (25 kDa), and ribonuclease A (13.7 kDa), was used. The void volume of the column was determined by using blue dextran 2000.

The isoelectric point (p*I*) of the purified enzyme was determined by isoelectric focusing electrophoresis (IEF) using homogeneous polyacrylamide gels (7.5% polyacrylamide with 3% cross-linkage) containing carrier ampholytes (3−9).[26]

Q-TOF2 Tandem Mass Spectrometry Sequencing. To determine the partial amino acid sequence by Q-TOF2 tandem mass spectrometry, the purified enzyme was subjected to SDS-PAGE. Protein band was excised from the gel and submitted for amino acid sequencing using high performance liquid chromatography−electrospray tandem mass spectrometry (HPLC-ESI-MS/MS) at National Center for Biomedical Analysis, Military Academy of Medical Sciences (Beijing, China). Mass spectral sequencing was performed using a Q-TOF II mass analyzer (Q-TOF2, Micromass Ltd., Manchester, UK). Peptide sequencing was performed using a palladium-coated borosilicate electrospray needle (Protana, Denmark). The mass spectrometer was used in positive ion mode with a source temperature of 80 °C, and a potential of 800 V was applied to the nanospray probe. MS/MS spectra were transformed using MaxEnt3 (MassLynx, Micromass), and amino acid sequences were interpreted manually using PepSeq (BioLynx, Micromass).

Effects of Environmental Factors on Enzyme Activity. The optimal temperature of the purified enzyme was determined by measuring the activity at different temperatures (16−60 °C) in sodium barbital buffer (pH 7.4). The thermal stability of the enzyme was determined by incubating the enzyme at different temperatures (23−60 °C) for 0.5 h in sodium barbital buffer (pH 7.4), and the residual activities were assayed.

To determine the optimal pH of the purified fibrinolytic enzyme, the enzyme activity was assayed at 37 °C in different buffers within the range of pH 6.8−8.2. pH stability of the purified enzyme was determined by incubating the enzyme in different buffers ranging from pH 3−12 for 1 h, and the residual activities were assayed by fibrin plate method. The buffers used were: citrate−phosphate (pH 3.0−7.0), barbital sodium−chlorhydric acid buffer (pH 8.0−9.0), Na_2CO_3−$NaHCO_3$ (pH 9.5−10.5), and Na_2HPO_4−NaOH buffer (pH 11.0−12.0).

Effects of various factors such as (1) metal ions (Cu^{2+}, Co^{2+}, K^+, Fe^{3+}, Fe^{2+}, Ca^{2+}, Mg^{2+}, Mn^{2+}, Na^+, and Zn^{2+}) at a concentration of 5 mM at 37 °C for 18 h; (2) protease inhibitors such as pepstatin, PMSF (phenylmethyl sulfonyl fluoride), aprotinin, TPCK (*N*-α-tosyl-L-phenyl alanine chloromethyl ketone), SBTI (soybean trypsin inhibitor), Lys and metal chelator EDTA (ethylenediamine tetraacetic acid) at concentrations of 2.0 and 10 mM (2.5 and 10 mM in case of EDTA and Lys) at 37 °C for 10 min; (3) various protective agents and other reagents (5 mmol/L reduced glutathione, 5 mmol/L oxidized glutathione, 20 mmol/L cysteine, 0.5% β-mercaptoethanol, 1%, w/v, bovine serum albumin, 1% gelatin, 1% peptone), organic substances (10%, v/v, acetone, 10% glycerol), and denaturants (urea and SDS) at 37 °C for 4 h on the activity were determined as above.

Simulated Gastric and Blood Environment Effect on Enzyme Activity. To prepare simulated gastric juice solution, 10% HCl solution (pH 3.0) was first autoclaved (121 °C, 15 min), cooled down to 37 °C, and mixed with pepsin (1 g per 100 mL). Simulated blood solution (Clorox solution, commonly used for mammalian heart perfusion test) was prepared by dissolving 0.9 g NaCl, 0.042 g KCl, 0.024 g $CaCl_2$, 0.02 g $NaHCO_3$, and 0.2 g glucose into 100 mL deionized water and stored at 4 °C until further use.

The activity of the enzyme in simulated gastric juice and simulated blood was tested in six different combinations:

(1) 100 μL of water + 50 μL of purified enzyme;
(2) 50 μL of artificial gastric juice + 50 μL of broth + 50 μL of purified enzyme;
(3) 50 μL of artificial gastric juice + 50 μL of H_2O + 50 μL of purified enzyme;

DOI: 10.1021/jf505717e
J. Agric. Food Chem. 2015, 63, 2215−2224

(4) 50 μL of artificial gastric juice + 50 μL of 10% maltose + 50 μL of purified enzyme;
(5) 50 μL of artificial gastric juice + 25 μL of broth + 25 μL of 10% maltose + 50 μL of purified enzyme;
(6) 100 μL of Clorox solution + 50 μL of purified enzyme.

Simulated gastric and Clorox solutions were added to the purified enzyme separately and incubated at 37 °C for 4 h. The effect of simulated gastric juice in the presence of protein and carbohydrate was also evaluated. The residual activities were measured by standard fibrin plate method.

Storage Stability of Purified Enzyme. *1. Impact of Freeze−Thawing on Storage of the Purified Enzyme.* Purified fibrinolytic enzyme (0.151 mg/mL) was stored at −20 °C and −70 °C, and repeated freeze−thawing was carried out for 2, 4, 6, 8, 11, 13, 15, and 17 times and the residual enzyme activity was determined.

2. Effect of Stabilizers on Storage Stability of the Purified Enzyme. To appropriate volume of purified enzyme (0.066 mg/mL), an equal volume of different concentrations of glycerol and sucrose (5%, 10%, 15%, 20%) were added, mixed, and stored at 4 °C refrigerator for 1 week. The residual activity was measured by standard assay.

3. Long-Term Storage Stability of the Purified Enzyme. The purified enzyme (both in liquid (0.151 mg/mL) and lyophilized forms) was stored at different temperatures (25 °C, 4 °C, −20 °C, −80 °C) for 1 day, 2 days, 1, 2, 3, 4, and 7 weeks, and 1 year. The residual activities were determined.

Measurement of Thrombin Activity of the Purified Enzyme. Thrombin activity of the purified enzyme was measured as follows. First, 40 μL of different concentrations of fibrinogen (10, 20, 40, 80, and 100 mg/mL) was mixed with 10 μL of the enzyme (0.075 mg/mL), and then the clotting time was recorded. Bovine thrombin (500 U/mL) was used as a positive control.

Activation of Plasminogen (Plasminogen Activator Activity). Activation of plasminogen by the purified enzyme was analyzed by fibrin plate method. Fibrin plates were prepared as described earlier. Usually, commercially available fibrinogen contains traces of plasminogen, so the plasminogen-free plates were prepared by using similar method but were heated at 85 °C for 30 min to inactivate plasminogen. The presence of plasminogen activity was measured by difference in area of lytic zone in two different plates.

In Vitro Dissolution of Blood Clots by the Purified Enzyme. To 0.4890 g of blood clot, 500 μL (0.075 mg/mL) of enzyme solution was added and incubated at 37 °C for 6 h. Samples at different time intervals, 10, 20, 40, 60, 90, 120, 180, 240, 300, and 360 min, were centrifuged briefly at 3000 rpm for 30 s, the supernatant was transferred, and the residual clot weight was recorded. The clot was redissolved in the supernatant, and the reaction was continued for further dissolution. Finally the rate of clot dissolution was calculated as follows:

$$\text{clot dissolution rate} = [(\text{clot weight before dissolving} - \text{clot weight after dissolving}) / \text{clot weight before dissolving}] \times 100\%$$

Fibrin(ogen)olytic Activity of the Enzyme. *Human Blood Fibrinogen Degradation.* Fibrinogenolytic activity was measured by a modified fibrinogenolytic assay.[27] Fibrinogen (23 μL of 2% human fibrinogen in 0.05 mol/L Tris-HCl buffer (pH 7.6)) was mixed with the purified enzyme (23 μL of 0.075 mg/mL) and incubated at 37 °C for different time intervals (1 min, 5 min, 15 min, 25 min, 1 h, 1.5 h, 2 h, 4 h, and 24 h). After the indicated time intervals, aliquots were transferred onto ice and analyzed by SDS-PAGE to examine the cleavage patterns of the fibrinogen chains.

Fibrin Degradation. Fibrinolytic activity was measured by a modified fibrinolytic assay. To 23 μL of fibrinogen (2% human fibrinogen in 0.05 mol/L Tris-HCl buffer (pH 7.6)), 10 μL of thrombin was added. After coagulation, 23 μL of purified enzyme (0.075 mg/mL) was added and incubated at 37 °C for different time intervals (3 min, 6 min, 15 min, 25 min, 1 h, 1.5 h, 2 h, 4 h, and 24 h). After the indicated time intervals, aliquots were transferred onto ice and analyzed by SDS-PAGE to examine the cleavage pattern of the fibrin.

Analysis of In Vitro Fibrinolytic and Anticoagulant Effect. To study the fibrinolytic and anticoagulant effect in vitro, purified enzyme (0.075 mg/mL), fibrinogen (Fbg 10 mg/mL), and thrombin (Tb, 0.5 U/μL) were mixed in three ways as follows:

(1) Human fibrinogen + thrombin (clot formation time was recorded) + purified enzyme (clot dissolution time was recorded).
(2) Human fibrinogen (37 °C for 5 min) + purified enzyme and Tb mixture; subsequently incubated in 37 °C (time required for clot formation and complete dissolution was recorded).
(3) Human fibrinogen + purified enzyme (incubated at 37 °C water bath for 5 min) + Tb.

The samples were incubated at 37 °C, and the time required for clot formation and dissolution were recorded. The degradation patterns of the samples were analyzed by SDS-PAGE. Fibrinogen was used as control.

Proteolytic Effect of Purified Enzyme on Blood Proteins. The effect of purified enzyme on blood protein components was studied by incubating purified enzyme (23 μL) with equal volume of human serum albumin (HSA) (15 mg/mL), human immunoglobulin G (IgG), and human thrombin at 37 °C for 4 h. Samples were analyzed by electrophoresis.

RESULTS

Purification and Characterization of Fibrinolytic Enzyme. A submerged culture method was developed to prepare fibrinolytic enzyme. The fibrinolytic enzyme extract was first subjected to 20% ammonium sulfate precipitation. The precipitated materials were discarded, and after buffer exchange, the supernatant was subjected to hydrophobic interaction chromatography on phenyl sepharose FF column; the active fractions were pooled and further purified by cation exchange chromatography, followed by Superdex 75 gel filtration chromatography (Figure 1). An overall yield of 4.0% was obtained with 41.3-fold increase in purity. The specific activity of the purified enzyme was 1682 U/mg. A summary of purification steps is presented in Table 1.

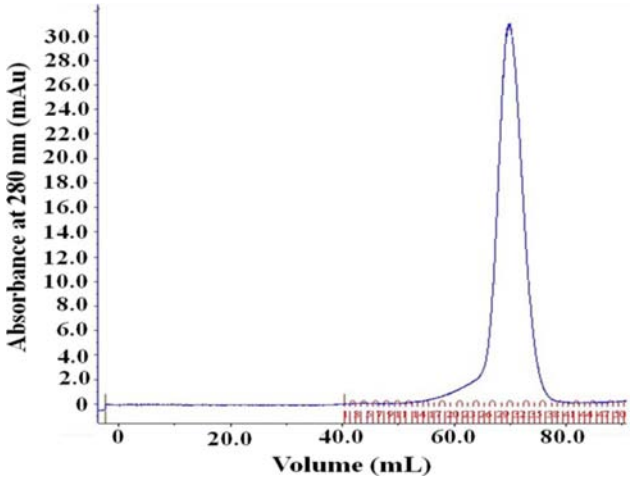

Figure 1. Purification of fibrinolytic enzyme from *Cordyceps militaris* by using Superdex 75 gel filtration chromatography column.

The purified fibrinolytic enzyme appeared to be a single homogeneous band on SDS-PAGE (Figure 2a). The molecular weight of the purified enzyme was determined under native and denatured conditions. Its molecular weight was determined to

DOI: 10.1021/jf505717e
J. Agric. Food Chem. 2015, 63, 2215−2224

Table 1. Summary of Purification Steps of Fibrinolytic Enzyme from *Cordyceps militaris*

purification step	volume (mL)	protein (mg)	activity (U)	recovery (%)	specific activity (U/mg)	fold
culture supernatant	40	118.6	4822.9	100	40.7	1
20% $(NH_4)_2SO_4$ precipitation	39	47.8	3547.3	73.6	74.3	1.8
phenyl-Sepharose HP	78	4.0	2500.1	51.8	632.8	15.5
CM-Sepharose FF	68	1.4	1228.7	25.5	893.8	22
Superdex 75	16	0.1	193.0	4.0	1682	41.3

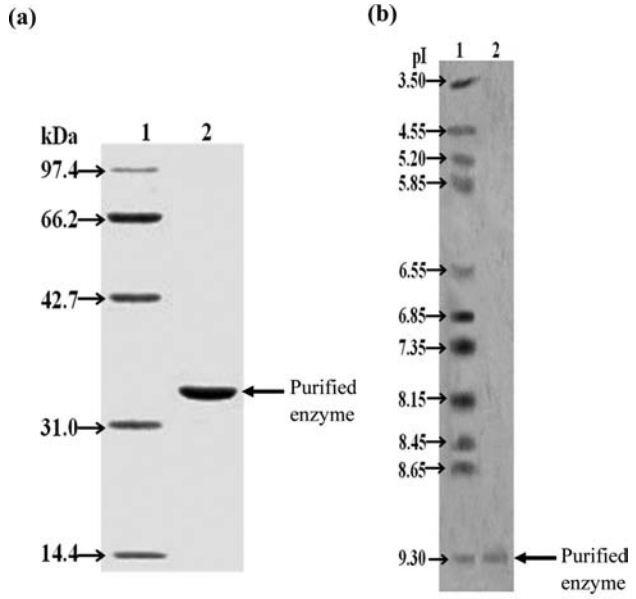

Figure 2. Analysis of the purified fibrinolytic enzyme. (a) SDS-PAGE under reducing denaturing conditions. Lane 1, molecular weight marker; lane 2, purified enzyme. (b) Isoelectric focusing (IEF). Lane 1, p*I* marker; lane 2, purified enzyme.

be 32 kDa by both gel filtration chromatography (data not shown) and SDS-PAGE (Figure 2a), indicating that the enzyme is monomeric in nature. The isoelectric point (p*I*) of the purified enzyme was determined to be 9.3 ± 0.2 (Figure 2b). The purified enzyme was found to be a glycoprotein as identified by Molish test with a carbohydrate content of 0.98% (w/v).

The partial amino acid sequences of the purified enzyme were determined by Q-TOF2 mass spectrometer. Three internal peptides were obtained and their amino acid sequences are APQALTVAAVGATWAR, EKNVGSTVNLLSYDGNK, and TDATSVLLDGYNVSAVNDLVAK. All the three peptides were analyzed using NCBI-BLAST database for sequence similarity with earlier reported fibrinolytic enzymes, and the results are summarized in Table 2.

Effects of Environmental Factors on Enzyme Activity. The optimal pH of the purified enzyme was 7.4 (Figure 3a) and exhibited stability at pH ranging from pH 6.0 to 11.0 (Figure 3b). The enzyme exhibited maximum activity at 37 °C (Figure 3c) and showed thermostability in the temperature range of 23−60 °C and was highly stable up to 47 °C, retaining >80% of its activity when incubated for 30 min (Figure 3d). Enzyme activity and thermostability decreased slowly above 50 °C.

Effect of various metal ions, protease inhibitors, and other reagents on fibrinolytic activity of the purified enzyme was also studied. The activity was strongly inhibited by Fe^{3+} (46.7%) but was not affected by Fe^{2+} (94.5%), however, the activity was enhanced by Ca^{2+} (131.9%) and Cu^{2+} (114.1%) at a concentration of 5 mM (Table 3). The enzyme activity was strongly inhibited by serine protease inhibitors and aspartic protease inhibitor but not by chymotrypsin inhibitor and metalloprotease inhibitor (Table 4). These results indicated that metal ion is not present in the active site of the enzyme and is not involved in enzyme activity.

The enzyme activity was inhibited by −SH group reactive agents, which indicated that the sulfhydryl group of the enzyme was necessary for its activity. BSA (80.5% activity) slightly inhibited the enzyme activity, while gelatin (120% activity) and peptone (127% activity) enhanced the enzyme activity (Table 5).

Stability Studies of the Purified Enzyme. The enzyme was found to be highly stable even after repeated cycles of freeze−thawing. This property is very useful during industrial

Table 2. Comparison of Internal Peptide Fragments of Fibrinolytic Enzyme from *Cordyceps militaris* with Earlier Reported Proteases

source	position of first amino acid	sequence[a]	identity (%)	positives (%)	accession no.
peptide 1		**APQALTVAAVGATWAR**			**present study**
Cordyceps militaris CM01	283	APQAITVAAVGATWAR	94	93	XP_006670629.1
Beauveria bassiana ARSEF 2860	283	APQAITVAAVNSEWSR	69	68	XP_008593638.1
Colletotrichum orbiculare MAFF 240422	260	APQAITVGAVDASW	71	71	ENH77499.1
peptide 2		**EKNVGSTVNLLSYDGNK**			**present study**
Cordyceps militaris CM01	381	NVGSTVNLLSYNGN	93	100	XP_006670629.1
Beauveria bassiana ARSEF 2860	381	NVGKTVNLLSYNGN	86	92	XP_008593638.1
peptide 3		**TDATSVLLDGYNVSAVNDLVAK**			**present study**
Cordyceps militaris CM01	210	TADTSVILDGYN-WAVNDIVAK	73	72	XP_006670629.1
Trichoderma harzianum	226	TSVILDGYN-WAVNDIVSK	74	73	CAL25580.1
Colletotrichum fioriniae PJ7	223	TSVILDGYN-WAVNDIATK	68	68	XP_007602907.1

[a]Identical amino acid sequences are underlined.

DOI: 10.1021/jf505717e
J. Agric. Food Chem. 2015, 63, 2215−2224

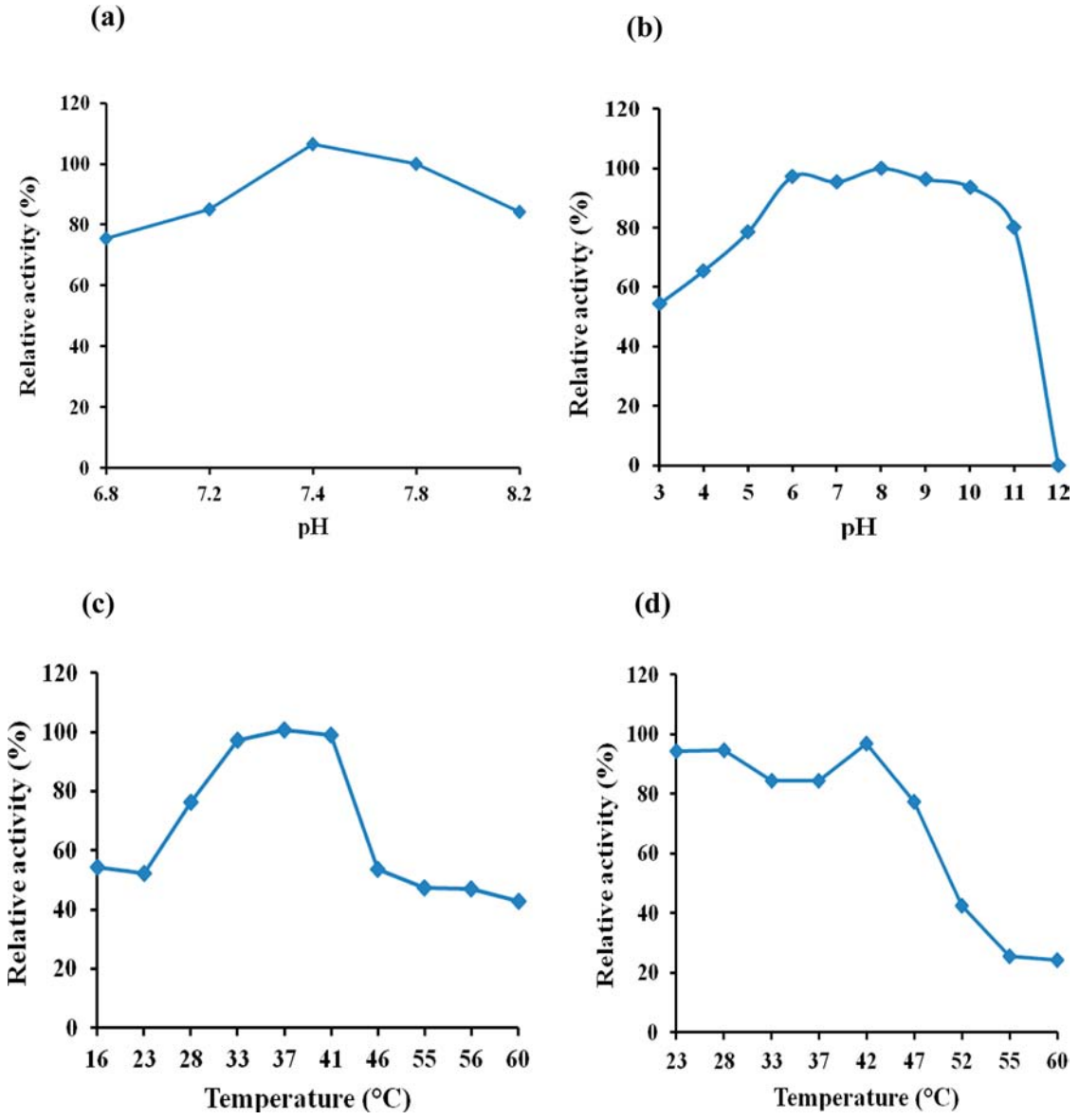

Figure 3. Effect of pH and temperature on fibrinolytic activity of the enzyme. (a) Optimal pH of the purified enzyme was checked at 37 °C in 20 mM of different buffers: citrate−phosphate (pH 3.0−7.0), barbital sodium−chlorhydric acid buffer (pH 8.0−9.0), Na_2CO_3−$NaHCO_3$ (pH 9.5−10.5), and Na_2HPO_4−NaOH buffer (pH 11.0−12.0). (b) For pH stability, the enzyme was incubated at 37 °C for 1 h over range of pH buffers and the residual activities were determined. (c) Optimal temperature of the purified enzyme was determined at different temperatures (16−60 °C) in sodium barbital buffer (pH 7.4). (d) For temperature stability, the enzyme was incubated at different temperatures (23−60 °C) for 0.5 h, in sodium barbital buffer (pH 7.4), and the residual activities were measured by standard fibrin plate method.

Table 3. Effect of Various Metal Ions on Fibrinolyitc Activity of Purified Enzyme

metal ion (5 mM)	residual activity (%)
control	100
Cu^{2+}	114.1
Fe^{2+}	94.5
Fe^{3+}	46.7
Zn^{2+}	101.7
Co^{2+}	103.1
K^{+}	112.5
Na^{+}	91.2
Mg^{2+}	110.3
Ca^{2+}	131.9
Mn^{2+}	104.3

production and clinical applications of the enzyme. The effect of stabilizers such as glycerol and sucrose on storage stability of the purified enzyme was also investigated. The enzyme was stable for 1 week at 4 °C in the presence of 15% glycerol without any loss of activity (data not shown). Sucrose did not exhibit any protective role at the same experimental conditions as glycerol.

Stability of the purified enzyme both in liquid and lyophilized forms was studied. The enzyme was stable in liquid form up to 1 day at 25 and 4 °C, while in lyophilized form, the enzyme was stable after one month of storage at same temperature (25 and 4 °C), retaining 78% and 83% of its initial activity, respectively. Storage of both the forms at −20 °C and −80 °C did not result in loss of any activity up to one month.

The stability of the enzyme was further analyzed after 14 months of storage. The liquid form of enzyme was stable and

DOI: 10.1021/jf505717e
J. Agric. Food Chem. 2015, 63, 2215−2224

Table 4. Effect of Protease Inhibitors on Fibrinolytic Activity of Purified Enzyme

inbihitor	concentration (mmol/L)	activity (%)
control		100
EDTA	2.5	103.7
	10	86.6
Lys	2.5	115.1
	10	133.0
TPCK	2	83.3
	10	90.7
SBTI	2	50.3
	10	47.0
PMSF	2	0
	10	0
aprotinine	2	0
	10	0
pepstatin	2	0

Table 5. Effect of Various Reagents on Fibrinolytic Activity of Purified Enzyme

reagent	concentration	residual activity (%)
control		100
reduced glutathione	5 mmol/L	0
oxidized glutathione	5 mmol/L	0
cysteine	20 mmol/L	34.0
β-mercaptoethanol	0.5%	0
bovine serum albumin (BSA)	1%	80.5
gelatin	1%	120.3
peptone	1%	127.1
acetone	10%	39.3
glycerol	30%	93.3
SDS	0.1%	0
urea	8 M	0

retained 56% and 76% of its activity when stored at −20 °C and −80 °C for 14 months. Meanwhile, the lyophilized form of enzyme was highly stable at 4 °C, −20 °C, and −80 °C for the same period of time and retained 62%, 83%, and 101% of its activity, respectively.

Simulated Gastric and Blood Environment Effect on Enzyme. As shown in Figure 4a, the enzyme lost its activity completely after 4 h of incubation in gastric juice (lane 3) and retained ∼60% of its relative activity in the presence of protein broth (lane 2) or protein broth and maltose (lane 5). Maltose did not show any protective effect (lane 4). The enzyme also tolerated simulated blood environment (Clorox solution); 60% of its relative activity was retained after 4 h of incubation. Therefore, the enzyme should be administered after a meal or intravenously; the loss of the enzyme activity after 4 h of incubation implied its possible advantage over the current fibrinolytic agents associated with bleeding due to excessive plasmin activity.

Determination of Thrombin-Like Activity of Purified Enzyme. The coagulation time required for clotting at different concentrations of human fibrinogen by bovine thrombin is 3−4 min. Thrombin specifically hydrolyzes Aα and Bβ subunits of fibrinogen and forms insoluble fibrin clot. The purified enzyme was unable to clot fibrinogen even at the highest concentrations of 100 mg/mL, indicating that the enzyme did not have thrombin-like activity but acts directly on fibrin clots (data not shown).

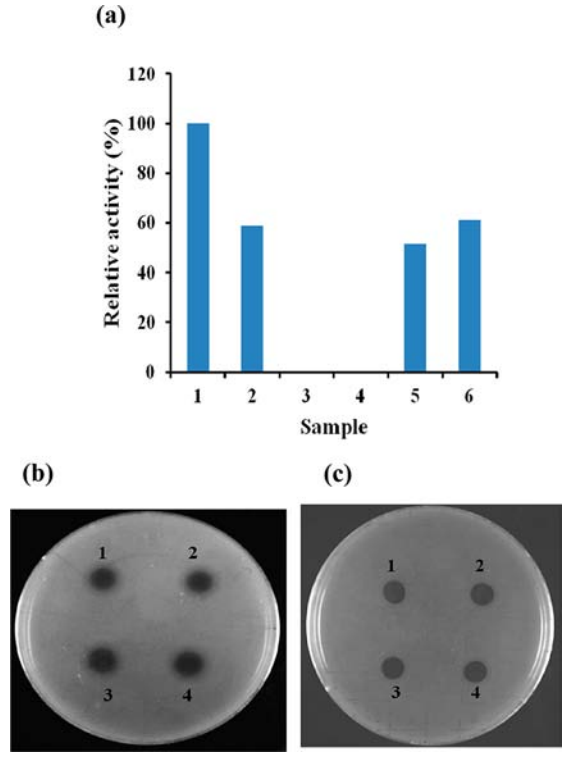

Figure 4. (a) Effect of simulated gastric and blood environments on purified enzyme. The activity of the enzyme in simulated gastric juice and simulated blood was tested in six different combinations. Lane 1, enzyme in water (control); lane 2, enzyme in artificial gastric juice and protein broth; lane 3, enzyme in artificial gastric juice; lane 4, enzyme in artificial gastric juice and maltose; lane 5, enzyme in artificial gastric juice, maltose and protein broth; lane 6, enzyme in Clorox solution. (b) Analysis of plasminogen activation by purified fibrinolytic enzyme on plasminogen-free fibrin plate and (c) activation of plasminogen by purified fibrinolytic enzyme on plasminogen-rich fibrin plate: 10 μL each of the purified enzyme was placed at four spots (1−4) on each plate and incubated at 37 °C for 6 h. Activity was quantified by measuring the area of lysis (1−4 circles) and compared between plasminogen-free and rich plates.

Activation of Plasminogen (Plasminogen Activator Activity). Plasminogen activator activity of the purified enzyme was examined. The purified enzyme did not act as plasminogen activator because the area of diameter of the lytic circle was almost similar in both plasminogen and plasminogen-free fibrin plates (Figure 4b,c).

In Vitro Dissolution of Blood Clots by the Purified Enzyme. The in vitro effect of purified enzyme on dissolution of blood clots, and its dissolution rate was measured at different time intervals (Table 6). The purified enzyme could dissolve the blood clots; the dissolution substantially increased at prolonged incubation time, and the clots completed disappeared within 6 h (Table 6).

Fibrin(ogen)olytic Activity of Purified Enzyme. The enzyme exhibited fibrin(ogen)olytic activity and the degradation patterns of fibrin(ogen) by the purified enzyme were analyzed by SDS-PAGE (Figure 5a,b). In control, fibrinogen was separated into Aα, Bβ, and γ chains. When fibrinogen was incubated with the purified enzyme, the Aα band disappeared first, followed by the Bβ and γ bands. This indicates that the enzyme degraded the Aα chain of fibrinogen first, followed by the Bβ and γ chains. The Aα chain was degraded within 5 min of incubation, while the Bβ and γ chains were degraded in 1 h

DOI: 10.1021/jf505717e
J. Agric. Food Chem. 2015, 63, 2215−2224

Table 6. Analysis of Dissolution of Blood Clots by Purified Enzyme at Different Time Intervals

time (min)	weight (g)	dissolution rate (%)
0	0.4890	0
10	0.4597	6.0
20	0.4290	12.3
40	0.4079	16.6
60	0.3745	23.4
90	0.3347	31.6
120	0.1887	61.4
180	0.1647	66.3
240	0.1277	73.9
300	0.1001	79.5
360	0.0956	80.5

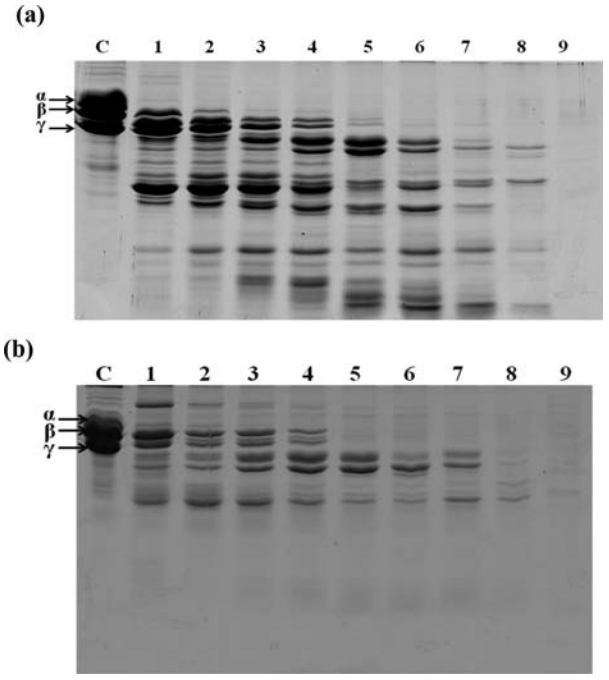

Figure 5. Analysis of cleavage pattern of fibrin(ogen) by purified enzyme. (a) SDS-PAGE analysis of reduced human fibrinogen after digestion by the purified enzyme; lane C, control; lanes 1−9, degradation pattern of fibrinogen at different time intervals of 1 min, 5 min, 15 min, 25 min, 1 h, 1.5 h, 2 h, 4 h, and 24 h, respectively. (b) SDS-PAGE analysis of reduced human fibrin after digestion by the purified enzyme; lane C, control; lanes 1−9, degradation pattern of fibrinogen at different time intervals of 3 min, 6 min, 15 min, 25 min, 1 h, 1.5 h, 2 h, 4 h, and 24 h, respectively.

after incubation (Figure 5a). This implies that the cleavage sites of Aα and Bβ chains were different from thrombin. The low molecular weight degradation products increased with incubation time.

The fibrin degradation pattern by the purified enzyme was also analyzed (Figure 5b). The fibrin α-chain was hydrolyzed within 3 min, followed by the γ−γ chain in 25 min of incubation. The β chain was hydrolyzed slowly and degraded completely in 1 h.

Analysis of in Vitro Fibrinolytic and Anticoagulant Effect. When fibrinogen and thrombin were premixed and then the enzyme was added, the time required for formation of clot was 9.75 s, and for dissolution it was 3 min 20 s. Although the clot was dissolved completely, the subunits of the fibrin were not degraded completely as shown in SDS-PAGE (Figure 6a); the α-subunit was degraded completely, while β and γ subunits were still visible.

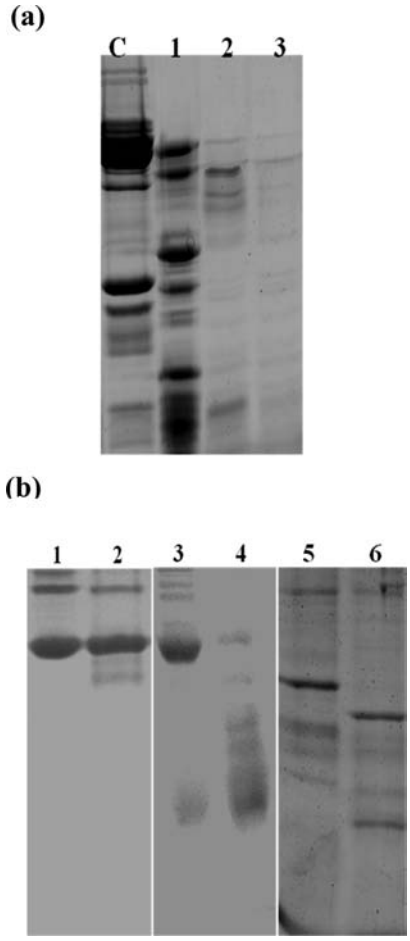

Figure 6. (a) In vitro fibrinogen degradation and anticoagulant effect of purified enzyme. Lane C, control; lane 1, Fbg and Tb were premixed and the enzyme was added after the formation of the fibrin clot (1st combination); lane 2, fibrinogen was first preactivated, then purified enzyme and thrombin mixture were added (2nd combination); lane 3, human fibrinogen was premixed with purified enzyme (3rd combination). (b) Effect of purified enzyme on blood proteins. Lanes 1, 3, and 5 represent positive controls of human serum albumin (HSA), human IgG, and human thrombin, respectively; lanes 2, 4, and 6 represent their respective degradation patterns by the enzyme.

When fibrinogen was first preactivated and then the purified enzyme and thrombin were added, it took 1 min 41 s for clot formation, which was much longer than the first combination (9.75 s). However, the newly formed fibrin clot was dissolved by the enzyme within a short period of 2 min 15 s, which was significantly shorter than first combination (3 min 20 s). The difference in time required for clot formation, and dissolution could be due to the fact that both processes might have occurred simultaneously in the system. Degree of degradation of each subunit of the fibrin between two reactions was further confirmed by SDS-PAGE (Figure 6a, lane 2). As shown in Figure 6a, lane 3, human fibrinogen subunit was thoroughly hydrolyzed; as a result, no observable large protein bands could be seen on the gel.

Effect of Purified Enzyme on Blood Plasma Proteins. The effect of purified enzyme on different blood plasma

DOI: 10.1021/jf505717e
J. Agric. Food Chem. 2015, 63, 2215−2224

proteins was studied. As shown in Figure 6b, human IgG and serum albumin were partially hydrolyzed by the enzyme. It also degraded human thrombin to some extent (Figure 6b).

DISCUSSION

In this study, a novel fibrinolytic enzyme from the mushroom, *Cordyceps militaris*, was produced by submerged culture fermentation. During fermentation, soybean cake was used as a major component of the culture medium, which is different from that of other reports.[29] The enzyme was purified to homogeneity by using combination of various chromatographic steps. The molecular weight of the purified enzyme was 32 kDa. The molecular weight of mushroom fibrinolyic enzymes are in the range of 17−100 kDa.[28] Our value is similar to the enzyme purified from *Pleurotus ostreatus* mycelia (32 kDa)[17] but is smaller than that of fibrinolytic enzyme from *Flammulina velutipes* (37 kDa) and *Cordyceps militaris* (52 kDa).[7,20] The molecular weight of the purified enzyme is not similar to any of the reported fibrinolytic enzymes from *Cordyceps* sp.[3,18,20,29] The isoelectric point (p*I*) of the purified enzyme was determined to be 9.3 ± 0.2, which is higher than the fibrinolytic enzymes from *Cordyceps militaris* (8.1) and *Rhizopus chinensis* 12 (8.5).[3,26] The partial amino acid sequences of the purified enzyme were determined by Q-TOF2 mass spectrometer. Peptides 1, 2, and 3 exhibited 94%, 93%, and 73% similarity with alkaline serine protease, Alp1, from *Cordyceps militaris* CM01, respectively (accession no. XP_006670629.1) (Table 2).

Mushroom fibrinolytic enzymes exhibited optimal activity in the range of pH 5.0−10.0.[28] The optimal pH of the purified enzyme for the fibrinolytic activity is 7.4, which is the physiological pH of humans. Its optimum pH is similar to fibrinolytic enzymes from fruiting bodies of *Cordyceps militaris* and *Tricholoma saponaceum*[15,20] but higher than that of *Flammulina velutipes*, *Armillaria mellea*, and *Schizophyllum commune* enzymes.[5,7,16] The enzyme exhibited maximal activity at 37 °C, which is the same as the enzyme purified from fruiting bodies of *Cordyceps militaris*[20] but higher than the enzyme purified from *Armillaria mellea*, *Flammulina velutipes*, and *Cordyceps militaris*.[7,16,18] Mushroom fibrinolytic enzymes have optimal activity at temperatures ranging from 20 to 60 °C.[28]

The enzyme activity was strongly inhibited by serine protease inhibitors and aspartic protease inhibitor but not by chymotrypsin inhibitor and metalloprotease inhibitor. Our results are similar to the fibrinolytic enzyme from *Cordyceps militaris*[20] but are in contrast to other fibrinolytic enzymes from fruiting bodies of Korean *Cordyceps militaris* where the enzyme activity was strongly inhibited by TPCK, EDTA, and metal ions.[3,18] Most fibrinolytic enzymes purified from mushrooms are inhibited by the metal chelator EDTA.[5,7,17,30] On the basis of their inhibitory specificities, mushroom fibrinolytic enzymes are classified into two groups, viz. serine proteases (those inhibited by PMSF, SBTI, aprotinin) and metalloproteases (those inhibited by EDTA). Therefore, the purified fibrinolytic enzyme from this study is a serine protease. SDS and urea strongly inhibited the enzyme activity, indicating that these reagents might have denatured the enzyme.

Glycerol and sucrose are used as thermoprotective agents for storage of proteins or enzymes. The cryoprotective effect of sucrose on stability of purified enzyme was found to be weaker than glycerol. Therefore, it is recommended to add 15% glycerol for improving its storage stability. Results from stability studies indicate that the liquid form of enzyme stored at 25 and 4 °C was stable only for a short time, and the rate of loss of activity of freeze-dried powder was less than that of solution form. The lyophilized powder of the enzyme can be stored for more than one year at −80 °C. After one year of storage at −20 °C, the enzyme was more stable in freeze-dried powder, retaining more than 80% of its activity as compared to the liquid enzyme solution where it lost about half of its activity. Therefore, it is recommended that the purified enzyme be lyophilized and stored in a deep freezer for long-term storage (more than one year). For the first time, stability of a purified fibrinolytic enzyme from mushrooms was studied and reported.

The enzyme retained 60% of its relative activity in the presence of an appropriate protein solution (broth) which acts as a protective agent. It also tolerated simulated blood environment (Clorox solution). Therefore, the enzyme should be administered after a meal or intravenously; the loss of the enzyme activity after 4 h of incubation implied its possible advantage over the current fibrinolytic agents associated with bleeding due to excessive plasmin activity. Fibrinolytic enzyme from fermented shrimp paste was resistant to the digestive enzymes, pepsin and trypsin; and tolerated in vitro physiological conditions of stomach and small intestine models for 1 h.[6]

Fibrinolytic enzymes degrade thrombus in two ways, either by degrading fibrin directly or by indirectly degrading fibrin through activation of plasminogen into plasmin.[5] The purified enzyme in this study did not act as plasminogen activator because the area of diameter of the lytic circle was almost similar in both plasminogen and plasminogen-free fibrin plates. In plasminogen-free plates, the lytic circles are not condensed and appeared slightly larger than the plasminogen plates. It is possible that pretreatment of fibrin plates at high temperature might have changed the fibrin structure, which resulted in less condensed lytic zone. These preliminary results indicate that *Cordyceps militaris* fibrinolytic enzyme is a plasmin-like protein, which can degrade fibrin directly, but not a plasminogen activator, which can participate in thrombolysis. These results are dissimilar to the earlier reported fibrinolytic enzymes from *Schizophyllum commune* and *Bacillus* sp., which exhibited enhanced activities in plasminogen rich plates.[5,9,10]

The purified enzyme could dissolve the blood clots; the dissolution substantially increased at prolonged incubation time, and the clots completely disappeared within 6 h (Table 6). Similar result was reported for fibrinolytic enzyme purified from *Bacillus subtilis* DC33.[9] Our study showed for the first time the presence of thrombolytic activity in mushroom fibrinolytic enzyme.

Degradation of fibrin(ogen) by purified enzyme was studied. Fibrinolytic enzymes from *Cordyceps militaris* and *Flammulina velutipes* also exhibited similar degradation patterns.[7,20] In addition, the enzyme can hydrolyze fibrin(ogen) chains more quickly than the fibrinolytic enzyme from fruiting bodies of Korean *Cordyceps militaris* (requires 4 h for complete degradation).[3] However, some fibrinolytic enzymes cannot hydrolyze all three chains of fibrin(ogen). It was reported that fibrinolytic enzyme from *Bacillus* sp. could hydrolyze only Bβ and γ-chains of fibrinogen.[10] Fibrinolytic enzymes from the mushrooms *Armillariella mellea* and *Tricholoma saponaceum* have been shown to hydrolyze Aα and Bβ chains of fibrinogen with equal efficiency, but γ-chain was resistant to hydrolysis.[14,15] It is noteworthy that the purified enzyme in this study can hydrolyze all three chains of fibrinogen more efficiently and quickly.

DOI: 10.1021/jf505717e
J. Agric. Food Chem. 2015, 63, 2215−2224

During in vitro fibrinolytic and anticoagulant studies when human fibrinogen was premixed with the purified enzyme, the enzyme degraded human fibrinogen. As a result, fibrinogen was not activated by thrombin, or even if activated it could no longer have the capacity to cross-link required for clot formation, which was further observed by electrophoresis (Figure 6a). As shown in Figure 6a, lane 3, human fibrinogen subunit was thoroughly hydrolyzed; as a result, no observable large protein bands could be seen on the gel. These results indicate that the purified enzyme could act as an anticoagulant as well as a fibrinolytic agent. It could suppress the formation of blood clots during coagulation process and has the potential to develop into a novel thrombolytic drug. The fibrinolytic enzyme from fermented shrimp paste also exhibited similar kinds of characteristics.[6]

Human IgG and serum albumin were partially hydrolyzed by the enzyme. IgG, the main human immunoglobulin, constitutes about 70% of human plasma globulin, which is the most important antibody in the primary immune response. Human serum albumin is the main component in the formation of the osmotic pressure of plasma gum and plays an important role in maintaining normal body fluid distribution, blood volume, and blood pressure. Thrombin is the most important clotting factor in the process of thrombosis. It also degraded human thrombin to some extent (Figure 6b). These results indicate that during normal fibrin clot formation, thrombin activity can also be inhibited and the enzyme can prevent thrombosis. Similar degradation was observed for the fibrinolytic enzyme from *Bacillus subtilis* DC33.[9] Therefore, the use of this enzyme for fibrinolytic therapy might cause some mild undesirable effects such as partial degradation of human IgG and serum albumin but can also prevent thrombosis by hydrolyzing thrombin. In contrast to the present results, the fibrinolytic enzyme purified from fermented shrimp paste, fruiting bodies of mushrooms *Armillariella mellea* and *Tricholoma saponaceum*, did not show any proteolytic effect on the blood proteins.[6,14,15]

To conclude, a 32 kDa novel fibrinolytic enzyme with specific activity of 1682 U/mg was purified from *Cordyceps militaris*. The optimal condition for this enzyme was at human physiological pH (7.4) and temperature (37 °C). As a plasmin-like protein, this enzyme could degrade fibrin directly and cleaved α-chains more efficiently than β- and γ-chains. It degraded thrombin, which indicates that it can act as an anticoagulant and prevent thrombosis. Intravascular thrombosis is one of the major reasons of cardiovascular diseases. Hence, the enzyme may be applied as a potential therapeutic agent for treating thrombosis.

AUTHOR INFORMATION

Corresponding Authors

*For X.Z.: phone, +86-04522738168; fax, +86-04522725454; E-mail, zhengxiqun@126.com.

*For J.W.: E-mail, jwu3@ualberta.ca.

Funding

This work was supported by National Natural Science Foundation of P. R. China (NSFC) (no. 31171744), Natural Science Foundation of Heilongjiang province (no. ZD201305), P. R. China, and Program for Young Teachers Scientific Research at Qiqihar University (2012k-Z08).

Notes

The authors declare no competing financial interest.

ABBREVIATIONS USED

BSA, bovine serum albumin; SDS-PAGE, sodium dodecyl sulfate polyacrylamide gel electrophoresis; EDTA, ethylenediamine tetracetic acid; TPCK, *N*-tosyl-L-phenylalanine chloromethyl ketone; SBTI, soybean trypsin inhibitor; PMSF, phenylmethane sulfonyl fluoride

REFERENCES

(1) Mine, Y.; Wong, A. H.; Jiang, B. Fibrinolytic enzymes in Asian traditional fermented foods. *Food Res. Int.* **2005**, *38*, 243−250.

(2) Peng, Y.; Yang, X.; Zhang, Y. Microbial fibrinolytic enzymes: an overview of source, production, properties, and thrombolytic activity in vivo. *Appl. Microbiol. Biotechnol.* **2005**, *69* (2), 126−132.

(3) Choi, D. B.; Cha, W. S.; Park, N.; Kim, H. W.; Lee, J. H.; Park, J. S.; Park, S. S. Purification and characterization of a novel fibrinolytic enzyme from fruiting bodies of Korean *Cordyceps militaris*. *Bioresour. Technol.* **2011**, *102*, 3279−3285.

(4) Wu, B.; Wu, L.; Chen, D.; Yang, Z.; Luo, M. Purification and characterization of a novel fibrinolytic protease from *Fusarium* sp. CPCC480097. *J. Ind. Microbiol. Biotechnol.* **2009**, *36*, 452−459.

(5) Park, I. S.; Park, J. U.; Seo, M. J.; Kim, M. J.; Lee, H. H.; Kim, S. R.; Kang, B. W.; Choi, Y. H.; Joo, W. H.; Jeong, Y. K. Purification and biochemical characterization of a 17 kDa fibrinolytic enzyme from *Schizophyllum commune*. *J. Microbiol.* **2010**, *48* (6), 836−841.

(6) Wong, K. A. H.; Mine, Y. Novel fibrinolytic enzyme in fermented shrimp paste, a traditional Asian fermented seasoning. *J. Agric. Food Chem.* **2004**, *52*, 980−986.

(7) Park, S. E.; Li, M. H.; Kim, J. S.; Sapkota, K.; Kim, J. E.; Choi, B. S.; Yoon, Y. H.; Lee, J. C.; Lee, H. H.; Kim, C. S.; Kim, S. J. Purification and characterization of a fibrinolytic protease from a culture supernatant of *Flammulina velutipes* mycelia. *Biosci., Biotechnol., Biochem.* **2007**, *71* (9), 2214−2222.

(8) Sumi, H.; Hamada, H.; Tsushima, H.; Mihara, H.; Muraki, H. A novel fibrinolytic enzyme (Nattokinase) in the vegetable cheese *Natto*, a typical and popular soybean food in the Japanese diet. *Experientia* **1987**, *43*, 1110−1111.

(9) Wang, C. T.; Ji, B. P.; Li, B.; Nout, R.; Li, P. L.; Ji, H.; Chen, L. F. Purification and characterization of a fibrinolytic enzyme of *Bacillus subtilis* DC33, isolated from Chinese traditional *Douchi*. *J. Ind. Microbiol. Biotechnol.* **2006**, *33* (9), 750−758.

(10) Hua, Y.; Jiang, B.; Mine, Y.; Mu, W. M. Purification and characterization of a novel fibrinolytic enzyme from *Bacillus* sp. nov. sk006 isolated from an Asian traditional fermented shrimp paste. *J. Agric. Food Chem.* **2008**, *56*, 1451−1457.

(11) Choi, N. S.; Song, J. J.; Chung, D. M.; Kim, Y. J.; Maeng, P. J.; Kim, S. H. Purification and characterization of a novel thermo acid-stable fibrinolytic enzyme from *Staphylococcus* sp. strain AJ isolated from Korean salt-fermented anchovy-joet. *J. Ind. Microbiol. Biotechnol.* **2009**, *36*, 417−426.

(12) Waseer, S. P. Medicinal mushrooms as a source of antitumor and immunomodulating polysaccharides. *Appl. Microbiol. Biotechnol.* **2002**, *60*, 258−274.

(13) Lee, S. H.; Hwang, H. S.; Yun, J. W. Production of polysaccharides by submerged mycelial culture of entomopathogenic fungus *Cordyceps takaomontana* and their apoptotic effects on human neuroblastoma cells. *Korean J. Chem. Eng.* **2009**, *26* (4), 1075−1083.

(14) Kim, J. H.; Kim, Y. S. A fibrinolytic metalloprotease from the fruiting bodies of an edible mushroom *Armillariella mellea*. *Biosci., Biotechnol., Biochem.* **1999**, *63*, 2130−2136.

(15) Kim, J. H.; Kim, Y. S. Characterization of a metalloenzyme from a wild mushroom *Tricholoma saponaceum*. *Biosci., Biotechnol., Biochem.* **2001**, *65* (2), 356−362.

(16) Lee, S. Y.; Kim, J. S.; Kim, J. E.; Sapkota, K.; Shen, M. H.; Kim, S.; Chun, H. S.; Yoo, J. C.; Choi, H. S.; Kim, M. K.; Kim, S. J. Purification and characterization of fibrinolytic enzyme from cultured mycelia of *Armillaria mellea*. *Protein Expression Purif.* **2005**, *43* (1), 10−17.

DOI: 10.1021/jf505717e
J. Agric. Food Chem. 2015, 63, 2215−2224

(17) Shen, M. H.; Kim, J. S.; Sapkota, K.; Park, S. E.; Choi, B. S.; Kim, S.; Lee, H. H.; Kim, C. S.; Chun, H. S.; Ryoo, C. I.; Kim, S. J. Purification, characterization, and cloning of fibrinolytic metalloprotease from *Pleurotus ostreatus* mycelia. *J. Microbiol. Biotechnol.* **2007**, *17* (8), 1271−1283.
(18) Cui, L.; Dong, M. S.; Chen, X. H.; Jiang, M.; Lv, X.; Yan, G. A novel fibrinolytic enzyme from *Cordyceps militaris*, a Chinese traditional medicinal mushroom. *World J. Microbiol. Biotechnol.* **2008**, *24*, 483−489.
(19) Ng, T. B.; Wang, H. X. Pharmacological actions of *Cordyceps*, a prized folk medicine. *J. Pharm. Pharmacol.* **2005**, *57*, 1509−1519.
(20) Kim, J. S.; Sapkota, K.; Park, S. E.; Choi, B. S.; Kim, S.; Nguyen, T. H.; Kim, C. S.; Choi, H. S.; Kim, M. K.; Chun, H. S.; Park, Y.; Kim, S. J. A fibrinolytic enzyme from the medicinal mushroom *Cordyceps militaris*. *J. Microbiol.* **2006**, *44*, 622−631.
(21) Pandee, P.; Kittikul, A. H.; Masahiro, O.; Dissara, Y. Production and properties of a fibrinolytic enzyme by *Schizophyllum commune* BL23. *Songklankarin J. Sci. Technol.* **2008**, *30* (4), 447−453.
(22) Astrup, T.; Mullertz, S. The fibrin plate method for estimating fibrinolytic activity. *Arch. Biochem. Biophys.* **1952**, *40*, 346−351.
(23) Lowry, O. H.; Rosebrough, N. J.; Farr, A. L.; Randall, R. J. Protein measurement with the Folin phenol reagent. *J. Biol. Chem.* **1951**, *193*, 264−275.
(24) Yemm, E. W.; Willis, A. J. The estimation of carbohydrate in plant extracts by anthrone. *Biochem. J.* **1954**, *57* (3), 508−514.
(25) Laemmli, U. K. Cleavage of structural proteins during the assembly of the head of bacteriophage T4. *Nature* **1970**, *227*, 680−686.
(26) Liu, X. L.; Du, L. X.; Lu, F. P.; Zheng, X. Q.; Xiao, J. Purification and characterization of a novel fibrinolytic enzyme from *Rhizopus chinensis* 12. *Appl. Microbiol. Biotechnol.* **2005**, *67*, 209−214.
(27) Koh, Y. S.; Chung, K. H.; Kim, D. S. Biochemical characterization of a thrombin-like enzyme and a fibrinolytic serine protease from snake (*Agkistrodon saxatilis*) venom. *Toxicon* **2001**, *39* (4), 555−560.
(28) Lu, C. L.; Chen, S. N. Fibrinolytic enzymes from medicinal mushrooms. In *Protein Structure*; Faraggi, E., Ed.; InTech: Rijeka, Croatia, 2012; pp 337−363.http://www.intechopen.com/books/protein-structure/fibrinolytic-enzymes-from-medicinal-mushrooms.
(29) Li, H. P.; Hu, Z.; Yuan, J. L.; Fan, H. D.; Chen, W.; Wang, S. J.; Zheng, S. S.; Zheng, Z. L.; Zou, G. L. A novel extracellular protease with fibrinolytic activity from the culture supernatant of *Cordyceps sinensis*: purification and characterization. *Phytother. Res.* **2007**, *21* (12), 1234−1241.
(30) Lee, S. Y.; Kim, J. S.; Kim, J. E.; Sapkota, K.; Shen, M. H.; Kim, S.; Chun, H. S.; Yoo, J. C.; Choi, H. S.; Kim, M. K.; Kim, S. J. Purification and characterization of fibrinolytic enzyme from cultured mycelia of *Armillaria mellea*. *Protein Expression Purif.* **2005**, *43* (1), 10−17.

DOI: 10.1021/jf505717e
J. Agric. Food Chem. 2015, 63, 2215−2224

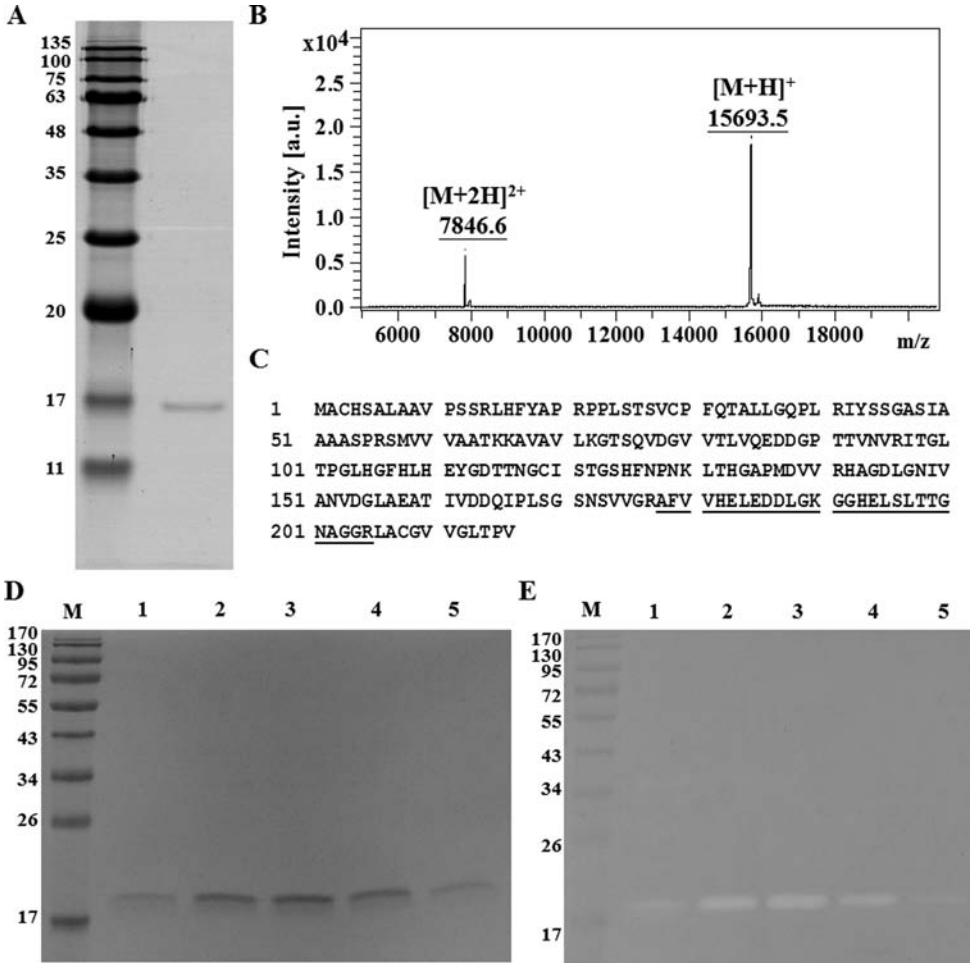

Figure 1. Purification and identification of SOD from *Piper betle* leaf (PBL). (A) Apparent homogeneity of the purified protein (right lane) detected by SDS-PAGE and Coomassie blue staining. Protein marker (left lane) with molecular mass (kD) is indicated. (B) MALDI-TOF analysis showing the purified protein with a molecular mass of 15.7 kDa. (C) The predicted sequence of Cu/Zn SOD from *Zantedeschia aethiopica*. The sequences of two adjacent tryptic peptides near the C-terminus are underlined. (D) and (E) Native gel examination of the five collected fractions from DEAE-cellulose chromatography by Coomassie staining (D) and zymography (E).

Purification of the PBL Protein of Interest. Unless otherwise indicated, the following protein purification protocol was performed at room temperature and initiated by homogenizing PBL in 3 volumes of buffer A (20 mM Tris/HCl, pH 7.0). The homogenate was filtrated with 4-layer cheesecloth and centrifuged at 13 000 rpm for 20 min at 4 °C, and the clear supernatant was filtrated again to remove insoluble residue on the surface of the supernatant. The proteins in the clear supernatant were fractionated with 80% ammonium sulfate and centrifuged to collect the precipitate. The precipitate was redissolved in buffer A and dialyzed against buffer A (50X volume) overnight. After repeating the dialysis step, the sample was loaded onto a DEAE-cellulose column pre-equilibrated with buffer A. The column was then washed with buffer A until the eluent was colorless, as judged with vision. The proteins in the column were eluted in the linear gradient with 1 M NaCl in buffer A, and the protein eluent was subjected to 15% SDS-PAGE (8 × 10 cm^2) at 110 V for 2 h. The fractions containing the protein of interest were pooled and diluted 5-fold with buffer A. The diluted sample was repeatedly subjected to the above-mentioned DEAE-cellulose chromatography to purify the protein of interest, except 0.2 M NaCl replaced the 1 M NaCl in the linear gradient. The molecular mass of the purified protein was determined in the linear mode using MALDI-TOF-TOF MS, as previously described.[13]

Protein Identification by nano-LC-Q-TOF-MS/MS. The protein band on the SDS-PAGE gel was excised, followed by in-gel digestion and peptide extraction according to the protocol previously described.[14] Analysis of the tryptic peptides was performed using an nano-LC-MS/MS system. The peptides were separated using an Ultimate 3000 LC RSLC nanoLC system (Dionex-Thermo Scientific, Chelmsford, MA, U.S.A.), and the mass spectrometry (MS) results were acquired with a quadrupole time-of-flight (Q-TOF) mass spectrometer (maXis impact, Bruker Daltonics Inc. Bremen, Germany). The sample was injected into a C_{18} trapping column (Acclaim PepMap100:100 μm × 2 cm, Dionex-Thermo Scientific, Chelmsford, MA, U.S.A.), connected with a C_{18} nano column (Acclaim PepMap RSLC, 75 μm × 15 cm, Dionex-Thermo Scientific, Chelmsford, MA, U.S.A.) to separate peptides. The mass spectrometer was operated by a captive spray source with a spray voltage of 1400 V, and the MS were acquired from 50 to 2000 m/z. The three most intense ions with charge states between 2 and 3 in each survey scan were selected for the MS/MS experiment. The MS/MS data were acquired from 50 to 2000 m/z. The peak list of MS spectra was processed by DataAnalysis v.4.1 software (Bruker Daltonics Inc. Bremen, Germany), and the extracted peak list was searched against the Swiss-Prot database (release 2011727) using MASCOT v.2.2.04 (Matrix Science, London, England).

SOD Zymography and Activity Assay. The following protocol for SOD zymography was conducted as described by Shukla et al.[15] with a slight modification. Gel electrophoresis is conducted exactly as the above-mentioned SDS-PAGE protocol, except the absence of SDS in the native gel. The native gel was then soaked twice in distilled water with gentle shaking for 30 min per time. The gel was

DOI: 10.1021/jf505753d
J. Agric. Food Chem. 2015, 63, 2225−2232

subsequently incubated in 0.28 mM nitro-blue tetrazolium (NBT) solution in the dark with gentle shaking for 20 min. The gel was then immersed in HEPES buffer (50 mM, pH 7.9) with 28 mM TEMED and 28 μM riboflavin and gentle shaken in the dark for 15 min. A white band on the gel gradually appeared after exposure to light.

Activity assay of SOD was conducted exactly as that suggested by the manufacturer. Reduction of WST-1 with superoxide anion, the product of xanthine oxidase-catalyzed reaction, was blocked in the presence of SOD. Absorbance at 450 nm was measured to determine the inhibition rate. In the experiment, 50- and 200-fold dilution for the crude extract and purified SOD, respectively, was used to perform activity assay. One unit/mL of activity was defined as 50% of inhibition rate calculated from the protocol in the kit.

Identifying the Mediator of SOD Dimerization by HPLC and LC-MS/MS. Areca nut or PBL alone was chewed in the oral cavity, and the oral extracts were then collected and centrifuged. The small-molecule components in the clear supernatant were filtrated using Microcon 3 concentrator, followed by HPLC analysis using a LiChroCART column (4 × 250 mm^2) (Merck & Co., Inc., Whitehouse Station, NJ). The mobile phases of ddH_2O and acetonitrile were used in a linear gradient at a flow rate of 1 mL/min, and 1.5 mL of eluent was manually collected in each tube. The LC-MS/MS analysis was conducted exactly as previously described.[13]

Measurement of Hydrogen Peroxide in the Oral Extract. (+)-Catechin (0.5 mM) and 3 μL oral extract, from different preparations were mixed in a 200 μL Tris/HCl (0.1M, pH 7.0) reaction solution. No additional peroxidase was required because peroxidase is present in both areca nuts and PBL. In the presence of hydrogen peroxide, peroxidase catalyzed catechin oxidation to form a product that exhibited absorbance at 475 nm and was measured spectrophotometrically.[13]

SDDC (a Cu/Zn SOD-specific inhibitor) was employed to evaluate whether SOD was responsible for production of hydrogen peroxide. It was conducted similarly except preincubation of catechin with 5-mM SDDC in Tris/HCl buffer for 5 min. After addition of the oral extract, absorbance at 475 nm was measured spectrophotometrically.

RESULTS

Identification of the Purified PBL Protein of Interest as Cu/Zn SOD. As depicted in Figure 1A, a functionally unknown protein in PBL was purified to apparent homogeneity using repetitive DEAE-cellulose chromatography. It appeared to be monomeric according to the results of SDS-PAGE (Figure 1A) with a 15.7-kDa molecular mass as determined by MALDI-TOF analysis (Figure 1B). The protein was identified as Cu/Zn SOD. Sequence identities were recognized in two adjacent tryptic peptides, both of which were mapped to the C-terminal region of Cu/Zn SOD from *Zantedeschia aethiopica*, as shown in Figure 1C. Zymography of the native gel clearly established the protein's SOD activity (Figure 1E). The pattern of Coomassie staining (Figure 1D) indicated that PBL SOD is monomeric at neutral pH. The process represented about 80-fold purification, obtained from comparison of specific activity between the crude extract (60 U/mg) and purified SOD (4700 U/mg).

SOD Dimerization in the Betel Nut Oral Extract. Zymography was used to examine the status of the SOD in the betel nut oral extract (BPS oral extract). Unexpectedly, the results showed nearly complete conversion of SOD monomer to the dimeric form in all 6 oral extracts (Figure 2A, arrowhead in lanes 1−6). Clearly, SOD was readily dimerized in the alkaline condition caused by slaked lime. Oral extract obtained after chewing PBL combined with areca nut in the absence of slaked lime (BP oral extract) induced SOD dimerization but to a much lesser extent than BPS oral extract (Figure 2A, lanes 7−9). The conversion was also observed using betel nut

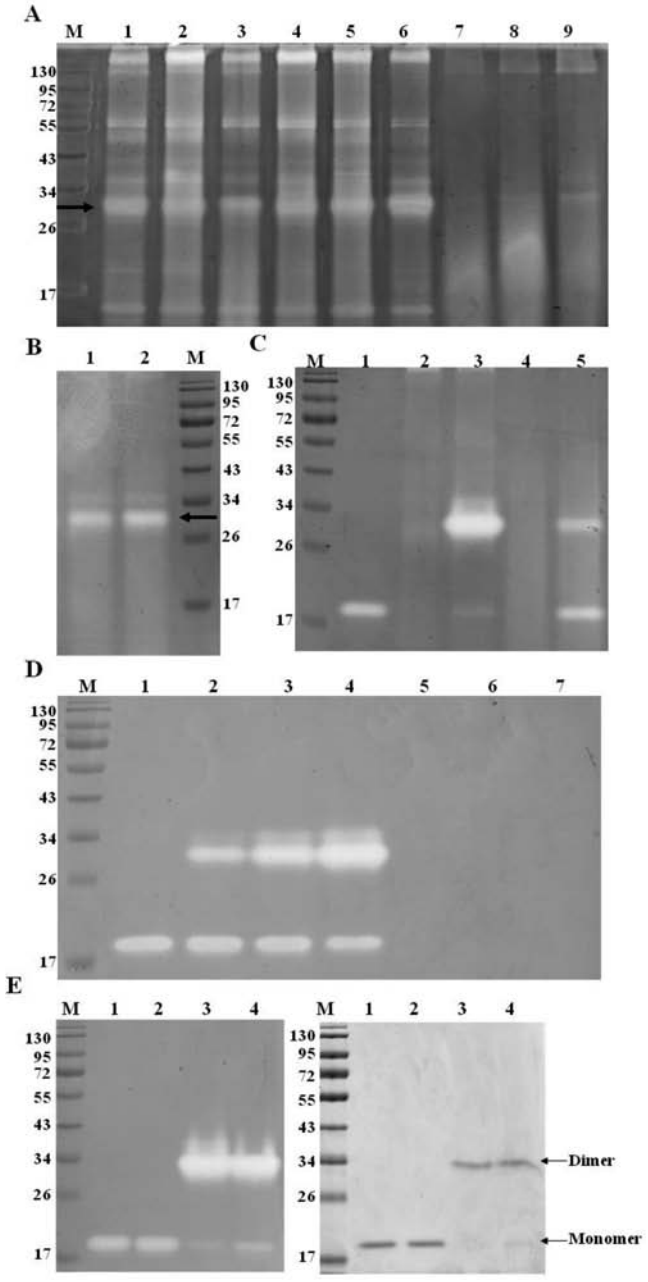

Figure 2. SOD dimerization induced by slaked lime. (A) Zymographic detection of SODs in the oral extract. The oral extract collected after chewing betel nut with slaked lime (BPS oral extract, lanes 1−6) or without slaked lime (BP oral extract, lanes 7−9). Equal volumes of BPS and BP oral extracts were analyzed, and the SOD dimer of interest is indicated by the arrowhead on the left. (B) The presence of SOD dimer in the betel nut homogenate. Betel nut was homogenized with Tris/HCl buffer (20 mM, pH 7.0) instead of oral chewing, and two doses of the homogenate (lanes 1 and 2) were used in a zymographic assay of SOD dimerization (arrowhead on the right). (C) The effect of BPS and BP oral extracts on SOD dimerization. Dimerization was assessed by mixing the purified SOD with a small amount of BPS (lane 3) or BP (lane 5) oral extract, as compared with an equal amount of enzyme alone (lane 1). Lanes 2 and 4 show BPS and BP oral extracts alone. (D) The effect of slaked lime on SOD dimerization. Slaked lime from a betel nut was dissolved in 10 mL ddH_2O and centrifuged, and the clear supernatant was used immediately. Increasing amounts of the supernatant were mixed with a given amount of SOD (lanes 2−4) to assess SOD dimerization, as compared with the enzyme control (lane 1). Lanes 5−7 show the

DOI: 10.1021/jf505753d
J. Agric. Food Chem. 2015, 63, 2225−2232

Figure 2. continued

supernatants alone corresponding to lanes 2−4, respectively. (E) The assessment of SOD dimerization was performed by separately mixing SOD with an equal volume of water (lane 1), 0.1 M Tris/HCl (pH 7, lane 2), 0.1 M Tris/HCl (pH 8.8, lane 3), or the slaked lime supernatant described above (lane 4). The left and right panels show zymography and Coomassie staining, respectively, with the monomer and dimer indicated.

homogenate (Figure 2B, arrowhead), which was derived from homogenizing the betel nut with neutral buffer rather than chewing betel nut in the oral cavity.

In the presence of a small amount of BPS oral extract with a lower SOD activity (lane 2 of Figure 2C), the purified SOD remarkably dimerized and possessed at least a 5-fold increase in activity (lane 3) as compared with an equal amount of the monomeric SOD with low activity at neutral pH (lane 1). The addition of a small amount BP oral extract exerted the same effect on SOD dimerization, although to a lesser extent (lane 5). The disappearance of the monomeric SOD in Figure 2A,B is believed to be due to SOD dimerization in the presence of slaked lime.

Next, the effect of slaked lime on SOD dimerization was studied. No dimerization was observed with SOD alone (Figure 2D, lane 1), but slaked lime induced SOD dimerization in a dose-dependent manner (Figure 2D, lanes 2−4). Usage of the supernatants, which contained even smaller amounts of slaked lime, resulted in no detectable SOD activity (lanes 5−7). BPS oral extract, which contains slaked lime, is alkaline (pH 8.9), and BP oral extract lacking slaked lime is acidic (pH 5.78). As shown in Figure 2E, the addition of alkaline solution to monomeric SOD induced SOD dimerization (lane 3 of both panels), mirroring the action of slaked lime (lane 4 of both panels), whereas the addition of neutral buffer had no effect (lane 2 of both panels).

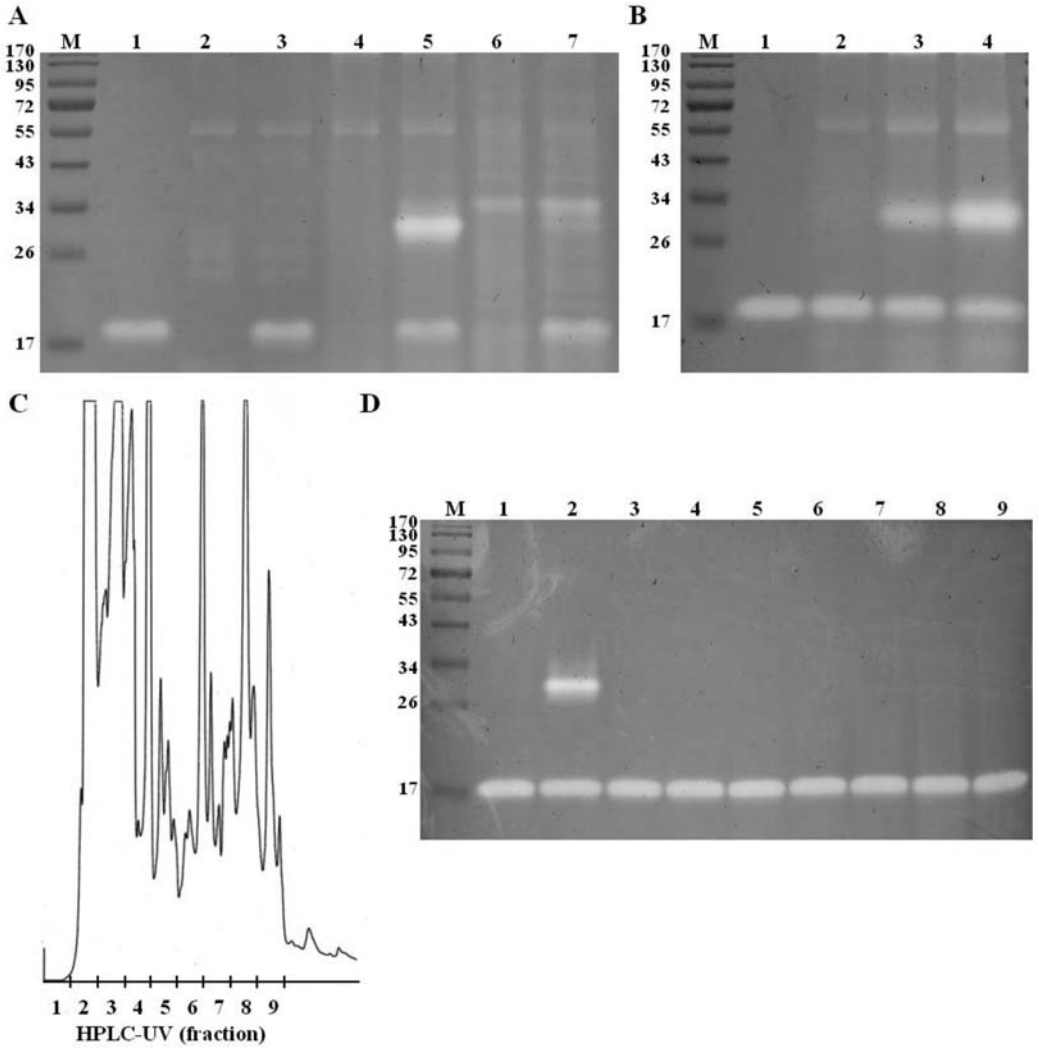

Figure 3. Mediator of SOD dimerization distinct from slaked lime. (A) The component in areca nut that mediates SOD dimerization. The assessment was performed by mixing SOD with saliva (lane 3), areca-nut (AN) oral extract (lane 5), or PBL oral extract (lane 7) and comparing with an equal amount of enzyme control (lane 1). Lanes 2, 4, and 6 show the controls for saliva and AN and PBL oral extracts, respectively. (B) The effect of AN oral extract on SOD dimerization. The effect of increasing amounts of AN oral extract (lanes 2−4) was compared with that of the enzyme control (lane 1). (C) HPLC chromatogram for small-molecule components in AN oral extract. The small-molecule components in AN oral extract were filtrated using Microcon 3, followed by HPLC analysis. The collected fraction for each time interval is shown at the bottom. (D) Each collected fraction, indicated at the top, was speed-vacuum-dried, and mixed with SOD to determine which fraction was able to mediate SOD dimerization.

DOI: 10.1021/jf505753d
J. Agric. Food Chem. 2015, 63, 2225−2232

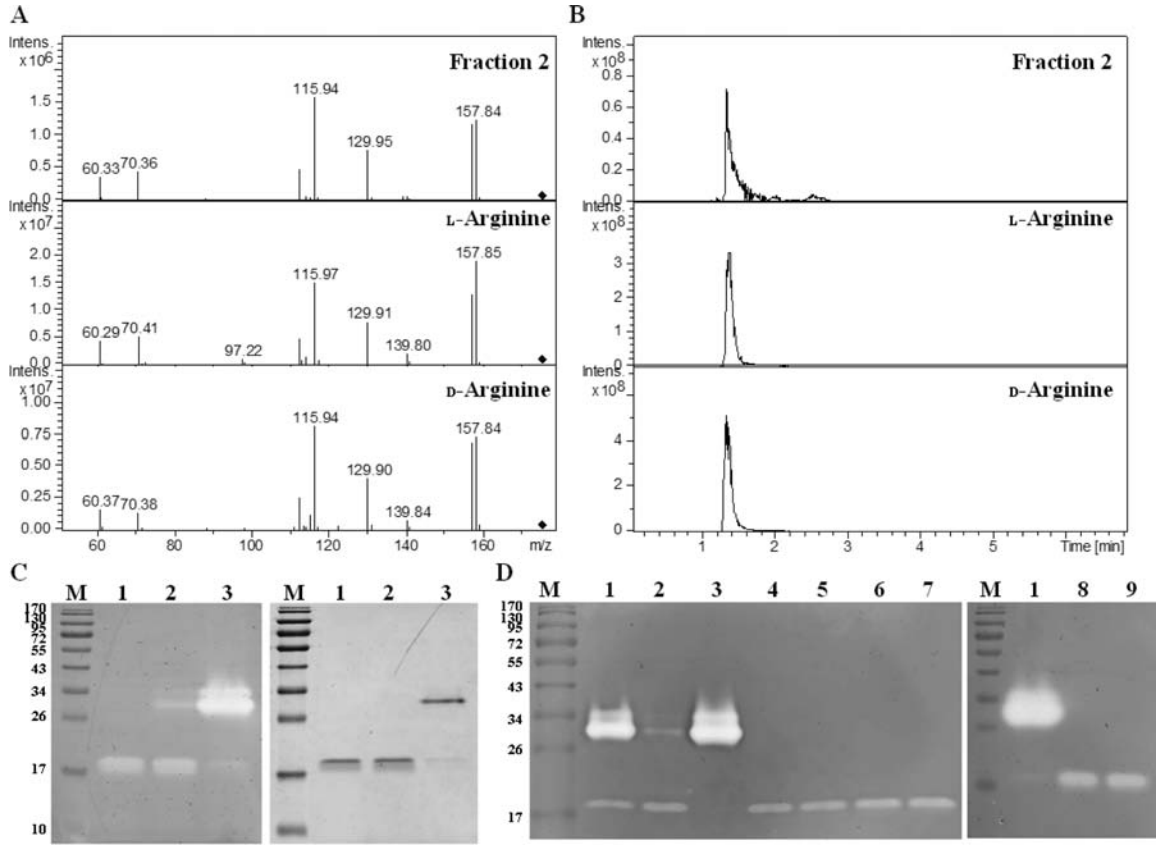

Figure 4. Identification of the mediator in areca nut as arginine. (A) and (B) MS/MS spectrum (A) and extracted ion chromatogram (EIC) (B) of the active component in fraction 2 (upper panel) compared with that of L- and D-arginine (middle and lower panels). (C) The effect of L-arginine on SOD dimerization. SOD dimerization was evaluated in the presence 10 and 20 mM L-arginine (lanes 2 and 3) by zymography (left panel) and Coomassie staining (right panel) and compared with that observed with an equal amount of enzyme control (lane 1). (D) The assessment was extended to D-arginine (lanes 2 and 3) and other basic amino acids, including lysine (lanes 4 and 5), histidine (lanes 6 and 7), and citrulline (lanes 8 and 9). A final concentration of 10 mM (lanes 2, 4, 6, and 8) and 20 mM (lanes 3, 5, 7, and 9) of each amino acid was used, as compared with 20 mM L-arginine (lane 1).

Contribution of Arginine in Areca Nut to SOD Dimerization. An additional component in areca nut distinct from slaked lime contributes to SOD dimerization. When oral extract obtained by chewing areca nut alone was added, dimerization was still observed, although to a less extent than that initiated by slaked lime (Figure 3A, lane 5 vs lane 4). No conversion was detected with the saliva control (lane 3 vs lane 2) or oral extract after chewing PBL alone (lane 7 vs lane 6). However, the oral extract after chewing areca nut alone in an acidic environment stimulated dimerization in a dose-dependent manner (Figure 3B), reminiscent of slaked lime. Furthermore, HPLC analysis revealed a complicated pattern with numerous components in the microcon-3 filtrate of the active oral extract (Figure 3C). The manually collected fractions were examined, and the ability to induce SOD dimerization was stringently restricted to fraction 2 (Figure 3D).

The MS/MS spectrum of the active component in fraction 2 with m/z 175 in the positive mode (Figure 4A, upper panel) was equivalent to that of L- and D-arginine (Figure 4A, middle and lower panels). As expected, the analysis of the extracted ion chromatogram (EIC) revealed the same retention time for the active component and both enatiomers of arginine (Figure 4B). As was observed for the enzyme control, 10 mM L-arginine exerted a faint effect that was insufficient to induce dimerization as examined by zymography and Coomassie staining (Figure 4C, lanes 1 and 2 in both panels). In contrast, a nearly complete conversion to the dimeric form occurred in the presence of 20 mM L-arginine (Figure 4C, lane 3 in both panels). Furthermore, D-arginine conferred a similar effect on SOD dimerization (Figure 4D, lanes 2 and 3 compared with Figure 4C, lanes 2 and 3). The absolute specificity of arginine in this process was also reflected in the fact that the other two basic amino acids histidine and lysine as well as arginine-analogous citrulline all lacked the ability to induce SOD dimerization (Figure 4D, lanes 4–9).

Production of Hydrogen Peroxide in the Betel Nut Oral Extract. The nearly complete dimerization of SOD in the presence of betel nut oral extract greatly increased its enzymatic activity, potentially resulting in the production of substantial amounts of hydrogen peroxide in the oral cavity. An absorbance increase in response to catechin was observed only with the BPS oral extract (left three bars of Figure 5A); very little change of absorbance occurred with the BP oral extract (middle three bars), clearly indicating the presence of hydrogen peroxide in the BPS oral extract. The increased absorbance was regenerated when hydrogen peroxide was produced in large quantities (right three bars), indicating little or no production of hydrogen peroxide in the BP oral extract.

To clarify the source of hydrogen peroxide, additional oral extracts were prepared by chewing PBL or areca nut in the presence of slaked lime and are referred to as PS and BS oral

DOI: 10.1021/jf505753d
J. Agric. Food Chem. 2015, 63, 2225−2232

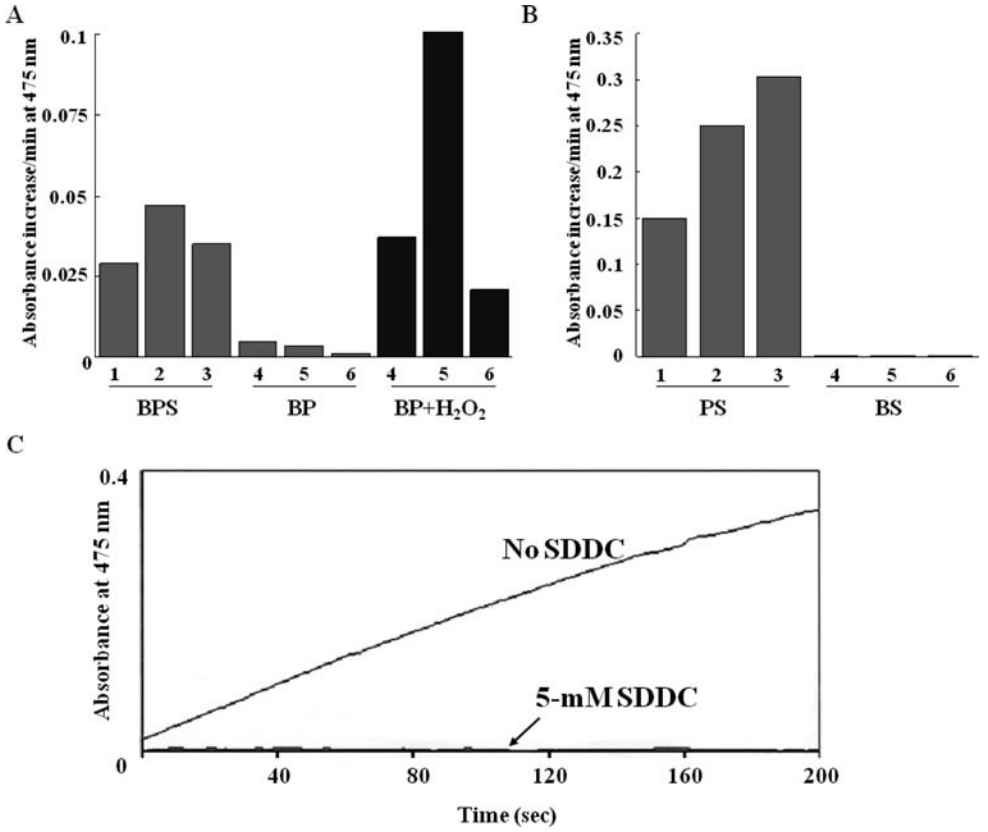

Figure 5. PBL as the source of hydrogen peroxide. (A) BPS and BP oral extracts (left and middle three bars) evaluated for their ability to oxidize catechin. Hydrogen peroxide was used as a control, demonstrating the extremely small amount of hydrogen peroxide in the BP oral extracts (right three bars). (B) PS and BS oral extracts (left and right three bars) were prepared to determine the source of hydrogen peroxide. (C) Continuity for hydrogen peroxide production in the PS oral extract. Formation of hydrogen peroxide immediately ceased in the presence of SDDC, an SOD inhibitor.

extracts, respectively. As depicted in Figure 5B, a significant change in absorbance was only detected when PS was present, i.e., the SOD in PBL was involved in the production of hydrogen peroxide. SOD may be the primary source for the generation of hydrogen peroxide, as supported by the fact that addition of SDDC immediately blocked the ability of PS oral extract to oxidize catechin (Figure 5C).

DISCUSSION

SOD dimerization and enhancement of enzymatic activity has been previously reported in other studies, using recombinant SOD of sweet potato.[16] Unlike other plant SODs, which exist in an equilibrium of monomers and dimers at neutral pH,[16,17] purified PBL SOD was entirely monomeric (Figure 1D,E) and existed in the same form within the cell. When chewing betel nut, the presence of slaked lime exerted two significant effects. First, in the presence of slaked lime, significantly more proteins were extracted compared with using oral extract from chewing betel nut alone (Figure 2A). The protein(s) were mainly derived from PBL rather than the areca nut, with trace amounts of proteins that included peroxidase as the major protein constituent.[13] Furthermore, the SOD of interest in the experiment was completely converted to the dimeric form in the presence of slaked lime, greatly enhancing its enzymatic activity in the oral cavity.

SOD dimerization was further augmented by arginine in the areca nut, i.e., arginine was a distinct mediator of SOD dimerization. The involvement of arginine in SOD dimerization was also reported by Klatt et al.[18] Furthermore, SOD dimerization in the BP oral extract (Figure 2C, lane 5) was most likely due to the presence of arginine in the areca nut. Previous experiments in animals and cell cultures have demonstrated that arginine plays a role in preventing toxicity such as that induced by free radicals[19,20] and may act through the synthesis of nitric oxide. These studies also revealed that arginine treatment alters the activities of antioxidant enzymes. Among them, the increased SOD activity[20] might be attributed to the formation of SOD dimers. Based on our results, the increased SOD activity may be independent of nitric oxide formation (Figure 4C). Despite the protective roles of arginine and SOD, the simultaneous presence of both components in the oral cavity resulted in harmful effects, such as the production of hydrogen peroxide as described below. The self-association of arginine molecules in aqueous solution demonstrated its striking ability to stabilize proteins and prevent protein aggregation.[21] Arginine monomers have been reported to hydrogen-bond to each other, forming a large cluster.[22] The charged amino acids on the surface of SOD may interact with arginine in a cluster and concomitantly link two molecules of SOD together.

Plant SODs play a defensive role by detoxifying superoxide radical to oxygen and hydrogen peroxide,[23] and numerous studies have demonstrated the protective role of plant Cu/Zn SODs against oxidative stress.[24,25] There is increasing evidence establishing hydrogen peroxide as a tumor promoter in carcinogenesis development.[26,27] In this study, PBL together

DOI: 10.1021/jf505753d
J. Agric. Food Chem. 2015, 63, 2225−2232

with the aid of slaked lime facilitated hydrogen peroxide production in the oral cavity (Figure 5A) in response to SOD. The antioxidants catechin and epicatechin in areca nut were in turn oxidized by hydrogen peroxide in the reaction catalyzed by peroxidases of both PBL and areca nut.[13] In this case, both antioxidants were completely consumed and undetectable in the BPS oral extract, as shown in the Supporting Information (Figure S1). In contrast, both antioxidants were still present in the BP oral extract due to the low concentration of hydrogen peroxide.

The hypothesis that hydrogen peroxide attacks and damages oral tissue is clearly supported by other reports, demonstrating hydrogen peroxide as a mediator of inflammation.[28,29] It was noteworthy that the formation of hydrogen peroxide in the oral cavity was immediately blocked by adding the inhibitor SDDC (Figure 5C), i.e., SOD activity was blocked and thus the production of H_2O_2 was prevented. This clearly indicates that hydrogen peroxide is continuously produced when betel nut is chewed uninterrupted, as is the case with most consumers. Nair et al. reported the effect of slaked lime on the production of reactive oxygen species (ROS) and its involvement in the development of oral cancer.[30,31] Taken together with our results, we conclude that slaked lime mediates the production of ROS, which is subsequently converted to hydrogen peroxide via SOD action. Therefore, we conclude that PBL SOD plays a role in oral carcinogenesis through the continuous formation of hydrogen peroxide in the oral cavity.

■ ASSOCIATED CONTENT

Supporting Information

Figure showing the detection of antioxidants catechin and epicatechin in the BPS and BP oral extracts. This material is available free of charge via the Internet at http://pubs.acs.org.

■ AUTHOR INFORMATION

Corresponding Authors

*Tel.: +886 4 22840837 ext 215. Fax:+ 886 4 22862073. E-mail: ylin@dragon.nchu.edu.tw (Y.-C.L.).

*Tel.: +886 4 22053366 ext 2103. Fax: +886 4 22053764. E-mail: hcho@mail.cmu.edu.tw (H.-C.H.).

Notes

The authors declare no competing financial interest.

■ ABBREVIATIONS USED

SOD, superoxide dismutase; DART-MS, direct analysis in real time mass spectrometry; PBL, *Piper betle* leaf; SA, sinapinic acid; SDDC, sodium diethyldithiocarbamate trihydrate; HCCA, α-cyano-4-hydroxycinnamic acid; DEAE, diethylaminoethyl; BPS, betel nut with slaked lime; BP, betel nut without slaked lime; PS, PBL with slaked lime; BS, areca nut with slaked lime; AN, areca-nut

■ REFERENCES

(1) Rathee, J. S.; Patro, B. S.; Mula, S.; Gamre, S.; Chattopadhyay, S. Antioxidant activity of *piper betel* leaf extract and its constituents. *J. Agric. Food Chem.* **2006**, *54*, 9046−9054.

(2) Bajpai, V.; Sharma, D.; Kumar, B.; Madhusudanan, K. P. Profiling of *Piper betle* Linn. cultivars by direct analysis in real time mass spectrometric technique. *Biomed. Chromatogr.* **2010**, *24*, 1283−1286.

(3) Nalina, T.; Rahim, Z. H. A. The crude aqueous extract of *Piper betle* L. and its antibacterial effect towards *Streptococcus mutans*. *Am. J. Biotechnol. Biochem.* **2007**, *3*, 10−15.

(4) Murata, K.; Nakao, K.; Hirata, N.; Namba, K.; Nomi, T.; Kitamura, Y.; Moriyama, K.; Shintani, T.; Iinuma, M.; Matsuda, H. Hydroxychavicol: a potent xanthine oxidase inhibitor obtained from the leaves of betel, *Piper betle*. *J. Nat. Med.* **2009**, *63*, 355−359.

(5) Pandey, A.; Bani, S.; Dutt, P.; Suri, K. A. Modulation of Th1/Th2 cytokines and inflammatory mediators by hydroxychavicol in adjuvant induced arthritic tissues. *Cytokine* **2010**, *49*, 114−121.

(6) Young, S. C.; Wang, C. J.; Lin, J. J.; Peng, P. L.; Hsu, J. L.; Chou, F. P. Protection effect of piper betel leaf extract against carbon tetrachloride-induced liver fibrosis in rats. *Arch. Toxicol.* **2007**, *81*, 45−55.

(7) Bhide, S. V.; Shivapurkar, N. M.; Gothoskar, S. V.; Ranadive, K. J. Carcinogenicity of betel quid ingredients: feeding mice with aqueous extract and the polyphenol fraction of betel nut. *Br. J. Cancer* **1979**, *40*, 922−926.

(8) Rai, M. P.; Thilakchand, K. R.; Palatty, P. L.; Rao, P.; Rao, S.; Bhat, H. P.; Baliga, M. S. Piper betel Linn (betel vine), the maligned Southeast Asian medicinal plant possesses cancer preventive effects: time to reconsider the wronged opinion. *Asian Pac. J. Cancer Prev.* **2011**, *12*, 2149−2156.

(9) Ko, Y. C.; Huang, Y. L.; Lee, C. H.; Chen, M. J.; Lin, L. M.; Tsai, C. C. Betel quid chewing, cigarette smoking and alcohol consumption related to oral cancer in Taiwan. *J. Oral Pathol. Med.* **1995**, *24*, 450−453.

(10) Hossain, Md. M.; Pervin, F.; Absar, N. Purification, characterization and N-terminal sequence analysis of Betel leaf (*Piper betle*) invertase. *J. Chin. Chem. Soc.* **2011**, *58*, 389−397.

(11) Shovon, M. S.; Sharma, S. C. D.; Roy, N. Purification, characterization and effect of physico-chemical agents on the stability of β-galactosidase from betel leaves. *J. Biosci.* **2010**, *18*, 108−115.

(12) Gupta, S.; Gupta, S. M.; Sane, A. P.; Kumar, N. Chlorophyllase in *Piper betle* L. has a role in chlorophyll homeostasis and senescence dependent chlorophyll breakdown. *Mol. Biol. Rep.* **2012**, *39*, 7133−7142.

(13) Liu, Y. C., Chen, C. J., Lee, M. R., Li, M., Hsieh, W. T., Chung, J. G., Ho, H. C. Peroxidase as the Major Protein Constituent in Areca Nut and Identification of Its Natural Substrates. *J. Evidence-Based Complementary Altern. Med.* **2013**, Article ID 412851.

(14) Chang, C. T.; Liao, H. Y.; Chang, C. M.; Chen, C. Y.; Chen, C. H.; Yang, C. Y.; Tsai, F. J.; Chen, C. J. Oxidized ApoC1 on MALDI-TOF and glycated-ApoA1 band on gradient gel as potential diagnostic tools for atherosclerotic vascular disease. *Clin. Chim. Acta* **2013**, *420*, 69−75.

(15) Shukla, M. R.; Yadav, R.; Desai, A. Catalase and superoxide dismutase double staining zymogram technique for *Deinococcus* and *Kocuria* species exposed to multiple stresses. *J. Basic Microbiol.* **2009**, *49*, 593−597.

(16) Lin, C. T.; Lin, M. T.; Chen, Y. T.; Shaw, J. F. Subunit interaction enhances enzyme activity and stability of sweet potato cytosolic Cu/Zn-superoxide dismutase purified by a His-tagged recombinant protein method. *Plant Mol. Biol.* **1995**, *28*, 303−311.

(17) Lin, C. T.; Kuo, T. J.; Shaw, J. F.; Kao, M. C. Characterization of the dimer-monomer equilibrium of the papaya Copper/Zinc superoxide dismutase and its equilibrium shift by a single amino acid mutation. *J. Agric. Food Chem.* **1999**, *47*, 2944−2949.

(18) Klatt, P.; Schmidt, K.; Lehner, D.; Glatter, O.; Bächinger, H. P.; Mayer, B. Structural analysis of porcine brain nitric oxide synthase reveals a role for tetrahydrobiopterin and L-arginine in the formation of an SDS-resistant dimer. *EMBO J.* **1995**, *14*, 3687−3695.

(19) Das, B.; Mandal, S.; Chaudhuri, K. Role of arginine, a component of aqueous garlic extract, in remediation of sodium arsenite induced toxicity in A375 cells. *Toxicol. Res.* **2014**, *3*, 191−196.

(20) Saad, E. A. Kidney response to L-arginine treatment of carbon tetrachloride-induced hepatic injury in mice. *Nat. Sci.* **2013**, *5*, 1−6.

(21) Shukla, D.; Trout, B. L. Interaction of Arginine with Proteins and the Mechanism by Which It Inhibits Aggregation. *J. Phys. Chem. B* **2010**, *114*, 13426−13438.

DOI: 10.1021/jf505753d
J. Agric. Food Chem. 2015, 63, 2225−2232

(22) Zhang, D.; Wu, L.; Koch, K.; Cooks, R. Arginine clusters generated by electrospray ionization and identified by tandem mass spectrometry. *Eur. J. Mass Spectrum.* **1999**, *5*, 353−361.
(23) Bowler, C.; Van Camp, W.; Van Montagu, M.; Inzé, D. Superoxide dismutase in plants. *Crit. Rev. Plant Sci.* **1994**, *13*, 199−218.
(24) Gupta, A. S.; Heinen, J. L.; Holaday, A. S.; Burke, J. J.; Allen, R. D. Increased resistance to oxidative stress in transgenic plants that overexpress chloroplastic Cu/Zn superoxide dismutase. *Proc. Natl. Acad. Sci. U.S.A.* **1993**, *90*, 1629−1633.
(25) Gupta, A. S.; Webb, R. P.; Holaday, A. S.; Allen, R. D. Overexpression of Superoxide Dismutase Protects Plants from Oxidative Stress (Induction of Ascorbate Peroxidase in Superoxide Dismutase-Overexpressing Plants). *Plant Physiol.* **1993**, *103*, 1067−1073.
(26) Weitzman, S. A.; Weitberg, A. B.; Stossel, T. P.; Schwartz, J.; Shklar, G. Effects of hydrogen peroxide on oral carcinogenesis in hamsters. *J. Periodontol.* **1986**, *57*, 685−688.
(27) Huang, R. P.; Peng, A.; Hossain, M. Z.; Fan, Y.; Jagdale, A.; Boynton, A. L. Tumor promotion by hydrogen peroxide in rat liver epithelial cells. *Carcinogenesis* **1999**, *20*, 485−492.
(28) Misawa, M.; Arai, H. Airway inflammatory effect of hydrogen peroxide in guinea pigs. *J. Toxicol. Environ. Health.* **1993**, *38*, 435−448.
(29) Schalkwijk, J.; van den Berg, W. B.; van de Putte, L. B.; Joosten, L. A. An experimental model for hydrogen peroxide induced tissue damage: effect on cartilage and other articular tissues. *Int. J. Tissue React.* **1987**, *9*, 39−43.
(30) Nair, U. J.; Friesen, M.; Richard, I.; MacLennan, R.; Thomas, S.; Bartsch, H. Effect of lime composition on the formation of reactive oxygen species from areca nut extract in vitro. *Carcinogenesis* **1990**, *11*, 2145−2148.
(31) Nair, U. J.; Obe, G.; Friesen, M.; Goldberg, M. T.; Bartsch, H. Role of lime in the generation of reactive oxygen species from betel-quid ingredients. *Environ. Health Perspect.* **1992**, *98*, 203−205.

DOI: 10.1021/jf505753d
J. Agric. Food Chem. 2015, 63, 2225−2232

vitro, suggesting a method for the semisynthesis of brain-targeted flavan-3-ol metabolites.[7] Of the 12 enzymes tested, UGT1A9 was the most efficient, and this enabled us to generate 3′-*O*-methyl-EC-5-*O*-glucuronide to 50% overall yield.[7]

In the present study, we have extended the above approach, in combination with chemical methylation of C and EC with iodomethane, to generate authentic standards of the C and EC metabolites found in the plasma and brains of rats treated with GSPE. The structures of the metabolites were rigorously identified, and we present a robust, validated protocol for the measurement of the levels of these compounds in animal fluids.

MATERIALS AND METHODS

Materials. Uridine 5′-diphospho (UDP)-glucuronosyl transferase enzymes (recombinant or as mouse microsomes), buffers, and UDP-glucuronic acid were purchased from BD Biosciences (San Diego, CA). (−)-Epicatechin, (+)-catechin, DBU (1,8-diazabicyclo[5.4.0]-undec-7-ene), and iodomethane were from Sigma-Aldrich, St Louis, MO. 3′- and 4′-*O*-Methyl epicatechin were purchased from Nacalai USA, Inc. (San Diego, CA).

Chemical Methylation of C/EC. (Epi)catechin (1 g) was dissolved in 240 mL of dimethylformamide in a 1 L bottle, and the bottle was saturated with nitrogen gas for 5 min. DBU (14 mL) and iodomethane (300 mL) were then added and mixed well, and the solution was resaturated with nitrogen gas for 30 s. The bottle was capped and placed at 40 °C in the dark for 3 h. The reaction was then quenched by the addition of 400 mL of methanol with mixing. The solution was dried under nitrogen and resuspended in high-performance liquid chromatography (HPLC)-grade methanol for HPLC analysis and purification.

Large-Scale Purification of Methylated C/EC. Methylated (epi)catechins were purified on a large scale using a Biotage Isolera flash chromatography system equipped with a 10 g SNAP C18 cartridge at a flow rate of 18 mL/min, monitoring at 280 nm with a UV/vis detector. The sample in methanol was added to the column via a preloading concentrator disc. Solvent A was milli-Q water, and solvent B was HPLC-grade acetonitrile. The column was equilibrated at 5% B, and the gradient for elution was as follows: isocratic at 5% B for 12 column volumes (CVs) or 180 mL; from 5% B to 13% B in 48 CVs or 720 mL; from 13% B to 100% B in 4 CVs or 60 mL; then washed in 100% B for 20 CVs or 300 mL. Fractions were collected in 16 CV or 240 mL fractions.

Glucuronidation of EC and Methyl-C/EC and Purification of the Products. The glucuronidation reaction was performed at room temperature, and the mixture consisted of 210 μL of purified water, 40 μL of UGT Reaction Mix Solution A (containing UDP-glucuronic acid, BD Biosciences), 100 μL of UGT Reaction Mix Solution B (containing $MgCl_2$, Tris-HCl buffer, and alamethicin, BD Biosciences), 10 μL of 20 mM (epi)catechin derivative, and 120 μL of human UGT1A9 (for EC and methyl-EC) or pooled male mouse liver microsomes (5 mg protein per mL) (for C and methyl-C). After 6 h, an additional 40 μL of UGT Reaction Mix Solution A, 40 μL of Reaction Mix Solution B, 120 μL of UGT1A9 or mouse microsomes, and 10 μL of 20 mM (epi)catechin derivative were added. Then, at 12 h, a further 40 μL of UGT Reaction Mix Solution A and 120 μL of UGT1A9 or mouse microsomes were added. The reactions were stopped after 24 h by the addition of 400 μL of methanol containing 3% of 85% phosphoric acid. The solvent was removed under nitrogen gas, and the aqueous fractions were desalted using a Waters Sep-Pak Plus C18 cartridge. The cartridge was first washed with 10 mL of methanol, followed by 20 mL of water. The sample (5 mL) was loaded onto the cartridge, then washed twice with 5 mL of water, and finally eluted twice with 5 mL of methanol. The sample was dried under nitrogen and then resuspended in a small volume of methanol for HPLC purification. Product peaks were partially purified on the analytical HPLC, and the solvent was removed under nitrogen gas. The aqueous fractions were then acidified to 1% phosphoric acid final concentration and desalted using a Waters Sep-Pak Plus C18 cartridge. The methanol was dried under nitrogen, and the fractions were analyzed for comparison to products found in the plasma of mice/rats fed the monomer-enriched GSPE fraction. All samples were dissolved in 100 μL of acidified water and acetonitrile (4:1, v/v) and further analyzed by HPLC coupled to LC-TOF-MS (see below).

HPLC for Analysis and Purification of C/EC Metabolites. HPLC analysis and purification of (epi)catechin derivatives were performed on an Agilent HP1200 HPLC, monitoring at 280 nm. The HPLC with ChemStation software version B.02.01.SRI was equipped with a G1322A degasser, a G1311A quaternary pump, a G1367B autosampler, a G1316A thermostatic column compartment, and a G1315C diode array detector. A Varian Metasil 5 Basic C18 250 × 4.6 mm column was used for analytical and micropreparative HPLC on the Agilent HPLC system. Analytical and preparative HPLC were performed using the following gradient: isocratic at 5% B for 5 min; 5% B to 10% B in 5 min; 10% B to 17% B in 15 min; 17% B to 23% B in 5 min; then 23% B to 50% B in 35 min. Alternatively, a shorter method was used that retained the same gradient except that the last step gradient was from 23% B to 28% B in 5 min, reducing the run time by 30 min. Solvent A was 1% phosphoric acid in Milli-Q water, and solvent B was HPLC-grade acetonitrile. The flow rate was 1 mL/min.

Solid-Phase Extraction (SPE) of C and EC Metabolites from Rodent Plasma. Rodent plasma samples were obtained from a previous pharmacokinetic study using GSPE[4] that received approval from the Animal Care and Use Committee at Purdue University. Plasma aliquots from control animals (no GSPE) and treated animals (with GSPE) that were collected at sacrifice were thawed from −80 °C storage and quickly pooled separately at Purdue University. These control and GSPE plasma samples were then realiquoted into individual vials and refrozen at −80 °C until analysis. For target assessment purposes, typical plasma was diluted 5-fold with blank plasma to produce low-dose plasma. Blank, low, and normal plasma samples were then used for analytical validation at Purdue University, and a parallel set of samples was sent to the University of North Texas for cross-lab validation.

Samples of frozen plasma were thawed at room temperature, and 300 μL of acidified saline (9g of NaCl in 1 L of 0.1% v/v formic acid/H_2O) were added to 200 μL of plasma with vortex mixing. A SPE cartridge (30 mg Oasis HLB column, Waters Co, Milford, MA) was activated by addition of 1 mL of MeOH followed by 1 mL of DI H_2O, after which the plasma/saline mixture was loaded. The loaded SPE column was first washed with 1 mL of 1.5 M formic acid, followed by 1 mL of 95:5 v/v water/MeOH, and the eluate was discarded. Metabolites were then eluted with 2 mL of 0.1% v/v formic acid/MeOH.

Extraction recovery was assessed in a pilot experiment by spiking 10 μL of ethyl gallate stock solution (10 μM) into freshly thawed plasma samples prior to extraction and analysis. Extraction recovery was found to be 96.0 ± 3.1%. Following validation of recovery, ethyl gallate was used as a daily internal standard (10 μL of stock 10 μM solution) added to the eluates from solid-phase extraction prior to samples being dried under vacuum (<50 mmHg) at 37 °C. The residues were resuspended in 160 μL of 0.1% v/v formic acid/H_2O + 40 μL of 0.1% v/v formic acid/acetonitrile, sonicated for 10 s, vortex-mixed for 10 s, and then transferred to centrifuge tubes, which were centrifuged at 18 000*g* for 5 min to remove any particulates. The clear supernatants were carefully transferred to 300 μL HPLC vials for analysis.

The ability of this extraction method to account for potential matrix effects was assessed by comparing the response of individual metabolite standards in the presence or absence of blank plasma extracted matrix. Briefly, standards of C and its major metabolites in GSPE rodent plasma at 50, 100, and 500 nM were resuspended either in pure solvent (160 μL of 0.1% v/v formic acid/H_2O + 40 μL of 0.1% v/v formic acid/acetonitrile—Standard) or in resolubilized blank plasma extracted by SPE (Standard + Matrix). By comparison of response between standards injected with or without plasma matrix, an estimate of matrix effects was established by using the following equation: % matrix effect (% ME) = (peak area of standard with

DOI: 10.1021/jf505922b
J. Agric. Food Chem. 2015, 63, 2233−2240

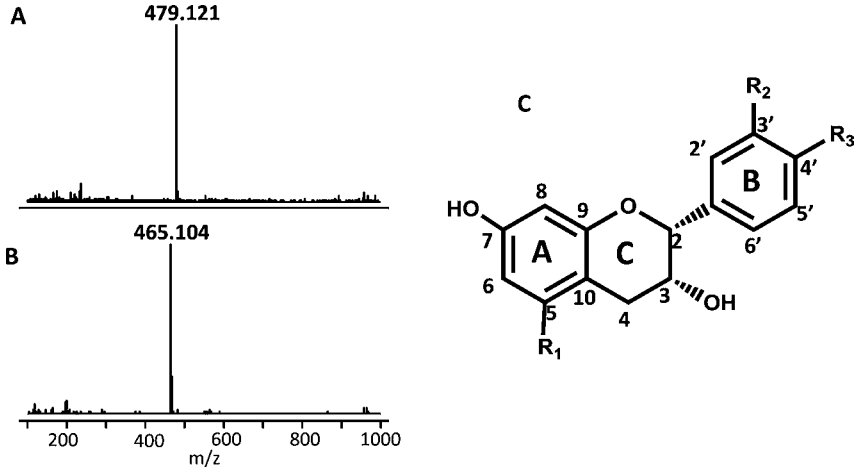

Figure 1. Flavan-3-ol derivatives in rodent plasma. (A, B) Representative mass spectra of unknown metabolites in rodent plasma obtained on a LC/TOF system with a recording range of 100−1000 *m/z*. The mass spectrum of (A) is consistent with the mass of methyl-C/EC glucuronide, while that of (B) is consistent with C/EC glucuronide. (C) Structure of 2,3-*cis*-flavan-3-ols. Epicatechin, R1 = R2 = R3 = OH; 3′-*O*-methyl-epicatechin-5-*O*-*β*-D-glucuronide, R1 = glucuronic acid, R2 = OMe, R3 = OH.

matrix−peak area of pure standard)/(peak area of pure standard) × 100.[8]

NMR Analysis. NMR spectroscopy was performed using a Bruker Avance DRX 500 MHz spectrometer equipped with a cryoprobe. The metabolites were dissolved in CD_3OD (99.96% atom D; Sigma, St. Louis, MO) and then transferred to a 5 mm Shigemi tube (Wilmad Glass, Vineland, NJ).

HPLC/MS Analysis of C/EC Metabolites from Rodent Plasma. *(1). LC-TOF-MS for Unknown Metabolite Characterization.* Separation was achieved on an Agilent 1100 HPLC system using a Waters XBridge BEH shield RP-C18 XP (2.1 × 100 mm 2.5 μm) column following a 2 μm frit filter. The column and autosampler were maintained at 40 and 10 °C, respectively. Mobile phase A was 0.1% v/v formic acid/water and B was 0.1% v/v formic acid/acetonitrile. A linear gradient for elution was used at a constant flow rate of 0.26 mL/min. Initial conditions, 5% B; 0−12 min, 5−15% B; 12−18 min, hold at 15% B; 18−24 min, 15−40% B; 24−30 min, 40−50% B; 30−31 min, 50−5% B; 31−36 min, hold at 5% B to reset gradient. Injection volume was set to 10 μL. Mass spectra of flavan-3-ol metabolites were obtained using an Agilent 6200 time-of-flight (TOF) mass spectrometer, with negative mode electrospray ionization, using a mass range of 100−1000 *m/z* and an acquisition rate of 1.4 spectra/s. Source parameters were as follows: gas temperature = 350 °C, drying gas = 9 L/min, nebulizer pressure = 35 psi, capillary potential = 3500 V, fragmentor voltage = 145 V, skimmer voltage = 60 V, and OCT 1 RF Vpp = 250 V.

(2). LC-MS/MS for Metabolite Quantification. Separation was achieved on an Agilent 1200 HPLC system as described in the previous section, except for the gradient conditions as follows: initial conditions, 10% B; 0−9 min, 10−35% B; 9−10 min, 35−65% B; 10−12 min, 65−10% B; 12−16 min, hold at 10% B to reset gradient. Analytes were quantified using tandem mass spectrometry (MS/MS) with an Agilent 6460 triple quadrupole with electrospray ionization (ESI) in negative mode using selected reaction monitoring (SRM) mass transitions. Collision energy was 17 eV. Acquisition multiple reaction monitorings (MRMs) were as follows: C/E, 289 → 245 *m/z*; C/E glucuronide, 465 → 289 *m/z*; methyl C/E glucuronide, 479 → 303 *m/z*; ethyl gallate, 197 → 169 *m/z*. All mass transitions used a dwell time of 200 ms and a fragmentor voltage of 135 V. Source parameters were as follows: gas temperature = 350 °C, gas flow = 11 L/min, nebulizer pressure = 30 psi, sheath gas temperature = 350 °C, sheath gas flow = 11 L/min, capillary potential = 3500 V, and nozzle voltage = 1000 V. Intraday repeatability was assessed by extracting and analyzing pooled plasma *n* = 5 times. Interday reproducibility was determined across *n* = 5 days using aliquot pooled plasma. Repeatability and reproducibility were determined as relative coefficient of variation (% CV) as calculated by standard deviation/mean × 100. Limit of detection (LOD) was defined as signal-to-noise ratio (S/N) = 3, and limit of quantification (LOQ) was defined as S/N = 5. Both values were obtained by producing serial dilutions of parent nonmetabolized compounds and metabolites. Data are presented as mean ± standard deviation. S/N was calculated using MassHunter software using the peak-to-peak method.

(3). Second Site Validation. Samples were analyzed using a Waters Xevo-TQ mass spectrometer interfaced with a Waters Acquity ultra-performance liquid chromatography (UPLC) system. Sample preparation and LC parameters were according to the original protocol above. Mass spectrometry source parameters were as follows: ESI, negative mode; capillary voltage, 2 kV; source temperature, 150 °C; sheath gas flow, 800 L/h; desolvation temperature, 400 °C; cone voltage, 28 V. Acqusition MRMs were as follows: C/EC glucuronide, 456 → 289 *m/z*, collision energy 22; C/EC methyl glucuronide, 479 → 303 *m/z*, collision energy 22; ethyl gallate, 197 → 169 *m/z*, collision energy 16. Dwell time was 200 ms.

RESULTS AND DISCUSSION

Metabolites of Flavan-3-ols in Rat Plasma and Strategy for Generation of Standards. Multiple metabolites derived from the flavan-3-ols C (2,3-*trans*) and EC (2,3-*cis*) are found in mouse or rat plasma following the feeding of monomer-enriched GSPE. LC-MS analysis has indicated that these compounds are primarily glucuronides of C/EC or methyl-C/EC[4] (Figure 1A, B). One of the most abundant metabolites in plasma was previously identified by micro-NMR as 3′-*O*-methyl-EC-5-*O*-*β*-D-glucuronide (Figure 1C),[7] and we have developed a semisynthetic route to this compound.[7] Because of the low levels of the metabolites, as well as the need to develop a robust method for their quantitation, we decided to develop semisynthetic routes to the remaining compounds.

Our strategy for generation of standards of the other C/EC metabolites found in rat plasma was to (1) synthesize methyl derivatives of C and EC; (2) subject the (methylated) C and EC to enzymatic glucuronidation; (3) compare LC-MS mobility and fragmentation pattern of the synthetic compound to those of the metabolites in plasma; and (4) scale up the synthesis of compounds that match those in plasma and confirm their structures by NMR.

Methylation of C and EC. Although 3′-and 4′-*O*-methyl-EC are commercially available, they are expensive (synthetic 4′-

DOI: 10.1021/jf505922b
J. Agric. Food Chem. 2015, 63, 2233−2240

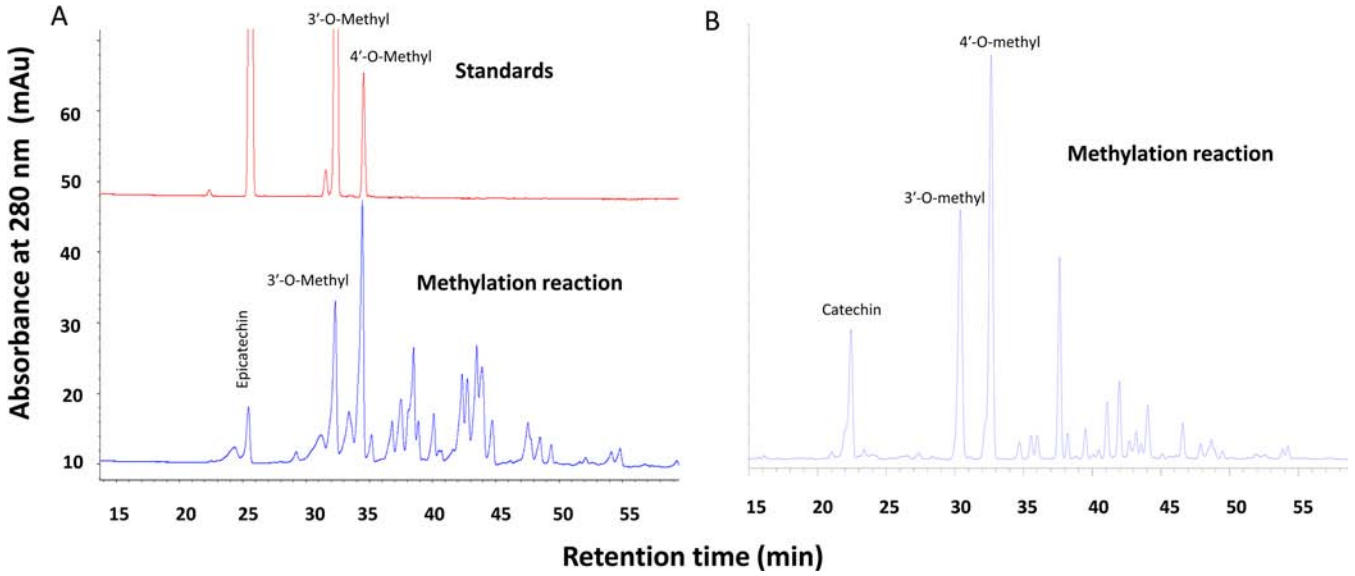

Figure 2. *O*-Methylation of epicatechin (A) and catechin (B) by reaction with iodomethane. HPLC traces show the multiple products formed, with the 3′- and 4′-*O*-methyl derivatives identified by comparison to authentic standards.

O-methyl-EC currently costs over 1 000 Euros per mg; tebubio, Le Perray-en-Yvelines, France). We have previously explored the methylation of EC using catechol-*O*-methyltransferase from porcine liver;[7] this leads predominantly to the 3′-*O*-methyl derivatives. Although this method was effective (and is a useful approach if it is desired to incorporate radiolabel in the methyl group through incubation with labeled methyl donor S-adenosyl-L-methionine), it is also relatively expensive, and we therefore investigated the cheaper alternative of chemical methylation of the core flavan-3-ols with iodomethane, using previously established procedures.[9] This approach leads to generation of multiple methylated products from both C and EC (Figure 2), with the more complex multimethylated products constituting a larger proportion of the reaction products with longer incubation times. However, because the different products and isomers can easily be separated by preparative HPLC, and because of the low cost of the starting materials, this method proved effective for generation of 3′- and 4′-*O*-monomethyl derivatives of both C and EC, suitable for subsequent glucuronidation. The methylated EC derivatives were authenticated by comparison to the commercial standards. Standards are not available for the methyl-C derivatives; identity was first inferred based on the retention times of the corresponding EC derivatives and subsequently confirmed (for the 3′-*O*-methyl derivative) by NMR of the resulting glucuronidated products (see below). Optimization of reaction conditions, particularly reaction time, resulted in maximum yields of 3′-*O*-methyl-C/EC of ∼20%. The methylated compounds were purified by chromatography using a Biotage Isolera system.

Glucuronidation of (Methyl)-C/EC and Matching of Synthetic Compounds to Metabolites in Plasma. Human recombinant glucuronosyltransferase UGT1A9, in the presence of UDP-glucuronic acid, converts EC to a number of products, the major one being the 3′-*O*-glucuronide (a compound not found in the plasma of rats or mice fed GSPE), with minor amounts of the 5-*O*-glucuronide (a minor metabolite in the plasma).[7] 3′-*O*-Methyl-EC is efficiently converted by UGT1A9 to 3′-*O*-methyl-EC-5-*O*-glucuronide (a major plasma metabolite). The other compounds in plasma appear to be derivatives of C. We therefore investigated conditions (reaction times, enzyme and substrate concentrations, and supplementation of reaction mixtures with additional enzyme/substrate) for the optimal glucuronidation of methylated and nonmethylated C by mammalian glucuronosyltransferases and UDP-glucuronic acid, as previously described for EC.[7] In contrast to EC, we found that pooled male mouse microsomes were more efficient at glucuronidation of C and its derivatives than was recombinant UGT1A9, resulting in two major products initially named CG14 and CG18 based on their approximate retention times by HPLC (Figure 1A in Supporting Information). CG14 and CG18 were further purified by preparative HPLC (Figure 1B in Supporting Information). Both compounds possessed a molecular ion of 465 and matched peaks in the plasma of rats fed GSPE: CG14 was a minor component (Figure 1C in Supporting Information), whereas CG18 corresponded to the second most abundant metabolite (Figure 1D in Supporting Information).

In a similar manner, glucuronidation of (presumed) 3′-*O*-methyl-C by mouse microsomes in the presence of UDP-glucuronic acid led to the formation of multiple products of which two, with retention times of 19 and 24 min and molecular ions of 479 (MCG19 and MCG24), matched metabolites in the rat plasma. Glucuronidation products of (presumed) 4′-*O*-methyl-C did not match any of the compounds found in plasma. Figure 3 summarizes the matches between the synthetic (methyl)-C's and plasma-derived metabolites and indicates the diagnostic major fragmentation products of the molecular ions.

Structural Characterization of C and EC Metabolites. We have previously reported the structural characterization of 3′-*O*-methyl-EC-5-*O*-glucuronide.[7] To elucidate the structures of CG14, CG18, MCG19, and MCG24, 2D NMR experiments using HSQC (heteronuclear single quantum coherence spectroscopy), HMBC (heteronuclear multiple bond correlation spectroscopy), and NOESY (nuclear Overhauser effect spectroscopy) were performed. The spectral data (chemical shifts) for the four compounds are shown in Table 1, and ^{1}H, HSQC, HMBC, and NOESY data are shown in Figures 2–8 in Supporting Information. The glucuronic acid moiety was

DOI: 10.1021/jf505922b
J. Agric. Food Chem. 2015, 63, 2233−2240

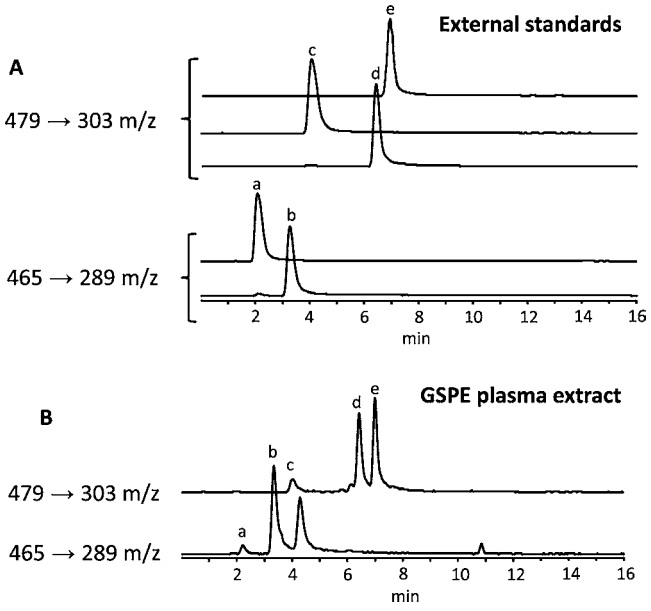

Figure 3. Chromatographic separation and identification of C/EC metabolites for each mass transition. Peak identification: (a) CG14, C-glucuronide; (b) CG18, C-glucuronide; (c) MCG24, 3′-*O*-methyl-C-glucuronide; (d) MCG19, 3′-*O*-methyl-C-glucuronide; (e) 3′-*O*-methyl-EC-5-*O*-glucuronide.

assigned to the 7 position on (+)-C for CG-14 and MCG-19 based on the presence of a HMBC cross-peak between the anomeric proton (H-1″) and C-7 (Figure 7 in Supporting Information). The assignment on CG-18 and MCG-24 was to the 5 position due to a HMBC cross-peak between H-1″ and C-5 (Figure 4 in Supporting Information). The methyl group was assigned to the 3′ position on MCG-19 and MCG-24 due to a NOESY cross-peak between H-2′ and the methoxy group, confirming the identity of the precursor as 3′-*O*-methyl-C (Figure 8 in Supporting Information). Figure 4 summarizes the structures of the four C metabolites, and its caption provides further description of how the positions of methylation and glucuronidation were assigned.

Several previous studies have reported the presence of PAC metabolites in blood plasma after feeding animals with PA preparations or foods rich in PACs.[10−13] The metabolites were partially identified as sulfonated, glucuronidated, and/or methylated derivatives of EC and C,[11,14−16] with most studies focusing on the EC derivatives. Definitive structures, particularly with respect to the position of glucuronidation, were not systematically assigned for many of the biologically relevant metabolites. The present systematic approach to the synthesis and identification of predominant plasma-derived metabolites of flavan-3-ols present in plasma of rodents dosed with GSPE provides a blueprint for the development of improved methods for the evaluation of bioavailability of plant polyphenols, as well as a source of standard target molecules for evaluating modes of action.

Cross-Validated Analytical Method for Determining Plasma Levels of C and EC Metabolites. LC-MS using an Agilent 6460 Triple Quadrupole system was selected as the analytical method to determine the levels of C and EC metabolites in samples of plasma from rats fed GSPE, due in part to the sensitive and selective nature of this method as well as the broad application of this method in the literature.[17−19] Initially, the linear dynamic range for each molecule (C, EC, two C-glucuronides, two methyl-C-glucuronides, and one methyl-EC-glucuronide) was determined for concentrations ranging over 4 orders of magnitude (pM−μM), with the lowest concentrations in the 250−650 pM range. The linear dynamic range was observed to be excellent (Table 2) and provides the ability to quantify these compounds across a range of concentrations typical in biological fluids and tissues. Metabolites were extracted from plasma by solid-phase extraction as described in Materials and Methods. Measurement of effects of matrix and plasma concentration (Table 1 in Supporting Information) and intraday and interday variability (Tables 2 and 3 in Supporting Information) revealed the method to be highly robust and efficient at limiting ion suppression or other matrix effects commonly reported, but rarely accounted for, in analysis of biological samples.[20−22] As expected, there was a greater matrix effect (ME) at lower concentrations. The % ME when measuring C ranged from −7.84% at 500 nM to −20.7% at 50 nM. The ME for MCG24 ranged from −13.5% at 500 nM to −23.0% at 50 nM. Finally, the ME for CG18 ranged from −13.1% at 500 nM to −15.7% at 50 nM. Because metabolites appear in rodent plasma at

Table 1. NMR Spectral Data (Chemical Shifts) for CG14, CG18, MCG19, and MCG24

	chem. shift (ppm)			chem. shift (ppm)			chem. shift (ppm)			chem. shift (ppm)	
CG-14 position	^{1}H	^{13}C	MCG-19 position	^{1}H	^{13}C	MCG-24 position	^{1}H	^{13}C	CG-18 position	^{1}H	^{13}C
2	4.59	82.55	2	4.63	82.54	2	4.62	83.04	2	4.59	82.53
3	3.97	68.17	3	4.01	68.29	3	4.13	66.49	3	4.05	66.31
4a	2.87	28.04	4a	2.90	30.88	4a	2.61	27.08	4a	3.00	28.35
4b	2.53		4b	2.54		4b	2.17		4b	2.60	
6	6.25	96.94	6	6.22	96.94	6	6.34	97.49	6	6.27	96.76
8	6.15	96.81	8	6.14	96.59	8	6.00	98.08	8	6.01	97.97
2′	6.83	114.86	2′	6.97	111.46	2′	6.96	111.61	2′	6.81	114.83
5′	6.71	120.27	OMe	3.84	55.83	OMe	3.83	56.40	5′	6.70	115.75
6′	6.76	115.62	5′	6.79	115.42	5′	6.77	115.97	6′	6.75	115.50
1″	4.83	102.06	6′	6.83	121.44	6′	6.85	121.21	1″	4.84	102.23
2″	3.45	74.23	1″	4.84	102.03	1″	4.82	102.81	2″	3.48	74.43
3″	3.44	77.27	2″	3.48	74.06	2″	3.50	74.60	3″	3.48	77.43
4″	3.53	72.98	3″	3.43	74.42	3″	3.49	77.94	4″	3.55	73.12
5″	3.77	76.16	4″	3.56	72.65	4″	3.55	73.71	5″	3.81	76.57
			5″	3.87	76.13	5″	3.69	76.59			

DOI: 10.1021/jf505922b
J. Agric. Food Chem. 2015, 63, 2233−2240

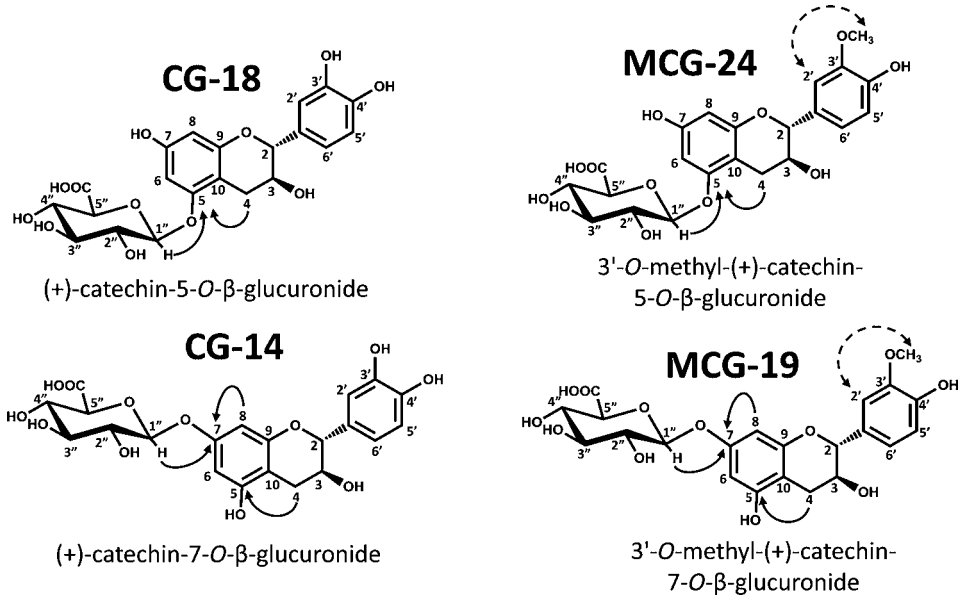

Figure 4. Structures assigned to CG14, CG18, MCG19, and MCG24. The glucuronic acid moiety was able to be assigned to the 7 position on (+)-catechin for CG-14 and MCG-19 based on the presence of a HMBC cross-peak between the anomeric proton (H-1″) and C-7. The chemical shift of C-7 was determined by a HMBC cross-peak between H-8 and C-7. Further support of this connectivity was provided by the absence of a cross-peak between H-1″ and C-5 (chemical shift determined by a cross-peak between H-4 and C-5). The assignment on CG-18 and MCG-24 was to the 5 position due to a HMBC cross-peak between H-1″ and C-5. The methyl group was assigned to the 3′ position on MCG-19 and MCG-24 due to a NOESY cross-peak between H-2′ and the methoxy group. HMBC is designated by a solid arrow, and NOESY is designated by a dashed arrow.

Table 2. Linear Dynamic Ranges for the Quantitation of (Methyl)catechin and (Methyl)epicatechin Glucuronides by LC-MS/MS

compound	range	regression line	linearity (R^2)	LOQ (S/N = 5) MOC	LOD (S/N = 3) MOC
C	5 nM−50 μM	$y = 7 \times 10^{09}x + 528.31$	0.9997	138.9 pmol	55.5 pmol
EC	5 nM−50 μM	$y = 7 \times 10^{09}x + 689.79$	0.9997	106.4 pmol	48.4 pmol
3′OMe-EC-5-*O*-glucr	250pM−2.5 μM	$y = 5 \times 10^{11}x - 3699.8$	0.9998	2.05 fmol	1.07 fmol
CG18	500pM−10 μM	$y = 4 \times 10^{11}x + 403.99$	0.9999	10.6 fmol	3.41 fmol
CG14	500pM−10 μM	$y = 6 \times 10^{11}x - 16601$	0.9998	3.68 fmol	1.2 fmol
MCG19	650pM−10 μM	$y = 2 \times 10^{11}x + 12580$	0.9990	5.80 fmol	2.80 fmol
MCG24	500pM−20 μM	$y = 4 \times 10^{11}x - 31920$	0.9994	4.70 fmol	1.03 fmol

∼300−400 nM after repeated dosing of GSPE, using the SPE procedure results in underestimating metabolites by ∼13%.

The Horwitz ratio (HorRat), a well-recognized normalized performance parameter that provides a measure of laboratory precision, was calculated for individual metabolites based on the equations described by Horwitz and Albert.[23] HorRat values ranging from 0.13 to 1.29 indicated the high reproducibility of this method. While lower values of the HorRat (0.13−0.21) do fall outside of the generally accepted range, it is important to note that these were for minor metabolites (C-7-*O*-glucuronide, 3′-*O*-Me-C-7-*O*-glucuronide, and 3′-*O*-Me-EC-7-*O*-glucuronide). Comparatively, values for major metabolites identified in this method, (C-5-*O*-glucuronide and 3′-*O*-Me-C-5-*O*-glucuronide) were 1.29 and 0.51, respectively. Overall these data are consistent with that of a highly reproducible analytical method.

Calculated LOD (defined as 3:1 signal/noise) ranged from 1.03 to 3.41 fmol on column for metabolites of C and EC compared to 55.5 and 48.4 pmol on column for the parent compounds C and EC, respectively. This suggests the potential for more efficient ionization of metabolites relative to parent compounds. These values translated to LOQs of 2.1−10.6 fmol on-column or ∼11−53 fmol per mL of plasma for metabolites.

Finally, the analyses were repeated at a second site, using the same column and separation parameters, but a different mass spectrometer (see Materials and Methods). The C and EC metabolites in the plasma were resolved by HPLC with very similar profiles to those recorded previously (compare Figure 9 in Supporting Information and Figure 3). Calibration with authentic standards resulted in absolute values and standard deviations that closely matched the results from the first site analyses, with the exception of MCG24 (3′-*O*-methyl-C-5-*O*-glucuronide), which was determined based on calibration with the corresponding 7-*O*-glucuronide (Table 4 in Supporting Information). It was observed that the C and EC metabolites were unstable in thawed plasma samples, as recently reported elsewhere,[24] such that reproducible results were only obtained if the samples were injected onto the HPLC within a few hours. Samples left at room temperature were almost totally degraded after 3 days.

Advantages and Disadvantages of the Present Approach. Alternative approaches for identifying metabolites of flavan-3-ols in biological fluids have either generated standard compounds by chemical synthesis[9] or attempted to identify the compounds directly from the fluids;[14−16,25] most of these previous approaches have only unequivocally identified a

DOI: 10.1021/jf505922b
J. Agric. Food Chem. 2015, 63, 2233−2240

subset of the metabolites present. A recent study has reported the chemical synthesis and full characterization of a complete range of EC glucuronides and sulfates.[24] Such compounds will be of great value for future studies on bioavailability, although their chemical synthesis is complex, requiring as a starting point the availability of a complete series of orthogonally protected EC derivatives.

The present study has combined a semisynthetic/biosynthetic scheme with matching of compounds to authentic metabolites. Although the glucuronosyl transferase enzymes are not completely regiospecific, their mammalian origin means that they can generate physiologically relevant metabolites, and the matching of synthetic compounds to plasma metabolites prior to final purification means that only those metabolites that are physiologically relevant are pursued. Furthermore, an enzymatic strategy has advantages for the facile introduction of radiolabel, for example, in the methyl (from S-adenosyl-L-methionine) or glucuronide (from UDP-glucuronic acid) moieties, should labeled compounds be required for mechanism of action studies or analytical internal standards. The limiting steps from a cost perspective are the price of the enzymes, which cannot be recycled, and the cost of UDP-glucuronic acid. Now that standards of all glucuronidated metabolites are available for subsequent identification of products, this problem could be circumvented by a total biological synthesis using recombinant enzymes expressed in *E. coli*, as we have previously shown for synthesis of flavonol and isoflavone glucosides.[26] It should be noted that the present work does not address the sulfated derivatives that also arise from mammalian metabolism of flavan-3-ols, particularly in humans.[27]

■ ASSOCIATED CONTENT

Supporting Information

Supplemental figures: Figure 1, glucuronidation of catechin by mouse microsomes in the presence of UDP-glucuronic acid, as well as comparison of major products to metabolites of catechin in plasma from rats fed GSPE; Figure 2, ^{1}H NMR spectrum of catechin glucuronide CG-18; Figure 3, ^{1}H NMR spectrum of methyl catechin glucuronide MCG-24; Figure 4, HSQC and HMBC spectra of CG-18 and MCG-24; Figure 5, ^{1}H NMR spectrum of methyl catechin glucuronide MCG-19; Figure 6, ^{1}H NMR spectrum of catechin glucuronide CG-14; Figure 7, HSQC and HMBC spectra of CG-14 and MCG-19; Figure 8, NOESY spectra of methylcatechin glucuronide MCG-19; Figure 9, chromatographic separation and identification of C/EC metabolites for each mass transition in the second site validation experiment; Table 1, target assessment (plasma dilutions) and matrix effects for quantitation of catechin and epicatechin metabolites in rat plasma by LC-MS; Table 2, intraday variability for quantitation of catechin and epicatechin metabolites in rat plasma by LC-MS, n = 5; Table 3, interday variability for quantitation of catechin and epicatechin metabolites in rat plasma by LC-MS; Table 4, quantitation of catechin and epicatechin metabolites in rat plasma (nmol/L) by LC-MS in the second site validation experiment, n = 5. This material is available free of charge via the Internet at http://pubs.acs.org.

■ AUTHOR INFORMATION

Corresponding Author

*E-mail: Richard.Dixon@unt.edu. Phone: +1-940-565-2308. Fax: +1-580-224-6692.

Funding

This work was supported by National Institutes of Health grant 5 PO1 AT004511-05 Administrative Supplement to G.P. and by the University of North Texas and Purdue University. This material is also the result of work supported in part with resources and the use of facilities at the James J. Peters Veterans Affairs Medical Center, Bronx, NY. In addition, GMP holds a Career Scientist Award in the Research and Development unit and is the Director of the Basic and Biomedical Research and Training Program, GRECC, James J. Peters Veterans Affairs Medical Center. We acknowledge that the contents of this manuscript do not represent the views of the U.S. Department of Veterans Affairs or the United States Government. B.W.R. is supported by National Science Foundation grant DGE-1333468.

Notes

The authors declare no competing financial interest.

■ ABBREVIATIONS USED

GSPE, grape seed polyphenol extract; PAC, proanthocyanidin; C, (+)-catechin; EC, (−)-epicatechin; DBU, 1,8-diazabicyclo-[5.4.0]undec-7-ene; UGT, uridine diphosphate glycosyltransferase; CV, column volume; SPE, solid-phase extraction; DI, deionized; LC-TOF-MS, liquid chromatography/time-of-flight mass spectrometry; MRM, multiple reaction monitoring; NMR, nuclear magnetic resonance; SRM, selective reaction monitoring; HSQC, heteronuclear single quantum coherence spectroscopy; HMBC, heteronuclear multiple bond correlation spectroscopy; NOESY, nuclear Overhauser effect spectroscopy; LOD, limit of detection; LOQ, limit of quantitation

■ REFERENCES

(1) Ishikawa, T.; Suzukawa, M.; Ito, T.; Yoshida, H.; Ayaori, M.; Nishiwaki, M.; Yonemura, A.; Hara, Y.; Nakamura, H. Effect of tea flavonoid supplementation on the susceptibility of low-density lipoprotein to oxidative modification. *Am. J. Clin. Nutr.* **1997**, *66*, 261−266.

(2) Guo, W.; Kong, E.; Meydani, M. Dietary polyphenols, inflammation, and cancer. *Nutr. Cancer* **2009**, *61*, 807−810.

(3) Dixon, R. A. Natural products and disease resistance. *Nature* **2001**, *411*, 843−847.

(4) Wang, J.; Ferruzzi, M. G.; Ho, L.; Blount, J.; Janle, E.; Arrieta-Cruz, I.; Sharma, V.; Cooper, B.; Lobo, J.; Simon, J. E.; Zhang, C.; Cheng, A.; Qian, X.; Pavlides, C.; Dixon, R. A.; Pasinetti, G. M. Brain-targeted proanthocyanidin metabolites for Alzheimer's disease treatment. *J. Neurosci.* **2012**, *32*, 5144−5150.

(5) Wang, J.; Ho, L.; Zhao, W.; Ono, K.; Rosensweig, C.; Chen, L.; Humala, N.; Teplow, D. B.; Pasinetti, G. M. Grape-derived polyphenolics prevent Aβ oligomerization and attenuate cognitive deterioration in a mouse model of Alzheimer's disease. *J. Neurosci.* **2008**, *28*, 6388−6392.

(6) Sharma, V.; Zhang, C.; Pasinetti, G. M.; Dixon, R. A. Fractionation of grape seed proanthocyanidins for bioactivity assessment. In *Recent Advances in Phytochemistry: Biological Activity of Phytochemicals*; Gang, D. R., Ed.; Springer: New York, 2010; Vol. *41*, pp 33−46.

(7) Blount, J. W.; Ferruzzi, M. G.; Raftery, D.; Pasinetti, G. M.; Dixon, R. A. Enzymatic synthesis of substituted epicatechins for bioactivity studies in neurological disorders. *Biochem. Biophys. Res. Commun.* **2011**, *417*, 457−461.

(8) Ćirić, A.; Prosen, H.; Jelikić-Stankov, M.; Đurđević, P. Evaluation of matrix effect in determination of some bioflavonoids in food samples by LC−MS/MS method. *Talanta* **2012**, *99*, 780−790.

(9) Gonzalez-Manzano, S.; Gonzalez-Paramas, A.; Santos-Buelga, C.; Duenas, M. Preparation and characterization of catechin sulfates,

DOI: 10.1021/jf505922b
J. Agric. Food Chem. 2015, 63, 2233−2240

glucuronides, and methylethers with metabolic interest. *J. Agric. Food Chem.* **2009**, *57*, 1231−1238.
(10) Baba, S.; Osakabe, N.; Natsume, M.; Muto, Y.; Takizawa, T.; Terao, J. In vivo comparison of the bioavailability of (+)-catechin, (−)-epicatechin and their mixture in orally administered rats. *J. Nutr.* **2001**, *131*, 2885−2891.
(11) Baba, S.; Osakabe, N.; Natsume, M.; Yasuda, A.; Takizawa, T. Cocoa powder enhances the level of antioxidative activity in rat plasma. *Br. J. Nutr.* **2000**, *84*, 673−680.
(12) Feng, W. Metabolism of green tea catechins: an overview. *Curr. Drug Metab.* **2006**, *7*, 755−809.
(13) Spencer, J.; Schroeter, H.; Rechner, A.; Rice-Evans, C. Bioavailability of flavan-3-ols and procyanidins: Gastrointestinal tract influences and their relevance to bioactive forms in vivo. *Antioxid. Redox Signaling* **2001**, *3*, 1023−1039.
(14) Abd-el-Mohsen, M.; Kuhnle, G.; Rechner, A.; Schroeter, H.; Rose, S.; Jenner, P.; Rice-Evans, C. Uptake and metabolism of epicatechin and its access to the brain after oral ingestion. *Free Radical Biol. Med.* **2002**, *33*, 1693−1702.
(15) Piskula, M.; Terao, J. Accumulation of (−)-epicatechin metabolites in rat plasma after oral administration and distribution of conjugation enzymes in rat tissues. *J. Nutr.* **1998**, *128*, 1172−1178.
(16) Spencer, J. Role of flavonoids in the diet metabolism of tea flavonoids in the gastrointestinal tract. Proceedings of the third international scientific symposium on tea and human health. *J. Nutr.* **2003**, *133*, 3255S−3261S.
(17) Tsang, C.; Auger, C.; Mullen, W.; Bornet, A.; Rouanet, J. M.; Crozier, A.; Teissedre, P. L. The absorption, metabolism and excretion of flavan-3-ols and procyanidins following the ingestion of a grape seed extract by rats. *Br. J. Nutr.* **2005**, *94*, 170−81.
(18) Urpi-Sarda, M.; Monagas, M.; Khana, N.; Lloracha, L.; Lamuela-Raventósa, R. M.; Jáureguib, O.; Estruch, R.; Izquierdo-Pulidoa, M.; Andrés-Lacueva, C. Targeted metabolic profiling of phenolics in urine and plasma after regular consumption of cocoa by liquid chromatography-tandem mass spectrometry. *J. Chromatogr. A* **2009**, *1216.43*, 7258−7267.
(19) Roura, E.; Andres-Lacueva, C.; Estruch, R.; Lourdes Mata Bilbao, M.; Izquierdo-Pulido, M.; Lamuela-Raventos, R. M. The effects of milk as a food matrix for polyphenols on the excretion profile of cocoa (−)-epicatechin metabolites in healthy human subjects. *Br. J. Nutr.* **2008**, *100*, 846−51.
(20) Matuszewski, B. K.; Constanzer, M. L.; Chavez-Eng, C. M. Strategies for the assessment of matrix effect in quantitative bioanalytical methods based on HPLC-MS/MS. *Anal. Chem.* **2003**, *75*, 3019−3030.
(21) Li, L.; Liang, S.; Du, F.; Li, C. Simultaneous quantification of multiple licorice flavonoids in rat plasma. *J. Am. Soc. Mass Spectrom.* **2007**, *18*, 778−782.
(22) Gardana, C.; Guarnieri, S.; Riso, P.; Simonetti, P.; Porrini, M. Flavanone plasma pharmacokinetics from blood orange juice in human subjects. *Br. J. Nutr.* **2007**, *98*, 165−172.
(23) Horwitz, W.; Albert, R. The Horwitz ratio (HorRat): A useful index of method performance with respect to precision. *J. AOAC Int.* **2006**, *89*, 1095−109.
(24) Zhang, M.; Jagdmann, G. E., Jr.; Van Zandt, M.; Sheeler, R.; Beckett, P.; Schroeter, H. Chemical synthesis and characterization of epicatechin glucuronides and sulfates: bioanalytical standards for epicatechin metabolite identification. *J. Nat. Prod.* **2013**, *76*, 157−69.
(25) Natsume, M.; Osakabe, N.; Oyama, M.; Sasaki, M.; Baba, S.; Nakamura, Y.; Osawa, T.; Terao, J. Structures of (−)-epicatechin glucuronide identified from plasma and urine after oral ingestion of (−)-epicatechin: Differences between human and rat. *Free Radical Biol. Med.* **2003**, *34*, 840−849.
(26) He, X.-Z.; Li, W.-S.; Blount, J. W.; Dixon, R. A. Regioselective synthesis of plant flavonoid glycosides in *E. coli*. *Appl. Microbiol. Biotechnol.* **2008**, *80*, 253−260.
(27) Ottaviani, J. I.; Momma, T. Y.; Kuhnle, G. K.; Keen, C. L.; Schroeter, H. Structurally related (−)-epicatechin metabolites in humans: Assessment using de novo chemically synthesized authentic standards. *Free Radical Biol. Med.* **2012**, *52*, 1403−1412.

DOI: 10.1021/jf505922b
J. Agric. Food Chem. 2015, 63, 2233−2240

Table 1. List of Asteraceae Plant Essential Oils Tested

common name of essential oil	scientific name	source	part	country of origin
Artemisia afra	*Artemisia afra*	Jinarome	flowering plant	South Africa
Artemisia arborescens	*Artemisia arborescens*	Oshadhi	flowering plant	Morocco
chamomile blue	*Chamomilla matricaria*	Oshadhi	blossoms	Nepal
chamomile roman	*Anthemis nobilis*	Oshadhi	blossoms	France
chamomile wild	*Ormensis multicaulis*	Oshadhi	blossoms	Morocco
chrysantheme abs.	*Chrysanthemum morifolium*	Oshadhi	leaves	India
costus root	*Saussurea lappa*	Oshadhi	roots	India
davana	*Artemisia pallens*	Jinarome	leaves	India
elecampane roots	*Inula racemosa*	Oshadhi	roots	India
erigeron	*Coniza canadensis*	Oshadhi	flowering plant	Canada
Eriocephalus punctulatus	*Eriocephalus punctulatus*	Oshadhi	flowering plant	South Africa
Helichrysum bracteiferum	*Helichrysum bracteatum*	Oshadhi	blossoms	South Africa
helichrysum (Immortella)	*Helichrysum angustifolium*	Oshadhi	blossoms	Croatia
santolina	*Santolina chamaecyparissus*	Oshadhi	plant	Spain
tagetes extra-s	*Tagetes minuta*	Oshadhi	blossoms	Egypt
tarragon	*Artemisia dracunculus*	Oshadhi	plant	France

(90%) were purchased from Sigma-Aldrich (Milwaukee, WI, USA). Camphor (>97%), terpinen-4-ol (99%), γ-terpinene (97%), and *p*-cymene (95%) was purchased from Fluka (Buchs, Switzerland). β-Caryophyllene (>90%), (+)-α-pinene (95%), and β-pinene (94%) were obtained from Tokyo Kasei (Tokyo, Japan). Acetone (99.8%) was purchased from Merck. Dichlorvos (purity 98.6%) was purchased from Chem Service (West Chester, PA, USA), and deltamethrin (purity 96.8%) was supplied from Dongbu Farm Hannong (Seoul, Republic of Korea).

Insects. German cockroaches, *B. germanica*, were reared in plastic boxes (54.3 × 18.8 × 36.3 cm, $L \times W \times H$) without exposure to any insecticide. The cockroaches were supplied with water from a glass flask fitted with a cotton stopper and dried mouse food (Purina feed). The cockroaches were maintained at 25 ± 1 °C and 60% RH (relative humidity) under a 16:8 h light:dark cycle.

Gas Chromatography. Gas chromatography (GC) analysis of *Artemisia arborescens*, santolina, and tarragon oils was carried out using an Agilent 7890A (Agilent Technologies, Santa Clara, CA, USA), equipped with DB-1MS or HP-INNOWAX columns (30 m × 0.25 mm internal diameter [i.d.]; film thickness, 0.25 μm; J&W Scientific, Folsom, CA, USA) and a flame ionization detector (FID). Retention times of essential oil components were compared with those of authentic compounds. The oven temperature of the gas chromatograph was programmed as isothermal at 40 °C for 1 min, raised at a rate of 6 °C/min to 250 °C, and maintained at 250 °C for 4 min. Helium was used as the carrier gas at a flow rate of 1.5 mL/min. Retention indices were obtained in relation to a homologous series of *n*-alkanes (C_7−C_{20}; DB-1MS), (C_8−C_{22}; HP-INNOWAX) under the same gas chromatography operating conditions. Further identification of oil constituents was confirmed by increasing the integrated area by coinjection with oil and standard samples.

Gas Chromatography−Mass Spectrometry. Constituents of Asteraceae plant essential oils were also analyzed using a tandem gas chromatograph (Agilent 7890A) mass spectrometer (Agilent 5975C MSD) (GC-MS) (Agilent Technologies). A DB-5MS column (30 m × 0.25 mm i.d.; film thickness, 0.25 μm; J&W Scientific) was used, and the column oven temperature program was the same as used for GC-FID analysis. Helium was used as the carrier gas at a flow rate of 1.0 mL/min. The effluent of the column was introduced directly into the source of the MS via a transfer line (250 °C). Ionization was attained using electron impact (70 eV; source temperature, 230 °C). The scan range was 41−400 amu. Most components of the plant essential oils were tentatively confirmed by comparing the mass spectra of each peak with those of standard samples in the NIST MS library. NMR spectra were obtained on a Varian UI 500 NMR spectrometer (500 MHz for ^{1}H spectra and 125 MHz for ^{13}C spectra) at Korean Basic Science Institute using TMS as an internal standard.

Isolation and Identification of β-Thujone and Artemisia Ketone. To isolate β-thujone, 1 mL of *A. arborescens* oil was chromatographed on a SiO_2 column (Wakogel 200; Wako Pure Chemicals, Osaka, Japan) eluting with a diethyl ether−hexane gradient. β-Thujone and camphor coeluted with 10:90 (ether:hexane) solution. This mixture was rechromatographed on a 10% $AgNO_3$-impregnated SiO_2 column, and β-thujone eluted with 10% ether−hexane solution in 98.9% purity (395 mg). Artemisia ketone was isolated from santolina oil. Santolina oil (1 mL) was chromatographed on a SiO_2 column eluting with a diethyl ether−hexane gradient. Artemisia ketone (purity 80%) was isolated with 10:90 (ether: hexane) solution. To obtain pure artemisia ketone, the 10% ether fraction was rechromatographed on a SiO_2 column eluting with 1:99 ether:hexane. The purity of isolated artemisia ketone (245 mg) was 98.6%. Isolated β-thujone and artemisia ketone were subjected to NMR analysis and were used for bioassays.

Synthesis of β-Phellandrene. β-Phellandrene (purity 98.2%) was synthesized in the laboratory and was subjected to bioassay. The synthesis procedure and NMR data have been well documented in our previous study.[16]

Fumigant Toxicity Test. The fumigant toxicity of Asteraceae plant essential oils and their constituents was determined using a glass cylinder (diameter, 9.5 cm; height, 19 cm) with a wire sieve installed 9.5 cm above the bottom. Asteraceae plant essential oils or their components were applied to a paper disk (8 mm, Advantec). The treated paper disk was transferred to the bottom lid of the glass cylinder. The lid of the glass cylinder was sealed with Para-film to prevent the leakage of the oil or constituents (Pechiney Plastic Packaging Company, Chicago, IL, USA). Ten adult male or female German cockroaches were placed on the sieve, which prevented direct contact of the cockroaches with the test oils and constituents. Test cockroaches were maintained at 25 ± 1 °C and 60% RH. Mortality was determined 48 h after treatment. All treatments were replicated 4 times.

Contact Toxicity Test. The appropriate dose of Asteraceae plant essential oil or individual constituents was dissolved in acetone. Adult male and female German cockroaches were anesthetized using CO_2, and the oils or constituents in acetone were topically applied to the abdomen of adult male and female German cockroaches with a microapplicator (Burkard, U.K.). Control insects received only acetone (1 μL). Treated adults (10 adults/replication) were transferred to Petri dishes (diameter, 9.5 cm; height, 2 cm), which were maintained at 25 ± 1 °C and 60% RH. Mortality was determined 24 h after treatment. Each assay was replicated 5 times.

Acetylcholinesterase Inhibition. Crude protein was obtained from two adult male and female cockroaches. Adult cockroaches were soaked in 0.1 M Tris-HCl mixed with 0.02 M NaCl, 0.5% Triton X-100 (pH 7.8), and a protease inhibitor cocktail (Sigma-Aldrich, St. Louis, MO, USA), and then they were ground using a glass tissue grinder (Wheaton Industries Inc., Millville, NJ, USA) in ice. The ground

DOI: 10.1021/jf505927n
J. Agric. Food Chem. 2015, 63, 2241−2248

Table 2. Fumigant Toxicity of 16 Asteraceae Plant Essential Oils against Adult of German Cockroaches

plant essential oils	mortality (%, mean ± SE, $N = 40$[a])								
	male					female			
	20[b]	10	5	2.5	1.25	20	10	5	2.5
Artemisia afra	70 ± 4.1 bc[c]	2.5 ± 2.5 c	–[d]	–	–	17.5 ± 7.5 cd	–	–	–
Artemisia arborescens	100 a	60 ± 12.9 b	15.0 ± 6.5 b	–	–	25 ± 6.5 bc	–	–	–
chamomile blue	2.5 ± 2.5 ef	–	–	–	–	0 d	–	–	–
chamomile roman	85.0 ± 5.0 ab	22.5 ± 8.5 c	–	–	–	25.0 ± 6.5 bc	–	–	–
chamomile wild	57.5 ± 2.5 c	10 ± 4.1 c	–	–	–	0 d	–	–	–
chrysantheme abs.	7.5 ± 4.8 def	–	–	–	–	0 d	–	–	–
costus root	0 f	–	–	–	–	0 d	–	–	–
davana	27.5 ± 7.5 de	–	–	–	–	35 ± 2.9 bc	–	–	–
elecampane roots	60 ± 4.1 bc	0 c	–	–	–	42.5 ± 2.5 b	0 b	–	–
erigeron	0 f		–	–	–	0 d	–	–	–
Eriocephalus punctulatus	30 ± 4.1 d	2.5 ± 2.5 c	–	–	–	0 d	–	–	–
Helichrysum bracteiferum	5 ± 5.0 def	–	–	–	–	0 d	–	–	–
helichrysum (Immortella)	0 f	–	–	–	–	0 d	–	–	–
santolina	100 a	22.5 ± 9.6 c	–	–	–	37.5 ± 4.8 bc	2.5 ± 2.5 b	–	–
tagetes extra-s	0 f	–	–	–	–	0 d	–	–	–
tarragon	100 a	100 a	100 a	90	15.0 ± 6.5	100 a	100 a	50 ± 14.1	10 ± 8.2
control	0 f	0 c	0 b	0	0	0 d	0 b	0	0
	$F_{16,51} = 145.810$ $p < 0.0001$	$F_{8,27} = 36.054$ $p < 0.0001$	$F_{2,9} = 209.400$ $p < 0.0001$			$F_{16,51} = 67.796$ $p < 0.0001$	$F_{3,12} = 1574.333$ $p < 0.0001$		

[a]Number of insects tested. [b]mg/filter paper. [c]Means within a column followed by the same letters are not significantly different (Scheffé's test). [d]Not tested.

Table 3. Contact Toxicity of 16 Asteraceae Plant Essential Oils against Adult of German Cockroaches

plant essential oils	mortality (%, mean ± SE, $N = 50$[a])				
	male			female	
	2[b]	1	0.5	2	1
Artemisia afra	70 ± 9.5 bcde[c]	16 ± 2.4 cd	–[d]	30 ± 10.5 cdef	
Artemisia arborescens	82 ± 5.8 abc	42 ± 10.2 bc	6 ± 4.0 b	26 ± 4.0 cdef	
chamomile blue	74 ± 8.0 abcd	16 ± 5.1 cd	–	16 ± 4.0 def	
chamomile roman	12.5 ± 3.7 hi	–	–	14 ± 5.1 ef	
chamomile wild	96 ± 2.4 ab	54 ± 6.8 b	16 ± 4.0 ab	48 ± 9.7 bcd	18 ± 3.7 abc
chrysantheme abs.	42 ± 4.9 efg	14 ± 4.0 cd	–	24 ± 10.8 cdef	
costus root	46 ± 6.8 defg	24 ± 7.5 bcd	–	20 ± 6.3 def	
davana	58 ± 7.3 cdefg	18 ± 2.0 cd	–	38 ± 8.0 bcde	
elecampane roots	66 ± 6.8 cdef	6 ± 2.4 d	–	30 ± 5.5 cdef	
erigeron	50 ± 6.3 defg	50 ± 5.5 b	12 ± 5.8 b	16 ± 2.4 def	
Eriocephalus punctulatus	32 ± 3.7 gh	–	–	20 ± 8.4 def	
Helichrysum bracteiferum	98 ± 2.0 ab	30 ± 8.4 bcd	–	30 ± 8.4 cdef	
helichrysum (Immortella)	98 ± 2.0 ab	50 ± 3.2 b	20 ± 6.3 ab	54 ± 7.5 bc	6 ± 4.0 bc
santolina	100 a	86 ± 9.3 a	12 ± 8.0 b	70 ± 4.5 ab	32 ± 2.0 a
tagetes extra-s	40 ± 10.5 fgh	0 d	–	6 ± 2.4 ef	
tarragon	100 a	100 a	44 ± 11.2 a	100 a	14 ± 2.4 b
control	0 i	0 d	0 b	0 f	0 c
	$F_{16,68} = 66.609$ $p < 0.0001$	$F_{14,60} = 51.721$ $p < 0.0001$	$F_{7,32} = 5.891$ $p < 0.0001$	$F_{16,68} = 31.488$ $p < 0.0001$	$F_{4,20} = 18.750$ $p < 0.0001$

[a]Number of insects tested. [b]mg/adult. [c]Means within a column followed by the same letters are not significantly different (Scheffé's test). [d]Not tested.

cockroach extract was centrifuged at 17000*g* for 15 min at 4 °C to eliminate insect tissue debris. The concentration of crude protein was measured by the Bradford protein assay using BSA as the standard protein. The AChE inhibition activity was evaluated using the modified Ellman method.[17] Test chemicals were dissolved in acetone to give a concentration of 100 mg/mL. Mixtures of 1 μL of test compound and 79 μL of crude cockroach protein were placed in 96-well microplates, which were incubated for 10 min at rt (room temperature). The control

DOI: 10.1021/jf505927n
J. Agric. Food Chem. 2015, 63, 2241−2248

Table 4. Chemical Analysis of *Artemisia arborescens*, Santolina, and Tarragon Oils

		retention index		composition rate (%)			
no.	compound	DB-1	Innowax	*Artemisia arborescens*	santolina	tarragon	identification
1	α-pinene	929	1020	2.33	–[a]	1.46	GC, GC-MS
2	camphene	941	1064	2.51	–	–	GC, GC-MS
3	sabinene	964	1122	4.21	8.99	–	GC, GC-MS
4	β-pinene	969	1107	–	8.84	–	GC, GC-MS
5	β-myrcene	982	1165	7.22	11.46	–	GC, GC-MS
6	*p*-cymene	1011	1273	2.09	–	–	GC, GC-MS
7	β-phellandrene	1019	1209	–	25.67	–	GC, GC-MS
8	limonene	1020	1200	–	–	4.87	GC, GC-MS
9	*cis*-ocimene	1027	1238	–	–	3.02	GC, GC-MS
10	artemisia ketone	1043	1350	–	31.20	–	GC, GC-MS, NMR
11	γ-terpinene	1049	1247	2.28	–	–	GC, GC-MS
12	β-thujone	1095	1444	43.72	–	–	GC, GC-MS, NMR
13	camphor	1117	1519	22.93	–	–	GC, GC-MS
14	terpinen-4-ol	1160	1611	3.03	–	–	GC, GC-MS
15	estragole	1174	1676	–	–	88.7	GC, GC-MS
16	β-caryophyllene	1415	1600	2.56	–	–	GC, GC-MS
	sum			92.88	86.16	98.10	

[a]Not detected.

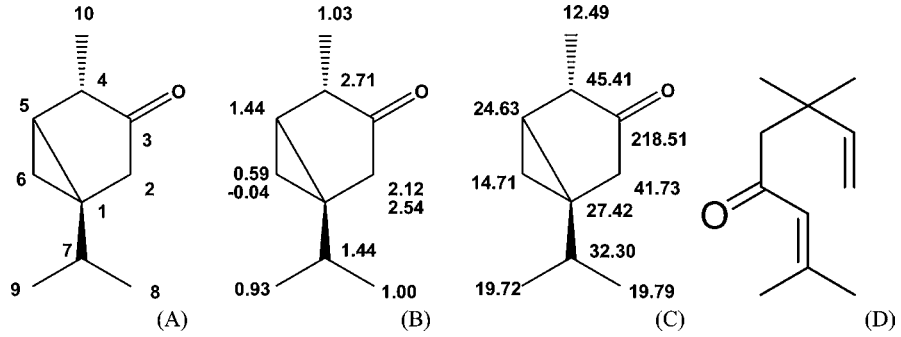

Figure 1. Chemical structure (A), ^{1}H NMR (B), and ^{13}C NMR (C) chemical shift values of β-thujone, and chemical structure of artemisia ketone (D).

received acetone only. 10 μL of acetylthiocholine iodide (ASChI, 10 mM) and 10 μL of 5,5′-dithiobis(2-nitrobenzoic acid) (DTNB, 4 mM) were added to the mixtures of test compounds and crude protein. AChE activity was evaluated by estimating the initial velocity (V_0) for 20 min at 30 s intervals at 405 nm and rt using an iMark microplate absorbance reader (Bio-Rad, Hercules, CA, USA). The primary AChE inhibition assay was replicated at least 3 times. The percentage inhibition of each chemical was calculated according to the following formula:

$$\text{inhibn act. (\%)} = 100 - [(V_0 \text{ of chemical treatment} / V_0 \text{ of control treatment}) \times 100]$$

To determine the IC_{50} value of β-phellandrene, the following concentrations of β-phellandrene were used: 1, 0.5, 0.2, 0.1, and 0.05 mg/mL. All treatments were replicated 3 times at each concentration. The AChE inhibition activity was evaluated according to the formula described above, and the IC_{50} was determined by probit analysis.[18]

Statistical Analysis. Percentage mortality and primary AChE inhibition rates were transformed to arcsine square-root values for analysis of variance. Treatment mean values were compared and analyzed using Scheffé's test.[18] Mean (±SE) values of untransformed data are reported.

RESULTS AND DISCUSSION

Fumigant and Contact Toxicities of Plant Essential Oils. Fumigant and contact toxicities of 16 Asteraceae plant essential oils varied according to oil type and dose (Table 2). *Artemisia arborescens*, santolina, and tarragon essential oils exhibited 100% fumigant toxicity against male German cockroaches at 20 mg/filter paper. The fumigant toxicity of tarragon was 100% at 10 and 5 mg/filter paper, but declined to 90% at 2.5 mg/filter paper. Fumigant toxicities of *Artemisia arborescens*, and santolina were 60% and 22.5% at 10 mg/filter paper, respectively. Chamomile roman showed 85% mortality at 20 mg/filter paper, but declined to 22.5% at 10 mg/filter paper. Other oils showed moderate or weak fumigant toxicity against male German cockroaches. In a test with female German cockroaches, only tarragon showed potent fumigant toxicity at 20 mg/filter paper. Fumigant toxicities of tarragon against female German cockroaches were 100% and 50% at concentrations of 10 and 5 mg/filter paper, respectively. Other oils exhibited moderate or weak toxicity against female German cockroaches at 20 mg/filter paper. In contact toxicity tests, santolina and tarragon essential oils showed 100% insecticidal activity against adult male German cockroaches at 2 mg/♂ (Table 3). Insecticidal activities of tarragon and santolina were 100% and 86% at 1 mg/♂, but were reduced to 44% and 12% at 0.5 mg/♂, respectively. *Helichrysum bracteiferum*, helichrysum (Immortella), and chamomile wild exhibited 98%, 98%, and 96% mortality against male German cockroaches at 2 mg/♂, but declined to 30%, 50%, and 54% at 1 mg/♂, respectively. Contact toxicities of other oils against male German cockroaches were less than 85% at 2 mg/♂. In tests with female cockroaches, tarragon and santolina exhibited 100% and 70% mortality at 2 mg/♀,

DOI: 10.1021/jf505927n
J. Agric. Food Chem. 2015, 63, 2241−2248

Table 5. Fumigant Toxicity of Constituents from *Artemisia arborescens*, Santolina, and Tarragon Oils against Adult of German Cockroaches

	mortality (%, mean ± SE, $N = 40^a$)											
	male					female						
compounds	20[b]	10	5	2.5	1.25	20	10	5	2.5	1.25
artemisia ketone	27.5 ± 4.8 b[c]	–[d]	–	–	–	15 ± 2.9 bc	–	–	–	–
camphene	7.5 ± 2.5 bc	–	–	–	–	10 ± 7.1 bc	–	–	–	–
camphor	22.5 ± 7.5 bc	–	–	–	–	10 ± 11.5 bc	–	–	–	–
β-caryophyllene	0 c	–	–	–	–	0 c	–	–	–	–
estragole	100 a	100 a	100 a	100	67.5 ± 5.0 b	100 a	100 a	80 ± 16.3 b	40 ± 29.4 b	2.5 ± 5.0 b
cis-ocimene	82.5 ± 4.8 a	35.0 ± 2.9 b	22.5 ± 22.2 b	–	–	12.5 ± 4.8 bc	–	–	–	–
β-phellandrene	100 a	20.0 ± 4.1 b	–	–	–	47.5 ± 15.5 b	10 ± 4.1 bc	–	–	–
β-thujone	100 a	90.0 ± 5.8 a	12.5 ± 4.8 b	–	–	100 a	17.5 ± 4.8 b	–	–	–
dichlorvos	100 a	100 a	100 a	100	100 a	100 a	100 a	100 a	100 a	100 a
control	0 c	0 b	0 b	0	0 c	0 c	0 c	0 c	0 c	0 b
	$F_{9,30} = 148.745$ $p < 0.0001$	$F_{5,18} = 43.145$ $p < 0.0001$	$F_{4,15} = 82.436$ $p < 0.0001$	–	$F_{2,9} = 1249.0$ $p < 0.0001$	$F_{9,30} = 54.071$ $p < 0.0001$	$F_{4,15} = 317.526$ $p < 0.0001$	$F_{2,9} = 126.0$ $p < 0.0001$	$F_{2,9} = 35.077$ $p < 0.0001$	$F_{2,9} = 1561.0$ $p < 0.0001$

[a]Number of insects tested. [b]mg/filter paper. [c]Means within a column followed by the same letters are not significantly different (Scheffé's test). [d]Not tested.

respectively, while the other oils exhibited less than 55% mortality at 2 mg/♀. Many plant essential oils have been reported to exhibit fumigant or contact toxicity against German cockroaches.[8−10,12,13] Yeom et al.[8] reported that plant essential oils belonging to Apiaceae exhibited potent fumigant and contact toxicity against German cockroaches. Alzogaray et al.[19] and Yeom et al.[9] also investigated the insecticidal activities of plant essential oils belonging to Myrtaceae. However, fumigant and contact toxicities of the plant essential oils used in this study against German cockroaches have not been reported in any other study.

Chemical Constituents of Plant Essential Oils. The chemical compositions of *Artemisia arborescens*, santolina, and tarragon essential oils are shown in Table 4. The most abundant components of *Artemisia arborescens* were β-thujone (43.72%) followed by camphor (22.93%), β-myrcene (7.22%), sabinene (4.21%), terpinen-4-ol (3.03%), β-caryophyllene (2.56%), camphene (2.51%), α-pinene (2.33%), γ-terpinene (2.28), and *p*-cymene (2.09%). Artemisia ketone (31.20%), β-phellandrene (25.67%), β-myrcene (11.46%), sabinene (8.99%), and β-pinene (8.84%) were detected as the main constituents in santolina oil. Estragole (88.75%) was identified as the most abundant compound in tarragon oil followed by limonene (4.87%), *cis*-ocimene (3.02%), and α-pinene (1.46%). Chemical analyses of *Artemisia arborescens*, santolina, and tarragon essential oils have been reported previously in other studies.[20−22] While the main components of these oils were similar to those previous reports, there were some differences in minor components and composition quantities. Beyrouthy et al.[20] reported that β-thujone (68.5%), chamazulene (12.3%), terpinen-4-ol (1.5%), myrcene (1.1%), linalool and *cis*-thuyanol-4-ol (1%), α-thujone (0.9%), and sabinene (0.8%) were detected as the main components of *Artemisia arborescens.* Chamazulene, linalool, *cis*-thuyanol-4-ol, and α-thujone were not detected in our study. The difference of some oil components and composition amount could be attributed to the origin of *Artemisia arborescens.* Beyrouthy et al.[20] and we used *Artemisia arborescens* essential oils from Lebanon and Moroco, respectively. Artemisia ketone, camphor, and β-phellandrene were analyzed as the main compounds in santolina oil by Demirci et al.,[21] while camphor was not detected in our study. Arabhosseini et al.[22] analyzed the constituents of French tarragon oil and found estragole, methyl eugenol, ocimene, and sabinene as the main constituents. In our study, the amount of estragole was higher, and methyl eugenol and sabinene were not identified. Galambosi and Peura[23] suggested that constituents of plant essential oils differ widely according to production conditions such as harvesting date and storage time, as well as climatic or edaphic factors.

Isolation and Identification of β-Thujone and Artemisia Ketone. Based on ^{1}H- and ^{13}C NMR, DEPT, ^{1}H−^{1}H COSY, and HMQC, each signal of β-thujone was assigned as shown in Figure 1. β-Thujone: ^{13}C (ppm) 12.49 (C10, $-CH_3$), 14.71 (C6, $-CH_2$), 19.72 (C9, $-CH_3$), 19.79 (C8, $-CH_3$), 24.63 (C5, −CH), 27.42 (C1, -C), 32.30, (C7, −CH), 41.73 (C2, $-CH_2$), 45.41 (C4,-CH), 218.51 (C3, -C═O); ^{1}H (ppm) −0.04 (6a, 1H, dd, J = 5.5, 4), 0.59 (6b, 1H, tq, J = 7, 2), 1.00 (8, 3H, d, J = 7), 1.03 (10, 3H, d, J = 7), 1.44 (5, 7, 2H, m), 2.12 (2a, 1H, d, J = 18.5), 2.54 (2b, 1H, d, J = 18.5, 2), 2.71 (4, 1H, m). Chemical shift values of the proton at C6 of α-thujone and β-thujone were reported as 0.12 and −0.05 ppm, respectively.[24] ^{1}H NMR analysis of the isolated thujone showed only a chemical shift value at −0.05 ppm. Thus, the isolated thujone was determined

DOI: 10.1021/jf505927n
J. Agric. Food Chem. 2015, 63, 2241−2248

Table 6. Contact Toxicity of Constituents from Santolina and Tarragon Essential Oils against Adult of German Cockroaches

	mortality (%, mean ± SE, $N = 50^a$)			
	male			female
compounds	1[b]	0.5	0.25	1
artemisia ketone	74 ± 11.7 ab[c]	30.0 ± 3.1 b	–	40 ± 4.5 b
camphene	4 ± 2.4 d	–[d]	–	0 e
camphor	16 ± 4.0 cd	–	–	0 e
β-caryophyllene	46 ± 6.8 bc	22 ± 3.7 b	–	0 e
estragole	100 a	100 a	34 ± 7.5 b	20 ± 3.2 cd
cis-ocimene	42 ± 7.3 bc	22 ± 7.3 b	–	6 ± 2.4 de
β-phellandrene	56 ± 2.4 b	10 ± 4.5 bc	–	26. ± 4.0 bc
deltamethrin	100 a	100 a	100 a	100 a
control	0 d	0 c	0 c	0 e
	$F_{8,36} = 48.784$ $p < 0.0001$	$F_{6,28} = 124.354$ $p < 0.0001$	$F_{2,12} = 138.5$ $p < 0.0001$	$F_{8,36} = 186.404$ $p < 0.0001$

[a]Number of insects tested. [b]mg/adult. [c]Means within a column followed by the same letters are not significantly different (Scheffé's test). [d]Not tested.

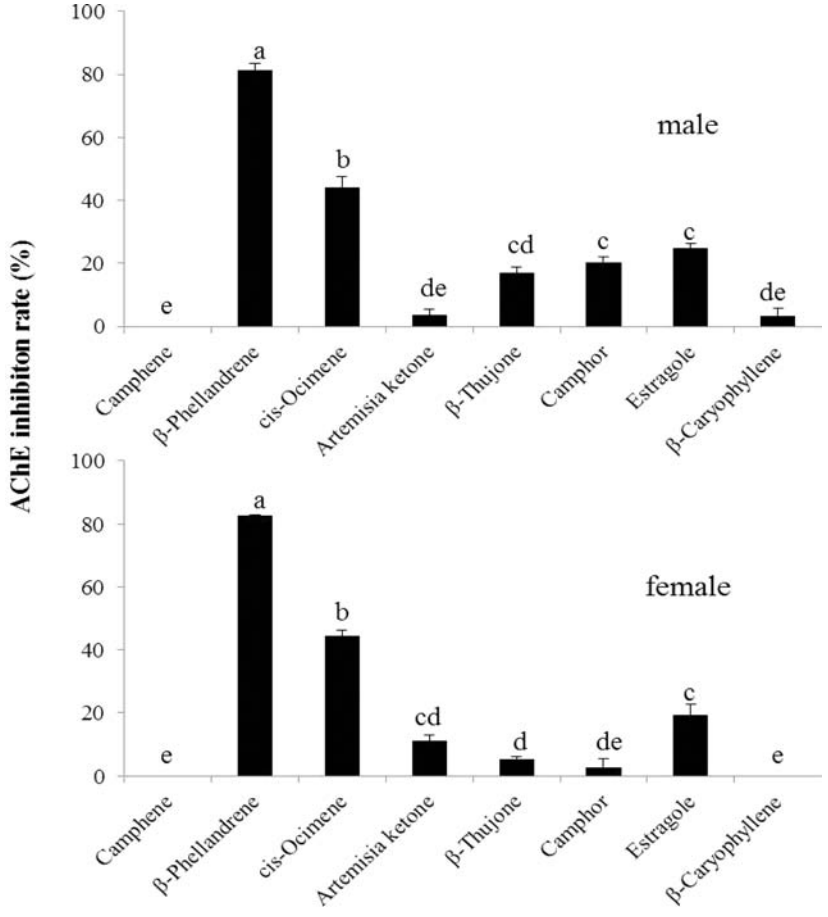

Figure 2. *Blatella germanica* acetylcholinesterase inhibition rates of constituents identified in essential oils from *Artemisia arborescens*, santolina, and tarragon oils at 1 mg/mL. Mean values corresponding to each treatment with different letters are significantly different from one another (male: $F_{7,16} = 109.235$, $p < 0.0001$, female, $F_{7,16} = 230.853$, $p < 0.0001$, Scheffé's test).

Table 7. IC_{50} Values of β-Phellandrene against Adult German Cockroach Acetylcholinesterase Activity

	male				female			
compounds	IC_{50} (mg/mL)	slope	95% cl[a]	χ^2	IC_{50} (mg/mL)	slope	95% cl	χ^2
β-phellandrene	0.30	2.19 ± 0.16	0.26–0.34	2.95	0.28	1.82 ± 0.14	0.24–0.34	0.29

[a]Confidence limit.

to be β-thujone. NMR data of artemisia ketone was assigned in our previous study.[25]

Fumigant and Contact Toxicities of Individual Constituents. The fumigant and contact toxicities of individual

DOI: 10.1021/jf505927n
J. Agric. Food Chem. 2015, 63, 2241–2248

constituents from *Artemisia arborescens*, santolina, and tarragon essential oils are shown in Tables 5 and 6. Fumigant or contact toxicities of α-pinene, β-pinene, β-myrcene, *p*-cymene, limonene, γ-terpinene, and terpinen-4-ol were not tested in this study, because their toxicities to German cockroaches have been reported in our previous studies.[8,9] In a fumigant toxicity test, estragole was the most toxic component to adult males. Fumigant toxicities of estragole were 100% and 67.5% at 2.5 and 1.25 mg/filter paper, respectively. β-Thujone, β-phellandrene, and *cis*-ocimene showed 100%, 100%, and 82.5% fumigant toxicity against adult males at 20 mg/filter paper, but their activities were reduced to 90%, 20%, and 35% at 10 mg/filter paper, respectively. Other compounds showed weak activity. In tests with adult females, estragole exhibited 100% fumigant toxicity at 20 and 10 mg/filter paper, but its toxicity was reduced to 80% and 40% at 5 and 2.5 mg/filter paper, respectively. The fumigant toxicity of β-thujone was 100% at 20 mg/filter paper, but was reduced to 17.5% at 10 mg/filter paper. Other compounds showed moderate or weak toxicity at 20 mg/filter paper. In a contact toxicity test, only estragole exhibited potent activity against adult males. The contact toxicity of estragole was 100% at 1 and 0.5 mg/♂, but was reduced to 34% at 0.25 mg/♂. Artemisia ketone produced 74% mortality at 1 mg/♂, but the mortality decreased to 30% at 0.5 mg/♂. Other compounds exhibited moderate or weak contact toxicity. In a contact toxicity test with female German cockroaches, all test compounds showed moderate or weak toxicity at 1 mg/♀. However, fumigant or contact toxicity of all test compounds was weaker than that of conventional pesticides such as dichlorvos and deltamethrin (Tables 5 and 6). Insecticidal activities of phytochemicals from plant essential oils against German cockroaches have been reported in several studies.[8−10,13] Yeom et al.[8,9] reported fumigant and contact toxicities of constituents from Apiaceae and Myrtaceae plant essential oils. They found that carvone, 1,8-cineole, *trans*-dihydrocarvone, cumminaldehyde, *trans*-anethole, *p*-cymene, γ-terpinene, carvacrol, thymol, carveol, terpinen-4-ol, terpinolene, and α-terpinene demonstrated potent fumigant or contact toxicities against male and female German cockroaches. Philips et al.[10] and Philips and Appel[13] also tested fumigant and contract toxicities of phytochemicals from plant essential oils including carvacrol, 1,8-cineole, *trans*-cinnamaldehyde, citronellic acid, eugenol, geraniol, limonene, linalool, menthone, α-pinene, β-pinene, and thymol. In our study, estragole showed the most potent fumigant toxicity to male and female German cockroaches and contact toxicity to male German cockroaches. Estragole is the main constituent of basil oil, and its insecticidal activity against fruit flies (*Ceratitis capitata*, *Bactrocera dorsalis*, *Bactrocera cucurbitae*), maize weevil (*Sitophilus zeamais*), azuki bean weevil (*Callosobruchus chinensis*), rice weevil (*Sitophilus oryzae*), and cigarette beetle (*Lasioderma serricorne*) have been reported in several studies.[26−28] However, this is the first report on its fumigant and contact toxicity against adult German cockroaches. Many studies have identified β-thujone and β-phellandrene as components of plant essential oils.[20,21] However, there are few reports on their insecticidal activity because they are not commercially available.[29]

In this study, adult male German cockroaches were more susceptible than adult female German cockroaches to plant essential oils and their constituents. The weight of female German cockroaches (average weight of 20 females was 104.9 mg) was about twice that of the male German cockroaches (54.2 mg). This weight difference may be the main reason for the different susceptibility to test oils and their constituents. Lee et al.[30] also found that weight differences between male and female German cockroaches affected the insecticide susceptibility to synthetic insecticides such as organophosphates, carbamates, and pyrethroids.

Primary AChE Inhibition Assay and IC_{50} Determination. AChE inhibition by artemisia ketone, camphene, camphor, β-caryophyllene, estragole, *cis*-ocimene, and β-phellandrene was determined, since inhibition activities of the other constituents were reported in our previous study.[8,9] The primary inhibition activities of various isolated constituents against German cockroach acetylcholinesterase are summarized in Figure 2. β-Phellandrene gave the highest inhibition (81.28%), followed by *cis*-ocimene (44.10%) and estragole (25.04%) (Figure 2). Inhibition activities of the other compounds were less than 20%. In the primary inhibition assay, only β-phellandrene showed >50% inhibition. IC_{50} values of β-phellandrene against male and female acetylcholinesterase were 0.30 and 0.28 mg/mL, respectively (Table 7). Insect acetylcholinesterase inhibition activity of many phytochemicals has been investigated in several studies.[16,25,31−38] German cockroach AChE inhibition activity of phytochemicals from plant essential oils has also been studied by Yeom et al.[8,9] They reported that insecticidal activity of carvacrol and dihydrocarvone correlated with their ability to inhibit German cockroach acetylcholinesterase. However, there was no relationship between AChE inhibition and most other active compounds. In our study, only β-phellandrene showed potent AChE inhibition activity, while most of the other active compounds revealed moderate or weak inhibition activity. Seo et al.[25] reported that β-phellandrene exhibited potent AChE inhibition activity against Japanese termites. The results of our study and other research indicate that insecticidal activity of β-phellandrene correlates with its ability to inhibit AChE. Although the mode of action of phytochemicals from plant essential oils has been reported by some research groups to include AChE, a definitive mechanism has yet to be completely established.[8,9,16,25,31,39,40]

Our results indicate that Asteraceae plant essential oils and their components can be used as fumigants or spray-type control agents against German cockroaches. However, further studies including safety of the oils and their constituents to humans and nontarget organisms, formulations, and their modes of action are necessary for practical use of Asteraceae plant essential oils and their constituents as novel cockroach-control agents.

AUTHOR INFORMATION

Corresponding Author

*(Tel: +82-2-880-4751. Fax: +82-2-873-3560. E-mail: parkik1@snu.ac.kr.

Author Contributions

‡H.-J.Y. and C.-S.J. contributed equally to this work.

Funding

This work was supported by a Research Resettlement Fund for the new faculty of Seoul National University (Project No.: 500-20140209) and a grant from Korea Forest Service (Project No.: S111414L080110) to I.-K.P.

Notes

The authors declare no competing financial interest.

REFERENCES

(1) Schal, C.; Hamilton, R. L. Integrated suppression of synanthropic cockroaches. *Annu. Rev. Entomol.* **1990**, *35*, 521−551.

DOI: 10.1021/jf505927n
J. Agric. Food Chem. 2015, 63, 2241−2248

(2) Wirtz, R. A. Allergic and toxic reactions to nonstinging arthropods. *Annu. Rev. Entomol.* **1984**, *29*, 47−69.
(3) Rust, M. K.; Reierson, D. A.; Ziechner, B. C. Relationship between insecticide resistance and performance in choice tests of field collected German cockroaches (Dictyoptera: Blattellidae). *J. Econ. Entomol.* **1993**, *86*, 1124−1130.
(4) Chang, K. S.; Jung, J. S.; Park, C.; Lee, H. I.; Lee, W. G.; Lee, D. K.; Shin, E. H. Insecticide susceptibility and resistance of *Blattella germanica* (Blattaria: Blattellidae) in Seoul, Republic of Korea, 2007. *Entomol. Res.* **2009**, *39*, 243−247.
(5) Chang, K. S.; Shin, E. H.; Jung, J. S.; Park, C.; Ahn, Y. J. Monitoring for insecticide resistance in field-collected populations of *Blattella germanica* (Blattaria: Blattellidae). *J. Asia-Pac. Entomol.* **2010**, *13*, 309−312.
(6) Bang, J. R.; Lee, H. R.; Kim, J. W. Studies on the insecticide resistance of the German cockroach (*Blattella germanica* L.) II. Resistant development and cross resistance. *Korean J. Appl. Entomol.* **1993**, *32*, 129−133.
(7) Chang, K. S.; Ahn, Y. J. Fumigant activity of (*E*)-anethole in *Illicium verum* fruit against *Blattella germanica*. *Pest Manage. Sci.* **2001**, *58*, 161−166.
(8) Yeom, H. J.; Kang, J. S.; Kim, G. H.; Park, I. K. Insecticidal and acetylcholine esterase inhibition activity of Apiaceae plant essential oils and their constituents against adults of German cockroach (*Blattella germanica*). *J. Agric. Food Chem.* **2012**, *60*, 7194−7203.
(9) Yeom, H. J.; Kang, J. S.; Kim, S. W.; Park, I. K. Fumigant and contact toxicity of Myrtaceae plant essential oils and blends of their constituents against adults of German cockroach (*Blattela germanica*) and their acetylcholinesterase inhibitory activity. *Pestic. Biochem. Physiol.* **2013**, *107*, 200−206.
(10) Phillips, A. K.; Appel, A. G.; Sims, S. R. Topical toxicity of essential oils to the German cockroach (Dictyoptera: Blattellidae). *J. Econ. Entomol.* **2010**, *103*, 448−459.
(11) Yoon, C.; Kang, S. H.; Yang, J. O.; Noh, D. J.; Indiragandhi, P.; Kim, G. H. Repellent activity of citrus oils against the cockroaches *Blattella germanica, Periplaneta americana* and *P. fuliginosa*. *J. Pestic. Sci.* **2009**, *34*, 77−88.
(12) Appel, A. G.; Gehret, M. J.; Tanley, M. J. Repellency and toxicity of mint oil to American and German cockroaches (Dictyoptera: Blattidae and Blattellidae). *J. Agric. Urban Entomol.* **2001**, *18*, 149−156.
(13) Phillips, A. K.; Appel, A. G. Fumigant toxicity of essential oils to the German cockroach (Dictyoptera: Blattellidae). *J. Econ. Entomol.* **2010**, *103*, 781−790.
(14) Park, H. M.; Kim, J.; Chang, K. S.; Kim, B. S.; Yang, Y. J.; Kim, G. H.; Shin, S. C.; Park, I. K. Larvicidal activity of Myrtaceae essential oils and their components against *Aedes aegypti*, acute toxicity on *Daphnia magna*, and aqueous residue. *J. Med. Entomol.* **2011**, *48*, 405−410.
(15) Park, H. M.; Park, I. K. Larvicidal activity of *Amyris balsamifera, Daucus carota* and *Pogostemon cablin* essential oils and their components against *Culex pipiens pallens*. *J. Asia-Pac. Entomol.* **2012**, *15*, 631−634.
(16) Kang, J. S.; Kim, E.; Lee, S. H.; Park, I. K. Inhibition of acetylcholinesterases of the pinewood nematode, *Bursaphelenchus xylophilus*, by phytochemicals from plant essential oils. *Pestic. Biochem. Physiol.* **2013**, *105*, 50−56.
(17) Ellman, G. L.; Courtney, K. D.; Andres, V.; Featherstone, R. M. A new and rapid colorimetric determination of acetylcholinesterase activity. *Biochem. Pharmacol.* **1961**, *7*, 88−95.
(18) SAS Institute. *SAS/STAT User's Guide, Version 9.1.3*; SAS Institute: Cary, NC, 2004.
(19) Alzogaray, R. A.; Lucia, A.; Zerba, E. N.; Masuh, H. M. Insecticidal activity of essential oils from eleven *Eucalyptus spp*. And two hybrids: lethal and sublethal effects of their major components on *Blattella germanica*. *J. Econ. Entomol.* **2011**, *104*, 595−600.
(20) Beyrouthy, M. E.; Arnold-Apostolides, N.; Labaki, M.; Cazier, F.; Najm, S.; Abouaïs, A. Chemical composition of the essential oil of the *Artemisia arborescens* L. growing wild in Lebanon. *Lebanese Sci. J.* **2011**, *12*, 71−78.
(21) Demirci, B.; Özek, T.; Baser, K. H. C. Chemical composition of *Santolina chamaecyparissus* L. essential oil. *J. Essent. Oil Res.* **2000**, *12*, 625−627.
(22) Arabhosseini, A.; Padhye, S.; van Beek, T. A.; van Boxtel, A. J.; Huisman, W.; Posthumus, M. A.; Müller, J. Loss of essential oil of tarragon (*Artemisia dracunculus* L.) due to drying. *J. Sci. Food. Agric.* **2006**, *86*, 2543−2550.
(23) Galambosi, B.; Peura, P. Agrobotanical feature and oil content of wild and cultivated forms of caraway (*Carum carvi* L.). *J. Essent. Oil Res.* **1996**, *8*, 389−397.
(24) Tori, K. Conformations of α-thujone and β-thujone. *Chem. Pharm. Bull.* **1964**, *12*, 1439−1446.
(25) Seo, S. M.; Kim, J.; Kang, J.; Koh, S. H.; Ahn, Y. J.; Kang, K. S.; Park, I. K. Fumigant toxicity and acetylcholinesterase inhibitory activity of 4 Asteraceae plant essential ols and their constituents against Japanese termite (*Reticulitermes speratus* Kolbe). *Pestic. Biochem. Physiol.* **2014**, *113*, 55−61.
(26) Chang, C. L.; Cho, I. K.; Li, Q. Insecticidal activity of basil oil, *trans*-anethole, estragole, and linalool to adult fruit flies of *Ceratitis capitata*, *Bactrocera dorsalis*, and *Bactrocera cucurbitae*. *J. Econ. Entomol.* **2009**, *102*, 203−209.
(27) Wang, C. F.; Yang, K.; Zhang, H. M.; Cao, J.; Fang, R.; Liu, Z. L.; Du, S. S.; Wang, Y. Y.; Deng, Z. W.; Zhou, L. Components and insecticidal activity against the maize weevils of *Zanthoxylum schinifolium* fruits and leaves. *Molecules* **2011**, *16*, 3077−3088.
(28) Kim, D. H.; Ahn, Y. J. Contact and fumigant activities of constituents of *Foeniculum vulgare* fruit against three coleopteran stored-product insects. *Pest Manage. Sci.* **2001**, *57*, 301−306.
(29) Szolyga, B.; Gnilka, R.; Szczepanik, M.; Szumny, A. Chemical composition and insecticidal activity of *Thuja occidentalis* and *Tanacetum vulgare* essential oils against larvae of the lesser mealworm, *Alphitobius diaperinus*. *Entomol. Exp. Appl.* **2014**, *151*, 1−10.
(30) Lee, C. Y.; Yap, H. H.; Chong, N. L. Insecticide toxicity on the adult German cockroach, *Blattella germanica* (L.) (Dictyoptera: Blattellidae). *Malays. J. Sci.* **1996**, *17A*, 1−9.
(31) Kim, S. W.; Kang, J. S.; Park, I. K. Fumigant toxicity of Apiaceae essential oils and their constituents against *Sitophilus oryzae* and their acetylcholinesterase inhibitory activity. *J. Asia-Pac. Entomol.* **2013**, *16*, 443−448.
(32) Gracza, L. Molecular pharmacological investigation of medicinal plant substances II. Inhibition of acetylcholinesterase by monoterpene derivatives in vitro. *Z. Naturforsch.* **1985**, *40C*, 151−153.
(33) Grundy, D. L.; Still, C. C. Inhibition of acetylcholinesterase by pulegone-1,2-epoxide. *Pestic. Biochem. Physiol.* **1985**, *3*, 383−388.
(34) Miyazawa, M.; Watanabe, H.; Kameoka, H. Inhibition of acetylcholinesterase activity by monoterpenoids with a *p*-menthane skeleton. *J. Agric. Food Chem.* **1997**, *45*, 677−679.
(35) Ryan, M. F.; Byrne, O. Plant-insect coevolution and inhibition of acetylcholinesterase. *J. Chem. Ecol.* **1988**, *14*, 1965−1975.
(36) Abdelgaleil, S. A. M.; Mohamed, M. I. E.; Badway, M. E. I.; El-arami, S. A. A. Fumigant and contact toxicities of monoterpenes to *Sitophilus oryzae* (L.) and *Tribolium castaneum* (Herbst) and their inhibitory effects on acetylcholinesterase activity. *J. Chem. Ecol.* **2009**, *35*, 518−525.
(37) Lee, S. E.; Lee, B. H.; Choi, W. S.; Park, B. S.; Kim, J. G.; Campbell, B. C. Fumigant toxicity of volatile natural products from Korean spices and medicinal plants towards the rice weevil, *Sitophilus oryzae* (L). *Pest Manage. Sci.* **2001**, *57*, 548−553.
(38) Anderson, J. A.; Coats, J. R. Acetylcholinesterase inhibition by nootkatone and carvacrol in arthropods. *Pestic. Biochem. Physiol.* **2012**, *102*, 124−128.
(39) Enan, E. E. Insecticidal activity of essential oils: octopaminergic sites of action. *Comp. Biochem. Physiol.* **2001**, *130C*, 320−325.
(40) Enan, E. E. Molecular and pharmacological analysis of an octopamine receptor from American cockroach and fruit fly in response to plant essential oils. *Arch. Insect Biochem. Physiol.* **2005**, *59*, 161−171.

DOI: 10.1021/jf505927n
J. Agric. Food Chem. 2015, 63, 2241−2248

consuming ATP. The CK/PCr system is a buffer for short-term energy supply in tissues and cells with high and rapidly changing energy consumption, like skeletal and heart muscles (up to 94% of total body CR) and brain cells.[19] A male person weighing 70 kg has a total CR pool of approximately 120 g, from which 2% per day is nonenzymatically converted to creatinine at a constant rate. Creatinine is rapidly excreted via the kidneys into the urine. This daily loss of CR of about 2 g/day has to be replaced either endogenously by de novo synthesis or exogenously with the diet.[20]

Meat contains CR in amounts of 4 to 5 g/kg,[21] indicating that for nonvegetarians, approximately half of the daily requirement of creatine is covered by the diet. Vegetarians solely depend on the endogenous synthesis to replace excreted creatine. Concentrations of CR in serum and erythrocytes of subjects regularly consuming meat were significantly higher when compared to vegetarians (male subjects, serum 41 ± 19 vs 25 ± 19 μmol/L, erythrocytes 370 ± 72 μmol/L vs 270 ± 41 μmol/L).[22]

Studies point to an active transport of CR from plasma into erythrocytes, but the biological role of CR in erythrocytes remains enigmatic.[23] Dietary supplementation with large doses of CR is common, particularly for athletes, but scientific data pointing to ergogenic effects are still ambiguous.[24,25] In this context it is noteworthy that CR is intensively discussed in recent years as a therapeutic supplement for patients suffering from muscle, neuron, and brain disorders.[26−28] To date, however, no explanations of possible effects of CR on a molecular level have been provided.

Creatine shows structural analogy to aminoguanidine and arginine referring to the guanidine moiety (Figure 1). The reaction between MG and aminoguanidine or arginine, respectively, is well characterized. MG-H1 (methylglyoxal-derived hydroimidazolone 1, Figure 1) is a quantitatively important AGE, resulting from the reaction of MG with the guanidino side chain of peptide-bound arginine.[2] To the best of our knowledge, however, there are no studies investigating the reaction between MG and CR. We, therefore, hypothesized that CR should react with MG under physiological conditions to CR-specific dicarbonyl adducts similar to peptide-bound arginine.

Following incubation experiments in order to prove the carbonyl-trapping activity of CR, a hydromidazolone as a creatine-specific methylglyoxal adduct was isolated and quantified in urine samples of healthy volunteers. Considering the relatively high plasma levels of CR in comparison to MG, we postulate that CR, formed endogenously and/or applied via dietary sources, may constitute a "natural" trapping agent for MG in vivo.

MATERIALS AND METHODS

Chemicals and Materials. Creatine monohydrate was from Applichem (Darmstadt, Germany); creatinine was from Merck (Darmstadt, Germany); ammonium acetate was from Grüssing (Filsum, Germany); acetic acid was from Roth (Karlsruhe, Germany); ion-exchange material AG Resin 1-X8 was from Bio-Rad (Hercules, CA); *o*-phenylenediamine, silical gel (63−200 μm particle size), and methylglyoxal (40% solution in water) were from Sigma-Aldrich (Steinheim, Germany); HPLC gradient grade acetonitrile and methanol were from VWR Prolabo (Leuven, Belgium); and LC-MS grade acetonitrile was from Fisher (Loughborough, U.K.). All other chemicals were purchased from standard suppliers and were of the highest purity available. Water for preparation of buffers and solutions was obtained with a Purelab plus purification system (USFilter, Ransbach-Baumbach, Germany). Water for solutions used for LC-MS/MS analysis was distilled twice in the presence of potassium permanganate. Artificial urine was prepared according to the literature.[29]

Urine Samples. Eight healthy, nonvegetarian volunteers (age 21−25 years, 5 women and 3 men) and 7 healthy, vegetarian volunteers (age 21−23 years, 5 women and 2 men, 5 ovo-lacto-vegetarian and 2 vegan) had to collect their 24 h urine (8:00 a.m. until 8:00 a.m. the following day) for 1 day, and had to record a nutritional protocol. All participants were normoglycemic (fasting blood sugar ≤ 5.5 mmol/L) and were of normal body weigth (body mass index ≤ 25.0 kg/m^2).

In an orienting intervention study, one healthy, nonvegetarian volunteer (32 years, female) followed a controlled ovo-lacto-vegetarian diet for 7 days (wash-out period). At the last day (day 1 of the intervention study), 24 h urine was collected (8:00 a.m. until 8:00 a.m. the following day). Vegetarian diet was continued for a further 7 days (days 2−8), but additionally 2 g of creatine ("Creapure", creatine monohydrate, Olimp Laboratories, Dębica, Poland) was consumed daily after lunch (supplementation period). At the last day of the supplementation period (day 8), again 24 h urine was collected.

Isolation of *N*-(4-Methyl-5-oxo-1-imidazolin-2-yl)sarcosine (MG-HCr). 12.5 mmol of creatine monohydrate and 12.5 mmol of methylglyoxal in 125 mL of 0.1 M sodium phosphate buffer, pH 7.4, were incubated for 2 d at 60 °C. To remove nonreacted creatine via flash chromatography, the incubation mixture was dried in vacuo and the residue dissolved in 5 mL of a mixture of acetonitrile/methanol/water (6/4/2, v/v/v). This was applied to a glass column (dimensions 3.0 × 30 cm) filled with 70 g of silica gel with particle size 63−200 μm. Elution was performed with 1400 mL of a mixture of acetonitrile/methanol/water (6/4/2, v/v/v). The fractions were characterized by HPLC-UV-MS/MS, and fractions eluting between 140 and 460 mL containing a peak with the mass transition 186 → 87 were pooled. Solvents were removed under vacuum. To remove further byproducts, the residue was subjected to anion exchange chromatography. A column (2.5 × 8 cm) filled with AG Resin 1-X8 in acetate form was used and eluted with 300 mL each of 0.01, 0.05, 0.10, 0.15, and 0.20 M acetic acid. The fraction size was 10 mL, and a fraction collector (RediFrac, Pharmacia Biotech, Uppsala, Sweden) with a flow rate of 0.5 mL/min was used. Fractions eluting with 0.1 M acetic acid containing a peak with the mass transition 186 → 87 were pooled, dried under vacuum, washed with distilled water, dried by lyophilization, and characterized.

N-(4-Methyl-5-oxo-1-imidazolin-2-yl)sarcosine (MG-HCr): ESI-TOF-MS, positive mode, $[M+H^+]$ m/z 186.09; UV spectroscopy, λ_{max} (1.0 mM ammonium acetate, pH 5.5, acetonitrile/water, 75/25, v/v) 226 nm (log ε = 4.09); elemental analysis, $C_7H_{11}N_3O_3$ (MW = 185.18), calculated, C 45.40%, H 5.99%, N 22.69%, O 25.92%; found, C 41.65%, H 6.28%, N 20.11%; content = 88.6%, based on nitrogen (traces of acetate and methanol were visible in NMR spectra). Yield = 52 mg (molar yield = 2.0%).

Model Incubations under Physiological Conditions. Solutions of MG (10 mM) and CR (100 mM), respectively, in phosphate buffer (100 mM, pH 7.4) were prepared. Five milliliters of the CR solution was mixed with 5 mL of the MG solution in glass tubes, resulting in a 10-fold excess of CR. The mixtures were incubated at 37 °C, and aliquots were taken at defined times (0 h, 1 h, 2 h, 4 h, and 24 h). For the analysis of CR, creatinine, and MG-HCr, 200 μL aliquots were immediately frozen until analysis. For analysis of MG, aliquots of 500 μL were instantly used for derivatization and pipetted into vials containing 150 μL of phosphate buffer (500 mM, pH 6.5) and 150 μL of *o*-phenylenediamine solution (1% in phosphate buffer). Derivatization was done overnight for 16 h under exclusion of light.[30] The incubations were performed in triplicate. As control, MG was incubated in the absence of CR and CR in the absence of MG, respectively, to monitor stability of the compounds during the incubation.

Analysis of *N*-(4-Methyl-5-oxo-1-imidazolin-2-yl)sarcosine (MG-HCr), Creatine, and Creatinine in Model Incubations and Urine Samples by HPLC-ESI-DAD-MS/MS. The HPLC system consisted of a degasser, a pump, an autosampler, and a diode array

DOI: 10.1021/jf505998z
J. Agric. Food Chem. 2015, 63, 2249−2256

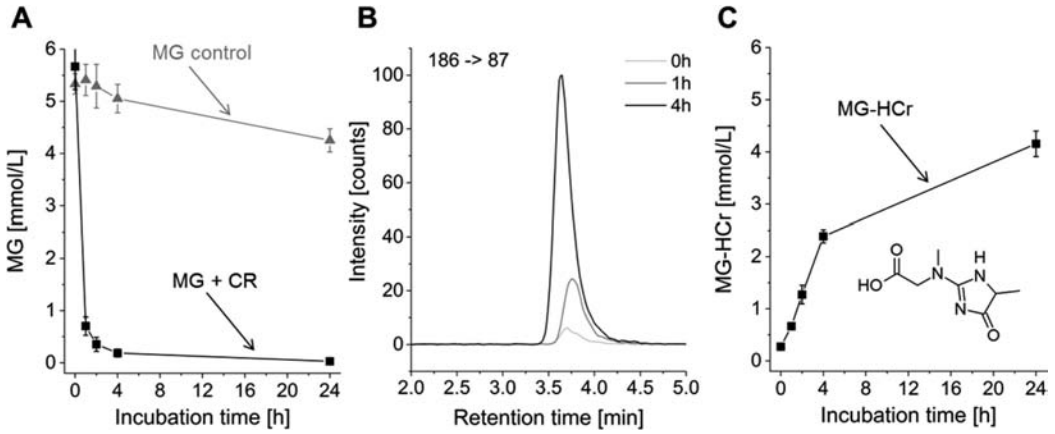

Figure 2. (A) Physiological model incubations of methylglyoxal in the presence of creatine and MG control sample. MG was analyzed after derivatization with *o*-phenylenediamine via RP-HPLC-UV.[30] Incubations were done in triplicate. (B) Formation of a new peak in the incubation of MG with CR with the transition 186 → 87 analyzed by HPLC-ESI-DAD-MS/MS. (C) MG-HCr concentration in the incubation of MG and CR. MG-HCr was quantitated via HPLC-ESI-DAD-MS/MS at UV = 226 nm.

detector, all from Agilent Technologies 1200 series (Boeblingen, Germany). For MS/MS measurements, a Triple Quad LC/MS 6410 from Agilent Technologies was used. For separation a column SeQuant ZIC-HILIC (3.5 μm, 100 Å, PEEK 150 × 2.1 mm; Merck KGaA, Darmstadt, Germany) was used. Elution was performed at 25 °C with a flow rate of 0.2 mL/min with the following starting conditions: 100% solvent A (1.0 mM ammonium acetate in water/acetonitrile 25:75, v/v, pH 5.5) and 0% solvent B (4.65 mM ammonium acetate in water/acetonitrile 70:30 v/v, pH 6.8). This solvent composition was held for 11 min (isocratic elution) followed by an increase of solvent B to 100% within 1 min and held for 8 min, followed by an equilibration at starting conditions for 11 min. Detection wavelengths were 214, 226, and 236 nm for CR, MG-HCr, and creatinine, respectively. For analysis of model incubations 1 μL and for analysis of urine samples 5 μL were injected into the HPLC system.

Single ion monitoring (SIM) was performed from 1 to 11 min in positive mode for *m*/*z* 186 with 200 ms dwell time, fragmentor voltage 115 V, gas temperature 350 °C, gas flow 11 mL/min, and nebulizer pressure 35 psi.

Product ion scans were recorded from 1 to 11 min with the precursor ions *m*/*z* 186 for MG-HCr, *m*/*z* 132 for creatine, and *m*/*z* 114 for creatinine, applying the conditions as described above. The ranges of product ions were set from *m*/*z* 50 to 200 with a scan time of 200 ms, a fragmentor voltage of 115 V, and collision energy of 25 eV.

Measurements of MG-HCr were performed using multiple reaction monitoring mode (MRM) in positive mode. The mass transition 186 → 87 was used for quantitation of MG-HCr with fragmentor voltage and collision energy of 115 V and 20 eV, respectively and a dwell time of 150 ms. For qualification purposes the mass transitions 186 → 140 and 186 → 69 were monitored.

In model incubations, MG-HCr was analyzed without further sample preparation except filtration (0.2 μm) and dilution (1:1000 with solvent A) as described above for the HPLC-ESI-DAD-MS/MS method. Identification of MG-HCr was realized via MS/MS detection and quantitation via UV detection (226 nm) with an external calibration using authentic MG-HCr reference material (see above).

Urine samples were centrifuged (4 °C, 10,000 rpm, 10 min), and 250 μL was deproteinized with 750 μL of acetonitrile at 4 °C for 20 min. After centrifugation (4 °C, 10,000 rpm, 10 min) and filtration (0.2 μm) the solution was employed to standard addition. Quantification via standard addition was necessary to avoid interference due to matrix effects. Urine samples of vegetarians were diluted 3 + 2 and urine samples of nonvegetarians 1 + 4 with 10 μL of MG-HCr standard solution and 10 or 30 μL of solvent A (1.0 mM ammonium acetate in water/acetonitrile 25:75, v/v, pH 5.5), respectively. For standard addition each urine was spiked with four ascending concentrations of MG-HCr resulting in 5 samples per urine including the nonspiked urine (instead of MG-HCr standard solution 10 μL of water was added). MG-HCr stock solution (35 mmol/L) was prepared from the above-described synthesized reference material. This solution was diluted to 0.70, 0.35, 0.18, and 0.07 μmol/L with water, respectively. Each was added to the urine samples. For analysis 5 μL of the spiked urine samples was injected into the HPLC-ESI-DAD-MS/MS. MG-HCr was detected via MS/MS and creatinine via UV at 236 nm. The quantitation of creatinine was realized via external calibration with commercially available reference material. Analysis of urine samples was done in duplicate.

The limits of detection (LOD) and quantification (LOQ) in urine were calculated as the concentrations of the analyte necessary to show a peak at a signal-to-noise ratio of 3 and 10, respectively. For determination of method precision, one urine sample was applied to replicate analysis on different days (n = 5). Recovery of MG-HCr was calculated from the slope of the recovery function after spiking a urine with ascending MG-HCr concentrations (resulting in the same MG-HCr levels as in the standard addition method) before sample workup (n = 5).

Quantitation of Methylglyoxal in Model Incubations by RP-HPLC with UV Detection. Analysis of MG in the model incubations was carried out as previously published.[30] Derivatization with *o*-phenylenediamine to the corresponding quinoxaline was realized immediately after withdrawal from the reaction mixture to scavenge the residual MG.

Mass Spectrometry. For mass spectrometric analyses, a PerSeptive Biosystems Mariner time-of-flight mass spectrometry instrument equipped with an electrospray ionization source (ESI-TOF-MS, Applied Biosystems, Stafford, TX, USA) working in the positive mode was used. Calibration of the mass scale was established using a mixture of bradykinin, angiotensin I, and neurotensin. After appropriate dilution with 1% formic acid in 50% acetonitrile, the sample was injected into the ESI source by a syringe pump at a flow rate of 5 L/min. Spray tip potential, nozzle potential, quadrupole RF voltage, and detector voltage were adjusted to 4812, 80, 1000, and 2400 V, respectively.

Ultraviolet (UV) Spectroscopy. Absorption spectra were recorded on a Specord S100 diode array spectrophotometer (Carl Zeiss, Jena, Germany) with a wavelength accuracy of ±1 nm. The compound was dissolved in 1.0 mM ammonium acetate, pH 5.5, in acetonitrile/water (75/25, v/v) at a concentration of 100 μM. The maxima and molar coefficient of extinction were calculated using quartz cuvettes 115-QS (Hellma, Müllheim, Germany) of 10.00 mm path length.

Nuclear Magnetic Resonance (NMR) Spectroscopy. ^{1}H and ^{13}C NMR spectra were recorded on an AVANCE III instrument (Bruker, Rheinstetten, Germany) at 400 and 100 MHz, respectively. Substances were resolved in 750 μL of deuterium oxide for analysis.

DOI: 10.1021/jf505998z
J. Agric. Food Chem. 2015, 63, 2249−2256

Assignments of ^{1}H and ^{13}C signals are based on $^{1}H-^{1}H$ COSY (correlation spectroscopy), HSQC (heteronuclear single quantum coherence), HMBC (heteronuclear multiple bond correlation), and DEPT (distortionless enhancement by polarization transfer) experiments. A NOESY (nuclear Overhauser enhancement spectroscopy) experiment for carbon−proton couplings and a HMBC (heteronuclear multiple bond correlation) experiment for nitrogen−proton couplings were performed in addition to the above-mentioned 2D experiments on a Bruker Avance III instrument at 600 MHz (^{1}H), 150 MHz (^{13}C), and 61 MHz (^{15}N). All chemical shifts are given in parts per million (ppm), those of protons relative to the internal HOD signal (4.80 ppm), those of carbon atoms relative to external standard tetramethylsilane, and those of nitrogen atoms relative to external standard urea.

Elemental Analysis. To know the purity of the isolated compound used as standard material, elemental analysis data were obtained on an Elementar Vario Micro Cube CHNS elemental analyzer (Hanau, Germany). The purity of the isolated compound was calculated as the percentage of nitrogen in the preparation divided by the theoretical percentage of nitrogen of the target substance and expressed in percent by weight.

Statistical Treatment. Comparisons of means between the daily urinary excretions of the different days were examined with Student's *t* test. *P* values ≤0.05 were considered significant (two-tailed) using OriginPro 8.6.

RESULTS AND DISCUSSION

Incubation of methylglyoxal in the presence of a 10-fold excess of creatine under physiological conditions resulted in a rapid decrease of the carbonyl compound (Figure 2 A). After 1 h of incubation at 37 °C, only 13% of the initial concentration could be detected as free MG, and after 24 h nearly complete derivatization of MG was observed. In control samples, MG and CR incubated individually remained stable (Figure 2 A). No creatinine formation was detectable using HPLC-DAD within 24 h. After prolonged incubation for 4 d, creatinine formation accounted for only 2% of the initial CR concentration (data not shown). Therefore, it can be concluded that reactive MG is quantitatively trapped by the guanidino compound CR.

From incubation mixtures containing equimolar amounts of MG and CR, the major reaction product was isolated by flash chromatography and semipreparative ion-exchange chromatography. For the isolated compound, a relative molecular mass M_r of 185.08 ($[M + H]^+$ m/z = 186.09) was determined via ESI-TOF-MS. This corresponds to the addition of one molecule of MG to one molecule of CR with the loss of one molecule of water and formation of a methylglyoxal-derived hydroimidazolone of creatine, namely, *N*-(4-methyl-5-oxo-1-imidazolin-2-yl)sarcosine (Figure 3). The supposed structure for MG-HCr was unequivocally confirmed with ^{1}H NMR and ^{13}C NMR experiments as well as two-dimensional NMR (Table 1 and Figure 3). In the ^{1}H NMR and ^{13}C NMR spectra (except for C-2 in ^{13}C NMR) all signals were doubled, indicating two dominating tautomeric forms in a ratio of 40:60 (A:B) based on proton intensities in the ^{1}H spectrum. The signals were assigned to the two tautomers each using the resonance in ^{1}H-^{1}H COSY and HMBC as well as the intensity relation in the ^{1}H experiment.

Results from ^{1}H NMR showed 4 different signals. The intensities indicated two methyl, one methylene, and one methine group. The singlets of one methyl group and the methylene group were assigned to C-8 and C-9 of the creatine backbone. The second methyl signal was split into a doublet and showed a vicinal coupling to the quartet of the methine

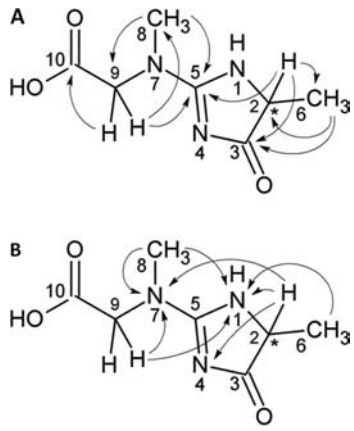

Figure 3. Structural formula of *N*-(4-methyl-5-oxo-1-imidazolin-2-yl)sarcosine (MG-HCr). Arrows indicate the relevant (A) carbon−proton or (B) nitrogen−proton long-range connectivities from HMBC spectra.

group. The $^{1}H,^{1}H$ COSY experiment showed only one resonance confirming the connection of the methyl group at C-6 and the methine H at C-2. In the ^{13}C NMR spectra, seven signals appeared, which were assigned to three quarternary, one methylene, and three methyl or methine carbon atoms by DEPT measurement. The HSQC experiment confirmed these results and allowed the interpretation of C-6 and C-8 as methyl groups, C-2 as methine group, and C-9 as methylene group. To confirm the position of the quarternary carbon atoms, a HMBC experiment was accomplished, which resulted in the assignment shown in Figure 3. The C-10 of the carboxyl group and the C-5 of the guanidino group are connected to the creatine backbone. By contrast, C-3 showed resonance with the protons of C-2 and C-6. Taking the resonance of C-2 and C-6 protons with C-5 into account, the hydroimidazolone substructure is highly likely. In consequence of the inflexible heterocyclic hydroimidazolone structure, the NOESY experiment showed only cross peaks of the protons of C-2 with C-6 and C-8 with C-9. An additional $^{1}H-^{15}N$ HMBC experiment resulted in cross peaks of the proton at C-2 with all nitrogen atoms N-1, N-4, and N-7, also verifying the heterocyclic hydroimidazolone structure.

As mentioned above, doubled signals indicating two tautomeric forms were observed. At present, the NMR data do not allow a definite assignment to two of five predictable tautomeric forms of the hydroimidazolone moiety (possible structures are shown in the Supporting Information). However, participation of all tautomers considering an enol at C-2/C-3 is implausible (compare structures **IV** and **V**, Supporting Information), because this would be indicated by the disappearance of the proton signal at C-2 due to a quantitative H−D exchange in the solvent D_2O. For the methylglyoxal-derived hydroimidazolone of arginine, two tautomers and the appearance of the keto-imine and the keto-amine structure in a ratio 2:1 were postulated as well, supported by NMR experiments.[31] This points to structures **I** and **II** (see Supporting Information). Although one report on X-ray analysis of the compound shown in Figure 3 can be found in the literature,[32] to the best of our knowledge, formation of MG-HCr as a specific reaction product from MG and creatine has not been described yet, although the reaction of guanidino moieties with oxoaldehydes is well-known.[33,34]

DOI: 10.1021/jf505998z
J. Agric. Food Chem. 2015, 63, 2249−2256

Table 1. ^{15}N, ^{13}C, and ^{1}H NMR Spectroscopic Data and Results of 2D NMR Experiments of *N*-(4-Methyl-5-oxo-1-imidazolin-2-yl)sarcosine (MG-HCr)[a]

			Coupling			
				HMBC[c]		
Assigment of N or C atom (Figure 3)	δ_N/ppm or δ_C/ppm[b]	δ_H/ppm	$^{1}H-^{1}H$ COSY	$^{1}H-^{13}C$	$^{1}H-^{15}N$	$^{1}H-^{13}C$ NOESY[c]
1[d]	A −278.6; B −277.2					
2	A + B[e] 56.09 (CH)	pseudo quintet: A 4.47 (q, 1H, J = 7.2 Hz); B 4.49 (q, 1H, J = 7.2 Hz)	6	3; 5; 6	1; 4; 7	6
3	A 179.11 (C_i); B 179.51 (C_i)					
4[d]	A + B[e] −303.3					
5	A 157.75 (C_i); B 158.18 (C_i)					
6	A + B[e] 15.63 + 15.67 (CH_3)	A 1.48 (d, 3H, J = 7.2 Hz); B 1.50 (d, 3H, J = 7.2 Hz)	2	2; 3	1	2
7[d]	A + B[e] −297.0					
8	A 38.35 (CH_3); B 37.10 (CH_3)	A 3.22 (s); B 3.18 (s)		5; 9	1; 7	9
9	A 53.62 (CH_2); B 54.71 (CH_2)	A 4.08 (s); B 4.11 (s)		5; 8; 10	1; 7	8
10	A 172.41 (C_i); B 172.90 (C_i)					

[a]A and B represent tautomers. [b]Type of signal deduced from ^{13}C DEPT measurement is given in parentheses. [c]Couplings from the corresponding hydrogen atoms are denoted. [d]^{15}N signal dedicated from HMBC coupling. [e]These signals are not resolved.

To further characterize the scavenging reaction between MG and CR, samples of different time points were analyzed with regard to the possible formation of MG-HCr. With proceeding incubation time, one peak at mass transition 186 → 87 increased in the chromatograms (Figure 2 B). This peak could be assigned to the compound MG-HCr by comparing retention time and fragmentation pattern of product ion scan of MG-HCr reference material (see Figure II in the Supporting Information). Quantitative data obtained for MG-HCr in the incubation mixtures via external calibration are shown in Figure 2 C. After 24 h, the concentration of MG-HCr in the incubation samples was quantitated with 4.2 ± 0.2 mmol/L (Figure 2 C). Initial MG concentration (t = 0 h) was 5.6 ± 0.4 mmol/L, indicating that 75% of MG had been reacted with CR to MG-HCr. Compared with the decrease in MG (Figure 2 A), the formation of MG-HCr (Figure 2 C) is somewhat delayed. This can be explained with the proposed reaction mechanism (Figure 4), in which the conversion to the hydroimidazolone in the last reaction step should be rate-determining.[35]

The fast and quantitative scavenging of MG by CR can be compared with the scavenging capacity of other guanidino compounds such as aminoguanidine[17] and acetylarginine.[35] At present, no studies have been performed to investigate a possible reaction between CR and MG under physiological conditions. The reaction between creatinine and reducing carbohydrates was studied regarding the taste modulating effects of the formed compounds in meat. From these reaction mixtures, a MG-derived creatinine compound was isolated and quantitated in urine after meat ingestion.[36,37]

Our results show that CR reacts with MG under physiological conditions resulting in MG-HCr as the main reaction product. The excellent trapping capacity of CR in vitro for the reactive oxoaldehyde MG points to a possible biological role of CR in vivo. As described in the Introduction, oral administration of aminoguanidine (AG) was found to suppress pathophysiological consequences of diabetes in animal experiments via dicarbonyl scavenging, but exhibited adverse side effects in human studies.[17,18] Plasma concentrations of AG

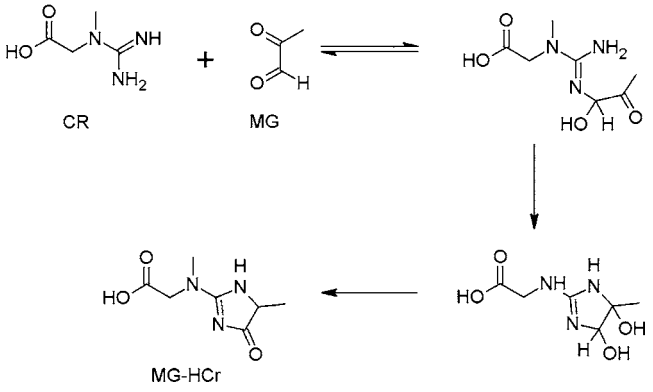

Figure 4. Proposed reaction mechanism for the reaction of creatine (CR) with methylglyoxal (MG) to *N*-(4-methyl-5-oxo-1-imidazolin-2-yl)sarcosine (MG-HCr) via the Schiff base and the dihydroxyimidazolidine. Formation of the hydroimidazolone of creatine should be rate determining.[35]

between 10 to 50 μmol/L were necessary to induce pharmacologically relevant effects.[38] In this context it is noteworthy that normal serum concentration of CR in men (nonvegetarian) is 41 ± 19 μmol/L.[22] Therefore, it can be hypothesized that naturally occurring CR may have MG trapping effects in vivo, leading to continuous formation and excretion of MG-HCr.

To support this hypothesis, a method was established for the quantitation of MG-HCr in urine samples of vegetarians and nonvegetarians, based on hydrophilic interaction chromatography (HILIC) to separate polar compounds.[21] Sensitive detection was realized via tandem mass spectrometry. SIM chromatograms were recorded at m/z 186, the pseudomolecular ion of MG-HCr ($[M + H]^+$). Using HILIC column material, it turned out that the retention time of MG-HCr was considerably dependent on the ionic milieu of the injected sample solution. For identification in urine samples, MG-HCr reference material was therefore dissolved in artificial urine,

DOI: 10.1021/jf505998z
J. Agric. Food Chem. 2015, 63, 2249−2256

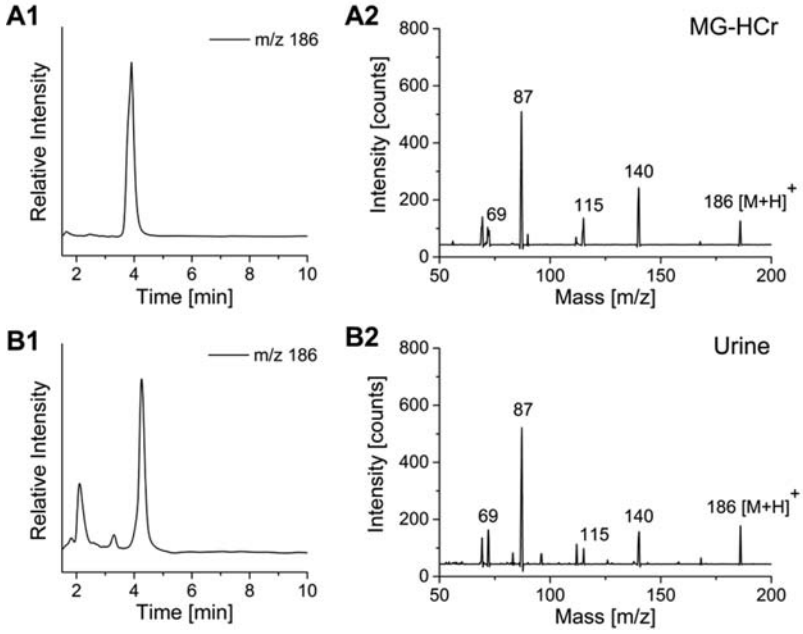

Figure 5. Identification of MG-HCr by HPLC-ESI-MS/MS. SIM chromatograms of the synthesized MG-HCr reference material in artificial urine[29] (A1) and a urine sample (B1) at m/z = 186, respectively. Product ion patterns after fragmentation of the peak at 3.9 min of the MG-HCr standard (A2) and the peak at 4.3 min of the urine sample (B2) with m/z = 186.

thus simulating the average composition of urine including salts, urea, and organic acids.[29] Assignment of the peak in the SIM chromatogram of a urine sample (Figure 5B1) to MG-HCr was confirmed first of all chromatographically by comparing the retention times of the target compound in artificial urine and urine (compare Figures 5A1 and 5B1). Retention time of the main peak in the chromatogram of the urine sample with m/z 186 (4.3 min in Figure 5 B1) differed slightly from that of the peak in the chromatogram of the MG-HCr reference material (3.9 min in Figure 5A1). Depending on the ionic milieu (artificial urine, dilution of the urine), retention time for MG-HCr could vary within 0.5 min on the applied HILIC column. The shifts in retention time of the peak in the urine samples were verified by standard addition (data not shown). Unequivocal identification was accomplished based on the corresponding mass spectra. In Figures 5A2 and 5B2, the product ion patterns after fragmentation (product ion scan) of the peak with m/z = 186 of a MG-HCr standard solution in artificial urine and of a urine sample are displayed, respectively. The two fragmentation patterns were identical and showed the same distinct signals (Figures 5A2 and 5B2). Thus, unambiguous identification of MG-HCr in urine was achieved.

With the applied chromatographic system, a sufficient retardation of the polar compound MG-HCr as well as separation from creatine and creatinine was possible (see Figure III, Supporting Information). Standard addition curves in the concentration range of 0.07−0.7 μmol/L showed linearity (R^2 > 0.99) for MG-HCr. The limit of detection (LOD) and limit of quantitation (LOQ) were calculated from the signal-to-noise ratio. LOD in urine was 0.01 μmol/L, and LOQ was 0.05 μmol/L. Method precision, expressed as relative standard deviation of replicate analysis of a urine sample (n = 5), was 8.6%. Repeated recovery experiments (n = 5), where urine samples were spiked before sample workup, showed a recovery of 81.6 ± 5.5%, calculated from the slope of the recovery function. The validation parameters of the standard addition method indicate a reliable method for accurate quantitation of MG-HCr in urine. The developed method should be easily transferred to other biological matrices as, for example, plasma.

Using this method, MG-HCr in 24 h urine samples of 15 healthy volunteers (7 vegetarians, 8 nonvegetarians) was analyzed. The participants followed their own individual diet and collected their 24 h urine for 1 day. Data for urinary excretion of MG-HCr are shown in Figure 6 A. Daily MG-HCr

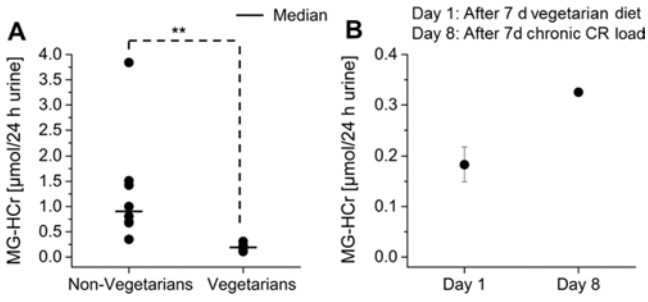

Figure 6. (A) 24 h urinary excretion of MG-HCr of 8 nonvegetarians and 7 vegetarians healthy volunteers. Comparisons of means were examined using Student's t test. **, P < 0.01 (significant). (B) Urinary excretion of MG-HCr into 24 h urine of 1 person (nonvegetarian) during a creatine intervention study. Day 1: after 7 days of vegetarian diet (wash-out period). Day 8: after 7 days of creatine supplementation (2 g daily after lunch). Error bars give the standard error of the mean (n = 2).

excretion of nonvegetarians ranged from 0.35 to 3.84 μmol/24 h urine (median: 0.90 μmol/24 h urine) and of vegetarians from 0.11 to 0.31 μmol/24 h urine (median: 0.19 μmol/24 h urine). The urinary excretion between nonvegetarians and vegetarians differed significantly (P < 0.01). Based on the dietary recordings and taking literature data of CR in food into account,[39−41] it turned out that the estimated intake of CR with the daily diet of the vegetarians was significantly lower when compared with the nonvegetarians (0−0.3 mmol/day vs 1.3−

DOI: 10.1021/jf505998z
J. Agric. Food Chem. 2015, 63, 2249−2256

12.2 mmol/day). Therefore, MG-HCr detectable in urine of vegetarians must be due to formation in vivo. The higher amount of creatine taken up with the daily diet of non-vegetarians should lead to higher plasma concentrations of the guanidino compound which may trap more MG and thus can induce an increased excretion of MG-HCr in urine samples of nonvegetarians.

To further strengthen this hypothesis, urinary excretion of one healthy volunteer (nonvegetarian) was measured after being for 7 days on a vegetarian diet (day 1, Figure 6 B). This wash-out period was followed by a supplementation period, in which for 7 days 2 g of CR per day was consumed after lunch. This amount of CR corresponds to an ingestion of about 500 g of meat.[21] After 7 days on a vegetarian diet, MG-HCr increased from 0.18 ± 0.03 μmol/24 h urine (day 1, Figure 6B), which is in the range of the vegetarians shown in Figure 6A, to 0.33 ± 0.01 μmol/24 h urine (day 8, Figure 6B). This significant increase of MG-HCr excretion following an oral load with creatine clearly demonstrates that trapping of MG in vivo can be increased by dietary means. On the other hand, however, it cannot be excluded that excretion of MG-HCr at least partly can result from an oral uptake of the reaction product with heated meat and subsequent renal excretion. At present, no data about the occurrence of MG-HCr in meat are available. Corresponding studies are currently underway in our laboratory.

In conclusion, with the identification of MG-HCr, the specific reaction product formed from MG and CR under physiological conditions, and its unambiguous quantitation in urine, we provide evidence for a new physiological role of creatine. Our results suggest that dietary intake of CR and resulting increased plasma concentrations may provide a natural "safety mechanism" for the trapping of highly reactive dicarbonyl compounds. This mechanism could be of special importance in situations in which the body has to deal with pathophysiologically increased amounts of dicarbonyl compounds ("carbonyl stress"), for instance in diabetic patients. Furthermore, our findings may shed light on the question why erythrocytes accumulate CR, but do not use the guanidino compound for their energy metabolism. As mentioned in the Introduction, concentrations of CR in erythrocytes are about 10-fold higher compared to blood serum, and subjects consuming meat have higher concentrations of CR in erythrocytes and serum compared to vegetarians.[22,23] Taking into account that erythrocytes produce energy solely by the glycolysis of glucose and lactic acid fermentation of the resulting pyruvate,[42] significant amounts of MG are continuously formed as byproduct, which have to be metabolized, in particular by the glyoxalase system. Additionally, the arginine residues of hemoglobin nonenzymatically trap MG via formation of MG-H1.[2] It is conceivable that CR may significantly contribute to the detoxification of MG in particular in erythrocytes. Acting this way, CR could retard the formation of advanced glycation end products (AGEs) and thus delay those long-term consequences of diabetes and aging, which are commonly attributed to AGE formation in vivo. As another aspect, CR may positively contribute to MG-linked neurological disorders.[13,14] If this hypothesis can be confirmed, dietary intake of CR via meat or supplements may constitute a so far overlooked nutritional benefit.

■ ASSOCIATED CONTENT

Ⓢ Supporting Information

Figure I, possible tautomeric forms of *N*-(4-methyl-5-oxo-1-imidazolin-2-yl)sarcosine (MG-HCr). Figure II, identification of MG-HCr by HPLC-ESI-MS/MS in the model incubation of CR and MG. Figure III, HPLC-ESI-MS/MS and HPLC-UV chromatograms of a MG-HCr standard and a urine sample. This material is available free of charge via the Internet at http://pubs.acs.org.

■ AUTHOR INFORMATION

Corresponding Author

*Tel: +49-351-463-34647. Fax: +49-351-463-34138. E-mail: Thomas.Henle@chemie.tu-dresden.de.

Author Contributions

†J.L. and J.D. contributed equally to this work.

Notes

The authors declare no competing financial interest.

■ ACKNOWLEDGMENTS

We thank Dr. Uwe Schwarzenbolz, Institute of Food Chemistry, for the ESI-TOF-MS measurements. We appreciate the support of the members of the Chair of Inorganic Coordination Chemistry (Group of Professor Jan Weigand), namely, Sivathmeehan Yogendra, Maximilian Donath, and Stephen Schulz, who recorded NMR spectra and provided the elemental analysis. We are grateful to the members of the Institute of Organic Chemistry, namely, Dr. Margit Gruner and Dr. Tilo Lübken, for recording further NMR spectra.

■ ABBREVIATIONS USED

AGE, advanced glycation end product; AG, aminoguanidine; CK, creatine kinase; CR, creatine; LOD, limit of detection; LOQ, limit of quantification; MG, methylglyoxal; MG-HCr, methylglyoxal-derived hydroimidazolone of creatines, namely, *N*-(4-methyl-5-oxo-1-imidazolin-2-yl)sarcosine; PCr, phosphocreatine; SIM, selected ion monitoring; t_R, retention time

■ REFERENCES

(1) Phillips, S. A.; Thornalley, P. J. The formation of methylglyoxal from triose phosphates. Investigation using a specific assay for methylglyoxal. *Eur. J. Biochem.* **1993**, *212*, 101−115.

(2) Rabbani, N.; Thornalley, P. J. Methylglyoxal, glyoxalase 1 and the dicarbonyl proteome. *Amino Acids* **2012**, *42*, 1133−1142.

(3) Henning, C.; Liehr, K.; Girndt, M.; Ulrich, C.; Glomb, M. A. Extending the spectrum of α-dicarbonyl compounds in vivo. *J. Biol. Chem.* **2014**, *289*, 28676−28688.

(4) Rabbani, N.; Thornalley, P. J. Measurement of methylglyoxal by stable isotopic dilution analysis LC-MS/MS with corroborative prediction in physiological samples. *Nat. Protoc.* **2014**, *9*, 1969−1979.

(5) Ahmed, N. Advanced glycation endproducts - role in pathology of diabetic complica-tions. *Diabetes Res. Clin. Pract.* **2005**, *67*, 3−21.

(6) Degen, J.; Hellwig, M.; Henle, T. 1,2-Dicarbonyl compounds in commonly consumed foods. *J. Agric. Food Chem.* **2012**, *60*, 7071−7079.

(7) Degen, J.; Vogel, M.; Richter, D.; Hellwig, M.; Henle, T. Metabolic transit of methyglyoxal. *J. Agric. Food Chem.* **2013**, *61*, 10253−10260.

(8) Degen, J.; Beyer, H.; Heymann, B.; Hellwig, M.; Henle, T. Dietary influence on urinary excretion of 3-deoxyglucosone and its metabolite 3-deoxyfructose. *J. Agric Food. Chem.* **2014**, *62*, 2449−2456.

(9) Hellwig, M.; Henle, T. Baking, ageing, diabetes: a short history of the Maillard reaction. *Angew. Chem., Int. Ed.* **2014**, *53*, 10316−10329.

DOI: 10.1021/jf505998z
J. Agric. Food Chem. 2015, 63, 2249−2256

(10) Miyata, T.; Sugiyama, S.; Saito, A. Kurokawa. Reactive carbonyl compounds related uremic toxicity ("carbonyl stress"). *Kidney Int.* **2001**, *78*, S25−S31.
(11) Henle, T.; Miyata, T. Advanced glycation end products in uremia. *Adv. Renal Replacement Ther.* **2003**, *10*, 321−331.
(12) Mittelmaier, S.; Niwa, T.; Pischetsrieder, M. Chemical and physiological relevance of glucose degradation products in peritoneal dialysis. *J. Renal Nutr.* **2012**, *22*, 181−185.
(13) Arai, M.; Yuzawa, H.; Nohara, I.; Ohnishi, T.; Obata, N.; Iwayama, Y.; Haga, S.; Toyota, T.; Ujike, H.; Ichikawa, T.; Nishida, A.; Tanaka, Y.; Furukawa, A.; Aikawa, Y.; Kuroda, O.; Niizato, K.; Izawa, R. Nakamura. Enhanced carbonyl stress in a subpopulation of schizophrenia. *Arch. Gen. Psychiatry* **2010**, *67*, 589−597.
(14) Srikanth, V.; Westcott, B.; Forbes, J.; Phan, T. G.; Beare, R.; Venn, A.; Pearson, S.; Greenaway, T.; Parameswaran, V.; Münch, G. Methylglyoxal, cognitive function and cerebral atrophy in older people. *J. Gerontol., Ser. A* **2013**, *68*, 68−73.
(15) Godfrey, L.; Yamada-Fowler, N.; Smith, J.; Thornalley, P. J.; Rabbani, N. Arginine-directed glycation and decreased HDL plasma concentration and functionality. *Nutr. Diabetes* **2014**, DOI: 10.1038/nutd.2014.31.
(16) Engelen, L.; Stehouwer, C. D.; Schalkwijk, C. G. Current therapeutic interventions in the glycation pathway: evidence from clinical studies. *Diabetes, Obes. Metab.* **2013**, *15*, 677−689.
(17) Thornalley, P. J. Kinetics and mechanism of the reaction of aminoguanidine with the alpha-oxoaldehydes glyoxal, methylglyoxal, and 3-deoxyglucosone under physiological conditions. *Biochem. Pharmacol.* **2000**, *60*, 55−65.
(18) Thornalley, P. J. Use of aminoguanidine (Pimagedine) to prevent the formation of advanced glycation endproducts. *Arch. Biochem. Biophys.* **2003**, *419*, 31−40.
(19) Wyss, M.; Kaddurah-Daouk, R. Creatine and creatinine metabolism. *Physiol. Rev.* **2000**, *80*, 1107−1213.
(20) Persky, A. M.; Brazeau, G.; Hochhaus, G. Pharmacokinetics of the dietary supplement creatine. *Clin. Pharmacokinet.* **2003**, *42*, 557−574.
(21) Mora, L.; Sentandreu, M. A.; Toldrá, F. Hydrophilic chromatographic determination of carnosine, anserine, balenine, creatine, and creatinine. *J. Agric. Food Chem.* **2007**, *55*, 4664−4669.
(22) Delanghe, J.; Deslypere, J. P.; Debuyzere, M.; Robbrecht, J.; Wieme, R.; Vermeulen, A. Normal reference values for creatine, creatinine and carnitine are lower in vegetarians. *Clin. Chem.* **1989**, *35*, 1802−1803.
(23) Jiao, Y.; Okumiya, T.; Saibara, T.; Tsubosaki, E.; Matsumura, H.; Park, K.; Sugimoto, K.; Kageoka, T.; Sasaki, M. An enzymatic assay for erythrocyte creatine as an index of the erythrocyte life time. *Clin. Biochem.* **1998**, *31*, 59−65.
(24) Branch, C. D. Effect of creatine supplementation on body composition and performance: a meta-analysis. *Int. J. Sport Nutr. Exercise Metab.* **2003**, *13*, 198−226.
(25) Brosnan, J. T. Creatine: endogenous metabolite, dietary, and therapeutic supplement. *Annu. Rev. Nutr.* **2007**, *27*, 241−261.
(26) Kley, R. A.; Tarnopolsky, M. A.; Vorgerd, M. Creatine for treating muscle disorders. *Cochrane Database Syst. Rev.* **2013**, DOI: 10.1002/14651858.CD004760.pub4.
(27) Pastula, D. M.; Moore, D. H.; Bedlack, R. S. Creatine for amyotrophic lateral sclerosis/motor neuron disease. *Cochrane Database Syst. Rev.* **2010**, DOI: 10.1002/14651858.CD005225.pub2.
(28) Allen, P. J. Creatine metabolism and psychiatric disorders: Does creatine supplementation have therapeutic value? *Neurosci. Biobehav. Rev.* **2012**, *36*, 1442−1462.
(29) Brooks, T.; Keevil, C. W. A simple artificial urine for the growth of urinary pathogens. *Lett. Appl. Microbiol.* **1997**, *24*, 203−206.
(30) Mavric, E.; Wittmann, S.; Barth, G.; Henle, T. Identification and quantification of methylglyoxal as the dominant antibacterial constituent of Manuka (Leptospermum scoparium) honeys from New Zealand. *Mol. Nutr. Food Res.* **2008**, *52*, 483−489.
(31) Henle, T.; Walter, A. W.; Haeßner, R.; Klostermeyer, H. Detection and identification of a protein-bound imidazolone resulting from the reaction of arginine residues and methylglyoxal. *Z. Lebensm.-Unters. Forsch.* **1994**, *199*, 55−58.
(32) Shima, K.; Ishikawa, K.; Izawa, K.; Suzuki, E. Crystal Structure of N-(4-Methyl-5-oxo-1-imidazolin-2-yl)sarcosine Monohydrate. *Anal. Sci.* **1998**, *14*, 1185−1186.
(33) Sopio, R.; Lederer, M. Reaction of 3-deoxypentosulose with N-methyl- and N,N-dimethylguanidine as model reagents for protein-bound arginine and for creatine. *Z. Lebensm.-Unters. Forsch.* **1995**, *201*, 381−386.
(34) Thornalley, P. J.; Battah, S.; Ahmed, N.; Karachalis, N.; Agalou, S.; Babaei-Jadidi, R.; Dawnay, A. Quantitative screening of advanced glycation endproducts in cellular and extracellular proteins by tandem mass spectrometry. *Biochem. J.* **2003**, *375*, 581−592.
(35) Lo, T. W.; Westwood, M. E.; McLellan, A. C.; Selwood, T.; Thornalley, P. J. Binding and modification of proteins by methylglyoxal under physiological conditions. *J. Biol. Chem.* **1994**, *269*, 32299−322305.
(36) Kunert, C.; Walker, A.; Hofmann, T. Taste modulating N-(1-methyl-4-oxoimidazolidin-2-ylidene) α-amino acids formed from creatinine and reducing carbohydrates. *J. Agric. Food Chem.* **2011**, *59*, 8366−8374.
(37) Kunert, C.; Skurk, T.; Frank, O.; Lang, R.; Hauner, H.; Hofmann, T. Development and application of a stable isotope dilution analysis for the quantitation of advanced glycation end products of creatinine in biofluids of type 2 diabetic patients and healthy volunteers. *Anal. Chem.* **2013**, *85*, 2961−2969.
(38) Nyengaard, J. R.; Chang, K.; Berhorst, S.; Reiser, K. M.; Williamson, J. R.; Tilton, R. G. Discordant effect of guanidines on renal structure and function and on regional vascular dysfunction and collagen changes in diabetic rats. *Diabetes* **1997**, *46*, 94−106.
(39) Balsom, P. D.; Söderlund, K.; Ekblom, B. Creatine in Humans with Special Reference to Creatine Supplementation. *Sports Med.* **1994**, *18*, 268−280.
(40) Harris, R. C.; Lowe, J. A.; Warnes, K.; Orme, C. E. The concentration of creatine in meat, offal and commercial dog food. *Res. Vet. Sci.* **1997**, *62*, 58−62.
(41) Del Campo, G.; Gallego, B.; Berregi, I.; Casado, J. A. Creatinine, creatine and protein in cooked meat products. *Food Chem.* **1998**, *63*, 187−190.
(42) van Wijk, R.; van Solinge, W. W. The energy-less red blood cell is lost: erythrocyte enzyme abnormalities of glycolysis. *Blood* **2005**, *106*, 4034−4042.

DOI: 10.1021/jf505998z
J. Agric. Food Chem. 2015, 63, 2249−2256

microfractionation coupled with microplate-based biochemical detection, also known as high-resolution bioassay,[10] and (ii) state-of-the-art high-performance liquid chromatography−solid-phase extraction−nuclear magnetic resonance spectroscopy (HPLC−SPE−NMR).[11−13] The combination of the two with high-resolution mass spectrometry, that is, high-resolution bioassay/HPLC−HRMS−SPE−NMR, has already proven successful for fast and efficient analysis of monoamine oxidase A inhibitors,[14] antioxidants,[15−17] α-amylase inhibitors,[4] and fungal plasma membrane H^+-ATPase inhibitors.[18] In this work, microplate-based high-resolution α-glucosidase profiling combined with HPLC−HRMS−SPE−NMR[19,20] have been used for identification of α-glucosidase inhibitors direct from crude extracts of a series of plants in order to investigate their potential use as future functional foods and/or to identify new T2D drug leads.

EXPERIMENTAL PROCEDURES

Chemicals. Analytical-grade methanol (99.9%), methanol-d_4, α-glucosidase type I (EC 3.2.1.20, from *Saccharomyces cerevisiae*, lyophilized powder), *p*-nitrophenyl α-D-glucopyranoside (≥99.9%), dimethyl sulfoxide (DMSO; ≥99.5%), sodium dihydrogen phosphate dihydrate, disodium hydrogen phosphate, sodium azide, acarbose, and quercetin were purchased from Sigma−Aldrich (St. Louis, MO). Analytical-grade ethyl acetate (99.8%) and acetonitrile (99.9%), as well as sodium hydroxide (35%), were purchased from VWR International (Radnor, PA), whereas formic acid (98−100%) was from Merck (Darmstadt, Germany). Water was purified by 0.22 μm membrane filtration and deionization (Millipore, Billerica, MA).

Plant Material. In total, 24 plants were bought in local stores in Denmark, Sweden, and Lebanon in March−April 2014 (Table 1). Fresh plant material was washed with tap water and sun-dried or oven-dried at 40 °C (Termaks, TS5410, Bergen, Norway) for 5 days. Dried material was ground in a mill, and the pulverized plant material was extracted with ethyl acetate and methanol by shaking on a Lab Dancer (IKA, Germany) for 3 min, followed by sonication at room temperature for 2 h. Details of amount of plant material and volume of extraction solvent are listed in Table S1 in Supporting Information. The extracts were passed through syringe filters with a pore size of 0.4 μM and subsequently evaporated to dryness by a stream of nitrogen gas. Percentage yields based on the dried starting materials are listed in Table S1 in Supporting Information. The dried extracts were kept at −18 °C until use.

Table 1. Names and Place of Purchase of Plant Species Included in This Work

family	plant species[a]	common name	purchased
Actinidiaceae	*Actinidia deliciosa*	kiwi	Denmark
Amaryllidaceae	*Allium ascalonicum*	shallot	Denmark
Amaryllidaceae	*Allium sativum*	garlic	Denmark
Apiaceae	*Cuminum cyminum*	cumin	Denmark
Apiaceae	*Foeniculum vulgare*	fennel	Denmark
Apiaceae	*Pimpinella anisum*	anise	Denmark
Brassicaceae	*Brassica juncea*	green mustard cabbage	Denmark
Compositae	*Gundelia tournefortii*	tumble thistle	Sweden
Compositae	*Scorzonera suberosa*	yemlik[b]	Denmark
Lamiaceae	*Thymus vulgaris*	thyme	Lebanon
Lauraceae	*Cinnamomum zeylanicum*	cinnamon	Denmark
Leguminosae	*Cassia angustifolia*	senna	Denmark
Leguminosae	*Glycine max*	soybean	Denmark
Leguminosae	*Glycyrrhiza glabra*	liquorice	Denmark
Leguminosae	*Lupinus albus*	white lupin	Lebanon
Leguminosae	*Tamarindus indica*	Indian date	Lebanon
Piperaceae	*Piper nigrum*	black pepper	Denmark
Polygonaceae	*Rheum palmatum*	Turkish rhubarb	Lebanon
Polygonaceae	*Rheum rhabarbarum*	rhubarb	Denmark
Polygonaceae	*Rumex acetosa*	sheep sorrel	Denmark
Ranunculaceae	*Nigella sativa*	black caraway	Denmark
Rhamnaceae	*Frangula alnus*	alder buckthorn	Denmark
Solanaceae	*Capsicum frutescens*	chili	Denmark
Urticaceae	*Urtica dioica*	stinging nettle	Denmark

[a]Purchased March−April 2014. [b]Turkish name.

α-Glucosidase Assay. A 0.1 M phosphate buffer was prepared by dissolving 2.65 g of $NaH_2PO_4{\cdot}2H_2O$, 4.70 g of Na_2HPO_4, and 0.10 g of NaN_3 in 500 mL of Milli-Q water and adjusting to pH 7.5 with 2 N sodium hydroxide. Enzyme solution was prepared by dissolving 1.3 mg of 15.8 units/mg α-glucosidase from *S. cerevisiae* in 10 mL of phosphate buffer, resulting in an enzyme activity of 2 units/mL. Substrate solution of 1.0 mM was prepared by dissolving 60.2 mg of *p*-nitrophenyl α-D-glucopyranoside (*p*-NPG) in 20 mL of phosphate buffer. The contents of all wells in the microplates were dissolved in 10 μL of DMSO, and 165 μL of phosphate buffer and 5 μL of α-glucosidase solution were added. After the samples were shaken for 2 min and preincubated at 28.1 °C for 10 min, 20 μL of 10 mM *p*-NPG solution was added to start the reaction. The absorbance was measured at 405 nm every 30 s for 35 min. Incubation and absorbance measurements were performed with a Multiscan FC microplate photometer with built-in shaker and incubator (Thermo Scientific, Waltham, MA). For data acquisition, SkanIt version 2.5.1 software (Thermo Scientific, Waltham, MA) was used. The absorbance readings for the samples were compared with a control, which consisted of the same materials except extract. The percentage of enzyme inhibition was calculated by

$$\%\ \text{inhibition} = \frac{\left(\text{slope}_{405}^{\text{control}} - \text{slope}_{405}^{\text{extract}}\right)}{\text{slope}_{405}^{\text{control}}} \times 100$$

Dilution series consisting of 10−16 dilutions of extracts dissolved in 0.1 M phosphate buffer were prepared for IC_{50} determination. Thus, 200 μL aliquots of each concentration in the dilution series were added to 96-well microplates in triplicate, and after evaporation overnight (Savant SPD121P concentrator coupled with a RVT400 refrigerated vapor trap and an OFP-400 oil free pump, Thermo Scientific, Waltham, MA), the α-glucosidase assay was performed by the method described above. Dose−response curves and IC_{50} values were obtained by use of GraphPad Prism (version 6.00.283).

HPLC Analysis. Dried extracts were redissolved in methanol and filtered (Q-Max RR 13 mm 0.45 μm Nylon, Frisenette, Denmark). HPLC analyses of the extracts were performed on an Agilent 1200 series chromatograph consisting of a G1311A quaternary pump, a G1322A degasser, a G1316A thermostated column compartment, a G1315C photodiode-array detector, a G1367C high-performance autosampler, and a G1364C fraction collector (Santa Clara, CA). Separations were performed with a Phenomenex Luna $C_{18}(2)$ column (150 × 4.6 mm i.d., 3 μm particle size, 100 Å pore size) maintained at 40 °C. HPLC solvent A consisted of water−acetonitrile 95:5 with 0.1% formic acid added, and solvent B consisted of acetonitrile−water 95:5 with 0.1% formic acid added. For all samples, 5 μL of extract was injected and separated by use of the following gradient elution profile at 0.5 mL/min: 0 min, 0% B; 30 min, 100% B; 35 min, 100% B; 36 min, 0% B; 42 min, 0% B. The chromatograms were monitored at 210, 230, 254, 270, 310, and 360 nm. The chromatographic system was controlled by Agilent ChemStation revision B.03.02 software.

Removal of Tannins. Tannins were removed from methanol extracts of *C. zeylanicum* and *R. palmatum* by use of 500 mg Oasis HLB cartridges (Waters, Milford, MA). The extracts were dissolved in 5% aqueous methanol at a concentration of 50 mg/mL. The cartridges were preconditioned with 7 mL of methanol and subsequently equilibrated with 7 mL of Milli-Q water. Cartridges were loaded with 0.5 mL of extract, washed with 7 mL of 5% aqueous methanol, eluted with 7 mL of methanol, and re-equilibrated with 7 mL of water. This

DOI: 10.1021/jf506297k
J. Agric. Food Chem. 2015, 63, 2257−2263

procedure was performed repeatedly in series until the entire volume of the samples had been used. The methanol extracts were evaporated on a rotary evaporator, weighed, and stored at −18 °C until use.

High-Resolution α-Glucosidase Profiling. Methanol extracts of *R. palmatum* (201.3 mg/mL, injection volume 5 μL, fractionation of 5−35 min in 176 wells), *C. zeylanicum* (161.7 mg/mL, injection volume 20 μL, fractionation of 9−36 min in 176 wells), and *R. rhababarum* (14.4 mg/mL, injection volume 20 μL, fractionation of 2−33 min in 176 wells) were separated on a Phenomenex C_{18}(2) Luna column (150 × 4.6 mm, 3 μm, 40 °C, 0.5 mL/min) with the following elution gradient: 0 min, 0% B; 30 min, 100% B; 35 min, 100% B; 36 min, 0% B; and 42 min, 0% B. Ethyl acetate extracts of *R. palmatum* (68.5 mg/mL, injection volume 2 μL, fractionation of 3−25 min in 176 wells) was separated under above conditions with the following elution gradient: 0 min, 20% B; 3 min, 20% B; 15 min, 80% B; 16 min, 100% B; 30 min, 100% B; 35 min. 20% B; and 41 min, 20% B. Ethyl acetate extracts of *A. ascalonicum* (68.5 mg/mL, injection volume 5 μL, fractionation of 9−36 min in 176 wells) and *C. zeylanicum* (36.1 mg/mL, injection volume 2 μL, fractionation of 3−25 min in 176 wells) were separated with the following elution gradient: 0 min, 0% B; 30 min, 100% B; 35 min, 100% B; 36 min 0% B; and 42 min, 0% B. Microplates were evaporated to dryness under reduced pressure in a SPD121P Savant SpeedVac, and α-glucosidase inhibitory activity was assessed for each well as described above. Inhibition of α-glucosidase activity was plotted against chromatographic retention time to give a high-resolution biochromatogram.

HPLC−HRMS−SPE−NMR Analyses. HPLC−HRMS−SPE−NMR analyses of *A. ascalonicum*, *C. zeylanicum,* and *R. palmatum* were performed on a system consisting of an Agilent 1200 chromatograph comprising quaternary pump, degasser, thermostated column compartment, autosampler, and photodiode-array detector (Santa Clara, CA); a Bruker microTOF-Q II mass spectrometer (Bruker Daltonik, Bremen, Germany) equipped with an electrospray ionization (ESI) source and operated via a 1:99 flow splitter; a Knauer Smartline K120 pump for postcolumn dilution (Knauer, Berlin, Germany), a Spark Holland Prospekt 2 SPE unit (Spark Holland, Emmen, The Netherlands); a Gilson 215 liquid handler equipped with a 1 mm needle for automated filling of 1.7 mm NMR tubes, and a Bruker Avance III 600 MHz NMR spectrometer (^{1}H operating frequency 600.13 MHz) equipped with a Bruker SampleJet sample changer and a cryogenically cooled gradient inverse triple-resonance 1.7 mm TCI probe-head (Bruker Biospin, Rheinstetten, Germany). A solution of sodium formate clusters was injected in the beginning of each run to enable internal mass calibration. The HPLC eluate was diluted with Milli-Q water at a flow rate of 1.5 mL/min prior to trapping on 10 × 2 mm i.d. Resin GP [general purpose, 5−15 μm, spherical shape, poly(divinylbenzene) phase] SPE cartridges (Spark Holland, Emmen, The Netherlands), based on absorption thresholds at 254 nm. Before trapping, the cartridges were preconditioned with 500 μL of MeCN followed by 500 μL of H_2O. Thus, four analytes were trapped from ethyl acetate extract of *A. ascalonicum* peel (10 repetitive separations of 10 μL of a 51.64 mg/mL sample; elution profile 0 min, 0% B; 30 min, 100% B; 35 min, 100% B; 36 min 0% B; and 42 min, 0% B). Eight analytes were trapped from ethyl acetate extract of *R. palmatum* root (10 repetitive separations of 5 μL of a 68.5 mg/mL sample; elution profile 0 min, 20% B; 3 min, 20% B; 15 min, 80% B; 16 min, 100% B; 30 min, 100% B; 35 min, 20% B; and 42 min, 20% B). Five peaks were trapped from ethyl acetate extract of *C. zeylanicum* bark (five repetitive separations of 10 μL of a 36.1 mg/mL sample; elution profile: 0 min, 0% B; 30 min, 100% B; 35 min, 100% B; 36 min 0% B; and 42 min, 0% B). Loaded cartridges were dried with pressurized N_2 gas for 45 min and eluted with 30 μL of methanol-d_4 into 1.7 mm o.d. NMR tubes (Bruker Biospin, Karlsruhe, Germany) by use of a Gilson 215 liquid handler (Gilson, Middleton, WI). Separations were controlled by Bruker Hystar version 3.2 software, automated filling of NMR tubes was controlled by PrepGilsonST version 1.2 software, and automated NMR acquisition was controlled by Bruker IconNMR version 4.2 software.

NMR Experiments. All NMR spectra were recorded in methanol-d_4 at 300 K. ^{1}H chemical shifts were referenced to the residual solvent signal (δ 3.31). One-dimensional ^{1}H NMR spectra were acquired in automation (temperature equilibration to 300 K, optimization of lock parameters, gradient shimming, and setting of receiver gain) with 30° pulses, 3.66 s interpulse intervals, and 64K data points and multiplied with an exponential function corresponding to line broadening of 0.3 Hz prior to Fourier transform. Phase-sensitive double quantum filtered correlation spectroscopy (DQF-COSY) spectra were recorded using a gradient-based pulse sequence with a 20 ppm spectral width and 2k × 256 data points (processed with forward linear prediction to 1k data points). Multiplicity-edited heteronuclear single quantum coherence (HSQC) spectra were acquired with the following parameters: spectral width 20 ppm for ^{1}H and 165 ppm for ^{13}C, 2K × 256 data points (processed with forward linear prediction to 1K data points), and 2.0 s relaxation delay. Heteronuclear multiple-bond correlation (HMBC) spectra were optimized for $^nJ_{C,H}$ = 10 Hz and acquired with the following parameters: spectral width 20 ppm for ^{1}H and 222 ppm for ^{13}C, 2K × 128 data points (processed with forward linear prediction to 1K data points), and 1.5 s relaxation delay.

RESULTS AND DISCUSSION

This work aimed at identifying α-glucosidase inhibitors in plants by use of microplate-based high-resolution α-glucosidase inhibition profiling combined with HPLC−HRMS−SPE−NMR. Thus, a total of 24 different plants, primarily edible and well-known species, were purchased at local stores in Denmark, Sweden, and Lebanon (Table 1). The plants were distributed in 14 different families, with most species belonging to Leguminosae. The dried plant materials were extracted with methanol and ethyl acetate, and the crude extracts were assessed for α-glucosidase inhibitory activity. Table 2 lists IC_{50} values of methanol and ethyl acetate extracts of all samples. Six samples—methanol extracts of *C. zeylanicum*, *R. rhabarbarum* (peel), and *R. palmatum* (root) and ethyl acetate extracts of *C. zeylanicum*, *A. ascalonicum* (peel), and *R. palmatum* (root)—show IC_{50} values below 20 μg/mL. In comparison, the IC_{50} value of Acarbose reference standard is 0.47 ± 0.02 mg/mL. IC_{50} curves of these six extracts and Acarbose are shown in Figure S1 and high-resolution α-glucosidase inhibition profiles of methanol extracts of *C. zeylanicum* (bark), *R. rhabarbarum* (peel), and *R. palmatum* (root) are shown in Figures S2−S4, respectively, in Supporting Information. From the broad hump from approximately 8−30 min observed in the HPLC chromatograms in Figures S2−S4, it is evident that the methanol extracts of *C. zeylanicum* (bark), *R. rhabarbarum* (peel), and *R. palmatum* (root) contain tannins. It is also evident that this tannin hump is correlated with high α-glucosidase inhibition. Polyphenols, such as tannins, have been found to react with the α-glucosidase enzyme by accelerating the sedimentation of protein, which may cause the high level of inhibition,[21] that is, giving false-positive results. To investigate whether the methanol extracts of *C. zeylanicum* (bark) and *R. palmatum* (root) contain specific α-glucosidase inhibitors, tannins were removed by solid-phase extraction on Oasis HLB columns. The samples were subsequently assessed by analytical-scale HPLC to monitor the efficiency of tannin removal, and α-glucosidase inhibitory activities were measured for tannin-free samples. This showed IC_{50} values of 1.57 μg/mL for *C. zeylanicum* (bark) and 7.41 μg/mL for *R. palmatum* (root) (IC_{50} curves in Figure S5 in Supporting Information). Thus, the IC_{50} values were still below the inclusion criterion of 20 μg/mL chosen for this study, which indicated that tannin-free methanol extracts of *C. zeylanicum* (bark) and *R. palmatum* (root) must contain specific α-glucosidase inhibitors.

DOI: 10.1021/jf506297k
J. Agric. Food Chem. 2015, 63, 2257−2263

Table 2. α-Glucosidase Inhibitory Activity of Methanol and Ethyl Acetate Extracts

		IC_{50}[a] ± SD (mg/mL)	
plant species	plant part	MeOH extract	EtOAc extract
A. deliciosa	peel	0.18 ± 0.01	2.77 ± 2.4
A. deliciosa	fruit	21.71 ± 0.98	nd (61.6)
A. ascalonicum	peel	0.047 ± 0.04	0.012 ± 0.002
A. ascalonicum	peeled bulb	1.078 ± 0.09	0.035 ± 0.01
A. ascalonicum	whole bulb	0.97 ± 0.01	0.052 ± 0.01
A. sativum	bulb	3.60 ± 0.4	2.51 ± 0.5
B. juncea	leaves	0.34 ± 0.2	0.21 ± 0.02
C. frutescens	fruit	13.19 ± 5.4	2.12 ± 0.4
C. angustifolia	fruit	nd (17.0)	8.86 ± 0.2
C. zeylanicum	bark	0.0090 ± 0.0002	0.018 ± 0.0006
C. cyminum	seeds	1.07 ± 0.06	28.31 ± 2.1
F. vulgare	seeds	3.12 ± 0.3	3.015 ± 0.2
F. alnus	bark	0.56 ± 0.2	0.21 ± 0.03
G. max	beans	6.48 ± 1.5	12.83 ± 4.0
G. glabra	root	0.092 ± 0.009	1.033 ± 0.2
G. tournefortii	aerial parts	12.32 ± 0.73	nd (56.2)
L. albus	seeds/beans	nd (41.2)	28.30 ± 5.6
N. sativa	seeds	0.055 ± 0.04	0.10 ± 0.005
P. anisum	seeds	15.97 ± 3.0	6.27 ± 0.1
P. nigrum	fruit	1.36 ± 0.3	0.43 ± 0.06
R. rhabarbarum	peel	0.013 ± 0.002	0.24 ± 0.01
R. rhabarbarum	peeled stick	4.94 ± 1.1	0.21 ± 0.01
R. palmatum	root	0.014 ± 0.0001	0.016 ± 0.0002
R. acetosa	leaves	0.76 ± 0.2	0.20 ± 0.1
S. suberosa	leaves	nd (115.1)	nd (24.8)
T. indica	beans	0.062 ± 0.005	6.052 ± 0.3
T. vulgaris	leaves	0.83 ± 0.2	0.36 ± 0.008
U. dioica	leaves	nd (134.7)	1.060 ± 1.002

[a]Measured in triplicate. Acarbose standard IC_{50} = 0.47 ± 0.02 mg/mL. nd = not determined; that is, no significant inhibition above maximum possible concentration given in parentheses.

High-Resolution α-Glucosidase Inhibition Assay and HPLC−HRMS−SPE−NMR Analyses. Careful inspection of HPLC chromatograms of the tannin-free methanol extracts and ethyl acetate extracts of *C. zeylanicum* (bark) and *R. palmatum* (root) showed that the ethyl acetate extracts contained more or less the same analytes but with a flatter baseline of the chromatogram due to the absence of tannins. Thus, it was decided to perform high-resolution α-glucosidase inhibition assay/HPLC−HRMS−SPE−NMR analyses with ethyl acetate extracts of *A. ascalonicum* (peel), *R. palmatum* (root), and *C. zeylanicum* (bark). The α-glucosidase inhibition profiles of *A. ascalonicum* peel (Figure 1), *R. palmatum* root (Figure 3), and *C. zeylanicum* bark (Figure 4) allowed pinpointing of HPLC peaks correlated with bioactivity and thus allowed identification of the individual metabolites responsible for the activity by subsequent HPLC−HRMS−SPE−NMR analysis, as detailed below.

Allium ascalonicum. The high-resolution α-glucosidase inhibition profile of ethyl acetate extract of *A. ascalonicum* is shown below its corresponding HPLC chromatogram at 254 nm in Figure 1. The chromatogram shows several well-separated peaks but only four of these, peaks 1−4, are correlated with α-glucosidase inhibition in the inhibition profile. HPLC−HRMS−SPE−NMR analysis of peaks 1−4 allowed identification of the corresponding compounds **1**−**4** as

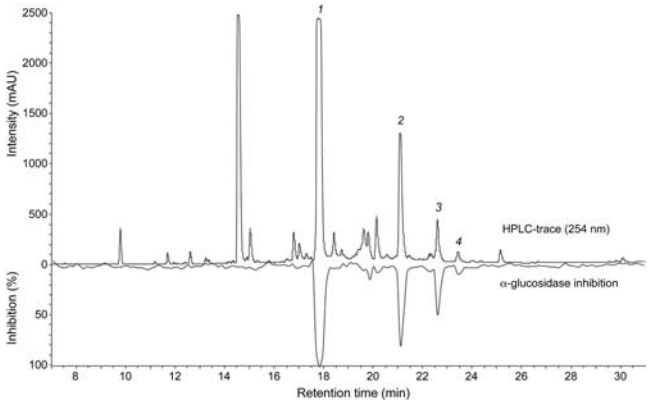

Figure 1. High-resolution α-glucosidase inhibition profile of ethyl acetate extract of *A. ascalonicum* peel with overlaid HPLC chromatogram at 254 nm. Peaks numbered 1−4 (corresponding to compounds **1**−**4**) correlated with α-glucosidase inhibition and were analyzed by HPLC−HRMS−SPE−NMR [Phenomenex C_{18}(2) Luna column, 150 × 4.6 mm, 3 μm, 40 °C, elution rate 0.5 mL/min; elution gradient 0 min, 0% B; 30 min, 100% B; 35 min, 100% B; 36 min 0% B; and 42 min, 0% B; microfractionation from 7 to 31 min in 176 wells].

quercetin (**1**) as well as the dimer (**2**), trimer (**3**), and tetramer (**4**) of quercetin (see Figure 2).

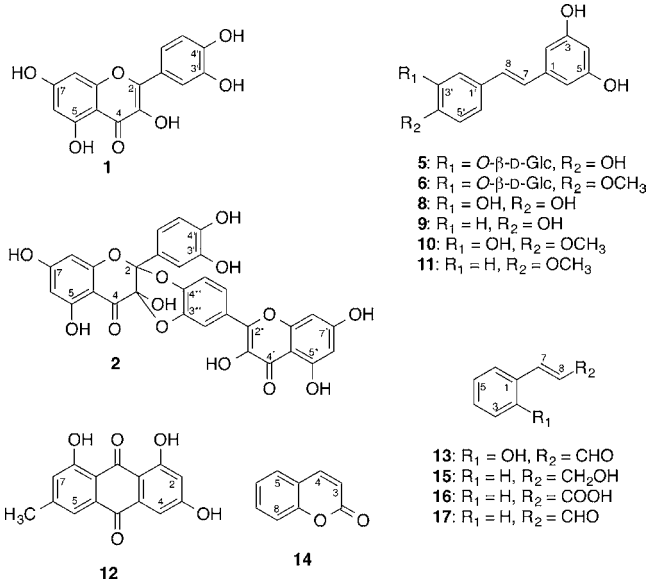

Figure 2. Structures of compounds identified in *A. ascalonicum*, *R. palmatum*, and *C. zeylanicum*.

HRMS of **1** and **2** showed *m*/*z* values of 303.0518 and 603.0760, in agreement with $[M + H]^+$ for molecules with the formulas $C_{15}H_{10}O_7$ and $C_{30}H_{18}O_{14}$, respectively. Comparison with ^{1}H NMR data from literature confirmed **1** to be quercetin[22] and **2** to be the dimer of quercetin formed by a Diels−Alder-related mechanism.[23,24] ^{1}H NMR data obtained in the HPLC−HRMS−SPE−NMR mode are given in Supporting Information Table S2.

HRMS analysis of **3** and **4** in negative-ion mode showed *m*/*z* values of 901.0862 and 1201.1154, in agreement with $[M - H]^-$ for molecules with the formulas $C_{45}H_{26}O_{21}$ and $C_{60}H_{34}O_{28}$, respectively. The ^{1}H NMR data acquired in HPLC−HRMS−SPE−NMR mode suggested the presence of a trimer and a tetramer, respectively, but the quality of the

DOI: 10.1021/jf506297k
J. Agric. Food Chem. 2015, 63, 2257−2263

spectra did not allow unambigous assignment of all ^{1}H resonances. Therefore, peaks 3 and 4 were isolated by preparative-scale HPLC (along with peaks 1 and 2) for NMR analysis. Furthermore, **1**−**4** were investigated by HPLC−ESI(−)−MS/MS with a range of collision energies to oberve daughter ions corresponding to neutral loss of the individual dioxane-linked quercetin monomers in a reverse Diels−Alder reaction (Q_{rDiAl}; m/z 300) (Supporting Information, Table S2). For both **2** and **3**, the main daughter ion was m/z 299, corresponding to $[Q_{rDiAl} - H]^-$, while for **3** a weak daughter ion of m/z 601 was also observed, corresponding to $[M - Q_{rDiAl}\text{-}H]^-$. The trimer (**3**) of quercetin has previously been reported from scales of *Allium cepa*,[23] but this is the first report on its α-glucosidase inhibitory activity. The fragmentation pattern of **4** showed the presence of an intense ion at 901 ($[M - Q_{rDiAl}\text{-}H]^-$) together with the daughter ions observed for **3**, that is, $[M - 2Q_{rDiAl} - H]^-$ and $[M - 3Q_{rDiAl} - 2H - H]^-$, corresponding to sequential loss of three quercetin moieties for **4**. Thus, **4** is a quercetin tetramer. Please refer to Supporting Information Figure S6 for the proposed ESI(−)-MS/MS fragmentation of **4**. Due to the complexity of the NMR spectra with increasing number of quercetin monomers, the NMR data of **3** and **4** did not allow unambiguous structural identification and full assignment of all NMR resonances of the quercetin trimer and tetramer. Thus, formation of the dioxane linkages in **3** and **4** via a Diels−Alder mechanism could occur via ether bond formation involving C-2 and C-3 on one quercetin and C-3′ and C-4′ on a second quercetin unit (i.e., C_2−O−$C_{3'}$ and C_3−O−$C_{4'}$ ether bonds) or the opposite (i.e., C_2−O−$C_{4'}$ and C_3−O−$C_{3'}$ ether bonds). We are awaiting access to ultra-high-field NMR facilities (>900 MHz) to conduct these structural studies, which will be published in an independent paper.

It has previously been shown that a wide range of 4-oxoflavonoids are present in onions, with quercetin monoglucosides and quercetin diglucosides accounting for 80% of the total flavonoids in the onion bulb.[25] It has, however, also been shown that autohydrolysis during storage, heating, and other kinds of processing cause degradation of quercetin monoglucosides and quercetin diglucosides into quercetin.[26,27] This is why the flavonoid content of onion scales, that is, the outer dry layer of onions, differs from the content of the onion bulb. The scales are rich in dimers and trimers of quercetin,[23] and these compounds are suggested to be formed by a Diels−Alder mechanism.[28] In recent years it has been shown that extracts of other *Allium* species have α-glucosidase inhibitory activity; for example, *N*-*p*-coumaroyltyramine in *Allium fistulosum*[29] and quercetin in *A. cepa*,[30] as well as a quercetin dimer,[31] are potent α-glucosidase inhibitors. In this work it was shown that the relative α-glucosidase inhibitory activities observed for the extract of scales of *A. ascalonicum* is **1** > **2** > **3** > **4** on the basis of the α-glucosidase inhibition profile. This correlates well with the intensity of the corresponding peaks, **1** > **2** > **3** > **4**, but further pharmacological characterization is needed for in-depth understanding of their mode of action. However, the current work shows the potential of scales of *A. ascalonicum*, a production side stream in the food industry, as a future functional food for management of T2D.

Rheum palmatum. The high-resolution α-glucosidase inhibition profile and corresponding HPLC chromatogram of ethyl acetate extract of *R. palmatum* are shown in Figure 3. The chromatogram shows more than 30 well-separated peaks, and eight of these are correlated with α-glucosidase inhibition. These peaks were numbered 5−12 and were subsequently

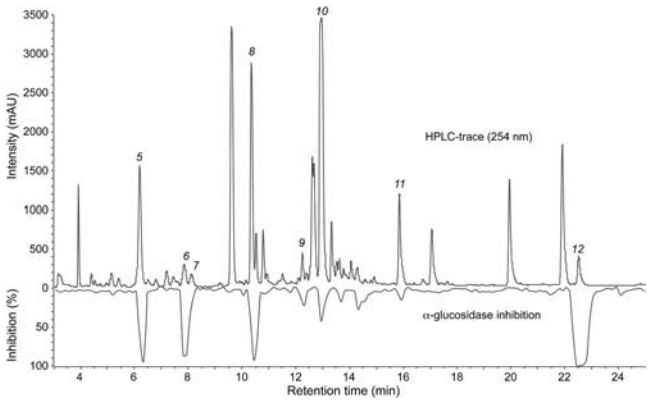

Figure 3. High-resolution α-glucosidase inhibition profile of ethyl acetate extract of *R. palmatum* with overlaid HPLC chromatogram at 254 nm. Peaks numbered 5−12 (corresponding to compounds **5**−**12**) correlated with α-glucosidase inhibition and were therefore analyzed by HPLC−HRMS−SPE−NMR. [Phenomenex C_{18}(2) Luna column, 150 × 4.6 mm, 3 μm, 40 °C, elution rate 0.5 mL/min; elution gradient 0 min, 20% B; 3 min, 20% B; 15 min, 80% B; 16 min, 100% B; 30 min, 100% B; 35 min, 20% B; and 36 min, 20% B; microfractionation from 3 to 25 min in 176 wells].

subjected to HPLC−HRMS−SPE−NMR analysis. HRMS and ^{1}H NMR data are given in Table S3 (Supporting Information), and this allowed identification of (*E*)-piceatannol 3′-*O*-β-D-glucopyranoside (**5**),[32] (*E*)-rhapontigenin 3′-*O*-β-D-glucopyranoside (**6**),[33] (*E*)-piceatannol (**8**),[34] (*E*)-resveratrol (**9**),[32] (*E*)-rhapontigenin (**10**),[32] desoxyrhapontigenin (**11**),[32] and emodin (**12**),[35] in agreement with NMR data from the cited papers. The structures of **5**, **6**, and **8**−**12** are shown in Figure 2. The amount and purity of the material eluted as peak 7 was too low to allow identification of the constituent(s) of this peak.

R. palmatum radix is an important ingredient in traditional Chinese medicine and is known to contain anthraquinones (hydroxyanthracenes), stilbenes, flavonoids, phenolic acids, tannins, and calcium oxalate.[32] *R. palmatum* radix is used as a laxative and has also been shown to contain two stilbene glucosides, 4′-*O*-methylpiceid and rhapontin, with α-glucosidase inhibitory activity.[36] This paper shows that *R. palmatum* contains several other analytes that also possess α-glucosidase inhibitory activity. However, the maximum allowed dose of *R. palmatum* is restricted to a dose providing 30 mg of hydroxyanthracene glycosides daily,[37] and use for more than 1−2 weeks requires medical supervision. Thus, a selective extraction protocol that omits the hydroxyanthracene glycosides is needed for prolonged use of *R. palmatum* root as a future functional food for type 2 diabetics.

Cinnamomum zeylanicum. As seen in Supporting Information Figure S2, the α-glucosidase inhibitory activity of methanol extract of cinnamon bark is correlated with the broad hump of tannins eluting at 10−30 min. The ethyl acetate extract is almost devoid of this tannin hump while maintaining α-glucosidase inhibitory activity (18.0 ± 0.6 μg/mL), albeit with a slightly higher IC_{50} value than for the methanol extract of cinnamon bark (9.0 ± 2.0 μg/mL).

The high-resolution biochromatogram of the ethyl acetate extract is shown in Figure 4, and it is clearly devoid of major peaks showing α-glucosidase inhibition. However, the areas around 18.5−19.5 and 21−23.5 min show repeatedly weak and broad inhibition profiles of up to 20% inhibition in separate experiments (data not shown). On the basis of HRMS and ^{1}H

DOI: 10.1021/jf506297k
J. Agric. Food Chem. 2015, 63, 2257−2263

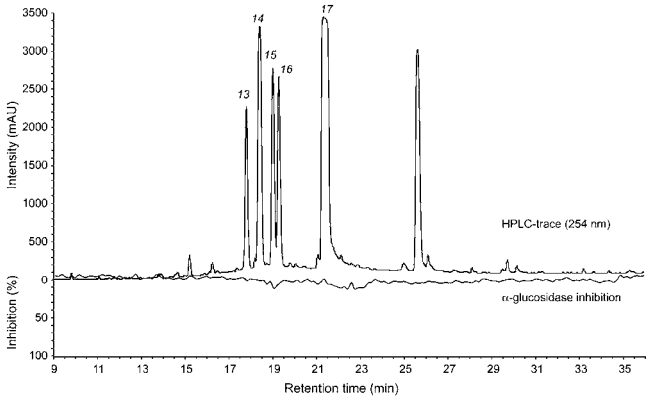

Figure 4. High-resolution α-glucosidase inhibition profile of ethyl acetate extract of *C. zeylanicum* with overlaid HPLC chromatogram at 254 nm. Peaks numbered 13−17 (corresponding to compounds **13**−**17**) were analyzed by HPLC−HRMS−SPE−NMR. [Phenomenex C_{18}(2) Luna column, 150 × 4.6 mm, 3 μm, 40 °C, elution rate 0.5 mL/min; elution gradient: 0 min, 0% B; 30 min, 100% B; 35 min, 100% B; 36 min, 0% B; and 42 min, 0% B; microfractionation from 9 to 36 min in 176 wells].

NMR data obtained in HPLC−HRMS−SPE−NMR mode (Table S4, Supporting Information), the compounds eluted as peaks 13−17 were assigned as (*E*)-2-hydroxycinnamaldehyde (**13**),[38] coumarin (**14**),[39] (*E*)-cinnamyl alcohol (**15**),[40] (*E*)-cinnamic acid (**16**),[41] and (*E*)-cinnamaldehyde (**17**).[42] Extract of cinnamon has previously been shown to inhibit α-glucosidase and lower postprandial glucose in diabetic rats,[43,44] but IC_{50} values of cinnamic acid (>5 mM)[45] and cinnamaldehyde (~225 μM)[46] against α-glucosidase are moderate to high. Thus, the observed α-glucosidase inhibitory effect of methanol as well as ethyl acetate extract of *C. zeylanicum* is likely to be a combined effect of tannins and one or more weak to moderate inhibitors.

In conclusion, quercetin (**1**) and its dimer (**2**), trimer (**3**), and tetramer (**4**) from *A. ascalonicum* as well as (*E*)-piceatannol 3′-*O*-β-D-glucopyranoside (**5**), (*E*)-rhapontigenin 3′-*O*-β-D-glucopyranoside (**6**), (*E*)-piceatannol (**8**), and emodin (**12**) from *R. palmatum* are responsible for the major α-glucosidase inhibitory activity of ethyl acetate extracts of the two plants. This shows that *A. ascalonicum* and *R. palmatum* hold potential as future functional foods, but further studies for investigation of optimal preparation procedures and seasonal variations, as well as in vivo activity and safety of optimized preparations, are needed.

■ ASSOCIATED CONTENT

Supporting Information

Six figures showing IC_{50} curves of extracts with IC_{50} values below 20 μg/mL, high-resolution biochromatograms of selected plants, and proposed fragmentation of quercetin tetramer **4**, and four tables listing extraction yields and HRMS and ^{1}H NMR data for identified compounds. This material is available free of charge via the Internet at http://pubs.acs.org.

■ AUTHOR INFORMATION

Corresponding Author

*Telephone +45 35336177; fax +45 35336001; e-mail ds@sund.ku.dk.

Author Contributions

†K.T.K., C.Ö., and A.B. contributed equally and performed the majority of the experimental work.

Funding

HPLC equipment used for high-resolution bioassay profiles was obtained via a grant from The Carlsberg Foundation. The 600 MHz HPLC−HRMS−SPE−NMR system used in this work was acquired through a grant from Apotekerfonden af 1991, The Carlsberg Foundation, and the Danish Agency for Science, Technology and Innovation via the National Research Infrastructure funds.

Notes

The authors declare no competing financial interest.

■ ACKNOWLEDGMENTS

Arife Önder (University of Copenhagen) is acknowledged for technical assistance, and Gülhan Özdemir and Najwa Khalil are gratefully acknowledged for obtaining the majority of the plant samples included in this work.

■ REFERENCES

(1) International Diabetes Federation. IDF Diabetes Atlas, 6th ed., 2013. ISBN: 2-930229-85-3. Online version at http://www.idf.org/diabetesatlas; accessed December 5, 2014.

(2) Israili, Z. H. Advances in the treatment of type 2 diabetes mellitus. *Am. J. Ther.* **2011**, *18*, 117−152.

(3) Marcovecchio, M. L.; Lucantoni, M.; Chiarelli, F. Role of chronic and acute hyperglycemia in the development of diabetes complications. *Diabetes Technol. Ther.* **2011**, *13*, 389−394.

(4) Okutan, L.; Kongstad, K. T.; Jäger, A. K.; Staerk, D. High-resolution α-amylase assay combined with high-performance liquid chromatography−solid-phase extraction−nuclear magnetic resonance spectroscopy for expedited identification of α-amylase inhibitors: Proof of concept and α-amylase inhibitor in cinnamon. *J. Agric. Food Chem.* **2014**, *62*, 11465−11471.

(5) van de Laar, F. A.; Lucassen, P. L.; Akkermans, R. P.; van de Lisdonk, F. H.; Rutten, G. E.; Van Weel, C. Alpha-glucosidase inhibitors for patients with type 2 diabetes: Results from a cochrane systematic review and meta-analysis. *Diabetes Care* **2005**, *28*, 154−163.

(6) van de Laar, F. A.; Lucassen, P. L. B. J.; Akkermans, R. P.; Van de Lisdonk, E. H.; De Grauw, W. J. C. Alpha-glucosidase inhibitors for people with impaired glucose tolerance or impaired fasting blood glucose. *Cochrane Database Syst. Rev.* **2006**, No. 4, No. CD005061, DOI: 10.1002/14651858.CD005061.pub2.

(7) Kawamori, R.; Tajima, N.; Iwamoto, Y.; Kashiwagi, A.; Shimamoto, K.; Kaku, K. Voglibose for prevention of type 2 diabetes mellitus: a randomised, double-blind trial in Japanese individuals with impaired glucose tolerance. *Lancet* **2009**, *373*, 1607−1614.

(8) Fujisawa, T.; Ikegami, H.; Inoue, K.; Kawabata, Y.; Ogihara, T. Effect of two alpha-glucosidase inhibitors, voglibose and acarbose, on postprandial hyperglycemia correlates with subjective abdominal symptoms. *Metab., Clin. Exp.* **2005**, *54*, 387−390.

(9) Clissold, S. P.; Edwards, C. Acarbose: A preliminary review of its pharmacodynamics and pharmacokinetic properties and therapeutic potential. *Drugs* **1988**, *3*, 214−243.

(10) Giera, M.; Heus, F.; Janssen, L.; Kool, J.; Lingeman, H.; Irth, H. Microfractionation revisited: A 1536 well high resolution screening assay. *Anal. Chem.* **2009**, *81*, 5460−5466.

(11) Sprogøe, K.; Stærk, D.; Jäger, A. K.; Adsersen, A.; Hansen, S. H.; Witt, M.; Landbo, A.-K. R.; Meyer, A. S.; Jaroszewski, J. W. Targeted natural product isolation guided by HPLC-SPE-NMR: constituents of *Hubertia* species. *J. Nat. Prod.* **2007**, *70*, 1472−1477.

(12) Sprogøe, K.; Stærk, D.; Ziegler, H. L.; Jensen, T. H.; Holm-Møller, S. B.; Jaroszewski, J. W. Combining HPLC-PDA-MS-SPE-NMR with circular dichroism for complete natural product character-

DOI: 10.1021/jf506297k
J. Agric. Food Chem. 2015, 63, 2257−2263

ization in crude extracts: Levorotatory gossypol in *Thespesia danis*. *J. Nat. Prod.* **2008**, *71*, 516−519.
(13) Johansen, K. T.; Wubshet, S. G.; Nyberg, N. T.; Jaroszewski, J. W. From retrospective assessment to prospective decisions in natural product isolation: HPLC-SPE-NMR analysis of *Carthamus oxyacantha*. *J. Nat. Prod.* **2011**, *74*, 2454−2461.
(14) Grosso, C.; Jäger, A. K.; Staerk, D. Coupling of a high-resolution monoamine oxidase-A inhibitor assay and HPLC-SPE-NMR for advanced bioactivity profiling of plant extracts. *Phytochem. Anal.* **2013**, *24*, 141−147.
(15) Agnolet, S.; Wiese, S.; Verpoorte, R.; Staerk, D. Comprehensive analysis of commercial willow bark extracts by new technology platform: Combined use of metabolomics, high-performance liquid chromatography-solid-phase extraction-nuclear magnetic resonance spectroscopy and high-resolution radical scavenging assay. *J. Chromatogr., A* **2012**, *1262*, 130−137.
(16) Wiese, S.; Wubshet, S. G.; Nielsen, J.; Staerk, D. Coupling HPLC-SPE-NMR with a microplate-based high-resolution antioxidant assay for efficient analysis of antioxidants in food: Validation and proof-of-concept study with caper buds. *Food Chem.* **2013**, *141*, 4010−4018.
(17) Wubshet, S. G.; Nyberg, N. T.; Tejesvi, M. V.; Pirttilä, A. M.; Kajula, M.; Mattila, S.; Staerk, D. Targeting high-performance liquid chromatography-high-resolution mass spectrometry-solid-phase extraction-nuclear magnetic resonance analysis with high-resolution radical scavenging profiles - bioactive secondary metabolites from the endophytic fungus *Penicillium namyslowskii*. *J. Chromatogr., A* **2013**, *1302*, 34−39.
(18) Kongstad, K. T.; Wubshet, S. G.; Johannesen, A.; Kjellerup, L.; Winther, A.-M. L.; Jäger, A. K.; Staerk, D. High-resolution screening combined with HPLC−HRMS−SPE−NMR for identification of fungal plasma membrane H^+-ATPase inhibitors from plants. *J. Agric. Food Chem.* **2014**, *62*, 5595−5602.
(19) Schmidt, J. S.; Lauridsen, M. B.; Dragsted, L. O.; Nielsen, J.; Staerk, D. Development of a bioassay-coupled HPLC-SPE-*tt*NMR platform for identification of α-glucosidase inhibitors in apple peel (*Malus* × *domestica* Borkh.). *Food Chem.* **2012**, *135*, 1692−1699.
(20) Wubshet, S. G.; Schmidt, J. S.; Wiese, S.; Staerk, D. High-resolution screening combined with HPLC-HRMS-SPE-NMR for identification of potential health-promoting constituents in sea aster and searocket New nordic food ingredients. *J. Agric. Food Chem.* **2013**, *61*, 8616−8623.
(21) Chen, Y.-G.; Li, P.; Li, P.; Yan, R.; Zhang, X.-Q.; Wang, Y.; Zhang, X.-T.; Ye, W.-C.; Zhang, Q.-W. α-Glucosidase inhibitory effect and simultaneous quantification of three major flavonoid glycosides in *Microctis folium*. *Molecules* **2013**, *18*, 4221−4232.
(22) Schmidt, B.; Jaroszewski, J. W.; Bro, R.; Witt, M.; Stærk, D. Combining PARAFAC analysis of HPLC-PDA profiles and structural characterization using HPLC-PDA-SPE-NMR-MS experiments: commercial preparations of St. John's wort. *Anal. Chem.* **2008**, *80*, 1978−1987.
(23) Ly, T. N.; Hazama, C.; Shimoyamada, M.; Ando, H.; Kato, K.; Yamauchi, R. Antioxidative compounds from the outer scales of onion. *J. Agric. Food Chem.* **2005**, *53*, 8183−8189.
(24) Mohamad, G. A. Alliuocide G, a new flavonoid with potent α-amylase inhibitory activity from *Allium cepa* L. *ARKIVOC* **2008**, No. xi, 202−209.
(25) Rohdes, M. J. C.; Price, K. R. Analytical problems in the study of flavonoid compounds in onions. *Food Chem.* **1996**, *57*, 113−117.
(26) Price, K. R.; Bacon, J. R.; Rhodes, M. J. C. Effect of storage and domestic processing on the content and composition of flavonol glucosides in onion (*Allium cepa*). *J. Agric. Food Chem.* **1997**, *45*, 938−942.
(27) Schmidt, J. S.; Nyberg, N. T.; Staerk, D. Assessment of constituents in *Allium* by multivariate data analysis, high-resolution α-glucosidase inhibition assay and HPLC-SPE-NMR. *Food Chem.* **2014**, *161*, 192−198.
(28) Krishnamachari, V.; Levine, L. H.; Paré, P. W. Flavonoid oxidation by the radical generator AIBN: A unified mechanism for quercetin radical scavenging. *J. Agric. Food Chem.* **2002**, *50*, 4357−4363.
(29) Nishioka, T.; Watanabe, J.; Kawabata, J.; Niki, R. Isolation and activity of *N*-*p*-coumaroyltyramine, an α-glucosidase inhibitor in Welsh onion (*Allium fistulosum*). *Biosci. Biotechnol. Biochem.* **1997**, *61*, 1138−1141.
(30) Kim, S.-H.; Jo, S.-H.; Kwon, Y.-I.; Hwang, J.-K. Effects of onion (*Allium cepa* L.) extract administration on intestinal α-glucosidases activities and spikes in postprandial blood glucose levels in SD rats model. *Int. J. Mol. Sci.* **2011**, *12*, 3757−3769.
(31) Zhang, C.; Dong, S.; Chen, K.; Duan, L.; Wu, X.; Zhao, Y.; Zheng, H. Medicinal application of quercetin dipolymer flavanoids to preparation of glycosidase enzyme inhibitors. Chinese Patent CN102000059, 2012.
(32) Ngoc, T. M.; Minh, P. T. H.; Hung, T. M.; Thuong, P. T.; Lee, I.; Min, B.-S.; Bae, K. Lipoxygenase inhibitory constituents in rhubarb. *Arch. Pharm. Res.* **2008**, *31*, 598−605.
(33) Kashiwada, Y.; Nonaka, G.-I.; Nishioka, I. Studies of rhubarb (rhei rhizoma). VI. Isolation and characterization of stilbenes. *Chem. Pharm. Bull.* **1984**, *32*, 3501−3517.
(34) Han, S. Y.; Bang, H. B.; Lee, H. S.; Hwang, J. W.; Choi, D. H.; Yang, D. M.; Jun, J.-G. A new synthesis of stilbene natural product piceatannol. *Bull. Korean Soc. Chem.* **2008**, *29*, 1800−1802.
(35) Danielsen, K.; Aksnes, D. W.; Francis, G. W. NMR study of some anthraquinones from rhubarb. *Magn. Reson. Chem.* **1992**, *30*, 359−360.
(36) Kubo, I.; Mural, Y.; Soediro, I.; Soetarno, S.; Sastrodihardjo, S. Efficient isolation of glycosidase inhibitory stilbene glucosides from *Rheum palmatum*. *J. Nat. Prod.* **1991**, *54*, 1115−1118.
(37) Committee on Herbal Medicinal Products, European Medicine Agency. Community herbal monograph on *Rheum palmatum* L. and *Rheum officinale* Baillon, Radix, 2007; http://www.ema.europa.eu/ema/.
(38) Kwon, B.-M.; Cho, Y.-K.; Lee, S.-H.; Nam, J.-Y.; Bok, S.-H.; Chun, S.-K.; Kim, J.-A.; Lee, I.-R. 2′-Hydroxycinnaldehyde from stem bark of *Cinnamomum cassia*. *Planta Med.* **1996**, *62*, 183−184.
(39) Scognamiglio, M.; Fiumano, V.; D'Abrosca, B.; Esposito, A.; Choi, Y. H.; Verporte, R.; Fiorentino, A. Chemical interactions between plants in mediterranean vegetation: The influence of selected plant extracts on *Aegilops geniculata* metabolome. *Phytochemistry* **2014**, *106*, 69−85.
(40) Duan, Y.; Bai, R.; Tian, J.; Chen, L.; Yan, X. Hydrogenation of aldehydes and ketones to corresponding alcohols with methylamine borane in neat water. *Synth. Commun.* **2014**, *44*, 2555−2564.
(41) Shi, H.; Xie, D.; Yang, R.; Cheng, Y. Synthesis of caffeic acid phenethyl ester derivatives, and their cytoprotective and neuritogenic activities in PC12 cells. *J. Agric. Food Chem.* **2014**, *62*, 5046−5053.
(42) Fujita, N.; Tanaka, E.; Murata, M. Cinnamaldehyde inhibits phenylalanine ammonia-lyase and enzymatic browning of cut lettuce. *Biosci. Biotechnol. Biochem.* **2006**, *70*, 672−676.
(43) Shihabudeen, H. M. S.; Priscilla, D. H.; Thirumurugan, K. Cinnamon extract inhibits a-glucosidase activity and dampens postprandial glucose excursion in diabetic rats. *Nutr. Metab.* **2011**, *8*, 46.
(44) Adisakwatana, S.; Lerdsuwankij, O.; Poputtachai, U.; Minipun, A.; Suparpprom, C. Inhibitory activity of cinnamon bark species and their combination effect with acarbose against intestinal α-glucosidase and pancreatic α-amylase. *Plant Foods Hum. Nutr.* **2011**, *66*, 143−148.
(45) Adisakwattana, S.; Sookkongwaree, K.; Roengsumran, S.; Petsom, A.; Ngamrojnavanich, N.; Chavasiri, W.; Deesamer, S.; Yibchok-anun, S. Structure-activity relationships of trans-cinnamic acid derivatives on α-glucosidase inhibition. *Bioorg. Med. Chem. Lett.* **2004**, *14*, 2893−2896.
(46) Ngadiwiyana, I.; Nor Basid, A. P.; Dan Purbowatiningrum, R. S. Potency of cinnamaldehyde of cinnamon oil as an antidiabetic compound. *Indones. J. Pharm.* **2011**, *22*, 9−14.

DOI: 10.1021/jf506297k
J. Agric. Food Chem. 2015, 63, 2257−2263

mass spectrometry (LC/MS), we established the chemical profile of phytosterols in WB. Furthermore, the structure−activity relationship (SAR) of sterol oxides against the growth of human colon cancer cells was discussed on the basis of both purified and synthesized compounds **1**−**8** and **13**.

MATERIALS AND METHODS

Materials. Cholesterol, β-sitosterol, stigmasterol, and pregnenolone were purchased from Sigma (St. Louis, MO) or Thermo Fisher Scientific (Waltham, MA). Anhydrous reactions were carried out in oven-dried glassware under a nitrogen atmosphere unless otherwise noted. Analytical (250 μm thickness, 2−25 μm particle size) and preparative thin layer chromatography (TLC) plates (1000 μm thickness, 2−25 μm particle size) were purchased from Sigma (St. Louis, MO) and Sorbent Technologies (Atlanta, GA), respectively. Sephadex LH-20 was purchased from Sigma (St. Louis, MO). Medium pressure column chromatography was carried out over reverse phase silica gel (60 Å, Sigma, St. Louis, MO), equipped with LabAlliance Series I pump and Spectra/chrom fraction collector CF-2. LC/MS-grade solvents and other reagents were obtained from Thermo Fisher Scientific (Waltham, MA). HCT-116 and HT-29 human colon cancer cells were obtained from American Type Tissue Culture (Manassas, VA). McCoy's 5A medium was purchased from Thermo Fisher Scientific (Waltham, MA). Fetal bovine serum (FBS) and penicillin/streptomycin were purchased from Gemini Bio-Products (West Sacramento, CA). MTT (3-(4,5-dimethylthiaxol-2-yl)-2,5-diphenyltetrazolium bromide) was procured from Calbiochem-Novabiochem (San Diego, CA). Apoptag Plus Peroxydase *In Situ* Apoptosis Detection Kit was purchased from Millipore (Billerica, MA).

Preparation of Sterol-Enriched Fraction from WB. Eight fractions (F1−F8) were obtained from WB oil, as described in our previous study.[11] Briefly, wheat bran, provided by ConAgra Food Ingredients Company, was extracted by 95% ethanol at 40 °C for 24 h to give an ethanol extract. After evaporation, the ethanol residue was then suspended in water and partitioned with ethyl acetate (EA). After removal of EA in vacuo, the WB oil was obtained. The WB oil was subjected to column chromatography (CC) over a normal phase silica gel eluted with a mixture of hexane and EA, affording F1−F8, which are stored at −80 °C until analysis. Phytosterols could be detected in both F7 and F8. In order to avoid the analytical interference from ARs in F7, we enriched sterols from F8. Specifically, part of F8 (6.0 g) was subjected to reverse phase (RP) C_{18} silica gel medium pressure CC (30 mm × 360 mm, 60 Å) eluted with 50% methanol, methanol, and methanol containing 0.2% formic acid (FA). Sphingolipids remained in acidic methanol eluate. The neutral methanol fraction was further loaded on Sephadex LH-20 CC eluted with 50% ethanol and ethanol. The ethanol eluates were evaporated *in vacuo*, giving the sterol-enriched fraction (2.0 g).

Purification of Oxyphytosterols 1−4 from Sterol-Enriched Fraction and Their NMR Data. Repeated purification of the sterol-enriched fraction (1.0 g) by RP C_{18} silica gel medium pressure CC eluted with methanol, giving stigmast-4-en-6β-ol-3-one (**1**) (4 mg), stigmast-4,22-dien-6β-ol-3-one (**2**) (6 mg), stigmast-5-en-3β-ol-7-one (**3**) (8 mg), and stigmast-5,22-dien-3β-ol-7-one (**4**) (5 mg).

*Stigmast-4-en-6β-ol-3-one (**1**) as a White Solid.* ^{1}H NMR (700 MHz, Py-d5) δ 1.64 (1H, m, H-1a), 1.92 (1H, m, H-1b), 2.45 (1H, m, H-2a), 2.60 (1H, m, H-2b), 6.07 (1H, s, H-4), 4.57 (1H, m, H-6), 1.28 (1H, m, H-7a), 2.21 (1H, m, H-7b), 2.30 (1H, m, H-8), 0.91 (1H, m, H-9), 1.48 (2H, m, H-11), 1.17 (1H, m, H-12a), 2.04 (1H, m, H-12b), 1.02 (1H, m, H-14), 1.16 (1H, m, H-15a), 1.65 (1H, m, H-15b), 1.27 (1H, m, H-16a), 1.88 (1H, m, H-16b), 1.17 (1H, m, H-17), 0.74 (3H, s, H-18), 1.57 (3H, s, H-19), 1.43 (1H, m, H-20), 1.02 (3H, d, *J* = 6.6 Hz, H-21), 1.14 (1H, m, H-22a), 1.43 (1H, m, H-22b), 1.28 (2H, m, H-23), 1.02 (1H, m, H-24), 1.71 (1H, m, H-25), 0.89 (3H, d, *J* = 6.5 Hz, H-26), 0.91 (3H, d, *J* = 6.5 Hz, H-27), 1.32 (2H, m, H-28), and 0.92 (3H, t, *J* = 6.6 Hz, H-29); ^{13}C NMR (175 MHz, Py-d5) δ 37.9 (t, C-1), 35.4 (t, C-2), 200.1 (s, C-3), 126.3 (d, C-4), 170.3 (s, C-5), 70.3 (d, C-6), 40.1 (t, C-7), 30.7 (d, C-8), 54.5 (d, C-9), 38.9 (s, C-10), 21.7 (t, C-11), 40.4 (t, C-12), 43.2 (s, C-13), 56.7 (d, C-14), 25.0 (t, C-15), 29.0 (t, C-16), 56.6 (d, C-17), 12.5 (q, C-18), 20.0 (q, C-19), 36.8 (d, C-20), 19.4 (q, C-21), 34.6 (t, C-22), 26.9 (t, C-23), 46.5 (d, C-24), 30.0 (d, C-25), 19.6 (q, C-26), 20.4 (q, C-27), 23.9 (t, C-28), and 12.6 (q, C-29); positive ESIMS, *m*/*z* 429 $[M + H]^+$.

*Stigmast-4,22-dien-6β-ol-3-one (**2**) as a White Solid.* ^{1}H NMR (700 MHz, Py-d5) δ 6.07 (1H, s, H-6), 5.24 (1H, dd, *J* = 15.2, 8.8 Hz, H-22), 5.09 (1H, dd, *J* = 15.2, 8.8 Hz, H-23), 4.56 (1H, m, H-6), 2.61 (1H, m), 2.46 (1H, m), 2.28−2.18 (2H, m), 2.09 (1H, m), 2.01 (1H, m), 1.93 (1H, m), 1.78 (1H, m), 1.68−1.41 (5H, m), 1.37−1.0 (10H, m), 1.57 (3H, s, H-19), 1.12 (3H, d, *J* = 6.6 Hz, H-21), 0.94 (3H, t, *J* = 6.5 Hz, H-29), 0.92 (3H, d, *J* = 6.5 Hz, H-27), 0.89 (3H, d, *J* = 6.5 Hz, H-26), and 0.76 (3H, s, H-18); ^{13}C NMR (175 MHz, Py-d5) δ 200.1 (s, C-3), 170.3 (s, C-5),139.2 (d, C-22), 130.0 (d, C-23), 126.3 (d, C-4), 73.0 (d, C-6), 56.7, 56.5, 54.6, 51.9, 43.0, 41.2, 40.2, 40.1, 38.8, 37.9, 35.1, 32.6, 30.7, 29.7, 26.1, 25.0, 21.9, 21.7, 21.6, 20.0, 19.6, 13.0 (q, C-29), and 12.7 (q, C-18); positive ESIMS, *m*/*z* 427 $[M + H]^+$.

*7-Keto-β-sitosterol (**3**) as a White Solid.* ^{1}H NMR (600 MHz, CD_3OD + $CDCl_3$) δ 5.64 (1H, s, H-6), 3.56 (1H, m, H-3), 2.48−2.45 (1H, m), 2.40−2.32 (2H, m), 2.29−2.25 (1H, m), 2.06−2.03 (1H, m), 1.98−1.95 (1H, m), 1.90−1.88 (2H, m), 1.69−1.46 (6H, m), 1.37−1.00 (13H, m), 1.21 (3H, s, H-19), 0.93 (3H, d, *J* = 6.5 Hz, H-21), 0.85 (3H, t, *J* = 7.3 Hz, H-29), 0.83 (3H, d, *J* = 6.8 Hz, H-27), 0.81 (3H, d, *J* = 6.8 Hz, H-26), and 0.70 (3H, s, H-18); ^{13}C NMR (150 MHz, CD_3OD + $CDCl_3$) δ 204.5 (s, C-7), 168.7 (s, C-5), 126.2 (d, C-6), 70.9 (d, C-3), 55.8 (d, C-17), 51.1 (d, C-14), 51.1 (d, C-9), 46.9, 46.4, 44.1, 42.5, 39.7, 39.4, 37.3, 37.1, 34.9, 31.6, 30.1, 29.4, 27.2, 27.0, 23.9, 22.1, 20.2 (q, C-27), 19.5 (q, C-26), 19.4 (q, C-21), 17.7 (q, C-19), 12.4 (q, C-29), and 12.3 (q, C-18); positive ESIMS, *m*/*z* 429 $[M + H]^+$.

*7-Keto-stigmasterol (**4**) as a White Solid.* ^{1}H NMR (600 MHz, CD_3OD + $CDCl_3$) δ 5.63 (1H, s, H-6), 5.15 (1H, dd, *J* = 15.1, 8.7 Hz, H-23), 5.01 (1H, dd, *J* = 15.1, 8.7 Hz, H-22), 3.56 (1H, m, H-3), 2.48−2.45 (1H, m), 2.40−2.34 (1H, m), 2.31−2.24 (2H, m), 2.07−1.99 (2H, m), 1.97−1.94 (1H, m), 1.90−1.87 (1H, m), 1.75−1.71 (1H, m), 1.62−1.38 (7H, m), 1.34−1.10 (7H, m), 1.20 (3H, s, H-19), 1.01 (3H, d, *J* = 6.7 Hz, H-21), 0.83 (3H, d, *J* = 6.4 Hz, H-27), 0.79 (3H, t, *J* = 7.3 Hz, H-29), 0.78 (3H, d, *J* = 6.4 Hz, H-26), and 0.70 (3H, s, H-18); ^{13}C NMR (150 MHz, CD_3OD + $CDCl_3$) δ 204.4 (s, C-7), 168.5 (s, C-5), 139.0 (d, C-22), 130.3 (d, C-23), 126.1 (d, C-6), 70.6 (d, C-3), 55.6 (d, C-17), 52.2, 51.0, 50.9, 46.2, 43.8, 42.3, 41.1, 39.4, 39.3, 37.2, 32.7, 31.4, 29.8, 27.1, 26.1, 21.9, 21.8 (q, C-27), 21.4 (q, C-26), 19.4 (q, C-21), 17.7 (q, C-19), 12.6 (q, C-29), and 12.6 (q, C-18); positive ESIMS, *m*/*z* 427 $[M + H]^+$.

General Procedure A for the Synthesis of Sterol Acetates. A mixture of sterols (1.0 equiv), acetic anhydride (Ac_2O) (10.0 equiv), and pyridine (Py) (50.0 equiv) was incubated at 37 °C overnight. The solvent was removed *in vacuo*. The residue was reconstituted in ethyl acetate (EA), washed with water, dried over Na_2SO_4, and filtered. The filtration was evaporated off, and the residue was subjected to a short pad of Celite, eluting with a mixture of hexane/EA (20:1), to give sterol acetates.

General Procedure B for the Synthesis of 7-Ketosterol Acetates. Chromium trioxide (CrO_3) (15.0 equiv) was suspended in dry dichloromethane (DCM) and stirred for 30 min at −20 °C. 3,5-Dimethylpyrazole (15.0 equiv) was added in one portion, and the reaction mixture was stirred for 30 min at −20 °C. Sterol acetates (1.0 equiv) were added, and the mixture was stirred at −20 °C and allowed to warm up to room temperature (rt) overnight. EA was then added, and the brown suspension was filtered through Celite. The filtration was concentrated, and the residue was purified by CC or pre-TLC to give 7-ketosterol acetates.

General Procedure C for the Synthesis of 7-Ketosterols. LiOH (4.0 equiv) was added at rt to a stirred solution of 7-ketosterol acetates (1.0 equiv) in THF/MeOH/H_2O (3:1:1). The resulting mixture was stirred at rt for 2 h. The organic solvents were evaporated, and the residue was diluted with water, and extracted with EA. The organic layer was washed with water and brine, dried over Na_2SO_4, and concentrated *in vacuo*. The residue was purified by pre-TLC to give 7-ketosterols.

DOI: 10.1021/jf506361r
J. Agric. Food Chem. 2015, 63, 2264−2276

General Procedure D for the Synthesis of 7β-Hydroxysterols. A suspension of 7-ketosterols (1.0 equiv) and cerium chloride heptahydrate (4.0 equiv) in methanol was stirred at 0 °C for 10 min. Sodium borohydride (2.5 equiv) was added to the suspension, and the mixture was stirred at rt for 4−18 h. The reaction solution was partitioned between water and EA. The organic layer was washed with water and brine, dried over Na_2SO_4, and concentrated under reduced pressure. The residue was purified by pre-TLC to give 7β-hydrolxysterols.

General Procedure E for the Synthesis of 3-*O*-(4-Acetoxyferuloyl)-oxysterols. *trans*-4-Acetoxy ferulic acid (1.1 equiv) and 7-oxysterols (1.0 equiv) were dissolved in dry DCM at 0 °C. DCC (3.0 equiv) and DMAP (2.5 equiv) were added, and the mixture was stirred at rt for 6 h. The solid that formed was filtered off, and the solution was washed with water, 10% HOAc, and again with water. The organic extracts were dried over Na_2SO_4 and concentrated *in vacuo*. The residue was purified by pre-TLC to give 3-*O*-(4-acetoxyferuloyl)-oxysterols.

General Procedure F for the Synthesis of Oxysterol Ferulates. 3-*O*-(4-Acetoxyferuloyl)-oxysterols (1.0 equiv) was dissolved in a mixture of DCM/MeOH (2:1, 3 mL). K_2CO_3 (0.2 equiv) was added, and the mixture was stirred at rt for 5 h. The reaction was quenched by adding a saturated aqueous NH_4Cl solution. The organic layers were separated, washed with water and brine, dried over Na_2SO_4, and concentrated under reduced pressure. The residue was purified by pre-TLC (H/E = 3:1) to give oxysterol ferulates.

Synthesis of Sterol Oxides 3−8. *β-Sitosterol Acetate (**22**).* Procedure A was followed by using β-sitosterol (414 mg, 1.0 mmol), Ac_2O (0.94 mL, 10.0 mmol), and Py (4.07 mL, 50.0 mmol), giving the title compound (456 mg, yield: 100%) as a white solid: positive ESIMS, m/z 457 $[M + H]^+$.

*Stigmasterol Acetate (**23**).* Procedure A was followed by using stigmasterol (412 mg, 1.0 mmol), Ac_2O (0.94 mL, 10.0 mmol), and Py (4.07 mL, 50.0 mmol), giving the title compound (454 mg, yield: 100%) as a white solid: ^{1}H NMR (600 MHz, $CDCl_3$) δ 5.39 (1H, d, J = 4.7 Hz, H-6), 5.16 (1H, dd, J = 15.1, 8.6 Hz, H-23), 5.03 (1H, dd, J = 15.1, 8.6 Hz, H-22), 4.62 (1H, m, H-3), 2.35−2.31 (2H, m), 2.10−1.95 (4H, m), 2.05 (3H, s, OAc-3), 1.90−1.85 (2H, m), 1.76−1.68 (1H, m), 1.62−1.39 (10H, m), 1.32−1.12 (5H, m), 1.11−0.92 (4H, m), 1.14 (3H, s, H-19), 1.13 (3H, d, J = 6.7 Hz, H-21), 0.86 (3H, d, J = 6.4 Hz, H-27), 0.82 (3H, t, J = 7.3 Hz, H-29), 0.81 (3H, d, J = 6.4 Hz, H-26), and 0.71 (3H, s, H-18); positive ESIMS, m/z 455 $[M + H]^+$.

*Cholesterol Acetate (**24**).* Procedure A was followed by using cholesterol (386 mg, 1.0 mmol), Ac_2O (0.94 mL, 10.0 mmol), and Py (4.07 mL, 50.0 mmol), giving the title compound (428 mg, yield: 100%) as a white solid: ^{1}H NMR (600 MHz, $CDCl_3$) δ 5.36 (1H, d, J = 5.0 Hz, H-6), 4.59 (1H, m, H-3), 2.34−2.28 (2H, m), 2.04−1.93 (2H, m), 2.03 (3H, s, OAc-3), 1.88−1.78 (3H, m), 1.65−1.40 (8H, m), 1.38−1.20 (4H, m), 1.18−0.90 (9H, m), 1.02 (3H, s, H-19), 0.90 (3H, d, J = 6.5 Hz, H-21), 0.86 (3H, d, J = 6.6 Hz, H-27), 0.85 (3H, d, J = 6.6 Hz, H-26), and 0.66 (3H, s, H-18); positive ESIMS, m/z 429 $[M + H]^+$.

*7-Ketositosterol Acetate (**25**).* Procedure B was followed by using β-sitosterol acetate (**25**) (200 mg, 0.44 mmol), CrO_3 (658 mg, 6.58 mmol), and dimethylpyrazole (632 mg, 6.58 mmol) in dry DCM (20 mL). The resulting residue was purified by pre-TLC (H/E = 8:1) to give the title compound (138 mg, yield: 67%) as a white solid: positive ESIMS, m/z 471 $[M + H]^+$.

*7-Ketostigmasterol Acetate (**26**).* Procedure B was followed by using stigmasterol acetate (**26**) (454 mg, 1.0 mmol), CrO_3 (1.5 g, 15.0 mmol), and dimethylpyrazole (1.44 g, 15.0 mmol) in dry DCM (50 mL). The resulting residue was purified by CC (H/E = 15:1, 10:1, and 8:1) to give the title compound (269 mg, yield: 57%) as a white solid: ^{1}H NMR (600 MHz, $CDCl_3$) δ 5.68 (1H, H-6), 5.16 (1H, dd, J = 15.1, 8.6 Hz, H-23), 5.01 (1H, dd, J = 15.1, 8.6 Hz, H-22), 4.70 (1H, m, H-3), 2.55−2.51 (1H, m), 2.47−2.42 (1H, m), 2.39−2.33 (1H, m), 2.24−2.20 (1H, m), 2.04−1.93 (4H, m), 2.03 (3H, s, OAc-3), 1.79−1.48 (7H, m), 1.41−1.10 (8H, m), 1.20 (3H, s, H-19), 1.01 (3H, d, J = 6.7 Hz, H-21), 0.83 (3H, d, J = 6.3 Hz, H-27), 0.79 (3H, t, J = 7.3 Hz, H-29), 0.78 (3H, d, J = 6.3 Hz, H-26), and 0.68 (3H, s, H-18); positive ESIMS, m/z 469 $[M + H]^+$.

*7-Ketocholesterol Acetate (**27**).* Procedure B was followed by using cholesterol acetate (**27**) (428 mg, 1.0 mmol), CrO_3 (1.5 g, 15.0 mmol), and dimethylpyrazole (1.44 g, 15.0 mmol) in dry DCM (50 mL). The resulting residue was purified by CC (H/E = 15:1, 10:1, and 8:1) to give the title compound (260 mg, yield: 60%) as a white solid: ^{1}H NMR (600 MHz, $CDCl_3$) δ 5.69 (1H, s, H-6), 4.70 (1H, m, H-3), 2.55−2.51 (1H, m), 2.48−2.35 (2H, m), 2.26−2.18 (1H, m), 2.07−1.82 (4H, m), 2.06 (3H, s, OAc-3), 1.71−1.47 (5H, m), 1.40−0.99 (13H, m), 1.20 (3H, s, H-19), 0.91 (3H, d, J = 6.5 Hz, H-21), 0.86 (3H, d, J = 6.6 Hz, H-27), 0.85 (3H, d, J = 6.6 Hz, H-26), and 0.67 (3H, s, H-18); positive ESIMS, m/z 443 $[M + H]^+$.

*7-Ketositosterol (**3**).* Procedure C was followed by using 7-keto-β-sitosterol acetate (100 mg, 0.21 mmol) and LiOH (20 mg, 0.84 mmol) in THF/MeOH/H_2O (3:1:1, 5 mL). The resulting residue was purified by pre-TLC (H/E = 2:1) to give the title compound (**3**) (90 mg, yield: 100%).

*7-Ketostigmasterol (**4**).* Procedure C was followed by using 7-keto-stigmasterol acetate (181 mg, 0.39 mmol) and LiOH (37 mg, 1.55 mmol) in THF/MeOH/H_2O (3:1:1, 5 mL). The resulting residue was purified by pre-TLC (C/M = 20:1) to give the title compound (**4**) (166 mg, yield: 100%).

*7β-Hydroxysitosterol (**5**).* Procedure D was followed by using 7-keto-β-stigmasterol (**3**) (30 mg, 0.07 mmol), $CeCl_3{\cdot}7H_2O$ (104 mg, 0.28 mmol), and $NaBH_4$ (7 mg, 0.18 mmol) in MeOH (3 mL). The mixture was stirred at rt for 18 h. The residue was purified by pre-TLC (C/M = 20:1) to give the title compound (**5**) (17 mg, yield: 57%) as a white solid: ^{1}H NMR (600 MHz, CD_3OD + $CDCl_3$) δ 5.24 (1H, s, H-6), 3.72 (1H, d, J = 8.0 Hz, H-7), 3.41 (1H, m, H-3), 2.26−2.18 (2H, m), 2.04−2.02 (1H, m), 1.87−1.78 (4H, m), 1.70−1.66 (1H, m), 1.55−1.33 (6H, m), 1.32−0.99 (13H, m), 1.06 (3H, s, H-19), 0.94 (3H, d, J = 6.5 Hz, H-21), 0.86 (3H, t, J = 7.4 Hz, H-29), 0.84 (3H, d, J = 6.8 Hz, H-27), 0.83 (3H, d, J = 6.8 Hz, H-26), and 0.72 (3H, s, H-18); ^{13}C NMR (150 MHz, CD_3OD + $CDCl_3$) δ 144.0 (s, C-5), 127.4 (d, C-6), 73.7 (d, C-7), 72.1 (d, C-3), 57.7 (d, C-17), 56.8 (d, C-14), 50.0, 47.2, 44.0, 42.5, 41.2, 41.0, 38.2, 37.5, 37.4, 35.1, 32.2, 30.3, 29.6, 27.3, 27.1, 24.1, 22.2, 20.2 (q, C-27), 19.5 (q, C-26), 19.4 (q, C-21), 19.3 (q, C-19), 12.3 (q, C-29), and 12.3 (q, C-18); positive ESIMS, m/z 431 $[M + H]^+$.

*7β-Hydroxystigmasterol (**6**).* Procedure D was followed by using 7-keto-stigmasterol (**4**) (100 mg, 0.23 mmol), $CeCl_3{\cdot}7H_2O$ (350 mg, 0.94 mmol), and $NaBH_4$ (22 mg, 0.58 mmol) in MeOH (5 mL). The mixture was stirred at rt for 6 h. The residue was purified by pre-TLC (C/M = 20:1) to give the title compound (**6**) (50 mg, yield: 50%) as a white solid: ^{1}H NMR (600 MHz, CD_3OD + $CDCl_3$) δ 5.24 (1H, s, H-6), 5.16 (1H, dd, J = 15.1, 8.8 Hz, H-23), 5.03 (1H, dd, J = 15.1, 8.8 Hz, H-22), 3.71 (1H, d, J = 8.2 Hz, H-7), 3.42 (1H, m, H-3), 2.29−2.20 (2H, m), 2.06−1.99 (2H, m), 1.87−1.69 (4H, m), 1.58−1.36 (7H, m), 1.31−1.11 (9H, m), 1.06 (3H, s, H-19), 1.03 (3H, d, J = 6.7 Hz, H-21), 0.85 (3H, d, J = 6.3 Hz, H-27), 0.81 (3H, t, J = 7.1 Hz, H-29), 0.80 (3H, d, J = 6.3 Hz, H-26), and 0.73 (3H, s, H-18); ^{13}C NMR (150 MHz, CD_3OD+$CDCl_3$) δ 144.0 (s, C-5), 139.7 (d, C-22), 130.5 (d, C-23), 127.3 (d, C-6), 73.7 (d, C-7), 72.0 (d, C-3), 57.7 (d, C-17), 56.7, 52.7, 50.0, 43.8, 42.4, 41.8, 41.1, 40.8, 38.2, 37.5, 33.1, 32.2, 30.3, 27.3, 26.5, 22.2, 21.9 (q, C-27), 21.5 (q, C-26), 19.5 (q, C-21), 19.4 (q, C-19), 12.7 (q, C-29), and 12.6 (q, C-18); positive ESIMS, m/z 429 $[M + H]^+$.

*7-Ketocholesterol (**7**).* Procedure C was followed by using 7-keto-cholesterol acetate (260 mg, 0.61 mmol) and LiOH (59 mg, 2.44 mmol) in THF/MeOH/H_2O (3:1:1, 5 mL). The resulting residue was purified by pre-TLC ($CHCl_3$/MeOH = 15:1) to give the title compound (**7**) (223 mg, yield: 91%) as a white solid: ^{1}H NMR (600 MHz, CD_3OD + $CDCl_3$) δ 5.63 (1H, s, H-6), 3.55 (1H, m, H-3), 2.48−2.45 (1H, m), 2.41−2.35 (2H, m), 2.30−2.26 (1H, m), 2.06−2.04 (1H, m), 1.98−1.96 (1H, m), 1.90−1.87 (2H, m), 1.63−1.46 (5H, m), 1.39−0.99 (13H, m), 1.22 (3H, s, H-19), 0.94 (3H, d, J = 6.4 Hz, H-21), 0.87 (3H, d, J = 6.6 Hz, H-27), 0.86 (3H, d, J = 6.6 Hz, H-26), and 0.71 (3H, s, H-18); ^{13}C NMR (150 MHz, CD_3OD + $CDCl_3$) δ 204.5 (s, C-7), 168.8 (s, C-5), 126.3 (d, C-6), 71.0 (d, C-3), 56.1 (d,

DOI: 10.1021/jf506361r
J. Agric. Food Chem. 2015, 63, 2264−2276

C-17), 51.3 (d, C-14), 51.2 (d, C-9), 46.5, 44.2, 42.6, 40.6, 39.9, 39.5, 37.5, 37.3, 36.9, 31.7, 29.5, 29.0, 27.3, 24.9, 23.2 (q, C-27), 23.0 (q, C-26), 22.2, 19.4 (q, C-21), 17.1 (q, C-19), and 12.4 (q, C-18); positive ESIMS, m/z 401 $[M + H]^+$.

*7β-Hydroxycholesterol (**8**).* Procedure D was followed by using 7-keto-cholesterol (**7**) (100 mg, 0.26 mmol), $CeCl_3{\cdot}7H_2O$ (388 mg, 1.04 mmol), and $NaBH_4$ (25 mg, 0.65 mmol) in MeOH (8 mL). The mixture was stirred at rt for 4 h. The residue was purified by pre-TLC (C/M = 15:1) to give the title compound (**8**) (58 mg, yield: 58%) as a white solid: ^{1}H NMR (600 MHz, CD_3OD+$CDCl_3$) δ 5.24 (1H, s, H-6), 3.72 (1H, d, J = 8.2 Hz, H-7), 3.42 (1H, m, H-3), 2.27−2.18 (2H, m), 2.05−2.02 (1H, m), 1.89−1.78 (4H, m), 1.56−1.25 (10H, m), 1.18−0.99 (9H, m), 1.06 (3H, s, H-19), 0.93 (3H, d, J = 6.5 Hz, H-21), 0.87 (3H, d, J = 6.6 Hz, H-27), 0.86 (3H, d, J = 6.6 Hz, H-26), and 0.71 (3H, s, H-18); ^{13}C NMR (150 MHz, CD_3OD + $CDCl_3$) δ 143.9 (s, C-5), 127.3 (d, C-6), 73.6 (d, C-7), 72.0 (d, C-3), 57.6 (d, C-17), 56.9 (d, C-14), 49.9, 43.9, 42.4, 41.1, 40.9, 40.6, 38.2, 37.4, 37.3, 37.0, 32.2, 29.6, 29.0, 27.2, 24.9, 23.2 (q, C-27), 23.0 (q, C-26), 22.2, 19.5 (q, C-21), 19.4 (q, C-19), and 12.4 (q, C-18); positive ESIMS, m/z 403 $[M + H]^+$.

Synthesis of Sterol Ferulates 13 and 13a. *3-O-(4-Acetoxyferuloyl)-7β-hydroxycholesterol (**28**).* *trans*-4-Acetoxy ferulic acid was prepared followed procedure A by using *trans*-ferulic acid (582 mg, 3.0 mmol), Ac_2O (2.8 mL, 30.0 mmol), and Py (12 mL, 150 mmol). The mixture was incubated at 37 °C overnight. The organic solvent was removed *in vacuo* to give *trans*-4-acetoxy ferulic acid (700 mg, yield: 100%) as a white solid: ^{1}H NMR (600 MHz, $CDCl_3$) δ 7.73 (1H, d, J = 15.9 Hz, H-1), 7.14 (1H, d, J = 8.1 Hz, H-6′), 7.12 (1H, s), 7.06 (1H, d, J = 8.1 Hz, H-6′), 6.39 (1H, d, J = 15.9 Hz, H-2), 3.87 (3H, s, OCH_3-3′), and 2.32 (3H, s, OAc-4′); positive ESIMS, m/z 237 $[M + H]^+$.

Procedure E was followed by using *trans*-4-acetoxy ferulic acid (20 mg, 0.08 mmol), 7β-hydroxycholesterol (31 mg, 0.08 mmol), DCC (50 mg, 0.24 mmol), and DMAP (24 mg, 0.2 mmol) in dry DCM (1 mL). The resulting residue was purified by pre-TLC (H/E = 4:1) to give the title compound (21 mg, yield: 42%) as a white solid: ^{1}H NMR (600 MHz, $CDCl_3$) δ 5.34 (1H, s, H-6), 4.75 (1H, m, H-3), 3.86 (1H, d, J = 8.3 Hz, H-7), 2.48−2.32 (2H, m), 2.15−0.99 (24H, m), 1.06 (3H, s, H-19), 0.93 (3H, d, J = 6.5 Hz, H-21), 0.87 (3H, d, J = 6.5 Hz, H-27), 0.86 (3H, d, J = 6.5 Hz, H-26), 0.70 (3H, s, H-18), and 4-acetyl ferulate [7.62 (1H, d, J = 15.9 Hz, H-7′), 7.10 (1H, d, J = 8.1 Hz, H-6′), 7.09 (1H, s, H-2′), 7.04 (1H, d, J = 8.1 Hz, H-5′), 6.35 (1H, d, J = 15.9 Hz, H-8′), 3.85 (3H, s, OMe-3′), and 2.31 (3H, s, OAc-4′)]; positive ESIMS, m/z 621 $[M + H]^+$.

*3-O-(4-Acetoxyferuloyl)-7-ketocholesterol (**29**).* Procedure E was followed by using *trans*-4-acetoxy ferulic acid (18 mg, 0.075 mmol), 7-keto-cholesterol (20 mg, 0.05 mmol), DCC (31 mg, 0.15 mmol), and DMAP (16 mg, 0.13 mmol) in dry DCM (1 mL). The resulting residue was purified by pre-TLC (H/E = 4:1) to give the title compound (18 mg, yield: 58%) as a white solid: ^{1}H NMR (600 MHz, $CDCl_3$) δ 5.72 (1H, s, H-6), 4.85 (1H, m, H-3), 2.64−2.61 (1H, m), 2.56−2.51 (1H, m), 2.42−2.38 (1H, m), 2.26−2.21 (1H, m), 2.08−1.98 (2H, m), 1.93−1.87 (1H, m), 1.77−1.74 (1H, m), 1.58−1.48 (5H, m), 1.37−0.99 (13H, m), 1.20 (3H, s, H-19), 0.92 (3H, d, J = 6.5 Hz, H-21), 0.85 (3H, d, J = 6.5 Hz, H-27), 0.84 (3H, d, J = 6.5 Hz, H-26), 0.68 (3H, s, H-18), and 4-acetyl ferulate [7.63 (1H, d, J = 15.9 Hz, H-7′), 7.10 (1H, d, J = 8.2 Hz, H-6′), 7.09 (1H, s, H-2′), 7.04 (1H, d, J = 8.2 Hz, H-5′), 7.35 (1H, d, J = 15.9 Hz, H-8′), 3.84 (3H, s, OMe-3′), and 2.31 (3H, s, OAc-4′)]; positive ESIMS, m/z 619 $[M + H]^+$.

*7-Ketocholesterol Ferulate (**13**).* Procedure F was followed by using 3-*O*-(4-acetoxyferuloyl)-7-ketocholesterol (15 mg, 0.024 mmol) and K_2CO_3 (0.52 mg, 0.0049 mmol) in DCM/MeOH (2:1, 3 mL). The residue was purified by pre-TLC (H/E = 3:1) to give the title compound **13** (10 mg, yield: 71%) as a white solid: ^{1}H NMR (600 MHz, $CDCl_3$) δ 5.72 (1H, s, H-6), 4.84 (1H, m, H-3), 2.65−2.51 (2H, m), 2.44−2.37 (1H, m), 2.28−2.20 (1H, m), 2.10−1.85 (4H, m), 1.80−1.48 (3H, m), 1.40−1.20 (8H, m), 1.18−0.99 (6H, m), 1.23 (3H, s, H-19), 0.91 (3H, d, J = 6.5 Hz, H-21), 0.86 (3H, d, J = 6.5 Hz, H-27), 0.85 (3H, d, J = 6.5 Hz, H-26), 0.68 (3H, s, H-18), and ferulate moiety [7.60 (1H, d, J = 15.8 Hz, H-7′), 7.06 (1H, d, J = 8.2 Hz, H-6′), 7.02 (1H, s, H-2′), 6.90 (1H, d, J = 8.2 Hz, H-5′), 6.26 (1H, d, J = 15.8 Hz, H-8′), and 3.92 (3H, s, OMe-3′)]; ^{13}C NMR (150 MHz, $CDCl_3$) δ 202.0 (s, C-7), 164.0 (s, C-5), 126.7 (d, C-6), 72.1 (d, C-3), 54.8, 50.0, 49.8, 45.4, 43.1, 39.5, 38.7, 38.4, 37.9, 36.2, 36.1, 35.7, 28.5, 28.0, 27.5, 26.3, 23.8, 22.8 (q, C-27), 22.6 (q, C-26), 21.2, 18.9 (q, C-21), 17.3 (q, C-19), 12.0 (q, C-18), and ferulate moiety [166.4 (s, C═O, C-9′), 148.0 (s, C-4′), 146.8 (s, C-3′), 145.1 (d, C-7′), 126.9 (s, C-1′), 123.1 (d, C-6′), 115.4 (d, C-8′), 114.7 (d, C-5′), 109.3 (d, C-2′), and 55.9 (q, OMe-3′)]; positive ESIMS, m/z 577 $[M + H]^+$.

*7β-Hydroxycholesterol Ferulate (**13a**).* Procedure F was followed by using 3-*O*-(4-acetoxyferuloyl)-7β-hydroxycholesterol (21 mg, 0.034 mmol) and K_2CO_3 (1.0 mg, 0.0068 mmol) in DCM/MeOH (2:1, 3 mL). The residue was purified by pre-TLC (H/E = 3:1) to give the title compound **13a** (16 mg, yield: 80%) as a white solid: ^{1}H NMR (600 MHz, $CDCl_3$) δ 5.34 (1H, s, H-6), 4.76 (1H, m, H-3), 3.87 (1H, d, J = 7.8 Hz, H-7), 2.48−2.37 (2H, m), 2.05−1.79 (5H, m), 1.70−1.22 (10H, m), 1.18−0.99 (9H, m), 1.09 (3H, s, H-19), 0.93 (3H, d, J = 6.5 Hz, H-21), 0.87 (3H, d, J = 6.5 Hz, H-27), 0.86 (3H, d, J = 6.5 Hz, H-26), 0.70 (3H, s, H-18), and ferulate moiety [7.60 (1H, d, J = 15.9 Hz, H-7′), 7.06 (1H, dd, J = 8.2, 1.6 Hz, H-6′), 7.03 (1H, d, J = 1.6 Hz, H-2′), 6.91 (1H, d, J = 8.2 Hz, H-5′), 6.27 (1H, d, J = 15.9 Hz, H-8′), and 3.92 (3H, s, OMe-3′)]; ^{13}C NMR (150 MHz, $CDCl_3$) δ 142.5 (s, C-5), 126.3 (d, C-6), 73.4 (d, C-7), 73.3 (d, C-3), 55.8 (d), 55.4 (d), 48.2, 42.9, 40.8, 39.6, 39.5, 37.8, 36.7, 36.6, 36.2, 35.7, 28.5, 28.0, 27.9, 26.4, 23.8, 22.8 (q, C-27), 22.6 (q, C-26), 21.0, 19.2 (q, C-19), 18.8 (q, C-19), 11.8 (q, C-18), and ferulate moiety [166.6 (s, C═O, C-9′), 147.9 (s, C-4′), 146.7 (s, C-3′), 144.7 (d, C-7′), 127.0 (s, C-1′), 123.1 (d, C-6′), 115.9 (d, C-8′), 114.7 (d, C-5′), 109.3 (d, C-2′), and 55.9 (q, OMe-3′)]; positive ESIMS, m/z 579 $[M + H]^+$.

Synthesis of Aza-oxysterols 7a and 8a. *Pregnenolone Acetate (**30**).* Procedure A was followed by using pregnenolone (1.58 g, 10.0 mmol) and Ac_2O (4.7 mL, 50.0 mmol) in Py (20 mL), giving the title compound (3.58 g, yield: 100%) as a white solid: ^{1}H NMR (600 MHz, $CDCl_3$) δ 5.35 (1H, m, H-6), 4.32 (1H, m, H-3), 2.58−2.52 (2H, m), 2.39−2.31 (1H, m), 2.23−2.12 (1H, m), 2.12 (3H, s, H-21), 2.04 (3H, s, OAc-3), 2.0−1.2 (16H, m), 1.37 (3H, s, H-19), and 0.64 (3H, s, H-18); positive ESIMS, m/z 359 $[M + H]^+$.

*20-Aza-cholesterol Acetate (**31**).* Pregnenolone acetate (358 mg, 1.0 mmol) was dissolved in 10 mL of methanol, and isopentylamine (522 mg, 6.0 mmol) was added. pH value of the solution was adjusted to around 6 by adding HOAc (1.0 mL). Then, 10 mL of THF and $NaBH_3CN$ (82 mg, 1.1 mmol) in methanol (2 mL) were added, and the reaction mixture was stirred under reflux overnight. After evaporation *in vacuo*, the resulted residue was resuspended in 10 mL of water, and the pH was adjusted to 8 by 10% Na_2CO_3 solution. The solution was extracted with DCM (10 mL × 3), washed with water (10 mL) and brine (10 mL), dried over Na_2SO_4, and concentrated under reduced pressure. The residue was purified by CC (H/E = 5:1; H/E/TEA = 5:1:0.1 and 3:1:0.1) to give the title compound (446 mg, yield: 85%) as a colorless gum: ^{1}H NMR (600 MHz, $CDCl_3$) δ 5.37 (1H, m, H-6), 4.60 (1H, m, H-3), 2.90−2.75 (1H, m, H-20), 2.38−2.28 (2H, m, H-23), 2.05 (3H, s, OAc-3), 2.02−1.92 (1H, m), 1.90−1.80 (2H, m), 1.75−1.41 (12H, m), 1.40−1.10 (8H, m), 1.01 (3H, s, H-19), 0.98−0.84 (9H, m, H-21, H-26 and H-27), and 0.73 (3H, s, H-18); positive ESIMS, m/z 430 $[M + H]^+$.

*7-Keto-20-aza-cholesterol Acetate (**32**).* Procedure B was followed by using 20-aza-cholesterol acetate (446 mg, 1.04 mmol), CrO_3 (1.56 g, 15.6 mmol), and dimethylpyrazole (1.50 g, 15.6 mmol) in dry DCM (50 mL). The mixture was stirred at rt for 6 h. After addition of EA, the mixture was filtered through a short pad of Celite eluted by a mixture of EA and TEA (30:1), and the filtration was concentrated *in vacuo*. The resulted residue was purified by CC (H/E = 5:1; H/E/TEA = 5:1:0.1 and 3:1:0.1) to give the title compound (314 mg, yield: 68%) as a yellow gum: ^{1}H NMR (600 MHz, $CDCl_3$) δ 5.70 (1H, m, H-6), 4.71 (1H, m, H-3), 2.98−2.80 (1H, m, H-20), 2.58−2.41 (2H, m, H-23), 2.30−2.10 (2H, m), 2.05 (3H, s, OAc-3), 2.02−1.20 (19H, m), 1.18 (3H, s, H-19), 0.98−0.84 (9H, m, H-21, H-26 and H-27), and 0.75 (3H, s, H-18); positive ESIMS, m/z 444 $[M + H]^+$.

*7-Keto-20-aza-cholesterol (**7a**).* Procedure C was followed by using 7-keto-20-aza-cholesterol acetate (314 mg, 0.71 mmol) and

DOI: 10.1021/jf506361r
J. Agric. Food Chem. 2015, 63, 2264−2276

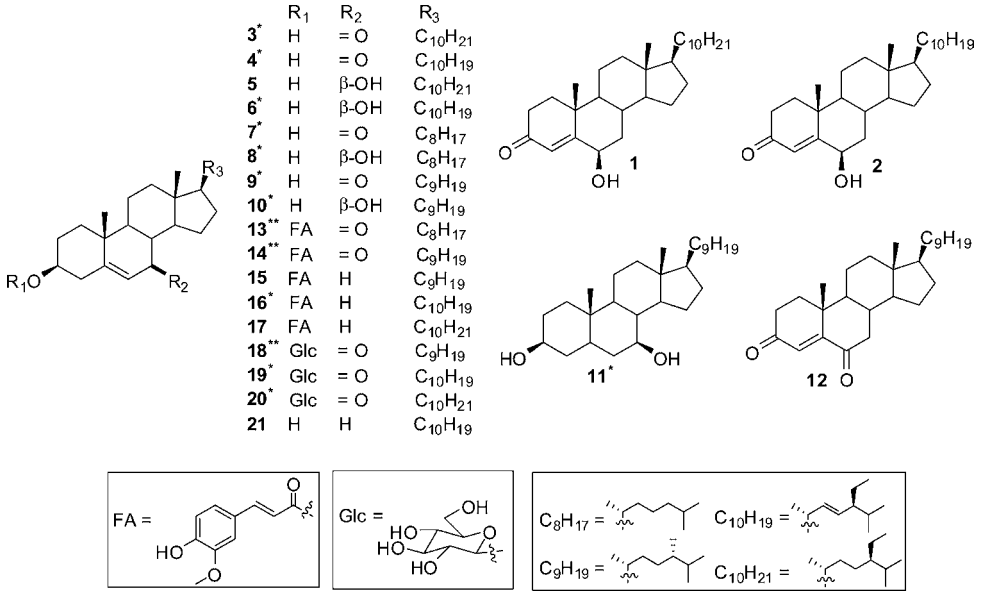

Figure 1. Structures of steroids **1**−**21** identified from wheat bran extract. *Reported in wheat bran for the first time. **New compounds.

LiOH (68 mg, 2.84 mmol) in THF/MeOH/H_2O (3:1:1, 5 mL). The mixture was stirred at rt for 1 h. After removal of the organic solvent, the residue was partitioned between water (5 mL) and DCM (5 mL). DCM extracts were washed with water and brine, dried over Na_2SO_4, and concentrated *in vacuo*. The residue was purified by CC (H/E/TEA = 5:1:0.5, 3:1:0.5, 2:1:0.5, and 1.5:1:0.5) to give the title compound (**7a**) (240 mg, yield: 85%) as a white solid: ^{1}H NMR (700 MHz, $CDCl_3$) δ 5.69 (1H, s, H-6), 3.67 (1H, m, H-3), 2.97−2.86 (1H, m, H-20), 2.53−2.49 (2H, m, H-23), 2.41−2.38 (1H, m), 2.25−2.21 (1H, m), 1.96−1.87 (2H, m), 1.85−1.77 (2H, m), 1.70−1.66 (2H, m), 1.64−1.58 (2H, m), 1.57−1.50 (1H, m), 1.45−1.21 (10H, m), 1.18 (3H, s, H-19), 0.94 (3H, d, J = 6.5 Hz, H-21), 0.93 (6H, d, J = 6.5 Hz, H-26/27), and 0.78 (3H, s, H-18); positive ESIMS, m/z 402 $[M + H]^+$.

*7β-Hydroxy-20-aza-cholesterol (**8a**).* Procedure D was followed by using 7-keto-20-aza-cholesterol (**7a**) (284 mg, 0.71 mmol), $CeCl_3 \cdot 7H_2O$ (1.59 g, 4.26 mmol), and $NaBH_4$ (108 mg, 2.84 mmol) in MeOH (10 mL) at −10 °C. The mixture was stirred at −10 °C for 5 min and quenched with water (1 mL). After removal of most of the organic solvent, the residue was partitioned between water (10 mL) and DCM (10 mL). DCM extracts were washed, dried, and concentrated. The resulted residue was purified by CC (H/E/TEA = 5:1:0.1, 2:1:0.1, 2:1:0.5, and 1:1:0.5) to give the title compound (**8a**) (100 mg, yield: 35%) as a white solid: ^{1}H NMR (700 MHz, $CDCl_3$) δ 5.27 (1H, s, H-6), 3.83 (1H, d, J = 8.1 Hz, H-7), 3.54 (1H, m, H-3), 2.99 (1H, m, H-20), 2.88 (1H, m, H-23a), 2.68 (1H, m, H-23b), 2.35−2.31 (1H, m), 2.28−2.22 (1H, m), 1.98−1.83 (5H, m), 1.66−1.57 (4H, m), 1.53−1.46 (4H, m), 1.42−1.30 (4H, m), 1.25−1.16 (4H, m), 1.16 (3H, s, H-19), 0.94 (3H, d, J = 6.7 Hz, H-21), 0.93 (3H, d, J = 6.5 Hz, H-27), 0.92 (3H, d, J = 6.5 Hz, H-26), and 0.73 (3H, s, H-18); ^{13}C NMR (175 MHz, $CDCl_3$) δ 143.5 (s, C-5), 125.6 (d, C-6), 73.3 (d, C-7), 71.3 (d, C-3), 63.2 (d, C-20), 55.2 (d, C-17), 48.1, 45.9, 43.5, 42.9, 41.7, 40.6, 37.7, 37.5, 37.0, 36.6, 31.5, 28.2, 26.7, 26.3, 22.6, 22.4 (q, C-26/27), 20.8 (q, C-21), 19.1 (q, C-19), and 12.7 (q, C-18); positive ESIMS, m/z 404 $[M + H]^+$.

LC/MS Analysis. LC/MS analysis was carried out with a Thermo-Finnigan Spectra System consisting of an Accela high speed MS pump, an Accela refrigerated autosampler, and an LCQ Fleet ion trap mass detector (Thermo Electron, San Jose, CA) incorporated with an electrospray ionization (ESI) interface. A Gemini-NX C_{18} column (150 mm × 3.0 mm i.d., 5 μm, Phenomenex) was used to analyze authentic sterol oxides and the sterol-enriched fraction with a flow rate of 0.3 mL/min. The binary mobile phase system consisted of water with 0.2% acetic acid (AA) as phase A and methanol with 0.2% AA as phase B. The column was eluted by a gradient progress (80 to 90% B from 0 to 10 min; 90 to 95% B from 10 to 20 min; 95−99% B from 20 to 30 min; 99−100% B from 30 to 45 min; 100% B from 45 to 65 min, and then 80% B from 65 to 70 min). The injection volume was 10 μL for each sample. The column temperature was maintained at 20 °C. To optimize the mass spectrometric parameters, each standard dissolved in methanol (10 μM) was infused in the ESI source by a syringe pump (flow rate 10 μL/min) and analyzed in positive ion mode. The optimized parameters for analysis of oxyphytosterols are capillary voltage 16 V, spray voltage 4.6 kV, tube lens offset 70 V, capillary temperature 260 °C, and sheath gas (nitrogen) flow rate 25 (arbitrary units). The structural information on compounds **1**−**21** were obtained by tandem mass spectrometry (MS/MS) through collision-induced dissociation (CID) with a relative collision energy setting of 35%. Data acquisition was performed with Xcalibur version 2.0 (Thermo Electron, San Jose, CA).

Nuclear Magnetic Resonance (NMR). ^{1}H, ^{13}C NMR, and two-dimensional (2-D) NMR spectra were recorded on a Bruker AVANCE 600 or 700 MHz spectrometer (Bruker Inc., Silberstreifen, Rheinstetten, Germany). Compounds were analyzed in $CDCl_3$, CD_3OD, or pyridine-d_5. Multiplicities are indicated by s (singlet), d (doublet), t (triplet), q (quartet), and br (broad). The ^{13}C NMR spectra are proton decoupled.

MTT Assay. Cell growth inhibition was determined by a 3-(4,5-dimethylthiazol-2-yl)-2,5-diphenyltetrazolium bromide (MTT) colorimetric assay.[21] Human colon cancer cells HCT-116 and HT-29 were plated in 96-well microtiter plates with 5000 cells/well and allowed to attach for 24 h at 37 °C. The test compounds in dimethyl sulfoxide (DMSO) were added to cell culture medium to the desired final concentrations (final DMSO concentrations for control and treatments were 0.1%). After the cells were cultured for 24 h, the medium was aspirated, and cells were treated with 200 μL fresh medium containing 2.41 mmol/L MTT. After incubation for 3 h at 37 °C, the medium containing MTT was aspirated, 100 μL of DMSO was added to solubilize the formazan precipitate, and plates were shaken gently for an hour at room temperature. Absorbance values were derived from the plate reading at 550 nm on a Biotek microtiter plate reader (Winooski, VT). The reading reflected the number of viable cells and was expressed as a percentage of viable cells in the control. Both HCT-116 and HT-29 cells were cultured in McCoy's 5A medium. All of the above media were supplemented with 10% fetal bovine serum, 1% penicillin/streptomycin, and 1% glutamine, and the cells were kept in a 37 °C incubator with 95% humidity and 5% CO_2.

Apoptotic Assay. The Cell Death Detection ELISA (enzyme-linked immunoabsorbant assay) Plus kit from Roche (Mannheim, Germany) was used. HCT-116 and HT-29 cells were seeded in 96-well plates at

DOI: 10.1021/jf506361r
J. Agric. Food Chem. 2015, 63, 2264−2276

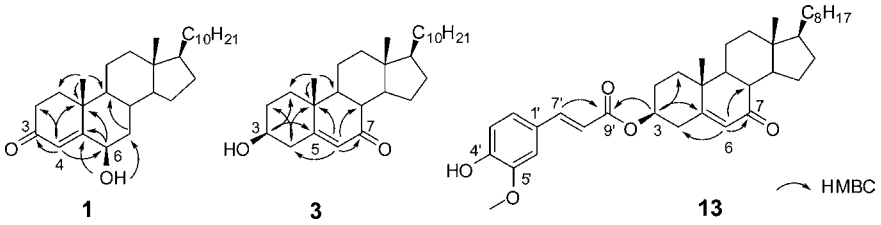

Figure 2. Key HMBC correlations (↷) of compounds **1**, **3**, and **13**.

Table 1. ESI-MS and ESI-MS^n (n = 2−3) Fragment Ions of Steroids (1−21) in Wheat Bran

no.	Rt (min)	$[M + H]^+$	MS^2	MS^3
1	24.8	429	**429**/411 $[M - H_2O + H]^+$ (B), 393 $[M - 2H_2O + H]^+$	**411**/393 (B), 295, 271, 253, 185, 171, 155
				393/309, 281 (B), 269, 253, 239, 215
2	24.5	427	**427**/409 $[M - H_2O + H]^+$ (B), 391 $[M - 2H_2O + H]^+$, 271	**409**/223
				391/223
3	24.1	429	**429**/411 $[M - H_2O + H]^+$ (B), 393 $[M - 2H_2O + H]^+$	**411**/393 (B), 315, 295, 271, 253, 175
				393/337, 295, 267, 253 (B), 239, 225, 199, 157
4	22.5	427	**427**/409 $[M - H_2O + H]^+$ (B), 391 $[M - 2H_2O + H]^+$, 271	**409**/391 (B), 293, 279, 251, 237, 227, 215
				391/335, 293, 251 (B), 237, 211, 197, 183, 159
5	23.7	431	**431**/413 $[M - H_2O + H]^+$ (B), 395 $[M - 2H_2O + H]^+$	**413**/395 (B), 287, 255
				395/311, 283, 255, 241 (B), 227, 213, 185, 173
6	21.6	429	**429**/411 $[M - H_2O + H]^+$ (B), 393 $[M - 2H_2O + H]^+$	**411**/393 (B), 350, 295, 271, 255, 175
				393/267, 239 (B), 201, 185
7	20.8	401	**401**/383 $[M - H_2O + H]^+$ (B), 365 $[M - 2H_2O + H]^+$	**383**/365 (B), 271, 253, 241, 163
				365/295, 281, 253 (B), 239, 225, 211, 199, 157
8	20.7	403	**403**/385 $[M - H_2O + H]^+$ (B), 367 $[M - 2H_2O + H]^+$	**385**/367 (B), 261, 247, 214, 159
				367/241, 201 (B), 159
9	22.2	415	**415**/397 $[M - H_2O + H]^+$ (B), 379 $[M - 2H_2O + H]^+$	**397**/379 (B), 271, 253
				379/323, 295, 267, 253 (B), 239, 225, 199, 157
10	22.1	417	**417**/399 $[M - H_2O + H]^+$ (B), 381 $[M - 2H_2O + H]^+$	**399**/381 (B)
				381/311, 241 (B), 229, 159
11	19.6	413	**413**/395 $[M - H_2O + H]^+$ (B), 377 $[M - 2H_2O + H]^+$	**395**/377 (B)
				377/349, 293, 277, 251 (B), 157
12	21.7	419	**419**/401 $[M - H_2O + H]^+$ (B), 383 $[M - 2H_2O + H]^+$, 274	**401**/383 (B), 261
				383/285, 255, 243 (B), 213
13	26.8	577	**577**/383 $[M - 194 + H]^+$ (B), 251, 191	**383**/365 (B), 301, 271, 257, 247, 217, 197, 157
14	28.2	591	**591**/397 $[M - 194 + H]^+$, 251, 219, 167	**397**/379 (B), 301, 287, 271, 253, 203
15	25.7	577	**577**/383 $[M - 194 + H]^+$	**383**/301, 273, 257, 243, 229, 215, 203, 157
16	26.1	589	**589**/395 $[M - 194 + H]^+$	**395**/353, 339, 311, 297, 255, 159
17	27.6	591	**591**/397 $[M - 194 + H]^+$, 251, 219, 191, 159	**397**/341, 315, 285, 257, 243, 203, 161
18	17.4	577	**577**/559, 415 $[M - 162 + H]^+$, 397 $[M - 180 + H]^+$ (B) 397/379 (B), 281, 271	**415**/397
19	17.6	589	**577**/571, 427 $[M - 162 + H]^+$, 409 $[M - 180 + H]^+$ (B)	**409**/391 (B), 376, 349, 335, 285, 273, 255, 223
20	18.9	591	**591**/573, 429 $[M - 162 + H]^+$, 397 $[M - 180 + H]^+$ (B), 371	**411**/393 (B), 351, 309, 287, 269
21	17.9	413	**413**/395, 301 (B), 201, 189, 171, 159	**395**/349, 325, 311 (B), 215, 175

3000 cells/well and incubated at 37 °C in 5% CO_2 incubator. After 24 h, fresh media supplemented with DMSO (control), **5**, **6**, **7**, or **8** (5, 10, 20, or 30 μM; final DMSO concentration for control and treatments was 0.1%) were added to the wells. After 48 h, the microplate was centrifuged for 10 min at 1200 rpm, and the supernatant was removed. Then, 200 μL of the lysis buffer was added in each well, and the microplate was incubated for 30 min at room temperature. The plate was then centrifuged for 10 min at 1200 rpm, and 20 μL of the supernatant was transferred to streptavidin-coated microwells. ELISA assay was performed according to manufacturer's instruction. Absorbance in each well was measured at 405 nm in absorbance units (AU), and the enrichment factor (EF) in small nucleosomes was calculated with the formula EF = $AU_{(treated)}/AU_{(DMSO)}$. The experiment was repeated independently to confirm the results.

Statistical Analysis. For simple comparisons between two groups, two-tailed Student's t-test was used. A p-value of less than 0.05 was considered statistically significant in all the tests.

RESULTS

Structural Elucidation of Oxyphytosterols 1−4. The chemical investigation on the sterol-enriched fraction yielded two unusual 3-ketophytosterols **1** and **2**, and two 7-ketophytosterols **3** and **4** (Figure 1). Compound **1** had a molecular formula of $C_{29}H_{48}O_2$ based on positive ESI-MS at m/z 411 $[M - H_2O + H]^+$ and NMR data. One tertiary proton adjacent to oxygen atom, one olefinic proton and six methyl groups in the ^{1}H NMR spectrum of **1**, and a ketone group, four double bond signals, and an oxygenated tertiary carbon in the ^{13}C NMR spectrum of **1**, suggested **1** is oxyphytosterol.[22]

DOI: 10.1021/jf506361r
J. Agric. Food Chem. 2015, 63, 2264−2276

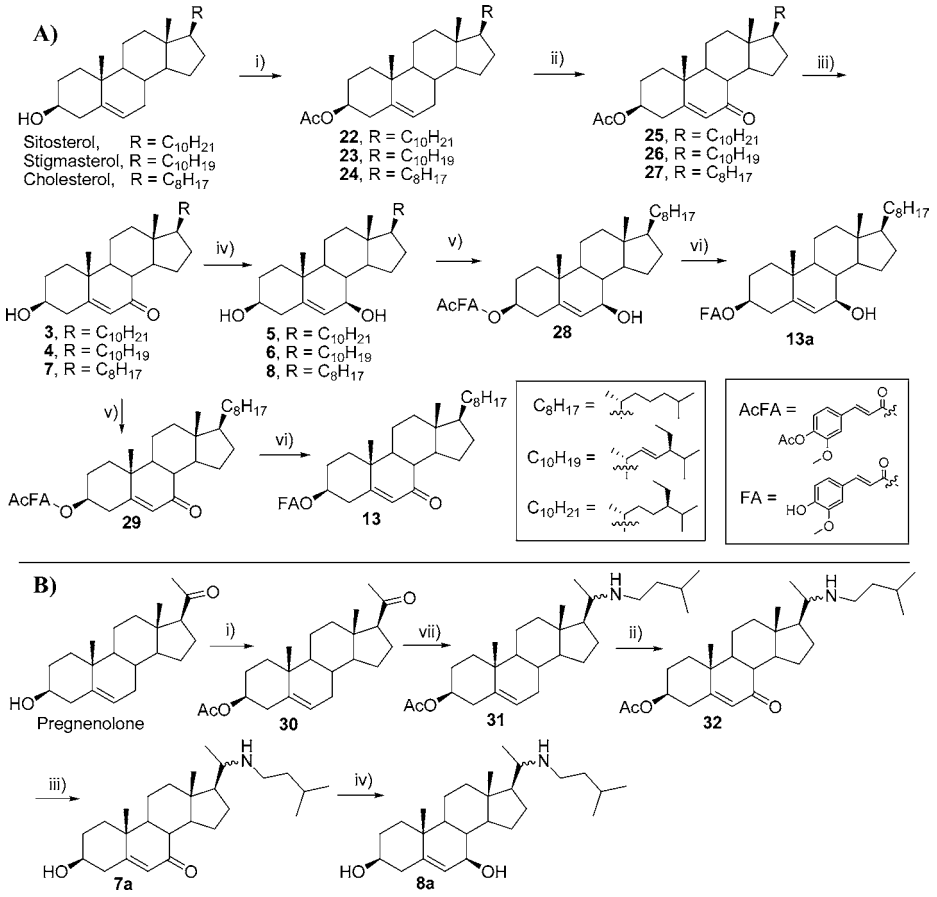

Figure 3. Synthesis of (A) sterol oxides **3**–**8** and oxysterol ferulates **13** and **13a**, and (B) 20-aza-oxysterols **7a** and **8a**. Reagents and conditions: (i) Ac_2O, Py, 37 °C, 18 h; (ii) CrO_3, 3,5-dimethylpyrazole, DCM, −20 °C to rt; (iii) LiOH, THF/MeOH/H_2O, rt; (iv) $CeCl_3{\cdot}7H_2O$, $NaBH_4$, MeOH; (v) 4-acetoxy ferulic acid, DCC, DMAP, DCM, 0 °C to rt, 18 h; (vi) K_2CO_3, DCM/MeOH, rt; (vii) isopentylamine, $NaBH_3CN$, HOAc, MeOH/THF, reflux, 18 h.

Heteronuclear multiple bond correlation (HMBC) established a partial structure of 4-en-6-ol-3-one in **1** (Figure 2). The fragment ion at m/z 253/393/429 $[M - 2H_2O - C_{10}H_{20} + H]^+$ in the MS^3 spectra of **1** (Table 1), corresponding to the loss of two water molecules followed by the cleavage of the side chain, further confirmed **1** as being stigmast-4-en-6β-ol-3-one, as previously described in extracts of wheat straw.[23]

Compound **2** possessed a molecular formula of $C_{29}H_{46}O_2$ based on positive ESI-MS at m/z 409 $[M - H_2O + H]^+$ and NMR data. Its ^1H and ^{13}C NMR data were very similar to those of **1** except for additional olefinic signals [δ_H 5.09 (1H, dd, J = 15.2, 8.8 Hz) and δ_H 5.24 (1H, dd, J = 15.2, 8.8 Hz); and δ_C 130.0 (d) and δ_C 139.2 (s)] in **2**, indicating **2** is stigmast-4,22-dien-6β-ol-3-one, as previously described in extracts of wheat straw.[23]

Compound **3** had the same molecular formula of $C_{29}H_{48}O_2$ to that of **1** based on positive ESI-MS at m/z 411 $[M - H_2O + H]^+$ and NMR data. The ^1H and ^{13}C NMR spectra of **3** were similar to those of **1**, suggesting **3** is also an oxyphytosterol. HMBC correlations established a partial structure of 5-en-3-ol-7-one in **3** (Figure 2). The fragment ion at m/z 253/393/429 $[M - 2H_2O - C_{10}H_{20} + H]^+$ in the MS^3 spectra of **3**, corresponding to the loss of two water molecules followed by the side chain, further confirmed **3** as being stigmast-5-en-3β-ol-7-one, namely 7-ketositosterol, as previously reported from marine sponges.[24] This is the first report of 7-ketositosterol **3** in WB.

Compound **4** had a molecular formula of $C_{29}H_{46}O_2$ based on positive ESI-MS at m/z 409 $[M - H_2O + H]^+$ and NMR data. Its ^1H and ^{13}C NMR data were very similar to those of **3** except for additional olefinic signals [δ_H 5.01 (1H, dd, J = 15.1, 8.7 Hz) and δ_H 5.15 (1H, dd, J = 15.1, 8.7 Hz); and δ_C 130.3 (d) and δ_C 139.0 (d)] in **4**, indicating **4** is an oxidation product of stigmasterol. Fragment ion at m/z 251/391/427 $[M - 2H_2O - C_{10}H_{20} + H]^+$ in the MS^3 spectra of **4** (Table 1), following the same fragmentation patterns as **3**, established **4** as being stigmast-5,22-dien-3β-ol-7-one, namely 7-ketostigmasterol, as previously described elsewhere.[25] This is the first report of 7-ketostigmasterol **4** in WB as well.

Synthesis of Sterol Oxides 3–8, Sterol Ferulates 13 and 13a, and Aza-oxysterols 7a and 8a. Sterol oxides **3**–**8** were synthesized in house in quantities, following the method of McCarthy with some modifications (Figure 3A).[26] Briefly, acetylation of sterols yielded sterol acetates **22**–**24**. The acetates were treated by the combination of chromium trioxide and dimethylpyrazole to give 7-ketosterol acetates **25**–**27**. After hydrolysis using lithium hydroxide, 7-ketosterols **3**, **4**, and **7** were obtained. Luche reduction of 7-ketosterols afforded 7β-hydroxysterols **5**, **6**, and **8**. Coupling reaction of 7-ketocholesterol **7** with 4-acetoxy ferulic acid utilizing *N*,*N*′-dicyclohexylcarbodiimide (DCC) and 4-dimethylaminopyridine (DMAP) followed by deacetylation yielded 7-ketocholesterol ferulate **13**. Likewise, 7β-hydroxycholesterol ferulate **13a** was obtained from 7β-hydroxycholesterol **8**. The synthesis of aza-

DOI: 10.1021/jf506361r
J. Agric. Food Chem. 2015, 63, 2264−2276

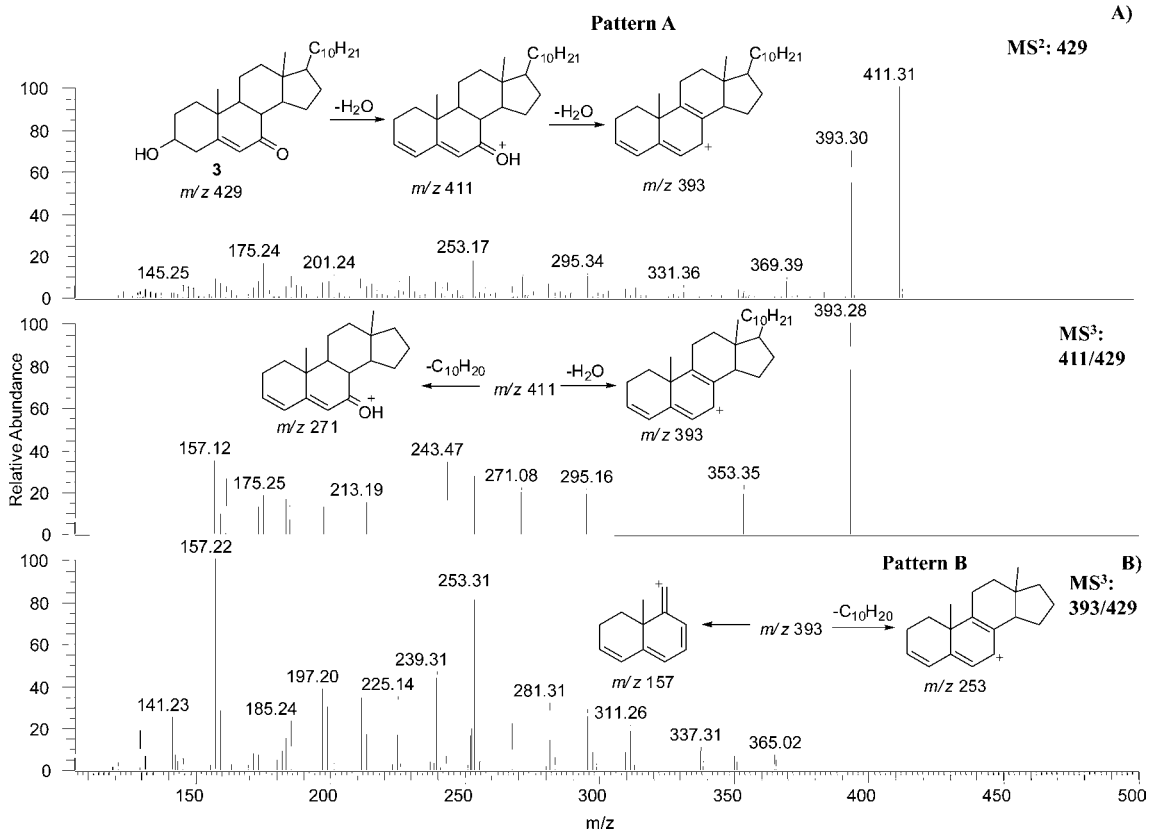

Figure 4. ESI/MS^n (n = 2−3) spectra and fragmentation patterns of compound **3**. (A) Fragmentation pattern A: loss of two water molecules from parent ion forms a stable resonance structure with the positive charge at the C-7 position in MS^2 spectra. (B) Fragmentation pattern B: cleavage of the side chain at the C17−C20 bond in the fragments obtained from pattern A via hydrogen shifts and inductive cleavages produces a typical daughter ion in MS^3 spectra.

oxysterols **7a** and **8a** was illustrated in Figure 3B. Reductive amination of pregnenolone acetate **30** with isopentylamine catalyzed by $NaBH_3(CN)$ in MeOH/THF at pH 6 produced 20-aza-cholesterol acetate **31**.[27] Oxidation of **31** by chromium trioxide followed by treatment with lithium hydroxide afforded 7-keto-20-aza-cholesterol **7a** with a yield of 60%. Luche reduction of **7a** gave 7β-hydroxyl-20-aza-cholesterol **8a** with a yield of 35%. This is the first report of synthesis for 7-keto-20-aza-cholesterol **7a** and 7β-hydroxy-20-aza-cholesterol **8a**.

Characterization of Synthetic Sterol Oxides 5−8, Sterol Ferulates 13 and 13a, and Aza-oxysterols 7a and 8a. Compound **5** was reduced from 7-ketositosterol **3**. Its molecular ion at m/z 431 $[M + H]^+$ is two mass units higher than that of **3**, indicating **5** is the reduction product of **3**. The appearance of one additional signal adjacent to oxygen atom [δ_H 3.72 (1H, d, J = 8.0 Hz) and δ_C 73.7 (d)] in **5** confirmed the conversion of the carbonyl group in **3** into the hydroxyl group in **5**. The fragment ion at m/z 241/395/431 $[M - 2H_2O - C_{10}H_{20} - CH_2 + H]^+$ in the MS^3 spectra of **5** (Table 1), corresponding to the loss of two water molecules followed by the side chain and one methyl group, further supported that **5** was stigmast-5-en-3β,7β-diol, namely, 7β-hydroxysitosterol, as previously reported in wheat flour.[18] Likewise, compound **6** was the product of the reduction of **4** and subsequently established as being stigmast-5,22-dien-3β,7β-diol, namely, 7β-hydroxystigmasterol, as previously reported elsewhere.[25]

Compound **7**, owning a molecular formula of $C_{27}H_{44}O_2$ based on positive ESI-MS at m/z 383 $[M - H_2O + H]^+$ and NMR data, was synthesized from cholesterol. Its ^{1}H and ^{13}C NMR data were very similar to those of **3**, suggesting **7** is an oxidation product of cholesterol. The fragment ion at m/z 253/365/401 $[M - 2H_2O - C_8H_{16} + H]^+$ in the MS^3 spectra of **7** (Table 1), in agreement with the loss of two water molecules followed by the side chain, provided **7** as cholest-5-en-3β-ol-7-one, namely, 7-ketocholesterol, as previously described in marine sponges.[24] Likewise, compound **8**, as the reduction product of **7**, was elucidated as being cholest-5-en-3β,7β-diol, namely 7β-hydroxycholesterol, as previously reported in marine sponges.[24]

Compound **13**, possessing a molecular formula of $C_{37}H_{52}O_5$ based on its positive ESI-MS at m/z 383 $[M - C_{10}H_{10}O_4 + H]^+$ and NMR data, was a ferulic acid conjugate of **7**. HMBC correlation between H-3 (δ_H 4.84) and the carbonyl group (C-9′) of ferulate (δ_C 166.4) established the linkage at C-3 between ferulate moiety and 7-ketocholesterol (Figure 2). The fragment ion at m/z 383/577 $[M - C_{10}H_{10}O_4 + H]^+$ in the MS^2 spectra of **13**, corresponding to the loss of a ferulic acid moiety, further confirmed **13** as being 7-ketocholesterol ferulate. Compound **13a** was synthesized by the coupling reaction of ferulic acid with **8**. Its NMR spectra were similar to those of **13** except for an additional oxygenated signal [δ_H 3.87 (1H, d, J = 7.8 Hz) and δ_C 73.4 (d)], coinciding **13a** being 7β-hydroxycholesterol ferulate.

Compound **7a**, having a molecular formula of $C_{26}H_{43}NO_2$ based on its positive ESI-MS at m/z 402 $[M + H]^+$ and NMR data, was synthesized from pregnenolone through four steps. The ^{1}H NMR spectra of **7a** was similar to that of 7-ketocholesterol **7**. The major difference is the appearance of

DOI: 10.1021/jf506361r
J. Agric. Food Chem. 2015, 63, 2264−2276

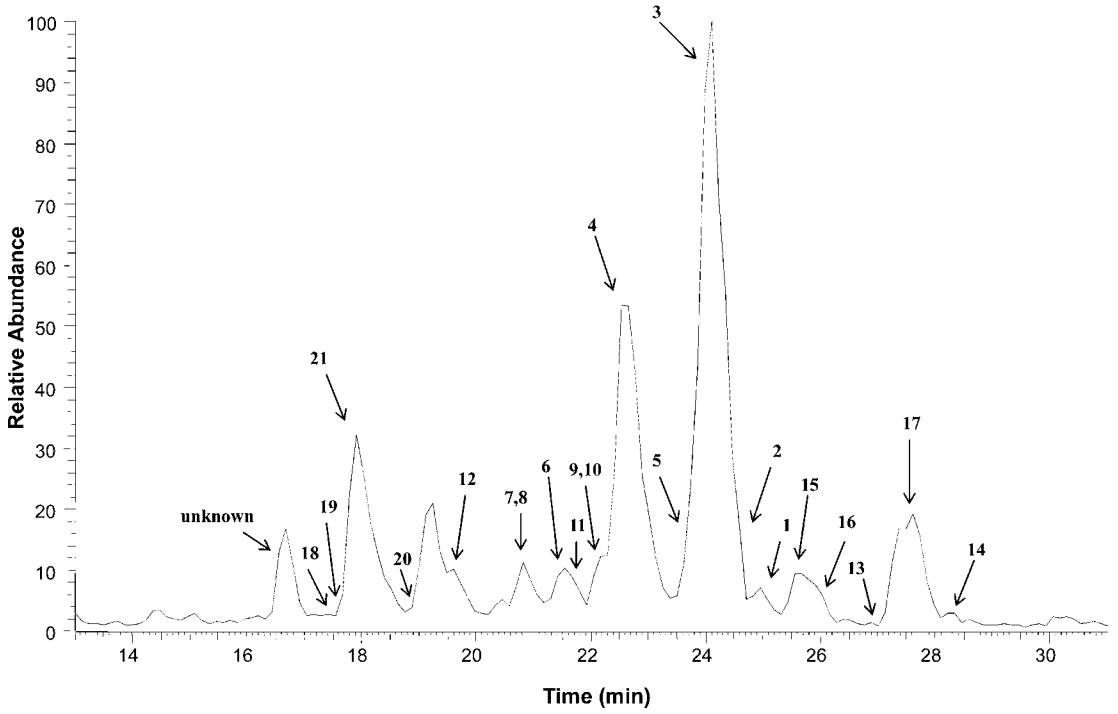

Figure 5. Chemical profile of steroids **1**–**21** in wheat bran extract generated from positive HPLC-ESI/MS^n (n = 2–3).

two multiplets at δ_H 2.97–2.86 (1H, m, H-20) and δ_H 2.53–2.49 (2H, m, H-23) in **7a** compared to those of **7**, indicating **7a** is 7-keto-20-aza-cholesterol. Compound **8a** was the reductive product of **7a**. The ^1H and ^{13}C NMR spectra of **8a** showed an additional oxygenated signal [δ_H 3.83 (1H, d, J = 8.1 Hz) and δ_C 73.3 (d)] compared to **7a**, suggesting **8a** is 7β-hydroxy-20-aza-cholesterol.

Fragmentation Patterns of Authentic Sterol Oxides. There are two major fragmentation patterns of the authentic 7-ketosterols **3**, **4**, and **7** (Table 1) under ESI positive ionization mode, as exemplified by compound **3** in Figure 4, pattern A): loss of two water molecules from parent ion forms a stable resonance structure with the positive charge at C-7 position in MS^2 spectra (Figure 4A), and pattern B): cleavage of the side chain at the C17–C20 bond in the fragments obtained from pattern A via hydrogen shifts and inductive cleavages produces a typical daughter ion in MS^3 spectra (Figure 4B). These fragmentation patterns are consistent with the conclusions that Jiang et al. reported previously.[28] The observation from 7β-hydroxysterols **5**, **6**, and **8** led to a characteristic fragmentation pattern C: the cleavage of the side chain followed by an additional methyl group in the fragments obtained from pattern A gives characteristic tertiary daughter ions in MS^3 spectra (Table 1).

Identification of Steroids 1–21 in WB by LC-ESI/MS^n Spectra. Oxyphytosterols **1**–**4** were isolated from WB extract and identified by NMR experiments. Sterol oxides **5**–**8** and **13** in WB were recognized by comparison of their retention times and tandem mass spectra with those of the synthetic standards (Table 1). Compounds **9**–**12** and **14**–**20** were tentatively elucidated in WB based on the analysis of their tandem mass spectra, referring to fragmentation patterns observed from known standards (Table 1 and Figure 4). Stigmasterol **21** was confirmed in WB by comparison with its commercial authentic standard.

As per the knowledge obtained above, compound **9** had two peak ions with loss of H_2O at m/z 397 $[M - H_2O + H]^+$ and 379 $[M - 2H_2O + H]^+$ in its MS^2 spectra (pattern A), and one daughter ion with loss of the alkyl side chain at m/z 253 $[M - 2H_2O - C_9H_{18} + H]^+$ in its MS^3 spectra (pattern B) (Table 1), indicating that **9** is campest-5-en-3β-ol-7-one, namely 7-ketocampesterol.[29] Compound **10**, with two peak ions at m/z 399 $[M - H_2O + H]^+$ and 381 $[M - 2H_2O + H]^+$ in its MS^2 spectra (pattern A), and one major daughter ion at m/z 241 $[M - 2H_2O - C_9H_{18} - CH_2 + H]^+$ in its MS^3 spectra (pattern C) (Table 1), was identified as campest-5-en-3β,7β-diol, namely, 7β-hydroxycampesterol.[29] Similarly, compound **11**, having two peak ions at m/z 395 $[M - H_2O + H]^+$ and 377 $[M - 2H_2O + H]^+$ in its MS^2 spectra (pattern A), and one tertiary ion at m/z 251 $[M - 2H_2O - C_9H_{18} + H]^+$ in its MS^3 spectra (pattern B), was proposed as ergost-4-en-3,6-dione, as reported previously in wheat straw.[30] Compound **12** owned two peak ions at m/z 401 $[M - H_2O + H]^+$ and 383 $[M - 2H_2O + H]^+$ in its MS^2 spectra (pattern A), and one daughter ion at m/z 243 $[M - 2H_2O - C_9H_{18} - CH_2 + H]^+$ in its MS^3 spectra (pattern C), and was tentatively suggested as ergostane-3β,7β-diol, as described previously elsewhere.[31]

Compound **14**, with a base peak at m/z 397 $[M - C_{10}H_{10}O_4 + H]^+$ in its MS^2 spectra and a major ion at m/z 379 $[M - C_{10}H_{10}O_4 - H_2O + H]^+$ in its MS^3 spectra, had similar fragmentation patterns (loss of ferulic acid moiety) as that of analogue **13** (Table 1), indicating **14** is a sterol ferulate. The molecular weight of **14** at m/z 591 $[M + H]^+$ was 14 mass units higher than that of **13**, suggesting that **14** is 7-ketocampesterol ferulate, which has never been reported before. In a similar manner, compounds **15**–**17**, with major peak ions at m/z 383 $[M - C_{10}H_{10}O_4 + H]^+$, 395 $[M - C_{10}H_{10}O_4 + H]^+$, and 397 $[M - C_{10}H_{10}O_4 + H]^+$ in their respective MS^2 spectra, corresponding to loss of ferulic acid moiety, were identified as campesterol ferulate **15**, stigmasterol ferulate **16**, and sitosterol ferulate **17**, respectively. Of these, campesterol ferulate **15** and

DOI: 10.1021/jf506361r
J. Agric. Food Chem. 2015, 63, 2264–2276

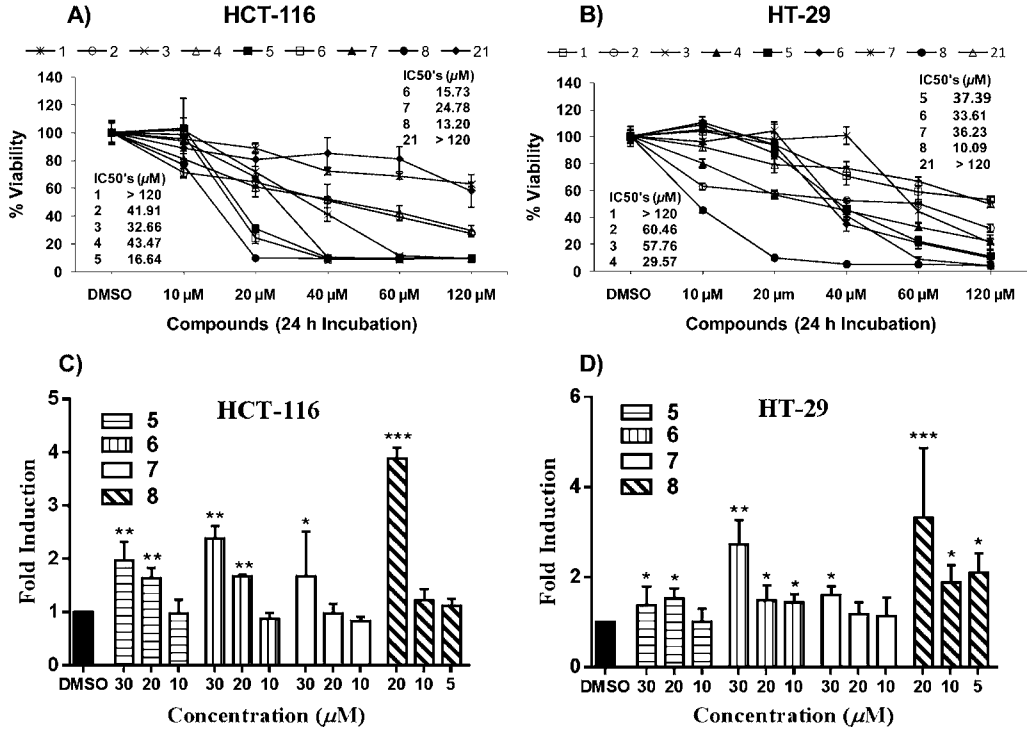

Figure 6. Growth inhibition of sterol oxides **1**–**8** and unoxidized stigmasterol **21** against human colon cancer cells HCT-116 (A) and HT-29 (B), and effects of sterol oxides **5**–**8** on the induction of apoptosis in human colon cancer cells HCT-116 (C) and HT-29 (D). MTT assays: cells were treated with 10, 20, 40, 60, and 120 μM concentrations of the test compounds for 24 h in the presence of 10% FBS and 1% streptomycin/penicillin at 37 °C. Bar, standard error (n = 6). ELISA assays: cells were incubated with test compounds or DMSO for 48 h, upon which a Roche Apoptosis kit was applied to the wells and apoptosis was quantified and expressed as fold induction against the DMSO control. Bar, standard error; *, $p < 0.05$; **, $p < 0.01$; ***, $p < 0.0001$. All statistical tests are unpaired Student t-test, 2 tailed, compared to DMSO.

sitosterol ferulate **17** have been reported in WB previously,[19] whereas stigmasterol ferulate **16** was here described in WB for the first time. Peak ions at m/z 415 $[M - 162 + H]^+$ and 397 $[M - 180 + H]^+$ in MS^2 spectra of **18** corresponded to the loss of a hexanose. Moreover, peak ion at m/z 379 $[M - 180 - H_2O + H]^+$ in its MS^3 spectra, similar to the fragmentation of 7-ketocampesterol **9**, tentatively suggested that **18** is 3-*O*-glucopyranosyl-7-ketocampesterol, which has never been reported before. Compound **19**, bearing two peak ions at m/z 427 $[M - 162 + H]^+$ and 409 $[M - 180 + H]^+$ in its MS^2 spectra and one peak ion at m/z 391 $[M - 180 - H_2O + H]^+$ in its MS^3 spectra, was therefore proposed as 3-*O*-glucopyranosyl-7-ketostigmasterol, as reported previously in *Rosa laevigata*.[32] Similarly, parent ion at m/z 591 $[M + H]^+$ of **20** was 14 mass units higher than that of **18**, indicating that **20** is 3-*O*-glucopyranosyl-7-ketositosterol, as described previously in *Rosa laevigata*.[32]

Consequently, a total of 21 steroids **1**–**21** were identified and characterized from WB extract, using NMR experiments, chemical synthesis approaches, and LC-ESI/MS^n techniques, eventually leading to a comprehensive profile of steroids in WB, as shown in Figure 5. Among them, 7-ketositosterol **3** and 7-ketostigmasterol **4** were found to be the major oxyphytosterols in WB.

***In Vitro* Cytotoxic Activity.** Two human colon cancer cell lines HCT-116 and HT-29 were treated with eight sterol oxides **1**–**8** and the nonoxidized stigmasterol **21**, with concentrations ranging from 0 to 120 μM. Seven sterol oxides **2**–**8** were found to be active against the growth of both HCT-116 and HT-29 human colon cancer cells (Figure 6A,B). Nonoxidized stigmasterol was inactive in both cells (IC_{50} >120 μM, Figure 6A,B). Unusual 3-ketophytosterols **1** and **2** were less active than 7-ketophytosterols **3**, **4**, and **7** in both cancer cell lines, indicating an entity of 3-ol-5-en-7-one in the structure is more favorable for anticancer activity than a 6-ol-4-en-3-one. In HCT-116 cell lines, 7β-hydroxycholesterol **8** was found to be the most active compound with an IC_{50} value of 13.20 μM, followed by 7β-hydroxystigmasterol **6** (IC_{50}: 15.73 μM), 7β-hydroxylsitosterol **5** (IC_{50}: 16.64 μM), 7-ketocholesterol **7** (IC_{50}: 24.78 μM), 7-ketositosterol **3** (IC_{50}: 32.66 μM), and 7-ketostigmasterol **4** (IC_{50}: 43.47 μM) (Figure 6A). The reduction products **5**, **6**, and **8** showed 2-fold higher inhibitory effects than their respective 7-keto precursors **3**, **4**, and **7** (Figure 6A), suggesting that an entity of 5-en-3,7-diol in the structure greatly increases the activity compared to an partial structure of 3-ol-5-en-7-one. 7β-Hydroxycholesterol **8**, with eight carbons in the alkyl side chain, showed a better inhibitory effect than 7β-hydroxysterols **5** and **6**, both bearing 10 carbons in alkyl side chains, indicating that increasing the numbers of carbon in the alkyl side chain decreases the activity. In HT-29 cell lines, 7β-hydroxycholesterol **8** also showed the most potency with IC_{50} value of 10.09 μM (Figure 6B). Whereas the rest of the sterol oxides **2**–**7** showed moderate inhibitory effects, and IC_{50} values ranged from 29.57 to 60.46 μM (Figure 6B). Notably, the two major oxyphytosterols **3** and **4** found in WB exerted great antiproliferative property in both cancer cell lines, indicating that oxyphytosterols may contribute to the observed chemopreventive effects of WB.

We also measured the growth inhibitory effects of the ferulate conjugates of sterols, 7-ketocholesterol ferulate **13** and 7β-hydroxycholesterol ferulate **13a**. Our results indicated that they were inactive in both cell lines (IC_{50}'s > 60 μM),

DOI: 10.1021/jf506361r
J. Agric. Food Chem. 2015, 63, 2264–2276

indicating a free hydroxyl group at C-3β in both entities of 3-ol-5-en-7-one, and 5-en-3,7-diol plays a crucial role in the observed activity.

In order to increase the polarity of oxyphytosterols, we synthesized two aza-oxysterols **7a** and **8a** by introducing an −NH group into C-20 in the side chain of oxysterols **7** and **8**, respectively. In HT-29 cells, MTT assays showed that **7a** exerted a similar activity (IC_{50}: 35.33 μM) to that of **7** (IC_{50}: 36.23 μM), and the activity of **8a** was attenuated while still remaining active (IC_{50}: 54.26 μM), compared to **8** (IC_{50}: 10.09 μM). In HCT-116 cells, the activities of both aza-oxysterols **7a** and **8a** were decreased (IC_{50} > 60 μM for both) compared to oxysterols **7** and **8**.

Induction of Apoptosis in Colon Cancer Cells. Apoptosis is a mechanism often responsible for the induction of cell death in response to internal or external stress. In order to clarify whether oxyphytosterols exert antiproliferative properties via a pathway of apoptosis, we tested the four most active sterol oxides **5**−**8** for apoptotic effects in human colon cancer cells HCT-116 and HT-29. The results are summarized in Figure 6C,D. In HCT-116 cells, compounds **5**−**7** showed significant apoptotic effects at the concentration of 30 μM (Figure 6C), while compound **8** exerted significant apoptotic effect at an even low concentration (20 μM) compared to DMSO control. In particular, the induction of apoptosis by **8** was significantly superior to those of the remaining **5**−**7** at the same concentration (20 μM). In HT-29 cells, compound **8** was also found to be the most potent agent to induce apoptosis (Figure 6D). Compound **6** displayed a significant apoptotic effect at the concentration of 30 μM (Figure 6D). Compounds **5** and **7** showed more or less apoptotic effects at the concentration of 30 μM.

DISCUSSION

In the present study, we outlined a comprehensive chemical profile of steroids in WB. Notably, we observed that 17 (**1**−**14** and **18**−**20**) out of 21 steroids (**1**−**21**) in WB are sterol oxides. This suggests that WB or whole grain wheat may be a dietary source of oxyphytosterols.[33] Daily consumption of whole grain wheat or diet supplemented with WB allows oxyphytosterols to contribute to health effects of the whole grain. Interestingly, three oxidation products of cholesterol, **7**, **8**, and **13**, were also found in WB as minor components. This observation could be demonstrated by the fact that many plants contain cholesterol both in free and esterified forms.[34,35] In addition, it is worth emphasizing that most phytosterols are present in WB in oxidized form or ferulate conjugates in this study, and stigmasterol is the only free plant sterol detected in WB so far.

Phytosterols are liable to oxidation giving rise to a family of oxyphytosterols. Thus, oxyphytosterols are most often present in the proximity of their parent compounds phytosterols. The two main pathways elucidated for oxidation of sterols are enzymatic oxidations and nonenzymatic oxidations. Upon exposure to reactive oxygen and free radical species, or radiation, ring oxidation products are formed.[36,37] Side chain oxidation is believed to be due mainly to enzymatic reactions, the principal enzymes including cytochrome P450 monooxygenases, dehydrogenases, epoxidases, and hydroxylases.[36,37] Physiological effects of cholesterol oxidation products have been well-documented.[38] However, the biological data on oxyphytosterols is relatively scarce. Most reports available so far suggest that oxyphytosterols possess cytotoxic effects *in vitro* and *in vivo*, cholesterol- and lipid-lowering effects, antidiabetic properties, and anti-inflammatory activities.[39] The main barrier to progress in this area was the lack of availability of individual oxyphytosterols. In the present study, nine sterol oxides **1**−**8** and **13** obtained in quantities from direct purification or chemical synthesis enabled us to evaluate them for their antiproliferative properties. MTT assays showed that seven sterol oxides **2**−**8** exerted significant inhibitory effects against human colon cancer cells HCT-116 and HT-29, compared to the parent stigmasterol **21**. Our results demonstrated that sterol oxides in WB may greatly participate in the observed chemopreventative properties of the grain as an active ingredient.

It is known that phytosterols are hardly absorbed (<15%) in human and only low amounts circulate in plasma.[40] Absorption of phytosterols occurs under the same conditions as that of cholesterol and other lipids. Phytosterol solubilization into intestinal mixed micelles is a prerequisite to be absorbed from the lumen, due to their excessive hydrophobicity.[33] Concerning the relative higher polarity of oxyphytosterols than phytosterols, oxyphytosterols may be better absorbed than their nonoxidized counterparts. Studies on the *in vivo* absorption of oxidized phytosterols in rats found that oxyphytosterols may be better absorbed than their nonoxidized counterparts.[41,42] However, there is no study on the bioavailability of oxyphytosterols in humans. Whether or not oxyphytosterols are more bioavailable than phytosterols in humans is a topic of future study.

It has been previously reported that aza-sterols exerted great growth inhibitory effects against human colon cancer cells HT-29,[27,43] leading us to hypothesize that oxyphytosterols with a hydrophilic amino group on the side chain might have improved inhibitory potencies. In this study, we introduced an NH group into position C-20 on the side chain of oxysterols **7** and **8**, giving rise to 20-aza-oxysterols **7a** and **8a**, respectively. Our results showed that the polar aza-oxysterols **7a** and **8a** mostly retained the antiproliferative properties of their respective counterparts **7** and **8**, at least in human colon cancer cells HT-29. This finding led to a strategy to modify oxyphytosterols for better absorption and enhanced anticancer activity in the future study.

In conclusion, we purified four oxyphytosterols **1**−**4** from WB extract, synthesized five sterol oxides **5**−**8** and **13**, and identified a total of 21 steroids **1**−**21** in WB extract using LC-ESI/MS^n techniques based on analysis of their own tandem mass spectra or direct comparison with the authentic references. Among them, three sterol oxides **13**, **14**, and **18** are novel compounds, and 14 compounds **3**, **4**, **6**−**11**, **13**, **14**, **16**, and **18**−**20** were reported in WB for the first time. It is also the first report of the complete NMR data (^{1}H and ^{13}C NMR) for 3-ketophytosterols **1** and **2**. MTT assays showed that seven sterol oxides **2**−**8** exerted significant antiproliferative effects, with oxysterol **8** being the most active compound in both HCT-116 and HT-29 human colon cancer cells. ELISA assays demonstrated that sterol oxides **5**−**8** could induce cell death through apoptosis pathway. Study on SAR of sterol oxides revealed that (1) an entity of 3-ol-5-en-7-one in the structure is more favorable for anticancer activity than a partial structure of 6-ol-4-en-3-one; (2) an entity of 5-en-3,7-diol in the structure greatly increases the activity compared to 3-ol-5-en-7-one; (3) a free hydroxyl group at C-3β in an entity of 3-ol-5-en-7-one or 5-en-3,7-diol plays a crucial role in the observed activity; and (4) a lipophilic side chain of eight carbons in length yields the optimal activities.

DOI: 10.1021/jf506361r
J. Agric. Food Chem. 2015, 63, 2264−2276

AUTHOR INFORMATION

Corresponding Author

*Phone: 704-250-5710. Fax: 704-250-5709. E-mail: ssang@ncat.edu or shengminsang@yahoo.com.

Funding

The authors are grateful for financial support from USDA-NIFA Grant 2012-38821-20012 to S.S.

Notes

The authors declare no competing financial interest.

REFERENCES

(1) Aune, D.; Norat, T.; Romundstad, P.; Vatten, L. J. Whole grain and refined grain consumption and the risk of type 2 diabetes: a systematic review and dose-response meta-analysis of cohort studies. *Eur. J. Epidemiol.* **2013**, *28*, 845−858.

(2) Lillioja, S.; Neal, A. L.; Tapsell, L.; Jacobs, D. R., Jr. Whole grains, type 2 diabetes, coronary heart disease, and hypertension: Links to the aleurone preferred over indigestible fiber. *Biofactors* **2013**, *39*, 242−258.

(3) Ochoa-Aviles, A.; Verstraeten, R.; Lachat, C.; Andrade, S.; Van Camp, J.; Donoso, S.; Kolsteren, P. Dietary intake practices associated with cardiovascular risk in urban and rural Ecuadorian adolescents: A cross-sectional study. *BMC Public Health* **2014**, *14*, 939.

(4) Ortiz-Martinez, M.; Winkler, R.; Garcia-Lara, S. Preventive and therapeutic potential of peptides from cereals against cancer. *J. Proteomics* **2014**, *111C*, 165−183.

(5) Kyro, C.; Skeie, G.; Loft, S.; Landberg, R.; Christensen, J.; Lund, E.; Nilsson, L. M.; Palmqvist, R.; Tjonneland, A.; Olsen, A. Intake of whole grains from different cereal and food sources and incidence of colorectal cancer in the Scandinavian HELGA cohort. *Cancer, Causes Control* **2013**, *24*, 1363−1374.

(6) Aune, D.; Chan, D. S.; Lau, R.; Vieira, R.; Greenwood, D. C.; Kampman, E.; Norat, T. Dietary fibre, whole grains, and risk of colorectal cancer: Systematic review and dose-response meta-analysis of prospective studies. *BMJ (Br. Med. J.)* **2011**, *343*, d6617.

(7) World Cancer Research Fund/American Institute for Cancer Research. *Continuous Update Project Report. Food, Nutrition, Physical Activity and the Prevention of Colorectal Cancer*; 2011.

(8) Slavin, J. Why whole grains are protective: Biological mechanisms. *Proc. Nutr. Soc.* **2003**, *62*, 129−134.

(9) Reddy, B. S.; Hirose, Y.; Cohen, L. A.; Simi, B.; Cooma, I.; Rao, C. V. Preventive potential of wheat bran fractions against experimental colon carcinogenesis: implications for human colon cancer prevention. *Cancer Res.* **2000**, *60*, 4792−4797.

(10) Sang, S.; Ju, J.; Lambert, J. D.; Lin, Y.; Hong, J.; Bose, M.; Wang, S.; Bai, N.; He, K.; Reddy, B. S.; Ho, C. T.; Li, F.; Yang, C. S. Wheat bran oil and its fractions inhibit human colon cancer cell growth and intestinal tumorigenesis in Apc(min/+) mice. *J. Agric. Food Chem.* **2006**, *54*, 9792−9797.

(11) Zhu, Y.; Conklin, D. R.; Chen, H.; Wang, L.; Sang, S. 5-Alk(en)ylresorcinols as the major active components in wheat bran inhibit human colon cancer cell growth. *Bioorg. Med. Chem.* **2011**, *19*, 3973−3982.

(12) Zhu, Y.; Soroka, D. N.; Sang, S. Structure elucidation and chemical profile of sphingolipids in wheat bran and their cytotoxic effects against human colon cancer cells. *J. Agric. Food Chem.* **2013**, *61*, 866−874.

(13) Lagarda, M. J.; Garcia-Llatas, G.; Farre, R. Analysis of phytosterols in foods. *J. Pharm. Biomed. Anal.* **2006**, *41*, 1486−1496.

(14) AbuMweis, S. S.; Jones, P. J. Cholesterol-lowering effect of plant sterols. *Curr. Atheroscler. Rep.* **2008**, *10*, 467−472.

(15) Grattan, B. J., Jr. Plant sterols as anticancer nutrients: Evidence for their role in breast cancer. *Nutrients* **2013**, *5*, 359−387.

(16) Moghadasian, M. H.; McManus, B. M.; Godin, D. V.; Rodrigues, B.; Frohlich, J. J. Proatherogenic and antiatherogenic effects of probucol and phytosterols in apolipoprotein E-deficient mice: Possible mechanisms of action. *Circulation* **1999**, *99*, 1733−1739.

(17) Bouic, P. J. The role of phytosterols and phytosterolins in immune modulation: a review of the past 10 years. *Curr. Opin. Clin. Nutr. Metab. Care* **2001**, *4*, 471−475.

(18) Nourooz-Zadeh, J.; Appelqvist, L. Isolation and quantitative determination of sterol oxides in plant-based foods: Soybean oil and wheat flour. *J. Am. Oil Chem. Soc.* **1992**, *69*, 288−293.

(19) Iwatsuki, K.; Akihisa, T.; Tokuda, H.; Ukiya, M.; Higashihara, H.; Mukainaka, T.; Iizuka, M.; Hayashi, Y.; Kimura, Y.; Nishino, H. Sterol ferulates, sterols, and 5-alk(en)ylresorcinols from wheat, rye, and corn bran oils and their inhibitory effects on Epstein-Barr virus activation. *J. Agric. Food Chem.* **2003**, *51*, 6683−6688.

(20) Prinsen, P.; Gutierrez, A.; Faulds, C. B.; del Rio, J. C. Comprehensive study of valuable lipophilic phytochemicals in wheat bran. *J. Agric. Food Chem.* **2014**, *62*, 1664−1673.

(21) Mosmann, T. Rapid colorimetric assay for cellular growth and survival: Application to proliferation and cytotoxicity assays. *J. Immunol. Methods* **1983**, *65*, 55−63.

(22) Kontiza, I.; Abatis, D.; Malakate, K.; Vagias, C.; Roussis, V. 3-Keto steroids from the marine organisms Dendrophyllia cornigera and Cymodocea nodosa. *Steroids* **2006**, *71*, 177−181.

(23) Monteiro Gaspar, E. M. M. S.; Chaves Das Neves, H. J. Unusual steroids in allelopathic extracts of wheat straw. *Proc.—Plant Growth Regul. Soc. Am.* **1995**, *22*, 78−80.

(24) Notaro, G.; Piccialli, V.; Sica, D. New steroidal hydroxyketones and closely related diols from the marine sponge *Cliona copiosa*. *J. Nat. Prod.* **1992**, *55*, 1588−1594.

(25) Foley, D. A.; O'Callaghan, Y.; O'Brien, N. M.; McCarthy, F. O.; Maguire, A. R. Synthesis and characterization of stigmasterol oxidation products. *J. Agric. Food Chem.* **2010**, *58*, 1165−1173.

(26) McCarthy, F. O.; Chopra, J.; Ford, A.; Hogan, S. A.; Kerry, J. P.; O'Brien, N. M.; Ryan, E.; Maguire, A. R. Synthesis, isolation and characterisation of beta-sitosterol and beta-sitosterol oxide derivatives. *Org. Biomol. Chem.* **2005**, *3*, 3059−3065.

(27) Xie, W.; Peng, H.; Kim, D. I.; Kunkel, M.; Powis, G.; Zalkow, L. H. Structure-activity relationship of aza-steroids as PI-PLC inhibitors. *Bioorg. Med. Chem.* **2001**, *9*, 1073−1083.

(28) Jiang, X.; Ory, D. S.; Han, X. Characterization of oxysterols by electrospray ionization tandem mass spectrometry after one-step derivatization with dimethylglycine. *Rapid Commun. Mass Spectrom.* **2007**, *21*, 141−152.

(29) Gao, J.; Yue, Q.; Ji, Y.; Cheng, B.; Zhang, X. Novel synthesis strategy for the preparation of individual phytosterol oxides. *J. Agric. Food Chem.* **2013**, *61*, 982−988.

(30) del Rio, J. C.; Prinsen, P.; Gutierrez, A. A comprehensive characterization of lipids in wheat straw. *J. Agric. Food Chem.* **2013**, *61*, 1904−1913.

(31) Allevi, P.; Anastasia, M.; Colombo, D.; Fiecchi, A. Hydroboration of 5 alpha-ergost-8-en-3 beta-ol. *Steroids* **1989**, *54*, 133−143.

(32) Fang, J. M.; Wang, K. C.; Cheng, Y. S. Steroids and triterpenoids from *Rosa laevigata*. *Phytochemistry* **1991**, *30*, 3383−3387.

(33) Garcia-Llatas, G.; Rodriguez-Estrada, M. T. Current and new insights on phytosterol oxides in plant sterol-enriched food. *Chem. Phys. Lipids* **2011**, *164*, 607−624.

(34) Johnson, D. F.; Bennett, R. D.; Heftmann, E. Cholesterol in higher plants. *Science* **1963**, *140*, 198−199.

(35) Behrman, E. J.; Gopalan, V. Cholesterol and plants. *J. Chem. Educ.* **2005**, *82*, 1791−1793.

(36) Smith, L. L. Review of progress in sterol oxidations: 1987−1995. *Lipids* **1996**, *31*, 453−487.

(37) Smith, L. L. Cholesterol autoxidation 1981−1986. *Chem. Phys. Lipids* **1987**, *44*, 87−125.

(38) Schroepfer, G. J., Jr. Oxysterols: Modulators of cholesterol metabolism and other processes. *Physiol. Rev.* **2000**, *80*, 361−554.

(39) Hovenkamp, E.; Demonty, I.; Plat, J.; Lutjohann, D.; Mensink, R. P.; Trautwein, E. A. Biological effects of oxidized phytosterols: A review of the current knowledge. *Prog. Lipid Res.* **2008**, *47*, 37−49.

(40) Chan, Y. M.; Varady, K. A.; Lin, Y.; Trautwein, E.; Mensink, R. P.; Plat, J.; Jones, P. J. Plasma concentrations of plant sterols:

DOI: 10.1021/jf506361r
J. Agric. Food Chem. 2015, 63, 2264−2276

Physiology and relationship with coronary heart disease. *Nutr. Rev.* **2006**, *64*, 385−402.
(41) Tomoyori, H.; Kawata, Y.; Higuchi, T.; Ichi, I.; Sato, H.; Sato, M.; Ikeda, I.; Imaizumi, K. Phytosterol oxidation products are absorbed in the intestinal lymphatics in rats but do not accelerate atherosclerosis in apolipoprotein E-deficient mice. *J. Nutr.* **2004**, *134*, 1690−1696.
(42) Grandgirard, A.; Sergiel, J. P.; Nour, M.; Demaison-Meloche, J.; Ginies, C. Lymphatic absorption of phytosterol oxides in rats. *Lipids* **1999**, *34*, 563−570.
(43) Xie, W.; Peng, H.; Zalkow, L. H.; Li, Y. H.; Zhu, C.; Powis, G.; Kunkel, M. 3Beta-hydroxy-6-aza-cholestane and related analogues as phosphatidylinositol specific phospholipase C (PI-PLC) inhibitors with antitumor activity. *Bioorg. Med. Chem.* **2000**, *8*, 699−706.

DOI: 10.1021/jf506361r
J. Agric. Food Chem. 2015, 63, 2264−2276

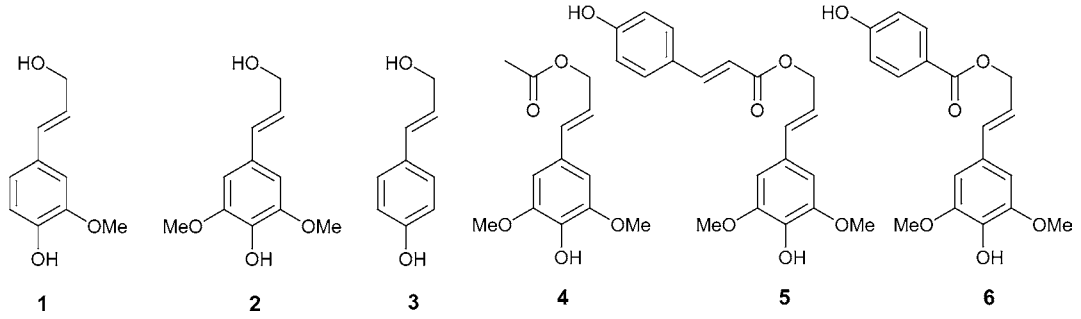

Figure 1. Traditional monolignols **1**–**3** and nontraditional monolignols **4**–**6**.

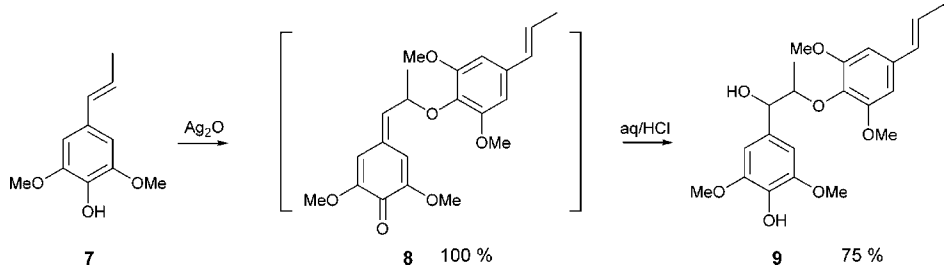

Figure 2. Ag_2O-mediated oxidative coupling of a syringyl-type monomer by Zanarotti.[13]

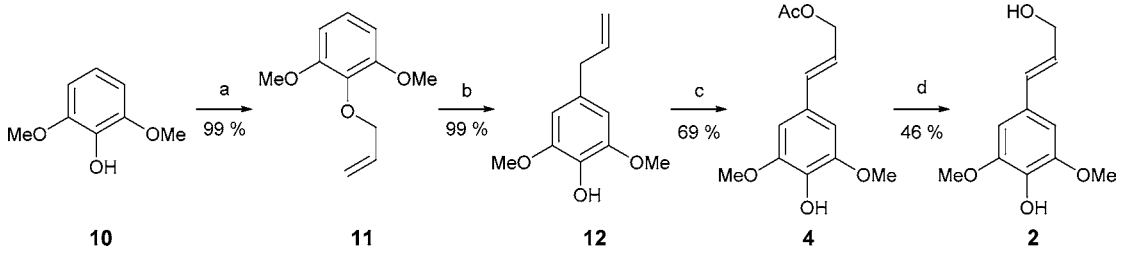

Figure 3. Synthesis of sinapyl acetate and sinapyl alcohol. Reaction conditions: (a) allyl bromide, K_2CO_3, *n*-Bu_4NI, DMF; (b) neat, under Ar, 200 °C; (c) Ag_2O, benzene, and then acetic acid/sodium acetate; (d) $LiAlH_4$, THF, −10 °C.

of phenols. The oxidative coupling of a syringyl-type phenol **7** by Ag_2O was reported to produce the *β-O*-4-coupled dimeric product **9** in 75% yield (Figure 2).[13] We expected that Ag_2O may be more suitable than HRP/peroxide to investigate the formation of *β-O*-4 structures by the oxidative coupling of syringyl-type monolignols.

MATERIALS AND METHODS

General. All chemicals were purchased from Wako (Osaka, Japan) and used as received without any purification. ^1H and ^{13}C NMR spectra were recorded with a Bruker AVANCE II 400 FT-NMR (400 MHz) or a Bruker AMX500 FT-NMR (500 MHz) spectrometer in $CDCl_3$ or acetone-d_6 with tetramethylsilane (TMS) as an internal standard. Chemical shifts (δ) and coupling constants are reported in δ values (ppm) and hertz, respectively. Assignments of *erythro* and *threo* isomers were made by the comparison of chemical shifts with the similar lignin model compounds. ESI-MS spectra were recorded on an 1100 LC-MSD spectrometer (Agilent Technology, Santa Clara, CA, USA). High-resolution ESI-ToF-MS was done with a Bruker micrOTOF. Biomimetic oxidations of sinapyl alcohol and sinapyl acetate were carried out at least twice during the isolation process of reaction products. The isolated yields of the reaction products were calculated on the basis of one set of reactions described below.

Synthesis of Sinapyl Alcohol and Sinapyl Acetate. Sinapyl alcohol, **2**, and sinapyl acetate, **4**, were synthesized from 2,6-dimethoxyphenol, **10**, as shown in Figure 3.[14]

*2-(Allyloxy)-1,3-dimethoxybenzene, **11**:* To a stirred solution of 2,6-dimethoxyphenol, **10** (5 g, 32.4 mmol), in *N*,*N*-dimethylformamide (DMF; 50 mL) under argon were added allyl bromide (98%, 3.5 mL, 38.9 mmol), potassium carbonate (6.72 g, 48.7 mmol), and tetra-*n*-butyl ammonium iodide (1.2 g, 3.24 mmol) at room temperature. The reaction mixture was kept at 50 °C for 3.5 h. The reaction mixture was filtered, diluted with ethyl acetate, washed with brine, dried over Na_2SO_4, and concentrated to dryness in vacuo. The product was purified on a silica gel column with ethyl acetate/hexane (1:4, v/v) to afford a syrup, **11** (6.0 g, 95%): ^1H NMR (400 MHz, $CDCl_3$) δ 3.85 (6H, s, OCH_3), 4.52 (2H, dt, J = 6.1, 1.1 Hz, $OCH_2CH{=}CH_2$), 5.18 (1H, ddt, J = 10.3, 1.6, 1.1 Hz, $OCH_2CH{=}CH_2$), 5.30 (1H, dq, J = 17.2, 1.6 Hz, $OCH_2CH{=}CH_2$), 6.12 (1H, ddt, J = 17.2, 10.3, 6.1 Hz, $-CH_2CH{=}CH_2$), 6.58 (2H, d, J = 8.4 Hz, C2,6-H), 6.99 (1H, t, J = 8.4 Hz, C1-H); ^{13}C NMR (400 MHz, $CDCl_3$) δ 56.1 (OCH_3), 74.1 ($OCH_2CH{=}CH_2$), 105.4 (C2,6), 117.6 ($OCH_2CH{=}CH_2$), 123.6 (C1), 134.6 ($OCH_2CH{=}CH_2$), 136.9 (C4), 153.8 (C3,5); ESI-MS (m/z) 217 ($[M + Na]^+$, 100); high-resolution ESI-ToF-MS, calculated for $C_{11}H_{14}NaO_3^+$, 217.0835, found 217.0839.

*4-Allyl-2,6-dimethoxyphenol, **12**:* Compound **11** (8 g, 41.2 mmol) was placed in a stainless steel autoclave and heated at 200 °C under stirring for 6 h. The product was purified on a silica gel column with ethyl acetate/hexane (1:4, v/v) to afford a syrup, **12** (8.0 g, 97%): ^1H NMR (400 MHz, $CDCl_3$) δ 3.31 (2H, br d, J = 6.7 Hz, α), 3.86 (6H, s, OCH_3), 5.04–5.12 (2H, m, γ), 5.95 (1H, ddt, J = 17.0, 10.0, 6.7 Hz, β), 6.41 (2H, s, C2,6-H); ^{13}C NMR (400 MHz, $CDCl_3$) δ 40.4 (α), 56.3 (OCH_3), 105.2 (C2,6), 115.8 (γ), 131.1 (C1), 133.0 (C4), 137.7 (β), 147.0 (C3, 5); ESI-MS (m/z) 217 ($[M + Na]^+$); high-resolution ESI-ToF-MS, calculated for $C_{11}H_{14}O_3Na^+$ 217.0835, found, 217.0843.

*(E)-3-(4-Hydroxy-3,5-dimethoxyphenyl)allyl acetate, **4**:* To a stirred solution of $AgNO_3$ (2.1 g, 12.4 mmol) in H_2O (12.4 mL) was

DOI: 10.1021/jf506111q
J. Agric. Food Chem. 2015, 63, 2277–2283

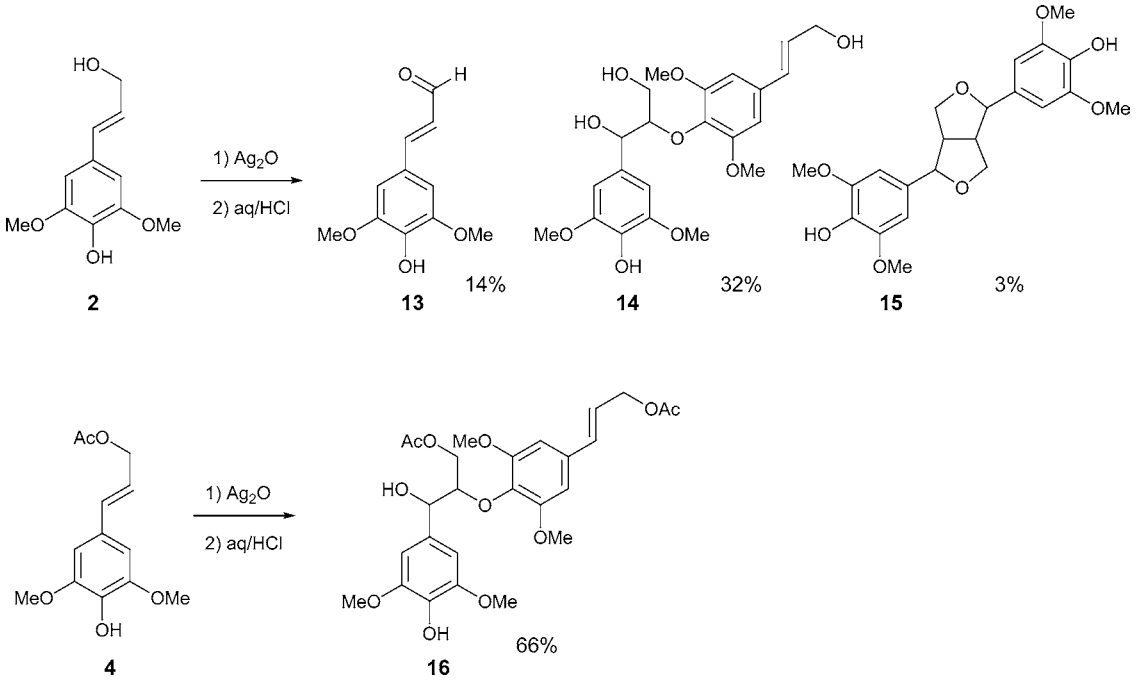

Figure 4. Ag_2O-mediated oxidative coupling of sinapyl alcohol and sinapyl acetate.

added dropwise aqueous NaOH (0.54 g, 13.5 mmol) solution in H_2O (4.9 mL) at room temperature. The reaction mixture was kept for 5 min; it was then filtered and dried under vacuum to afford Ag_2O. To a solution of compound **12** (1.0 g, 5.15 mmol) in benzene (20 mL) was added all of the freshly prepared Ag_2O at room temperature. The reaction mixture was kept for 30 min with vigorous stirring. The reaction mixture in benzene was filtered through Celite into a flask containing acetic acid (25 mL) and sodium acetate (2 g) at room temperature. The reaction mixture was kept for 30 min. The reaction mixture was filtered and concentrated to dryness in vacuo. The product was purified on a silica gel column with ethyl acetate/hexane (1:1, v/v) to afford a syrup (0.9 g, 69%): ^{1}H NMR (400 MHz, $CDCl_3$) δ 2.10 (3H, s, $COCH_3$), 3.91 (6H, s, OCH_3), 4.71 (2H, dd, J = 6.6, 1.1 Hz, γ), 6.16 (1H, dt, J = 15.8, 6.6 Hz, β), 6.57 (1H, br d, J = 15.8 Hz, α), 6.64 (2H, s, C2,6-H); ^{13}C NMR (400 MHz, $CDCl_3$) δ 21.2 ($CO\underline{C}H_3$), 56.4 (OCH_3), 65.4 (γ), 103.6 (C2,6), 121.3 (β), 127.9 (C1), 134.8 (α), 135.2 (C4), 147.3 (C3,5), 171.1 ($COCH_3$); high-resolution ESI-TOF-MS, calculated for $C_{13}H_{16}O_5Na^+$ 275.0890, found 275.0899.

Sinapyl alcohol, 2: To a stirred suspension of lithium aluminum hydride (61 mg, 1.61 mmol) in dry THF (10 mL) at −10 °C under argon was added dropwise a solution of compound **4** (200 mg, 0.79 mmol) in dry THF (1.5 mL). The solution was kept at the same temperature for 1.5 h. To the reaction mixture was added ethyl acetate (0.5 mL) to stop the reaction, and wet THF (0.5 mL), cold water (4 mL), and CH_2Cl_2 (3 mL) were then added. The water phase was neutralized with a 10% $KHSO_4$ solution and extracted with CH_2Cl_2. The organic layer was dried with Na_2SO_4 and concentrated to 3 mL under vacuum. Hexane was added to the solution, and sinapyl alcohol, **2**, was crystallized in the cold to afford light yellow crystals (76 mg, 46%): ^{1}H NMR (400 MHz, $CDCl_3$) δ 3.90 (6H, s, OCH_3), 4.31 (2H, br s, γ), 6.24 (1H, dt, J = 15.8, 5.8 Hz, β), 6.52 (1H, br d, J = 15.8 Hz, α), 6.63 (2H, s, C2,6-H); ^{13}C NMR (400 MHz, $CDCl_3$) δ 56.3 (OCH_3), 63.8 (γ), 103.3 (C2,6), 126.6 (β), 128.2 (C1), 131.5 (α), 134.8 (C4), 147.1 (C3, 5).

Oxidative Coupling of Sinapyl Alcohol. To a stirred solution of compound **2** (100 mg, 0.476 mmol) in 1,4-dioxane (3 mL) under argon was added freshly prepared Ag_2O (111 mg, 0.479 mmol). The reaction mixture was kept for 1 h under vigorous stirring in the dark. The reaction mixture in 1,4-dioxane was filtered through Celite into a flask containing concentrated HCl (0.35 mL), H_2O (20 mL), and THF (10 mL) at room temperature. The reaction mixture was kept under stirring for 1.5 h and then neutralized by adding $NaHCO_3$. The reaction mixture was diluted with ethyl acetate, washed with brine, dried over Na_2SO_4, and concentrated to dryness in vacuo. The product was purified on a silica gel column with ethyl acetate/hexane (3:1, v/v) to afford five fractions. Sinapyl aldehyde, **13** (14 mg, 14%), was obtained from fraction 1. Both the *erythro* and *threo* isomers of syringyl glycerol-β-sinapyl alcohol, **14** (34 mg, 32%), and syringaresinol, **15** (<3 mg, 3%), were obtained from fraction 5 by thin layer chromatography (TLC) with methanol/CH_2Cl_2 (1:19, v/v). Sinapyl aldehyde, **13**: ^{1}H NMR (500 MHz, acetone-d_6) δ 3.92 (6H, s, OCH_3), 6.69 (2H, dd, J = 15.8, 7.7 Hz, β), 7.08 (2H, s, C2,6-H), 7.55(1H, d, J = 15.8 Hz, α), 9.64 (1H, d, J = 7.7 Hz, γ). Syringyl glycerol-β-sinapyl alcohol, **14**, chemical shifts and coupling constants were determined for *erythro* and *threo* mixtures: ^{1}H NMR (500 MHz, acetone-d_6) *erythro* δ 3.41 (1H, γ), 3.81 (OCH_3), 3.85 (1H, γ), 3.90 (OCH_3), 4.18 (1H, m, β), 4.24 (2H, br d, J = 5.2 Hz, γ'), 4.37 (1H, α-OH), 4.99 (1H, α), 6,39 (2H, dt, J = 15.9, 5.2 Hz, β'), 6.57 (1H, br d, J = 15.9 Hz, α'), 6.72 (2H, s, C2,6-H or C2′,6′-H), 6.82 (2H, s, C2,6-H or C2′,6′-H); *threo* δ 3.33 (1H, γ), 3.67 (1H, γ), 3.80 (OCH_3), 3.92 (OCH_3), 3.95 (1H, m, β), 4.99 (1H, α), 6.39 (2H, dt, J = 15.9, 5.2 Hz, β'), 6.56 (1H, br d, J = 15.9 Hz, α'), 6.77 (2H, s, C2,6-H or C2′,6′-H), 6.82 (2H, s, C2,6-H or C2′,6′-H); ^{13}C NMR (400 MHz, acetone-d_6) *erythro*/*threo* δ 56.7 (OCH_3), 61.0 (γ), 63.2 (γ'), 73.7 (α), 74.3 (α), 88.2 (β), 89.9 (β), 104.6, 104.7, 104.9, 105.6, 129.9, 131.0, 132.8, 132.5, 134.8, 136.2, 148.5, 154.1, 154.3; high-resolution ESI-TOF-MS m/z (M + Na)$^+$ calculated for $C_{22}H_{28}O_9Na^+$ 459.1626, found 459.1647. Syringresinol, **15**: ^{1}H NMR (500 MHz, acetone-d_6) δ 3.10 (2H, m, β) 3.82−3.85 (2H, m, γ), 3.84 (6H, s, OCH_3), 4.23 (2H, m, γ), 4.67 (2H, d, J = 3.8 Hz, α), 6.69 (4H, s, C2,6-H); ^{13}C NMR (500 MHz, acetone-d_6) δ 55.3 (β), 56.6 (OCH_3), 72.3 (γ), 86.8 (α), 104.4 (C2,6), 133.2 (C1), 136.2 (C4), 148.7 (C3,5); high-resolution ESI-TOF-MS m/z (M + Na)$^+$ calculated for $C_{22}H_{26}O_8Na^+$ 441.1520, found 441.1565.

Oxidative Coupling of Sinapyl Acetate. To a stirred solution of compound **4** (100 mg, 0.396 mmol) in 1,4-dioxane (3 mL) under argon was added freshly prepared Ag_2O (100 mg, 0.43 mmol). The reaction mixture was kept under vigorous stirring for 20 min in the dark. The reaction mixture in 1,4-dioxane was filtered through Celite into a flask containing concentrated HCl (0.35 mL), H_2O (20 mL), and THF (10 mL) at room temperature. The reaction mixture was

DOI: 10.1021/jf506111q
J. Agric. Food Chem. 2015, 63, 2277−2283

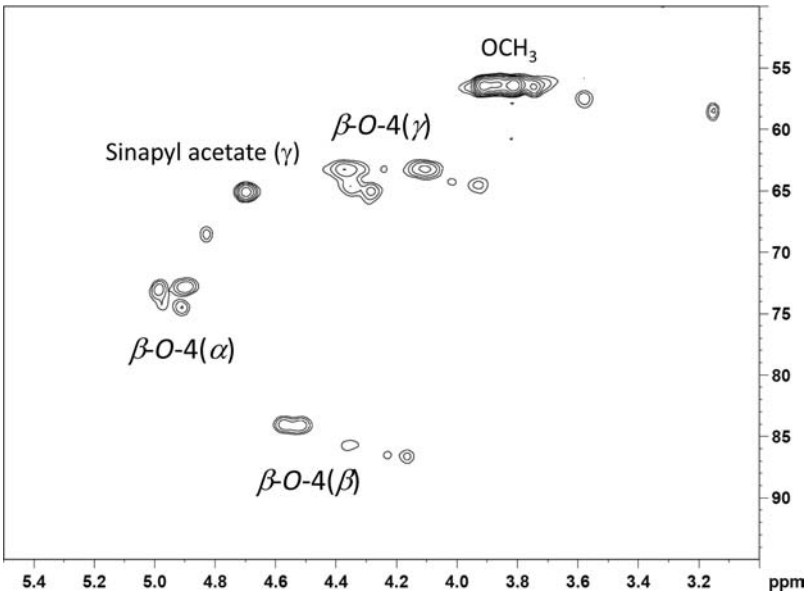

Figure 5. HSQC NMR spectrum of oligomeric products formed form the Ag_2O-mediated oxidative coupling of sinapyl acetate.

kept for 30 min under stirring and was then neutralized by adding $NaHCO_3$. The reaction mixture was diluted with ethyl acetate, washed with brine, dried over Na_2SO_4, and concentrated to dryness in vacuo. The product was purified on a silica gel column with ethyl acetate/hexane (2:1, v/v) to afford five fractions. Fraction 4 (18 mg, 18%) was mainly composed of *β-O*-4 oligomeric products, as was confirmed by the HSQC NMR spectra. The *β-O*-4-coupled dimers *erythro*-**16** (50 mg, 48%) and *threo*-**16** (19 mg, 18%) were obtained from fractions 2 and 3, respectively, by TLC with ethyl acetate/hexane/benzene (10:5:1, v/v/v).

*erythro-**16**:* ^{1}H NMR (500 MHz, acetone-d_6) δ 1.87 (3H, s, $COCH_3$), 2.04 (3H, s, $COCH_3$), 3.81 (6H, s, OCH_3), 3.91 (6H, s, OCH_3), 4.09 (1H, dd, J = 11.8, 3,3 Hz, γ), 4.36 (1H, m, γ), 4.53 (1H, m, β), 4.70 (2H, dd, J = 6.3, 1.0 Hz, γ'), 4.91 (1H, m, α), 6.36 (1H, dt, J = 15.9, 6.3 Hz, β'), 6.66 (1H, dt, J = 15.9 Hz, α'), 6.69 (2H, s, C2,6-H or C2′,6′-H), 6.86 (2H, s, C2,6-H or C2′,6′-H); ^{13}C NMR (400 MHz, acetone-d_6) δ 20.8 ($CO\underline{C}H_3$), 20.9 ($CO\underline{C}H_3$), 56.7 (OCH_3), 63.5 (γ), 65.4 (γ'), 73.1 (α), 84.5 (β), 104.6 (C2,6 or C2′,6′), 104.9 (C2,6 or C2′,6′), 124.4 (β'), 131.6 (C1, C1′, C4, or C4′), 133.5 (C1, C1′, C4, or C4′), 134.4 (α'), 136.0 (C1, C1′, C4, or C4′), 136.5 (C1, C1′, C4, or C4′), 148.6 (C3,5 or C3′,5′), 154.5 (C3,5 or C3′,5′), 170.9 ($\underline{C}OCH_3$); high-resolution ESI-TOF-MS m/z $(M + Na)^+$ calculated for $C_{26}H_{32}O_{11}Na^+$ 543.1837, found 543.1811.

*threo-**16**:* ^{1}H NMR (500 MHz, acetone-d_6) δ 1.96 (3H, s, $COCH_3$), 2.04 (3H, s, $COCH_3$), 3.79 (6H, s, OCH_3), 3.89 (6H, s, OCH_3), 3.93 (1H, dd, J = 11.9, 4.2 Hz, γ), 4.22 (1H, m, β), 4.33 (1H, dd, J = 11.9, 3.3 Hz, γ), 4.69 (2H, dd, J = 6.2, 1.0 Hz, γ'), 4.91 (1H, m, α), 6.35 (1H, dt, J = 15.9, 6.2 Hz, β'), 6.65 (1H, d, J = 15.9 Hz, α'), 6.73 (2H, s, C2,6-H or C2′,6′-H), 6.85 (2H, s, C2,6-H or C2′,6′-H); ^{13}C NMR (400 MHz, acetone-d_6) δ 20.8 ($CO\underline{C}H_3$), 20.9 ($CO\underline{C}H_3$), 56.6 (OCH_3), 56.7 (OCH_3), 64.8 (γ), 65.3 (γ'), 74.7 (α), 86.7 (β), 104.9 (C2,6 or C2′,6′), 105.4 (C2,6 or C2′,6′), 124.4 (β'), 132.1 (C1, C1′, C4, or C4′), 133.4 (C1, C1′, C4, or C4′), 134.3 (α'), 136.4 (C1, C1′, C4, or C4′), 137.8 (C1, C1′, C4, or C4′), 148.5 (C3,5 or C3′,5′), 154.0 (C3,5 or C3′,5′), 170.8 ($\underline{C}OCH_3$), 170.9 ($\underline{C}OCH_3$); high-resolution ESI-TOF-MS m/z $(M + Na)^+$ calculated for $C_{26}H_{32}O_{11}Na^+$ 543.1837, found 543.1820.

Computational Calculations of Sinapyl Acetate and Sinapyl Alcohol Radicals. Computational calculations were conducted with Spartan ’08 Win (Wavefunction, Inc., Irvine, CA, USA). Conformational analyses of the radicals were performed with the standard conformer search program in Spartan ’08 using PM3 semiempirical calculations. The conformers obtained were further optimized at the UB3LYP/6-31G* level of theory to identify the lowest energy conformers. Single-point energy calculations of the conformers were performed at the same level to obtain electrostatic charges and spin densities based on natural population analysis. Solvent effects were added to the energy calculations using the POSTSOLVENT command based on the SM8 model in Spartan ’08.

RESULTS AND DISCUSSION

Synthesis of Sinapyl Acetate and Sinapyl Alcohol. Sinapyl acetate, **4**, and sinapyl alcohol, **2**, were synthesized from 2,6-dimethoxyphenol, **10**, by the reported procedure (Figure 3).[14] The allylation of compound **10** was performed with allyl bromide and potassium carbonate in dimethyl formaldehyde (DMF) to afford compound **11** in 99% yield. The Claisen rearrangement of compound **11** in a sealed tube under argon at 200 °C gave compound **12** in 99% yield.[15] Compound **12** was treated with freshly prepared Ag_2O in benzene, and the suspension was filtered through Celite to give a vinyl quinone methide intermediate. The benzene solution of the formed vinyl quinone methide was poured into acetic acid/sodium acetate to give sinapyl acetate, **4**, in 69% yield.[14] The acetyl group in compound **4** was removed by lithium aluminum hydride to give sinapyl alcohol, **2**, in 46% yield.

Table 1. Calculated Spin Densities of Sinapyl Alcohol and Sinapyl Acetate Radicals

	sinapyl alcohol radical	sinapyl acetate radical
C1	0.2216	0.2216
C2	−0.1007	−0.1028
C3	0.1802	0.1824
C4	0.0337	0.0310
C5	0.1532	0.1549
C6	−0.0933	−0.0957
Cα	−0.0841	−0.0845
Cβ	0.1797	0.1767
Cγ	−0.0078	−0.0080
O3	0.0750	0.0781
O4	0.3597	0.3611
O5	0.0607	0.0634
Oγ	0.0003	0.0001

DOI: 10.1021/jf506111q
J. Agric. Food Chem. 2015, 63, 2277−2283

Table 2. Calculated Electrostatic Charges of Carbon and Oxygen Atoms in Sinapyl Alcohol and Sinapyl Acetate Radicals

	sinapyl alcohol radical			sinapyl acetate radical		
solvent	none	1,4-dioxane	water	none	1,4-dioxane	water
C1	0.3958	0.3983	0.4162	0.3714	0.3839	0.4017
C2	−0.5513	−0.5480	−0.5579	−0.5422	−0.5479	−0.5550
C3	0.3014	0.2962	0.2941	0.3028	0.3102	0.3040
C4	0.2888	0.2880	0.2802	0.2851	0.2775	0.2688
C5	0.2811	0.2881	0.2876	0.2930	0.3062	0.3091
C6	−0.5268	−0.5376	−0.5503	−0.5313	−0.5461	−0.5599
Cα	−0.2147	−0.2133	−0.2294	−0.1869	−0.1974	−0.2184
Cβ	−0.1883	−0.1953	−0.1656	−0.1714	−0.1619	−0.1194
Cγ	0.1344	0.1579	0.1521	0.0289	0.0067	−0.0271
O3	−0.1972	−0.1913	−0.2022	−0.1896	−0.1908	−0.2024
O4	−0.4326	−0.4313	−0.4664	−0.4272	−0.4244	−0.4605
O5	−0.2160	−0.2162	−0.2279	−0.2128	−0.2133	−0.2256
Oγ	−0.5779	−0.5824	−0.6039	−0.3887	−0.3847	−0.3834

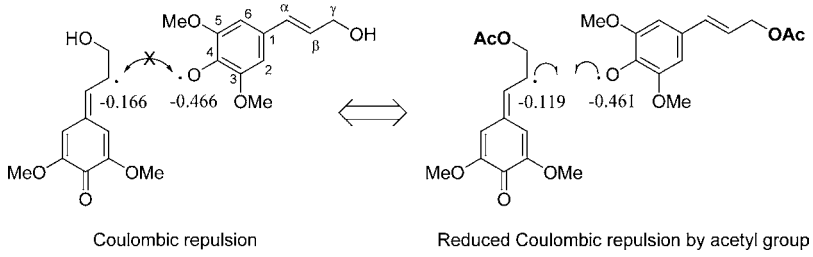

Figure 6. Reduced negative charges by acetyl group result in the high yield of β-*O*-4 products.

Oxidative Coupling of Sinapyl Alcohol and Sinapyl Acetate by Silver Oxide. The oxidative coupling of lignin-related monomers by Ag_2O was first carried out by Zanarotti.[13] The oxidation of a syringyl-type monomer, 2,6-dimethoxy-4-(prop-1-en-1-yl)phenol, **7**, in dry benzene or in dry methylene chloride quantitatively yielded quinone methide **8**, which was further hydrated with aqueous acid to produce the β-*O*-4-coupled dimeric product **9** (C−O-coupled dimer) in 75% yield (Figure 2).[13] Later, this procedure was applied to the oxidative coupling of a guaiacyl-type monomer, coniferyl alcohol.[16] The reaction products from coniferyl alcohol were different from those from the syringyl-type monomer. In methylene chloride, the β-5-coupled dimer was formed as a major product in 50% yield, whereas in a two-phase methylene chloride/water (1:1, v/v) solution, the β-β-coupled dimer was the major product in 25% yield.[16] Both the β-5 and β-β dimers were C−C-coupled products.

On the other hand, the oxidative coupling of sinapyl alcohol, **2**, a typical syringyl-type monomer, by Ag_2O has not been reported. Alternatively, $FeCl_3$ has been used for the oxidative coupling of sinapyl alcohol, **2** in 1,4-dioxane, which gave the β-*O*-4-coupled dimer **14** in 28% isolated yield.[17] In this investigation, sinapyl alcohol, **2**, was treated with Ag_2O in 1,4-dioxane, and the resultant quinone methide was further hydrated with aqueous hydrochloric acid (HCl)/tetrahydrofuran (THF) solution.[18] The Ag_2O oxidation of sinapyl alcohol, **2**, produced sinapyl aldehyde, **13**, in 14% yield, the β-*O*-4-coupled dimer **14** in 32% yield, the β-β-coupled dimer (syringaresinol, **15**) in 3% yield, and other unidentified oligomeric products (Figure 4). The yield of the β-*O*-4-coupled dimer from the Ag_2O oxidation of sinapyl alcohol was a little higher than the yield reported for $FeCl_3$ oxidation. The oxidative coupling of phenols by Ag_2O has been reported to preferentially form C−O-coupled products, whereas $FeCl_3$ leads to C−C-coupled products.[19]

We examined the Ag_2O-mediated oxidative coupling of the γ-acetylated monomer sinapyl acetate, **4**, to elucidate the effect of the γ-acetyl group on the oxidative coupling of sinapyl alcohol. The Ag_2O oxidation of sinapyl acetate, **4**, in benzene preferentially formed *erythro* and *threo* isomers of the β-*O*-4-coupled dimer, **16**, in 39% yield. In 1,4-dioxane, the selectivity for β-*O*-4-coupled products became even higher. The yield of the *erythro* and *threo* isomers of the β-*O*-4-coupled dimer was 66% (Figure 4). Oligomeric products with predominantly β-*O*-4 structures (Figure 5) were also obtained in 18% yield. However, nontraditional tetrahydrofuran-type β-β-coupled products[10] were not detected by the NMR analysis. These results showed that the Ag_2O-mediated oxidative coupling of sinapyl acetate preferentially formed β-*O*-4 linkages. The yield of the β-*O*-4-coupled products from sinapyl acetate was much higher than that from sinapyl alcohol. The oxidation of the hydroxyl group at the γ-position was completely prevented by the acetyl group in sinapyl acetate, which partially contributed to the high yield of β-*O*-4 products from sinapyl acetate.

Computational Calculations of Atomic Spin Densities and Charges of Sinapyl Radicals. To further understand the effect of the acetyl group at the γ-position in sinapyl acetate, computational calculations based on density functional theory (DFT) were performed. The atomic spin densities of phenoxy radicals derived from sinapyl acetate and sinapyl alcohol are shown in Table 1. The spin densities show that the unpaired electrons are mainly located at C1, C3, C5, Cβ, and O4 in both sinapyl acetate and sinapyl alcohol radicals. The spin densities of these radicals are the highest at O4, which is agreement with the reported data for sinapyl alcohol radical.[20] The C1, C3, and C5 sites are not considered to be important coupling sites in sinapyl alcohol radicals. Thus, the most reactive coupling sites

DOI: 10.1021/jf506111q
J. Agric. Food Chem. 2015, 63, 2277−2283

are Cβ and O4 in both sinapyl acetate and sinapyl alcohol radicals. The radical coupling at Cβ and Cβ produces β-β linkages, whereas coupling at Cβ and O4 produces β-O-4 linkages. The spin densities of carbon and oxygen atoms in sinapyl acetate and sinapyl alcohol radicals are quite similar to each other. The acetyl group at the γ-position did not significantly affect the localization of the unpaired electron in the sinapyl alcohol radical. These results indicate that the modification of the localization of the unpaired electron cannot explain the preferential formation of β-O-4-coupled products by the oxidative coupling of sinapyl acetate.

The charge density at each atom in monolignol radicals is also important for the coupling reaction of the radicals.[20] The electrostatic charges of all carbon and oxygen atoms in sinapyl acetate and sinapyl alcohol radicals are shown in Table 2. The solvent effects of water and 1,4-dioxane were also added to the calculation of the electrostatic charges. These data show that Cβ and O4 were negatively charged in the sinapyl alcohol and sinapyl acetate radicals. As the two radicals approach each other, their negative charges result in Coulombic repulsion between the Cβ and O4 positions.[20] The data show that the negative charge at the Oγ position in the sinapyl acetate radical was much smaller than that in the sinapyl alcohol radical. This result can be reasonably explained by the fact that acyl groups, such as the acetyl group, are electron-withdrawing groups. It is interesting to note that the electron-withdrawing effects of the acetyl group are active even at the Cβ position in the sinapyl acetate radical. The negative charge at Cβ in the sinapyl acetate radical was significantly smaller than that in the sinapyl alcohol radical. This tendency was more obvious when solvent effects were considered in the calculations. The differences in the electrostatic charges at Cβ between the sinapyl acetate and sinapyl alcohol radicals were 0.033 e in 1,4-dioxane and 0.052 e in water. These results suggest that the Coulombic repulsion between the Cβ and O4 positions was significantly reduced by the γ-acetyl group (Figure 6), which resulted in the high yield of β-O-4-coupled products from the oxidative coupling of sinapyl acetate.

In conclusion, compared to the biomimetic oxidative coupling of sinapyl alcohol, the biomimetic oxidative coupling of sinapyl acetate by silver oxide preferentially formed β-O-4-coupled products. Computational calculations showed that the γ-acetyl group significantly decreased the negative charge at Cβ in the sinapyl acetate radical. The Coulombic repulsion between Cβ and O4 seems to be reduced when two sinapyl acetate radicals approach each other. These results suggest that acylated monolignols preferentially couple at Cβ and O4, resulting in the high frequency of β-O-4 structures in highly acylated lignins.

AUTHOR INFORMATION

Corresponding Author

*(T.K.) Phone: +81-766-56-7500 (ext. 567). Fax: +81-766-56-2498. E-mail: takao@pu-toyama.ac.jp.

Funding

Part of this work was supported by JSPS KAKENHI Grant 24658156.

Notes

The authors declare no competing financial interest.

ACKNOWLEDGMENTS

We are grateful to Yuka Nonaka and Junko Kawabata, graduates of the Department of Biotechnology, Toyama Prefectural University, for their contributions to the preliminary experiments of this investigation.

ABBREVIATIONS USED

DFT, density functional theory; HRP, horseradish peroxidase; HSQC, heteronuclear single-quantum coherence

REFERENCES

(1) Sjöström, E. Lignin. In *Wood Chemistry: Fundamentals and Applications*; Academic Press: San Diego, CA, USA, 1993; pp 71−89.

(2) Kishimoto, T.; Uraki, Y.; Ubukata, M. Easy synthesis of β-O-4 type lignin related polymers. *Org. Biomol. Chem.* **2005**, *3*, 1067−1073.

(3) Kishimoto, T.; Uraki, Y.; Ubukata, M. Chemical synthesis of β-O-4 type artificial lignin. *Org. Biomol. Chem.* **2006**, *4*, 1343−1347.

(4) Kishimoto, T.; Uraki, Y.; Ubukata, M. Synthesis of β-O-4-type artificial lignin polymers and their analysis by NMR spectroscopy. *Org. Biomol. Chem.* **2008**, *6*, 2982−2987.

(5) Ralph, J.; Landucci, L. L. NMR of lignins. In *Lignin and Lignans: Advances in Chemistry*; Heitner, C., Dimmel, D. R., Schmidt, J. A., Eds.; CRC Press: New York, 2010; pp 137−244.

(6) Ralph, J. An unusual lignin from kenaf. *J. Nat. Prod.* **1996**, *59*, 341−342.

(7) del Río, J.; Rencoret, J.; Marques, G.; Gutiérrez, A.; Ibarra, D.; Santos, J.; Jiménez-Barbero, J.; Zhang, L.; Martínez, Á. Highly acylated (acetylated and/or *p*-coumaroylated) native lignins from diverse herbaceous plants. *J. Agric. Food Chem.* **2008**, *56*, 9525−9534.

(8) Villaverde, J. J.; Li, J.; Ek, M.; Ligero, P.; de Vega, A. Native lignin structure of *Miscanthus* × *giganteus* and its changes during acetic and formic acid fractionation. *J. Agric. Food Chem.* **2009**, *57*, 6262−6270.

(9) Kishimoto, T.; Chiba, W.; Saito, K.; Fukushima, K.; Uraki, Y.; Ubukata, M. Influence of syringyl to guaiacyl ratio on the structure of natural and synthetic lignins. *J. Agric. Food Chem.* **2010**, *58*, 895−901.

(10) Lu, F.; Ralph, J. Novel tetrahydrofuran structures derived from β-β-coupling reactions involving sinapyl acetate in Kenaf lignins. *Org. Biomol. Chem.* **2008**, *6*, 3681−3694.

(11) Lu, F.; Ralph, J.; Morreel, K.; Messens, E.; Boerjan, W. Preparation and relevance of a cross-coupling product between sinapyl alcohol and sinapyl *p*-hydroxybenzoate. *Org. Biomol. Chem.* **2004**, *2*, 2888−2890.

(12) Tanahashi, M.; Takeuchi, H.; Higuchi, T. Dehydrogenative polymerization of 3,5-disubstituted *p*-coumaryl alcohols. *Wood Res.* **1976**, *61*, 44−53.

(13) Zanarotti, A. Synthesis and reactivity of lignin model quinone methide. Biomimetic synthesis of 8-O-4′ neolignan. *J. Chem. Res., Synop.* **1983**, 306−307.

(14) Zanarotti, A. Preparation and reactivity of 2,6-dimethoxy-4-allyliden-2,5-cyclohexadien-1-one (vinyl quinone methide). A novel synthesis of sinapyl alcohol. *Tetrahedron Lett.* **1982**, *23*, 3815−3818.

(15) Jing, X.; Gu, W.; Bie, P.; Ren, X.; Pan, X. Total synthesis of (±)-eusiderin K and (±)-eusiderin J. *Synth. Commun.* **2001**, *31*, 861−867.

(16) Quideau, S.; Ralph, J. A biomimetic route to lignin model compound via silver(I) oxide oxidation. 1. Synthesis of dilignols and non-cyclic benzyl aryl ethers. *Holzforschung* **1994**, *48*, 12−22.

(17) Alam, S.; Suzuki, T.; Katayama, T. Formation of optically active *erythro*-syringylglycerol-8-*O*-4′-(sinapyl alcohol) ethers from achiral monolignols with enzyme preparations of higher plant. *Middle-East J. Sci. Res.* **2010**, *6*, 340−345.

(18) Hawkes, G. E.; Smith, C. Z.; Utley, H. P.; Chum, H. Key structural feature of acetone-soluble phenol-pulping lignins by ^{1}H and ^{13}C NMR spectroscopy. *Holzforschung* **1986**, *40* (Suppl.), 115−123.

(19) Cotelle, P.; Vezin, H. The reaction of methyl isoferulate with $FeCl_3$ or Ag_2O − hypothesis on the biosynthesis of lithospermic acids

DOI: 10.1021/jf506111q
J. Agric. Food Chem. 2015, 63, 2277−2283

and related nor and neolignans. *Tetrahedron Lett.* **2003**, *44*, 3289−3292.
(20) Shigematsu, M.; Masamoto, H. Solvent effects on the electronic state of monolignol radicals as predicted by molecular orbital calculations. *J. Wood Sci.* **2008**, *54*, 308−301.

DOI: 10.1021/jf506111q
J. Agric. Food Chem. 2015, 63, 2277−2283

genome allows the differentiation of even closely related genotypes.[6,22] For example, Ganopoulos et al.[23] were successful in discriminating 21 Greek sweet cherry cultivars by genotyping nine genic SNP loci. Moreover, a sufficient number of SNPs for varietal origin detection can be identified by analyzing relatively short DNA sequences. Reale et al.[24] did the first work describing SNP marker development for olive cultivar identification and identified 22 SNPs with only 3440 bp (base pair) of olive genic sequence. Thus, they observed a high frequency of SNP occurrence (1 SNP per 156 bp). Using a total of 11 markers, 8 of which were SNP derived, Reale et al.[24] discriminated 47 olive accessions. Following Reale et al.,[24] Consolandi et al.[25] used 17 SNP loci to differentiate 49 olive varieties that are commonly cultivated in the Mediterranean region and developed a SNP-based ligation detection assay for varietal origin detection. The efficiency of the SNP-based ligation detection assay was displayed on eight monovarietal olive oils from Italy, Spain, France, and Portugal.[1]

Restriction profile-based genotyping, either referred to as CAPS or PCR-RFLP (PCR-restriction fragment length polymorphism), has been successfully used in a number of DNA-based food authentication studies. Dooley et al.[26] were able to discriminate ten white fish species by using three PCR-RFLP assays that target a 464 bp region of the *Cytochrome b* gene. In addition, the reproducibility of the assays was displayed by an interlaboratory study that involves five different food control laboratories in the United Kingdom. Spaniolas et al.[27] described a single SNP-based PCR-RFLP assay that allows the discrimination of Arabica and Robusta coffee samples. Bazakos et al.[21] were first to display the effectiveness of a PCR-RFLP (restriction fragment length polymorphism) approach to identify the varietal origin of olive oils based on their SNP alleles. The authors were able to discriminate eight olive varieties using five SNPs and showed the usefulness of this approach on five Greek monovarietal olive oils.

Turkey is among the world's leading olive producers and ranks fourth with 1 676 000 tonnes (t) of total production, following Spain (7 875 000 t), Italy (3 022 886 t), and Greece (2 000 000 t).[28] According to statistics released by the International Olive Oil Council, Turkey ranked fifth in olive oil production in the harvest year 2011/2012 after Spain, Italy, Greece, and Syria.[29] Turkish olive cultivars such as Ayvalik, Memecik, Gemlik, and Nizip Yaglik are known for their oils with distinctive sensory features.[30] In a limited number of studies, DNA markers were used for the molecular characterization of Turkish olive cultivars.[31−34] However, there is no report on the use of molecular markers for establishing DNA barcodes of Turkish monovarietal olive oils. The aim of this work was to discriminate commonly cultivated Turkish olive varieties using the fewest possible SNP markers and to standardize SNP-based molecular assays that complement the shortcomings of conventional analytical approaches in resolving the traceability of premium monovarietal olive oils.

MATERIALS AND METHODS

Plant Material and Oil Samples. Leaf and oil samples of 17 commonly cultivated Turkish olive varieties were used in this study. Leaf samples of each olive variety were collected from three individual plants. Cultivar names and primary usage information are provided in Table 1. Leaf samples and filtered monovarietal oils produced by a laboratory-scale mill were obtained from the Olive Research Institute (Izmir, Turkey). Commercial olive oil samples were obtained from a retail market.

Table 1. Olive Varieties Used in The Study

olive variety	common usage[a]	region of cultivation
Memecik	oil	southern Aegean
Gemlik (Trilye)	table/oil	Marmara
Ayvalik	oil	northern Aegean
Uslu	oil/table	southern Aegean
Erdek Yaglik	table/oil	Marmara
Kilis Yaglik	oil	southeast Anatolia
Nizip Yaglik	oil	southeast Anatolia
Tesbih Celebi	oil	southeast Anatolia
Tekirdag Siyah Salamura	table/oil	Marmara
Domat	table/oil	Aegean
Yun Celebi	oil/table	southeast Anatolia
Cekiste	table/oil	Aegean
Mavi	oil	southeast Anatolia
Sinop No:5	oil	Black Sea
Patos	oil/table	Black Sea
Maraş No:7	oil	southeast Anatolia
Saurani	oil	Mediterranean

[a]Primary usage is indicated first for the varieties that have both uses.

DNA Isolation. DNA from the leaf tissue of three replicate plants was isolated from 200 mg of liquid nitrogen-frozen ground leaf tissue using a CTAB method.[35] For isolating DNA from monovarietal olive oil samples, Wizard Magnetic DNA Purification System for Food (Promega Corp., Madison, WI) was used according to the manufacturer's instructions. The concentration of DNA from leaf and oil samples was measured using a Qubit 2.0 Fluorometer (Life Technologies, Thermo Fisher Scientific Inc., Waltham, MA) with dsDNA BR Assay Kit (Life Technologies). DNA integrity was checked on a 1.5% agarose gel.

Primer Design, Sequencing, and SNP Identification. Primers that amplify targets from the *Cycloarthenol synthase* and *Lupeol synthase* genes were designed on the basis of the partial coding sequences Genbank Acc. No. AY847065 and AY847066, respectively (http://www.ncbi.nlm.nih.gov/genbank) (Table 2). The primer design process was carried out using Primer3 software.[36] The primers Cyc6-F and Lup1-F&R were previously reported by Bazakos et al.[21] (Table 2). Primers that target the *Anthocyanidin synthase* (Ant-F&R), *Calcium binding protein* (Cbp-F&R), and *Chalcone synthase* (Chs-F&R) genes were reported by Consolandi et al.[1] (Table 2).

Leaf DNA from the 17 olive varieties was used for dye-terminator sequencing reactions. Sequencing targets were amplified in 20 μL reaction mixtures containing 1X PCR buffer, 1.5 mM $MgCl_2$, 0.25 mM of each deoxyribonucleotide triphosphate (dNTP) (Promega Corp.), 1 U Taq polymerase, 0.25 μM of each primer, and 5 ng template DNA. Thermal cycling conditions consisted of one cycle of initial denaturation for 10 min at 94 °C, followed by 35 cycles of 94 °C for 30 s, 57 °C for 30 s, 72 °C for 45 s, with a final extension step of 10 min at 72 °C. For each olive variety, PCR reactions were performed in five replicates and combined during the purification step with the DNA Clean & Concentrator-5 Kit (Zymo Research, Irvine, CA). Purified PCR products were used as template in dye-terminator sequencing reactions, prepared using GenomeLab DTCS Quick Start Kit (Beckman Coulter, Brea, CA) according to the manufacturer's instructions. Sequencing reaction thermal cycling conditions were 30 cycles of 96 °C 20 s, 50 °C 20 s, 60 °C 4 min. The reaction mixture for each amplicon was then purified using ZR DNA Sequencing Clean-up Kit (Zymo Research), resuspended in 30 μL of sample loading solution (Beckman Coulter), and run on a Beckman CEQ8800 capillary electrophoresis device using the LFR-c method (injection voltage 2.0 kV for 10−15 s, separation temperature 60 °C, separation voltage 7.4 kV, separation time 45 min). Sequence peaks were visualized by Beckman CEQ8800 software version 8.0 (Beckman Coulter), and SNP detection was done by visual inspection of sequence peaks from different varieties.

DOI: 10.1021/acs.jafc.5b00090
J. Agric. Food Chem. 2015, 63, 2284−2295

Table 2. List of Primers Used for SNP Identification and Genotyping[a]

primer[b] name	sequence (5′ to 3′)	product size	assay name	SNP alleles	motif[c] (5′ to 3′)
*Ant-F**	GCCCAGCAACAAGTGAGTATG	274 bp	SNP3-HphI	C/T	GG**T**GA
*Ant-R**	GACCCATTTTCCCTCACAGA				
*Cbp-F**	CAGGAATTCCAAGCCTTCAG	328 bp	SNP6-EagI	C/G	CGG**C**CG
*Cbp-R**	GCTCGACGGATGAGATCAAT				
*Chs-F**	TCGGAGATTACTGCGGTTACTT	297 bp	SNP2-BsgI	C/T	**CT**GCAC
*Chs-R**	CTAGAGGCTGGAATGCTTCA				
Cyc1-F	TTTGCTCCCAGGTCATTA	165 bp			
Cyc1-R	GGATGCTGTAGCATGACA				
Cyc2-F	TGGTTTGCCTTTTCATTT	168 bp	SNP4-Hpy166II	C/T	GTNNA**C**
Cyc2-R	ACCAAATTCTTCCCCAAG				
Cyc3-F	AGCTTGGGGAAGAATTTGGTC	198 bp			
Cyc3-R	ATATCGCCTGGGCAATCCTC				
Cyc4-F	TCTTTTCTTTAGGCGGTTC	173 bp			
Cyc4-R	AGGTGGAAACATCACAATG				
Cyc5-F	AACAGCAATTGTTGGTGAA	163 bp	SNP5-HindIII	C/T	AAG**C**TT
Cyc5-R	ATCCCTTTCCGAAAACAA				
Cyc6-F**	TTCTGTTGTTTTCGGAAAGG	220 bp			
Cyc6-R	TGGAGCCATCTTTTTCCAAT				
Lup1-F**	GCAACTCAAATGAATGAATC	125 bp			
Lup1-R**	TCTAAGAAACGGACTTGCTAT				
Lup2-F	AGTAGCATACCCTGTGTTTC	204 bp			
Lup2-R	TTGCTTGTTGGGTAGAAGAT				
Lup3-F	ACCCTGTGTTTCGATTTGCT	107 bp	SNP1-HpyCH4III	A/T	ACNG**T**
Lup3-R	ATGCAGGTTATTTTCTTTCATCA				

[a]Unless indicated otherwise, primers were designed in this study. [b]Single asterisk indicates primers reported by Consolandi et al. (2008). Double asterisks indicate primers reported by Bazakos et al. (2012). Primers used in CAPS assays are given in italics. [c]Nucleotides in bold indicate SNP loci in motifs.

Design and Application of the CAPS Assays for SNP Genotyping. Sequences obtained by the dye-terminator method were analyzed with the NEBcutter Version 2.0 software (http://tools.neb.com/NEBcutter2/) (New England Biolabs Inc., Ipswich, MA) for the allelic variants of each SNP identified. SNPs with alleles that alter recognition motifs of restriction enzymes were selected for genotyping by a restriction digestion-based analysis.

Fragments that harbor SNP loci were amplified in 20 μL reaction mixtures containing 1X PCR buffer, 1.5 mM $MgCl_2$, 0.25 mM of each deoxyribonucleotide triphosphate (dNTP) (Promega Corp.), 1 U Taq polymerase, 0.25 μM of each primer, and 5 ng of olive leaf DNA or 5 ng of oil DNA stock solution as template. Thermal cycling conditions consisted of one cycle of initial denaturation for 10 min at 94 °C, followed by 40 cycles (35 cycles for leaf DNA) of 94 °C for 30 s, 57 °C for 30 s, 72 °C for 45 s, with a final extension step of 10 min at 72 °C. PCR products were directly subjected to restriction digestion without any purification step. Digestion reaction mixtures of the CAPS assays (Table 2) contained 20 μL of PCR product, 1 μL of restriction enzyme (New England Biolabs Inc.), and 2.5 μL of CutSmart reaction buffer (New England Biolabs Inc.) in a total volume of 25 μL. Reaction mixtures of the enzyme EagI involved NEBuffer 3.1 instead of the CutSmart buffer, and 0.25 μL of *S*-adenosylmethione was added to the BsgI reaction mixtures. Incubation temperature was constant (37 °C) for all enzymes, and incubation time was standardized as 6 h. Following the incubation step, digestion fragments were run on a Qiaxcel Advanced capillary electrophoresis system (Qiagen, Valencia, CA) using a Qiaxcel DNA High Resolution Kit (Qiagen). QX DNA Size Marker 25−500bp, v2.0 (Qiagen) was used as the size standard, and QX Alignment Marker 15 bp/600 bp (Qiagen) was used for aligning the size standard fragments. The high resolution run method OM800 was applied with a sample injection time of 20 s. QIAxcel ScreenGel Software (Qiagen) was used for the visualization of the digestion profiles. The six CAPS assays developed in this work were applied on the oil DNA of each olive variety in three replicates.

Statistical Analysis. The frequency of each SNP allele was determined by calculating the proportion of the occurrence of the allele to the total number of alleles at a given SNP locus. Probability of identity for individual SNP loci and the combined, multilocus probability of identity were calculated according to Paetkau et al.[37] Allelic error was calculated according to Pasqualone et al.[38]

RESULTS

SNP Identification by Sequencing. Five olive genes, *Anthocyanidin synthase* (*Ant*), *Calcium binding protein* (*Cbp*), *Chalcone synthase* (*Chs*), *Cycloarthenol synthase* (*Cyc*), and *Lupeol synthase* (*Lup*), were targeted for SNP identification by sequencing. Leaf genomic DNA from the 17 olive varieties (Table 1) was used as template for the dye-terminator sequencing reactions. Total lengths of the sequencing targets from *Cyc*, *Lup*, *Cbp*, *Chs*, and *Ant* genes were 1087 (six amplicons), 436 (three amplicons), 328 (one amplicon), 297 (one amplicon), and 274 bp (one amplicon), respectively (Table 2). Sequencing of these 12 PCR amplicons that spanned 2422 bp of coding sequence resulted in the identification of 17 SNPs, corresponding to a frequency of 1 SNP per 142.5 bp of coding sequence. Among these SNPs, five, one, two, six, and three SNPs were identified in the *Ant*, *Cbp*, *Chs*, *Cyc synthase*, and *Lup* sequences, respectively.

Design of CAPS Assays for SNP Genotyping. In order to develop a restriction digestion-based SNP genotyping strategy, sequences obtained from the five olive genes by dye-terminator method were analyzed to identify SNPs that reside in restriction enzyme recognition motifs. In the analysis, allelic variants were taken into account for each SNP, so that restriction enzymes with allele-dependent digestion patterns could be identified. As a result, allelic variants of 12 of the 17 SNP loci (71%) were found to alter restriction enzyme recognition motifs. CAPS assays were designed for each SNP

DOI: 10.1021/acs.jafc.5b00090
J. Agric. Food Chem. 2015, 63, 2284−2295

Table 3. Genotypes of the 17 Olive Varieties for the SNPs Used for Constructing the Cultivar Origin Identification Key

olive variety	SNP1-HpyCH4III	SNP2-BsgI	SNP3-HphI	SNP4-Hpy166II	SNP5-HindIII	SNP6-EagI
Memecik	TA	CC	CC	TT	CC	GG
Gemlik(Trilye)	TA	CC	CT	TC	CC	GG
Ayvalik	AA	CT	CT	TC	CC	GG
Uslu	TT	CC	CT	TT	CT	GG
Erdek Yaglik	TA	CC	CT	TC	CC	GG
Kilis Yaglik	TA	CC	CC	TT	CT	GC
Nizip Yaglik	AA	CT	CC	TT	CC	GG
Tesbih Celebi	TA	CC	CC	TT	CT	GC
Tekirdag SS[a]	TA	CC	CT	TC	CC	GG
Domat	TA	CC	CT	TT	CT	GG
Yun Celebi	AA	CC	CT	TT	CC	GC
Cekiste	AA	CC	CC	TT	CC	GG
Mavi	TA	CT	CT	TT	CT	GC
Sinop No:5	TT	CC	CC	TT	CT	GC
Patos	TA	CC	CT	TC	CT	GG
Maraş No:7	TA	CC	CC	TT	CT	GG
Saurani	AA	CT	CT	TT	CC	GG

[a]Variety name Tekirdag Siyah Salamura is abbreviated as Tekirdag SS.

and applied on leaf DNA from three replicate plants for SNP verification (data not shown). The assays involved amplification of the PCR product that harbored the SNP, restriction digestion of the amplicon with the appropriate restriction enzyme, and visualization of the digestion pattern with capillary electrophoresis. Out of the 12 CAPS assays, a subset of six was sufficient to provide the discrimination power to distinguish 17 olive varieties. As a result, those six assays (Table 2) were used to establish an identification key for the monovarietal olive oils.

SNP1, identified in the *Lup* gene, had A and T variants. On the basis of SNP1 alleles, the olive varieties were separated into three groups (Table 3). A total of 5 varieties were homozygous for the A allele, 10 varieties were heterozygous carrying both A and T alleles, and 2 varieties were homozygous for the T allele. The T allele of SNP1 resulted in an intact HpyCH4III recognition motif, while the A allele disrupted the motif. As a result, genotypes homozygous for the T allele were distinguished by a homozygous digestion pattern with two restriction fragments, whereas genotypes homozygous for the A allele produced a single undigested fragment. Heterozygous genotypes yielded a three fragment digestion pattern with two digestion fragments and the undigested amplicon (Figures 2−4). SNP2, identified in the *Chs* sequence, separated the olive varieties into two groups. While 13 homozygous genotypes carried only the C allele, the remaining four genotypes were heterozygous and carried C and T alleles (Table 3). The C allele disrupted the recognition site for the restriction enzyme BsgI, leading to a single undigested fragment for homozygous genotypes. In contrast, heterozygous genotypes carried one copy of the intact BsgI restriction site and were distinguished by a three fragment digestion pattern in the capillary electropherograms (Figures 2−4). SNP3 was identified in the *Ant* sequence and allowed separation of olive varieties into two groups. Genotypes homozygous for SNP3 (seven varieties) carried only the C allele (Table 3) and were distinguished by a single undigested fragment. Whereas, due to the presence of the T allele, heterozygous genotypes (ten varieties) (Table 3) carried one copy of an intact HphI recognition motif and produced a three fragment HphI digestion pattern (Figures 2−5). SNP4 and SNP5 were both identified in sequences from the *Cyc* gene. Olive genotypes were either homozygous (TT) (12 varieties) or heterozygous (TC) (5 varieties) for the SNP4 locus (Table 3). Homozygous genotypes were distinguished by a homozygous Hpy166II digestion pattern with two restriction fragments. Because the C allele disrupted the recognition motif for the enzyme, heterozygous genotypes were identified by three fragments in their capillary electropherograms (Figures 3 and 4). SNP5 separated olive varieties into two groups of nine homozygous (CC) and eight heterozygous (TC) genotypes (Table 3). Homozygous genotypes (CC) displayed a homozygous digestion pattern with two HindIII digestion fragments in their capillary electropherograms. Heterozygous genotypes (TC) were distinguished by a three fragment digestion pattern including the two digestion fragments and the undigested amplicon (Figures 3 and 4). Olive varieties were either homozygous (GG) (12 varieties) or heterozygous (CG) (five varieties) for SNP6, identified in the *Cbp* gene (Table 3). Because the G allele disrupted the EagI recognition motif, homozygous genotypes displayed a single undigested fragment in their capillary electropherograms. Heterozygous genotypes carrying one copy of an intact EagI recognition site were characterized by a three fragment restriction pattern (Figure 4). Allelic frequencies of the six SNP loci used for the discrimination of the olive varieties are given in Table 4.

Fingerprinting Monovarietal Olive Oils Using SNP-Based CAPS Markers. Among the six SNPs used to design CAPS assays, combinations that involved two, three, four, or five SNPs were sufficient to discriminate the olive varieties (Figure 1). Therefore, variable sets of CAPS assays were applied to the oil DNA samples of the 17 varieties. SNP1-HpyCH4III assay was common in the discriminatory assay combinations for all varieties. However, different combinations of the remaining five assays (SNP2-BsgI, SNP3-HphI, SNP4-Hpy166II, SNP5-HindIII, and SNP6-EagI) were used for the identification of the olive varieties.

Only two SNPs were sufficient to discriminate Uslu, Mavi, and Sinop No:5 varieties. Discrimination of both Uslu and Sinop No:5 oils involved using the SNP1-HpyCH4III and SNP3-HphI assay combination (Figure 2). The SNP2-BsgI assay was used instead of SNP3-HphI for the discrimination of the Mavi variety (Figure 2). Identification of the varieties, Nizip Yaglik, Yun Celebi, and Cekiste, involved using three SNPs. A

DOI: 10.1021/acs.jafc.5b00090
J. Agric. Food Chem. 2015, 63, 2284−2295

Table 4. Allele Frequency, Informativeness, and Reproducibility of the Six SNP Markers, Expressed as Probability of Identity and Allelic Error, Respectively

SNP locus	AF[a]		PI[b]	AE[c]
	T	A		
SNP1	0.41	0.59	0.383	0.000
	C	T		
SNP2	0.88	0.12	0.649	0.000
	C	T		
SNP3	0.71	0.29	0.428	0.000
	C	T		
SNP4	0.15	0.85	0.593	0.000
	C	T		
SNP5	0.76	0.24	0.475	0.000
	G	C		
SNP6	0.85	0.15	0.593	0.000
multilocus PI			0.018	

[a]AF, allele frequency. [b]PI, probability of identity. [c]AE, allelic error.

common set of CAPS assays (SNP1-HpyCH4III, SNP2-BsgI, and SNP3-HphI) was used to discriminate the monovarietal oils of these varieties (Figure 2). The varieties Memecik, Ayvalik, Domat, and Saurani could be discriminated from the rest using four SNPs. Ayvalik, Domat, and Saurani oils were discriminated using an identical set of assays that included SNP1-HpyCH4III, SNP2-BsgI, SNP3-HphI, and SNP4-Hpy166II (Figure 3) whereas the SNP5-HindIII assay was required instead of SNP4-Hpy166II for the discrimination of Memecik oil (Figure 3). Among the 17 commonly cultivated Turkish olive varieties included in this work, two groups of cultivars were suggested as synonyms by the experts of the Olive Research Institute (Izmir, Turkey) based on long-term agromorphological observations. In agreement with these observations, the genotypes of the two groups of varieties were identical for all of the 17 SNPs identified in this study (data not shown). However, further detailed molecular genetic characterization would confirm whether the two groups of olive varieties are actually synonyms. The first group of varieties that are suggested as synonyms was Gemlik, Erdek, and Tekirdag Siyah Salamura. A combination of five CAPS assays (SNP1-HpyCH4III, SNP2-BsgI, SNP3-HphI, SNP4-Hpy166II, and SNP5-HindIII) allowed the discrimination of these three monovarietal oils from the rest of the collection (Figure 4). The second group of varieties suggested as synonyms was Kilis Yaglik and Tesbih Celebi. By using a set of five CAPS assays (SNP1-HpyCH4III, SNP2-BsgI, SNP3-HphI, SNP5-HindIII, and SNP6-EagI), the oils of these two varieties were discriminated from the rest of the monovarietal olive oils (Figure 4). Olive varieties Patos and Maras No:7 were also distinguished from the rest using five SNPs. Thus, a set of five assays (SNP1-HpyCH4III, SNP2-BsgI, SNP3-HphI, SNP4-

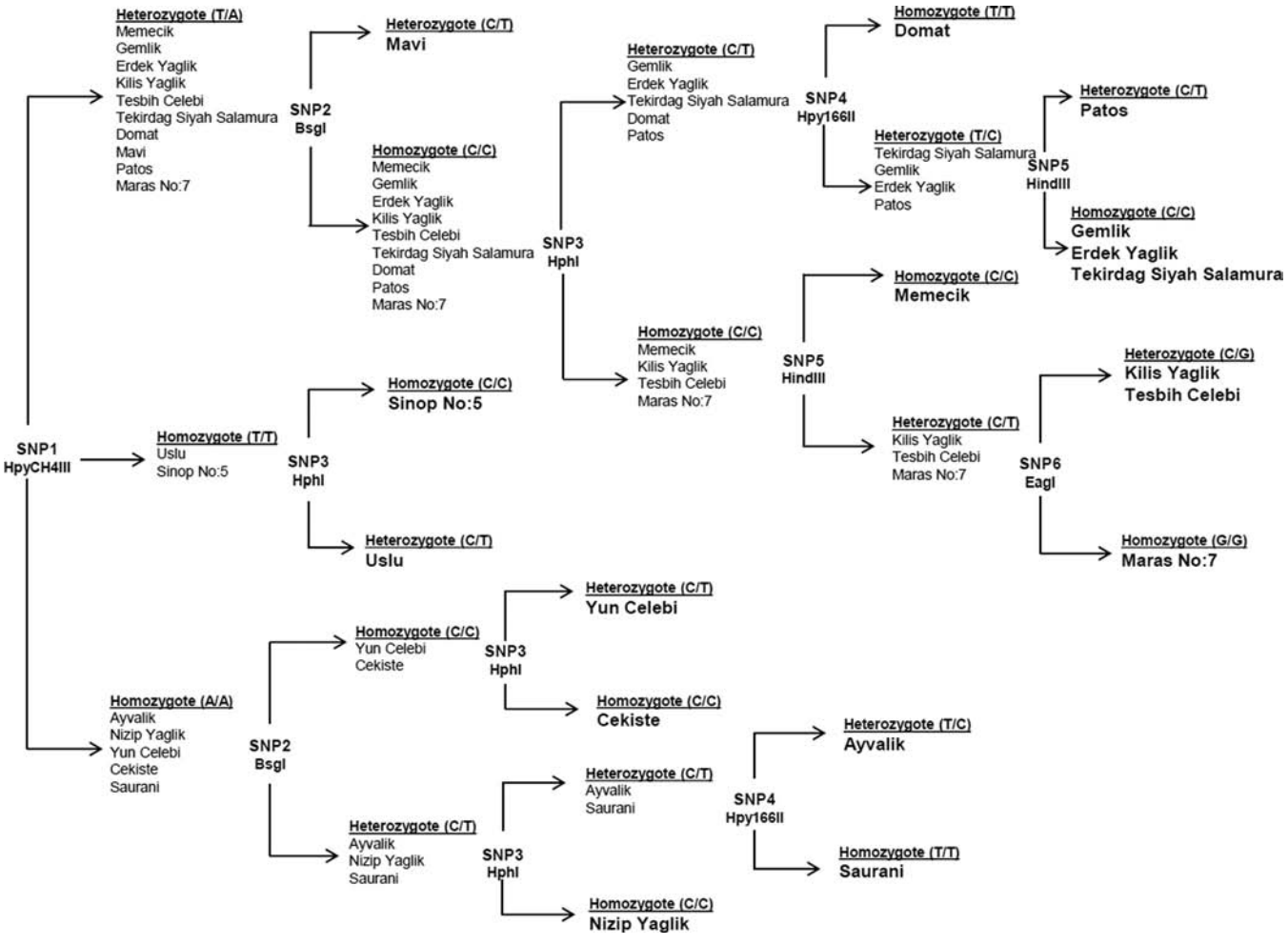

Figure 1. Identification key displaying the discrimination of Turkish olive cultivars according to SNP-based CAPS assays.

DOI: 10.1021/acs.jafc.5b00090
J. Agric. Food Chem. 2015, 63, 2284−2295

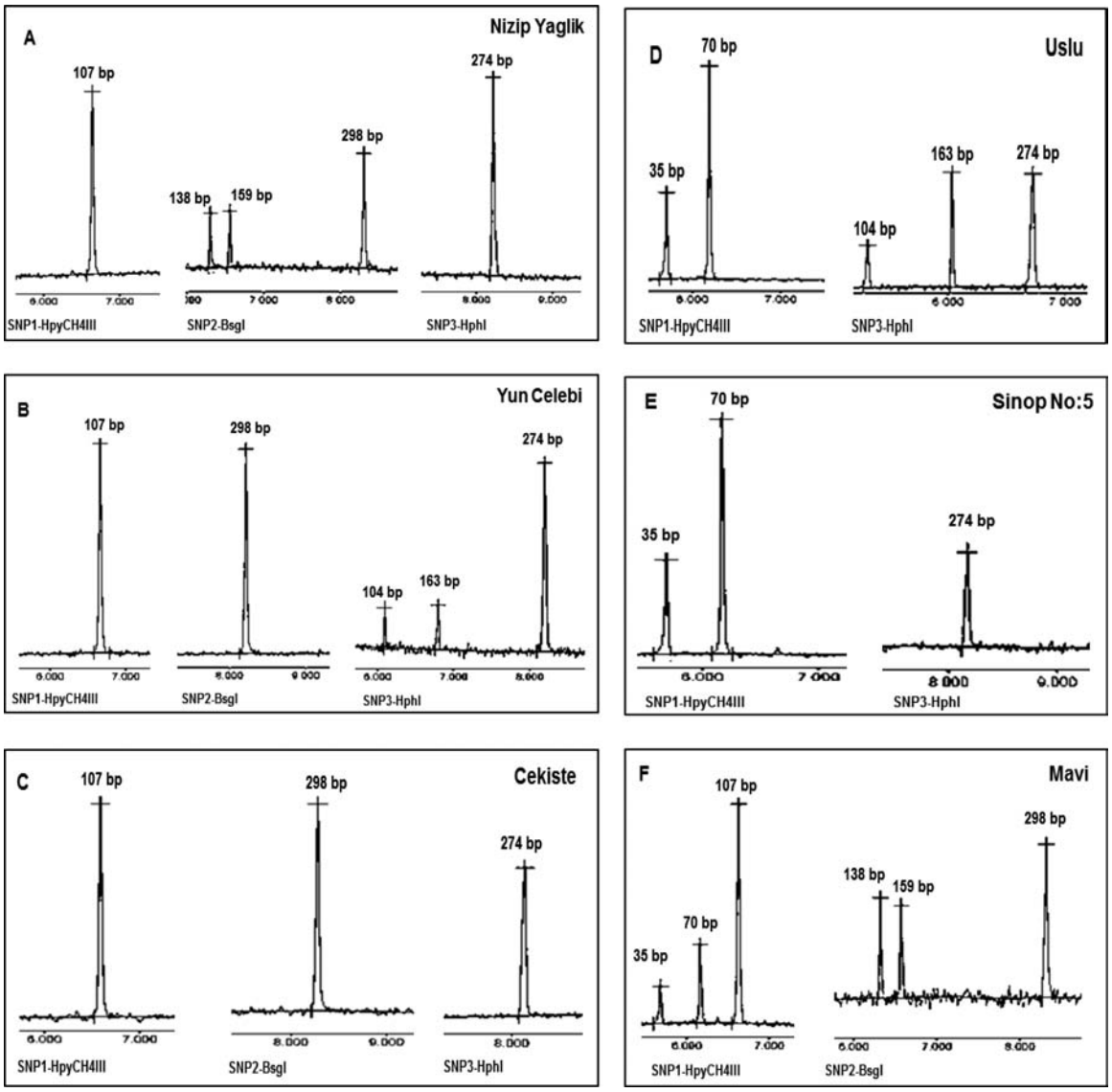

Figure 2. Electrophoretic patterns obtained by SNP-based CAPS assays for the monovarietal olive oils discriminated by two or three SNPs. Each capillary electropherogram displays the result of a SNP-based CAPS assay: A, Nizip Yaglik; B, Yun Celebi; C, Cekiste; D, Uslu; E, Sinop No:5; F, Mavi.

Hpy166II, and SNP5-HindIII) was used for the discrimination of Patos oil (Figure 4), while the SNP6-EagI assay was interchanged with the SNP4-Hpy166II assay for the discrimination of Maras No:7 oil (Figure 4).

Application of the SNP-Based CAPS Markers for Detecting Olive Oil Mixtures and Commercial Oil Samples. We tested the usefulness of our CAPS assays in identifying olive oil admixtures. For this purpose, we used oil from the Memecik and Uslu varieties, both of which are commonly cultivated in the South Aegean region of Turkey. We prepared admixtures of Memecik and Uslu oils at different ratios, extracted DNA from those admixtures, and applied the SNP3-HphI assay to determine if we could detect the contribution of DNA from the Uslu oil in the admixtures. When applied on the Memecik variety, the SNP3-HphI assay yielded a single, undigested fragment (Figure 3). Because Uslu was heterozygous for SNP3, application of the same assay yielded a three-fragment digestion pattern when applied on the oil of this variety (Figure 2). Therefore, any digestion fragment alongside the undigested band would be proof of an impurity in a Memecik oil sample. The olive oil samples prepared for the admixture detection assay contained 50%, 40%, 30%, 20%, and 10% of Uslu oil added to Memecik oil. In order to assess the limit of detecting olive oil admixtures confidently, SNP3-HphI assay was carried out in three replicates on each DNA sample. As a result of the analysis, we successfully detected Uslu oil contribution down to a limit of 20% (Figure 5). Because the admixture with 10% Uslu oil was detected only once out of the three replicate analyses, a 10% contribution by an undeclared variety was considered to be below the limit of detection of the CAPS analysis (data not shown).

We further tested the applicability of the SNP-based CAPS markers on two commercial olive oil samples. While sample no. 1 had its cultivar origin declared on the label as "Memecik", sample no. 2 was not labeled as a monovarietal product. A DNA concentration of approximately 2 ng/μL was measured by fluorometer for both of the commercial samples, which constituted a sufficient quantity of template DNA for further PCR amplifications. The entire set of six CAPS assays (Table 2) was applied on DNA from both samples in three replicates.

DOI: 10.1021/acs.jafc.5b00090
J. Agric. Food Chem. 2015, 63, 2284−2295

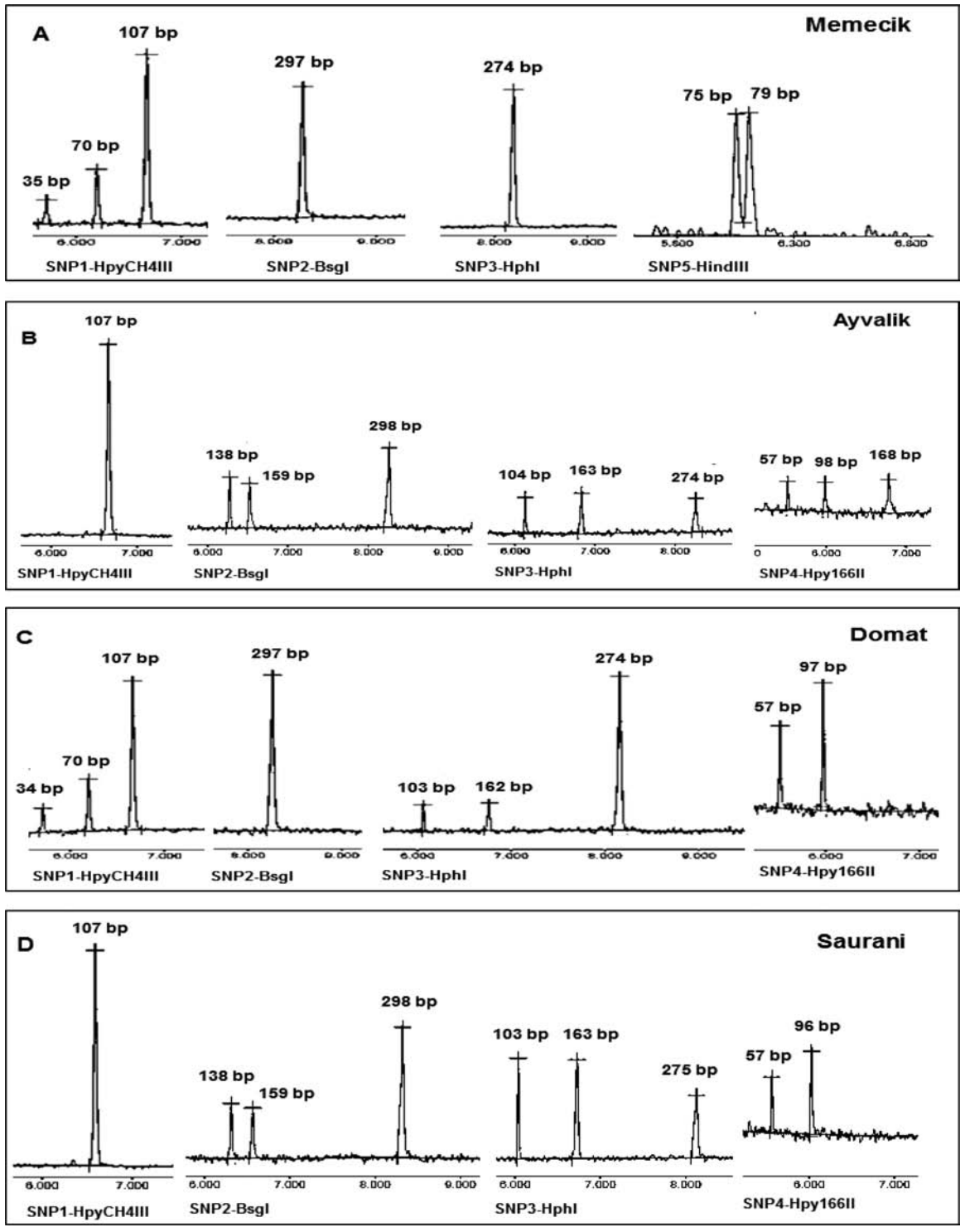

Figure 3. Electrophoretic patterns obtained by SNP-based CAPS assays for the monovarietal olive oils discriminated by four SNPs. Each capillary electropherogram displays the result of a SNP-based CAPS assay: A, Memecik; B, Ayvalik; C, Domat; D, Saurani.

For sample no. 1, the digestion profiles resulting from the six assays (Figure 6) were in agreement with the genotype of the Memecik variety (Table 2), and did not provide any evidence to suspect the declared varietal origin of the product. In case of sample no. 2, the digestion profiles obtained from the six assays (Figure 7) matched the combined SNP genotypes of none of the 17 varieties (Table 2). In addition, the result of the SNP2-BsgI assay (Figure 7) excluded the four varieties, Ayvalik, Nizip Yaglik, Mavi, and Saurani, as these varieties were heterozygous for this locus. As a result, it was concluded that either the cultivar origin of sample no. 2 was not represented in the set of 17 varieties or the product was a mixture of the oils from different varieties. The latter seemed to be a more viable explanation, because sample no. 2 was not declared as a monovarietal product on the label and the genotypes included in this work represent the most commonly cultivated Turkish olive varieties.

DOI: 10.1021/acs.jafc.5b00090
J. Agric. Food Chem. 2015, 63, 2284−2295

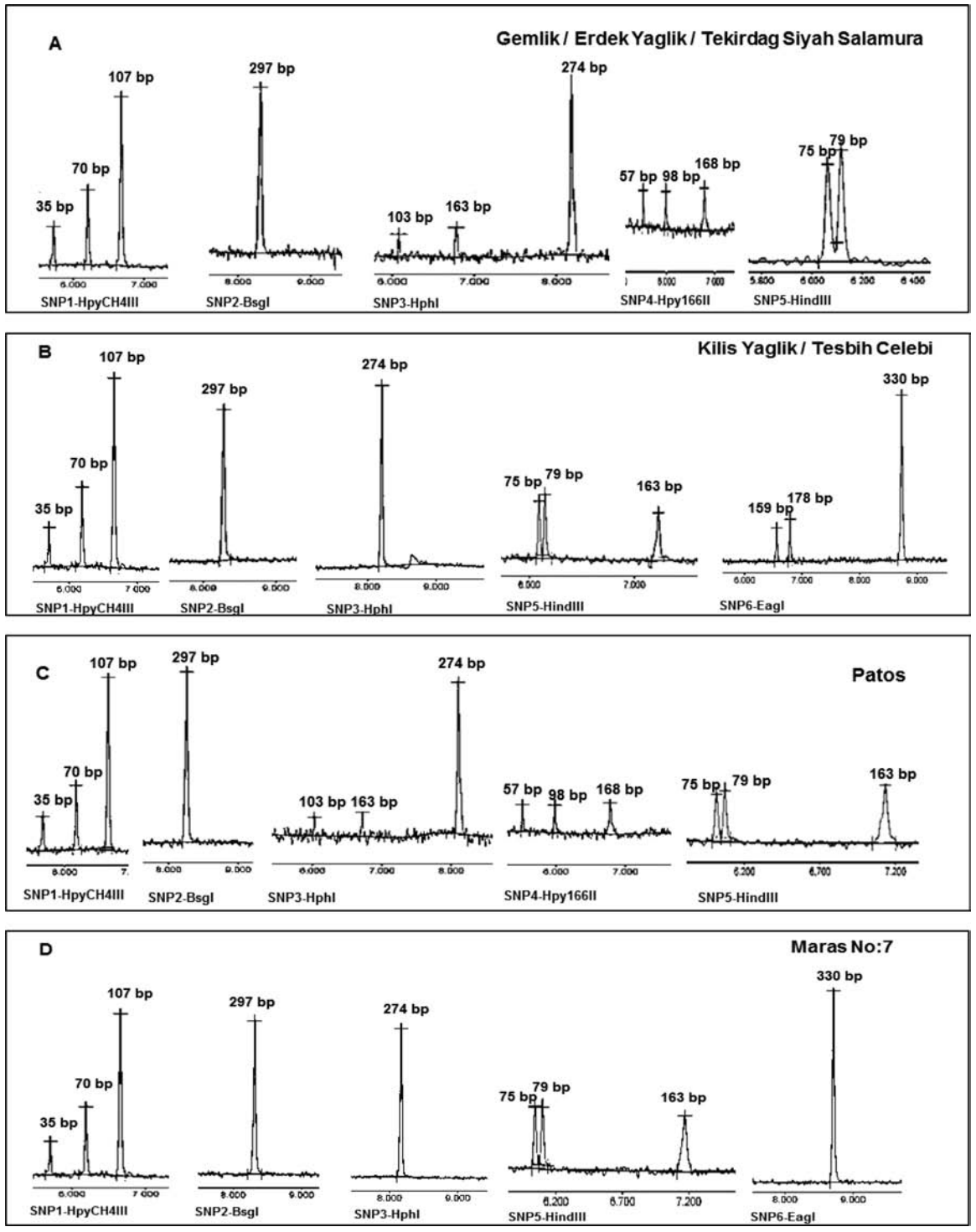

Figure 4. Electrophoretic patterns obtained by SNP-based CAPS assays for the monovarietal olive oils discriminated by five SNPs. Each capillary electropherogram displays the result of a SNP-based CAPS assay: A, Gemlik, Erdek Yaglik, Tekirdag Siyah Salamura; B, Kilis Yaglik, Tesbih Celebi; C, Patos; D, Maras No:7.

DISCUSSION

As an agro-food product with great economic value, virgin olive oil is an attractive target for adulteration and mislabeling. While olive oils with mislabeled cultivar origin do not constitute a health threat, traceability protocols to verify the authenticity of genuine products should be established to protect basic consumer rights. Several researchers reported that the chemical composition of oil extracted from the same olive variety is highly affected by climatic conditions,[9] agricultural practices,[10,11] time of harvest,[12] extraction procedure, and packaging and storage conditions.[13] In contrast, DNA-based assays are not influenced by compositional variations due to external effects. Therefore, either alone[21] or in combination with analytical chemistry methods,[2] DNA-based assays are increasingly used to authenticate monovarietal olive oils. The recovery of a sufficient quantity and quality of DNA is a key step in the success in

DOI: 10.1021/acs.jafc.5b00090
J. Agric. Food Chem. 2015, 63, 2284−2295

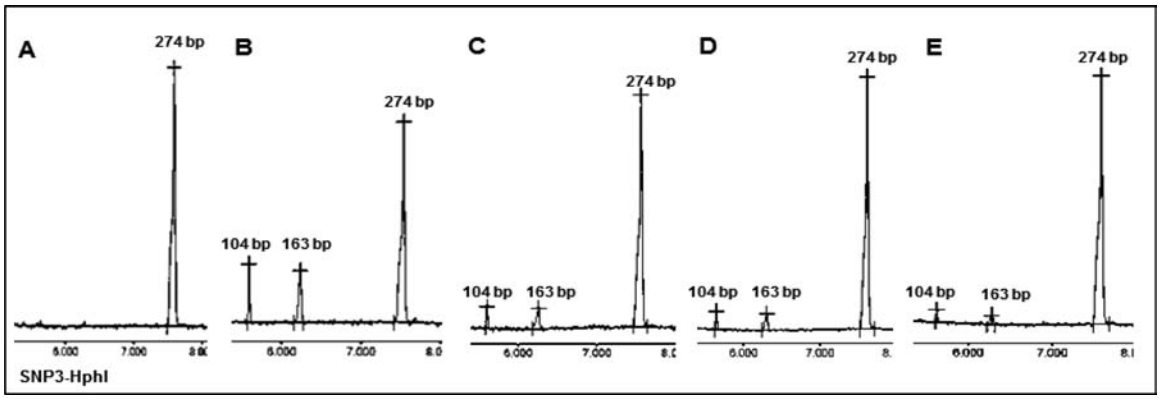

Figure 5. Capillary electropherograms displaying the results of SNP3-HphI assay applied on olive oil admixtures: A, 100% Memecik oil; B, 50% Memecik oil/50% Uslu oil; C, 60% Memecik oil/40% Uslu oil, D, 70% Memecik oil/30% Uslu oil; E, 80% Memecik oil/20% Uslu oil.

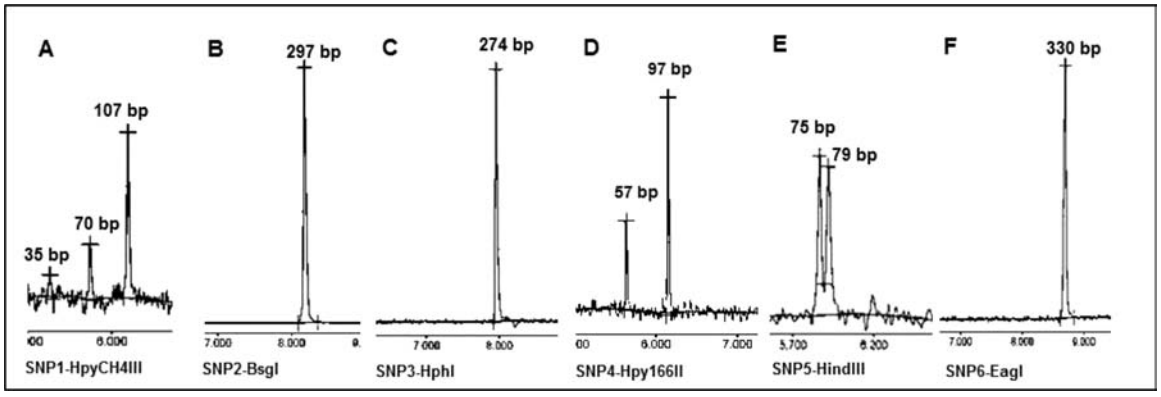

Figure 6. Capillary electropherograms displaying the results of the SNP1-HpyCH4III, SNP2-BsgI, SNP3-HphI, SNP4-Hpy166II, SNP5-HindIII, and SNP6-EagI assays applied on commercial sample no. 1.

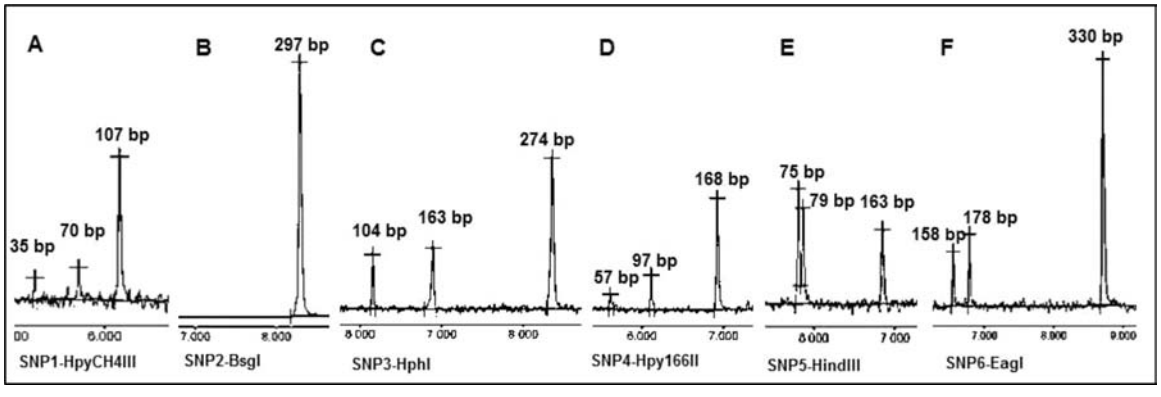

Figure 7. Capillary electropherograms displaying the results of the SNP1-HpyCH4III, SNP2-BsgI, SNP3-HphI, SNP4-Hpy166II, SNP5-HindIII, and SNP6-EagI assays applied on commercial sample no. 2.

DNA-based olive oil authentication. Different authors recommend various commercial kits or in-house protocols.[1,16,17,39] When we compared different commercial kits and an in-house CTAB based protocol, we found that commercial kits are faster and more consistent in yielding amplifiable DNA from olive oil samples. While a DNA concentration that ranges between 100−200 ng/μL was obtained from olive leaf samples with the CTAB[35] method, the DNA extracted using the same method from oil samples was often below the limit of detection of the fluorometer. In contrast, commercial kits were consistent in yielding a DNA concentration of 2−4 ng/μL from the oil samples, with no visible sign of degradation on the agarose gel. Therefore, our experience suggests using food-specific commercial kits to ensure successful downstream applications.

We used SNP markers in our study as their abundance in the genome makes them ideal for identifying differences between closely related genotypes.[6] The SNP frequency we identified in olive coding sequences (1 SNP per 142.5 bp) was similar to the results of Reale et al.,[24] who reported a frequency of 1 SNP per 156 bp in the *Cycloarthenol synthase*, *Lupeol synthase*, and *Cu−Zn-superoxide dismutase* genic sequences. The high frequency of single nucleotide polymorphisms identified in olive coding sequences suggests that olive germplasm harbors a high level of genotypic diversity. Indeed, Belaj et al.[40] reported high genetic

DOI: 10.1021/acs.jafc.5b00090
J. Agric. Food Chem. 2015, 63, 2284−2295

diversity in both local olive germplasm and collections of cultivars representing different cultivation regions. Despite clonal propagation, a high genetic variability is not unexpected in olive because *Olea europaea* L. is an outcrossing species and interfertile with oleasters (wild olives).[40,41] Among the six SNPs used in the identification key, three were reported in previous work. SNP2, identified in the *Chalcone synthase* gene, was reported by Consolandi et al.[25] SNP5, identified in the *Cycloarthenol synthase* gene, was also reported by Consolandi et al.,[25] and Bazakos et al.[21] In addition, we found that the SNP in the *Calcium binding protein* gene, first described by Reale et al.,[24] was also polymorphic in Turkish germplasm and is referred to as SNP6 in this study. These results demonstrate that SNPs in olive coding sequences are conserved across the geography of olive distribution and can be useful for estimating ancestral alleles via phylogenetic analysis.

Restriction digestion-based SNP genotyping is a highly reproducible strategy, producing results that are not prone to variable interpretation in different hands. Very high reproducibility is due to the fact that genotyping is based on observing digestion patterns and does not involve any fluorescence signal intensity measurements or fragment size comparisons. In addition, there is no requirement for SNP-specific probe design or sophisticated equipment.[42] Regular PCR primers are sufficient for the application of SNP-based CAPS assays. Restriction enzymes recognizing a wide variety of sequence motifs are available, making restriction digestion-based SNP genotyping a highly feasible strategy. In this work, a high proportion (70%) of the identified SNPs were amenable to genotyping by CAPS strategy, and only six CAPS assays were sufficient to reach our aim of establishing an identification key for 17 monovarietal olive oils. According to long-term observation of agromorphological traits, two groups of varieties included in this work were suggested as synonyms by the experts of the Olive Research Institute (Izmir, Turkey). The first group of putative synonyms consisted of Gemlik, Erdek Yaglik, and Tekirdag Siyah Salamura, while the second group included Kilis Yaglik and Tesbih Celebi (personal communication). These varieties were included in our analysis in order to investigate if the DNA-based assay produced false positive results by identifying clones as distinct varieties. As a result, we found that the putative synonyms carried identical alleles for the 17 SNP loci identified in five genes, and they were grouped as indistinguishable varieties in the identification key (Figure 1). This result can be attributed to the fact that the SNP loci identified in this work reside in coding sequences. However, performing a detailed molecular genetic characterization involving markers from both coding and noncoding regions may result in distinguishing the putatively synonymous varieties.

When we applied SNP-based CAPS assays on monovarietal olive oils, we were able to obtain the expected digestion profiles. Indeed, SNP-based CAPS analysis proved highly reproducible, and produced identical banding patterns in all three replicate experiments. As a result, the allelic error was found to be 0.000 for the six SNP-based CAPS markers (Table 4). As expected for SNP markers due to their biallelic nature,[23] the multilocus probability of identity value of the SNP loci was moderately low (0.018). By following the identification key (Figure 1) introduced in this work, the cultivar origins of oils from the 17 Turkish olive varieties can be identified and authenticated. Given that the genotypes included in this work represent the most commonly cultivated olive varieties in Turkey, we expect that the variety-specific assay combinations would largely meet the expectations of the Turkish olive oil industry for authenticating high-economic value, premium monovarietal olive oils.

The ultimate goal of cultivar origin detection analyses is to determine if the origin of an oil sample is true to its labeling. Therefore, such an assay should enable the detection of undeclared impurities in a sample. Due to the fact that both the adulterant and the adulterated food commodity are extremely similar materials, the detection of mislabeled cultivar origin is a challenging task, making it attractive for unscrupulous manufacturers or vendors to gain profit from such fraudulent practice.[6,8] In addition, it is reasonable to expect that fruits of varieties cultivated in the same region are commonly processed together for oil extraction, leading to unintended mislabeling of cultivar origin. Thus, in addition to establishing a cultivar origin identification key, it was important for us to test the ability of our SNP-based CAPS assays to detect olive oil admixtures. The Memecik and Uslu varieties were specifically chosen for this kind of analysis as the oil of the Memecik variety is well-known for its sensory qualities and its area of cultivation (South Aegean region of Turkey) overlaps with that of Uslu. Therefore, we can expect that fruits of these two varieties are commonly used together for oil production. On the basis of our analysis, we could successfully detect a minimum of 20% Uslu oil mixed with Memecik oil (Figure 5). We consider this to be a good threshold of detection because, due to economic concerns, fraud generally involves much higher proportions of adulterants. However, it must be remembered that our method does not allow quantification of admixtures and that the use of different percent admixtures was solely to determine the threshold of detection.

To our knowledge, this is the first report that describes the utilization of SNP-based CAPS assays for the detection of admixtures of oils from different olive varieties. Moreover, this is the first time that SNP markers were applied on Turkish olive oils for establishing a varietal identification key and detecting olive oil admixtures. The applicability of the CAPS assays on commercial olive oil samples was also demonstrated. In addition to their use for addressing the authenticity issues of monovarietal olive oils, the CAPS assays introduced in this work will find several uses including olive tree certification, germplasm characterization, and preservation studies.

AUTHOR INFORMATION

Corresponding Author

*E-mail: samidoganlar@iyte.edu.tr. Phone: +902327507313.

Funding

This study was supported by Grant 1334 STZ 2012/1 from Republic of Turkey, Ministry of Science, Industry and Technology, with the contributions of Özaltın Agricultural Enterprises Industry and Commerce Inc., and Genmar Diagnostic Company. We are grateful to the Olive Research Institute (Izmir, Turkey) for providing oil and leaf samples.

Notes

The authors declare no competing financial interest.

REFERENCES

(1) Consolandi, C.; Palmieri, L.; Severgnini, M.; Maestri, E.; Marmiroli, N.; Agrimonti, C.; Baldoni, L.; Donini, P.; De Bellis, G.; Castiglioni, B. A procedure for olive oil traceability and authenticity: DNA extraction, multiplex PCR and LDR–universal array analysis. *Eur. Food Res. Technol.* **2008**, *227*, 1429–1438.

DOI: 10.1021/acs.jafc.5b00090
J. Agric. Food Chem. 2015, 63, 2284–2295

(2) Pasqualone, A.; Di Rienzo, V.; Blanco, A.; Summo, C.; Caponio, F.; Montemurro, C. Characterization of virgin olive oil from Leucocarpa cultivar by chemical and DNA analysis. *Food Res. Int.* **2012**, *47*, 188−193.
(3) Agrimonti, C.; Vietina, M.; Pafundo, S.; Marmiroli, N. The use of food genomics to ensure the traceability of olive oil. *Trends Food Sci. Technol.* **2011**, *22*, 237−244.
(4) Owen, R. W.; Giacosa, A.; Hull, W. E.; Haubner, R.; Würtele, G.; Spiegelhalder, B.; Bartach, H. Olive-oil consumption and health: the possible role of antioxidants. *Lancet Oncol.* **2000**, *1*, 107−112.
(5) Perez-Jimenez, M.; Besnard, G.; Dorado, G.; Hernandez, P. Varietal tracing of virgin olive oil based on plastid DNA variation profiling. *PLoS One* **2013**, *8*, e70507.
(6) Costa, J.; Mafra, I.; Oliveira, M. B. P. P. Advances in vegetable oil authentication by DNA-based markers. *Trends Food Sci. Technol.* **2012**, *26*, 43−55.
(7) Woolfe, M.; Primrose, S. Food forensics: using DNA technology to combat misdescription and fraud. *Trends Biotechnol.* **2004**, *5*, 222−226.
(8) Ulberth, F.; Buchgraber, M. Authenticity of fats and oils. *Eur. J. Lipid Sci. Technol.* **2000**, *102*, 687−694.
(9) Aguilera, M. P.; Beltrán, G.; Ortego, D.; Fernández, A.; Jiménez, A.; Uceda, M. Characterisation of virgin olive oil of Italian olive cultivars: 'Frantoio' and 'Leccino', grown in Andalusia. *Food Chem.* **2005**, *89*, 387−391.
(10) Gómez-Rico, A.; Salvador, M. D.; Moriana, A.; Pérez, D.; Olmedilla, N.; Ribas, F.; Freagapane, G. Influence of different irrigation strategies in a traditional Cornicabra cv. olive orchard on virgin olive oil composition and quality. *Food Chem.* **2007**, *100*, 568−578.
(11) Erel, R.; Kerem, Z.; Ben-Gal, A.; Dag, A.; Schwartz, A.; Zipori, I.; Basheer, L.; Yermiyahu, U. Olive (*Olea europaea* L.) tree nitrogen status is a key factor for olive oil quality. *J. Agric. Food Chem.* **2013**, *61*, 11261−11272.
(12) Dag, A.; Kerem, Z.; Yogev, N.; Zipori, I.; Lavee, S.; Ben-David, E. Influence of time of harvest and maturity index on olive oil yield and quality. *Sci. Hortic.* **2011**, *127*, 358−366.
(13) Ben-Hassine, K.; Taamalii, A.; Ferchichi, S.; Mlaouah, A.; Benincasa, C.; Romano, E.; Flamini, G.; Lazzez, A.; Grati-kamoun, N.; Perri, E.; Malouche, D.; Hammami, M. Physicochemical and sensory characteristics of virgin olive oils in relation to cultivar, extraction system and storage conditions. *Food Res. Int.* **2013**, *54*, 1915−1925.
(14) Madesis, P.; Ganopoulos, I.; Bosmali, I.; Tsaftaris, A. Barcode high resolution melting analysis for forensic uses in nuts: A case study on allergenic hazelnuts (*Corylus avellana*). *Food Res. Int.* **2013**, *50*, 351−360.
(15) Ganopoulos, I.; Bazakos, C.; Madesis, P.; Kalaitzis, P.; Tsaftaris, A. Barcode DNA high-resolution melting (Bar-HRM) analysis as a novel close-tubed and accurate tool for olive oil forensic use. *J. Sci. Food. Agric.* **2013**, *93*, 2281−2286.
(16) Breton, C.; Claux, D.; Metton, I.; Skorski, G.; Bervillé, A. Comparative study of methods for DNA preparation from olive oil samples to identify cultivar SSR alleles in commercial oil samples: Possible forensic applications. *J. Agric. Food Chem.* **2004**, *52*, 531−537.
(17) Testolin, R.; Lain, O. DNA extraction from olive oil and PCR amplification of microsatellite markers. *J. Food Sci.* **2005**, *70*, c108−c112.
(18) Pasqualone, A.; Montemurro, C.; Summo, C.; Sabetta, W.; Caponio, F.; Blanco, A. Effectiveness of microsatellite DNA markers in checking the identity of protected designation of origin extra virgin olive oil. *J. Agric. Food Chem.* **2007**, *55*, 3857−3862.
(19) Martins-Lopes, P.; Gomes, S.; Santos, E.; Guedes-Pinto, H. DNA markers for Portuguese olive oil fingerprinting. *J. Agric. Food Chem.* **2008**, *56*, 11786−11791.
(20) Raieta, K.; Muccillo, L.; Colantuoni, V. A novel reliable method of DNA extraction from olive oil suitable for molecular traceability. *Food Chem.* **2014**, *172*, 596−602.
(21) Bazakos, C.; Dulger, A. O.; Uncu, A. T.; Spaniolas, S.; Spano, T.; Kalaitzis, P. A SNP-based PCR-RFLP capillary electrophoresis analysis for the identification of the varietal origin of olive oils. *Food Chem.* **2012**, *134*, 2411−2418.
(22) Khlestkina, E. K.; Salina, E. A. SNP markers: Methods of analysis, ways of development, and comparison on an example of common wheat. *Russ. J. Genet.* **2006**, *42*, 585−594.
(23) Ganopoulos, I.; Tsaballa, A.; Xanthopoulou, A.; Madesis, P.; Tsaftaris, A. Sweet cherry cultivar identification by high-resolution-melting (HRM) analysis using gene-based SNP markers. *Plant Mol. Biol. Rep.* **2013**, *31*, 763−768.
(24) Reale, S.; Doveri, S.; Díaz, A.; Angiolillo, A.; Lucentini, L.; Pilla, F.; Martín, A.; Donini, P.; Lee, D. SNP-based markers for discriminating olive (*Olea europaea* L.) cultivars. *Genome* **2006**, *49*, 1193−1205.
(25) Consolandi, C.; Palmieri, L.; Doveri, S.; Maestri, E.; Marmiroli, N.; Reale, S.; Lee, D.; Baldoni, L.; Tosti, N.; Severgnini, M.; De Bellis, G.; Castiglioni, B. Olive variety identification by ligation detection reaction in a universal array format. *J. Biotechnol.* **2007**, *129*, 565−574.
(26) Dooley, J. J.; Sage, H. D.; Clarke, M-A. L.; Brown, H. M.; Garrett, S. D. Fish species identification using PCR-RFLP analysis and lab-on-a-chip capillary electrophoresis: Application to detect white fish species in food products and an interlaboratory study. *J. Agric. Food Chem.* **2005**, *53*, 3348−3357.
(27) Spaniolas, S.; May, S. T.; Bennett, M. J.; Tucker, G. A. Authentication of coffee by means of PCR-RFLP analysis and lab-on-a-chip capillary electrophoresis. *J. Agric. Food Chem.* **2006**, *54*, 7466−7470.
(28) FAOSTAT. *Production Statistics 2013*. URL http://faostat.fao.org/site/567/DesktopDefault.aspx?PageID=567#ancor (date accessed October 10, 2014).
(29) IOC. *World Olive Oil Figures*. URL http://www.internationaloliveoil.org/estaticos/view/131-world-olive-oil-figures (date accessed October 10, 2014).
(30) Ocakoglu, D.; Tokatli, F.; Ozen, B.; Korel, F. Distribution of simple phenols, phenolic acids and flavonoids in Turkish monovarietal extra virgin olive oils for two harvest years. *Food Chem.* **2009**, *113*, 401−410.
(31) Ercisli, S.; Barut, E.; Ipek, A. Molecular characterization of olive cultivars using amplified fragment length polymorphism markers. *GMR, Genet. Mol. Res.* **2009**, *8*, 414−419.
(32) Isik, N.; Doganlar, S.; Frary, A. Genetic diversity of Turkish olive varieties assessed by simple sequence repeat and sequence-related amplified polymorphism markers. *Crop Sci.* **2011**, *51*, 1646−1654.
(33) Ipek, A.; Barut, E.; Gulen, H.; Ipek, M. Assessment of inter- and intracultivar variations in olive using SSR markers. *Sci. Agric.* **2012**, *69*, 327−335.
(34) Kaya, H. B.; Cetin, O.; Kaya, H.; Sahin, M.; Sefer, F.; Kahraman, A.; Tanyolac, B. SNP discovery by Illumina-based transcriptome sequencing of the olive and genetic characterization of Turkish olive genotypes revealed by AFLP, SSR and SNP markers. *PLoS One* **2013**, *8*, e73674.
(35) Doyle, J. J.; Doyle, J. E. Isolation of plant DNA from fresh tissue. *Focus* **1990**, *12*, 13−15.
(36) Rozen, S.; Skaletsky, H. Primer3 on the WWW for general users and for biologist programmers. In *Methods in Molecular Biology: Bioinformatics Methods and Protocols*, Krawetz, S., Misener, S., Eds.; Humana Press: Totowa, NJ, 2000; Vol. *132*, pp 365−386.
(37) Paetkau, D.; Calwert, W.; Stirling, I.; Strobeck, C. Microsatellite analysis of population structure in Canadian polar bears. *Mol. Ecol.* **1995**, *4*, 347−354.
(38) Pasqualone, A.; Di Rienzo, V.; Nasti, R.; Blanco, A.; Gomes, T.; Montemurro, C. Traceability of Italian protected designation of origin (PDO) table olives by means of microsatellite molecular markers. *J. Agric. Food Chem.* **2013**, *61*, 3068−3073.
(39) Busconi, M.; Foroni, C.; Corradi, M.; Bongiorni, C.; Cattapan, F.; Fogher, C. DNA extraction from olive oil and its use in the identification of the production cultivar. *Food Chem.* **2003**, *83*, 127−134.
(40) Belaj, A.; Dominguez-García, M. C.; Atienza, S. G.; Urdíroz, M. N.; De la Rosa, R.; Satovic, Z.; Martín, A.; Kilian, A.; Trujillo, I.;

DOI: 10.1021/acs.jafc.5b00090
J. Agric. Food Chem. 2015, 63, 2284−2295

Valpuesta, V.; Del Río, C. Developing a core collection of olive (Olea europaea L.) based on molecular markers (DArTs, SSRs, SNPs) and agronomic traits. *Tree Genet. Genomes* **2012**, *8*, 365−378.
(41) Belaj, A.; Muńoz-diez, C.; Baldoni, L.; Porceddu, A.; Barranco, D.; Satovic, Z. Genetic diversity and population structure of wild olives from the north-western Mediterranean assessed by SSR markers. *Ann. Bot.* **2007**, *100*, 449−458.
(42) Spaniolas, S.; Bazakos, C.; Tucker, G. A.; Bennet, M. J. Comparison of SNP-based detection assays for food analysis: Coffee authentication. *J. AOAC Int.* **2014**, *97*, 1114−1120.

DOI: 10.1021/acs.jafc.5b00090
J. Agric. Food Chem. 2015, 63, 2284−2295

filling period,[20,21] collectively, might maintain normal yields. Salt concentrations above the tolerable threshold would compromise these adaptive processes and lead to lower productivity.[20] It is especially devastating when imposed at grain filling, since at this terminal phase of the lifecycle, the plant has fewer compensatory mechanisms to mitigate the buildup of salt in sensitive tissues.[9,20] The results are increased floret sterility, increased percentage of partially filled and unfilled grain, and lower yield.[3,8,17,22,23] Because of the multiplicity of factors that determine plant response to salinity the outcome may not always be predictable.

Rice growth environment also strongly dictates grain postharvest attributes since the grain is consumed whole with minimal processing.[3,24,25] Starch is the main grain reserve in rice accumulating up to 50−90% of dry weight with protein contributing 5−12% to the total.[26] Starch molecular composition and structure are the major quality determinants influencing grain visual, textural, nutritional, and taste attributes, but protein can also impact sensory properties.[15,26,27]

The effects of heat and drought on rice quality have been widely reported, but data on salinity are limited.[3] Some studies show that moderate to high concentrations (EC 4−8 dS/m^2) of salt reduce amylose[6,7,14] and modulate rice texture, pasting properties, and gel consistency.[6,14,28] These functional changes may be due to disruptions in the grain starch-to-storage protein ratio, amylose content, amylopectin glucan chain distribution, the lipids associated with amylose, starch granule crystallinity, and particle size distribution;[3,29−31] however, other than amylose content, most of these parameters have not been investigated.

Because of the importance of rice as a global commodity, and the potential threat of increasing soil salinity to rice production, a better understanding of how salinity affects rice quality and yield is needed. To work toward this goal we took a comprehensive view of how timing and severity of salinity stress can change some aspects of rice productivity and grain sensory quality. Plants were grown in a controlled greenhouse setting to eliminate extraneous, confounding factors.[3] Nipponbare was used, as it is the model rice ecotype, which should permit comparison with other published research.[32,33] Salinity (NaCl) was imposed at the seedling stage in one batch of rice, and at the reproductive stage in another as we anticipated differences in plant response with the differential timing of salt application.[3] This would also enable greater comparison and interpretability with the limited published data on salinity effects on grain quality, which usually adopt one approach, e.g., salt applied at the seedling stage[6,7] or during grain filling.[12,14] Two salt concentrations, EC 2 and 4 dS/m^2, were used to induce a mild and moderate salt stress rather than a nonagronomic "salt shock".[23] This was intended to allow us to examine plant adaptive responses that could be obscured by a rapid onset of senescence. Finally, we aimed to connect changes in grain sensory parameters to modifications occurring in the starch at the molecular level. Collectively these data could provide a nuanced overview of how grain parameters respond to salinity stress.

MATERIALS AND METHODS

Plant Growth Conditions. Rice (*Oryza sativa* L.) cv. Nipponbare were grown in a greenhouse in Davis, CA, from May to October 2013 in 5″ pots with a mixture of UC potting mix (1 peat moss: 1 coarse sand (v:v)) and perlite 9:1 (v:v) each containing Osmocote 17-7-12 controlled release fertilizer (B&T Grower Supply, Inc., Forest Hill, LA) flooded with water. Salt stress was imposed by adding either 20 or 40 mM NaCl to achieve EC values of 2 and 4 dS/m^2 either at 4-weeks after transplanting (V5 stages, ref 34), described here as Seedling EC2 and Seedling EC4, or at anthesis (R8 stage, ref 34), described here as Anthesis EC2 and Anthesis EC4. The control plants were grown without the addition of NaCl and were maintained at EC0. Once all filled seeds were hardened, the water was drained, and plants were kept in pots for another 7 days before the panicles were harvested. The EC was maintained at 2 and 4 (±15% variation) dS/m^2 until harvest (see Supporting Information Figure S1).

Plant Productivity and Seed Characteristics. The number of panicles per plant, 100-grain weight, total grain weight per plant, and seed fertility (expressed as number of fully filled seeds per 100 seeds) were calculated. To examine seed morphology in a high throughput manner, approximately 150 grains were placed on a scanner, and an image of 600 dpi was taken and then used as an input for WinSeedle (Regents Instrument Inc., Canada). Grain length, width, width-to-length ratio, perimeter, surface area, and volume were recorded.

Starch and Reducing Sugar Measurements. A half-gram of milled grains was homogenized to a fine powder using a Thomas Wiley Mini-Mill (Thomas Scientific, Swedesboro, NJ). Sugars were extracted from the grain by boiling 100 mg of milled flour samples three times in 80% (v/v) ethanol. Ethanol was removed by drying the soluble fraction in a speedvac, and the residue was reconstituted in 300 μL of water. Starch was analyzed from the ethanol-insoluble residue by digesting to glucose as previously described.[35] Reducing sugars in the reconstituted sample soluble fraction, as well as glucose digested from starch, were analyzed using 3,5-dinitrosalicylic acid.[36]

Starch Purification and Analysis. Starch was extracted as described in ref 37 except that 15 g of seeds was used. The samples were homogenized in a blender, and the homogenate was filtered through 4 layers of Miracloth. *Amylose* was assayed on 10 mg of purified starch using the Megazyme amylose/amylopectin determination kit (Wickson, Ireland).[36] *Amylopectin branch chain-length distribution* was analyzed by high-performance anion-exchange chromatography (HPAEC) as previously described.[38] *Thermal analyses* were done by differential scanning calorimetry (DSC), with the method modified from ref 39. Starch slurries with a water-to-starch ratio of 3:1 (∼15 mg) were hermetically sealed in a large volume stainless steel pan, and equilibrated overnight at room temperature prior to analysis. An empty stainless steel pan was used as a reference. The sample and reference pans were scanned from 30 to 120 °C at a heating rate of 10 °C/min. *Particle size analysis* was done as described in ref 40. *Pasting properties* of 8% (w/v) starch slurry was measured by AR1000-N Rheometer (TA Instrument, New Castle, DE). The temperature profile for the rheometer, which simulates the temperature profile of a Rapid Visco-Analyzer (RVA), was as follows: hold at 50 °C for 1 min, heat to 95 °C over 4.5 min, hold at 95 °C for 3 min, cool to 50 °C over 4.5 min, and finally hold at 50 °C for 1 min. The experiments were done in triplicate.

Total Protein and Nitrogen Content and SDS-PAGE Profile of Grain Flour. Protein and nitrogen (N) contents were assayed using the AOAC Kjeldahl method.[41] To analyze grains storage protein, 40 mg of flour was homogenized in 700 μL of sodium dodecyl sulfate−urea solution overnight and then centrifuged at 7000 *g* for 5 min.[42] Then, 5 μL of supernatant was loaded onto 10% (w/v) precast bis-tris sodium dodecyl sulfate polyacrylamide gel electrophoresis (SDS-PAGE) gel (Invitrogen, Carlsbad, CA) and subjected to electrophoresis. Coomassie Brilliant Blue R-250 (Bio-Rad, Hercules, CA) was used to stain the separated proteins, which were visualized using an AlphaImager (Alpha Innotech, San Leandro, CA). The density of each band was measured using ImageJ (NIH, Bethesda, MA).[43]

Statistical and Multivariate Analysis. A one-way analysis of variance (ANOVA) was used to determine statistically significant differences in means between treatments. A Tukey−Kramer post hoc test was calculated when statistical differences were observed. A minimum of 3, but typically 5−10, biological replicates were used. Differences were deemed to be statistically significant when $P \leq 0.05$. Partial-least squares discriminant analysis (PLS-DA) was done

DOI: 10.1021/jf503948p
J. Agric. Food Chem. 2015, 63, 2296−2304

Table 1. Productivity of Nipponbare Rices Grown under Different Salinity Conditions[a]

treatment	EC (dS/m^2)	panicle no.	% fertility	100 grain wt (g)	total grain wt (g)
control	0	10.3 ± 0.26 b	87.8 ± 0.84 a	2.24 ± 0.02 a	28.79 ± 1.49 a
seedling	2	**12.5 ± 0.60 a**	86 ± 2.60 a	2.38 ± 0.07 a	31.27 ± 2.38 a
	4	11.7 ± 0.54 a,b	80.4 ± 4.51 a,b	2.09 ± 0.11 a,b	26.81 ± 1.21 a,b
anthesis	2	9.6 ± 0.34 b	80 ± 2.02 a,b	2.11 ± 0.05 a,b	28.14 ± 1.19 a
	4	9.3 ± 0.42 b	**70.8 ± 3.41 b**	**1.91 ± 0.09 b**	**20.51 ± 1.95 b**

[a]Values are means ± SEM. Means within each column with different superscripts and presented in bold are significantly different ($P \leq 0.05$) by Tukey's test ($n = 10$).

following data normalization via logarithmic transformation using Metaboanalyst online tool (TMIC, Canada).[44]

RESULTS AND DISCUSSION

The aim of this work was to determine how salinity affects rice productivity and grain quality. These parameters both determine market value and acceptance of novel rice varieties.[14,27,45] Quality parameters encompass not only the physical appearance of the caryopsis, but also the biochemical composition of the grain, and most importantly the physicochemical properties of the endosperm protein and especially starch, as they are the major determinants of rice eating quality.[27] The study also aimed to investigate plants grown in the greenhouse settings where the EC was controlled (Supporting Information Figure S1) in order to achieve clear understanding of how salt impacts grain parameters.

Effect of Saline Soils on Yields and Grain Characteristics. *Plant Productivity.* Changes in rice agronomic yields were assessed by measuring grain weight, caryopsis fertility, and the number of panicles per plant (Table 1). Small and green unfilled caryopses were visible in all salt treatments except the Seedling EC2 (Figure 1). Decreases in fertility, total grain weight, and 100-grain weight were only statistically significant in the Anthesis EC4 treatment (Table 1). These results were similar to those in a study where EC 3.2 and 4.6 dS/m^2-treated rice led to reductions in grain weight.[16] Reductions of up to 98% in caryopsis weights[6,7,12] and increases in the fraction of unfilled spikelets[12] under high salt (5−8 dS/m^2) have been reported. The occurrence of unfilled seeds was suggested to be due to reduced activity of starch synthase and decreased translocation of soluble carbohydrate as a result of loss of Na^+/K^+ homeostasis in floral organs.[12] Pollen sterility and changes in floral structure may also have contributed to the floret sterility[21] in the Anthesis EC4 treatment. Conversely, Zeng et al. (2001) showed that total grain weight and grain fertility were enhanced when salinity (EC 1.8, 3.2, and 4.6 dS/m^2) was imposed at the booting stage.[16] However, unlike the present study, salinity stress was episodic, only imposed for 20 days after which soil EC was restored to control levels until harvest, perhaps accounting for the positive effects on productivity.[16]

Figure 1. Rice seeds from control and salinity-treated plants at harvest. There are 100 random seeds of each treatment shown. Several infertile unfilled seeds, as shown by green hull color, were seen in the Seedling 4 dS/m^2, and in the Anthesis treatments from both salt concentrations. The grains from these treatments were also smaller than those from the control and Seedling 2 dS/m^2 treatment (see Table 1).

Panicle numbers for the control and both anthesis treatments were not different, while it was enhanced (12%) in the Seedling EC2 treatment (Table 1). This has not been reported in any previous study, and thus requires further investigation to determine whether a mild stress had a stimulatory effect on floral primordia initiation. Since fertility, total grain weight, and 100-grain weight were not affected by the mild level of salt stress, this suggests an agronomically beneficial adaptive response of the plants. From a practical point of view, it should be possible to design experiments to determine the use of low quality irrigation water, or saline soils up to 2 dS/m^2 for rice irrigation purposes, as this treatment has minimal repercussions for rice growth in the greenhouse setting

Grain Characteristics. Grain physical appearance and dimensions are an important indicator of the marketability of rice as they are readily obvious to purchasers;[45] however, the length and shape of the rice kernels also affect kernel milling, cooking, and sensory properties.[46] Here, we showed that prolonged exposure to NaCl throughout development affected grain dimensions (Table 2). Seedling EC4 plants had lower grain volume compared to the control. This could indicate changes in cell number in the lemma and palea because the size of the outer glume greatly restricts the dimension of dehulled rice endosperms.[47] Seedling EC2 plants had increased grain length and surface area (Figure 1 and Table 2). This may be perceived negatively in some Asian markets.[15] On the contrary, a decrease in grain length of two indica rice cultivars has been reported for plants grown in a higher degree of salinity (EC 5−

Table 2. Caryopsis Characteristics of Rices Grown under Different Salinity Conditions[a]

treatment	EC (dS/m^2)	length (mm)	width (mm)	width-to-length ratio	perimeter (mm)	surface area (mm^2)	volume (mm^3)
control	0	4.99 ± 0.04 b	2.98 ± 0.02 a	0.60 ± 0.003 a	13.25 ± 0.09 b	26.11 ± 0.30 b	23.56 ± 0.38 a
seedling	2	**5.14 ± 0.03 a**	2.99 ± 0.02 a	**0.58 ± 0.002 b**	**13.56 ± 0.08 a**	**27.06 ± 0.30 a**	24.53 ± 0.42 a
	4	5.02 ± 0.02 b	2.93 ± 0.01 a	**0.59 ± 0.004 b**	13.27 ± 0.05 b	25.88 ± 0.13 b	**22.98 ± 0.22 b**
anthesis	2	5.12 ± 0.02 a,b	2.98 ± 0.01 a	**0.58 ± 0.003 b**	**13.52 ± 0.05 a**	26.79 ± 0.11 a,b	24.21 ± 0.13 a
	4	5.07 ± 0.02 a,b	2.96 ± 0.01 a	**0.58 ± 0.003 b**	13.41 ± 0.04 a,b	26.39 ± 0.14 a,b	23.68 ± 0.24 a

[a]Values are means ± SEM. Means within each column with different superscripts and presented in bold are significantly different ($P \leq 0.05$) by Tukey's test ($n = 6$). Approximately 100 seeds were scanned for each technical replicates.

DOI: 10.1021/jf503948p
J. Agric. Food Chem. 2015, 63, 2296−2304

Table 3. Storage Product Composition of Rice Caryopses Grown under Different Salinity Conditions[a]

treatment	EC (dS/m^2)	reducing sugar content (mg gFW^{-1})	starch content (mg gFW^{-1})	N content (%)	protein content (%)	amylose content (%)
control	0	0.13 ± 0.03 a	291.65 ± 6.18 b	1.21 ± 0.05 b	7.18 ± 0.29 b	14.53 ± 0.67 a
seedling	2	0.14 ± 0.02 a	317.57 ± 4.38 b	1.14 ± 0.02 b	6.80 ± 0.14 b	15.59 ± 0.55 a
	4	0.09 ± 0.02 a	**386.85 ± 10.77 a**	1.20 ± 0.04 b	7.14 ± 0.22 b	13.51 ± 0.84 a
anthesis	2	0.19 ± 0.03 a	**405.39 ± 13.77 a**	1.27 ± 0.00 b	7.56 ± 0.05 b	13.63 ± 0.72 a
	4	0.15 ± 0.03 a	319.67 ± 3.98 b	**1.45 ± 0.03 a**	**8.62 ± 0.18 a**	14.69 ± 0.18 a

[a]Values are means ± SEM. Means within each column with different superscripts and presented in bold are significantly different ($P \leq 0.05$) by Tukey's test ($n = 4$ for starch, sugar, and N content analyses; $n = 3$ for amylose content and particle size analyses).

6 dS/m^2),[6] again emphasizing that plant response is genotype and environment sensitive.

Grain Storage Product Composition. *Starch, Sugar, and Amylose Contents and Starch Particle Size Distribution.* The major grain carbohydrates are starch, sugars, and amylose. Starch dictates yield, while amylose content is one of the major properties determining rice sensory quality.[48] Differences in starch granule size also influence starch functionality,[49,50] and grain sugars could increase due to stress-induced starch breakdown and may influence taste.[51] Here we found no difference in reducing sugar content (Table 3). Interestingly, we found that the Seedling EC4 and the Anthesis EC2 treatments increased the percentage of starch in the rice flour (Table 3) as well as in each caryopsis (Supporting Information Table S1). These increases in starch content stand in sharp contrast to rice grown under stronger saline conditions (EC 4–8 dS/m^2) which reduced endosperm starch[6,14] even in greenhouse grown rice such as ours.[6] Salt enhances starch accumulation in tomato fruits by elevating ADP-glucose pyrophosphorylase (AGPase) activity, a key enzyme in starch biosynthesis.[52] In rice, expression level of the leaf large and small AGPase subunits also increased in response to salinity.[53] However, whether AGPase transcript level and enzyme activity increase in the endosperm in a similar way to that seen in tomato under salinity is worth determining.

Surprisingly, the percentage of amylose in starches from plants exposed to salinity, including those that had increased starch contents, did not differ from that of the control (Table 3). Reductions in amylose exposed to high salt concentration (EC 4–8 dS/m^2) at the reproductive stages have been reported;[6,14] however, in one study, salinity exposure at the seedling stage had to be as high as 6–8 dS/m^2 for amylose content to decrease.[7] The particle size distribution of starch grains was also not affected by salt stress (Supporting Information Table S2). Because salinity stress exposure was associated with increased starch content and no change in the percentage of amylose or starch granule size distribution, it is tempting to speculate that salinity may have altered some aspects of starch biosynthesis such as starch granule initiation and amylose biosynthesis.

Protein and N Content. Rice grain protein and N contents can be increased by salinity stress.[11] In this study, the protein and N content in the flour from the Anthesis EC4 treatment was significantly higher than that of the flours from other growth conditions (Table 3). SDS-PAGE profiles of these grains confirmed that the glutelin and prolamin contents were greatly enhanced (Figure 2). Similarly, six rice cultivars grown under 2.5 dS/m^2 salinity were found to have higher protein content with major contributions from glutelin.[11] When the protein content was expressed relative to starch content (data not shown), the starch:protein ratio of the Anthesis EC4 sample was lower compared to the control, thus potentially

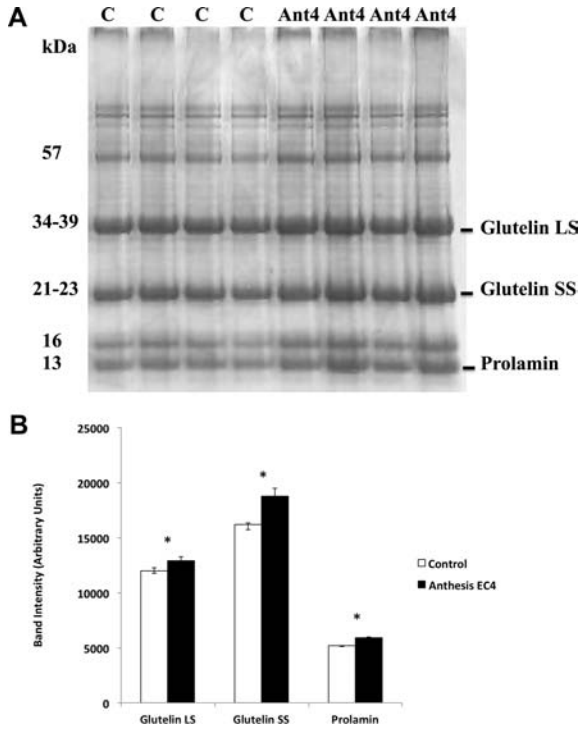

Figure 2. Analysis of grain storage proteins extracted from flour of Control and Anthesis EC4 treatments. (A) SDS-PAGE showing the bands of the glutelin large subunit (LS), glutelin small subunit (SS), and prolamin. (B) Densitometry plot showing the relative content of these rice storage proteins. Values are means ±SEM. Means of each pair of columns with a star are significantly different ($P \leq 0.05$) by Student's *t*-test ($n = 4$).

affecting rice cooking and sensory properties.[54] Removing proteins from rice flours increases the water availability for starch and results in a less viscous product;[54] therefore, the Anthesis EC4 caryopsis, once cooked, might become firmer due to reduced water availability for starch granule swelling and glucan leaching. This high protein-induced hardness in cooked rice may be further amplified because caryopsis amylose content was unchanged (Table 3).[6] However, to determine this, the retrogradation property of the endosperm starch must also be considered.

When expressed on a mg per grain basis, caryopsis protein and starch levels in the Anthesis EC4 treatment were not different from the control (Supporting Information Table S1). The lack of congruency in protein expressed on an equal mass basis versus on a per grain basis suggests differences in reserve allocation and partitioning to the grain due to salinity. Moreover, while grain starch was enhanced in the Seedling EC4 and Anthesis EC2 treatments, the protein accumulation remained stable (Supporting Information Table S1). This

DOI: 10.1021/jf503948p
J. Agric. Food Chem. 2015, 63, 2296–2304

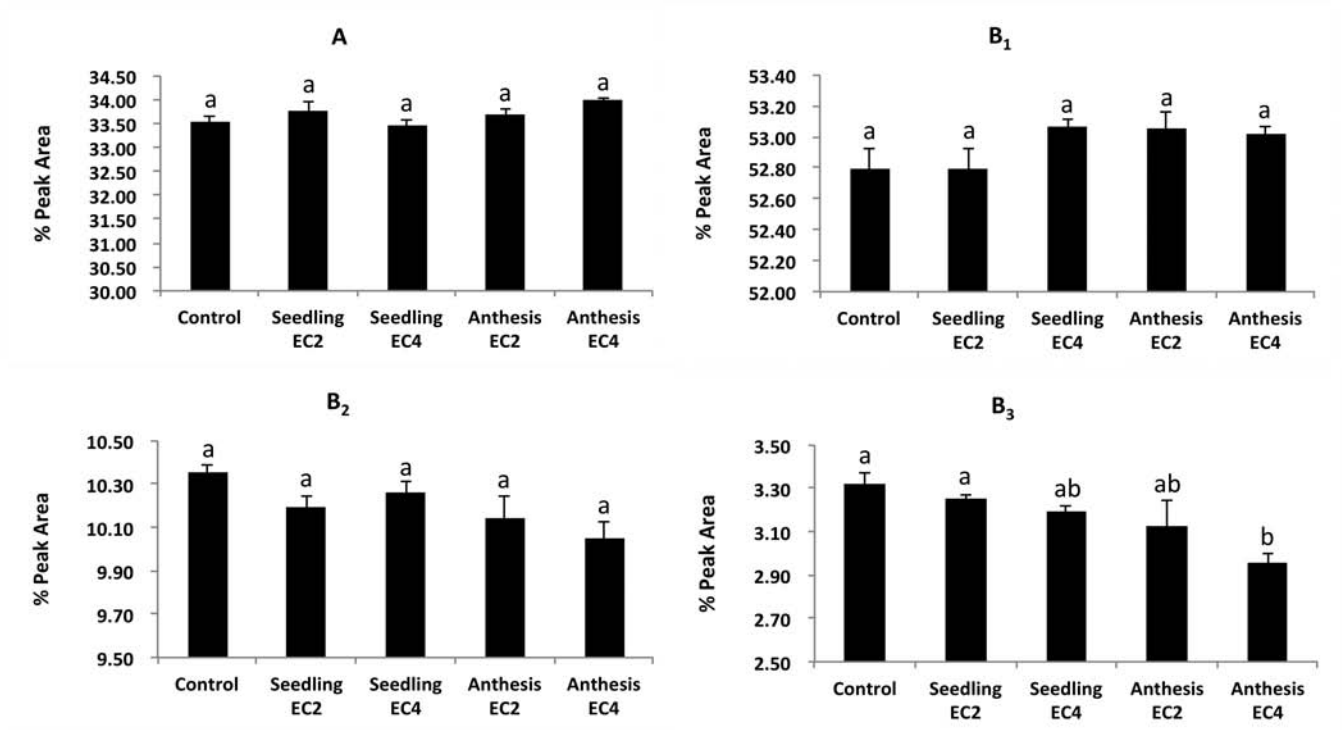

Figure 3. Branch chain length distribution of rice amylopectin of different classes. Starch was digested with isoamylase, and the digested starch was then separated by HPAEC. The distributions of branch chain lengths were categorized into A class (DP 6−12), B_1 class (DP 13−24), B_2 class (DP 25−36), and B_3 class (DP ≥ 37). Values are means ± SEM. Means of each column with different superscripts are significantly different ($P \leq 0.05$) by Tukey's test ($n = 4$).

Table 4. Gelatinization Properties of Rice Starches Analyzed by DSC[a]

treatment	EC (dS/m^2)	onset temp (°C)	peak temp (°C)	conclusion temp (°C)	temp range (°C)	enthalpy (J/g)
control	0	61.30 ± 0.36 a	67.41 ± 0.47 a	74.02 ± 0.46 a	12.71 ± 0.63 a	14.62 ± 0.40 a
seedling	2	60.22 ± 0.29 a	**65.69 ± 0.24 b**	**72.04 ± 0.18 b**	11.81 ± 0.38 a	13.28 ± 0.38 a
	4	59.56 ± 0.60 a	65.81 ± 0.50 a,b	**71.95 ± 0.62 b**	12.39 ± 0.17 a	15.66 ± 1.03 a
anthesis	2	60.41 ± 0.22 a	**65.60 ± 0.40 b**	72.63 ± 0.36 a,b	12.23 ± 0.31 a	15.50 ± 0.50 a
	4	60.07 ± 0.39 a	**65.35 ± 0.27 b**	**70.81 ± 0.44 b**	**10.74 ± 0.50 b**	14.24 ± 0.33 a

[a]Values are means ± SEM. Means within each column with different superscripts and presented in bold are significantly different ($P \leq 0.05$) by Tukey's test ($n = 4$).

Table 5. Pasting Properties of Rice Starches[a]

treatment	EC (dS/m^2)	pasting temp (°C)	peak viscosity (Pa s)	peak temp (°C)	breakdown (Pa s)	final viscosity (Pa s)	setback (Pa s)
control	0	62.85 ± 0.15 a	0.76 ± 0.08 a	89.83 ± 1.46 a	0.39 ± 0.08 a	0.75 ± 0.06 a	0.38 ± 0.07 a
seedling	2	62.14 ± 0.15 a	0.58 ± 0.03 a	92.02 ± 0.40 a	0.23 ± 0.03 a	**0.51 ± 0.03 b**	**0.15 ± 0.03 b**
	4	62.18 ± 0.21 a	0.74 ± 0.08 a	90.45 ± 0.60 a	0.36 ± 0.08 a	0.65 ± 0.06 a	0.26 ± 0.07 a
anthesis	2	62.53 ± 0.16 a	0.64 ± 0.04 a	91.50 ± 0.29 a	0.25 ± 0.03 a	**0.56 ± 0.04 b**	**0.15 ± 0.03 b**
	4	**61.66 ± 0.28 b**	0.55 ± 0.01 a	91.53 ± 0.39 a	0.22 ± 0.03 a	**0.50 ± 0.02 b**	**0.17 ± 0.02 b**

[a]Values are means ± SEM. Means within each column with different superscripts and presented in bold are significantly different ($P \leq 0.05$) by Tukey's test ($n = 4$).

suggests that, under these two salinity conditions, starch and protein accumulation were differently regulated.

Starch Molecular Structure and Functionality. *Amylopectin Branch Chain-Length Distribution.* Amylopectin fine structure is an important contributor of starch functionality as its branch chain-length distribution is shown to relate to starch crystalline structure[55] and pasting properties.[56] There was no difference in distribution pattern of the branch chains of different degrees of polymerization among all treatment groups (Supporting Information Figure S2), suggesting no notable effect of salinity on the overall amylopectin chain-length profile. However, when the glucan chain lengths were categorized into discrete classes (A class, DP 6−12; B_1 class, DP 13−24; B_2 class, DP 25−36; and B_3 class, DP ≥ 37),[55] differences were found in the Anthesis EC4 treatment, which had a reduced proportion of the long chains (i.e., DP ≥ 37) (Figure 3).

Starch Gelatinization Properties. DSC enables the heat of gelatinization of a starch−water suspension to be observed as a well-defined endotherm peak.[57] Salt stress reduced both the peak and conclusion temperatures, while the temperature range was smallest in the Anthesis EC4 among others (Table 4). The enthalpy of the system nevertheless did not vary among all

DOI: 10.1021/jf503948p
J. Agric. Food Chem. 2015, 63, 2296−2304

treatments (Table 4). The DSC analysis also reveals the thermal behavior of the amylose−lipid complex melting, which can alter starch functionality.[58] There was no significant difference in the melting profiles of all treatments, except for the Anthesis EC4 treatment, where a significant reduction in onset temperature of melting was found (Supporting Information Table S3). This suggests only a slight difference in strength and amount of lipid complexes with amylose as a result of salinity, and is in agreement with the finding that amylose content was unchanged due to saline conditions in this study.

Starch Pasting Properties. The pasting behavior of a starch/water mixture is measured as a change in viscosity resistance of the mixture to controlled shear as the temperature is increased and decreased.[59] The rheometer-simulated RVA pasting profile showed that Anthesis EC4 starch formed a paste at slightly lower temperatures than the control starch (Table 5 and Figure 4), while the pasting temperatures of other treatments did not

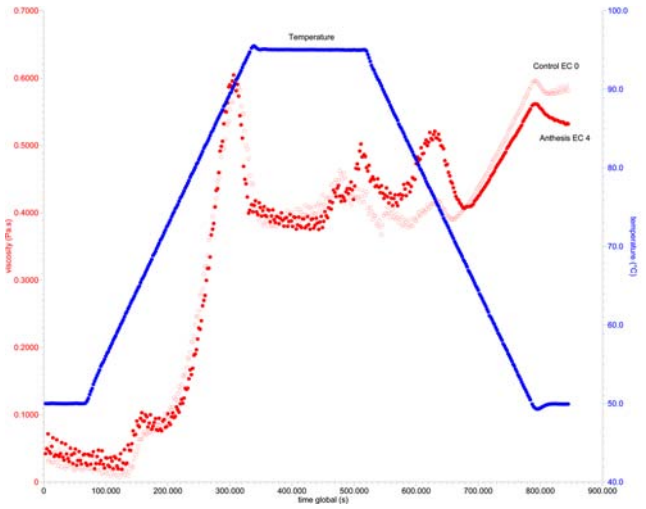

Figure 4. Pasting profiles of starches from Control and Anthesis 40 dS/m^2 NaCl-treated plants. An 8% (w/w) starch slurry was analyzed on the rheometer-simulated RVA platform. The temperature profile is shown in the figure.

deviate from that of the control sample. The same was shown in the study by Peiris et al.[7] with rice exposed to EC values ranging from 2 to 4 dS/m^2. The lower pasting temperature of the Anthesis EC4 starch may be explained by the diminished proportion of the long chains of amylopectin (Table 5), as these long chains could contribute to maintenance of starch granule integrity during the pasting process.[56] The peak viscosity and setback of most of the salt treatments were also lower than those of the control (Table 5), suggesting that the integrity of the gel network was compromised, thus reducing the occurrence of starch retrogradation.[60]

Multivariate Analysis. The PLS-DA algorithm is a supervised method that uses multiple linear regression analyses to identify maximum covariance between measured variables and treatments. In other words, the variation *within* groups is reduced in order to maximize differences *among* groups. The measured variables are summarized into a smaller number of variables called "scores" which then were plotted on the 2D-plots.[61] Here, PLS-DA was used to analyze the behavior of all variables measured in this study (Figure 5A), of the agronomic variables (Figure 5B), and of the grain composition and starch

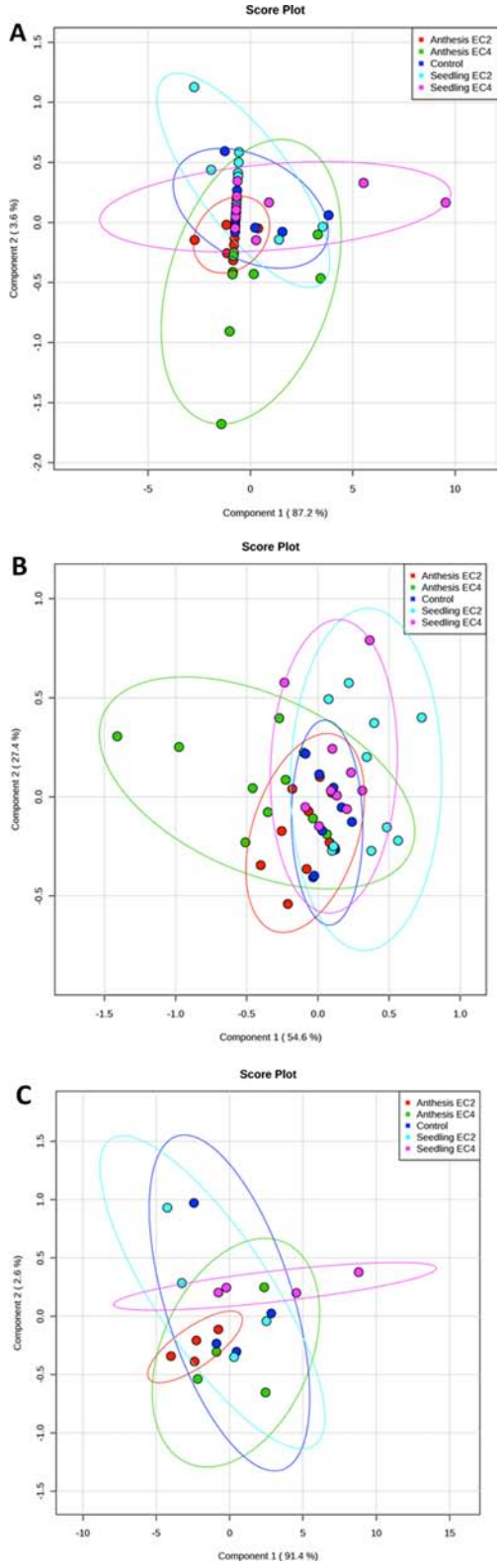

Figure 5. Partial-least squares discriminant analysis (PLS-DA) of measured variables. (A) PLS-DA plot of all variables in this study. (B) Agronomic yield and grain characteristic variables. (C) Grain composition and starch functionality variables. Each of the 3−10 replicates was individually plotted, and the samples were projected onto 2D-plots showing the first 2 principal components (PCs). Each PC captures maximum variation of the data set, where PC1 retains the most variation and PC2 captures the second most level of variation.[62] The confidence ellipses represent 95% confidence intervals of the data.

DOI: 10.1021/jf503948p
J. Agric. Food Chem. 2015, 63, 2296−2304

functionality variables (Figure 5C) in order to illustrate the separation between different groups of treatments. Although there were significant changes ($P < 0.05$) in the individual data sets of both agronomical and grain composition and starch functionality measurements, the multivariate analysis revealed that, when considered together, the variables behaved similarly among all the treatments as no distinct separation between treatment groups was observed (Figure 5A). Some separation could be seen between the Seedling EC2 Anthesis EC4 treatments when only the agronomical variables were taken into account (Figure 5B), but separation disappeared when grain composition and starch functionality parameters were simultaneously assessed (Figure 5C). Some separation between Anthesis EC2 and Seedling EC4 treatments however was observed when considering grain composition and starch functionality variables (Figure 5C). This implies that the impacts of different salinity levels applied at different developmental stages were not profound, at least in this greenhouse-based experimental setting in which other potential environmental variables were reduced.

This study aimed to understand and differentiate the prolonged and isolated effects at the grain filling stage of both mild and high salinity on the yield, and compositional and functionality components of rice grains. Overall, the changes were most pronounced in the high salinity treatment applied at the reproductive stages. Rice grown under both prolonged treatments seemed to have adapted to the salinity, but to different extents; that is, Seedling EC2 appeared to have morphological adaptation, while Seedling EC4 plants modulated their carbon flux to the developing kernels. Applying salt at Anthesis had a direct but opposite effect on grain filling process: Anthesis EC2 may have accelerated grain filling, resulting in higher starch accumulation, while Anthesis EC4 was compromised in its adaptability to the imposed salinity level, which was reflected in diminished agronomic yields and starch content. Although multivariate analysis of the data showed that the 2 and 4 dS/m^2 NaCl did not have profound effects on rice starch molecular composition regardless of the time of treatment application, there were still measurable changes in starch thermal and pasting properties, which were only limited to the most affected treatment (i e. Anthesis EC4). Overall, this study demonstrated the complexity of rice responses to timing and severity of salinity stress.

■ ASSOCIATED CONTENT

Supporting Information

Tables S1, S2, and S3 and Figures S1 and S2. This material is available free of charge via the Internet at http://pubs.acs.org.

■ AUTHOR INFORMATION

Corresponding Author

*E-mail: dmbeckles@ucdavis.edu. Phone: 1 (530) 754-4779. Fax: 1 (530) 752-9659.

Present Address

[⊥]Department of Agronomy, Faculty of Agriculture at Kamphaeng Saen, Kasetsart University, Nakhonpathom 73140, Thailand.

Funding

This work was supported by Hatch Project # CA-D-PLS-2164-H (D.M.B.). M.T. thanks the Royal Thai Government and Henry A. Jastro Graduate Research Award for funding.

Notes

The authors declare no competing financial interest.

■ ACKNOWLEDGMENTS

We thank Peter Colowit and Dr. Tom Tai for use of the WinSeedle program, Dr. Raul Piedrahita for use of the particle size analyzer, Dr. Jorge Dubcovsky for access to the Mini-mill, and Yoseph Murtanu for his assistance in Table of Contents graphic design.

■ ABBREVIATIONS USED

ADP-glucose pyrophosphorylase, AGPase; degree of polymerization, DP; differential scanning calorimetry, DSC; electrical conductivity, EC; high-performance anion-exchange chromatography, HPAEC; nitrogen, N; partial-least squares discriminant analysis, PLS-DA; rapid viscosity analysis, RVA; sodium chloride, NaCl; sodium dodecyl sulfate polyacrylamide gel electrophoresis, SDS-PAGE

■ REFERENCES

(1) FAOSTAT. Production of cereals and their share in the world 2004. *FAO Statistics Yearbook*; 2009, Vol. *1*.

(2) Yang, L. X.; Wang, Y. L.; Dong, G. C.; Gu, H.; Huang, J. Y.; Zhu, J. G.; Yang, H. J.; Liu, G.; Han, Y. The impact of free-air CO2 enrichment (FACE) and nitrogen supply on grain quality of rice. *Field Crops Res.* **2007**, *102*, 128−140.

(3) Beckles, D. M.; Thitisaksakul, M. How environmental stress affects starch composition and functionality in cereal endosperm. *Starch-Starke* **2014**, *66*, 58−71.

(4) Munns, R.; Tester, M. Mechanisms of salinity tolerance. *Annu. Rev. Plant Biol.* **2008**, *59*, 651−681.

(5) Pattanagul, W.; Thitisaksakul, M. Effect of salinity stress on growth and carbohydrate metabolism in three rice (Oryza sativa L.) cultivars differing in salinity tolerance. *Indian J. Exp. Biol.* **2008**, *46*, 736−742.

(6) Siscar-Lee, J. J. H.; Juliano, B. O.; Qureshi, R. H.; Akbar, M. Effect of saline soil on grain quality of rices differing in salinity tolerance. *Plant Foods Hum. Nutr.* **1990**, *40*, 31−36.

(7) Peiris, B. D.; Siegel, S. M.; Senadhira, D. Chemical characteristics of grains of rice (Oryza-Sativa-L) cultivated in saline media of varying ionic composition. *J. Exp. Bot.* **1988**, *39*, 623−631.

(8) Lutts, S.; Kinet, J. M.; Bouharmont, J. Changes in plant response to NaCl during development of rice (Oryza sativa L) varieties differing in salinity resistance. *J. Exp. Bot.* **1995**, *46*, 1843−1852.

(9) Mittler, R.; Blumwald, E. Genetic engineering for modern agriculture: challenges and perspectives. *Annu. Rev. Plant Biol.* **2010**, *61*, 443−462.

(10) Grattan, S. R.; Zeng, L.; Shannon, M. C.; Roberts, S. R. Rice is more sensitive to salinity than previously thought. *Calif. Agric.* **2002**, *56*, 189−198.

(11) Baxter, G.; Zhao, J.; Blanchard, C. Salinity alters the protein composition of rice endosperm and the physicochemical properties of rice flour. *J. Sci. Food Agric.* **2011**, *91*, 2292−2297.

(12) Abdullah, Z.; Khan, M. A.; Flowers, T. J. Causes of sterility in seed set of rice under salinity stress. *J. Agron. Crop Sci.* **2001**, *187*, 25−32.

(13) Yeo, A. R.; Yeo, M. E.; Flowers, S. A.; Flowers, T. J. Screening of rice (Oryza-Sativa-L) genotypes for physiological characters contributing to salinity resistance, and their relationship to overall performance. *Theor. Appl. Genet.* **1990**, *79*, 377−384.

(14) Rao, P. S.; Mishra, B.; Gupta, S. R. Effects of soil salinity and alkalinity on grain quality of tolerant, semi-tolerant and sensitive rice genotypes. *Rice Sci.* **2013**, *20*, 284−291.

(15) Calingacion, M.; Laborte, A.; Nelson, A.; Resurreccion, A.; Concepcion, J. C.; Daygon, V. D.; Mumm, R.; Reinke, R.; Dipti, S.; Bassinello, P. Z.; Manful, J.; Sophany, S.; Lara, K. C.; Bao, J. S.; Xie, L. H.; Loaiza, K.; El-hissewy, A.; Gayin, J.; Sharma, N.; Rajeswari, S.;

DOI: 10.1021/jf503948p
J. Agric. Food Chem. 2015, 63, 2296−2304

Manonmani, S.; Rani, N. S.; Kota, S.; Indrasari, S. D.; Habibi, F.; Hosseini, M.; Tavasoli, F.; Suzuki, K.; Umemoto, T.; Boualaphanh, C.; Lee, H. H.; Hung, Y. P.; Ramli, A.; Aung, P. P.; Ahmad, R.; Wattoo, J. I.; Bandonill, E.; Romero, M.; Brites, C. M.; Hafeel, R.; Lur, H. S.; Cheaupun, K.; Jongdee, S.; Blanco, P.; Bryant, R.; Lang, N. T.; Hall, R. D.; Fitzgerald, M. Diversity of global rice markets and the science required for consumer-targeted rice breeding. *PLoS One* **2014**, *9*.

(16) Zeng, L.; Shannon, M. C.; Lesch, S. M. Timing of salinity stress affects rice growth and yield components. *Agric. Water Manage.* **2001**, *48*, 191−206.

(17) Roessner, U.; Beckles, D. M. Metabolomics for salinity research. In *Plant Salt Tolerance: Methods and Protocols (Method in Molecular Biology)*; Shabala, S., Cuin, T. A., Eds.; Humana Press: New York City, 2012.

(18) Heenan, D. P.; Lewin, L. G.; Mccaffery, D. W. Salinity Tolerance in rice varieties at different growth-stages. *Aust. J. Exp. Agric.* **1988**, *28*, 343−349.

(19) Schmidt, R.; Caldana, C.; Mueller-Roeber, B.; Schippers, J. H. M. The contribution of SERF1 to root-to-shoot signaling during salinity stress in rice. *Plant Signaling Behav.* **2014**, *9*, e27540.

(20) Munns, R. Genes and salt tolerance: bringing them together. *New Phytol.* **2005**, *167*, 645−663.

(21) Lutts, S.; Kinet, J. M.; Bouharmont, J. Changes in plant response to NaCl during development of rice (Oryza sativa L.) varieties differing in salinity resistance. *J. Exp. Bot.* **1995**, *46*, 1843−1852.

(22) Thitisaksakul, M.; Jiménez, R. C.; Arias, M. C.; Beckles, D. M., Effects of environmental factors on cereal starch biosynthesis and composition. *J. Cereal Sci.* **2012**, *56*, 67−80.

(23) Shavrukov, Y. Salt stress or salt shock: which genes are we studying? *J. Exp. Bot.* **2013**, *64*, 119−127.

(24) Sun, M. M.; Abdula, S. E.; Lee, H. J.; Cho, Y. C.; Han, L. Z.; Koh, H. J.; Cho, Y. G. Molecular Aspect of Good Eating Quality Formation in Japonica Rice. *PLoS One* **2011**, *6*, e18385.

(25) Yamakawa, H.; Hirose, T.; Kuroda, M.; Yamaguchi, T. Comprehensive expression profiling of rice grain filling-related genes under high temperature using DNA microarray. *Plant Physiol.* **2007**, *144*, 258−277.

(26) Chen, Y.; Wang, M.; Ouwerkerk, P. B. F. Molecular and environmental factors determining grain quality in rice. *Food Energy Secur.* **2012**, *1*, 111−132.

(27) Sun, M. M.; Abdula, S. E.; Lee, H. J.; Cho, Y. C.; Han, L. Z.; Koh, H. J.; Cho, Y. G., Molecular Aspect of Good Eating Quality Formation in Japonica Rice. *PLoS One* **2011**, *6*.

(28) Grattan, S. R.; Zeng, L.; Shannon, M. C.; Roberts, S. R. Rice is more sensitive to salinity than previoulsy thought. *Calif. Agric.* **2002**, *56*, 189−198.

(29) Radhika Reddy, K.; Zakiuddin Ali, S.; Bhattacharya, K. R. The fine structure of rice-starch amylopectin and its relation to the texture of cooked rice. *Carbohydr. Polym.* **1993**, *22*, 267−275.

(30) Ramesh, M.; Zakiuddin Ali, S.; Bhattacharya, K. R. Structure of rice starch and its relation to cooked-rice texture. *Carbohydr. Polym.* **1999**, *38*, 337−347.

(31) Wani, A. A.; Singh, P.; Shah, M. A.; Schweiggert-Weisz, U.; Gul, K.; Wani, I. A. Rice starch diversity: effects on structural, morphological, thermal, and physicochemical properties—a review. *Compr. Rev. Food Sci. Food Saf.* **2012**, *11*, 417−436.

(32) Venu, R. C.; Sreerekha, M. V.; Madhav, M. S.; Nobuta, K.; Mohan, K. M.; Chen, S. B.; Jia, Y. L.; Meyers, B. C.; Wang, G. L. Deep transcriptome sequencing reveals the expression of key functional and regulatory genes involved in the abiotic stress signaling pathways in rice. *J. Plant Biol.* **2013**, *56*, 216−231.

(33) Schmidt, R.; Schippers, J. H.; Welker, A.; Mieulet, D.; Guiderdoni, E.; Mueller-Roeber, B., Transcription factor OsHsfC1b regulates salt tolerance and development in Oryza sativa ssp japonica. *AoB Plants* **2012**, pls011.

(34) Counce, P. A.; Keisling, T. C.; Mitchell, A. J. A uniform, objective, and adaptive system for expressing rice development. *Crop Sci.* **2000**, *40*, 436−443.

(35) Luengwilai, K.; Beckles, D. M., Climacteric ethylene is not essential for initiating chilling injury in tomato (Solanaum lycorpesicon L.) cv. Ailsa Caig. *J. Stored Prod. Postharvest Res.* **2010**, *1*, 1−8.

(36) Tanadul, O.; VanderGheynst, J. S.; Beckles, D. M.; Powell, A. L. T.; Labavitch, J. M. The impact of elevated CO2 concentration on the quality of algal starch as a potential biofuel feedstock. *Biotechnol. Bioeng.* **2014**, *111*, 1323−1331.

(37) Lumdubwong, N.; Seib, P. A. Rice starch isolation by alkaline protease digestion of wet-milled rice flour. *J. Cereal Sci.* **2000**, *31*, 63−74.

(38) Chun, A. Effects of temperature during grain filling on quality and starch properties in rice. Ph.D. Thesis, Seoul National University, Republic of Korea, 2009.

(39) Luengwilai, K.; Tananuwong, K.; Shoemaker, C. F.; Beckles, D. M. Starch molecular structure shows little association with fruit physiology and starch metabolism in tomato. *J. Agric. Food Chem.* **2010**, *58*, 1275−1282.

(40) Hazard, B.; Zhang, X. Q.; Colasuonno, P.; Uauy, C.; Beckles, D. M.; Dubcovsky, J. Induced mutations in the starch branching enzyme II (SBEII) genes increase amylose and resistant starch content in durum wheat. *Crop Sci.* **2012**, *52*, 1754−1766.

(41) AOAC. *Official Methods of Analysis*; Association of Official Analytical Chemists: Rockville, MD, 2006.

(42) Iida, S.; Amano, E.; Nishio, T. A rice (Oryza sativa L.) mutant having a low content of glutelin and a high content of prolamine. *Theor. Appl. Genet.* **1993**, *87*, 374−378.

(43) Schneider, C. A.; Rasband, W. S.; Eliceiri, K. W. NIH Image to ImageJ: 25 years of image analysis. *Nat. Methods* **2012**, *9*, 671−675.

(44) Xia, J. G.; Mandal, R.; Sinelnikov, I. V.; Broadhurst, D.; Wishart, D. S. MetaboAnalyst 2.0-a comprehensive server for metabolomic data analysis. *Nucleic Acids Res.* **2012**, *40*, W127−W133.

(45) Fitzgerald, M. A.; McCouch, S. R.; Hall, R. D. Not just a grain of rice: The quest for quality. *Trends Plant Sci.* **2009**, *14*, 133−139.

(46) Luo, Y.; Zhu, Z.; Chen, N.; Duan, B.; Zhang, L. Grain types and related quality characteristics of rice in China. *Zhongguo Shuidao Kexue* **2003**, *18*, 135−139.

(47) Shomura, A.; Izawa, T.; Ebana, K.; Ebitani, T.; Kanegae, H.; Konishi, S.; Yano, M. Deletion in a gene associated with grain size increased yields during rice domestication. *Nat. Genet.* **2008**, *40*, 1023−1028.

(48) Tian, Z. X.; Qian, Q.; Liu, Q. Q.; Yan, M. X.; Liu, X. F.; Yan, C. J.; Liu, G. F.; Gao, Z. Y.; Tang, S. Z.; Zeng, D. L.; Wang, Y. H.; Yu, J. M.; Gu, M. H.; Li, J. Y. Allelic diversities in rice starch biosynthesis lead to a diverse array of rice eating and cooking qualities. *Proc. Natl. Acad. Sci. U.S.A.* **2009**, *106*, 21760−21765.

(49) Chiotelli, E.; Le Meste, M. Effect of small and large wheat starch granules on thermomechanical behavior of starch. *Cereal Chem.* **2002**, *79*, 286−293.

(50) Vasanthan, T.; Bhatty, R. S. Physicochemical properties of small- and large-granule starches of waxy, regular, and high-amylose barleys. *Cereal Chem.* **1996**, *73*, 199−207.

(51) Smyth, D. A.; Prescott, H. E. Sugar content and activity of sucrose metabolism enzymes in milled rice grain. *Plant Physiol.* **1989**, *89*, 893−896.

(52) Yin, Y.-G.; Kobayashi, Y.; Sanuki, A.; Kondo, S.; Fukuda, N.; Ezura, H.; Sugaya, S.; Matsukura, C. Salinity induces carbohydrate accumulation and sugar-regulated starch biosynthetic genes in tomato (Solanum lycopersicum L. cv. 'Micro-Tom') fruits in an ABA- and osmotic stress-independent manner. *J. Exp. Bot.* **2009**, erp333.

(53) Boriboonkaset, T.; Theerawitaya, C.; Yamada, N.; Pichakum, A.; Supaibulwatana, K.; Cha-um, S.; Takabe, T.; Kirdmanee, C. Regulation of some carbohydrate metabolism-related genes, starch and soluble sugar contents, photosynthetic activities and yield attributes of two contrasting rice genotypes subjected to salt stress. *Protoplasma* **2013**, *250*, 1157−1167.

(54) Martin, M.; Fitzgerald, M. A. Proteins in rice grains influence cooking properties! *J. Cereal Sci.* **2002**, *36*, 285−294.

DOI: 10.1021/jf503948p
J. Agric. Food Chem. 2015, 63, 2296−2304

(55) Hanashiro, I.; Abe, J.-i.; Hizukuri, S. A periodic distribution of the chain length of amylopectin as revealed by high-performance anion-exchange chromatography. *Carbohydr. Res.* **1996**, *283*, 151−159.
(56) Jane, J.; Chen, Y. Y.; Lee, L. F.; McPherson, A. E.; Wong, K. S.; Radosavljevic, M.; Kasemsuwan, T. Effects of amylopectin branch chain length and amylose content on the gelatinization and pasting properties of starch. *Cereal Chem. J.* **1999**, *76*, 629−637.
(57) Stevens, D.; Elton, G. Thermal properties of the starch/water system part I. Measurement of heat of gelatinisation by differential scanning calorimetry. *Starch-Stärke* **1971**, *23*, 8−11.
(58) Biliaderis, C. G.; Page, C. M.; Slade, L.; Sirett, R. R. Thermal behavior of amylose-lipid complexes. *Carbohydr. Polym.* **1985**, *5*, 367−389.
(59) Copeland, L.; Blazek, J.; Salman, H.; Tang, M. C. M. Form and functionality of starch. *Food Hydrocolloids* **2009**, *23*, 1527−1534.
(60) Jane, J.; Chen, Y. Y.; Lee, L. F.; McPherson, A. E.; Wong, K. S.; Radosavljevic, M.; Kasemsuwan, T. Effects of amylopectin branch chain length and amylose content on the gelatinization and pasting properties of starch1. *Cereal Chem. J.* **1999**, *76*, 629−637.
(61) Xia, J.; Psychogios, N.; Young, N.; Wishart, D. S. MetaboAnalyst: a web server for metabolomic data analysis and interpretation. *Nucleic Acids Res.* **2009**, *37*, W652−W660.
(62) Stamova, B. S.; Roessner, U.; Suren, S.; Laudencia-Chingcuanco, D.; Bacic, A.; Beckles, D. M. Metabolic profiling of transgenic wheat over-expressing the high-molecular-weight Dx5 glutenin subunit. *Metabolomics* **2009**, *5*, 239−252.

NOTE ADDED AFTER ASAP PUBLICATION

This paper was published ASAP on February 12, 2015, with an error in references 22, 33, 35, and 52. The corrected version reposted on February 17, 2015.

DOI: 10.1021/jf503948p
J. Agric. Food Chem. 2015, 63, 2296−2304

pomegranate seeds and almond have been studied by different researchers,[7−9] to the best of our knowledge, no investigation is available on the bioactive and physicochemical properties of those byproducts in detail and no investigation has been focused on the properties of extracts of walnut. Therefore, this study was aimed to investigate the physicochemical (crude fat, protein, fiber, mineral, phenolic, and fatty acid contents, volatile composition, and color properties), antimicrobial (against *Staphylococcus aureus*, *Listeria monocytogenes*, *Escherichia coli* O157:H7, and *Salmonella* Typhimurium), and bioactive (hydrolyzable tannin, total phenolic, and flavonoid contents) properties and volatile composition of those byproducts in detail. The results of the present study could provide information about where these byproducts could be used in the food industry to achieve economic gain.

MATERIALS AND METHODS

Materials. Oil byproducts obtained by cold pressing of grape, walnut, pomegranate, and almond seeds were provided from Oneva Food Co, Istanbul, Turkey, and were coded as GOB, WOB, POB, and AOB, respectively. Air-dried and powdered samples were subsequently transferred to the laboratory and stored in damp-proof plastic bags at room temperature until being analyzed.

Physicochemical Properties. *Determination of Color, Browning Index (BI), and Bulk Density.* The color properties of the byproducts were measured using a colorimeter (Konica Minolta, CR-400, Mississauga, ON, Canada), and the color values were expressed as *L* (whiteness/darkness), *a* (redness/greenness), and *b* (yellowness/blueness). BI analysis was carried out according to a method described by Palombo et al.[10] Briefly, absorbance values of the centrifuged clear filtrates were measured at 420 and 550 nm by spectrophotometer (8453E UV−vis spectroscopy system and Agilent, USA). Distilled water was used as the blank, and the BI, which was expressed as optical density/g dry solids, was calculated as

$$\text{browning index (BI)} = A_{420} - A_{520} \quad (1)$$

where A_{420} and A_{520} are absorbance values of the samples measured at 420 and 520 nm, respectively. Bulk density of the byproducts was determined according to method described by Chegini and Ghobadian.[11]

Determination of Dry Matter, Oil, Protein, Crude Fiber, and Ash Contents. Dry matter, ash, protein, crude fiber, and oil contents of the byproducts were determined according to the method reported by official procedures.[12] Dry matter contents of the samples were analyzed by drying at 105 °C for 4 h in a drying oven (FN 120, Nuve, Ankara, Turkey). Ash content was determined by incineration of the samples at 550 °C for 6 h, whereas protein content was tested using an automatic nitrogen analyzer (FP 528, Leco, USA), on the basis of the Dumas method. Total protein contents were calculated by multiplying the obtained nitrogen values by 6.25. Crude fiber contents of the samples were determined using an automatic fiber analyzer (ANKOM Technology Corp., Fairport, NY, USA). The oil contents of the byproducts was determined using a Soxhlet extraction system in which hexane were used as a solvent.

Determination of Water Activity and pH Values. A water activity meter (AquaLab, 2.0, USA) was used for determining the water activity of the samples. Samples were placed into plastic cups to cover the surface and transferred into the equipment. The results were measured at 25 °C. The pH of the sample was measured with a pH meter (WTW-Inolab, Weilheim, Germany) in a suspension of 10% (w/v) powder in distilled water at 25 °C.

Determination of Fatty Acid Composition. The fatty acid composition of the extracted oil samples was determined using fatty acid methyl ester (FAME) according to the method described by Yalcin et al.[13] To determine the fatty acid composition of the samples, the samples were subjected to an oil extraction procedure by hexane using a Soxhlet extraction system for 6 h. A GC (Agilent 6890, Agilent, USA) equipped with a FID and 100 × 0.25 mm i.d. HP-88 column was used. Injection block temperature was adjusted to 250 °C. The oven temperature was held at 103 °C for 1 min, heated to 170 °C at 6.5 °C/min and from 170 to 230 °C for 12 min at 2.5 °C/min, and then held at 230 °C for 5 min. Helium was used as a carrier gas with a flow rate 2 mL/min; the split rate was 1/50.

Determination of Mineral Composition. Mineral analysis of the samples was performed according to the method described by AOAC with some modifications.[14] Half a gram of the sample was weighed into Teflon microwave digestion vessel and incorporated with 5 mL of concentrated nitric acid and 1 mL of hydrogen peroxide. Vessels were covered and placed into a microwave oven. The initial oven temperature was adjusted to 25 °C, then heated to 90 °C for 5 min, from 90 to 120 °C at 6 °C/min, and from 120 to 150 °C at 6 °C/min, finally increased to 175 °C at 6 °C/min, and held at this temperature for 5 min. After the vessels cooled, clear digested samples were transferred to 50 mL volumetric flasks and diluted to the mark with deionized water. Minerals were determined using a PerkinElmer AAS 700 in flame mode. The following wavelengths and slit widths were used to quantify minerals: calcium, wavelength 422.7, slit, 0.7 H; sodium, wavelength 589.0, slit 0.2 H; iron, wavelength 248.3, slit 0.2 H; zinc, wavelength 213.9, slit 0.7 H; manganese, wavelength 279.5, slit 0.2 H; potassium, wavelength 766.5, slit 0.7 H; magnesium, wavelength 285.2, slit 0.7 H; copper, wavelength 324.8, slit 0.7 H.

Bioactive Properties. *Extraction Procedure.* Methanol was used for the extraction of the bioactive compounds from the byproducts. During the extraction process, 1 g of the sample was weighed into the test tube and mixed with 10 mL of methanol. The mixture was stirred by vortex and then by a shaker for 1 h at ambient temperature (Simsek Labor Teknik, Ankara, Turkey). Following the extraction process, the solution was centrifuged on a Universal 320 centrifuger (Hettich, Germany) at 5000g for 5 min, and the supernatants were filtered using a 0.45 μm filter (Sartorious Stedim Biotech, Gottingen, Germany). Obtained extracts were kept at −18 °C for further analysis.

Determination of Total Phenolic Content (TPC). TPC of the methanolic extracts was determined according to the modified method described by Singleton and Rossi.[15] TPC was determined at 760 nm by a spectrophotometer (Agilent 8453E UV−vis spectroscopy system) using Folin−Ciocalteu's phenol reagent. TPCs of the samples were calculated as milligrams of gallic acid equivalents (GAE) per 100 g of dried samples.

Determination of Total Flavonoid Content (TFC). TFC of the methanolic extracts was determined according to the method described by Zhinsen et al.[16] TFC was determined spectrophotometrically at 510 nm. The results were expressed as milligrams of catechin (CE) per 100 g of dried sample.

Determination of Total Hydrolyzable Tannin Content (HTC). The total HTC of the methanolic extracts was determined according to the method of Willis and Allen.[17] The absorbance of the samples was recorded at 550 nm, and the results were calculated as mg of tannic acid (TA) per 100 g of dried sample.

Determination of Phenolic Composition. The phenolic profile of the samples was determined according to the modified method described by Schieber et al.[18] using a HPLC system (Shimadzu, Kyoto, Japan) equipped with a DGU-20A5 degasser, an LC-20AT gradient pump, an SIL-20A autosampler, a CTO-10AS VP column oven, and an SPD-M20A diode array detection (DAD) system. The column used was a Luna, 5 μm, C18 100A (250 × 4.6 mm) from Phenomenex (Torrance, CA, USA). Column temperature was set to 25 °C. Mobile phase A was 2% (v/v) acetic acid prepared in double-distilled water; eluent B was 0.5% acetic acid in double-distilled water and acetonitrile (50:50, v/v). The gradient was as follows: from 90 to 55% of A within 40 min, from 55 to 0% of A within 5 min, and returning to the initial 90% A within 5 min. Between each analysis 15 min of equilibration treatment (90% of A) was performed. The flow rate was 1 mL/min, and the injection volume was 20 μL.

Antibacterial Activity. Antibacterial activity was assessed using the extracts of the byproducts prepared for determination of bioactive properties. Four bacterial strains were used to assess antibacterial activity of the extracts of oil byproducts, two Gram-positive (*Staphylococcus aureus* ATCC 25923 and *Listeria monocytogenes*

DOI: 10.1021/jf504390t
J. Agric. Food Chem. 2015, 63, 2305−2313

Table 1. Physical Properties of the Oil Byproducts[a]

sample[b]	color values			BI[c]	bulk density
	L	*a*	*b*		
WOB	48.33 ± 0.01b	8.45 ± 0.01c	22.11 ± 0.04b	0.520 ± 0.001a	1.33 ± 0.00d
POB	42.01 ± 0.02c	10.15 ± 0.03b	23.27 ± 0.02a	0.221 ± 0.000b	1.47 ± 0.02b
GOB	43.41 ± 0.02c	12.72 ± 0.02a	18.19 ± 0.03c	0.074 ± 0.000c	1.37 ± 0.00c
AOB	68.39 ± 0.01a	5.71 ± 0.01d	18.76 ± 0.04c	0.042 ± 0.000d	1.53 ± 0.00a

[a]Different lower case letters show differences between the samples (n = 3). The results are expressed as the mean ± SD. [b]WOB, walnut seed oil byproduct; POB, pomegranate seed oil byproduct; GOB, grape seed oil byproduct; AOB, almond seed oil byproduct. [c]BI, browning index.

Table 2. Chemical Properties of the Oil Byproducts[a]

sample[b]	dry matter (%)	protein (%)	oil (%)	crude fiber (%)	ash (%)	pH	a_w
WOB	90.55 ± 0.04c	34.09 ± 1.01b	10.11 ± 0.36b	6.65 ± 0.17c	4.50 ± 0.15b	5.52 ± 0.05b	0.498 ± 0.006a
POB	93.71 ± 0.49a	24.33 ± 0.49c	12.57 ± 0.36a	25.10 ± 1.08b	3.30 ± 0.06c	4.43 ± 0.00c	0.431 ± 0.003c
GOB	93.47 ± 0.46a	9.38 ± 0.23d	4.82 ± 0.33d	45.83 ± 0.66a	3.07 ± 0.02d	4.25 ± 0.11d	0.391 ± 0.011d
AOB	92.41 ± 0.02b	49.05 ± 1.03a	8.83 ± 0.52c	5.87 ± 0.30d	5.72 ± 0.01a	6.14 ± 0.02a	0.486 ± 0.001b

[a]Different lower case letters show differences between the samples (n = 3). The results are expressed as the mean ± SD. [b]WOB, walnut seed oil byproduct; POB, pomegranate seed oil byproduct; GOB, grape seed oil byproduct; AOB, almond seed oil byproduct.

ATCC 19118) and two Gram-negative bacteria (*Escherichia coli* O157:H7 ATCC 33150 and *Salmonella enteric* subsp. *enteric* serovar Typhimurium ATCC 14028). All bacterial strains were activated twice in nutrient broth (Merck, Darmstadt, Germany), and inocula were prepared by 18 h culture in nutrient broth at 37 °C.

The agar diffusion method was used to determine the antibacterial effect on the basis of the method described by Özkan et al.[19] For this aim, autoclaved nutrient agar (Merck) was inoculated with each 18 h bacterial strain, targeting a final cell concentration of 10^6–10^7 CFU/mL at 43–45 °C and poured in Petri plates. After the solidification of agar, four wells were made in the agar using sterile cork pores (4 mm). A 50 μL of different concentrations (50%, 20% and 4% v:v in 95% ethanol) of the extracts was pipetted in each well. 95% ethanol was used as the negative control. Petri plates were incubated at 37 °C for 24h. The antibacterial activity was expressed as the mean of inhibition diameters (mm) produced by the extract minus that for the negative control.

Volatile Composition. The volatile profile of the oil byproducts was determined using a gas chromatography–mass spectrometry (Agilent 7890A GC system, Agilent Technologies, Avondale, AZ, USA) using a mass selective detector (Agilent Technologies) and DB-WAX column (60 m × 0.250 mm i.d.; film thickness, 0.25 μm). The oven temperature was adjusted to 40 °C for 10 min, then heated to 110 °C at 3 °C/min, from 110 to 150 °C at 4 °C/min, and from 150 to 210 °C at 10 °C/min, finally increased to 210 °C/min and held for 15 min. Helium was used as a carrier gas with a flow rate of 1.0 mL/min, and the voltage of the electron ionization detector was 70 eV. The compounds adsorbed by the SPME fiber (75 μm, 23 ga, carboxen/polydimethylsiloxane (CAR/PDMS)) (Supelco, Bellefonte, PA, USA) at 40 °C for 1 h were desorbed from the injection port for 15 min at 50 °C in the splitless mode. The compounds were identified by comparison with spectra from the libraries Flavor 2, NIST 05, and Wiley 7n. Analyses were conducted in duplicate.

Statistical Analysis. All of the results were expressed as the mean ± SD. ANOVA was performed to determine the differences among the samples using the SPSS Statistical Software Program (SPSS Statistics 17.0, Armonk, NY, USA). The Duncan multiple-comparison test was conducted to determine the differences between the parameters at the probability level of 0.05.

RESULTS AND DISCUSSION

Physicochemical Properties. *Physical Properties.* Color (L, a, b), BI, and bulk density values of the oil byproducts are shown in Table 1. As can be seen in Table 1, L, a, and b values of the byproducts were found between 42.01 and 68.39, between 5.71 and 12.72, and between 18.19 and 23.27, respectively. Color values of the WOB, POB, and GOB samples were very close to each other; however, those of AOB, especially L and a values, were quite different from the others. As known, the color of a certain food is one of the main factors affecting its consumer preference. Use of different additives may change color properties of foods. In this respect, these oil byproducts, if they are used, may affect foods' color. Color of the byproducts is related with pigments, carotenoids, and phenolic pigments (anthocyanins, flavonols, and proanthocyanins). Therefore, variation in type or amount of these compounds results in different color values. BI values of the byproducts analyzed in the present study changed between 0.042 and 0.520. Browning of the food and agricultural material and their byproducts occurs by the formation of some colored pigments due to enzymatic and nonenzymatic reaction and concentration changes The highest BI value belonged to WOB, whereas AOB had the lowest BI. In addition to color properties, bulk densities of the samples were also analyzed. Bulk density of the cold-pressed oil byproducts were found between 1.33 and 1.53. Because powder forms of these byproducts could be used for any aim, their bulk density values are also important in this respect. Among the samples, WOB had the lowest bulk density value, indicating that it can be compressed easily when compared with the others.

Some Chemical Properties. Chemical properties of the oil byproducts are presented in Table 2. pH and a_w values of the samples ranged from 4.25 to 6.14 and from 0.391 to 0.498, respectively. Dry matter contents of the byproducts were very close to each other and varied between 90.55 and 93.71%. Protein contents of the samples varied over a wide range, from 9.38 to 49.05%. Among the samples, AOB had the highest protein content followed by WOB, POB, and GOB, respectively. As seen from the results, WOB, POB, and AOB had significant amounts of protein; therefore, they might be used to enrich the protein content of different food products. Cam et al.[20] added pomegranate byproducts to ice cream and reported that ice cream samples enriched with byproducts had higher protein content than control ice cream. Enrichment of different food products with AOB could be preferred because it has high protein content and almond proteins can provide all essential amino acids except for methionine in quantities equal to or greater than recommended by the FAO.[21]

DOI: 10.1021/jf504390t
J. Agric. Food Chem. 2015, 63, 2305–2313

Table 3. Fatty Acid Composition (Percent) of the Oils Extracted from the Cold Press Oil Byproducts[a]

fatty acid[b]	WOB[c]	POB[c]	GOB[c]	AOB[c]
C14:0	nd[d]	0.31 ± 0.00a	0.14 ± 0.00c	0.20 ± 0.00b
C16:0	7.81 ± 0.02c	4.40 ± 0.02d	8.65 ± 0.03a	8.35 ± 0.01b
C18:0	3.99 ± 0.03b	2.76 ± 0.01c	4.29 ± 0.03a	1.73 ± 0.01d
C18:1	20.12 ± 0.06b	6.28 ± 0.02d	18.67 ± 0.29c	60.18 ± 0.01a
C18:2	57.33 ± 0.11b	8.75 ± 0.02d	67.50 ± 0.24a	28.79 ± 0.01c
C18:3ω3	10.75 ± 0.00a	1.08 ± 0.00b	nd	nd
C18:3ω6	nd	76.42 ± 0.07a	0.76 ± 0.01b	0.75 ± 0.00b
SFA	11.80ab	7.47c	13.08a	10.28b
MUFA	20.12b	6.28c	18.67b	60.18a
PUFA	68.08b	86.25a	68.26b	29.54c

[a]Different lower case letters show differences between the samples (n = 3). The results are expressed as the mean ± SD. [b]C14:0, butyric acid; C16:0, palmitic acid; C18:0, stearic acid; C18:1, oleic acid; C18:3ω3, linolenic acid; C18:3ω6, conjugated linolenic acid; SFA, saturated fatty acid; MUFA, monounsaturated fatty acid; PUFA, polyunsaturated fatty acid. [c]WOB, walnut seed oil byproduct; POB, pomegranate seed oil byproduct; GOB, grape seed oil byproduct; AOB: Almond seed oil byproduct. [d]nd, not detected.

Table 4. Mineral Composition (Milligrams per 100 g of Sample) of Cold Press Oil Byproducts[a]

mineral	WOB[b]	POB[b]	GOB[b]	AOB[b]
K	1171.5 ± 3.5b	920.6 ± 1.9c	832.3 ± 0.1d	1473.4 ± 0.1a
Ca	665.7 ± 3.4b	439.08 ± 3.0c	670.0 ± 0.5b	895.8 ± 0.1a
P	377.2 ± 10.8b	192.6 ± 1.4c	83.27 ± 0.06d	522.3 ± 0.0a
S	187.4 ± 1.4b	119.5 ± 0.3c	53.09 ± 0.00d	255.5 ± 0.0a
Mg	437.6 ± 3.4b	146.7 ± 1.7d	179.4 ± 6.7c	536.1 ± 0.3a
Fe	11.31 ± 1.04a	9.84 ± 2.97a	4.47 ± 0.00b	10.94 ± 0.00a
Si	29.91 ± 2.31a	13.72 ± 0.63b	9.91 ± 0.00c	7.57 ± 0.00d
Al	26.94 ± 1.72a	16.38 ± 0.26b	13.12 ± 0.00c	11.75 ± 0.00d
Cl	38.75 ± 1.91b	77.95 ± 0.35a	5.75 ± 0.07d	13.80 ± 0.00c
Mn	10.41 ± 1.04a	2.12 ± 0.24c	2.75 ± 0.38c	5.56 ± 0.44b
Cu	<1	<1	<1	<1
Zn	6.57 ± 0.06b	3.60 ± 0.11c	2.69 ± 0.17d	7.25 ± 0.23a
Sr	7.14 ± 0.18a	1.61 ± 0.36c	1.86 ± 0.00c	5.66 ± 0.00b
Na	18.96 ± 0.58b	15.21 ± 0.10c	8.56 ± 0.00d	19.96 ± 0.00a
Rb	1.46 ± 0.00c	1.69 ± 0.19b	1.37 ± 0.00d	4.30 ± 0.00a

[a]Different lower case letters show differences between the samples (n = 2). The results are expressed as the mean ± SD. [b]WOB, walnut seed oil byproduct; POB, pomegranate seed oil byproduct; GOB, grape seed oil byproduct; AOB, almond seed oil byproduct.

Oil Content and Fatty Acid Composition. Oil contents of the byproducts ranged from 4.82 to 12.57%. Except for GOB, the other seed byproducts had approximately 10% oil, indicating a relatively low cold-pressing yield, which can be considered as a general problem for cold press oil industry. The high oil content of the byproducts could lead to problems due to oxidation of oil, which might cause some problems during storage of the byproducts or food products enriched with them. However, as will be seen in subsequent sections, this problem might be prevented due to the high phenolic composition of the samples. The fatty acid composition of the oils extracted from the byproducts is presented in Table 3. As seen from Table 3, significant differences were observed among the fatty acid compositions of the oil byproducts. The dominant fatty acid of the oil extracted from GOB was found to be C18:2, followed by C18:1, C16:0, and C18:0, respectively. The saturated fatty acid content of the GOB was determined as 13.08%. Mono- and polyunsaturated fatty acid contents were found as 18.67 and 68.26%, respectively. Beveridge et al.[22] studied the fatty acid composition of oil extracted from different grape seed varieties with supercritical carbon dioxide extraction, and they revealed that saturated and mono- and polyunsaturated fatty acid compositions of the oils ranged between 11.21 and 13.85%, between 12.77 and 18.59%, and between 68.10 and 73.67%, respectively. As seen, our results were in accordance with the literature findings. The oil extracted from AOB contained the fatty acid types in decreasing order C18:1, C18:2, C16:0, C18:0, C18:3n6, and C14:0. The findings of the present study were in accordance with the previous study.[23] The fatty acid profile of POB oil is also presented in Table 3, and the most abundant fatty acid determined was C18:3n6, which was followed by C18:2, C18:1, C16:0, C18:0, C18:3n3, and C14:0, respectively. POB oil comprised saturated and mono- and polyunsaturated fatty acids in concentrations of 7.47, 6.48, and 86.25%, respectively. C18:3 was found as the dominant fatty acid in POB oil. The results of the present study were consistent with the findings of Fadavi et al.,[24] who reported that saturated and mono- and polyunsaturated fatty acid contents of the 25 different pomegranate seed oils varied between 4.8 and 26.8%, between 0.4 and 17.4%, and between 55.8 and 92.1%, respectively. C18:2 was determined as the dominant fatty acid in WOB oil when compared to the other fatty acid types, which was consistent with the study in which saturated and mono- and polyunsaturated fatty acid contents of walnut seed oil were reported to be 11.76, 15.28, and 72.96%, respectively.[23] As expected, slight differences

DOI: 10.1021/jf504390t
J. Agric. Food Chem. 2015, 63, 2305−2313

Table 5. Antibacterial Activity of Cold Press Oil Byproducts[a] against Selected Foodborne Pathogens[b]

	inhibition zone (mm)			
extract concn (%)	*S.* Typhimurium	*E. coli* O157:H7	*L. monocytogenes*	*S. aureus*
almond oil byproduct				
4	nz[c]	nz	7.00 ± 0.00a	nz
20	nz	6.00 ± 0.00b	10.50 ± 0.71a	7.00 ± 0.21
50	9.50 ± 0.71b	10.00 ± 0.00b	20.50 ± 0.71a	16.00 ± 1.41a
pomegranate oil byproduct				
4	7.00 ± 0.00a	6.00 ± 0.00a	7.00 ± 0.00a	nz
20	10.00 ± 0.00a	8.00 ± 0.00a	9.50 ± 0.71a	nz
50	15.50 ± 0.71a	16.00 ± 1.41a	12.00 ± 0.00b	8.00 ± 0.00b

[a]Grape and walnut extracts did not show antibacterial activity against any of the bacteria. [b]Different lower case letters show differences between the studied extract concentration levels for each bacterial strain (n = 3). The results are expressed as the mean ± SD. [c]No inhibition zone was observed.

among the results of the present study and previous studies were observed for each byproduct oil, which might be resulted from genetic and environmental factors such as production year and growing location.[25] As known, consumption of vegetable oils is currently increasing due to their high polyunsaturated fatty acid content, which possesses a natural preventive role in cardiovascular diseases and promotes reduction of total and HDL cholesterol.[26] Therefore, enrichment of different foods with these oil byproducts could be suggested regarding their fatty acid composition, which also gains economic benefit as well as health benefit.

Crude Fiber Contents. The crude fiber contents of the byproducts varied between 5.87 and 45.83% as shown in Table 2. Among the byproducts analyzed in the present study, the highest crude fiber content was observed in GOB (45.83%), whereas POB, WOB, and AOB had crude fiber in concentrations of 25.10, 6.65, and 5.87%, respectively. As known, sufficient dietary fiber consumption could reduce the risk of cardiovascular disease, colon cancer, and obesity.[27] Hereby, consumption of the dietary fiber enriched products is very important for the health of people of all ages. Enrichment of the food products with GOB or POB should be suggested considering the beneficial effects of dietary fiber. Moreover, these byproducts can be used as a new source for the production of different dietary fiber types, which can provide important economic benefit because in recent years people tend to consume products with high fiber content. Chau and Huang[28] reported that products rich in dietary fibers have attracted attention as food ingredients and have encouraged researchers to search out new fiber sources.

Determination of Total Ash and Mineral Composition. Ash contents of the oil byproducts varied between 3.07 and 4.50%. AOB had the highest ash content followed by WOB, POB, and GOB, respectively. The mineral composition profile of the byproducts analyzed is summarized in Table 4. GOB was found to be a rich source of potassium (832.27 mg/100 g sample) and calcium (670.03 mg/100 g sample). AOB and WOB samples had significant amounts of potassium, calcium, phosphorus, sulfur, and magnesium. POB was rich in potassium, calcium, phosphorus, and sulfur. In general, all of the byproducts were rich in macroelements, namely, potassium, calcium, phosphorus, and magnesium, whereas these elements were all the most abundant minerals found in AOB. These byproducts also contained dietary trace minerals (iron, manganese, copper, and zinc) in different quantities. As known, calcium is required for bone growth, nerve and muscle functions, and protection against high blood pressure; phosphorus for bone growth, acid base balance, and structure of nucleic acids; magnesium also for bone growth and regular functions of nervous and muscular system; and potassium for regulation of blood pressure and muscular contraction. Among the trace elements, iron is required for use of oxygen in the body, building of blood cells, and structuring of hemoglobin and copper for absorption of iron, structuring of hemoglobin, and production of energy. For these reasons, people of all ages require these minerals to keep their healthy life and, in this respect, incorporation of the oil byproducts into different food products has the potential to improve their nutritional quality by enriching their mineral profile. For instance, if any AOB is incorporated to any food product in concentrations of 1%, it provides approximately 12.07 mg of potassium, 8.96 mg of calcium, 5.22 mg of phosphorus, and 2.56 mg of sulfur per 100 g of food to the person consuming this enriched food product. As seen, enrichment of the products with these byproducts can induce significant increase in mineral composition.

Antibacterial Activity. In this study, almond and pomegranate extracts showed antibacterial activity, whereas grape and walnut extracts showed no antibacterial activity against any pathogenic bacteria tested. Table 5 shows the antibacterial activity of AOB and POB as inhibition zone. As can be seen from the table, AOB showed no antibacterial activity on tested microorganisms except *L. monocytogenes* at the lowest concentration. It is also clear from the table that the antibacterial activity of the AOB and POB extracts was concentration dependent, and lower concentrations of the extracts exhibited weak or no antibacterial activity. AOB extract was more effective against Gram-positive bacteria (*L. monocytogenes* and *S. aureus*) than POB extract, whereas stronger antibacterial activity on Gram-negative *S.* Typhimurium and *E. coli* O157:H7 was exhibited by pomegranate. Baydar et al.[29] reported that grape bagasse extracts did not show antibacterial activity against 15 bacteria. They also stated that lower concentrations of grape seed extracts were ineffective. Hammer et al.[30] showed that sweet almond (*Prunus dulcis*) oil did not inhibit any organisms even at the highest concentration, which was 2.0% oil. De et al.[31] reported antimicrobial activity of pomegranate seeds against *Bacillus subtilis*, *E. coli*, and *Saccharomyces cerevisiae*. The peel extract has shown highest antimicrobial activity compared to other extracts, whereas the seed extracts exhibited variable antimicrobial activities to the bacteria except for *Bacillus coagulans*. It can be understood from the literature that the antimicrobial activity of plant extracts depends on several factors such as plant part, extraction method, solvent used, and extract concentration.

Bioactive Properties. *Total TPC, TFC, and HTC Contents.* Figure 1 represents TPC, TFC, and HTC values of the oil

DOI: 10.1021/jf504390t
J. Agric. Food Chem. 2015, 63, 2305−2313

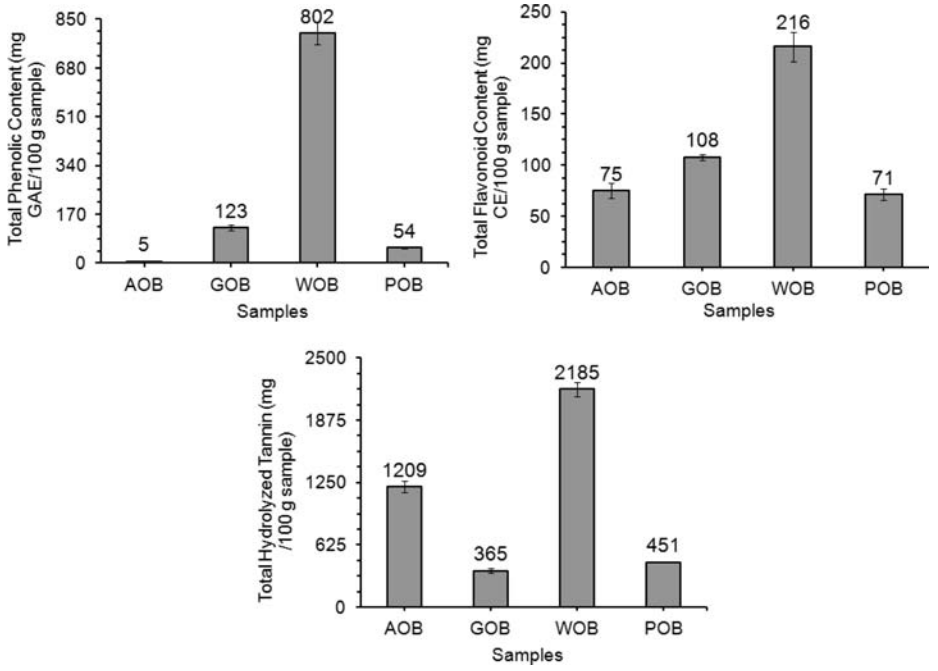

Figure 1. Total phenolic, flavonoid, and hydrolyzed tannin contents of the byproducts. AOB, almond seed oil byproduct; GOB, grape seed oil byproduct; WOB, walnut seed oil byproduct; POB, pomegranate seed oil byproduct.

Table 6. Phenolic Composition (Parts per Million) of Cold Press Oil Byproducts[a]

compound	WOB[b]	POB[b]	GOB[b]	AOB[b]
gallic acid	58.84 ± 5.04a	2.90 ± 0.40d	3.78 ± 0.10c	49.79 ± 1.29b
gallocatechin	1067.2 ± 64.5b	120.2 ± 1.5d	295.4 ± 26.7c	1321.5 ± 24.9a
epigallocatechin	71.51 ± 7.36b	40.93 ± 2.61c	366.5 ± 12.4a	77.96 ± 6.43b
catechin	24.94 ± 2.18a	8.95 ± 0.85c	2.79 ± 0.54d	14.17 ± 1.92b
chlorogenic acid	79.60 ± 2.11a	7.54 ± 0.10b	5.98 ± 0.14c	1.10 ± 0.11d
epicatechin	689.0 ± 45.9a	402.9 ± 4.2b	91.83 ± 2.37c	9.00 ± 0.25d
p-coumaric acid	202.4 ± 5.2b	349.8 ± 18.6a	11.50 ± 3.95d	47.13 ± 2.08c
quercetin	394.5 ± 33.0a	300.2 ± 17.4b	7.43 ± 1.06d	54.71 ± 3.01c
resveratrol	71.34 ± 1.86a	4.37 ± 0.45c	3.65 ± 0.62c	16.42 ± 1.42b
catechin gallate	159.4 ± 1.7a	7.42 ± 0.48b	0.53 ± 0.07d	2.45 ± 0.45c
quercetin hydrate	1.40 ± 0.22d	2.37 ± 0.18c	3.33 ± 0.40b	4.24 ± 0.14a
kaempferol	4.00 ± 0.46c	11.59 ± 0.44b	15.32 ± 1.65a	3.28 ± 0.15d

[a]Different lower case letters show differences between the samples (n = 2). The results are expressed as the mean ± SD. [b]WOB, walnut seed oil byproduct; POB, pomegranate seed oil byproduct; GOB, grape seed oil byproduct; AOB, almond seed oil byproduct.

byproduct extracts. TPC values of the samples varied from 5.21 to 801.89 mg GAE/100 g. TFC and HTC values of samples were found to be 71−216 mg CE/100 g and 364.97−2184.60 mg TA/100 g, respectively. Among the extracts, WOB extract had the highest TPC, TFC, and HTC levels.

Grape seeds have attracted considerable attention due to high abundance of bioactive compounds, especially various types of phenolics. It has been reported that grape seed contains higher levels of phenolics than skin and pulp.[32] As expected, TPC of GOB was found to be lower than those of their studies, probably caused by the cold-pressing process. The TPC value of GOB was also lower than that of the grape wine byproducts previously reported in the literature.[33] Growth environment of grape cultivars might also influence their TPC values. The TFC value of GOB was comparable with that of grape skin, whereas it was higher than that of the grape pulp as reported in the literature.

In the present study, considerable amounts of the bioactive compounds were found in the walnut waste obtained after cold press oil processing (Figure 1). It was reported that walnut bioactive compounds have antioxidant activity and potential beneficial health effects such as anti-inflammatory, antimutagenic, and antiatherogenic.[34] Almond HTC was reported to be 54.7 mg EA and 27.4 mg GA 100 g^{-1} for different almond varieties.[35] It was reported that tannins and other phenolic compounds found in almond could be beneficial for health due to their antioxidant and anti-inflammatory effects.[35]

Pomegranate seeds are byproducts of pomegranate fruits. In the present study, moderate levels of bioactive compounds were found in POB as compared to other byproducts (Figure 1). It can be concluded that byproducts analyzed in this study could be considered as valuable waste materials, which may have potential food applications due to the presence of high amounts of bioactive compounds.

Phenolic Profile of the Byproducts. Rather than TPC, distribution of the specific phenolics in a certain medium is very important due to balanced intake of essential materials into the body. Phenolic distribution may vary depending on several

DOI: 10.1021/jf504390t
J. Agric. Food Chem. 2015, 63, 2305−2313

Table 7. Major Volatile Compounds of the Oil Byproducts (Percent)[a]

no.	compound	WOB	POB	GOB	AOB
		Terpenes			
1	limonene	90.2 ± 0.8b	93.7 ± 1.0a	93.7 ± 0.7a	93.6 ± 1.2a
2	myrcene	1.23 ± 0.03b	1.32 ± 0.07b	1.22 ± 0.03b	1.56 ± 0.07a
3	α-pinene	0.26 ± 0.00b	0.26 ± 0.01b	nd[b]	0.35 ± 0.02a
4	β-pinene	1.29 ± 0.11a	1.16 ± 0.09a	0.83 ± 0.03b	0.84 ± 0.05b
5	γ-terpinene	0.11 ± 0.00b	0.11 ± 0.00b	0.20 ± 0.01a	0.18 ± 0.00a
6	terpinolene	0.21 ± 0.01a	0.15 ± 0.00c	0.19 ± 0.00b	0.18 ± 0.02ab
7	8,9-epoxy-*p*-menth-1-ene	0.59 ± 0.04a	nd	nd	0.12 ± 0.00b
8	*p*-cymene	0.22 ± 0.00	nd	nd	nd
9	1,5,8-*p*-methatriene	0.15 ± 0.01	nd	nd	nd
10	α-terpinene	nd	nd	0.15	nd
11	3,8-*o*-methatriene	nd	nd	0.17	nd
12	6-acetoxy-1,4-dimethylbicyclohept-3-ene	0.46 ± 0.02	nd	nd	nd
13	*trans*-2,3-epoxydecahydronaphthalene	nd	nd	0.26	nd
	total terpenes	94.75b	96.73a	96.74a	96.87a
		Other Compounds			
1	nonanal	nd	0.13 ± 0.02a	0.11 ± 0.00a	0.11 ± 0.00a
2	*cis*-limonene oxide	0.43 ± 0.01a	0.20 ± 0.01c	nd	0.30 ± 0.02b
3	*trans*-limonene oxide	1.22 ± 0.04a	0.20 ± 0.00b	nd	1.14 ± 0.08a
4	3-cyclohexene-1-acetaldehyde	0.18 ± 0.01a	nd	nd	0.11 ± 0.00b
5	citral	2.45 ± 0.12a	0.21 ± 0.02b	nd	0.18 ± 0.01b
6	2-cyclohexen-1-one	0.26 ± 0.01	nd	nd	nd
7	ethylcyclooctane	0.29 ± 0.01	nd	nd	nd
8	cyclohexanone	0.15 ± 0.01	nd	nd	nd
9	2-cyclohexene-1-propanal	0.27 ± 0.01	nd	nd	nd
10	ethenylcyclohexane	0.30 ± 0.02	nd	nd	nd
11	phenethyl alcohol	nd	0.31 ± 0.00a	0.20 ± 0.01b	nd
12	*trans*-2,4-nonadienal	nd	0.28 ± 0.02	nd	nd
13	ethyl octanoate	nd	0.46 ± 0.03b	0.67 ± 0.02a	nd
14	phenethyl acetate	nd	0.20 ± 0.00	nd	nd
15	ethyl decanoate	nd	0.20 ± 0.01	nd	nd
16	*n*-hexadecane	nd	0.12 ± 0.00	nd	nd
17	2-propyl-2-heptanal	nd	0.10 ± 0.00	nd	nd
18	*trans*-2,4-decadienal	nd	0.21 ± 0.01	nd	nd
19	tetracyclodecane	nd	nd	0.19 ± 0.01	nd
20	carvone	nd	nd	0.10 ± 0.00	nd
21	2,2,4,6,6-pentamethylheptane	nd	nd	0.19 ± 0.01	nd
22	2,2,9-trimethyldecane	nd	nd	0.25 ± 0.01	nd
23	ethyl laurate	nd	nd	0.11 ± 0.00	nd
24	2,2-dimethyldecane	nd	nd	0.39 ± 0.04	nd
	total other compounds	5.55a	2.62b	1.54d	1.84c

[a]Different lower case letters show differences between the samples (n = 2). The results are expressed as the mean ± SD. Volatiles of the oil byproducts in concentrations <0.1% are not mentioned in the table. [b]nd, not detected.

factors such as plant origin, cultivar, harvesting time, and soil types. In this study, phenolic compositions of the cold press oil byproducts are presented in Table 6. As expected, distribution and ratios of phenolic compounds were variable and influenced from the origin of the byproducts. Epigallocatechin, gallocatechin, and epicatechin were the predominant phenolics in GOB (Table 6). Epicatechin was also found to be the most abundant phenolic compound in the grape seed extracts as reported by Baydar et al.[36] Gallocatechin was found to be the major phenolic among the AOB phenolics. Gallic acid, epigallocatechin, and *p*-coumaric acid were determined to be the other major phenolics detected in AOB (Table 6). Epicatechin had the highest level of phenolics in POB followed by *p*-coumaric acid, quercetin, and gallocatechin. There were slight differences between *p*-coumaric acid, quercetin, and gallocatechin contents of POB (Table 6). Gallocatechin was the highest phenolic in WOB, whereas epicatechin and quercetin were the other major phenolics found in WOB. WOB contained higher levels of catechin, chlorogenic acid, and resveratrol than the other byproducts (Table 6). Ellagitannins (ETs) have been reported to be the main phenolic compounds found in the seed of *Juglans regia*.[37] Gallotannins and ellagitannins, which are classified as hydrolyzable tannins, were also reported to be at high amounts in the walnut kernel.[38]

DOI: 10.1021/jf504390t
J. Agric. Food Chem. 2015, 63, 2305−2313

Volatile Composition. Approximately 35 different volatile compounds were identified in the oil byproducts. However, their concentrations >0.1% are shown in Table 7. As seen from Table 7, terpenes were found as the predominant volatile compounds of the byproducts. Terpenes were composed of 95% of the volatile compounds. Total terpene contents of AOB and POB were found to be similar ($p > 0.05$). Among the volatile compounds identified, limonene, which is a terpene, was found to be a major compound in all of the samples analyzed with amounts ranging from 90.2 to 93.7%. The highest limonene level was determined in POB and GOB, whereas the lowest was in WOB. Limonene is known as a natural and functional monoterpene. Limonene is considered as safe (GRAS) and used as a flavoring agent and food preservative.[39] Gerhäuser et al.[40] reported bactericidal, antioxidant, chemopreventative, and therapeutic activities of limonene. Therefore, the use of these byproducts that are rich in limonene in the different food products may be important for human health. In addition, the oil byproducts had myrcene and β-pinene compounds in concentrations that ranged between 1.22 and 1.56% and between 0.84 and 1.29%, respectively. *trans*-Limonene oxide is another volatile compound found in AOB and WOB with concentrations >1.0%. In addition, the percentage of citral in WOB was determined as 2.45%.

In conclusion, in the cold press edible oil industry, remarkable amounts of byproducts arise after production of the oil. Recovery of these products is important regarding economical gain. Determination of physicochemical and functional properties of the products is crucial to reveal their recovery potential in terms of economic and health aspects. In the present study, physicochemical and bioactive properties, fatty acid and mineral composition, antibacterial activity, and volatile profiles of the cold press oil byproducts of almond, walnut, grape seed, and pomegranate were determined. In general, the byproducts were found to possess significant amounts of protein and bioactive compounds including phenolic compounds, flavonoids, and tannins. GOB and POB had significant amounts of crude fiber, which gained them importance to be evaluated as new sources of dietary fiber. Extracts of almond and pomegranate showed considerable antibacterial activity against the pathogenic bacteria tested, indicating their antimicrobial potential, whereas grape and walnut did not have any inhibitory effect. Limonene was the most abundant volatile component of all the byproducts. In conclusion, this study revealed that pomegranate, walnut, grape seed, and almond cold press oil byproducts had valuable potentials and qualifications from different aspects to be used in different areas of the food industry for enrichment purposes of food materials.

AUTHOR INFORMATION

Corresponding Author

*(S. Karasu) E-mail: skarasu@yildiz.edu.tr. Phone: 090 212 383 4580. Fax: 090 212 383 4571.

Notes

The authors declare no competing financial interest.

REFERENCES

(1) Lutterodt, H.; Luther, M.; Slavin, M.; Yin, J.-J.; Parry, J.; Gao, J.-M.; Yu, L. Fatty acid profile, thymoquinone content, oxidative stability, and antioxidant properties of cold-pressed black cumin seed oils. *LWT—Food Sci. Technol.* **2010**, *43*, 1409—1413.

(2) Deferne, J.-L.; Pate, D. W. *J. Ind. Hemp* **1996**, *3*, 4—7.

(3) Zheng, Y.-l.; Wiesenborn, D.; Tostenson, K.; Kangas, N. Screw pressing of whole and dehulled flaxseed for organic oil. *J. Am. Oil Chem. Soc.* **2003**, *80*, 1039—1045.

(4) Lowe, E. D.; Buckmaster, D. R. Dewatering makes big differences in compost strategies. *BioCycle* **1995**, *36*, 78—82.

(5) Arvanitoyannis, I. S. 1 — Potential and representatives for application of environmental management system (EMS) to food industries. In *Waste Management for the Food Industries*; Arvanitoyannis, I. S., Ed.; Academic Press: Amsterdam, The Netherlands, 2008; pp 3—38.

(6) Sagdic, O.; Ozturk, I.; Yilmaz, M. T.; Yetim, H. Effect of grape pomace extracts obtained from different grape varieties on microbial quality of beef patty. *J. Food Sci.* **2011**, *76*, M515—M521.

(7) Amarowicz, R.; Troszynska, A.; Shahidi, F. Antioxidant activity of almond seed extract and its fractions. *J. Food Lipids* **2005**, *12*, 344—358.

(8) Baydar, N. G.; Sagdic, O.; Ozkan, G.; Cetin, S. Determination of antibacterial effects and total phenolic contents of grape (*Vitis vinifera* L.) seed extracts. *Int. J. Food Sci. Technol.* **2006**, *41*, 799—804.

(9) Singh, R. P.; Chidambara Murthy, K. N.; Jayaprakasha, G. K. Studies on the antioxidant activity of pomegranate (*Punica granatum*) peel and seed extracts using in vitro models. *J. Agric. Food Chem.* **2001**, *50*, 81—86.

(10) Palombo, R.; Gertler, A.; Saguy, I. A simplified method for determination of browning in dairy powders. *J. Food Sci.* **1984**, 1609—1613.

(11) Chegini, G. R.; Ghobadian, B. Effect of spray-drying conditions on physical properties of orange juice powder. *Drying Technol.* **2005**, *23*, 657—668.

(12) AOAC. *Official Methods of Analysis Association of Official Analytical Chemists*; Washington, DC, USA, 2000.

(13) Yalcin, H.; Ozturk, I.; Tulukcu, E.; Sagdic, O. Effect of γ-irradiation on bioactivity, fatty acid compositions and volatile compounds of clary sage seed (*Salvia sclarea* L.). *J. Food Sci.* **2011**, *76*, C1056—C1061.

(14) AOAC. *Official Methods of Analysis*, 16th ed.; Washington, DC, USA, 1995; official method 985.35.

(15) Singleton, V. L.; Rossi, A. Colorimetry of total phenolics with phosphomolybdic-phosphotungstic acid reagents. *Am. J. Enol. Vitic.* **1965**, 144—158.

(16) Zhinsen, J.; Mengcheng, T.; Jianming, W. The determination of flavonoid contents in mulberry and their scavenging effects on superoxide radicals. *Food Chem.* **1999**, *64*, 555—559.

(17) Willis, R. B.; Allen, P. R. Improved method for measuring hydrolyzable tannin using potassium iodate. *Analyst* **1998**, *127*, 435—439.

(18) Schieber, A.; Keller, P.; Carle, R. Determination of phenolic acids and flavonoids of apple and pear by high-performance liquid chromatography. *J. Chromatogr., A* **2001**, *910*, 265—273.

(19) Özkan, G.; Sagdiç, O.; Göktürk Baydar, N.; Kurumahmutoglu, Z. Antibacterial activities and total phenolic contents of grape pomace extracts. *J. Sci. Food Agric.* **2004**, *84*, 1807—1811.

(20) Cam, M.; Erdogan, F.; Aslan, D.; Dinc, M. Enrichment of functional properties of ice cream with pomegranate by-products. *J. Food Sci.* **2013**, *78*, C1543—C1550.

(21) Esteban, R. M.; Lopezandreu, F. J.; Carpena, O. Protein extractability of almond (*Prunus amygdalus* Batsch) seed. *J. Sci. Food Agric.* **1985**, *36*, 485—490.

(22) Beveridge, T. H. J.; Girard, B.; Kopp, T.; Drover, J. C. G. Yield and composition of grape seed oils extracted by supercritical carbon dioxide and petroleum ether: varietal effects. *J. Agric. Food Chem.* **2005**, *53*, 1799—1804.

(23) Venkatachalam, M.; Sathe, S. K. Chemical composition of selected edible nut seeds. *J. Agric. Food Chem.* **2006**, *54*, 4705—4714.

(24) Fadavi, A.; Barzegar, M.; Hossein Azizi, M. Determination of fatty acids and total lipid content in oilseed of 25 pomegranates varieties grown in Iran. *J. Food Compos. Anal.* **2006**, *19*, 676—680.

DOI: 10.1021/jf504390t
J. Agric. Food Chem. 2015, 63, 2305—2313

(25) Amaral, J. S.; Cunha, S. C.; Santos, A.; Alves, M. R.; Seabra, R. M.; Oliveira, B. P. P. Influence of cultivar and environmental conditions on the triacylglycerol profile of hazelnut (*Corylus avellana* L.). *J. Agric. Food Chem.* **2006**, *54*, 449−456.
(26) Melgarejo, P.; Artes, F. Total lipid content and fatty acid composition of oilseed from lesser known sweet pomegranate clones. *J. Sci. Food Agric* **2000**, *80*, 1452−1454.
(27) Marlett, J. A. In *Handbook of Dietary Fibre*; Cho, S. S., Ed.; Dekker: New York, 2001; pp 17−30.
(28) Chau, C. F.; Huang, Y. L. Characterization of passion fruit seed fibres − a potential fibre source. *Food Chem.* **2004**, *85*, 189−194.
(29) Baydar, N. G.; Özkan, G.; Sağdiç, O. Total phenolic contents and antibacterial activities of grape (*Vitis vinifera* L.) extracts. *Food Control* **2004**, *15*, 335−339.
(30) Hammer, K. A.; Carson, C. F.; Riley, T. V. Antimicrobial activity of essential oils and other plant extracts. *J. Appl. Microbiol.* **1999**, *86*, 985−990.
(31) De, M.; De, A. K.; Banerjee, A. B. Antimicrobial screening of some Indian spices. *Phytother. Res.* **1999**, *13*, 616−618.
(32) Yilmaz, Y.; Toledo, R. T. Major flavonoids in grape seeds and skins: antioxidant capacity of catechin, epicatechin, and gallic acid. *J. Agric. Food Chem.* **2004**, *52*, 255−260.
(33) Lachman, J.; Hejtmánková, A.; Hejtmánková, K.; Horníčková, Š.; Pivec, V.; Skala, O.; Dědina, M.; Přibyl, J. Towards complex utilisation of winemaking residues: characterisation of grape seeds by total phenols, tocols and essential elements content as a by-product of winemaking. *Ind. Crops Prod.* **2013**, *49*, 445−453.
(34) Tapia, M. I.; Sanchez-Morgado, J. R.; Garcia-Parra, J.; Ramirez, R.; Hernandez, T.; Gonzalez-Gomez, D. Comparative study of the nutritional and bioactive compounds content of four walnut (*Juglans regia* L.) cultivars. *J. Food Compos. Anal.* **2013**, *31*, 232−237.
(35) Xie, L.; Roto, A. V.; Bolling, B. W. Characterization of ellagitannins, gallotannins, and bound proanthocyanidins from California almond (*Prunus dulcis*) varieties. *J. Agric. Food Chem.* **2012**, *60*, 12151−12156.
(36) Baydar, N. G.; Babalik, Z.; Turk, F. H.; Cetin, E. S. Phenolic composition and antioxidant activities of wines and extracts of some grape varieties grown in Turkey. *Tarim Bilim. Derg.* **2011**, *17*, 67−76.
(37) Fukuda, T.; Ito, H.; Yoshida, T. Antioxidative polyphenols from walnuts (*Juglans regia* L.). *Phytochemistry* **2003**, *63*, 795−801.
(38) Regueiroa, J.; Sánchez-González, C.; Vallverdú-Queraltb, A.; Simal-Gándara, J. Comprehensive identification of walnut polyphenols by liquid chromatography coupled to linear ion trap−Orbitrap mass spectrometry. *Food Chem.* **2014**, *152*, 340−348.
(39) Sun, J. D-Limonene: safety and clinical applications. *Altern. Med. Rev.* **2007**, *12*, 259−264.
(40) Gerhäuser, C.; Klimo, K.; Heiss, E.; Neumann, I.; Gamal-Eldeen, A.; Knauft, J.; Liu, G.-Y.; Sitthimonchai, S.; Frank, N. Mechanism-based in vitro screening of potential cancer chemopreventive agents. *Mutat. Res. Fundam. Mol. Mech. Mutagen.* **2003**, *523*−*524*, 163−172.

DOI: 10.1021/jf504390t
J. Agric. Food Chem. 2015, 63, 2305−2313

chosen because it contains a high protein amount.[14] Macromolecules were purified following the preparative method proposed by Van Sluyter et al.[15] with some modifications. Ten liters of wine were treated with 4 g/L PVPP (Sigma-Aldrich, Milan, Italy) and 1.5 g/L charcoal (Sigma-Aldrich, Milan, Italy) for 24 h at 15 °C in order to remove most of the polyphenols. The wine was then filtered with GF/A filters (Whatman, Kent, U.K.) and finally at 0.45 μm with cellulose acetate membranes (Sartorius AG, Göttingen, Germany), and it was then brought to pH 3.0 with HCl. Aliquots of 5 L were loaded at 8 mL/min on a S-Sepharose column (5 × 14 cm) (Pharmacia, Uppsala, Sweden) previously equilibrated in trisodium citrate buffer 30 mM pH 3.0. After washing with two column volumes with the same buffer, proteins were eluted with a gradient of NaCl from 0 to 1 M. Both the flow through (containing the unbound material, i.e., mainly polysaccharides) and the pool of the eluted peaks (representing the total proteins) were ultrafiltered at 3 kDa with an Amicon 8400 apparatus (Sartorius), then dialyzed on regenerated cellulose membrane (3.5 kDa, Cellu-Sep) against water and finally freeze-dried. Five liters of the same wine were used for the purification of two main wine proteins (chitinase and the thaumatin-like protein VVTL1). In this case, the fractions obtained after cation exchange separation on S-Sepharose were diluted in 1.25 M ammonium sulfate and further purified by hydrophobic interaction chromatography (HIC) on a phenyl-sepharose HP column (GE-Healthcare) as follows. After washing the column with 1.25 M ammonium sulfate in 50 mM sodium citrate, pH 5.0, proteins were eluted with a 110 min linear gradient up to 100% 50 mM sodium citrate, pH 5.0. The peaks obtained with this second step were dialyzed against water (3.5 kDa MWCO) and freeze-dried. The purity and identity of the fractions were assessed by RP-HPLC[15] and SDS-PAGE.[16]

Aroma Extraction. Fermentative compounds and grape volatiles were extracted from a dry Moscato bianco wine (vintage 2011) produced in the Colli Euganei (Veneto, Italy) not previously treated with bentonite by using the method previously reported for wines and model wine solutions.[17] This type of wine was chosen because of its high content of primary aroma compounds. Aliquots of 500 mL were spiked with 4 mL of 1-heptanol (442 mg/L) as the internal standard, and extracted 3 × 50 mL with dichloromethane (Carlo Erba, Milano, Italy). Extraction was carried out under agitation for 15 min each time. The organic phase containing the aroma compounds was collected and washed 3 × 30 mL with 5% $NaHCO_3$ to remove the acidic compounds by salification and shift into aqueous phase. After dehydration with anhydrous sodium sulfate, dichloromethane was filtered on blue ribbon filters 589/3 (Whatman, U.K.). The extract was concentrated first using a Vigreux column and finally under nitrogen flow. This extract was then used for the reconstitution experiments in model wine solution.

Fifty milliliters of the clear supernatant of each reconstituted sample were used for the extraction of the aroma compounds remaining after bentonite treatment. The samples were spiked with 400 μL of 1-decanol 450 mg/L as the internal standard and extracted 3 × 15 mL with dichloromethane. After dehydration with anhydrous sodium sulfate and filtration as previously described, the extracts were concentrated with a Vigreux column (l = 40 cm) to approximately 3 mL and adjusted to 1 mL under nitrogen flow before GC/MS analysis.

Stability Test. The purified proteins were suspended at 100 mg/L in model wine (tartaric acid 5 g/L, ethanol 12%, pH 3.2) or in a ultrafiltered Manzoni bianco wine (3.5 kDa). Bentonite Nucleobent (EVER, Pramaggiore, Italy) was prepared at 5% (w/v) in water for 24 h, and then different amounts (5, 10, 15 g/hL, final concentrations) were added to the wine protein solution. After 1 h at room temperature, the solutions were filtered at 0.45 μm on cellulose acetate membrane (Sartorius). In order to assess the bentonite dose necessary to reach the protein stability, the protein solutions prepared in ultrafiltered wine were subjected to the heat test as reported by Pocock and Rankine.[18] Briefly, the samples were heated at 80 °C for 6 h, followed by incubation at 4 °C for 12 h; then, the turbidity was measured with a nefelometer (HACH). When the difference in the turbidity measured before and after the heating was less than 2 NTU the sample could be considered stable. For the samples prepared in model solution, the dose of bentonite necessary for stabilization was instead calculated as the amount able to reduce the protein content below 20 mg/L.

Determination of the Protein Content. The protein content was measured according to Vincenzi et al.[19] First, proteins were precipitated from 1 mL of wine with 10 μL of SDS 10% followed by 250 μL of KCl 1 M. The pellets were dissolved in 1 mL of distilled water and quantified by the Smith method,[20] using the BCA-200 protein assay kit (Pierce, Rockford, IL) according to the manufacturer instructions. The calibration curve was prepared by using serial dilution of bovine serum albumin (BSA, Sigma, Milan, Italy) in water.

Electrophoresis. Electrophoretic analyses were performed according to Laemmli.[21] Samples to be analyzed were dissolved in a 0.5 M Tris-HCl pH 6.8 buffer containing 15% (v/v) glycerol (Sigma-Aldrich, Milano, Italy), 1.5% (w/v) SDS (Bio-Rad laboratories, Segrate, Italy), and 4% β-mercaptoethanol (Sigma-Aldrich, Milano, Italy) and heated at 100 °C for 5 min before loading. For both fractions (bound and unbound material), 20 μg of lyophilized powder were loaded in each lane. Electrophoresis was performed in a Mini-Protean III apparatus (Bio-Rad, Hercules, CA) with T = 14% (acrylamide/N,N′ metylen-bis(acrylamide) 29:1; Fluka, Milan, Italy) gels. The molecular weight standard proteins were Broad Range Molecular Weight Markers (Bio-Rad, Hercules, CA). After electrophoresis, gels were stained for 18 h with colloidal Coomassie and then destained with water for 24 h. The Periodic Acid−Schiff (PAS) method was used to stain glycoproteins as described by Segrest and Jackson.[22]

Reconstitution Experiments. The concentrated extract was diluted in model wine to reach a concentration of the aroma compounds equal to that found in the original Moscato wine. Then, 10 g/hL of bentonite alone or 100 mg/L of proteins followed by 10 g/hL of bentonite were added to 55 mL of this solution. An additional experiment with 100 mg/L of proteins and 200 mg/L of the S-Sepharose unbound fraction followed by 10 g/hL bentonite was performed. Each experiment was done in triplicate.

The reconstituted samples were stored at 10 °C (in closed containers) for 12 h and centrifuged (5000g, 5 min, 15 °C), then 50 mL of clear supernatant was recovered and used for the aroma extraction. A second experiment was performed using four selected ethyl esters instead of the total aroma extract. Esters were ethyl hexanoate, octanoate, decanoate, and dodecanoate at 1167, 1102, 1035, and 1145 μg/L, respectively, dissolved in model wine. In this case, the treatments were performed as above, but adding the purified wine chitinase and thaumatin-like protein (TLP) separately (both at 100 mg/L) before treating the solution with 10 g/hL of bentonite. Each treatment was done in triplicate.

GC/MS Analysis. Gas chromatography/mass spectrometry (GC/MS) analysis was performed using a 6850 gas chromatography system (Agilent Technologies, Santa Clara, CA, US), equipped with a fused silica HP-INNOWax polyethylene glycol capillary column (30 m × 0.25 mm, 0.25 μm inner diameter) (Agilent Technologies, Santa Clara, CA, U.S.A.), coupled with HP 5975C mass spectrometer and 7693A automatic liquid sampler injector (Agilent Technologies, Santa Clara, CA, U.S.A.). Oven temperature program: 40 °C isothermal for 1 min, heating 2 °C/min until 160 °C, 3 °C/min until 230 °C, 230 °C isothermal for 15 min. Other experimental conditions: injector temperature, 230 °C; carrier gas, helium at flow rate of 1.2 mL/min; sample volume injected, 1 μL splitless injection; transfer line temperature, 250 °C; quadrupole temperature, 150 °C; mass range, m/z 35−550.

Compounds identification was performed by using the spectral libraries NIST Mass (rev08) Spectral Database and the homemade CRA-VIT database. For some compounds, the identification was confirmed on the basis of GC retention times of pure standards. For the other compounds the Kovats retention index on PEG stationary phase was calculated by using a standard mixture of C11−C32 aliphatic hydrocarbons. The concentration of compounds was calculated as μg/L of internal standard 1-decanol.

Statistical Analysis. Data were analyzed by XLSTAT program. Significance was determined at $P < 0.05$ or $P < 0.01$ by ANOVA followed by Fisher LSD comparison test.

DOI: 10.1021/jf505657h
J. Agric. Food Chem. 2015, 63, 2314−2320

RESULTS AND DISCUSSION

The distinct effect of bentonite and proteins on the removal of wine aroma compounds was first studied in wine model solution. Total wine proteins were extracted from a Manzoni Bianco wine, using a preparative procedure previously described.[15] The wine proteins bound to the cation exchange (SCE) resin were recovered as a whole, whereas the unbound material (flow through, FT) was collected separately. SDS-PAGE analysis followed by staining for proteins (Figure 1A)

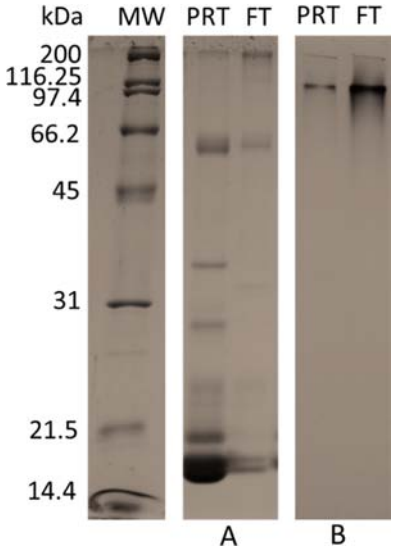

Figure 1. SDS-PAGE analysis of Manzoni Bianco wine molecules retained (PRT) or not retained (FT) on the cation exchange resin. The gels were stained with colloidal Coomassie (A) or Periodic Acid–Schiff (B). Standard molecular weight are reported on the left.

and sugars (Figure 1B) confirmed that FT was mainly composed of high molecular weight glycans, with only small contamination by two proteins of 65 and 18 kDa, which can be identified as the grape invertase and thaumatin-like protein, respectively—these latter components being similar to those retained by the SCE resin. On the contrary, the SCE bound material showed to be composed mainly of proteins. Nitrogen analysis confirmed that the protein content (as N × 6.25) in the SCE bound fraction was more than 70%, whereas that in the FT was about 10%, a percentage corresponding to that present in yeast mannoproteins.[23]

The protein concentration of 100 mg/L in the model solution was chosen for the experiments because this quantity falls in the typical range (20–250 mg/L) for white wines before bentonite treatment.[19,24]

Preliminary tests with increasing doses of bentonite (5, 10, and 15 g/hL) were performed to determine the amount necessary for stabilization. Different tests are available to assess wine stability and one of the most used is the heat test, in which the wine proteins are heat-denatured and the induced turbidity is measured by nephelometry. Since this test does not work in model wine,[25] the residual protein content after bentonite treatment was taken as the parameter to be considered for protein stability. The limit for stability was set at less than 20 mg/L of protein.[26] To reach this quantity, the dose of 10 g/hL of bentonite was necessary, which reduced the protein content to about 5 mg/L (Figure 2).

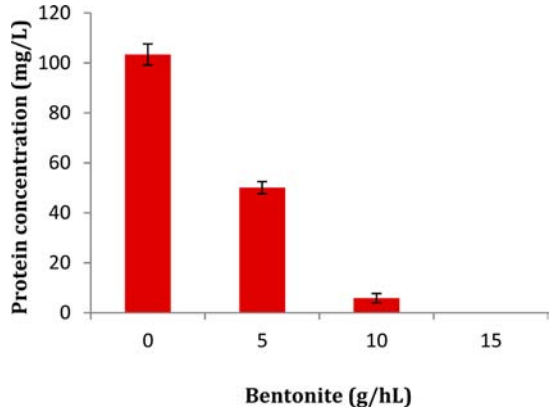

Figure 2. Protein concentration in model wine containing 100 mg/L of wine proteins and treated with increasing amount of bentonite.

Effect of Bentonite in the Presence of Total Wine Proteins and Aromas. Bentonite (10 g/hL) was then used to treat the model solution containing the wine aroma compounds, both in the presence and absence of added wine proteins. The use of such "reconstituted wine" allowed to study separately the direct effect of bentonite and that of the proteins removed by bentonite on the aroma composition. Differently from other papers, in which the effect of bentonite was studied only on selected molecules,[9,11] in these experiments all the volatile compounds extracted from an aromatic wine were examined, allowing to study the interactions among aroma molecules, bentonite, and proteins in a simple system. In addition, the use of a model solution allowed to exclude potential side interactions among the components of interest and other compounds present in wine. For example, polyphenols can modify the aroma volatility or bind to proteins,[27,28] thus potentially interfering in the interaction of proteins with aromas or bentonite. As a matter of fact, in our case, to completely remove 100 mg/L of wine proteins added to the ultrafiltered wine (containing all compounds with MW < 3000 Da), it was necessary to use at least the double of the bentonite needed to eliminate the same quantity of proteins from the model wine solution (data not shown).

Although it constitutes a simplification compared to the real wine, this approach allow to study in a direct way the interactions among aromas, bentonite, and proteins. In detail, the quantity of the different aroma compounds was determined in the model solutions before and after treatment with 10 g/L of bentonite, allowing to understand which are the aroma components directly removed by this treatment. Then, in order to establish the contribution of the phenomenon of protein removal by bentonite on aroma depletion, the same experiment was performed with the aroma solution containing 100 mg/L of added wine proteins. The average contents of fermentative (Table 1) and grape-deriving (Table 2) aroma compounds of the control sample (before the addition of bentonite) were compared to those remaining after treatment with bentonite alone and in the presence of added wine proteins.

In general, it can be observed that the treatment with bentonite resulted in a significant removal of various compounds, in particular ethyl esters and fatty acids (Table 1). For the ethyl esters, the longer was the hydrocarbon chain, the greater was the removal (Table 1), ranging from a loss of 20% for ethyl butanoate to 84% for ethyl dodecanoate. This relation between hydrocarbon chain length and rate of removal

DOI: 10.1021/jf505657h
J. Agric. Food Chem. 2015, 63, 2314–2320

Table 1. Fermentative Volatile Compounds Detected in Model Wine Solutions after Treatment with Bentonite, Bentonite + Proteins, Bentonite + Proteins + Mannoproteins (Three Replicate Treatments)[a]

compds. (μg/L extract)	LRI_{calc}[b]	control	bentonite	bentonite + proteins	bentonite + proteins + mannoproteins
ethyl butanoate[a]		175	141	162	151
2-methyl-1 -propanol[a]		929	987	1019	1081
isoamyl acetate	1128	2043	1725	1734	1746
2+3-methyl-1-butanol	1220	33375	35817	37328	37648
ethyl hexanoate	1236	620 A	373 B	343 B	374 B
3-methyl-3-buten-1-ol	1247	25	25	27	24
1-pentanol	1250	10	9	11	11
hexyl acetate	1272	137 A	91 B	30 B	90 B
3-hydroxy-2-butanone	1278	15	13	14	20
4-methyl-1-pentanol	1312	16	26	37	27
3-methyl-2-buten-1-ol	1318	6	6	6	7
3-methyl-1-pentanol	1322	57	53	57	53
ethyl lactate	1342	990	971	1044	1107
1-hexanol	1352	232	229	244	252
trans-3-hexen-1-ol	1362	6	6	6	6
3-ethoxy-1-propanol	1369	9	8	9	10
cis-3-hexen-1-ol	1380	27	26	28	29
trans-2-hexen-1-ol	1412	2	2	2	2
ethyl octanoate	1433	443 A	147 B	117 B	123 B
ethyl 3-hydroxybutanoate	1509	139	132	138	140
γ-butyrolactone	1604	637	613	629	654
ethyl decanoate	1633	129 A	37 B	16 B	25 B
2-furanmethanol	1657	3	3	3	4
diethylsuccinate	1670	365	356	360	349
2-phenylethyl acetate	1797	1210	1139	1126	1195
ethyl dodecanoate	1838	53 A	9 B	11 B	24 B
diethyl hydroxysuccinate	2033	256	243	245	250
octanoic acid	2067	161	145	123	166
ethyl hexadecanoate	2249	118 A	29 B	44 B	57 B
decanoic acid	2280	1465 A	1093 AB	353 B	1156 B
ethyl octadecanoate	2453	80 A	15 B	20 B	26 B
dodecanoic acid	2497	118 A	27 B	16 B	33 B

[a]Concentrations are expressed as μg/L internal standard (1-decanol). Compounds with different letters are significantly different ($p < 0.05$). Identification based on purchased reference compounds. [b]LRI_{calc}: linear retention index calculated on INNOWax capillary column.

would indicate an involvement of hydrophobicity in determining the interaction. However, because of the hydration of the inorganic cations on the exchange sites, the bentonite surface is recognized as hydrophilic, making the clay ineffective as sorbent for organic compounds.[29] It has, however, already been demonstrated by many authors that ethyl esters have high affinity for bentonite probably due to involvement of other weak forces, such as van der Waals attractions and hydrogen bonding. For example, Dif et al.[30] demonstrated that in aqueous solutions hydrophobic compounds tend to be "pushed" to the adsorbent surface of Na-bentonite.

The addition of proteins before the bentonite treatment did not cause statistically significant effects ($p < 0.05$) in the different aroma compounds content (data not shown). However, a general tendency toward an increased removal of the ethyl esters by bentonite could be observed when the wine proteins were present (Table 1). This additional ester removal was probably due to the fact that these aroma compounds were bound to the proteins, confirming a previous hypothesis.[7,31]

In the case of fatty acids (which are important precursors of aromatic esters), significant effect of bentonite was observed for the removal of decanoic and dodecanoic acids but not for octanoic acid, for which the electrostatic repulsion with the negative charge of bentonite may predominate on the interactions due to hydrophobicity. It has already been suggested that bentonite can interact with fatty acids in grape juices[31,32] thus explaining the increase of the fermentation time when bentonite is used before yeast inoculation.

As for ethyl esters, the presence of wine proteins increased the loss of the long chain fatty acids, in particular decanoic, although these differences were not statistically significant (Table 1).

The effect of addition to the samples of the S-Sepharose unbound fraction, which was mainly constituted by sugar-containing macromolecules (Figure 1) attributable to the yeast mannoproteins was also studied. Since mannoproteins can bind some wine aroma compounds (such as ethyl hexanoate, β-ionone, 1-hexanol, and isoamyl acetate[8,33,34]) and mannoprotein removal from wine by bentonite is low,[35] an improved retention of aroma compounds in wine during bentonite fining can be expected. However, the addition of this fraction showed no significant effects on the quantity of aroma compounds remaining in the solution after bentonite treatment (Table 1).

Considering the aroma compounds deriving from grapes, the overall effect of bentonite on monoterpenes was low and not significant ($p < 0.05$), with the exception of β-damascone (Table 2). These results seems not fully match with the literature, because losses of terpenols due to bentonite

DOI: 10.1021/jf505657h
J. Agric. Food Chem. 2015, 63, 2314−2320

Table 2. Volatile Compounds of Grape Origin Detected in Model Wine Solutions after Treatment with Bentonite, Bentonite + Proteins, Bentonite + Proteins + Mannoproteins (Three Replicate Treatments)[a]

compds. (μg/L extract)	LRI_{calc}[b]	control	bentonite	bentonite + proteins	bentonite + proteins + mannoproteins
			Terpenols		
cis-furan linalool oxide	1461	58	47	56	55
linalool	1548	429	405	416	420
ho-trienol	1607	86	81	85	85
α-terpineol	1685	223	220	224	221
trans-pyran linalool oxide	1725	222 A	210 A	222 A	152 B
cis-pyran linalool oxide	1757	55 AB	63 A	68 A	44 B
$\sum$ pyran linalool oxide		276 A	274 A	290 A	196 B
citronellol	1763	38	26	27	32
nerol	1792	74	70	71	71
geraniol	1857	155	150	149	147
diendiol I	1947	243	221	237	244
endiol	1978	47	43	45	43
diendiol II	2127	37	37	39	37
hydroxycitronellol	2201	99	89	92	82
trans-8-hydroxylinalool	2269	35	32	36	39
hydroxygeraniol	2303	49	40	48	51
cis-8-hydroxylinalool	2304	20	18	21	22
$\sum$ 8-hydroxylinalool		55	50	56	62
geranic acid	2344	82	68	69	53
			Benzenoids		
benzaldehyde	1504	81 A	79 A	74 A	59 B
benzeneacetaldehyde	1626	13 A	8 AB	7 AB	6 B
acetophenone	1628	59	55	53	49
benzyl alcohol	1863	1999	1964	2067	2018
2-phenylethanol	1897	18435	19042	19615	16468
vanillin	2545	9	9	7	6
methylvanillate	2590	91	92	94	96
acetovanillone	2620	36	36	30	43
homovanillic acid	2829	82	85	90	90
			Norisoprenoids		
3-hydroxy-β-damascone	2514	37 A	23 B	29 AB	26 B
3-oxo-α-ionol	2606	38	38	43	42
vomifoliol	3128	5	4	5	5

[a]Concentrations are expressed as μg/L internal standard (1-decanol). Compounds with different letters are significantly different ($p < 0.05$). [b]LRI_{calc}: linear retention index calculated on INNOWax capillary column.

treatments were previously observed.[12,36] However, in those experiments, bentonite doses higher than those used in this study (10 g/hL) were employed. For example in Albarino wine added with 60 g/hL of bentonite a loss of 13% of total terpenes was observed,[12] while in Falanghina treated with 80 g/hL of bentonite (but also with potassium caseinate, gelatin, silica gel, and charcoal), losses of total free and bound terpenols were found, corresponding to 23% in must and 31−36% in wine.[36]

When the wine proteins were added to the aroma solution before the treatment with bentonite, no effect on the terpenols or on the other aromas of grape origin was found (Table 2). These results suggest that wine proteins of grape origin have little or no effect on the depletion of grape-deriving aroma after bentonite fining. On the contrary, the addition of the sugar-containing S-Sepharose unbound fraction provoked, in combination with bentonite and wine proteins, a significant removal of few aromatic compounds, such as linalol and benzaldehyde. Because that chromatographic fraction was likely to comprise most of the mannoproteins, these results would indicate a certain effect of these yeast compounds on the aroma composition of bentonite-treated wines, confirming previous studies performed on wines aged on yeast lees.[8,33,34]

Effect of Bentonite in the Presence of Selected Ethyl Esters and Purified Wine TLP and Chitinase. Due to the importance of ethyl esters in determining the wine aroma, the effects of bentonite fining on four selected ethyl esters were studied in presence and absence of two individual proteins purified from wine. These proteins, a class IV chitinase and a thaumatin-like protein (VVTL1) have been described as the main components in wines.[37] When used alone, bentonite confirmed to have high affinity for the ethyl esters, with an effect which increased with the length of their carbon chain (from 20% of removal for hexanoate to 84% of removal for dodecanoate) (Figure 3). In this simplified system, the removal percentage was lower than in the previous experiment, especially for ethyl hexanoate and octanoate. This was probably due to the higher initial concentration of the esters in comparison to that of total wine aroma extract (from about the double for ethyl hexanoate to around 20-fold for ethyl dodecanoate). However, an effect of other compounds present in the wine extract could not be excluded. In any case, a reduction of the ethyl esters in wines treated with a relatively low bentonite dose can be expected.

DOI: 10.1021/jf505657h
J. Agric. Food Chem. 2015, 63, 2314−2320

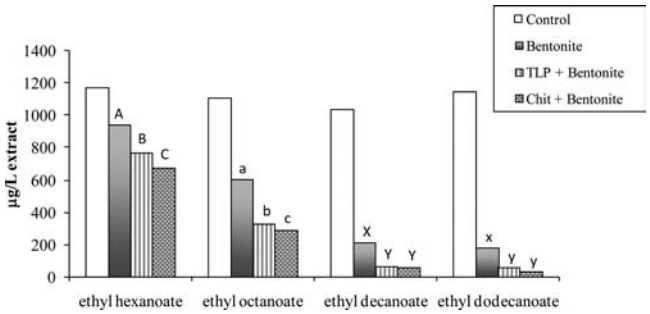

Figure 3. Mean content of ethyl esters found in the model wine treated with bentonite alone or in the presence of 100 mg/L of thaumatin-like protein or chitinase. Samples with different letters are significantly different ($p < 0.01$).

The two wine proteins, individually added at 100 mg/L before the treatment with bentonite, showed a synergistic effect with the clay, increasing significantly ($p < 0.01$) the amount of esters removed from the solution (Figure 3). The intensity of this effect was higher than that observed in the previous experiments, when total wine proteins and aroma were used (Table 1). The differences between the two experiments could be attributed to the higher initial concentration of the selected aroma molecules in the simplified model and/or to an interference caused by the other aroma compounds present in the more complex wine extract.

Compared to the bentonite alone, the additional removal increased from hexanoate to octanoate, then started to slowly decrease for the other two esters with longer chain. The maximum of this phenomenon was observed for ethyl octanoate in the presence of chitinase.

The more interesting results of this second experiment were the differences between the effect of the two proteins on the aroma removal. The mean value of ester depletion in the presence of chitinase was ever slightly higher than that observed when TLP was added, even though these differences were not statistically significant ($p < 0.01$). It has to be highlighted that for the esters tested the overall aroma removal in combination with bentonite almost ever reached values higher than 70%, thus potentially masking a possible difference between the two proteins. As a matter of fact, for ethyl hexanoate, for which the overall aroma removal was less intense (below 50%) the greater binding to chitinase in comparison with TLP became highly significant ($p < 0.01$).

An indication of the relative hydrophobicity of the two proteins can be roughly deduced from the elution order on the Phenyl Sepharose column (not showed). The conductivity of the solution at which the elution of chitinase starts (136 mS) is lower than that necessary to elute TLP (145−148 mS) thus highlighting the greater surface hydrophobicity of the former protein, confirming previous studies on wine proteins.[38] Considering the different affinity of chitinase and TLP for ethyl esters of varying length, the idea that hydrophobic forces are involved in the interactions between aroma compounds and proteins is further supported.

This study showed that in general bentonite has low effect on the loss of terpenes. Instead more evident effects were observed on ethyl esters: in addition, proteins showed synergistic effect with bentonite by increasing losses from ethyl octanoate to ethyl decanoate, as confirmed by a study on model wine solutions of the four esters. Contrarily to what it was expected from literature data,[8,33,34,35] the mannoprotein addition had no significant effect in reduction of ethyl esters, and only a small protective effect on some terpenols.

In conclusion, the data here reported confirm that the individual proteins of grape origin that can be found in wine can interact at least with the fermentative esters, thus contributing to the loss of aroma when those proteins are removed by bentonite fining. This conclusion supports previously reported hypotheses.[7] However, the described phenomena, which can be seen using a simple reconstituted system containing a single protein (grape TLP or chitinase) and a few esters, seem to have only small effects with a more complex system comprising the pools of the wine proteins and aroma compounds, indicating that the main responsible for the aroma losses after bentonite fining is the direct adsorption of the aroma molecules on the clay. This absorption, however, at least in the experimental condition here used, concerns mainly the fermentative aroma compounds, whereas those deriving from the grape are generally not affected. These results can be of great interest for the oenologist, because they suggest that bentonite fining could have a lower impact on the aroma quality when used before fermentation, which is when the fermentative aromas are still to be produced.

AUTHOR INFORMATION

Corresponding Author

*Fax: +39 0438 453744. Phone: +39 0438 453052. E-mail: simone.vincenzi@unipd.it.

Notes

The authors declare no competing financial interest.

REFERENCES

(1) Bayly, F. C.; Berg, H. W. Grape and wine proteins of white wine varietals. *Am. J. Enol. Vitic.* **1967**, *24*, 18−32.

(2) Hsu, J. C.; Heatherbell, D. A. Heat-unstable proteins in wine. I. Characterization and removal by bentonite fining and heat treatement. *Am. J. Enol. Vitic.* **1987**, *38*, 11−16.

(3) Waters, E. J.; Wallace, W.; Williams, P. J. Identification of heat-unstable wine proteins and their resistance to peptidases. *J. Agric. Food Chem.* **1992**, *40*, 1514−1519.

(4) Dawes, H.; Boyes, S.; Keene, J.; Heatherbell, D. Protein instability of wines: Influence of protein isoelectric point. *Am. J. Enol. Vitic.* **1994**, *45*, 319−326.

(5) Esteruelas, M.; Poinsaut, P.; Sieczkowski, N.; Manteau, S.; Fort, M. F.; Canals, J. M.; Zamora, F. Characterization of natural haze protein in sauvignon white wine. *Food Chem.* **2009**, *113*, 28−35.

(6) Sauvage, F. X.; Bach, B.; Moutounet, M.; Vernhet, A. Proteins in white wines: Thermo-sensitivity and differential adsorption by bentonite. *Food Chem.* **2010**, *118*, 26−34.

(7) Lambri, M.; Dordoni, R.; Silva, A.; De Faveri, D. M. Effect of bentonite fining on odor-active compounds in two different white wine styles. *Am. J. Enol. Vitic.* **2010**, *61*, 225−233.

(8) Voilley, A.; Lamer, C.; Dubois, P.; Feuillat, M. Influence of macromolecules and treatments on the behavior of aroma compounds in a model wine. *J. Agric. Food Chem.* **1990**, *38*, 248−251.

(9) Lubbers, S.; Voilley, A.; Charpentier, C.; Feuillat, M. Mise en evidence d'interactions entre les macromolecules et les aromes du vin. Influence des traitments de clarification sur la qualité aromatique du vin. *Rev. Fr. Oenol.* **1993**, *33*, 12−18.

(10) Sanborn, M.; Edwards, C. G.; Ross, C. F. Impact of fining on chemical and sensory properties of Washington state chardonnay and gewurztraminer wines. *Am. J. Enol. Vitic.* **2010**, *61*, 31−41.

(11) Lambri, M.; Dordoni, R.; Silva, A.; De Faveri, D. M. Odor-active compound adsorption onto bentonite in a model white wine solution. *Chem. Eng. Trans.* **2013**, *32*, 1741−1746.

(12) Armada, L.; Falqué, E. Repercussion of the clarification treatment agents before the alcoholic fermentation on volatile

DOI: 10.1021/jf505657h
J. Agric. Food Chem. 2015, 63, 2314−2320

composition of white wines. *Eur. Food Res. Technol.* **2007**, *225*, 553−558.
(13) Lubbers, S.; Charpentier, C.; Feuillat, M. Etude de la rétention de composés d'arôme par les bentonites en moût, vin et milieux modèles. *Vitis* **1996**, *35*, 59−62.
(14) Vincenzi, S.; Marangon, M.; Tolin, S.; Curioni, A. Protein evolution during the early stages of white winemaking and its relations with wine stability. *Austr. J. Grape Wine Res.* **2011**, *17*, 20−27.
(15) Van Sluyter, S. C.; Marangon, M.; Stranks, S. D.; Neilson, K. A.; Hayasaka, Y.; Haynes, P. A.; Menz, R. I.; Waters, E. J. Two-step purification of pathogenesis-related proteins from grape juice and crystallization of thaumatin-like proteins. *J. Agric. Food Chem.* **2009**, *57*, 11376−11382.
(16) Vincenzi, S.; Curioni, A. Anomalous electrophoretic behavior of a chitinase isoform from grape berries and wine in glycol chitin-containing SDS-PAGE gels. *Electrophoresis* **2005**, *26*, 60−63.
(17) Andujar-Ortiz, I.; Moreno-Arribas, M. V.; Martín-Álvarez, P. J.; Pozo-Bayón, M. A. Analytical performance of three commonly used extraction methods for the gas chromatography−mass spectrometry analysis of wine volatile compounds. *J. Chromatogr. A* **2009**, *1216*, 7351−7357.
(18) Pocock, K. F.; Rankine, B. C. Heat test for detecting protein instability in wine. *Aust. Wine Brew. Spirit Rev.* **1973**, *91*, 42−43.
(19) Vincenzi, S.; Mosconi, S.; Zoccatelli, G.; Dalla Pellegrina, C.; Veneri, G.; Chignola, R.; D. B. Peruffo, A.; Curioni, A.; Rizzi, C. Development of a new procedure for protein recovery and quantification in wine. *Am. J. Enol. Vitic.* **2005**, *56*, 182−187.
(20) Smith, P. K.; Krohn, R. I.; Hermanson, G. T.; Mallia, A. K.; Gartner, F. H.; Provenzano, M. D.; Fujimoto, E. K.; Goeke, N. M.; Olson, B. J.; Klenk, D. C. Measurement of protein using bicinchoninic acid. *Anal. Biochem.* **1985**, *150*, 76−85.
(21) Laemmli, U. K. Cleavage of structural protein during the assembly of head of bacteriophage T4. *Nature* **1970**, *227*, 680−685.
(22) Segrest, J. P.; Jackson, R. L. Molecular weight determination of glycoproteins by polyacrylamide gel electrophoresis in sodium dodecyl sulfate. *Methods Enzymol.* **1972**, *28*, 54−63.
(23) Gonçalves, F.; Heyraud, A.; de Pinho, M. N.; Rinaudo, M. Characterization of white wine mannoproteins. *J. Agric. Food Chem.* **2002**, *50*, 6097−6101.
(24) Monteiro, S.; Piçarra-Pereira, M. A.; Mesquita, P. R.; Loureiro, B.; Teixeira, A.; Ferreira, R. B. The wide diversity of structurally similar wine proteins. *J. Agric. Food Chem.* **2001**, *49*, 3999−4010.
(25) Pocock, K. F.; Alexander, G. M.; Hayasaka, Y.; Jones, P. R.; Waters, E. J. Sulfate—A candidate for the missing essential factor that is required for the formation of protein haze in white wine. *J. Agric. Food Chem.* **2007**, *55*, 1799−1807.
(26) Pocock, K.; Waters, E. J. The effect of secondary fermentation and aging on yeast lees in bottles on protein stability of sparkling wines. *AWRI Tech. Rev.* **2005**, *158*, 8−14.
(27) Dufour, C.; Bayonove, C. L. Interactions between wine polyphenols and aroma substances. An insight at the molecular level. *J. Agric. Food Chem.* **1999**, *47*, 678−684.
(28) Mitopoulou, A.; Hatzidimitriou, E.; Paraskevopoulou, A. Aroma release of a model wine solution as influenced by the presence of non-volatile components. Effect of commercial tannin extracts, polysaccharides, and artificial saliva. *Food Res. Int.* **2011**, *44*, 1561−1570.
(29) He, H.; Frost, R. L. Application of near infrared spectroscopy for the determination of adsorbed p-nitrophenol on HDTMA organoclay-implications for the removal of organic pollutants from water. *Spectrochim. Acta, Part A* **2008**, *69*, 835−841.
(30) Dif, M.; Blel, W.; Sire, O. New physico-chemical regeneration process of CIP solutions. *Chem. Eng. Trans.* **2012**, *29*, 829−834.
(31) Lambri, M.; Dordoni, R.; Silva, A.; De Faveri, D. M. Comparing the impact of bentonite addition for both must clarification and wine fining on the chemical profile of wine from Chambave Muscat grapes. *Int. J. Food Sci. Technol.* **2012**, *47*, 1−12.
(32) Weiss, K. C.; Bisson, L. F. Effect of bentonite treatment of grape juice on yeast fermentation. *Am. J. Enol. Vitic.* **2002**, *53*, 28−36.
(33) Lubbers, S.; Charpentier, C.; Feuillat, M.; Voilley, A. Influence of yeast walls on the behavior of aroma compounds in a model wine. *Am. J. Enol. Vitic.* **1994**, *45*, 29−33.
(34) Chalier, P.; Angot, B.; Delteil, D.; Doco, T.; Gunata, Z. Interactions between aroma compounds and whole mannoprotein isolated from *Saccharomyces cerevisiae* strains. *Food Chem.* **2007**, *100*, 22−30.
(35) Rodrigues, A.; Ricardo Da Silva, J. M.; Lucas, C.; Laureano, O. Influence of fining and tartaric stabilisation procedures on white wine mannoprotein content. *S. Afr. J. Enol. Vitic.* **2012**, *33*, 88−94.
(36) Moio, L.; Ugliano, M.; Gambuti, A.; Genovese, A.; Piombino, P. Influence of clarification treatment on concentration of selected free varietal aroma compounds and glycoconjugates in Falanghina (*Vitis vinifera L.*) must and wine. *Am. J. Enol. Vitic.* **2004**, *55*, 7−12.
(37) Waters, E. J.; Shirley, N. J.; Williams, P. J. Nuisance proteins of wine are grape pathogenesis related proteins. *J. Agric. Food Chem.* **1996**, *44*, 3−5.
(38) Marangon, M.; Van Sluyter, S.; Haynes, P. A.; Waters, E. J. Grape and wine proteins: Their fractionation by hydrophobic interaction chromatography and identification by chromatography and proteomic analysis. *J. Agric. Food Chem.* **2009**, *57*, 4415−4425.

DOI: 10.1021/jf505657h
J. Agric. Food Chem. 2015, 63, 2314−2320

or different roasting grades, and the presence of defects on roasted coffee and to estimate the shelf life of packaged coffee.[33−39] Furthermore, the electronic nose system was applied on EC to determine the best time for packaging[40] of coffee grounds, to discriminate the coffee from different production countries and roasting degrees,[24] and to classify beans, grounds, and brew of commercial coffee blends.[41] Particularly, in this work, the authors reported that a correct distinction of the brews was not statistically significant.

On the basis of the above considerations, the purpose of this paper was to study the changes of the EC during extraction to obtain useful information for the better management of the brew quality. More specifically, the main objective was to use the electronic nose system to study the changes of the overall aromatic profile of EC, taking into account the extraction time and the grinding level of coffee powder as independent variables.

MATERIALS AND METHODS

Raw Materials and EC Preparation. Roasted coffee beans (medium-dark roasting: L^* = 21.50, a^* = 5.92) were supplied from ESSSE caffè S.p.A. (Anzola dell'Emilia, Bologna, Italy). The beans were ground by an automatic grinder with flat grinding blades (model Super Jolly coffee grinder for a grocery, Mazzer, Italy) having eight levels of grinding: 1 for the finest and 8 for the coarsest. Water "Leggera" (Gaudianello S.p.A., Italy) used for brew preparation was locally purchased. Table 1 reports the main physical and chemical characteristics of the water as specified on the label, except the pH value, which was experimentally measured. EC samples were prepared using an EC machine mod. V220 (Vibiemme, Italy) with filter holder monodose applied the following experimental conditions: 7.0 g of ground coffee, a 60 mm of holder filter diameter, pressure on the upper surface of ground coffee cake of 1500 g, water temperature of 92 °C, and 9 atm of relative pressure. According to scientific literature, these conditions may be considered as the most common for EC preparation.[7,8,11−13,42] Instead, the value of pressure was chosen on the basis of preliminary experiments in which different weights were used to press ground coffee.

Table 1. Physicochemical Characteristics of Mineral Water "Leggera" (Gaudianello, Italy) as Listed on the Label of the Bottle

analytical parameter	value
pH	7.30[a]
conductivity at 20 °C (μS/cm)	510
total residue at 180 °C (TDS) (mg/L)	416
silica (SiO_2) (mg/L)	105
potassium (K^+) (mg/L)	32
calcium (Ca^{2+}) (mg/L)	46
magnesium (Mg^{2+}) (mg/L)	14
chloride (Cl^-) (mg/L)	26
sulfate (SO_4^{2-}) (mg/L)	14
bicarbonate (HCO^{3-}) (mg/L)	306
nitrate (NO^{3-}) (mg/L)	4

[a]Mean value of six samples measured in triplicate.

Experimental Design. EC samples were always prepared within 3 min from the grinding of beans, which was performed at three levels, 6, 6.5, and 7, corresponding to fine, fine−coarse, and coarse coffee grounds, respectively. The choice of these grinding levels was performed on the basis of preliminary experiments, in which the particle size distribution of the ESSSE caffè S.p.A. coffee grounds commonly used in the bars was determined. Once the variability of coffee grounds was defined, we did choose the grinding levels that enabled us to express the differences well in terms of particle size distribution commonly detectable in the bars. Then, the particle size distribution for each grinding level was described shaking 100 g of coffee grounds with four sieves (600, 400, 250, and 180 μm) until a constant weight. Table 2 shows the percentage of distribution of the particle sizes for each grinding level.

Table 2. Distribution (%) of Particle Size in Each Grinding Grade of Coffee Powder (Mean Values ± Standard Deviation)

	grinding grade		
particle size (μm)	6	6.5	7
>600	0.21 ± 0.11	0.68 ± 0.22	2.93 ± 0.53
400 < X < 600	5.69 ± 1.26	13.80 ± 0.82	33.87 ± 1.63
250 < X < 400	32.00 ± 4.89	47.15 ± 14.12	35.64 ± 1.88
180 < X < 250	52.60 ± 6.12	37.18 ± 14.10	26.42 ± 1.07
<180	9.52 ± 3.21	1.19 ± 1.02	1.15 ± 0.85

Each EC sample was divided into three fractions (F) collecting the brews obtained in the first 8 s (Ft1), from 9 to 16 s (Ft2), and from 17 to 24 s (Ft3) of extraction. These extraction times were chosen by dividing in three fractions the time necessary to prepare a regular coffee that is 25 s. The extraction times were measured using a digital timer. The regular EC of 25 mL, from each grinding level, was prepared measuring the volume of brew through a graduate cylinder. At least 20 replicates were performed for each espresso, obtaining a total of 240 samples.

Physical and Chemical Analyses. The pH of the samples was measured by a pH-meter model Basic 20 (Crison, Allen) previously calibrated with three buffers at pH 4.00, 7.00, and 9.00. Also, acidity was measured by titration of 25 mL of coffee brew at room temperature with 0.1 N NaOH until pH of 7.00.[43] The total solids content was measured gravimetrically by drying about 3 mL of EC at 105 °C until a constant weight.[44]

The caffeine content was measured using the method described by Skoog et al.,[45] with some modifications. Each EC brew (fractions and regular coffee) was previously filtered with 0.22 μm nylon filter (Olim Peak, Teknokroma Anlítica, Spain) and directly injected (injection volume = 20 μL) into a high-performance liquid chromatography (HPLC) binary pump (Waters model 1525, Milford, MA) equipped with a detector set at 254 nm (Waters model 2487, Milford, MA). Peak separation was achieved on a C_{18} column (Hibar 125-4 with LiChrospher 100, 5 μm) at 25 °C, using a mobile phase (v/v) of water (74%), methanol (25%), and acetic acid (1%) (J.T.Baker) previously seeped through a filter in cellulose acetate of 0.45 μm (VWR International, Radnor, PA) and submitted to an ultrasound pulse (Elmasonic S 60 H, Elma Schmidbauer GmbH, Germany) for 20 min to remove the air. The flow rate of pump was 0.9 mL/min. The concentration was calculated using the equation obtained by the linear regression of external caffeine standards at different concentrations (Sigma-Aldrich, St. Louis, MO), and the results were expressed as milligrams per milliliter.

Determination of the Aromatic Profile by the Electronic Nose System. The aromatic profile was characterized by an electronic nose system αFOX Sensor Array System 2000 (Alpha M.O.S., Toulouse, France) equipped with six metal oxide semiconductor sensors (T30/1, T70/2, P10/1, P10/2, P40/1, and PA/2) and an autosampler model HS 100 (Alpha M.O.S., Toulouse, France). The sensors measure the changes of the electrical resistance generated by the adsorption−desorption of the volatile organic compounds. Dry air with impurities specified as H_2O < 5 ppm, C_nH_m < 5 ppm, $O_2 + N_2$ > 99.95%, and O_2 = 20 ± 1% was used as carrier gas using a flow rate of 150 mL/min. A total of 1 mL of each coffee sample was placed in vials of 10 mL, sealed with a rubber stopper, and maintained in an oven at 87 °C in agitation at 300 rpm for 3 min before the injection of 500 μL. A flow rate of 150 mL/min was used for the analysis. The sensor responses were detected every 1 s for a total time, t, of 300 s (a total of 300 points for each sample). The response of the sensors was

DOI: 10.1021/jf505691u
J. Agric. Food Chem. 2015, 63, 2321−2327

Table 3. Physicochemical Parameters of EC Samples (Mean Values ± Standard Deviation)

sample	grinding grade	volume of brew[a] (mL)	pH[a]	titrable acidity[a] (mL of NaOH/mL of EC)	total solids[a] (mg/mL)	caffeine[a] (mg/mL)
Ft1	6	16.239 ± 3.579 c	5.180 ± 0.017 a	0.329 ± 0.064 a	74.615 ± 0.013 a	4.982 ± 0.624 a
	6.5	28.858 ± 2.318 b	5.237 ± 0.047 a	0.272 ± 0.012 a	69.699 ± 0.010 a	4.359 ± 0.919 a
	7	41.847 ± 1.701 a	5.233 ± 0.031 a	0.121 ± 0.010 b	34.632 ± 0.002 b	2.431 ± 0.338 b
Ft2	6	14.661 ± 2.009 c	5.467 ± 0.068 c	0.0573 ± 0.010 a	17.056 ± 0.003 a	1.288 ± 0.247 a
	6.5	22.920 ± 3.579 b	6.023 ± 0.130 b	0.016 ± 0.004 b	8.530 ± 0.001 b	0.832 ± 0.231 a
	7	55.904 ± 1.889 a	6.790 ± 0.159 a	0.003 ± 0.001 b	2.681 ± 0.001 c	0.305 ± 0.023 b
Ft3	6	14.614 ± 1.113 c	5.893 ± 0.199 c	0.025 ± 0.014 a	9.175 ± 0.002 a	0.645 ± 0.148 a
	6.5	21.295 ± 2.227 b	6.510 ± 0.160 b	0.003 ± 0.001 b	3.783 ± 0.001 b	0.296 ± 0.115 b
	7	48.016 ± 1.113 a	7.213 ± 0.058 a		1.079 ± 0.001 b	0.176 ± 0.011 b
regular coffee	6	25	4.983 ± 0.419 a	0.254 ± 0.008 a	50.640 ± 7.354 a	4.179 ± 0.209 a
	6.5	25	5.177 ± 0.021 a	0.243 ± 0.006 a	55.115 ± 4.747 a	4.014 ± 0.163 a
	7	25	5.163 ± 0.021 a	0.180 ± 0.009 b	44.342 ± 0.745 a	3.212 ± 0.267 b

[a]Different letters indicate statistically significant differences among grinding grade ($p < 0.05$, Tukey's test).

expressed as R_t/R_0, where R is the resistance of the sensor and the subscripts 0 and t refer to the initial value and each time t. After each analysis, the system was purged for 240 s with filtered air before a new injection to allow for re-establishment of the instrument baseline.

Statistical Analysis. For each grinding grade, significant differences among physicochemical parameters of the fractions and the regular coffee were determined by one-way analysis of variation (ANOVA). Tukey's test ($p < 0.05$) was used to highlight significant differences.

Principal component analysis (PCA) was performed on the data of the odor profile to discriminate the samples on the basis of their aromatic profile. The analysis was performed using as experimental data the values of maximum intensity detected by each sensor. Statistical analysis was performed using STATISTICA, version 10 (StatSoft. Inc., Tulsa, OK).

RESULTS AND DISCUSSION

Table 3 shows the main chemical attributes of the regular EC samples as well as each fraction of the brew collected as a function of the extraction time. The pH values of the regular coffee were not significantly different ($p > 0.05$), exhibiting values ranging between 4.983 ± 0.419 and 5.177 ± 0.021; these results were in accordance with the data reported from Parenti et al.[46] but slightly lower than the values reported from Andueza et al.[7] and Caporaso et al.,[47] who showed average values of ∼5.6 and ∼5.8, respectively.

Similar results were observed for titrable acidity for which only the samples obtained using a grinding level of 7 showed values significantly lower than the others. Moreover, taking into account the total solid content, no differences were observed ($p > 0.05$), stating that the three grinding grades did not affect this parameter for the regular EC samples. Our results showed values ranging between 44.342 ± 0.745 and 55.115 ± 4.747 mg/mL, which were in accordance with Parenti et al.,[46] who showed a total solid content of 59.48 mg/mL. However, a high variance in the total solids content of EC has been reported in the literature.[7,8,47]

Caffeine contents of the regular EC between 3.212 ± 0.267 and 4.179 ± 0.209 mg/mL were observed. These values were higher than those reported by Caporaso et al.[47] and Parenti et al.,[46] which showed values always lower than 2.44 mg/mL.

Although our results showed some discrepancies when compared to other authors, our findings may be considered within the natural variance of the chemical composition of EC brews. As well-known, the EC may be affected by several variables, such as roasting grade, mixture of roasted coffee varieties, water temperature, etc.[3−7] In addition, the volume of EC, which considerably affects the chemical composition of brew, is often highly variable among the scientific publications.[7,8,46,47]

However, from Table 3, the analysis of the changes in chemical attributes of the three fractions of EC showed structured variations. The pH values significantly increased as a function of the fraction of brew for each grinding grade. Of course, this result may be caused from the progressive reduction of organic acids still contained in the coffee grounds during the solid−liquid extraction. Moreover, in comparison to the pH values obtained from different grinding grades while keeping the same fraction constant, no significant differences ($p > 0.05$) were observed for the Ft1 samples, while a significant increase ($p < 0.05$) was observed for the second (Ft2) and third (Ft3) fractions of EC. These results were probably caused by a dilution effect because the increase of the grinding grade significantly affected the percolation rates with values of 1.66 ± 0.19, 2.89 ± 0.59, and 6.51 ± 0.26 mL/s when grinding levels of 6, 6.5, and 7 were used, respectively. More specifically, the increase of the percolation rate could be caused by the effect of the different particle size distributions (as reported in Table 2) on the microstructure of the coffee cake. A higher porosity and/or better percolation pathway, which are expected when increasing the grinding grade, could improve the extraction rate. However, because the pH values of the first fraction of EC samples were practically constant, it is possible to suppose that the major amount of organic acids was extracted in the first 8 s of percolation. Similar observations may be performed for titrable acidity, total solids, and caffeine contents, for which a progressive decrease was observed as a function of the coffee fractions and the grinding grade. Particularly, for caffeine content, the HPLC diagram of Ft1, Ft2, and Ft3 samples obtained using a grinding level of 6 is reported in Figure 1, showing the caffeine content decreasing as a function of the extraction time in the range of 5.231 and 0.749 mg/mL.

The study of the aromatic profile of each fraction of the EC and regular coffee obtained using different grinding grades is reported in Figures 2−5.

Figure 2 shows the loading plot of the sensors, which contributes to the discrimination of samples as well as the factor coordinates of the fractions of EC prepared with the three grinding grades. PC1 accounted for 98.77% of the variation of samples, while PC2 accounted for 1.01%, stating that the first two PCs allowed us to explain accurately the variation of the aroma profile of EC samples (99.78%). All of

DOI: 10.1021/jf505691u
J. Agric. Food Chem. 2015, 63, 2321−2327

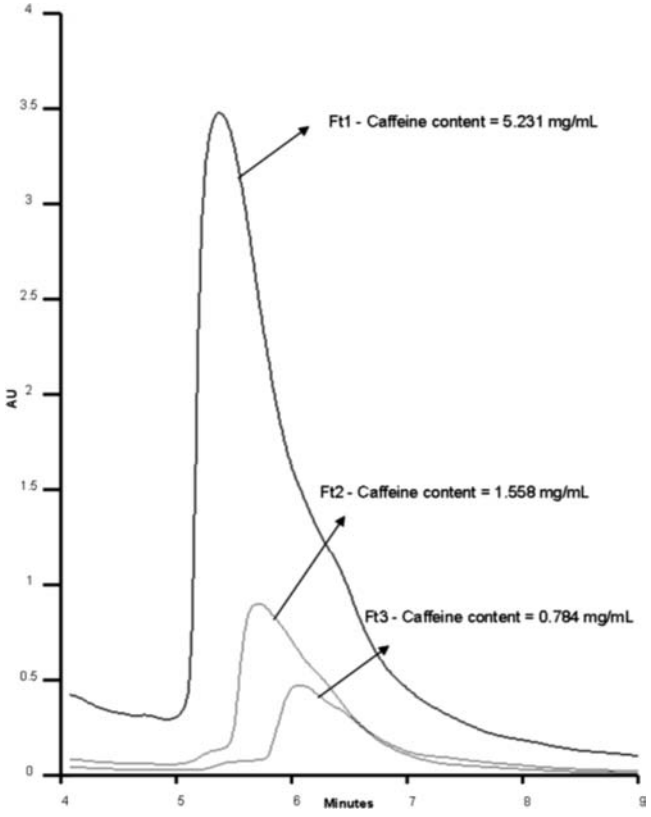

Figure 1. HPLC diagram of caffeine contents for each fraction (Ft1, Ft2, and Ft3) from grinding level 6 (fine).

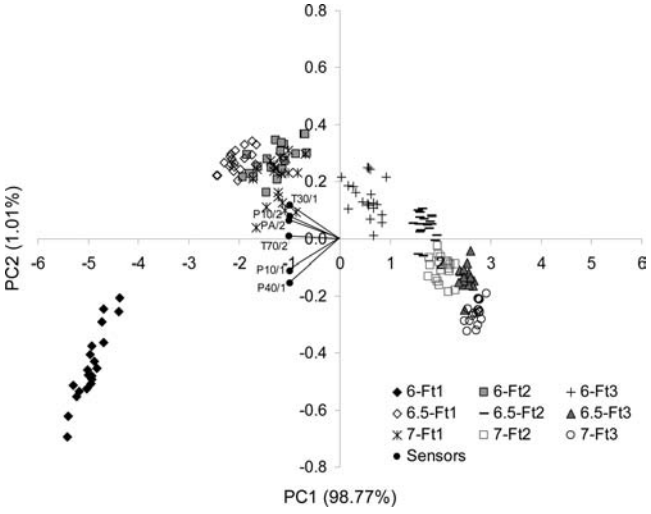

Figure 2. Principal component projection of the loading plot of the six sensors and score plot of EC samples in different experimental conditions.

the sensors have been significant for detecting differences in terms of odor compounds of EC samples. More specifically, the sensors T30/1, P10/2, PA/2, and T70/2 showed the highest contribution in the discrimination of the majority of samples with the exception of the sample 6-Ft1, which was better recognized by the sensors P10/1 and P40/1. Particularly, the sample 6-Ft1 was clearly separated from the other coffee fractions, stating that, during the first 8 s of percolation with the finest coffee grounds, a significantly different aromatic profile was developed. However, the samples 6-Ft2 and 6-Ft3 were

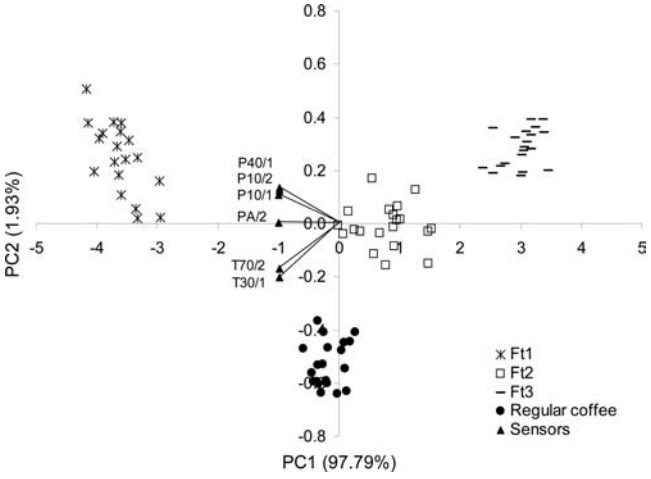

Figure 3. Principal component projection of the loading plot of six sensors and score plot of the fractions and regular coffee (25 mL) obtained from grinding grade 6.

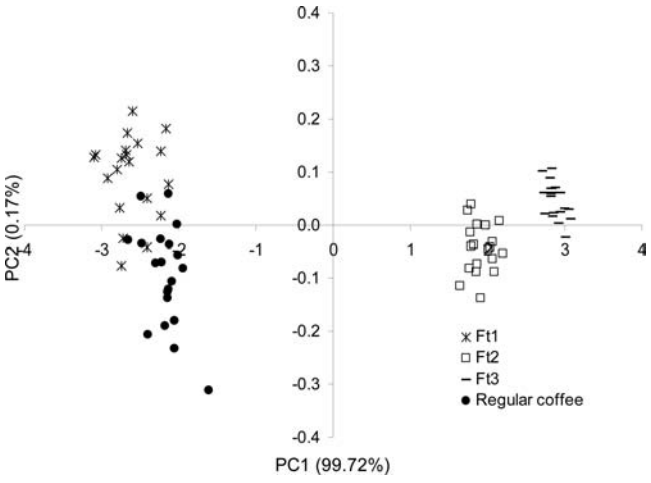

Figure 4. Principal component projection of the score plot of fractions and regular coffee (25 mL) obtained from grinding grade 6.5 (fine−coarse).

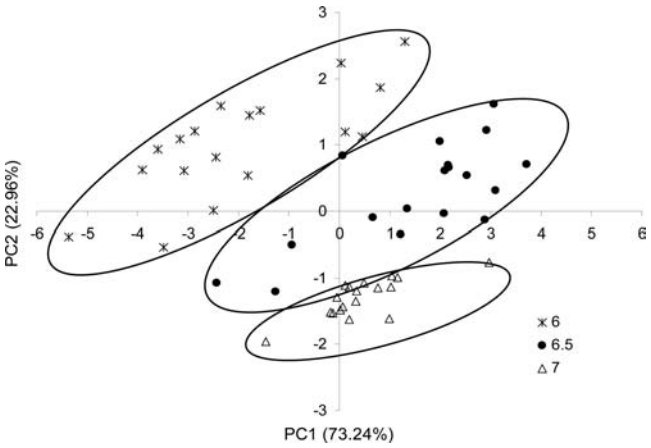

Figure 5. Principal component projection of the score plot of regular coffee (25 mL) obtained from three grinding grades (6, 6.5, and 7).

also well-discriminated, but their differences were better highlighted from the responses of the other four sensors.

DOI: 10.1021/jf505691u
J. Agric. Food Chem. 2015, 63, 2321−2327

Table 4. Maximum Intensity of Signal Sensors of EC Prepared in Different Experimental Conditions (Mean Values ± Standard Deviation)

grinding grade	sample	T30/1	P10/1	P10/2	P40/1	T70/2	PA/2
6	Ft1	0.561 ± 0.011	0.404 ± 0.014	0.553 ± 0.013	0.348 ± 0.013	0.563 ± 0.016	0.685 ± 0.016
	Ft2	0.377 ± 0.022	0.262 ± 0.013	0.398 ± 0.018	0.224 ± 0.011	0.321 ± 0.026	0.436 ± 0.029
	Ft3	0.246 ± 0.018	0.209 ± 0.008	0.312 ± 0.013	0.183 ± 0.006	0.187 ± 0.017	0.288 ± 0.021
6.5	Ft1	0.430 ± 0.015	0.286 ± 0.008	0.428 ± 0.010	0.243 ± 0.007	0.388 ± 0.019	0.493 ± 0.016
	Ft2	0.173 ± 0.011	0.175 ± 0.004	0.235 ± 0.007	0.156 ± 0.004	0.130 ± 0.009	0.189 ± 0.009
	Ft3	0.099 ± 0.006	0.156 ± 0.004	0.194 ± 0.005	0.142 ± 0.003	0.073 ± 0.004	0.121 ± 0.007
7	Ft1	0.381 ± 0.014	0.261 ± 0.010	0.383 ± 0.019	0.226 ± 0.009	0.327 ± 0.016	0.416 ± 0.023
	Ft2	0.151 ± 0.015	0.169 ± 0.005	0.200 ± 0.010	0.153 ± 0.004	0.115 ± 0.012	0.148 ± 0.012
	Ft3	0.084 ± 0.009	0.154 ± 0.005	0.170 ± 0.006	0.141 ± 0.004	0.066 ± 0.006	0.093 ± 0.006
6	regular coffee	0.453 ± 0.013	0.285 ± 0.007	0.401 ± 0.009	0.244 ± 0.006	0.424 ± 0.017	0.477 ± 0.014
6.5		0.419 ± 0.010	0.275 ± 0.006	0.396 ± 0.012	0.237 ± 0.005	0.376 ± 0.013	0.450 ± 0.016
7		0.410 ± 0.007	0.281 ± 0.005	0.402 ± 0.007	0.243 ± 0.004	0.364 ± 0.009	0.452 ± 0.009

When the three fractions of ECs prepared with the grinding grade 6.5 were considered (6.5-Ft1, 6.5-Ft2, and 6.5-Ft3), a good discrimination was observed in the direction of the sensors T30/1, P10/2, and PA/2, which gave the most important contribution for detecting significant differences in the aroma profile of these samples. Similarly, the three fractions of the samples obtained from the coarse coffee grounds (7-Ft1, 7-Ft2, and 7-Ft3) were well-discriminated from the above three sensors. These results confirmed that there is a significant change in the type and/or amount of volatiles of EC during extraction. Moreover, significant differences were also observed among the three grinding grades used for preparing coffee brews. When the grinding grade was increased for each fraction of EC (Ft1, Ft2, and Ft3), the samples were well-discriminated, proving that the use of different grinding grades may significantly modify the aromatic profile of coffee brew. Again, it is reasonable to suppose that this result was caused by a different level of extraction as a consequence of the variation in the particle size distribution of coffee grounds. Particularly, the particle sizes become smaller as the solid−liquid surface becomes greater, and as previously reported, the percolation rate is lower. Of course, the greater solid−liquid surface could have increased the amount of volatiles extracted from coffee grounds. From Figure 2, it is possible to observe that the sample 6-Ft2 cannot be discriminated from the samples 6.5-Ft1 and 7-Ft1, stating that the coffee brew extracted from 9 to 16 s using the finest coffee grounds showed a similar aromatic profile to the brews obtained during the first 8 s of extraction with the medium−coarse and coarse coffee grounds. According to our results, Clarke[48] and Andueza et al.[7] reported that the coffee brews prepared with coarse coffee grounds showed the lowest aromatic profile. Bhurmiratana et al.[49] demonstrated that the grinding of roasted coffee beans increased the surface area and, consequently, influenced the release of aromatic compounds. Again, these results support the idea that different aromatic profiles of EC may be obtained when different grinding grades are used and/or when the extraction time is not constant.

With the aim to better compare the difference in aromatic profiles among the fractions of EC and regular coffee, Figures 3 and 4 show the results of principal component analysis (PCA) for samples prepared with grinding grades of 6 and 6.5, respectively. In all cases, PC1 accounted for more than 97% of the variance of the samples, while PC2 explained a maximum of 1.93%. Considering the samples prepared with a grinding grade of 6, a clear discrimination of each of the three fractions was observed (Figure 3). Again, these differences could be a result of a dilution effect because of the progressive reduction of the chemical substances and volatiles still contained in the coffee grounds, going forward with the extraction time of coffee brew. However, the regular coffee of 25 mL seems to have an aromatic profile comparable to the second fraction of the brew collected from 9 to 16 s of extraction. This is in accordance with the above results; particularly, by considering the flow rate of 1.66 mL/s, ∼15 s is the time necessary to obtain a regular coffee of 25 mL, which is in the range of time for obtaining an EC cup with all Ft1 and part of Ft2 samples. Probably, the dilution effect produced by the addition of Ft2 to Ft1 led the regular EC to have an aromatic profile similar to the Ft2 sample only. Similarly, Nicoli et al.[15] and Severini et al.[16] observed a progressive reduction of chemical and aromatic concentrations in the consecutive fractions of EC and moka coffee.

When grinding grades of 6.5 and 7 were used for EC preparation, a good discrimination was again observed among the three different fractions of the brew. Nevertheless, by considering PC1 axis, where the maximum variance explained resides, regular coffee appeared to be practically overlapped with the Ft1 sample when using a grinding grade of 6.5 (Figure 4), while the regular coffee was slightly separated when a grinding grade of 7 was used (data not shown). Again, considering the volume of brew of 28.858 ± 2.318 and 41.847 ± 1.701 mL (Table 3) measured for grinding grades 6.5-Ft1 and 7-Ft1, respectively, it is reasonable to suppose that these fractions showed similar and lower concentrations of odor compounds, respectively, when compared to the regular coffee (25 mL). Some studies supported our results, showing that the fine grade produced a low volume of coffee brew with respect to a coarse grinding level.[6,7] In addition, Clarke and Macrae[4] reported that the brews obtained with fine-ground coffee exhibited the highest extraction of soluble solids and volatile compounds, while Andueza et al.[7] found that the particle size is inversely related to the extraction of organic acids and the sensorial aromatic perception.

In Figure 5, the results of PCA obtained by analyzing the regular coffee only achieved from different grinding levels are shown. In this case, both the PCs had a significant contribution in the discrimination of samples, with PC1 accounting for 73.24% and PC2 accounting for 22.96%. The three types of regular coffee were well-distinguished, proving that different aromatic profiles were obtained by preparing a cup of coffee of 25 mL using coffee powder with different grinding levels; nevertheless, in comparison to the difference observed among

DOI: 10.1021/jf505691u
J. Agric. Food Chem. 2015, 63, 2321−2327

each fraction, the three types of regular coffee appeared to be nearest. According to the previous results, the regular coffee prepared with fine−coarse and coarse coffee grounds contain the entire Ft1 sample and only a small part of it, respectively, while using the fine coffee grounds, the regular coffee contains both fractions Ft1 and Ft2. Under this consideration, it can be stated that the regular coffee collected the majority of odor compounds.

Table 4 shows the maximum value of the responses of each sensor to the volatiles of EC samples. A reduction of the response of all sensors as a function of the fractions of EC brew was observed for each grinding grade. As reported from several authors, the reduction of the intensity of the response of the sensors may be related to the concentration of aromatic compounds.[37,50] Similarly, the reduction observed in Table 4 for EC samples may be related to a decrease of the volatile concentration in the brew because of the dilution effect discussed above. The maximum response observed for the Ft1 samples confirmed the hypothesis that the maximum extraction of odor molecules occurs during the first few seconds of the percolation process. For all grinding levels, the reduction of sensor intensity was more pronounced from Ft1 to Ft2, while the gap between Ft2 and Ft3 appeared practically negligible. For the regular EC (25 mL), only slight variations in the response of each sensor were observed, confirming the low differences in terms of the aromatic profile, as highlighted in Figure 5.

In conclusion, the chemical attributes and aromatic profiles of EC were proven to be significantly affected by the extraction time and grinding grade of coffee powder. Particularly, the majority of organic acids, solids, and caffeine contained in the coffee grounds was extracted during the first 8 s of percolation. Also, using the electronic nose system, it was possible to prove that both extraction time and grinding level significantly affect the overall aromatic profiles of EC samples; indeed, through PCA, a high discrimination was obtained among the brew fractions and grinding levels. This result highlights the importance of making more efforts on the control of these two variables in the bar with the aim to ensure a constant aromatic quality of EC served every day.

AUTHOR INFORMATION

Corresponding Author

*Telephone: +39-0881-589222. E-mail: carla.severini@unifg.it.

Notes

The authors declare no competing financial interest.

ACKNOWLEDGMENTS

The authors gratefully acknowledge ESSSE Caffè S.p.A. for providing coffee samples. Arcangela Del Mastro and Ofelia Alessandrino (University of Foggia) are acknowledged for their support during the experiments.

REFERENCES

(1) Illy, E.; Navarini, L. Neglected food bubbles: The espresso coffee foam. *Food Biophys.* **2011**, *6*, 335−348.

(2) Illy, A.; Viani, R.; Suggi Liverani, F. *Espresso Coffee: The Science of Quality*; Elsevier Academic Press: San Diego, CA, 2005; pp 16−19.

(3) Sivetz, M.; Desrosier, N. W. *Coffee Technology*; AVI Publishing Company, Inc.: Westport, CT, 1979

(4) *Coffee, Volume 2: Technology*; Clarke, R. J., Macrae, R., Eds.; Elsevier Applied Science: London, U.K., 1987.

(5) Lerici, C. R.; Dalla Rosa, M.; Nicoli, M. C.; Severini, C. Influences of processing conditions on the properties of coffee beverage. In: *Trends in Food Processing II*; Ghee, A. H., Ed.; Institute of Food Science and Technology: Singapore, 1987; pp 94−98.

(6) Lingle, T. R. *The Coffee Brewing Handbook*; Specialty Coffee Association: Long Beach, CA, 1996.

(7) Andueza, S.; Maeztu, L.; Pascual, L.; Ibáñez, C.; de Peña, M. P.; Cid, C. Influence of extraction temperature on the final quality of espresso coffee. *J. Sci. Food Agric.* **2003**, *83*, 240−248.

(8) Andueza, S.; Maeztu, L.; Dean, B.; de Peña, M. P.; Bello, J.; Cid, C. Influence of water pressure on the final quality of Arabica espresso coffee. Application of multivariate analysis. *J. Agric. Food Chem.* **2002**, *50*, 7426−7431.

(9) Andueza, S.; de Peña, M. P.; Cid, C. Chemical and sensorial characteristics of espresso coffee as affected by grinding and torrefacto roast. *J. Agric. Food Chem.* **2003**, *51*, 7034−7039.

(10) Romani, S.; Severini, C.; Fiore, A. G. Quality of "espresso" coffee: A study performer through Italian coffee shop. *Proceedings of 20th International Conference on Coffee Science (ASIC)*; Bangalore, India, Oct 11−15, 2004.

(11) Severini, C.; Derossi, A.; De Pilli, T.; Del Mastro, A.; Alessandrino, O. Modelling espresso coffe preparation. *Proceedings of 25th International Conference of Coffee Science (ASIC)*; Armenia, Colombia, Sept 8−13, 2014.

(12) Severini, C.; Romani, S.; Cevoli, C.; Derossi, A. Quality "in cup" of espresso coffee: Data from over ten years of investigation. *Proceedings of 24th International Conference of Coffee Science (ASIC)*; San Josè, Costa Rica, Nov 11−16, 2012; pp 201−208.

(13) Caprioli, G.; Cortese, M.; Cristalli, G.; Maggi, F.; Odello, L.; Ricciutelli, M.; Sagratini, G.; Sirocchi, V.; Tomassoni, G.; Vittori, S. Optimization of espresso machine parameters through the analysis of coffee odorants by HS-SPME−GC/MS. *Food Chem.* **2012**, *135*, 1127−1133.

(14) Navarini, L.; Cappuccio, R.; Suggi-Liverani, F.; Illy, A. Espresso coffee beverage: Classification on texture terms. *J. Texture Stud.* **2004**, *35* (5), 525−541.

(15) Nicoli, M. C.; Dalla Rosa, M.; Lerici, C. R.; Severini, C. Caratteristiche chimiche dell'estratto di caffè. Nota 1: Cinetiche di estrazione della caffeina e delle sostanze solide. *Ind. Aliment.* **1987**, *26*, 467−471.

(16) Severini, C.; Mastrocola, D.; Nicoli, M. C.; Dalla Rosa, M. C. Caratteristiche chimiche dell'estratto di caffè. Nota 2: Cinetica di estrazione delle sostanze volatili. *Ind. Aliment.* **1988**, *27*, 537−540.

(17) López-Galilea, I.; Fournier, N.; Cid, C.; Guichard, E. Changes in headspace volatile concentrations of coffee brews caused by the roasting process and the brewing procedure. *J. Agric. Food Chem.* **2006**, *54*, 8560−8566.

(18) Gloess, A. N.; Schonbachler, B.; Klopprogge, B.; D'Ambrosio, L.; Chatelain, K.; Bongartz, A.; Strittmatter, A.; Rast, M.; Yeretzian, C. Comparison of nine common coffee extraction methods: Instrumental and sensory analysis. *Eur. Food Res. Technol.* **2013**, *236*, 607−627.

(19) Sunarharum, W. B.; Williams, D. J.; Smyth, H. E. Review. Complexity of coffee flavor: A compositional and sensory perspective. *Food Res. Int.* **2014**, *62*, 315−325.

(20) Mestdagh, F.; Davide, T.; Chaumonteuil, M.; Folmer, B.; Blank, I. The kinetics of coffee aroma extraction. *Food Res. Int.* **2014**, *63*, 271−274.

(21) Maeztu, L.; Sanz, C.; Andueza, S.; Paz, M. P. D.; Bello, J.; Cid, C. Characterization of espresso coffee aroma by static headspace GC−MS and sensory flavor profile. *J. Agric. Food Chem.* **2001**, *49* (11), 5437−5444.

(22) Sanz, C.; Maeztu, L.; Zapelena, M. J.; Bello, J.; Cid, C. Profiles of volatile compounds and sensory analysis of three blends of coffee: Influence of different proportions of Arabica and Robusta and influence of roasting coffee with sugar. *J. Sci. Food Agric.* **2003**, *82*, 840−847.

(23) Huang, L. F.; Wu, M. J.; Zhong, K. J.; Sun, X. J.; Liang, Y. Z.; Dai, Y. H.; Huang, K. L.; Guo, F. Q. Fingerprint developing of coffee

DOI: 10.1021/jf505691u
J. Agric. Food Chem. 2015, 63, 2321−2327

flavor by gas chromatography−mass spectrometry and combined chemometrics methods. *Anal. Chim. Acta* **2007**, *588*, 216−223.
(24) Michisita, T.; Akiyama, M.; Hirano, Y.; Ikeda, M.; Sagara, Y.; Araki, T. Gas chromatography/olfactometry and electronic nose analyses of retronasal aroma of espresso and correlation with sensory evaluation by artificial neural network. *J. Food Sci.* **2010**, *75*, S477−89.
(25) Peris, M.; Escuder-Gilabert, L. A 21st century technique for food control: Electronic noses. *Anal. Chim. Acta* **2009**, *638*, 1−15.
(26) Nagle, H. T. The how and why of electronic noses. *IEEE Spectrum* **1998**, 22−33.
(27) Shilbayeh, N.; Iskandarani, M. Discrimination of perfumes using an electronic nose system. *WSEAS Trans. Circuits Syst.* **2003**, *2* (4), 820−825.
(28) Loutfi, A.; Coradeschi, S.; Mani, G. K.; Shankar, P.; Rayappan, J. B. B. Electronic noses for food quality: A review. *J. Food Eng.* **2015**, *144*, 103−111.
(29) Pearce, T. C.; Schiffman, S. S.; Nagle, H. T.; Gardner, J. W. *Handbook of Machine Olfaction: Electronic Nose Technology*; Wiley-VCH Verlag GmbH & Co. KGaA: Weinheim, Germany, 2003.
(30) Berna, A. Review. Metal oxides sensors for electronic noses and their application to food analysis. *Sensors* **2010**, *10*, 3882−3910.
(31) Aishima, T. Aroma discrimination by pattern recognition analysis of responses from semiconductor gas sensor array. *J. Agric. Food Chem.* **1991**, *39*, 752−756.
(32) Pornpanomchai, C.; Jurangboon, K.; Jantarasee, K. Instant coffee classification by electronic noses. *Proceedings of the 2nd International Conference on Mechanical and Electronics Engineering (ICMEE)*; Kyoto, Japan, Aug 1−3, 2010; Vol. *1*, pp 10−13.
(33) Ulmer, H.; Mitrovics, J.; Noetzel, G.; Wiemar, U.; Gopel, W. Odours and flavours identified with hybrid modular sensor systems. *Sens. Actuators, B* **1992**, *43*, 24−33.
(34) Gardner, W. J.; Shurmer, H. V.; Tan, T. T. Application of an electronic nose to the discrimination of coffees. *Sens. Actuators, B* **1992**, *6*, 71−75.
(35) Tan, T. T.; Loubet, F.; Labreche, S.; Amine, H. Quality control of coffee using the FOX4000 electronic nose. *Proceedings of the IEEE International Symposium on Industrial Electronics (ISIE'97)*; Guimaraes, Portugal, July 7−11, 1997; pp 140−145.
(36) Pardo, M.; Sberveglieri, G. Coffee analysis with an electronic nose. *IEEE Trans. Instrum. Meas.* **2002**, *51*, 1334−1339.
(37) Shilbayeh, N.; Iskandarani, M. Z. Quality control of coffee using an electronic nose system. *Am. J. Appl. Sci.* **2004**, *1*, 129−35.
(38) Falasconi, M.; Pardo, M.; Sberveglieri, G.; Riccò, I.; Bresciani, A. The novel EOS^{835} electronic nose and data analysis for evaluating coffee ripening. *Sens. Actuators, B* **2005**, *110*, 73−80.
(39) Rodriguez, J.; Durán, C.; Reyes, A. Electronic nose for quality control of Colombian coffee through the detection of defects in "cup tests". *Sensors* **2010**, *10*, 36−46.
(40) Falasconi, M.; Pardo, M.; Sberveglieri, G.; Nardini, F.; Della, T.; Bresciani, A. The novel EOS^{835} electronic nose sniffs out the Italian espresso coffee quality. *Proc. IEEE Sens. 2003, IEEE Int. Conf. Sens., 2nd* **2003**, 26−29.
(41) Pardo, M.; Niederjaufner, G.; Benussi, G.; Comini, E.; Faglia, G.; Sberveglieri, G.; Holmberg, M.; Lundstrom, I. Data preprocessing enhances the classification of different brands of espresso coffee with an electronic nose. *Sens. Actuators, B* **2000**, *69*, 397−403.
(42) Petracco, M. Technology IV: Beverage preparation: Brewing trends for the new millennium. In *Coffee Recent Developments*; Clarke, R. J., Vitzthum, O. G., Eds.; Blackwell Science: Oxford, U.K., 2001; pp 140−164.
(43) Gloess, A. N.; Vietri, A.; Wieland, F.; Smrke, S.; Schönbächler, B.; Sánchez López, J. A.; Petrozzi, S.; Bongers, S.; Koziorowski, T.; Yeretzian, C. Evidence of different flavour formation dynamics by roasting coffee from different origins: On-line analysis with PTR-ToF-MS. *Int. J. Mass Spectrom.* **2014**, *365−366*, 324−337.
(44) AOAC International. *Official Method 968.11 Moisture (Loss on Drying in Roasted Coffee. Vaccum Oven Method 1)*, 17th ed.; AOAC International: Rockville, MD, 2000.
(45) Skoog, D. A.; Holler, F. J.; Crouch, S. R. Determination of caffeine in beverages by high performance liquid chromatography. *Principles of Instrumental Analysis*, 6th ed.; Harcourt Brace College Publishers: Orlando, FL, 2007; Chapters 26 and 28.
(46) Parenti, A.; Guerrini, L.; Masella, P.; Spinelli, S.; Calamai, L.; Spugnoli, P. Comparison of espresso coffee brewing techniques. *J. Food Eng.* **2014**, *121*, 112−117.
(47) Caporaso, N.; Genovese, A.; Canela, M. D.; Civitella, A.; Sacchi, R. Neapolitan coffee brew chemical analysis in comparison to espresso, moka and American brews. *Food Res. Int.* **2014**, *61*, 152−160.
(48) Clarke, R. J. Extraction. In *Coffee, Volume 2: Technology*; Clarke, R. J., Macrae, R., Eds.; Elsevier Applied Science: London, U.K., 1987; pp 109−144.
(49) Bhumiratana, N.; Adhikari, K.; Chambers, E., IV. Evolution of sensory aroma attributes from coffee beans to brewed coffee. *LWT—Food Sci. Technol.* **2011**, *44*, 2185−2192.
(50) Iskandarani, M. A.; Shilbayeh, N. F. Design and analysis of a smart multi purpose electronic nose system. *J. Computer Sci.* **2005**, *1* (1), 63−71.

DOI: 10.1021/jf505691u
J. Agric. Food Chem. 2015, 63, 2321−2327

addition, no studies investigating this treatment on Tempranillo grapevines have been found. Tempranillo is the most cultivated red grape variety in Spain, accounting for around 21.5% of the total wine-growing surface in 2011. Moreover, it is the dominant red grape variety in Spanish aged wines. Therefore, improving its phenolic content would be of enological interest in order to enhance its aging potential. According to the literature, all the experiments conducted under vineyard conditions investigated the effect of direct applications of MeJ to clusters. Cluster application requires a previous defoliation in order to achieve correct distribution of the applied product. In contrast, foliar application is a costless and easier technique due to the fact that a previous defoliation is not required. Therefore, the aim of this paper was to evaluate the influence of MeJ foliar application to Tempranillo grapevines on grape and wine phenolic composition.

MATERIALS AND METHODS

Reagents and Standards. All solvents (methanol, acetonitrile, and formic acid) were of HPLC quality, and all chemicals were analytical grade (>99%) unless otherwise stated and were purchased from Panreac (Barcelona, Spain). Water was of Milli-Q quality (Millipore, Bedford, MA). Methyl jasmonate and Tween 80 were purchased from Sigma−Aldrich (Madrid, Spain). Trolox (6-hydroxy-2,5,7,8-tetramethylchroman-2-carboxylic acid) and DPPH radical (diphenyl-1-picrylhydracyl) were purchased from Fluka Chemie (Buchs, Switzerland). Folin−Ciocalteu reagent was purchased from Merck (Darmstadt, Germany). The following commercial standards were purchased from Sigma−Aldrich: (−)-epicatechin, (+)-catechin, rutin, quercetin, quercetin 3-*O*-glucoside, quercetin 3-*O*-galactoside, kaempferol, myricetin, piceatannol, *trans*-resveratrol, *trans*-piceid, gallic acid, protocatechuic acid, caffeic acid, *p*-coumaric acid, ferulic acid, and caftaric acid. Malvidin 3-*O*-glucoside was purchased from Extrasynthèse (Genay, France).

Plant Material, Foliar Treatments, and Vinification. The study was conducted in 2013 in the experimental vineyard of La Grajera, located in the northern region of La Rioja (Spain). Vines were grafted onto R-110 rootstock and the vineyard was managed under a conventional soil tillage management system. The soil was classified as Typic Calcixerept according to the American Soil Taxonomy. In 2013, the annual precipitation was 569.3 mm, and the average annual temperature was 17.7 °C. Methyl jasmonate (MeJ) was applied to Tempranillo (*Vitis vinifera* L.) grapevines. To carry out the treatments, aqueous solutions at a concentration of 10 mM MeJ were prepared with Tween 80 as wetting agent (0.1% v/v). Control plants were sprayed with aqueous solution of Tween 80 alone. The applications of MeJ and control were carried out twice, at veraison and 1 week later. For each application, 200 mL/plant were sprayed over leaves. Treatments were carried out in triplicate with three vines for each replicate and arranged in a randomized block design.

Grapes were harvested at their optimum technological maturity. From each treatment, about 150 berries were separated and frozen at −20 °C in order to determine their monomeric phenolic composition. Grapes were destemmed and crushed, and oenological parameters were determined in the musts.

The alcoholic fermentation was performed following the method described by Sampaio et al.[24] Grapes from each replicate (group of three plants) were elaborated separately. Three kilograms of pomace (must, seed, and skin) was introduced into 4 L glass bottles. Potassium metabisulfite was added to the samples to give a final total SO_2 concentration of 50 mg/L, and then the must was inoculated with commercial *Saccharomyces cerevisiae* strain Uvaferm VRB (Lallemand, St. Simon, France) (25 g/hL). The must was fermented at a controlled temperature of 25 °C. The end of the alcoholic fermentation was determined by measuring the reducing sugars. Wine enological parameters were then analyzed and aliquots of each wine were frozen and stored at −20 °C until analyses of monomeric phenolic compounds were carried out.

Enological Parameters of Musts and Wines. °Brix was determined by refractometry, pH, total acidity, malic acid, and potassium were determined in musts according to ECC official methods,[25] while tartaric acid was determined following the Rebelein method.[26] Wines were characterized by determining alcoholic degree, pH, total acidity, malic acid, lactic acid, volatile acidity, hue, color intensity (CI), and Folin−Ciocalteu index (FCI) according to ECC official methods[25] and tartaric acid by the Rebelein method.[26] Total phenolics were determined as total polyphenol index (TPI) by spectrophotometric absorbance at 280 nm after previous dilution of samples.[27] Total anthocyanins were determined by bleaching with sulfur dioxide,[27] and total tannins were determined following the method described by Ribéreau-Gayon et al.[28] Ionized anthocyanins were determined according to Glories,[29] and polymerization index was calculated according to Ruiz.[30]

Field treatments were performed in triplicate and a wine was made from each replicate, so the results of these enological parameters are the average of analyses of three samples (n = 3).

Determination of Total Antioxidant Activity in Wines. Total antioxidant activity in wines was determined according to the DPPH method, which evaluates the radical-scavenging activity of the sample.[31] The analysis was performed following the methodology described by Nixdorf and Hermosín-Gutiérrez.[32] Briefly, 100 μL of wine, previously diluted 5% (v/v) in methanol, were added to 2.9 mL of a 0.06 mM DPPH methanolic solution. The percentage absorbance decrease was measured after 25 min at 515 nm. Results were compared to a Trolox calibration curve set for the range of 0.10−0.80 mM. Results were expressed as millimoles of Trolox equivalents per liter of wine (mmol of TE/L).

Determination of Grape and Wine Low-Molecular-Weight Phenolic Compounds. *Extraction of Grape Phenolics.* Grape phenolic compounds were extracted according to the following method. About 50 g of each frozen grape sample was weighed and immersed into 50 mL of aqueous methanol solution (50% v/v), and the pH of the solvent was adjusted to pH 2 with formic acid (>96%). Grapes were then homogenized by Ultra-Turrax T-18 (IKA, Staufen, Germany) at high speed (18 000 rpm) for 1 min, producing a smooth paste. Then samples were macerated in an ultrasonic bath (JP Selecta, Barcelona, Spain) for 10 min and were centrifuged at 5000 rpm at 10 °C for 10 min. A second extraction of the resulting pellets was completed with the same volume of the solvent mixture (50 mL). The supernatants were combined and the volume was annotated. Each sample was transferred to vials and stored at −20 °C until HPLC analyses were carried out.

Sample Preparation for Analysis of Non-Anthocyanin Phenolic Compounds. Due to the fact that anthocyanins are present in high quantities in red grape and wine, other phenolic compounds might be masked during the chromatographic separation and identification. An extraction on PCX solid-phase extraction (SPE) cartridges (500 mg, 6 mL; Bond Elut Plexa, Agilent, Palo Alto, CA) containing a mixture of reverse-phase and cation-exchanger materials allowed the isolation of non-anthocyanin phenolic compounds. Cartridges were placed in the extraction system (Vac Elut 20 station from Varian, Palo Alto, CA). The separation was achieved following the method proposed by Castillo-Muñoz et al.[33] First, grape extracts (3 mL) were diluted with 9 mL of 0.1 N HCl. In the case of wine samples, 3 mL of wine were diluted with 3 mL of 0.1 N HCL. The PCX SPE cartridges were previously conditioned with 5 mL of methanol and 5 mL of water. Then diluted samples were passed through the PCX SPE cartridges and a washing step was carried out with 5 mL of 0.1 N HCl and 5 mL of water. The non-anthocyanin phenolic compound fraction was eluted with 3 × 5 mL of methanol. Adsorbed anthocyanins were removed by passing 2 × 5 mL of 2% ammonia in 80% methanol, then 3 × 5 mL of 2% hydrochloric acid in 80% methanol and finally 5 mL of water. The latter step also regenerates the cationic exchange sites for reuse of the cartridges. The non-anthocyanin phenolic compound fraction was dried in a rotary evaporator (35 °C) and resolved in 1.5 mL of 20% (v/v) aqueous methanol solution. The anthocyanin-free fraction was used to analyze non-anthocyanin phenolic compounds

DOI: 10.1021/jf5060672
J. Agric. Food Chem. 2015, 63, 2328−2337

(flavonols, hydroxycinnamic and hydroxybenzoic acids, stilbenes, and flavan-3-ols).

Analysis of Phenolic Compounds by HPLC-DAD. Phenolic compounds were analyzed by reverse-phase HPLC on an Agilent 1260 Infinity chromatograph, equipped with a diode-array detector (DAD) coupled to an Agilent Chem Station. Injection of samples was carried out after filtration (0.22 μm, Easyprep, Quebec, Canada). Separation was achieved on a LiCrospher 100 RP-18 reversed-phase column (250 × 4.0 mm; 5 μm packing; Agilent) with precolumn LiChrospher 100 RP-18 (4 × 4 mm; 5 μm packing; Agilent), both thermostated at 40 °C. A flow rate of 0.63 mL/min was established.

Chromatographic Conditions. Chromatographic conditions were based on Castillo-Muñoz et al.[34] In the case of anthocyanin analysis, 10 μL of sample (grape extract or wine) was injected. Eluents used were (A) acetonitrile/water/formic acid (3:88.5:8.5 v/v/v) and (B) acetonitrile/water/formic acid (50:41.5:8.5 v/v/v). The linear solvents' gradient for anthocyanin analysis was as follows: 0 min, 6% B; 15 min, 30% B; 30 min, 50% B; 35 min, 60% B; 38 min, 60% B; 46 min, 6% B. For analysis of non-anthocyanin phenolic compound fractions, the injection volume was 20 μL. Eluents were (A) acetonitrile/water/formic acid (3:88.5:8.5 v/v/v), (B) acetonitrile/water/formic acid (50:41.5:8.5 v/v/v), and (C) methanol/water/formic acid (90:1.5:8.5 v/v/v). The linear solvents' gradient for non-anthocyanin analysis was as follows: 0 min, 4% B and 0% C; 7 min, 4% B and 0% C; 38 min, 17% B and 13% C; 52 min, 30% B and 20% C; 52.5 min, 40% B and 30% C; 57 min, 50% B and 50% C; 58 min, 50% B and 50% C; 65 min, 4% B and 0% C.

Identification of phenolic compounds was carried out according to retention times of pure compounds and UV−vis data obtained from authentic standards and/or published in previous studies.[34,35] Phenolic compounds were quantified according to the DAD chromatograms recorded at 520 nm (anthocyanins), 360 nm (flavonols), 320 nm (hydroxybenzoic and hydroxycinnamic acids and stilbenes), and 280 nm (flavanols) and calibration graphs of the respective standards ($R^2 > 0.999$). When a standard was not available, quantification was made according to the calibration graph of the most similar compound. Hence, malvidin 3-*O*-glucoside was used for anthocyanins, quercetin 3-*O*-glucoside was used for flavonols, *trans*-caftaric acid was used for free hydroxycinnamic acids and the corresponding tartaric esters, catechin was used for procyanidins B1 and B2, epicatechin was used for epigallocatechin, and *trans*-piceid and *trans*-resveratrol were used for their respective *cis* isomers. Concentrations in grape samples were expressed as milligrams per weight of grape (mg/kg) while concentrations in wines were expressed as milligrams per liter of wine (mg/L).

Field treatments were performed in triplicate and a wine was made from each replicate, so results for phenolic compounds correspond to the average of analyses of three samples ($n = 3$).

Statistical Analysis. Statistical procedures were performed with SPSS version 21.0 statistical package for Windows (Chicago, IL). Data for the different determinations were processed by analysis of variance (ANOVA). Significant differences between means were determined by use of the Duncan test at $p \leq 0.05$.

RESULTS AND DISCUSSION

Enological Parameters. Results for grape enological parameters are summarized in Table 1. All samples presented normal values of these parameters for Tempranillo grapes from La Rioja.[36] No significant differences were found between control grapes and those from grapevines foliar treated with MeJ. Ruiz-García et al.[37] studied the application of MeJ at the same concentration as our study on clusters from different clones of Monastrell and observed that, in general, grapes from the MeJ treatment were very similar to the control grapes. Moreover, in a 2-year study in which Monastrell clusters were sprayed with the same dose of MeJ, the authors observed that the effect on total acidity, pH, and tartaric and malic acid content varied from one year to another.[22] The latter finding might suggest that the influence of MeJ application on grape physicochemical parameters could therefore depend on climatic conditions as well.

Table 1. Enological Parameters of Grape Berries from Control Grapevines and from Grapevines Treated with Methyl Jasmonate[a]

	control	MeJ-treated
weight of 100 berries (g)	232 ± 25 a	225 ± 5 a
°Brix	23.2 ± 0.8 a	22.3 ± 0.3 a
pH	3.30 ± 0.02 a	3.33 ± 0.04 a
total acidity[b] (g/L)	8.42 ± 0.19 a	8.53 ± 0.40 a
tartaric acid (g/L)	6.16 ± 0.11 a	6.23 ± 0.03 a
malic acid (g/L)	4.26 ± 0.36 a	4.40 ± 0.28 a
potassium (mg/L)	1635 ± 110 a	1583 ± 58 a

[a]Since the treatments were performed in triplicate, all parameters are listed with their standard deviation ($n = 3$). For each row, values with the same letters are not significantly different between the samples ($p \leq 0.05$). [b]As grams of tartaric acid per liter.

Physicochemical parameters of wines are shown in Table 2. All wines presented values within the usual ranges reported for young Tempranillo red wines from La Rioja region.[38] Significant differences between control wines and wines obtained from treated grapevines appeared to be related to phenolic composition. Control wines showed lower color intensity (CI) than wines from MeJ treatment. This result could be explained by a higher proportion of ionized anthocyanins in MeJ-treated wines than in control ones (Table 2). In this respect, this parameter is correlated with colored anthocyanin content. Moreover, the values obtained for Folin−Ciocalteu index (FCI) were higher in the case of wines from MeJ-treated grapevines than in control wines, suggesting that those wines had a greater phenolic content. In accordance with our results, Ruiz-García et al.[22] found that application of

Table 2. Enological Parameters and Total Antioxidant Activity of Control Wine and Wine Made from Grapevines Treated with Methyl Jasmonate[a]

	control	MeJ-treated
alcoholic degree (% v/v)	13.4 ± 0.6 a	12.7 ± 0.0 a
pH	3.69 ± 0.08 a	3.63 ± 0.08 a
total acidity[b] (g/L)	7.50 ± 0.04 a	7.45 ± 0.29 a
tartaric acid (g/L)	1.95 ± 0.13 a	1.98 ± 0.01 a
malic acid (g/L)	3.82 ± 0.15 a	3.95 ± 0.23 a
lactic acid[c] (g/L)	0.05 ± 0.03 a	0.09 ± 0.00 a
volatile acidity (g/L)	0.26 ± 0.09 a	0.18 ± 0.04 a
hue	0.50 ± 0.03 a	0.44 ± 0.01 a
color intensity (CI)	11.54 ± 0.46 a	15.66 ± 0.42 b
Folin−Ciocalteu index	43.3 ± 2.3 a	50.7 ± 0.6 b
total polyphenol index (TPI)	51.86 ± 3.20 a	59.71 ± 2.50 a
total anthocyanins (mg/L)	992 ± 77 a	1122 ± 82 a
ionized anthocyanins (mg/L)	216 ± 15 a	306 ± 17 b
total tannins (mg/mL)	2.50 ± 0.28 a	3.57 ± 0.64 a
polymerization index	1.33 ± 0.09 a	1.62 ± 0.10 b
total antioxidant activity[d] (mmol of TE/L)	5.60 ± 0.34 a	5.89 ± 0.19 a

[a]Since the treatments were performed in triplicate, all parameters are listed with their standard deviation ($n = 3$). For each row, values with different letters are significantly different between the samples ($p \leq 0.05$). [b]As grams of tartaric acid per liter. [c]As grams of acetic acid per liter. [d]As millimoles of Trolox equivalents per liter of wine.

DOI: 10.1021/jf5060672
J. Agric. Food Chem. 2015, 63, 2328−2337

Table 3. Individual Anthocyanin Content in Tempranillo Grape Berries and Wines from Control Grapevines and from Grapevines Treated with Methyl Jasmonate[a]

	anthocyanin content			
	grape berries (mg/kg)		wines (mg/L)	
	control	MeJ-treated	control	MeJ-treated
delphinidin 3-glc	256.94 ± 27.77 a	324.98 ± 20.85 a	57.80 ± 8.67 a	87.21 ± 5.44 b
cyanidin 3-glc	84.28 ± 26.65 a	142.75 ± 15.07 a	7.03 ± 2.34 a	12.66 ± 1.20 a
petunidin 3-glc	164.80 ± 8.63 a	197.27 ± 1.24 b	63.22 ± 8.01 a	83.19 ± 0.09 b
peonidin 3-glc	115.37 ± 23.96 a	180.74 ± 1.32 b	25.11 ± 6.37 a	41.77 ± 0.73 b
malvidin 3-glc	342.44 ± 38.68 a	364.48 ± 39.13 a	210.18 ± 19.92 a	228.15 ± 14.81 a
delphinidin 3-acglc	4.49 ± 0.10 a	4.68 ± 0.58 a	5.37 ± 0.70 a	6.31 ± 0.00 a
cyanidin 3-acglc	0.83 ± 0.17 a	1.19 ± 0.06 a	0.23 ± 0.01 a	0.21 ± 0.00 a
petunidin 3-acglc	2.85 ± 0.26 a	2.94 ± 0.52 a	2.86 ± 0.24 a	3.19 ± 0.11 a
peonidin 3-acglc	0.20 ± 0.06 a	0.16 ± 0.06 a	0.79 ± 0.15 a	1.10 ± 0.04 a
malvidin 3-acglc	5.82 ± 1.56 a	5.12 ± 1.18 a	6.72 ± 1.38 a	6.39 ± 0.54 a
delphinidin 3-cmglc	24.37 ± 2.11 a	26.36 ± 1.92 a	6.90 ± 1.38 a	9.02 ± 1.05 a
cyanidin 3-cmglc	7.99 ± 1.27 a	11.70 ± 0.47 b	2.34 ± 0.38 a	4.16 ± 0.40 b
petunidin 3-cmglc	15.49 ± 2.82 a	15.67 ± 1.78 a	5.54 ± 1.20 a	6.65 ± 0.28 a
peonidin 3-cmglc	11.85 ± 1.51 a	15.88 ± 0.28 b	4.66 ± 0.84 a	7.41 ± 0.21 b
malvidin 3-*cis*-cmglc	0.97 ± 0.51 a	0.79 ± 0.13 a	0.46 ± 0.15 a	0.41 ± 0.01 a
malvidin 3-*trans*-cmglc	42.64 ± 14.34 a	37.95 ± 6.41 a	21.08 ± 6.82 a	21.47 ± 1.15 a
malvidin 3-cfglc	0.48 ± 0.16 a	0.31 ± 0.15 a	0.20 ± 0.07 a	0.23 ± 0.06 a
total anthocyanins	1082 ± 34 a	1333 ± 15 b	420 ± 40 a	520 ± 7 b
vitisin A			1.57 ± 0.20 a	1.59 ± 0.28 a
vitisin B			1.47 ± 0.09 a	1.68 ± 0.02 b

[a]Nomenclature abbreviations: glc, glucoside; acglc, acetylglucoside; cmglc, *trans-p*-coumaroylglucoside; cfglc, caffeoylglucoside. Since the treatments were performed in triplicate, all parameters are listed with their standard deviation ($n = 3$). For each row, values with different letters are significantly different between the samples ($p \leq 0.05$).

MeJ to Monastrell clusters led to wines with better chromatic characteristics [i.e., higher total anthocyanin content, total phenol index (TPI), and CI]. The same research group found that the application of MeJ together with another elicitor (benzothiadiazole) led to wines with higher TPI and CI.[39] Moreover, Fernández-Marín et al.[21] showed that application of MeJ to Syrah clusters resulted in darker wines with higher anthocyanin content at press moment, although no differences were found after bottling. On another note, our results showed that polymerization index in wine increased with the application of MeJ to grapevine (Table 2). This parameter measures the stability of anthocyanins against sulfur dioxide, providing information about anthocyanin polymerization and thus wine color stability.[30] In this respect, the results suggest that greater color stability could be found in wines made from grapevines treated with MeJ. For the remaining parameters, no significant differences were found between the samples. Indeed, no significant differences were observed regarding total antioxidant activity estimated by the DPPH assay. In contrast, Ruiz-García et al.[39] observed that wine antioxidant capacity, estimated by 2,2′-azinobis(3-ethylbenzothiazoline-6-sulfonic acid) (ABTS) assay, increased with application of a combination of MeJ and benzothiadiazole.

Effects of Methyl Jasmonate Foliar Application. *Anthocyanin Compounds.* The HPLC analysis identified 17 anthocyanins in grape samples (Table 3). The 3-*O*-glucosides (3-glc) of delphinidin, cyanidin, petunidin, peonidin, and malvidin were identified, together with their acetyl (3-acglc) and *trans-p*-coumaroyl (3-cmglc) derivatives. In addition, *cis-p*-coumaroyl (*cis*-3-cmglc) and caffeoyl derivatives (3-cfglc) of malvidin were also identified. The concentrations of individual anthocyanins found in all samples were within the ranges described for Tempranillo grapes in previous studies.[40,41] Thus, malvidin 3-*O*-glucoside and its derivatives were the dominant anthocyanin type in all samples, accounting for 40% of total anthocyanins. Nonacylated anthocyanins represented around 90% of all anthocyanins. Among acylated anthocyanins, *p*-coumaroyl derivatives were dominant (87% of all acylated anthocyanins), which is typical for this grape variety.[40]

Foliar application of MeJ to grapevine led to a significant enhancement of anthocyanin synthesis by the plant. Consequently, grapes from this treatment showed higher content of 3-*O*-glucosides of petunidin and peonidin and *trans-p*-coumaroyl derivatives of cyanidin and peonidin (Table 3). Total anthocyanin concentration, calculated as the sum of individual anthocyanin contents, was increased 23% due to foliar treatment. The improvement of anthocyanin content seems to be an expected outcome from MeJ application, as it has been reported in previous studies. In this respect, Ruiz-García et al.[22] observed that application of MeJ to Monastrell clusters led to increases of around 16% of total anthocyanin content. In a recent study, application of the same dose of MeJ to different clones of Monastrell also resulted in an increase of anthocyanin content in most of the clones.[37] Similar results were reported by Fernández-Marín et al.,[21] who treated clusters of Syrah with MeJ and found that total anthocyanin content

DOI: 10.1021/jf5060672
J. Agric. Food Chem. 2015, 63, 2328−2337

Table 4. Individual Flavonol Content in Tempranillo Grape Berries and Wines from Control Grapevines and from Grapevines Treated with Methyl Jasmonate[a]

	flavonol content			
	grape berries (mg/kg)		wines (mg/L)	
	control	MeJ-treated	control	MeJ-treated
myricetin 3-glcU	1.59 ± 0.33 a	2.20 ± 0.77 a	1.54 ± 0.16 a	1.91 ± 0.05 a
myricetin 3-gal	0.72 ± 0.43 a	0.87 ± 0.11 a		
myricetin 3-glc	18.76 ± 2.68 a	22.63 ± 0.01 a	13.38 ± 2.28 a	17.90 ± 0.04 a
quercetin 3-gal	0.57 ± 0.29 a	1.01 ± 0.46 a		
quercetin 3-glcU	4.60 ± 1.30 a	6.43 ± 2.76 a	2.45 ± 0.46 a	3.63 ± 0.81 a
quercetin 3-glc	6.20 ± 1.31 a	11.13 ± 3.03 a	3.00 ± 0.31 a	6.55 ± 1.17 b
quercetin 3-rut	0.39 ± 0.13 a	0.52 ± 0.33 a		
laricitrin 3-glc	2.03 ± 0.63 a	2.30 ± 0.15 a	1.09 ± 0.11 a	1.23 ± 0.12 a
kaempferol 3-gal	0.18 ± 0.06 a	0.34 ± 0.17 a		
kaempferol 3-glcU	0.16 ± 0.04 a	0.20 ± 0.01 a		
kaempferol 3-glc	0.77 ± 0.40 a	1.61 ± 0.80 a	0.03 ± 0.03 a	0.16 ± 0.02 b
isorhamnetin 3-gal	0.11 ± 0.03 a	0.13 ± 0.02 a		
isorhamnetin 3-glc	0.40 ± 0.10 a	0.80 ± 0.18 b	0.22 ± 0.04 a	0.39 ± 0.01 b
syringetin 3-glc	0.71 ± 0.23 a	0.89 ± 0.00 a	0.81 ± 0.13 a	0.92 ± 0.14 a
free myricetin			4.77 ± 0.45 a	5.91 ± 0.00 b
free quercetin			2.52 ± 0.21 a	2.86 ± 0.41 a
free laricitrin			0.10 ± 0.01 a	0.10 ± 0.01 a
free kaempferol			0.33 ± 0.04 a	0.48 ± 0.08 a
free isorhamnetin			0.19 ± 0.01 a	0.19 ± 0.001 a
free syringetin			0.11 ± 0.03 a	0.20 ± 0.05 a
total flavonols	37.19 ± 7.34 a	51.06 ± 8.26 a	30.54 ± 2.59 a	42.42 ± 0.11 b

[a]Nomenclature abbreviations: glcU, glucuronide; gal, galactoside; glc, glucoside; rut, rutinoside. Since the treatments were performed in triplicate, all parameters are listed with their standard deviation ($n = 3$). For each row, values with different letters are significantly different between the samples ($p \leq 0.05$).

was increased 11% in comparison with control grapes. Moreover, induction of anthocyanin synthesis has also been observed in cell cultures of *V. vinifera* cv. Gamay Fréaux[20] and in studies in which MeJ was applied in combination with another elicitor, benzothiadiazole,[39] as well as in different works with other fruits such as raspberry[17] or apple.[18] Enhancement of anthocyanin synthesis seems to be explained by the accumulation of different enzymes involved in the phenylpropanoid pathway.[19] In this sense, it has been reported that grapevines may respond to MeJ application by activating gene expression of enzymes responsible for phenolic biosynthesis such as phenylalanine ammonia lyase, chalcone synthase, stilbene synthase, UDP-glucose:flavonoid-*O*-transferase, proteinase inhibitors, and chitinase, with subsequent accumulation of anthocyanins and stilbenes in grapevine cell cultures.[20]

Regarding wine analysis, in addition to the 17 anthocyanins found in grapes, two pyranoanthocyanins, vitisins A and B, were identified (Table 3). Formation of the latter compounds occurs during alcoholic fermentation by reaction of malvidin 3-*O*-glucoside with pyruvic acid (vitisin A) or with acetaldehyde (vitisin B).[42] Similarly to grape analysis, malvidin derivatives were the most abundant type of anthocyanin, and *p*-coumaroyl anthocyanins were the dominant acylated form.

Higher anthocyanin levels found in grapes from MeJ treatment were reflected in the corresponding wines (Table 3). Thus, wines made from treated grapevines exhibited higher content of 3-*O*-glucosides of delphinidin, petunidin, and peonidin and higher content of *trans*-*p*-coumaroyl 3-*O*-glucosides of cyanidin and peonidin, as well as vitisin B. Furthermore, total anthocyanin content in wines from MeJ treatment increased 24% with respect to control wine. The latter finding is partly in contrast with results obtained with spectrophotometric measurement of total anthocyanins in wine (Table 2). That measure revealed no significant differences between the samples even though a higher value (around 13%) was found in MeJ wines. Ruiz-García et al.[22] also observed discrepancies between HPLC and spectrophotometric analyses regarding anthocyanin concentration. These authors suggested that differences between the two analyses were explained by the analytical method. In any case, other analysis related to wine color (i.e., CI and ionized anthocyanin content) showed higher values for MeJ wines than for control wines. Moreover, results of individual analyses of wine anthocyanins are also in accordance with those obtained in the analysis of grapes (Table 3) showing a similar increase in total anthocyanin content. Ruiz-García et al.[22] also found that MeJ application improved wine total anthocyanin content determined by HPLC.

Anthocyanins play an important role in grape and wine quality since they are the main compounds responsible for red

DOI: 10.1021/jf5060672
J. Agric. Food Chem. 2015, 63, 2328−2337

Table 5. Individual Flavanol Content in Tempranillo Grape Berries and Wines from Control Grapevines and from Grapevines Treated with Methyl Jasmonate[a]

	flavanol content			
	grape berries (mg/kg)		wines (mg/L)	
	control	MeJ-treated	control	MeJ-treated
procyanidin B1	13.95 ± 2.95 a	15.49 ± 0.25 a	13.16 ± 1.93 a	17.84 ± 0.78 a
epigallocatechin	1.39 ± 0.49 a	1.06 ± 0.15 a	12.16 ± 0.97 a	12.51 ± 1.66 a
catechin	65.51 ± 2.40 a	66.43 ± 14.40 a	43.90 ± 3.00 a	46.23 ± 4.60 a
procyanidin B2	17.58 ± 2.57 a	16.47 ± 1.58 a	6.60 ± 1.47 a	6.86 ± 0.40 a
epicatechin	34.75 ± 2.69 a	34.51 ± 3.88 a	18.60 ± 2.21 a	19.69 ± 0.12 a
epicatechin 3-gallate	9.61 ± 0.97 a	10.52 ± 0.69 a	0.38 ± 0.23 a	0.72 ± 0.33 a
total flavanols	142.78 ± 8.39 a	144.48 ± 20.97 a	94.81 ± 6.42 a	103.84 ± 2.76 a

[a]Since the treatments were performed in triplicate, all parameters are listed with their standard deviation ($n = 3$). For each row, values with the same letter are not significantly different between the samples ($p \leq 0.05$).

wine color. Wine color is the first feature perceived by the consumer, and consequently, improvements on this parameter may have a substantial impact on wine tasting and quality. Our results suggest that grape and wine anthocyanic composition of Tempranillo variety was improved following foliar treatment with MeJ, which could be of great enological importance.

Flavonol Compounds. Table 4 shows individual flavonol content of grape and wine samples. HPLC analysis indicated the presence of 14 flavonols in all samples. Derivatives of the two major forms in Tempranillo grape berries, myricetin and quercetin, were identified, accounting together for 85% of total flavonols. Derivatives of the other four flavonol structures naturally present in *V. vinifera* grape berries were also identified: laricitrin, kaempferol, isorhamnetin, and syringetin derivatives. Results indicated the presence of all 3-*O*-glucosides (3-glc), although 3-*O*-glucuronides (3-glcU) and 3-*O*-galactosides (3-gal) of myricetin, quercetin, and kaempferol were detected too. In addition, quercetin 3-*O*-rutinoside (3-rut) and isorhamnetin 3-*O*-galactoside (3-gal) were identified. There is little research on grape flavonols in comparison with anthocyanins. In this respect, flavonol levels in our study seemed to be in accordance with the scarce literature on this topic, which reports an important proportion of myricetin- and quercetin-type flavonols in Tempranillo grape berries.[43]

There were not significant differences between control grape samples and those from MeJ foliar treatment except for the content of isorhamnetin 3-*O*-glucoside, which was higher in samples from MeJ treatment (Table 4). Isorhamnetin-type flavonols are formed by gradual methoxylation of quercetin during grape ripening.[33] As can be seen from Table 3, peonidin 3-*O*-glucoside and its coumaroylated form were found in higher proportion in grapes from MeJ treatment. Therefore, results seem to suggest that MeJ application had a marked effect on the methoxylated forms of disubstituted flavonoids (i.e., peonidin and isorhamnetin). In this respect, flavonols are closely related to anthocyanins since they share a big part of their biosynthetic pathway. However, our results seem to indicate that MeJ application had less influence on flavonol compounds than on anthocyanin composition. In accordance with our study, Ruiz-García et al.[37] observed that flavonol content was normally unaffected by MeJ treatment. As well as this, although Ruiz-García et al.[22] reported an increase in grape anthocyanin content in the two years of their study, total flavonol content was improved only in the second year. Therefore, it appears that improvement of anthocyanin synthesis by MeJ application does not necessarily imply a significant induction of flavonol synthesis. Based then on the results, it seems as if MeJ application favors the activity of specific enzymes for anthocyanin synthesis [e.g., dihydroflavonol 4-reductase (DFR) or flavonoid 3-glucosyltransferase (UFGT)], while in contrast it does not significantly favor the activity of specific enzymes for flavonol synthesis [i.e., flavonol synthase (FLS)].

Regarding wine analysis, flavonol glycosides are hydrolyzed during fermentation, releasing their corresponding aglycons.[33,43] In this respect, the aglycons from six possible structures were identified: myricetin, quercetin, laricitrin, kaempferol, isorhamnetin, and syringetin (Table 4). Moreover, some glycosides that had been quantified in grape were not identified in wine (3-*O*-galactosides of myricetin, quercetin, kaempferol, and isorhamnetin, as well as quercetin 3-*O*-rutinoside and kaempferol 3-*O*-glucuronide). These compounds were present in small concentrations in grape samples. Consequently, their hydrolysis during vinification decreased their concentration in wine, making them undetectable. Moreover, Castillo-Muñoz et al.[33] stated that 3-*O*-glucosides of mono- and disubstituted flavonols (i.e., kaempferol, quercetin, and isorhamnetin) appeared to be easily hydrolyzed. Furthermore, in our study, syringetin 3-*O*-glucoside appeared to be the less hydrolyzed compound, which might be an expected outcome according to Hermosín-Gutiérrez et al.[43] As seen in grape analysis, myricetin- and quercetin-type flavonols were the dominant type of flavonols in wine samples, accounting for around 90% of all total flavonols, followed by laricitrin- and syringetin-type flavonols. In agreement with previous studies,[43] isorhamnetin- and kaempferol-type flavonols were minor compounds in wine.

In general, more significant differences for these compounds were observed between wine samples than between grape samples. Thus, wines obtained from grapevines treated with MeJ showed higher total flavonol content in comparison with control wines (Table 4). This result was probably due to differences in individual concentrations of quercetin 3-*O*-glucoside and free myricetin, which were quantitatively important in the wine samples, apart from kaempferol 3-*O*-glucoside. Moreover, as seen in grape analysis, isorhamnetin 3-*O*-glucoside was also found in a higher concentration in wines from MeJ treatment than in control ones. Since grape samples from control and MeJ treatment had shown similar flavonol levels, the slight differences occurring between wines might be

DOI: 10.1021/jf5060672
J. Agric. Food Chem. 2015, 63, 2328−2337

Table 6. Non-Flavonoid Compounds in Tempranillo Grape Berries and Wines from Control Grapevines and from Grapevines Treated with Methyl Jasmonate[a]

	non-flavonoid content			
	grape berries (mg/kg)		wines (mg/L)	
	control	MeJ-treated	control	MeJ-treated
	Hydroxybenzoic Acids			
gallic acid	0.41 ± 0.17 a	0.38 ± 0.05 a	17.48 ± 2.05 a	19.88 ± 1.03 a
protocatechuic acid			3.60 ± 0.55 a	4.33 ± 0.01 a
	Hydroxycinnamic Acids			
trans-caftaric acid	8.95 ± 1.35 a	9.69 ± 2.08 a	47.57 ± 2.83 a	48.10 ± 6.33 a
trans- + *cis*-coutaric acids	9.04 ± 1.35 a	9.01 ± 1.36 a	46.82 ± 5.15 a	51.16 ± 6.81 a
trans-fertaric acid	0.68 ± 0.01 a	0.67 ± 0.00 a	1.94 ± 0.18 a	2.16 ± 0.09 a
cis-fertaric acid	0.21 ± 0.01 a	0.25 ± 0.00 a		
caffeic acid			6.83 ± 1.21 a	9.21 ± 0.58 a
p-coumaric acid			2.07 ± 0.31 a	2.55 ± 0.19 a
ferulic acid			0.93 ± 0.22 a	1.27 ± 0.04 a
total hydroxycinnamic acids	18.89 ± 2.67 a	19.62 ± 3.44 a	106.15 ± 7.64 a	114.45 ± 12.63 a
	Stilbenes			
trans-piceid	0.65 ± 0.17 a	3.65 ± 0.58 b	1.74 ± 0.31 a	5.39 ± 1.44 b
cis-piceid	0.39 ± 0.10 a	1.30 ± 0.06 b	0.34 ± 0.15 a	0.87 ± 0.59 a
trans-resveratrol	0.13 ± 0.05 a	0.13 ± 0.01 a	0.63 ± 0.14 a	1.31 ± 0.54 a
cis-resveratrol	0.10 ± 0.01 a	0.09 ± 0.00 a	0.18 ± 0.02 a	0.26 ± 0.08 a
total stilbenes	1.26 ± 0.33 a	5.17 ± 0.61 b	2.98 ± 0.54 a	7.83 ± 2.65 b

[a]Since the treatments were performed in triplicate, all parameters are listed with their standard deviation ($n = 3$). For each row, values with different letters are significantly different between the samples ($p \leq 0.05$).

attributed to higher flavonol extractability when MeJ was applied. Schwarz et al.[44] reported that prefermentation addition to the must of a flavonol compound, rutin, favored anthocyanin extraction during winemaking due to the formation of copigmentation complexes. On account of this, it could be hypothesized that grapes richer in anthocyanin compounds, such as those from MeJ treatment, may lead to wines richer not only in anthocyanins but also in flavonols. In contrast to our results, Ruiz-García et al.[22] found that MeJ application to Monastrell clusters had no influence on wine total flavonol content. However, the latter authors found that wine flavonol content increased with application of another elicitor, benzothiadiazole.[39]

Flavanol Compounds. Results of grape and wine flavanol analysis are shown in Table 5. Catechin was the major flavanol compound in grapes, followed by epicatechin. The results showed that MeJ foliar application did not affect flavanol synthesis since MeJ-treated grape samples exhibited similar flavanol levels to those found in control grape samples. There are only a few works in the literature that studied the influence of MeJ application on flavanol composition in grapes or in other fruits. Shafiq et al.[18] observed that preharvest MeJ application to red blush apples increased skin catechin and epicatechin content, although results depended upon the time of application. Ruiz-García et al.[22] found that skin proanthocyanidin content was increased by MeJ application, while on the other hand, there was barely any difference regarding seed tannin content between control and treated samples. Moreover, the latter research group stated that MeJ application could lead to different results depending on the treated clone.[37] In some clones, tannin synthesis might be favored at the expense of anthocyanin synthesis, while other clones could show the opposite behavior. In our study, Tempranillo grapes treated with MeJ have shown a significant enhancement of anthocyanin compounds while no differences have been observed in terms of flavanol composition.

As seen in grape analysis, catechin and epicatechin were the most abundant compounds in wines, accounting together for around 65% of the total flavanols identified (Table 5). Both wines showed a similar flavanol composition, suggesting that MeJ foliar application did not influence this group of flavonoids. Therefore, our results confirm those obtained from grape analysis, which showed no differences between control grapes and grapes from the foliar treatment. Similarly, Fernández-Marín et al.[21] did not observe any difference concerning total flavanol content between control wines and wines elaborated from Syrah clusters treated with MeJ. Moreover, Ruiz-García et al.[22] observed that the application of MeJ to Monastrell clusters led to an increase in the total amount of flavanols in the second year of the study, whereas no effect from MeJ application was noticed in the first year.

Non-Flavonoid Compounds. Non-flavonoid grape and wine composition is shown in Table 6. Gallic acid was the only hydroxybenzoic acid identified in grape samples. Hydroxycinnamic acids in grapes are esterified with tartaric acid.[45] *trans*-Caftaric and *trans*- + *cis*-coutaric acids were the dominant hydroxycinnamic acids. As for stilbenes, *trans*-piceid was the most abundant stilbene in grape samples, representing around 51% of total stilbene content.

Hydroxybenzoic and hydroxycinnamic acid content in grapes was independent of MeJ foliar application, since no differences were observed between the concentration found in control grapes and that found in grapes from treated grapevines (Table 6). In contrast, a marked increase in stilbene concentration was observed after MeJ foliar treatment. The synthesis of both piceid isomers was enhanced by this application: *trans*-piceid was 5.6-fold increased while the cis isomer was 3.3-fold increased. On the other hand, *trans*- and *cis*-resveratrol were not affected by MeJ foliar treatment. All the same, total stilbene content was 3-fold increased. Induction of stilbene formation seems to be an expected outcome, as it has been reported in several works. Ruiz-García et al.[37] observed that MeJ

DOI: 10.1021/jf5060672
J. Agric. Food Chem. 2015, 63, 2328−2337

application normally leads to an increase in stilbene concentration (up to 5-fold increase depending on the clone). Syrah clusters treated with MeJ were richer in different stilbenes than untreated clusters at the harvest moment.[21] Moreover, *trans*-resveratrol content increased at ripening in Barbera grapes treated by cumulative MeJ applications.[23] Apart from this, Belhadj et al.[20] observed an accumulation of total piceids (*trans*- and *cis*-piceids) in Gamay Fréaux cell suspensions treated with MeJ alone or in combination with sucrose. Furthermore, they found that different genes involved in the biosynthesis of polyphenols were upregulated by MeJ application. In a previous study conducted by the latter research group,[19] Cabernet Sauvignon leaves treated with MeJ showed an accumulation of enzymes responsible for stilbene formation (e.g., stilbene synthase). Therefore, our results confirm those previously reported for other grape varieties and obtained in different conditions. Elicitors may reduce the use of conventional fungicides by preventing the attack of certain pathogens through the induction of plant defense responses.[14,19] Accumulation of phytoalexins (e.g., stilbenes) is one of the plant responses to elicitor perception.[46] Thus, treated grapevines in our study seemed to activate the synthesis and accumulation of stilbene compounds. In contrast, the absence of significant differences regarding phenolic acids seems to be related to the different biosynthetic pathway of these compounds. Results suggest that MeJ application may favor the biosynthetic pathway of anthocyanins (also flavonols in a lesser extent) and stilbenes, while it seemed to have little effect on phenolic acid synthesis.

Concerning wine analysis, protocatechuic acid was identified together with gallic acid (Table 6). As expected, hydrolysis of the hydroxycinnamoyl tartaric acids during alcoholic fermentation released the corresponding free acids, enabling us to identify caffeic, *p*-coumaric, and ferulic acids. Still, *trans*-caftaric and *trans*- + *cis*-coutaric acids remained as the major hydroxycinnamic acid derivatives in the wine samples. As for stilbenes, like in grapes, *trans*-piceid was the major compound in wine, representing around 60% of total stilbene compounds. Moreover, the average *trans*-piceid/*trans*-resveratrol ratio decreased from 5.74 in grapes to 2.70 in wines, probably due to hydrolysis of *trans*-piceid to *trans*-resveratrol during the alcoholic fermentation.[46]

It was confirmed that samples from MeJ foliar treatment showed a higher concentration of total stilbenes and *trans*-piceid, while the effect on other non-flavonoid compounds was less evident. In particular, it could be of interest that wine made from treated grapevines showed a similar concentration of nonesterified hydroxycinnamic acids (caffeic, *p*-coumaric, and ferulic acids) to the control wine. These compounds are ethylphenol precursors, and therefore they could be involved in ethylphenol formation and subsequent wine alteration, especially during barrel aging.[47] This might be a noteworthy outcome, taking into account that Tempranillo grapes are normally used for producing aged wines.[48] Despite this fact, it should be also taken into account that hydroxycinnamic acids are also precursors in the formation of hydroxyphenyl pyranoanthocyanins, which are anthocyanin-derived pigments that contribute to wine color stability.[49] Regarding stilbenes, *trans*-piceid content was 3 times higher in wines from MeJ foliar treatment than in control wines. Moreover, total stilbene content was increased 163% in wines obtained from grapevines treated with MeJ in comparison with control wines. The increase in wine total stilbene concentration is in good agreement with previous works, which have shown that MeJ application in the vineyard could result in an improvement of wine stilbene content. In this respect, Fernández-Marín et al.[21] found that total stilbene content was increased in wine, both at press and bottle moments, with the application of MeJ to Syrah clusters. In recent years, research on stilbenes has become very popular due to their importance for human health.[50] Therefore, foliar application of MeJ to Tempranillo grapevines could be an interesting tool in order to enhance wine health-promoting properties.

Our results describe for the first time the effect of MeJ foliar application on the phenolic composition of Tempranillo grape and wine. Grape and wine phenolic content was increased in the samples from MeJ treatment in comparison with control samples. Anthocyanin content was increased in both grape and wine by MeJ application. Similarly, wine color-related parameters were also improved as a consequence of MeJ application. Apart from this, stilbene synthesis was enhanced by MeJ application, as stilbene content was increased in both grape and wine. The effect of MeJ application was less evident on flavonols, although total flavonol content was higher in wines from MeJ treatment than in control wines. For the remaining parameters, there were not significant differences between control and MeJ samples. It should be taken into account that foliar application does not require a previous defoliation, which, in contrast, is necessary when the application is carried out directly on clusters. Therefore, this paper has shown that foliar application of MeJ could be an easy and interesting viticultural practice in order to increase the phenolic content of grapes. Furthermore, it could improve as well the wine color and its health-promoting properties.

AUTHOR INFORMATION

Corresponding Author

*Telephone +34 941291833; fax +34 941291392; e-mail Teresa.GardeCerdan@gmail.com or teresa.garde@icvv.es.

Funding

We are grateful for financial support given by the Gobierno de La Rioja to R-08-13 project. J.P. thanks Gobierno de La Rioja for the formation grant, and I.L.-A. and T.G.-C. thank INIA-Gobierno de La Rioja for contracts.

Notes

The authors declare no competing financial interest.

REFERENCES

(1) Jackson, R. S. Grapevine structure and function. In *Wine Science: Principles and Applications*, 3rd ed.; Elsevier: San Diego, CA, 2008; pp 50−107.

(2) Gómez-Míguez, M.; González-Manzano, S.; Escribano-Bailón, M. T.; Heredia, F. J.; Santos-Buelga, C. Influence of different phenolic copigments on the color of malvidin 3-glucoside. *J. Agric. Food Chem.* **2006**, *54*, 5422−5429.

(3) Zhang, B.; Liu, R.; He, F.; Zhou, P.-P.; Duan, C.-Q. Copigmentation of malvidin-3-*O*-glucoside with five hydroxybenzoic acids in red wine model solutions: Experimental and theoretical investigations. *Food Chem.* **2015**, *170*, 226−233.

(4) Del Rio, D.; Rodriguez-Mateos, A.; Spencer, J. P. E.; Tognolini, M.; Borges, G.; Crozier, A. Dietary (poly)phenolics in human health: structures, bioavailability, and evidence of protective effects against chronic diseases. *Antioxid. Redox Signaling* **2013**, *18*, 1818−1892.

(5) Gómez-Alonso, S.; Collins, V. J.; Vauzour, D.; Rodríguez-Mateos, A.; Corona, G.; Spencer, J. P. E. Inhibition of colon adenocarcinoma cell proliferation by flavonols is linked to a G2/M cell cycle block and reduction in cyclin D1 expression. *Food Chem.* **2012**, *130*, 493−500.

DOI: 10.1021/jf5060672
J. Agric. Food Chem. 2015, 63, 2328−2337

(6) Gonzalo-Diago, A.; Dizy, M.; Fernández-Zurbano, P. Taste and mouthfeel properties of red wines proanthocyanidins and their relation to the chemical composition. *J. Agric. Food Chem.* **2013**, *61*, 8861−8870.
(7) Gonzalo-Diago, A.; Dizy, M.; Fernández-Zurbano, P. Contribution of low molecular weight phenols to bitter taste and mouthfeel properties in red wines. *Food Chem.* **2014**, *154*, 187−198.
(8) Pérez-Magariño, S.; González-San José, M. L. Evolution of flavanols, anthocyanins, and their derivatives during the aging of red wines elaborated from grapes harvested at different stages of ripening. *J. Agric. Food Chem.* **2004**, *52*, 1181−1189.
(9) Portu, J.; López-Giral, N.; López, R.; González-Arenzana, L.; González-Ferrero, C.; López-Alfaro, I.; Santamaría, P.; Garde-Cerdán, T. Different tools to enhance grape and wine anthocyanin content. In *Handbook of Anthocyanins: Food Sources, Chemical Applications and Health Benefits*; Warner, L. M., Ed.; Nova Science Publishers, Inc.: New York, 2015; pp 51−88.
(10) Balint, G.; Reynolds, A. G. Impact of exogenous abscisic acid on vine physiology and grape composition of Cabernet Sauvignon. *Am. J. Enol. Vitic.* **2013**, *64*, 74−87.
(11) Berli, F. J.; Fanzone, M.; Piccoli, P.; Bottini, R. Solar UV-B and ABA are involved in phenol metabolism of *Vitis vinifera* L. Increasing biosynthesis of berry skin polyphenols. *J. Agric. Food Chem.* **2011**, *59*, 4874−4884.
(12) Pardo-García, A. I.; Martínez-Gil, A. M.; Cadahía, E.; Pardo, F.; Alonso, G. L.; Salinas, M. R. Oak extract application to grapevines as a plant biostimulant to increase wine polyphenols. *Food Res. Int.* **2014**, *55*, 150−160.
(13) Ruiz-García, Y.; Gómez-Plaza, E. Elicitors: A tool for improving fruit phenolic content. *Agriculture* **2013**, *3*, 33−52.
(14) Delaunois, B.; Farace, G.; Jeandet, P.; Clément, C.; Baillieul, F.; Dorey, S.; Cordelier, S. Elicitors as alternative strategy to pesticides in grapevine? Current knowledge on their mode of action from controlled conditions to vineyard. *Environ. Sci. Pollut. Res.* **2014**, *21*, 4837−4846.
(15) Rohwer, C. L.; Erwin, J. E. Horticultural applications of jasmonates: A review. *J. Hortic. Sci. Biotechnol.* **2008**, *83*, 283−304.
(16) Wang, S. Y.; Bowman, L.; Ding, M. Methyl jasmonate enhances antioxidant activity and flavonoid content in blackberries (*Rubus* sp.) and promotes antiproliferation of human cancer cells. *Food Chem.* **2008**, *107*, 1261−1269.
(17) Wang, S. Y.; Zheng, W. Preharvest application of methyl jasmonate increases fruit quality and antioxidant capacity in raspberries. *Int. J. Food Sci. Technol.* **2005**, *40*, 187−195.
(18) Shafiq, M.; Singh, Z.; Khan, A. S. Time of methyl jasmonate application influences the development of 'Cripps Pink' apple fruit colour. *J. Sci. Food Agric.* **2013**, *93*, 611−618.
(19) Belhadj, A.; Saigne, C.; Telef, N.; Cluzet, S.; Bouscaut, J.; Corio-Costet, M.-F.; Mérillon, J.-M. Methyl jasmonate induces defense responses in grapevine and triggers protection against *Erysiphe necator*. *J. Agric. Food Chem.* **2006**, *54*, 9119−9125.
(20) Belhadj, A.; Telef, N.; Saigne, C.; Cluzet, S.; Barrieu, F.; Hamdi, S.; Mérillon, J.-M. Effect of methyl jasmonate in combination with carbohydrates on gene expression of PR proteins, stilbene and anthocyanin accumulation in grapevine cell cultures. *Plant Physiol. Biochem.* **2008**, *46*, 493−499.
(21) Fernández-Marín, M. I.; Puertas, B.; Guerrero, R. F.; García-Parrilla, M. C.; Cantos-Villar, E. Preharvest methyl jasmonate and postharvest UVC treatments: increasing stilbenes in wine. *J. Food Sci.* **2014**, *79*, C310−C317.
(22) Ruiz-García, Y.; Romero-Cascales, I.; Gil-Muñoz, R.; Fernández-Fernández, J. I.; López-Roca, J. M.; Gómez-Plaza, E. Improving grape phenolic content and wine chromatic characteristics through the use of two different elicitors: Methyl jasmonate versus benzothiadiazole. *J. Agric. Food Chem.* **2012**, *60*, 1283−1290.
(23) Vezzulli, S.; Civardi, S.; Ferrari, F.; Bavaresco, L. Methyl jasmonate treatment as a trigger of resveratrol synthesis in cultivated grapevine. *Am. J. Enol. Vitic.* **2007**, *58*, 530−533.
(24) Sampaio, T. L.; Kennedy, J. A.; Vasconcelos, M. C. Use of microscale fermentations in grape and wine research. *Am. J. Enol. Vitic.* **2007**, *58*, 534−539.
(25) ECC. Commission Regulation No. 2676/90 concerning the establishment of common analytical methods in the sector of wine. *Off. J. Eur. Commun.* **1990**, *L272*(3), 1−192.
(26) Lipka, Z.; Tanner, H. Une nouvelle méthode de dosage du acide tartarique dans les moûts, les vins et autres boissons (selon Rebelein). *Rev. Suisse Vitic. Arboric. Hortic.* **1974**, *6*, 5−10.
(27) Ribéreau-Gayon, P.; Stonestreet, E. Determination of anthocyanins in red wine. *Bull. Soc. Chim. Fr.* **1965**, *9*, 2649−2652.
(28) Ribéreau-Gayon, J.; Peynaud, E.; Ribéreau-Gayon, P.; Sudraud, P. *Sciences et Techniques du Vin*; Dunod: Paris, 1976.
(29) Glories, Y. Recherches sur la Matière Colorante des Vins Rouges. Ph.D. Thesis, Université de Bordeaux II, France, 1978.
(30) Ruiz, M. *La Crianza del Vino Tinto desde la Perspectiva Vitícola*; AMV Ediciones: Madrid, Spain, 1999.
(31) Brand-Williams, W.; Cuvelier, M. E.; Berset, C. Use of a free radical method to evaluate antioxidant activity. *LWT—Food Sci. Technol.* **1995**, *28*, 25−30.
(32) Nixdorf, S. L.; Hermosín-Gutiérrez, I. Brazilian red wines made from the hybrid grape cultivar Isabel: Phenolic composition and antioxidant capacity. *Anal. Chim. Acta* **2010**, *659*, 208−215.
(33) Castillo-Muñoz, N.; Gómez-Alonso, S.; García-Romero, E.; Hermosín-Gutiérrez, I. Flavonol profiles of *Vitis vinifera* red grapes and their single-cultivar wines. *J. Agric. Food Chem.* **2007**, *55*, 992−1002.
(34) Castillo-Muñoz, N.; Fernández-González, M.; Gómez-Alonso, S.; García-Romero, E.; Hermosín-Gutiérrez, I. Red-color related phenolic composition of Garnacha Tintorera (*Vitis vinifera* L.) grapes and red wines. *J. Agric. Food Chem.* **2009**, *57*, 7883−7891.
(35) Lago-Vanzela, E. S.; Da-Silva, R.; Gomes, E.; García-Romero, E.; Hermosín-Gutiérrez, I. Phenolic composition of the edible parts (flesh and skin) of Bordô grape (*Vitis labrusca*) using HPLC-DAD-ESI-MS/MS. *J. Agric. Food Chem.* **2011**, *59*, 13136−13146.
(36) López-Alfaro, I.; González-Arenzana, L.; López, N.; Santamaría, P.; López, R.; Garde-Cerdán, T. Pulsed electric field treatment enhanced stilbene content in Graciano, Tempranillo and Grenache grape varieties. *Food Chem.* **2013**, *141*, 3759−3765.
(37) Ruiz-García, Y.; Romero-Cascales, I.; Bautista-Ortín, A. B.; Gil-Muñoz, R.; Martínez-Cutillas, A.; Gómez-Plaza, E. Increasing bioactive phenolic compounds in grapes: Response of six Monastrell grape clones to benzothiadiazole and methyl jasmonate treatments. *Am. J. Enol. Vitic.* **2013**, *64*, 459−465.
(38) Avizcuri-Inac, J.-M.; Gonzalo-Diago, A.; Sanz-Asensio, J.; Martínez-Soria, M.-T.; López-Alonso, M.; Dizy-Soto, M.; Echávarri-Granado, J.-F.; Vaquero-Fernández, L.; Fernández-Zurbano, P. Effect of cluster thinning and prohexadione calcium applications on phenolic composition and sensory properties of red wines. *J. Agric. Food Chem.* **2013**, *61*, 1124−1137.
(39) Ruiz-García, Y.; Gil-Muñoz, R.; López-Roca, J. M.; Martínez-Cutillas, A.; Romero-Cascales, I.; Gómez-Plaza, E. Increasing the phenolic compound content of grapes by preharvest application of abcisic acid and a combination of methyl jasmonate and benzothiadiazole. *J. Agric. Food Chem.* **2013**, *61*, 3978−3983.
(40) Gómez-Alonso, S.; García-Romero, E.; Hermosín-Gutiérrez, I. HPLC analysis of diverse grape and wine phenolics using direct injection and multidetection by DAD and fluorescence. *J. Food Compos. Anal.* **2007**, *20*, 618−626.
(41) Diago, M. P.; Ayestarán, B.; Guadalupe, Z.; Poni, S.; Tardáguila, J. Impact of prebloom and fruit set basal leaf removal on the flavonol and anthocyanin composition of Tempranillo grapes. *Am. J. Enol. Vitic.* **2012**, *63*, 367−376.
(42) Bakker, J.; Timberlake, C. F. Isolation, identification, and characterization of new color-stable anthocyanins occurring in some red wines. *J. Agric. Food Chem.* **1997**, *45*, 35−43.
(43) Hermosín-Gutiérrez, I.; Castillo-Muñoz, N.; Gómez-Alonso, S.; García-Romero, E. Flavonol profiles for grape and wine authentication. In *Progress in Authentication of Food and Wine*; Ebeler, S. E., Takeoka,

DOI: 10.1021/jf5060672
J. Agric. Food Chem. 2015, 63, 2328−2337

G. R., Winterhalter, P., Eds.; ACS Symposium Series; American Chemical Society: Washington, DC, 2011; pp 113−129.
(44) Schwarz, M.; Picazo-Bacete, J. J.; Winterhalter, P.; Hermosín-Gutiérrez, I. Effect of copigments and grape cultivar on the color of red wines fermented after the addition of copigments. *J. Agric. Food Chem.* **2005**, *53*, 8372−8381.
(45) Rentzsch, M.; Wilkens, A.; Winterhalter, P. Non-flavonoid phenolic compounds. In *Wine Chemistry and Biochemistry*; Moreno-Arribas, M. V., Polo, M. C., Eds.; Springer: New York, 2009; pp 509−527.
(46) Bavaresco, L.; Mattivi, F.; de Rosso, M.; Flamini, R. Effects of elicitors, viticultural factors, and enological practices on resveratrol and stilbenes in grapevine and wine. *Mini-Rev. Med. Chem.* **2012**, *12*, 1366−1381.
(47) Schopp, L. M.; Lee, J.; Osborne, J. P.; Chescheir, S. C.; Edwards, C. G. Metabolism of nonesterified and esterified hydroxycinnamic acids in red wines by *Brettanomyces bruxellensis*. *J. Agric. Food Chem.* **2013**, *61*, 11610−11617.
(48) Garde-Cerdán, T.; Lorenzo, C.; Carot, J. M.; Jabaloyes, J. M.; Esteve, M. D.; Salinas, M. R. Statistical differentiation of wines of different geographic origin and aged in barrel according to some volatile components and ethylphenols. *Food Chem.* **2008**, *111*, 1025−1031.
(49) Rentzsch, M.; Schwarz, M.; Winterhalter, P.; Hermosín-Gutiérrez, I. Formation of hydroxyphenyl-pyranoanthocianins in Grenache wines: Precursor levels and evolution during aging. *J. Agric. Food Chem.* **2007**, *55*, 4883−4888.
(50) Guerrero, R. F.; García-Parrilla, M. F.; Puertas, B.; Cantos-Villar, E. Wine resveratrol and health: A review. *Nat. Prod. Commun.* **2009**, *4*, 635−658.

DOI: 10.1021/jf5060672
J. Agric. Food Chem. 2015, 63, 2328−2337

Table 1. Relative Decrease (Percent)[a] in the Intensity of Estimated and Measured ESR Signal Values for the Mixtures of Insoluble Grains and Beverages Rich in Antioxidants

	mixture volume					
	100 μL		150 μL		200 μL	
mixture[b]	estimated	measured	estimated	measured	estimated	measured
IW + GT	23.0 ± 1.1a	41.1 ± 1.0b	31.7 ± 0.4a	48.8 ± 1.4b	42.1 ± 1.1a	55.5 ± 0.3b
IW + RW	20.8 ± 1.1a	35.0 ± 0.2b	28.7 ± 0.4a	44.1 ± 0.7b	37.4 ± 1.1a	51.9 ± 0.2b
IW + PJ	19.4 ± 0.5a	26.0 ± 2.9a	27.1 ± 1.3a	35.0 ± 1.7b	37.8 ± 1.6a	44.5 ± 4.5a
IW + ESP	18.8 ± 2.9a	34.3 ± 6.1a	26.0 ± 0.7a	47.9 ± 2.2b	37.0 ± 0.8a	55.4 ± 5.1b
IO + GT	25.8 ± 1.3a	47.8 ± 0.3b	32.2 ± 1.2a	64.5 ± 0.3b	40.0 ± 0.8a	77.7 ± 3.4b
IO + RW	23.6 ± 1.3a	35.1 ± 3.7a	29.3 ± 1.2a	48.1 ± 0.7b	35.3 ± 0.8a	58.2 ± 2.6b
IO + PJ	22.2 ± 0.6a	36.1 ± 3.0b	27.6 ± 2.0a	49.0 ± 1.4b	35.7 ± 1.3a	58.3 ± 6.2b
IO + ESP	21.6 ± 3.1a	47.3 ± 6.2b	26.5 ± 1.5a	57.0 ± 3.8b	34.9 ± 0.5a	66.4 ± 4.5b
IR + GT	27.5 ± 1.5a	41.6 ± 2.0b	35.4 ± 0.3a	63.9 ± 5.4b	43.3 ± 1.0a	69.5 ± 3.5b
IR + RW	25.3 ± 1.4a	40.3 ± 0.6b	32.5 ± 0.3a	50.3 ± 3.7b	38.5 ± 1.0a	51.4 ± 3.8b
IR + PJ	23.9 ± 0.8a	45.0 ± 6.1b	30.8 ± 1.1a	52.0 ± 0.7b	39.0 ± 1.6a	67.5 ± 1.9b
IR + ESP	23.3 ± 3.2a	40.2 ± 1.7b	29.7 ± 0.6a	57.9 ± 0.5b	38.2 ± 0.7a	60.5 ± 0.1b

[a]Different letters indicate the statistical significance of difference at $p < 0.05$ for each estimated−measured pair. [b]IW, insoluble wheat; IR, insoluble rye; IO, insoluble oat; GT, green tea; RW, red wine; PJ, pomegranate juice; ESP, espresso.

(−)-epicatechin gallate, (−)-epigallocatechin gallate, chlorogenic acid, resveratrol, 6-hydroxy-2,5,7,8-tetramethylchroman-2-carboxylic acid (Trolox), iron(III) chloride, adenosine 5′-diphosphate sodium salt (ADP), methanol, chloroform, hexane, and ethanol were purchased from Sigma-Aldrich Chemie (Steinheim, Germany). L-(+)-Ascorbic acid, monopotassium phosphate, and glycine were purchased from Merck (Darmstadt, Germany). All solvents used were of analytical grade, unless otherwise stated. Water was purified through a Millipore Q-plus purification train (Millipore Corp., Bedford, MA, USA).

Grains and Beverages. All grain varieties used were purchased from a local market in Ankara, Turkey. Green tea, pomegranate juice, roasted coffee beans, and red wine were of food grade and purchased in Copenhagen, Denmark. Green tea was prepared by brewing 3 g of green tea with 100 mL of hot water for 15 min, and espresso was prepared in a kitchen-type coffee machine, Titanium Gaggia, at the seventh level of the dose control knob.

Preparation of the Insoluble Fractions of Grains. Ground whole grains were washed according to the procedure described by Çelik et al.[24] to remove water, alcohol, and lipid-soluble fractions. Washed grains were freeze-dried, ground with a ceramic mortar to obtain a fine powder, and passed through a sieve (Endecotts Test Sieve, London, UK) of 40 mesh size (425 μm). The final insoluble powder was tested and found to be free of soluble antioxidant compounds. It was kept under 4 °C prior to experiments.

Preparation of Liposomes. Liposomes were prepared with minor modifications[25] according to the method described by Tirmenstein et al.[26] Forty milligrams of phosphatidylcholine was dissolved in chloroform and evaporated to dryness under nitrogen flow. The phosphatidylcholine residue was subsequently rehydrated with 5 mL of 50 mM sodium phosphate buffer (PB) (pH 7.4) and vortexed. The suspension was sonicated at 100 W with 30 s intervals 10 times to yield a white homogeneous suspension of multilamellar liposomes. Between the intervals, the suspension was left to cool in an ice bath for at least 2 min. The sonicated suspension was centrifuged at 16000*g* for 30 min, and the supernatant containing the liposomes was collected. The liposomes were stored under 4 °C for 1 week before experimental studies to increase the level of lipid hydroperoxides (about 5−10% of the phosphatidylcholine). These will react with Fe^{3+} to produce free radicals.

Peroxidation of Liposomes. Liposomes prepared 1 week prior to measurement were pipetted into a 96-well transparent plate as 10 μL for each well and mixed with 50 μL of sample dilutions or standard solution (Trolox), whereas Milli-Q water was used as zero sample. Sample dilutions were prepared at 500, 100, 50, and 10 μM for pure antioxidant compounds, 1:500, 1:1000, 1:5000, and 1:10000 dilutions with water for beverages, and 10, 5, 1, and 0.5 mg/mL aqueous solutions for insoluble and whole grains. Mixtures of insoluble grains with beverages/pure antioxidant solutions were prepared by combining two different concentrations of grains (10 and 5 mg/mL) with two different concentrations of beverages (1:500, 1:1000) or pure solutions (500 and 100 μM) at a ratio of 1:1 to give 50 μL sample. Because aldehydes generated by lipid peroxidation can react with amines to produce fluorescent products, glycine was added to the reaction medium as glycine ascorbate buffer (GAB), which was prepared as 50 mM potassium phosphate buffer (PPB) with 100 mM glycine and 450 μM ascorbate at pH 7.4, for 120 μL per well. Background wells were made by pipetting GAB buffer instead of liposome and samples. Lipid peroxidation was initiated by introducing 20 μL of an oxidizing agent composed of 25 μM $FeCl_3$ in 50 mM PPB (pH 7.4) with 1 mM ADP.

The plate was inserted into the plate reader of a Tecan fluorometer immediately after addition of oxidizing agent. The lag phase before the onset of oxidation was measured for 4 h at 37 °C (excitation at 360 nm, emission at 460 nm) in 10 min intervals, and samples were analyzed in triplicate.

Inhibition of lipid oxidation was calculated by using the formula

$$\text{inhibition of lipid oxidation (\%)} = 100 - (\text{AUC}_{\text{sample}}/\text{AUC}_{\text{control}}) \times 100$$

where $\text{AUC}_{\text{sample}}$ is the area under the curve of sample containing antioxidant as measured in the well and $\text{AUC}_{\text{control}}$ is the area under the curve measured for the control well. To avoid differences originating from different starting levels of oxidation, all fluorescent values were subtracted from the lowest value, considering the lowest point as zero, and the AUC was calculated by the trapezoid rule.

Scavenging of Fremy's Salt Radical. The scavenging of Fremy's salt radical was determined with minor modifications according to the method described by Rødjter et al.[27] For insoluble and whole grains, 10, 15, or 20 mg of sample was mixed with 1 mL of Milli-Q water and 200 μL of a solution of Fremy's salt (1.64 mM) in 25% saturated sodium carbonate solution. For pure antioxidant solutions (10 μM) and beverages (1:1000 diluted) 100, 150, and 200 μL of sample was used instead of 10, 15, and 20 mg. Combinations of insoluble grains with beverages/pure antioxidant solutions were made in the ratio of 10 mg:100 μL, and then 100, 150, and 200 μL of sample from the prepared mixture was added into the reaction medium as described for beverages and pure solutions above. Six minutes after the mixing, ESR spectra were recorded with a MiniScope MS200 ESR spectrometer (Magnettech GmbH, Berlin, Germany). The measurements were carried out with the following settings: BO field, 3366.90 G; sweep

DOI: 10.1021/acs.jafc.5b00009
J. Agric. Food Chem. 2015, 63, 2338−2343

Table 2. Relative Decrease (Percent)[a] in the Intensity of Estimated and Measured ESR Signal Values for Mixtures of Insoluble Grains with Solutions of Pure Antioxidants

	mixture volume					
	100 μL		150 μL		200 μL	
mixture[b]	estimated	measured	estimated	measured	estimated	measured
IW + CGA	17.2 ± 0.2a	31.6 ± 0.3b	26.8 ± 0.8a	47.1 ± 0.0b	38.9 ± 1.7a	55.1 ± 3.5b
IW + EC	34.9 ± 0.3a	88.0 ± 0.7b	43.3 ± 0.5a	91.0 ± 0.7b	52.1 ± 0.6a	90.7 ± 0.0b
IW + ECG	20.2 ± 0.7a	50.7 ± 6.3b	29.5 ± 0.6a	63.6 ± 5.2b	39.5 ± 0.8a	87.3 ± 9.0b
IW + EGC	18.2 ± 0.6a	40.3 ± 4.4b	29.4 ± 0.6a	54.6 ± 3.4b	39.1 ± 0.9a	60.6 ± 4.3b
IW + EGCG	22.4 ± 1.0a	87.7 ± 0.4b	31.8 ± 1.2a	89.6 ± 0.4b	42.9 ± 1.2a	91.5 ± 0.9b
IW + RES	14.5 ± 1.3a	33.8 ± 2.6b	24.8 ± 2.6a	42.4 ± 1.7b	32.6 ± 1.5a	52.9 ± 0.0b
IO + CGA	20.1 ± 0.4a	42.3 ± 0.4b	27.3 ± 1.6a	51.9 ± 1.7b	36.8 ± 1.4a	70.9 ± 4.1b
IO + EC	37.7 ± 0.4a	88.7 ± 0.6b	43.8 ± 1.2a	89.5 ± 0.0b	50.0 ± 0.3a	92.8 ± 1.1b
IO + ECG	23.0 ± 0.9a	49.9 ± 3.5b	30.1 ± 1.3a	64.0 ± 0.0b	37.4 ± 0.5a	84.1 ± 0.0b
IO + EGC	21.0 ± 0.8a	46.2 ± 0.0b	29.9 ± 1.3a	56.8 ± 1.0b	37.0 ± 0.6a	60.0 ± 5.2b
IO + EGCG	25.2 ± 1.1a	88.8 ± 0.5b	32.3 ± 1.9a	91.6 ± 0.3b	40.8 ± 0.9a	92.8 ± 0.0b
IO + RES	17.4 ± 1.4a	35.7 ± 2.9b	25.4 ± 3.3a	48.3 ± 6.5b	30.5 ± 1.2a	53.0 ± 4.9b
IR + CGA	21.8 ± 0.5a	51.5 ± 2.3b	30.5 ± 0.7a	65.1 ± 9.2b	40.0 ± 1.6a	72.8 ± 3.6b
IR + EC	39.4 ± 0.6a	88.3 ± 0.3b	47.0 ± 0.4a	92.5 ± 2.8b	53.2 ± 0.5a	92.6 ± 0.2b
IR + ECG	24.7 ± 1.1a	55.9 ± 2.9b	33.3 ± 0.5a	68.7 ± 4.9b	40.7 ± 0.7a	74.9 ± 6.2b
IR + EGC	22.7 ± 1.0a	46.1 ± 2.1b	33.2 ± 0.4a	59.8 ± 1.4b	40.3 ± 0.8a	72.1 ± 0.0b
IR + EGCG	26.9 ± 1.3a	89.7 ± 0.5b	35.6 ± 1.9a	91.3 ± 0.9b	44.0 ± 0.9a	92.6 ± 0.7b
IR + RES	19.0 ± 1.6a	33.7 ± 1.9b	28.6 ± 2.5a	45.5 ± 5.6a	33.7 ± 1.4a	60.3 ± 3.5b

[a]Different letters indicate the statistical significance of difference at $p < 0.05$ for each estimated−measured pair. [b]IW, insoluble wheat; IR, insoluble rye; IO, insoluble oat; CGA, chlorogenic acid; EC, epicatechin; ECG, epicatechin gallate; EGC, epigallocatechin; EGCG, epigallocatechin gallate; RES, resveratrol.

Table 3. Estimated and Measured Relative Inhibition Values (Percent)[a] of Lipid Oxidation for Different Mixture Combinations of Insoluble Grains with Beverages Rich in Antioxidants

	inhibition of lipid oxidation for different mixture combinations (%)							
	5 mg/mL of insoluble grain				10 mg/mL of insoluble grain			
	1:500 dilute beverage		1:1000 dilute beverage		1:500 dilute beverage		1:1000 dilute beverage	
mixture[b]	estimated	measured	estimated	measured	estimated	measured	estimated	measured
IW + GT	36.8 ± 2.7a	83.5 ± 3.5b	30.3 ± 2.6a	53.5 ± 3.7b	38.8 ± 1.9a	83.9 ± 0.7b	32.4 ± 1.8a	55.0 ± 1.4b
IW + RW	21.6 ± 3.1a	51.7 ± 3.6b	9.4 ± 2.5a	38.8 ± 3.8b	23.7 ± 2.4a	47.2 ± 2.5b	11.4 ± 1.7a	33.1 ± 3.9b
IW + PJ	9.5 ± 2.8a	25.5 ± 1.2b	−1.3 ± 2.6a	16.5 ± 2.2b	11.5 ± 2.1a	27.4 ± 4.6b	0.7 ± 1.9a	13.4 ± 4.2b
IW + ESP	12.8 ± 2.9	49.8 ± 3.4b	3.3 ± 2.2a	42.1 ± 0.2b	14.8 ± 2.1a	44.5 ± 2.9b	5.3 ± 1.5a	39.2 ± 4.1b
IO + GT	39.1 ± 1.9a	82.5 ± 2.8b	32.6 ± 1.8a	63.3 ± 3.6b	43.1 ± 1.0a	86.7 ± 0.9b	36.7 ± 0.9a	54.0 ± 3.8b
IO + RW	23.9 ± 2.3a	34.9 ± 2.4b	11.7 ± 1.7a	36.8 ± 2.3b	28.0 ± 1.4a	49.5 ± 2.3b	15.7 ± 0.8a	45.0 ± 0.0b
IO + PJ	11.8 ± 2.1a	25.7 ± 1.4b	1.0 ± 1.9a	10.3 ± 1.5b	15.8 ± 1.2a	30.7 ± 3.0b	5.0 ± 1.0a	20.0 ± 2.5b
IO + ESP	15.1 ± 2.1a	47.0 ± 1.4b	5.6 ± 1.5a	28.0 ± 2.0b	19.1 ± 1.2a	41.0 ± 4.5b	9.6 ± 0.6a	33.7 ± 3.1b
IR + GT	32.7 ± 1.4a	81.1 ± 1.3	26.2 ± 1.3a	68.5 ± 0.5b	42.8 ± 0.7a	77.8 ± 2.4b	36.4 ± 0.6a	60.2 ± 2.4b
IR + RW	17.5 ± 1.8a	49.8 ± 0.5b	5.3 ± 1.2a	34.3 ± 2.0b	27.7 ± 1.2a	57.6 ± 2.0b	15.4 ± 0.6a	37.7 ± 2.4b
IR + PJ	5.4 ± 1.5a	28.0 ± 4.2b	−5.4 ± 1.3a	24.1 ± 1.2b	15.5 ± 0.9a	23.0 ± 2.5b	4.7 ± 0.7a	18.9 ± 2.7b
IR + ESP	8.7 ± 1.6a	59.2 ± 0.5b	−0.8 ± 0.9a	34.6 ± 1.6b	18.8 ± 1.0a	58.8 ± 4.8b	9.3 ± 0.3a	33.0 ± 3.0b

[a]Different letters indicate the statistical significance of difference at $p < 0.05$ for each estimated−measured pair. [b]IW, insoluble wheat; IR, insoluble rye; IO, insoluble oat; GT, green tea; RW, red wine; PJ, pomegranate juice; ESP, espresso.

width, 49.82 G; sweep time, 60 s; smooth, 0; steps, 4096; number, 1 pass; modulation, 1000 mG; Mw atten, 10 dB; gain, 2; E,1.

Statistical Analysis. The analytical data were reported as the mean ± standard deviation of duplicate independent measurements. The significance of mean differences was determined by independent Samples *t* test using SPSS version 17.0.

RESULTS AND DISCUSSION

Antioxidant Activity Measurement by ESR Spectroscopy Assay. Table 1 gives the relative decrease (%) in the intensity of measured and estimated ESR signal values for the mixtures of insoluble grains and beverages rich in antioxidants. The antioxidant activities of samples were determined as their ability to reduce the stable Fremy's salt radical as measured by ESR spectrometer. Diamagnetic reduction products are formed, which are ESR-invisible, when antioxidant compounds scavenge Fremy's salt radicals, leading to a decrease in the ESR signal.[27] The percentage decrease in the intensity of ESR signal was determined for insoluble grains, beverages, and pure antioxidant compounds separately, and the decrease in the ESR signal for combinations of grains with beverages/pure antioxidant solutions was calculated by using these data. At the same time, the experiments were performed for combinations of grains with beverages/pure antioxidant solutions. Estimated

DOI: 10.1021/acs.jafc.5b00009
J. Agric. Food Chem. 2015, 63, 2338−2343

Table 4. Estimated and Measured Relative Inhibition Values (Percent)[a] of Lipid Oxidation for Different Mixture Combinations of Insoluble Grains with Solutions of Pure Antioxidants

	inhibition of lipid oxidation for different mixture combinations (%)							
	5 mg/mL of insoluble grain				10 mg/mL of insoluble grain			
	100 μM pure compound		500 μM pure compound		100 μM pure compound		500 μM pure compound	
mixture[b]	estimated	measured	estimated	measured	estimated	measured	estimated	measured
IW + CGA	37.7 ± 2.6a	66.9 ± 4.0b	42.7 ± 2.2a	93.8 ± 0.5b	39.7 ± 1.9a	61.3 ± 3.5b	44.7 ± 1.5a	93.3 ± 2.6b
IW + EC	34.9 ± 2.4a	88.3 ± 0.9b	40.2 ± 2.2a	94.5 ± 0.6b	36.9 ± 1.7a	89.6 ± 0.5b	42.3 ± 1.4a	93.6 ± 1.9b
IW + ECG	41.7 ± 3.0a	94.6 ± 2.5b	41.8 ± 2.6a	96.5 ± 0.8b	43.7 ± 2.2a	96.4 ± 0.3b	43.8 ± 1.8a	94.7 ± 1.6b
IW + EGC	42.2 ± 2.4a	90.7 ± 1.1b	39.9 ± 3.4a	83.7 ± 1.4b	42.0 ± 1.7a	89.6 ± 0.2b	41.2 ± 2.7a	56.7 ± 6.5b
IW + EGCG	42.2 ± 2.1a	91.5 ± 1.4b	42.2 ± 2.1a	96.5 ± 1.3b	44.3 ± 1.4a	93.5 ± 3.1b	44.3 ± 1.4a	94.2 ± 1.7b
IO + CGA	40.0 ± 1.9a	60.3 ± 4.2b	45.0 ± 1.4a	93.9 ± 1.7b	40.0 ± 1.0a	59.6 ± 3.9b	49.0 ± 0.5a	94.7 ± 0.5b
IO + EC	37.2 ± 1.6a	88.7 ± 2.6b	42.5 ± 1.4a	92.4 ± 3.7b	41.2 ± 0.7a	89.2 ± 1.7b	46.6 ± 0.5a	95.8 ± 0.7b
IO + ECG	44.0 ± 2.2a	93.6 ± 2.2b	44.1 ± 1.8a	94.2 ± 0.3b	48.0 ± 1.3a	95.6 ± 0.7b	48.1 ± 0.9a	92.7 ± 0.7b
IO + EGC	42.3 ± 1.7a	91.8 ± 1.3b	41.5 ± 2.6a	91.9 ± 1.7b	46.3 ± 0.7a	91.5 ± 1.0b	45.5 ± 1.7a	93.2 ± 1.6b
IO + EGCG	44.5 ± 1.3a	96.4 ± 0.5b	44.5 ± 1.4a	97.1 ± 0.0b	48.6 ± 0.4a	96.4 ± 0.9b	48.5 ± 0.5a	100.0 ± 2.5b
IR + CGA	33.6 ± 1.3a	62.4 ± 0.9b	38.6 ± 0.9a	94.9 ± 0.7b	43.7 ± 0.7a	63.0 ± 3.9b	48.7 ± 0.3a	94.7 ± 0.5b
IR + EC	30.8 ± 1.1a	84.0 ± 4.7b	36.1 ± 0.9a	94.4 ± 0.3b	40.9 ± 0.5a	90.5 ± 1.1b	46.2 ± 0.3a	92.6 ± 1.0b
IR + ECG	37.6 ± 1.7a	94.4 ± 3.9b	37.7 ± 1.2a	97.4 ± 2.3b	47.7 ± 1.1a	96.4 ± 1.4b	47.8 ± 0.6a	96.9 ± 3.3b
IR + EGC	35.8 ± 1.1a	89.2 ± 1.5b	35.0 ± 2.1a	91.8 ± 1.0b	46.0 ± 0.5a	89.7 ± 0.9b	45.2 ± 1.5a	90.2 ± 2.6b
IR + EGCG	38.1 ± 0.8a	93.4 ± 2.1b	38.1 ± 0.8a	92.7 ± 3.8b	48.3 ± 0.2a	90.4 ± 6.9b	48.2 ± 0.2a	92.3 ± 1.9b

[a]Different letters indicate the statistical significance of difference at $p < 0.05$ for each estimated−measured pair. [b]IW, insoluble wheat; IR, insoluble rye; IO, insoluble oat; CGA, chlorogenic acid; EC, epicatechin; ECG, epicatechin gallate; EGC, epigallocatechin; EGCG, epigallocatechin gallate.

data were obtained by summing the halves of the percentage decreases (%) in the intensities of ESR signals separately measured for the concentrations/dilutions of insoluble grains and beverages/pure antioxidant compounds, which were used to make 1:1 combination.

In general, an almost linear relationship was observed between the mixture volume added to the reaction medium and estimated/measured values of decrease in the ESR signals. The measured values of decrease in the intensity of ESR signals were significantly higher than the estimated ones for combinations of almost all insoluble grains with all beverages used, pointing toward a clear synergistic effect ($p < 0.05$). Among beverages, green tea showed the highest synergistic effect, whereas pomegranate juice showed the lowest one with all grain varieties. For insoluble grains the synergistic effect was highest for oat and lowest for wheat (Table 1).

Table 2 gives the relative decrease (%) in the intensity of measured and estimated ESR signal values for the mixtures of insoluble grains and pure antioxidants. It is clear from the results that replacing pure antioxidant solutions for antioxidant-rich beverages as the source of soluble antioxidants did not change the synergistic behavior observed between insoluble grains and soluble antioxidants. Particularly, the percentage decrease in the ESR signals measured with EC and EGCG was remarkably higher, pointing toward a stronger synergism. This result becomes meaningful, considering that EC and EGCG are the main antioxidants in green tea. Overall, the results suggested that both pure antioxidants and beverages rich in soluble antioxidants are effective synergistic agents of DF-bound antioxidants.

Prevention of Lipid Oxidation in Liposomes. The insoluble grains, beverages, and pure antioxidant solutions and combinations of insoluble grains with beverages/pure antioxidant solutions were also tested for their ability to inhibit lipid oxidation in a liposome system. Because liposomes allow investigations of both water and lipid-soluble antioxidants in the same system, it can be considered as a proper model of biological membranes.[28]

Table 3 gives estimated and measured inhibition of lipid oxidation (%) for different mixture combinations of insoluble grains with beverages rich in antioxidants. The potential inhibition of lipid oxidation values was estimated by summing the halves of the inhibition data (%) separately measured for the concentrations/dilutions of insoluble grains and pure antioxidant solutions/beverages, which were used to make a 1:1 combination. The inhibition of lipid oxidation measured for real combinations was significantly higher than those estimated for all beverage-insoluble grain combinations, showing a clear synergistic effect in agreement with the ESR assay results ($p < 0.05$). Espresso showed the highest synergistic effect among beverages, whereas oat was the most efficient synergist among insoluble grains. The combinations of insoluble grains with beverages had a slightly higher synergistic effect at low concentration of insoluble grains: the antioxidant activities of 5 mg−500 μM and 5 mg−100 μM combinations were higher than those of 10 mg−500 μM and 10 mg−100 μM combinations, respectively. The reason may most probably be the pro-oxidative behavior of insoluble grains in the liposome system due to the chain-carrying effect of DF phenolate groups.

In the liposome system, the antioxidant behavior of insoluble grains shifted to the pro-oxidant side, in contrast to the results obtained in the ESR assay, whereas the antioxidant role of beverages and pure antioxidant solutions remained the same (the results are not shown for single measurements of both insoluble and soluble antioxidants in the paper). The primary reason for this situation may be the metal ions, which are added to the liposomes from the fiber. Because ascorbate is present in the system, which is known to promote oxidation in the presence of metals, added metals from any source could explain the situation. In addition, it can be explained by the fact that the antioxidant activity depends not only on the chemical activity of the antioxidant molecules but also on the microenvironment of the reaction media.[29,30] Besides, the structure of antioxidants

DOI: 10.1021/acs.jafc.5b00009
J. Agric. Food Chem. 2015, 63, 2338−2343

such as ferulic acid bound in insoluble grains shows these to be more hydrophobic than the water-soluble antioxidants used, a difference that may restrict their interaction with the hydrophilic surfaces of liposomes. The DF phenolates may also create an environment for a chain-carrying effect due to the ease with which they form free radicals.[31]

Table 4 gives the estimated and measured inhibition of lipid oxidation (%) for different mixture combinations of insoluble grains with pure antioxidants. The combinations of insoluble grains with pure antioxidant solutions exerted the same synergistic behavior in liposome systems as for the insoluble grain−beverage combinations, low concentrations of insoluble grains causing a slightly higher synergistic effect. Among pure antioxidants, EC showed the highest synergetic effect, whereas CGA was the least effective with all insoluble grain types. It is a fact that ferulic acid is the dominant form of antioxidant bound to insoluble dietary fiber matrix. Its structural resemblance to CGA might be the reason for the pro-oxidant behavior of insoluble grains.

A proposed mechanism of the synergetic interaction between DF-bound antioxidants and soluble antioxidants is explained in Figure 1 for radical scavenging confirmed by ESR-based

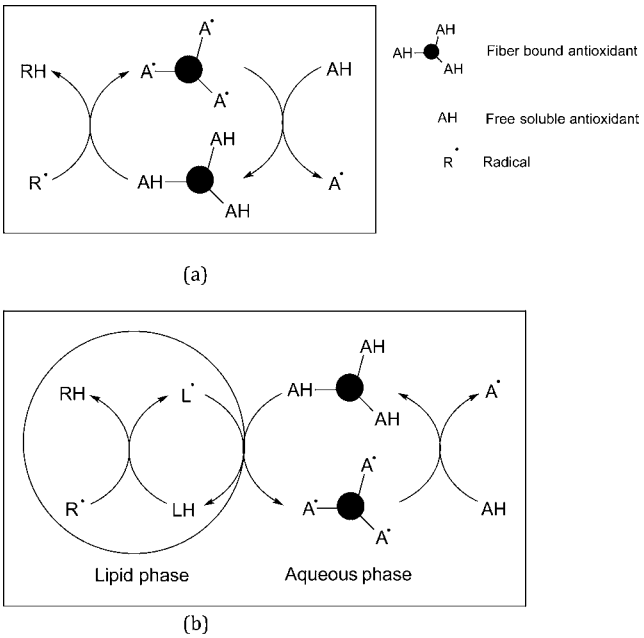

Figure 1. Synergistic antioxidant mechanism of dietary fiber bound antioxidants via regeneration by free soluble antioxidants: (a) radical scavenging confirmed by ESR-based Fremy's salt stable radical measurement; (b) inhibition of lipid oxidation in the liposome system confirmed by spectrophotometric measurement.

Fremy's salt stable radical measurement (a) and inhibition of lipid oxidation in a liposome system confirmed by spectrophotometric measurement (b). According to this proposal, in a medium containing stable radicals (i.e., Fremy's salt), an insoluble DF-bound antioxidant will scavenge a free radical, becoming an antioxidant radical itself. At this time, if soluble antioxidants exist in the medium, they will regenerate the DF-bound antioxidant, leading it to scavenge free radicals again. In the liposome system, an initiating factor (oxidizing agent in our experiment) will promote oxidation of the lipid phase, creating a lipid radical, which will revert to its original form via gaining one hydrogen from a DF-bound antioxidant, leading it to become a radical itself. At this point, if soluble antioxidants exist in the medium, they will regenerate the DF-bound antioxidant, leading it to exert its antioxidant effect against lipid oxidation.

If we want to adapt the proposed mechanism to the human GI tract, we should consider the metabolism of DF-bound antioxidants first. When we consume cereal products, the bound antioxidants, which exert their health effects already in the mouth, will part from the soluble fraction at the upper GI tract, bypass the digestion there, and reach the colon intact bound to the DF matrix. Then the colonic microbiota can start a slow and continuous release of bound antioxidants from the fiber matrix via fermentation. The antioxidants released will start to scavenge the radicals that are naturally found in the colon and create a healthy antioxidant environment there, at the expense of the antioxidants, which become radicals.

At this point, if free soluble antioxidants are available in the colon environment, they will react with the DF-bound antioxidant radicals to regenerate the bound antioxidant radicals and will help to maintain the healthy antioxidant environment created (soluble antioxidants will react with DF-bound antioxidants in any part of the GI tract as well). In this way, the advantage of soluble antioxidants will also increase and be prolonged in contrast to a sudden peak in plasma antioxidant capacity followed by rapid disappearance as normally seen.

As a result of the reaction between DF-bound antioxidants and soluble antioxidants, either synergistic or additive or antagonistic effects will occur. Within this framework, the potential synergistic effect has been investigated in the present study. According to the results, a clear synergism was observed between DF-bound antioxidants and frequently consumed beverages as well as pure antioxidant solutions tested at two different stages of oxidation. The synergistic effects of the materials tested differed due to the different stages of oxidation under investigation; that is, green tea showed the highest synergistic effect in the ESR assay, whereas espresso showed the highest synergistic effect in the liposome assay. In addition, synergetic effects of different combinations changed depending not only on the type of antioxidant compounds present and their concentration but also on the ratios at which they are mixed as mentioned in an earlier study of Zanfini et al.[32] For example, green tea catechins, which were found to be good synergists in this study, can also enhance lipid peroxidation and create an antagonistic effect.[33] However, the clear synergism demonstrated for green tea and its phenolic antioxidant with DF-bound antioxidants is also in good agreement with the result of other studies.[34]

In conclusion, the presence of the synergistic effect between DF-bound antioxidants and soluble antioxidants, which is evidenced by this study, is important because of its possibility to occur in the GI tract. The synergistic effect was demonstrated both for the capacity of the antioxidants as radical scavengers and for the formation of secondary lipid oxidation products. This work will constitute the basis for future studies exploring the synergistic behavior of DF-bound antioxidants with water-soluble antioxidants.

AUTHOR INFORMATION

Corresponding Author

*(V.G.) Phone: +90 312 2977108. Fax: +90 312 2992123. E-mail: vgokmen@hacettepe.edu.tr.

Notes

The authors declare no competing financial interest.

DOI: 10.1021/acs.jafc.5b00009
J. Agric. Food Chem. 2015, 63, 2338−2343

REFERENCES

(1) Belderok, B. Developments in bread-making processes. *Plant Food Hum. Nutr.* **2000**, *55*, 1−14.

(2) Lambo, A. M.; Oste, R.; Nyman, M. E. Dietary fibre in fermented oat and barley β-glucan rich concentrates. *Food Chem.* **2005**, *89*, 283−293.

(3) Saura-Calixto, F. Dietary fiber as a carrier of dietary antioxidants. *J. Agric. Food Chem.* **2011**, *59*, 43−49.

(4) Mellen, P. B.; Walsh, T. F.; Herrington, D. M. Whole grain intake and cardiovascular disease: a meta-analysis. *Nutr. Metab. Cardiovasc.* **2007**, *18*, 283−290.

(5) de Munter, J. S. L.; Hu, F. B.; Spiegelman, D.; Franz, M.; van Dam, R. M. Whole grain, bran, and germ intake and risk of type 2 diabetes: a prospective cohort study and systematic review. *PLoS Med.* **2007**, *48*, No. e261.

(6) Melanson, K. J.; Angelopoulos, T. J.; Nguyen, V. T.; Martini, M.; Zukley, L.; Lowndes, J.; Dube, T. J.; Fiutem, J. J.; Yount, B. W.; Rippe, J. M. Consumption of whole-grain cereals during weight loss: effects on dietary quality, dietary fibre, magnesium, vitamin B-6, and obesity. *J. Am. Diet. Assoc.* **2006**, *106*, 1380−1388.

(7) Jacobs, D.; Marquart, L.; Slavin, J.; Kushi, L. Whole grain intake and cancer: an expanded review and meta-analysis. *Nutr. Cancer* **1998**, *30*, 85−96.

(8) Erkkila, A. T.; Herrington, D. M.; Mozaffarian, D.; Lichtenstein, A. H. Cereal fibre and whole-grain intake are associated with reduced progression of coronary-artery atherosclerosis in post-menopausal women with coronary artery disease. *Am. Heart J.* **2005**, *150*, 94−101.

(9) Jacobs, D. R.; Pereira, M. A.; Meyer, K. A.; Kushi, L. H. Fibre from whole grains, but not refined grains is inversely associated with all-cause mortality in older women: the Iowa Women's Health Study. *J. Am. Coll. Nutr.* **2000**, *19*, 326S−330S.

(10) Jensen, M. K.; Koh-Banerjee, P.; Hu, B. F.; Franz, M.; Sampson, L.; Grønbaek, M.; Rimm, E. B. Intakes of whole grains, bran, and germ and the risk of coronary heart disease in men. *Am. J. Clin. Nutr.* **2004**, *80*, 1492−1499.

(11) Koh-Banerjee, P.; Franz, M.; Sampson, L.; Liu, S.; Jacobs, D. R., Jr.; Spiegelman, D.; Willett, W.; Rimm, E. Changes in wholegrain, bran, and cereal fibre consumption in relation to 8-y weight gain among men. *Am. J. Clin. Nutr.* **2004**, *80*, 1237−1245.

(12) Vitaglione, P.; Aurora, N.; Fogliano, V. Cereal dietary fibre: a natural functional ingredient to deliver phenolic compounds into the gut. *Trends Food Sci. Technol.* **2008**, *19*, 451−463.

(13) Griendling, K. K.; FitzGerald, G. A. Oxidative stress and cardiovascular injury: Part II: Animal and human studies. *Circulation* **2003**, *108*, 2034−2040.

(14) Rao P, S.; Kalva, S.; Yerramilli, A.; Mamidi, S. Free radicals and tissue damage: role of antioxidants. *Free Radical Antioxid.* **2011**, *1*, 2−7.

(15) Haliwell, B. Antioxidants in human health and disease. *Annu. Rev. Nutr.* **1996**, *16*, 33−50.

(16) Diplock, A. T. Antioxidants and disease prevention. *Mol. Aspects Med.* **1994**, *15*, 293−376.

(17) Esterbauer, H.; Gebicki, J.; Puhl, H.; Jurgens, G. The role of lipid peroxidation and antioxidants in oxidative modification of LDL. *Free Radical Biol. Med.* **1992**, *13*, 341−390.

(18) Bryans, J. A.; Judd, P. A.; Ellis, P. R. The effect of consuming instant black tea on postprandial plasma glucose and insulin concentrations in healthy humans. *J. Am. Coll. Nutr.* **2007**, *26*, 471−477.

(19) Rondini, L.; Peyrat-Maillard, M. N.; Marsset-Baglieri, A.; Fromentin, G.; Durand, P.; Tome, D.; Prost, M.; Berset, C. Bound ferulic acid from bran is more bioavailable than the free compound in rat. *J. Agric. Food Chem.* **2004**, *52*, 4338−4343.

(20) Uri, N. Mechanisms of autoxidation. In *Autoxidation and Antioxidants*; Lundberg, W. O., Ed.; Wiley: New York, 1961.

(21) Graversen, H. B.; Becker, E. M.; Skibsted, L. H.; Andersen, M. L. Antioxidant synergism between fruit juice and alpha-tocopherol. A comparison between high phenolic black chokeberry (*Aronia melanocarpa*) and high ascorbic blackcurrant (*Ribes nigrum*). *Eur. Food Res. Technol.* **2008**, *226*, 737−743.

(22) Miller, N. J.; Rice-Evans, C. Antioxidant activities of flavonoids as bioactive components of food. *Biochem. Soc. Trans.* **1996**, *24*, 790−794.

(23) Roberts, W. G.; Gordon, M. H. Determination of the total antioxidant activity of fruits and vegetables by a liposome assay. *J. Agric. Food Chem.* **2003**, *51*, 1486−1493.

(24) Çelik, E. E.; Gökmen, V.; Fogliano, V. Soluble antioxidant compounds regenerate the antioxidants bound to insoluble parts of foods. *J. Agric. Food Chem.* **2013**, *61*, 10329−10334.

(25) De Gobba, C.; Tompa, G.; Otte, J. Bioactive peptides from caseins released by cold active proteolytic enzymes from *Arsukibacterium ikkense*. *Food Chem.* **2014**, *165*, 205−215.

(26) Tirmenstein, M. A.; Pierce, C. A.; Leraas, T. L.; Fariss, M. W. A fluorescence plate reader assay for monitoring the susceptibility of biological samples to lipid peroxidation. *Anal. Biochem.* **1998**, *265*, 246−252.

(27) Rødjter, A.; Skibsted, L. H.; Andersen, M. L. Antioxidative and prooxidative effects of extracts made from cherry liqueour promace. *Food Chem.* **2006**, *99*, 6−14.

(28) Altunkaya, A.; Eleonora, M. C.; Gökmen, V.; Skibsted, L. H. Antioxidant activity of lettuce extract (*Lactuca sativa*) and synergism with added phenolic antioxidants. *Food Chem.* **2009**, *115*, 163−168.

(29) Liu, Z. Q.; Yu, W.; Liu, Z. L. Antioxidative and prooxidative effects of coumarin derivatives on free radical initiated and photosensitized peroxidation of human low-density lipoprotein. *Chem. Phys. Lipids* **1999**, *103*, 125−135.

(30) Yu, W.; Lin, Z. Q.; Liu, Z. L. Antioxidant effect of coumarin derivatives on free radical initiated and photosensitized peroxidation of linoleic acid in micelles. *J. Chem. Soc., Perkin Trans. 2* **1999**, 969−974.

(31) Çelik, E. E.; Gökmen, V. Investigation of the interaction between soluble antioxidants in green tea and insoluble dietary fiber bound antioxidants. *Food Res. Int.* **2014**, *63*, 266−270.

(32) Zanfini, A.; Corbini, G.; La Rosa, C.; Dreassi, E. Antioxidant activity of tomato extracts and interactions between carotenoids and α-tocopherol in synthetic mixtures. *Food Sci. Technol.−LEB* **2010**, *43*, 67−72.

(33) Niki, E. Lipid antioxidants: how they may act in biological systems. *Br. J. Cancer Suppl.* **1987**, *55*, 153−157.

(34) Terao, J.; Piskula, M.; Yao, Q. Protective effect of epicatechin, epicatechin gallate, and quercetin on lipid-peroxidation in phospholipid-bilayers. *Arch. Biochem. Biophys.* **1994**, *308*, 278−284.

DOI: 10.1021/acs.jafc.5b00009
J. Agric. Food Chem. 2015, 63, 2338−2343

Table 1. Nutritional Values of *P. stratiotes* (% of dry mass)

	this study	ref 5	ref 63	ref 64	ref 9	ref 65[a]	ref 66	ref 1	ref 67	ref 15
N			2.2				2.1			
K	2.3	3.3	4.7							
P	0.3	0.6		0.9		0.5	0.2			
Ca	2.8	0.5		2.8		1.5				
PO_4			0.4							
Na	0.3	1.4								
crude protein		21		20	14	11		14	15	
crude fat		3.8		4.2		2.3				
crude fiber		19		13	22	7				
ash		17		27	30	15				34
nitrates		1.3								
polyphenols		2.1								
lignin							9.1			
calories (cal g^{-1})					3.8					
dry matter (% of FW)		5.3	7.1			7.7				

[a]Only total amounts in fresh mass were given in the original work. Values listed above were recalculated on dry mass.

hyperaccumulative properties for several risk elements such as Cd, Hg, and Pb.[13] Whereas the Pb concentration in conventional plants is usually very low, Pb levels in PS growing on polluted areas can increase by up to 1.48[14] and 15.76 mg kg^{-1}.[15] Moreover, after cultivation in a 1 mmol L^{-1} Pb solution, an incredibly high Pb concentration of 203 g kg^{-1} was observed[16] under artificial conditions.

EU Directive 2002/32/EC[17] set the maximal permissible limits for Pb in green fodder at 30 mg kg^{-1}. However, even slightly increased levels of this metal in forage crops may negatively affect the health of both animal and human consumers because Pb is toxic to the organism, even when absorbed in small amounts. Recently, it has been demonstrated that the trace element toxicity of food is dependent on more than just their total concentration. With regard to the risk of feed intake, the bioaccesssibility and bioavailability of trace elements are crucial factors. Bioaccessibility (BAC) is theoretically the amount of substance that is soluble in the gastrointestinal environment, i.e., fraction that is released from the matrix into the gastrointestinal tract during the digestion process and, thus, becomes available for intestinal absorption and can enter the bloodstream.[18] Bioavailability (BAV) is the general term used to describe the absorption of a contaminant into the body of an exposed subject. Absolute bioavailability (ABAV) is the proportion of the contaminant in the administered dose that is absorbed into the test organism.

To evaluate bioaccessible fractions of contaminants, several *in vitro* approaches have been developed in attempts to mimic the effects of the digestion process in mammals. Generally, these approaches are commonly called simulated *in vitro* gastrointestinal extraction procedures. The physiologically based extraction test (PBET), an *in vitro* test system for predicting the bioavailability of metals from a solid matrix, is the most widely used to date. The PBET was designed primarily to evaluate the absolute risk element bioavailability from contaminated soil in the digestive tracts of children.[19] However, various modifications of this original technique have recently been made. With regard to risk element bioaccessibility in animal and human food, the PBET was previously used to determine bioaccessible portions of both essential and toxic elements in contaminated plant samples,[20,21] seaweed,[22] medicinal plants,[23] raw vegetables,[24] uncooked rice,[25] cooked vegetable soup,[26] walnuts,[27] and mussel tissue.[28] However, to the best of our knowledge, both the BAC and BAV of trace elements have never been evaluated simultaneously in any phyto hyperaccumulators, including *P. stratiotes*.

Because data concerning the total concentrations of both essential and risk elements in contaminated plant material provide little information about the possible nutritional values and toxic effects of this kind of forage, the PBET can be a useful tool in assessing the potential risk of its diet intake. Nevertheless, the results of *in vitro* procedures should always be accompanied and confirmed by *in vivo* trials. Therefore, the aims of this study were as follows: (i) to determine the potential bioaccessibility and real bioavailability of both essential and risk elements from *P. stratiotes* and (ii) to determine the effect of *P. stratiotes* biomass feed intake on the accumulation of elements in mammalian organisms. For this purpose, an *in vitro* PBET using artificial digestive solutions was conducted, followed by an *in vivo* feeding trial on laboratory rats. In the course of this experiment, essential (Cu, Fe, Mn, and Zn) and risk (Pb) element levels were determined within a simulated gastrointestinal tract and within several rat tissues (liver, kidney, muscle, bone, and intestinal wall).

MATERIALS AND METHODS

Chemicals. Nitric acid (65%, p.a. ISO, Merck), H_2O_2 (30%, TraceSelect, Fluka), an ASTASOL-CZ9098MN1 standard solution (Analytika, CR), ammonium dihydrogen phosphate GR (Merck), and certified reference material BRC 12-02-01 (bovine liver) were used in this study.

Apparatus. An MWS-3+ microwave digestion system (Berghof Products+Instruments) was equipped with Teflon digestion vessel DAP-60S.

An atomic absorption spectrometer with electrothermal atomization (ET-AAS, Varian AA 280Z) with graphite tube atomizer GTA 120 and a PSD 120 programmable sample dispenser was used. The inductively coupled plasma-atomic emission spectrometry (ICP-OES) (Varian VistaPro) instrument was equipped with a two-channel peristaltic pump, a Struman-Masters spray chamber, and a V-groove pneumatic nebulizer made of inert material.

***In Vitro* Evaluation of Bioaccessibility.** The PBET[20] was performed to assess bioaccessible portions of elements in the gastrointestinal tract as follows.

Gastric Solution (1 L volumetric flask). Pepsin (1.25 g), citric acid (0.5 g), malate (0.5 g), lactic acid (0.84 mL), and acetic acid (1 mL) were mixed with deionized water. The pH of the mixture was adjusted with concentrated HCl to 2.5 ± 0.05. Then 0.5 g of sample was mixed

DOI: 10.1021/jf5058099
J. Agric. Food Chem. 2015, 63, 2344−2354

in an 85 mL polypropylene bottle with 50 mL of the prepared gastric solution. The bottle was placed in a shaker bath at 37 °C and shaken for 1 h at 150 rpm. After centrifugation, a 5 mL aliquot was taken off and measured for element content.

Pancreatic Solution. Five milliliters of the fresh gastric solution was added to the remaining reaction mixture, and the pH was adjusted to 7 with a saturated $NaHCO_3$ solution. Later, 25 mg of pancreatin and 87.5 mg of bile salts were added. The sample was again shaken in the bath for 2 h and centrifuged, and the extract was then measured. The element contents in the extracts were determined by ICP-OES. Bioaccessible portions of Cu, Fe, Mn, Zn, and Pb were expressed as a percentage of total element concentration in both the control diet and *P. stratiotes* biomass.

***In Vivo* Evaluation of Bioavailability.** *Experimental Animals and Diet.* Adult male Wistar rats (*Rattus norvegicus*) were used as models for bioavailability evaluation. The animals were obtained from a commercial supplier (Institute of Physiology of the AS CR, Prague, Czech Republic) and randomly divided into two groups based on plant material intake: CO, commercial diet only (n = 6); PS, *P. stratiotes* intake (n = 9). The rats were placed separately into plastic metabolic cages (TecniPlast) and left to acclimatize for 7 days. They were kept in controlled conditions (temperature of 22 ± 2 °C, 12/12 h light/dark cycle), given commercial feed, and allowed to drink tap water *ad libitum*.

A complete feed mixture for SPF breeding rats was purchased from a commercial supplier (Velaz s.r.o.) and used as a control diet. The nutritional values, as declared by the manufacturer, are as follows: moisture, 12.5%; nitrogenous compounds, 24%; fiber, 4.4%; fat, 3.4%; ash, 6.8%; lysin, 14 g; methionine, 4.8 g; Ca, 11 g; P, 7.2 g; Na, 1.8 g; Cu, 20 mg; Se, 0.38 mg of dry weight. The PS-supplemented diet was prepared as follows. *P. stratiotes* specimens were cultivated in a Pb-enriched medium under greenhouse conditions.[29] Harvested biomass was dried. Dry mass was ground to a fine powder, and each single dose (25 mg) was then weighed and thoroughly mixed with 25 g of commercial feed. These batches were administered to rats daily for a period of 6 weeks. The PS biomass constituted approximately 0.1% of the feed ration. Data concerning feed consumption were recorded daily (see Table 3), whereas individual animal weight gains were recorded twice a week (Figure 1).

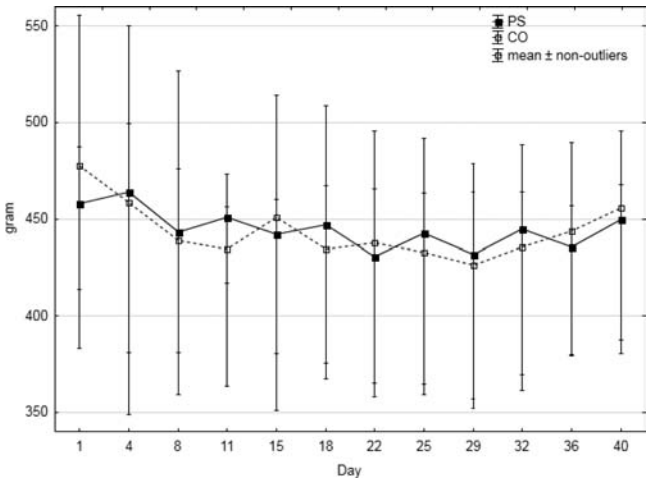

Figure 1. Weight gains of experimental animals.

All experiments with laboratory animals were conducted in compliance with the current laws of the Czech Republic (Act No. 246/1992 coll. on Protection Animals against Cruelty) and EC Directive 86/609/EEC. The experimental project was approved by the committee of the Ministry of Education, Youth and Sports, Czech Republic (approval code MSMT-31220/2014-7). Animal care was supervised by authorized personnel: Zuzana Čadková, Ph.D., recipient of the Central Commission for Animal Welfare Certificate CZ 02201.

Element Analysis of Rat Tissues. At the end of feeding trial, experimental animals were euthanized. Individual autopsies were conducted with Teflon instruments to obtain appropriate tissue samples (liver, kidney, testes, duodenal wall, femoral muscle, and bone) for element analyses. All tissues were weighed, properly washed in redistilled water, placed into Petri dishes, and stored at −20 °C until they underwent chemical analysis. Prior to element analysis, tissue samples (except bones) were freeze-dried and microwave digested in an acid-based mixture using the MWS-3+ microwave digestion system (Berghof Products+Instruments). The ET-AAS technique was used to determine element concentrations in all digested tissue samples of control groups, as well as in the liver, muscle, testes, and intestinal wall of PS-exposed groups.[30] The calibration curve for the measurement was prepared using the standard ASTASOL-CZ9098MN1 solution (Analytika). The evaluation of the obtained data was conducted using a standard addition method, and ammonium dihydrogen phosphate GR (Merck) was used as a matrix modifier. Samples with elevated Pb levels (kidneys and bones), along with the total element content in the PS biomass and in the control diet, were analyzed using ICP-OES (Varian VistaPro). Certified reference material BRC 12-02-01 (bovine liver) was simultaneously analyzed under the same conditions to assess analytical data quality (Table 2). Experimental data were adjusted

Table 2. Analytical Data Quality Assessment[a]

	CRM-BCR 12-02-01 certified value ($\mu g\ g^{-1}$) (mean ± SD)	CRM-BCR 12-02-01 determined value ($\mu g\ g^{-1}$) (mean ± SD)
Cu	26.3 ± 1.6	23.3 ± 3.0
Fe	495 ± 28	427 ± 51
Mn	7.6 ± 0.5	6.2 ± 0.5
Pb	0.71 ± 0.08	0.75 ± 0.09
Zn	162 ± 6.0	157 ± 5.5

[a]SD, standard deviation. CRM-BCR 12-02-01, certified reference material (bovine liver).

using the mean element concentrations in blanks (±3 standard deviations of blanks), which were prepared under the same conditions as were the tissue samples. Tissue samples were analyzed in two replicates, which were averaged for subsequent statistical processing. The relative element concentration in rat tissues was expressed in milligrams per kilogram of dry weight.

Total Element Levels in Rat Tissues. Total amounts of particular elements that accumulated in rat tissues (Table 3) were determined

Table 3. Total Feed Consumption and Element Intake during the *in Vivo* Trial[a]

	CO	PS
total feed consumption	1011[b]	992[c]
total Cu intake	0.023	0.022
total Fe intake	0.348	0.341
total Mn intake	0.114	0.112
total Zn intake	0.079	0.078
total Pb intake	0.002	0.037

[a]Mean values in grams per rat. [b]Total of 100% commercial diet for laboratory rodents ST1. [c]Total of 99.9% commercial diet for laboratory rodents ST1 + 0.1% of *P. stratiotes* dry mass.

using the element concentrations (milligrams per kilogram of fresh weight) together with the weight coefficient of individual rat tissues,[31] according to the following formula:

$$TEAT_{(mg)} = EC_{[mg\ (kg\ of\ FW^{-1})]} \times \text{animal weight}_{(kg)} \times SOWC \times 10^{-2}$$

where TEAT is the total element amount in tissue, EC the element concentration, FW the fresh weight, and SOWC the specific organ weight coefficient.[31]

DOI: 10.1021/jf5058099
J. Agric. Food Chem. 2015, 63, 2344−2354

Additionally, portions [$P_{(\%)}$] of the total Pb intake that accumulated in particular animal tissues were determined according to the folowing formula:

$$P_{(\%)} = \mathrm{TEAT}_{(mg)}/\mathrm{TI}_{(mg)} \times 100$$

where TI is the total intake.

Statistical Procedure. Data obtained from the *in vitro* PBET were assessed via Statistica version 12[32] using a Student's *t* test for dependent variables. Results of the *in vivo* feeding trial (differences in element tissue accumulations between animals from CO and PS groups) were analyzed using R version 3.1.1.[33] Because of the small number of animals used in our experiment (n = 15) and a significant number of potential interactions, we used separate tests for each monitored element. The basic *lme* model tested the general influence of a fixed effect "group" (CO vs PS) with control for a random effect "animal" with a nested factor "organ". The influence of individual animal variability was tested using AIC value comparison between a model that includes factor "animal" and a simplified model without this factor. In all cases (Cu, Fe, Mn, Pb, and Zn), AIC differences exceeded 50, favoring the simpler model. Finally, after factorial ANOVA with factors "group" and "organ", post hoc Tukey HSD tests were used to determine effect of diet (CO vs PS) on element concentrations in particular organs. An analogical approach was used for evaluation of differences in TAET values between PS and CO animals. To fit normality, data were log-transformed before applying the statistical models. However, to show the patterns more clearly, original values are presented in graphs and tables. The threshold for statistical significance was set at α = 0.05.

RESULTS

During the course of our experiment, the supplementing of daily feed rations with 0.1% PS dry mass did not significantly affect animal weight gains [*t* test, CO vs PS group (see Figure 1)]. The individual variance was mainly caused by nonuniform initial animal weights at the beginning of the experiment. Figure 1 shows that individual variation actually decreased during the feeding trial.

Total and Extracted Element Concentrations. Artificially cultivated *P. stratiotes* dry mass contained Fe, Mn, and Pb concentrations significantly higher than those of the control pellet feed. All three element concentrations were also significantly higher in the medium that simulated the gastric phase of PS digestion (pepsin extraction). In the artificial intestinal environment (pancreatin extraction), the PS digest showed significantly higher concentrations of all of the monitored elements, Cu, Fe, Mn, Zn, and Pb (Table 4).

***In Vitro* Bioaccessibility.** The PBET revealed that extraction of an element from PS biomass during the digestive process differs from that of conventional feed (Figures 2 and 3). In control feed, the BAC (%) of the majority of the monitored elements (Cu, Mn, Zn, and Pb) was higher (25−53%) in the gastric phase than in the intestinal fluid (9−20%). The most significant decrease was observed for Zn, a >5-fold decrease (from 53% in GP to 9% in IP). Fe BAC (%) from control feed showed a trend that was the opposite of those of previous elements. It was extremely low in GP (1%) and increased to 5% in a simulated intestinal environment. In PS biomass, the BAC (%) of all essential elements decreased significantly during the transition from the gastric phase (5−73%) to the intestinal phase (3−31%). As with control feed BAC, Fe BAC in PS was very low (5% in GP and 3% in IP), and Zn BAC dropped considerably (from 73 to 31%). Unlike control feed digestion, PS fed digestion exhibited almost twice the Pb BAC levels in the intestinal fluid (9%) as in the gastric phase (5%).

Table 4. Results (mean ± SD) of the *in Vitro* Experiment

	control feed (n = 3)	*P. stratiotes* (n = 3)	*t* test p value
	Total Element Concentration [mg (kg of DW)$^{-1}$]		
Cu	23 ± 5.3	25 ± 0.6	0.502
Fe	344 ± 24	991[a] ± 79	<0.001
Mn	113 ± 0.4	295[a] ± 25	<0.001
Zn	79 ± 6.5	73 ± 11	0.456
Pb	1.9 ± 0.4	14349[a] ± 1720	<0.001
	Element Concentration in the Gastric Phase (mg kg^{-1})		
Cu	5.5 ± 1.4	6.5 ± 0.2	0.307
Fe	3.7 ± 1.2	53[a] ± 1.4	<0.001
Mn	39 ± 9.4	122[a] ± 2.1	<0.001
Zn	40 ± 9.7	52 ± 0.3	0.103
Pb	0.5 ± 0.1	700[a] ± 19	<0.001
	Element Concentration in the Intestinal Phase (mg kg^{-1})		
Cu	4.4 ± 0.1	6.1[a] ± 0.2	<0.001
Fe	18 ± 1.6	32[a] ± 1.3	<0.001
Mn	16 ± 1.5	70[a] ± 2.4	<0.001
Zn	7.4 ± 0.7	22[a] ± 0.9	<0.001
Pb	0.2 ± 0.02	1319[a] ± 49	<0.001

[a]Significant differences (p < 0.001) between control feed and *P. stratiotes* biomass determined by a *t* test.

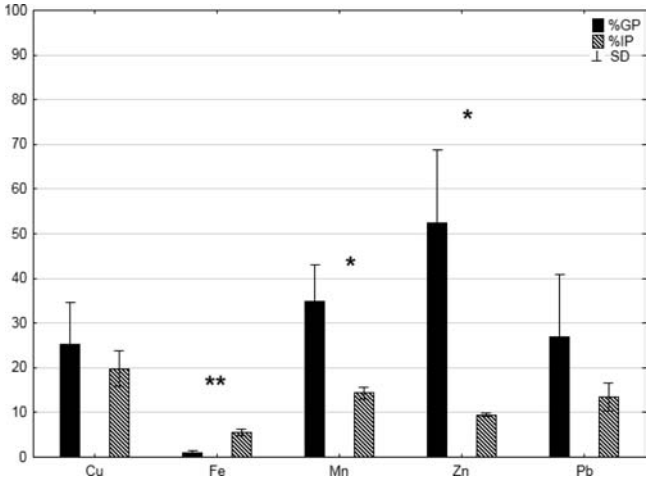

Figure 2. Control feed BAC (%) in gastric and intestinal phases of the PBET: GP, gastric phase; IP, intestinal phase; SD, standard deviation. Significant differences between GP and IP (*p < 0.05; **p < 0.01) determined by a pairwise *t* test.

***In Vivo* Bioavailability.** The accumulation of an element in rat tissues was expressed in two ways: (i) relative concentration in milligrams per kilogram of dry weight (DW) (Table 5) and (ii) total amount in milligrams (TEAT) (Figures 4A−F and 5). PS biomass intake affected element biokinetics in a rat. Supplementing the diet with Pb-loaded PS caused a significant increase in the total level of Pb accumulation (*lme*; F = 38.332; p < 0.0001). Compared to those of the CO group, the most intensive Pb growths were observed in bones (Tukey HSD test; p < 0.0001), kidneys (Tukey HSD test; p < 0.0001), and livers (Tukey HSD test; p < 0.0001). With regard to the Pb distribution in PS exposed animals (Table 6), the greatest portion of Pb accumulated in the skeleton (0.6%). Conversely, significantly lower (*lme*; F = 5.385; p < 0.05) Fe levels were observed in animals fed PS. Overall concentrations of Zn (*lme*; F = 3.94; p = 0.069), Mn (*lme*; F = 0.963; p = 0.344), and Cu (*lme*; F = 2.420; p = 0.144) were equal in both tested groups.

DOI: 10.1021/jf5058099
J. Agric. Food Chem. 2015, 63, 2344−2354

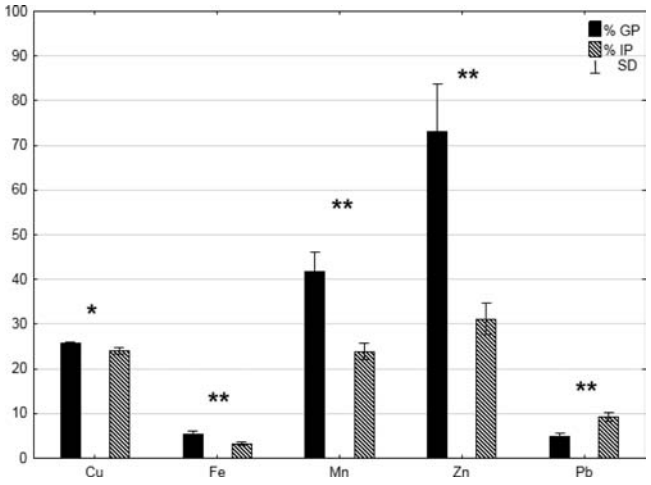

Figure 3. *P. stratiotes* biomass BAC (%) in gastric and intestinal phases of the PBET: GP, gastric phase; IP, intestinal phase; SD, standard deviation. Significant differences between GP and IP (*$p < 0.05$; **$p < 0.01$) determined by a pairwise t test.

Intestinal element levels were mainly influenced by diet because the intestinal walls of animals exposed to PS biomass had significantly smaller amounts of all monitored essential elements: Zn (Tukey HSD test; $p < 0.01$), Mn (Tukey HSD test; $p < 0.001$), Cu (Tukey HSD test; $p < 0.05$), and Fe (Tukey HSD test; $p < 0.0001$). With regard to TAET results, PS dietary intake reduced total Cu amounts in skeletons (Tukey HSD test; $p < 0.0001$) and increased Mn amounts in musculatures (Tukey HSD test; $p < 0.0001$). Zn levels in the testes of animals fed PS were considerably lower than in those of animals fed CO; however, the limit for statistical significance was not achieved (Tukey HSD test; $p = 0.09$).

DISCUSSION

***In Vitro* Bioaccessibility of Essential Elements.** In our experiment, the BAC (%) of Cu, Mn, and Zn in both analyzed types of feeds decreased significantly during the transition from the gastric phase to the intestinal phase. A similar trend can be found in the results of previous studies.[24,34] This decrease is most likely due to the fact that BAC of these elements correlates negatively with pH levels.[35] As with our results, previous study[20] concerning various leafy vegetables demonstrated the higher BAC of Mn and Zn in the gastric phase when compared to intestinal BAC. However, Cu BAC differs greatly between various matrices and extraction phases in several other works.[20,36,37] This variability may be related to Cu complexation with a wide spectrum of organic ligands that have various levels of degradability. On the basis of a high variability in previous *in vitro* BAC results summarized in Table 7, we can conclude that the identical microelements in different biological materials are bound to compounds with various grades of degradability for digestive enzymes. However, this presumption has to be verified through specific studies. Therefore, a particular extraction method as well as matrix characteristics should always be taken into account when assessing BAC. A generalization of this complex issue can lead to inaccuracy.

The behavior of iron in a simulated gastrointestinal tract differs considerably from that of Cu, Mn, and Zn. With regard to Fe in conventional plants, it usually has a very low BAC (only a few percent) under simulated stomach conditions; this is most likely due to the high content of phytates and phytosterols, which strongly bind Fe in an acidic environment. Subsequently, Fe BAC is enhanced in the artificial small intestine because Fe forms soluble complexes with chelating compounds, which are released in the intestinal juices during digestion. Because the most intensive nutrient absorption takes place in the small intestine, Fe BAC enhancement is crucial for sufficient Fe intake within the organism.

However, with regard to Fe extractability, a trend that is the opposite to that of a conventional plant was detected in phyto hyperaccumulators in a recent study[21] as well as in the experiment presented here. The reasons for this may be as follows. (1) Fe in hyperaccumulating plants may be bound to specific compounds, which have low solubility under intestinal conditions, or (2) elevated levels of risk elements in hyperaccumulating plants may reduce the extent of the transition of Fe from the gastrointestinal tract, which is due to antagonistic actions in intestinal fluids. Nevertheless, there is a lack of supporting information concerning this topic in the scientific literature, and the real reason for reduced Fe BAC from phyto hyperaccumulators under intestinal conditions must be elucidated. Even so, our current findings indicate that considerable consumption of these plant species could lead to a latent risk of severe Fe deficiency.

***In Vitro* Bioaccessibility of Pb.** Pb is generally considered to have a very low solubility. The main part of Pb in plant material is organically bound in the form of strong complexes

Table 5. Relative Element Concentrations[a] in Rat Tissues (milligrams per kilogram of dry weight)

organ	group	Cu	Fe	Mn	Zn	Pb
liver	CO	3.29 ± 0.38	203 ± 36.6	1.76 ± 0.16	23.9 ± 4.83	0.19 ± 0.16
	PS	3.79 ± 0.91	187 ± 23.4	1.95 ± 0.38	21.2 ± 2.81	1.06 ± 0.44[d]
kidney	CO	6.88 ± 1.39	104 ± 18.9	0.72 ± 0.14	24.9 ± 7.02	0.65 ± 0.75
	PS	7.56 ± 2.25	78.4 ± 7.31	0.73 ± 0.06	21.6 ± 2.21	6.34 ± 3.43[d]
bone	CO	0.64 ± 0.29	46.8 ± 15.5	0.32 ± 0.09	106 ± 50.1	0.14 ± 0.07
	PS	0.33 ± 0.08	37.7 ± 10.6	0.26 ± 0.05	106 ± 11.5	7.10 ± 4.21[d]
muscle	CO	1.17 ± 1.09	25.8 ± 12.2	0.13 ± 0.10	16.4 ± 12.3	0.05 ± 0.04
	PS	0.97 ± 0.34	18.0 ± 4.86	0.19 ± 0.08	14.0 ± 3.03	0.14 ± 0.08
intestine	CO	2.20 ± 0.30	26.9 ± 5.84	2.29 ± 1.15	33.2 ± 7.77	0.07 ± 0.02
	PS	1.24 ± 0.32[b]	11.2 ± 1.75[d]	1.06 ± 0.23[d]	17.9 ± 4.57[c]	0.25 ± 0.11[b]
testes	CO	1.76 ± 0.13	32.2 ± 7.65	0.31 ± 0.08	29.9 ± 7.39	0.08 ± 0.05
	PS	1.46 ± 0.25	25.1 ± 10.8	0.29 ± 0.10	20.3 ± 4.00	0.18 ± 0.18

[a]Values expressed as means ± SD. [b]Significant differences between CO and PS group (Tukey HSD tests). $p < 0.05$. [c]Significant differences between CO and PS group (Tukey HSD tests). $p < 0.01$. [d]Significant differences between CO and PS group (Tukey HSD tests). $p < 0.001$.

DOI: 10.1021/jf5058099
J. Agric. Food Chem. 2015, 63, 2344−2354

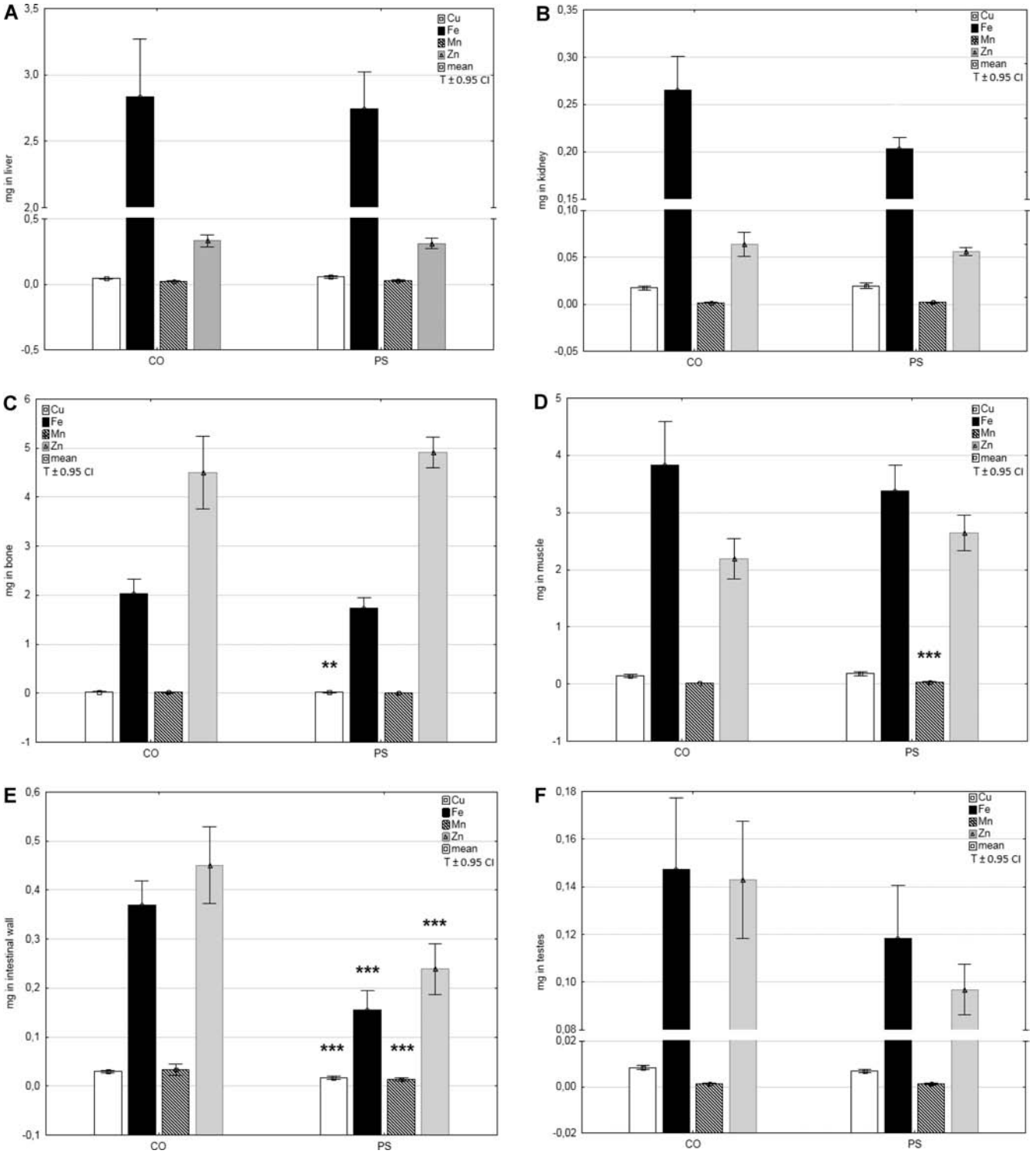

Figure 4. (A) Total essential elements in livers. (B) Total essential elements in kidneys. (C) Total essential elements in skeletons. (D) Total essential elements in musculatures. (E) Total essential elements in intestinal walls. (F) Total essential elements in testes. Significant differences between CO and PS groups (**$p < 0.01$; ***$p < 0.001$) based on factorial ANOVA and post hoc Tukey HSD tests.

(biomacromolecules), which are not dissociated even in a stomach environment.[27] Up to 99% of Pb can be insoluble because of chelation with polyphenols, phytosterols, or di- and monoacylglycerols.[38] When the Pb bioaccessible fractions from PS were compared to those from other biological materials (Table 7), considerably low levels (5−9%) were observed in our experiment. This may be due to relatively high polyphenol content in *P. stratiotes*, which was previously reported.[11,39]

According to previous studies,[21,24,40] Pb BAC is usually higher in the stomach than in the small intestine. This is due to the oxidation of elementary Pb forms at low pH levels. Pb dissolution in an acidic stomach environment is strongly pH-dependent[42] because the extent of dissolution is decreased by

DOI: 10.1021/jf5058099
J. Agric. Food Chem. 2015, 63, 2344−2354

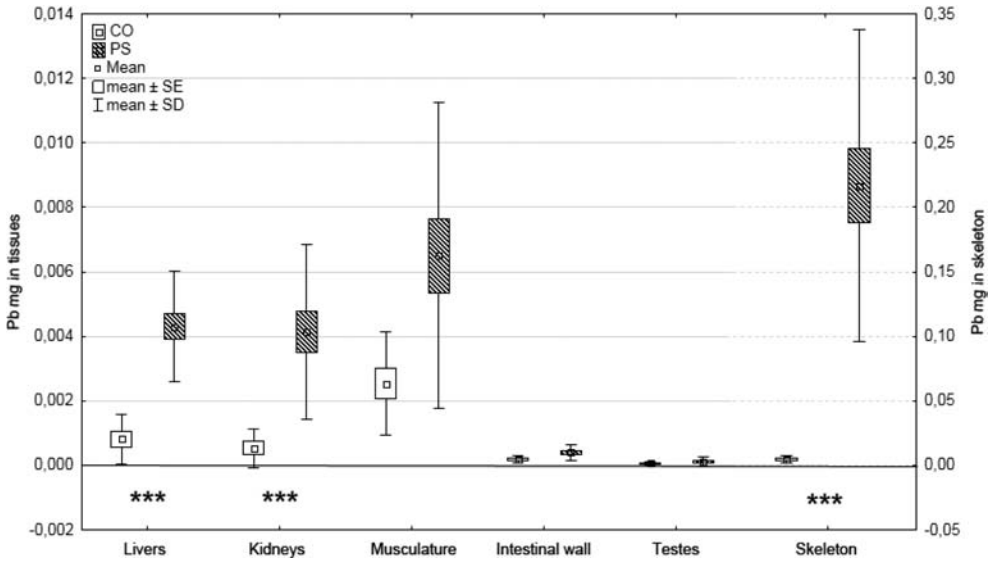

Figure 5. Total Pb in rat tissues. Significant differences between CO and PS groups (***$p < 0.001$) based on factorial ANOVA and post hoc Tukey HSD tests. Please note the different scale of skeleton Pb values.

Table 6. Accumulation of Pb in the Body from a PS diet (expressed as a percent of total Pb intake)

tissue	total Pb intake[a] (mg)	estimated tissue mass[a] (g)	element concentration[a] [mg (kg of FW)$^{-1}$]	portion of Pb intake (%)
intestinal wall	36 ± 3	13.9 ± 1.03	0.03 ± 0.02	0.0001
testes		4.95 ± 0.36	0.02 ± 0.03	0.0001
liver		14.7 ± 1.65	0.25 ± 0.13	0.01
kidney		2.70 ± 0.20	1.22 ± 0.94	0.01
musculature		197 ± 14.5	0.03 ± 0.02	0.02
skeleton		48.1 ± 3.55	3.59 ± 2.89	0.6
total				0.64

[a]Values are expressed as means ± SD.

65% when the stomach pH is increased from 1.3 to 2.5.[41] Under neutral-pH intestinal conditions, BAC can drop by around 70%. This is most likely due to reactions such as precipitation and re-adsorption, which are responsible for losses of soluble Pb.[35,43] Moreover, Pb can also be re-adsorbed on solid residues in chyme.[27]

The Pb BAC pattern of control feed in our experiment was in accordance with this presumption. On the contrary, Pb BAC from PS biomass under intestinal conditions was twice as high as that in an artificial stomach environment. Similar results regarding elevated intestinal BAC were observed in leafy and root vegetables and in mussels.[20,28] An enhanced Pb BAC level from PS in the small intestine poses a risk of excessive absorption into the exposed organism.

***In Vivo* Bioavailability of Essential Elements.** Total concentrations of essential elements detected in PS biomass are in good agreement with the previously defined metal composition of conventional plants.[44] The total Fe and Mn concentrations were significantly higher in PS biomass than in control feed. Moreover, simulated gastric as well as intestinal PS extracts exhibited higher concentrations of all essential elements when compared to those of the control feed. Regardless, there was no general elevation in tissue microelement concentrations detected in PS-fed animals. This is most likely due to two factors. First, essential element homeostasis in mammalian organisms allows a wide range of element intake without any marked effects. Second, the selected level of PS added to the diet (0.1%) was too low, and the experimental period (40 days) was too short to produce relevant changes.

In our experiment, the *in vivo* BAV was evaluated in two ways: (i) based on the final tissue Pb concentrations, which is actually one of standard methods for BAV evaluation, and (ii) based on total Pb amounts (TEAT), which were accumulated throughout the entire organ structure using the organ weight coefficient.[31] This represents a new and unique approach to BAV assessment. A principal advantage of this approach is the fact that it reflects individual weights of exposed animals. Moreover, our results showed that TEAT is able to detect differences in biokinetics of specific elements more sensitively than the conventional method.

Generally, animals fed PS biomass exhibited predominantly lower essential element levels in the tissues than did the control group (Figure 4A–F). Cu TEATs detected in the skeletons of PS animals were significantly lower than those in the CO group. This may be due to element interaction in the digestive tract, because a high intake of Fe, Zn, and/or Mn can interfere with Cu absorption and reduce the rate of transit of Cu through the intestinal wall.[45,46] The decreased Zn TEAT observed in the testes of PS-fed animals can pose a serious health problem because adequate Zn levels are crucial for an antioxidant defense of this organ. An interesting result of our study was that the intestinal wall of the animals exposed to PS biomass had significantly smaller amounts of all monitored essential elements. Such reduction most likely reflects some kind of imbalance in the absorption process. A suppressed transport of essential elements may be related to one of the following: (i) Pb competition for protein binding sites in the intestinal epithelium,[47] (ii) the inhibitory activities of *Pistia* tannins on digestive enzymes,[39] and (iii) reduced essential element absorption caused by the presence of phytic acids.[48,49]

***In Vivo* Bioavailability of Pb.** Despite extremely high total Pb concentrations in PS biomass and high Pb concentrations extracted into artificial gastrointestinal fluids, the BAV fractions of this element detected in rat bodies were rather low. After a 40 day feeding trial, <1% of the administered Pb dose was stored in monitored rat tissues (see Table 6). However,

DOI: 10.1021/jf5058099
J. Agric. Food Chem. 2015, 63, 2344−2354

Table 7. Comparison of Cu, Fe, Mn, Zn, and Pb BAC (%) in Different Organic Matrices

material	digestion phase	Cu	Fe	Mn	Zn	Pb	ref
control feed	gastric	25	1	35	53	26	this experiment
	intestinal	20	5	14	9	13	
P. stratiotes	gastric	25	5	41	73	5	
	intestinal	24	3	23	31	9	
Bacopa monnieri	gastric	17	6.5	69	33	13	21
	intestinal	45	2	32	12	7	
marked vegetable	gastric	33			51	30	24
	intestinal	11			27	12	
mussels (CMR)	gastric	24		45		0	28
	intestinal	67		40		9	
mussels from polluted area	gastric	33		44		18	
	intestinal	33		25		10	
tea leaves (CRM)	gastric	5		52			34
	intestinal	UDL[a]		5			
lettuce leaves	gastric			64	45		
	intestinal			10	7		
spinach leaves	gastric	24		16	7		
	intestinal	UDL[a]		9	5		
radish roots	gastric			46	21		
	intestinal			32	9		
tea leaves (CRM)	gastric	17	0.2	58	40	8	20
	intestinal	33	1.5	21	26	12	
spinach leaves (CMR)	gastric	44	20	47	57	31	
	intestinal	40	33	37	32	28	
lettuce leaves	gastric	30	7.5	48	45	17	
	intestinal	48	43	36	36	42	
spinach leaves	gastric	30	14	41	44	19	
	intestinal	51	36	44	32	22	
radish roots	gastric	29	29	44	32	13	
	intestinal	45	43	48	56	47	
carrot roots	gastric	41	29	41	38	17	
	intestinal	41	48	48	50	38	
hazelnuts	gastric	25	4.5	68	28	8	27
	intestinal	14	22	78	60	UDL[a]	
walnuts	gastric	80	4.5	21	15	UDL[a]	
	intestinal	62	23	39	60	UDL[a]	
macroalga *Zostera marina*	gastric	1			3.5	0.25	37
	intestinal	3.5			<1	<0.05	
cocoa powder	gastric					5.6	68
	intestinal					10	
cooked vegetable soup	total BAC		24−31	15−20	25−34		26
Indian herbal medicine and minerals	total BAC					33	40

[a]UDL, under the detection limit.

according to the current evaluations of the Joint FAO/WHO Expert Committee on Food Additives,[50] there is no safe threshold limit for Pb intake, and even a negligible portion of this toxic metal can produce harmful effects. With regard to Pb absolute bioavailability (ABAV), our findings are consistent with the results of soil-bound Pb ABAV based on bone and liver data.[51] A higher ABAV (approximately 3%) can be estimated on the basis of blood Pb values. Even though we did not determine blood Pb levels in our experiment, we could expect a pattern similar to those described in the study mentioned above. Blood Pb-based ABAV tends to be overestimated because blood Pb levels comprise also the Pb fractions, which are initially absorbed from the gut into the bloodstream but could eventually be excreted from the body through bile or urine.

The risk of Pb intoxication due to contaminated forage is usually low because the uptake of Pb from soil is limited in most terrestrial plants, including vegetables.[52] However, excessive Pb concentrations have often been detected in aquatic plants and weeds because many of these species have hyperaccumulative properties.[53−58] We detected elevated Pb concentrations in all monitored tissues of PS-fed animals, with the greatest increases observed in bones, kidneys, and livers. Therefore, the consumption of phyto hyperaccumulator biomass by both animals and humans can pose a serious toxic risk.

Pb levels in artificially cultivated PS biomass used in our experiment greatly exceeded the maximal allowable limit for animal feed in the European Union (10 mg of Pb kg^{-1}) and the United States (30 mg of Pb kg^{-1}). Therefore, this plant material could not be used as a single-component animal feed, and a low

DOI: 10.1021/jf5058099
J. Agric. Food Chem. 2015, 63, 2344−2354

level of supplementation (0.1%) was required in our experiment. However, with regard to the application of PS as animal feed, even the wild specimen *P. stratiotes*, which grows in some polluted areas, exhibits unacceptable Pb concentrations (15.76 mg kg^{-1}).[15] Therefore, potential forage plants that grow on polluted sites and artificially affected water bodies should be properly tested for risk element load before being processed for feeding purposes.

Comparison of BAC and BAV Results. A direct comparison of BAC and BAV results still remains questionable. The majority of previous studies focused on accidental dietary intake of soil-bound risk elements. Therefore, we are compelled to derive information from such studies. The partial correlations between *in vitro* BAC and *in vivo* BAV of soil-bound As, Cd, and Pb were previously demonstrated in young swine models.[42,59,60] However, when *in vitro* Pb BAC results were directly compared with *in vivo* BAV for swine, only two physiologically based extraction methods provided measurements that were within the accepted margin of error.[35]

We observed a similar trend in our experiment, wherein potential BAC fractions of particular elements differed from those determined in rat tissues. The results of the *in vitro* PBET indicated a high accessibility of all monitored elements form PS biomass; however, the supplementation level was most likely too low to cause significant effects in the *in vivo* model. With regard to human health risk assessment, an IVG method must always be correlated with an acceptable *in vivo* model.[61]

Because element (essential as well as toxic) absorption occurs primarily in the small intestine, there is a scientific basis for the relationship between intestinal BAC and potential BAV. Therefore, the determination of BAC in the intestinal compartment should be considered relevant for assessing the risk of element intake from the gastrointestinal tract. BAC determined in the stomach compartment results in a physiologically irrelevant relative BAV factor, which probably overestimates the actual fraction that is available for intestinal metal absorption.[62]

In summary, several important findings should be mentioned. BAC and BAV were compared in both conventional animal feed and phyto hyperaccumulator biomass for the first time. Using the *in vitro* PBET, we demonstrated that the digestive process of phyto hyperaccumulator biomass differed from that of conventional feed. *P. stratiotes* exhibited high concentrations of certain essential elements (Fe and Mn), and it could be potentially used in feedstuff. However, when this kind of plant grows in polluted areas, it can absorb extremely large amounts of risk elements. Therefore, consumption of such material poses a serious toxic risk. Additionally, our study revealed that high levels of risk elements (primarily Pb) in phyto hyperaccumulator biomass can affect essential element absorption from the gastrointestinal tract as well as element biokinetics inside an organism. The results of our experiment indicated heterogeneity between potential bioaccessibility determined *in vitro* and estimated bioavailability determined *in vivo*; this was because large bioaccessible fractions of elements from PS did not lead to elevated element concentrations in animal tissues. An important innovative aspect of this study is the application of a new method for ABAV evaluation based on the total element amount in specific organs or whole organ systems. Using TEAT, we were able to detect differences in element biokinetics between PS and CO groups more accurately. On the basis of the disparity between *in vitro* BAC and *in vivo* BAV in our study, we can recommend the following general approach. The PBET should be used primarily as a basic step for the identification of risk elements with high bioaccessibility in the digestive tract. Because *in vitro* methods are less expensive, less complicated, and less laborious than *in vivo* tests, this step allows us to specify potentially dangerous elements in animal fodder. Subsequently, once elements with high bioaccessibility are specified, only their bioavailability needs to be confirmed via more demanding *in vivo* trials.

AUTHOR INFORMATION

Corresponding Author

*Department of Zoology and Fisheries, FAFNR, CULS Prague, Kamycka 957, Prague 6, 165 21 Czech Republic. Phone: +420 224 383 451. E-mail: cadkova@af.czu.cz.

Funding

This study was financially supported by GAČR Project 13-18154S and the University-wide internal grant agency of the Czech University of Life Sciences, Prague, (CIGA 20142030).

Notes

The authors declare no competing financial interest.

ACKNOWLEDGMENTS

We gratefully acknowledge Brian Kavalir (Ontario, Canada) for his proofreading services.

ABBREVIATIONS USED

PS, *P. stratiotes*; BAC, bioaccessibility; BAV, bioavailability; ABAV, absolute bioavailability; PBET, physiologically based extraction test; SPF, specific pathogens free; CO, control; TEAT, total element amount in tissue; TI, total intake; EC, element concentration; FW, fresh weight; SOWC, specific organ weight coefficient; DW, dry weight; GP, gastric phase; IP, intestinal phase; AIC, Akaike's Information Criterion

REFERENCES

(1) Sharma, B. M.; Sridhar, M. K. C. The productivity of *Pistia stratiotes* L in a eutrophic lake. *Environ. Pollut., Ser. A* **1981**, *24* (4), 277−289.

(2) Tepe, Y.; Türkmen, M.; Türkmen, A. Assessment of heavy metals in two commercial fish species of four Turkish seas. *Environ. Monit. Assess.* **2008**, *146*, 277−284.

(3) Türkmen, A.; Türkmen, M.; Tepe, Y.; Çekiç, M. Metals in tissues of fish from Yelkoma Lagoon, northeastern Mediterranean. *Environ. Monit. Assess.* **2010**, *168* (1−4), 223−230.

(4) Türkmen, M.; Türkmen, A.; Tepe, Y. Comparison of Metals in Tissues of Fish from Paradeniz Lagoon in the Coastal Area of Northern East Mediterranean. *Bull. Environ. Contam. Toxicol.* **2011**, *87* (4), 381−385.

(5) Banerjee, A.; Matai, S. Composition of Indian Aquatic Plants in Relation to Utilization as Animal Forage. *J. Aquat. Plant Manage.* **1990**, *28*, 69−73.

(6) Global Invasive Species Database. http://www.issg.org/database, 2005 (accessed November 10, 2014).

(7) CABI Switzerland Annual Report. http://www.cabi.org, Delémont, Switzerland, 2011 (accessed November 10, 2014).

(8) Edwards, P. In *Food Potential of Aquatic Macropythes. Inclarm Studies and Reviews*; International Center for Living Aquatic Resources Management: Manila, The Philippines, 1980; Vol. 5, p 51.

(9) Ayoade, G. O.; Sharma, B. M.; Sridhar, M. K. C. Trails of *Pistia-stratiotes* L as animal feed. *J. Aquat. Plant Manage.* **1982**, *20*, 56−57.

(10) Chantiratikul, A.; Atiwetin, P.; Chantiratikul, P. Feasibility of Producing Selenium-Enriched Water Lettuce (*Pistia stratiotes* L.). *J. Biol. Sci.* **2008**, *8* (3), 644−648.

DOI: 10.1021/jf5058099
J. Agric. Food Chem. 2015, 63, 2344−2354

(11) Dewanji, A. Amino Acid Composition of Lea Proteins Extracted from Some Aquatic Weeds. *J. Agric. Food Chem.* **1993**, *41*, 1232−1236.
(12) Dewanji, A.; Matai, S. Nutritional Evaluation of Leaf Protein Extracted from Three Aquatic Plants. *J. Agric. Food Chem.* **1996**, *44*, 2162−2166.
(13) Odjegba, V. J.; Fasidi, I. O. Accumulation of trace elements by *Pistia stratiotes*: Implications for phytoremediation. *Ecotoxicology* **2004**, *13* (7), 637−646.
(14) Yasar, A.; Khan, M.; Tabinda, A. B.; Hayya, M.; Zaheer, A. Percentage uptake of heavy metals of different macrophytes in stagnant and flowing textile effluent. *J. Anim. Plant Sci.* **2013**, *23* (6), 1709−1713.
(15) Sridhar, M. K. C. Trace element composition of *Pistia stratiotes* L. in polluted lake in Nigeria. *Hydrobiologia* **1986**, *131*, 273−276.
(16) Vesely, T.; Trkal, L.; neuberg, M.; Szakova, J.; Drabek, O.; Tejnecky, V.; Balikova, M.; Tlustos, P. Removal of Al, Fe and Mn by *Pistia stratiotes* L. and its stress response. *Centr. Eur. J. Biol.* **2012**, *7* (6), 1037−1045.
(17) Directive 2002/32/EC of the European Parliament and of the Council of 7 May 2002 on undesirable substances in animal feed.
(18) Oomen, A. G.; Hack, A.; Minekus, M.; Zeijdner, E.; Cornelis, C.; Schoeters, G.; Verstraete, W.; Van de Wiele, T.; Wragg, J.; Rompelberg, C. J. M.; Sips, A. J. A. M.; Van Wijnen, J. H. Comparison of five in vivo digestion models to study the bioaccessibility of soil contaminants. *Environ. Sci. Technol.* **2002**, *36* (15), 3326−3334.
(19) Ruby, M. V.; Davis, A.; Link, T. E.; Schoof, R.; Chaney, R. L.; Freeman, G. B.; Bergstrom, P. Development of an in-vitro screening-test to evaluate the in-vivo bioaccessibility of ingested mine-waste lead. *Environ. Sci. Technol.* **1993**, *27* (13), 2870−2877.
(20) Intawongse, M.; Dean, J. R. Use of the physiologically-based extraction test to assess the oral bioaccessibility of metals in vegetable plants grown in contaminated soil. *Environ. Pollut.* **2008**, *152*, 60−72.
(21) Lavu, R. V. S.; Pradas, M. N. V.; Pratti, V. L.; Meißner, R.; Rinklebe, J.; Van De Wiele, T.; Tack, F.; Laing, G. D. Trace Metals Accumulation in *Bacopa monnieri* and Their Bioaccessibility. *Planta Med.* **2013**, *79* (12), 1081−1083.
(22) Laparra, J. M.; Velez, D.; Montoro, R.; Barbera, R.; Farre, R. Bioaccessibility of inorganic arsenic in raw and cocked *Hizikia fusiforme* seaweed. *Appl. Organomet. Chem.* **2004**, *18* (12), 662−669.
(23) Jayawardene, I.; Saper, R.; Lupoli, N.; Sehgal, A.; Wright, R. O.; Amarasiriwardena, C. Determination of *in vitro* bioaccessibility of Pb, as, Cd and Hg, in selected traditional Indian medicines. *J. Anal. At. Spectrom.* **2010**, *25* (8), 1275−1282.
(24) Hu, J.; Wu, F.; Wu, S.; Cao, Z.; Lin, X.; Wong, M. H. Bioaccessibility, dietary expsure and human risk assessment of heavy metals from market vegetables in Honk Kong revealed with *in vitro* gastrointestinal model. *Chemosphere* **2013**, *91*, 455−461.
(25) Yang, L. S.; Zhang, X. W.; Li, Y. H.; Li, H. R.; Wang, Y.; Wang, W. Y. Bioaccessibility and Risk Assessment of Cadmium from Uncooked Rice Using an In Vitro Digestion Model. *Biol. Trace Elem. Res.* **2012**, *145* (1), 81−86.
(26) Zheng, F. Y.; Chen, L. H.; Li, S. X.; Qiu, Y. Q. Effect of edible plants combination on mineral bioaccessibility and bioavailability, using in vitro digestion and liposome-affinity extraction. *Food Res. Int.* **2013**, *53*, 174−179.
(27) Arpadjan, S.; Momchilova, S.; Venelinov, T.; Blagoeva, E.; Nikolova, M. Bioaccessibility of Cd, Cu, Fe, Mn, Pb and Zn in Hazelnut and Walnut Kernels Investigated by an Enzymolysis Approach. *J. Agric. Food Chem.* **2013**, *61*, 6086−6091.
(28) Navarro, P.; Arana, G.; Etxebarria, N.; Dean, J. R. Evaluation of the physiologically based extraction test as an indicator of metal toxicity in mussel tissue. *Anal. Chim. Acta* **2008**, *622*, 126−132.
(29) Čadková, Z.; Szaková, J.; Miholová, D.; Válek, P.; Pacáková, Z.; Vadlejch, J.; Langrová, I.; Jankovská, I. Faecal Excretion Dynamic during Subacute Oral Exposure to Different Pb Species in *Rattus norvegicus*. *Biol. Trace Elem. Res.* **2013**, *152* (2), 225−232.
(30) Mader, P.; Szaková, J.; Miholová, D. Classical dry ashing of biological and agricultural materials. Part II. Losses of analytes due to their retention in an insoluble residue. *Analusis* **1998**, *26*, 121−129.
(31) Hunder, G.; Javdani, J.; Elsenhans, B.; Schumann, K. Use of γ-spectrometry for simultaneous of Pb-210, As-73, Cd-109, Hg-203 and Fe-59 distribution and excretion in rats at low doses. *Toxicology* **2000**, *150* (1−3), 69−82.
(32) *STATISTICA*, version 12.0; StatSoft: Tulsa, OK, 2013.
(33) R Development Core Team. *R: A language and environment for statistical computing*; R Foundation for Statistical Computing: Vienna, 2014.
(34) Intawongese, M.; Dean, J. R. *In-vitro* testing for assessing oral bioaccessibility of trace metals in soil and food samples. *Trends Anal. Chem.* **2006**, *25* (9), 876−886.
(35) Koch, I.; Reimer, K. J.; Bakker, M. I.; Basta, N. T.; Cave, M. R.; Denys, S.; Dodd, M.; Hale, B. A.; Irwin, R.; Lowney, Y. W.; Moore, M. M.; Paquin, V.; Rasmussen, P. E.; Repaso-Subang, T.; Stephenson, G. L.; Siciliano, S. D.; Wragg, J.; Zagury, G. J. Variability of bioaccessibility results using seventeen different methods on a standard reference material, NIST 2710. *J. Environ. Sci. Health, Part A: Toxic/Hazard. Subst. Environ. Eng.* **2013**, *48* (6), 641−655.
(36) Crews, H. M.; Burrell, J. A.; MvWeeny, D. J. Preliminary enzymolysis studies on trace element extractability from food. *J. Sci. Food Agric.* **1983**, *34* (9), 997−1004.
(37) Turner, A.; Hambling, J. Bioaccessibility of Trace Metals in Sediment, Macroalga and Antifouling Paint to the Wild Mute Swan, *Cygnus color*. *Water, Air, Soil Pollut.* **2012**, *223*, 2503−2509.
(38) Arpadjan, S.; Çelik, G.; Taşkesen, S.; Güçer, Ş. Arsenic, cadmium and lead in medicinal herbs and their fraction. *Food Chem. Toxicol.* **2008**, *46*, 2871−2875.
(39) Mandal, S.; Ghosh, K. Inhibitory effect of *Pistia* tannin on digestive enzymes of Indian major carps: An in vitro study. *Fish Physiol. Biochem.* **2010**, *36*, 1171−1180.
(40) Koch, I.; Moriarty, M.; House, K.; Sui, J.; Cullen, W. R.; Saper, R. B.; Reimer, K. J. Bioaccessibility of lead and arsenic in traditional Indian medicines. *Sci. Total Environ.* **2011**, *409*, 4545−4552.
(41) Pelfrêne, A.; Wterlot, Ch.; Douay, F. In vitro digestion and DGT techniques for estimating cadmium and lead bioavailability in contaminated soils: Influence of gastric juice pH. *Sci. Total Environ.* **2011**, *409*, 5076−5085.
(42) Ruby, M. V.; Davis, A.; Schoof, R.; Eberle, S.; Sellstone, C. M. Estimation of lead and arsenic bioavailability using a physiologically based extraction test. *Environ. Sci. Technol.* **1996**, *30* (2), 422−430.
(43) Charlesworth, S.; De Miguel, E.; Ordóñez, A. A review of the distribution of particulate trace elements in urban terrestrial environments and its application to considerations of risk. *Environ. Geochem. Health* **2011**, *33*, 103−123.
(44) Market, B. The biological system of the elements (BSE) for terrestrial plants (Glycomphytes). *Sci. Total Environ.* **1994**, *155* (3), 221−228.
(45) Johnson, P. J. Factors Affecting Cooper Absorption in Humans and Animals. In *Copper Bioavailability and Metabilosm*; Kies, C., Ed.; Advances in Experimental Medicine and Biology; Springer: Dallas, 1989; Vol. *258*, pp 71−79.
(46) Sandstroëm, B. Micronutrient interactions: Effects on absorption and bioavailability. *Br. J. Nutr.* **2001**, *85* (2), 181−185.
(47) Morrison, J. N.; Quarterman, J. The relationship between iron status and lead absorption in rats. *Biol. Trace Elem. Res.* **1987**, *14* (1−2), 115−126.
(48) Likuski, H. J. A.; Forbes, R. M. Mineral utilization in rat. 4. Effects of calcium and phytic acid on utilization of dietary zinc. *J. Nutr.* **1965**, *85* (3), 230−234.
(49) Davies, N. T.; Nightinagle, R. Effects of phytate on intestinal-absorption and secretion of zinc, and whole-body retention of Zn, cooper, iron and manganese in rats. *Br. J. Nutr.* **1975**, *34* (2), 243−258.
(50) Joint FAO/WHO Expert Committee on Food Additives. http://www.fao.org/food/food-safety-quality/scientific-advice/jecfa/en/, 2011 (accessed November 10, 2014).
(51) Freeman, G. B.; Johnson, J. D.; Liao, S. C.; Feder, P. I.; Davis, A. O.; Ruby, M. V.; Schoof, R. A.; Chaney, R. L.; Bergstrom, P. D. Absolute bioavailability of lead acetate and mining waste lead in rats. *Toxicology* **1994**, *91* (2), 151−163.

DOI: 10.1021/jf5058099
J. Agric. Food Chem. 2015, 63, 2344−2354

(52) Xu, D.; Zhou, P.; Zhan, J.; Gao, Y.; Dou, Ch.; Sun, Q. Assessment of trace metal bioavailability in garden soils and health risks via consumption of vegetables in the vicinity of Tongling mining area, China. *Ecotoxicol. Environ. Saf.* **2013**, *90*, 103−111.
(53) Deng, H.; Ye, Z. H.; Wong, M. H. Accumulation of lead, zinc, copper and cadmium by 12 wetland plant species thriving in metal-contaminated sites in China. *Environ. Pollut.* **2004**, *132*, 29−40.
(54) Drzewiecka, K.; Borowiak, K.; Mleczek, M.; Zawada, I.; Golinsky, P. Cadmium and lead accumulation in two littoral plants of five lakes in Poznan, Poland. *Acta Biol. Cracov., Ser. Bot.* **2010**, *52* (2), 59−68.
(55) Kastratovic, V.; Krivokapic, S.; Durovic, D.; Blagojevic, N. Seasonal changes in metal accumulation and distribution in the organs of *Phragmites australis* (common reed) from Lake Skadar, Montenegro. *J. Serb. Chem. Soc.* **2013**, *78* (8), 1241−1258.
(56) Matache, M. L.; Marin,C.; Rozylowicz, L.; Tudorache, A. Plants accumulating heavy metals in the Danube River wetlands. *Journal of Environmental Health Science and Engineering.* **2013**, *11*, No. 39.
(57) Pourkhabbaz, A. R.; Pourkhabbaz, H. R.; Khazaei, T.; Behravesh, S.; Ebrahimpour, M. Assessment of heavy metal accumulation in Anzali wetland, Iran, using a submerged aquatic plant, *Ceratophyllum demersum*. *Afr. J. Aquat. Sci.* **2011**, *36* (3), 261−265.
(58) Wang, Z.; Yao, L.; liu, G.; Liu, W. Heavy metals in water, sediments and submerged macrophytes in ponds around the Dianchi Lake, China. *Ecotoxicol. Environ. Saf.* **2014**, *107*, 200−206.
(59) Rodriguez, R. R.; Basta, N. T. An in vitro gastrointestinal method to estimate bioavailable arsenic in contaminated soils and soils media. *Environ. Sci. Technol.* **1999**, *33* (4), 642−649.
(60) Schroder, J. L.; Basta, N. T.; Si, J. T.; Casteel, S. W.; Evans, T.; Payton, M. In vitro gastrointestinal method to estimate relative bioavailable cadmium in contaminated soil. *Environ. Sci. Technol.* **2003**, *37* (7), 1365−1370.
(61) U.S. Environmental Protection Agency. http://www.epa.gov/roe/, 2007 (accessed November 10, 2014).
(62) Oomen, A. G.; Brandon, E. F. A.; Swartjes, F. A.; Lijzen, J. P. A.; Sips, A. J. A. M. How can information on oral bioavailability improve human health risk assessment for lead-contaminated soils? Implementation and scientific basis. *Epidemiology* **2006**, *17* (6), S40.
(63) Henry-Silva, G. G.; Camargo, A. F. M.; Pezzato, L. E. Digestibilidade aparente de macrófitas aquáticas pela tilápia-do-nilo (*Oreochromis niloticus*) e qualidade da áqua em relação às concentrações de nutrientes. *Rev. Bras. Zootec.* **2006**, *35* (3), 641−647.
(64) Wheeler, G. S.; Van, T. K.; Center, T. D. Herbivore Adaptations to a Low-Nutrient Food: Weed Biological Control Specialist *Spodoptera pectinicornis* (Lepidoptera: Noctuidae) Fed the Floating Aqatic Plant *Pistia stratiotes*. *Environ. Entomol.* **1998**, *27* (2), 993−1000.
(65) Khare, C. P. *Pistia*. In *Indian Herbal Remedies: Rational Western Therapy, Ayurvedic, and Other Traditional Usage, Botany*; Khare, C. P., Ed.; Springer: Berlin, 2004; pp 372.
(66) Tripathi, P.; Kumar, R.; Sharma, A. K.; Mishra, A.; Gupta, R. *Pista stratiotes* (Jalkumbhi). *Pharmacogn. Rev.* **2010**, *4* (8), 153−160.
(67) Martínez, F. S.; Franceschini, M. C.; Poi, A. Preferencia alimentaria de *Neochetina eichhorniae* (Coleoptera: Curculionidae) en plantas acuáticas de diferente valor nutritivo. *Rev. Colomb. Entomol.* **2013**, *39* (1), 81−87.
(68) Mounicou, S.; Szpunat, J.; Andrey, D.; Blacke, C.; Lobinski, R. Development of a sequential enzymolysis approach for the evaluation of the bioaccessibility of Cd and Pb from cocoa. *Analyst* **2002**, *127* (12), 1638−1641.

DOI: 10.1021/jf5058099
J. Agric. Food Chem. 2015, 63, 2344−2354

have a higher rate than in Europe. Past studies about decreasing Cs accumulation in crops in Fukushima dominantly focused on the effect of K fertilization on Cs mobility in the soil−plant system.[4,26,27] However, more studies should set out to establish the elemental network to associate the Cs (and Sr) with other essential and nonessential elements, not only K and Ca, to clarify how regulatory mechanisms of Cs, Sr, and other elements interact, because the regulation in plants of a given ion uptake is decided by not only competitive ions but the balance of multiple ions.

In a previous study we concluded that the varietal effect of the genus *Amaranthus* brings about a significant difference in radiocesium uptake and transfer from soil.[28] In the present study we further present a phylogenetic analysis of interspecies difference in nutrient and trace element concentrations and establish the ionomic interactions between Cs, Sr, and other elements in amaranth shoots among 33 varieties of *Amaranthus* species.

MATERIALS AND METHODS

Plant Materials and Growth Conditions. A field experiment was conducted in Iino located in the suburbs of Fukushima city (37°39 N, 140°32 E). The sites were 50.9 km northwest from the Fukushima 1 Nuclear Power Plant, and the field was cultivated in 2011. Soil type was gray lowland soil based on the classification of cultivated soils in Japan.[29] The contamination level of the soil by ^{134}Cs and ^{137}Cs was 2769 ± 141 Bq/kg (average ± SE). Thirty-three *Amaranthus* species were adopted including 10 local varieties (Table 1 in ref 28). All of the seeds were sown in vermiculite on June 30, 2012, and then transplanted to the field on July 14, 2012. The plot area was 120 m^2 (12 m × 10 m), and the soil was sampled for the chemical analysis before transplanting and the data for soil characteristics of the field are shown (Table 2 in ref 28). To avoid possible interaction between ions during radiocesium transport by root, only nitrogen fertilizer in the form of ammonium sulfate was applied at a rate of 100 kg N ha^{-1}, and the plants were then cultivated at a 15 cm depth. Twenty plants for each examined plant variety or species were transplanted at 70 cm × 50 cm planting density.

Sampling and Analysis. Plant samples were harvested on October 6, 2012, with three replications (two to three individuals in each replication) for each variety or species, and then the aboveground shoot was separated from the roots. Plant samples were dried at 70 °C for 1 week and then mercerized by a stainless grinder. After drying and milling, 50 mg shoot samples were digested with 2 mL of 61% HNO_3 (EL grade; Kanto Chemical, Tokyo) in a tube at 110 °C in a DigiPREP apparatus (SCP Science, Quebec, Canada) for 3 h, and 0.5 mL of hydrogen peroxide (semiconductor grade; Santoku Chemical, Tokyo, Japan) was added two times at a 30 min interval as an oxidant and heated at 110 °C until the solution became clear. After cooling to room temperature, tubes were filled to 15 mL with 2% HNO_3, and concentrations of 23 elements (P, K, Mg, Ca, Mn, Fe, Cu, Zn, B, Mo, Ni, Sr, Cr, Al, Ba, Cd, As, Na, Co, Se, Li, Rb, and Cs) in the digests were analyzed by an inductively coupled plasma mass spectrometer (ICP-MS) (Elan, DRC-e; PerkinElmer, Waltham, MA, USA). The ICP multielement standard solution IV (Merck, Tokyo, Japan) was used as standard for ionomic determination.

Statistical Analysis. To visualize the differences of the 23 mineral elements in 33 amaranthus varieties, descriptive statistics, one-way variance (ANOVA), correlation analysis, and principal component analysis (PCA) were performed using SPSS 18.0. For statistical differences between elemental compositions for the cultivars, ANOVA was conducted, and the ratio of variance between groups to variance within groups was used to estimate the variation caused by varieties. For correlation analysis Pearson correlation coefficients and Student's *t* test were applied to identify the significant correlations between mineral elements. A conservative *p* value limit of 0.001 was used to confirm whether the correlation is significant. The overall accumulations of 23 elements were profiled by PCA. The varimax with Kaiser normalization was used as rotation method.

RESULTS AND DISCUSSION

Statistics and Variation of Mineral Elements Contents in Amaranth Shoot among 33 Different Varieties. In this study, shoot element concentrations varied by 6 orders of magnitude from 0.073 μg g^{-1} for Cs to 34.15 mg g^{-1} for K, in the order K > Ca > P > Mg > Mn > Rb > Al > B > Fe > Na > Sr > Ba > Zn > Ni > Cu > Co > Cr > Cd > Li > As > Mo > Se > Cs (Figure 1). Cs accumulation was the lowest among 23 elements, which is probably related to the low available Cs concentration in soil and the high affinity of Cs to the clays.[8,11,30] The affinity of cations to clays in soil follows the order $Cs^+ > NH_4^+ > K^+ > Na^+ > Ca^{2+}$.[30]

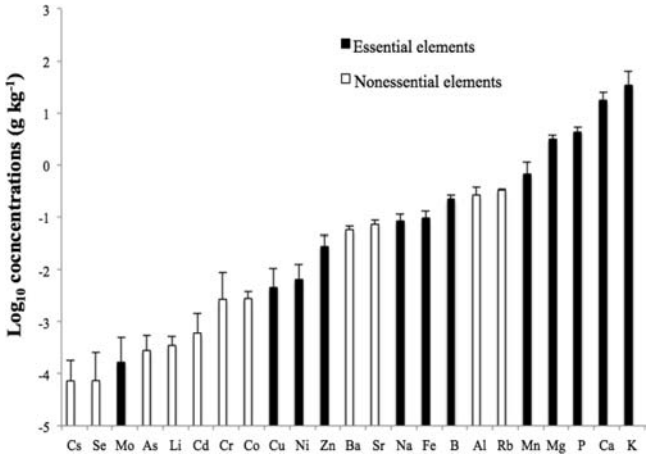

Figure 1. Average concentration of 23 mineral elements in shoots of 33 varieties of *Amaranthus* (n = 3 for each variety). Black columns represent the essential elements, and white columns represent nonessential elements. (Na is also regarded as an essential element in this research as Na is an indispensible part of growth of C4 plants including amaranths.)

The results of varietal difference contributed to the variation of elements, and descriptive statistics were presented in Table 1. Significant difference (p < 0.001) between different varieties was detected in all of the elements excluding Se. The relatively smaller phylogenetic variation in shoot Se was concordant with previous studies.[31,32] The remaining variation for a given element corresponding to differences besides species was likely caused by soil and climatic factors, sampling depth of field, or uneven distribution of trace elements in the field.[32] To quantify the varietal variance affecting each mineral element, the ratio of variance between groups to total variance was calculated and ranged from 53.64% for Se to 99.14% for Cr. Cr revealed the largest varietal variance, approaching 100%, and the largest ratio of maximum to minimum as well as CV (coefficient of variation, ratio of standard deviation of all cultivars to mean of all cultivars) was also observed in Cr. Although no metabolic activity involving Cr is known in plants, even within the same genotype there are differences in root exudates influencing the soil microbe community and element availability in the soil.[33,34] Environmental factors may also have important effects, such as the specific soil characteristics and uneven distribution of nonessential elements in the field. Whereas there is variation associated with genotypes across the entire elemental composition, the varied degree as measured by the ratio of

DOI: 10.1021/jf5058777
J. Agric. Food Chem. 2015, 63, 2355−2363

Table 1. Varietal Variation in Element Concentrations in Shoots among 33 Cultivars[a] (n = 99)

	variety difference (%)	F^b	max	min	ratio	mean	SD
Cs	65.53	3.92*	0.00015	0.00002	8.87	0.000073	0.000024
As	86.66	13.4*	0.00089	0.00002	38.76	0.00028	0.00019
Rb	81.29	8.96*	0.11	0.02	5.15	0.057	0.020
Al	86.41	13.11*	1.16	0.10	11.32	0.33	0.25
Fe	78.89	7.71*	1.08	0.021	51.46	0.27	0.20
Ba	68.55	4.50*	0.15	0.016	9.38	0.086	0.027
Ni	93.34	28.90*	0.021	0.0017	13.00	0.0047	0.0039
P	80.19	8.35*	7.26	2.67	2.72	4.35	0.90
K	91.10	21.11*	81.99	6.36	12.90	34.15	16.28
Ca	83.99	10.82*	29.09	9.02	3.22	17.79	3.99
Mg	81.07	8.834*	5.33	2.16	2.47	3.11	0.54
Mn	79.13	7.82*	1.34	0.23	5.70	0.66	0.24
Cu	76.12	6.58*	0.012	0.0032	3.76	0.0066	0.0015
Zn	85.25	11.92*	0.12	0.041	2.82	0.073	0.015
Mo	79.04	7.78*	0.00069	0.000052	13.30	0.00017	0.00014
B	89.56	17.69*	0.040	0.013	2.98	0.027	0.0061
Na	92.69	26.14*	1.35	0.064	20.94	0.22	0.26
Co	89.03	16.74*	0.008	0.0008	10.02	0.0027	0.0015
Se	53.64	2.39	0.00022	0.00001	31.52	0.000074	0.000039
Sr	75.49	6.35*	0.15	0.045	3.24	0.094	0.019
Li	83.24	10.24*	0.00077	0.00004	17.81	0.00035	0.00017
Cr	99.14	238.04*	0.031	0.00013	251.40	0.0028	0.0054
Cd	87.32	14.20*	0.00114	0.00026	4.45	0.00061	0.00016

[a]Values reported are the partition of variance for the cultivar difference (ratio % of variance between groups to total variance); F values generated from the ANOVA with Tukey test; maximum (max), minimum (min), mean with the unit of μg g^{-1}; max/min (ratio) and standard deviation (SD) of elemental accumulation in shoot for mineral elements. [b]*, $P < 0.001$.

the maximum to the minimum concentration or by the CV is highly element dependent (Table 1; Figure 2). The CV in

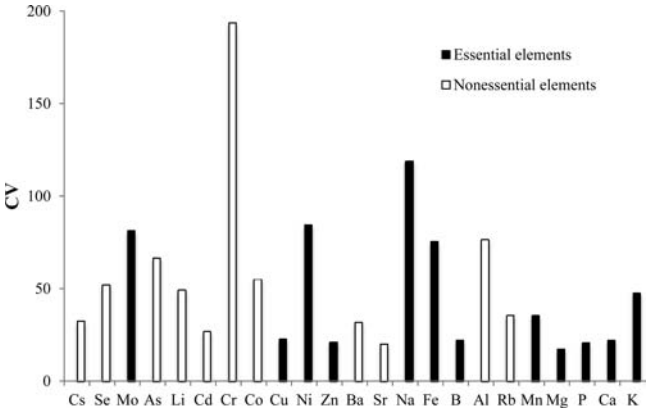

Figure 2. Relationship between mean concentration of elements in plants and their coefficients of variation (CV).

response to the variety effect increased in the order Mg < P < Sr < Zn < B < Ca < Cu < Cd < Ba < Cs < Mn < Rb < K < Li < Se < Co < As < Fe < Al < Mo < Ni < Na < Cr. The CV of macronutrients including P, K, Ca, and Mg varied <50%, whereas Na and Cr had CVs >100%. The pattern of CV of shoot minerals is consistent with the stability of limiting elements hypothesis: the CVs of Mg, Ca, P, B, Zn, and Cu (the essential elements) are <25%, whereas the CVs of As, Cr, Co, and Al were >50% and Cr approximated to 200%, becoming the most sensitive element of amaranths grown on the field subject to radionuclide contamination.

On the other hand, the CVs of seven elements (Mg, Ca, Mg, B, Sr, Zn, and Cu) were <25%, but only Sr belongs to nonessential elements. Both the CV and variety variance of Sr were higher than those for Cs, Ba, and Se. Meanwhile, variety difference of Cs was lower than all elements excluding Se. These results indicate that the amaranths are less sensitive to the accumulation of Cs and Sr than most other mineral elements to the species level. In contrast with Cs, the analogues K and Na showed relatively higher variety difference and CV. These results illustrate K and Na were unstably distributed in the shoot of different varieties of *Amaranthus*. Compared to the alkali metal elements, the variety diversity was more consistent for alkali earth metals and Ca, Mg, Sr, and Ba, which all showed relatively lower CV (<50%). The relatively stable intervarietal alterations for Cs and Sr within the *Amaranthus* genus coordinate with the larger range of investigations. According to meta-analysis for 27 plant species, it was concluded that the intervarietal variation at the ratio of the maximum to minimum of concentrations for a given crop species ranged from 1.0 to 6.3 for Cs and from 1.0 to 4.5 for Sr,[35] which is similar to the ratio within the genus of *Amaranthus* in this study and relatively lower than that of many other mineral elements. In conclusion, phylogenetic variation for Cs and Sr within genus was lower than the essential elements of their analogues, which suggests the essential elements of groups I and II in the periodic table are more sensitive to genetic difference than their alternative nonessential elements. Moreover, within the *Amaranthus* genus the lower interspecies difference of alkali earth metals (Ca, Mg, Sr, and Ba) than of some alkali metals (K and Na) suggests the elemental accumulation in shoot is independent of the mother rock composition of minerals. However, Ca and Mg have higher phylogenetic variation above family than K and Na.[32]

Among the 23 elements, the Rb concentration was higher than all elements excluding P, K, Ca, Mg, and Mn, but there is an unknown role for Rb in plant nutrition. As the analogue of

DOI: 10.1021/jf5058777
J. Agric. Food Chem. 2015, 63, 2355−2363

Table 2. Correlation Coefficients for Shoot Composition of Mineral Elements in 33 Varieties of Amaranths

	P	K	Ca	Mg	Fe	Mn	Cu	Zn	Mo	B	Ni	Na	Cs	Rb	Co	Se	Al	As	Li	Sr	Ba	Cd	Cr
P	–																						
K	NS	–																					
Ca	0.44*[a]	NS	–																				
Mg	0.45*	NS	0.86*	–																			
Fe	NS	NS	NS	NS	–																		
Mn	0.54*	NS	0.74*	0.58*	−0.36*	–																	
Cu	0.55*	NS	0.51*	0.46*	NS	0.51*	–																
Zn	0.39*	NS	0.50*	0.44*	−0.34*	0.42*	0.42*	–															
Mo	NS	NS	NS	NS	NS	NS	NS	NS	–														
B	NS	NS	0.60*	0.67*	−0.49*	0.46*	NS	0.65*	**	–													
Ni	NS	−0.44*	NS	NS	0.85*	NS	NS	NS	0.40*	−0.54*	–												
Na	NS	NS	0.50*	0.56*	NS	NS	NS	NS	0.52*	NS	ns	–											
Cs	NS	NS	NS	NS	0.39*	NS	NS	NS	NS	NS	0.37*	NS	–										
Rb	0.38*	NS	NS	NS	NS	0.41*	NS	NS	NS	NS	NS	NS	0.49*	–									
Co	NS	−0.38*	NS	NS	NS	0.68*	0.39*	NS	NS	NS	NS	NS	NS	NS	–								
Se	NS	NS	NS	NS	NS	NS	NS	0.40*	NS	NS	NS	NS	NS	0.43*		–							
Al	NS	−0.44*	NS	NS	0.86*	NS	NS	NS	NS	−0.53*	0.95*	NS	0.40*	NS	NS	NS	–						
As	NS	NS	NS	NS	NS	0.50*	NS	NS	NS	NS	NS	NS	0.60*	0.37*	0.75*	NS	NS	–					
Li	NS	−0.38*	NS	NS	0.66*	NS	NS	NS	0.40*	−0.37*	0.72*	0.45*	NS	−0.38*	NS	NS	0.79*	0.38*	–				
Sr	NS	NS	0.79*	0.69*	NS	0.46*	NS	0.55*	NS	0.62*	NS	NS	NS	NS	NS	NS	NS	NS	NS	–			
Ba	NS	NS	NS	0.59*	NS	NS	0.37*	NS	NS	NS	NS	NS	−0.38*	NS	NS	NS	NS	NS	NS	0.58*	–		
Cd	0.40*	−0.36*	0.73*	NS	NS	0.56*	0.43*	0.63*	NS	0.68*	−0.40*	NS	NS	NS	NS	NS	0.36*	NS	NS	0.68*	NS	–	
Cr	NS	NS	−0.39*	NS	0.69*	NS	NS	NS	0.49*	−0.49*	0.90*	NS	NS	NS	NS	NS	0.75*	NS	0.45*	NS	NS	0.42*	–

[a]Coefficients are derived from Pearson correlation analysis. NS, not significant; *, $P < 0.001$.

J. Agric. Food Chem. 2015, 63, 2355−2363 DOI: 10.1021/jf5058777

Table 3. Significantly Highest and Lowest Accumulating Varieties for Each Element[a]

	P	K	Ca	Mg	Fe	Mn	Cu	Zn	Mo	B	Ni	Na
sig H[b]	7	1	24	23	17	12	10	10	17	27	17	23
sig L	17	9	17	20	NS	20	20	3	10	17	19	NS
	20								11			

	Cs	Rb	Co	Se	Al	As	Li	Sr	Ba	Cd	Cr
sig H	12	6	12	30	17	12	16	24	16	28	17
	17							28			
sig L	25	16	2	17	NS	23	4	3	3	17	14
		17				25		17			
		20				26					

[a]Numbers represent the variety exhibited in Table1 of reference13. On the basis of ANOVA with Tukey's test, significantly highest/lowest varieties for each element were selected no more than three, and if there were over five varieties showing significant extreme values, the NS would be shown in this table. [b]Sig H means significantly highest and sig L, significantly lowest.

Cs, the Rb concentration was also relatively constant across species with lower CV and ratio of maximum to minimum concentration. This stable distribution in different varieties in amaranths was similar to Cs, but dissimilar to K, which coincides with the previous study that Rb concentration in the shoot mainly depends on soil chemical and physical properties, rather than variety difference.[31] In addition, Cs^+ and Rb^+ uptake are mediated by K transport systems because K^+, Rb^+, and Cs^+ have comparable physical−chemical characteristics owing to similar radii of their hydrated ions.[35,36]

Interactions between Mineral Elements. The homeostatic mechanisms that control the levels of different elements are reported interconnected, and certain interconnections could be detected across species.[20,37] The correlation analysis among elements in 33 varieties of *Amaranthus* was therefore investigated (Table 2).

In this study, positive correlations were identified between K, Na, and Li and Cs and Rb in the first group and between Mg, Ca, and Sr in the second group. Fe, Ni, Ba, Al, As, and Rb showed significant correlations with Cs, but among them only Fe and Ni are of essential role in plant nutrition, which suggested the Cs uptake was more readily affected by some nonessential elements. The absence of significant correlations between K and Cs coordinates with the previous study.[38,39] Whereas it has been reported that K and Cs enter root cells through the same molecular mechanisms and Cs uptake could be effectively strengthened in K-deficient solution,[40,41] the correlation between K and Cs was still insignificant. It has been proposed that the lack of this correlation is consistent with the constitutive expression of some selective K^+ transporters such as AKT1, which was unlikely to contribute significantly to Cs^+ uptake from the soil solutions with high concentration of Ba^{2+}, Ca^{2+}, or La^{3+},[42] and the expression of other proteins catalyzing the nonspecific absorption of Cs^+ and K^+ are regulated by varietal factors including the K^+ status of the plant.[41,43] The internal translocation rate of Cs is slower than that of K in rice shoot, and the distribution of Cs in grain and nonedible parts also diverges from that of K.[44] Therefore, the physiological reasons why K fertilization is against the transfer of Cs from soil to plant should separate from the transport inside the plant and associate with the block effect of K on Cs influx into root by cation exchanging from soil because K can occupy the absorption site of Cs in root.

Moreover, there was a recent report that Cs accumulation in yeast and plants could be specifically inhibited by the SNARE protein (Sec22p/SEC22) without interrupting K homeostasis in *Saccharomyces cerevisiae*, and the mechanism may be caused by raising nonselective cations storage to vacuole.[45] In the evaluation of taxonomic variation of shoot Cs concentration, it was speculated that the plants able to hyperaccumulate Cs, including amaranths, were all of halophytes with less selectivity to nonessential elements to meet their cation demands.[2] In addition, the partition of excessive quantities of cations in cell vacuole is an effective energy-efficient method for generating an osmotic potential for rapid cell expansion and growth.[46] Therefore, the interactions between Cs and its remarkably correlated cationic elements in vacuole are likely to be responsible for the higher Cs concentration in amaranths rather than only by cutting off the K supply.

In addition, among elements significantly correlated with Cs, As was the sole anion and displayed the highest coefficient with Cs (Table 2). It has been reported that *Athyrium yokoscense* not only displayed the highest TF (translocation factor) value of radiocesium (0.703) among 99 herbs grown on a radiocesium-contaminated field but also hyperaccumulated As from mine soil with elevated concentrations of As and heavy metallic ions.[47,48] These results indicate that the mutual promotion may exist for taking up As and Cs into plants. The findings from some previous studies may be helpful to explain the regulation of As on Cs that the significant decline in essential elements was associated with increasing As in rice grain.[49,50] Furthermore, Ba was the unique element showing a significantly negative association with Cs. This correlation probably resulted from the blocking of Ba^{2+} on the channel for Cs^+ xylem loading to aboveground tissues. The termed K^+-selective outward-rectifying channels (KORC) facilitate K^+ efflux from root cells and are permeable to Cs^+, but are inhibited by extracellular Ba^{2+} because the gene encoding the typical KORC is down-regulated by Ba^{2+} at millimolar concentrations.[51] This negative correlation between Ba and Cs also suggests the importance of long-distance transport for Cs accumulation in shoot of amaranths. In conclusion, the absence of correlations between K and Cs in amaranth shoot suggests that the competition between K and Cs mainly occurs in soils, and the negative correlation between Ba and Cs suggests that Ba is a key element to inhibit the internal Cs transport in shoot. As Ba^{2+} repressed Cs^+ translocation by obstructing the K transporters (AKT1) or pathway (KORC),[42,51] K availability in growth medium possibly played an important role in the interaction between Ba and Cs in the shoot.

Significant correlations between Ca, Mg, Mn, Zn, B, Ba, Cd, and Sr were detected, and all of the coefficients were positive. Compared with the relationship between K and Cs, the

DOI: 10.1021/jf5058777
J. Agric. Food Chem. 2015, 63, 2355−2363

relationship between Ca and Sr was much more pronounced (Ca presented the highest coefficient with Sr), which concurs with many previous findings in other plant species.[32,35,52] It has been reported that the interaction between Ca and Sr concentration in shoots is consistent with reduced transport selectivity due to a greater contribution of apoplastic movement of these elements in plants.[51] However, if the countermeasures to decrease Sr uptake are considered on the basis of this directly proportional correlation between Ca and Sr, the intake of Ca by humans may be compromised in varieties with low Sr accumulation. The positive correlation between Sr^{2+} and many bivalent ions possibly depends on the shared nonselective cation channels, including Ca^{2+}-ATPase, ZIP, and YSL family of transport proteins, in xylem transport.[23,53] Besides the bivalent cationic ions, B was the unique anion to significantly correlate with Sr. Bivalent cations are often transported in the xylem by complexation with organic acids,[23] but the relationship between B and Sr was little reported. It is probably related to the cation−anion balance, but the exact mechanism requires more studies.

Identification of Extreme Varieties. Because of the large genetic variance observed in a majority of elements and the fold-ranges of CVs for certain elements, potential candidate varieties for accumulating extremely high or low status of elements are prone to be identified. As shown in Table 3 (see the serial number of varieties in Table 1 of ref 13), varieties were identified with the significant highest value for all elements and significant lowest value for all elements excluding Fe, Al, and Na. Particularly some varieties showed the same extreme for more than one element with the significantly highest or lowest concentration, which relates to complicated elemental correlations. Variety 12 accumulated the significantly highest Cs, Mn, As, and Co in shoot. Variety 25 displayed the strongest resistance for Cs accumulation in shoot among 33 varieties, and it also restricted the As accumulation with the highest efficiency, which is possibly associated with the result that As was the element with the highest correlation coefficient with Cs. Therefore, the countermeasures to prevent As uptake may be also beneficial for Cs resistance, such as increasing P fertilization. Variety 17 showed extreme promotion for the accumulations of Cs, Fe, Ni, Al, Cr, and Mo and extreme inhibition for accumulations of Ca, Sr, Cd, Se, P, Rb, and B. Interestingly, Cs and Rb exhibited significant positive correlation, but in variety 17 the accumulations of Cs and Rb diverged. This result implies that although a positive correlation between Rb and Cs was demonstrated, the up-regulation on Rb^+ uptake may be still beneficial for restricting more Cs^+ influx into the shoot. The accumulation of Rb^+, rather than Cs^+, was remarkably high in amaranth shoot because it was ranked $K^+ > Rb^+ > Cs^+$, with a relative ratio of 468386:7818:1, which coincides with the previous study on the mobility of K, Cs, and Rb within the soil−ectomycorrhizal system.[37] In that study, the fungi showed a high preferential uptake of Rb and K compared with Cs, and it was reported that the mechanism of Cs uptake by fungi was similar to that of Rb, whereas the K uptake mechanism may be different. However, research on the relationship between Rb and Cs accumulation in shoot was quite scarce. On the basis of the inference from the extreme accumulation of variety 17, the much larger preference of amaranths on Rb may provide new insight into the regulation on Cs uptake. In addition, the significantly highest Cs and lowest Sr both appeared in variety 17. In the present study, Sr and Cs did not show significant correlation, which coordinates with a large proportion of past studies.[35,52] This specific accumulation in variety 17 probably resulted from the greatly different uptake mechanisms and functions of their analogous elements K and Ca. This result poses a challenge for the selection of low-accumulating varieties owing to the exhibition of low accumulation of one radionuclide but not necessarily of the other. Variety 17 may be a potential plant material for studying the relationship between Cs and Sr accumulation in shoots.

The significantly highest concentrations of Sr and Ca were both detected in variety 24, which showed the role of Ca on Sr accumulation in shoot again. The significantly highest concentrations of Sr and Cd were both detected in variety 28. The significantly lowest concentrations of Sr, Ba, and Zn were all observed in variety 3. All of the varieties, excluding variety 17, showed that the extreme accumulation for Sr must be associated with other bivalent cationic elements, and Ca was not the only choice.

Profiling the Ionome in 33 *Amaranthus* Varieties. PCA succeeded in reducing the number of variables by clustering the elements with close interactions into the novel principal component (PC) and explained their contributions to the genetic variance, respectively (Tables 4 and 5). A total of 23 elements of 33 varieties were subjected to PCA, and these 23 original variables were converted to a set of linearly uncorrelated 6 PCs that totally contributed 83.7% of total variance of elements among species (Table 4). The PC where the elements exposed the highest loading score can define the according elements. In this study, PC1 accounted for 23.2% of the highest total variance and was mainly affected by Ni, Al, Fe, Cr, Li, Mo, and Ca. Notably, PC2 explained 20.3% of total

Table 4. Rotated Component Matrix of Different Elements Loading Score in Different PCs[a]

	PC1 (23.2%)	PC2 (20.3%)	PC3 (12.4%)	PC4 (10.1%)	PC5 (9.1%)	PC6 (8.6%)
Ni	**0.96**	−0.20	−0.02	−0.05	−0.06	0.09
Al	**0.94**	−0.18	0.05	0.05	−0.15	0.12
Fe	**0.88**	−0.18	0.05	−0.01	−0.22	−0.08
Cr	**0.86**	−0.25	−0.06	−0.21	0.11	−0.02
Li	**0.76**	0.25	0.02	−0.05	−0.41	0.30
Mo	**0.53**	0.40	−0.06	−0.49	0.08	−0.23
Ca	−0.23	**0.88**	0.04	0.06	0.22	0.21
Mg	−0.17	**0.85**	−0.06	−0.02	0.31	0.00
Sr	−0.07	**0.84**	−0.11	0.48	−0.04	0.02
Na	0.22	**0.76**	−0.17	−0.45	−0.17	0.00
Cd	−0.30	**0.75**	−0.04	0.26	0.25	−0.09
B	−0.51	**0.59**	0.02	0.30	0.16	−0.19
Mn	−0.30	**0.55**	0.37	0.00	0.35	0.47
Cs	0.35	−0.20	**0.82**	−0.27	0.04	−0.03
Rb	−0.41	0.07	**0.74**	0.05	0.20	−0.06
As	0.13	−0.01	**0.78**	−0.02	−0.01	0.53
Se	−0.35	0.18	**0.53**	0.41	0.34	0.04
Ba	0.08	0.10	−0.20	**0.81**	0.09	−0.27
Zn	−0.29	0.33	0.03	**0.58**	0.48	0.12
P	−0.33	0.17	0.13	0.05	**0.78**	0.04
Cu	0.10	0.43	0.20	0.13	**0.69**	0.16
Co	−0.04	0.06	0.41	−0.07	0.23	**0.83**
K	−0.41	0.01	0.26	0.14	0.07	**−0.71**

[a]Boldfaced entries represent the most dominant score of each element in the PC.

DOI: 10.1021/jf5058777
J. Agric. Food Chem. 2015, 63, 2355−2363

Table 5. Factor Loading Scores of 33 Varieties in Different PCs

variety	PC1	PC2	PC3	PC4	PC5	PC6	variety	PC1	PC2	PC3	PC4	PC5	PC6
1	−0.44	−0.34	−0.12	0.27	0.36	−1.39	18	1.74	−0.41	−0.50	−0.22	−0.44	0.07
2	−0.29	−0.77	0.91	−0.91	0.92	−1.86	19	−0.90	−0.95	−0.33	−0.67	−0.27	−0.03
3	−0.70	−1.66	−0.11	−2.38	−1.11	−0.09	20	−0.88	−1.73	−1.51	−0.88	−1.84	0.40
4	−0.89	−0.67	0.75	−0.11	0.92	−0.97	21	0.24	1.94	0.12	−1.41	0.04	−0.69
5	−0.29	−0.20	1.77	0.00	−0.67	−1.48	22	−0.18	0.91	−1.21	0.02	−0.20	0.78
6	0.50	−0.64	1.79	0.18	0.30	−0.32	23	−0.06	2.36	−1.06	−1.49	0.61	−0.15
7	−0.50	−0.41	0.98	0.10	1.95	0.33	24	0.71	2.82	−0.10	−1.32	−0.48	−0.72
8	−0.02	0.51	0.82	0.54	−2.36	0.93	25	−0.44	−0.61	−2.30	0.39	1.45	0.53
9	−0.06	−0.03	0.31	−0.36	−0.86	2.37	26	−0.15	−0.14	−1.39	0.39	1.35	−0.05
10	0.56	0.21	0.58	1.11	1.52	1.99	27	−0.82	−0.15	−0.02	−0.02	−0.70	−0.67
11	1.40	−0.42	0.75	1.28	−0.30	0.56	28	−0.17	1.47	0.11	0.99	−0.94	−0.26
12	−0.53	0.12	2.29	−1.51	0.83	2.52	29	−0.32	0.33	0.28	1.26	0.37	−0.57
13	−0.83	0.08	−0.86	−0.21	0.82	1.36	30	−0.44	0.09	0.52	1.14	0.11	−0.43
14	−0.63	−0.52	−1.21	0.33	0.01	−0.15	31	−0.18	−0.02	0.15	0.90	−0.35	−0.61
15	−0.04	0.30	−0.91	1.29	0.38	−0.41	32	−0.26	0.18	0.22	1.22	0.27	−0.52
16	1.66	−0.29	−0.42	1.53	−1.74	0.25	33	−0.81	−0.10	0.12	−0.06	−0.80	−0.18
17	4.04	−1.68	−0.44	−1.72	0.85	−0.52							

variance and was dominantly incorporated by Sr and many of its significantly correlated elements, excluding Na. PC3 revealed 12.4% of the total variance and summed up the set of Cs and its significantly correlated elements, Rb, As, and Se.

In Table 5, the component score coefficient matrix of different varieties shows the relative accumulations of different elements in plants. The mean value of factor loading score is 0, and the positive value means the score is higher than the average level individual. It is noted that variety 12 not only accumulated the significantly highest Cs in shoot but also obtained the highest loading scores in PC3 and PC6 and the second lowest score in PC4. Besides variety 12, the variety with loading score of PC3 higher than 1 was detected only in varieties 4 and 5. On the other hand, variety 25 accumulated the lowest Cs and loading scores in PC3 among 33 varieties. Additionally, variety 17 exhibited the highest loading score in PC1 and higher than variety 13 at the second place in the ranking of loading score in PC1 by 1.4-fold. Variety 9 presented uniquely positive values in all PCs. Conversely, variety 3, with the lowest concentration of Sr in shoot, showed a negative loading score in all PCs, which means any of the loading scores in PCs was lower than the mean value.

PC3 is important with respect to Cs accumulation because it collected Cs and the significantly correlated elements As, Rb, and Se in the same set. Variety 12 obtained the highest loading score in both PC3 and PC6 dominated by positive Co and negative K quantification and the second lowest loading score in PC4 dominated by Ba and Zn quantifications. As a result, greater Cs deposited in the shoot of variety 12 may be achieved by increasing the absorption of Co, Cs, Rb, As, and other elements positively correlated with Cs and diminishing the K, Zn, and Ba, the potentially competitive or antagonistic ion flux into plants. It has been reported that a lack of K supply would result in the decrease of vacuolar K^+ concentrations and further lower osmotic potential,[23,37] which is beneficial for nonselective assimilation of minerals, especially for Rb^+ and Cs^+, owing to their chemical similarity. It could be speculated that K^+ starvation in the vacuole could probably push the flux of cations including Rb^+ and Cs^+ to vacuole to maintain the osmotic potential and limit the absorption of Ba^{2+} to be unobstructed in xylem transport, which is consistent with the loading score of variety 12 in PC3, PC4, and PC6.

Variety 17 revealed another similar mechanism for efficiently taking up Cs. It gained the highest loading score in PC1 that accounted for 23.2% of the highest total variance and was mainly affected by Ni, Al, Fe, Cr, Li, and Mo, among which Ni, Al, and Fe were significantly correlated with Cs. Meanwhile, the lowest loading score in PC2 and second lowest loading score in PC4 were achieved by variety 17. PC2 and PC4 were dominantly affected by B, Na, Ca, Mg, Sr, Ba, Zn, Cd, and Mn. These elements, excluding Na, were all significantly correlated with Sr and played an indicative role for Sr accumulation. There is no competitive relationship between monovalent ion and bivalent ion, so this pattern of elemental composition possibly derives from the regulation of plant on overall ionomic uptake. It was demonstrated that the inward-rectifying potassium channels (KIR) in the plasma membranes, also permeable for Cs^+, are inhibited by millimolar concentrations of Ba^{2+} and Ca^{2+}.[50] Although significant correlation was not detected between Cs^+ and any of the bivalent cations, the particular ionomic characteristic in variety 17 may be of importance to associate Cs and Sr. Varieties 12 and 17 both took up more Cs by promoting the influx of elements positively correlated with Cs into shoot, but the former decreased the K and Ba uptake and the latter inhibited the accumulation of Rb, Sr, and significantly correlated elements of Sr in shoot.

On the basis of these results, K fertilization may be a feasible countermeasure against radiocesium uptake in K-deficient soils in Fukushima, because grown under K deficiency the sudden K supply would inhibit the flux of Rb^+ and Cs^+ into root to a great degree and adequate K storage in vacuoles would limit the uploading of Ba^{2+} into xylem transport to maintain the Ba^{2+} concentration in shoot at millimole level to repress the upward transport of Cs^+.[35,39,51] In addition, vermiculates, zeolites, and bentonites may be splendid selections as well because many cations including K^+, Ca^{2+}, and Mg^{2+} are contained in them. The application of these minerals to achieve the radiocesium retention has been demonstrated successfully in some previous studies.[24,54−56] It was proved that manure application led to the inhibition of the upward translocation of Cs to soybean seed and improved the accumulation of Cd, Ba, Co, and Zn, which coordinates with the inference in this study.[17] In addition, because among elements the highest positive coefficient for Cs was detected between Cs and As and variety 33 accumulated

DOI: 10.1021/jf5058777
J. Agric. Food Chem. 2015, 63, 2355−2363

both the lowest Cs and As, the countermeasures to inhibit As uptake may be beneficial for resistance of Cs translocation to the shoot.

AUTHOR INFORMATION

Corresponding Author

*(T.S.) Mail: Agricultural Radiation Research Center, NARO Tohoku Agricultural Research Center, 50 AzaHarajyukuminami, Arai, Fukushima 960-2156, Japan. Phone: +81-24-593-1310. Fax: +81-24-593- 2155. E-mail: shinano@affrc.go.jp.

Funding

A portion of this study was supported by the Mitsui & Co., Ltd., Environment Fund.

Notes

The authors declare no competing financial interest.

ACKNOWLEDGMENTS

We are thankful for the supply of amaranthus seeds (origin of U.S. National Plant Germplasm System) by Dr. David Brenner, Iowa State University, Plant Introduction Station, through the U.S. National Plant Germplasm System and also appreciate the supply of *A. retroflexus* and several local-variety seeds by Dr. Mutsumi Yamagami, Institute for Environmental Sciences, and the Mexico and K4 lines from Dr. Naoki Ogata, National Institute of Crop Science. We are grateful to Drs. Tetsuro Mimura, Mari Mimura, Chiyo Komiyama, and Akira Kitamura (Kobe University) for assistance with radioisotope measurements. We also thank Atsuko Uchida, NARO Hokkaido Agricultural Research Center, for sample preparation.

REFERENCES

(1) Silva-Sanchez, C.; Barba de la Rosa, A. P.; León-Galván, M. F.; De Lumen, B. O.; De León-Rodríguez, A.; González de Mejía, E. Bioactive peptides in amaranth (*Amaranthus hypochondriacus*) seed. *J. Agric. Food Chem.* **2008**, *56*, 1233−1240.

(2) Broadley, M. R.; Willey, N. J.; Mead, A. A method to assess taxonomic variation in shoot cesium concentration among flowering plants. *Environ. Pollut.* **1999**, *106*, 341−349.

(3) Willey, N. J.; Tang, S.; Watt, N. R. Predicting inter-taxa differences in plant uptake of cesium-134/137. *J. Plant Qual.* **2005**, *34* (5), 1478−1489.

(4) Ohmori, Y.; Kajikawa, M.; Nishida, S.; Tanaka, N.; Kobayashi, N.; Tanoj, K.; Furukawa, J.; Fujiwara, T. The effect of fertilization on cesium concentration of rice grown in a paddy field in Fukushima prefecture in 2011 and 2012. *J. Plant Res.* **2014**, *137*, 67−71.

(5) Dushenkov, S.; Mikheev, A.; Prokhnevsky, A.; Ruchko, M.; Sorochinsky, B. Phytoremediation of radiocesium-contaminated soil in the vicinity of Chernobyl, Ukraine. *Environ. Sci. Technol.* **1999**, *33*, 469−475.

(6) Balanov, M. I.; Bruk, G. Y.; Golikov, V. Y.; Barkovsky, A. N.; Kravtsova, E. M.; Kravtosova, O. S.; Mubasarov, A. A.; Shutov, V. N.; Travnikova, I. G.; Howard, B. J.; Brown, J. E.; Strand, P. Assessement of current exposre of the population living in the Techa River Basin from radioactive releases of the Mayak facility. *Health Phys.* **2007**, *92*, 134−147.

(7) Ivanov, Y. A.; Lewyckyj, N.; Levchuk, S. E.; Prister, B. S.; Firsakova, S. K.; Arkhipov, N. P.; Kruglov, S. V.; Alexakhin, R. M.; Sandalls, J.; Askbrant, S. Migration of ^{137}Cs and ^{90}Sr from chernobyl fallout in Ukrainian, Belarussian and Russian soils. *J. Environ. Radioact.* **1997**, *35* (1), 1−21.

(8) Zhu, Y. G.; Smolders, E. Plant uptake of radiocesium: a review of mechanisms, regulation and application. *J. Exp. Bot.* **2000**, *51*, 1635−1645.

(9) Kanter, U.; Hauser, A.; Michalke, B.; Draxl, S.; Schaffner, A. R. Caesium and strontium accumulation in shoots of *Arabidopsis thaliana*: genetic and physiological aspects. *J. Exp. Bot.* **2010**, *61*, 3995−4009.

(10) Tsukada, H.; Takeda, A.; Takahashi, T.; Hasegawa, H.; Hisamatsu, S. I.; Inaba, J. Uptake and distribution of ^{90}Sr and stable Sr in rice plants. *J. Environ. Radioact.* **2005**, *81* (2), 221−231.

(11) Smolders, E.; Tsukada, H. The transfer of radiocesium from soil to plants: mechanisms, data, and perspectives for potential countermeasures in Japan. *Integr. Environ. Assess. Manage.* **2011**, *7* (3), 379−381.

(12) Braodley, M. R.; White, P. J. Some elements are more equal than others: soil-to-plant transfer of radiocaesium and radiostrontium, revisited. *Plant Soil* **2012**, *355*, 23−27.

(13) Camps, M.; Rigol, A.; Hillier, S.; Vidal, M.; Rauret, G. Quantitative assessment of the effects of agricultural practices designed to reduce Cs-137 and Sr-90 soil-plant transfer in meadows. *Sci. Total Environ.* **2004**, *332*, 23−38.

(14) Guillaume, T.; Chawla, F.; Steinmann, P.; Gobat, J. M.; Froidevaux, P. Disparity in ^{90}Sr and ^{137}Cs uptake in Alpine plants: phytogenetic effect and Ca and K availability. *Plant Soil* **2012**, *355* (1−2), 29−39.

(15) Roca, M. C.; Vallejo, V. R. Effect of soil potassium and calcium on caesium and strontium uptake by plant roots. *J. Environ. Radioact.* **1995**, *28* (2), 141−159.

(16) Maiga, A.; Diallo, D.; Bye, R.; Paulsen, B. S. Determination of some toxic and essential metal ions in medicinal and edible plants from Mali. *J. Agric. Food Chem.* **2005**, *53* (6), 2316−2321.

(17) Sha, Z. M.; Oka, N.; Watanabe, T.; Dulbert, B.; Okazaki, K.; Osaki, M.; Shinano, T. Ionome of soybean seed affected by previous cropping with mycorrhizal plant and manure application. *J. Agric. Food Chem.* **2012**, *60* (38), 9543−9552.

(18) Aguilar, E. G.; Cantarelli, M. A.; Marchevsky, E. J.; Escudero, N. L.; Camiña, J. M. Multielemental analysis and classification of amaranth seeds according to their botanical origin. *J. Agric. Food Chem.* **2011**, *59* (17), 9059−9064.

(19) Salt, D. E.; Baxter, I.; Lahner, B. Ionomics and the study of the plant ionome. *Annu. Rev. Plant Biol.* **2008**, *59*, 709−733.

(20) Baxter, I.; Hermans, C.; Lahner, B.; Yakubova, E.; Tikhonova, M.; Verbruggen, N.; Chao, D. Y.; Salt, D. E. Biodiversity of mineral nutrient and trace elements accumulation in *Arabidopsis thaliana*. *PLoS One* **2012**, *7* (4), No. e35121.

(21) Buescher, E.; Achberger, T.; Amusan, I.; Giannini, A.; Ochsenfeld, C.; Rus, A.; Lahner, B.; Hoekenga, O.; Yakubova, E.; Harper, J. F.; Guerinot, M. L.; Zhang, M.; Salt, D. E.; Baxter, I. R. Natural genetic variation in selected populations of *Arabidopsis thaliana* is associated with ionomic differences. *PLoS One* **2010**, *5* (6), No. e11081.

(22) Shtangeeva, I.; Alber, D.; Bukalis, G.; Stanik, B.; Zepezauer, F. Multivariate statistical analysis of nutrients and trace elements in plants and soil from northwestern Russia. *Plant Soil.* **2009**, *322*, 219−228.

(23) Rigol, A.; Riog, M.; Vidal, M.; Rauret, G. Sequential extractions for the study of radiocaesium and radiostrontium dynamics in mineral and organic soils from Western Europe and Chernobyl areas. *Environ. Sci. Technol.* **1999**, *33*, 887−895.

(24) Vidal, M.; Camps, M.; Grebenshikova, N.; Sanzharova, N.; Ivanov, Y.; Vandecasteele, C.; Shand, C.; Rigol, A.; Firsakova, S.; Fesenko, S.; Levchuk, S.; Cheshire, M.; Saura, T.; Rauret, G. Soil- and plant-based countermeasures to reduce ^{137}Cs and ^{90}Sr uptake by grasses in natural meadoes: the REDUP project. *J. Environ. Radioact.* **2001**, *56*, 139−156.

(25) Konoplev, A. V.; Viktorova, N. V.; Virchenko, E. P.; Popov, V. E.; Bulgakov, A. A.; Desmet, G. M. Influence of agricultural countermeasures on the ratio of different chemical forms of radionuclides in soil and soil solution. *Sci. Total Environ.* **1993**, *137* (1−3), 147−162.

(26) Fujimura, S.; Yoshioka, K.; Saito, T.; Sato, M.; Sato, M.; Sakuma, Y.; Muramatsu, Y. Effects of applying potassium, zeolite and vermiculite on the radiocesium uptake by rice plants grown in paddy

DOI: 10.1021/jf5058777
J. Agric. Food Chem. 2015, 63, 2355−2363

field soils collected from Fukushima prefecture. *Plant Prod. Sci.* **2013**, *16*, 166−170.
(27) Kubo, K.; Nemoto, K.; Kobayashi, H.; Kuriyama, Y.; Harada, H.; Matsunami, H.; Eguchi, T.; Kihou, N.; Ota, Takeshi.; Keitoku, S.; Kimura, T.; Shinano, T. Analyses and countermeasures for decreasing radioactive cesium in buckwheat in areas affected by the nuclear accident in 2011. *Field Crops Res.* **2015**, *170*, 40−46.
(28) Shinano, T.; Watanabe, T.; Chu, Q.; Osaki, M.; Kobayashi, D.; Okouchi, T.; Matsunami, H.; Nagata, O.; Okazaki, K.; Nakamura, T. Varietal difference in radiocesium uptake and transfer from radiocesium deposited soils in the genus *Amaranthus*. *Soil Sci. Plant Nutr.* **2014**, *60*, 1−9.
(29) Cultivated Soil Classification Committee: Classification of cultivated soil in Japan, third approximation. *Misc, Publ, Nat. Agro-Environ. Sci.* **1995**, *17*, 1−79 (in Japanese).
(30) Staunton, S.; Roubaud, M. Absorption of Cs on montmorillonite and illite: effect of charge compensating cation, ionic strength, concentration of Cs, K and fulvic acid. *Clays. Clay Miner.* **1997**, *45*, 251−260.
(31) White, P. J.; Bowen, H. C.; Parmaguru, P.; Fritz, M.; Spracklen, W. P.; Spidy, R. E.; Meacham, M. C.; Harriman, M.; Trueman, L. J.; Smith, B. M.; Thomas, B.; Broadley, M. R. Interactions between selenium and sulphur nutrition in *Arabidopsis thaliana*. *J. Exp. Bot.* **2004**, *55*, 1927−1937.
(32) Watanabe, T.; Broadley, M. R.; Jansen, S.; White, P. J.; Takada, J.; Satake, K.; Tkamatsu, T.; Tuah, S. J.; Osaki, M. Evolutionary control of leaf element composition in plants. *New Phytol.* **2007**, *174*, 516−523.
(33) Rengel, Z.; Damon, P. M. Crops and genotypes differ in efficiency of potassium uptake and use. *Physiol. Plant.* **2008**, *133* (4), 624−636.
(34) Micallef, S. A.; Shiaris, M. P.; Colón-Carmona, A. Influence of *Arabidopsis thaliana* accessions on rhizobacterial communities and natural variation in root exudates. *J. Exp Bot.* **2009**, DOI: 10.1093/jxb/erp053.
(35) Penrose, B.; Bereford, N. A.; Broadley, M. R.; Crout, N. M. J. Inter-varietal variation in caesium and strontium uptake by plants: a meta-analysis. *J. Environ. Radioact.* **2015**, *139*, 103−117.
(36) Taylor, D. M.; Gillis, T. M. Correlation of biokinetic behavior and physicochemical parameters within chemical families: alkali metals and lanthanides. *Radiat. Prot. Dosimetry* **1994**, *53*, 183−186.
(37) Vinichuk, M.; Mårtensson, A.; Rosén, K. Inoculation with arbuscular mycorrhizae does not improve ^{137}Cs uptake in crops grown in the Chernobyl region. *J. Environ. Radioact.* **2013**, *126*, 14−19.
(38) White, P. J.; Broadley, M. R.; Thompson, J. A.; McNicol, J. W.; Crawley, M. J.; Poulton, P. R.; Johnston, A. E. Testing the distinctness of shoot ionomes of angiosperm families using the Rothamsted Park Grass Continuous Hay Experiment. *New Phytol.* **2012**, *196* (1), 101−109.
(39) Braodley, M. R.; White, P. J. Some elements are more equal than others: soil-to-plant transfer of radiocaesium and radiostrontium, revisited. *Plant Soil* **2012**, *355*, 23−27.
(40) Isaure, M. P.; Fraysse, A.; Deves, G.; Le Lay, P.; Fayar, B.; Susini, J.; Bourguignon, J.; Ortega, R. Micro-chemical imaging of cesium distribution in *Arabidopsis thaliana* plant and its interaction with potassium and essential trace elements. *Biochimie* **2006**, *88*, 1583−1590.
(41) Qi, Z.; Hampton, C. R.; Shin, R.; Barkla, B. J.; White, P. J.; Schachtman, D. P. The high affinity K^+ transporter AtHAK5 plays a physiological role in planta at very low K^+ concentrations and provides a caesium uptake pathway in *Arabidopsis*. *J. Exp. Bot.* **2008**, *59*, 595−607.
(42) Broadley, M. R.; Escobar-Gutierrez, A. J.; Bowen, H. C.; Willey, N. J.; White, P. J. Influx and accumulation of Cs^+ by the *akt1* mutant of *Arabidopsis thaliana* (L.) Heynh. lacking a dominant K^+ transport system. *J. Exp. Bot.* **2001**, *52*, 839−844.
(43) Hampton, C. R.; Bowen, H. C.; Broadley, M. R.; Hammond, J. P.; Mead, A.; Payne, K. A.; Pritchard, J.; White, P. J. Cesium toxicity in *Arabidopsis*. *Plant Physiol.* **2004**, *136*, 3824−3837.
(44) Tsukada, H.; Hasegawa, H.; Hisamatsu, S.; Yamasaki, S. Rice uptake and distributions of radioactive ^{137}Cs, stable ^{133}Cs and K from soil. *Environ. Pollut.* **2002**, *117* (3), 403−409.
(45) Draxi, S.; Muller, J.; Li, W. B.; Michalke, B.; Scherb, H.; Hense, B. A.; Chiersch, J.; Kanter, U.; Schaffner, A. R. Caesium accumulation in yeast and plants is selectively repressed by loss of the SNARE Sec22p/SEC22. *Nat. Commun.* **2013**, DOI: 10.1038/ncomms3092.
(46) Ahmad, I.; Maathuis, F. J. M. Cellular and tissue distribution of potassium: physiological relevance, mechanisms and regulation. *J. Plant Physiol.* **2014**, *171* (9), 708−714.
(47) Brown, G. R.; Cummings, S. P. Potassium uptake and retention by *Oceanomonas baumannii* at low water activity in the presence of phenol. *FEMS Microbiol. Lett.* **2001**, *205* (1), 37−41.
(48) Yamashita, J.; Enomoto, T.; Yamada, M.; Ono, T.; Hanafusa, T.; Nagamatsu, T.; Sonoda, S.; Yamamoto, Y. Estimation of soil-to-plant transfer factors of radiocesium in 99 wild plant species grown in arable lands 1 year after the Fukushima 1 nuclear power plant accident. *J. Plant Res.* **2014**, *127*, 11−22.
(49) Norton, G. J.; Dasgupta, T.; Islam, M. R.; Islam, S.; Deacon, C. M.; Zhao, F. J.; Stroud, J. L.; Mcgrath, S. P.; Feldmann, J.; Price, A. H.; Meharg, A. A. Arsenic influence on genetic variation in grain trace-element nutrient content in Bengal Delta grown rice. *Environ. Sci. Technol.* **2010**, *44* (21), 8284−8288.
(50) Williams, P. N.; Islam, S.; Islam, R.; Jahiruddin, M.; Adomako, E.; Soliaman, A. R. M.; Rahman, G. K. M. M.; Lu, Y.; Deacon, C.; Zhu, Y. G.; Meharg, A. A. Arsenic limits trace mineral nutrition (selenium, zinc, and nickel) in Bangladesh rice grain. *Environ. Sci. Technol.* **2009**, *43* (21), 8430−8436.
(51) White, P. J.; Broadley, M. R. Mechanisms of caesium uptake by plants. *New Phytol.* **2000**, *147*, 241−256.
(52) Ariyama, K.; Nishida, T.; Noda, T.; Kadokura, M.; Yasui, A. Effects of fertilization, crop year, variety, and provenance factors on mineral concentrations in onions. *J. Agric. Food Chem.* **2006**, *54* (9), 3341−3350.
(53) Song, W. Y.; Choi, K. S.; Kim, D. Y.; Geisler, M.; Park, J.; Vincenzetti, V.; Schellenberg, M.; Kim, S. H.; Lim, Y. P.; Noh, E. W.; Lee, Y.; Martinoia, E. *Arabidopsis* PCR2 is a zinc exporter involved in both zinc extrusion and long-distance zinc transport. *Plant Cell* **2010**, *22*, 2237−2252.
(54) Van, T. K.; Kang, Y.; Fukui, T.; Sakurai, K.; Iwasaki, K.; Aikawa, Y.; Phuong, N. M. Arsenic and heavy metal accumulation by *Athyruim yokoscense* from contaminated soils. *Soil Sci. Plant Nutr.* **2006**, *52*, 701−710.
(55) Valke, E.; Elsen, A.; Cremers, A. The use of zeolites as amendments in radiocaesium- and radiostrontium-contaminated soils: a soil-chemical approach. 4. A potted soil experiment to verify laboratory-based predictions. *Zeolites* **1997**, *18*, 225−231.
(56) Atun, G.; Bodur, N. Retention of Cs on zeolite, bentonite and their mixtures. *J. Radioanal. Nucl. Chem.* **2002**, *253*, 275−279.

DOI: 10.1021/jf5058777
J. Agric. Food Chem. 2015, 63, 2355−2363

JOURNAL OF AGRICULTURAL AND FOOD CHEMISTRY

Addition/Correction

pubs.acs.org/JAFC

Correction to Fermentative Conditions Modulating Sweetness in Dry Wines: Genetics and Environmental Factors Influencing the Expression Level of the *Saccharomyces cerevisiae HSP12* Gene

Axel Marchal,* Philippe Marullo, Cécile Durand, Virginie Moine, and Denis Dubourdieu

J. Agric. Food Chem. **2015**, *63* (1), 304−311. DOI: 10.1021/jf504408t

There was a mistake in the caption of Figure 5A. The names of the yeast strains attributed to sweetness intensities were shuffled. The right attribution can be found in Figure 5 below.

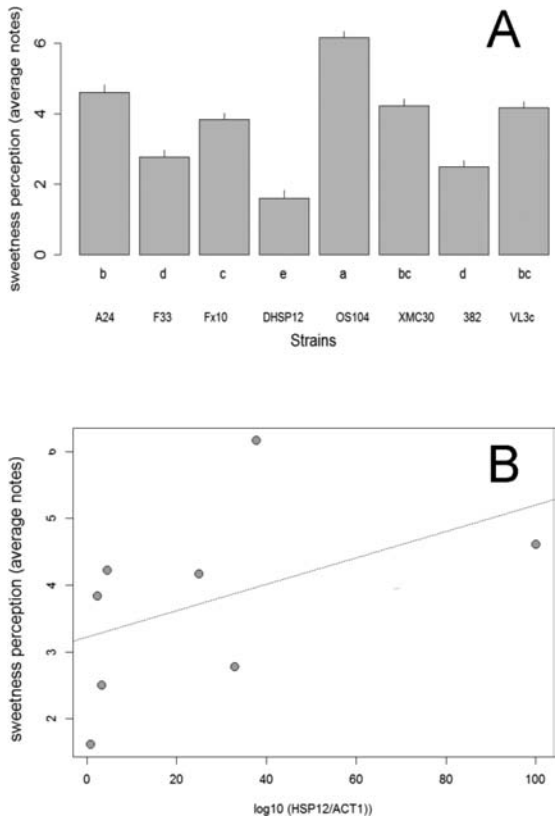

Figure 5. Wine in contact with lees obtained from different yeast strains showed marked difference in sweetness perception. (A) A wine without Hsp12p was obtained by fermenting a Merlot juice with Δ°hsp12. Yeast biomass of eight different strains was added to this wine, and aging on lees was carried out at 32 °C for 10 days. This biomass was collected from fermenting cells at 46 g/L of CO_2 produced. After wine centrifugation, a panel tasted the modalities, and the sweetness intensity was rated on a scale from 0 to 7. Error bars indicates the standard error of 17 notes. A two-way analysis of variance was used to estimate the strain effect ($Y = \mu + \text{strain}^i + \text{panel}^j + \varepsilon^{ij}$). The letters below the box plot indicate groups with a statistical difference according to the linear model used (Duncan test $\alpha = 0.05$). (B) Relationship between sweetness perception and expression level of *HSP12* (Kendall correlation test, $T = 22$, p value = 0.0601).

Published: February 17, 2015

ACS Publications © 2015 American Chemical Society

DOI: 10.1021/acs.jafc.5b00815
J. Agric. Food Chem. 2015, 63, 2364−2364

JOURNAL OF AGRICULTURAL AND FOOD CHEMISTRY

Addition/Correction

pubs.acs.org/JAFC

Correction to A Survey of Tremtone, Dehydrotremetone, and Structurally Related Compounds in *Isocoma* spp. (Goldenbush) in the Southwestern United States

Stephen T. Lee,* Daniel Cook, T. Zane Davis, Dale R. Gardner, Robert L. Johnson, and Clinton A. Stonecipher

J. Agric. Food Chem. **2015**, *63* (3), 872−879. DOI: 10.1021/jf505423h

Several of the values contained in the original version of Table 2 are incorrect due to a calculation error, and are corrected in the revised table by multiplying the previously published values by 8. Tremetone, **1**, and 7-isopentenyloxycoumarin, **5**, from the Red Rock, Mesa, Kingman, and Wickenburg Sites and 3-oxyangeloyltremetone, **3**, from the Tuba City Site have been corrected in the revised table and are greater by a factor of 8. The corrected table appears below.

Table 2. Concentrations of Tremetone, 1, Dehydrotremetone, 2, 3-Oxyangeloyltremetone, 3, 4-Hydroxy-3-(3-methyl-2-butenyl)acetophenone, 4, and 7-Isopentenyloxycoumarin, 5, in *Isocoma* spp. Field Collections[a]

	av compd concentration[b] ± SD (n = 10), μg/mg dry weight				
Isocoma spp./site	**1**	**2**	**3**	**4**	**5**
I. pluriflora					
Pecos	0.4 ± 0.3	2.6 ± 0.7	4 ± 1		
Carlsbad	0.16 ± 0.09	0.8 ± 0.2	1.9 ± 0.7		
I. tenuisecta					
Tuscon	0.2 ± 0.1	1.7 ± 0.5	2 ± 1	*0.4 ± 0.4*	*1.1 ± 0.4*
Red Rock	0.9 ± 0.6	0.7 ± 0.5	1.3 ± 0.9	*0.09 ± 0.1*	*0.8 ± 0.4*
I. azteca					
Newcomb	6 ± 2	0.8 ± 1	2 ± 3	*0.7 ± 0.4*	
Tsaya	8 ± 2	0.0004 ± 0.001	0.5 ± 0.3	*0.8 ± 0.4*	
I. acradenia					
Mesa	8 ± 1	1.0 ± 0.4	1.1 ± 0.9	*0.4 ± 0.4*	*0.8 ± 0.3*
Kingman	3 ± 2	4 ± 2	4 ± 2	*1 ± 1*	*0.8 ± 0.1*
Wickenburg	9 ± 3	1.1 ± 0.5	1.2 ± 0.7	*0.6 ± 0.4*	*0.7 ± 0.2*
I. rusbyi					
Marble Canyon	0.7 ± 0.6	0.6 ± 0.6	4 ± 1	*0.07 ± 0.03*	*0.4 ± 0.3*
Tuba City	2 ± 1		4 ± 1	*0.02 ± 0.02*	*0.07 ± 0.1*
Holbrook	2 ± 1	2 ± 2	7 ± 4	*0.13 ± 0.07*	

[a] n = 10 for all sites except Pecos, Carlsbad, and Marble Canyon, where n = 9. [b] The concentrations in italics are expressed in tremetone equivalents.

Published: February 20, 2015

ACS Publications © 2015 American Chemical Society

DOI: 10.1021/acs.jafc.5b00819
J. Agric. Food Chem. 2015, 63, 2365−2365

Table 1. Distribution of the Three Main Food Folate Pools, 5-CH_3-H_4folate, Formyl Folate,[a] and Unsubstituted Folate,[b] in Some Nonfortified Foods[c]

food sample	5-CH_3-H_4folate (%)	formyl folate (%)	unsubstituted folate		Σ of unsubstituted folate (%)	folic acid equivalents (μg/100 g^{FW})
			H_4-folate (%)	folic acid (%)		
baker's yeast, dry	61.0	18.7	20.3	nd[e]	20.3	3520 ± 60[25]
pig liver (CRM 487)[d]	33.4	20.2	27.4	19.1	46.5	1443 ± 13[29]
wheat germ	<10	81	<1	10	~10	285[30]
wheat bran	13.5	77	10	nd	10	118[25]
wholemeal rye flour	12.7	79.5	5.8	nd	5.8	63.5[25]
wholemeal wheat flour	10.6	62.7	9.8	17	26.8	40[25]
rice, unpolished	~48	~40	~6	~6	~12	44.4 ± 2.9[22,34]
spinach, raw	76−88	5−34	0−19	nd	0−19	96−159[31]
spinach, raw	46−54	20−23	23−33	na	23−33	155−178[32]
spinach, raw	73	26	0.5	na	0.5	117[30]
chickpeas, dry	37.7	49.0	9.6	3.8	13.4	282[30]
peas, green	74.7	12.8	10.8	1.2	12.0	96[30]
Savoy cabbage	61.2	28.2	10	<1	~10	163[30]
broccoli	67.6	16.3	16.0	nd	16.0	125 ± 10[33]
romaine lettuce	41.4	46.3	2.5	nd	2.5	219 ± 14[33]
carrot	81.2	8.6	10.2	nd	10.2	76 ± 10[33]
potato, raw	~30	~42	~12	~16	~28	24 ± 0.23[89]

[a]Formyl folate = sum of 5-HCO-H_4folate, 10-HCO-H_4folate, and 5,10-CH^+-H_4folate. [b]Unsubstituted folate = sum of H_4folate, H_2folate, folic acid, and converted 5,10-CH_2-H_4folate. [c]Expressed in percentage (%) of total folate calculated as folic acid equivalents per 100 g fresh weight (FW). All data are based on deconjugated folates determined by LC-MS or LC-MS/MS. [d]Lyophilized certified reference material (CRM). [e]nd, not detected.

intestinal mucosa and finally intracellularly, especially in the liver, first to H_2folate and subsequently to H_4folate.[9,12]

Immediately upon intracellular entrance, H_4folate participates in the biosynthesis of polyglutamate forms, usually up to five to seven residues, to be retained within cells and subcellular compartments. Polyglutamated folates are the preferred coenzymes involved in C1 metabolism. Chain elongation increases the anionic nature of folate coenzymes by providing α-carboxyl charges and decreases affinity for membrane carriers, thus impairing folate diffusion through hydrophobic barriers.[19] The polyglutamated H_4folate molecules accept C1 groups supplied from the catabolism of certain amino acids such as glycine, serine, and histidine or from the catabolism of purines. The C1 groups are donated enzymatically to be included in the nucleotide synthesis of DNA and RNA and in the methylation of homocysteine to methionine. After donation of their C1groups, the substituted folates regenerate to polyglutamate forms of H_4folate or H_2folate and are then ready to accept new C1 groups.[2,9,10]

OCCURRENCE IN FOOD

Plant foods are the major source of folate because they can synthesize folate. This biosynthesis route has already been explored for biofortification of tomato fruit and rice with 25- and 50-fold increases in folate content, respectively.[21,22] Other types of bioprocessing to enhance dietary folate are germination, sprouting, malting, or fermentation based on yeast or lactic acid bacteria (LAB) or both. Bioprocessing is commonly used for the manufacture of bread, yogurt, buttermilk, beer, and wine.[23−26] Good dietary sources of native folate include liver, legumes, green leafy vegetables, citrus fruit and juice, certain berries, cereals, and egg.[17] Mandatory or voluntary fortification with folic acid is also common mostly as prophylaxis against neural tube defects because women of fertile age throughout the world have difficulties meeting the daily folate recommendations during pregnancy and lactation.[27]

Most of the folate information in food databases originates from microbiological assays (MA), which give information only on the total folate content determined after deconjugation. During the past decades, chromatographic methods have been developed that can separate the different folate vitamers. Such studies have shown 5-CH_3-H_4folate to be the major native food folate form, followed by the formyl folates. Overall, unsubstituted folates are ranked as the third folate pool in diet. Table 1 gives an overview of deconjugated native folates in monoglutamate forms that have been determined in food using chromatographic methods, for example, high-performance liquid chromatography (HPLC) or ultrahigh-performance liquid chromatography (UHPLC). Only data based on HPLC and highly selective detectors such as mass spectrometry (MS) are displayed in Table 1.[22,25,28−34]

Dietary folates are divided into 5-CH_3-H_4folate, sum of formyl folates, and two individual unsubstituted folates, H_4folate and folic acid. H_2folate is not recorded because it is too labile to be determined. Folic acid is included as a stable degradation product of H_4folate and H_2folate. Baker's dry yeast is one of the richest dietary sources of folate, containing about 3 mg total folate/100 g, of which H_4folate constitutes ~25%.[28] Another rich dietary folate source is liver, where H_4folate occurs in similar proportions as 5-CH_3-H_4folate, and is thus the second most common group there.[29] Other good dietary sources of folate and H_4folate are legumes and green leafy vegetables such as spinach and cabbage, in which H_4folate constitutes about 10−20%.[30−33] Cereal fractions also contain H_4folate, usually below 10% (Table 1). Folic acid as a degradation product of H_4folate and H_2folate is occasionally but not regularly found in low concentrations, up to 25% of total folate in cereal fractions (whole grain flour, bran).[22,25,30,34] Apart from the "natural" presence of folic acid in certain foods, folic acid can also be added as a mandatory or voluntary food fortificant, especially to flours of wheat and corn, bread, fruit juices, and infant foods.

DOI: 10.1021/jf504987n
J. Agric. Food Chem. 2015, 63, 2367−2377

CHEMICAL PROPERTIES OF UNSUBSTITUTED FOLATES

Background information about chemical properties is essential to understand the stability and conversions of unsubstituted folates during food handling and analysis. All folates comprise a pteridine coupled via a carbon−nitrogen (C^9−N^{10}) bond to pABG, which in turn is coupled via an amide bond through its carboxyl moiety to the amino group of L-glutamic acid. The pteridine moiety of folates can exist in three oxidation states: fully oxidized (folic acid) or as the reduced 7,8-dihydrofolate (H_2folate) or 5,6,7,8-tetrahydrofolate (H_4folate). H_4folate is the coenzymatically active form of the vitamin that accepts, transfers, and donates C1 groups, attached either at the N^5 or N^{10} position or by bridging these positions.[9,35,36] The C1 groups also differ in their oxidation state, with folates existing as derivatives of formate (5-formyl-H_4folate, 10-formyl-H_4folate, 5,10-methenyl-H_4folate, and 5-formimino-H_4folate), methanol (5-methyl-H_4folate), or formaldehyde (5,10-methylene-H_4folate).[16] In addition to these structural variables, most naturally occurring folates exist as γ-linked polyglutamate conjugates, with chain lengths typically in the range of five to seven glutamate residues.[9] The chemical structures of unsubstituted folates are displayed in Figure 1.

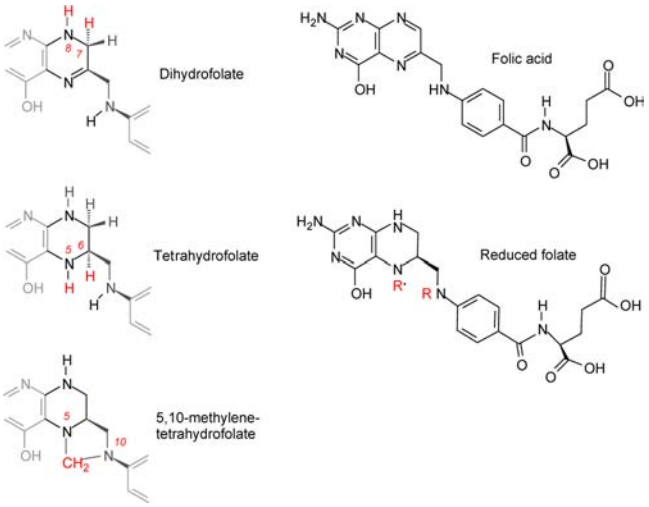

Figure 1. Structures of folic acid and the native monoglutamate folate forms.

Folates are ionogenic and amphoteric molecules, which exist in cationic, anionic, or zwitterionic form depending on pH. The pH ranges, in which the various ionizable groups of unsubstituted folates are predominantly (>50%) charged, are displayed in Figure 2.[37−41] Ionogenic groups of particular significance in the pH values relevant to foods and biological systems are the N^5 position of H_4folate (basic pK_a = 4.8) and the glutamate carboxyl groups (acidic α pK_a = 3.5; γ pK_a = 4.8). Folates undergo changes in ionic forms as a function of pH, which in part explains the pH dependency of folate solubility and the stability and behavior during chromatographic separation.[9,38−41]

Folates generally have minimum solubility in the mildly acidic pH range (e.g., pH 2−4), monocationic and neutral species predominating, whereas solubility generally increases in proportion to the pH above this range, mainly zwitterionic and anionic species. The solubility of folates in aqueous solutions is low due to the pteridine part. An increase in temperature and

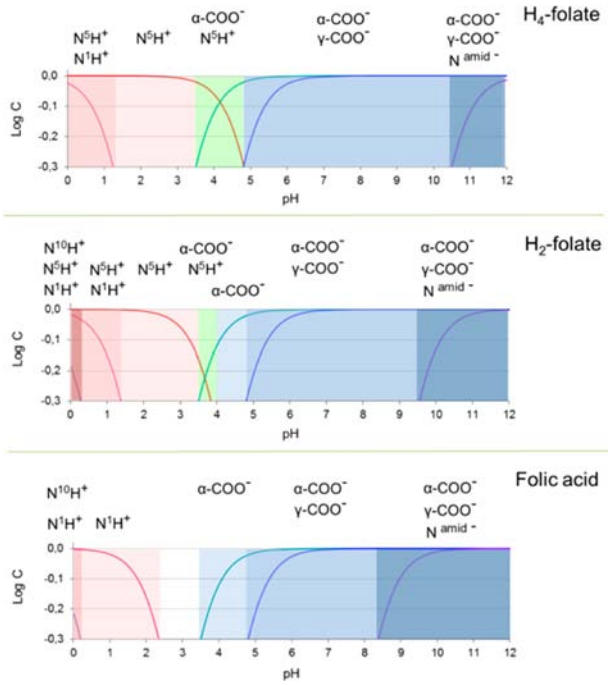

Figure 2. Ionized groups present in unsubstituted folates at different pH ranges and their pK_a values. pH ranges where they are predominantly charged, 50% or more, are displayed by color. pK_a values for each group are displayed where their log C curves cross the x-axis. For pK_a values displayed in a table, see Patring et al.[37]

the presence of ions from buffers or salts increase the solubility.[9,35,36]

UV light, air, and heating destroy the molecules by oxidation if not protected by antioxidants.[41] Early works show that the effect of pH on the stability of reduced unsubstituted folates is U-shaped with the highest stability observed between pH 1−2 and 8−12, whereas the stability is lowest between pH 4 and 6.[9,41−43] However, even at these favorable pH intervals, H_4folate and H_2folate are extremely unstable with half-lives of losses in bioactivity below 5 h.[9] Folic acid, the oxidized form, is much more stable than reduced unsubstituted folates. Its stability also depends on pH and it is stable under neutral and alkaline conditions, but less stable in acidic conditions (pH <5).[44−48] All three unsubstituted folates are sensitive to UV light. For more details on the stability of the unsubstituted folates, see Table 2.[36,43,46−54]

DEGRADATION BY AUTOXIDATION

All unsubstituted folates undergoing autoxidation are split in their C^9−N^{10} bond into biologically inactive products. Figure 3 gives an overview of the pathways and the major autoxidation products identified in the oxidation carried out in the presence of UV light, air, or oxygen *and in the absence of antioxidants*.[7,15,45,55,56] The major products are pABG and various substituted pterins, ultimately converted into pterins under release of formaldehyde. Classical work has shown that the oxidative degradation of solutions of H_4folate first produces a quinonoid isomer of H_2folate as intermediate. At acidic pH, this quinonoid is oxidized to pABG and 7,8-dihydropterin under release of formaldehyde. This dihydropterin is then further oxidized to pterins. At alkaline conditions, the quinonoid-H_2folate is converted to H_2folate, which is further oxidized to pABG and 6-formyltetrapterin, followed by the

DOI: 10.1021/jf504987n
J. Agric. Food Chem. 2015, 63, 2367−2377

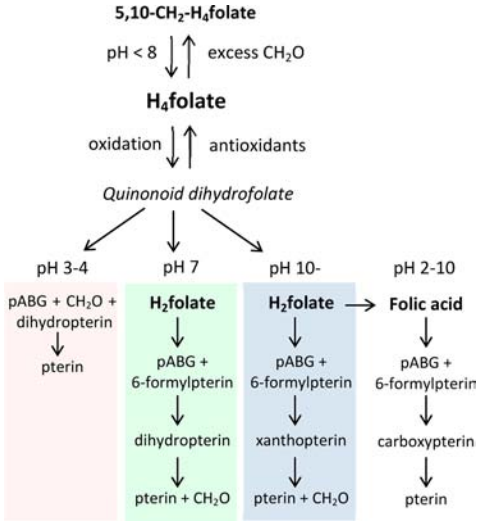

Figure 3. Pathways for interconversion between H_4folate and 5,10-CH_2-H_4folate and degradation of unsubstituted folates exposed to air at ambient temperature;[15,55,56] degradation of folic acid in the presence of light or UV irradiation.[44−46,48]

formation of xanthopterin and formaldehyde.[15,55,56]Irradiation of folic acid with UV light first produces pABG and pterine-6-carboxyaldehyde, which is converted to 6-carboxylic acid and finally to the decarboxylated 2-amino-4-hydroxypteridine.[45−48]

MECHANISMS OF AUTOXIDATION

The pH-dependent oxidation, affecting the rates and type of products, has drawn attention to the role of ionization and protonation of the zwitterion folate/folic acid as a mechanism.[15,38] Akhtar and co-workers studied the effect of pH in the pH range 2−10 on photodecomposition of folic acid.[46,47] According to their results folic acid exhibited best stability at highly alkaline pH 10.0, whereas its stability was lowest and susceptibility to photolysis was highest in the acidic range (pH 2−4). This clearly showed that photolysis of folic acid is a pH-dependent reaction and occurs more rapidly at low pH when folic acid exists predominantly as a neutral species. More recently, Martin et al. proposed a mechanism of photolysis of folic acid where UV radiation at 350−400 nm caused formation of pterin radicals, which were then oxidized to the known photoproduct 6-carboxypterin.[57]

According to early studies, steric hindrance is another phenomenon affecting the oxidative sensitivity of unsubstituted folates. H_4folates with substituents at the N^5 position, that is, 5-CH_3-H_4folate and 5-HCO-H_4folate, exhibit much higher stability than unsubstituted H_4folate. This suggests that the stabilization effect of the N^5 methyl group or the N^5 formyl group is, at least in part, due to steric hindrance in restricting the access of oxygen or other oxidants to the pteridine ring. The stabilizing effect of the substituent is presumably due to the effect of the one-carbon substituent in interfering with the formation of resonance forms involved in oxidative degradation.[15,55]

DEGRADATION PRODUCTS IN THE PRESENCE OF ANTIOXIDANTS

In the presence of antioxidants and while protected against UV light, the unsubstituted folates are protected against oxidation. Depending on the combination and concentration of antioxidants, pH, time, and temperature, the oxidation of H_4folates is either fully or partly prevented. Antioxidants decrease the rate of oxidative degradation, making it possible to detect even early biologically active oxidation products of H_4folate, such as H_2folate and folic acid. Hence, a mixture of these forms appears together with pABG and various pterins in foods during processing, cooking, storage, or analytical conditions (see Figure 3).[13,14,58]

Thiols, for example, 2-mercaptoethanol (MCE) and 2,3-dimercaptopropanol (BAL), were the first antioxidants to be shown to retard the oxidation of H_4folate.[59,60] In a classical work, Blakley[60] found BAL to be a better antioxidant than MCE. Later, the combination of thiols with ascorbate was found to be the most effective in protecting H_4folate. Wilson and Horne[58] were the first group to combine the use of ascorbate and MCE as antioxidants during food folate analysis. Today, combinations of 1−2% ascorbate with MCE or BAL are commonly used to stabilize H_4folate during determination by HPLC.

Although MCE is the most commonly used and inexpensive thiol in combination with ascorbic acid/ascorbate to protect H_4folate during food analysis, it is less effective and more toxic than other thiols such as BAL, 1,4-dithiothreitol (DTT), or 2-thiobarbituric acid (TBA).[22,61] Patring et al.[61] compared the combination of ascorbate (2%) and four different antioxidants (MCE, DTT, BAL, and TBA), all at 0.1%, on the stability of H_4folate solutions boiled for 1 h. BAL, DTT, and TBA were all capable of protecting >96% of H_4folate in three different buffers varying between pH 5.1 and 7.85. DTT was the most effective antioxidant in acetate buffer (pH 5), DTT and BAL were the most effective in phosphate buffer (pH 6.1), and BAL and TBA were the most effective in HEPES/CHES buffer, pH 7.85, whereas MCE was the least effective in all buffers compared to the other thiols (degradation range 7−12%). Recently, De Brouwer and co-workers found DTT in concentration of 0.5% to be as efficient as BAL when using phosphate buffer pH 7.2.[22] Thereby, these three antioxidants (BAL, DTT, and TBA) should be considered as more efficient and environmentally friendly substitutes for MCE in modern analytical methods for folate analysis, including AOAC methods.

H_4folate is easier to stabilize by proper combination of antioxidants than H_2folate because the initial/primary oxidation product of H_4folate is quinonoid-H_2folate, which can be reduced back to H_4folate by antioxidants.[35] This step is the only one that could be reversible in the oxidation chain of H_4folate, which means that once H_2folate has been formed, it is further oxidized to folic acid or to degradation products such as pABG and pterins (see Figure 3). Several studies have reported between 12 and 30% of folic acid formation from H_2folate under analytic conditions in the pH range 2.6−7.4.[13,14,58,62] As mentioned in a previous section (Occurrence in Food), H_2folate is usually not analyzed in foods due to its high instability. H_2folate seems to require much higher concentrations of antioxidants than H_4folate to be protected.[42,63]

MECHANISM OF ANTIOXIDANT PROTECTION AGAINST OXIDATION

Reducing agents such as ascorbic acids and thiols exert multiple protective effects on folates through their action as oxygen scavenger, reducing agent, and free radical scavenger. The degradation of unsubstituted folates via a free radical mechanism has been proposed by several groups.[15,55,56,64] Thomas et al.[48] suggested that singlet oxygen, probably

DOI: 10.1021/jf504987n
J. Agric. Food Chem. 2015, 63, 2367−2377

Table 2. Stability of Unsubstituted Folate According to the Literature

Folic Acid
At 20 °C and 65% relative humidity, solid folic acid has a decomposition rate of 1% per year.[54]
Extensive degradation of solutions of folic acid at room temperature is induced by sunlight, UV, or visible light. This photolysis increases in rate at pH <5.[46,47]
Solutions of folic acid are stable for up to 10 h at 100 °C in the pH range 5−12, light-protected and without antioxidants, but the stability decreases at pH values <5.[43]
H_2folate
H_2folate in powder is stable for up to 1 year if stored at −20 °C in oxygen-free sealed tubes.[36]
The extent of degradation of a stock solution of H_2folate in Tris buffer, at pH 7.3, containing 0.3 M MCE and stored at 0 °C, is only 2.3% in 10 h.[50]
H_2folate is oxidized 40 times faster at pH 4 than at pH 7. At pH 9.5, H_2folate appears to be relatively stable.[49]
Although H_2folate is relatively unstable at pH 4.0−7.0, addition of thiols and ascorbic acid appears to retard oxidation. MCE in concentration 5−10 mM is sufficient to prevent decomposition of H_2folate solutions.[50]
H_4folate
H_4folate is relatively stable dry in ampules at −20 °C[51]
The rate of degradation of an unprotected solution of H_4folate increases 5-fold from 0 °C to room temperature. Increasing the temperature from 23 to 37 °C increases the rate of decomposition another 5-fold.[51]
H_4folate in phosphate buffer (pH 7.5) loses half its activity in 40 min at 23 °C. MCE at a concentration of 0.01 M or bubbling with N_2 gas protects H_4folate for >90 min.[52]
H_4folate is stable in anaerobic conditions at room temperature.[36]
Aqueous solutions of H_4folate stored at room temperature undergo 90% degradation in 4 h, the lability being influenced by pH and the buffer.[42]
Aqueous solutions of H_4folate are rapidly degraded. After 5 min at room temperature, a 1 mM (6*R*,*S*)-H_4folate-3HCl solution is degraded by >10% in the presence of air. After 45 min, it is degraded by about 25%. Solutions should be made as concentrated as possible, in oxygen-free water, with lowest possible pH, and used immediately.[51]
At 100 °C, solutions of H_4folate have a half-life of 2.25 min.[53]

produced by electronically excited states of folic acid molecule, is the oxidant agent that starts the degradation reaction. Further support for free radical mechanisms is the finding that riboflavin (vitamin B_2) sensitizes the photodegradation of folic acid, leading to the deactivation of the vitamin.[45,47] In addition, transition metal ions such as Fe^{3+} or Cu^{2+}, recognized for their involvement in free radical mechanisms, have been found to catalyze the oxidation of H_4folate.[55]

INTERCONVERSIONS BETWEEN H_4FOLATE AND 5,10-METHYLENE-H_4FOLATE

H_4folate rapidly and reversibly condensates with formaldehyde (in ∼30-fold excess) in aqueous solutions at room temperature, forming 5,10-methylenetetrahydrofolate (5,10-CH_2-H_4folate (see Figure 3).[35,65] This is an example of interconversion reaction because it includes a reversible conversion between two bioactive folate vitamers. The N^5−N^{10}-bridged compound is found to be more stable against chemical oxidation than H_4folate, but its stability depends on an excess of formaldehyde.[11,35,65] Without excess of formaldehyde, the stability of 5,10-CH_2-H_4folate is strongly pH dependent; 5,10-CH_2-H_4folate appears to be completely stable at pH 9.5 or above, in either the presence or absence of antioxidants. As soon as the pH decreases to neutral pH, 5,10-CH_2-H_4folate dissociates rapidly, within 15 min, back to H_4folate and formaldehyde, and heating enhances the rate of the dissociation.[65,66]

5,10-CH_2-H_4folate is one of the C1 derivatives of H_4folate used for enzymatic methylation of uridinylate to thymidinylate, a key step for DNA synthesis. Hence 5,10-CH_2-H_4folate is a native folate form that could be present in intact living cells. Because 5,10-CH_2-H_4folate requires either alkaline pH (>8) or an excess of formaldehyde to remain stable, this form is not likely to occur in foods because the pH of food is generally neutral or slightly acidic. Hence, 5,10-CH_2-H_4folate most probably converts to H_4folate or its degradation products in food samples or both.

There is only one recorded condition in food analysis when formaldehyde can be formed in excess with potential to interconvert H_4folate into 5,10-CH_2-H_4folate. When Wilson and Horne[14] boiled aqueous solutions of H_4folate for 10 min in a buffer (pH 7.8) containing 2% sodium ascorbate, 5,10-CH_2-H_4folate was formed in a yield of 25%. The authors were able to show that heating of ascorbate led to its thermal degradation followed by the formation of formaldehyde, which converted H_4folate into 5,10-CH_2-H_4folate. This conversion did not occur *without heating*; neither did formation of formaldehyde. More recently, this interconversion was confirmed by de Brouwer et al. using HPLC and MS detection.[62] This emphasizes the need to combine thiols and ascorbate during heat extraction, which is also common practice today in folate determination. The inhibitory effect of adding thiols is a formation of hemithioacetal with formaldehyde, thereby preventing the reaction between formaldehyde and H_4folate.[58,66,67]

STABILITY OF UNSUBSTITUTED FOLATE IN THE FOOD CHAIN

Because H_4folate is the most vulnerable folate form, one could expect high losses of H_4folate in the food chain, especially after heat treatment such as thermal processing or cooking. Hence, the richest dietary sources of H_4folate should occur in raw foods with intact cell structure, where it may be bound and stabilized by proteins. A folate binding protein (FBP) is present in milk. By adding FBP to labile folate forms in model systems, H_4folate has been shown to become significantly stabilized.[68]

As soon as the cell integrity is compromised by freezing and thawing, mechanical stress, or thermal processing, H_4folate starts to oxidize unless protected by native antioxidants such as ascorbic acid or being bound to proteins and other cell constituents. Note that iron and copper ions leaking from process equipment or process water are pro-oxidative.[41]

Baker's yeast, in compressed or dried form, still contains viable cells and is therefore an example of a food ingredient with intact cell structure. It contains about 25% of its total

DOI: 10.1021/jf504987n
J. Agric. Food Chem. 2015, 63, 2367−2377

folate as H_4folate (Table 1). When dry baker's yeast was stored in room temperature during 45 days, H_4folate was stable. In contrast, compressed baker's yeast stored in a refrigerator (5 °C) lost 40% of H_4folate after 17 days. Drying of yeast reduced the content of H_4folate because the content of H_4folate was considerably higher in compressed baker's yeast prior to storage, but these differences reduced progressively with storage time.[28]

Cereal fractions contain about 10% of its folate as H_4folate. During breadmaking, yeast and fermentation could add further H_4folate. However, several studies indicate undetectable levels of H_4folate in bread; instead they often report the occurrence of folic acid, ranging from a few percent to 50% of total folate.[25,69,70] The breads in these studies were not made from folic acid fortified flours. Hence, the folic acid most probably originates from oxidation of unsubstituted reduced folates as well as from 5,10-CH_2-H_4folate during fermentation and oven baking.

Green vegetables are mostly blanched and frozen before being cooked and served. Their content of ascorbate and possibly other antioxidants could protect the H_4folate from being oxidized, but losses by leakage could occur. In one study by Stea and co-workers broccoli and green peas were investigated after different thermal processes.[71] Blanching did not reduce H_4folate, but, in general, these vegetables retained only up to half of their H_4folate after other thermal treatments, for example, steam cooking, microwaving, boiling, and reheating. In a recent study on the effects of industrial processing on folate content in green vegetables, Delchier et al. found leakage to be a major cause behind folate losses.[72]

Some losses of dietary folates by leakage and/or degradation seem inevitable in the food chain.[71,72] Therefore, it is of utmost importance to avoid further degradation and conversions of unsubstituted folates during the analytical procedure as outlined in the following section.

STABILIZATION DURING DIFFERENT STEPS OF THE ANALYTICAL PROCEDURE

Analytical techniques used to determine folate content are biological, such as microbiological and competitive-binding methods, or chemical, such as HPLC methods.[9,12,18,73] The microbiological assay (MA) utilizes the nutritional requirement of a microorganism (*Lactobacillus rhamnosus*), which exhibited high response to all bioactive folate forms in monoglutamic or diglutamic forms including biologically active interconversion products. Hence, MA gives the sum of all bioactive forms, that is, total folate.[9] There are standard methods assessed in collaborative studies established for microbiological assays, for fortified infant formula, for cereals, and for foodstuffs.[74−76] A disadvantage of the MA is the overall time needed for analysis, almost 2 days, during which the samples are kept at 37 °C, which emphasizes the need for optimal protection by antioxidants.

The competitive binding assay, using a folate-binding protein and a radiolabeled folate to compete with the folate to be determined, also gives total folate content. The Biacore method, certified by AOAC for folic acid determinations, uses a folate binding protein isolated from bovine milk and measures the amount of vitamin with plasma surface resonance technique.[77] However, the folate-binding protein does not have the same affinity to the various folate forms.[78,79] Therefore, these methods are appropriate only if it is possible to calibrate against the same form of folate as the one present in the sample, such as folic acid in fortified foods. They are less useful for food analysis with more complex matrices and several combinations of folate forms.

However, if the focus of interest is on the individual folate forms, chromatographic methods such as HPLC, UHPLC, or LC-MS, which separate and detect the different forms on the basis of their chemical properties, have to be used. Figure 4 gives a schematic overview of the analytical methods for folate determination in foods. All methods include the following steps: extraction, deconjugation, cleanup by filtration and centrifugation, and detection/quantification.[80] The chromatographic methods often include additional cleanup by affinity chromatography or solid phase extraction (SPE). It is beyond the scope of this paper to go into all analytical details about chromatography-based methods for determination of food folates. Instead, we refer to recent reviews.[12,18,30,62,73,81−83]

To obtain reliable analytical results, the stabilization of unsubstituted folates, especially H_4folate, is of great importance. In Table 3 we summarize the most crucial factors in the stabilization of unsubstituted folates during analytical procedure. As seen from Table 3, it is possible to efficiently stabilize unsubstituted folates by using the following protection strategies:

- protection from UV light, oxygen, and catalysts of free radical reactions such as iron and copper ions throughout the analytical procedure;
- avoidance of repeated freeze−thaw cycles of food samples, food extracts, and stock solutions;
- choice of lower temperature and shorter time for each analytical step everywhere it does not compromise the yield of folates;
- use of combination of two antioxidants, ascorbic acid/ascorbate and a thiol (BAL, DTT, or TBA).

Sampling, Storage, and Homogenization. To obtain reliable analytical results, good laboratory practice of sampling and storage of food samples is important, by protecting them from UV light, air, and high temperatures. Storage should preferably be carried out at −80 °C. Once the samples are homogenized, they should be dissolved in buffers of neutral pH containing two antioxidants, usually 1−2% ascorbic acid/ascorbate and a thiol to protect H_4folate from oxidative degradation.[58−61] Further storage after homogenization should be avoided because repeated freezing and thawing results in the degradation of H_4folate.[61]

Extraction and Deconjugation. Three major procedures are used to extract folate from the food matrix: heat treatment, enzymatic extraction, or a combination of heat and enzymatic treatments. Most studies use neutral pH during extraction and other enzyme treatments. Heat treatment is usually done by boiling in a water bath (100 °C for 10 min)[73,81] or heating (75 °C for 1 h),[80,85] when using HPLC methods, or by autoclave (120 °C/15 min), when applying MA.[74−76] The enzymatic extraction is commonly performed at 37 °C for 1−4 h by adding protease and/or amylase to the sample and terminating each enzyme treatment by boiling (5 min).[73,81] The combination of two antioxidants, ascorbic acid and thiol, is crucial during sample extraction to protect the labile H_4folate from oxidative degradation as well as to prevent interconversion of H_4folate into 5,10-CH_2-H_4folate caused by formaldehyde formed from ascorbic acid when heated.[14] Three thiols, BAL, TBA, and DTT, have been shown to be highly efficient for these purposes, whereas the most commonly used, MCE,

DOI: 10.1021/jf504987n
J. Agric. Food Chem. 2015, 63, 2367−2377

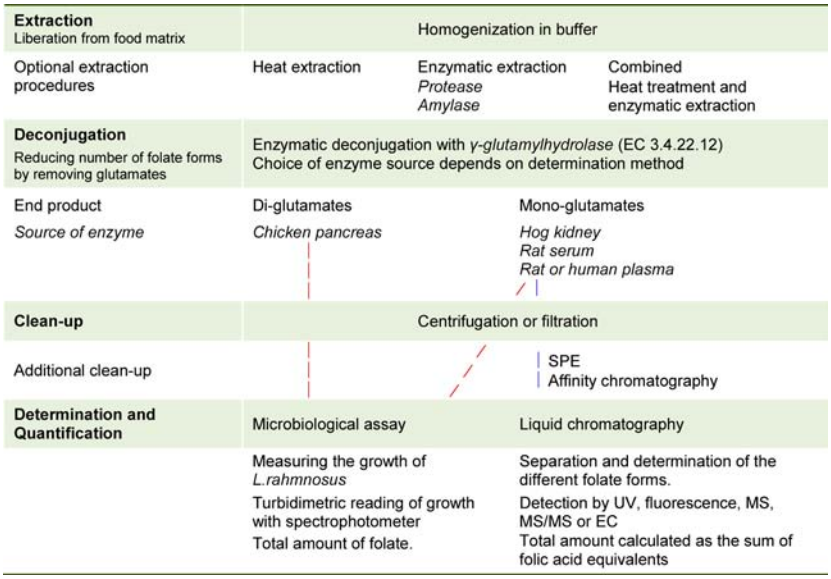

Figure 4. Schematic overview of analytical methods for folate determination in foods modified from refs 12, 18, 78, and 81.

appeared to be the least efficient.[61] Besides efficiency, the toxicity and environmental risks should also be considered when choosing thiol to stabilize H_4folate. From this point of view, the nontoxic TBA is the best choice followed by low-toxic DTT and BAL.[22,61]

To limit the amount of forms for determination, mono- or diglutamates are achieved by enzymatic deconjugation of the glutamate residues. Choice of conjugase (γ-glutamyl hydrolase) source depends on the method of determination used. For HPLC it is necessary to use a conjugase source, usually rat plasma, human plasma, or hog kidney conjugase with monoglutamates as the end product, whereas the bacteria in the MA can use the diglutamates produced by chicken pancreas as well.[86] The duration of deconjugation procedure usually varies from 2 to 3 h to overnight incubation at 37 °C, followed by inactivation by 5 min of boiling.[81] In addition to the mammal-based conjugase sources hitherto used, Diaz de la Garza's group recently evaluated two recombinant γ-glutamyl hydrolases from *Arabidopsis thaliana*.[87] These enzymes were far more efficient in hydrolyzing folate polyglutamates in plant food samples compared with rat plasma; in fact, the deconjugation time could be shortened to 0.5−1 h. Moreover, the recombinants also seemed to be less sensitive toward conjugase inhibitors present in certain plant extracts.[87] The repeated heating and relatively long time of incubation during deconjugation (overnight incubation is most common for MA) emphasize the need to optimize the antioxidative protection of H_4folate, as mentioned above for the extraction enzymes. Moreover, blanks need to be included for all enzymes added in the assay to subtract their endogenous folate content.

Storage of food extracts after heating and deconjugation should be avoided. Tamura and co-workers showed that storage at −70 °C for a few months caused considerable degradation of H_4folate (~60%) in food extracts.[88] Patring and co-workers also observed losses of native H_4folate in yeast extract stored at −22 °C for 4 weeks.[61] With 2% sodium ascorbate and 0.1% MCE the losses amounted to 53%, whereas the replacement of MCE with BAL reduced losses to only 19%. De Brouwer and co-workers reported stabilities of 63.7−77.7% for native H_4folate in rice extract stored at 4 °C for 36 h, whereas the stability was >95% when stored at −20 or −80 °C with one freeze−thaw cycle.[22,31] Van Daele and co-workers used 1% ascorbic acid and 0.5% DTT for stabilization of folates in standard solutions and potato extracts. They reported stability >90% for H_4folate solution when stored at 4 °C for 24 h in the autosampler or at −20 °C with three freeze−thaw cycles.[89]

Cleanup by SPE or Affinity Chromatography. Chromatographic methods are more sensitive to interfering substances and have higher demands on sample cleanup than MA. SPE can be used both to remove interfering substances and to concentrate the analyte. Affinity chromatography cleanup using folate-binding protein applied on columns can be used to increase sensitivity. However, different affinities to the various folate forms may easily lead to considerable losses of folate forms with low affinity.[18]

Folates are eluted by acidic buffers, and affinity chromatography causes the most pronounced acidification by operating close to pH 2 during the 10−20 min the elution takes. SPE-based cleanup procedures using strong-anion exchange (SAX) cartridges elute the folates by sodium acetate solution containing sodium chloride salt (5 or 10%) and ascorbic acid (1%), which keeps the pH close to 5. However, it is still important to use antioxidants in optimal amounts and UV light protection to prevent oxidation and degradation of reduced unsubstituted folates, especially if the samples are stored in a refrigerator or autosampler overnight until subjected into HPLC. For instance, Kirsch and co-workers[13] studied the stability of individual folate standards stored at 4 °C during 24 h in buffers of different pH values (2.6, 3.4, and 7.0) containing 0.1% ascorbic acid. The main interconversion products were presented for each folate form based on UHPLC-MS/MS analysis. H_4folate showed minor interconversion (<5%) into H_2folate and folic acid, whereas H_2folate showed degradation at acidic conditions and interconversion (12.7−16.7%) to folic acid.

Chromatographic Separation by HPLC and UHPLC. No antioxidants are present in the mobile phase during chromatographic separation, which makes folates unprotected against oxidation. Moreover, column temperatures might vary between 20 and 35 °C in HPLC[28,30] and 60 °C in UHPLC.[34,89] The extent to which acid-catalyzed oxidations of unsubstituted folates occur at this stage of analysis has received little attention

DOI: 10.1021/jf504987n
J. Agric. Food Chem. 2015, 63, 2367−2377

Table 3. Crucial Factors in the Stabilization of Unsubstituted Folates during All Steps of the Analytical Procedure[a]

factor	analytical steps	protection strategies
presence of oxygen	all	degass with nitrogen or argon
UV light	all	protect from UV light, e.g., by using yellow filter on lamps or yellow lamps
freeze–thaw cycle	storage of food samples	avoid multiple freeze–thaw cycles, no more than one
	storage of food *extracts* prior to analysis	avoid freeze–thaw step, use storage at 4 °C instead
presence of impurities	all	use reagents of high purity, avoid presence of pro-oxidative catalysts, e.g., copper and iron ions
		check the purity of folate standards and correct concentrations of stock solutions for purity[84]
temperature	storage of food *samples* prior sample pretreatment	as low a temperature as possible, −80 °C[22,34,88]
	storage of stock solutions	−80 °C
	extraction by heat treatment	as low a temperature as possible, e.g., 75 °C instead of 100 °C[61,85]
	storage of food *extracts* prior to analysis	4–6 °C
	separation on HPLC column	avoid using elevated column temperatures if possible[61,90]
	detection by UV followed by fluorescence	use UV-DAD detector with efficient cooling system
time	storage of samples and extracts	as short as possible
	extraction by heat treatment and/or enzymes	as short as possible
	deconjugation	as short as possible, avoid overnight incubation
	separation on the HPLC column	shorter retention times are preferable
oxidation	preparation of stock and working solutions, extraction and elution buffer.	use a combination of two antioxidants, ascorbic acid/ascorbate and TBA, for MA or ascorbic acid/ascorbate and BAL or DTT for HPLC methods
	all steps of sample pretreatment	make fresh working solutions on daily basis

[a]Only H_4folate and folic acid are considered, because there are no studies presenting data on H_2folate or the conversion product 5,10-CH_2-H_4folate in foods due obviously to their lack of stability as already discussed in the sections above.

over the years. Strandler and co-workers found a concentration-dependent stability of H_4folate under these conditions, pH around 3 and a temperature of 35 °C.[90] At a concentration of 5 μg/mL the losses of H_4folate were 20% after 30 min, whereas at a lower concentration of 0.5 μg/mL H_4folate was degraded completely after 10 min.[90] Usually the concentrations of H_4folate in injected standard and food extracts are in the range of 1–50 ng/mL, that is, much lower than those studied by Strandler and co-workers (for references, see Table 1). This indicates a considerable risk for losses of H_4folate during the passage of the chromatographic column, which can lead to deviations from linearity in the lower region of calibration curve and false-negative results for H_4folate. Therefore, special consideration should be given to the on-column stability of H_4folate in the development and optimization of new HPLC or UHPLC methods to determine folates in view of the concentration-dependent stability of H_4folate. Shorter retention time and lower column temperature are preferable to improve the on-column stability of H_4folate.

HPLC or UHPLC with Different Detectors. When using HPLC, the choice of calibrants becomes more crucial because only the forms that are used as calibrants can be identified in the sample. Due to interconversion and stability problems, there are limitations to which folate forms can be found in food extracts, and this has been reviewed in previous sections of this review. Determination can be made by using UV, fluorescence, MS, or electrochemical detection.[12,73,81,82] The reduced folates have native fluorescence of different intensities and wavelength maxima.[91] Folic acid does not fluorescence and is better determined with UV detection.[81] This means that a combination of UV and fluorescence detection at different excitation/emission wavelengths is necessary to quantify all folate forms. When using both detectors connected in sequence (UV detector followed by fluorescence detector), special attention should be paid to the stability of H_4folate during the passage of UV detector flow cell because of the high risk for degradation of H_4folate due to UV light and increased temperature in the flow cell. The stability check can be performed by comparing the fluorescence response for H_4folate with and without UV detector connected before the fluorescence detector. If the fluorescence response for H_4folate is lower without the UV detector, this indicates that there are losses of H_4folate in the UV detector flow cell. In such a case it is preferable to use split and connect detectors in parallel.

Higher specificity is achieved by using mass spectrometric detectors. Analytes are ionized, giving a specific mass to charge pattern, and folates can be determined in both positive and negative modes.[28] Quantification is usually performed with external calibration in HPLC methods when using UV and fluorescence detection. In methods with mass spectrometric detection the use of stable isotopes as internal standards, such as deuterium-labeled ($^2H_4$)[31]or ^{13}C-labeled ($^{13}C_5$) isotopes of folates,[22,89] can considerably improve the relative recovery, but it cannot affect the absolute recovery.[92] Although the *relative recovery* of H_4folate is about 100%, the *absolute recovery* may be much lower, about 37–70%,[22,30,33,34,89] which may lead to negative false results for H_4folate if concentrations in food samples are close to the limit of quantification. Moreover, the use of internal standards or external standards will not correct for oxidations or conversions into other bioactive folate forms during analysis, as recently discussed by Ringling and Rychlik,[30] for instance, when native 5,10-CH_2-H_4folate dissociates to

DOI: 10.1021/jf504987n
J. Agric. Food Chem. 2015, 63, 2367–2377

H_4folate and H_4folate is oxidized to H_2folate and folic acid. Hence, conversions and oxidations may cause some overestimations of H_4folate and folic acid because the changes are not exactly the same in the food matrix as in the standards.

It is important to consider that the bioactive unsubstituted folates analyzed in foods, H_4folate and folic acid, reflect the sum of oxidative and interconversion changes of H_4folate, H_2folate, and 5,10-CH_2H_4folate originally present in the intact cells of vegetable, animal, or microbiological origin such as yeast and LAB. In addition, folic acid in foods either depends on the oxidation of H_4folate or H_2folate or is a consequence of supplementation/fortification or both. Analysts monitoring folic acid content in fortified foods need to consider that parts of the analyzed folic acid could be due to oxidation of unsubstituted reduced folates or conversion from 5,10-CH_2-H_4folate to H_4folate and its further oxidation. Also worth mentioning is that the relatively stable folic acid in fortified foods might be underestimated due to photodecomposition if not protected from UV light during sample pretreatment. When it comes to UV light sensitivity, both oxidized and reduced folates are sensitive to degradation.

AUTHOR INFORMATION

Corresponding Author

*(H.S.S.) Phone: +4618175757. Fax: +4618105848. E-mail: hans@slv.se.

Notes

The authors declare no competing financial interest.

ABBREVIATIONS USED

5-CH_3-H_4folate	5-methyltetrahydrofolate
5-HCO-H_4folate	5-formyltetrahydrofolate
10-HCO-H_4folate	10-formyltetrahydrofolate
10-HCO-H_2folate	10-formyldihydrofolate
10-HCO-folic acid	10-formylfolic acid
5,10-CH^+-H_4folate	5,10-methenyltetrahydrofolate
5,10-CH_2-H_4folate	5,10-methylenetetrahydrofolate
AOAC	Association of Analytical Chemists
BAL	2,3-dimercapto-1-propanol
C1	one-carbon
CHES	2-(*N*-cyclohexylamino)ethanesulfonic acid
CH_2O	formaldehyde
DAD	diode array detector
DTT	1,4-dithiothreitol
ECD	electrochemical detection
FBP	folate binding protein
FW	fresh weight
H_2folate	dihydrofolate
H_4folate	tetrahydrofolate
HEPES	*N*-(2-hydroxyethyl)-piperazine-*N*-2-ethanesulfonic acid
IS	internal standard
LAB	lactic acid bacteria
MA	microbiological assay
MCE	2-mercaptoethanol
NTD	neural tube defect
pABG	*p*-aminobenzoylglutamic acid
SAX	strong anion exchange
SPE	solid phase extraction
TBA	2-thiobarbituric acid
UHPLC	ultrahigh-performance liquid chromatography

REFERENCES

(1) MRC. Vitamin Study Research Group. Prevention of neural tube defects: results of the Medical Research Council Vitamin Study. *Lancet* **1991**, *338*, 131−137.

(2) Lucock, M. Folic acid: nutritional biochemistry, molecular biology, and role in disease processes. *Mol. Gen. Metab.* **2000**, *71*, 121−138.

(3) Clarke, R.; Halsey, J.; Bennett, D.; Lewington, S. Homocysteine and vascular disease: review of published results of the homocysteine-lowering trials. *J. Inherit. Metab. Dis.* **2011**, *34*, 83−91.

(4) De-Regil, L.; Fernández-Gaxiola, A.; Dowswell, T.; Peña-Rosas, J. Effects and safety of periconceptional folate supplementation for preventing birth defects. *Cochrane Database Systematic Rev.* **2010**, *10*, CD007950.

(5) WCRF/AICR (World Cancer Research Fund/American Institute for Cancer Research Publisher). Food, nutrition, physical activity and the prevention of cancer: a global perspective; Washington DC, USA; www.dietandcancerreport.org (accessed March 2014).

(6) Durga, J.; van Boxtel, M. P. J.; Schouten, E. G.; Kok, F. J.; Jolles, J.; Katan, M. B.; Verhoef, P. Effect of 3-year folic acid supplementation on cognitive function in older adults in the FACIT trial: a randomised, double blind, controlled trial. *Lancet* **2007**, *369*, 208−216.

(7) Qin, X.; Cui, Y.; Shen, L.; Sun, N.; Zhang, Y.; Li, J.; Xu, X.; Wang, B.; Xu, X.; Huo, Y.; Wang, X. Folic acid supplementation and cancer risk: a meta-analysis of randomized controlled trials. *Int. J. Cancer* **2013**, *133*, 1033−1041.

(8) Wien, T. N.; Pike, E.; Wisløff, T.; Staff, A.; Smeland, S.; Klemp, M. Cancer risk with folic acid supplements: a systematic review and meta-analysis. *BMJ Open* **2012**, 2e000653, DOI: 10.1136/bmjopen-2011-005.

(9) Gregory, J. F. Chemical and nutritional aspects of folate research: analytical procedures, methods of folate synthesis, stability, and bioavailability of dietary folates. In *Advances in Food and Nutrition Research*; Kinsella, J. E., Ed.; Academic Press: New York, 1989; pp 1−101.

(10) Nelson, D. L.; Cox, M. M. Chapter 22.2. Biosynthesis of amino acids. In *Lehninger Principles of Biochemistry*, 5th ed.; Freeman: New York, 2008; pp 882−897.

(11) Hawkes, J. G.; Villota, R. Folates in foods: reactivity, stability during processing, and nutritional implications. *Crit. Rev. Food Sci. Nutr.* **1989**, *28*, 439−538.

(12) Ball, G. F. M. Folate. In *Vitamins in Foods: Analysis, Bioavailability, and Stability*; Ball, G., Ed.; CRC Press: Boca Raton, FL, USA, 2006; pp 231−273.

(13) Kirsch, S. H.; Knapp, J.-P.; Herrmann, W.; Obeid, R. Quantification of key folate forms in serum using stable-isotope dilution ultra performance liquid chromatography-tandem mass spectrometry. *J. Chromatogr., B* **2010**, *878*, 68−75.

(14) Wilson, S. D.; Horne, D. W. Evaluation of ascorbic acid in protecting labile folic acid derivatives. *Proc. Natl. Acad. Sci. U.S.A.* **1983**, *80*, 6500−6504.

(15) Reed, L. S.; Archer, M. C. Oxidation of tetrahydrofolic acid by air. *J. Agric. Food Chem.* **1980**, *28*, 801−805.

(16) Eto, I.; Krumdieck, C. L. Determination of three different pools of reduced one-carbon-substituted folates: I. A study of the fundamental chemical reactions. *Anal. Biochem.* **1980**, *109*, 167−184.

(17) USDA National Nutrient Database for Standard Reference, release 25; Nutrient Data Laboratory Home Page, 2012; http://www.ars.usda.gov/ba/bhnrc/ndl.

(18) Quinlivan, E. P.; Hanson, A. D.; Gregory, J. F. The analysis of folate and its metabolic precursors in biological samples. *Anal. Biochem.* **2006**, *348*, 163−184.

(19) Ravanel, S.; Douce, R.; Rébeille, F. Metabolism of folates in plants. In *Advances in Botanical Research*; Rebeille, F., Douce, R., Eds.; Academic Press: London, UK, 2011; Vol. 59, pp 67−106.

(20) Hanson, A. D.; Gregory, J. F. Folate biosynthesis, turnover, and transport in plants. *Annu. Rev. Plant Biol.* **2011**, *62*, 105−125.

DOI: 10.1021/jf504987n
J. Agric. Food Chem. 2015, 63, 2367−2377

(21) Díaz de la Garza, R. I.; Gregory, J. F., III; Hanson, A. D. Folate biofortification of tomato fruit. *Proc. Natl. Acad. Sci. U.S.A.* **2007**, *104*, 4218−4222.
(22) De Brouwer, V.; Storozhenko, S.; Van de Steene, J. C.; Wille, S. M. R.; Stove, C. P.; van der Straeten, D.; Lambert, W. E. Optimisation and validation of a liquid chromatography-tandem mass spectrometry method for folates in rice. *J. Chromatogr., A* **2008**, *1215*, 125−132.
(23) Jägerstad, M.; Piironen, V.; Walker, C.; Ros, G.; Carnovale, E.; Holasova, M.; Nau, H. Increasing natural food folates through bioprocessing and biotechnology. *Trends Food Sci.Technol.* **2005**, *16*, 298−306.
(24) Koehler, P.; Hartmann, G.; Wieser, H.; Rychlik, M. Changes of folates, dietary fiber, and proteins in wheat as affected by germination. *J. Agric. Food Chem.* **2007**, *55*, 4678−4683.
(25) Patring, J.; Wandel, M.; Jägerstad, M.; Frølich, W. Folate content of Norwegian and Swedish flours and bread analysed by use of liquid chromatography-mass spectrometry. *J. Food Compos. Anal.* **2009**, *22*, 649−656.
(26) Kariluoto, S.; Edelmann, M.; Herranen, M.; Lampi, A.-M.; Shmelev, A.; Salovaara, H.; Korhola, M.; Piironen, V. Production of folate by bacteria isolated from oat bran. *Int. J. Food Microbiol.* **2010**, *143*, 41−47.
(27) FFI (Food Fortification Initiative); http://www.ffinetwork.org (accessed January 2015).
(28) Patring, J. D. M.; Jastrebova, J. A. Application of liquid chromatography-electrospray ionisation mass spectrometry for determination of dietary folates: effects of buffer nature and mobile phase composition on sensitivity and selectivity. *J. Chromatogr., A* **2007**, *1143*, 72−82.
(29) Vishnumohan, S.; Arcot, J.; Pickford, R. Naturally-occurring folates in foods: method development and analysis using liquid chromatography−tandem mass spectrometry (LC−MS/MS). *Food Chem.* **2011**, *125*, 736−742.
(30) Ringling, C.; Rychlik, M. Analysis of seven folates in food by LC−MS/MS to improve accuracy of total folate data. *Eur. Food Res.Technol.* **2013**, *236*, 17−28.
(31) Freisleben, A.; Schieberle, P.; Rychlik, M. Specific and sensitive quantification of folate vitamers in foods by stable isotope dilution assays using high-performance liquid chromatography-tandem mass spectrometry. *Anal. Bioanal. Chem.* **2003**, *376*, 149−156.
(32) Zhang, G. F.; Storozhenko, S.; Van der Straeten, D.; Lambert, W. E. Investigation of the extraction behavior of the main monoglutamate folates from spinach by liquid chromatography−electrospray ionization tandem mass spectrometry. *J. Chromatogr., A* **2005**, *1078*, 59−66.
(33) Wang, C.; Riedl, K. M.; Schwartz, S. J. Fate of folates during vegetable juice processing — deglutamylation and interconversion. *Food Res. Int.* **2013**, *53*, 440−448.
(34) De Brouwer, V.; Storozhenko, S.; Stove, C. P.; Van Daele, J.; Van der Straeten, D.; Lambert, W. E. Ultra-performance liquid chromatography-tandem mass spectrometry (UPLC-MS/MS) for the sensitive determination of folates in rice. *J. Chromatogr., B* **2010**, *878*, 509−513.
(35) Blakley, R. L. The Biochemistry of folic acid and related pteridines. In *Frontiers of Biology*; North Holland Publishing: Amsterdam, The Netherlands, 1969; pp 1−99.
(36) Temple, C., Jr.; Montgomery, J. A. Chemical and physical properties of folic acid and reduced derivatives. In *Folates and Pterins*; Blakley, R. L., Benkovic, S. J., Eds.; Wiley: New York, 1984; Vol. 1, pp 62−104.
(37) Patring, J.; Lanina, S. A.; Jastrebova, J. A. Applicability of alkyl-bonded ultra-pure silica stationary phases for gradient reversed-phase HPLC of folates with conventional and volatile buffers under highly aqeous conditions. *J. Sep. Sci.* **2006**, *29*, 889−904.
(38) Kallen, R. G.; Jencks, W. P. The dissociation constants of tetrahydrofolic acid. *J. Biol. Chem.* **1966**, *241*, 5845−5850.
(39) Kallen, R. Tetrahydrofolic acid and formaldehyde. In *Methods in Enzymology*; Wright, D. M. A. L., Ed.; Academic Press: New York, 1971; Vol. 66, pp 705−716.
(40) Poe, M. Acidic dissociation constants of folic acid, dihydrofolic acid, and methotrexate. *J. Biol. Chem.* **1977**, *25*, 3724−3728.
(41) Gregory, J. F. Vitamins. In *Food Chemistry*; Damodaran, S., Parkin, K. L., Fennema, O. R., Eds.; Dekker: New York, 2008; pp 498−503.
(42) O'Broin, J.; Temperley, I.; Brown, J.; Scott, J. Nutritional stability of various naturally occurring monoglutamate derivatives of folic acid. *Am. J. Clin. Nutr.* **1975**, *28*, 438−444.
(43) Paine-Wilson, B.; Chen, T. S. Thermal destruction of folacin: effect of pH and buffer ions. *J. Food Sci.* **1979**, *44*, 717−722.
(44) Mnkeni, A. P.; Beveridge, T. Thermal destruction of pteroylglutamic acid in buffer and model food systems. *J. Food Sci.* **1982**, *47*, 2038−2041.
(45) Lowry, O. H.; Bessey, O. A.; Crawford, E. J. Photolytic and enzymatic transformations of pteroylglutamic acid. *J. Biol. Chem.* **1949**, *180*, 389−398.
(46) Akhtar, M. J.; Khan, M. A.; Ahmad, I. Photodegradation of folic acid in aqueous solution. *J. Pharm. Biomed. Anal.* **1999**, *19*, 269−275.
(47) Akhtar, J. M.; Khan, A. M.; Ahmad, I. Effect of riboflavin on the photolysis of folic acid in aqueous solution. *J. Pharm. Biomed. Anal.* **2000**, *23*, 1039−1044.
(48) Thomas, A. H.; Suárez, G.; Cabrerizo, F. M.; Martino, R.; Capparelli, A. L. Study of the photolysis of folic acid and 6-formylpterin in acid aqueous solutions. *J. Photochem. Photobiol. A: Chem.* **2000**, *135*, 147−154.
(49) Poe, M. Dihydrofolate reductase from a methotrexate-resistant strain of *Escherichia coli:* dihydrofolate monooxygenase activity. *Biochem. Biophys. Res. Commun.* **1973**, *54*, 1008−1014.
(50) Hillcoat, B. L.; Nixon, P. F.; Blakley, R. L. Effect of substrate decomposition on the spectrophotometric assay of dihydrofolate reductase. *Anal. Biochem.* **1967**, *21*, 178−189.
(51) Schircks laboratories data sheets on folic acid (16.203) dihydrofolic acid (16.206) and tetrahydrofolic acid (16.207).
(52) Scrimgeour, K. G. Methods for reduction, stabilization, and analyses of folates. In *Methods in Enzymology*; Donald, B., McCormick, L. D. W., Eds.; Academic Press: New York, 1980; Vol. 66, pp 517−523.
(53) Chen, T. S.; Cooper, R. G. Thermal destruction of folacin: effect of ascorbic acid, oxygen and temperature. *J. Food Sci.* **1979**, *44*, 713−716.
(54) Tripet, F. Y.; Kesselring, U. W. Stability of solid folic acid in relation to temperature and humidity. *Pharm. Acta Helv.* **1975**, *50*, 318−322.
(55) Blair, J. A.; Pearson, A. J. Kinetics and mechanism of the autoxidation of the 2-amino-4-hydroxy-5,6,7,8-tetrahydropteridines. *J. Chem. Soc., Perkin Trans. 2* **1974**, *1*, 80−88.
(56) Blair, J. A.; Farrar, G. Chapter 6. Oxidation of tetrahydrofolates and tetrahydrobiopterin by molecular oxygen. In *Atmospheric Oxidation and Antioxidants*; Scott, G., Ed.; Elsevier: Amsterdam, The Netherlands, 1993; pp 171−182.
(57) Martin, C. B.; Walker, D.; Soniat, M. Density functional theory study of possible mechanisms of folic acid photodecomposition. *J. Photochem. Photobiol. A: Chem.* **2009**, *208*, 1−6.
(58) Wilson, S. D.; Horne, D. W. High-performance liquid chromatographic determination of the distribution of naturally occurring folic acid derivatives in rat liver. *Anal. Biochem.* **1984**, *142*, 529−535.
(59) Osborn, M. J.; Huennekens, F. M. Enzymatic reduction of dihydrofolic acid. *J. Biol. Chem.* **1958**, *233*, 969−974.
(60) Blakley, R. L. Spectrophotometric studies on the combination of formaldehyde with tetrahydropteroylglutamic acid and other hydropteridines. *Biochem. J.* **1960**, *74*, 71−82.
(61) Patring, J. D. M.; Johansson, M.; Yazynina, E.; Jastrebova, J. Evaluation of impact of different antioxidants on stability of dietary folates during food sample preparation and storage of extracts prior to analysis. *Anal. Chim. Acta* **2005**, *553*, 36−42.
(62) De Brouwer, V.; Zhang, G. F.; Storozhenko, S.; Straeten, D. V.; Lambert, W. E. pH stability of individual folates during critical sample

DOI: 10.1021/jf504987n
J. Agric. Food Chem. 2015, 63, 2367−2377

preparation steps in prevision of the analysis of plant folates. *Phytochem. Anal.* **2007**, *18*, 496−508.
(63) Zakrezewski, S. F. Evidence for the chemical interaction between 2-mercaptoethanol and tetrahydrofolate. *J. Biol. Chem.* **1966**, *241*, 2957−2961.
(64) Pearson, A. J. Kinetics and mechanisms of the autooxidation of tetrahydropterins. *Chem. Ind.* **1974**, 233−239.
(65) Osborn, M. J.; Talbert, P. T.; Huennekens, F. M. The structure of "active formaldehyde" (N^5,N^{10}-methylene tetrahydrofolic acid). *J. Am. Chem. Soc.* **1960**, *82*, 4921−4927.
(66) Blakley, R. L. The reaction of tetrahydropteroylglutamic acid and related hydropteridines with formaldehyde. *Biochem. J.* **1959**, *72*, 707−710.
(67) Kallen, R. G.; Jencks, W. P. The mechanism of the condensation of formaldehyde with tetrahydrofolic acid. *J. Biol. Chem.* **1966**, *241*, 5851−5863.
(68) Jones, M. L.; Nixon, P. F. Tetrahydrofolates are greatly stabilized by binding to bovine milk folate-binding protein. *J. Nutr.* **2002**, *132*, 2690−2694.
(69) Pfeiffer, C. M.; Rogers, L. M.; Gregory, J. F. Determination of folate in cereal-grain food products using trienzyme extraction and combined affinity and reversed-phase liquid chromatography. *J. Agric. Food Chem.* **1997**, *45*, 407−413.
(70) Konings, E. J.; Roomans, H. H.; Dorant, E.; Goldbohm, R. A.; Saris, W. H.; van den Brandt, P. A. Folate intake of the Dutch population according to newly established liquid chromatography data for foods. *Am. J. Clin. Nutr.* **2001**, *73*, 765−776.
(71) Stea, T. H.; Johansson, M.; Jägerstad, M.; Frølich, W. Retention of folates in cooked, stored and reheated peas, broccoli and potatoes for use in modern large-scale service systems. *Food Chem.* **2007**, *101*, 1095−1107.
(72) Delchier, N.; Ringling, C.; Le Grandois, J.; Aoudé-Werner, D.; Galland, R.; Georgé, S.; Rychlik, M.; Renard, C. Effects of industrial processing on folate content in green vegetables. *Food Chem.* **2013**, *139*, 815−824.
(73) Nollet, L. M. L.; Toldra, F. *Food Analysis by HPLC*, 3rd ed.; CRC Press: Boca Raton, FL, USA, 2012.
(74) *Official Methods of Analysis of AOAC INTERNATIONAL (2003) 17th Ed.*, AOAC INTERNATIONAL: Gaithersburg, MD, USA, Official Method **992.05**.
(75) *Official Methods of Analysis of AOAC INTERNATIONAL (2005) 18th Ed.*, AOAC INTERNATIONAL: Gaithersburg, MD, USA. Official Method **2004.05**.
(76) CEN, EN 14131:2003 Foodstuffs. Determination of folate by microbiological assay, 2003.
(77) Boström Caselunghe, M.; Lindeberg, J. Biosensor-based determination of folic acid in fortified food. *Food Chem.* **2000**, *70*, 523−532.
(78) Stralsjo, L.; Arkbage, K.; Witthoft, C.; Jagerstad, M. Evaluation of a radioprotein-binding assay (RPBA) for folate analysis in berries and milk. *Food Chem.* **2002**, *79*, 525−534.
(79) Nygren-Babol, L.; Jägerstad, M. Folate-binding protein in milk: a review of biochemistry, physiology, and analytical methods. *Crit. Rev. Food Sci. Nutr.* **2012**, *52*, 410−425.
(80) Strandler, H. S. *Determination of Folate for Food Composition Data*, Swedish University of Agricultural Sciences, Uppsala, Sweden, 2012.
(81) Eitenmiller, R. R.; Ye, L.; Landen, W. O. Chapter 10. Folate and folic acid. In *Vitamin Analysis for the Health and Food Sciences*, 2nd ed.; CRC Press: Boca Raton, FL, USA, 2008; pp 443−505.
(82) Bagley, P. J.; Selhub, J. Analysis of folate form distribution by affinity followed by reversed-phase chromatography and electrochemical detection. *Clin. Chem.* **2000**, *46*, 404−411.
(83) Jägerstad, M.; Jastrebova, J. Occurrence, stability, and determination of formyl folates in foods. *J. Agric. Food Chem.* **2013**, *61*, 9758−9768.
(84) van den Berg, H.; Finglas, P. M.; Bates, C. FLAIR intercomparisons on serum and red cell folate. *Int. J. Vitam. Nutr. Res.* **1994**, *64*, 288−293.
(85) Yazynina, E.; Johansson, M.; Jagerstad, M.; Jastrebova, J. Low folate content in gluten-free cereal products and their main ingredients. *Food Chem.* **2008**, *111*, 236−242.
(86) Tamura, T.; Shin, Y. S.; Williams, M. A.; Stokstad, E. L. R. *Lactobacillus casei* response to pteroylpolyglutamates. *Anal. Biochem.* **1972**, *49*, 517−521.
(87) Ramos-Parra, P. A.; Urrea-Lopez, R.; Diaz de la Garza, R. I. Folate analysis in complex food matrices: use of a recombinant *Arabidopsis* γ-glutamyl hydrolase for folate deglutamylation. *Food Res. Int.* **2013**, *54*, 177−185.
(88) Tamura, T.; Mizuno, Y.; Johnston, K. E.; Jacob, R. A. Food folate assay with protease, α-amylase, and folate conjugase treatments. *J. Agric. Food Chem.* **1997**, *45*, 135−139.
(89) van Daele, J.; Blancquaert, D.; Kiekens, F.; van Der Straeten, D.; Lambert, W. E.; Stove, C. P. Folate profiling in potato (*Solanum tuberosum*) tubers by ultrahigh-performance liquid chromatography−tandem mass spectrometry. *J. Agric. Food Chem.* **2014**, *62*, 3092−3100.
(90) Strandler, H. S.; Axelsson, M.; Jastrebova, J. Food folate analysis by HPLC; effects of on-column degradation and interconversion of folates. Presented at the 1st International Vitamin Conference, Copenhagen, Denmark, 2010.
(91) Gounelle, J. C.; Ladjimi, H.; Prognon, P. A rapid ans specific extraction procedure for folate determination in rat liver and analysis by high-performance liquid chromatography with fluorometric detection. *Anal. Biochem.* **1989**, *176*, 406−411.
(92) Wieling, J. LC-MS-MS experiences with internal standards. *Chromatographia* **2002**, *55*, S107−S113.

NOTE ADDED AFTER ASAP PUBLICATION

This article published February 26, 2015 with errors in the TOC graphic, Figure 2, and Figure 3. The corrected files reposted February 27, 2015.

DOI: 10.1021/jf504987n
J. Agric. Food Chem. 2015, 63, 2367−2377

Table 1. Stages of Development of Tomato Fruits Exposed for Different Number of Days to High Temperature (DHT)

stage of development	description	DHT[a]
1	flowering	44
2	diam[b] ≤ 30 mm	36
3	diam ≤ 40 mm	27
4	diam ≤ 50 mm	22
5	diam ≤ 60 mm	16
6	green fruit fully developed	6

[a]DHT are mean values for each treatment, with a maximum variability of ±3 days. [b]Diameter.

replicates per treatment were randomly collected, each one constituted by ten fruits. After the physical parameters had been determined, fruits belonging to the same sample were cut into small pieces (using the whole fruit), powdered with liquid N_2, and kept at −80 °C until subsequent analysis.

For the extraction of vitamin C, samples were homogenized with EDTA (St. Louis, MO, USA), 0.05% (w/v), and dithiothreitol (Sigma-Aldrich, Steinheim, Germany). Vitamin C, measured as the sum of ascorbic acid and dehydroascorbic acid, was analyzed using liquid chromatography equipped with a triple quadrupole mass spectrometer detector (Agilent Series 1200, Santa Clara, CA, USA) according to the methodology developed by Fenoll et al.[10] For accurate quantification of the samples, the standard addition approach was performed. Ascorbic acid standard was purchased from Sigma-Aldrich (Sigma-Aldrich, Steinheim, Germany) (purity >99%).

Carotenoids were extracted according to the method of Böhm[11] with methanol/tetrahydrofuran (1/1, v/v) containing 0.1% BHT (Sigma-Aldrich, St. Louis, MO, USA) and using β-apo-8′-carotenal (Sigma-Aldrich, St. Louis, MO, USA) as internal standard. Carotenoids were determined using a Hewlett-Packard model 1100 HPLC system (Waldbronn, Germany) equipped with a photodiode array UV/vis detector. Separation was achieved in a 250 mm × 4.6 mm i.d., 3 μm Prontosil C_{30} column (Bischoff, Leonberg, Germany) with methanol (solvent A) and methyl *tert*-butyl ether (solvent B) as mobile phase. All the solvents (HPLC grade) were supplied by Fisher Chemical (Loughborough, U.K.). The gradient procedure was as follows: (1) initial conditions 15% solvent B and 85% solvent A, (2) a 10 min linear gradient to 15% solvent B, (3) a 20 min linear gradient to 90% solvent B. Elution was performed at a solvent flow rate of 1.3 mL/min with an injection volume of 20 μL and detection at 287 nm for phytoene, 347 nm for phytofluene, and 444 nm for other carotenoids and internal standard. Carotenoids in the samples were identified by comparison of retention times and UV−vis absorptions with those of the corresponding standard or with those reported in the literature. In addition, *cis* isomers were identified based on their absorption at near 330 or 360 nm and by the *Q* ratio, defined as the height ratio of the *cis* peak to the main absorption peak, as previously reported in the literature. The major compounds were identified using commercially available external standards of carotenoids (DHI LAB, Hoersholm, Denmark), except for phytoene and phytofluene, which were expressed as β-carotene equivalents.

The results were statistically analyzed using IBM SPSS Statistic 21 by analysis of variance (ANOVA) and Tukey's test for differences between means.

RESULTS AND DISCUSSION

Fruit mean weight and equatorial and longitudinal diameter decreased as a result of the increased temperature (32 °C) (Table 2). These weight and size losses were proportional to the period of exposure to the stress, except in the case of fruits exposed to high temperature from flowering (stage 1), which showed fruit weights and sizes similar to those of the control fruits. The results obtained at this first stage could have been due to the higher incidence of flower abortion as a feedback controlling mechanism to prevent an excessive sink/source ratio.[12] The reproductive process has previously been shown to be more sensitive to high temperature stress than vegetative growth. In addition, even within the different development stages of a fruit, certain stages are more sensitive. Thus, high temperature stress increased the tendency for younger flowers to abort due to shrunken pollen grain, failure of anther dehiscence, and an irregularly arranged endothecium and epidermis.[13] Therefore, the higher incidence of flower abortion caused by high temperatures would only affect trusses in development stage 1 (truss 6), leading to an increase in the mean weight of the remaining fruits, and thus compensating the weight loss resulting from temperature stress. In addition, the increased total soluble content in fruit from the stage 1 treatment (Table 2) could be explained as a concentration effect due to a decreased sink/source ratio. No treatment effect was observed in the fruit water content.

The Hunter parameter related to red (a^*) decreased as a result of high temperature in fruits subjected to the stress from the fully developed green fruit stage (6 DHT). Similarly, in a previous study, the redness of tomato decreased when fruits were ripened off-vine at 32 °C, as a result of the inhibition of lycopene synthesis.[8] In our study, the negative effect of high temperature on the red color diminished as the period of exposure to the stress increased. Moreover, in fruits grown 36 and 44 days under high temperature, the value of a^* increased above that obtained in control fruits.

The analysis of metabolites in control fruits was initially carried out separately in individual trusses (from 3 to 6). However, no differences between trusses were observed in any

Table 2. Mean Weight, Equatorial Diameter, Longitudinal Diameter, Color Hunter Parameters (L^*, a^*, and b^*), Total Soluble Solids, and Water Content (WC) of Tomato Fruits under Different Exposure Periods at 32 °C[a]

	days under high temperature						
	0	6	16	22	27	36	44
MW[b] (g)	83.5 cd	85.7 d	78.1 abcd	67.2 abc	60.9 a	63.5 ab	79.5 bcd
eq diam[c] (mm)	60.1 bc	60.7 bc	57.1 bc	55.4 ab	50.5 a	55.5 a	60.0 c
long. diam[d] (mm)	42.0 b	42.1 b	41.7 b	39.1 ab	37.5 a	37.7 ab	43.8 b
L^*	35.5 a	36.5 a	35.3 a	36.2 a	36.1 a	36.5 a	38.2 b
a^*	15.1 ab	13.0 a	13.6 a	15.8 b	16.4 b	18.6 c	26.3 d
b^*	13.3 a	14.5 ab	13.5 a	14.6 ab	14.2 ab	15.0 b	17.1 c
TSS[e] (°Brix)	4.2 ab	4.0 a	4.1 ab	4.0 ab	4.2 ab	4.6 bc	4.8 c
WC[f] (%)	94.1	94.6	94.87	94.9	95.5	93.5	94.0

[a]Different letters in the same column indicate significant differences between means according to Tukey's test. Values are means (n = 6). [b]Mean weight. [c]Equatorial diameter. [d]Longitudinal diameter. [e]Total soluble solids. [f]Water content.

DOI: 10.1021/jf505507h
J. Agric. Food Chem. 2015, 63, 2378−2382

of the studied metabolites (carotenoids and vitamin C), and so the results of the control treatment are presented as the mean values for the different trusses. The fact that no differences were observed between trusses in control plants can be attributed to (i) fruits from different trusses were collected from different plants, and therefore no modification of the sink/source ratio was influenced by previous harvest before sampling, and (ii) in the growth chamber, where the photoperiod remained unaltered throughout the growing period, differences between trusses are are much less likely to occur than in natural conditions.

The effect of high temperature on vitamin C concentration depended on the duration and timing of the stress (Figure 1).

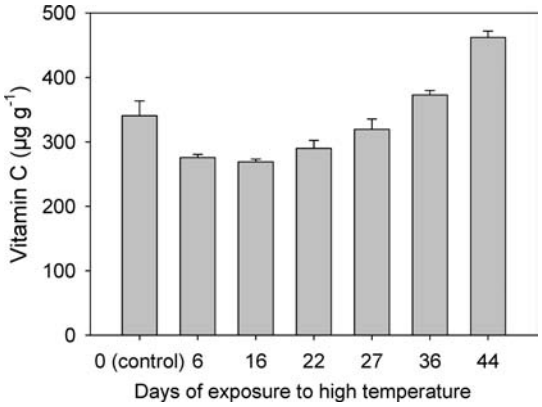

Figure 1. Vitamin C concentration in fruits exposed to temperature stress (32 °C) during increasing time periods. Bars are mean values ± SE (n = 6).

In fruits subjected to 32 °C from the advanced development stages (stage 6 and stage 5, equivalent to 6 and 16 DHT, respectively), vitamin C concentration decreased with regard to control fruits. The negative effect of high temperature on vitamin C decreased as the period of exposure to the stress increased. Thus, fruits grown at a high temperature for 36 days (from stage 4) showed a similar vitamin C content to control fruits. Moreover, increasing the exposure period up to 44 days led to an increase in the vitamin C concentration to above the values obtained in control fruits.

The stress caused by high temperatures leads to an alteration of the composition of the fruit through modifications at physiological, biochemical, and molecular levels. At plant level, the increased temperature changes the distribution of photoassimilates among plant organs, increasing biomass translocation to fruits at the expense of vegetative growth.[12] On the other hand, temperatures above the optimum values can directly alter metabolite synthesis/degradation processes. In particular, ascorbate accumulation is limited by high temperatures, which reduce ascorbate synthesis and/or favor ascorbate degradation through oxidation due to intensified ascorbate peroxidase and ascorbate oxidase activities and a depression of the enzyme dehydroascorbate reductase.[14]

The increase of vitamin C concentration observed after longer periods at high temperature suggests an adaptation of the plant metabolism to high temperature and/or a restoration of the ascorbate synthesis processes during the time intervals in which the temperature decreases along the photoperiod (night). Finally, the vitamin C content was higher in fruit exposed to a high temperature from flowering than in control fruits, probably due to a concentration effect as a result of a decreased sink/source ratio due to increased flower abortion. A concentration effect cannot be attributed to the lower fruit water content since no differences in this parameter were observed between treatments.

The carotenoids identified and quantified in the tomato samples by HPLC were phytoene, phytofluene, *all-trans*-lycopene, 13-*cis*-lycopene, 5-*cis*-lycopene, lutein, *all-trans*-γ-carotene, *all-trans*-β carotene, 9-*cis*-β-carotene, 13-*cis*-β-carotene, and violaxanthin (Figure 2). The increased temperature,

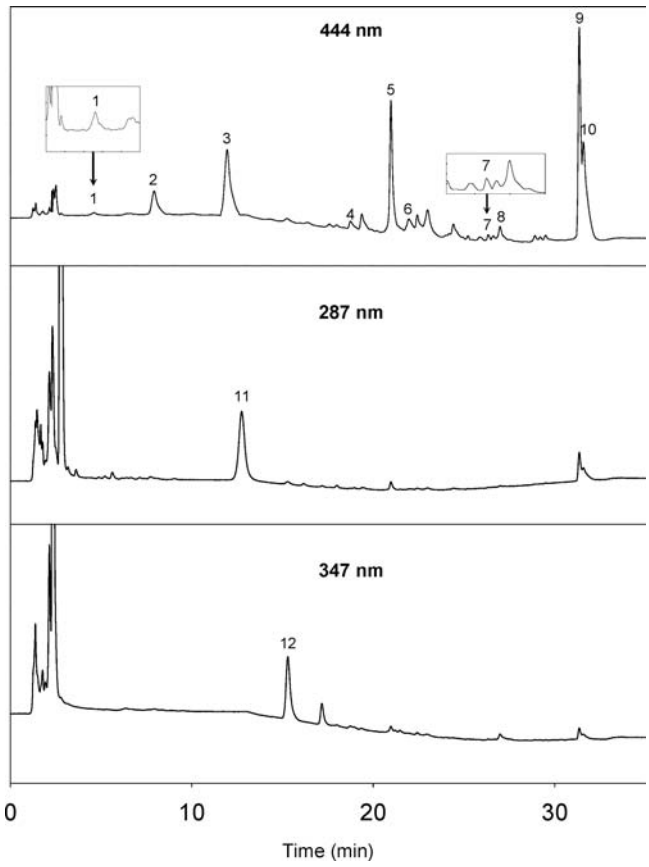

Figure 2. HPLC-DAD chromatogram of carotenoids in cv. Velasco recorded at 444, 287, and 347 nm. Peak identification: (1) violaxanthin, (2) lutein, (3) internal standard, (4) 13-*cis*-β-carotene, (5) *all-trans*-β-carotene, (6) 9-*cis*-β-carotene, (7) *all-trans*-γ-carotene, (8) 13-*cis*-lycopene, (9) *all-trans*-lycopene, (10) 5-*cis*-lycopene, (11) phytoene, and (12) phytofluene.

when imposed in the fully developed green fruit stage (stage 5), lowered the concentration of total lycopene (calculated as the sum of *all-trans*, 13-*cis*, and 5-*cis* lycopene isomers) in the mature fruit (Figure 3A). This decrease was accompanied by a decrease in the concentration of phytoene and phytofluene (precursors) and an increase in lutein (product) (Table 2 and Figure 4). At earlier stages, the inhibitory effect of temperature on the accumulation of lycopene and its precursors and the stimulatory effect on lutein decreased in proportion to the length of exposure to 32 °C. In the case of fruit subjected to high temperatures since flowering, the phytoene and lycopene concentrations reached higher levels than those observed in the control fruits. Unlike lycopene, the total β-carotene concentration (calculated as the sum of *all-trans*-, 9-*cis*-, and 13-*cis*-β-carotene isomers) was not affected by the temperature increase (Figure 3B). Furthermore, the concentrations of γ-carotene and

DOI: 10.1021/jf505507h
J. Agric. Food Chem. 2015, 63, 2378−2382

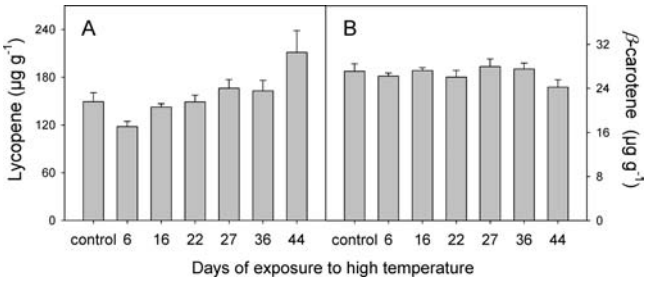

Figure 3. Total lycopene (A) and total β-carotene (B) concentrations in fruits exposed to temperature stress (32 °C) during increasing time periods. Bars are mean values ± SE (n = 6).

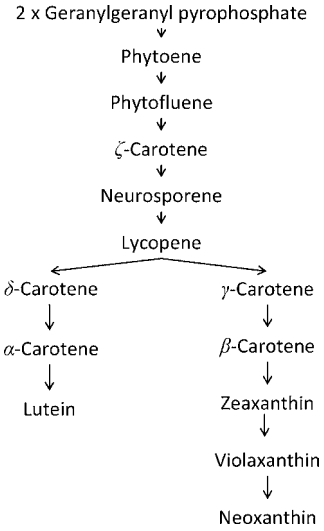

Figure 4. Summary of carotenoid biosynthesis.

violaxanthin decreased in proportion to the time of exposure to heat stress.

According Gautier et al.,[8] the enzyme phytoene synthase (PSY), responsible for the formation of phytoene from two molecules of geranylgeranyl diphosphate (GGPP), plays a key role in regulating the biosynthesis of carotenoids. PSY is inhibited by temperature increases, especially at the transcriptional level.[15,16] This inhibition could explain the observed decrease in the concentration of phytoene, phytofluene, and its product lycopene in fruits subjected to a high temperature for a short period (stage 5). Some authors suggest that the decrease in lycopene as a result of temperature increase may be due to a degradation of this compound toward the formation of β-carotene.[8] However, our results also suggest a degradation of lycopene toward the formation of lutein.

The feedback control mechanisms and metabolic channeling between each branch of the isoprenoid pathway play a key role in the final concentration of each compound.[17] Thus, the fact that the concentration of β-carotene was stable could be linked, on the one hand, to the increased degradation of lycopene and γ-carotene and, on the other, to the decreased catabolism of β-carotene into the formation of violaxanthin, which would also explain the observed decrease in the concentration of the latter compound.

An increasing time of exposure to temperature stress reduced the negative effect of temperature on the concentration of phytoene, phytofluene, lycopene, and lutein, suggesting, similarly to that observed in the case of vitamin C, an adaptation of the plant metabolism to high temperature and/or the restoration of carotenoid synthesis processes during the time intervals in which the temperature decreases along the photoperiod. The increase in the total carotenoid content observed in fruits from the stage 1 treatment (Table 3) could also be attributed to a concentration effect resulting from a lower sink/source ratio.

In addition to these metabolic changes in the isoprenoid biosynthesis route, temperature stress led to an increase in the concentration of the 13-*cis* isomer of β-carotene and lycopene. The formation of *cis* isomers from the *all-trans* form as a result of increased temperature has previously been described.[18] Different lycopene isomers were shown to have different stabilities (5-*cis* ≥ *all-trans* ≥ 9-*cis* ≥ 13-*cis* > 15-*cis* > 7-*cis* > 11-*cis*) due to their molecular energy.[19] Although the *cis* forms are more unstable, *cis*-lycopene isomers have been shown to be more bioavailable than *trans*-lycopene probably because of their shorter length and low tendency to form aggregates, which confers greater solubility.[20,21]

In conclusion, the effect of increased temperature on fruit development and on the concentrations of vitamin C and carotenoids depended closely on the development stage at which the stress was first imposed. In general, increased temperature negatively affected fruit weight and size propor-

Table 3. Carotenoid Concentration (μg g^{-1}FW) in Tomato Fruits Exposed to High Temperature (32 °C) during Increasing Time Periods[a]

	days of exposure at high temperature (DHT)						
compound	0	6	16	22	27	36	44
phytoene	16.8 c	8.5 a	9.9 ab	11.4 ab	13.5 bc	22.7 d	24.4 d
phytofluene	7.8 bc	4.2 a	5.1 ab	5.4 ab	6.2 ab	6.3 ab	6.7 c
all-trans-lycopene	100.4 b	78.5 a	94.9 ab	99.3 ab	111.3 b	107.2 b	143.6 c
13-*cis*-lycopene	4.8 a	5.2 ab	6.6 abc	6.4 abc	7.1 bc	8.5 c	9.3 d
5-*cis*-lycopene	3.3 b	1.9 a	1.8 a	2.2 ab	1.8 a	2.2 ab	1.9 ab
lutein	11.2 a	12.8 ab	13.8 b	13.2 ab	13.4 ab	13.7 b	12.2 ab
all-trans-γ-carotene	3.2 c	2.8 bc	2.8 bc	2.3 ab	2.1 a	1.9 a	2.0 a
all-trans-β-carotene	25.7	24.6	25.2	24.2	25.9	24.5	21.6
9-*cis*-β-carotene	0.6	0.6	0.7	0.6	0.7	0.7	0.5
13-*cis*-β-carotene	0.9 a	1.0 ab	1.3 cd	1.2 ab	1.4 cd	1.4 cd	1.3 d
violaxanthin	3.1 d	3.0 cd	2.5 bcd	2.5 bc	2.2 b	1.8 b	1.1 a
total carotenoids	177.8 ab	143.1 a	164.6 ab	168.7 ab	185.6 b	190.9 bc	224.6 c

[a]Different letters in the same column indicate significant differences between means.

DOI: 10.1021/jf505507h
J. Agric. Food Chem. 2015, 63, 2378−2382

tionally to the length of exposure. However, tomatoes subjected to the stress from the flowering stage showed similar weights and sizes to control fruits, due to a higher incidence of flower abortion and the subsequent weight increase in the remaining fruits. As regards nutritional quality, exposure to the increased temperature of 32 °C over a short period of time (beginning when fruit were in the last developing stages) caused a decrease of the concentration of vitamin C and lycopene but did not affect the β-carotene concentration. Changes in the concentrations of other carotenoids can be explained by possible metabolic channeling between the different isoprenoid biosynthetic pathway branches.

The negative effect of high temperature on vitamin C and lycopene diminished as the period of exposure to the stress increased, reaching values similar to those obtained in control fruits, or even higher if fruits were under temperature stress since flowering. These results show the ability of the tomato plants to adapt to temperature stress, being able to restore the concentrations of these metabolites after longer periods at high temperature. These results contribute to a better understanding of the effect of increased air temperature, as may be expected as a result of global warming, on the functional quality of tomato, allowing a more precise evaluation of temperature stress on the vitamin C and carotenoid concentrations of the fruit.

AUTHOR INFORMATION

Corresponding Author

*Instituto Murciano de Investigación y Desarrollo Agrario y Alimentario (IMIDA), c/ Mayor s/n, La Alberca, 3150 Murcia, Spain. E-mail: mpilar.flores@carm.es. Phone: +34 968 366804. Fax: +34 968 366792.

Funding

This research has been supported by INIA (Project RTA2010-00119-00-00 and a predoctoral fellowship).

Notes

The authors declare no competing financial interest.

ACKNOWLEDGMENTS

The authors are grateful to Inmaculada Garrido González, Juana Cava Artero, and María V. Molina Menor for technical assistance.

REFERENCES

(1) Vadez-Morales, M.; Espinosa-Alonso, L. G.; Espinoza-Torres, L. C.; Delgado-Vargas, F.; Medina-Godoy, S. Phenolic content and antioxidant and antimutagenic activities in tomato peel, seeds, and byproducts. *J. Agric. Food Chem.* **2014**, *62*, 5281−5289.

(2) Smirnoff, N.; Conklin, P. L.; Loewus, F. A. Biosynthesis of ascorbic acid in plants: A renaissance. *Annu. Rev. Plant Biol.* **2001**, *52*, 437−467.

(3) Leonardi, C.; Ambrosino, P.; Esposito, F.; Fogliano, V. Antioxidative activity and carotenoid and tomatine contents in different typologies of fresh consumption tomatoes. *J. Agric. Food Chem.* **2000**, *10*, 4723−4727.

(4) Mein, J. R.; Lian, F.; Wang, X.-D. Biological activity of lycopene metabolites: implications for cancer prevention. *Nutr. Rev.* **2008**, *66*, 667−683.

(5) Sommerburg, O.; Keunen, J. E. E.; Bird, A. C.; van Kuijk, F. Fruits and vegetables that are sources for lutein and zeaxanthin: the macular pigment in human eyes. *Br. J. Ophthalmol.* **1998**, *82*, 907−910.

(6) Riso, P.; Visioli, F.; Grande, S.; Guarnieri, S.; Gardana, C.; Simonetti, P.; Porrini, M. Effect of a tomato-based drink on markers of inflammation, immunomodulation, and oxidative stress. *J. Agric. Food Chem.* **2006**, *54*, 2563−2566.

(7) Bita, C. E.; Zenoni, S.; Vriezen, W. H.; Mariani, C.; Pezzotti, M.; Gerats, T. Temperature stress differentially modulates transcription in meiotic anthers of heat-tolerant and heat-sensitive tomato plants. *BMC Genomics* **2011**, *12*, 384.

(8) Gautier, H.; Diakou-Verdin, V.; Benard, C.; Reich, M.; Buret, M.; Bourgaud, F.; Poessel, J. L.; Caris-Veyrat, C.; Genard, M. How does tomato quality (sugar, acid, and nutritional quality) vary with ripening stage, temperature, and irradiance? *J. Agric. Food Chem.* **2008**, *56*, 1241−1250.

(9) Intergovernmental panel on climate change. Third Assessment Report—Climate Change 2001: Synthesis Report. http://www.ipcc.ch.

(10) Fenoll, J.; Martinez, A.; Hellin, P.; Flores, P. Simultaneous determination of ascorbic and dehydroascorbic acids in vegetables and fruits by liquid chromatography with tandem-mass spectrometry. *Food Chem.* **2011**, *127*, 340−344.

(11) Bohm, V. Use of column temperature to optimize carotenoid isomer separation by C-30 high performance liquid chromatography. *J. Sep. Sci.* **2001**, *24*, 955−959.

(12) de Koning, A. N. M. Quantifying the responses to temperature of different plant processes involved in growth and development of glasshouse tomato. *Acta Hortic.* **1996**, *406*, 99−104 http://www.actahort.org/books/406/406_9.htm.

(13) Sato, S.; Peet, M. M.; Thomas, J. F. Determining critical pre- and post-anthesis periods and physiological processes in *Lycopersicon esculentum* Mill. exposed to moderately elevated temperatures. *J. Exp. Bot.* **2002**, *53*, 1187−1195.

(14) Rosales, M. A.; Ruiz, J. M.; Hernandez, J.; Soriano, T.; Castilla, N.; Romero, L. Antioxidant content and ascorbate metabolism in cherry tomato exocarp in relation to temperature and solar radiation. *J. Sci. Food Agric.* **2006**, *86*, 1545−1551.

(15) Bramley, P. M. Regulation of carotenoid formation during tomato fruit ripening and development. *J. Exp. Bot.* **2002**, *53*, 2107−2113.

(16) Fraser, P. D.; Bramley, P. M. The biosynthesis and nutritional uses of carotenoids. *Prog. Lipid Res.* **2004**, *43*, 228−265.

(17) Poiroux-Gonord, F.; Bidel, L. P. R.; Fanciullino, A.-L.; Gautier, H.; Lauri-Lopez, F.; Urban, L. Health benefits of vitamins and secondary metabolites of fruits and vegetables and prospects to increase their concentrations by agronomic approaches. *J. Agric. Food Chem.* **2010**, *58*, 12065−12082.

(18) Takehara, M.; Nishimura, M.; Kuwa, T.; Inoue, Y.; Kitamura, C.; Kumagai, T.; Honda, M. Characterization and thermal isomerization of (*all-E*)-lycopene. *J. Agric. Food Chem.* **2014**, *62*, 264−269.

(19) Chasse, G. A.; Mak, M. L.; Deretey, E.; Farkas, I.; Torday, L. L.; Papp, J. G.; Sarma, D. S. R.; Agarwal, A.; Chakravarthi, S.; Agarwal, S.; Rao, A. V. An ab initio computational study on selected lycopene isomers. *J. Mol. Struct.: THEOCHEM* **2001**, *571*, 27−37.

(20) Melendez-Martinez, A. J.; Paulino, M.; Stinco, C. M.; Mapelli-Brahm, P.; Wang, X. D. Study of the time-course of *cis*/*trans* (Z/E) isomerization of lycopene, phytoene, and phytofluene from tomato. *J. Agric. Food Chem.* **2014**, *62*, 12399−12406.

(21) Boileau, A. C.; Merchen, N. R.; Wasson, K.; Atkinson, C. A.; Erdman, J. W. *Cis*-lycopene is more bioavailable than *trans*-lycopene in vitro and in vivo in lymph-cannulated ferrets. *J. Nutr.* **1999**, *129*, 1176−1181.

DOI: 10.1021/jf505507h
J. Agric. Food Chem. 2015, 63, 2378−2382

Table 1. Agronomic Measures of Different Varieties of Corn Forage Grown with or without Irrigation

	cultivar	variety	plants/ha	DM (%)	moisture (%)	DM yield (T/ha)	days to tasseling	days to silking
irrigation	Pioneer	P2501	79688	40.6	59.5	18.6	74.3	75.8
		P39m26	79948	48.7	51.3	15.6	62.0	71.8
		P7443	78646	47.1	52.9	18.0	68.5	74.3
	Hyland	HL3085	68229	39.8	60.2	13.4	66.5	73.3
		HLBaxxos	74740	40.8	59.3	16.6	73.0	76.5
		HLR219	78646	41.4	58.6	18.3	74.0	76.0
		HLSR22	80209	36.2	63.8	20.0	76.8	78.8
	Pickseed	Silex BT	72656	37.5	62.5	18.3	72.8	76.5
mean			76595	41.5	58.5	17.4	71.0	75.3
dry land	Pioneer	P2501	74219	39.6	60.4	17.2	75.5	77.8
		P39m26	70052	46.2	53.8	13.8	63.8	73.3
		P7443	71354	42.7	57.4	12.5	69.8	75.8
	Hyland	HL3085	68229	38.2	61.8	14.7	74.0	78.8
		HLBaxxos	73438	41.9	58.1	13.9	67.5	73.8
		HLR219	71355	39.8	60.3	15.9	74.8	77.5
		HLSR22	69010	35.0	65.1	14.0	78.3	81.5
	Pickseed	Silex BT	71615	36.3	63.7	15.3	72.5	77.5
mean			71159	39.9	60.1	14.6	72.0	77.0
statistical analysis								
SEM			1991	0.82	0.82	0.55	0.46	0.44
P	irrigation		<0.0001	0.0003	0.0003	<0.0001	<0.0001	<0.0001
	variety		0.004	<0.0001	<0.0001	<0.0001	<0.0001	<0.0001
	variety × irrigation		0.045	0.09	0.09	<0.0001	<0.0001	<0.0001
contrast	Pioneer vs Hyland		0.02	<0.0001	<0.0001	0.74	<0.0001	<0.0001
	Pioneer vs Pickseed		0.04	<0.0001	<0.0001	0.06	<0.0001	<0.0001
	Hyland vs Pickseed		0.59	0.001	0.001	0.03	0.20	1.00

MATERIALS AND METHODS

Corn Cultivation, Experimental Design, and Sampling. Eight varieties were collected from the Canada−Saskatchewan Irrigation Diversification Centre, Agriculture and Agri-Food Canada (Outlook, SK, Canada; 51°30′ N, 107°03′ W). These varieties were Pioneer 2501 (P2501), Pioneer 39m26 (P39m26), Pioneer 7443 (P7443; Pioneer Hi-Bred International Inc., Johnston, IA, USA); Hyland 3083 (HL3083), Hyland Baxxos (HLBaxxos), Hyland R219 (HLR219), Hyland SR22 (HLSR22; Hyland Seeds, Blenheim, ON, Canada); and Silex BT (Pickseed Canada Inc., Nipawin, SK, Canada). This experiment was designed as a randomized complete block design. All of the varieties were arranged with four plots (blocks) with a total of 64 plots. The plot size was 6 m × 1.7 m with seeding rate of 600 kernels per plot on May 20, 2012. For the irrigated plots, irrigation was started at the end of July and ended in mid-September at 25 mm per week according to the practical standard. For the dry land plots, no irrigation was performed. The precipitation from seeding date to harvesting date was 192 mm. When the moisture content of corn forage of the entire plot reached 65−70%, the forage was ready for harvest. Harvests were carried out at the same time (September 28, 2012) with a kemper chopper (Champion 1200, Denmark) for all corn plots. Cutting height was set at 10 cm above the ground.

Agronomic Measurement. The numbers of corn plants in each plot, tassel initiation, and silk initiation were recorded during the experiment. On the harvesting day, the corn forages of the entire plot were chopped and weighed with a built-in scale in the chopper before unloading onto the ground. Approximately 500 g of fresh chopped plant from each plot was sealed in a plastic sample bag for the determination of DM according to AOAC Official Method 930.15.[18] In addition, chopped forage samples of around 1 kg for each treatment were collected, dried in a forced-air oven at 55 °C for 72 h, and ground through 1.0 mm screen (Retsch ZM-1; Brinkmann Instruments, Mississauga, ON, Canada) for further analyses.

Basic Chemical Profile with Near-Infrared Reflectance (NIR) Spectroscopy System. The air-dried forage samples were scanned using a NIR system (Foss InfraXact, Hilleroed, Denmark) at the University of Saskatchewan (SK, Canada) for measurements of DM, organic matter (OM), crude protein (CP), crude fiber (CF), and ether extract (EE) based on internal available calibration curves in the NIR system. Approximately 50 g of forage sample was used under the analysis model of plant (forage) material in NIR system. Spectra were collected in the visible (vis) and NIR regions in reflectance (ca. 1850−570 nm), within 60 s by a monochromator-based NIR system in triplicates. Both spectrophotometer operation and data acquisition were performed by ISIscan Software IS-2200 (FOSS Analytical, Hilleroed, Denmark).

Carbohydrate and Protein Molecular Structures by ATR-FT-MIR Spectroscopy. The spectral scans (within mid-IR region ca. 4000−800 cm^{-1}) of ground forage samples (0.5 mm) were performed using a JASCO FT/IR 4200 with ATR (JASCO Corp., Tokyo, Japan) at the University of Saskatchewan. In the present study, both protein- and carbohydrate-related molecular structures were revealed by 128 co-added scans at a resolution of 4 cm^{-1}. The parameters related to carbohydrate molecular structures included peak heights of total carbohydrate (CHO, peak baseline ca. 1198−800 cm^{-1}; three peaks fell into this region, named CHO first, second, and third peaks centered at 1154, 1103, and 1033 cm^{-1}, respectively), cellulosic compounds (CELC, peak baseline ca. 1290−1180 cm^{-1}) centered at 1240 cm^{-1}, and lignin (peak baseline ca. 1525−1490 cm^{-1}) centered at 1512 cm^{-1}. The protein spectral parameters involved protein amide I, amide II, and its secondary structures such as α-helix and β-sheet; all of the protein peaks were identified within the baseline ca. 1696−1488 cm^{-1} and the peaks centered at 1610, 1538, 1652, and 1629 cm^{-1}, respectively. More detailed information about peak identification can be found in previous publications.[19,20] Then the spectral analysis was carried out using OMNIC 7.2 software (Spectra Tech., Madison, WI, USA).

Principal Component Analysis (PCA). Multivariate spectral analyses−PCA was performed using Statistica 8.0 software (StatSoft Inc., Tulsa, OK, USA) within the NIR fingerprint spectra ca. 1850−570 nm on each corn variety to clarify whether there was any

DOI: 10.1021/jf505911a
J. Agric. Food Chem. 2015, 63, 2383−2391

Table 2. Chemical and Nutrition Profile Derived from NIR Spectral Analysis of Different Varieties of Corn Forage Grown with or without Irrigation

	cultivar	variety	OM (% DM)	protein (% DM)	CF (% DM)	EE (% DM)
irrigation	Pioneer	P2501	94.97	9.51	11.73	1.17
		P39m26	94.59	8.58	10.52	1.10
		P7443	94.60	9.17	10.38	1.18
	Hyland	HL3085	95.00	10.18	11.25	1.28
		HLBaxxos	94.95	8.91	13.54	1.01
		HLR219	95.40	9.76	11.89	1.17
		HLSR22	94.51	10.14	14.78	0.90
	Pickseed	Silex BT	94.93	10.29	12.43	1.16
mean			94.87	9.57	12.07	1.12
dry land	Pioneer	P2501	93.97	9.57	12.67	1.01
		P39m26	94.35	8.95	11.10	1.20
		P7443	93.88	9.36	11.52	0.99
	Hyland	HL3085	95.04	10.00	12.52	1.04
		HLBaxxos	94.08	9.76	10.28	1.27
		HLR219	94.78	9.76	10.97	1.25
		HLSR22	94.04	10.81	14.17	0.86
	Pickseed	Silex BT	95.30	10.70	13.02	1.23
mean			94.43	9.88	12.03	1.10
statistical analysis						
SEM			0.289	0.200	0.459	0.051
P	irrigation		0.002	0.002	0.87	0.52
	variety		0.001	<0.0001	<0.0001	<0.0001
	variety × irrigation		0.19	0.19	<0.0001	<0.0001
contrast	Pioneer vs Hyland		0.03	<0.0001	<0.0001	0.76
	Pioneer vs Pickseed		0.002	<0.0001	<0.0001	0.03
	Hyland vs Pickseed		0.08	0.0004	0.36	0.02

molecular structural relationship between irrigated and nonwatered corn forages. The application of PCA in feedstuff molecular structure research has been described clearly by Yu,[21] which was also referred to in the current study.

Statistical Analysis. The treatment design was 8 × 2 factorial design with 8 corn forage varieties and 2 treatments (irrigation and nonirrigation). The experiment design was randomized complete block design (RCBD). The data of the agronomic measurements and basic chemical profile as well as carbohydrate and protein spectral data in corn forages were statistically analyzed using the Mixed Model procedure of SAS 9.2, and the model was

$$Y_{ijkl} = \mu + F_i + I_j + F_i \times I_j + B_k + e_{ijkl}$$

where Y_{ijkl} is the observation of the dependent variable *ijkl*; μ is the fixed effect of population mean of the variable; F_i is a fixed effect of corn forage variety (i = 8; P2501, P39m26, P7443, HL3085, HLBaxxos, HLR219, HLSR22, and Silex BT), I_j is a fixed effect of irrigation (j = 2; irrigation and dryland), $F_i \times I_j$ is a fixed effect of interaction between factor F at level i and factor I at level j; B_k is a random block effect; and e_{ijkl} is the random error associated with the observation *ijkl*.

The three assumptions of the RCBD were (1) residual errors are normally distributed; (2) there were common variances among the treatments; and (3) block effects are normally distributed. For normality tests, Proc Univariate of SAS with Normal Plot option was used. For the common variance, treatment ID against residue pattern was checked.

Multiple treatment comparisons were performed using the Tukey–Kramar test. Statistical significance was declared and detected at $P < 0.05$, whereas trends were declared at $P \leq 0.10$.

RESULTS AND DISCUSSION

Agronomic Characteristics. Table 1 shows the agronomic features of different varieties of corn forage response to irrigation. Forage plant number was significantly affected ($P < 0.05$) by the interaction of irrigation and variety. The number of HLSR22 plants grown with irrigation was at the highest level, whereas that of HL3085 (with or without irrigation) was at the lowest level. Most of our data fell into the optimum density range of 79,000−143,000 plants per hectare, which is considered to have maximum forage yields.[22,23] A significant difference (P = 0.0003) on DM content of corn forage was found between irrigation and no water use treatments. The plants grown with irrigation treatment had 4% more DM than those grown on dry land. Limited water supply in the growing stage leads to deficient water content in the soil, and this deficit strongly hinders nutrient uptake by the roots and delays physiological processes for the growth and development of plants.[24] Additionally, the drier soil may slow or even block rooting,[25] transpiration, photosynthetic rates, and nutrient transportation from roots to shoots.[26−28] A positive effect of irrigation on crop DM accumulation was also reported by numerous researchers previously.[11,26,29] Cultivar Pioneer had the greatest DM concentration with an average of 45.4%, followed by Hyland (39.5%) and Pickseed (37.5%). In regard to DM yield, it interacted ($P < 0.0001$) with irrigation regimen and corn variety. The DM yield of HLSR22 cultivated on irrigated land reached 20 tons (per hectare), which was at the highest level among treatments. Our result was in agreement with several studies[11,30,31] in which increased DM yield of forage was highly associated with higher level of irrigation. The timings of tassel initiation and silk initiation were also changed among corn varieties grown with and without water treatment. The interaction of irrigation and variety was significant, and the earliest tassel and silk initiations were found in P39m26 grown

DOI: 10.1021/jf505911a
J. Agric. Food Chem. 2015, 63, 2383−2391

Table 3. Peak Intensity Measures from FTIR Univariate Spectral Data Analysis of Different Varieties of Corn Forage Grown with or without Irrigation

	cultivar	variety	CHO first peak	CHO second peak	CHO third peak	cellulosic compounds	lignin	protein amide I	protein amide II	α-helix	β-sheet
	peak position:[a]		~1154 cm^{-1}	~1103 cm^{-1}	~1033 cm^{-1}	~1240 cm^{-1}	~1512 cm^{-1}	~1610 cm^{-1}	~1538 cm^{-1}	~1652 cm^{-1}	~1629 cm^{-1}
irrigation	Pioneer	P2501	0.0220	0.0624	0.1010	0.0076	0.0040	0.0298	0.0205	0.0127	0.0142
		P39m26	0.0212	0.0553	0.0923	0.0067	0.0039	0.0259	0.0195	0.0102	0.0106
		P7443	0.0224	0.0564	0.0946	0.0066	0.0041	0.0268	0.0194	0.0110	0.0113
	Hyland	HL3085	0.0218	0.0579	0.0960	0.0065	0.0045	0.0298	0.0211	0.0132	0.0140
		HLBaxxos	0.0218	0.0585	0.0955	0.0081	0.0039	0.0282	0.0196	0.0115	0.0128
		HLR219	0.0227	0.0610	0.0999	0.0075	0.0042	0.0303	0.0214	0.0124	0.0134
		HLSR22	0.0210	0.0591	0.0954	0.0077	0.0042	0.0296	0.0204	0.0132	0.0146
	Pickseed	Silex BT	0.0212	0.0585	0.0954	0.0082	0.0037	0.0276	0.0189	0.0111	0.0125
mean			0.0218	0.0587	0.0963	0.0074	0.0041	0.0285	0.0201	0.0119	0.0129
dry land	Pioneer	P2501	0.0202	0.0576	0.0936	0.0077	0.0035	0.0238	0.0164	0.0098	0.0106
		P39m26	0.0207	0.0554	0.0924	0.0081	0.0053	0.0264	0.0203	0.0092	0.0093
		P7443	0.0196	0.0543	0.0892	0.0068	0.0037	0.0241	0.0179	0.0086	0.0094
	Hyland	HL3085	0.0206	0.0562	0.0924	0.0075	0.0050	0.0277	0.0203	0.0107	0.0110
		HLBaxxos	0.0195	0.0524	0.0854	0.0061	0.0038	0.0248	0.0179	0.0107	0.0113
		HLR219	0.0206	0.0564	0.0918	0.0075	0.0046	0.0271	0.0196	0.0106	0.0110
		HLSR22	0.0183	0.0549	0.0877	0.0070	0.0042	0.0258	0.0186	0.0110	0.0118
	Pickseed	Silex BT	0.0196	0.0567	0.0898	0.0072	0.0038	0.0279	0.0197	0.0107	0.0120
mean			0.0199	0.0555	0.0903	0.0072	0.0042	0.0259	0.0189	0.0102	0.0108
statistical analysis											
SEM			0.00079	0.00207	0.00345	0.00031	0.00039	0.00114	0.00095	0.00050	0.00057
P	irrigation		<0.0001	0.003	0.001	0.20	0.32	<0.0001	0.004	<0.0001	<0.0001
	variety		0.34	0.23	0.503	0.02	0.003	0.01	0.048	<0.0001	<0.0001
	variety × irrigation		0.84	0.83	0.89	<0.0001	0.07	0.051	0.10	0.11	0.16
contrast	Pioneer vs Hyland		0.60	0.89	0.65	0.58	0.19	0.002	0.06	<0.0001	<0.0001
	Pioneer vs Pickseed		0.34	0.67	0.67	0.09	0.25	0.07	0.64	0.10	0.01
	Hyland vs Pickseed		0.54	0.73	0.89	0.03	0.04	0.82	0.42	0.050	0.60

[a]Protein amide data unit, IR absorbance unit; the protein peak baseline, ca. 1696−1488 cm^{-1}; carbohydrate (CHO) peak baseline, ca. 1198−800 cm^{-1}; cellulosic compounds peak baseline, ca. 1290−1180 cm^{-1}; lignin peak baseline, ca. 1525−1490 cm^{-1}.

J. Agric. Food Chem. 2015, 63, 2383−2391
DOI: 10.1021/jf505911a

in wetter plots, which were around 16 and 10 days prior to the latest one, HLSR22 cultivated on dry land. Such findings partially complied with previous results of NeSmith and Ritchie[32] and Abrecht and Carberry,[33] who reported that delays in crop phenology could be expected with severe water deficits.

Basic Chemical Profile Derived from NIR Spectral Analysis. The contents of OM, CP, CF, and EE in different varieties of corn forage grown with and without irrigation are shown in Table 2. Both growing conditions (irrigated or not; $P = 0.002$) and corn variety ($P = 0.001$) significantly affected OM content. Compared with corn grown on dry land, corn grown with water stress had 0.44% unit higher OM content, which partially corresponded to the recent result of Jahanzad et al.,[5] who found the ash content (=100 − OM) followed a declining trend as irrigation levels increased in two forage sorghum cultivars named Speedfeed and Pegah. Within three cultivars, Pioneer had a higher OM content than Hyland and Pickseed, and the latter two were similar to each other. Also, this result was not far from the observation reported by Abeysekara et al.[34] The concentration of CP plays an important role in forage quality and ruminant feed nutrition.[35] In the current research, the CP contents in different kinds of corn forage were strongly influenced by irrigation conditions ($P = 0.002$). A progressive rise in CP concentration was found in the corn forage grown on dry land. As for the effect of various irrigation regimens on CP accumulation in crops, previous studies showed inconsistent results. Some researchers reported an improved CP content in forage as water deficit intensified, which might result from nitrogen accumulation in drier soil,[7,36,37] the breakdown in plant protein molecules,[36] or the decrease in amino acids incorporated into protein,[38,39] which were also supported by our data. In contrast, certain increased levels of CP concentration in alfalfa were found in wetter cultivated spots.[40,41] Distinctively, Nielsen[11] found that the CP levels showed inconsistent variation from year to year (2001−2008) in soybean forages under four irrigation treatments.[11] The possible reasons for these controversial results might be partly associated with the precipitation conditions as well as nitrogen fertilizer supply as reviewed by Peyraud and Astigarraga.[42] Additionally, the CP concentrations varied ($P < 0.05$) among different cultivars. The averaged CP content of Pickseed was 10.5%, which was at the highest level, whereas that of Pioneer was at the lowest level (9.19%); an intermediate level (9.92%) was observed in the Hyland cultivar. The CP values in Pioneer and Hyland were much greater than those found in a very recent publication[34] in which these two cultivars had similar CP contents (averaged at 7.1% DM). This variation might be related to different growing years between two studies (2011 vs 2012) as discussed by Nielsen.[11] The variation might be also due to the analysis methods: NIR in this study versus wet chemical analysis. As for the carbohydrate composition like CF in the corn forages, there was a significant interaction between irrigation treatment and corn variety. Regardless of irrigated or dry plots, HLSR22 had the greatest the content of CF, whereas HLBaxxos grown on dry land had the lowest concentration. Compared with Hyland and Pickseed, which were similar to each other ($P = 0.36$), cultivar Pioneer had the lowest level of CF content. However, the average value for CF was only 12.1% DM, which was markedly lower than the value in the Dairy One Forage Database.[43] In this database, the ranges of CF content of crops accumulated from 2000 to 2013 are 18.3−23.7%. The possible reason for these inconsistent results might be related to the different growing conditions such as climate, fertilizer application, and water use or different biological stage of corn crops at harvesting time or different chemical analysis methods (NIR vs wet chemical analysis). Additionally, the EE content was highly affected by the interaction of corn variety and irrigation implementation. The average EE concentration in corn forages was 1.11% DM, and this value was slightly beyond the range of 1.4−1.8% DM reported by Abeysekara et al.,[34] who worked on the corn forages obtained from Pioneer and Hyland.

Spectral Characteristics of Corn Forage. Table 3 gives the carbohydrate and protein molecular structural characteristics for eight varieties of corn forage grown in both irrigated and dry plots. The CHO first peak (ca. 1154 cm^{-1}), second peak (ca. 1103 cm^{-1}), and third peak (ca. 1033 cm^{-1}) exhibited significant differences ($P < 0.05$) between corn forages cultivated on wet and dry lands. The CHO peak intensity of crops under irrigation treatment was approximately 1.1-fold that of the plants grown on dry land. No variation could be found among varieties or cultivars ($P > 0.05$). Irrigation treatment interacted with corn variety on mid-IR absorbance of cellulosic compounds (CELC), and the greatest and weakest intensities were observed on Silex BT grown with water stress (0.0082 IR unit) and HLBaxxos cultivated on dry plot (0.0061 IR unit), respectively. All of these chemical functional groups' spectral intensities are related to carbohydrate structure makeup. Our results indicated that irrigations implication and corn forage variety affected carbohydrate molecular structure makeup. The peak intensity of lignin was not altered by irrigation treatment ($P > 0.05$). Moreover, among three cultivars, Pickseed had the highest IR value on CELC and the lowest value on lignin, whereas Hyland displayed the opposite features and Pioneer was intermediate. There is no literature published on the effect of irrigation on spectral characteristics of corn forage, and therefore we did not have any data to compare with. However, our results indicated that carbohydrate structure makeup in corn variety differed and irrigation implication had a significant impact on carbohydrate structure makeup.

Studying the structure of proteins leads to an understanding of the components that make up a whole protein. An understanding of the structure of the whole protein is often vital to understanding its digestive behavior and nutritive quality. Protein secondary structures include mainly α-helix and β-sheet. The percentage of these two structures in protein secondary structures influences protein nutritive value because protein structure affects access to gastrointestinal digestive enzymes, which affect protein value. All of the protein spectral parameters were significantly influenced by both irrigation treatment and corn forage variety but without any interaction. The crops treated with water stress had 6.5−19.7% stronger peak intensities ($P < 0.05$) on protein amide I, amide II, α-helix, and β-sheet. These differences in FTIR spectral traits indicated that water use during growing period did influence structural conformations of corn forage, which might be highly related to nutritive values as shown in Table 2. Also, the protein structural features varied among corn varieties or cultivars. P3085 and HLR219 showed the highest amide I peak height, whereas P7443 exhibited the lowest peak height and the remaining five were in the middle. This might be one possible explanation of the variation in CP content (Table 2). If these eight varieties of corn forage were ranked on the basis of protein secondary structural profiles (α-helix and β-sheet), HL3085, HLR219, and HLSR22 showed the greatest values of α-helix; besides these

DOI: 10.1021/jf505911a
J. Agric. Food Chem. 2015, 63, 2383−2391

Table 4. Peak Intensity Ratios of Different Varieties of Corn Forage Grown with or without Irrigation

	cultivar	variety	CHO third peak: CELC	CHO third peak: lignin	CELC: lignin	amide I:II	α-helix:β-sheet	CHO third peak: amide I	amide I: lignin	amide II: lignin
irrigation	Pioneer	P2501	13.54	25.74	1.94	1.45	0.90	3.39	7.56	5.20
		P39m26	13.83	25.08	1.81	1.33	0.96	3.59	6.95	5.21
		P7443	14.55	27.17	1.88	1.39	0.98	3.61	7.29	5.19
	Hyland	HL3085	14.98	22.85	1.53	1.42	0.94	3.22	7.07	4.96
		HLBaxxos	11.91	25.24	2.18	1.44	0.90	3.41	7.38	5.12
		HLR219	13.49	24.06	1.79	1.42	0.93	3.29	7.28	5.12
		HLSR22	12.75	22.83	1.85	1.45	0.91	3.22	7.08	4.89
	Pickseed	Silex BT	11.79	26.30	2.26	1.46	0.88	3.46	7.58	5.19
mean			13.35	24.91	1.91	1.42	0.92	3.40	7.27	5.11
dry land	Pioneer	P2501	12.29	27.37	2.24	1.45	0.92	3.94	6.94	4.77
		P39m26	11.59	22.77	1.94	1.34	1.06	3.61	6.07	4.43
		P7443	13.17	24.98	1.90	1.34	0.90	3.71	6.75	5.00
	Hyland	HL3085	12.52	20.08	1.60	1.37	0.99	3.36	5.88	4.24
		HLBaxxos	13.97	22.71	1.64	1.38	0.96	3.45	6.60	4.77
		HLR219	13.63	22.79	1.71	1.39	0.98	3.41	6.52	4.63
		HLSR22	12.68	21.06	1.67	1.39	0.93	3.39	6.22	4.48
	Pickseed	Silex BT	12.52	47.53	3.99	1.43	0.90	3.24	15.56	9.94
mean			12.80	26.16	2.09	1.39	0.96	3.51	7.57	5.28
statistical analysis										
SEM			0.406	5.049	0.427	0.019	0.027	0.077	1.719	0.997
P	irrigation		0.01	0.60	0.38	0.0002	0.003	0.001	0.73	0.72
	variety		0.0002	0.045	0.01	<0.0001	<0.0001	<0.0001	0.046	0.055
	variety × irrigation		<0.0001	0.19	0.23	0.31	0.01	<0.0001	0.10	0.08
contrast	Pioneer vs Hyland		0.72	0.28	0.36	0.01	0.39	<0.0001	0.85	0.72
	Pioneer vs Pickseed		0.003	0.004	0.001	<0.0001	0.001	<0.0001	0.001	0.001
	Hyland vs Pickseed		0.001	0.0002	<0.0001	0.01	0.004	0.94	0.0003	0.0003

three varieties, P2501 and Silex BT were also at the greatest level for β-sheet intensity. Then, P39m26 exhibited the smallest peak intensity for both α-helix and β-sheet. Hyland had greater IR absorbance of amide I, α-helix, and β-sheet than Pioneer. Such results were not completely coincident with recent findings of Abeysekara et al.,[34] who reported that only protein amide II peak height significantly differed between Pioneer and Hyland. In fact, varieties P7443 and HLBaxxos were also used in their study. Even so, they displayed quite different profiles of protein structure. This interesting phenomenon might be attributed to different growing years between these two research studies (2011 vs 2012).

Peak height ratios of eight varieties of corn forage in irrigated and dry lands are presented in Table 4. Irrigation treatment and corn varieties interacted significantly to affect peak height ratios of CHO third peak to CELC, α-helix to β-sheet, and CHO third peak to amide I. Among different cultivars, the ratios of CHO third peak to lignin, CELC to lignin, and amide I to lignin as well as amide II to lignin showed a similar trend that Pickseed had much higher values ($P < 0.05$) than the other two cultivars ,which were not far from each other. Height ratio of amide I to amide II was remarkably modified ($P = 0.0002$) by irrigation treatment. Compared with the crops under water stress (1.42), corn forage on dry land had a smaller ratio value (1.39). These results implied that molecular structures in corn forages did not remain constant, and they could be altered by growing conditions such as irrigation implementation. Again, few studies were directed to the effect of different irrigation conditions on spectral ratio profiles of crops, so no results we can be referred to. However, as we discussed earlier, during the growing period, the plants need to take up nutrients and essential elements by ion transportation from soil to roots, from roots to stems, and from stems to leaves for their growth and development. Water is the best transmission medium for the whole process, so the soil water deficit could cause reduced transpiration, poor efficiency of nutrient transportation, and delayed cell elongation,[28,44,45] which might lead to a poor development of molecular conformation in the plants.

Additionally, although differences in peak intensity were statistically significant among treatments, the variation ranges were generally narrow. According to our knowledge, Fourier transform infrared (FTIR) spectroscopy has already been successfully applied to detect structural differences induced by transgenic modification,[46] heat treatment,[14,15] bioethanol processing,[16,17,47] and climate changes such as frost damage.[48] Then on the basis of our findings mentioned above, even small variations existed in structural makeup of corn forages grown on wet and dry soil could also be detected by this powerful and accurate spectroscopic technique.

Information on molecular structural makeup in forage in relation to nutrient availability is very limited or unknown. Future study is needed to see how structural changes and how structural makeup are affected by irrigation and corn variety and how structural changes affect nutrient utilization and availability. This is a novel research area in feed research.

Principal Component Analysis within the Near-Infrared Region (Figure 1). The detailed principal, variable selections, variable reduction, distance method, matrix method, principal components selection, and explanation of hierarchical cluster analysis and principal component analysis in feed structural research have been explained previously.[21] In the study, we used synchrotron-based FTIR microspectroscopy as an example. The main purpose of PCA and CLA analyses is to detect treatment differences based on structural spectral data at

DOI: 10.1021/jf505911a
J. Agric. Food Chem. 2015, 63, 2383−2391

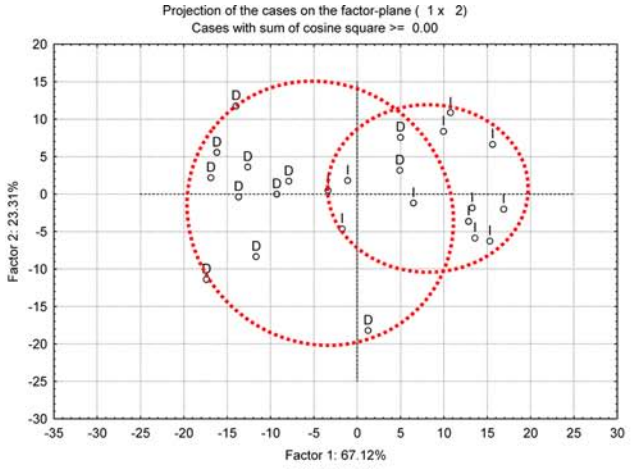

(1) P2501

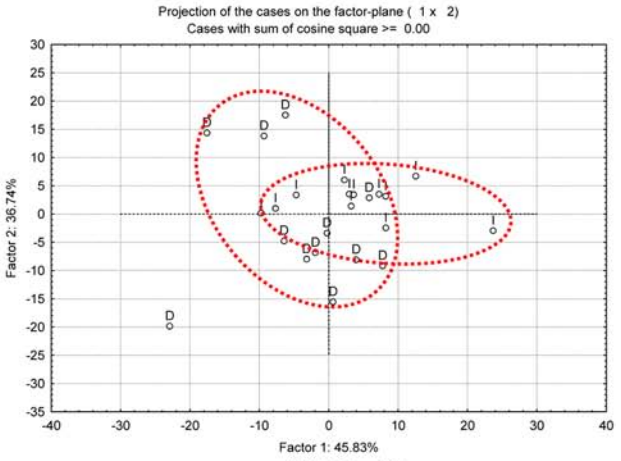

(2) P39m26

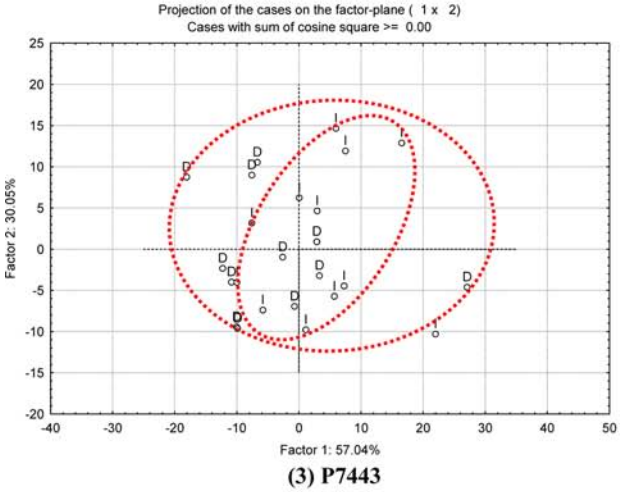

(3) P7443

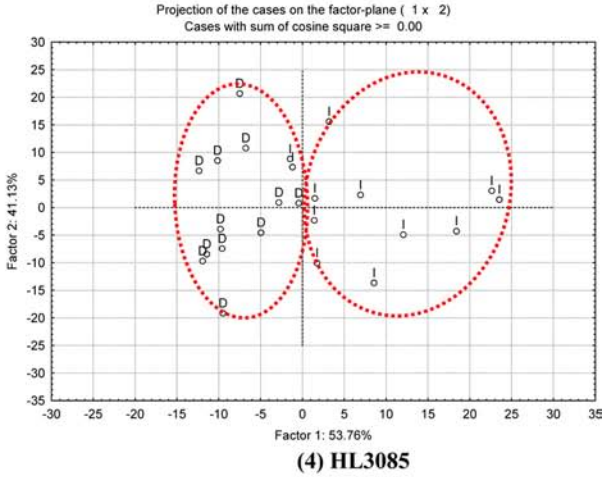

(4) HL3085

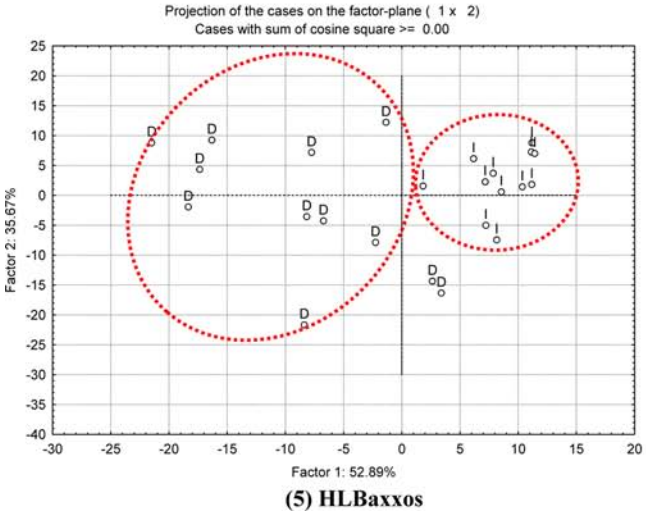

(5) HLBaxxos

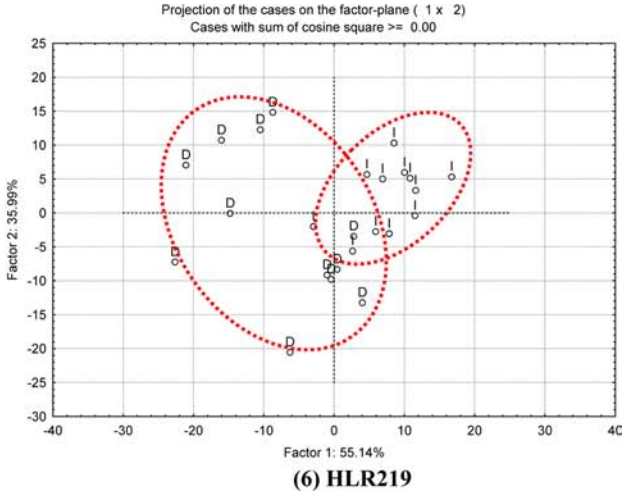

(6) HLR219

Figure 1. continued

DOI: 10.1021/jf505911a
J. Agric. Food Chem. 2015, 63, 2383−2391

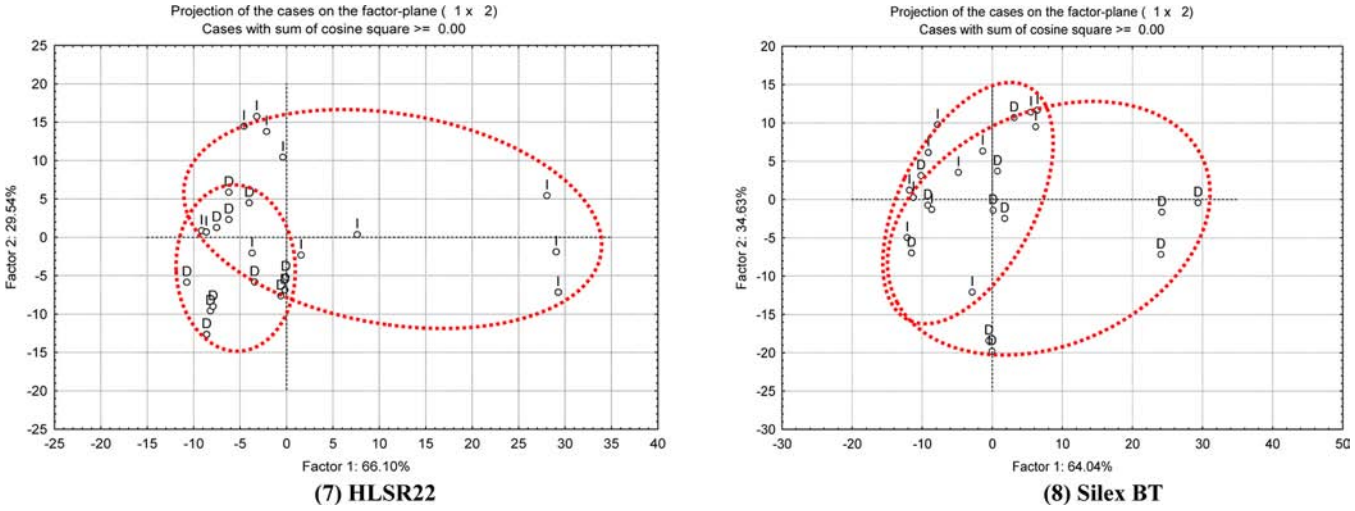

Figure 1. Principal component analysis within the NIR region (1842−570 nm) between irrigated (I) and dry (D) land corn forages.

fingerprint regions. If varieties form different clusters and groups, this indicated the structural difference between varieties.

NIR spectroscopy is performed on the basis of molecular information and combination vibrations, and every item should have its particular scanning spectrum within the detection region. In our study, to clarify whether irrigation treatment brings out any internal changes in molecular structural conformation, we selected all of the spectral data (ca. 1842−570 nm) of each corn variety obtained from the NIR system for PCA. For this multivariate analysis, the first and second principal components explained 45.83−67.12 and 23.31−41.13%, respectively, of the total variance in PCA figures. As can be seen from the figures, only for the varieties HL3085 and HLBaxxos could the structural makeup of the forage cultivated under water stress be almost distinguished from that grown on dry land. For the remaining six varieties, targeted plants from wet and dry experimental plots could not be grouped into separate ellipses owing to the produced heavy overlapping of groups. These results indicated that for most varieties, internal structural relationships in molecular makeup were exhibited between irrigated corn forage and that grown on dry land.

All of the results shown above might lead one to conclude that irrigation treatment was an influential factor in terms of agronomic measures and chemical compositions as well as molecular structural parameters over different kinds of corn forage. As for DM, OM, and CP contents as well as most spectral parameters, the well-watered plant was quite different from that cultivated on dry land. Moreover, water use interacted with corn variety on most agronomic features and CF and EE contents as well as some spectral data such as CELC peak intensity, peak ratios of CHO third peak to CELC, α-helix to β-sheet, and CHO third peak to amide I. Also, significant differences were often observed among three cultivars on these measured parameters. Multivariate results from PCA indicated some structural similarities existed between two treated corn forages with the exception of HL3085 and HLBaxxos. Further study on the optimum level of irrigation for corn forage cultivation might be helpful in semiarid regions such as western Canada.

AUTHOR INFORMATION

Corresponding Author

*(P.Y.) Phone: (306) 966-4132. Fax: (306) 966-4151. E-mail: peiqiang.yu@usask.ca.

Present Address

⊥College of Animal Sciences and Technology, Northeast Agricultural University, Harbin China.

Funding

Research projects of the feed research chair group of Professor Dr. Peiqiang Yu are supported by grants from the Ministry of Agriculture Strategic Research Chair Program, the Saskatchewan Agricultural Development Fund (ADF), the Natural Sciences and Engineering Research Council of Canada (NSERC), SaskCanola, the Thousand-Talent-People Research Program and University Innovation Team "Veterinary Biotechnology" (TD12-5019, Tianjin), Saskatchewan Forage Network (SNK), SaskMilk, and Western Grain Research Foundation (WGRF).

Notes

The authors declare no competing financial interest.

ACKNOWLEDGMENTS

We gratefully acknowledge the vital assistance in corn forage sample supply by Garry Hnatowich at Canada−Saskatchewan Irrigation Diversification Centre (Outlook, SK, Canada) and valuable advice and guidance from Dr. David Christensen. We thank Zhiyuan Niu for kind assistance in sampling and laboratory analysis in this study.

REFERENCES

(1) Coors, J. G.; Lauer, J. G. Silage corn. In *Specialty Corns*, 2nd ed.; Hallauer, A. R., Ed.; CRC Press: Boca Raton, FL, USA, 2001; pp 347−392.

(2) Khan, N.; Theodoridou, K.; Yu, P. Chapter 5. Role of fiber in dairy nutrition and health. In *Dietary Fiber: Production Challenges, Food Sources and Health Benefits*; Clemens, M. E., Ed.; Nova Science Publishers: New York, 2015; pp 69−91, ISBN 978-1-63463-655-1.

(3) Khan, N. A.; Yu, P.; Ali, M.; Cone, J. W.; Hendriks, W. H. Invited Review: Nutritive value of maize silage in relation to dairy cow performance and milk quality. *J. Food Agric. Sci. (England)* **2015**, *95*, 238−252.

(4) Statistics Canada, Historical Overview of Canadian Agriculture, 1976−1996, Statistics Canada, Catalog 93-359-XPB, 1997.

DOI: 10.1021/jf505911a
J. Agric. Food Chem. 2015, 63, 2383−2391

(5) Roth, G.; Undersander, D.; Allen, M.; Ford, S.; Harrison, J.; Hunt, C.; Lauer, J.; Muck, R.; Soderlund, S. *Corn Silage Production, Management and Feeding*; American Society of Agronomy: Madison, WI, USA, 1995; p 21, ISSN 0021-8561.
(6) Nielsen, D. C.; Vigil, M. F.; Benjamin, J. G. Forage yield response to water use for dryland corn, millet, and triticale in the central great plains. *Agron. J.* **2006**, *98*, 992−998.
(7) Janhanzad, E.; Jorat, M.; Moghadam, H.; Sadeghpour, A.; Chaichi, M.-R.; Dashtaki, M. Response of a new and a commonly grown forage sorghum cultivar to limited irrigation and planting density. *Agric. Water Manage.* **2013**, *117*, 62−69.
(8) Tahir, S. M. Fertilizers alleviate moisture stress. In *17th Coll. Int. Potash Institute, Farm Mechanization for Profit*; Worth, B., Xin, J., Eds.; Granada Publishing: London, UK, 1983; 269 pp.
(9) House, L. R. *A Guide to Sorghum Breeding*; International Crops Research Institute for Semiarid Tropics: Patancheru, India, 1985; pp 344−502.
(10) Saeed, J. A. M.; El-Nadi, A. H. Forage sorghum yield and water use efficiency under variable irrigation. *Irrig. Sci.* **1998**, *18*, 67−71.
(11) Nielsen, D. C. Forage soybean yield and quality response to water use. *Field Crop Res.* **2011**, *124*, 400−407.
(12) Fereres, E.; Soriano, M. A. Deficit irrigation for reducing agricultural water use. *J. Exp. Bot.* **2006**, *58*, 147−159.
(13) Van Soest, P. J. Environment and forage quality. In *Proceedings, Cornell Nutrition Conference for Feed Manufacturers*, Rochester, NY, 1996; pp 224−238.
(14) Doiron, K. J.; Yu, P.; McKinnon, J. J.; Christensen, D. A. Heat-induced protein structures and protein subfractions in relation to protein degradation kinetics and intestinal availability in dairy cattle. *J. Dairy Sci.* **2009**, *92*, 3319−3330.
(15) Abeysekara, S.; Yu, P. Response and sensitivity of lipid related molecular structure to wet and dry heating in canola tissue. *Spectrochim. Acta Part A: Mol. Biomol. Spectrosc.* **2012**, *90*, 63−71.
(16) Zhang, X.; Yu, P. Using ATR-FT/IR molecular spectroscopy to detect effects of blend DDGS inclusion level on the molecular structure spectral and metabolic characteristics of the proteins in hulless barley. *Spectrochim. Acta Part A: Mol. Biomol. Spectrosc.* **2012**, *95*, 53−63.
(17) Zhang, X.; Yu, P. Relationship of carbohydrate molecular spectroscopic features in combined feeds to carbohydrate utilization and availability in ruminants. *Spectrochim. Acta Part A: Mol. Biomol. Spectrosc.* **2012**, *92*, 225−233.
(18) AOAC. *Official Methods of Analysis*; Association of Official Analytical Chemists: Washington, DC, USA, 1990.
(19) Xin, H.; Falk, K. C.; Yu, P. Studies on *Brassica carinata* seed. 1. Protein molecular structure in relation to protein nutritive values and metabolic characteristics. *J. Agric. Food Chem.* **2013**, *61*, 10118−10126.
(20) Liu, N.; Yu, P. Molecular clustering, interrelationships and carbohydrate conformation in hull and seeds among barley cultivars. *J. Cereal Sci.* **2011**, *53*, 379−383.
(21) Yu, P. Applications of hierarchical cluster analysis (CLA) and principal component analysis (PCA) in feed structure and feed molecular chemistry research, using synchrotron-based Fourier transform infrared (FTIR) microspectroscopy. *J. Agric. Food Chem.* **2005**, *53*, 7115−7127.
(22) Graybill, J. S.; Cox, W. J.; Otis, D. J. Yield and quality of forage maize as influenced by hybrid, planting date, and plant density. *Agron. J.* **1991**, *83*, 559−564.
(23) Jones, R. M.; Sanderson, M. A.; Read, J. C.; Lovell, A. C. Management of corn for silage production in south central USA. *J. Prod. Agric.* **1995**, *8*, 175−180.
(24) Payero, J. O.; Tarkalson, D. D.; Irmak, S.; Davison, D.; Petersen, J. L. Effect of timing of a deficit-irrigation allocation on corn evapotranspiration, yield, water use efficiency and dry mass. *Agric. Water Manage.* **2009**, *96*, 1387−1397.
(25) Bathke, G. R.; Gassel, D. K.; Hargrove, W. L.; Porter, P. M. Modification of soil physical properties and root growth response. *Soil Sci.* **1992**, *154*, 316−329.
(26) Turner, N. C. Stomatal behavior and water status of maize, sorghum, and tobacco under field conditions. II. At low soil water potential. *Plant Physiol.* **1974**, *55*, 360−365.
(27) Masle, J.; Passiour, J. B. The effect of soil strength on the growth of young wheat plants. *Aust. J. Plant Physiol.* **1987**, *14*, 643−656.
(28) Kramer, O. J. K.; Boyer, J. S. *Water Relations of Plant and Soils*; Academic Press: New York, 1995.
(29) Ertek, A.; Kara, B. Yield and quality of sweet corn under deficit irrigation. *Agric. Water Manage.* **2013**, *129*, 138−144.
(30) Berenguer, M. J.; Faci, J. M. Sorghum (*Sorghum bicolor* L. Moench) yield compensation processes under different plant densities and variable water supply. *Eur. J. Agron.* **2001**, *15*, 43−55.
(31) Vasilakoglou, I.; Dhima, K.; Karagiannidis, N.; Gatsis, T. Sweet sorghum productivity for bio-fuels under increased soil salinity and reduced irrigation. *Field Crop Res.* **2011**, *120*, 38−46.
(32) NeSmith, D. S.; Ritchie, J. T. Effects of soil water-deficits during tassel emergence on development and yield component of maize (*Zea mays*). *Field Crop Res.* **1992**, *28*, 251−256.
(33) Abrecht, D. G.; Carberry, P. S. The influence of water deficit prior to tassel initiation on maize growth, development and yield. *Field Crop Res.* **1993**, *31*, 55−69.
(34) Abeysekara, S.; Christensen, D. A.; Niu, Z.; Theodoridou, K.; Yu, P. Molecular structure, chemical and nutrient profiles, and metabolic characteristics of the proteins and energy in new cool-season corn varieties harvested as fresh forage for dairy cattle. *J. Dairy Sci.* **2013**, *96*, 6631−6643.
(35) Assefa, G.; Ledin, I. Effect of variety, soil type and fertilizer on the establishment, growth, forage yield, quality and voluntary intake by cattle of oats and vetches cultivated in pure stands and mixtures. *Anim. Feed Sci. Technol.* **2001**, *92*, 95−111.
(36) Haberle, J.; Svoboda, P.; Raimanova, I. The effect of post-anthesis water supply on grain nitrogen concentration and grain nitrogen yield of winter wheat. *Plant Soil Environ.* **2008**, *54*, 304−312.
(37) Pessarakli, M. M.; Morgan, P. V.; Gilbert, J. Dry-matter yield, protein synthesis, starch, and fiber content of barley and wheat plants under two irrigation regimes. *J. Plant Nutr.* **2005**, *28*, 1227−1241.
(38) Von Mothes, K. *Encyclopedia of Plant Physiology*; Springer Verlag: Berlin, Germany, 1956; pp 656−664.
(39) Kahane, I.; Poljakoff-Mayber, A. Effect of substrate salinity on the ability for protein synthesis in pea roots. *Plant Physiol.* **1968**, *43*, 1115−1119.
(40) Halim, R. A.; Buxton, D. R.; Hattendorf, M. J.; Carlson, R. E. Crop water stress index and forage quality relationships in alfalfa. *Agron. J.* **1990**, *82*, 906−909.
(41) Deetz, D. A.; Jung, H. G.; Buxton, D. R. Water-deficit effects on cell-wall composition and in vitro degradability of structural polysaccharides from alfalfa stems. *Crop Sci.* **1996**, *36*, 383−388.
(42) Peyraud, J. L.; Astigarraga, L. Review of the effect of nitrogen fertilization on the chemical composition, intake, digestion and nutritive value of fresh herbage: consequences on animal nutrition and N balance. *Anim. Feed Sci. Technol.* **1998**, *72*, 235−259.
(43) Dairy One; http://www.dairyone.com/forage/feedcomp/Main_GetResults.asp.
(44) Heyn, A. N. J. The physiology of cell elongation. *Bot. Rev.* **1940**, *6*, 515−574.
(45) Vaadia, Y.; Rane, F. C.; Hagen, R. M. Plant water deficits and physiological process. *Annu. Rev. Plant Physiol.* **1961**, *12*, 265−292.
(46) Yu, P.; Jonker, A.; Gruber, M. Molecular basis of protein structure and nutritive value in proanthocyanidin-enhanced Lc-transgenic alfalfa using synchrotron-radiation FTIR microspectroscopy. *Spectrochim. Acta A: Mol. Biomol. Spectrosc.* **2009**, *73*, 846−853.
(47) Yu, P.; Niu, Z.; Damiran, D. Protein molecular structures and protein fraction profiles of new co-products of bioethanol production: a novel approach. *J. Agric. Food Chem.* **2010**, *58*, 3460−3464.
(48) Xin, H.; Zhang, X.; Yu, P. Using synchrotron radiation-based infrared microspectroscopy to reveal microchemical structure characterization: frost damaged wheat vs. normal wheat. *Int. J. Mol. Sci.* **2013**, *14*, 16706−16718.

DOI: 10.1021/jf505911a
J. Agric. Food Chem. 2015, 63, 2383−2391

Table 1. Different Methods of Detection Pyrethroids

methodology	detection limit	detection rate (%)	advantages	disadvantages
this method	9.17−60 nM L^{-1}	61.4−106.2	high sensitivity, simplicity, speed, convenience, efficiency	immaturity, boundedness
Huang et al.[15]	2.1−6.9 ng kg^{-1}	73.4−120.1	accuracy, high sensitivity	multistep, time-consuming, expensive instruments
Deme et al.[16]	0.01−1 μg kg^{-1}	62−110	accuracy, high sensitivity	multistep, complexity, time-consuming, expensive instruments,
Esteve-Turrillas et al.[17]	0.08−5.4 μg kg^{-1}	84−120	accuracy, high sensitivity	multistep, complexity, time-consuming, expensive instruments
Ma and Chen[34]	3.5 ng kg^{-1}	82.4−101.7	accuracy, high sensitivity	multistep, complexity, time-consuming, inaccuracy
Song et al.[37]	5−10 μM L^{-1}	97.8−103.5	convenience, efficiency, simplicity	time-consuming, boundedness, complexity, immaturity

pyrethroids from soil with microwave-aided extraction (MAE) methodology. Although such methods are quite accurate, they depend on multistep sample cleanup procedures and result in relatively expensive and time-consuming processes. Thus, the exploitation of novel functional materials for the simple, rapid, and highly sensitive detection of trace pyrethroid insecticides remains a challenge, especially in complicated sample matrices.

A promising way to achieve the tailored selective detection of analytes is to use molecularly imprinted polymers (MIPs). Because the MIPs can be easily prepared with low cost, in addition to their greater stability, the molecularly imprinted materials will attract more and more people.[18−24] In our research group, Pan and co-workers have synthesized molecularly imprinted polymers based on magnetic halloysite nanotube composites with selective recognition of 2,4,6-trichlorophenol.[25] Xu and co-workers synthesized thermally responsive magnetic molecularly imprinted polymers for selective removal of antibiotics from aqueous solution.[26] Obviously, compared with the traditional separation−enrichment method, MIPs with selective recognition ability can separate the target molecule conveniently and effectively, excluding the influence of any other structural analogues. Moreover, the method to prepare MIPs is simple. Also, MIPs, with good reproducibility, can be stored easily.[27−29] The excellent performance of molecularly imprinted polymers allows them to be widely used in many fields.[30−32] Shi et al.[33] concentrated pyrethroid selectivity from aquaculture water with molecularly imprinted solid phase extraction methodology and detected pyrethroid with GC. Ma and Chen[34] prepared a magnetic surface molecularly imprinted polymer based on carbon nanotube, which adsorbed LC selectively. However, as to the level of molecular imprinting technique, it is still a challenge for us to find a more convenient and effective way to detect pyrethroid pesticide residues in the environment.

The fluorescence detection method is efficient, simple, and sensitive. It has great potential in the field of analyzing samples quickly. Compared with HPLC, it has advantages in solvent consumption, sample pretreatment, and test time. We can design an experiment to adapt the molecular imprinting technology to fluorescence detection, to take advantage of the recognition and capture ability of MIPs to make target molecules be adsorbed on MIPs selectively, in order that they can be separated with interfering substances, and then the fluorescence analyzer can be used to detect fluorescence. For the reason that it contains fluorescent nanomaterials during the synthesizing process of molecularly imprinted polymerization, the fluorescence intensity will quench after the reaction of target molecules and MIPs.[35] Zhao et al. have synthesized composite quantum dots molecularly imprinted polymer (QDs@MIP) nanospheres for specific recognition and direct fluorescent quantification of pesticides in aqueous media.[36] Song et al.[37] prepared porous silica fluorescent nanospheres recognizing LC in aqueous media efficiently. We make the comparison of this method and other methods in Table 1. As shown in the table, the method of detection of LC has some advantages compared with the others. This method not only has the advantages of high sensitivity, simplicity, efficiency, speed, and convenience but also could deal with complex samples. The interference of coexisting substance in specimen material can be eliminated by this coupling technology, and the selectivity of molecular imprinting can be combined with the high sensitivity of fluorescence detection. As a result, we get a new detection and analysis method.

In this study, fluorescent molecularly imprinted polymers (SiO_2@FITC-APTS@MIPs) were proposed for the analysis of LC based on the LC-resulted fluorescence quenching of the fluorescent dye anchored on the MIP polymer, which was covalently coated on the surface of SiO_2 via a surface molecular imprinting process. We chose Chinese spirit as a practical sample, a kind of distilling liquor unique to China. Chinese spirit is a popular drink in China for its special aroma. The main raw material of Chinese spirit is grain. However, pyrethroid is a kind of broad-spectrum insecticide for these agricultural products. Therefore, not only can the Chinese spirit as a sample reveal the detection levels of SiO_2@FITC-APTS@MIPs in complex samples but also the SiO_2@FITC-APTS@MIPs can be a steppingstone to detect additional practical samples in the future. On the whole, through the experiment of the fluorescence detection of LC in Chinese spirits, we can see that the SiO_2@FITC-APTS@MIPs have a broad prospect in the food safety analysis field.

EXPERIMENTAL PROCEDURES

Materials. Tetraethyl orthosilicate (TEOS, AR), divinylbenzene (DVB, AR), and fluorescein 5(6)-isothiocyanate (FITC, AR) were all purchased from Aladdin Reagent Co., Ltd. (Shanghai, China). 3-Aminopropyltriethoxysilane (APTS, AR) was purchased from Energy Chemical (Shanghai, China). Acrylamide (AM, AR), acetonitrile, and ammonium hydroxide were all purchased from Sinopharm Chemical Reagent Co., Ltd. (Shanghai, China). 2,2′-Azobis(isobutyronitrile) (AIBN, AR) was obtained from Tianjin Guangfu Fine Chemical Research Institute (Tianjin, China). All of the pyrethroid pesticides, LC, β-cyfluthrin (BC), esfenvalerate (FE), and bifenthrin (BI), were obtained from Yingtianyi Standard Sample Co. (Beijing, China), and the corresponding chemical structures of the pyrethroids are displayed in Figure 5. Doubly distilled water was used for cleaning processes.

Instrument. Infrared spectra (4000−400 cm^{-1}) were recorded on a Nicolet NEXUS-470 FT-IR apparatus (USA). The morphologies of SiO_2@FITC-APTS@MIPs/SiO_2@FITC-APTS@NIPs were observed by a scanning electron microscope (SEM, JEOL, JSM-7001F) and a

DOI: 10.1021/jf5043823
J. Agric. Food Chem. 2015, 63, 2392−2399

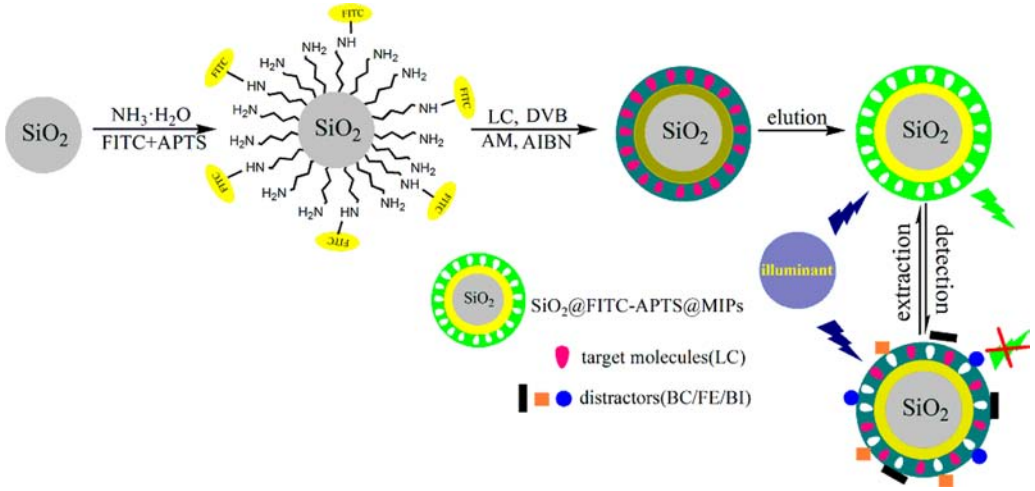

Figure 1. Schematic illustration for the preparation of SiO_2@FITC-APTS@MIPs.

transmission electron microscope (TEM, JEOL, JEM-2100). Fluorescence intensity was measured by using a Cary Eclipse fluorescence spectrophotometer (Varian, USA). UV−vis adsorption spectra were obtained with a UV−vis spectrophotometer (UV-2450, Shimadzu, Japan). Laser confocal microscopy images of SiO_2@FITC-APTS@MIPs samples were observed using a TCS SP5 II confocal microscope (Leica, Germany) with a 488 nm solid state laser light source. Transient fluorescence spectra were measured on a QuantaMaster 40 spectrofluorometer (Photon Technology International, USA). TGA of the samples was performed for powder samples (about 10 mg) using a Diamond TG/DTA instruments (PerkinElmer, USA) under a nitrogen atmosphere up to 1000 °C with a heating rate of 10 °C min^{-1}.

Preparation of SiO_2 and SiO_2@FITC-APTS. Silica has been widely used as substrate material due to its chemical stability and the property of easy modification.[38] First, SiO_2 beads were prepared according to the stöver process.[39,40] Typically, 2.0 mL of $NH_3{\cdot}H_2O$ was dissolved in 25 mL of ethanol and 25 mL of double-distilled water in a 100 mL round-bottom flask by sonication for 15 min. Then, 2.0 mL of TEOS was slowly added into the flask sequentially. The mixture was allowed to react for 24 h at room temperature under a continuous stirring of 1000 rpm. The resulting product was separated from the solvent by centrifuge and washed rotationally by ethanol and double-distilled water several times.

Typically, 40 mg of FITC was dissolved in 2.0 mL of APTS in a 10 mL test tube for 48 h in darkness at room temperature under continuous stirring of 800 rpm first. The reaction formula is shown in Figure S1 in the Supporting Information. After the reaction for 24 h, we obtained a FITC-APTS mixture.[41] Then SiO_2 beads was scattered in 100 mL of ethanol by sonication in a 250 mL brown round-bottom flask, and 5.0 mL of $NH_3{\cdot}H_2O$ and 30 mL of double-distilled water were added into the flask. Then the mixture was slowly added into the flask sequentially and allowed to react for 24 h in darkness at room temperature under continuous stirring of 1000 rpm. The resulting SiO_2@FITC-APTS was separated from the solvent by centrifuge and was repeatedly washed.

Synthesis of SiO_2@FITC-APTS@MIPs and SiO_2@FITC-APTS@NIPs. The synthesis of SiO_2@FITC-APTS@MIPs via a multistep precipitation polymerization procedure is illustrated in Figure 1. The first and second steps were narrated in the above. The third step was to prepare the preassemble solution. Typically, LC (0.50 g, 1.0 mmol) and AM (0.2840 g, 4.0 mmol) were dissolved with 20 mL of acetonitrile in a 50 mL beaker under the dark environment for 1.0 h. Then 200 mg of SiO_2@FITC-APTS beads was added into a 250 mL brown round-bottom flask and scattered in 70 mL of acetonitrile by sonication for 1.0 h. After this, the mixture (LC and AM) was poured into the flask, and 0.8 mL of DVB was added into the flask at the same time. The mixture was degassed in an ultrasonic bath for 10 min and sparged with oxygen-free nitrogen for 10 min. Then, the flask was submerged in a thermostatically controlled oil bath, which was in stirring condition, and the stirring rate was 1200 rpm. After the temperature was increased from room temperature to 60 °C within 30 min, free radical initiator AIBN (about 0.02 g) was added into the flask, and then the temperature was maintained at 60 °C for a further 24 h. After the reaction, the SiO_2@FITC-APTS@MIPs beads were collected from the reaction medium by centrifuge, and the product was rinsed several times with ethanol and double-distilled water. After that, the beads were eluted with 100 mL of acetic acid/methanol (10:90, v/v) to remove LC templates by Soxhlet extractor. Finally, after 5 days of elution, the product SiO_2@FITC-APTS@MIPs were obtained, which were dried under vacuum for 12 h at 40 °C. In principle, the methods of preparing SiO_2@FITC-APTS@NIP beads and SiO_2@FITC-APTS@MIPs were the same, the only difference being that the former lacked the LC template.

RESULTS AND DISCUSSION

Characterization of SiO_2@FITC-APTS@MIPs and SiO_2@FITC-APTS@NIPs. The products of SiO_2, SiO_2@FITC-APTS, and SiO_2@FITC-APTS@MIPs were investigated by FT-IR spectroscopy (Supporting Information, Figure S2). SiO_2 (Figure S2a) spheres displayed the characteristic signals of Si−O at 473 and 803 cm^{-1}, and they were attributed to symmetric stretching vibration and bending vibration, respectively. The strong and broad peak around 1103 cm^{-1} indicated Si−O−Si asymmetric stretching. These results suggested that the tetraethyl orthosilicate successfully condensed into silicon dioxide by hydrolysis. Compared with the infrared data of pure SiO_2, the SiO_2@FITC-APTS (Figure S2b) displayed the characteristic peak of amino groups at 1403 cm^{-1}.[42] The presence of bands around 2926 cm^{-1} suggested the aliphatic C−H stretching.[43] These facts showed the presence of amine ligands on the surface of SiO_2. As shown in Figure S2c, para-substituted benzene surface deformation vibration was about 832 cm^{-1}, meta-substituted benzene surface deformation vibration was about 712 cm^{-1}, and 794 and 900 cm^{-1} were the characteristic peaks of divinylbenzene. The characteristic peaks of the benzene ring frame vibration at about 1606 cm^{-1} and C═O stretching vibration of amide at 1683 cm^{-1} indicated that the MIPs layer had been successfully compounded on the surface of SiO_2@FITC-APTS.

To ascertain the synthesizing of materials further, UV−vis spectra of SiO_2@FITC-APTS@MIPs, SiO_2@FITC-APTS, FITC-APTS, APTS, FITC, and SiO_2 were measured as

DOI: 10.1021/jf5043823
J. Agric. Food Chem. 2015, 63, 2392−2399

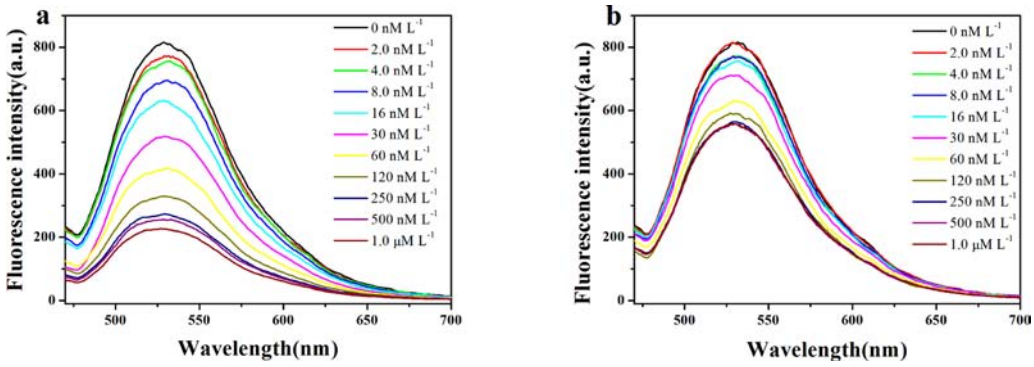

Figure 2. Response of SiO_2@FITC-APTS@MIPs (a) and SiO_2@FITC-APTS@NIPs (b) to LC in the concentration range from 0 to 1.0 μM L^{-1}.

shown in Figure S3 in the Supporting Information. The figure showed that pure SiO_2 (purple) and APTS (green) almost have no visible absorption peaks. The solution of FITC (yellow) displayed two visible absorption peaks at 455 and 485 nm, whereas the FITC−APTS conjugates (blue) showed only one visible absorbance at 502 nm, indicating that a strong interaction occurred between APTS and FITC molecules. In the meantime, the dispersive liquid of SiO_2@FITC-APTS (red) showed nearly a visible absorption peak at 505 nm. The solution of SiO_2@FITC-APTS@MIPs (black) showed a strong absorption peak at 505 nm. From the above phenomenon, we found that the FITC−APTS conjugates, directly and successfully, grafted on the surface of SiO_2 by the means of APTS condensation.

The SiO_2@FITC-APTS@MIPs (black) dispersive liquid displayed the visible absorption peak of dye FITC with the λ_{max} at 506 nm, whereas the pure SiO_2 showed scarcely any visible absorption as indicated in Figure S4 of the Supporting Information. The fluorescence spectra of SiO_2@FITC-APTS@MIPs (blue) dispersive liquid displayed a green fluorescence emission with λ_{max} at 531 nm (excited at 450 nm), which is identical to the emission spectra of the dye FITC.

The size and shape of SiO_2 and SiO_2@FITC-APTS@MIPs were examined by SEM and TEM techniques. The SEM and TEM images of SiO_2 beads are shown in Figure 5a,c. It can be observed that the diameter of pure SiO_2 was about 300 nm. It can be seen that the pure SiO_2 was dispersed fully before polymerization; that is to say, it had the good monodispersity. The size and shape of SiO_2@FITC-APTS@MIPs are shown in Figure 5b,d. After being coated with FITC−APTS and MIPs, the diameter of the SiO_2@FITC-APTS@MIPs increased to about 500 nm, and the grain size was increased about 100 nm. As shown in the inset of Figure 5d, it was clearly observed that the product of SiO_2@FITC-APTS@MIPs beads had an approximately spherical shape and good monodispersity. It is observed that the product of SiO_2@FITC-APTS@MIPs not only keeps the spherical morphology but also still has good monodispersity after polymerization. On the whole, it was confirmed that the SiO_2@FITC-APTS@MIPs beads with core−shell structure had been successfully prepared.

The fluorescent images of SiO_2@FITC-APTS and SiO_2@FITC-APTS@MIPs were observed by confocal laser scanning microscope. Excitation wavelength and emission wavelength were 488 and 525 nm, respectively. Apparently, SiO_2@FITC-APTS@MIPs had strong fluorescence emission. As can be seen from the diagram, the monodispersity of SiO_2@FITC-APTS (a) and SiO_2@FITC-APTS@MIPs (b) did not change greatly before or after aggregation. The molecularly imprinted polymer still had the better monodispersity, and there is no serious reunion, which contributes to detection of the target molecule.

Figure S7 of the Supporting Information shows the TGA of SiO_2@FITC-APTS@MIPs and SiO_2@FITC-APTS@NIPs. It can be observed that the weight losses of SiO_2@FITC-APTS@MIPs and SiO_2@FITC-APTS@NIPs before 900 °C were ∼71.52 and ∼71.91%, respectively. The slight weight difference may be attributed to crystal water. The whole thermogravimetric process could be divided roughly into three stages. First, the temperature was before 100 °C, due to the loss interior water of crystallization. Second, the temperature was started at 350−500 °C, and weight losses of SiO_2@FITC-APTS@MIPs and SiO_2@FITC-APTS@NIPs were about 56.40 and 57.12%, respectively. The second weight loss stage can be ascribed to the polymerization of organic matter decomposition. The third weight loss stage started at 500−920 °C, during which the weight losses of SiO_2@FITC-APTS@MIPs and SiO_2@FITC-APTS@NIPs were 15.12 and 14.79%, respectively. This might be the reason for thermal decomposition of the modification of FITC-APTS. We could draw the conclusions that, first, the curves of imprinting and nonimprinting are almost the same. Second, polymers were grafted onto the surface of SiO_2 particles successfully, and the amounts of loss and use were equal. Finally, better temperature resistance of obtained products proved that thermal decomposition at room temperature does not readily occur.

Fluorescence Detection of SiO_2@FITC-APTS@MIPs Beads. All luminescence experiments were carried out at room temperature. The fluorescence spectrophotometer was used to monitor the fluorescence intensity of different molecularly imprinted polymers with the excitation wavelength of 450 nm. The samples of SiO_2@FITC-APTS@MIPs beads (50 mg) were dispersed in 100 mL alcohol solutions, which were prepared for spectrum measurement. Afterward, we prepared LC solution of different concentration ranges (0−1.0 μM L^{-1}). Then 5.0 mL of the sample solutions was poured into various concentrations of the 5.0 mL LC solution. Before spectrum measurement, the mixture of samples solution was stirred thoroughly. The fluorescence quenching efficiency of the SiO_2@FITC-APTS@MIPs beads with LC was calculated by Stern−Volmer equation, and the linear relationship could be described by $(F_0/F - 1)$ versus the concentration (nM L^{-1}). The same procedure was performed for the SiO_2@FITC-APTS@NIPs.

From the data in Figure 2a, it can be seen that with the increase of concentration of LC, the fluorescence intensity became weaker and weaker, and the reduced degree of fluorescence intensity in SiO_2@FITC-APTS@MIPs was

DOI: 10.1021/jf5043823
J. Agric. Food Chem. 2015, 63, 2392−2399

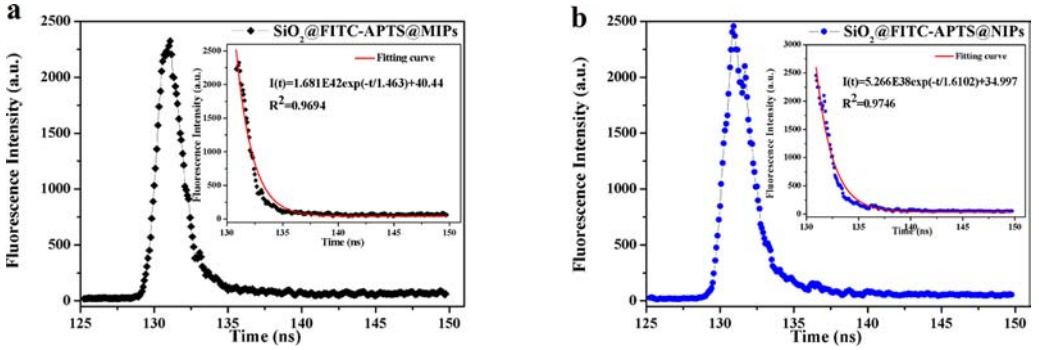

Figure 3. Transient fluorescence spectra of SiO_2@FITC-APTS@MIPs (a) and SiO_2@FITC-APTS@NIPs (b), for which the excitation wavelengths are 450 nm. Time-resolved fluorescence curves SiO_2@FITC-APTS@MIPs and SiO_2@FITC-APTS@NIPs are illustrated.

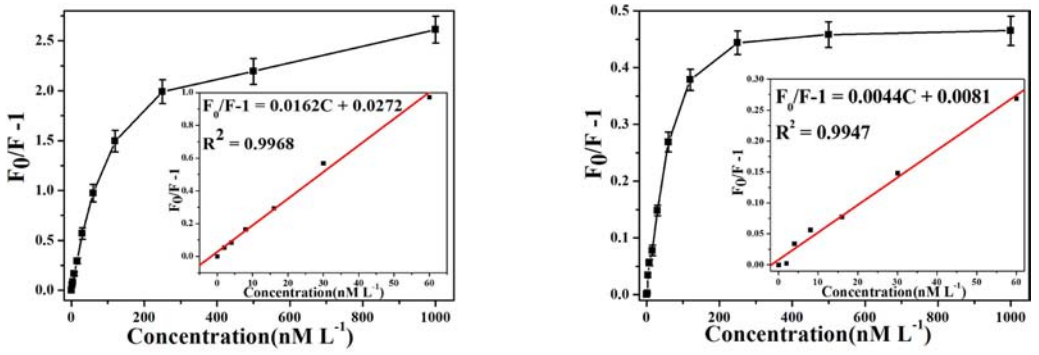

Figure 4. Fluorescence quenching efficiency changed according to LC concentration. (Insets) Linear equations of SiO_2@FITC-APTS@MIPs (a, left) and SiO_2@FITC-APTS@NIPs (b, right).

notably higher than that of the SiO_2@FITC-APTS@NIPs (Figure 2b). Therefore, we found that SiO_2@FITC-APTS@MIPs could detect the LC by fluorescence quenching. However, when the concentration of LC was between 250 and 1000 nM L^{-1}, the fluorescence intensity change was no longer apparent. As shown in Figure 2b, the fluorescence intensity changed, but it was of small amplitude along with the concentration of LC increasing. The fluorescence intensities of the SiO_2@FITC-APTS@MIPs and SiO_2@FITC-APTS@NIPs were important data to evaluate the selectivity and sensitivity of the materials obtained. It was illustrated that the spatial adsorption sites could be incorporated into the SiO_2@FITC-APTS@MIPs matrix, but a slightly in SiO_2@FITC-APTS@NIPs. In addition, it was also confirmed that the SiO_2@FITC-APTS@MIPs beads had been produced successfully.

The transient fluorescence spectra of SiO_2@FITC-APTS@MIPs and SiO_2@FITC-APTS@NIPs are displayed in Figure 3. The time-resolved fluorescence curves are illustrated in Figures. Decay in the fluorescence intensity (I) with time (t) was fitted by an exponential function

$$I(t) = A \exp(-t/\tau)$$

where τ is the lifetime and A is the amplitude.

As can be seen from Figure 3, the obvious fluorescence decay was found clearly illustrated. The two decay curves were fitted by exponential function. The nolinear equations of SiO_2@FITC-APTS@MIPs (Figure 3a) and NIPs (Figure 3b) were $I(t)$ = 1.681E42 exp($-t$/1.463) + 40.44 and $I(t)$ = 5.266E38 exp($-t$/1.6102) + 34.997, and the corresponding correlation coefficients (R^2) were R^2 = 0.9694 and R^2 = 0.9746, respectively. From the equations, we found that the lifetimes of SiO_2@FITC-APTS@MIPs and NIPs are τ = 1.463 ns and τ_0 = 1.610 ns, respectively.

Generally speaking, a collision would happen between fluorophor and quencher. This kind of collision may be a dynamic collision,[44] but it may also be an optical collision[45] for the dimolecule was in the excited state. To investigate the fluorescence quenching mechanism of SiO_2@FITC-APTS@MIPs with LC, the quenching efficiency of SiO_2@FITC-APTS@MIPs was evaluated by the Stern−Volmer equation, as follows:

$$F_0/F = 1 + K_{SV}C = 1 + K_q\tau_0 C \quad (1)$$

F_0 is the initial fluorescence intensity without analyte. F is the fluorescence intensity with the concentration of analyte. K_{SV} is the Stern−Volmer quenching constant in units of L mol^{-1}. C is the concentration of molecular targets. K_q is the rate constant of the bimolecular quenching process in units of L mol^{-1} s^{-1}. τ_0 is the lifetime without quenching agent.

We did reproducibility experiments three times and acquired Figure 4 by their average. As shown in Figure 3a, LC, the concentration range of which was 0−60 nM L^{-1}, could have a good linear relationship with fluorescence intensity. The linear equation of SiO_2@FITC-APTS@MIPs was $F_0/F - 1$ = 0.0162C + 0.0272, and the corresponding correlation coefficient was R^2 = 0.9968. The limit of detection is evaluated using LOD = $3\sigma/S$ and is found to be 9.17 nM L^{-1}, where σ is the standard deviation of the blank signal and S is the slope of the linear calibration plot. From Figure 4a, we could see that the concentration range of analyte was 0−60 nM L^{-1}. From Figure 4b, we could see the linear equation of fluorescence intensity and the concentration of LC (also from 0 to 60 nM L^{-1}) was $F_0/F - 1$ = 0.0044C + 0.0081, with R^2 = 0.9947.

DOI: 10.1021/jf5043823
J. Agric. Food Chem. 2015, 63, 2392−2399

When it surpassed the range of linear concentration, the slope of quenching became gentle. When the concentration was >250 nM L^{-1}, the quenching rate almost reached saturation.

The lifetimes are quite different whether the quenching agent exists or not. We found another kind of representation of the Stern−Volmer equation according to eq 1

$$\tau_0/\tau = 1 + K_{SV}C = 1 + K_q\tau_0 C \quad (2)$$

where τ is the lifetime with quenching agent.

According to eq 2, we found the relationship $K_{SV} = K_q\tau_0$. Now we know τ_0 = 1.6102 ns, which does not exist for quenching agent, and K_{SV} = 0.0044 L mol^{-1} via the above linear equation of SiO_2@FITC-APTS@NIPs. Therefore, $K_{q(NIPs)}$ = 3.792E6 L mol^{-1} s^{-1} was calculated by the equation. $K_{q(MIPs)}$ = 1.107E7 L mol^{-1} s^{-1} by the same method. K_q is the rate constant of the bimolecular quenching process, which represents bimolecular encountering frequency orders of magnitude. The rate constant (K_q) of maximum diffusion-controlled dynamic quenching, which is between the quenching agent and fluorescent molecule, is 2.0E10 L mol^{-1} s^{-1}.[46] The K_q in this study is always <2.0E10 L mol^{-1} s^{-1}, so the reason for fluorescence quenching is dynamic quenching. Due to many specific binding sites existing in the fluorescent molecularly imprinted polymer because $K_{q(MIPs)}$ (1.107E7 L mol^{-1} s^{-1}) > $K_{q(NIPs)}$ (3.792E6 L mol^{-1} s^{-1}), the fluorescent molecularly imprinted polymer is more likely to cause the fluorescence quenching phenomenon than fluorescent molecularly non-imprinted polymer. That is to say, the fluorescent molecularly imprinted polymer is more likely to occur with bimolecular dynamic collision, thereby producing dynamic quenching. We could draw the conclusion that the molecularly imprinted polymer not only had a high quenching rate but also a wide linear range. The obtained high quenching efficiency of the SiO_2@FITC-APTS@MIPs resulted from specific recognition sites for template molecule created during the course of imprinting.

Selectivity Determination. To measure the selectivity of the SiO_2@FITC-APTS@MIPs beads further, we made a comparison between the potential interference of several structurally related compounds (BC, FE, and BI) and LC. The SiO_2@FITC-APTS@MIPs beads were added to 10 mL of ethanol solutions containing 30 nM L^{-1} of BC, FE, and BI, respectively. The mixture was stirred for 1.0 h at the room temperature. The fluorescence intensity was detected by the fluorescence spectrophotometer, and $[(F_0/F) - 1]$ was calculated with the fluorescent data.

As shown in Figure S8a in the Supporting Information, the fluorescence quenching intensity of SiO_2@FITC-APTS@MIPs for LC was much lower than that of the structural analogues. It showed that only LC could adapt to the recognition sites in SiO_2@FITC-APTS@MIPs rather than other structural analogues, which could generate more fluorescence quenching efficiency. However, SiO_2@FITC-APTS@NIPs had a lower fluorescence quenching rate than the imprinting in Figure S8b. Other structural analogues were the same as LC, and their fluorescence quenching rates were all low. In conclusion, the fluorescence quenching of SiO_2@FITC-APTS@NIPs was invisible, because there were nonspecific recognition sites in SiO_2@FITC-APTS@NIPs.

As shown in Figure 5, the chemical structures of each structural analogue are displayed. We could see from Figure 5 that the fluorescence quenching efficiency of SiO_2@FITC-APTS@MIPs for LC was much higher than that of other

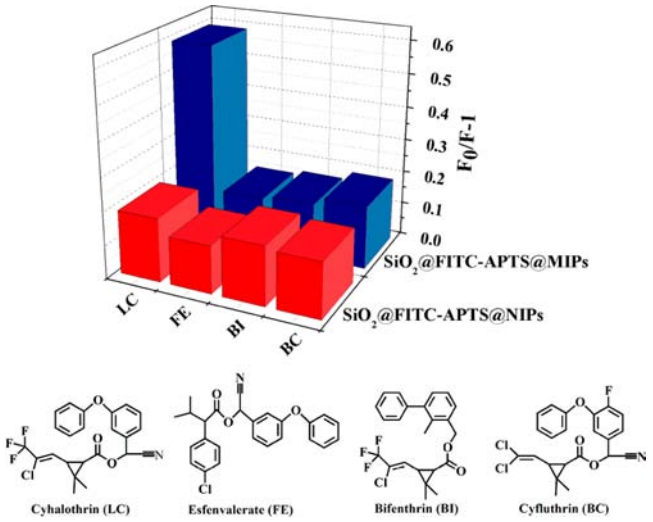

Figure 5. Quenching amount of SiO_2@FITC-APTS@MIPs and NIPs by different kinds of 30 nM L^{-1} pyrethroid pesticides and the chemical structures of each pyrethroid pesticide.

structural analogues. The results showed that SiO_2@FITC-APTS@MIPs had good selectivity for λ-cyhalothrin and none of the competitors being evaluated led to any significant fluorescence quenching rate. It can be proved that the SiO_2@FITC-APTS@MIPs beads provided high selectivity for LC, which was produced for the reason that there were specific recognition sites of LC in SiO_2@FITC-APTS@MIPs.

To further the investigation of how the competitive analogue affects the fluorescence quenching, BC, FE, and BI, these three competitive pesticides, were added into LC solution to form blend solutions, and the concentrations of λ-cyhalothrin and the competitive pesticides were all 30 nM L^{-1}. As can be seen from Figure 6, these three competitive pesticides could not obviously interfere with the fluorescence intensity of SiO_2@FITC-APTS@MIPs and NIPs. As can be seen from Figure 6a, the addition of structural analogues had almost no effect on the detection of LC. The last complex sample (LC, BC, BI, and FE) had too many structural analogues, so the SiO_2@FITC-APTS@MIPs could not detect the LC very well. The SiO_2@FITC-APTS@NIPs may be for the same reason in Figure 6b. From what had been discussed above, we could draw the conclusion that the SiO_2@FITC-APTS@MIPs provided high selectivity for LC, and it had good anti-interference for structural analogues. That is to say, the product of SiO_2@FITC-APTS@MIPs can identify the target molecule from the complex samples very well.

Application to Water Sample Analysis. To assess the applicability of SiO_2@FITC-APTS@MIPs beads in three water samples, we collected the distilled water and tap water from the laboratory, and we bought the Chinese spirits from a supermarket in China. We selected four concentrations to evaluate the applicability of SiO_2@FITC-APTS@MIPs beads and got the recovery by parallel measurement five times. The 5.0 mL water sample was added into 5.0 mL of LC solution (0−500 nM L^{-1}) and analyzed by the procedure mentioned above. Table 2 lists the corresponding results. The results showed that the SiO_2@FITC-APTS@MIPs had a good recovery in the linear concentration range, regardless of whether it was water sample or Chinese spirits. The recovery is smaller and smaller beyond the linear concentration range. The Chinese spirit sample is relatively complex, but it still has a

DOI: 10.1021/jf5043823
J. Agric. Food Chem. 2015, 63, 2392−2399

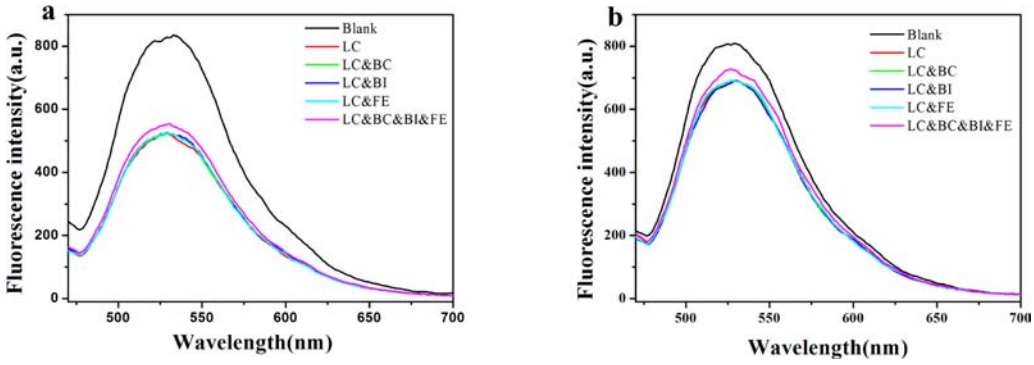

Figure 6. Quenching amount of SiO_2@FITC-APTS@MIPs (a) and SiO_2@FITC-APTS@NIPs (b) by different kinds of 30 nM L^{-1} pyrethroid pesticides.

Table 2. Recovery of LC-Spiked Water Samples Using the Proposed Sensor

sample	test	LC added (nM)	LC found[a] (nM)	recovery (%)
distilled water	1	0	0	
	2	8	7.9 ± 0.2	98.8 ± 2.5
	3	60	60.5 ± 0.9	100.8 ± 1.5
	4	500	386 ± 2.8	77.2 ± 0.56
tap water	1	0	0.1 ± 0.1	
	2	8	8.3 ± 0.4	103.8 ± 5.0
	3	60	61.4 ± 1.2	102.3 ± 2.0
	4	500	371 ± 3.9	74.2 ± 0.78
Chinese spirits	1	0	0.2 ± 0.1	
	2	8	8.5 ± 0.5	106.2 ± 6.2
	3	60	62.8 ± 2.9	104.6 ± 4.8
	4	500	307 ± 5.1	61.4 ± 1.0

[a]Average of five measurements.

good recovery. This suggests that the SiO_2@FITC-APTS@MIPs could analyze LC in Chinese spirit samples. The results clearly establish that the SiO_2@FITC-APTS@MIPs can attain good recovery and can be effectively applied in the detection of LC in Chinese spirits.

To appraise the detection for SiO_2@FITC-APTS@MIPs beads with interferences further, we selected a better recovery of concentration (60 nM L^{-1}) to assess the applicability of SiO_2@FITC-APTS@MIPs. The Chinese spirit sample 5.0 mL was added into 5.0 mL of LC solution (60 nM L^{-1}) and analyzed according to the procedure mentioned above. The recovery of the Chinese spirit sample was obtained by carrying out parallel measurements five times. Table 3 lists the corresponding results. As shown, all recoveries were >100%. The existence of error is allowed. The concentration of the

Table 3. Interferences in LC Detection in Chinese Spirits

	LC added (nM)					
test	LC	BC	BI	FE	LC found[a] (nM)	recovery (%)
1	60	0	0	0	62.1 ± 0.6	103.5 ± 1.0
2	60	60	0	0	63.3 ± 0.5	105.5 ± 0.8
3	60	0	60	0	63.2 ± 0.6	105.3 ± 1.0
4	60	0	0	60	63.4 ± 0.4	105.7 ± 0.7
5	60	60	60	60	64.2 ± 0.8	107 ± 1.3

[a]Average of five measurements.

fluorescent molecularly imprinted polymers in 60 nM L^{-1} is the maximum detectable concentration in the linear interval area. At the same time, the fluorescence quenching is the strongest. First, there are acids, aldehydes, ketones, aldehydes, aromatics, and other compounds in Chinese spirits. The feeble fluorescence quenching of the fluorescent molecularly imprinted polymers was caused by certain compounds in the Chinese spirits, thus resulting in the recovery becoming larger. Because the chemical structures of other competitive pyrethroids are similar to that of the target molecule, these other competitive pyrethroids also can produce certain fluorescence quenching of fluorescent molecularly imprinted polymer. However, it is not the main reason for the fluorescence quenching. Therefore, we found that the recovery would become larger with the increasing kinds of pyrethroid. On the whole, the results showed that the recovery has almost no change with single distracters. Although the recovery of the last test with three distractors is not as good as before, it still has relatively stable recovery. On the whole, the SiO_2@FITC-APTS@MIPs can attain satisfactory recovery in complex Chinese spirits.

To appraise the regeneration for SiO_2@FITC-APTS@MIPs beads, 60 nM L^{-1} LC solutions were first prepared. One hundred milligrams of SiO_2@FITC-APTS@MIPs beads was added into 100 mL of LC solution and incubated for 2.0 h before fluorescence measurement. After the test, the SiO_2@FITC-APTS@MIPs beads containing LC were washed with methanol−acetic acid solution, collected by centrifuge, and rinsed with ethanol. As shown in Figure S9 in the Supporting Information, the SiO_2@FITC-APTS@MIPs beads have certified that they can be reused five times without remarkable loss of signal intensity.

Conclusion. In summary, by combining a surface imprinting technique and fluorescent polymers, core−shell submicrometer SiO_2@FITC-APTS@MIPs on the surface of SiO_2 beads, which can be applied to the selective detection of LC, were synthesized. The unique aspects of SiO_2@FITC-APTS@MIPs, such as molecular recognition, fast separation, and fluorescence detection of target molecule were realized and discussed in detail. The adsorption of LC was detected by fluorescence spectrophotometer, and, using the Stern−Volmer equation, analyzed for fluorescence intensity. It is noteworthy that the SiO_2@FITC-APTS@MIPs not only have fluorescence property but also have quick detection, high fluorescence intensity, and good selective recognition for the target molecule. The experimental results showed the fluorescence quenching efficiency of SiO_2@FITC-APTS@MIPs for LC was

DOI: 10.1021/jf5043823
J. Agric. Food Chem. 2015, 63, 2392−2399

much higher than that of the structurally analogous composite and the SiO_2@FITC-APTS@NIPs, and it illustrated that the adsorption capacity and selectivity of the SiO_2@FITC-APTS@MIPs for the target molecule were good. From the SiO_2@FITC-APTS@MIPs detected LC in Chinese spirit samples, it can be seen that the SiO_2@FITC-APTS@MIPs not only has the advantage of high selectivity of molecular imprinting technique but also has the advantage of high sensitivity. On the whole, the present studies not only provide a new way to actualize selectively fluorescent detection of pyrethroid pesticides but also improve the potential application of molecularly imprinted polymers in the analysis field.

■ ASSOCIATED CONTENT

Supporting Information

Detailed experimental characterization for polymers such as the fluorescent equation, measurements, and additional figures (FT-IR, UV−vis spectra, CLSM images, thermal gravity analysis, results of competitive and regenerative experiments). This material is available free of charge via the Internet at http://pubs.acs.org.

■ AUTHOR INFORMATION

Corresponding Author

*(Y.Y.) Phone: +86 0511 88791800. E-mail: yys@mail.ujs.edu.cn.

Funding

This work was financially supported by the National Natural Science Foundation of China (No. 21107037, 21176107, 21407064, 21407057, 21277063, and 21346004), the Natural Science Foundation of Jiangsu Province (No. BK2011461 and BK2011514), the National Postdoctoral Science Foundation (No. 2013M530240), the Postdoctoral Science Foundation funded Project of Jiangsu Province (No. 1202002B), Programs of Senior Talent Foundation of Jiangsu University (No. 12JDG090), and Ph.D. Innovation Programs Foundation of Jiangsu Province (No. CXZZ13_0681).

Notes

The authors declare no competing financial interest.

■ REFERENCES

(1) Seenivasan, S.; Muraleedharan, N. N. *Food Chem. Toxicol.* **2009**, *47*, 502−505.
(2) Gong, J. L.; Gong, F. C.; Kuang, Y.; Zeng, G. M.; Shen, G. L.; Yu, R. Q. *Anal. Bioanal. Chem.* **2004**, *379*, 302−307.
(3) Bradberry, S. M.; Cage, S. A.; Proudfoot, A. T.; Vale, J. A. *Toxicol. Rev.* **2005**, *24* (2), 93−106.
(4) Guo, Y. R.; Liang, X.; Wang, Y. Y.; Liu, Y. H.; Zhu, G. N.; Gui, W. J. *J. Appl. Polym.* **2013**, *128*, 4014−4022.
(5) (a) Barro, R.; Garcia-Jares, C.; Llompart, M.; Cela, R. *J. Chromatogr. Sci.* **2006**, *44*, 430−437. (b) Reigart, J. R.; Roberts, J. R. *Recognition and Management of Pesticide Poisonings*, 5th ed.; U.S. Environment Protection Agency (EPA): Washington, DC, USA, 1999.
(6) Sicbaldi, F.; Sarra, A.; Mutti, D.; Bo, P. F. *J. Chromatogr., A* **1997**, *765*, 13−22.
(7) Lehotay, S. J.; Lightfield, A. R.; Harman-Fetcho, J. A.; Donoghue, D. J. *J. Agric. Food Chem.* **2001**, *49*, 4589−4596.
(8) Pang, G. F.; Fan, C. L.; Chao, Y. Z.; Zhao, T. S. *J. Chromatogr., A* **1994**, *667*, 348−353.
(9) Fernández-Gutiérrez, A.; Martínez-Vidal, J. L.; Arrebola, F. J.; Gonzalez-Casado, A.; Vílchez, J. L. *Fresenius' J. Anal. Chem.* **1998**, *360*, 568−572.
(10) López-López, T.; Gil-Garcia, M. D.; Martínez-Vidal, J. L.; Martínez-Galera, M. *Anal. Chim. Acta* **2001**, *447*, 101−111.
(11) Pasha, A.; Vijayashankar, Y. N. *Analyst* **1993**, *118*, 777−778.
(12) Patil, V. B.; Sevalkar, M. T.; Padalikar, S. V. *Analyst.* **1992**, *117*, 75−76.
(13) Argauer, R. J.; Eller, K. I.; Pfeil, R. M.; Brown, R. *J. Agric. Food Chem.* **1997**, *45*, 180−184.
(14) Ramesh, A.; Balasubramanian, M. *Analyst* **1998**, *123*, 1799−1802.
(15) Huang, X. H.; Zhao, X. H.; Lu, X. T.; Tian, H. P.; Xu, A. J.; Liu, Y.; Jian, Z. *J. Chromatogr., B* **2014**, *967*, 1−7.
(16) Deme, P.; Azmeera, T.; Devi, L. A. P.; Jonnalagadda, P. R.; Prasad, R. B. N.; Vijaya Sarathi, U. V. R. *Food Chem.* **2014**, *142*, 144−151.
(17) Esteve-Turrillas, F. A.; Pastor, A.; Guardia, M. D. L. *Anal. Bioanal. Chem.* **2006**, *384* (3), 801−809.
(18) Gao, D. M.; Zhang, Z. P.; Wu, M. H.; Xie, C. G.; Guan, G. J.; Wang, D. P. *J. Am. Chem. Soc.* **2007**, *129* (25), 7859−7866.
(19) Haupt, K.; Mosbach, K. *Chem. Rev.* **2000**, *100*, 2495−2504.
(20) Zimmerman, S. C.; Wendland, M. S.; Rakow, N. A.; Zharov, I.; Suslick, K. S. *Nature* **2002**, *418*, 399−403.
(21) Mertz, E.; Zimmerman, S. C. *J. Am. Chem. Soc.* **2003**, *125* (12), 3424−3425.
(22) Katz, A.; Davis, M. E. *Nature* **2000**, *403*, 286−289.
(23) Bass, J. D.; Katz, A. *Chem. Mater.* **2003**, *15* (14), 2757−2763.
(24) Xie, C. G.; Liu, B. H.; Wang, Z. Y.; Gao, D. M.; Guan, G. J.; Zhang, Z. P. *Anal. Chem.* **2008**, *80* (2), 437−443.
(25) Pan, J. M.; Yao, H.; Xu, L. C.; Ou, H. X.; Huo, P. W.; Li, X. X.; Yan, Y. S. *J. Phys. Chem. C* **2011**, *115*, 5440−5449.
(26) Xu, L. C.; Pan, J. M.; Dai, J. D.; Li, X. X.; Hang, H.; Cao, Z. J.; Yan, Y. S. *J. Hazard. Mater.* **2012**, *48*−*56*, 233−234.
(27) Jenkins, A. L.; Uy, O. M.; Murray, G. M. *Anal. Chem.* **1999**, *71* (2), 373−378.
(28) Ansell, R. J.; Mosbach, K. *Analyst* **1998**, *123* (7), 1611−1616.
(29) Levi, R.; McNiven, S.; Piletsky, S. A.; Cheong, S. H.; Yano, K.; Karube, I. *Anal. Chem.* **1997**, *69* (11), 2017−2021.
(30) Kong, X.; Gao, R. X.; He, X. W.; Chen, L. X.; Zhang, Y. K. *J. Chromatogr., A* **2012**, *1245*, 8−16.
(31) Gao, R. X.; Su, X. Q.; He, X. W.; Chen, L. X.; Zhang, Y. K. *Talanta* **2011**, *83* (3), 757−764.
(32) Gao, R. X.; Kong, X.; Su, F. H.; He, X. W.; Chen, L. X.; Zhang, Y. K. *J. Chromatogr., A* **2010**, *1217* (52), 8095−8102.
(33) Shi, X.; Liu, J.; Sun, A.; Chen, J. *J. Chromatogr., A* **2012**, *1227*, 60−66.
(34) Ma, G.; Chen, L. *J. Chromatogr. A* **2014**, *1329*, 1−9.
(35) Feng, H.; Wang, N. Y.; Trans, T. T. T.; Yuan, L. J.; Li, J. Z.; Cai, Q. Y. *Sens. Actuators, B−Chem.* **2014**, *195*, 266−273.
(36) Zhao, Y. Y.; Ma, Y. X.; Li, H.; Wang, L. Y. *Anal. Chem.* **2012**, *84*, 386−395.
(37) Song, Z. L.; Liu, C. B.; Pan, J. M.; Yan, Y. S.; Wei, X.; Meng, M. J.; Yu, P.; Gao, L.; Dai, J. D.; Lin, S. *Anal. Methods* **2014**, *6*, 915−923.
(38) Li, Y. L.; Cui, Z. M.; Li, D. P.; Li, H. B. *Sens. Actuators, B−Chem.* **2011**, *155* (2), 878−883.
(39) Stober, W.; Fink, A. *J. Colloid Interface Sci.* **1968**, *26*, 62−69.
(40) Chen, S. L.; Yuan, G. M.; Hu, C. T. *Powder Technol.* **2011**, *207* (1−3), 232−237.
(41) Imhof, A.; Megens, M.; Engelberts, J. J.; Lang de, D. T. N.; Sprik, R.; Vos, W. L. *J. Phys. Chem. B* **1999**, *103* (9), 1408−1415.
(42) Li, H. L.; Perkas, N.; Li, Q. L.; Gofer, Y.; Koltypin, Y.; Gedanken, A. *Langmuir* **2003**, *19* (24), 10409−10413.
(43) Wang, H. F.; He, Y.; Ji, T. R.; Yan, X. P. *Anal. Chem.* **2009**, *81* (4), 1615−1621.
(44) Ganter, M. A.; Uicker, J. J. *J. Mech. Des.* **1986**, *108* (4), 549−555.
(45) Coggeshall, N. D.; Saier, E. L. *J. Chem. Phys.* **2004**, *15* (1), 65−71.
(46) Ware, W. R. *J. Phys. Chem.* **1962**, *66*, 455−458.

DOI: 10.1021/jf5043823
J. Agric. Food Chem. 2015, 63, 2392−2399

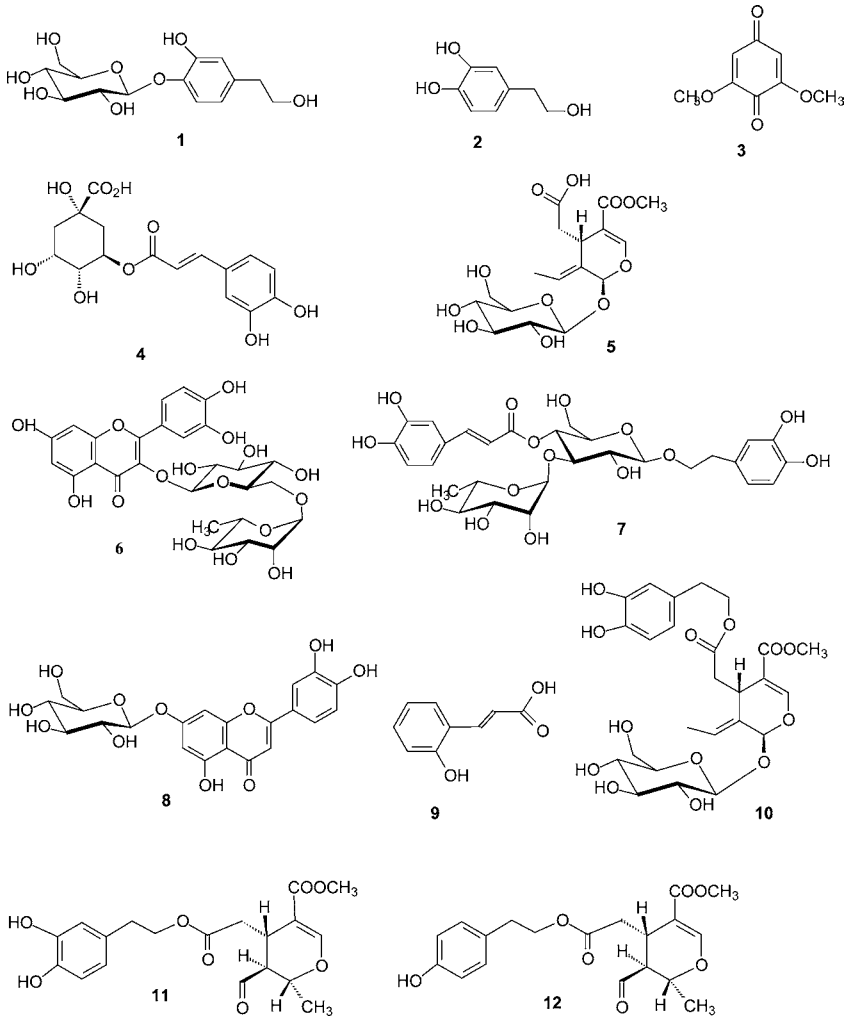

Figure 1. Structures of the studied compounds.

which contain very low amounts of oleuropein,[9] dry salt processing leads to a higher concentration of oleuropein,[5] highlighting the critical role of processing in the chemical composition of finished olives.[4] California-style black ripe olive processing methods involve harvesting olives before complete maturity (green). The raw olives are either directly treated with lye to remove bitterness or preserved in an acidic brine solution (0.2−0.4% calcium chloride, pH < 4.0) until they can be lye-treated and processed. A mild fermentation may occur during the initial brine storage. This style of processing results in olives with the lowest levels of oleuropein and bitterness.[10]

Herein, we describe a rapid ultrahigh-pressure liquid chromatography (UHPLC) triple-quadrupole tandem mass spectrometry (QqQ MS/MS) method using dynamic multiple reaction monitoring (dMRM) for the measurement of a range of key bitter and bioactive constituents in olives. The method was applied for the simultaneous quantitation of hydroxytyrosol-4-*O*-glucoside (**1**), hydroxytyrosol (**2**), 2,6-dimethoxy-*p*-benzoquinone (**3**), chlorogenic acid (**4**), oleoside-11-methyl ester (**5**), rutin (**6**), verbascoside (**7**), luteolin-7-*O*-glucoside (**8**), *o*-coumaric acid (**9**), oleuropein (**10**), oleuropein aglycone monoaldehydic form (**11**), and ligstroside aglycone monoaldehydic form (**12**) (Figure 1) in three different varieties of fresh and processed olives cured using either dry salt or California-style black ripe processing methods.

MATERIALS AND METHODS

Chemicals. High-performance liquid chromatography (HPLC)-grade formic acid, acetonitrile, hexane, and methanol were obtained from Fisher Scientific (Fair Lawn, NJ).

Samples. Dry salt-cured Throuba Thassos olives were purchased from a local market in Davis, CA, and the producer was contacted for processing conditions. The Throuba Thassos olives were treated with 40% dry salt for 2 months. After curing, the olives were washed with water and dried at ambient temperature for 2−3 days before packaging. Dry salt Mission olives were purchased directly from the grower/processor at the local farmers' market in Davis, CA. According to the producer, the olives were treated with dry salt (1:1, w/w) for 3 months. After curing, the olives were washed with water and sun-dried. California-style black ripe olives were prepared using fresh Manzanilla olives collected in early October 2011 in Davis, CA. The fresh samples were analyzed on the day that they were collected. California-style black ripe olives were produced using typical commercial processing.[11] Briefly, the olives were prepared by immersion in a 1−2% sodium hydroxide solution over 3 consecutive days until the lye penetrated the cuticle layers, 1−2 mm of the pulp, and the pit. During the intervals between lye treatments, the fruit was suspended in water, in which air is bubbled for 24 h. Oxygen is required for the black color formation, an oxidation reaction that results from the oxidation and polymerization of *o*-diphenols, mainly hydroxytyrosol and caffeic acid. A ferrous gluconate solution (0.1%, w/v) was added for 24 h to fix the developed black color. Olives were then rinsed with water to neutralize the solution. Olives were packed in a 3% sodium chloride solution and sterilized at 121 °C for 15 min.

DOI: 10.1021/jf506367e
J. Agric. Food Chem. 2015, 63, 2400−2405

Table 1. Mass Spectra Acquisition Properties of 12 Constituents Quantitated in Olive Fruit[a]

compound	compound name	mass	precursor ion	product ion	fragmentor voltage	collision energy	retention time
1	hydroxytyrosol 4-*O*-glucoside	316.12	315	153	115	12	1.55
2	hydroxytyrosol	154.06	153.1	123	100	8	2.15
3	2,6-dimethoxy-*p*-benzoquinone	168.04	169	141	110	12	3.4
4	chlorogenic acid	354.1	353.1	191	95	12	3.9
5	oleoside-11-methyl ester	404.13	403	223	90	10	4.25
6	rutin	610.15	609.1	300	220	40	4.55
7	verbascoside	624.21	623.2	161	210	36	4.92
8	luteolin-7-*O*-glucoside	448.1	447.1	285	135	16	5.55
9	*o*-coumaric acid	164.05	163	119	80	8	6.18
10	oleuropein	540.18	539.2	275.1	165	20	6.3
11	oleuropein aglycone monoaldehyde form	378.13	377.1	307	105	4	8.95
12	ligstroside aglycone monoaldehyde form	362.14	361.1	291.1	95	8	9.18

[a]All compounds were monitored in negative mode with the exception of compound 3, which was monitored in positive mode.

Reference Compounds. Hydroxytyrosol, oleuropein, rutin, chlorogenic acid, and *o*-coumaric acid were purchased from Extrasynthese (Genay, France), and their purity as stated by the supplier was >98%. Hydroxytyrosol-4-*O*-glucoside, luteolin-7-*O*-glucoside, verbascoside, oleoside-11-methyl ester, 2,6-dimethoxy-*p*-benzoquinone, oleuropein, and ligstroside aglycones were isolated after chromatographic purification from olives. The identity and purity of the isolated compounds was established using nuclear magnetic resonance (NMR) spectroscopy and, in all cases, was >95%.

Extraction and Sample Preparation. A random sampling of 20−30 olives was separated into three sub-samples. Each sub-sample was homogenized individually. A 10 g (wet weight) sample of olive pulp was removed and extracted immediately with 25 mL of MeOH/H_2O (4:1, v/v) in an ultrasonic bath for 45 min at 25 °C. A 25 mL aliquot of hexane was added for oil removal, and the mixture was shaken for 30 s. The supernatant was separated with centrifugation at 4000 rpm for 3 min. The hexane phase was removed, and a 1 mL aliquot of the MeOH/H_2O phase was filtered through a 0.45 μm filter (EMD Millipore, Billerica, MA), diluted with H_2O (1:50), and injected into the liquid chromatography−mass spectrometry (LC−MS).

UHPLC−MS/MS Analysis. Analysis of the 12 phenolic and secoiridoid compounds was performed on a 1290 Infinity UHPLC interfaced to a 6460 QqQ MS/MS with electrospray ionization (ESI) via Jet Stream technology (Agilent Technologies, Santa Clara, CA). The UHPLC was equipped with a binary pump with an integrated vacuum degasser (G4220A), an autosampler (G4226A) with a thermostat (G1330B), and a thermostated column compartment (G1316C). The column used was a 150 × 2.1 mm inner diameter, 2.7 μm, Poroshell 120 EC-C18 (Agilent Technologies, Santa Clara, CA). The mobile phase consisted of 0.1% formic acid in water (A) and acetonitrile (B) with the following gradient program: 0−2.5 min, 10% B; 2.5−3.0 min, 10−25% B; 3.0−6.0 min, 25% B; 6.0−7.5 min, 25−40% B; 7.5−8.5 min, 40−95% B; and 8.5−9.5 min, 95% B. The flow rate was 0.4 mL/min, and the injection volume was 1.0 μL.

Negative and positive ESI modes were used. The drying gas temperatures and flow rate were 250 °C and 8 L/min, respectively. The sheath gas temperature and flow rate were 350 °C and 11 L/min, respectively, and the nebulizer gas pressure was 45 psi. The capillary voltage was 3.5 kV for positive and negative modes, and the nozzle voltage was 0 and 1.5 kV for positive and negative modes, respectively.

Dynamic MRM mode was used to analyze olive phenolic and secoiridoid compounds. A cycle time of 500 ms was used. Dwell times were automatically set using cycle time and peak overlap. Precursor ions and product ions were identified and optimized using MassHunter Optimizer (Agilent Technologies). A summary of the precursor ions and product ions used for quantitation is given in Table 1.

Calibration Curves. Standard stock solutions of 1.0 mg/mL were prepared in methanol. Stock solutions were diluted in MeOH/H_2O (4:1, v/v) to give a concentration ranging from 0.001 to 50 μg/mL. Stock solutions were used to identify the linear range for quantitation (LRQ), limit of detection (LOD; S/N > 3), and limit of quantitation (LOQ; S/N > 10) for each analyte. Olive samples were spiked to give concentrations of analytes at 0.002, 0.02, 0.2, 1, 2, and 5 mg/g of olive by diluting appropriate volumes of the stock standard solutions with MeOH/H_2O (4:1, v/v) and mixing with 10.0 g of olive flesh (cv. Manzanilla) after California-style black ripe processing. This olive matrix was selected because it presented the lowest concentrations of the analytes, making the construction of the calibration curves easier. The area of each analyte was measured in a blank matrix standard and then again after the addition of a known amount of standard analyte to the matrix. The difference in area measured for each analyte peak, before and after spiking, was directly correlated with the spiked amount to construct the calibration curve.

Method Validation. The method was checked for the linearity, precision [calculated as the relative standard deviation % (RSD %)], accuracy [evaluated as the relative percentage error % (Er %)], and sensitivity [defined by the limit of detection (LOD) and limit of quantitation (LOQ)].

RESULTS AND DISCUSSION

A UHPLC−QqQ MS/MS method using dynamic MRM was developed to quantitate a range of bitter and biologically active

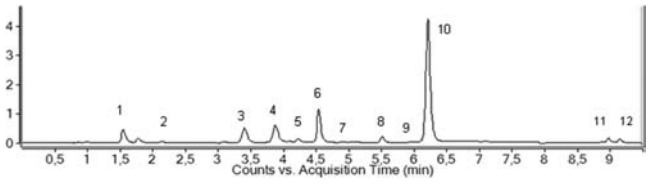

Figure 2. Total ion chromatogram of a mixture of the studied compounds. The numbers assigned to each peak correspond to each of the studied compounds.

phenolic and secoiridoid compounds in table olives. This method offers improved sensitivity, selectivity, and throughput (<10 min/run) in comparison to previously reported methods, as reviewed by Segura-Carretero et al.[12] The usefulness of the new method was demonstrated in the simultaneous quantitation of a broad range of phenolic and secoiridoid compounds in fresh and finished olive products generated by dry salt or California-style debittering methods. Rapid reliable methods for the quantitation of hydroxytyrosol, oleuropein, and their derivatives is of special interest because these compounds have been recently recognized by the European Union (EU) as agents protecting low-density lipoprotein (LDL) oxidation and, thus, offering cardiovascular protection.[13] Currently, this health claim is recognized only for olive oil. To date, several gas

DOI: 10.1021/jf506367e
J. Agric. Food Chem. 2015, 63, 2400−2405

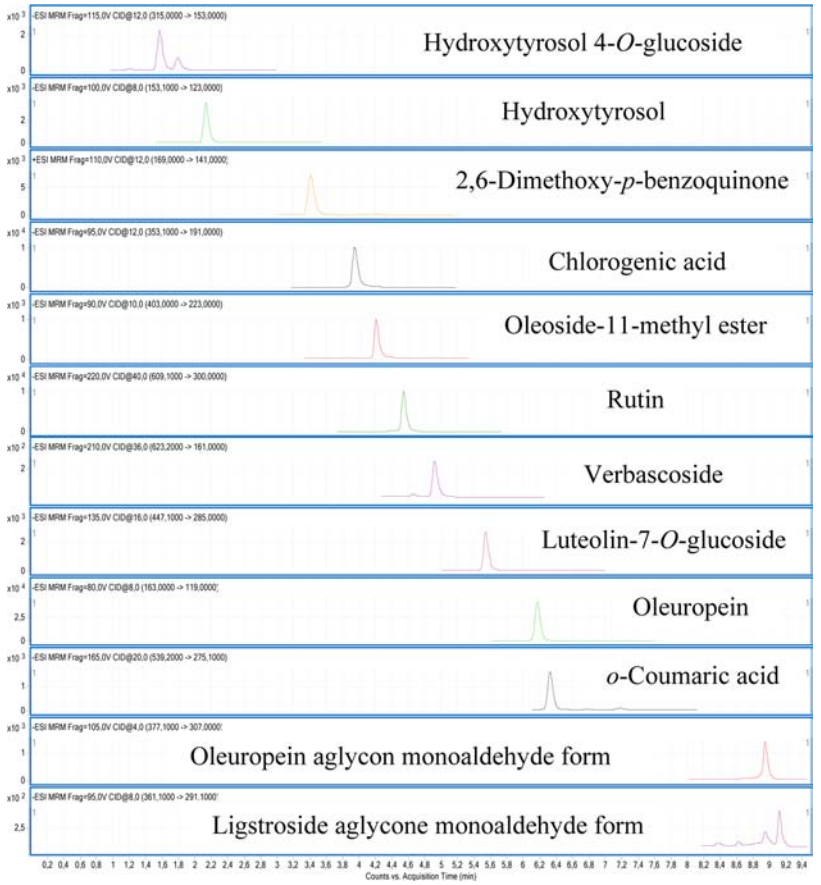

Figure 3. MRM-extracted chromatograms for each quantitated compound from a Mission olive sample.

Table 2. Concentration of Studied Compounds Expressed as Microgram Per Gram of Flesh (Wet Weight), Mean Values of Three Measurements

compound	compound name	Throuba Thassos dry salt	Mission dry salt	Manzanilla fresh	Manzanilla California style
1	hydroxytyrosol 4-*O*-glucoside	263.5 ± 19.1	1890.4 ± 150.5	163.5 ± 15.5	73.1 ± 5.5
2	hydroxytyrosol	195.1 ± 7.8	633.8 ± 55.1	894.5 ± 45.2	210.0 ± 18.8
3	2,6-dimethoxy-*p*-benzoquinone	7.0 ± 0.5	14.9 ± 1.2	916.9 ± 61.3	7.4 ± 0.6
4	chlorogenic acid	3.8 ± 0.2	20.8 ± 1.4	40.8 ± 3.7	ND[a]
5	oleoside-11-methyl ester	4238.1 ± 333.4	1393.8 ± 60.1	231.4 ± 19.9	7.9 ± 0.5
6	rutin	38.2 ± 2.5	194.8 ± 14.7	278.1 ± 20.5	ND
7	verbascoside	156.1 ± 10.1	14.9 ± 1.3	66.5 ± 6.1	ND
8	luteolin-7-*O*-glucoside	11.9 ± 1.0	276.3 ± 11.4	279 ± 18.3	4.5 ± 0.3
9	oleuropein	1459.5 ± 100.1	516.2 ± 44.3	9186.4 ± 530.2	36.7 ± 3.1
10	*o*-coumaric acid	ND	2.0 ± 0.5	1.8 ± 0.3	ND
11	oleuropein aglycone monoaldehyde form	50 ± 4.3	379.3 ± 30.2	2126 ± 190.1	ND
12	ligstroside aglycone monoaldehyde form	ND	74.6 ± 6.1	465.1 ± 34.8	ND

[a]ND = not detected.

chromatography/mass spectrometry (GC/MS), HPLC−ultraviolet (UV), or LC/MS methods are available for monitoring phenolic and secoiridoid compounds in olive products (e.g., olive oil, olive leaves, and olive fruits).[12] The GC/MS methods require derivatization and long analysis times (30−120 min).[14] The HPLC−UV methods have low sensitivity (e.g., LOQ = 1 μg/mL for hydroxytyrosol[5]) and are limited by long chromatographic separation times (20−100 min).[12] Additionally, in some cases, HPLC−UV methods are unable to resolve overlapped peaks,[15] making the simultaneous quantitation of numerous compounds difficult, especially in short separation times. Rapid LC/MS methods have been applied to unprocessed olives but are restricted to the quantitation of oleuropein and hydroxytyrosol.[16,17] A HPLC−Orbitrap MS/MS method for quantitation of nine compounds in fresh olives was recently reported.[18] The HPLC−Orbitrap and current UHPLC−QqQ methods present similar LODs and LOQs for oleuropein, hydroxytyrosol, oleuropein aglycone, and ligstroside aglycone, the only four common compounds studied using the two methods; however, the Orbitrap method presented a longer analysis time (31 min), and the quantitation range was restricted to higher concentrations (e.g., 1000−50 000 ng/mL compared to 100−12 500 ng/mL for oleuropein aglycone and 500−20 000 ng/mL versus 50−6250 ng/mL for hydroxytyr-

DOI: 10.1021/jf506367e
J. Agric. Food Chem. 2015, 63, 2400−2405

osol). Moreover, the HPLC−Orbitrap method relies on calibration curves that were constructed by dilution of standard compounds in a different solvent (acetonitrile) than the solvent used for the dilution of the real samples (methanol and water). Extraction or dilution of oleocanthal and oleacein using methanol can have a negative impact on their levels as recently reported[19,20] and has the potential to impact other compounds (e.g., oleuropein aglycone and ligstroside aglycone) because these two compounds easily isomerize[20] and require well-controlled conditions for accurate measurements.

Recovery from the olive matrix varied. At high concentrations of added standards (1−5 ppm), recoveries were 85−95%, whereas at low concentrations (0.1−0.5 ppm), recoveries were 50−60%. For this reason, it was necessary to use calibration curves constructed with the addition of known amounts to olive matrix, instead of calibration curves constructed with pure compounds in solution. The method was checked for linearity, precision, accuracy, LOD, and LOQ, and the results were satisfactory. These results show that the method can be efficiently used for the measurement of target analytes. Intraday precision (repeatability) was in all cases <10%.

Special care was taken during the extraction to reduce the risk of enzymatic degradation of sensitive compounds, such as oleuropein and other glucosides, and for this purpose, the olive pulp was extracted immediately after crushing. However, specific experiments examining the role of the sample preparation procedure on the formation of aglycones were not performed.

A total ion chromatogram with all studied compounds (Figure 2) and a representative MRM-extracted chromatogram of Mission olives (Figure 3) demonstrate clearly resolved peaks. Although this study focused on quantitation of 12 targeted compounds, we were able to tentatively identify isomers, such as hydroxytyrosol-1-*O*-glucoside (1.8 min) and luteolin-4-*O*-glucoside (5.95 min), as well as tyrosol glucoside (salidroside), tyrosol, caffeic acid, and methoxytyrosol (data not shown). Tyrosol does not ionize well in ESI mode and, therefore, can only be quantitated at high concentrations. Because the levels of tyrosol were below the level of quantitation, it was not included in this study.

The levels of the 12 secoiridoid and phenolic compounds measured in fresh and California-style black ripe processed Manzanilla olives are given in Table 2. The levels of oleuropein (9186 ± 530 μg/g), oleuropein aglycone monoaldehyde (2126 ± 190 μg/g), and hydroxytyrosol (894.5 ± 45.2 μg/g) were measured in fresh olives (wet weight). After California-style black ripe processing, only hydroxytyrosol, hydroxytyrosol-4-*O*-glucoside, and oleuropein could be detected in levels of 210.0 ± 18.8, 73.1 ± 5.5, and 36.7 ± 3.1 μg/g wet weight, respectively. All of the other compounds presented concentrations lower than 10 μg/g wet weight. Chlorogenic acid, rutin, verbascoside, *o*-coumaric acid, oleuropein aglycone, and ligstroside aglycone could not be detected. These data indicate that California-style black ripe olive processing methods lead to significant reductions in the levels of the secoridoid and phenolic compounds evaluated in this study. This finding is in accordance with previous reports on phenolic compound change during California-style processing;[5] however, herein, a larger range of compounds was evaluated and with higher sensitivity.

In contrast to California-style olives, the dry salt Mission and Throuba Thassos olives presented relatively higher amounts of almost all studied compounds. For example, in Mission and Throuba Thassos olives, the levels were of oleuropein (516.2 ± 44.3 and 1459.5 ± 100.1 μg/g of wet weight), oleoside methyl ester (1393.8 ± 60.1 and 4238.1 ± 333.4 μg/g of wet weight), hydroxytyrosol (633.8 ± 55.1 and 195.1 ± 7.8 μg/g of wet weight), and hydroxytyrosol glucosides (1890.4 ± 150.5 and 263.5 ± 19.1 μg/g of wet weight) (Table 2). These findings support dry salt debittering methods as being advantageous for the retention of polyphenolic and secoiridoid constituents in table olives,[3] and they are not restricted to a specific variety; two commercial samples of two cultivars of different geographic origins presented similar retention of the targeted compounds.

The information presented herein demonstrates wide variation in the composition of a range of key bioactive phenolics in olives that is dependent upon both the variety and processing method used to create the olive product, and these factor need to be considered when developing possible health claims for table olives and their products.

■ ASSOCIATED CONTENT

Supporting Information

Linearity range, r^2, accuracy, LOD, and LOQ values for each compound in solution. This material is available free of charge via the Internet at http://pubs.acs.org.

■ AUTHOR INFORMATION

Corresponding Author

*Telephone: +30210-7274052. E-mail: emelliou@pharm.uoa.gr.

Notes

The authors declare no competing financial interest.

■ ACKNOWLEDGMENTS

The authors thank Charoenprasert Suthawan for preparing the California-style black ripe olives and Dr. Susan Ebeler and Cary Doyle of the Food Safety and Measurement Facility for analytical support. The authors also thank Dan Flynn, Executive Director of the UC Davis Olive Center, for helping to identify sources of the fresh olives and Dianne Madison for providing the dry salt Mission olives.

■ REFERENCES

(1) International Olive Council. Focus on table olives: World estimates for 2012/13. *Int. Olive Counc. Mark. Newsl.* **2013**, *73*, 1.

(2) Garrido Fernández, A.; Fernández Diez, M. J.; Adams, M. R. *Table Olives*; Chapman & Hall: London, U.K., 1997.

(3) Boskou, D. Phenolic compounds in olives and olive oil. *Olive Oil Minor Constituents and Health*; CRC Press (Taylor & Francis Group): Boca Raton, FL, 2008.

(4) Charoenprasert, S.; Mitchell, A. Factors influencing phenolic compounds in table olives (*Olea europaea*). *J. Agric. Food Chem.* **2012**, *60*, 7081−7095.

(5) Zoidou, E.; Melliou, E.; Gikas, E.; Tsarbopoulos, A.; Magiatis, P.; Skaltsounis, A. L. Identification of Throuba Thassos, a traditional Greek table olive variety, as a nutritional rich source of oleuropein. *J. Agric. Food Chem.* **2010**, *58*, 46−50.

(6) Kailis, S.; Harris, D. *Producing Table Olives*; Landlinks Press: Collingwood, Australia, 2007.

(7) Romero, C.; Brenes, M.; Yousfi, K.; García, P.; García, A.; Garrido, A. Effect of cultivar and processing method on the contents of polyphenols in table olives. *J. Agric. Food Chem.* **2004**, *52*, 479−484.

(8) Ramírez, E.; García-García, P.; de Castro, A.; Romero, C.; Brenes, M. Debittering of black dry-salted olives. *Eur. J. Lipid Sci. Technol.* **2013**, *11*, 1319−1324.

DOI: 10.1021/jf506367e
J. Agric. Food Chem. 2015, 63, 2400−2405

(9) Mantzouridou, F.; Tsimidou, M. Z. Microbiological quality and biophenol content of hot air-dried Thassos cv. table olives upon storage. *Eur. J. Lipid Sci.Technol.* **2011**, *113*, 786−795.
(10) Marsilio, V.; Campestre, C.; Lanza, B. Phenolic compounds change during California-style ripe olive processing. *Food Chem.* **2001**, *74*, 55−60.
(11) Charoenprasert, S.; Mitchell, A. Influence of California-style black ripe olive processing on the formation of acrylamide. *J. Agric. Food Chem.* **2014**, *62*, 8716−8721.
(12) Segura-Carretero, A.; Carrasco-Pancorbo, A.; Bendini, A.; Cerretani, L.; Fernández-Gutiérrez, A.; Analytical determination of polyphenols in olive oil. In *Olives and Olive Oil in Health and Disease Prevention*; Preedy, V. R., Watson, R. R., Eds.; Academic Press: San Diego, CA, 2010; Chapter 56, pp 509−523.
(13) European Food Safety Authority (EFSA).. Scientific opinion on the substantiation of health claims related to polyphenols in olive and protection of LDL particles from oxidative damage. *EFSA J.* **2011**, *9*, 2033.
(14) Carrasco-Pancorbo, A.; Cerretani, L.; Bendini, A.; Segura-Carretero, A.; Gallina-Toschi, T.; Fernández-Gutiérrez, A. Analytical determination of polyphenols in olive oils. *J. Sep. Sci.* **2005**, *28*, 937−858.
(15) Vinha, A. F.; Ferreres, F.; Silva, B. M.; Valentão, P.; Gonçalves, A.; Pereira, J. A.; Oliveira, M. B.; Seabra, R. M.; Andrade, P. B. Phenolic profiles of Portuguese olive fruits *Olea europaea* L.: Influences of cultivar and geographical origin. *Food Chem.* **2005**, *89*, 561−568.
(16) Bouaziz, M.; Jemai, H.; Khabou, W.; Sayadi, S. Oil content, phenolic profiling and antioxidant potential of Tunisian olive drupes. *J. Sci. Food Agric.* **2010**, *90*, 1750−1758.
(17) Jemai, H.; Bouaziz, M.; Sayadi, S. Phenolic composition, sugar contents and antioxidant activity of tunisian sweet olive cuitivar with regard to fruit ripening. *J. Agric. Food Chem.* **2009**, *57*, 2961−2968.
(18) Kanakis, P.; Termentzi, A.; Michel, T.; Gikas, E.; Halabalaki, M.; Skaltsounis, A. L. From olive drupes to olive oil. An HPLC−Orbitrap-based qualitative and quantitative exploration of olive key metabolites. *Planta Med.* **2013**, *79*, 1576−1587.
(19) Karkoula, E.; Skantzari, A.; Melliou, E.; Magiatis, P. Direct measurement of oleocanthal and oleacein levels in olive oil by quantitative ^{1}H NMR. Establishment of a new index for the characterization of extra virgin olive oils. *J. Agric. Food Chem.* **2012**, *60*, 11696−11703.
(20) Karkoula, E.; Skantzari, A.; Melliou, E.; Magiatis, P. Quantitative measurement of major secoiridoid derivatives in olive oil using qNMR. Proof of the artificial formation of aldehydic oleuropein and ligstroside aglycone isomers. *J. Agric. Food Chem.* **2014**, *62*, 600−607.

DOI: 10.1021/jf506367e
J. Agric. Food Chem. 2015, 63, 2400−2405

quantitative results.[26] Despite this, it presents a great difficulty in determining Na^+ due to the generation of Auger electrons, which decreases the fluorescence yield and limits its use in quantitative analysis of this element.[27] In addition to this effect, scattering effects of radiation such as Rayleigh, Compton, and Raman, also occur.[27−29] This situation requires specially designed tools for quantification, such as the fundamental parameters method (FP). The FP method is considered the state of the art in the correction of these effects and has the ability to apply theoretical corrections for the interelemental effect.[30−33] An example of FP use is the metal determination in rice samples[34] or in medicinal plants.[35]

Multivariate analysis, also known as chemometric tools, can also be employed, such as principal component analysis (PCA), which can reduce the size of the original data set. Furthermore, it is possible to recognize trends, outliers, and, most importantly, variables.[36−38] In the literature, examples are found of XRF and chemometric tools combination used to recognize similarities between samples, such as in honey bee.[39]

Calibration models can also be constructed by establishing a quantitative relationship between the information provided by the equipment and the properties of interest. Partial least squares (PLS) regression[40] performs predictions for sample values that have no previous classification,[41,42] being an important tool in analytical chemistry and also in industrial process control.[43] This strategy was employed to determine the energy value of flour and breakfast cereals;[44] to calibrate acidity, alcohol, and sucrose in *cachaça*;[45] to determine TiO_2 in toothpastes;[46] and for quality parameters of sugar cane,[47] always without reagent consumption and waste generation.

The goal of this study is to quantify the amounts of Na and K in samples of table salt (refined and marine) and low-sodium salt by EDXRF to compare three different quantification methodologies: the FP method, univariate calibration, and multivariate regression models by PLS.

MATERIALS AND METHODS

Samples. In the study, 21 samples of table salt were used. The samples were acquired in supermarkets and natural food stores in Campinas, SP, Brazil. The types, numbers of samples of each class, and the codes used for each brand are shown in Table 1.

Table 1. Types, Numbers of Samples, and Brands of Table Salt Used in the Study for the Na^+ and K^+ Determinations

salt type	no. of samples	brands
refined	8	RS1, RS2, RS3, RS4, RS5, RS6, RS7, RS8
low-sodium	7	LS1, LS2, LS3, LS4, LS5, LS6, LS7
marine	6	MS1, MS2, MS3, MS4, MS5, MS6

Samples of ca. 10 g were ground with a mortar and pestle, dried at 150 °C for 24 h, and stored in a desiccator prior to analysis. Specific cells were completely filled with salt (Chemplex 1300 cells with Chemplex 2.5 mm thick Mylar film) for EDXRF analysis in the spectrometer. The same treatment was used for the standards construction using analytical grade NaCl (Merck, Rio de Janeiro, Brazil) and KCl (Vetec, Rio de Janeiro, Brazil).

Fourteen standards with various concentrations of Na^+ and K^+ were prepared, in duplicate, by the mixing of NaCl and KCl. The standards were weighed on an analytical balance to five decimal places and comprise the ranges from 0 to 39 g/100 g of Na (0−100 g/100 g NaCl) and from 0 to 52 g/100 g for K (0−100 g/100 g KCl).

Irradiation Conditions. An EDXRF spectrometer (Shimadzu EDX700) with a rhodium target X-ray tube and a Si(Li) detector was used. The applied voltage for the X-ray tube was 50 kV; the detector dead time, 25%; collimator, 5 mm; and irradiation time, 500 s. The scanning range was from 0 to 20 keV with energy steps of 0.01 keV.

Experimental Data Processing. For peak areas and background signal calculations for Na and K analytical curves were used the programs WinSPEDAC 2.2 and WinQxas 1.30 (International Atomic Energy Agency).[48]

Fundamental parameters results were calculated by Shimadzu EDX700 software, version DXP-700E 1.00.

Matlab 7.0 (MathWorks) and PLSToolbox 4.0 (Eigenvector Research) were used to carry out PCA and PLS. The only preprocessing employed was data mean centering.

RESULTS AND DISCUSSION

Fundamental Parameters Determination. The FP method has the ability to resolve interferences caused by interelemental effects, especially in not very complex samples, such as table salt. However, this advantage is overcome by the nature of the elements Na, K, and Cl, which have atomic numbers of <22. The results for the NaCl and KCl standards concentration have deviations from the expected stoichiometric ratio (Table 2).

The results show that the FP quantification is not satisfactory, and other approaches are required to determine the salt composition, such as calibration by characteristic peak areas of the elements.

Determination by Peak Area Calculation. Figure 1a shows the overlapped EDXRF spectra of all standards, refined salt (RS), marine salt (MS), and low-sodium salt (LS) samples. The region from 0 to 4 keV, which contains the Na, K, and Cl characteristic Kα peaks, is shown in Figure 1b.

With the values of the calculated areas by WinQxas 1.30 program, a calibration curve was constructed for Na^+ (Figure 2a) through the directly proportional relationship between intensity (cps/μA) and standards concentration (g/100 g).

The low fluorescence intensity of Na leads to a low value of the slope (0.037). Nevertheless, there is a reasonable correlation between the obtained data, as shown by the regression coefficient value (r = 0.974).

The same treatment was performed for K, whose Kα peak areas (3.31 keV) were measured and plotted (Figure 2b). Again, data showed good correlation for the element (r = 0.992).

Finally, Na^+ and K^+ concentrations in refined, marine, and low-sodium salts samples were estimated. The calculated values

Table 2. Comparison of the Na, K, and Cl Contents Calculated for FP in Standards Obtained by Mixing Pure NaCl and KCl (n = 3)

	NaCl		KCl	
	Na	Cl	K	Cl
expected (g/100 g)	39	61	52	48
FP (g/100 g)	26.5 ± 0.4	72.6 ± 0.1	70.02 ± 0.04	29.94 ± 0.04
difference (%)	−32	19	35	−38

DOI: 10.1021/jf504941z
J. Agric. Food Chem. 2015, 63, 2406−2412

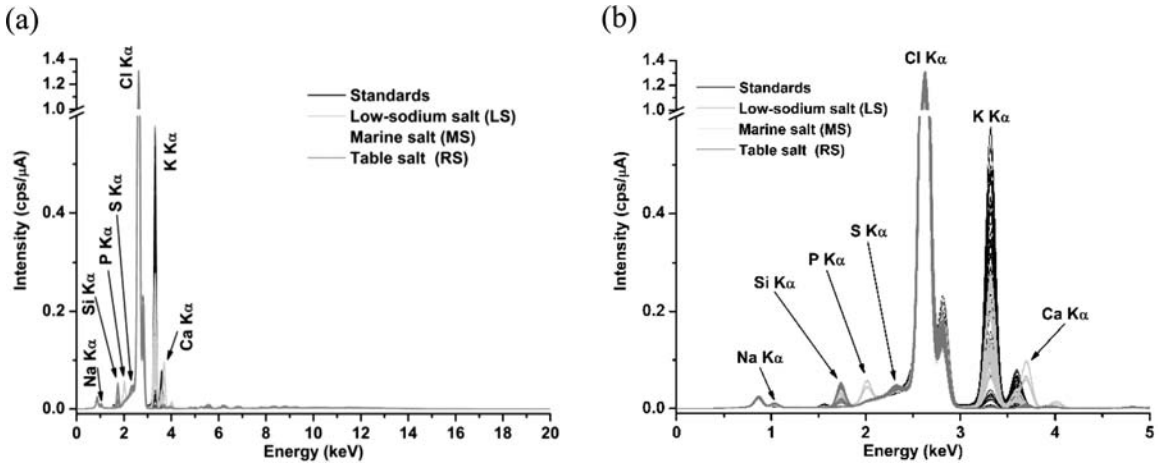

Figure 1. Overlapped XRF spectra of (a) all standards and samples of table salt (RS), marine salt (MS), and low-sodium salt (LS) and (b) 0−4 keV region.

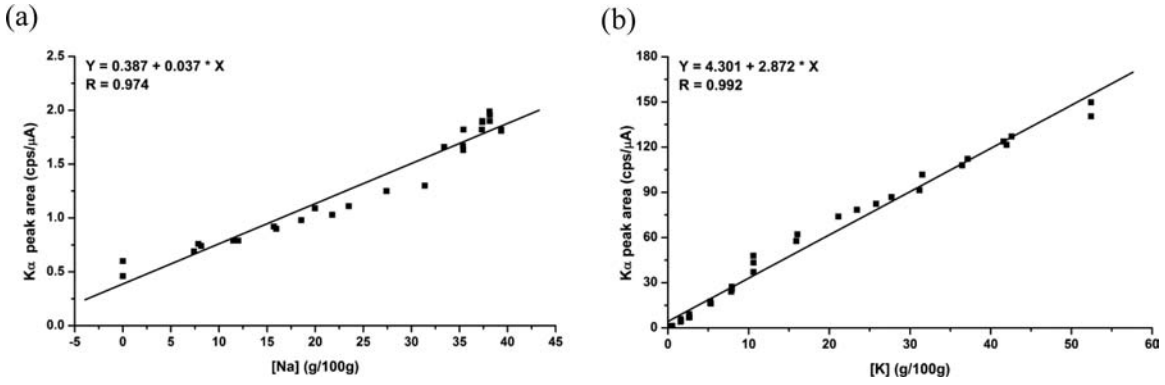

Figure 2. Analytical curves constructed for (a) Na and (b) K with characteristic Kα peak areas (n = 3).

Table 3. Na^+ Concentrations in Refined and Marine Salt Samples and Na^+ and K^+ Concentrations Calculated for the Low-Sodium Salt Samples from Constructed Analytical Curves (n = 9)

table salt	Na^+ (g/100 g)	marine salt	Na^+ (g/100 g)	low-sodium salt	Na^+ (g/100 g)	K^+ (g/100 g)
RS1	41 ± 1	SM1	37 ± 1	LS1	28 ± 3	13 ± 2
RS2	41 ± 3	SM2	36 ± 1	LS2	28 ± 3	7.9 ± 0.2
RS3	37 ± 2	SM3	39 ± 1	LS3	34 ± 7	7 ± 1
RS4	37 ± 1	SM4	37 ± 3	LS4	32 ± 8	7 ± 1
RS5	35 ± 1	SM5	36 ± 2	LS5	24 ± 6	18 ± 1
RS6	42 ± 2	SM6	38 ± 2	LS6	17 ± 4	22 ± 1
RS7	38 ± 1			LS7	28 ± 2	6 ± 2
RS8	39 ± 3					

for the Na element in table and marine salt samples were close to theoretical value for pure NaCl, which was 39 g/100 g (Table 3).

Apparently, table salts have higher levels of Na^+ than marine salts, once the refining process removes other elements such as Ca or Mg. Moreover, the salts have various origins and undergo different industrial processes, resulting in changes in the concentrations.

With respect to K in the low-sodium salt, there is a great variation in the sample concentration: from 6 ± 2 to 22 ± 1 g/100 g (Table 3). This may occur due to a manufacturer option to add other elements or compounds to reduce the Na^+ content. In low-sodium salt samples, the Na^+ reduction ranged from 13 to 58%.

Chemometric Analysis. The univariate calibration difficulties, that is, the difficulties in spectral manipulation for net intensity peak determination, and high levels of Na^+ in low-sodium salt samples led us to the use of chemometric tools as an alternative method for salt quantification. The standards and samples spectral data have 2048 intensity values related to each energy channel, with energies between 0 and 20 keV and resolution of 0.01 keV. Spectral data were mean centered, and the models were built with the software Matlab 7.0 (MathWorks) and PLSToolbox 4.0 (Eigenvector Research). In the statistical multivariate analysis 21 samples for PCA models were employed: 8 of refined salt, 6 of marine salt, and 7 of low-sodium salt, thus assembling a (21 × 2048) matrix. For the PLS models, 14 NaCl + KCl standards were made in duplicate. From this set, 7 were used for Na external validation and the

DOI: 10.1021/jf504941z
J. Agric. Food Chem. 2015, 63, 2406−2412

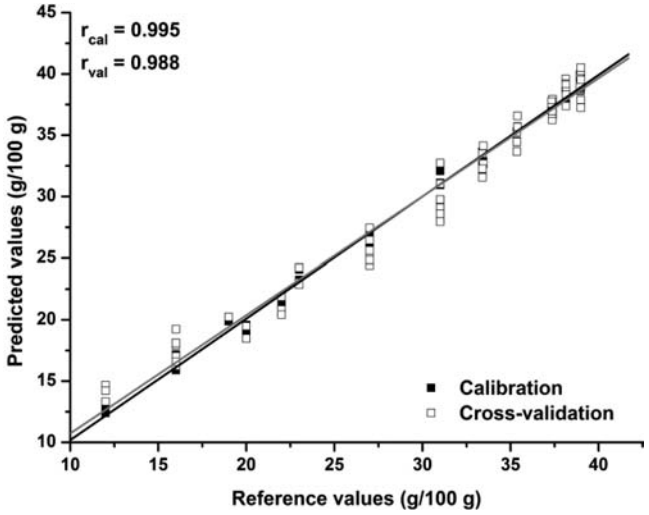

Figure 3. Correlation curves for reference and predicted values of Na^+ standards for calibration and internal validation (cross-validation) of the PLS model (n = 3).

Table 4. Na^+ Reference and Predicted Values with Mean Prediction Errors in External Validation Using the PLS Model

standard	reference value (g/100 g)	predicted value (g/100 g)	error (%)
2	39.3	41 ± 1	5
3	38.2	38 ± 1	2
5	35.4	36.3 ± 0.9	3
6	33.4	32.6 ± 0.5	2
7	31	30.69 ± 0.08	1
10	20	19.6 ± 0.4	2
12	11	13.5 ± 0.9	22

Table 5. Na^+ Contents in Commercial Table Salt, Marine Salt, and Low-Sodium Salt Samples Determined by PLS Model

table salt		marine salt		low-sodium salt	
sample	Na^+ (g/100 g)	sample	Na^+ (g/100 g)	sample	Na^+ (g/100 g)
RS1	33 ± 1	MS1	32.7 ± 0.9	LS1	26 ± 1
RS2	31.1 ± 0.5	MS2	32.1 ± 0.7	LS2	37.7 ± 0.5
RS3	32.2 ± 0.7	MS3	32.1 ± 0.7	LS3	26 ± 1
RS4	43.5 ± 0.5	MS4	43 ± 1	LS4	27.8 ± 0.9
RS5	44.5 ± 0.5	MS5	31.3 ± 0.5	LS5	23.3 ± 0.6
RS6	43 ± 1	MS6	43.5 ± 0.4	LS6	27 ± 1
RS7	42.2 ± 0.7			LS7	40 ± 2
RS8	42 ± 1				

other 7 for K validation. Finally, the 21 real samples were quantified in the PLS model performed with the spiked standards. Therefore, for multivariate analysis the spectral data are not manipulated but used as obtained after a simple preprocessing step.

PCA allowed the classification of the marine and table salts due to their Cl content and also due to some physical characteristics, such as moisture, particle size, and minor elements composition. For some samples the presence of an anti-humectant agent also allowed a differentiation. Detailed PCA discussion is presented in the Supporting Information.

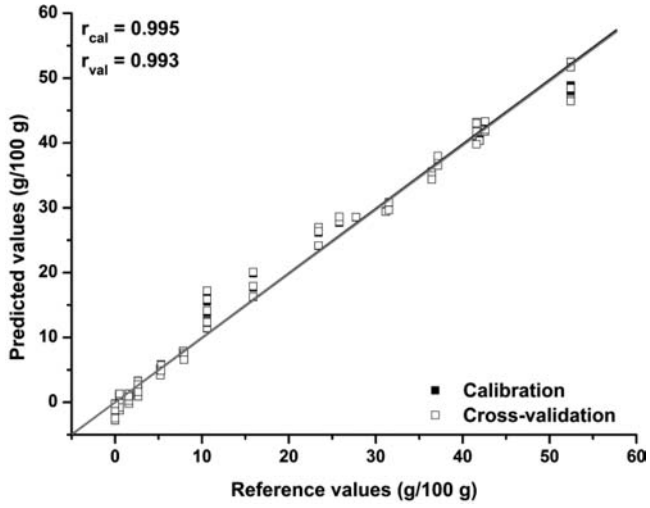

Figure 4. Correlation curves between reference and predicted values of K^+ standards for calibration and internal validation (cross-validation) of the PLS model (n = 3).

Table 6. K^+ Reference and Predicted Values with Mean Prediction Errors in External Validation Using the PLS Model (n = 3)

standard	reference value (g/100 g)	predicted value (g/100 g)	error (%)
3	1.56	not detected	
5	5.26	5 ± 1	14
6	7.89	8.7 ± 0.4	10
8	16.0	21 ± 1	30
9	21.1	24 ± 1	15
10	25.8	28.0 ± 0.3	8
11	31.5	33.3 ± 0.9	6

Table 7. K^+ Contents in Commercial Low-Sodium Salt Samples Determined by PLS Model

sample	K^+ (g/100 g)
LS1	33 ± 2
LS2	7 ± 1
LS3	30 ± 2
LS4	30 ± 2
LS5	39.8 ± 0.7
LS6	21.7 ± 0.9
LS7	8 ± 2

Na^+ Quantification by PLS. After the qualitative results of PCA, the next step was to build a PLS calibration model for Na and K. Spectral data were mean-centered, and the choice of latent variables number (LV) was performed based on the root-mean-square error of cross-validation (RMSECV) and the amount of accumulated information for each LV.

Five LVs were chosen on the basis of the variables contribution presented in the loadings graphs, and correlation curves were constructed for Na^+ values (measured and predicted) for calibration and cross-validation (RMSECV 1.286, cumulative variance in X 99.65%, cumulative variance in Y 99.08%). The values of correlation coefficients for calibration (r_{cal} = 0.995) and cross-validation (r_{val} = 0.988) show a good model correlation ability (Figure 3).

Table S1 in the Supporting Information shows the average values and prediction errors associated with the internal

DOI: 10.1021/jf504941z
J. Agric. Food Chem. 2015, 63, 2406−2412

Table 8. Comparison of Na^+ Contents Obtained by the Univariate Method (Peak Area) and Multivariate Method (PLS) for Table Salt and Marine Salt and Na^+ and K^+ Contents for Low-Sodium Salt

	Na^+ (g/100 g)			Na^+ (g/100 g)			Na^+ (g/100 g)		K^+ (g/100 g)	
table salt	univariate	PLS	marine salt	univariate	PLS	low-sodium salt	univariate	PLS	univariate	PLS
RS1	41 ± 1	33 ± 1	MS1	37.4 ± 0.4	32.7 ± 0.9	LS1	28 ± 3	26 ± 1	13 ± 2	33 ± 2
RS2	41 ± 3	31.1 ± 0.5	MS2	36 ± 1	32.1 ± 0.7	LS2	28 ± 3	38 ± 1	7.9 ± 0.2	7 ± 1
RS3	37 ± 2	32.2 ± 0.7	MS3	39 ± 1	32.1 ± 0.7	LS3	34 ± 7	26 ± 1	7 ± 1	30 ± 2
RS4	36.8 ± 0.7	43.5 ± 0.5	MS4	37 ± 3	43 ± 1	LS4	32 ± 8	28 ± 1	7 ± 1	30 ± 2
RS5	35.4 ± 0.7	44.5 ± 0.5	MS5	36 ± 2	31.3 ± 0.5	LS5	24 ± 6	23.3 ± 0.6	17.8 ± 0.6	39.8 ± 0.7
RS6	42 ± 2	43 ± 1	MS6	38 ± 2	43.5 ± 0.4	LS6	17 ± 4	27 ± 1	22 ± 1	21.7 ± 0.9
RS7	38 ± 1	42.2 ± 0.7				LS7	28 ± 2	40 ± 2	6 ± 2	8 ± 2
RS8	39 ± 3	42 ± 1								

calibration of the model, with most of the errors being below 10%. Only standard 12 shows an average error of 16%, probably because it displays the lowest content of Na^+, resulting in a difficult adjustment by the model. From an analysis of the errors, it is observed that in the range equivalent to samples—from pure NaCl (39% Na) by low-sodium salt samples (19% Na) concentration—they are acceptable (<10%).

Another tool for model evaluation is the use of an external validation step, as shown in Table 4. Again the model was suitable for Na^+ quantification in table salt samples, with errors exceeding a value of 5% in only one of the standards. This standard has a Na^+ concentration of 11 g/100 g, lower than all of the commercial samples.

The model was used to predict the Na values in 21 commercial samples (Table 5). In the refined salt samples (RS1−RS8), the levels found are placed between 31.1 ± 0.5 and 44.5 ± 0.5 g/100 g, with most samples having a higher content than pure NaCl, 39 g/100 g. This trend was observed only in 33% of marine salt (MS1−MS6) samples. These results emphasize the difficulty of determining light elements by XRF.

Finally, with regard to low-sodium salt, the PLS model indicated that Na^+ reduction, which should be at least 50%, was observed only for the LS5 sample (60%). The calibration capability (RMSEC) and prediction of cross-validation (RMSECV) were evaluated, being 0.811 and 1.286 g/100 g, respectively, whereas the *t* test concluded that systematic errors in the model are not significant, because t_{bias} calculated (0.069) was lower than t_{bias} tabulated (1.994).

K^+ Quantification by PLS. Similarly, a model for K was constructed, and calculated values of RMSECV and accumulated variance in *X* and *Y* led to the choice of four LVs (RMSECV 2.040, cumulative variance in *X* 99.78%, cumulative variance in *Y* 98.93%).

Table S2 in the Supporting Information presents the absolute prediction average errors for the internal validation (cross-validation), with larger errors for samples that have lower concentrations of element (standard 2, 3, and 4). In samples with concentration >23 g/100 g, the errors did not exceed 10%. This indicates the possibility to use the model for table salt samples with reduction of 50% of Na^+ by adding KCl.

Graphics of measured and predicted K^+ values were constructed for the calibration and cross-validation (Figure 4). The model has good correlation ability, as indicated by the correlation coefficients of calibration (r_{cal} = 0.995) and cross-validation (r_{val} = 0.993).

For external validation samples, errors are <10% for standards 10 and 11, with 25.8 and 31.5 g/100 g, respectively (Table 6).

Again, the model shows good calibration capability (RMSEC) and prediction of cross-validation (RMSECV), being 1.811 and 2.040 g/100 g, respectively. The *t* test concluded that systematic errors in the model are not significant, because t_{bias} calculated (0.180) was lower than t_{bias} tabulated (1.990).

Finally, the model for quantifying K^+ concentration was applied in seven commercial low-sodium salt samples with values from 7 ± 1 to 39.8 ± 0.7 g/100 g (Table 7).

Samples LS3 and LS4 (same brand but different batches) exhibit good agreement; on the other hand, this is not the case with LS1 and LS2 and LS5 and LS6 (from the same supplier). This discrepancy could be credited to the option of manufacturers to add other compounds rather than KCl or variations in the manufacturing process or raw materials. Taking into account these concentration variations in samples of the same suppliers and high deviation of the calibration, the method must be employed with reservations for determining K^+ in low-sodium salts.

Comparison of the Employed Methods. Table 8 shows a comparison of Na^+ levels in refined and marine salts, and in most cases some discrepancies between values occur. These differences may be positive or negative, with no apparent trend being detected. The same comparison was made for K^+.

For sea salt there is a reasonable correlation for Na, whereas for K in low-sodium salt the differences are more pronounced. The best results for Na in PLS can be attributed to a possible enhancement of the source scattering, because it is more susceptible to the effect for being a lighter element than K. A *t* test stated that there are no significant differences in the methods for Na quantification, because the calculated value (0.296) is lower than the tabulated value (2.086) for a confidence level of 95%.

The determination of Na^+ and K^+, due to their characteristics, are hard tasks to be achieved by XRF. The FP method, which considers all of the element signals present in the sample, is more subject to variations and deviations and sometimes is impracticable. The univariate method with peak area calibration is, in this specific case, a more interesting alternative, even though the several steps to manipulate the spectral data to obtain the net intensity area of the peaks demands longer analysis times. With respect to the time of the data preprocessing, chemometrics is faster than the univariate method because the spectra are used as obtained.

DOI: 10.1021/jf504941z
J. Agric. Food Chem. 2015, 63, 2406−2412

■ ASSOCIATED CONTENT

Supporting Information

PCA results for refined, marine, and low-sodium salt and scores and loadings graphics (Figures S1−S4). This material is available free of charge via the Internet at http://pubs.acs.org.

■ AUTHOR INFORMATION

Corresponding Author

*(F.L.M.) Phone: 55 42 3629 8129. Fax: 55 42 3629 8130. E-mail: fmelquiades@unicentro.br.

Funding

This research was funded by the Conselho Nacional de Desenvolvimento Científico e Tecnológico (CNPq) and Fundação de Amparo à Pesquisa do Estado de São Paulo (FAPESP).

Notes

The authors declare no competing financial interest.

■ ACKNOWLEDGMENTS

We thank André F. P. Biajoli for English evaluation and valuable critical analysis.

■ REFERENCES

(1) American Heart Association. Sodium and salt; http://www.heart.org/HEARTORG/GettingHealthy/NutritionCenter/HealthyDietGoals/Sodium-Salt-or-Sodium-Chloride_UCM_303290_Article.jsp (accessed Oct 28, 2014).

(2) ANVISA. Decreto 75.697/75; http://portal.anvisa.gov.br/wps/wcm/connect/1e2de70047457a74871ad73fbc4c6735/DECRETO_75697_1975.pdf?MOD=AJPERES (accessed Oct 28, 2014).

(3) INMETRO. Sal Refinado; http://www.inmetro.gov.br/consumidor/produtos/sal.asp (accessed Oct 28, 2014).

(4) INMETRO. Sal para Consumo Humano; http://www.inmetro.gov.br/consumidor/produtos/sal2.asp (accessed Oct 28, 2014).

(5) ANVISA. RDC no. 28; http://portal.anvisa.gov.br/wps/wcm/connect/c7624300474588a49268d63fbc4c6735/RDC_28.pdf?MOD=AJPERES (accessed Oct 28, 2014).

(6) Vinodkumar, M.; Rajagopalan, S. Multiple micronutrient fortification of salt and its effect on cognition in Chennai school children. *Asia Pac. J. Clin. Nutr.* **2007**, *16*, 505−511.

(7) Vinodkumar, M.; Rajagopalan, S. Multiple micronutrient fortification of salt. *Eur. J. Clin. Nutr.* **2009**, *63*, 437−445.

(8) Whitford, G. M. Fluoride metabolism when added to salt. *Schweiz. Monatsschr. Zahnmed.* **2005**, *115*, 675−678.

(9) Tramini, P. Salt fluoridation in France since 1986. *Schweiz. Monatsschr. Zahnmed.* **2005**, *115*, 656−658.

(10) Gillespie, G. M.; Baez, R. Development of salt fluoridation in the Americas. *Schweiz. Monatsschr. Zahnmed.* **2005**, *115*, 663−669.

(11) Bürgi, H.; Zimmermann, M. B. Salt as a carrier of iodine in iodine deficient areas. *Schweiz. Monatsschr. Zahnmed.* **2005**, *115*, 648−650.

(12) ANVISA. RDC no. 130; http://portal.anvisa.gov.br/wps/wcm/connect/583e21804745936f9b5fdf3fbc4c6735/RDC_130_2003.pdf?MOD=AJPERES (accessed Oct 28, 2014).

(13) Portal Brasil. Hipertensão atinge 24,3% da população adulta; http://www.brasil.gov.br/saude/2013/11/hipertensao-atinge-24-3-da-populacao-adulta (accessed Oct 28, 2014).

(14) Brown, I. J.; Tzoulakit, I.; Candeias, V.; Elliott, P. Salt intakes around the world: implications for public health. *Int. J. Epidemiol.* **2009**, *38*, 791−813.

(15) Sarno, F.; Claro, R. M.; Levy, R. B.; Bandoni, D. H.; Ferreira, S. R. G.; Monteiro, C. A. Estimativa de consumo de sódio pela população brasileira, 2002−2003. *Rev. Saude Publ.* **2009**, *43*, 219−225.

(16) WHO/FAO. *Diet, Nutrition and the Prevention of Chronic Diseases*; Report of a joint WHO/FAO expert consultation; Technical Report Series 916; World Health Organization: Geneva, Switzerland, 2003.

(17) ANVISA. Portaria no. 54/MS/SNVS; http://www.anvisa.gov.br/legis/portarias/54_95.htm (accessed Oct 28, 2014).

(18) Frank, R. L.; Mickelsen, O. Sodium-potassium chloride mixtures as table salt. *Am. J. Clin. Nutr.* **1969**, *22*, 464−470.

(19) Sarkkinen, E. S.; Kastarinen, M. J.; Niskanen, T. H.; Karjalainen, P. H.; Venäläinen, T. M.; Udani, J. K.; Niskanen, L. K. Feasibility and antihypertensive effect of replacing regular salt with mineral salt − rich in magnesium and potassium − in subjects with mildly elevated blood pressure. *Nutr. J.* **2011**, *10*, 1−9.

(20) Houston, M. C. The importance of potassium in managing hypertension. *Curr. Hypertens. Rep.* **2011**, *13*, 309−317.

(21) Chang, H.; Hu, Y.; Yue, C. J.; Wen, Y.; Yeh, W.; Hsu, L.; Tsai, S.; Pan, W. Effect of potassium-enriched salt on cardiovascular mortality and medical expenses of elderly men. *Am. J. Clin. Nutr.* **2006**, *83*, 1289−1296.

(22) Banerjee, G. Determination of sodium and potassium in salt by atomic absorption spectrophotometry or potassium by gravimetry with tetraphenyl boron. *Fresenius' J. Anal. Chem.* **1974**, *270*, 288.

(23) Goodney, D. E. Determination of sodium in salt substitute by flame emission spectrometry. *J. Chem. Educ.* **1982**, *59*, 875−876.

(24) Inczédy, J.; Lengyel, T.; Ure, A. M. *Compendium of Analytical Nomenclature (Definitive Rules 1997) − The Orange Book*, 3rd ed.; Blackwell Science: Oxford, UK, 1998.

(25) Jenkins, R.; De-Vries, J. L. *Practical X-Ray Spectrometry*, 2nd ed.; Springer-Verlag: New York, 1970.

(26) Bertin, E. P. *Principles and Practice of X-Ray Spectrometric Analysis*; Plenum Press: New York, 1970.

(27) Jenkins, R. *X-Ray Fluorescence*, 2nd ed.; Wiley-Interscience: New York, 1999

(28) Van Gysel, M.; Lemberge, P.; Van Espen, P. Description of compton peaks in energy-dispersive X-ray fluorescence spectra. *X-Ray Spectrom.* **2003**, *32*, 139−147.

(29) Mizuno, Y.; Ohmura, Y. Theory of X-ray raman scattering. *J. Phys. Soc. Jpn.* **1967**, *22*, 445−449.

(30) Pavlinsky, G. V.; Dukhanin, A. Y.; Baranov, E. O.; Portnoy, A. Y. Theory of the implementation of the fundamental parameter method for the X-ray fluorescence determination of low-atomic-number elements. *J. Anal. Chem.* **2006**, *61*, 654−661.

(31) Sherman, J. The theoretical derivation of fluorescent X-ray intensities from mixtures. *Spectrochim. Acta, Part B* **1955**, *7*, 283−306.

(32) Shiraiwa, T.; Fujino, N. Theoretical calculation of fluorescent X-ray intensities in fluorescent X-ray spectrochemical analysis. *Jpn. J. Appl. Phys.* **1966**, *5*, 886−899.

(33) Bilbrey, D. B.; Bogart, G. R.; Leyden, D. E.; Harding, A. R. Comparison of fundamental parameters programs for quantitative X-ray fluorescence spectrometry. *X-Ray Spectrom.* **1988**, *17*, 63−73.

(34) Teixeira, A. P.; Quintella, C. M.; Korn, M. G. A.; Fernandes, A. P.; Castro, M. T. P. O. Determinação de Mn e Zn em arroz empregando espectrometria de fluorescência de raios X de energia dispersiva. *Quim. Nova* **2012**, *35*, 1133−1136.

(35) Shaltout, A. A.; Moharram, M. A.; Mostafa, N. Y. Wavelength dispersive X-ray fluorescence analysis using fundamental parameter approach of *Catha edulis* and other related plant samples. *Spectrochim. Acta, Part B* **2012**, *67*, 74−78.

(36) Geladi, P. Chemometrics in spectroscopy. Part 1. Classical chemometrics. *Spectrochim. Acta, Part B* **2003**, *58*, 767−782.

(37) Wold, S.; Esbensen, K.; Geladi, P. Principal component analysis. *Chemom. Intell. Lab. Syst.* **1987**, *2*, 37−52.

(38) Massart, D. L.; Vandeginste, B. G. M.; Buydens, L. M. C.; De-Jong, S.; Lewi, P. J.; Smeyers-Verbeke, J. *Handbook of Chemometrics and Qualimetrics − Part A*; Elsevier: Amsterdam, The Netherlands, 1997.

(39) Enrich, C.; Boeykens, S.; Caracciolo, N.; Custo, G.; Vásquez, C. Honey characterization by total reflection X-ray fluorescence: evaluation of environmental quality and risk for the human health. *X-Ray Spectrom.* **2007**, *36*, 215−220.

(40) Otto, M. *Chemometrics*; Wiley: Weinheim, Germany, 1999.

DOI: 10.1021/jf504941z
J. Agric. Food Chem. 2015, 63, 2406−2412

(41) Martens, H.; Naes, T. *Multivariate Calibration*; Wiley: New York, USA, 1996.
(42) Geladi, P.; Kowalski, B. R. Partial least-squares regression: a tutorial. *Anal. Chim. Acta* **1986**, *185*, 1−17.
(43) Beebe, K. R.; Pell, R. J.; Seasholtz, M. B. *Chemometrics: A Practical Guide*; Wiley: New York, 1998.
(44) Terra, J.; Antunes, A. M.; Prado, M. A.; Bueno, M. I. M. S. Energy value determinations of industrialized foods: the potential of using X-ray spectroscopy and partial least squares. *X-Ray Spectrom.* **2010**, *39*, 167−175.
(45) Alexandre, T. L.; Goraieb, K.; Bueno, M. I. M. S. Quality control of beverages using XRS allied to chemometrics: determination of fixed acidity, alcohol and sucrose contents in Brazilian cachaça and cashew juice. *X-Ray Spectrom.* **2010**, *39*, 285−290.
(46) Schwab, N. V.; Da-Col, J. A.; Terra, J.; Bueno, M. I. M. S. Fast direct determination of titanium dioxide in toothpastes by X-ray fluorescence and multivariate calibration. *J. Braz. Chem. Soc.* **2012**, *23*, 546−554.
(47) Melquiades, F. L.; Bortoleto, G. G.; Marchiori, L. F. S.; Bueno, M. I. M. S. Direct determination of sugar cane quality parameters by X-ray spectrometry and multivariate analysis. *J. Agric. Food Chem.* **2012**, *60*, 10755−10761.
(48) International Atomic Energy Agency. http://www-naweb.iaea.org/napc/physics/ps/soft.htm (accessed Oct 28, 2014).

DOI: 10.1021/jf504941z
J. Agric. Food Chem. 2015, 63, 2406−2412

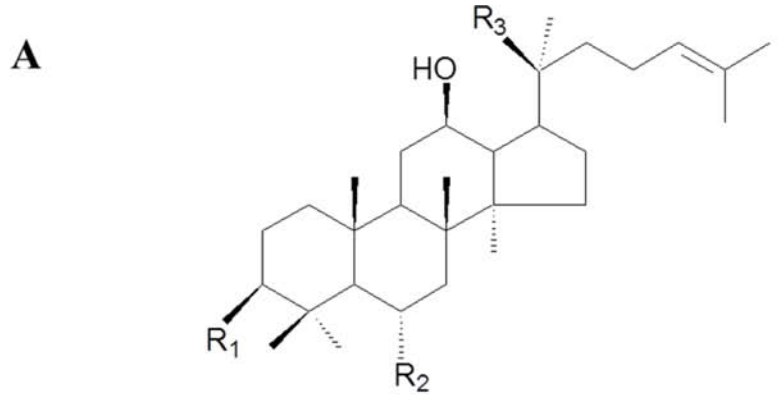

Compound	R1	R2	R3
Notoginsenoside R1 (**1**)	-OH	-O-Glc-(2-1)-Xyl	-O-Glc
Ginsenoside Rg1 (**2**)	-OH	-O-Glc	-O-Glc
Ginsenoside Re (**3**)	-OH	-O-Glc-(2-1)-Rha	-O-Glc
Ginsenoside Rb1 (**4**)	-O-Glc-(2-1)-Glc	-H	-O-Glc-(6-1)-Glc
Ginsenoside Rd (**5**)	-O-Glc-(2-1)-Glc	-H	-O-Glc

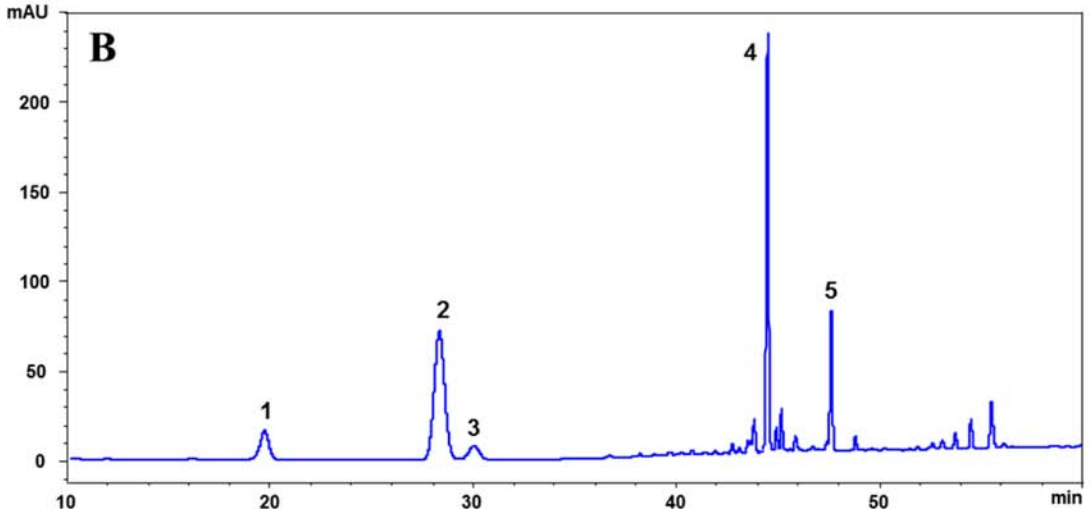

Figure 1. Chemical structures of notoginsenoside R1, ginsenoside Rg1, Re, Rb1 and Rd (A), and representative HPLC-UV chromatogram of PNS. HPLC was performed using an Agilent Zorbax Extend-C18 (250 × 4.6 mm i.d.,5 μm) and an Agilent Zorbax Extend-C18 guard columns (12.5 × 4.6 mm i.d.,5 μm) at 40 °C. The mobile phase consisted of water (a) and acetonitrile (b) using the following gradient program: 0−30 min, 18−19%b; 30−40 min, 19−31%b; 40−60 min, 31−70%b. Flow rate was kept at 1.5 mL/min, the detection wavelength was set at 203 nm, and the sample injection volume was 10 μL. Peaks: 1, notoginsenoside R1; 2−5, ginsenosides Rg1, Re, Rb1, and Rd, respectively. Glc, β-D-glucose; Rha, α-L-rhamnose; Xyl, β-D-xylose.

rated fatty acids,[12] have been shown to possess protective effects against ethanol-induced liver injury. Root of *Panax notoginseng* (Burk.) F. H. Chen, also called as Sanqi in Chinese, is a highly valued medicinal herbs that has been traditionally applied to clinic for preventive and therapeutic purposes, especially for cardiovascular diseases and hepatic diseases, either alone or in combination.[13] *P. notoginseng* is contained in several famous Chinese traditional formulas, such as "*Pian Zi Huang*", which is used for the treatment of virus hepatitis. *P. notoginseng* has also been widely used for a variety of medicinal cuisines for the diverse purposes, including soup, stew, and beverage. Dammarane-type triterpene saponins are generally considered to be the major bioactive constituents in *P. notoginseng*.[13,14] An increasing number of in vivo and in vitro studies have demonstrated that *P. notoginseng* and its saponins exerted extensively beneficial effects on several systems, including hematological,[15] immune,[16] cardiovascular,[17] central nervous,[18] and endocrine systems.[19] However, the effect of *P. notoginseng* saponins (PNS) on ethanol-induced liver injury has not been fully elucidated.

A mouse model of acute alcohol consumption could be used to investigate the early effects of alcohol-induced liver injury and is well-suited to mimicking acute alcohol administration, with blood ethanol concentrations, behavioral effects, and physiological changes comparable to those of binge drinking in humans.[20] In the present study, the protective effect of PNS on

DOI: 10.1021/jf502990n
J. Agric. Food Chem. 2015, 63, 2413−2422

acute ethanol-induced liver injury and its underlying molecular mechanisms were investigated in a mouse model of binge drinking.

MATERIALS AND METHODS

Chemicals. *Panax notoginseng* saponins (PNS) was purchased from International Laboratory Inc. (San Francisco, CA, U.S.A.) with the labeled purity of over 95%. Authentic saponins, including notoginsenoside R1, ginsenosides Rg1, Re, Rb1, and Rd, were purchased from National Institute for the Control of Pharmaceutical and Biological Products (Beijing, P.R. China) and their structures are shown in Figure 1A. Absolute ethanol (99.9%) was the product of Sigma-Aldrich (St Louis, MO, U.S.A.). The preparations were made fresh every time before the commencement of the experiment. HPLC-grade acetonitrile was purchased from Merck KGaA (Darmstadt, Germany), and deionized water was prepared by a Milli-Q purification system (Millipore, Bedford, MA, U.S.A.). All other chemicals were of analytical grade.

HPLC Analysis of PNS. To ensure the consistency of its efficacy, the commercial PNS was analyzed by high-performance liquid chromatography (HPLC) as previously developed chromatographic conditions.[17,21,22] Briefly, the analysis was achieved using an Aglient 1100 series HPLC apparatus (Palo Alto, CA, USA). An Zorbax Extend-C18 (250 × 4.6 mm i.d., 5 μm) and an Zorbax Extend-C18 guard columns (12.5 × 4.6 mm i.d., 5 μm) were used at a column temperature of 40 °C. The mobile phase consisted of water (A) and acetonitrile (B) using the following gradient program: 0−30 min, 18−19% B; 30−40 min, 19−31% B; 40−60 min, 31−70% B. Flow rate was kept at 1.5 mL/min, analyte was detected at 203 nm, and the sample injection volume was 10 μL.

Animals and Treatments. All the animal procedures were approved by Animal Ethics Committee, Institute of Chinese Medical Sciences, University of Macau (Approval No. AEC-13-002), and every effort was made to minimize animal suffering. Male C57BL/6 mice, weighting 25−30g, were purchased from Laboratory Animal Services Center, the Chinese University of Hong Kong (Hong Kong, China). Mice were maintained on individually ventilated cage (IVC) system in a temperature (22.5 ± 0.5 °C) and humidity (50 ± 5%) controlled rooms with a 12 h light/dark cycle and allowed free access to water and standard lab chow. After 2 weeks acclimation, all mice were randomly divided into four groups (i.e., control group, ethanol group, and two PNS treatment groups). A mouse model of binge drinking was used to induce acute ethanol-induced liver injury. Low-dose and high-dose group animals were orally administered PNS at doses of 100 and 300 mg/kg BW, respectively for 7 days prior to ethanol challenge, at the same time, mice in control and ethanol groups received an equal volume of water. On day 8, mice received three acute doses of 60% (v/v) ethanol (4.7 g/kg BW) in water every 12 h by oral gavage. Control mice were treated with an isocaloric maltose solution to eliminate the difference in energy between the control and ethanol groups. The used ethanol dose had shown to cause significant liver injury, as described in our previous study.[12] At 4 h after the last administration, mice were sacrificed and their blood samples, whole livers, and epididymal fats were immediately collected. The portion of tissues from the same lobe of liver in each mouse was embedded in OCT (frozen tissue matrix) for histological analysis. The remaining liver tissue and epididymal fat were stored at −80 °C until analyzed.

Measurement of Serum Aminotransferase Levels. Serum biochemical markers (e.g., alanine aminotransferase (ALT) and aspartate aminotransferase (AST)) are commonly used to indicate liver injury.[23] To examine the effect of PNS on acute ethanol-induced hepatotoxicity, serum levels of ALT and AST were determined by using commercial spectrophotometric kits (Nanjing Jiancheng Bioengineering Institute, Nanjing, China) according to the manufacturer's instructions.

Histological Assay. The embedded liver sample slices were processed by standard Oil Red O staining procedure. Briefly, liver cryostat sections (8 μm) were fixed with 4% phosphate-buffered paraformaldehyde (pH = 7.4), stained with Oil Red O (Sigma-Aldrich, St Louis, MO, U.S.A.) and counterstained with hematoxylin (Sigma-Aldrich). The stained sections were examined and recorded by an Olympus CX-31 light microscopy with CCD camera (Olympus Crop, Tokyo, Japan).

Measurement of Serum and Hepatic Triglyceride Contents. Triglyceride levels in serum and liver samples were quantitatively determined by a Triglyceride Quantification Kit (Beijing BHKT Clinical Reagent Co., Ltd., Beijing, China) following the manufacturer's protocol. For hepatic triglyceride assay, 50 mg of liver tissue was homogenized in 450 μL of chloroform/methanol solution (2:1, v/v). After extraction for 24 h at 4 °C, 500 μL 0.9% NaCl was added to each sample. Samples were then centrifuged at 2000 rpm for 15 min, and the organic phase (lower) was removed to a new tube and dried under nitrogen gas. The resulting residue was dissolved in 100 μL phosphate-buffered saline containing 1% Triton X-100 and the triglyceride contents were then determined by using a Triglyceride Quantification Kit. The value of hepatic triglyceride content was normalized to wet tissue weight and expressed as mg/g of liver. Serum triglyceride levels of mice were also examined by the identical kit.

Determination of Hepatic ROS, MDA, SOD, and GSH Levels. Liver tissue was homogenized in 19 volumes of cold radioimmunoprecipitation assay buffer (RIPA buffer, Beyotime Institute of Biotechnology, Nanjing, China) and the tissue homogenate (5%, w/v) was prepared. After centrifugation at 12500*g* for 20 min at 4 °C, the supernatant was collected for the measurement of hepatic superoxide dismutase (SOD) activity, and the levels of reactive oxygen species (ROS), malondialdehyde (MDA), and glutathione (GSH) using commercial Superoxide Dismutase Assay Kit, Reactive Oxygen Species Detection Assay Kit, Malondialdehyde Assay Kit, and Reduced Glutathione Assay Kit (Nanjing Jiancheng Institute, China), respectively, according to the manufacturer's instructions. The values were normalized to hepatic total protein.

Measurement of Hepatic Cytokines. Hepatic TNF-α and IL-6, were quantified using commercial TNF-α and IL-6 ELISA kits. Briefly, 50 mg of liver tissue was homogenized in 450 μL PBS containing 0.5% Triton X-100 and 1% phenylmethylsulfonyl fluoride (PMSF) protease inhibitor (Thermo Scientific), then centrifugated at 12 000*g* for 10 min.[24] The levels of TNF-α and IL-6 in the supernatant were respectively examined by using Mouse TNF-α and IL-6 ELISA MAX Standard kits (BioLegend Inc., San Diego, CA, U.S.A.). The values were normalized to total protein and expressed as pg/mg of protein.

Measurement of Adipose Tissue Lipolysis. Lipolysis of adipose tissue was measured as free fatty acid (FFA) released into the culture medium ex vivo. Briefly, fresh epididymal adipose tissue explants were washed in culture plates with prewarmed Dulbecco's PBS containing 100 U/mL penicillin and 100 mg/mL streptomycin. After removing possible blood vessels and connective tissues, approximate 30 mg of adipose tissue was transferred to 12-well plates, cut into small pieces, and cultured in 2 mL DMEM supplemented with L-glutamine (2 mM), penicillin (50 U/mL), streptomycin (50 mg/mL), and 2% fatty acid-free bovine serum albumin for 2 h. FFA released into the culture medium was measured by using a Fatty Acid Quantification Kit (Biovision, Milpitas, CA) according to its manufacturer's instruction. The FFA in serum was also determined using the same kit.

Western Blotting Analysis. Total proteins were extracted from liver and epididymal adipose tissue using RIPA buffer containing 1% phenylmethanesulfonylfluoride (Beyotime Institute of Biotechnology) and 1% phosphatase inhibitor cocktail. Protein concentrations were measured with Pierce BCA Protein Assay Kit (Thermo Fisher Scientific Inc., Rockford, IL, U.S.A.). Aliquots containing 60 μg protein samples were separated by electrophoresis on 8% or 10% SDS-PAGE gel and transferred onto a polyvinylidene fluoride (PVDF) membranes. After blocking with 5% nonfat dry milk in Tris-buffered saline with 0.1% Tween-20 (TBST) for 1h at room temperature, the membranes were immunoblotted with primary antibodies, including CYP2E1 (1:500; Abcam, Cambridge, U.K.), HSL (1:1000; Cell Signaling Technology, Danvers, MA), Phospho-HSL (1:1000; Cell Signaling Technology) and GAPDH (1:1500; Cell Signaling Technology) at 4 °C for overnight. HSL antibody can recognize both phosphorylated HSL and unphosphorylated HSL, and phospho-

DOI: 10.1021/jf502990n
J. Agric. Food Chem. 2015, 63, 2413−2422

HSL antibody specifically recognized the phosphorylated HSL. After three 10 min washings in TBST, the membranes were incubated with second antibody HRP-linked antimouse IgG (1:3000; Cell Signaling Technology) at room temperature for 1 h. The protein bands were visualized by using Amersham ECL Select Western Blotting Detection Reagent (GE Healthcare Bio-Sciences., Piscataway, NJ, U.S.A.) under in Bio-Rad ChemiDoc XRS System (Bio-Rad Laboratories, Inc., Hercules, CA, U.S.A.), and quantified by densitometry analysis using Quantity One software (Bio-Rad).

Real Time-PCR Analysis. Total RNA was extracted from liver using Trizol reagent (Life Technologies Corp., Grand Island, NY, U.S.A.) and cDNA was synthesized using a random primer and TaqMan Reverse Transcription Reagents Kit (Life Technologies). The sequences of CD36 (forward: 5′-ATGGGCTGTGAT CGGAACTG-3′; reverse: 5′-GTCTTCCCAATAAGCATGTCTCC-3′) and β-actin (forward: 5′-GGCTGTATTCCCCTCCATCG-3′; reverse: 5′-CCAGTTGGTAACAATGCCATGT-3′) were obtained from the Primer Bank (http://pga.mgh.harvard.edu/primerbank). Real Time-PCR reactions were performed by using SYBR Green PCR Master Mix in an Applied Biosystems 7500 Real-Time PCR System (Life Technologies) and normalized to β-actin content.

Statistical Analysis. Data was expressed as mean ± standard deviation (SD). Student's t-test was used for between-group comparison using GraphPad Prism 5.0 software. The levels of significance was considered at $P < 0.05$.

RESULTS

Saponin Composition of PNS. The commercial PNS from *P. notoginseng* contains a number of different dammarane triterpene saponins. In order to ensure quality consistency of the tested sample and experimental reproducibility, the chemical characteristics of PNS was profiled using the previously developed HPLC-UV method (Figure 1B).[17,21,22] Notoginsenoside R1, ginsenosides Rg1, Re, Rb1, and Rd were well identified by comparing the retention times of the peaks with those of the reference compounds eluted under the same chromatographic conditions, and their individual concentrations were determined to be 8.1%, 32.0%, 3.9%, 33.4%, and 7.4% of PNS, respectively.

Body Weight, Liver Weight, and Liver Index. The body weight, liver weight, and liver index (liver weight/body weight, %) were compared across four groups and were shown in Table 1. Three doses of ethanol administration and PNS treatment did not affect animal body weight and liver weight, when compared to control group. However, the liver index in ethanol group was remarkably increased by 9.0%, the most plausible explanation was that alcohol exposure caused the lipid accumulation in the liver. This increase was prevented by PNS treatments, especially by high-dose PNS (300 mg/kg BW) treatment. Low-dose PNS (100 mg/kg BW) showed a decreasing tendency compared to ethanol group, but there was no significant difference.

Table 1. Effects of PNS on Body Weight, Liver Weight and Liver Index (Liver Weight/Body Weight, %) in Ethanol-Treated Mice[a]

	control	ethanol	ethanol + PNS (100 mg/kg)	ethanol + PNS (300 mg/kg)
body weight (g)	28.2 ± 0.9	28.0 ± 2.3	26.9 ± 1.4	26.9 ± 3.0
liver weight (g)	1.12 ± 0.09	1.21 ± 0.08	1.16 ± 0.08	1.11 ± 0.14
liver index (%)	3.98 ± 0.38	4.34 ± 0.16[b]	4.29 ± 0.17	4.11 ± 0.19[c]

[a]Data are expressed as mean ± SD ($n = 6$). [b]$P < 0.01$, compared to the control group. [c]$P < 0.05$, compared to the ethanol group.

PNS Attenuated Acute Ethanol-Induced Hepatoxicity. ALT and AST are released from the cytoplasm of hepatocytes that have suffered structural damage. Their serum activities were most commonly used as reliable primary indicators for clinical monitoring of liver injury.[8] As shown in Figure 2, serum

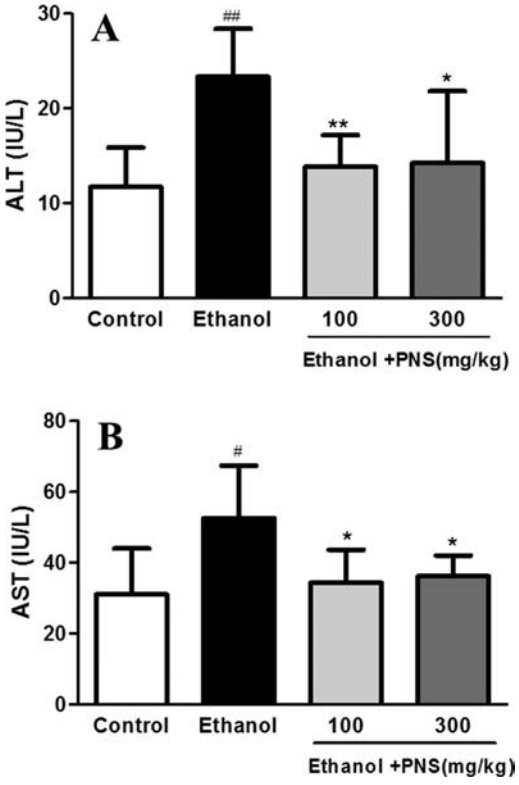

Figure 2. Effects of PNS on acute ethanol-induced changes in serum enzyme activities of (A) ALT and (B) AST. Value represents means ± SD ($n = 6$). IU/L, International Unit per liter; $^{\#}P < 0.05$ and $^{\#\#}P < 0.01$ compared to the control group; $^{*}P < 0.05$ and $^{**}P < 0.01$, compared to the ethanol group.

levels of ALT and AST in ethanol group were significantly increased by 100% (23.4 ± 5.0 vs 11.7 ± 4.1) and 69.1% (52.6 ± 14.9 vs 31.1 ± 12.9), respectively, over those in control group. However, it was also apparent that the pretreatment with PNS, either low-dose or high-dose, was effective in suppressing the acute ethanol-induced liver injury by decreasing the levels of serum ALT and AST activities. Nevertheless, this suppressive effect on ethanol-induced injury did not appear in dose dependent manner.

PNS Prevented Acute Ethanol-Induced Lipid Accumulation in Liver. To assess the effect of PNS on hepatic steatosis induced by acute ethanol intake, hepatic lipid accumulation was qualitatively examined by Oil Red O staining and quantitatively determined by a triglyceride quantification kit. After three doses of ethanol administration via oral gavage, mice from both the ethanol groups and ethanol + PNS groups exhibited obvious accumulation of neutral lipid droplets in their livers when compared to control group, as illustrated by Oil Red O staining (Figure 3A–D). The lipid droplets in the livers of PNS-treated groups were much smaller and fewer than those

DOI: 10.1021/jf502990n
J. Agric. Food Chem. 2015, 63, 2413−2422

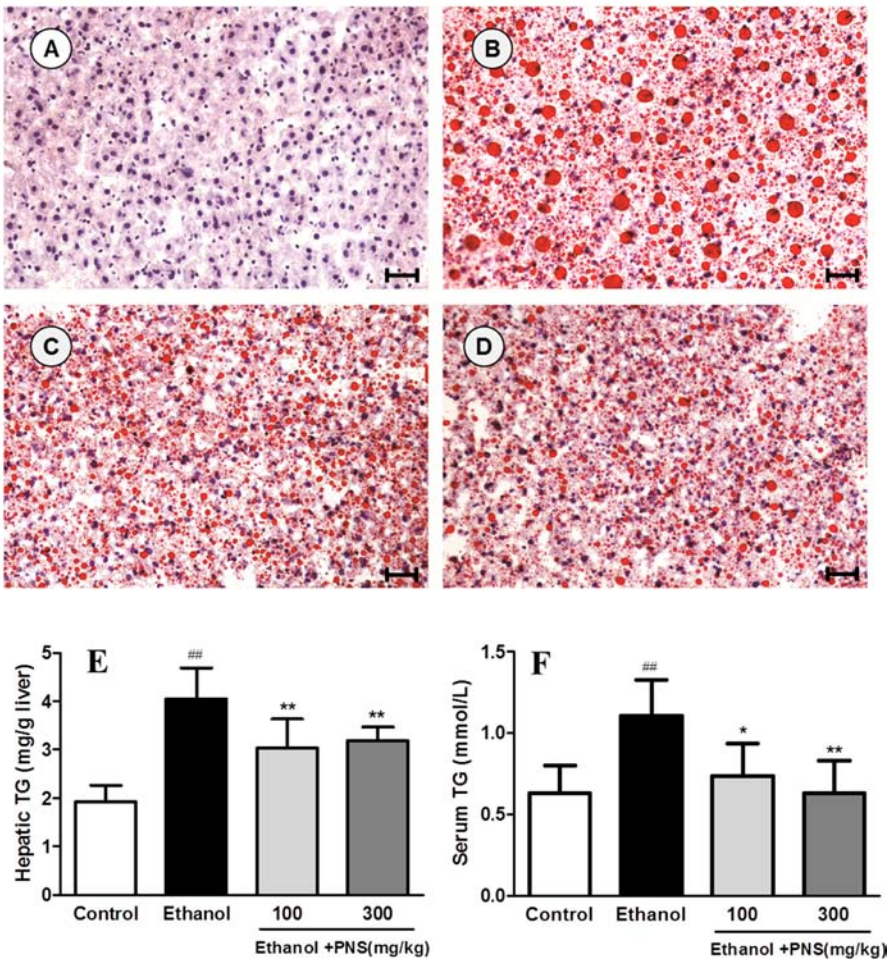

Figure 3. PNS suppressed acute ethanol-induced hepatic lipid accumulation. Representative Oil Red O-stained sections of the livers from (A) control, (B) ethanol group, (C) ethanol + PNS (100 mg/kg BW), and (D) ethanol + PNS (300 mg/kg BW) (400 × magnification; scale bars, 25 μm); (E) hepatic triglyceride levels; and (F) serum triglyceride levels. Value represents means ± SD (n = 6). $^{\#\#}P < 0.01$, compared to control group; $^{*}P < 0.05$, $^{**}P < 0.01$, compared to ethanol group.

in the ethanol group. Quantitative analysis confirmed the histological results by demonstrating that acute ethanol gavage dramatically increased the hepatic triglyceride content in mice, and this elevation was significantly diminished by pretreatment of PNS at dose of 100 mg/kg or 300 mg/kg (Figure 3E). In addition, serum triglyceride levels in PNS-treated mice were significantly lower when compared to that of ethanol group (Figure 3F). These data clearly indicated that PNS could effectively acute ethanol-induced liver injury, at least in part, through reversing hepatic lipid accumulation.

Effect of PNS on WAT Lipolysis and Hepatic Fatty Acid Uptake. To gain insight into the mechanisms underlying inhibitory effect of PNS on acute ethanol-induced hepatic steatosis, we examined the lipolysis capacity of white adipose tissue (WAT) and the expressions of the related gene involved in fatty acid transportation from adipose tissue to liver. Lipolysis capacity was determined by incubating freshly isolated epididymal WAT. As shown in Figure 4A, adipose explants from alcohol-fed mice showed a significant increase in FFA release during 2 h incubation, in comparison to control group. Pretreatment with PNS completely abolished the increased FFA release from epididymal WAT induced by ethanol intake. These results were consistent with the change in serum FFA level, PNS could prevent the serum FFA content elevated by acute ethanol consumption (Figure 4B). Hormone-sensitive lipase (HSL) is the rate-limiting enzyme for lipolysis of triglyceride in adipose tissue, and the activity of HSL is primarily regulated by phosphorylation−dephosphorylation reactions.[25] Therefore, the protein expression levels of total HSL and phosphorylated HSL (p-HSL) in epididymal WAT were examined by Western blotting analysis. As shown in Figure 4C and D, acute ethanol exposure obviously up-regulated the protein expressions of p-HSL and total HSL, as well as p-HSL/HSL ratio, which were suppressed by PNS. Our results suggested that pretreatment with PNS improved the acute ethanol-induced WAT dysfunction, which was associated with inhibiting the expressions of p-HSL and total HSL.

CD36 is a major fatty acid translocase for hepatic fatty acid uptake.[26] The transcriptional levels of CD36 in liver tissue were also examined by real-time PCR analysis. Acute ethanol feeding significantly increased the mRNA expression of CD36 in liver, which was normalized by PNS (Figure 4E). These data suggested that PNS might decrease the elevation of hepatic fatty acid uptake stimulated by ethanol feeding.

PNS Relieved Ethanol-Mediated Oxidative Stress. The term oxidative stress characterizes an imbalance between endogenous prooxidants (e.g., ROS) and antioxidants (e.g., SOD and GSH), ROS has a great potential to react with lipids,

DOI: 10.1021/jf502990n
J. Agric. Food Chem. 2015, 63, 2413−2422

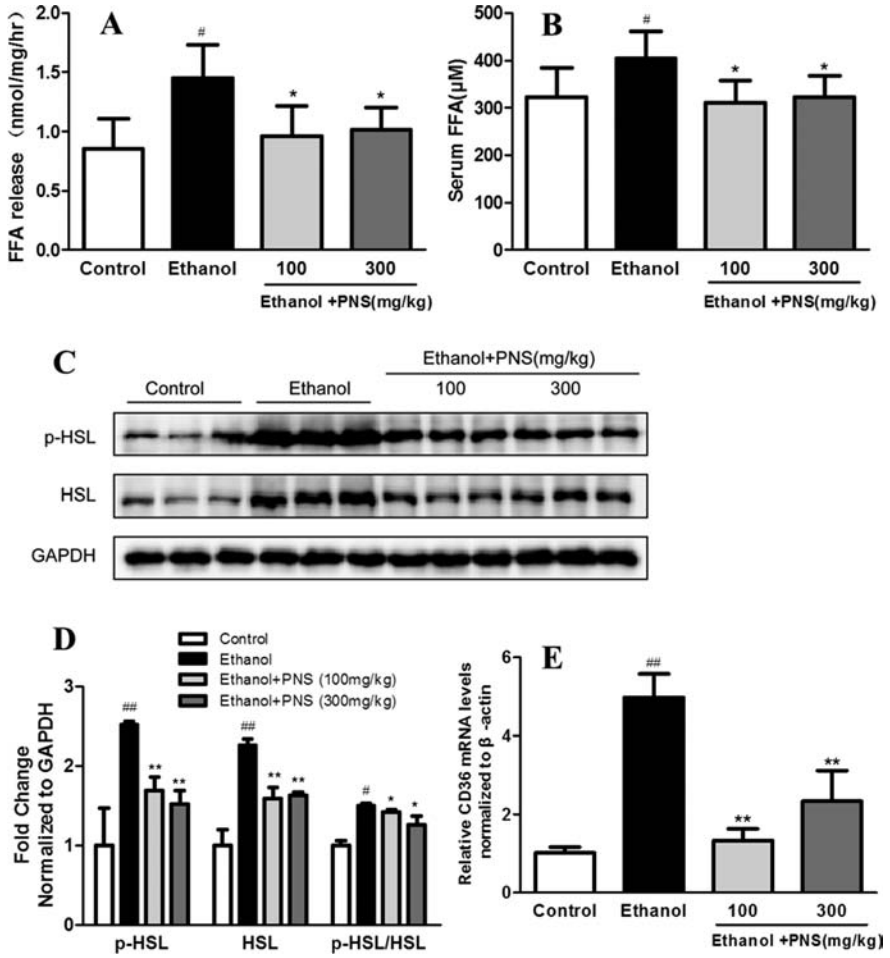

Figure 4. PNS ameliorated acute ethanol-induced dysfunctional lipid metabolism at WAT-liver axis. (A) Fatty acid release from epididymal WAT ex vivo; (B) serum FFA levels; (C) Immunoblot analysis of HSL and p-HSL proteins related to lipolysis in epididymal WAT. (D) The immunoblot bands were quantified by densitometry analysis, and ratio to GAPDH was calculated by setting the value of controls as one. (E) Real-time PCR analysis of hepatic CD36 gene related to fatty acid uptake. Value represents means ± SD (n = 6 in A and B; n = 3 in C; n = 4 in E). $^{\#}P < 0.05$ and $^{\#\#}P < 0.01$, compared to the control group; $^{*}P < 0.05$ and $^{**}P < 0.01$, compared to the ethanol group.

Table 2. Effects of PNS on Hepatic ROS, MDA, GSH, and SOD in Ethanol-Treated Mice[a]

meas.	control	ethanol	ethanol + PNS (100 mg/kg)	ethanol + PNS (300 mg/kg)
ROS (unit/μg protein)	80.3 ± 4.2	87.0 ± 4.3[b]	76.3 ± 3.8[e]	79.2 ± 3.4[e]
MDA (nmol/mg protein)	1.39 ± 0.08	3.41 ± 0.74[c]	1.69 ± 0.11[e]	1.67 ± 0.25[e]
GSH (μmol/g protein)	18.4 ± 1.92	5.10 ± 1.12[c]	16.3 ± 4.10[e]	17.5 ± 1.46[e]
SOD (U/mg protein)	163 ± 13.2	147 ± 6.9[b]	170 ± 1.7[e]	182 ± 14.8[e]

[a]Data are expressed as mean ± SD (n = 6). [b]$P < 0.01$ and. [c]$P < 0.01$ compared to the control group. [d]$P < 0.05$ and. [e]$P < 0.01$, compared to the ethanol group.

leading to lipid peroxidation (LPO), which results in cell membrane damage. Malonyldialdehyde (MDA), an principal product of LPO, has been widely used as indicator of LPO and a marker for the status of oxidative damage.[27] To evaluate the effects of PNS on acute ethanol-mediated oxidative stress, the productions of ROS and MDA, and the GSH levels, as well as SOD activity in liver were measured and shown in Table 2. Three doses ethanol administration significantly increased hepatic ROS and MDA levels by 8.3% ($p < 0.05$) and 148% ($p < 0.01$), respectively, when compared to those in control mice. Pretreatment with PNS at doses of 100 mg/kg and 300 mg/kg significantly inhibited the elevation of hepatic ROS by 12.3% and 8.9%, and MDA by 50.6% and 50.4%, respectively. These results were consistent with the changes in serum levels of ALT and AST (Figure 2) that are primary indicators for liver injury. Conversely, three doses of ethanol intake resulted in the decreases of the antioxidant parameters, such as hepatic GSH content and SOD activity, both low-dose and high-dose of PNS remarkably ameliorated the depletion of GSH and SOD.

To understand the mechanism of the attenuation of ethanol-mediated oxidative stress by PNS, protein expression of CYP2E1, a major contributor to ROS production, was examined by immunoblot analysis. As shown in Figure 5, three doses of ethanol gavage remarkably increased the protein expression of CYP2E1 by 87.1% in comparison to control group. This elevation of CYP2E1 expression was inhibited significantly by PNS in a dose-dependent manner. Our results suggested that the protective effect of PNS on ethanol-

DOI: 10.1021/jf502990n
J. Agric. Food Chem. 2015, 63, 2413−2422

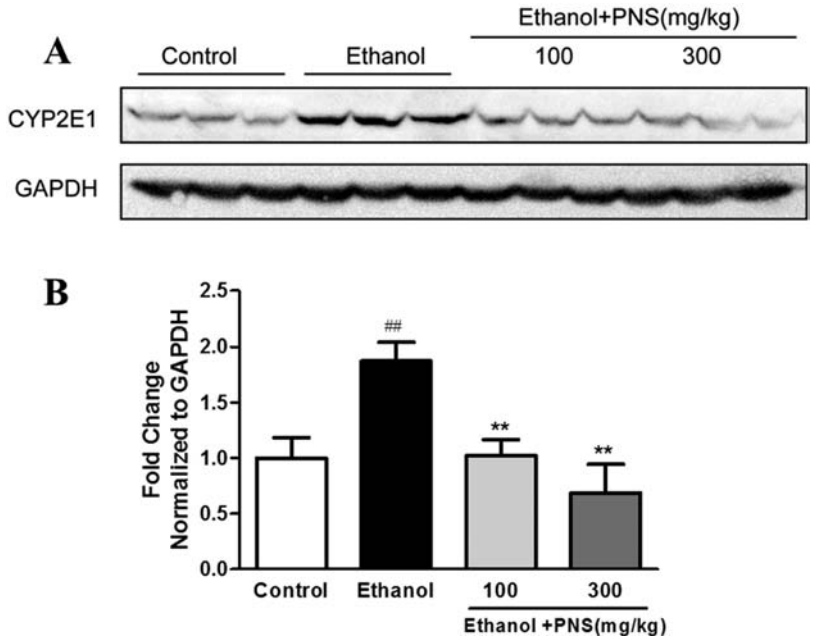

Figure 5. Effect of PNS on protein expression of cytochrome P450 2E1 (CYP2E1) in liver. (A) Immunoblot analysis; (B) quantification of the data from part A by densitometry analysis using a Quantity One software. Data are means ± SD (n = 3). $^{\#\#}P < 0.01$, compared to the control group; $^{**}P < 0.01$, compared to the ethanol group.

mediated oxidative stress was associated with down-regulation of CYP2E1 in liver.

PNS Reduced the Production of Hepatic Inflammatory Cytokines. To examine the effect of PNS treatment on acute ethanol-induced inflammatory cytokines, the hepatic levels of TNF-α and IL-6 were measured using commercial ELISA kits. As shown in Figure 6, the production of both TNF-α and IL-6 were significantly increased in the livers of ethanol group, compared to those in the control group. These increases were attenuated by PNS treatment at dose of either 100 mg/kg or 300 mg/kg.

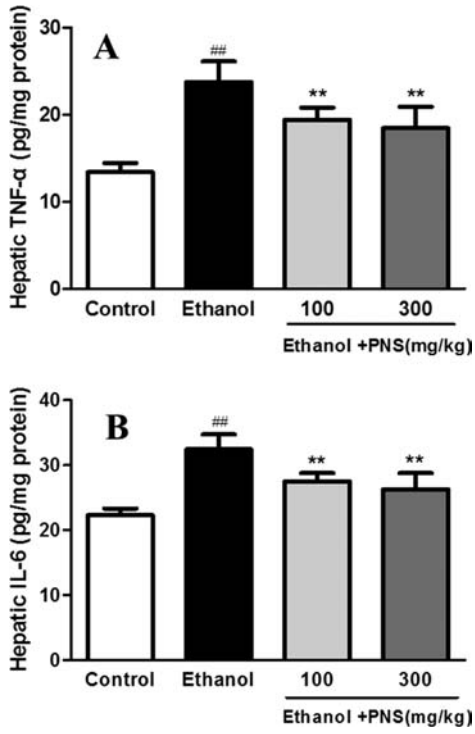

Figure 6. PNS treatment inhibited hepatic productions of inflammatory cytokines (A) TNF-α and (B) IL-6. Values represent means ± SD (n = 6) and are normalized to microgram protein content. $^{\#\#}P < 0.01$, compared to the control group; $^{**}P < 0.01$, compared to the ethanol group.

DISCUSSION

Despite the economic burden of ALD and its serious effect on public health, there are few satisfactory therapeutic approaches to prevent or reverse the progression of ALD.[1] In recent years, much attention has been paid to bioactive components from herbal medicines for the prevention and treatment of ALD.[8] In the present study, the effect of PNS treatment on acute ethanol-induced liver injury was investigated using a binge drinking mouse model. Our results demonstrated that pretreatment of PNS markedly ameliorated liver injury induced by three doses of ethanol. This protective effect was associated with the reduced hepatic lipid accumulation and decreased ethanol-mediated oxidative stress.

Hepatic steatosis, characterized by excessive triglyceride accumulation in the cytoplasm of hepatocytes, is the earliest stage in the progression of ALD and most common response of liver to acute or chronic alcohol exposure. The excessive lipids dominate the cytoplasmic space of the hepatocytes, which greatly affect cellular function and make the hepatocytes susceptible to hepatotoxins, such as lipopolysaccharide (LPS),[28] and oxidative stress.[4] Thus, the suppression of hepatic lipid accumulation during alcohol consumption might block further liver injury. Our data demonstrated that PNS treatment significantly decreased acute ethanol-induced hepatic steatosis, as described by Oil Red O staining and quantification of hepatic triglycerides. An increasing number of studies have indicated that chronic alcohol exposure for weeks stimulates adipose tissue lipolysis and elevates hepatic fatty acid uptake capability, leading to the increased fatty acid influx to the liver, which also involved in pathogenesis of alcoholic steatosis.[4,5] However, the

DOI: 10.1021/jf502990n
J. Agric. Food Chem. 2015, 63, 2413−2422

role of this effect in hepatic steatosis induced by acute alcohol intake has not been addressed yet. Increasing hepatic de novo lipogenesis has been considered to be mainly responsible for hepatic lipid accumulation in acute ethanol consumption model. However, it appears that there is not enough time to express a series of lipogenic genes to biosynthesize the large amount of triglyceride from glucose in such short-term. Adipose tissue derived-fatty acids influx to the liver might be a more important and economical contributor to acute ethanol-induced hepatic steatosis. Our results demonstrated, for the first time, that our mouse model of alcohol binge drinking by gavaging three doses every 12 h, stimulated adipose tissue lipolysis and elevated hepatic fatty acid uptake, which could be prevented by PNS treatment. In order to further reveal the underlying molecular mechanisms, the expressions of the related genes in adipose and liver tissues were examined. HSL is a key rate-limiting enzyme responsible for hydrolyzing triacylglycerols, diacylglycerols, and monoacylglycerols to release the fatty acid in adipose tissue, and activated via phosphorylation by PKA, acyclic AMP-dependent kinase.[29] CD36 is a key transport protein involved in regulating the uptake of fatty acids across the plasma membrane in hepatocytes. Our data indicated that PNS could normalize the increased protein levels of total HSL and phosphorylated HSL and inhibited the augmented mRNA expression of hepatic CD36 induced by acute ethanol exposure, which mainly contributed to its inhibitory effect on adipose tissue lipolysis and hepatic fatty acid uptake, respectively. These effects of PNS might contribute to its protective effect against ethanol-induced hepatic injury.

The importance of oxidative stress in ethanol-induced liver injury and the pathogenesis of ALD is now well recognized.[6] Both acute and chronic alcohol exposure increases the production of ROS, including superoxide, hydroxyl radical and hydrogen peroxide, leading to oxidative stress in the liver. Ethanol-induced ROS production appears to be toxic to hepatocytes because it reacts with most cellular macromolecules by causing DNA damage, denaturing proteins, and increasing lipid peroxidation of cellular membrane.[30] In addition, ethanol-mediated oxidative stress also depleted endogenous antioxidative defenses, including enzymatic and nonenzymatic antioxidants.[31] SOD is an important endogenous antioxidant enzyme involved in ROS elimination and serves as the first line of defense against oxidative damage.[32] GSH, a nonenzymatic antioxidant, acts as a direct ROS scavenger and the substrate of GSH-related detoxifying and antioxidant enzymes.[33] Our results demonstrated that PNS not only could decrease the production of hepatic ROS induced by three doses of ethanol but also ameliorated the depletion of antioxidants, including SOD and GSH. ROS triggered oxidative stress usually showed an increase in MDA levels, an end-product of lipid peroxidation.[27] Generally, ROS has a great potential to react with lipids, particularly polyunsaturated fatty acids, which results in cell membrane damage. Thus, MDA has been widely used as indicator of lipid peroxidation and a marker for the status of oxidative stress. In our study, PNS prevented the elevation of hepatic MDA levels induced by acute ethanol intake, indicating the decrease lipid peroxidation in the liver. In order to further investigate the mechanisms underlying the antioxidative stress effect of PNS, the expression of CYP2E1 in liver was examined. CYP2E1 has been considered to be a major contributor to ethanol-induced oxidative stress and to ethanol induced liver injury. The expression and activity of CYP2E1 are elevated by alcohol intake, which catalyzes conversion of ethanol to acetaldehyde in the presence of iron, and causes ROS overproduction.[34] The results of present study indicated that pretreatment with PNS inhibited the ethanol-induced elevation of hepatic CYP2E1 expression, which contributed to its antioxidative stress effect.

Several inflammatory cytokines play a crucial role in the progression of ALD, especially from hepatic steatosis to steatohepatitis, which is featured by the presence of inflammatory infiltrate and hepatocyte damage.[35] It was well-known that oxidative stress also stimulates the release of these cytokines and amplify the inflammation response to cause further liver damage.[36] TNF-α and IL-6, mainly produced by sensitized Kupffer cells and the recruited monocytes, have been widely considered to be the most important cytokines in alcohol induced liver injury.[35] Besides inflammatory and cytotoxic effects, TNF-α also increases fatty acid de novo synthesis by stimulating the maturation of transcription factor sterol regulatory element binding protein-1c (SREBP-1c).[37] The results from this study showed that PNS reduced hepatic production of the inflammatory cytokines, TNF-α and IL-6, and also contributed to its protective effect on acute ethanol-induced liver injury.

In pharmacological evaluation of PNS, it is important to understand not only its chemical components but also which PNS-derived compounds circulate considerably in plasma after dosing. After oral administration of the aqueous extract of *P. notoginseng*, 20(*S*)-protopanaxadiol, 20(*S*)-protopanaxatriol, and their oxidized metabolites, as well as compound K represent major circulating forms of ginsenosides through the ginsenoside deglycosylation by the colonic microflora and sapogenin oxidation by enterohepatic cytochrome P450 enzymes in rats and human.[38,39] In this study, the protective effects of PNS against acute ethanol-induced liver injury might be attributed to these deglycosylated products of ginsenosides in bloodstream.

Taken together, the pretreatment with PNS effectively attenuated acute ethanol-induced liver injury. This protective effect might be associated with ameliorating hepatic steatosis and reducing ethanol-mediated oxidative stress. Our findings suggested that PNS had the potential to be developed to an effective preventable agent in acute ethanol-induced liver injury.

AUTHOR INFORMATION

Corresponding Author

*Tel: +853-8822 4680. E-mail: jbwan@umac.mo.

Author Contributions

[§]R.-B.D. and K.T. contributed equally to this work.

Notes

The authors declare no competing financial interest.

ACKNOWLEDGMENTS

This study was supported by the grants from the Research Committee of the University of Macau (MYRG123-ICMS12 and MYRG111-ICMS13 to J.B. Wan) and from Macao Science and Technology Development Fund (010/2013/A1 to J.-B. Wan).

ABBREVIATIONS USED

ALD, alcoholic liver disease; ALT, alanine aminotransferase; AMP, adenosine monophosphate; AST, aspartate aminotransferase; CD36, cluster of differentiation 36 or fatty acid

DOI: 10.1021/jf502990n
J. Agric. Food Chem. 2015, 63, 2413−2422

translocase 36; CYP2E1, cytochrome P450 2E1; DMEM, Dulbecco's modified Eagle's medium; ELISA, enzyme-linked immunosorbent assay; FFA, free fatty acid; GAPDH, glyceraldehyde 3-phosphate dehydrogenase; GSH, glutathione; HPLC, high-performance liquid chromatography; HRP, horseradish peroxidase; HSL, hormone-sensitive lipase; IgG, immunoglobulin G; IL-6, Interleukin 6; IVC, individually ventilated cage; LPO, lipid peroxidation; LPS, lipopolysaccharide; MDA, malondialdehyde; PBS, phosphate buffered saline; PCR, polymerase chain reaction; p-HSL or phospho-HSL, phosphorylation of hormone-sensitive lipase; PKA, protein kinase A; PNS, *Panax notoginseng* saponins; PVDF, polyvinylidene fluoride; RIPA, radio immunoprecipitation assay; ROS, reactive oxygen species; SD, standard deviation; SOD, superoxide dismutase; SREBP-1c, sterol regulatory element binding protein-1c; TBST, Tris-buffered saline with Tween-20; TNF-α, tumor necrosis factor alpha; TG, triglyceride; VLDL, very low-density lipoprotein; WAT, white adipose tissue

REFERENCES

(1) Altamirano, J.; Bataller, R. Alcoholic liver disease: Pathogenesis and new targets for therapy. *Nat. Rev. Gastroenterol. Hepatol.* **2011**, *8*, 491−501.

(2) Bataller, R.; Brenner, D. A. Liver fibrosis. *J. Clin. Invest.* **2005**, *115*, 209−218.

(3) Day, C. P.; James, O. F. Hepatic steatosis: innocent bystander or guilty party? *Hepatology* **1998**, *27*, 1463−1466.

(4) Zhong, W.; Zhao, Y.; Tang, Y.; Wei, X.; Shi, X.; Sun, W.; Sun, X.; Yin, X.; Sun, X.; Kim, S.; McClain, C. J.; Zhang, X.; Zhou, Z. Chronic alcohol exposure stimulates adipose tissue lipolysis in mice: Role of reverse triglyceride transport in the pathogenesis of alcoholic steatosis. *Am. J. Pathol.* **2012**, *180*, 998−1007.

(5) Kang, L.; Chen, X.; Sebastian, B. M.; Pratt, B. T.; Bederman, I. R.; Alexander, J. C.; Previs, S. F.; Nagy, L. E. Chronic ethanol and triglyceride turnover in white adipose tissue in rats: Inhibition of the anti-lipolytic action of insulin after chronic ethanol contributes to increased triglyceride degradation. *J. Biol. Chem.* **2007**, *282*, 28465−28473.

(6) Koch, O. R.; Pani, G.; Borrello, S.; Colavitti, R.; Cravero, A.; Farre, S.; Galeotti, T. Oxidative stress and antioxidant defenses in ethanol-induced cell injury. *Mol. Aspects Med.* **2004**, *25*, 191−198.

(7) Stewart, S.; Jones, D.; Day, C. P. Alcoholic liver disease: New insights into mechanisms and preventative strategies. *Trends Mol. Med.* **2001**, *7*, 408−413.

(8) Ding, R. B.; Tian, K.; Huang, L. L.; He, C. W.; Jiang, Y.; Wang, Y. T.; Wan, J. B. Herbal medicines for the prevention of alcoholic liver disease: a review. *J. Ethnopharmacol.* **2012**, *144*, 457−465.

(9) Kim, S. J.; Lee, S. M. Effect of baicalin on toll-like receptor 4-mediated ischemia/reperfusion inflammatory responses in alcoholic fatty liver condition. *Toxicol. Appl. Pharmacol.* **2012**, *258*, 43−50.

(10) Yuan, G. J.; Gong, Z. J.; Zhou, X. R.; Zhang, P.; Sun, X. M.; Li, X. Epigallocatechin-3-gallate ameliorates alcohol-induced liver injury in rats. *Int. J.Mol. Sci.* **2006**, *7*, 204−219.

(11) Yang, X.; Dong, C.; Ren, G. Effect of soyasaponins-rich extract from soybean on acute alcohol-induced hepatotoxicity in mice. *J. Agric. Food Chem.* **2011**, *59*, 1138−1144.

(12) Huang, L. L.; Wan, J. B.; Wang, B.; He, C. W.; Ma, H.; Li, T. W.; Kang, J. X. Suppression of acute ethanol-induced hepatic steatosis by docosahexaenoic acid is associated with downregulation of stearoyl-CoA desaturase 1 and inflammatory cytokines. *Prostaglandins. Leukot. Essent. Fatty Acids* **2013**, *88*, 347−353.

(13) Wan, J. B.; Wang, Y. T.; Li, S. P. *Panax notoginseng* (Sanqi). In *Pharmacological Activity-Based Quality Control of Chinese Herbs*; Li, S. P., Wang, Y. T., Eds.; Nova Science Publishers, Inc.: New York, 2008; pp 179−203.

(14) Wan, J. B.; Chen, Y.; Li, P.; Huang, W. H.; Zhang, Q. W. Saponins from Panax Species: Chemistry, Isolation, and Analysis. In *Saponins: Properties, Applications, and Health Benefits*; Koh, R., Tay, I., Eds.; Nova Science Publishers, Inc.: New York, 2012; pp 51−98.

(15) White, C. M.; Fan, C.; Chow, M. An evaluation of the hemostatic effect of externally applied notoginseng and notoginseng total saponins. *J. Clin. Pharmacol.* **2000**, *40*, 1150−1153.

(16) Sun, H.; Ye, Y.; Pan, Y. Immunological-adjuvant saponins from the roots of *Panax* notoginseng. *Chem. Biodivers.* **2005**, *2*, 510−515.

(17) Wan, J. B.; Lee, S. M.; Wang, J. D.; Wang, N.; He, C. W.; Wang, Y. T.; Kang, J. X. Panax notoginseng reduces atherosclerotic lesions in ApoE-deficient mice and inhibits TNF-α-induced endothelial adhesion molecule expression and monocyte adhesion. *J. Agric. Food Chem.* **2009**, *57*, 6692−6697.

(18) Liu, J. W.; Tian, S. J.; de Barry, J.; Luu, B. Panaxadiol glycosides that induce neuronal differentiation in neurosphere stem cells. *J. Nat. Prod.* **2007**, *70*, 1329−1334.

(19) Chan, R. Y.; Chen, W. F.; Dong, A.; Guo, D.; Wong, M. S. Estrogen-like activity of ginsenoside Rg1 derived from *Panax notoginseng*. *J. Clin. Endocrinol. Metab.* **2002**, *87*, 3691−3695.

(20) Carson, E. J.; Pruett, S. B. Development and characterization of a binge drinking model in mice for evaluation of the immunological effects of ethanol. *Alcohol.: Clin. Exp. Res.* **1996**, *20*, 132−138.

(21) Wan, J. B.; Li, S. P.; Chen, J. M.; Wang, Y. T. Chemical characteristics of three medicinal plants of the *Panax* genus determined by HPLC-ELSD. *J. Sep. Sci.* **2007**, *30*, 825−832.

(22) Wan, J. B.; Lai, C. M.; Li, S. P.; Lee, M. Y.; Kong, L. Y.; Wang, Y. T. Simultaneous determination of nine saponins from Panax notoginseng using HPLC and pressurized liquid extraction. *J. Pharm. Biomed. Anal.* **2006**, *41*, 274−279.

(23) Sherman, K. E. Alanine aminotransferase in clinical practice. A review. *Arch. Int. Med.* **1991**, *151*, 260−265.

(24) Borovikova, L. V.; Ivanova, S.; Zhang, M.; Yang, H.; Botchkina, G. I.; Watkins, L. R.; Wang, H.; Abumrad, N.; Eaton, J. W.; Tracey, K. J. Vagus nerve stimulation attenuates the systemic inflammatory response to endotoxin. *Nature* **2000**, *405*, 458−462.

(25) Krintel, C.; Morgelin, M.; Logan, D. T.; Holm, C. Phosphorylation of hormone-sensitive lipase by protein kinase A in vitro promotes an increase in its hydrophobic surface area. *FEBS J.* **2009**, *276*, 4752−4762.

(26) He, J.; Lee, J. H.; Febbraio, M.; Xie, W. The emerging roles of fatty acid translocase/CD36 and the aryl hydrocarbon receptor in fatty liver disease. *Exp. Biol. Med.* **2011**, *236*, 1116−1121.

(27) Li, G.; Ye, Y.; Kang, J.; Yao, X.; Zhang, Y.; Jiang, W.; Gao, M.; Dai, Y.; Xin, Y.; Wang, Q.; Yin, Z.; Luo, L. l-Theanine prevents alcoholic liver injury through enhancing the antioxidant capability of hepatocytes. *Food Chem. Toxicol.* **2012**, *50*, 363−372.

(28) Yang, S.; Lin, H.; Diehl, A. M. Fatty liver vulnerability to endotoxin-induced damage despite NF-kappaB induction and inhibited caspase 3 activation. *Am. J. Physiol. Gastrointest. Liver Physiol.* **2001**, *281*, G382−392.

(29) Jaworski, K.; Sarkadi-Nagy, E.; Duncan, R. E.; Ahmadian, M.; Sul, H. S. Regulation of triglyceride metabolism. IV. Hormonal regulation of lipolysis in adipose tissue. *Am. J. Physiol. Gastrointest. Liver Physiol.* **2007**, *293*, G1−4.

(30) Wu, D.; Cederbaum, A. I. Oxidative stress and alcoholic liver disease. *Semin. Liver Dis.* **2009**, *29*, 141−154.

(31) Yu, B. P. Cellular defenses against damage from reactive oxygen species. *Physiol. Rev.* **1994**, *74*, 139−162.

(32) Wu, D.; Cederbaum, A. I. Alcohol, oxidative stress, and free radical damage. *Alcohol. Res. Health* **2003**, *27*, 277−284.

(33) Yao, P.; Li, K.; Song, F.; Zhou, S.; Sun, X.; Zhang, X.; Nussler, A. K.; Liu, L. Heme oxygenase-1 upregulated by Ginkgo biloba extract: Potential protection against ethanol-induced oxidative liver damage. *Food Chem. Toxicol.* **2007**, *45*, 1333−1342.

(34) Jimenez-Lopez, J. M.; Cederbaum, A. I. CYP2E1-dependent oxidative stress and toxicity: role in ethanol-induced liver injury. *Expert Opin. Drug Metab. Toxicol.* **2005**, *1*, 671−685.

(35) Yoon, S. J.; Koh, E. J.; Kim, C. S.; Zee, O. P.; Kwak, J. H.; Jeong, W. J.; Kim, J. H.; Lee, S. M. Agrimonia eupatoria protects against

DOI: 10.1021/jf502990n
J. Agric. Food Chem. 2015, 63, 2413−2422

chronic ethanol-induced liver injury in rats. *Food Chem. Toxicol.* **2012**, *50*, 2335−2341.
(36) Albano, E. Free radical mechanisms in immune reactions associated with alcoholic liver disease. *Free Radic. Biol. Med.* **2002**, *32*, 110−114.
(37) Lawler, J. F., Jr.; Yin, M.; Diehl, A. M.; Roberts, E.; Chatterjee, S. Tumor necrosis factor-α stimulates the maturation of sterol regulatory element binding protein-1 in human hepatocytes through the action of neutral sphingomyelinase. *J. Biol. Chem.* **1998**, *273*, 5053−5059.
(38) Liu, H.; Yang, J.; Du, F.; Gao, X.; Ma, X.; Huang, Y.; Xu, F.; Niu, W.; Wang, F.; Mao, Y.; Sun, Y.; Lu, T.; Liu, C.; Zhang, B.; Li, C. Absorption and disposition of ginsenosides after oral administration of *Panax notoginseng* extract to rats. *Drug Metab. Dispos.* **2009**, *37*, 2290−2298.
(39) Hu, Z.; Yang, J.; Cheng, C.; Huang, Y.; Du, F.; Wang, F.; Niu, W.; Xu, F.; Jiang, R.; Gao, X.; Li, C. Combinatorial metabolism notably affects human systemic exposure to ginsenosides from orally administered extract of *Panax notoginseng* roots (Sanqi). *Drug Metab. Dispos.* **2013**, *41*, 1457−1469.

DOI: 10.1021/jf502990n
J. Agric. Food Chem. 2015, 63, 2413−2422

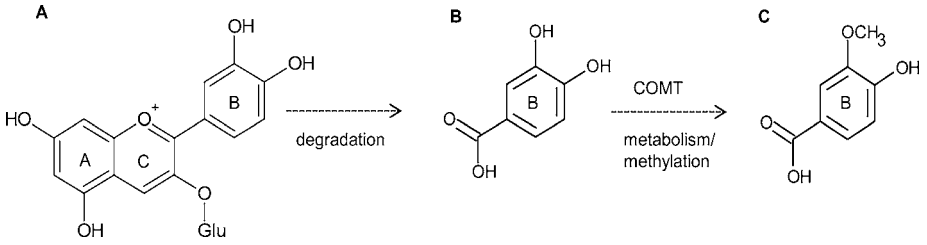

Figure 1. Chemical structures of the anthocyanin cyanidin-3-glucoside (A), its B-ring degradation product protocatechuic acid (B), and the mono-*O*-methylated metabolite of protocatechuic acid, vanillic acid (C). COMT, catechol *O*-methyltransferase.

solutions were prepared in dimethyl sulfoxide (DMSO) and stored at −80 °C. Fetal bovine serum (FBS, heat-inactivated) was purchased from Biosera (Ringmer, U.K.), and tumor necrosis factor-alpha (TNF-α), TRIzol reagent, and SuperScript II Reverse Transcriptase were obtained from Life Technologies (Paisley, U.K.).

Precision 2× real-time PCR MasterMix with SYBRGreen was obtained from PrimerDesign Ltd. (Southampton, U.K.). Custom primer sets for human NOX2, NOX4, $p22^{phox}$, $p47^{phox}$, and $p67^{phox}$ were supplied by PrimerDesign Ltd., and custom primers for human HO-1 (HMOX-1) by Life Technologies. Primer sequences are provided as Supporting Information (Table S1).

NuPAGE sample reducing agent and LDS sample buffer were purchased from Life Technologies, and Precision Plus Protein Dual Color standards were purchased from Bio-Rad Laboratories, Inc. (Hemel Hempstead, U.K.).

Cell Culture. Early passage, pooled HUVECs were purchased from TCS Cellworks (Buckingham, U.K.) and used between passages 2 and 4. Cells were routinely cultured in large vessel endothelial cell growth medium (TCS CellWorks) at 37 °C and 5% CO_2. HUVECs were subcultured using 0.025% trypsin and 0.01% ethylenediaminetetraacetic acid (EDTA) (TCS CellWorks).

Cryopreserved, second passage, single donor HCAECs were purchased from PromoCell GmbH (Heidelberg, Germany) and used between passages 3 and 6. Cells were routinely cultured in endothelial cell medium MV (PromoCell GmbH) at 37 °C and 5% CO_2. HCAECs were subcultured using 0.04% trypsin and 0.03% EDTA (PromoCell GmbH).

Cytotoxicity Assay. The maximal level of flavonoids and flavonoid metabolites reported in the systemic circulation is generally below 10 μM,[1] hence this concentration was the maximum in vitro concentration utilized in the present study. Cell viability following exposure to 10 μM of treatment compounds was determined using cell proliferation reagent WST-1 (Roche Applied Science, Burgess Hill, U.K.) in accordance with the manufacturer's protocol. The assay was conducted using fibronectin-coated microplates seeded with HUVECs at a density of ∼10,000 cells/well, and subsequently grown to confluence as determined by light microscopy. After incubation with treatment compounds for 24 h, 10 μL of WST-1 reagent was added to each well, and plates were incubated for a further 4 h. Absorbance was measured at 440−450 nm using a microplate reader [Fluostar/Polarstar Optima, BMG Labtech (Aylesbury, U.K.)].

Nitrite/Nitrate Assay and eNOS Enzyme-Linked Immunosorbent Assay (ELISA). Fibronectin-coated 24-well plates were seeded with HUVECs at a density of ∼30,000 cells/well, and cells were grown to confluence. Cells were then cultured in the absence or presence of treatment compounds (0.1, 1, or 10 μM) for 24 h; after which supernatants were removed and stored at −80 °C. Cells were washed once with warm phosphate-buffered saline (PBS) and then harvested in trypsin/EDTA and trypsin-blocking solution. Cell suspensions were stored at −80 °C until lysis. Nitric oxide production was assessed using a colorimetric microplate assay (Cayman Chemical Company Nitrate/Nitrite Colorimetric Assay Kit from Cambridge Bioscience, Cambridge, U.K.) according to the manufacturer's instructions. The average intra-assay coefficient of variation (CV) was 6.63% ± 1.10% (mean ± SD, n = 3), and the interassay CV was 2.38% (n = 3). Quantification of eNOS in HUVEC lysates was performed with the Quantikine Human eNOS Immunoassay (R&D Systems, Abingdon, U.K.) according to the manufacturer's instructions. The average intra-assay CV was 4.67% ± 1.86% (mean ± SD, n = 3), and the interassay CV was 6.10% (n = 3).

Stimulated Superoxide Production Assay. Superoxide production was assessed using a modified cytochrome *c* assay.[20,21] The modified assay utilized fibronectin-coated 24-well plates seeded with HUVECs at a density of ∼50,000 cells/well, and grown to confluence, after which cells were washed once with warm Medium 199 (supplemented with 2% FBS) and incubated for 16−18 h. Cells were then washed once with warm PBS and incubated for 6 h in supplemented phenol-red free Medium 199 (Invitrogen, Paisley, U.K.) with 0.1 μM angiotensin II, 30 μM ferricytochrome *c*, and 0.1, 1, or 10 μM of the treatment compounds or 5 μM VAS2870 (selective NOX inhibitor[22]), in the presence or absence of 65 units of superoxide dismutase (SOD). Aliquots of cell supernatants were subsequently transferred to a 96-well microplate for measurement of absorbance at 550 nm. Culture plates were frozen at −80 °C for protein extraction.

Direct Cytochrome *c* Reduction. Direct reduction of cytochrome *c* was assessed by coincubation of treatment compounds in cell-free extracts at concentrations of 2, 20, 200, and 2000 μM with 20 μM cytochrome *c* in PBS at 37 °C, as described previously for catechols and quinols.[23] The spontaneous reduction of cytochrome *c* was monitored kinetically at 550 nm over 2 h. Cytochrome *c* reduction was quantified using the millimolar extinction coefficient for reduced cytochrome *c* (29.5 mM cm^{-1}).

Superoxide Production. Cell-free superoxide production by xanthine/xanthine oxidase was measured using a previously described method.[21] Briefly, 200 μM of cytochrome *c*, 0.1 U/mL xanthine oxidase, and 200 μM xanthine was added to 1, 10, 100, and 1000 μM of the treatment compounds in 50 mM sodium phosphate buffer (pH 7.4). The reaction kinetics of cytochrome *c* was monitored at 550 nm at 25 °C over 15 min (to reaction plateau). Superoxide generated was determined by subtracting the rate of cytochrome *c* reduction (increase in absorbance at 550 nm) in the presence of SOD versus parallel incubations in the absence of SOD.

Stimulated NOX Isoform/Subunit Gene Expression Assay. Twenty-four well plates (SPL Life Sciences) coated with fibronectin were seeded with HUVECs at a density of ∼30,000 cells/well and the cells grown to confluence. Culture medium was then aspirated, and the cells were incubated for 16−18 h in M199 supplemented with 2% FBS. Thereafter, the cells were incubated for 4 h in supplemented M199 alone (basal), or medium with 0.1 μM angiotensin II in the presence or absence of 0.1, 1, or 10 μM vanillic acid. After incubation, the plates were either frozen at −80 °C or used for RNA extraction.

Stimulated $p47^{phox}$ Protein Expression Assay. Six-well plates (SPL Life Sciences) coated with fibronectin were seeded with HUVECs or HCAECs at a density of 100,000 cells/well, and cells were grown to confluence. Culture medium was then aspirated, and the cells were incubated for 16−18 h in M199 supplemented with 2% FBS (HUVECs only). Cells were subsequently incubated for 5 h in supplemented M199 alone (basal), or medium with 20 ng/mL TNF-α in the presence or absence of 0.1, 1, or 10 μM vanillic acid. After incubation, medium was aspirated from all wells, and the plates frozen at −80 °C until protein extraction.

Endothelial HO-1 Expression Assay. Expression of HO-1 mRNA/protein was assessed using fibronectin-coated 6-well plates (SPL Life Sciences) seeded with HUVECs or HCAECs at a density of

DOI: 10.1021/jf5041993
J. Agric. Food Chem. 2015, 63, 2423−2431

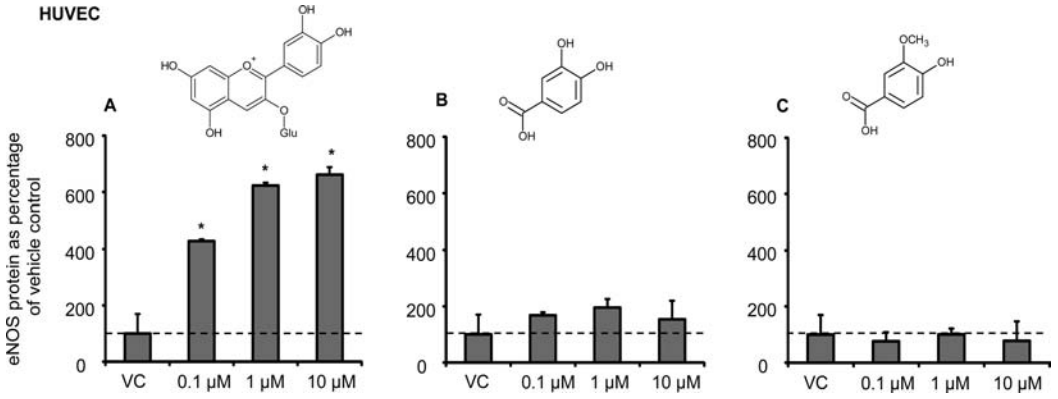

Figure 2. Modulation of endothelial eNOS expression (as quantified by ELISA of cell lysates) following 24 h incubation of HUVECs with vehicle control [0.05% DMSO in supplemented culture medium] (VC) or 0.1−10 μM cyanidin-3-glucoside (A), protocatechuic acid (B), and vanillic acid (C). Data are graphed as mean eNOS protein as percentage of vehicle control (designated as 100% and marked by dashed line); mean ± SD (n = 3). *Significant difference versus vehicle control (p < 0.05).

~100,000 cells/well, and grown to ~70% confluence. Culture medium was then aspirated, and the cells were incubated for 6 h in supplemented culture medium alone (basal), or medium with 10 ng/mL phorbol 12-myristate 13-acetate (PMA, positive control), vehicle control (0.005% DMSO; HUVECs only), or 0.1, 1, or 10 μM vanillic acid. After incubation, medium was aspirated from all wells and the plates either frozen at −80 °C or used for RNA or protein extraction.

Reverse Transcription−Quantitative Polymerase Chain Reaction. RNA was extracted from cells using TRIzol reagent, according to the manufacturer's instructions; and 1 μg of each sample was utilized in a reverse transcription reaction with SuperScript II. Analysis of gene expression was performed using the Applied Biosystems 7500 Real time PCR System (Life Technologies; 7500 software version 2.0) with SYBRGreen detection. Typically, 25 ng of cDNA was amplified with 300 nM of the appropriate primer set. Following enzyme activation at 95 °C for 10 min, 50 cycles of denaturation (15 s at 95 °C) and data collection (60 s at 60 °C) were performed. Relative changes in gene expression were quantified using the comparative C_t method.[24] Optimal stably expressed human reference genes for normalization of C_t data were identified using a geNormPLUS kit with primer sets for six genes (PPIA, PRDM4, UBE2D2, UBE4A, TWY1, VIPAS39) supplied by PrimerDesign Ltd.

Immunoblot Analysis of Endothelial NOX Isoform/Subunit and HO-1 Expression. Cells were harvested and lysed with 1% IGEPAL (octylphenoxy polyethoxyethanol, CA-630), 150 mM NaCl, 20 mM Tris, and 10% glycerol (pH 8.0), supplemented with protease inhibitors (Roche Complete Protease Inhibitor Cocktail). Plates were incubated with lysis buffer for 0.5 h at 4 °C, and recovered solutions were subjected to cell disruption by oscillation (50 Hz for 5 min with Qiagen TissueLyser LT). After centrifugation at 13,000 rpm (15 min at 4 °C) the protein content of the supernatants was assayed using the Pierce BCA Protein Assay Kit (Fisher Scientific U.K. Ltd., Loughborough, U.K.) according to the manufacturer's instructions.

For SDS−PAGE, cell lysates were reduced using 50 mM dithiothreitol. Briefly, 15−25 μg of protein was loaded onto a 4% polyacrylamide stacking gel, and separated across a 10% resolving gel (at 25 mA for 1 h) prior to semidry transfer to Immobilon-FL PVDF membrane (Millipore, Watford, U.K.) at 200 mA for 1.5 h. Membranes were blocked for 1 h at room temperature and incubated overnight (at 4 °C) with chicken polyclonal anti-glyceraldehyde-3-phosphate dehydrogenase (GAPDH, Millipore) or goat polyclonal anti-actin (Santa Cruz Biotechnology, Inc., California, USA); and either rabbit polyclonal anti-gp91phox (Millipore), rabbit polyclonal anti-NOX4 (Abcam, Cambridge, U.K.), rabbit polyclonal anti-$p47^{phox}$ (Santa Cruz Biotechnology, Inc., or Abcam), or rabbit polyclonal anti-HO-1 (Abcam). Membranes were then washed prior to incubation with either donkey anti-chicken IgG (IR dye 680 LT) or donkey anti-goat IgG (IR dye 680) and goat anti-rabbit IgG (IR dye 800 CW) (Li-Cor, Cambridge, U.K.) for 1 h at room temperature. Membranes were washed and subsequently imaged and quantified using an Odyssey Infrared Imaging System (Li-Cor; Application Software version 3.0.21).

Statistical Analysis. Analysis of variance (ANOVA) with LSD post hoc test was performed using SPSS software (IBM, New York, USA) version 18 for Windows. Significance was determined at the 5% level relative to basal or the assay control. Three biological replicates for each control or treatment were utilized for analysis unless otherwise noted. Means of biological replicates were represented graphically, with error bars denoting standard deviation from the mean. For each control or treatment in the stimulated superoxide production assay, mean absorbance ratio (550 nm/620 nm) in the presence of SOD (n = 3) was subtracted from individual absorbance ratio values in the absence of SOD (n = 3), to correct for cytochrome c reduction owing to generated superoxide. Mean SOD-corrected absorbance ratio for each treatment was then represented graphically as percentage of that for the angiotensin II control.

RESULTS

Endothelial Cytotoxicity. All treatments were screened for cytotoxicity at a concentration of 10 μM, representing the highest concentration used in subsequent bioactivity investigations. No significant effects (p > 0.05) on endothelial cell viability were observed following a 24 h incubation of HUVECs with 10 μM of any treatment compound (data not shown).

Endothelial NO Production. Cyanidin-3-glucoside and the phenolic derivatives protocatechuic acid and vanillic acid did not significantly alter endothelial NO production as measured by levels of NO decomposition products (nitrite and nitrate) in HUVEC supernatants (Supporting Information, Figure S1). Resveratrol (100 μM) and PMA (10 nM) were used as positive controls to confirm the sensitivity of the assay and elicited significant increases in total nitrite and nitrate (>270% above basal levels).

eNOS Expression in Cultured HUVECs. Significant upregulation of eNOS (p < 0.001) was observed following 24 h incubation of HUVECs with 0.1, 1, and 10 μM cyanidin-3-glucoside (~4−7-fold increase; Figure 2A). No significant alteration in eNOS levels was observed at any concentration of protocatechuic acid (Figure 2B) or vanillic acid (Figure 2C).

Stimulated Endothelial Superoxide Production. The generation of superoxide anion was confirmed using a previously reported NOX inhibitor VAS2870,[22] in the presence and absence of angiotensin II, where coincubation with

DOI: 10.1021/jf5041993
J. Agric. Food Chem. 2015, 63, 2423−2431

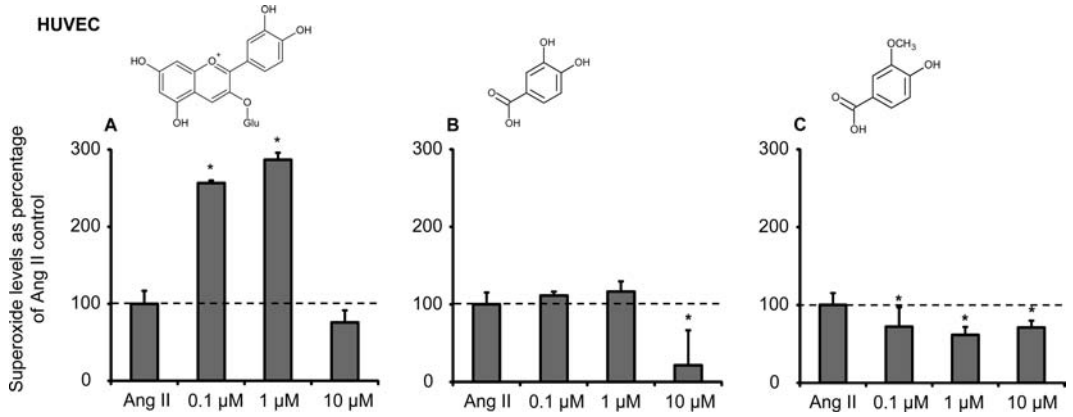

Figure 3. Modulation of angiotensin II (Ang II)-stimulated HUVEC superoxide production by 0.1−10 μM cyanidin-3-glucoside (A), protocatechuic acid (B), or vanillic acid (C). Superoxide production was quantified by reduction of extracellular ferricytochrome *c*. Data are graphed as SOD-corrected mean absorbance (OD) ratio (550 nm/620 nm) as percentage of Ang II control (designated as 100% and marked by dashed line); mean ± SD (n = 3). *Significant difference versus Ang II stimulated control (p < 0.05).

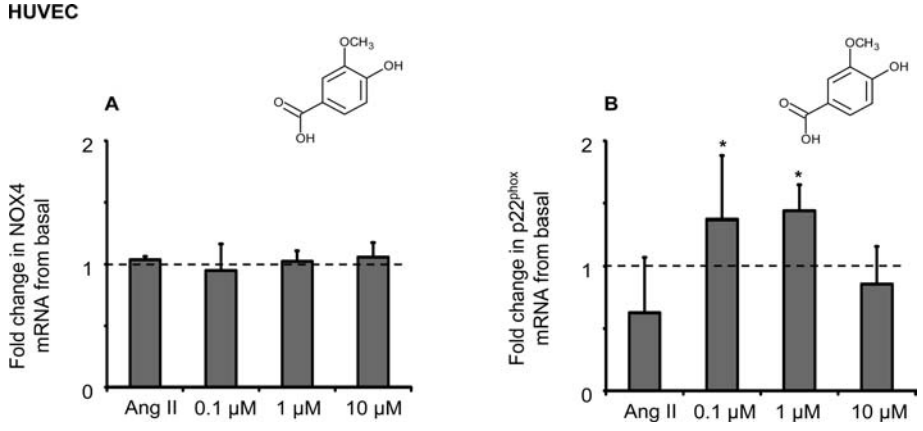

Figure 4. Modulation of HUVEC NOX4 (A) or $p22^{phox}$ (B) mRNA levels following 4 h incubation with 0.1 μM angiotensin II control (Ang II), or Ang II with 0.1 μM, 1 μM, or 10 μM vanillic acid, presented as fold change versus unstimulated cells (basal; designated as 1 and marked by dashed line). Relative quantification was performed by RT-qPCR using the comparative C_t method, incorporating the geometric mean of reference genes UBE4A and VIPAS39 as the normalization factor. Data are graphed as mean ± SD (n = 3). *Significant difference versus Ang II stimulated control (p < 0.05).

VAS2870 significantly reduced superoxide production (p < 0.01) (Supporting Information, Figure S2).

Significantly elevated superoxide levels were detected following incubation of cells with 0.1 μM and 1 μM cyanidin-3-glucoside (∼3-fold increase; Figure 3A), relative to the angiotensin II stimulated control. A significant decrease in superoxide (p < 0.001) was induced by protocatechuic acid, at 10 μM (∼5-fold decrease; Figure 3B), while vanillic acid elicited statistically significant reductions (p < 0.05) in superoxide at all concentrations examined (∼2-fold decrease at 1 μM; Figure 3C). A linear dose−response relationship was not evident for any treatment. Control experiments were conducted to exclude possible confounding through direct reduction of cytochrome *c*, or scavenging of NOX-derived superoxide radicals, by the treatments. There was no significant impact on cytochrome *c* reduction (≤0.02 nmol h^{-1}) or superoxide levels (75−106% of control) during incubations with treatment compounds at concentrations up to 10 μM in cell-free systems.

Stimulated Endothelial Gene Expression of NOX Isoforms and Subunits. Vanillic acid was examined for effects on stimulated endothelial gene expression of the NOX2 and NOX4 isoforms, and the associated subunits $p22^{phox}$, $p47^{phox}$, and $p67^{phox}$. Real time PCR melt curve data indicated non-specific amplification for NOX2, $p47^{phox}$, and $p67^{phox}$ primer sets (data not shown); therefore relative quantification of gene expression was performed for NOX4 and $p22^{phox}$ only. Coincubation of HUVECs with angiotensin II and vanillic acid (0.1, 1, and 10 μM) for 4 h elicited no significant differences in NOX4 mRNA compared to the angiotensin II control (p > 0.05; Figure 4A). A statistically significant (p < 0.05) upregulation of $p22^{phox}$ mRNA levels was observed with vanillic acid at 0.1 μM and 1 μM (Figure 4B).

Stimulated Endothelial Protein Expression of NOX Isoforms and Subunits. The modulation of NOX2 and NOX4 isoforms by vanillic acid was further characterized at the protein level. Following angiotensin II stimulation, weak immunoreactive bands corresponding to NOX2 were visualized by immunoblotting of endothelial lysates, such that quantification of bands by densitometry was not possible (data not shown). By contrast, angiotensin II-induced upregulation of NOX4 expression was observed, although this was not significantly modulated (p > 0.05) by coincubation of cells with angiotensin II and vanillic acid at any concentration examined (0.1−10 μM) (Figure 5).

DOI: 10.1021/jf5041993
J. Agric. Food Chem. 2015, 63, 2423−2431

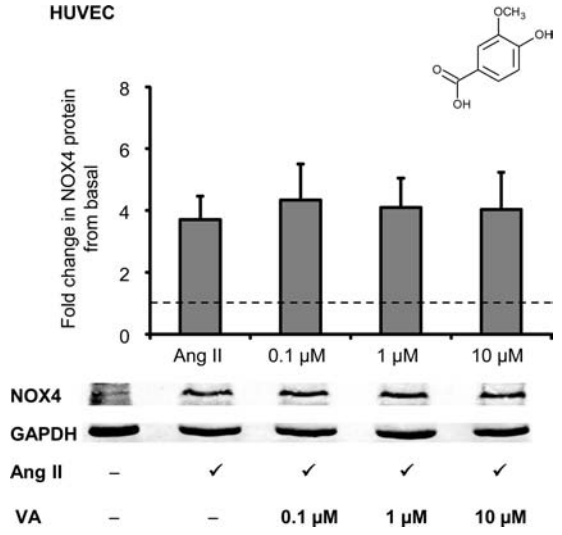

Figure 5. Expression of NOX4 protein in cell lysates from unstimulated HUVECs (basal) and following 6 h incubation with 0.1 μM angiotensin II (Ang II), or Ang II with 0.1 μM, 1 μM, or 10 μM vanillic acid (VA). Glyceraldehyde-3-phosphate dehydrogenase (GAPDH) was utilized as a loading control for immunoblotting of cell lysates. Graphs show fold increase in NOX4 expression relative to basal (designated as 1 and marked by dashed line), after quantification by densitometry and normalization to loading control (mean ± SD, n = 5).

The effect of vanillic acid on stimulated protein expression of the key NOX2 subunit p47^{phox} was also investigated as a possible mechanism of NOX inhibition. Following coincubation of HUVECs with 20 ng/mL TNF-α and increasing concentrations of vanillic acid (0.1, 1, or 10 μM) for 5 h, a trend toward decreased p47^{phox} expression was observed relative to TNF-α alone (Figure 6A), although these changes were not statistically significant (p = 0.06 at 1 μM and 10 μM vanillic acid). A confirmatory experiment was conducted using the HCAEC model, but here no effect was detected on TNF-α stimulated p47^{phox} expression (p > 0.05; Figure 6B).

Endothelial HO-1 Expression. Modulation of HO-1 expression by vanillic acid was examined as a putative indirect mechanism of NOX inhibition. Incubation of HUVECs with the protein kinase C activator PMA (at 10 ng/mL) for 6 h induced a significant increase in basal HO-1 mRNA levels (p < 0.001 versus vehicle control; Figure 7). Vanillic acid, at concentrations of 0.1, 1, and 10 μM, elicited a concentration-dependent elevation in endothelial HO-1 mRNA (~1.6-fold versus unstimulated cells with 10 μM vanillic acid), with a trend toward significance compared to vehicle control (p = 0.1) at 10 μM (Figure 7). Trends toward elevated expression of HO-1 protein in HUVECs were also observed following a 6 h incubation with PMA (~1.9-fold increase versus unstimulated

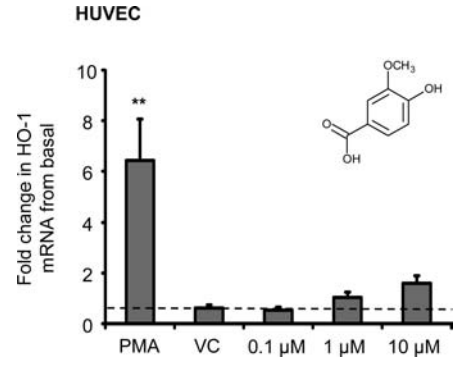

Figure 7. Modulation of HUVEC HO-1 mRNA levels following 6 h incubation with vehicle control (VC, 0.005% DMSO), 10 ng/mL phorbol 12-myristate 13-acetate (PMA), or 0.1 μM, 1 μM, or 10 μM vanillic acid, presented as fold change versus untreated (basal) cells (designated as 1 and marked by dashed line). Relative quantification was performed by RT-qPCR using the comparative C_t method, incorporating the geometric mean of human reference genes TYW1 and PPIA as the normalization factor. Data are graphed as mean ± SD (n = 3). *Significant difference versus vehicle control (*p < 0.01).

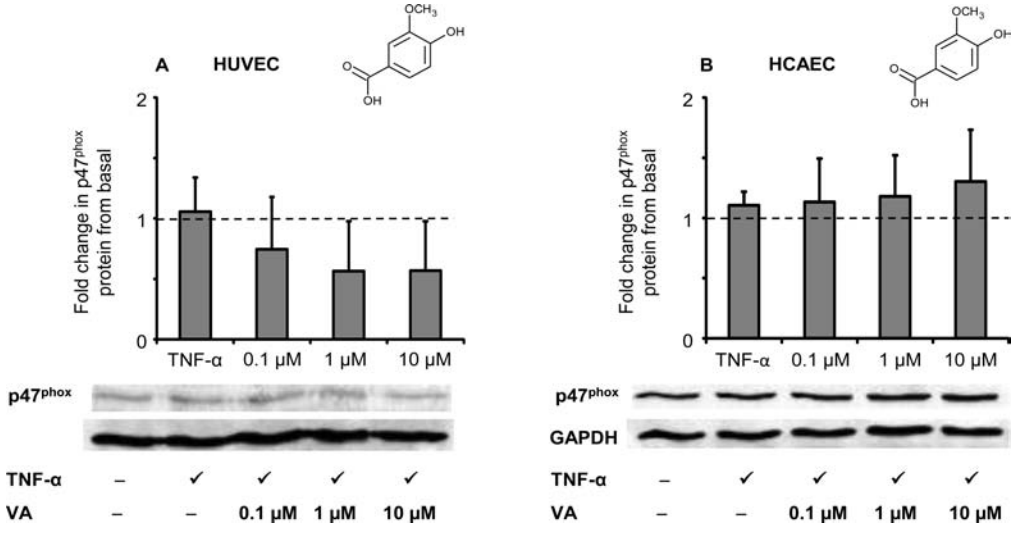

Figure 6. Expression of p47^{phox} protein in HUVEC (A) or HCAEC (B) lysates from unstimulated cells (basal) and following 5 h incubation with 20 ng/mL TNF-α, or TNF-α with 0.1 μM, 1 μM, or 10 μM vanillic acid. Glyceraldehyde-3-phosphate dehydrogenase (GAPDH) was utilized as a loading control for immunoblotting of cell lysates. Graphs show fold increase in p47^{phox} expression relative to basal (designated as 1 and marked by dashed line), after quantification by densitometry and normalization to loading control. Data are graphed as mean ± SD (n = 5 for HUVECs and n = 4 for HCAECs).

DOI: 10.1021/jf5041993
J. Agric. Food Chem. 2015, 63, 2423−2431

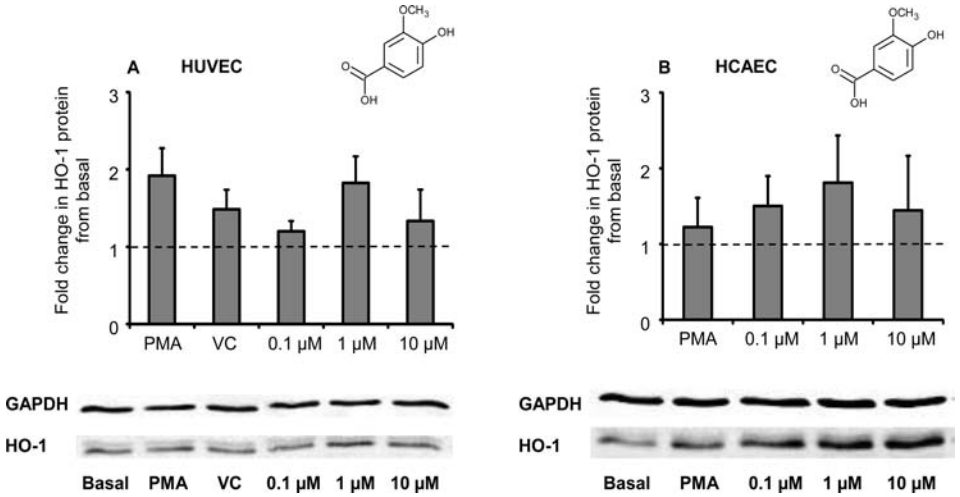

Figure 8. Expression of HO-1 protein in HUVEC (A) or HCAEC (B) lysates from untreated cells (basal) and following 6 h incubation with 10 ng/mL phorbol 12-myristate 13-acetate (PMA), vehicle control (VC, 0.005% DMSO; HUVECs only), or 0.1 μM, 1 μM, or 10 μM vanillic acid. Glyceraldehyde-3-phosphate dehydrogenase (GAPDH) was utilized as a loading control for immunoblotting of cell lysates. Graphs show fold increase in HO-1 expression relative to basal (designated as 1 and marked by dashed line), after quantification by densitometry and normalization to loading control. Data are graphed as mean ± SD (n = 4).

cells) or vanillic acid (~1.8-fold increase at 1 μM vanillic acid) relative to the vehicle control (p = 0.07 and p = 0.1 respectively; Figure 8A). Since the vehicle control (0.005% DMSO) also appeared to upregulate HO-1 protein, vanillic acid was prepared directly in aqueous solution for use in the HCAEC model, to exclude any vehicle-related effects. Expression of HO-1 protein was slightly elevated following a 6 h incubation with PMA in the HCAEC model (~1.2-fold increase versus unstimulated cells; Figure 8B). An apparent upregulation of HO-1 protein was observed at all concentrations of vanillic acid tested (Figure 8B), with a trend toward significance at 1 μM (~1.8-fold increase; p = 0.07) relative to basal.

DISCUSSION

The low bioavailability of parent anthocyanins suggests that their bioactivity in vivo is mediated by phenolic metabolites, which have recently been reported as the main circulating species following anthocyanin consumption.[17−19] Here, we report that phenolic metabolites appear to modulate vascular endothelial cell function through alternative mechanisms to those previously described for parent anthocyanins. In the present study, the parent anthocyanin increased eNOS expression, whereas phenolic derivatives had no effect. However, these metabolites elicited reductions in superoxide production, which could subsequently decrease scavenging of NO. Recent studies by Czank et al. (2013) and de Ferrars et al. (2014) have confirmed a physiologically appropriate range for anthocyanin metabolites in humans of 0.1−10 μM,[17−19] and the present study assessed potential mechanisms of activity at these concentrations. Indeed, following consumption of 500 mg of ^{13}C-labeled cyanidin-3-glucoside, a serum C_{max} of 1.85 μM has been reported for vanillic acid, with 1 μM concentrations persisting for up to 24 h,[19] suggesting that phenolic derivatives of anthocyanins may be present in the systemic circulation at low micromolar levels for at least 18−24 h after ingestion of parent anthocyanins. Based on our findings, physiologically relevant levels of anthocyanin metabolites are likely to act indirectly to maintain vascular homeostasis, through induction of HO-1 and decreased endothelial superoxide generation, as opposed to directly stimulating eNOS activity and NO production.

Endothelium-derived NO is a key component of vascular homeostasis,[11] and prior in vitro studies have described both upregulation and activation of the eNOS enzyme by anthocyanins (including cyanidin-3-glucoside) in cultured endothelial cells at concentrations ranging from 0.001 μM up to 250 μM.[7,8,13] Interestingly, in the present study we observed differential bioactivity for cyanidin-3-glucoside relative to its phenolic acid derivatives. Specifically, no treatment compounds significantly modulated endothelial NO production, however, cyanidin-3-glucoside significantly upregulated eNOS protein levels, while the phenolic derivatives remained inactive (Figure 2).

NOX enzymes represent a major source of reactive oxygen species in the vasculature,[12,25] and anthocyanin metabolites could act as endothelial NOX inhibitors, based on previously reported structure−activity studies.[21] In the current study, differential bioactivity was again observed for cyanidin-3-glucoside relative to its phenolic acid derivatives. A significant elevation in superoxide levels was elicited by cyanidin-3-glucoside; and in contrast, both protocatechuic acid and vanillic acid significantly reduced superoxide levels (Figure 3). While previous reports have described superoxide scavenging[26] and direct cytochrome c reduction[27] elicited by flavonoids, such activity is reported at much higher concentrations (~40−100 μM) than those used in the current investigation (≤10 μM), and control experiments in cell-free incubations confirmed negligible superoxide scavenging or direct cytochrome c reduction by the treatments. High concentrations of phenolic compounds in culture medium have also been reported to result in the generation of hydrogen peroxide,[28] which could potentially interfere with assay methodologies; however, only minimal hydrogen peroxide formation has previously been reported for delphinidin (at 10 μM),[28] which is one of the most reactive anthocyanins.[29] Therefore, data from cell-free experiments in the current study indicate that the treatment compounds do not directly scavenge superoxide radicals, as negligible activity was observed, and the present findings likely

DOI: 10.1021/jf5041993
J. Agric. Food Chem. 2015, 63, 2423−2431

reflect reduced endothelial superoxide generation as opposed to radical scavenging.

The phenolic derivative vanillic acid (the methylated metabolite of protocatechuic acid) was subsequently selected to explore mechanisms potentially underlying the observed reductions in superoxide production. In the present study, vanillic acid at a concentration of 1 μM significantly reduced endothelial superoxide levels, which is comparable to the C_{max} value reported by Czank et al. (2013) for ^{13}C-labeled phase II conjugates of protocatechuic acid (2.35 μM) following ingestion of ^{13}C-labeled cyanidin-3-glucoside.[17] Steffen et al. (2008) have previously described NOX inhibitory activity of vanillic acid in disintegrated HUVECs (IC_{50} = 8.1 μM), with minimal direct superoxide scavenging activity in a cell-free system (IC_{50} > 100 μM),[21] which was confirmed by the absence of direct superoxide scavenging by vanillic acid in the present study.

NOX4 is reported to be the major vascular endothelial isoform,[30,31] producing mainly hydrogen peroxide;[32] and while NOX4-derived hydrogen peroxide would not act to limit NO bioavailability,[33] it might induce vasodilation through hyperpolarization independently of NO activity.[34] In contrast NOX2 generates superoxide[35] and may have a key role in regulating vascular function.[32,36] Both NOX2 and NOX4 associate with the integral membrane protein $p22^{phox}$,[37] but activation of NOX2 follows the recruitment of additional cytosolic proteins including $p47^{phox}$ ("organizer" subunit) and $p67^{phox}$ ("activator" subunit).[37,38] Modulation of the expression of NOX2 and NOX4 isoforms, and associated subunits ($p22^{phox}$, $p47^{phox}$, and $p67^{phox}$) by vanillic acid was therefore explored using RT-qPCR. Coincubation of angiotensin II with vanillic acid elicited no significant changes in levels of endothelial NOX4 mRNA relative to angiotensin II alone (Figure 4A). However, a significant upregulation of $p22^{phox}$ mRNA levels was observed with 0.1 and 1 μM vanillic acid (Figure 4B), while we were unable to assess transcriptional modulation of the superoxide-generating NOX2 isoform, or $p47^{phox}$ and $p67^{phox}$. Therefore, the effects of vanillic acid on the stimulated expression of NOX2 and $p47^{phox}$, and also NOX4, were explored at the protein level.

There was no significant modulation of stimulated NOX4 protein expression by vanillic acid (Figure 5), indicating that this particular metabolite does not affect endothelial NOX4 protein. NOX2 expression was more difficult to discern by immunoblotting of cell lysates, which may reflect low mRNA/protein expression in vascular cells, and/or poor antibody specificity, although upregulation of NOX2 in HUVECs following angiotensin II stimulation has been previously reported.[20] Interestingly, the observed elevation in $p22^{phox}$ mRNA induced by vanillic acid did not appear to be associated with increased NOX4 or NOX2 protein levels. Modulation of $p47^{phox}$ protein expression was examined as a possible mechanism of NOX2 inhibition, and here a trend was observed toward downregulation of $p47^{phox}$ protein following coincubation with TNF-α and vanillic acid (Figure 6A). Interestingly, in the HCAEC model, vanillic acid did not modulate stimulated $p47^{phox}$ expression (Figure 6B), and thus vanillic acid does not appear to significantly alter $p47^{phox}$ levels (under the present conditions) and therefore affect NOX2 activity by this mechanism. However, the anthocyanidin delphinidin has recently been reported to inhibit $p47^{phox}$ translocation and NOX activity in human dermal fibroblasts,[39] suggesting another potential mechanism by which anthocyanins and/or their degradation products could modulate NOX function.

Upregulation of HO-1 has been reported to inhibit NOX function;[14,15] and previous studies have described induction of HO-1 expression by anthocyanins and/or their metabolites in human endothelial cells.[13,40] For example, Nrf2 nuclear translocation and HO-1 expression in cultured HUVECs was elicited by serum samples obtained from healthy subjects following ingestion of 160 mg of purified anthocyanins, which may reflect activity of anthocyanin metabolites as opposed to parent compounds.[40] Moreover, delphinidin-3-glucoside has previously been reported to enhance survival of murine hepatocytes exposed to a cytotoxic concentration of epigallocatechin-3-gallate through upregulation of HO-1 mRNA levels.[41] Endothelial homeostasis is maintained through the action of vasodilators such as NO, however NO bioactivity is diminished by radicals such as $O_2^{\bullet-}$ which are produced through activation of NOX.[9,12] Anthocyanin metabolites could potentially indirectly maintain vascular homeostasis by inducing HO-1, with subsequent inhibition of NOX activity, thus reducing the scavenging of NO by NOX-derived superoxide.[14,15,40] Therefore, the potential indirect effect of vanillic acid on NOX activity was explored by assessing modulation of endothelial HO-1 expression. Following exposure of HUVECs to vanillic acid, elevated HO-1 mRNA levels were observed in what appeared to be a concentration-dependent response (Figure 7), with a trend toward significance relative to the vehicle control (at 10 μM vanillic acid). Likewise, vanillic acid increased HUVEC HO-1 protein expression (Figure 8A), and densitometric analysis indicated a trend toward significance at 1 μM. The vehicle control also appeared to moderately upregulate HO-1, reflecting previously reported studies in HUVECs with low concentrations of DMSO (0−0.8%).[42] As such, vanillic acid was prepared directly in aqueous solution for investigation in the HCAEC model, where a similar trend for upregulation of HO-1 protein was evident (at 1 μM; Figure 8B), suggesting an inverted U-shaped dose response.

A possible limitation of the current investigation was the use of HUVECs as an in vitro model. While HUVECs are widely used for research concerning general properties of endothelial cells,[43] an arterial endothelial cell type may be more appropriate for studies investigating the potential modulation of NOX activity in relation to endothelial dysfunction. Thus, as part of the current investigation confirmatory studies were conducted for potential modulation of $p47^{phox}$/HO-1 expression, using HCAECs as a more physiologically representative endothelial model. Furthermore, in the present study there was no effect of cyanidin-3-glucoside on endothelial NO production (Supporting Information, Figure S1), despite a previous report of activation of eNOS by cyanidin-3-glucoside at concentrations of ≤5 μM in HUVECs.[7] It is possible that assessing eNOS activity by investigating enzyme phosphorylation, as described previously for blackcurrant anthocyanins in a HUVEC model,[44] could have provided further information as to the effects of treatment compounds upon eNOS. NO production was clearly increased by PMA and resveratrol in control experiments, indicating adequate assay sensitivity for the detection of NO-derived nitrite/nitrate in aqueous solution. It is however possible that the assay was not sensitive enough to detect subtle changes in nitrite/nitrate. Interestingly, and with the possible exception of the upregulation of eNOS by cyanidin-3-glucoside, linear dose−response relationships were not observed for any treatment in the current investigation,

DOI: 10.1021/jf5041993
J. Agric. Food Chem. 2015, 63, 2423−2431

suggesting differential bioactivity of anthocyanins and their metabolites across dose ranges, as described previously for cyanidin-3-glucoside.[8] However, as only three concentrations of the treatment compounds were assessed in the current study, it is not possible to draw definitive conclusions regarding dose−response relationships, and a wider dosage range is required to confirm our observations.

Another limitation of the present study was the poor qPCR specificity observed for NOX2, $p47^{phox}$, and $p67^{phox}$, which precluded determination of relative changes in expression for these transcripts. Previously reported studies have suggested low or no endothelial expression of NOX2 mRNA,[30,45] and low expression of $p47^{phox}$ and $p67^{phox}$ mRNA in HUVECs.[30] Moreover, minimal changes were detected in NOX4 gene expression, and $p47^{phox}$ protein expression, following stimulation with angiotensin II or TNF-α respectively, although limited upregulation of $p47^{phox}$ was consistent in both HUVEC and HCAEC models.

In the present study, cyanidin-3-glucoside significantly upregulated endothelial expression of eNOS as previously reported for unmetabolized anthocyanins,[8,13] however the phenolic acid derivatives were not active. By contrast, both the degradation product protocatechuic acid and its phase II metabolite vanillic acid significantly reduced endothelial superoxide levels, whereas the parent anthocyanin did not. These data suggest a differential bioactivity of anthocyanins relative to their phenolic derivatives. Our findings therefore indicate that anthocyanins may directly stimulate eNOS, eliciting improved endothelial function; however, when anthocyanins are metabolized, this direct effect upon eNOS is lost. Nevertheless, their metabolites could maintain vascular homeostasis through indirectly preserving NO bioactivity, by mechanisms involving NOX or HO-1. It must be noted that Czank et al. (2013) identified 16 phenolic metabolites of cyanidin-3-glucoside in human serum,[17] which should all be investigated for potential vascular bioactivity in future studies. Indeed, preliminary data from ongoing studies in our laboratory suggest that protocatechuic acid, and protocatechuic acid in combination with vanillic acid, upregulate HO-1 protein expression in rat aortic smooth muscle cells in vitro (data not shown).

In conclusion, there was no direct effect of vanillic acid on endothelial protein expression of eNOS or NOX isoforms in the present investigation, whereas HO-1 protein was modestly increased, indicating different mechanisms of bioactivity for phenolic derivatives relative to parent anthocyanins. This also suggests a potential indirect activity of anthocyanin metabolites in maintaining vascular homeostasis in vivo.

■ ASSOCIATED CONTENT

Supporting Information

Primer sequences for custom primer sets (human HMOX-1, NOX2, NOX4, $p22^{phox}$, $p47^{phox}$, and $p67^{phox}$) and Figures S1 and S2. This material is available free of charge via the Internet at http://pubs.acs.org.

■ AUTHOR INFORMATION

Corresponding Author

*Faculty of Medicine and Health Sciences, Department of Nutrition, Norwich Medical School, University of East Anglia, Norwich NR4 7UQ, U.K. E-mail: Colin.Kay@uea.ac.uk. Tel: +44 (0)1603 591236.

Present Addresses

[†]M.E.: GFA, Ely, Cambridgeshire CB7 4EX, U.K.

[‡]C.C.: Telethon Kids Institute, University of Western Australia, West Perth, Western Australia.

[§]G.M.W.: Department of Clinical Biochemistry, Oxford University Hospitals, Oxford.

Funding

This study was supported by two UK Biotechnology and Biological Sciences Research Council (BBSRC) CASE studentships (M.E. and G.M.W.) in partnership with GlaxoSmithKline (U.K.).

Notes

The authors declare no competing financial interest.

■ ACKNOWLEDGMENTS

The authors would like to thank Ilde Rodriguez-Ramiro and Emily Warner (Department of Nutrition, Norwich Medical School, University of East Anglia) for their work on the bioactivity of flavonoids and phenolic metabolites in rat aortic smooth muscle cells (supported by the BBSRC Diet and Health Research Industry Club; BB/H004963/1, BB/I006028/1).

■ ABBREVIATIONS USED

Ang II, angiotensin II; ANOVA, analysis of variance; CV, coefficient of variation; DMSO, dimethyl sulfoxide; EDTA, ethylenediaminetetraacetic acid; ELISA, enzyme-linked immunosorbent assay; eNOS, endothelial nitric oxide synthase; FBS, fetal bovine serum; GAPDH, glyceraldehyde-3-phosphate dehydrogenase; HCAEC, human coronary artery endothelial cell; HO-1, heme oxygenase-1; HUVEC, human umbilical vein endothelial cell; NADPH, reduced nicotinamide adenine dinucleotide phosphate; NO, nitric oxide; NOX, NADPH oxidase; $O_2^{\bullet-}$, superoxide; PBS, phosphate-buffered saline; PMA, phorbol 12-myristate 13-acetate; SOD, superoxide dismutase; TNF-α, tumor necrosis factor-alpha; VA, vanillic acid

■ REFERENCES

(1) Crozier, A.; Jaganath, I. B.; Clifford, M. N. Dietary phenolics: chemistry, bioavailability and effects on health. *Nat. Prod. Rep.* **2009**, *26*, 1001−43.

(2) Cassidy, A.; O'Reilly, E. J.; Kay, C.; Sampson, L.; Franz, M.; Forman, J.; Curhan, G.; Rimm, E. B. Habitual intake of flavonoid subclasses and incident hypertension in adults. *Am. J. Clin. Nutr.* **2010**, *93*, 338−47.

(3) Mink, P. J.; Scrafford, C. G.; Barraj, L. M.; Harnack, L.; Hong, C. P.; Nettleton, J. A.; Jacobs, D. R., Jr. Flavonoid intake and cardiovascular disease mortality: a prospective study in postmenopausal women. *Am. J. Clin. Nutr.* **2007**, *85*, 895−909.

(4) McCullough, M. L.; Peterson, J. J.; Patel, R.; Jacques, P. F.; Shah, R.; Dwyer, J. T. Flavonoid intake and cardiovascular disease mortality in a prospective cohort of US adults. *Am. J. Clin. Nutr.* **2012**, *95*, 454−64.

(5) Zhu, Y.; Xia, M.; Yang, Y.; Liu, F.; Li, Z.; Hao, Y.; Mi, M.; Jin, T.; Ling, W. Purified Anthocyanin Supplementation Improves Endothelial Function via NO-cGMP Activation in Hypercholesterolemic Individuals. *Clin. Chem.* **2011**, *57*, 1524−33.

(6) Rodriguez-Mateos, A.; Rendeiro, C.; Bergillos-Meca, T.; Tabatabaee, S.; George, T. W.; Heiss, C.; Spencer, J. P. Intake and time dependence of blueberry flavonoid−induced improvements in vascular function: a randomized, controlled, double-blind, crossover intervention study with mechanistic insights into biological activity. *Am. J. Clin. Nutr.* **2013**, *98*, 1179−91.

DOI: 10.1021/jf5041993
J. Agric. Food Chem. 2015, 63, 2423−2431

(7) Xu, J. W.; Ikeda, K.; Yamori, Y. Cyanidin-3-glucoside regulates phosphorylation of endothelial nitric oxide synthase. *FEBS Lett.* **2004**, *574*, 176−80.
(8) Xu, J. W.; Ikeda, K.; Yamori, Y. Upregulation of endothelial nitric oxide synthase by cyanidin-3-glucoside, a typical anthocyanin pigment. *Hypertension* **2004**, *44*, 217−22.
(9) Higashi, Y.; Noma, K.; Yoshizumi, M.; Kihara, Y. Endothelial function and oxidative stress in cardiovascular diseases. *Circ. J.* **2009**, *73*, 411−8.
(10) Wever, R.; Stroes, E.; Rabelink, T. J. Nitric oxide and hypercholesterolemia: a matter of oxidation and reduction? *Atherosclerosis* **1998**, *137* (Suppl.), S51−60.
(11) Naseem, K. M. The role of nitric oxide in cardiovascular diseases. *Mol. Aspects Med.* **2005**, *26*, 33−65.
(12) Bonomini, F.; Tengattini, S.; Fabiano, A.; Bianchi, R.; Rezzani, R. Atherosclerosis and oxidative stress. *Histol. Histopathol.* **2008**, *23*, 381−90.
(13) Sorrenti, V.; Mazza, F.; Campisi, A.; Di Giacomo, C.; Acquaviva, R.; Vanella, L.; Galvano, F. Heme oxygenase induction by cyanidin-3-O-beta-glucoside in cultured human endothelial cells. *Mol. Nutr. Food Res.* **2007**, *51*, 580−6.
(14) Jiang, F.; Roberts, S. J.; Datla, S.; Dusting, G. J. NO modulates NADPH oxidase function via heme oxygenase-1 in human endothelial cells. *Hypertension* **2006**, *48*, 950−7.
(15) Datla, S. R.; Dusting, G. J.; Mori, T. A.; Taylor, C. J.; Croft, K. D.; Jiang, F. Induction of Heme Oxygenase-1 In Vivo Suppresses NADPH Oxidase-Derived Oxidative Stress. *Hypertension* **2007**, *50*, 636−42.
(16) Vitaglione, P.; Donnarumma, G.; Napolitano, A.; Galvano, F.; Gallo, A.; Scalfi, L.; Fogliano, V. Protocatechuic acid is the major human metabolite of cyanidin-glucosides. *J. Nutr.* **2007**, *137*, 2043−8.
(17) Czank, C.; Cassidy, A.; Zhang, Q.; Morrison, D. J.; Preston, T.; Kroon, P. A.; Botting, N. P.; Kay, C. D. Human metabolism and elimination of the anthocyanin, cyanidin-3-glucoside: a ^{13}C-tracer study. *Am. J. Clin. Nutr.* **2013**, *97*, 995−1003.
(18) de Ferrars, R. M.; Cassidy, A.; Curtis, P.; Kay, C. D. Phenolic metabolites of anthocyanins following a dietary intervention study in post-menopausal women. *Mol. Nutr. Food Res.* **2014**, *58*, 490−502.
(19) de Ferrars, R. M.; Czank, C.; Zhang, Q.; Botting, N. P.; Kroon, P. A.; Cassidy, A.; Kay, C. D. The pharmacokinetics of anthocyanins and their metabolites in humans. *Br. J. Pharmacol.* **2014**, *171*, 3268−82.
(20) Rueckschloss, U.; Quinn, M. T.; Holtz, J.; Morawietz, H. Dose-dependent regulation of NAD(P)H oxidase expression by angiotensin II in human endothelial cells: protective effect of angiotensin II type 1 receptor blockade in patients with coronary artery disease. *Arterioscler., Thromb., Vasc. Biol.* **2002**, *22*, 1845−51.
(21) Steffen, Y.; Gruber, C.; Schewe, T.; Sies, H. Mono-O-methylated flavanols and other flavonoids as inhibitors of endothelial NADPH oxidase. *Arch. Biochem. Biophys.* **2008**, *469*, 209−19.
(22) Stielow, C.; Catar, R. A.; Muller, G.; Wingler, K.; Scheurer, P.; Schmidt, H. H.; Morawietz, H. Novel Nox inhibitor of oxLDL-induced reactive oxygen species formation in human endothelial cells. *Biochem. Biophys. Res. Commun.* **2006**, *344*, 200−5.
(23) Saleem, M. M.; Wilson, M. T. Kinetic studies on the reduction of cytochrome c. Reaction with dihydroxy conjugated compounds (catechols and quinols). *Biochem. J.* **1982**, *201*, 433−44.
(24) Schmittgen, T. D.; Livak, K. J. Analyzing real-time PCR data by the comparative C(T) method. *Nat. Protoc.* **2008**, *3*, 1101−8.
(25) Bedard, K.; Krause, K. H. The NOX family of ROS-generating NADPH oxidases: physiology and pathophysiology. *Physiol. Rev.* **2007**, *87*, 245−313.
(26) Taubert, D.; Breitenbach, T.; Lazar, A.; Censarek, P.; Harlfinger, S.; Berkels, R.; Klaus, W.; Roesen, R. Reaction rate constants of superoxide scavenging by plant antioxidants. *Free Radical Biol. Med.* **2003**, *35*, 1599−607.
(27) Skemiene, K.; Rakauskaite, G.; Trumbeckaite, S.; Liobikas, J.; Brown, G. C.; Borutaite, V. Anthocyanins block ischaemia-induced apoptosis in the perfused heart and support mitochondrial respiration potentially by reducing cytosolic cytochrome c. *Int. J. Biochem. Cell Biol.* **2012**, *45*, 23−9.
(28) Long, L. H.; Hoi, A.; Halliwell, B. Instability of, and generation of hydrogen peroxide by, phenolic compounds in cell culture media. *Arch. Biochem. Biophys.* **2010**, *501*, 162−9.
(29) Woodward, G.; Kroon, P.; Cassidy, A.; Kay, C. Anthocyanin stability and recovery: implications for the analysis of clinical and experimental samples. *J. Agric. Food Chem.* **2009**, *57*, 5271−8.
(30) Ago, T.; Kitazono, T.; Ooboshi, H.; Iyama, T.; Han, Y. H.; Takada, J.; Wakisaka, M.; Ibayashi, S.; Utsumi, H.; Iida, M. Nox4 as the Major Catalytic Component of an Endothelial NAD(P)H Oxidase. *Circulation* **2004**, *109*, 227−33.
(31) Takac, I.; Schroder, K.; Brandes, R. P. The Nox Family of NADPH Oxidases: Friend or Foe of the Vascular System? *Curr. Hypertens. Rep.* **2011**, *14*, 70−8.
(32) Brown, D. I.; Griendling, K. K. Nox proteins in signal transduction. *Free Radical Biol. Med.* **2009**, *47*, 1239−53.
(33) Brandes, R. P.; Takac, I.; Schroder, K. No Superoxide−No Stress?: Nox4, the Good NADPH Oxidase! *Arterioscler., Thromb., Vasc. Biol.* **2011**, *31*, 1255−7.
(34) Ray, R.; Murdoch, C. E.; Wang, M.; Santos, C. X.; Zhang, M.; Alom-Ruiz, S.; Anilkumar, N.; Ouattara, A.; Cave, A. C.; Walker, S. J.; Grieve, D. J.; Charles, R. L.; Eaton, P.; Brewer, A. C.; Shah, A. M. Endothelial Nox4 NADPH Oxidase Enhances Vasodilatation and Reduces Blood Pressure In Vivo. *Arterioscler., Thromb., Vasc. Biol.* **2011**, *31*, 1368−76.
(35) Brandes, R. P.; Weissmann, N.; Schroder, K. NADPH oxidases in cardiovascular disease. *Free Radical Biol. Med.* **2010**, *49*, 687−706.
(36) Schroder, K. Isoform specific functions of Nox protein-derived reactive oxygen species in the vasculature. *Curr. Opin. Pharmacol.* **2010**, *10*, 122−6.
(37) Sumimoto, H.; Miyano, K.; Takeya, R. Molecular composition and regulation of the Nox family NAD(P)H oxidases. *Biochem. Biophys. Res. Commun.* **2005**, *338*, 677−86.
(38) Drummond, G. R.; Selemidis, S.; Griendling, K. K.; Sobey, C. G. Combating oxidative stress in vascular disease: NADPH oxidases as therapeutic targets. *Nat. Rev. Drug Discovery* **2011**, *10*, 453−71.
(39) Lim, T.-G.; Jung, S. K.; Kim, J.-e.; Kim, Y.; Lee, H. J.; Jang, T. S.; Lee, K. W. NADPH oxidase is a novel target of delphinidin for the inhibition of UVB-induced MMP-1 expression in human dermal fibroblasts. *Exp. Dermatol.* **2013**, *22*, 428−30.
(40) Cimino, F.; Speciale, A.; Anwar, S.; Canali, R.; Ricciardi, E.; Virgili, F.; Trombetta, D.; Saija, A. Anthocyanins protect human endothelial cells from mild hyperoxia damage through modulation of Nrf2 pathway. *Genes Nutr.* **2013**, *8*, 391−9.
(41) Inoue, H.; Maeda-Yamamoto, M.; Nesumi, A.; Murakami, A. Delphinidin-3-O-galactoside protects mouse hepatocytes from (−)-epigallocatechin-3-gallate-induced cytotoxicity via up-regulation of heme oxygenase-1 and heat shock protein 70. *Nutr. Res. (N.Y.)* **2012**, *32*, 357−64.
(42) Liang, C.; Xue, Z.; Cang, J.; Wang, H.; Li, P. Dimethyl sulfoxide induces heme oxygenase-1 expression via JNKs and Nrf2 pathways in human umbilical vein endothelial cells. *Mol. Cell. Biochem.* **2011**, *355*, 109−15.
(43) Baudin, B.; Bruneel, A.; Bosselut, N.; Vaubourdolle, M. A protocol for isolation and culture of human umbilical vein endothelial cells. *Nat. Protoc.* **2007**, *2*, 481−5.
(44) Edirisinghe, I.; Banaszewski, K.; Cappozzo, J.; McCarthy, D.; Burton-Freeman, B. M. Effect of Black Currant Anthocyanins on the Activation of Endothelial Nitric Oxide Synthase (eNOS) in Vitro in Human Endothelial Cells. *J. Agric. Food Chem.* **2011**, *59*, 8616−24.
(45) Alvarez, E.; Rodino-Janeiro, B. K.; Ucieda-Somoza, R.; Gonzalez-Juanatey, J. R. Pravastatin counteracts angiotensin II-induced upregulation and activation of NADPH oxidase at plasma membrane of human endothelial cells. *J. Cardiovasc. Pharmacol.* **2010**, *55*, 203−12.

DOI: 10.1021/jf5041993
J. Agric. Food Chem. 2015, 63, 2423−2431

$CD44^+$ or $CD133^+$,[17] and CSCs that have survived chemotherapeutic drug treatment can be obtained using their drug-resistance feature.[3,10] In addition, using the induction of epithelia to mesenchymal transition (EMT) in tumor cells, the specific tumor cell population that exhibits stemness after dedifferentiation can be obtained.[18]

Gupta et al.[19] showed that salinomycin selectively kills CSCs and effectively inhibits BCSC survival and mammosphere formation. These results showed that specific inhibition of mammosphere formation might be regarded as an effective measure for breast cancer treatment. Because therapeutic drugs, such as paclitaxel, doxorubicin, docetaxel, and cyclophosphamide, are already used to target breast cancer, development of an adjuvant therapy to target CSCs from natural products that are highly safe, do not have side effects, and can strengthen the effect of chemotherapeutic drugs should be a feasible strategy for breast cancer treatment.[12]

6-Gingerol (6-G) is the most abundant polyphenolic compound in ginger (*Zingiber officinalis*); after dehydration, 6-G becomes 6-shogaol (6-S), which has higher physiological activities. 6-S is the source of the pungent constituent of ginger; it can attenuate neuroinflammation and cognitive deficits[20] and induce colon cancer cell apoptosis through the induction of reactive oxygen species (ROS) production and activation of the caspase pathway.[21] Weng et al.[22] showed that 6-S and 6-G inhibit the invasive characteristics of liver cancer cells. Pterostilbene (PTE), which is extensively present in blueberries and grapes, is a dimethylated analogue of resveratrol and a natural antibacterial substance.[23] Simoni et al.[24] confirmed that PTE can effectively induce apoptosis in HL-60 leukemia cells and can inhibit the invasion and metastasis functions of HepG2 liver cancer cells through the inhibition of the expression of NF-κB and AP-1 transcriptional factors and MMP-9.[23] Nobiletin (5,6,7,8,3′,4′-hexamethoxyflavone, NOL) and 5-hydroxy-3,6,7,8,3′,4′-hexamethoxyflavone (5-HF) are both flavonoids in citrus fruits; previous studies have confirmed that they have antitumor potentials, such as the inhibition of tumor cell invasion and promotion of apoptosis.[25,26]

Modern chemotherapies are designed to prevent the local recurrences of primary tumors and the distant metastases of tumor cells. However, the effective doses of many chemotherapeutics cause severe side effects. There is considerable interest in the discovery and investigation of more potent anticancer stemness compounds to prevent and delay cancer recurrence. Important attributes of an ideal inhibitor would be easy obtainment, absorption, and excretion, little or none toxicity, and the absence of serious side effects. Naturally occurring polyphenols such as 6-G, 6-S, 5-HF, NOL, and PTE should, therefore, be ideal candidates for reducing cancer stemness. Although previous paper have described the antitumor activities of the above phytochemicals, no studies have been made of their selective cytotoxic effects on CSCs and their parental cancer cells. In the field of CSC studies, BCSCs were discovered early and could be identified using cell surface antigens. Therefore, there are detailed reports on the isolation and identification of CSCs that can be referenced. On the basis of these reports, this study aimed to investigate the effects of 6-S, 6-G, PTE, NOL, and 5-HF on BCSC proliferation and clarify the underlying molecular mechanisms.

MATERIALS AND METHODS

Chemicals. 6-G and 6-S were isolated and purified as previously described.[27] 5-HF and NOL were synthesized according to the previous method.[28] PTE was synthesized according to the method reported by Pettit et al.[29] Epidermal growth factor (EGF), basic fibroblast growth factor (bFGF), human leukemia inhibitory factor (hLIF), insulin-transferrin-sodium selenite supplement (ITSS), 3-(4,5-dimethylthiazol-2-yl)-2,5-diphenyltetrazolium bromide (MTT), fish gelatin, anti-β-actin antibody, HEPES buffer, Tween-20, and sodium bicarbonate were purchased from Sigma Chemical Co. (St. Louis, MO, USA). The protein assay kit and Tris-base were obtained from Bio-Rad (Hercules, CA, USA). B27 supplement, Dulbecco's modified Eagle's medium/Ham's F-12 (DMEM/F12) medium, Roswell Park Memorial Institute (RPMI) 1640 medium, fetal bovine serum (FBS), trypsin-EDTA, propidium iodide (PI), and penicillin–streptomycin were purchased from Invitrogen (Carlsbad, CA, USA). The nuclear/cytosol fractionation kit was purchased from BioVision (Milpitas, CA, USA). Dimethyl sulfoxide (DMSO) was obtained from Merck Co. (Darmstadt, Germany). Anti-phospho-GSK3β (ser9), anti-notch, anti-STAT3, anti-phospho-STAT3, anti-survivin, and anti-Sonic-hedgehog antibodies were obtained from Millipore (Bedford, MA, USA). Anti-β-catenin, anti-phospho-β-catenin (Ser33/37/Thr41), anti-mTOR, anti-phospho-mTOR, anti-Akt, and anti-phospho-Akt (ser473) antibodies were purchased from Cell Signaling Technology (Beverly, MA, USA). Anti-cyclin D1, anti-c-Myc, and anti-GSK3 antibodies were obtained from Santa Cruz Biotechnology Inc. (Santa Cruz, CA, USA). Anti-CD44-PE and anti-CD24-FITC antibodies were obtained from Biolegend (San Diego, CA, USA), and the horseradish peroxidase-conjugated anti-mouse secondary antibody was obtained from Bethyl Laboratories Inc. (Montgomery, TX, USA).

Cell Line and Culture. The MCF-7 human breast adenocarcinoma cell line was obtained from the Bioresource Collection and Research Center (BCRC 60436; Food Industry Research and Development Institute) and was cultured in DMEM supplemented with 10% v/v FBS in a humidified atmosphere of 95% air and 5% CO_2. The medium was changed three times per week. The MCF-7 cells were estrogen receptor positive and characterized as having a low metastatic phenotype.

BCSC Isolation and Culture. MCF-7 cells were detached and resuspended in PBS containing 1% FBS and 1% penicillin/streptomycin (10^6 cells/100 μL). Combinations of fluorochrome-conjugated monoclonal antibodies against human CD44 (FITC) and CD24 (PE) or their respective isotype controls were added to the cell suspension at concentrations recommended by the manufacturer and incubated at 4 °C in the dark for 30 min. Cells were analyzed and sorted on an FACSAria Cell Sorter unit (Becton Dickinson, San Jose, CA, USA), using PI as a viable stain. BCSCs were gated on low side scatter, low-to-moderate forward scatter, and low PI. The $CD44^+/CD24^{-/low}$ phenotype was used to identify and isolate BCSCs, according to a previous study.[30] For data acquisition, at least 10000 events were analyzed. The purity and viability of isolated cells were routinely >98%, as determined by trypan blue dye exclusion. The sorted BCSCs were cultured in stem cell medium (SCM, DMEM/F12 medium containing B27 supplement, 10 ng/mL EGF, bFGF, and ITSS) without FBS.

Mammosphere Formation. Sorted cells were plated on ultralow attachment plates (Corning, Acton, MA, USA) at a density of 20000 viable cells per milliliter and a density of 1000 cells per milliliter for subsequent passages. Cells were grown in SCM as described above. Mammospheres were collected by gentle centrifugation (800 rpm) after 7–10 days and were dissociated enzymatically (10 min in 0.05% trypsin) and mechanically, using a fire-polished Pasteur pipet. The cells obtained from dissociation were passed through a 40 μm sieve and analyzed microscopically for single cellularity. Cells plated at low densities (1000 cells/mL) were grown in conditioned medium from high-density sorted cultures in suspension.

Soft Agar for Anchorage-Independent Growth Assay. BCSCs were harvested and seeded in six-well plates (5×10^4 cells/well) coated with 0.6% agarose. Anchorage-independent growth was assessed after incubation for 10–14 days in culture medium with or without the tested phytochemicals (0, 25, and 50 μM), which was replaced every 2 days. The plates were stained with 0.005% crystal

DOI: 10.1021/acs.jafc.5b00002
J. Agric. Food Chem. 2015, 63, 2432–2441

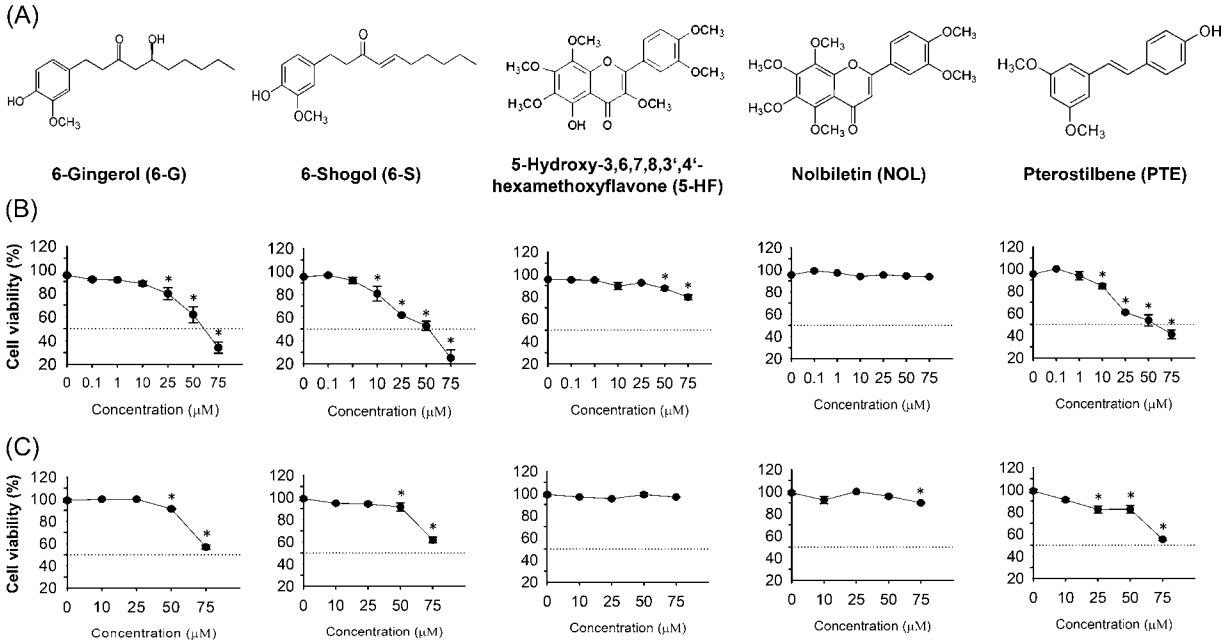

Figure 1. Selective cytotoxicity of 6-gingerol (6-G), 6-shogaol (6-S), 5-hydroxy-3,6,7,8,3′,4′-hexamethoxyflavone (5-HF), nobiletin (NOL), and pterostilbene (PTE) (A) against the $CD44^+/CD24^-$ cell population of MCF-7 cells (B) and MCF7 human breast cancer cells (C). MCF-7 cells or MCF7 $CD44^+/CD24^-$ cells were treated with 0−75 μM of the tested compounds for 72 h. The reported values are the mean ± SD (n = 3); ∗, p < 0.01, indicates significant differences compared with the control group.

violet, and the colonies were counted manually under a microscope and imaged.

Western Blotting. BCSCs were treated with 6-S or PTE for 4−24 h. After treatment, the cell lysates and nuclear fractions were prepared using a nuclear/cytosol fractionation kit. The protein concentrations of the cell lysate and nuclear fractions were estimated with the Bio-Rad DC protein assay using BSA as the standard. Total proteins (25−50 μg) were separated by SDS-PAGE using a 10% polyacrylamide gel and then transferred onto a nitrocellulose membrane. The membrane was blocked with 1% fish gelatin in PBS with 0.05% Tween 20 (pH 7.2) for 1 h. The membranes were then incubated with primary antibodies (1:1000) at 4 °C overnight, followed by incubation with a horseradish peroxide-linked secondary antibody (1:10000). The protein bands were visualized using the ChemiLucent ECL Detection System (Millipore) and the Biospectrum AC Imaging System (UVP, Upland, CA, USA). The expression levels of the proteins of interest were normalized to the expression of β-actin. The intensity of the chemiluminescence signal was quantified using the UVP VisionWorksLS Image Acquisition and Analysis software.

Statistical Analyses. Each experiment was performed in triplicate. The results are expressed as the mean ± SD. The statistical analyses were performed using SAS software, and the variances were assessed using ANOVAs. Significant differences (p < 0.05) between the means were identified by Duncan's multiple-range tests.

RESULTS

Cytotoxic Effects of the Selected Phytochemicals on BCSCs. This study selected five phytochemicals, 6-G, 6-S, 5-HF, NOL, and PTE (Figure 1A), to evaluate with regard to their cytotoxicity on MCF-7 BCSCs ($CD44^+/CD24^-$ subpopulations of MCF-7 cells) and MCF-7 breast cancer cells using the trypan blue assay. The results showed that, of the above five phytochemicals tested at doses of 0.1−75 μM, the IC_{50} values of 6-G, 6-S, and PTE on BCSCs were 50, 25, and 25 μM, respectively (Figure 1B), which was more significant than their effects on MCF-7 parental cells (Figure 1C). Of note, none of these compounds had a cytotoxic effect on primary cultured rat hepatocytes at a concentration of 25 μM for the same time frame (Supporting Information). These results indicated that 6-S and PTE had potent selective toxic effects on BCSCs. Subsequent experiments evaluated the effects of 6-S and PTE on BCSC characteristics.

6-S and PTE Induce Changes in Cell Morphology and Mammosphere-Forming Capacity of BCSCs. The images of cell morphology in Figure 2A show that after a 6 h treatment with 6-S or PTE, cell necrosis phenomena, such as membrane injury and bleb formation, were induced in BCSCs. Mammosphere formation is an important indicator of BCSC differentiation. After BCSCs were treated with 6-S or PTE for 72 h, robust mammosphere disruptions were induced (Figure 2B, left panel), and the number of mammospheres was effectively reduced (Figure 2B, right panel). In addition, this study further simulated a nutrient-deficient or -sufficient environment using SCM without FBS or RPMI 1640 medium containing 10% FBS, respectively, to investigate the effects of 6-S and PTE on mammospheres under different FBS concentrations. The results showed that large BCSC mammospheres were easily induced in a nutrient-deficient environment, whereas mammospheres were at a dormant status in a nutrient-sufficient environment. Under culture conditions without FBS, PTE more effectively reduced the volume of mammospheres than 6-S and promoted their disintegration; however, in an environment containing FBS, neither compound had any influence on mammospheres (Figure 2C).

Effects of 6-S or PTE Combined with Paclitaxel on the Differentiated BCSC Population. This study cultured BCSCs in RPMI medium containing 10% FBS to promote differentiation to observe the effects of the chemotherapeutic drug paclitaxel on the differentiated BCSC population when combined with either 6-S or PTE. Figure 3A shows that 10 nM paclitaxel had significant cytotoxic effects on the differentiated BCSC populations; however, this cytotoxicity was not increased when the dose was increased to 50 nM (Figure 3A, p > 0.05). It is worth noting that 6-S and PTE (Figure 3B) already doubled

DOI: 10.1021/acs.jafc.5b00002
J. Agric. Food Chem. 2015, 63, 2432−2441

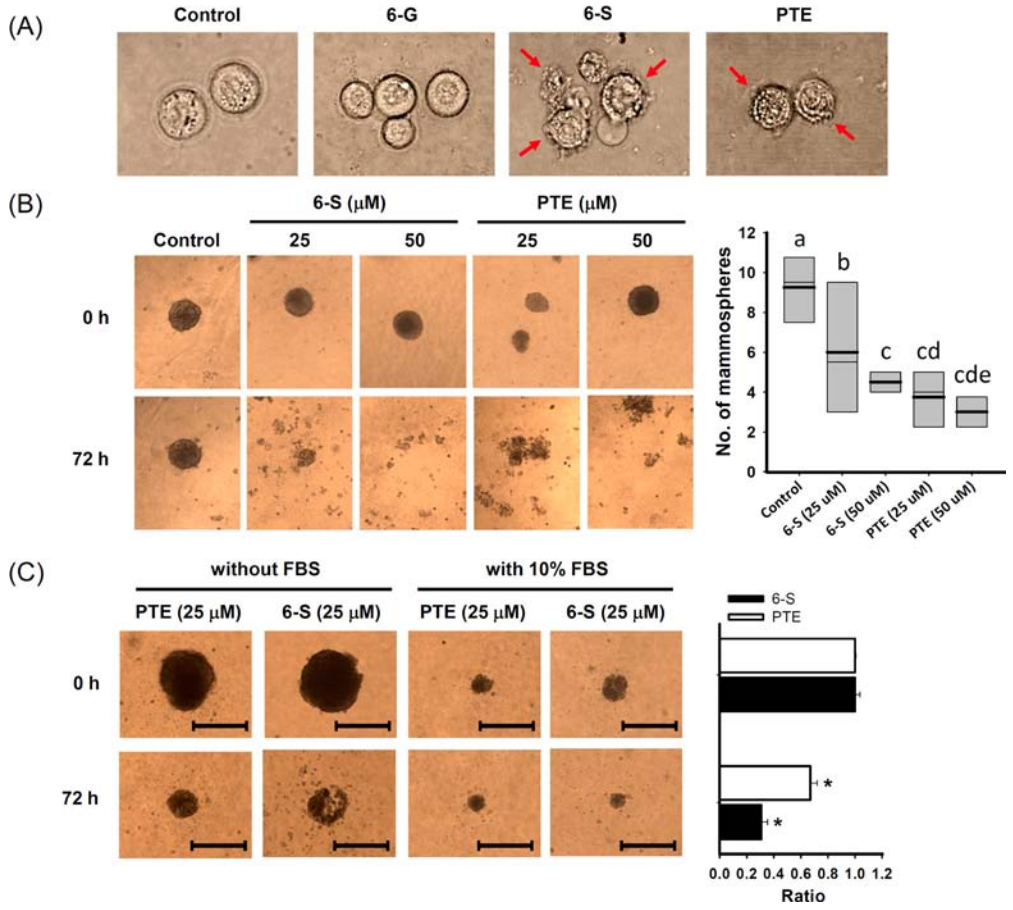

Figure 2. Effects of 6-G, 6-S, and PTE on BCSC morphology, mammosphere formation, and colony formation. (A) Images show the morphology of BCSCs treated with 100 μM of the tested compounds for 6 h (400×). The red arrows indicate blebs on the cell surface. (B) The left-side panels of the figure show mammosphere morphology changes for 0 and 72 h (40×). The right-side panels represent the number of mammospheres (line indicates the median). The cells were treated with 25 or 50 μM 6-S and PTE for 72 h (n = 4). The boxes represent the 25th to 75th percentiles, and horizontal lines within the box represent mean (bold) and median (thin) values, respectively. The bars with different letters are significantly different from each other in individual assays ($p < 0.05$). (C) Images show the morphology of mammospheres that were cultured in stem cell medium without FBS and in RPMI medium plus 10% FBS (40×). The cells were grown in 0.3% soft agar for 14 days and then treated with 25 μM 6-S and PTE for a further 72 h. The right-side panel represents the quantified size of the mammospheres in the left panel. The reported values are the mean ± SD (n = 3); *, $p < 0.05$, indicates significant differences from the control group. BCSCs, breast cancer stem cells.

the cytotoxicity of chemotherapeutic drugs on the differentiated BCSC populations at low doses (0.5 and 10 μM; Figure 3C); therefore, they may increase the antitumor effects of chemotherapeutic drugs.

Effects of 6-S and PTE on the Expression of CD44/CD24 Surface Markers on BCSCs. It is known that the degree of breast cancer cell malignancy is closely associated with the expression of $CD44^+/CD24^-$ on stem cells.[30] When the CD44 surface antigen is activated, breast cancer cell populations evolve into cell populations that have increased invasiveness. This study used flow cytometry to observe the effects of 6-S or PTE on stem cell surface antigen expression in BCSCs. The cell population in the $CD44^+/CD24^-$ quadrant was the BCSC population, whereas the cell population in the $CD44^-/CD24^-$ quadrant was the cell population that had lost stemness. Figure 4 shows that after culture of 6-S or PTE (25 μM) with BCSCs for 72 h, the number of BCSCs was inhibited, and the number of cells that did not have stemness was significantly increased ($p < 0.05$). The maintenance of BCSC stemness was inhibited through a decrease in CD44 expression.

Effects of 6-S and PTE on the Hedgehog Signaling Pathway in BCSCs. The hedgehog signal transduction pathway and β-catenin transcription activity can regulate the differentiation and self-renewal of CSCs.[31] Many studies have regarded the hedgehog pathway as an important indicator for the suppression of drug resistance in CSCs and tumor recurrence. This study cultured BCSCs in SCM with 6-S or PTE (5 and 25 μM) for 4, 8, and 24 h and analyzed the changes in the expression levels of hedgehog, phospho-Akt, Akt, phospho-GSK3β, and GSK3β. The results showed that 6-S (Figure 5A) and PTE (Figure 5B) effectively inhibited hedgehog protein expression and Akt and GSK3β phosphorylation ($p < 0.05$).

Effects of 6-S and PTE on β-Catenin Phosphorylation and Downstream Protein Expression in BCSCs. The Wnt/β-catenin signaling transduction pathway is very important for the maintenance of CSC stemness. Studies have indicated that β-catenin activation is an important target for regulation of CSC differentiation and inhibition of tumor recurrence. In this study, BCSCs were treated with 6-S or PTE (5 and 25 μM) for 4, 8, and 24 h to analyze the changes in the expression of phospho-β-catenin, β-catenin, cyclin D1, and c-Myc. The results showed that 6-S (Figure 6A) and PTE (Figure 6B), at a concentration of 25 μM, significantly induced β-catenin

DOI: 10.1021/acs.jafc.5b00002
J. Agric. Food Chem. 2015, 63, 2432−2441

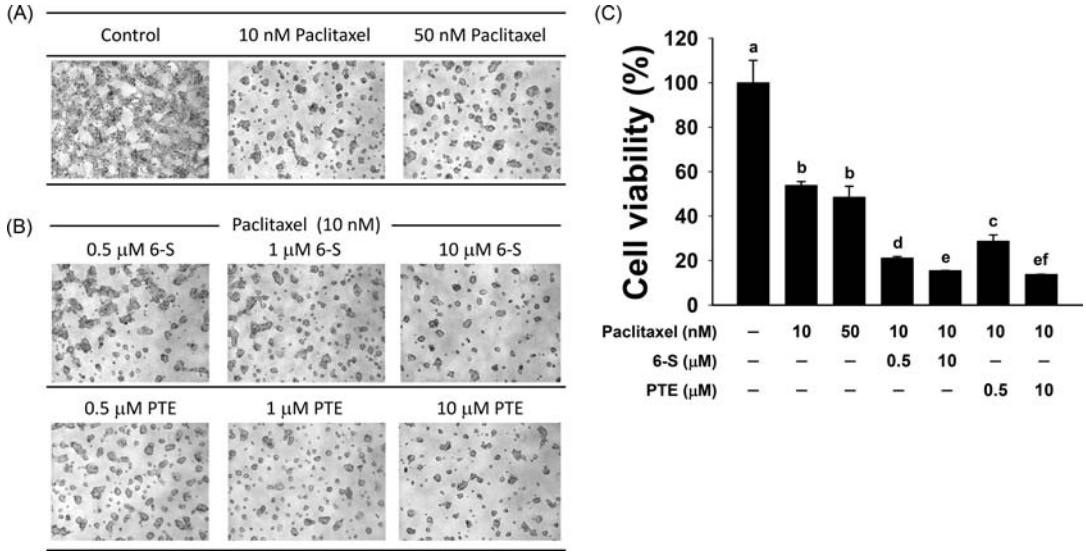

Figure 3. Effects of paclitaxel with or without 6-S and PTE on cell morphology and viability of differentiated BCSCs. BCSCs were first cultured in RPMI medium plus 10% FBS for 7 days to simulate differentiation. Cells were then treated with different concentrations of paclitaxel (A) and 10 nM paclitaxel plus 6-S or 10 nM paclitaxel plus PTE (B) for 72 h. (C) Quantified cell viability in groups A and B. The reported values are the mean ± SD (n = 3). Bars with different letters are significantly different from each other in individual assays (p < 0.05).

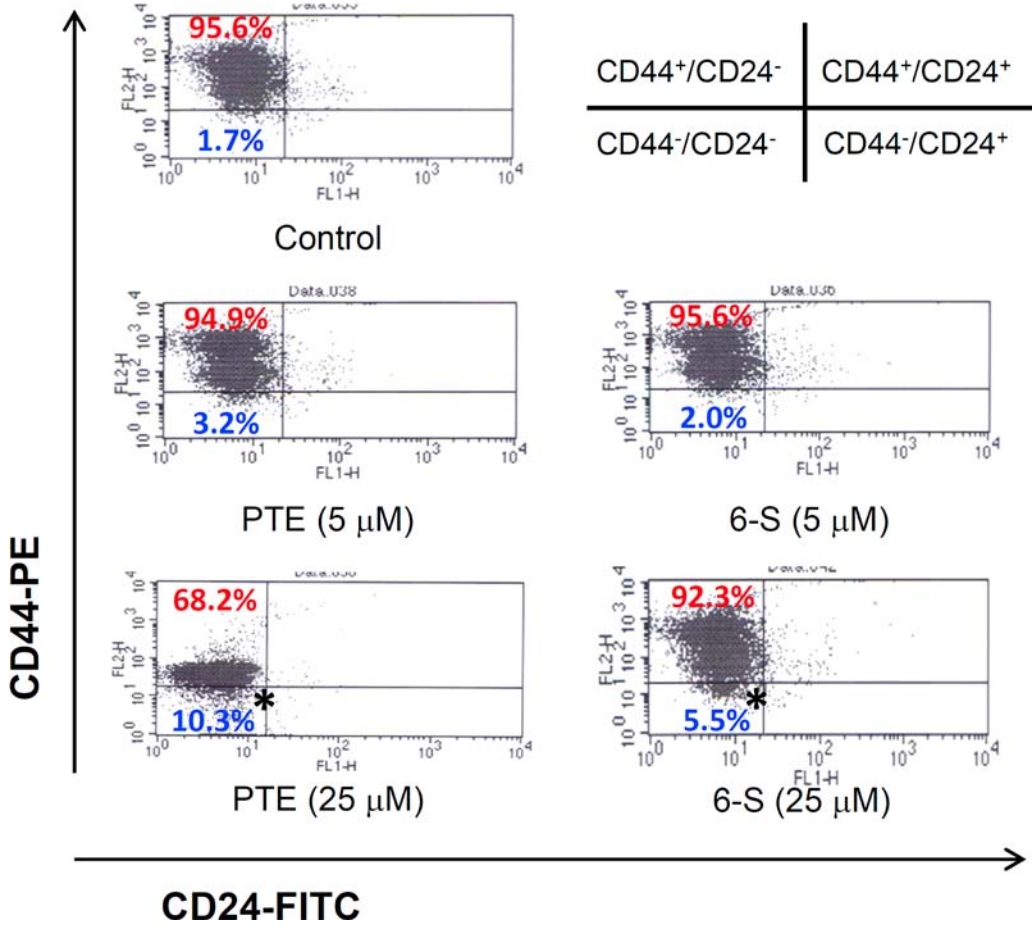

Figure 4. Effects of 6-S and PTE on the expression of the cell surface marker CD44/CD24 in BCSCs. The cells were treated with 0−25 μM 6-S and PTE for 72 h. FITC/PE double-stained cells were analyzed by flow cytometry. Cells that were $CD44^+/CD24^-$ represent the BCSC population. Cells with $CD44^-/CD24^-$ represent a loss of stemness. *, p < 0.05, indicates significant differences compared with the control group.

phosphorylation to increase its degradation and inhibit protein expression of cyclin D1 and c-Myc (p < 0.05). Therefore, 6-S and PTE both effectively increased the level of β-catenin phosphorylation and inhibited the expression of the downstream cyclin D1 and c-Myc proteins; the inhibitory effect of PTE was more significant.

DOI: 10.1021/acs.jafc.5b00002
J. Agric. Food Chem. 2015, 63, 2432−2441

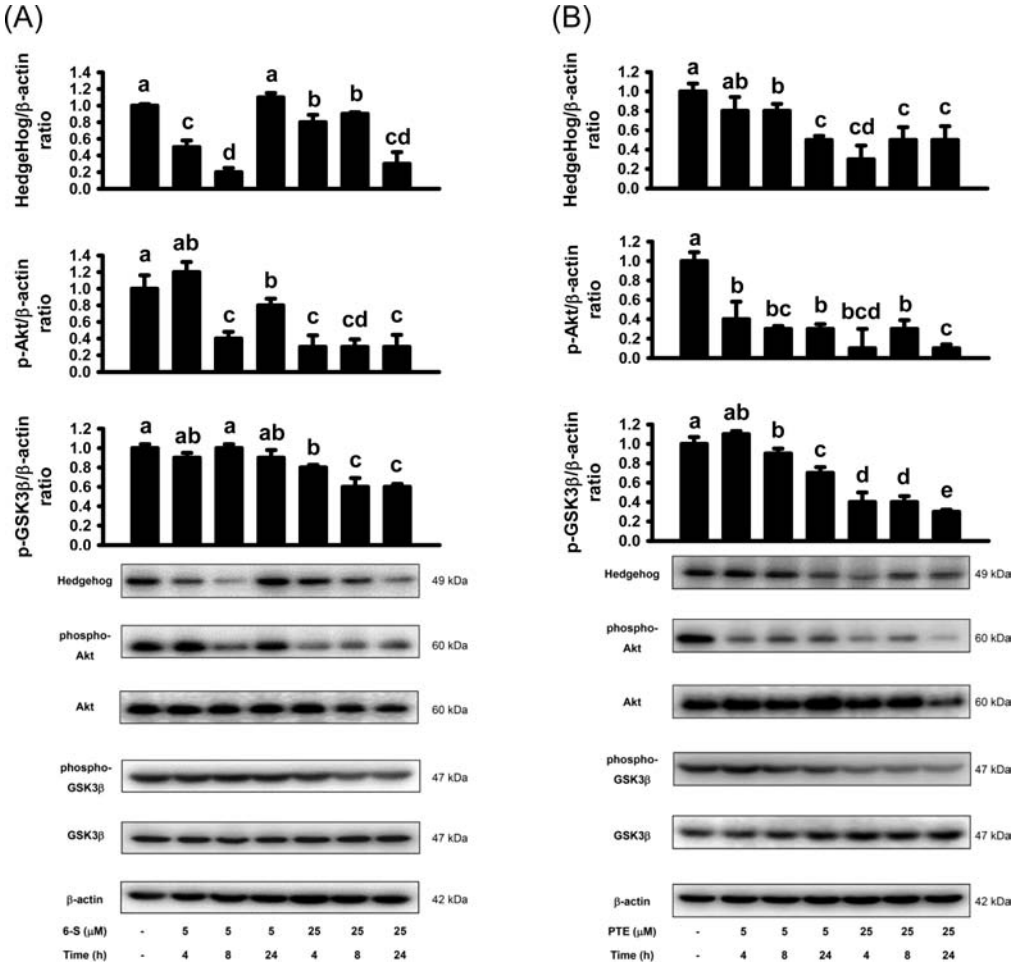

Figure 5. Effects of 6-S (A) and PTE (B) on protein expression of hedgehog signaling in BCSCs. Cells were treated with 25 μM of tested compounds for 4, 8, and 24 h, respectively. The relative density was compared with the control. All experiments were performed in duplicate and repeated at least three times. Quantitative data are expressed as the mean ± standard deviation. Bars with different letters are significantly different from each other in individual assays ($p < 0.05$).

DISCUSSION

General stem cells have the ability to differentiate into many different cells. However, abnormal stem cells will develop into abnormal cell populations. These abnormal stem cells are CSCs. Because CSCs can survive in a nutrient- and oxygen-deficient environment and have drug resistance, they are considered one reason that cancer cannot be completely cured.

Phytochemicals have been discovered to have antioxidant, anti-inflammatory, and antitumor activities. Because their side effects can be milder than those of chemotherapeutic drugs, they have been extensively applied and investigated in clinical cancer studies.[12] For example, citrus fruits are rich in NOL and 5-HF, which have been discovered in previous studies to have anti-invasion activity against cancer cells and can inhibit colon cancer proliferation and induce apoptosis.[32] The study by Weng et al.[22] showed that the active ingredients of ginger, 6-G and 6-S, and the component of berries, PTE, inhibit liver cancer cell metastasis. Our previous studies showed that 6-S and PTE inhibit invadopodia formation in breast cancer cells and inhibit invasive metastasis.[33] Therefore, these two phytochemicals, 6-S and PTE, might have excellent antitumor potential. This study selected the above phytochemicals to investigate their effects on the suppression of BCSC survival and mammosphere formation as well as the effects of complementary chemotherapeutic drugs on BCSCs. The antitumor activity and the molecular mechanism of 6-S and PTE were also clarified.

A review of the study by Gupta et al.[19] and many other papers showed that because BCSCs have the feature of self-renewal and might produce drug resistance, during the screening of compounds that can inhibit BCSC survival, the culture time should be estimated to at least the third generation. Therefore, 72 h was selected as the culture time in this study to investigate the effects of these compounds. The MCF-7 breast cancer cells and the human BCSCs isolated from MCF-7 cells using $CD44^{+}/CD24^{-/low}$ were treated with different concentrations (0−75 μM) of 5-HF, 6-G, 6-S, NOL, and PTE to evaluate their effects on cell survival. 6-S and PTE demonstrated the highest cytotoxicity levels against BCSCs. After BCSCs were treated with 25 μM 6-S or PTE for 72 h, the cell survival rate was reduced to <50%. However, treatment of MCF-7 breast cancer cells with these two chemicals at 25 μM (LD50) for 72 h showed that the cell survival rates were both maintained above 80%. Next, after BCSCs were treated with 6-G at 50 μM for 72 h, the cell survival rate was also reduced to 50%, whereas under the same concentration and time, the survival rate of treated MCF-7 cells was maintained at 90% (Figure 1B,C). Therefore, these three compounds might have the potential to specifically inhibit BCSCs. Further treatment of cells with these three compounds at a concentration of 25 or

DOI: 10.1021/acs.jafc.5b00002
J. Agric. Food Chem. 2015, 63, 2432−2441

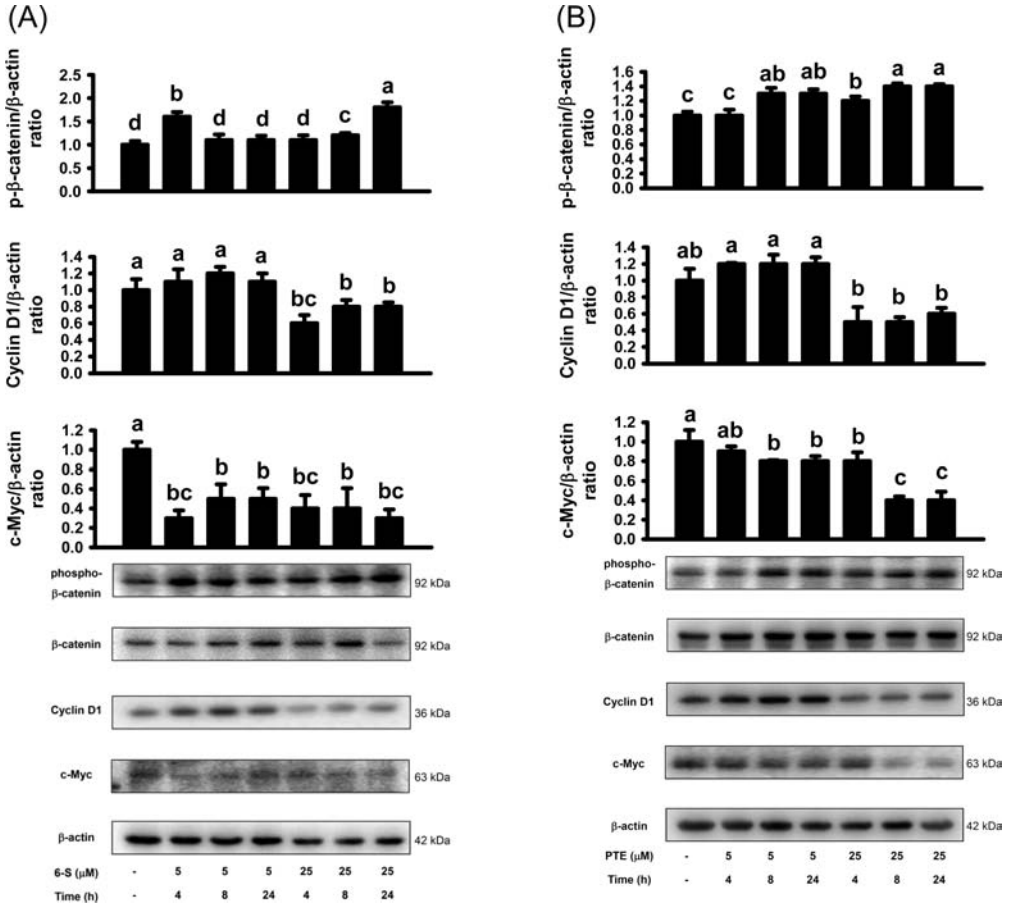

Figure 6. Effect of 6-S (A) and PTE (B) on protein expression of β-catenin, c-Myc, and cyclin D1 in BCSCs. The cells were treated with 25 μM of tested compounds for 4, 8, and 24 h, respectively. The relative density was compared with the control. All experiments were performed in duplicate and repeated at least three times. Quantitative data are expressed as the mean ± standard deviation. Bars with different letters are significantly different from each other in individual assays ($p < 0.05$).

100 μM showed that 6-S and PTE promoted bleb formation on the surface of BCSCs within 3−6 h, whereas 6-G did not cause bleb formation under the same conditions (Figure 2A). Therefore, it was speculated that 6-S and PTE had the most potential to inhibit BCSCs. Because their influences on the regulation of intracellular signaling proteins might start between 3 and 6 h, subsequent experiments selected 4, 8, and 24 h as controls.

CSCs have self-renewal and high differentiation potentials. Their growth does not require serum, their number in cell populations is small, and they are present as an unstable suspension. In in vitro cultured BCSCs, they aggregate into floating clumps to facilitate attached differentiation. These clumps are called spheroids and are specifically called mammospheres in breast cancer cells. Mammospheres form a functional mammary tree after long-term culture. Studies have shown that treatment of sulforaphane (5 μM) with BCSC-like cells isolated using ALDH for 7 days effectively reduced the size of mammospheres.[34] Kakarala et al.[35] treated mammospheres with curcumin or piperine and obtained similar results. The results of this study in Figure 2B,C confirmed that 6-S and PTE reduced the size and number of mammospheres.

There are already several drugs in clinical use with excellent treatment effects on breast cancer such as cyclophosphamide, paclitaxel, doxorubicin, and docetaxel; therefore, current treatment strategies that target CSCs might supplement chemodrugs to achieve the goal of eliminating breast cancer.[3,12] Therefore, the present study referenced the method of Lee et al.[36] to add serum into the BCSC culture to promote cell differentiation to simulate the condition of tumor recurrence and growth. Next, 6-S, PTE, and paclitaxel were cultured with this cell population for 72 h to observe whether these two compounds and paclitaxel had a synergistic effect on the suppression of tumor growth. The results in Figure 3 show that although paclitaxel (10 and 50 nM) had toxicity on the differentiated cell population of BCSCs, the effect was not dose dependent ($p > 0.05$). Of note, 6-S and PTE had auxiliary effects on paclitaxel to reduce the survival of that cell population. Studies have shown that the combination of curcumin (10 μM) and paclitaxel (10 μM) significantly reduced tumor size in nude mice, decreased MMP-9 expression in tumor, and promoted breast cancer cell apoptosis.[37] The study by Aggarwal et al.[38] also indicated that curcumin (50 μM), which is a polyphenolic compound similar to the samples used in this study, assists paclitaxel (10 μM) in reducing the survival rate of breast cancer MDA-MB435 cells by 80%.

The present study demonstrated that 6-S and PTE inhibit BCSCs from forming mammospheres and have synergistic effects with paclitaxel. To confirm the mechanism underlying the regulation of BCSC characteristics by these two compounds, further investigation was performed on whether the signaling pathway of BCSCs to maintain their self-renewal was affected by 6-S and PTE. CSCs are identified using different cell surface antigens; for example, BCSCs have been

DOI: 10.1021/acs.jafc.5b00002
J. Agric. Food Chem. 2015, 63, 2432−2441

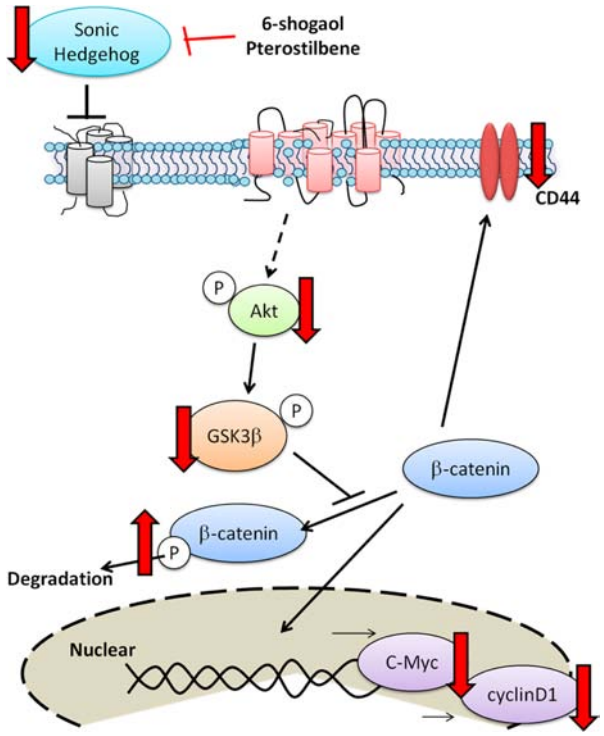

Figure 7. Schematic representation of the mechanisms of action by 6-S and PTE in the inhibition of BCSC stemness. 6-S and PTE mediate CD44 expression through the reduction of hedgehog and β-catenin in BCSCs. 6-S and PTE lead to reduced expression of hedgehog, inhibit the phosphorylation of Akt and GSK3β, and decrease the translocation of β-catenin, followed by the down-regulation of CD44, c-Myc, and cyclin D1 expression.

isolated using $CD44^{+}/CD24^{-/low}$ expression on the cell surface of MCF-7 cells.[5] The decrease of CD44 expression reduced the tumorigenicity of BCSCs in vivo; thus, it was speculated that CD44 expression is associated with the maintenance of stemness.[39] Therefore, this study cultured 6-S or PTE with BCSCs for 72 h to observe their influences on CD44 and CD24 cell surface antigens. Figure 4 shows that 6-S and PTE effectively decreased the expression of CD44. This result was similar to the results of So et al.,[40] who used a novel Gemini vitamin D analogue, BXL0124. Recent studies also showed that caffeic acid phenethyl ester, a derivative of the natural polyphenolic compound caffeic acid, reduces the percentage of CSCs in the MDA-MB231 cell line to inhibit CSC proliferation.[41] Studies have also shown that acetaminophen induces BCSC differentiation, decreases CD44 expression, and causes these cells to lose tumorigenicity in nude mice.[42]

It is known that hedgehog, Notch, PI3K/Akt, and Wnt/β-catenin are associated with self-renewal of cells and stem cell survival in normal organs or embryonic stem cells.[12] Studies have indicated that these signaling pathways might also participate in the maintenance of the stemness of $CD44^{+}/CD24^{-/low}$ BCSCs.[13] CSCs play very important roles in the recurrence and growth of many tumors, whereas Wnt/β-catenin is associated with CSC differentiation. In many antitumor (such as lung cancer and brain cancer) studies that have targeted CSCs, the inhibition of intracellular concentration and the transcription activity of β-catenin were used as a target.[10,43] Hope et al.[44] used a low dose of resveratrol to regulate β-catenin transcription activities and achieved the inhibition of the differentiation of many liver cancer cells to prevent the aggravation of liver cancer. Therefore, inhibition of the transcription activity of β-catenin might successfully inhibit CSCs to produce drug resistance and promote tumor recurrence.[45]

Studies showed that the EMT pathway can induce tumor cells to produce CSCs with stemness; therefore, if EMT activation could be inhibited through the TGF-β or Wnt signaling pathways, then CSC proliferation could be reduced. The EMT pathway is induced by the Twist and Snail proteins. Twist can inhibit the phosphorylation of the downstream β-catenin and Snail proteins through the promotion of phosphorylation of Akt (Ser 473) and GSK3β (Ser 9) to increase CD44 expression and achieve the goal of maintaining stemness. In addition, Twist can also inhibit E-cadherin activation and its ability to bind β-catenin, which further inhibits cell invasion and metastasis.[39] The regulation of Akt and GSK3β is also affected by the hedgehog signaling pathway. Sonic hedgehog interacts with its transmembrane receptor patched to release smoothed protein to further activate PI3K and Akt, thus promoting GSK3β phosphorylation and reducing its activity. When GSK3β activity decreased, β-catenin phosphorylation is reduced, and its degradation pathway is suppressed; at the same time, CG44 expression is increased. Excess β-catenin translocates into the nucleus to promote cell proliferation and differentiation and then interacts with the TCF/LEF complex to transcribe cyclin D1 and c-Myc. Furthermore, the levels of phosphorylated Akt, phosphorylated GSK3β, and β-catenin in mammospheres are all significantly higher than those in general attachment-type tumor cells.[46] Introduction of the Akt inhibitor perifosine (orally active alkylphosphocholine) into mammary stem cells or progenitor cells promotes β-catenin phosphorylation. Therefore, this study focused on whether 6-S and PTE had inhibitory effects on the signaling pathways that maintained the above CSC characteristics.

Results in this study showed that treatment of BCSCs with 6-S (5 μM) for 8 h significantly decreased hedgehog expression and Akt phosphorylation. 6-S at a concentration of 25 μM significantly decreased hedgehog expression and Akt phosphorylation after 4 h, and this effect was stably maintained for 24 h (Figure 5A). Figure 6A shows that treatment of BCSCs with 6-S (25 μM) for 8 h increased β-catenin phosphorylation and caused its degradation. Further observation of the expression of downstream cyclin D1 and c-Myc proteins also showed that 6-S at a concentration of 25 μM triggered down-regulation of cyclin D1 and c-Myc within 4 h. A previous study treated a polyphenolic compound, curcumin (50 μM), with MDA-MB435 breast cancer cells and showed that the expression of cyclin D1 and c-Myc proteins was inhibited.[38]

The results in Figure 5B show that PTE cultured with BCSCs significantly inhibited hedgehog expression and Akt phosphorylation. In addition, with regard to GSK3β activity, PTE reduced the levels of GSK3β phosphorylation. At 25 μM, PTE increased β-catenin phosphorylation and promoted its degradation (Figure 6B). Further observation of the downstream cyclin D1 and c-Myc protein expression showed that PTE also effectively reduced the expression of these two proteins. The study by Lepourcelet et al.[47] also observed that the two natural compounds isolated from fungi, PKF115-584 and CGF049090 (5 μM), significantly inhibited the intracellular concentrations of β-catenin and the expression of cyclin D1 and c-Myc proteins.

DOI: 10.1021/acs.jafc.5b00002
J. Agric. Food Chem. 2015, 63, 2432−2441

In summary, the increased phosphorylation of β-catenin by 6-S and PTE might be through the reduction of hedgehog protein expression and Akt and GSK3β phosphorylation, thus reducing the expression of downstream c-Myc and cyclin D1 proteins (Figure 7). Therefore, 6-S and PTE activated β-catenin degradation to reduce CD44 activity and affect the maintenance of stemness of CSCs to further induce the loss of tumorigenicity of these BCSCs.

■ ASSOCIATED CONTENT

Supporting Information

Supplemental Figure 1. This material is available free of charge via the Internet at http://pubs.acs.org.

■ AUTHOR INFORMATION

Corresponding Author

*(G.C.Yen) Mail: Department of Food Science and Biotechnology, National Chung Hsing University, 250 Kuokuang Road, Taichung 40227, Taiwan. Phone: +886 4 2287 9755. Fax: +886 4 2285 4378. E-mail: gcyen@nchu.edu.tw.

Funding

This research work was supported in part by the Ministry of Science and Technology (MOST99-2628-B005-002-MY3), Taiwan, and the Ministry of Education, Taiwan, under the ATU plan.

Notes

The authors declare no competing financial interest.

■ REFERENCES

(1) Quintana, E.; Shackleton, M.; Sabel, M. S.; Fullen, D. R.; Johnson, T. M.; Morrison, S. J. Efficient tumour formation by single human melanoma cells. *Nature* **2008**, *456*, 593−598.

(2) Ye, J.; Wu, D.; Wu, P.; Chen, Z.; Huang, J. The cancer stem cell niche: cross talk between cancer stem cells and their microenvironment. *Tumour Biol.* **2014**, *35*, 3945−3951.

(3) Yi, S. Y.; Hao, Y. B.; Nan, K. J.; Fan, T. L. Cancer stem cells niche: a target for novel cancer therapeutics. *Cancer Treat. Rev.* **2013**, *39*, 290−296.

(4) Bonnet, D.; Dick, J. E. Human acute myeloid leukemia is organized as a hierarchy that originates from a primitive hematopoietic cell. *Nat. Med.* **1997**, *3*, 730−737.

(5) Al-Hajj, M.; Wicha, M. S.; Benito-Hernandez, A.; Morrison, S. J.; Clarke, M. F. Prospective identification of tumorigenic breast cancer cells. *Proc. Natl. Acad. Sci. U.S.A.* **2003**, *100*, 3983−3988.

(6) Singh, S. K.; Clarke, I. D.; Terasaki, M.; Bonn, V. E.; Hawkins, C.; Squire, J.; Dirks, P. B. Identification of a cancer stem cell in human brain tumors. *Cancer Res.* **2003**, *63*, 5821−5828.

(7) Kim, C. F.; Jackson, E. L.; Woolfenden, A. E.; Lawrence, S.; Babar, I.; Vogel, S.; Crowley, D.; Bronson, R. T.; Jacks, T. Identification of bronchioalveolar stem cells in normal lung and lung cancer. *Cell* **2005**, *121*, 823−835.

(8) Li, C.; Heidt, D. G.; Dalerba, P.; Burant, C. F.; Zhang, L.; Adsay, V.; Wicha, M.; Clarke, M. F.; Simeone, D. M. Identification of pancreatic cancer stem cells. *Cancer Res.* **2007**, *67*, 1030−1037.

(9) O'Brien, C. A.; Pollett, A.; Gallinger, S.; Dick, J. E. A human colon cancer cell capable of initiating tumour growth in immunodeficient mice. *Nature* **2007**, *445*, 106−110.

(10) Clarke, M. F.; Fuller, M. Stem cells and cancer: two faces of Eve. *Cell* **2006**, *124*, 1111−1115.

(11) Li, F.; Tiede, B.; Massagué, J.; Kang, Y. Beyond tumorigenesis: cancer stem cells in metastasis. *Cell Res.* **2007**, *17*, 3−14.

(12) Kawasaki, B. T.; Hurt, E. M.; Mistree, T.; Farrar, W. L. Targeting cancer stem cells with phytochemicals. *Mol. Interv.* **2008**, *8*, 174−184.

(13) Pardal, R.; Clarke, M. F.; Morrison, S. J. Applying the principles of stem-cell biology to cancer. *Nat. Rev. Cancer* **2003**, *3*, 895−902.

(14) Dontu, G.; Abdallah, W. M.; Foley, J. M.; Jackson, K. W.; Clarke, M. F.; Kawamura, M. J.; Wicha, M. S. In vitro propagation and transcriptional profiling of human mammary stem/progenitor cells. *Genes Dev.* **2003**, *17*, 1253−1270.

(15) Deleyrolle, L. P.; Reynolds, B. A. Isolation, expansion, and differentiation of adult mammalian neural stem and progenitor cells using the neurosphere assay. *Methods Mol. Biol.* **2009**, *549*, 91−101.

(16) Hurt, E. M.; Kawasaki, B. T.; Klarmann, G. J.; Thomas, S. B.; Farrar, W. L. $CD44^+$ $CD24^-$ prostate cells are early cancer progenitor/stem cells that provide a model for patients with poor prognosis. *Br. J. Cancer* **2008**, *98*, 756−765.

(17) Bhat-Nakshatri, P.; Appaiah, H.; Ballas, C.; Pick-Franke, P.; Goulet, R., Jr.; Badve, S.; Srour, E. F.; Nakshatri, H. SLUG/SNAI2 and tumor necrosis factor generate breast cells with $CD44^+/CD24^-$ phenotype. *BMC Cancer* **2010**, *6* (10), 411.

(18) Valent, P.; Bonnet, D.; Wöhrer, S.; Andreeff, M.; Copland, M.; Chomienne, C.; Eaves, C. Heterogeneity of neoplastic stem cells: theoretical, functional, and clinical implications. *Cancer Res.* **2013**, *73*, 1037−1045.

(19) Gupta, P. B.; Onder, T. T.; Jiang, G.; Tao, K.; Kuperwasser, C.; Weinberg, R. A.; Lander, E. S. Identification of selective inhibitors of cancer stem cells by high-throughput screening. *Cell* **2009**, *138*, 645−659.

(20) Moon, M.; Kim, H. G.; Choi, J. G.; Oh, H.; Lee, P. K.; Ha, S. K.; Kim, S. Y.; Park, Y.; Huh, Y.; Oh, M. S. 6-Shogaol, an active constituent of ginger, attenuates neuroinflammation and cognitive deficits in animal models of dementia. *Biochem. Biophys. Res. Commun.* **2014**, *449*, 8−13.

(21) Pan, M. H.; Hsieh, M. C.; Kuo, J. M.; Lai, C. S.; Wu, H.; Sang, S.; Ho, C. T. 6-Shogaol induces apoptosis in human colorectal carcinoma cells via ROS production, caspase activation, and GADD 153 expression. *Mol. Nutr. Food Res.* **2008**, *52*, 527−537.

(22) Weng, C. J.; Wu, C. F.; Huang, H. W.; Ho, C. T.; Yen, G. C. Anti-invasion effects of 6-shogaol and 6-gingerol, two active components in ginger, on human hepatocarcinoma cells. *Mol. Nutr. Food Res.* **2010**, *54*, 1618−1627.

(23) Pan, M. H.; Chiou, Y. S.; Chen, W. J.; Wang, J. M.; Badmaev, V.; Ho, C. T. Pterostilbene inhibited tumor invasion via suppressing multiple signal transduction pathways in human hepatocellular carcinoma cells. *Carcinogenesis* **2009**, *30*, 1234−1242.

(24) Simoni, D.; Roberti, M.; Invidiata, F. P.; Aiello, E.; Aiello, S.; Marchetti, P.; Baruchello, R.; Eleopra, M.; Di Cristina, A.; Grimaudo, S.; Gebbia, N.; Crosta, L.; Dieli, F.; Tolomeo, M. Stilbene-based anticancer agents: resveratrol analogues active toward HL60 leukemic cells with a non-specific phase mechanism. *Bioorg. Med. Chem. Lett.* **2006**, *16*, 3245−3248.

(25) Chen, C.; Ono, M.; Takeshima, M.; Nakano, S. Antiproliferative and apoptosis-inducing activity of nobiletin against three subtypes of human breast cancer cell lines. *Anticancer Res.* **2014**, *34*, 1785−1792.

(26) Pan, M. H.; Lai, Y. S.; Lai, C. S.; Wang, Y. J.; Li, S.; Lo, C. Y.; Dushenkov, S.; Ho, C. T. 5-Hydroxy-3,6,7,8,3′,4′-hexamethoxyflavone induces apoptosis through reactive oxygen species production, growth arrest and DNA damage-inducible gene 153 expression, and caspase activation in human leukemia cells. *J. Agric. Food Chem.* **2007**, *55*, 5081−5091.

(27) Pan, M. H.; Hsieh, M. C.; Hsu, P. C.; Ho, S. Y.; Lai, C. S.; Wu, H.; Sang, S.; Ho, C. T. 6-Shogaol suppressed lipopolysaccharide-induced up-expression of iNOS and COX-2 in murine macrophages. *Mol. Nutr. Food Res.* **2008**, *52* (12), 1467−1477.

(28) Li, S.; Lo, C. Y.; Ho, C. T. Hydroxylated polymethoxyflavones and methylated flavonoids in sweet orange (*Citrus sinensis*) peel. *J. Agric. Food Chem.* **2006**, *54* (12), 4176−4185.

(29) Pettit, G. R.; Grealish, M. P.; Jung, M. K.; Hamel, E.; Pettit, R. K.; Chapuis, J. C.; Schmidt, J. M. Antineoplastic agents. 465. Structural modification of resveratrol: sodium resverastatin phosphate. *J. Med. Chem.* **2002**, *45* (12), 2534−2542.

DOI: 10.1021/acs.jafc.5b00002
J. Agric. Food Chem. 2015, 63, 2432−2441

(30) Fillmore, C. M.; Kuperwasser, C. Human breast cancer cell lines contain stem-like cells that self-renew, give rise to phenotypically diverse progeny and survive chemotherapy. *Breast Cancer Res.* **2008**, *10* (2), R25.
(31) Curtin, J. C.; Lorenzi, M. V. Drug discovery approaches to target Wnt signaling in cancer stem cells. *Oncotarget* **2010**, *1* (7), 552−566.
(32) Meiyanto, E.; Hermawan, A. Anindyajati Natural products for cancer-targeted therapy: citrus flavonoids as potent chemopreventive agents. *Asian Pac. J. Cancer Prev.* **2012**, *13* (2), 427−436.
(33) Hong, B. H.; Wu, C. H.; Yeh, C. T.; Yen, G. C. Invadopodia-associated proteins blockade as a novel mechanism for 6-shogaol and pterostilbene to reduce breast cancer cell motility and invasion. *Mol. Nutr. Food Res.* **2013**, *57* (5), 886−895.
(34) Li, Y.; Zhang, T.; Korkaya, H.; Liu, S.; Lee, H. F.; Newman, B.; Yu, Y.; Clouthier, S. G.; Schwartz, S. J.; Wicha, M. S.; Sun, D. Sulforaphane, a dietary component of broccoli/broccoli sprouts, inhibits breast cancer stem cells. *Clin. Cancer Res.* **2010**, *16* (9), 2580−2590.
(35) Kakarala, M.; Brenner, D. E.; Korkaya, H.; Cheng, C.; Tazi, K.; Ginestier, C.; Liu, S.; Dontu, G.; Wicha, M. S. Targeting breast stem cells with the cancer preventive compounds curcumin and piperine. *Breast Cancer Res. Treat.* **2010**, *122* (3), 777−785.
(36) Lee, J.; Kotliarova, S.; Kotliarov, Y.; Li, A.; Su, Q.; Donin, N. M.; Pastorino, S.; Purow, B. W.; Christopher, N.; Zhang, W.; Park, J. K.; Fine, H. A. Tumor stem cells derived from glioblastomas cultured in bFGF and EGF more closely mirror the phenotype and genotype of primary tumors than do serum-cultured cell lines. *Cancer Cell* **2006**, *9* (5), 391−403.
(37) Kang, H. J.; Lee, S. H.; Price, J. E.; Kim, L. S. Curcumin suppresses the paclitaxel-induced nuclear factor-κB in breast cancer cells and potentiates the growth inhibitory effect of paclitaxel in a breast cancer nude mice model. *Breast J.* **2009**, *15* (3), 223−229.
(38) Aggarwal, B. B.; Shishodia, S.; Takada, Y.; Banerjee, S.; Newman, R. A.; Bueso-Ramos, C. E.; Price, J. E. Curcumin suppresses the paclitaxel-induced nuclear factor-κB pathway in breast cancer cells and inhibits lung metastasis of human breast cancer in nude mice. *Clin. Cancer Res.* **2005**, *11* (20), 7490−7498.
(39) Li, J.; Zhou, B. P. Activation of β-catenin and Akt pathways by Twist are critical for the maintenance of EMT associated cancer stem cell-like characters. *BMC Cancer* **2011**, *11*, 49.
(40) So, J. Y.; Lee, H. J.; Smolarek, A. K.; Paul, S.; Wang, C. X.; Maehr, H.; Uskokovic, M.; Zheng, X.; Conney, A. H.; Cai, L.; Liu, F.; Suh, N. A novel Gemini vitamin D analog represses the expression of a stem cell marker CD44 in breast cancer. *Mol. Pharmacol.* **2011**, *79* (3), 360−367.
(41) Omene, C. O.; Wu, J.; Frenkel, K. Caffeic acid phenethyl ester (CAPE) derived from propolis, a honeybee product, inhibits growth of breast cancer stem cells. *Invest. New Drugs* **2012**, *30* (4), 1279−1288.
(42) Takehara, M.; Hoshino, T.; Namba, T.; Yamakawa, N.; Mizushima, T. Acetaminophen-induced differentiation of human breast cancer stem cells and inhibition of tumor xenograft growth in mice. *Biochem. Pharmacol.* **2011**, *81* (9), 1124−1135.
(43) Holland, J. D.; Klaus, A.; Garratt, A. N.; Birchmeier, W. Wnt signaling in stem and cancer stem cells. *Curr. Opin. Cell Biol.* **2013**, *25* (2), 254−264.
(44) Hope, C.; Planutis, K.; Planutiene, M.; Moyer, M. P.; Johal, K. S.; Woo, J.; Santoso, C.; Hanson, J. A.; Holcombe, R. F. Low concentrations of resveratrol inhibit Wnt signal throughput in colon-derived cells: implications for colon cancer prevention. *Mol. Nutr. Food Res.* **2008**, *52* (Suppl. 1), S52−S61.
(45) Yao, H.; Ashihara, E.; Maekawa, T. Targeting the Wnt/β-catenin signaling pathway in human cancers. *Expert Opin. Ther. Targets* **2011**, *15* (7), 873−887.
(46) Korkaya, H.; Paulson, A.; Charafe-Jauffret, E.; Ginestier, C.; Brown, M.; Dutcher, J.; Clouthier, S. G.; Wicha, M. S. Regulation of mammary stem/progenitor cells by PTEN/Akt/β-catenin signaling. *PLoS Biol.* **2009**, *7* (6), No. e1000121.
(47) Lepourcelet, M.; Chen, Y. N.; France, D. S.; Wang, H.; Crews, P.; Petersen, F.; Bruseo, C.; Wood, A. W.; Shivdasani, R. A. Small-molecule antagonists of the oncogenic Tcf/β-catenin protein complex. *Cancer Cell* **2004**, *5* (1), 91−102.

DOI: 10.1021/acs.jafc.5b00002
J. Agric. Food Chem. 2015, 63, 2432−2441

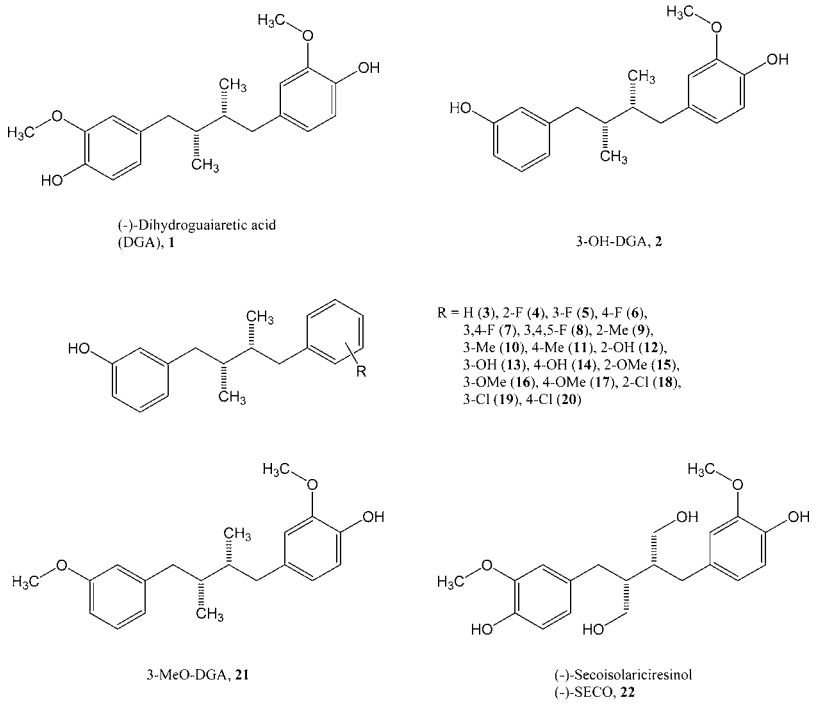

Figure 1. Structures of (−)-dihydroguaiaretic acid, **1**; its 3-OH derivatives, **2**−**20**; 3-OMe-DGA derivative **21**; and secoisolariciresinol **22**.

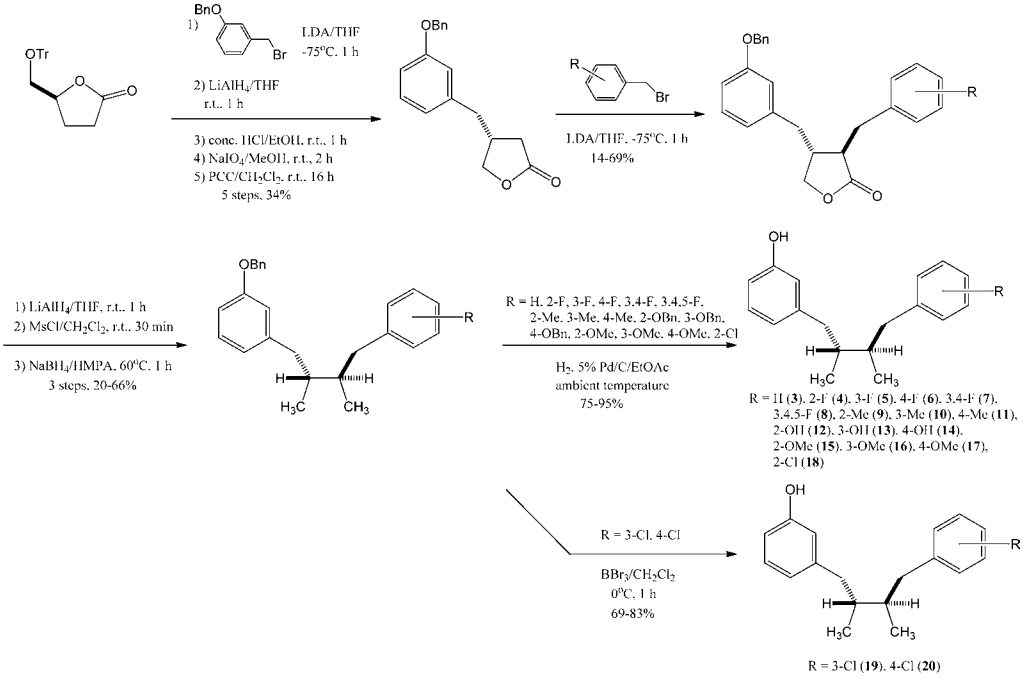

Figure 2. Synthetic scheme of compounds **3**−**20**.

lignans.[9] The synthetic scheme is shown in Figure 2, which was fundamentally the same as the earlier report.[7] Compounds **4**−**18** were obtained from (*R*)-3-(3-benzyloxybenzyl)-4-butanolide and the corresponding substituted benzyl bromide (preparation for hydroxybenzyl derivatives **12**−**14** needs a benzyloxybenzyl bromide to be deprotected in the final step) by employing the same method described for the synthesis of **3**. Compound **20** was synthesized using the preparation procedure of compound **19**. Compounds **21** and **22** were our stock samples.

Synthesis of Derivatives. *(8R,8′R)-Lignan-3-ol* ***3***. To a solution of lithium diisopropylamide (2.10 mmol) in tetrahydrofuran (THF, 10 mL) was added a solution of (*R*)-3-(3-benzyloxybenzyl)-4-butanolide (0.50 g, 1.77 mmol; see the preparation method in the Supporting Information) in THF (10 mL), and then the resulting solution was stirred at −70 °C for 30 min before addition of a solution of benzyl bromide (0.30 g, 1.75 mmol) in THF (5 mL). After the reaction solution was stirred at −70 °C for 1 h, saturated (sat.) aqueous (aq) NH_4Cl solution and ethyl acetate (EtOAc) were added. The organic solution was separated, washed with brine, dried (Na_2SO_4), and concentrated. The residue was applied to silica gel column chromatography (EtOAc/hexane = 1/3). To an ice-cooled suspension of $LiAlH_4$ (14 mg, 0.37 mmol) in THF (5 mL) was added a solution of the obtained compound in THF (5 mL). The resulting reaction mixture was stirred at room temperature for 30 min, and then sat. aq

DOI: 10.1021/jf504816a
J. Agric. Food Chem. 2015, 63, 2442−2448

$MgSO_4$ and K_2CO_3 were added. The mixture was stirred at room temperature for 30 min. After filtration of the mixture, the filtrate was concentrated. To an ice-cooled solution of the residue and Et_3N (0.54 mL, 3.87 mmol) in CH_2Cl_2 (5 mL) was added MsCl (0.30 mL, 3.88 mmol). After the reaction mixture was stirred at room temperature for 30 min, H_2O and CH_2Cl_2 were added. The organic solution was separated, dried (Na_2SO_4), and concentrated. A solution of the residue and $NaBH_4$ (90 mg, 2.38 mmol) in hexamethylphosphoric triamide (HMPA, 5 mL) was heated at 60 °C for 30 min before additions of sat. aq NH_4Cl solution and EtOAc. The organic solution was separated, washed with brine, dried (Na_2SO_4), and concentrated. A reaction mixture of the residue and 5% Pd/C (0.20 g) in EtOAc (10 mL) was stirred under H_2 gas at the ambient temperature for 2 h before filtration. The filtrate was concentrated, and then the residue was applied to silica gel column chromatography (EtOAc/hexane = 1/5) to give **3** (40 mg, 0.16 mmol, 9% in 5 steps) as a colorless oil, $[\alpha]^{20}_D$ = −29 (*c* 0.5, $CHCl_3$); ^{1}H NMR (400 MHz, $CDCl_3$) δ: 0.82 (3H, d, *J* = 6.4 Hz), 0.84 (3H, d, *J* = 6.4 Hz), 1.78−1.82 (2H, m), 2.38 (1H, dd, *J* = 13.3, 8.0 Hz), 2.43 (1H, dd, *J* = 12.5, 8.2 Hz), 2.60 (1H, dd, *J* = 12.5, 6.2 Hz), 2.64 (1H, dd, *J* = 13.3, 6.5 Hz), 4.77 (1H, s), 6.51 (1H, m), 6.62−6.67 (2H, m), 7.09−7.13 (2H, m), 7.13 (1H, d, *J* = 7.2 Hz), 7.17 (1H, m), 7.24−7.27 (2H, m). ^{13}C NMR (100 MHz, $CDCl_3$) δ: 14.0, 37.8, 38.1, 41.2, 41.4, 112.5, 115.8, 121.6, 125.6, 128.1, 129.1, 129.2, 141.6, 143.6, 155.3. EIMS *m*/*z* (%): 254 (M^+, 62), 108 (100), 91 (73). HRMS (EI) *m*/*z*: calcd for $C_{18}H_{22}O$, 254.1672; found, 254.1665.

(8R,8′R)-2′-Fluorolignan-3-ol ***4***. Yield of 31% through 5 steps as a colorless oil, $[\alpha]^{20}_D$ = −33 (*c* 0.8, $CHCl_3$); ^{1}H NMR (400 MHz, $CDCl_3$) δ: 0.84 (3H, d, *J* = 6.7 Hz), 0.85 (3H, d, *J* = 6.8 Hz), 1.69−1.82 (2H, m), 2.37 (1H, dd, *J* = 13.5, 8.7 Hz), 2.46 (1H, dd, *J* = 13.4, 8.6 Hz), 2.61 (1H, dd, *J* = 13.5, 6.0 Hz), 2.69 (1H, dd, *J* = 13.4, 6.0 Hz), 4.72 (1H, s), 6.54 (1H, m), 6.63 (1H, dd, *J* = 8.0, 2.7 Hz), 6.67 (1H, d, *J* = 7.6 Hz), 6.96−7.04 (2H, m), 7.06−7.17 (3H, m). ^{13}C NMR (100 MHz, $CDCl_3$) δ: 14.0, 34.1, 37.4, 38.2, 41.1, 112.5, 115.1 (d, *J* = 22.8 Hz), 115.8, 121.6, 123.7 (d, *J* = 3.1 Hz), 127.3 (d, *J* = 7.8 Hz), 128.4 (d, *J* = 15.4 Hz), 129.3, 131.3 (d, *J* = 5.1 Hz), 143.6, 155.3, 161.3 (d, *J* = 244.3 Hz). ^{19}F NMR (376 MHz, $CDCl_3$) δ: −119.1. EIMS *m*/*z* (%): 272 (M^+, 15), 109 (100). HRMS (EI) *m*/*z*: calcd for $C_{18}H_{21}OF$, 272.1576; found, 272.1571.

(8R,8′R)-3′-Fluorolignan-3-ol ***5***. Yield of 23% through 5 steps as a colorless oil, $[\alpha]^{20}_D$ = −31 (*c* 0.9, $CHCl_3$); ^{1}H NMR (400 MHz, $CDCl_3$) δ: 0.82 (6H, d, *J* = 6.3 Hz), 1.76−1.80 (2H, m), 2.38 (1H, dd, *J* = 13.7, 8.3 Hz), 2.41 (1H, dd, *J* = 13.7, 8.3 Hz), 2.58 (1H, dd, *J* = 13.6, 6.0 Hz), 2.62 (1H, dd, *J* = 13.6, 6.1 Hz), 4.88 (1H, s), 6.55 (1H, m), 6.63−6.67 (2H, m), 6.79 (1H, d, *J* = 10.0 Hz), 6.83−6.90 (2H, m), 7.11 (1H, dd, *J* = 7.8, 7.7 Hz), 7.19 (1H, m). ^{13}C NMR (100 MHz, $CDCl_3$) δ: 13.9, 14.0, 37.86, 37.90, 41.07, 41.14, 112.5, (d, *J* = 21.1 Hz), 112.6, 115.7 (d, *J* = 21.8 Hz), 115.8, 121.6, 124.7 (d, *J* = 2.6 Hz), 129.3, 129.4 (d, *J* = 8.3 Hz), 143.4, 144.2, (d, *J* = 7.3 Hz), 155.3, 162.8 (d, *J* = 244.9 Hz); ^{19}F NMR (376 MHz, $CDCl_3$) δ: −114.1. EIMS *m*/*z* (%): 272 (M^+, 61), 108 (100). HRMS (EI) *m*/*z*: calcd for $C_{18}H_{21}OF$, 272.1576; found, 272.1575.

(8R,8′R)-4′-Fluorolignan-3-ol ***6***. Yield of 14% through 5 steps as a colorless oil, $[\alpha]^{20}_D$ = −34 (*c* 0.4, $CHCl_3$); ^{1}H NMR (400 MHz, $CDCl_3$) δ: 0.81 (3H, d, *J* = 6.7 Hz), 0.83 (3H, d, *J* = 6.6 Hz), 1.72−1.79 (2H, m), 2.37 (1H, dd, *J* = 12.8, 5.9 Hz), 2.40 (1H, dd, *J* = 12.8, 5.5 Hz), 2.58 (1H, dd, *J* = 13.4, 6.7 Hz), 2.64 (1H, dd, *J* = 13.4, 6.6 Hz), 4.79 (1H, s), 6.55 (1H, m), 6.63−6.67 (2H, m), 6.90−6.96 (2H, m), 7.00−7.08 (2H, m), 7.11 (1H, dd, *J* = 7.8, 7.7 Hz). ^{13}C NMR (100 MHz, $CDCl_3$) δ: 13.87, 13.93, 37.8, 38.2, 40.5, 41.2, 112.6, 114.8 (d, *J* = 21.0 Hz), 115.8, 121.6, 129.3, 130.2 (d, *J* = 7.7 Hz), 137.1, (d, *J* = 3.0 Hz), 143.5, 155.3, 161.1 (d, *J* = 242.6 Hz); ^{19}F NMR (376 MHz, $CDCl_3$) δ: −119.0. EIMS *m*/*z* (%): 272 (M^+, 24), 109 (100). HRMS (EI) *m*/*z*: calcd for $C_{18}H_{21}OF$, 272.1576; found, 272.1573.

(8R,8′R)-3′,4′-Difluorolignan-3-ol ***7***. Yield of 2% through 5 steps as a colorless oil, $[\alpha]^{20}_D$ = −22 (*c* 0.3, $CHCl_3$); ^{1}H NMR (400 MHz, $CDCl_3$) δ: 0.82 (6H, d, *J* = 6.7 Hz), 1.70−1.76 (2H, m), 2.38 (1H, dd, *J* = 13.6, 8.3 Hz), 2.39 (1H, dd, *J* = 13.3, 8.2 Hz), 2.57 (1H, dd, *J* = 13.3, 6.4 Hz), 2.58 (1H, dd, *J* = 13.6, 6.4 Hz), 4.78 (1H, s), 6.56 (1H, m), 6.64−6.66 (2H, m), 6.77 (1H, m), 6.86 (1H, m), 7.02 (1H, ddd, *J* = 10.3, 8.3, 8.3 Hz), 7.12 (1H, dd, *J* = 7.81, 7.78 Hz). ^{13}C NMR ($CDCl_3$) δ: 13.8, 13.9, 37.8, 37.9, 40.5, 41.2, 112.7, 115.8, 116.7 (d, *J* = 16.6 Hz), 117.5 (d, *J* = 16.5 Hz), 121.5, 124.7 (dd, *J* = 5.7, 3.5 Hz), 129.3, 138.5 (*J* = 5.1, 4.2 Hz), 143.4, 148.6 (dd, *J* = 245.1, 12.6 Hz), 150.0 (dd, *J* = 248.6, 14.9 Hz), 155.3. ^{19}F NMR (376 MHz, $CDCl_3$) δ: −139.8, −143.5. EIMS *m*/*z* (%): 290 (M^+, 44), 127 (66), 108 (100). HRMS (EI) *m*/*z*: calcd for $C_{18}H_{20}OF_2$, 290.1481; found, 290.1476.

(8R,8′R)-3′,4′,5′-Trifluorolignan-3-ol ***8***. Yield of 29% through 5 steps as a colorless oil, $[\alpha]^{20}_D$ = −16 (*c* 0.5, $CHCl_3$); ^{1}H NMR (400 MHz, $CDCl_3$) δ: 0.821 (3H, d, *J* = 6.7 Hz), 0.824 (3H, d, *J* = 6.6 Hz), 1.68−1.76 (2H, m), 2.35 (1H, dd, *J* = 13.7, 8.2 Hz), 2.39 (1H, dd, *J* = 13.4, 8.1 Hz), 2.56 (1H, dd, *J* = 13.7, 6.3 Hz), 2.57 (1H, dd, *J* = 13.4, 6.4 Hz), 4.80 (1H, s), 6.57 (1H, m), 6.65−6.69 (4H, m), 7.13 (1H, dd, *J* = 7.83, 7.75 Hz). ^{13}C NMR (100 MHz, $CDCl_3$) δ: 13.7, 13.9, 37.6, 37.8, 40.7, 41.1, 112.7, 115.8, 121.5 129.4, 137.2 (d, *J* = 110.1 Hz), 138.5 (d, *J* = 133.6 Hz), 143.2, 150.8 (d, *J* = 252.8 Hz), 150.9 (d, *J* = 244.4 Hz), 155.4. ^{19}F NMR (376 MHz, $CDCl_3$) δ: −136.5, −165.7. EIMS *m*/*z* (%): 308 (M^+, 40), 145 (58), 108 (100). HRMS (EI) *m*/*z*: calcd for $C_{18}H_{19}OF_3$, 308.1386; found, 308.1381.

(8R,8′R)-2'a-Homolignan-3-ol ***9***. Yield of 18% through 5 steps as a colorless oil, $[\alpha]^{20}_D$ = −46 (*c* 0.5, $CHCl_3$); ^{1}H NMR (400 MHz, $CDCl_3$) δ: 0.82 (3H, d, *J* = 6.8 Hz), 0.89 (3H, d, *J* = 6.7 Hz), 1.76 (1H, m), 1.84 (1H, m), 2.19 (3H, s), 2.39 (1H, br d, *J* = 13.5 Hz), 2.42 (1H, br d, *J* = 13.5 Hz), 2.58 (1H, dd, *J* = 13.6, 7.5 Hz), 2.63 (1H, dd, *J* = 13.6, 5.8 Hz), 4.73 (1H, s), 6.48 (1H, m), 6.62 (1H, dd, *J* = 8.1, 2.3 Hz), 6.66 (1H, d, *J* = 7.6 Hz), 7.03 (1H, m), 7.08−7.09 (4H, m). ^{13}C NMR (100 MHz, $CDCl_3$) δ: 13.8, 14.3, 19.4, 36.3, 38.3, 38.8, 41.0, 112.5, 115.7, 121.5, 125.5, 125.7, 129.3, 130.0, 130.2, 136.3, 139.8, 143.6, 155.3. EIMS *m*/*z* (%): 268 (M^+, 97), 121 (28), 108 (100). HRMS (EI) *m*/*z*: calcd for $C_{19}H_{24}O$, 268.1828; found, 268.1830.

(8R,8′R)-3'a-Homolignan-3-ol ***10***. Yield of 11% through 5 steps as a colorless oil, $[\alpha]^{20}_D$ = −32 (*c* 0.3, $CHCl_3$); ^{1}H NMR (400 MHz, $CDCl_3$) δ: 0.826 (3H, d, *J* = 6.7 Hz), 0.832 (3H, d, *J* = 6.7 Hz), 1.76−1.85 (2H, m), 2.32 (3H, s), 2.37 (1H, dd, *J* = 13.5, 5.2 Hz), 2.39 (1H, dd, *J* = 13.5, 5.1 Hz), 2.59 (1H, br d, *J* = 13.5 Hz), 2.61 (1H, br d, *J* = 13.5 Hz), 4.80 (1H, br s), 6.53 (1H, m), 6.63 (1H, dd, *J* = 8.1, 2.1 Hz), 6.67 (1H, d, *J* = 7.6 Hz), 6.89−6.90 (2H, m), 6.99 (1H, d, *J* = 7.5 Hz), 7.11−7.14 (2H, m). ^{13}C NMR (100 MHz, $CDCl_3$) δ: 14.0, 14.1, 21.4, 37.8, 38.0, 41.16, 41.23, 112.5, 115.8, 121.6, 126.1, 126.3, 128.0, 129.2, 129.8, 137.6, 141.6, 143.6, 155.3. EIMS *m*/*z* (%): 268 (M^+, 47), 108 (100). HRMS (EI) *m*/*z*: calcd for $C_{19}H_{24}O$, 268.1828; found, 268.1823.

(8R,8′R)-4'a-Homolignan-3-ol ***11***. Yield of 8% through 5 steps as a colorless oil, $[\alpha]^{20}_D$ = −23 (*c* 0.6, $CHCl_3$); ^{1}H NMR (400 MHz, $CDCl_3$) δ: 0.81 (3H, d, *J* = 6.6 Hz), 0.82 (3H, d, *J* = 6.7 Hz), 1.74−1.83 (2H, m), 2.31 (3H, s), 2.35 (1H, dd, *J* = 13.6, 6.0 Hz), 2.38 (1H, dd, *J* = 13.6, 6.0 Hz), 2.60 (1H, dd, *J* = 13.6, 6.1 Hz), 2.61 (1H, dd, *J* = 13.6, 6.1 Hz), 4.75 (1H, s), 6.52 (1H, m), 6.62 (1H, dd, *J* = 8.1, 2.4 Hz), 6.66 (1H, d, *J* = 7.6 Hz), 6.97 (2H, d, *J* = 7.9 Hz), 7.05 (2H, d, *J* = 7.9 Hz), 7.09 (1H, dd, *J* = 7.83, 7.78 Hz). ^{13}C NMR ($CDCl_3$) δ: 13.97, 13.99, 21.0, 37.8, 38.2, 40.9, 41.2, 112.5, 115.8, 121.6, 128.8, 128.9, 129.2, 135.0, 138.5, 143.6, 155.3. EIMS *m*/*z* (%): 268 (M^+, 38), 107 (74), 105 (100). HRMS (EI) *m*/*z*: calcd for $C_{19}H_{24}O$, 268.1828; found, 268.1827.

(8R,8′R)-Lignane-2′,3-diol ***12***. Yield of 6% through 5 steps as a colorless oil, $[\alpha]^{20}_D$ = −40 (*c* 0.5, $CHCl_3$); ^{1}H NMR (400 MHz, $CDCl_3$) δ: 0.83 (3H, d, *J* = 6.7 Hz), 0.85 (3H, d, *J* = 6.8 Hz), 1.80−1.92 (2H, m), 2.39 (1H, dd, *J* = 13.4, 8.2 Hz), 2.42 (1H, dd, *J* = 13.4, 8.4 Hz), 2.59 (1H, dd, *J* = 13.6, 6.5 Hz), 2.66 (1H, dd, *J* = 13.6, 6.1 Hz), 4.91 (1H, s), 5.04 (1H, s), 6.52 (1H, m), 6.63 (1H, dd, *J* = 8.0, 2.3 Hz), 6.67 (1H, d, *J* = 7.5 Hz), 6.71 (1H, d, *J* = 7.8 Hz), 6.83 (1H, dd, *J* = 7.8, 7.5 Hz), 7.02−7.06 (2H, m), 7.04 (1H, dd, *J* = 7.8, 7.7 Hz). ^{13}C NMR (100 MHz, $CDCl_3$) δ: 14.0, 14.1, 35.5, 36.3, 38.0, 41.1, 112.5, 115.3, 115.7, 120.6, 121.7, 127.0, 127.6, 129.3, 131.2, 143.6, 153.6, 155.2. EIMS *m*/*z* (%): 270 (M^+, 73), 107 (100). HRMS (EI) *m*/*z*: calcd for $C_{18}H_{22}O_2$, 270.1621; found, 270.1624.

(8R,8′R)-Lignane-3,3′-diol ***13***. Yield of 25% through 5 steps as colorless crystals, mp 67−68 °C, $[\alpha]^{20}_D$ = −14 (*c* 0.8, $CHCl_3$); ^{1}H NMR (400 MHz, $CDCl_3$) δ: 0.81 (6H, d, *J* = 6.7 Hz), 1.77 (2H, m), 2.40 (2H, dd, *J* = 13.6, 7.4 Hz), 2.53 (2H, dd, *J* = 13.6, 7.1 Hz), 5.49 (2H, s), 6.53 (2H, m), 6.65−6.68 (4H, m), 7.11 (2H, dd, *J* = 7.8, 7.7

DOI: 10.1021/jf504816a
J. Agric. Food Chem. 2015, 63, 2442−2448

Hz). ^{13}C NMR (100 MHz, $CDCl_3$) δ: 13.9, 36.8, 41.1, 112.7, 115.8, 121.8, 129.3, 143.5, 155.2. EIMS m/z (%): 270 (M^+, 76), 107 (100). HRMS (EI) m/z: calcd for $C_{18}H_{22}O_2$, 270.1621; found, 270.1623.

(8R,8′R)-Lignane-3,4′-diol **14**. Yield of 10% through 5 steps as a colorless oil, $[\alpha]^{20}_D$ = −38.0 (c 0.4, $CHCl_3$); ^{1}H NMR (400 MHz, $CDCl_3$) δ: 0.81 (6H, d, J = 6.7 Hz), 1.68−1.79 (2H, m), 2.36 (1H, dd, J = 13.5, 7.9 Hz), 2.37 (1H, dd, J = 13.5, 8.1 Hz), 2.53 (1H, dd, J = 13.5, 6.9 Hz), 2.55 (1H, dd, J = 13.5, 6.7 Hz), 5.40 (1H, s), 5.41 (1H, s), 6.50 (1H, m), 6.63−6.67 (2H, m), 6.73 (2H, m), 6.93 (2H, m), 7.10 (1H, dd, J = 7.78, 7.81 Hz). ^{13}C NMR ($CDCl_3$) δ: 13.85, 13.93, 37.3, 38.0, 40.4, 41.2, 112.6, 115.0, 115.7, 121.6, 129.2, 130.0, 133.8, 143.6, 153.3, 155.3. EIMS m/z (%): 270 (M^+, 87), 107 (100). HRMS (EI) m/z: calcd for $C_{18}H_{22}O_2$, 270.1621; found, 270.1618.

(8R,8′R)-2′-Methoxylignan-3-ol **15**. Yield of 24% through 5 steps as a colorless oil, $[\alpha]^{20}_D$ = −46 (c 0.6, $CHCl_3$); ^{1}H NMR (400 MHz, $CDCl_3$) δ: 0.81 (3H, d, J = 6.8 Hz), 0.85 (3H, d, J = 6.6 Hz), 1.76−1.88 (2H, m), 2.38 (1H, dd, J = 13.6, 8.9 Hz), 2.40 (1H, dd, J = 13.1, 8.3 Hz), 2.59 (1H, dd, J = 13.6, 6.7 Hz), 2.67 (1H, dd, J = 13.1, 6.1 Hz), 3.72 (3H, s), 4.86 (1H, s), 6.50 (1H, m), 6.62 (1H, dd, J = 8.1, 2.2 Hz), 6.66 (1H, d, J = 7.5 Hz), 6.81 (1H, d, J = 8.1 Hz), 6.85 (1H, dd, J = 7.5, 7.4 Hz), 7.04 (1H, dd, J = 7.3, 1.8 Hz), 7.09 (1H, dd, J = 7.9, 7.8 Hz), 7.16 (1H, ddd, J = 7.7, 7.7, 1.8 Hz). ^{13}C NMR ($CDCl_3$) δ: 14.1, 14.2, 35.7, 36.1, 38.0, 41.1, 55.1, 110.3, 112.4, 115.7, 120.1, 121.6, 126.8, 129.1, 130.2, 130.7, 143.9, 155.3, 157.7. EIMS m/z (%): 284 (M^+, 99), 121 (100), 107 (53). HRMS (EI) m/z: calcd for $C_{19}H_{24}O_2$, 284.1777; found, 284.1771.

(8R,8′R)-3′-Methoxylignan-3-ol **16**. Yield of 18% through 5 steps as a colorless oil, $[\alpha]^{20}_D$ = −31 (c 0.5, $CHCl_3$); ^{1}H NMR (400 MHz, $CDCl_3$) δ: 0.83 (6H, d, J = 6.7 Hz), 1.76−1.84 (2H, m), 2.39 (1H, dd, J = 13.9, 8.0 Hz), 2.42 (1H, dd, J = 13.8, 8.0 Hz), 2.55−2.63 (2H, m), 3.78 (3H, s), 4.98 (1H, s), 6.52 (1H, m), 6.63−6.65 (2H, m), 6.68 (1H, d, J = 7.8 Hz), 6.71−6.75 (2H, m), 7.10 (1H, dd, J = 7.81, 7.78 Hz), 7.17 (1H, dd, J = 7.9, 7.7 Hz). ^{13}C NMR (100 MHz, $CDCl_3$) δ: 13.9, 14.0, 37.4, 37.6, 41.1, 41.4, 55.2, 110.9, 112.6, 114.8, 115.8, 121.6, 121.7, 129.0, 129.2, 143.3, 143.5, 155.4, 159.3. EIMS m/z (%): 284 (M^+, 99), 121 (100), 107 (53). HRMS (EI) m/z: calcd for $C_{19}H_{24}O_2$, 284.1777; found, 284.1773.

(8R,8′R)-4′-Methoxylignan-3-ol **17**. Yield of 3% through 5 steps as a colorless oil, $[\alpha]^{20}_D$ = −36 (c 0.3, $CHCl_3$); ^{1}H NMR (400 MHz, $CDCl_3$) δ: 0.815 (3H, d, J = 6.7 Hz), 0.820 (3H, d, J = 6.6 Hz), 1.72−1.82 (2H, m), 2.36 (1H, br d, J = 13.5 Hz), 2.38 (1H, br d, J = 13.5 Hz), 2.55−2.61 (2H, m), 3.79 (3H, s), 4.87 (1H, s), 6.53 (1H, m), 6.63 (1H, dd, J = 8.4, 2.6 Hz), 6.66 (1H, d, J = 7.0 Hz), 6.81 (2H, m), 7.00 (2H, m), 7.11 (1H, dd, J = 7.81, 7.78 Hz). ^{13}C NMR ($CDCl_3$) δ: 13.9, 14.0, 35.7, 38.2, 40.4, 41.2, 55.3, 112.5, 113.5, 115.8, 121.6, 129.2, 129.9, 133.7, 143.6, 155.3, 157.5. EIMS m/z (%): 284 (M^+, 46), 121 (100). HRMS (EI) m/z: calcd for $C_{19}H_{24}O_2$, 284.1777; found, 284.1778.

(8R,8′R)-2′-Chlorolignan-3-ol **18**. Yield of 4% through 5 steps as a colorless oil, $[\alpha]^{20}_D$ = −37 (c 0.5, $CHCl_3$); ^{1}H NMR (400 MHz, $CDCl_3$) δ: 0.83 (3H, d, J = 6.9 Hz), 0.88 (3H, d, J = 6.7 Hz), 1.84 (1H, m), 1.91 (1H, m), 2.38 (1H, dd, J = 13.5, 8.6 Hz), 2.51 (1H, dd, J = 13.4, 8.8 Hz), 2.62 (1H, dd, J = 13.5, 6.3 Hz), 2.81 (1H, dd, J = 13.4, 5.7 Hz), 4.89 (1H, s), 6.56 (1H, m), 6.63 (1H, dd, J = 8.0, 2.4 Hz), 6.67 (1H, d, J = 7.6 Hz), 7.09−7.15 (4H, m), 7.31 (1H, m). ^{13}C NMR ($CDCl_3$) δ: 13.8, 14.2, 36.6, 38.4, 38.8, 41.0, 112.5, 115.8, 121.5, 126.3, 127.1, 129.2, 129.4, 131.3, 134.3, 139.2, 143.5, 155.3. EIMS m/z (%): 288 (M^+, 37), 125 (55), 108 (100). HRMS (EI) m/z: calcd for $C_{18}H_{21}OCl$, 288.1282; found, 288.1288.

(8R,8′R)-3′-Chlorolignan-3-ol **19**. (8*R*,8′*R*)-3-Benzyloxy-3′-chlorolignane was obtained from (*R*)-3-(3-benzyloxybenzyl)-4-butanolide and 3-chlorobenzyl bromide by employing the same method described for the synthesis of **3**. To a solution of (8*R*,8′*R*)-3-benzyloxy-3′-chlorolignane (0.10 g, 0.35 mmol) in CH_2Cl_2 (5 mL) was added BBr_3 (0.049 mL, 0.52 mmol) at −10 °C, and then the reaction solution was stirred at −10 °C for 30 min before addition of sat. aq $NaHCO_3$ solution. The organic solution was separated, washed with brine, and dried (Na_2SO_4). Concentration followed by silica gel column chromatography (EtOAc/hexane = 1/4) gave the title compound (69 mg, 0.24 mmol, 32% in 5 steps) as a colorless oil, $[\alpha]^{20}_D$ = −32 (c 0.9, $CHCl_3$); ^{1}H NMR (400 MHz, $CDCl_3$) δ: 0.819 (3H, d, J = 6.6 Hz), 0.824 (3H, d, J = 6.6 Hz), 1.74−1.82 (2H, m), 2.37 (1H, dd, J = 13.6, 7.9 Hz), 2.39 (1H, dd, J = 13.6, 8.0 Hz), 2.59 (1H, dd, J = 13.6, 8.0 Hz), 2.60 (1H, dd, J = 13.6, 8.6 Hz), 4.85 (1H, s), 6.55 (1H, m), 6.65 (1H, dd, J = 7.6, 2.8 Hz), 6.66 (1H, d, J = 7.2 Hz), 6.96 (1H, m), 7.08 (1H, m), 7.10−7.19 (3H, m). ^{13}C NMR ($CDCl_3$) δ: 13.9, 14.0, 37.78, 37.82, 41.0, 41.1, 112.6, 115.8, 121.6, 125.8, 127.2, 129.0, 129.32, 129.34, 133.8, 143.4, 143.7, 155.3. EIMS m/z (%): 288 (M^+, 25), 125 (29), 108 (100). HRMS (EI) m/z: calcd for $C_{18}H_{21}OCl$, 288.1282; found, 288.1283.

(8R,8′R)-4′-Chlorolignan-3-ol **20**. Yield of 18% through 5 steps as a colorless oil, $[\alpha]^{20}_D$ = −25 (c 0.5, $CHCl_3$); ^{1}H NMR (400 MHz, $CDCl_3$) δ: 0.81 (3H, d, J = 6.7 Hz), 0.82 (3H, d, J = 6.7 Hz), 1.73−1.79 (2H, m), 2.37 (1H, dd, J = 13.6, 5.5 Hz), 2.39 (1H, dd, J = 13.6, 5.7 Hz), 2.58 (1H, dd, J = 13.4, 6.6 Hz), 2.59 (1H, dd, J = 13.4, 6.7 Hz), 4.72 (1H, s), 6.54 (1H, m), 6.64 (1H, dd, J = 7.9, 2.6 Hz), 6.65 (1H, d, J = 7.3 Hz), 6.96 (2H, d, J = 8.3 Hz), 7.11 (1H, dd, J = 7.8, 7.8 Hz), 7.21 (2H, m). ^{13}C NMR ($CDCl_3$) δ: 13.89, 13.94, 37.8, 38.0, 40.7, 41.2, 112.6, 115.8, 121.6, 128.2, 129.3, 130.3, 131.3, 140.0, 143.4, 155.3. EIMS m/z (%): 288 (M^+, 17), 125 (27), 108 (100). HRMS (EI) m/z: calcd for $C_{18}H_{21}OCl$, 288.1282; found, 288.1285.

Insects. Eggs of the common house mosquito *Culex pipiens* were purchased from Sumika Techno Service Co., Ltd. (Hyogo, Japan), and reared. Larvae were maintained at 25 °C under a photoperiod of 12 h of light and 12 h of darkness.

Evaluation of the Larvicidal Activity. The larvicidal activity of the test compounds was evaluated according to our earlier report.[7] Briefly, 20 larvae (10 larvae released in 1 mL of water × 2 tubes) were prepared for each concentration, and the lethal concentration for inducing death in 50% of mosquito larvae [LC_{50} (M)] 24 h after applying the compound was calculated by probit analysis.[10] The acute toxic symptom at the concentration of 2.5 × 10^{-4} M was also monitored within 2 h using the same procedure. The insecticidal assay was performed in triplicate. Dimethylsulfoxide (DMSO) at the concentration of 0.5% demonstrated no adverse effect on mosquitoes. Imidacloprid was employed as a positive control.

Evaluation of the Inhibitory Activity of the Chemicals on the O_2 Consumption of the Mitochondrial Fraction. The O_2 consumption inhibitory activity was measured for compound **6**, inducing the highest acute toxic symptom in the present study, as well as for the reference compounds **1** ((−)-DGA) and **2** (3-OH-DGA). To compare **1**, **2**, and **6**, the inhibitory activities of 3-methoxy-DGA derivatives (3-OMe-DGA) and (−)-secoisolariciresinol ((−)-SECO) (compounds **21** and **22** in Figure 1), whose LC_{50} values were 4.73 × 10^{-5} and >45 × 10^{-5} M (mortality is 0% at this concentration), respectively,[7] were also evaluated. In 10 mL of the ice cold buffer A (3 mM Tris-HCl buffer (pH 7.4) containing 0.25 M sucrose and 1 mM EDTA), 2.8 g of rat liver was homogenized, followed by centrifugation (500*g*, 10 min, 4 °C). The resultant pellet was suspended in buffer A, and the solution was centrifuged (8,000*g*, 10 min, 4 °C; two times) to get the mitochondrial fraction (resuspended in buffer A). After the protein concentration of the fraction was measured by the Bradford Reagent (Sigma) with bovine serum albumin as the standard, it was adjusted to 5 mg/mL using buffer A. The prepared mitochondrial fraction was kept at −80 °C before use.

In each well of a 96-well microplate (Nunc F96 MicroWell black polystyrene plate, Thermo Fisher Scientific K. K., Yokohama, Japan) were added 1 μL of DMSO solution containing each test sample, 50 μL of buffer B (3 mM Tris-HCl buffer (pH 7.4) containing 0.25 M sucrose, 1 mM EDTA, and 125 mM succinic acid disodium salt), 50 μL of buffer C (3 mM Tris-HCl buffer (pH 7.4) containing 0.25 M sucrose, 1 mM EDTA, and 8.25 mM ADP), 100 μL of MitoXpress probe solution (Luxcel Biosciences, Ltd., Cork, Ireland; 0.1 μM of the solution diluted by buffer A), and 50 μL of the mitochondrial fraction. The DMSO solutions without any samples and 160 μM NaCN were employed as the negative and positive controls, respectively. After addition of 100 μL of the mineral oil into each well, the fluorescence intensity was recorded by using the fluorescence microplate reader (SH-8000Lab, Corona electric Co., Ltd., Hitachinaka, Japan) in the time-dependent manner (time-resolved mode; 30 °C, 3.3 min intervals

DOI: 10.1021/jf504816a
J. Agric. Food Chem. 2015, 63, 2442−2448

for 99 min, excitation 380 nm, emission 650 nm, and 100 μs as the delay and gate times.). The final concentrations of the test samples other than SECO **22** were set to 4, 40, 120, and 200 μM. SECO was applied at the concentration of 3.98×10^{-3} M. The slope of the intensity over time for each curve was calculated, and the concentration, which induced the mean value of the slope values of the positive and negative controls, was defined as the EC_{50} value (M). The assay was performed in triplicate or more (n = 3–5).

RESULTS AND DISCUSSION

LC_{50} values of the synthesized lignan derivatives are shown in Table 1. Compared with the activity of (−)-DGA and SECO (LC_{50} values were ca. $3.5–4.5 \times 10^{-5}$ M), that of the unsubstituted compound **3** was somewhat low (7×10^{-5} M). The fluorinated compounds **4**–**8** showed a higher activity than the unsubstituted compound **3**. The 2-F derivative **4** showed the highest activity, 3.5-fold higher than that of compound **3**. Differing potency among the positions of the substituents was not observed (compounds **4**–**6**), and the potency of multiple substituted derivatives (compounds **7** and **8**) did not differ from that of the monofluorinated compounds. Among the methylated compounds **9**–**11**, 3-Me and 4-Me derivatives (compounds **10** and **11**) were 2- and 4-fold less potent, respectively, than 2-Me derivative (compound **9**), which was almost equipotent to the fluorinated compounds. The 4-OH derivative **14** showed higher potency than the other OH derivatives **12** and **13**, and the 3-OMe derivative **16** showed higher potency than that of the other positioned OMe derivatives **15** and **17**. The replacement of a fluorine atom of compounds **4**–**6** with a chlorine atom retained the high activity. The ratio of the highest activity (2-F **4**, 2.01×10^{-5} M) to the lowest (4-Me **11**, 12.1×10^{-5} M) was 6, demonstrating that the effect of the substituent at the 7′ phenyl moiety on activity was not as large when a compound had the 3-OH phenyl ring at the 7 position, regardless of the physicochemical properties of the substituents, such as electron-withdrawing/donating and hydrophilic/hydrophobic features.

Table 1. Larvicidal Activity against *Culex pipiens* of 3-OH DGA Derivatives 24 h after the Sample Application (LC_{50} (M), Mean ± SEM)[a]

		insecticidal activity			insecticidal activity
no.		LC_{50} ($\times 10^{-5}$ M)	no.		LC_{50} ($\times 10^{-5}$ M)
1	(−)-DGA	3.52 ± 0.56 a	**11**	4-Me	12.1 ± 0.44 b
2	3-OH-DGA	4.57 ± 1.27 a	**12**	2-OH	7.94 ± 0.15 ab
3	H	7.12 ± 1.39 ab	**13**	3-OH	8.24 ± 2.24 ab
4	2-F	2.01 ± 0.49 a	**14**	4-OH	4.97 ± 0.69 a
5	3-F	2.56 ± 0.50 a	**15**	2-OMe	5.93 ± 1.99 ab
6	4-F	3.66 ± 1.08 a	**16**	3-OMe	2.74 ± 0.58 a
7	3,4-F	2.50 ± 0.24 a	**17**	4-OMe	4.63 ± 1.29 a
8	3,4,5-F	2.37 ± 0.26 a	**18**	2-Cl	2.52 ± 0.26 a
9	2-Me	3.03 ± 0.95 a	**19**	3-Cl	2.23 ± 0.16 a
10	3-Me	6.13 ± 2.99 ab	**20**	4-Cl	2.56 ± 0.33 a

[a]Data are represented as mean and standard error of mean (n = 3). Not significantly different from each other when labeled with the same letters (one-way ANOVA, Tukey; $P < 0.05$; PRISM software 5.0). The LC_{50} value of imidacloprid (positive control) was $2.66 \pm 0.52 \times 10^{-7}$ M (n = 3).

For all of the synthesized compounds, their acute toxic symptom against the larvae of the mosquitoes was observed (Figure 3). The unsubstituted derivative **3** was equipotent to 3-OH DGA **2** (Figure 3A). Among the derivatives with an ortho-substituted phenyl group (Figure 3B), the 2-F derivative **4** induced complete death of the larvae within 1 h, whereas the 2-OH derivatives **18** induced a mortality of only 60% in 2 h [62 ± 12% (n = 3)]. The other ortho-substituted compounds (2-Me, 2-OMe, and 2-Cl) showed almost the same curves as one

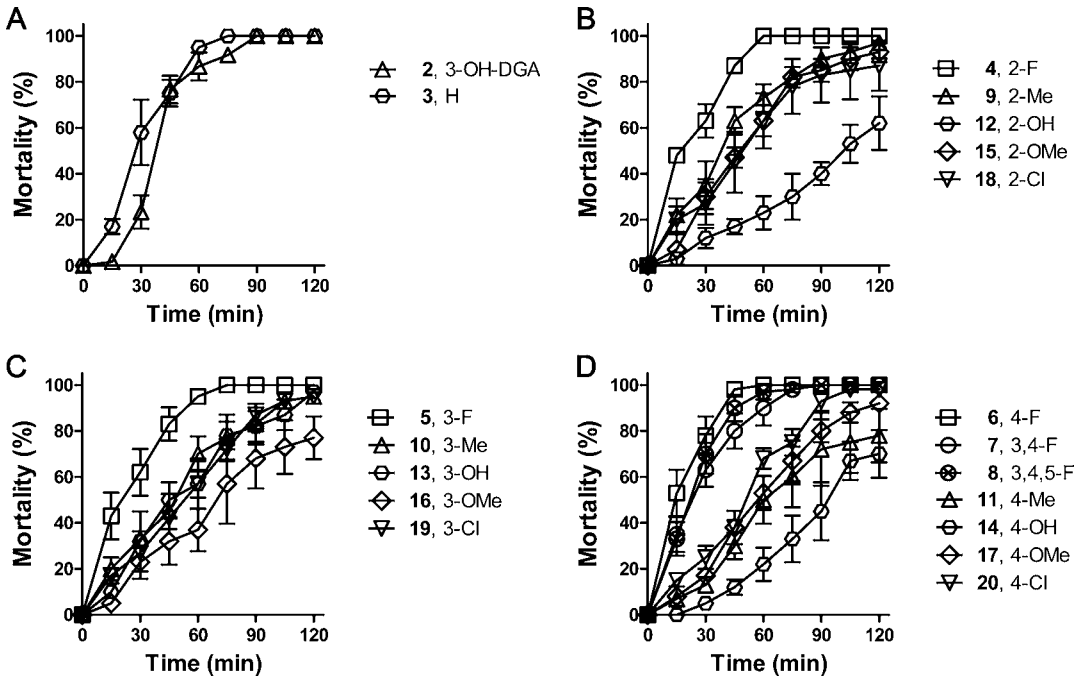

Figure 3. Time-dependent curves of the acute larvicidal activity against *Culex pipiens* of the test chemicals within 2 h. No adverse effect on mosquitoes was observed in the control within 2 h. (A) 3-OH-DGA **2** and the unsubstituted **3**, (B) ortho-substituted phenyl derivatives **4**, **9**, **12**, **15**, and **18**, (C) meta-substituted phenyl derivatives **5**, **10**, **13**, **16**, and **19**, and (D) para-substituted phenyl derivatives **6**, **11**, **14**, **17**, and **20** and multifluorinated derivatives **7** and **8**.

DOI: 10.1021/jf504816a
J. Agric. Food Chem. 2015, 63, 2442–2448

another. Among the meta-substituted compounds (Figure 3C), the 3-F derivative **5** killed all of the mosquitoes at 75 min, showing some delay compared with the 2-F derivative. The 3-OMe derivative **16** did not completely kill the mosquitoes even after 120 min [mortality, 77 ± 9% (n = 3)]. Among the para-substituted compounds (Figure 3D), 4-F derivative **6** killed almost all larvae within 45 min, showing the fastest larvicidal activity among all of the synthesized compounds. The 4-OH derivative **14** killed 70% of mosquitoes at 120 min [mortality, 70 ± 10% (n = 3)]. Compound **2**, inducing high mortality within 1 h (Figure 3A), has 3-OMe as well as 4-OH groups, although the compound having either the 3-OMe or 4-OH group took much more time to kill the mosquito larvae. The reason why compound **2** induced the acute toxic symptom remains unclear, but the multiple substituents may exert a synergistic effect. The multifluorine-substituted derivatives **7** and **8** killed most of the mosquitoes within 1 h; the same effectiveness was observed for the monofluorinated derivatives. Replacement of a fluorine atom of compounds **4**–**6** with a chlorine atom (compounds **18**–**20**) reduced the speed of killing of the mosquito larvae (for example, ca. 100% mortality induced by the 4-Cl derivative **20** was observed 90–105 min after application), suggesting that electron-withdrawing groups do not always induce rapid toxicity. Ultimately, the unsubstituted derivative **3** and fluorinated compounds **4**–**8** were found to exhibit higher toxicity than the others, suggesting that smaller substituents better promote acute toxicity. The 3-OMe derivative **16**, which did not kill mosquitoes perfectly within 2 h, showed higher insecticidal activity (Table 1), suggesting that acute toxicity is not the primary factor for inducing high insecticidal activity.

In search of clues to the mode of action of the active lignan derivatives, we investigated whether or not compounds **1**, **2**, **6** (selected for most acute toxicity), **21** (selected for exerting almost the same insecticidal activity as compounds **2** and **6**, but not acute toxicity), and **22** (selected for exerting neither insecticidal activity nor acute toxicity) were able to suppress the O_2 consumption of the mitochondrial fraction, associated with the respiratory system (Table 2). All of the insecticidal compounds tested in the O_2 consumption assay were found to show suppressive activity at almost the same concentration, whether they induced acute toxic symptom or not. (−)-SECO **22** did not suppress the O_2 consumption even at the 50-fold higher concentration. Although a good correlation between the insecticidal (LC_{50}) and O_2 consumption (IC_{50}) activities was not observed (data not shown), the insecticidal lignan derivatives suppressed the O_2 consumption of the mitochondrial fraction in vitro, suggesting that their insecticidal activity was associated, at least in part, with the inhibition of the respiratory system. Compounds **1** and **21**, which did not kill mosquito larvae within 2 h, may take more time to reach target sites in insects, probably owing to their hydrophobicity. As insecticides and acaricides, mitochondrial electron transport inhibitors, such as tebufenpyrad and Fenpyroximate (targeting complex I), have been developed,[11] and investigation of the novel structure of complex I inhibitors has been reported.[12] In the present study, it remains unclear how the synthesized lignan derivatives suppressed the O_2 consumption in the mitochondrial fraction; however, it has been reported that a partially demethylated DGA (2,3-dimethyl-1-(3,4-dihydroxyphenyl)-4-(4-hydroxy-3-methoxyphenyl)butane) showed inhibitory activity toward mitochondrial succinoxidase and the NADH-oxidase enzyme system,[13] suggesting that the present lignan derivatives also inhibit mitochondrial electron transport.

Table 2. Oxygen Consumption Inhibitory Activity of (−)-DGA Derivatives (IC_{50} (M), Mean ± SEM)

		oxygen consumption inhibitory activity[a]	insecticidal activity	acute toxicity
no.		IC_{50} ($\times 10^{-5}$ M)	LC_{50} at 24 h ($\times 10^{-5}$ M)	mortality at 45 min (%)
1	(−)-DGA	6.89 ± 2.69 (n = 4)	3.52 ± 0.56[b]	0
2	3-OH-DGA	6.78 ± 2.41 (n = 5)	4.57 ± 1.27[b]	83 ± 4.4
6	4-F	4.03 ± 0.83 (n = 3)	3.66 ± 1.08[c]	98 ± 1.7
21	3-OMe-DGA	5.08 ± 1.52 (n = 4)	4.73 ± 1.46[b]	0
22	(−)-SECO	>398 (n = 3)	>45[b]	0

[a]The IC_{50} value of NaCN (positive control) was 3.66 ± 0.02 × 10^{-6} M (n = 3). [b]Cited from ref 7. [c]Cited from Table 1.

In summary, we identified 3-OH-DGA derivatives, in particular, monofluorinated 3-OH-DGA derivatives, showing insecticidal activity as well as acute toxicity against the larvae of the mosquito, *C. pipiens*. Some of the compounds were found to inhibit the O_2 consumption of the mitochondrial fraction, suggesting that they inhibit the respiratory system. The insecticidal activity of these natural lignan-based compounds was lower than that of imidacloprid, one of the most famous commercial neuroactive insecticides (LC_{50} value of imidacloprid was 2.66 ± 0.52 × 10^{-7} M (n = 3)). But the simple structure of the compounds inducing acute larvicidal activity and structure–activity relationship elucidated in the present study should be available for further structural modification, leading to novel and useful vector-control agents.

■ ASSOCIATED CONTENT

Supporting Information

Preparation method for (*R*)-3-(3-benzyloxybenzyl)-4-butanolide. This material is available free of charge via the Internet at http://pubs.acs.org.

■ AUTHOR INFORMATION

Corresponding Author

*Tel.: +81-89-946-9846. Fax: +81-89-977-4364. E-mail: syamauch@agr.ehime-u.ac.jp.

Funding

We are grateful to Marutomo Co. for financial support.

Notes

The authors declare no competing financial interest.

■ ACKNOWLEDGMENTS

Part of this study was performed at the INCS (Johoku station) of Ehime University.

■ REFERENCES

(1) Henrick, C. A. Methoprene. *J. Am. Mosq. Control Assoc.* **2007**, *23*, 225–239.

(2) Dame, D. A.; Wichterman, G. J.; Hornby, J. A. Mosquito (*Aedes taeniorhynchus*) resistance to methorprene in an isolated habitat. *J. Am. Mosq. Control Assoc.* **1998**, *14*, 200–203.

(3) Cornel, A. J.; Stanich, M. A.; McAbee, R. D.; Mulligan, F. S. High level methoprene resistance in the mosquito *Ochlerotatus nigromaculis* (Ludlow) in Central California. *Pest Manage. Sci.* **2002**, *58*, 791–798.

DOI: 10.1021/jf504816a
J. Agric. Food Chem. 2015, 63, 2442–2448

(4) Baumann, P.; Clark, M. A.; Baumann, L.; Broadwell, A. H. *Bacillus sphaericus* as a mosquito pathogen: Properties of the organism and its toxins. *Microbiol. Rev.* **1991**, *55*, 425−436.
(5) Charles, J. F.; Nielson-LeRoux, C.; Delecluse, A. *Bacillus sphaericus* toxins: Molecular biology and mode of action. *Annu. Rev. Entomol.* **1996**, *41*, 451−472.
(6) el-Bendary, M. A. *Bacillus thuringiensis* and *Bacillus sphaericus* biopesticides production. *J. Basic Microbiol.* **2006**, *46*, 158−170.
(7) Nishiwaki, H.; Hasebe, A.; Kawaguchi, Y.; Akamatsu, M.; Shuto, Y.; Yamauchi, S. Larvicidal activity of (−)-dihydroguaiaretic acid derivatives against *Culex pipiens*. *Biosci. Biotechnol. Biochem.* **2011**, *75*, 1735−1739.
(8) Wukirsari, T.; Nishiwaki, H.; Hasebe, A.; Shuto, Y.; Yamauchi, S. First discovery of insecticidal activity of 9,9′-epoxylignane and dihydroguaiaretic acid against houseflies and the structure−activity relationship. *J. Agric. Food Chem.* **2013**, *61*, 4318−4325.
(9) Moss, G. P. Nomenclature of lignans and neolignans (IUPAC recommendations 2000). *Pure Appl. Chem.* **2000**, *72*, 1493−1523.
(10) Finney, D. J. *Probit analysis*, 2nd ed.; Cambridge University Press: London, 1952.
(11) Schuler, F.; Casida, J. E. The insecticide target in the PSST subunit of complex I. *Pest Manage. Sci.* **2001**, *57*, 932−940.
(12) Song, H.; Liu, Y.; Xiong, L.; Li, Y.; Yang, N.; Wang, Q. Design, synthesis, and insecticidal evaluation of new pyrazole derivatives containing imine, oxime ether, oxime ester, and dihydroisoxazoline groups based on the inhibitor binding pocket of respiratiory complex I. *J. Agric. Food Chem.* **2013**, *61*, 8730−8736.
(13) Heiser, R. W.; Cheng, C. C.; Pardini, R. S. Inhibition of mitochondrial electron transport by partially demethylated dihydroguaiaretic acid. *Pharmacol. Res. Commun.* **1977**, *9*, 917−925.

DOI: 10.1021/jf504816a
J. Agric. Food Chem. 2015, 63, 2442−2448

are responsible for the immune stimulatory activity of YFWGE.[26,28] Furthermore, Tuscano et al.[29] showed that YFWGE contains proteins (polypeptides) with molecular weights of 5−100 kilodaltons (kd) that are active in inhibiting the proliferation of cancer cells. Thus, there is interest in developing wheat germ using biotechnology with lactic acid bacteria and yeast.

Although wheat germ fermentation has been widely studied, there is little information about the anticarcinogenic activity of wheat germ extract fermented with lactic acid bacteria. In 2013, lactic acid bacteria isolated from wheat germ were characterized and selected on the basis of technological performance to be used as starters for fermenting wheat germ, and an Italian researcher found that the fermented wheat germ extract could inhibit the growth of the colorectal cancer cell lines HT-29, HCT-8, and DLD-1.[30] However, only the benzoquinones of the fermentation extracts were analyzed, and thus further research is needed on other anticarcinogenic components.

In this study, we evaluate the anticarcinogenic activities of *Lactobacillus plantarum* dy-1 fermented wheat germ extracts (LFWGE), including the growth inhibition and induction of apoptosis via the Caspase-3 signaling pathway in the human colon cancer HT-29 cell line. In addition, some of the compounds in LFWGE were analyzed and identified.

MATERIALS AND METHODS

Materials and Chemicals. The fresh wheat germ was purchased from Shandong Yongle of China. The moisture, ash, and fat content were determined according to the Approved Methods of the American Association of Cereal Chemists.[31] The crude protein content (Kjeldahl method) was measured with a semiautomatic Kjeldahl apparatus (K355, Buchi, Switzerland) and a Metrohm 877 Titrino Plus Automatic Titrator (Switzerland). A conversion factor of 5.70 was used. The lactobacillus strain *Lactobacillus plantarum* dy-1 was previously isolated by authors. HT-29 colon cancer cells were provided by the Cell Bank at the Chinese Academy of Sciences in Shanghai. Foetal bovine serum and McCOY'S 5A medium were purchased from GIBCO. Trypsin-EDTA was purchased from Beyotime. Annexin V-FITC, propidium iodide (PI), Hoechst dye 33342, penicillin, chloramphenicol, 2,6-dimethoxybenzoquinone, gallic acid, Folin-Ciocalteu reagent, coomassie brilliant blue R250, and bovine serum albumin were purchased from Sigma-Aldrich, Inc. (Supelco, Bellefonte, PA). The MTT (3-(4, 5-dimethylthiazol-2-yl)-2, 5-diphenyltetrazolium bromide), sephadex G-50, and sephacryl S-200 were purchased from Shanghai Chuangsai Scientific Instrument Limited Co. (Shanghai, China). All of the other reagents and solvents were purchased from Sinopharm Chemical Reagent Co. Ltd. (Shanghai, China) and were of either analytical or chromatographic grade.

Preparation of the Extracts. *Lactobacillus plantarum* dy-1 was used as the starter culture in the direct vat set fermentation, which was previously isolated from pickles by authors. Its preservation number is CGMCC NO. 6016 in the Chinese Common Microbe Bacterial Preservation Administration Center database. *Lactobacillus plantarum* dy-1 was cultivated in MRS, treated with a protective agent (20% skim milk, 10% fucose, 14% monosodium glutamate, 6% sorbitol, and 6% vitamin C), and lyophilized to powder. The wheat germ was crushed and passed through a 100-mesh sieve. A 200 g portion of wheat germ powders, 1.4 L of distilled water, and 4 g of freeze-dried fungus powder containing *Lactobacillus plantarum* dy-1 (cell density 4×10^8 cfu/g) were shaken and incubated at 30 °C for 24 h in a microbiological incubator. After fermentation, the solution was centrifuged at 12 000 *g* for 15 min at 4 °C using a refrigerated centrifuge (Jouan, France), and then the supernatant was freeze-dried into a powder (LFWGE) using a vacuum freeze-dryer (Marin Christ, Germany). For the unfermented wheat germ, 200 g of powder was extracted with 1.4 L of distilled water at room temperature for 3 h in shaking tables. The supernatant was collected by centrifuging, and then freeze-dried into a powder (WGE) under the same conditions as the fermented wheat germ. This step was repeated six times for analysis. The freeze-dried samples were stored in sealed containers at −20 °C for further analysis. The extraction yield was calculated by the following equation: extraction yield (%) = [weight of freeze-dried powder/weight of WG (g)] × 100.

Extraction of Benzoquinones and HPLC Analysis. The benzoquinones were extracted and analyzed using the following procedure. About 0.5 g of WGE or LFWGE was dissolved into 50 mL of double-distilled water and subjected three times to extraction by shaking with 25 mL of chloroform ($CHCl_3$).[32] The $CHCl_3$ layers were pooled, washed three times with distilled water, and dried over anhydrous Na_2SO_4. The solvent was evaporated to dryness by rotary evaporation at 40 °C. The residue was redissolved in 5 mL of $CHCl_3$ and filtered through a 0.22 μm filter membrane. The filtrate was analyzed by a high performance liquid chromatography (HPLC) system consisting of an Äkta purifier HPLC equipped with shim-pack VP-ODS (250 mm × 4.6 mm, 5 μm) and an ultraviolet detector operating at 288 nm. The mobile phase was a water/methyl alcohol mixture (80:20, v/v), with the flow rate and sample injection volume fixed at 1 mL/min and 20 μL, respectively. The temperature was 25 °C. 2,6-Dimethoxybenzoquinone (Sigma) dissolved in 100% $CHCl_3$ was used as reference to assign retention times and generate the calibration curve

Determination of the Protein Content and SDS-PAGE Analysis of the Extracts. The protein content of the extracts was determined using the Kjeldahl method. A conversion factor of 5.70 was used.

The size and purity of the extracted protein were analyzed by sodium dodecyl sulfate-polyacrylamide gel electrophoresis (SDS-PAGE), which was performed as follows. The aqueous solutions of LFWGE and WGE were mixed with a quarter volume of sample buffer (10% SDS, 0.5% bromophenol blue, 0.25 M Tris-HCl, pH 6.8, 50% glycerin, and 5% β-mercaptoethanol) and heated in a water bath at 100 °C for 5 min. After centrifugation (6000 × *g* for 10 min), 10 μL of the supernatant was electrophoresed with 12% gel concentration and mini-cell apparatus (Bio-Rad) at 20 mA for 3 h and stained with Coomassie brilliant blue R-250 for 2 h followed by destaining using methanol/acetic acid/water at a ratio of 10:7.5:82.5. A GS-800 calibrated densitometer (Bio-Rad) was used to scan the gel.

Separation and Identification of Proteins in the LFWGE. The components of the LFWGE, which were concentrated by precipitation with solid ammonium sulfate to 80−90% saturation, were separated and purified. After being centrifuged (12 000 *g* for 15 min at 4 °C), the precipitate was redissolved in distilled water and dialyzed (molecular weight cut off: 8000−10000 Da) against distilled water at 4 °C for 48 h (renewal of distilled water every other 4−8 h), and finally freeze-dried. Then, the freeze-dried powder was dissolved in phosphate buffer (pH 7.2, 10 mmol/L), and the solution was passed through a sephadex G-50 column (1.6 cm × 50 cm) in series with a sephacryl S-200 (1.6 cm × 50 cm) column at 1 mL/min equilibrated and eluted with phosphate buffer (pH 7.2, 10 mmol/L). The eluent was monitored at 280 nm by UV absorbance, and fractioned peaks were collected, dialyzed against distilled water, and freeze-dried for the assay of anticarcinogenic activity. The anticarcinogenic fractions of the eluent were analyzed by liquid chromatography and tandem mass spectrometry (LC-MS/MS) analysis at the Institute of Biochemistry and Cell Biology, Shanghai Institutes for Biological Sciences (SIBS) of the Chinese Academy of Sciences (CAS).

RP-HPLC was performed using a surveyor LC system (Thermo Finnigan, San Jose, CA) on a C18 column (RP, 180 μm × 150 mm, BioBasic C18, 5 μm, Thermo Hypersil-Keystone). The pump flow rate was 2 μL/min. Mobile phase A was 0.1% formic acid in water, and mobile phase B was 0.1% formic acid in acetonitrile. The protein mixtures were eluted using a gradient of 5−65% B over 30 min. The mass spectral data were acquired on an LTQ linear ion trap mass spectrometer (Thermo Finnigan) equipped with an electrospray interface operated in positive ion mode. The temperature of the heated capillary was set at 200 °C. A voltage of 3.2 kV applied to the ESI needle resulted in a distinct signal. The mass spectrometer was set so that one full MS scan was followed by three MS/MS scans on the three most intense ions from the MS spectrum with the following Dynamic

DOI: 10.1021/acs.jafc.5b00041
J. Agric. Food Chem. 2015, 63, 2449−2457

Exclusion TM settings: repeat count, 2; repeat duration, 0.5 min; exclusion duration, 2.0 min.

Determination of the Total Phenols Content. The total phenol content in WGE and LFWGE was determined using the Folin-Ciocalteu method, slightly modified according to Heimler et al.[33] About 0.5 g of WGE or LFWGE was weighed in a 100 mL volumetric flask and dissolved in 40% ethanol aqueous solution. Then, 1 mL of the solution was added to 4 mL of deionized water and 1 mL of Folin-Ciocalteu reagent in glass test tubes. After the mixture was shaken, 10 mL of a 7% aqueous Na_2CO_3 solution was added, and the mixture was shaken once again. The final volume was adjusted to 20 mL with distilled water. After 90 min of reaction at 45 °C, the absorbance at 765 nm using a spectrophotometer (model UV-9600, Rayleigh, Beijing, China) with water as a blank was measured and used to calculate the phenol content, with gallic acid as a standard. The total phenol amount was expressed as gallic acid equivalent (GAE, mg gallic acid/g sample) through the calibration curve of gallic acid. The calibration curve ranged from 20 to 100 μg/mL (R^2 = 0.9924).

Determination and Extraction of the Total Sugar Content. The total polysaccharide content was determined by the phenol-sulfuric acid method with slight modifications.[34] First, 2 mL of the sample solution was vortex-mixed with 1 mL of 5% phenol in water before rapidly adding 5 mL of concentrated sulfuric acid. After 30 min of standing at room temperature, the absorbance of the sample solution was measured at 490 nm against the blank, which was prepared by substituting distilled water for the sample solution. Aqueous glucose solutions of different concentrations (5, 10, 20, 40, 80, and 160 μg/mL) were used for the standards. The results were expressed as grams of glucose per 100 g of extract.

Crude polysaccharides were extracted with hot water from the LFWGE. The extraction procedure was as follows. First, 25 g of LFWGE was dissolved in 150 mL of double-distilled water, heated at 100 °C for 10 min and then filtered. The clear solution was concentrated in a rotary evaporator under reduced pressure at 50 °C. Then, the concentrated solution was precipitated by the addition of absolute ethanol (4 times the volume of concentrated solution) at 4 °C, followed by centrifugation at 4800 × *g* (20 min) to yield the crude polysaccharides. Then, the deproteinization of the crude polysaccharides was performed using the Sevag method.[35] Finally, the polysaccharide samples were freeze-dried into a powder.

Determination of Lactic Acid Content. The lactic acid content in the LFWGE was determined by high performance liquid chromatography (HPLC). The samples were dissolved in distilled water (about 1.0 mg/mL) and filtered through a 0.45 μm PTFE membrane filter. The WGE or LFWGE was analyzed by a Shimadzu LC-20A HPLC system (Shimadzu Corp., Kyoto, Japan) equipped with a photodiode array (PDA). The operating conditions included a shim-pack VP-ODS C-18 (250 mm × 4.6 mm, 5 μm) column (Shimadzu Corp., Kyoto, Japan), a mobile phase of 3% methanol/0.01 mol/L K_2HPO_4 (pH 2.5), a volume injection of 20 μL, a flow rate of 0.8 mL/min, and detection at 210 nm at 25 °C. The standard curves for lactic acid (Sangon Biotech Co., Ltd., Shanghai, China) were used to quantify the acid.

Cell Lines and Cell Culture. The human colon cancer cell line HT-29 was used for experimentation and obtained from the Shanghai Institutes for Biological Sciences (SIBS) of the Chinese Academy of Sciences (CAS). The HT-29 cells were cultured as monolayers with up to 80% confluence in McCOY'S 5A supplemented with 10% heat-inactivated fetal calf serum and 1% penicillin/streptomycin at 37 °C and 5% CO_2 in humidified air. Cell counts were determined using a microcell counter CC-108 (Sysmex, Kobe, Japan), and cells in a logarithmic phase of growth were used for all of the studies described below.

Growth Inhibition Assay. Cell growth was determined by the MTT (3-(4, 5-dimethylthiazol-2-yl)-2, 5-diphenyltetrazolium bromide) assay.[5] The HT-29 cells were placed in 96-well plates 24 h before treatment. Following treatment with 125−4000 μg/mL of LFWGE (adjustment of pH to 7.0 with 0.1 M NaOH) and WGE (control), the proliferation activity of the cells was tested after 24, 48, and 72 h of incubation. Following treatment with 12.5−100 μg/mL of 2,6-dimethoxy benzoquinone (standard), 25−200 μg/mL of protein fraction, 250−4000 μg/mL of sugar, and 25−100 μg/mL of lactic acid (standard), respectively, the proliferation activity of the cells was measured after 24 h of incubation.

Absorbance was measured at 490 nm using a Multiskan Spectrum (Thermo Electron Corp., Asheville, NC). Cell viability was expressed as a percentage of the control culture value, which was considered to be 100% viable.

Cell Cycle Distribution Analysis. The HT-29 cells (0.4×10^6 per mL) were seeded in 6-well culture plates and incubated with increasing concentrations of LFWGE [0 (double-distilled water), 0.2, 0.4, 0.8 mg/mL] at 37 °C under cell culture conditions. After 48 h, the cells were harvested and suspended in 5 mL of cold PBS, centrifuged (500 g for 10 min), and resuspended and fixed in 3 mL of cold ethanol (70%) for overnight at 4 °C. After washing twice with cold PBS, RNase A and propidium iodide were added to a final concentration of 50 μg/mL each. The sample was then incubated at 4 °C for 30−60 min before measurement. The cells were analyzed on a flow cytometer (Beckman Coulter), and the cell cycle distribution was calculated with the ModFit LT software (Verity Software House, Topsham, ME).

Hoechst Dye 33342 Staining. The HT-29 cells (0.4×10^6 per mL) were seeded in 12-well culture plates and exposed to 1 mg/mL concentrations of LFWGE for 48 h. Hoechst 33342 was added directly to the cells to a final concentration of 5 μg/mL. After 15 min at room temperature in the dark, the cells were visualized with a Leica DMR XA fluorescence microscope (Leica Microsystems Wetzlar GmbH, Wetzlar, Germany) equipped with the appropriate filters for Hoechst 33342 to determine the nuclear morphological changes.

Assessment of Apoptosis by Flow Cytometry. Apoptosis was determined with an apoptosis kit (Sigma). The procedure was performed according to the manufacturer's instructions. Briefly, after treatment with different concentrations (0.25, 0.5, 1, 2, and 4 mg/L) of LFWGE for 24, 48, and 72 h, the HT-29 cells were harvested and collected by centrifugation. The cells were washed with ice-cold PBS and resuspended in the binding buffer at a concentration of 10^6 cells/mL. Then, 500 μL of cell suspension was mixed with 5 μL of annexin V-FITC and 10 μL of propidium iodide (PI) solution. The mixtures were incubated for 10 min at 4 °C and protected from exposure to light. The fluorescence of the cells was analyzed by flow cytometry. Approximately 2×10^4 cells were tested for each histogram by flow cytometry.

Quantitative PCR. Approximately 2×10^7 HT-29 cells were lysed in Trizol Reagent. Total RNA was prepared according to the manufacturer's instructions (Takara, Japan). To remove the genomic DNA, 5 μg of total RNA was treated with 5U RNase-free DNaseI for 30 min at 37 °C. After the DNase treatment, the RNA were incubated at 65 °C for 10 min. RNA integrity was assessed by an Agilent 2100 Bioanalyzer (Agilent Technologies, Palo Alto, CA). Quantitative PCR was used to generate RNA with two sharp ribosomal 18S and 28S bands. First-strand cDNA synthesis was carried out on 2 μg of the total RNA from each sample with the PrimeScript RT Master Mix (Takara, Japan) first-strand synthesis kit for RT-PCR according to the manufacturer's instructions. Experimental wells containing 25 μL of SYBR Green PCR Master Mix (Takara, Japan) were run using north tube plates. Quantitative PCR was conducted on the iCycler according to the SYBR Green method. Forward and reverse primers were designed using the tools available through the MIT Whitehead Institute web page. The primer sequences were as follows: caspase-3(F) AACCTCAGGGAAACATTCAG, caspase3(R) GGCTCAGAAGCACACAAAC; caspase8(F) GGATGCCTTGATGTTATTCC, caspase8(R) AGTTCCCTTTCCATCTCCTC; caspase9(F) TTCCCAGGTTTGTTTCCTG, caspase9(R) ACCCTAAGCAGGAGGGACTG; caspase7(F) GAAGAGGCTCCTGGTTTGTG, caspase7(R) TCATGGAAGTGTGGGTCATC; actin(F) AGCGAGCATCCCCCAAAGTT, and actin(R) GGGCACGAAGGCTCATCATT. Quantitative PCR amplification for all of the caspases included preincubation at 94 °C for 6 min, followed by 38 cycles at 95 °C for 5 s, 57 °C for 45 s, and 72 °C for 30 s. The relative expression of mRNA was calculated using the $2^{-\Delta\Delta Ct}$ method.[36]

DOI: 10.1021/acs.jafc.5b00041
J. Agric. Food Chem. 2015, 63, 2449−2457

Caspase-3 Activity. The caspase-3 activity was determined using a caspase-3 activity kit (Nanjing Jiancheng Bioengineering Research Institute, Nanjing, China). Cell lysates were prepared after their respective treatment with various designated procedures, and the assays were performed on 96-well microtiter plates by incubating 10 μL of cell lysate protein per sample in 80 μL reaction buffer (1% NP-40, 20 mM Tris-HCl (PH 7.5), 137 mM Nad, and 10% glycerol) containing 10 μL of caspase-3 substrate (Ac-DEVD-pNA) (acetyl-Asp-Glu-Val-Asp p-nitroanilide) (2 mM). The lysates were incubated at 37 °C for 4 h. The samples were measured with an ELISA reader at an absorbance of 405 nm by a spectrophotometer.

Statistical Analysis. All of the statistical analyses were accomplished by using SPSS Statistics software version 17.0 (SPSS, Chicago, IL). Analysis of variance (ANOVA) was used to test for differences between the means.

RESULTS AND DISCUSSION

Yield and Chemical Composition of the Extracts. The composition of raw wheat germ was as follows: moisture 12.48 ± 0.46%, crude protein (N × 5.70) 37.88 ± 0.24% of dry matter (d.m.); fat 11.91 ± 0.34% of d.m.; and ash 7.68 ± 0.09% of d.m. In this experiment, the yields of the aqueous extract of LFWGE and WGE were 22.19 ± 1.32% and 40.02 ± 1.82%, respectively.

Table 1 presents the composition of LFWGE and WGE. As shown, WGE contained 32.90 ± 0.57% of crude protein and 43.05 ± 1.23% of total sugar. After 24 h of incubation with *Lactobacillus plantarum* dy-1 (initial cell density 4 × 10^8 cfu/g) at 30 °C (the optimum fermentation condition according to some preliminary work for antitumor activity), the protein in LFWGE slightly increased to 34.36 ± 0.23% and the sugar decreased to 33.04 ± 1.03%. In addition, the total phenol content of WGE was 20.81 ± 0.11 mg/g (expressed as the gallic acid equivalent, mg gallic acid/g dried extract). The total phenol content of LFWGE was to 28.48 ± 0.16 mg/g. Lactic acid was not detectable in WGE, whereas 27.7 ± 1.2 mg/g of lactic acid was found in LFWGE.

Table 1. Main Composition (% Dry-Weight) of LFWGE and WGE[a]

composition	WGE	LFWGE
2, 6-dimethoxybenzoquinone (μg/g)	33.85 ± 2.85	181.10 ± 4.56
protein (%, w/w)	32.90 ± 0.57	34.36 ± 0.23
total phenols (mg gallic acid/g)	20.81 ± 0.11	28.48 ± 0.16
total sugar (%, w/w)	43.05 ± 1.23	33.04 ± 1.03
lactic acid (mg/g)	0	27.7 ± 1.2

[a]The results are expressed as the mean (±SD), n = 3.

Due to the difficulty of buying 2-methoxy benzoquinone in China, 2,6-dimethoxybenzoquinone was selected as the analysis target. The 2,6-dimethoxybenzoquinone content in WGE and LFWGE was then determined by $CHCl_3$ selective extraction and HPLC analysis. WGE contained 2, 6-dimethoxybenzoquinone at a concentration of 33.82 ± 2.85 μg/g. After fermentation, the concentration of 2, 6-dimethoxybenzoquinone in LFWGE increased to 181.10 ± 4.56 μg/g (Table 1). This result shows that the fermentation had a significant effect on the 2,6-dimethoxybenzoquinone content of the aqueous extract of wheat germ, which may be attributable to the release of benzoquinones present in wheat germ as glucosides, as found by Rizzello et al.[30] and Yoo et al.[37]

Inhibition of Cell Proliferation in LFWGE-Treated HT-29 Cells. To examine the effects of LFWGE and WGE on cell growth, their inhibitory capacity against HT-29 colon cancer cells was assessed using the MTT assay. Logarithmically growing HT-29 cells were seeded at a concentration of 3 × 10^4 cells per mL, and then HT-29 colon cancer cells were treated with different concentrations of LFWGE and WGE (0.125−4 mg/mL) for 24, 48, and 72 h. As shown in Figure 1, WGE hardly inhibited cell proliferation in the HT-29 cells. However, with increasing concentrations of LFWGE, an increasing inhibition of cell proliferation in HT-29 cells was observed, with different degrees of potency between incubation times. The IC_{50} value was defined as the concentration at which the cell proliferation was inhibited by 50% of the control cells. LFWGE inhibited the growth of HT-29 cells in a dose- and time-dependent manner with IC_{50} values of 1.288, 0.6397, and 0.5435 mg/mL, respectively. These results indicate that LFWGE displays anticarcinogenic activity in HT-29 colon cancer cells.

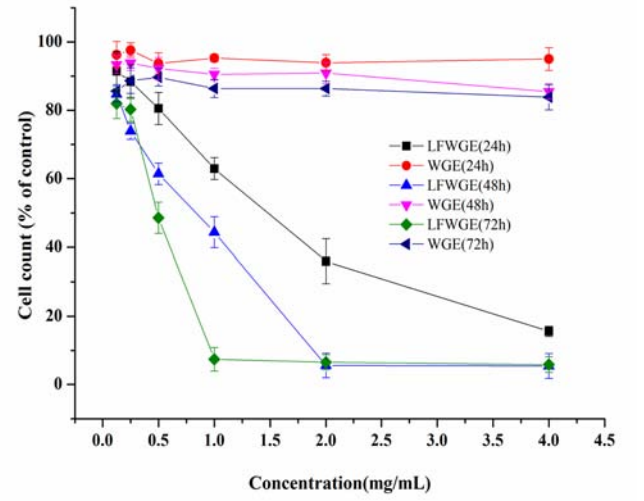

Figure 1. HT-29 cell proliferation in response to LFWGE and WGE treatment. Colon cell cultures were treated with increasing doses of LFWGE as indicated on the x axis. Cell proliferation was determined by formazan dye uptake and expressed as a percent of untreated control cell proliferation. Mean ± SD, n = 8.

Several studies have described the promising anticarcinogenic activity of a yeast (*Saccharomyces cerevisiae*) fermented wheat germ extract (Avemar), which is attributed to two quinones: 2,6-dimethoxybenzoquinone (2,6-DMBQ) and 2-methoxy benzoquinone (2-MBQ).[27,28] Yoo et al.[37] and Rizzello et al.[31] also demonstrated that both benzoquinones could be obtained from wheat germ using lactic acid bacteria fermentation. The HT-29 cells were treated with multiple levels of 2,6-DMBQ isolated from LFWGE to determine the dose-dependent response to this compound. The results obtained, shown in Table 2, show that the cell proliferation inhibition rate increased with the concentration. However, combined with the results of LFWGE treatment and 2,6-DMBQ content, we found that the proliferation of HT-29 cell was inhibited not only by benzoquinones. Therefore, further research on other functional components is still needed.

Some studies have also exploited the potential of specific low molecular proteins or polypeptides to reduce or inhibit the growth or proliferation of a cancer cell.[29] Proteins played a role in this study, and their effects on the cancer cells by isolated protein fractions from LFWGE were analyzed. Electrophoresis (SDS-PAGE) of WGE and LFWGE was performed to obtain

DOI: 10.1021/acs.jafc.5b00041
J. Agric. Food Chem. 2015, 63, 2449−2457

Table 2. Inhibition Effect of the Fraction on the Proliferation of HT-29 Cells[a]

concentration (μg/mL)	inhibition (%)
Control	
0	
2,6-Dimethoxy Benzoquinone	
100	78.58 ± 5.40
50	70.54 ± 3.32
25	69.57 ± 4.72
12.5	35.38 ± 2.71
Protein Peak1	
200	88.6 ± 2.85
100	56.8 ± 2.64
50	51.0 ± 1.98
25	28.4 ± 1.25
Protein Peak2	
200	0.9 ± 0.14
100	2.3 ± 0.045
50	−1.2 ± 0.012
25	1.1 ± 0.044
Sugar	
4000	2.6 ± 0.15
2000	0.5 ± 0.10
1000	9.9 ± 0.36
500	10.01 ± 0.15
250	7.5 ± 0.14
Lactic Acid	
100	5.40 ± 0.58
50	2.70 ± 0.88
25	1.30 ± 0.45

[a]The results are expressed as the mean (±SD), $n = 6$.

information on the molecular weight and distribution patterns of the protein components (Figure 2a,b). Protein bands were observed distinctly between 15 and 120 kDa in WGE, and between 15 and 40 kDa in LFWGE.

The extracted proteins were isolated and purified by sephadex G-50 and sephacryl S-200 gel filtration. To improve the separation efficiency, series columns were adopted. A typical elution profile is shown in Figure 3. The elution profile

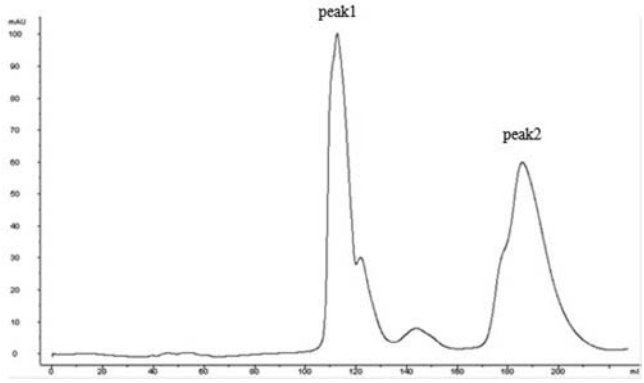

Figure 3. Chromatography of LFWGE on Sephadex G-50 column and sephacryl S-200 column. Eluent: phosphate buffer (pH 7.2, 10 mmol/L); flow rate, 1 mL/min.

was reproducible and revealed two main peaks (due to collection and detection difficulties, other smaller peaks were ignored). Among them, the peak1 fraction indicated the highest anticarcinogenic activity inhibiting the growth of HT-29 cells with 88.6% in 200 μg/mL (Table 2). An LC-MS/MS analysis was carried out for peak 1, and 21 proteins were observed and identified by searching against the NCBInr viridiplantae protein database. The active proteins were added to those listed in Table 3.

In addition, to determine which sugars in LFWGE might be at work, sugars were extracted and treated on HT-29 cells to

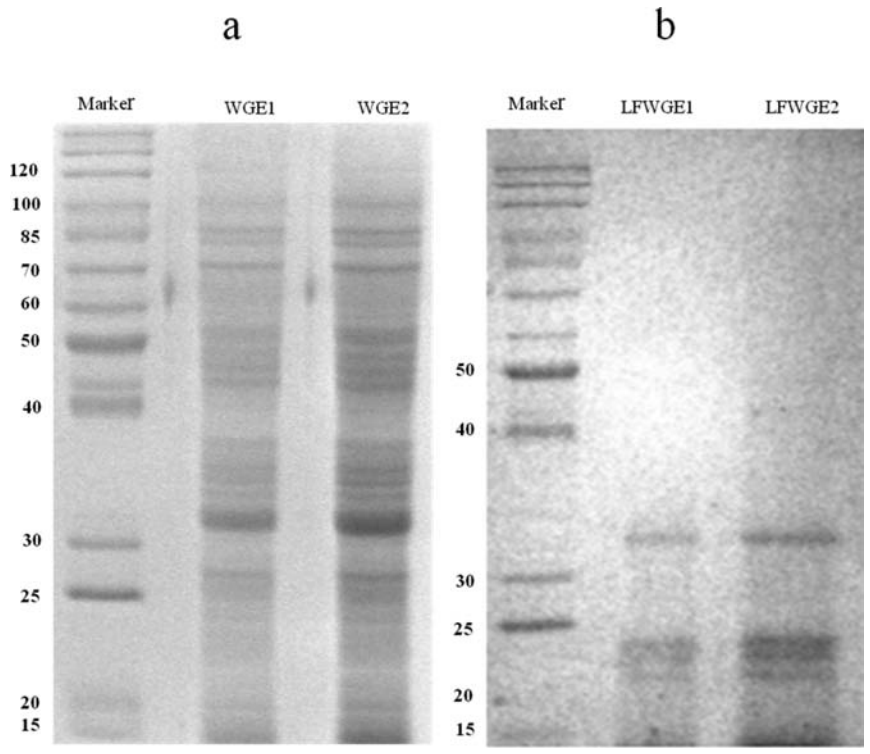

Figure 2. SDS-PAGE patterns of proteins in WGE and LFWGE: WGE1 (0.1 mg), WGE2 (0.2 mg), LFWGE1 (0.1 mg), LFWGE2 (0.2 mg).

DOI: 10.1021/acs.jafc.5b00041
J. Agric. Food Chem. 2015, 63, 2449−2457

Table 3. Identification of the Proteins of Triticum Aestivum in Peak1

proteins	number(s) and sequence(s) of corresponding peptide(s)	NCBI amino acid no.
peroxidase1	7 peptides: 33−42, rglsfdfyrr; 61−72, kdiglaaglllrl; 126−142, rgavvscadilalaard; 167−190, rqdvlsdlpapssnvpsllallrp; 218−235, rlf prpdptinpp flarl; 253−270, rtpnvfdnqyyvdlvnre; 268−292, reglfvsdqdlftnditrpiverf	AAM88383.1 (GI:22001285)
crystal structure of the *Triticum aestivum* xylanase inhibitor-i in complex with *Aspergillus niger* xylanase-i	5peptides: 135−160, rgstgvaglansglalpaqvasaqkv; 219−238, rvpvpegalatggvmlstrl; 271−287, raveavapfgvcydtkt; 342−365, rapavilggaqmedfvldfdmekk; 366−381, rlgfs rlphftgcggl	1T6G (GI:55669877)
xylanase inhibitor 725ACC	4 peptides: 156−181, rgstg vagladsglalpaqvasaqkv; 266−279, rdvyrplvdaftka; 364−387, rapavilggaqmedfvl dfdmekk; 393−403, rlphftgcggl	ABU55392.1 GI:156186243
unnamed protein product	4 peptides: 55−66, reiaiaaglvri; 132−161, raaivasgg ptfpvplgnldslapasqdkv; 182−202, rglgdvadlvalsgahtigrs; 232−251, rlqnldvvtpdlfdngyyka	CBC68269.1 GI:257651497
serpin	4 peptides: 32−62, ksaasnaafspvslhsalsllaagagsatrd; 171−182, klvlanalyfkg; 289−302, kisfgieasdllkc; 328−355, rvssvfhqafvevneqgteaaastaikm	ACN59483.1 GI:224589266
low molecular weight glutenin subunit	2 peptides: 209−228, kvflqqqcspvampqslars; 260−276, raiiysivlqeqqqvrg	ACA63852.1 GI:169666907
xylanase inhibitor, partial	2 peptides: 37−51, rsdvyrpfitafdra; 57−73, kvaavapfelcydsskl	ACO55043.1 GI:226427708
endochitinase	2 peptides: 207−230, raigtdllnnpdlvatdatvsfkt; 264−284, rvpgygvitniingglecgrg	CAA53626.1 GI:416029
LMW glutenin pGM107	2 peptides: 184−203, kvflqqqcspvampqslars; 310−325, rilptmcsvnvplyrt	AAS66085.1 GI:45477539
class II Chitinase	3 peptides: 78−111, revaaflaqtshettggwatapdgafawgycfkq; 153−176, raigvdllsnpdlvatdptvsfkt; 244−266, rycdilgvgygdnldcynqrpfa	AAX83262.1 GI:62465514
0.19 dimeric α-amylase inhibitor, partial	2 peptides: 39−54, rdccqqlahisewcrc; 100−117, rlpivvdasgdgayvckd	AAV39514.1 GI:54778501
putative avenin-like a precursor	1peptides: 91−125, rcqavcsvaqiimrqqqgqsfgqpqqqvpveimrm	CAJ32654.1 GI:89143120
recname: full = cytochrome C	1peptides: 99−109, radliaylkka	P00068.1 GI:118040
monomeric α-amylase inhibitor, partial	1peptides: 1−15, sgpwswcdpatgykv	ABO45971.1 GI:134034581
recname: full = Serpin-Z2A; AltName: full = TriaeZ2a; AltName: full = WSZ2a	2peptides: 171−182, rlvlgnalyfkg; 288−300, kisfgieasdllk	Q9ST57.1 GI:75313847
Bp2A protein, partial	1peptides: 198−208, kmkaleiaert	ABO40343.1 GI:133872552
root peroxidase	1peptides: 110−125, kqtvscadiltvaard	ACF70704.1 GI:194425589
R2R3MYB transcriptional factor	1peptides: 39−49, slpsaagllrc	AEG64799.1 GI:334145749
BAX.2	1peptides: 19−42, rlprpyhgggpe pddgvlllgrrg	ACN81638.1 GI:225193978
alternative oxidase	1peptides: 64−91, kdnvastaaataeamqaakagavqaake	BAB88646.1 GI:19912727
histone deacetylase HDAC2	1peptides: 253−270, kgavhvatphpakkagkt	ABG43091.1 GI:109716218

trace any activity. The result showed no anticarcinogenic activity (Table 2).

It is important to note that the pH was adjusted to 7.0 with 0.1 M of NaOH in vitro treated with LFWGE to eliminate the influence of low pH, which was attributed to the production of lactic acid during fermentation. The effect of lactic acid in the HT-29 cell lines was studied, but the result showed that it had no significant effect on the HT-29 cells (Table 2).

Cell Cycle Distribution after Treatment with LFWGE. To further confirm the proliferation inhibiting effect of LFWGE on HT-29 cells, the cell cycle distribution was analyzed by flow cytometry. Preliminary experiments have shown that while the cells die within 72 h, they do not change significantly for 24 h, so 48 h treatment was selected. The effect of LFWGE on the cell cycle distribution of HT-29 cells is shown in Figure 4. In the control cells, the cell cycle pattern remained constant over time. After 48 h of incubation with increasing doses of LFWGE, the percentage of cells in each phase was as follows: G_0/G_1 phase (DNA presynthetic phase), 61.2%, 70.2%, and 80.8%; S phase (DNA synthesis phase), 28.4%, 25%, and 14.8%; G_2/M phase (DNA postsynthetic and mitosis phases), 10.5%, 4.78%, and 4.34%, respectively. Overall, a broad peak appeared in the G_0/G_1 region with a significant decrease in the S cycle phase. Therefore, LFWGE halted the cell cycle transition of HT-29 cells in the G_0/G_1 phase of the cell cycle, resulting in the depletion of G_2/M phase cells. Studies have shown that Avemar also stops the cell cycle transition of HT-29 cells in the G_0/G_1 phase of the cell cycle and halts the cell cycle transition of HL-60 cells in the G_2/M phase of the cell cycle.[38]

Induction of Apoptosis by LFWGE. To evaluate the effect of LFWGE on the induction of apoptosis, the HT-29 cells were incubated with 0.25, 0.5, 1, 2, and 4 mg/mL of LFWGE for 24, 48, and 72 h, and then double stained with annexin V-FITC and PI, followed by quantitative flow cytometry analysis. The results confirmed that LFWGE induced the apoptosis of HT-29 cells, which was positively correlated with LFWGE dose

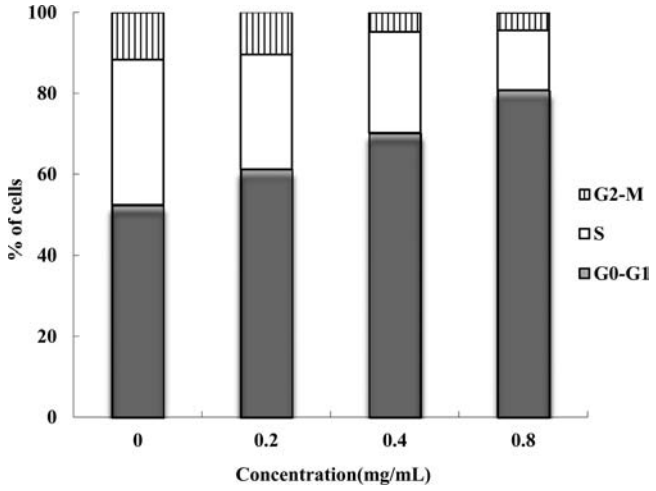

Figure 4. HT-29 cell cycle changes in response to LFWGE treatment (48 h). HT-29 cell cultures were treated with increasing doses of LFWGE as indicated on the right column, and cell cycle distribution was determined using flow cytometry after PI staining, and expressed as a percent of G_0/G_1, S, and G_2/M cycle phases. The DNA histograms show that LFWGE induced a dose-dependent decrease in the S cycle phase, whereas there was a significant expansion of the G_0/G_1 cycle phase consistent with an increase in the number of apoptotic HT-29 cell figures. Analysis by flow cytometry showed the distinct signals and cell frequencies associated with the arrested cell cycle status as described under the Results and Discussion section (n = 6).

DOI: 10.1021/acs.jafc.5b00041
J. Agric. Food Chem. 2015, 63, 2449−2457

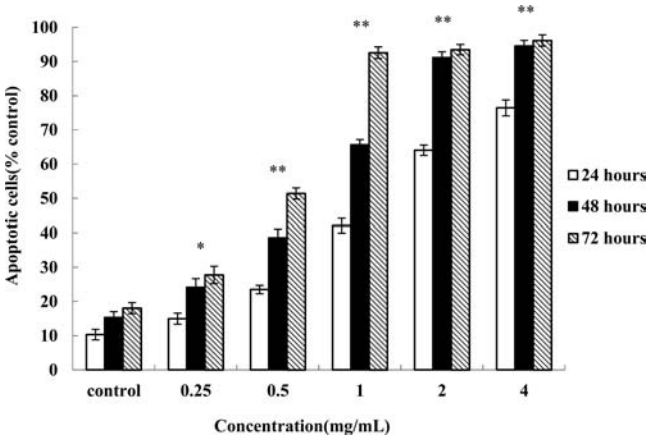

Figure 5. HT-29 cell apoptosis in response to LFWGE treatment. HT-29 cell cultures were treated with increasing doses of LFWGE as indicated on the *x* axis, and the number of apoptotic HT-29 cell was determined using flow cytometry after PI and annexin V staining. Mean ± SD $n = 3$, *, $p < 0.05$, **, $p < 0.01$.

and incubation time (Figure 5). The cells were double stained with annexin V-FITC and propidium iodide and analyzed by flow cytometry to examine the distribution of late and early apoptotic cells. The control cells demonstrated normal cell viability without significant cell apoptosis. In contrast, after treatment with 1 mg/mL of LFWGE, the portion of normal cells was only 2.6%, whereas the proportion of early apoptotic cells was 68.4% and that of late apoptotic cells was 28.9%. From these results, we found that LFWGE functions similarly to Avemar. It has been previously shown that Avemar treatment leads to an increase in apoptosis.[31,39] However, with regard to potency, the former is more effective than the latter.

Cell death in multicellular organisms exhibits two patterns: necrosis and apoptosis. Apoptosis is a process of programmed cell death characterized by various biochemical and morphological changes, including cell shrinkage, chromatin condensation, internucleosomal DNA fragmentation and the formation of "apoptotic bodies".[40] To further elucidate apoptotic cell death due to the exposure of HT-29 cells to LFWGE, the cells were stained with Hoechst dye 33342 and examined using a Leica DMR XA fluorescence microscope. As shown in Figure 6, the

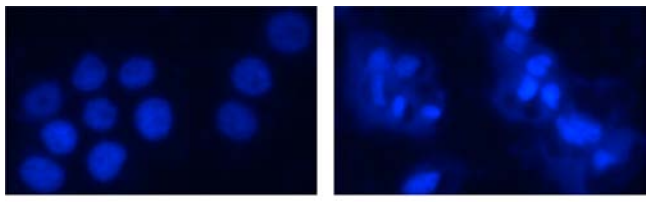

Figure 6. Effect of LFWGE treatment on the nuclear morphological changes of HT-29 cells: (a) control cells; (b) cells treated with 1 mg/mL LFWGE for 72 h. The medium was removed, and the cells were incubated with 5 μg/mL Hoechst for 15 min at room temperature in the dark. Stained solution was washed out, and cells were visualized under fluorescence microscopy (200×).

control cells exhibited intact and round-shaped nuclei characterized by a diffused chromatin structure (a). In contrast, exposure to 1 mg/mL of LFWGE for 72 h significantly altered the HT-29 cell morphology; that is, the nucleus exhibited condensed chromatin (b), which is characteristic of apoptotic cells. Moreover, combined with the cell cycle distribution, we found that the cell nuclei of early apoptotic cells were pycnoid or round-bead shaped, whereas those of late apoptotic cells appeared to have apoptotic bodies (Figure 7).

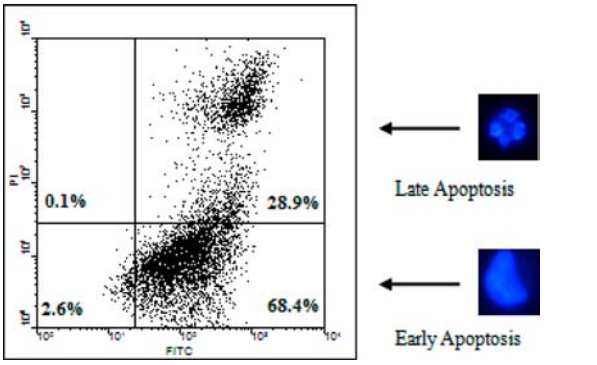

Figure 7. HT-29 cell early apoptosis and late apoptosis in response to LFWGE treatment using flow cytometry. HT-29 cell cultures were treated with 1 mg/mL LFWGE (72 h), and the formation of early apoptotic and late apoptotic HT-29 cell figures was determined using PI and Annexin V-FITC staining. The majority (68.4%, right bottom quadrant) of HT-29 cells exhibited early apoptosis as indicated by the limited nuclear fragmentation. Late apoptosis/necrosis was present in 28.9% (right upper quadrant) of HT-29 cells with advanced nuclear fragmentation and limited staining, while the frequency of normal cells dropped to 2.6% as observed in the left bottom quadrant of the flow cytometry screen ($n = 6$).

Role of Caspases in the Apoptotic Effect of LFWGE. Apoptosis is a well-controlled process involving a programmed set of cellular events partially mediated by caspases, which are the cysteine aspartate proteases involved in apoptosis that lead to the loss of cellular structure and function, phosphatidylserine exposure, and ultimately cell death.[41] Initiator caspases, such as caspases-2, -8, and -9, are closely linked to pro-apoptotic signals.[42] The effector caspases-3, -6, and -7 cleave cytoskeletal and nuclear proteins to induce apoptosis.[43,44] We therefore approached the question of caspases involvement in HT-29 cell processes by assaying the transcriptional regulation of caspases mRNA. The RNA purity was quantified by spectrophotometer with a OD260/280 ratio of 1.8 to 2.0 for all specimens. The RNA integrity was determined by 1% agarose gel electrophoresis, yielding two sharp ribosomal 18S and 28S bands. The expression of caspase-3, caspase-7, caspase-8, and caspase-9 was presented as $2^{-\Delta\Delta Ct}$. Caspase-3, caspase-7, caspase-8, and caspase-9 mRNA expression at 48 h after the addition of 0.4 and 0.8 mg/mL of LFWGE was detected by qPCR. Following the treatment of the HT-29 cells with increasing doses of LFWGE, the mRNA expression levels of caspase-3 ($F = 163.59$, $P = 0.000$), caspase-7 ($F = 504.491$, $P = 0.000$), caspase-8 ($F = 403.52$, $P = 0.000$) and caspase-9 ($F = 1465.930$, $P = 0.000$) significantly increased compared with the control group (Figure 8).

Caspase-3 is an executioner caspase activated by multiple pathways[45] that has been shown to increase with Avemar treatment.[32] The treatment of HT-29 cells with 0.4, 0.8, and 1.5 mg/mL of LFWGE for 48 h induced a dose-dependent activation of caspase-3. LFWGE induced a detectable increase in caspase-3 activity after 48 h of treatment, showing a 1.6-, 2.6-, and 4.08-fold increase, respectively (Figure 9). Therefore, growth inhibition and the induction of apoptosis in tumor

DOI: 10.1021/acs.jafc.5b00041
J. Agric. Food Chem. 2015, 63, 2449−2457

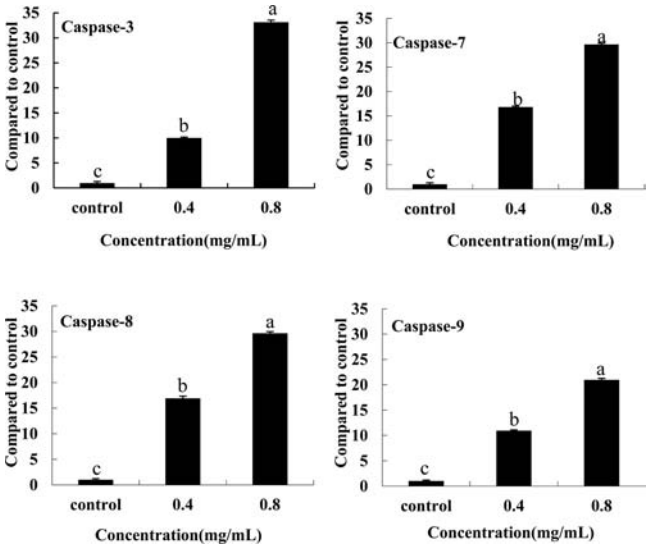

Figure 8. Caspase-3, caspase-8, caspase-9, and caspase-7 mRNA expression analysis following treatment of HT-29 cells with LFWGE (0.4 mg/mL, 0.8 mg/mL) for 48 h. The differences in expression after treatment with the various concentrations of LFWGE were calculated using the ANOVA method. $n = 6$.

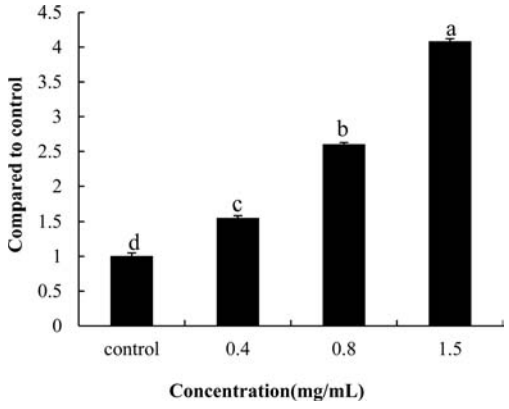

Figure 9. LFWGE activation of caspase-3 in HT-29 cells. HT-29 cells were treated in medium with 0.4, 0.8, and 1.5 mg/mL of LFWGE for 48 h, and then caspase-3 activity was estimated. Values are presented as the mean ± SD, and expressed as fold increase over the pre-treatment level (experimental/control). $n = 6$.

cells may be associated with the increased expression of caspases.

In conclusion, our findings confirm the value of LFWGE as a natural product with anticarcinogenic properties. LFWGE as a strong regulator is able to inhibit the growth of HT-29 cells and induce apoptosis in vitro. Further research is required to identify which components or which group of low molecular weight proteins are the most pronounced functional ingredients. In addition, the results indicate the possible involvement of a coordinated caspases response to induce apoptosis. On the basis of our data, LFWGE might warrant further investigation in the prevention or treatment of human colon cancer.

AUTHOR INFORMATION

Corresponding Author

*Phone: +86-511-88797202. Fax: +86-511-88780201. E-mail: ydong@mail.ujs.edu.cn.

Funding

This study was supported by the priority academic program development of Jiangsu Higher education institutions and the Industry-academic joint technological innovations funded project of Jiangsu province (BY2012172).

Notes

The authors declare no competing financial interest.

ACKNOWLEDGMENTS

We express our gratitude to Jiangsu University Analysis and Test Center for providing the technical assistance in flow cytometry analysis. We also would like to thank our colleagues in School of Food and Biological Engineering who provided assistance in this study.

ABBREVIATIONS USED

kd, kilodaltons; LFWGE, aqueous extract of fermented wheat germ with *Lactobacillus plantarum* dy-1; WGE, aqueous extract of raw wheat germ; SFWG, sourdough fermented wheat germ; YFWGE, yeast fermented wheat germ extract; SDS-PAGE, sodium dodecyl sulfate-polyacrylamide gel electrophoresis; PI, propidium iodide; MTT, 3-(4,5-dimethylthiazol-2-yl)-2,5-diphenyltetrazolium bromide; ANOVA, analysis of variance

REFERENCES

(1) Ploeg, M.; Aben, K.; Kiemeney, L. A. The present and future burden of urinary bladder cancer in the world. *World J. Urol.* **2009**, *27*, 289−293.

(2) Johanning, G. L.; Wang-Johanning, F. Efficacy of a medical nutriment in the treatment of cancer. *Altern. Ther. Health Med.* **2007**, *13*, 56−63.

(3) Olie, R. A.; Simoes-Wust, A. P.; Baumann, B.; Leech, S. H.; Fabbro, D.; Stahel, R. A.; Zangemeister-Wittke, U. A novel antisense oligonucleotide targeting survivin expression induces apoptosis and sensitizes lung cancer cells to chemotherapy. *Cancer Res.* **2000**, *60*, 2805−2809.

(4) Kim, J. M.; Kim, J. S.; Yoo, H.; Choung, M. G.; Sung, M. K. Effects of black soybean [glycine max (l.) merr.] seed coats and its anthocyanidins on colonic inflammation and cell proliferation in vitro and in vivo. *J. Agric. Food Chem.* **2008**, *56*, 8427−8433.

(5) Zou, Y. P.; Chang, S. Effect of black soybean extract on the suppression of the proliferation of human AGS gastric cancer cells via the induction of apoptosis. *J. Agric. Food Chem.* **2011**, *59*, 4597−4605.

(6) Liu, R. H. Potential synergy of phytochemicals in cancer prevention: mechanism of action. *J. Nutr.* **2004**, *134* (12 Suppl.), 3479S−3485S.

(7) Judson, P. L.; Al Sawah, E.; Marchion, D. C.; Xiong, Y.; Bicaku, E.; Zgheib, N. B.; Chon, H. S.; Stickles, X. B.; Hakam, A.; Wenham, R. M.; Apte, S. M.; Gonzalez-Bosquet, J.; Chen, D. T.; Lancaster, J. M. Characterizing the efficacy of fermented wheat germ extract against ovarian cancer and defining the genomic basis of its activity. *Int. J. Gynecol. Cancer* **2012**, *22*, 960−967.

(8) Duh, P.; Chen, Z.; Lee, S.; Lin, T.; Wang, Y.; Yen, W.; Kuo, L.; Chu, H. Antiproliferative activity and apoptosis induction of eucalyptus citriodora resin and its major bioactive compound in melanoma b16f10 cells. *J. Agric. Food Chem.* **2012**, *60*, 7866−7872.

(9) Brandolini, A.; Vidal, A. M. H. Wheat germ: Not only a by-product. *Int. J. Food Sci. Nutr.* **2012**, *63*, 71−74.

(10) Ge, Y. Q.; Sun, A. D.; Ni, Y. Y.; Cai, T. Y. Some nutritional and functional properties of defatted wheat germ protein. *J. Agric. Food Chem.* **2000**, *48*, 6215−6218.

(11) Eisenmenger, M.; Dunford, N. T. Bioactive components of commercial and supercritical carbon dioxide processed wheat germ oil. *J. Am. Oil Chem. Soc.* **2008**, *85*, 55−61.

DOI: 10.1021/acs.jafc.5b00041
J. Agric. Food Chem. 2015, 63, 2449−2457

(12) Gnanasambandam, R.; Zayas, J. F. Quality characteristics of meat batters and frankfurters containing wheat germ protein flour. *J. Food Qual.* **1994**, *1*, 129−142.
(13) Hassan, H. M. M.; Afify, A. S.; Basyiony, A. E.; Ahmed, G. T. Nutritional and functional properties of defatted wheat protein isolates. *Aust. J. Basic Appl. Sci.* **2010**, *4*, 348−358.
(14) Ge, Y. Q.; Sun, A. D.; Ni, Y. Y.; Cai, T. Y. Study and development of a defatted wheat germ nutritive noodle. *Eur. Food Res. Technol.* **2001**, *212*, 344−348.
(15) Arshad, M. U.; Anjum, F. M.; Zahoor, T. Nutritional assessment of cookies supplemented with defatted wheat germ. *Food Chem.* **2007**, *102*, 123−128.
(16) Bansal, S.; Sudha, M. L. Nutritional, microstructural, rheological and quality characteristics of biscuits using processed wheat germ. *Int. J. Food Sci. Nutr.* **2011**, *62*, 474−479.
(17) Xu, B.; Zhou, S. L.; Miao, W. J.; Gao, C.; Cai, M. J.; Dong, Y. Study on the stabilization effect of continuous microwave on wheat germ. *J. Food Eng.* **2013**, *117*, 1−7.
(18) Rizzello, C. G.; Nionelli, L.; Coda, R.; De Angelis, M.; Gobbetti, M. Effect of sourdough fermentation on stabilisation, and chemical and nutritional characteristics of wheat germ. *Food Chem.* **2010**, *119*, 1079−1089.
(19) Poutanen, K.; Flander, L.; Katina, K. Sourdough and cereal fermentation in a nutritional perspective. *Food Microbiol.* **2009**, *26*, 693−699.
(20) Rathore, S.; Salmeron, I.; Pandiella, S. S. Production of potentially probiotic beverages using single and mixed cereal substrates fermented with lactic acid bacteria cultures. *Food Microbiol.* **2012**, *30*, 239−244.
(21) Arrigoni, E.; Jorger, F.; Kolloffel, B.; Roulet, I.; Herensperger, M.; Meile, L.; Amado, R. In vitro fermentability of a commercial wheat germ preparation and its impact on the growth of bifidobacteria. *Food Res. Int.* **2002**, *35*, 475−481.
(22) Rizzello, C. G.; Nionelli, L.; Coda, R.; Di Cagno, R.; Gobbetti, M. Use of sourdough fermented wheat germ for enhancing the nutritional, texture and sensory characteristics of the white bread. *Eur. Food Res. Technol.* **2010**, *230*, 645−654.
(23) Rizzello, C. G.; Cassone, A.; Coda, R.; Gobbetti, M. Antifungal activity of sourdough fermented wheat germ used as an ingredient for bread making. *Food Chem.* **2011**, *127*, 952−959.
(24) Telekes, A.; Resetar, A.; Balint, G.; Blazso, G.; Falkay, G.; Lapis, K.; Raso, E.; Szende, B.; Ehrenfeld, M.; Shoenfeld, Y.; Hidvegi, M. Fermented wheat germ extract (avemar) inhibits adjuvant arthritis. *Autoimmunity, Pt B: Novel Applications of Basic Research* **2007**, *1110*, 348−361.
(25) Mueller, T.; Jordan, K.; Voigt, W. Promising cytotoxic activity profile of fermented wheat germ extract (avemar (r)) in human cancer cell lines. *J. Exp. Clin. Cancer Res.* **2011**, *30*, 42−48.
(26) Mueller, T.; Voigt, W. Fermented wheat germ extract - nutritional supplement or anticancer drug? *Nutr. J.* **2011**, *10*, 89−94.
(27) Telekes, A.; Hegedus, M.; Chae, C. H.; Vekey, K. Avemar (wheat germ extract) in cancer prevention and treatment. *Nutr. Cancer* **2009**, *61*, 891−899.
(28) Hidvegi, M.; Raso, E.; Tomoskozi, F. R.; Lapis, K.; Szende, B. Effect of MSC on the immune response of mice. *Immunopharmacology* **1999**, *41*, 183−186.
(29) Tuscano, J.; Lau, D.; O'Donnell, R.; Ma, Y. P. Fermented wheat germ proteins (FWGP) for the treatment of cancer. WO patent 135580A2, 2010.
(30) Rizzello, C. G.; Mueller, T.; Coda, R.; Reipsch, F.; Nionelli, L.; Curiel, J. A.; Gobbetti, M. Synthesis of 2-methoxy benzoquinone and 2,6-dimethoxybenzoquinone by selected lactic acid bacteria during sourdough fermentation of wheat germ. *Microb. Cell Fact.* **2013**, *12*, 105−113.
(31) AACC. *Approved Methods of the American Association of Cereal Chemistry*, 10th ed.; AACC: Eagon, Minnesota, 2002.
(32) Kim, M. H.; Jo, S. H.; Ha, K. S.; Song, J. H.; Jang, H. D.; Kwon, Y. I. Antimicrobial activities of 1, 4-benzoquinones and wheat germ extract. *J. Microbiol. Biotechnol.* **2010**, *20*, 1204−1209.
(33) Heimler, D.; Vignolini, P.; Isolani, L.; Arfaioli, P.; Ghiselli, L.; Romani, A. Polyphenol content of modern and old varieties of triticum aestivum l. and t. durum desf. grains in two years of production. *J. Agric. Food Chem.* **2010**, *58*, 7329−7334.
(34) Shang, D.; Zhang, J.; Wen, L.; Li, Y.; Cui, Q. Preparation, characterization, and antiproliferative activities of the Se-containing polysaccharide SeGLP-2B-1 from Se-enriched Ganoderma lucidum. *J. Agric. Food Chem.* **2009**, *57*, 7737−7742.
(35) Zha, X. Q.; Xiao, J. J.; Zhang, H. N.; Wang, J. H.; Pan, L. H.; Yang, X. F.; Luo, J. P. Polysaccharides in Laminaria japonica (LP): Extraction, physicochemical properties and their hypolipidemic activities in diet-induced mouse model of atherosclerosis. *Food Chem.* **2012**, *134*, 244−252.
(36) Livak, K. J.; Schmittgen, T. D. Analysis of relative gene expression data using real-time quantitative PCR and the 2-ΔΔCT method. *Methods* **2001**, *25*, 402−408.
(37) Yoo, J. G.; Kim, M. D. Production of 2-methoxy-1,4-benzoquinone (2-MBQ) and 2,6-dimethoxy-1,4-benzoquinone (2,6-DMBQ) from wheat germ using lactic acid bacteria and yeast. *Food Eng. Prog.* **2010**, *14*, 292−298.
(38) Comin-Anduix, B.; Boros, L. G.; Marin, S.; Boren, J.; Callol-Massot, C.; Centelles, J. J.; Torres, J. L.; Agell, N.; Bassilian, S.; Cascante, M. Fermented wheat germ extract inhibits glycolysis/pentose cycle enzymes and induces apoptosis through poly (ADP-ribose) polymerase activation in Jurkat T-cell leukemia tumor cells. *J. Biol. Chem.* **2002**, *277*, 46408−46414.
(39) Illmer, C.; Madlener, S.; Horvath, Z.; Saiko, P.; Losert, A.; Herbacek, I.; Grusch, M.; Krupitza, G.; Fritzer-Szekeres, M.; Szekeres, T. Immunologic and biochemical effects of the fermented wheat germ extract Avemar. *Exp. Biol. Med.* **2005**, *230*, 144−149.
(40) Wyllie, A. H.; Kerr, J. F.; Currie, A. R. Cell death: The significance of apoptosis. *Int. Rev. Cytol.* **1980**, *68*, 251−306.
(41) Shi, Y. G. Mechanisms of caspase activation and inhibition during apoptosis. *Mol. Cell* **2002**, *9*, 459−470.
(42) Matsui, T.; Ramasamy, K.; Ingelsson, M.; Fukumoto, H.; Conrad, C.; Frosch, M. P.; Irizarry, M. C.; Yuan, J.; Hyman, B. T. Coordinated expression of caspase 8, 3 and 7 mRNA in temporal cortex of Alzheimer disease: relationship to formic acid extractable abeta42 levels. *J. Neuropathol Exp. Neurol.* **2006**, *65*, 508−515.
(43) Degterev, A.; Boyce, M.; Yuan, J. Y. A decade of caspases. *Oncogene* **2003**, *22*, 8543−8567.
(44) Ashkenazi, A.; Dixit, V. M. Death receptors: Signaling and modulation. *Science* **1998**, *281*, 1305−1308.
(45) Stennicke, H. R.; Jurgensmeier, J. M.; Shin, H.; Deveraux, Q.; Wolf, B. B.; Yang, X.; Zhou, Q.; Ellerby, H. M.; Ellerby, L. M.; Bredesen, D.; Green, D. R.; Reed, J. C.; Froelich, C. J.; Salvesen, G. S. Pro-caspase-3 is a major physiologic target of caspase-8. *J. Biol. Chem.* **1998**, *273*, 27084−27090.

DOI: 10.1021/acs.jafc.5b00041
J. Agric. Food Chem. 2015, 63, 2449−2457

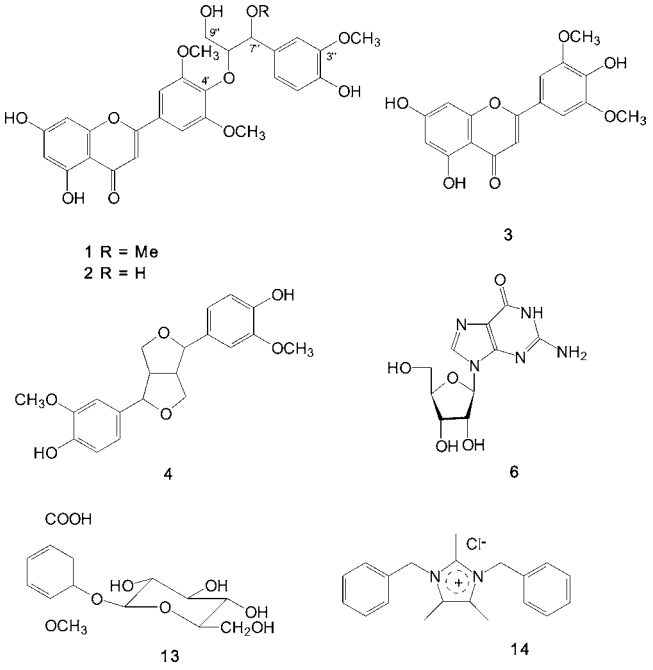

Figure 1. Structures of compounds **1**–**4**, **6**, **13**, and **14**.

acetonitrile and increased to 95% acetonitrile over 40 min and then increased to 100% acetonitrile over 5 min. At the end of the run, 100% of acetonitrile was allowed to flush the column for 5 min, and an additional 10 min of post run time was set to allow for equilibration of the column with the starting eluant. The UV detector was set at 280 nm wavelength, and the column temperature was ambient.

Plant Material. The roots of maca, *L. meyenii*, were collected from the Andean mountains of Peru. The species was identified using a HPLC method by comparison with an authentic sample. A voucher specimen (MA10205) was deposited in the Herbarium of Naturex, Inc.

Extraction and Isolation of *L. meyenii* Constituents. Two different extracts were prepared before isolation. The first extraction was carried out with 20 kg of maca root powder, which was extracted by H_2O three times (50 L × 3) at room temperature. The extract was concentrated (4.3 kg) and chromatographed on the column of CG 161 resin (Rohm and Haas, Philadelphia, PA, USA) (27 L, 26 cm × 180 cm), eluting with a H_2O/EtOH (1:0, 9:1, 3:1, 2:1, 1:1, 0:1) solvent system. A volume of 3 L was used in each step, and 1 L was collected as one fraction (named I fractions). The 90% H_2O/EtOH eluates (I 4–6, 78 g) were column chromatographed (CC) on an FPX 66 (Rohm and Haas, Inc.) (2.0 L, 12 cm × 50 cm) and eluted with H_2O/EtOH (1:0, 9:1, 3:1, 2:1, 1:3, 0:1) solvent system. Four liters of solvent was used in each step, and 1.0 L was collected as a fraction (named II fractions). A total of 24 fractions were collected and concentrated. These fractions were separately and repeatedly subjected to CC over MCI GEL CHP-20P (Mitsubishi Kasei Co.) and/or Sephadex LH-20

Table 1. ^{1}H and ^{13}C NMR and HMBC Data for 1 and 2 (CD_3OD)[a]

1				2			
no.	δ_H	δ_C	HMBC (H to C)	no.	δ_H	δ_C	HMBC (H to C)
1				1			
2		165.0 s		2		165.0 s	
3	6.57 s	105.6 d	2, 4, 10, 1′ ROE: 2′, 6′	3	6.56 s	105.6 d	2, 4, 10, 1′ ROE: 2′, 6′
4		183.6 s		4		183.7 s	
5		163.0 s		5		163.1 s	
6	6.13 s	100.2 d	5, 7, 8, 10	6	6.12 s	100.2 d	5, 8, 10, 9″
7		166.0 s		7		166.1 s	
8	6.39 s	95.2 d	7, 9, 10	8	6.36 s	95.2 d	3, 4, 7, 9, 10, 9″
9		159.2 s		9		159.2 s	
10		105.5 s		10		105.4 s	
1′		127.4 s		1′		127.5 s	
2′	7.06 s	104.7 d	2, 1′, 3′, 4′, 6′	2′	7.07 s	104.8 d	2, 1′, 3′, 4′, 6′
3′		154.6 s		3′		154.7 s	
4′		140.2 s		4′		140.4 s	
5′		154.6 s		5′		154.7 s	
6′	7.06 s	104.7 d	2, 1′, 2′, 4′, 5′	6′	7.07 s	104.8 d	2, 1′, 2′, 4′, 5′
3′,5′-OCH_3	3.83 s	56.7 q	3′ or 5′ ROE: 2′, 6′	3′,5′-OCH_3	3.85 s	56.8 q	3′ or 5′ ROE: 2′, 6′, 7″, 8″
1″		131.0 s		1″		133.7 s	
2″	6.89 br s	112.0 d	3″, 4″, 6″	2″	6.97 d (1.6)	111.5 d	3″, 4″, 6″, 7″
3″		148.8		3″		148.6 s	
4″		147.2		4″		146.9	
5″	6.75 br s	115.6 d	1″, 2″, 3″	5″	6.72 d (8.0)	115.6 d	
6″	6.80 m	122.0	1″, 3″, 4″, 7″	6″	6.79 dd (8.0, 1.6)	120.8 d	1″, 2″, 3″, 4″, 7″
7″	4.46 d (6.0) *threo* form	83.7 d	1″, 2″, 6″, 8″, 9″, 7″-OCH_3	7″	4.91 d (4.4) *erythro* form	74.2 d	2″, 6″, 8″, 7″-OCH_3
8″	4.43 m	86.6 d		8″	4.41m	87.5 d	
9″	3.92 dd (12.0, 4.4) 3.73 dd (12.0, 3.2)	61.7 t		9″	3.89 dd (12.0, 4.4) 3.65 dd (12.0, 3.2)	61.9 t	
3″-OCH_3	3.81 s	56.3 q	3″ ROE: 2″	3″-OCH_3	3.80 s	56.4 q	3″ ROE: 2″
7″-OCH_3	3.89 s	56.8 q					

[a]Carbon multiplicities were determined by DEPT experiments (s, C; d, CH; t, CH_2; q, CH_3); figures in parentheses denote *J* values (hertz).

DOI: 10.1021/acs.jafc.5b00219
J. Agric. Food Chem. 2015, 63, 2458–2463

(Sigma Chemical Co., St. Louis, MO, USA) (100 mL, 2.5 cm × 40 cm) and eluted with a gradient H_2O/MeOH solvent system to yield **6** (33 mg from fractions II 5−6, t_R = 6.0 min in HPLC), **7** (35 mg from fractions II 5−6, t_R = 9.8 min), **8** (27 mg from fractions II 7−9, t_R = 10.3 min), **12** (25 mg from fractions II 10−12, t_R = 13.8 min), and **13** (5 mg from fractions II 5−6, t_R = 6.2 min). The 75% H_2O/EtOH fractions (I 7−9, 22g) from CG 161 resin were CC on FPX 66 using the same condition as described above and produced III serial fractions. These fractions were separately and repeatedly subjected to CC over MCI GEL CHP-20P and/or Sephadex LH-20 using gradient H_2O/MeOH to yield **9** (16 mg from fractions III 10−11, t_R = 12.0 min), **10** (156 mg from fractions III 8−9, t_R = 17.7 min), and **11** (162 mg from fractions III 12−14, t_R = 10.8 min). The second extraction was performed using 120 kg of maca roots. The air-dried root powder was extracted with H_2O twice (800 L × 2) at room temperature. After the H_2O extract was drained, the remaining roots were extracted with 95% EtOH three times (800 L × 3). The EtOH solutions were combined and concentrated under reduced pressure to yield ethanol extract (6.1 kg), which was suspended in H_2O and successively partitioned with hexane and EtOAc (10 L × 3). The EtOAc phase was concentrated (528 g) and CC on silica gel (2.5 kg, 12 cm × 50 cm), using a step gradient solvent system of hexane/acetone (10:1, 5:1, 2:1, 1:1, 0:1). In each step, 5 L of solvent was used and 1 L was collected as a fraction. Factions 12−18 were combined and concentrated (23 g) and were CC on polyamide resin (Sigma Chemical Co., St. Louis, MO, USA) (500 mL, 3.5 cm × 60 cm) using a H_2O/EtOH as solvent system (1:0, 10:1, 5:1, 3:1, 2:1, 1:1, 1:2, 0:1). A total of 1.5 L was used in each step, and 0.5 L was collected as one fraction (named IV fractions). These fractions were further CC over MCI GEL CHP-20P and/or Sephadex LH-20 and eluted with a gradient H_2O/MeOH system to yield **1** (21 mg from fractions IV 13−15, t_R = 28.0 min), **2** (17 mg from fractions IV 9−12, t_R = 25.1 min), **3** (2 mg from fractions IV 9−12, t_R = 28.5 min), **4** (3 mg from fractions IV 9−12, t_R = 13.9 min), and **5** (5 mg from fractions IV 16−19, t_R = 19.5 min).

NMR and ESI-MS of Flavonoids. *Tricin 4′-O-[threo- β-guaiacyl-(7″-O-methyl)-glyceryl] ether (**1**):* yellow amorphous powder; $C_{28}H_{28}O_{11}$; $[\alpha]_D^{25}$ −0.9° (*c* 1.00, MeOH); UV (MeOH) λ_{max} (log ε) 215, 272, 340 nm; IR (amorphous powder) ν_{max} 3316, 1595, 1419, 1182, 1025 cm^{-1}; ^1H and ^{13}C NMR data, see Table 1; HRESIMS *m*/*z* 541.1647 $[M + H]^+$ (calculated for $C_{28}H_{29}O_{11}$, 541.1639).

*Tricin 4′-O-(erythro-β-guaiacyl-glyceryl) ether (**2**):* yellow amorphous powder; $C_{27}H_{26}O_{11}$; $[\alpha]_D^{25}$ −0.9° (*c* 0.90, MeOH); UV (MeOH) λ_{max} (log ε) 205, 270, 338 nm; ^1H and ^{13}C NMR data, see Table 1; HRESIMS *m*/*z* 527.1553 $[M + H]^+$ (calculated for $C_{27}H_{27}O_{11}$, 527.1542).

*Tricin (**3**):* yellow amorphous powder; $C_{17}H_{14}O_7$; ^1H NMR (400 MHz, CD_3OD) δ 6.42 (1H, s, H-3), 6.18 (1H, d, *J* = 2.0 Hz, H-8), 5.98 (1H, d, *J* = 2.0 Hz, H-6), 7.18 (2H, s, H-2′ and 6′H), 3.91 (6H, s, 3′ and 5′-OCH_3); ^{13}C NMR (100 MHz, CD_3OD) δ 166.1 (C-2), 104.3 (C-3), 183.7 (C-4), 163.1 (C-5), 100.2 (C-6), 165.8 (C-7), 95.2 (C-8), 159.3 (C-9), 104.5 (C-10), 122.5 (C-1′), 105.0 (C-2′ and 6′), 149.5 (C-3′ and 5′), 141.0 (C-4′), 56.8 (C-3′ and 5′-OCH_3); HRESIMS *m*/*z* 331.0811 $[M + H]^+$ (calculated for $C_{17}H_{15}O_7$, 331.0818).

*Pinoresinol (**4**):* white amorphous powder; $C_{20}H_{22}O_6$; ^1H NMR (400 MHz, CD_3OD) δ 6.93 (2H, d, *J* = 1.2 Hz, H-2 $ 2′), 6.75 (2H, d, *J* = 8.0 Hz, H-5 and 5′), 6.80 (2H, dd, *J* = 8.0, 2.0 Hz, H-6 and 6′), 4.69 (2H, d, *J* = 4.4 Hz, H-7 and 7′), 3.12 (2H, dd, *J* = 6.4, 4.4 Hz, H-8 and 8′), 4.21 (2H, dd, *J* = 8.8, 6.8 Hz, H-9 and 9′), 3.81 (2H, dd, *J* = 8.8, 5.2 Hz, H-9 and 9′), 3.84 (6H, s, 3′ and 3″-OCH_3); ^{13}C NMR (100 MHz, CD_3OD) δ 133.7 (C-1 and 1′), 110.9 (C-2 and 2′), 149.1 (C-3 and 3′), 147.3 (C-4 and 4′), 116.0 (C-5 and 5′), 120.0 (C-6 and 6′), 87.5 (C-7 and 7′), 55.3 (C-8 and 8′), 72.6 (C-9 and 9′), 56.3 (C-3′ and 3″-OCH_3); HRESIMS *m*/*z* 359.1489 $[M + H]^+$ (calculated for $C_{20}H_{23}O_6$, 359.1495).

*4-Hydroxycinnamic acid (**5**):* white powder; $C_9H_8O_3$; ^1H NMR (400 MHz, CD_3OD) δ 7.40 (2H, d, *J* = 8.8 Hz, H-2 and 6), 6.76 (2H, d, *J* = 8.8 Hz, H-3 and 5), 7.56 (1H, d, *J* = 16.4 Hz, H-7), 6.24 (1H, d, *J* = 16.4 Hz, H-8); ^{13}C NMR (100 MHz, CD_3OD) δ 127.1 (C-1), 131.1 (C-2 and 6), 116.8 (C-3 and 5), 161.1 (C-4), 146.6 (C-7), 115.5 (C-8), 171.1 (C-9); ESI-MS (negative) *m*/*z* 163 $[M - H]^-$, $C_9H_7O_3$.

*Guanosine (**6**):* white powder; $C_{10}H_{13}N_5O_5$; ^1H NMR (400 MHz, DMSO-d_6) δ 7.93 (1H, s, H-8), 5.67 (H, d, *J* = 4.4 Hz, H-1′), 4.39 (1H, br s, H-2′), 4.07 (1H, br s, H-3′), 3.84 (1H, br s, H-4′), 3.69 (1H, d, *J* = 11.2 Hz, H-5′a), 3.51 (1H, d, *J* = 11.2 Hz, H-5′b); ^{13}C NMR (100 MHz, DMSO-d_6) δ 157.0 (C-1), 116.4 (C-2), 151.4 (C-3), 153.5 (C-5), 136.0 (C-8), 86.4 (C-1′), 73.6 (C-2′), 70.3 (C-3′), 85.2 (C-4′), 61.8 (C-5′); ESI-MS (positive) *m*/*z* 284 $[M + H]^+$, $C_{10}H_{14}N_5O_5$.

*Glucotropaeolin (**7**):* white powder; $C_{14}H_{18}NO_9S_2K$; ^1H NMR (400 MHz, CD_3OD) δ 7.38 (2H, d, *J* = 7.6 Hz, H-2 and 6), 7.32 (2H, dd, *J* = 7.6, 0.8 Hz, H-3 and 5), 7.22 (1H, t, *J* = 7.2 Hz, H-4), 4.45 (H, d, *J* = 9.2 Hz, H-7a), 4.22 (H, d, *J* = 9.2 Hz, H-7b), 4.63 (H, br s, H-1′), 4.03 (H, d, *J* = 16.0 Hz, H-6′a), 3.82 (H, d, *J* = 16.0 Hz, H-6′b), 3.57 (H, dd, *J* = 10.0, 2.4 Hz, H-4′), 3.07−3.23 (3H, m, H-2′, 3′, and 5′); ^{13}C NMR (100 MHz, CD_3OD) δ 137.4 (C-1), 129.3 (C-2 and 6), 129.9 (C-3 and 5), 128.2 (C-4), 39.6 (C-7), 160.7 (C-8), 82.8 (C-1′), 74.1 (C-2′), 79.3 (C-3′), 71.1 (C-4′), 82.2 (C-5′), 62.7 (C-6′); ESI-MS (negative) *m*/*z* 408 $[M - H]^-$, $C_{14}H_{17}NO_9S_2$.

*Desulfoglucotropaeolin (**8**):* white powder; $C_{14}H_{19}NO_6S$; ^1H NMR (400 MHz, CD_3OD) δ 7.30 (2H, overlapped, H-2 and 6), 7.27 (2H, overlapped, H-3 and 5), 7.20 (1H, overlapped, H-4); ^{13}C NMR (100 MHz, CD_3OD) δ 138.0 (C-1), 128.8 (C-2 and 6), 129.4 (C-3 and 5), 127.6 (C-4), 39.0 (C-7), 153.4 (C-8), 82.1 (C-1′), 74.0 (C-2′), 79.0 (C-3′), 70.8 (C-4′), 81.7 (C-5′), 62.3 (C-6′); ESI-MS (negative) *m*/*z* 328 $[M - H]^-$, $C_{14}H_{18}NO_6S$.

*3-Hydroxybenzylisothiocyanate (**9**):* white powder; C_8H_7NOS; ^1H NMR (400 MHz, CD_3OD) δ 6.72 (1H, s, H-2), 6.64 (1H, dd, *J* = 8.0, 2.8 Hz, H-4), 7.09 (1H, t, *J* = 8.0 Hz, H-5), 6.73 (H, dd, *J* = 8.0, 2.8 Hz, H-6), 3.40 (2H, s, H-7); ^{13}C NMR (100 MHz, CD_3OD) δ 138.2 (C-1), 117.0 (C-2), 158.6 (C-3), 114.8 (C-4), 130.5 (C-5), 121.3 (C-6), 43.4 (C-7), 177.1 (C-8); ESI-MS (negative) *m*/*z* 163 $[M - H]^-$, C_8H_6NOS.

*Malic acid benzoate (**10**):* white powder; $C_{11}H_{10}O_6$; ^1H NMR (400 MHz, CD_3OD) δ 7.97 (2H, d, *J* = 8.0 Hz, H-2 and 6), 7.56 (2H, t, *J* = 7.2 Hz, H-3 and 5), 7.41 (1H, m, H-4), 5.61 (1H, dd, *J* = 7.2, 4.8 Hz, H-2′), 3.01 (2H, t, *J* = 4.0 Hz, H-3′); ^{13}C NMR (100 MHz, CD_3OD) δ 130.2 (C-1), 130.6 (C-2 and 6), 134.7 (C-3 and 5), 129.5 (C-4), 167.1 (C-7), 173.1 (C-1′), 70.3 (C-2′), 36.9 (C-3′), 172.4 (C-4′); ESI-MS (negative) *m*/*z* 237 $[M - H]^-$, $C_{11}H_9O_6$.

*5-(Hydroxymethyl)furfural (**11**):* colorless oil; $C_6H_6O_3$; ^1H NMR (400 MHz, CD_3OD) δ 9.52 (1H, s, H-6), 7.38 (1H, d, *J* = 3.6 Hz, H-2), 6.57 (1H, d, *J* = 3.6 Hz, H-2), 4.60 (2H, s, H-5); ^{13}C NMR (100 MHz, CD_3OD) δ 153.8 (C-1), 124.9 (C-2), 110.9 (C-3), 163.1 (C-4), 57.6 (C-5); ESI-MS (negative) *m*/*z* 125 $[M - H]^-$, $C_6H_5O_3$.

*D-Phenylalanine (**12**):* white powder; $C_9H_{10}NO_2$; ^1H NMR (400 MHz, CD_3OD) δ 7.33 (5H, m, H-2, 3, 4, 5, and 6), 3.26 (H, dd, *J* = 15.2, 5.2 Hz, H-7a), 3.03 (H, dd, *J* = 15.2, 8.8 Hz, H-7b), 3.85 (1H, dd, *J* = 8.8, 5.2 Hz, H-8); ^{13}C NMR (100 MHz, CD_3OD) δ 135.6 (C-1), 130.0 (C-2 and 6), 130.4 (C-3 and 5), 128.7 (C-4), 37.2 (C-7), 55.5 (C-8), 171.8 (C-9); ESI-MS (negative) *m*/*z* 164 $[M - H]^-$, $C_9H_{10}NO_2$.

*Vanillic acid 4-O-β-D-glucoside (**13**):* white powder; $C_{14}H_{18}O_9$; ^1H NMR (400 MHz, CD_3OD) δ 7.56 (1H, s, H-2), 7.16 (1H, d, *J* = 8.0 Hz, H-5), 7.60 (1H, d, *J* = 8.0 Hz, H-6), 3.86 (3H, s, 3-OCH_3), 5.00 (H, d, *J* = 7.2 Hz, H-1′), 3.52 (1H, m, H-2′), 3.40 (1H, m, H-3′), 3.48 (1H, m, H-4′), 3.45 (1H, m, H-5′), 3.89 (1H, m, H-6′a), 3.67 (1H, dd, *J* = 12.0, 4.8 Hz, H-6′b); ^{13}C NMR (100 MHz, CD_3OD) δ 126.1 (C-1), 114.1 (C-2), 150.1 (C-3), 151.8 (C-4), 116.1 (C-5), 124.7 (C-6), 169.7 (C-7), 56.6 (3-OCH_3), 101.8 (C-1′), 74.6 (C-2′), 77.7 (C-3′), 71.1 (C-4′), 78.2 (C-5′), 62.3 (C-6′); ESI-MS (negative) *m*/*z* 329 $[M - H]^-$, $C_{14}H_{17}O_9$.

Cell Culture and Chemicals. The COLO 205 cell lines were isolated from human colon adenocarcinoma (ATCC CCL-222). Human promyelocytic leukemia (HL-60) cells were obtained from American Type Culture Collection (Rockville, MD, USA). The human HepG2 hepatocellular carcinoma cell lines (BCRC 60025) were obtained from the Food Industry Research and Development Institute (Hsinchu, Taiwan). COLO 205 and HL-60 cell lines were grown at 37 °C in 5% CO_2 atmosphere in RPMI. Hep G2 cells were grown in

DOI: 10.1021/acs.jafc.5b00219
J. Agric. Food Chem. 2015, 63, 2458−2463

Dulbecco's minimal essential medium (DMEM) supplemented with 10% heat-inactivated fetal calf serum (Gibco BRL, Grand Island, NY, USA), 100 units/mL of penicillin, and 100 μg/mL of streptomycin and kept at 37 °C in a humidified atmosphere of 5% CO_2 in air. Selected compounds were dissolved in dimethyl sulfoxide (DMSO). Propidium iodide was obtained from Sigma Chemical Co. (St. Louis, MO, USA).

Determination of Cell Viability. Cell viability was assayed by 3-(4,5-dimethylthiazol-2-yl)-2,5-diphenyltetrazolium bromide (MTT) assay.[15] Briefly, human cancer cells were plated at a density of 1×10^5 cells/mL into 24-well plates. After overnight growth, cells were pretreated with various concentrations of test compounds for 24 h. The final concentration of dimethyl sulfoxide (DMSO) in the culture medium was <0.05%.[27,29] At the end of treatment, 30 μL of MTT was added, and the cells were incubated for a further 4 h. Cell viability was determined by scanning with an enzyme-linked immunosorbent assay reader with a 570 nm filter.

Nitrite Assay. The RAW 264.7 cells are treated with selected compounds and LPS or LPS alone. The supernatants are harvested, and the amount of nitrite, an indicator of NO synthesis, is measured by use of the Griess reaction. Briefly, supernatants (100 μL) are mixed with the same volume of Griess reagent (1% sulfanilamide in 5% phosphoric acid and 0.1% naphthylethylenediamine dihydrochloride in water) in duplicate on 96-well plates. After incubation at room temperature for 10 min, absorbance at 570 nm is measured with an ELISA reader (Thermo Labsystems Multiskan Ascent, Kaikki Oikeudet, Finland).

RESULTS AND DISCUSSION

The air-dried roots of *L. meyenii* were extracted with H_2O and subsequently with 95% EtOH to provide two extracts. The separation was conducted by using a combination of column chromatography on CG 161, FPX 66, silica gel, MCI GEL CHP-20P, and Sephadex LH-20, and a total of 13 compounds were isolated from the two extracts, including two flavonolignans, tricin 4′-*O*-[*threo*-β-guaiacyl-(7″-*O*-methyl)-glyceryl] ether (**1**)[36] and tricin 4′-*O*-(*erythro*-β-guaiacyl-glyceryl) ether (**2**),[35] and one flavonoid, tricin (**3**),[28] together with pinoresinol (**4**),[17] 4-hydroxycinnamic acid (**5**), guanosine (**6**), glucotropaeolin (**7**),[25,30] desulfoglucotropaeolin (**8**),[31] 3-hydroxybenzylisothiocyanate (**9**),[25,32] malic acid benzoate (**10**),[25] 5-(hydroxymethyl)furfural (**11**), D-phenylalanine (**12**), and vanillic acid 4-*O*-β-D-glucopyranoside (**13**).[33] Compounds **1**−**3**, **5**, **6**, **8**, **9**, **11**, and **13** were for the first time isolated from this plant. All of the structures were established by spectroscopic methods, including ^{1}H, ^{13}C NMR, DEPT, 2D correlation spectroscopy, MS, HRESIMS, and chemical properties. The known compounds were identified by NMR data compared with those reported in the literature. Compounds **7**, **8**, **11**, and **12** were identified by direct comparison with commercial standards.

Compound **1** was obtained as a yellow amorphous powder. Its molecular formula, $C_{28}H_{28}O_{11}$, was established on the basis of HRESIMS (*m*/*z* 541.1742 $[M + H]^+$, calcd for $C_{28}H_{29}O_{11}$, 541.1710). The IR spectrum showed the OH absorption (3316 cm^{-1}) and aromatic rings (1615, 1595 cm^{-1}). The UV spectrum of **1** exhibited maximum absorptions at 215, 272, and 340 nm, typical for a flavone derivative. The ^{13}C NMR spectrum revealed the presence of 28 carbon signals, including a conjugated ketonic carbon (δ 183.6), 20 aromatic or olefinic (δ 95.2−166.0), 4 methoxy (δ 56.3, 56.7, 56.7, and 56.8), 2 oxygenated methine (δ 86.6 and 83.7), and 1 oxygenated methylene carbon signals (δ 61.7). These signals correspond to a methoxy and one phenylpropanoid-substituted flavonoid of **1**. The ^{1}H NMR spectrum contained signals of a 3′,4′,5′-trihydroxy substituted B-ring at δ 7.06 (2H, s, H-2′, 6′), and it was confirmed by the observed long-range correlations of H-2′ (6′) with C-2 (δ 165.0), C-1′ (δ 127.4), C-3′ (5′) (δ 154.6), C-4′ (δ 140.2), and C-6′ (2′) (δ 104.7) in the gHMBC spectrum. The signal at δ 6.57 (1H, s, H-3) was assigned to H-3 on the basis of its long-range correlations with C-2, C-4 (δ 183.6), C-10 (δ 105.5), and C-1′ in the gHMBC spectrum, as well as NOE correlation of H-3 with H-2′ (6′) in the ROESY spectrum. Two broad singlets at δ 6.39 and 6.13 were assigned to be H-8 and H-6, respectively, in the 5,7-dihydroxy-substituted A-ring. The assignments were confirmed by the long-range correlations of H-8 with C-7 (δ 166.0), C-9 (δ 159.2), and C-10 and of H-6 with C-5 (δ 163.0), C-7, C-8 (δ 95.2), and C-10 in the gHMBC spectrum, respectively. The correlations of two *O*-methyl protons at δ 3.83 (6H, s, OCH_3) with C-3′ (5′) (δ 154.6) in the gHMBC spectrum, as well as the NOE correlations with H-2′ (6′) in the ROESY spectrum, indicated that two methoxy groups were substituted at C-3′ and 5′. Thus, the flavone moiety was identified as 5,7,4′-trihydroxy-3′,5′-dimethoxyflavone (tricin). Additional NMR data showed the existence of a guaiacylglycerol moiety by the presence of an ABX spin system in ^{1}H NMR at δ 6.75 (1H, br s, H-5″), 6.80 (1H, dd, *J* = 4.8, 1.6 Hz, H-6″), and 6.89 (1H, d, *J* = 1.6 Hz, H-2″) for the guaiacyl part and signals at δ 4.46 (1H, d, *J* = 6.0 Hz, H-7″), 4.43 (1H, m, H-8″), 3.92 (1H, dd, *J* = 12.0, 4.4 Hz, H-9″), and 3.73 (1H, dd, *J* = 12.0, 3.2 Hz, H-9″) for the glycerol part. The methoxy group in guaiacyl was confirmed by the observed correlation between the *O*-methyl protons at δ 3.81 (3H, s, OCH_3) and C-3″(δ 148.8) in the gHMBC and NOE correlation between the methoxy protons and H-2″ in the ROESY spectrum, respectively. The fourth methoxy group (δ 3.89) (3H, s, OCH_3) was located at C-7″, because a 9.5 ppm downfield shift for C-7″ (δ 83.7) in **1** was observed, when compared to compound **2**, where C-7″ (δ 74.2) was hydroxyl group substituted.[34,35] The linkage between the moieties of tricin and guaiacylglycerol was suggested through 4′-O-C-8″, as the signals of C-3′, 5′ (δ 154.6) of **1** showed a 5.1 ppm downfield shift compared with those of tricin (**3**) at C-3′, 5′ (δ 149.5). Very similar chemical shifts of C-8″ and C-9″ of **1** to those found in **2** and literature data[34] were in accord with the above suggestion. The coupling constant of $J_{H\text{-}7'',H\text{-}8''}$ for **1** was 6.0 Hz in methanol-d_6, corresponding to a *threo* form of chiral centers at C-7″ and C-8″ based on empirical observation.[35,36] Therefore, **1** was identified to be tricin 4′-*O*-[*threo*-β-guaiacyl-(7″-*O*-methyl)-glyceryl] ether, and **2** was idenfied to be tricin 4′-*O*-(erythro-β-guaiacyl-glyceryl) ether, two flavonolignan compounds from *L. meyenii*. The complete ^{1}H and ^{13}C NMR assignments are given in Table 1.

Compounds **1**−**3** and lepidiline B (**14**, previously isolated from *L. meyenii*)[26] were tested with regard to their effects on nitrite production in LPS-activated macrophages. As shown in Table 2, when RAW 264.7 cells were treated with test compounds at 40 μg/mL and LPS (100 ng/mL), the potency of inhibitory effect on nitrite production showed the sequence

Table 2. Effects of 1−3 and 14 on LPS-Induced Nitrite Production in RAW 264.7 Macrophage

	1	2	3	14
control	0.3 ± 0.6	0.3 ± 0.6	0.3 ± 0.6	0.3 ± 0.6
LPS	27.2 ± 3.0	27.2 ± 3.0	27.2 ± 3.0	27.2 ± 3.0
20 μg/mL	12.5 ± 1.2	24.2 ± 1.2	21.9 ± 1.9	6.3 ± 2.2
40 μg/mL	1.7 ± 0.4	24.5 ± 2.3	16.8 ± 0.6	4.3 ± 1.9

DOI: 10.1021/acs.jafc.5b00219
J. Agric. Food Chem. 2015, 63, 2458−2463

1 > **14** > **3** > **2**, where **1** and **14** significantly inhibited NO production. The four compounds were also assayed for cytotoxicity in HL-60, Hep G2, and COLO 205 cell lines. Compounds **1**, **3**, and **14** showed moderate to weak effect against HL-60 cells with IC_{50} values of 40.4, 52.1, and 52.0 μM, respectively, whereas no cytotoxicity was observed for these compounds in Hep G2 and COLO 205 cell lines (Table 3).

Table 3. Effect of Different Compounds on the Growth of Various Human Cancer Cells[a]

	IC_{50} (μM) for cell line		
compound	HL-60	Hep G2	COLO 205
1	40.4 ± 1.9	>100	>100
2	>100	>100	>100
3	52.1 ± 3.7	>100	>100
14	52.0 ± 1.1	>100	>100
doxorubicin[b]	4.64 ± 0.05	4.82 ± 0.05	16.12 ± 1.49

[a]Cells were treated with various concentrations of selected compounds for 24 h. Cell viability then was determined by the MTT assay as described. Each experiment was independently performed three times and expressed as the mean ± SE. [b]Positive control compound.

Compound **14** was previously reported against the UMUC3, PACA2, MDA231, and FDIGROV cell lines with ED_{50} values of 6.47, 1.38, 1.66, and 5.26 μg/mL, respectively.[25] The three isolated flavonoids in the present investigation all consist of a tricin unit. Tricin, which exists as glycoside in rice bran and other grass species, has been considered as a potential cancer chemopreventive agent in humans.[37] Some other isolated compounds in the current study have also been reported to possess different biological activities.

AUTHOR INFORMATION

Corresponding Author

*(N.B.) Phone: 0086-29-88305682. Fax: 0086-29-88302223. E-mail: nsbai@nwu.edu.cn.

Funding

We thank Naturex Inc. for funding this project.

Notes

The authors declare no competing financial interest.

ACKNOWLEDGMENTS

We thank Dr. Baoning Su, Wuxi Pharma Inc., for collaboration on the HRESIMS analyses and valuable suggestions for the chemical structural identification.

REFERENCES

(1) Johns, T. The anu and the maca. *J. Ethnobiol.* **1981**, *1*, 208−212.
(2) Zheng, B. L.; He, K.; Kim, C. H.; Rogers, L.; Shao, Y.; Huang, Z. Y.; Lu, Y.; Yan, S. J.; Qien, L. C.; Zheng, Q. Y. Effect of a lipidic extract from *Lepidium meyenii* on sexual behavior in mice and rats. *Urology* **2000**, *55*, 598−602.
(3) Cicero, A. F.; Bandieri, E.; Arletti, R. *Lepidium meyenii* Walp. improves sexual behaviour in male rats independently from its action on spontaneous locomotor activity. *J. Ethnopharmacol.* **2001**, *75*, 225−229.
(4) Cicero, A. F. G.; Piacente, S.; Plaza, A.; Sala, E.; Arletti, R.; Pizza, C. Hexanic maca extract improves rat sexual performance more effectively than methanolic and chloroformic maca extracts. *Andrologia* **2002**, *34*, 177−179.
(5) Ruiz-Luna, A. C.; Salazar, S.; Aspajo, N. J.; Rubio, J.; Gasco, M.; Gonzales, G. F. *Lepidium meyenii* (maca) increases litter size in normal adult female mice. *Reprod. Biol. Endocrinol.* **2005**, *3*, 16.
(6) Zheng, B. L.; He, K.; Hwang, Z. Y.; Lu, Y.; Yan, S. J.; Kim, C. H.; Zheng, Q. Y. Effect of aqueous extract from *Lepidium meyenii* on mouse behavior in forced swimming test. In *Quality Management of Nutraceuticals*; Ho, C. T., Zheng, Q. Y., Eds.; American Chemical Society: Washington, DC, USA, 2002; pp 90−100.
(7) López-Fando, A.; Gómez-Serranillos, M. P.; Iglesias, I.; Lock, O.; Upamayta, U. P.; Carretero, M. E. *Lepidium peruvianum* chacon restores homeostasis impaired by restraint stress. *Phytother. Res.* **2004**, *18*, 471−474.
(8) Rubio, J.; Caldas, M.; Dávila, S.; Gasco, M.; Gonzales, G. F. Effect of three different cultivars of *Lepidium meyenii* (maca) on learning and depression in ovariectomized mice. *BMC Complement. Altern. Med.* **2006**, *6* (23), 1−7.
(9) Gonzales, G. F.; Gasco, M.; Córdova, A.; Chung, A.; Rubio, J.; Villegas, L. Effect of *Lepidium meyenii* (maca) on spermatogenesis in male rats acutely exposed to high altitude (4340 m). *J. Endocrinol.* **2004**, *180*, 87−95.
(10) Zhang, Y.; Yu, L.; Ao, M.; Jin, W. Effect of ethanol extract of *Lepidium meyenii* Walp. on osteoporosis in ovariectomized rat. *J. Ethnopharmacol.* **2006**, *105*, 274−279.
(11) Gonzales, G. F.; Vasquez, V.; Rodriguez, D.; Maldonado, C.; Mormontoy, J.; Portella, J.; Pajuelo, M.; Villegas, L.; Gasco1, M. Effect of two different extracts of red maca in male rats with testosterone-induced prostatic hyperplasia. *Asian J. Androl.* **2007**, *9*, 245−251.
(12) Meissner, H. O.; Mrozikiewicz, P.; Bobkiewicz-Kozlowska, T.; Mscisz, A.; Kedzia, B.; Lowicka, A.; Reich-Bilinska, H.; Kapczynski, W.; Barchia, I. Hormone-balancing effect of pre-gelatinized organic maca (*Lepidium peruvianum* Chacon). (I) Biochemical and pharmacodynamic study on maca using clinical laboratory model on ovariectomized rats. *Int. J. Biomed. Sci.* **2006**, *2*, 260−272.
(13) Rubio, J.; Qiong, W.; Liu, X.; Jiang, Z.; Dang, H.; Chen, S.-L.; Gonzales, G. F. Aqueous extract of black maca (*Lepidium meyenii*) on memory impairment induced by ovariectomy in mice. *Evidence-Based Complement. Altern. Med.* **2011**, No. 253958.
(14) Vecera, R.; Orolin, J.; Skottová, N.; Kazdová, L.; Oliyarnik, O.; Ulrichová, J.; Simánek, V. The influence of maca (*Lepidium meyenii*) on antioxidant status, lipid and glucose metabolism in rat. *Plant Foods Hum. Nutr.* **2007**, *62*, 59−63.
(15) Gonzales, G. F.; Cordova, A.; Gonzales, C.; Chung, A.; Vega, K.; Villena, A. *Lepidium meyenii* (maca) improved semen parameters in adult men. *Asian J. Androl.* **2001**, *3*, 301−303.
(16) Gonzales, G. F.; Córdova, A.; Vega, K.; Chung, A.; Villena, A.; Góñez, C.; Castillo, S. Effect of *Lepidium meyenii* (maca) on sexual desire and its absent relationship with serum testosterone levels in adult healthy men. *Andrologia* **2002**, *34*, 367−372.
(17) Gonzales, G. F.; Córdova, A.; Vega, K.; Chung, A.; Villena, A.; Góñez, C. Effect of *Lepidium meyenii* (maca), a root with aphrodisiac and fertility-enhancing properties, on serum reproductive hormone levels in adult healthy men. *J. Endocrinol.* **2003**, *176*, 163−168.
(18) Zenico1, T.; Cicero, A. F.; Valmorri1, L.; Mercuriali, M.; Bercovich, E. Subjective effects of *Lepidium meyenii* (maca) extract on well-being and sexual performances in patients with mild erectile dysfunction: a randomised, double-blind clinical trial. *Andrologia* **2009**, *41*, 95−99.
(19) Meissner, H. O.; Mscisz, A.; Reich-Bilinska, H.; Kapczynski, W.; Mrozikiewicz, P.; Bobkiewicz-Kozlowska, T.; Kedzia, B.; Lowicka, A.; Barchia, I. Hormone-balancing effect of pre-gelatinized organic maca (*Lepidium peruvianum* Chacon). (II) Physiological and symptomatic responses of early-postmenopausal women to standardized doses of maca in double blind, randomized, placebo-controlled, multi-centre clinical study. *Int. J. Biomed. Sci.* **2006**, *2*, 360−374.
(20) Meissner, H. O.; Mscisz, A.; Reich-Bilinska, H.; Mrozikiewicz, P.; Bobkiewicz-Kozlowska, T.; Kedzia, B.; Lowicka, A.; Barchia, I. Hormone-balancing effect of pre-gelatinized organic maca (*Lepidium peruvianum* Chacon). (III) Clinical responses of early-postmenopausal women to maca in double blind, randomized, placebo-controlled,

DOI: 10.1021/acs.jafc.5b00219
J. Agric. Food Chem. 2015, 63, 2458−2463

crossover configuration, outpatient study. *Int. J. Biomed. Sci.* **2006**, *2*, 375−394.
(21) Zheng, B. L.; Kim, C. H.; Wolthoff, S.; He, K.; Rogers, L.; Shao, Y.; Zheng, Q. Y. U.S. Patent 6,267,995, 2001.
(22) Muhammad, I.; Zhao, J.; Dunbar, D. C.; Khan, I. A. Constituents of *Lepidium meyenii* 'maca'. *Phytochemistry* **2002**, *59*, 105−110.
(23) Zhao, J.; Muhammad, I.; Dunbar, D. C.; Mustafa, J.; Khan, I. A. New alkamides from maca (*Lepidium meyenii*). *J. Agric. Food Chem.* **2005**, *53*, 690−693.
(24) Dini, I.; Tenore, G. C.; Dini, A. Glucosinolates from maca (*Lepidium meyenii*). *Biochem. Syst. Ecol.* **2002**, *30*, 1087−1090.
(25) Piacente, S.; Carbone, V.; Plaza, A.; Zampelli, A.; Pizza, C. Investigation of the tuber constituents of maca (*Lepidium meyenii* Walp.). *J. Agric. Food Chem.* **2002**, *50*, 5621−5625.
(26) Cui, B. L.; Zheng, B. L.; He, K.; Zheng, Q. Y. Imidazole alkaloids from *Lepidium meyenii*. *J. Nat. Prod.* **2003**, *66*, 1101−1103.
(27) Mosmann, T. Rapid colorimetric assay for cellular growth and survival: application to proliferation and cytotoxicity assays. *J. Immunol. Methods* **1983**, *65*, 55−63.
(28) Kuwabara, H.; Mouri, K.; Otsuka, H.; Kasai, R.; Yamasaki, K. Tricin from a Malagasy Connaraceous plant with potent antihistaminic activity. *J. Nat. Prod.* **2003**, *66*, 1273−1275.
(29) Carpinella, M. C.; Giorda, L. M.; Ferrayoli, C. G.; Palacios, S. M. Antifungal effects of different organic extracts from *Melia azedarach* L. on phytopathogenic fungi and their isolated active components. *J. Agric. Food Chem.* **2003**, *51*, 2506−2511.
(30) Prestera, T.; Fahey, J. W.; Holtzclaw, W. D.; Abeygunawardana, C.; Kachinski, J. L.; Talalay, P. Comprehensive chromatographic and spectroscopic methods for the separation and identification of intact glucosinolates. *Anal. Biochem.* **1996**, *239*, 168−179.
(31) Kiddle, G.; Bennett, R. N.; Botting, N. P.; Davidson, N. E.; Robertson, A. A.; Wallsgrove, R. M. High-performance liquid chromatographic separation of natural and synthetic desulphoglucosinolates and their chemical validation by UV, NMR and chemical ionization-MS methods. *Phytochem. Anal.* **2001**, *12*, 226−242.
(32) Fahey, J. W.; Zalcmann, A. T.; Talalay, P. The chemical diversity and distribution of glucosinolates and isothiocyanates among plants. *Phytochemistry* **2001**, *56*, 5−51.
(33) Sakushima, A.; Coskun, M.; Maoka, T. Hydroxybenzoic acids from *Boreava orientalis*. *Phytochemistry* **1995**, *40*, 257−261.
(34) Bouaziz, M.; Veitch, N. C.; Grayer, R. J.; Simmonds, M. S. J.; Damak, M. Flavonolignans from *Hyparrhenia hirta*. *Phytochemistry* **2002**, *60*, 515−520.
(35) Nakajima, Y.; Yun, Y. S.; Kunugi, A. Six new flavonolignans from *Sasa veitchii* (Carr.) Rehder. *Tetrahedron* **2003**, *59*, 8011−8015.
(36) Jung, L. H.; Lee, D. Y.; Cho, J. G.; Lee, S. M.; Kang, H. C.; Seo, W. D.; Kang, H. W.; Kim, J. Y.; Baek, N. I. A new flavonolignan from the aerial parts of *Oryza sativa* L. inhibits nitric oxide production in RAW 264.7 macrophage cells. *J. Korean Soc. Appl. Chem.* **2011**, *54*, 865−870.
(37) Verschoyle, R. D.; Greaves, P.; Cai, H.; Borkhardt, A.; Broggini, M.; D'Incalci, M.; Gescher, A. J. Preliminary safety evaluation of the putative cancer chemopreventive agent tricin, a naturally occurring flavone. *Cancer Chemother. Pharmacol.* **2006**, *57* (1), 1−6.

DOI: 10.1021/acs.jafc.5b00219
J. Agric. Food Chem. 2015, 63, 2458−2463

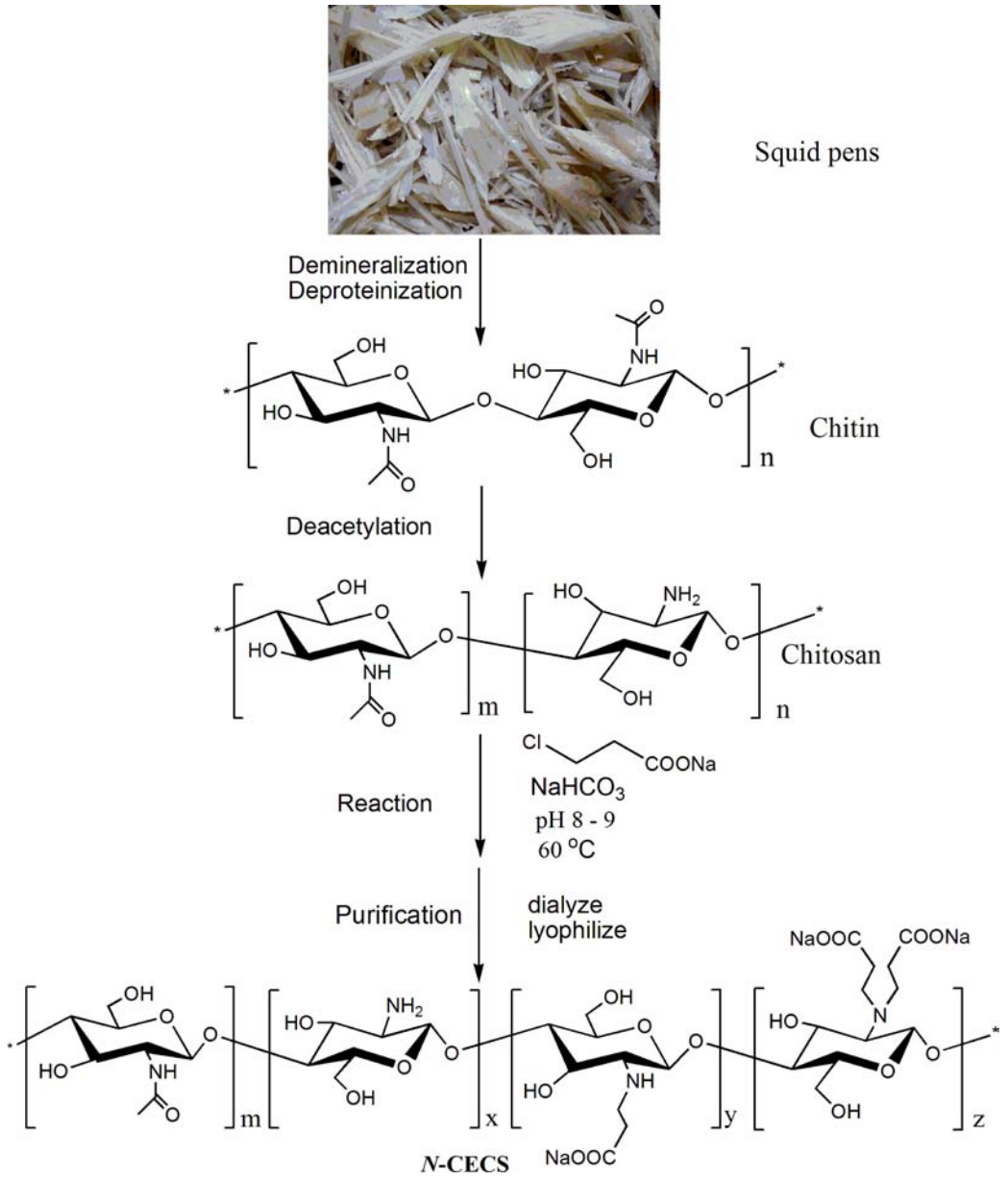

Figure 1. Preparation of water-soluble *N*-CECS.

can be synthesized via Michael-type 1,4-conjugate addition[24−26] or alkylation by halocarboxylic acids in neutral or mild alkaline conditions.[21,22]

Reactive oxygen species (ROS) have a wide variety of pathological effects, including in cancer, cardiovascular disease, diabetes, and atherosclerosis.[27] Antioxidants can reduce oxidative damage by scavenging ROS or preventing the generation of ROS. The use of synthetic antioxidants, such as butylated hydroxyanisole, *tert*-butylhydroquinone, and propyl gallate, is strictly regulated because of their potential health hazards. Recently, the antioxidant activity of chitosan and its derivatives have attracted the most attention in replacing synthetic species because of their nontoxic nature and natural abundance.[8,10,28,29] Furthermore, the extent to which carboxyethyl groups have been added to the polymer chain will directly affect the properties of CECS. However, to the best of our knowledge, there have been very few attempts to evaluate the relationship between the biochemical activities of *N*-CECS and their different degrees of carboxyethyl substitution.

In this paper, chitosan was prepared by alkaline N-deacetylation of squid pen *β*-chitin, and three *N*-(2-carboxyethyl)chitosans (*N*-CECS) with different degrees of substitution (DS) of carboxyethyls were synthesized to investigate the effect of substituting groups on the antioxidant activity and bile acid binding capacity. The antioxidant activity of *N*-CECS was investigated by scavenging 2,2′-azinobis(3-ethylbenzothiazoline-6-sulfonic acid) (ABTS) radicals ($ABTS^{\bullet+}$) and superoxide anion radicals ($^{\bullet}O_2^-$) and reducing power. In addition, the *in vitro* bile acid binding capacity of the derivatives was evaluated.

MATERIALS AND METHODS

Materials. Squid pens were provided by Hangzhou Baokai Biochemical Co., Ltd. (Hangzhou, China). 3-Chloropropionic acid, sodium bicarbonate, sodium acetate trihydrate, ferrous sulfate, bile acid (derived from taurocholate), furfual, nitro blue tetrazolium (NBT), phenazine methosulfate (PMS), ABTS, potassium ferricyanide [$K_3Fe(CN)_6$], reduced nicotinamide adenine dinucleotide (NADH), and

DOI: 10.1021/jf505581n
J. Agric. Food Chem. 2015, 63, 2464−2471

trichloroacetic acid were purchased from Aladdin Reagent Co., Ltd. (Shanghai, China). Sodium phosphate monobasic monohydrate, sodium phosphate dibasic anhydrous, and acetic acid were purchased from Sangon Biotech Co., Ltd. (Shanghai, China). All other chemicals were of analytical grade and used without further purification. All water used in the extraction and analysis was distilled and deionized.

Preparation of Chitosan from Squid Pens. The preparation of chitosan from squid pens was carried out using the method by Huang et al.[8] Chitosan with a degree of deacetylation of more than 90% was prepared from squid pens with a viscosity average molecular weight of 6.5×10^5 Da.

Preparation of *N*-CECS. *N*-CECS was synthesized as described by Skorik et al.[21]and Kogan et al.[22] According to Figure 1, chitosan (2 g) was dissolved in water (140 mL) containing 3-chloropropionic acid for 1 h. An amount of $NaHCO_3$ equivalent to the 3-chloropropionic was added to the dissolved chitosan in batches, which was stirred for an additional 30 min to remove the excess CO_2 (pH ~ 6.5). After stirring at 60 °C for 6 h, $NaHCO_3$ (6 g) was added, and after 1−2 h, the pH of the mixture was adjusted to be 8.5 by adding 10% NaOH. When the reaction was complete, the product was filtered and precipitated in ethanol and the precipitant was subsequently dissolved in water (20 mg/mL). The solution was acidified to pH 1−2 with concentrated HCl. The product was then dialyzed using a regenerated cellulose membrane (molecular weight cutoff of 3500) against distilled water for 2−3 days and lyophilized to obtain purified *N*-CECS. The sample was kept in a refrigerator for 4 °C.

Characterization of *N*-CECS Derivatives. Fourier transform infrared (FTIR) spectra of chitosan and *N*-CECS were obtained using a Bruker FTIR spectrometer (Vertex 70, Bruker Optik GmbH, Ettlingen, Germany). ^1H and ^{13}C nuclear magnetic resonance (NMR) spectra of *N*-CECS were recorded on a Bruker AVANCE III 500 MHz using D_2O as the solvent operating at 25 °C. Determination of the DS was estimated by the integrals of $\delta(-CH_2COOH)$ in the amino group from the following equation:

$$\mathrm{DS} = \frac{y + 2z}{x + y + z} \tag{1}$$

where x corresponds to the mole fraction of no carboxyethylated glucosamine units, y is the mole fraction of mono-carboxyethylated glucosamine units, and z is the mole fraction of di-carboxyethylated glucosamine units.

The X-ray diffraction (XRD) spectra of the samples in powder form were performed by a X-ray scattering diffractometer (X'Pert PRO, PANalytical, Netherlands) with Cu Kα 185 radiation (λ = 1.5444) in the range of 5−40° (2θ) at a voltage of 40 kV and current of 40 mA. To minimize the influence of the uneven surface of samples on the diffraction angle, each *N*-CECS was pressed into a 0.8 mm thick pellet with 10 MPa of pressure.

The CHN elemental analysis of chitosan and *N*-CECS was performed on a Vario El cube CHNOS elemental analyzer (Elementar Analysensysteme GmbH, Hanau, Germany). The degree of deacetylation (DDA) value of chitosan samples was calculated from the following equation:[30]

$$\mathrm{DDA}\ (\%) = \frac{6.857 - C/N}{1.714} \tag{2}$$

DS was designated as the average number of carboxyethyl groups on each D-glucosamine. It was calculated as C (%)/N (%)

$$\mathrm{DS} = \frac{14}{36}\frac{[C/N(\mathrm{CECS}) - 5.14]}{\mathrm{DDA}\ (\%)} \tag{3}$$

where the C/N is a percentage ratio of these elements in the derivative and in the original chitosan. The constant 5.14 is the C/N value of chitosan at a deacetylation degree of 100%. There were two hydrogen atoms on each amino group, which could be substituted by the carboxyethyl groups. When the hydrogen atoms of $-NH_2$ on chitosan were fully substituted, the DS of *N*-CECS was 200%.

Estimation of *N*-CECS Water Solubility. The water solubility of *N*-CECS at various pH values was determined by a turbidity measurement.[31] An aqueous solution of *N*-CECS (2 mg/mL, pH 1.5) was prepared; NaOH solution (10 M) was added to adjust the pH. The transmittance of the solutions at different pH values was recorded on a METASH UV-5500PC spectrophotometer at 600 nm.

Bile Acid Binding Capacity Assay. The bile acid binding capacity of *N*-CECS was investigated *in vitro* using the method by Muzzarelli et al.[32] and Zhao et al.,[10] with minor modifications. An aliquot of the sample (1 mL, 10 mg/mL) was mixed with 0.4 mL of 5 mg/mL bile acid, and the mixtures were adjusted to a total volume of 5 mL with distilled water. The mixtures were incubated for 2 h at 37 °C and then filtered. The resulting samples (1 mL) were mixed with 1 mL of 1% (w/v) furfural and 13 mL of 45% (v/v) sulfuric acid. The samples were then incubated for 20 min at 70 °C, and the absorbance was measured at 605 nm.

ABTS Radical Scavenging Ability. The radical scavenging activity of *N*-CECS toward ABTS was measured on the basis of the method by Prouillac et al.[33] and Re et al.,[34] with some modifications. Briefly, the ABTS radical cation ($ABTS^{\bullet+}$) was generated by mixing an ABTS diammonium salt solution (7.4 mM in water) with the same volume of potassium persulfate aqueous solution (2.6 mM). The mixture was kept in the dark overnight until the reaction was complete. The working solution was prepared by diluting the ABTS stock solution in phosphate-buffered saline (PBS) solution (0.1 M, pH 7.4) to an absorbance of 0.7 at 734 nm. The free radical scavenging activity was assessed by mixing the $ABTS^{\bullet+}$ working solution (0.8 mL) with *N*-CECS solution (0.2 mL) and shaking for 30 s. After reaction for 20 min, the scavenging activity was calculated according to the following equation:

$$\text{scavenging effect}\ (\%) = \left(1 - \frac{A_{\mathrm{sample}}}{A_{\mathrm{control}}}\right) \times 100 \tag{4}$$

where A_{control} was the absorbance of the initial concentration of $ABTS^{\bullet+}$ (distilled water instead of sample) and A_{sample} was the absorbance of the remaining concentration of $ABTS^{\bullet+}$ in the presence of *N*-CECS. The EC_{50} value (mg/mL) is the effective concentration at which $ABTS^{\bullet+}$ radicals were scavenged by 50%.

Superoxide Radical Scavenging Ability. The superoxide scavenging ability of *N*-CECS was assessed by the method of Zhao et al.[10] and Yuan et al.[35] Each sample (2−10 mg/mL, 0.2 mL) were mixed separately with 0.2 mL of NADH (471.6 μM) and 0.2 mL of NBT (342.5 μM) in 0.05 M Tris−HCl buffer (pH 8.0). The reaction was initiated by adding 0.2 mL of PMS solution (163 μM) to the mixture and then incubated at 25 °C for 5 min, and the absorbance at 560 nm was measured against blank samples. In control, the sample was substituted with Tris−HCl buffer (0.05 M, pH 8.0). Decreased absorbance of the reaction mixture indicated increased superoxide anion scavenging activity.

Reducing Power Measurement. The reducing power of *N*-CECS samples was measured as described by Huang et al.[36] The reaction mixture contained different concentrations of *N*-CECS samples (0.2 mL), 0.2 M sodium phosphate buffer at pH 6.6 (0.2 mL), and 1% (w/v) potassium ferricyanide (0.2 mL). The mixtures were blended well and incubated for 20 min at 50 °C. Then, 10% (w/v) trichloroacetic acid (0.2 mL) was added to the mixtures and centrifuged at 4000 rpm for 10 min. The supernatant (0.5 mL) was mixed with distilled water (0.5 mL) and 0.1% (w/v) ferric chloride solution (0.1 mL). The absorbance values were determined at 700 nm. Increased absorbance of the reaction mixture indicated an increased reducing power.

Statistical Analysis. All of the analyses were performed at least in triplicate. Each experimental data point represents the mean from three independent experiments. The deviation from the mean at the 95% significance level was used for statistical analysis.

RESULTS AND DISCUSSION

Characterization of *N*-CECS. The preparation process and reaction conditions of *N*-CECS with different DS from squid pens are shown in Figure 1. Infrared spectroscopy has been

DOI: 10.1021/jf505581n
J. Agric. Food Chem. 2015, 63, 2464−2471

used to determine the structure of chitosan and *N*-CECS.[26,37] Figure 2 displays the FTIR spectrum of chitosan and *N*-CECS.

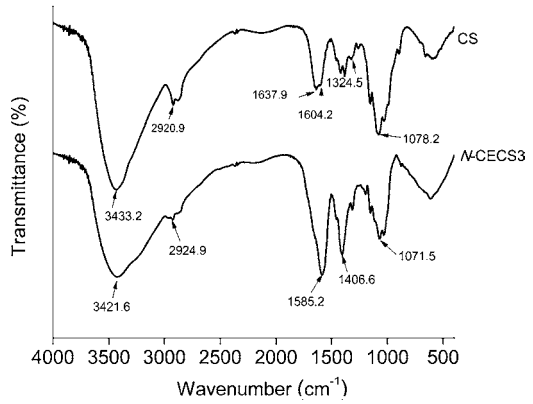

Figure 2. FTIR spectra of chitosan (CS) and *N*-CECS. The DS value of *N*-CECS was 1.41 by ^{1}H NMR.

Both characteristic peaks for chitosan at 3433 and 1078 cm^{-1} could be attributed to the O−H and C−O stretching vibrations, respectively. After carboxyethylation, two new bands at 1585 and 1407 cm^{-1} were observed. These were characteristic peaks of the stretching vibration of asymmetric and symmetric carboxyl groups, respectively.[10,38] Therefore, the FTIR data suggested that carboxyethyl groups were present in the derivative.

To compare the crystalline properties between the different samples, the XRD patterns of chitosan, *N*-CECS1, *N*-CECS2, and *N*-CECS3 are depicted in Figure 3. The peak registered

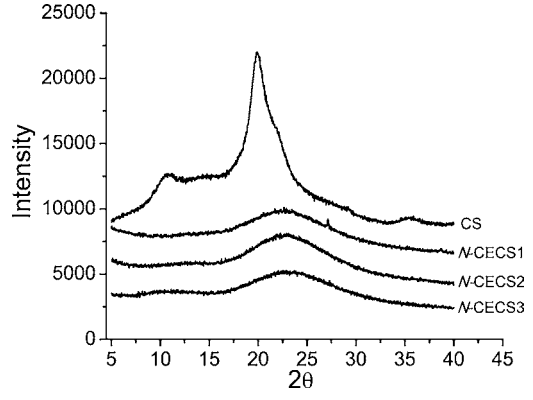

Figure 3. XRD patterns of chitosan (CS) and *N*-CECS with different DS. DS values of *N*-CECS1, *N*-CECS2, and *N*-CECS3 calculated by ^{1}H NMR were 0.88, 1.06, and 1.41, respectively.

near 19.90° highlights the relatively regular crystal lattice of chitosan. In comparison to unmodified chitosan, the X-ray patterns of *N*-CECS samples exhibit some changes to both their diffraction angles and peak intensity. The peak intensity registered near 19.90° decreased and shifted to a higher 2θ value (22.70°). The rigid crystalline structure of chitosan is mostly maintained by the intra- and intermolecular hydrogen bonds.[39]

The introduction of carboxyethyl groups disturbed the crystal domain of chitosan because of the high steric hindrance. Thus, the peaks of the crystal associated with chitosan were weakened and broadened. The change in these characteristic XRD peaks demonstrated that chitosan transited from a crystalline structure to an amorphous state through the carboxyethylation process.

The chemical structure of *N*-CECS was further characterized by ^{1}H and ^{13}C NMR spectroscopies. Figures 4 and 5 show typical ^{1}H and ^{13}C NMR spectra of the reaction product, respectively. Mono- and dicarboxyethylated amines are distinguishable on the spectrum because of the two different chemical shifts of $-CH_2COONa$ (2.56 and 2.80 ppm). The ^{13}C NMR spectrum of *N*-CECS showed as expected chemical shifts of carbonyl atoms of carboxyethyl (179.54 ppm), α-methylene of carboxyethyl of $GlcNR_2$ (33.51 ppm), and α-methylene of carboxyethyl of GlcNHR (36.39 ppm). The spectrum was comparable to literature reports.[21,22] The ^{1}H and ^{13}C NMR spectra further prove the substitution of the carboxyethyl group onto the amino groups of the chitosan backbone. Skorik et al.[22] reported that the chemoselectivity of chitosan carboxyalkylation arose from the mild alkaline reaction conditions. This makes it possible to differentiate the reactivity of $-OH$ and $-NH_2$ groups. Mild conditions (pH 8−9) facilitated alkylation of chitosan exclusively on the amino groups.

The high substitution found on the amino groups could hardly be achieved via Michael addition reaction.[24−26,40,41] Moreover, the structure of *N*-CECS was different from that of *N,O*-(2-carboxyethyl)chitosan (*N,O*-CECS); methylene of the carboxyethyl group substituted on C-6 also existed in the ^{1}H NMR spectrum of *N,O*-CECS in addition to the carboxyethylation of the amide group.[37] The DS values were calculated by ^{1}H NMR and elemental analysis (Table 1). The data showed that the DS values from ^{1}H NMR were similar to those from elemental analysis.

Water Solubility. Carboxyalkylation of chitosan can greatly improve its water solubility. Figure 6 illustrates the solubility of *N*-CECS with different DQ values at different pH values. The solubility of all *N*-CECS samples decreased with the increase of pH, and the corresponding pH of *N*-CECS1, *N*-CECS2, and *N*-CECS3 with minimum solubility is 5.6, 4.1, and 3.3, respectively. Further increasing the pH, however, led to a drastic increase in solubility and finally plateaued.

Figure 6 also showed good water solubility of all *N*-CECS above pH 6.5, but chitosan has poor solubility at pH > 6.5. The possible explanation for this phenomenon might be that the solubility of polyampholytes is the lowest at the isoelectric point (pI), all *N*-CECS samples with an amino group and a carboxyethyl group are polyampholytes, and pI of all *N*-CECS is different. When negative charge in the *N*-CECS structure increases upon introduction of carboxyethyl groups, the corresponding pI of *N*-CECS decreased. *N*-CECS had a more amorphous structure than chitosan, but the pI of *N*-CECS has a positive correlation with the pH of the minimum solubility.

***In Vitro* Bile Acid Binding Capacity.** The *in vitro* bile acid binding capacities of *N*-CECS are shown in Table 1. The binding capacity of *N*-CECS1, *N*-CECS2, and *N*-CECS3 against bile acid was 27.2, 36.9, and 0 mg/g (1.9-, 2.6-, and 0-fold higher than chitosan), respectively.

Previous reports have showed that the charge−charge interactions are the major force between the anionic bile acid and the bile acid sequestrants.[36,42] In comparison to native chitosan, the introduction of carboxyethyl groups severely disrupted the inner structure of *N*-CECS. The ability of *N*-CECS to form hydrogen bonds declined sharply; that is, the amino groups were activated, which increases the bile acid binding capacity. When a negative charge in the *N*-CECS structure increased above a certain level upon the introduction

DOI: 10.1021/jf505581n
J. Agric. Food Chem. 2015, 63, 2464−2471

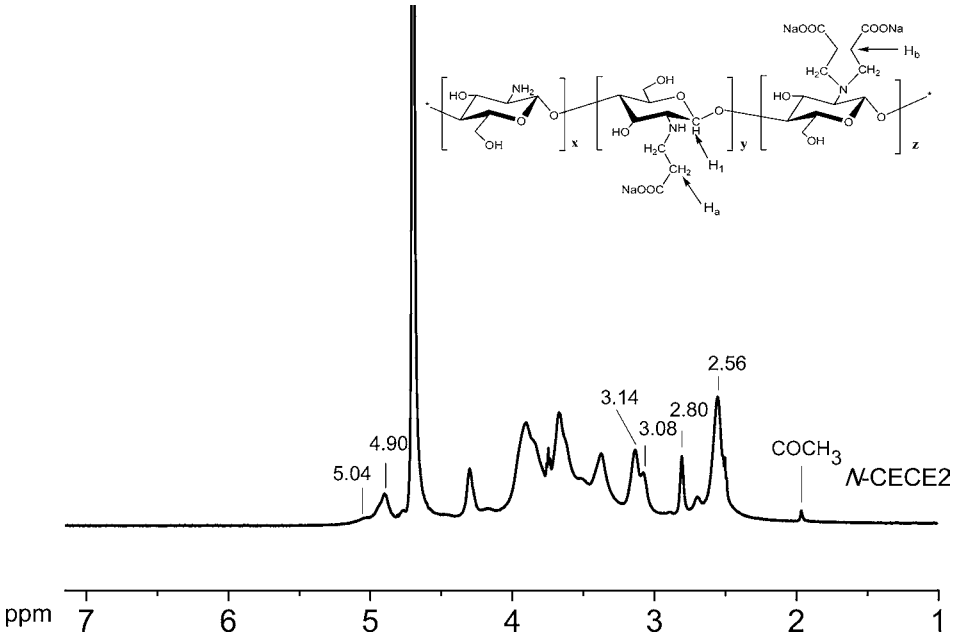

Figure 4. ^{1}H (500 MHz) NMR spectroscopy (δ, ppm) of *N*-CECS2 solution in D_2O: 2.56 (−CH_2COONa of GlcNHR, H_a), 2.80 (−CH_2COONa of GlcNR_2, H_b), 3.08 (H-2 of GlcNH_2), 3.14 (H-2 of GlcNHR), 4.90 (H-1 of GlcNHR), and 5.04 (H-1 of GlcNR_2). The DS value of *N*-CECS2 was 1.06 by ^{1}H NMR.

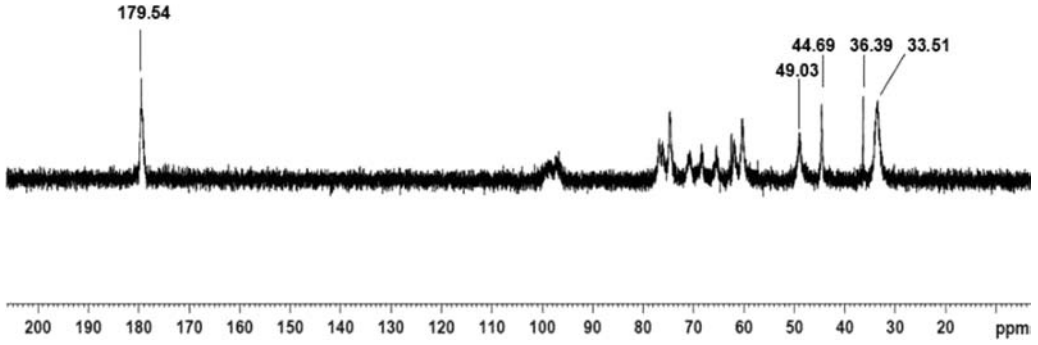

Figure 5. ^{13}C (125 MHz) NMR (δ, ppm) spectroscopy of *N*-CECS3 in D_2O at 25 °C: 33.51 (CH_2COONa of GlcNR_2), 36.39 (CH_2COONa of GlcNHR), 44.69 (NCH_2 of GlcNHR), 49.03 (NCH_2 of GlcNHR_2), 60.29−62.53 (C-2 and C-6), 65.51−76.82 (C-3, C-4, and C-5), 96.8−98.93 (C-1), and 179.54 (COONa). The DS value of *N*-CECS3 was 1.41 by ^{1}H NMR.

Table 1. Reaction Conditions, DS, and Bile Acid Binding Capacity of *N*-CECS

product	reagent ratio[a]	reaction time (h)	*N* (%)	*C* (%)	*H* (%)	*C*/*N*	DS[b]	*x*/*y*/*z*[c]	DS[d]	BA[e]
chitosan			7.72	40.24	6.56	5.20				14.0
N-CECS1	5	6	5.08	37.92	6.10	7.45	0.91	0.16:0.80:0.04	0.88	27.2
N-CECS2	5	15	4.78	37.98	5.94	7.94	1.12	0.07:1.06:1.41	1.06	36.9
N-CECS3	10	120	4.10	37.74	5.33	9.22	1.62	0.00:0.59:0.41	1.41	0

[a]The molar ratio of 3-chloropropionic acid/D-glucosamine. [b]DS was calculated per D-glucosamine residue of chitosan by elemental analysis. [c]See Figure 1. [d]DS was calculated per D-glucosamine residue of chitosan by ^{1}H NMR spectrum, DS = $(y + 2z)/(x + y + z)$. [e]Bile acid (BA) binding capacity (mg/g).

of carboxyethyl groups, the significant decrease in the bile acid binding capacity could be caused by ionic repulsion because of its anionic characteristics. Moreover, the solubility improvement of *N*-CECS also enhances its biological activity, including bile acid binding capacity.[43] Thus, *N*-CECS with enhanced bile acid binding capacity may be used as an ingredient in the pharmaceutical industry to possibly reduce cholesterol and blood pressure.

Scavenging Effect on ABTS Radicals. The ABTS free radicals have been widely used for testing the preliminary radical scavenging capacity of plant extracts or antioxidants.[44] ABTS radical scavenging is an electron-transfer reaction; the addition of antioxidants to the preformed radical cation $ABTS^{\bullet+}$ reduces ABTS. This extent of the reaction and the kinetics depends upon the antioxidant activity, the concentration of the antioxidant, and the duration of the reaction.[33] The scavenging activities of *N*-CECS toward ABTS radicals with varying DS and concentrations are shown in Figure 7. Figure 7 showed that the scavenging ability of *N*-CECS toward ABTS radicals improved as a function of concentrations. The

DOI: 10.1021/jf505581n
J. Agric. Food Chem. 2015, 63, 2464−2471

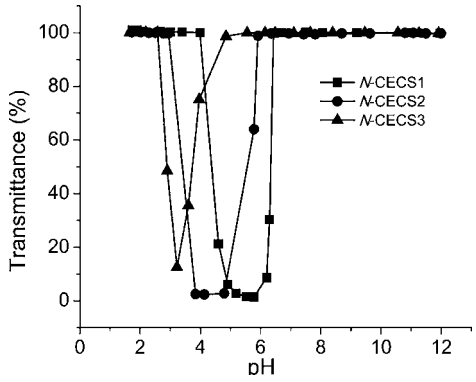

Figure 6. pH dependence of *N*-CECS water solubility with different DS. DS values of *N*-CECS1, *N*-CECS2, and *N*-CECS3 calculated by ^{1}H NMR were 0.88, 1.06, and 1.41, respectively.

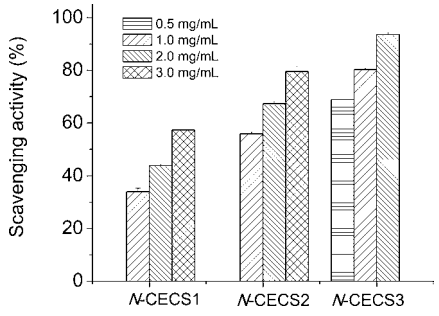

Figure 7. Scavenging effect of *N*-CECS with different DS toward ABTS radicals. DS values of *N*-CECS1, *N*-CECS2, and *N*-CECS3 calculated by ^{1}H NMR were 0.88, 1.06, and 1.41, respectively.

EC_{50} values of *N*-CECS1, *N*-CECS2, and *N*-CECS3 toward the ABTS radical were 1.83, 1.23, and 0.33 mg/mL, respectively. The data indicated that the addition of carboxyethyl groups to chitosan improved its scavenging activities against the ABTS radicals.

The hydroxyl group of chitosan and its derivatives plays an important role in scavenging the ABTS radicals.[17] The formation of inter- and intramolecular hydrogen bonds in chitosan inhibited the reaction of ABTS radicals with the active hydroxyl groups. In comparison to chitosan, the inner structure of *N*-CECS was severely disrupted by the introduction of hydrophilic *N*-carboxyethyl groups. The ability to form hydrogen bonds declined sharply; that is, more active hydroxyl groups in the *N*-CECS polymer chains were exposed. As the DS increased, the numbers of active hydroxyl groups in *N*-CECS increased. Thus, there were better scavenging abilities by *N*-CECS samples with a higher DS than *N*-CECS samples with a lower DS.

Cheng et al.[16] reported that the scavenging of ABTS radicals by hydroxypropyl chitosan (HPCS) with different DS (0.42−2.25) were below 40% at 10 mg/mL. Huang et al.[17] showed that the scavenging of ABTS radicals by *N*-(2-hydroxy)propyl-3-trimethylammonium chitosan chloride (HTCC) with different DS (0.77−1.06) was below 35% at 5 mg/mL. In comparison to HTCC and HPCS chitosans, *N*-CECS was more effective in ABTS radical scavenging activity.

Superoxide Radical Scavenging Activity. The superoxide anion formed in almost all aerobic cells is known to be very harmful to cellular components and is a precursor of more reactive oxidative species, such as single oxygen and hydroxyl radicals.[44,45] Figure 8 depicts the scavenging activities of *N*-CECS with varying DS and concentrations on superoxide radicals. The scavenging effect of all forms of *N*-CECS toward superoxide radical correlated well with their concentrations. The correlation between the carboxyethyl content (DS) of *N*-CECS and their superoxide radical scavenging activity was positive. At 10 mg/mL, the scavenging effect on superoxide radicals of *N*-CECS1, *N*-CECS2, and *N*-CECS3 was 42.08, 45.92, and 50.44%, respectively. The corresponding EC_{50} values (mg/mL) were 13.32, 11.52, and 9.75. In comparison to the previously reported EC_{50} value for chitosan (14.58 mg/mL),[10] *N*-CECS was more effective than chitosan at eliminating superoxide radicals.

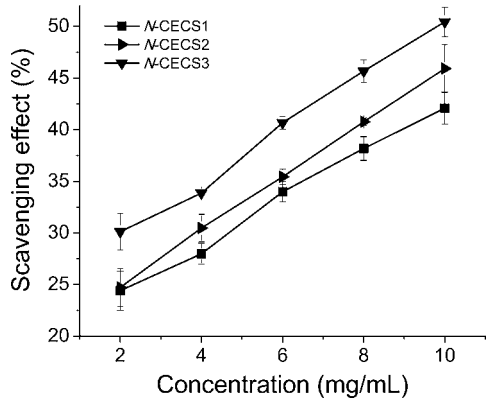

Figure 8. Scavenging effect of *N*-CECS with different DS toward superoxide radicals. DS values of *N*-CECS1, *N*-CECS2, and *N*-CECS3 calculated by ^{1}H NMR were 0.88, 1.06, and 1.41, respectively.

Chitosan has two hydroxyl groups and one amino group in its basic unit. Polysaccharides with scavenging effects toward superoxide anion all have one or more alcohol or phenolic hydroxyl groups. The formation of hydrogen bonds in chitosan inhibited the reaction of superoxide anion with the active hydroxyl groups in the polymer chains.[8,10] After etherification, more hydroxyl groups are activated, and this is helpful for enhancing the scavenging effect toward the superoxide radical. As an electron-donating group, the carboxyethyl group may enhance the electron cloud density of the active hydroxyl group in the *N*-CECS polymer chain. Thus, the electron-donating activity of *N*-CECS increased, and the scavenging effect on superoxide anion increased, when the DS increased from 0.88 to 1.41. We conclude that *N*-CECS may be an antioxidant based on its ability to scavenge ABTS and superoxide radicals.

Reducing Power. Figure 9 depicts the reducing power of *N*-CECS with different DS values using the potassium ferricyanide reduction method. As shown in Figure 9, the reducing power of *N*-CECS correlated well with increasing the concentration. However, the correlation between the carboxyethyl content (DS) of *N*-CECS and reducing power was not positive. At 6 mg/mL, the absorbance values of *N*-CECS1, *N*-CECS2, and *N*-CECS3 were 0.049, 0.064, and 0.032, respectively. Huang et al.[8] reported that, at 2 mg/mL, the reducing power of low-molecular-weight (LMW) chitosans was more than 0.50. In comparison to LMW chitosans, it seems that *N*-CECS has poor reducing power. Previous studies have shown direct correlation between the antioxidant activities and the reducing power of certain plant extracts.[37,46,47] The reducing properties are generally associated with the presence of reductones that break the free radical chain by donating a hydrogen atom.[44] The reducing power of *N*-CECS suggested

DOI: 10.1021/jf505581n
J. Agric. Food Chem. 2015, 63, 2464−2471

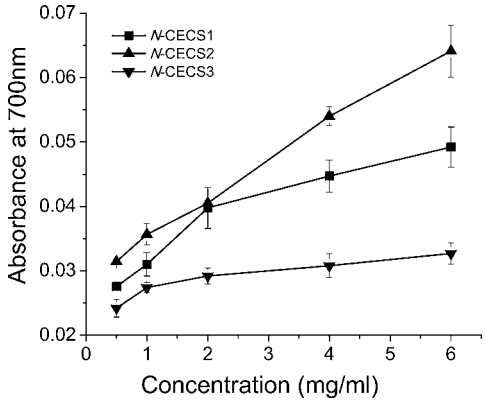

Figure 9. Reducing power of *N*-CECS with different DS. DS values of *N*-CECS1, *N*-CECS2, and *N*-CECS3 calculated by ^{1}H NMR were 0.88, 1.06, and 1.41, respectively.

that it was likely to contribute insignificantly toward the observed antioxidant effect.

AUTHOR INFORMATION

Corresponding Authors

*Telephone/Fax: +86-571-85070392. E-mail: zjhzmjw@163.com.

*Telephone: +86-571-87953161. Fax: +86-571-87951982. E-mail: meilh@zju.edu.cn.

Funding

This work was supported by the Science and Technology Department of Zhejiang Province of the People's Republic of China (2008C14067), the Interdisciplinarity Research Program of Zhejiang University of Science and Technology (2013JC10Y), the International Science and Technology Cooperation Program of China (2010DFA34370), and the International Science and Technology Cooperation Program of Zhejiang (2013C14012).

Notes

The authors declare no competing financial interest.

ACKNOWLEDGMENTS

The authors thank Professor Yury A. Skorik at St. Petersburg State Chemical Pharmaceutical Academy (Russia) for providing the help in synthesizing *N*-CECS.

ABBREVIATIONS USED

ABTS, 2,2′-azinobis(3-ethylbenzothiazoline-6-sulfonic acid); *N*-CECS, *N*-carboxyethylated chitosan; XRD, X-ray diffraction; DS, degree of substitution; NMR, nuclear magnetic resonance; FTIR, Fourier transform infrared

REFERENCES

(1) Rinaudo, M. Chitin and chitosan: Properties and applications. *Prog. Polym. Sci.* **2006**, *31*, 603−632.

(2) Muzzarelli, R. A. A. Carboxymethylated chitins and chitosans. *Carbohydr. Polym.* **1988**, *8*, 1−21.

(3) Minke, R.; Blackwell, J. The structure of α-chitin. *J. Mol. Biol.* **1978**, *120*, 167−181.

(4) Hajji, S.; Younes, I.; Ghorbel-Bellaaj, O.; Hajji, R.; Rinaudo, M.; Nasri, M.; Jellouli, K. Structural differences between chitin and chitosan extracted from three different marine sources. *Int. J. Biol. Macromol.* **2014**, *65*, 298−306.

(5) Kurita, K.; Tomita, K.; Tada, T.; Ishii, S.; Nishimura, S. I.; Shimoda, K. Squid chitin as a potential alternative chitin source: Deacetylation behavior and characteristic properties. *J. Polym. Sci., Part A: Polym. Chem.* **1993**, *31*, 485−491.

(6) Kurita, K.; Ishii, S.; Tomita, K.; Nishimura, S. I.; Shimoda, K. Reactivity characteristics of squid β-chitin as compared with those of shrimp chitin: High potentials of squid chitin as a starting material for facile chemical modifications. *J. Polym. Sci., Part A: Polym. Chem.* **1994**, *32*, 1027−1032.

(7) Kurita, K. Controlled functionalization of the polysaccharide chitin. *Prog. Polym. Sci.* **2001**, *26*, 1921−1971.

(8) Huang, J.; Zhao, D. K.; Hu, S.; Mao, J. W.; Mei, L. H. Biochemical activities of low molecular weight chitosans derived from squid pens. *Carbohydr. Polym.* **2012**, *87*, 2231−2236.

(9) Jayakumar, R.; Chennazhi, K. P.; Muzzarelli, R. A. A.; Tamura, H.; Nair, S. V.; Selvamurugan, N. Chitosan conjugated DNA nanoparticles in gene therapy. *Carbohydr. Polym.* **2010**, *79*, 1−8.

(10) Zhao, D. K.; Huang, J.; Hu, S.; Mao, J. W.; Mei, L. H. Biochemical activities of N,O-carboxymethyl chitosan from squid cartilage. *Carbohydr. Polym.* **2011**, *85*, 832−837.

(11) Muzzarelli, R. A. A.; Morganti, P.; Morganti, G.; Palombo, P.; Palombo, M.; Biagini, G.; Mattioli Belmonte, M.; Giantomassi, F.; Orlandi, F.; Muzzarelli, C. Chitin nanofibrils/chitosan glycolate composites as wound medicaments. *Carbohydr. Polym.* **2007**, *70*, 274−284.

(12) Muzzarelli, R. A. A. Chitins and chitosans for the repair of wounded skin, nerve, cartilage and bone. *Carbohydr. Polym.* **2009**, *76*, 167−182.

(13) Kofuji, K.; Qian, C. J.; Nishimura, M.; Sugiyama, I.; Murata, Y.; Kawashima, S. Relationship between physicochemical characteristics and functional properties of chitosan. *Eur. Polym. J.* **2005**, *41*, 2784−2791.

(14) Ong, S. Y.; Wu, J.; Moochhala, S. M.; Tan, M. H.; Lu, J. Development of a chitosan-based wound dressing with improved hemostatic and antimicrobial properties. *Biomaterials* **2008**, *29*, 4323−4332.

(15) Shelma, R.; Sharma, C. P. Development of lauroyl sulfated chitosan for enhancing hemocompatibility of chitosan. *Colloid Surf. B-Biointerfaces* **2011**, *84*, 561−570.

(16) Cheng, Z. H.; Huang, J.; Hu, S.; Jiang, C. J.; Ge, Q.; Lai, H. W.; Gong, J. Y.; Sun, P. L.; Mao, J. W.; Mei, L. H. Effects of hydroxypropyl degree on physiochemical activities of chitosan from squid pens. *Int. J. Biol. Macromol.* **2014**, *65*, 246−251.

(17) Huang, J.; Cheng, Z. H.; Xie, H. H.; Gong, J. Y.; Lou, J.; Ge, Q.; Wang, Y. J.; Wu, Y. F.; Liu, S. W.; Sun, P. L.; Mao, J. W. Effect of quaternization degree on physiochemical and biological activities of chitosan from squid pens. *Int. J. Biol. Macromol.* **2014**, *70*, 545−550.

(18) Wan, A. J.; Xu, Q.; Sun, Y.; Li, H. L. Antioxidant activity of high molecular weight chitosan and N,O-quaternized chitosans. *J. Agric. Food Chem.* **2013**, *61*, 6921−6928.

(19) Ouchi, T.; Nishizawa, H.; Ohya, Y. Aggregation phenomenon of PEG-grafted chitosan in aqueous solution. *Polymer* **1998**, *39*, 5171−5175.

(20) Jimtaisong, A.; Saewan, N. Utilization of carboxymethyl chitosan in cosmetics. *Int. J. Cosmet. Sci.* **2014**, *36*, 12−21.

(21) Skorik, Y. A.; Gomes, C. A. R.; Vasconcelos, M. T. S. D.; Yatluk, Y. G. *N*-(2-Carboxyethyl)chitosans: Regioselective synthesis, characterisation and protolytic equilibria. *Carbohydr. Res.* **2003**, *338*, 271−276.

(22) Kogan, G.; Skorik, Y. A.; Žitňanová, I.; Križková, L.; Ďuračková, Z.; Gomes, C. A. R.; Yatluk, Y. G.; Krajčovič, J. Antioxidant and antimutagenic activity of *N*-(2-carboxyethyl)chitosan. *Toxicol. Appl. Pharmacol.* **2004**, *201*, 303−310.

(23) Lee, Y. M.; Shin, E. M.; Noh, S. T. Pervaporation separation of water−ethanol through modified chitosan membranes, II. Carboxymethyl, carboxyethyl, cyanoethyl, and amidoxime chitosan membranes. *Angew. Makromol. Chem.* **1991**, *192*, 169−181.

(24) Sashiwa, H.; Yamamori, N.; Ichinose, Y.; Sunamoto, J.; Aiba, S. I. Chemical modification of chitosan 17a: Michael reaction of chitosan with acrylic acid in water. *Macromol. Biosci.* **2003**, *3*, 231−233.

DOI: 10.1021/jf505581n
J. Agric. Food Chem. 2015, 63, 2464−2471

(25) Sashiwa, H.; Yamamori, N.; Ichinose, Y.; Sunamoto, J.; Aiba, S. Michael reaction of chitosan with various acryl reagents in water. *Biomacromolecules* **2003**, *4*, 1250−1254.
(26) Sashiwa, H.; Shigemasa, Y.; Roy, R. Novel N-alkylation of chitosan via Michael type reaction. *Chem. Lett.* **2000**, *8*, 862−863.
(27) Willett, W. C. Diet and health: What should we eat? *Science* **1994**, *264*, 532−537.
(28) Castagnino, E.; Francesca Ottaviani, M.; Cangiotti, M.; Morelli, M.; Casettari, L.; Muzzarelli, R. A. A. Radical scavenging activity of 5-methylpyrrolidinone chitosan and dibutyryl chitin. *Carbohydr. Polym.* **2008**, *74*, 640−647.
(29) Muzzarelli, R. A. A.; Boudrant, J.; Meyer, D.; Manno, N.; DeMarchis, M.; Paoletti, M. G. Current views on fungal chitin/chitosan, human chitinases, food preservation, glucans, pectins and inulin: A tribute to Henri Braconnot, precursor of the carbohydrate polymers science, on the chitin bicentennial. *Carbohydr. Polym.* **2012**, *87*, 995−1012.
(30) Jiang, X.; Chen, L.; Zhong, W. A new linear potentiometric titration method for the determination of deacetylation degree of chitosan. *Carbohydr. Polym.* **2003**, *54*, 457−463.
(31) Ding, F. Y.; Shi, X. W.; Li, X. X.; Cai, J.; Duan, B.; Du, Y. M. Homogeneous synthesis and characterization of quaternized chitin in NaOH/urea aqueous solution. *Carbohydr. Polym.* **2012**, *87*, 422−426.
(32) Muzzarelli, R. A. A.; Orlandini, F.; Pacetti, D.; Boselli, E.; Frega, N. G.; Tosi, G.; Muzzarelli, C. Chitosan taurocholate capacity to bind lipids and to undergo enzymatic hydrolysis: An in vitro model. *Carbohydr. Polym.* **2006**, *66*, 363−371.
(33) Prouillac, C.; Vicendo, P.; Garrigues, J. C.; Poteau, R.; Rima, G. Evaluation of new thiadiazoles and benzothiazoles as potential radioprotectors: Free radical scavenging activity in vitro and theoretical studies (QSAR, DFT). *Free Radical Biol. Med.* **2009**, *46*, 1139−1148.
(34) Re, R.; Pellegrini, N.; Proteggente, A.; Pannala, A.; Yang, M.; Rice-Evans, C. Antioxidant activity applying an improved ABTS radical cation decolorization assay. *Free Radical Biol. Med.* **1999**, *26*, 1231−1237.
(35) Yuan, H. M.; Zhang, W. W.; Li, X. G.; Lü, X. X.; Li, N.; Gao, X. L.; Song, J. M. Preparation and in vitro antioxidant activity of κ-carrageenan oligosaccharides and their oversulfated, acetylated, and phosphorylated derivatives. *Carbohydr. Res.* **2005**, *340*, 685−692.
(36) Huang, J.; Chen, W. W.; Hu, S.; Gong, J. Y.; Lai, H. W.; Liu, P.; Mei, L. H.; Mao, J. W. Biochemical activities of 6-carboxy-β-chitin derived from squid pens. *Carbohydr. Polym.* **2013**, *91*, 191−197.
(37) Cai, Z. S.; Song, Z. Q.; Yang, C. S.; Shang, S. B.; Yin, Y. B. Synthesis, characterization and antibacterial activity of quaternized *N,O*-(2-carboxyethyl) chitosan. *Polym. Bull.* **2009**, *62*, 445−456.
(38) Kong, X. P. Simultaneous determination of degree of deacetylation, degree of substitution and distribution fraction of −COONa in carboxymethyl chitosan by potentiometric titration. *Carbohydr. Polym.* **2012**, *88*, 336−341.
(39) Xiao, B.; Wan, Y.; Wang, X. Y.; Zha, Q. C.; Liu, H. M.; Qiu, Z. Y.; Zhang, S. M. Synthesis and characterization of *N*-(2-hydroxy)-propyl-3-trimethyl ammonium chitosan chloride for potential application in gene delivery. *Colloid Surf. B-Biointerfaces* **2012**, *91*, 168−174.
(40) Pestov, A. V.; Kodess, M. I.; Matochkina, E. G.; Yatluk, Y. G. Selective mono-N-2-carboxyethylation of chitosan in the presence of magnesium halides. *Carbohydr. Polym.* **2011**, *86*, 783−788.
(41) Zhou, Y. S.; Yang, H. J.; Liu, X.; Mao, J.; Gu, S. J.; Xu, W. L. Electrospinning of carboxyethyl chitosan/poly(vinyl alcohol)/silk fibroin nanoparticles for wound dressings. *Int. J. Biol. Macromol.* **2013**, *53*, 88−92.
(42) Daggy, B. P.; O'Connell, N. C.; Jerdack, G. R.; Stinson, B. A.; Setchell, K. D. Additive hypocholesterolemic effect of psyllium and cholestyramine in the hamster: Influence on fecal sterol and bile acid profiles. *J. Lipid Res.* **1997**, *38*, 491−502.
(43) Wang, Y. J.; Yu, Y. Z.; Mao, J. W. Carboxymethylated β-glucan derived from *Poria cocos* with biological activities. *J. Agric. Food Chem.* **2009**, *57*, 10913−10915.
(44) Xie, M. H.; Hu, B.; Wang, Y.; Zeng, X. X. Grafting of gallic acid onto chitosan enhances antioxidant activities and alters rheological properties of the copolymer. *J. Agric. Food Chem.* **2014**, *62*, 9128−9136.
(45) Sun, T.; Yao, Q.; Zhou, D. X.; Mao, F. Antioxidant activity of *N*-carboxymethyl chitosan oligosaccharides. *Bioorg. Med. Chem. Lett.* **2008**, *18*, 5774−5776.
(46) Xing, R. E.; Liu, S.; Guo, Z. Y.; Yu, H. H.; Wang, P. B.; Li, C. P.; Li, Z. E.; Li, P. C. Relevance of molecular weight of chitosan and its derivatives and their antioxidant activities in vitro. *Bioorg. Med. Chem.* **2005**, *13*, 1573−1577.
(47) Duh, P. D.; Tu, Y. Y.; Yen, G. C. Antioxidant activity of water extract of Harng Jyur (*Chrysanthemum morifolium* Ramat). *LWT—Food Sci. Technol.* **1999**, *32*, 269−277.

DOI: 10.1021/jf505581n
J. Agric. Food Chem. 2015, 63, 2464−2471

Table 1. ^{1}H NMR Data (600 MHz, $CDCl_3$) for Compounds 1−9 (δ in ppm, J in Hz)

	1	2	3	4	5	6	7	8	9
3a	1.80 (dd, 7.2, 13.5)	1.78 (dd, 6.6, 13.2)	1.79 (dd, 7.2, 13.5)	1.77 (dd 6.6, 13.2)	1.79 (dd 6.6, 13.2)	1.79 (dd,7.2, 13.8)	1.75 (dt,6.6, 13.2)	1.84 (m)	1.79 (dd, 6.6, 13.5)
3b	1.75 (dd, 7.2, 13.5)	1.75 (dd, 6.6, 13.2)	1.75 (dd, 7.2, 13.5)	1.74 (dd 6.6, 13.2)	1.75 (dd 6.6, 13.2)	1.75 (dd, 7.2, 13.8)	1.78 (dt, 6.6, 13.2)	1.85 (m)	1.75 (dd, 6.6, 13.5)
4	2.70 (td, 3.0, 7.2)	2.75 (dt, 6.6, 13.8)	2.69 (td, 2.4, 7.2)	2.75 (dd 6.6, 14.1)	2.70 (td 4.8, 6.6)	2.75 (dd, 7.2, 14.4)	2.75 (dt, 6.6, 13.8)	2.66 (m)	2.70 (t, 6.6)
5	6.39 (dd, 2.4, 3.0)		6.39 (d, 2.4)		6.39 (d, 3.0)				6.39 (d, 2.4)
7	6.48 (d, 2.4)	6.62 (s)	6.48 (d, 2.4)	6.63 (s)	6.48 (d, 3.0)	6.63 (s)	6.62 (s)	6.59 (br s)	6.48 (d, 2.4)
1′a	1.64 (m)	1.63 (m)	1.55 (m)	1.55 (m)	1.82 m	1.61 (m)	1.56 (m)	1.53 (m)	1.63 (m)
1′b	1.55 (m)	1.56 (m)	1.62 (m)	1.63 (m)	1.55 m	1.55 (m)	1.63 (m)	1.21 (m)	1.56 (m)
2′a	2.11 (m)	2.13 m	2.1 (m)	2.10 (m)	2.10 m	2.10 (m)	2.13 (m)	1.95 (m)	2.12 (m)
2′b								1.85 (m)	
3′	5.17 (brt, 6.6)	5.17 (brt, 7.2)	5.13 (brt, 6.6)	5.15 (brt, 7.2)	5.11 (brt, 7.2)	5.10 (brt, 7.2)	5.13 (brt, 6.6)	5.13 (t, 6.6)	5.14 (t, 6.6)
5′a	1.98 (m)	1.98 (m)	1.97 (m)	1.98 (m)	1.96 m	1.96 (m)	1.96 (m)	2.11 (m)	2.15 (m)
5′b								1.80 (m)	1.92 (m)
6′a	2.08 (m)	2.07 (m)	2.06 (m)	2.06 (m)	2.05 (dd, 7.2, 7.8)	2.05 (m)	2.05 (m)	1.13 (m)	1.32 (m)
6′b								1.99 (m)	1.67 (m)
7′	5.13 (brt, 6.6)	5.13 (brt, 7.2)	5.13 (brt, 6.6)	5.15 (brt 7.2)	5.11 (brt, 7.2)	5.13 (brt, 7.2)	5.12 (brt, 6)	5.08 (brt, 7.2)	1.61 (m)
9′a	2.22 (m)	2.22 (m)	2.26 (m)	2.27 (m)	2.22 (brt, 7.8)	2.22 (m)	2.28 (t, 7.8)	2.14 (m)	5.23 (s)
9′b	2.06 (m)	2.07 (m)	2.02 (m)	2.02 (m)				2.10 (m)	
10′a	1.58 (m)	1.41 (m)	1.41 (m)	1.41 (m)	2.53 (brt, 7.8)	2.53 (m)	2.63 (t, 7.8)	1.45 (dt, 3.6, 7.2)	2.25 (m)
10′b	1.44 (m)	1.58 (m)	1.51 (m)	1.51 (m)					1.97 (m)
11′	3.36 (br d, 10.2)	3.36 (brd, 10.8)	3.29 (brd, 10.2)	3.43 (dt, 2.4, 10.8)				3.31 (m)	3.45 (m)
12′					2.61 (m)	2.61 (m)			
13′	1.20 (s)	1.20 (s)	1.12 (s)	1.12 (s)	1.09 (d, 6.6)	1.08 (d, 6.6)	1.38 (overlap)	1.37 (s)	0.81 (s)
14′	1.16 (s)	1.15 (s)	1.09 (s)	1.09 (s)	1.09 (d, 6.6)	1.09 (d, 6.6)	1.38 (overlap)	1.24 (s)	0.94 (s)
15′	1.59 (brs)	1.59 (brs)	1.59 (brs)	1.59 (brs)	1.59 (brs)	1.59 (brs)	1.61 (brs)	1.58 (brs)	1.71 (brs)
16′	1.60 (brs)	1.60 (brs)	1.58 (brs)	1.58 (brs)	1.59 (brs)	1.59 (brs)	1.59 (brs)	1.03 (brs)	1.61 (brs)
17′	1.26 (s)	1.27 (s)	1.26 (s)	1.26 (s)	1.26 (s)	1.27 (s)	1.27 (s)	1.37 (s)	1.27 (s)
18′	2.13 (s)	2.10 (s)	2.13 (s)	2.11 (s)	2.13 (s)	2.11 (s)	2.10 (s)	2.11 (s)	2.13 (s)
19′		3.78 (s)	3.22 (s)	3.78 (s)		3.78 (s)	3.78 (s)		
20′				3.22 (s)					

J. Agric. Food Chem. 2015, 63, 2472−2478
DOI: 10.1021/jf5056387

Table 2. ^{13}C NMR Data (150 MHz, $CDCl_3$) for Compounds 1−9

	1	2	3	4	5	6	7	8	9
2	75.2	74.9	75.3	74.9	75.3	74.9	74.8	74.9	75.2
3	31.3	30.6	31.4	30.6	31.3	30.6	30.6	32.5	31.3
4	22.4	17.4	24.1	17.4	22.4	17.4	17.4	17.8	24.1
4a	121.2	114.3	121.2	114.3	121.3	114.3	114.3	110.3	120.2
5	112.6	142.3	112.6	142.2	112.6	142.3	142.3	132.5	112.6
6	147.7	140.7	147.8	140.7	147.7	140.7	140.3	147.0	147.7
7	115.6	115.0	115.6	114.9	115.6	114.9	115.0	123.4	115.6
8	127.3	122.3	127.3	122.3	127.3	122.3	122.3	116.0	127.3
8a	145.9	145.4	145.9	145.4	145.9	145.4	145.4	148.8	145.9
1′	39.4	39.6	39.4	39.6	39.5	39.7	39.6	34.0	39.4
2′	22.1	22.1	22.1	22.1	22.1	22.1	22.1	21.1	22.1
3′	124.5	124.4	124.3	124.2	124.4	124.3	124.4	124.6	124.7
4′	134.9	135.0	134.9	135.1	134.9	135.0	134.9	137.1	135.3
5′	39.5	39.6	39.6	39.6	39.5	39.5	39.5	38.4	41.9
6′	26.4	26.4	26.6	26.6	26.5	26.5	26.5	29.4	27.0
7′	125.0	125.0	124.5	124.5	124.6	124.6	125.1	127.1	48.7
8′	134.9	134.9	135.0	134.9	133.2	133.8	133.3	133.9	137.0
9′	36.7	36.8	36.8	36.8	33.5	33.5	33.1	34.1	118.3
10′	29.6	29.7	29.6	29.6	39.1	39.1	34.3	32.2	31.7
11′	78.3	78.3	76.3	76.8	214.8	214.6	214.1	72.0	75.0
12′	73.0	73.0	76.8	77.4	40.8	40.8	76.2	83.2	38.0
13′	26.3	26.4	20.7	20.7	18.2	18.2	26.4	21.3	16.0
14′	23.2	23.2	18.9	18.8	18.2	18.2	26.4	24.3	25.2
15′	15.9	15.9	15.9	15.9	16.1	16.1	15.8	17.4	22.4
16′	15.8	15.8	15.9	15.8	15.8	15.9	16.1	15.9	16.0
17′	24.0	23.9	24.1	23.9	24.1	23.9	23.9	25.9	22.6
18′	16.1	15.9	16.1	16.0	16.1	15.8	15.9	15.3	16.1
19′		60.5	49.0	60.6		60.6	60.5		
20′				49.0					

applied on silica gel 60 (Merck, 230−400 mesh), Sephadex LH-20 (Amersham Pharmacia Biotech), and Li Chroprep RP-18 (Merck, 40−63 μm).

The EtOAc-soluble portion (65 g) was subjected to a silica gel column in gradient elution of mixed solvent compoed of *n*-hexane−EtOAc−MeOH and led to 25 fractions (E1−E25). Fraction E11 (640 mg) was separated via another silica gel column with hexane−ethyl acetate mixture as the eluent to obtain 15 subfractions (E11-1−E11-15). Fraction E10 (642 mg) was fractionated by a Sephadex LH-20 column (100% acetone) to give nine subfractions (E10-1−E10-9). Compound **1** (7 mg) was purified by LH-20 chromatography (100% acetone) from subfraction E11-10 (228 mg) together with eight portions (E11-10-1−E11-10-8). Compounds **2** (7 mg), **3** (4 mg), and **7** (2 mg) were, respectively, isolated form fractions E11-10-3, E10-5, and E10-7 by C-18 reverse-phase chromatography with MeOH−H_2O (7:3−1:0); besides, six subfractions (E10-7-1−E10-7-6) were obtained. Moreover, compounds **4** (2 mg) and **8** (1 mg) were isolated from subfraction E10-7-3 and subjected to silica gel column purification and by reverse-phase HPLC (MeOH/H_2O = 85:15). On the other hand, the nonpolar section, hexane layer, was separated in the same way as the EtOAc−solution part, and 10 fractions (H1−H10) were given. Fraction H8 was reapplied to a silica gel column using *n*-hexane−EtOAc mixtures in stepwise-increasing polarity to fractionate 14 segments (H8-1−H8-14). The subfraction H8-11 (3.5 g) was further purified through an Amberlite XAD-2 column (100% MeOH), a Toyopearl HW-40F column, and a RP-HPLC column (MeOH/H_2O = 85:15), resulting in compounds **5** (4 mg), **6** (2 mg), and **9** (9 mg).

*Litchtocotrienol A (**1**).* **1** was a colorless oil. CD (MeOH, c = 0.12, nm (ε)) 212 (−1.09), 225 (+14.33), 291 (−0.83). $[\alpha]^{25}_{D}$ −75 (c = 0.2, $CHCl_3$). UV (MeOH) λ_{max} 297 (log ε = 3.0) nm. IR (KBr): 3391, 1609, 1472 cm^{-1}. ^1H NMR (600 MHz, $CDCl_3$) and ^{13}C NMR (150 MHz, $CDCl_3$) spectroscopic data are listed in Tables 1 and 2, respectively. HRESIMS $[M + Na]^+$ m/z 453.2962 (calcd for $C_{27}H_{42}O_4Na$, 453.2975). IUPAC name: (*S*,6*E*,10*E*)-13-((*R*)-6-hydroxy-2,8-dimethylchroman-2-yl)-2,6,10-trimethyltrideca-6,10-diene-2,3-diol.

*Litchtocotrienol B (**2**).* **2** was a colorless oil. CD (MeOH, c = 0.12, nm (ε)) 211 (+7.41), 278 (−0.49). $[\alpha]^{25}_{D}$ +85 (c = 0.2, $CHCl_3$). UV (MeOH) λ_{max} 294 (log ε = 3.0) nm. IR (KBr): 3424, 1482, 3424 cm^{-1}. ^1H NMR (600 MHz, $CDCl_3$) and ^{13}C NMR (150 MHz, $CDCl_3$) spectroscopic data are listed in Tables 1 and 2, respectively. HRESIMS $[M + Na]^+$ m/z 483.3085 (calcd for $C_{28}H_{44}O_5Na$, 483.3081). IUPAC name: (*S*,6*E*,10*E*)-13-((*R*)-6-hydroxy-5-methoxy-2,8-dimethylchroman-2-yl)-2,6,10-trimethyltrideca-6,10-diene-2,3-diol.

*Litchtocotrienol C (**3**).* **3** was a colorless oil. CD (MeOH, c = 0.12) nm (ε) 216 (+11.99), 285 (−0.99). $[\alpha]^{25}_{D}$ −63 (c = 0.11, $CHCl_3$). UV (MeOH) λ_{max} 296 (log ε = 3.0) nm. IR (KBr):3358 and 1471 cm^{-1}. ^1H NMR (600 MHz, $CDCl_3$) and ^{13}C NMR (150 MHz, $CDCl_3$) spectroscopic data are listed in Tables 1 and 2, respectively. HRESIMS $[M + Na]^+$ m/z 467.3128 (calcd for $C_{28}H_{44}O_4Na$, 467.3132). IUPCA name: (*R*)-2-((*S*,3*E*,7*E*)-11-hydroxy-12-methoxy-4,8,12-trimethyltrideca-3,7-dien-1-yl)-2,8-dimethylchroman-6-ol.

*Litchtocotrienol D (**4**).* **4** was a colorless or yellow oil. CD (MeOH, c = 0.12) nm (ε) 207 (+6.45), 278 (−1.18). $[\alpha]^{25}_{D}$ −72 (c = 0.11, $CHCl_3$). UV (MeOH) λ_{max} 293 (log ε = 3.0) nm. IR (KBr): 3429 and 1479 cm^{-1}. ^1H NMR (600 MHz, $CDCl_3$) and ^{13}C NMR (150 MHz, $CDCl_3$) spectroscopic data are listed in Tables 1 and 2, respectively. HRESIMS $[M + Na]^+$ m/z 497.3219 (calcd for $C_{29}H_{46}O_5Na$, 497.3227). IUPAC name: (*R*)-2-((*S*,3*E*,7*E*)-11-hydroxy-12-methoxy-4,8,12-trimethyltrideca-3,7-dien-1-yl)-5-methoxy-2,8-dimethylchroman-6-ol

*Litchtocotrienol E (**5**).* **5** was a yellow oil. CD (MeOH, c = 0.12, nm (ε)) 212 (−3.03), 256 (+0.35), 291 (−0.30). $[\alpha]^{25}_{D}$ +44 (c = 0.2, $CHCl_3$). UV (MeOH) λ_{max} 296 (log ε =2.9) nm. IR (KBr): 3415, 1705, 1467 cm^{-1}. ^1H NMR (600 MHz, $CDCl_3$) and ^{13}C NMR (150 MHz, $CDCl_3$) spectroscopic data are listed in Tables 1 and 2,

DOI: 10.1021/jf5056387
J. Agric. Food Chem. 2015, 63, 2472−2478

respectively. HRESIMS $[M + Na]^+$ m/z 435.2861 (calcd for $C_{27}H_{40}O_3Na$, 435.2870). IUPAC name: (6*E*,10*E*)-13-((*R*)-6-hydroxy-2,8-dimethylchroman-2-yl)-2,6,10-trimethyltrideca-6,10-dien-3-one.

*Litchtocotrienol F (**6**).* **6** was a yellow oil. CD (MeOH, c = 0.12, nm (ε)) 207 (+6.46), 278 (−1.19). $[\alpha]^{25}_D$ +45 (c = 0.2, $CHCl_3$). UV (MeOH) λ_{max} 293 (log ε = 2.9) nm. IR (KBr): 3425, 1708, 1475 cm^{-1}. ^1H NMR (600 MHz, $CDCl_3$) and ^{13}C NMR (150 MHz, $CDCl_3$) spectroscopic data are listed in Tables 1 and 2, respectively. HRESIMS $[M + Na]^+$ m/z 465.2962 (calcd for $C_{28}H_{42}O_4Na$, 465.2975). IUPAC name: (6*E*,10*E*)-13-((*R*)-6-hydroxy-5-methoxy-2,8-dimethylchroman-2-yl)-2,6,10-trimethyltrideca-6,10-dien-3-one.

*Litchtocotrienol G (**7**).* **7** was a yellow oil. CD (MeOH, c = 0.11, nm (ε)) 210 (−3.79), 2.49 (+1.04), 2.91 (−0.39). $[\alpha]^{25}_D$ +83 (c = 0.12, $CHCl_3$). UV (MeOH) λ_{max} 292 (log ε = 2.5) nm. IR (KBr): 3417, 1708, 1454 cm^{-1}. ^1H NMR (600 MHz, $CDCl_3$) and ^{13}C NMR (150 MHz, $CDCl_3$) spectroscopic data are listed in Tables 1 and 2, respectively. HRESIMS $[M + Na]^+$ m/z 481.2910 (calcd for $C_{28}H_{42}O_5Na$, 481.2924). IUPAC name: (6*E*,10*E*)-2-hydroxy-13-((*R*)-6-hydroxy-5-methoxy-2,8-dimethylchroman-2-yl)-2,6,10-trimethyltrideca-6,10-dien-3-one.

*Macrolitchtocotrienol A (**8**).* **8** was a yellow oil. CD (MeOH, c = 0.12, nm (ε)) 220 (−70.42), 282 (−2.68). $[\alpha]^{25}_D$ −54.0 (c = 0.1, $CHCl_3$). UV (MeOH) λ_{max} 293 (log ε = 2.6) nm. IR (KBr): 3410, 1475 cm^{-1}. ^1H NMR (600 MHz, $CDCl_3$) and ^{13}C NMR (150 MHz, $CDCl_3$) spectroscopic data are listed in Tables 1 and 2, respectively. HRESIMS $[M + Na]^+$ m/z 451.2820 (calcd for $C_{27}H_{40}O_4Na$, 451.2819). IUPAC name: (1^2R,4*E*,8*E*,12*S*)-1^2,1^8,5,9,13,13-hexamethyl-1^3,1^4-dihydro-1^2H-14-oxa-1(2,6)-chromenacyclotetradecaphane-4,8-diene-1^5,12-diol.

*Cyclolitchtocotrienol A (**9**).* **9** was a yellow oil. CD (MeOH, c = 0.12, nm (ε)) 216 (+15.48), 267 (−0.91). $[\alpha]^{25}_D$ −13.5 (c = 0.1, $CHCl_3$). UV (MeOH) λ_{max} 293 (log ε = 3.0) nm. IR (KBr): 3410, 1469 cm^{-1}. ^1H NMR (600 MHz, $CDCl_3$) and ^{13}C NMR (150 MHz, $CDCl_3$) spectroscopic data are listed in Tables 1 and 2, respectively. HRESIMS $[M - H]^-$ m/z 411.2891 (calcd for $C_{27}H_{39}O_3Na$, 411.2894). IUPAC name: (*R*)-2-((*E*)-6-((1*R*,5*S*)-5-hydroxy-2,6,6-trimethylcyclohex-2-en-1-yl)-4-methylhex-3-en-1-yl)-2,8-dimethylchroman-6-ol.

In Vitro Cytotoxicity Assay. The cytotoxicity assays for these new isolated litchtocotrienols against HepG2 2.2.1.5 (human hepatocellular carcinoma cells) obtained from Prof. Pei-Jer Chen of National Taiwan University and AGS (ATCC CRL 1739; human gastric adenocarcinoma) were estimated by the 3-(4,5-dimethylthiazol-2-yl)-2,5-diphenyltetrazolium bromide (MTT) colorimetric method.[21,22] Briefly, 10% FBS dilution of cancer cells was loaded in 96-well plates and then incubated for 24 h to allow for attaching to the microtiter plate. Pure compounds in different concentrations (2−20 μg/mL) and positive control (doxorubicin and 5-fluorouracil) treated on cancer cells and then hatched at 37 °C in a 5% CO_2 incubator for 24 h. After incubation, the medium was removed from each well and added 100 μL of MTT (dissolved in PBS) at 37 °C for 1 h, and then MTT crystals were washed away by DMSO. Finally, each plate was measured by a plate reader at 570 nm, and the cytotoxic intensity of each compound was determined by the OD values.

RESULTS AND DISCUSSION

The structures of the isolated compounds were determined by extensive spectroscopic analysis, including nuclear magnetic resonance (NMR), high-resolution mass spectroscopy (HR-ESIMS), UV, IR, and circular dichroism (CD) techniques.

Compound **1**, Figure 1, was obtained as a colorless oil. The molecular formula, $C_{27}H_{42}O_4$ with 7 degrees of unsaturation, was deduced from the pseudo-molecular ion (m/z 453.2962, $[M + Na]^+$ calcd for 453.2975) in HRESIMS. The IR spectrum showed the absorptions of the hydroxyl group (3394 cm^{-1}) and aromatic ring (1609 cm^{-1}). The ^1H NMR spectrum (Table 1) exhibited six tertiary methyl signals at δ_H 1.16, 1.20, 1.26, 1.59, 1.60, and 2.13 and five methine resonances at δ_H 3.36 (br d, J = 10.2 Hz), 5.13 (br t, J = 6.6 Hz), 5.17 (br t, J = 6.6 Hz), 6.39 (d, J = 2.4 Hz), and 6.48 (d, J = 2.4 Hz). In the DEPT NMR spectra, 27 signals were categorized into six methyl carbons at δ_C 15.8, 15.9, 16.1, 23.2, 24.0, and 26.3, eight methylene carbons at δ_C 22.1, 22.4, 26.4, 29.6, 31.3, 36.7, 39.4, and 39.5, five methine carbons at δ_C 78.3, 112.6, 115.6, 124.5, and 125.0, and eight quaternary carbons at δ_C 73.0, 75.2, 121.2, 127.3, 134.9, 134.9, 145.9, and 147.7 (Table 2). Four sections (**I**−**IV**, Supporting Information) were established from key cross-peaks in the COSY spectrum (H-3/H-4, H-1′/H-2′/H-3′, H-5′/H-6′/H-7′, H-9′/H-10′/H-11′). In the HMBC spectrum, the correlations of H-5 with C-4a (δ_C 121.2), C-6 (δ_C 147.7), C-7 (δ_C 115.6), and C-8a (δ_C 145.9) and that of Me-18′ with C-8 (δ_C 127.3), C-7, and C-8a revealed that compound **1** possessed a *m*-cresol structure. In addition, the ^1H−^{13}C heteronuclear correlations of Me-17′ with the oxygenated quaternary carbon C-2 (δ_C 75.2), C-3 (δ_C 31.3), and C-1′ (δ_C 39.4) as well as that of H-4 with C-4a plus the segment **I** extend the *m*-cresol to a chromanol ring moiety. Likewise, fragments **II**−**IV** combined with the HMBC correlations of the methyl protons at Me-16′ with C-3′ (δ_C 124.5), C-4′ (δ_C 134.9), and C-5′ (δ_C 39.5), Me-15 with C-7′ (δ_C 125.0), C-8′ (δ_C 134.9), and C-9′ (δ_C 36.7), and two geminal methyls Me-13′ and Me-14′ both showed correlations with C-11′ (δ_C 78.3) and C-12′(δ_C 73.0), indicating a long linear geranyl portion connected with 2,3-pentanediol. Therefore, the planar structure of **1**, which pertained to the δ-tocotrienol skeleton, was assigned as litchtocotrienol A.[23−27]

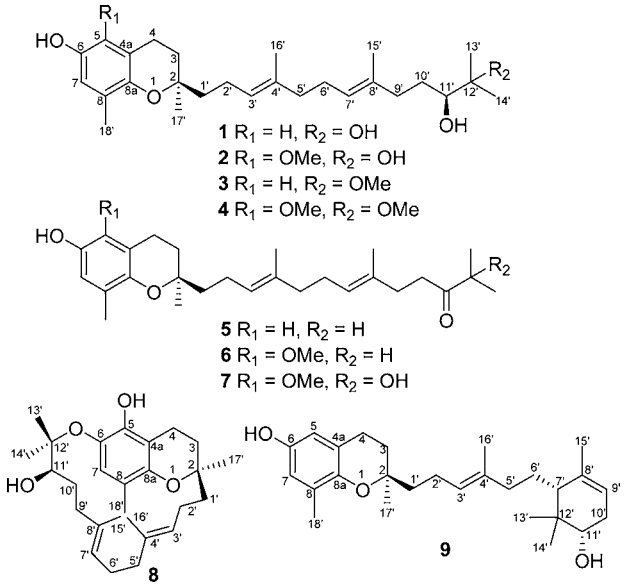

Figure 1. Structures of compounds **1**−**9** from the leaves of *L. chinensis*.

The configuration of **1** was determined mainly from NOESY correlations and the circular dichroism (CD) spectrum. The carbon resonances of two vinyl methyls Me-15′ (δ_C 15.9) and Me-16′ (δ_C 15.8) combined with the NOESY cross-peaks of H-1′/H-3′/H-5′ and H-2′/Me-16′/H-5′/H-7′ explained the *E* geometry for the $\Delta^{3'4'}$ and $\Delta^{7'8'}$ double bonds. Besides, the *R* configuration of C-11′ was assigned by comprehensive comparison of NMR data with that of (1*R*, 2*R*, 4*S*, 17*R*)-loba-8,10,13(15)-triene-17,18-diol.[28,29] Additionally, the absolute configuration of the chiral center at C-2 was suggested by CD observation. The negative Cotton effect at 291 ($\Delta\varepsilon$ −0.83)

DOI: 10.1021/jf5056387
J. Agric. Food Chem. 2015, 63, 2472−2478

nm in the CD spectrum indicated that **1** has the *R* configuration at C-2.[30,31]

Compound **2** possessed a pseudomolecular ion peak at *m/z* 483.3085 by HRESIMS, appropriate for a molecular formula of $C_{28}H_{44}O_5$. The same units of unsaturation and similar ^1H and ^{13}C NMR data (Tables 1 and 2) to **1** disclosed that these two structures pertain to the same litchtocotrienol-type framework, and thus, **2** is an analogue of **1**. The difference between **1** and **2** was an aromatic proton H-5 (δ_H 6.39) in **1** and a methoxyl group (δ_H 3.78) in **2**. The actual structure was confirmed by key HMBC correlations of H-4 (δ_H 2.75), H-7 (δ_H 6.62), and H_3-19′ (δ_H 3.78) with C-5 (δ_C 142.3). The similar NOESY correlations suggested the same configuration of the hydroxylated farnesyl tail in **2**. Moreover, the negative CD curve at 278 ($\Delta\varepsilon$ −0.49) nm assigned the *R* chirality of C-2.[30,31] Consequently, compound **2** was named litchtocotrienol B, a 5-methoxyl analogue of litchtocotrienol A.

Compound **3** was isolated as colorless oil, and the HRESIMS of **3** afforded a $[M + Na]^+$ ion at *m/z* 467.3128, implying the molecular formula $C_{28}H_{44}O_4$ and 7 indices of unsaturation. ^1H and ^{13}C NMR spectra of **3** were similar to those of **1**, and the formula difference indicated that **3** has a homologous structure. Moreover, the extra methyl protons at δ_H 3.22 and the same counts of each carbon multiplicities showing in the DEPT analyses indicated that **3** was a methylated derivative of **1**. The HMBC correlation of *O*-methyl (δ_H 3.22) with the quaternary carbon C-12′ (δc 76.8) pointed the evident position at the end of the side chain. Equally, the negative CD band allowed the *R* assignment at C-2. On the basis of the above data, the structure of **3** was elucidated as (*R*)-2-((*S*,3*E*,7*E*)-11-hydroxy-12-methoxy-4,8,12-trimethyltrideca-3,7-dien-1-yl)-2,8-dimethylchroman-6-ol, designated as litchtocotrienol C.

The molecular formula of **4** was calculated as $C_{29}H_{46}O_5$ with 7 degrees of unsaturation deducing from the HR-ESIMS. The similar UV, IR, and NMR spectra suggested that compound **4** possessed the same litchtocotrienol skeleton. Comprehensive analyses and comparisons of NMR data of compounds **2**−**4** showed that **4** differed from **2** by one aliphatic methoxy (δ_H 3.22, δ_C 49.0) and from **3** by one aromatic methoxy signal (δ_H 3.78, δ_C 60.6). In the HMBC spectrum, the methyl protons of OMe-5 (δ_H 3.78, 3H, s) were associated with C-5 (δ_C 142.2) while OMe-12′ corresponded with C-12′ (δ_C 76.8). These two essential HMBC correlations evidenced that compound **4** performed 12′-*O*-methylation of **2**, while it acted as a 5′-*O*-methylated mimic of **3** and thus was given the name litchtocotrienol D.

On the basis of the characteristics of IR and NMR data and HR-ESIMS information (*m/z* 435.2861, $[M + Na]^+$), compound **5** was identified as a δ-tocotrienol analogue with a molecular formula $C_{27}H_{40}O_3$ (8 degrees of unsaturation). The main structural difference from previous litchtocotrienols **1**−**4** was that compound **5** contained a ketone group according to the IR vibration at 1705 cm^{-1} and the downfield carbon signal at δ_C 214.8. After ^1H, ^{13}C, and DEPT NMR analyses, compound **5** was composed of two methyl groups instead of one methoxyl group. The COSY fragment of Me-13′/H-12′/Me-14′ along with the long rang $^1H-^{13}C$ associations of H-9′, H-10′, H-12′, Me-13′, and Me-14′ with C-11′ (δ_C 214.8) inferred an isopropyl group unit adjacent to a ketone group (C-11′). The configuration of **5** was determined from interpretation of NOESY and CD spectra. The *E* stereochemistry of two olefins at the side chain was assigned by the presence of the NOESY correlations of H-2′/Me-16′ and H-6′/Me-15′. The 2*R* configuration was determined by comparison of the CD spectrum with that of **1** and the literature.[31] Thus, compound **5** was identified as (6*E*,10*E*)-13-((*R*)-6-hydroxy-2,8-dimethylchroman-2-yl)-2,6,10-trimethyltrideca-6,10-dien-3-one, and the name litchtocotrienol E was given.

The HR-ESIMS spectrum of compound **6** exhibited a pseudo-molecular ion at *m/z* 465.2962 $[M + Na^+]$, consistent with a molecular formula of $C_{28}H_{42}O_4$ (8 degrees of unsaturation). The IR spectrum of **6** showed a similar absorbance to that of **5**, including functional groups of hydroxyl (3425 cm^{-1}) and ketone (1708 cm^{-1}), suggesting that **6** was an analogue of **5**. By comparing the NMR data, the methine H-5 on the benzene moiety in **5** was substituted by a methoxyl group (OMe-19′) in **6**, which was also confirmed by the HMBC correlation from OMe-19′ (δ_H 3.78) to C-5 (δ_C 142.3). The 2*R* configuration at the dihydropyran ring was corroborated by the CD measurement (278 nm, −1.19) and compared with that of **1**. Thus, the structure of litchtocotrienol F was unambiguously established.

Compound **7** possessed a molecular formula of $C_{28}H_{42}O_5$ with 8 units of unsaturation by deducing from the HR-ESIMS peak at *m/z* 481.2910 $[M + Na]^+$. The specific NMR peaks (six methyls and a *m*-cresol) revealed that **7** also possessed a chromanol ring moiety with a side chain containing three double bonds. Except the geranyl part, the quaternary carbon resonance at δ_C 214.1 and the IR absorption at 1699 cm^{-1} indicated that the third sp^2-hybridized carbon was a ketone functionality as compounds **5** and **6**. The protons of H-4, H-7, and Me-19′ corresponded with C-5 in the HMBC spectrum, suggesting a 5-methoxyl modification. Meanwhile, the HMBC correlations of both Me-13′ and Me-14′ with the oxygenated quaternary carbon C-12′ (δ_C 76.2) and that of H-9′, H-10′, Me-13′, and Me-14′ with carbonyl carbon C-11′ (δ_C 214.1) evidenced that the side chain ended in a 2-hydroxyl isobutanone. Finally, it gave the name litchtocotrienol G to compound **7**, a 12′-hydroxylated derivate of **2**.

Compound **8** was obtained as a colorless oil and had a molecular ion peak at *m/z* 451.2820 $[M + Na]^+$ (calcd for 451.2819) in HRESIMS, corresponding to the molecular formula $C_{27}H_{40}O_4$ and 8 degrees of unsaturation. The IR and ^1H and ^{13}C NMR spectra of **8** revealed that **8** should be a derivative of itchtocotrienol without ketone structure. Similarly, the gross structure of **8** was mainly established by the COSY correlations of H-3/H-4, H-1′/H-2′/H-3′, H-5′/H-6′/H-7′, and H-9′/H-10′/H-11′ connected by the HMBC correlations of the methyl protons at Me-16′ with C-3′ (δ_C 124.6), C-4′ (δ_C 137.1), and C-5′ (δ_C 38.4) and Me-15′ with C-7′ (δ_C 127.1), C-8′ (δ_C 133.9), and C-9′ (δ_C 34.1). Furthermore, the HMBC correlations of two terminal methyl protons (Me-13′and Me-14′) with C-11′ (δ_C 72.0) and C-12′ (δ_C 83.2) indicated the linear prenyl chain attached to a 2, 3-pentanediol group via C-11′. Thus far, seven degrees of unsaturation were applied; an extra ring was required for compound **8**. There are four possible ether arrangements for cycling through an oxygen bridge (C-5 or C-6 connected with C-11′ or C-12′) by considering of ^1H and ^{13}C NMR data. The absence of the proton−carbon correlations of H-11′ with C-5 or C-6 inferred that either the ring was formed via the linkage between C-5 and C-12′ or that between C-6 and C-12′. This problem was solved by the presence of the key NOESY correlation (Figure 2) of H-7/Me-14′ which only appeared in the ether linkage crossing C-6 and C-12′. Therefore, the planar structure of **8** was identified

DOI: 10.1021/jf5056387
J. Agric. Food Chem. 2015, 63, 2472−2478

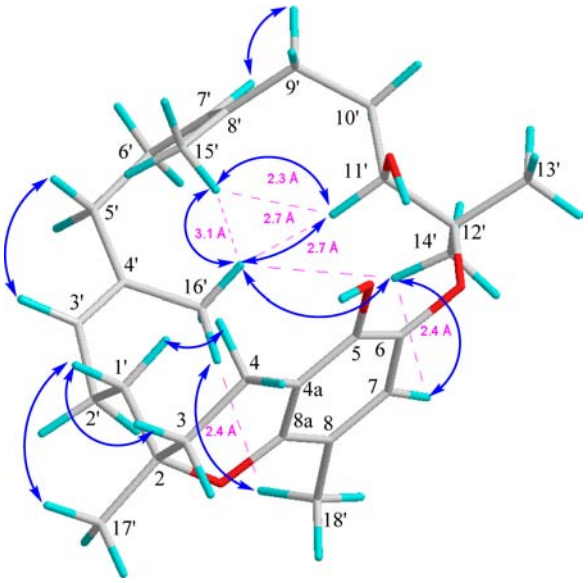

Figure 2. Selected NOESY correlations of **8**.

as the δ-tocotrienol skeleton and occupied an unusual oxacyclicnonadecane ring.

The configuration of **8** was determined mainly from the NOESY correlations and circular dichroism. The CD spectrum of **8** exhibited the negative Cotton effect at 282 ($\Delta\varepsilon$ −2.67) nm, indicating 2*R* chiral center.[23−27,31] Thus, it was assumed that Me-17′ of **8** favored the α orientation as those naturally occurring chromane derivatives and the prenyl chain was on the β face. The NOESY correlations of H-3′/H-5′and H-7′/H-9′ could assign the *E* geometry of the double bonds. Importantly, H-11′, Me-14′, Me-15′, and Me-18′ showed the dipolar couplings with Me-16′ (Figure 2), which had a quasi-equatorial orientation and was upfield shifted to δ_H 1.03 by anisotropic effects from the benzene ring, confirming the existence of this macrocyclic structure, and revealed the α orientation of H-11′. Thus, the whole structure of **8** was elucidated and named cyclolitchtocotrienol A.

Compound **9** had the molecular formula $C_{27}H_{40}O_3$ with 8 indices of unsaturation by measuring the HR-ESIMS. Analysis of ^{13}C NMR data showed 10 olefinic signals which revealed that compound **9** contained a tricyclic ring system. The ^1H NMR spectrum exhibited two characteristic methine signals at δ_H 6.39 (d, *J* = 2.8 Hz) and 6.48 (d, *J* = 2.8 Hz) coupled with the HMQC spectrum as well as the UV maximal absorption at 293 nm (log ε = 3.0), revealing the presence of a hydroquinone-type moiety.[32] The $^1H-^1H$ COSY spectrum of **9** showed four segments similar to that in **1** and with the aid of key correlations in the HMBC spectrum (H-4, H-5, and H-7/C-8a; Me-18′/C-7, C-8, and C-8a; Me-17′/C-1′, C-2, and C-3; H-4/C-2, C-4a, and C-5; Me-16′/C-3′, C-4′, and C-5′), illustrating the chromanol moiety attached with the first isoprene unit (C-1′∼C-5′) via C-2. However, the proton sequence III revealed H-5′/H-6′ connecting to an aliphatic proton H-7′ rather than to an olefinic one and H-10′/H-11′ corresponding to a sp^2 methine proton H-9′ not a sp^3 methylene, and the HMBC correlations of Me-15′/C-7′, C-8′, and C-9′ indicated that the last double bond was located at $\Delta^{8/9'}$ and suggested the presence of an additional ring at the prenyl portion. Incorporating with the long-range heteronuclear couplings of H-7′ with C-8′, C-9′, and C-11′ as well as of Me-13′ and Me-14′ with C-7′, C-11′ and C-12′ allowed the accomplishment of the rest of the structure containing the third ring, a trimethylcyclohexenol. Consequently, the planar structure of cyclolitchtocotrienol A was established as a new chromane meroditerpene.

The CD curve of **9** showing a negative Cotton effect at 267 nm proved the absolute 2*R* of **9**. The NOESY correlations of H-7′ and H-10′b/H-11′, H-11′/Me-13′ indicated that these protons were at the same β position. On the other hand, the NOESY cross-peak of H-10′a/Me-14′ showed the α orientation of H-10′a and Me-14′. Furthermore, the β orientation of both H-7′ and H-11′ was identified by the ^1H and ^{13}C NMR signal comparisons of **9** and camelliol C, which also contained a trimethylcyclohexenol portion.[33] On the basis of above interpretation, the configuration of **9** was unambiguously established as 2*R*, 7′*R**, and 11′*S**.

Human hepatocellular carcinoma (HepG2 2.2.15) and human gastric epithelial (AGS) cells were chosen to test the in vitro cytotoxicity of the isolated compounds. The results (Table 3) showed that compounds **1**−**8** exhibited minor cytotoxic activities against HepG2 2.2.15 and AGS cells line.

Table 3. Cytotoxicity of 1−8 on Tumor Cell Lines, IC_{50} (μM)

compound	HepG2	AGS	compound	HepG2	AGS
1	11.11	10.91	**6**	12.30	49.24
2	14.18	32.02	**7**	34.13	43.24
3	22.66	24.20	**8**	16.52	NT[a]
4	NT[a]	26.76	5-fluorouracil[b]	62.9	
5	10.71	27.36	doxorubicin[b]		11.0

[a]Not tested. [b]Used as positive control.

As for the bioassay of anti-HepG2 2.2.15 cells, litchtocotrienol C (C-12′ methylated form of **1**) was 2 times less potent than that of **1**, but litchtocotrienol B (5-methoxylated form of **1**) possessed slightly weaker anti-HepG2 activity than **1**. A similar situation was observed between compounds **5** with **7** and between **5** with **6**. The above findings suggested that the functional groups at position C-12′ rather than at the chromanol ring moiety were important for the cytotoxicity against HepG2 cells of δ-tocotrienol-type compounds. As for the bioassay of anti-AGS cells, litchtocotrienols B and C were about 3 and 2 times less potent than that of **1**, respectively. In addition, compounds **6** and **7** (5-methoxylated form of **5**) were both 2 times less potent than that of **5**. These results suggested that the functional groups at position C-5 of δ-tocotrienol-type compounds were important for anti-AGS cell activities.

■ ASSOCIATED CONTENT

Supporting Information

NMR, HRESIMS, CD spectra, and selected HMBC and COSY correlations for new compounds. This material is available free of charge via the Internet at http://pubs.acs.org.

■ AUTHOR INFORMATION

Corresponding Author

*Tel.: +886-4-2205-3366 (ext. 1633). Fax: +886-4-2207-1500. E-mail: choumasa@mail.cmu.edu.tw.

Author Contributions

▽Yu-Chi Lin and Jia-Chen Chang contributed equally to this work.

DOI: 10.1021/jf5056387
J. Agric. Food Chem. 2015, 63, 2472−2478

Notes

The authors declare no competing financial interest.

■ ACKNOWLEDGMENTS

This research was supported by grants from the National Science Council, Taiwan (NSC98-2321-B-039-001-MY3, NSC98-2621-B-039-002-MY3, NSC99-2622-B-039-003-CC3, and NSC98-2324-B-039-002), awarded to C.-H.C., and NCKU-D102-38B05. We appreciate the donation of HepG 2.2, 2.15 by Academician Prof. P. J. Chen of National Taiwan University. Additionally, technical assistance with NMR and MS data analyses from both Proteomics Research Core Laboratory, Office of Research & Development at China Medical University and National Chung Hsing University is greatly acknowledged.

■ REFERENCES

(1) Sarni-Manchado, P.; Le Roux, E.; Le Guerneve, C.; Lozano, Y.; Cheynier, V. Phenolic composition of litchi fruit pericarp. *J. Agric. Food Chem.* **2000**, *48*, 5995−6002.

(2) Kong, F.; Zhang, M.; Liao, S.; Yu, S.; Chi, J.; Wei, Z. Antioxidant activity of polysaccharide-enriched fractions extracted from pulp tissue of *Litchi chinensis* sonn. *Molecules* **2010**, *15*, 2152−2165.

(3) Wang, X.; Yuan, S.; Wang, J.; Lin, P.; Liu, G.; Lu, Y.; Zhang, J.; Wang, W.; Wei, Y. Anticancer activity of *litchi* fruit pericarp extract against human breast cancer in vitro and in vivo. *Toxicol. Appl. Pharmacol.* **2006**, *215*, 168−178.

(4) Zhao, M.; Yang, B.; Wang, J.; Liu, Y.; Yu, L.; Jiang, Y. Immunomodulatory and anticancer activities of flavonoids extracted from litchi (*Litchi chinensis* Sonn.) pericarp. *Int. Immunopharmacol.* **2007**, *7*, 162−166.

(5) Ma, Q.; Xie, H.; Li, S.; Zhang, R.; Zhang, M.; Wei, X. Flavonoids from the pericarps of *Litchi chinensis*. *J. Agric. Food Chem.* **2014**, *62*, 1073−1078.

(6) Jing, Y.; Huang, L.; Lv, W.; Tong, H.; Song, L.; Hu, X.; Yu, R. Structural characterization of a novel polysaccharide from pulp tissues of *Litchi chinensis* and its immunomodulatory activity. *J. Agric. Food Chem.* **2014**, *62*, 902−911.

(7) Jiang, G.; Lin, S.; Wen, L.; Jiang, Y.; Zhao, M.; Chen, F.; Prasad, K. N.; Duan, X.; Yang, B. Identification of a novel phenolic compound in litchi (*Litchi chinensis* Sonn.) pericarp and bioactivity evaluation. *Food Chem.* **2013**, *136*, 563−568.

(8) Xu, X.; Xie, H.; Wang, Y.; Wei, X. A-type proanthocyanidins from lychee seeds and their antioxidant and antiviral activities. *J. Agric. Food Chem.* **2010**, *58*, 11667−11672.

(9) Sakurai, T.; Nishioka, H.; Fujii, H.; Nakano, N.; Kizaki, T.; Radak, Z.; Izawa, T.; Haga, S.; Ohno, H. Antioxidative effects of a new lychee fruit-derived polyphenol mixture, oligonol, converted into a low-molecular form in adipocytes. *Biosci. Biotechnol. Biochem.* **2008**, *72*, 463−476.

(10) Gangehei, L.; Ali, M.; Zhang, W.; Chen, Z.; Wakame, K.; Haidari, M. Oligonol a low molecular weight polyphenol of lychee fruit extract inhibits proliferation of influenza virus by blocking reactive oxygen species-dependent ERK phosphorylation. *Phytomedicine* **2010**, *17*, 1047−1056.

(11) Choi, Y. Y.; Maeda, T.; Fujii, H.; Yokozawa, T.; Kim, H. Y.; Cho, E. J.; Shibamoto, T. Oligonol improves memory and cognition under an amyloid β(25−35)-induced Alzheimer's mouse model. *Nutr. Res. (N.Y.)* **2014**, *34*, 595−603.

(12) Noh, J. S.; Kim, H. Y.; Park, C. H.; Fujii, H.; Yokozawa, T. Hypolipidaemic and antioxidative effects of oligonol, a low-molecular-weight polyphenol derived from lychee fruit, on renal damage in type 2 diabetic mice. *Br. J. Nutr.* **2010**, *104*, 1120−1128.

(13) Jun, N.; Maremi, S. U.; Kentaro, K.; Koji, W.; Hajime, F. Amelioration of abdominal obesity by low-molecular-weight polyphenol (Oligonol) from lychee. *J. Funct. Foods* **2009**, *1*, 341−348.

(14) Wang, C. M.; Jhan, Y. L.; Yen, L. S.; Su, Y. H.; Chang, C. C.; Wu, Y. Y.; Chang, C. I.; Tsai, S. Y.; Chou, C. H. The allelochemicals of litchi leaf and its potential as natural herbicide in weed control. *Allelopathy J.* **2013**, *32*, 157−174.

(15) Castellain, R. C.; Gesser, M.; Tonini, F.; Schulte, R. V.; Demessiano, K. Z.; Wolff, F. R.; Delle-Monache, F.; Netz, D. J.; Cechinel-Filho, V.; de Freitas, R. A.; de Souza, M. M.; Meyre-Silva, C. Chemical composition, antioxidant and antinociceptive properties of *Litchi chinensis* leaves. *J. Pharm. Pharmacol.* **2014**, in press.

(16) You, C. S.; Sontag, T. J.; Swanson, J. E.; Parker, R. S. Long-chain carboxychromanols are the major metabolites of tocopherols and tocotrienols in A549 lung epithelial cells but not HepG2 cells. *J. Nutr.* **2005**, *135*, 227−232.

(17) Guan, F.; Li, G.; Liu, A. B.; Lee, M. J.; Yang, Z.; Chen, Y. K.; Lin, Y.; Shih, W.; Yang, C. S. δ- and γ-tocopherols, but not α-tocopherol, inhibit colon carcinogenesis in azoxymethane-treated F344 rats. *Cancer Prev. Res.* **2012**, *5*, 644−654.

(18) Ju, J.; Picinich, S. C.; Yang, Z.; Zhao, Y.; Suh, N.; Kong, A. N.; Yang, C. S. Cancer-preventive activities of tocopherols and tocotrienols. *Carcinogenesis* **2010**, *31*, 533−542.

(19) Tan, B. Appropriate spectrum vitamin E and new perspectives on desmethyl tocopherols and tocotrienols. *J. Am. Nutraceutical Assoc.* **2005**, *8*, 35−42.

(20) Yap, W. N.; Zaiden, N.; Tan, Y. L.; Ngoh, C. P.; Zhang, X. W.; Wong, Y. C.; Ling, M. T.; Yap, Y. L. Id1, inhibitor of differentiation, is a key protein mediating anti-tumor responses of gamma-tocotrienol in breast cancer cells. *Cancer Lett.* **2010**, *291*, 187−199.

(21) O'Toole, S. A.; Sheppard, B. L.; McGuinness, E. P. J.; Gleeson, N. C.; Yoneda, M.; Bonnar, J. The MTS assay as an indicator of chemosensitivity/resistance in malignant gynaecological tumours. *Cancer Detect. Prev.* **2003**, *27*, 47−54.

(22) Hsu, Y. M.; Weng, J. R.; Huang, T. J.; Lai, C. H.; Su, C. H.; Chou, C. H. Solanum torvum inhibits *Helicobacter pylori* growth and mediates apoptosis in human gastric epithelial cells. *Oncol. Rep.* **2010**, *23*, 1401−1405.

(23) de Mesquita, M. L.; Araújo, R. M.; Bezerra, D. P.; Filho, R. B.; de Paula, J. E.; Silveira, E. R.; Pessoa, C.; de Moraes, M. O.; Costa Lotufo, L. V.; Espindola, L. S. Cytotoxicity of δ-tocotrienols from *Kielmeyera coriacea* against cancer cell lines. *Bioorg. Med. Chem.* **2011**, *19*, 623−630.

(24) Jang, K. H.; Lee, B. H.; Choi, B. W.; Lee, H. S.; Shin, J. Chromenes from the Brown Alga *Sargassum siliquastrum*. *J. Nat. Prod.* **2005**, *68*, 716−723.

(25) Seo, Y.; Park, K. E.; Kim, Y. A.; Lee, H. J.; Yoo, J. S.; Ahn, J. W.; Lee, B. J. Isolation of tetraprenyltoluquinols from the brown alga *Sargassum thunbergii*. *Chem. Pharm. Bull.* **2006**, *54*, 1730−1733.

(26) Seo, Y.; Park, K. E.; Nam, T. J. Isolation of a new chromene from the brown alga *Sargassum thunbergii*. *Bulletin-Korean Chemical Society* **2007**, *28*, 1831−1833.

(27) Makoto, I.; Natsuko, T.; Tomoyo, H.; Takayuki, M.; Jun, M.; Haruo, S. New Chromane Derivatives Isolated from the Brown Alga *Sargassum micracanthum*. *Chem. Pharm. Bull.* **2008**, *56*, 124−128.

(28) Edrada, R. A.; Proksch, P.; Wray, V.; Witte, L.; van Ofwegen, L. Four new bioactive lobane diterpenes of the soft coral *Lobophytum pauciflorum* from Mindoro, Philippines. *J. Nat. Prod.* **1998**, *61*, 358−361.

(29) Nagaoka, H.; Iwashima, M.; Miyahara, M.; Yamada, Y. Synthesis of (1R,2R,4S,17R)-loba-8,10,13(15)-triene-17,18-diol, a marine diterpene. *Chem. Pharm. Bull.* **1992**, *40*, 556−558.

(30) Crabbé, P. *Chem. Ind.* **1969**, *27*, 917−918.

(31) Mazzini, F.; Pescitelli, G.; Di Bari, L.; Netscher, T.; Salvadori, P. Circular dichroism of tocopherols versus tocotrienols. *Chirality* **2009**, *21*, 35−43.

(32) Whittle, K. J.; Dunphy, P. J.; Pennock, J. F. The isolation and properties of δ-tocotrienol from *Hevea latex*. *Biochem. J.* **1966**, *100*, 138−145.

(33) Mariya, D. K.; William, K. W.; David, A. L.; Allie, C. O.; Seiichi, P. T. M. Arabidopsis camelliol C synthase evolved from enzymes that make pentacycles. *Org. Lett.* **2007**, *9*, 5223−5226.

DOI: 10.1021/jf5056387
J. Agric. Food Chem. 2015, 63, 2472−2478

whole broth of A. camphorata are not well-defined in high-fat diet (HFD)-induced diabetic mice.

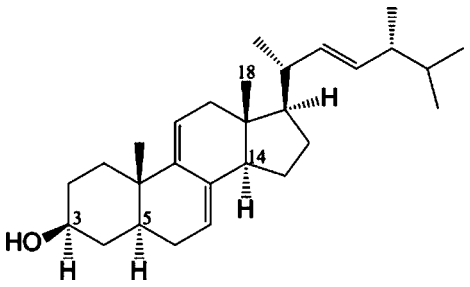

Figure 1. Structure of ergostatrien-3β-ol (EK100).

Glucose transporter 4 (GLUT4) is a key regulator of whole-body glucose homeostasis.[8] Both insulin and exercise induce a translocation of glucose transporter GLUT4 from intracellular storage compartments toward the plasma membrane in adipocytes and skeletal muscle cells, allowing the cell to take up glucose.[8,9] Impairment of GLUT4 expressions, GLUT4 translocation, and/or insulin signaling may affect insulin-stimulated glucose uptake, which would result in insulin resistance and hyperglycemia.[10] Thus, therapeutic strategies based on enhancing GLUT4 expressions may facilitate drug discovery.

AMP-activated protein kinase (AMPK) is a key regulator of glucose and lipid metabolism. Because glucose and lipid metabolism is dysregulated in type 2 diabetes mellitius,[11] AMPK modulators have been proposed to be promising therapies. Metformin is also known to activate AMPK and stimulate human skeletal muscle, promote GLUT4 membrane translocation, and stimulate insulin-independent glucose uptake.[12]

Thiazolidinediones (TZDs) such as rosiglitazone are antidiabetic peroxisome proliferator-activated receptor (PPAR) γ agonists. PPARγ activator like TZDs decrease blood glucose levels.[13] Rosiglitazone does not stimulate insulin secretion. Rosiglitazone was approved for glycemic control in people with type 2 diabetes. Rosiglitazone directly targets insulin resistance and increases peripheral glucose uptake, thus improving glycemic control. The modes of action of rosiglitazone mainly contributed to the insulin-sensitizing effect and GLUT4 levels.[14]

Fenofibrate is an activator of PPARα[15] and has been used for the management of hypertriglyceridemia for many years.[16] PPARα is a key regulator of genes associated with lipid metabolism, which results in a decrease in circulating triglycerides and fatty acids via modulation of many target genes involved in lipogenesis, fatty acid oxidation, and energy expenditure.[17]

The model of C57BL/6J mouse that was fed a high fat-diet (HFD) is a robust and efficient model for early type 2 diabetes.[18] The C57BL/6J mouse is susceptible not only to HFD-induced marked increases in adipose tissue mass but also to pronounced insulin resistance, hyperlipidemia, hyperinsulinemia, hypertriglycemia, and hypercholesterolemia.[19] Metformin is a widely used antidiabetic agent in the treatment of type 2 diabetes mellitius.[11] Metformin activates AMPK in both hepatocyte and skeletal muscle.[11,20] Nevertheless, metformin causes few adverse effects, including lactic acidosis, and this drug is regarded as a potential treatment for type 1 and type 2 diabetes. TZDs not only activate AMPK through a signal pathway that is different from metformin but also further activate AMPK.[21] This influence in plasma adipocytokine concentration is associated with a decrease in accumulation in the liver and improvement in insulin resistance.[21] Thus, Rosi was chosen as a positive control for comparison with the antidiabetic effects of EK100. Phosphorylation of Thr 172 of α subunits is essential for AMPK activity.[22] Therefore, HFD-fed mouse models are chosen to address the effect and mode of action of EK100 on AMPK activity and GLUT4 content, and to compare with Rosi and Feno. As a possible molecular mechanism of EK100, the target gene expressions involved in antidiabetes and antihyperlipidemia in peripheral tissues were also investigated.

MATERIALS AND METHODS

Chemicals. A hemoglobin A_{1c} kit was obtained from BioSystems S.A. (Barcelona, Costa Brava, Spain). GLUT4, structural proteins GAPDH and β-actin were purchased from Santa Cruz Biotechnology (Santa Cruz, CA, USA); phospho-AMPK was obtained from Abcam Inc. (Cambridge, MA, USA); phospho-Akt, total AMPK, and total Akt were from Cell Signaling Technology, Inc. (Danver MA, USA); the BCA protein assay kit was from Thermo Scientific (Rockford, IL, USA); and the ECL reagent kit was from GE Healthcare BioSciences (Buckinghamshire, UK). Secondary antibody antirabbit was from Jackson ImmunoResearch Laboratories, Inc. (West Grove, PA, USA).

Fungus Material. The freeze-dried powder of *A. camphorata* submerged whole broth was provided by the Biotechnology Center of Grape King Inc., Chung-Li City, Taiwan.

Isolation and Determination of the Active Compound. The freeze-dried powder of *A. camphorata* of the submerged whole broth (1.6 kg) was extracted three times with methanol (16 L) at room temperature (1 day each). The methanol extract was evaporated *in vacuo* to obtain a brown residue, which was suspended in H_2O (1 L) and then partitioned (three times) with 1 L of ethyl acetate. The EtOAc fraction (95 g) was chromatographed on silica gel and eluted with mixtures of hexane and EtOAc to increase polarity and further purified with high performance liquid chromatography (HPLC). EK100 (5.4 g) was eluted with 10% EtOAc in hexane, and recrystallization with EtOH.[23]

Experimental Animals. The experiments were conducted under the guidelines of the Institutional Animal Care and Use Committee of Central Taiwan University of Science and Technology. As previously described,[24−26] four-week-old male C57BL/6J mice (n = 63) was purchased from the National Laboratory Animal Breeding and Research Center, Ministry of Science and Technology. After 1-week of acclimatization, mice were designed to initiate the study, and the study lasted for 12 weeks. First, mice were divided randomly into two groups (the control (CON) group (n = 9), which received a low-fat diet (Diet 12450B, Research Diets, Inc., New Brunswick, NJ, USA), and the high-fat diet (HFD)-fed group (n = 54), which was fed a 45% high-fat diet (Diet 12451, Research Diets, Inc.)). After 8 weeks of diet induction, HFD-treated mice were further randomly subdivided into six groups (n = 9 per group), receiving EK100 (10, 20, 40 mg/kg/day body wt) or fenofibrate (Feno; purchased from Sigma Chemical Co, St Louis, and administrated at a dose of 250 mg/kg/day body wt) or rosiglitazone (Rosi; 1% methylcellulose 10 mg/kg body weight, obtained from GlaxoSmithKline Product No: BRL49653 C) or vehicle by oral gavages one time per day for another 4 weeks and still on high-fat diet. The CON group and high-fat control (HF) group were given with vehicle only. The low-fat diet consisted of fat 10%, whereas the high-fat diet (HFD) consisted of fat 45% (of total energy, % kcal). The compositions of the experimental diets are shown as described.[24] At the end of the study, food was deprived from the animals (from 10 p.m. to 10 a.m.). On the next day, the mice were sacrificed, and blood and tissue were collected for analysis. Livers, skeletal muscles, and white adipose tissues (WATs) (including epididymal, mesenteric and retroperitoneal WAT) were excised and weighed, and then

DOI: 10.1021/acs.jafc.5b00073
J. Agric. Food Chem. 2015, 63, 2479−2489

Table 1. Primers Used in This Study

Gene	Primer sequence	PCR product (bp)	Annealing temp (°C)
PEPCK	F: CTACAACTTCGGCAAATACC R: TCCAGATACCTGTCGATCTC (Seq No. NM_011044.2)	330	52
G6 Pase	F: GAACAACTAAAGCCTCTGAAAC R: TTGCTCGATACATAAAACACTC (Seq No. NM_008061.3)	350	50
Adiponectin	F:TCTTCTACAACCAACAGAATCA R:GTATCATGGTAGAGAAGGAAGC (Seq No. NM_009605.4)	324	50.5
PPARα	F: ACCTCTGTTCATGTCAGACC R: ATAACCACAGACCAACCAAG (Seq No. NM_011144)	352	55
SREBP1c	F: GGCTGTTGTCTACCATAAGC R: AGGAAGAAACGTGTCAAGAA (Seq No. NM_011480)	219	50
DGAT2	F: AGTGGCAATGCTATCATCATCGT R: AAGGAATAAGTGGGAACCAGATCA (Seq No. NM_026384.3)	149	50
apo C-III	F: CAGTTTTATCCCTAGAAGCA R: TCTCACGACTCAATAGCTG (Seq No. NM_023114.3)	349	47
SREBP2	F: ATATCATTGAAAAGCGCTAC R: ATTTTCAAGTCCACATCACT (Seq No. AF289715.2)	256	47
apo A-I	F: ACATATATAGACCAGGGAAGAA R: AAACTGGGACACATAGTCTCT (Seq No. NM_009692.3	246	50.5
GAPDH	F: TGTGTCCGTCGTGGATCTGA R: CCTGCTTCACCACCTTCTTGA (Seq No. NM_031144	99	55

immediately stored in a freezer at −80 °C. Heparin (30 units/mL) (Sigma) was added to blood samples. Plasma samples were collected by centrifugation at 1600*g* for 15 min at 4 °C within 30 min, and plasma was obtained for insulin and leptin level analysis.

Body Weight, Body Weight Gain, and Food Intake Analysis. Throughout the study, body weight and food intake were daily recorded at the same time. Body weight gain is defined as the difference between 1 day and the next day. The pellet food was weighed and placed in a cage food container. After 24 h, the remaining food was weighed and the crumbs were collected as much as possible. Based on the difference between 1 day and the next day, the daily food intake was calculated.

Blood Glucose and Glycated Hemoglobin (HbA1c) Levels and Biochemical Analysis. Blood samples (0.8 mL) were collected from the retro-orbital sinuses of fasting mice, and glucose level was measured by the glucose oxidase method (model 1500; Sidekick Glucose Analyzer; YSI Inc., Yellow Springs, OH, USA). Percent HbA_{1c} was detected with a Hemoglobin A_{1c} kit (BioSystems S.A., Barcelona, Spain). Plasma triglycerides (TG), total cholesterol (TC), free fatty acids (FFA), high-density lipoprotein cholesterol (HDL-C), and low-density lipoprotein cholesterol (LDL-C) were determined using commercial assay kits (Triglycerides-E test, Cholesterol-E test, and FFA-C test, Wako Pure Chemical, Osaka, Japan; HDL-C-test and LDL-C-test, Roche Diagnostics GmbH, Indianapolis, USA) according to their instructions. A mouse insulin ELISA kit (Sibayagi, Gunma, Japan) and mouse leptin ELISA kit (Morinaga, Yokohama, Japan) were used to measure blood insulin and leptin levels, respectively.

Histopathological Examination. A portion of the collected epididymal WAT and liver tissue was fixed with formalin (200 g/kg) neutral buffered solution and embedded in paraffin. Sections (8 μm) were cut and stained with hematoxylin and eosin. A microscope (Leica, DM2500) and Leica Digital camera (DFC-425-C) were used for microscopic examination and images taken, respectively.

Hepatic Lipids Measurements. Hepatic lipids were extracted as previously described.[25] Liver sample (0.375 g) was homogenized with 1 mL of distilled water for 5 min for the hepatic lipid extraction and analyzed using a triglycerides kit as used for serum lipids.

Relative Quantization of mRNA Indicating Gene Expression Analysis. The experiment was performed as in a previously described protocol.[24−27] Total RNA from the liver tissue was isolated with a Trizol reagent (Molecular Research Center, Inc., Cincinnati, OH, USA) according to the manufacturer's directions. Total RNA (1 μg) was reverse transcribed to cDNA with 5 μL of Moloney murine leukemia virus reverse transcriptase (Epicenter, Madison, WI, USA) as a previously described protocol.[24−27] The polymerase chain reaction (PCR) was performed in a final 25 μL containing 1 U Blend Taq-Plus (TOYOBO, Japan), 1 μL of the RT first-strand cDNA product, 10 μM of each forward (F) and reverse (R) primer, 75 mM Tris-HCl (pH 8.3) containing 1 mg/L Tween 20, 2.5 mM dNTP, and 2 mM $MgCl_2$. The primers are shown in Table 1. The products were run on 2% agarose gels and stained with ethidium bromide. The relative density of the band was evaluated using AlphaDigiDoc 1201 software (Alpha Innotech Co., San Leandro, CA, USA). All of the measured PCR products were normalized to the amount of cDNA of GAPDH in each sample.

Western Blotting Analysis. Protein extractions and immunoblots for the determination of GLUT4, phospho-AMPK (Thr172), and phospho-Akt (Ser 473) proteins were carried out on frozen skeletal muscle and liver tissue from mice, which follows a previous paper.[25−27] Additionally, GLUT4 was carried out on frozen skeletal muscle from mice, and the total membrane fractions were collected with buffer and centrifuged as a previously described.[28−30] The protein contents of GLUT4, phospho-AMPK, phospho-Akt, total AMPK, and total Akt were detected by blotting. Western blotting had been determined as described elsewhere.[25−28] Subsequently, antibodys were detected using horseradish peroxidase linked to a goat anti-IgG rabbit secondary

DOI: 10.1021/acs.jafc.5b00073
J. Agric. Food Chem. 2015, 63, 2479−2489

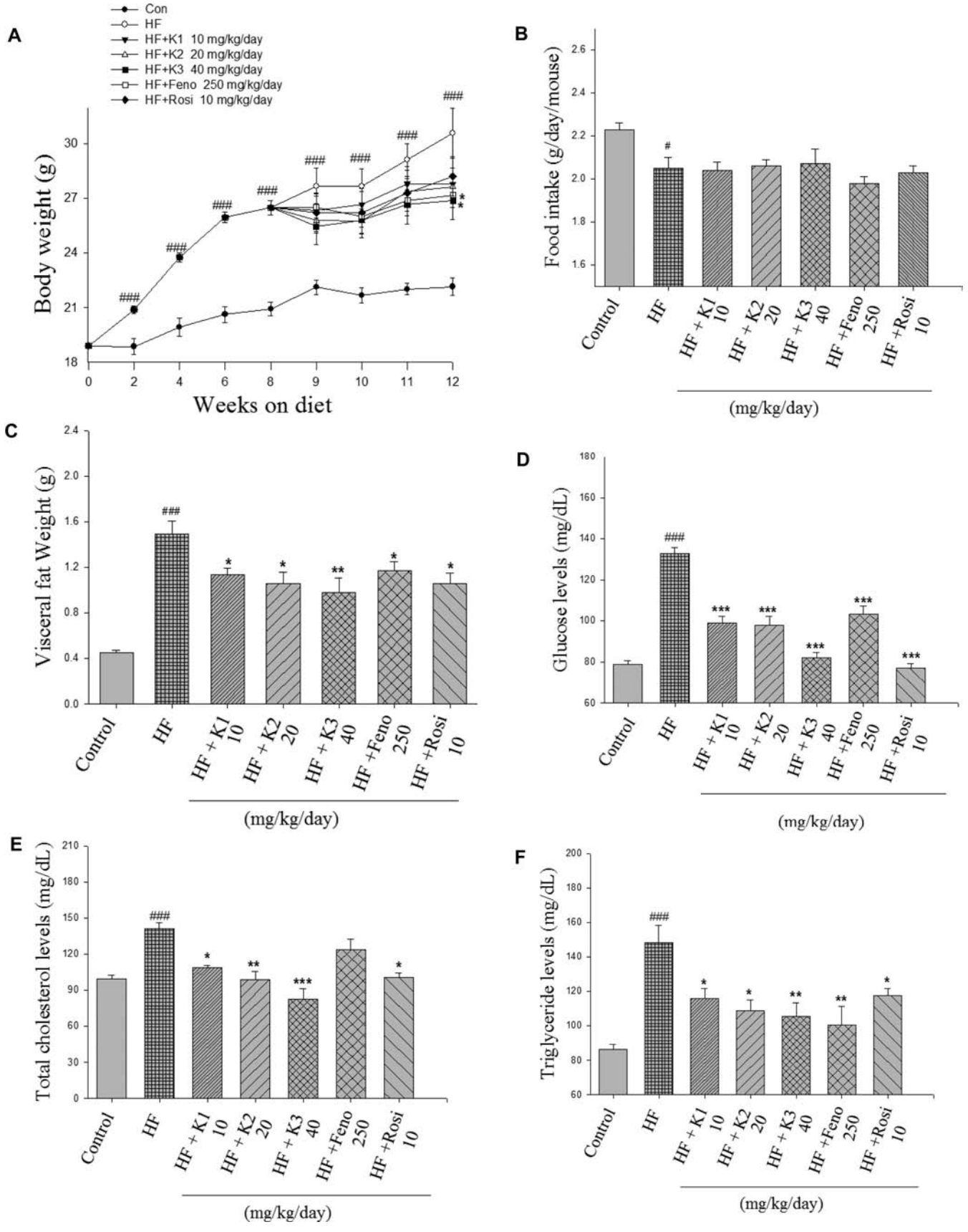

Figure 2. continued

DOI: 10.1021/acs.jafc.5b00073
J. Agric. Food Chem. 2015, 63, 2479−2489

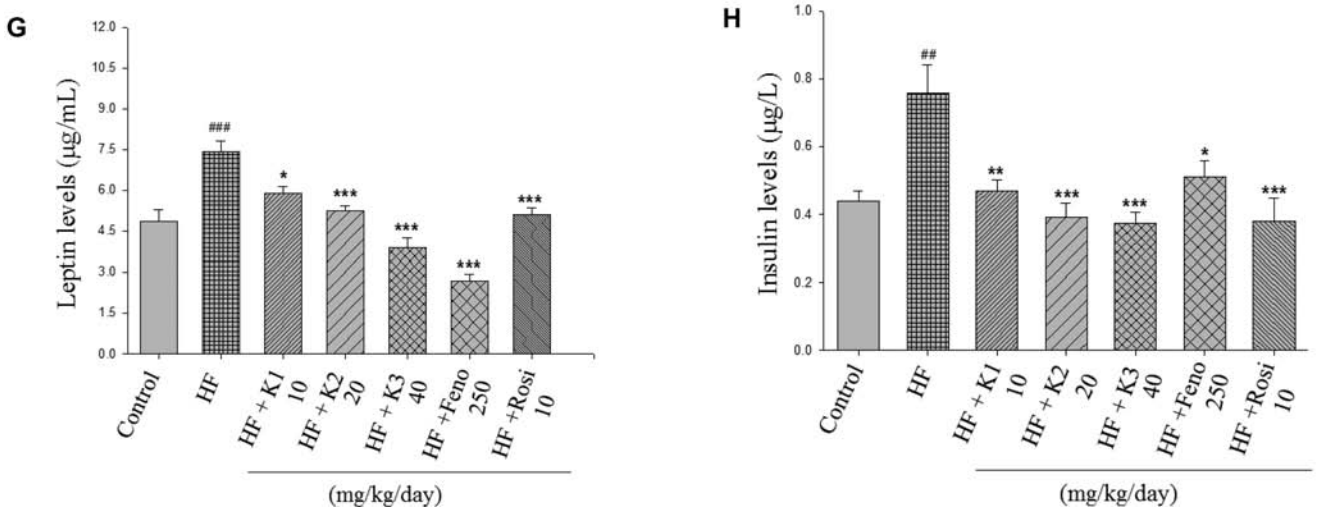

Figure 2. Effects of ergostatrien-3β-ol (EK100) on (A) body weight, (B) food intake, (C) visceral fat, (D) blood glucose levels, (E) total cholesterol levels, (F) triglycerides levels, (G) leptin levels, and (H) insulin levels at week 12. Mice were fed with 45% high-fat diet (HF) or low-fat diet (CON) for 12 weeks. After 8 weeks of induction, the HF mice were treated with vehicle, or ergostatrien-3β-ol (EK100), or fenofibrate (Feno) or rosiglitazone (Rosi) accompanied by HF diet for 4 weeks. All values are means ± SE (n = 9). $^{\#}$ P < 0.05, $^{\#\#}$ P < 0.01, and $^{\#\#\#}$ P < 0.001 compared with the control (CON) group; * P < 0.05, ** P < 0.01, and *** P < 0.001 compared with the high-fat plus vehicle (HF) group by ANOVA. Ergostatrien-3β-ol (EK100): K1:10, K2:20, K3:40 mg/kg body wt; Feno: fenofibrate (250 mg/kg body weight); Rosi: rosiglitazone (10 mg/kg body wt). WAT, white adipose tissue; visceral fat represented epididymal WAT plus retroperitoneal WAT.

Table 2. Absolute Tissue Weights, Liver Lipid, Blood HbA1c, and Other Parameters[a] in HFD-Mice Treated Orally with Ergostatrien-3β-ol (EK100)

Parameter	CON	HF	HF+K1	HF+K2	HF+K3	HF+Feno	HF+Rosi
			10[b]	20[b]	40[b]	250[b]	10[b]
			Absolute Tissue Weight (g)				
EWAT	0.391 ± 0.016	1.103 ± 0.092$^{\#\#\#}$	0.853 ± 0.031*	0.774 ± 0.057*	0.736 ± 0.070*	0.924 ± 0.069	0.813 ± 0.069*
MWAT	0.197 ± 0.015	0.341 ± 0.032$^{\#\#\#}$	0.276 ± 0.032	0.276 ± 0.032	0.244 ± 0.024*	0.295 ± 0.009	0.257 ± 0.019*
RWAT	0.061 ± 0.006	0.391 ± 0.041$^{\#\#\#}$	0.281 ± 0.016*	0.283 ± 0.025*	0.243 ± 0.041*	0.249 ± 0.028*	0.244 ± 0.042*
Skeletal muscle	0.462 ± 0.021	0.744 ± 0.051	0.781 ± 0.034	1.167 ± 0.045*	1.351 ± 0.153***	0.569 ± 0.069	0.737 ± 0.094
BAT	0.123 ± 0.009	0.190 ± 0.010$^{\#\#}$	0.160 ± 0.007	0.143 ± 0.016*	0.144 ± 0.013*	0.142 ± 0.012*	0.175 ± 0.018
Liver (g)	0.827 ± 0.017	0.839 ± 0.025	0.813 ± 0.025	0.819 ± 0.025	0.796 ± 0.041	1.046 ± 0.033***	0.816 ± 0.038
weight gain (g)	1.21 ± 0.23	3.96 ± 1.24$^{\#}$	1.30 ± 0.39	1.13 ± 0.20	0.37 ± 0.38*	0.69 ± 0.63*	1.71 ± 0.56
			Liver Lipids				
total lipid (mg/g)	57.6 ± 2.8	97.2 ± 6.0$^{\#\#\#}$	72.4 ± 3.7**	68.0 ± 4.5**	65.4 ± 4.2**	63.8 ± 4.7**	65.1 ± 5.3**
triacylglycerol (μmol/g)	35.6 ± 3.7	80.3 ± 7.3$^{\#\#\#}$	57.3 ± 5.5**	44.5 ± 4.7***	43.7 ± 6.6***	48.4 ± 5.6***	44.5 ± 3.2***
			Blood Profiles				
FFA (meq/L)	0.99 ± 0.09	1.35 ± 0.11$^{\#\#}$	1.06 ± 0.10*	1.05 ± 0.09*	1.03 ± 0.05**	0.94 ± 0.08**	1.00 ± 0.09*
HbA1c (%)	5.5 ± 0.6	9.3 ± 0.5$^{\#\#\#}$	5.8 ± 0.7**	5.7 ± 0.5***	5.1 ± 0.3***	6.4 ± 0.7**	6.2 ± 0.4**
HDL-C (mg/dL)	84.9 ± 3.9	65.3 ± 3.1$^{\#\#\#}$	82.2 ± 3.9**	83.0 ± 2.0***	83.8 ± 1.6***	80.3 ± 4.5**	73.1 ± 5.8
LDL-C (mg/dL)	107.1 ± 7.7	130.5 ± 20.0	112.4.0 ± 7.4	103.7 ± 10.8	86.8 ± 11.5**	105.8 ± 10.4	86.7 ± 7.7**

[a]All values are means ± SE (n = 9). $^{\#}$ P < 0.05, $^{\#\#}$ P < 0.01, and $^{\#\#\#}$ P < 0.001 compared with the control (CON) group; * P < 0.05, ** P < 0.01, and *** P < 0.001 compared with the high-fat plus vehicle (distilled water) (HF) group. Ergostatrien-3β-ol (EK100): K1:10, K2:20, K3:40 mg/kg body wt; Feno: fenofibrate (250 mg/kg body wt); Rosi: rosiglitazone (10 mg/kg body wt). BAT, brown adipose tissue; RWAT, retroperioneal white adipose tissue; MWAT, mesenteric white adipose tissue; FFA, plasm free fatty acid. [b]Dose (mg/kg/day)

antibody and visualized using an ECL system. The density blotting was analyzed using Alpha Easy FC software (Alpha Innotech Corp., Randburg, South Africa). Structural proteins GAPDH and β-actin were obtained by stripping the nitrocellulose membrane proteins of liver and skeletal muscle, respectively.

Statistical Analysis. All results were presented as mean and standard error. Whenever possible, data were subjected to analysis of variance, followed by Dunnett's multiple range tests, using SPSS software (SPSS Inc., Chicago, IL, USA). P < 0.05 was considered to be statistically significant.

RESULTS

Body Weight, Food Intake, and Tissue Weight. All group mice begin with similar mean body weights (18.9 ± 0.2 g). Mice on HFD for 12 weeks displayed significantly greater increases in body weight and body weight gain compared to CON littermates (Figure 2A and Table 2). Administration of K3 and Feno displayed resistance to bodyweight gain. HF mice consume high-fat diets much less than CON littermates (Figure 2B). All the EK100-, Feno- and Rosi-treated mice and HF mice consume high-fat diets similarly. Feeding a HFD displayed a

DOI: 10.1021/acs.jafc.5b00073
J. Agric. Food Chem. 2015, 63, 2479−2489

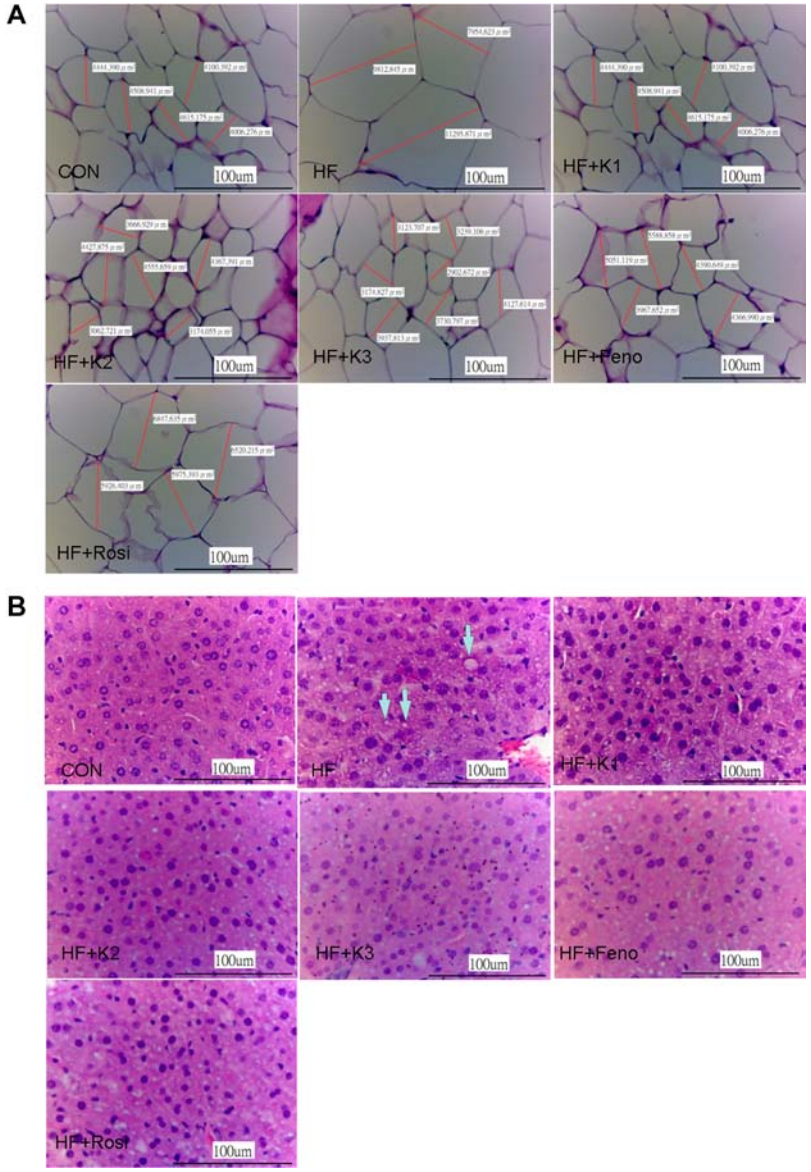

Figure 3. Effects of ergostatrien-3β-ol (EK100) on (A) epididymal WAT and (B) liver tissue morphology in the low-fat (CON), high-fat (HF), HF + K1, HF + K2, HF + K3, or HF + Feno, or HF + Rosi groups. Pictures of hematoxylin and eosin-stained sections of (A) epididymal adipocytes (Magnification: 10 (ocular) × 20 (object lens)) from mice fed with EK100. The appearance of adipocyte is polyhedral and displayed the string-like cytosol surrounded by a vacuole (H&E stain); and (B) liver tissue (Magnification: 10 (ocular) × 20 (object lens)) from mice fed with EK100. The high-fat diet induced the hepatic ballooning degeneration in the HF group as compared with the CON group. The ballooning degeneration is a form of liver parenchymal cell death, and the nucleolus was squeezed into the other side of the named balloon (as the arrow indicates). Each presented image is typical and representative of nine mice. Ergostatrien-3β-ol (EK100): K1:10, K2:20, K3:40 mg/kg body wt; Feno: fenofibrate (250 mg/kg body wt); Rosi: rosiglitazone (10 mg/kg body wt).

marked increase in weights of absolute adipose tissues (epididymal, visceral fat, mesenteric and retroperitoneal WAT) (Table 2 and Figure 2C). The K1-, K2-, K3-, Feno-, and Rosi-treated mice displayed a decrease in weights of retroperitoneal WAT and visceral fat. The K1-, K2-, K3-, and Rosi-treated mice reduced weights of epididymal WAT. The K3- and Rosi-treated mice display less mesenteric WAT weights. The brown adipose tissue (BAT) mass was decreased in K2-, K3- and Feno-treated mice. The K2- and K3-treated mice showed an increase in skeletal muscle mass. Feno-treated mice showed a marked increase in liver weight (Table 2).

Blood Glucose and HbA1c Levels. After 8 weeks on HFD, HF mice displayed the hyperglycemia evidence compared with the CON mice ($P < 0.001$). Administration of K1, K2, K3, Feno, and Rosi significantly reduced blood glucose levels ($P < 0.001$, $P < 0.001$, $P < 0.001$, $P < 0.001$, $P < 0.001$, respectively) (Figure 2D). The percent of hemoglobin was evaluated nonenzymatically (percent HbA1c) as an integrated measure of long-term blood glucose regulation. Blood levels of HbA1c were significantly greater in the HF group than in the CON group. Treatment with K1, K2, K3, Feno, and Rosi decreased HbA1c levels in blood (Table 2).

Blood Lipid and Hepatic Lipid. HFD caused increases in blood total cholesterol (TC), triglyceride (TG), and free fatty acid (FFA) (Figure 2E and F and Table 2). The K1-, K2-, K3-, and Rosi-treated mice lowered TC levels ($P < 0.05$, $P < 0.01$, $P < 0.001$, $P < 0.05$, respectively). The K1-, K2-, K3-, Feno-, and Rosi-treated mice decreased TG level. The K1-, K2-, K3-,

DOI: 10.1021/acs.jafc.5b00073
J. Agric. Food Chem. 2015, 63, 2479−2489

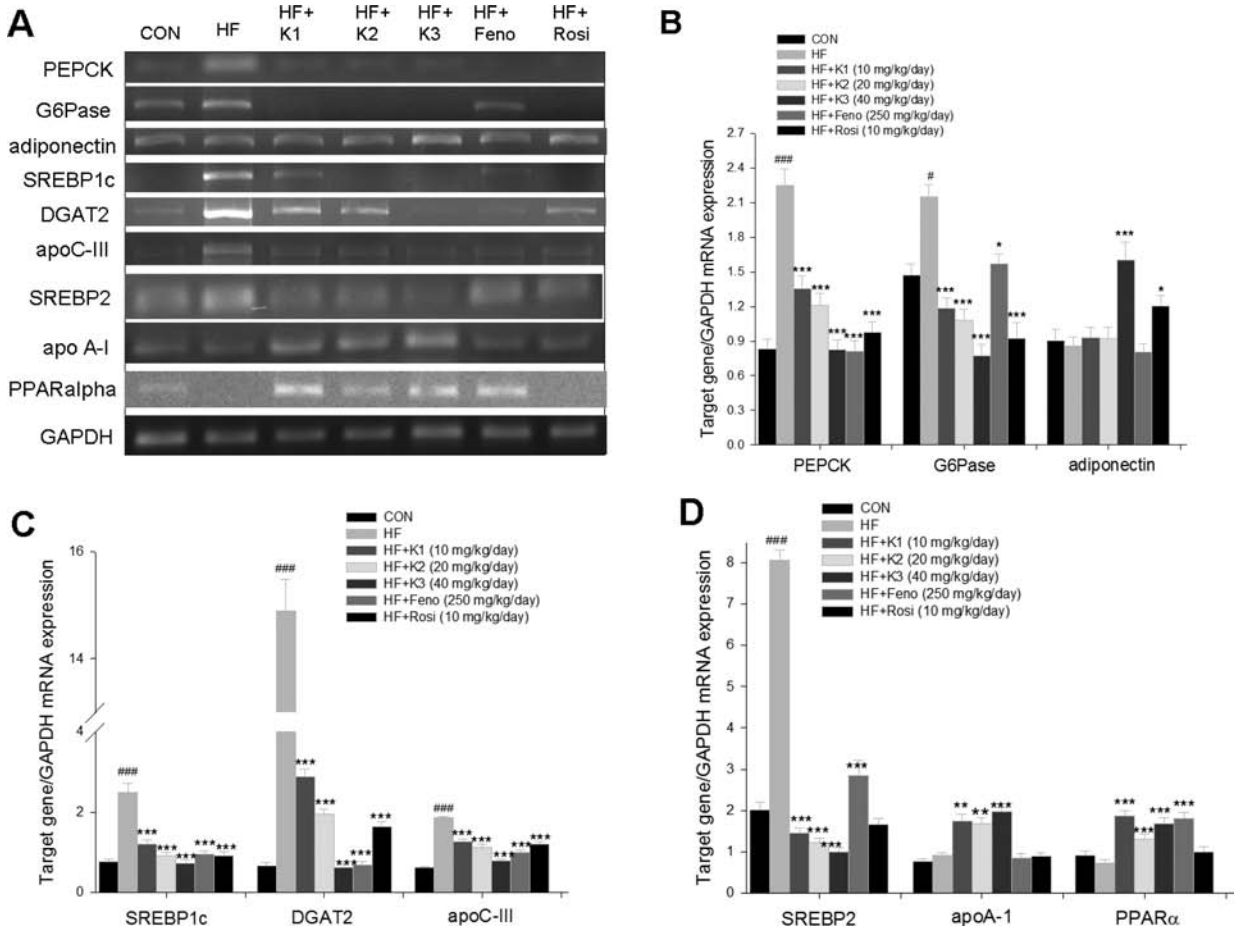

Figure 4. Semiquantitative RT-PCR analysis on PEPCK, G6 Pase, adiponectin, SREBP1c, DGAT2, apo C-III, SREBP2, apo A-I, and PPARα mRNA expression in liver tissue of the mice receiving ergostatrien-3β-ol (EK100) by oral gavage for 4 weeks. All values are means ± SE (n = 9). $^{\#}$ $P < 0.05$ and $^{\#\#\#}$ $P < 0.001$ compared with the control (CON) group; * $P < 0.05$, ** $P < 0.01$, and *** $P < 0.001$ compared with the high-fat plus vehicle (HF) group. Ergostatrien-3β-ol (EK100): K1:10, K2:20, K3:40 mg/kg body wt; Feno: fenofibrate (250 mg/kg body wt); Rosi: rosiglitazone (10 mg/kg body wt). Total RNA (1 μg) isolated from tissue was reverse transcripted by MMLV-RT, 10 μL of RT products were used as templates for PCR. Signals were quantitated by image analysis; each value was normalized by GAPDH.

Feno-, and Rosi-treated mice showed decreased FFA concentrations. The K1-, K2-, K3-, and Feno-treated mice increased high-density lipoprotein cholesterol (HDL-C) levels (Table 2). The K3- and Rosi-treated mice displayed a decrease in low-density lipoprotein cholesterol (LDL-C) level. HFD caused increases in the total lipids of liver and concentrations of triacylglycerol, while treatment with K1, K2, K3, Rosi, and Feno displayed marked decreases in these phenomena (Table 2).

Blood Leptin and Insulin Levels. Blood leptin and insulin levels were greater in the HF group than in the CON group (Figure 2G and H). The K1-, K2-, K3-, Feno-, and Rosi-treated mice displayed a decrease in blood leptin and insulin levels.

Histopathology Examination. Feeding a HFD induced hypertrophy of adipocytes (the average areas of adipocytes in the HF group and CON group are 9604.2 ± 281.3 and 3797.5 ± 412.9 μm^2, respectively), whereas mice treated with K1 (4204.0 ± 131.5 μm^2), K2 (3535.7 ± 340.2 μm^2), K3 (3458.9 ± 30.7 μm^2), and Feno (4175.4 ± 322.9 μm^2) showed significantly lower hypertrophy. The average area of the Rosi-treated mice is 5598.6 ± 162.7 μm^2 (Figure 3A). Feeding a HFD induced ballooning degeneration of hepatocyte. Administration of K1, K2, K3, Feno, and Rosi decreased the ballooning degeneration (Figure 3B).

Targeted Gene mRNA Expressions in Liver Tissue. The HFD induced higher expression levels of phosphoenol pyruvate carboxykinase (PEPCK), glucose-6-phosphatase (G6 Pase), sterol regulatory element binding protein 1c (SREBP1c), acyl-coenzyme A: diacylglycerol acyltransferase 2 (DGAT2), apolipoprotein C-III (apo C-III), and SREBP2 in the HF group than in the CON group. Administration of K1, K2, K3, Feno, and Rosi showed a decreased mRNA level of PEPCK, G6 Pase, SREBP1c, DGAT2, apo C-III, and SREBP2. K3- and Rosi-treated mice increased the mRNA level of adiponectin. The K1-, K2-, and K3-treated mice show increased mRNA levels of apolipoprotein A-I (apo A-I). Administration of K1, K2, K3, and Feno increased the mRNA level of PPARα (Figure 4).

Western Blotting of GLUT4, phospho-Akt (Ser 473)/ total Akt, and Phospho- AMPK (Thr172) Proteins. The levels of GLUT4 and phospho-Akt/total Akt were lower in HF mice than in CON mice. K1-, K2-, K3-, Feno-, and Rosi-treated mice show increased muscular GLUT4 protein contents ($P < 0.01$, $P < 0.01$, $P < 0.001$, $P < 0.05$, $P < 0.001$, respectively). Administration of K1, K2, K3, and Rosi displayed higher levels of phospho-Akt/total Akt than in HF mice. The mice on HFD showed decreased phospho-AMPK in liver tissue and skeletal muscle. The protein contents of phospho-AMPK were

DOI: 10.1021/acs.jafc.5b00073
J. Agric. Food Chem. 2015, 63, 2479−2489

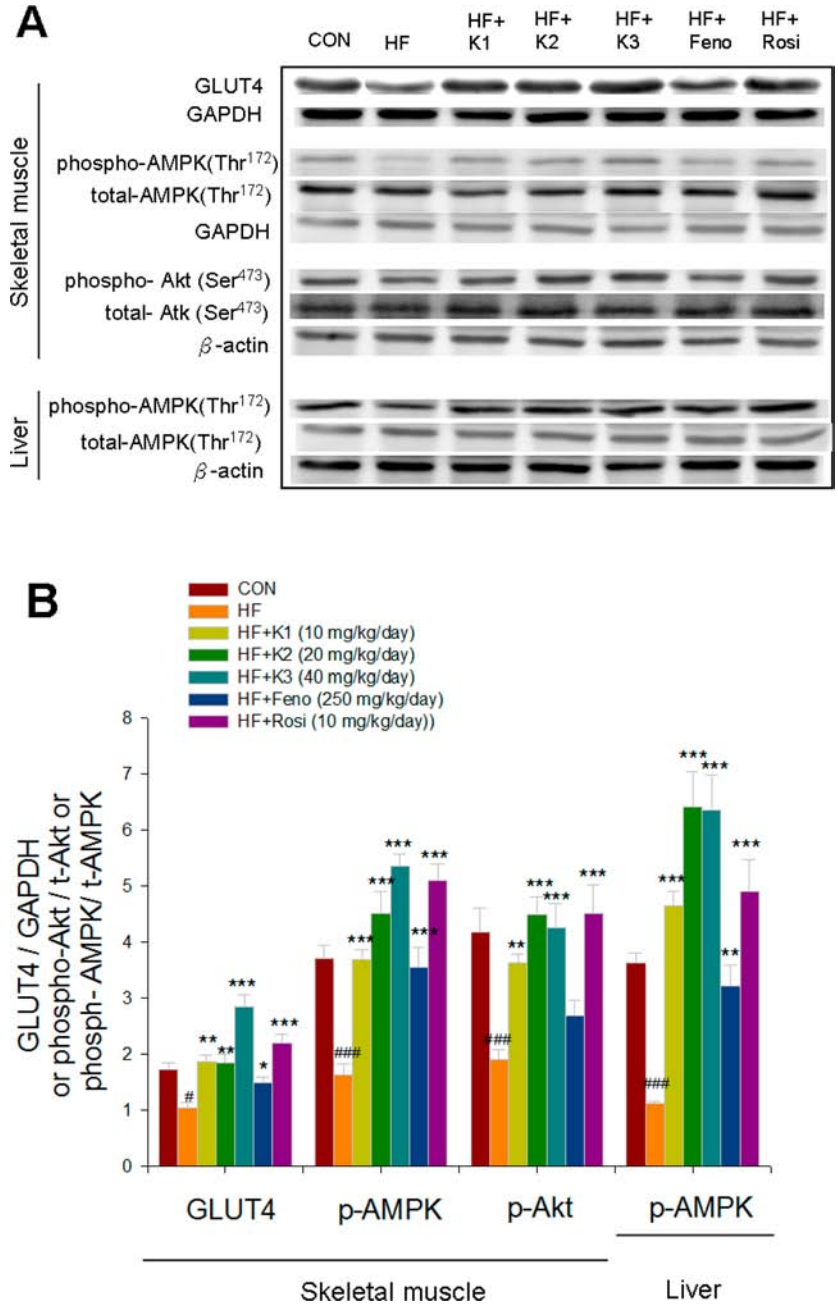

Figure 5. Protein contents of GLUT4, phospho-AMPK (Thr172)/total AMPK, and phospho-Akt/total Akt in skeletal muscle and phospho-AMPK (Thr172)/total AMPK in liver tissue of the mice receiving ergostatrien-3β-ol (EK100) by oral gavage for 4 weeks. Protein was separated by 12% SDS-PAGE detected by Western blot. All values are means ± SE (n = 9). $^{\#}$ $P < 0.05$ and $^{\#\#\#}$ $P < 0.001$ compared with the control (CON) group; * $P < 0.05$, ** $P < 0.01$, and *** $P < 0.001$ compared with the high-fat plus vehicle (HF) group. Ergostatrien-3β-ol: K1:10, K2:20, K3:40 mg/kg body wt; Feno: fenofibrate (250 mg/kg body wt); Rosi: rosiglitazone (10 mg/kg body wt).

significantly increased in the K1-, K2-, K3-, Feno-, and Rosi-treated groups in liver tissue ($P < 0.001$, $P < 0.001$, $P < 0.001$, $P < 0.01$, $P < 0.001$, respectively) and in skeletal muscle ($P < 0.001$, $P < 0.001$, $P < 0.001$, $P < 0.001$, $P < 0.001$, respectively) (Figure 5).

DISCUSSION

The present study demonstrated that EK100-treated mice displayed effectively lower blood glucose and circulating triglyceride levels. In this study, high-fat feeding induces hyperglycemia and hyperinsulinemia. EK100 treatment significantly decreased blood glucose levels and makes mice resistant to HFD-induced hyperinsulinemia, suggesting EK100 displayed increased insulin sensitivity or efficiency. In the present study, Rosi and Feno caused reduced blood glucose level, consistent with earlier observations.[13,29] Moreover, the level of blood glycosylated HbA1c, which is a maker of long-term control of blood glucose, is also significantly decreased. On the other hand, HFD caused an increase in circulating triglyceride and total cholesterol levels, which were consistent with earlier studies,[19] while they were significantly lowered in EK100-treated mice. These data reinforce that EK100 is effective to improve insulin resistance and dyslipidemia in a mouse model of Type 2 diabetes and dyslipidemia. The

DOI: 10.1021/acs.jafc.5b00073
J. Agric. Food Chem. 2015, 63, 2479−2489

physiological relevance of these findings is supported by the increased skeletal muscular GLUT4 contents and activation of AMPK in both skeletal muscle and liver tissue.

To ascertain whether EK100 regulates glucose utilization, we evaluated the membrane protein contents of GLUT4 in skeletal muscle because glucose uptake is primarily mediated by skeletal muscle. Levels of GLUT4 movement to the plasma membrane were assessed, as it is an essential step for insulin-responsive glucose in skeletal muscle that becomes defective in insulin resistance.[8] All EK100-treated mice display an enhancement of muscular GLUT4 protein; moreover, EK100 (K3) and Rosi treatment displayed approximately 2.7-fold and 2.1-fold enhancement, respectively, implying that EK100 treated mice are indeed hypersensitive to insulin and exhibit antidiabetic activity. Rosi has been shown to act as an insulin sensitizer.

The apparent insulin sensitivity of EK100-treated mice prompted our interest in EK100 regulation of GLUT4 and Akt. There are two principal mechanisms involved in promoting tranlocation of GLUT4 to the plasma membrane, including insulin signaling through the phosphatidylinositol 3′ kinase (PI3-kinase)/Akt pathway and the AMPK pathway.[8] Previous findings showed that a mutation in the gene encoding Akt2/PK Bβ resulted in severe insulin resistance,[30] establishing Akt2/PK Bβ as a key protein in the maintenance of euglycemia. To explore the mechanism of enhanced GLUT4 proteins by EK100, we measured phosphorylation of Akt levels in skeletal muscle. We observed that EK100 manifested elevated phosphorylation of Akt levels in skeletal muscle, implying that the enhanced GLUT4 proteins by EK100 appear to be in part mediated by the insulin signaling pathway through increased phosphorylation of Akt.

The phosphorylation of the AMPK pathway is another major regulator of GLUT4 translocation during exercise or in response to some antidiabetic agents such as AICAR and metformin.[8] In this study, we found that EK100-treated mice manifest elevated phosphorylation of AMPK levels in both skeletal muscle and liver tissue. Metformin is used for the treatment of type 2 diabetes due to increased skeletal muscular glucose uptake and reduced hepatic glucose production.[11,20] The present results demonstrated that EK100-treated mice were protected from HFD-induced hyperglycemia by AMPK activities and GLUT4 proteins. Whether skeletal muscular activation of AMPK by EK100 is responsible for overall GLUT4 regulation, the potential mechanisms require further investigation of the phosphorylation of AS160.

PEPCK and G6 Pase are key rate-limiting enzymes of gluconeogenesis.[31] The liver of diabetic rats showed a significant increase in the activities of G6 Pase.[31] Over-expression of PEPCK enzyme in mice results in symptoms of type 2 diabetes. The published research further showed that activation of AMPK in turn inhibited the expression of the hepatic gluconeogenic genes PEPCK and G6 Pase.[32] Activation of AMPK has been implicated in metformin action in hepatocytes.[11] Metformin decreases hyperglycemia primarily by suppressing glucose production by the liver (hepatic gluconeogenesis).[20] EK100-treated mice elicited decreased expressions of PEPCK and G6 Pase. Thus, the antidiabetic effect of EK100 is possibly partly due to down-regulation of PEPCK and G6 Pase. Collectively, this study demonstrated that EK100 caused glucose lowering by AMPK activation in both liver tissue and skeletal muscle, besides its ability to increase glucose uptake in skeletal muscle, possibly by down-regulations of PEPCK to inhibit hepatic glucose production.

Our second goal was to determine the molecular mechanism of EK100-mediated hypolipidemic effects. Fenofibrate, a PPARα agonist, has been recommended to reduce circulating triglycerides.[17] In this study, Feno displayed a decrease of the circulating TG level by 47.9%, while Rosi decreased the circulating TG level less. EK100 showed a moderate reduction in levels of TG. PPARα agonist is known to down-regulate numerous genes involved in lipid synthesis. PPARα ligands (such as fibrates) reduce the expression of apo C-III gene,[33] thus resulting in a hypotriglyceridemic effect. PPARα has been shown to regulate lipid metabolism and fatty acid oxidation. SREBP-1c plays a key role in the activation of lipogenic enzyme expression, fatty acid synthesis and triglyceride accumulation,[34] and it plays the role of PPARα in SREBP- mediated regulation of lipogenic genes.[35] In this study, EK100-treated mice displayed an increase in expressions of PPARα but a reduction in SREBP1c and DGAT2 mRNA. DGAT2 is known to catalyze the final step in the synthesis of triglycerides.[36] Therefore, the down-regulation of DGAT2 seems to be responsible for the hepatic triglyceride output, thus resulting in a decrease in blood TG. These findings further confirmed that EK100 displayed hypolipidemic activity partly via regulation of genes associated with fatty acid oxidation and lipogenesis.

K3-treated mice showed reduced body weight, which primarily reflects decreased fat accumulation with reduced weight of epididymal adipose tissue (EWAT) as well as decreased weight of visceral fat. Although their body weight was lower, K3-treated mice show increased skeletal muscle mass. These findings were consistent with an earlier report,[37] which revealed that increased Akt signaling resulted in muscle hypertrophy, increased insulin sensitivity, and resistance to HFD-induced weight gain. Akt activation is a common feature of the diverse model of increased insulin sensitivity. Both reduced obesity and increased Akt signaling may elicit the improved insulin sensitivity of the K3-treated mice.

Histology investigation has revealed that EK100 treatment lowered the area of adipocytes. Because circulating TG level is fluctuating and liver is the major organ responsible for metabolizing fat, presumably EK100 reflected the movement of fat from adipose tissue to liver by increasing hepatic lipid metabolism, which led to reduced adipocyte size and nearly invisible liver lipid droplets.

It was observed that EK100 decreased blood TC and TG levels while it increased HDL-C concentrations. Moreover, only K3-treated mice displayed a decrease in LDL-C levels. PPARα agonists are known to reduce LDL-C and increase HDL-C. In this study, Feno-treated mice reduced adiposity[17] and displayed no changes in total cholesterol (TC) and LDL-C levels, but increased HDL-C concentrations, consistent with an earlier study.[38] The difference between EK100 and Feno is that EK100-treated mice show significantly decreased TC levels whereas Feno-treated mice display unchanged levels in this manifest hypercholesterolemia animal model.

An additional mechanism that plays a role in the hypolipidemic effect was also examined. In this study, EK100-treated mice displayed reduced blood TC levels and decreased SREBP2 expression, since SREBP2 plays a major role in the regulation of cholesterol synthesis,[39] implying that the potential mechanism of EK100 was involved in SREPB2 on the inhibitory action of cholesterol synthesis. PPARα ligands are used widely to lower serum TG and to increase HDL-C in patients with obesity and dyslipidemia.[40] In this study, EK100 enhanced both HDL-C levels and apo A-I expression. HDL-C

DOI: 10.1021/acs.jafc.5b00073
J. Agric. Food Chem. 2015, 63, 2479−2489

is positively associated with a decreased risk of coronary heart disease (CHD). Since apo A-I has been reported to be synthesized by liver cells[41] and the major apolipoproteins of HDL-C are apo A-I and apo A-II,[42] the observed increase in HDL-C level by EK100 was presumably mediated by enhanced hepatic apo A-I production. These data are important because they suggest that EK100 treatment resulted in elevated HDL-C concentration, a known physiological consequence that may be useful in cardiovascular events.

In conclusion, EK100 exhibited not only lowered blood glucose levels accompanied by decreased HbA1c and ameliorated insulin resistance but also diminished blood TC and TG levels. EK100 exerted significantly increased GLUT4 protein in skeletal muscle, which enhanced glucose uptake; moreover, EK100 increased phosphorylation of AMPK in liver and reduced PEPCK and G6 Pase expressions, which decreased hepatic glucose production, leading to exertion of an antihyperglycemic effect. On the other hand, EK100 enhanced hepatic expressions of PPARα (fatty acid oxidation) and reduced SREBP1c (lipogenesis), thus resulting in lowering circulating TG levels. Moreover, EK100 reduced hepatic expressions of SREBP2 while it enhanced apo A-I and thus contributed to a decrease in blood TC and a rise in the plasma HDL-C level. Our results reinforce that EK100 will have therapeutic potential in treating type 2 diabetes associated with hyperlipidemia.

AUTHOR INFORMATION

Corresponding Author

* (C.-C.S.) Phone: +886-4-22391647 ext. 3978. Fax: +886-4-22394256. E-mail: ccshih@ctust.edu.tw.

Funding

Financial support for this study was partly by CMU under the Aim for Top University Plan of the Ministry of Education, Taiwan, and partly by Taiwan Ministry of Health and Welfare Clinical Trial and Research Center of Excellence (MOHW103-TDU-B-212-113002).

Notes

The authors declare no competing financial interest.

ABBREVIATIONS USED

AMPK, AMP-activated protein kinase; apo A-I, apolipoprotein A-I; apo C−III, apolipoprotein C-III; BAT, brown adipose tissue; CON, control; DGAT, acyl-coenzyme A:diacylglycerol acyltransferase; EWAT, epididymal white adipose tissue; fenofibrtae, Feno; FFA, free fatty acid; GAPDH, glyceraldehyde-3-phosphate dehydrogenase; G6 Pase, glucose-6-phosphatase; GLUT4, glucose transporter 4; HbA1c, glycated hemoglobin; HDL-C, high-density lipoprotein cholesterol; HF, high-fat control; LDL-C, low-density lipoprotein cholesterol; PEPCK, phosphenolpyruvate carboxykinase; PPAR, peroxisome proliferator-activated receptor; Rosi, rosiglitazone; RT-PCR, reverse transcription-polymerase chain reaction; SREBP, sterol regulatory element binding protein; TC, total cholesterol; TG, triglyceride; WAT, white adipose tissue

REFERENCES

(1) O'Rahilly, S.; Turner, R. C.; Matthews, D. R. Impaired pulsatile secretion of insulin in relatives of patients with non-insulin-dependent diabetes. *N. Engl. J. Med.* **1988**, *318*, 1225−1230.

(2) Thresher, J. S.; Podolin, D. A.; Wei, Y.; Mazzeo, R. S.; Pagliassotti, M. J. Comparison of the effects of sucrose and fructose on insulin action and glucose tolerance. *Am. J. Physiol. Regul. Integr. Comp. Physiol.* **2000**, *279*, R1334−R1340.

(3) Geethangili, M.; Tzeng, Y. M. Review of pharmacological effects of *Antrodia camphorata* and its bioactive compounds. *Evidence-Based Compl. Altern. Med.* **2011**, *2011*, No. 212641.

(4) Yeh, C. T.; Rao, Y. K.; Yao, C. J.; Yeh, C. F.; Li, C. H.; Chuang, S. E.; Luong, J. H.; Lai, G. M.; Tzeng, Y. M. Cytotoxic triterpenes from *Antrodia camphorata* and their mode of action in HT-29 human colon cancer cells. *Cancer Lett.* **2009**, *285*, 73−79.

(5) Huang, G. J.; Huang, S. S.; Lin, S. S.; Shao, Y. Y.; Chen, C. C.; Hou, W. C.; et al. Analgesic effects and the mechanisms of anti-inflammation of ergostatrien-3beta-ol from *Antrodia camphorata* submerged whole broth in mice. *J. Agric. Food Chem.* **2010**, *58*, 7445−7452.

(6) Wang, G. J.; Tseng, H. W.; Chou, C. J.; Tsai, T. H.; Chen, C. T.; Lu, M. K. The vasorelation of *Antrodia camphorata* mycelia: Involvement of endothelial Ca^{2+}-NO-cAMP pathway. *Life Sci.* **2003**, *73*, 2769−2783.

(7) Song, T. Y.; Yen, G. C. Protective effects of fermented filtrate from *Antrodia camphorata* in submerged culture against CCl_4-induced hepatic toxicity in rats. *J. Agric. Food Chem.* **2003**, *51*, 1571−1577.

(8) Huang, S.; Czech, M. P. The GLUT4 glucose transporter. *Cell Metab.* **2007**, *5*, 237−252.

(9) Bryant, N. J.; Govers, R.; James, D. E. Regulated transport of the glucose transporter GLUT4. *Nat. Rev. Mol. Cell Biol.* **2002**, *3*, 267−277.

(10) Watson, R. T.; Pessin, J. E. Intracellular organization of insulin signaling and GLUT4 translocation. *Recent Prog. Horm. Res.* **2001**, *56*, 175−193.

(11) Zhou, G.; Myers, R.; Li, Y.; Chen, Y.; Shen, X.; Fenyk-Melody, J.; Wu, M.; Ventre, J.; Doebber, T.; Fujii, N.; Musi, N.; Hirshman, M. F.; Goodyear, L. J.; Möller, D. E. Role of AMP-activated protein kinase in mechanism of metformin action. *J. Clin. Invest.* **2001**, *108*, 1167−1174.

(12) Musi, N.; Hirshman, M. F.; Nygren, J.; Svanfeldt, M.; Bavenholm, P.; Rooyackers, O.; Zhou, G.; Williamson, J. M.; Ljunqvist, O.; Efendic, S.; Möller, D. E.; Thorell, A.; Goodyear, L. J. Metformin increases AMP-activated protein kinase activity in skeletal muscle od subjects with type 2 diabetes. *Diabetes* **2002**, *51*, 2074−2081.

(13) Rangwala, S. M.; Lazar, M. A. Peroxisome proliferator-activated receptor gamma in diabetes and metabolism. PPAR gamma, glucose homeostasis. *Trends Pharmacol. Sci.* **2004**, *25*, 331−336 Review..

(14) Martinez, L.; Berenguer, M.; Bruce, M. C.; Le Marchand-Brustel, Y.; Govers, R. Rosiglitazone increases cell surface GLUT4 levels in 3T3-L1 adipocytes through an enhacement of endosomal recycling. *Biochem. Pharmacol.* **2010**, *79*, 1300−1309.

(15) Kersten, S.; Desvergne, B.; Wahli, W. Roles of PPARs in health and disease. *Nature* **2000**, *405*, 421−424.

(16) Farnier, M.; Bonnefous, F.; Debbas, N.; Irvine, A. Comparative efficacy and safety of micronised fenofibrate and simvastatin in patients with primary type IIa or IIb hyperlipidemia. *Arch. Int. Med.* **1994**, *154*, 441−449.

(17) Srivastava, R. A. K.; Jahagirdar, R.; Azhar, S.; Sharma, S.; Bisgaier, C. L. Peroxisome proliferator-activated receptor-α—selective ligand reduces adiposity, improves insulin sensitivity, and inhibits atherosclerosis in LDL receptor-deficient mice. *Mol. Cell. Biochem.* **2006**, *285*, 35−50.

(18) Winzell, M. S.; Ahrèn, B. The high-fat diet mouse: a model for studying mechanisms and type 2 diabetes. *Diabetes* **2004**, *53* (Suppl. 3), S215−219.

(19) Petro, A. E.; Cotter, J.; Cooper, D. A.; Peters, J. C.; Surwit, S. J.; Surwit, R. S. Fat, carbohydrate and calories in the development of diabetes and obesity in the C57BL/6J mouse. *Metabolism* **2004**, *53*, 454−457.

(20) Viollet, B.; Guigas, B.; Sanz Garcia, N.; Leclerc, J.; Foretz, M.; Andreelli, F. Cellular and molecular mechanisms of metformin: an overview. *Clin. Sci. (London)* **2012**, *122*, 253−270.

DOI: 10.1021/acs.jafc.5b00073
J. Agric. Food Chem. 2015, 63, 2479−2489

(21) Fryer, L. G.; Parbu-Patel, A.; Patel, A. The anti-diabetic drugs rosiglitazone and metformin stimulate AMP-activated protein kinase through distinct signaling pathways. *J. Biol. Chem.* **2002**, *277*, 25226−25232.
(22) Stein, S. C.; Woods, A.; Jones, N. A.; Davison, M. D.; Carling, D. The regulation of AMP-activated protein kinase by phosphorylation. *Biochem. J.* **2000**, *345*, 437−443.
(23) Shao, Y. Y.; Chen, C. C.; Wang, H. Y.; Chiu, H. L.; Hseu, T. H.; Kuo, Y. H. Chemical constituents of *Antrodia camphorata* submerged whole broth. *Nat. Prod. Res.* **2008**, *22*, 1151−1157.
(24) Shih, C. C.; Lin, C. H.; Lin, W. L. Effects of *Momordica charantia* on insulin resistance and visceral obesity in mice on high-fat diet. *Diabetes Res. Clin. Pract.* **2008**, *81*, 134−143.
(25) Shih, C. C.; Lin, C. H.; Wu, J. B. *Eriobotrya japonica* improves hyperlipidaemia and reverses insulin resistance in high-fat-fed mice. *Phytother. Res.* **2010**, *24*, 1769−1780.
(26) Shih, C. C.; Ciou, J. L.; Lin, C. H.; Wu, J. B.; Ho, H. Y. Cell suspension culture of *Eriobotrya japonica* regulates the diabetic and hyperlipidemic signs of high-fat-fed mice. *Molecules* **2013a**, *18*, 2726−2753.
(27) Wu, J. B.; Kuo, Y. H.; Lin, C. H.; Ho, Y. H.; Shih, C. C. Tormentic acid, a major component of suspension cells of *Eriobotrya japonica,* suppresses high-fat diet-induced diabetes and hyperlipidemia by glucose transporter 4 and AMP-activated protein kinase phosphorylation. *J. Agric. Food Chem.* **2014**, *62*, 10717−10726.
(28) Shih, C. C.; Lin, C. H.; Lin, W. L.; Wu, J. B. *Momordica charantia* extract on insulin resistance and the skeletal muscle GLUT4 protein in fructose-fed rats. *J. Ethnopharmacol.* **2009**, *123*, 82−90.
(29) Damci, T.; Tatliagac, S.; Osar, Z.; Ilkova, H. Fenofibrate treatment is associated with better glycemic control and lower serum leptin and insulin levels in type 2 diabetic patients with hypertriglyceridemia. *Eur. J. Inter. Med.* **2003**, *14*, 357−360.
(30) George, S.; Rochford, J. J.; Wolfrum, C.; et al. A family with severe insulin resistance and diabetes due to a mutation in AKT2. *Science* **2004**, *304*, 1325−1328.
(31) Berg, J. M.; Tymoczko, J. L.; Stryer. L. Glycolysis and glyconeogenesis. In *Stryer Biochemistry*; Berg, J. M., Tymoczko, J. L., Eds.; Freeman: New York, 2001; pp 425−464.
(32) Mithieux, G.; Guignot, L.; Bordet, J. C.; Wiernsperger, N. Intrahepatic mechanisms underlying the effect of metformin in decreasing basal glucose production in rats fed a high-fat diet. *Diabetes* **2002**, *51*, 139−143.
(33) Staels, B.; Dallongeville, J.; Auwerx, J.; Schoonjans, K.; Leitersdorf, E.; Fruchart, J.-C. Mechanism of action of fibrates on lipid and lipoprotein metabolism. *Circulation* **1998**, *98*, 2088−2093.
(34) Shimano, H.; Yahagi, N.; Amemiya-Kudo, M.; Hasty, A. H.; Osuga, J.; Tamura, Y.; Shionoiri, F.; Iizuka, Y.; Ohashi, K.; Harada, K.; Gotoda, T.; Ishibashi, S.; Yamada, N. Sterol regulatory element-binding protein-1 as a key transcription factor for nutritional induction of lipogenic enzyme genes. *J. Biol. Chem.* **1999**, *274*, 35832−35839.
(35) Patel, D. D.; Knight, B. L.; Wiggins, D.; Humphreys, S. M.; Gibbons, G. F. Disturbances in the normal regulation of SREBP-sensitive genes in PPAR alpha-deficient mice. *J. Lipid Res.* **2001**, *42*, 328−337.
(36) Cases, S.; Stone, S. J.; Zhou, P.; Yen, E.; Tow, B.; Lardizabal, K. D.; Voelker, T.; Farese, R. V., Jr. Cloning of DGAT2, a second mammalian diacylglycerol acyltransferase, and related family members. *J. Biol. Chem.* **2001**, *276*, 38870−38876.
(37) Izumiya, Y.; Hopkins, T.; Morris, C.; Sato, K.; Zeng, L.; Viereck, J.; Hamilton, J. A.; Ouchi, N.; LeBrasseur, N. K.; Walsh, K. Fast/Glycolytic muscle fiber growth reduces fat mass and improves metabolic parameters in obese mice. *Cell Metab.* **2008**, *7*, 159−172.
(38) Srivastava, R. A. K. Fenofibrate ameliorates diabetic and dyslipidemic profiles in KKAy mice partly via down-regulation of *11β-HSD1*, *PEPCK* and *DGAT2*. Comparison of PPAR*α*, PPAR*γ*, and liver x receptor agonists. *Eur. J. Pharmacol.* **2009**, *607*, 258−263.
(39) Shimano, H.; Shimomura, I.; Hammer, R. E.; Herz, J.; Goldstein, J. L.; Brown, M. S.; Horton, J. D. Elevated levels of SREBP-2 and cholesterol synthesis in livers of mice homozygous for a targeted disruption of the SREBP-1 gene. *J. Clin. Invest.* **1997**, *100*, 2115−2124.
(40) Staeles, B.; Fruchart, J. C. Therapeutic roles of peroxisome proliferator-activated receptor agonists. *Diabetes* **2005**, *54*, 2460−2470.
(41) Eggerman, T. L.; Hoeg, J. M.; Meng, M. S.; Tombragel, A.; Bojanovski, D.; Brewer, H. B., Jr. Differential tissue-specific expression of human apoA-I and apoA-II. *J. Lipid Res.* **1991**, *32*, 821−828.
(42) Gordon, D. J.; Probstfield, J. L.; Garrison, R. J.; Neaton, J. D.; Castelli, W. P.; Knoke, J. D.; Jacobs, D. R., Jr.; Bangdiwala, S.; Tyroler, H. A. High-density lipoprotein cholesterol and cardiovascular disease: four prospective American studies. *Circulation* **1989**, *79*, 8−15.

DOI: 10.1021/acs.jafc.5b00073
J. Agric. Food Chem. 2015, 63, 2479−2489

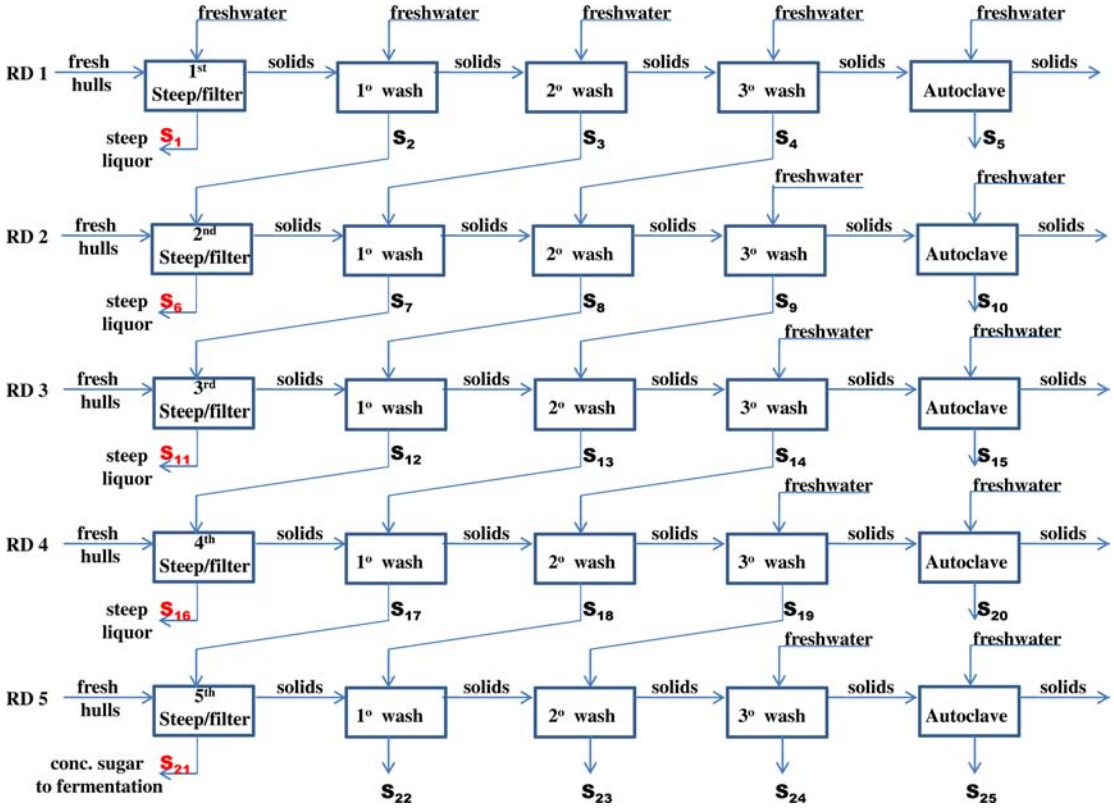

Figure 1. Laboratory extraction scheme utilized to mimic countercurrent extraction.

Quantitative Sugar Extraction. Sugar quantification was achieved by modification of the method of Sequeira and Lew[2] by using three successive blender extractions (Ninja NJ600 Professional Blender) each time using fresh, hot tap water (50 °C) and 1 min of blending time at 5% solids. Liquid/solids separation was accomplished using Whatman no. 4 filter paper in a pressurized air filter (OFI Testing Equipment, model 140-31) operated just above atmospheric pressure to force as much liquor out of the hulls as possible yet not create channeling. The final extraction via autoclave (L30 cycle) ensured that all sugars were quantified and on average released about 5% of additional free sugars.

The sugars and sugar alcohols were then analyzed by HPLC (Agilent 1200 series) equipped with a binary pump, an HPX-87P (Bio-Rad) column, and an RI detector. Mobile phase was water, flow rate was 0.5 mL/min, the column compartment was heated to 85 °C to enhance separation, and the RI detector was operated at its maximum of 55 °C. External calibration was used to quantify the free sugars and sugar alcohols (glucose, sucrose, fructose, xylose, inositol, and sorbitol). Each analysis was performed in triplicate.

Analysis of Filter Cake. The spent almond hulls (insoluble material after extraction) were dried and subjected in triplicate to standard analysis for quantification of the cell wall carbohydrate polymer composition by Wiley milling to pass a 40-mesh screen followed by dissolution of the polymeric materials in 3% H_2SO_4.[16] The insoluble residue after acid hydrolysis was measured gravimetrically and fired in the muffle furnace at 550 °C for 6 h to quantify acid-insoluble ash and organic matter. A 1 mL aliquot of the liquid fraction was neutralized with $CaCO_3$ and centrifuged to remove insoluble salts, and the resulting neutral solution was analyzed by HPLC. The system and operating conditions were identical to those described above for free fermentable sugars, but the external calibration standard set consisted of cell wall sugar residues (glucose, xylose, galactose, arabinose, mannose).

Optimizing Solids Content, Water Recovery, and Pectinase Application Experiments. Solids content was varied from 5 to 20% with incubation for either 1 h or overnight time periods. The almond hulls were diluted with 50 °C tap water to the specified solids content in the blender and milled for 1 min to reduce particle size and initiate swelling. After transfer to an Erlenmeyer flask, the hulls suspension was incubated according to the desired time period at 50 °C in an orbital incubator shaker (Amerex Instruments, Inc., model SK-747R) at 150 rpm. At the end of the incubation period, filtration was performed using the pressure filter, and the resulting filtrate was weighed for water recovery and sampled for analysis of sugar content by HPLC.

For the pectinase application experiments two approaches were taken. First, the almond hulls were milled at 20% solids content for 1 min followed by the addition of pectinase from *Aspergillus aculeatus* (Pectinex, Sigma-Aldrich). The pectinase content was varied from 0 to 0.75% (w/v), the mixture was incubated with orbital shaking (150 rpm) for 1 h, and then the filtration/analysis as described above was performed to obtain the experimental results. Second, the identical procedure of milling was performed, and then the pectinase (0.5% w/v) was added and the incubation time varied from 0 to 60 min. Again, experimental workup was identical to previous analyses.

Countercurrent Extraction. Figure 1 depicts the concept of countercurrent extraction in which the solvent (water) and the solid matrix (almond hulls) contact each other in opposite flow directions. In this case, a 1 h steep followed by filtration and then three rapid extraction (wash) stages recovered the bulk of the free sugars. Fresh water was introduced in the final extraction (third wash stage), and the third filtrate from the final stage was cascaded forward to serve as wash water for the prior (second) wash stage. The wash water cascaded forward becomes progressively higher in sugar concentration as the solid phase is washed free of sugars as it moves through the extraction process. The filtrate from the first wash stage is the dilution water for the steep process, and the isolated steep liquor is the concentrated sugar product.

The countercurrent experiment consisted of five rounds of extraction as described in the previous paragraph. Specifically, the fresh hulls (40 g, db) were diluted to 20% solids with 50 °C tap water, milled for 1 min in a blender, and transferred to an Erlenmeyer flask along with 0.5% (w/v) pectinase, and then the flask was placed in an

DOI: 10.1021/jf5048332
J. Agric. Food Chem. 2015, 63, 2490−2498

incubator at 50 °C for 1 h. After the steep process, the solids were filtered over the pressure filter apparatus. The filtrate (S_1, Figure 1), termed the steep liquor, was saved as sugar concentrate. For the first round of processing only, the hulls were resuspended in 200 mL of hot tap water, blended for 1 min, and refiltered in the same apparatus. This process was repeated a total of three times, and the filtrates produced were saved to serve as wash water (labeled S_2, S_3, and S_4, respectively) in the following round of extractions. In this way a feed-forward recycle loop was created between previous and subsequent rounds of extraction.

For each of the subsequent four rounds of extraction, the procedure was identical to that described above except that the dilution water for the steep and the first two washing stages was the filtrates produced in the preceding round of extraction (in this case S_2, S_3, and S_4 for the steep, first and second wash stages for round 2, respectively). In all cases the third (final stage) wash water was hot tap water. A final L30 autoclave cycle followed by a final filtration quantified the total sugar in the almond hull sample and accounted for variability in the feedstock. The filter cake after the final filtration was weighed and dried to complete the mass and water balances. Both internal and external mass balances were performed to estimate equilibrium sugar concentrations and also to calculate recovery efficiencies. Sugar concentrations were quantified by HPLC as described above.

Large Batch. To obtain a large volume of sugar concentrate for fermentation studies, 1 kg of almond hulls was suspended at 10% solids content and milled in a Waring blender for 1 min, transferred to a Fernbach flask, along with 0.5% (w/v) pectinase, and incubated for 1 h at 50 °C. In the case of large scale sugar concentrate production, the hulls were hand squeezed using grade 60 cheesecloth (Fisher) for solids retention. The filtrate was recovered and weighed, whereas the solids were weighed, analyzed for TS, and discarded. The filtrate was used to wet the next round of almond hulls with the charge of hulls determined to be 10% solids on a filtrate basis. This procedure of concentrating was used until sufficient sugar concentration was achieved.

Ethanol Fermentation. Fermentation was performed using an overnight seed culture of *Saccharomyces cerevisiae* D5A (ATCC 200062) with 0.0125 g of dry yeast added to 50 mL of seed media. Sterilized culture media (autoclaved for 20 min at 121 °C) consisted of glucose (150 g/L), yeast extract (7.5 g/L), ammonium sulfate (22.5 g/L), dipotassium phosphate (15 g/L), and magnesium sulfate heptahydrate (3 g/L).[17] The pH of this seed media was adjusted to 4.5, with temperature maintained at 30 °C under gentle mixing (200 rpm) using a shaker incubator. Growth of this seed culture was completed after glucose concentration fell below 2 g/L. Inocula from the seed culture were rinsed twice by centrifuging at 4500 rpm for 10 min, decanting the supernatant, resuspending cells in the same volume of distilled water, and repeating this process. Resuspended cells ($^1/_{10}$th dilution) were used to inoculate the concentrated sugar solutions supplemented with 1% yeast extract and 2% peptone and sterilized for 20 min at 121 °C. The fermentations were incubated for 24 h at 30 °C with glucose and ethanol concentrations monitored by HPLC.

Distillation. The ethanol was recovered by simple distillation to leave behind a thin stillage stock solution for high-rate anaerobic digestion. Specifically, a 2 L distilling flask in an electric heating mantle was filled half full (1 L volume) with broth containing ~7.5% (v/v) ethanol. Under low heat, the broth was heated so as to cause the ethanol to evaporate and rise into the fractional condensing column providing high-efficiency separation of the ethanol. The vapor phase azeotrope was cooled via a water jacket and recovered in a flask containing activated carbon and molecular sieves to remove volatiles and residual water. The solution retained in the distilling flask was saved as the thin stillage and used for biogas production.

Anaerobic Digestion of the Thin Stillage. A 1 L upflow attached-growth anaerobic reactor was utilized to determine the biomethane potential (BMP) and the anaerobic biodegradability of the thin stillage. The reactor was packed with biological filter media (Eheim Substrat Pro biological filter media, Eheim, Germany) and had a working volume of 720 mL. The system also contained a separatory funnel modified to serve as an in-line clarifier external to the reactor to collect sloughed biomass and also to allow for removal and wasting of accumulated solids and filtrate. In all, the total system volume was 1.07 L. Flow rate (20 mL/min) was controlled via a peristaltic pump with an overall system turnover of slightly less than 55 min. Flow to the reactor was in the upflow direction to an internal overflow weir for a total contact time of 36 min per reactor pass. The weir overflow fed by gravity to the separatory funnel, and the clarifier overflowed to the pump inlet to complete the flow loop. The reactor was jacketed for temperature control, which was maintained at 37 °C via a circulating water bath. Gas flow was collected in a calibrated 9 L gas accumulator filled with 10 N KOH to strip CO_2 from the biogas so that only CH_4 was stored. CH_4 produced was measured by volume displacement of a free floating inner cylinder within the accumulator and measurement of the height the cylinder was raised.

The reactor was populated by settling 250 mL of an anaerobic culture from a nursery reactor and inoculating the biological filter media with the supernatant. The culture was established on the attached growth medium with a glucose solution to increase population prior to the introduction of the thin stillage. The reactor was then acclimated to the thin stillage for an additional month before BMP was estimated by feeding weekly over a 7 week period. Known volumes of concentrated thin stillage were diluted with RO H_2O to create a stock feed. The feed was then sampled to obtain a diluted soluble chemical oxygen demand COD (SCOD) content and fed to the reactor. SCOD was performed with a Chemetrics COD kit using their midrange tubes and heated with a HACH meter (model CR2200). COD was measured using a UV−vis spectrophotometer (Molecular Devices M2) and calibrated using 1000 and 10000 ppm of COD standards (A-7301 and A-7310, respectively, from Chemetrics).

RESULTS AND DISCUSSION

Physical Properties of Fresh Almond Hulls and Measurement of Soluble Sugars. Nonpareil almond hulls were used for all of the following experiments and determined to be 80% total solids (TS). Nonpareil hulls were reported previously to be of low contaminant content;[5] however, for this study, the hulls were hand sorted to ensure 100% hull content in all samples. The ash content was 3.5% (Table 1).

It is known that almond hulls contain free fermentable sugars (sucrose, glucose, fructose) and nonfermentable sugars and

Table 1. Compositional Analysis of the Almond Hulls Used in This Study Compared to Literature Values[a]

	dry hulls	soluble	insoluble	lit. values[ref]
fermentable sugars	37.3 (1.1)	37.3		21.2[3]−24.5[2]
sucrose	5.2 (0.6)	5.2		5.3[2]−10.6[3]
glucose	16.3 (0.6)	16.3		5.8[3]−10.4[2]
fructose	15.9 (0.2)	15.9		4.8[3]−8.8[2]
nonfermentable sugars	9.0 (0.3)	9.0		4.8[3]−7.1[2]
xylose	0.6 (0.03)	0.6		
inositol	2.5 (0.1)	2.5		2.1[3]−2.5[2]
sorbitol	5.9 (0.4)	5.9		2.7[3]−4.6[2]
total sugars	46.3 (1.4)	46.3		25.6−31.6[2,3,18]
ash	3.5 (0.2)	2.1	1.4	6.1−12.8[4,19−22]
cellulose/starch	6.6 (0.6)		6.6	9.0−15.5[4,19−22]
hemicellulose	6.0 (0.3)		6.0	6.9−10.0[4,20−22]
lignin (acid insolubles)	12.3 (0.6)		12.3	4.1−15.4[4,19−22]
unknown	25.3	13.1	12.1	
total weight	100.1	61.5	38.4	

[a]Moisture content for the hulls was 80%. Standard errors are listed in parentheses next to each subcomponent.

DOI: 10.1021/jf5048332
J. Agric. Food Chem. 2015, 63, 2490−2498

sugar alcohols (xylose, inositol, sorbitol).[2,3,14] The four-step procedure used here achieved total sugar levels >30% higher than reported in the previous literature (reported in Table 1 for comparison). Literature values for sucrose contents range from 5.3 to 10.6%,[2,3] comparable to or higher than the current results (5.2%, Table 1). Inositol values are similar to the reported values (~2%), whereas the sorbitol levels measured here are slightly higher (5.9 vs 2.7−4.6%). The quantitative difference between techniques is expressed in this analysis as marked increases in the contents of glucose and fructose, 16.3 and 15.9%, respectively. Reported literature values range from 5.8 to 10.4% for glucose and from 4.8 to 8.8% for fructose.[2,3] Enhancement of the glucose and fructose contents could in part be a result of the decomposition of sucrose (a dimer of glucose and fructose) into its monomeric components but does not completely account for the difference. The difference may also be attributed to variety or breeding, changes in agricultural approaches, location, environmental conditions, sensitivity of analysis, higher degree of quantitation, or other factors. In total for the almond hulls analyzed here, fermentable sugar (FS) content is 37% and total sugar plus sugar alcohol content is 46%. Total extractable sugar plus sugar alcohol contents reported by the previous studies range from 25.6 to 31.5%[2,3,18] (Table 1).

The free fermentable sugars comprise 75% of the soluble components of the almond hulls with the remainder being soluble ash (3.4%) and unknown compounds (21.3%), comprised in part by the following categories: tannins, polyphenols, fats, proteins, pectins, gums, and other polysaccharides (Table 1).[4]

Characterization of the Insoluble Fraction (Spent Almond Hulls). The structural carbohydrate composition was determined by acid hydrolysis of the spent almond hulls (residual almond cake) after hot water extraction. Analysis of the residue assuming no losses during extraction indicates that the dry raw hulls contain 6.6% cellulose, 6.0% hemicellulose, and 12.3% lignin (acid-insoluble fraction). The cellulose and hemicellulose contents are slightly lower than previous results from dairy forage analysis (12.8 and 9.0%, respectively, on average), and the lignin content is slightly higher in this analysis (12.3%) versus an average of 10% reported previously.[4,19−22]

In total, 68% of the spent almond hulls is readily identifiable based upon cell wall analysis and ash content and, overall, 74.7% of the total almond hull content is identified by the procedures utilized here (Table 1).

Practical Solids Content and Water Recovery. Commercial ethanol production requires a high sugar concentration for fermentation, because high sugar levels result in sufficient alcohol content to make distillation economical.[23] The hulls were first subjected to a steeping process at 1 h and overnight time periods to determine maximum practical solids content and maximum achievable sugar recovery. The extent to which the fermentable sugars may be recovered is a function of the free water availability due to the absorptive capacity of the hulls and the equilibrium sugar concentration. Almond hulls are highly hydrophilic and can absorb and retain 10−15 times their weight in water. The initial steeping step involves wetting of the hulls and, as a result a substantial proportion of the solvent (and solute), remains with the solid phase, thus reducing extraction efficiency. Figure 2 shows the results at various solids content for the 1 h and overnight periods. As can be seen, low solids (5%) and overnight extraction result in 74% recovery of the free sugars but at very low concentration (17.6 g/L FS or 22.4 g/L TS). In all other cases, overnight sugar recovery was equal to or lower than that for the 1 h steep duration due to lower water recovery resulting from complete saturation of the almond hulls. Additionally, sugar concentrations were equivalent over the two time frames, suggesting a 1 h steep was sufficient to achieve equilibration of the free and absorbed solutes. At 20% solids content and a 1 h steep, sugar concentration (65 g/L FS) was sufficiently high to use this as a basis for a multistage extraction process.

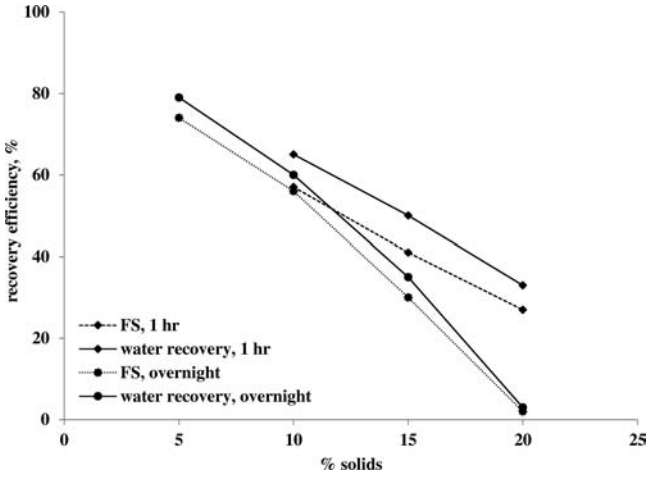

Figure 2. Effect of solids content and extraction duration on free fermentable sugar and free water recovery.

Pectinase Application. It has been reported previously that almond hulls contain pectin[4,24] or pectin-like hydrocolloids. Many fruit-processing operations include the use of pectinase to control the viscosity, improve liquids/solids separation, and clarify juice products.[25] Pectin is located in the primary cell wall and middle lamella and provides firmness or compression rigidity to the fruit.[26] Almond hulls have a tremendous propensity to absorb and hold water, in part due to the pectin molecules, making free sugar extraction and disposal of the residuals more difficult. As a result, pectinase applications were explored to improve sugar extraction and water recovery. The enzyme cocktail used in this study contains methyl esterases and polygalacturonases as well as small amounts of hemicellulases and cellulases, all of which can contribute to the breakdown of the cell wall to facilitate fermentable sugar extraction.

Almond hulls were steeped at 20% solids loading at 50 °C for 1 h with pectinase enzymes at application rates ranging from 0 to 0.75% (w/v). After a 1 h steep with no enzyme, the entire volume of water was absorbed by the control (i.e., no steep liquor available). Steep liquor recovery improves to 26% of applied with 0.25% pectinase application and then increases only slightly (34%) at the higher enzyme dosages. It is likely that the enzyme application removes the rigid, hydrophilic pectin material, decreasing the absorptivity of the hull, making more free water available, and facilitating equilibration of the free and absorbed solutes. Figure 3a illustrates how the maximum sugar extraction levels are directly tied to water recovery. Higher sugar recovery rates require additional extraction stages. Figure 3a also shows that the sugar yield after steep liquor recovery and first extraction (wash) improves 36% over the control with just 0.10% enzyme application and improves to 76% at 0.75% application. In total, at sufficient

DOI: 10.1021/jf5048332
J. Agric. Food Chem. 2015, 63, 2490−2498

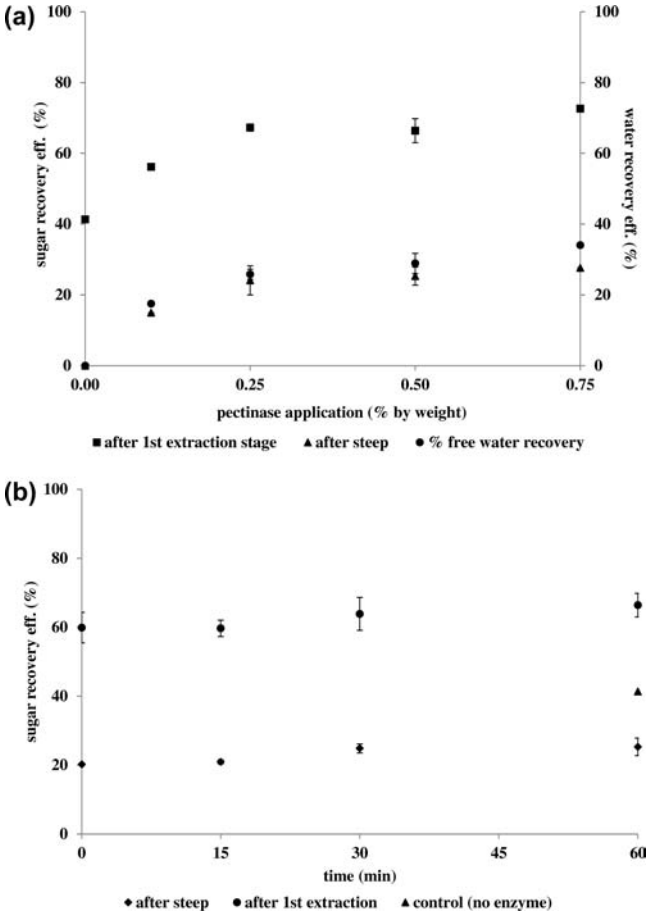

Figure 3. (a) Effect of pectinase application on the efficiency of sugar recovery through steep and first wash stage. Steeping was performed at 50 °C for 60 min. (b) Improvement in sugar recovery with pectinase treatments (0.5% w/v) over time.

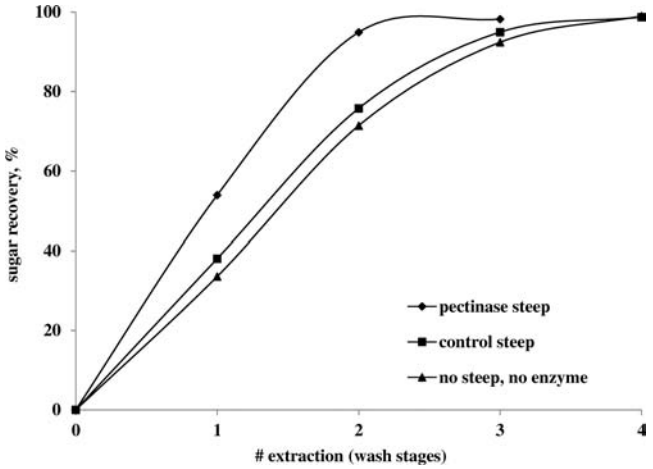

Figure 4. Free sugar extraction with and without pectinase enzyme application and steeping. When applied, enzyme application was 0.5% (w/v) and steep time was 60 min at 50 °C.

enzyme application rates, sugar recovery after steeping and first-stage washing is ~70%.

To examine the benefits of steep time, enzyme application was maintained at 0.5% (w/v) and steep time varied. Figure 3b shows sugar yields in the steep liquor increase only slightly (from 20 to 25%) over steep time varying from 0 to 60 min. The data indicate that equilibration occurs rather quickly, at least during the initial contact of the almond hulls with the solvent as milling in the blender reduces particle size. The apparent benefit of the pectinase is that it reduces the swelling capacity of the hulls and maintains a free volume during the wetting process so that recovery of free sugars can occur after saturation of the hulls is achieved. In comparison to the control (60 min with no enzyme), sugar recovery after steep liquor recovery and first-stage extraction increases 60%, and this is due to the reduction in the water-retaining capacity of the hulls. Over the time curve the enhancement of sugar recovery is less because equilibration between free and absorbed solute is quickly achieved. As a result, it may be acceptable to shorten steep time and reduce overall processing time.

Figure 4 shows the effects of steeping and pectinase additions versus the control (no enzyme, no equilibration time). The control solubilizes the readily available soluble sugars, but contact time is not sufficient for diffusion of water into hulls. As such, a fair volume of water is recovered through filtration but with fairly low sugar concentration (46 g/L FS). Steeping with no enzyme produces a more concentrated product (88 g/L FS), but very little free water is available after a single stage and the total sugar recovery is similar to the control. Only slightly more sugar is recovered by steeping without pectinase application (38% recovery vs 34%) than for no equilibration time. The two curves mirror each other in slope as the hulls become saturated and sugar extraction is equivalent because structurally the hulls remain similar. After three extraction stages, 96 and 93% of sugar was recovered, respectively, for steeping without enzyme and no steep options. An additional stage recovers 99% of the sugar in both of these cases.

The pectinase steeped hulls release significant volumes of free water and fermentable sugars, resulting in a high sugar concentration in the steep liquor (74 g/L FS). Hence, much more sugar is recovered in the first stage of extraction. Figure 4 also shows that enzyme application under ideal conditions (fresh wash water) results in complete sugar recovery in three filtration steps and that 96% recovery is already achieved after only two filtrations. Enhanced sugar recovery is important in commercial processing to reduce the number of stages required for recovery of product and also to maximize the product concentration. As a result, the application of pectinase is beneficial to accelerate sugar recovery, produce higher volumes of free water at high solids processing conditions, and produce higher fermentable sugar concentrations.

Countercurrent Extraction of Free Fermentable Sugars. On the basis of the above results a series of experiments were devised to mimic countercurrent extraction of soluble sugars, analogous to a diffuser, which is used in the food-processing industry for extraction of sugars. The counter flowing water is fresh at its inlet point and progressively increases in sugar concentration as it contacts sugar-rich hulls (Figure 1). The process involves (1) diffusion of the lower strength solvent (water) into the substrate, (2) dissolution and equilibration of soluble components, and (3) forced displacement of the free water and solubles by low-pressure filtration (extraction).

Five rounds of extraction were performed to reproduce the concentration of sugars analogous to the countercurrent extraction process. Round 1 utilized fresh water as the wash water and produced a steep liquor, S_1 (84 g/L total sugar and sugar alcohol concentration) and a battery of filtrates (S_2, S_3,

DOI: 10.1021/jf5048332
J. Agric. Food Chem. 2015, 63, 2490−2498

S_4) to serve as wash water in the subsequent rounds. S_2 served as the dilution water for the fresh almond hulls in round 2, carrying along with it a total sugar concentration of 39 g/L total sugars (30 g/L FS). By mass balance, the equilibrium sugar content in the round 2 steep liquor (S_6) was calculated as the sugar input divided by the total of the free and absorbed water and should be 115 g/L total sugars. By measurement of the filtrate (S_6, Figure 1), the actual concentration was 117 g/L (91 g/L FS), indicating that the steep process was adequate for equilibration. The first wash stage consists of suspension of the almond hull cake in the second filtrate from round 1 extraction (S_3, Figure 1) for the duration of milling (1 min) followed by filtration. Interestingly, the observed sugar concentration in S_7 (56 g/L total sugar, 44 g/L FS) was predicted by the equilibrium sugar calculation, indicating that the contact time during milling in the blender was sufficient for equilibration. Observed values were consistently in sync with predicted values (± 10%) throughout, especially with the more concentrated filtrates. Dilute filtrates had a larger percent difference but were close in value for g/L total sugar. Throughout the entirety of the study, the free fermentable sugar content was 0.78 g per g of total sugar extracted, which demonstrates that no preferential extraction of one type of sugar or sugar alcohol is occurring.

Figure 5 shows the average efficiency of sugar recovery by each individual extraction stage and the cumulative average

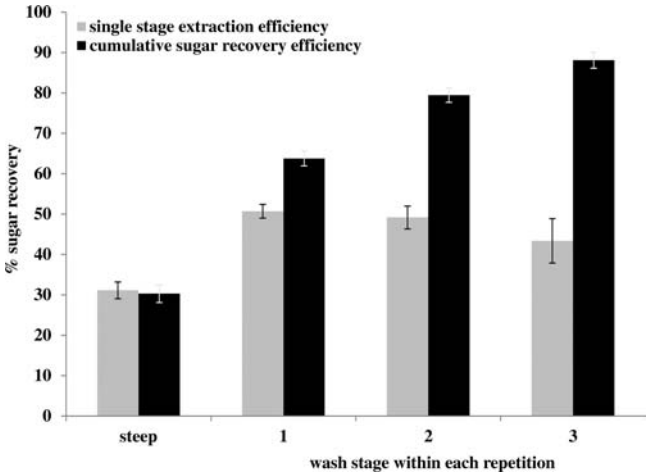

Figure 5. Sugar recovery efficiency for individual extraction stages within countercurrent extraction repetitions (gray bars); average cumulative sugar recovery within repetition (black bars).

across the three wash stages. Efficiency is lowest during the steep stage as the hulls are saturating, and the free water recovery yields are lower. On average, 70% of the steep water is retained within the hulls. Because the yield of extractable sugar is dependent upon free water recovery, it follows that sugar recovery is only ~30% on average (see Figure 2a). After steeping, the hulls are saturated and the process equilibrates, whereby extraction stage efficiencies vary from 51 to 49 to 43% in the first to third stages, respectively. The efficiency is defined as the total sugar in the filtrate divided by the total sugar in the solid matrix and the wash solution. The first and second stage sugar recoveries are closely related to water recovery yields; however, the third stage strays somewhat from this relationship. Specifically, the average water recovery from the third wash stage was 60%; however, the average sugar recovery yield was only 43%. At this point, the average particle size is small after four 1 min milling treatments and a 1 h enzyme steep. The deviation from the water recovery relationship may indicate that displacement is incomplete, the residual sugar is difficult to completely extract, or the final autoclave cycle causes some minor depolymerization of hemicelluloses.

Figure 5 also depicts cumulative extraction efficiency defined as the total cumulative sugar recovery combined over the steep and three extraction stages divided by the total sugar input with the solid hulls and recycled wash water. On average, the cumulative recovery was 88% and varied between 83 and 93% over the five repetitions. The data show that although the extraction efficiencies per repetition do not decrease with increasing sugar concentrations (i.e., rounds 4 and 5), larger amounts of sugar are not extracted through three wash stages as the feedback wash loop contains larger amounts of sugar than are actually input with the hulls. Including the recycled sugars in the efficiency calculation, repetitions 4 and 5 are 83 and 88% efficient, respectively. However, using the calculation of losses divided by input with the fresh hulls would return values of 78 and 69%. The lingering sugar with the residue after three extraction stages and high sugar concentrations throughout indicates that a fourth extraction stage may be useful to achieve better sugar recovery.

Five consecutive countercurrent extractions were performed to concentrate the soluble sugars in the product; however, equilibrium was not quite reached by this point. After a single round of extraction, the concentrated sugar product contained 65 g/L FS (84 g/L total sugars), and after round 5, the product contained 131 g/L FS (169 g/L total sugars) (Figure 6). The

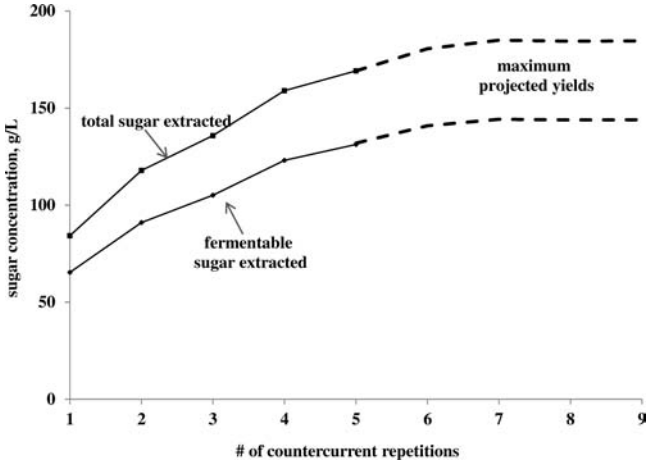

Figure 6. Total sugars and free fermentable sugars extracted per countercurrent repetition. Solid line represents laboratory data; dashed lines represent theoretical yields based upon modeling using measured extraction efficiencies.

results demonstrate that countercurrent extraction is efficient for producing a high free fermentable sugar concentration for fermentation to alcohol. In practice, the sugar concentration would increase until equilibrium is achieved through the system, and this would be the operational target. On the basis of the extraction efficiencies, the point of equilibrium was estimated as depicted by the dashed line extensions in Figure 6. Calculations indicate that two additional rounds of extraction would bring the concentrated product close to an equilibrium point of 184 g/L TS (144 g/L FS), which would mark the highest concentration that can be achieved through countercurrent extraction.

DOI: 10.1021/jf5048332
J. Agric. Food Chem. 2015, 63, 2490−2498

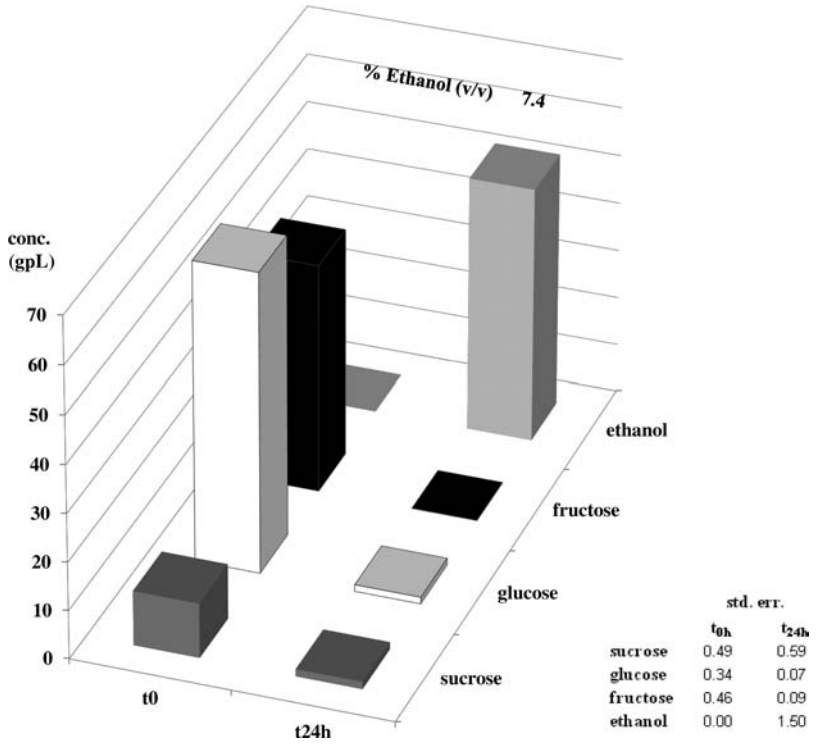

Figure 7. Fermentation of high sugar concentrate steep liquor to ethanol. Glucose and fructose were completely converted, and sucrose was 87 % converted. Ethanol yields were 86% of theoretical. Beer concentration averaged 7.4% (v/v).

Table 2. Data from the Anaerobic Fermentation of Almond Hull Thin Stillage to Biogas

feed	SCOD added (g)	SCOD destroyed (g)	% removal eff	CH_4 yield (mL/g $SCOD_{destroyed}$)	SCOD effluent (mg SCOD/L)
1	5.71	5.15	90	263	1230
2	4.74	4.24	90	280	1253
3	4.97	4.40	88	278	1377
4	4.97	4.44	89	291	1429
5	4.13	3.97	96	392	1069
6	4.34	3.68	85	276	1312
7	4.30	3.92	91	300	1238
av	4.74	4.26	90	297	1273
σ			3.3	43	117
SE			1.3	16	44

Filter cake residues were collected and analyzed for moisture content and percent of original almond hull remaining. The average solids content of the spent almond hull cake was 9.2%, and overall the average recovery of solids was 28.5% of the original almond hull input, about 10% lower than the quantification assay. Discrepancies could be related to pectinase application or additional handling.

Fermentation of Soluble Sugars to Alcohol. The countercurrent extraction experiment demonstrates that the sugar concentration in the steep liquor and wash filtrates can be progressively enhanced providing data for estimation of the maximum producible sugar concentrations. The countercurrent experiment, however, utilized small product volumes, with insufficient quantity to carry out a significant, reproducible fermentation experiment. Accordingly, a large extraction starting with 1 kg of almond hulls was undertaken to ultimately produce a large volume of high sugar product for fermentation experiments. Sugar content was monitored until the total sugar content was 178 g/L (140 g/L fermentable sugars). Figure 7 shows the average results of fermentation of the sugar solution after a 24 h conversion period. The yields were an average of 86% of the theoretical ethanol (using four replicate experiments) and an average of 7.4% (v/v) ethanol concentration in the resulting beer. Furthermore, mass balance on the fermentable sugars shows a nearly complete utilization of both glucose and fructose and an average of 87% utilization of the sucrose in solution. Inhibitors such as furfural, HMF, and acetic acid were tracked but were not present in any appreciable concentration.

Anaerobic Fermentation of Thin Stillage to Methane. The beer was subjected to overhead distillation to separate and purify the ethanol but also to create a thin stillage for further analysis. The thin stillage was analyzed for SCOD content and stored in the refrigerator for further use. A total of 60−70% of the almond hull was solubilized during the extraction process, whereas the fermentable sugars utilizable by the yeast comprise only slightly more than half of this content. As a result, the beer has an amber color and a very high SCOD content (233,250

DOI: 10.1021/jf5048332
J. Agric. Food Chem. 2015, 63, 2490−2498

mg/L), thus making it a very good candidate for biogas production.

A 1 L mesophilic upflow attached growth anaerobic reactor (AGR) packed with biological filter media and equipped with an internal overflow weir was commissioned to analyze the biodegradability and biomethane potential (BMP) of the thin stillage. To measure BMP, the reactor was batch fed with a 1 week retention time to allow for complete decomposition of the feed substrate, although decomposition typically took <72 h. The organic loading rate (0.67 g/L day) was intentionally held low for the BMP analysis over a 1 week hydraulic retention time (HRT).

The reactor was acclimated over 1 month to allow for a stable culture with constant pH. The reactor was then operated over a 7 week period on the thin stillage, and the average biomethane yield was 297 mL CH_4/g SCOD destroyed, with an average SCOD feed destruction of 90% (Table 2). Background SCOD levels remained stable throughout operation, declining to levels comparable to the initial SCOD concentration prior to feeding. indicating nearly complete destruction. Volatile fatty acids were tracked but did not accumulate, and the inositol and sorbitol in the feed were completely degraded. The alkalinity remained high (~2500 mg $CaCO_3$ eq/L) in conjunction with a pH that averaged 7.1−7.3. Effluent SCOD levels were 1.2−1.5 g/L SCOD. Overall, it appears that the thin stillage is very amenable to biogas production.

Bioenergy Potential of Soluble Components of Almond Hulls. On the basis of the Nonpareil almond hulls used here, it can be estimated that the theoretical ethanol potential on a dry ton basis is 64 gal (242 L). On the basis of sugar recovery and fermentation efficiencies, the realistic ethanol potential is 49 gal (185 L)/t hulls (db). This result is higher than previously reported (39 gal, 148 L)[18] but is in alignment with the higher fermentable sugar contents that were detected in this study. In addition, this study estimated the biomethane potential per gram of SCOD destroyed. Estimating the biomethane potential on a per tonne basis was done on the basis of the amount of hulls used for preparing the bulk solution for fermentation, which is roughly estimated at 75 m^3 CH_4/t of fresh hulls (db). In total, 1 t of hulls can provide a minimum of 6700 MJ of locally produced bioenergy with the breakout being 58% of the energy arising from ethanol and 42% from biogas.

In conclusion, almond hulls are a major California agricultural residue and contain very high levels of free fermentable sugars and other carbohydrates that can be made available for a number of uses, including locally produced transportation fuels such as bioethanol and biogas. Via an optimization analysis, the maximum practical solids concentration (20%) that could be utilized for effective sugar extraction with both acceptable water recovery yields and sugar concentrations was determined. Sugar extraction is directly related to the ability to recover free water because the equilibrium relationship between the free and absorbed water limits the recovery potential of the soluble sugar in any one extraction stage. Small additions (~0.5% w/v) of pectinase can reduce the absorptive capacity of the hulls and improve the subsequent additional free water recovery thereby aiding sugar recovery, especially in the initial extraction stages.

High solids (20%) countercurrent extraction was utilized to extract and accumulate the free fermentable sugars for further use. The initial free fermentable sugar concentrate increased from 65 g/L fermentable sugars after one round of extraction to 131 g/L after five rounds of extraction as a result of the applied countercurrent approach. Extraction efficiency was high, 88% overall; however, the number of extraction stages within each round of extraction would ideally be extended one or two wash stages as the sugars concentrate in the recycle loop.

The beer produced from fermentation of the concentrated steep liquor had an average ethanol content of 7.4% (v/v), well within a range that is acceptable for economic distillation. Fermentation efficiencies were high (86%), and the fermentation was complete in <24 h. The thin stillage after distillation was rich in SCOD (233 g/L) and was fed to an attached growth reactor for the measurement of biomethane potential. The biomethane potential was determined to be 297 mL/g SCOD destroyed, the efficiency in SCOD destruction was 90%, and the effluent SCOD concentrations were low (1.2 g/L SCOD). Overall, it was estimated that almond hulls are capable of delivering a minimum of 185 L EtOH/t of fresh hulls (db) and approximately 75 m^3 CH_4/t of fresh hulls (db).

AUTHOR INFORMATION

Corresponding Author

*(K.M.H.) Phone: (510) 559-5929. Fax: (510) 559-5675. E-mail: kevin.holtman@ars.usda.gov.

Funding

We thank the Almond Hullers and Processors Association (AHPA) for financial support under Trust Fund Cooperative Agreement 58-5325-2-140.

Notes

The authors declare no competing financial interest.

ACKNOWLEDGMENTS

We thank the Almond Hullers and Processors Association (AHPA), especially Kelly Covello from AHPA, for facilitating almond hull collection.

REFERENCES

(1) *2012 Almond Almanac*; Almond Board of California: Modesto, CA, USA, 2012.

(2) Sequeira, R. M.; Lew, R. B. The carbohydrate composition of almond hulls. *J. Agric. Food Chem.* **1970**, *18*, 950−951.

(3) Saura-Calixto, F.; Cañellas, J.; García-Raso, J. Gas chromatographic analysis of sugars and sugar-alcohols in the mesocarp, endocarp, and kernel of almond fruit. *J. Agric. Food Chem.* **1984**, *32*, 1018−1020.

(4) Saura-Calixto, F.; Cafiellas, J.; Garcia-Raso, J. Contents of detergent-extracted dietary fibers and composition of hulls, shells, and teguments of almonds (*Prunus amygdalus*). *J. Agric. Food Chem.* **1983**, *31*, 1255−1259.

(5) Offeman, R. D.; Holtman, K. M.; Covello, K. M.; Orts, W. J. Almond hulls as a biofuels feedstock: variations in carbohydrates by variety and location in California. *Ind. Crops Prod.* **2014**, *54*, 109−114.

(6) Rabinowitz, I. Increasing the inositol yield from almond hulls. U.S. Patent 5,064,762, 1991.

(7) Rabinowitz, I. Extraction of products from almond fruit. U.S. Patent 4,997,489, 1991.

(8) Rabinowitz, I. Enhanced production from almond hulls of products such as inositol and inositol phosphates. U.S. Patent Appl. US20040018599, 2004.

(9) Rabinowitz, I. Edible food produced such as sports beverages, health drinks, fruit bars, jams and jellies. U.S. Patent Appl. US20020132031, 2002.

(10) *Biorefineries − Industrial Processes and Products. Status Quo and Future Directions*; Kamm, B., Gruber, P. R., Kamm, M., Eds.; Wiley-VCH: Weinheim, Germany, 2006; Vol. 1.

DOI: 10.1021/jf5048332
J. Agric. Food Chem. 2015, 63, 2490−2498

(11) Perry, R. H.; Green, D. W.; Maloney, J. O. *Perry's Chemical Engineers' Handbook*, 7th ed.; McGraw-Hill: New York, 1997.
(12) Asadi, M. *Beet-Sugar Handbook*; Wiley: Hoboken, NJ, USA, 2006; p 866.
(13) Rabinowitz, I. Method of producing aqueous extracts from almond hulls. U.S. Patent 6,716,465, 2004.
(14) Cruess, W. V. Almond meats and hulls: new and improved uses for larger-sized meats and for hulls subjects of investigations. *Calif. Agric.* **1949**, *3* (12), 6−12.
(15) APHA; AWWA; WPCF. *Standard Methods for the Examination of Water and Wastewater*, 16th ed.; Franson, M. H., Ed.; American Public Health Association: Washington, DC, USA, 1985; pp 99−100.
(16) Dence, C. W. The determination of lignin. In *Methods in Lignin Chemistry*; Lin, S. Y., Dence, C. W., Eds.; Springer: Berlin, Germany, 1992; pp 33−61.
(17) Selig, M.; Weiss, N.; Ji, Y. Enzymatic saccharification of lignocellulosic biomass. NREL/TP-510-42629, 2008.
(18) Cruess, W. V.; Kilbuck, J. H.; Hahl, E. Utilization of almond hulls. *Fruit Prod. J.* **1947**, *26*, 363−373.
(19) Aguilar, A. A.; Smith, N. E.; Baldwin, R. L. Nutritional value of almond hulls for dairy cows. *J. Dairy Sci.* **1984**, *67*, 97−103.
(20) Fadel, J. G. Evaluation of chemical composition, optical density measurements and in sacco disappearance of two commodities under controlled moisture and heating conditions. *Anim. Feed Sci. Technol.* **1992**, *36*, 13−27.
(21) Norollahi, H.; Kamalzadeh, A.; Karimi, A. Determination of chemical composition and digestibility of almond hull. *Acta Hortic.* **2006**, *726*, 591−593.
(22) Yalchi, T.; Kargar, S. Chemical composition and in situ ruminal degradability of dry matter and neutral detergent fiber from almond hulls. *J. Food, Agric. Environ.* **2010**, *8*, 781−784.
(23) Madson, P. W.; Lococo, D. B. Recovery of volatile products from dilute high-fouling process streams. *Appl. Biochem. Biotechnol.−Part A* **2000**, *84*−*86*, 1049−4061.
(24) Coffin, D. R.; Fishman, M. L. Physical and mechanical properties of highly plasticized pectin/starch films. *J. Appl. Polym. Sci.* **1994**, *54*, 1311−1320.
(25) Kashyap, D. R.; Vohra, P. K.; Chopra, S.; Tewari, R. Applications of pectinases in the commercial sector: a review. *Bioresour. Technol.* **2001**, *77*, 215−227.
(26) Willats, W. G. T.; Mccartney, L.; Mackie, W.; Knox, J. P. Pectin: cell biology and prospects for functional analysis. *Plant Mol. Biol.* **2001**, *47*, 9−27.

DOI: 10.1021/jf5048332
J. Agric. Food Chem. 2015, 63, 2490−2498

enzymatic treatments to remove cross-links, and new cross-links being formed. An overview of tanning chemistry has been presented.[6] Some aspects of chemical treatments of skins and their effect on structure have been observed previously with liming of skins (increasing the pH with calcium hydroxide) showing a decrease in the D-spacing of collagen.[7] Dehydration of parchment has been shown to result in a decrease in collagen D-spacing from 64.5 to 60.0 nm.[8] Pickling and retanning agents have been shown to swell collagen fibers at low pH.[9] At low ionic strength and nonisoelectric pH, charge-dependent interactions (screening and selective ion adsorption) are prevalent in maintaining the collagen architecture,[10] which is also reflected in the greater thermal stability of collagen at low pH[11] and in the elastic response of collagen.[12]

In this work, we use SAXS to investigate the changes that take place in the microstructure of leather through the different stages of processing from skin to leather. The structural basis of these changes at the level of the collagen fibrils is not fully understood and forms the basis of this investigation.

EXPERIMENTAL PROCEDURES

Ovine pelts were obtained from 5-month-old, early-season New Zealand Romney cross lambs. Samples were removed from the same skin during several stages of processing at or near the "official sampling position" (OSP).[13] These stages were termed fresh green, salted, pickled, pretanned, wet blue, retanned, dry crust, and dry crust staked. Cross sections were cut parallel to the backbone and as close together as possible. The samples, except for dry crust and dry crust staked, all had high moisture contents because these were taken during processing.

Conventional beamhouse and tanning processes were used to generate the leather. A pelt was depilated using a caustic treatment, and then the residual keratinaceous material was removed. The pelt was washed, pretanned, and degreased using 4% (w chemical/w limed leather for all percent chemical additions unless otherwise stated) Tetrapol LTN (Shamrock Group) and 2% Zoldine ZE (The Dow Co.). Sodium formate was added followed by sodium bicarbonate, which was gradually added to increase the pH to 7.5−8. The pickled pelt was then chrome tanned.

The resulting "wet blue" pelt was first neutralized, then washed, and retanned using 2% w/w synthetic retanning agent (Tanicor PW, Clariant, Germany) and 3% w/w vegetable tanning material (mimosa, Tanac, Brazil). Fat liquor was added at a concentration of 6% by weight of wet leather and the leather processed at 50 °C for 45 min. Finally, the leather was fixed by the addition of 0.5% w/w formic acid and processed for 30 min followed by draining and washing.

Tear strengths of the leathers were tested using standard methods.[14,15] Samples (strips 1 × 50 mm) were tested on an Instron 4467. "Dry" samples were conditioned at 23 °C and 50% relative humidity for 24 h before testing following the standard method.[16] "Wet" samples were in contact with free liquid up to the point at which they were tested.

Diffraction patterns were recorded on the Australian Synchrotron SAXS/WAXS beamline, utilizing a high-intensity undulator source. Energy resolution of 10^{-4} was obtained from a cryo-cooled Si (111) double-crystal monochromator, and the beam size (fwhm focused at the sample) was 250 × 80 μm, with a total photon flux of about 2 × 10^{12} ph s^{-1}. All diffraction patterns were recorded with an X-ray energy of 11 keV using a Pilatus 1 M detector with an active area of 170 × 170 mm and a sample-to-detector distance of 3371 mm. Exposure time for diffraction patterns was 1 s, and data processing was carried out using SAXS15ID software.[17] The partially processed leather samples were sandwiched between kapton tape to prevent drying and mounted for X-ray analysis.

A custom-built stretching apparatus was built for in situ SAXS measurements as described elsewhere.[18] Strips of leather, 1 × 30 mm, cut from the OSP, were mounted horizontally without tension and without slack, with a measured separation between the jaws, typically of 15 mm. SAXS patterns were taken through the full thickness of the sample and the force and extension information recorded. The sample was stretched by 1 mm and was maintained at this extension for 1 min before patterns were recorded. This process was repeated with the sample stretched a further 1 mm each time until the sample failed.

Orientation index (OI) is defined as (90° − OA)/90°, where OA is the azimuthal angle range that contains 50% of the microfibrils centered at 180°. OI is used to give a measure of the spread of microfibril orientation (an OI of 1 indicates the microfibrils are completely parallel to each other; an OI of 0 indicates the microfibrils are completely randomly oriented). The OI is calculated from the spread in azimuthal angle of the most intense D-spacing peak (at around 0.059−0.060 $Å^{-1}$).[19]

The D-spacing was determined from Bragg's law by taking the center of a Gaussian curve fitted to the sixth-order diffraction peak of an integrated intensity plot for each spectrum.

RESULTS

Orientation Index Changes. The OI of the corium region is higher than that of the grain region throughout all of the processing stages (Figure 1). Whereas there is considerable variation in the OI during processing, the OI of the final staked dry crust leather is fairly similar to that of the fresh green skin so that overall there is not a large change in OI.

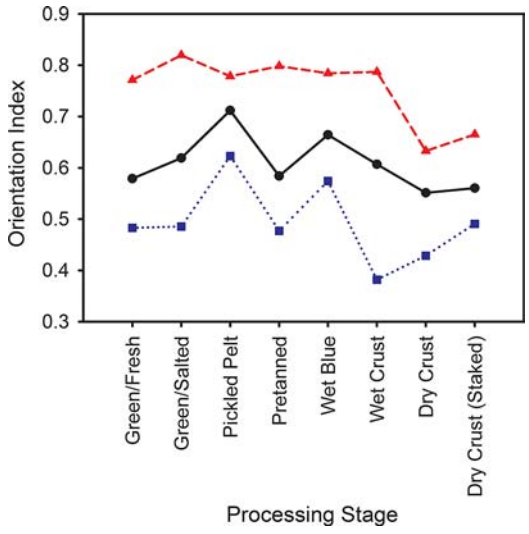

Figure 1. Variation in orientation index for all stages of processing: (red triangles) corium; (blue squares) grain; (black circles) average.

Orientation Index and Thickness. The thickness of the skin or leather varies by a factor of >2 during processing. With this variation of thickness there is a change in OI (Figure 2). The stages appear to be in two groups with the dry samples (salted, pretanned, dry crust, and dry crust staked) in one group of lower OI, which decreases with increasing thickness, and the wet samples (pickled, wet blue, retanned, and fresh green) in another group of higher OI that decreases with increasing thickness.

D-Spacing with Processing and pH. Significant changes are observed in the D-spacing of the collagen fibrils with the application of each process step (Figure 3). Both the corium and the grain regions of the leather have similar D-spacings and are similarly affected by the processing. The most significant change in D-spacing occurs with pretanning, when there is a contraction of the D-spacing of 1.4−1.5 nm (2%). The pH of the solutions in which each process takes place does not appear

DOI: 10.1021/jf506357j
J. Agric. Food Chem. 2015, 63, 2499−2505

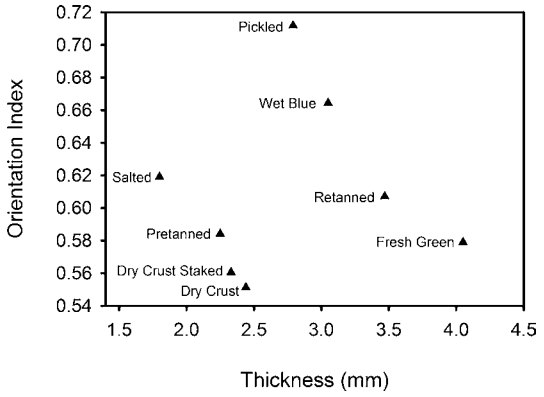

Figure 2. Fibril orientation index versus thickness.

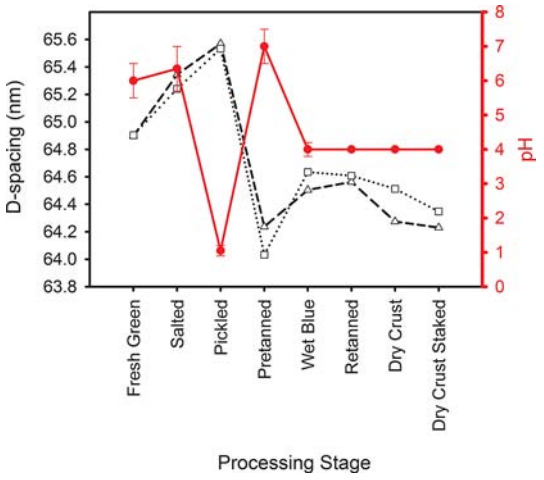

Figure 3. Variation in D-spacing and pH between different stages of processing prior to stretching: (triangles) corium; (squares) grain; (circles) pH.

to correlate with the D-spacing (Figure 4). For fresh green and salted skins the pH was measured by a surface probe rather

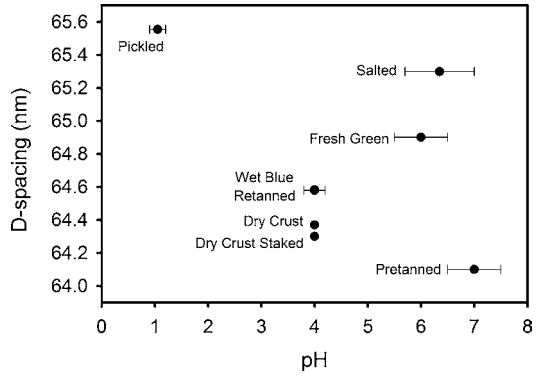

Figure 4. Variation of D-spacing with pH (wet blue and retanned points are coincident).

than the process liquor as used in the later stages. Although there is not a correlation of D-spacing with pH, it appears that there is a relationship between D-spacing and the moisture content. The three dry samples have a lower D-spacing than the wet samples.

Orientation Index and pH. The OI appears to be correlated with pH (Figure 5) (linear regression: $r^2 = 0.335$, $t = -1.74$, $P = 0.133$). However, as discussed later in the paper, we believe this correlation is not a causal relationship.

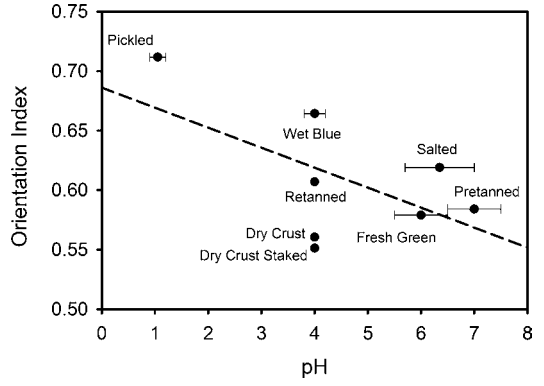

Figure 5. Correlation of OI with pH.

D-Spacing and Orientation Index. A correlation is observed between OI and D-spacing (Figure 6). The

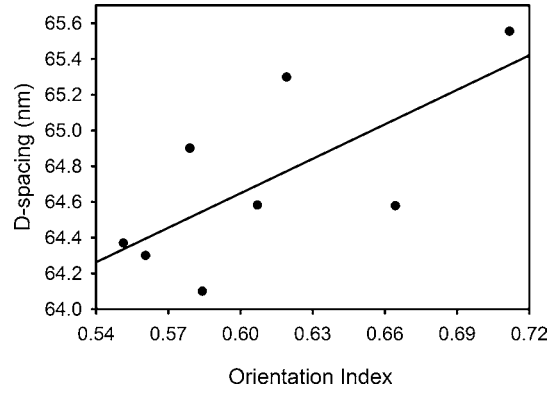

Figure 6. D-spacing versus OI for samples of different stages of processing when held without tension.

correlation is statistically significant (linear regression: $r^2 = 0.485$, $t = 2.4$, $P = 0.055$). However, as is discussed later in the paper, we believe this correlation is not a causal relationship.

Stress–Strain. Stress–strain curves were measured in situ at the synchrotron during SAXS data collection (Figure 7). The samples were not of a uniform width, so an absolute comparison of the modulus of elasticity from these curves is not possible. However, it is possible in a very general way to compare the shapes of the curves. Most of the samples show a toe region, with an initial lower elastic modulus, followed by a linear region.

Orientation Index and D-Spacing with Mechanical Stretching. There is an increase in D-spacing as the skin or leather samples are stretched (Figure 8). This increase in D-spacing is a measure of the stress being transferred to the individual fibrils, causing their length to increase. An increase in OI on stretching is also found (Figure 9) as the collagen fibrils realign in the direction of the applied force (values for the D-spacing and OI changes are found in the Supporting Information). At every stage of the leather processing, a strain applied to the samples results in an increase in OI.

DOI: 10.1021/jf506357j
J. Agric. Food Chem. 2015, 63, 2499–2505

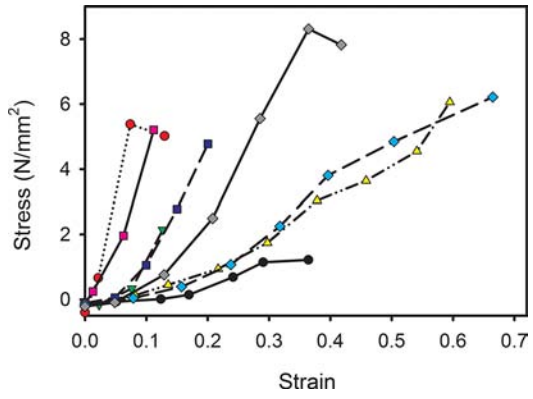

Figure 7. Stress−strain curves for each process stage, performed in situ concurrently with the SAXS measurement (not normalized for sample width or thickness): (black circles) fresh green; (red circles) salted; (green downward triangles) pickled; (yellow upward triangles) pretanned; (magenta squares) wet blue; (blue squares) retanned; (turquoise diamonds) dry crust; (gray diamonds) dry crust staked.

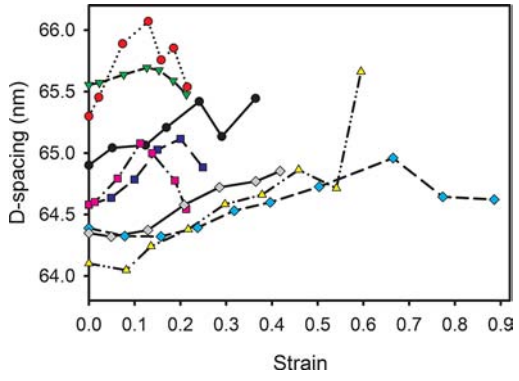

Figure 8. Changes in collagen D-spacing as samples of partially processed skin are stretched: (black circles) fresh green; (red circles) salted; (green downward triangles) pickled; (yellow upward triangles) pretanned; (blue squares) wet blue; (magenta squares) retanned; (turquoise diamonds) dry crust; (gray diamonds) dry crust staked.

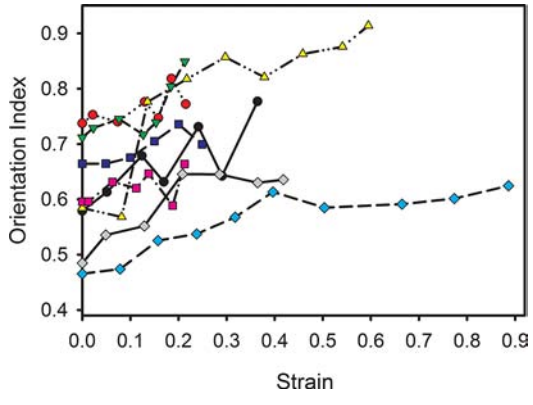

Figure 9. Changes in collagen fibril OI as samples of partially processed skin are stretched: (black circles) fresh green; (red circles) salted; (green downward triangles) pickled; (yellow upward triangles) pretanned; (blue squares) wet blue; (magenta squares) retanned; (turquoise diamonds) dry crust; (gray diamonds) dry crust staked.

DISCUSSION

We have measured the changes to the structure and arrangement of collagen fibrils in skin during several stages of the chemical processing to form leather. These build a picture of what happens in the process of transforming skin to leather.

Model of Orientation Index Change with Thickness. At the different stages of the processing of skin to leather, the thickness of the skin varies, at times becoming thicker and at other times thinner. The variation in thickness amounted to a factor of 2.25. If the collagen fibrils are not lying flat, then as the thickness of the leather increases, the angle of these fibrils to the plane of leather will increase (Figure 10). This will cause a change in OI. We have therefore developed a model for the change in OI with thickness changes. This enables us to determine how much of the OI change is due just to the change in thickness and how much is due to other factors.

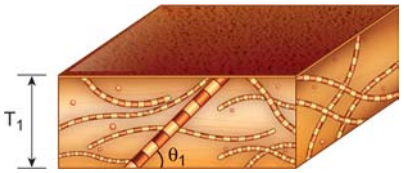

Figure 10. Illustration of the change in collagen fibril angle θ_1 to the plane of leather as the thickness T_1 of the leather changes.

The range of fiber angles in a sample is given by the OI, which is derived from the orientation angle, OA.[1] OA is defined as the subtended angle that contains half the fibrils; that is, it satisfies eq 1.

$$0.5 = \frac{\int_{\theta=-\mathrm{OA}/2}^{\theta=\mathrm{OA}/2} \theta N \, \mathrm{d}\theta}{\int_{\theta=-90^\circ}^{\theta=90^\circ} \theta N \, \mathrm{d}\theta} \quad (1)$$

N is the number of fibrils, and θ is the fiber angle (relative to the plane of the leather). In practice, this is determined from the SAXS diffraction pattern by the integrated intensity versus azimuthal angle for one of the D-spacing diffraction peaks, eq 2:

$$0.5 = \frac{\int_{\phi=-\mathrm{OA}/2}^{\phi=\mathrm{OA}/2} \phi I \, \mathrm{d}\phi}{\int_{\phi=-90^\circ}^{\phi=90^\circ} \phi I \, \mathrm{d}\phi} \quad (2)$$

I is the diffraction intensity of a selected D-spacing diffraction peak above a fitted background, and φ is the azimuthal angle of the diffracted X-rays.

OI is derived from OA by eq 3.

$$\mathrm{OI} = \frac{1 - \mathrm{OA}}{\mathrm{OA}} \quad (3)$$

Therefore, for perfect alignment in the reference direction, which is normally the plane of a piece of leather or skin, OI = 1; for no alignment or completely isotropic fibrils, OI = 0; and for perfect alignment at right angles to the reference direction, OI = −1.

If a sample of leather containing a fiber expands in thickness uniformly, and the fiber is at an angle θ_1 from the base (Figure 10), then the new angle of the fiber, θ_2, depends on the change in thickness by eq 4.

$$\frac{T_2}{T_1} = \frac{\tan \theta_2}{\tan \theta_1} \quad (4)$$

T_1 is the original thickness, and T_2 is the new thickness.

Rearranging eq 4 for θ_2 gives the new angle of the fiber after the leather has increased in thickness:

DOI: 10.1021/jf506357j
J. Agric. Food Chem. 2015, 63, 2499−2505

$$\theta_2 = \tan^{-1}\left(\frac{T_2}{T_1}\tan\theta_1\right) \quad (5)$$

It is then possible to calculate a transformed OA after stretching. The OA defines the subtended angle of 50% of the fibers. Therefore, fibers that have an initial angle from the reference angle of greater than half the OA will, after transformation, still have an angle greater than the transformed OA; fibers that have an initial angle lower than half the OA will, after transformation, still have an angle lower than half the transformed OA. In other words, the 50% inside the OA will remain inside the OA, the 50% outside the OA will remain outside the OA. Therefore, it is only necessary to calculate the transformation by eq 5 of the angle that is the OA to calculate the new OA that represents the new fiber distribution.

As an illustration of the extent of this change, for thickness changes similar to those observed here, some values are listed in Table 1. Note that expanding the thickness sufficiently results in an alignment of fibers vertically (negative OI).

Table 1. Calculated Change in Orientation Index of Collagen Fibrils for Different Thicknesses of Material

	new OI when		
starting OI	T_2/T_1 = 1.5	T_2/T_1 = 2.0	T_2/T_1 = 2.5
0.00	−0.25	−0.41	−0.52
0.10	−0.16	−0.33	−0.44
0.20	−0.05	−0.23	−0.36
0.30	0.05	−0.13	−0.26
0.40	0.17	−0.01	−0.15
0.50	0.29	0.12	−0.02
0.60	0.42	0.27	0.13
0.70	0.56	0.43	0.31
0.80	0.70	0.61	0.52
0.9	0.85	0.80	0.75
1	1.00	1.00	1.00

We did also consider how the OI might be affected by the area change to the leather, with wet stages generally of larger area than dry stages. This expansion of area would influence the OI in the opposite sense to the thickness change. However, the area change of the skin is small, <5%, and can be neglected compared with the >100% change in the thickness.

With the thickness taken into account, the OI now reflects any underlying structural changes that take place during the chemical and mechanical processing of skin to leather. The OI has therefore been recalculated for each sample using the thinnest sample, the salted skin, as the reference, and the adjusted results are presented in the following analysis.

Orientation Index and Water. Once the effect of thickness on the OI is removed, it can be seen that the samples fall into two groups (Figure 11). There are the fresh green, pickled, wet blue, and retanned materials. These all have a high OI (corrected for thickness relative to salted) of around 0.8. These samples are all wet. The pretanned, dry crust, and dry crust staked all have a corrected OI of around 0.67. These samples are all dry. The salted skin also has a low OI, of 0.62, and it is also a dry sample. Therefore, the factor that separates the high OI from the low OI materials is the wetness of the samples. When these collagen materials are dried, the OI decreases. Although it might be tempting to ascribe this to a crimping of the collagen fibrils as the materials dry, which would result in a lower OI, crimping in not observed in skin (unlike in tendon or pericardium,[20] for example). Therefore, by removing the thickness effect, we have been able to identify that there is a fundamental change between wet and dry stages, but we have not determined the mechanism of this change. It is suggested that a possible mechanism could be the space filling that results from hydration creates a hindrance to the movement of fibrils and leads to a higher OI at higher moisture contents. At lower moisture contents there is more space available for fibers to bend and adjust themselves into positions resulting in lower OI.

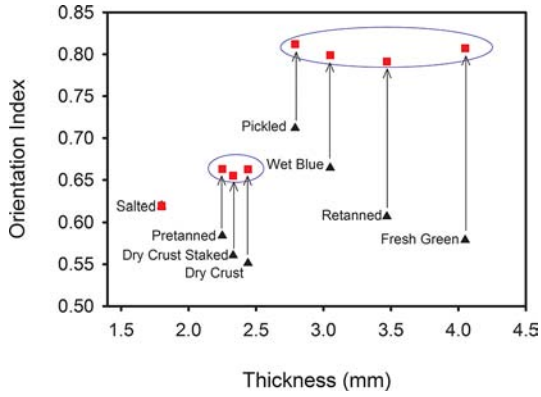

Figure 11. Fibril orientation index versus thickness: (black triangles) measured OI; (red squares) calculated OI adjusted for thickness changes (relative to salted).

D-Spacing and Orientation Index. Once the OI is corrected for thickness effects, there is no longer a statistically significant correlation between D-spacing and OI (Supporting Information, Figure S1) (linear regression: $r^2 = 0.109$, $t = 0.855$, $P = 0.426$). It is known that the result of straining leather is a straightening or alignment of the fibrils (an increase in OI) and that D-spacing measures the stress applied to individual fibrils.[18] A correlation between OI and D-spacing during different stages of processing would have suggested that these were both due to changes in internal strain in leather: when strain is released, D-spacing decreases and OI decreases. However, this was not observed here.

D-Spacing and Water. It was found that the D-spacing is lower in the dry samples by 0.38 nm; wet samples, which include fresh green, pickled, wet blue, and retanned, have an average D-spacing of 64.90 (σ = 0.46) nm, whereas dry samples, which include salted, pretanned, dry crust, and dry crust staked, have an average D-spacing of 64.52 (σ = 0.53) nm. It has previously been shown by X-ray diffraction and by atomic force microscopy that the D-spacing is moisture dependent with a reduction in D-spacing on drying.[8,21−24] This is believed to be due to the collapse of the gap and overlap regions and the partial shearing of unit cell contents within the gap region upon loss of water.[21]

D-Spacing and pH. It is perhaps a little surprising that D-spacing is not affected by pH. The D-period is affected both by the length of the tropocollagen units and by the way these tropocollagen units are assembled into the collagen fibril. The length of these structures is partially determined by the length of the hydrogen bonds between collagen molecules within the tropocollagens and by hydrophobic interactions between tropocollagen units. pH can affect hydrogen bonding, which, in collagen and other proteins, relies on a polar interaction between specific functional groups on amino acids.[10,11]

DOI: 10.1021/jf506357j
J. Agric. Food Chem. 2015, 63, 2499−2505

Mechanisms for fibril elongation by chemical treatments have previously been discussed,[20,25] and it appears that pH does not have an impact here.

Orientation Index and pH. Once the OI is corrected for thickness, it is apparent that there is no correlation between OI and pH (Supporting Information, Figure S2) (linear regression: r^2−0.0215, t = 0.488, P = 0.22). These instead fall into two groups: low OI for dry samples and high OI for wet samples, irrespective of the pH conditions.

Response to Strain. We found that when strain was applied to the samples, both the OI and D-spacing increased. It has previously been shown that upon stretching of leather, collagen fibrils first realign and then lengthen (an increase in the OI followed by an increase in the D-spacing)[18] and that collagen fibrils are very resilient with a high Poisson's ratio.[26] In pretanned, dry crust, and dry crust staked samples, the OI increased first after the first few increments in strain, and then the D-spacing increased with the further strain. These samples form a cluster at an OI of approximately 0.67 following thickness correction. The D-spacing of the wet samples (fresh green, pickled, wet blue, and retanned) increased with the first application of strain. These wet samples form a cluster with an OI of about 0.80. It is possible for the dry group to undergo more realignment with strain than the wet group because the dry samples have a lower OI initially and therefore more scope for change. Therefore, in the wet samples, because less realignment is possible, the strain was taken on by the individual collagen fibrils sooner, as shown by the immediate increase in D-spacing.

Cross-Linking. In the process of treating skin to produce leather, naturally present cross-links are removed and new cross-links are formed. The natural glycosaminoglycan cross-links are removed in the liming and bating stages so that the processed skin, known as pickled, should have fewer cross-links. New cross-links are added at the pretanned and wet blue stages. Although there have been studies on the effects of cross-linking on fibril alignment, there have been mixed conclusions drawn about the influence of cross-linking. It has been suggested that cross-links may stabilize a network structure (with fewer aligned fibrils)[27,28] and that removal of cross-links may destabilize the network structure, leading to fibrils becoming more aligned.[28] However, such behavior is not observed here during processing, where some of the cross-linking would be expected to be removed by the end of the pickled stage, and then cross-links are added by the completion of the wet blue stage.

We have found that although processing results in changes in OI, this is not a fundamental redistribution of fibrils but is rather a decrease in OI that occurs as the thickness increases and also (independently of thickness) as the water content increases. This understanding may be useful for relating structural changes that occur during different stages of processing to the development of the final physical characteristics of leather. For example, if fibril orientation is critical to strength in certain leathers, the structural relationship that should exist between the fresh skin and the final leather is now known, and it is possible to seek to maintain this characteristic during processing or modify it appropriately.

■ ASSOCIATED CONTENT

Ⓢ Supporting Information

Detailed tables of D-spacing changes in processing stages of leather with strain, OI changes in processing stages of leather with strain OI, and variation of D-spacing with OI and pH. This material is available free of charge via the Internet at http://pubs.acs.org.

■ AUTHOR INFORMATION

Corresponding Author

*(R.G.H.) E-mail: r.haverkamp@massey.ac.nz.

Funding

The New Zealand Synchrotron Group provided travel funding. The work was supported by a grant from the Ministry of Business, Innovation, and Employment.

Notes

The authors declare no competing financial interest.

■ ACKNOWLEDGMENTS

This research was undertaken on the SAXS/WAXS beamline at the Australian Synchrotron, Victoria, Australia. Sue Hallas of Nelson assisted with editing.

■ REFERENCES

(1) Basil-Jones, M. M.; Edmonds, R. L.; Allsop, T. F.; Cooper, S. M.; Holmes, G.; Norris, G. E.; Cookson, D. J.; Kirby, N.; Haverkamp, R. G. Leather structure determination by small angle X-ray scattering (SAXS): cross sections of ovine and bovine leather. *J. Agric. Food Chem.* **2010**, *58*, 5286−5291.

(2) Sturrock, E. J.; Boote, C.; Attenburrow, G. E.; Meek, K. M. The effect of the biaxial stretching of leather on fibre orientation and tensile modulus. *J. Mater. Sci.* **2004**, *39*, 2481−2486.

(3) Kronick, P. L.; Buechler, P. R. Fiber orientation in calfskin by laser-light scattering or X-ray-diffraction and quantitative relation to mechanical-properties. *J. Am. Leather Chem. Assoc.* **1986**, *81*, 221−230.

(4) Sasaki, N.; Odajima, S. Stress-strain curve and youngs modulus of a collagen molecule as determined by the x-ray diffaction technique. *J. Biomech.* **1996**, *29*, 655−658.

(5) Liao, J.; Yang, L.; Grashow, J.; Sacks, M. S. Molecular orientation of collagen in intact planar connective tissues under biaxial stretch. *Acta Biomater.* **2005**, *1*, 45−54.

(6) Covington, A. D. Modern tanning chemistry. *Chem. Soc. Rev.* **1997**, *26*, 111−126.

(7) Maxwell, C. A.; Wess, T. J.; Kennedy, C. J. X-ray diffraction study into the effects of liming on the structure of collagen. *Biomacromolecules* **2006**, *7*, 2321−2326.

(8) Wess, T. J.; Orgel, J. P. Changes in collagen structure: drying, dehydrothermal treatment and relation to long term deterioration. *Thermochim. Acta* **2000**, *365*, 119−128.

(9) Bulo, R. E.; Siggel, L.; Molnar, F.; Weiss, H. Modeling of bovine type-I collagen fibrils: interaction with pickling and retanning agents. *Macromol. Biosci.* **2007**, *7*, 234−240.

(10) Ciferri, A. Charge-dependent and charge-independent contributions to ion-protein interaction. *Biopolymers* **2008**, *89*, 700−709.

(11) Zanaboni, G.; Rossi, A.; Onana, A. M. T.; Tenni, R. Stability and networks of hydrogen bonds of collagen triple helical structure: influence of pH and chaotropic nature of three anions. *Matrix Biol.* **2000**, *19*, 511−520.

(12) Grant, C. A.; Brockwell, D. J.; Radford, S. E.; Thomson, N. H. Tuning the elastic modulus of hydrated collagen fibrils. *Biophys. J.* **2009**, *97*, 2985−2992.

(13) IULTCS. *Leather − Chemical, physical and Mechanical and Fastness Tests − Sampling Location*; ISO: Geneva, Switzerland, 2002; ISO 2418:2002.

(14) Williams, J. M. V. IULTCS (IUP) test methods − Measurement of tear load-double edge tear. *J. Soc. Leather Technol. Chem.* **2000**, *84*, 327−329.

(15) IULTCS. *Leather − Physical and Mechanical Tests − Determination of Tear Load−- Part 2: Double Edge Tear*; ISO: Geneva, Switzerland, 2002; BS EN ISO 3377-2:2002(E).

DOI: 10.1021/jf506357j
J. Agric. Food Chem. 2015, 63, 2499−2505

(16) IULTCS. *Leather − Physical and Mechanical Tests − Sample Preparation and Conditioning*; ISO: Geneva, Switzerland, 2012; ISO 2419:2012.
(17) Cookson, D.; Kirby, N.; Knott, R.; Lee, M.; Schultz, D. Strategies for data collection and calibration with a pinhole-geometry SAXS instrument on a synchrotron beamline. *J. Synchrotron Radiat.* **2006**, *13*, 440−444.
(18) Basil-Jones, M. M.; Edmonds, R. L.; Norris, G. E.; Haverkamp, R. G. Collagen fibril alignment and deformation during tensile strain of leather: a SAXS study. *J. Agric. Food Chem.* **2012**, *60*, 1201−1208.
(19) Basil-Jones, M. M.; Edmonds, R. L.; Cooper, S. M.; Haverkamp, R. G. Collagen fibril orientation in ovine and bovine leather affects strength: a small angle X-ray scattering (SAXS) study. *J. Agric. Food Chem.* **2011**, *59*, 9972−9979.
(20) Sizeland, K. H.; Wells, H. C.; Higgins, J. J.; Cunanan, C. M.; Kirby, N.; Hawley, A.; Haverkamp, R. G. Age dependant differences in collagen fibril orientation of glutaraldehyde fixed bovine pericardium. *BioMed. Res. Int.* **2014**, *2014*, No. 189197.
(21) Wess, T. J.; Purslow, P. P.; Kielty, C. M. X-ray diffraction studies of fibrillin-rich microfibrils: effects of tissue extension on axial and lateral packing. *J. Struct. Biol.* **1998**, *122*, 123−127.
(22) Kemp, A. D.; Harding, C. C.; Cabral, W. A.; Marini, J. C.; Wallace, J. M. Effects of tissue hydration on nanoscale structural morphology and mechanics of individual type I collagen fibrils in the Brtl mouse model of Osteogenesis Imperfecta. *J. Struct. Biol.* **2012**, *180*, 428−438.
(23) Brodsky, B.; Eikenberry, E. F.; Cassidy, K. An unusual collagen periodicity in skin. *Biochim. Biophys. Acta* **1980**, *621*, 162−166.
(24) Price, R. I.; Lees, S.; Kirschner, D. A. X-ray diffraction analysis of tendon collagen at ambient and cryogenic temperatures: role of hydration. *Int. J. Biol. Macromol.* **1997**, *20*, 23−33.
(25) Sizeland, K. H.; Wells, H. C.; Norris, G. E.; Edmonds, R. L.; Kirby, N.; Hawley, A.; Mudie, S.; Haverkamp, R. G. Collagen D-spacing and the effect of fat liquor addition. *J. Am. Leather Chem. Assoc.* **2015**, *110*, 66−71.
(26) Wells, H. C.; Sizeland, K. H.; Kayed, H. R.; Kirby, N.; Hawley, A.; Mudie, S. T.; Haverkamp, R. G. Poisson's ratio of collagen fibrils measured by SAXS of strained bovine pericardium. *J. Appl. Phys.* **2015**, *117*, No. 044701.
(27) Deb Choudhury, S.; Haverkamp, R. G.; DasGupta, S.; Norris, G. E. Effect of oxazolidine E on collagen fibril formation and stabilization of the collagen matrix. *J. Agric. Food Chem.* **2007**, *55*, 6813−6822.
(28) Kayed, H. R.; Sizeland, K. H.; Kirby, N.; Hawley, A.; Mudie, S. T.; Haverkamp, R. G. Collagen cross linking and fibril alignment in pericardium. *RSC Adv.* **2015**, *5*, 3611−3618.

DOI: 10.1021/jf506357j
J. Agric. Food Chem. 2015, 63, 2499−2505

into reasons for possible physical and viscosity changes observed in *t,t* CLA-rich eggs.

Previous egg enrichment studies either report the modified fatty acid composition relative to control eggs, or determine changes in egg quality. Correlations between egg quality alterations and fatty acid composition are rarely reported. The aim of this experiment was to investigate the effects of *t,t* CLA enrichment on egg quality during a typical shelf life of 30 days refrigerated storage. In addition, correlations between CLA-egg yolk fatty acid composition and any resulting quality or viscosity changes were also explored. The objectives were to determine the effect of *t,t* CLA-rich soy oil in feed on egg yolk viscosity and yolk quality during refrigerated storage. Yolk quality parameters that were investigated included yolk weight, yolk index, moisture content, pH, and vitelline membrane strength.

EXPERIMENTAL SECTION

Materials. All solvents used for sample preparation were analytical grade. The fatty acid methyl ester (FAME) internal standard and long chain polyunsaturated FAME standards used were purchased from Supelco (Bellefonte, PA).

Methods. *CLA–Rich Soy Oil Production.* A 18% CLA-rich soybean oil used in the feeding trial was produced by linoleic acid photoisomerization using a pilot scale unit and method of Jain and Proctor.[13] The refined, bleached and deodorized (RBD) soybean oil was provided by Riceland Foods (Stuttgart, AR).

Feeding and Egg Production. Feed Preparation. CLA oil produced by photoisomerization (18% CLA) was combined with RBD soybean oil to produce treatment oils containing 15%, 10%, 5%, 2.5% and 0% CLA. The fatty acid composition for the soybean oil and CLA oil are provided in Table 1. The feed used for the study was a pelleted commercial corn and soybean meal-based finisher diet provided by Cobb-Vantress (Siloam Springs, AR). Feed was formulated without meat or animal byproducts to meet or exceed minimum NRC (1994) standards for all ingredients. Treatment diets were produced by adding 10% (wt.) soy oil or CLA oil to the standard commercial feed and combined using a Hobart stand mixer.

Table 1. Fatty Acid Composition of Refined, Bleached, and Deodorized (RBD) Soy Oil before Photoisomerization, and Resulting CLA-Rich Soy Oil after 12 h Photoisomerization

Fatty acid	RBD Soy oil (g FA/100 g oil)	CLARSO (g FA/100 g oil)
Palmitic acid C16:0	12.2 ± 0.05	12.2 ± 0.02
Palmitoleic acid C16:1	0.09 ± 0.001	0.09 ± 0.001
Stearic acid C18:0	4.12 ± 0.04	4.24 ± 0.02
Oleic acid C18:1	25.0 ± 0.05	25.9 ± 0.06
Linoleic acid C18:2	55.0 ± 0.07	36.5 ± 0.05
Linolenic acid C18:3	3.54 ± 0.02	3.59 ± 0.02
cis-9,*trans*-11 CLA	ND[1]	1.64 ± 0.01
trans-9,*cis*-11 & *cis*-10,*trans*-12 CLA	ND	2.14 ± 0.02
trans-10, *cis*-12 CLA	ND	1.27 ± 0.01
trans, *trans* CLA	ND	13.1 ± 0.02
Total CLA	ND	18.15 ± 0.03

[1]Not detected.

Diet Administration. Animal procedures were approved by the University of Arkansas Institutional Animal Care and Use Committee (Protocol # 13033). One hundred single-comb white leghorn chicks were reared under standard commercial conditions. At 25 weeks, 60 hens were randomly chosen and assigned to single bird cages in blocks of 5 birds each, separated by 2 empty cages. All hens received the same standard commercial finisher diet until the feeding trial began at 33 weeks. Each soybean oil diet (15%, 10%, 5%, 2.5% and 0% CLA) was randomly assigned to 2 blocks of 5 birds each, resulting in 10 birds receiving each treatment diet. The remaining two hen blocks continued to receive standard commercial feed without additional soybean oil and served as a standard control group.

Egg Collection. After 12 days of treatment feed administration, eggs were collected daily, counted, and labeled with cage number and date for 20 days. Eggs were stored in a walk in cooler at 4 °C. Eggs used for analysis were refrigerated for either 0, 5, 10, 20, or 30 days prior to analysis.

Fatty Acid Analysis. Yolk Lipid Extractions. Total yolk lipids were extracted from quadruplicate eggs from each treatment and storage duration [$N = 120$] using a rapid hexane/isopropanol method.[17] A 0.5 g yolk sample was collected in a 7 mL glass vial and dissolved in 5 mL hexane/isopropanol (1:1, v/v), vortexed for 5 min, and allowed to settle. The liquid containing the lipid extract was decanted into a 50 mL plastic centrifuge tube and used for subsequent FAME preparation.

Fatty Acid Analysis as FAMEs. Fatty acid methyl esters (FAMEs) were prepared from all extractions using a rapid, micro FAMEs preparation method modified for the volume of lipid extract solution.[18] Decanted extraction samples in 50 mL centrifuge tubes were combined with 0.5 mL of a prepared 1% (wt.) heptadecanoic acid (C17:0) methyl ester solution in hexane. Then 1 mL of toluene and 4 mL of 0.5 M sodium methoxide in methanol were added to each tube. The centrifuge tubes were placed in a h 50 °C water bath for 10 min with constant agitation and then removed and cooled at ambient temperature for 2 min. Glacial acetic acid, 0.2 mL, was added to each tube to inhibit sodium hydroxide formation. Five mL of distilled water was added, followed by 2 mL of hexane. The tubes were vortexed for 2 min and then the immiscible layers were allowed to separate. The upper layer was pipetted out and dried over anhydrous sodium sulfate for 15–20 s.

Duplicate fatty acid profiles were obtained for each lipid extraction by GC with a SP 2560 fused silica capillary column (100 m × 0.25 mm i.d. × 2 μm film thickness; Supelco Inc. Bellefonte, PA), and a flame ionization detector (FID model 3800, Varian, Walnut Creek, CA). Samples of 3.0 μL were injected by autosampler. The FID settings were as follows: oven temp = 250 °C; sensitivity = 12, He gas = 30 mL/min, H2 = 31 mL/min, air = 296 mL/min, and over program time = 111 min. Total fatty acid composition, CLA concentration and CLA isomer concentration were calculated by the following equation:

$$[\%\text{fatty acid}] = ([\text{HME}] \times \text{sample peak area} \times \text{relative response factor})/\text{HME peak area}$$

The position of double bonds in CLA-rich soybean oil produced by photoisomerization[13] were previously determined by silver ion HPLC.[14] Fatty acid percent concentration were converted to mmoles of fatty acid/100 g yolk based on the molar mass of each fatty acid and lipid extract as constituting 32% of total yolk weight.

Statistical Analysis. Data were analyzed by ANOVA in response to dietary CLA concentration. Tukey's test was used to compare treatment means, which were deemed significant a $p \leq 0.05$. P-values comparing individual treatments were determined using orthogonal contrast analysis.

Viscosity Analysis. Triplicate yolks from all six treatment groups (standard control, soy control, 15%, 10%, 5%, and 2.5% CLA) were analyzed in duplicate as either freshly laid yolks (0 day), or after 20 or 30 day refrigerated storage [$N = 54$]. In addition, triplicate control, soy control, and CLA-rich eggs containing the highest dietary CLA concentration were analyzed in duplicate after 5 and 10 days of refrigerated storage [$N = 18$]. An AR-2000 Rheometer was used for viscosity analysis.[19] Each yolk sample was vortexed for 20 s and 2 aliquots of yolk were dispensed from a 1 mL auto pipet on the lower rheometer plate. A 40 mm diameter sand-blasted geometry was applied to the sample surface at a constant shear rate of 100 s^{-1}. The initial plate temperature was stabilized at 4 °C for 2 min and then heated at a constant rate of 10 °C/min until a final temperature of 60 °C was reached. Sheer stress (Pa) measurements were recorded 100x

DOI: 10.1021/jf504759w
J. Agric. Food Chem. 2015, 63, 2506–2513

Table 2. Egg Yolk Total CLA Concentration and Polyunsaturated Fatty Acid Concentrations from Hens Fed Either a Standard Control Diet or a Diet Enriched with 10% Soybean Oil [N = 120][a]

Yolk polyunsaturated fatty acids	Control yolk 0% CLA	Soy control yolk 0% CLA	0.5 mmol CLA (per 100 g yolk)	0.9 mmol CLA (per 100 g yolk)	2 mmol CLA (per 100 g yolk)	2.7 mmol CLA (per 100 g yolk)
trans, trans CLA	0 ± 0e	0 ± 0e	0.21 ± 0.01d	0.43 ± 0.02c	1.11 ± 0.06b	1.43 ± 0.18a
cis-9, *trans*-11 CLA	0 ± 0e	0 ± 0e	0.14 ± 0.01a	0.15 ± 0.01a	0.13 ± 0.01a	0.15 ± 0.02a
trans-9, *cis*-11 & *cis*-10, *trans*-12 CLA	0 ± 0e	0 ± 0e	0.08 ± 0.001d	0.17 ± 0.01c	0.31 ± 0.01b	0.41 ± 0.04a
trans-10, *cis*-12 CLA	0 ± 0e	0 ± 0e	0.07 ± 0.01d	0.14 ± 0.01c	0.36 ± 0.02b	0.55 ± 0.06a
cis-11, *trans*-13 CLA	0 ± 0e	0 ± 0e	0.01 ± 0.001d	0.03 ± 0.002c	0.07 ± 0.006b	0.11 ± 0.01a
Linoleic acid	16.97 ± 0.67b	28.03 ± 0.9a	27.46 ± 0.53a	27.77 ± 0.77a	27.51 ± 0.66a	26.2 ± 0.67a
Linolenic acid	0.31 ± 0.03c	0.87 ± 0.05a	0.81 ± 0.04ab	0.78 ± 0.05ab	0.77 ± 0.03ab	0.69 ± 0.06b
Arachidonic acid	0.17 ± 0.01a	0.13 ± 0.04a	0 ± 0a	0 ± 0a	0 ± 0a	0.13 ± 0.13a
Eicospentaneoic acid	1.75 ± 0.14ab	1.91 ± 0.05a	1.75 ± 0.04ab	1.66 ± 0.04ab	1.67 ± 0.03ab	1.43 ± 0.13b
Docosahexaneoic acid	0.47 ± 0.01de	0.95 ± 0.04a	0.8 ± 0.02b	0.69 ± 0.01bc	0.6 ± 0.01cd	0.45 ± 0.05e
Total PUFA	19.68 ± 0.77b	31.9 ± 0.95a	31.34 ± 0.55a	31.82 ± 0.82a	32.54 ± 0.71a	31.56 ± 0.7a

[a]Soybean oils had 0% (soy control), 2.5%, 5%, 10% or 15% CLA concentrations. Concentrations are expressed as mmol of fatty acid per 100 g yolk. Connecting letters within the same row indicate significant differences in fatty acid concentration.

per minute. Viscosity was calculated as shear stress divided by the constant sheer rate.

Statistical Analysis. Yolk viscosity data has been determined to fit the Power Law in the temperature range of 4°- 60 °C, and can be adequately modeled by a nonlinear exponential 3-parameter model that describes the asymptote, viscosity at initial temperature, and decay rate (eq 1).[20] Parameter estimates were compared by analysis of means at an alpha level of 0.05 in response to storage duration and CLA concentration.

$$\text{Viscosity} = A + B \times e^{(C \times \text{Temp})} \quad \text{(eq 1)}$$

where A = asymptote, B = scale, and C = decay rate.

Correlations between viscosity at 4 °C and fatty acid compositions were determined for 0, 20, and 30 day eggs. Correlation values 0.30 and above indicate a weak linear relationship, values 0.50 and above indicate a moderate linear relationship, and values above 0.70 indicate a strong linear relationship. If the value is negative the paired items are inversely correlated.

Egg Quality Analysis. Egg Yolk Physical Properties. Duplicate eggs from duplicate treatment blocks were analyzed fresh (0 day), or after 20 or 30 days of refrigerated storage. Whole egg weights were measured and recorded, followed by yolk weights, which were weighed after being gently rolled on a Kim-wipe to remove any adhering albumen and chalazae. Yolk index (YI), defined as the ratio of yolk height to diameter, was measured using a caliper and recorded.

Vitelline Membrane Strength (VMS). The force required to puncture through the yolk vitelline membrane was determined using TA-XT2i Texture analyzer equipped with a 5 kg load cell and a 1 mm probe.[27] The probe was calibrated at 18 mm above the platform. The test speed was set at 3.2 mm/s and distance target mode was 13 mm. The peak force (g) was recorded as VMS for quadruplicate eggs from each treatment group on each refrigerated storage duration.

Yolk pH and Moisture Content. Yolk pH was measured in triplicate on day 0, 20, and 30 d eggs. Yolk moisture content was determined gravimetrically in duplicate eggs during the 30 d refrigerated. Yolks were dried in an oven at 100 °C for 20 h.[21]

Statistical Analysis. Data were analyzed according to a split-plot design, with dietary CLA concentration as the whole plot and duration of egg storage as the subplots, to determine main effects of dietary CLA and duration of storage, and their interactions. Tukey's test was used to compare treatment and main effect means, as appropriate. When dietary CLA by refrigeration duration interactions were observed, comparisons among treatments were made. Otherwise, comparisons were made among main means.

RESULTS AND DISCUSSION

Fatty Acid Analysis. Total yolk CLA, CLA isomers and PUFA concentrations are presented in Table 2. Egg yolk total CLA increased linearly as dietary CLA levels increased (mmol CLA/g yolk = 0.05 + 0.18 g CLA/kg feed, R^2 = 0.8). *trans, trans* CLA was the most abundant isomer in all CLA-rich yolks, and increased linearly in response to total CLA in the diet (mmol *t,t* CLA/g yolk = 0.02 + 0.1 g CLA/kg feed, R^2 = 0.77). Yolks with the lowest CLA concentration had 42% of CLA in *t,t* form, while yolks with the greatest CLA levels had 53% in *t,t* form. The *c*-9, *t*-11 CLA concentration was similar in all CLA yolks, but its proportion of total CLA decreased from 28% to only 5% in response to higher CLA levels in the diet. The proportion of *t*-10, *c*-12 to total CLA was similar in all CLA yolks at about 15%, and its concentration increased linearly with CLA in the diet (mmol *t*-10,*c*-12 CLA/g yolk = −0.02 + 0.04 g CLA/kg feed, R^2 = 0.80). All other CLA isomers maintained similar proportions of total CLA, and increased linearly in response to dietary concentration. However, previous studies reported that the *cis*-9, *trans*-11 CLA isomer was preferentially incorporated in CLA yolks, whereas the *t*-10, *c*-12 incorporation was less efficient.[2] In contrast, when *t,t* CLA-rich soybean oil was used in the feed, *t,t* CLA was preferentially incorporated, followed by *t*-10, *c*-12.

Linoleic and linolenic acid concentrations were similar in all eggs produced from soy oil-rich diets, and were significantly greater than the standard control yolks ($p < 0.001$). While standard control egg yolks had the greatest arachidonic acid (AA) concentration at 0.17 mmol/100 g yolk, AA levels in the other treatment yolks had such a large variation that no significant differences could be determined relative to control yolks. Eicosapentaneoic acid (EPA) concentration was greatest in yolks from the soy control diet, but its concentration decreased significantly with increasing CLA concentration ($p < 0.001$). However, yolks containing 0.5 mmol of CLA per 100 g yolk contained a similar amount of EPA when compared with standard control eggs. Docosahexaneoic acid (DHA) concentration was also greatest in soy control yolks and decreased with increasing CLA concentration ($p \leq 0.003$). However, DHA levels in egg yolks with the greatest CLA concentration were similar to DHA levels in standard control egg yolks ($p = 0.60$).

DOI: 10.1021/jf504759w
J. Agric. Food Chem. 2015, 63, 2506−2513

Table 3. Egg Yolk Total Saturated and Monounsaturated Fatty Acid Concentrations from Hens Fed Either a Standard Control Diet or Diets Enriched with 10% Soybean Oil [N = 120][a]

Yolk saturated fatty acids	Control yolk 0% CLA	Soy control yolk 0% CLA	0.5 mmol CLA (per 100 g yolk)	0.9 mmol CLA (per 100 g yolk)	2 mmol CLA (per 100 g yolk)	2.7 mmol CLA (per 100 g yolk)
Myristic acid	0.41 ± 0.01a	0.3 ± 0.01c	0.33 ± 0.01bc	0.39 ± 0.02ab	0.46 ± 0.03a	0.47 ± 0.02a
Palmitic acid	29.08 ± 0.38c	26.16 ± 0.33d	28.47 ± 0.23c	29.65 ± 0.36bc	30.67 ± 0.4ab	31.93 ± 0.65a
Stearic acid	11.55 ± 0.27c	12.52 ± 0.3c	14.97 ± 0.36b	16.19 ± 0.38ab	17.92 ± 0.38a	17.77 ± 0.74a
Eicosanoic acid	0.19 ± 0.18a	0.02 ± 0.01a	0.01 ± 0a	0.01 ± 0a	0.02 ± 0a	0.08 ± 0.05a
Tot sat fatty acids	41.22 ± 0.4c	38.99 ± 0.45d	43.77 ± 0.37bc	46.24 ± 0.51b	49.07 ± 0.42a	50.25 ± 1.3a
Yolk monounsaturated fatty acids	**Control yolk 0% CLA**	**Soy control yolk 0% CLA**	**0.5 mmol CLA (per 100 g yolk)**	**0.9 mmol CLA (per 100 g yolk)**	**2 mmol CLA (per 100 g yolk)**	**2.7 mmol CLA (per 100 g yolk)**
Palmitoleic acid	3.02 + 0.1a	1.48 + 0.03b	1.32 + 0.08bc	1.14 + 0.05cd	1.05 + 0.05cd	1.04 + 0.05d
Oleic acid	48.71 + 0.72a	40.01 + 0.63b	35.99 + 0.48c	33.35 + 0.66c	29.99 + 0.63d	30.12 + 1.26d
Tot monounsat fatty acids	51.73 + 0.66a	41.49 + 0.64b	37.31 + 0.53c	34.48 + 0.65c	31.04 + 0.65d	31.16 + 1.29d

[a]Soybean oils had 0% (soy control), 2.5%, 5%, 10% or 15% CLA concentrations. Concentrations are expressed as mmol of fatty acid per 100 g yolk. Connecting letters within the same row indicate significant differences in fatty acid concentration.

Table 4. Egg Yolk Viscosity Variable Estimates Described by the Exponential Decay Model, Which Includes R^2 Value for Each Viscosity Curve, Initial Viscosity at 4°C, Asymptote (lowest part of curve), and Average Decay Rate[a]

	Control yolk	Soy control yolk	0.5 mmole yolk	0.9 mmole CLA yolk	2.0 mmole yolk	2.7 mmole yolk
Day 0 Egg yolks	*Model R^2 = 0.85*					
Asymptote (Pa·s)	0.09 ± 0.05b	0.24 ± 0.03a	0.27 ± 0.03a	0.2 ± 0.02a	0.21 ± 0.02a	0.28 ± 0.02a
Initial Viscosity at 4°C (Pa·s)	1.82 ± 0.04d	2.04 ± 0.04d	2.22 ± 0.05c	1.77 ± 0.06d	2.41 ± 0.05b	3.74 ± 0.07a
Decay rate	-0.04 ± 0.00a	-0.05 ± 0.003a	-0.06 ± 0.003b	-0.07 ± 0.005b	-0.07 ± 0.003b	-0.08 ± 0.002c
Egg yolks stored for 5 days	*Model R^2 = 0.93*					
Asymptote (Pa·s)	0.20 ± 0.02a	0.14 ± 0.02b	---	---	---	0.14 ± 0.02b
Initial Viscosity at 4°C (Pa·s)	1.87 ± 0.03b	1.58 ± 0.03c	---	---	---	3.01 ± 0.04a
Decay rate	-0.05 ± 0.002a	-0.04 ± 0.003b	---	---	---	-0.06 ± 0.002c
Egg yolks stored for 10 days	*Model R^2 = 0.82*					
Asymptote (Pa·s)	0.21 ± 0.02a	0.19 ± 0.03a	---	---	---	0.31 ± 0.02a
Initial Viscosity at 4°C (Pa·s)	1.80 ± 0.05b	1.77 ± 0.03b	---	---	---	3.20 ± 0.08a
Decay rate	-0.05 ± 0.004a	-0.05 ± 0.004a	---	---	---	-0.08 ± 0.003b
Egg yolks stored for 20 days	*Model R^2 = 0.82*					
Asymptote (Pa·s)	0.12 ± 0.02c	0.10 ± 0.02c	0.20 ± 0.02b	0.08 ± 0.02c	0.20 ± 0.02b	0.33 ± 0.02a
Initial Viscosity at 4°C (Pa·s)	0.72 ± 0.03c	0.80 ± 0.03c	1.45 ± 0.04c	1.17 ± 0.03b	2.52 ± 0.04a	2.86 ± 0.04a
Decay rate	-0.06 ± 0.007a	-0.05 ± 0.006a	-0.06 ± 0.004a	-0.05 ± 0.004a	-0.06 ± 0.002a	-0.07 ± 0.002a
Egg yolks stored for 30 days	*Model R^2 = 0.80*					
Asymptote (Pa·s)	0.08 ± 0.02a	0.5 ± 0.02a	0.04 ± 0.02a	0.09 ± 0.01a	0.07 ± 0.01a	0.07 ± 0.01a
Initial Viscosity at 4°C (Pa·s)	0.99 ± 0.03b	0.95 ± 0.02b	0.62 ± 0.04c	1.0 ± 0.02b	1.29 ± 0.02a	1.29 ± 0.02a
Decay rate	-0.05 ± 0.003a	-0.05 ± 0.003a	-0.05 ± 0.004a	-0.07 ± 0.003b	-0.06 ± 0.002b	-0.06 ± 0.002b
Effects Test	**Prob > F**					
Yolk Type	<0.0001*					
Storage	<0.0001*					
Yolk Type*Storage	<0.0001*					

[a]Yolks were stored at 4 °C prior to analysis. Variable estimates were compared by analysis of means at 0.05 alpha-level for each storage duration. Connecting letters within the same row indicate significant differences from the model mean.

Previous studies have reported significantly lower long chain PUFA levels in CLA-rich eggs and have deemed this effect undesirable.[1,2,8] Ahn et al. reported a decrease in AA concentration from 3.7% to 2.7% of total FA when hens were fed 2.5% CLA, while Chamruspollert et al. reported a more dramatic drop in AA levels from 3.9% to 2.6% of total FA from hens fed 2.5% CLA.[1,8] However, this consequence of CLA enrichment seemed to be lessened using the *t,t* CLA-rich soybean oil, as standard control yolks contained 1.7% AA of total FA while CLA-rich yolks produced from 1.5% CLA in the diet lowered AA concentration to 1.4% of total FA (0.13 mmol CLA/100 g yolk). Likewise, Szymczyk and Pisulewski reported a DHA decrease from 1.4% to 0.2% of total FA with 2% CLA present in the diet.[2] However, DHA levels in CLA-rich yolks and control yolks were not significantly different in this study. The reduction of these fatty acids and subsequent increase in stearic acid has been attributed to stearoyl-coenzyme A desaturase inhibition in the liver.[22,23] This lesser decrease in DHA may be preferable, when compared with eggs produced from feeding *cis,trans* mixtures.

DOI: 10.1021/jf504759w
J. Agric. Food Chem. 2015, 63, 2506−2513

Table 3 presents yolk saturated and monounsaturated fatty acid levels. Egg yolk total saturated fatty acid (SFA) content significantly increased as yolk total CLA concentration increased ($p < 0.001$), while soy control egg yolks had significantly lower saturated fat levels in comparison to standard control yolks ($p = 0.02$). Previous CLA feeding trials using *cis,trans* isomer mixtures observed a 34% increase in SFA levels with only 0.5% CLA in the diet.[7] However, CLA-rich soybean oil raised SFA levels by only 28% with 1.5% CLA in the diet, relative to soy control yolks.

Table 3 also shows that egg yolk monounsaturated fatty acid (MUFA) concentration decreased significantly in yolks produced from all soy oil diets. The MUFA decrease became more substantial as yolk CLA concentration increased. Previous studies reported a 32% drop in MUFA concentrations.[7] This study determined only 25% decrease in MUFA concentration in yolks containing the greatest CLA concentrations, relative to the control yolks. The overall trends in fatty acid composition modifications are similar to previous reports with a significant increase in saturated fatty acids and subsequent decrease in monounsaturated fatty acids.[1,2,4,5] However, *t,t* CLA-rich soybean oil reduced these changes relative to previous studies.

Viscosity analysis. *Fresh Egg Yolks.* Table 4 shows the initial viscosity, asymptote (lowest part of curve), and average decay rate. Supplemental Figure 1 shows the differences in viscosity among yolks on days 0, 20, and 30. On day 0 yolks containing 2.7 mmol of CLA had significantly greater initial viscosity than all other yolk types ($p < 0.05$). However, initial yolk viscosity was not consecutively lowered with respect to decreasing yolk CLA concentration. For example, egg yolks containing 0.9 mmol CLA displayed a significantly lower initial viscosity compared to all other yolks. Analysis of means revealed that fresh egg yolks from soybean oil-enriched diets displayed viscosities that leveled off at similar values (asymptote) while standard control yolk leveled off at a significantly lower viscosity. The viscosity decay rates were faster in response to increasing yolk CLA concentration, while control and soy control yolks displayed similar decay rates.

Correlations between initial viscosity and fatty acid composition in day 0 yolks revealed that viscosity was moderately correlated with total SFA ($R = 0.43$) and CLA concentration ($R = 0.54$), and moderately inversely correlated with EPA concentration ($R = -0.57$). The fatty acid composition shows that EPA concentrations in 0.9 and 2.0 mmol CLA yolks are similar, and that they drop significantly in 2.7 mmol CLA yolks. It is not completely apparent why 0.9 mmol CLA yolks displayed such a low initial viscosity compared to all other yolks, but it may be due to a synergistic effect of EPA and CLA levels, along with a SFA level that is not significantly different from control yolks.

Egg Yolks Refrigerated for 5 days. After 5 days of refrigeration CLA yolks have a significantly greater initial viscosity of 3 Pa·s than control yolks with an initial viscosity of 1.9 Pa·s, while soy control yolks had a significantly lower initial viscosity at 1.6 Pa·s than control yolks. The viscosity decay rate was significantly faster in CLA yolks, followed by soy control, and control yolks. Control yolk viscosity had a greater asymptote than CLA or soy control yolks, which had similar asymptotes.

Egg Yolks Refrigerated for 10 days. CLA yolks continued to have significantly greater initial viscosities in comparison to both the control and soy control yolks. However, both CLA and soy control yolks stored for 10 days had initial viscosities that were actually greater than their 5 day old counterparts. Although asymptote estimates provided by modeling indicate that CLA yolk levels off at a greater viscosity than control yolks, the statistical significance was not apparent from analysis of means. Viscosity decay rates were similar between control yolks, while CLA yolk viscosity decreased significantly more quickly in response to increasing temperature.

Egg Yolks Refrigerated for 20 days. Decreases in yolk initial viscosity seem to correspond to decreasing CLA concentration, but 0.9 mmol CLA yolks exhibited lower initial viscosity than 0.5 mmol CLA yolks. Control yolks, soy control yolks, and 0.9 mmol CLA yolks leveled off at similar viscosities, while all other CLA yolks displayed significantly greater asymptote values. Decay rates were similar among all yolk types. Correlations on viscosity and fatty acid profile from day 20 yolks revealed that viscosity was strongly correlated with CLA concentration ($R = 0.81$), total SFA ($R = 0.74$), and palmitic acid concentration ($R = 0.72$), and had a strong inverse correlation with oleic acid concentration ($R = -0.72$). In addition, initial viscosity was moderately inversely correlated with EPA concentration ($R = -0.69$). It seems that as storage duration increases, CLA and saturated fat concentration were correlated with increasing yolk viscosity, while oleic and EPA concentration were negatively correlated with viscosity.

Egg Yolks Refrigerated for 30 days. Yolks containing 2.0 and 2.7 mmol CLA exhibited nearly identical viscosity trends and have significantly greater initial viscosities than all other yolk types. Control, soy control, and 0.9 mmol CLA yolks have similar initial viscosities, while 0.5 mmol yolks exhibit significantly lower initial viscosity than all other yolk types. All viscosities level off at similar levels regardless of CLA concentration. Multivariate analysis revealed only slight correlations between viscosity and fatty acid composition, namely, myristic acid ($R = 0.46$), palmitic acid ($R = 0.35$), CLA ($R = 0.36$), and a slight inverse correlation with DHA ($R = -0.38$).

In both control and soy control yolks, viscosity is similar during the first 10 days of refrigerated storage, and then a significant decrease is observed after 20 days refrigeration. Alternatively, the CLA-rich yolks have a significantly greater overall viscosity, and a marked decrease in viscosity is only apparent after 30 days of refrigeration. It may be that changes in viscosity after 30 days storage were more influenced by changes in other yolk quality parameters, such as moisture content and pH, rather than fatty acid composition.

CLA yolks containing the greatest CLA enrichment were considerably more viscous at low temperatures and retained their thickness for a longer storage duration. This effect may be advantageous in the preparation of mayonnaises and salad dressing recipes, where commercial products' microbial safety is more likely controlled by the acidity of the product, rather than a heat treatment. However, this increased viscosity was not solely a function of increased CLA concentration, but rather the distinct fatty acid composition changes that were a result of CLA enrichment. It was anticipated that the greater viscosities in CLA-rich yolks would be most highly correlated with saturated fatty acid content because a previous study identified significantly increased concentrations of saturated triacylglycerol species.[16] However, a relationship between SFA and viscosity was only apparent after the yolks had been refrigerated for 20 days. It seems that yolk viscosity was a collective effect of the fatty acid composition, not just one specific type of fatty acid.

DOI: 10.1021/jf504759w
J. Agric. Food Chem. 2015, 63, 2506−2513

Table 5. CLA-Rich, Soybean Oil-Rich, and Standard Control Egg Yolk Quality Parameters Were Measured in Quadruplicate on Each Storage Duration[a]

Whole Egg Weight				Vitelline Membrane Strength			
Yolk Type	0 Days in Storage	20 Days in Storage	30 Days in Storage	Yolk Type	0 Days in Storage	20 Days in Storage	30 Days in Storage
Control	64.8 ± 2.31a	66.7 ± 2.1a	68.8 ± 0.6a	***Control***	5.28 ± 0.1a	3.96 ± 0.8ab	3.88 ± 0.1ab
Soy Control	62.7 ± 0.8a	62.3 ± 0.5b	62.3 ± 0.7b	***Soy Control***	5.34 ± 0.2a	2.68 ± 0.9b	2.08 ± 0.6b
0.5 mmole CLA	62.1 ± 3.68a	62.1 ± 1.9b	60.3 ± 0.6b	***0.5 mmole CLA***	5.18 ± 0.1a	3.40 ± 0.9ab	4.36 ± 0.7a
0.9 mmole CLA	61.4 ± 1.23a	59.3 ± 0.9b	58.6 ± 0.7b	***0.9 mmole CLA***	4.44 ± 0.1b	3.76 ± 0.6ab	4.74 ± 0.8a
2.0 mmole CLA	56.9 ± 1.27b	60.0 ± 1.1b	60.0 ± 1.5b	***2.0 mmole CLA***	4.20 ± 0.1b	3.28 ± 1ab	3.92 ± 1.0ab
2.7 mmole CLA	59.0 ± 0.83a	55.8 ± 0.4c	55.8 ± 0.6c	***2.7 mmole CLA***	4.46 ± 0.2b	4.9 ± 0.2a	3.48 ± 0.9ab
Effects Test	**Prob > F**			**Effects Test**	**Prob > F**		
Yolk Type	0.0094*			Yolk Type	0.58		
Storage	0.98			Storage	0.008*		
Yolk Type*Storage	0.36			Yolk Type*Storage	0.037*		

Yolk Weight				Yolk pH			
Yolk Type	0 Days in Storage	20 Days in Storage	30 Days in Storage	Yolk Type	0 Days in Storage	20 Days in Storage	30 Days in Storage
Control	18.7 ± 0.6ab	20.2 ± 1.8a	18.8 ± 0.17a	***Control***	*6.21 ± 0.1a*	*5.96 ± 0.12ab*	*6.08 ± 0.01b*
Soy Control	19.8 ± 0.4a	19.9 ± 0.8a	18.5 ± 0.74a	***Soy Control***	6.23 ± 0.1a	5.91 ± 0.15ab	6.31 ± 0.03b
0.5 mmole CLA	18.2 ± 1.1ab	18.9 ± 0.3a	18.1 ± 1.06a	***0.5 mmole CLA***	6.21 ± 0.2a	5.88 ± 0.07ab	6.05 ± 0.01b
0.9 mmole CLA	17.9 ± 0.4ab	18.7 ± 0.6a	18.3 ± 0.52a	***0.9 mmole CLA***	6.22 ± 0.1a	5.62 ± 0.02b	7.17 ± 0.35a
2.0 mmole CLA	16.0 ± 0.2b	19.0 ± 0.6a	17.9 ± 0.25a	***2.0 mmole CLA***	6.20 ± 0.05a	6.32 ± 0.1a	7.29 ± 0.09a
2.7 mmole CLA	17.2 ± 0.6ab	18.0 ± 0.7a	18.9 ± 0.49a	***2.7 mmole CLA***	6.20 ± 0.1a	6.43 ± 0.18a	7.5 ± 0.18a
Effects Test	**Prob > F**			**Effects Test**			
Yolk Type	0.0061*			Yolk Type	1		
Storage	0.038*			Storage	<0.0001*		
Yolk Type*Storage	0.27			Yolk Type*Storage	<0.0001*		

Yolk index				Moisture Content			
Yolk Type	0 Days in Storage	20 Days in Storage	30 Days in Storage	Yolk Type	0 Days in Storage	20 Days in Storage	30 Days in Storage
Control	*0.4 ± 0.01a*	*0.35 ± 0.03ab*	*0.44 ± 0.01a*	***Control***	*48.1 ± 0.5a*	*47.4 ± 0.54b*	*46.4 ± 0.38c*
Soy Control	0.4 ± 0.01a	0.36 ± 0.05ab	0.44 ± 0a	***Soy Control***	46.9 ± 0a	47.7 ± 0.62b	48.7 ± 0.38bc
0.5 mmole CLA	0.4 ± 0a	0.35 ± 0.03ab	0.45 ± 0.02ab	***0.5 mmole CLA***	47.5 ± 1.48a	48.4 ± 1.71ab	48.6 ± 0.06bc
0.9 mmole CLA	0.39 ± 0.01a	0.38 ± 0.01a	0.42 ± 0.01ab	***0.9 mmole CLA***	47.0 ± 1.56a	48.0 ± 1.06ab	50.6 ± 0.73ab
2.0 mmole CLA	0.4 ± 0.03a	0.37 ± 0.02ab	0.37 ± 0.01b	***2.0 mmole CLA***	47.5 ± 0.62a	50.0 ± 0.08ab	51.8 ± 0.86a
2.7 mmole CLA	0.38 ± 0.01a	0.34 ± 0.02b	0.42 ± 0.01ab	***2.7 mmole CLA***	47.2 ± 0.62a	51.4 ± 1.83a	53.2 ± 0.08a
Effects Test	**Prob > F**			**Effects Test**	**Prob > F**		
Yolk Type	0.48			Yolk Type	0.98		
Storage	< 0.0001*			Storage	<0.0001*		
Yolk Type*Storage	0.17			Yolk Type*Storage	0.008*		

[a]Connecting letters within the same column identify values with no significant difference at the 0.05 α-level.

Yolks with most CLA enrichment had the greatest viscosity. The viscosity changes during refrigeration at 4 °C indicate that CLA eggs that have been stored up to 20 days may provide improved food texture, mouth feel characteristics compared to fresh control eggs. This would enhance the viscosity of mayonnaises and salad dressings, custard desserts, and sauces, which is the most desirable sensory attribute by consumers.[24]

Egg Quality Analysis. *Egg Yolk Physical Properties.* Table 5 shows whole egg weights of day 0 eggs, and eggs refrigerated for 20 and 30 days. Day 0 eggs showed the greatest variability in whole egg weight, so no statistical differences could be determined. However, during refrigeration all egg weight variability decreased. Inclusion of control soy oil and CLA soy oil in the diet significantly reduced whole egg weights, relative to hens fed the unmodified control diet (p = 0.009), despite the additional metabolizable energy added with soy oil supplementation. Eggs containing the most CLA (2.7 mmol/100 g yolk) had significantly lower whole egg weights after 20 and 30 days storage. However, all other CLA-rich egg weights were not significantly different from the soy control eggs (p = 0.65). Storage time did not have a significant effect overall on whole egg weights (p = 0.98). However, eggs produced from control soy oil or CLA-soy oil diets seemed to lose weight during storage while control yolks' total weight increased during storage. As an egg ages, it loses moisture and CO_2 through the shell pores, and both loses are dependent on storage temperature and relative humidity. While the decrease in total egg weight may be due to non-CLA soy fatty acids, CLA seemed to enhance this weight loss effect and may have some influence on how the egg is transpiring during storage. Other studies have reported conflicting results on total egg weight. Suksombat et al. (2006) reported significant egg weight decreases with CLA, while another study determined no difference among CLA and control yolk weights.[5,8]

Table 5 shows the yolk weights of control and CLA-rich eggs as analyzed at 0, 20, and 30 days of storage. Egg yolks containing 2.0 mmol of CLA were significantly smaller than soy control yolks (p = 0.006). However, all other CLA yolk weights were not significantly different from both control yolks. After 20 and 30 days of storage no significant differences could be determined among yolk types. CLA-rich soy oil prevented yolk weight reduction that has been previously reported from *cis, trans* CLA supplementation.[5]

There were no differences in yolk index (YI) at day 0 across in treatments, so YI was unaffected by CLA-rich soy oil supplementation (p = 0.60, Table 5). After 20 days there were no differences in yolk indices (p = 0.73). After 30 days of storage YI the only significant difference was that the 2.0 mmol CLA yolk YI were smaller than the controls. CLA-rich yolks have been previously reported to affect YI in comparison with control yolks.[6] However, this study determined that changes in YI were more dependent on storage time than CLA content. In contrast, previous findings reported the effect of CLA but did not account for normal storage time and temperatures. For example Kim et al. stored eggs at −50 °C, which may have altered YI, as yolks irreversibly gel during freezing.[6] Schafer et al. observed very tall CLA yolks and larger YI than control yolks but did not indicate egg storage time, which would produce very different results from those reported in our study.[29]

DOI: 10.1021/jf504759w
J. Agric. Food Chem. 2015, 63, 2506−2513

Vitelline Membrane Strength. At day 0 VMS was greatest in control, soy control, and yolks containing 0.5 mmol of CLA ($p < 0.001$, Table 5). After 20 days eggs with the highest CLA had the strongest VMS, while control yolks has the weakest VMS. After 30 days of refrigeration yolks containing 0.5 and 0.9 mmol CLA had the strongest VMS, followed by 2.0 mmol CLA, standard control, and 2.7 mmol CLA yolks, while soy control yolks were still significantly weaker.

CLA incorporation maintained VMS up to 20 days, while diets containing unmodified soy oil resulted in weaker membranes after 5 days (data not shown). Vitelline membrane strength has been reported in omega-3 eggs, but not in previous CLA feeding trials. CLA-rich yolks with 2.7 mmol CLA did have significantly lower membrane strengths at day 0 and were maintained through day 20. After 30 days 2.7 mmol CLA yolks were significantly stronger than soy control eggs. Yolks containing 0.5 and 0.9 mmol CLA had the greatest VMS after 30 days of refrigeration. An omega-3 egg study determined that these designer eggs had significant decreases in vitelline membrane strength, resulting in shorter shelf life.[25] The fact that CLA yolks VMS increased during storage may be beneficial for shelf life and storage.

Yolk pH and Moisture Content. Yolk pH was similar in all day 0 egg yolks at 6.2 (Table 5). After 20 days of refrigerated storage, both types of control yolks, and the two lower CLA yolk concentrations had not changed significantly, while the 2.0 and 2.7 mmol CLA yolks had pH values above 6.3. After 30 days in refrigeration, control yolks and yolks containing 0.5 mmol CLA had pH at 6.08 and 6.05, respectively, while the yolks containing greater levels of CLA had pH all above 7.15. These changes in pH were similar to previous yolk CLA enrichment reports.[7]

Table 5 shows changes in yolk moisture content during 30 days of refrigeration. Yolk moisture content was similar among day 0 eggs regardless of CLA concentration at 47−48%, and increased significantly in response to refrigerated storage ($p < 0.001$). This increase was significantly greater as yolk CLA concentration increased ($p = 0.008$). Yolks containing the three greatest CLA concentrations had moisture contents of 53% after 30 days of refrigeration, while both control and soy control yolks and 0.5 mmol CLA yolks had moisture contents slightly lower than 49%.

Both pH and moisture content increased with increased yolk CLA concentrations, which has been speculated to be due to increased permeability through the vitelline membrane.[7] However, other CLA egg studies have reported some pink discoloration in the albumen after refrigeration, and have also attributed the effect to membrane permeability.[26] This effect was not observed from *trans, trans* CLA eggs up to 30 days. Further investigations on the vitelline membrane physiochemical and structural properties may provide further insight into the aging and shelf life of both CLA and standard eggs.

This study reported increase in saturated fatty acid in CLA eggs, relative to conventional eggs but not to the same degree as described in previous studies.[1,2,5] Viscosity and VMS have not been previously reported in CLA eggs. Both determinations were greater than those of the control yolks, and these qualities were preserved longer throughout storage. These enhanced qualities may benefit egg shelf life and provide advantages in prepared egg based dressings and sauces. The study did not find changes in CLA yolk weights or yolk indices, relative to controls. In contrast, other studies report CLA eggs had smaller yolk weights and larger yolk indices relative to conventional eggs, but storage conditions were either unspecified or different from those in this study. Egg yolk viscosity and VMS in CLA eggs is worthy of further study, as they may affect egg quality and have food processing applications.

■ ASSOCIATED CONTENT

Supporting Information

This material is available free of charge via the Internet at http://pubs.acs.org.

■ AUTHOR INFORMATION

Corresponding Author

*E-mail: aproctor@uark.edu.

Notes

The authors declare no competing financial interest.

■ REFERENCES

(1) Chamruspollert, M.; Sell, J. L. Transfer of dietary conjugated linoleic acid to egg yolks of chicken hens. *Poult. Sci.* **1999**, *78*, 1138−1150.

(2) Szymczyk, B.; Pisulewski, P. M. Effects of dietary conjugated linoleic acid on fatty acid composition and cholesterol content of hen egg yolks. *Br. J. Nutr.* **2003**, *90*, 93−99.

(3) Shang, X. G.; Wang, F. L.; Li, D. F.; Yin, J. D.; Li, J. Y. Effects of dietary conjugated linoleic acid on the productivity of laying hens and egg quality during refrigerated storage. *Poult. Sci.* **2004**, *83*, 1688−1695.

(4) Raes, K.; Huyghebaert, D.; Smet, S.; Nollet, L.; Arnoutsm, S.; Demeyer, D. The deposition of conjugated linoleic acids in eggs of laying hens fed diets varying in fat level and fatty acid profile. *J. Nutr.* **2002**, *132*, 182−189.

(5) Suksombat, W.; Samitayotin, S.; Lounglawan, P. Effects of conjugated linoleic acid supplementation in layer diet on fatty acid compositions of egg yolk and layer performances. *Poult. Sci.* **2006**, *85*, 1603−1609.

(6) Kim, J. H.; Hwangbo, J.; Choi, N. J.; Park, H. G.; Yoon, D. H.; Park, E. W.; Kim, Y. J. Effect of dietary supplementation with conjugated linoleic acid, with oleic, linoleic, or linolenic acid, on egg quality characteristics and fat accumulation in the egg yolk. *Poult. Sci.* **2007**, *86*, 1180−1186.

(7) Aydin, R.; Pariza, M. W.; Cook, M. E. Olive oil prevents the adverse effects of dietary conjugated linoleic acid on chick hatchability and egg quality. *J. Nutr.* **2001**, *131*, 800−806.

(8) Ahn, D. U.; Sell, J. L.; Jo, C.; Chamruspollert, M.; Jeffrey, M. Effect of dietary conjugated linoleic acid on the quality characteristics of chicken eggs during refrigerated storage. *Poult. Sci.* **1999**, *78*, 922−928.

(9) Shah, U.; Baum, J. I.; Proctor, A. A New Perspective on trans, trans Conjugated Linoleic Acid (CLA), an Overlooked CLA Isomer. *J. Am. Oil Chem. Soc.* **2014**, 521−524.

(10) Beppu, F.; Hosokawa, M.; Tanaka, L.; Kohno, H.; Tanaka, T.; Miyashita, K. Potent Inhibitory effect of trans-9, trans-11 isomer of conjugated linoleic acid on the growth of human colon cancer cells. *J. Nutr. Biochem.* **2006**, *17*, 830−36.

(11) Islam, M.; Kim, Y.; Jang, W.; Lee, S.; Kim, H.; Kim, S.; Kim, J.; Ha, Y. A mixture of trans,trans Conjugated Linoleic Acid Induces Apoptosis in MCF-7 Human Breast Cancer Cells with Reciprocal Expression of Bax and BCl-2. *J. Agric. Food Chem.* **2008**, *56*, 5970−5976.

(12) Lee, Y.; Heuvel, J. Inhibition of macrophage adhesion activity by 9 trans, 11 trans- conjugated linoleic acid. *J. Nutr. Biochem.* **2010**, *21*, 490−497.

(13) Jain, V. P.; Proctor, A.; Lall, R. Pilot-Scale Production of Conjugated Linoleic Acid-Rich Soy Oil by Photoirradiation. *J. Food Sci.* **2008**, *73*, 183−192.

DOI: 10.1021/jf504759w
J. Agric. Food Chem. 2015, 63, 2506−2513

(14) Shah, U.; Proctor, A.; Lay, J. O., Jr; Moon, K. Determination of CLA trans, trans positional isomerism in CLA-rich soy oil by GC−MS and silver ion HPLC. *J. Am. Oil Chem. Soc.* **2012**, *8*, 979−985.
(15) Gilbert, W.; Gadang, V.; Proctor, A.; Jain, V.; Devareddy, L. Trans, trans Conjugated Linoleic Acid Enriched Soybean Oil Reduces Fatty Liver and Lowers Serum Cholesterol in Obese Zucker Rats. *Lipids* **2011**, *46*, 961−968.
(16) Shinn, S.; Liyanage, R.; Lay, J.; Proctor, A. Improved fatty acid analysis of conjugated linoleic acid-rich egg yolk triacylglycerols and phospholipid species. *J. Agric. Food Chem.* **2014**, *62*, 6608.
(17) Shinn, S. E.; Proctor, A. Rapid Lipid extraction from egg yolks. *J. Am. Oil Chem. Soc.* **2012**, *90*, 367−369.
(18) Lall, R. K.; Proctor, A.; Jain, V. P. A Rapid, Micro FAME Preparation Method for Vegetable Oil Fatty Acid Analysis by Gas Chromatography. *J. Am. Oil Chem. Soc.* **2009**, *86*, 309−314.
(19) Ruan, C. M.; Proctor, A. Physicochemical Properties of Conjugated Linoleic Acid-Rich Soy Oil. *J. Am. Oil Chem. Soc.* **2014**, *91*, 49−54.
(20) Ibarz, A.; Sintes, J. Rheology of egg yolk. *J. Texture Stud.* **1989**, *20*, 161−167.
(21) AOAC International. *Official methods of analysis of AOAC International*; AOAC International: 1995.
(22) Lee, K. N.; Pariza, M. W.; Ntambi, J. M. Conjugated linoleic acid decreases hepatic stearoyl-CoA desaturase mRNA expression. *Biochem. Biophys. Res. Commun.* **1998**, *248*, 817−821.
(23) Shang, X. G.; Wang, F. L.; Li, D. F.; Yin, J. D.; Li, X. J.; Yi, G. F. Effect of dietary conjugated linoleic acid on the fatty acid composition of egg yolk, plasma and liver as well as hepatic stearoyl-coenzyme A desaturase activity and gene expression in laying hens. *Poult. Sci.* **2005**, *84*, 1886−1892.
(24) Weenen, H.; Van Gemert, L. J.; Van Doorn, J. M.; Dijksterhuis, G. B.; De Wijk, R. A. Texture and mouthfeel of semisolid foods: commercial mayonnaises, dressings, custard desserts and warm sauces. *J. Texture Stud.* **2003**, *34*, 159−179.
(25) Dunn-Horrocks, S.; Pichardo-Fuchs, M.; Lee, J.; Ruiz-Feria, C.; Creger, C.; Hyatt, D.; Stringfellow, K.; Sanchez, M.; Farnell, M. Effect of Omega-3 Enriched Layer Rations on Egg Quality. *Int. J. Poult. Sci.* **2011**, *10*, 8−11.
(26) Abou-Ashour, A. M.; Edwards, H. M., Jr. Effect of dietary Sterculia foetida oil on pink-white discoloration and fatty acid distribution in stored eggs. *J. Nutr.* **1970**, *100*, 757−766.
(27) Caudill, A. B.; Curtis, P. A.; Anderson, K. E.; Kerth, L. K.; Oyarazabal, O.; Jones, D. R.; Musgrove, M. T. The effects of commercial cool water washing of shell eggs on Haugh unit, vitelline membrane strength, aerobic microorganisms, and fungi. *Poult. Sci.* **2010**, *87*, 160−168.
(28) Kirunda, D. F. K.; McKee, S. R. Relating quality characteristics of aged eggs and fresh eggs to vitelline membrane strength as determined by a texture analyzer. *Poult. Sci.* **2000**, *79*, 1189−1193.
(29) Schäfer, K.; Männer, K.; Sagredos, A.; Eder, K.; Simon, O. Incorporation of dietary linoleic and conjugated linoleic acids and related effects on eggs of laying hens. *Lipids* **2001**, *36*, 1217−1222.

DOI: 10.1021/jf504759w
J. Agric. Food Chem. 2015, 63, 2506−2513

tion is available on Pickering emulsions stabilized by the particles of biological origin, such as cellulose nanocrystals,[17] chitin nanocrystals,[18] phytosterol,[19] modified starch,[20] and zein colloid particles.[16,21] Those works focused mainly on the fabrication and physical performances of the emulsions; little is known about their oxidant stability.

Zein, a prolamin, is the major storage protein in corn or maize. It contains sharply defined hydrophobic and hydrophilic domains at its surface and is capable of self-assembly to form a wide variety of mesostructures.[22] Zein particles have been studied for delivery and encapsulation,[23] but their use as Pickering emulsifiers are still limited. Theoretically, the Pickering emulsifiers should remain insoluble in both phases and remain intact over the lifetime of the emulsions.[12,16] Therefore, zein particles with partial wettability possesses promising potential in the manufacture of food-grade Pickering emulsions. de Folter et al. reported that zein particles (approximately 80 nm) were able to stabilize oil-in-water emulsions, but emulsion stability should be improved because free oil appeared after 3 days of storage.[21] Zein has a high proportion of apolar amino acid (>50%); as a result, the surface of zein particles seems quite hydrophobic. They tend to aggregate in the aqueous circumstance and are hard to arrange at the oil−water interface, leading to unstable Pickering emulsions. Some pertinent strategy should be utilized to tune the surface wettability of zein particles so as to form stable Pickering emulsions, for example, the interaction between proteins and polysaccharides.

Curcumin, a hydrophobic polyphenol with yellow color, is a major constituent extracted from the dried root of turmeric, the rhizome of the herb *Curcuma longa*.[24] It is an effective and potent antioxidant.[25] In addition, curcumin is a fluorophore, and its fluorescence can be monitored by excitation by an argon laser at 488 nm.[26] Curcumin was encapsulated in silica nanoparticle stabilized Pickering emulsion to study its fat during storage and simulated digestion.[27] In this paper, we demonstrate the fabrication of stable, soap-free, and edible Pickering emulsions based on fully natural renewable resources using protein/polysaccharide complex particles. This work attempted to protect lipid droplets of emulsions from peroxidation via manipulating the emulsions' interfacial framework using the Pickering mechanism and interface cargo of antioxidant. For this purpose, dual-function particles acting as Pickering emulsifier and interfacial transport vehicles of curcumin (a model antioxidant) were fabricated via a simple co-assembly approach. We propose a novel strategy to target accumulation of antioxidants at the interface via dual-function particles and compare the oxidative stability of encapsulated corn oil via either shell or core antioxidant. Pickering emulsions were characterized by confocal laser scanning microscopy (CLSM), particle size distribution, zeta potential, and physical stability measurements. The oxidative status of the samples was assessed by monitoring the formation of primary and secondary products during thermally accelerated oxidation storage. In addition, a schematic illustration of the formation pathway of zein/CH complex particle (ZCP)-stabilized antioxidant emulsions was proposed to correlate the oxidative stability of Pickering emulsions with their interfacial architecture.

MATERIALS AND METHODS

Materials. Zein (product Z 3625) and chitosan were purchased from Sigma Chemical Co. (St. Louis, MO, USA). According to the manufacturer, the molecular weight of the chitosan was approximately 500 kDa and the degree of deacetylation was 90%. Fluorescent dyes including Nile Red, Nile Blue A, and fluoresceine 5(6)-isothiocyanate mixed isomers (FITCs) were obtained from Sigma-Aldrich, Inc. (St. Louis, MO, USA). Chitosan was labeled by FITCs to check its distribution in emulsions. In short, the FITC solution (in ethanol) was added to chitosan solution, and FITC-labeled chitosan was precipitated using 0.2 mol L^{-1} NaOH and obtained via centrifugation (4000*g* 15 min) after 1 h of incubation at 40 °C. The unreacted FITC was removed before freeze-drying by dialysis against deionized water under darkness until no free FITCs were detected. 1,1,3,3-Tetramethoxypropane, thiobarbituric acid, and trichloroacetic acid were purchased from Sinopharm Chemical Reagent Co. Ltd. (Shanghai, China). Corn oil was purchased from a local supermarket (Guangzhou, China). All other chemicals used were of analytical grade.

Solution Preparation. Zein stock solutions was produced by dissolving 10.0 g of zein powder in 100 mL of aqueous ethanol binary solvent (70 v/v %). Curcumin-loaded zein solutions were prepared by adding curcumin to the preceding zein solutions at curcumin-to-zein ratios of 1:100, 1:50, and 1:20, respectively. Chitosan (CH) solutions were produced by dispersing 0.5 g of chitosan powder into 100 mL of 1% acetic acid under magnetic stirring overnight to facilitate chitosan hydration.

Particle Synthesis. Dual-function ZCP (or ZCP-cur) was fabricated via a so-called antisolvent procedure. All operations were at room temperature. Curcumin-loaded zein solutions were trickled into CH solutions within 2 min under shearing at 5000 rpm using an Ultraturax T10 homogenizer. After another 10 min of shearing, the remaining ethanol in the particle dispersions was removed by an RV 10 digital rotary evaporator (IkA-Works Inc., Staufen, Germany). Finally, the zein and CH concentrations in the dispersion were 7 and 0.35%, respectively. The plain ZCP was produced according to the same procedure without curcumin addition. Particle size, shape, and ζ-potential of fresh ZCP and ZCP-cur dispersions were characterized prior to the emulsion preparation.

Preparation of Pickering Emulsion. The preceding ZCP and ZCP-cur were utilized to prepare Pickering emulsions, ZCP-stabilized emulsions (ZCPEs), and ZCP-cur stabilized emulsions (ZCP-curEs). All emulsions were prepared using an oil−water ratio of 50:50. In brief, 5 mL of corn oil was added to 5 mL of the particles suspensions in a glass vial, and the resultant mixtures were sheared using an Ultraturax T10 homogenizer (IkA-Works Inc.) at 6000 rpm for 5 min at room temperature to yield the Pickering emulsions. For ZCPE-cur, curcumin was incorporated in corn oil at curcumin-to-zein ratios of 1:100, 1:50, and 1:20, respectively, prior to the emulsion preparation.

Zeta-Potential Measurements. Zeta potentials of the complex particle dispersions and Pickering emulsions were determined by a Zetasizer Nano (Malvern Instruments Ltd., Worcestershire, UK) at room temperature. Each value represents the average of at least three independent trials.

Contact Angle Measurements. Three-phase contact angle (θ) measurements were measured using an OCA 20 AMP (Dataphysics Instruments GmbH, Germany) equipped with a high-speed video camera. Colloid particle dispersions were freeze-dried to yield particle powders that were compressed to produce tablets of 13 mm in diameter and 2 mm in thickness. The tablets were then immersed in corn oil bath, and 2 μL of Milli-Q water was deposited gently on the tablets using a high-precision injector. The drop image was photographed using the high-speed video camera at a rate of 10 pictures per second, and the LaPlace−Young equation was utilized to fit the profile data of the droplet to calculate the θ. Measurements were averaged over at least 10 droplets.

Morphology Observation. Topographic structures of ZCP were analyzed by a Zeiss Merlin Field emission scanning electron microscope (Zeiss, Oberkochen, German). The freeze-dried ZCP powers were utilized to investigate their morphological attributes, and they were loosely glued onto a conductive adhesive mounted on a stainless steel stage. Subsequently, they were coated with a thin (<20 nm) conductive gold and platinum layer using a sputter coater (Hummer XP, Anatech, Union City, CA, USA). Representative SEM images were reported.

DOI: 10.1021/jf505227a
J. Agric. Food Chem. 2015, 63, 2514−2524

Particle Size Distribution of Pickering Emulsion. Droplet size distributions of the Pickering emulsion were measured immediately after the emulsification and after 2 and 7 weeks of storage at room temperature, using a Mastersizer 2000 (Malvern Instruments Ltd.). The samples were diluted in deionized water at 2000 rpm until an obscuration rate of 10% was obtained. The Mie theory was applied by considering the following optical properties for corn oil droplets: a refractive index of 1.330 and absorption of 0.001. Volume mean diameter ($D_{4,3}$) and surface mean diameter ($D_{3,2}$) parameters were calculated from particle size profiles of the Pickering emulsions according to eqs 1 and 2, respectively.

$$D_{4,3} = \frac{\sum n_i d_i^4}{\sum n_i d_i^3} \quad (1)$$

$$D_{3,2} = \frac{\sum n_i d_i^3}{\sum n_i d_i^2} \quad (2)$$

n_i is the number of droplets of a determined size range, and d_i is the droplet diameter.

Stability Test. *Long-Term Storage Stability.* Pickering emulsions were sealed in glass test tubes for 7 weeks at room temperature. Droplet size and size distributions as well as visual appearance of the emulsions were monitored periodically.

Centrifugation Stability. Emulsion stability was checked by centrifugation for 30 min at 5500 *g*, and the thickness of the creaming layer was measured with a digital caliper.[17]

Creaming Stability. The creaming stability of the emulsions was analyzed via creaming index (CI).[28] Emulsion samples were poured into glass tubes (2.8 cm in diameter 7.5 cm in height), and the tubes were sealed to prevent moisture evaporation. The samples were monitored for 7 weeks. The CI values were calculated according to eq 3

$$\mathrm{CI}\ (\%) = H_s/H_e \quad (3)$$

where H_s is the serum layer height and H_e is the total emulsion height.

Confocal Laser Scanning Microscopy. CLSM experiments were performed according to the procedure of Ma et al.,[29] using a Leica TCS SP5 CSLM (Leica Microsystems Inc., Heidelberg, Germany). Various specimens of the Pickering emulsions were dyed with a mixed fluorescent dye solution consisting of 1 mg mL^{-1} Nile Red and 1 mg mL^{-1} Nile Blue A (in isopropyl alcohol). The dyed emulsions were put on concave slides, and then the concave slides were covered with coverslips. Finally, glycerol was coated around the coverslips to seal the samples. The fluorescent dyes were excited by either an argon laser at 488 nm for Nile Red or a helium neon (He−Ne) laser at 633 nm for Nile Blue A. In addition, curcumin fluorescence was monitored by exciting by an argon laser at 488 nm,[26] reflecting its distribution within the Pickering emulsions. FITC-labeled chitosan was utilized to synthesize ZCPs and yield Pickering emulsion, and FITC fluorescence was visualized using an argon laser at 488 nm to explore the role of chitosan in the formation of ZCP-stabilized Pickering emulsions.

Lipid Oxidation Measurements. The fresh emulsions (10 mL) were immediately placed in a sealed screw-cap glass tube and kept in an oven for 22 days at 40 °C to accelerate oxidation of corn oil. An aliquot of 0.5 mL of emulsions was periodically taken out to determine the primary and secondary oxidant products.

Primary Lipid Oxidation Products. Lipid hydroperoxide, as the marker of primary products of lipid oxidation, was measured according to the procedure described by Tong et al.[30] An aliquot of 200 mg of the Pickering emulsions was mixed with 1.5 mL of isooctane/2-propanol (3:1, v/v) by vortexing (10 s, three times), and the organic phase was isolated by centrifugation (2000*g*, 5 min). An aliquot of 0.2 mL the resultant supernatant was admixed to 2.8 mL of methanol/1-butanol (2:1, v/v) solution, followed by 15 μL of 3.94 M ammonium thiocyanate and 15 μL of ferrous iron solution. Ferrous iron solution was prepared by mixing $BaCl_2$ and $FeSO_4$ to final concentrations of 0.132 and 0.144 mol L^{-1}, respectively. After 20 min of incubation, the absorbance of the solutions was read at 510 nm using an UV−visible spectrophotometer (UV-2300, TianMei Techcomp Limited., Shanghai, China). Hydroperoxide concentrations were calculated from the standard curve of hydrogen peroxide.

Secondary Lipid Oxidation Products. The secondary oxidation products were monitored via the thiobarbituric acid reactive substances (TBARS) protocol.[30] This approach was developed to quantify malondialdehyde (MDA), one of two marked biproducts of lipid peroxidation. In brief, an aliquot (0.2 mL) of the Pickering emulsions after accelerated storage for 22 days was admixed with 1.8 mL of deionized water and 4.0 mL of thiobarbituric acid (TBA) solution, which was prepared by dissolving 15 g of trichloroacetic acid (15% w/v) and 0.375 g of TBA (0.375%) in 100 mL of 0.25 mol L^{-1} HCl. The resulting mixtures were heated for 15 min in a boiling water bath and then cooled to room temperature using tap water. Finally, the mixture was centrifuged at 2000*g* for 15 min. The MDA−TBA adducts formed from the reaction of the MDA in the emulsion samples with the TBA reagent were detected colorimetrically, and the absorbance was read at 532 nm. The MDA concentrations were calculated from a standard curve made from 1,1,3,3-tetraethoxypropane.

Hexanal Measurements. An aliquot (8 mL) of fresh emulsions was put into 10 mL headspace vials, and the vials were sealed with silicone rubber Teflon caps using a crimper. After thermally accelerated storage (40 °C, 22 days) in a dark oven, the headspace hexanal of the Pickering emulsion specimens was determined using a Trace DSQ II GC-MS (Thermo-Fisher Scientific, Waltham, MA, USA) according to the procedures of Panya et al.[31] and Wan et al.[32] In brief, solid phase microextraction (PME) trials were performed as follows. A 75 μm stable flex PME fiber (carboxen/polydimethylsiloxane, Supelco, Bellefonte, PA, USA) was inserted in the sample headspace through a vial septum, and the PME process was continued for 10 min at 55 °C. The PME fiber was desorbed in the GC detector at a split ratio of 1:10 (250 °C, 3 min). GC analysis of the headspace hexanal was carried out using a TR-5MS capillary column (30 m × 25 mm × 0.25 μm). The temperatures of the injector, flame ionization detector, and oven were 250, 250, and 60 °C, respectively. Test time was set at 15 min. Triplicate tests were performed for each emulsion sample.

Statistics. Statistical analyses were performed using an analysis of variance (ANOVA) procedure of the SPSS 13.0 statistic analysis program, and the differences between means of the trials were detected by a least significant difference (LSD) test ($P < 0.05$).

RESULTS AND DISCUSSION

Wetting Properties. The wettability of the particles at the interface plays a crucial role in the formation of stable Pickering emulsions. The partial wettability attributes can facilitate efficient packing of particles at the oil−water interface to form steric hindrance against droplet coalescence. Contact angle measurement (CAM) was a potent technique for evaluating the wetting properties of a surface. The wetting properties of ZCP were investigated by measuring three-phase contact angles (θ) of ZCP films that were immersed in corn oil. Figure 1 shows typical images of water droplets deposited to zein films immersed in corn oil. The θ of zein particles without chitosan was 112.73 ± 1.29°. This result may be associated with the nature of zein possessing >50% hydrophobic amino acid. The decrease in the θ of the ZCP indicates a successful surface coating of zein particles with chitosan (Figure 1). The association between chitosan and zein particles at acidic pH via weak electrostatic interaction between the positively charged amino of chitosan and the nonprotonated carboxyl groups of zein at acidic pH (~3.5) caused an increase in the free amino and hydroxyl group at the surface of zein particles, thereby lessening their hydrophobic characteristics. The θ data (about 82°) clearly demonstrated that the ZCP at CH-to-zein ratios of 1:20 and 1:10 are potentially suitable materials as Pickering emulsifier to yield oil-in-water Pickering emulsions. In contrast, the θ values of the ZCP at the CH-to-zein ratio of 1:50 did not situate between chitosan-free zein particles and

DOI: 10.1021/jf505227a
J. Agric. Food Chem. 2015, 63, 2514−2524

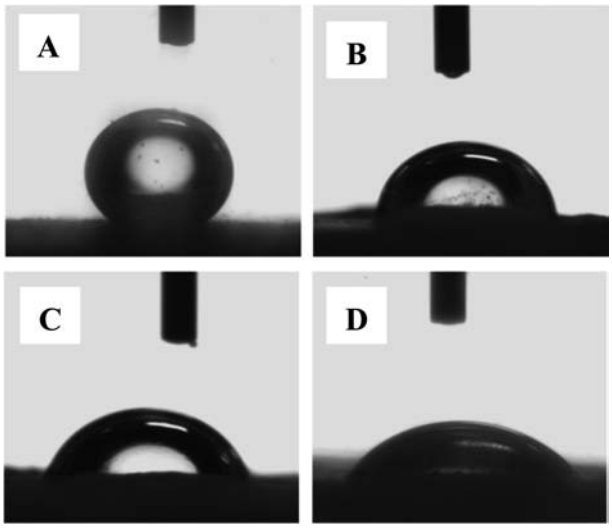

Figure 1. Typical three-phase contact angles (θ) of ZCP films as a function of CH-to-zein ratios: (A) plain zein; (B) 1:10; (C) 1:20; (D) 1:50.

ZCP with the CH-to-zein ratios of 1:10 and 1:20. The underlying mechanism for this phenomenon was unknown, but it was repeatable. Furthermore, in other experiments, we utilized *n*-tetradecane to replace corn oil and found a similar phenomenon. In this work, the ZCPs produced at a CH-to-zein ratio of 1:20 were utilized to fabricate Pickering emulsions.

Particle Size Characterization of ZCP and ZCP-cur. Figure 2B shows typical droplet size distribution of ZCP and ZCP-cur. The ZCP showed a nearly monomodal droplet size distribution, and the position of the maxima appeared at 1−2 μm, which was consistent with morphological observation by the SEM (Figure 2C). Curcumin loading changed the size distributions of the particles from a nearly narrow monomodal (ZCP) to bimodal (ZCP-cur) patterns, and two overlay peaks at 0.9 and 8−10 μm were observed in the size distribution profiles (Figure 2B). This phenomenon indicated that curcumin loading affected the self-assembly process of amphiphilic zein. Concomitantly, the $D_{3,2}$ and $D_{4,3}$ were calculated to reflect quantitatively the changes in the size of ZCP due to the curcumin additions. Curcumin loadings did not cause marked alterations in the $D_{3,2}$ and $D_{4,3}$ of the ZCP (Table 1). In theory, the desorption energy of particles can easily reach several thousands of k_BT (T, absolute temperature; k_B, Boltzmann constant) even for nanoscale particles at the oil−water interface.[33] This suggests that once the solid particles are absorbed at the interface, they are anchored irreversibly. Furthermore, the larger the particles, the more the detachment energy.[13] Therefore, micrometer-sized ZCPs possess a promising potential to form stable Pickering emulsions with food-grade status once they are absorbed at the oil−water interface.

Table 1. Mean Particle Size and Zeta Potentials of Zein/CH Particles Loaded with Various Curcumin Concentrations[a]

particle type	cur/zein ratio	$D_{3,2}$ (μm)	$D_{4,3}$ (μm)	zeta potential (mV)
ZCP[b]	0	1.58 ± 0.51	6.03 ± 0.38	64.0 ± 1.6
ZCP-cur[c]	1:100	1.73 ± 0.33	6.14 ± 1.92	64.9 ± 1.9
ZCP-cur[c]	1:50	1.81 ± 0.11	5.15 ± 0.35	61.7 ± 0.5
ZCP-cur[c]	1:20	2.07 ± 0.35	5.64 ± 0.58	57.3 ± 1.9

[a]Values are expressed as the means and standard deviations of three measurements. [b]ZCP, zein/CH complex particles. [c]ZCP, zein/CH complex particles with various curcumin loadings.

Zeta potentials of ZCPs with or without curcumin ranged from 57.3 ± 1.9 to 63 ± 1.6 mV (Table 1), implying the presence of strong electrostatic repulsion among lipid droplets stabilized by zein/CH microspheres. The correlation between effective Pickering stabilization and particle flocculating conditions was well-established experimentally,[34] and it was also confirmed theoretically.[35] ZCPs flocculated after 12 h of storage at room conditions to form a deposit layer at the bottom of the glass tube (Figure 2A), supporting the formation of stable Pickering emulsions.

Physical Performance of Pickering Emulsions. Emulsion type (either o/w or w/o) was deduced by observing what happened when a drop of emulsions was added to either oil or water. ZCP-stabilized Pickering emulsion rapidly dispersed when it was added to water, confirming that it is an o/w emulsion.

Visual Appearance. Figure 3 shows the visual appearance of the Pickering emulsions stabilized by ZCP and ZCP-cur. Visual inspection revealed the fresh emulsions remained homogeneous without noticeable sign of creaming or phase separation. ZCP-stabilized Pickering emulsions were milky white, whereas the emulsion color changed from milky white to yellow upon incorporation of curcumin, irrespective of curcumin locations and/or concentrations (ZCP-curE and/or ZCPE-cur) (Figure 3). A lipid droplet-enriched cream layer gradually appeared as a

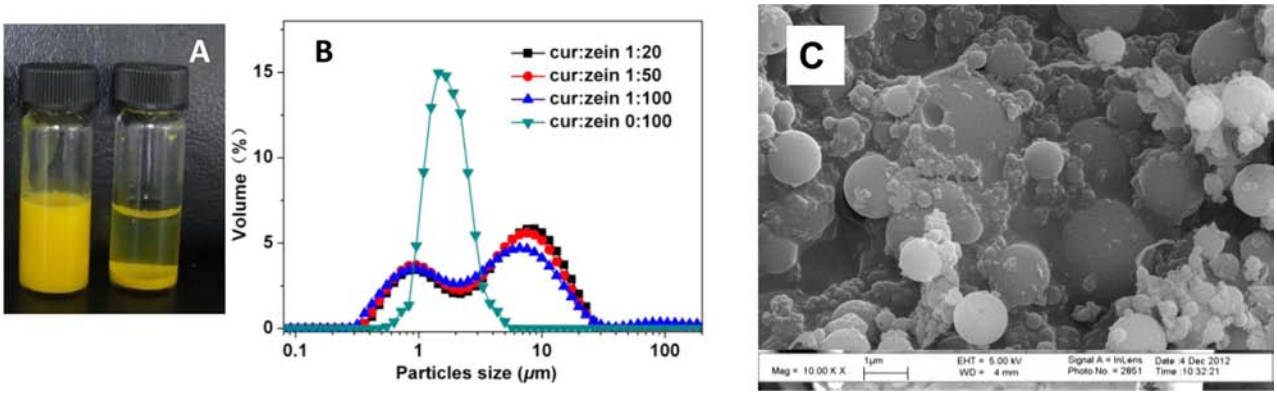

Figure 2. Visual appearance (A), particle size distributions (B), and topography (C) of the ZCP. (A) Fresh ZCP dispersion (left) and after 12 h of storage (right).

DOI: 10.1021/jf505227a
J. Agric. Food Chem. 2015, 63, 2514−2524

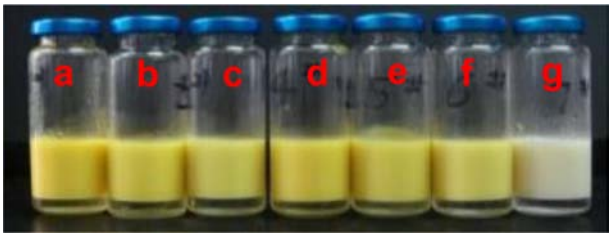

Figure 3. Visual appearance of Pickering emulsions stabilized by ZCP or ZCP-cur: (a–c) ZCP-curE at curcumin-to-zein ratios of 1:100, 1:50, and 1:20, respectively; (d–f) ZCPE-cur at curcumin-to-zein ratios of 1:100, 1:50, and 1:20, respectively; (g) ZCPE.

result of gravitational separation of the emulsion samples during the storage.[36] After 5 h of storage, the interface was positioned at a height of 3–4 mm for ZCPE, ZCPE-cur, and ZCP-curE. After 2 weeks, the height slightly increased to 15 mm, corresponding to about 30% of the height of raw emulsions, and the height of the interface reached a plateau for all emulsions. Interestingly, the creaming of the encapsulated droplets did not lead to irreversible flocculation and completely disappeared after gentle shaking. In contrast, de Folter et al. fabricated zein nanoparticles (about 80 nm)-stabilized Pickering emulsion and reported the height slightly increased to 45% after 2 weeks of storage and free oil occurred after 3 days of storage.[21] Therefore, ZCP-stabilized Pickering emulsions were more stable than the plain zein particle-stabilized emulsion.

Long-Term Stability of Emulsions. Long-term stability is a prerequisite property for emulsions used in various fields. Selected droplet size distributions of the emulsions are shown in Figure 4, and detailed surface mean diameters ($D_{3,2}$) of Pickering emulsions a function of storage times are listed in Table 2. ZCPE showed a multimodal droplet size distribution, and the maxima appeared at 10–20 μm (Figure 4). A minor peak at about 1 μm may pertain to the remaining ZCP in the continuous phase, and a peak at ~1000 μm can be attributed to the presence of multiple emulsion phenomena in ZCP-stabilized emulsions, confirmed by CLSM technique (Figure 6A,C). The peak at ~1000 μm disappeared after 2 weeks of storage at room temperature, whereas the others remained nearly unaffected after storage for 2 weeks and longer for various emulsions. Concomitantly, the mean particle size was used to quantitatively characterize the size of Pickering emulsion over the storage for 7 weeks, reflecting that all preparations were micrometer-sized. The $D_{3,2}$ of ZCPE was 14.87 ± 1.45 μm. ZCPE-cur and ZCP-curE had similar particle sizes (Table 2). The $D_{3,2}$ values of these emulsions were stable for 7 weeks (Table 2), reflecting that no coalescence occurs during the storages.

Centrifugation Stability. Centrifugation accelerates the creaming process of emulsions, forcing the droplets to concentrate. The excess water is then excluded from the emulsion, leading to close packing conditions. The creaming index after the centrifugation was used to reflect their physical stabilities. After centrifugation at 4000*g*, the CI was about 44% for tested emulsions, which was higher than that after 1 week of storage (23.8–25%) and 7 weeks of storage (28.5–30.0%) (Table 3), reflecting that excess water was excluded from the emulsion in the course of centrifugation. In addition, the deposit was detected at the bottom of the centrifugal tube, reflecting the ZCP in the Pickering emulsions was excess (Figure 5). However, the tested emulsions were not "broken up", indicating that the emulsions resisted the stress induced by the centrifugation.

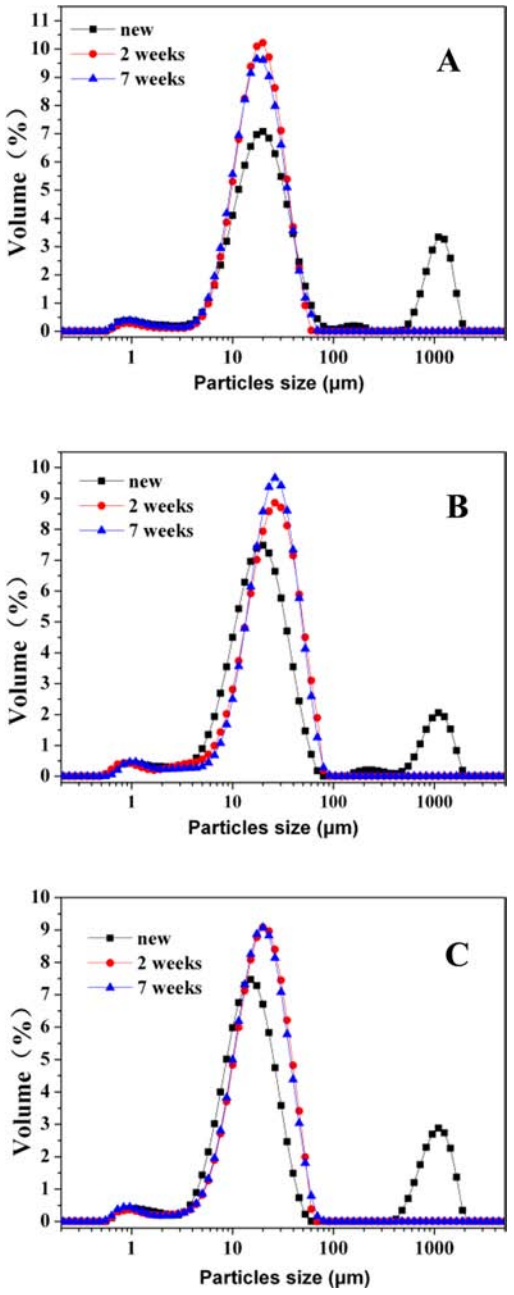

Figure 4. Typical particle size distribution of the emulsions stabilized by ZCP or ZCP-cur at selected storage times: (A) ZCP-stabilized emulsions (ZCPE); (B) emulsions stabilized by ZCP-cur (ZCP-curE) at a curcumin-to-zein ratio of 1:50; (C) ZCP-stabilized emulsions via loading curcumin (ZCPE-cur) at a curcumin-to-zein ratio of 1:50.

Microstructure. The morphological structure of emulsions, including interfacial characteristics (composition, thickness, and integrality) and the distribution of antioxidant within the emulsions, determined to some degree their physical performance and oxidant stability. It can be evaluated by the CLSM technique by the linkage of fluorescence labeling and electronic microscopy. Figure 6A shows overlay fluorescence micrographs of ZCP-stabilized emulsions. Micrographs were taken of the same area during selective excitation with either Nile Red (oil, green) or Nile Blue A (zein, red). Green fluorescence from Nile Red lay in the spherical droplets, and there were obvious red

DOI: 10.1021/jf505227a
J. Agric. Food Chem. 2015, 63, 2514–2524

Table 2. Mean Droplet Size ($D_{3,2}$) of Oil-in-Water Emulsions Stabilized with Zein/CH Particles, as a Function of Curcumin Amounts and Adding Strategy[a]

		$D_{3,2}$			
emulsion type	cur/zein ratio	fresh emulsion	1 week	7 weeks	zeta potential (mV)
ZCPE[b]	0	14.87 ± 1.45	11.92 ± 0.68	12.65 ± 0.57	62.4 ± 2.4
ZCP-curE[c]	1:100	11.77 ± 0.69	11.18 ± 0.88	12.19 ± 0.72	56.6 ± 7.1
ZCP-curE[c]	1:50	10.61 ± 0.51	10.75 ± 0.56	11.94 ± 0.31	62.2 ± 3.8
ZCP-curE[c]	1:20	11.08 ± 0.90	12.23 ± 0.69	12.97 ± 1.54	64.2 ± 2.6
ZCPE-cur[d]	1:100	12.11 ± 0.42	9.870 ± 0.48	12.08 ± 0.42	66.5 ± 0.8
ZCPE-cur[d]	1:50	11.71 ± 0.97	11.96 ± 0.55	13.38 ± 0.76	60.6 ± 5.7
ZCPE-cur[d]	1:20	10.73 ± 0.75	11.59 ± 0.71	12.38 ± 0.48	63.0 ± 1.7

[a]Values are expressed as the means and standard deviations of three measurements. [b]ZCPE, Pickering emulsions stabilized by the ZCP. [c]ZCP-curE, Pickering emulsions stabilized by dual-function ZCP-cur. [d]ZCPE-cur, ZCP-stabilized Pickering emulsions loaded with curcumin in oil core.

Table 3. Creaming Index of Pickering Emulsion after Long-Term Storage and Centrifugation Treatment

	creaming index (%)		
emulsion type	centrifugation	1 week	7 weeks
ZCPE[a]	43.8	25.0	28.5
ZCPE-cur[b]	43.5	26.3	31.3
ZCP-curE[b]	44.3	23.8	30.0

[a]ZCPE, Pickering emulsions stabilized by ZCP (zein/CH colloid particles). [b]ZCPE-cur, ZCP-stabilized Pickering emulsions loaded with curcumin. [b]ZCP-curE, Pickering emulsions stabilized by dual-function ZCP-cur.

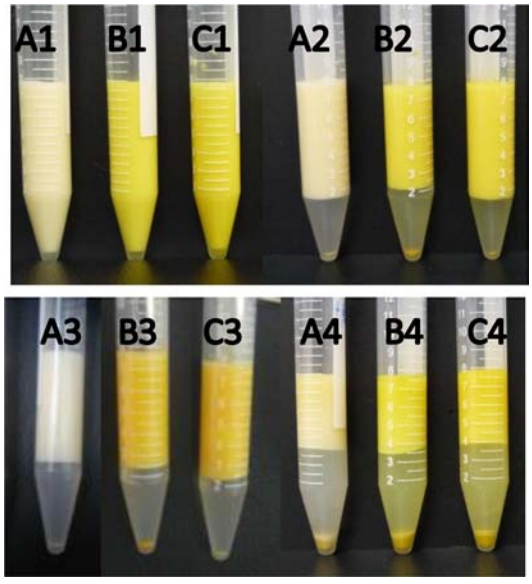

Figure 5. Digital photographs of corn oil-in-water emulsions stabilized by the ZCP with various curcumin loading approaches: (A) Pickering emulsion (ZCPE); (B) Pickering emulsion stabilized by ZCP-cur (ZCP-curE); (C) ZCPE with curcumin loading in oil core (ZCPE-cur). The numbers within the figure, 1−4, represent fresh, 1 week, 7 weeks, and centrifugation at 4000*g* for 2 min, respectively.

circles around spherical droplets (Figure 6A), further confirming that an o/w emulsion was formed when the ZCP was utilized as Pickering emulsifier (θ = 82°, Figure 1). This result is consistent with previous findings that particles with θ < 90° yield an o/w emulsion.[37] Droplet sizes of the emulsions ranged between 5 and 50 μm, evidenced by the results determined by Mastesizer 2000 (Figure 4). In general, full coverage by solid particles is not necessary to produce stable Pickering emulsions.[11,38] Figure 6A2 shows the blowup of a single lipid droplet of Pickering emulsion, displaying the intact and thick ZCP shells coating the surface of spherical droplets. This kind of interface framework contributed to the aforementioned stabilization phenomena of the Pickering emulsions and gave them a promising potential against lipid oxidation via physical barrier of particle-based interfacial membrane.

Curcumin fluorescence was excited by an argon laser at 488 to distinguish its distribution within the emulsions. In this work, the dual-function particles (ZCP-cur) were produced via a co-assembly approach, and the utilization of ZCP-cur as particulate emulsifier resulted in a targeted accumulation of curcumin at the oil−water interfaces, evidenced by the presence of obvious blue circles around emulsion droplets (black) (Figure 6B). In contrast, curcumin was distributed uniformly within the interior of dispersed droplets when it was admixed to corn oil prior to the emulsification (Figure 6C). The distribution of curcumin within the Pickering emulsions played a key role in the oxidant stability of the emulsions.

Primary and Secondary Oxidative Products of Pickering Emulsions. Corn oil is labile to oxidation because its fatty acids consist of >56% linoleic acid and about 30% oleic acid.[39] The oxidative stability of corn oil-in-water Pickering emulsions was evaluated by monitoring the formation of the complementary markers during thermally accelerated storage.

Lipid Hydroperoxides (LP). LP concentration was determined to reflect the initial lipid oxidation rate of the emulsions. Figure 7A displays the LP concentrations of ZCP-stabilized Pickering emulsions (ZCPEs) as a function of incubation time. They increased gradually from 0.95 ± 0.30 mmol/kg of oil (fresh) to 18.57 ± 0.24 and 49.05 ± 0.63 mmol/kg of oil after 9 and 22 days of storage at 40 °C, respectively. Comparatively, ZCP was more effective in inhibiting lipid oxidation of the emulsions than protein-type emulsifiers or protein/polysaccharide complex, for example, soy protein, whey protein, and soy protein isolate (SPI)/pectin.[32,40] LP concentrations in the WPI- and SPI-stabilized emulsions increased to 113.2 and 205.5 mmol/kg of oil, respectively, after 185 h (7−8 days) of storage at 37 °C.[40] Wan et al. fabricated complex interfaces of SPI and stevioside (STE) micelles and reported the hydroperoxides of the emulsions were about 120 mmol/kg oil after 21 days of storage at 37 °C.[32] The phenomena may be attributed to the interfacial characteristics of ZCPEs in which network fabrics of zein/CH complex particles at the surface of spherical droplets were confirmed via CLSM technique (Figure 7A). Similarly, the peroxide value (PV) of Pickering emulsion stabilized by microcrystalline cellulose (MCC) or modified starch (MS)

DOI: 10.1021/jf505227a
J. Agric. Food Chem. 2015, 63, 2514−2524

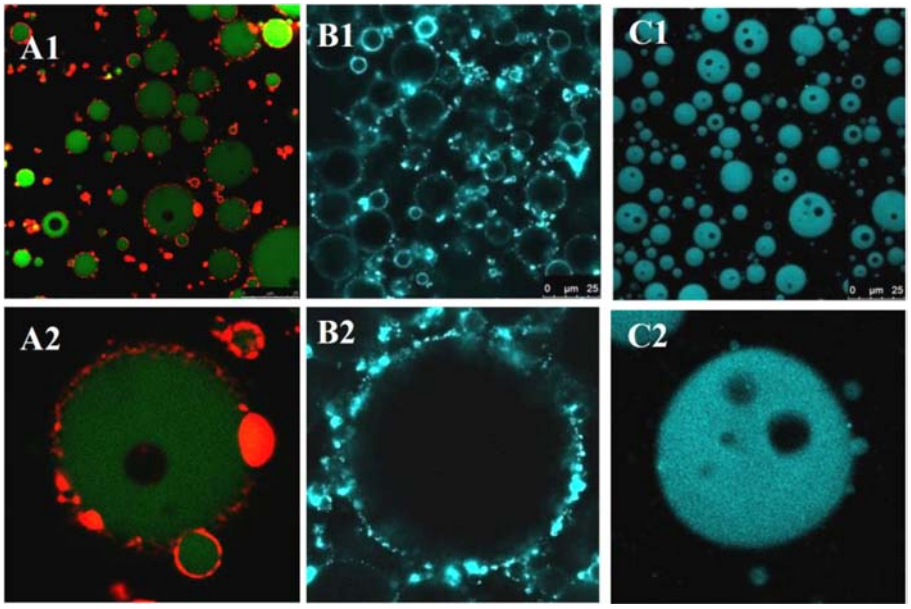

Figure 6. CLSM images of Pickering emulsions: (A1, A2) ZCP-stabilized emulsions (ZCPE) (corn oil was stained with Nile Red, and zein was stained by Nile Blue A; the fluorescent dyes were excited at 488 nm for Nile Red (green) and at 633 nm for Nile Blue A (red)); (B1, B2) emulsions stabilized by ZCP-cur (ZCP-curE) at a curcumin-to-zein ratio of 1:50 (curcumin fluorescence was monitored by excitation by an argon laser at 488 nm (blue)); (C1, C2) ZCP-stabilized emulsions via loading curcumin (ZCPE-cur) at a curcumin-to-zein ratio of 1:50 (curcumin fluorescence was monitored by excitation at 488 nm (blue)).

increased to 8−20 mM after 7 days of incubation at 40 °C, in a particle concentration- and type-dependent manner.[41,42] Therefore, particle-stabilized emulsions can restrict the formation of primary oxidant products, and ZCP is a suitable particulate emulsifier to form stable Pickering emulsions with depressed initial oxidant rate.

The oxidative stability of the emulsions depended on the curcumin locations. Curcumin was found to be an effective and potent antioxidant in different in vitro assays.[25] The antioxidant activity of curcumin incorporated into the droplet's shell of the ZCPE was compared with that of it admixed into the oil phase prior to the emulsification. Dual-function particles serving as a particulate emulsifier and interfacial cargo of curcumin were fabricated via a simple co-assembly approach, and the targeted accumulation of curcumin at the interface was achieved using the dual-function particles (ZCP-cur) (Figure 7A). As a consequence, antioxidant interfacial shells around spherical droplets were formed, endowing the emulsions with improved oxidative stability. The LP decreased by approximately 50% from 49.05 (ZCPE) to 20.14−24.14 (ZCP-curE) mmol/kg oil after 22 days of storage at 40 °C depending on the curcumin loadings within the ZCP (Figure 7A). In contrast, the LP of Pickering emulsions decreased slightly from 49.05 (ZCPE) to 25.46−40.89 (ZCPE-cur) by directly admixing curcumin in corn oil before the emulsification (Figure 7A). Therefore, fabrication of antioxidant interface via dual-function ZCP is a promising approach to enhance further the oxidant stability of ZCPE.

Secondary Oxidant Products. Measuring the secondary products of lipid peroxidation is one of the most widely accepted assays for the oxidative stability of emulsions.[43] MDA, a marker of secondary oxidative products, was monitored by TBARS assay. Figure 7B displays MDA content of the ZCPEs after 22 days of storage at 40 °C. The MDA value of the emulsion was 53.99 ± 6.04 μmol/kg oil. Comparatively, ZCPs were more effective in inhibiting lipid oxidation of the emulsions than biopolymers, for example, protein-type or protein/polysaccharide complex emulsifiers. The MDA of SPI-stabilized emulsions was about 20 mmol/kg oil under accelerated storage at 50 °C for 10 days.[7] Lomova et al. fabricated the emulsions stabilized by complex interface of BSA and biocompatible polyelectrolytes and reported the MDA of the emulsion ranged from 40 to 100 mmol/kg oil during storage for 0−15 days at 37 °C.[1] The MDA of ZCPE were lower than those of the preceding emulsions by 2−3 orders of magnitude. The irreversible adsorption of ZCP at the interface resulted in submicrometer interfacial barriers, restricting the interactions between LP at the interface and pro-oxidants (e.g., Fe^{2+}) in the continuous phase via steric hindrance. In addition, strongly positive ZCP shells around dispersed droplets did have an advantage over negatively charged emulsions regarding the oxidative stability.

To further clarify the influence of antioxidant locations on the oxidative stability of the Pickering emulsions, the MDAs of the emulsions with shell curcumin or core curcumin were analyzed and compared. CLSM trials confirmed the targeted accumulation of curcumin at the oil−water interfaces via the cargo of the ZCP (Figure 7B), producing antioxidant interface shells around spherical droplets. The interfacial frameworks markedly enhanced oxidative stability of the emulsions. The MDA decreased by approximately 50% from 53.99 (ZCPE) to 24.57−33.34 μmol/kg oil (ZCP-curE) after 22 days of storage at 40 °C in a loading-dependent manner (Figure 7B). In contrast, the MDA decreased slightly from 53.99 (ZCPE) to 32.37−37.83 μmol/kg oil (ZCPE-cur) after 22 days of incubation at 40 °C when curcumin was directly incorporated within the dispersed droplets (Figure 7B). Hence, the formation of the antioxidant shell around dispersed droplet surfaces appears to be an advantageous strategy to protect emulsified oil against oxidation rather than admixing antioxidants into oil core.

DOI: 10.1021/jf505227a
J. Agric. Food Chem. 2015, 63, 2514−2524

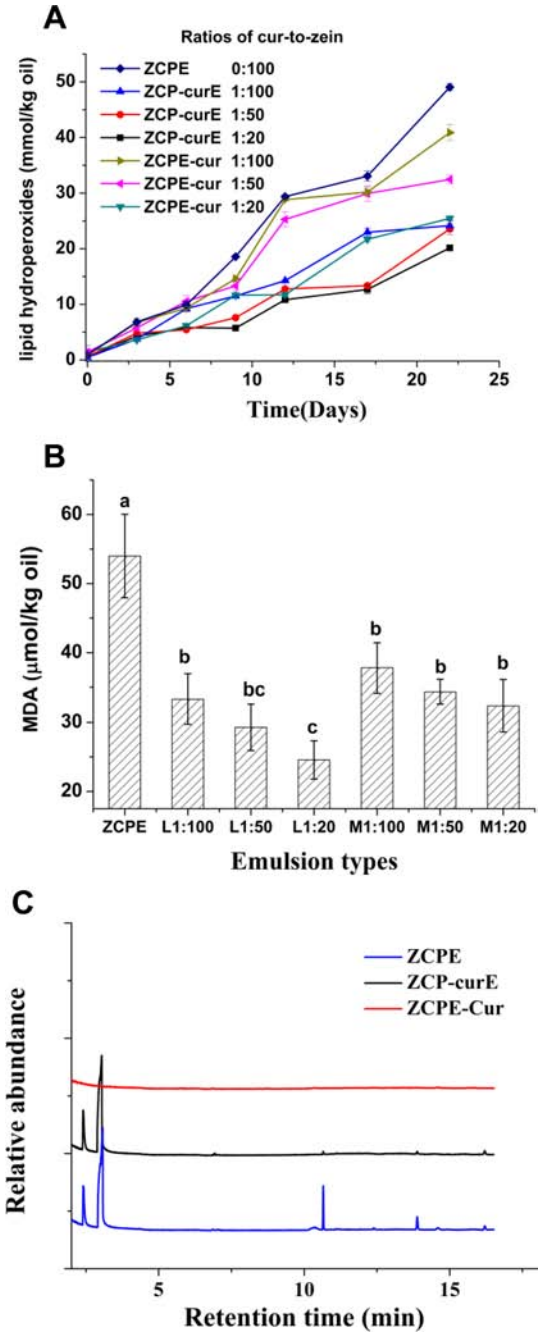

Figure 7. Primary and secondary oxidant products of Pickering emulsions under accelerated storages at 40 °C: (A) LP content; (B) MDA content (L1:100, L1:50, and L1:20 represent ZCP-curE at three curcumin/zein ratios; M1:100, M1:50, and M1:20 represent ZCPE-cur at three curcumin/zein ratios; different characters (a–c) on the columns represent significant difference); (C) hexanal content.

Headspace Hexanal. There was a complex mixture for secondary lipid oxidation products, and hexanal, a volatile compound, is another marker of secondary oxidation products. The hexanal level of Pickering emulsions was analyzed by headspace gas chromatography (Figure 7C). In our laboratory, hexanal content in SPI and SPI–resveratrol emulsions was analyzed using headspace gas chromatography, confirming the presence of an identified hexanal peak at approximately 7 min for the emulsions after 21 days of storage.[32] The situation changes drastically when ZCPs were utilized as the particulate emulsifier, where no hexanal was detected in headspace gas chromatography of the Pickering emulsions using the preceding protocol for SPI and SPI–resveratrol emulsions (Figure 7C). Furthermore, the smell of rancidity did not appear as well. These results were consistent with the TBARS assay (Figure 7B) where the MDA values of ZCP emulsions were markedly lower than those of the emulsions stabilized by SPI or complex polyelectrolytes.[1,7] Thus, headspace hexanal analysis provided further evidence that ZCP effectively improved the oxidative stability of emulsions. As expected, there was no detectable headspace hexanal peak in headspace gas chromatography of ZCPE-cur and ZCP-curE after 22 day storage at 40 °C (Figure 7C).

Schematic Illustration. The interfacial architecture is a determined factor for the oxidant stability of the emulsions. Fabrication of Pickering emulsions is a promising strategy to improve the oxidative stability of the emulsions via the formation of dense particle-based interfacial layers, providing a physical barrier against the pro-oxidants. The MDA value of ZCPE was lower than that of the emulsions stabilized by the biopolymers by 2–3 orders of magnitude.[1,7] Concomitantly, no detectable hexanal peak in headspace gas chromatography appeared for the ZCPE after 22 days of storage at 40 °C. Curcumin is an effective and potent antioxidant; the introduction of curcumin further enhanced the oxidative stability of the emulsions, depending on curcumin loadings and locations (Figure 7). Especially, the targeted migration of curcumin at the oil–water interfaces was put into practice when ZCP was utilized as the interface delivery of curcumin, further slowing the lipid oxidation in the emulsions (Figure 7).

Herein, a schematic diagram for the formation pathway of ZCP-stabilized antioxidant Pickering emulsions is proposed to correlate the oxidative stability and physical performance of the Pickering emulsions with their interface frameworks, so as to elucidate the possible mechanism for excellent physical and oxidative stability for ZCP-stabilized Pickering emulsions (Figure 8). Chitosan, a pH responsive polymer, is not a conventionally good emulsifier. It is able to in situ self-assemble at pH >6.0 to form nanoparticles or micrometer-sized floccular precipitates, and these aggregates can adsorb at the oil–water interface to yield Pickering emulsions.[44] Demulsification happened when the pH of the emulsions was adjusted to 6.0 or lower, indicating chitosan has low surface activity at acidic pH.[44] In this work, ZCP-stabilized Pickering emulsions were fabricated at pH 3.5, at which chitosan possesses low surface activity. To shed light on the role of chitosan in emulsion formation and performance, we performed additional experiments using FITC-labeled chitosan to produce ZCP. Unexpectedly, the CLSM photograph indicated that chitosan formed a network on the surface of dispersed droplets in the Pickering emulsions at acidic pH. It has been proposed that the steric particle-based barrier in Pickering emulsions is not a simple bilayer or monolayer, but a network of particles, adsorbed at the oil–water interface.[11,45] This phenomenon was also observed in our Pickering emulsions in which ZCPs assemble through the bridging flocculation of chitosan to form dense particle-based networks at the oil–water interface (Figures 5 and 9). The zeta potentials were 64.0 ± 1.6 and 62.4 ± 2.4 for ZCP and ZCPEs, respectively (Tables 1 and 2). The cations' screening effect also contributed to depressed oxidative degradation of emulsified lipid in the Pickering emulsions. This kind of interface framework endowed the emulsions with predominant oxidative stability.

DOI: 10.1021/jf505227a
J. Agric. Food Chem. 2015, 63, 2514–2524

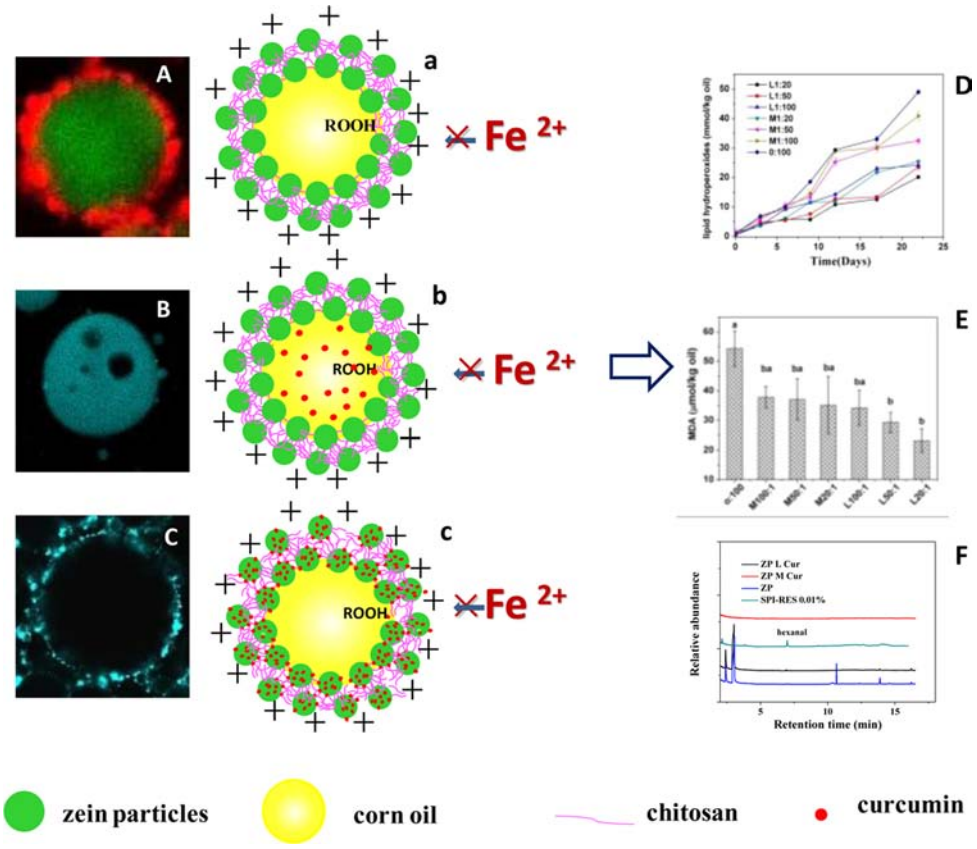

Figure 8. Schematic diagram for the formation pathway of ZCP-stabilized antioxidant Pickering emulsions proposed to relate oxidative stability and physical performance of the emulsions with their interface frameworks. Fe^{2+} was utilized as a representative pro-oxidant.

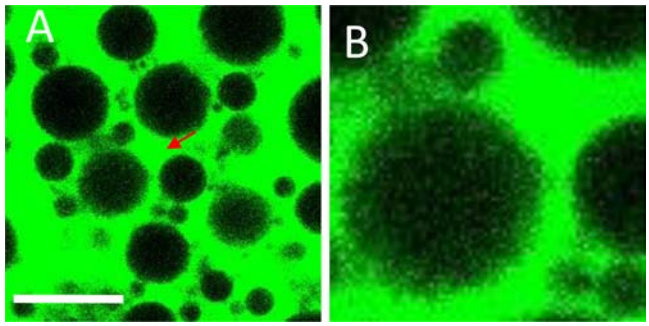

Figure 9. CLSM images of Pickering emulsions stabilized by zein/FITC-labeled chitosan particles. FITC fluorescence was visualized using an argon laser at 488 nm (green) to explore the distribution of chitosan within the emulsions. Panel B is an amplified image of panel A at the arrow.

To further enhance the oxidative stability of the emulsions, curcumin was introduced into the emulsions via shell antioxidant and core antioxidant approaches (Figures 7 and 8B,C). In the case of the shell antioxidant approach, curcumin-loaded ZCPs (ZCP-cur) were used to form antioxidant shells around the dispersed droplets. In addition to static hindrance and electrostatic effect of interfacial shells formed by the ZCPs, the targeted accumulation of curcumin, a natural antioxidant within the interface layer, may give them antioxidant capacity via chelating metallic ion (e.g., Fe^{2+}) activity and scavenging free highly reactive radicals such as alkoxyl and peroxyl radicals. Therefore, the oxidative stability of Pickering emulsion was further improved in a dose-dependent manner (Figure 7). In the case of core antioxidant, curcumin was added to the oil phase prior to the emulsification. Curcumin was distributed uniformly with the interior of dispersed oil droplets (Figure 6C). Both LP and MDA concentrations decreased slightly when compared with those of the ZCPE (Figure 7A,B). The incorporation of curcumin in the dispersed oil phase retards the lipid peroxidation via mainly chain-breaking mechanism of curcumin targeting radicals formed inside the oil core during the course of lipid autoxidization. As expected, the formation of the antioxidant interface appears to be a promising strategy to protect emulsified oil against oxidation rather than admixing antioxidants into the oil core.

Conclusion. Novel edible Pickering emulsions stabilized by zein/chitosan complex particles were fabricated to enhance oxidative stability of the emulsions. ZCPs were more effective in inhibiting lipid oxidation of the emulsions than the biopolymers, and the MDA values of ZCPE were lower than that of the biopolymer-stabilized emulsions by 2−3 orders of magnitude. The introduction of curcumin in Pickering emulsions further improved the oxidative stability of the emulsions in a curcumin location-dependent manner. Especially, the formation of antioxidant interface via interfacial cargo of curcumin markedly enhanced the oxidative stability of the emulsions. Interestingly, no detectable hexanal peak appeared in the headspace gas chromatography of the Pickering emulsions. The CLSM photograph confirmed the formation of dense ZCP-based networks at the oil−water interface, a typical Pickering-type steric barrier. The novel interfacial architecture of Pickering emulsions stabilized by dual-function ZCP-cur gave them excellent physical performance and

DOI: 10.1021/jf505227a
J. Agric. Food Chem. 2015, 63, 2514−2524

oxidative stability. Some other factors (e.g., bulk viscosity, free ZCCP) are also important to the physical and oxidative stability of Pickering emulsions; their roles are worth addressing in future works. A schematic illustration of the formation pathway of ZCP-stabilized antioxidant emulsions was proposed to correlate the oxidative stability of the Pickering emulsions with their interfacial architectures. This study opens a promising pathway for producing antioxidant emulsions via the combination of Pickering stabilization mechanism and interfacial cargo of antioxidant.

AUTHOR INFORMATION

Corresponding Authors

*(S.-W.Y.) Phone: +86-2087114262. Fax: (+86)-20-87114263. E-mail: feysw@scut.edu.cn.

*(X.-Q.Y.) Phone: +86-2087114262. Fax: (+86)-20-87114263. E-mail: fexqyang@scut.edu.cn.

Funding

This work was partially supported by the project supported by the National Natural Science Foundation of China (21406077, 31471628), the Research Fund for Excellent Doctoral Dissertations of Guangdong Province (sybzzxm201219), and the Research Funds for Zhu-Jiang Science and Technology Nova Program, Guangzhou. We appreciate financial support by the Fundamental Research Funds for the Central Universities (SCUT 2014ZG0021, 2013ZM0065).

Notes

The authors declare no competing financial interest.

REFERENCES

(1) Lomova, M. V.; Sukhorukov, G. B.; Antipina, M. N. Antioxidant coating of micronsize droplets for prevention of lipid peroxidation in oil-in-water emulsion. *ACS Appl. Mater. Interfaces* **2010**, *2*, 3669−3676.

(2) Leuratti, C.; Singh, R.; Lagneau, C.; Farmer, P. B.; Plastars, J. P.; Marnett, L. J.; Shuker, D. E. G. Determination of malondialdehyde-induced DNA damage in human tissues using an immunoslot blot assay. *Carcinogenesis* **1998**, *19*, 1919−1924.

(3) McClements, D. J.; Decker, E. A. Lipid oxidation in oil-in-water emulsions: impact of molecular environment on chemical reactions in heterogeneous food systems. *J. Food Sci.* **2000**, *65*, 1270−1282.

(4) Chaiyasit, W.; Elias, R. J.; McClements, D. J.; Decker, E. A. Role of physical structures in bulk oils on lipid oxidation. *Crit. Rev. Food Sci. Nutr.* **2007**, *47*, 299−317.

(5) Horn, A. F.; Wulff, T.; Nielsen, N. S.; Jacobsen, C. Effect of α-lactalbumin and β-lactoglobulin on the oxidative stability of 10% fish oil-in-water emulsions depends on pH. *Food Chem.* **2013**, *141*, 574−581.

(6) Guzey, D.; McClements, D. J. Formation, stability and properties of multilayer emulsions for application in the food industry. *Adv. Colloid Interface Sci.* **2006**, *128−130*, 227−248.

(7) Huang, P. H.; Lu, H. T.; Wang, Y. T.; Wu, M. C. Antioxidant activity and emulsion-stabilizing effect of pectic enzyme treated pectin in soy protein isolate-stabilized oil/water emulsion. *J. Agric. Food Chem.* **2011**, *59*, 9623−9628.

(8) Silvestre, M. P. C.; Chaiyasit, W.; Brannan, R. G.; McClements, D. J.; Decker, E. A. Ability of surfactant headgroup size to alter lipid and antioxidant oxidation in oil-in-water emulsions. *J. Agric. Food Chem.* **2000**, *48*, 2057−2061.

(9) Chaiyasit, W.; Silvestre, M. P. C.; McClements, D. J.; Decker, E. A. Ability of surfactant hydrophobic tail group size to alter lipid oxidation in oil-in-water emulsions. *J. Agric. Food Chem.* **2000**, *48*, 3077−3080.

(10) Binks, B. P., Horozov, T. S,Eds. *Colloidal Particles at Liquid Interfaces*; Cambridge University Press: Cambridge, UK, 2006.

(11) Dickinson, E. Food emulsions and foams: stabilization by particles. *Curr. Opin. Colloid Interface Sci.* **2010**, *15*, 40−49.

(12) Rousseau, D. Trends in structuring edible emulsions with Pickering fat crystals. *Curr. Opin. Colloid Interface Sci.* **2013**, *18*, 283−291.

(13) Lam, S.; Velikov, K. P.; Velev, O. D. Pickering stabilization of foams and emulsions with particles of biological origin. *Curr. Opin. Colloid Interface Sci.* **2014**, *19*, 490−500.

(14) Dickinson, E. Use of nanoparticles and microparticles in the formation and stabilization of food emulsions. *Trends Food Sci. Technol.* **2012**, *24*, 4−12.

(15) Dickinson, E. Stabilising emulsion-based colloidal structures with mixed food ingredients. *J. Sci. Food Agric.* **2013**, *93*, 710−721.

(16) Gao, Z. M.; Yang, X. Q.; Wu, N. N.; Wang, L. J.; Wang, J. M.; Guo, J.; Yin, S. W. Protein based Pickering emulsion and oil gel prepared by complexes of zein colloidal particles and stearate. *J. Agric. Food Chem.* **2014**, *62*, 2672−2678.

(17) Kalashnikova, I.; Bizot, H.; Cathala, B.; Capron, I. New Pickering emulsions stabilized by bacterial cellulose nanocrystals. *Langmuir* **2011**, *27*, 7471−7479.

(18) Tzoumaki, V. M.; Moschakis, T.; Kiosseoglou, V.; Biliaderis, G. C. Oil-in-water emulsions stabilized by chitin nanocrystal particles. *Food Hydrocolloids* **2011**, *25*, 1521−1529.

(19) Liu, F.; Tang, C. H. Phytosterol colloidal particles as Pickering stabilizers for emulsions. *J. Agric. Food Chem.* **2014**, *62*, 5133−5141.

(20) Yusoff, A.; Murray, B. S. Modified starch granules as particle-stabilizers of oil-in-water emulsions. *Food Hydrocolloids* **2011**, *25*, 42−55.

(21) de Folter, J. W. J.; van Ruijvena, M. W. M.; Velikov, K. P. Oil-in-water Pickering emulsions stabilized by colloidal particles from the water-insoluble protein zein. *Soft Matter* **2012**, *8*, 6807−6815.

(22) Wang, Y.; Padua, G. W. Nanoscale characterization of zein self-assembly. *Langmuir* **2012**, *28*, 2429−2435.

(23) Patel, A.; Hu, Y.; Tiwari, J. K.; Velikov, K. P. Synthesis and characterisation of zein−curcumin colloidal particles. *Soft Matter* **2010**, *6*, 6192−6199.

(24) Anand, P.; Sundaram, C.; Jhurani, S.; Kunnumakkara, A. B.; Aggarwal, B. B. Curcumin and cancer: an "old-age" disease with an "age-old" solution. *Cancer Lett.* **2008**, *267*, 133−164.

(25) Tuba, A. K.; İlhami, G. Antioxidant and radical scavenging properties of curcumin. *Chem.−Biol. Interact.* **2008**, *174*, 27−37.

(26) O'Toole, M. G.; Henderson, R. M.; Soucy, P. A.; Fasciotto, B. H.; Hoblitzell, P. J.; Keynton, R. S.; Ehringer, W. D.; Gobin, A. S. Curcumin encapsulation in submicrometer spray-dried chitosan/Tween 20 particles. *Biomacromolecules* **2012**, *13*, 2309−2314.

(27) Tikekar, R. V.; Pan, Y. J.; Nitin, N. Fate of curcumin encapsulated in silica nanoparticle stabilized Pickering emulsion during storage and simulated digestion. *Food Res. Int.* **2013**, *51*, 370−377.

(28) Keowmaneechai, E.; McClements, D. J. Influence of EDTA and citrate on physicochemical properties of whey protein-stabilized oil-in-water emulsions containing $CaCl_2$. *J. Agric. Food Chem.* **2002**, *50*, 7145−7153.

(29) Ma, W.; Tang, C. H.; Yin, S. W.; Yang, X. Q. Fabrication and characterization of kidney bean (*Phaseolus vulgaris* L.) protein isolate chitosan composite films at acidic pH. *Food Hydrocolloids* **2013**, *31*, 237−247.

(30) Tong, L. M.; Sasaki, S.; McClements, D. J.; Decker, A. Antioxidant activity of whey in a salmon oil emulsion. *J. Food Sci.* **2000**, *65*, 1325−1329.

(31) Panya, A.; Laguerre, M.; Lecomte, J.; Villeneuve, P.; Weiss, J.; McClements, D. J.; Decker, E. A. Effects of chitosan and rosmarinate esters on the physical and oxidative stability of liposomes. *J. Agric. Food Chem.* **2010**, *58*, 5679−5684.

(32) Wan, Z. L.; Wang, J. M.; Wang, L. Y.; Yang, X. Q.; Yuan, Y. Enhanced physical and oxidative stabilities of soy protein-based emulsions by incorporation of a water-soluble stevioside−resveratrol complex. *J. Agric. Food Chem.* **2013**, *61*, 4433−4440.

(33) Binks, B. P. Particles as surfactants − similarities and differences. *Curr. Opin. Colloid Interface Sci.* **2002**, *7*, 21−41.

DOI: 10.1021/jf505227a
J. Agric. Food Chem. 2015, 63, 2514−2524

(34) Binks, B. P.; Rodrigues, J. A. Enhanced stabilization of emulsions due to surfactant-induced nanoparticle flocculation. *Langmuir* **2007**, *23*, 7436−7439.
(35) Salari, J. W. O.; Leermakers, F. A. M.; Klumperman, B. Pickering emulsions: wetting and colloidal stability of hairy particles − a self-consistent field theory. *Langmuir* **2011**, *27*, 6574−6583.
(36) McClements, D. J. *Food Emulsions: Principles, Practices, and Techniques*, 2nd ed.; CRC Press: Boca Raton, FL, USA, 2005.
(37) Vignati, E.; Piazza, R.; Lockhart, T. P. Pickering emulsions: interfacial tension, colloidal layer morphology, and trapped-particle motion. *Langmuir* **2003**, *19*, 6650−6656.
(38) Binks, B. P.; Clint, J. H.; Mackenzie, G.; Simcock, C.; Whitby, C. P. Naturally occuring spore particles at planar fluid interfaces and in emulsions. *Langmuir* **2005**, *21*, 8161−8167.
(39) Baur, F. J.; Brown, J. B. The fatty acids of corn oil. *J. Am. Chem. Soc.* **1945**, *67*, 1899−1890.
(40) Hu, M.; Mcclements, D. J.; Decker, E. A. Lipid oxidation in corn oil-in-water emulsions stabilized by casein, whey protein isolate, and soy protein isolate. *J. Agric. Food Chem.* **2003**, *51*, 1696−1700.
(41) Kargar, M.; Fayazmanesh, K.; Alavi, M.; Spyropoulos, F.; Norton, I. T. Investigation into the potential ability of Pickering emulsions (food-grade particles) to enhance the oxidative stability of oil-in-water emulsions. *J. Colloid Interface Sci.* **2012**, *366*, 209−215.
(42) Kargar, M.; Spyropoulos, F.; Norton, I. T. The effect of interfacial microstructure on the lipid oxidation stability of oil-in-water emulsions. *J. Colloid Interface Sci.* **2011**, *357*, 527−533.
(43) Gidez, L. I.; Miller, G. J.; Burstein, M.; Slagle, S.; Eder, H. A. Separation and quantitation of subclasses of human plasma high density lipoproteins by a simple precipitation procedure. *J. Lipid Res.* **1982**, *2*, 1206−1223.
(44) Liu, H.; Wang, C. Y.; Zou, S. W.; Wei, Z. J.; Tong, Z. Simple, reversible emulsion system switched by pH on the basis of chitosan without any hydrophobic modification. *Langmuir* **2012**, *28*, 11017−11024.
(45) Wongkongkatep, P.; Manopwisedjaroen, K.; Tiposoth, P.; Archakunakorn, S.; Pongtharangkul, T.; Suphantharika, M.; Honda, K.; Hamachi, I.; Wongkongkatep, J. Bacteria interface pickering emulsions stabilized by self-assembled bacteria−chitosan network. *Langmuir* **2012**, *28*, 5729−5736.

DOI: 10.1021/jf505227a
J. Agric. Food Chem. 2015, 63, 2514−2524

Ethanol, Glycerol, Acetic Acid, and Lactic Acid. These compounds were quantified by using a HPLC-RI (PerkinElmer, Flexar) system equipped with Aminex column (HPX-87H, 300 mm × 7.8 mm; Bio-Rad) under isocratic conditions (40 °C) at a flow of 0.5 mL min^{-1} of 2.5 mM H_2SO_4.

Fermentable Sugars. Fermentable sugars were analyzed by high-performance anion exchange chromatography (HPAEC) (Dionex ICS-3000) with pulse amperometric detection (PAD) using a CarboPac PA-1 (4 mm × 250 mm) analytical column and a CarboPac PA-1 (4 mm × 50 mm) guard column at 30 °C (Dionex Corp, Sunnyvale, CA, USA). The system was equilibrated with 100 mM NaOH. After injection of a 100 μL filtered (0.45 μm), diluted sample, 100 mM NaOH was run through the column (5 min). Separation was achieved with a gradient (1 mL min^{-1}) of 100−300 mM NaOH in 3 min and then 300−250 mM NaOH + 75 mM sodium acetate in 15 min, and a final washing step with 100 mM NaOH + 300 mM sodium acetate and 300 mM NaOH. The flow rate was 1 mL min^{-1}. The results were confirmed by MSQ detection (HPAEC-MS) using a CarboPac PA200 (3 mm × 250 mm) with a CarboPac PA200 guard (3 mm × 50 mm) column (Dionex) with a configuration as described by Bruggink et al.[4] and a gradient as described by Mikkelson et al.[5]

Hop-Derived Bitter Compounds. For quantitation of 96 hop-derived bitter compounds, beer samples were degassed by ultrasonification and filtered (0.45 μm), and an aliquot (5 μL) was analyzed by HPLC-MS/MS_{MRM} as reported recently.[6,7]

Yeast-Derived Flavor Compounds. These compounds in bottle A56 and reference beers were determined by GC analysis as described[8] and those in bottle C49 by headspace-GC-MS. 1-Butanol was used as internal standard. Samples (4 mL) of C49 were filtered (0.45 μm) and incubated at 60 °C for 30 min, and then 1 mL was injected (splitless; 260 °C; flow = 14.9 mL min^{-1}) into a gas chromatograph (Agilent 6890 series; Palo Alto, CA, USA) combined with an MS detector (Agilent 5973 Network MSD, USA) and an SPME autosampler (Combipal, Varian Inc., USA). Analytes were separated on a BPX5 capillary column (60 m × 0.25 mm with phase thickness = 1.0 μm; SGE Analytical Science Pty Ltd., Australia). The carrier gas was helium (1.7 mL min^{-1}). The temperature program was 50 °C for 3 min, 10 °C min^{-1} to 100 °C, 5 °C min^{-1} to 140 °C, 15 °C min^{-1} to 260 °C, and then isothermal elution for 1 min. MSD was operated in electron impact mode at 70 eV, in the full scan mode (m/z 40−550). The ion source temperature was 230 °C, and the interface was 280 °C. Compounds were identified by comparison with authentic standards and the mass spectra in Palisade Complete 600 K Mass Spectral Library (Palisade Mass Spectrometry, USA) and were quantified using standard curves.

Total Vicinal Diketones (VDKs). VDKs were measured according to Analytica-EBC method 9.10.[3]

Carbonyl Compounds. Carbonyl compounds were analyzed as oximes by using GC-ECD as described by Ojala et al.[9] To 5 mL beer samples were added 500 μL of 0.4% (w/v) PFBOA (*O*-(2,3,4,5,6-pentafluorobenzyl)hydroxylamine hydrochloride) solution and 100 μL of internal standard (benzaldehyde; 0.1% v/v). Samples were then incubated at room temperature for 2 h. Reaction was stopped by adding 100 μL of 9 M H_2SO_4, and oximes were extracted into 2 mL of hexane. Samples (2 μL, split injection 12.5:1) were analyzed using GC-ECD (Agilent 6890 Series). Analytes were separated in constant flow mode with helium as carrier gas (1.2 mL min^{-1}) on a DP-5 capillary column (30 m × 0.32 mm) with a phase thickness of 0.50 μm (Agilent). The injector was kept at 260 °C, and the ECD was kept at 300 °C. The temperature program was 100 °C for 2 min, 8 °C min^{-1} to 250 °C, and a 5 min hold. Compounds were identified with authentic standards and quantified with standard calibration curves.

Short-Chain Fatty Acids. Short-chain fatty acids were extracted with diethyl ether from 4 mL of acidified beer samples as described by Schooley et al.[10] Internal standard was heptanoic acid (C7). Diethyl ether extracts (2 μL, splitless injection) were analyzed by GC-FID (Agilent 6890 series). Analytes were separated on a DP-FFAP capillary column (30 m × 0.32 mm; phase thickness = 0.25 μm; Agilent). The carrier gas was helium (2.7 mL min^{-1}). The injector and FID were at 250 °C. The temperature program was 50 °C for 3 min, 25 °C min^{-1} to 100 °C, 10 °C min^{-1} to 240 °C, and a 10 min hold. Compounds were quantified using authentic standards.

Bound and Free Phenolic Acids (PAs). Beer samples (250 μL) were mixed with 2 M NaOH (1.1 mL, for hydrolysis of bound PAs) or water (1.1 mL, for free PAs). After 16 h in the dark, samples were acidified with 5 M HCl and extracted with ethyl acetate (3 × 2 mL). The extracts were dried under nitrogen and residues dissolved in 0.5 mL of methanol, filtered, and used to quantify free and total PAs by ultraperformance liquid chromatography (UPLC). Portions (200 μL) of the methanol samples were dried and dissolved in 30 μL of dichloromethane (DCM) and derivatized with MSTFA (*N*-methyl-*N*-trimethylsilyltrifluoroacetamide, Pierce, Rockford, IL, USA; 25 μL, 80 °C for 20 min) for GC-MS analysis of minor PAs.

Volatile Phenols. Beer samples (0.5 mL) were vortexed, spiked with heptadecanoic acid (10 μg), and extracted with DCM (2 × 4 mL). The separated DCM extracts were dried under nitrogen and redissolved in 100 μL of DCM. Half (50 μL) of each extract was trimethylsilylated with MSTFA (25 μL, 80 °C for 20 min). Underivatized and derivatized samples were both analyzed by GC-MS.

Phenolic compounds were analyzed using UPLC and GC-MS. A Waters Acquity UPLC was equipped with a Waters Acquity BEH C18 column (1.7 μm, 2.1 × 100 mm) combined with a VanGuard pre-column (2.1 × 5 mm 1.7 μm). The solvent was 5% formic acid and acetonitrile. Flow was 0.43 mL min^{-1}. The proportion of acetonitrile was increased linearly from 5 to 90% in 9 min and returned to 5% in 2 min. The diode array detector was used at 190−600 nm. Ferulic, sinapic, and *p*-coumaric acids were quantified at 320 nm by using standard curves of authentic compounds (0.1−100 μg mL^{-1}). For GC-MS analyses, an Agilent 7890A GC was equipped with a 5975C mass selective detector and Rtx-5MS silica capillary column (15 m, 0.25 mm i.d., phase thickness of 0.25 μm (Restek, Bellefonte, PA, USA)). The oven temperature was increased from 70 °C (1 min) at 10 °C min^{-1} to 270 °C (4 min). The split ratio was 25:1, and the samples were injected by a Gerstel Maestro MPS 2 sampling system (Gerstel GmbH & Co.KG, Mühlheim an der Ruhr, Germany). Data were collected in the full scan mode (m/z 40−600). Compounds were identified by retention times and library comparison (NIST '08, Scientific Instrument Services, Inc., Ringoes, NJ, USA).

Protein Content. Proteins were precipitated from beers (400−500 μL) with acetone (1600 μL) at −20 °C. Precipitates from centrifugation (720*g*, 5 min) were dissolved in 25 μL of rehydration buffer (2 M thiourea, 7 M urea, 0.5% Triton-X-100, 0.5% Pharmalyte 3−10) and assayed by 2-D Quant Kit (GE Healthcare UK Limited, Buckinghamshire, UK) with bovine serum albumin as standard.

Amino Acids. Total and free amino acids were analyzed with Mass TRAK Amino Acid Analysis Application Solution (Waters, Milford, MA, USA). Samples for total amino acids were hydrolyzed in 6 N HCl at 110 °C for 20 h and then dried under nitrogen, dissolved in 200 μL of water, redried, and dissolved in 200 μL of 0.1 N HCl. Hydrolyzed and untreated samples (10 μL) were mixed with internal standard (10 μL of 250 μM norvaline) and derivatized (AccQ·Fluor reagent kit; Waters). AccQ·Fluor reagent (20 μL) and boric acid buffer (70 μL) were added, and the mixture was vortexed for 60 s. UPLC-MS analysis involved an Acquity UPLC system (Waters) with a diode array detector. Chromatography involved an Acquity Mass TRAK (2.1 × 150 mm, 1.7 μm) column (Waters) at 43 °C. The injection volume was 2.0 μL. Separation was achieved by gradient elution with 10% (v/v) Amino Acid Analysis Concentrate A in water and Amino Acid Analysis Eluent B at 0.4 mL min^{-1}, monitoring the effluent at 260 nm.

RESULTS

Bottles. Bottles A56 (Figure 1) and C49 were similar brown glass bottles, 245 mm high including the 80 mm neck. The diameters increased from 85 mm at the base to 90 mm at the shoulder. The necks were about 37 mm in diameter. The bases had conical depressions about 40 mm deep (as in traditional wine bottles). Bottle A56 showed no signs of sand abrasion or glass corrosion (Risto Aalto, Riikka Alvik, Markku Annila, Ulla Klemelä, and Kaisa Koivisto, personal communication). It

DOI: 10.1021/jf5052943
J. Agric. Food Chem. 2015, 63, 2525−2536

Figure 1. Bottle A56.

appeared to have been mouth blown while revolving in a cylindrical mold, which shaped the wall (marks from the mold were visible on the wall). The bottle's mouth was apparently formed by wrapping strips of hot glass round the cut neck. No labels remained on either bottle. Both bottles were closed with rather coarse-grained corks that protruded several millimeters out of the necks.

Bubbles of gas, presumably CO_2, formed during sampling, producing a light foam. Both beers were bright golden yellow, with little haze. Both beers smelt of autolyzed yeast, dimethyl sulfide, Bakelite, burnt rubber, over-ripe cheese, and goat, with phenolic and sulfury notes. As the samples warmed to room temperature, the smell of hydrogen sulfide disappeared and that of butyric acid (particularly strong in C49) strengthened.

Physicochemical Analyses. Compared to modern beers, the shipwreck beers contained similar levels of potassium but 15−60-fold more sodium (Table 1), presumably derived from seawater. This may have diluted the beers up to 30%. Ethanol contents were low (2.8−3.2% ABV) compared to typical modern lagers and ales. The mass ratios of glycerol/ethanol were 4.5% for both shipwreck beers, which is typical for a yeast fermentation product. Both beers were acidic, with pH about 1 unit below modern values. The color strengths were in the range of modern ales and lagers (and much lower than those of porters or stouts). Bitterness was lower in A56 (9.9 IBU, corresponding to a modern light lager) and higher in C49 (16 IBU). Sulfur dioxide was not detected in A56 (not tested in C49): original sulfur dioxide would probably be oxidized over the 170 years under water. FAN was low (61 mg L^{-1}) for A56 but normal (114 mg L^{-1}) for C49. Protein levels (5−7 mg L^{-1}) were very low in both beers.

Table 1. Physicochemical Properties of Shipwreck Beers

property	unit	beer A56	beer C49	modern beers[a]
ethanol	ABV[b] (% v/v)	2.8	3.2	3−6
glycerol	g L^{-1}	1.0	1.1	1−2
pH		3.18	3.39	3.9−4.5
color	EBC[c] units	8.9	10.5	2−27
bitterness	IBU[d]	9.9	16	6−30
apparent extract	°Plato	1.32	3.10	1−5
real extract	°Plato	2.24	3.98	3−6
SO_2 (sulfite)	mg L^{-1}	<0.4	NA[f]	0−10
FAN[e]	mg L^{-1}	61	114	40−250
protein	mg L^{-1}	5−7	5−7	200−500
glucose	g L^{-1}	1.35	9.8	0
fructose	g L^{-1}	<0.04	<0.04	0
sucrose	g L^{-1}	<0.04	<0.04	0
maltose	g L^{-1}	0.14	1.2	0.0−2.5
maltotriose	g L^{-1}	0.073	0.11	0.0−3.0
Na^+ (sodium)	mg L^{-1}	1200	890	20−60
K^+ (potassium)	mg L^{-1}	440	510	500

[a]Results for shipwreck beers A56 and C49 are compared with typical values for modern ales and lagers. Concentrations are for the beer "as is", i.e., values have not been normalized to a standard ethanol concentration. [b]ABV, alcohol by volume. [c]EBC, European Brewing Convention. [d]IBU, International Bitterness Unit. [e]FAN, free amino nitrogen. [f]NA, not analyzed.

Fermentable Sugars. A small amount of maltose was present in A56 and much more in C49, which contained more maltose than is typical in modern beers (Table 1). Both shipwreck beers contained less maltrotriose than maltose, whereas modern beers contain more maltotriose than maltose.[11] Both beers, especially C49, contained unexpectedly large amounts of glucose (glucose is usually consumed completely early in fermentation). Fructose and sucrose were not detected in either shipwreck beer. Like glucose, these sugars are consumed in early fermentation (their presence would suggest deliberate sweetening).

Apparent extracts (1.32 °Plato for A56 and 3.10 °Plato for C49) were at the low end of the range for modern ales and lagers (Table 1). Real extracts, calculated from the apparent extracts and ethanol concentrations, were 2.24 °Plato (A56) and 3.98 °Plato (C49). Total carbohydrate levels were not measured, but the difference between real extracts and residual sugars and salts suggests that starch was still present at about 17 g L^{-1} (A56) and 25 (C49) g L^{-1}.

Hop Components. The shipwreck beers contained small amounts of some iso-α-acids, which are considered the key bitter compounds in beer (Table 2). Among these iso-α-acids, *cis*-isohumulone and *cis*-isocohumulone were found in both beers, whereas additional isomers were detectable in C49 only. Besides the iso-α-acids, some of their degradation products such as tri- and tetracyclic degradation products, allo-iso-α-acids, scorpiohumols, and the tricyclohumolactols were detected (Table 2). These compounds are formed upon beer aging by an acid-catalyzed degradation of iso-α-acids.[12−14] In addition, hulupone and hulupinic acid were found as degradation products of hop β-acids. Only small amounts of xanthohumol, isoxanthohumol, and 6- and 8-prenylnaringenin were detected, although their presence was unequivocally confirmed. Hydroperoxides of allo-iso-α-acids, tricyclic degradation products of β-acids, and hydroperoxides and hydroxides of tricyclolupones are known hop derivatives,[12−14] but were not detected in either shipwreck beer. Their absence is, however, not unexpected as they are susceptible to chemical degradation from autoxidation and acid-catalyzed reactions. A series of oxidation products of α-, iso-α-, and β-acids such as humulinons, allohumulonhydroxides, and humulinic acids was detected in C49 but not in A56. Most other hop-derived compounds present in A56 were detected in C49 at higher concentrations. The higher concentration of most hop components in C49 than in A56 agrees with the more pronounced bitterness of C49 (Table 1).

Yeast-Derived Flavor Compounds. Yeasts produce compounds that contribute to the flavor of fermented beverages. Some of these compounds were analyzed in the

DOI: 10.1021/jf5052943
J. Agric. Food Chem. 2015, 63, 2525−2536

Table 2. Hop-Derived Bitter Taste Compounds

compound	A56 (μmol L^{-1})	C49 (μmol L^{-1})	substance group
phloroisobutyrophenone	0.03	0.01	precursors of desoxyhumulones
phloroisovalerophenone	nd[a]	nd	
o-prenylphloroisobutyrophenone	nd	nd	
o-prenylphloroisovalerophenone	nd	nd	
desoxycohumulone	0.12	nd	precursors of α- and β-acids
desoxyhumulone	0.03	nd	
desoxyadhumulone	nd	nd	
humulone	nd	0.05	α-acids
adhumulone	nd	nd	
cohumulone	nd	nd	
prähumulone	nd	nd	
adprähumulone	nd	nd	
posthumulone	nd	nd	
humulinone	nd	0.65	oxidation products of α-acids
adhumulinone	nd	0.20	
cohumulinone	nd	0.52	
cis-isohumulone	0.29	0.72	iso-α-acids
cis-isoadhumulone	nd	0.44	
cis-isocohumulone	0.27	0.69	
cis-isoprähumulone	nd	nd	
cis-isoposthumulone	nd	0.29	
trans-isohumulone	nd	1.02	
trans-isoadhumulone	nd	0.39	
trans-isocohumulone	nd	nd	
trans-isoprähumulone	nd	nd	
trans-isoposthumulone	nd	nd	
cis-alloisohumulone	0.24	0.57	allo-iso-α-acids
cis-alloisoadhumulone	nd	nd	
cis-alloisocohumulone	0.20	0.51	
trans-alloisohumulone	nd	nd	
trans-alloisoadhumulone	nd	nd	
trans-alloisocohumulone	nd	nd	
cis-alloisohumulonhydroperoxide	nd	nd	hydroperoxides of allo-iso-α-acids
cis-alloisoadhumulonhydroperoxide	nd	nd	
cis-alloisocohumulonhydroperoxide	nd	nd	
trans-alloisohumulonhydroperoxide	nd	nd	
trans-alloisoadhumulonhydroperoxide	nd	nd	
trans-alloisocohumulonhydroperoxide	nd	nd	
cis-alloisohumulonhydroxide	nd	8.37	hydroxides of allo-iso-α-acids
cis-alloisoadhumulonhydroxide	nd	21.29	
cis-alloisocohumulonhydroxide	nd	10.27	
trans-alloisohumulonhydroxide	nd	6.89	
trans-alloisoadhumulonhydroxide	nd	8.20	
trans-alloisocohumulonhydroxide	nd	2.56	
tricyclocohumol	2.31	7.76	tricyclic degradation products of iso-α-acids
tricyclohumol	2.59	8.65	
tricycloadhumol	0.82	2.88	
tricyclocohumene	nd	0.36	
tricyclohumene	nd	0.46	
tricycloadhumene	nd	nd	
isotricyclocohumene	nd	4.91	
isotricyclohumene	nd	4.56	
isotricycloadhumene	nd	1.48	

DOI: 10.1021/jf5052943
J. Agric. Food Chem. 2015, 63, 2525−2536

Table 2. continued

compound	A56 (μmol L^{-1})	C49 (μmol L^{-1})	substance group
tetracyclocohumol	1.60	4.24	tetracyclic degradation products of iso-α-acids
tetracyclohumol	1.98	1.24	
tetracycloadhumol	0.59	4.86	
tricyclocohumolactol	0.35	0.90	tricyclic degradation products of iso-α-acids
tricyclohumolactol	0.33	1.25	
tricycloadhumolactol	0.40	0.60	
scorpiohumol	0.17	nd	tricyclical degradation products of iso-α-acids
sorpioadhumol	nd	nd	
sorpiocohumol	0.26	0.23	
cis-cohumulinic acid	nd	0.12	oxidation products of iso-α-acids
cis-humulinic acid	nd	0.24	
cis-adhumulinic acid	nd	0.11	
trans-cohumulinic acid	nd	0.21	
trans-humulinic acid	nd	0.36	
trans-hdhumulinic acid	nd	0.19	
lupulone	nd	nd	β-acids
adlupulone	nd	nd	
colupulone	nd	nd	
postlupulone	nd	nd	
prälupulone	nd	nd	
adprälupulone	nd	nd	
cohulupone	24.26	68.43	oxidation products of β-acids
hulupone	8.07	17.84	
adhulupone	3.35	9.38	
hulupinic acid	15.55	59.01	oxidation product of hulupones
nortricyclocolupone	nd	nd	tricyclic degradation products of β-acids
nortricyclolupone	nd	nd	
dehydrotricyclocolupone	nd	nd	
dehydrotricyclolupone	nd	nd	
dehydrotricycloadlupone	nd	nd	
tricyclocolupone	nd	nd	
tricyclolupone	nd	nd	
tricycloadlupone	nd	nd	
peroxytricyclocolupone	nd	nd	hydroperoxides of tricyclolupones
peroxytricyclolupone	nd	nd	
peroxytricycloadlupone	nd	nd	
hydroxytricyclocolupone	nd	nd	hydroxides of tricyclolupones
hydroxytricyclolupone	nd	nd	
hydroxytricycloadlupone	nd	nd	
xanthohumol	0.002	0.005	chalconaringenine
isoxanthohumol	0.004	0.167	flavonoids
6-prenylnaringenin	<0.001	0.004	
8-prenylnaringenin	<0.001	0.002	

[a]nd, not detected.

shipwreck beers and six reference beers. Results were normalized to a standard ethanol concentration of 35 g L^{-1}. The (normalized) concentrations of most compounds in the shipwreck beers were within or close to the range found in the reference beers (Figure 2). However, there were exceptions. Acetaldehyde, with a Tb (taste threshold in beer) of 25 mg L^{-1} (unless stated otherwise, taste thresholds in beer and flavor descriptions are from Meilgaard[15]) and a green leaf flavor, was

DOI: 10.1021/jf5052943
J. Agric. Food Chem. 2015, 63, 2525−2536

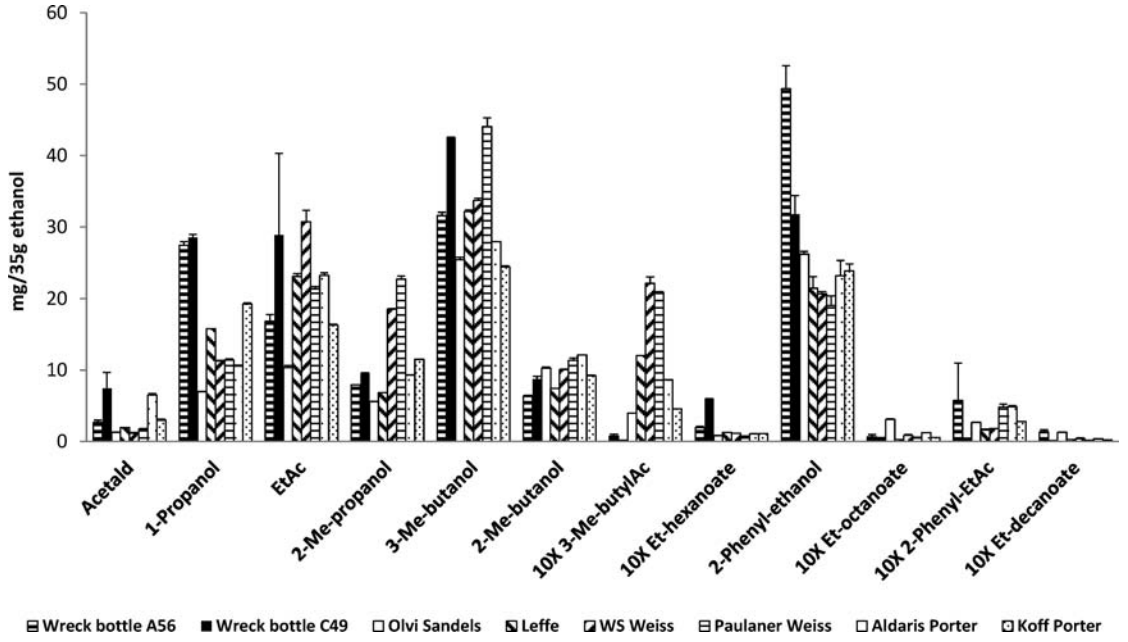

Figure 2. Yeast-derived flavor compounds in shipwreck and six modern reference beers. Concentrations are normalized to an ethanol concentration of 35 g L^{-1}. Actual ethanol concentrations (g L^{-1}) were as follows: A56, 22.2; C49, 25.6; Olvi Sandels, 37.4; Leffe Brune, 49.7; Weihenstephan Hefe Weissbier, 45.0; Paulaner Hefe Weissbier, 43.8; Aldaris Porter, 54.3; and Koff Porter, 59.2. Abbreviations are acetald, acetaldehyde; EtAc, ethyl acetate; 2-Me-propanol, 2-methylpropanol; 3-Me-butanol, 3-methylbutanol; 2-Me-butanol, 2-methylbutanol; 3-Me-butylAc, 3-methylbutyl acetate; Et-hexanoate, ethyl hexanoate; Et-octanoate, ethyl octanoate; 2-Phenyl-EtAc, 2-phenylethyl acetate; Et-decanoate, ethyl decanoate. Where indicated (10 X), the concentrations of some compounds have been multiplied by 10. Results are averages of duplicate or triplicate analyses, and error bars show the SDs.

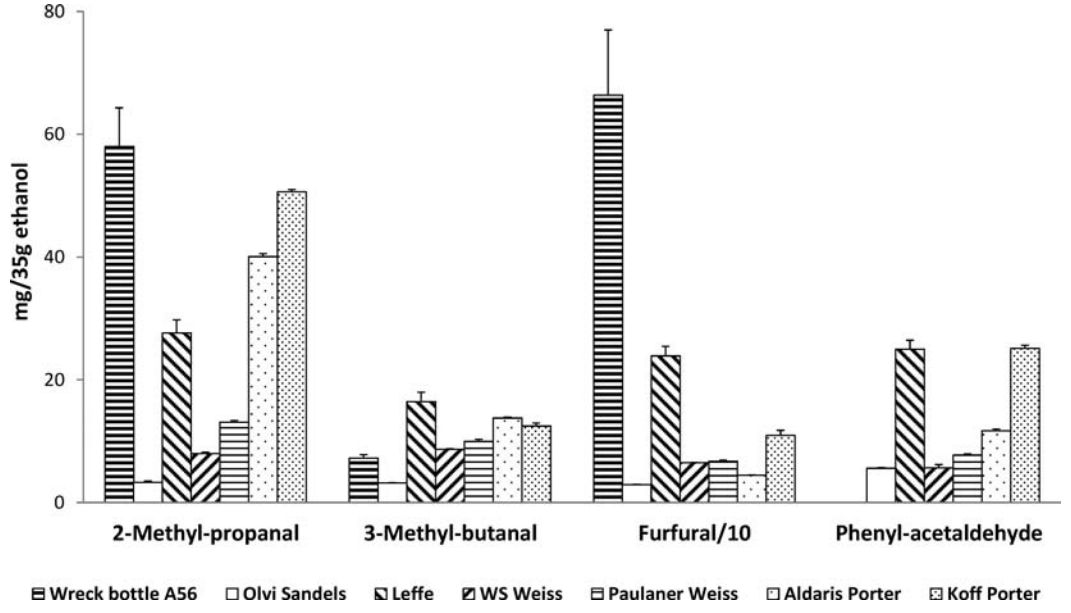

Figure 3. Carbonyl concentrations in shipwreck beer A56 and six reference beers. Concentrations are normalized to an ethanol concentration of 35 g L^{-1} (see Figure 2). Furfural/10 indicates the furfural concentration divided by 10. Results are averages of two or (wreck bottle A56) three determinations, and error bars show the SDs.

relatively high in C49 as was 1-propanol (Tb = 800 mg L^{-1}; alcohol) in both shipwreck beers. 3-Methylbutyl acetate (Tb = 1.6 mg L^{-1}; banana) was markedly low in both shipwreck beers. Ethyl hexanoate (Tb = 0.23 mg L^{-1}; apple) was high in both shipwreck beers, especially C49. Ethyl decanoate (Tb = 0.9 mg L^{-1}; sweet apple) was high in A56 (and also in the beer Olvi Sandels). 2-Phenylethanol (Tb = 125 mg L^{-1}; rose) was high in A56 and slightly high in C49. 2-Phenylethyl acetate (Tb = 3.8 mg L^{-1}; rose) was possibly high in A56, but low in C49.

Carbonyl Compounds. Two vicinal diketones, which are also yeast-derived and can cause a buttery or butterscotch-like flavor considered unacceptable in lagers but appreciated in some ales, were measured in A56 and the reference beers. Normalized concentrations of diacetyl (Tb = 150 μg L^{-1}) were 36 μg L^{-1} for A56 compared to 15 μg L^{-1} for Olvi Sandels and

DOI: 10.1021/jf5052943
J. Agric. Food Chem. 2015, 63, 2525−2536

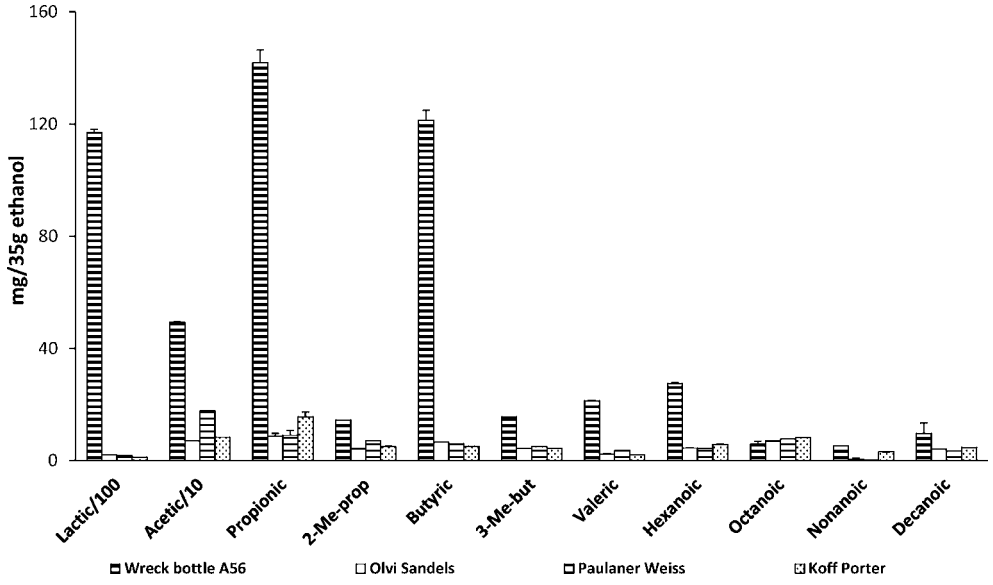

Figure 4. Organic acid concentrations in shipwreck beer A56 and three reference beers. Concentrations are normalized to an ethanol concentration of 35 g L^{-1} (see Figure 2). Abbreviations are Lactic/100, lactic acid divided by 100; Acetic/10, acetic acid divided by 10; 2-Me-prop, 2-methylpropionic acid; 3-Me-but, 3-methylbutyric acid. Results are averages of duplicate determinations. Error bars show half the range.

Table 3. Phenolic Compounds[a]

	A56	C49	Olvi Sandels	Paulaner Weiss	Koff Porter
hydroxycinnamic acids					
total ferulic acid	7.5	9.4	9.4	10.3	12.3
free ferulic acid	1.8 (24%)	1.4 (15%)	2.5 (27%)	<0.004 (0%)	0.88 (7%)
total sinapic acid	0.92	1.2	2.1	4.1	2.3
free sinapic acid	0.14 (16%)	0.11 (9%)	0.46 (22%)	0.21 (5%)	0.31 (14%)
total *p*-coumaric acid	1.3	1.5	1.5	0.44	1.5
free *p*-coumaric acid	0.87 (67%)	1.0 (67%)	1.2 (78%)	0.06 (15%)	0.93 (61%)
total caffeic acid	1.3	1.2	0.40	0.21	0.93
hydroxybenzoic acids					
total syringic acid	0.77	0.75	0.55	0.82	0.37
total vanillic acid	2.1	3.4	1.0	1.1	1.3
other aromatic					
total 4-hydroxyphenylacetic acid	2.0	2.1	0.93	0.67	0.95
ferulic acid-derived					
total 4-vinlyguaiacol	0.16	0.04	0.07	0.87	0.04
total 4-ethylguaiacol	<0.008	<0.014	<0.005	<0.004	<0.006
sinapic acid-derived					
total 4-vinylsyringol	0.08	0.014	0.03	0.17	0.05
other phenolic					
total 4-hydroxyphenyl ethanol	6.7	10.2	7.9	13.7	6.8

[a]Concentrations (mg L^{-1}) are averages of two analyses and normalized to an ethanol concentration of 35 g L^{-1}. Values in parentheses denote the percentage of free, unbound compound with respect to the total concentration for that particular compound.

34−64 μg L^{-1} for the other reference beers. Pentanedione (Tb = 900 μg L^{-1}) was low in A56 (7 μg L^{-1}) and was below the average concentration (14 μg L^{-1}) found in the reference beers. The levels of four other carbonyl compounds in shipwreck beer A56 and the reference beers are compared in Figure 3 (not measured in C49). All of the beers contained between 3.2 μg L^{-1} (Olvi Sandels) and 16.5 (Leffe Brune) μg L^{-1} 3-methylbutanal (Tb = 600 μg L^{-1}; unripe banana). There was greater variation for the other carbonyls. For 2-methylpropanal (Tb = 1000 μg L^{-1}; banana, melon) reference beers contained between 3.3 μg L^{-1} (Olvi Sandels) and 51 (Koff Porter) μg L^{-1}, whereas the shipwreck beer contained 58 μg L^{-1}. Phenylacetaldehyde (Tb = 1600 μg L^{-1}; hyacinth) could not be detected in the shipwreck beer and was between 5.7 μg L^{-1} (Weihenstephan Weissbier) and 25 (Koff Porter) μg L^{-1} in the reference beers. Furfural (Tb = 150 mg L^{-1}) ranged between 29 μg L^{-1} (Olvi Sandels) and 240 (Koff Porter) μg L^{-1} in the references and was much higher (664 μg L^{-1}), but still below threshold, in the shipwreck beer.

Organic Acids. Several fatty acids were measured in shipwreck beer A56 and three reference beers (Figure 4). The (normalized) concentration of lactic acid (Tb = 400 mg L^{-1}; acid) was extremely high (11.7 g L^{-1}) in A56 (and 10.5 g L^{-1} in C49; not shown in Figure 4) compared to the reference beers (100−200 mg L^{-1}). Acetic acid (Tb = 175 mg L^{-1}; vinegar) levels were also relatively high: 70−180 mg L^{-1} in the

DOI: 10.1021/jf5052943
J. Agric. Food Chem. 2015, 63, 2525−2536

reference beers compared with 493 mg L^{-1} in A56 and 542 mg L^{-1} in C49 (not shown in Figure 4). The other measured organic acids were present at much lower concentrations in the reference beers (0.2−16 mg L^{-1}). A56 contained higher levels of most of these acids, including about 20-fold more butyric acid (Tb = 2.2 mg L^{-1}; buttery, sweaty) and 15-fold more propionic acid (Tb = 150 mg L^{-1}; vinegar).

Phenolics. Several phenolic compounds were measured in the shipwreck beers and three reference beers (Table 3). Among these five beers, the wheat beer, Paulaner Weiss, was exceptional. It contained at least 5-fold more 4-vinylguaiacol and 2-fold more 4-vinylsyringol than any other beer and exhibited the highest concentrations of sinapic acid and 4-hydroxyphenylethanol and the lowest concentrations of *p*-coumaric, caffeic, and 4-hydroxyphenylacetic acids. The proportions of free compared to total hydroxycinnamic acids were much smaller (0% ferulic, 5% sinapic, and 15% *p*-coumaric) for Paulaner Weiss than for all other beers (7−17% ferulic, 9−22% sinapic, and 61−78% *p*-coumaric). The shipwreck beers more closely resembled the other references, Olvi Sandels (a lager) and Koff Porter. Total concentrations of phenolic acids in the shipwreck beers were within ±60% of those in the Olvi Sandels and/or Koff Porter references, except that vanillic and 4-hydroxyphenylacetic acids were 2−3-fold higher in the shipwreck beers. A56 contained more 4-vinylguaiacol than the Olvi Sandels and Koff Porter references, but much less than Paulaner Weiss. 4-Ethylguaiacol was below the limit of quantification in all beers.

Amino Acids. After acid hydrolysis, the main (total) amino acids in shipwreck beers were glutamate/glutamic acid, proline, and glycine (Table 4). The amino acid composition of the shipwreck beers was similar to that of modern commercial beers,[16] except that shipwreck beers had relatively more proline and alanine and less asparagine/aspartic acid. Proline was the main free amino acid in both shipwreck beers. The amino acid profiles of the two beers were similar, but C49 had a higher proportion of free glycine and a smaller proportion of free threonine and proline than A56. Differences of the same magnitude are found between different modern beers.[17]

Table 4. Amino Acid Profiles with (Total Amino Acids) and without (Free Amino Acids) Acid Hydrolysis

	total amino acids (%)		free amino acids (%)	
	A56	C49	A56	C49
alanine	9.6	9.6	12.2	12.9
arginine	1.9	1.8	3.2	3.0
aspartic acid + asparagine	5.1	4.9	5.8	5.0
cysteine	0.4	0.3	0.0	0.0
glutamic acid + glutamine	22.0	23.1	7.4	6.7
glycine	11.6	13.0	9.6	14.8
histidine	1.3	1.7	1.1	1.8
isoleucine	2.0	2.0	1.3	1.8
leucine	3.3	3.4	3.7	4.0
lysine	3.1	3.0	2.1	2.2
methionine	0.7	0.5	1.2	1.4
phenylalanine	2.4	2.5	3.1	3.2
proline	22.7	21.1	35.5	29.5
serine	4.6	4.8	4.0	5.5
threonine	3.4	2.2	2.5	0.0
tyrosine	1.5	1.2	1.7	2.0
valine	4.5	4.9	5.7	6.2
total	100.0	100.0	100.0	100.0

DISCUSSION

The overall shape and detailed features of bottles A56 and C49 indicate a high-quality technology that was not yet used in Finland in 1840, but had been used to manufacture beer bottles for two or three decades in central and northern Europe (personal communication; Risto Aalto, Riikka Alvik, Markku Annila, Ulla Klemelä, and Kaisa Koivisto). The presence of hop components (extensively degraded), maltose, and maltotriose identifies the bottles' contents as beers. The higher concentrations of hop components in beer C49 than in A56 cannot be explained by different degrees of chemical degradation or dilution by seawater and indicates that the bottles contained two different beers. Both shipwreck beers contained too little protein (Table 1) to permit protein identification by 2D gel electrophoresis. Most of the original protein was probably hydrolyzed (e.g., by proteolytic activity of lactic acid bacteria) and partially consumed by microorganisms during aging (both beers contained large numbers of dead bacteria and yeast). Peptides that may have been liberated by hydrolysis and still present in the beer would not have been detected in the protein assay employed as the acetone precipitation step is much less efficient for peptides than for proteins. The amino acid profiles of both beers were broadly similar to those of modern commercial beers (Table 4) and clearly different from, for example, that of apple cider.[18] Features such as the relatively high free proline content are consistent with the raw material being cereal grain but do not distinguish between barley and wheat, which have very similar amino acid profiles.[16] Furthermore, the amino acid profiles of the shipwreck beers have been disturbed by the activity of microbial contaminants.

The presence of hop-derived bitter compounds confirms the use of hops for bittering the beers. Kettle-boiling induces the transformation of α-acids to iso-α-acids and that of β-acids to hulupones.[6] The lack of α- and β-acids and the presence of iso-α-acids and hulupones therefore indicate that hops were added to the worts before kettle-boiling. The amounts of *cis*-iso-α-acids were higher than those of the corresponding *trans*-iso-α-acids, which is in line with the higher stability of *cis*-iso-α-acids and literature findings that *trans*-iso-α-acids are readily transformed into tri- and tetracyclocohumols, scorpiohumols, and tricyclolactohumols by proton catalysis during aging of beer.[7] Compared to modern beers, rather high amounts of these four compounds were detected; for example, 7.76 and 4.24 μmol L^{-1} of tri- and tetracyclocohumol were found in C49 compared to 1.00 and 0.46 μmol L^{-1} in a fresh Pilsner-type beer.[7] The high levels of these aging products can be explained by the low pH and long "reaction time" in the shipwreck. Interestingly, the unexpectedly large amounts of β-acid degradation products hulupones and hulupinic acid are consistent with old hop varieties containing higher levels of β-acids than modern varieties, which have been bred to maximize the α-acid content.

The lack of hydroxides and hydroperoxides of iso-α- and β-acids in beer A56 indicates that the degradation of the hop components was primarily driven by proton-catalyzed reactions rather than by autoxidation involving oxygen. In contrast, beer C49 contained oxidation products of α-, iso-α-, and β-acids such as hydroxides of allo-iso-α-acids, hulupones, and humulinic acids, clearly indicating autoxidation of hop

DOI: 10.1021/jf5052943
J. Agric. Food Chem. 2015, 63, 2525−2536

components during aging. These differences may be due partly to ingress of air after bottling of C49 but also suggest that the two beers originated from different batches of hops.

Both shipwreck beers contained much more sodium than is usual in beers. Presumably either Na^+ ions diffused into the beers through the cork or seawater entered the bottles. Assuming average concentrations during the last 170 years of 3000 mg Na L^{-1} and 100 mg K L^{-1} in the sea around the wreck at 50 m depth (Baltic salinity varies with time, location, and depth[19]), the beers may have been diluted with seawater by up to about 30%. Concentrations of other analytes may be too low by up to 30% from this cause alone. This may account for the low levels of ethanol in the beers. Concentrations in Figures 2−4 and Table 3 are normalized to 35 g ethanol L^{-1}, which corrects for simple dilution and provides a more meaningful comparison with the reference beers.

The predominant organoleptic properties of both shipwreck beers were unpleasant (acidic, salty, burnt, sulfury, etc.). These negative qualities masked any fruitiness, maltiness, or hopiness. The levels of several organic acids were unusually high in the shipwreck beers (Figure 4), which presumably caused their low pH (Table 1) and vinegary, goaty, and soured milk flavors. Optical and electron microscopy revealed numerous bacteria in both beers and four species of (non-spore-forming) lactic acid bacteria were recovered by cultivation (R, Juvonen, M. Raulio, A. Wilhelmson, and E. Storgårds, E; manuscript in preparation). The organic acids found in the beers can be produced by bacterial activity (e.g., lactic acid bacteria can produce several volatile fatty acids as well as larger amounts of lactic and acetic acids[20−22]). In the 1840s, "microbiological hygiene" was a matter of trial and error with empirical experience but no scientific basis. Flavors now known to be caused by bacteria may have been intended (as for Belgian Geuze beers) or production faults. In either case, the bacterial activity continued after the shipwreck and eventually produced unacceptably large amounts of organic acids. The presence of live, non-spore-forming bacteria means that vegetative cells have been metabolizing continuously, albeit slowly, for about 170 years.

Compared to modern beers,[11] beer A56 contained less maltose and both beers contained much less maltotriose and relatively high concentrations of glucose (Table 1). A plausible explanation is that after the initial (yeast-driven) fermentation, contaminating microbes excreted enzymes (e.g., amyloglucosidase) able to degrade residual carbohydrates to glucose. This glucose supply probably supported the growth and fermentative activity of lactic acid bacteria and other microbes. As conditions deteriorated (e.g., acidity increasing), the production of glucose exceeded the fermentative capacity of the remaining viable microbes, and glucose began to accumulate. This hypothesis would explain the high glucose and low maltotriose in the shipwreck beers, but does not immediately explain the relatively high maltose in beer C49.

Despite the unpleasant organoleptic features probably resulting from bacterial spoilage, chemical analyses revealed profiles of yeast-derived flavor compounds broadly similar to those of modern beers (Figure 2). There were some notable peculiarities. Both beers contained very little 3-methylbutyl acetate, but rather high levels of 2-phenylethanol and 1-propanol; A56 contained a high level of 2-phenylethyl acetate, but C49 contained very little; A56 (but not C49) contained a high level of ethyl decanoate and C49 especially contained a high level of ethyl hexanoate. A problem is to determine how much these results reflect the original character of the two beers rather than chemical changes during 170 years at about 4 °C. To our knowledge, there are no studies of the chemical stability of beer over such a long time. Vanderhaegen et al.[23] studied the stability of top-fermented beer for 6 months at 0, 20, or 40 °C. Rates of change were very temperature-sensitive. Many compounds that changed markedly in 6 months at 20 or 40 °C were stable at 0 °C. The amounts of ethyl acetate and 3-methylbutyl acetate decreased by 25 and 60%, respectively, at 40 °C, but did not change at 0 °C. Thus, possibly both shipwreck beers originally contained only little 3-methylbutyl acetate, an important flavor component (banana) of modern beers. More probably, its concentration has decreased during the long aging. Lambic beers contain little 3-methylbutyl acetate, and this is thought to result from the activity of an esterase produced by *Dekkera* (*Brettanomyces*) yeasts during the lambic fermentation.[24] Considering the lack of ethylphenol compounds in the beers, it may be more likely that an esterase derived from lysed *Saccharomyces* cells contributed to the loss of 3-methylbutyl acetate.[25]

Vanderhaegen et al.[23] found that ethyl hexanoate, octanoate, and decanoate in beer decreased rapidly during storage at 20 or 40 °C, and ethyl octanoate and decanoate decreased by 10 and 25% during 6 months at 0 °C. Malfliet et al.[26] observed similar lowering of flavor compound concentrations in a range of modern beers stored at 30 °C for 60 days or at 22 °C for 9 months. Thus, the original levels of ethyl hexanoate in both shipwreck beers and of ethyl decanoate in beer A56 were probably at least as high as shown in Figure 2 and would have contributed fruity (apple) flavors to the fresh beers. Ethyl hexanoate was above its taste threshold[15] of 0.2 mg L^{-1} in both beers. However, if an appropriate esterase was present, these esters could, instead, have been formed in the bottles from ethanol and hexanoic and decanoic acids produced by spoilage micro-organisms, so that the levels in Figure 2 may overestimate those of the fresh beers.

The level of 1-propanol may have been increased by metabolic interactions of lactic acid bacteria. *Lactobacillus buchneri* can convert lactate into 1,2-propanediol, which *Lactobacillus diolivorans* can further convert into 1-propanol and propionic acid.[21,2728]

We did not find long-term stability studies for phenylethanol. Malfliet et al.[26] noted that the phenylethyl acetate concentration was lowered by 10−20% during aging, possibly explaining the relatively low level of this compound compared to the phenylethanol in beer C49. The phenylethanol concentration in A56 shipwreck beer (Figure 2) was nearly twice that of modern beers but still below the taste threshold[15] of 125 mg L^{-1}. Phenylethyl acetate in beer A56 (0.68 mg L^{-1}), although higher than in the reference beers (Figure 2), was below its taste threshold[15] (3.8 mg L^{-1}). It is known that compounds present in concentrations below their taste threshold concentrations can still contribute to the general flavor of beers because of synergistic effects,[15] so that in typical modern beers phenylethanol and phenylethyl acetate contribute to the general floral flavor, rather than imparting a specific rose flavor. Yet, the higher concentrations of these compounds in one or both shipwreck beers may have introduced clearer rose notes. At least sake strains of *S. cerevisiae* can evolve to produce high levels of phenylethanol.[29,30,46] Unusually high levels of phenylalanine in the wort can also result in higher phenylethanol levels.[31−33] Moreover, increased uptake of phenylalanine occurs at higher temperatures[34] and may contribute to higher concentrations of phenylethanol in wines

DOI: 10.1021/jf5052943
J. Agric. Food Chem. 2015, 63, 2525−2536

fermented at higher temperatures.[35] Fermentation temperatures were poorly controlled in the 1840s and may have been relatively high during the summer. However, high phenylethanol concentrations might also have been caused by non-*Saccharomyces* yeasts in the brewing process. In the 1840s, pure yeast cultures were an unknown concept. Top fermentation was still the principal method. Fermentations were performed in open, wooden vessels that provided good attachment surfaces for microbes and were difficult to clean. Fermentations were open to airborne contamination and were pitched with the entire microbiota collected from a previous fermentation by skimming. This could have included several yeasts that today are classified as brewery contaminants, including *Dekkera* spp., *Kluyveromyces marxianus* and *Hanseniaspora* spp. that can produce high levels of phenylethanol.[33,36−41]

The level of total diacetyl (i.e., free diacetyl plus its α-acetolactic acid precursor) in beer A56 was within the typical range for beer, whereas the total pentanedione concentration was low (these two vicinal diketones were not analyzed in beer C49). In contrast to that, Vanderhaegen et al.[23] found large increases in diacetyl (3-fold at 0 °C; 50-fold at 40 °C) and pentanedione (30% at 0 °C and 8-fold at 40 °C) during storage of top-fermented beer for 6 months. Apparently this did not happen during aging of beer A56. Rather, this beer may have initially contained low levels of α-acetolactate and the 2,3-pentanedione precursor α-acetohydroxybutyrate, but a high fermentation temperature and low pH due to bacterial activity in the open fermentation vessels could have favored rapid oxidative decarboxylation of the α-acetohydroxy acids and prompted yeast-catalyzed reduction of the resulting vicinal diketones to the corresponding, flavor-neutral alcohols.

Shipwreck beer A56 contained slightly more 2-methylpropanal than the two reference porters but much more than the lager (Olvi Sandels) (Figure 3). 2-Methylpropanal increases during aging, and levels in the A56 beer are similar to those in pale lagers aged for 6 months at 22 °C[26] The level of 3-methylbutanal in A56 was about twice that in Olvi Sandels, but less than that found in modern wheat beers and porters. Levels of 3-methylbutanal can increase 6-fold (reaching 21−43 μg L^{-1}) during storage of top-fermented beers and lagers, especially in the presence of oxygen.[23,26] The relatively low value for 3-methylbutanal in beer A56 suggests that this bottle did not contain much oxygen or that the reactions leading to its formation were very slow at deep Baltic sea temperatures (approximately 4 °C). This assumption is clearly supported by the fact that, in contrast to beer C49, no hop-derived oxidation products of the α-, iso-α-, or β-acids were detected in beer A56.

Furfural is formed during aging of beers.[23] However, its level was less than that (2500 μg L^{-1}) reached during aging of a modern ale for 6 months at 40 °C[23] and much less than the reported taste threshold in beer[15] (150,000 μg L^{-1}). Yet, A56 contained much more furfural (660 μg L^{-1}) than any of the reference beers and very much more than a modern lager (29 μg L^{-1} for the Olvi Sandels). It might also have been formed thermally during mashing. Presumably the mash and wort were heated over an open fire, requiring very effective stirring to prevent burning of local patches of mash against the inner wall of the pot. Whether the resulting burnt flavor (not necessarily from furfural itself) was perceived as positive or negative is unclear.

We have no information about the stability of phenolic compounds in beer at about 4 °C. Still, the concentrations of phenolic compounds remaining in the shipwreck beers were similar to those found in a bottom-fermented lager (Olvi Sandels) and top-fermented porter (Koff Porter) but differed from those in a modern wheat beer (Paulaner Weiss). Paulaner Weiss contained 5−20-fold more 4-vinylguaiacol (clove flavor) than the shipwreck beers and much smaller proportions of the free forms of ferulic, sinapic, and *p*-coumaric acids (Table 3). 4-Vinylguaiacol is formed by decarboxylation of (free) ferulic acid catalyzed by phenylacrylic decarboxylase (Pad1). Pad1 is absent from bottom-fermenting (lager) strains of brewer's yeast[42] but present in some top-fermenting strains (including all tested strains used for production of wheat beers[42]) and in *Brettanomyces* (*Dekkera*) yeasts[44] and some lactic acid bacteria.[45] Table 3 results suggest that all of the free ferulic acid in Paulaner Weiss has been decarboxylated to 4-vinylguaiacol, but that, in contrast, most of the microorganisms responsible for the fermentation of the shipwreck beers did not produce active Pad1. The small amounts of 4-vinylguaiacol found in the shipwreck beers and the other two reference beers may derive from thermal degradation of ferulic acid during wort boiling.[43] The very small amounts of 4-ethylguaiacol in both shipwreck beers (Table 3) suggest that *Dekkera* spp. did not contribute significantly to their fermentation, because these yeasts produce large amounts of ethylphenols.[43] Levels of total and free ferulic acid are in agreement with those reported by Vanbeneden et al.[43] for 58 beers of many types (bound, 11.4 ± 2.6 mg L^{-1}; free, 1.3 ± 0.8 mg L^{-1}), except that the concentration of free ferulic acid in Paulaner Weiss was lower than in many wheat beers (0.81 ± 0.44; $n = 9$).

In summary, these two about 170-year-old bottles contained two different beers, one (C49) more strongly hopped than the other (A56) with the low α-acid yielding hop varieties common in the 19th century. Both beers exhibited typical profiles of yeast-derived flavor compounds and of phenolics. Present knowledge of the long-term chemical and microbiological stability of these compounds is not adequate to assess how closely the observed profiles indicate the original flavor of the beers. The flavors of these compounds were hidden by very high levels of organic acids, probably produced by bacterial spoilage. The composition of the microbial mixture used to produce these beers is unclear, but it probably did not include many strains producing the Pad1 enzyme responsible for the volatile phenols characteristic of wheat beers. Pad1 activity is common in wild yeast, and its absence suggests that the yeasts employed were domesticated rather than wild.[47]

AUTHOR INFORMATION

Corresponding Author

*(B.G.) Phone: + 358 20 722 6603. E-mail: brian.gibson@vtt.fi.

Funding

We thank the Regional Government of Åland and the Stallhagen Brewery, Åland, for financial support and for permission to publish.

Notes

The authors declare no competing financial interest.

ACKNOWLEDGMENTS

We thank Ulla Klemelä and Riikka Alvik (The Maritime Museum of Finland, Kotka), Kaisa Koivisto (The Finnish Glass Museum, Riihimäki), Risto Aalto, and Markku Annila for their expert examination of the glass bottle A56 and suggestions regarding its date and provenance. We thank Silja Home and Hannele Sweins for serving on the taste panel. We also thank

DOI: 10.1021/jf5052943
J. Agric. Food Chem. 2015, 63, 2525−2536

Maarit Kivilompolo for the amino acid analyses and Markku Honkala for Na and K analyses. We gratefully acknowledge the technical assistance of Aila Siltala, Eero Mattila, and Tarja Wikström as well as a critical reading of the manuscript and valuable comments by Esko Pajunen. We thank the Regional Government of Åland and the Stallhagen Brewery, Åland, for providing the shipwreck beer samples

REFERENCES

(1) Thomas, K. The Story of Flag Porter; http://www.darwinbrewery.com/FlagPorterHistory.PDF, 9.2.2013.
(2) Pryde, J.; Conner, J.; Jack, F.; Lancaster, M.; Meek, L.; Owen, C.; Paterson, R.; Steele, G.; Strang, F.; Woods, J. Sensory and chemical analysis of "Shackleton's" Mackinlay scotch whisky. *J. Inst. Brew.* **2011**, *117*, 156−165.
(3) European Brewery Convention. *Analytica-EBC*; Fachcerlag Hans Carl: Nürnberg, Germany, 2007.
(4) Bruggink, C.; Maurer, R.; Herrmann, H.; Cavalli, S.; Hoefler, F. Analysis of carbohydrates by anion exchange chromatography and mass spectrometry. *J. Chromatogr., A* **2005**, *1085*, 104−109.
(5) Mikkelson, A.; Maaheimo, H.; Hakala, T. K. Hydrolysis of konjac glucomannan by *Trichoderma reesei* mannanase, EGI and EGII for the production of glucomannooligosaccharides. *Carbohydr. Res.* **2013**, *372*, 60−68.
(6) Haseleu, G.; Lagemann, A.; Stephan, A.; Intelmann, D.; Dunkel, A.; Hofmann, T. Quantitative sensomics profiling of hop-derived bitter compounds throughout a full-scale beer manufacturing process. *J. Agric. Food Chem.* **2010**, *58*, 7930−7939.
(7) Intelmann, D.; Haseleu, G.; Dunkel, A.; Lagemann, A.; Stephan, A.; Hofmann, T. Comprehensive sensomics analysis of hop-derived bitter compounds during storage of beer. *J. Agric. Food Chem.* **2011**, *59*, 1939−1953.
(8) Huuskonen, A.; Markkula, T.; Vidgren, V.; Lima, L.; Mulder, L.; Geurts, W.; Walsh, M.; Londesborough, J. Selection from industrial lager strains of variants with improved fermentation performance in very-high-gravity worts. *Appl. Environ. Microbiol.* **2010**, *76*, 1563−1573.
(9) Ojala, M.; Kotiaho, T.; Siirilä, J.; Sihvonen, M.-L. Analysis of aldehydes and ketones from beer as *O*-(2,3,4,5,6-pentaflurobenzyl)-hydroxylamine derivatives. *Talanta* **1994**, *41*, 1297−1309.
(10) Schooley, D. L.; Kubiak, F. M.; Evans, J. V. Capillary gas chromatographic analysis of volatile and non-volatile organic acids from biological samples as the t-butyldimethylsilyl derivatives. *J. Chromatogr. Sci.* **1985**, *23*, 385−390.
(11) Panchal, C. J.; Stewart, G. G. Utilization of wort carbohydrates. *Brew. Dig.* **1979**, *44*, 26−48.
(12) Intelmann, D.; Kummerlowe, G.; Haseleu, G.; Desmer, N.; Schulze, K.; Frohlich, R.; Frank, O.; Luy, B.; Hofmann, T. Structures of storage-induced transformation products of the beer's bitter principles, revealed by sophisticated NMR spectroscopic and LC-MS techniques. *Chemistry* **2009**, *15*, 13047−13058.
(13) Intelmann, D.; Demmer, O.; Desmer, N.; Hofmann, T. ^{18}O Stable isotope labeling, quantitative model experiments, and molecular dynamics simulation studies on the transspecific degradation of the bitter tasting iso-α-acids of beer. *J. Agric. Food Chem.* **2009**, *57*, 11014−11023.
(14) Intelmann, D.; Hofmann, T. On the autoxidation of bitter-tasting iso-α-acids in beer. *J. Agric. Food Chem.* **2010**, *58*, 5059−5067.
(15) Meilgaard, M. C. Flavor chemistry of beer. II. Flavor and threshold of 239 aroma volatiles. *Tech. Q. MBAA* **1975**, *12*, 151−168.
(16) Dale, C. J.; Young, T. W.; Brewer, S. Amino acid analysis of beer polypeptides. *J. Inst. Brew.* **1989**, *95*, 89−97.
(17) Kabelóva, I.; Dvoráková, M.; Cízková, H.; Dostálek, P.; Melzoch, K. Determination of free amino acids in beers: a comparison of Czech and foreign brands. *J. Food Compos. Anal.* **2008**, *21*, 736−741.
(18) Suárez Valles, B.; Palacios García, N.; Rodríguez Madrera, R.; Picinelli Lobo, A. Influcence of yeast strain and aging time on free amino acid changes in sparkling ciders. *J. Agric. Food Chem.* **2005**, *53*, 6408−0413.
(19) Olsonen, R., Ed. *FIMR Monitoring of the Baltic Sea Environment − Annual Report 2007*; MERI − Report Series of the Finnish Institute of Marine Research 62; 2008; ISBN 978-951-53-3034-5.
(20) Corsetti, A.; Gobbetti, M.; Rossi, J.; Damiani, P. Antimould activity of sourdough lactic acid bacteria: identification of a mixture of organic acids produced by *Lactobacillus sanfrancisco* CB1. *Appl. Microbiol. Biotechnol.* **1998**, *50*, 253−256.
(21) Krooneman, J.; Faber, F.; Alderkamp, A. C.; Oude Elferink, S. J. H. W.; Driehuis, F.; Cleenwerck, I.; Swings, J.; Gottschall, J. C.; Vancanneyt, M. *Lactobacillus diolivorans* sp. nov., a 1,2-propanediol-degrading bacterium isolated from aerobically stable maize silage. *IJSEM* **2002**, *52*, 639−646.
(22) Escamilla-Hurtado, M. L.; Valdés-Matinez, S. E.; Soriani-Santos, J.; Gómez-Pliego, R.; Verde-Calvo, J. R.; Reyes-Dorantes, A.; Tomasini-Campocosio, A. Effect of culture conditions on production of butter flavor compounds by *Pediococcus pentosaceus* and *Lactobacillus acidophilus* in semi-solid maize-based cultures. *Int. J. Food Microbiol.* **2005**, *105*, 305−316.
(23) Vanderhaegen, B.; Neven, H.; Coghe, S.; Verstrepen, K. J.; Verachtert, H.; Derdelinckx, G. Evolution of chemical and sensory properties during aging of top-fermented beer. *J. Agric. Food Chem.* **2003**, *51*, 6782−6790.
(24) Spaepen, M.; Verachtert, H. Esterase activity in the genus *Brettanomyces*. *J. Inst. Brew.* **1982**, *88*, 11−17.
(25) Neven, H.; Delvaux, F.; Derdelinckx, G. S. Flavor evolution of top fermented beers. *Master Brew. Assoc. Am. Tech. Q.* **1997**, *34*, 115−118.
(26) Malfliet, S.; Van Opstaele, F.; De Clippeleer, J.; Syryn, E.; Goiris, K.; De Cooman, L.; Aerts, G. Flavour instability of pale lager beers: determination of analytical markers in relation to sensory ageing. *J. Inst. Brew.* **2008**, *114*, 180−192.
(27) Moll, M. *Beers and Coolers*; Springer-Verlag: New York, 1994; p 510.
(28) Oude Elferink, S. J. H. W.; Krooneman, J.; Gottschall, J. C.; Spoelstra, S. F.; Faber, F.; Alderkamp, A. C.; Driehuis, F. Anaerobic conversion of lactic acid to acetic acid and 1,2-propanediol by *Lactobacillus buchneri*. *Appl. Environ. Microbiol.* **2001**, *67*, 125−132.
(29) Akita, O.; Ida, T.; Obata, T.; Hara, S. Mutants of *Saccharomyces cerevisiae* producing a large quantity of β-phenylethyl alcohol and β-phenylethyl acetate. *J. Ferm. Bioeng.* **1990**, *69*, 125−128.
(30) Fukuda, K.; Watanabe, M.; Asano, K.; Ueda, H.; Ohta, S. Breeding of a brewing yeast producing a large amount of β-phenylethyl alcohol and β-phenylethylacetate. *Agric. Biol. Chem.* **1990**, *54*, 269−271.
(31) Hernàndez-Orte, P.; Cacho, J.; Ferreira, V. Relationship between varietal amino acid profile of grapes and wine aromatic composition. Experiments with model solutions and chemometric study. *J. Agric. Food Chem.* **2002**, *50*, 2891−2899.
(32) Hernàndez-Orte, P.; Ibarz, M. J.; Cacho, J.; Ferreira, V. Effect of the addition of ammonium and amino acids to musts of Airen variety on aromatic composition and sensory properties of the obtained wine. *Food Chem.* **2005**, *89*, 163−174.
(33) Trinh, T. T. T.; Woon, W. Y.; Curran, P.; Liu, S.-Q. Effect of L-isoleucine and L-phenylalanine addition of aroma compound formation during longan juice fermentation by a co-culture of *Saccharomyces cerevisiae* and *Williopsis saturnus*. *S. Afr. J. Enol. Vitic.* **2010**, *31*, 116−124.
(34) Beltran, G.; Rozes, N.; Mas, A.; Guillamon, J. M. Effect of low-temperature fermentation on yeast nitrogen metabolism. *World J. Microbiol. Biotechnol.* **2007**, *23*, 809−815.
(35) Molina, A. M.; Sweigers, J. H.; Varela, C.; Pretorius, I. S.; Agosin, E. Influence of wine fermentation temperature on the synthesis of yeast-derived volatile aroma compounds. *Appl. Microbiol. Biotechnol.* **2007**, *77*, 675.
(36) Fabre, C. E.; Duviau, V. J.; Blanc, P. J.; Goma, G. Identification of volatile flavour compounds obtained in culture of *Kluyveromyces marxianus*. *Biotechnol. Lett.* **1995**, *17*, 1207−1212.

DOI: 10.1021/jf5052943
J. Agric. Food Chem. 2015, 63, 2525−2536

(37) Garavaglia, J.; Hickmann Flores, S.; Pizzolato, T. M.; do Carmo Peralba, M.; Ayub, M. A. Z. Bioconversion of L-phenylalanine into 2-phenylethanol by *Kluyveromyces marxianus* in grape must cultures. *World J. Microbiol. Biotechnol.* **2007**, *23*, 1273−1279.
(38) Moreira, N.; Mendes, F.; Hogg, T.; Vasconcelos, I. Alcohols, esters and heavy sulphur compounds production by pure and mixed cultures of apiculate wine yeasts. *Int. J. Food Microbiol.* **2005**, *103*, 285−294.
(39) Moreira, N.; Pina, C.; Mendes, F.; Couto, J. A.; Hogg, T.; Vasconcelos, I. Volatile compounds contribution of *Hanseniaspora guilliermondii* and *Hanseniaspora uvarum* during red wine vinifications. *Food Control* **2011**, *22*, 662−667.
(40) Viana, F.; Gil, J. V.; Vallés, S.; Manzanares, P. Increasing the levels of 2-phenylethyl acetate in wine through the use of a mixed culture of *Hanseniaspora osmophila* and *Saccharomyces cerevisiae*. *Int. J. Food Microbiol.* **2009**, *135*, 68−74.
(41) Wittman, C.; Hans, M.; Bluemke, W. Metabolic physiology of aroma-producing *Kluyveromces marxianus*. *Yeast* **2002**, *19*, 1351−1363.
(42) Coghe, S.; Benoot, K.; Delvaux, F.; Vanderhaegen, B.; Delvaux, F. R. Ferulic acid release and 4-vinylguaiacol formation during brewing and fermentation: indications for feruloyl esterase activity in *Saccharomyces cerevisiae*. *J. Agric. Food Chem.* **2004**, *52*, 602−608.
(43) Vanbeneden, N.; Gils, F.; Delvaux, F.; Delvaux, F. R. Formation of 4-vinal and 4-ethyl derivatives from hydroxycinnamic acids: Occurrence of volatile phenolic flavour compounds in beer and distribution of Pad1-activity among brewing yeasts. *Food Chem.* **2008**, *107*, 221−230.
(44) Chatonnet, D.; Dasnoy, S.; Collin, S. Identification of a stale-beer-like odorant in extracts of naturally aged beers. *J. Sci. Food Agric.* **1992**, *60*, 165−178.
(45) Lindsay, R. F.; Priest, F. G. Decarboxylation of substituted cinnamic acids by Enterobacteria − influence on beer flavour. *J. Appl. Bacteriol.* **1975**, *39*, 181−187.
(46) Fukuda, K.; Watanabe, M.; Asano, K. Altered regulation of aromatic amino acid biosynthesis in β-phenylethyl-alcohol-over-producing mutants of sake yeast *Saccharomyces cerevisiae*. *Agric. Biol. Chem.* **1990**, *54*, 3151−3156.
(47) Steensels, J.; Verstrepen, K. J. Taming wild yeast: potential of conventional and nonconventional yeasts in industrial fermentations. *Annu. Rev. Microbiol.* **2014**, *68*, 61−80.

DOI: 10.1021/jf5052943
J. Agric. Food Chem. 2015, 63, 2525−2536

Table 1. The feeding experiment was approved by the Iowa State University Institutional Animal Care and Use Committee (IACUC).

Table 1. Concentrations of Annatto and α-Tocopherol in Supplemented Diets

diet	annatto[a] (ppm)	α-tocopherol[b] (TC, ppm)
control	0	0
T3 100	100	0
T3 500	500	0
T3 2000	2000	0
TC 200	2000	200
TC 600	2000	600
TC 1000	2000	1000

[a]Annatto tocotrienols: total tocotrienols, 74.5% (δ-tocotrienol 89.2%, γ-tocotrienol 10.8%, and other tocotrienols/tocopherols <1%). [b]α-Tocopherol: 96.6%

The base diet met the NRC nutrient recommendations.[17] The hens were randomly assigned to a treatment and were kept in an environment similar to that of most modern industry laying facilities. The average temperature was 25 °C and the average relative humidity was 40%. The lighting was on for 16 h and off the remaining 8 h of the day. Three hens were placed in each cage (experimental unit, EU) with 30 cages (10 stacks with 3 tiers per stack) total. Only 28 cages were needed to house the 84 laying hens; two cages were not used due to air velocity difference and failure of eggs to roll to the front, causing breakage. There were seven treatments diets (Table 1) with four replicates (4 EUs) for each treatment, thus 12 hens per treatment diet. Upon arrival to the new environment, the hens were given a week of acclimation. No mortalities occurred during this study.

Feed Mixing. A horizontal mixer (Precision horizontal batch mixer; H.C. Davis Sons Mfg Co., Inc., Bonner Springs, KS) combined the base diet for 30 min. To mix the supplements into the base diet, the appropriate amount of annatto and/or α-tocopherol was weighed and then was mixed into a small amount of the base diet to ensure it was well incorporated. This mixture was then added to more feed and mixed well with a Hobart mixer (model H-600; Hobart, Troy, OH). This portion was then incorporated into the entire diet portion with the same horizontal mixer that was used to mix the base diet. Feed was stored at refrigeration temperatures (4 °C) away from light and taken to the experimental site daily, where hens were fed and watered ad libitum throughout the entire study. Daily measurements taken precisely every 24 h were feed disappearance and egg production. Hen body weight was taken weekly as an indicator if the hens were eating properly.

Egg Sampling and Storage. The eggs were collected daily for the first 2 weeks and weekly for the remaining 5 weeks. Eggs were taken from 2 days and pooled (i.e., day 1 and day 2 eggs are referred to day 2 eggs in this study). The sampling days were 2 (1−2 days), 4 (3−4 days), 6 (5−6 days), 8 (7−8 days), 10 (9−10 days), 12 (11−12 days), 14 (13−14 days), 21 (20−21 days), 28 (27−28 days), 35 (34−35 days), 42 (41−42 days), and 49 (48−49 days). For sample preparation, the egg yolks were carefully separated from the albumen and rolled on a paper towel to ensure only yolk was taken. The yolks from one cage over 2 days were homogenized manually, and a sample was taken and stored at −4 °C until further analyses were carried out. The frozen egg yolks were then freeze-dried (Virtis Genesis 25LE) for at least 72 h to remove the moisture by sublimation to preserve the lipids.

Physical and Sensory Properties of Eggs and Egg Yolks. The quality of the eggs collected was measured at every sampling time by using a high-accuracy digital egg tester DET6000 (Nabel, Japan). The measurements taken included whole egg weight (grams), eggshell strength (newtons), egg yolk color (yolk color fan, YCF), Haugh unit (calculated from albumen height), and eggshell thickness (millimeters). The YCF taken objectively by this instrument is based on tristimulus values standardized by the 1931 CIE colormetric according to the instrument manual.

Trained Sensory Panel Evaluation on Egg Yolk. To determine whether and how different the treatment eggs (days 35 and 36) were from the control, nine panelists were trained in four training sessions to evaluate the egg yolk for yolk color (less to more yellow), moistness (low to high), smoothness (lumpy to smooth), chalkiness or mouth drying (none to intense), savory egg yolk flavor (none to intense), bitterness (none to intense), and off-flavor (none to intense) on a 15 cm line scale. To calibrate the panelists to these attributes, anchors were used and included egg yolks from the extreme diets (control, T3 2000, and TC 1000) for each scale, YCF for yolk color, and quinine solution for bitterness. For sample preparation, eggs were hard-boiled and consistently cooled by refrigeration, followed by cutting in half and serving to the panelists, cut side down, on a plate labeled with a random 3-digit code in a random order to minimize bias. The four replicates were evaluated on four separate days with panelists' scores averaged on each day.

For all remaining analyses, the egg yolk was carefully separated from the albumen and analysis was conducted on only the egg yolk. Viscosity was measured on the raw separated egg yolks collected from day 47 by use of a Haake RS 150 rheometer (ThermoOrion, Karlsruhe, Germany). This measurement was taken as explained in Walker et al.[2]

Chemical Properties of Egg Yolks. *Total Egg Yolk Moisture.* Total moisture was measured by drying 2 g of yolk in an aluminum dish for 4−5 h at 105 °C as stated in AOAC Standard Method 922.06. This measurement was done on day 28 yolks after they were homogenized.

Egg Yolk Lipid Extraction. Freeze-dried egg yolk samples were ground with a mortar and pestle to reduce particle size, and the yolk was a fine powder. About 0.5 g of the ground freeze-dried yolk powder was accurately weighed into a glass vial and mixed with 5.0 mL of chloroform/methanol (2:1 v/v), similar to the procedure of Folch et al.[18] The vials were capped and manually shaken for 30 s to ensure full dispersion of the solid in the solvent. The vials were placed in a shaker at ambient temperature overnight and then centrifuged to obtain a clear layer. Approximately 2 mL of the supernatant was filtered through a 0.45 μm filter [polytetrafluoroethylene, PTFE] with a glass syringe. The filtrate (1.0 mL) was taken precisely and placed in a preweighed glass vial, and the solvent was evaporated with a nitrogen evaporator to prevent lipid oxidation. To ensure all of the residual solvent was removed, the samples were placed in a vacuum oven at ambient temperature overnight. The vials were weighed to calculate total oil extracted. The oil was then dissolved in HPLC-grade hexanes and stored in an explosion-proof −20 °C freezer until further analyses were carried out, including HPLC quantification of tocopherols and tocotrienols.

Egg Yolk Phospholipid Composition. ^{31}P NMR was used to determine the phospholipid profile for day 21 egg yolk samples. After the egg yolk oil was extracted, a small sample (80−120 mg) of oil was taken and prepared as explained by Yao and Jung.[19] These samples were analyzed for phospholipid content and class composition in the egg yolk oil.

Egg Yolk Fatty Acid Composition. A small sample of egg yolk oil from day 49 was converted to fatty acid methyl esters (FAME) by mixing the lipid with 1 mL of 1 M sodium methoxide at ambient temperature for 5 h. The reaction was stopped by adding 3 mL of deionized (DI) water. Hexanes (2 mL) were added to extract the FAME to the top layer. The FAME samples were then analyzed by gas chromatography (GC; Hewlett-Packard 5890 series II) with a FID detector and a capillary column from Supelco (Bellefonte, PA; SP-2340, 60 m long × 0.25 mm internal diameter ×0.2 μm film thickness). Parameters used for GC quantification were injector and detector temperature of 250 °C and oven temperature-programmed to start at 100 °C and rise 4 °C/min to finish at 240 °C. The flow of gases was set as in Walker et al.[2] A standard solution of FAME (Nu-Check Prep Inc. GC reference standard 566) was used to identify fatty acid peaks in the egg yolk lipid samples.

DOI: 10.1021/jf505536u
J. Agric. Food Chem. 2015, 63, 2537−2544

Table 2. Hen Performance and Laying Rate for Diets with Different Levels of Annatto Tocotrienol and α-Tocopherol Supplementation[a]

diet[b]	daily feed disappearance (g·day^{-1}·hen^{-1})	laying rate (%)	weekly hen weight[c] (kg·hen^{-1})
control	103.16 ± 6.28 B	94.56 ± 0.96	1.50 ± 0.02
T3 100	107.85 ± 5.05 A	94.90 ± 2.86	1.49 ± 0.03
T3 500	107.43 ± 4.75 A	97.62 ± 3.26	1.50 ± 0.03
T3 2000	108.28 ± 4.87 A	94.73 ± 2.96	1.48 ± 0.04
TC 200	107.14 ± 6.49 A	96.94 ± 2.39	1.48 ± 0.03
TC 600	107.54 ± 5.20 A	94.39 ± 3.66	1.50 ± 0.03
TC 1000	106.76 ± 6.39 A	96.43 ± 1.70	1.49 ± 0.02
significance[d]	*	NS	NS

[a]Values are means ± standard deviations for $n = 4$. Different letters (comparing all treatments) in the same column indicate significant differences at the 95% confidence level. [b]Diets are detailed in Table 1. Tocotrienols (T3) = ppm of annatto; α-tocopherol (TC) = ppm of α-tocopherol with constant 2000 ppm of annatto. [c]Hen weights were taken weekly and averaged over 7 weeks. [d]NS, not significant at 5%.

Table 3. Egg and Egg Yolk Quality Properties and Sensory Attributes of Boiled Eggs from Laying-Hen Diets with Different Levels of Annatto Tocotrienol and α-Tocopherol Supplementation[a]

diet[b]	whole egg weight (g)	egg yolk weight (g)	egg shell strength (N)	yolk color, YFC	Haugh unit, HU	egg shell thickness (mm)	yolk viscosity (kg/s·m)
control	59.71 ± 2.03	14.47 ± 0.22	37.37 ± 1.84	4.9 ± 0.07	89.44 ± 1.09	0.36 ± 0.01	0.93 ± 0.19 A
T3 100	59.87 ± 1.33	14.71 ± 0.31	39.87 ± 3.00	4.9 ± 0.19	89.47 ± 1.42	0.36 ± 0.01	0.74 ± 0.12 A,B
T3 500	59.14 ± 1.43	14.49 ± 0.38	37.44 ± 3.45	5.0 ± 0.14	89.70 ± 2.28	0.35 ± 0.01	0.59 ± 0.10 B
T3 2000	59.74 ± 0.65	14.70 ± 0.16	37.48 ± 3.17	5.1 ± 0.18	87.35 ± 1.45	0.35 ± 0.01	0.65 ± 0.12 B
TC 200	59.44 ± 1.07	14.64 ± 0.14	40.69 ± 3.06	5.2 ± 0.14	86.96 ± 2.10	0.37 ± 0.01	0.50 ± 0.14 B
TC 600	60.32 ± 1.16	14.89 ± 0.14	36.39 ± 1.38	5.1 ± 0.15	87.88 ± 1.13	0.35 ± 0.01	0.63 ± 0.07 B
TC 1000	59.58 ± 0.84	14.42 ± 0.48	38.92 ± 1.52	5.0 ± 0.16	88.84 ± 1.57	0.35 ± 0.01	0.69 ± 0.06 A,B
significance[c]	NS	NS	NS	NS	NS	NS	*

diet[b]	yellow color	moistness	smoothness	chalk/mouth drying	savory yolk flavor	bitterness	off-flavor
control	6.3 ± 0.6 B	5.2 ± 0.9	8.6 ± 1.0	5.5 ± 1.2	5.7 ± 0.2 A,B	0.3 ± 0.4	0.2 ± 0.3
T3 100	6.8 ± 0.7 A,B	5.6 ± 1.4	9.5 ± 1.2	4.1 ± 0.4	5.5 ± 0.3 A,B	0.1 ± 0.1	0.2 ± 0.2
T3 500	6.9 ± 0.3 A,B	6.3 ± 1.4	8.9 ± 0.6	4.4 ± 0.4	5.3 ± 1.1 A,B	0.6 ± 0.6	0.5 ± 0.5
T3 2000	7.5 ± 0.2 A,B	6.2 ± 1.2	8.2 ± 1.2	4.0 ± 1.5	6.5 ± 1.0 A	0.4 ± 0.3	0.1 ± 0.1
TC 200	8.3 ± 1.0 A	5.7 ± 0.4	8.9 ± 0.9	4.5 ± 0.4	6.4 ± 0.5 A	0.6 ± 0.9	0.1 ± 0.1
TC 600	8.3 ± 0.9 A	5.4 ± 0.9	9.1 ± 0.9	4.6 ± 0.4	6.7 ± 0.5 A	0.8 ± 0.9	0.1 ± 0.1
TC 1000	6.7 ± 0.4 A,B	5.2 ± 1.0	8.6 ± 0.6	5.2 ± 0.5	4.4 ± 0.5 B	0.1 ± 0.1	0.5 ± 0.6
significance[c]	**	NS	NS	NS	**	NS	NS

[a]Values are means ± standard deviations for $n = 4$. Different letters (comparing all treatments) in the same column indicate significant differences at the 99% confidence level. [b]Diets are detailed in Table 1. Tocotrienols (T3) = ppm of annatto; α-tocopherol (TC) = ppm of α-tocopherol with constant 2000 ppm of annatto. [c]NS, not significant at 1% for **, and at 5% for *.

Vitamin E Content in Egg Yolk. Egg oil was dissolved in an appropriate volume of HPLC-grade hexanes to obtain vitamin E isomers in the quantifiable region. HPLC was run as explained in Walker et al.[2] Concentrations of tocopherols and tocotrienols were determined by normal-phase HPLC with a Luna 3 μm NH_2 100 Å, 150 mm × 3.0 mm column (Phenomenex, Torrance, CA) and fluorescence detection. The separation was achieved isocratically with a mobile phase of 98% hexanes and 2% 2-propanol.

Vitamin E Transfer Efficiency to Egg Yolk. Transfer efficiency was calculated on the basis of the maximum concentration reached for each treatment (all of these occurred at approximately day 10). For this calculation, the amount of supplement that theoretically could have been completely or 100% transferred (i.e., the amount of supplement provided from feed daily) was calculated from supplement composition (Table 1), daily feed consumption, laying rate, and egg yolk weight. The ratio of the value quantified to the theoretical value calculated on the basis of complete transfer is the transfer efficiency, expressed as a percentage.

Egg Yolk Cholesterol Quantification. To quantify total cholesterol in the egg yolks, a Wako Cholesterol E (Mountain View, CA) kit was used. The procedure was carried out as instructed, with 2 mg of freeze-dried egg yolk (weighed with an analytical balance) mixed with the color reagent provided by the kit. This mixture was shaken and allowed to react for 15 min at 37 °C, ensuring that all of the yolk was uniformly dispersed in solution for blue pigment formation. The samples were centrifuged to settle the egg yolk particle, and the liquid was carefully pipetted into a cuvette. The cuvette was read on a spectrophotometer (Beckman Coulter DU 720 UV/vis spectrophotometer) at 600 nm, with DI water as a blank. A standard curve was constructed each time samples were measured, by use of the standard cholesterol provided in the kit, to quantify the cholesterol in the egg yolks.

Statistical Analysis. Statistical analysis was done with JMP Pro (version 10, SAS Institute Inc., Cary, NC). One-way analysis of variance (ANOVA) was used for mean comparisons, and all-pairwise comparisons were done by use of Tukey's honest significant difference (HSD) at $p = 0.01$ (sensory and fatty acid data) or $p = 0.05$ (all other data).

RESULTS AND DISCUSSION

Hen Production Performance. The daily feed disappearance, weekly laying rate (100 × eggs produced/hens in cage), and weekly averaged hen body weight are shown in Table 2. No significant differences were found among treatments in the laying rate or hen body weight. The laying rate was over 90% for all diets, similar to that reported in literature.[2,13,20] All hens on treatment diets consumed significantly more feed than those

DOI: 10.1021/jf505536u
J. Agric. Food Chem. 2015, 63, 2537−2544

on the control diet, with no differences among treatments, indicating that the annatto additive caused the hens to consume more feed even at the lowest concentration.

Annatto has a potent red-orange color from bixin and norbixin carotenoids present and is traditionally used in many industries for coloring various products. But due to the low lighting in the environment, broad-spectrum sight of the laying hens,[21] and low concentration of supplement in the feed with very subtle visual change in color of feed, the cause for the higher feed disappearance is not believed to be associated with the color of the additive. The pure annatto supplement used was tasted by the researchers, and it had a bitter and fruity taste. Its addition to the feed may have made the feed more palatable to the laying hens, causing an increase in the average amount of feed consumed. Chickens have been shown to be sensitive to salty or bitter substances.[22] Not knowing how the laying hens perceive the annatto supplement, it is difficult to know exactly what caused this increase. The hens consuming more feed but not producing more eggs would lead to higher production costs. The egg is considered to be the gold standard for protein;[23] thus increasing the cost of production is not desirable for the industry or egg consumers. A potential application of this supplementation may be for broiler chickens for more rapid muscle growth. Kudo et al.[24] found that broiler chickens had the highest number of taste buds over layer type and Rhode Island Red type. The higher feed consumption likely can lead to faster rate of growth and meat production.

Physical and Sensory Properties of Eggs and Egg Yolks. No significant differences were found in whole egg weight, egg yolk weight, egg shell strength, yolk color, Haugh unit (HU), or egg shell thickness averaged over time (Table 3). It was expected that there would be minimal changes in the physical and quality properties due to the supplements. All HUs on average were greater than 72, indicating that the eggs produced in this feeding study were AA eggs by USDA grading standards,[25] and the HUs were similar to those found in literature.[2,26] Significant differences were found in yolk viscosity, with many of the treatment diets (T3 500, T3 2000, TC 200, and TC 600) being significantly lower than the control.

Kirunda et al.[27] also reported inconsistent and lower measurements for viscosity of yolk from diets with vitamin E supplementation. Environmental or storage conditions may cause changes in viscosity, that is, increasing storage time decreases viscosity,[28] but all eggs were exposed to the same environmental and storage conditions. In the study of Walker et al.,[2] the only significant difference in yolks from hens supplemented with palm toco concentrate and astaxanthin was the emulsification capacity, with a significant decrease upon increased level of supplementation. It is uncertain why a decrease in emulsification capacity was seen in the egg yolks, but it was thought to be due to changes in egg yolk protein and lipid interactions. A similar change could have occurred in this study due to feed supplementation. Egg yolk is a complex system with a large amount of water, lipoproteins, and free proteins. Understanding the changes in viscosity will require further compositional and microstructural studies of the yolk, which are beyond the scope of this work. Nonetheless, such changes in viscosity may impact the egg yolk functionality and its applications.

Trained Sensory Panel Evaluation on Egg Yolk. A trained sensory panel was carried out to determine what changes were perceived by a trained sensory panel. No significant differences were perceived in moistness, smoothness, chalkiness/mouth drying, bitterness, or off-flavor (Table 3). It is interesting to note that a general trend is seen that as the moistness increased, the viscosity decreased, although not significantly. Although the annatto supplement had bitter, astringent, and fruity flavors, these flavors of the pure annatto extract were not transferred to the eggs based on the trained sensory panelist's evaluation. Panelists did perceive the yolks of the TC 200 and TC 600 diets to be significantly more yellow than those of the control. The egg yolk color measured instrumentally (Table 3) did not show any significant differences in the color of the raw egg, indicating that cooking of the eggs may have enhanced the difference in yellow color of the yolk. The scale set by panelists was a narrow range in yellow color with the extremes not being unacceptable to a consumer, indicating although a change in yolk color in some of the supplemented diets was perceived, it was not seen as a negative quality. Some consumers prefer a more intense yellow or paler yellow egg yolk. Preferences in egg yolk color also vary with geographical and cultural differences, with many consumers associating a certain color of egg yolk with level of quality and safety of the eggs.[29,30] Other studies had shown an increase in the yellow color of egg yolks with annatto supplementation,[20,29] but the levels of supplementation in this study were much lower, thus showing much less of an effect on yolk color. The savory yolk flavor was perceived to be lowest in the TC 1000 diet, but the level of change is not expected to be unacceptable to consumers.

Chemical Properties of Egg Yolks. *Total Egg Yolk Moisture.* There was no significant difference among the treatment diets for moisture content (48.30−48.84%). Moisture content of an egg yolk can vary with breeds of chicken, but 48−49% moisture is consistent with the dry solids content of 52−53% reported by Varadarajulu and Cunningham.[31] Generally, 50% moisture content is accepted for an egg yolk,[32] and the values found in this study were comparable to this.

Because significant differences were found in viscosity, it was expected that there would be differences in moisture content. Many of the treatments had lower viscosity values than the control, indicating a thinner yolk, which would be attributed to higher moisture; but this was not observed.

Egg Yolk Lipid Content. There was no significant difference among the treatment diets for egg yolk lipid content (63.43−64.34% dry basis, db). The total lipid found in the egg yolks was slightly higher than that found in literature of 62.5% dry basis.[32] It was assumed that the modification of the Folch[16] lipid extraction procedure of not using a water wash step would leave extractable proteins in the lipid extract, thus causing the increase. However, when the traditional Folch wash was carried out for the same egg yolk samples, the results were similar to those measured with the modified method.

Egg Yolk Phospholipid Composition. ^{31}P NMR was performed to determine the weight percent of phospholipids for egg yolks from day 21. Peaks in the NMR spectrum were identified by methodology from Yao and Jung.[19] No significant differences were found among treatment diets in any of the phospholipids. The major phospholipids detected were phosphatidylcholine (74.74−75.54%) and phosphatidylethanolamine (19.00−20.25%), which are expected in egg yolk. The total phospholipid in the yolk lipid (21.11−24.94%) was comparable with that reported in literature.[2,32] Other minor phospholipids in the egg yolk samples were phosphatidylinositol (0.82−1.48%), lysophosphatidylcholine (1.22−1.44%),

DOI: 10.1021/jf505536u
J. Agric. Food Chem. 2015, 63, 2537−2544

sphingomyelin (1.90−2.47%), and lysophosphatidylethanolamine (0.59−0.80%). Phospholipids have many applications in the food industry[33] and are important biological molecules in maintaining a healthy body.[34]

Egg Yolk Fatty Acid Composition. The fatty acids detected in day 49 yolk samples were 16:0 (24.37−26.26%), 16:1 (2.04−2.57%), 18:0 (9.29−10.05%), 18:1 (39.53−40.92%), 18:2 (15.91−17.05%), 20:4 (1.88−2.19%), and 22:6 (0.48−0.60). There were no significant differences in any of the fatty acids reported across the treatment diets, and the percentages found are similar to those reported in literature.[2,32,35]

Vitamin E Content in Egg Yolk. After 10 days of feeding the supplement diets, a steady state of nutrient transfer of vitamin E to the egg yolk was reached, as shown in Figure 1, the same as reported by Walker et al.[2] The forms of vitamin E reported in the figure include α-tocopherol, γ-T3, and δ-T3 because these are the major forms of vitamin E in the supplements added to the feed. It is evident from the kinetics of transfer shown in Figure 1 that α-tocopherol was transferred at a much higher rate than either γ- or δ-T3, even when supplemented in similar amounts.

To understand how the additives were transferred to the yolk, measurements after steady state (day 10 and after) were averaged and compared, as shown in Table 4. Diets without α-tocopherol supplementation (control, T3 100, T3 500, and T3 2000) were not significantly different, with similar amounts of α-tocopherol as reported by the USDA Nutrient Database.[36] There is α-tocopherol in the base diet, and the amount found and transfer efficiencies are the same across these treatments. As expected, the amount of α-tocopherol in the egg yolks significantly increased as the amount of α-tocopherol added to the feed increased. At steady state, γ-T3 was the highest in T3 2000, showing that α-tocopherol did decrease the amount of γ-T3 transferred, but this was not significant until the use of highest level of α-tocopherol (TC 1000). This outcome indicates that when α-tocopherol is present at a high concentration, it lowers the amount of γ-T3 transferred to the egg yolk from the feed.

δ-T3 was significantly higher in diets supplemented with 2000 ppm of annatto, with none of the diets supplemented with α-tocopherol being significantly different from T3 2000. Therefore, α-tocopherol did not impact the transfer of δ-T3 as it did for γ-T3, and this is believed to be due to the differences and similarities of structure between the various forms of vitamin E. γ-T3 is more structurally similar to α-tocopherol (three methyl groups) with two methyl groups on the ring structure, but δ-T3 has only one methyl group on the phenolic ring.[3] α-Tocopherol is reported to interfere with absorption of T3s with a dose−response relationship,[37] and this is believed to be due to how the various forms of vitamin E are inherently transported and distributed.

When the supplement diets without α-tocopherol were compared, T3 500 and T3 2000 diets were significantly higher in γ- and δ-T3 than the control, and they were different from each other. Thus, it is possible to increase γ- and δ-T3 in the egg yolks with increasing annatto supplementation, although this was not proportional to its concentration in the feed and the quantity transferred is not very high.

Vitamin E Transfer Efficiency to Egg Yolks. α-Tocopherol was transferred much more efficiently (21.19−49.17%) to the egg yolk than either γ-T3 (0.50−0.96%) or δ-T3 (0.74−0.93%), as reported in Table 5. Significant decreases in the transfer efficiency of α-tocopherol were observed when it was supplemented at higher concentration. Decreases in γ-T3 transfer efficiencies were observed after supplementation passed

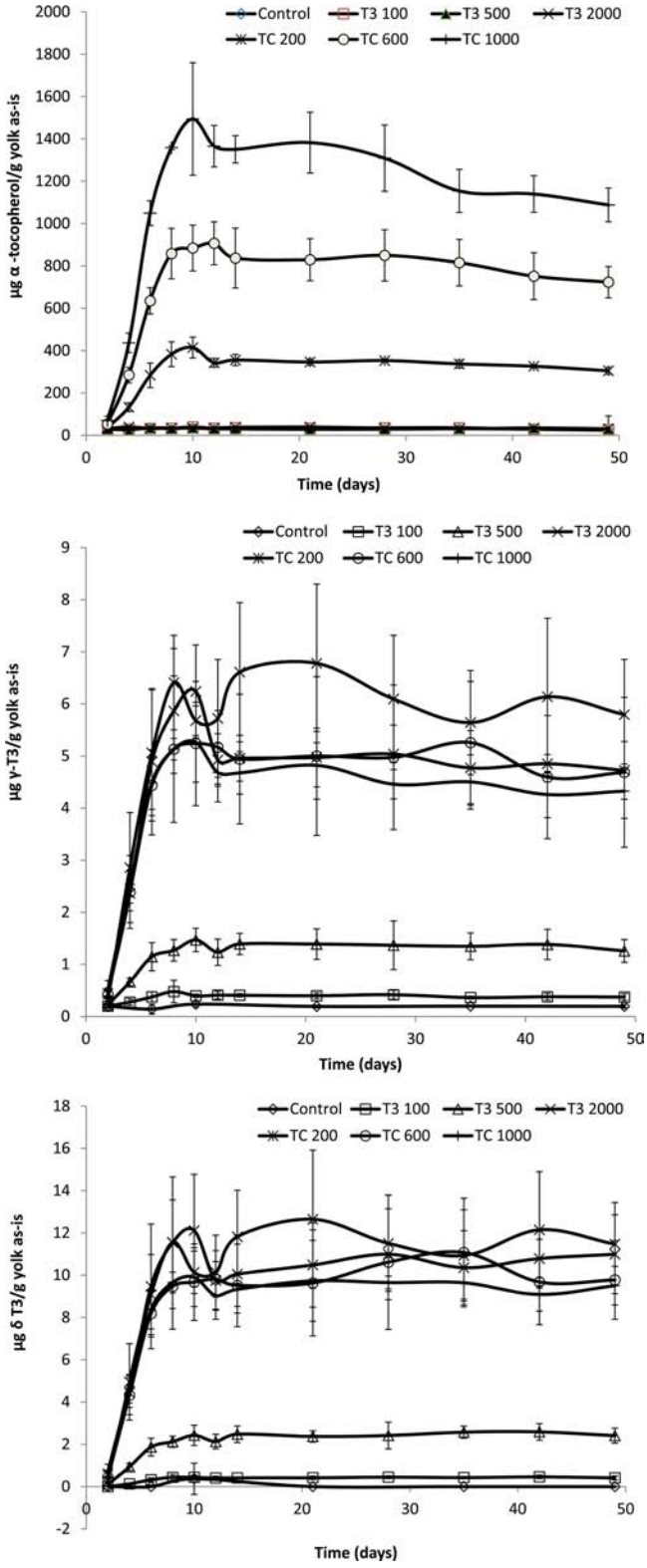

Figure 1. Kinetics of (top) α-tocopherol, (middle) γ-T3, and (bottom) δ-T3 accumulation in egg yolk over 7-week feeding period, showing means and standard deviation bars (n = 4). Diets are detailed in Table 1. T3 = ppm of annatto; TC = ppm of α-tocopherol with constant 2000 ppm of annatto.

DOI: 10.1021/jf505536u
J. Agric. Food Chem. 2015, 63, 2537−2544

Table 4. Average Concentration of Vitamin E Isomers in Egg Yolks after Reaching Steady State (Days 10−49) from Diets with Different Levels of Annatto Tocotrienol and α-Tocopherol Supplementation[a]

diet[b]	α-TC (μg/g of yolk as-is)	γ-T3 (μg/g of yolk as-is)	δ-T3 (μg/g of yolk as-is)
control	29.15 ± 6.39 D	0.21 ± 0.01 C, c	0.09 ± 0.18 B, c
T3 100	33.64 ± 2.62 D	0.39 ± 0.04 C, bc	0.43 ± 0.06 B, c
T3 500	30.71 ± 3.04 D	1.35 ± 0.23 C, b	2.43 ± 0.32 B, b
T3 2000	34.21 ± 3.66 D, δ	6.06 ± 0.95 A, a	11.35 ± 1.84 A, a
TC 200	347.49 ± 4.71 C, γ	5.06 ± 0.49 AB	10.69 ± 1.81 A
TC 600	824.63 ± 94.56 B, β	4.98 ± 1.16 AB	9.97 ± 1.91 A
TC 1000	1285.40 ± 94.96 A, α	4.62 ± 0.36 B	9.49 ± 0.56 A
significance	*	*	*

[a]Values are means of values from day 10, 12,14, 21, 28, 35, 42, and 49 ± standard deviations for $n = 4$. Different uppercase letters (comparing all treatments), lowercase letters (comparing control, T3 100, T3 500, and T3 2000), and Greek letters (comparing T3 2000, TC 200, TC 600, and TC 1000) in the same column indicate significant differences at the 95% confidence level. [b]Diets are detailed in Table 1. Tocotrienols (T3) = ppm of annatto; α-tocopherol (TC) = ppm of α-tocopherol with constant 2000 ppm of annatto.

Table 5. Transfer Efficiency of Vitamin E Isomers into Egg Yolks from Feed with Different Levels of Annatto Tocotrienol and α-Tocopherol Supplementation[a]

diet[b]	α-TC	γ-T3	δ-T3
control	39.50 ± 5.01 A	N/A	N/A
T3 100	46.89 ± 7.82 A	0.96 ± 0.32 A	0.74 ± 0.45
T3 500	41.60 ± 5.71 A	0.60 ± 0.12 A,B	0.81 ± 0.49
T3 2000	49.17 ± 7.62 A, α	0.67 ± 0.12 A,B	0.93 ± 0.54
TC 200	26.91 ± 2.19 B, β	0.56 ± 0.08 B	0.90 ± 056
TC 600	21.19 ± 2.52 B, β	0.53 ± 0.10 B	0.79 ± 0.44
TC 1000	21.42 ± 3.16 B, β	0.50 ± 0.06 B	0.80 ± 0.47
significance[c]	*	*	NS

[a]Values are means at maximum value ± standard deviations for $n = 4$. Different uppercase letters (comparing all treatments), and Greek letters (comparing T3 2000, TC 200, TC 600, and TC 1000) in the same column indicate significant differences at the 95% confidence level. [b]Diets are detailed in Table 1. Tocotrienols (T3) = ppm of annatto; α-tocopherol (TC) = ppm of α-tocopherol with constant 2000 ppm of annatto. [c]NS, not significant at 5%.

100 ppm, but the efficiency was not impacted by added α-tocopherol.

The transfer efficiency for α-tocopherol was much higher than that reported by Walker et al.[2] (9.9%) and very similar to that reported by Walde et al.[13] (39.59−44.78%). Efficiency decreased as more α-tocopherol was added. This decrease indicates that there was a leveling off, possibly due to saturation of the α-tocopherol transfer protein (αTTP) in the liver that is an important step in the uptake of vitamin E, especially α-tocopherol.

Tocotrienols had been shown to have poor absorption and transfer to egg yolks in the literature previously;[2,13] thus low transfer efficiencies were not unexpected. The transfer efficiency of γ-T3 was higher than those reported by both Walker et al.[2] (<about 0.1%) and Walde et al.[13] (0.37−0.40%). δ-T3 was transferred at a level higher than that reported by Walker et al. and Walde et al. (about 0%).

α-Tocopherol was more efficiently transferred to the yolk and this was expected due to the presence of an αTTP in the liver, which preferentially binds α-tocopherol, making it more bioavailable.[4] When the highest T3 diet, T3 2000, is compared with the TC diets, no significant differences are found, indicating that adding more α-tocopherol did not impact the transfer efficiency of γ-T3. This can also be seen in δ-T3, with no significant differences among the treatment diets. This trend was expected because α-tocopherol dominated the αTTP, causing the T3s to be mostly excreted. Overall, it was observed that annatto T3s were not well absorbed, with high concentration detected in the manure (manuscript under review), showing a need for a better carrier system or matrix to transport T3s into the body.

Egg Yolk Cholesterol Quantification. The amount of cholesterol in day 2, 21, and 49 yolks was determined spectrophotometrically, and the results are shown in Table 6.

Table 6. Cholesterol Content of Day 2, 21, and 49 Egg Yolks from Diets with Different Levels of Annatto Tocotrienol and α-Tocopherol Supplementation[a]

	cholesterol (mg/g of yolk as-is)		
diet[b]	day 2	day 21	day 49
control	14.62 ± 1.64	14.61 ± 1.22	14.87 ± 0.49
T3 100	14.71 ± 1.74	15.80 ± 2.93	15.21 ± 1.71
T3 500	14.09 ± 1.32	14.60 ± 1.13	14.37 ± 1.03
T3 2000	15.18 ± 1.41	14.37 ± 1.03	14.46 ± 0.25
TC 200	13.68 ± 0.96	13.20 ± 1.50	13.49 ± 0.92
TC 600	14.90 ± 0.68	15.52 ± 1.43	13.52 ± 0.45
TC 1000	14.71 ± 1.43	13.24 ± 1.21	13.94 ± 1.42
significance[c]	NS	NS	NS

[a]Values are means ± standard deviations for $n = 4$. [b]Diets are detailed in Table 1. Tocotrienols (T3) = ppm of annatto; α-tocopherol (TC) = ppm of α-tocopherol with constant 2000 ppm of annatto. [c]NS, not significant at 5%.

This method was a modification that used a cholesterol quantification kit designed for biological samples, especially blood serum. To validate this method, various tests were performed to ensure it was accurate and appropriate. With the freeze-dried egg yolk being a mass of solid particles, the concern was length of time for the reaction to reach completion. A time-lapse study was done to ensure that all cholesterol present in the egg yolk powder reacted fully. It was observed that at 15 min (3 times longer than required by kit), the ratio of absorbance to mass of freeze-dried egg yolk reached a constant, and it did not change significantly after 15 min.

When an average of the egg yolk weights (14.61 g/yolk) is used, the range of cholesterol in the yolks was 192−231 mg/yolk. This amount is in general consistent with values reported in the literature.[39−41] Kazmierska et al.[41] discussed how different techniques for quantifying cholesterol gave slightly different results. For this reason, AOCS saponification and then GC method (Ca 6b-53) was done on selected treatments

DOI: 10.1021/jf505536u
J. Agric. Food Chem. 2015, 63, 2537−2544

(control and T3 2000) to compare the amount of cholesterol quantified. No significant differences were detected among treatments. However, it was noted that the kit used in this study resulted in 18.37−20.63% higher values than the AOCS saponification and GC method, possibly due to complete quantification of all cholesterol forms. The kit method in this study allowed for detection of both free cholesterol and cholesterol ester, with the enzyme cholesterol ester hydrolase freeing cholesterol esters to allow for total quantification.

It is well-known that cholesterol ester takes longer to free the cholesterol during saponification compared to the hydrolysis of other lipid ester bonds.[42] It is not well understood how the amount of cholesterol changes (i.e., hydrolysis of ester or degradation of the free sterol) under conditions of heat and high pH during saponification. Busch and King[43] reported that cholesterol was heat-labile at 45 °C in the presence of 1 M KOH, which are conditions typically milder than that used in various cholesterol quantification procedures. Egg yolks were reported to have 10−15% of the cholesterol present as esters.[44] If the ester hydrolysis was incomplete or there was free cholesterol degradation during the saponification, the standard AOCS method would lead to an underestimation of the total cholesterol content.

In reporting the amount of cholesterol in an egg, it is important to specify the weight size class of the egg (peewee, small, medium, large, extra-large, or jumbo).[25] The average egg weight found in this study was 59.69 ± 0.37 g (with shell). According to the USDA Nutrient Database,[36] a large egg is 50 g and an extra-large egg is 56 g at a minimum without shell, so it is most appropriate to use the USDA grading manual[25] (weights with shells included) to categorize the eggs with shell in this study. According to these standards, the eggs in this study are large eggs. USDA reports the yolk of a large egg to be 17 g, much larger than the average in this study (14.61 g). Our yolk weight is very accurate because any attached egg albumen outside the yolk was removed with paper towels. It is evident that, based on weight for the large egg class and its yolk size as determined in this study, the amount of cholesterol reported by the USDA nutrient database, 184 mg/large yolk or 12.6 mg cholesterol/g of yolk as-is, is lower than that found in this study, 14.4 mg cholesterol/g of yolk as-is average across all treatments and days. The reasons for this difference are discussed above.

No significant cholesterol reductions over the feeding study were seen across treatment diets. Walde et al.[13] found a 4% or 6% reduction in diets supplemented with barley or palm T3s, respectively, but this trend was not seen in our study. A key difference in our study and the study by Walde et al.[13] is the form and amount of T3s present in the sources. Barley had mixed tocopherols and T3s, with α-T3 being the dominant form. Palm also contained mixed tocopherols, with γ-T3 being the dominant molecule. Even though egg from this study can contain up to a similar level of total T3 (~100 μg/egg) as that of Walde et al., we did not observe cholesterol reduction. Harder et al.[15] also observed lower cholesterol content in eggs with higher levels of supplemented annatto in the feed, particularly above 1.5% supplementation. However, there was no information on the T3 content in the annatto. Nonetheless, McGonigle et al.[16] observed no significant difference in the cholesterol content in eggs when feed was supplemented with annatto, similar to the observation in this study.

T3s have been shown to lower cholesterol levels in many studies.[5−12] Yu et al.[12] showed that supplementation with 50−2000 ppm of δ- and γ-T3 in young female chickens caused decreases in total serum cholesterol (32%), LDL levels (66%), and triacylglycerols (TAGs), with minimal changes to HDL cholesterol. In our study, blood samples were taken from the hens at day 49 of our feeding trial (37 weeks old), and they also showed no significant changes in lipid chemistry (total cholesterol, HDL, and TAGs; data reported in Hansen et al., manuscript under review). We do not know the cause of the different outcomes, but we thought that the use of young female birds versus adult laying hens may play a role in these differences.

In summary, annatto and α-tocopherol supplements did not significantly impact most of the hen performance indicators and quality parameters of the resulting egg yolks. Significant differences were found in daily feed disappearance, egg yolk viscosity, sensory yolk color, and savory yolk flavor and in the amount and transfer efficiency of various forms of vitamin E in the egg yolks. On the basis of both data over time and transfer efficiencies at the maximum value for α-tocopherol, γ-T3, and δ-T3, it is evident that α-tocopherol is much better transferred to hen egg yolks and does play some role in how the other forms of vitamin E are absorbed. This study confirms that the T3s cannot be substantially transferred in hen's body and yolk, even when there is no significant amount of α-tocopherol present to compete with the binding protein. This study illustrates that by changing what is in laying-hen feed, it is possible to change the nutrients in an egg, but only when the physiology of the animals allows. Novel approaches have to be designed to overcome the physiology barrier in order to make the hens more efficiently transfer the T3s to the egg. With a better delivery system, it may be possible to observe a cholesterol reduction effect of T3s in egg.

■ ASSOCIATED CONTENT

Ⓢ Supporting Information

One table listing composition of base diet fed to laying hens for 7 weeks. This material is available free of charge via the Internet at http://pubs.acs.org.

■ AUTHOR INFORMATION

Corresponding Author

*Telephone 515-294-5448; fax 515-294-8181; e-mail tongwang@iastate.edu.

Funding

We thank American River Nutrition for funding this work and providing the annatto used to supplement the laying-hen feed. We also thank ADM for providing the α-tocopherol used to supplement the laying-hen feed.

Notes

The authors declare no competing financial interest.

■ ACKNOWLEDGMENTS

The work done in this project would not have been possible without the many who graciously volunteered their time. Matthew Hansen, Dr. John C. Fuller Jr., Charlwit Kulchaiyawat, and Tao Fei all played a vital role in having a successful feeding study.

■ REFERENCES

(1) Yao, L.; Wang, T.; Persia, M.; Horst, R.; Higgins, M. Effects of vitamin D_3-enriched diet on egg yolk vitamin D_3 content and yolk quality. *J. Food Sci.* **2013**, *78* (2), 178−183.

DOI: 10.1021/jf505536u
J. Agric. Food Chem. 2015, 63, 2537−2544

(2) Walker, L.; Wang, T.; Xin, H.; Dolde, D. Supplementation of laying-hen feed with palm tocos and algae astaxanthin for egg yolk nutrient enrichment. *J. Agric. Food Chem.* **2012**, *60*, 1989−1999.
(3) Sontag, T.; Parker, R. Influence of major structural features of tocopherols and tocotrienols on their ω-oxidation by tocopherol-ω-hydroxylase. *J. Lipid Res.* **2007**, *48*, 1090−1098.
(4) Traber, M. Molecular mechanisms of vitamin E transport. *Annu. Rev. Nutr.* **1999**, *19*, 343−355.
(5) Yang, Z.; Lee, M.; Sang, S.; Yang, C. Bioavailability and metabolism of tocotrienols. In *Tocotrienols Vitamin E Beyond Tocopherols*, 2nd ed.; Tan, B., Watson, R., Preedy, V., Eds.; CRC Press: Boca Raton, FL, 2013; pp 37−51.
(6) Qureshi, A.; Burger, W.; Peterson, D.; Elson, C. The structure of an inhibitor of cholesterol biosynthesis isolated from barley. *J. Biol. Chem.* **1986**, *261* (23), 10544−10550.
(7) Pearce, B.; Parker, R.; Deason, M.; Qureshi, A.; Wright, J. Hypocholesteolemic activity of synthetic and natural tocotrienols. *J. Med. Chem.* **1992**, *35*, 3595−3606.
(8) Parker, R.; Pearce, B.; Clark, R.; Gardon, D.; Wright, J. Tocotrienols regulate cholesterol production in mammalian cells by post-transcriptional suppression of 3-hydroxy-3-methylglutaryl-coenzyme A reductase. *J. Biol. Chem.* **1993**, *268* (15), 11230−11238.
(9) Qureshi, A.; Mo, H.; Packer, L.; Peterson, D. Isolation and identification of novel tocotrienols from rice bran with hypocholesterolemic, antioxidant, and antitumor properties. *J. Agric. Food Chem.* **2000**, *48*, 3130−3140.
(10) Qureshi, A.; Peterson, D. The combined effects of novel tocotrienols and lovastatin on lipid metabolism in chickens. *Atherosclerosis* **2001**, *156*, 39−47.
(11) Qureshi, A.; Peterson, D.; Hasler-Rapacz, J.; Rapacz, J. Novel tocotrienols of rice bran suppress cholesterogenesis in hereditary hypercholesterolemic swine. *J. Nutr.* **2001**, *131*, 223−230.
(12) Yu, S.; Thomas, A.; Gapor, A.; Tan, B.; Qureshi, N.; Qureshi, A. Dose-response impact of various tocotrienols on serum lipid parameters in 5-week-old-female-chickens. *Lipids* **2006**, *41*, 453−461.
(13) Walde, C.; Drotleff, A.; Ternes, W. Comparision of dietary tocotrienols from barley and palm oils in hen's egg yolk: Transfer efficiency, influence of emulsification, and effect on egg cholesterol. *J. Sci. Food Agric.* **2014**, *94* (4), 810−818.
(14) Frega, N.; Mozzon, M.; Bocci, F. Identification and estimation of tocotrienols in the annatto lipid fraction by gas chromatography-mass spectrometry. *J. Am. Oil Chem. Soc.* **1998**, *75* (12), 1723−1727.
(15) Harder, M.; Canniatti-Brazaca, S.; Coelhe, A.; Savino, V.; Franco, C. Cholesterol and iron availability in the yolk of laying hens feed with annatto (*Bixa orellana*). *Animal* **2007**, *1*, 477−482.
(16) McGonigle, K.; McCracken, K. Study of the effects of annatto (*Bixa orellana*) and *Yucca schidegera* on cholesterol content and yolk colour. *Br. Poult. Sci.* **2002**, *43*, S41−S42.
(17) NRC, National Research Council. *Nutrient requirements of poultry*, 9th ed.; National Academy Press: Washington, DC, 1994.
(18) Folch, J.; Lees, M.; Sloane Stanley, G. A simple method for the isolation and purification of total lipids from animal tissues. *J. Biol. Chem.* **1957**, *226*, 497−509.
(19) Yao, L.; Jung, S. ^{31}P NMR phospholipid profiling of soybean emulsion recovered from aqueous extraction. *J. Agric. Food Chem.* **2010**, *58*, 4866−4872.
(20) Garcia, E.; Molino, A.; Goncalves, H.; Junqueira, O.; Pelicia, K.; Osera, R.; Duarte, K. Gound annatto seeds (*Bixa orellana L.*) in sorghum-based commercial layer diets and their effects on performance, egg quality, and yolk pigmentation. *Braz. J. Poult. Sci.* **2010**, *12* (4), 259−264.
(21) Wineland, M. Fundamentals of managing light for poultry. In *Commercial Chicken Meat and Egg Production*, 5th ed.,; Bell, D., Weaver, W., Eds.; Kluwer Academic Publishers: Dordrecht, The Netherlands, 2002; pp 129−148.
(22) Webster, B. Behavior of chickens. In *Commercial Chicken Meat and Egg Production*, 5th ed.; Bell, D., Weaver, W., Eds.; Kluwer Academic Publishers: Dordrecht, The Netherlands, 2002; pp 71−86.
(23) Iowa Egg Council. Available at http://iowaegg.org/#sthash.HH5porln.wxzK2AeQ.dpbs (last accessed October 2014).
(24) Kudo, K.; Nishimura, S.; Tabata, S. Distribution of taste buds in layer-type chickens: Scanning electron microscopic observations. *Anim. Sci. J.* **2008**, *79*, 680−685.
(25) Department of Agriculture. *Egg-Grading Manual*; U.S. Department of Agriculture: Washington, DC, 2000; Vol. *75*.
(26) Franchini, A.; Sirri, F.; Tallarico, N.; Minelli, G.; Iaffaldano, N.; Meluzzi, A. Oxidative stability and sensory and functional properties of eggs from laying hens fed supranutritional doses of vitamins E and C. *Poult. Sci.* **2002**, *81*, 1744−1750.
(27) Kirunda, D.; Scheideler, S.; McKee, S. The efficacy of vitamin E (DL-α-tocopheryl acetate) supplementation in hen diets to alleviate egg quality deterioration associated with high temperature exposure. *Poult. Sci.* **2001**, *80*, 1378−1383.
(28) Devera, L.; Nedomova, S.; Buchar, J. Influence of storing time and temperature on viscosity of an egg yolk. *J. Food Eng.* **2010**, *96*, 266−269.
(29) Ofosu, I.; Appiah-Nkansah, E.; Owusu, L.; Apea-Bah, F.; Oduro, I.; Ellis, W. Formulation of annatto feed concentrate for layers and the evaluation of egg yolk color preference of consumers. *J. Food Biochem.* **2010**, *34*, 66−77.
(30) Williams, W. Origin and impact of color on consumer preference for food. *Poult. Sci.* **1992**, *71*, 744−746.
(31) Varadarajulu, P.; Cunningham, F. A study of selected characteristics of hens' egg yolk. Influence of breed, strain, and age of bird. *Poult. Sci.* **1972**, *51*, 1327−1331.
(32) Anton, M. Composition and structure of hen egg yolk. In *Bioactive Egg Compounds*; Huopalahti, R., López-Fandiño, R., Anton, M., Schade, R., Eds.; Springer: Berlin and New York, 2007; pp 1−5.
(33) Restuccia, D.; Spizzirri, U.; Puoci, F.; Cirillo, G.; Vinvi, G.; Picci, N. Determination of phospholipids in food samples. *Food Rev. Int.* **2012**, *28*, 1−46.
(34) Kullenberg, D.; Taylor, L.; Schneider, M.; Massing, U. Health effects of dietary phospholipids. *Lipids Health Dis.* **2012**, *11* (3), 1−16.
(35) QPFC Kewpie Corp. Egg yolk lecithin pl-30S egg yolk oil; Kewpie Corp. Fine Chemical Division: Tokyo, Japan, 2010.
(36) USDA Nutrient Database, Agricultural Research Service, U.S. Department of Agriculture: Full Report (All Nutrients): 01123, Egg, whole, raw, fresh. Available at http://ndb.nal.usda.gov/ndb/foods/show/112?fg=&man=&lfacet=&count=&max=&sort=&qlookup=&offset=&format=Full&new=&measureby= (last accessed September 2014).
(37) Qureshi, A.; Pearce, B.; Nor, R.; Gapor, A.; Peterson, D.; Elson, C. Dietary α-tocopherol attenuates the impact of γ-tocotrienol on hepatic 3-hydroxy-3-methylglutaryl coenzyme a reductase activity in chickens. *J. Nutr.* **1996**, *126*, 389−394.
(38) Campo, J. Comparative yolk cholesterol content in four Spanish breeds of hens, an F_2 cross, and a white leghorn population. *Poult. Sci.* **1995**, *74*, 1061−1066.
(39) Bair, W.; Marion, W. Yolk cholesterol in eggs from various avian species. *Poult. Sci.* **1978**, *57*, 1260−1265.
(40) Golzar, S.; Ahbab, M.; Fani, A.; Hajbaei, A.; Ceylan, N.; Cooper, R. Egg yolk fatty acid profile of avian species − influence on human nutrition. *J. Anim. Physiol. Anim. Nutr.* **2013**, *97*, 27−38.
(41) Kazmierska, M.; Jarosz, B.; Korzeniowska, M.; Trziszka, T.; Dobrzanski, Z. Comparative analysis of fatty acid profile and cholesterol content of egg yolks of different bird species. *Polym. J. Food Nutr. Sci.* **2005**, *55* (14), 69−73.
(42) Christie, W.; Han, X. Preparation of derivatives of fatty acids. In *Lipid Analysis*, 4th ed.; The Oily Press: Bridgwater, England, 2010; pp 145−146.
(43) Busch, T.; King, A. Stability of cholesterol, 7-ketocholesterol, and beta-sitosterol during saponification: Ramifications for artifact monitoring of sterol oxide products. *J. Am. Oil Chem. Soc.* **2010**, *87*, 955−962.
(44) Bitman, J.; Wood, D. Cholesterol and cholesteryl esters of eggs from various avian species. *Poult. Sci.* **1980**, *59*, 2014−2023.

DOI: 10.1021/jf505536u
J. Agric. Food Chem. 2015, 63, 2537−2544

QDs. A conventional bulk polymerization was adopted to construct the MIP layer on the QDs for production of sesamol recognition sites in the prepared optosensing imprinted polymers. The MIPs and QDs acted as the recognition and response elements, respectively, and a spectrofluorometer was used as the signal output element in the process of experiment. The advantages of this experiment are easy preparation, portability, and simple and rapid operation.

MATERIALS AND METHODS

Materials and Reagents. Sesamol, piperonal (PN), *tert*-butylhydroquinone (TBHQ), and *tert*-butylhydroxyanisole (BHA) were obtained from Acros Organics (Morris Plains, NJ, USA). Other chemicals used for the MIP synthesis were the functional monomer methacrylic acid (MAA) and the cross-linker ethylene glycol dimethacrylate (EGDMA), which were purchased from Sigma-Aldrich (Shanghai, China), and 2,2-azobis(isobutyronitrile) (AIBN, 99%), which was purchased from Tianjin Kermel Chemical Reagents Co., Ltd. (Tianjin, China). CdSe/ZnS QDs were purchased from Jiayuan (Wuhan, China). Anhydrous ethanol and chloroform were of analytical reagent grade from Tianjin No. 1 Chemical Reagent Factory (Tianjin, China). Refined sesame oil was obtained from a local factory.

Characterization. Fluorescence measurements were performed on an F-2500 spectrofluorometer (Hitachi, Japan) equipped with a quartz cell (1 cm × 1 cm). It was carried out with the excitation wavelength of 280 nm with a recording emission range of 500−650 nm, and the slit widths of the excitation and emission were both 2.5 nm. UV−vis spectra (200−800 nm) were recorded on the Cary 50-Bio UV spectrometer (Victoria, Australia). Scanning electron microscopy (SEM, SU1510, Hitachi, Japan) was employed to observe the surface morphology and microstructure of synthetic material. Transmission electron microscope (TEM) images were obtained on a 2010 FEF microscope (JEOL, Tokyo, Japan). Samples for TEM were obtained by drying droplets of the sample in absolute alcohol on a 300-mesh Cu grid coated with a lacey carbon film.

Preparation of the Optosensing Chip. One-step polymerization was used to fabricate the optosensing material of MIP-coated CdSe/ZnS QDs. Under dark conditions, sesamol template molecule (1.0 mmol) and CdSe/ZnS QDs (0.05 mmol) were, respectively, dissolved in chloroform (5.0 mL). The functional monomer MAA (8.0 mmol) was added, and the solution was stirred for 30 min. Then cross-linker EGDMA (25 mmol) and free radical initiator AIBN (45 mg) were added. After the mixture had been stirred for another 30 min, it was sealed and thermally initiated in a water bath at 60 °C for 20 h. After the polymerization, the polymers were ground to powder using a mortar and then sieved through a 200-mesh sieve. The template molecule of sesamol was removed by Soxhlet extraction with 200 mL of methanol until sesamol was no longer detected and then put in a vacuum dryer at 40 °C for 10 h. The optosensing materials of MIP-coated CdSe/ZnS QDs were obtained. The nonmolecularly imprinted polymers (NIPs) were prepared using the same procedure but without addition of sesamol. The optosensing material of MIP- or NIP-coated (0.5 mg) CdSe/ZnS QDs was transferred to a chitosan solution (0.5%, 5 mL) and ultrasonicated for a few minutes to yield a 0.1 mg/mL suspension that was dropped (10 μL) onto the surface of a commercial 9 MHz AT-cut quartz crystal with polished Au electrodes to prepare the optosensing chip.

Selectivity Experiments of Sesamol by the Optosensing Chip. Selectivity experiments were carried out using PN as a sesamol structural analogue and TBHQ and BHA as structural and functional analogues for sesamol in sesame oil. The prepared optosensing chip was put into the quartz cell containing anhydrous ethanol solution (3 mL) and then dropped into the different concentrations of analyte for spectrofluorometer analysis.

Analysis of Sesame Oil Samples. The sesame oil samples (0.1 g) were spiked with sesamol at three different levels: 5, 10, and 20 μg g^{-1}, respectively. The oil/sesamol mixture was left to stand for 12 h, and then it was dissolved in anhydrous ethanol (10 mL). Three milliliters was removed and put into a quartz cell before the optosensing chip was added for spectrofluorometer analysis.

Statistical Analysis. The results were expressed in terms of standard deviation for three independent determinations. Student's t test was applied to calculate the significant difference between values.

RESULTS AND DISCUSSION

Fabrication of an Optosensing Chip for Sesamol. We propose a one-step synthetic strategy for the optosensing imprinted materials of MIP-coated CdSe/ZnS QDs and then drop it on the surface of a commercial 9 MHz AT-cut quartz crystal to prepare an optosensing chip. The general scheme for the synthesis process is illustrated in Figure 1. Typically, CdSe/ZnS QDs are wrapped in MIPs by cross-linking the functional monomers (MAA) and cross-linker (EGDMA). Subsequently, the carboxyl groups of MAA reacted with the phenolic hydroxyl groups of the template molecules (sesamol) via hydrogen bonding. The sesamol molecules were extracted from the prepolymer using 200 mL of methanol to decompose the hydrogen bond, yielding distinct sesamol binding sites. Prior to the removal of the sesamol, the fluorescence intensity of the MIP-coated QDs was about 64.3% of that from NIP-coated QDs, but after removal of the sesamol, the fluorescence intensity of the MIP-coated QDs increased to 98.3% of that from NIP-coated QDs (Figure 2). These results indicated the facile and effective removal of the sesamol from the starting material. Finally, the optosensing material was put into a chitosan solution to form a uniform suspension after it was dropped on the surface of a chip. To verify the effects of the chitosan solution on the recognition

Figure 1. Schematic illustration of the preparation of the optosensing chip.

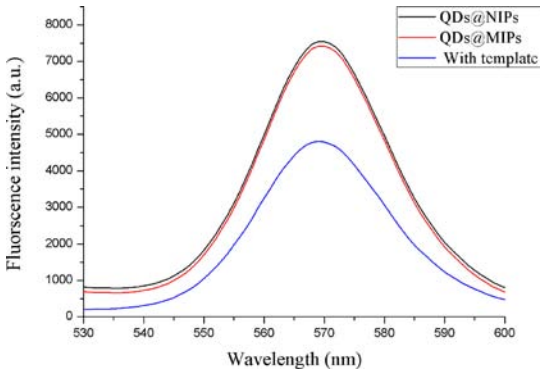

Figure 2. Fluorescence spectra of the optosensing materials of QDs@NIPs, QDs@MIPs, and QDs@MIPs with template.

DOI: 10.1021/jf505790c
J. Agric. Food Chem. 2015, 63, 2545−2549

site of MIPs, the same amounts of MIPs were added to absorb the same concentration of sesamol in the presence or absence of chitosan. The role of chitosan was to locate for the prepared materials on the surface of the sensing chip. The fluorescence intensities of the two samples were nearly the same, as shown in Figure S1 (Supporting Information), which indicated that the chitosan solution did not affect the adsorption properties of MIPs.

Characterization of QDs and Optosensing Imprinted Material. The TEM image of the initial CdSe/ZnS QDs (Supporting Information, Figure S2a) indicates a uniform size and distribution. The SEM image of the MIP-coated CdSe/ZnS QDs (Supporting Information, Figure S2b) reveals a spherical morphology with a larger particle size than that of the initial CdSe/ZnS QDs. This indicated that the MIPs layer coated the surface of the CdSe/ZnS QDs.

Reacting Mechanism of the Optosensing Chip for Sesamol. The fluorescence intensity of the optosensing chip decreased significantly in the presence of sesamol and recovered after the sesamol was extracted. A charge transfer from QDs to sesamol is responsible for the fluorescence quenching of the CdSe/ZnS QDs. Such a charge-transfer mechanism has also been suggested by Tu et al.[24] The UV absorption band of sesamol is close to the band gap of the CdSe/ZnS QDs as revealed by the absorption spectra (Figure 3), the charges of the conductive

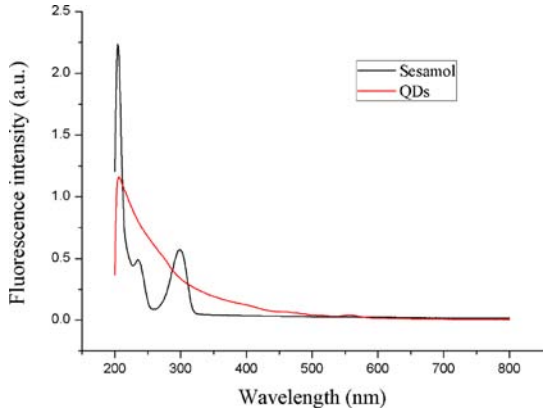

Figure 3. UV−vis spectra of sesamol solution and the optosensing material.

bands of the CdSe/ZnS QDs can transfer to the lowest unoccupied molecular orbital of the UV band of sesamol molecules. There is no spectral overlap between the absorption spectrum of the sesamol species and the emission spectrum of the QDs.

Analytical Figures of the Optosensing Chip for the Fluorescence Detection of Sesamol. The fluorescence quenching in this system followed the Stern−Volmer equation as shown in Figure 4

$$F_0/F = 1 + K_{SV}[C] \quad (1)$$

where F_0 and F are the fluorescence intensity of QDs in the absence and presence of sesamol, respectively, K_{SV} is the Stern−Volmer constant, and [C] is the quencher concentration. This equation was used to quantify the different quenching constants in this research, and the ratio of K_{SV} of the MIPs and NIPs ($K_{SV,MIPs}/K_{SV,NIPs}$) was defined as the imprinting factor to evaluate the selectivity of the optosensing chip.

To further evaluate the analytical performance of the optosensing chip, the detection limit and linear range were investigated. The optosensing chip exhibits linear fluorescent quenching for sesamol in the concentration range from 2.4×10^{-6} to 1.2×10^{-3} mol L^{-1} with a correlation coefficient of 0.9976 and $F_0/F = 0.0014Q + 1.5594$ (where Q is the concentration of sesamol in μmol L^{-1}). The detection limit, which was calculated as the concentration of sesamol that quenched 3 times the standard deviation of the blank signal and then divided by the slope of the standard curve, was 7.2×10^{-8} mol L^{-1}. Finally, the relative standard deviation for five repeated measurements of 4.8×10^{-4} mol L^{-1} sesamol was 2.2%.

Specificity of the Optosensing Chip. The performance of the optosensing chip was further demonstrated by competitive binding experiment. PN as a structural analogue for sesamol and TBHQ and BHA as structural and functional analogues in sesame oil were involved to evaluate the specificity of the optosensing chip. As shown in Figure 5a, the changes in fluorescence intensity of MIP-coated QDs for sesamol were much greater than those for PN, TBHQ, and BHA, owing to the high selectivity and specificity of MIPs. The result demonstrated that the recognition of MIP-coated QDs is based on the interactions of the size, shape, and functionality of the template. Therefore, sesamol was strongly bound to the particles and caused a significant change of fluorescence intensity. When sesamol was not existent, the adsorption capacity of the optosensing chip for the analogues was obvious. This demonstrated that the optosensing chip could be applied to the analysis of similar structure, when sesamol did not exist in the real sample. Furthermore, the changes in fluorescence intensity for the MIP-coated QDs were much higher than those for the NIP-coated QDs. This indicated that the imprinted cavities allowed the sesamol to access the receptor sites by the removal of the template, during the preparation process.

The competitive binding experiment was performed by fixing the concentration of sesamol and increasing the concentration of PN. As shown in Figure 5b, the changes in fluorescence intensity were not obvious by the increase of the ratio of $C_{PN}/C_{Sesamol}$. Although the same hydrogen bond formed between PN and MAA, because of a structure similar to that of sesamol, the adsorption capacity for PN was much lower than that for sesamol.

Reproducibility of the Optosensing Chip. The advantage of the optosensing chip is good reproducibility, and it can be used repeatedly. The reproducibility of the optosensing chip was investigated by measuring the fluorescence intensity response in a seamol at a concentration of 4.8×10^{-4} mol L^{-1}. After each measurement, the chip was washed with methanol/acetic acid (9:1, v/v) to remove the analyte molecules. The relative standard deviation (RSD) for the five repeated analyses was 2.2%, indicating a good reproducibility.

Application of the Optosensing Chip to the Detection of Sesamol in Sesame Oil Samples. The developed fluorescence method based on the optosensing chip of MIP-coated CdSe/ZnS QDs was applied to determine sesamol in sesame oil samples. For this purpose, sesame oil samples from a local factory were determined to be free of sesamol by the HPLC method. Because of the complex oil samples, the available interferences affecting the application performance of the optosensing chip were unpredictable. A recovery study was carried out on the samples spiked with 5, 10, and 20 μg g^{-1} sesamol to evaluate the accuracy for sesamol determination in real samples by the developed fluorescence method (Table 1).

DOI: 10.1021/jf505790c
J. Agric. Food Chem. 2015, 63, 2545−2549

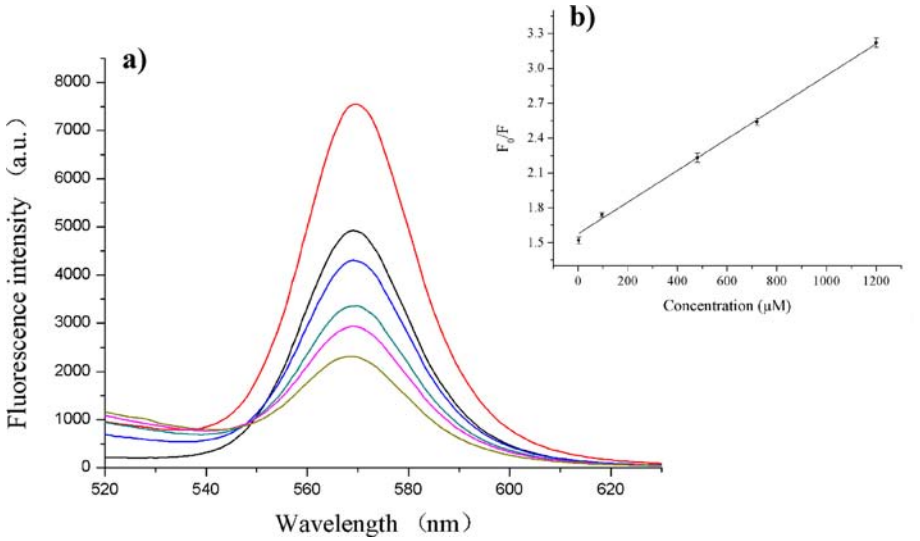

Figure 4. (a) Fluorescence spectra of the optosensing chip with the increasing concentrations of sesamol. (b) Effect of sesamol concentration on the fluorescence intensity of the optosensing chip.

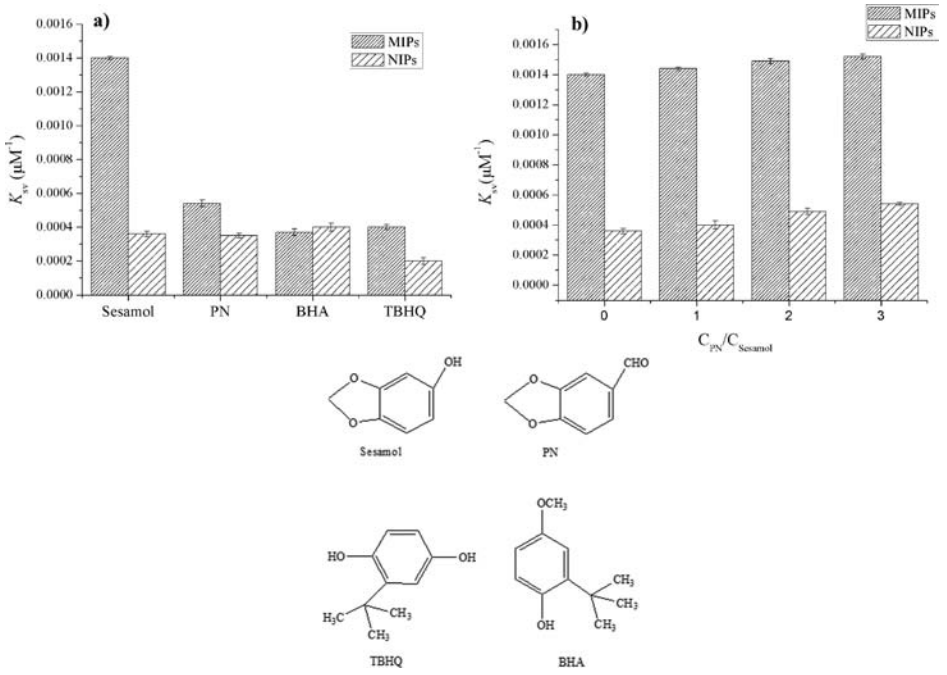

Figure 5. (a) Specificity of the optosensing chip for sesamol, PN, TBHQ, and BHA. (b) Effect of the competitive analogue PN on the binding of template sesamol on the optosensing chip.

Table 1. Spiked Recovery Results for the Determination of Sesamol in Sesame Oil Samples (RSD%, n = 3)

spike level (μg g^{-1})	theor level (μg g^{-1})	determined[a] (mean ± SD; n = 3, μg g^{-1})	recovery (%)
5	1.5	1.48 ± 0.17	98.7
10	3	3.07 ± 0.09	102.3
20	6	5.69 ± 0.32	94.8

[a]Determined results are not significantly different with spike levels ($t < t_{0.05}$). Values given are the means of three samples ± standard deviation.

The recoveries ranging from 94.8 to 102.3% showed the ability of our optosensing chip to provide accurate measures of sesamol concentrations in real sesame oil samples. The imprinting factor, which is calculated as the ratio of $K_{SV,MIPs}$ to $K_{SV,NIPs}$, was 3.9 for sesamol, indicating an efficient imprinting.

The practicality of the developed optosensing chip method was validated by a comparison with the totally independent technique of HPLC, with a UV detector. Sesamol was detected by absorbance at 294 nm. The results of spike−recovery test by HPLC-UV are shown in Table S1 (Supporting Information). Student's t test was applied to calculate the significant difference between the developed method and HPLC-UV. The result of statistical analysis was 1.9 (less than $t_{0.05}$), which indicated that the difference of the two methods was not significant. This was consistent with the developed fluorescence method of optosensing chip based on MIP-coated CdSe/ZnS QDs.

Conclusions. In summary, a novel method for the detection of sesamol based on an optosensing chip is developed in this

DOI: 10.1021/jf505790c
J. Agric. Food Chem. 2015, 63, 2545−2549

study. It was successfully applied to analyze sesamol in real sesame oil samples, without prior separation or derivatization processes and without large-scale instrumentation, using only a simple spectrofluorometer. Although the optosensing analytical method is still in its infancy, the simple preparation, high selectivity, low cost, and simple sample pretreatment processes make this technique attractive.

■ ASSOCIATED CONTENT

Supporting Information

Figures S1 and S2 and Table S1. This material is available free of charge via the Internet at http://pubs.acs.org.

■ AUTHOR INFORMATION

Corresponding Author

*(J.W.) Phone: +86 10-68984545. Fax: +86 10-68985456. E-mail: wangjing@th.btbu.edu.cn.

Funding

This work was supported by National Natural Science Foundation of China (No. 31271976), the Importation and Development of High-Caliber Talents Project of Beijing Municipal Institutions (No. CIT&TCD20130309 and IDHT20130506), and the Food Quality and Safety Platform of Beijing Municipal Education Commission.

Notes

The authors declare no competing financial interest.

■ REFERENCES

(1) Lee, W. J.; Su, N. W.; Lee, M. H.; Lin, J. T. Assessment of authenticity of sesame oil by modified Villavecchia test and HPLC-ELSD analysis of triacylglycerol profile. *Food Res. Int.* **2013**, *53*, 195−202.

(2) Suja, K. P.; Jayalekshmy, A.; Arumughan, C. Free radical scavenging behavior of antioxidant compounds in sesame in DPPH system. *J. Agric. Food Chem.* **2004**, *52*, 912−915.

(3) Uchida, M.; Nakajn, S.; Toyoshima, M. Antioxidative effect of sesamol and related compounds on lipid peroxidation. *Biol. Pharm. Bull.* **1996**, *19*, 623−626.

(4) Hsu, D. Z.; Chen, K. T.; Li, Y. H.; Chuang, Y. C.; Liu, M. Y. Sesamol delay mortality and attenuates hepatic injury after cecal ligation and puncture in rats: role of oxidative stress. *Shock* **2006**, *25*, 528−532.

(5) Hsu, D. Z.; Li, Y. H.; Chu, P. Y.; Chien, S. P.; Chuang, Y. C.; Liu, M. Y. Attenuation of endotoxin-induced oxidative stress and multiple organ injury by 3,4-methylenedioxyphenal in rats. *Shock* **2006**, *25*, 300−305.

(6) Ohta, S.; Suzuki, M.; Sato, N.; Kamogawa, A.; Shinoda, M. Protective effects of sesamol and its related compounds on carbon tetrachloride induced liver injury in rats. *Yakugaku Zasshi* **1994**, *114*, 901−910.

(7) Kaur, I. P.; Saini, A. Sesamol exhibits antimutagenic activity against oxygen species mediated mutagenicity. *Mutat. Res.*. **2000**, *470*, 71−76.

(8) Kapadia, G. J.; Azuine, M. A.; Tokuda, H.; Takasaki, M.; Mukainaka, T.; Konoshima, T.; Nishino, H. Chemopreventive effect of resveratrol, sesamol, sesame oil and sunflower oil in the Epstein-Barr virus early antigen activation assay and the mouse skin two state carcinogenesis. *Pharmacol. Res.* **2002**, *45*, 499−505.

(9) Liu, Z.; Xiang, Q.; Du, L.; Song, G.; Wang, Y.; Liu, X. The interaction of sesamol with DNA and cytotoxicity, apoptosis, and localization in HepG2 cells. *Food Chem.* **2013**, *141*, 289−296.

(10) Sun, W.; Xiao, R. Determination of sesamol in sesame oil by anion exchange solid phase extraction coupled with HPLC. *Anal. Methods−U.K.* **2014**, *6*, 6432−6436.

(11) Wang, X.; Pan, J.; Guan, W.; Zou, X.; Huo, P.; Yan, Y.; Hu, W. Selective recognition of sesamol using molecularly imprinted polymers containing magnetic wollastonite. *J. Sep. Sci.* **2011**, *34*, 3287−3294.

(12) Bhargava, R. N.; Gallaghar, D.; Hong, X.; Nurmikko, A. Optical properties of manganese-doped nanocrystals of ZnS. *Phys. Rev. Lett.* **1994**, *72*, 416−419.

(13) Bruchez, M.; Moronne, M.; Gin, P.; Weiss, S.; Alivisatos, A. P. Semiconductor nanocrystals as fluorescent biological labels. *Science* **1998**, *281*, 2013−2016.

(14) Chan, W. C. M.; Nie, S. Quantum dot bioconjugates for ultrasensitive nonisotopic detection. *Science* **1998**, *281*, 2016−2018.

(15) Lan, G. Y.; Lin, Y. W.; Huang, Y. F.; Chang, H. T. Photo-assisted synthesis of highly fluorescent ZnSe(S) quantum dots in aqueous solution. *J. Mater. Chem.* **2007**, *17*, 2661−2666.

(16) Lin, C. I.; Joseph, A. K.; Chang, C. K.; Lee, Y. D. Molecularly imprinted polymeric film on semiconductor nanoparticles analyte detection by quantum dot photoluminescence. *J. Chromatogr., A* **2004**, *1027*, 259−262.

(17) Lin, C. I.; Joseph, A. K.; Chang, C. K.; Lee, Y. D. Synthesis and photoluminescence study of molecularly imprinted polymers appended onto CdSe/ZnS core-shells. *Biosens. Bioelectron.* **2004**, *20*, 127−131.

(18) Chen, Y. P.; Wang, D. N.; Yin, Y. M.; Wang, L. Y.; Wang, X. F.; Xie, M. X. Quantum dots capped with dummy molecularly imprinted film as luminescent sensor for the determination of tetrabromobisphenol A in water and soils. *J. Agric. Food Chem.* **2012**, *60*, 10472−10479.

(19) Li, H. B.; Li, Y. L.; Cheng, J. Molecularly imprinted silica nanospheres embedded CdSe quantum dots for highly selective and sensitive optosensing of pyrethroids. *Chem. Mater.* **2010**, *22*, 2451−2457.

(20) Stringer, R. C.; Gangopadhyay, S.; Grant, S. Detection of nitroaromatic explosives using a fluorescent-labeled imprinted polymer. *Anal. Chem.* **2010**, *82*, 4015−4019.

(21) Liu, H. L.; Fang, G. Z.; Li, C. M.; Pan, M. F.; Liu, C. C.; Fan, C.; Wang, S. Molecularly imprinted polymer on ionic liquid-modified CdSe/ZnS quantum dots for the highly selective and sensitive optosensing of tocopherol. *J. Mater. Chem.* **2012**, *22*, 19882−19887.

(22) Liu, H.; Fang, G.; Zhu, H.; Li, C.; Liu, C.; Wang, S. A nove lionic liquid stabilized molecularly imprinted optosensing material based on quantum dots and graphene oxide for specific recognition of vitamin E. *Biosens. Bioelectron.* **2013**, *47*, 127−132.

(23) Liu, H.; Fang, G.; Zhu, H.; Wang, S. Application of molecularly imprinted polymer appended onto CdSe/ZnS quantum dots for optosensing of tocopherol in rice. *Food Anal. Methods* **2014**, *7*, 1443−1450.

(24) Tu, R.; Liu, B.; Wang, Z.; Gao, D.; Wang, F.; Fang, Q.; Zhang, Z. Amine-capped ZnS-Mn^{2+} nanocrystals for fluorescence detection of trace TNT explosive. *Anal. Chem.* **2008**, *80*, 3458−3465.

DOI: 10.1021/jf505790c
J. Agric. Food Chem. 2015, 63, 2545−2549

Myofibrils were isolated according to the method of Park et al.[13] Thawed and minced muscle was homogenized by blending for 30 s in an ultraturrax with 4 volumes (w/v) of a cold isolation buffer (10 mM sodium phosphate buffer, 0.1 M NaCl, 2 mM $MgCl_2$, and 1 mM ethylene glycol tetraacetic acid (EGTA), pH 7.0). The muscle homogenate was centrifuged at 2000*g* for 15 min, and the supernatant was discarded. The myofibril pellet was washed two more times with 4 volumes of the same isolation buffer using the same blending and centrifugation conditions as indicated above. The myofibril pellet was then washed three more times with 4 volumes of 0.1 M NaCl under the same conditions as above except that, in the last wash, the myofibril suspension was filtered through a strainer to remove connective tissue, and its pH was adjusted to 6.0 with 0.1 N HCl prior to centrifugation. The isolated myofibrillar proteins were stored in a tightly capped bottle, kept on ice, and used within 24 h. The protein concentration of the myofibril pellet was measured by the biuret method[15] using bovine serum albumin (BSA) as standard.

The myofibrillar proteins were oxidized under meat-processing conditions according to the method of Estévez et al.[16] Briefly, the isolated myofibrillar proteins were suspended in 15 mM piperazine-*N*,*N*-bis(2-ethanesulfonic acid) (PIPES) buffer (pH 6.0) containing 0.6 M NaCl (total volume = 30 mL; 20 mg protein/mL). The suspensions were oxidized with 0.01 mM $FeCl_3$, 0.1 mM ascorbic acid, and 1 mM H_2O_2 (final concentration). Three doses of $NaNO_2$ (0, 100, or 1000 mg $NaNO_2$/kg protein) were added, and the samples were incubated at 37 °C for 7 days with constant stirring. After 30 min (without incubation at 37 °C) and 4 and 7 days, suspensions were divided in aliquots of 1.2 mL and stored at −80 °C until analysis. Myofibrillar proteins suspended in PIPES buffer without oxidants or $NaNO_2$ were used as nonoxidized control.

Raw Porcine Patties. Lean porcine longissimus muscles were purchased from a local slaughterhouse at 2 days post mortem. Three treatments were considered: 0, 18, or 180 mg of $NaNO_2$ per kilogram patty. In the basic formulation, the ingredients were as follows: 500 g of meat, 35 g of distilled water, 8.5 g of sodium chloride, and 0, 0.01, or 0.1 g of $NaNO_2$. The muscles were trimmed of visible fat and connective tissue and subsequently diced into approximately 5 g pieces. The meat was ground in a grinder (Omega T-12) equipped with a 10 mm plate. NaCl and $NaNO_2$ were dissolved in the distilled water and immediately added to the meat. After mixing of the batter by hand, the mixture was ground once more with a 3.5 mm plate. Nine patties of 40 g were prepared per treatment. Three patties were immediately vacuum-packed and stored at −80 °C until analysis (day 0). The six remaining patties were wrapped in an oxygen-permeable film and subjected to illuminated chilled display (4 °C, 1000 lx). After 4 and 7 days of display, three patties were vacuum-packed and stored at −80 °C until analysis. The entire patty manufacturing and display process was performed in duplicate.

Chemical Analyses. *Proximate Composition.* Dry matter, crude protein, and crude fat contents were analyzed on two unexposed patties per treatment according to ISO 1442-1973, ISO 937-1978, and ISO 1444-1973 methods, respectively. Results were expressed as grams per 100 g of fresh matter. The pH was measured using a glass pH-electrode.

Thiol Concentration. The thiol concentration was determined in the isolated myofibrillar proteins and patties after derivatization by Ellman's reagent, 5,5′-dithiobis(2-nitrobenzoic acid) (DTNB), adopted from Jongberg et al.[5] An aliquot of 1.2 mL myofibrillar protein suspension was defrosted and centrifuged for 20 min at 2000*g*. The supernatant was carefully discarded, and 1.0 mL of 0.1 M tris(hydroxymethyl)aminomethane (TRIS) buffer (pH 8.0) was added to the pellet, vortexed, and centrifuged at 2000*g* for 20 min. After the supernatant had been discarded, 1.0 mL of TRIS buffer was added to the pellet, and everything was transferred to a test tube. The microtube was rinsed twice with 1 mL of TRIS buffer, which was also transferred to the test tube. Three milliliters of 10% sodium dodecyl sulfate (SDS) in 0.1 M TRIS buffer (pH 8.0) was added, and the proteins were dissolved by 1 h of incubation in a water bath heated to 80 °C. After cooling, samples were centrifuged at 1400*g* for 10 min, and the thiol concentration of the supernatant was analyzed. For the raw patties, 2 g was homogenized with 50 mL of 5% SDS buffer. The proteins were dissolved by 1 h of incubation in a water bath heated to 80 °C. After cooling, samples were filtered, and the filtrate was used for further analysis. For both the myofibrillar proteins and the patties, 2 mL of 0.1 M TRIS buffer (pH 8.0) and 0.5 mL of 10 mM DTNB dissolved in 0.10 M TRIS buffer (pH 8.0) were added to 0.5 mL of sample. For each sample a blank was included containing 0.5 mL of sample and 2.5 mL of 0.10 M TRIS buffer (pH 8.0). A solution containing 0.5 mL of 5% SDS in TRIS buffer (pH 8.0), 0.5 mL of 10 mM DTNB, and 2.0 mL of 0.1 M TRIS buffer (pH 8.0) was used as reagent blank. All mixtures were protected against light and allowed to react for exactly 30 min. The absorbance was measured spectrophotometrically at 412 nm, and the thiol concentration was calculated using the formula of Lambert−Beer (ε_{412} = 14000 M^{-1} cm^{-1}) and expressed in nanomoles of thiol per milligram of protein. The blank samples were used to determine the protein content. Protein content was analyzed spectrophotometrically at 280 nm using a BSA standard curve.

Protein Carbonyl Content. The protein carbonyl content of the isolated myofibrillar proteins and patties was determined by derivatization with 2,4-dinitrophenylhydrazine (DNPH) as described by Levine et al.[17] with some modifications. An aliquot of 1.2 mL of myofibrillar protein suspension was defrosted and centrifuged for 20 min at 2000*g*. The pellet was then resuspended in 1 mL of phosphate buffer (20 mM, pH 6.5), and four aliquots of 0.2 mL were taken. For the raw patties, 3 g of meat with 30 mL of phosphate buffer (20 mM, pH 6.5 containing 0.6 M NaCl) was homogenized and four aliquots of 0.2 mL were taken. All aliquots were treated with 1 mL of ice-cold trichloroacetic acid (TCA, 10%) to precipitate the proteins. The samples were left for 15 min in an ice bath, and after centrifugation at 2000*g* for 30 min, the supernatant was discarded. Another milliliter of ice-cold TCA (10%) was added, and the above-mentioned procedure was repeated. For both the myofibrillar protein isolates and the patty pellets, two aliquots were treated with 0.5 mL of 10 mM DNPH dissolved in 2.0 M HCl, and two aliquots were treated with 0.5 mL of 2.0 M HCl (blank). The samples were placed on a vortex (350 rpm) for 1 h covered from light to derivatize. Subsequently, 0.5 mL of ice-cold 20% TCA was added, vortexed, and placed on ice for 15 min before centrifugation at 2000*g* for 20 min, after which the supernatant was discarded. Excess DNPH was removed by three washings with 1.0 mL of ethanol/ethyl acetate (1:1 v/v), vortexing, and centrifuging at 2000*g* for 20 min. After every wash, the supernatant was discarded. Following the final wash, excess solvent was removed by leaving the samples for 15 min under the hood. The pellets were dissolved in 1.0 mL of 6.0 M guanidine hydrochloride in 20 mM phosphate buffer (pH 6.5) and placed on a vortex (350 rpm) for 30 min covered from light. The final solution was centrifuged at 9500*g* for 10 min to remove insoluble material. The carbonyl concentration (nmol/mg protein) was calculated from the absorbance at 280 and 370 nm of the samples using the equation[17]

$$\frac{C_{\text{hydrazone}}}{C_{\text{protein}}} = \frac{A_{370}}{\varepsilon_{\text{hydrazone},370} \times (A_{280} - A_{370} \times 0.43)} \times 10^6$$

where $\varepsilon_{\text{hydrazone},370}$ is 22000 M^{-1} cm^{-1} and the carbonyl concentrations obtained from the blanks were subtracted from the contribution obtained from the corresponding treated sample.

Protein Solubility. Changes in solubility of the myofibrillar protein suspension were measured according to the method of Liu et al.[18] with minor modifications. Protein solubility was defined as the protein concentration in the supernatant, after centrifugation at 5000*g* (for 15 min), divided by the protein concentration of the original myofibril suspension. The protein concentration was determined according to the biuret method[15] using BSA as standard and expressed as milligrams of soluble protein per 100 mg of protein. For the patties, 3 g of meat was homogenized with 30 mL of NaCl (0.015 M). The concentration of the obtained protein solution was determined using the biuret method after centrifugation at 2000*g* for 10 min. Results were expressed as milligrams of solubilized protein per gram of meat.

DOI: 10.1021/jf505775u
J. Agric. Food Chem. 2015, 63, 2550−2556

3-Nitrotyrosine. The 3-nitrotyrosine content was quantified spectrophotometrically after alkalinization in both the myofibrillar protein isolates and patties according to the method of Fontana et al.[19] with some modifications. Aliquots of 1.2 mL of myofibrillar protein isolates were defrosted, and two aliquots of 0.5 mL were taken. After centrifugation at 2000*g* for 30 min, the supernatant was carefully discarded. For the raw patties, 3 g of meat with 30 mL of phosphate buffer (20 mM, pH 6.5 containing 0.6 M NaCl) was homogenized, and two aliquots of 0.2 mL were treated with 1 mL of ice-cold TCA (10%). The samples were left for 15 min in an ice bath, and after centrifugation at 2000*g* for 30 min, the supernatant was discarded. Another milliliter of ice-cold TCA (10%) was added, and the above-mentioned procedure was repeated. To both the myofibrillar protein and patty pellets was added 1 mL of guanidine−HCl (6 M). After 1 h on a vortex, 0.6 mL was transferred into a microtube, an equal amount of bicarbonate buffer (0.2 M, pH 10.5) was added, and the samples were centrifuged at 9500*g* for 10 min. The 3-nitrotyrosine content was quantified spectrophotometrically at 430 nm, using 3-nitro-L-tyrosine as standard. The total protein content was quantified at 280 nm using BSA as standard. Results were expressed as nanomoles of 3-nitrotyrosine per milligram of protein.

Lipid Oxidation. Malondialdehyde, a secondary lipid oxidation product, was determined in the patties following a thiobarbituric acid reactive substances (TBARS) method using extraction with perchloric acid.[3] Malondialdehyde forms a colored complex with thiobarbituric acid, which was determined spectrophotometrically at 532 nm. Five grams of minced patty was dispensed in a plastic tube and homogenized with 30 mL of perchloric acid (0.6 M) and 1 mL of butylhydroxytoluene (1.5% (w/v) in ethanol). The homogenate was filtered, and 5 mL aliquots were mixed with 1 mL of thiobarbituric acid (6 mM) in test tubes. The test tubes were placed in a boiling water bath for 35 min. After cooling, the absorbance was measured at 532 nm. The standard curve was prepared using 1,1,3,3-tetramethoxypropane, and results were expressed as milligrams of malonaldehyde per kilogram of patty.

Statistical Analysis. Statistical analysis was performed using SPSS version 22. Two-way analysis of variance (ANOVA) was used to evaluate the main effects "display time" and "$NaNO_2$" and their interaction term. Differences between treatments were tested using Tukey's post hoc test operating at a 5% level of significance.

RESULTS

Proximate Composition of the Patties. Across treatments, the mean pH, dry matter, and fat and protein contents of the patties were respectively 5.40 ± 0.03, 25.5 ± 0.4 g/100 g patty, 1.35 ± 0.23 g/100 g patty, and 19.9 ± 0.6 g/100 g patty. No treatment effects were observed ($p > 0.05$).

Protein Carbonyl Content. Seven days of induced in vitro oxidation resulted in an approximately 10-fold higher content of carbonyl compounds in the isolated myofibrillar proteins when compared to the nonoxidized myofibrillar proteins (Figure 1A). The addition of sodium nitrite affected the formation of carbonyl compounds after 30 min of induced oxidation as significantly higher carbonyl concentrations were found in the samples treated with 1000 mg/kg $NaNO_2$ compared to the treatment without $NaNO_2$. However, this effect was not observed after 4 and 7 days of induced oxidation (Figure 1A). For the patties, on average significantly lower carbonyl concentrations were found across days of display in patties treated with 180 mg/kg sodium nitrite compared to 0 and 18 mg/kg (Table 1); however, within each day of display no significant differences were observed (Figure 1B). The carbonyl concentrations of the patties did not change significantly during the whole period of illuminated chilled display (Table 1).

Protein Thiol Groups. From the moment the oxidants were added to the isolated myofibrillar proteins, the thiol concentrations decreased 4-fold compared to the nonoxidized myofibrillar proteins (Figure 2A). During the following 7 days no further decrease of thiol groups was observed, and the addition of sodium nitrite did not affect the thiol content (Table 1). Across treatments, the thiol content of the patties decreased significantly during illuminated chilled display (Table 1). The addition of 180 mg $NaNO_2$/kg resulted at days 4 and 7 of illuminated display in significantly lower thiol concentrations compared to the other two treatments (Figure 2B).

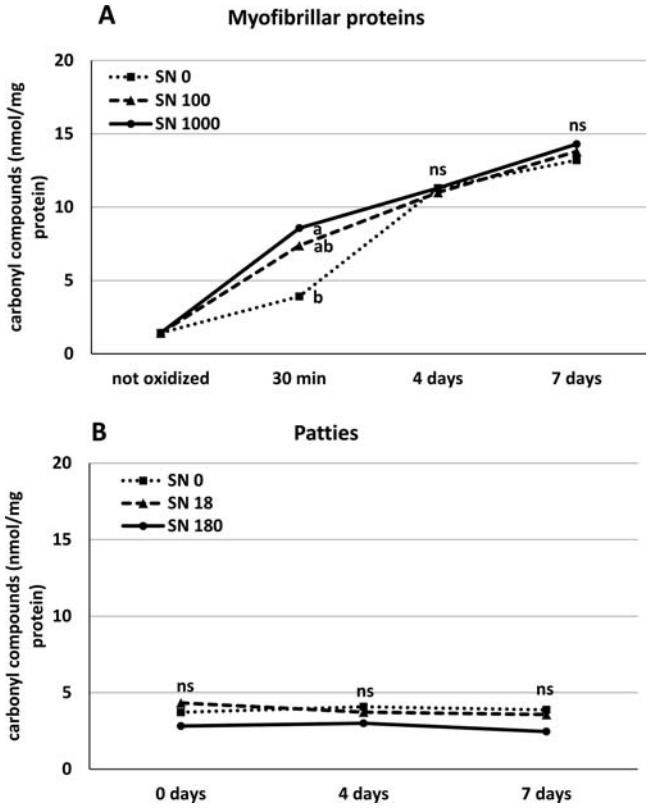

Figure 1. Effect of nitrite dose (SN, mg/kg) on protein carbonyl compounds (nmol/mg protein) in (A) myofibrillar protein isolates during Fenton reagent-induced oxidation ($n = 3$) and in (B) raw patties during illuminated chilled display ($n = 6$). ns, not significant; a, b, values within a display day with different letters are significantly different ($p < 0.05$).

Protein Solubility. The protein solubility of the isolated myofibrillar proteins after 30 min of induced oxidation was 2-fold higher compared to the nonoxidized myofibrillar proteins, probably because of the added NaCl (Figure 3A). The protein solubility decreased significantly in the myofibrillar protein isolates during in vitro oxidation and in the patties during illuminated chilled display (Table 1). No effect of nitrite on protein solubility was found for either the isolated myofibrillar proteins or the patties (Figure 3 and Table 1).

3-Nitrotyrosine. The 3-nitrotyrosine content of the isolated myofibrillar proteins remained constant during the experiment, except for 2-fold lower 3-nitrotyrosine concentrations in samples treated with 100 and 1000 mg $NaNO_2$/kg after 30 min of induced oxidation (Figure 4A). The 3-nitrotyrosine content of the patties was not affected by the added sodium nitrite content (Figure 4B) or by the display period (Table 1).

Lipid Oxidation. A significant increase of TBARS values was observed during illuminated chilled display for the

DOI: 10.1021/jf505775u
J. Agric. Food Chem. 2015, 63, 2550−2556

Table 1. Significance Values for the Main Effects of "Nitrite", "Display Time", and Their Interaction Term on the Protein and Lipid Chemical Markers

	carbonyl compounds	thiol groups	protein solubility	3-nitrotyrosine	TBARS
myofibrillar protein isolates					
nitrite	0.037	0.257	0.053	0.105	–[a]
time	<0.001	0.115	<0.001	<0.001	–
nitrite × time	ns[b]	ns	ns	0.015	–
patties					
nitrite	0.003	<0.001	0.347	0.166	<0.001
time	0.653	<0.001	<0.001	0.317	<0.001
nitrite × time	ns	ns	ns	ns	<0.001

[a]–, not analyzed. [b]ns, not significant ($p > 0.05$).

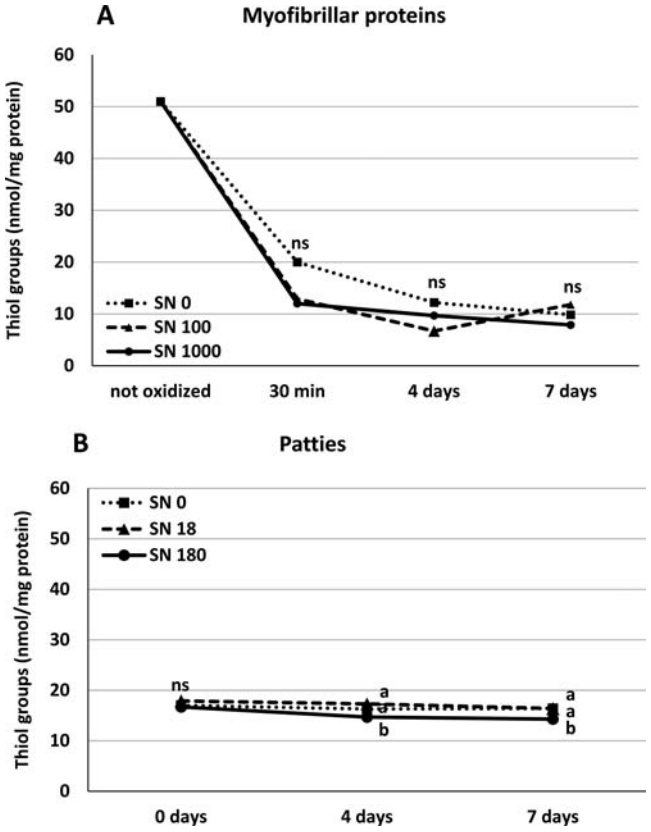

Figure 2. Effect of nitrite dose (SN, mg/kg) on protein thiol groups (nmol/mg protein) in (A) myofibrillar protein isolates during Fenton reagent-induced oxidation (n = 3) and in (B) raw patties during illuminated chilled display (n = 6). ns, not significant; a, b, different letters within display day indicate significant differences ($p < 0.05$).

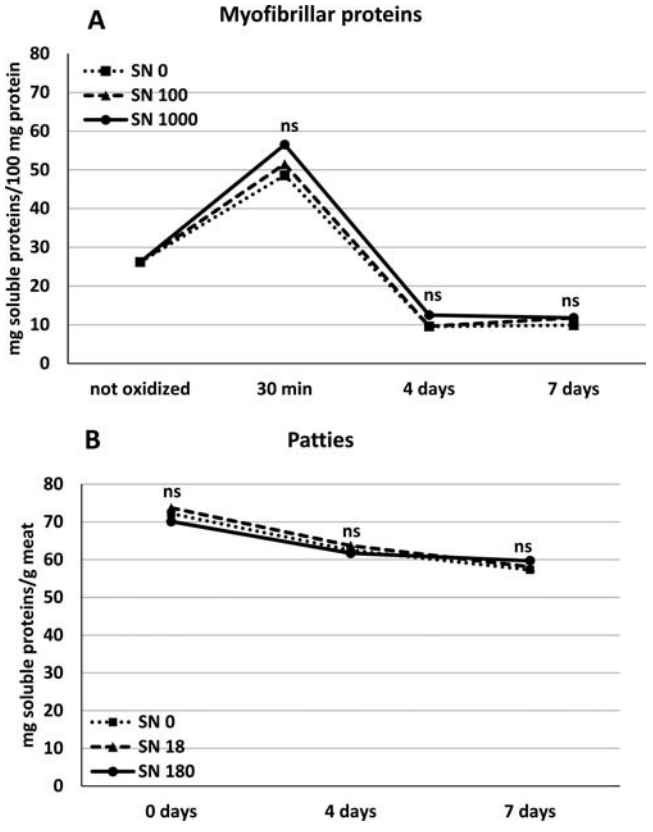

Figure 3. Effect of nitrite dose (SN, mg/kg) on protein solubility in (A) myofibrillar protein isolates (mg soluble protein/100 mg protein) during Fenton reagent-induced oxidation (n = 3) and in (B) raw patties (mg soluble protein/g meat) during illuminated chilled display (n = 6). ns, values within a display day are not significantly different ($p > 0.05$).

untreated samples, whereas no increase was found in any nitrite-treated samples (Figure 5).

DISCUSSION

This study investigated the effect of sodium nitrite on protein oxidation and nitration in two different meat model systems. In the myofibrillar protein isolates, 100 and 1000 mg $NaNO_2$/kg protein was used, which corresponds approximately to the addition of 20 and 200 mg of $NaNO_2$ to 1 kg of lean meat (assuming a dry matter content of 20%).

$NaNO_2$ has antioxidant activity against lipid oxidation, which is mostly explained by its ability to break the radical chain processes after its conversion to nitric oxide and by chelating iron, a known oxidation promoter.[20] As the mechanism behind the oxidation of proteins is believed to proceed via a free radical chain reaction similar to that of lipid oxidation,[1] it can be hypothesized that $NaNO_2$ will act as an antioxidant against protein oxidation. On the other hand, $NaNO_2$ could also act as pro-oxidant because, after its reduction to nitric oxide, peroxynitrite can be formed by reacting with a superoxide anion. Peroxynitrite can induce lipid oxidation in food systems and [21] protein oxidation in vivo[22] and can cause discoloration of muscle foods by oxidizing oxymyoglobin.[23] Although nitrite showed the expected antioxidant effect against lipid oxidation in the patties, no clear pro- or antioxidant effect against protein oxidation was found in the present study. According to Rubbo et al.,[24] the pro-oxidant versus antioxidant outcome of nitric oxide critically depends on the relative concentrations of

DOI: 10.1021/jf505775u
J. Agric. Food Chem. 2015, 63, 2550–2556

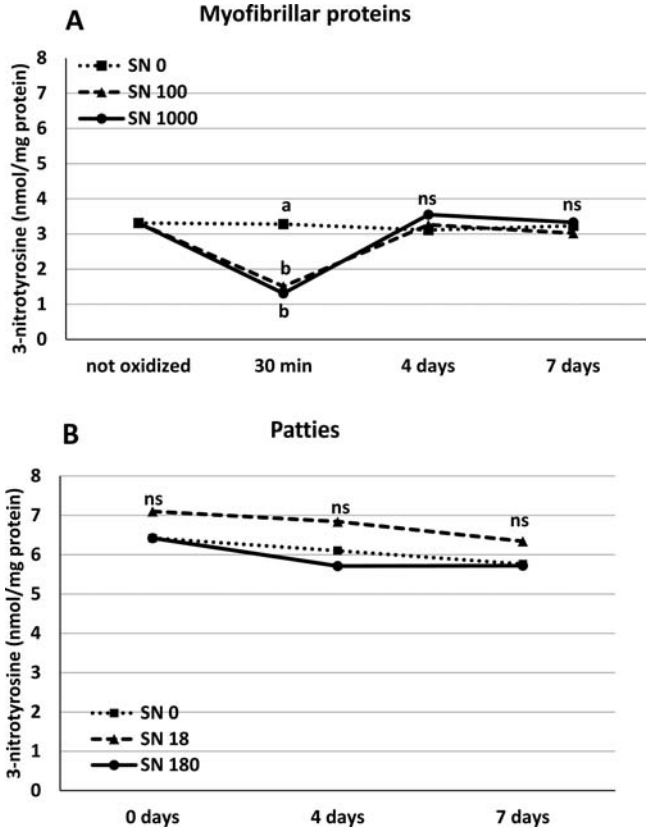

Figure 4. Effect of nitrite dose (SN, mg/kg) on protein nitration (3-nitrotyrosine, nmol/mg protein) in (A) myofibrillar protein isolates during Fenton reagent-induced oxidation (n = 3) and in (B) raw patties during illuminated chilled display (n = 6). ns, not significant; a, b, different letters within display day indicate significant differences (p < 0.05).

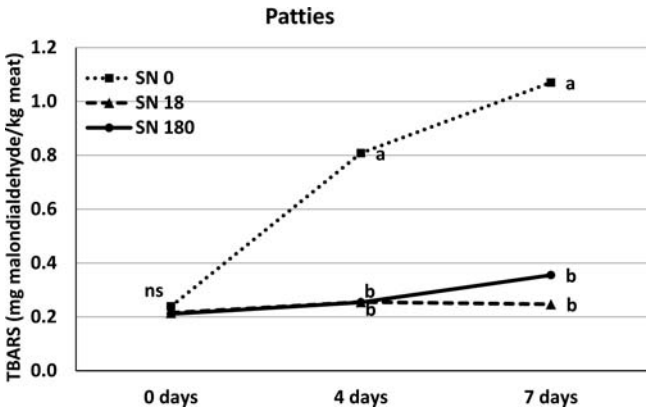

Figure 5. Effect of nitrite dose (SN, mg/kg) on lipid oxidation (TBARS, mg malondialdehyde/kg meat) in raw patties after illuminated chilled display (n = 6). ns, not significant; a, b, different letters within display day indicate significant differences (p < 0.05).

individual reactive species such as superoxide anions, hydrogen peroxides, and hydroxyl radicals.

These reactive species are abundantly present in in vitro oxidation systems, which could explain the pro-oxidative effect of sodium nitrite on the formation of carbonyl compounds in the isolated myofibrillar proteins, 0.5 h after the addition of the oxidants. Similar to the present results, Villaverde et al.[25] observed a fast pro-oxidant effect of nitrite on protein carbonylation immediately after the addition of nitrite to a meat batter. As discussed by these authors, nitrite is an efficient pro-oxidant as it is able to initiate oxidative reactions by abstracting an electron from a sensitive molecule[20] and to form reactive nitrogen species that could initiate oxidative reactions in meat systems.[26] In addition, the sodium nitrite and pro-oxidants were added simultaneously in the present study, which could have affected the reaction pathways of nitrite. Furthermore, the intensity of the induced oxidation could have masked the pro-oxidant effect of nitrite in isolated myofibrillar proteins at later time points. Villaverde et al.[12] reported a negligible effect of sodium nitrite on the α-aminoadepic semialdehyde content of isolated myofibrillar proteins after 4 days of induced oxidation in a similar in vitro system, which is in accordance with the present results. In the patties, sodium nitrite may first react with other meat components before oxidation during illuminated chilled display occurs, possibly explaining why a different effect of nitrite was found in the isolated myofibrillar proteins compared to the patties. For example, nitrite can react with myoglobin, resulting in nitrosylmyoglobin,[27] which appears to be active as an antioxidant both through dissociation of nitric oxide and through direct reaction with activated oxygen species.[20] In addition, nitric oxide can react with the free radical intermediates of lipid oxidation, and these compounds can function both as nitric oxide donors and as antioxidants.[28] The oxidation of thiol groups leads to a series of complex reactions resulting in the formation of various oxidized products such as sulfenic acid, sulfinic acid, and disulfide cross-links.[1] In addition, Sullivan and Sebranek[27] found decreasing thiol groups with increasing ingoing sodium nitrite and attributed this to the formation of S-nitrosothiol groups. A lower thiol content was therefore expected in the sodium nitrite-treated samples, which was observed in the patties with 180 mg/kg sodium nitrite, but not in the myofibrillar isolates. It is likely that the intensity of the induced oxidation, which resulted in an overall large loss of thiol groups, masked this effect. The values obtained for protein solubility, progress of protein carbonyl formation, and loss in thiol groups in induced in vitro oxidation of the isolated myofibrillar proteins compare well with the observations of respectively Liu et al.,[18] Estévez and Heinonen,[14] and Liu and Xiong.[29] The effects are greater compared to those usually found in real meat products, as the concentrations of oxidants applied in a model system are designed to stimulate oxidation.

It is not clear whether the addition of sodium nitrite affected the 3-nitrotyrosine content post mortem, and additional investigations are necessary to explore the occurrence of 3-nitrotyrosine in muscle foods and its potential influence on the quality. An increase in 3-nitrotyrosine content in the sodium nitrite-treated samples was hypothesized, but conversely a decrease was seen in the myofibrillar protein isolates after 30 min of induced oxidation. This was rather unexpected, especially because after 4 days of induced oxidation the 3-nitrotyrosine content reached its basal value again. It can be speculated that the simultaneous increase in carbonyl compounds plays a role; however, this has to be further investigated. The present findings suggest that 3-nitrotyrosine is not a good marker for protein oxidation in cured meat products, but on the contrary, Villaverde et al.[12] did find higher amounts of 3-nitrotyrosine in myofibrillar protein isolates treated with sodium nitrite. In that study, similar oxidation conditions were applied as in the present study, but with considerably higher concentrations of nitrite. Also, ascorbic acid

DOI: 10.1021/jf505775u
J. Agric. Food Chem. 2015, 63, 2550−2556

was added to the isolates in our study. Villaverde et al.[12] reported that ascorbate can inhibit the nitrosation of myofibrillar proteins dose-dependently. Furthermore, the quantification of 3-nitrotyrosine was performed at a higher pH than in the study of Villaverde et al.[12] (10.5 versus 3.5). According to Yang et al.[30] tyrosine and nitrotyrosine both exhibit an absorption peak at 280 nm, and nitrotyrosine has an additional peak at 430 nm in basic solutions (pH ≥9.5) and at 357 nm in acidic solutions (pH ≤3.5). In the present study, the analysis was carried out at basic conditions to reduce the risks of artifacts, as the nitration of tyrosine under acidic conditions in the presence of only trace quantities of nitrite has been reported.[31]

One item to be further explored is the variation between animals and between muscles of the basal 3-nitrotyrosine content. It is therefore interesting to quantify the 3-nitrotyrosine content as nanomoles of 3-nitrotyrosine per milligram of meat protein instead of reporting band intensities from Western blots. The occurrence of 3-nitrotyrosine in muscle proteins is a result of oxidative stress in vivo,[22] so basal levels of 3-nitrotyrosine in the porcine patties as well as in the myofibrillar protein isolates were expected. Stagsted et al.[11] found significantly higher basal concentrations of 3-nitrotyrosine in meat of chickens fed a low antioxidant diet compared to chickens fed a low antioxidant diet in combination with corn. As 3-nitrotyrosine may affect the structure and function of proteins,[32] it was hypothesized that 3-nitrotyrosine could be a marker for protein oxidation in cured meat products, affecting the quality of muscle foods. From the present results, however, it can be concluded that nitrite curing has no effect on the 3-nitrotyrosine content during chilled display.

In conclusion, sodium nitrite did not reveal clear pro- or antioxidant effects against protein oxidation in different meat models. 3-Nitrotyrosine was present in untreated meat proteins, but whether other compounds and process conditions influence its occurrence post mortem and whether this is a suitable marker for protein oxidation in processed meat remain to be elucidated.

AUTHOR INFORMATION

Corresponding Author

*(S.D.S.) Phone: +32 (0)9 264 90 03. Fax: +32 (0)9 264 90 99. E-mail: Stefaan.DeSmet@UGent.be.

Notes

The authors declare no competing financial interest.

ACKNOWLEDGMENTS

We gratefully acknowledge D. Baeyens, S. Coolsaet, and E. Claeys for their skilled technical support.

ABBREVIATIONS USED

DNPH, 2,4-dinitrophenylhydrazine; DTNB, 5,5′-dithiobis(2-nitrobenzoic acid); EGTA, ethylene glycol tetraacetic acid; PIPES, piperazine-*N*,*N*-bis(2-ethanesulfonic acid); TBARS, thiobarbituric acid reactive substances; TCA, trichloroacetic acid; TRIS, tris(hydroxymethyl)aminomethane; SDS, sodium dodecyl sulfate

REFERENCES

(1) Lund, M. N.; Heinonen, M.; Baron, C. P.; Estevez, M. Protein oxidation in muscle foods: a review. *Mol. Nutr. Food Res.* **2011**, *55*, 83−95.

(2) Zhang, W.; Xiao, S.; Ahn, D. U. Protein oxidation: basic principles and implications for meat quality. *Crit. Rev. Food Sci. Nutr.* **2012**, *53*, 1191−1201.

(3) Ventanas, S.; Estevez, M.; Tejeda, J. F.; Ruiz, J. Protein and lipid oxidation in *Longissimus dorsi* and dry cured loin from Iberian pigs as affected by crossbreeding and diet. *Meat Sci.* **2006**, *72*, 647−655.

(4) Vossen, E.; Utrera, M.; De Smet, S.; Morcuende, D.; Estévez, M. Dog rose (*Rosa canina* L.) as a functional ingredient in porcine frankfurters without added sodium ascorbate and sodium nitrite. *Meat Sci.* **2012**, *92*, 451−457.

(5) Jongberg, S.; Torngren, M. A.; Gunvig, A.; Skibsted, L. H.; Lund, M. N. Effect of green tea or rosemary extract on protein oxidation in Bologna type sausages prepared from oxidatively stressed pork. *Meat Sci.* **2013**, *93*, 538−546.

(6) Villaverde, A.; Morcuende, D.; Estévez, M. Effect of curing agents on the oxidative and nitrosative damage to meat proteins during processing of fermented sausages. *J. Food Sci.* **2014**, *79*, C1331−C1342.

(7) Vossen, E.; Doolaege, E. H.; Moges, H. D.; De Meulenaer, B.; Szczepaniak, S.; Raes, K.; De Smet, S. Effect of sodium ascorbate dose on the shelf life stability of reduced nitrite liver pâtés. *Meat Sci.* **2012**, *91*, 29−35.

(8) Arendt, B.; Skibsted, L. H.; Andersen, H. J. Antioxidative activity of nitrite in metmyoglobin induced lipid peroxidation. *Z. Lebensm.-Unters. Forsch.* **1997**, *204*, 7−12.

(9) Stadtman, E. R.; Levine, R. L. Protein oxidation. *Ann. N.Y. Acad. Sci.* **2000**, *899*, 191−208.

(10) Souza, J. M.; Peluffo, G.; Radi, R. Protein tyrosine nitration-functional alteration or just a biomarker? *Free Radical Biol. Med.* **2008**, *45*, 357−366.

(11) Stagsted, J.; Bendixen, E. k.; Andersen, H. J. Identification of specific oxidatively modified proteins in chicken muscles using a combined immunologic and proteomic approach. *J. Agric. Food Chem.* **2004**, *52*, 3967−3974.

(12) Villaverde, A.; Parra, V.; Estévez, M. Oxidative and nitrosative stress induced in myofibrillar proteins by a hydroxyl-radical generating system: impact of nitrite and ascorbate. *J. Agric. Food Chem.* **2014**, *62*, 2158−2164.

(13) Park, D.; Xiong, Y. L.; Alderton, A. L. Concentration effects of hydroxyl radical oxidizing systems on biochemical properties of porcine muscle myofibrillar protein. *Food Chem.* **2006**, *101*, 1239−1246.

(14) Estévez, M.; Heinonen, M. Effect of phenolic compounds on the formation of α-aminoadipic and γ-glutamic semialdehydes from myofibrillar proteins oxidized by copper, iron, and myoglobin. *J. Agric. Food Chem.* **2010**, *58*, 4448−4455.

(15) Gornall, A. G.; Bardawill, C. J.; David, M. M. Determination of serum proteins by means of the biuret reaction. *J. Biol. Chem.* **1949**, *177*, 751−766.

(16) Estévez, M.; Ollilainen, V.; Heinonen, M. Analysis of protein oxidation markers α-aminoadipic and γ-glutamic semialdehydes in food proteins using liquid chromatography (LC)-electrospray ionization (ESI)-multistage tandem mass spectrometry (MS). *J. Agric. Food Chem.* **2009**, *57*, 3901−3910.

(17) Levine, R. L.; Williams, J. A.; Stadtman, E. P.; Shacter, E. Carbonyl assays for determination of oxidatively modified proteins. In *Methods in Enzymology, Oxygen Radicals in Biological Systems, Part C*; Lester, P., Ed.; Academic Press: New York, 1994; Vol. 233, pp 346−357.

(18) Liu, Z.; Xiong, Y. L.; Chen, J. Identification of restricting factors that inhibit swelling of oxidized myofibrils during brine irrigation. *J. Agric. Food Chem.* **2009**, *57*, 10999−11007.

(19) Fontana, M.; Blarzino, C.; Pecci, L. Formation of 3-nitrotyrosine by riboflavin photosensitized oxidation of tyrosine in the presence of nitrite. *Amino Acids* **2012**, *42*, 1857−1865.

(20) Skibsted, L. H. Nitric oxide and quality and safety of muscle based foods. *Nitric Oxide* **2011**, *24*, 176−183.

DOI: 10.1021/jf505775u
J. Agric. Food Chem. 2015, 63, 2550−2556

(21) Brannan, R. G.; Connolly, B. J.; Decker, E. A. Peroxynitrite: a potential initiator of lipid oxidation in food. *Trends Food Sci. Technol.* **2001**, *12*, 164−173.
(22) Tiago, T.; Aureliano, M.; Gutiérrez-Merino, C. Effects of reactive oxygen and nitrogen species on actomyosin and their implications for muscle contractility. In *Free Radicals in Biology and Medicine*; Gutiérrez-Merino, C., Leeuwenburgh, C., Eds.; Research Signpost: Scarborough, Canada, 2008; pp 1−19.
(23) Connolly, B. J.; Decker, E. A. Peroxynitrite induced discoloration of muscle foods. *Meat Sci.* **2004**, *66*, 499−505.
(24) Rubbo, H.; Radi, R.; Trujillo, M.; Telleri, R.; Kalyanaraman, B.; Barnes, S.; Kirk, M.; Freeman, B. A. Nitric oxide regulation of superoxide and peroxynitrite-dependent lipid peroxidation. Formation of novel nitrogen-containing oxidized lipid derivatives. *J. Biol. Chem.* **1994**, *269*, 26066−26075.
(25) Villaverde, A.; Ventanas, J.; Estévez, M. Nitrite promotes protein carbonylation and Strecker aldehyde formation in experimental fermented sausages: are both events connected? *Meat Sci.* **2014**, *98*, 665−672.
(26) Honikel, K. O. The use and control of nitrate and nitrite for the processing of meat products. *Meat Sci.* **2008**, *78*, 68−76.
(27) Sullivan, G. A.; Sebranek, J. G. Nitrosylation of myoglobin and nitrosation of cysteine by nitrite in a model system simulating meat curing. *J. Agric. Food Chem.* **2012**, *60*, 1748−1754.
(28) Nicolescu, A. C.; Reynolds, J. N.; Barclay, L. R.; Thatcher, G. R. Organic nitrites and NO: inhibition of lipid peroxidation and radical reactions. *Chem. Res. Toxicol.* **2004**, *17*, 185−196.
(29) Liu, G.; Xiong, Y. L. Oxidatively induced chemical changes and interactions of mixed myosin, β-lactoglobulin and soy 7S globulin. *J. Sci. Food Agric.* **2000**, *80*, 1601−1607.
(30) Yang, H.; Zhang, Y.; Pöschl, U. Quantification of nitrotyrosine in nitrated proteins. *Anal. Bioanal. Chem.* **2010**, *397*, 879−886.
(31) Duncan, M. W. A review of approaches to the analysis of 3-nitrotyrosine. *Amino Acids* **2003**, *25*, 351−361.
(32) Kuo, W. N.; Kreahling, J. M.; Shanbhag, V. P.; Shanbhag, P. P.; Mewar, M. Protein nitration. *Mol. Cell. Biochem.* **2000**, *214*, 121−129.

DOI: 10.1021/jf505775u
J. Agric. Food Chem. 2015, 63, 2550−2556

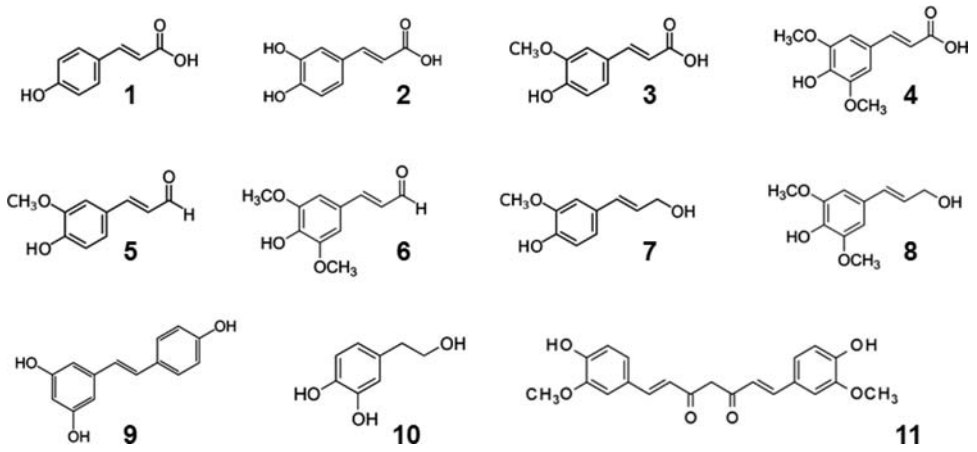

Figure 1. Phenolic compounds tested in this study: **1**, *p*-coumaric acid, **2**, caffeic acid, **3**, ferulic acid, **4**, sinapic acid, **5**, coniferaldehyde, **6**, sinapaldehyde, **7**, coniferyl alcohol, **8**, sinapyl alcohol, **9**, resveratrol, **10**, hydroxytyrosol, **11**, curcumin.

promising natural compounds are well-known plant constituents, such as resveratrol from grapes,[14] curcumin from turmeric,[15] hydroxytyrosol from olive,[16] as well as ubiquitous lignin-related phenylpropanoids.[17,18] Interestingly, the latter group acts as natural surface-functionalizing materials, impregnating the plant cell wall and conferring antimicrobial activity upon it in case of pathogen attack.[19] Using natural phenolic compounds as a basis for active food-contact surfaces is still in its infancy. Rhim and Ng[20] proposed to use nanocomposite technology to produce environmentally friendly antimicrobial food packaging and food-contact surfaces by blending nanolignin with biodegradable polymers. This approach proved feasible in the textile industry when fabrics with antimicrobial activity were produced by adding lignin nanoparticles to the fiber.[21] To the best of our knowledge, no screening of various phenolic compounds for their potential as functionalizing ingredients for antimicrobial surfaces has been performed until now.

Curcumin (1,7-bis(4-hydroxy-3-methoxyphenyl)-1,6-heptadiene-3,5-dione), a natural phenylpropanoid dimer, is one of the promising candidates for the role of a natural food-grade surface-functionalizing phenolic compound. It is an active principle of turmeric *Curcuma longa* L. used as a traditional spice and folk medicine in South and South-East Asia and Middle East. Curcumin exhibits various biological activities including antiproliferative, antioxidant, and wound healing effects[22] and has a self-affirmed "Generally Recognized as Safe" (GRAS) status.[23] Curcumin possesses antibacterial properties against a number of Gram-positive and Gram-negative bacteria.[15,24] However, poor water solubility limits the application of curcumin as antimicrobial agent in its native form. Reduction of the particle size down to the nanorange markedly improved water dispersibility and antimicrobial efficacy of curcumin.[25] Nanoparticles of curcumin (nanocurcumin) having a size distribution in the range of 2−40 nm prepared by a wet-milling technique were more effective than regular curcumin against *S. aureus*, *B. subtilis*, *E. coli*, *P. aeruginosa*, *Penicillium notatum*, and *Aspergillus niger*. Transmission electron microscopy revealed permeation of nanocurcumin particles inside the Gram-positive bacteria followed by cell wall disintegration and eventually cell death. In spite of the unique combination of antimicrobial potency, food origin, and health benefits, no attempts have been taken until now to use curcumin for developing antimicrobial food-contacting surfaces. However, curcumin impregnation conferred antimicrobial activity to wool fabric.[26]

Polydiacetylene (PDA) vesicles are a novel carrier system for hydrophobic materials poorly soluble in water, such as anticancer drug paclitaxel based on plant component taxol.[27] Incorporation of a polymerizable diacetylene into the lipid bilayer greatly improves the stability of the vesicles compared with the conventional liposomes. Furthermore, the PDA vesicles can be covalently bound to the surface of solid substrates such as glass.[28] Dogra et al.[29] studied the interaction of glucose-tagged PDA vesicles (either giant or nanoscale-sized) with *E. coli* as a model of molecular recognition mechanisms. However, to the best of our knowledge, this system has not been used so far for delivery of antimicrobial activity and for construction of antimicrobial active surfaces.

The ultimate goal of this research was developing novel antimicrobial food-contact materials based on phenylpropanoids or related natural compounds. In order to reach this goal, the work comprised the following steps: (a) selecting the most promising antimicrobial compound; (b) building PDA nanovesicles functionalized with the selected compound; (c) binding the vesicles to a glass surface; (d) testing the antimicrobial activity of the vesicles, both suspended and immobilized, toward Gram-positive and Gram-negative bacteria, as well as toward yeast.

MATERIALS AND METHODS

Chemicals. The phenolic compounds and methyl-*β*-cyclodextrin (MBCD, MW 1331) were supplied by Sigma-Aldrich Israel (Rehovot, Israel). If not specified differently, other solvents and chemicals were from Fisher Scientific, Fair Lawn, NJ. 1-(3-(Dimethylamino)propyl)-3-ethylcarbodiimide hydrochloride and 10,12-pentacosadiynoic acid were from GFS Chemicals, Columbus OH, and 1,2-dimyristoyl-*sn*-glycero-3-phosphocholine (DMPC) was from Avanti Polar Lipids, Alabaster, AL. Nutrient media were purchased from BD Difco Laboratories, Detroit, MI, except for the nutrient yeast dextrose broth (NYDB) that was prepared using nutrient broth (Difco), yeast extract (Pronadisa Conda, Madrid, Spain), and D-(+)-glucose (Merck, Darmstadt, Germany) in amounts of 0.8, 0.5, and 1.0 g per 1 L water, respectively.

Screening Antimicrobial Activity of MBCD-Encapsulated Phenolic Compounds. *Microencapsulation of Phenolic Compounds.* The following phenolic compounds were tested in this study: *p*-coumaric acid, caffeic acid, ferulic acid, sinapic acid, coniferaldehyde, sinapaldehyde, coniferyl alcohol, sinapyl alcohol, hydroxytyrosol, resveratrol, and curcumin (Figure 1). Equal volumes of a 20 mM

DOI: 10.1021/jf505442w
J. Agric. Food Chem. 2015, 63, 2557−2565

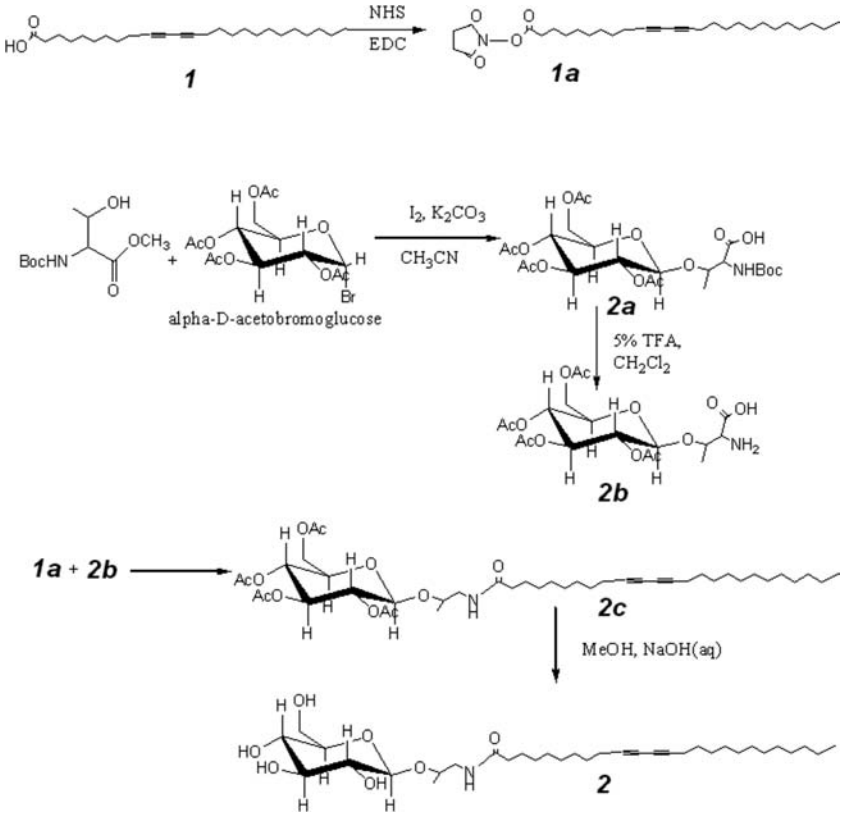

Figure 2. Synthesis of diacetylene monomers. Monomers: ***1***, 10,12-pentacosadiynoic acid, ***1a***, NHS-tagged diacetylene monomer, ***2***, glucose-tagged diacetylene monomer.

ethanolic solution of a phenolic compound tested and a 20 mM aqueous solution of MBCD were mixed and stirred for 2 h on a magnetic stirrer at room temperature. Ethanol was removed from the mixture by evaporation under vacuum to half-volume (Rotavapor R-124, Buchi, Flawil, Switzerland). The nonencapsulated residue of the phenolic compound was removed by filtration through a sterile 0.45 μ Millex filter with Durapore membrane (Millipore, Cork, Ireland). The obtained filter-sterilized aqueous dispersion of the phenolic−MBCD complex (Ph−MBCD) was kept in a refrigerator until use. The concentration of the phenolic compound in the Ph−MBCD was determined by diluting the aqueous dispersion with ethanol in a ratio of 1:9 and measuring its absorbance with an Ultrospec 2100 pro spectrophotometer (Amersham Biosciences, Piscataway NJ) at a characteristic wavelength in comparison with the calibration curve of the compound in 90% ethanol. In particular, wavelengths of 262 and 425 nm were used for curcumin quantification.

Assay of the Antimicrobial Activity of MBCD-Encapsulated Phenolic Compounds. Cells of *E. coli* (ATCC 25922) were grown overnight in LB broth (Lennox) liquid medium, separated from the medium by centrifugation, washed with sterile water, and resuspended in a fresh double-strength LB medium to reach an optical density of 0.2 at a wavelength of 600 nm. The bacterial suspensions were further diluted 1:1 with aqueous Ph−MBCD dispersions and sterile water to obtain various concentrations of phenolics but the same initial *E. coli* dilution. The bacterial suspensions were aseptically pipetted into the wells of a 96-well microplate, 0.2 mL per plate, and incubated for 20 h at 27 °C in an EnSpire multilabel plate reader (PerkinElmer, Waltham MA, USA) with hourly 10 s shaking. The experiments were run in triplicate and in addition to treatments (viable *E. coli* + Ph−MBCD) included blanks (nutrient medium without *E. coli* + Ph−MBCD), positive controls (viable *E. coli* + nutrient medium and MBCD without phenolics), and negative controls (*E. coli* killed by boiling + Ph−MBCD). The bacterial growth was registered by hourly measurement of turbidity as optical density at 600 nm and evaluated as added area under the growth curve (AAUC) during the whole cultivation period (20 h). Growth inhibition was calculated as AAUC reduction (%) in the presence of a given phenolic concentration compared with a positive control without phenolics. The half-maximal inhibitory concentration (IC_{50}) was determined as a concentration required for 50% growth inhibition and minimum inhibitory concentration (MIC) as the lowest concentration resulting in complete growth prevention. A similar technique was used for evaluating the effect of curcumin−MBCD complex on yeast *Saccharomyces cerevisiae* growth, except for using the NYDB instead of the LB medium.

Synthesis of Diacetylene Monomers. The synthesis procedures are schematically presented in Figure 2.

Synthesis of N-Hydroxysuccinimide (NHS)-Tagged Diacetylene Monomer. NHS (0.348 g, 3.0 mmol) was added to a solution of 10,12-pentacosadiynoic acid ***1*** (1.00 g, 2.7 mmol) in 20 mL of anhydrous dichloromethane (DCM), followed by adding 1-(3-(dimethylamino)propyl)-3-ethylcarbodiimide hydrochloride (0.570 g, 3.1 mmol) to the same solution. The solution was stirred at room temperature for 2 h followed by rotary evaporation of the solvent. The residue was extracted with diethyl ether and washed with water three times. The organic layer was dried with magnesium sulfate for 0.5 h and then filtered. The solvent was removed by rotary evaporation to give a white solid powder of NHS-tagged diacetylene monomer ***1a*** (1.18g, 93%).

Synthesis of Glucose-Tagged Diacetylene Monomer. Synthesis of ***2a.*** N-Boc-L-threonine (2.65 g, 12.0 mmol), acetobromoglucose (2.46 g, 6.0 mmol), and potassium carbonate (1.24 g, 9.0 mmol) were dissolved in 40 mL of dry acetonitrile under argon atmosphere with stirring for 10 min. Iodine (2.28 g, 9.0 mmol) was then added against a flow of argon. The glassware was then sealed and stirred at room temperature with the exclusion of light for 6 h. A saturated sodium thiosulfate aqueous solution was added to the above stirring solution, until the deep red color had disappeared, leaving a slightly yellow solution. The insoluble residual potassium carbonate was removed by filtration. The filtrate was concentrated to 1/4 of its original volume under reduced pressure on a rotary evaporator. DCM (40 mL) was

DOI: 10.1021/jf505442w
J. Agric. Food Chem. 2015, 63, 2557−2565

added to the mixture, and the solution was extracted with sodium bicarbonate aqueous solution (5% w/v, 50 mL) one time, followed by brine (50 mL) two times; the organic layer was dried over magnesium sulfate. The crude products were purified by flash chromatography using a glass column packed with silica gel and a gradient solvent system hexane/ethyl acetate 10:1 to 1:4. The major fraction was collected and evaporated in vacuum to a white solid ***2a***; yield 1.75 g, 53%.

*Synthesis of **2b**.* The product ***2a*** (1.5 g, 2.73 mmol) was dissolved in 20 mL of anhydrous DCM under argon. Trifluoroacetic acid (1.0 mL, 13.01 mmol) was then added dropwise to it, and the solution was stirred at room temperature for 3 h. The process was monitored by TLC until no starting materials were detected. The solvent was evaporated under reduced pressure to give a viscous liquid ***2b***.

*Synthesis of **2c**.* Triethylamine (1.49 mL, 10.6 mmol) and a solution of ***2b*** (0.867 g, 1.93 mmol) in 10 mL of anhydrous DCM were added to a solution of ***1a*** (1.0 g, 2.12 mmol) in 20 mL of anhydrous DCM. After stirring over 36 h, the solvent was removed by rotary evaporation. The residue was redissolved in 20 mL of DCM, and then it was washed with the following solutions: 1 M HCl aqueous solution (twice), saturated sodium bicarbonate solution (twice), and saturated sodium chloride solution (once). The organic layer was dried with magnesium sulfate, filtered, and evaporated to give crude semisolid. The crude products were purified by flash chromatography (silica gel, chloroform/methanol 20:1). Compound ***2c*** was obtained as a white powder (1.102 g, 75%).

*Synthesis of **2**.* Compound ***2c*** (1.0 g, 1.31 mmol) was dissolved in 50 mL of methanol containing 0.05 N sodium methanolate and was stirred at room temperature overnight. Ion exchange resin was added to the solution until the pH $\leq$ 6 was reached. The solution was filtered, and the solvent was removed by rotary evaporation to get a white solid. The crude products were purified by flash chromatography (silica gel, chloroform/methanol 2:1). Compound ***2*** (glucose-tagged diacetylene monomer) was obtained as a white powder (0.389 g, 50%).

Preparation and Characteristic of Curcumin-Functionalized PDA Nanovesicles. Curcumin was used for preparing functionalized nanovesicles due to its superior antimicrobial potency shown in preliminary screening tests.

Self-Assembly of Curcumin-Functionalized Nanovesicles. A mixture containing 10,12-pentacosadiynoic acid, glucose-tagged and NHS-tagged diacetylene monomers, and DMPC in a ratio of 4:4:2:1 was dissolved in chloroform in a round-bottom flask, and the solvent was then evaporated completely to yield a thin film of monomers. The film was hydrated with a saturated aqueous solution of curcumin and sonicated at 76 °C for 15 min using a probe sonicator (Vibra-cell Model CV 33, Sonics & Materials, Inc., Newton, CN, USA). Sonication resulted in vesicle formation and inclusion of curcumin in the hydrophobic bilayer of the vesicles. The dispersion was then passed through a 0.8 μm nylon filter (Whatman, Inc., Piscataway, NJ, USA) to remove the lipid aggregates and cooled at 4 °C overnight to promote self-assembly of the monomers. The obtained filtrate was optically clear. Free curcumin was removed by dialysis using a Spectra/Por Biotech Cellulose Ester membrane, MWCO 100 000 (Fisher Scientific International, Inc., Hampton, NH, USA) preliminarily soaked in deionized water for 15 min. The final dispersion was collected in a vial covered with aluminum foil. Curcumin concentration in the vesicle dispersion was determined spectrophotometrically after its dilution in ratio (1:9) with ethanol using the extinction coefficient of 59 500 M^{-1} cm^{-1} in 90% ethanol at 425 nm. Typically, the curcumin concentration in the dispersion varied within the range 0.1−0.5 mM.

Binding Curcumin-Functionalized Nanovesicles to Glass Surface. The nanovesicles, with or without curcumin, were bound to the surface of silanized glass slides through amidization between the amine groups of the aminosilane and the NHS head groups of PDA-NHS. Glass slides, 25 × 25 mm, were cleaned by sonication in acetone for 10 min, dried under argon for 5 min, and treated with freshly prepared Piranha solution (70% H_2SO_4, 30% H_2O_2) for 30 min. The cleaned slides were rinsed with copious amounts of distilled water and dried under vacuum. Silanization was performed at room temperature by immersing the glass slides in 4% aminosilane solution, 1% acetic acid, and 95% ethanol under continuous stirring for 4 h at room temperature. The silanized glass slides were then cleaned with ethanol for about 10 min, baked at 110 °C overnight, and brought back to room temperature. Slides were dipped in curcumin nanovesicle dispersion for 1 h and then kept in vacuum desiccator overnight.

Spectroscopic Measurements and Atomic Force Microscopy. UV−vis absorption spectra of all of the samples were recorded at room temperature using a PerkinElmer Lambda 25 (spectral slit width 1 nm) UV/vis spectrometer using a cuvette of 1 cm path length. Fluorescence emission spectra of all of the samples were recorded at room temperature using a PerkinElmer Lambda 55 (spectral slit width 1 nm) luminescence spectrometer (PerkinElmer, Waltham MA, USA). The samples were excited at 350 nm, and emission was recorded in 360−650 nm range.

The topology of nanovesicles on glass surfaces was investigated by atomic force microscopy (AFM) using a TopoMetrix TMX 1010 Explorer instrument (TopoMetrix/Veeco Instruments, Santa Clara CA) in tapping mode using antimony-doped silicon tip. The largest scanning area was 80 × 80 μm, and the highest z resolution of the instrument was 0.2 nm. The samples were prepared by applying nanovesicle dispersion on a mica or glass surface, followed by overnight drying under vacuum.

The transmission electron microscopy (TEM) images of liposomes were obtained after staining the liposomes with 2% phosphotungstic acid using a Hitachi S-7100 TEM instrument (Hitachi HTA, Inc., Schaumburg, IL, USA) operating at an accelerating voltage of 100 kV. The liposome samples were deposited onto Formvar-coated copper grids (Ted Pella, Inc., Redding CA, USA) for obtaining TEM images.

Visualization of Nanovesicle Contact with E. coli Cells. In order to visualize the contact of nanovesicles with *E. coli* cells, the vesicles were tagged with Sulforhodamine 101 (SR-101) having red emission and *E. coli* was stained with 4′,6-diamidino-2-phenylindole (DAPI) having blue emission as described in the previous publication.[29] A DAPI filter (excitation and emission band widths 349 ± 25 and 459 ± 25 nm, respectively) and a 41004 Texas Red filter (exciting and emitting band widths 527−567 and 605−682 nm, respectively) were used for capturing blue and red emission.

Testing the Antimicrobial Activity of Curcumin-Functionalized Nanovesicles. The cultures of *E. coli* W 1485 and *Bacillus cereus* ATCC 14579 were grown on tryptic soy broth (TSB) medium at 37 °C for 12 h and harvested by centrifugation (Beckman J2-M1, Schaumburg, IL, USA) for 10 min at 5500*g* and 4 °C. The pellet was suspended in 50 mL of phosphate buffer saline (PBS) at pH 7.0. Serial dilutions were made and plated onto tryptic soy agar (TSA) plates for colony-forming units (CFU) enumeration.

The antibacterial activity of suspended and glass-bound curcumin-functionalized nanovesicles (CFN) was studied by the shake flask assay method in comparison with vesicles containing no curcumin (control). Two milliliters of the vesicle dispersion was added into the sterile conical flask containing 23 mL of PBS. For studying the antimicrobial activity of CFN-coated glass slides they were placed in a sterile conical flask containing 50 mL of PBS at pH 7.0. Glass slides coated with nanovesicles without curcumin served as control. A 1 mL amount of test culture suspension was pipetted into the flask, which brought the initial cell density of the cell suspension to approximately 10^5 CFU mL^{-1}. Flasks were incubated in a gyratory water bath shaker (New Brunswick Scientific, Edison, NJ) at 36 °C for 48 h. Viable bacteria in the flasks at different time intervals were counted by plating aliquots of serial dilutions onto TSA media and incubating for 18−24 h at 35 °C.

A similar approach was used for evaluating the effect of curcumin-containing nanovesicles on the survival of yeast *S. cerevisiae* in nongrowing medium (PBS at pH 7.4), except for using NYDB for initial growing of the *S. cerevisiae* culture and potato dextrose agar amended with 100 ppm chloramphenicol for plating. The incubation duration was extended to 120 h.

Statistics. Bacterial counts (CFU mL^{-1}) were obtained from three replicates, and resulting means were converted to $\log_{10}$ CFU mL^{-1}.

DOI: 10.1021/jf505442w
J. Agric. Food Chem. 2015, 63, 2557−2565

Resulting $\log_{10}$ CFU mL^{-1} reduction values were compared by analysis of variance (ANOVA) and Tukey's HSD (honestly significant difference) tests using SAS 9.2 software (SAS Institute Inc., Cary, NC).

RESULTS

Active Principle Selection: Curcumin as a Promising Antimicrobial Compound. The phenolic compounds tested varied greatly in their inhibitory activity toward *E. coli*. Just a few compounds having 4-hydroxy-3-methoxy substituents demonstrated a complete inhibition of *E. coli* growth at concentrations tested: curcumin, coniferaldehyde, and ferulic acid (Table 1). Within the series with the same substituents the activity declined in the order aldehyde > acid ≫ alcohol. Curcumin showed by far the highest inhibitory effect among the compounds tested. An example of the curcumin effect on *E. coli* proliferation is presented in Figure 3. At 0.2 mM curcumin reduced the growth rate of *E. coli* approximately by one-half, while 0.4 mM curcumin resulted in full arrest of bacterial proliferation, so that the growth curve overlapped with that of the dead culture. The growth of the yeast *S. cerevisiae* was also inhibited by the MBCD-encapsulated curcumin with an IC_{50} value of 0.67 mM (data not shown). No growth inhibition was shown by MBCD at 5 mM, the highest concentration tested. Curcumin was chosen as the promising active principle for further research.

Table 1. Inhibitory Activity of MBCD-Encapsulated Phenolic Compounds toward *E. coli*

compound	group	substitution	IC_{50} (mM)	MIC (mM)
p-coumaric acid	phenylpropanoid acid	4-hydroxy	9.2	n.d.[a]
caffeic acid	phenylpropanoid acid	3,4-dihydroxy	8.3	>13
ferulic acid	phenylpropanoid acid	4-hydroxy-3-methoxy	4.4	6.4
sinapic acid	phenylpropanoid acid	4-hydroxy-3,5-dimethoxy	7.9	n.d.
coniferaldehyde	phenylpropanoid aldehyde	4-hydroxy-3-methoxy	3.0	6.8
sinapaldehyde	phenylpropanoid aldehyde	4-hydroxy-3,5-dimethoxy	5.6	n.d.
coniferyl alcohol	phenylpropanoid alcohol	4-hydroxy-3-methoxy	13.6	n.d.
sinapyl alcohol	phenylpropanoid alcohol	4-hydroxy-3,5-dimethoxy	16.0	n.d.
hydroxytyrosol	phenylethanoid alcohol	3,4-dihydroxy	10.5	n.d.
resveratrol	stilbenoid	3,5,4′-trihydroxy	6.1	n.d.
curcumin	phenylpropanoid dimer	4-hydroxy-3-methoxy	0.17	0.4

[a]MIC was evaluated only when complete inhibition was reached; n.d., not determined.

Characteristics of Curcumin-Functionalized Nanovesicles. Curcumin-functionalized nanovesicles (CFN) were prepared as described in Materials and Methods. The particle dimensions were in a range of 50−400 nm (Figure 4). The polymerized PDA nanovesicles containing no curcumin were characterized by absorption peaks at 590 and 640 nm, while the ethanolic curcumin solution had maximal absorption at 428 nm (Figure 5A and 5B, respectively). Both PDA and curcumin characteristic maxima were presented in the absorption spectrum of CFN (Figure 5C).

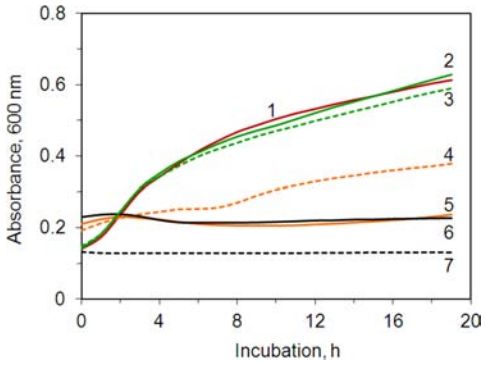

Figure 3. Effects of curcumin and MBCD concentrations on *E. coli* growth. Curves designation: (1) no additives (control); (2) 5 mM MBCD; (3) 2.5 mM MBCD; (4) 0.2 mM curcumin + 2.5 mM MBCD; (5) 0.4 mM curcumin + 5 mM MBCD; (6) 0.4 mM curcumin + 5 mM MBCD (thermally inactivated culture); (7) no additives (thermally inactivated culture). Curves 1−5 correspond to viable *E. coli* culture.

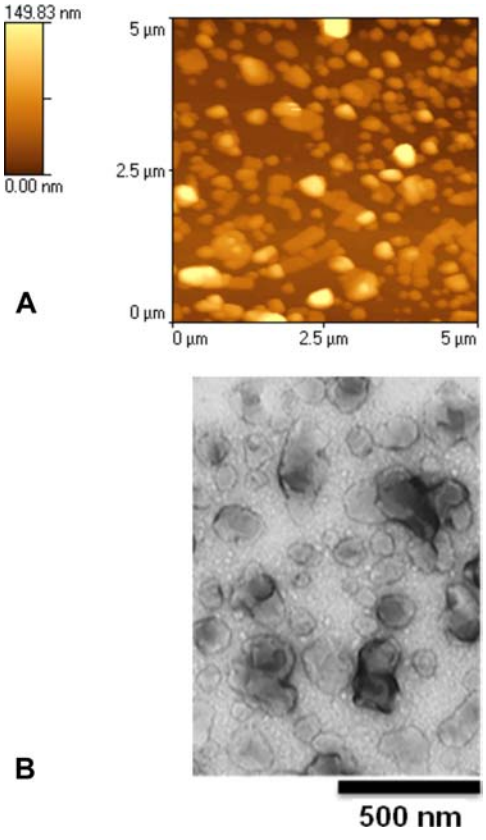

Figure 4. AFM (A) and TEM (B) images of the PDA nanovesicles.

Indication of curcumin location within the nanovesicles could be obtained from comparing the fluorescence emission spectrum of CFN with the emission spectra of curcumin in solvents of different polarities. Figure 6 represents the emission spectra of curcumin dissolved in hexane, toluene, chloroform, tetrahydrofuran, ethanol, and water whose dielectric constant values at 20 °C were 1.89, 2.38, 4.81, 7.52, 25.30, and 80.10, respectively.[30] In agreement with the literature,[31] polar solvents tended to shift the curcumin emission maxima toward higher wavelength. The comparison indicated that at least part of the CFN-associated curcumin was located in relatively nonpolar medium having a dielectric constant between 4.8 and 7.5, rather

DOI: 10.1021/jf505442w
J. Agric. Food Chem. 2015, 63, 2557−2565

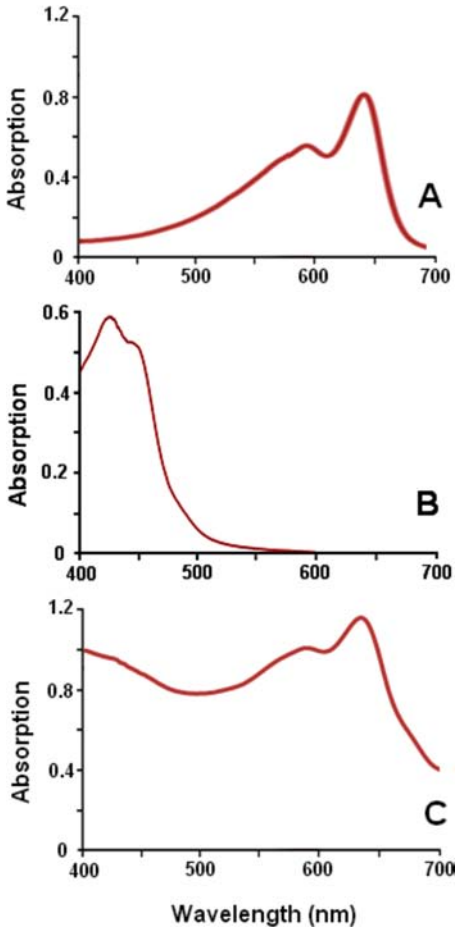

Figure 5. Absorption spectra of PDA vesicles without curcumin (A), ethanolic solution of curcumin (B), and curcumin-functionalized PDA vesicles (C).

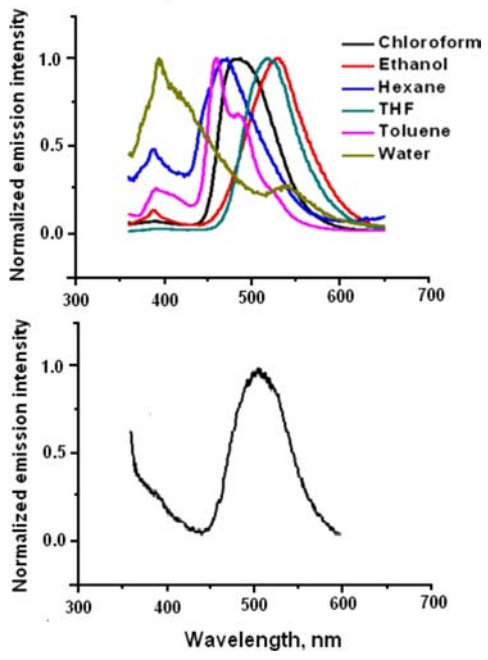

Figure 6. Emission spectra of curcumin in solvents of different polarity (top) and of the CFN-enclosed curcumin (bottom).

than in aqueous environment. The presented dielectric constant range was comparable with that of polymerized PDA.[32] It can be suggested that due to its hydrophobicity curcumin molecules tend to concentrate in the lipophilic bilayer of the nanovesicle.

Interaction of Free and Surface-Bound CFN with Bacteria. When brought in contact with *E. coli*, the nanovesicles tended to bind to the bacterial surface as shown in Figure 7, presenting a fluorescent micrograph of SR-101-tagged nanovesicles (red) and DAPI-stained *E. coli* nucleoid (blue). As shown previously, this binding was due to the presence of covalently bound receptor (glucose) in the bilayer of the nanovesicles.[29]

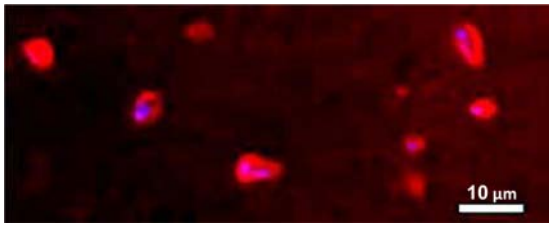

Figure 7. Fluorescence micrograph of SR-101-tagged nanovesicles (red emission) bound to the surface of *E. coli* stained with DAPI (blue emission in the nucleoid region).

The CFN demonstrated bactericidal activity toward both Gram-negative (*E. coli*) and vegetative cells of Gram-positive (*B. cereus*) bacteria, reducing their counts in phosphate-buffered saline (PBS) at pH 7.0 from 5 log to an undetectable level within 8 h (Figure 8). Only limited activity (not more than 1 log reduction) was observed against yeast (data not shown).

The attachment of CFN to glass slides rendered antibacterial activity to their surface. Incubation of *E. coli* with CFN-bound glass resulted in a reduction in its viable counts by 2.5 log CFU mL^{-1} (Figure 9A). With *B. cereus*, fast viability decline was observed within 4 h of incubation with the coated glass (Figure 9B). The reduction was 1.3 log CFU mL^{-1} without curcumin and 2.5 log CFU mL^{-1} in the presence of curcumin. No significant changes in viable counts of *B. cereus* occurred during further incubation. In parallel, the formation of spores was observed in *B. cereus* cultures, both in the presence of curcumin and in the control.

DISCUSSION

Within the series of phenylpropanoids with the same substitution pattern, the activity decreased in the order aldehyde > acid ≫ alcohol. Curcumin, with two carbonyl groups and "double coniferaldehyde" structure, also apparently obeyed this trend. Similar tendencies in the activity of phenylpropanoids against several microorganisms were demonstrated by Barber et al.,[17] except for curcumin behavior that was not analyzed by those authors. Prevalence of curcumin over monomeric phenylpropanoids (e.g., ferulic acid) in anticancer and antiviral activity was demonstrated by Huang et al.[33] and Bourne et al.,[34] respectively. It was reported that the antibacterial effect of curcumin may be related, in particular, to inhibition of assembly and polymerization of the citoskeletal protein FtsZ playing a role in prokaryote cell division.[24,35] Kaur et al.[35] located the binding site of curcumin to the FtsZ molecule and stressed the potential of curcumin for the development of novel antimicrobials.

DOI: 10.1021/jf505442w
J. Agric. Food Chem. 2015, 63, 2557−2565

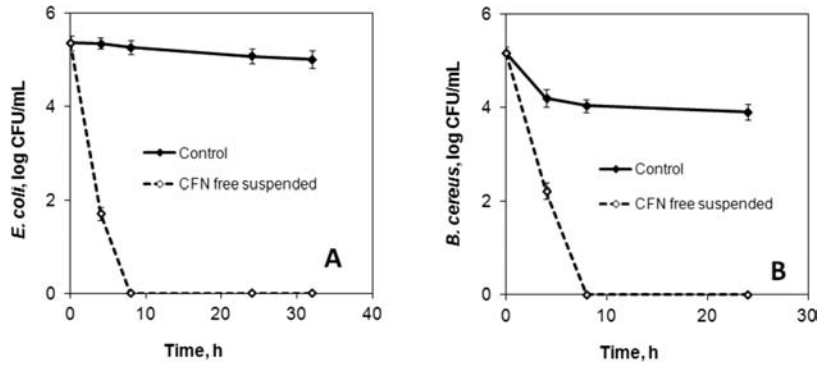

Figure 8. Viable counts of *E. coli* (A) and *B. cereus* (B) in PBS. Dashed lines: free-suspended CFN (0.25 mM curcumin). Solid lines: particles without curcumin (control).

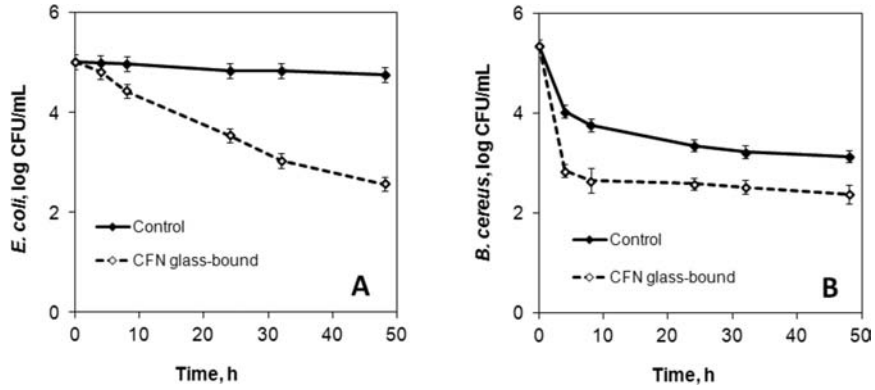

Figure 9. Viable counts of *E. coli* (A) and *B. cereus* (B) in PBS. Dashed lines: CFN-coated glass slides (approximately 1 μg curcumin per cm^2). Solid lines: glass slides coated with nanoparticles without curcumin (control).

Our suggestion about localization of curcumin within the membrane bilayer region rather than in more polar environments of the vesicle's cavity or interface region is in agreement with the report of Kunwar et al.[36] concerning phospholipid liposomes. Similarly, Sun et al.[37] investigated the interaction of curcumin with bilayer lipid membranes of giant unilamellar vesicles and came to the conclusion that curcumin initially binds to the interface and then is eventually inserted into the nonpolar hydrocarbon region.

Interaction of CFN-enclosed curcumin with bacterial membranes deserves further investigation in order to understand the mode of its antimicrobial action. Several possible mechanisms were proposed for liposome–bacterial cell interaction.[38] The two most relevant alternatives are (a) a fusigenic mechanism based on the merger of liposome bilayer with the cellular membrane releasing the vesicle content inside the cell[38] and (b) the "collision" mechanism, including intermembrane transfer of lipophilic materials without disruption of membranes.[39] Considering the strongly lipophilic character of curcumin and its bilayer localization, we suggest that the collision mechanism prevails in the mode of action of CFN. Since this mechanism is not associated with membrane disruption, it may allow longer functional durability of the CFN-coated surfaces.

To the best of our knowledge, this is the first report of curcumin-functionalized active antimicrobial surfaces. Obviously, physical contact of these surfaces with microbial cells was necessary for realization of their bactericidal potential. Inclusion of glucose in the interface layer of the vesicles facilitated their binding with bacteria based on ligand–receptor interaction.[29] On the other hand, the shake flask assay might not ensure optimal contact of bacteria suspended in the whole PBS volume with the CFN-coated glass. These contact limitations might result in certain reduction of efficacy of glass-bound vs free-suspended CFN toward *E. coli*. Sporulation of *B. cereus* caused by contact with nanovesicle-coated glass (with or without addition of curcumin) might affect the results obtained with this species. An optimal standardized procedure for testing the antimicrobial activity of active surfaces has yet to be developed. At any rate, the trials have shown a significant count reduction of both Gram-negative and Gram-positive bacteria caused by the contact with CFN-coated glass as compared with glass coated with nanovesicles without curcumin. On the other hand, further optimization of the nanovesicle efficacy is needed.

In summary, this study has demonstrated the advantages of curcumin as a potent natural antibacterial compound far exceeding other phenolic compounds tested. This activity was retained after inclusion of curcumin in liposome-type PDA nanovesicles and further covalent binding of the vesicles to glass surface. Thus, for the first time active antimicrobial surfaces functionalized by the natural food-grade compound curcumin were prepared. The activity of the curcumin-functionalized surfaces was demonstrated toward both Gram-negative (*E. coli*) and Gram-positive (*B. cereus*) bacteria. After efficacy optimization, this approach can be implemented, without imposing a health risk, for controlling microbial growth and preventing cross-contamination and biofilm formation on food-contacting surfaces (equipment, utensils, packaging) used in the food industry and home cooking.

DOI: 10.1021/jf505442w
J. Agric. Food Chem. 2015, 63, 2557–2565

■ ASSOCIATED CONTENT

Supporting Information

NMR spectra of intermediate and final products formed during synthesis of diacetylene monomers as shown in Figure 2. This material is available free of charge via the Internet at http://pubs.acs.org.

■ AUTHOR INFORMATION

Corresponding Author

*Tel.: +972-3-9683609; Fax +972-3-9683622; E-mail: vrodov@agri.gov.il.

Present Address

⊥Navneet Dogra: Department of Chemical & Environmental Engineering, School of Engineering & Applied Science, Yale University, 55 Prospect Street, New Haven, Connecticut 06511, United States.

Funding

This research was supported by the US-Israel Binational Agricultural Research and Development (BARD) Grants US-4471-11F and US-4680-13C. Contribution from the Agricultural Research Organization, The Volcani Center, Bet Dagan, Israel, No 705/14.

Notes

The authors declare no competing financial interest.

■ ACKNOWLEDGMENTS

The authors are grateful to David P. Clark, Department of Microbiology at Southern Illinois University in Carbondale, for providing stock cultures of *E. coli* and *B. cereus*.

■ ABBREVIATIONS USED

AAUC, added area under the curve; AFM, atomic force microscopy; CFN, curcumin-functionalized nanovesicles; CFU, colony-forming units; DAPI, 4′,6-diamidino-2-phenylindole; DCM, dichloromethane; DMPC, 1,2-dimyristoyl-*sn*-glycero-3-phosphocholine; IC_{50}, half-maximal inhibitory concentration; MBCD, methyl-β-cyclodextrin; MIC, minimum inhibitory concentration; NHS, *N*-hydroxysuccinimide; NYDB, nutrient yeast dextrose broth; PBS, phosphate buffer saline; PDA, polydiacetylene; TEM, transmission electron microscopy; TSA, tryptic soy agar; TSB, tryptic soy broth

■ REFERENCES

(1) Gillespie, I. A.; O'Brien, S. J.; Adak, G. K.; Ward, L. R.; Smith, H. R. Foodborne general outbreaks of *Salmonella enteritidis* phage type 4 infection, England and Wales, 1992−2002: where are the risks? *Epidemiol. Infect.* **2005**, *133*, 795−801.

(2) Page, K.; Wilson, M.; Parkin, I. P. Antimicrobial surfaces and their potential in reducing the role of the inanimate environment in the incidence of hospital-acquired infection. *J. Mater. Chem.* **2009**, *19*, 3819−3831.

(3) Appendini, P.; Hotchkiss, J. H. Review of antimicrobial food packaging. *Innovative Food Sci. Emerg. Technol.* **2002**, *3*, 113−126.

(4) Onnis-Hayden, A.; Hsu, B. B.; Klibanov, A. M.; Gu, A. Z. An antimicrobial polycationic sand filter for water disinfection. *Water Sci. Technol.* **2011**, *63*, 1997−2003.

(5) Quintavalla, S.; Vicini, L. Antimicrobial food packaging in meat industry. *Meat Sci.* **2002**, *62*, 373−380.

(6) Sharma, V. K.; Yngard, R. A.; Lin, Y. Silver nanoparticles: green synthesis and their antimicrobial activities. *Adv. Colloid Interface Sci.* **2009**, *145*, 83−96.

(7) Grass, G.; Rensing, C.; Solioz, M. Metallic copper as an antimicrobial surface. *Appl. Environ. Microbiol.* **2011**, *77*, 1541−1547.

(8) Kurt, P.; Wood, L.; Ohman, D. E.; Wynne, K. J. Highly effective contact antimicrobial surfaces via polymer surface modifiers. *Langmuir* **2007**, *23*, 4719−4723.

(9) Madkour, A. E.; Dabkowski, J. M.; Nusslein, K.; Tew, G. N. Fast disinfecting antimicrobial surfaces. *Langmuir* **2009**, *25*, 1060−1067.

(10) Tiller, J. C.; Liao, C. J.; Lewis, K.; Klibanov, A. M. Designing surfaces that kill bacteria on contact. *Proc. Natl. Acad. Sci. U.S.A.* **2001**, *98*, 5981−5985.

(11) Lin, J.; Qiu, S.; Lewis, K.; Klibanov, A. M. Bactericidal properties of flat surfaces and nanoparticles derivatized with alkylated polyethylenimines. *Biotechnol. Prog.* **2002**, *18*, 1082−1086.

(12) Lee, S. B.; Koepsel, R. R.; Morley, S. W.; Matyjaszewski, K.; Sun, Y.; Russell, A. J. Permanent, nonleaching antibacterial surfaces. 1. Synthesis by atom transfer radical polymerization. *Biomacromolecules* **2004**, *5*, 877−882.

(13) Poverenov, E.; Shemesh, M.; Gulino, A.; Cristaldi, D. A.; Zakin, V.; Yefremov, T.; Granit, R. Durable contact active antimicrobial materials formed by a one-step covalent modification of polyvinyl alcohol, cellulose and glass surfaces. *Colloids Surf. B: Biointerfaces* **2013**, *112*, 356−361.

(14) Filip, V.; Plockova, M.; Smidrkala, J.; Spickova, Z.; Melzoch, K.; Schmidt, S. Resveratrol and its antioxidant and antimicrobial effectiveness. *Food Chem.* **2003**, *83*, 585−593.

(15) Parvathy, K. S.; Negi, P. S.; Srinivas, P. Antioxidant, antimutagenic and antibacterial activities of curcumin-β-diglucoside. *Food Chem.* **2009**, *115*, 265−271.

(16) Furneri, P. M.; Piperno, A.; Sajia, A.; Bisignano, G. Antimycoplasmal activity of hydroxytyrosol. *Antimicrob. Agents Chemother.* **2004**, *48*, 4892−4894.

(17) Barber, M. S.; McConnell, V. S.; Decaux, B. S. Antimicrobial intermediates of the general phenylpropanoid and lignin specific pathways. *Phytochemistry* **2000**, *54*, 53−56.

(18) Cruz, J. M.; Dominguez, J. M.; Dominguez, H.; Parajo, J. C. Antioxidant and antimicrobial effects of extracts from hydrolysates of lignocellulosic materials. *J. Agric. Food Chem.* **2001**, *49*, 2459−2464.

(19) Ascensao, A. R. F. D. C. de; Dubery, I. A. Soluble and wall-bound phenolics and phenolic polymers in *Musa acuminata* roots exposed to elicitors from *Fusarium oxysporum* f.sp cubense. *Phytochemistry* **2003**, *63*, 679−686.

(20) Rhim, J. W.; Ng, P. K. W. Natural biopolymer-based nanocomposite films for packaging applications. *Crit. Rev. Food Sci. Nutr.* **2007**, *47*, 411−433.

(21) Zimniewska, M.; Kozłowski, R.; Batog, J. Nanolignin modified linen fabric as a multifunctional product. *Mol. Cryst. Liq. Cryst.* **2008**, *484*, 409−416.

(22) Maheshwari, R. K.; Singh, A. K.; Gaddipati, J.; Srimal, R. C. Multiple biological activities of curcumin: A short review. *Life Sci.* **2006**, *78*, 2081−2087.

(23) ChromaDex. *99% Pure Curcumin*; ChromaDex: Irvine, CA, 2012, 4 p.

(24) Rai, D.; Singh, J. K.; Roy, N.; Panda, D. Curcumin inhibits FtsZ assembly: an attractive mechanism for its antibacterial activity. *Biochem. J.* **2008**, *410*, 147−155.

(25) Bhawana; Basniwal, R. K.; Buttar, H. S.; Jain, V. K.; Jain, N. Curcumin nanoparticles: preparation, characterization, and antimicrobial study. *J. Agric. Food Chem.* **2011**, *56*, 2056−2061.

(26) Han, S.; Yang, Y. Antimicrobial activity of wool fabric treated with curcumin. *Dyes Pigm.* **2005**, *64*, 157−161.

(27) Guo, C.; Liu, S.; Dai, Z.; Jiang, C.; Li, W. Polydiacetylene vesicles as a novel drug sustained-release system. *Colloid. Surf. B: Biointerfaces* **2010**, *76*, 362−365.

(28) Shim, H. Y.; Lee, S. H.; Ahn, D. J.; Ahn, K. D.; Kim, J. M. Micropatterning of diacetylenic liposomes on glass surfaces. *Mater. Sci. Eng.: C* **2004**, *24*, 157−161.

(29) Dogra, N.; Li, X.; Kohli, P. Investigating ligand-receptor interactions at bilayer surface using electronic absorption spectroscopy and fluorescence resonance energy transfer. *Langmuir* **2012**, *28*, 12989−12998.

DOI: 10.1021/jf505442w
J. Agric. Food Chem. 2015, 63, 2557−2565

(30) In *CRC Handbook of Chemistry and Physics*, 91st ed.; Haynes, W. M., Ed.; CRC Press: Boca Raton, FL, 2010; 2610 pp.
(31) Lakowicz, J. R. *Principles of Fluorescence Spectroscopy*, 2nd ed.; Kluwer Academics: New York, 1999; Chapter 13, 692 pp.
(32) Haraguchi, M.; Okamoto, T.; Hayashi, H.; Hasegawa, T.; Akamatsu, T.; Fukui, M.; Koda, T.; Takeda, K. Real-time observation of the dielectric constant variation of evaporated polydiacetylene films during photopolymerization and photochromic transitions. *Thin Solid Films.* **1998**, *331*, 39−44.
(33) Huang, M. T.; Smart, R. C.; Wong, C. Q.; Conney, A. H. Inhibitory effect of curcumin, chlorogenic acid, caffeic acid, and ferulic acid on tumor promotion in mouse skin by 12-O-tetradecanoylphorbol-13-acetate. *Cancer Res.* **1988**, *48*, 5941−5946.
(34) Bourne, K. Z.; Bourne, N.; Reising, S. F.; Stanberry, L. R. Plant products as topical microbicide candidates: assessment of in vitro and in vivo activity against herpes simplex virus type 2. *Antiviral Res.* **1999**, *42*, 219−226.
(35) Kaur, S.; Modi, N. H.; Panda, D.; Roy, N. Probing the binding site of curcumin in *Escherichia coli* and *Bacillus subtilis* FtsZ − A structural insight to unveil antibacterial activity of curcumin. *Eur. J. Med. Chem.* **2010**, *45*, 4209−4214.
(36) Kunwar, A.; Barik, A.; Pandey, R.; Priyadarsini, K. I. Transport of liposomal and albumin loaded curcumin to living cells: an absorption and fluorescence spectroscopic study. *Biochim. Biophys. Acta: Gen. Subj.* **2006**, *1760*, 1513−1520.
(37) Sun, Y.; Lee, C. C.; Hung, W. C.; Chen, F. Y.; Lee, M. T.; Huang, H. W. The bound states of amphipathic drugs in lipid bilayers: study of curcumin. *Biophys. J.* **2008**, *95*, 2318−2324.
(38) Pignatello, R.; Nicolosi, D.; Nicolosi, V. M. Fusogenic liposomes as new carriers to enlarge the spectrum of action of antibiotic drugs against Gram-negative bacteria. In *Science Against Microbial Pathogens: Communicating Current Research and Technological Advances*; Mendez-Vilas, A., Ed.; Formatex Res. Center: Badajoz, Spain, 2011; pp 52−60.
(39) Fahr, A.; van Hoogevest, P.; May, S.; Bergstrand, N.; Leigh, M. L. S. Transfer of lipophilic drugs between liposomal membranes and biological interfaces: Consequences for drug delivery. *Eur. J. Pharm. Sci.* **2005**, *26*, 251−265.

DOI: 10.1021/jf505442w
J. Agric. Food Chem. 2015, 63, 2557−2565

for which the European Commission has issued "indicative" levels for the presence of acrylamide.[18]

The European food industry has devised many strategies for reducing acrylamide formation by modifying food processing. These have been compiled in a "*Toolbox*" produced by Food Drink Europe.[19] Analysis of manufacturers' data on acrylamide levels in potato chips in Europe showed a clear, statistically significant downward trend for mean levels of acrylamide from 763 (±91.1) μg/kg (parts per billion) in 2002 to 358 (±2.5) μg/kg in 2011, a decrease of 53% (±13.5), which was taken as evidence of the effectiveness of the "*Toolbox*".[20] However, the effect of seasonality arising from the influence of potato storage on acrylamide levels was evident in the study, and this was consistent with the results of a study that had analyzed samples of commercial potatoes in the United Kingdom from harvest through 9 months of storage,[21] showing the difficulty of processing a variable raw material to give a consistently low acrylamide level in the product. In the United States, the Food and Drug Administration has developed an "action plan" with a number of goals, including identifying means to reduce exposure. A North American perspective on the issue and the response to it has been given by Bethke and Bussan.[22]

Reducing the acrylamide-forming potential of potatoes and making it more consistent would be a great help to the food industry. In the United States, The J. R. Simplot Co. has recently begun to market a low-acrylamide biotech potato variety that has reduced activity of an asparagine synthetase gene (*ASN1*), two genes encoding enzymes of starch breakdown, phosphorylase L (*PhL*), and starch-associated R1 (*R1*), as well as a gene (*PPO5*) encoding polyphenol oxidase, an enzyme involved in bruising.[23,24] There is currently no possibility of such an approach being taken in Europe, but plant and agronomic science still have an important part to play, for example, through the identification and production of crop genotypes that stay consistently low in acrylamide-forming potential through a range of environments and conditions, including storage, and the development of best crop management practice.[25]

Conditions and length of storage are clearly aspects of potato management that can be optimized to keep acrylamide-forming potential as low as possible, and nutrition is another, with nitrogen availability, for example, increasing the acrylamide-forming potential of most varieties but decreasing it in some, whereas sulfur application reduces glucose concentrations and mitigates the effect of high nitrogen application in some varieties.[26] In this study, the impact of a third aspect of potato management, irrigation, was assessed, and the related issue of the effect of severe drought stress was investigated. The results showed water availability to have profound effects on the free amino acid and sugar concentrations and acrylamide-forming potential of potatoes. Lack of irrigation in the field and severe drought stress imposed in a glasshouse both brought about significant but different changes in composition, and different genotypes were affected in dissimilar fashion by the same treatment, indicating that there is no single, unifying potato tuber drought stress response.

MATERIALS AND METHODS

Chemicals. Ethanol (95% v/v, analytical grade) (Thermo Fisher Scientific UK Ltd., Loughborough, UK), HCl (Corning Life Science; supplied by Sigma-Adrich Company Ltd., Poole, UK), and acrylamide-$^{13}C_3$ (Sigma-Adrich Co. Ltd., Poole, UK) were used. KOH for IC chromatography (Thermo Fisher Scientific UK Ltd.), amino acid standards (Phenomenex, Torrence, CA, USA), isotopically labeled amino acids (Cambridge Isotope Laboratories, Inc., Andover, MA, USA), and helium (high purity) (BOC Industrial Gases, Sheffield, UK) were also acquired.

Commercial Potato Samples. Tubers from five varieties of potatoes (*S. tuberosum*) grown commercially in the United Kingdom in 2011 were provided by Higgins Group (Doncaster, UK). They came from adjacent irrigated and not-irrigated fields in Herefordshire and Shropshire in western England and from Norfolk in eastern England, water being supplied to the irrigated plants when required in the judgment of the farm manager. The potatoes were planted in April and harvested between late September and early November 2011. Nitrogen, phosphate, and potassium fertilizer was applied at levels recommended in the *Fertiliser Manual* (RB209),[27] which takes into account soil type and intrinsic soil nutrient levels. In all cases, irrigated and not-irrigated plots received the same fertilizer treatment. After harvest, the potatoes were kept in a commercial potato store at 8.5–9.5 °C, in line with normal UK practice, until analysis in January 2012. The varieties were Hermes, Markies, and Ramos, considered to be drought-tolerant, and Lady Claire and Saturna, which are drought-sensitive. Replication was derived from randomly sampling five tubers from each plot.

Glasshouse Experiment. A split-plot experiment in two blocks was set up in four deep troughs (2 m long × 0.625 m wide × 0.55 m deep), consisting of a two-variety (Saturna and Markies) by two-treatment (watered and drought-stressed) factorial. Two containers formed a block, one for watered and one for drought-stressed main-plot treatment. Each main plot was further divided into six split-plots, with three tubers of each of the two varieties being planted on February 16, 2012, one tuber per split-plot. All split-plots were sealed compartments in the container to maintain watered and drought-stressed conditions and prevent leakage between compartments. Day temperature was maintained at 18 °C and night temperature at 16 °C; supplementary lighting was used to provide the plants with a 16 h day. The troughs were filled with compost (Rothamsted mixture, requiring no additional fertilizer) on top of a 2.5 cm layer of J. Arthur Bower's Hydroleca (lightweight clay aggregate beads; William Sinclair Horticulture Ltd., Lincoln, UK) to allow efficient drainage.

Water was supplied automatically through a drip-feed for 3 min per day from the day of planting. On April 25 (68 days after planting) the plants began to flower, a developmental change that coincides closely with tuber initiation. At this point, watering to the drought treatment plants was reduced to 1 min per day and again on May 18 (91 days after planting) to 1 min per week. On June 7 (111 days after planting) the supply to the watered plants was increased to 6 min per day, and on September 6 (202 days after planting) watering to all plants was ceased to encourage senescence. Leaf water potential at mid-day was measured in a pressure chamber (PMS Instrument Co., Corvallis, OR, USA) to ensure that the plants for which water was withheld were drought-stressed. The plants were harvested on September 27, 2012 (223 days after planting).

Free Amino Acid and Sugar Concentrations. Free amino acids and sugars were measured as described previously.[21] Flour was prepared from individual freeze-dried tubers, and free amino acids were derivatized and then analyzed by gas chromatography–mass spectrometry (GC-MS) using an Agilent 5975 system (Agilent, Santa Clara, CA, USA). Note that arginine cannot be measured using this system, whereas cysteine concentrations were too low to measure accurately. Sugar concentrations were measured using a Dionex ion chromatography system with a 250 × 4 mm Carbopac PA1 column (Dionex Corp., Sunnyvale, CA, USA), operated using Chromeleon software, also as described previously.[21]

Acrylamide Formation. Acrylamide was measured in cooked potato flour after heating to 160 °C for 20 min. The analysis was performed by liquid chromatography–tandem mass spectrometry (LC-MS/MS) using an Agilent 1200 high-performance liquid chromatography (HPLC) system with a 6410 triple-quadrupole mass spectrometer with electrospray ion source in positive ion mode, as previously described.[21]

DOI: 10.1021/jf506031w
J. Agric. Food Chem. 2015, 63, 2566–2575

Statistical Analyses. The method of Residual Maximum Likelihood (REML) as implemented in *GenStat* (16th ed., VSN International Ltd., Hemel Hempstead, UK) was used to fit a linear mixed model to the data on the $\log_e$ scale, this transformation ensuring constant variance across the variety by treatment combinations. The analysis tested (F tests) the main effects and interactions between factors. For the field experiment, these factors were variety nested in type (drought-tolerant and -sensitive) and irrigation/nonirrigation, whereas random effects of location had to be accounted for. In the glasshouse experiment, the factors were variety and treatment (drought-stressed or watered), with blocks, main-plots, and split-plots being the random effects. Significant ($p < 0.05$, F test) terms for inspection were disseminated by considering differences between means of biological interest in terms of the standard error of the difference (SED) values on the relevant degrees of freedom (df). The least significant difference (LSD) was therefore used to judge significance at the 5% level.

For further inspection of the data, Pearson's correlation coefficients (r) were calculated between all pairs of responses, for the full data set and also for data pertaining to the separate treatments (irrigated and not-irrigated; watered or drought-stressed). These correlations were tested for significance using F tests.

RESULTS AND DISCUSSION

Effect of Irrigation on Tuber Composition in Five Potato Varieties Grown on Commercial Farms in the United Kingdom in 2011. Potato varieties Ramos, Lady Claire, Saturna, Hermes, and Markies were grown in three regions of the United Kingdom, namely, Herefordshire and Shropshire in western England and Norfolk in eastern England, under irrigated and not-irrigated conditions. The meteorological data for the United Kingdom in 2011 are available from the UK Meteorological Office: http://www.metoffice.gov.uk/climate/uk/2011/. Notable features of that year for England were a very warm and dry spring (the mean temperature for April was 3.5 °C above average), giving way to a rather cool summer with rainfall close to the average, although regionally variable. Eastern England, including Norfolk, where the Markies samples came from, was very dry in the spring, but the dry spell broke in June.

Data were obtained from tuber samples on free amino acids (excluding arginine, which cannot be measured by the method used, and cysteine, which was present at concentrations lower than would be required to allow reliable measurement) and the sugars glucose, fructose, and sucrose. Total amino acid content was calculated along with the ratio of free asparagine to total free amino acid concentration, a parameter that was identified as potentially related to acrylamide formation in a study that modeled the kinetics of acrylamide formation in French fry production.[28] Total sugar content was also calculated along with the sum of glucose and fructose as reducing sugars (potatoes contain very little maltose, and this was not measured). Data on acrylamide formation in heated flour were also obtained for analysis. The complete data set is given in Supporting Information Tables S1–S3.

The data were subjected to REML analysis following a $\log_e$ transformation to ensure constant variance across the variety by treatment (irrigated versus not irrigated) combinations. The results are shown in Table 1. There was a significant interaction ($p < 0.05$, F test) between treatment and variety nested in type for proline, tryptophan, glucose, total reducing sugars, and acrylamide. There was also a significant ($p < 0.05$, F test) interaction of type with treatment for free glutamine and the ratio of free asparagine to total free amino acids, indicating that the drought-tolerant and -sensitive varieties responded differently to irrigation with respect to these parameters. There were significant ($p < 0.05$, F test) varietal differences, nested in type, for free alanine, glycine, leucine, threonine, serine, γ-aminobutyric acid (GABA), asparagine, aspartic acid, glutamic acid, phenylalanine, glutamine, lysine, tyrosine, total free amino acids, the ratio of free asparagine to total free amino acids, and fructose. There was also a main effect ($p = 0.001$, F test) of treatment for fructose and a main effect of type ($p < 0.001$, F test) for free valine, isoleucine, and methionine. The relevant means, standard error of the difference between means (SED) (df), and least significant difference (LSD) (5%) values for comparisons are given in Table 2.

Table 2a shows the relevant means for the different varieties nested in type. Saturna had significantly different ($p < 0.05$, LSD) and lower concentrations of free alanine, glycine, threonine, serine, GABA, glutamine, lysine, and total free amino acids than the other varieties. The drought-tolerant varieties generally had greater concentrations of most free

Table 1. p Values Denoting Significance of Main Effects and Interactions of Treatment Factors in Linear Mixed Model (REML) Analyses of Measured Variables for Five Varieties of Potatoes Grown, with or without Irrigation, on Commercial Farms in the United Kingdom in 2011[a]

	type	treatment	type × variety	type × treatment	type × variety × treatment
amino acids					
alanine	<0.001	0.796	**0.004**	0.434	0.715
glycine	<0.001	0.867	**<0.001**	0.059	0.782
valine	**<0.001**	0.225	0.468	0.614	0.803
leucine	0.006	0.115	**0.003**	0.738	0.584
isoleucine	**<0.001**	0.407	0.106	0.682	0.656
threonine	<0.001	0.632	**0.005**	0.693	0.509
serine	<0.001	0.598	**<0.001**	0.302	0.885
γ-aminobutyric acid	0.712	0.834	**<0.001**	0.057	0.752
proline	<0.001	<0.001	<0.001	0.903	**<0.001**
asparagine	0.047	0.088	**0.014**	0.919	0.786
aspartic acid	0.123	0.165	**<0.001**	0.139	0.958
methionine	**<0.001**	0.828	0.067	0.762	0.630
glutamic acid	<0.001	0.513	**0.006**	0.557	0.374
phenylalanine	<0.001	0.187	**0.004**	0.198	0.316
glutamine	<0.001	0.350	**<0.001**	0.021	0.893
lysine	<0.001	0.830	**0.006**	0.568	0.201
tyrosine	0.001	0.485	**<0.001**	0.287	0.111
tryptophan	0.011	0.420	<0.001	0.643	<0.001
total amino acids	<0.001	0.180	**<0.001**	0.178	0.762
asparagine/total amino acids	<0.001	0.480	**<0.001**	**0.001**	0.104
sugars					
glucose	0.165	<0.001	<0.001	0.605	<0.001
fructose	<0.001	**0.001**	**<0.001**	0.577	0.064
sucrose	0.065	0.642	0.129	0.149	0.482
reducing sugars	<0.001	<0.001	<0.001	0.994	0.010
total sugars	0.288	0.586	0.057	0.091	0.147
acrylamide	0.017	<0.001	<0.001	0.485	**<0.001**

[a]Variety is nested within type (drought-tolerant and -sensitive), and the × indicates the interaction between the treatment factors type and variety, type and treatment (irrigated or not irrigated), and type, variety, and treatment. P values in bold indicate the significant ($p < 0.05$, F test) terms that were selected for inspection (significant values not in bold were superseded by more complex terms in the ANOVA).

DOI: 10.1021/jf506031w
J. Agric. Food Chem. 2015, 63, 2566–2575

Table 2. Comparison of Means for Free Amino Acids, Sugars and Acrylamide Formation for Five Varieties of Potatoes Grown, with and without Irrigation, on Commercial Farms in the UK in 2011

(a) Log_e Means (n = 10), Standard Error of the Difference (SED), Degrees of Freedom (df), and Least Significant Difference (LSD) at the 5% Level of Significance for Comparison of Means for Variables with Only a Main Effect ($p < 0.05$, F Test) of Variety Nested within Type (Drought-Tolerant and -Sensitive)[a]

	type × variety						
	sensitive		tolerant				
	Lady Claire	Saturna	Hermes	Markies	Ramos	SED/SE (df)	LSD (5%)
amino acids							
alanine	0.986 (2.680)	−0.029 (0.971)	1.922 (6.835)	1.804 (6.074)	1.898 (6.673)	0.2562 (40)	0.5179
glycine	0.042 (1.043)	−0.737 (0.479)	0.390 (1.477)	0.913 (2.492)	0.895 (2.447)	0.1796 (40)	0.3629
leucine	−0.017 (0.983)	−0.070 (0.932)	0.708 (2.030)	0.051 (1.052)	0.107 (1.113)	0.1789 (40)	0.3617
threonine	1.021 (2.776)	0.422 (1.525)	1.657 (5.244)	1.822 (6.184)	1.560 (4.759)	0.1684 (40)	0.3404
serine	1.460 (4.306)	0.368 (1.445)	1.661 (5.265)	2.020 (7.538)	1.944 (6.987)	0.2136 (40)	0.4317
γ-aminobutyric acid	3.137 (23.03)	1.367 (3.924)	2.216 (9.171)	2.259 (9.574)	2.134 (8.449)	0.2022 (40)	0.4087
asparagine	4.729 (113.18)	4.563 (95.87)	4.613 (100.79)	5.049 (155.87)	4.811 (122.85)	0.1347 (40)	0.2722
aspartic acid	3.261 (26.08)	2.772 (15.99)	2.946 (19.03)	3.204 (24.63)	3.281 (26.60)	0.1247 (40)	0.2520
glutamic acid	2.564 (12.99)	2.316 (10.14)	2.648 (14.13)	3.149 (23.31)	2.739 (15.47)	0.1550 (40)	0.3132
phenylalanine	0.366 (1.442)	0.449 (1.567)	1.381 (3.979)	0.556 (1.744)	1.027 (2.793)	0.2118 (40)	0.4281
glutamine	4.401 (81.53)	3.127 (22.81)	4.032 (56.37)	4.380 (79.84)	4.398 (81.29)	0.1747 (40)	0.3530
lysine	−0.030 (0.970)	−1.310 (0.270)	0.380 (1.462)	0.060 (1.062)	0.130 (1.139)	0.3450 (40)	0.6980
tyrosine	−1.287 (0.276)	−1.023 (0.360)	0.295 (1.343)	−0.808 (0.446)	−0.975 (0.377)	0.2949 (40)	0.5961
total amino acids	5.717 (303.99)	5.117 (166.83)	5.538 (254.17)	5.898 (364.31)	5.862 (351.43)	0.1415 (40)	0.2860
asparagine/total amino acids	−0.988 (0.372)	−0.554 (0.575)	−0.924 (0.397)	−0.848 (0.428)	−1.052 (0.349)	0.0593 (40)	0.1198
sugars							
fructose	−5.069 (6)	−4.060 (17)	−4.072 (17)	−3.405 (48)	−3.378 (34)	0.2846 (39)	0.5756
sucrose					−0.436 (647)	0.034 (39)	
total sugars					−0.343 (710)	0.033 (39)	

(b) Log_e Means, Number of Observations in Means, Standard Error of the Difference (SED), Degrees of Freedom (df), and Least Significant Difference (LSD) at the 5% Level of Significance for Comparison of Means for Variables with a Type ($p < 0.05$, F Test) Effect Only

	type			
amino acid	sensitive	tolerant	SED (df)	LSD (5%)
valine	1.546, 20 (4.693)	2.316, 30 (10.14)	0.1266 (40)	0.2559
isoleucine	0.212, 20 (1.236)	0.978, 30 (2.659)	0.1273 (40)	0.2573
methionine	−0.072, 20 (0.931)	1.122, 30 (3.071)	0.1352 (40)	0.2733

(c) Log_e Means, Number of Observations in Means, Standard Error of the Difference (SED), Degrees of Freedom (df), and Least Significant Difference (LSD) at the 5% Level of Significance for Comparison of Means for Variables with a Type (Drought-Tolerant and -Sensitive) by Treatment ($p < 0.05$, F Test) Effect

	treatment					
	irrigated		not irrigated			
amino acid	sensitive	tolerant	sensitive	tolerant	SED (df)	LSD (5%)
glutamine	3.979, 10 (53.46)	4.214, 15 (67.63)	3.550, 10 (34.81)	4.326, 15 (75.64)	0.1747[b] (40)	0.3530
					0.1595[c] (40)	0.3223
					0.1426[d] (40)	0.2882
asparagine/total amino acids	−0.865, 10 (0.421)	−0.901, 15 (0.406)	−0.677, 10 (0.508)	−0.982, 15 (0.375)	0.0593[b] (40)	0.1198
					0.0541[c] (40)	0.1094
					0.0484[d] (40)	0.0978

(d) Log_e Means (n = 5), Standard Error of the Difference (SED), Degrees of Freedom (df), and Least Significant Difference (LSD) at the 5% Level of Significance for Comparison of Means for Variables with Significant Interaction of Treatment with Variety Nested within Type (Drought-Tolerant and -Sensitive) ($p < 0.05$, F Test)

variety	treatment	proline	tryptophan	glucose	reducing sugars	acrylamide
Lady Claire[e]	irrigated	1.343 (3.831)	−0.070 (0.932)	−3.888 (20)	−3.510 (30)	0.557 (1.745)
Saturna[e]	irrigated	0.625 (1.868)	−3.140 (0.043)	−2.865 (57)	−2.493 (83)	1.156 (3.177)
Hermes	irrigated	1.777 (5.912)	−1.110 (0.330)	−3.310 (37)	−2.862 (57)	0.726 (2.067)
Markies	irrigated	2.846 (17.22)	−0.800 (0.449)	−4.135 (16)	−2.803 (61)	0.758 (2.134)
Ramos	irrigated	1.950 (7.029)	−1.510 (0.221)	−2.399 (91)	−1.789 (167)	0.873 (2.394)
Lady Claire[e]	not irrigated	3.062 (21.37)	−1.880 (0.153)	−4.459 (12)	−4.065 (17)	0.482 (1.619)
Saturna[e]	not irrigated	0.793 (2.210)	−1.910 (0.148)	−3.753 (23)	−3.339 (35)	0.852 (2.344)
Hermes	not irrigated	1.976 (7.214)	−0.780 (0.458)	−3.658 (26)	−3.210 (40)	0.678 (1.970)
Markies	not irrigated	2.925 (18.63)	−1.330 (0.264)	−4.025 (18)	−2.956 (52)	0.700 (2.014)
Ramos	not irrigated	4.650 (104.58)	−1.570 (0.208)	−3.992 (18)	−3.384 (34)	0.244 (1.276)

DOI: 10.1021/jf506031w
J. Agric. Food Chem. 2015, 63, 2566−2575

Table 2. continued

(d) Log_e Means (n = 5), Standard Error of the Difference (SED), Degrees of Freedom (df), and Least Significant Difference (LSD) at the 5% Level of Significance for Comparison of Means for Variables with Significant Interaction of Treatment with Variety Nested within Type (Drought-Tolerant and -Sensitive) ($p < 0.05$, F Test)

variety	treatment	proline	tryptophan	glucose	reducing sugars	acrylamide
SED (df)		0.4358 (40)	0.4670 (40)	0.2425 (39)	0.3109 (39)	0.0863 (40)
LSD (5%)		0.8808	0.9440	0.4905	0.6288	0.1745

[a]The grand mean (n = 50) and corresponding standard error (SE) are given for sucrose and total sugars, these having no effects at all. Back-transformed means (mmol per kg for amino acids and mg per kg for sugars) are given in parentheses. [b]Comparing means having 10 replicates. [c]Comparing means having 10 replicates with means having 15 replicates. [d]Comparing means having 15 replicates. [e]Drought-sensitive varieties.

amino acids than the drought-sensitive varieties and were more consistent as a group, although Hermes had significantly different ($p < 0.05$, LSD) and lower free glycine, aspartic acid, and total free amino acids and greater leucine and tyrosine than Markies and Ramos. Markies had the highest concentration of free asparagine, significantly different ($p < 0.05$, LSD) from Lady Claire, Saturna, and Hermes but not from Ramos. However, Saturna had the greatest ratio of free asparagine to total free amino acids, significantly different ($p < 0.05$, LSD) from the other varieties. Markies and Ramos had the greatest fructose, significantly different ($p < 0.05$, LSD) from the other three varieties.

The two types (drought-tolerant and -sensitive) differed significantly ($p < 0.05$, F test) as a whole, regardless of within-type (varietal) influence, only in that the tolerant varieties showed greater concentrations of valine, isoleucine, and methionine (Table 2b), but there was an interaction between type and treatment (Table 2c): free glutamine was significantly different ($p < 0.05$, LSD) and lower in the not-irrigated samples than the irrigated for the drought-sensitive varieties but higher for the drought-tolerant varieties, whereas the ratio of free asparagine to total free amino acids was significantly different ($p < 0.05$, LSD) and higher in the not-irrigated samples than the irrigated samples for the drought-sensitive varieties but slightly lower for the drought-tolerant varieties.

There were more effects from the interaction between treatment and variety nested in type (Table 2d), indicating that the varieties responded differently to irrigation. There was a higher concentration of proline in the not-irrigated conditions for all varieties but significantly so ($p < 0.05$, LSD) for Lady Claire and Ramos, the latter having a tremendous increase of 13.9-fold from 7.02 mmol/kg with irrigation to 104.58 mmol/kg without irrigation. An increase in proline concentration in response to drought and other treatments that cause osmotic stress has been observed in many plant species and has led to the hypothesis that it is not just a symptom of stress but part of the stress response, decreasing cell osmotic potential and thereby increasing turgor while decreasing plant water potential. This hypothesis has been reviewed in detail (and with some skepticism) by Lawlor.[29] The results of the present study would support an increase in free proline concentration being part of the response to drought stress, except that the varietal type was not well-associated with the quantity of increased proline, because Lady Claire is known to be drought-sensitive, whereas Ramos is drought-tolerant. The tryptophan concentration also suggested a differential response to irrigation for the varieties: the concentration was significantly different ($p < 0.05$, LSD) and higher for Saturna in the not-irrigated than in the irrigated sample, but significantly different ($p < 0.05$, LSD) and lower for Lady Claire.

Drought stress has also been shown to bring about an interconversion of simple sugars and complex carbohydrates, such as starch and fructan, in some plant species, and, as with proline, an increase in the concentration of simple sugars has been proposed to act as an osmotic protectant.[2,5] However, in this study, the glucose concentration was significantly different ($p < 0.05$, LSD) and lower in the not-irrigated samples for Lady Claire, Saturna, and Ramos and also substantially lower for Hermes, although slightly increased for Markies. Similar results were seen for total reducing sugars, albeit with Markies now showing a decrease.

There was no significant effect of the treatment, either on its own or interacting with type or variety nested in type, on the concentration of the other acrylamide precursor, free asparagine ($p = 0.088$, F test), but the indication was for an increase in all five varieties, with 124.84 mmol/kg in the not-irrigated samples and 107.66 mmol/kg in the irrigated samples, a 1.16-fold difference.

Acrylamide formation was lower for all varieties without irrigation and significantly so ($p < 0.05$, LSD) for Saturna (by 0.262 mg/kg on average) and Ramos (by 1.118 mg/kg on average). Previous studies have shown the relationship between precursor concentration and acrylamide formation in potato to be complex,[30] but glucose concentration has been a major factor in determining the acrylamide-forming potential in most of the data sets that have been obtained.[21,26,28,30−32] The correlation ($r = 0.625$, $p < 0.001$) between glucose concentration and acrylamide formation in this data set is shown in Figure 1A, and the lower glucose concentration in the not-irrigated samples was almost certainly responsible for the reduced acrylamide formation observed (Table 2d). There were also positive although not strong correlations with sucrose ($r = 0.304$, $p = 0.034$), total reducing sugars ($r = 0.492$, $p < 0.001$), and total sugar ($r = 0.458$, $p = 0.001$).

Free asparagine concentration has also been shown to contribute positively to the variance in acrylamide formation in some data sets,[21,30,33,34] but the correlation here was weak and negative ($r = -0.328$, $p = 0.022$). There was, however, a striking nonlinear relationship ($r = -0.589$, $p < 0.001$) of decreased acrylamide with increased proline (Figure 1B), with the very high proline concentrations brought about by nonirrigation, particularly in Ramos (Table 2d), being associated with reduced acrylamide formation. Proline has been shown to inhibit acrylamide formation in model systems[35] but is usually present in potatoes at much lower concentrations than asparagine, so the data presented here are the first to suggest that this could occur in a food matrix.

Effect of Drought Stress on Tuber Composition in Two Potato Varieties Grown in a Glasshouse. To apply a more controlled and severe drought stress, an experiment was conducted in a glasshouse. Two varieties, Markies, which is drought-tolerant, and Saturna, which is drought-sensitive, were selected for the study. For the plants to be able to develop a full-size root system and form tubers without physical

DOI: 10.1021/jf506031w
J. Agric. Food Chem. 2015, 63, 2566−2575

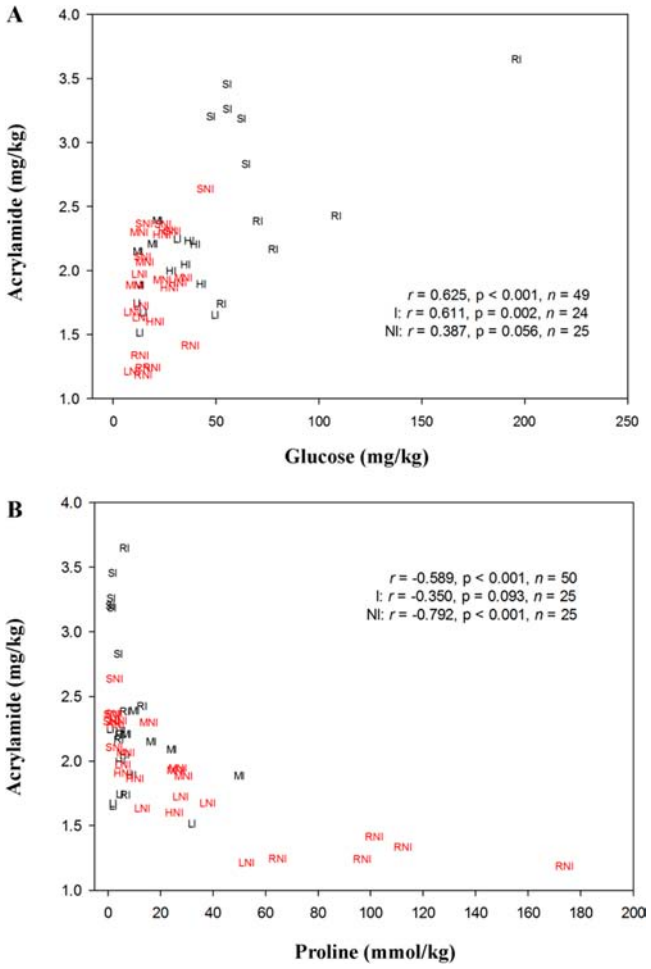

Figure 1. Graphs showing the correlation between glucose (A) and proline (B) concentrations and acrylamide formation in potato flour heated to 160 °C for 20 min. The flour was prepared from five varieties of potatoes grown, with and without irrigation, on commercial farms in the United Kingdom in 2011. The varieties were Hermes (H), Lady Claire (L), Markies (M), Ramos (R), and Saturna (S). Points on the graphs from irrigated potatoes are denoted I in black, whereas those for not-irrigated potatoes are denoted NI in red. The Pearson correlation coefficients (r), corresponding p values (F test), and number of pairs of observations (n) are given on the graphs.

restriction, the plants were grown in deep troughs filled with compost over a 2.5 cm layer of beads to allow drainage. A randomized, split-plot design was used, and drought stress was applied by reducing watering to half of the plants (drought) and maintaining it for the others (watered) (see Materials and Methods for details).

Watering of the drought plants was reduced after 68 days, at which point the plants were beginning to tuberize, and tubers were harvested after 7 months, when the plants were beginning to senesce. In previous glasshouse experiments on potato, the life cycle from planting to harvest has been 12 weeks,[34] the difference being that the plants were grown in pots containing vermiculite so that feeding with minerals could be controlled. In the present study, growing the plants in sufficient depth of compost to allow full root development resulted in a life cycle duration much more similar to that in the field in the United Kingdom.

Leaf water potential (LWP) at mid-day was monitored to ensure that the plants for which water was being withheld were drought-stressed. At the beginning of the treatment, LWP ranged from 4 to 6 MPa for Saturna and from 6 to 7.5 MPa for Markies. After 3 weeks of the treatment, the range of LWP for watered Saturna was 4.5−5.5 MPa and for watered Markies, 3.5−5.5 MPa, whereas the range in drought-stressed Saturna had risen to 8.5−10.5 MPa and for Markies, 10−11 MPa. These levels were maintained until the plants began to senesce.

Data were obtained on concentrations of free amino acids (once again without arginine and cysteine) and sugars (glucose, fructose, and sucrose). Total free amino acid content was calculated along with the ratio of free asparagine to total free amino acid content. Total sugar content was also calculated along with the sum of glucose and fructose as reducing sugars. Data on acrylamide formation in heated flour were also obtained for analysis. The full data set is given in Supporting Information Tables S4−S6.

REML was applied to the data on the $\log_e$ scale, this transformation ensuring constant variance across the variety by treatment combinations. The results are given in Table 3.

Table 3. p Values Denoting Significance of Main Effects of Drought Stress and Variety and Interactions between the Two in Linear Mixed Model (REML) Analyses of Measured Variables for Two Varieties of Potato Grown in a Glasshouse with Water Provided or Withheld[a]

	stress	variety	stress × variety
amino acids			
alanine	0.345	**0.011**	0.775
glycine	0.178	**0.005**	0.869
α-aminobutyric acid	**0.007**	0.926	0.362
valine	0.853	0.116	**0.028**
leucine	0.823	0.001	**0.005**
isoleucine	0.916	**0.007**	0.087
threonine	0.185	0.116	0.878
serine	0.469	0.231	0.728
γ-aminobutyric acid	0.092	0.222	0.826
proline	0.238	**0.025**	0.159
asparagine	**0.036**	0.849	0.953
aspartic acid	0.239	0.520	0.709
methionine	0.984	0.123	0.333
glutamic acid	0.301	0.213	0.234
phenylalanine	0.937	**<0.001**	0.067
glutamine	0.822	**0.004**	0.937
ornithine	0.074	0.071	0.417
lysine	0.911	**<0.001**	0.079
histidine	0.209	0.012	**0.020**
tyrosine	0.885	<0.001	**0.019**
tryptophan	0.795	**0.018**	0.158
total amino acids	0.062	0.222	0.884
asparagine/total amino acids	0.249	**0.007**	0.531
sugars			
glucose	0.534	**0.013**	0.297
fructose	0.963	0.813	0.457
sucrose	0.240	0.220	0.859
reducing sugars	0.391	**0.021**	0.376
total sugars	0.266	0.146	0.965
acrylamide	0.178	0.257	0.176

[a]The × indicates the interaction between the factors: drought stress (stress) and variety. p values in bold indicate the significant ($p < 0.05$, F test) terms for inspection.

DOI: 10.1021/jf506031w
J. Agric. Food Chem. 2015, 63, 2566−2575

Table 4. Comparison of Means for Free Amino Acids, Sugars and Acrylamide Formation for Two Varieties of Potato Grown in a Glasshouse with Water Provided (Watered) Or Withheld (Drought)

(a) Log_e Means (n = 12), Standard Error of the Difference (SED), Degrees of Freedom (df), and Least Significant Difference (LSD) at the 5% Level of Significance for Comparison of Means for Free Amino Acids and Sugars with Only a Main Effect (p < 0.05, F Test) of Variety[a]

	variety			
	Markies	Saturna	SED/SE (df)	LSD (5%)
amino acids				
alanine	2.63 (13.87)	1.94 (6.96)	0.231 (13)	0.499
glycine	1.85 (6.36)	1.17 (3.22)	0.206 (13)	0.466
isoleucine	0.96 (2.61)	1.95 (7.03)	0.311 (13)	0.673
threonine	1.89 (6.62)		0.099 (13)	
serine	2.68 (14.60)		0.108 (13)	
γ-aminobutyric acid	3.29 (26.76)		0.075 (13)	
proline	3.78 (43.82)	2.90 (18.17)	0.347 (13)	0.750
aspartic acid	3.34 (28.16)		0.100 (13)	
methionine	0.82 (2.27)		0.131 (13)	
glutamic acid	0.660 (1.93)		0.117 (13)	
phenylalanine	−0.07 (0.93)	1.56 (4.76)	0.368 (13)	0.795
glutamine	4.54 (93.69)	3.82 (45.60)	0.206 (13)	0.446
ornithine	0.22 (1.25)		0.164 (13)	
lysine	1.43 (4.18)	2.12 (8.31)	0.161 (13)	0.348
tryptophan	−1.30 (0.27)	0.03 (1.03)	0.487 (12)	1.060
total amino acids	6.18 (482.99)		0.065 (10)	
asparagine/total free amino acids	−1.06 (0.35)	−0.91 (0.40)	0.046 (10)	0.103
sugars				
glucose	5.44 (230.44)	4.68 (107.77)	0.266 (13)	0.574
fructose	3.62 (37.34)		0.159 (13)	
sucrose	7.14 (1261.43)		0.147 (13)	
reducing sugars	5.65 (284.29)	5.01 (149.90)	0.244 (13)	0.528
total sugars	7.30 (1480.30)		0.141 (13)	

(b) Log_e means (n = 12), Standard Error of the Difference (SED), Degrees of Freedom (df), and Least Significant Difference (LSD) at the 5% Level of Significance for Comparison of Means for Amino Acids and Sugars with Only a Main Effect (p < 0.05, F Test) of Stress[b]

	treatment			
amino acid	drought	watered	SED (df)	LSD (5%)
α-aminobutyric acid	−1.00 (0.37)	−1.19 (0.30)	0.002 (1)	0.027
asparagine	5.49 (242.26)	4.88 (132.03)	0.035 (1)	0.442

(c) Log_e Means (n = 6), Standard Error of the Difference (SED), Degrees of Freedom (df), and Least Significant Difference (LSD) at the 5% Level of Significance for Comparison of Means for Amino Acids and Sugars with an Interaction (p < 0.05, F Test) between Variety and Stress[c]

	treatment					
	Markies		Saturna			
amino acid	drought	watered	drought	watered	SEC (df)	LSD (5%)
valine	2.36 (10.59)	2.92 (18.54)	3.36 (28.79)	2.73 (15.33)	0.338 (13)	0.731
					0.288 (7)	0.670
leucine	0.27 (1.31)	0.75 (2.12)	1.87 (6.49)	0.92 (2.51)	0.300 (13)	0.648
					0.846 (1)	8.108
histidine	1.04 (2.83)	0.64 (1.90)	2.16 (8.67)	0.69 (1.99)	0.288 (13)	0.662
					0.378 (2)	1.665
tyrosine	−1.61 (0.20)	−0.85 (0.43)	1.29 (3.63)	0.08 (1.08)	0.519 (13)	1.122
					1.296 (1)	11.543

(d) Log_e Means (n = 6) for Acrylamide, Glucose, Fructose, Sucrose, Reducing Sugars, and Total Sugars[d]

	treatment				
	Markies		Saturna		
response	drought	watered	drought	watered	grand mean, SE
acrylamide	7.534 (1871)	7.954 (2847)	7.573 (1945)	7.535 (1872)	7.649 (2099), 0.090
glucose	5.780 (324)	5.110 (166)	4.730 (113)	4.630 (103)	5.060 (158), 0.149
fructose	3.560 (35)	3.750 (43)	3.710 (41)	3.460 (32)	3.620 (37), 0.159
sucrose	7.510 (1826)	7.100 (1212)	7.22 (1366)	6.72 (829)	7.140 (1261), 0.147
reducing sugars	5.930 (376)	5.380 (217)	5.060 (158)	4.960 (143)	5.330 (206), 0.137
total sugars	7.700 (2208)	7.290 (1466)	7.330 (1525)	6.890 (982)	7.300 (1480), 0.141

DOI: 10.1021/jf506031w
J. Agric. Food Chem. 2015, 63, 2566−2575

Table 4. continued

[a]The grand mean (n = 24) and corresponding standard error (SE) are given for amino acids and sugars with no effects of variety or stress. Back-transformed means (mmol per kg for amino acids and mg per kg for sugars) are given in parentheses. [b]Back-transformed means (mmol per kg) are given in parentheses. [c]The first SED and LSD of each pair in the table are for comparison of the varieties in either drought or control condition; the second SED and LSD of each pair are for all other comparisons. Back-transformed means (mmol per kg) are given in parentheses. [d]There was no significant (p < 0.05, F test) effect of stress for acrylamide or sugars (Table 3), but the full means table is included here for inspection. Back-transformed means (mg per kg for sugars and μg per kg for acrylamide) are given in parentheses.

There was an interaction (p < 0.05, F test) between stress and variety for free valine, leucine, histidine, and tyrosine. There was a main effect (p < 0.05, F test) of stress only for α-aminobutyric acid (AABA) and asparagine. There was a main effect (p < 0.05, F test) of variety only for free alanine, glycine, isoleucine, proline, phenylalanine, glutamine, lysine, tryptophan, the ratio of free asparagine to total free amino acids, glucose, and reducing sugars. There was no significant (p < 0.05, F test) effect of either stress or variety for acrylamide.

The relevant means and SED (df) and LSD (5%) values for metabolites showing a main effect of variety only are given in Table 4a. Markies had significantly different (p < 0.05, F test) and greater concentrations of free alanine, glycine, proline, and glutamine, as well as glucose and reducing sugars, than Saturna. Meanwhile, Saturna had significantly different (p < 0.05, F test) and greater concentrations of free isoleucine, phenylalanine, lysine, and tryptophan and a greater ratio of free asparagine to total free amino acids than Markies.

Two free amino acids, asparagine and AABA, showed a significant effect (p < 0.05, F test) of the treatment alone (in other words, the two varieties responded in similar fashion) (Table 4b). AABA concentration was somewhat greater in the potatoes from drought-stressed than watered plants, but free asparagine was almost doubled, from 132.03 to 242.26 mmol/kg. Four other free amino acids, valine, leucine, histidine, and tyrosine, showed an effect of the stress interacting with variety (in other words, the varieties responded differently) (Table 4c). For free valine, Saturna showed a substantial increase under the stress, whereas Markies had a considerable decrease, so that the difference between the varieties was significant (p < 0.05, LSD) under stress. A similar effect was seen for leucine and tyrosine. For histidine there was an increase under the stress for both varieties, but more so for Markies (4.4-fold), giving a significant (p < 0.05, LSD) difference between the varieties under the stress condition.

Proline concentration increased in both varieties in response to drought but, in contrast to the field-grown potatoes, the response was not statistically significant (p = 0.238, F test, for the main effect of stress and p = 0.159, F test, for the variety by stress interaction). There was also no overall significant effect of the treatment on sugar concentrations or acrylamide formation, but Table 4d gives the means for information. Markies showed considerably less acrylamide in the drought than in the watered condition (consistent with the result of the field study), whereas Saturna showed slightly more. For Saturna, the increase in acrylamide formation could be explained by increases in glucose and fructose. However, in Markies glucose was substantially higher in the drought samples than in the watered samples (Table 4d), and, given that free asparagine concentration was also almost doubled in the drought-stressed samples compared with the watered (Table 4b), the reduction in acrylamide formation is surprising. Fructose concentration did decrease in drought-stressed Markies, and fructose has been shown to be more reactive than glucose in kinetic modeling of acrylamide formation in French fries.[28] Nevertheless, the fact that both total reducing sugar and free asparagine concentration rose in Markies in response to drought stress but acrylamide formation declined does suggest that other factors were involved, and this requires further study.

Another notable aspect of the study was that lack of irrigation to commercial, field-grown potatoes, destined for the food chain, resulted in statistically significant changes in composition, even in the temperate United Kingdom in a year with not-unusual levels of rainfall. This is an example of the potential impact of environmental and management factors on crop composition, nutritional value, and processing properties.[2] Furthermore, the changes caused by lack of irrigation in the field were different in some respects from those brought about by more extreme drought stress imposed in the glasshouse. The most striking contrast between the effects of the moderate and more extreme stress was in the change in free asparagine concentration, which did not differ with statistical significance in the irrigated versus not-irrigated field samples but which showed a big increase in response to drought stress in the glasshouse.

The accumulation of free asparagine has been observed in diverse plant species in response to a range of abiotic stresses,[36] and, of course, this has potential implications for food safety.[2] Free proline, an increase in the concentration of which is also associated with abiotic stress, did not increase significantly in response to drought in the glasshouse experiment, but did in the field. Proline has been shown to increase in concentration in the leaves of drought-stressed potato plants,[37,38] with more accumulating in drought-sensitive than -tolerant genotypes. However, drought tolerance has also been suggested to be dependent on root growth rather than responses in the leaves.[39] The subject is reviewed comprehensively by Monneveux et al.,[40] but, as is generally the case with effects of stresses such as drought on plants, physiological studies have focused on the vegetative parts of the plant and the ability of the plant to survive the stress, not on the composition of the tubers. Unfortunately, the field data on Ramos, which showed a massive change in proline concentration in tubers in response to lack of irrigation, was not available in time to have included this variety in the glasshouse experiment. The increase in proline concentration in Ramos in the field was far greater than in the other varieties, showing that different genotypes of potato are affected in dissimilar fashion by the same abiotic stress. Consequently, the study did not identify a unifying potato tuber drought stress response.

The differing responses of the potatoes to lack of irrigation in the field and severe drought stress imposed in a glasshouse support the growing realization among plant physiologists that mild and extreme stresses may provoke very different responses in plants. This was discussed by Hancock et al.[41] in the context of temperature stress responses in potato, drawing on hypotheses put forward by Skirycz et al.[42] and Cramer et

DOI: 10.1021/jf506031w
J. Agric. Food Chem. 2015, 63, 2566−2575

al.[43] The results of the present study are consistent with this new paradigm.

Implications for Commercial Potato Production. Although the field and glasshouse experiments produced different responses and raised new questions about the relationship between precursor concentration and acrylamide formation, the effect of irrigation in the field on acrylamide formation during processing was clear: irrigation led to an increase in acrylamide formation. It must be borne in mind that the study concerned samples from one harvest year. Nevertheless, it would be sensible for potato farmers to irrigate only if necessary to maintain the health and yield of the crop.

■ ASSOCIATED CONTENT

Ⓢ Supporting Information

Free amino acid and sugar concentrations and acrylamide formed in heated flour. This material is available free of charge via the Internet at http://pubs.acs.org.

■ AUTHOR INFORMATION

Corresponding Author

*(N.G.H.) Fax: +44 1582 763010. E-mail nigel.halford@rothamsted.ac.uk.

Funding

The study was financially supported by the Biotechnology and Biological Sciences Research Council (BBSRC) of the United Kingdom and industry partners through the Sustainable Arable LINK program "Producing Low Acrylamide Risk Potatoes" (http://www.acrylamide-potato.org.uk/). Rothamsted Research receives grant-aided support from the BBSRC.

Notes

The authors declare no competing financial interest.

■ ACKNOWLEDGMENTS

We are grateful to Simon Pyper of Higgins Group, Doncaster, UK, for providing the field-grown potatoes.

■ REFERENCES

(1) Curtis, T. Y.; Postles, J.; Halford, N. G. Reducing the potential for processing contaminant formation in cereal products. *J. Cereal Sci.* **2014**, *59*, 382−392.

(2) Halford, N. G.; Curtis, T. Y.; Chen, Z.; Huang, J. Darwin Review: Effects of abiotic stress and crop management on cereal grain composition: implications for food quality and safety. *J. Exp. Bot.* **2015**, *66*, 1145−1156.

(3) Nursten, H. E. *The Maillard Reaction*; Royal Society of Chemistry: Cambridge, UK, 2005.

(4) Mottram, D. S. The Maillard reaction: source of flavor in thermally processed foods. In *Flavors and Fragrances: Chemistry, Bioprocessing and Sustainability*; Berger, R. G., Ed.; Springer-Verlag: Berlin, Germany, 2007; pp 269−284.

(5) Halford, N. G.; Curtis, T. Y.; Muttucumaru, N.; Postles, J.; Mottram, D. S. Sugars in crop plants. *Ann. Appl. Biol.* **2011**, *158*, 1−25.

(6) Mottram, D. S.; Wedzicha, B. L.; Dodson, A. T. Acrylamide is formed in the Maillard reaction. *Nature* **2002**, *419*, 448−449.

(7) Stadler, R. H.; Blank, I.; Varga, N.; Robert, F.; Hau, J.; Guy, P. A.; Robert, M.-C.; Riediker, S. Acrylamide from Maillard reaction products. *Nature* **2002**, *419*, 449−450.

(8) Zyzak, D. V.; Sanders, R. A.; Stojanovic, M.; Tallmadge, D. H.; Eberhart, B. L.; Ewald, D. K.; Gruber, D. C.; Morsch, T. R.; Strothers, M. A.; Rizzi, G. P.; Villagran, M. D. Acrylamide formation mechanism in heated foods. *J. Agric. Food Chem.* **2003**, *51*, 4782−4787.

(9) Granvogl, M.; Jezussek, M.; Koehler, P.; Schieberle, P. Quantitation of 3-aminopropionamide in potatoes − a minor but potent precursor in acrylamide formation. *J. Agric. Food Chem.* **2004**, *52*, 4751−4757.

(10) Granvogl, M.; Schieberle, P. Thermally generated 3-aminopropionamide as a transient intermediate in the formation of acrylamide. *J. Agric. Food Chem.* **2006**, *54*, 5933−5938.

(11) Claus, A.; Weisz, G. M.; Schieber, A.; Carle, R. Pyrolytic acrylamide formation from purified wheat gluten and gluten-supplemented wheat bread rolls. *Mol. Nutr. Food Res.* **2006**, *50*, 87−93.

(12) International Agency for Research on Cancer. *Some Industrial Chemicals*; IARC Monographs on the Evaluation of Carcinogenic Risks to Humans 60;International Agency for Research on Cancer (IARC): Lyon, France, 1994.

(13) Friedman, M. Chemistry, biochemistry and safety of acrylamide. A review. *J. Agric. Food Chem.* **2003**, *51*, 4504−4526.

(14) Taeymans, D.; Wood, J.; Ashby, P.; Blank, I.; Studer, A.; Stadler, R. H.; Gonde, P.; Van Eijck, P.; Lalljie, S.; Lingnert, H.; Lindblom, M.; Matissek, R.; Muller, D.; Tallmadge, D.; O'Brien, J.; Thompson, S.; Silvani, D.; Whitmore, T. A review of acrylamide: an industry perspective on research, analysis, formation and control. *Crit. Rev. Food Sci. Nutr.* **2004**, *44*, 323−347.

(15) EFSA CONTAM Panel (EFSA Panel on Contaminants in the Food Chain). Scientific Opinion on Acrylamide in Food. *EFSA J.* **2014**, DOI: 10.2903/j.efsa.20YY.NNNN.

(16) Joint FAO/WHO Expert Committee on Food Additives (JECFA). *Safety Evaluation of Certain Contaminants in Food*; WHO Food Additives Series 63; FAO JECFA Monographs 8; World Health Organization: Geneva, Switzerland, 2011.

(17) European Food Safety Authority. Results on acrylamide levels in food from monitoring years 2007−2009 and exposure assessment. *EFSA J.* **2011**, *9*, 2133.

(18) European Commission. Commission recommendation of 8 November 2013 on investigations into the levels of acrylamide in food; European Commission, Brussels, Belgium, 2013.

(19) Food Drink Europe. *Acrylamide Toolbox 2013*; Food Drink Europe: Brussels, Belgium, 2013.

(20) Powers, S. J.; Mottram, D. S.; Curtis, A.; Halford, N. G. Acrylamide concentrations in potato crisps in Europe from 2002 to 2011. *Food Addit. Contam.: Part A* **2013**, *30*, 1493−1500.

(21) Halford, N. G.; Muttucumaru, N.; Powers, S. J.; Gillatt, P. N.; Hartley, L.; Elmore, J. S.; Mottram, D. S. Concentrations of free amino acids and sugars in nine potato varieties: effects of storage and relationship with acrylamide formation. *J. Agric. Food Chem.* **2012**, *60*, 12044−12055.

(22) Bethke, P. C.; Bussan, A. J. Acrylamide in processed potato products. *Am. J. Potato Res.* **2013**, *90*, 403−424.

(23) Rommens, C. M.; Yan, H.; Swords, K.; Richael, C.; Ye, J. Low-acrylamide French fries and potato chips. *Plant Biotechnol. J.* **2008**, *6*, 843−853.

(24) Chawla, R.; Shakya, R.; Rommens, C. M. Tuber-specific silencing of asparagine synthetase-1 reduces the acrylamide-forming potential of potatoes grown in the field without affecting tuber shape and yield. *Plant Biotechnol. J.* **2012**, *10*, 913−924.

(25) Halford, N. G.; Curtis, T. Y.; Muttucumaru, N.; Postles, J.; Elmore, J. S.; Mottram, D. S. The acrylamide problem: a plant and agronomic science issue. *J. Exp. Bot.* **2012**, *63*, 2841−2851.

(26) Muttucumaru, N.; Powers, S. J.; Elmore, J. S.; Mottram, D. S.; Halford, N. G. Effects of nitrogen and sulfur fertilization on free amino acids, sugars and acrylamide-forming potential in potato. *J. Agric. Food Chem.* **2013**, *61*, 6734−6742.

(27) *Fertiliser Manual* (2011), *Fertiliser Manual* (RB209), 8th ed. with 2011 errata; www.defra.gov.uk.

(28) Parker, J. K.; Balagiannis, D. P.; Higley, J.; Smith, G.; Wedzicha, B. L.; Mottram, D. S. Kinetic model for the formation of acrylamide during the finish-frying of commercial French fries. *J. Agric. Food Chem.* **2012**, *60*, 9321−9331.

(29) Lawlor, D. W. Genetic engineering to improve plant performance under drought: physiological evaluation of achievements, limitations, and possibilities. *J. Exp. Bot.* **2013**, *64*, 83−108.

DOI: 10.1021/jf506031w
J. Agric. Food Chem. 2015, 63, 2566−2575

(30) Muttucumaru, N.; Powers, S. J.; Briddon, A.; Elmore, J. S.; Mottram, D. S.; Halford, N. G. Evidence for the complex relationship between the concentrations of free amino acids, sugars and acrylamide-forming potential in potato. *Ann. Appl. Biol.* **2011**, *164*, 286−300.
(31) Amrein, T. M.; Bachmann, S.; Noti, A.; Biedermann, M.; Barbosa, M. F.; Biedermann-Brem, S.; Grob, K.; Keiser, A.; Realini, P.; Escher, F.; Amadò, R. Potential of acrylamide formation, sugars, and free asparagine in potatoes: a comparison of cultivars and farming systems. *J. Agric. Food Chem.* **2003**, *51*, 5556−5560.
(32) Becalski, A.; Lau, B. P.-Y.; Lewis, D.; Seaman, S. W.; Hayward, S.; Sahagian, M.; Ramesh, M.; Leclerc, Y. Acrylamide in French fries: influence of free amino acids and sugars. *J. Agric. Food Chem.* **2004**, *52*, 3801−3806.
(33) Elmore, J. S.; Mottram, D. S.; Muttucumaru, N.; Dodson, A. T.; Parry, M. A.; Halford, N. G. Changes in free amino acids and sugars in potatoes due to sulfate fertilization, and the effect on acrylamide formation. *J. Agric. Food Chem.* **2007**, *55*, 5363−5366.
(34) Shepherd, L. V. T.; Bradshaw, J. E.; Dale, M. F. B.; McNicol, J. W.; Pont, S. D. A.; Mottram, D. S.; Davies, H. V. Variation in acrylamide producing potential in potato: segregation of the trait in a breeding population. *Food Chem.* **2010**, *123*, 568−573.
(35) Koutsidis, G.; Simons, S. P. J.; Thong, Y. H.; Haldoupis, Y.; Mojica-Lazaro, J.; Wedzicha, B. L.; Mottram, D. S. Investigations on the effect of amino acids on acrylamide, pyrazines, and Michael addition products in model systems. *J. Agric. Food Chem.* **2009**, *57*, 9011−9015.
(36) Lea, P. J.; Sodek, L.; Parry, M. A.; Shewry, P. R.; Halford, N. G. Asparagine in plants. *Ann. Appl. Biol.* **2007**, *150*, 1−26.
(37) Vasquez-Robinet, C.; Mane, S. P.; Ulanov, A. V.; Watkinson, J. I.; Stromberg, V. K.; De Koeyer, D.; Schafleitner, R.; Willmot, D. B.; Bonierbale, M.; Bohnert, H. J.; Grene, R. Physiological and molecular adaptations to drought in Andean potato genotypes. *J. Exp. Bot.* **2008**, *59*, 2109−2123.
(38) Schafleitner, R.; Gaudin, A.; Gutierrez Rosales, R. O.; Alvarado Aliaga, C. A.; Bonierbale, M. Proline accumulation and real time PCR expression analysis of genes encoding enzymes of proline metabolism in relation to drought tolerance in Andean potato. *Acta Physiol. Plant.* **2007**, *29*, 19−26.
(39) Puértolas, J.; Ballester, C.; Elphinstone, D.; Dodd, I. C. Two potato (*Solanum tuberosum*) varieties differ in drought tolerance due to differences in root growth at depth. *Funct. Plant Biol.* **2014**, *41*, 1107−1118.
(40) Monneveux, P.; Ramírez, D. A.; Pino, M. T. Drought tolerance in potato (*S. tuberosum* L.). Can we learn from drought tolerance research in cereals? *Plant Sci.* **2013**, *205−206*, 76−86.
(41) Hancock, R. D.; Morris, W. L.; Ducreux, L. J. M.; Morris, J. A.; Usman, M.; Verall, S. R.; Fuller, J.; Simpson, C. G.; Zhang, R.; Hedley, P. E.; Taylor, M. A. Physiological, biochemical and molecular responses of the potato (*Solanum tuberosum* L.) plant to moderately elevated temperature. *Plant Cell Environ.* **2014**, *37*, 439−450.
(42) Skirycz, A.; Vandenbroucke, K.; Clauw, P.; Maleux, K.; De Meyer, B.; Dhondt, S.; Pucci, A.; Gonzalez, N.; Hoeberichts, F.; Tognetti, V. B.; Galbiati, M.; Tonelli, C.; van Breusegem, F.; Vuylsteke, M.; Inze, D. Survival and growth of *Arabidopsis* plants given limited water are not equal. *Nat. Biotechnol.* **2011**, *29*, 212−214.
(43) Cramer, G. R.; Urano, K.; Delrot, S.; Pezzotti, M.; Shinozaki, K. Effects of abiotic stress on plants: a systems biology perspective. *BMC Plant Biol.* **2011**, *11*, 163.

DOI: 10.1021/jf506031w
J. Agric. Food Chem. 2015, 63, 2566−2575

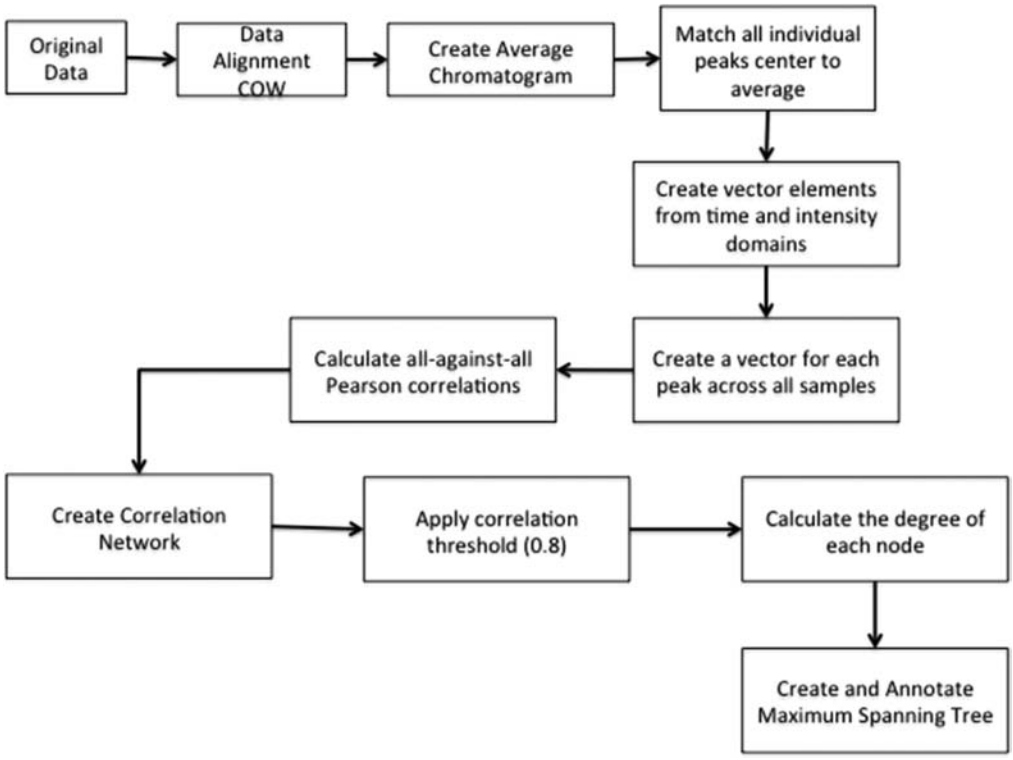

Figure 1. Flowchart for kinetic network reconstruction.

constructed from the peaks found in the total ion current (TIC). Some nodes of the network were subsequently identified and quantified in forced-aged wines (wines stored on different conditions of oxygen and temperature) to determine their kinetic parameters

MATERIALS AND METHODS

Reagents. Chemicals and standards were obtained from Sigma-Aldrich, USA (high-purity grade, >99.0%). Dichloromethane and anhydrous sodium sulfate were obtained from Merck, Darmstadt, Germany.

Wine Material. Thirty-four samples of Port wine with ages between 1 and 129 years were used. All wines were matured in oak barrels and were made following the standard traditional winemaking procedures for Port wine. For the isothermal protocol, 16 L of Port wine made on the year of the experiment (without any oak contact) with pH 3.4, a dissolved-oxygen concentration of 2.5 mg/L, a free-SO_2 level of 17 mg/L, a reducing-sugars level of 105 g/L, and 20.5% alcohol were used in order to determine kinetic parameters.

Isothermal Protocol. Kinetics for each compound detected in Port wine were followed using an isothermal storage method in order to determine the effects of oxygen and temperature. Isothermal storage was carried out at different temperatures (20, 30, 35, and 40 °C) and a series of sequential oxygen saturations inside a hermetically sealed vessel (0 to 10 saturations). Oxygen treatments included 0 (F1), 3 (F2), 5 (F3), and 10 (F4) saturations. Each combination of oxygen/temperature conditions was carried out in glass vessels containing 500 mL of wine. Oxygen saturation was achieved by stirring the sample for roughly 1 h, until an oxygen concentration of about 8−9 mg/L was reached. The F1 group was never supplemented with O_2. F2 was saturated on days 14, 35, and 56. F3 was saturated in the beginning of the experiment and at days 14, 28, 42, and 56. F4 was saturated with O_2 on days 0, 14, 21, 28, 35, 42, 49, 56, and 63.

This forced-aging protocol was carried out in duplicate. For logistical reasons, not all samples were analyzed by GC-MS, but rather the replicate was used as a crosscheck procedure.

Measurements of Dissolved Oxygen. Oxygen concentrations were measured using a Fibox 3 LCD fiber optic oxygen transmitter, a polymer optical fiber, and planar oxygen-sensitive spots (5 mm sensor spots PSt3) from PreSens Precision Sensing GmbH (Germany). The sensor was positioned in the center of the vessel (500 mL) where it remained in contact with the wine at all times.

Chemical Analysis. The extraction procedure was based on the one described by Silva Ferreira et al.[5] Briefly, 50 mL samples of Port were spiked with 50 μL of 3-octanol in a hydro alcoholic solution (1:1, v/v) at 427 mg/L as the internal standard and 5 g of anhydrous sodium sulfate. The wine was extracted twice with 5 mL of dicloromethane. The two organic phases obtained were blended and dried over anhydrous sodium sulfate. Two milliliters of this organic extract was concentrated to 0.4 mL under a nitrogen stream.

GC-MS Analysis. Extracts were analyzed using a Varian 450 gas chromatograph, equipped with a mass detector using Varian 240-MS and Saturn GC-MS workstation software, version 5.51. The injector port was heated to 220 °C. The split vent was opened after 30 s. The carrier gas was helium C-60 (Gasin, Portugal) at a 1 mL/min constant flow. The oven temperature was set at 40 °C for 1 min, then increased at 2 °C/min to 220 °C, and held for 30 min. All mass spectra were acquired in the electron-impact (EI) mode. The ion-trap temperatures were 230, 45, and 170 °C. The mass range was m/z 33−350, with a scan rate of 6 scans/s. The emission current was 50 μA, and the electron multiplier was set in relative mode to autotune procedure. The maximum ionization time was 25000 μs, with an ionization storage level of m/z 35. The injection volume was 1 μL, and the analysis was carried out in full-scan mode. Compound identification was achieved from comparisons of mass spectra obtained from the sample with those from pure standards injected under the same conditions, via comparisons of the Kovats indices and the mass spectra present in NIST 05 MS Library Database.

Statistical Analysis. Statistical analysis and the developed methodology involving the experimental data were carried out with R 2.12.1 for Mac, using the following packages: (i) classical multivariate analysis library (mva), (ii) main library of Venables and Ripley's (MASS), (iii) Harrell miscellaneous (Hmisc), and (iv) R-base packages (R-Project, 2012).

DOI: 10.1021/jf5055084
J. Agric. Food Chem. 2015, 63, 2576−2581

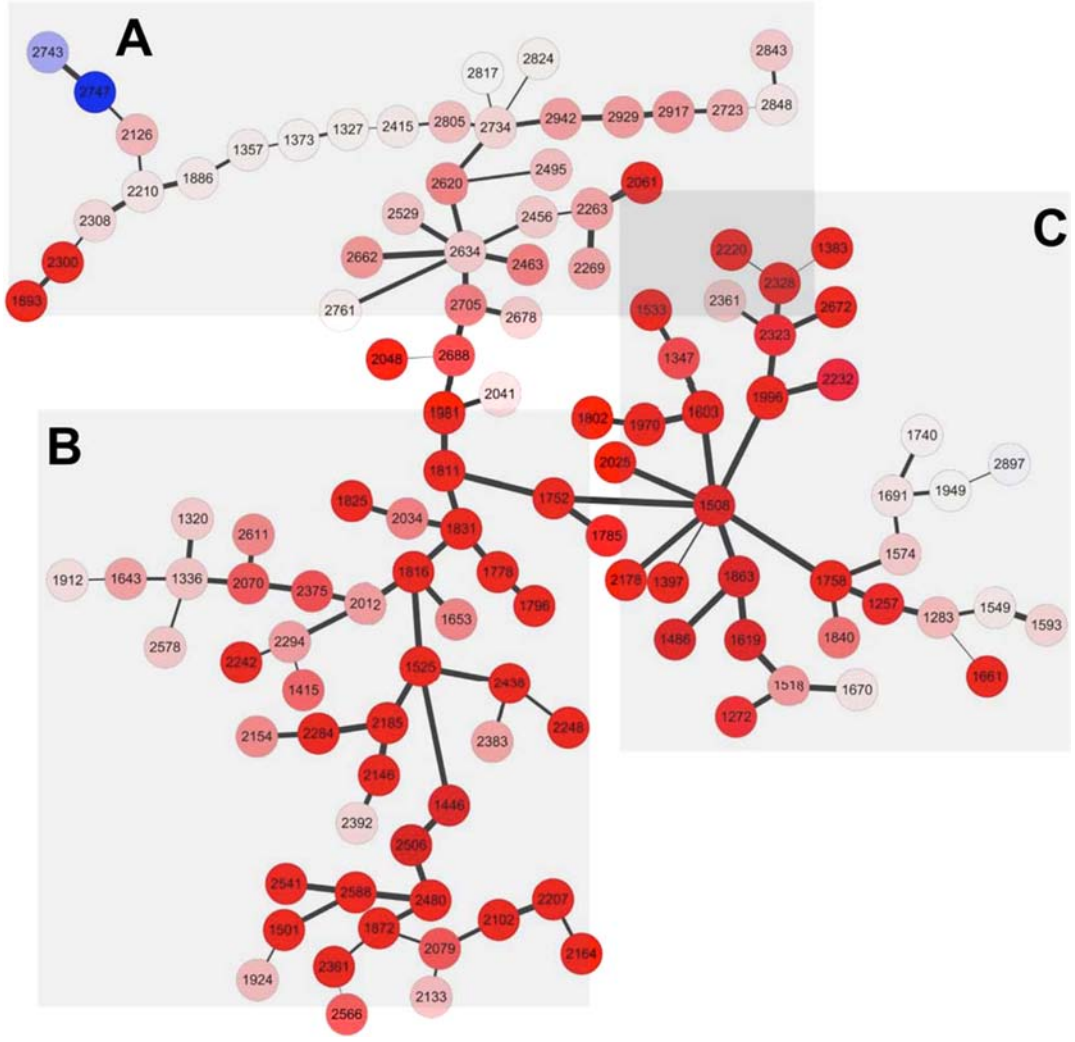

Figure 2. GC-MS putative kinetic network.

Data Preprocessing. The ASCII file of chromatographic data obtained from each sample was extracted, and a matrix was created containing all of the chromatograms. The intensities were normalized by dividing each value by the intensity of the internal standard (3-octanol). All of the m/z channels were normalized to total intensity to yield a total ion current (TIC) chromatogram for each sample. The resulting data set was then imported into The UnscramblerX 10.1 (Camo, Sweden), where the first stage of the alignment of chromatograms was carried out using Correlation Optimized Warping (COW).[6] The saturated peaks were then removed and the baseline corrected. The resulting matrix (GC-MS-TIC matrix) was then used for multivariate data analysis as described in the statistical analysis section.

KINETIC NETWORK RECONSTRUCTION

To reconstruct the underlying kinetic network, the fingerprint needed to be further compressed to a single value for each putative molecule detected by GC-MS. Thus, each chromatographic peak needed to be replaced with a single value for the intensity and retention time at the apex of each peak; therefore, a more refined alignment procedure was required. This was achieved as illustrated in Figure 1. Briefly, an "average" chromatogram was created by taking the mean of the values at each elution point in the GC-MS-TIC matrix. The wavelet method of Du et al.,[7] which was originally developed for peak-calling in peptide mass-spec data, was adapted for finding peak centers in chromatographic data, and a Mexican-hat wavelet was used to determine the location of all of the peaks in the average and sample chromatograms. A custom-built Perl program was integrated with the R-based wavelet method to achieve this. The distances between the locations of all of the peaks in each sample chromatogram and the locations of the peaks in the average chromatogram were calculated. It was observed that there was a correlation between peak height and the amount of peak-center shift that occurred across chromatograms; thus, we devised a two-step process for aligning sample peaks to those of the average chromatogram. If the (internal-standard-normalized) height of the average peak was greater than 2 and the distance to the nearest sample peak was less than 0.3 min, then the intensity value of the sample peak was assigned as the sample value at the average peak location. However, if the (internal-standard-normalized) height of the average peak was less than 2 and the distance to the nearest sample peak was less than 0.15 min, then the intensity value of the sample peak was assigned as the sample value at the average peak retention time. This algorithm was implemented in Perl.

As a result of this process, a new matrix was created that contained the retention time of all peaks in the average chromatogram and the intensity values of all of the peak centers from each sample aligned to these average retention times. Thus, a vector was created for each peak (presumably representing a compound) across all samples. A total correlation comparison

DOI: 10.1021/jf5055084
J. Agric. Food Chem. 2015, 63, 2576−2581

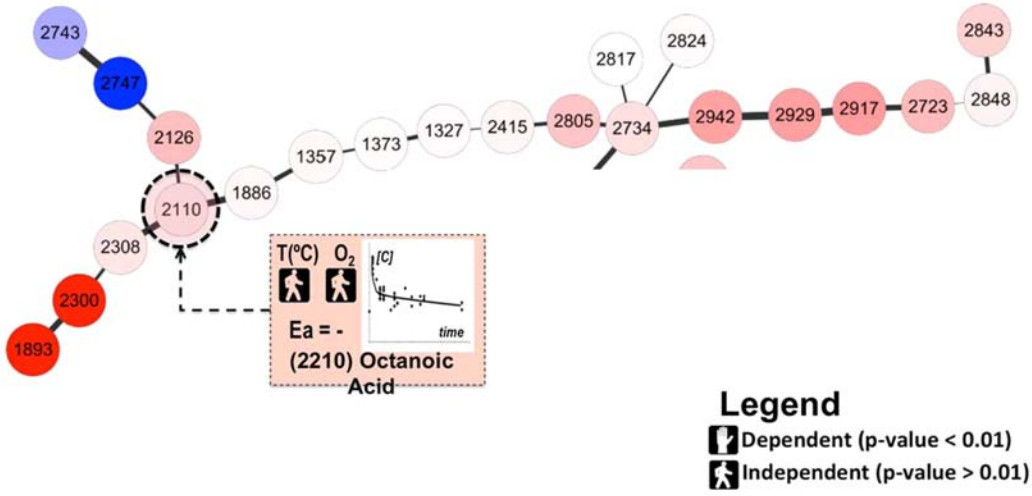

Figure 3. Putative kinetic network, branch A identification: 2210, octanoic acid; 1886, hexanoic acid; and 2308, decanoic acid.

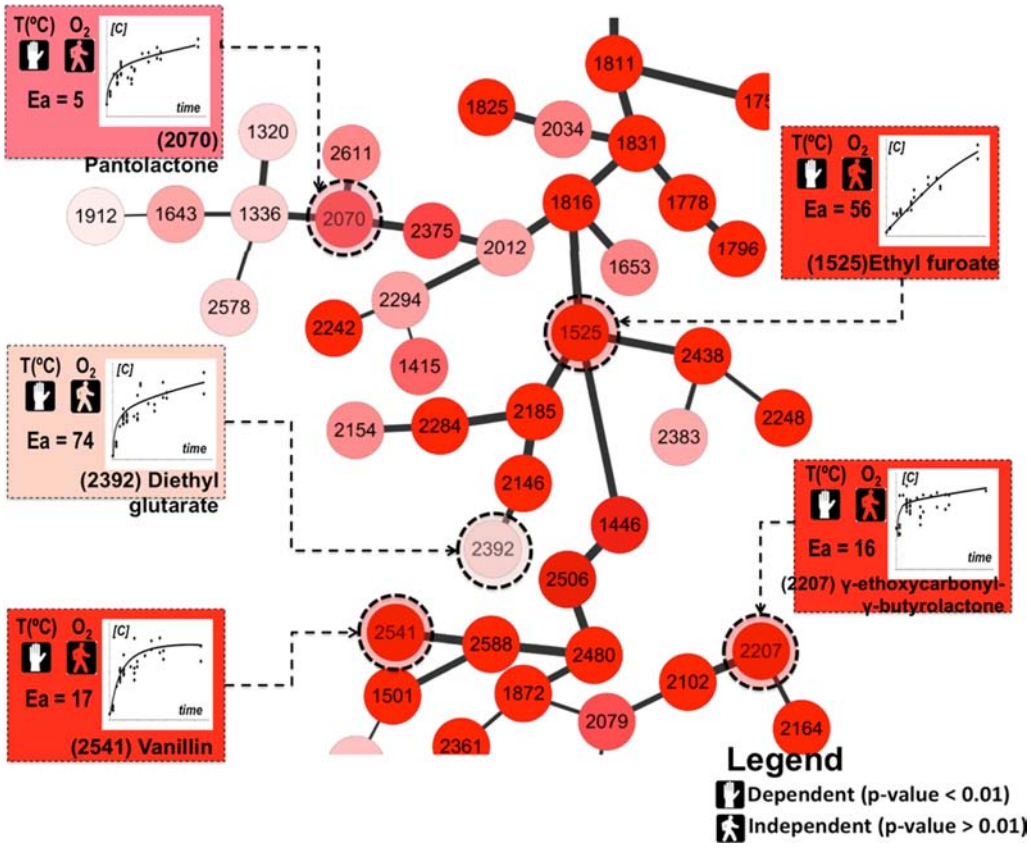

Figure 4. Putative kinetic network, branch B: 2070, pantolactone; 2392, diethylglutarate; 2541, vanillin; 2207, γ-ethoxycarbonyl-γ-butyrolactone; and 1525, ethyl furoate.

was done calculating the Pearson correlation among each and every peak vector. As such, one is able to track the increase or decrease of compounds (peaks) during the aging process and determine the correlative relationships among them. We applied a Pearson-correlation threshold of 0.8 and represented the remaining relationships as a mathematical graph in order to form a correlation network with the nodes representing peaks and the edges weighted with the Pearson correlations among the peak vectors. To reconstruct the most likely kinetic network underlying the set of chemical reactions involved in the aging process, a maximum-spanning tree was created by transforming the edge weights into inverse correlations (by taking the difference between the number 1 and the absolute correlation values) and the subsequent use of a minimum-spanning tree (mst) algorithm[8] on the this inverse correlation network. A minimum-spanning tree represents the shortest possible path through a graph and, as such, selects for the smallest inverse correlation (i.e., highest correlation) pairs among all nodes in the network. The resulting networks were visualized in Cytoscape.[9]

Kinetic Parameters. Nonlinear regression for model fitting was carried out on all data, using a one-step methodology,[10] by maximizing the likelihood function for all temperatures and using

DOI: 10.1021/jf5055084
J. Agric. Food Chem. 2015, 63, 2576−2581

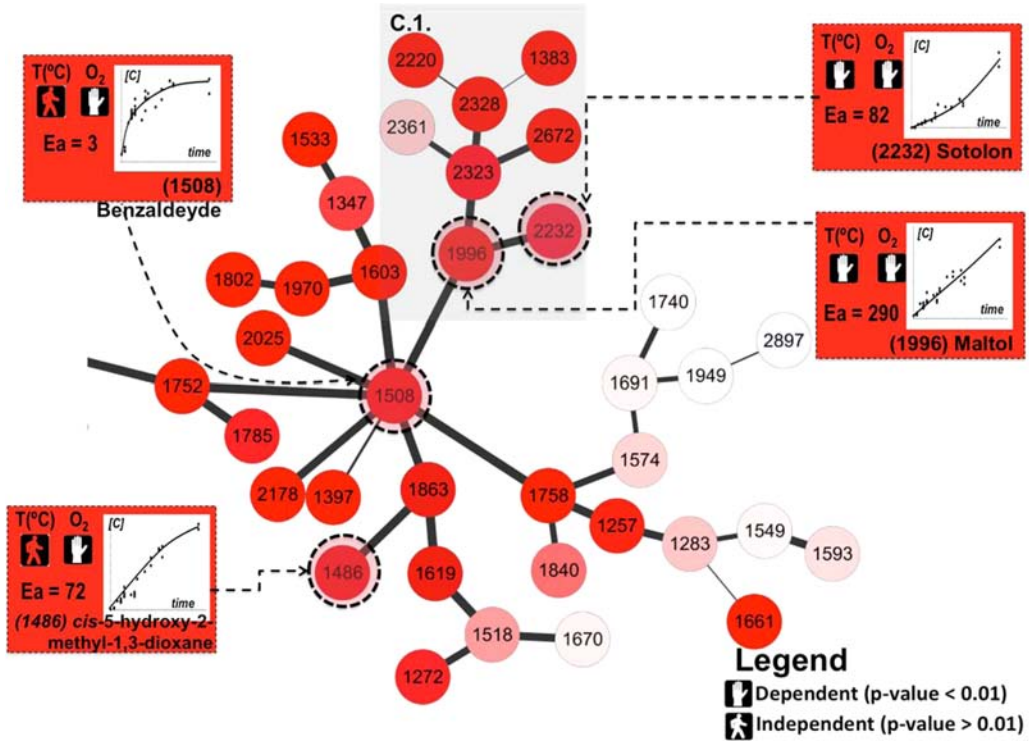

Figure 5. Putative kinetic network, branch C: 2232, sotolon; 1508, benzaldehyde; 1486, *cis*-5-hydroxy-2-methyl-1,3-dioxane; 1996, maltol; C.1., sub-branch related with oxygen and temperature.

bootstrap sampling to estimate the prediction residuals sum of squares (PRESS) criterion.[11,12] The lack-of-fit test was carried out to determine the adequacy of the regression model, and the studentized effect was studied at a 5% confidence level.

The general rate law for compound formation is

$$r = \frac{\mathrm{d}[\mathrm{compound}]}{\mathrm{d}t} = k_{\mathrm{obs}} * [\mathrm{compound}]$$

Therefore, the kinetic rate may follow the Arrhenius behavior with temperature.

$$k_{\mathrm{app}} = k_{\mathrm{ref}} \exp\left[-\frac{E_{\mathrm{a}}}{R}\left(\frac{1}{T} - \frac{1}{T_{\mathrm{ref}}}\right)\right]$$

where k_{ref} (day^{-1}) is the kinetic rate at the reference temperature T_{ref} (Kelvin), E_{a} represents the Arrhenius activation energy (J mol^{-1}), and R is the universal gas constant (Joule mole^{-1} Kelvin^{-1}).

Statistical analysis and the developed methodology involving the experimental data were carried out with R 2.12.1 for MAC using R-base packages (R-Project).

All the calculated kinetic models have p values below 0.05.

RESULTS AND DISCUSSION

Figure 2 shows the maximum-spanning tree derived from the correlation network among all peaks. Each node represents the center of a peak (Kovats index), and each edge represents the best correlation among the peaks. Fold changes between 1- and 129-year-old wines were calculated for each peak and the nodes colored accordingly, with shades of red representing increasing concentration and shades of blue representing decreasing concentration. The thickness of each edge has been scaled to represent the level of correlation (thicker lines mean higher correlation values). It was possible to observe three main branches indicated as A, B, and C.

It was observed that branch A (Figure 3) included compounds such as hexanoic (1886), octanoic (2110), and decanoic (2308) acids that cluster together. The ANOVA on perturbed wines shows that acids are not dependent on temperature or oxygen. In fact, because acid concentration during wine aging is regulated by the esterification/hydrolysis between the acid and the corresponding ester, acids may be formed as a result of hydrolysis, be lost through chemical esterification, or remain at a near-constant equilibrium concentration depending on their initial, post-fermentation levels.[13] When the system is in balance, there is a constant correlation between the concentrations of the substances present, governed by the mass action law.

Branch B (Figure 4) contains two compounds that are demonstrated to be highly sensitive to temperature as a result of their high activation energy (HMF (2506) and furfural (1446)), which suggests that the other compounds in the branch may also be sensitive to temperature. A summary of the ANOVA results is present on each figure as well as the time of expression of each compound identified. All the compounds identified tend to increase during aging, and ANOVA shows that significant differences were established across the temperature conditions, meaning that the compounds identified were all dependent on temperature. It is possible to observe three sub-branches apparently related to activation energy. The sub-branches of vanillin (2541), γ-ethoxycarbonyl-γ-butyrolactone (2207), diethyl tartrate (2361), and triethyl citrate (2480) have an E_{a} between 16 and 36 kJ/mol. The organic acid esters, diethyl tartrate (2361) and triethyl citrate (2480), tend to increase as a result of the high concentration of the respective acids (tartaric and citric acids), by the reaction between the acid and the ethanol (esterification reaction). According to Ribéreau-Gayon and Peynoud,[14] polyprotic acids such as tartaric, citric, and malic

DOI: 10.1021/jf5055084
J. Agric. Food Chem. 2015, 63, 2576−2581

acid esterified more rapidly than the monoprotic acids acetic, propanoic, and butanoic acid, and temperature accelerates the reaction. γ-Ethoxycarbonyl-γ-butyrolactone (2207) is a lactone that probably results from glutamic acid or related compounds and is dependent on wine aging, contributing a cherry aroma to wine.[15] The formation of the lactone is an esterification reaction. Vanillin (2541) is a phenolic aldehyde related with barrel aging. Its sensitivity to temperature in wines that were not subject to wood contact is still unknown. Diethyl glutarate (2392) and ethyl-2-furoate (1525) are located in a second sub-branch. These two compounds have activation energies of 74 and 56 kJ/mol, respectively, which are higher than those present in the posterior sub-branch. Ethyl-2-furoate (1525) is also dependent on temperature, and its formation is related to the Maillard reaction. In summary, this branch contains compounds related to temperature, and it would appear that there is an association between network location and activation energy.

Branch C (Figure 5) contains compounds related to oxidation, such as benzaldehyde (1508) (formed by the oxidation of benzyl alcohol), dioxanes (1486 and 1863), and dioxolanes (1619) (formed by the reaction of ethanal and glycerol). One region of this branch (C.1., Figure 5) seems to indicate a correlation between sotolon (2232) and 3-hydroxy-2-methyl-4H-pyran-4-one (1996, maltol). These two compounds have somewhat similar chemical structures (i.e., a furanone and a pyranone, respectively), and both have a very sweet aroma, normally classified in the same group of aromas with flavors of burnt sugar, caramel, and maple. However, the sensorial impact of each compound occurs at different orders of magnitude, parts per billion for sotolon and parts per million for maltol.

Sotolon is dependent on temperature and oxygen, which suggests that maltol is dependent on the same parameters; in fact, the ANOVA indicates that the compound is sensitive to both parameters and has a very high activation energy when compared to sotolon. This suggests that maltol is much more sensitive to temperature than sotolon. Yaylayan et al. observed that maltol formation is related to 1-deoxyosone, an important intermediary of the Maillard reaction.[16] However, there are no studies on the impact of oxidation on its formation.

Other compounds present in sub-branch C.1. (Figure 5) appear to be connected to sotolon and maltol. These compounds are probably dependent on oxygen and temperature, and their identification could be useful in the unraveling of the connection between the Maillard mechanism and oxidation.

These observations would seem to validate the assumptions made that compounds grouped on the same branch of the network have the same time of expression and consequently the same kinetic order. It was also observed that compounds grouped together are sensitive to the same technological parameter.

We believe that this network-driven approach to the study of large kinetic systems is proving to be a useful tool for identifying putative compounds of interest and for mechanistic hypothesis generation that can subsequently be tested experimentally. We would recommend that this type of chemiomics approach become a standard workflow for the future investigation of complex chemical systems.

AUTHOR INFORMATION

Corresponding Author

*Phone: +351 22 558 0001. Fax: +351 22 509 0351. E-mail: asferreira@porto.ucp.pt.

Funding

This research was funded by the project "Wine Metrics: Revealing the Volatile Molecular Feature Responsible for the Wine Like Aroma a Critical Task Toward the Wine Quality Definition." (PTDC/AGR-ALI/121062/2010) and partially supported by ESB/UCP plurianual funds through the POS-Conhecimento Program that includes FEDER funds through the program COMPETE (Programa Operacional Factores de Competitividade), national funds through FCT (Fundação para a Ciência e a Tecnologia), the Wine Industry Network of Expertise and Technology (Winetech IWBT BI 13/01), the Technology and Human Resources Programme, and the South African National Science Foundation.

Notes

The authors declare no competing financial interest.

REFERENCES

(1) Martins, R. C.; Monforte, A. R.; Silva Ferreira, A. Port Wine Oxidation Management: A Multiparametric Kinetic Approach. *J. Agric. Food Chem.* **2013**, *61*, 5371−5379.

(2) Courant, F.; Antignac, J.-P.; Monteau, F.; Le Bizec, B. Metabolomics as a Potential New Approach for Investigating Human Reproductive Disorders. *J. Proteome Res.* **2013**, *12*, 2914−2920.

(3) Cevallos-Cevallos, J. M.; Reyes-De-Corcuera, J. I.; Etxeberria, E.; Danyluk, M. D.; Rodrick, G. E. Metabolomic analysis in food science: a review. *Trends Food Sci. Technol.* **2009**, *20*, 557−566.

(4) Jacobson, D.; Monforte, A. R.; Silva Ferreira, A. C. Untangling the chemistry of Port wine aging with the use of GC-FID, multivariate statistics and network reconstruction. *J. Agric. Food Chem.* **2013**, *61*, 2513−2521.

(5) Silva Ferreira, A. C.; Barbe, J.-C.; Bertrand, A. 3-Hydroxy-4,5-dimethyl-2(5H)-furanone: A Key Odorant of the Typical Aroma of Oxidative Aged Port Wine. *J. Agric. Food Chem.* **2003**, *51*, 4356−4363.

(6) Gong, F.; Liang, Y.-Z.; Fung, Y.-S.; Chau, F.-T. Correction of retention time shifts for chromatographic fingerprints of herbal medicines. *J. Chromatogr., A* **2004**, *1029*, 173−183.

(7) Du, P.; Kibbe, W. A.; Lin, S. M. Improved peak detection in mass spectrum by incorporating continuous wavelet transform-based pattern matching. *Bioinformatics* **2006**, *22*, 2059−2065.

(8) Dijkstra, E. W. A note on two problems in connection with graphs. *Numer. Math.* **1959**, *1*, 269−271.

(9) Shannon, P.; Markiel, A.; Ozier, O.; Baliga, N. S.; Wang, J. T.; Ramage, D.; Amin, N.; Schwikowski, B.; Ideker, T. Cytoscape: A Software Environment for Integrated Models of Biomolecular Interaction Networks. *Genome Res.* **2003**, *13*, 2498−2504.

(10) Arabshahi, A.; Lund, D. B. Considerations in calculating kinetic parameters from experimental data. *J. Food Process Eng.* **1985**, *7*, 239−251.

(11) Hastie, T.; Tibshirami, R. Discriminant adaptative nearest neighbour classification. *IEEE Trans. Pattern Anal. Mach. Intell.* **1996**, *18*, 607−616.

(12) Bates, D. M.; Watts, D. G. *Non-linear Regression Analysis and its Applications*. John Wiley & Sons: New York, 1998.

(13) Baig, S.; Rehman, F. Signal Modeling Using Singular Value Decomposition. In *Advances in Computer, Information, and Systems Sciences, and Engineering*; Elleithy, K., Sobh, T., Mahmood, A., Iskander, M., Karim, M., Eds.; Verlag: The Netherlands, 2006; pp 31−37.

(14) Ramney, D.; Ough, C. S. Volatile ester hydrolysis or formation during storage of model solutions of wines. *J. Agric. Food Chem.* **1980**, *28*, 928−934.

(15) Wurz, R. E. M.; Kepner, R. E.; Webb, A. D. The Biosynthesis of Certain Gamma-Lactones from Glutamic Acid by Film Yeast Activity on the Surface of Flor Sherry. *Am. J. Enol. Vitic.* **1988**, *39*, 234−238.

(16) Yaylayan, V. A.; Mandeville, S. Stereochemical Control of Maltol Formation in Maillard Reaction. *J. Agric. Food Chem.* **1994**, *42*, 771−775.

DOI: 10.1021/jf5055084
J. Agric. Food Chem. 2015, 63, 2576−2581

JOURNAL OF AGRICULTURAL AND FOOD CHEMISTRY

Addition/Correction

pubs.acs.org/JAFC

Correction to In Vitro Bioaccessibility of Carotenoids, Flavonoids, and Vitamin C from Differently Processed Oranges and Orange Juices [*Citrus sinensis* (L.) Osbeck]

Julian K. Aschoff, Sabrina Kaufmann, Onur Kalkan, Sybille Neidhart, Reinhold Carle, and Ralf M. Schweiggert*

J. Agric. Food Chem. **2015**, *63* (2), 578−587. DOI: 10.1021/jf505297t

In our paper, the dietary fiber contents of the test foods are shown in Table 3 to demonstrate their reduction upon dejuicing of fresh oranges. The values were shown in "g/100 g of dry weight (DW)", although the footnote stated "g/100 g of fresh weight (FW)". Consequently, on page 583, we erroneously compared the dietary fiber content of orange (DW) to that of tomato (FW). We calculated the dietary fiber level of oranges per g/100 FW (**2.2 g/100 g FW**), which should be used for this comparison instead.

This correction does not affect the validity of our discussion.

Published: February 25, 2015

ACS Publications © 2015 American Chemical Society

DOI: 10.1021/acs.jafc.5b00991
J. Agric. Food Chem. 2015, 63, 2582−2582

Table 1. Characterization of Soils Used for Incubation Experiments

site name	altitude (m asl)	land use	soil type	sand (%)	silt (%)	clay (%)	pH ($CaCl_2$)	organic carbon (%)	soil moisture[a] (% w/w) (% of MWHC)[b]
Realp	2120	alpine pasture	clay	12.2	39.0	48.8	4.0	18.1	63−64
									59−60
Neualp	955	fertilized pasture	sandy loam	59.5	20.8	19.7	5.5	4.2	31−32
									39−40
Dübendorf	440	arable land	loam	40.5	32.3	27.2	7.2	1.9	19−20
									37−39

[a]Soil moisture varied slightly from experiment to experiment due to different water volumes used for spiking. [b]Maximum water-holding capacity.

expressed as haloxyfop"),[7] and residue enforcement methods (e.g., the German official multiresidue method)[8] do not address enantiomer composition. Moreover, the fate of individual stereoisomers in soil is not well understood. Although the rapid enantiomerization of several FOPs, for example, fluazifop, diclofop, and fenoxaprop, in soil was previously described,[3,9−11] a deeper insight into the mechanism and actual conversion rates are still missing.

In this paper, we describe an enantioselective analytical method used to isolate milligram quantities of single enantiomers of haloxyfop (both acid and methyl ester) based on HPLC as well as a method for the enantioselctive analysis of these compounds in soil extracts based on GC-MS. The latter was also used to analyze the compounds in plant extracts as reported in our companion paper.[12] Our results confirm the rapid hydrolysis of haloxyfop-methyl (Ha-me) to haloxyfop (Ha-acid) in soil. We then examine the rapid and preferential interconversion and further degradation of Ha-acid in soil as determined by incubating the racemic compound and the pure *R*- and *S*-enantiomers. Three different soils are used to determine if soil properties have any influence on the enantioselectivity of transformation. Control experiments in sterile soil are performed to determine whether the conversion is biologically mediated. A hypothesis on the mechanism of conversion in soil is postulated on the basis of H−D exchange experiments and mass spectrometric analysis. Mathematic modeling is applied to derive kinetic parameters for *R*/*S* interconversion and degradation in soil.

MATERIALS AND METHODS

Reference Materials. Racemic haloxyfop-methyl and haloxyfop-P-methyl (*rac*-Ha-me and *R*-Ha-me; 99.2 and 99.1%, respectively) were obtained from Dow AgroSciences, Hitchin, UK, and *rac*-haloxyfop (*rac*-Ha-acid, 99.8%) was from Riedel de Haen, Seelze, Germany. Pure *R*- and *S*-enantiomers of Ha-me and Ha-acid were isolated from the racemates by enantioselective HPLC (see below). *rac*-Fluazifop (*rac*-Fl-acid, 94.5%, from Dr. Ehrenstorfer, Augsburg, Germany) and *rac*-fluazifop-methyl (*rac*-Fl-me), prepared by methylation of *rac*-Fl-acid using diazomethane (see below), were used as internal standards. For CAS names of the various compounds used, see Supporting Information Table S2.

Semipreparative Isolation of *R*- and *S*-Enantiomers of Ha-me and Ha-acid. Pure *R*- and *S*-enantiomers of Ha-me were prepared from the racemic compound in milligram quantities by enantioselective HPLC according to a method published by CIPAC.[13] The enantiomers were separated on a silica gel column coated with cellulose tricinnamate (Chiralcel OK, 25 cm × 4 mm, 10 μm particle size; Daicel Chemical Industries, Osaka, Japan) at ambient temperature using heptane/isopropanol/methanol (85:5:10) as eluent at a flow rate of 1 mL/min and UV detection at 280 nm. *R*- and *S*-enantiomers of Ha-me eluted baseline separated after 6.7 and 8.8 min, respectively, with peak widths of 1.0 and 1.5 min (chromatogram, see Supporting Information Figure S5).

Pure enantiomers of Ha-acid were prepared using the same column and heptane/isopropanol/acetic acid (95:5:0.1) as eluent at a flow rate of 1 mL/min and UV detection at 280 nm. *R*- and *S*-Ha-acid eluted baseline separated after 13.5 and 20.4 min, respectively (peak widths of 4 and 6 min; chromatogram see Supporting Information Figure S6). A total of 10 injections of *rac*-Ha-me and *rac*-Ha-acid (0.5 mg in 100 μL), respectively, were made, and fractions were collected at the exit of the UV detector while the UV trace was observed. The pooled fractions contained approximately 2 mg of each enantiomer with >99% enantiomeric purity as determined by enantioselective GC-MS after methylation with diazomethane when appropriate (see below). Isolated enantiomers were stored in mobile phase until used for incubation experiments. Aliquots were then evaporated to dryness and redissolved in spiking solution (water or water/methanol, see below).

Incubation of Ha-me and Ha-acid in Soil. Soil samples were collected at sampling locations in close proximity to those of the Swiss soil monitoring network (NABO, www.bafu.admin.ch/boden). The soils were selected to cover a wide range of properties, in particular pH and organic carbon (Table 1). Standard equipment was used for sampling soil from the top 10 cm. The soils were kept in the dark at ≈4 °C for no more than 6 months prior to use.

Portions of 2 mm sieved, field-moist soil (100 g) were spread on glass dishes, and the test substance was applied using a small spray bottle (1−2 mL of an aqueous solution containing 100 μg per enantiomer of Ha-acid). For experiments with Ha-me (only with soil Neualp), the spike solution contained 30% methanol as cosolvent to increase the solubility (note the solubility of Ha-me in water is 9.1 mg/L[7]). The resulting spike levels were 1 μg enantiomer/g moist soil and thus high enough to allow for reliable quantification down to 1% of the initial concentration. This spike level is somewhat higher than the concentrations expected from typical application rates in the field of up to 160 g/ha (0.21 μg/g assuming uniform incorporation in the top 5 cm soil layer and a bulk density of 1.5 g/cm^3) but is not expected to affect soil microorganisms. Separate experiments were carried out with racemic compounds and with pure *R*- and *S*-enantiomers. The soils were then thoroughly mixed, transferred to Erlenmeyer flasks, closed with air-permeable cellulose plugs, and incubated at 20 °C in the dark for up to 4 days. The moisture of the soils (24−174 g water/100 g dry soil, corresponding to 37−60% of the maximum water-holding capacity) was regularly checked by weighing and kept constant by the addition of distilled water. At appropriate time intervals, aliquots of 10 g of soil were removed for extraction and analysis.

Sterile Control Experiments. Abiotic transformation of Ha-acid was studied using a γ-irradiated soil (soil Dübendorf, Table 1) as sterile control. Portions of 200 g of soil in closed screw-cap glass jars were exposed for a few hours to γ-irradiation (dosimeter controlled total dose of 30 kGy) from a commercial ^{60}Co source (Leoni Studer-Hard, Däniken, Switzerland). The glass jars were kept tightly closed after irradiation until the start of the incubation experiments to ensure sterile conditions. Spiking was done in the same way as for the nonsterile soils except that the soil was kept in the glass jars during spiking. Nevertheless, sterile conditions were broken upon spiking. As the incubation experiments lasted for only a few days, this was not expected to allow for restoration of any substantial biological activity in the soil.

H−D Exchange Experiments. Three 100 g portions of 2 mm sieved, field-moist soil (Neualp, Table 1) were spread on glass dishes

DOI: 10.1021/jf505241t
J. Agric. Food Chem. 2015, 63, 2583−2590

and allowed to dry to approximately 50% of their initial water content. The evaporated water was replaced by dropwise addition of deuterium oxide (Fluka, Buchs, Switzerland) to achieve an approximate 1:1 ratio of H_2O/D_2O. As D_2O can be toxic to soil microorganisms, a larger proportion was avoided. The soils were then spiked in the same way as the other soils (separate experiments with *rac*-Ha-acid and with pure *R*- and *S*-enantiomers). Soil moisture was maintained by the addition of a 1:1 mixture of distilled water and deuterium oxide.

Extraction and Derivatization. Soil samples from experiments with Ha-acid (10 g) were collected from the incubation vessels in 20 mL glass scintillation vials. Immediately after weighing, 10 mL of methanol and 100 μL of a methanolic solution of *rac*-Fl-acid (0.1 μg/μL) were added and the vials closed and vigorously shaken by hand for approximately 1 min and then stored at −20 °C until further processed (typically within 1 day). The vials were centrifuged at a relative centrifugal force (RCF) of 720 for 5 min (rotor with a radius of 16 cm, 2000 rpm), and the clear supernatants were removed into 30 mL glass vials, diluted with 10 mL of distilled water, and acidified to pH ≈1 by the addition of 4 drops of 5 M sulfuric acid. The extracts were then partitioned twice with 5 mL of dichloromethane, and the combined organic extracts were allowed to evaporate to dryness overnight in a fume hood. The extracts were then redissolved in a few drops of methanol and methylated by the addition of approximately 300 μL of an ethereal diazomethane solution until the yellow color of the diazomethane persisted (see ref 14 and cautionary note therein). The reaction mixtures were allowed to stand for 15 min and then carefully evaporated to dryness in a stream of air, and the dry residues were dissolved in 5 mL of hexane. An aliquot of 1 μL was used for GC-MS analysis. Absolute recoveries over the extraction and derivatization procedure, determined in soil Neualp, were 71% for both Fl-acid and Ha-acid, respectively (spike level, 1 μg/g moist soil). This indicates that both compounds show very similar behavior and that Fl-acid is thus an appropriate internal standard for Ha-acid. The method precision, expressed as relative standard deviation of multiple extractions, on average was 3.2% (range, from 0.3 to 5.9%).

In exploratory experiments with Ha-me, the same extraction procedure was used. In contrast to the experiments with Ha-acid, prior to the extraction the soil samples were fortified with 10 μg of *rac*-Fl-acid in 100 μL of methanol and 10 μg of *rac*-Fl-me in 100 μL of ethyl acetate as internal standards. The samples were derivatized with diazoethane (for a description of the preparation, see ref 12) rather than diazomethane, to allow for the simultaneous determination of parent Ha-me as well as Ha-acid formed during incubation. An aliquot of 1 μL was used for GC-MS analysis. Absolute recoveries over the extraction and derivatization procedure were 68 and 71% for Fl-me and Ha-me, respectively (spike level, 1 μg/g moist soil).

Several control experiments were conducted to ensure that no artifacts were produced during extraction and derivatization. Selected samples were spiked only with Fl-acid and then derivatized with diazomethane or diazoethane to confirm that no (<1%) ethyl ester was formed upon methylation and vice versa. Samples spiked only with Fl-me were derivatized with diazoethane to confirm that no transesterification occurred (<1% Fl-et present in ethylated soil extract dissolved in ethyl acetate). Finally, soils freshly spiked with single isomers of Ha-me and Ha-acid were processed to confirm that no hydrolysis and no enantiomerization occurred during sample preparation.

Enantioselective GC-MS Analysis. A Quattro Micro GC-MS/MS system (Waters Corp., Milford, MA, USA) connected to a HP6890N gas chromatograph (Agilent Technologies, Santa Clara, CA, USA) fitted with a PAL autosampler (CTC Analytics, Zwingen, Switzerland) was used in the electron ionization (EI, 70 eV, 180 °C) mode. Full-scan EI mass spectra (m/z 35−435, 0.5 s/scan, nominal mass resolution) were recorded for analyte detection and identification. Analysis of the methyl and ethyl esters was carried out in the selected ion monitoring mode for optimum sensitivity (cycle time = 0.5 s) using the m/z values listed in Table 2.

A custom-made 20 m GC column coated with OV 1701 containing 15% (w/w) permethyl-β-cyclodextrin with a film thickness of 0.1 μm (BGB Analytics, Boeckten, Switzerland) was used for separation. The

Table 2. GC-MS Masses Used for Determination of Target Compounds, Retention Times of the Enantiomers, and Chromatographic Resolution Achieved with the Permethyl-β-Cyclodextrin Column

target compound	m/z (all M^+)	retention times (min)	resolution
fluazifop-methyl (Fl-me)	341.1	38.5/38.7	1.4
fluazifop-ethyl (Fl-et)	355.1	39.9/40.1	1.3
haloxyfop-methyl (Ha-me)	375.1	41.3/41.5	1.3
haloxyfop-D_1-methyl	376.1	41.3/41.5	1.3
haloxyfop-ethyl (Ha-et)	389.1	42.7/42.9	1.2

GC conditions were as follows: split/splitless injection (240 °C, 48 s splitless time); temperature program, 50 °C for 2 min, increase to 120 °C at a rate of 25 °C/min and to 220 °C (upper temperature limit for this type of columns) at 2 °C/min. Helium was used as carrier gas at a flow rate of 2 mL/min. The column showed excellent stability, low bleed, and good and constant, nearly baseline, resolution of Ha-me, Ha-et, Fl-me, and Fl-et enantiomers (Table 2).

Kinetic Evaluation of Experimental Data. All kinetic analyses of experiments were performed using the modeling software Aquasim, version 2.1b.[15] Degradation and isomerization were implemented as first-order processes based on the conceptual model given in Figure 2,

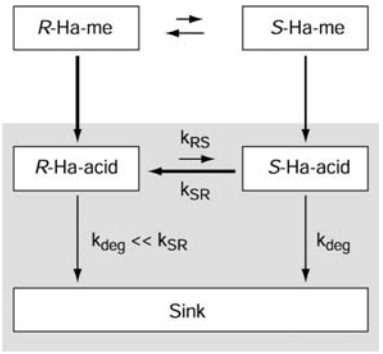

Figure 2. Reaction scheme and definitions of reaction rate constants used in the model calculations. The shaded area highlights the portion that was covered by model calculations.

and the corresponding rate constants were determined by fitting the modeled curves to measured data. The rate equations used for curve fitting were

$$d[S]/dt = k_{RS} \times [R] - (k_{SR} + k_{deg}) \times [S]$$

$$d[R]/dt = k_{SR} \times [S] - (k_{RS} + k_{deg}) \times [R]$$

Initial enantiomer concentrations were not fixed, but were fitted as additional parameters, with the following exceptions: the initial concentration of *S*-Ha-acid in the experiment with enantiopure *R*-Ha-acid was set to zero (and vice versa), and equal initial concentrations of *R*- and *S*-Ha-acid were assumed in the experiments with *rac*-Ha-acid.

Fitting was done in several steps. First, all rate constants, including separate degradation rate constants for each enantiomer, were fitted individually for each experiment. This approach did not yield satisfying solutions for the degradation rate constants because isomerization (particularly $S \rightarrow R$) is substantially faster than degradation. It is thus not possible to determine whether the *S*- or the *R*-enantiomer is more rapidly degraded because a small change in the isomerization rate constants would compensate for that difference. Therefore, a more robust fitting approach was used assuming that both enantiomers are degraded with an equal rate constant, k_{deg}. Isomerization rate constants k_{RS} and k_{SR}, respectively, were fitted for each soil simultaneously with data from the experiments with *rac*-Ha-acid and the pure *R*- and *S*-

DOI: 10.1021/jf505241t
J. Agric. Food Chem. 2015, 63, 2583−2590

enantiomers, using the enantiomer fractions[16] ([R]/([R] + [S]) and [S]/([R] + [S]), respectively) rather than individual concentrations as fit targets. The fitted values for k_{RS} and k_{SR} were then fixed, and k_{deg} values were determined for each individual experiment by fitting of the total concentrations (sum of *R*- and *S*-enantiomers).

RESULTS AND DISCUSSION

Analytical Considerations. For the sensitive and accurate enantioselective determination of Ha-me and Ha-acid in soil, chiral GC with mass spectrometric detection was used. Ha-acid and Fl-acid (internal standard) were converted to the respective methyl esters using diazomethane. In the initial experiments with Ha-me, selected samples were derivatized with diazo*ethane* to allow for simultaneous detection of Ha-acid (as ethyl ester) and Ha-me. Experiments with sterile soil showed that the extraction and derivatization procedures did not change the enantiomer ratios of Ha-acid.

Several chiral GC columns were evaluated for resolution of haloxyfop and fluazifop enantiomers. Whereas a dimethyl-*tert*-butyldimethylsilyl-*β*-cyclodextrin column had shown excellent enantiomer resolution of various phenoxypropionic acid herbicides,[17] this selector was found to provide insufficient chromatographic resolution of haloxyfop and fluazifop enantiomers. Eventually, a column coated with OV 1701 containing 15% (w/w) permethyl-*β*-cyclodextrin provided best resolution and allowed elution of the target analytes below 200 °C and, thus, well below the temperature limit of the column of 220 °C (Figure 3).

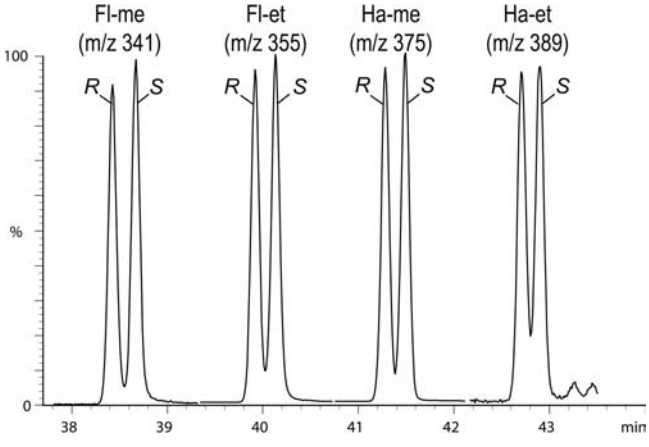

Figure 3. EI SIM chromatograms of racemic reference compounds of the methyl and ethyl esters of fluazifop (internal standard) and haloxyfop, analyzed on the enantioselective permethyl-*β*-cyclodextrin column.

The same enantiomer elution order (*R* prior to *S*) was observed for Ha-me, Ha-et, and Fl-me on this chiral selector. It is interesting to note that the same elution order was observed for ibuprofen, when considering its reverted absolute configuration at the *α*-carbon atom (*S* prior to *R*).[18] This indicates a common principle toward chiral recognition of the propionic acid moiety by this cyclodextrin derivative.

Whereas the enantiomer composition of Ha-acid was expected to change during incubation, the racemic fluazifop, serving as an internal standard, theoretically should always show enantiomer ratios of 1:1. The actual ratios for *rac*-Fl-acid (analyzed as methyl and ethyl esters) on a new GC column were indeed very close to 1:1, but with aging of the column, they were shifted toward a small excess in the later eluted *S*-enantiomer (Figure 3), which is commonly observed in enantioselective GC. In this particular case, the shift of apparent peak area ratios was small (approximately 0.9:1.1), and it was not due to peak tailing. Using the observed apparent ratio of the internal standard it was possible to apply a correction factor to the experimental data and thus to obtain accurate enantiomer ratios for haloxyfop.

Exploratory Soil Incubations of Ha-me. In initial experiments, *rac*-Ha-me or its pure enantiomers were incubated for 0, 2, and 4 h in soil Neualp (Table 1). In Figure 4 we show

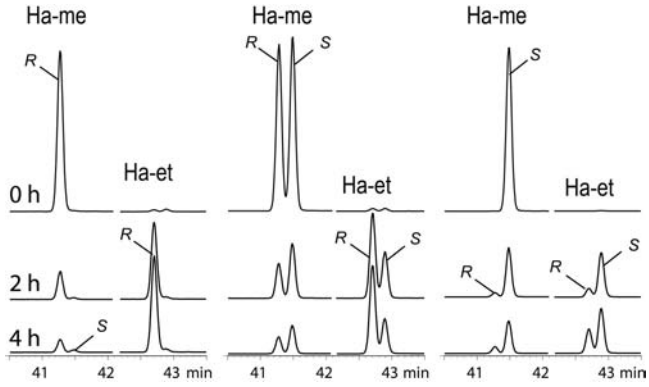

Figure 4. EI SIM chromatograms (*m*/*z* 375 + 389) of extracts of soil Neualp spiked with *R*- (left), *rac*- (middle), and *S*-Ha-me (right) immediately after spiking (top) and 2 h (middle) and 4 h later (bottom). Signals are normalized to the peaks for Fl-me used as internal standard. Note the rapid disappearance of Ha-me and the concurrent formation of Ha-acid (analyzed as ethyl ester).

chromatograms from these incubations. In all three experiments, Ha-me rapidly disappeared with half-lives of <2 h, and approximately 75% of the applied Ha-me was transformed to Ha-acid. The chromatograms from the incubation with *rac*-Ha-me indicate that degradation is enantioselective with faster dissipation of the *R*-enantiomer (residual composition, $R < S$). Degradation of the enantiopure compounds was associated with formation of small amounts of the antipode, indicating that enantiomerization occurred, although at a much slower rate compared to degradation.

This initial set of experiments confirmed that rapid degradation of Ha-me was leading to Ha-acid, consistent with previous studies.[7,19] Indeed, the 0 h ("quasi-zero") samples already showed the presence of some small amounts of free acid (analyzed as ethyl esters, Figure 4), whereas standards of Ha-me contained no detectable amounts of free acid. Apparently, the short time (a few minutes) required for preparation (spiking, mixing of soil, sampling) was sufficient to form free acid by hydrolysis of the methyl ester. In the 2 h sample, then, the presence of acid was significant, thus clearly indicating rapid hydrolysis of the methyl ester to the free acid. In a review,[20] the properties of microbial carboxy esterases were described and enantioselective cleavage of, for example, substituted phenoxypropionic acids was reported. Apparently, these esterases are widespread in soil microbiology, which could explain the fast ester cleavage of Ha-me.

Closer inspection of the signals for Ha-acid (analyzed as its ethyl ester) in Figure 4, from incubation of *rac*- and particularly from *S*-Ha-me, indicates that the proportion of *R*-Ha-acid formed is larger than would be expected from the stereochemical composition of the precursor. Furthermore, the proportion of the *R*-enantiomer increases from the 2 h to the

DOI: 10.1021/jf505241t
J. Agric. Food Chem. 2015, 63, 2583−2590

4 h sample. This indicates that Ha-acid enantiomers formed in soil are rapidly interconverted, with preference for the *R*-enantiomer. This interconversion appears to be faster than the actual degradation of Ha-acid, as its impact on the enantiomer composition is clearly observed. As Ha-acid is the active metabolite of Ha-me and is present in soil much longer than Ha-me, its enantiomer composition determines the residual herbicidal activity. Therefore, we investigated the degradation and enantiomerization of Ha-acid in soil in more detail.

Incubation of *rac*-, *R*-, and *S*-Ha-acid in Three Different Soils. Separate incubation experiments were conducted with racemic and enantiopure Ha-acid to investigate possible enantioselective degradation as well as conversion of one enantiomer to the other. From the experiment with Ha-me it was expected that changes in enantiomeric composition are fast. Therefore, short initial sampling intervals of 4 h were chosen, except for soil Dübendorf (Table 1), for which 1 day intervals were used.

In all three soils, the enantiomer composition of spiked Ha-acid changed rapidly as indicated by the chromatograms shown in Figure 5. In fact, the enantiomer ratio after 8 h of incubation was almost independent of the initial enantiomer composition. The change in composition was faster than the overall dissipation of Ha-acid in soil. It involved the formation of *R*-from *S*-Ha-acid and, to a lesser degree, also the reverse reaction. The enantiomer composition eventually approached a steady state, where the concentration of the *R*-enantiomer was about 10 times that of the *S*-enantiomer. The composition in the three soils, expressed as enantiomer fraction (here defined as concentration of *S*-enantiomer divided by total concentration), is shown in Figure 6. From the curves it is suggested that the final enantiomer composition is independent of the initial composition and very similar in all three soils, whereas the rate at which this composition was achieved differed slightly (curve fitting, see below).

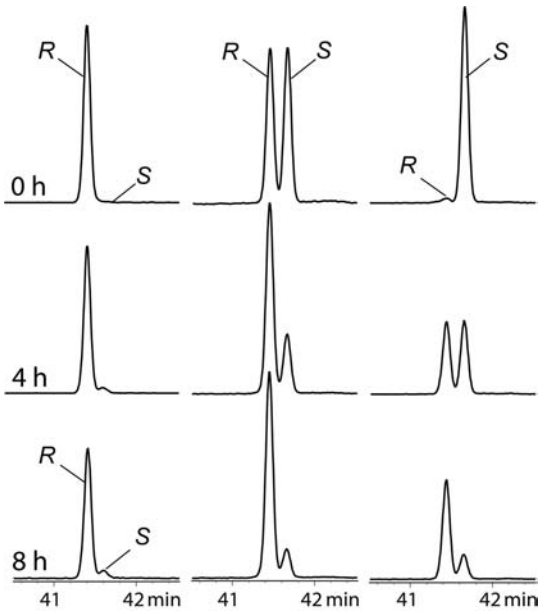

Figure 5. EI SIM chromatograms (m/z 375) of extracts of soil Neualp spiked with *R*- (left), *rac*- (middle), and *S*-Ha-acid (right) immediately after spiking (top) and 4 h (middle) and 8 h later (bottom), analyzed after methylation. Signals are normalized to the peaks for fluazifop used as internal standard. Note the rapid disappearance of *S*-Ha-acid and the concurrent formation of the *R*-enantiomer.

In the sterile soil, no degradation and no change in enantiomer composition were observed over the first 4 days of incubation, indicating that degradation as well as enantiomerization in soil are microbially mediated processes. After prolonged incubation, some conversion was observed, probably due to regrowth of microorganisms as sterile conditions were broken with spiking and sampling.

Kinetic Modeling of Degradation and Enantiomerization of Ha-acid in Soils. The experimental data in the three nonsterile soils were fitted using the conceptual model shown in Figure 2. In total, three rate constants were fitted to describe the conversion of *R*- to *S*-Ha-acid and vice versa, as well as overall degradation. The actual degradation of Ha-acid was found to be much slower than enantiomerization. Consequently, the degradation rate constants could not be fitted individually for each enantiomer and were thus assumed to be equal for *R*- and *S*-Ha-acid. This does not necessarily mean that the enantiomers were degraded equally quickly, but rather that any differences in degradation rates would be compensated by the rapid enantiomerization.

As an example, the fitting of degradation and enantiomerization of Ha-acid in soil Neualp is shown in Figure 7, where the fitted curves describe the observed behavior (formation and dissipation of enantiomers as well as overall degradation) correctly. The kinetic parameters thus derived for this and the two other soils are shown in Table 3. Overall, degradation was faster in soil Neualp (half-lives = ln $2/k_{deg}$, 2.3−4.0 days) than in the other two soils (6.0−9.3 days). Degradation in the experiments with *rac*-Ha-acid was consistently slower than in experiments with the pure enantiomers. This may be due to the fact that *rac*-Ha-acid was spiked with a slightly lower water volume, and the soil was thus a little less moist (Table 1).

The rate constants for conversion of *R*- to *S*-Ha-acid (k_{RS}) were only somewhat higher than the degradation rate constants in the same soils, whereas the rate constants for the reverse reaction were substantially (≈20 times) higher.

Due to rapid enantiomerization, a steady-state enantiomeric composition was achieved within 1−2 days of incubation (Figure 6). From the enantiomerization rate constans (k_{RS} and k_{SR}) equilibrium constants (K_{enant}) for the enantiomerization of Ha-acid can be calculated as

$$K_{enant} = k_{RS}/k_{SR}$$

The value of K_{enant} corresponds to the enantiomer ratio S/R at steady state. As shown in Table 3, the values for K_{enant} ranged from 0.061 to 0.082 and were thus very similar in all three soils.

This is in contrast to the situation when a chiral compound is degraded enantioselectively, but with no apparent enantiomerization, such as with the chiral fungicide metalaxyl.[21] In that case, the enantiomer ratio (ER) changes with incubation time according to the equation

$$\ln(ER) = \ln(ER_0) - \Delta k \times t$$

where Δk is the difference of the degradation rate constants of the two enantiomers and ER_0 is the enantiomer ratio at time zero. This equation indicates that the enantiomer ratio will not reach a steady state at any given time.

In a recent paper on diclofop-methyl,[10] a herbicide that is structurally closely related to Ha-me, the authors used the above equation to evaluate their experimental data. However, they did not take into consideration the rapid enantiomeriza-

DOI: 10.1021/jf505241t
J. Agric. Food Chem. 2015, 63, 2583−2590

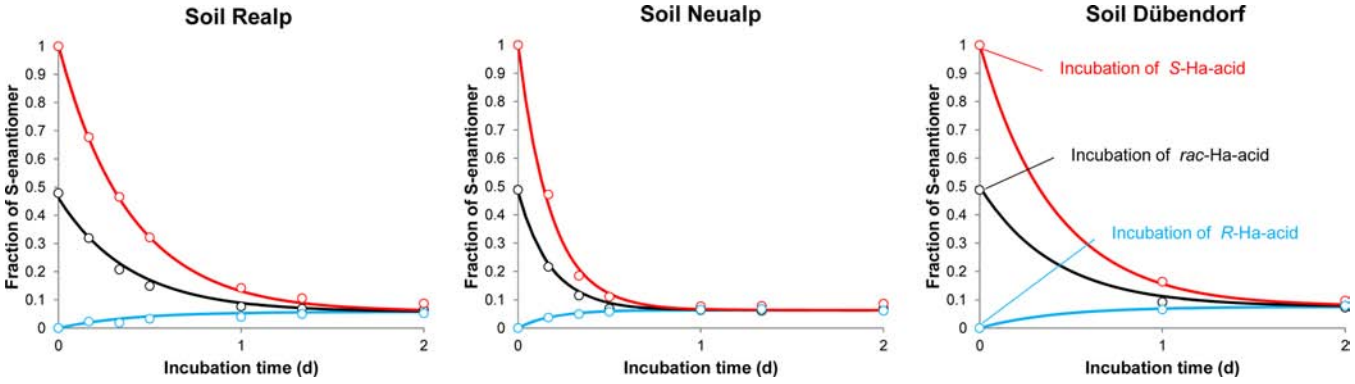

Figure 6. Change of enantiomeric composition of Ha-acid in soils, expressed as enantiomer fraction (concentration of *S*-enantiomer divided by total concentration) during incubation of racemic and enantiopure Ha-acid. Lines indicate the fitted curves. Note that the final composition is independent of the initially applied substance.

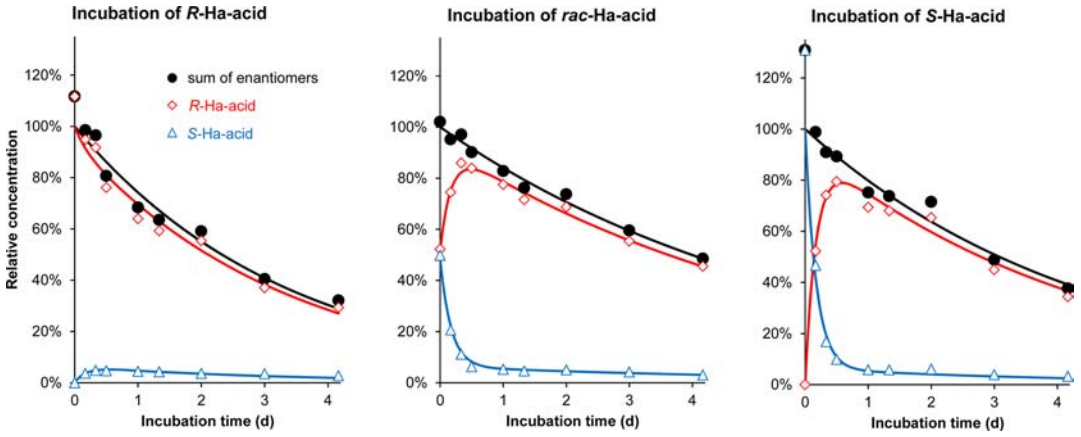

Figure 7. Concentrations of *R*-, *S*-, and total Ha-acid in soil Neualp after spiking of *R*- (left), *rac*- (middle), and *S*-Ha-acid (right). Curves were fitted according to the conceptual model shown in Figure 2.

Table 3. Degradation and Enantiomerization Rate Constants (± Standard Deviation Calculated by the Software) of Ha-acid in Three Soils Determined in Experiments with *rac*-Ha-acid and the Pure *R*- and *S*-Enantiomers Using the Kinetic Scheme Shown in Figure 2[a]

soil	spiked with	k_{deg} (day^{-1})	k_{RS} (day^{-1})	k_{SR} (day^{-1})	k_{RS}/k_{SR}
Dübendorf	*R*-Ha-acid	0.103 ± 0.012	0.184 ± 0.015	2.25 ± 0.11	0.082 ± 0.008
	rac-Ha-acid	0.080 ± 0.012			
	S-Ha-acid	0.115 ± 0.013			
Neualp	*R*-Ha-acid	0.298 ± 0.029	0.353 ± 0.086	5.21 ± 0.46	0.068 ± 0.018
	rac-Ha-acid	0.173 ± 0.017			
	S-Ha-acid	0.225 ± 0.020			
Realp	*R*-Ha-acid	0.107 ± 0.002	0.147 ± 0.073	2.40 ± 0.26	0.061 ± 0.031
	rac-Ha-acid	0.074 ± 0.022			
	S-Ha-acid	0.113 ± 0.028			

[a]Note that k_{deg} values were fitted for each experiment individually, whereas k_{RS} and k_{SR} were fitted simultaneously for all experiments with a particular soil.

tion of diclofop acid. To test the applicability of our approach for evaluation of Ha-acid to other, similar cases, we used the data for diclofop acid from ref 10 and applied the same conceptual model as for Ha-acid to derive the kinetic parameters. The resulting plots and kinetic parameters are shown in the Supporting Information (Figures S1−S4; Table S1). Indeed, acceptable fits for diclofop acid were obtained in this way from those previously published data.

Comparison of Haloxyfop Behavior in Soil with That of Other Phenoxy Acids. Isomerization of chiral pesticides in the environment was described for numerous compounds from different chemical families.[22] Rapid conversion of enantiomers with clear preference for the *R*-enantiomer was also observed for other FOPs, for example, for fluazifop,[9] diclofop,[3,10] and fenoxaprop.[3] It is also consistent with field experiments with Ha-me, where it was shown that the efficacy of the substance against weeds depended strongly on the enantiomeric

DOI: 10.1021/jf505241t
J. Agric. Food Chem. 2015, 63, 2583−2590

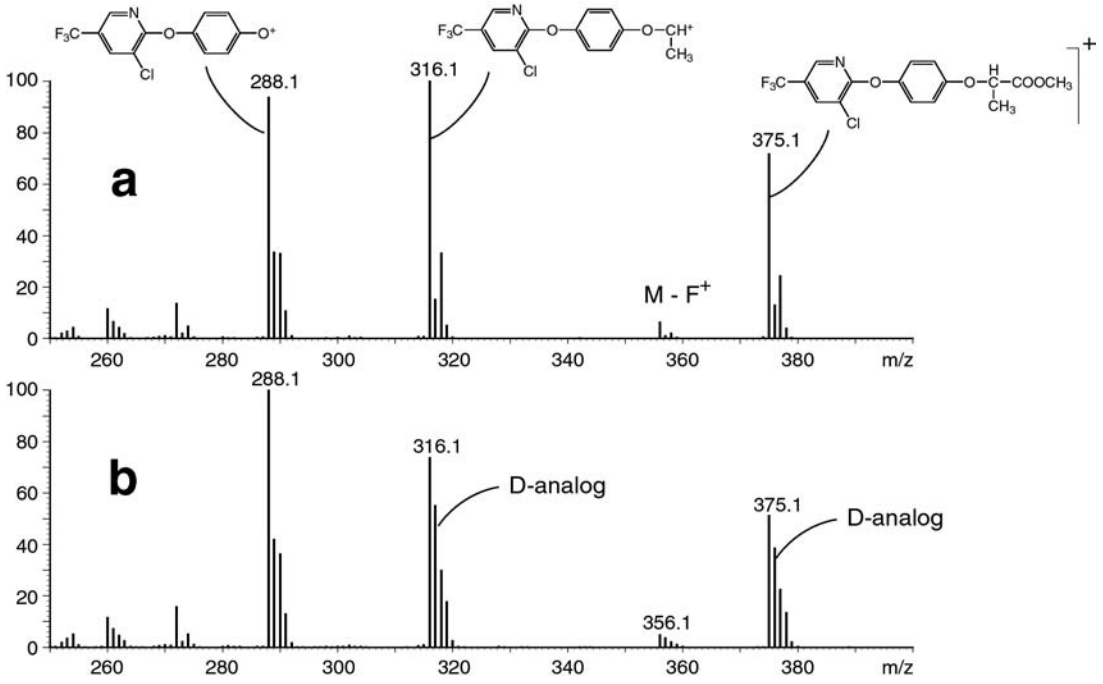

Figure 8. Partial mass spectra of (a) Ha-me (reference compound) and of (b) Ha-acid after 4 h of incubation in soil in the presence of D_2O and subsequent methylation. Note the incorporation of a single deuterium into Ha-acid as indicated by the changed isotope profiles of the molecular and the major ions at m/z 375 and 316, respectively (panel b).

composition when applied postemergent (thus applied to the leaves), whereas it was practically independent of the enantiomeric composition when applied pre-emergent (and is thus taken up from soil).[11] In the latter study, residues extracted from soil 7 days after application of Ha-me consisted mainly of *R*-Ha-acid.

Conversion of enantiomers was also observed for phenoxypropionic acid herbicides such as mecoprop and dichlorprop.[17,23] However, in contrast to our results with Ha-acid, degradation appeared to be faster than enantiomerization.[17] The enantioselectivity of degradation/enantiomerization of mecoprop and dichlorprop varied over a wide range and apparently changed with soil pH values (see ref 24 and references therein), whereas no pH dependence with respect to the preferential formation of the *R*-enantiomer was observed with Ha-acid in the three soils studied here.

Mechanistic Considerations from H−D Exchange Experiments. Full-scan MS clearly indicated the incorporation of deuterium when Ha-acid was incubated in soil where water was partially replaced with D_2O (H/D ratio of about 1:1). The EI mass spectra of Ha-me (Figure 8), Ha-et, and Fl-me are very similar in that all three show intense molecular ions and agree in their major fragmentation pathways. Ha-me (M^+ = 375) and Ha-et (M^+ = 389) yield the same major fragment ions at m/z 316 (loss of $COOCH_3$ and $COOC_2H_5$, respectively) and m/z 288 (loss of $CHCH_3COOCH_3$ and $CHCH_3COOC_2H_5$, respectively). No significant differences were observed in the spectra of the enantiomers.

As shown in Figure 8, the mass spectrum of Ha-acid after incubation in D_2O-containing soil and analyzed as methyl ester clearly shows changed isotopic patterns of M^+ (note increased signal of m/z 376) and for the main fragment ion at m/z 316 (increased signal of m/z 317) due to the incorporation of a single D into the molecule. The exact location of D was deduced from the fact that the isotopic pattern of fragment ion m/z 288 (loss of the complete propionic acid side chain) was still the same as with the native compound. This locates the D label at one of two carbons (C-2 or C-3) of the propionic acid moiety, most likely at C-2 (the methin-H), in the same sense as was observed with the propionic acid herbicide mecoprop.[23] The amount of D incorporation, estimated from the signal intensities at m/z 375 and 376 and when corrected for ^{13}C contributions, was about 35%.

The H−D exchange presumably follows a scheme such as outlined in Figure 9 via a planar transitional enolate structure

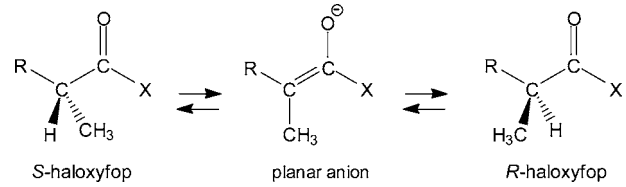

Figure 9. Proposed mechanism for the conversion of the enantiomers of Ha-me and Ha-acid in soil. "X" depicts a methoxy, a hydroxy, or a possible intermediate coenzyme A ester, analogous to that proposed for aryl propionic acid isomerization in mammalian metabolism.[6]

(back/front addition of H/D). However, the exchanged proton located next to the carboxylic acid moiety is only weakly acidic. Consequently, this reaction requires enzymatic activity such as in biologically active soils. For APAs it was shown that epimerization proceeds via formation of a coenzyme A thioester.[6] The enzyme that catalyzes epimerization of the coenzyme A esters of APAs in rats (2-arylpropionyl-coenzyme A epimerase) was isolated from rat liver[25] and was subsequently shown to be closely related, if not identical, to the 2-methylacyl-coenzyme A racemases present in peroxisomes and mitochondria,[26] which are involved in the metabolism of branched-chain fatty acids.[27] Although the epimerase is not enantioselective,

DOI: 10.1021/jf505241t
J. Agric. Food Chem. 2015, 63, 2583−2590

the net formation of an excess of one enantiomer results from enantioselective formation of the coenzyme A thioester.[6]

It is interesting to note that in the WHO JMPR evaluation of haloxyfop[28] the reviewer concluded that in mammals Ha-me undergoes rapid ester cleavage in vivo, followed by an equally rapid and almost complete conversion of *S*- to *R*-Ha-acid. There seems to be a striking similarity in the findings from the studies in rodents, dogs, and monkeys with our finding of the rapid transformations of Ha-me and Ha-acid in biologically active soils. This may indicate that the same biochemical processes are involved in soil as in mammalian conversion of haloxyfop enantiomers, and these may even be very closely related to those involved in the conversion of APA enantiomers.

In contrast to these similarities in behavior of Ha-acid enantiomers in mammalian and soil metabolism, no conversion of Ha-acid enantiomers and no enantioselectivity in degradation of Ha-me or Ha-acid were found in plants.[12] Consequently, the residues in plants most likely reflect the stereoisomer composition of the compound that was applied (uptake by leaves) or that was formed in soil (root uptake).

■ ASSOCIATED CONTENT

Supporting Information

Figures S1−S6 and Tables S1 and S2. This material is available free of charge via the Internet at http://pubs.acs.org.

■ AUTHOR INFORMATION

Corresponding Author

*(T.P.) E-mail: thomas.poiger@agroscope.admin.ch. Phone: +41 58 460 6289. Fax: +41 58 460 6341.

Notes

The authors declare no competing financial interest.

■ REFERENCES

(1) Cobb, A. H.; Reade, J. P. H. *Herbicides and Plant Physiology*, 2nd ed.; Wiley-Blackwell: Chichester, UK, 2010.

(2) Herbicide Resistance Action Committee (HRAC) Classification of herbicides according to site of action. http://www.hracglobal.com/ (accessed Feb 23, 2015).

(3) Wink, O.; Luley, U. Enantioselective transformation of the herbicides diclofop-methyl and fenoxaprop-ethyl in soil. *Pestic. Sci.* **1988**, *22*, 31−40.

(4) Hoppe, H. H.; Zacher, H. Inhibition of fatty-acid biosynthesis in isolated bean and maize chloroplasts by herbicidal phenoxy-phenoxypropionic acid-derivatives and structurally related compounds. *Pestic. Biochem. Physiol.* **1985**, *24*, 298−305.

(5) Kantoci, D.; Wechter, W. J. Calculation of inversion half-lives of aryl propionic acid class nonsteroidal antiinflammatory drugs. *J. Clin. Pharmacol.* **1996**, *36*, 500−504.

(6) Wechter, W. J. Drug chirality − on the mechanism of R-aryl propionic-acid class NSAIDs − epimerization in humans and the clinical implications for the use of racemates. *J. Clin. Pharmacol.* **1994**, *34*, 1036−1042.

(7) European Food Safety Authority (EFSA). Conclusion on the peer review of the pesticide risk assessment of the active substance haloxyfop-P (haloxyfop-R). *EFSA J.* **2009**, *7*, 1348.

(8) Bundesamt für Verbraucherschutz und Lebensmittelsicherheit BVL, Multimethode zur Bestimmung von Pflanzenschutzmittelrückständen in pflanzlichen Lebensmitteln mittels GC-MS(/MS) oder LC-MS/MS nach Acetonitril-Extraktion/Verteilung und Aufreinigung mittels dispersiver SPE (QuEChERS). In *Methodensammlung BVL*, L 00.00-115 ed.; 2007.

(9) Bewick, D. W. Stereochemistry of fluazifop-butyl transformations in soil. *Pestic. Sci.* **1986**, *17*, 349−356.

(10) Diao, J. L.; Xu, P.; Wang, P.; Lu, Y. L.; Lu, D. H.; Zhou, Z. Q. Environmental behavior of the chiral aryloxyphenoxypropionate herbicide diclofop-methyl and diclofop: enantiomerization and enantioselective degradation in soil. *Environ. Sci. Technol.* **2010**, *44*, 2042−2047.

(11) Gerwick, B. C.; Jackson, L. A.; Handly, J.; Gray, N. R.; Russell, J. W. Preemergence and postemergence activities of the (R) and (S) enantiomers of haloxyfop. *Weed Sci.* **1988**, *36*, 453−456.

(12) Buerge, I. J.; Bächli, A.; Heller, W. E.; Keller, M.; Poiger, T. Environmental behavior of the chiral herbicide haloxyfop. 2. Unchanged enantiomer composition in blackgrass (*Alopecurus myosuroides*) and garden cress (*Lepidium sativum*). *J. Agric. Food Chem.* **2015**, DOI: 10.1021/jf50242f.

(13) Collaborative International Pesticides Analytical Council (CIPAC) Normal phase HPLC method (CIPAC/4618) for the determination of haloxyfop-P-methyl in TC and EC formulations (ISBN 902951521); http://www.cipac.org/ (accessed Feb 23, 2015).

(14) Vogel, A. I. *Vogel's Textbook of Practical Organic Chemistry*, 5th ed.; Longman Scientific and Technical: Harlow, UK, 1989.

(15) Reichert, P. Aquasim − a tool for simulation and data-analysis of aquatic systems. *Water Sci. Technol.* **1994**, *30*, 21−30.

(16) Harner, T.; Wiberg, K.; Norstrom, R. Enantiomer fractions are preferred to enantiomer ratios for describing chiral signatures in environmental analysis. *Environ. Sci. Technol.* **2000**, *34*, 218−220.

(17) Müller, M. D.; Buser, H.-R. Conversion reactions of various phenoxyalkanoic acid herbicides in soil. 1. Enantiomerization and enantioselective degradation of the chiral 2-phenoxypropionic acid herbicides. *Environ. Sci. Technol.* **1997**, *31*, 1953−1959.

(18) Buser, H.-R.; Poiger, T.; Müller, M. D. Occurrence and environmental behavior of the chiral pharmaceutical drug ibuprofen in surface waters and in wastewater. *Environ. Sci. Technol.* **1999**, *33*, 2529−2535.

(19) Smith, A. E. Transformation and persistence of the herbicide [C-14]haloxyfop-methyl in soil under laboratory conditions. *J. Agric. Food Chem.* **1985**, *33*, 972−976.

(20) Bornscheuer, U. T. Microbial carboxyl esterases: classification, properties and application in biocatalysis. *FEMS Microbiol. Rev.* **2002**, *26*, 73−81.

(21) Buser, H.-R.; Müller, M. D.; Poiger, T.; Balmer, M. E. Environmental behavior of the chiral acetamide pesticide metalaxyl: Enantioselective degradation and chiral stability in soil. *Environ. Sci. Technol.* **2002**, *36*, 221−226.

(22) Katagi, T. Isomerization of chiral pesticides in the environment. *J. Pestic. Sci.* **2012**, *37*, 1−14.

(23) Buser, H.-R.; Müller, M. D. Conversion reactions of various phenoxyalkanoic acid herbicides in soil. 2. Elucidation of the enantiomerization process of chiral phenoxy acids from incubation in a D_2O/soil system. *Environ. Sci. Technol.* **1997**, *31*, 1960−1967.

(24) Buerge, I. J.; Poiger, T.; Müller, M. D.; Buser, H.-R. Enantioselective degradation of metalaxyl in soils: chiral preference changes with soil pH. *Environ. Sci. Technol.* **2003**, *37*, 2668−2674.

(25) Reichel, C.; Brugger, R.; Bang, H.; Geisslinger, G.; Brune, K. Molecular cloning and expression of a 2-arylpropionyl-coenzyme A epimerase: a key enzyme in the inversion metabolism of ibuprofen. *Mol. Pharmacol.* **1997**, *51*, 576−582.

(26) Schmitz, W.; Helander, H. M.; Hiltunen, J. K.; Conzelmann, E. Molecular cloning of cDNA species for rat and mouse liver α-methylacyl-CoA racemases. *Biochem. J.* **1997**, *326*, 883−889.

(27) Lloyd, M. D.; Darley, D. J.; Wierzbicki, A. S.; Threadgill, M. D. α-Methylacyl-CoA racemase − an "obscure" metabolic enzyme takes centre stage. *FEBS J.* **2008**, *275*, 1089−1102.

(28) Renshaw, D. W.; Tasheva, M. Haloxyfop (including haloxyfop-*R* and haloxyfop-*R* methyl ester). In *Pesticide Residues in Food − 2006, Part II - Toxicological Evaluations*; Joint FAO/WHO Meeting on Pesticide Residues; 2006; pp 315−354.

DOI: 10.1021/jf505241t
J. Agric. Food Chem. 2015, 63, 2583−2590

enantiomer composition was not changed. Unfortunately, later sampling was not performed. "Chiral stability" of the enantiomers of diclofop and quizalofop was also observed in studies with freshwater algae.[22,23] A further study was conducted with cole.[24] After foliar treatment, diclofop-methyl and diclofop-acid were both degraded enantioselectively with a preference for the *S*-enantiomers. However, since no experiments were performed with pure enantiomers, no conclusion could be made on possible interconversion.

No experimental data are currently available on the behavior of the enantiomers of haloxyfop-methyl in plants (chemical structure, see Figure 1). In the European registration process, it

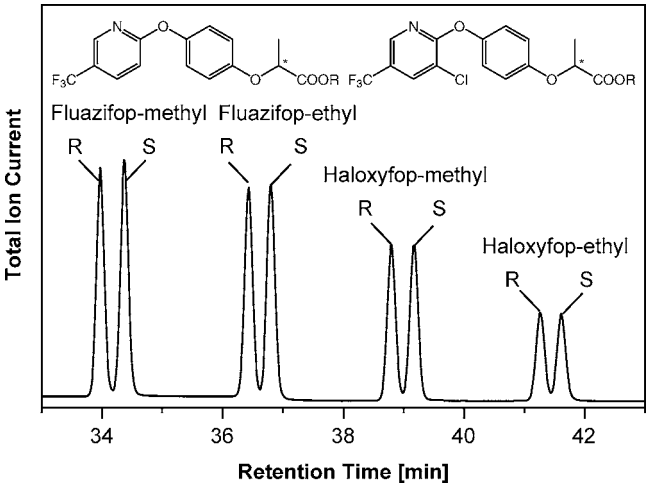

Figure 1. Reconstructed ion chromatogram of eight mass traces showing the elution of the enantiomers of haloxyfop-methyl (concentrations, 1.7 mg/g plant dry weight), haloxyfop-acid (analyzed as ethyl-ester, 1.0 mg/g), and the corresponding internal standards (fluazifop) in an ethylated extract from blackgrass, sampled 24 h after treatment with *rac*-haloxyfop-methyl. Nonenantioselective metabolism was observed for both methyl-ester and acid.

was concluded that "due to the lack of isomeric specificity of the [...] analytical methods, any possible stereochemical inversion in either direction in food of plant and animal origin could not be detected".[25] The selective herbicide is used for the postemergent control of annual and perennial grasses in sugar beet, fodder beet, oilseed rape, potatoes, vegetables, sunflowers, soya beans, vines, strawberries, and other dicotyledonous crops.[26,27] Haloxyfop-methyl is absorbed by leaves and roots and is metabolized to haloxyfop-acid and conjugates with glucose and other sugars.[27]

The present study aims at filling this data gap with regard to metabolism in plants. Our enantiomer-specific, gas chromatographic method allowed us to investigate the enantioselectivity of degradation of haloxyfop-methyl and haloxyfop-acid in plants. Possible interconversion of enantiomers was studied by using pure *R*-haloxyfop-methyl. For our experiments, we selected blackgrass as a typical weed that is controlled with haloxyfop-methyl and garden cress as a dicotyledonous plant that is not sensitive to the herbicide and, from an experimental point of view, was easy to cultivate. The herbicide was applied to the aerial parts of the plants in a way that excluded root uptake so that processes in leaves and shoots could be studied.

MATERIALS AND METHODS

Chemicals and Reagents. Racemic haloxyfop-methyl (purity, 97.5%; CAS name, see Supporting Information, Table S2 in ref 15), racemic haloxyfop-acid (99.5%), and racemic fluazifop-acid (94.5%) were from Ehrenstorfer, Augsburg, Germany. Haloxyfop-P-methyl (99.3%), racemic fluazifop-methyl (97.4%), N-nitroso-N-ethylurea (containing 2% acetic acid as stabilizer), and the nonionic detergent Tween 60 were from Sigma-Aldrich, Steinheim, Germany. A blank formulation (EF-1400) was obtained from Dow AgroSciences, Norfolk, UK. CIPAC standard water D with a hardness of 342 ppm and a pH of 6.9 was prepared as described in ref 28. The mineral fertilizer Kristalon Red Acid was from Yara, Oslo, Norway. LP0013 Agar Technical (No. 3) was purchased from Oxoid, Basingstoke, UK.

Plants. Seeds of blackgrass, *Alopecurus myosuroides* (LS-Number Fors000021), were from Appels Wilde Samen, Darmstadt, Germany, and garden cress, *Lepidium sativum* (UFA 50280), was from Fenaco, Winterthur, Switzerland. The plants were grown on agar, which was either poured on sterile polystyrene Petri dishes (diameter, 9 cm) or filled into 40 mL clear glass vials (diameter, 2.8 cm, Figure 2). Agar-

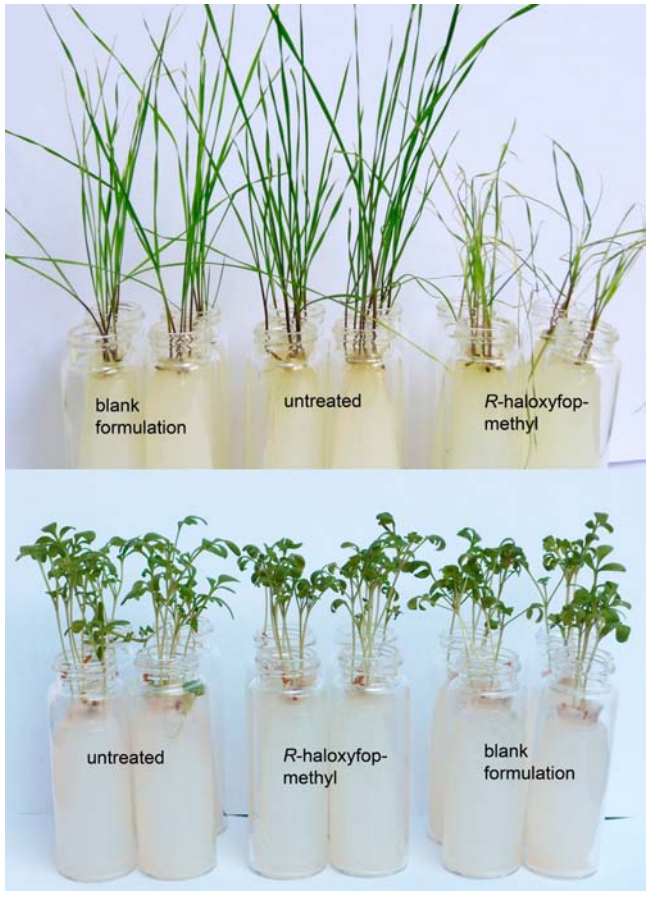

Figure 2. Blackgrass (top) and garden cress (bottom) 96 h after treatment with formulated *R*-haloxyfop-methyl, a blank formulation, and grown without treatment. The herbicide has selective activity on true grasses (*Poaceae*).

medium for Petri dishes was prepared with tap water at a concentration of 12 g/L, the medium for vials with a nutrient solution (0.1% Kristalon Red Acid, pH ≈ 7) at a concentration of 15 g/L. Agar was autoclaved at 121 °C for 15 min.

The germination rate of blackgrass after 1 week was about 30−40%. Therefore, seeds were first sown on agar plates, and germinated seedlings were then transplanted into agar vials. In a clean air bench, 25 seeds were spread on each plate and covered with a polystyrene lid. To suppress growth of fungi in the agar, blackgrass seeds were first

DOI: 10.1021/jf505242f
J. Agric. Food Chem. 2015, 63, 2591−2596

disinfected. For that, seeds were placed into a tea strainer and dipped in aqueous acetic acid (7%, with addition of ∼1 g/L of the surfactant Tween 60) for 15 min. Thereafter, the seeds were thoroughly rinsed in tap water for 2 h. After sowing, the agar plates were kept in a greenhouse chamber at 80% relative humidity and a temperature of ∼25 °C (day) or ∼18 °C (night). The seedlings were exposed to natural sunlight (November−January at 47° N, attenuated by the windows of the greenhouse) and, as necessary, artificial light (high pressure sodium lamps, type Master SON-T PIA Plus 400 W, Philips) to give a total irradiance of ∼250 W/m^2 (photoperiod, 14 h per day). After about 7 days, five seedlings were transplanted into a 40 mL glass vial filled with nutrient agar (planting depth of seeds, ∼5 mm; the roots of the seedlings were completely pushed into the agar). These vials were kept in the greenhouse for another 10 days. After this time, the grass seedlings typically had developed three leaves with a length of ∼10−15 cm.

Garden cress was directly sown into the glass vials since germination was nearly 100%. Five seeds were placed ∼3 mm deep into the nutrient agar. After 7 days in the greenhouse, the cress seedlings had two leaves (cotyledons) and shoot lengths of ∼4−7 cm.

Herbicide Application on Blackgrass. Haloxyfop-methyl has a low water solubility of 9 mg/L at 25 °C.[27] To improve its solubility in the application solution and its uptake by weeds, commercial herbicides (e.g., Gallant) additionally contain adjuvants, aromatic solvents, and emulsifiers. For our experiments, we dissolved ∼50 mg of racemic haloxyfop-methyl (or ∼25 mg *R*-haloxyfop-methyl) in ∼400 mg blank formulation, an emulsifiable concentrate with the code EF-1400 (composition confidential). This solution was then mixed with 30 mL of CIPAC standard water D. The resulting, milky emulsion thus contained 1.6 g/L *rac*-haloxyfop-methyl or 0.8 g/L *R*-haloxyfop-methyl. Assuming that 200 L are sprayed per hectare, these concentrations correspond to application rates of 320 g/ha *rac*-haloxyfop-methyl or 160 g/ha *R*-haloxyfop-methyl, the latter being the currently approved, maximum application rate in Switzerland. For a preliminary experiment, an application solution was prepared with haloxyfop-methyl, composed of $[R]$:$[S]$ = 2:1, at a concentration of 1.5 g/L (note that, based on the label, the test substance should have been racemic). To investigate possible herbicidal effects of the adjuvants, the blank formulation was also diluted with CIPAC water as described above but without the addition of haloxyfop-methyl.

The application method was designed to ensure that the herbicide is only taken up through leaves (and not by roots via agar) and that it is distributed as evenly as possible on the leaves. For that, the grass leaves were inserted overhead into an empty test tube (160 mm × 16 mm), which was then filled with application solution. Within less than 5 s, the leaves were pulled out of the test tube, and the application solution was allowed to drip off the leaves, still overhead (we assume that the tips of the leaves received somewhat higher amounts of active substance and formulation). After 2 min, the treated plants were placed into a climate chamber at 21−22 °C and 65% relative humidity and illuminated by two types of lamps simulating natural sunlight (three tubular low-pressure mercury-vapor fluorescent lamps, type TL40*W*/05, Philips, emitting radiation between 300 and 460 nm; and three tubular fluorescent lamps, type F40*W*/125-RS, Sylvania, emitting radiation between 400 and 650 nm). Grass leaf samples were collected immediately after application and 2, 5, 24, 32, 48, 72, and 96 h later. At each sampling time, five leaves were harvested and extracted as described later. Extractions and analyses were performed in triplicate at all time-points.

Herbicide Application on Garden Cress. For garden cress, a more diluted application solution was prepared (reason, see Results and Discussion section): ∼6 mg of racemic haloxyfop-methyl (or ∼3 mg of *R*-haloxyfop-methyl) was dissolved in ∼50 mg of EF-1400 and mixed with 30 mL of CIPAC standard water D (resulting concentrations, 0.2 g/L *rac*-haloxyfop-methyl or 0.1 g/L *R*-haloxyfop-methyl). The cress leaves were directly dipped into the application solution, pulled out within less than 5 s, and allowed to drip off overhead for 2 min. Then, the plants were placed into the climate chamber (conditions as described for blackgrass). Leaf samples were taken immediately after application and 2, 5, 24, 32, 48, 72, and 96 h later (in triplicate). All leaves of a particular vial were used for extraction.

Extraction. The harvested plant material was cut into pieces of ∼2 cm and extracted with 10 mL of methanol containing 10 μg of racemic fluazifop-methyl and fluazifop-acid as internal standards (chemical structures, see Figure 1). Extraction was facilitated by sonication for at least 5 min or until visually all chlorophyll was extracted and the leaves were bleached. An aliquot of the extract was then removed for spectrophotometric analysis of chlorophyll a at wavelengths of 665, 652, and 750 nm, as described in ref 29. With tweezers, the bleached leaves were removed from the extract and dried in an oven at 60 °C for 1 h to determine their dry weight (3−6 mg per five blackgrass leaves, 6−18 mg per five cress plants, depending on their age).

Ethylation of Haloxyfop-Acid, Cleanup. To analyze haloxyfop-acid and fluazifop-acid by GC−MS, it was necessary to derivatize. Ethylation was considered appropriate as it allowed, in contrast to methylation, distinction of haloxyfop-methyl and -acid, analyzed as ethyl ester. Prior to derivatization, the methanolic extract was reduced to a volume of ∼100 μL on a heating plate (80 °C) with a gentle flow of N_2. The concentrated extract was acidified with 2−3 drops of 0.5% trifluoroacetic acid in methanol. Haloxyfop-acid and fluazifop-acid were then derivatized by addition of ∼750 μL of diazoethane in methyl *tert*-butyl ether (MTBE).

Diazoethane was prepared as follows. In a 50 mL glass bottle, 1.5 g of N-nitroso-N-ethylurea was dissolved in 30 mL of MTBE and placed on ice. To this solution, 6 mL of 40% aqueous potassium hydroxide was added, and the bottle was loosely covered so that gas formed during reaction could escape. After gas formation had ceased (∼1 h), the orange colored organic layer containing the diazoethane was transferred to a 50 mL glass bottle containing a few potassium hydroxide pellets and stored in the freezer (−20 °C) until use (usually within 1 week). Note that diazoethane is toxic by inhalation and by contact with skin or eyes, and thus, all handling was strictly done in a fume hood. Likewise, the compound is explosive, and contact with sharp glassware must be avoided. Prior to disposal of any waste, excess diazoethane was reacted with dilute acetic acid in methanol.

No methyl ester was formed from ethylation of the acid in methanol/MTBE. After derivatization and evaporation of the solvents, the residues were dissolved in ∼100 μL of ethyl acetate. For cleanup, the derivatized extract was passed through a silica mini-column (5 mm i.d. Pasteur pipet filled with ∼60 mm of silica gel 60, Merck, Darmstadt, Germany, dried at 140 °C for 24 h, deactivated with 5% water, and topped with 10 mm of anhydrous sodium sulfate). The analytes were eluted with 10 mL of ethyl acetate. The eluate was carefully concentrated with a gentle flow of N_2 and mild heating to a final volume of 1 mL and quantitatively transferred into a 2 mL autosampler glass vial.

Enantioselective GC−MS Analysis. The enantiomers of haloxyfop-methyl, haloxyfop-ethyl, and the corresponding internal standards (fluazifop-methyl and fluazifop-ethyl) were separated on a chiral GC column coated with permethyl-β-cyclodextrin (15%) in OV1701 (BGB 171, 20 m, 0.25 mm i.d., 0.15 μm film, BGB, Boeckten, Switzerland). GC conditions were as follows: 1 μL split/splitless injection (240 °C, initial 48 s splitless); temperature program, 70 °C, 2 min isothermal, 25 °C/min to 150 °C, 1 °C/min to 200 °C, isothermal hold at 220 °C; constant flow, 2 mL/min helium. The GC was coupled to a Voyager single quadrupole MS (Finnigan, Manchester, UK) operated in electron impact ionization (70 eV, 180 °C) and selected-ion-monitoring mode. Haloxyfop-methyl, haloxyfop-ethyl, fluazifop-methyl, and fluazifop-ethyl were quantified using the ions m/z 375 (316 and 288 for confirmatory purposes), 389 (316, 288), 341 (282, 254), and 355 (282, 254), respectively. The enantiomer resolution of the four analytes was ∼1.3, 1.2, 1.4, and 1.3, respectively (defined as $R = 2\,(t_{r2} - t_{r1})/(w_1 + w_2)$, where t_{ri} is the retention time of enantiomer i, and w_i is the width at the base of peak i). A representative chromatogram of a plant extract is shown in Figure 1. The elution order of the enantiomers was *R* prior to *S* for all compounds as determined with pure reference substances. Quantification was based on peak area ratios relative to the internal standards

DOI: 10.1021/jf505242f
J. Agric. Food Chem. 2015, 63, 2591−2596

and in reference to suitable standard solutions of the racemic compounds. For more details on the analytical method, see ref 15.

RESULTS AND DISCUSSION

Rapid Ester Cleavage of Haloxyfop-Methyl to Haloxyfop-Acid in Blackgrass. After application on blackgrass, *rac*-haloxyfop-methyl was rapidly metabolized to haloxyfop-acid, the herbicidally active compound (Figure 3a). Within 24 and

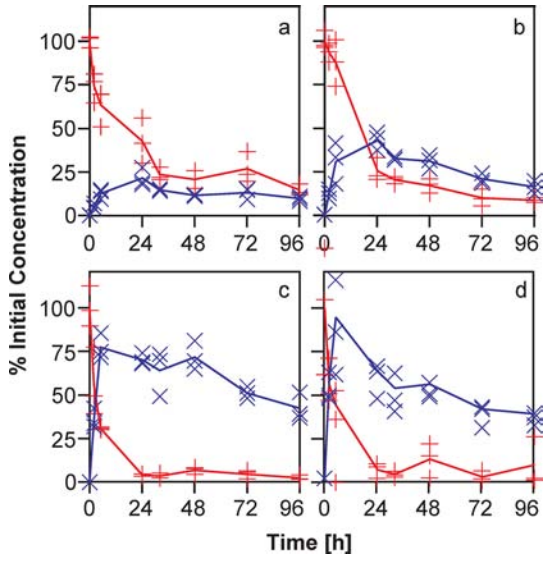

Figure 3. Metabolism of haloxyfop-methyl and haloxyfop-acid in blackgrass (a,b) and garden cress (c,d) after treatment with *rac*-haloxyfop-methyl (a,c) or *R*-haloxyfop-methyl (b,d). Symbols depict individual concentration data for haloxyfop-methyl (+) and haloxyfop-acid (×); the lines connect mean concentrations of three replicates. Residues are based on plant dry weight and those of the metabolite in parent equivalents. The enantiomer composition remained constant throughout the experiments.

32 h, concentrations of haloxyfop-methyl decreased by more than 50% and 75%, respectively (residues based on plant dry weight). Residues of haloxyfop-acid reached a maximum of ∼22% (parent equivalents) 24 h after treatment, which suggested that the acid was further metabolized (or that other primary metabolites were formed besides). Moreover, plant growth also resulted in somewhat lower concentrations (dilution effect, less than a factor of two).

After 32 h, metabolism of parent and metabolite slowed down considerably (Figure 3a). At the same time, the treated grass showed first withering symptoms (see Figure 2 for grass treated with *R*-haloxyfop-methyl). Within about 1 week, the leaves turned completely brown. Concurrently, the chlorophyll a content decreased from ∼20 mg/g (dry weight) before treatment to less than 3 mg/g 96 h after treatment (data not shown). In the control experiment, where blackgrass was treated with blank formulation, without the active compound, no striking herbicidal injuries were observed. Only the leaf tips slightly turned brown, whereas untreated grass showed no symptoms at all (Figure 2).

Nonenantioselective Metabolism of Haloxyfop-Methyl and Haloxyfop-Acid in Blackgrass. The enantiomer composition of haloxyfop-methyl in blackgrass did not change within the 96-h duration of the experiment (Figure 1). The enantiomer fraction (defined as EF = $[R]/([R] + [S])$, where $[R]$ and $[S]$ are the concentrations of *R*- and *S*-haloxyfop-methyl, respectively) varied between 0.48 and 0.51, which indicated that metabolism was nonenantioselective. The enantiomer composition of the acid metabolite also remained constant within 96 h, which suggested that not only the formation, but also the further transformation was non-enantioselective (Figure 1). EF values ranged from 0.47−0.54. Enantiomer fractions showed clearly less variation than the concentrations of the individual enantiomers since it was not possible to apply the test substance in a way to ensure that all plants received exactly the same amount of herbicide (see Materials and Methods section), whereas the enantiomer composition in the application solution was, of course, reproducible.

"Chiral Stability" of Haloxyfop-Methyl and Haloxyfop-Acid in Blackgrass. After application of *rac*-haloxyfop-methyl on blackgrass, residues thus remained racemic. However, the observed, constant enantiomer fractions of 0.5 may, in principle, also be the result of a fast racemization in the leaves. To investigate a possible interconversion of enantiomers, further blackgrass plants were treated with pure *R*-haloxyfop-methyl. These experiments confirmed that no *S*-haloxyfop-methyl and no *S*-haloxyfop-acid were formed from the corresponding *R*-enantiomers. The plant extracts only contained traces of the *S*-enantiomers that were already present in the reference material (∼1%). The opposite process, conversion of the *S*- into the *R*-enantiomers, could also be excluded since metabolism was nonenantioselective in experiments with the racemic herbicide. Therefore, additional experiments with pure *S*-haloxyfop-methyl were not performed as they were not considered necessary.

Appearance and degree of necrosis symptoms and reduction of the chlorophyll a content were similar after treatment with *R*-haloxyfop-methyl as in the experiments with *rac*-haloxyfop-methyl (Figure 2). Note that the same amount of the *R*-enantiomer was applied (*R*-haloxyfop is the herbicidally active form).

Concentration-Dependent Formation of Haloxyfop-Acid. The rate of degradation/dissipation of *R*-haloxyfop-methyl was similar to that of *rac*-haloxyfop-methyl (Figure 3a,b). However, in the experiments with pure *R*-haloxyfop-methyl, concentrations of *R*-haloxyfop-acid reached a maximum of ∼43% (parent equivalents), which is twice as high as in the corresponding experiments with the racemic compound (∼22%). In a further experiment, where blackgrass was treated with haloxyfop-methyl, composed of $[R]:[S]$ = 2:1, the maximum concentration of the acid was just between the above values, ∼32% (data not shown). A simple explanation for these differences in relative formation cannot be given as it is obviously not due to preferential conversion of enantiomers nor due to obvious differences in senescence. Formation of the acid may, however, depend on the concentration of applied haloxyfop-methyl. Indeed, when considering further data from experiments with garden cress (see below), which were conducted with clearly lower herbicide concentrations, a good correlation was found between maximum formation of haloxyfop-acid and initial concentration of haloxyfop-methyl in the leaves (Figure 4). Nonetheless, the underlying biochemical explanation for this observation remains unclear.

Phytotoxic Injuries on Garden Cress Caused by the Blank Formulation. Haloxyfop has selective activity on true grasses (*Poaceae*) but no activity on other monocotyledonous and dicotyledonous plants.[12] Garden cress was selected as representative dicotyledonous plant since it has a high

DOI: 10.1021/jf505242f
J. Agric. Food Chem. 2015, 63, 2591−2596

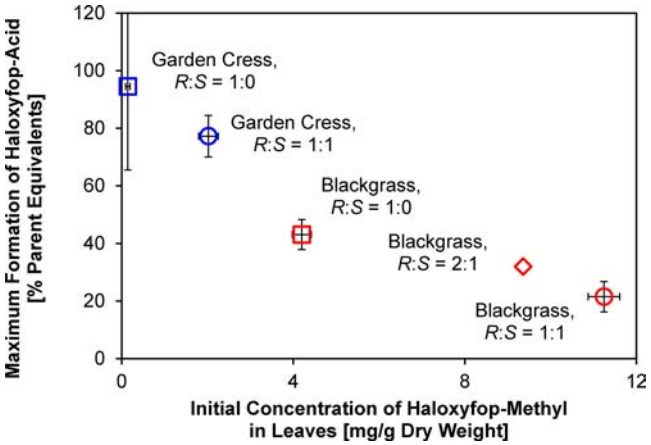

Figure 4. Maximum formation of haloxyfop-acid in experiments with blackgrass and garden cress treated with haloxyfop-methyl at different concentrations and enantiomer composition in the application solution; thus, different initial concentration in the leaves. Error bars indicate the standard deviation of three replicate experiments. The maximum formation of haloxyfop-acid is given in parent equivalents in relation to the mean initial concentration in the leaves. Note that these values are not corrected for plant growth.

germination rate and can easily be cultivated. In preliminary experiments, garden cress was treated with the same solution/emulsion of formulated haloxyfop-methyl as used for blackgrass. However, the plants showed severe withering symptoms already after 24 h. The control experiment, in which plants were treated with blank formulation only, indicated that the observed phytotoxicity was caused by the formulation rather than by haloxyfop. The amount of water used to dilute the formulated herbicide was chosen as it would be done in agricultural practice, but we assume that with the treatment procedure (dipping of leaves in the application solution to avoid uptake by roots), considerably higher amounts of active substance and adjuvants were finally applied to the leaves than with a spray application under normal field conditions. Therefore, a more diluted application solution (8×) was prepared for the definitive experiments with garden cress. Phytotoxic injuries were now clearly reduced, and only the most tender leaves showed minor symptoms. After 96 h, treated (formulation with and without haloxyfop-methyl) and untreated cress plants looked quite similar (Figure 2).

Nonenantioselective Metabolism of Haloxyfop-Methyl and Haloxyfop-Acid in Garden Cress. In garden cress, metabolism of haloxyfop-methyl was faster than in blackgrass, with a half-life of ∼3 h (Figure 3c,d for treatment with *rac*- and *R*-haloxyfop-methyl). However, the residues of the methyl-ester did not decline further between 24 and 96 h after treatment. Apparently, this small residue fraction (<10%) is not available for metabolism, for example, it may be associated with lipophilic waxes in the cuticle of the leaves.

Maximum formation of the acid metabolite was observed already 5 h after treatment (Figure 3c,d). Up to ∼95% (average of three replicates) was formed from *R*-haloxyfop-methyl and ∼77% from the racemic compound. The correlation shown in Figure 4 suggests that maximum formation depends on the initial concentration of haloxyfop-methyl in the leaves (see Discussion section above). In experiments with garden cress, variability of the measured concentrations in the three replicates was quite high, in particular at early sampling times (Figure 3c,d). In bent leaves (Figure 2), small droplets of application solution adhered instead of a homogeneous, thin film, and consequently, application to cress leaves was less reproducible than with blackgrass. After 5 h, the concentration of the acid slowly decreased (Figure 3c,d) not only due to further metabolism, but also of course due to plant growth.

In experiments with *rac*-haloxyfop-methyl applied on garden cress, the enantiomer fractions ranged from 0.44−0.57 for the parent compound and from 0.47−0.52 for the acid metabolite. The EF values thus slightly deviated from 0.50, in particular, at low residue levels of haloxyfop-methyl but without a clear temporal trend. Again, in experiments with *R*-haloxyfop-methyl, no formation of *S*-haloxyfop-methyl and *S*-haloxyfop-acid was observed, which suggests that metabolism of parent and metabolite was not or only slightly enantioselective and that no conversion of enantiomers occurred.

Remarkable Contrast Between Chiral Stability in Plants and Rapid Interconversion of Enantiomers of Haloxyfop-Acid in Soil. Our experiments with blackgrass and garden cress showed that the enantiomer composition of haloxyfop-methyl and its major metabolite haloxyfop-acid was not changed in plants either by enantioselective metabolism or by interconversion of enantiomers. Blackgrass is susceptible to the herbicide, whereas the dicotyledonous garden cress is not susceptible. These findings with regard to chiral stability can thus probably be generalized to most mono- and dicotyledonous plants. Consequently, it may be expected that residues in crops have the same enantiomer composition as in the applied product provided that the compound is applied postemergent and primarily taken up through leaves. In rotational and succeeding crops, uptake of haloxyfop-acid from soil occurs via roots, and potential residues should then predominantly contain the *R*-enantiomer. However, because of the relatively fast degradation of the acid in soils (typical half-lives under field conditions, 5−27 days[25]), measurable residues would only be expected when the succeeding crop is planted shortly after application of the herbicide, for example, after failure of the preceding crop.

Chiral stability in plants strongly contrasts the observed, rapid conversion of *S*- to *R*-haloxyfop-acid in soils[12,15] and mammals.[25] In soils, this transformation is biologically mediated (probably via deprotonation at the methine carbon[7,15]), whereas in plants, apparently, no such enzymes are present or accept haloxyfop-acid as substrate. It was speculated that in plants, enzyme-mediated interconversion of enantiomers of chiral pesticides is less common than in soil,[7] but at the same time, it was also stated that more plant metabolism studies would be needed to support such a conclusion.

The present study shows that the use of the herbicidally active, pure *R*-haloxyfop-methyl rather than the racemic compound is advantageous from an environmental perspective. It allows 50% lower application rates at similar field performance, results in lower residues in crops and environment, and may lead to fewer side effects on nontarget organisms.

AUTHOR INFORMATION

Corresponding Author

*E-mail: ignaz.buerge@agroscope.admin.ch; phone: +41 58 460 6383; fax: +41 58 460 6341.

Notes

The authors declare no competing financial interest.

DOI: 10.1021/jf505242f
J. Agric. Food Chem. 2015, 63, 2591−2596

■ ACKNOWLEDGMENTS

We thank Dow AgroSciences for providing the blank formulation and N. Fernandez (Agroscope) for support in the laboratory.

■ REFERENCES

(1) Ariëns, E. J.; van Rensen, J. J. S.; Welling, W. *Stereoselectivity of Pesticides, Biological and Chemical Problems*; Elsevier: Amsterdam, 1988; Vol. *1*, p 544.

(2) Garrison, A. W.; Gan, J.; Liu, W. Chiral Pesticides: Stereoselectivity and Its Consequences. *ACS Symposium Series*; American Chemical Society: Washington, DC, 2011; Vol. *1085*, p 225.

(3) Magrans, J. O.; Alonso-Prados, J. L.; Garcia-Baudin, J. M. Importance of Considering Pesticide Stereoisomerism—Proposal of a Scheme To Apply Directive 91/414/EEC Framework to Pesticide Active Substances Manufactured as Isomeric Mixtures. *Chemosphere* **2002**, *49*, 461−469.

(4) Garrison, A. W. Probing the Enantioselectivity of Chiral Pesticides: Enantiomer-Specific Formulations Could Decrease Pesticide Use and Protect the Environment from Unintended Effects. *Environ. Sci. Technol.* **2006**, *40*, 16−23.

(5) Ulrich, E. M.; Morrison, C. N.; Goldsmith, M. R.; Foreman, W. T. Chiral Pesticides: Identification, Description, and Environmental Implications. *Rev. Environ. Contam. Toxicol.* **2012**, *217*, 1−74.

(6) Regulation (EC) No 1107/2009 of the European Parliament and of the Council. *Official Journal of the European Union* **2009**, *24.11.2009*, L 309/50.

(7) Katagi, T. Isomerization of Chiral Pesticides in the Environment. *J. Pestic. Sci.* **2012**, *37*, 1−14.

(8) Schneiderheinze, J. M.; Armstrong, D. W.; Berthod, A. Plant and Soil Enantioselective Biodegradation of Racemic Phenoxyalkanoic Herbicides. *Chirality* **1999**, *11*, 330−337.

(9) Müller, M. D.; Buser, H.-R. Conversion Reactions of Various Phenoxyalkanoic Acid Herbicides in Soil. 1. Enantiomerization and Enantioselective Degradation of the Chiral 2-Phenoxypropionic Acid Herbicides. *Environ. Sci. Technol.* **1997**, *31*, 1953−1959.

(10) Buser, H.-R.; Müller, M. D. Conversion Reactions of Various Phenoxyalkanoic Acid Herbicides in Soil. 2. Elucidation of the Enantiomerization Process of Chiral Phenoxy Acids from Incubation in a D2O/Soil System. *Environ. Sci. Technol.* **1997**, *31*, 1960−1967.

(11) Dicks, J. W.; Slater, J. W.; Bewick, D. W. PP 005—The *R*-Enantiomer of Fluazifop-butyl. *Proc. - Br. Crop Prot. Conf.—Weeds* **1985**, 271−280.

(12) Gerwick, B. C.; Jackson, L. A.; Handly, J.; Gray, N. R.; Russell, J. W. Preemergence and Postemergence Activities of the (*R*) and (*S*) Enantiomers of Haloxyfop. *Weed Sci.* **1988**, *36*, 453−456.

(13) Cartwright, D. The Synthesis, Stability, and Biological Activity of the Enantiomers of Pyridyloxyphenoxypropionates. *Proc. - Br. Crop Prot. Conf.—Weeds* **1989**, 707−716.

(14) Diao, J.; Xu, P.; Wang, P.; Lu, Y.; Lu, D.; Zhou, Z. Environmental Behavior of the Chiral Aryloxyphenoxypropionate Herbicide Diclofop-methyl and Diclofop: Enantiomerization and Enantioselective Degradation in Soil. *Environ. Sci. Technol.* **2010**, *44*, 2042−2047.

(15) Poiger, T.; Müller, M. D.; Buser, H.-R.; Buerge, I. J. Environmental Behavior of the Chiral Herbicide Haloxyfop (I): Rapid and Preferential Interconversion of the Enantiomers in Soil. *J. Agric. Food Chem.* **2015**, DOI: 10.1021/jf505241t.

(16) Secor, J.; Cséke, C. Inhibition of Acetyl-CoA Carboxylase Activity by Haloxyfop and Tralkoxydim. *Plant Physiol.* **1988**, *86*, 10−12.

(17) Turner, J. A.; Pernich, D. J. Origin of Enantiomeric Selectivity in the Aryloxyphenoxypropionic Acid Class of Herbicidal Acetyl-Coenzyme A Carboxylase (ACCase) Inhibitors. *J. Agric. Food Chem.* **2002**, *50*, 4554−4566.

(18) Zhang, H.; Tweel, B.; Tong, L. Molecular Basis for the Inhibition of the Carboxyltransferase Domain of Acetyl-Coenzyme A Carboxylase by Haloxyfop and Diclofop. *Proc. Natl. Acad. Sci. U.S.A.* **2004**, *101*, 5910−5915.

(19) Tao, J.; Zhang, G.; Zhan, A.; Zheng, L.; Cao, S. Study on the Enantioselectivity Inhibition Mechanism of Acetyl-Coenzyme A Carboxylase toward Haloxyfop by Homology Modeling and MM-PBSA Analysis. *J. Mol. Model.* **2012**, *18*, 3783−3792.

(20) Nestler, H. J.; Bieringer, H. Synthesis and Herbicidal Activity of the D- and L-Methyl 2-[4-(2,4-dichlorophenoxy)-phenoxy]-propionate Enantiomers. *Z. Naturforsch.* **1980**, *85b*, 366−371.

(21) Shimabukuro, R. H.; Hoffer, B. L. Enantiomers of Diclofop-methyl and Their Role in Herbicide Mechanism of Action. *Pestic. Biochem. Phys.* **1995**, *51*, 68−82.

(22) Cai, X.; Liu, W.; Sheng, G. Enantioselective Degradation and Ecotoxicity of the Chiral Herbicide Diclofop in Three Freshwater Alga Cultures. *J. Agric. Food Chem.* **2008**, *56*, 2139−2146.

(23) Zhang, X.; Wang, S.; Wang, Y.; Xia, T.; Chen, J.; Cai, X. Differential Enantioselectivity of Quizalofop Ethyl and Its Acidic Metabolite: Direct Enantiomeric Separation and Assessment of Multiple Toxicological Endpoints. *J. Hazard Mater.* **2011**, *186*, 876−882.

(24) Gu, X.; Lu, Y.; Wang, P.; Dang, Z.; Zhou, Z. Enantioselective Degradation of Diclofop-methyl in Cole (*Brassica chinensis* L.). *Food Chem.* **2010**, *121*, 264−267.

(25) European Food Safety Authority. Conclusion on the Peer Review of the Pesticide Risk Assessment of the Active Substance Haloxyfop-P (Haloxyfop-R). *EFSA J.* **2009**, *7*, 1348.

(26) Botte, M. C.; Ambolet, B.; Sturm, K. Haloxyfop-*R*, A New Selective Post Emergence Herbicide for Grass Weeds Control in Main Broad Crops and Vineyard. *Proc. 15th Columa Conf.* **1992**, *1*, 397−404.

(27) Tomlin, C. D. S. *The Pesticide Manual*, 15th ed.; The British Crop Protection Council: Alton, UK, 2009.

(28) Dobrat, W.; Martijn, A. *CIPAC Handbook - Physicochemical Methods for Technical and Formulated Pesticides*; Collaborative International Pesticides Analytical Council (CIPAC): Oxfordshire, UK, 1995; Vol. *F*, p 472.

(29) Porra, R. J.; Thompson, W. A.; Kriedemann, P. E. Determination of Accurate Extinction Coefficients and Simultaneous Equations for Assaying Chlorophylls a and b Extracted with Four Different Solvents: Verification of the Concentration of Chlorophyll Standards by Atomic Absorption Spectroscopy. *Biochim. Biophys. Acta* **1989**, *975*, 384−394.

DOI: 10.1021/jf505242f
J. Agric. Food Chem. 2015, 63, 2591−2596

excessively large amount of highly soluble nitrogen compounds. As SRF/CRF release their nutrients slowly and gradually during all vegetation seasons, they need to be applied only once, greatly reducing both time and energy consumption. A better and more efficient use of nutrients can lead both to a reduction of waste material produced by the fertilizer industry and to a reduction in natural gas consumption.

One of the drawbacks of CRFs, particularly polymer-coated CRFs, is that after nutrient consumption, a considerable amount of nonfunctional polymer remains in the soil, amounting to approximately 50 kg/ha per year.[4] It should be kept in mind in that context that the average consumption of nutrients (NPK) in the European Union is approximately 100 kg/ha per year. One possible solution that has not yet been implemented on a large scale is to produce CRF using biodegradable materials,[13] either natural materials or biosynthetic materials manufactured from renewable raw materials. Among the various biodegradable materials used for this purpose, starch and its derivatives seem to be the most extensively investigated,[14,15] although cellulose and its derivatives,[16−18] chitosan,[19,20] and polylactic acid[21] have also recently been examined for this application as described in the literature.

All of the products with prolonged nutrient release, available on the market, including commercially successful ones such as Osmocote, Multicote, Meister, Nutricote, Basacote, or Polyon, are manufactured with the use of polymers that are not biodegradable. The objective of this research was to obtain materials with controlled-release properties by coating granules of a mineral fertilizer with a layer of biodegradable aliphatic copolymer of poly(butylene succinate) and a butylene ester of dilinoleic acid (PBS/DLA) using an immersion method, to characterize the prepared materials, and to evaluate the nutrient release kinetics. As far as we know this kind of copolyester (PBS/DLA) has not been used in the preparation of controlled-release fertilizer; however, copolyesters of succinic acid with starch[22] and maleic anhydride[23] have been evaluated as biodegradable matrix materials for the controlled release of bacterial fertilizers.

MATERIALS AND METHODS

Materials. The source of active, mineral, macronutrient components (nitrogen, phosphorus, potassium) for this experiment was the commercial, granulated, multicomponent fertilizer NPK(S) 6−20−30−(7). This fertilizer contains at least 92% of particles within the range of 2−5 mm. Its bulk density is approximately 0.9−1.0 kg/dm^3. For the experiment, the granule fraction with a diameter of 3−4 mm was selected.

The fertilizer was commercially produced according to the Dorr-Oliver method.[24] The mixture of phosphoric and sulfuric acid was neutralized in the saturator with ammonia to obtain monoammonium phosphate and ammonium sulfate slurry, which was then granulated in the blunger with potassium chloride and small amounts of magnesium carbonate as a filler. Fertilizer granules were dried, crushed, sieved, and conditioned to obtain the final product. The contents of the three main components of the fertilizer, namely, nitrogen (5.9 wt % N-NH_4^+), phosphorus (19.8 wt % total P_2O_5, 18.2 wt % water-soluble P_2O_5), and potassium (29.5 wt % K_2O), were determined by potentiometry with an Orion 9512 ion selective electrode (Thermo Fisher Scientific, Beverly, MA, USA), spectrophotometry with a Spekol 11 instrument (Carl Zeiss, Oberkochen, Germany) and emission flame photometry with a BWB-1 instrument (BWB Technologies, Newbury, UK), respectively. These measured contents of the mineral components are consistent with the data declared by the fertilizer producer.

The aliphatic copolymer of PBS and a butylene ester of DLA (PBS/DLA) was used as a coating material. The aliphatic copolyester was synthesized through direct melt polycondensation in the presence of 1,4-butanediol.[25] This copolyester is a multiblock thermoplastic elastomer composed of soft sequences containing flexible chains of butylene ester of DLA and PBS as hard segments. The obtained copolymer contains 60 wt % PBS and 40 wt % DLA. This material was shown to be biodegradable in biodegradation tests carried out on thin polymer films (60 × 60 × 0.5 mm) under controlled conditions at 50 °C for 3 months in a mixture of sand and compost, according to the previously reported procedure.[26] The weight losses of the PBS/DLA copolyester were approximately 5 wt % after 1 month, 8 wt % after 2 months, and 10 wt % within 3 months of incubation;[25] however, there are reports on complete biodegradation of PBS and PBS blends with various organic materials.[22,23,27]

Despite the fact that the use of PBS/DLA in the preparation of controlled-release fertilizers may bring many benefits, especially in the context of environment protection, it should be kept in mind that PBS is not a cost-effective material. The price of commercially available PBS is approximately 5.4−5.6 euro/kg, and it is comparable with other synthetic biodegradable polyesters[28] but slightly higher than the price of biobased, biodegradable polymers from natural resources and several times higher than the price of conventional, not biodegradable synthetic polymers. The high price of PBS, being the main obstacle of its possible acceptance as a fertilizer component, can be lowered by the preparation of PBS blends with various organic materials from natural resources, for example, with dilinoleic acid.

Preparation. The granules of the multicomponent fertilizer in the 3−4 mm fraction were weighed and coated with a layer of biodegradable copolyester of PBS/DLA by the immersion method. For this purpose, appropriate amounts of solid polymer were dissolved, gradually and with the use of a magnetic stirrer, in appropriate amounts of chloroform (preferably 10 ± 0.1 g of PBS/DLA and 90 ± 0.1 g of chloroform) to obtain a 10 wt % solution. Fertilizer granules were placed separately as a monolayer on the stainless steel wire cloth (opening size = 1.6 mm × 1.6 mm) and dipped into the solution, with a contact time of 2−3 s, at a constant temperature of 25 °C, and then dried at 60 °C to evaporate the solvent residue. Repeating this dipping/drying procedure controlled and determined the amount of polymer layer coating the granules. After preparation, the coated fertilizer granules were weighed again. This method was used to prepare materials with various polymer to fertilizer (P/F) mass ratios.

Methods. The morphology of the polymer-coated granules and the thickness of the coating layers were examined using an SU8020 scanning electron microscope with cold field emission and a resolving power of 1.3 nm (Hitachi High-Technologies Corp., Tokyo, Japan) coupled with an energy dispersive NSS 312 X-ray analyzer (Thermo Fisher Scientific, Madison, WI). Granules of the prepared fertilizer materials were mechanically polished to achieve a flat cross section and then placed on double-sided adhesive tape kept on an aluminum stub. Granules were sprayed with a thin conductive film of chromium in a Q150T ES turbo-pumped sputter coater (Quorum Technologies, Laughton, UK). Coated fertilizers were observed at an accelerating voltage of 138 eV. Cross sections through the granules of the prepared fertilizer materials were recorded at a magnification of 20×. The thickness of the polymer layers was measured at a magnification of 100×. EDX mapping was also performed.

XRD experiments were performed on an X'Pert PRO powder diffractometer (PANalytical, Almelo, The Netherlands) with a proportional detector, computer-aided data acquisition, and a copper lamp as an X-ray radiation source. The XRD patterns were recorded over the 2θ range from 10 to 60°.

The mechanical strength of the prepared material granules was measured using a commercial table-top Zwick/Roell Z2.5 strength-testing machine (Zwick GmbH, Ulm, Germany) with the TestExpert II ver. 2.2 software. The granules were individually compressed in the radial direction between two rigid plates with a maximum testing force F_{max} of 2.5 kN at a constant crosshead test speed of 10 mm/s. The load at which the granule fractured was recorded as the crushing

DOI: 10.1021/acs.jafc.5b00518
J. Agric. Food Chem. 2015, 63, 2597−2605

strength. For each sample, a total of 25 parallel measurements were carried out. Crushing strength was normalized to the granule diameter and compared with the mechanical properties of a commercial fertilizer.

Nutrient release from the prepared fertilizer materials was measured over time in water. A sample of the prepared material (preferably five granules, weighed with the accuracy of 0.0001 g) was placed in a plastic cap beaker with 50 ± 0.5 mL of distilled water. The sample was incubated at a constant temperature of 25 ± 0.5 °C. After 1 h of incubation, the solution was decanted and the beaker was again filled with 50 ± 0.5 mL of distilled water. This procedure was repeated after 3, 6, and 24 h and after 3, 5, 7, 14, 21, and 28 days. Spectrophotometric and potentiometric methods were used to determine the amounts of released phosphates and ammonium, respectively.

The overall release of water-soluble mineral components of the fertilizer was also monitored and analyzed with the use of a CPC 505 pH/conductivity meter with temperature compensation (Elmetron, Zabrze, Poland). Polymer-coated granules with a given polymer to fertilizer ratio (P/F) were placed into distilled water at ambient temperature, and the conductivity was measured automatically every hour for 6 days (144 h). At the end of the experiment, the granules were mechanically crushed to determine the final conductivity value.

Data analysis software system STATISTICA version 10.0 was used to evaluate descriptive statistics, that is, standard deviation and standard error. To describe experimental data related to nutrient release experiments with model lines, OriginPro 8 software was used.

RESULTS AND DISCUSSION

Morphology and Structure. Granules of the NPK fertilizer are initially of regular, spherical shape and uniform light gray to dark gray color. No permanent caking of the fertilizer granules is observed: they are hard, although when subjected to adequate crushing force, they can be easily crumbled into small pieces that can then be milled into a powder. XRD measurements (Figure 1) demonstrate that the

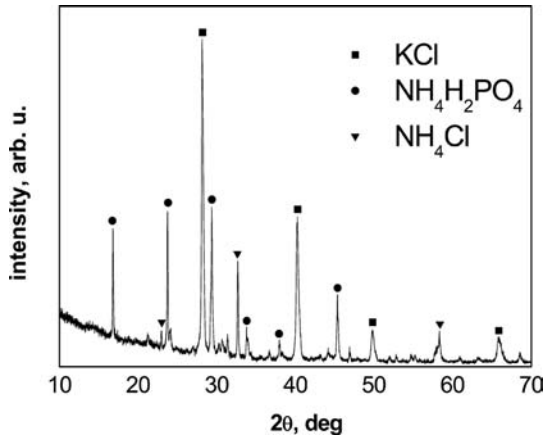

Figure 1. XRD image of the commercial, multicomponent fertilizer NPK(S) 6−20−30−(7).

NPK fertilizer includes nitrogen, phosphorus, and potassium mainly in the form of dihydrogen ammonium phosphate, ammonium chloride, and potassium chloride. Nonetheless, as the multicomponent NPK fertilizer is an example of a complex fertilizer, some small amounts of additional compounds resulting from reactions between initial substrates may also be observed and identified.

Fertilizer granules were coated with PBS/DLA copolyester by the immersion method to create over 40 samples of materials with different polymer to fertilizer mass ratios and with various layer thicknesses. The mass ratio of polymer to fertilizer P/F was determined on the basis of the mass balance of the process. Fertilizer materials have been obtained with mass ratios P/F ranging from 0.18 to 0.26. The fertilizer granules are completely covered with the polymer. The prepared materials consist of a fertilizer core surrounded by an inert polymer layer. The surface of the prepared materials is uniform, dense, and compact. There are no visible cracks or fractures on the material surfaces. The degree of coverage of granules with the polymer, that is, the polymer to fertilizer mass ratio, increased with the number of immersion cycles and the contact time.

Cross-sectional SEM images of the NPK fertilizer granules covered with PBS/DLA at two different polymer to fertilizer mass ratio extremes of 0.18 and 0.26 are presented in Figure 2.

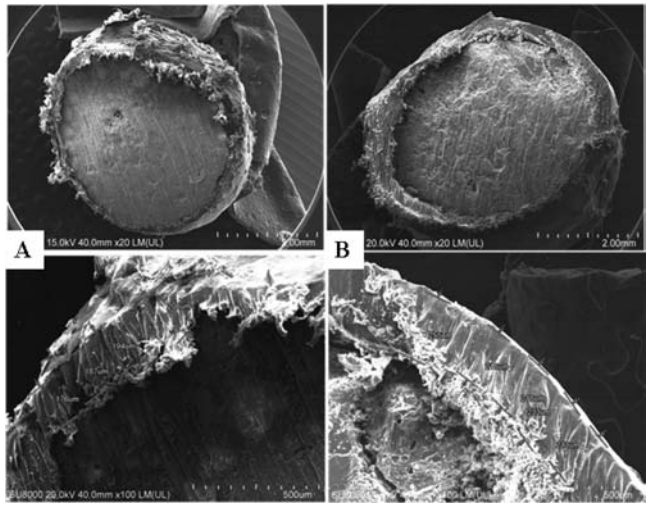

Figure 2. SEM images of the fertilizer granules coated with PBS/DLA with extreme polymer to fertilizer mass ratios: (A) P/F = 0.18; (B) P/F = 0.26.

As the thickness of the layer varies around the granule, 20 measurements were made to ensure accurate evaluation, with 5 measurements for every quarter of the granule cross section. On the basis of the performed measurements, the mean value of the polymer coating thickness was determined to be 190.4 μm (with a standard deviation of 9.21 and a standard error of 2.06) in the case of the material with P/F = 0.18 (Figure 2A) and 231.2 μm (with a standard deviation of 8.81 and a standard error of 1.97) in the case of the material with the mass ratio P/F = 0.26 (Figure 2B).

The distribution of elements in the prepared materials was characterized using a scanning electron microscope coupled with the energy dispersive X-ray analyzer. The EDX mapping of the cross section of the material with P/F = 0.18 is presented in Figure 3. The EDX analysis demonstrates that only carbon and oxygen are present in the polymer coating layer. This observation is consistent with the chemical composition of the polymer used in the experiment. The structure of the formed layer is rather homogeneous, with carbon and oxygen atoms spread quite uniformly throughout the layer. The EDX analysis demonstrates that the components of the polymer coating do not penetrate into the granule core, which appears to be quite heterogeneous. The EDX mapping exhibits areas with higher concentrations of potassium (red dots) and chlorine (bright pink dots). The increased incidence of these

DOI: 10.1021/acs.jafc.5b00518
J. Agric. Food Chem. 2015, 63, 2597−2605

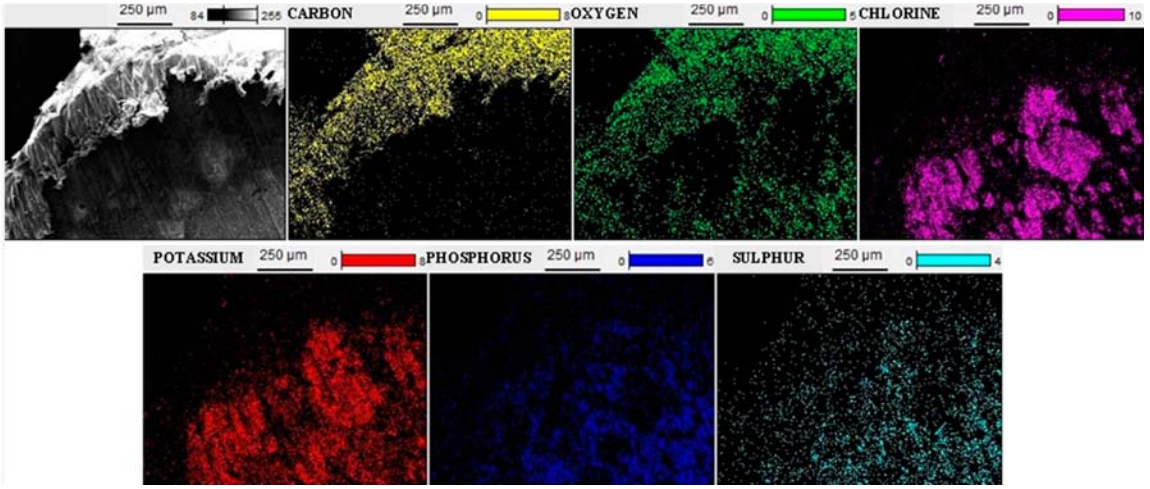

Figure 3. EDX mapping of the elements for the material with polymer to fertilizer mass ratio P/F = 0.18. Elements correspond to the color code indicated at the top of each panel.

elements results from the presence of larger particles of potassium chloride in those places. It is expected that the concentrations of oxygen (green dots) and phosphorus (dark blue dots), as the components of ammonium phosphate salts, are significantly lower in these areas. The EDX mapping also indicates that small amounts of sulfur (light blue dots) are spread evenly throughout the granule. Setting aside the location and arrangement of the elements in the granule core, the EDX analysis demonstrates that fertilizer components from the granule core do not pass into the polymer layer. To confirm that observation, a granule covered with a polymer layer was cut in half and the mineral components of the fertilizer were rinsed off with water. A meticulous and thorough inspection of the polymer layer revealed no differences in appearance between the inside and outside surfaces of the layer.

To investigate whether any interactions occur between the fertilizer components and the polymer material used to cover the granules, XRD analysis was also performed. The XRD spectra of the prepared materials (not presented here) were compared with the spectrum of the initial NPK fertilizer. These spectra are highly similar, with no differences observed in the position and intensity of the peaks between the spectra of the prepared materials and the initial NPK fertilizer. All recorded peaks can be assigned only to the fertilizer components. On the basis of the fact that no new peaks are present in the spectra of the prepared materials, no new phases are formed during the coating process. Therefore, the interactions between the fertilizer components of the granule and the polymer layer components are physical but not chemical in nature.

Mechanical Properties. Crushing strength was measured for samples of prepared materials with the lowest and highest polymer to fertilizer mass ratios of 0.18 and 0.26, respectively, and for the initial NPK fertilizer. For each sample, 25 parallel measurements were performed, and the mean value of the crushing strength was then calculated. The dependence of the crushing strength on deformation for the polymer-coated materials and for the initial NPK fertilizer are presented in Figure 4.

Fertilizers can be considered typical materials with a brittle failure mode. Fertilizer granules are porous, containing various mineral compounds with many flaws, dislocations, and crystal edges.[29,30] Any discontinuity in the fertilizer granule bulk should be treated as a defect and the reason for the stress

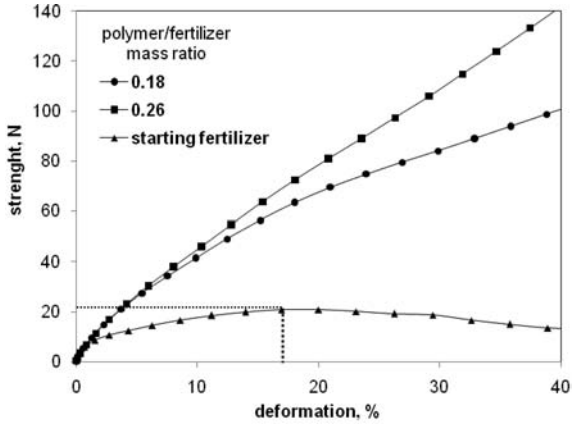

Figure 4. Crushing strength as a function of deformation for materials with different polymer to fertilizer mass ratios and for the uncoated, starting NPK fertilizer.

concentration. The mechanical damage to the fertilizer granule results from brittle failure due to an abrupt disastrous increase of a decisive defect under tensile stress induced in the material bulk. In the case of the initial NPK fertilizer, fracture or, rather, cracking of the granule occurred at the crushing strength of 21 N, with the mean deformation of 17% (Figure 4). The obtained crushing strength (21 N) corresponds to a pressure of 2.1 kg/granule and is comparable with the literature data for various granulated fertilizer compounds: urea, 1.5−3.5 kg/granule; triple superphosphate (TSP), 1.5−3 kg/granule; monoammonium phosphate (MAP), 2−3 kg/granule; or ammonium sulfate, 1.5−2.5 kg/granule.[31] Compared with the starting NPK fertilizer, polymer-coated granules exhibited significantly higher resistance toward the crushing force (Figure 4). For both prepared and examined materials, the crushing force continuously increased with deformation up to 50%, and no fracture or cracking of the samples was observed. The crushing force reached the value of almost 170 N in the case of the material with the polymer to fertilizer mass ratio of 0.26, and 120 N for the material with the polymer to fertilizer mass ratio of 0.18. On the basis of the experiments and dependencies presented here, it is not possible to determine the maximum crushing strength for the prepared polymer-coated materials because of their ductile properties. Instead of a brittle failure,

DOI: 10.1021/acs.jafc.5b00518
J. Agric. Food Chem. 2015, 63, 2597−2605

only a plastic deformation of these samples can be observed, evidently within the deformation region from 0 to 50%.

Nutrient Release. All prepared polymer-coated materials were tested in water-release experiments. This kind of approach (nutrient release in water) is fully acceptable: several papers using that approach have been published recently.[16,18,32−35] Nutrient release in water and nutrient release in soil are quite different aspects of the topic. Undoubtedly, field experiments are necessary in the further and final assessment of the product, but these experiments will be addressed in another paper. Besides, as it was clearly indicated in the relevant references,[16,36] nutrient release in soil can be easily predicted from release experiments performed in water, although the nutrient release rate depends on the medium used, with the fastest release rate observed in water, followed by water-saturated sand and, finally, sand.[36]

Figure 5 presents the results of the investigation of phosphate release from the prepared polymer-coated materials

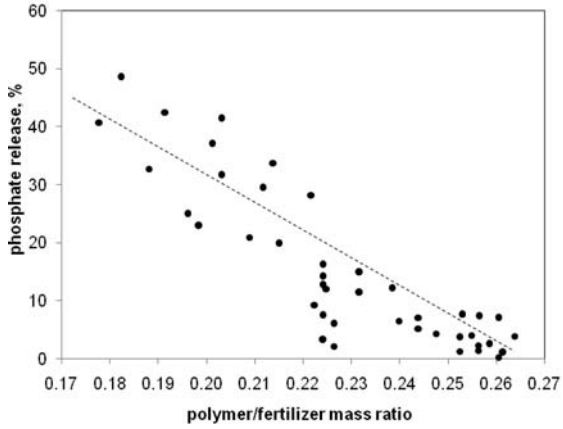

Figure 5. Release of phosphates versus the polymer to fertilizer mass ratio P/F after 24 h.

over 24 h. The data presented here show that for the group of materials with polymer to fertilizer mass ratios in the range from approximately 0.23 to 0.26, <15% of phosphates is released within 24 h. Additionally, long-term release experiments have demonstrated that the release of phosphate from this group of materials is <75% within 28 days. On the other hand, for the group of materials with polymer to fertilizer mass ratios of <0.23, >15% of phosphates are released within 24 h. Solely on the basis of these phosphate release results, the materials prepared here with polymer to fertilizer mass ratios ranging from approximately 0.23 to 0.26 meet the first and second criteria of controlled-release fertilizers, whereas those with mass ratios of <0.23 do not.

A series of papers[36−39] reported that the release rate of phosphates is lower than those of K, N-NH_4^+, and N-NO_3^-. There is no consensus as to the margin of that discrepancy. In some experiments, the release rate of phosphates was 45−70% slower than that of nitrates,[36] but only a 10% difference was observed in another study.[38] The presence of strong interactions among nutrients in the fertilizer granule and differences in nutrient solubility could lead to this observed difference in release rate.[36] Generally, the phosphate release rate can be treated as a "bottleneck" for overall nutrient release. The kinetics of chemical processes are known to be controlled by their slowest steps. The release of phosphates from controlled-release fertilizers is the slowest step; therefore, their release rate determines the overall nutrient release from that type of material. To define controlled-release fertilizers, however, rather than knowing which fertilizer component is released most slowly, it is important to know which is released most quickly or to determine the overall nutrient release rate.

Additional experiments have been conducted to more accurately assess the release properties of the materials prepared here. The release of ammonium and phosphate ions for the sample of prepared material with the highest mass ratio of polymer to fertilizer (P/F = 0.26) is compared in Figure 6A.

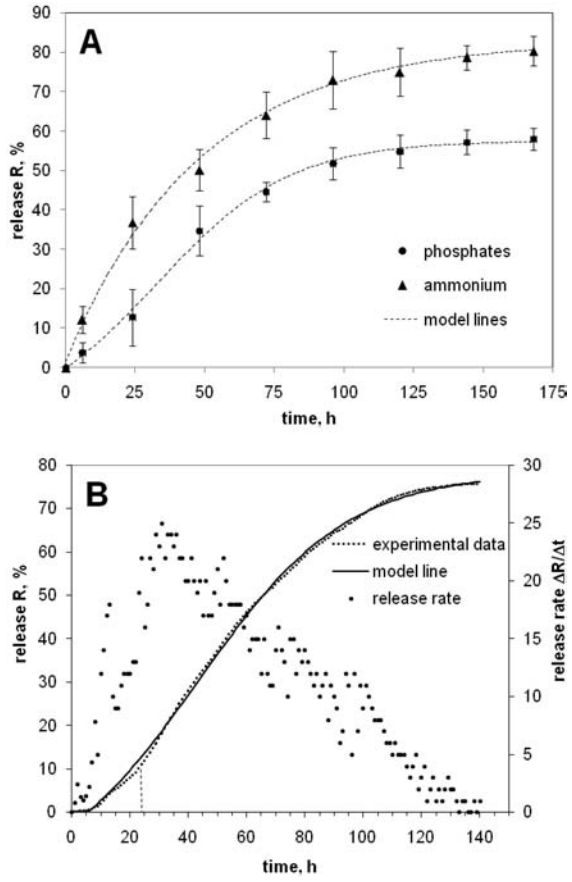

Figure 6. Comparison between the release of ammonium and phosphate ions (A) and the nutrient release measured by conductivity (B) for the sample of prepared material with the highest polymer to fertilizer mass ratio (P/F = 0.26).

Throughout the whole experiment, the release of phosphates is slower than the release of ammonium ions. However, the most significant difference in release is observed during the first 24 h. After that time, the cumulative release for phosphate and ammonium ions is 13 and 37%, respectively, whereas after 7 days it is 58 and 80%. The average difference between the release of phosphate and ammonium ions is 19%.

Figure 6B presents the results of nutrient release measured by conductivity for the sample of prepared material with the highest mass ratio of polymer to fertilizer (P/F = 0.26). The release of the mineral components of the fertilizer, R (%), was calculated according to the following equation, where σ_t represents the measured conductivity at time t and σ_F represents the final conductivity value:

DOI: 10.1021/acs.jafc.5b00518
J. Agric. Food Chem. 2015, 63, 2597−2605

$$R = \frac{\sigma_t \times 100}{\sigma_F} \quad (1)$$

Several studies have shown[36,40,41] that nutrient release from polymer-coated CRF can be described in three stages: lag period, linear stage, and decay period. In the experiment presented here (Figure 6B), the lag period is quite long. Placing the tangent line onto the experimental curve at the inflection point (31st hour) enables a rough estimate of the lag time, which is between 5 and 14 h. The linear stage of the release profile cannot be identified because the release rate constantly increases until the maximum release rate is reached at the 31st hour of the process. From that point, the release rate slowly decays, almost reaching zero after 140 h. Two further observations are worth mentioning. First, between hours 8 and 14, the release rate substantially increases, which might be related to the earlier differences in the release rates of fertilizer components. Second, after 24 h, the release of all water-soluble fertilizer components is approximately 11%, significantly below the limit of the first requirement of slow/controlled-release fertilizers.

On the basis of the experimental results presented here, the following conceptual model of nutrient release from the prepared fertilizer material can be proposed. At the very beginning of the process, after immersion of the polymer-coated fertilizer in water, water starts to diffuse through the polymer layer to penetrate the inner part of the granule. The fertilizer material is mainly composed of readily water-soluble compounds with similar water solubilities (KCl, 342 g/dm^3; NH_4Cl, 370 g/dm^3; $NH_4H_2PO_4$, 370 g/dm^3). The fertilizer components begin to dissolve in water. On the basis of the initial fertilizer composition and XRD measurement results (Figure 1), it is obvious that the same amounts of ammonium and phosphate ions result from the dissolution of dihydrogen ammonium phosphate. However, an additional amount of ammonium ions is present within the granule due to ammonium chloride dissolution. Therefore, it seems reasonable to conclude that the concentration of ammonium ions in the water-penetrated fertilizer granule is greater than the concentration of phosphate ions. Moreover, the concentration of phosphate ions is lower because slight amounts of phosphorus (approximately 8%) are bound up in the form of water-insoluble compounds. Differences in these ion concentrations may be one of the factors affecting nutrient release from polymer-coated fertilizer. Water-dissolved components of the fertilizer diffuse through the polymer layer outside the granule. As the driving force for diffusion depends on the component concentration gradient, the release of ammonium ions surpasses the release of phosphate ions. In discussing the release of ions (nutrients) from polymer-coated fertilizer, two other parameters should be considered, diffusion coefficients in water and ionic radii of nonhydrated and hydrated ions (Supporting Information, Table SI-A).[42−46] As the ionic potential $|Z_i|/r_i$ increases, where $|Z_i|$ is the absolute value of the charge of ion i and r_i is the crystal ionic radius of ion i, the ionic diffusion in water decreases. The reason for that dependence is that the hydration layer of the water molecules around the ion becomes thicker, thus hindering movement of the ion. The diffusion of phosphate ions in water is around 3 times less than the diffusion of ammonium ions in water, thus contributing to the slower release of phosphate ions from the polymer-coated granule.

Summarizing the previous considerations, both the observed discrepancy between the release of phosphate and ammonium ions (Figure 6A) and the substantial increase in the release rate between hours 8 and 14 of the process (Figure 6B) can be explained by the influence of nutrient concentration and diffusion properties of those nutrients in water. However, on the basis of the available experimental data, it is not possible to assess the mutual interaction of these factors in this phenomenon.

The release of phosphates and nutrients in general from the prepared polymer-coated materials depends on the polymer to fertilizer mass ratio (Figure 5). The phosphate release decreases as the mass ratio of polymer to fertilizer increases and as the layer thickness increases. The diffusion mechanism of the release can be noted as a reason for that correlation.[36] As the layer thickness increases, the value of the diffusion coefficient, D, decreases and the release process becomes increasingly hindered. The value of diffusion coefficient D through the polymer layer can be calculated according to the equation

$$D = \frac{h^2}{6 \times t_{lag}} \quad (2)$$

Taking the value of the polymer layer thickness (h = 231 μm) (Figure 2) and the value of the lag period (t_{lag} = 5−14 h) (Figure 6B) for the material with the highest polymer to fertilizer mass ratio (P/F = 0.26), the estimated value of diffusion coefficient D may be in the range of (0.176−0.494) × 10^{-8} cm^2/s. The diffusion coefficient through the polymer layer, D, is around 4 orders of magnitude smaller than the diffusion coefficient in water, D^0, presented earlier. The obtained D value refers to the diffusion of all water-soluble components of the fertilizer. We cannot provide detailed values for particular ions based on this experimental data, but this will be addressed in future research.

Note that all release experiments presented here were conducted in water. As mentioned earlier, nutrient release from polymer-coated controlled-release fertilizers is mainly controlled by diffusion. When materials with biodegradable polymer coatings are investigated in those conditions (water release experiments), the diffusion through the polymer layer has a critical impact on the release pattern. If the release experiments from materials coated with these biodegradable polymers were performed in soil, then some other factors and parameters would be important, especially microorganism-induced biodegradation of the polymer layer. Whereas microorganism-related biodegradation of the polymer layer and its influence on nutrient release are not addressed in the current work, that issue should be the topic of future research.

Figure 7 presents the results of 28 day release experiments for the polymer-coated materials with polymer to fertilizer mass ratios of 0.18, 0.20, 0.24, and 0.26 and the NPK fertilizer. During these experiments, the amounts of released phosphates were determined as a function of time at a constant temperature of 25 °C. The release of phosphates from the NPK fertilizer was very fast, with all phosphates released within 55−60 min. On the basis of the results presented here, all coated materials exhibit slower release of phosphates in comparison with the starting fertilizer.

Nutrient uptake by plants exhibits a sigmoidal relationship with the point in the plant's vegetation cycle.[3,4,46,47] Therefore, all experimental data presented related to nutrient release from the prepared polymer-coated materials were described and

DOI: 10.1021/acs.jafc.5b00518
J. Agric. Food Chem. 2015, 63, 2597−2605

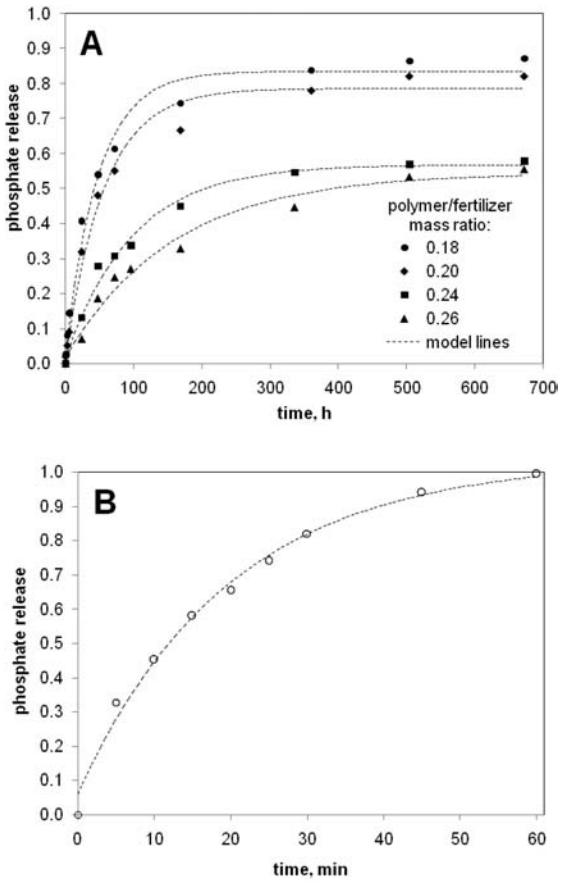

Figure 7. Release of phosphates within 28 days from (A) polymer-coated materials with polymer to fertilizer mass ratios of 0.18, 0.20, 0.24, and 0.26 amd (B) uncoated NPK fertilizer.

interpreted with a kinetic model. To interpret the kinetic data, a sigmoidal model equation was applied:

$$R = \frac{M_t}{M_\infty} = \frac{a - b}{1 + \exp\left(\frac{t - d}{c}\right)} + b \quad (3)$$

M_t/M_∞ is the fraction of nutrients released at time t and a, b, c, and d are the parameters of the sigmoidal equation.

The experimental data of nutrient release from the prepared polymer-coated materials and the predicted values calculated using the sigmoidal equation are compared in Figures 6 and 7. The sigmoidal model satisfactorily fits the experimental data, with the best result obtained for the experiment performed using the conductivity method (Figure 6B). On the basis of the applied sigmoidal model, the constants and correlation coefficients of the equations were determined and are given in Supporting Information Table SI-B.

The sigmoidal equation produces model lines that fit the experimental data very well as expressed by correlation coefficients. Keeping in mind the fact that the nutrient uptake by plants follows a sigmoidal curve and that the sigmoidal model has already been applied to describe controlled release,[48−50] the sigmoidal equation used in the present work satisfactorily predicts the release of phosphates from the prepared polymer-coated materials.

In conclusion, the new, innovative, biodegradable copolymer of poly(butylene succinate) and the butylene ester of saturated dilinoleic acid was successfully applied in the preparation of fertilizer materials with controlled and prolonged nutrient release. Multicomponent fertilizer granules can be coated with a polymer layer using the immersion method, which creates an incentive to use the process on a larger scale, for example, by spraying in a drum granulator or in the Wurster bed.

The obtained polymer-coated materials differ from each other in the layer thickness and the polymer to fertilizer mass ratio. The mass ratio of polymer to fertilizer ranged from 0.18 to 0.26, and the layer thickness ranged from 190 to 230 μm. The interactions between the fertilizer components of the granule and the polymer layer components were found to be physical rather than chemical in nature. The mechanical properties of the fertilizer granules coated with the copolyester layer are significantly better than those of the NPK fertilizer.

Release experiments have shown that polymer-coated materials with polymer to fertilizer mass ratios of 0.23−0.26 meet the requirements of controlled-release fertilizers. The overall nutrient release was <15% within 24 h and approximately 75% after 28 days, although the ammonium ion release during the first 24 h of the experiment was significantly higher than the release of phosphate ions. The concentrations of the mineral components inside the water-penetrated fertilizer granules and the diffusion properties of the nutrients in water have been indicated as the reasons for that discrepancy. Nutrient release from the polymer-coated materials decreased with the increasing layer thickness. The diffusion mechanism of release has been noted as a reason for that correlation. The diffusion coefficient through the polymer layer was estimated as $D = (0.176−0.494) \times 10^{-8}$ cm^2/s. The experimental kinetic data of nutrient release from the prepared polymer-coated materials have been accurately described using a sigmoidal model equation.

■ ASSOCIATED CONTENT

Supporting Information

Tables SI-A and SI-B. This material is available free of charge via the Internet at http://pubs.acs.org.

■ AUTHOR INFORMATION

Corresponding Author

*(K.L.) Phone: +48 91 449 4730. Fax: +48 91 449 4686. E-mail: klubkowski@zut.edu.pl.

Notes

The authors declare no competing financial interest.

■ REFERENCES

(1) Heffer, P.; Prud'homme, M. Fertilizer outlook 2014−2018, 82nd IFA Annual Conference, Sydney, 2014, pp 1−7; http://www.fertilizer.org/imis20/images/Library_Downloads/2014_ifa_sydney_summary.pdf?WebsiteKey=411e9724-4bda-422f-abfc-8152ed74f306&=404%3bhttp%3a%2f%2fwww.fertilizer.org%3a80%2fen%2fimages%2fLibrary_Downloads%2f2014_ifa_sydney_summary.pdf (accessed Jan 15, 2015).

(2) Hauck, R. D. Slow release and bio-inhibitor-amended nitrogen fertilizers. In *Fertilizer Technology and Use*; Engelstad, O. P., Ed.; SSSA: Madison, WI, USA, 1985; pp 293−322.

(3) Shaviv, A.; Mikkelsen, R. I. Controlled-release fertilizers to increase efficiency of nutrient use and minimize environmental degradation − a review. *Fert. Res.* **1993**, *35*, 1−12.

(4) Trenkel, M. E. *Slow- and Controlled-Release and Stabilized Fertilizers: An Option for Enhancing Nutrient Use Efficiency in Agriculture*; International Fertilizer Industry Association: Paris, France, 2010.

DOI: 10.1021/acs.jafc.5b00518
J. Agric. Food Chem. 2015, 63, 2597−2605

(5) Finck, A. Fertilizers and their efficient use. In *World Fertilizer Use Manual*; Halliday, D. J., Trenkel, M. E., Wichmann, W., Eds.; International Fertilizer Industry Association: Paris, France, 1992.
(6) Forman, D. Are the nitrates a significant risk factor in human cancer? *Cancer Surv.* **1989**, *8*, 443−458.
(7) Newbould, P. The use of nitrogen fertilizer in agriculture. Where do we go practically and ecologically? *Plant Soil* **1989**, *115*, 297−311.
(8) Cruse, M. J.; Liebman, M.; Raman, D. R.; Wiedenhoeft, M. H. Fossil energy use in conventional and low-external input cropping systems. *Agron. J.* **2010**, *102*, 934−941.
(9) Roberts, T. L. Improving nutrient use efficiency. *Turk. J. Agric. For.* **2008**, *32*, 177−182.
(10) Chien, S. H.; Prochnow, L. I.; Cantarella, H. Recent developments of fertilizer production and use to improve nutrient efficiency and minimize environmental impacts. *Adv. Agron.* **2009**, *102*, 267−322.
(11) Association of American Plant Food Control Officials (AAPFCO). *Official Publication 50, T-29*; Association of American Plant Food Control Officials: West Lafayette, IN, 1997.
(12) European Standard EN 13266. Slow-release fertilizers − determination of the release of the nutrients − method for coated fertilizers; European Committee for Standardization, Brussels, Belgium, 2001.
(13) Akelah, A. Novel utilizations of conventional agrochemicals by controlled release formulations. *Mater. Sci. Eng. C* **1996**, *4*, 83−98.
(14) Niu, Y.; Li, H. Controlled release of urea encapsulated by starch-*g*-poly(vinyl acetate). *Ind. Eng. Chem. Res.* **2012**, *51*, 12173−12177.
(15) El Diwani, G.; Motawie, N.; Shaarawy, H. H.; Shalaby, M. S. Nitrogen slow release biodegradable polymer based on oxidized starch prepared via electrogenerated mixed oxidants. *J. Appl. Sci. Res.* **2013**, *9*, 1931−1939.
(16) Perez-Garcia, S.; Fernandez-Perez, M.; Villafranca-Sanchez, M.; Gonzales-Pradas, E.; Flores-Cespedes, F. Controlled release of ammonium nitrate from ethylcellulose coated formulations. *Ind. Eng. Chem. Res.* **2007**, *46*, 3304−3311.
(17) Fernandez-Perez, M.; Garrido-Herrera, F. J.; Gonzalez-Pradas, E.; Villafranca-Sanchez, M.; Flores-Cespedes, F. Lignin and ethylcellulose as polymers in controlled release formulations of urea. *J. Appl. Polym. Sci.* **2008**, *108*, 3796−3803.
(18) Costa, M. M. E.; Cabral-Albuquerque, E. C. M.; Alves, T. L. M.; Pinto, J. C.; Fialho, R. L. Use of polyhydroxybutyrate and ethyl cellulose for coating of urea granules. *J. Agric. Food Chem.* **2013**, *61*, 9984−9991.
(19) Melaj, M. A.; Daraio, M. E. Preparation and characterization of potassium nitrate controlled-release fertilizers based on chitosan and xanthan layered tablets. *J. Appl. Polym. Sci.* **2013**, *130*, 2422−2428.
(20) Corradini, E.; de Moura, M. R.; Mattoso, L. H. C. A preliminary study of the incorporation of NPK fertilizer into chitosan nanoparticles. *eXPRESS Polym. Lett.* **2010**, *4*, 509−515.
(21) Wu, C.-S. Polylactide-based renewable composites from natural products residues by encapsulated film bag: characterization and biodegradability. *Carbohydr. Polym.* **2012**, *90*, 583−591.
(22) Wu, C.-S. Controlled release evaluation of bacterial fertilizer using polymer composites as matrix. *J. Controlled Release* **2008**, *132*, 42−48.
(23) Wu, C.-S. Promoting fertilizer use via controlled release of a bacteria-encapsulated film bag. *J. Agric. Food Chem.* **2010**, *58*, 6300−6305.
(24) Lutz, W. A. Production of ammonium phosphate. Patent US3310371, 1967.
(25) Kozłowska, A.; Gromadzki, M.; El Fray, M.; Štěpánek, P. Morphology evaluation of biodegradable copolyesters based od dimerized fatty acid studied by DSC, SAXS and WAXS. *Fibres Text. East. Eur.* **2008**, *16*, 85−88.
(26) Diamond, M. J.; Freedman, B.; Garibaldi, J. A. Biodegradable polyester films. *Int. Biodeterior. Biodegrad.* **2001**, *48*, 219−224.
(27) Reddy, M. M.; Mohanty, A. K.; Misra, M. Optimization of tensile properties thermoplastic blends from soy and biodegradable polyesters: Taguchi design of experiments approach. *J. Mater. Sci.* **2012**, *47*, 2591−2599.
(28) Changsha Green Mountain Chemical Co. Organic Products, Polybutylene succinate; http://greenmountchem.en.alibaba.com/product/526875229-213189775/Polybutylene_succinate.html (accessed Jan 15, 2015).
(29) Kelbaliyev, G. I.; Samedli, V. M.; Samedov, M. M.; Kasimova, R. K. Experimental study and calculation of the effect of intensifying additives on the strength of superphosphate granules. *Russ. J. Appl. Chem.* **2013**, *86*, 1478−1482.
(30) Nie, X.; Besant, R. W.; Evitts, R. W. An experimental study of moisture uptake and transport in a bed of urea particles. *Granul. Matter* **2008**, *10*, 301−308.
(31) Clayton, W. E. Physical properties of fertilizers. In *Modern Techniques in Fertilizer Distribution and Handling*; International Fertilizer Development Center: Muscle Shoals, AL, USA, 1995.
(32) Bortolin, A.; Aouada, F. A.; de Moura, M. R.; Ribeiro, C.; Longo, E.; Mattoso, L. H. C. Application od polysacharide hydrogels in adsorption and controlled-extended release of fertilizers processes. *J. Appl. Polym. Sci.* **2012**, *123*, 2291−2298.
(33) Calabria, L.; Vieceli, N.; Bianchi, O.; de Oliveira, R. V. B.; Filho, I. N.; Schmidt, V. Soy protein isolate/poly(lactic acid) injection-molded biodegradable blends for slow release of fertilizers. *Ind. Crops Prod.* **2012**, *36*, 41−46.
(34) Pereira, E. I.; Minussi, F. B.; da Cruz, C. C. T.; Bernardi, A. C. C.; Ribeiro, C. Urea-montmorillonite-extruded nanocomposites: a novel slow-release material. *J. Agric. Food Chem.* **2012**, *60*, 5267−5272.
(35) Bortolin, A.; Aouada, F. A.; Mattoso, L. H. C.; Ribeiro, C. Nanocomposite PAAm/methyl cellulose/montmorillonite hydrogel: evidence of synergetic effects for the slow release of fertilizers. *J. Agric. Food Chem.* **2013**, *61*, 7431−7439.
(36) Du, C.; Zhou, J.; Shaviv, A. Release characteristics of nutrients from polymer-coated compound controlled release fertilizers. *J. Polym. Environ.* **2006**, *14*, 223−230.
(37) Shoji, S.; Gandeza, A. T. *Controlled Release Fertilizers with Polyolefin Resin Coating*; Kanno Printing: Sendai, Japan, 1992.
(38) Huett, D. O.; Gogel, B. J. Longevities and nitrogen, phosphorus and potassium release patterns of polymer-coated controlled-release fertilizers at 30°C and 40°C. *Commun. Soil Sci. Plant Anal.* **2000**, *31*, 959−973.
(39) Shaviv, A. Advances in controlled release of fertilizers. *Adv. Agron.* **2000**, *71*, 1−49.
(40) Du, C.; Zhou, J.; Shaviv, A.; Wang, H. Mathematical model for potassium release from polymer-coated fertilizer. *Biosyst. Eng.* **2004**, *88*, 395−400.
(41) Du, C.; Tang, D.; Zhou, J.; Wang, H.; Shaviv, A. Prediction of nitrate release from polymer-coated fertilizers using an artificial neural network model. *Biosyst. Eng.* **2008**, *99*, 478−486.
(42) Li, J.-H.; Gregory, S. Diffusion of ions in sea water and in deep-sea sediments. *Geochim. Cosmochim. Acta* **1974**, *38*, 703−714.
(43) Gourary, B. S.; Adrian, F. J. Wave functions for electron-excess color centers in alkali halide crystals. *Solid State Phys.* **1960**, *10*, 127−247.
(44) Chua, K. S. Experimental multivalent ionic radii. *Nature* **1968**, *220*, 1317−1319.
(45) Conway, B. E. *Ionic Hydration in Chemistry and Biophysics (Studies in Physical & Theoretical Chemistry)*; Elsevier: New York, 1981.
(46) Shaviv, A. Controlled release fertilizers. *IFA International Workshop on Enhanced-Efficiency Fertilizers*, Frankfurt, Germany; International Fertilizer Industry Association: Paris, France, 2005.
(47) Shoji, S.; Takahashi, C. Innovative fertilization methods. In *Meister Controlled Release Fertilizer − Properties and Utilization*; Konno Printing: Sendai, Japan, 1999.
(48) Jarrell, W. M.; Boersma, L. Model for the release of urea by granules of sulphur-coated urea applied to soil. *Soil Sci. Soc. Am. J.* **1979**, *43*, 1044−1050.

DOI: 10.1021/acs.jafc.5b00518
J. Agric. Food Chem. 2015, 63, 2597−2605

(49) Shaviv, A.; Raban, S.; Zaidel, E. Modeling controlled nutrient release from polymer coated fertilizers: diffusion release from single granules. *Environ. Sci. Technol.* **2003**, *37*, 2251−2256.
(50) Shaviv, A.; Raban, S.; Zaidel, E. Modeling controlled nutrient release from a population of polymer coated fertilizers: statistically based model for diffusion release. *Environ. Sci. Technol.* **2003**, *37*, 2257−2261.

DOI: 10.1021/acs.jafc.5b00518
J. Agric. Food Chem. 2015, 63, 2597−2605

synthesized by a facile method with modifications. Synthesized CuNPs have been tested against mung bean plants and, as a comparison, a commercially available bulk counterpart, copper sulfate (CS) salt, is used under controlled laboratory condition. At 0.05 mg/L concentration, CS promotes plant growth and development as per earlier literature. It also elevates the function of photosynthetic machineries; the rate of carbon and nitrogen assimilation as Cu is known to be a cofactor in these metabolic processes.[10] CS treatment at or above 0.5 mg/L resulted in severe tissue injuries, causing reduction in growth, even death, of the plants.[11] Cu toxicity is a threat worldwide because of its tendency to produce harmful Cu chelates during interaction with soil colloids and nutrients, which are detrimental to the surrounding microflora.[12] In this study, we demonstrate a single-step designed encapsulation of CuNP within a biocompatible polymer to reduce its toxic response. Sustained release of nutrient interacts with biological sites, which controls the toxic response. Biochemical experiments have been carried out on isolated chloroplast (Chl) of mung bean plant treated with CuNPs, which demonstrates that CuNPs are more effective than CS to some extent. In a tandem process the effects of both nano and bulk counterpart of Cu in carbon and nitrogen assimilation have been checked. Interestingly, CuNP shows greater efficacy in contrast to CS. A series of biophysical techniques are used to confirm the bioavailability and uptake within the system. Oxidative stress markers, both antioxidative and non-antioxidative enzyme levels, show that CuNP does not inhibit any toxic response to the treated plant system. CuNP, both in physiological and biochemical aspects, worked significantly better than CS, which caused cellular toxicity because of dysfunctional metabolic pathways. The whole study is assisted by a probable mechanistic interpretation to outline its beneficial response. In light of these aforementioned analyses we envision CuNPs future prospect in crop management with reduced toxic response in contrast to its bulk counterpart. To the best of our knowledge this is the first effort to use biocompatible polymer-encapsulated CuNPs for augmentation of photosynthesis, elevated carbon and nitrogen assimilation, and improved morphological and physiological outputs within a plant system.

MATERIALS AND METHODS

CuNP Synthesis. Half a gram of copper sulfate was allowed to dissolve in 2 mL of water; to it was added 20 mL of PEG-200. The resultant mixture was sonicated in a sonication bath (100 Hz) for about 5 min to obtain a homogeneous dispersion. To the resultant dispersion was added dropwise an aqueous solution of sodium borohydride (0.1 M), and the reaction mixture was subjected to a microwave heating (450 W) until a characteristic reddish color was developed. Then the mixture was centrifuged and washed with ethanol three times to remove impurities and placed in a hot-air oven at 80 °C to obtain polymer-encapsulated CuNP.

Plant Material and Growth Conditions. Mung bean seeds (*Vigna radiata* var. Sonali) were purchased from Berhampur Pulse and Oil Research Centre. Seeds (20 seeds/replicate; 3 replicates in total) were washed in deionized double-distilled water and surface sterilized with 5% sodium hypochloride solution for about 20 min. Then the seeds were washed thoroughly with deionized double-distilled water and imbibed with the treatment solutions (control; CuNP 0.05, 0.1, 0.5, and 1 mg/L; CS 0.05, 0.1, 0.5, and 1 mg/L) in the dark for 4−6 h prior to the germination. Detailed growth conditions of plants are described in the Supporting Information (SI).

Morphological Parameters. Root and shoot lengths and fresh and dry weights of CuNP- and CS-treated plants were measured. Dry weight was recorded by drying the plants at 80 °C for 24 h.

Estimation of Photosynthetic Pigment Content. Control and treated leaves were centrifuged twice with 80% alkaline acetone at 6000*g* for 20 min, and chlorophyll content was estimated with the supernatant spectrophotometrically[13] in terms of micrograms of chlorophyll per gram of fresh tissue. Carotenoid was estimated according to the method of Davies with little modification,[14] and the data were expressed in terms of optical density (OD) per gram of fresh weight.

Isolation of Chloroplast. Mung bean leaves were homogenized in isolation buffer (330 mM mannitol, 30 mM HEPES, 2 mM EDTA, 3 mM MgCl, and 0.1% w/v BSA, pH 7.8).[15] The homogenate was filtered and centrifuged. Supernatant was further centrifuged at 1000*g* for 5 min at 4 °C.

Estimation of Fluorescence and Irradiance of Chloroplast by Photoluminescence (PL) Spectra. Chloroplast suspension contained 100 μM potassium phosphate buffer (pH 7.8), 2 μM NaCN, and 1.25 mM sucrose. The fluorescence spectra of the control and treated chloroplasts were recorded at 273 K under a 440 nm excitation wavelength. Photosynthesis versus irradiance (PI) of treated and untreated chloroplasts was calculated accordingly.[16]

Photoreduction Activities. The electron transport through the whole chain of photosynthesis was measured polarographically with an Oxygraph oxygen electrode (Hansatech Instruments, UK).[17] Oxygen evolution was assayed in a medium containing chloroplasts equivalent to 378 μg/mL of chlorophyll. Hill activity was measured according to the method of Vishniac.[18] Ferricyanide and nicotinamide adenine dinucleotide phosphate (NADP) reduction were determined by spectrophotometric methods.[19] Light-induced adenosine triphosphate (ATP) content of chloroplasts was measured by comparing the ATP level in the dark and after 1 min of illumination.[20]

Carbon Assimilation Assay. Chloroplast NADP-glyceraldehydes-3-phosphate dehydrogenase (GPDHase) activity was determined following the method of Taylor et al.[21] The enzyme was activated by a solution containing 0.2 M tricine (pH 8.4) and 20 mM ATP added to 0.1 mL of the solution containing the extracted enzymes. After 5 min, reaction medium (62.5 mM tricine (pH 8.4), 16 mM $MgCl_2$, 7.8 mM ATP, and 0.2 mM NADPH) was added to it. Fifty millimolar glycerate 3-P was then added to initiate the reaction and the oxidation of NADPH monitored at 340 nm. Fructose-1,6-bisphosphatase (FBPase) was activated by preincubation of enzyme extract with reaction medium (0.14 M tricine (pH 7.9), 14 mM $MgCl_2$, and 7 mM DTT). Sixty millimolar fructose-1,6-bisphosphate was added after 10 min and terminated after 15 min by the addition of 0.5 mL of 10% (w/v) TCA. This solution was cleared by centrifugation for 10 min at 12000*g* to determine the enzymatic activity. Ribulose-5-phosphate kinase (RBPase) activity was analyzed by 0.1 M tricine (pH 7.6) and 15 mM DTT for 1 h. After that, reaction medium (66 mM tricine (pH 7.6), 13 mM $MgC1_2$, 1.3 mM P-pyruvic acid, 1.3 mM ATP, 0.33 mM NADH, and 2 units each of phosphoriboisomerase, pyruvate kinase, and lactic dehydrogenase) was added. The reaction was initiated by 30 mM ribose-5-P and the oxidation of NADH monitored at 340 nm.

Nitrogen Metabolism. *Preparation of Leaf and Root Enzyme Extract.* Control and treated plants were homogenized at a ratio of 1:10 (w/v) in 50 mM phosphate buffer (pH 7.5) containing 2 mM EDTA, 1.5% (w/v) soluble casein, 2 mM DDT, and 1% (w/v) insoluble PVPP at cold temperature and centrifuged at 3000*g* for 5 min. Supernatant was again centrifuged at 30000*g* for 20 min. The extract was then used for enzymatic assays.

Determination of NO_3^-. Enzyme extract was added to a 10% salicyclic acid solution dissolved in 12 N sulfuric acid (w/v). NO_3^- content was measured as described by Cataldo et al.[22] The results were expressed as micromoles per gram of fresh weight.

Determination of Nitrate Reduction (NR) Activity. Enzyme extract was mixed in the reaction mixture containing 100 mM phosphate buffer (pH 7.5), 100 mM KNO_3, 10 mM cysteine, and 2 mM NADH. After 30 min of incubation at 30 °C, 1 M zinc acetate was added. The nitrite formed was determined at 540 nm, and NR activity was expressed as micromoles of NO_3^- formed per gram of fresh weight per hour.

Determination of Nitrite Reduction (NiR) Activity. To the reaction mixture (50 mM phosphate buffer (pH 7.5), 20 mM KNO_2, 5 mM methyl viologen (MV), 300 mM $NaHCO_3$) was added enzyme extract at

DOI: 10.1021/jf504614w
J. Agric. Food Chem. 2015, 63, 2606−2617

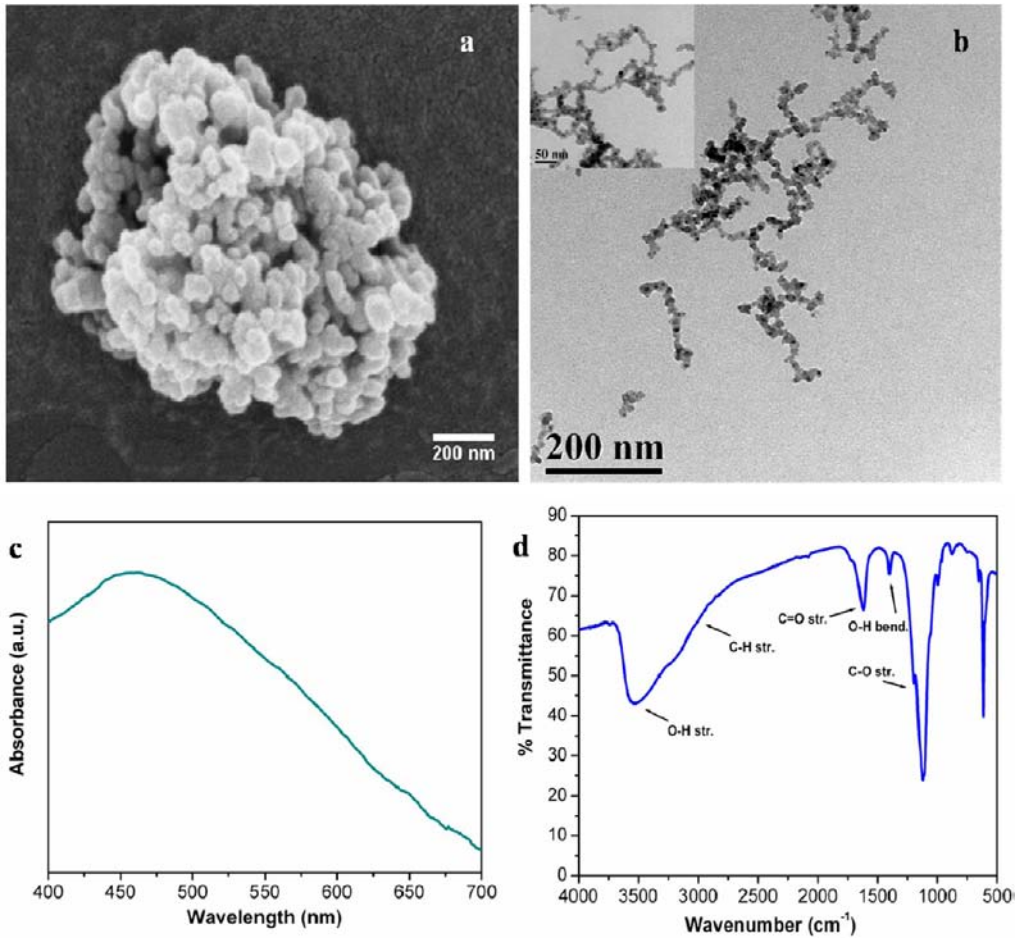

Figure 1. (a) FESEM image, (b) TEM image, (c) UV−vis spectra, and (d) FTIR spectra of CuNP.

30 °C. After 30 min, NiR activity was determined by the disappearance of NO_2^- from the reaction medium and expressed as micromoles of NO_2^- formed per gram of fresh weight per hour.

Determination of Glutamine Synthetase (GS) Activity. Enzyme extract was added in the reaction mixture containing 100 mM phosphate buffer (pH 7.5), 4 mM EDTA, 1 M sodium glutamate, 450 mM $MgSO_4 \cdot 7H_2O$, 300 mM hydroxylamine, and 100 mM ATP. The formation of glutamylhydroxamate was measured at 540 nm after complexing with acidified ferric chloride. GS activity was expressed as formed glutamylhydroxamate in grans of fresh weight per hour.

Determination of NADH-Glutamate Synthase (GOGAT) Activity. The reaction mixture contained 50 mM phosphate buffer (pH 7.5) with 0.1% (v/v) mercaptoethanol, 1 mM EDTA, 18.75 mM 2-oxoglutarate, 15 mM aminoxyacetate, 1.5 mM NADH, 75 mM L-glutamine, and enzyme extract. The decrease in absorbance was recorded for 5 min at 28 °C. The activity was expressed as micromoles of NAD per gram of fresh weight per hour.

Uptake of CuNP by Fluorescence Microscopy Study. CuNPs were amine functionalized and conjugated with fluorescein-B-isothiocyanate (FITC) for uptake study. Ultrathin cross sections of treated plant samples were fixed in 2% glutaraldehyde followed by washing in graded ethanol and observed under confocal microscope.[5]

Electron Micrographic Study. Transmission electron microscopy (TEM) and field emission scanning electron microscope (FESEM) of treated and untreated chloroplasts were performed for analyzing the interaction between chloroplast and CuNPs in photosynthesis. Chloroplasts were fixed with glutaraldehyde, stained with osmium tetraoxide, and washed in graded ethanol for observation under an electron microscope.

Cu Release Study by Inductively Coupled Plasma Optical Emission Spectroscopy (ICPOES). Cu release from CuNPs was monitored by using ICPOES at pH 7, that is, the pH of the plant growth medium. One hundred milliliters of CuNP dispersion of the aforementioned concentrations in Milli-Q water was allowed to stir for 24 h. The resultant dispersion was centrifuged and subjected to digestion in the presence of ultrapure nitric acid followed by estimation against a standard.[5]

Enzyme Assays Related to Oxidative Stress. Control and treated plants were ground in Tris-HCl buffer (pH 7.5) containing EDTA and polyvinylpyrrolidone followed by centrifugation at 0 °C. The supernatant was used for enzymatic assays. Superoxide dismutase (SOD) activity was estimated following a standard procedure.[23] Peroxidase (POD) activity was assayed according to the method of Chance et al.[24] The total peroxide content of plant tissue was estimated according to the method of Thurman et al.[25] Glutathione reductase (GR) was assayed according to the procedure of Wang.[26] Catalase (CAT) activity was assayed according to the method of Beers et al.[27] Activity of polyphenol oxidase (PPO) was assayed following standard methods.[28] Estimation of proline was done according to the method of Bates et al.[29] Phenol content was estimated according to the method of Malik et al.[30]

Estimation of Total Amino Acid (AA), Lipid, Protein, and Carbohydrate Contents. AA content in plant samples was estimated according to the ninhydrin method. Protein contents were estimated according to the method of Lowry et al. Lipid content was estimated according to the Bligh method. Total carbohydrate content was estimated following Loewus.

RESULTS AND DISCUSSION

Physicochemical Characterization of CuNP. Herein we demonstrated a designed synthesis of CuNPs encapsulated within a polymeric matrix followed by evaluation of its photosynthetic efficacy, carbon and nitrogen assimilation, and

DOI: 10.1021/jf504614w
J. Agric. Food Chem. 2015, 63, 2606−2617

Table 1. Effect of CuNP and CS on Morphology of 15-Day-Treated Mung Bean Plants (± SE, n = 25)[a]

treatment	control	0.05 mg/L	0.1 mg/L	0.5 mg/L	1 mg/L
root length (cm)					
CuNP	4.4 ± 0.23Aa	6.62 ± 0.189Ba	6.5 ± 0.048Ca	5.8 ± 0.097Da	5.63 ± 0.047Ea
CS	4.4 ± 0.23Ab	5.7 ± 0.08Bb	4.86 ± 0.159Cb	4 ± 0.11Db	3.14 ± 0.189Eb
shoot length (cm)					
CuNP	12.84 ± 0.034Aa	15.47 ± 0.166Ba	13.93 ± 0.137Ca	13.59 ± 0.08Da	12.87 ± 0.074Ea
CS	12.84 ± 0.034Ab	14.63 ± 0.241Bb	12.56 ± 0.095Cb	11.37 ± 0.09Db	8.728 ± 0.149Eb
fresh weight (g)					
CuNP	0.1 ± 0.001Aa	0.147 ± 0.003Ba	0.142 ± 0.002Ca	0.126 ± 0.004Da	0.132 ± 0.002Ea
CS	0.1 ± 0.001Ab	0.135 ± 0.002Bb	0.131 ± 0.002Cb	0.104 ± 0.006Db	0.09 ± 0.005Eb
dry weight (g)					
CuNP	0.013 ± 0.0008Aa	0.016 ± 0.0008Ba	0.014 ± 0.0004Ca	0.012 ± 0.0006Da	0.011 ± 0.0009 Ea
CS	0.013 ± 0.0008Ab	0.014 ± 0.0003Bb	0.012 ± 0.0002Cb	0.01 ± 0.0008Db	0.009 ± 0.0004Eb

[a]Capital letters change across the row owing to significance of respective pairwise treatments, whereas the lower case letters change down the column.

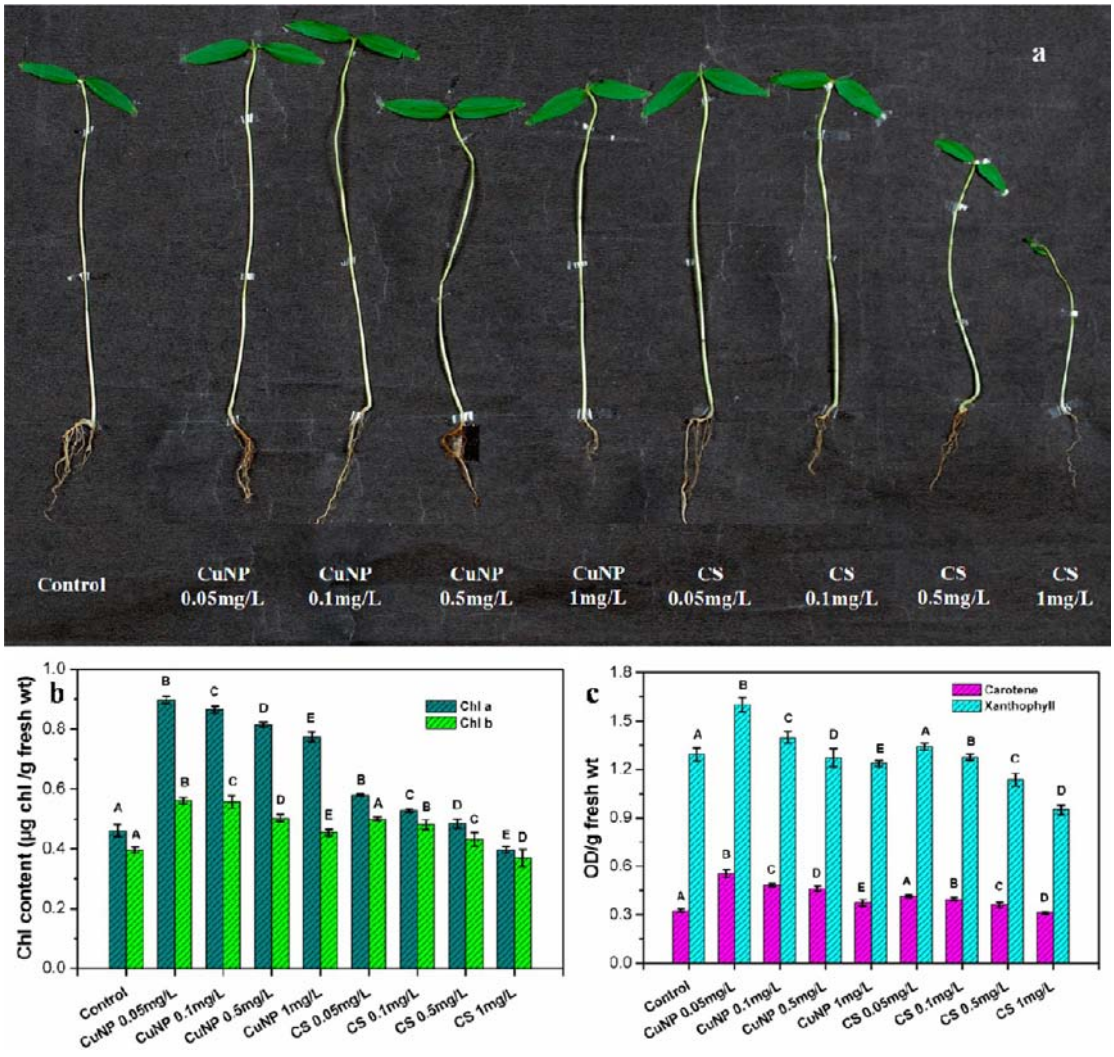

Figure 2. (a) Morphology of control and treated plants after 15 days of treatment. (b) CuNP and CS on chlorophyll content of 15-day-treated mung bean plants. Chlorophyll a, F = 76.5579, P < 0.000001; chlorophyll b, F = 464.8072, P < 0.0000001. (c) CuNP and CS on carotenoid content of 15-day-treated mung bean plants. Data represent the mean ± SE (n, no. of samples = 3). Carotene, F = 37.9368, P < 0.00001; xanthophyll, F = 75.1419, P < 0.00001. Within each type of treatment, mean pigment content (±SE, n = 3) followed by the same upper case letter is not significantly different for a particular dose; within each dose mean pigment content followed by the same lower case letter is not significantly different (Tukey–Kramer HSD test).

biosafety study in plant systems. In correlation bulk counterpart CS was also considered for a brief comparison. FESEM was used to evaluate the morphology of CuNPs, which justified spherical particles sheathed within a polymeric matrix (Figure 1a). TEM image showed that small spherical particles of almost 20 nm were formed during the synthesis (Figure 1b). In situ encapsulation of

DOI: 10.1021/jf504614w
J. Agric. Food Chem. 2015, 63, 2606−2617

CuNP within PEG-200 resulting in a chain-like unique morphology. This unique Cu nanochain array was composed of spherical CuNPs encapsulated within PEG-200 to yield a uniform dispersion, which was visible in the high-resolution image (Figure 1b, inset). It was well documented that the CuNP nanochain array was originally reddish; during synthesis a drastic blue to reddish coloration signified the formation of CuNP. A subsequent UV−vis absorbance at around 450−480 nm was noted, which also justified the formation of CuNPs (Figure 1c) and corroborated previous experimental findings. Polymeric encapsulation within PEG-200 resulted in suppression in crystallinity within CuNP in X-ray diffraction (XRD) pattern (SI, Figure S1). This amorphous nature of encapsulating agent was also consistent with the literature. Energy dispersive X-ray (EDX) analysis also justified that Cu is present as the main constituent. Additional peaks of impurities were avoided, which confirmed that CuNPs were obtained in their pure form (SI, Figure S2). The surface topology and height profile were obtained by atomic force microscopy (AFM). AFM image (SI, Figure S3) verified that the average height of the PEG-200 encapsulated CuNPs was 6−8 nm. Surface functionality of CuNPs was confirmed from Fourier transformed infrared (FTIR) spectra (Figure 1d). CuNPs were hydrophilic with the existence of surface hydroxyl and carbonyl/carboxyl groups. Spectral pattern confirmed C—H stretching, O—H bending, C═O stretching, and C—O stretching, which arose due to surface PEG-200 during encapsulation of CuNPs. A sustained release of 0.0136 ppm from predesigned 0.05 mg/L CuNP nanochain arrays after 24 h was noted by ICPOES under mimicking environment sealed inside a dialysis bag (SI, Figure S4). Sustained release of Cu from polymer-encapsulated nanochain array resulted in lower availability of Cu to the in vitro system in contrast to its bulk counterpart CS. As a result, toxicity symptoms were reduced to some extent in this smart designed nanochain array. Meanwhile, the hydrophilic character produced aqueous stability for the in vitro experiment. Altogether this paper claims well characterized, stable, polymer-encapsulated designed CuNPs to be useful for in vitro and in vivo plant experiments.

CuNPs at a Recommended Dose Promoted the Growth of 15-Day-Treated Mung Bean Plants. Cu is a known essential micronutrient in both algae and higher plants.[31] The bulk counterpart of CuNP, that is, CS, has now been extensively applied in the field to abate Cu-induced nutritional disorder. However, at or above certain concentration limits, it imparts toxicity to the plants, resulting in a decrease in plant yield; external toxic symptoms are the consequence of periodically or permanently changed cellular metabolism. Both CuNP and CS at different physiological doses were tested on mung bean plants, and several growth parameters were checked thereafter. In all cases, CuNPs worked better than CS in terms of root and shoot lengths and fresh and dry weights as noted in Table 1. Figure 2a shows the digital images of 15-day-treated plants in contrast to the control ones. Both CuNPs and CS had positive effects on plants at doses of 0.5 and 0.1 mg/L with respect to control, but beyond that dose, a plant's growth was affected by CS treatment. Plants are very sensitive to Cu toxicity, displaying metabolic disturbances and growth inhibition with Cu contents slightly higher than the normal levels in tissues. CuNP-treated plants were found to be healthy at all doses without any chlorotic or necrotic symptoms. Therefore, no significant abnormalities or stress response was noted in CuNP-treated sets; in fact, CuNPs exhibited growth promotion of the plants.

Increased Chlorophyll and Carotenoid Contents in CuNP-Treated Plants Even at a Dose of 1 mg/L. It is well established that in both Cu-deficient and -excess plants, a change in chlorophyll (Chl) content alters chloroplast structure and thylakoid membrane composition in leaves of spinach, rice, wheat, and bean in experimental growth conditions.[1] Cu interferes with the biosynthesis of the photosynthetic machinery modifying the pigment and protein compositions of photosynthetic membranes. This is attributed to the reduction of Chl content and subsequent substitution of the central Mg ion of Chl by Cu in vivo, leading to the inhibition of photosynthesis.[32] In our experiment in both Cu-deficient and CS-treated plants (at higher doses), similar results were observed. In the case of CuNP-treated plants, Chl-*a* content was increased specifically in all treatments, indicating CuNPs might have a momentous effect in photosynthesis, as chl-*a* is key player in the light-dependent photosynthetic pathway (Figure 2b). Carotenoid, the other important factor, which protects the photosynthetic machinery from any abiotic stress, was simultaneously checked. In CuNP-treated plants, both xanthophyll and carotene were found to be increased significantly with respect to its CS and the control (Figure 2c). Therefore, photosynthetic machinery was prevented from unnecessary external stress during CuNP treatment.

CuNP at 0.05 mg/L Enhanced the Activity of Light Reaction in Photosynthesis. In natural photosynthesis, incident light electronically excites a membrane-bound protein−pigment complex, called photosystem (PS). The photogenerated electrons are rapidly delivered to reaction centers (both PSI and PSII) with the help of antenna pigments along the electron transport chain (ETC) through a series of oxidizing agents for regenerating NADPH cofactors. These cofactors drive redox enzymatic reactions to synthesize organic compounds in the Calvin cycle.

At the initial stage of light-dependent reaction, some associated pigments, called antenna pigments, along with some light-harvesting proteins capture solar energy and transfer it to the reaction center. When the energy stored in chlorophylls in the excited state is rapidly dissipated by excitation transfer, the excited state is said to be quenched.[33] This quenching is believed to originate directly from the light-harvesting pigment bed and is influenced more by CuNP treatment than its bulk counterpart. Therefore, more intense energy transfer to the reaction center in the form of non-photosynthetic fluorescence was noted in CuNP treatment in contrast to CS treatment (SI, Figure S5). If the excited state of chlorophyll is not rapidly quenched by excitation transfer, it can react with molecular oxygen to form singlet oxygen. The extremely reactive singlet oxygen can damage many cellular components and hamper the photoefficiency of PSII. Photosynthesis irradiance (PI) response was evaluated (SI, Figure S6) to understand the relationship between CuNP and pigment efficiency in terms of energy capture and subsequent transfer of exciton. Enhancement in response curve after CuNP treatment with respect to control supported that CuNP did not encourage photochemical damage on PSII; the subsequent quenching (SI, Figure S6) was due to non-photosynthetic change during energy transfer. This initial stimulation after CuNP treatment provided a strong basis to trace out next sets of photochemical assays to address photosynthetic efficiency.

From the reaction center, the excited PSII transfers an electron to pheophytin. On the oxidizing site of PSII, it is rereduced by oxidation of water, generating molecular oxygen, which is a byproduct of photosynthesis. Pheophytin transfers electrons to a series of electron acceptors to cytochrome b_6f complex. A Cu−

DOI: 10.1021/jf504614w
J. Agric. Food Chem. 2015, 63, 2606−2617

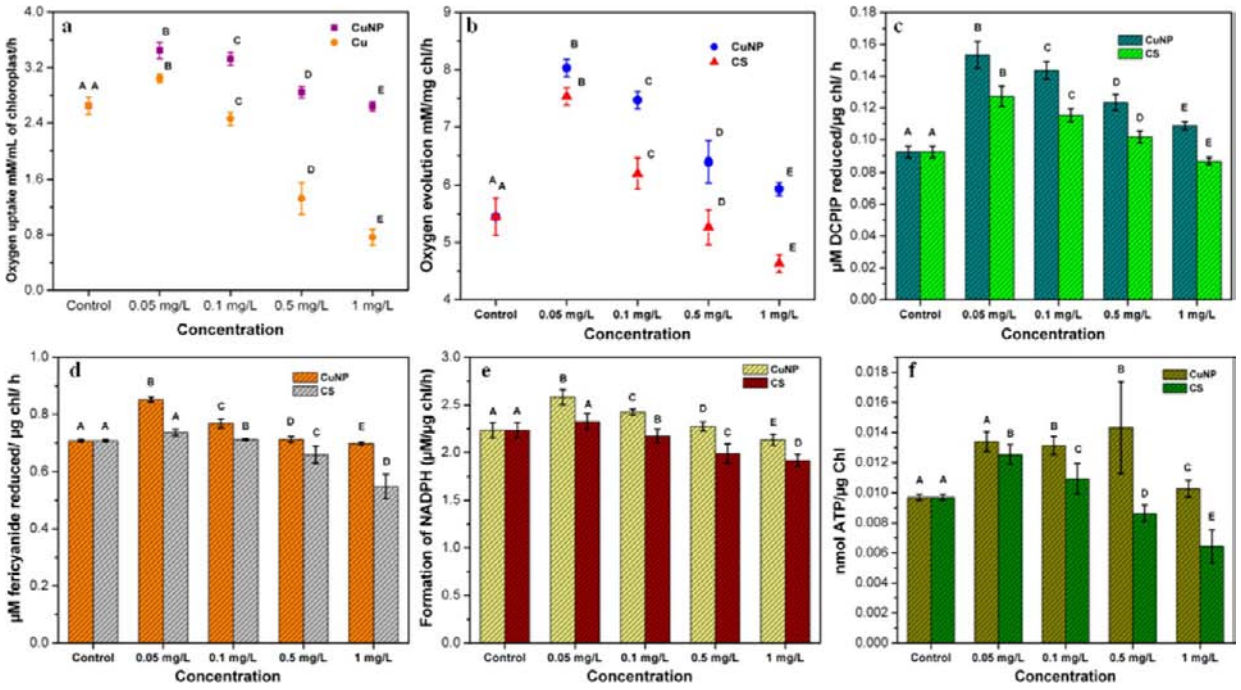

Figure 3. Polarographic and biochemical changes in photosynthetic pathway in CuNP and CS treated chloroplasts. (a) Polarographic changes in whole chain electron transport. $F = 44.558$, $P < 0.0001$. (b) Polarographic changes in oxygen evolution. $F = 57.9384$, $P < 0.00001$. (c) Hill reaction in treated chloroplasts. $F = 63.1117$, $P < 0.00001$. (d) Ferricyanide reduction. $F = 131.2841$, $P < 0.000001$. (e) NADP reduction. $F = 23.7879$, $P < 0.001$. (f) Activity of ATPase. $F = 6.0216$, $P < 0.001$. Within each type of treatment, mean data (± SE, $n = 3$) followed by the same upper case letter are not significantly different for a particular dose; within each dose, means followed by the same lower case letter are not significantly different (Tukey–Kramer HSD test).

Scheme 1. Illustration of Light Reaction

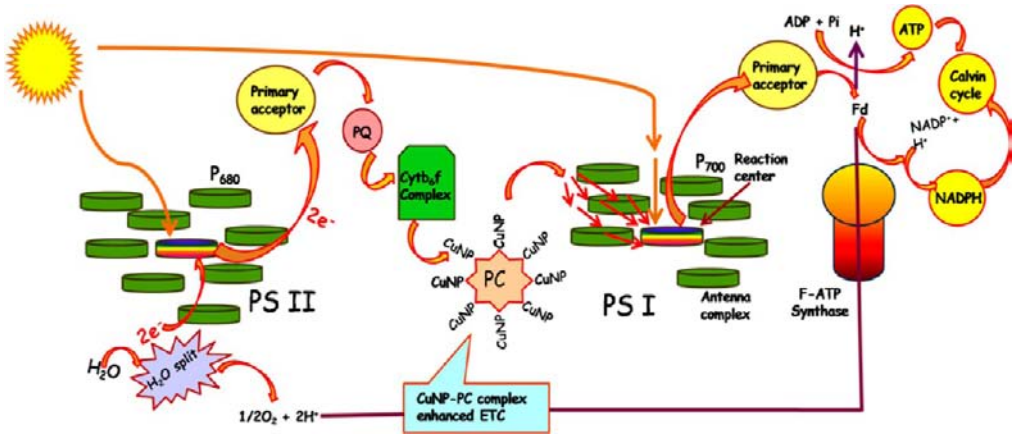

protein component, called plastocyanin, then transfers electrons from the cytochrome complex to PSI. Thereafter, a series of electron acceptors transfers electrons to produce NADPH, which is an essential component to be used in a later stage, that is, dark reaction of photosynthesis. Therefore, photosynthetic efficacy was measured in light of a series of biochemical reactions in the presence of different electron acceptors.

Cu, being a metalloprotein component of plastocyanin, induces structural changes in photosynthetic membrane leading to the inhibition of electron flux. As a result, at any alteration of doses, it inhibits sites of photosynthesis starting from the Hill reaction, that is, the processes of oxygen evolution, photosynthetic ET, and photophosphorylation to dark reaction. Excess Cu indirectly disturbs iron incorporation into Q_A–Fe sites in Chl, causing inhibition of PSII acceptor sites.[34] In our experiments, at higher doses of CS treated Chl showed impaired photosynthesis in all aspects of light reactions starting from the Hill reaction, whole chain ET, and PSI and PSII activity to photophosphorylation. CuNP at all doses was found to enhance light reaction, reducing the harmful effect of Cu deficiency and/or toxicity. Polarographic study for efficiency of whole chain electron transport (Figure 3a) and subsequent oxygen evolution (Figure 3b) in light reaction corroborated the previous results. The effect was maximum at the dose of 0.05 mg/L compared to CS counterpart in the Hill reaction (Figure 3c), ferricyanide reduction assay (PSII activity) (Figure 3d), and ferricyanide–NADP reduction (PSI activity) (Figure 3e).

Photophosphorylation is the process of converting energy from a light-excited electron into the pyrophosphate bond of an adenosine diphosphate (ADP) molecule. During water splitting the liberated proton is bypassed to the ATPase complex by a proton gradient to form ATP from ADP, which is an important

DOI: 10.1021/jf504614w
J. Agric. Food Chem. 2015, 63, 2606–2617

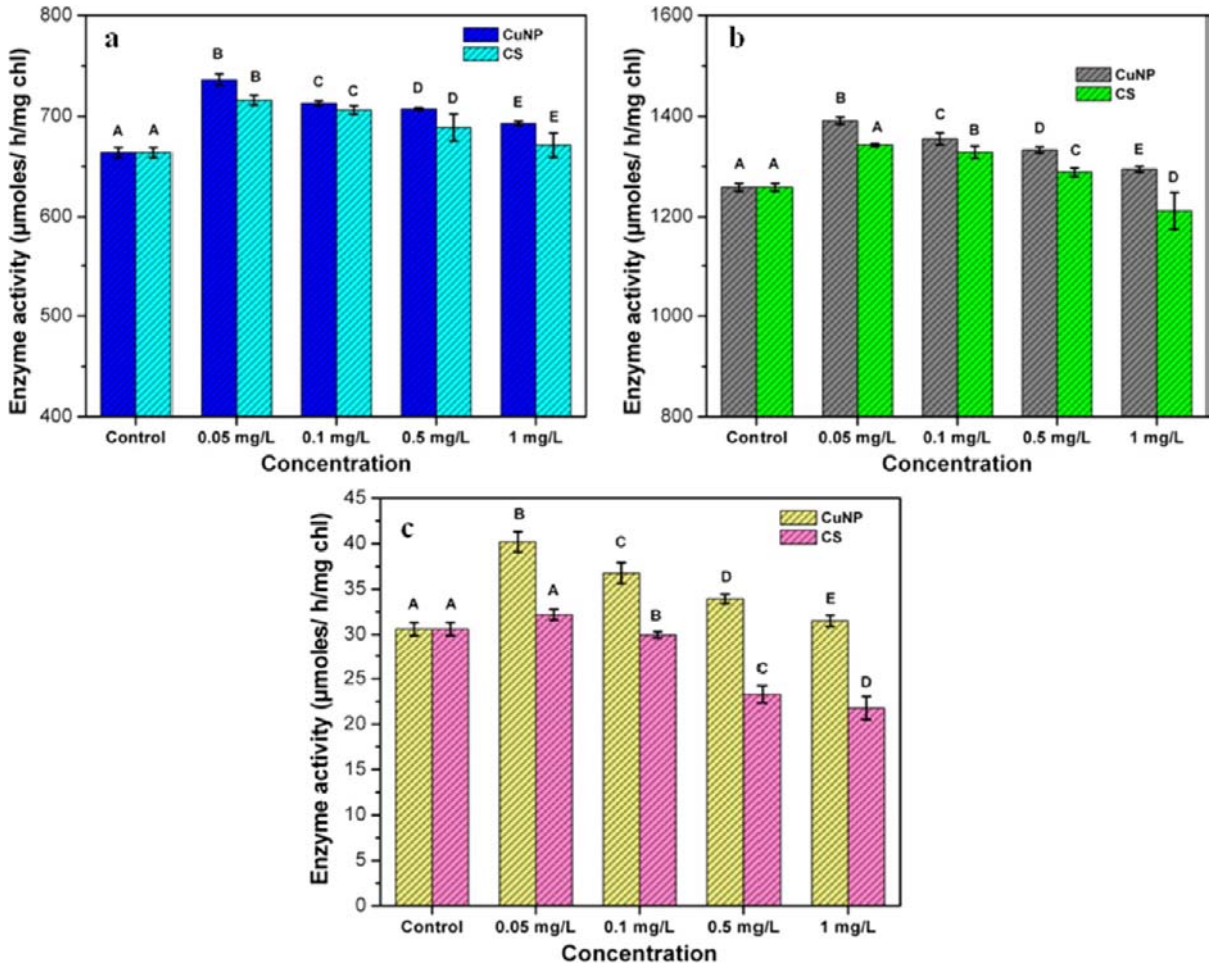

Figure 4. Changes in carbon assimilation in CuNP- and CS-treated chloroplasts. (a) GPDHase activity. $F = 149.1834$, $P < 0.0000001$. (b) RBPase activity. $F = 121.3573$, $P < 0.000001$. (c) FBPase activity. $F = 61.3766$, $P < 0.00001$. Within each type of treatment, mean data (± SE, $n = 3$) followed by the same upper case letter are not significantly different for a particular dose; within each dose, means followed by the same lower case letter are not significantly different (Tukey–Kramer HSD test).

material for dark reactions. In CuNP-treated Chl, ATP content was found to be greater than its bulk counterpart CS. No apparent toxicity was observed even at the highest dose of CuNP as noted in CS-treated Chl (Figure 3f).

In brief, when light falls on the green cells CuNP encouraged the energy packets present in the pigment bed to transfer the electron readily to the reaction center without hampering the pigment machinery, that is, PSII or PSI. CuNP positively enhanced the efficiency of chloroplast in light-mediated entire electron transfer process (30.29% more than control Chl when measured polarographically). It stimulated the PSII activity (20.5% more activity was observed with respect to control), resulting in greater oxygen evolution. CuNP also promoted the PSI activity probably because of its interaction between Cu–protein components, plastocyanin. As a result, photophosphorylation activity was also improved after CuNP treatment. CuNP thus modulated the entire light reaction positively with effective influence on electron transport chain along with phosphorylation activity as seen in Scheme 1.

CuNP Enhanced the Activity of Light-Regulating Enzymes in Dark Reaction of Photosynthesis. In light-independent reaction, CO_2 and water are enzymatically combined with a 5-C molecule to generate two molecules of a 3-C intermediate, which is reduced to carbohydrate by enzymatic reactions driven by ATP and NADPH generated photochemically. CuNP was found to facilitate the light–dark modulation providing an on–off switch for three key enzymes in the Calvin cycle, namely, fructose-1,6-bisphosphate phosphatase (FBPase), ribulose-5-phosphate kinase (RBPase), and NADP-glyceraldehyde-3-phosphate dehydrogenase (GPDHase). When CuNP-treated Chl was subjected to evaluation of GPDHase (Figure 4a), RBPase (Figure 4b), and FBPase activity (Figure 4c), it was noted that CuNP exhibited greater efficacy in contrast to its bulk counterpart CS. Interestingly, 0.05 mg/L was found to be most effective among all of the dosages, although CuNP had a strong influence on FBPase activity among these three enzymes. This result indicated that CuNP might play a pivotal role in the dark reaction of photosynthesis.

CuNP in Nitrogen Metabolism. Plant growth and photosynthetic ability can be improved by enhancing the nitrogen supply within the system, and therefore it is essential to evaluate the interactive effect of CuNP on nitrogen metabolism in the plant. The first step of this process is the reduction of nitrate in cytosol, and the reaction is catalyzed by nitrate reductase (NR), in which nitrate ion is converted to nitrite ion. Because nitrite is a highly reactive, potentially toxic ion, plant cells immediately transport the nitrite generated by NR from cytosol into chloroplastic leaves and plastids in roots.[35] Here, with the help of nitrite reductase (NiR), nitrite is transferred to ammonium ion. To avoid ammonium toxicity, plants rapidly convert

DOI: 10.1021/jf504614w
J. Agric. Food Chem. 2015, 63, 2606–2617

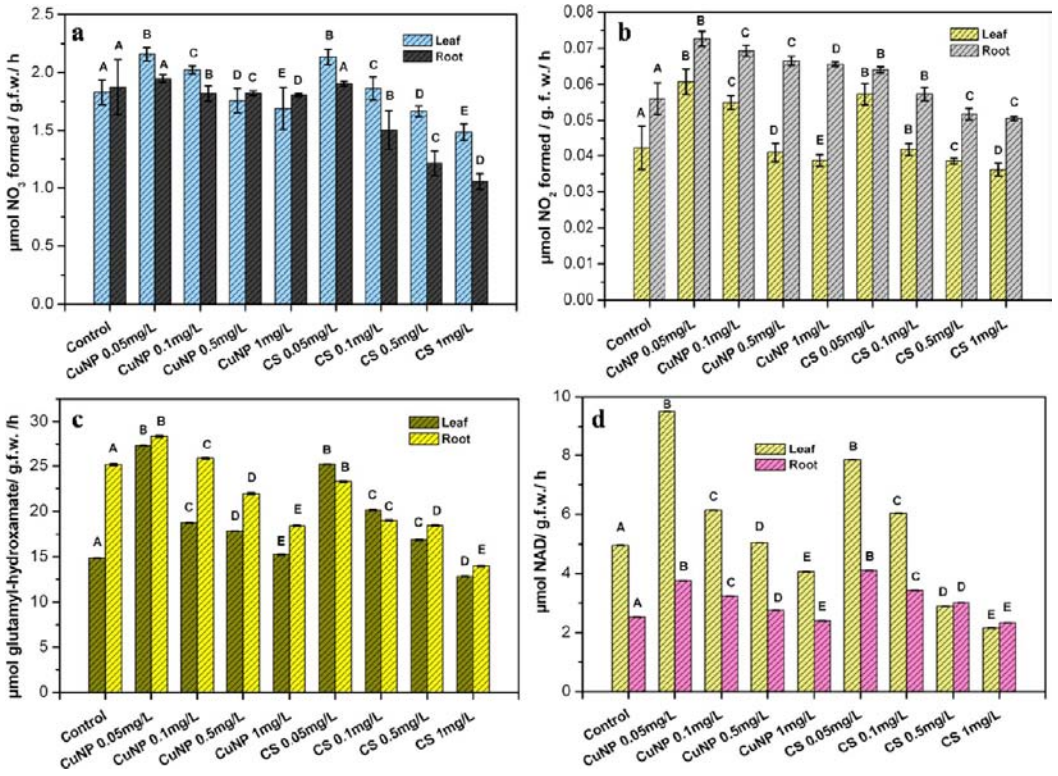

Figure 5. CuNP and CS on nitrogen metabolism on 15-day-treated mung bean plants. (a) NR activity. CuNP leaves, $F = 33.57$, $P < 0.0001$; CuNP roots, $F = 3.39$, $P < 0.1$; CS leaves, $F = 25.56$, $P < 0.001$; CS roots, $F = 7.44$, $P < 0.1$. (b) NiR activity. CuNP leaves, $F = 19.87$, $P < 0.001$; CuNP roots, $F = 19.51$, $P < 0.01$; CS leaves, $F = 10.12$, $P < 0.01$; CS roots, $F = 12.8$, $P < 0.01$. (c) GS activity. CuNP leaves, $F = 39.21$, $P < 0.000001$; CuNP roots, $F = 23.66$, $P < 0.01$; CS leaves, $F = 31.68$, $P < 0.000001$; CS roots, $F = 23.44$, $P < 0.001$. (d) GOGAT activity. CuNP leaves, $F = 20.02$, $P < 0.0001$; CuNP roots, $F = 122.23$, $P < 0.00001$; CS leaves, $F = 26.03$, $P < 0.0001$; CS roots, $F = 223.94$, $P < 0.000001$. Within each type of treatment, mean data (± SE, $n = 3$) followed by the same upper case letter are not significantly different for a particular dose; within each dose, means followed by the same lower case letter are not significantly different (Tukey–Kramer HSD test).

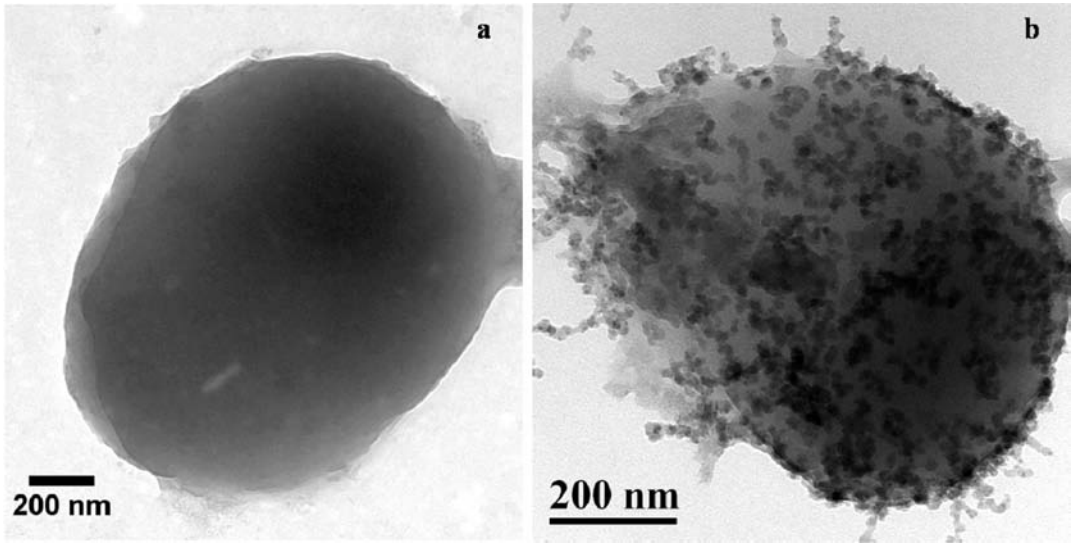

Figure 6. TEM images of (a) control and (b) CuNP-treated chloroplasts.

ammonium ion into amino acids (AAs) with the help of glutamine synthase (GS) and glutamate synthase (GOGAT). GS combines ammonium with glutamate to form glutamine, whereas GOGAT assimilates glutamine translocated from roots to leaves. Once assimilated into glutamate and glutamine, nitrogen is incorporated to AA via transamination reactions. Therefore, the activities of all four enzymes are imperative in nitrogen assimilation and can be stimulated by essential heavy metals.[36] In this paper, CuNP at modulated dose was found to be pertinent for use as an integral component in nitrogen fertilizer as it enhanced the activity of NR (Figure 5a), NiR (Figure 5b), GS (Figure 5c), and GOGAT (Figure 5d). Free nitrate ion concentration was much less in the system compared to the control (SI, Figure S7), ruling out the possibility of nitrate

DOI: 10.1021/jf504614w
J. Agric. Food Chem. 2015, 63, 2606−2617

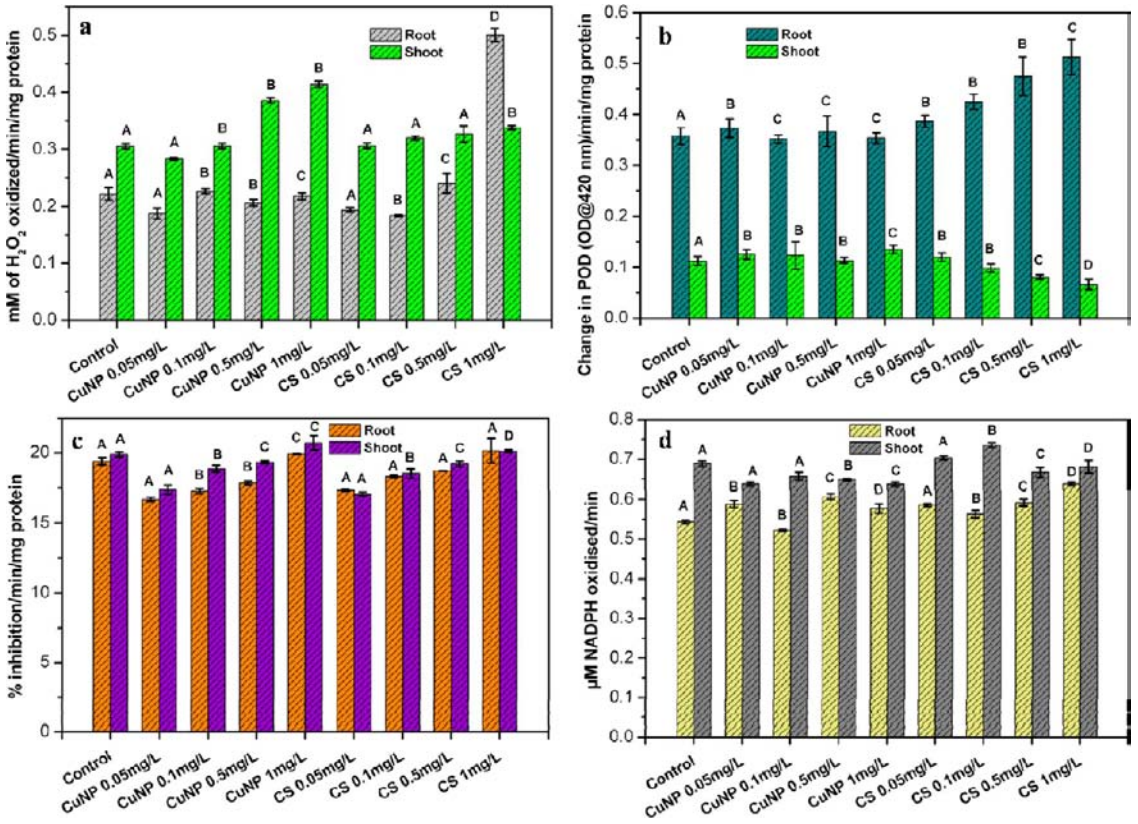

Figure 7. Changes in antioxidant enzymes in CuNP- and CS-treated plants. (a) CAT. Root, $F = 14.54$, $P < 0.001$; leaf, $F = 10.295$, $P < 0.01$. (b) POD. Root, $F = 4.428$, $P < 0.1$; leaf, $F = 10.5$, $P < 0.01$. (c) SOD. Root, $F = 16.73$, $P < 0.001$; leaf, $F = 34.125$, $P < 0.00001$. (d) GR. Root $F = 25.4324$, $P < 0.0001$; leaf, $F = 38.8256$, $P < 0.00001$. Within each type of treatment, mean data (± SE, $n = 3$) followed by the same upper case letter are not significantly different for a particular dose; within each dose, means followed by the same lower case letter are not significantly different (Tukey–Kramer HSD test).

toxicity leading to cellular injuries within the system. CuNP treatment at all doses worked better than the bulk counterpart at their respective concentrations. Therefore, it justified that CuNP might have a significant and implicit role in both photosynthesis and nitrogen metabolism as it offset all ominous effects of Cu toxicity caused in the agricultural sector.

Bioavailability and Uptake of CuNP. Due to strong binding of Cu by organic matter and other soil colloids, its mobility is severely restricted and the fraction of total Cu available for plant uptake is usually very low. Therefore, uptake and distribution of the CuNP within the plant system was important to execute the response. Compared to the bulk counterpart, availability of CuNP into the rhizosphere is expected to be very high because of its size, high surface by volume ratio, and unique physicochemical properties.[37] Bioavailability of CuNP within the plant sample was verified by confocal microscopy. To demonstrate its bioavailability, CuNP was conjugated with FITC following our previous study.[5] FITC-conjugated CuNP-treated mung bean plants were then observed under confocal microscopy. Leaf and root sections (SI, Figure S8a,b) demonstrated bright green color under confocal microscopy at 488 nm excitation wavelength, although the leaf section appeared to be brighter under confocal microscopy. A direct biomass distribution of CuNP-treated mung bean sample was observed by ICPOES as shown in the SI (Table S1). Distribution of Cu was greater in leaf than in root, which corroborated the confocal results as well.

We assessed the morphology of treated and control Chl by electron microscopy experiments. Treated samples retained similar spherical morphology under scanning electron microscopy (SEM). No significant alterations in morphology were observed in the post-treated samples (SI, Figure S9a). EDX analysis associated with SEM verified the presence of CuNP within the Chl (SI, Figure S9b). Finally, the TEM image demonstrated the presence of small-sized CuNPs over the surface of Chl without altering its uniform spherical morphology (Figure 6).

Consequently, excess Cu causes reduction of Chl content, connected with partial destruction of grana and considerable modification of lipid–protein composition in thylakoid membranes depending upon the duration of Cu action. As a consequence, we checked the morphology of root and leaf sections under a light microscope; no abnormalities in tissue anatomy were found, which corroborated the previous results. In root tissues, epi- and endodermis pericycle and vascular bundles were also normal in position and shape (SI, Figure S10). In leaves, spongy and palisade parenchyma were normal in position and shape with respect to control; even no sunken stomata were observed (SI, Figure S11). Therefore, we conclude CuNP is readily taken up by the root from rhizosphere and is subsequently transported to leaves via shoot. CuNPs did not impart any structural changes in the root or leaf tissue, not even to the Chl, signifying its compatibility with the plant system.

Mechanistic Interpretation or Mode of Action of CuNP. Under physiological processes in plants, Cu exists as the Cu^{2+}/Cu^{1+} system.[38] Cu acts as a structural element in regulatory proteins and participates in photosynthetic ETC, mitochondrial respiration, oxidative stress response, cell wall metabolism, and hormone signaling. In its absence, plants develop specific deficiency symptoms, which affect mostly the early devel-

DOI: 10.1021/jf504614w
J. Agric. Food Chem. 2015, 63, 2606–2617

opmental stages of plant and reproductive organs. Besides the redox properties, those make Cu an essential element also contributing to inherent toxicity. Redox cycling between Cu^{2+} and Cu^{1+} can trigger the production of highly toxic hydroxyl radicals with subsequent damage in nucleic acid, proteins, and other biomolecules. On the other hand, Cu has a strong affinity with thiols and can displace metals in proteins.[39] At the same time Cu is also prone to surface oxidation upon exposure to ambient condition. Therefore, we strategically encapsulated CuNP within a biocompatible polymer. Biocompatible polymer PEG-200 was already approved by the U.S. FDA for biomedical applications. This encapsulation prevented unnecessary leaching of Cu from the constituents and at the same time prevented oxidation of Cu under the conditions. Therefore, the recycling of Cu^{2+}/Cu^{1+} was controlled and a moderate amount of Cu would be released from the polymer matrix, ensuring no or little cellular damage within the system. Cu from CuNP was already noted by ICPOES as shown in Table 1 (SI). Meanwhile, Cu, being an inherent functional component of enzymatic reactions including the ETC pathway, nitrogen assimilation, CuNP was found to be enhanced and/or to modulate the significant biochemical pathways in the photosynthesis and nitrogen metabolism; a small but significant amount of released Cu from nanochain arrays was sufficient to execute the response.

Biosafety of CuNP in the Plant System. As CuNP enhanced the nitrogen assimilation and protected the cellular machinery from photochemical damages, it was obvious that the basic components of biomolecules such as protein, AA, reducing sugar, and total lipid content would be increased. The amount of reducing sugar was increased in all treated sets, although maximum efficacy was observed at 0.05 mg/L. Increase in sugar content, evidence of enhancement in photosynthesis, is shown in the SI (Figure S12a). Free AA content was elevated in CuNP-treated plants with respect to control and their respective bulk counterparts (SI, Figure S12b). This was possibly because of the modulatory effect of CuNP on nitrogen assimilation. CuNP directly or indirectly influenced many physiological processes, which were interconnected to photochemical reactions in nitrogen metabolism. Thereafter, protein (SI, Figure S12c) and total lipid content (SI, Figure S12d) were also increased in CuNP-treated plants compared to its control and bulk counterpart.

CuNP in Oxidative Stress. In plants, reactive oxygen species (ROS) are continuously produced as byproducts in various metabolic pathways localized in different cellular compartments. Under physiological steady-state conditions, these molecules are scavenged by different antioxidative defense components that are often confined to particular compartments.[40] Catalase (CAT) is involved in scavenging hydrogen peroxide during photorespiration and β-oxidation of fatty acids. In both leaves and roots CAT activity was unaltered after CuNP treatment with respect to control; however, at higher doses of CS, it was decreased at an alarming rate (Figure 7a). This result justified that even after CuNP treatment stress response was minimum. Peroxidase (POD) participates in developmental processes, ethylene biosynthesis, and defense. POD levels were almost unchanged between control and CuNP-treated sets, whereas CS showed drastic changes with respect to control (Figure 7b). Therefore, CuNP-treated plant tissues (both root and leaf) were not significantly altered, maintaining normal homeostasis into the metabolic system; ROS-mediated damage was insignificant. Superoxide dismutase (SOD) represents a group of multimeric metalloenzymes catalyzing the disproportion of superoxide free radical, generated by univalent reduction of molecular oxygen to hydrogen peroxide in different cellular compartments. No significant deviations of enzymatic activities with respect to control were observed at CuNP-treated plants at recommended doses as observed in Figure 7c. GR is a member of the flavoenzymes family, which catalyzes the NADPH-dependent reduction of glutathione disulfide to glutathione. In CuNP-treated sets GR levels showed minor alterations with respect to control, whereas CS showed drastic changes (Figure 7d). In both roots and leaves after CuNP treatment GR activities were increased with respect to control, but not in a dose-dependent manner because of the high affinity of Cu to bind with the −SH group of the protein moiety. Non-antioxidative protein components such as phenol (SI, Figure S13a), total peroxide (SI, Figure S13b), proline (SI, Figure S13c), and polyphenol oxidase (SI, Figure S13d) (PPO) were also determined as plants have general strategies to induce the activities of these non-antioxidative proteins to overcome the oxidative stress due to imposition of abiotic stress. Except proline, no abnormal activities were observed in CuNP-treated root and leaf tissues. Proline is a known stress marker, which counterbalances the detrimental effect of stress to maintain the equilibrium of the cellular machineries. Therefore, the elevated activities of proline in CuNP-treated sets helped to surpass the possible harmful effect of plants as enforced by the nanoparticle action. This ensured the protective baseline for the plant from any abiotic stress that had been impaired at high concentration of CS to the system. Direct exposure or release of Cu^{2+} from CS could result from oxidative stress and damage within cellular network, but deliberate embedding within a polymeric matrix resulted in controlled release of Cu from CuNP to yield the beneficial response as a micronutrient for crop management.

In a nutshell, biochemical and physiological implications as well as efficacy of newly synthesized polymer-encapsulated CuNP on plant systems had been established in comparison to its bulk counterpart CS. This not only promised to improve crop productivity by modulating photochemical pathway but also decimated the nutritional disorder by catalyzing the nitrogen assimilatory pathway and carbon assimilation. It reduced the toxicity issues developed by the commercially available salt CS, as it was biosafe at the physiological dosages used in these experiments. Ready uptake within the plant system verified its bioavailability; at the same time, strategic encapsulation within the biocompatible polymer matrix reduced the toxic response and ensured stability to some extent. At recommended dosages its efficacy in photosynthesis and biocompatibility were ensured in contrast to its bulk counterpart CS; cellular machineries were protected as well. Moreover, polymer-encapsulated CuNP might serve as a boon in the agricultural arena, being a suitable alternative of copper micronutrient, and hence it could be included in fertilizers amalgamated with other necessary macro- and micronutrients. We believe systematic modification in nanoparticle synthesis can lead to greater such beneficial response in the near future for crop management. Detailed toxicological profiling and thorough testing are also required prior to its commercialization, but it is an initial step that can provide a baseline for future research for sustainable development in agri-economics.

DOI: 10.1021/jf504614w
J. Agric. Food Chem. 2015, 63, 2606−2617

■ ASSOCIATED CONTENT

Supporting Information

Additional experimental details, references, figures, and table. This material is available free of charge via the Internet at http://pubs.acs.org.

■ AUTHOR INFORMATION

Corresponding Author

*(S.P.) E-mail: saheli.pra@gmail.com. Phone: +91-332577-3227. Fax: +91-332577-3049.

Funding

This work was generously supported by major grants from the Department of Biotechnology, Government of India (DBT) (Grants BT/PR15217/NNT/28/506/2011-2015; BT/BIPP0439/11/10). We are grateful to the National Agricultural Innovation Project (ICAR) (Grant NAIP/Comp-4/C3004/2008-2014), the National Fund (Indian Council of Agricultural Research) (Grant NFBSFARA/GB-2019/2011−2015; NFBSFARA/CA-4-15/2013-146), and ISI plan project funds (2008−2013) for providing financial support. S.M. is thankful to CSIR, New Delhi, for SRF. P.P. acknowledges a UGC-DSK postdoctoral fellowship.

Notes

The authors declare no competing financial interest.

■ ACKNOWLEDGMENTS

We acknowledge Ashim Dhar for his assistance during plant experiments.

■ REFERENCES

(1) Fernandes, J. C.; Henriques, F. S. Biochemical, physiological, and structural effects of excess copper in plants. *Bot. Rev.* **1991**, *57*, 246−273.

(2) Macsymiec, W. Effect of copper on cellular processes in higher plants. *Photosynthetica* **1997**, *34*, 321−342.

(3) Babu, T. S.; Marder, J. B.; Tripuranthakam, S.; Dixon, D. G.; Greenberg, B. M. Synergistic effects of a photooxidized polycyclic aromatic hydrocarbon and copper on photosynthesis and plant growth: evidence that in vivo formation of reactive oxygen species is a mechanism of copper toxicity. *Environ. Toxicol. Chem.* **2001**, *20*, 1351−1358.

(4) Pradhan, S.; Patra, P.; Das, S.; Chandra, S.; Mitra, S.; Dey, K. K.; Akbar, S.; Palit, P.; Goswami, A. Photochemical modulation of biosafe manganese nanoparticles on *Vigna radiata*: a detailed molecular, biochemical, and biophysical study. *Environ. Sci. Technol.* **2013**, *47*, 13122−13131.

(5) Yang, F.; Liu, C.; Gao, F.; Su, M.; Wu, X.; Zheng, L.; Hong, F.; Yang, P. The improvement of spinach growth by nano-anatase TiO_2 treatment is related to nitrogen photoreduction. *Biol. Trace Elem. Res.* **2007**, *119*, 77−88.

(6) Lin, D.; Xing, B. Phytotoxicity of nanoparticles: inhibition of seed germination and root growth. *Environ. Pollut.* **2007**, *150*, 243−250.

(7) Doshi, R.; Braida, W.; Christodoulatos, C.; Wazne, M.; O'Connor, G. Nano-aluminum: transport through sand columns and environmental effects on plants and soil communities. *Environ. Res.* **2008**, *106*, 296−303.

(8) Xiong, Z. T.; Liu, C.; Geng, B. Phytotoxic effects of copper on nitrogen metabolism and plant growth in *Brassica pekinensis* Rupr. *Ecotox Environ. Saf.* **2006**, *64*, 273−280.

(9) Dimkpa, C. O.; Mclean, J. E.; Latta, D. E.; Manangon, E.; Britt, D. W.; Johnson, W. P.; Boyanov, M. I.; Anderson, A. J. CuO and ZnO nanoparticles: phytotoxicity, metal speciation, and induction of oxidative stress in sand grown wheat. *J. Nanopart. Res.* **2012**, *14*, 1125 DOI: 10.1007/s11051-012-1125-9.

(10) Llorens, N.; Arola, L.; Bladé, C.; Mas, A. Effects of copper exposure upon nitrogen metabolism in tissue cultured *Vitis vinifera*. *Plant Sci.* **2000**, *160*, 159−163.

(11) Wong, M. H.; Bradshaw, A. D. A comparison of the toxicity of heavy metals, using root elongation of rye grass, *Lolium perenne*. *New Phytol.* **1982**, *91*, 255−261.

(12) Johnson, A. C.; Naresh. Influence of chelation on Cu distribution and barriers to translocation in *Lolium perenne*. *Environ. Sci. Technol.* **2013**, *47*, 7688−7695.

(13) Arnon, D. I. Copper enzymes in isolated chloroplasts. Polyphenol oxidase in *Beta vulgaris*. *Plant Physiol.* **1949**, *24* (1), 1−15.

(14) Davies, B. H. Analysis of carotenoid pigments. In *Chemistry and Biochemistry of Plant Pigments*; Goodwin, T. W., Ed.; Academic Press: New York, 1965.

(15) Heinemeyer, J.; Eubel, H.; Wehmhöner, D.; Jänsch, L.; Braun, H. P. Proteomic approach to characterize the supramolecular organization of photosystems in higher plants. *Phytochemistry* **2004**, *5*, 1683−1692.

(16) Lin, S. T.; Guan, B. T.; Chang, T. Y. Fitting photosynthesis irradiance response curves with nonlinear mixed-effects models. *Taiwan J. For. Sci.* **2008**, *23*, 55−69.

(17) Tripathy, B. C.; Mohanti, P. Zinc-inhibited electron transport of photosynthesis in isolated barley chloroplasts. *Plant Physiol.* **1980**, *66*, 1174−1178.

(18) Vishniac, W. Methods for study of the Hill reaction. *Methods Enzymology*; Colowick, S. P., Kaplan, N. O., Eds.; Academic Press: New York, 1957; Vol. 4, pp 342−343.

(19) Terry, N.; Huston, R. P. Effects of calcium on the photosynthesis of intact leaves and isolated chloroplasts of sugar beets. *Plant Physiol.* **1975**, *55*, 923−927.

(20) Wang, P.; Duan, W.; Takabayashi, A.; Endo, T.; Shikanai, T.; Ji-Yu, Y.; Hualing, M. Chloroplastic NAD(P)H dehydrogenase in tobacco leaves functions in alleviation of oxidative damage caused by temperature stress. *Plant Physiol.* **2006**, *141*, 465−474.

(21) Taylor, S. T.; Terry, N.; Huston, R. Limiting factors in photosynthesis, III. Effects of iron nutrition on the activities of three regulatory enzymes of photosynthetic carbon metabolism. *Plant Physiol.* **1982**, *70*, 1541−1543.

(22) Cataldo, D. A.; Haroon, M.; Schrader, L. E.; Young, V. L. Rapid colorimetric determination of nitrate in plant tissue by nitration of salicylic acid. *Commun. Soil Sci. Plant Anal.* **1975**, *6*, 71−80.

(23) Giannopolitis, C. N.; Ries, S. K. Superoxide dismutase I. Occurrence in higher plants. *Plant Physiol.* **1977**, *59*, 309−314.

(24) Chance, B.; Maehly, A. C. Assay of catalases and peroxidases. *Methods in Enzymology*; Colowick, S. P., Kaplan, N. O., Eds.; Academic Press: New York, 1955; Vol. 2, pp 764−775.

(25) Thurman, R. G.; Ley, H. G.; Scholz, R. Hepatic microsomal ethanol oxidation hydrogen peroxide formation and the role of catalase. *Eur. J. Biochem.* **1972**, *25*, 420−430.

(26) Wang, C. Y. Temperature preconditioning affects glutathione content and glutathione reductase activity in chilled zucchini squash. *J. Plant Physiol.* **1995**, *145*, 148−152.

(27) Beers, R. F. J. R.; Sizer, I. W. A spectrophotometric method for measuring the breakdown of hydrogen peroxide by catalase. *J. Biol. Chem.* **1952**, *195*, 133−140.

(28) Mayer, A. M.; Harel, E. Polyphenol oxidase in plants. *Phytochemistry* **1979**, *18*, 193−215.

(29) Bates, L. S.; Waldren, R. P.; Teare, I. D. Rapid determination of free proline for water-stress studies. *Plant Soil* **1973**, *39*, 205−207.

(30) Malik, C. P.; Singh, M. B. *Plant Enzymology and Histo-enzymology*; Kalyani Publishers: New Delhi, India, 1980; p 53.

(31) Baszyński, T.; Ruszkowska, M.; Król, M.; Tukendorf, A.; Wolińska, D. The effect of copper deficiency on the photosynthetic apparatus of higher plants. *Z. Pflanzenphysiol.* **1978**, *89*, 207−216.

(32) Stange, C.; Flores, C. Carotenoids and photosynthesis − regulation of carotenoid biosyntesis by photoreceptors. In *Advances in Photosynthesis − Fundamental Aspects*; Najafpour, M., Ed.; InTech Publishers: Rijeka, Croatia, 2012; ISBN 978-953-307-928-8.

(33) Maxwell, K.; Johnson, G. N. Chlorophyll fluorescence − a practical guide. *J. Exp. Bot.* **2000**, *51*, 659−668.

DOI: 10.1021/jf504614w
J. Agric. Food Chem. 2015, 63, 2606−2617

(34) Jegerschöld, C.; MacMillan, F.; Lubitz, W.; Rutherford, A. W. Effects of copper and zinc ions on photosystem II studied by EPR spectroscopy. *Biochemistry* **1999**, *38*, 12439−12445.
(35) Snowball, K.; Robson, A. D. The effect of copper on nitrogen fixation in subterranean clover (*Trifolium subterraneum*). *New Phytol.* **1980**, *S5*, 63−72.
(36) Abraham, Z. H. L.; Lowe, D. J.; Smith, B. E. Purification and characterization of the dissimilatory nitrite reductase from *Alcaligenes xylosoxidans* subsp. *xylosoxidans* (N.C.I.M.B. 11015): evidence for the presence of both type 1 and type 2 copper centres Cu in nitrogen metabolism. *Biochem. J.* **1993**, *295*, 587−593.
(37) Lee, W. M.; An, Y. J.; Yoon, H.; Kweon, H. S. Toxicity and bioavailability of copper nanoparticles to terrestrial plants *Phaseolus radiatus* (mungbean) and *Triticum aestivum* (wheat); plant agar test for water-insoluble nanoparticles. *Environ. Toxicol. Chem.* **2008**, *27*, 1915−1921.
(38) Manceau, A.; Nagy, K.; Marcu, M.; Lanson, M.; Geoffroy, N.; Jacquet, T.; Kirpichtchikova, T. Formation of metallic copper nanoparticles at the soil-root interface. *Environ. Sci. Technol.* **2008**, *42*, 1766−1772.
(39) Yruela, I. Copper in plants. *Braz. J. Plant Physiol.* **2005**, *17*, 145−156.
(40) Shigeoka, S.; Ishikawa, T.; Tamoi, M.; Miyagawa, Y.; Takeda, T.; Yabuta, Y.; Yoshimura, Y. Regulation and function of ascorbate peroxidase isoenzymes. *J. Exp. Bot.* **2002**, *53*, 1305−1319.

DOI: 10.1021/jf504614w
J. Agric. Food Chem. 2015, 63, 2606−2617

Table 1. Relevant Gene Information and Primers for Real-Time PCR Analysis

accession no.	gene name	description	primer sequence (5′ to 3′)
Cs7g31320.1	*AUX1*	auxin transporter protein 1	CGGTTGCCTGTGGTGATACACGGTGAAGCTGACCAAGAG
Cs6g07990.1	*LAX2*	auxin transporter-like protein 2	TTGTGTGGGAGAAGGTAATCGTGCGGAGTTGATAGGACCA
Cs2g16620.1	*PIN1*	auxin efflux carrier component 1	GCAGCAACAACAACAACAGCTCCTCCTTCAGAGACAGGTGA
Cs2g13710.1	*PIN-LIKES 2*	auxin efflux carrier component	CACACCCAAGACAGCAAATGAACGCTTTCACCCAATTCAG
Cs3g01570.1	*ARF1*	auxin response factor 1	AGTTGGGAGGGCTGTTGATTGACCACTTGCCACTTCTTGG
Cs7g19770.1	*ARF2*	auxin response factor 2	AATGAGGCAGCAGGGTAATGGGGCTTGTTCTTGGCTTGTA
Cs4g04520.1	*ARF5*	auxin response factor 5	CACTTCACCTTCCACAAACAACCAGATTGAGCCACTTCCTCTC
Cs2g09440.1	*ARF6*	auxin response factor 6	AGTCGGGTTCCTTCGGTAACATTAAAGCAGTCTATCACAC
Cs3g18940.1	*ARF17*	auxin response factor 17	TGCTTGAGGTTACTTGGGATGGGAGGGAATGCGGTATGAAG
Cs7g25670.1	*ARF18*	auxin response factor 18	GAAGTAAAGACACCCCACATCCAGAACCAGAACCATCAGAAG
Cs5g10820.1	*EXP1*	expansin-A1	AATGCTCTCCCAAACAATGCATGCCTCCCTTCCTACTGC
Cs8g18640.1	*EXP3*	expansin-A3	ACGGGTTCCGCTACTTCAACGCTCATCCAGCCAGTTCTTG
Cs7g29830.1	*EXP10*	expansin-A10	CAAGAGCAAAGGCAAAGACGGAAATGACCCTCCTCGCTTC
Cs1g05000.1	*Actin*	actin-7	CCAAGCAGCATGAAGATCAAATCTGCTGGAAGGTGCTGAG

four to six months. Finally, in Phase III, fruit growth is mostly arrested, and the fruit undergoes a nonclimacteric ripening process.[13] Therefore, the final sizes of citrus fruit are determined by both the cell number and the cell size, which are determined by the processes of cell division and cell expansion, respectively. Any perturbations to the two processes may cause alterations in final fruit size.[14]

Numerous studies have demonstrated that rootstocks exert a significant influence on fruit quality under diverse cultivation conditions. To gain insight into the potential mechanisms by which rootstocks influence fruit size, we investigated the effects of two citrus rootstocks on the fruit growth of 'Shatangju' mandarin. The rootstock genotypes chosen were Trifoliate orange (*Poncirus trifoliata* (L.) Raf.) and Canton lemon (*Citrus limonia* Osbeck), which are known to confer low and high scion vigor, respectively, in China.[15] We also conducted a hormone analysis and an expression-profiling study of the fruit from the two graft combinations.

MATERIALS AND METHODS

Plant Materials. This study was conducted at a commercial orchard in Yangchun, Guangdong Province, China (latitude 22°06′ N; longitude 111°42′ E; altitude 12.5 m). This area has a subtropical monsoon climate with a mean annual precipitation of 2380 mm, a mean annual temperature of 22.3 °C, and an annual mean of 1748.2 h of sunshine. The soil was classified as a red soil, with a pH of 5. The evaluated rootstocks were Trifoliate orange and Canton lemon, two rootstocks that are widely employed in China citrus production. Virus-free budwood of the 'Shatangju' mandarin was budded onto these rootstocks in January 2003, and the grafted plants were planted in spring 2004 at a spacing of 2.5 m × 3.0 m. The terms 'Shatangju'/Trifoliate orange and 'Shatangju'/Canton lemon are used to refer specifically to the 'Shatangju' mandarin grafted on either the Trifoliate orange rootstock or the Canton lemon rootstock, respectively. The experimental design was a randomized complete block with five replicates, and the experimental unit was a single tree per plot. Disease and pest control measures were performed according to an integrated pest management method.

Fruit quality was assessed from 2009 to 2012. Each year, 10 fruits were collected from each citrus tree in late December. For fruit quality analysis, the fruits were collected from the four quadrants of each plant, and the fruit fresh weight and fruit diameter were measured. The TSS content, which is expressed in °Brix, was assessed using a digital refractometer. The titratable acidity (TA) was determined by titration with 0.31 N NaOH. For the evaluations of tree growth in 2011 and 2012, the trunk diameter at 10 cm above the grafting line, the canopy volume, and the yield were measured. The canopy volume was calculated using the equation for one-half of a prolate spheroid.

For fruit growth analysis, five fruit samples per tree were collected in accordance with the following schedule: October 16, 2012; November 15, 2012; December 5, 2012; December 25, 2012; and January 13, 2013. The collected fruits were transported to the laboratory on dry ice and immediately separated into the peel and flesh components, frozen in liquid nitrogen, and stored at −80 °C until further analysis.

Cell-Size Measurements. Samples of 'Shatangju' mandarin fruits produced on the two rootstocks were collected on the designated sampling dates, and healthy peel sections along the equatorial region were removed and fixed in an FAA (formaldehyde, acetic acid, and ethanol) fixative. The fixed peel samples were dehydrated with ethanol and then embedded in paraffin according to the method previously described by Cajuste et al.[16] The embedded tissues were sliced into 8 μm sections and stained with a 0.5% hematoxylin staining solution. For each fruit, three to five sections of peel were analyzed. The cell diameter, as an indicator of cell size, was measured in the flavedo layer, which comprises the exocarp for a citrus fruit, excluding the outer epidermal layer and the oil-gland region. The mean cell size was calculated for each section.

Phytohormone Determinations. Fruit tissues were powdered in liquid nitrogen, extracted with 80% (v/v) methanol, containing 1 mM butylated hydroxy−toluene (BHT), for 4 h at 4 °C in the darkness, and then, centrifuged for 15 min at 6000 rpm before the supernatants were collected. The residue was extracted a second time as above, the supernatants were combined, and the volume was recorded. The supernatants were purified on a C18 Sep-Pak cartridge (Waters, Milford, MA, USA), evaporated to dryness in vacuum, and redissolved in a phosphate-buffered saline solution (pH 7.5). The contents of endogenous indole-3-acetic acid (IAA), zeatin riboside (ZR), gibberellins (GAs), and abscisic acid (ABA) were quantified by an enzyme-linked immunosorbent assay (ELISA) according to previously described procedures.[17,18] The ELISA kit was purchased from China Agricultural University. The absorbance of each well was measured at 490 nm using a Microplate Reader (Infinite M200, Tecan, Austria). Two replicates were performed for each measurement.

RNA Extraction and cDNA Synthesis. Total RNA was extracted from the frozen peel and pulp tissues of 'Shatangju' mandarin with TRIzol reagent according to the manufacturer's protocol (TaKaRa, Otsu, Japan), and was then treated with DNase I (TaKaRa). UV absorption spectrophotometry and gel electrophoresis were employed to assess RNA quality and quantity. Subsequently, single-stranded cDNA was synthesized from the extracted total RNA using oligo(dT) primers and M-MLV reverse transcriptase (TaKaRa) following the manufacturer's instructions.

Sequence Retrieval, Primer Design, and Quantitative Real-Time PCR Analysis. Gene sequences were retrieved from the NCBI (http://www.ncbi.nlm.nih.gov/) and orange genome bank (http://citrus.hzau.edu.cn/orange/index.php) by performing keyword searches as well as homology searches. All of the gene-specific primers for real-time polymerase chain reaction (PCR) were designed using the Primer

DOI: 10.1021/jf505843n
J. Agric. Food Chem. 2015, 63, 2618−2627

5 and BatchPrimer3 programs. The actin gene was used as a reference gene to normalize the expression of other genes. The primer sequences are listed in Table 1. Standard curves were created by analyzing a dilution series of mixed cDNA (spanning five orders of magnitude) to calculate the gene-specific PCR efficiency and the regression coefficient for each gene.

Quantitative real-time PCR was performed in 384-well plates in a LightCycler 480 instrument (Roche, Basel, Switzerland) using the LightCycler 480 SYBR Green I Master kit. Each reaction mixture contained 5 μL of SYBR Green I Master, 3.2 μL of PCR-grade water, 1 μL of cDNA, and 0.4 μL of each of the 10 μM forward and the 10 μM reverse gene-specific primers for a final volume of 10 μL. Quantitative real-time PCR analysis was performed using the manufacturer's recommended cycling parameters. The final relative expression levels of the target genes were calculated by the formula $2^{-\Delta\Delta CT}$.[19] Gene expression values represent the means of three biological replicates for each treatment.

Statistical Analysis. Data were subjected to a *t* test using the SPSS 18.0 software (SPSS Inc., Chicago, IL, USA), and the figures were created using OriginPro 8.5 (OriginLab Corporation, Northampton, MA, USA).

RESULTS AND DISCUSSION

Fruit Growth and Development. The choice of rootstock had a significant effect on tree vigor. The 'Shatangju' mandarin trees grafted on Canton lemon produced a greater canopy volume in both years and a larger trunk diameter (Table 2), which showed more vigorous growth compared with the trees that were grafted onto Trifoliate orange. The 'Shatangju' mandarin trees produced similar fruit yields on the two rootstocks (Table 2). Fruit quality was determined for each commercial harvest from 2009 to 2012 (fifth to seventh year after planting) (Table 3). Trees grafted on Canton lemon produced larger fruit in terms of fruit weight and fruit transverse diameter, which were 25% and 9% greater, respectively, than the corresponding values for the 'Shatangju'/Trifoliate orange fruits.

Table 2. Tree Size and Yield of 'Shatangju' Mandarin on Canton Lemon and Trifoliate Orange Rootstocks, Average of the Years 2011 and 2012[a]

rootstock	trunk diameter 10 cm above grafting line (cm)	canopy volume (m^3)	yield (kg)
Canton lemon	32.6 ± 1.6*	11.1 ± 0.4*	39.71 ± 4.1
Trifoliate orange	24.6 ± 0.4	9.05 ± 0.3	45.58 ± 4.2

[a]Data are means ± standard error of two years. Within a column, * indicates a significant difference on the basis of the independent-sample *t* test at $P < 0.05$.

Furthermore, the growth of 'Shatangju' mandarin fruit was significantly influenced by rootstocks (Figure 1). After a period during which the fruit weight steadily increased until December 5, the rate of increase becomes very slow, broadly resembling a flat line (constant weight) on 'Shatangju'/Trifoliate orange, resulting in a final fruit weight and size of only 68.3 g and 54.9 mm, respectively (Figure 1A, B). In contrast, the weight and size of fruits of 'Shatangju'/Canton lemon continued to increase linearly to approximately 86 g and 61 mm, respectively, which were approximately 26% and 11% heavier and larger than the corresponding 'Shatangju'/Trifoliate orange values (Figure 1A, B). No difference in fruit size was observed between the trees on both rootstocks before December, which is consistent with our previous investigation of the 2011 growing season (data not shown).

A classic example of the effect of rootstock on fruit size is provided by a comparison of sour orange and Rough lemon rootstocks. Fruits from trees grafted on Rough lemon were larger, compared to fruits from trees grafted on sour orange.[20] Other studies have also reported that fruits from trees grafted on vigorous rootstocks, such as Rangpur lime, 'Volkamer' lemon, and 'Orlando' tangelo, are generally larger than those produced by trees on dwarfing rootstocks, for example, Trifoliate orange.[2,5,8] Furthermore, 'Shatangju'/Trifoliate orange trees produced fruits with higher TSS contents and TA values. No significant effects of rootstock on other fruit quality characteristics such as seed number and peel thickness were observed (Table 3).

Studies have demonstrated that fruit size is correlated with the number of seeds per fruit[21] and the crop load.[22] Our results revealed that the seed numbers (Table 3) and the fruit yields (Table 2) did not differ significantly between the rootstocks, indicating that the effect of the citrus rootstock on the fruit size may be independent of any effect on the seed number or the fruit yield in this study.

Meanwhile, the mean size of the flavedo cells was determined in cross sections of the equatorial regions of the epicarp (Figure 1C). Differences in the fruit size can be attributed to differences in cell size, cell number, or the amount of intercellular space.[14] During the ripening period, the normal progression of cell expansion was arrested in the flavedo cells in the 'Shatangju'/Trifoliate orange, while the cell size of the 'Shatangju'/Canton lemon continued to increase linearly, which induced a 11.6% greater final cell diameter than 'Shatangju'/Trifoliate orange at the time of harvest (Figure 1C). In short, the results suggest that an enhancement of cell size, caused by increased cell enlargement, contributed greatly to the increase in the fruit size in 'Shatangju'/Canton lemon compared with 'Shatangju'/Trifoliate orange.

Hormone Levels. An increase in the IAA levels was observed in both the peel and the pulp of 'Shatangju'/Canton lemon after December 5, whereas the IAA levels in fruits of 'Shatangju'/Trifoliate orange remained stable, resulting in

Table 3. Mean Values of Fruit Quality Variables for 'Shatangju' Mandarin Grafted on Either Canton Lemon or Trifoliate Orange Rootstocks, for the Period from 2009−2012[a]

rootstock	fruit weight (g)	fruit transverse diameter (mm)	fruit vertical diameter (mm)	peel thickness (mm)	edible portion (%)	TSS (°Brix)	seed no. per fruit	TA (%)
Canton lemon	71.94 ± 3.0*	54.47 ± 1.2*	44.19 ± 0.9	2.31 ± 0.15	68.46 ± 1.6	10.67 ± 0.5*	14.37 ± 2.0	0.29 ± 0.02*
Trifoliate orange	57.55 ± 3.1	49.99 ± 1.5	41.81 ± 0.9	2.13 ± 0.12	70.84 ± 1.7	12.50 ± 0.3	12.71 ± 1.6	0.36 ± 0.02

[a]TSS, total soluble solids; TA, titratable acidity. Data are means ± standard error of four years. Within a column, * indicates a significant difference on the basis of the independent-sample *t* test at $P < 0.05$.

DOI: 10.1021/jf505843n
J. Agric. Food Chem. 2015, 63, 2618−2627

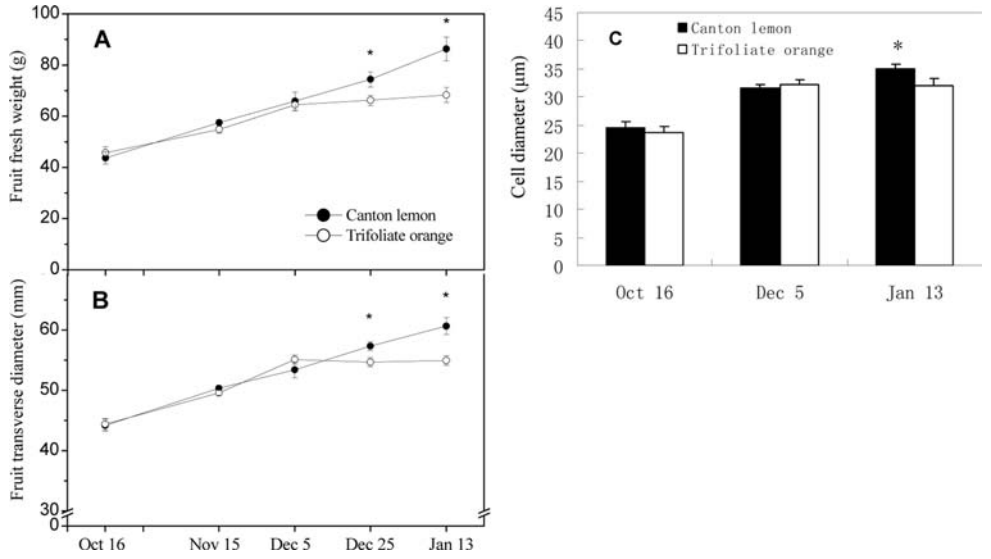

Figure 1. Comparison of fruit growth of 'Shatangju' mandarin grafted on two rootstocks during the 2012 growing season. (A) Fruit fresh weight. (B) Fruit transverse diameter. (C) Cell size for the equatorial region of the flavedo portion. Error bars show the standard error of five biological replicates. * indicates a significant difference on the basis of the independent-sample t test at $P < 0.05$.

significantly higher IAA concentrations in 'Shatangju'/Canton lemon during the ripening stage (Figure 2). The importance of auxins for fruit growth and maturation has been well established for a wide array of climacteric and nonclimacteric fruits. A number of studies have demonstrated that the IAA concentrations are typically high during the beginning of the cell expansion stage and then decline to low levels at the onset of ripening.[23,24] By drawing on literature, it is clear that auxins are responsible for the increase in cell enlargement in fruit tissues.[25−27] Applications of synthetic auxins after physiological drop have been demonstrated to increase late-stage citrus fruit growth and the final fruit size by affecting cell enlargement, rather than cell division, during juice vesicle development.[28,29]

Meanwhile, auxins may also play a relevant role in the control of fruit ripening.[30] Applications of exogenous auxin delayed fruit ripening.[31] For example, a preveraison auxin treatment delayed grape berry ripening, as measured by TSS, anthocyanins, and the onset of berry size increase, but increased the final fruit size.[32] Thus, we concluded that the higher IAA levels in fruits of 'Shatangju'/Canton lemon likely promoted cell enlargement, resulting in relatively larger fruit size during the later stages of fruit growth. Moreover, numerous studies have also described the effects of synthetic auxins on a range of citrus cultivars during the preharvest stage. Modise et al.[33] suggested that the preharvest application of synthetic auxin inhibits the natural fall of orange fruit and increases the weight of the fruits that are retained, but contrasting results were described by Almeida et al.,[34] who reported no significant effect of synthetic auxin on the fruit size.

GAs have been known for a long time for their role in fruit set and development and promote both cell division and expansion.[30] During the later stage of fruit development, the GA concentrations remained at a very low level after a decline in both tissues of 'Shatangju' mandarin fruit, and there was no difference in GA levels between the rootstocks (Figure 2). Meanwhile, the ZR concentrations in the fruit of 'Shatangju' mandarin decreased with ripening and were not significantly affected by the choice of rootstock except December 5 in the peel (Figure 2).

The ABA concentrations gradually increased in the peel during fruit development and ripening, and the ABA concentration was significantly greater in 'Shatangju'/Trifoliate orange after December 5 (Figure 2). In the pulp, the ABA concentration time series followed a flattened curve, and the ABA concentration of the peel from the 'Shatangju'/Trifoliate orange was greater compared with the peel from the 'Shatangju'/Canton lemon. The ABA level is usually very low in the unripe fruit but increases as a fruit ripens.[35,36] It was found that dwarfing rootstocks could induce higher ABA levels in the grafted trees.[37] So, the higher ABA level in the fruit of 'Shatangju'/Trifoliate orange may be attributed to a rootstock dwarfing effect induced by Trifoliate orange. ABA plays a positive role in fruit ripening, particularly for nonclimacteric fruit,[38] but exerts an inhibiting effect on plant growth.[39] Several studies have indicated that ABA, which serves as an antagonist to the other growth promoting hormones,[40,41] had a negative impact on cell division by blocking or slowing the cell cycle progression[42,43] and inhibited IAA-induced cell enlargement.[44,45] The higher ABA levels in 'Shatangju'/Trifoliate orange may inhibit the fruit growth and cell expansion through suppressing the synthesis of growth promoting hormones, such as GA and auxin.

Expression Levels of Auxin-Related Genes in the Fruit. Auxin is generally produced in the young developing regions of plants such as the shoot apex, emerging leaves, developing lateral roots, primary root tips, and developing seeds.[46] During the cell expansion stage of the fruit, auxin is transported from the seeds, which are an important site of auxin biosynthesis, to the fruit pedicel and the parent plant.[47] As fruits mature and the seeds become dormant, auxin biosynthesis and export from the seeds are inhibited, and the concentrations in the fruit decrease.[30,48] In this study, the final IAA concentrations in the seeds did not differ between the rootstocks (data not shown). Regarding the fruit, the explanation for the increased IAA levels in the fruits of 'Shatangju'/Canton lemon during the later stages of fruit growth is considered.

Auxin transport or distribution is known to passively occur through the bulk flow in the mature phloem and actively

DOI: 10.1021/jf505843n
J. Agric. Food Chem. 2015, 63, 2618−2627

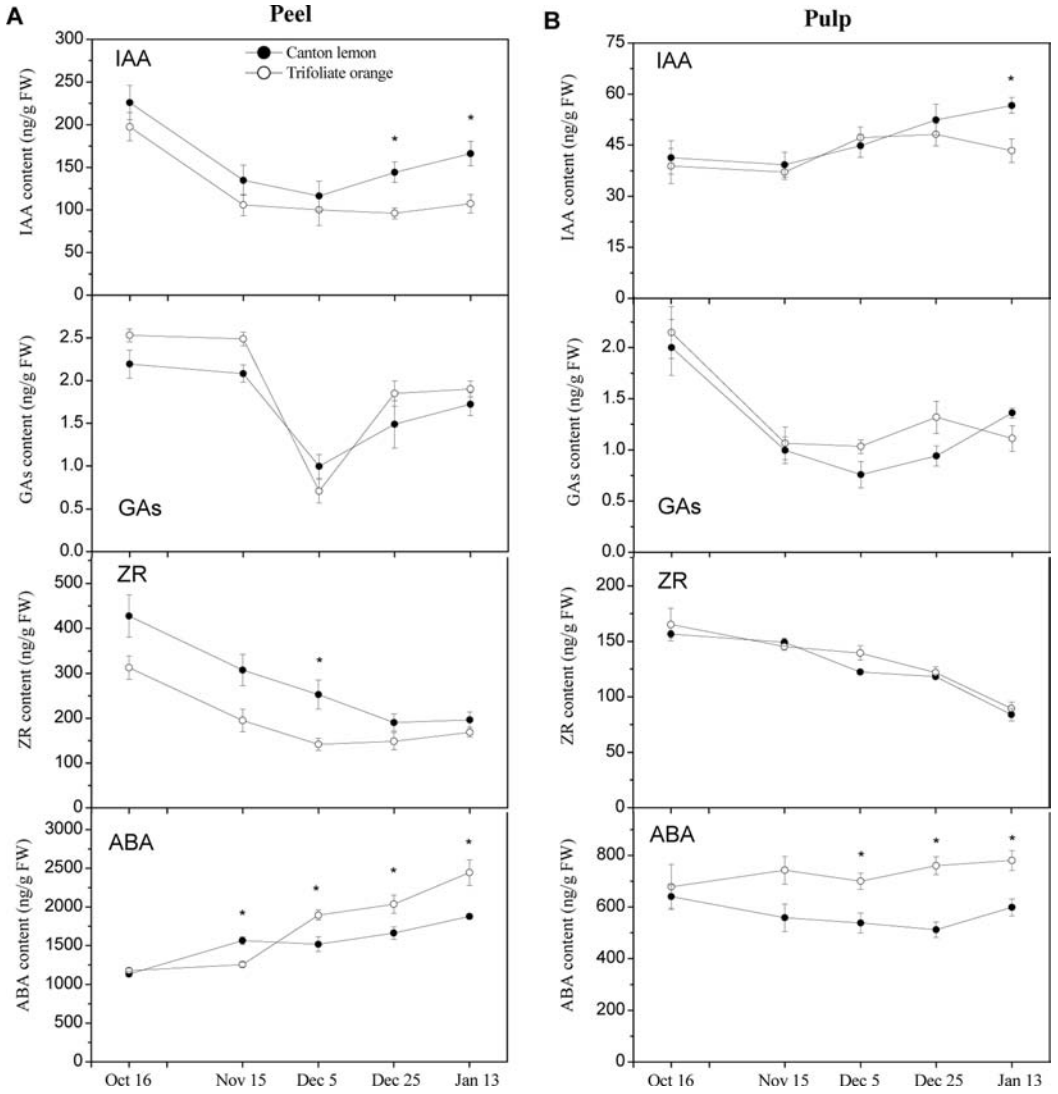

Figure 2. Hormone levels in the fruit of 'Shatangju' mandarin grafted on two rootstocks during the 2012 growing season. (A) Changes in hormone levels in the peel. (B) Changes in hormone levels in the pulp. Error bars show the standard error of five biological replicates. * indicates a significant difference on the basis of the independent-sample t test at $P < 0.05$.

through carrier-mediated cell-to-cell movement.[46,49] The PIN and AUX/LAX proteins have been suggested to function as the auxin efflux and influx carriers, respectively.[49] The results presented in Figure 3A demonstrate that the expression of *AUX1* and *LAX2* genes were upregulated and exhibited significantly higher levels in the peel of 'Shatangju'/Canton lemon at the later stage. The accumulation of AUX1 transcript was also markedly higher in the pulp of 'Shatangju'/Canton lemon (Figure 3B). In contrast, the majority of the PIN family genes was scarcely expressed in the 'Shatangju' mandarin except *PIN1* and *PIN-LIKES 2*, which showed considerably irregular expression patterns in the fruit, suggesting that, in fruit, the auxin influx may be promoted and may be greater than the auxin efflux at this stage. Previous studies have reported that AUX1 can regulate auxin transport between (and within) IAA source and sink tissues and facilitate auxin uptake in sink tissues.[50,51] *LAX3*, another homologous gene, has been suggested to maintain the auxin sink-strength in sink tissues.[52] Hence, we conclude that the higher IAA levels in fruits of 'Shatangju'/Canton lemon may be attributed to an increased IAA import from locations in the parent tree such as the leaves or roots.

To strengthen our understanding of the role of IAA in fruit development and ripening, the relative expression levels of ARFs were assessed by qPCR analyses (Figure 4). ARFs bind to auxin response elements (AuxREs) in the promoters of auxin-regulated genes and mediate auxin signaling by activating or repressing the transcription of these genes.[53] ARFs appear to act at the core of the auxin signal transduction pathway. When the auxin concentrations are low, ARFs dimerize with the Aux/IAA protein, resulting in the repression of auxin response genes. In contrast, higher auxin concentrations cause degradation of the Aux/IAA protein through the 26S proteasome and the release of ARF transcription factors to modulate the expression of early auxin response genes.[54] Recent studies have reported that ARFs are involved in the regulation of various aspects of fruit development.[48,55]

In this study, *ARF2* expression gradually decreased in fruits of 'Shatangju'/Canton lemon, whereas the pattern differed and the level of accumulation was significantly higher in 'Shatangju'/Trifoliate orange during the ripening period (Figure 4). A

DOI: 10.1021/jf505843n
J. Agric. Food Chem. 2015, 63, 2618−2627

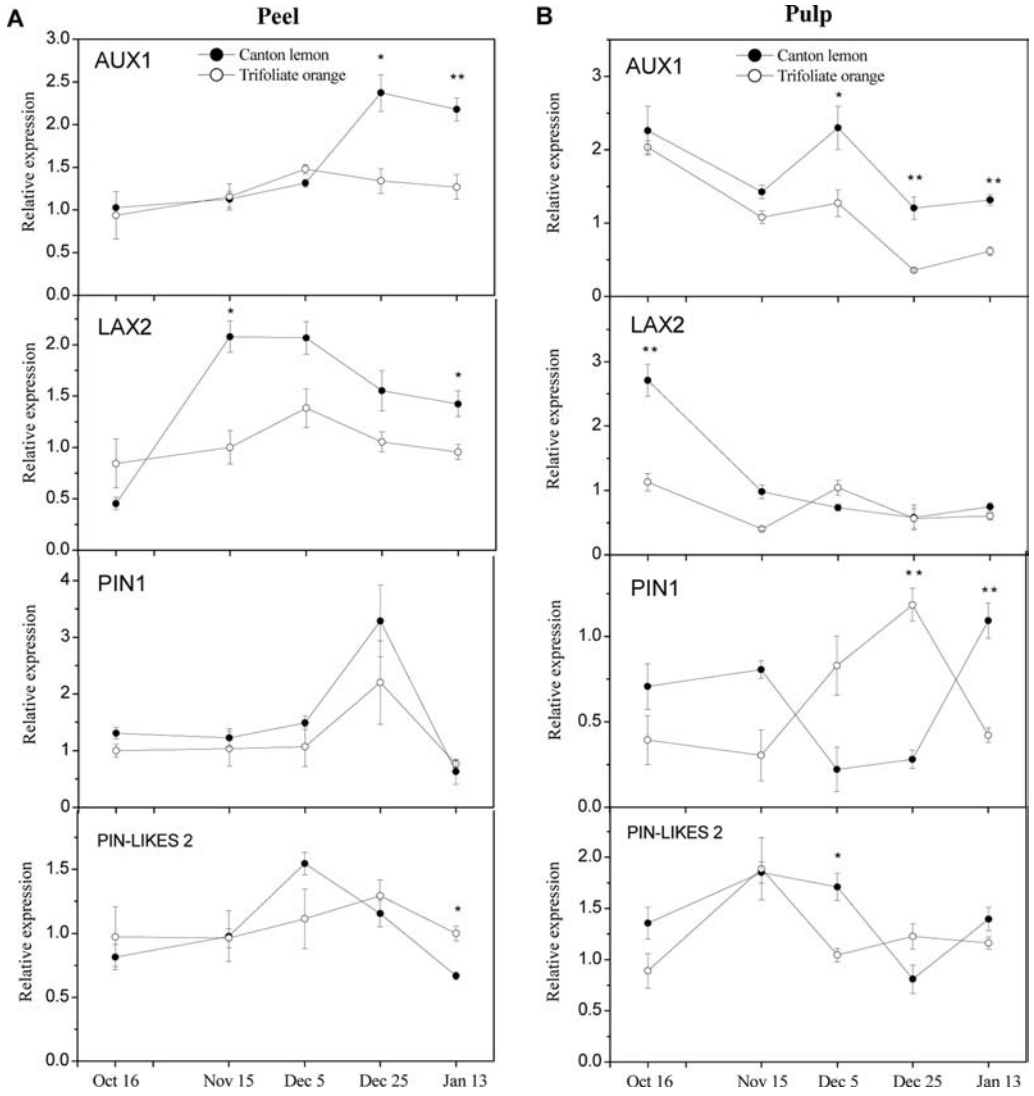

Figure 3. Expression levels of auxin transport genes in the fruit of 'Shatangju' mandarin grafted on two rootstocks during the 2012 growing season. (A) Expression levels in the peel. (B) Expression levels in the pulp. Error bars show the standard error of three biological replicates. * and ** indicate significant differences on the basis of the independent-sample *t* test at $P < 0.05$ and $P < 0.01$, respectively.

similar behavior was also observed for *ARF1*, which has been suggested to share redundant functions with *ARF2* in *Arabidopsis*.[56] In *Arabidopsis*, *arf2* mutants exhibit pleiotropic effects, including elongated hypocotyls and larger organ sizes because of the increases in cell division and cell expansion.[57] However, the role of the ARF2 protein in auxin signaling remains largely unknown. Several studies have reported that *arf2* mutations do not affect auxin signaling nor the endogenous free auxin content,[56,58] suggesting that *ARF2* does not participate in the auxin response pathway. ARF2 is thought to act as a transcriptional repressor and to have strong binding activity to synthetic auxin response elements.[59] ARF2 may mask the effect of AuxREs and prevent the binding of other ARFs, especially ARF transcriptional activators.[56,60]

Furthermore, in this study, the accumulation of *ARF6* transcripts increased with increasing ripening in the peel and pulp, and the transcript level was markedly higher in 'Shatangju'/Canton lemon during the later stages of fruit development (Figure 4), suggesting that *ARF6* may be involved in the regulation of 'Shatangju' mandarin fruit size. *ARF6* is believed to function as a transcriptional activator in *Arabidopsis*[59] and is a cleavage target of the microRNA miR167.[61] Devoghalaere et al.[48] reported that *ARF6* was upregulated in the later stage of apple fruit development, which is consistent with our study. The genetic marker developed from *ARF6* was also mapped to the fruit size QTL, although this marker is not the strongest in that region.[48] These results indicate that ARF genes are involved in the control of fruit size and that citrus rootstocks may modulate auxin signaling by affecting the ARF gene transcription levels in fruit, resulting in changes in fruit size.

Expansin Gene Expression Levels in Fruit. Expansins are cell-wall-loosening proteins that induce the hydrolysis of matrix polymers, enabling the extension of plant cell walls.[62] We evaluated the changes in expansin gene expression levels in 'Shatangju' mandarin grafted on two rootstocks because expansins have been suggested to play key roles in cell expansion and fruit softening during fruit growth and ripening.[63]

The accumulation patterns for EXP1 transcripts were similar for the peel and pulp of 'Shatangju' mandarin fruit (Figure 5). *EXP1* expression gradually increased before December 5 and

DOI: 10.1021/jf505843n
J. Agric. Food Chem. 2015, 63, 2618−2627

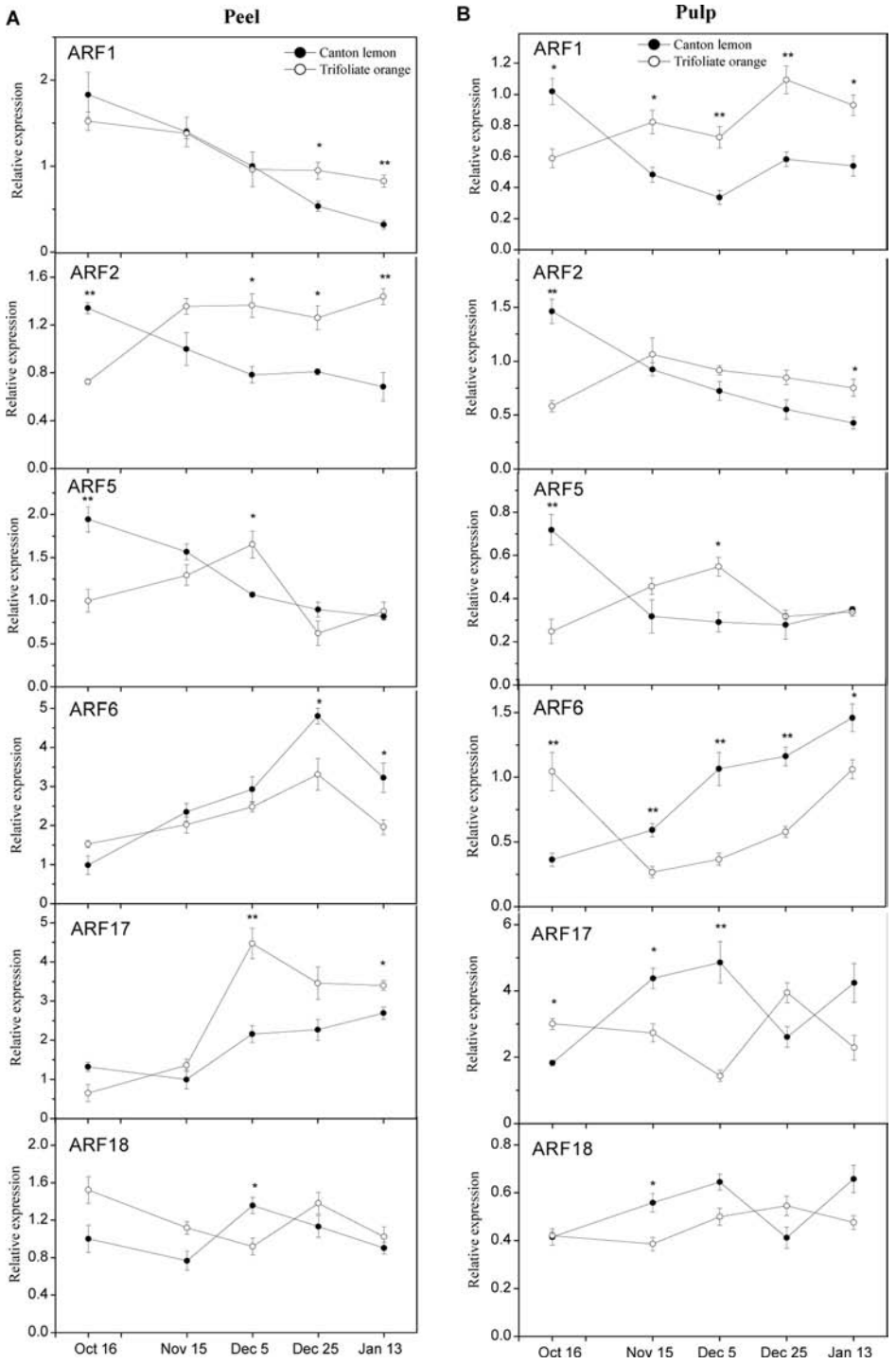

Figure 4. Expression levels of ARF genes in the fruit of "Shatangju" mandarin grafted on two rootstocks during the 2012 growing season. (A) Expression levels in the peel. (B) Expression levels in the pulp. Error bars show the standard error of three biological replicates. *and ** indicate significant differences on the basis of the independent-sample *t* test at $P < 0.05$ and $P < 0.01$ respectively.

then steadily decreased; at this time, the level of *EXP1* expression was greater in the fruit of 'Shatangju'/Canton lemon than in 'Shatangju'/Trifoliate orange in both tissues. The *EXP10* gene in the pulp was upregulated during the ripening period, and the expression levels were also higher in 'Shatangju'/Canton lemon at the later stage. The observed increase in *EXP1* expression levels was in accordance with the results of Rose et al.,[64] who reported that *EXP1* is specifically expressed in ripening tomato fruit, suggesting that expansins may contribute to cell wall disassembly and fruit softening. In addition, transgenic experiments have demonstrated increased cell elongation and organ dimensions in plants overexpressing *EXPA1*[65] or *EXP10*.[66] The *EXP3* expression patterns were irregular in the pulp, but the expression level in the peel was greater in 'Shatangju'/Canton lemon than in 'Shatangju'/Trifoliate orange (Figure 5). Hence, the larger fruit size of 'Shatangju'/Canton lemon is likely related to the higher activity of expansins, which function endogenously, because the activity

DOI: 10.1021/jf505843n
J. Agric. Food Chem. 2015, 63, 2618−2627

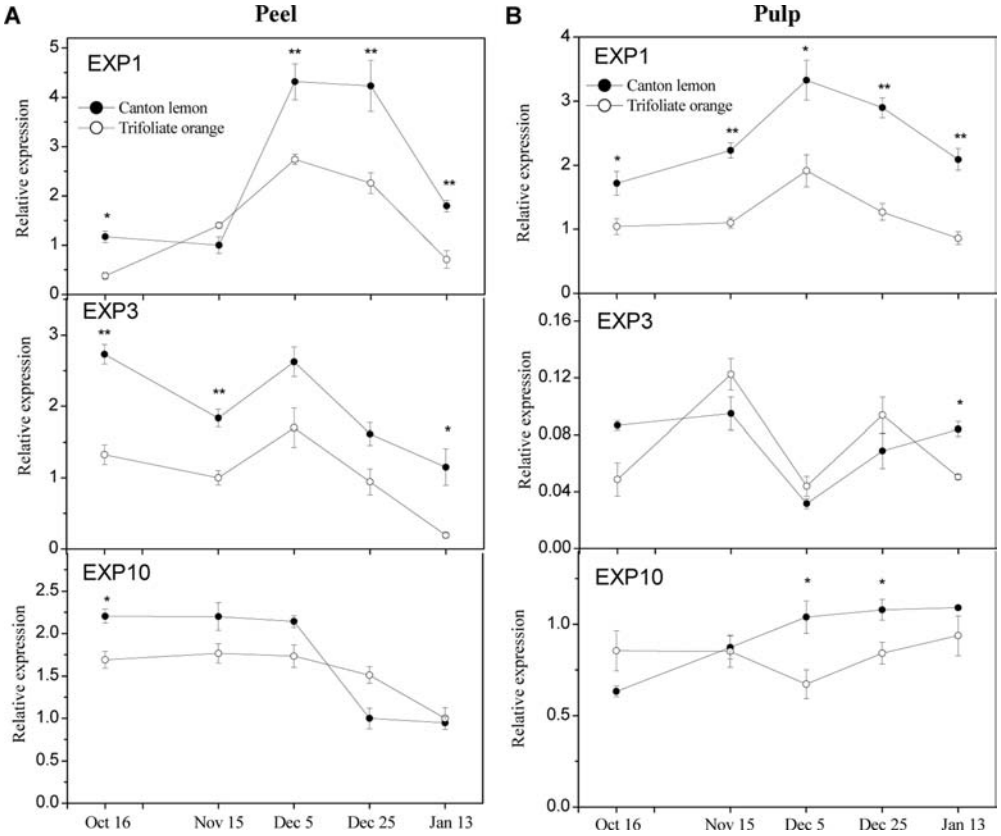

Figure 5. Expression levels of expansin genes in the fruit of 'Shatangju' mandarin grafted on two rootstocks during the 2012 growing season. (A) Expression levels in the peel. (B) Expression levels in the pulp. Error bars show the standard error of three biological replicates. * and ** indicate significant differences on the basis of the independent-sample *t* test at $P < 0.05$ and $P < 0.01$, respectively.

of cell-wall-loosening agents contribute to cell expansion. The reason for the change in expansin activity of citrus fruit on various rootstocks is obscure. However, the activity of expansins may be regulated by either auxin,[67] ethylene, or the cell wall pH.[68]

In conclusion, our results have demonstrated that citrus rootstocks exert a significant effect on fruit size through the regulation of cell size. The difference in fruit size was closely related to the increase in the IAA levels in the fruit of 'Shatangju'/Canton lemon, which may result from the enhanced IAA import from parent trees. Multiple ARF genes, such as the transcriptional repressors *ARF1* and *ARF2* and the transcriptional activator *ARF6*, were significantly affected by the choice of rootstock and may be involved in the control of the fruit size. Although the IAA level in the 'Shatangju' mandarin fruit is closely related to the fruit size control induced by rootstocks, further studies are needed to confirm this relationship on other scions that are grafted onto different rootstocks and to survey whether the application of synthetic auxins strengthens or weakens the rootstock effect on fruit growth regulation.

In addition, the ABA concentrations in the fruit of 'Shatangju'/Trifoliate orange were greater than those in 'Shatangju'/Canton lemon at the later stage of fruit development. The higher ABA levels in 'Shatangju'/Trifoliate orange may inhibit the fruit growth and cell expansion through suppression of the synthesis of growth promoting hormones. Moreover, our present results indicate that the larger fruit of 'Shatangju'/Canton lemon may be attributed to the enhanced cell expansion, which is achieved through increased cell wall loosening because of higher expansin gene transcript levels and through the concomitant higher water uptake associated with the more extensive rooting system of this vigorous rootstock. The results of this study imply that multiple pathways may influence citrus rootstocks regarding fruit growth, and an understanding of these mechanisms may optimize the production of high quality citrus fruits.

AUTHOR INFORMATION

Corresponding Authors

* (J. L.) Phone: +86 137 5177 4213; e-mail: 13751774213@139.com.

*(J. C.) Phone: +86 020-8528 6902; e-mail: cjzlxb@scau.edu.cn.

Author Contributions

‖Juan Li and Xiangyu Liu contributed equally to this work.

Funding

We are grateful to the Natural Science Foundation of Guangdong Province (S2013010013223), the National Natural Science Foundation of China (no. 31372008), the Training program of outstanding young teacher in Guangdong Province (no. yq2013095), and the Agricultural Industry Technology System of Fruit in Guangdong Province for financial support.

Notes

The authors declare no competing financial interest.

ABBREVIATIONS USED

TSS, total soluble solids; TA, titratable acidity; ARFs, auxin response factors; EXP, expansin; ELISA, enzyme-linked

DOI: 10.1021/jf505843n
J. Agric. Food Chem. 2015, 63, 2618−2627

immunosorbent assay; IAA, indole-3-acetic acid; ZR, zeatin riboside; ABA, abscisic acid

REFERENCES

(1) Liu, Y.; Heying, E.; Tanumihardjo, S. A. History, global distribution, and nutritional importance of citrus fruits. *Compr. Rev. Food Sci. Food Saf.* **2012**, *11* (6), 530−545.

(2) Shafieizargar, A.; Awang, Y.; Shukor Juraimi, A.; Othman, R. Yield and fruit quality of 'Queen' orange [*Citrus sinensis* (L) Osb.] grafted on different rootstocks in Iran. *Aust. J. Crop Sci.* **2012**, *6* (5), 777−783.

(3) Castle, W. S. Rootstock as a fruit quality factor in citrus and deciduous tree crops. *N. Z. J. Crop Hortic. Sci.* **1995**, *23* (4), 383−394.

(4) Benjamin, G.; Tietel, Z.; Porat, R. Effects of rootstock/scion combinations on the flavor of citrus fruit. *J. Agric. Food Chem.* **2013**, *61* (47), 11286−11294.

(5) Cantuarias-Avilés, T.; Mourão Filho, F. D. A. A.; Stuchi, E. S.; Da Silva, S. R.; Espinoza-Nuñez, E. Horticultural performance of 'Folha Murcha' sweet orange onto twelve rootstocks. *Sci. Hortic. (Amsterdam, Neth.)* **2011**, *129* (2), 259−265.

(6) Stenzel, N. M. C.; Neves, C. S. V. J.; Scholz, M. B. D. S.; Gomes, J. C. Comportamento da laranjera 'Folha Murcha' em sete porta-enxertos no noroeste do Paraná. *Rev. Bras. Frutic.* **2005**, *27*, 408−411.

(7) Tazima, Z. H.; Neves, C. S. V. J.; Yada, I. F. U.; Leite Júnior, R. P. Performance of 'Okitsu' Satsuma Mandarin on nine rootstocks. *Sci. Agric. (Piracicaba, Braz.)* **2013**, *70*, 422−427.

(8) Cantuarias-Avilés, T.; Mourão Filho, F. D. A. A.; Stuchi, E. S.; Silva, S. R. D.; Espinoza-Núñez, E. Tree performance and fruit yield and quality of 'Okitsu' Satsuma mandarin grafted on 12 rootstocks. *Sci. Hortic. (Amsterdam, Neth.)* **2010**, *123* (3), 318−322.

(9) Gre, L. B.; Magyar, Z.; López-Juez, E. New clues to organ size control in plants. *Genome Biol.* **2008**, *9* (7), 226.

(10) Gonzalez, N.; Beemster, G. T.; Inze, D. David and Goliath: What can the tiny weed Arabidopsis teach us to improve biomass production in crops? *Curr. Opin. Plant Biol.* **2009**, *12* (2), 157−64.

(11) Ariizumi, T.; Shinozaki, Y.; Ezura, H. Genes that influence yield in tomato. *Breed Sci.* **2013**, *63* (1), 3−13.

(12) Xu, Q.; Chen, L.; Ruan, X.; Chen, D.; Zhu, A.; Chen, C.; Bertrand, D.; Jiao, W.; Hao, B.; Lyon, M. P.; Chen, J.; Gao, S.; Xing, F.; Lan, H.; Chang, J.; Ge, X.; Lei, Y.; Hu, Q.; Miao, Y.; Wang, L.; Xiao, S.; Biswas, M. K.; Zeng, W.; Guo, F.; Cao, H.; Yang, X.; Xu, X.; Cheng, Y.; Xu, J.; Liu, J.; Luo, O. J.; Tang, Z.; Guo, W.; Kuang, H.; Zhang, H.; Roose, M. L.; Nagarajan, N.; Deng, X.; Ruan, Y. The draft genome of sweet orange (*Citrus sinensis*). *Nat. Genet.* **2012**, *45* (1), 59−66.

(13) Iglesias, D. J.; Cercós, M.; Colmenero-Flores, J. M.; Naranjo, M. A.; Ríos, G.; Carrera, E.; Ruiz-Rivero, O.; Lliso, I.; Morillon, R.; Tadeo, F. R.; Talon, M. Physiology of citrus fruiting. *Braz. J. Plant Physiol.* **2007**, *19*, 333−362.

(14) Guo, M.; Simmons, C. R. Cell number counts − The *fw2.2* and *CNR* genes and implications for controlling plant fruit and organ size. *Plant Sci.* **2011**, *181* (1), 1−7.

(15) Jiang, X. W.; Zeng, J. W.; Jiang, B.; Yi, G.; Shi, X. H. The effect of rootstocks on change of fruit quality and storage on tree of citrus reticulate 'Nianju'. *Acta Hortic. Sin.* **2012**, *02*, 349−354.

(16) Cajuste, J. F.; García-Breijo, F. J.; Reig-Armiñana, J.; Lafuente, M. T. Ultrastructural and histochemical analysis reveals ethylene-induced responses underlying reduced peel collapse in detached citrus fruit. *Microsc. Res. Tech.* **2011**, *74* (10), 970−979.

(17) Teng, N.; Wang, J.; Chen, T.; Wu, X.; Wang, Y.; Lin, J. Elevated CO_2 induces physiological, biochemical and structural changes in leaves of *Arabidopsis thaliana*. *New Phytol.* **2006**, *172* (1), 92−103.

(18) He, H. Y.; He, L. F.; Gu, M. H.; Li, X. F. Nitric oxide improves aluminum tolerance by regulating hormonal equilibrium in the root apices of rye and wheat. *Plant Sci.* **2012**, *183*, 123−30.

(19) Livak, K. J.; Schmittgen, T. D. Analysis of relative gene expression data using real-time quantitative PCR and the $2^{-\Delta\Delta CT}$ method. *Methods* **2001**, *25* (4), 402−408.

(20) Castle, W. S.; Tucker, D. P. H.; Krezdorn, A. H.; Youtsey, C. O. *Rootstocks for Florida Citrus*; University of Florida: Gainesville, FL, 1993.

(21) Ketsa, S. Effects of seed number on fruit characteristics of tangerine. *Seed* **2010**, *8* (16), 24.

(22) Stopar, M.; Bolcina, U.; Vanzo, A.; Vrhovsek, U. Lower crop load for cv. Jonagold apples. *J. Agric. Food Chem.* **2002**, *50* (6), 1643−1646.

(23) Buta, J. G.; Spaulding, D. W. Changes in indole-3-acetic acid and abscisic acid levels during tomato (*Lycopersicon esculentum* Mill.) fruit development and ripening. *J. Plant Growth Regul.* **1994**, *13* (3), 163−166.

(24) Zhang, X.; Luo, G.; Wang, R.; Wang, J.; Himelrick, D. G. Growth and developmental responses of seeded and seedless grape berries to shoot girdling. *J. Am. Soc. Hortic. Sci.* **2003**, *128* (3), 316−323.

(25) Teale, W. D.; Paponov, I. A.; Palme, K. Auxin in action: Signalling, transport and the control of plant growth and development. *Nat. Rev. Mol. Cell Biol.* **2006**, *7* (11), 847−859.

(26) Stern, R. A.; Flaishman, M.; Ben-Arie, R. Effect of synthetic auxins on fruit size of five cultivars of Japanese plum (*Prunus salicina* Lindl.). *Sci. Hortic. (Amsterdam, Neth.)* **2007**, *112* (3), 304−309.

(27) Gillaspy, G.; Ben-David, H.; Gruissem, W. Fruits: A developmental perspective. *Plant Cell* **1993**, *5* (10), 1439−1451.

(28) Agustí, M.; Almela, V.; Aznar, M.; El-Otmani, M.; Pons, J. Satsuma mandarin fruit size increased by 2,4-DP. *HortScience* **1994**, *29* (4), 279−281.

(29) El-Otmani, M.; Agustí, M.; Aznar, M.; Almela, V. Improving the size of 'Fortune' mandarin fruits by the auxin 2,4-DP. *Sci. Hortic. (Amsterdam, Neth.)* **1993**, *55* (3−4), 283−290.

(30) McAtee, P.; Karim, S.; Schaffer, R.; David, K. A dynamic interplay between phytohormones is required for fruit development, maturation, and ripening. *Front Plant Sci.* **2013**, *4*, 79.

(31) Davies, C.; Boss, P. K.; Robinson, S. P. Treatment of grape berries, a nonclimacteric fruit with a synthetic auxin, retards ripening and alters the expression of developmentally regulated genes. *Plant Physiol.* **1997**, *115* (3), 1155−1161.

(32) Bottcher, C.; Harvey, K.; Forde, C. G.; Boss, P. K.; Davies, C. Auxin treatment of pre-veraison grape (*Vitis vinifera* L.) berries both delays ripening and increases the synchronicity of sugar accumulation. *Aust. J. Grape Wine Res.* **2011**, *17* (1), 1−8.

(33) Modise, D. M.; Likuku, A. S.; Thuma, M.; Phuti, R. The influence of exogenously applied 2, 4-dichlorophenoxyacetic acid on fruit drop and quality of navel oranges (Citrus sinensis L.). *Afr. J. Biotechnol.* **2009**, *8* (10), 2131−2137.

(34) Almeida, I. M. L. D.; Rodrigues, J. D.; Ono, E. O. Application of plant growth regulators at pre-harvest for fruit development of 'PÊRA' oranges. *Braz. Arch. Biol. Technol.* **2004**, *47*, 511−520.

(35) Richardson, G. R.; Cowan, A. K. Abscisic acid content of *citrus* flavedo in relation to colour development. *J. Hortic. Sci. Biotechnol.* **1995**, *70* (5), 769−774.

(36) Setha, S. Roles of abscisic acid in fruit ripening. *Walailak J. Sci. Technol.* **2012**, *9* (4), 297−308.

(37) Yadava, U. L.; Dayton, D. F. The relation of endogenous abscisic acid to the dwarfing capability of East Malling apple rootstocks. *J. Am. Soc. Hortic. Sci.* **1972**, *97*, 701−705.

(38) Jia, H. F.; Chai, Y. M.; Li, C. L.; Lu, D.; Luo, J. J.; Qin, L.; Shen, Y. Y. Abscisic acid plays an important role in the regulation of strawberry fruit ripening. *Plant Physiol.* **2011**, *157* (1), 188−99.

(39) Jarret, R.; Gawel, N. Abscisic acid-induced growth inhibition of sweet potato (*Ipomoea batatas* L.) in vitro. *Plant Cell, Tissue Organ Cult.* **1991**, *24* (1), 13−18.

(40) Mahouachi, J.; Gómez-Cadenas, A.; Primo-Millo, E.; Talon, M. Antagonistic changes between abscisic acid and gibberellins in citrus fruits subjected to a series of different water conditions. *J. Plant Growth Regul.* **2005**, *24* (3), 179−187.

(41) Sun, J.; Li, C. Cross talk of signaling pathways between ABA and other phytohormones. In *Abscisic Acid: Metabolism, Transport and*

DOI: 10.1021/jf505843n
J. Agric. Food Chem. 2015, 63, 2618−2627

Signaling; Zhang, D.-P., Ed.; Springer: Dordrecht, Netherlands, 2014; pp 243−253.
(42) Smalle, J. The pleiotropic role of the 26S proteasome subunit RPN10 in Arabidopsis growth and development supports a substrate-Specific function in abscisic acid signaling. *Plant Cell* **2003**, *15* (4), 965−980.
(43) Swiatek, A.; Lenjou, M.; Van Bockstaele, D.; Inze, D.; Van Onckelen, H. Differential effect of jasmonic acid and abscisic acid on cell cycle progression in tobacco BY-2 cells. *Plant Physiol.* **2002**, *128* (1), 201−211.
(44) Tanada, T. Indoleacetic acid and abscisic acid antagonism: II. On the phytochrome-mediated attachment of barley root tips on glass. *Plant Physiol.* **1973**, *51* (1), 154−7.
(45) Gehring, C. A.; Irving, H. R.; Parish, R. W. Effects of auxin and abscisic acid on cytosolic calcium and pH in plant cells. *Proc. Natl. Acad. Sci. U.S.A.* **1990**, *87* (24), 9645−9.
(46) Michniewicz, M.; Brewer, P. B.; Friml, J. Polar auxin transport and asymmetric auxin distribution. *Arabidopsis Book* **2007**, *5*, e0108.
(47) Pattison, R. J.; Catala, C. Evaluating auxin distribution in tomato (*Solanum lycopersicum*) through an analysis of the *PIN* and *AUX/LAX* gene families. *Plant J.* **2012**, *70* (4), 585−98.
(48) Devoghalaere, F.; Doucen, T.; Guitton, B.; Keeling, J.; Payne, W.; Ling, T. J.; Ross, J. J.; Hallett, I. C.; Gunaseelan, K.; Dayatilake, G. A.; Diak, R.; Breen, K. C.; Tustin, D. S.; Costes, E.; Chagné, D.; Schaffer, R. J.; David, K. M. A genomics approach to understanding the role of auxin in apple (*Malus x domestica*) fruit size control. *BMC Plant Biol.* **2012**, *12*, 7.
(49) Petrasek, J.; Friml, J. Auxin transport routes in plant development. *Development* **2009**, *136* (16), 2675−88.
(50) Marchant, A.; Bhalerao, R.; Casimiro, I.; Eklof, J.; Casero, P. J.; Bennett, M.; Sandberg, G. AUX1 promotes lateral root formation by facilitating indole-3-acetic acid distribution between sink and source tissues in the Arabidopsis seedling. *Plant Cell* **2002**, *14* (3), 589−97.
(51) Vandenbussche, F.; Petrasek, J.; Zadnikova, P.; Hoyerova, K.; Pesek, B.; Raz, V.; Swarup, R.; Bennett, M.; Zazimalova, E.; Benkova, E.; Van Der Straeten, D. The auxin influx carriers AUX1 and LAX3 are involved in auxin-ethylene interactions during apical hook development in *Arabidopsis thaliana* seedlings. *Development* **2010**, *137* (4), 597−606.
(52) Swarup, K.; Benkova, E.; Swarup, R.; Casimiro, I.; Peret, B.; Yang, Y.; Parry, G.; Nielsen, E.; De Smet, I.; Vanneste, S.; Levesque, M. P.; Carrier, D.; James, N.; Calvo, V.; Ljung, K.; Kramer, E.; Roberts, R.; Graham, N.; Marillonnet, S.; Patel, K.; Jones, J. D.; Taylor, C. G.; Schachtman, D. P.; May, S.; Sandberg, G.; Benfey, P.; Friml, J.; Kerr, I.; Beeckman, T.; Laplaze, L.; Bennett, M. J. The auxin influx carrier LAX3 promotes lateral root emergence. *Nat. Cell Biol.* **2008**, *10* (8), 946−54.
(53) Guilfoyle, T. J.; Hagen, G. Auxin response factors. *Curr. Opin. Plant Biol.* **2007**, *10* (5), 453−460.
(54) Guilfoyle, T. Plant biology: Sticking with auxin. *Nature* **2007**, *446* (7136), 621−2.
(55) Kumar, R.; Tyagi, A. K.; Sharma, A. K. Genome-wide analysis of auxin response factor (ARF) gene family from tomato and analysis of their role in flower and fruit development. *Mol. Genet. Genomics* **2011**, *285* (3), 245−260.
(56) Okushima, Y.; Mitina, I.; Quach, H. L.; Theologis, A. AUXIN RESPONSE FACTOR 2 (ARF2): A pleiotropic developmental regulator. *Plant J.* **2005**, *43* (1), 29−46.
(57) Schruff, M. C.; Spielman, M.; Tiwari, S.; Adams, S.; Fenby, N.; Scott, R. J. The AUXIN RESPONSE FACTOR 2 gene of *Arabidopsis* links auxin signalling, cell division, and the size of seeds and other organs. *Development* **2006**, *133* (2), 251−61.
(58) Ellis, C. M.; Nagpal, P.; Young, J. C.; Hagen, G.; Guilfoyle, T. J.; Reed, J. W. *AUXIN RESPONSE FACTOR1* and *AUXIN RESPONSE FACTOR2* regulate senescence and floral organ abscission in *Arabidopsis thaliana*. *Development* **2005**, *132* (20), 4563−74.
(59) Ulmasov, T.; Hagen, G.; Guilfoyle, T. J. Dimerization and DNA binding of auxin response factors. *Plant J.* **1999**, *19* (3), 309−19.
(60) Lim, P. O.; Lee, I. C.; Kim, J.; Kim, H. J.; Ryu, J. S.; Woo, H. R.; Nam, H. G. Auxin response factor 2 (ARF2) plays a major role in regulating auxin-mediated leaf longevity. *J. Exp. Bot.* **2010**, *61* (5), 1419−30.
(61) Wu, M. F.; Tian, Q.; Reed, J. W. *Arabidopsis microRNA167* controls patterns of *ARF6* and *ARF8* expression, and regulates both female and male reproduction. *Development* **2006**, *133* (21), 4211−8.
(62) Cosgrove, D. J. Loosening of plant cell walls by expansins. *Nature* **2000**, *407*, 321−326.
(63) Kalamaki, M. S.; Powell, A. L. T.; Struijs, K.; Labavitch, J. M.; Reid, D. S.; Bennett, A. B. Transgenic overexpression of expansin influences particle size distribution and improves viscosity of tomato juice and paste. *J. Agric. Food Chem.* **2003**, *51* (25), 7465−7471.
(64) Rose, J. K.; Lee, H. H.; Bennett, A. B. Expression of a divergent expansin gene is fruit-specific and ripening-regulated. *Proc. Natl. Acad. Sci. U.S.A.* **1997**, *94* (11), 5955−60.
(65) Dal Santo, S.; Fasoli, M.; Cavallini, E.; Tornielli, G. B.; Pezzotti, M.; Zenoni, S. PhEXPA1, a *Petunia hybrida* expansin, is involved in cell wall metabolism and in plant architecture specification. *Plant Signaling Behav.* **2011**, *6* (12), 2031−2034.
(66) Cho, H. T.; Cosgrove, D. J. Altered expression of expansin modulates leaf growth and pedicel abscission in *Arabidopsis thaliana*. *Proc. Natl. Acad. Sci. U.S.A.* **2000**, *97* (17), 9783−8.
(67) Carrera, E.; Ruiz-Rivero, O.; Peres, L. E.; Atares, A.; Garcia-Martinez, J. L. Characterization of the procera tomato mutant shows novel functions of the SlDELLA protein in the control of flower morphology, cell division and expansion, and the auxin-signaling pathway during fruit-set and development. *Plant Physiol.* **2012**, *160* (3), 1581−96.
(68) Vreeburg, R. A. M.; Benschop, J. J.; Peeters, A. J. M.; Colmer, T. D.; Ammerlaan, A. H. M.; Staal, M.; Elzenga, T. M.; Staals, R. H. J.; Darley, C. P.; McQueen-Mason, S. J.; Voesenek, L. A. C. J. Ethylene regulates fast apoplastic acidification and expansin A transcription during submergence-induced petiole elongation in *Rumex palustris*. *Plant J.* **2005**, *43* (4), 597−610.

DOI: 10.1021/jf505843n
J. Agric. Food Chem. 2015, 63, 2618−2627

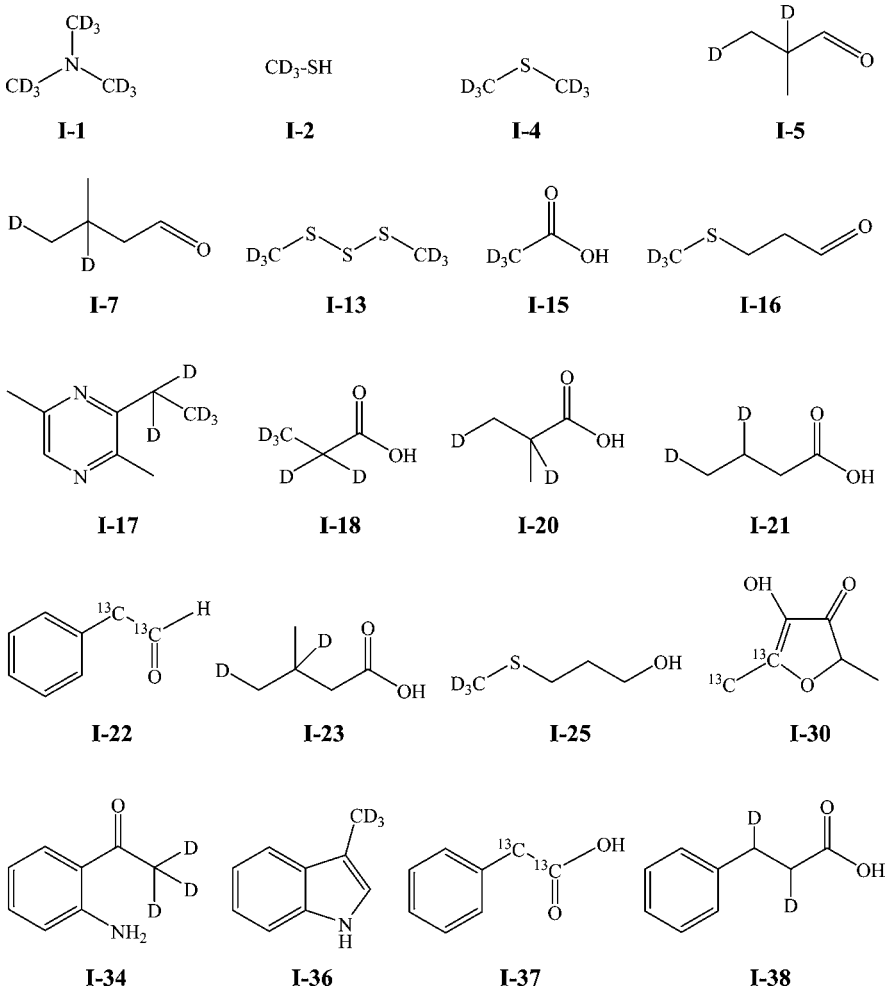

Figure 1. Structures for labeled standards used in stable isotope dilution assays.

concentration of each odorant as well as the matrix composition the product. This approach can be used to verify the results of instrumental analyses and reveal which odorants make the greatest contribution to the overall aroma of the product.

The aim of this study was to identify the key aroma components of premium commercial Thai fish sauce by application of the complementary GC−O techniques, aroma extract dilution analysis (AEDA), static headspace dilution analysis (SHDA), and by calculation of OAVs for predominant odorants based on accurate concentrations determined by SIDA. In addition, the impact of selected predominant odorants on the overall aroma of fish sauce was elucidated by aroma recombination and omission studies.

MATERIALS AND METHODS

Fish Sauce Samples. Two leading brands of commercial premium fish sauce (nam pla) were obtained from a local market (Bangkok, Thailand). They are referred to as fish sauce A (Rayong Fish Sauce Industry Co., Ltd., Rayong, Thailand) and fish sauce B (Marine Resources and Development Co., Ltd., Chantaburi, Thailand). Fish sauce A contained 23.99% (w/w) NaCl and 2.58% (w/w) total nitrogen, while NaCl and total nitrogen contents for fish sauce B were 24.85% (w/w) and 2.18% (w/w), respectively.

Reference Standard Compounds. The following chemicals (listed in Tables 2−7) were obtained from commercial sources given in parentheses: nos. **1**−**8**, **13**, **16**−**25**, **27**, **29**, **30**, and **33**−**38** (Sigma-Aldrich, St. Louis, MO); **15** (Fisher Scientific, Pittsburgh, PA); **28** (Firmenich, Princeton, NJ); **10** (Bedoukian Research Inc., Danbury, CT); **31** and **32** (TCI America, Portland, OR); **11** (Lancaster, Windham, NH). 2-Acetyl-1-pyrroline (no. **12**) was synthesized using the procedure described by Fuganti et al.,[9] and (*Z*)-1,5-octadien-3-one (no. **14**) was synthesized according to Lin et al.[10] Odorless deionized−distilled water was prepared by boiling glass-distilled water in an open flask until its volume was reduced by one-fourth of the original volume.

Isotopically Labeled Compounds. Structures for labeled standards used for quantification by stable isotope dilutions assays are provided in Figure 1. The following labeled compounds were obtained from commercial sources: [$^2H_9$]-trimethylamine (**I-1**), [$^2H_2$]-3-methylbutanal (**I-7**), [$^2H_3$]-acetic acid (**I-15**) (CDN, Pointe-Claire, Quebec, Canada); [$^2H_6$]-dimethyl sulfide (**I-4**) (Sigma-Aldrich); [$^2H_5$]-propanoic acid (**I-18**) (Cambridge Isotope Laboratories, Inc., Tewksbury MA); and [$^{13}C_2$]-2-phenylacetic acid (**I-37**) (Isotec, Miamisburg, OH).

The following labeled compounds were synthesized using previously published methods: [$^2H_3$]-methanethiol (**I-2**),[11] [$^2H_6$]-dimethyltrisulfide (**I-13**),[12] [$^2H_3$]-3-(methylthio)propanal (**I-16**),[12] [$^2H_5$]-3,6-dimethyl-2-ethylpyrazine (**I-17**),[13] [$^2H_2$]-butanoic acid (**I-21**),[14] [$^{13}C_2$]-phenylacetaldehyde (**I-22**),[15] [$^2H_2$]-3-methylbutanoic acid (**I-23**),[14] [$^{13}C_2$]-4-hydroxy-2,5-dimethyl-3(2*H*)-furanone (**I-30**),[16] [$^2H_3$]-*o*-aminoacetophenone (**I-34**),[17] and [$^2H_3$]-skatole (**I-36**).[18]

Synthesis. [2,3-$^2H_2$]-2-Methylpropanal (**I-5**) and [2,3-$^2H_2$]-2-methylpropanoic acid were synthesized from the corresponding labeled alcohol. The uniformly deuterium labeled alcohol was synthesized following a published procedure described for the synthesis of 5,6-[$^2H_2$]-hexan-1-ol[19] with some modifications.

DOI: 10.1021/jf5061248
J. Agric. Food Chem. 2015, 63, 2628−2638

[2,3-$^2H_2$]-2-Methylpropan-1-ol. Chlorotri(triphenylphosphine)-rhodium(I) (Wilkinson's catalyst; Sigma-Aldrich) (15 wt % of the alkenol; 0.45 g) and 2-methyl-2-propen-1-ol (Sigma-Aldrich; 2.5 g, 34.7 mmol) were placed in a pressure reactor equipped with stir bar and rubber septum. The reactor was sealed, then flushed for 5 min with deuterium gas (UHP grade 99.995%; isotopic enrichment 99.7%; Matheson Tri-Gas, Parsippany, NJ) using a needle placed below the surface of the solution. Reaction was carried out at 40 psi until the reaction was complete. The spent catalyst was removed by centrifugation. The target compound was purified by vacuum distillation.

Yield: 1.83 g (99% purity). MS-EI, *m/z* (%): 76 (11) (M+), 58 (5), 57 (7), 46 (5), 45 (100), 44 (64), 43 (59), 42 (42), 41 (13), 40 (13), 39 (8).

[2,3-$^2H_2$]-2-Methylpropanal (I-5). [2,3-$^2H_2$]-2-Methylpropan-1-ol (0.38 g; 5.0 mmol) in 2 mL of dichloromethane was added to a 10 mL suspension of pyridinium chlorochromate (Sigma-Aldrich) (1.2 g; 5.5 mmol) in dichloromethane. The mixture was stirred for 1.5 h at room temperature, and 20 mL of diethyl ether was added. The supernatant was decanted, and the residue was extracted with diethyl ether (3 × 5 mL) until the black gum became granular in consistency. The combined organic phase was filtered through a 10 g bed of Florisil (Sigma-Aldrich). The target compound (**I-5**) was purified by vacuum distillation prior to removal of solvent.

Yield: 0.18 g (92.2% purity). MS-EI, *m/z* (%): 75 (8) (M + 1), 74 (54) (M+), 73 (21), 58 (6), 59 (7), 45 (100), 44 (67), 43 (60), 42 (65), 40 (45), 39 (21).

[2,3-$^2H_2$]-2-Methylpropanoic Acid (I-20). [2,3-$^2H_2$]-2-Methylpropan-1-ol (1.0 g; 13 mmol) was added to a vigorously stirred solution of potassium permanganate (2.5 g, 16 mmol) dissolved in 50 mL of aqueous 0.15 M NaOH in a 200 mL flask. After 2 h, the mixture was acidified with 1 M HCl and then extracted with diethyl ether (3 × 20 mL). The ether layer was extracted with aqueous 0.5 M NaOH (3 × 20 mL). The NaOH extract was acidified with aqueous 4 M HCl and then extracted with ether (3 × 20 mL). The ether layer was washed with aqueous saturated NaCl (2 × 20 mL) and dried over anhydrous Na_2SO_4 (5 g). The target compound (**I-20**) was obtained after removal of the solvent.

Yield: 0.2552 g (98% purity). MS-EI *m/z* (%): 90 (8) (M+), 75 (15), 74 (19), 46 (6), 45 (100), 44 (11), 43 (29), 42 (20), 41 (6), 40 (9).

[2,3-$^2H_2$]-3-Phenylpropanoic Acid (I-38). The deuterated acid was synthesized from cinnamic acid using a modification of the procedure described above for synthesis of [2,3-$^2H_2$]-2-methylpropan-1-ol. Chlorotri(triphenylphosphine)rhodium(I) (Wilkinson's catalyst) (15 wt % of the alkenoic acid; 0.15 g) plus (*E*)-cinnamic acid (Eastman Kodak Co., Rochester, NY; 1.0 g; 34.7 mmol) and 5.0 mL of methanol-*d* (Sigma-Aldrich) were placed in a pressure reactor equipped with stir bar and rubber septum. The reactor was sealed then flushed for 5 min with deuterium gas (UHP grade 99.995%; isotopic enrichment 99.7%; Matheson Tri-Gas) using a needle placed below the surface of the solution. Reaction was carried out at 40 psi until the reaction was complete. The spent catalyst was removed by centrifugation and the solvent evaporated to yield the target compound (**I-38**).

Yield: 0.92 g (95% purity). MS-EI, *m/z* (%): 152 (42) (M+), 107 (15), 106 (43), 105 (22), 93 (9), 92 (100), 91 (16), 80 (5), 79 (10), 78 (13), 77 (6), 66 (8), 52 (6), 51 (10).

Sample Preparation. *Direct Solvent Extraction (DSE).* Fish sauce (20 g) plus 100 mL of odorless-distilled water was mixed well with 25 μL of an internal standard stock solution (1.15 μg/μL of 2-ethyl butyric acid in methanol as acidic fraction internal standard, 1.32 μg/μL of 2-methyl-3-heptanone, and 1.13 μg/μL of 2,4,6-trimethylpyridine in methanol as neutral/basic fraction internal standard). The pH was adjusted to ∼2.0 using 2 M HCl and extracted three times with diethyl ether (100 mL total volume). After the third extraction, the pH of sample was raised to ∼9.0 using 2 M NaOH and extracted three times with diethyl ether (100 mL total volume). The pooled solvent extract (200 mL) was concentrated to 50 mL using a Vigreux column in a 43 °C water bath.

Solvent-Assisted Flavor Evaporation (SAFE). Extracts prepared by DSE were subjected to SAFE to remove any nonvolatile materials, as previously described.[20] The SAFE extract was concentrated to 30 mL using a Vigreux column in a 43 °C water bath and separated into acidic (AF) and neutral/basic (NBF) fractions. The aroma extract (30 mL) was extracted with aqueous 0.1 M NaOH (3 × 20 mL), and the upper layer (diethyl ether) containing the neutral/basic volatiles fraction (NBF) was collected. The aqueous layers were pooled, acidified to pH ∼2.0 with 4 M HCl, saturated with NaCl, and then extracted with diethyl ether (3 × 20 mL). The upper layer containing the acidic volatiles (AF) was collected. The two fractions were washed twice with 15 mL of saturated NaCl solution to 10 mL using a Vigreux column and then dried over 2 g of anhydrous Na_2SO_4. Final volumes of extracts were concentrated using a gentle stream of nitrogen gas to 900 μL for AF and 100 μL for NBF. Extracts were stored in 2 mL glass vials at −70 °C until analysis.

Aroma Extract Dilution Analysis (AEDA). AF and NBF extracts were diluted by volume (1 part aroma extract to 2 parts solvent) in diethyl ether. Each dilution was analyzed by gas chromatography−olfactometry (GC−O) using a 6890 GC (Agilent Technologies, Inc., Palo Alto, CA) equipped with a flame ionization detector (FID) and olfactory detection port (DATU Technology Transfer, Geneva, NY). The sample (2 μL) was injected using direct cool-on-column mode (+3 °C temperature tracking). Separations were performed on polar (Rtx-Wax, 15 m × 0.32 mm i.d.; 0.5 μm film; Restek, Bellefonate, PA) and nonpolar (Rtx-5 SLIMS, 15 m × 0.32 mm i.d.; 0.5 μm film; Restek) columns. The GC oven temperature was programmed from 40 to 225 °C at a rate of 10 °C/min, with initial and final holding times of 5 and 20 min, respectively. Helium was used as the carrier gas at a constant flow rate of 2.2 mL/min. Column effluent was split 1:1 between the FID and the sniffing port using deactivated fused silica tubing (each 1 m × 0.25 mm i.d.; Restek). The FID and sniffing port were maintained at a temperature of 250 °C. GC−O was conducted by two experienced panelists. The flavor dilution factor (FD factor) for a compound was the highest dilution at which it was detected by GC−O. Other details of the procedure have been previously described.[21]

Static Headspace Dilution Analysis (SHDA). GC−O was conducted using a 6890 GC (Agilent Technologies, Inc.) equipped with an FID and olfactory detector port (ODP2; Gerstel, Inc., Germany). Fish sauce sample (5 g) was placed in a 250 mL round-bottom flask and sealed with a PTFE-lined septum. The flask was equilibrated at 40 °C for 30 min with agitation provided by a magnetic stir bar. Each headspace volume (25, 5, 1, 0.2, or 0.04 mL) was injected via a heated (50 °C) gastight syringe into a cooled injection system (CIS-4, Gerstel, Inc.) operating in the solvent vent mode [−120 °C (0.10 min hold) ramped at 12 °C/s to 260 °C (10 min hold); 50 mL/min initial vent flow (0.10 min hold), 1.10 min splitless time, 50 mL/min final split flow]. Separations were performed on Rtx-Wax (15 m × 0.53 mm i.d.; 1 μm film; Restek) and Rtx-5 columns (15 m × 0.53 mm i.d.; 1 μm film; Restek). The GC oven temperature was programmed from 35 to 225 °C at a rate of 6 °C/min, with initial and final holding times of 5 and 10 min, respectively. The FID and ODP2 temperatures were maintained at 250 °C. Column effluent was split 1:1 between the FID and ODP2 using deactivated fused silica tubing as described earlier. Other details of the procedure have been previously described.[21]

Gas Chromatography−Mass Spectrometry (GC−MS). The GC−MS analyses were performed using a 6890 GC/5973 mass selective detector (MSD; Agilent Technologies, Inc.) system. Each aroma extract (1 μL) was injected into a cooled injection system (CIS-4, Gerstel, Inc.) operating in the cold splitless-mode [−50 °C initial temperature (0.10 min hold); ramp rate 12 °C/s; 260 °C final temperature (10 min hold); 1.10 min valve-delay, the 50 mL/min vent flow]. Separations were performed on Stabilwax (30 m × 0.25 mm i.d.; 0.25 μm film; Restek) and Sac-5 columns (30 m × 0.25 mm i.d.; 0.25 μm film; Supleco, Bellefonte, PA). Helium was used as carrier gas at a constant rate of 1.0 mL/min. The GC oven temperature was programmed from 35 to 225 °C at a rate of 4 °C/min with initial and final holding times of 5 and 20 min, respectively. MSD conditions were: capillary direct interface temperature, 280 °C; ionization energy,

DOI: 10.1021/jf5061248
J. Agric. Food Chem. 2015, 63, 2628−2638

70 eV; mass range, 35−350 amu; electron multiplier voltage (Autotune +200 V); scan rate, 5.2 scans/s.

Headspace-Solid Phase Microextraction (H-SPME). For identification of highly volatile odorants, fish sauce sample (1 g) was placed in a 22 mL headspace vial and spiked with 5 μL of internal standards (1.15 μg/μL of 2-ethyl butyric acid, 1.32 μg/μL of 2-methyl-3-heptanone, and 1.13 μg/μL of 2,4,6-trimethylpyridine in methanol). The sample was sealed immediately with a PTFE-lined septum and preincubated at 40 °C for 10 min with agitation (500 rpm, 60 s on, 10 s off) using a MPS2 autosampler (Gerstel, Inc.). Then, a SPME fiber (50/30 μm DVB/carboxen/polydimethylsiloxane fiber; Supelco) was exposed to the vial headspace for 20 min. Then fiber was desorbed by splitless injection (injector temperature 260 °C; splitless time 4 min; vent flow 50 mL/min) into GC−MS system with the same settings as described above. The GC oven temperature was programmed from 35 to 225 °C at a rate of 6 °C/min with an initial and final holding time of 5 and 20 min, respectively.

Compound Identification. Compounds were tentatively identified by GC−O by comparing their retention indices (RIs) and odor properties with those of authentic reference compounds. Compounds were positively identified by comparing their RIs, odor properties, and mass spectra with authentic reference compounds. A homologous series of *n*-alkanes was used for determination of RIs according to the method of van den Dool and Kratz.[22]

Compound Quantification. For quantification of methanethiol (no. **2**), the concentration of the synthesized [$^2H_3$]-methanethiol was first determined by analysis using a 6890 GC−flame photometric detector (GC−FPD) system (Agilent Technologies, Inc.). Headspace volume of methanethiol (50−300 μL) or [$^2H_3$]-methanethiol (5 mL) were drawn by a gastight syringe and injected into 5 mL of methanol in 22 mL sealed headspace vials. Each methanolic sample (1 μL) was injected using hot split mode into an Rtx-Wax column (15 m × 0.53 mm i.d.; 1 um film; Restek). The concentration of [$^2H_3$]-methanethiol (13.7 μg/mL) in the stock solution was determined by comparing its peak area with a standard curve generated from known concentrations of methanethiol (seven levels, from 7.4 to 48.9 μg/mL). For analysis, fish sauce sample was spiked with an appropriate headspace volume of [$^2H_3$]-methanethiol and quantified by H-SPME as described above.

Other compounds in low abundance were quantified by H-SPME and DSE-SAFE as described above, respectively. Highly abundant compounds were analyzed by DSE as described above, except that a 5 g sample was first mixed with isotopically labeled compounds. Then sample was diluted and mixed well with 25 mL of odorless-distilled water. The sample was extracted three times with diethyl ether (60 mL total volume). The pooled solvent extract (60 mL) was evaporated to 10 mL using a Vigreux column in a 43 °C water bath, dried over 2 g of anhydrous Na_2SO_4, and further concentrated to 200 μL under nitrogen gas stream.

The selected ions and response factors of the target (unlabeled) and labeled compounds were determined by H-SPME-GC−MS and GC−MS as described above (Table 2). Response factor for each compound was determined by measuring five levels of defined mixtures of the respective labeled and unlabeled compounds. Concentration for each compound in fish sauce was calculated using the response factor and area of the selected ion and expressed as micrograms per kilogram (ppb). Odor-activity values (OAVs) were calculated by dividing the concentrations by the respective odor thresholds in water, obtained from literature.

Sensory Analysis. *Comparison of Fish Sauce and the Complete Fish Sauce Aroma Model.* Aroma profiling was done by descriptive sensory analysis as previously described.[21] One gram of fish sauce was dissolved in the matrix (10 mL of 0.1 M phosphate buffer, pH 5.6, 25% NaCl) and presented to panelists in 125 mL Nalgene PTFE wash bottles (Fisher, Pittsburgh, PA, USA) with siphon tubes removed from the caps. Bottles were covered with aluminum foil to prevent any visual bias and labeled with random three-digit codes. The 11-member panel (five males, six females, 20−48 years old) were asked to identify and define descriptive terms of fish sauce sample and to determine appropriate aroma references. Odor notes representing fish sauce samples were selected and included cheesy, potatoey, brothy/meaty, fishy/briny, malty, and sulfur (Table 1). Intensity of each reference material was rated on 15 cm universal scales, with intensity ratings of 0 and 15 corresponding to none and very intense, respectively (Table 1). Intensity ratings for the standards were used as calibration references for rating the intensities of the fish sauce samples and the aroma reconstitution models. The complete recombination models, consisting of 21 odorants, were prepared by mixing 1 mL of each stock solution (Table 3) in 10 mL of the aforementioned matrix based on the determined concentrations (Table 3). The panelists were asked to evaluate the intensities of each odor attribute in the fish sauce samples and models. Samples were evaluated in duplicate. Differences among samples were evaluated by analysis of variance with means separation using SPSS version 11 software (SPSS Inc., Chicago, IL).

Table 1. Attributes, References, and Rating for Sensory Descriptive Analysis of Fish Sauce

attribute	reference[a]	rating[b]
cheesy	0.1 g of parmesan cheese	9
potatoey	10 g of mashed potato	8
brothy/meaty	10 mL of a 1% yeast extract aqueous solution	5
fishy/briny	10 mL of a 100 ppb trimethylamine aqueous solution	8
malty	0.1 g of dark chocolate	8
sulfur	2 g of boiled Brussels sprouts	12

[a]Samples were presented in 125 mL PTFE bottles. [b]Aroma intensity was rated on a 15 cm universal scale, with intensity ratings of 0 and 15 corresponding to none and very, respectively.

Omission Experiments. Omission models were prepared in the same matrix described for the recombination models, except that various groups of compounds, namely acids, aldehydes, sulfur compounds, and low OVA compounds, were omitted from each model (Table 3). Sensory comparison of the omission models to the recombination (complete) models was performed using the R-index by ranking method.[23] Panelists were asked to rank the omission models on how different they were from the complete model, from most similar to least similar (n = 19; 5 males, 14 females). The degree of difference of each model compared against complete model was calculated using John Brown computations.[24]

RESULTS AND DISCUSSION

Identification of Odor-Active Compounds. Odor-active compounds from two brands of premium Thai fish sauce (A and B) were isolated by DSE/SAFE. To avoid interferences during GC−O, the aroma extracts were first separated into acidic (AF) and neutral/basic (NBF) fractions. The 29 compounds with $\log_3$FD factor of ≥1 were detected by AEDA, consisting of 11 acidic compounds (Table 4) and 18 neutral/basic compounds (Table 5). The AEDA results for the two fish sauce samples were similar. Compounds in AF with high $\log_3$FD values included acetic acid (vinegar), butanoic acid (cheesy), 3-methyl butanoic acid (cheesy, sweaty), 4-hydroxy-2,5-dimethyl-3(2*H*)-furanone (burnt sugar), 4-hydroxy-2-ethyl-5-methyl-3(2*H*)-furanone (burnt sugar), and 2-phenylacetic acid (rosy, plastic). These were regarded as the predominant acidic odorants based on their high $\log_3$FD factor (≥6). Likewise, predominant odorants in the NBF ($\log_3$FD factor ≥3) were 3-methylbutanal (malty, dark chocolate), 3-(methylthio)propanal (cooked potato), phenylacetaldehyde (rosy, plastic), and *o*-aminoacetophenone (musky, grape, stale).

In a previous study, 2-methylpropanal, 2-methylbutanal, 2-pentanone, 2-ethylpyridine, dimethyl trisulfide, 3-(methylthio)-propanal, and 3-methylbutanoic acid were reported with high FD factors and were regarded as principal contributors to the aroma of Thai fish sauce.[5] The results of the present study

DOI: 10.1021/jf5061248
J. Agric. Food Chem. 2015, 63, 2628−2638

Table 2. Selected Ions (m/z) and Response Factors Used in Stable Isotope Dilution Assays

no.[a]	compd	ion[b]	no.[c]	labeled compd	ion[b]	R_f[d]
1	trimethylamine	58	**I-1**	[$^2H_9$]-trimethylamine	66	0.57
2	methanethiol	48	**I-2**	[$^2H_3$]-methanethiol	51	0.96
4	dimethyl sulfide	62	**I-3**	[$^2H_6$]-dimethyl sulfide	68	4.27
5	2-methylpropanal	72	**I-4**	[$^2H_2$]-2-methylpropanal	74	2.13
6	2-methylbutanal	86	**I-7**[e]	[$^2H_2$]-3-methylbutanal	88	0.96
7	3-methylbutanal	86	**I-7**	[$^2H_2$]-3-methylbutanal	88	1.45
13	dimethyl trisulfide	126	**I-13**	[$^2H_6$]-dimethyl trisulfide	132	1.14
15	acetic acid	60	**I-15**	[$^2H_3$]-acetic acid	63	0.99
16	3-(methylthio)propanal	104	**I-16**	[$^2H_3$]-3-(methylthio)propanal	107	1.70
17	3,6-dimethyl-2-ethylpyrazine	135	**I-17**	[$^2H_5$]-3,6-dimethyl-2-ethylpyrazine	141	0.72
18	propanoic acid	74	**I-18**	[$^2H_5$]-propanoic acid	79	1.28
20	2-methylpropanoic acid	73	**I-20**	[$^2H_2$]-2-methylpropanoic acid	75	0.35
21	butanoic acid	88	**I-21**	[$^2H_2$]-butanoic acid	90	1.20
22	phenylacetaldehyde	120	**I-22**	[$^{13}C_2$]-phenylacetaldehyde	122	2.03
23	3-methylbutanoic acid	87	**I-23**	[$^2H_2$]-3-methylbutanoic acid	89	0.50
25	3-(methylthio)-1-propanol	106	**I-25**	[$^2H_3$]-3-(methylthio) propanol	109	1.07
30	4-hydroxy-2,5-dimethyl-3(2*H*)-furanone	128	**I-30**	[$^{13}C_2$]-4-hydroxy-2,5-dimethyl-3(2*H*)-furanone	130	0.95
34	*o*-aminoacetophenone	135	**I-34**	[$^2H_3$]-*o*-aminoacetophenone	138	1.65
36	skatole	130	**I-36**	[$^2H_3$]-skatole	133	0.37
37	2-phenylacetic acid	136	**I-37**	[$^{13}C_2$]-2-phenylacetic acid	138	0.76
38	3-phenylpropionic acid	150	**I-38**	[$^2H_2$]-3-phenylpropionic acid	152	0.96

[a]Numbers correspond to those in Tables 3−7 and Figures 1 and 2. [b]Selected ion. [c]The letter "I" indicates isotopically labeled compound. [d]Response factor. [e]A structurally similar compound was selected as the internal standard.

Table 3. Concentrations of High Purity Standard Compounds Used to Prepare Fish Sauce Models

			concn (μg/L)	
no.[a]	compd	% purity[b]	A model	B model
	Group 1, Acids[c]			
15	acetic acid[d]	99.9	4960000	4510000
18	propanoic acid[d]	99.4	99850	56100
20	2-methylpropanoic acid	99.5	6450	22400
21	butanoic acid	99.8	131500	308500
23	3-methylbutanoic acid	99.7	20050	95000
37	2-phenylacetic acid	99.3	2700	20600
38	3-phenylpropanoic acid	99.9	3600	1800
	Group 2, Aldehydes[e]			
5	2-methylpropanal	98.0	654	930
6	2-methylbutanal	95.8	376	906
7	3-methylbutanal	96.7	1360	1720
22	phenylacetaldehyde	99.3	177	184
	Group 3, Sulfur-Containing Compounds[e]			
2	methanethiol	99.5	62.5	62.5
4	dimethyl sulfide	99.6	41.1	11.4
13	dimethyl trisulfide	94.6	18.4	27.2
16	3-(methylthio)propanal	97.4	388	1138
25	3-(methylthio)-1-propanol	99.6	710	648
	Group 4, Low OAV Compounds[e]			
1	trimethylamine	99.9	0.860	1.34
17	3,6-dimethyl-2-ethylpyrazine	99.4	1.32	5.54
30	4-hydroxy-2,5-dimethyl-3(2*H*)-furanone	94.4	2600	2500
34	o-aminoacetophenone	99.8	4.02	3.00
36	skatole	99.6	0.474	0.482

[a]Numbers corresponded to those in Tables 2, 4−7. [b]Purity determined by GC−O and GC−FID analysis. [c]Stock solution prepared in water. [d]Compound was used neat. [e]Stock solution prepared in methanol.

confirm the importance of most of the above compounds, except for 2-pentanone and 2-ethylpyridine. Furthermore, 4-hydroxy-2,5-dimethyl-3(2*H*)-furanone, 4-hydroxy-2(or 5)-ethyl-5(or 2)-methyl-3(2*H*)-furanone, and 3-hydroxy-4,5-dimethyl-2(5*H*) furanone were identified for the first time as odor-active compounds in fish sauce.

4-Hydroxy-2,5-dimethyl-3(2*H*)-furanone has been found in many foods, including pineapple,[25] strawberry,[26] beef broth,[27]

DOI: 10.1021/jf5061248
J. Agric. Food Chem. 2015, 63, 2628−2638

Table 4. Predominant Acidic Odorants (Log_3FD factor ≥1) in Fish Sauce Determined by Aroma Extract Dilution Analysis

			RI[c]		log_3 FD factor[d]	
no.[a]	compd	odor[b]	Wax	Rtx-5	A	B
15	acetic acid[e]	sour	1433	nd[f]	6	6
18	propanoic acid[e]	cheesy, fecal	1514	nd	4	5
20	2-methylpropanoic acid[e]	cheesy, Swiss cheese	1550	804	4	6
21	butanoic acid[e]	cheesy	1611	829	8	9
23	3-methylbutanoic acid[e]	cheesy, sweaty	1654	893	7	9
30	4-hydroxy-2,5-dimethyl-3(2*H*)-furanone[e]	burnt sugar	2005	1078	6	6
31	4-hydroxy-2-ethyl-5-methyl-3(2*H*)-furanone[g]	burnt sugar	2056	1149	7	6
32	4-hydroxy-5-ethyl-2-methyl-3(2*H*)-furanone[g]	burnt sugar	2077	nd	2	nd
33	3-hydroxy-4,5-dimethyl-2(5*H*)-furanone[g]	curry, spicy	2173	1115	3	5
37	2-phenylacetic acid[e]	rosy, plastic	2515	1272	8	8
38	3-phenylpropanoic acid[e]	rosy	2590	1366	2	1

[a]Numbers correspond to those in Tables 2, 3, 5−7. [b]Odor quality as perceived during GC−O. [c]Retention indices were calculated from GC−O data; Wax, Rtx-Wax. [d]Flavor dilution (FD) factor determined on Rtx-Wax column. [e]Compound positively identified by comparing RIs, mass spectrum and odor properties with those of reference compound. [f]nd, not detected. [g]Compound tentatively identified by comparing RIs and odor properties with those of reference compound.

Table 5. Predominant Neutral/Basic Odorants (Log_3FD Factor ≥1) in Fish Sauce Determined by Aroma Extract Dilution Analysis

			RI[c]		Log_3FD factor[d]	
no.[a]	compd	odor[b]	Wax	Rtx-5	A	B
5	2-methylpropanal[g]	malty, dark chocolate	<900	nd[f]	0	2
6	2-methylbutanal[e]	malty, dark chocolate	904	nd	2	1
7	3-methylbutanal[e]	malty, dark chocolate	916	nd	3	3
10	(*Z*)-4-heptenal[g]	crabby, stale, fishy	1236	902	1	1
11	1-octen-3-one[g]	mushroom	1301	978	1	0
12	2-acetyl-1-pyrroline[g]	popcorn	1320	928	2	1
14	(*Z*)-1,5-octadien-3-one[g]	metallic	1380	988	1	0
16	3-(methylthio)propanal[e]	cooked potato	1452	908	6	4
17	3,6-dimethyl-2-ethylpyrazine[e]	roasted potato	1484	1068	2	2
19	(*E*)-2-nonenal[g]	stale, hay	1537	1162	0	1
22	phenylacetaldehyde[e]	rosy, plastic	1640	1048	4	4
25	3-(methylthio)-1-propanol[e]	potato	1712	985	0	1
27	2-acetyl-2-thiazoline[g]	popcorn	1760	1118	nd	1
28	(*E*)-*β*-damascenone[g]	floral, apple sauce	1826	1384	1	0
29	2-phenylethanol[e]	wine-like, rosy	1905	1122	1	1
34	*o*-aminoacetophenone[e]	musky, grape, stale	2202	1312	4	3
35	indole[e]	fecal	2428	1295	1	nd
36	skatole[e]	fecal	2480	1401	1	0

[a]Numbers corresponded to those in Tables 2−4, 6, 7. [b]Odor quality as perceived during GC−O. [c]Retention indices were calculated from GC−O data; Wax, Rtx-Wax. [d]Flavor dilution (FD) factor determined on Rtx-Wax column. [e]Compound positively identified by comparing RIs, mass spectrum, and odor properties with those of reference compound. [f]nd, not detected. [g]Compound tentatively identified by comparing RIs and odor properties with those of reference compound.

roasted almond,[28] and soy sauce.[29] It is a degradation product of an Amadori compound via 2,3-enolization, elongation by the Strecker aldehydes, and reduction of the resulting acetylformoin-type intermediates.[16] Its presence in fish sauce might be desirable because of its pleasant caramel/burnt sugar-like, sweet and fruity aroma note.

4-Hydroxy-2(or 5)-ethyl-5(or 2)-methyl-3(2*H*)-furanone and 3-hydroxy-4,5-dimethyl-2(5*H*)-furanone were tentatively identified and are likely to be the important compounds due to their low odor threshold values of 1.15 and 0.001 (*μ*g/L), respectively.[30] However, these two compounds were present in only trace levels and were not detected by GC−MS. Sasaki et al.[31] reported that 4-hydroxy-2(or 5)-ethyl-5(or 2)-methyl-3(2*H*)-furanone can be produced by yeast fermentation via the pentose-phosphate cycle. In addition, this compound was also formed through the Maillard reaction of pentose.[16] 3-Hydroxy-4,5-dimethyl-2(5*H*)-furanone is well-known as providing a spicy/curry aroma note and has been found in many food products.[30] This compound is reported for the first time as highly odor-active compound in fish sauce on the basis of its odor-activity in air (GC−O). Its presence in fish sauce might be desirable because of its seasoning (curry)-like aroma. It has been reported as a degradation product of threonine.[32] In addition, Kobayashi[33] reported that in sake and wine 3-hydroxy-4,5-dimethyl-2(5*H*)-furanone may be formed via aldol condensation of acetaldehyde and R-ketobutyric acid followed by lactonization.

Thirteen odorants were detected by SHDA of highly volatile compounds including two unknown compounds (Table 6). The highest FD factors (≥25) were found in methanethiol

DOI: 10.1021/jf5061248
J. Agric. Food Chem. 2015, 63, 2628−2638

Table 6. Predominant Odorants in Headspace of Fish Sauce Determined by Static Headspace Dilution Analysis

					FD factor[d]			
			RI[c]		A		B	
no.[a]	compd	odor[b]	Wax	Rtx-5	Wax	Rtx-5	Wax	Rtx-5
2	methanethiol[e]	rotten, sulfurous, cabbage	652	431	25	25	25	25
3	acetaldehyde[e]	pungent, sweet	698	<400	5	1	5	nd[f]
4	dimethyl sulfide[e]	corn	714	525	1	5	nd	nd
5	2-methylpropanal[e]	malty, dark chocolate	804	561	25	25	25	25
6	2-methylbutanal[e]	malty, dark chocolate	909	658	25	1	25	5
7	3-methylbutanal[e]	malty, dark chocolate		648		25		25
8	2,3-butanedione[e]	buttery	972	602	nd	1	1	1
9	*unknown*	fishy, rancid, stale	1160	815	1	1	1	1
13	dimethyl trisulfide[e]	rotten, sulfurous, cabbage	1371	970	25	5	5	5
15	3-(methylthio)propanal[e]	potato	1446	906	25	5	25	5
21	butanoic acid[e]	cheesy	1616	nd	5	nd	25	nd
24	2-methyl-(3-methyldithio)furan[g]	thiamin, meaty	1661	1176	1	1	5	1
26	*unknown*	rotten, sulfurous, cabbage	1727	1218	1	5	5	5

[a]Numbers corresponded to those in Tables 2−5, and 7. [b]Odor quality as perceived during GC−O. [c]Retention indices were calculated from GC−O data; Wax, Rtx-Wax. [d]FD factors of 1, 5, and 25 corresponding to headspace volumes of 25, 5, and 1 mL, respectively. [e]Compound positively identified by comparing RIs, mass spectrum, and odor properties with those of reference compound. [f]nd, not detected. [g]Compound tentatively identified by comparing RIs and odor properties with those of reference compound.

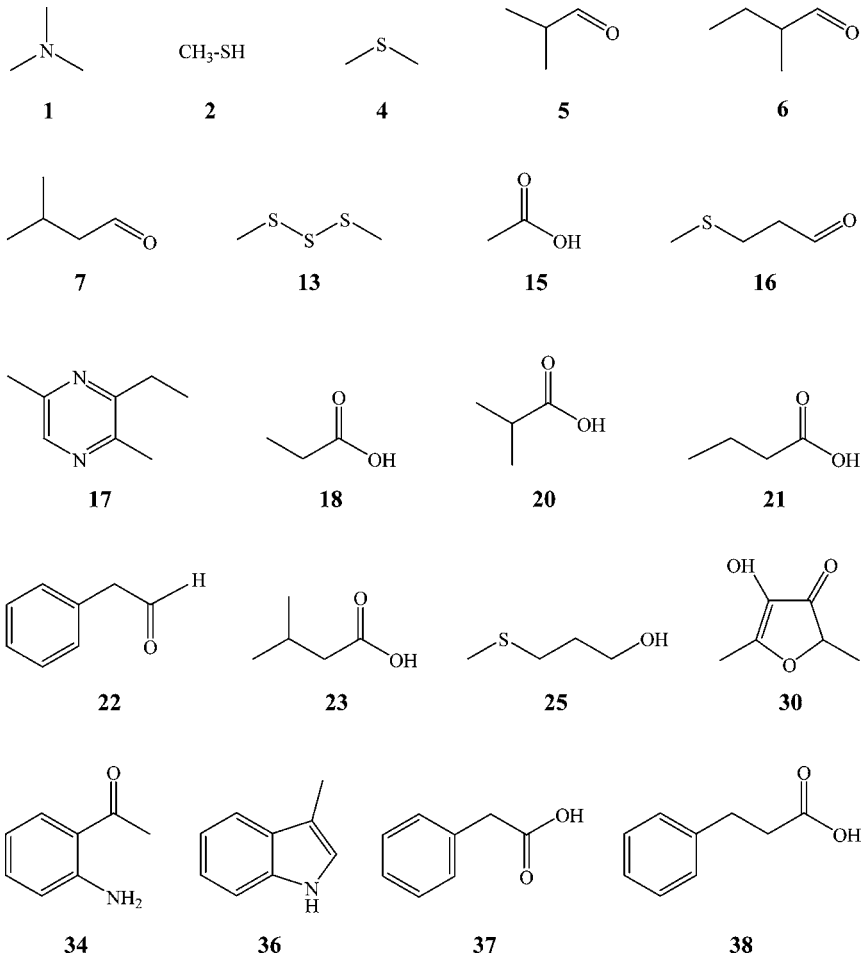

Figure 2. Structures for predominant odorants identified in fish sauce.

(rotten, sulfurous, cabbage), 2-methylpropanal (malty, dark chocolate), 2-methylbutanal (malty, dark chocolate), 3-methylbutanal (malty, dark chocolate), dimethyl trisulfide (rotten, sulfurous, cabbage), 3-(methylthio)propanal (cooked potato), and butanoic acid (cheesy). However, some compounds showed different FD factors on Rtx-Wax and Rtx-5 columns. High compound selectivity of the Rtx-Wax column favored detection of the more polar compounds. It should be noted that 2-methylbutanal and 3-methylbutanal could not be separated on an Rtx-Wax and, therefore, the FD-

DOI: 10.1021/jf5061248
J. Agric. Food Chem. 2015, 63, 2628−2638

Table 7. Concentrations and Odor-Activity Values (OAVs) of Predominant Odorants in Fish Sauce

		concn[b] (μg/kg)				OAV[d]	
no.[a]	compd	A	B	odor threshold[c] (μg/kg)	ref	A	B
1	trimethylamine[e]	0.84 (± 3.50)	1.28 (± 2.17)	0.47	46	1.80	2.72
2	methanethiol[e]	58.2 (± 1.81)	57.05 (± 1.30)	0.02	47	2910	2853
4	dimethyl sulfide[e]	40.2 (± 4.77)	10.14 (± 2.17)	0.3	48	134	34
5	2-methylpropanal[e]	620 (± 2.44)	900 (± 2.52)	1	49	620	900
6	2-methylbutanal[e]	347 (± 11.5)	852 (± 13.5)	3	50	116	284
7	3-methylbutanal[e]	1291 (± 10.3)	1661 (± 14.0)	0.2	50	6455	8305
13	dimethyl trisulfide[f]	17.5 (± 9.96)	25.64 (± 1.07)	0.01	50	1751	2564
15	acetic acid[g]	4963000 (± 2.72)	4506000 (± 1.85)	22000	50	226	205
16	3-(methylthio)propanal[f]	351(± 8.30)	1092 (± 14.8)	0.2	50	1755	5460
17	3,6-dimethyl-2-ethylpyrazine[f]	1.26 (± 6.54)	5.48 (± 8.57)	8.6	50	<1	<1
18	propanoic acid[g]	99870 (± 1.22)	561100 (± 3.22)	2000	50	50	281
20	2-methylpropanoic acid[g]	5660 (± 1.61)	22350 (± 1.21)	50	50	113	447
21	butanoic acid[g]	129300 (± 1.90)	307400 (± 1.07)	240	50	539	1281
22	phenylacetaldehyde[f]	172 (± 5.01)	180 (± 3.17)	4	50	43	45
23	3-methylbutanoic acid[g]	19570 (± 0.30)	94140 (± 2.64)	250	50	78	377
25	3-(methylthio)-1-propanol[f]	682 (± 5.62)	591 (± 2.92)	250	51	2.73	2.36
31	4-hydroxy-2,5-dimethyl-3(2*H*)-furanone[f]	2456 (± 5.31)	2351 (± 3.90)	31	52	79	76
34	*o*-aminoacetophenone[f]	4.01 (± 11.9)	2.87 (± 12.8)	0.2	50	20	14
36	skatole[f]	0.47 (± 16.5)	0.44 (± 17.7)	3	53	<1	<1
37	2-phenylacetic acid[f]	2675 (± 1.43)	20100 (± 1.62)	1000	54	2.68	20
38	3-phenylpropanoic acid[f]	3344 (± 1.85)	1865 (± 2.71)	*h*	*h*	*h*	*h*

[a]Number corresponded to those in Tables 2−6 and Figure 2. [b]Average concentration (± percent relative standard deviation) from triplicate determinations. [c]Orthonasal odor threshold in water. [d]Odor-activity value = concentration divided by odor detection threshold. [e]Concentration was determined by GC−MS combined with the following extraction technique: headspace solid-phase microextraction (H-SPME), [f]Concentration was determined by GC−MS combined with the following extraction technique: direct solvent extraction-solvent-assisted flavor evaporation (DSE-SAFE), or [g]Concentration was determined by GC−MS combined with the following extraction technique: direct solvent extraction (DSE). [h]Not available.

factors reported on the Rtx-Wax column are for the coeluted compounds.

Methanethiol, acetaldehyde, and dimethyl sulfide were not detected by AEDA. Because of their high volatility, these compounds might be coeluted with solvent and/or lost during the extraction and concentration procedures. Therefore, the aroma contribution of very volatile compounds were estimated by directly analyzing the headspace above fish sauce with decreased volumes. In addition, 2-methyl-(3-methyldithio)-furan was not detected by AEDA but tentatively identified by SHDA. This sulfur-containing furan contributed a thiamin/meaty aroma note and might play an important role in the overall aroma of fish sauce due to its very low odor threshold in water of 0.004 μg/L.[30] This compound has been considered as an odor-active compound in a beef-like flavor produced by extrusion of enzyme-hydrolyzed vegetable protein (E-HVP)[34] and yeast extract.[35] 2-Methyl-(3-methyldithio)furan can be formed via the reaction of 2-methyl-3-furanthiol with methanethiol or by Maillard reaction of ribose and cysteine.[36] This is the first report of 2-methyl-(3-methyldithio)furan as one of the potent odorants in the headspace of fish sauce. Alcohols and esters were also found in fish sauce samples, but they showed very low FD factors (data not shown). Thus, these compounds were not considered as important odor-active compounds and were, therefore, not quantified.

Quantitative Analysis of Selected Odorants. There were 21 odorants selected for quantification (Figure 2). The concentrations and odor-activity values (OAVs) of these odorants are presented in Table 7. The major volatile constituents of the premium Thai fish sauces were volatile short-chain fatty acids, namely acetic acid followed by butanoic acid, propanoic acid, and 3-methylbutanoic acid. Five volatile acids were previously reported in Malaysian fish sauce with acetic acid being the most abundant, followed by 3-methylbutanoic acid, 2-methylpropanoic acid, butanoic acid, and benzoic acid.[37] In addition, pentanoic acid, hexanoic acid, 2-methylheaxanoic acid, heptanoic acid, and octanoic acid have also been reported in fish sauce[7,37] However, these were not considered as odor-active compounds in this study. Other moderately abundant compounds in both fish sauces were 3-methylbutanal, 3-(methylthio)propanal, 2-methylpropanoic acid, 4-hydroxy-2,5-dimethyl-3(2*H*)-furanone, 2-phenylacetic acid, and 3-phenylpropanoic acid. On the other hand, trimethylamine, 3,6-dimethyl-2-ethylpyrazine, *o*-aminoacetophenone, and skatole were present at low concentrations (<10 μg/kg). Despite their low levels, these compounds might have a significant impact on fish sauce aroma because of their low odor detection threshold values.

Although AEDA is a useful technique for screening odor-active compounds, it does not provide information about the contribution of individual compounds to the overall aroma. Because compounds are extracted from the sample matrix with a solvent and volatilized during GC−O, these odorants are detected based on odor activity in air without considering interactions with the food matrix. For this reason, the use of OAVs may provide a better assessment of the odor activities of compounds as long as the quantitative data and the odor detection thresholds are accurate.

In this study, OAVs were calculated using odor detection thresholds determined in water, which was appropriate because fish sauce is mainly an aqueous product. Due to its low threshold, 3-methylbutanal had the highest OAV in both

DOI: 10.1021/jf5061248
J. Agric. Food Chem. 2015, 63, 2628−2638

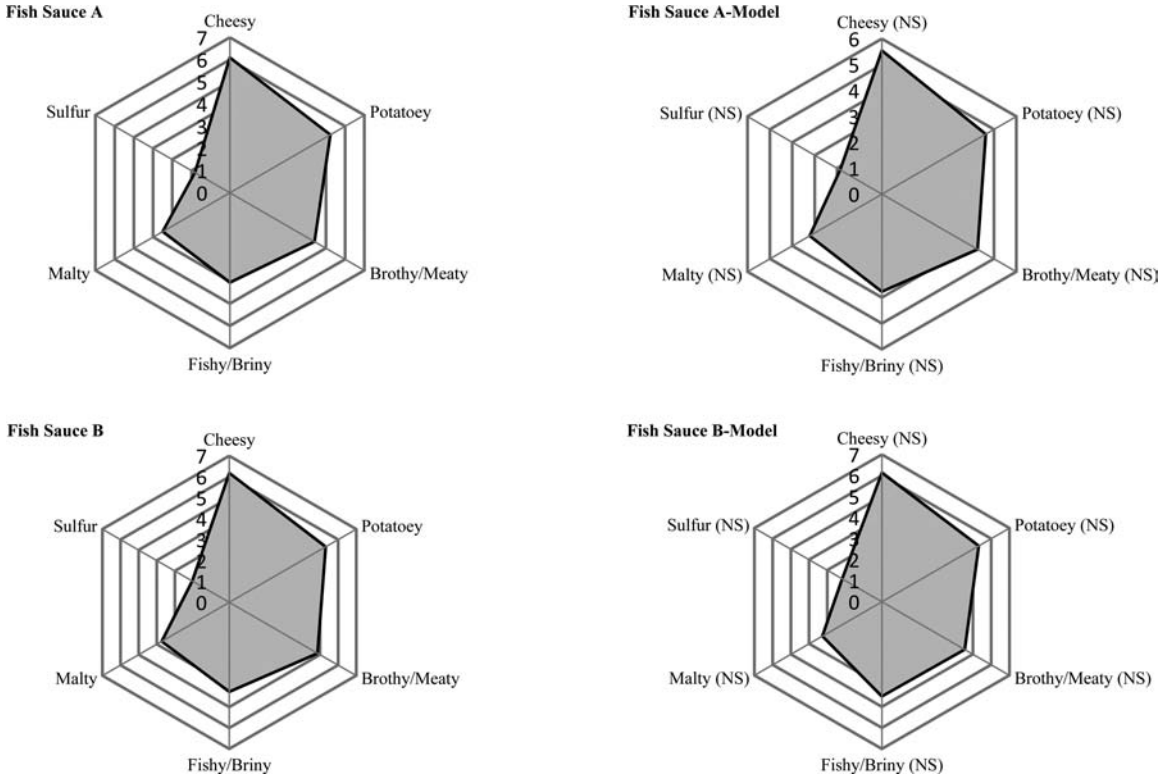

Figure 3. Sensory descriptive aroma profile comparison of fish sauces and recombination models. NS, not significantly different between fish sauce and the complete fish sauce model ($p > 0.05$).

samples despite its low abundance. In addition, high OAVs (>500) for methanethiol, 2-methylpropanal, dimethyl trisulfide, 3-(methylthio)propanal, and butanoic acid indicate the importance of these compounds in the overall aroma of premium Thai fish sauce. Certain volatile compounds, namely 3-methylbutanol, 2-methylbutanal, 3-methylbutanal, dimethyl disulfide, 3-(methylthio)propanal, 3-methylbutanoic acid, and benzaldehyde, have been previously reported to contribute to the characteristic aroma of Malaysian fish sauce.[37] Giri et al.[5] reported that butanoic acid had the highest OAV in premium Thai fish sauce, followed by 2-methylbutanoic acid, dimethyl trisulfide, 3-(methylthio)propanal, acetic acid, and trimethylamine. Shimoda et al.[38] reported that volatility of trimethylamine increased with pH. In this study, trimethylamine, due to its low OAVs, was of only minor importance to the overall aroma of both fish sauces.

Valine and leucine are precursors for 2-methylpropanal and 3-methylbutanal, respectively, which are formed via an amino acid catabolism pathway.[39] In addition, aldehydes can be formed by either enzymatic routes, including transamination and decarboxylation pathways, or by nonenzymatic reactions, such as the Strecker degradation.[40] Methionine is a precursor for 3-(methylthio)propanal, methanethiol, dimethyl sulfide, dimethyl disulfide, and dimethyl trisulfide.[41] Butanoic acid is likely to form by atmospheric oxidation of fish lipids,[29] and it also can be derived from amino acids via bacterial activity.[42] Halophilic bacteria can change the aroma profile of fish sauce. For example, *Tetragenococcus halophilus* has been shown to reduce dimethyl disulfide content in fish sauce.[43] Whereas, *Virgibacillus* sp. SK37 appeared to increase the content of 2-methylpropanal, 2-methylbutanal, 3-methylbutanal, acetic acid, and 2-methylpropanoic acid.[44]

The remaining odorants in Table 7 with OAVs > 100 may also be important aroma contributors. These include dimethyl sulfide, 2-methylbutanal, acetic acid, propanoic acid, 2-methylpropanoic acid, and 3-methylbutanoic acid. Because of their low OVAs (<1), 3,6-dimethyl-2-ethylpyradzine and skatole may contribute only slightly to the overall aromas of the two fish sauces.

Sensory Attributes of Fish Sauce and Aroma Model. Dougan and Haward[45] reported that three distinctive notes contributed to the odor of fish sauce were ammoniacal, cheesy, and meaty notes. In addition, burnt, fishy, sweaty, fecal, rancid, and nutty notes were found as distinctive notes for Thai fish sauce.[5,6] In this study, cheesy, malty, potatoey, brothy/meaty, fishy/briny, malty, and sulfur were the main aroma attributes detected in both fish sauces (Figure 3). Volatile short-chain fatty acids such as acetic acid, butanoic acid, 2-methlylpropanoic acid, 2/3-methylbutanoic, pentanoic acid, and heptanoic acid have been proposed to be responsible for the cheesy note of fish sauce.[5−7] Fukami et al.[6] found that four odor-active compounds contributing to the distinctive odor of Thai fish sauce were 2-methylpropanal, 2-methylbutanal, 2-ethylpyridine, and dimethyl trisulfide. 2-Ethylpyridine and dimethyl trisulfide contributed to fishy note. 2-Methylpropanal together with 2-methylbutanal and 2-ethylpyridine have been reported to contribute to meaty odor, whereas 2-methylpropanal, 2-methylbutanal, and 3-methylbutanal have been described as nutty odor in fish sauce.[5]

Intensities for all aroma attributes of both fish sauce samples were comparable to those of the respective reconstitution models (Figure 3, $p > 0.05$). These results demonstrate that the selection of odor-active compounds based on AEDA/SHDA were appropriate, and the results of quantitative experiments were highly accurate. Therefore, the reconstitution models were

DOI: 10.1021/jf5061248
J. Agric. Food Chem. 2015, 63, 2628−2638

considered to provide an accurate representation of the overall aroma of Thai premium fish sauce.

Omission Studies. Formulations for reconstitution and omission model mixtures are described in Table 7. Models in which either acids, aldehydes, or sulfur-containing compounds were omitted differed (α = 0.05) from the respective complete models (Table 8). The omission of sulfur-containing caused the most noticeable difference. This in agreement with the high OAVs determined for methanethiol, dimethyl trisulfide, and 3-(methylthio)propanal. Similarly, the omission of aldehydes and acids also caused significant differences. This is not surprising because these groups contained odorants with high OAVs, e.g., 3-methylbutanal in the aldehyde group and butanoic acid in the acids group. As expected, the models in which compounds with low OAV compounds were omitted did not differ from the complete models. This finding confirms that low OAV compounds, including trimethylamine, 3,6-dimethyl-2-ethylpyrazine, 4-hydroxy-2,5-dimethyl-3(2*H*)-furanone, *o*-aminoacetophenone, and skatole, had little influence on the overall aroma of fish sauce.

Table 8. R-Index Ranking Test Comparison of Complete Recombination Aroma Models Against Respective Omission Models

	R-index (significance)[a]	
comparison of complete model against	fish sauce A	fish sauce B
model with acids omitted	73.68*	78.95*
model with aldehydes omitted	73.68*	73.68*
model with sulfur compounds omitted	89.47*	84.21*
model with low OAV compounds omitted	63.16	63.16

[a]Degree of difference of each model against complete model (n = 19). *Significant difference from complete model at α = 0.05 (critical value, expressed in percentage; R-index 50% for two-tailed test, α = 0.05 and n = 19 is 20.97).

AUTHOR INFORMATION

Corresponding Author

*Phone: (217) 333-5803. Fax: (217) 333-1875. E-mail: cadwlldr@illinois.edu.

Funding

Partial support for this project was provided by the National Institute of Food and Agriculture, U.S. Department of Agriculture, under Project ILLU-698-366.

Notes

The authors declare no competing financial interest.

REFERENCES

(1) Lopetcharat, K.; Choi, Y. J.; Park, J. W.; Daeschel, M. D. Fish sauce products and manufacturing: a review. *Food Rev. Int.* **2001**, *17*, 65−88.

(2) Saisithi, P.; Kasemsarn, B.; Liston, J.; Dollar, A. M. Microbiology and chemistry of fermented fish. *J. Food Sci.* **1966**, *31*, 105−110.

(3) McIver, R. C.; Brooks, R. I.; Reineccius, G. A. Flavor of fermented fish sauce. *J. Agric. Food Chem.* **1982**, *30*, 1017−1020.

(4) Sanceda, N. G.; Kurata, T.; Arakawa, N. Study on the volatile compounds of fish sauce—shottsuru, nampla, and noucnam. *Agric. Biol. Chem.* **1986**, *50*, 1201−1208.

(5) Giri, A.; Osaka, K.; Okamoto, A.; Ohshima, T. Olfactometric characterization of aroma active compounds in fermented fish paste in comparison with fish sauce, fermented soy sauce and sauce products. *Food Res. Int.* **2010**, *43*, 1027−1040.

(6) Fukami, K.; Ishiyama, S.; Yaouramaki, H.; Masuzawa, T.; Nabeta, Y.; Endo, K.; Shimoda, M. Identification of distinctive volatile compounds in fish sauce. *J. Agric. Food Chem.* **2002**, *50*, 5412−5416.

(7) Pham, A. J.; Schilling, M. W.; Yoon, Y.; Kamadia, V. V.; Marshall, D. L. Characterization of fish sauce aroma-impact compounds using GC−MS, SPME-Osme-GCO, and Stevens' power law exponents. *J. Food Sci.* **2008**, *73*, 268−274.

(8) Schieberle, P.; Grosch, W. Quantitative analysis of aroma compounds in wheat and rye bread crusts using a stable isotope dilution assay. *J. Agric. Food Chem.* **1987**, *35*, 252−257.

(9) Fuganti, C.; Gatti, F. G.; Serra, S. A. general method for the synthesis of the most powerful naturally occurring Maillard flavors. *Tetrahedron* **2007**, *63*, 4762−4767.

(10) Lin, J.; Welti, D. H.; Vera, F. A.; Fay, L. B.; Blank, I. Synthesis of deuterated volatile lipid degradation products to be used as internal standards in isotope dilution assays. 2. Vinyl ketones. *J. Agric. Food Chem.* **1999**, *47*, 2822−2829.

(11) Guth, H.; Grosch, W. Identification of the character impact odorants of stewed beef juice by instrumental analyses and sensory studies. *J. Agric. Food Chem.* **1994**, *42*, 2862−2866.

(12) Sen, A.; Grosch, W. Synthesis of six deuterated sulfur containing odorants to be used as internal standards in quantification assays. *Z. Lebensm.-Unters.-Forsch.* **1991**, *192*, 541−547.

(13) Fang, M.; Cadwallader, K. R. Convenient synthesis of stable deuterium labeled alkyl pyrazines for use in stable isotope dilution assays. *J. Agric. Food Chem.* **2013**, *61*, 3580−3588.

(14) Kiatbenjakul, P.; Intarapichet, K.-O.; Cadwallader, K. R. Characterization of potent odorants in mail giant water bug (*Lethocerus indicus* Lep. and Serv.), an important edible insect of Southeast Asia. *Food Chem.* **2015**, *168*, 639−647.

(15) Schuh, C.; Schieberle, P. Characterization of the key aroma compounds in the beverage prepared from Darjeeling black tea: quantitative differences between tea leaves and infusion. *J. Agric. Food Chem.* **2006**, *54*, 916−924.

(16) Blank, I.; Fay, L. B.; Lakner, F. J.; Schlosser, M. Determination of 4-hydroxy-2,5-dimethyl-3(2*H*)-furnaone and 2(or 5)-ethyl-4-hydroxy-5(or 2)-methyl-3(2*H*)-furanone in pentose sugar-based Maillard model systems by isotope dilution assays. *J. Agric. Food Chem.* **1997**, *45*, 2642−2648.

(17) Dollman, B.; Wichmann, D.; Schmidt, A.; Koehler, H.; Schreier, P. Quantitative analysis of 2-aminoacetophenone in off-flavored wines by stable isotope dilution assay. *J. AOAC Int.* **1996**, *29*, 583−587.

(18) Schieberle, P.; Gassenmaier, K.; Guth, H.; Sen, A.; Grosch, W. Character impact odour compounds of different kinds of butter. *Lebensm. Wiss. Technol.* **1993**, *26*, 347−356.

(19) Lin, J.; Welti, D. H.; Vera, F. A.; Fay, L. B.; Blank, I. Synthesis of deuterated volatile lipid degradation products to be used as internal standards in isotope dilution assays. 1. Aldehydes. *J. Agric. Food Chem.* **1999**, *47*, 2813−2821.

(20) Rotsatchakul, P.; Chaiseri, S.; Cadwallader, K. R. Identification of characteristic aroma components of Thai fried chili paste. *J. Agric. Food Chem.* **2008**, *56*, 528−536.

(21) Zhou, Q.; Wintersteen, L.; Cadwallader, K. R. Identification and quantification of aroma-active components that contribute to the distinct malty flavor of buckwheat honey. *J. Agric. Food Chem.* **2002**, *50*, 2016−2021.

(22) van den Dool, H.; Kratz, P. D. A generalization of the retention index system including linear temperature programmed gas liquid partition chromatography. *J. Chromatogr.* **1963**, *11*, 463−471.

(23) Lorjaroenphon, Y.; Cadwallader, K. R.; Kim, H.; Lee, S.-Y. Evaluation of key odorants in chipotle pepper by quantitative analysis, calculation of odor-activity values and omission studies. In *Recent Highlights in Flavor Chemistry and Biology*; Deutsche Forschungsanstalt für Lebensmittelchemie: Garching, Germany, 2008; pp 191−200.

(24) O'Mahony, M. Understanding discrimination tests: a user-friendly treatment of response bias, rating and ranking R-index tests and their relationship to signal detection. *J. Sens. Stud.* **1992**, *7*, 1−47.

(25) Rodin, J. O.; Himel, R. M.; Silverstein, R. M.; Leeper, R. W.; Gortner, W. A. Volatile flavor and aroma components of pineapple. I.

DOI: 10.1021/jf5061248
J. Agric. Food Chem. 2015, 63, 2628−2638

Isolation and tentative identification of 2,5-dimethyl-4-hydroxy-3(2*H*)-furanone. *J. Food Sci.* **1965**, *30*, 280−285.
(26) Douillard, C.; Guichard, E. The aroma of strawberry (*Fragaria ananassa*): Characterization of some cultivars and influence of freezing. *J. Sci. Food Agric.* **1990**, *50*, 517−531.
(27) Tonsbeek, C. H. T.; Plancken, A. J.; van den Weerdhof, T. Components contributing to beef flavor. *J. Agric. Food. Chem.* **1968**, *16*, 1016−1021.
(28) Takei, Y.; Yamanishi, T. Flavor components of roasted almond. *Agric. Biol. Chem.* **1974**, *38*, 2329−2336.
(29) Steinhaus, P.; Schieberle, P. Characterization of the key aroma compounds in soy sauce using approaches of molecular sensory science. *J. Agric. Food Chem.* **2007**, *55*, 6262−6269.
(30) Rychlik, M.; Schieberle, P.; Grosch, W. In *Compilation of Odor Thresholds, Odor Qualities and Retention Indices of Key Food Odorants*; Deutsche Forschungsanstalt für Lebensmittelchemie: Garching, Germany, 1998.
(31) Sasaki, M.; Nunomura, N.; Matsudo, T. Biosynthesis of 4-hydroxy-2(or 5)-ethyl-5(or 2)-methyl-3(2*H*)-furanone by yeasts. *J. Agric. Food Chem.* **1991**, *39*, 934−938.
(32) Sulser, H.; Depizzol, J.; Büchi, W. A probable flavoring principle in vegetable-protein hydrolysates. *J. Food Sci.* **1967**, *32*, 611−615.
(33) Kobayashi, A. Sotolon. Identification, formation, and effects on flavor. In *Flavor Chemistry Trends and Developments*; Teranishi, R., Buttery, R. G., Shahidi, F., Eds.; ACS Symposium Series 388; American Chemical Society: Washington, DC, 1989; pp 49−59.
(34) Baek, H. H.; Kim, C. J.; Ahn, B. H.; Nam, H. S.; Cadwallader, K. R. Aroma extract dilution analysis of a beeflike process flavor from extruded enzyme-hydrolyzed soybean protein. *J. Agric. Food. Chem.* **2001**, *49*, 790−793.
(35) Mahadevan, K.; Farmer, L. Key odor impact compounds in three yeast extract pastes. *J. Agric. Food. Chem.* **2006**, *54*, 7242−7250.
(36) Mottram, D. S.; Whitfield, F. B. Maillard−lipid interactions in nonaqueous systems: volatiles from the reaction of cysteine and ribose with phosphatidylcholine. *J. Agric. Food. Chem.* **1995**, *43*, 1302−1306.
(37) Mohamed, H. N.; Man, Y. C.; Mustafa, S.; Manap, Y. A. Tentative identification of volatile flavor compounds in commercial Budu, a Malaysian fish sauce, using GC−MS. *Molecules* **2012**, *17*, 5062−5080.
(38) Shimoda, M.; Peralta, R. R.; Osajima, Y. Headspace gas analysis of fish sauce. *J. Agric. Food Chem.* **1996**, *44*, 3601−3605.
(39) Smit, B. A.; Engels, W. J. M.; Smit, G. Branched chain aldehydes: production and breakdown pathways and relevance for flavour in foods. *Appl. Microbiol. Biotechnol.* **2009**, *81*, 987−999.
(40) Ayad, E. H. E.; Verheul, A.; Engels, W. J. M.; Wouters, J. T. M.; Smit, G. Enhanced flavour formation by combination of selected lactococci from inductrial and artisanal origin with focus on completion of a metabolic pathway. *J. Appl. Microbiol.* **2001**, *90*, 59−67.
(41) Bonnarme, P.; Psoni, L.; Spinnler, H. E. Diversity of L-methionine catabolism pathways in cheese-ripening bacteria. *Appl. Environ. Microbiol.* **2000**, *66*, 5514−5517.
(42) Beddows, C. G.; Ardeshir, A. G.; bin Daud, W. J. Development and origin of volatile fatty acids in Budu. *J. Sci. Food Agric.* **1980**, *31*, 86−92.
(43) Udomsil, N.; Rodtong, S.; Choi, Y. J.; Hua, Y.; Yongsawatdigul, J. Use of *Tetragenococcus halophilus* as a starter culture for flavor improvement in fish sauce fermentation. *J. Agric. Food Chem.* **2011**, *59*, 8401−8408.
(44) Lapsongphon, N.; Cadwallader, K. R.; Rodtong, S.; Yongsawatdigul, J. Characterization of protein hydrolysis and odor-active compounds of fish sauce inoculated with *Virgibacillus* sp. SK37 under reduced salt content. *J. Agric. Food Chem.* **2013**, *61*, 6604−6613.
(45) Dougan, J.; Haward, G. E. Some flavoring constituents of fermented fish sauces. *J. Sci. Food Agric.* **1975**, *26*, 887−894.
(46) Amoore, J. E. Specific anosia and the concept of primary odours. *Chem. Senses Flavour* **1977**, *2*, 267−281.
(47) Guadagni, D. G.; Buterry, R. G.; Okano, S. Odour threshold of some organic compounds associated with food flavours. *J. Sci. Food Agric.* **1963**, *14*, 761−765.
(48) Buttery, R. G. Quantitative and sensory aspects of flavor of tomato and other vegetables and fruits. In *In Flavor Science-Sensible Prinziples and Techniques in Flavor Science*; Acree, T., Teranishi, R., Eds.; American Chemical Society: Washington, DC, 1993; pp 259−286.
(49) Guadagni, D. G.; Buttery, R. G.; Turnbaugh, J. G. Odor thresholds and similarity ratings of some potato chip compounds. *J. Sci. Food Agric.* **1972**, *23*, 1435−1444.
(50) Buttery, R. G.; Ling, L. C. Additional studies on flavor component of corn tortilla chips. *J. Agric. Food Chem.* **1998**, *46*, 2764−2769.
(51) Fritsch, H. T.; Schieberle, P. Identification based on quantitative measurements and aroma recombination of the character impact odorants in a Bavarian pilsner-type beer. *J. Agric. Food Chem.* **2005**, *53*, 7544−7551.
(52) Buttery, R. C.; Takeoka, G. R.; Krammer, G. E.; Ling, L. C. Furaneol: odor threshold and importance to tomato aroma. *J. Agric. Food Chem.* **1995**, *43*, 1638−1640.
(53) Moss, B. W.; Hawa, S. M.; Walker, N. Sensory Thresholds for skatole and indole. In *Colloques de l'INRA Measurement and Prevention of Boar Taint in Entire Male Pigs*; Bonneau, M., Ed.; INRA: Paris, France, 1993; pp 63−68.
(54) Carunchia Whetstine, M. E.; Cadwallader, K. R.; Drake, M. A. Characterization of aroma compounds responsible for the rosy/floral flavor in Cheddar cheese. *J. Agric. Food Chem.* **2005**, *53*, 3126−3132.

DOI: 10.1021/jf5061248
J. Agric. Food Chem. 2015, 63, 2628−2638

Table 1. Sample, Commercial Brand, Content, and Sample Code of the Juices and Nectars Employed in This Study

sample	brand	content	sample code
apple juice	Aliada	apple juice from concentrate	A1
	Hipercor	apple juice	A2
	Lambda	organic apple juice from concentrate	A3
	Homemade	squeezed apple juice	A4
	Tropicana	apple juice 100%, ascorbic acid	A5
	Auchan	apple juice	A6
	Consum	apple juice from concentrate with vitamin c	A7
	Vitafit	apple juice from concentrate	A8
grape juice	Don Simon	100% pure grape juice made from muscat grapes	G1
	Must Don Simon	juice from concentrate grape juice and citric acid	G2
	Must Greip	grape juice from concentrate, acid citric	G3
	Capel	grape juice from concentrate, water, CO_2, citric acid, ascorbic acid	G4
	Lambda	juice and pulp of organic grape	G5
	Consum	red grape juice, water, citric acid, ascorbic acid	G6
	Casón Histórico	white grape juice from concentrate	G7
	Casón Histórico	black grape juice from concentrate	G8
mandarin juice	Don Simon	100% pure mandarin juice, no pulp, rich in vitamin C	M1
	Aliada	100% squeezed tangerine juice	M2
	Auchan	mandarin juice	M3
	Hacendado	100% squeezed mandarin juice	M4
	Seleqtia (Eroski)	100% squeezed mandarin juice	M5
	Carrefour	100% squeezed mandarin juice	M6
	Consum	100% squeezed mandarin juice	M7
	El Corte Inglés	100% pure squeezed mandarin juice	M8
orange juice	Don Simón	100% squeezed orange juice without orange pulp	O1
	Pascual	100% squeezed orange juice and orange pulp	O2
	Don Simon	orange juice from concentrate	O3
	Homemade	squeezed orange juice	O4
	Juver	orange juice	O5
	Auchan	orange juice	O6
	Consum	orange juice from concentrate with vitamin C	O7
	El Corte Inglés	100% pure squeezed orange juice with pulp	O8
orange nectar	Don Simon	orange juice from concentrate (50%), water, citric acid, cyclamate, saccharin, ascorbic acid	ON1
	Aliada	orange juice from concentrate (50%), water, citric acid, acesulfame-K, aspartame, vitamins A, C, and E	ON2
	Minute Maid	orange juice from concentrate and pulp (65%), water, sugar	ON3
	Granini	orange juice from concentrate (55%), orange pulp (5%), water, sugar, vitamin C	ON4
	Kasfruit	orange juice from concentrate (50%), water, citric acid, vitamins C and E, cyclamate and saccharin	ON5
	Zumosol, Pascual	orange juice from concentrate and vitamin C	ON6
pineapple juice	Hipercor	pineapple juice	P1
	Vitafit	100% pineapple juice from concentrate	P2
	Auchan	pineapple juice, pectin	P3
	Hacendado	100% squeezed pineapple juice	P4
	Carrefour	100% squeezed pineapple juice	P5
	El Corte Inglés	pineapple juice	P6
	Rio d'Oro	pineapple juice from concentrate	P7
	Consum	100% squeezed pineapple juice	P8
pineapple nectar	Granini	pineapple juice (Smooth Cayenne) from concentrate (50%), water, sugar, citric acid, pectin, vitamin C	PN1
	Zumosol, Pascual	pineapple juice (50%) from concentrate, water, sugar, citric acid, vitamin C, pectin	PN2
	Granini	pineapple juice (Golden) from concentrate (50%), water, sugar, citric acid, pectin, vitamin C	PN3
	Juver	pineapple juice (50%) from concentrate, water, citric acid, ascorbic acid, sucralose, acesulfame-K, natural aroma	PN4
	Auchan	water, pineapple juice from concentrate (50%), glucose−fructose syrup, sugar, lemon juice from concentrate, pectin, ascorbic acid, natural aroma	PN5
	Kasfruit	pineapple juice from concentrate (50%), water, citric acid, pectin, vitamin C and E, cyclamate, and saccharin	PN6
multifruit juices	Don Simón	pineapple (55%) and grape (45%) juices from concentrates	B1
	Zumosol	pineapple (75%) and grape (25%) juices from concentrates	B2
	Don Simón	orange (70%) and grape (30%) juices from concentrates	B3

DOI: 10.1021/acs.jafc.5b00122
J. Agric. Food Chem. 2015, 63, 2639−2646

need for any derivatization step. For this purpose, a suitable background electrolyte (BGE) is added, CE separation being performed at pH > 12, where the hydroxyl groups of carbohydrates are ionized.[24−27,29,30]

In this work, an indirect capillary zone electrophoresis (CZE) method for the determination of sugars in several fruit juices and nectars was developed. The separation of carbohydrates was optimized in terms of an anionic chromophore (2,6-pyridine dicarboxylic acid, PDC) content in the BGE and in other CZE parameters. The carbohydrate and sodium cyclamate (Cyc, sweetener found in some nectars) content present in different fruit juices and nectars was obtained. Using sugar concentration ratios as predictors, a linear discriminant analysis (LDA) model to classify juices according to the type of fruit was constructed. Also, data treatment by multiple linear regression (MLR) was used to detect and quantify blends of pineapple and orange juices with grape juice.

MATERIALS AND METHODS

Chemicals and Samples. The following analytical grade reagents were used: sodium hydroxide (NaOH), D-fructose 1,6-biphosphate trisodium salt (internal standard, IS), 2,6-pyridine dicarboxylic acid (PDC), and cetyltrimethylammonium bromide (CTAB) (Sigma-Aldrich, St. Louis, MO). Deionized water (Barnstead deionizer, Sybron, Boston, MA) was also used. The analytical standards were sodium cyclamate (Cyc), glucose (Glu), fructose (Fru), sucrose (Suc), and sorbitol (Sor) (Sigma-Aldrich). Individual stock solutions of Cyc (0.3 g L^{-1}) and sugars (10 g L^{-1}) were prepared in water. The fruit juices and nectars employed in this study and their commercial brands are shown in Table 1.

To evaluate the possibility of detecting blends of fruit juices, binary mixtures containing different percentages of pineapple−grape and orange−grape juices were prepared. To improve the robustness of the MLR models, the mixtures were prepared using all the available fruit juices, which were randomly selected and mixed. For instance, for the pineapple−grape mixture, a total of 28 mixtures, four for each different percentage, which comprised between 0 and 100% pineapple, were performed. One more set of 28 mixtures containing the same percentages of orange juice was also prepared for the orange−grape mixture. Thus, a total of 56 mixtures were obtained.

Instrumentation and Procedures. An HP[3D] CE system (Agilent, Waldbronn, Germany) provided with a diode array spectrophotometric detector and uncoated fused-silica capillaries (Polymicro Technologies, Phoenix, AZ) of 48.5 cm length (40 cm effective length) × 50 μm id (375 μm od) was used. New capillaries were successively flushed with 1 and 0.1 M NaOH and water at 60 °C for 10 min each. Between runs, the capillary was flushed with the BGE for 4 min. The CZE optimal parameters employed in this study are summarized in Table 2. Data acquisition was performed with ChemStation Software (Rev.A.10.01, Agilent). Statistical data treatment was performed using SPSS (v. 15.0, Statistical Package for the Social Sciences, Chicago, IL).

Table 2. CZE Optimal Parameters Employed in This Study

sample injection	50 mbar × 6 s
separation voltage	25 kV
temperature	15 °C
BGE composition	10 mM PDC + 0.5 mM CTAB at pH 12.1

Sample Preparation. Fruit juice and nectar samples, previously refrigerated at 5 °C, were centrifuged at 10000 rpm for 10 min. The supernatant was properly diluted with water, and for quantification purposes, the IS at 250 mg L^{-1} was also added. All samples were injected three times.

RESULTS AND DISCUSSION

Optimization of Separation Conditions. In order to optimize sugar and Cyc separation, a test mixture containing the standards and the IS described in the Chemicals and Samples section was used. The initial BGE composition and separation conditions were adapted from the literature.[31] Thus, a BGE containing 20 mM PDC and 0.5 mM CTAB at pH 12.1 (at −25 kV and 20 °C) was initially tested in this study. Under these conditions (see Figure 1A), the Fru/Glu peak pair (peaks labeled as 2 and 3) was not baseline resolved, and a significant disturbance between Suc and Sor (peaks labeled as 4 and 5) was evidenced. Moreover, a relatively high signal-to-noise ratio was also observed. Thus, in order to improve sensitivity, peak efficiency, and resolution, the effect of PDC concentration in the BGE was first investigated. With a constant concentration of 0.5 mM CTAB in the BGE, the PDC concentration was varied between 5 and 20 mM (see Figure 1). Analysis time decreased when the PDC content was reduced due to an increase in EOF; however, when a 5 mM PDC (Figure 1D) was used, sensitivity was lower than that obtained with 10 mM (Figure 1C). Thus, this concentration was chosen as the best compromise between sensitivity, resolution, and analysis time.

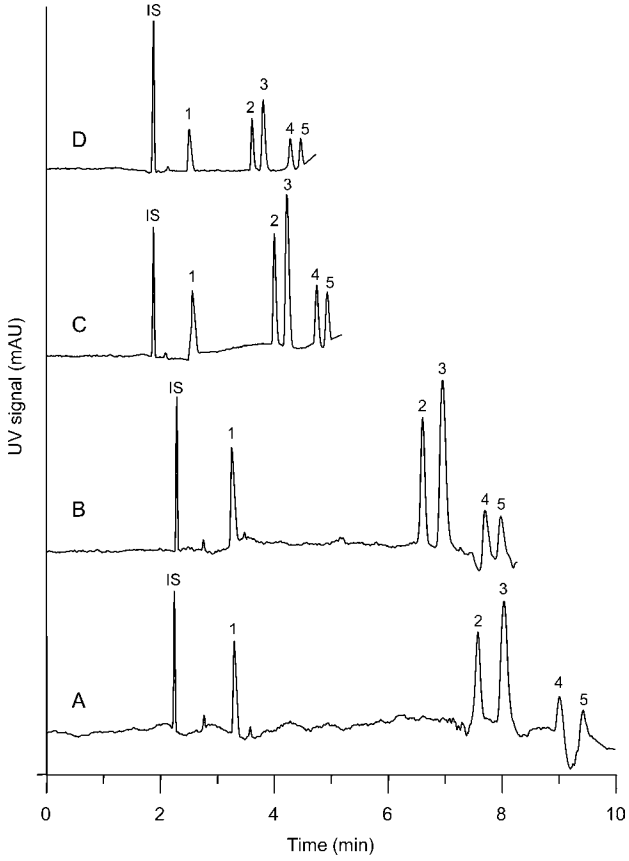

Figure 1. Influence of PDC content on the separation of analyte standards using a 20 mM (A), 15 mM (B), 10 mM (C), and 5 mM (D) PDC content in a BGE composed of 0.5 mM CTAB at pH 12.1. CZE conditions: Hydrodynamic injection, 50 mbar for 6 s; separation voltage, −25 kV at 20 °C; indirect detection, 575 nm (214 nm as reference). Peak identification: IS; 1, Cyc; 2, Fru; 3, Glu; 4, Suc; 5, Sor.

Next, the effect of temperature was studied. For this purpose, temperature was varied between 10 and 25 °C (see Figure S1 of Supporting Information). As it can be observed, analysis time

DOI: 10.1021/acs.jafc.5b00122
J. Agric. Food Chem. 2015, 63, 2639−2646

Table 3. Analytical Figures of Merit for the Determination of Sugars in Juice and Nectar Samples[a]

	intraday repeatability, RSD (%), n = 10		interday repeatability, RSD (%), n = 3							
analyte	peak area ratio	t_m	peak area ratio	t_m	sensitivity[b]	r^2	sensitivity (SA)	r^2 (SA)	LOD (μg mL^{-1})	LOQ (μg mL^{-1})
Cyc	0.71	0.12	1.34	0.61	0.0031	0.993	0.0032	0.993	11.6	38.3
Fru	0.94	0.17	1.56	0.89	0.0036	0.998	0.0036	0.997	12.2	40.3
Glu	1.01	0.17	1.62	0.91	0.0035	0.992	0.0036	0.992	13.4	44.2
Suc	1.21	0.23	2.29	1.23	0.0021	0.996	0.0020	0.996	17.8	58.7
Sor	1.33	0.27	2.45	1.42	0.0022	0.995	0.0023	0.996	18.1	59.7

[a] RSD relative standard deviation; t_m: migration time; r^2: regression coefficient; SA, standard addition; LOD: limit of detection; LOQ: limit of quantification. [b]Obtained from the slope of calibration curve constructed using peak area ratios (analyte area/IS area) vs analyte concentration (μg mL^{-1}).

decreased with increasing temperature due to a decrease in the buffer viscosity; however, a progressive loss in the resolution of the Suc/Sor peak pair (peaks labeled as 4 and 5) was also evidenced. Thus, a temperature of 15 °C was selected as the best compromise between analysis time and peak resolution.

After selection of the optimal temperature, the applied voltage for analyte separation was next optimized. For this purpose, different applied voltages, ranging from −15 to −30 kV, were applied. The separation voltage directly regulates migration time, also affecting peak resolution. When the applied voltage was lower than −25 kV, peak resolution decreased, while at a voltage of −30 kV, where resolution increased, a loss in peak efficiency (peak broadening) was evidenced (data not shown). Thus, as a compromise between peak resolution and efficiency, a voltage of −25 kV was selected for further studies.

On the other hand, hydrodynamic injection was selected since more reproducible results were obtained compared with electrokinetic injection. Injection time was varied between 2 and 10 s. Sensitivity increased when injection time was increased. However, more than 6 s resulted in no separation of Suc and Sor peaks. Consequently, an injection time of 6 s was selected as the optimum value.

Thus, the optimal separation conditions were BGE containing 10 mM PDC and 0.5 mM CTAB at pH 12.1, separation at −25 kV and 15 °C, injection of 50 mbar × 6 s (see Table 2). Under these conditions, the analyte standards were separated and quantified in less than 6 min with good resolutions (see Figure S1B, Supporting Information).

Performance Characteristics of the CZE Method. In order to significantly reduce the imprecision related to injection and ensure better reproducibility, the use of an IS in quantitative analysis is generally preferred.[32] Precision was determined by studying the intra- and interday repeatabilities of migration times and peak areas (analyte area/IS area) obtained by injecting the same 200 μg mL^{-1} solution for all analytes 6 times per day during 3 days (see Table 3). In all cases, the relative standard deviation (RSD) values were lower than 1.42% and 2.45% for migration times and peak areas, respectively.

External calibration curves of peak areas were constructed using the IS by injecting six standard solutions between 100 and 10000 μg mL^{-1} for Glu, Fru, Suc, and Sor, and between 50 and 500 μg mL^{-1} for Cyc. Straight lines with r^2 > 0.992 were obtained. The limits of detection (LOD) and limits of quantification (LOQ) were estimated for signal-to-noise ratios of 3 and 10, respectively. As observed in Table 3, LODs and LOQs ranged from 11.6 to 18.1 μg mL^{-1} and from 38.3 to 59.7 μg mL^{-1}, respectively. These values were comparable to those obtained by the CE methods with indirect photometric detection.[25,33−35]

Peak identification was performed by comparing migration times with those of the standards, and when necessary also by spiking the samples with the standards. Additionally, standard addition calibration curves were obtained by adding to the extracts at least four solutions with increasing concentrations up to 200 and 5000 μg mL^{-1} for Cyc and sugars, respectively. The curves were linear with r^2 > 0.992, and in all cases, the slope of calibration curve did not differ significantly from that obtained with the external calibration method. From these results, it can be concluded that no matrix effect was observed in the determination of these analytes in the fruit juices and nectars analyzed. Thus, external calibration curves were employed for analyte quantification in all analyzed samples.

Quantification of Sugars and Cyc in Fruit Juices and Nectars. Under the optimized conditions, all the fruit juices and nectars included in Table 1 were subjected to CZE analysis. Figure 2 shows representative CZE electropherograms of an apple (A), grape (B), and orange juices (C) and orange nectar (D). A summary of the contents found (expressed as minimum and maximum values in g L^{-1}) for the analyzed fruit juices and nectars is presented in Table 4. Some variability in the sugar levels can be observed among the analyzed samples, which was in accordance with previous studies.[7,36] Factors such as variety, climate and origin, maturity, and processing practices and storage, among others, can affect the sugar composition of juices. Apart from the sugar contents, the Fru/Glu ratio was also given in fruit juices. This ratio is a useful index for the evaluation of the product quality and authenticity in fruit juices.[2,14]

The Fru content in apple juices is typically two to three times higher than the Glu content.[5,14] Thus, the Glu levels should vary between 15 and 35 g L^{-1}, giving Glu/Fru ratios within the range of 0.3−0.5.[14] All apple juices analyzed (A1−A8) followed the reference guidelines of the Association of the Industry of Juices and Nectars (AIJN).[14] Sor was also used as an indicator of fruit juice authenticity, since its concentration differs over a large range between different fruits. For instance, high Sor levels are found in pears (10−25 g L^{-1}) and in apples (2.5−7 g L^{-1}), while no Sor or only low traces are found in grape and citrus fruits.[37] Thus, the appearance of Sor in samples not obtained from pear or apple could be a good marker of juice adulteration. On the other hand, grape juice did not contain any Suc, and the concentration range for Fru and Glu should be 60−110 g L^{-1}.[14] In our case, all fruit grape juices investigated (G1−G8) fell within this range. The Glu/Fru ratio in orange and mandarin juices is always less than 1, following all orange (O1−O8) and mandarin (M1−M8) juices the AIJN recom-

DOI: 10.1021/acs.jafc.5b00122
J. Agric. Food Chem. 2015, 63, 2639−2646

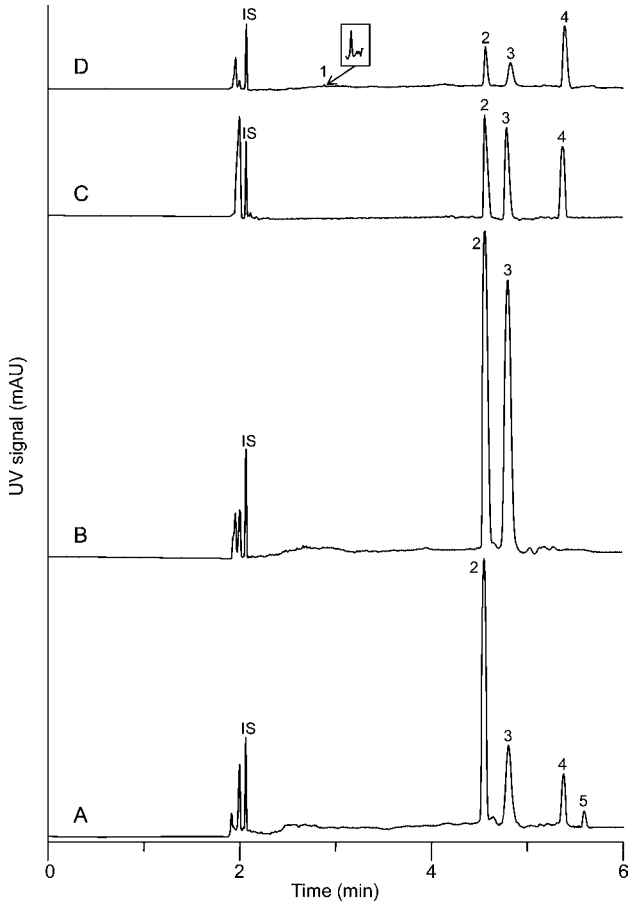

Figure 2. Representative electropherograms of apple juice (A), grape juice (B), orange juice (C), and orange nectar (D). CZE conditions: BGE composed of 10 mM PDC and 0.5 mM CTAB at pH 12.1; hydrodynamic injection, 50 mbar for 6 s; separation voltage, −25 kV at 15 °C. Other conditions as in Figure 1.

mendations. The levels of Fru and Glu in pineapple juice should be ranged between 15 and 40 g L^{-1}, whereas the concentration of Suc was within 25−80 g L^{-1}. A Fru/Glu ratio between 0.8 and 1.25 is commonly used as a good index of authenticity.[14] The pineapple juice samples (P1−P8) were in accordance with the AIJN criteria.

The determination of sugar composition in nectars was also performed (see Table 4). The contents of Fru and Glu were lower than those obtained with the orange and pineapple juices, which could be attributed to the addition of water to "fruit concentrate". According to the directive 2012/12/EU,[38] fruit nectars are a fermentable but unfermented product obtained by adding water and sugars or honey or both to the fruit juices, fruit juices from concentrate, concentrated fruit juices, or fruit purée or to a mixture of those products. The addition of sugars or honey is permitted up to 20% of the total weight of the finished product. Moreover, in most cases, the Suc content was higher than that found in authentic fruit juices (for samples ON3, ON4, PN1, PN2, and PN3), whereas in a few cases, low contents of Suc were found (samples ON1 and ON2). The presence of these large contents of Suc suggested that this sugar has been added in these samples.

Additionally, artificial sweeteners are allowed in nectars sold for dietetic purposes. The EU permitted cyclamates (Cyc) (E952, cyclamic acid, and its sodium and calcium salts) as sweeteners for a variety of food products, with a maximum acceptable level in fruit nectars of 250 mg L^{-1},[38] whereas for Codex GSFA the level is established at 400 mg kg^{-1}.[39] From the six orange nectars analyzed, only two samples (ON1 and ON5) contained Cyc (being consistent with that declared in their labels), but one sample (ON1) exceeded slightly the maximum levels allowed.

At the sight of the differences observed in sugar concentrations, the possibility of using these contents to distinguish fruit juices was considered. For this purpose, a graph of Fru/Glu versus Suc/total sugars was first tried. As shown in Figure 3, this plot was not able to discriminate between citrus

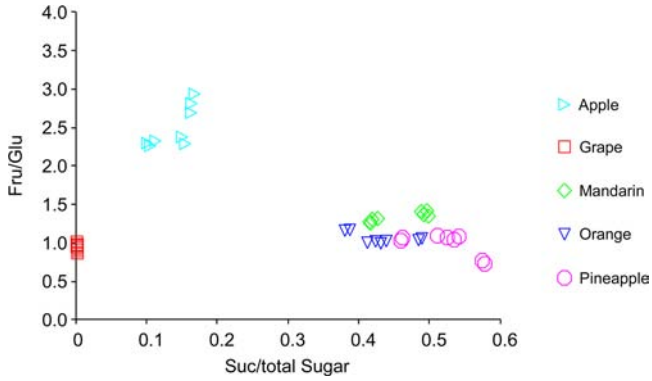

Figure 3. Graph of Fru/Glu versus Suc/total sugars of the studied fruit juices.

(orange and mandarin) and pineapple juices. Thus, in order to discriminate between juices obtained from different fruits, the construction of an LDA model was next considered.

Classification of Juices Obtained from Different Fruits by LDA: Evaluation of the Possibility of Detecting Juice Blends. LDA, a supervised classification technique, is widely recognized as an excellent tool to obtain vectors showing the maximal resolution between a set of previously defined categories. In LDA, vectors minimizing Wilks' lambda, λ_w, are

Table 4. Sugar and Cyc Contents[a] and Glu/Fru Ratio of the Juices and Nectars Used in This Study

	fruit type	Cyc	Fru	Glu	Suc	Sor	Glu/Fru ratio
juice	apple		60.2−81.0	17.9−35.3	7.2−24.1	4.1−7.2	0.27−0.44
	grape		81.1−108.9	75.4−104.0			1.02−1.07
	mandarin		29.5−40.1	22.5−32.8	45.6−53.7		0.7−0.8
	orange		22.0−31.5	18.6−31.5	22.5−49.7		0.84−0.98
	pineapple		23.3−35.4	21.1−32.9	39.2−80.1		0.93−0.96
nectar	orange	0−0.42	11.2−16.0	2.7−8.4	7.7−68.5		
	pineapple		14.9−25.1	12.5−17.4	66.6−96.7		

[a]Expressed in g L^{-1}.

DOI: 10.1021/acs.jafc.5b00122
J. Agric. Food Chem. 2015, 63, 2639−2646

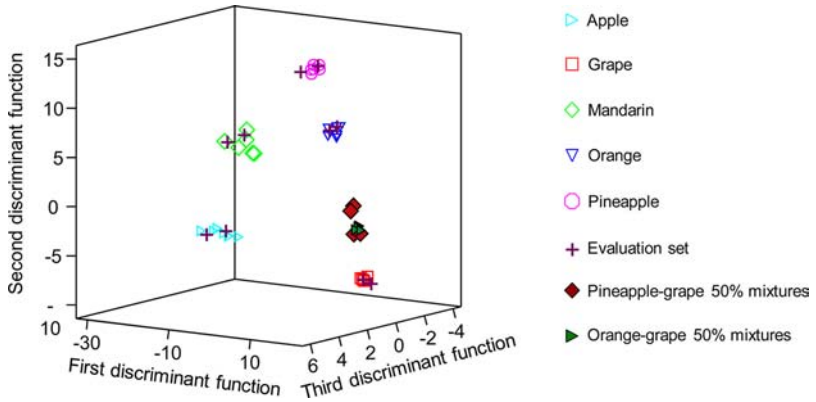

Figure 4. Score plot on an oblique plane of the three-dimensional space defined by the three first discriminant functions of the LDA model constructed to discriminate between juices obtained from different fruits. Evaluation set samples and fruit juice blends at a 50% level of each juice are labeled as indicated in figure legend.

obtained.[40] This parameter is calculated as the sum of squares of the distances between points belonging to the same category divided by the total sum of squares. Values of λ_w approaching zero are obtained with well-resolved categories, whereas overlapped categories make λ_w approach one. Up to $N - 1$ discriminant vectors are constructed by LDA, with N being the lowest value for either the number of predictors or the number of categories. The selection of the predictors to be included in the LDA models was performed using the SPSS stepwise algorithm. According to this algorithm, a predictor is selected when the reduction of λ_w produced after its inclusion in the model exceeds F_{in}, the entrance threshold of a test of comparison of variances or F test. However, the entrance of a new predictor modifies the significance of those predictors that are already present in the model. For this reason, after the inclusion of a new predictor, a rejection threshold, F_{out}, is used to decide whether one of the other predictors should be removed from the model. The process terminates when there are no predictors entering or being eliminated from the model. The default probability values of F_{in} and F_{out} of 0.05 and 0.10, respectively, were adopted.

Thus, for LDA, a data matrix was constructed using the concentration values of Table 4, divided by pairs, as original variables, in order to minimize the differences arising from the sugar concentrations found in the fruit juices considered in this study. This matrix contained 40 objects, which corresponded to all the fruit juices of Table 1, and six predictors, which were obtained by dividing each analyte concentration (Fru, Glu, Suc, and Sor) by the concentration of each one of the other analytes, taking into account that any pair of concentrations should be considered only once. A response column, containing the categories corresponding to the five fruit types, was added to this matrix. This matrix was divided in two groups of objects to constitute the training and evaluation sets. The training set was composed by 30 objects (6 juices × 5 fruit types), while the evaluation set was constituted by the remaining samples (10 objects).

When the LDA model was constructed, an excellent resolution between all the category pairs was achieved (Figure 4, $\lambda_w < 0.01$). The variables selected by the SPSS stepwise algorithm and the corresponding standardized coefficients of the model, showing the predictors with large discriminant capabilities, are given in Table 5. According to this table, the main concentration ratios selected by the algorithm to construct the LDA model corresponded to Suc/Fru and Suc/Glu. With this model and leave-one-out validation, all the objects of the training set were correctly classified. On the other hand, the prediction capability of the model was evaluated using the evaluation set. In this case, all the objects (represented with a cross symbol in Figure 4) were correctly assigned within a 95% probability level.

Table 5. Predictors Selected and Corresponding Standardized Coefficients of the LDA Model Constructed To Discriminate between Juices Obtained from Different Fruits

predictors[a]	f_1	f_2	f_3	f_4
Glu/Fru	3.17	−0.29	0.34	0.82
Suc/Fru	−4.61	1.34	−2.28	−0.89
Sor/Fru	−1.10	−0.39	−0.37	0.53
Suc/Glu	4.74	−0.34	2.68	1.28
Sor/Suc	2.44	−0.01	0.68	1.03

[a]Sugar concentration ratios.

The possibility of detecting fruit juice blends by LDA was also evaluated. For this purpose, different fruit juice mixtures (pineapple−grape and orange−grape), with a 50% content of each juice, were used to check whether the model is able to assign them to a category or whether, in contrast, the model is not able to assign them, which will demonstrate that those samples are juice blends. As it can be observed in Figure 4, pineapple−grape and orange−grape mixtures overlapped. However, in any case, any sample was assigned to any given category. Thus, it is demonstrated that the model is able to discriminate pure fruit juices from mixtures of them.

MLR Model Construction To Predict Blends of Fruit Juices. Finally, to evaluate the possibility of detecting different percentages of fruit juices in binary mixtures, two MLR models for pineapple−grape and orange−grape were constructed. To select the predictors used in the construction of MLR models, the SPSS stepwise algorithm with the default probability values of F_{in} and F_{out} of 0.05 and 0.10, respectively, was adopted. For MLR studies, calibration and external validation sets were constructed, one for each pair of fruit juices. The calibration matrices contained 21 objects (3 mixtures × 7 percentage levels), while the seven remaining mixtures were used as external validation set. These matrices contained also the six predictors and a response column with the pineapple or orange percentage. A plot showing the predicted versus the nominal fruit juice percentages for the two types of binary mixtures is shown in Figure 5. The predictors selected and their

DOI: 10.1021/acs.jafc.5b00122
J. Agric. Food Chem. 2015, 63, 2639−2646

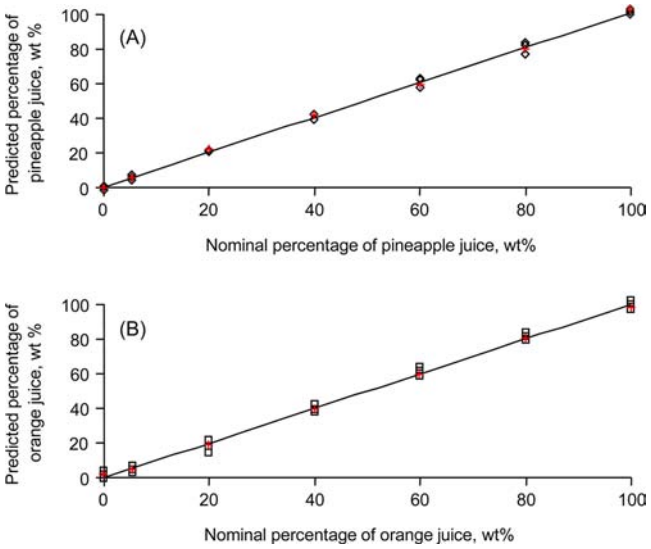

Figure 5. Predicted (MLR) versus nominal fruit juice percentages for (A) pineapple−grape and (B) orange−grape binary mixtures. External validation set samples are labeled with a cross symbol. The straight line is $y = x$.

corresponding nonstandardized model coefficients are given in Table 6. The regression coefficients and the average prediction errors (calculated as the sum of the absolute differences between expected and predicted fruit juice percentages divided by the number of predictions) are also provided. For both models using leave-one-out validation, the average prediction errors were lower than 4.0%. On the other hand, when the models were applied to the validation sets, an excellent prediction capability was observed (Figure 5, red cross symbols), the average validation errors being below 5.2%. The LODs (calculated as three times the standard deviation at 5% grape juice) are also given in Table 6. In both blend juices, these values were below 4.7%, which may be considered as a reasonable limit to discern between intentional addition and possible contamination because the same processing equipment was used for different juices. However, better LODs were found in the literature[1] using a metabolomics approach (with UPLC-QToF MS), which represented a high cost methodology (need for specialized ultrahigh pressure and MS systems). Finally, the commercially available mixtures of fruit juices were used to check whether the model was able to correctly predict the percentages stated in product labels. In all cases, the percentages found were consistent with the values indicated in the label, which clearly proved the usefulness of the MLR models constructed.

Table 6. Predictors Selected and Their Corresponding Nonstandarized Model Coefficients (coef.), Linear Regression Coefficients (R^2) and Average Prediction Errors (avg pred. error) Obtained for the MLR Models Constructed To Predict Binary Mixtures of Fruit Juices

binary mixture	predictor	coef.	R^2	avg pred. error (%)	LOD (%)
pineapple−grape	constant	278.42	0.990	3.8	4.7
	Suc/Fru	−490.50			
	Suc/Glu	413.09			
	Glu/Fru	−179.11			
orange−grape	constant	−285.15	0.997	3.2	3.7
	Glu/Fru	360.60			
	Suc/Fru	−938.29			
	Suc/Glu	875.33			

In summary, a fast, simple and reliable CZE method with indirect UV detection to determine sugars commonly present in several fruit juices and nectars has been established. The combination of CZE analysis with different chemometric tools (LDA and MLR) provides a simple way to classify juices from different fruits as well as to quantify different juice blends. Therefore, the present methodology provides an effective tool for quality control purposes in the juice industry and regulatory agencies.

■ ASSOCIATED CONTENT

Supporting Information

Influence of temperature on the separation of analyte standards. This material is available free of charge via the Internet at http://pubs.acs.org.

■ AUTHOR INFORMATION

Corresponding Author

*Dr. José Manuel Herrero-Martínez. Tel: +34 9635 44062. Fax: +34 9635 44436. E-mail: jmherrer@uv.es.

Funding

M.J. Lerma-García thanks the Generalitat Valenciana for a VALi+d postdoctoral contract. Work supported by Project CTQ 2014-52765-R (MINECO of Spain and FEDER funds) and Agilent Technologies Spain, S.L.

Notes

The authors declare no competing financial interest.

■ ACKNOWLEDGMENTS

The authors also thank Refresco Iberia, S.A.U., for supplying the fruit juice samples.

■ ABBREVIATIONS USED

CZE, capillary zone electrophoresis; Cyc, sodium cyclamate; PDC, 2,6-pyridine dicarboxylic acid; BGE, background electrolyte; LDA, linear discriminant analysis; Suc, sucrose; Glu, glucose; Fru, fructose; HPLC, high performance liquid chromatography; GC, gas chromatography; NaOH, sodium hydroxide; IS, internal standard; CTAB, cetyltrimethylammonium bromide; Sor, sorbitol; EOF, electroosmotic flow; LOD, limit of detection; LOQ, limit of quantification

■ REFERENCES

(1) Jandric, Z.; Roberts, D.; Rathor, M. N.; Abrahim, A.; Islam, M.; Cannavan, A. Assessment of fruit juice authenticity using UPLC−QToF MS: A metabolomics approach. *Food Chem.* **2014**, *148*, 7−17.

(2) Stander, M. A.; Kühn, W.; Hiten, N. F. Survey of South African fruit juices using a fast screening HILIC-MS method. *Food Addit. Contam., Part A* **2013**, *30*, 1473−1484.

(3) Saavedra, L.; García, A.; Barbas, C. Development and validation of a capillary electrophoresis method for direct measurement of isocitric, citric, tartaric and malic acids as adulteration markers in orange juice. *J. Chromatogr. A* **2000**, *881*, 395−401.

(4) Ashurst, P. R. *Chemistry and technology of soft drinks and fruit juices*, 2nd ed.; Blackwell Publishing Ltd: Oxford, U.K., 2005.

(5) Muntean, E. Simultaneous carbohydrate chromatography and unsuppressed ion chromatography in detecting fruit juices adulteration. *Chromatographia* **2010**, *71*, S69−S74.

DOI: 10.1021/acs.jafc.5b00122
J. Agric. Food Chem. 2015, 63, 2639−2646

(6) Simpkins, W.; Harrison, M. The state of the art in authenticity testing. *Trends Food Sci. Technol.* **1995**, *6*, 321−328.
(7) Fügel, R.; Carle, R.; Schieber, A. Quality and authenticity control of fruit purées, fruit preparations and jams − a review. *Trends Food Sci. Technol.* **2005**, *16*, 433−441.
(8) Ehling, S.; Cole, S. Analysis of organic acids in fruit juices by liquid chromatography-mass spectrometry: An enhanced tool for authenticity testing. *J. Agric. Food Chem.* **2011**, *59*, 2229−2234.
(9) Saavedra, L.; Rupérez, F. J.; Barbas, C. Capillary electrophoresis for evaluating orange juice authenticity: A study on Spanish oranges. *J. Agric. Food Chem.* **2001**, *49*, 9−13.
(10) Obón, J. M.; Díaz-García, M. C.; Castellar, M. R. Red fruit juice quality and authenticity control by HPLC. *J. Food Compos. Anal.* **2011**, *24*, 760−771.
(11) Díaz-García, M. C.; Obón, J. M.; Castellar, M. R.; Collado, J.; Alacid, M. Quantification by UHPLC of total individual polyphenols in fruit juices. *Food Chem.* **2013**, *138*, 938−949.
(12) Gómez-Ariza, J. L.; Villegas-Portero, M. J.; Bernal-Daza, V. Characterization and analysis of amino acids in orange juice by HPLC−MS/MS for authenticity assessment. *Anal. Chim. Acta* **2005**, *540*, 221−230.
(13) Yoon, J. H.; Kim, K.; Lee, D. S. Chemometric aspects of sugar profiles in fruit juices using HPLC and GC. *Bull. Korean Chem. Soc.* **1997**, *18*, 695−702.
(14) Association of the Industry of Juices and Nectars. Code of Practice for Evaluation of Fruit and Vegetable Juices, AIJN, Brussels, 2010.
(15) Martínez Montero, C.; Rodríguez Dodero, M. C.; Guillén Sánchez, D. A.; Barroso, G. C. Analysis of low molecular weight carbohydrates in food and beverages: A review. *Chromatographia* **2004**, *59*, 15−30.
(16) Kelly, J. F.; Downey, G. Detection of sugar adulterants in apple juice using Fourier Transform infrared spectroscopy and chemometrics. *J. Agric. Food Chem.* **2005**, *53*, 3281−3286.
(17) Karadeniz, F.; Eksi, A. Sugar composition of apple juices. *Eur. Food Res. Technol.* **2002**, *215*, 145−148.
(18) Pérez, A. G.; Olías, R.; Espada, J.; Olías, J. M.; Sanz, C. Rapid determination of sugars, nonvolatile acids, and ascorbic acid in strawberry and other fruits. *J. Agric. Food Chem.* **1997**, *45*, 3545−3549.
(19) Blanco-Gomis, D. In *Food Analysis by HPLC*; Mollet, L. M. L. Ed.; Marcel Dekker: New York, 2000; pp 482−484.
(20) Chinnici, F.; Spinabelli, U.; Riponi, C.; Amati, A. Optimization of the determination of organic acids and sugars in fruit juices by ion-exclusion liquid chromatography. *J. Food Compos. Anal.* **2005**, *18*, 121−130.
(21) Pereira, V.; Cámara, J. S.; Cacho, J.; Marques, J. C. HPLC-DAD methodology for the quantification of organic acids, furans and polyphenols by direct injection of wine samples. *J. Sep. Sci.* **2010**, *33*, 1204−1215.
(22) Morvai, M.; Molnár-Perl, I.; Knausz, D. Simultaneous gas—liquid chromatographic determination of sugars and organic acids as trimethylsilyl derivatives in vegetables and strawberries. *J. Chromatogr. A* **1991**, *552*, 337−344.
(23) Adams, M. A.; Chen, Z. L.; Landman, P.; Colmer, T. D. Simultaneous determination by capillary gas chromatography of organic acids, sugars, and sugar alcohols in plant tissue extracts as their trimethylsilyl derivatives. *Anal. Biochem.* **1999**, *266*, 77−84.
(24) Soga, T.; Ross, G. A. Simultaneous determination of inorganic anions, organic acids and metal cations by capillary electrophoresis. *J. Chromatogr. A* **1999**, *837*, 231−239.
(25) Soga, T.; Serwe, M. Determination of carbohydrates in food samples by capillary electrophoresis with indirect UV detection. *Food Chem.* **2000**, *69*, 339−344.
(26) Soga, T.; Imaizumi, M. Capillary electrophoresis method for the analysis of inorganic anions, organic acids, amino acids, nucleotides, carbohydrates and other anionic compounds. *Electrophoresis* **2001**, *22*, 3418−3425.
(27) Cebolla-Cornejo, J.; Valcárcel, M.; Herrero-Martínez, J. M.; Roselló, S.; Nuez, F. High efficiency joint CZE determination of sugars and acids in vegetables and fruits. *Electrophoresis* **2012**, *33*, 2416−2423.
(28) Hernández-Borges, J.; Rodríguez-Delgados, M. A.; Cifuentes, A. In *Chemometric Methods in Capillary Electrophoresis*; Hanrahan, G., Gomez, F. A. Eds.; John Wiley & Sons, Inc.: Hoboken, NJ, 2009.
(29) Klampfl, C. W.; Buchberger, W. Determination of low-molecular-mass organic acids by capillary zone electrophoresis. *TrAC, Trends Anal. Chem.* **1997**, *16*, 221−229.
(30) Doble, P.; Haddad, P. R. Indirect photometric detection of anions in capillary electrophoresis. *J. Chromatogr. A* **1999**, *834*, 189−212.
(31) Soga, T.; Heiger, D. N. Simultaneous determination of monosaccharides in glycoproteins by capillary electrophoresis. *Anal. Biochem.* **1998**, *261*, 73−78.
(32) Altria, K. D. Improved performance in capillary electrophoresis using internal standard. *LC·GC Eur.* **2002**, *15*, 588−584.
(33) Roselló, S.; Galiana-Balaguer, L.; Herrero-Martínez, J. M.; Maquieira, A.; Nuez, F. Simultaneous quantification of the main organic acids and carbohydrates involved in tomato flavour using capillary zone electrophoresis. *J. Sci. Food Agric.* **2002**, *82*, 1101−1106.
(34) Oliveira Fernandes, V. N.; Bellozi Fernandes, L.; Pereira Vasconcellos, J.; Vincenzi Jager, A.; Tonin, F. G.; Leal de Oliveira, M. A. Simultaneous analysis of aspartame, cyclamate, saccharin and acesulfame-K by CZE under UV detection. *Anal. Methods* **2013**, *5*, 1524−1532.
(35) Vaher, M.; Koel, M.; Kazarjan, J.; Kaljurand, M. Capillary electrophoretic analysis of neutral carbohydrates using ionic liquids as background electrolytes. *Electrophoresis* **2011**, *32*, 1068−1073.
(36) Pilando, L. S.; Wrolstad, L. E. Compositional profiles of fruit juice concentrates and sweetners. *Food Chem.* **1992**, *44*, 19−27.
(37) Dietrich, H.; Kruger-Steden, E.; Patz, C. D.; Will, F.; Rheinberger, A.; Hopf, I. Increase of sorbitol in pear and apple juice by water stress, a consequence of climatic change? *Fruit Process.* **2007**, No. Nov/Dec, 348−351.
(38) Directive 2012/12/EU, amending Council Directive 2001/112/EC relating to fruit juices and certain similar products intented for human consumption. Official Journal of the European Union, L115/1−L115/11.
(39) General Standard for Food Additives, Codex Alimentarius (GSFA, Codex STAN 192-1995), revision 2014.
(40) Vandeginste, B. G. M.; Massart, D. L.; Buydens, L. M. C.; De Jong, S.; Lewi, P. J.; Smeyers-Verbeke, J. *Data Handling in Science and Technology, Part B*; Elsevier Science: Amsterdam, The Netherlands, 1998; p 237.

DOI: 10.1021/acs.jafc.5b00122
J. Agric. Food Chem. 2015, 63, 2639−2646

Table 1. Conditions Used in Various Rounds of SELEX

round	selection	number of washings with binding buffer	number of elutions with elution buffer	eluate used in next round/cloning
1.	positive: BCM-7 beads	6	6	sixth eluate[a]
2.	positive: BCM-7 beads	5	5	fifth eluate[a]
3.	positive: BCM-7 beads	5	5	fifth eluate[a]
4.	positive: BCM-7 beads	6	6	sixth eluate[b]
	negative: magnetic beads			unbound from magnetic beads[a]
5.	positive: BCM-7 beads	5	5	fifth eluate[b]
	counter: BCM-5 beads			unbound from BCM-5 beads[a]
6.	positive: BCM-7 beads	5	5	fifth eluate[b]
	counter: BCM-9A1 beads			unbound from BCM-9A1beads[a]
7.	positive: BCM-7 beads	5	5	fifth eluate[b]
	counter: BCM-9A2 beads			unbound from BCM-9A2 beads[a]
8.	positive: BCM-7 beads	5	5	fifth eluate[a]
9.	positive: BCM-7 beads	5	5	fifth eluate[a]
10.	positive: BCM-7 beads	5	5	fifth eluate[c]

[a]Eluate used in next round of SELEX. [b]Fraction used in negative or counter selection. [c]Eluate used for cloning.

Conjugation of BCM-7, BCM-5, BCM-9A1, and BCM-9A2 Peptides to Magnetic Beads. BCM-7, BCM-5, BCM-9A1, and BCM-9A2 peptides (Technoconcept) were conjugated to tosyl activated Dynabeads M-280 (Invitrogen) as per manufacturer protocol. A 100 mM borate buffer was prepared by adding 6.18 g of boric acid in 800 mL of water. The pH was adjusted to 7.8 by 1 N NaOH; the final volume of the solution was made to be 1000 mL by the addition of water. A sample of 2×10^8 beads were washed four times with 100 mM borate buffer (pH 7.8). To the washed beads were added 100 μL of peptide (1 mg/mL in water); 50 μL of 100 mM borate buffer, pH 7.8; and 100 μL of 3.0 M ammonium sulfate (prepared in borate buffer, pH 7.8). The contents were incubated for 20 h at 37 °C. The unconjugated peptides were removed by washing the beads with borate buffer. The remaining sites on the beads were blocked by immersing beads in 0.5% bovine serum albumin (BSA) prepared in phosphate buffer saline (PBS), pH 7.4, for 1 h at 37 °C. After the blocking solution was removed, peptide conjugated beads were suspended in 0.1% BSA-PBS, pH 7.4, stored at 4 °C, and used within 15 days.

Amplification of ssDNA Library. A 500 ng sample of 72 nt long ssDNA (MW = 22 067 Da) library[19] (Integrative DNA technology, IDT) was amplified in 5 parallel reactions by PCR. This will essentially have $(500 \times 10^{-9})(6.023 \times 10^{23})/22\,067 = 1.36 \times 10^{13}$ molecules. Total randomness possible from 36 variable nucleotides in the 72 nt. long library will be $4^{36} = 4.7 \times 10^{21}$. However, the maximum randomness from a 500 ng library will be limited to 10^{13}. Each reaction mixture was composed of 50 mM $(NH_4)_2SO_4$, 100 mM Tris-HCl, 2.0 mM $MgCl_2$, 0.2 mM dNTPs, 100 ng of ssDNA library, 1.0 μM each of forward primer (5′-ATCCGTCACACCTGCTCT-3′) and phosphorylated reverse primer (5′-P-ATACGGGAGCCAACACCA-3′), and 1.5 U Taq DNA polymerase in a volume of 50 μL. The amplification conditions used are as follows: an initial heat activation step at 95 °C for 5 min and 30 cycles of 95 °C for 1 min, 55 °C for 1 min, 72 °C for 1 min, and an extension step of 2 min at 72 °C. Amplification of the library was confirmed by resolving PCR product on 3% agarose gel electrophoresis.

Conversion of dsDNA into ssDNA. Amplified PCR product without further purification was digested by λ exonuclease[20] (Fermentas) and digestion reaction was monitored on 3% agarose gel electrophoresis. After 100 min of digestion, the reaction was stopped by inactivating λ exonuclease, which was achieved by heating at 85 °C for 10 min. The product was purified by Qiax II gel extraction kit (Qiagen). The preparation (pure DNA) was stored at −20 °C until further use. On the day of SELEX, the contents were thawed and diluted with 100 μL of binding buffer (20 mM Tris HCl, 100 mM NaCl, 2.0 mM $MgCl_2$, 5.0 mM KCl, 1.0 mM $CaCl_2$, and 0.02% Tween 20, pH 7.6). The undigested reverse strands were further separated by snap cooling, which was achieved by heating of purified product at 90 °C for 15 min and immediately placing on ice for 5 min.[21]

SELEX. An amplified ssDNA library (10 μg) was incubated with BCM-7 conjugated beads (2×10^8) in 100 μL of binding buffer for 1 h at 28 °C with intermittent tapping of tubes to prevent settling of magnetic beads. Then, the beads were washed with 100 μL of binding buffer to remove unbound ssDNA, while bound ssDNA was eluted with elution buffer (20 mM Tris HCl, 10.0 mM EDTA, 3.5 M Urea, and 0.02% Tween 20, pH 8.0) at 80 °C for 10 min. Ten rounds of SELEX were performed to enrich target-specific oligonucleotides (aptamers). To enhance the specificity of the selected oligonucleotides, negative selector and counter selectors (BCM-5, BCM-9A1, and BCM-9A2 coated magnetic beads) were used. In negative selection, tosyl activated magnetic beads were blocked by 0.5% BSA (prepared in PBS) for 1 h at 37 °C. In each round of SELEX, ssDNA eluted from the last elution was amplified. Amplification conditions used are as follows: an initial heat activation step at 95 °C for 3 min and 17 cycles of 95 °C for 14 s, 55 °C for 23 s, 72 °C for 17 s, and an extension step of 2 min at 72 °C. The concentration of PCR product was determined by nanophotometer and was digested by addition of 10U λ exonuclease for every 2.0 μg of amplified product. The digested PCR product was purified by using Qiax II gel extraction kit, snap cooled, and used for the next round of SELEX. The conditions in various rounds of SELEX are provided in Table 1.

Enrichment of BCM-7 specific aptamer after each round of SELEX was evaluated by amplification of 1.0 μL of aliquot taken from each round of washings and elutions. The PCR reaction conditions used were the same as those mentioned above. The PCR product was confirmed by resolving on 3% agarose gel electrophoresis. The amount of DNA was calculated by gel analysis software (SynGene, Synoptis). The aptamers obtained after the last round of SELEX were amplified by using forward primer (5′-ATCCGTCACACCTGCTCT-3′) and reverse primer (5′-ATACGGGAGCCAACACCA-3′). The PCR product was inserted into pGEM T cloning vector (Promega). The recombinant vector was cloned into *Escherichia coli* (DH5α). A total of 41 clones were selected for sequencing (SciGenom).

Determination of Dissociation Constant. Prior to use, BCM-7 conjugated magnetic beads were washed and suspended in binding buffer. A 100 μL sample of 5−325 nM, 5(6)-carboxyfluorescein labeled aptamer (IDT) (prepared in binding buffer) was mixed with 50 μL of BCM-7 conjugated beads (1×10^8) for 1 h at 28 °C. Unbound aptamers were collected by five quick successive washing with binding buffer of 100 μL each. Bound aptamers were eluted with five successive treatments of beads with elution buffer of 100 μL each at 80 °C for 10 min.[22] The unbound and bound aptamers were separately pooled. Labeled aptamers were measured at 494 nm excitation and 520 nm emission wavelengths (Varian, Cary Eclipse Fluorescence Spectrophotometer). The dissociation constant (K_d) was calculated by nonlinear regression analysis using Graph Pad Prism 5 software.

Binding Selectivity of BCM-7 Apatmers. Selected aptamers were tested for their ability to bind with BCM-7/BCM-9A1/BCM-

DOI: 10.1021/acs.jafc.5b00007
J. Agric. Food Chem. 2015, 63, 2647−2653

9A2 by following the protocol as described by Niazi et al.[23] In brief, 500 ng of 5(6)-carboxyfluorescein labeled aptamer (dissolved in 100 μL of binding buffer) was mixed with 50 μL of peptide-coated beads (1×10^8) and incubated for 1 h at 28 °C. The unbound and bound aptamers were collected as mentioned above, and the fluorescence was measured.

Secondary Structure Prediction of Aptamers. Secondary structures of the aptamers were obtained by online program Mfold (http://mfold.rit.albany.edu/?q=mfold/DNA-Folding-Form) at 100 mM NaCl, 2.0 mM $MgCl_2$, and 28 °C to determine the possible interacting regions of the aptamers.

Gold Nanoparticles-Aptasensor. Gold nanoparticles (GNPs) were prepared by reduction of gold(III) chloride trihydrate (Sigma) by sodium citrate (Sigma).[24] The concentration of gold nanoparticles was calculated from the molar extinction coefficient value of 2.43×10^8 M^{-1} cm^{-1} at 520 nm[25] for 23 nm GNPs. A 20 μL sample of 100 μM aptamers was mixed with 10.0 mL of 5.0 nM GNPs suspended in water, and the mixture was incubated for 1 h[26,27] at 25 °C. Aptamer-coated GNPs were pelleted by centrifugation (8000 rpm, 20 min). The supernatant was discarded. The pelleted GNPs were resuspended in water. A 25 μL sample of varied concentration of BCM-7 from 1 to 30 μg/mL (prepared in water) were mixed with 200 μL of 5.0 nM aptamer-coated GNPs. After 1 h of incubation, 25 μL of 350 mM NaCl was added, and the contents were gently but quickly mixed. The color change of GNPs was recorded within 3 min.

Enzyme-Linked Aptamer-Sorbent Assay. Aptamers were evaluated for their potential use for the estimation of BCM-7 content using an enzyme-linked aptamer-sorbent assay. A 12 μL sample of 10 μM of each of five biotinylated aptamers (seq1, seq7, seq10, seqU4, and seqU5) (IDT), were mixed and further diluted by adding 1140 μL of 5X SSCT buffer (75 mM sodium citrate, 750 mM sodium chloride, and 0.05% Tween 20), pH 7.0. A 100 μL portion of the aptamer-mix was added to each well in a 96-well streptavidin coated plate (Nunc). After 1 h of incubation at room temperature, wells were washed three times with 2X SSCT (30 mM sodium citrate, 300 mM sodium chloride, and 0.05% Tween 20), pH 7.0 to remove unbound biotinylated aptamers. Then, wells were blocked by treating overnight with 1.5% BSA at 4 °C. Wells were washed three times with 1X phosphate saline buffer (PBS) at pH 7.4 to remove excess BSA. Then, 100 μL of BCM-7 at variable concentration (10−1000 ng/mL, prepared in water) were added, and the plate was incubated for 90 min at 25 °C. The wells were washed three times with 1X PBS at pH 7.4. Then, wells were treated with 1/2000 times diluted 100 μL of BCM-7-peroxidase conjugate (Merck) for 90 min at 25 °C. After incubation with conjugate, the plate was washed five times with 1X PBS, pH 7.4, to remove unbound BCM-7-peroxidase conjugate followed by addition of 100 μL of 3,3′,5,5′-tetramethylbenzidine (TMB) (Sigma). The plate was further incubated for 15 min at 37 °C, and then the reaction was stopped by adding 100 μL of 2 N HCl. The absorbance was recorded at 450 nm. in ELISA plate reader (BioTek).

Cross reactivity of individual BCM-7 specific aptamers (seq1, seq10, seq7, seqU5, seq3, seq4, seq6, seqU2, and seqU4) with BCM-5, BCM-9A1, and BCM-9A2 peptides was determined in a manner similar to that described above using 500 nM biotinylated BCM-7 aptamers and 500 ng/mL concentration of BCM-7/BCM-5/BCM-9A1/BCM-9A2 peptide.

BCM-7 aptamers (seqU4) were also evaluated for their possible use in development of ELASA method applicable to blood, urine, and β-casein digest. For this purpose, plasma (rat), urine (human), and β-casein digest (bovine) were spiked with BCM-7 peptide (3.2−200 μg/mL). A 15 mL sample of urine was treated with 50 μL (187 U) of urease at room temperature for 1 h to remove urea from urine; β-casein from bovine (sigma) was digested according to Jinsmaa and Yoshikawa protocol.[12] The 50 μL of urine or plasma or β-casein digest, 50 μL binding buffer, and 100 μL, 1/4000 times diluted BCM-7-peroxidase (diluted in binding buffer) were added simultaneously to each well. The 96-well plate was incubated for 90 min at room temperature and then subjected to peroxidase assay as described above.

RESULTS

Selection of Aptamers. An in vitro selection of ssDNA that binds to BCM-7 conjugated to tosyl activated magnetic beads by the SELEX process was conducted. DNA aptamers specific to BCM-7 were selected from a pool of 10^{13} random DNA library. A total of ten SELEX rounds including negative and counter selections made gradual enrichment of oligonucleotides. The percentage of ssDNA binding to BCM-7 from DNA pool was significantly increased with increasing the SELEX rounds. Before the fifth round of selection, the negative selection was performed by using magnetic beads. BCM-5, BCM-9A1, and BCM-9A2 counter selector peptides were used after SELEX round number 5, 6, and 7 respectively. The negative and counter selections were used to improve the specificity of aptamers for BCM-7. Sequences of inserts from 41 independent clones revealed a total of 15 different aptamers. Out of 15 aptamers, seq10, seq1, seqU1, seqU3, seqU4, seq7, and seq4 were present in 10, 6, 5, 4, 3, 3, and 2 of the independent clones, respectively (Table 2), indicating enrichment of aptamers. Thirteen aptamers were 72 nt long, and the remaining two aptamers (seq6 and seq9) were 71 nt long. Seq9 and seq10 aptamers have one base difference as seq9 lacked guanosine base at the 43rd position. Loss of one nucleotide in 71 nt long aptamer can happen during PCR amplification.

Dissociation Constant and Binding Selectivity Study of BCM-7 Specific Aptamers. The dissociation constant values of BCM-7 aptamers were in the range of 7.69−156.66 nM. Seq6 showed the lowest dissociation constant value (7.69 nM), while seq8 showed the highest value (156.66 nM) (Table 2).

Binding selectivity of nine aptamers, viz., seq1, seq10, seq7, seqU5, seq3, seq4, seq6, seqU2, and seqU4, toward BCM-7, BCM-9A1, and BCM-9A2 peptides was evaluated. In general, the binding of fluorescent labeled aptamers to BCM-7 was generally higher in comparison to BCM-9A1 or BCM-9A2 (Figure 1). Aptamers seq10, seqU5, seq4, seq6, seqU2, and seqU4 bind to a similar extent to BCM-9A1 and BCM-9A2. However, seq7 and seq3 aptamers cross-reacted preferably to BCM-9A1. Also, seq10, seq7, seqU5, and seqU4 aptamers exhibited lower cross-reaction with BCM-9A1 and BCM-9A2 (Figure 1).

Predicted Secondary Structure of BCM-7 Aptamers. Secondary structure of the selected aptamers was predicted by online program Mfold. Five structural motifs common in at least two aptamers were obtained by Mfold software (Figure 2 and Supporting Information). The selected aptamers were classified into six groups based on presence or absence of motifs (Table 3). Nine aptamers showed one common motif with at least one aptamer. The remaining six aptamers had no common motifs and hence were grouped in group 6. These motifs are present in the form of loops which are predominantly created by G-C linkage. For several aptamers, more than one Mfold structure were predicted. There are four aptamers in group 1, three aptamers in group 2, and two aptamers each in groups 3, 4, and 5. The remaining six aptamers which lacked conserved motif structure were grouped in group 6.

Recognition of BCM-7 by Aptamer-Coated Gold Nanoparticles. Selected aptamers from Mfold groups (seqU4, seq1, seqU5, seq10, seqU2, and seq7) were evaluated for their recognition at different concentrations of BCM-7 ranging from 1 to 30 μg/mL. The visible color change (pink to purple) in GNP was noted at 10−30 μg/mL concentration of

DOI: 10.1021/acs.jafc.5b00007
J. Agric. Food Chem. 2015, 63, 2647−2653

Table 2. Sequences of BCM-7 Specific Aptamers

aptamer name[a]	sequence (5′→3′)	sequence length (nt.)	no. of independent clones containing identified aptamer	K_d (nM) (mean ± SEM)
seq1(R)	ATACGGGAGCCAACACCATAAGTCTAAAAAACTGGGAGTAAACACAATGTGTATAGAGCAGGTGTGACGGAT	72	6	14 ± 1.16
seq2(F)	ATCCGTCACACCTGCTCTCCTCGAACTAGTTAGACCCTCCTCCAAGTCAACTTGTGGTGTTGGCTCCCGTAT	72	1	81 ± 8.08
seq3(R)	ATACGGGAGCCAACACCACTCTTATTTCCGGAAGTGGTTCTTCAACAGAGGAATAGAGCAGGTGTGACGGAT	72	1	18.77 ± 2.83
seq4(R)	ATACGGGAGCCAACACCAACAAAACTAGCAAATTAGAGCCGTATCGGAGCCTATAGAGCAGGTGTGACGGAT	72	2	141.26 ± 19.85
seq5(F)	ATCCGTCACACCTGCTCTCGAATAGAGTATTCGATACTGACTTTATTTACCGTCTGGTGTTGGCTCCCGTAT	72	1	10.23 ± 2.40
seq6(R)	ATACGGGAGCCAACACCAAAGTAAGATCATCACCCGGACGCGGACATAATAGGAGAGCAGGTGTGACGGAT	71	1	7.69 ± 1.68
seq7(R)	ATACGGGAGCCAACACCACACCAAGTTGACTTGGAGGAGGGTCTAACTAGTTCGAGGAGAGCAGGTGTGACGGAT	72	3	48.66 ± 5.78
seq8(R)	ATACGGGAGCCAACACCACACCACCAACATTATCAGAGTATGTTACTTATAGTGGTGGCAGAGCAGGTGTGACGGAT	72	1	156.66 ± 6.36
seq9(R)	ATACGGGAGCCAACACCACACCAGACGGTAAATAAAGTCAGTATCGATACTCTATTCGAGAGCAGGTGTGACGGAT	71	1	37.66 ± 4.66
seq10(R)	ATACGGGAGCCAACACCACAGACGGTAAATAAAGTCAGTATCGAGTACTCTATTCGAGAGCAGGTGTGACGGAT	72	10	37.53 ± 2.15
seqU1(F)	ATCCGTCACACCTGCTCTTGTAGGGTTCCCACACCCAATTCAGTTCCGTTAAACCATGGTGTTGGCTCCCGTAT	72	5	36.33 ± 2.33
seqU2(F)	ATCCGTCACACCTGCTCTCCCCGGCGTCCGTTTATTAGCAGACTTTGGCGGAATTGGTGTTGGCTCCCGTAT	72	1	41.85 ± 3.41
seqU3(R)	ATACGGGAGCCAACACCACACAACAAGATAAAGTATCAATCTGGTTGACGGACGTGAGAGCAGGTGTGACGGAT	72	4	21.43 ± 3.84
seqU4(R)	ATACGGGAGCCAACACCAATTCCGCCAAAGTCTGCTAATAAACGGACGCCGGGGAGAGCAGGTGTGACGGAT	72	3	23.11 ± 2.94
seqU5(F)	ATCCGTCACACCTGCTCTATACACATTGTGTTTACTCCCAGTTTTTTAGACTTATGGTGTTGGCTCCCGTAT	72	1	42 ± 2.30

[a]R or F in parentheses indicates aptamer generated from reverse strand or forward strand of amplified library, respectively.

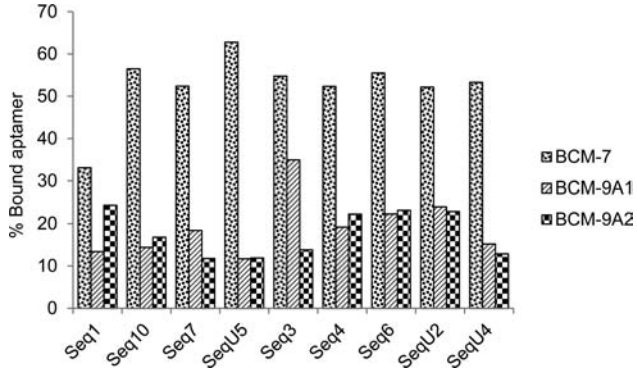

Figure 1. Percentage of bound aptamers for target peptide (BCM-7) and counter selector peptides (BCM-9A1 and BCM-9A2).

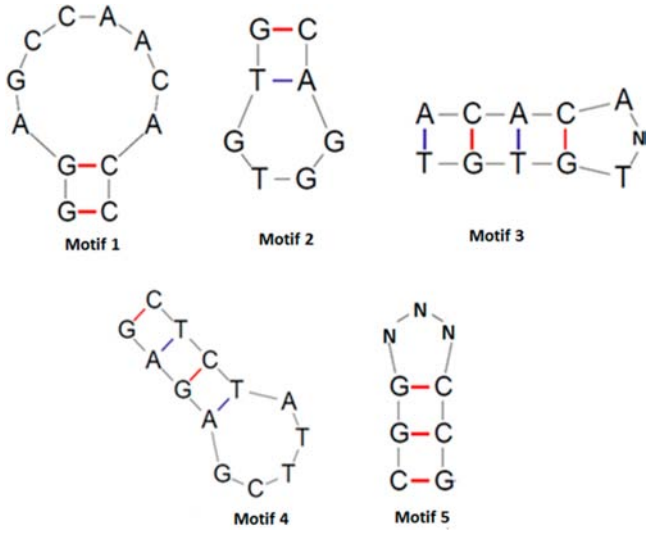

Figure 2. Five different motifs in BCM-7 aptamers. (N indicates any bases.)

Table 3. Groups of Aptamers

group	motif	name of aptamers[a]	K_d range (nM)
group 1	motif 1 5′GGAGCCAACACC 3′	seq1(5), seq4(3), seq6(2), and seqU4(4)	7.69−141.26
group 2	motif 2 5′CAGGTGTG 3′	seq1(5), seq6(2), and seq8(1)	7.69−156.66
group 3	motif 3 5′ ACACANTGTGT 3′	seq1(5) and seqU5(5)	14.71−42.0
group 4	motif 4 5′CTCTATTCGAGAG 3′	seq9(2) and seq10(2)	37.53−37.66
group 5	motif 5 5′ CGGNNNCCG 3′	seqU2(2) and seqU4(4)	41.85−23.11
group 6	no conserved motif	seq2(3), seq3(1), seq5(1), seq7(3), seqU1(2), and seqU3(2)	10.23−81.0

[a]Figure in parentheses indicates number of predicted structures.

BCM-7. A typical color change in "seqU4" coated GNP at different concentration of BCM-7 is shown in (Figure 3). The color change in other aptamers coated on GNPs in the presence of BCM-7 is shown in Supporting Information.

ELASA for BCM-7. The selected aptamers were evaluated for their binding to BCM-7 by ELASA method in a 96-well streptavidin coated plate. A mixture of five biotinylated

DOI: 10.1021/acs.jafc.5b00007
J. Agric. Food Chem. 2015, 63, 2647−2653

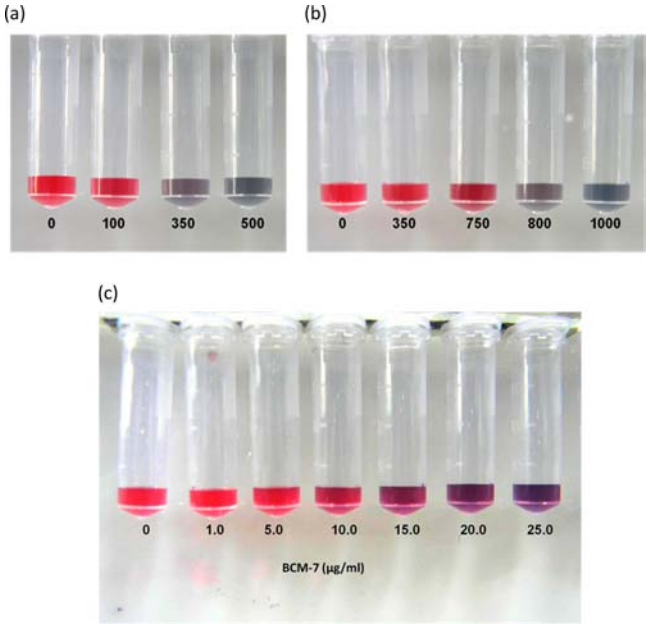

Figure 3. Color change in gold nanoparticles (GNPs): (a) NaCl addition at indicated concentrations (mM) to GNPs, (b) NaCl addition at indicated concentrations in mM to GNPs conjugated to aptamer (seqU4), and (c) color change in GNPs conjugated with aptamer (seqU4) on incubation with different concentrations (μg/mL) of BCM-7 and 350 mM NaCl.

aptamers (seq1, seq7, seq10, seqU4, and seqU5) was allowed to bind to the plate using biotin−avidin interaction. BCM-7 and BCM-7 peroxidase conjugate competed for limited amount of aptamer. There was an inverse relationship between peroxidase activity and BCM-7 concentration. The IC_{50} value was 250 ng/mL for BCM-7 (Figure 4a).

Cross recognition of selected nine aptamers to BCM-5, BCM-9A1, and BCM-9A2 peptides was also checked. In a 96-well plate format, BCM-7-peroxidase competed with BCM-5, BCM-7, BCM-9A1, or BCM-9A2. The extent of binding of these peptides is reflected in the extent of the drop in absorbance. For example, seqU5 aptamer has failed to recognize all the peptides including BCM-7. Seq7 has cross reacted with BCM-5, BCM-9A1, and BCM-9A2. Seq3, seq4, seq6, and seqU4 have shown lower cross-recognition among the nine aptamers tested (Figure 4b).

The ELASA method was used to evaluate whether aptamers could recognize spiked BCM-7 in biological fluids. Urine contains urea which may interfere in recognition of BCM-7 by aptamer; therefore, the urine sample was treated with urease before its use in ELASA. BCM-7-peroxidase competed with spiked BCM-7 present in urine, plasma, and β-casein digest samples as indicated by lowered absorbance with increasing concentration of BCM-7 (Figure 5). Results also suggest that some component of urine and plasma interferes in the assay (see absorbance value in corresponding control and blank samples) (Figure 5).

DISCUSSION

BCM-7 has been linked with certain noncommunicable diseases such as type I diabetes, coronary heart disease, schizophrenia, and autism; suitable ligands which can recognize BCM-7 are required for method development. This paper describes in vitro selection of aptamers that bind to BCM-7 with high affinity. Out of 15 aptamers, five aptamers are generated with forward primer while ten aptamers start with reverse primer. This

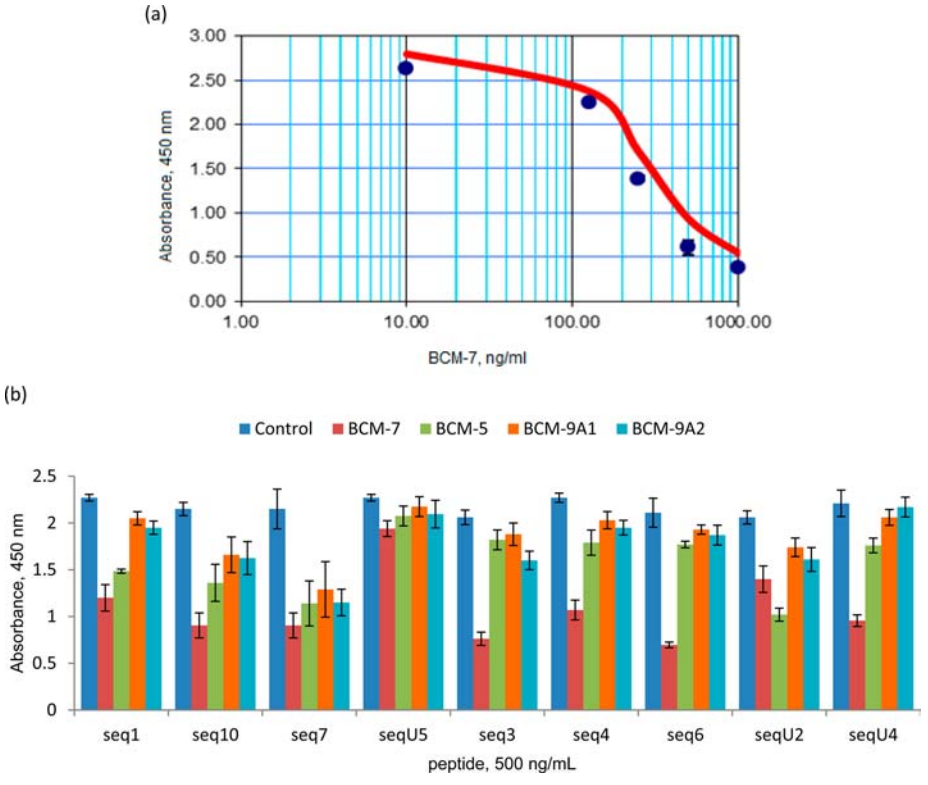

Figure 4. ELASA for BCM-7. The extent of displacement of the BCM-7 peroxidase conjugate by (a) BCM-7 peptide at different concentration and (b) BCM-7, BCM-5, BCM-9A1, and BCM-9A2 at fixed concentration.

DOI: 10.1021/acs.jafc.5b00007
J. Agric. Food Chem. 2015, 63, 2647−2653

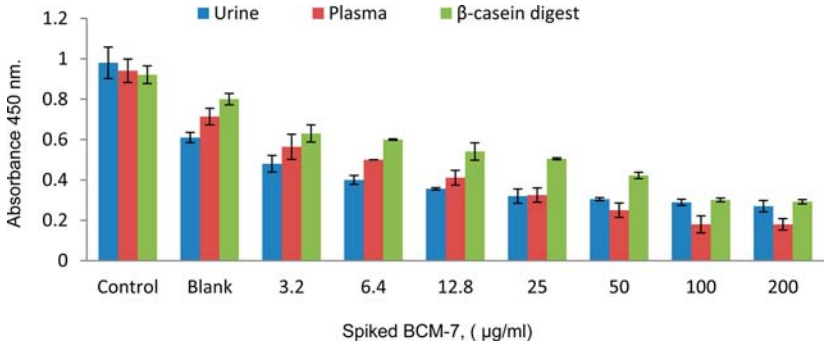

Figure 5. ELASA for BCM-7 in urine, plasma, and β-casein digest. "Control" and "blank" represent peroxidase activity in the absence of BCM-7 in binding buffer, urine, plasma, or β-casein digest, respectively.

clearly indicates that λ exonuclease was not able to fully digest the dsDNA. Available protocol for digestion of dsDNA by λ exonuclease requires prior purification of PCR product. However, there is a loss in yield that occurs during purification. In the present work, PCR product was digested with λ exonuclease without prior purification. This results in incomplete digestion. In fact, 13% dsDNA (GelQuant software) was found in DNA-digest by λ exonuclease, based on the intensity of dsDNA and ssDNA bands after their separation on agarose gel electrophoresis. Thus, the remaining dsDNA was converted to ssDNA by snap cool method.

The mean K_d values of forward strand aptamer (mean K_d = 42.0 nM) and reverse strand aptamers (mean K_d = 50.2 nM) suggest that both groups of aptamers have similar binding affinity for the target. The K_d values of repeat-aptamers were also compared with those of nonrepeat aptamers, and it was found that the mean K_d values of repeat-aptamers (mean K_d = 42.0 nM) were similar to that of nonrepeat aptamers (mean K_d = 49.5 nM).

Nine aptamers (seq1, seq10, seq7, seqU5, seq3, seq4, seq6, seqU2, and seqU4) were used for comparing their specificity in two different experimental designs (Figures 1 and 4b). The results suggest that the extent of cross reaction of aptamers with BCM-9A1 and BCM-9A2 was not similar and was dependent on the experimental format used. In one format, aptamer was labeled with 6-carboxyfluorescein, while in the other format, aptamers were labeled with biotin. Thus, it appears that modification of the aptamer with a label might result in structural changes which effect recognition of BCM-7 and cross reaction with BCM-9A1 and BCM-9A2. Also, it is to be noted that in the ELASA method aptamers are in an immobilized form, whereas in other experimental deigns using magnetic beads (binding selectivity), aptamers remain in the free form.

Gold nanoparticles (GNPs), a colorimetric-based method, was used to establish proof of principle of recognition of BCM-7 by aptamers. The aptamer-coated gold nanoparticles exhibited stability toward NaCl higher than that of naked GNPs. The enhanced stability is an indication of coating of aptamer on GNP surface because this results in enhanced negative charge on GNPs. Because of high affinity of aptamer for BCM-7, the later is removed from GNPs surface. Such GNPs lack enhanced stability and aggregate at lower NaCl concentration.

BCM-7-peroxidase competed with BCM-7 in spiked biological fluids in ELASA, suggesting that aptamers can work in the 96-well format. However, it appears that some component of urine and plasma interferes in the assay. Even the ELISA base method for assaying BCM-7 from urine requires prior extraction for determination of BCM-7 concentration.[15]

■ ASSOCIATED CONTENT

Supporting Information

Mfold structure of aptamers and photos of aptamers showing color change at different concentrations of BCM-7. This material is available free of charge via the Internet at http://pubs.acs.org.

■ AUTHOR INFORMATION

Corresponding Author

*Phone: +91184-2259129. E-mail: ys_rajput@rediffmail.com.

Notes

The authors declare no competing financial interest.

■ ACKNOWLEDGMENTS

Research funding and fellowship was provided by National Dairy Research Institute, Karnal-132001, India.

■ REFERENCES

(1) Ellington, A.; Szostak, J. *In vitro* selection of RNA molecules that bind specific ligands. *Nature* **1990**, *346*, 818−822.

(2) Chen, X.; Huang, Y.; Duan, N.; Wu, S.; Xia, Y.; Ma, X.; Zhu, C.; Jiang, Y.; Wang, Z. Screening and identification of DNA aptamers against T-2 toxin assisted by graphene oxide. *J. Agric. Food Chem.* **2014**, *62*, 10368−10374.

(3) Duan, N.; Wu, S.; Chen, X.; Huang, Y.; Xia, Y.; Ma, X.; Wang, Z. Selection and characterization of aptamers against *Salmonella typhimurium* using whole-bacterium systematic evolution of ligands by exponential enrichment (SELEX). *J. Agric. Food Chem.* **2013**, *61*, 3229−3234.

(4) He, J.; Liu, Y.; Fan, M.; Liu, X. Isolation and identification of the DNA aptamers target to acetamiprid. *J. Agric. Food Chem.* **2011**, *59*, 1582−1586.

(5) Wei, F.; Ho, C. M. Aptamer-based electrochemical biosensor for botulinum neurotoxin. *Anal. Bioanal. Chem.* **2009**, *393*, 1943−1948.

(6) Fernandez, E. G.; Álvarez, N. D. L. S.; Non, M. J. L. C.; Ordieres, A. J. M.; Blanco, B. T. N. Impedimetric aptasensor for tobramycin detection in human serum. *Biosens. Bioelectron.* **2011**, *26*, 2354−2360.

(7) Bonel, L.; Vidal, J. C.; Duato, P.; Castillo, J. R. An electrochemical competitive biosensor for ochratoxin A based on a DNA biotinylated aptamer. *Biosens. Bioelectron.* **2011**, *26*, 3254−3259.

(8) Luo, Y.; He, L.; Zhan, S.; Wu, Y.; Liu, L.; Zhi, W.; Zhou, P. Ultrasensitive resonance scattering (RS) spectral detection for trace tetracycline in milk using aptamer-coated nanogold (ACNG) as a catalyst. *J. Agric. Food Chem.* **2014**, *62*, 1032−1037.

(9) Zhu, Y.; Chandra, P.; Song, K. M.; Ban, C.; Shim, Y. B. Label-free detection of kanamycin based on the aptamer-functionalized

DOI: 10.1021/acs.jafc.5b00007
J. Agric. Food Chem. 2015, 63, 2647−2653

conducting polymer/gold nanocomposite. *Biosens. Bioelectron.* **2012**, *36*, 29−34.
(10) Vivekananda, J.; Kiel, J. L. Anti-francisella fularensis DNA aptamers detect tularemia antigen from different subspecies by aptamer-linked immobilized sorbent assay. *Lab. Invest.* **2006**, *86*, 610−618.
(11) Ng-Kwai-Hang, K.; Grosclaude, F. Genetic polymorphism of milk proteins: Relationships with production traits, milk composition and technological properties. *Adv. Dairy Chem. (3rd Ed.)* **2003**, *1*, 405−455.
(12) Jinsmaa, Y.; Yoshikawa, M. Enzymatic release of neocasomorphin and β-casomorphin from bovine β-casein. *Peptides* **1999**, *20*, 957−962.
(13) Cade, R.; Privette, M.; Fregly, M.; Rowland, N.; Zhongjie, S.; Zele, V.; Wagemaker, H.; Edelstein, C. Autism and schizophrenia: Intestinal disorders. *Nutr. Neurosci.* **2000**, *3*, 57−72.
(14) Beales, P.; Elliott, R.; Scott, F. A multi-centre blinded international trial of the effect of A^1 and A^2 β-casein variants on diabetes incidence in two rodent models of spontaneous Type I diabetes. *Diabetologia* **2002**, *45*, 1240−1246.
(15) Sokolov, O.; Kost, N.; Andreeva, O.; Korneeva, E.; Meshavkin, V.; Tarakanova, Y.; Dadayan, A.; Zolotarev, Y.; Grachev, S.; Mikheeva, I.; Varlamov, O.; Zozulya, A. Autistic children display elevated urine levels of bovinecasomorphin-7 immunoreactivity. *Peptides (New York, NY, U.S.)* **2014**, *56*, 68−71.
(16) Keating, A. F.; Smith, T. J.; Cairns, M. T. A note on the evaluation of a beta-casein variant in bovine breeds by allele-specific PCR and relevance to β-casomorphin. *Irish J. Agric. Food Res.* **2008**, *47*, 99−104.
(17) Barroso, A.; Dunner, S.; Canon, J. Technical note: Detection of bovine kappa-casein variants A, B, C, and E by means of polymerase chain reaction-single strand conformation polymorphism (PCR-SSCP). *J. Anim. Sci. (Savoy, IL, U.S.)* **1999**, *77*, 2629−2632.
(18) De Noni, I. Release of β-casomorphins 5 and 7 during simulated gastro-intestinal digestion of bovine β-casein variants and milk-based infant formulas. *Food Chem.* **2008**, *110*, 897−903.
(19) Bruno, J. G.; Carrillo, M. P.; Phillips, T. Development of DNA aptamers to a foot and mouth disease peptide for competitive FRET-based detection. *J. Biomol. Tech.* **2008**, *19*, 109−115.
(20) Citartan, M.; Tang, T. H.; Tan, S. C.; Gopinath, S. C. B. Conditions optimized for the preparation of single-stranded DNA (ssDNA) employing lambda exonuclease digestion in generating DNA aptamer. *World J. Microbiol. Biotechnol.* **2011**, *27*, 1167−1173.
(21) Chen, F.; Hu, Y.; Li, D.; Chen, H.; Zhang, X. L. CS-SELEX generates high-affinity ssDNA aptamers as molecular probes for Hepatitis C virus envelope glycoprotein E2. *PLoS One* **2009**, *4*, e8142.
(22) Stoltenburg, R.; Reinemann, C.; Strehlitz, B. FluMag-SELEX as an advantageous method for DNA aptamer selection. *Anal. Bioanal. Chem.* **2005**, *383*, 83−91.
(23) Niazi, J. H.; Lee, S. J.; Kim, Y. S.; Gu, M. B. Single strand DNA aptamers that selectively bind oxytetracycline. *Bioorg. Med. Chem.* **2008**, *16*, 1254−1261.
(24) Turkevitch, J.; Stevenson, P. C.; Hillier, J. A study of the nucleation and growth processes in the synthesis of colloidal gold. *Discuss. Faraday Soc.* **1951**, *11*, 55−75.
(25) Liu, X.; Atwater, M.; Wang, J.; Huo, Q. Extinction coefficient of gold nanoparticles with different sizes and different capping ligands. *Colloids Surf., B* **2007**, *58*, 3−7.
(26) Kim, Y. S.; Kim, J. H.; Kim, I. A.; Lee, S. J.; Jurng, J.; Gu, M. B. A novel colorimetric aptasensor using gold nanoparticle for a highly sensitive and specific detection of oxytetracycline. *Biosens. Bioelectron.* **2010**, *26*, 1644−1649.
(27) Song, M. K.; Jeong, E.; Jeon, W.; Cho, M.; Ban, C. Aptasensor for ampicillin using gold nanoparticle based dual fluorescence-colorimetric methods. *Anal. Bioanal. Chem.* **2012**, *402*, 2153−2161.

DOI: 10.1021/acs.jafc.5b00007
J. Agric. Food Chem. 2015, 63, 2647−2653

addition method is also not yet present in the literature. It works when the calibration graph was formed after the equivalent point because of dynamic quenching with excess iron(III) ions.

MATERIALS AND METHODS

Instrumentation. A PerkinElmer UV−vis dpectrophotometer and a PTI spectrofluorometer (QM 2006 model) were used to measure absorbance and fluorescence intensity, respectively. The excitation wavelength was 375 nm, and fluorescence emission spectra were recorded in the range of 400−650 nm with a slit width of 1.0 nm. A Jenway 3040 ion analyzer was used to measure the pH of the solutions.

Reagents. In all analytical measurements, pipets and vessels kept in dilute nitric acid at least overnight and subsequently washed three times with distilled water were used. Analytical grade chemicals and solvents were purchased from Merck (Darmstadt, Germany) and Fluka (Buch, Swetzerland). Stock solutions (1000 mg/L) of metal cations were prepared by dissolving an appropriate amount of nitrate salts in deionized water. Working standard solutions were obtained by appropriate dilution of these stock standard solutions. The buffer solutions (AVS Titrinorm, Merck Certipur) were purchased from Merck. Sandy soil standard (CRM-SA-C) was supplied from High-Purity Standards, Inc., and Mixed Polish Herbs standard (INCT-MPH-2) from Institute of Nuclear Chemistry and Technology. 2-(4-Fluorophenyl)-3-hydroxy-2,3-dihydroquinoline-4(1*H*)-one (Figure S1, Supporting Information) was prepared according to the literature. The synthetic procedure is described in the Supporting Information. A 2.6×10^{-3} mol/L solution of this compound was prepared by dissolving the appropriate amount of this ligand in 100 mL of methanol and was kept in a refrigerator at 4 °C for 1 week.

Samples. All food samples were purchased from local supermarkets and iron tablets from pharmacies in Trabzon, Turkey. The streamwater sample was collected from Değirmendere in Trabzon and was filtered through a 0.45 mm cellulose nitrate membrane. The vegetable samples were washed thoroughly with tap water and deionized water. Then, the samples were dried at 105 °C for 24 h and ground. Digestion of the dried samples (0.5 g) was carried out using 6.0 mL of HNO_3 and 2.0 mL of H_2O_2, and digestion of standard reference materials (0.5 g) was carried out using 1.5 mL of HNO_3, 4.5 mL of HCl, 1.0 mL of HF, and 2.0 mL of H_2O_2 in a closed microwave digestion system. After the microwave digestion process, the solutions were filtered through a 0.45 mm cellulose nitrate membrane and evaporated. Then, the volume was completed to 25 mL with deionized water. To digest the dried iron tablets, one iron tablet was dissolved in 60 mL of deionized water using an ultrasonic bath. Then, the temperature was set to 200 °C on the hot plate, and 3 mL of HNO_3 was added gradually. The solutions were filtered through a 0.45 mm cellulose nitrate membrane, and the final volume was completed to 25 mL with deionized water.

Optimum Conditions. Some parameters of the proposed method, such as solvent and concentration of ligand, solution pH, complexation time, and constant iron(III) concentration, were optimized. DMF, acetonitrile, THF, ethanol, and methanol were tested as a ligand solvent. Among these solvents, methanol was preferred because it is cheap and has high fluorescence intensity. A series of buffer solutions (pH from 2 to 10) was used to optimize solution pH. pH 7 was suitable for the study because of the high fluorescence intensity of the solution at this pH. Only 4 min was enough for complexation. Various constant iron(III) concentrations (0.2−3.0 mg/L) were tested to obtain accurate results with modified standard addition method. The optimum constant iron(III) concentration was 1.0 mg/L.

Proposed Method. The proposed method is based on fluorescence quenching of an azaflavanon-3-ol compound, which has been recently reported in the literature, with the iron(III) ion. A modified standard addition method was used to determine the iron content of food samples. Just like a standard addition method, it has not been reported in the literature according to our knowledge. One more tube (first tube) was used in this method. A certain amount of analyte and ligand was added to all tubes and the first tube. A certain amount of sample was added to all tubes, except for the first tube. The fluorescence intensities of the first tube containing the blank solution and the second tube and the slope of the calibration graph were used to calculate iron(III) concentration. The iron(III) complex has a lower fluorescence intensity compared to the free azaflavanon-3-ol ligand. After the iron(III) complex is formed, excess iron(III) ion (quencher) causes dynamic quenching of the complex, which is regular for increasing iron(III) concentration between 2.4 and 21.6 mg/L, and it is used to determine the iron content of the sample.

The modified standard addition method was used to determine the iron concentration in all samples. A constant amount of iron(III) (1 mg/L), 2 mL of ligand (1.3×10^{-5} M), and an aliquot sample solution were added to all tubes. Only the sample was not added to the first tube. Therefore, a blank solution without the sample in the first tube was prepared. Increasing amounts of iron were added to the third and next tubes. The pH of all solutions was set to 7 with citric acid buffer before the final volume was completed to 4 mL. Fluorescence intensity was measured at 503 nm for all solutions. The iron(III) concentration was calculated from eq 1

$$C_x = (F_0 - F_1)/m \quad (1)$$

where C_x is the iron concentration of the sample in the tubes, F_0 and F_1 are the fluorescence intensities of the first and second tubes, respectively, and m is the slope of the standard addition graph. According to this type of standard addition procedure, the difference between F_0 and F_1 is related to the iron concentration of the sample in the tubes. Figure S2 (Supporting Information) shows the standard addition graph for the determination of iron (2.5 mg/L) in spinach.

RESULTS AND DISCUSSION

When the ligand is excited at 375 nm, it gives a maximum emission band at 503 nm. Excitation and emission spectra of the ligand are given in Figure S3 (Supporting Information). Figure S4 (Supporting Information) shows the effects of Li^+, Na^+, K^+, Mg^{2+}, Ca^{2+}, Sr^{2+}, Ba^{2+}, Al^{3+}, Sn^{2+}, Pb^{2+}, Cr^{3+}, Mn^{2+}, Fe^{2+}, Fe^{3+}, Co^{2+}, Ni^{2+}, Cu^{2+}, Ag^+, Zn^{2+}, Cd^{2+}, and Hg^{2+} ions (1.3×10^{-4} M) on the fluorescence spectra of the ligand (1.3×10^{-5} M). As can be seen from Figure S4, there are moderate changes in the fluorescence intensity of the ligand for many ions, except for Fe^{2+} and Fe^{3+} ions. Al^{3+} causes a small shift in fluorescence spectra to short wavelength. However, spectrofluorometric titrations showed that there is no regular change for fluorescence intensity with increasing aluminum concentrations. In contrast, increasing Fe^{2+} and Fe^{3+} concentrations cause quenching on the fluorescence intensity of the ligand at 503 nm. Because the samples were digested in acidic media, iron(II) was oxidized to iron(III), and the method was based on quenching of the iron(III) ion.

Effect of pH. The effect of pH on the fluorescence intensity of the solution containing equivalent ligand and iron(III) (1.3×10^{-5} M) is shown in Figure S5 (Supporting Information). Citric acid−sodium hydroxide−hydrochloric acid, acetic acid−ammonium acetate, citric acid−sodium hydroxide, HEPES, and boric acid−sodium hydroxide−hydrochloric acid buffers were tested to set the pH of the solutions. As seen from Figure S5, the fluorescence intensity was satisfactorily high and nearly the same between pH 6 and 8. Iron determination was carried out with a variety of buffer solutions. The lowest relative error percent for the standard iron(III) solution was obtained for the citric acid buffer solution (pH 7). Therefore, this buffer solution was used for iron determination.

Effect of Reagent Concentration. To determine optimum reagent concentration, spectrofluorometric titrations were performed by using solutions of the ligand in the range from 5.0×10^{-5} to 2.6×10^{-6} M. The values of fluorescence intensity at 503 nm were plotted against the iron(III) concentration.

DOI: 10.1021/jf505336d
J. Agric. Food Chem. 2015, 63, 2654−2659

When 1.3×10^{-5} M ligand concentration was used, the highest R^2 value (0.9949) was obtained. Therefore, further studies were carried out at this concentration.

Effect of Constant Iron Concentration. The constant iron(III) concentration used in the modified standard addition method was optimized by changing from 0.2 to 3.0 mg/L. Measurements were carried out in Sandy Soil C and iron tablet 1 for 2.5 mg/L iron(III) concentration, and the results are shown in Table S1 (Supporting Information). As seen from Table S1, the low relative errors were 1.5 and 1.1% for 1 mg/L in the case of Sandy Soil C and iron tablet 1, respectively. Between constant iron concentrations of 1.3 and 2.0 mg/L, the RE% values were below 2.5. However, the lower concentration (1 mg/L) was preferred as the constant iron concentration.

Time before Measurement. The emission spectrum of the mixture containing an equivalent amount of iron(III) and the ligand (1.3×10^{-5} M) was obtained in the range of 1−15 min. It was seen that the fluorescence intensity did not change after 1 min (Figure S6, Supporting Information). There was very little change in the fluorescence intensity from 1.0 until 15 min, which means that a few minutes before the measurements was enough.

Composition and Stability of the Complex. The Job method was used to investigate the nature of the complex in methanol/water (1:1). The concentration of ligand and iron(III) was 2.6×10^{-6} M, and total solution volume was 4 mL. As seen from Figure S7 (Supporting Information), the plot of fluorescence intensity versus the ligand volume showed a break point at 2 mL, indicating that complex composition was 1:1. The conditional formation constant (log K ± standard deviation), calculated according to a known method[31] using the spectrofluorometric titration data ($N = 3$), was found to be 3.40 ± 0.09.

Effect of Foreign Ions. The potential interference due to common coexisting ions encountered in a natural sample was tested by adding these ions to the solution containing the equivalent ligand and iron(III) (1.3×10^{-5} M). The fluorescence intensity of the solution was compared with that of the solution containing only the ligand and iron(III). The tolerance limit was recognized at ±5% difference in the analytical signals. Ions Li^+, Na^+, K^+, Mg^{2+}, Ca^{2+}, Sr^{2+}, Ba^{2+}, Al^{3+}, Cr^{3+}, Sn^{2+}, Pb^{2+}, Zn^{2+}, Ni^{2+}, Co^{2+}, Cd^{2+}, Hg^{2+}, Ag^+, Cu^{2+}, Mn^{2+},OH^-, $C_2O_4^{2-}$, CO_3^{2-}, SO_4^{2-}, $S_2O_7^{2-}$, $Cr_2O_7^{2-}$, CrO_4^{2}, HCO_3^-, HSO_4^-, $H_2PO_4^-$, CN^-, SCN^-, HSO_4^-, F^-, Cl^-, Br^-, I^-, and CH_3COO^- were examined. As seen from Table S2 (Supporting Information), the effect of the tested foreign ions is negligible.

Quenching Mechanism. The Stern−Volmer relationship[32] (eq 2) expresses the efficiency of quenching of a fluorophore by a quencher.

$$F_0/F = 1 + K_{SV}[Q] \quad (2)$$

F_0 and F are the fluorescence intensities in the absence and presence of the quencher, respectively. K_{SV} is the Stern−Volmer quenching constant, and [Q] is the concentration of the quencher. If a system obeys the Stern−Volmer equation, a plot of F_0/F versus [Q] will give a straight line with a slope of K_{SV} and a y-axis intercept of 1. However, a positive deviation may be observed in the Stern−Volmer graph above a certain quencher concentration. In this case, both dynamic and static quenchings are efficient in the system.[33]

Figure S8 (Supporting Information) shows the Stern−Volmer plot of the iron(III)−ligand system. As seen from Figure S8, the F_0/F term linearly increased with increasing iron(III) concentration until 4×10^{-4} M, after which a positive deviation was observed. This result shows that both static and dynamic quenching exist in the system. As known, static quenching requires a ground state complex and is distinguished from dynamic quenching with temperature effect.[23] Dynamic quenching is a kind of collisional quenching, and quenching efficiency increases with increasing temperature. The inset of Figure S8 shows the temperature effect on fluorescence efficiency (F_0/F). As seen from the Figure S8 inset, the quenching efficiency does not increase with increasing temperature. Conversely, the lower fluorescence efficiency is observed when the temperature increases from 298 to 333 K. Therefore, it may be concluded from the consideration of Figure S8 that static quenching, proving a formation of complex between ligand and iron(III) ion, is effective in the fluorescence quenching.

Analytical Performance. An external calibration line based on fluorescence quenching of the 1.3×10^{-5} M ligand showed linearity within the concentration range of 1.4−21.6 mg/L. However, accuracy was not good in iron determination in samples using the external calibration graph. Because of this, a modified standard addition method was used in iron determination. The analytical performance data for the developed method under the optimized conditions are presented in Table S3 (Supporting Information).

The data given in Table S3 indicate that a linear relationship was found between the fluorescence intensity at 503 nm and the concentration of the iron(III) in the range of 2.4−21.6 mg/L. The correlation coefficient was 0.9949, indicating good linearity.

Table 1. Determination of Iron in Two Reference Materials ($N = 3$)

sample	found value	RSD%	certified value
Sandy Soil C	13.9	1.96	13.9
Mixed Polish Herbs	0.45	1.38	0.46

Table 2. Determination of Iron in Food Samples ($N = 3$)

	proposed method		standard method (ICP-OES)	
sample	value found	RSD%	value found	MU[a]
spinach	215.6	1.6	219.2	17.8
mint	642.7	0.7	648.4	52.5
rocket	615.7	1.4	607.0	49.2
purslane	136.3	0.3	135.7	11.0
dill	78.5	1.7	80.1	6.5
dry beans	102.6	0.6	102.9	8.3
red lentils	86.8	0.3	86.4	7.0

[a]Measurement uncertainty.

Table 3. Determination of Iron in Iron Tablet Samples ($N = 3$)

	proposed method		standard method (NMKL 161)	
sample	value found	RSD%	value found	SD
tablet 1	155.2	0.9	157.8	2.1
tablet 2	138.6	0.2	138.5	1.1

Table 4. Recovery Studies of Iron in the Streamwater Sample

Fe added (mg/L)	Fe found (mg/L) ± RSD%	recovery (%)
2.5	2.5 ± 0.8	98.8
5.0	5.0 ± 0.2	99.6
7.5	7.5 ± 0.3	99.6

DOI: 10.1021/jf505336d
J. Agric. Food Chem. 2015, 63, 2654−2659

Table 5. Analytical and Operational Parameters of the Proposed Method and Previously Reported Methods Based on Spectrofluorometry and Atomic Spectrometry

reagent, method	sample	sample preparation	procedures before measurement	pH	linear range (mg/L)	LOD (mg/L)	ref
2-(4-fluorophenyl)-3-hydroxy-2,3-dihydroquinoline-4(1*H*)-one, SF	rocket, dill, mint, spinach, purslane, red lentils, dry beans, and iron medicinal tablets	microwave-assisted digestion for food samples for about 20 min, wet digestion for iron medicinal tablets	modified standard addition method, waiting only 1−2 min before the measurement	7	2.40−2.60	0.81	PM
5-(8-hydroxy-2-quinolinylmethyl)-2,8-dithia-5-aza-2,6-pyridinophane, SF	rice, spinach, different water samples	left at 500 °C for 2 h, dissolving in nitric acid, dilution with an acetate buffer	preparation of a film, waiting >20 min to soak in buffer solution, and 5 min for fluorescence stability	5.5	33.6−0.006	0.0028	29
2-(2-hydroxyphenyl)-4(3*H*)-quinazolinone, SF	multivitamin tablets	dissolvied in aqua regia, heated to dryness, dilution to 10 mL with NaOAc−HOAc	preparation of an optode membrane and dried for 24 h before being used	2.5−4.5	0.04−7.80	0.005	26
2-pyridinecarbaldehyde−phenylenedihydrazone, SF	milk powder and jasmine tea	incineration for 270 and 60 min at 500 °C, for milk powder and jasmine tea, respectively	waiting 30 min for fluorescence stability	4.6	0.03−0.56	0.02	27
4-hydroxyquinoline, SF	bovine liver	acidic digestion	masking with KF, waiting 20 min for fluorescence stability		0.28−0.56	0.168	28
5-hydroxy-4-ethyl-5,6-dipyridin-2-yl-4,5-dihydro-2*H*-[1,2,4]-triazine-3-thione, FAAS	macaroni, wheat, flour, and some water samples	for food samples, dissolving concentrated HNO_3 and evaporation to dryness, oxidation with H_2O_2	SPE with the impregnated Amberlite XAD-16 resin, waiting for saturation for 2 h with the ligand solution, PF: 25	5.0		0.00459	11
zirconium(IV) hydroxide, FAAS	natural waters, coffee, fish, tobacco, black and green tea	digestion in microwave system for 26 min	coprecipitation with zirconium(IV), centrifugation for 15 min, dissolving the precipitate with 1 mL of concentrated HNO_3, PF: 25	8.0	0.25−5.0	0.00153	13
dimethyl (*E*)-2-[(*Z*)-1-acetyl)-2-hydroxy-1-propenyl]-2-butenedioate, FAAS	river water, rainwater, drinking water, and powdered milk	powdered milk charring at 300 °C for an hour, turned into ash overnight until becoming a grayish white color	extraction with modified octadecyl silica membrane disk using a vacuum, stripping iron(III) from the disk with EDTA solution, PF: 166	2.5	0.0400−1.0	0.0028	10
ammonium pyrolidine−dithiocarbamate−Chromosorb 102, $Ce(OH)_4$, FAAS or GFAAS	baking soda and baking powder samples	dissolving in a mixture of concentrated HNO_3 and distilled water before neutralization with NH_3	SPE with APDC-Chromosorb 102 and coprecipitation with $Ce(OH)_4$, PE: NA	6.00, 10.5	N.A	0.26, 0.12	12
8-oxyquinoline, FAAS	natural and mineral waters	complexation with 8-oxyquinoline solution	extraction of the complex to chloroform for 2 min	5.0	0.1−4.0	0.1	9

J. Agric. Food Chem. 2015, 63, 2654−2659
DOI: 10.1021/jf505336d

The LOD ($3 \times S_d/m$) and LOQ ($9 \times S_d/m$) were determined using the standard deviation of 11 measurements of the blank response (S_d) and the slope of the calibration line (m) according to IUPAC recommendations.

Accuracy. The accuracy of the proposed method was verified by analyzing two standard reference materials (CRM-SA-C Sandy Soil C and Mixed Polish Herbs INCT-MPH-2). A good agreement was found between obtained values and certified values (Table 1). Statistical analysis of the results using Student's t test shows no significant difference between obtained values and certified values. The calculated Student's t value (3.48) was less than the theoretical value (4.30) at a confidence level of 95%.

The food samples and two iron tablets were analyzed according to a modified standard addition method. Analysis of the same food samples was carried out by using a standard ICP-OES method, whereas standard NMKL 161 method was used to analyze iron tablets. The results are given in Tables 2 and 3. Statistical analysis of the results using Student's t test showed no significant difference between the results.

The accuracy was also tested by using a standard addition technique. The modified standard addition method was applied to a streamwater sample (Değirmendere, Trabzon) spiked at three iron(III) concentration levels, and recoveries between 98.9 and 99.6% were obtained (Table 4). The results showed that the proposed method can be applied for the determination of iron in foods, iron tablets, and water samples.

Comparison with Other Methods. A comparison of the analytical and operational parameters of the spectrofluorometric and atomic methods that are already present in the literature and the proposed method for the determination of Fe(III) is given in Table 5. Compared to previous methods, the proposed method is relatively time-saving and simpler.[10−13,26−29] Lower detection limits could be obtained by some atomic methods.[10,11,13] However, as seen from Table 5, time-consuming solid phase extraction and coprecipitation methods have been applied to separation and preconcentration of iron(III) ion in these studies. The preconcentration factors (PF) are given for these atomic methods in Table 5. Detection limits of some spectrofluorometric methods are also lower than the proposed method. However, sample preparation and treatment of these methods are more time-consuming than those of the proposed method (Table 5).

Advantages of the Proposed Method. The proposed method can be applied to various food samples and iron medicinal tablets. Sample digestion carried out in 20 min in a closed microwave system is not time-consuming compared with many methods in the literature (Table 5). There is no need either for the separation of iron(III) ion from sample solution or sample treatment stage before the measurement. A modified standard addition method handles probable matrix effects. A time of 1−2 min was sufficient before measurement to obtain a stable fluorescence response. Thus, this property of the proposed method is one of its advantages when compared to others (Table 5). The recovery studies showed that the proposed method can also be applied to water samples having proper iron(III) concentrations. Moreover, the used reagent is a kind of flavonoid compound. Flavonoids are known as useful compounds for the human body. In this context, it can be thought that the reagent is environmentally friendly. Spectrofluorometric methods are much cheaper compared with atomic methods. Consequently, these advantages make the proposed method time-saving, simple, and economic compared to several other methods in the literature.

■ ASSOCIATED CONTENT

Ⓢ Supporting Information

Synthesis of the ligand, excitation and emission spectra, and complexation and analytical performance data. This material is available free of charge via the Internet at http://pubs.acs.org.

■ AUTHOR INFORMATION

Corresponding Author

*(U.O.) Phone: +90 462 377 42 67. Fax: +90 462 325 31 96. E-mail: uocak@ktu.edu.tr.

Funding

This research was supported by Karadeniz Technical University, Scientific Research Foundation (Project 10481).

Notes

The authors declare no competing financial interest.

■ REFERENCES

(1) Beard, J.; Tobin, B. Iron status and exercise. *Am. J. Clin. Nutr.* **2000**, *72* (2), 594S−597S.

(2) Beinert, H.; Kennedy, M. C. Aconitase, a two-faced protein: enzyme and iron regulatory factor. *FASEB J.* **1993**, *7* (15), 1442−1449.

(3) Agarwal, K. N. Iron and the brain: neurotransmitter receptors and magnetic resonance spectroscopy. *J. Nutr.* **2001**, *85*, 147−150.

(4) Cherayil, B. J. The role of iron in the immune response to bacterial infection. *Immunol. Res.* **2011**, *50* (1), 1−9.

(5) Barnes, K. W.; Debrah, E. Determination of nutrition labeling education act minerals in foods by inductively coupled plasma-optical emission spectroscopy. *At. Spectrosc.* **1997**, *18*, 41−54.

(6) Da-Col, J. A.; Domene, S. M. A.; Pereira-Filho, E. R. Fast determination of Cd, Fe, Pb, and Zn in food using AAS. *Food Anal. Methods* **2009**, *2*, 110−115.

(7) Fakayode, S. O.; King, A. G.; Yakubu, M.; Mohammed, A. K.; Pollard, D. A. Determination of Fe content of some food items by flame atomic absorption spectroscopy (FAAS): a guided-inquiry learning experience in instrumental analysis laboratory. *J. Chem. Educ.* **2012**, *89*, 109−113.

(8) Jorhem, L.; Engman, J. Determination of lead, cadmium, zinc, copper, and iron in foods by atomic absorption spectrometry after microwave digestion: NMKL Collaborative Study. *J. AOAC Int.* **2000**, *83*, 1189−1203.

(9) Tautkus, S.; Steponeniene, L.; Kazlauskas, R. Determination of iron in natural and mineral waters by flame atomic absorption spectrometry. *J. Serb. Chem. Soc.* **2004**, *69* (5), 393−402.

(10) Khayatian, G.; Hassanpoor, S.; Nasiri, F.; Zolali, A. Preconcentration, determination and speciation of iron by solid-phase extraction using dimethyl (*E*)-2-[(*Z*)-1-acetyl)-2-hydroxy-1-propenyl]-2-butenedioate. *Quim. Nova* **2012**, *35*, 535−540.

(11) Tokalıoğlu, Ş.; Ergün, H.; Çukurovalı, A. Preconcentration and determination of Fe(III) from water and food samples by newly synthesized chelating reagent impregnated Amberlite XAD-16 resin. *Bull. Korean Chem. Soc.* **2010**, *31*, 1976−1980.

(12) Saracoğlu, S.; Divrikli, Ü.; Soylak, M.; Elçi, L. Determination of copper, iron, lead, cadmium, cobalt and nickel by atomic absorption spectrometry in baking powder and baking soda samples after preconcentration and separation. *J. Food Drug Anal.* **2002**, *10*, 188−194.

(13) Citak, D.; Tüzen, M.; Soylak, M. Simultaneous coprecipitation of lead, cobalt, copper, cadmium, iron and nickel in food samples with zirconium(IV) hydroxide prior to their flame atomic absorption spectrometric determination. *Food Chem. Toxicol.* **2009**, *47* (9), 2302−2307.

(14) Valeur, B.; Leray, I. Design principle of fluorescent molecular sensors for cation recognition. *Coord. Chem. Rev.* **2000**, *205*, 3−40.

(15) Veale, E. B.; Gunnlaugsson, T. Fluorescent sensors for ions based on organic structures. *Annu. Rep. Prog. Chem., Sect. B* **2010**, *106*, 376−406.

DOI: 10.1021/jf505336d
J. Agric. Food Chem. 2015, 63, 2654−2659

(16) Carter, K. P.; Young, A. M.; Palmer, A. E. Fluorescent sensors for measuring metal ions in living systems. *Chem. Rev.* **2014**, *114*, 4564−4601.
(17) Cha, K.-W.; Park, C.-I. Spectrofluorimetric determination of iron(III) with 2-pyridinecarbalddhyde-5-nitro-pyridylhydrazone in the presence of hexadecyltrimeth- ylammonium bromide surfactant. *Talanta* **1996**, *43*, 1335−1340.
(18) Jung, H. J.; Sing, N.; Lee, D. Y.; Jang, D. U. Single sensor for multiple analytes: chromogenic detection of I^- and fluorescent detection of Fe^{3+}. *Tetrahedron Lett.* **2010**, *51*, 3962−3965.
(19) Zhang, M.; Zheng, B.; Yuan, H.; Xiao, D. A spectrofluorimetric sensor based on grape skin tissue for determination of iron(III). *Bull. Chem. Soc. Ethiop.* **2010**, *24* (1), 31−37.
(20) Lee, D. Y.; Singh, N.; Jang, D. O. Fine tuning of a solvatochromic fluorophore for selective determination of Fe^{3+}: a new type of benzimidazole-based anthracene-coupled receptor. *Fuel* **2014**, *117*, 520−527.
(21) Feng, L.; Chen, Z.; Wang, D. Selective sensing of Fe^{3+} based on fluorescence quencing by 2,6-bis(benzoxazolyl)pyridine with β-cyclodextrin in neutral aqueous solution. *Spectrochim. Acta, Part A* **2007**, *66*, 599−603.
(22) Liping, L.; Zaihui, D.; Jiaoliang, W.; Qingjiao, L. Determination of Fe(III) by cephradine fluorescence quenching method. *Huagong Huanbao* **2008**, *28*, 549−552.
(23) Cha, K.-W.; Park, K.-W. Determination of iron(III) with salicylic acid by the fluorescence quenching method. *Talanta* **1998**, *46*, 1567−1571.
(24) Sayour, H. E. M.; Razek, T. M. A.; Fadel, K. F. Flow injection spectrofluorimetric determination of iron in industrial effluents based on fluorescence quenching of 1-naphtol-2-sulfonate. *J. Fluoresc.* **2011**, *21*, 1385−1391.
(25) Lin, W.; Long, L.; Yuan, L.; Cao, Z.; Feng, J. A novel ratiotmetric fluorescent Fe^{3+} sensor based on a phenanthroimidazole chromophore. *Anal. Chim. Acta* **2009**, *634*, 262−266.
(26) Zhang, X.-B.; Cheng, G.; Zhang, W.-J.; Shen, G.-L.; Yu, R.-Q. A fluorescence chemical sensor for Fe^{3+} based on blocking of intramolecular proton transfer of a quinazolinone derivative. *Talanta* **2007**, *71*, 171−177.
(27) Zhou, Q.; Liu, W.; Chang, L.; Chen, F. Spectral study of the interaction between 2-pyridinecarbaldehyde-P-phenyldihydrazone and ferric iron and its analytical application. *Spectrochim. Acta, Part A* **2012**, *92*, 78−83.
(28) Ragos, C. G.; Demertzis, M. A.; Issopoulos, P. B. A high-sensitive spectrofluorimetric method for the determination of micromolar concentrations of iron(III) in bovine liver with 4-hydroxyquinoline. *Farmaco* **1998**, *53*, 611−616.
(29) Shamsipur, M.; Sadeghi, M.; Garau, A.; Lippolis, V. An efficient and selective fluorescent chemical sensor based on 5-(8-hydroxy-2-quinolinylmethyl)-2,8-ditiha-5-aza-2,6-pyridinophane as a new fluoroionophore for determination of iron(III) ions. A novel probe for iron speciation. *Anal. Chim. Acta* **2013**, *761*, 169−177.
(30) Tavallali, H.; Nejabat, R. Effect of surfactant on spectrofluorimetric determination of Fe(III). *Asian J. Chem.* **2010**, *22*, 6663−6668.
(31) Bourson, J.; Valeur, B. Ion-responsive fluorescent compounds. 2. Cation-steered intramolecular charge transfer in a crowned merocyanine. *J. Phys. Chem.* **1989**, *93*, 3871−3876.
(32) Chen, R. F. Fluorescence of proteins and peptides. In *Practical Fluorescence*, 2nd ed.; Guilbault, G. G., Ed.; Dekker: New York, 1990; 595 pp.
(33) Behera, P. K.; Mukherjee, T.; Mishra, A. K. Simultaneous presence of static and dynamic component in the fluorescence quenching for substituted naphthalene-CCl_4 system. *J. Lumin.* **1995**, *65*, 131−136.

DOI: 10.1021/jf505336d
J. Agric. Food Chem. 2015, 63, 2654−2659

Action.[13] This protocol was integrated with a simulation of the final intestinal degradation step using porcine jejunal brush border membrane (BBM) vesicles.

MATERIALS AND METHODS

Chemicals. Enzymes used for in vitro human digestion were purchased from Sigma (St Louis, MO, USA) in line with those indicated by the Infogest protocol.[13] Urea, DTT, 2-(N-morpholino)ethanesulfonic acid (MES), Tris-HCl, *p*-toluene-sulfonyl-L-arginine methyl ester (TAME), sodium phosphate, ammonium bicarbonate, acetic acid, sulfosalicylic acid, trichloroacetic acid (TCA) and modified Lowry assay kit were from Sigma-Aldrich as well. Egg lecithin was from Lipid Products (Redhill UK). HPLC-grade solvents were from Merck (Whitehouse Station, NJ, USA). Electrophoresis reagents were all from Invitrogen (Carlsbad, CA, USA).

Pasta Cooking. A sample of a commercial brand of pasta (spaghetti type, 100% durum wheat semolina) was processed according to Hoebler et al.[14] Pasta (100 g) was cooked in 1.0 L of water (tap water) containing 3.5 g of NaCl for 10 min.

Whole Protein Extraction. An aliquot of raw pasta and cooked (undigested) pasta was ground, and whole protein was extracted twice in 1 mL of 7 M urea, 80 mmol/L Tris-HCl, pH 7.5, under magnetic stirring overnight at 4 °C. The sample was centrifuged at 10 000 g for 20 min. The surnatant was collected and desalted with Econo-Pac 10 DG columns (Biorad, Milan, Italy), eluting with 25 mmol/L ammonium bicarbonate. A modified Lowry method assay determined a protein concentration of 6.42 and 3.76 mg/mL for raw pasta and cooked pasta, respectively. Finally, samples were lyophilized and stored at −20 °C.

In Vitro Human Digestion. After cooking, the pasta was immediately subjected to in vitro simulated human digestion using the static model system as developed in the framework of the Infogest COST Action.[13] Simulated salivary fluid (SSF), simulated gastric fluid (SGF), and simulated intestinal fluid (SIF) were prepared according to the harmonized conditions.[13]

Oral Phase. Mastication was simulated by using a common manual mincer. A 5 g quantity of cooked pasta was mixed with 5 mL of SSF and minced for 2 min. SSF included 1500 U mL^{-1} of human salivary amylase.

Gastric Phase. The oral digesta was mixed with SGF (50:50 v/v); to this mixture was added gastric liposome (egg lecithin prepared in a vesicular form) up to a 0.17 mmol/L final concentration, 2000 U/mL of SGF porcine pepsin, and 80U/mL of SGF fungal lipase. The pH of the digesta was adjusted to 3, and the incubation was carried out for 2 h in a shaking incubator at 37 °C and 170 rpm. Samples were collected at different times (0, 30, 60, 90, and 120 min); the reaction was stopped by raising the pH to 7.0. Proteolysis was monitored by SDS-PAGE analysis.

Duodenal Phase. Gastric digesta (50:50 v/v) was added to the SIF containing 10 mmol/L bile salts (5 mmol/L sodium taurocholate, 5 mmol/L sodium glycodeoxycholate, and 1.8 mmol/L egg lecithin final concentration) and pancreatin. The amount of pancreatin added was calculated on the basis of the measured activity of trypsin, up to 100 U of trypsin/mL final volume. Trypsin activity was determined by TAME assay.[15] Each sample was incubated for 2 h in a shaking incubator at 37 °C. Aliquots were collected at different times (0, 5, 15, 30, 60, 90, and 120 min). The reaction was stopped by raising the pH to 10, and digestion was monitored by SDS-PAGE analysis.

Intestinal Brush Border Membrane Digestion. BBM enzymes (650 mU/mg) were obtained from pig jejunum according to the method described by Shirazi-Beechey et al.[16] Triplicate aliquots of each sample after duodenal digestion were diluted 2-fold with 0.1 mol/L sodium phosphate buffer, pH-adjusted to 7.2, and incubated for up to 4 h after BBM supplementation; the reaction was stopped by heating for 5 min in a boiling-water bath. Each sample (aliquots of 1 mL) was then chromatographed using an Econo-Pac 10 DG size-exclusion-chromatography (SEC) prepacked column (Bio-Rad Laboratories, Hercules, CA, USA) by eluting with 25 mmol/L Tris−HCl, pH 7.0, to separate the protein from the low MW peptide fraction. Effluents were collected in fractions of 1 mL and monitored by UV absorbance at 280 nm (Ultrospec 2100 pro, Amersham Biosciences). The peptide fractions (M_r < 6 kDa) were pooled and further desalted using Sep-Pak C18 prepacked cartridges (Waters, Milford, MA, USA), washed with aqueous 0.1% TFA (v/v), and eluted with 70% ACN (v/v)/0.1% TFA (v/v).

Analysis of Protein Recovered from the Pasta Cooking Water. After the pasta was cooked as described above, 250 mL of the cooking water was recovered and dialyzed overnight with a dialysis membrane (molecular weight cutoff = 3 kDa) against 0.1 M acetic acid. The sample was then lyophilized and resuspended in 1 mL of 50 mmol/L Tris-HCl, pH 7.5. The sample was further freed from low MW compounds by filtration through Econo-Pac 10 DG columns (Biorad) and eluted with 25 mmol/L ammonium bicarbonate, pH 8.5.

In Vitro Digestion of Salt Soluble Proteins. Salt-soluble proteins (albumin/globulin) were extracted from raw and cooked undigested pasta, according to the procedure described by Mamone et al.[17] Proteins were then digested by simulating gastric, pancreatic, and BBM in vitro digestion.[18] To confirm the stability of selected wheat albumins/globulins, in this case we used a simplified model of gastrointestinal digestion that minimized the presence of interfering compounds.[17]

SDS-PAGE Analysis. SDS-PAGE was performed on 15% or 4−20%-gradient gels run for 35 min at 200 V in MES buffer. Aliquots (1 mL) of oral−gastric and oral−gastric−duodenal (OGD) digesta were centrifuged at 4000 g for 20 min. The supernatant (75 μL) was with diluted 25 μL of NuPAGE LDS (Invitrogen) sample buffer (4×) containing DTT at a final concentration of 5 mmol/L. The pellet was resuspended in 100 μL NuPAGE LDS sample buffer (1×) containing 5 mmol/L DTT. Samples were heated for 10 min at 70 °C, and 20 μL of each gastric or duodenal fraction, respectively, was loaded into adjacent wells in the gel. Whole proteins (15 μg) extracted from raw and cooked undigested pasta were also run.

The gels were fixed with 50 mL of sulfosalicylic acid/TCA in a 10.5:36 ratio in 300 mL of water for 30 min, washed twice with water, and stained using colloidal Coomassie G250.

The protein bands of interest were excised from the gels with a scalpel, placed in Eppendorf tubes, washed twice with 50 μL of Milli-Q-purified water, and destained with 50 mmol/L ammonium bicarbonate in 50% (v/v) aqueous acetonitrile. The destained gel pieces were dehydrated by submersion in acetonitrile, dried under vacuum, and incubated on ice in 20 μL of 50 mmol/L ammonium bicarbonate containing 12 ng/μL trypsin. Gel pieces were allowed to rehydrate for 45 min. Afterward, the excess of trypsin solution was removed, and the protein bands were incubated overnight at 37°C. The tryptic digests were extracted in 40 μL of 50% acetonitrile/2.5% formic

DOI: 10.1021/jf505461x
J. Agric. Food Chem. 2015, 63, 2660−2667

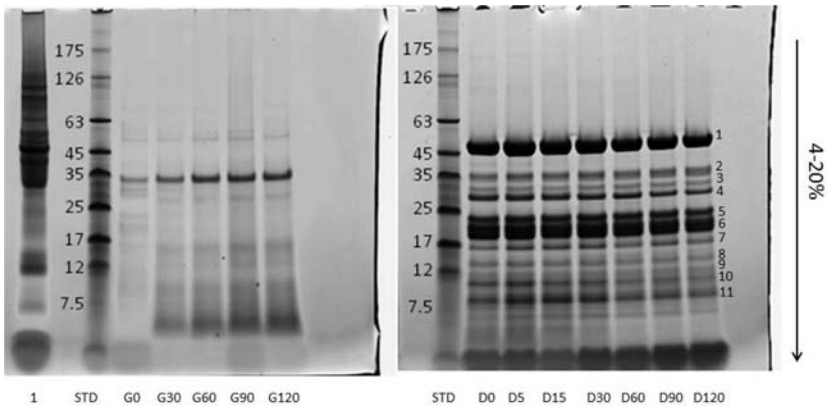

Figure 1. SDS PAGE (4−20%) analysis of gastric (left panel) and pancreatic (right panel) digestion of cooked pasta. MW markers (STD) are indicated on the left-hand side of each gel. Whole proteins from raw pasta were also run (1). The numbers on bottom denote the incubation times in minutes for gastric (G) and duodenal (D) digestion. Bands from D120 were cut and digested with trypsin for proteomic analysis.

acid and concentrated to a tenth of the original volume in a vacuum centrifuge before mass spectrometry analysis.

Western Blot Analysis. The proteins separated by SDS-PAGE (15%) were electroblotted onto nitrocellulose membranes (Transblot nitrocellulose, Bio-Rad) at 120 V for 60 min. The membrane was blocked for 1 h at room temperature using 5% nonfat milk in TBS-T (Tris saline buffer plus 0.05% Tween-20) for 1 h. The membranes were then incubated overnight at 4 °C with pooled sera (n = 8) of celiac subjects (age range = 5−36 years, average age = 24 years) or from healthy individuals (n = 4) as the negative controls, diluted 1/500 in TBS-T. Sera were pooled in order to average the individual variability of the immune response. After washing with TBS-T, monoclonal peroxidase-conjugated antihuman IgA antibody (Sigma) diluted in blocking solution (1/10 000) was applied to the membrane for 2 h at RT. The membrane was extensively rinsed with TBS-T (3 × 10 min) and finally with TBS (1 × 10 min) before development. The immunoreactive bands were detected using a chemiluminescence reagent (ECL Plus, GE Healthcare) and X-ray film (Kodak, Chalons/Saône, France).

Mass Spectrometry Analysis. Nanoflow LC-ESI MS/MS analysis was carried out using an Ultimate 3000 HPLC (Dionex, Sunnydale, CA, USA) instrument coupled to a Q-STAR mass spectrometer (Applied BioSystems, Framingham, USA). The eluents were (A) 5% ACN in 0.1% FA and (B) 80% ACN in 0.08% FA. The peptides were loaded into a C_{18} loading cartridge (LC Packings, USA) and separated with a C_{18} PepMap100 column (15 cm length, 75 μm ID and 300 Å [LC Packings]) using a 5−40% linear gradient of eluent B over 60 min at a constant flow rate of 300 nL/min. LC-MS/MS experiments were performed in the information-dependent acquisition (IDA) mode. The precursor ions were selected using the following MS to MS/MS switch criteria: ion m/z > 400, charge states = 2 to 4, intensity exceeding 15 counts, and ion tolerance of 50.0 mmu; former target ions were excluded for 30 s. CID was used to fragment the multiple-charged ions, and nitrogen was used as the collision gas. The raw spectra files were used to generate text files in Mascot generic file format (.mgf), which were submitted to the Mascot ver. 2.3 (http://www.matrixscience.com) and Batch-tag (Protein Prospector, University of California San Francisco, USA) search engines.

Tryptic peptides from SDS-PAGE bands were identified by Mascot (version 2.3) search engine using the following criteria: databases, NCBI and Uniprot; taxonomy, other green plants; type of search, MS/MS ion search; enzyme, trypsin; fixed modifications, carbamidomethyl; variable modifications, methionine oxidation and pyro-Glu formation through N-terminal loss of ammonia at Gln; mass values, monoisotopic; parent tolerance, 0.08 Da; MS/MS tolerance, 0.15 Da; number of maximum missed cleavages, 1.

Peptides released from OGD and BBM hydrolysis were identified using the Batch-Tag web tool Protein Prospector (http://prospector.ucsf.edu), taxonomically restricting the search to *Triticum*. The same search criteria used above were utilized. The resulting peptide identifications were validated by manual inspection of the MS/MS spectra. The peptide entries were considered identified when the measured molecular weight corresponded to the expected value and a sequence of at least three consecutive b or y ions occurred in the spectrum. For each of the protein/peptide fractions, nanoflow LC−MS/MS analyses were run in triplicate, and only matches occurring in all three analyses were included in the entry list.

RESULTS

Pasta proteins were digested using an in vitro static OGD digestion model that mimics human physiological conditions.[13] The digestion steps were carried out under simulated physiological conditions, including digestive enzymes and their activity as well as pH, lipid, and salt concentrations. Digestion times were selected according to the average transit time of chyme in the respective compartments. A more exhaustive justification of the conditions used is given in Minekus et al.[13] Our model also included an additional step with porcine intestinal BBM hydrolases that simulates peptide degradation at the level of the jejunum.[16] Assessment of the peptide stability relative to treatment with BBM peptidases has already demonstrated in vivo persistence, intended as in vitro−in vivo correspondence, because it supported the discovery of some of the most important determinants of CD.[5,19]

SDS-PAGE Analysis. The kinetics of simulated gastric digestion was assessed by SDS-PAGE (Figure 1). The protein patterns arising from digestion of pasta at 0−120 min were compared to the intact proteins extracted from raw undigested pasta. The pattern of the uncooked sample showed the typical protein components of *Triticum* wheat flour, which can be grouped into HMW-GS (65−90 kDa), ω-gliadins (44−55 kDa), LMW-GS (30−40 kDa), and α/β- and γ-gliadins (30−45 kDa).[20] Bands of albumins/globulins were also detected,

DOI: 10.1021/jf505461x
J. Agric. Food Chem. 2015, 63, 2660−2667

Table 1. Identification of Protein Bands Extracted from the Gel Shown on Figure 1

band label	accession number/protein abbreviation	protein name	species	MW (Da)	score	matched peptides
1	AMYP_PIG	pancreatic α-amylase	*Sus scrofa*	57791	431	17
2	CBPB1_PIG	carboxypeptidase B	*Sus scrofa*	47750	337	14
3	CBPA1_PIG	carboxypeptidase A1	*Sus scrofa*	47320	193	11
4	AMYP_PIG	pancreatic α-amylase	*Sus scrofa*	57791	157	7
5	TRYP_PIG	trypsin	*Sus scrofa*	25078	87	8
6	AMYP_PIG	pancreatic α-amylase	*Sus scrofa*	57791	74	6
7	TRYP_PIG	trypsin	*Sus scrofa*	25078	41	7
8	CBPB1_PIG	carboxypeptidase B	*Sus scrofa*	47750	74	5
9	TRYP_PIG	trypsin	*Sus scrofa*	25078	69	4
10	1AN1_E (gil3318722)	chain E, leech-derived tryptase inhibitor	*Sus Scrofa*	24142	61	4
11	P24296	nsLTP	*Triticum aestivum*	9494	101	5

including β-amylase(s) (60 kDa) and alpha-amylase/trypsin inhibitor (ATI) (14−16 kDa).[21]

In cooked pasta at the beginning of gastric digestion, wheat proteins were not detected except for a faint band, most likely because the proteins remained insoluble in the saline buffer or were still embedded in the starchy matrix of pasta (Figure 1, left panel). The main band at 35 kDa was identified as porcine pepsin by LC−MS/MS of tryptic-derived peptides (not shown). Because of its high concentration in SGF, pepsin masked the pasta proteinaceous material with similar molecular weight and interfered with data evaluation. The increased accumulation of low MW polypeptides (7−17 kDa) indicated the progressive degradation of proteins during digestion from 30 to 120 min. These polypeptides were made soluble by the proteolytic action of pepsin on the insoluble parent proteins.

After a 2 h incubation, the simulated gastric digests were subjected to simulated duodenal digestion, and aliquots were sampled over the 0−120 min time course for SDS-PAGE analysis (Figure 1, right panel). The progressive appearance of newly formed LMW polypeptides was the result of extensive hydrolysis by pancreatic enzymes. However, the complex protein pattern generated by the action of porcine pancreatin, used at such a high proteases-to-substrate ratio, could bias the clear detection of the products of digestion.[22]

Identification of Proteins Resistant to OGD Digestion. A proteomic approach was employed for the analysis of the polypeptides that survived the OGD digestion model. The numbered bands of the D120 lane were excised from the gel and selected for proteomic analysis (Figure 1, right panel). Except for the broad band at ∼5 kDa that escaped identification, the protein components were characterized by LC−MS/MS analysis. The list of significant protein hits from the Mascot search is shown in Table 1. No gluten polypeptides were detected, whereas the main bands were from pancreatic enzymes. The occurrence of multiple bands for a single enzyme is most likely due to autolysis or mutual digestion among pancreatin hydrolases. The large relative amount of pancreatin enzymes also complicated the identification of proteins that survived digestion.[22]

Non specific-lipid transfer protein (nsLTP), one of the metabolic proteins (albumins and globulins), was the only wheat-derived gene product identified. Neither any protein belonging to the albumin/globulin fraction nor gluten (gliadin and glutenin) was identified. These results indicated that with the exception of nsLTP the pasta proteins were digested relatively rapidly into small peptides that escaped detection by SDS-PAGE electrophoresis.

Analysis of IgA-Reactive Proteins in OGD Digesta. The immunoreactivity of the OGD digesta against the IgA antibodies in a sera pool of CD patients was assayed (Figure 2). The OGD digesta effluents (both collected at 2 h) were centrifuged, and the resulting soluble and insoluble fractions were run on SDS-PAGE for immunoblotting analysis. The total protein extracted from the cooked pasta before digestion was used as the positive control. The sera pool of healthy subjects did not bind to any band (not shown), confirming the specificity of the immunoreaction. As shown in Figure 2, the major IgA-reactive undigested proteins were detected between 30 and 97 kDa. The soluble gastric digesta (lane 3) showed a main immune-reactive band with an M_r of 45 kDa. Conversely, the distribution of IgA-binding proteins in the insoluble gastric sample (lane 2) was comparable with that of the total protein patterns (lane 1), indicating that the majority of the immunoreactive pasta proteins, in all likelihood composed of the gliadin fraction, were not solubilized and were pelleted by centrifugation. This might be a result of a chemically reversible heat-induced protein aggregation that occurs during pasta processing. Such aggregation can decrease protein solubility in the acidic gastric environment, as previously demonstrated.[23] However, after simulated OGD hydrolysis, only a few faint bands were still detected in both the insoluble (lane 4) and soluble (lane 5) fractions, indicating that the majority of IgA-binding proteins were degraded by pancreatic proteases.

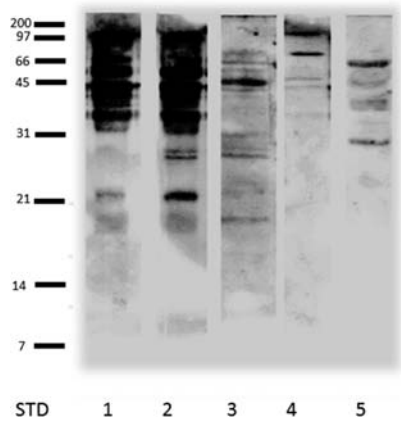

Figure 2. Western blot analysis of cooked pasta proteins against sera of celiac disease: whole proteins (lane 1), insoluble (lanes 2 and 4) and soluble (lanes 3 and 5) phases of gastric and intestinal digestion, respectively.

DOI: 10.1021/jf505461x
J. Agric. Food Chem. 2015, 63, 2660−2667

Identification of Pasta-Derived Peptides. To identify the most stable polypeptide sequences and to narrow the list of epitopes that are potentially involved in eliciting immune reactions, it is necessary to consider the action of intestinal BBM enzymes located on the polarized apical surface of the duodenal and jejunal enterocytes. The use of BBM enzymes is a fundamental step in assessing intestinal stability because the BBM enzyme mixture contains a series of endo- and exopeptidases with a range of different cleavage specificities that have significant effects in gradually shortening the surviving OGD peptides into di-, tri-, and oligopeptides as well as free amino acids. The OGD digesta were incubated with BBM enzymes purified from pig intestinal jejunum and then fractionated by SEC, allowing the separation of the large pasta polypeptides from the >6 kDa fraction (here referred to as the "peptide" fraction). The peptide fraction was analyzed via LC−MS/MS followed by software-assisted database searching. A comprehensive list of the 61 peptides surviving the digestion of pasta is reported in Table S1 (Supporting Information). The highest number of peptides arose from the γ-gliadin and LMW-glutenin proteins, which presented several motifs associated with the induction of CD. For instance, QGQGIIQPQQPA, QQPQQPFPQ, and PQQSFPQQQ fragments are generally classified among the main gliadin toxic motifs, commonly indicated as γ-II (or glia-γ30),[24−26] γ-VIIa,[25] and γ-I,[25] respectively.

The peptide α-gli 31−55 (LGQQQPFPPQQPYPQPQPFP-SQQPY), together with its shortened form, namely, α-gli 31−51, were also released in the digesta. This gliadin domain harbors the toxic motifs 31−43 and 44−55.[27] The potential stability of α-gli 31−55 under GI degradation has been already demonstrated in our previous studies.[18,28] The α-gli 56−68 peptide, largely used as a model peptide in CD investigations, was degraded into shorter fragments (i.e., QPFQPQLP and QPFQPQL), with lower immunogenicity compared to their parent peptide.[29,30] A few fragments arising from HMW By8 and Bx7 glutenin were also found, whereas β-amylase peptides were the only nongluten peptides identified. Most likely because of their prompt full digestion, no other peptides deriving from the soluble-protein fraction (albumins and globulins) occurred in detectable amounts. Nevertheless, the possibility that the overabundant amount of gluten-derived peptides suppressed the detection of low-abundance fragments of metabolic proteins can not be ruled out.

A more comprehensive characterization of the peptide fractions was severely challenged by a series of concomitant factors, including the extreme heterogeneity of the parent proteins, the possible heat-induced modifications of proteins, the nontryptic nature of the peptides, and the unpredictable cleavage specificity of protein hydrolysis resulting from the action of a pool of proteases and peptidases. Indeed, the faint MS/MS production of b- and y-series fragments and the abnormally intense internal-fragment ions, combined with the lack of amino acid constraints at the N- and C-terminal position, decreased the identification rate. Thus, although more than 200 peptides with M_r values between 400 and 6000 were detected in the LC−MS/MS chromatogram, two-thirds of these peptides remained unidentified due to low database scores.

Identification of Protein Lost in the Cooking Water. Because nsLTP was the only protein identified in the digested sample, we assumed that salt-soluble proteins might have leached into the water during the cooking process. To track the fate of expected and well-established potential allergens,[31] the proteins released into the cooking water were extracted and analyzed by SDS-PAGE (Figure 3). The protein profile was

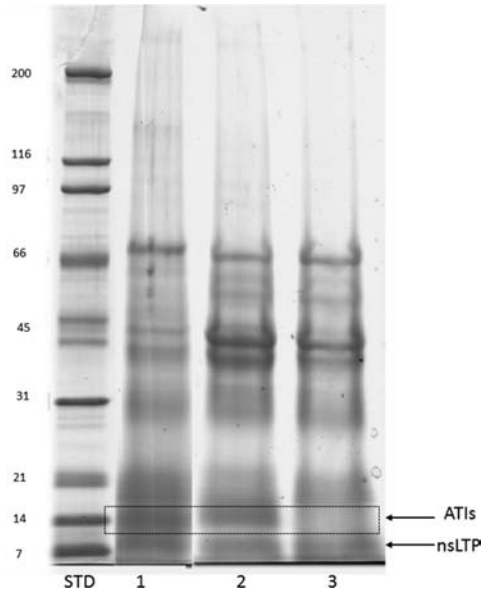

Figure 3. SDS-PAGE (15%) analysis of cooking-water protein (lane 1) and salt-soluble proteins extracted from raw (lane 2) and cooked (lane 3) pasta. MW markers (STD) are on the left. Arrows indicate the region of ATIs and nsLTP. ATIs were identified as ATIs -CM3 (gil 100834), -CM16 (P16851) and -CM2 (gil123956). nsLTP was identified as P16851.

compared to the salt-soluble fractions isolated from the raw and cooked (undigested) pasta. The identity of each polypeptide was assessed by proteomic analysis (not shown). Minor changes were observed among the individual fractions, indicating that only a part of the salt-soluble proteins were dispersed in the water during cooking. The bands at 9 kDa, corresponding to wheat nsLTP, were detected in all samples. A noticeable difference was due to the bands with an estimated M_r of 14 kDa, which were missing in the cooked pasta pattern (lane 3). These proteins, identified as ATI-CM3 (gil100834), -CM16 (P16851), and -CM2 (gil123956) and detected in the raw pasta sample (lane 2), were entirely retrieved in the cooking water (lane 1). This finding may explain why ATIs were not detected in the digesta as either whole proteins or peptides, despite their high abundance in flour and their relative stability to withstand hydrolysis, which is functionally ascribable to their role as protease inhibitors.

To confirm the digestion stability of ATIs, a simulated gastrointestinal digestion was performed specifically on the albumin/globulin fractions extracted from the raw and cooked pasta. In this case, the proteins were digested using a simplified model on a purified fraction[18] to minimize interference from both the matrix and high amount of pancreatin enzymes. SDS-PAGE analysis (Figure 4) showed the complete degradation of the albumins/globulins from raw pasta, with the exception of nsLTP and ATIs that both exhibited high resistance to proteases (lane 3). In contrast, in digested cooked pasta, nsLTP was the only salt-soluble protein still detectable (lane 4), whereas ATIs were no longer detected (lane 4). This experiment confirmed that ATIs, though resistant to digestion,

DOI: 10.1021/jf505461x
J. Agric. Food Chem. 2015, 63, 2660−2667

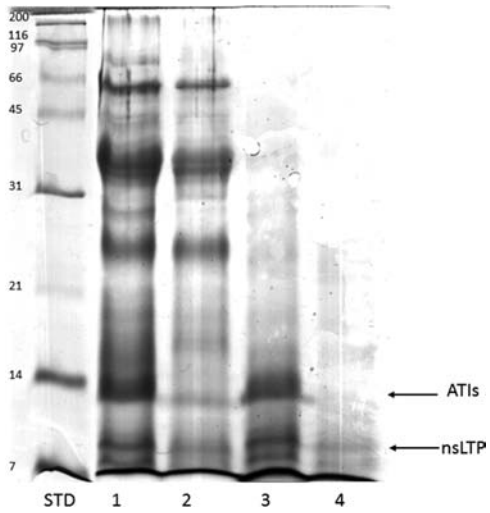

Figure 4. SDS-PAGE (15%) analysis of salt-soluble proteins before and after simulated GI digestion. Lanes 1 and 3, albumin/globulin proteins extracted from raw pasta before and after digestion, respectively. Lanes 2 and 4, albumin/globulin proteins extracted from cooked pasta before and after digestion, respectively. Arrows indicate the region of ATIs and nsLTP proteins. ATIs were identified as ATI-CM3 (gi|100834), -CM16 (P16851), and -CM2 (gi|123956). nsLTP was identified as P16851.

are lost in the cooking water so that nsLTP was the only salt-soluble protein found in the digested pasta (Figure 1).

DISCUSSION

The identification of the (poly)peptides surviving the in vitro model has important biochemical, immunochemical, and potentially allergenic implications. Previous attempts in this sense did not take into account the effect of the matrix in a real-food system,[18,28,32] which is expected to dramatically influence the accessibility of proteins to proteases as well as their susceptibility to hydrolysis, thereby contributing to the determination of the bioaccessibility, and hence the bioavailability, of wheat peptides. Alternatively, simplified digestion models that did not adequately mirror the physiological process of protein hydrolysis have been carried out on several wheat-based systems and may result in a poor in vitro−in vivo correspondence.[12]

In the present study, by accurately mimicking the human physiological conditions, we determined the effect of simulated digestion on proteins from pasta prepared according to ordinary home-cooking conditions. Although proteins are not affected by oral-phase hydrolysis, chewing and the action of human α-amylase are important to shear and break down the starch gel, so making the protein-cleavage sites accessible to proteolysis. However, a consistent pellet, containing particles of undigested pasta, was still evident after gastric digestion. SDS-PAGE and Western blot analysis showed that the majority of wheat proteins were not solubilized in the acidic environment of gastric juice and were resistant to pepsin action. This behavior is related to the heat-induced modifications of the wheat proteins.[7] As demonstrated in previous studies, thermal modifications occurring during industrial dehydration (i.e., up to 110 °C) and domestic cooking processes induce the aggregation of wheat proteins by disulfide bond formation and hydrophobic interactions, which combine with the intrinsically low water solubility of the gluten proteins.[23,33] In support of these data, HPLC analysis was carried out on the ethanol-extracted gliadins before and after cooking the pasta, as shown in Figure S1 (Supporting Information). Ethanol buffer extracts only monomeric gliadins that do not contain covalent cross-links.[3] Before cooking, the gliadin profile was somewhat similar to that of the gliadins extracted from flour, whereas the chromatogram dramatically changed after cooking. In particular, the peaks of ω-gliadins, which do not contain cysteine residues, were practically unaffected by cooking, whereas those relevant to α/β- and γ-gliadins significantly decreased after cooking, suggesting that these proteins underwent massive thermally induced aggregation (Figure S1).

Following the action of duodenal enzymes, the digesta became liquid, though highly viscous, as a result of the partial hydrolysis of starch by pancreatic α-amylase. After 2 h of simulated duodenal digestion, the wheat gluten proteins were almost completely degraded. Western blot analysis showed that few soluble and insoluble IgA-reactive bands resisted OGD digestion. These polypeptides were not identified by proteomic analysis, also as a consequence of the thermally induced protein modifications (i.e cross-linking, Maillard reaction, and deamidation).

The OGD digestion process releases immunologically active peptides that are able to reach the intestinal lumen and trigger immune responses in susceptible individuals. However, before crossing the gut epithelium, the peptides are further hydrolyzed by endo-/exopeptidases of BBM enterocytes, which typically degrade peptides to single amino acids or short di- or tripeptides. Because of their high percentage of proline residues, many gliadin and glutenin peptides are resistant to BBM digestion. The α-gliadin-derived 33-mer peptide, which is considered the most immunogenic and highly BBM-digestion-resistant peptide, was not detected because it is not expressed by *T. durum*, being characteristic of the D genome of *T. aestivum* (soft wheat).[19] However, several peptides containing epitopes that can trigger immune responses in CD patients were identified in the samples resulting from complete digestion. For instance, peptide 31−55, harboring toxic sequences 31−43 and 44−55, was found to be stable to digestion.[18,28] However, the repertoire of the pasta-derived OGD/BBM-digestion-resistant peptides still remains partial, as only approximately one-third of the peptides were clearly identified.

The incomplete identification can be primarily attributed to (i) the formation of high molecular mass peptides not easily detectable with the MS-based approaches, (ii) the incompleteness of wheat protein database annotation, (iii) intrinsic technical challenges, as explained in the Results section, and (iv) the very dynamic range of the components, which limits the identification of low-abundance peptides and is also due to ion-suppression effects. It has to be emphasized that in this research we used a representative commercial brand of pasta. The high genetic polymorphism of wheat cultivars might be a further source of heterogeneity and gluten-derived peptides could diverge to some extent if pasta samples produced with different wheat accession are analyzed.[34]

nsLTP was the only protein virtually unaffected by OGD digestion. This protein can elicit IgE-mediated sensitization in predisposed allergic individuals.[31] Previous reports demonstrated that nsLTP, along with other albumin/globulin proteins, is highly resistant to proteolysis especially those proteins functionally acting as proteases/inhibitors, such as ATIs.[35,36] These latter proteins were not found in cooked pasta because

DOI: 10.1021/jf505461x
J. Agric. Food Chem. 2015, 63, 2660−2667

they were almost completely dispersed in the cooking water. ATIs are known to be the major allergen responsible for baker's asthma.[6] In vitro studies demonstrated that ATIs could also play a major role in triggering the innate immune response in CD. More recently, it has been suggested that ATIs may fuel inflammation and immune reactions in other intestinal and nonintestinal immune disorders, in particular nonceliac gluten sensitivity.[37] This would indicate that pasta, as it is normally prepared, has a lower allergenic potency than raw flour and (probably) bakery products, and should be less toxic for gluten-related disorder patients who show symptoms after eating pasta. This finding is also in line with the results by De Gregorio et al.[7] who observed that the processing of wheat flour decreases the allergenic potency of the major salt-soluble wheat proteins (IgE-binding capacity) in the resulting food products.

In conclusion, we demonstrated that the proteins from cooked pasta are completely hydrolyzed during in vitro digestion, releasing gliadin and glutenin peptides that contain amino acid sequences harmful to CD patients. Among the wheat IgE allergens, nsLTP is highly resistant to both cooking and hydrolysis, whereas important allergen proteins such as ATIs are lost during pasta cooking.

The application of the harmonized static digestion model that mimics in vivo physiology provided new insights for establishing the evolution of wheat proteins during pasta processing, cooking, and digestion in humans. Thus, we also provide insights into the possible immunological implications and the possible effects of gluten resistant epitopes on human health.

■ ASSOCIATED CONTENT

Supporting Information

Supporting materials includeTable S1 and Figure S1. Table S1 displays a list of LMW peptides identified by LC−ESI-MS/MS. Figure S1 shows the HPLC analysis of gliadin extracted from pasta before and after cooking. This material is available free of charge via the Internet at http://pubs.acs.org.

■ AUTHOR INFORMATION

Corresponding Author

*E-mail: mamone@isa.cnr.it. Tel.: +39 0825 299521. Fax: +39 0825 781585.

Funding

The work at the Institute of Food Research was funded by the BBSRC through an Institute Strategic Programme Grant (research grant BB/J004545/1). The authors are participants of the EU-funded COST-action INFOGEST (COST FA 1005). The work at the Istituto di Scienze dell'Alimentazione, CNR, was in part supported by a dedicated grant from the Italian Ministry of Economy and Finance to CNR and ENEA for the project "Innovazione e sviluppo del Mezzogiorno Conoscenze Integrate per Sostenibilità ed Innovazione del Made in Italy Agroalimentare" - Legge n.191/2009.

Notes

The authors declare no competing financial interest.

■ ACKNOWLEDGMENTS

We are grateful to Dr. Carmen Gianfrani for providing human sera.

■ ABBREVIATIONS USED

ATI, α-amylase/trypsin inhibitor; BBM, brush border membrane; CD, Celiac disease; nsLTP, nonspecific lipid transfer protein; OGD, oral−gastric−duodenal; SGF, simulated gastric fluid; SIF, simulated intestinal fluid; SSF, simulated salivary fluid;

■ REFERENCES

(1) Cubadda, R. E.; Carcea, M.; Marconi, E.; Trivisonno, M. C. Influence of Gluten Proteins and Drying Temperature on the Cooking Quality of Durum Wheat Pasta. *Cereal Chem.* **2007**, *84*, 48−55.

(2) Shewry, P. R.; Tatham, A. S. Biotechnology of wheat quality. *J. Sci. Food Agric.* **1997**, *73*, 397−406.

(3) Shewry, P. R.; D'Ovidio, R.; Lafiandra, D.; Jenkins, J. A.; Mills, E. N. C.; Békés, F. Wheat grain proteins. In *Wheat: Chemistry and Technology*, 4th ed.; Khan, K., Shewry, P. R., Eds.; AACC Press: St Paul, MN, 2009; Vol. *8*, pp 223−298.

(4) Sollid, L. M. Molecular basis of celiac disease. *Annu. Rev. Immunol.* **2000**, *18*, 53−81.

(5) Hausch, F.; Shan, L.; Santiago, N. A.; Gray, G. M.; Khosla, C. Intestinal digestive resistance of immunodominant gliadin peptides. *Am. J. Physiol.: Gastrointest. Liver Physiol.* **2002**, *283*, G996.

(6) Tatham, A. S.; Shewry, P. R. Allergens in wheat and related cereal. *Clin. Exp. Allergy* **2008**, *38*, 1712−26.

(7) Wagner, M.; Morel, M. H.; Bonicel, J.; Cuq, B. Mechanisms of heat-mediated aggregation of wheat gluten protein upon pasta processing. *J. Agric. Food Chem.* **2011**, *13*, 3146−54.

(8) de Gregorio, M.; Armentia, A.; Díaz-Perales, A.; Palacín, A.; Duenas-Laita, A.; Martin, B.; Salecdo, G.; Sancehz-Monge, R. Salt-soluble proteins from wheat-derived foodstuffs show lower allergenic potency than those from raw flour. *J. Agric. Food Chem.* **2009**, *57*, 3325−30.

(9) Picariello, G.; Mamone, G.; Nitride, C.; Addeo, F.; Ferranti, P. Protein digestomics: integrated platforms to study food-protein digestion and derived functional and active peptides. *TrAC, Trends Anal. Chem.* **2013**, *52*, 120−134.

(10) De Zorzi, M.; Curioni, A.; Simonato, B.; Giannattasio, M.; Pasini, G. Effect of pasta drying temperature on gastrointestinal digestibility and allergenicity of durum wheat proteins. *Food Chem.* **2007**, *104*, 353−363.

(11) Petitot, M.; Brossard, C.; Barron, C.; Larré, C.; Morel, M. H.; Micard, V. Modification of pasta structure induced by high drying temperatures. Effects on the in vitro digestibility of protein and starch fractions and the potential allergenicity of protein hydrolysates. *Food Chem.* **2009**, *116*, 401−412.

(12) Prandi, B.; Faccini, A.; Tedeschi, T.; Cammerata, A.; Sgrulletta, D.; D'Egidio, M. G.; Galaverna, G.; Sforza, S. Qualitative and quantitative determination of peptides related to celiac disease in mixtures derived from different methods of simulated gastrointestinal digestion of wheat products. *Anal. Bioanal. Chem.* **2014**, *406*, 4765−75.

(13) Minekus, M.; Alminger, M.; Alvito, P.; Balance, S.; Bohn, T.; Bourlieu, C.; Carrière, F.; Boutrou, R.; Corredig, M.; Dupont, D.; Dufour, C.; Egger, L.; Golding, M.; Karakaya, S.; Kirkhus, B.; Le Feunteun, S.; Lesmes, U.; Macierzanka, A.; Mackie, A.; Marze, S.; McClements, D. J.; Ménard, O.; Recio, I.; Santos, C. N.; Singh, R. P.; Vegarud, G. E.; Wickham, M. S.; Weitschies, W.; Brodkorb, A. A standardised static *in vitro* digestion method suitable for food an international consensus. *Food Funct.* **2014**, *56*, 1113−24.

(14) Hoebler, C.; Karinthi, A.; Devaux, M. F.; Guillon, F. Physical and chemical transformations of cereal food during oraldigestion in human subjects. *Br. J. Nutr.* **1998**, *80*, 429−36.

(15) Hummel, B. C. A modified spectrophotometric determination of chymotrypsin, trypsin, and thrombin. *Can. J. Biochem. Physiol.* **1959**, *37*, 1393−1399.

(16) Shirazi-Beechey, S. P.; Davies, A. G.; Tebbutt, K.; Dver, J.; Ellis, A.; Taylor, C. J.; Fairclough, P.; Beechey, R. B. Preparation and properties of brush-border membrane vesicles from human small intestine. *Gastroenterology* **1990**, *98*, 676−85.

DOI: 10.1021/jf505461x
J. Agric. Food Chem. 2015, 63, 2660−2667

(17) Mamone, G.; Ferranti, P.; Chianese, L.; Scafuri, L.; Addeo, F. Qualitative and quantitative analysis of wheat gluten proteins by liquid chromatography and electrospray mass spectrometry. *Rapid Commun. Mass Spectrom.* **2000**, *14*, 897−904.
(18) Mamone, G.; Ferranti, P.; Rossi, M.; Roepstorff, P.; Fierro, O.; Malorni, A.; Addeo, A. Identification of a peptide from alpha-gliadin resistant to digestive enzymes: implications for celiac disease. *J. Chromatogr. B: Anal. Technol. Biomed. Life Sci.* **2007**, *855*, 236−241.
(19) Shan, L.; Molberg, Ø.; Parrot, I.; Hausch, F.; Filiz, F.; Gray, G. M.; Sollid, L. M.; Khosla, C. Structural basis for gluten intolerance in celiac sprue. *Science* **2002**, *297*, 2275−2279.
(20) Ferranti, P.; Mamone, G.; Picariello, G.; Addeo, F. Mass spectrometry analysis of gliadins in celiac disease. *J. Mass Spectrom.* **2007**, *42*, 1531−48.
(21) Weiss, W.; Huber, G.; Engel, K. H.; Pethran, A.; Dunn, M. J.; Gooley, A. A.; Görg, A. Identification and characterization of wheat grain albumin/globulin allergens. *Electrophoresis* **1997**, *18*, 826−833.
(22) Kopf-Bolanz, K. A.; Schwander, F.; Gijs, M.; Vergères, G.; Portmann, R.; Egger, L. Validation of an in vitro digestive system for studying macronutrient decomposition in humans. *J. Nutr.* **2012**, *142*, 245−250.
(23) Dexter, J. E.; Matsuo, R. R. Changes in spaghetti protein solubility during cooking. *Cereal Chem.* **1979**, *56*, 394−398.
(24) Vader, W.; Kooy, Y.; Van Veelen, P.; De Ru, A.; Harris, D.; Benckhuijsen, W.; Peña, S.; Mearin, L.; Drijfhout, J. W.; Koning, F. The gluten response in children with celiac disease is directed toward multiple gliadin and glutenin peptides. *Gastroenterology* **2012**, *122*, 1729−1737.
(25) Vader, L. W.; Stepniak, D. T.; Bunnik, E. M.; Kooy, Y. M.; de Haan, W.; Drijfhout, J. W.; Van Veelen, P. A.; Koning, F. Characterization of cereal toxicity for celiac disease patients based on protein homology in grains. *Gastroenterology* **2003**, *125*, 1105−1113.
(26) Qiao, S. W.; Bergseng, E.; Molberg, O.; Xia, J.; Fleckenstein, B.; Khosla, C.; Sollid, L. M. Antigen presentation to celiac lesion-derived T cells of a 33-mer gliadin peptide naturally formed by gastrointestinal digestion. *J. Immunol.* **2004**, *173*, 1757−1762.
(27) Maiuri, L.; Ciacci, C.; Ricciardelli, I.; Vacca, L. Association between innate response to gliadin and activation of pathogenic T cells in coeliac disease. *Lancet* **2003**, *362*, 30−37.
(28) Iacomino, G.; Fierro, O.; D'Auria, S.; Picariello, G.; Ferranti, P.; Liguori, C.; Addeo, F.; Mamone, G. Structural analysis and Caco-2 cell permeability of the celiac-toxic A-gliadin peptide 31−55. *J. Agric. Food Chem.* **2013**, *61*, 1088−96.
(29) Arentz-Hansen, E. H.; McAdam, S. N.; Molberg, O.; Kristiansen, C.; Sollid, L. M. Production of a panel of recombinant gliadins for the characterization T cell reactivity in coeliac disease. *Gut* **2000**, *46*, 46−51.
(30) Matysiak-Budnik, T. C.; Candalh, C.; Cellier, C.; Dugave, A.; Namane, T. Limited efficiency of prolyl-endopeptidase in the detoxification of gliadin peptides in celiac disease. *Gastroenterology* **2005**, *129*, 786−796.
(31) Pastorello, E. A.; Farioli, L.; Conti, A.; Pravettoni, V.; Bonomi, F.; Iametti, S.; Fortunato, D.; Scibilia, J.; Bindslev-Jensen, C.; Ballmer-Weber, B.; Robino, A. M.; Ortolani, C. Wheat IgE-mediated food allergy in European patients: α-amylase inhibitors, lipid transfer proteins and low-molecular-weight glutenins. Allergenic molecules recognized by double-blind, placebo-controlled food challenge. *Int. Arch. Allergy Immunol.* **2007**, *144*, 10−22.
(32) Shan, L.; Qiao, S. W.; Arentz-Hansen, H.; Molberg, Ø.; Gray, G. M.; Sollid, L. M.; Khosla, C. Identification and analysis of multivalent proteolytically resistant peptides from gluten: implications for celiac sprue. *J. Proteome Res.* **2005**, *4*, 1732−41.
(33) García, E.; Llorente, M.; Hernando, A.; Kieffer, R.; Wieser, H.; Méndez, E. Development of a general procedure for complete extraction of gliadins for heat processed and unheated foods. *Eur. J. Gastroenterol. Hepatol.* **2005**, *17*, 529−539.
(34) Prandi, B.; Bencivenni, M.; Faccini, A.; Tedeschi, T.; Dossena, A.; Marchelli, R.; Galaverna, G.; Sforza, S. Composition of peptide mixtures derived from simulated gastrointestinal digestion of prolamins from different wheat varieties. *J. Cereal Sci.* **2012**, *56*, 223−231.
(35) Asero, R.; Mistrello, G.; Roncarolo, D.; de Vries, S. C.; Gautier, M. F.; Ciurana, C. L.; Verbeek, E.; Mohammadi, T.; Knul-Brettlova, V.; Akkerdaas, J. H.; Bulder, I.; Aalberse, R. C.; van Ree, R. Lipid transfer protein: a pan-allergen in plant-derived foods that is highly resistant to pepsin digestion. *Int. Arch. Allergy Immunol.* **2001**, *124*, 67−69.
(36) Vassilopoulou, E.; Rigby, N.; Moreno, F. J.; Zuidmeer, L.; Akkerdaas, J.; Papadopoulos, N. G.; Saxoni-Papageorgiou, P.; van Ree, R.; Mills, C. Effect of *in vitro* gastric and duodenal digestion on the allergenicity of grape lipid transfer protein. *J. Allergy Clin. Immunol.* **2006**, *118*, 473−480.
(37) Junker, Y.; Zeissig, S.; Kim, S. J.; Barisani, D.; Wieser, H.; Leffler, D. A.; Zevallos, V.; Libermann, T. A.; Dillon, S.; Freitag, T. L.; Kelly, C. P.; Schuppan, D. Wheat amylase trypsin inhibitors drive intestinal inflammation via activation of toll-like receptor 4. *J. Exp. Med.* **2012**, *209*, 2395−2408.

DOI: 10.1021/jf505461x
J. Agric. Food Chem. 2015, 63, 2660−2667

Aspergillus niger, 300 AGU/g) were from Novozymes, Bagsvaerd, Denmark. The complex carbohydrase mixture Driselase (from Basidiomycetes), coniferaldehyde, sinapaldehyde, *p*-coumaric acid, borohydride exchange resin (2.5−5.0 mmol BH_4^-/g resin), acetyl bromide, diisobutylaluminum hydride, and the deuterated solvents were from Sigma-Aldrich, St. Louis, MO. Acetic anhydride, NaOH, NH_4Cl, Na_2HPO_4, NaH_2PO_4, and ethyl acetate were from Roth, Karlsruhe, Germany. Pyridine, glacial acetic acid, $MgSO_4$, HCl, methanol, dichloromethane, petroleum ether, *n*-hexane, 1,4-dioxane, ethanol, and acetone were obtained from VWR, Radnor, PA.

General. NMR analyses were performed on a Bruker (Rheinstetten, Germany) 250 MHz spectrometer using acetone-d_6 as solvent. NMR data of synthesized monolignols and their precursors were compared to those described in the lignin model database.[12] Solid-phase extraction (SPE) columns (Discovery, LC-SI, 500 mg/3 mL) were purchased from Supelco, Bellefonte, PA and Phenomenex, Torrance, CA (STRATA-X, polymeric reversed phase, 200 mg/3 mL). Filter papers were obtained from Macherey & Nagel, Düren, Germany (4−12 μm), and Roth, Karlsruhe, Germany (12−15 μm). GC analyses were carried out on a Shimadzu (Kyoto, Japan) GC-MS system (GC-2010plus, GC-MS-QP2010Ultra) using a 30 m × 0.25 mm, 0.25 μm Rtx-5MS column (Restek, Bellefonte, PA) and on a GC-FID system (GC-2010Plus) using a 30 m × 0.32 mm, 0.25 μm HP-5 column (Agilent, Santa Clara, CA).

Synthesis of Coniferyl and Sinapyl Alcohol. Coniferyl and sinapyl alcohols were synthesized from coniferaldehyde and sinapaldehyde as previously described.[13] In brief, coniferaldehyde/sinapaldehyde (205 mg/200 mg) were reduced in methanol (MeOH) (8 mL) by using a borohydride exchange resin (BER; 920 mg/770 mg), which was washed twice with 6 mL of MeOH before use. The reaction mixture was stirred at room temperature for 1 h/3 h. The resin was filtered off through glass wool, and the filtrate was evaporated. Cleanup was carried out using silica gel SPE columns: The columns were conditioned with 5 mL of ethyl acetate, the reaction mixture was applied in 5 mL of ethyl acetate, and the columns were eluted with 25 mL of ethyl acetate. Crystallization from dichloromethane/petroleum ether yielded pale yellow needles (57−67%) of coniferyl alcohol. Dichloromethane was added to the dried sinapyl alcohol, and the solution was kept in a freezer for several days. Since no crystallization was achieved, sinapyl alcohol was obtained as a yellow oil (67−95%).

Synthesis of *p*-Coumaryl Alcohol. *p*-Coumaryl alcohol was synthesized from *p*-coumaric acid in two steps as previously described.[14] Ethyl *p*-coumarate was prepared by stirring 1 g of *p*-coumaric acid and 5 mL of acetyl chloride in 50 mL of ethanol at room temperature for 17 h. After evaporation of the solvents, the procedure was repeated. The product was crystallized from ethyl acetate/petroleum ether. Ethyl *p*-coumarate was reduced using diisobutylaluminum hydride (DIBAL-H). Ethyl *p*-coumarate (640 mg) in 30 mL of toluene was ice cooled under nitrogen, and 12 mL of DIBAL-H was slowly added. The reaction mixture was stirred for 1 h, and the reaction was quenched by adding 5 mL of ethanol. The solvent was partially removed under reduced pressure, and 50 mL of water was added. The aqueous layer was extracted four times by using ethyl acetate. Pale yellow crystals of *p*-coumaryl alcohol (85−94%) were obtained by crystallization from dichloromethane/petroleum ether.

Synthesis of Diacetylated *p*-Coumaryl, Coniferyl, And Sinapyl Alcohols. Diacetylation of the three *p*-hydroxycinnamyl alcohols was carried out as described in the protocol of the DFRC method.[9] *p*-Hydroxycinnamyl alcohols (*p*-coumaryl alcohol, 162 mg; coniferyl alcohol, 189 mg; sinapyl alcohol, 216 mg), acetic anhydride (3.3 mL), and pyridine (3.2 mL) were stirred for 40 min at room temperature. The solvents were evaporated, and coevaporation was carried out using ethanol. The diacetylated compounds were obtained as yellow oils. For the synthesis of deuterium-labeled (hexadeuterated) *p*-hydroxycinnamyl alcohols acetic anhydride-d_6 was used. ^{1}H NMR (*p*-coumaryl diacetate-d_6), δ [ppm]: δ 7.50 (d, 2H, J = 8.6 Hz, H2/H6), 7.10 (d, 2H, J = 8.7 Hz, H3/H5), 6.71 (d, 1H, J = 16.0 Hz, Hα), 6.35 (dt, 1H, J = 16.0, 6.2 Hz, Hβ), 4.69 (dd, 2H, J = 6.2, 1.4 Hz, Hγ). ^{1}H NMR (coniferyl alcohol diacetate-d_6), δ [ppm]: δ 7.23 (s, 1H, H2), 7.02 (m, 2H, H5/H6), 6.69 (dt, 1H, J = 15.9, 1.3 Hz, Hα), 6.37 (dt, 1H, J = 15.9, 6.2 Hz, Hβ), 4.69 (dd, 2H, J = 6.2, 1.4 Hz, Hγ), 3.85 (s, 3H, OCH_3). ^{1}H NMR (sinapyl alcohol diacetate-d_6), δ [ppm]: δ 6.85 (s, 2H, H2/H6), 6.67 (dt, 1H, J = 15.9, 1.2 Hz, Hα), 6.39 (dt, 1H, J = 15.9, 6.2 Hz, Hβ), 4.69 (dd, 2H, J = 6.2, 1.3 Hz, Hγ), 3.81 (s, 6H, OCH_3).

Plant Material. All fruits and vegetables (pear (*Pyrus communis* L.), carrot (*Daucus carota* L. subsp. *sativus*), asparagus (*Asparagus officinalis* L.), and small radish (*Raphanus sativus* L. var. *sativus*), also known as European radish) were obtained from a local grocery store. Asparagus was peeled whereas pear, carrot, and European radish were used unpeeled; however, the cores of the pears were removed.

Preparation of Insoluble Fibers. All fruits and vegetables were freeze dried and milled to a particle size of <0.5 mm. Dried material (20 g) was suspended in 0.08 M sodium phosphate buffer pH 6.2 (200 mL), and 1.5 mL of α-amylase was added. The suspension was placed in a water bath (92 °C) for 20 min and shaken every 5 min. The samples were cooled to room temperature, and the pH was adjusted to 7.5 with 0.275 M NaOH. After adding 600 μL of protease, the samples were incubated for 30 min at 60 °C with continuous agitation. The samples were cooled down; the pH was adjusted to 4.5 with 0.375 M HCl and, after adding 700 μL of amyloglucosidase, incubated in a water bath for 30 min at 60 °C. The suspensions were filtered through filter paper (12−15 μm), and the residues were washed three times with hot water (60 °C), ethanol, and acetone and finally air dried under the fume hood. To remove small amounts of remaining lignin-like low molecular weight material, the insoluble fibers were further extracted with ethanol (8 h), ethyl acetate (8 h), and *n*-hexane (8 h) using a Soxhlet apparatus. Finally, the insoluble fibers were dried at 40 °C in a vacuum oven.

Enzyme Digestion. Insoluble fibers (1 g) were suspended in 100 mL of water and incubated with 60 mg of Driselase at 37 °C for 48 h. After inactivation of the enzymes (5 min, 100 °C), the samples were centrifuged for 10 min at 2500 rpm and washed twice with water, ethanol, and acetone. The residues were dried in a vacuum oven at 40 °C.

DFRC Method. The DFRC method was performed as described by Bunzel et al.[11] with minor modifications. About 10−25 mg (pear, 24 mg; radish, 11 mg; carrot and asparagus, 15 mg) of enzyme-digested insoluble dietary fiber were mixed with 7.5 mL of acetyl bromide reagent (acetyl bromide/glacial acetic acid, 20/80, v/v), and the mixture was stirred at 50 °C for 3 h. The solvent was removed by rotary evaporation, and 7.5 mL of acidic reduction solvent (dioxane/glacial acetic acid/water, 5/4/1, v/v/v) and about 50 mg of zinc dust were added. The mixture was stirred at room temperature for 40 min. This mixture, 10 mL of dichloromethane, and 10 mL of saturated NH_4Cl were transferred into a separatory funnel, and the internal standards (deuterium-labeled *p*-hydroxycinnamyl alcohol diacetates) were added. The amounts of added standard compounds depend on the dilution after sample cleanup (final internal standard concentration, 30 μM). The organic layer was separated, and extraction of the aqueous phase with 10 mL of dichloromethane was repeated twice. The combined organic layers were washed twice with 10 mL of saturated NH_4Cl and dried over $MgSO_4$. The mixture was filtered through filter paper (4−12 μm), and the solvent was evaporated.

For the acetylation step, 1.5 mL of dichloromethane, 200 μL of pyridine, and 200 μL of acetic anhydride were added to the residue. The mixture was stirred overnight, and the solvents were removed under reduced pressure (coevaporation with ethanol, 3×).

Sample Cleanup. The residue, which was obtained from the DFRC method, was dissolved in 1 mL of MeOH (ultrasonic bath). The mixture was centrifuged (3 min at 13 000 rpm), and the supernatant was removed and evaporated. The residue after evaporation was dissolved in 1 mL of MeOH/H_2O (40/60, v/v). Sample cleanup was carried out using polymeric reversed phase SPE tubes (conditioning with 3 mL of each MeOH and H_2O, application of the sample, washing with 3 mL of each H_2O and MeOH/H_2O (20/80, v/v), elution with 9 mL of MeOH), and the solvent was removed under reduced pressure.

DOI: 10.1021/jf506221p
J. Agric. Food Chem. 2015, 63, 2668−2673

Table 1. GC-MS Fragmentation Patterns of Diacetylated *p*-Coumaryl (HDiAc), Coniferyl (GDiAc), and Sinapyl (SDiAc) Alcohols and Their Hexadeuterated Compounds (d_6)[a]

compound	*m/z* (rel. intensity)
HDiAc	133 (100),[d] 149 (94), 192 (86),[c] 131 (65) 150 (65), 121 (53), 132 (45), 107 (41),[e] 134 (40), 105 (38), 103 (37), 234 (17),[b] 104 (15), 115 (15), 193 (12), 108 (7), 122 (6), 119 (6), 151 (5), 135 (5), 102 (5), 175 (5), 176(5)
HDiAc-d_6	150 (100), 134 (93),[d] 196 (80),[c] 132 (58), 122 (52), 133 (45), 152 (43), 135 (37), 106 (33), 104 (25), 109 (25), 103 (17), 240 (16),[b] 151 (13), 197 (12), 131 (11), 115 (11), 108 (10),[e] 105 (8), 123 (7), 116 (6), 102 (5), 120 (5), 149 (3)
GDiAc	222 (100),[c] 131 (77), 179 (51), 119 (37), 103 (36), 124 (26), 180 (25), 151 (24), 164 (20), 163 (19),[d] 147 (17), 162 (17), 137 (16),[e] 223 (13), 132 (11), 152 (10), 102 (8), 120 (8), 130 (8), 149 (7), 133 (7), 105 (7), 264 (7),[b] 104 (6), 148 (5), 115 (5)
GDiAc-d_6	226 (100),[c] 131 (76), 180 (61), 103 (33), 119 (29), 152 (27), 164 (21),[d] 165 (17), 148 (16), 182 (15), 126 (15), 227 (15), 120 (13), 139 (12), 163 (11), 181 (9), 270 (8),[b] 102 (8), 104 (8), 130 (8), 162 (7), 150 (7), 154 (7), 125 (7), 147 (6), 134 (5), 133 (5), 138 (4)[e]
SDiAc	252 (100),[c] 161 (35), 149 (30), 209 (28), 210 (18), 133 (17), 105 (17), 253 (14), 194 (14), 154 (13), 181 (13), 193 (13),[d] 131 (10), 121 (10), 162 (9), 103 (9), 177 (8), 182 (8), 192 (8), 167 (8), 118 (8), 106 (7), 119 (6), 115 (6), 147 (5), 135 (5), 179 (5), 132 (5), 134 (5), 107 (5), 294 (4),[b] 167 (1)[e]
SDiAc-d_6	256 (100),[c] 161 (32), 210 (31), 149 (27), 133 (15), 105 (15), 195 (15), 257 (15), 194 (13),[d] 182 (12), 212 (12), 162 (9), 131 (9), 103 (9), 121 (8), 156 (8), 150 (7), 118 (6), 193 (6), 115 (6), 184 (6), 132 (6), 119 (5), 106 (5), 211 (5), 178 (5), 164 (5), 300 (3),[b] 168 (3)[e]

[a]Only relative intensities ≥ 3% are shown. The *m/z* values chosen for selected-ion monitoring mode are underlined. [b]Molecular ion. [c]Fragment resulting from ketene loss from the molecular ion. [d]Fragment resulting from McLafferty rearrangement after ketene loss. [e]Benzylic cation fragment.

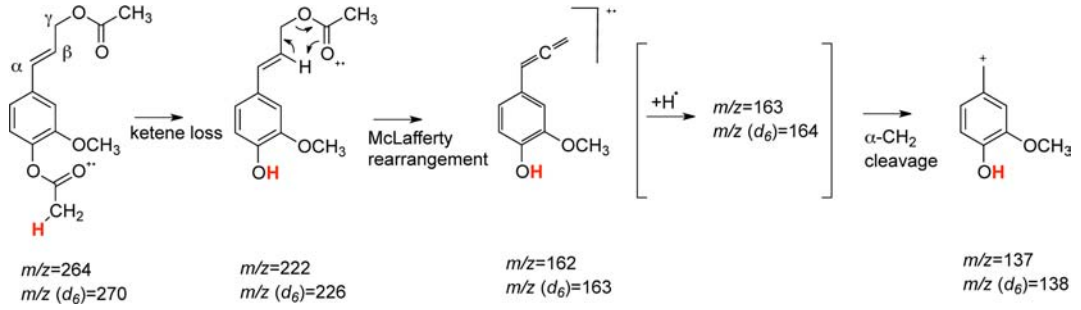

Figure 1. Characteristic fragmentations (EI-MS) of diacetylated coniferyl alcohol. *m/z* values of the products from the nondeuterated and the hexadeuterated (identified by the -d_6 descriptor in the figure) compounds resulting from ketene loss, McLafferty rearrangement, and α-CH_2 cleavage are indicated. Fragmentation reactions of diacetylated *p*-coumaryl and sinapyl alcohols are analogous.

GC-MS and GC-FID Analysis. DFRC monomers were separated and quantitated by GC-MS (EI) using He (1 mL/min) as carrier gas. GC conditions were as follows: initial column temperature 160 °C, ramped at 10 °C/min to 230 °C, ramped at 5 °C/min to 240 °C, ramped at 20 °C/min to 260 °C, ramped at 10 °C/min to 300 °C and held for 10 min; injector temperature 250 °C; split ratio 1/30. MS conditions were as follows: ion source temperature 220 °C, interface temperature 275 °C. Quantification was carried out in the selected-ion monitoring (SIM) mode using ions with the following *m/z*: *m/z* = 192/196 for *p*-coumaryl alcohol diacetate/*p*-coumaryl alcohol diacetate-d_6; *m/z* = 222/226 for coniferyl alcohol diacetate/coniferyl alcohol diacetate-d_6; *m/z* = 252/256 for sinapyl alcohol diacetate/sinapyl alcohol diacetate-d_6. Mass spectrometric detection was carried out only near the retention times of the compounds to avoid unnecessary contamination of the MS system.

GC-FID was used for analyzing low-lignin samples using the original DFRC protocol.[9] GC-FID conditions were as follows: He (1 mL/min) as carrier gas, injector temperature 220 °C, split ratio 1/10, detector temperature 310 °C. GC conditions: initial column temperature 160 °C, ramped at 5 °C/min to 210 °C, ramped at 2 °C/min to 280 °C, ramped at 10 °C/min to 310 °C, and held for 10 min.

Method Validation. Calibration curves were obtained from standard solutions (5−95 μM of the diacetylated hydroxycinnamyl alcohols) in MeOH. The deuterium-labeled internal standard compounds were added to the standard solutions (final concentration of the deuterium-labeled compounds, 30 μM). All solutions were measured in triplicate. The following validation parameters were tested: homogeneity of variances, detection limit (here signal-to-noise ratio of 5:1−10:1; see also Results and Discussion), quantification limit (here lowest calibration point used; see also Results and Discussion), linearity (residual plots, correlation coefficient). The recovery was estimated by comparing the peak area of ions from the hexadeuterated internal standard compounds obtained during sample application to the average peak area obtained from direct injection of the hexadeuterated internal standard compounds (concentration 30 μM) in the GC-SIM-MS sytem.

RESULTS AND DISCUSSION

GC-MS Fragmentation of Standard Compounds. GC-FID is routinely used to determine the ratios of diacetylated DFRC products. However, due to high levels of coeluting matrix compounds, peak identification and integration is often problematic, especially for low-lignin samples. GC-MS analysis in the SIM mode offers both higher selectivity and higher sensitivity. Ideally GC-SIM-MS is combined with using stable-isotope-labeled standard compounds. Here, by acetylation of the *p*-hydroxycinnamyl alcohols using perdeuterated acetic anhydride, six deuterium labels were incorporated into each of the three *p*-hydroxycinnamyl alcohol diacetates. A prerequisite for using the deuterium-labeled diacetates as internal standards is the occurrence of at least one main fragment that is different from the nonlabeled diacetates and thus can be used for quantification. Table 1 summarizes the EI-MS fragmentation patterns (70 eV) of the synthesized compounds. Generally, phenolic acetates lose ketene, which has also been described for lignin dimers.[15] During the loss of ketene one proton of the phenolic acetyl group remains with the parental molecule (Figure 1, using the example of diacetylated coniferyl alcohol). This explains the difference of four mass units between the ketene loss fragment of the nonlabeled (e.g., *m/z* = 222 for diacetylated coniferyl alcohol) and the corresponding hexadeuterated compounds (e.g., *m/z* = 226 for the deuterated

DOI: 10.1021/jf506221p
J. Agric. Food Chem. 2015, 63, 2668−2673

diacetylated coniferyl alcohol). The loss of m/z = 60 can be explained by a McLafferty rearrangement leading to cleavage of γ-acetates. Also, cleavage of α-CH_2 structures, leading to their corresponding benzylic cations, can be observed. In general, the fragments are comparable to those described in the literature,[10] but the intensities are different from literature data.

For coniferyl alcohol diacetate/coniferyl alcohol diacetate-d_6 (GDiAc/GDiAc-d_6) and sinapyl alcohol diacetate/sinapyl alcohol diacetate-d_6 (SDiAc/SDiAc-d_6) the base peak was chosen for GC-SIM-MS quantification. This was not possible for *p*-coumaryl alcohol diacetate (HDiAc) because the base peak of *p*-coumaryl alcohol diacetate-d_6 (HDiAc-d_6) occurs in the spectrum of the nondeuterated compound and vice versa. Thus, m/z = 192 and 196 were chosen to quantitate HDiAc and HDiAc-d_6, respectively. Figure 2 shows the GC-SIM-MS chromatogram of the synthesized standard compounds and their corresponding labeled compounds.

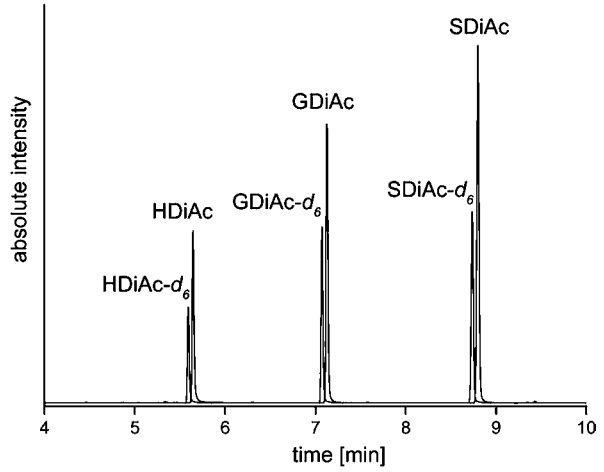

Figure 2. GC-MS chromatogram of the analysis of a standard mixture containing diacetylated *p*-coumaryl (HDiAc), coniferyl (GDiAc), and sinapyl (SDiAc) alcohols and their corresponding labeled compounds (d_6). Detection was carried out in selected-ion monitoring mode with m/z = 192/196 for HDiAc/HDiAc-d_6, m/z = 222/226 for GDiAc/GDiAc-d_6, and m/z = 252/256 for SDiAc/SDiAc-d_6.

Method Validation. The calibration curves of the three standard compounds were repeatedly analyzed in a range of 5−95 μM. Standard deviations of repeated injections were partially ≥20% depending on the concentration and/or day, suggesting less stable fragmentation. By using the corresponding deuterium-labeled compounds as internal standards to calculate the calibration curves, the standard deviations were more acceptable (0.1−2.0%). Thus, regression lines were obtained by plotting the area of analyte/area of internal standard [30 μM, see below] on the *y*-axis vs analyte concentration on the *x*-axis. The fact that less reproducible fragmentation can be corrected for by using the deuterated compounds as internal standards demonstrates the importance of internal standards that are structurally similar to the diacetylated DFRC products. For all calibration points an internal standard concentration of 30 μM was used, roughly representing the middle of the concentration range tested. The use of a fixed internal standard concentration implies a disadvantage that is, however, minor compared to the advantages of the method: The ready-to-analyze sample solutions need to contain the defined concentration of internal standards (30 μM). If absolutely no information about the lignin amount/composition of the sample is known or assessable, a preceding analysis of the sample material has to be performed. This additional performance is necessary to determine if and which final dilution is necessary to get the sample solution into the calibrated concentration range. Then, the concentration of the internal standard compounds added during sample preparation has to be adapted to this dilution.

Visual evaluation of the standard curves of the three acetylated monomers revealed that higher order polynomial regression may fit the data better than a linear regression. Therefore, a polynomial regression (second order) was used and confirmed by the correlation coefficient and residual analysis. Because homogeneity of variances at the highest and lowest concentration was not given, a weighted regression (with reduced chi^2, weighting factor 1/standard deviation^2) was used. The standard deviation of each calibration point was between 0.1% and 2.0% applying the parameters used. The most important validation parameters are shown in Table 2.

Table 2. Validation Parameters for the Calibration of *p*-Coumaryl Alcohol Diacetate (HDiAc), Coniferyl Alcohol Diacetate (GDiAc), and Sinapyl Alcohol Diacetate (SDiAc)[a]

	calibration equation (polynomial model)	correlation coefficient	LOD[b] [μM]	LOQ [μM]	recovery[c] (%)
HDiAc	$y = 0.00654 + 0.04094x + (8.59968 \times 10^{-5})x^2$	1.0000	0.007	5	99−142
GDiAc	$y = 0.00225 + 0.03314x + (1.2895 \times 10^{-4})x^2$	1.0000	0.001	5	68−185
SDiAc	$y = -0.00984 + 0.03872x + (1.553252 \times 10^{-4})x^2$	0.9997	0.05	5	77−179

[a]The corresponding deuterium-labeled compounds (final concentration: 30 μM) were used to correct for less stable fragmentation. The tested range was 5−95 μM for all three compounds. LOD, limit of detection; LOQ, limit of quantification. [b]Rough estimate due to less stable fragmentation (see text). [c]Estimated from the recovered area of the internal standard compounds added during sample preparation (see text).

Due to the less stable fragmentation of the analytes, the limits of detection and quantification (LOD, LOQ) determined via the signal-to-noise ratio are rather rough estimates than definite values. Also, due to the less stable fragmentation it was not possible to define exact concentrations with signal-to-noise ratios of 3:1 (LOD) or 9:1 (LOQ). Therefore, the LOD was defined by injecting standard solutions with decreasing concentrations in triplicate until a signal-to-noise ratio of about 5:1−10:1 was found in all three replicates. The limit of quantification was set as the lowest calibration point due to the mentioned problems in determining this validation parameter.

To test day-to-day reproducibility, the standard solutions were reinjected after 8 days and regression lines were compared. The calibration equations were similar, suggesting that the method was robust if performed as described. Also, the standard solutions were freshly prepared and analyzed. In this case, the regression lines vary in an acceptable way due to minor variations during solution preparation. These data suggest that a complete calibration with each sample set is not necessary. Instead, it is recommended to double check the regression lines by three calibration points before analysis of each sample set.

DOI: 10.1021/jf506221p
J. Agric. Food Chem. 2015, 63, 2668−2673

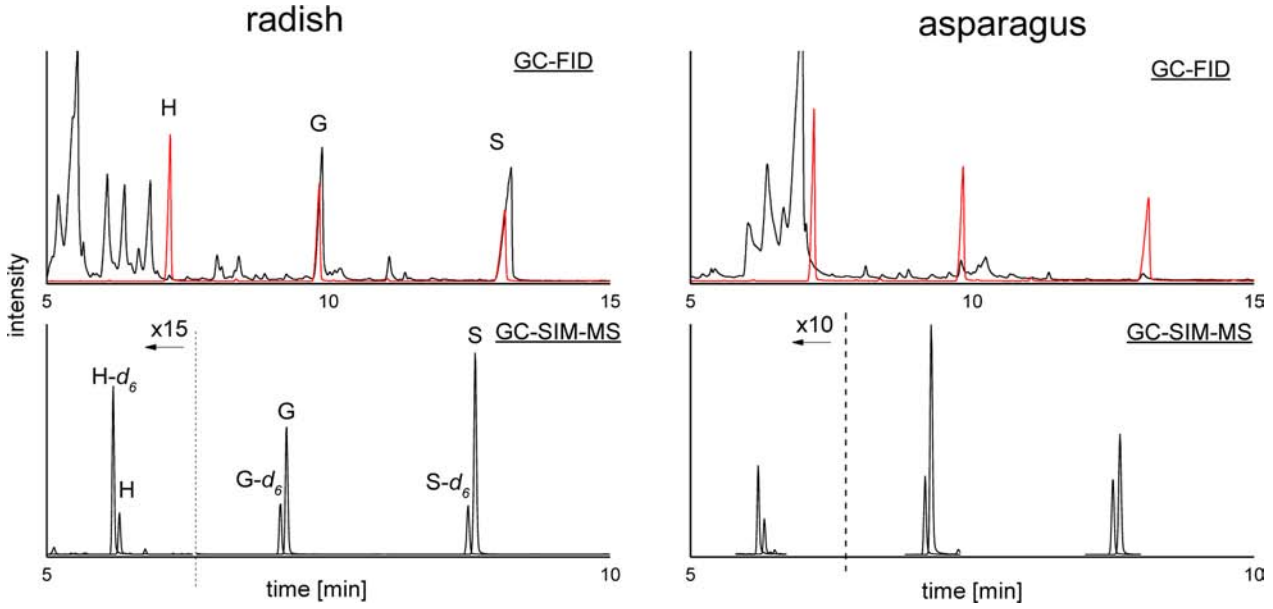

Figure 3. Comparison of chromatograms from derivatization followed by reductive cleavage (DFRC) products from radish (left) and asparagus (right). GC-FID chromatograms were obtained without modified sample cleanup. Colored lines represent the overlaid chromatograms of the standard compounds. GC-SIM-(selected-ion monitoring)-MS chromatograms were obtained by using the modified method. Peaks representing *p*-coumaryl alcohol diacetate and deuterated *p*-coumaryl alcohol diacetate are enlarged 15- (radish) and 10-fold (asparagus). HDiAc, *p*-hydroxyphenyl unit; G, guaiacyl unit; S, syringyl unit; d_6, hexadeuterated internal standard compounds.

Recoveries were estimated by using the analyzed areas of the internal standard compounds added before extraction of the liberated monomers during application of the method to low-lignin[11] samples (pear, radish, carrot, and asparagus, see below). Recovery rates were calculated by comparing these areas to the average areas of the deuterated internal standards obtained from direct injection of the internal standard solution (30 μM). It has to be kept in mind that the recovery rates determined here are only rough estimates due to one-point calibration without correcting this data point for fragmentation instabilities. The recovery rates were between 99% and 142% for HDiAc-d_6, 68−185% for GDiAc-d_6, and 77−179% for SDiAc-d_6. As described above, the standard deviations of repeated analyses of a single calibration point without adjustment for fragmentation instabilities using an internal standard are often ≥20% and can be up to 40%. However, despite large variations of the recovery rates due to noncorrected fragmentation instabilities, the average values demonstrate that major quantities of the liberated DFRC products are indeed analyzed after sample preparation and cleanup (see below). Furthermore, the MS fragmentation and detection does not seem to be suppressed significantly by matrix effects. In addition, the calculation of the actual monomer amount is not as important as the determination of the monolignol ratios. Because the DFRC method only cleaves β-O-4 linkages, the calculated ratios represent the monomers that are involved in these units. Because the β-O-4 linkages usually represent > 50% and up to 80% of the linkages in the lignin polymer the obtained ratios reflect well the composition of the lignin polymer. This has also been demonstrated by comparison of the G/S ratios of lignins from plant-based foods determined by the DFRC method with the G/S ratios of isolated lignins analyzed by 2D-NMR.[16]

Sample Cleanup. Sample cleanup is adapted to low-lignin samples to reduce the high matrix-derived content that can contaminate the GC-MS system. The original protocol describes a dissolution of the sample in dichloromethane after the acetylation step and before GC-MS analysis.[9] Dichloromethane dissolves the entire residue, i.e., DFRC products and (acetylated) matrix-derived components. Because the acetylated DFRC products are soluble in MeOH this solvent was chosen instead of dichloromethane to dissolve the DFRC residue after acetylation. Using MeOH leaves, conveniently, a large amount of matrix-derived components undissolved. Additionally, an SPE step was established for further cleanup. A polymeric reversed phase, which provides strong retention of aromatic compounds due to $\pi-\pi$ bonding interactions next to hydrogen bonding, was chosen as the stationary phase. The loading solution was MeOH/water (40/60, v/v), which was tested to completely dissolve the standard compounds. SPE conditions were tested by using a mixture of all standard compounds. The solution was loaded onto the column, which was washed and eluted in several steps using different volumes of H_2O and MeOH mixtures in different ratios. All eluates were collected separately and analyzed for DFRC products.

The results showed that loading in MeOH/H_2O (40/60, v/v) and washing with H_2O and MeOH/H_2O (20/80, v/v) result in a loss of about 1% of the standard compounds. Also, the recovery rates of the internal standard compounds (68−185% depending on the determined monomer) as determined during application of the sample cleanup on different plant-based food samples reveal applicability of the chosen conditions for complex, high-matrix samples.

Application. The developed method was applied to fibers from four plant-based food samples: pear, radish, carrot, and asparagus. The enzymatic digestion of the extracted fibers by using an enzyme mixture capable of digesting cell wall polysaccharides is recommended because it reduces the sample matrix load, which contaminates the MS system. Figure 3 shows the chromatograms of radish and asparagus DFRC products measured by GC-FID (original DFRC protocol[9]) or GC-SIM-MS (modified sample cleanup). The GC-FID

DOI: 10.1021/jf506221p
J. Agric. Food Chem. 2015, 63, 2668−2673

chromatogram reveals the existence of a large amount of matrix from low-lignified samples, complicating the identification and/or quantification of the acetylated DFRC products. Using the newly developed GC-SIM-MS method these problems are minimized.

The results from the application of the DFRC method to food samples are summarized in Table 3. To characterize the lignin composition H:G:S proportions and G/S ratios were calculated. The insoluble dietary fiber lignin of carrots shows a high G/S ratio (ca. 38) and can be classified as a G-rich lignin. In contrast, lignins from pear, radish, and asparagus are characterized by balanced G/S ratios. These values are generally comparable to literature data.[11] Smaller differences can be explained by different maturation stages of the used samples and methodological differences. Furthermore, by using the GC-SIM-MS method, H units were detected in quantifiable amounts in all samples analyzed. In comparison to G and S units, the amounts were low, with the exception of carrot lignin with an H/S ratio of 0.87. Bunzel et al.[11] could detect quantifiable amounts of H units from lignins of radish only. Although differences in the plant materials are possible, the detection of minor amounts of H units in this study is most likely due to the increased selectivity and sensitivity of the newly developed stable-isotope dilution GC-MS approach.

Table 3. Monolignol Composition of Fibers from Pear, Radish, Carrot, and Asparagus Determined by the Derivatization Followed by Reductive Cleavage (DFRC) Method with Modified Sample Cleanup and GC-Selected-Ion Monitoring (SIM)-MS Analysis[a]

	H:G:S [mol %]	ratio G/S	ratio G/S from literature[11]
pear	0.18:53.28:46.54	1.15 (±0.03)	0.6 (±0.04)
radish	1.29:44.75:53.96	0.80 (±0.14)	1.5 (±0.18)
carrot	2.32:94.97:2.71	35.24 (±2.45)	38.8 (±6.11)
asparagus	0.85:67.04:32.11	2.10 (±0.17)	3.3 (±0.28)

[a]Ratios of H (*p*-hydroxyphenyl unit), G (guaiacyl unit), and S (syringyl unit) were determined as percentages on a molar basis. G/S ratios are calculated on molar basis too. Each sample was measured in duplicate. Uncertainties of measurement are indicated in brackets as range/2. For quantification, the hexadeuterated internal standards were used at a concentration of 30 μM.

AUTHOR INFORMATION

Corresponding Author

*Tel.: +4972160842936. E-mail: mirko.bunzel@kit.edu.

Funding

This work was funded by a fellowship from the Carl-Zeiss Foundation.

Notes

The authors declare no competing financial interest.

ABREVIATIONS USED

BER, borohydride exchange resin; DFRC, derivatization followed by reductive cleavage; DIBAL-H, diisobutylaluminum hydride; H, *p*-hydroxyphenyl unit; HDiAc, *p*-coumaryl alcohol diacetate; G, guaiacyl unit; GDiAc, coniferyl alcohol diacetate; LOD, limit of detection; LOQ, limit of quantification; MeOH, methanol; S, syringyl unit; SDiAc, sinapyl alcohol diacetate; SIM, selected ion monitoring; SPE, solid-phase extraction

REFERENCES

(1) Ralph, J.; Lundquist, K.; Brunow, G.; Lu, F.; Kim, H.; Schatz, P. F.; Marita, J. M.; Hatfield, R. D.; Ralph, S. A.; Christensen, J. H.; Boerjan, W. Lignins: natural polymers from oxidative coupling of 4-hydroxyphenylpropanoids. *Phytochem. Rev.* **2004**, *3*, 29−60.

(2) Boerjan, W.; Ralph, J.; Baucher, M. Lignin biosynthesis. *Annu. Rev. Plant Biol.* **2003**, *54*, 519−546.

(3) Baucher, M.; Monties, B.; Van, M. M.; Boerjan, W. Biosynthesis and genetic engineering of lignin. *Crit. Rev. Plant Sci.* **1998**, *17*, 125−197.

(4) Slavin, J. Fiber and prebiotics: mechanisms and health benefits. *Nutrients* **2013**, *5*, 1417−1435.

(5) Funk, C.; Weber, P.; Thilker, J.; Grabber, J. H.; Steinhart, H.; Bunzel, M. Influence of lignification and feruloylation of maize cell walls on the adsorption of heterocyclic aromatic amines. *J. Agric. Food Chem.* **2006**, *54*, 1860−1867.

(6) Funk, C.; Braune, A.; Grabber, J. H.; Steinhart, H.; Bunzel, M. Model studies of lignified fiber fermentation by human fecal microbiota and its impact on heterocyclic aromatic amine adsorption. *Mutat. Res.* **2007**, *624*, 41−48.

(7) Harris, P. J.; Triggs, C. M.; Roberton, A. M.; Watson, M. E.; Ferguson, L. R. The adsorption of heterocyclic aromatic amines by model dietary fibers with contrasting compositions. *Chem.-Biol. Interact.* **1996**, *100*, 13−25.

(8) Lapierre, C.; Monties, B.; Rolando, C. Thioacidolysis of lignin - comparison with acidolysis. *J. Wood Chem. Technol.* **1985**, *5*, 277−292.

(9) Lu, F.; Ralph, J. Derivatization followed by reductive cleavage (DFRC method), a new method for lignin analysis: protocol for analysis of DFRC monomers. *J. Agric. Food Chem.* **1997**, *45*, 2590−2592.

(10) Lu, F.; Ralph, J. DFRC method for lignin analysis. 1. New method for β-aryl ether cleavage: lignin model studies. *J. Agric. Food Chem.* **1997**, *45*, 4655−4660.

(11) Bunzel, M.; Seiler, A.; Steinhart, H. Characterization of dietary fiber lignins from fruits and vegetables using the DFRC method. *J. Agric. Food Chem.* **2005**, *53*, 9553−9559.

(12) Ralph, S. A.; Ralph, J.; Landucci, L. L. NMR database of lignin and cell wall model compounds. http://ars.usda.gov/Services/docs.htm?docid=10491, 2004.

(13) Kim, H.; Ralph, J. Simplified preparation of coniferyl and sinapyl alcohols. *J. Agric. Food Chem.* **2005**, *53*, 3693−3695.

(14) Quideau, S.; Ralph, J. Facile large-scale synthesis of coniferyl, sinapyl, and *p*-coumaryl alcohol. *J. Agric. Food Chem.* **1992**, *40*, 1108−1110.

(15) Peng, J.; Lu, F.; Ralph, J. The DFRC method for lignin analysis. Part 4. Lignin dimers isolated from DFRC-degraded loblolly pine wood. *J. Agric. Food Chem.* **1998**, *46*, 553−560.

(16) Bunzel, M.; Ralph, J. NMR characterization of lignins isolated from fruit and vegetable insoluble dietary fiber. *J. Agric. Food Chem.* **2006**, *54*, 8352−8361.

DOI: 10.1021/jf506221p
J. Agric. Food Chem. 2015, 63, 2668−2673

example, the following (peak area) percentages have been reported: sabinene (42−63%), α-phellandrene (37−63%), linalool (30−68%), and β-pinene (35−78%).[9−12] On the other hand, at least four terpenes have been reported with consistently predominate (+)-enantiomers, viz., α-pinene (60−90%), terpinen-4-ol (65−70%), α-terpineol (70−78%), and limonene (58−62%).[9−13] No clear standard has been developed primarily due to the limited number of investigations and samples. The measurement of chiral ratios of TTO components is demanding and often requires the use of multidimensional GC or NMR with lanthanide shift reagents. These techniques are labor intensive and require extensive operator expertise.

Chemometrics has increasingly found applications in quality control of natural products. It can be used to extract chemically relevant information out of large quantities of chemical data to provide a better way to represent and display the information as well as a better understanding of the chemical system. Two chemometric approaches are usually applied: the targeted approach selectively analyzes a subset of compounds, while the nontargeted approach provides a holistic analysis of the entire chemical data set. Chemometrics has been used extensively[14−18] for the analysis of infrared and mass spectra of essential oils. However, this data analysis tool has not been used to validate TTOs or commercial products based on GC/MS data with conventional or chiral columns.

The inherent complexity and variability within plants and essential oils pose challenges in the identification and quantification of specific chemical compounds as quality control parameters. The need exists for the development of chemical analysis techniques and data analysis tools that can profile the whole chemical system including those components present at very low concentration levels. As part of an ongoing research program on authentication, safety, and quality control of phytochemicals, the present investigation was carried out employing the aforementioned conventional and chiral GC/MS systems combined with chemometric analyses to assess the quality of tea tree oils and commercial products. The study involved a large number (n = 104) of samples divided into two categories, viz., known provenance essential oils and commercial products of unknown provenance. Thus, an independent norm from the chiral analysis for a given set of samples could be established for comparison purposes. The objectives of the current investigation were to employ the three previously discussed techniques in the investigation of an extensive set of TTOs and commercial products. This holistic approach will be used to identify TTO and commercial samples that do not represent the common terpinen-4-ol type of tea tree oil.

MATERIALS AND METHODS

Sample Information. Fifty-seven known provenance tea tree oil samples (A1−14, A17−40, A48−64, A84, and A90) were obtained by steam distillation of *Melaleuca alternifolia*. Oils A15 and 16 were obtained from the steam distillation of *M. linariifolia* and *M. dissitiflora*, respectively. Forty-three commercial samples that claimed to be tea tree oil samples (A41−44, A46, A47, A65−83, A85−89, A92, and A100−110) were purchased from various foreign sources. The provenance of these samples was unknown. Sample A45 was sold as synthetic tea tree oil, and A99 was sold as synthetic terpinen-4-ol. All TTOs and commercial products were collected by the Australian Tea Tree Industry Association (ATTIA, Casino NSW, Australia). Specimens of all samples are deposited at the botanical repository of the National Center for Natural Products Research (NCNPR), University of Mississippi.

Reagents and Standards. GC-grade n-hexane and the reference standards α-thujene (**1**), α-pinene (**2**), β-pinene (**4**), myrcene (**5**), α-phellandrene (**6**), α-terpinene (**7**), p-cymene (**8**), limonene (**10**), γ-terpinene (**11**), terpinolene (**12**), and terpinen-4-ol (**13**) (listed in Table 1 and Figure S1, Supporting Information) were purchased from Sigma-Aldrich. A mixture of a series of n-alkanes (C_9H_{20} to $C_{22}H_{46}$) was used for the determination of the retention indices, and the alkane standards were purchased from PolyScience Corp. The analytical standard n-tridecane ($C_{13}H_{28}$) was selected as the internal standard and obtained from PolyScience Corp. The enantiomeric compounds of α-pinene, limonene, terpinen-4-ol, and α-terpineol were purchased from Sigma-Aldrich.

Table 1. Twenty Most Abundant Compounds in the Tea Tree Oil Sample (A-22) by Conventional GC/MS Analysis

no.	compound	retention index	literature value[17] (methyl silicone column)	% peak area (ISO)
1	α-thujene	925	931	
2	α-pinene	931	939	1−6
3	sabinene	965	972	trace−3.5
4	β-pinene	969	978	
5	myrcene	983	986	
6	α-phellandrene	996	1002	
7	α-terpinene	1009	1016	5−13
8	p-cymene	1011	1016	0.5−8
9	1,8-cineole	1019	1025	trace−15
10	limonene	1021	1025	0.5−1.5
11	γ-terpinene	1052	1056	10−28
12	terpinolene	1083	1081	1.5−5
13	terpinen-4-ol	1172	1175	30−48
14	α-terpineol	1182	1185	1.5−8
15	aromadendrene	1452	1475	trace−3
16	*allo*-aromadendrene	1471		
17	ledene	1503	1484	trace−3
18	δ-cadinene	1526	1524	trace−3
19	globulol	1568		trace−1
20	viridiflorol	1577	1588	trace−1

Sample Preparation. Five microliter samples were diluted in 1 mL of n-hexane. The selected internal standard ($C_{13}H_{28}$) was added to each sample solution at a constant concentration.

Chromatography Instruments and Conditions. *Conventional GC/MS Analyses.* Gas chromatographic analysis was performed on an Agilent 7890 GC instrument equipped with an Agilent 5975C mass-specific detector and an Agilent 7693 autosampler. An Agilent J&W HP-1 fused silica capillary column (60 m × 0.25 mm i.d.) coated with a 0.25 μm film of cross-linked 100% dimethyl-polysiloxane was used with helium as the carrier gas at a constant pressure of 24 psi. In a typical analysis, the oven was held for 2 min at 50 °C and then programmed at 2.0 °C/min to 180 °C. The post run was set at 250 °C for 5 min to clean up the column. The injector temperature was 250 °C. The split ratio was set to 25:1. Duplicate injections were made for each sample.

For the scan measurements, the spectra were recorded at 70 eV from m/z 35 to 450. Compound identification involved comparison of the spectra with the databases (Wiley and NIST) using a probability-based matching algorithm. Further identification was based on the relative retention indices compared with the literature and the reference standards purchased from commercial sources.

Chiral GC/MS Analyses. The same instrument setting used for the conventional GC/MS analysis was applied for the chiral GC/MS analysis. The chiral GC/MS column was an Agilent J&W HP-Chiral-20β (30 m × 0.25 mm, i.d.) coated with a 0.25 μm film of 20% β-cyclodextrin in (35%-phenyl)-methylpolysiloxane. Helium was used as a carrier gas. The flow rate was 1 mL/min for the first 27 min and then programmed at 0.2−3 mL/min for the rest of the experiment. In a typical chiral analysis, the oven was held for 10 min at 50 °C and programmed at 3.0 °C/min to 100 °C, 2.0 °C/min to 140 °C, and then 4.0 °C/min to 180 °C in the last step. The injector temperature was 250 °C. The split ratio

DOI: 10.1021/acs.jafc.5b00147
J. Agric. Food Chem. 2015, 63, 2674−2682

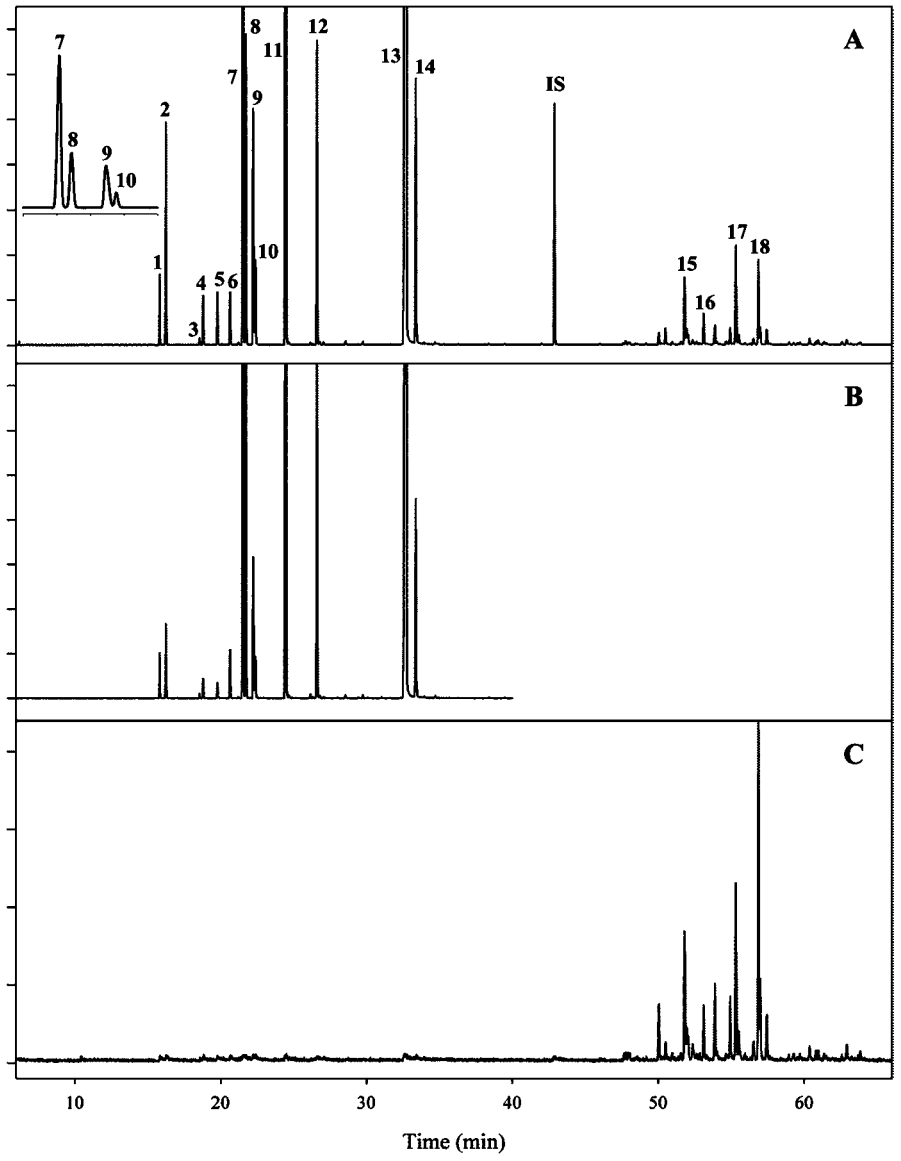

Figure 1. GC/MS chromatograms of sample A-22. (A) Total ion chromatogram (m/z 35−450). (B) Extracted ion chromatogram (m/z 136) for monoterpenes. (C) Extracted ion chromatogram (m/z 204) for sesquiterpenes.

was set to 40:1. Duplicate injections were made for each sample. The mass spectra were recorded at 70 eV from m/z 40 to 550.

Chemometric Analysis. The GC/MS data were acquired by Agilent MSD Productivity ChemStation software (E.02.02). Extraction of the GC/MS data was performed using the NIST Automated Mass Spectral Deconvolution and Identification Software (AMDIS). Ions were extracted as entities characterized by retention time (t_R), peak intensity, and mass to charge ratio (m/z). The ELU file format required for the chemometric analysis was created by AMDIS for each sample and then exported into the Mass Profiler Professional software (MPP, version B.12.05, Agilent Technologies).

A holistic nontargeted approach was used for the preprocessing of GC/MS data using the full spectra which allows for unbiased analysis. The initial stage involved baseline correction, data smoothing, and peak alignment. Various minimum abundance settings and compound quality score filter parameters were examined; 5000 counts and a score of 20 were finally selected for the entities extraction in the entire experiment time window for the minimum absolute abundance and minimum quality score, respectively. Alignment of retention time with a tolerance retention time window of 0.15 min and similarity of spectral pattern was carried out across the entire sample set. The internal standard selected for GC/MS analysis was applied for normalization of the peak intensity to account for the differences in the abundances of each compound. A list of 634 entities obtained from the MPP software was exported to SIMCA (version 12) for chemometric analysis. Principal component analysis (PCA) was performed for a quick overview of the data. A sample class predictive model (PCA-class) based on the TTO samples that met the ISO standards was constructed. The class predictive model was cross-validated and then applied to evaluate the remainder of the samples in the TTO data set.

RESULTS AND DISCUSSION

Typical chromatograms of a TTO sample obtained from GC/MS with a conventional stationary phase (HP-1) and a chiral stationary phase (HP-Chiral-20B) are shown in Figures 1 and 2, respectively. The assignment of the 20 components and their corresponding retention indices in the conventional chromatogram as well as the concentration limits regulated by ISO standards are listed in Table 1. Table S1, Supporting Information, gives the (peak area percentage) analysis results for the 20 compounds listed in Table 1 with the conventional GC stationary phase. Table S2, Supporting Information, gives the results from chiral analyses.

DOI: 10.1021/acs.jafc.5b00147
J. Agric. Food Chem. 2015, 63, 2674−2682

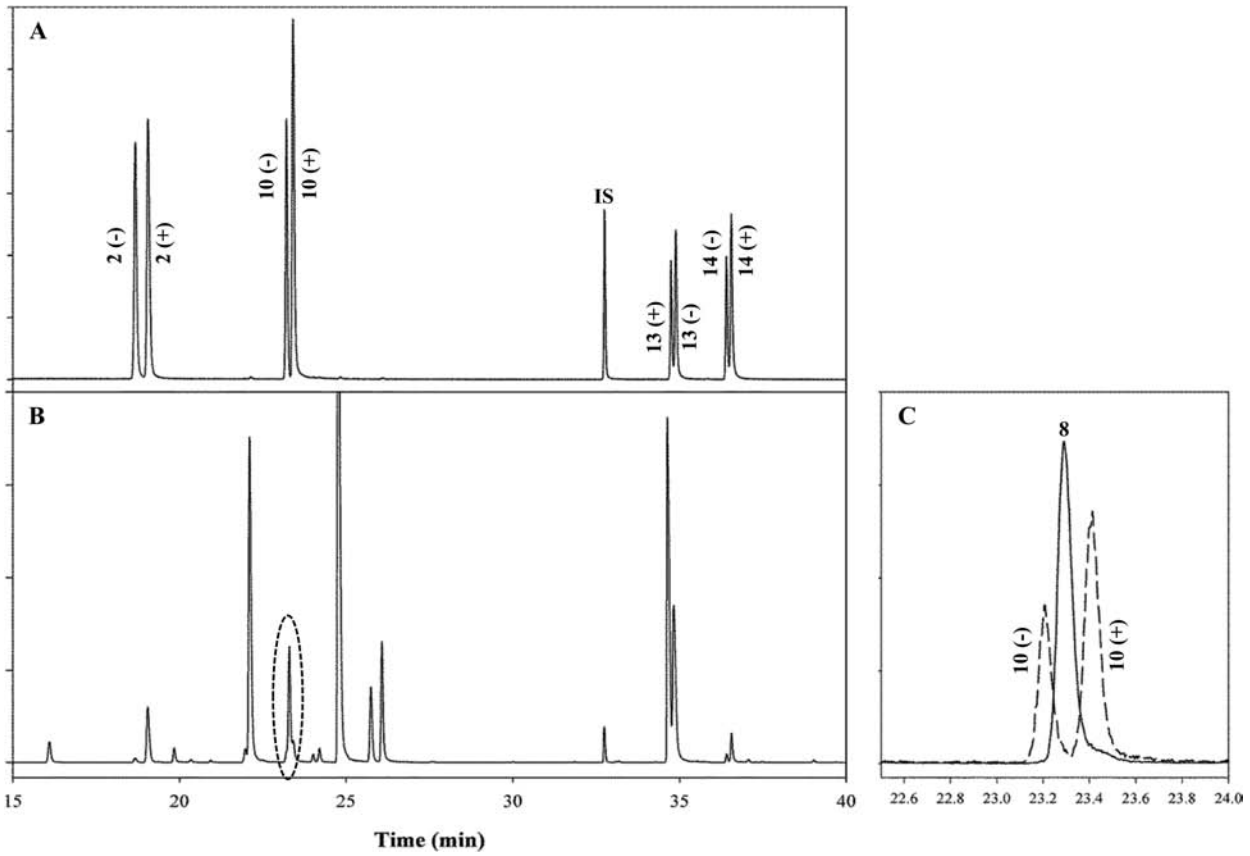

Figure 2. Chromatograms of chiral GC/MS analysis for the major enantiomers in TTOs. (A) Mixture of standards. (B) Sample A-1. (C) Extracted ion chromatograms. Dashed line (EIC at m/z 68) illustrates the detection of (+)/(−) limonene. Solid line (EIC at m/z 134) illustrates the detection of *p*-cymene.

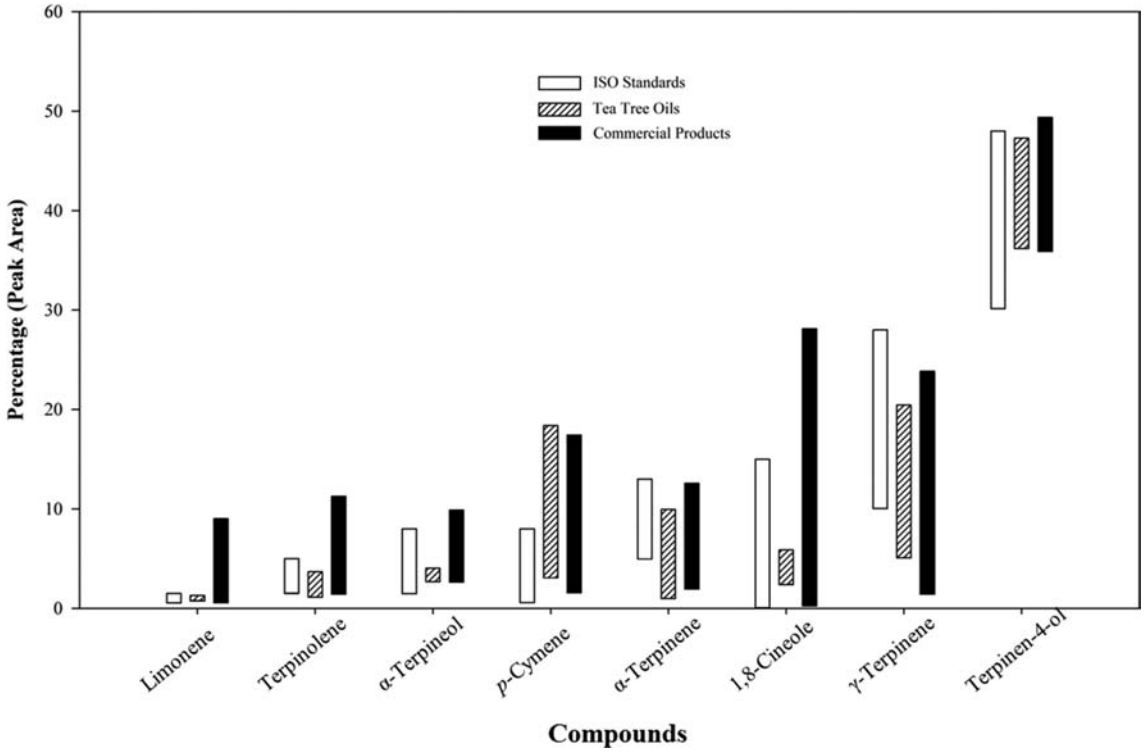

Figure 3. Comparison of upper and lower limits of the major terpenes in tea tree oils, commercial products, and ISO standards. Synthetic samples A45, A99, and the samples of *M. linariifolia* (A15) and *M. dissitiflora* (A16) were not included.

DOI: 10.1021/acs.jafc.5b00147
J. Agric. Food Chem. 2015, 63, 2674−2682

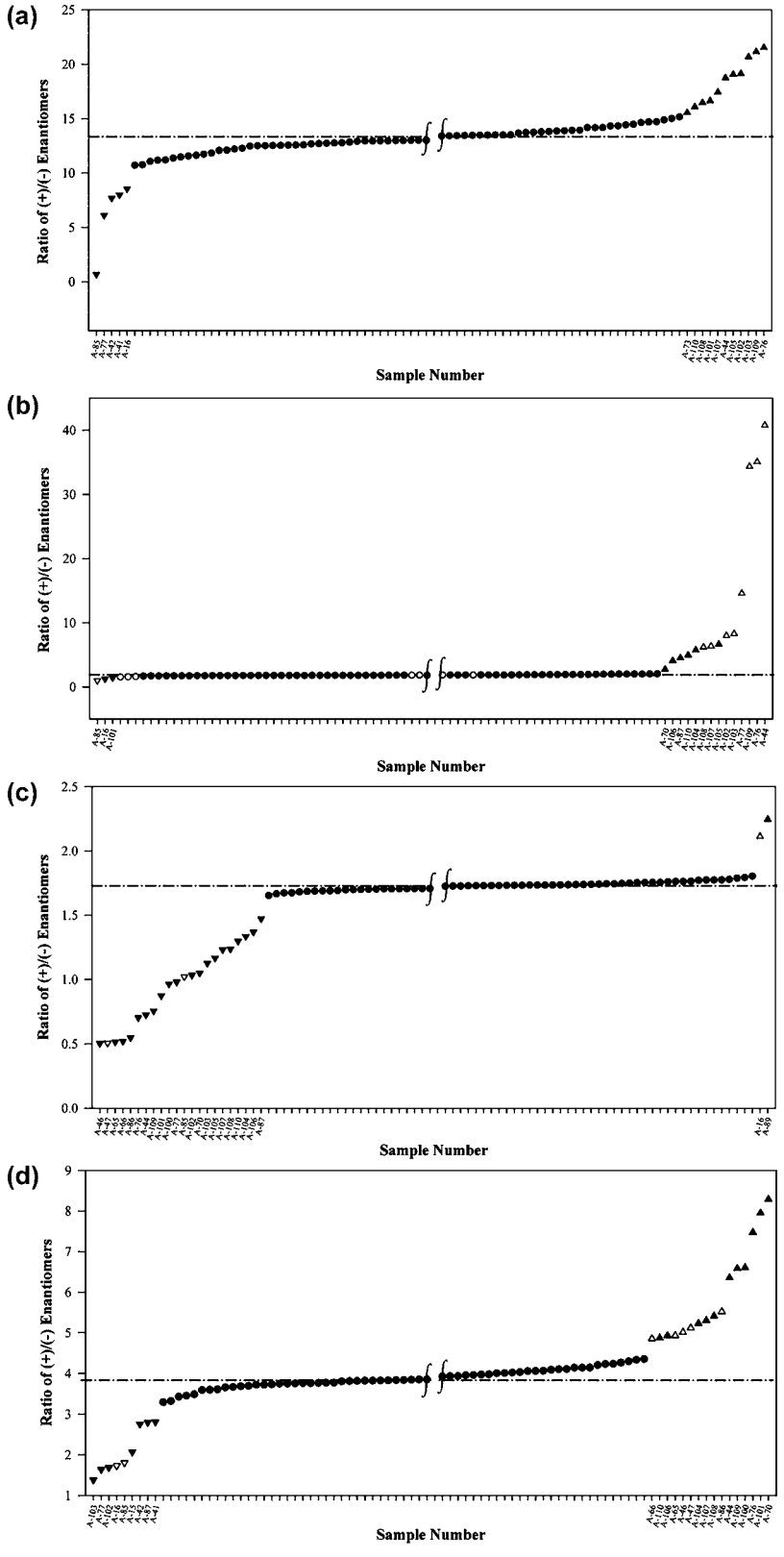

Figure 4. (A) Chiral analysis results for α-pinene. Gap in the data represents the omission of 15 points with the average enantiomeric ratio. Samples that displayed an enantiomeric ratio greater/less than the average of TTOs ± three times the standard deviation (SD) are shown as ▲/▼ in the figure. (B) Chiral analysis results for limonene. Data points shown with open symbols represent samples that did not meet ISO standards. (C) Chiral analysis results for terpinen-4-ol. (D) Chiral analysis results for α-terpineol.

Conventional GC/MS Analyses: Comparison with ISO Standards. *Known Provenance Tea Tree Oil Samples.* Figure 3 shows the concentration ranges of the eight major ISO-specified terpenes and related alcohols and ethers along with the ranges of concentration specified by ISO 4730-2004. The measured concentration ranges for the same components in the

DOI: 10.1021/acs.jafc.5b00147
J. Agric. Food Chem. 2015, 63, 2674−2682

ATTIA TTO samples are also shown in the figure. The compounds that were outside the ISO standards are marked in gray in Table S1, Supporting Information. Fourteen of 57 TTO samples did not meet at least one of the ISO standards, even though all of the oils were ISO compliant when distilled as evidenced by certificates of analysis obtained by ATTIA immediately after distillation. The primary problems were excess *p*-cymene and diminished α- and γ-terpinene as well as terpinolene concentrations. Auto-oxidation was probably responsible for most of the observed deviations.[19] Aside from the four probe solutes involved in the generation of *p*-cymene, all of the TTOs were within ISO standards for the other 10 solutes.

The analytical results for the five sesquiterpenes specified in the ISO standards are included in the tables; however, their concentrations were always less than 3%. Their low concentrations and relatively high variability and uncertainty limited their use as verification probes.

Commercial Samples. In Table S1, Supporting Information, the TTO and commercial samples that did not meet the ISO standards are marked in gray. Samples A45 and A99 were labeled as synthetic TTO and synthetic terpinen-4-ol, respectively. These synthetic samples both contained about 95% terpinen-4-ol along with low concentrations of α- and γ-terpinene and *p*-cymene. Twenty-three other commercial samples did not meet ISO standards. The major problems were an excess of limonene (16 samples), α-terpineol (7 samples), or *p*-cymene (11 samples). A lower number of samples was deficient in α-terpinene (7 samples), γ-terpinene (4 samples), and terpinen-4-ol (3 samples).

On the basis of solely the ISO standards, 49% of the commercial TTO samples were not qualified to be sold as "tea tree oils" on the commercial market. This raises the question whether or not the ISO standards alone are sufficient to positively identify oils and commercial products that actually contain Australian "terpinen-4-ol type" tree oil. The most common secondary test for TTO quality evaluation involves the analysis of chiral components.

Chiral GC/MS Analyses. A complete chiral analysis was carried out for the entire data set for four terpenes with predominately (+)-enantiomer for which standards were available, viz., α-pinene, limonene, terpinen-4-ol, and α-terpineol. The results for all of the chiral solutes are given in Table S2, Supporting Information.

Resolution of limonene enantiomers from *p*-cymene has proven to be a difficult problem in many investigations of the chiral components of TTOs.[10,12,13] *p*-Cymene has been reported to coelute with (+)-limonene[10,12] or (−)-limonene.[13] Two-dimensional GC has been used to overcome this problem.[11,12] In the current study, *p*-cymene (**8**) was found to elute between (−)- and (+)-limonene (**10**) as shown in Figure 2. The mass spectrum for limonene shows a base peak at *m*/*z* 68 (isoprenyl), while the spectrum for *p*-cymene is barren in this mass region. Thus, selected ion monitoring at *m*/*z* 68 was used to differentiate limonene from *p*-cymene (*m*/*z* 134) as shown in the inset (C) of Figure 2.

Known Provenance Tea Tree Oil Samples. The enantiomeric ratios +/− for all of the known provenance essential oil samples were calculated and used as the norm for evaluation of the commercial samples. The tea tree oil samples showed consistent enantiomeric ratios. The averages and standard deviations were 13.0 (±0.8), 1.83 (±0.08), 1.72 (±0.03), and 3.86 (±0.03) for α-pinene, limonene, terpinen-4-ol, and α-terpineol, respectively. The chiral ratios of α-pinene, limonene, terpinen-4-ol, and α-terpineol for all of tea tree oils and commercial products are shown in Figure 4A−D. The lines in the plots are the averages for the enantiomeric ratios of just the known provenance oil samples. Incomplete resolution of enantiomers skewed the results toward the later eluting enantiomer, i.e., the (+)-enantiomer for all compounds except α-terpineol. The effect was especially obvious for the components at the highest concentration and lowest resolution, viz., the alcohols. Better resolution could be obtained with dilute samples or higher split ratio but with an unacceptable loss of sensitivity.

The analyses of a large number of samples allowed the establishment of a characteristic +/− chiral ratio, i.e., the average of the TTO data, without regard to previously published data. Outliers could be identified by their "distance" from the average. Thus, the absolute value of the chiral ratio was less important than the deviation of a sample from the norm of the TTO data set.

Commercial Samples. Except for the synthetic samples, all of the ATTIA samples met the ISO standards (1−6%) for α-pinene. Figure 4A shows the chiral results and outliers for α-pinene. The data are given as the ratio (+/−)-enantiomers rather than percentages because it was easier to identify outliers with ratios rather than percentages. Mosandl[11] reported ratios of 6−10, Southwell reported a ratio of 9.3,[6] and Leach[13] reported a ratio of 9. The average value for α-pinene in Table S2, Supporting Information, was 13.0. Outliers were identified as samples that displayed an enantiomeric ratio greater than the average plus three times the standard deviation (SD). These points are shown as ▲ in the figure. The same criterion was used to determine outliers below the average minus three times the SD (▼). The chiral results did not show a clear plateau. This compound is ubiquitous in many natural products, and the concentration range was low, so this probe solute is not satisfactory for quality control of TTO products.

The chiral results for limonene are illustrated in Figure 4B. The ratio of (+/−)-isomers in TTO has been reported as 1.4−1.6 by Mosandl[11] and 1.7 by Shellie.[12] In the present study, the average value for the limonene data was 1.83 for the 57 TTO samples, all of which met the ISO standards (0.5−1.5%). Four commercial samples, viz., A44, A76, A77, and A109, contained almost exclusively (+)-limonene. Samples A16, A85, and 101 contained a racemic mixture of limonene enantiomers. Ten other samples contained primarily the (+)-isomer but in concentrations higher than the average of all samples. Of the 17 samples that were outliers for the limonene chirality, 9 were also outliers for the ISO standards. The samples that did not meet ISO standards are shown as open data points in the figures.

Terpinen-4-ol or 4-terpineol is a major, characteristic component of TTO (30−48%) and the basis for the so-called terpinen-4-ol type of TTO. Previous literature reports the chiral ratios for terpinen-4-ol in TTO range from 2.17,[2] 1.96,[9] 2.13−2.57,[10] 1.78−2.23,[11] 2.22,[12] and 1.88.[13] The average of the data for terpinen-4-ol in Table S2, Supporting Information, was 1.72. The results are shown in Figure 4C. Only two samples (A16 and A89) displayed an excess of the (+)-enantiomer. However, 22 samples had measured ratios significantly less than the average of the full data set. Because of the broad range of concentration (30−48%) for terpinen-4-ol specified in the ISO document, only three samples (A16, A47, and A85), other than the two synthetic samples, did not meet the ISO standards for terpinen-4-ol.

The two synthetic samples (A45 and A99) both gave measured +/− ratios of ∼0.3 compared to the average of 1.72 for the natural essential oil samples. Thus, a low enantiomeric ratio for

DOI: 10.1021/acs.jafc.5b00147
J. Agric. Food Chem. 2015, 63, 2674−2682

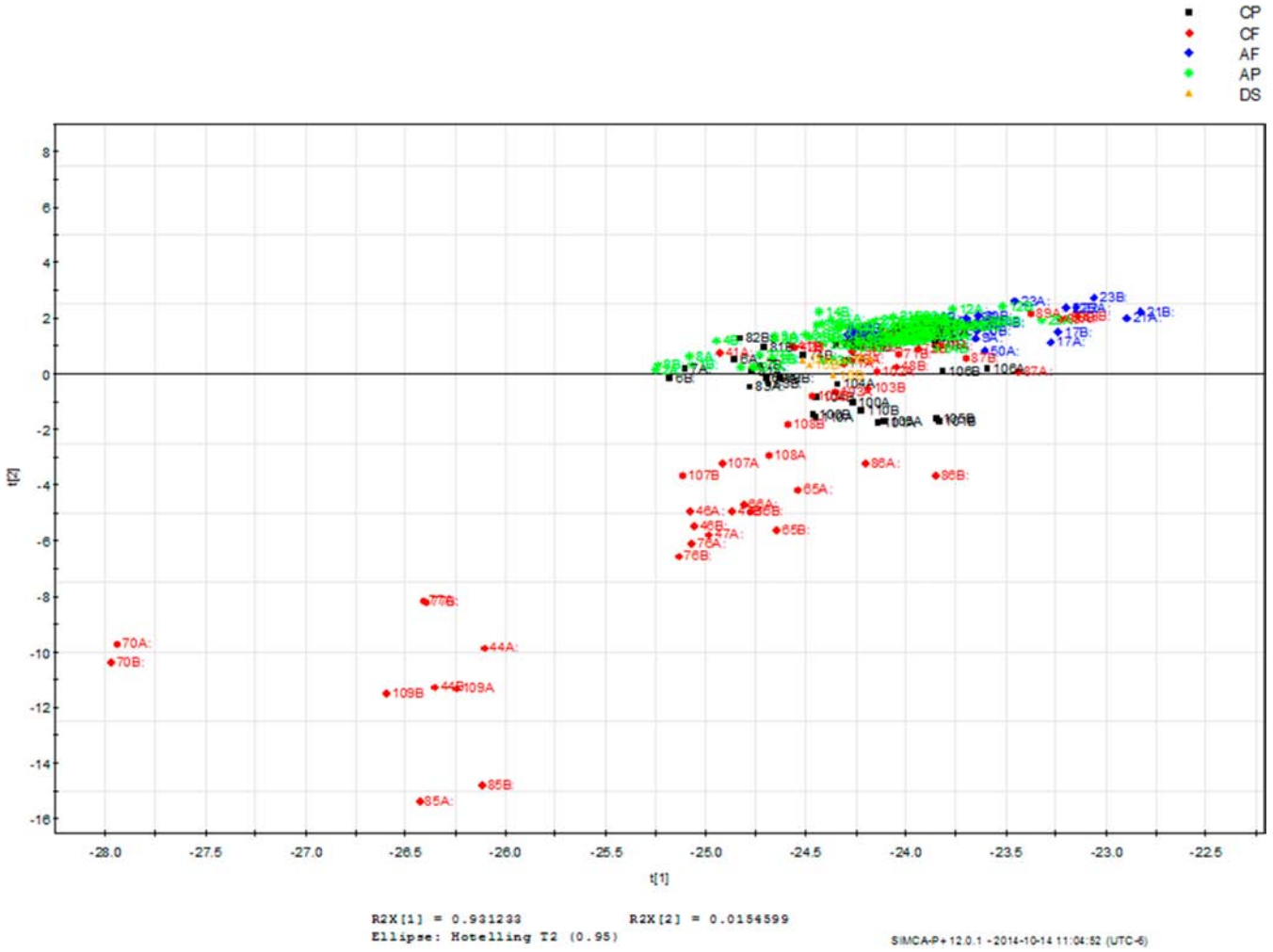

Figure 5. PCA score plot of the TTOs and commercial products. CP: Commercial samples met ISO standards. CF: Commercial samples failed to meet ISO standards. AF: TTOs failed to meet ISO standards. AP: TTOs met ISO standards. DS: Different species (A15 and A16).

this component may be a clear indication of substitution or adulteration in commercial products.

The results for the chiral analysis for α-terpineol are shown in Figure 4D. The previously measured chiral ratios for α-terpineol in TTOs were 2.92,[2] 3.31,[9] 2.85−3.35,[10] 2.65,[12] and 2.94.[13] The average for all of the TTO samples in Table S2, Supporting Information, was 3.86. Sixteen samples had excessively high +/− ratios, while nine displayed excessively low ratios. With this probe solute, there were seven samples (shown in Figure 4D as open data points) that did not meet the ISO composition standards and were outliers from the average value in the chiral analyses. Thus, this solute may provide a method for the detection of unacceptable commercial products that would not be detected with the ISO standards alone.

Chiral analysis can be used to identify commercial samples that are unacceptable in chiral distribution but satisfactory in chemical composition (chemotype). However, chiral GC is difficult. Baseline resolution between enantiomers is hard to achieve and even more difficult to maintain especially with complex samples such as natural products. Thus, chiral analysis alone is possibly not the optimum method for evaluating or validating commercial TTO products.

Chemometric Analyses. Chiral analysis is based only on limited probe solutes such as α-pinene, limonene, terpinen-4-ol, and α-terpineol. GC/MS analysis is a more holistic approach utilizing information concerning all of the components in a TTO or commercial sample. However, three-dimensional GC/MS data sets are difficult to interpret because of their sheer size. For example, in the present study with 104 samples, ca. 50 components with a mass range of 500 amu, the data set contained over 2 million points. Chemometric pattern recognition techniques, such as principal component analysis, are valuable tools for reducing the complexity of such data sets.

The GC/MS results normalized to the internal standard, $C_{13}H_{28}$, were subjected to PCA, in which all observations and variables are present. The scores plot for the entire data set is shown in Figure 5. The summary of the fit of the model is displayed with R^2X (cum) [R^2X shows the percentage of variance in the data that is explained by a particular component, R^2X(cum) sums up the R^2X as they accumulate with an increase in the number of components] and Q^2 (cum) [indicates the predictive ability of the model]. In total the PCA describes 93.1% of the variation (R^2X) in the data with a Q^2 of 93.0% for the first component indicating good prediction properties of the model. The first two components explain 96.0% of the variables. The R^2 and Q^2 plot for the PCA is given in Figure S2, Supporting Information. In this case, PCA provides an overview of the data and identifies the trends, groups, and strong outliers.

Class prediction analysis has proven to be a valuable technique in characterization and authentication of traditional medicinal

DOI: 10.1021/acs.jafc.5b00147
J. Agric. Food Chem. 2015, 63, 2674−2682

plants. The class prediction model allows assigning new samples into previously determined groups in an unbiased fashion. This workflow would be very useful for the QC of natural products and dietary supplements because the batch samples can be automatically acquired, processed, and class predicted. In the current investigation, all known provenance TTOs that met the ISO standards cluster in a single group (green) in the PCA score plot (Figure 5). The chiral ratios of α-pinene, limonene, terpinen-4-ol, and α-terpineol for the tea tree oil samples in this group were also within the ranges of norms. Thus, this group of samples was used to construct a class predictive model (PCA-class). The PCA-class model was cross-validated and used to evaluate all commercial samples and the TTO samples that did not meet the ISO standards. The R^2 and Q^2 values for the PCA class model (Figure S3, Supporting Information) were 95.5% and 95.4%, respectively. The results given in Table S3, Supporting Information, provide a confidence measure to the prediction, PModXPS+. This value shows the probability of the predicted observations belonging to the model. Observations with a probability of belonging less than 5% (PModXPS+ < 0.05) are considered to be outliers of the class predictive model and dissimilar to the observations used to build the model. In particular, there were several commercial products that met the ISO specifications but displayed unusual enantiomeric ratios (A100, A101, A104−106, and A110); those commercial products were also identified as outliers by the class prediction model. Additionally, there were TTOs and commercial products (A9, A17, A21−23, A48, A-50, and A-79) that met the chiral specifications but did not meet the ISO standards; they were also outliers identified by the PCA class prediction model. The results from the class prediction model and the outliers identified by different methods are summarized in Table S3, Supporting Information.

In conclusion, both chiral and conventional GC/MS analysis can be used to identify abnormal commercial tea tree oil products. Four chiral components, viz., α-pinene, limonene, terpinen-4-ol, and α-terpineol, were utilized for chiral analysis of the TTO samples. These compounds are major components of terpinen-4-ol type oils. Chiral analysis based on these four probes could be used to identify unsatisfactory, adulterated, substituted, or otherwise unusual commercial TTO products.

Analysis of three-dimensional GC/MS data along with chemometrics can also be used to isolate outliers in commercial samples. In this investigation, the outliers identified by chiral analysis coincided with the outliers identified by the class predictive model for all of the TTO components.

■ ASSOCIATED CONTENT

Supporting Information

Percentage of major compounds in tea tree oil samples and commercial products; enantiomeric percentage of four terpenes; results from PCA-class model prediction and outliers identified by ISO specifications, chiral analysis, and class prediction model; chemical structures of 20 major compounds present in tea tree oil (*M. alternifolia*); summary of R^2X and Q^2 for the PCA; summary of R^2X and Q^2 for the PCA-class model. This material is available free of charge via the Internet at http://pubs.acs.org.

■ AUTHOR INFORMATION

Corresponding Author

*Tel.: +1-662-915-7821. Fax: +1-662-915-7989. E-mail: ikhan@olemiss.edu.

Funding

This research was supported in part by "Science-Based Authentication of Dietary Supplements" funded by the Food and Drug Administration grant number 1U01FD004246-04 and the United States Department of Agriculture, Agricultural Research Service, Specific Cooperative Agreement number 58-6408-1-603 amendment 04.

Notes

The authors declare no competing financial interest.

■ ACKNOWLEDGMENTS

We thank Agilent Technologies for provision of the instrumentation and MPP software. Appreciation is also extended to Tony Larkman and the Australian Tea Tree Industry Association (ATTIA) for provision of the tea tree oils and commercial samples.

■ REFERENCES

(1) European Commission, Scientific Committee on Consumer Products. Opinion on tea tree oil. Adopted Dec 16, 2008; p 34; http://ec.europa.eu/health/ph_risk/committees/04_sccp/docs/sccp_o_160.pdf (Feb, 23, 2015).

(2) Wong, Y. F.; Davies, N. W.; Chin, S.-T.; Larkman, T.; Marriott, P. J. Enantiomeric distribution of selected terpenes for authenticity assessment of Australian *Melaleuca alternifolia* oil. *Ind. Crops Prod.* **2015**, *67*, 475−483.

(3) Chudleigh, P.; Simpson, S. Economic evaluation of investment in the tea tree oil R&D program, 2010; https://rirdc.infoservices.com.au/items/10-212 (Feb 23, 2015).

(4) International Standard ISO-4730. Oil of *Melaleuca*, terpinen-4-ol type (tea tree oil), 2004.

(5) Hammer, K. A.; Carson, C. F.; Riley, T. V.; Nielsen, J. B. A review of the toxicity of *Melaleuca alternifolia* (tea tree) oil. *Food Chem. Toxicol.* **2006**, *44*, 616−625.

(6) Southwell, I. Tea tree constituents. *Tea tree-the genus Melaleuca*; CRC Press: Boca Raton, FL, 1999; pp 29−62.

(7) Carson, C. F.; Riley, T. V. Safety, efficacy and provenance of tea tree (*Melaleuca alternifolia*) oil. *Contact Dermatitis* **2001**, *45*, 65−7.

(8) Brophy, J. J.; Davies, N. W.; Southwell, I. A.; Stiff, I. A.; Williams, L. R. Gas chromatographic quality control for oil of *Melaleuca* terpinen-4-ol type (Australian tea tree). *J. Agric. Food Chem.* **1989**, *37*, 1330−5.

(9) Sciarrone, D.; Ragonese, C.; Carnovale, C.; Piperno, A.; Dugo, P.; Dugo, G.; Mondello, L. Evaluation of tea tree oil quality and ascaridole: A deep study by means of chiral and multi heart-cuts multidimensional gas chromatography system coupled to mass spectrometry detection. *J. Chromatogr. A* **2010**, *1217*, 6422−6427.

(10) Shellie, R.; Mondello, L.; Dugo, G.; Marriott, P. Enantioselective gas chromatographic analysis of monoterpenes in essential oils of the family Myrtaceae. *Flavour Fragrance J.* **2004**, *19*, 582−585.

(11) Kreck, M.; Scharrer, A.; Bilke, S.; Mosandl, A. Enantioselective analysis of monoterpene compounds in essential oils by stir bar sorptive extraction (SBSE)-enantio-MDGC-MS. *Flavour Fragrance J.* **2002**, *17*, 32−40.

(12) Shellie, R.; Marriott, P.; Cornwell, C. Application of comprehensive two-dimensional gas chromatography (GC × GC) to the enantioselective analysis of essential oils. *J. Sep. Sci.* **2001**, *24*, 823−830.

(13) Leach, D. N.; Wyllie, S. G.; Hall, J. G.; Kyratzis, I. Enantiomeric composition of the principal components of the oil of *Melaleuca alternifolia*. *J. Agric. Food Chem.* **1993**, *41*, 1627−32.

(14) Tankeu, S.; Vermaak, I.; Kamatou, G.; Viljoen, A. Vibrational spectroscopy as a rapid quality control method for *Melaleuca alternifolia* Cheel (tea tree oil). *Phytochem. Anal* **2014**, *25*, 81−88.

(15) Sandasi, M.; Kamatou, G. P. P.; Baranska, M.; Viljoen, A. M. Application of vibrational spectroscopy in the quality assessment of Buchu oil obtained from two commercially important *Agathosma* species (Rutaceae). *S. Afr. J. Bot.* **2010**, *76*, 692−700.

DOI: 10.1021/acs.jafc.5b00147
J. Agric. Food Chem. 2015, 63, 2674−2682

(16) Juliani, H. R.; Kapteyn, J.; Jones, D.; Koroch, A. R.; Wang, M.; Charles, D.; Simon, J. E. Application of near-infrared spectroscopy in quality control and determination of adulteration of African essential oils. *Phytochem. Anal.* **2006**, *17*, 121−128.
(17) Jalali-Heravi, M.; Zekavat, B.; Sereshti, H. Characterization of essential oil components of Iranian geranium oil using gas chromatography-mass spectrometry combined with chemometric resolution techniques. *J. Chromatogr. A* **2006**, *1114*, 154−163.
(18) Sandasia, M.; Kamatoua, G. P. P.; Gavaghanb, C.; Baranskac, M.; Viljoena, A. M. A quality control method for geranium oil based on vibrational spectroscopy and chemometric data analysis. *Vib. Spectrosc.* **2011**, *57*, 242−247.
(19) Davies, N. W. Gas chromatographic retention indices of monoterpenes and sesquiterpenes on methyl silicone and Carbowax 20M phases. *J. Chromatogr.* **1990**, *503*, 1−24.

DOI: 10.1021/acs.jafc.5b00147
J. Agric. Food Chem. 2015, 63, 2674−2682

NMR Analysis. NMR spectra were measured with a JNM-A400 spectrometer (JEOL, Japan). The NMR spectra (^{1}H, ^{13}C, DEPT, COSY, CHSHF, HMBC) of isolated inositols were measured with D_2O and 3-(trimethylsilyl)propionic acid sodium salt as an internal standard.

Extraction and Separation of Inositols from Plants. Ten grams of each plant was homogenized in 100 mL of 80% EtOH for 1 min with a Polytron (Kinematica AG, Switzerland) at room temperature. After filtration of the mixture with a filter paper under suction, the residue was re-extracted twice with 100 mL of 80% EtOH. Filtrates were combined and concentrated to dryness with a rotary evaporator under vacuo. The dried filtrate was dissolved in 20 mL of water and extracted three times with 10 mL of *n*-pentane to remove chlorophyll. The water solution was concentrated to remove *n*-pentane and made up to 50 mL with water. One milliliter of the solution was passed through an ODS cartridge (⌀ 1 × 1 cm, BondElut C18, Varian) equilibrated with water after washing thoroughly with MeOH. The pass-through fraction was charged to a Dowex 1 × 4 column ($^-$OH type, ⌀ 0.6 × 3.5 cm) connected to an ODS cartridge. The cartridge was washed with 3 mL of water. The eluate was successively passed through the Dowex small column. After removal of the ODS cartridge, the Dowex column was further washed with 4 mL of water. Eluates (total 8 mL) were combined and made up to 10 mL with water. Twenty-five microliters of the solution containing inositols was analyzed by HPAE-PAD. Extraction and separation of inositols from each plant and HPAE-PAD analysis were carried out twice and the contents of inositols averaged.

Isolation and Identification of Inositols. Several inositols were isolated from the remaining solutions of the above crude extracts and used in the preparation of samples for the HPAE-PAD analyses. The extract solutions were charged to a Wakosil ODS (C18, Tokyo, Japan) column (⌀ 2 × 10 cm) and washed with water. The pass-through fractions were concentrated and further separated with a Dowex 1 × 4 column ($^-$OH type, ⌀2 × 10 cm). Water elutes were fractionated into 5 g each and eluates of each fraction detected by spotting on a TLC plate, spraying 40% sulfuric acid to spots, and heating the plates at 105 °C. Fractions containing inositols were concentrated and lyophilized. Chemical structures of isolates were identified by comparison with NMR spectra of authentic samples or the literature.[11−21]

Determination of Hydroxyl Radical Scavenging Activity. The hydroxyl radical scavenging activities of inositols were determined by adding them to a generating/detecting system and observing their competition with the detector.[9] Hydroxyl radicals were generated from ascorbate and detected by their ability to hydroxylate salicylic acid.[9,10,22] The reaction mixture contained 150 mM K-Pi buffer (pH 7.4), 0.26 mM ascorbic acid, 0.15 mM Fe(III)−EDTA, 0.6 mM H_2O_2, 2 mM sodium salicylate, and 20 mM inositol or other compound in a total volume of 2 mL. After incubation for 60 min at 25 °C, hydroxylated salicylate was extracted and spectrophotometrically determined by the following methods. To the reaction mixture were added 0.5 mL of 2.0 M HCl saturated NaCl and 2 mL of diethyl ether, and then the solution was mixed with a Vortex mixer for 30 s. After removal of the upper ether layer, hydroxylated salicylate was re-extracted with 2 mL of diethyl ether. The combined ether layer was evaporated to dryness at 50 °C with N_2 gas. To the residues dissolved in 0.25 mL of deionized water were added 0.125 mL of 10% (w/v) trichloroacetic acid dissolved in 0.5 M HCl, 0.25 mL of 10% (w/v) sodium tungstate, and 0.25 mL of 0.5% (w/v) sodium nitrite. After standing for 5 min, 0.5 mL of 0.5 M KOH and 1.375 mL of deionized water was added to the solution, and absorbances were measured at 510 nm. Assays for each compound were carried out four times, and the inhibitory activities on salicylate hydroxylation by hydroxyl radicals were averaged.

RESULTS AND DISCUSSION

Separation and Determination of Inositols by HPAE-PAD. Chair conformations of *myo*-inositol, *chiro*-inositol, and *scyllo*-inositol including ononitol, sequoyitol, and pinitol are indicated in Figure 1. Inositols contain six hydrogen atoms. In the *scyllo*-inositol (c), the bonds of hydrogen atoms are all axial, whereas those of the hydrogen atoms at the 2-position in *myo*-inositol (a) and at the 1- and 6-positions in *chiro*-inositol (b) are equatorial. Ononitol and pinitol are methylated compounds consisting of *myo*-inositol at the OH of the 4-position and *chiro*-inositol at the OH of the 3-position. The five compounds having similar structures were well separated by HPAE-PAD with a Dionex CarboPac MA1 column (Figure 2). 5-*O*-Methyl-*myo*-inositol (sequoyitol) and *β*-D-methyl-glucose (d), however, had the same retention times as ononitol and *scyllo*-inositols,

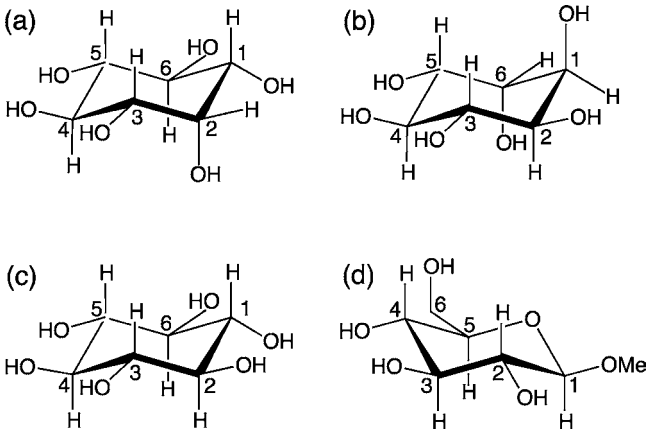

Figure 1. Structures of *myo*-inositol (a), *chiro*-inositol (b), *scyllo*-inositol (c), and *β*-D-methyl-glucose (d). O-methylated compounds at the 4-and 5-positions in (a) and at the 3-position in (b) are ononitol, sequoyitol, and pinitol, respectively.

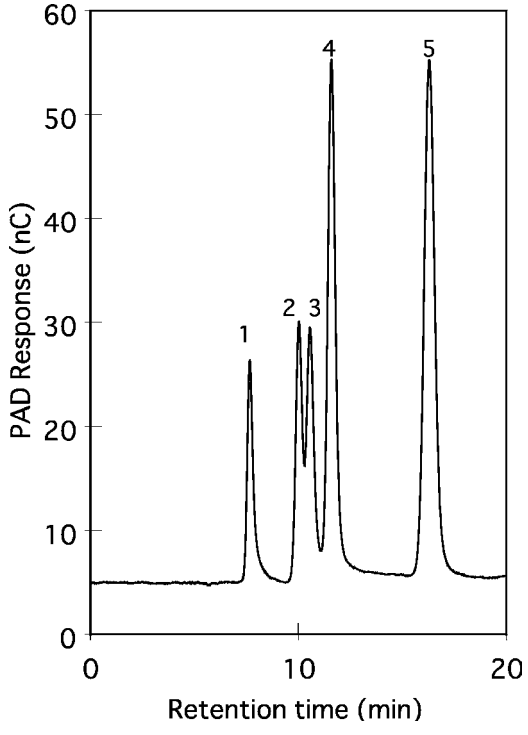

Figure 2. Separation of inositols by HPAE-PAD. Peaks: 1, ononitol or sequoyitol (retention time, 7.7 min); 2, pinitol (10.0 min); 3, *myo*-inositol (10.6 min); 4, *scyllo*-inositol or *β*-D-methyl-glucose (11.6 min); 5, *chiro*-inositol (16.3 min). Additionally, retention time of glucose was 37.4 min. See the details of the separation conditions under Materials and Methods.

DOI: 10.1021/jf5041367
J. Agric. Food Chem. 2015, 63, 2683−2688

Table 1. Content of Inositols in Familiar Plants[a]

plant	content of inositols (mg/100 g FW)					moisture (g/100 g FW)
	ononitol	pinitol	*myo*-inositol	*scyllo*-inositol	*chiro*-inositol	
soybean (*Glycine max*)						
young leaf	12.6	269.7	–	1.8	4.8	82.47
young bean	–	46.6	48.0	–	6.1	68.29
white clover (*Trifolium repens*)						
leaf	63.6	286.9	70.2	(30.1)[b]	–	83.64
stem	50.1	421.1	–	(110.3)[b]	–	92.04
red clover (*Trifolium pratense*)						
leaf	59.4	387.7	126.2	(18.9)[b]	–	77.12
stem	46.4	458.1	22.6	(65.1)[b]	–	88.33
bush clover (*Lespedeza bicolor*)						
leaf	39.0	452.5	26.7	–	19.0	77.23
locust tree (*Robinia pseudoacacia*)						
young leaf	350.0	625.1	–	–	–	74.63
flower	95.8	269.1	–	–	–	87.28
wisteria (*Wisteria nutt*)						
young leaf	34.8	259.0	26.5	–	–	78.51
flower	–	214.8	15.1	–	–	86.69
kudzu (*Pueraria lobata*)						
young vine	–	212.1	–	–	–	85.97
dandelion (*Taraxacum officinale*)						
young leaf	–	–	80.9	–	141.3	84.66
flower	–	–	173.8	–	191.3	84.40
sticky mouse-ear (*Cerastium glomeratum*)						
stem and leaf	166.2	260.0	22.3	2.5	7.0	86.48
chickweed (*Stellaria media*)						
stem and leaf	11.3	274.7	–	–	6.8	89.86
ginkgo (*Ginkgo biloba*)						
young leaf	(287.0)[c]	332.0	49.1	–	–	80.42
Japanese mallotus (*Mallotus japonicus*)						
young leaf	–	–	19.2	–	156.4	74.97

[a]Underlined values were identified by NMR analyses. –, undetected. [b]In clover, β-D-methyl-glucose was detected instead of *scyllo*-inositol. [c]In gingko, sequoyitol (5-*O*-methyl-*myo*-inositol) was detected instead of ononitol.

respectively (Figure 2), under our HPLC conditions. By PAD, we were able to determine the sugars and cyclitols in the amounts of 10 pmol, without modifications.[7]

Identification of Inositols by NMR. In Table 1, the compounds with the values underlined were all identified by ^{1}H and ^{13}C NMR analyses after the isolations, which were completed by using Wakosil ODS and Dowex 1 × 4 columns as indicated under Materials and Methods. The yields of most isolates in Table 1 were >40%. The ^{1}H NMR spectra in Figure 3 are distinguishable from each other for identifications. The H-2 position in *myo*-inositol, the H-1 and H-6 positions in *chiro*-inositol, and those in their methylated compounds were equatorial (Figure 1). Signals of these protons were detected at approximately 4.0 ppm (Figure 3A–E). Proton signals of methoxyl groups were observed at 3.6 ppm in methylated compounds (Figure 3B,C,E). Methylations of the hydroxyl groups in *myo*-inositol and *chiro*-inositol changed the chemical shifts of the axial protons, especially H-4 of B, H-5 of C, and H-3 of E showed low frequencies. By comparing the signal patterns of the ^{1}H NMR spectra in pinitol, ononitol, and sequoyitol, we were able to identify each of them easily. Furthermore, the spectrum of β-D-methyl-glucose is similar to that of the methylated inositols, but the existences of anomeric proton of H-1 (about 4.4 ppm) and 2 protons of H-6 are remarkably different from the inositols (Figure 3E). On the other hand, the signals of protons and carbon atoms were each observed as one signal (3.35 and 76.4 ppm, respectively) in authentic *scyllo*-inositol, the structure of which is symmetric (Figure 1).

^{1}H NMR and ^{13}C NMR Spectral Data. The spectra of *myo*-inositol, D-*chiro*-inositol, D-pinitol, and β-D-methyl-glucose were in agreement with those of the authentic samples and data in the literature.[11−21] The NMR spectral data of methylated inositols were assigned as follows:

Ononitol: ^{1}H NMR (400 MHz, D_2O) δ 4.05 (1H, t, J = 2.8 Hz, H-2), 3.67 (1H, t, J = 5.6 Hz, H-6), 3.63 (1H, t, J = 5.6 Hz, H-3), 3.60 (3H, s, 4-OMe), 3.49 (1H, dd, J = 10.0, 2.8 Hz, H-1), 3.39 (1H, t, J = 9.2 Hz, H-4), 3.36 (1H, t, J = 9.2 Hz, H-5); ^{13}C NMR (100 MHz, D_2O) δ 85.3 (C-4), 76.5 (C-5), 75.3 (C-6), 75.1 (C-2), 73.8 (C-1), 73.4 (C-3), 62.6 (OMe).[12,15]

Sequoyitol: ^{1}H NMR (400 MHz, D_2O) δ 4.05 (1H, t, J = 2.8 Hz, H-2), 3.71 (2H, t, J = 10.0 Hz, H-4, H-6), 3.60 (3H, s, 5-OMe), 3.55 (2H, dd, J = 10.0, 2.8 Hz, H-1, H-3), 3.07 (1H, t, J = 9.6 Hz, H-5); ^{13}C NMR (100 MHz, D_2O) δ 87.0 (C-5), 74.8 (C-2), 74.5 (C-4, C-6), 73.9 (C-1, C-3), 62.4 (OMe).[14]

D-Pinitol: ^{1}H NMR (400 MHz, D_2O) δ 4.01 (2H, m, H-1, H-6), 3.82 (1H, dd, J = 10.0, 2.0 Hz, H-5), 3.77 (1H, dd, J = 10.0, 2.0 Hz, H-2), 3.66 (1H, t, J = 10.0 Hz, H-4), 3.60 (3H, s, 3-OMe), 3.35 (1H, t, J = 10.0 Hz, H-3); ^{13}C NMR (100 MHz, D_2O) δ 85.6 (C-3), 74.9 (C-4), 74.5 (C-1 or C-6), 74.3 (C-6 or C-1), 73.4 (C-2), 72.6 (C-5), 62.5 (OMe).[13]

DOI: 10.1021/jf5041367
J. Agric. Food Chem. 2015, 63, 2683−2688

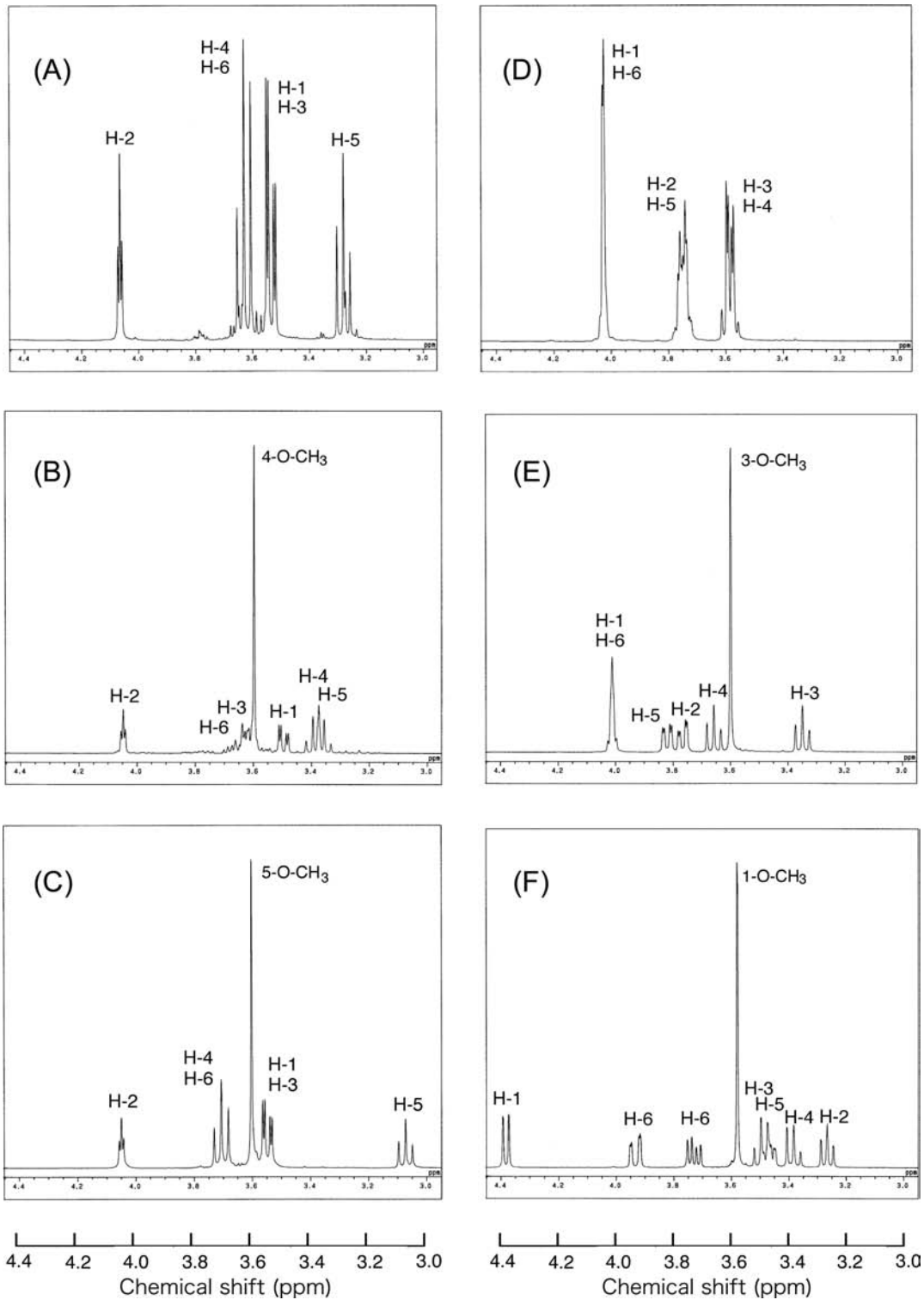

Figure 3. ^{1}H NMR spectra of several isolates: (A) *myo*-inositol from young leaf of dandelion; (B) ononitol from stem and leaf of sticky mouse-ear; (C) sequoyitol from young leaf of ginkgo; (D) *chiro*-inositol from young leaf of Japanese mallotus; (E) pinitol from stem and leaf of chickweed; (F) *β*-D-methyl-glucose from stem of white clover. As compared with these spectra, only one signal was observed at 3.35 ppm in the spectrum of authentic *scyllo*-inositol.

Content of Inositols in the Familiar Plants. The content of inositols in 45 kinds of edible plants from 23 families was investigated. Table 1 shows that 12 familiar plants contain large amounts of *myo*-inositol, *chiro*-inositol, and their methylated compounds. Soybean, white, red and bush clovers, locust tree, wisteria, and kudzu, which are all Fabaceae plants, contained pinitol of 200−600 mg/100 g fresh weight. Similar amounts of pinitol were found in sticky mouse-ear, chickweed, and ginkgo, whereas dandelion and Japanese mallotus contained large amounts of nonmethylated type *chiro*-inositol. Kim et al.[6] reported that total *chiro*-inositol contents in 100 g dry weight of carob pod, *Bougainvillea*, soy whey, and soybean oligosacchar-

DOI: 10.1021/jf5041367
J. Agric. Food Chem. 2015, 63, 2683−2688

ides were 4.0, 2.0, 2.0, and 1.74 g, respectively. A comparison with moisture contents showed 100 g dry weights of pinitol for young leaves of soybean, stems of white clover, stems of red clover, young leaves of locust tree, sticky mouse-ear, and chickweed were 1.54, 5.29, 3.93, 2.46, 1.92, and 2.71 g, respectively. On the other hand, peaks of ononitol were detected in Fabaceae plants and sticky mouse-ear, especially in the young leaves of locust trees. In ginkgo a peak of ononitol was detected, but this compound was identified as sequoyitol by NMR analysis after isolation. Similarly, in the peaks of *scyllo*-inositol detected in white and red clovers by HPAE-PAD, *β*-D-methyl-glucose was detected. In plants the accumulation of pinitol is commonly thought to be beneficial for stress adaptation and stabilization of membranes against osmotic alternations.[13] Furthermore, the plants used in this study were collected in the spring, suggesting that plants accumulate large amounts of inositols as cryoprotectants to protect themselves against the winter cold.[8] Furthermore, Adams et al. reported an apparent correlation in the postharvest longevity of flowers and content of inositols, particularly D-pinitol.[7] Pinitol content of flower petals from carnation was 7.2 mg/g FW.[7] It is presumed that pinitol is biosynthesized from *myo*-inositol via ononitol or sequoyitol.[15,23,24] In dandelion and Japanese mallotus (Table 1), it is suggested that some *myo*-inositol remains without methylation and that ononitol has already been epimerized and demethylated to be *chiro*-inositol, whereas pinitol in ginkgo, which belongs to gymnosperm, seems to be synthesized via sequoyitol.[15,23,24] In the plants not shown in Table 1, 4.9 mg/100 g FW of ononitol, 19.0 mg/100 g FW of pinitol, and 3.4 mg/100 g FW of *myo*-inositol in ice plant (*Mesembryanthemum crystallinum*) and 40.8 mg/100 g FW of pinitol and 27.9 mg/100 g FW of *myo*-inositol in *Artemisia indica* were detected. Furthermore, 160−210 mg/100 g FW of *myo*-inositol was detected in the leaves of *Cercidiphyllum japonicum*, *Lonicera japonica*, *Morus alba*, and *Diospyros kaki*. Furthermore, dandelion and Japanese mallotus (Table 1) contained 191.3 (or 141.3) mg/100 g FW and 156.4 mg/100 g FW of *chiro*-inositol, respectively. These high contents are compared to the other plants in Table 1. The sprouts of mung bean are reported to contain 5.79 mg/g DW or less of *chiro*-inositol,[25] which is not more than half the content of dandelion or almost the same as Japanese mallotus.

Hydroxyl Radical Scavenging Activity of Inositols. Table 2 shows the inhibitory effects of *myo*-inositol, *scyllo*-inositol, *chiro*-inositol, their methylated inositols, and several other compounds on salicylate hydroxylation by hydroxyl radicals. Inhibition with *myo*-inositol and *scyllo*-inositol was approximately 55%. Inhibition by *chiro*-inositol, mannitol, sorbitol, and glucose was about 65%. Furthermore, inhibitory activities of pinitol, ononitol, sequoyitol, and *β*-D-methyl-glucose were about 75%, which are higher than those of their native compounds by 10−20%. These results indicate that the methylated compounds have high activities for hydroxyl radical scavenging. On the other hand, substantial amounts ranging from 2.5 to 6.5 mM of *myo*-inositol, *chiro*-inositol, and *scyllo*-inositol were detected in mouse blood plasma after oral administration of 1 g/kg BW of three inositols.[26] This suggests that inositols can function as strong hydroxyl radical scavengers in the human body.

Applications in Our Daily Lives. This study showed that plants containing large amounts of inositols are commonly grown as well-known plants (Table 1). Boiled young soybeans are very often eaten in Japan, so people can ingest pinitol in their daily lives. However, the young leaves of soybean can be easily used for fried foods and soups. Young vines of kudzu are grown in spring to summer. Other Fabaceae plants such as clovers and locust trees are found everywhere and can be easily used. Furthermore, dandelion, sticky mouse-ear, and chickweed are weeds that are useful for human health. Leaves of ginkgo tree, dandelion, and kaki are already used as herbal teas in Japan. Other than eating plants, extracts from plants with boiled water are useful for cooking. Kim et al.[6] isolated pinitol from soy whey and carob pod and indicated that oral administration of soy pinitol and carob pinitol (10 mg/kg) decreased blood glucose by 15% at 2−6 h in streptozotocin-induced diabetic rats. This study demonstrated that pinitol can be beneficial in controlling blood glucose in an animal model of diabetes mellitus. On the other hand, considerable amounts of *myo*-inositol, *chiro*-inositol, and their methylated compounds, which are effective hydroxyl radical scavengers (Table 2), may be incorporated into the blood.[26] These results indicate that inositols play very important roles for protecting humans from stresses. Although we did not examine the physiological functions of inositols from the plants in this study, isolates from our plants likely have the same functions as those from soy whey and carob pod. Ingesting these plants is expected to provide good effects for human health. The familiar edible plants in this study may be more easily available and economical sources of inositols.

Table 2. Inhibitory Effect of Various Compounds on Salicylate Hydroxylation by Hydroxyl Radicals

compound	inhibition[a] (%)
myo-inositol	54.5 ± 3.8
scyllo-inositol	56.2 ± 1.5
chiro-inositol	66.0 ± 1.0
pinitol (3-*O*-methyl-*chiro*-inositol)	75.6 ± 1.3
ononitol (4-*O*-methyl-*myo*-inositol)	74.9 ± 1.7
sequoyitol (5-*O*-methyl-*myo*-inositol)	76.4 ± 1.2
mannitol	65.8 ± 2.0
sorbitol	66.9 ± 1.3
glucose	64.3 ± 2.4
β-D-methyl-glucose	75.7 ± 1.2
proline	22.3 ± 3.3
glycinebetaine	0.5 ± 3.4

[a]Inhibition (%) is expressed as $(1 - P/C) \times 100$, where P is A_{510} in the salicylate hydroxylation reaction with inositols or other compounds and C is A_{510} in the control reaction without those compounds; values are means ± SD.

■ ASSOCIATED CONTENT

Supporting Information

NMR spectra (^{1}H, DEPT, and COSY) of several isolates in Figure 3. This material is available free of charge via the Internet at http://pubs.acs.org.

■ AUTHOR INFORMATION

Corresponding Author

*(O.N.) Phone: +81-29-853-4933. Fax: +81-29-853-4605. E-mail: negishi.osamu.gf@u.tsukuba.ac.jp.

Notes

The authors declare no competing financial interest.

DOI: 10.1021/jf5041367
J. Agric. Food Chem. 2015, 63, 2683−2688

■ ACKNOWLEDGMENTS

We thank Hokko Chemical Industry Co., Ltd. for supplying authentic inositols.

■ REFERENCES

(1) Bates, S. H.; Jones, R. B.; Bailey, C. J. Insulin-like effect of pinitol. *Br. J. Pharmacol.* **2000**, *130*, 1944−1948.
(2) Choi, M. S.; Lee, M. K.; Jung, U. J.; Kim, H. J.; Do, G. M.; Park, Y. B.; Jeon, S. M. Metabolic response of soy pinitol on lipid-lowering, antioxidant and hepatoprotective action in hamsters fed-high fat and high cholesterol diet. *Mol. Nutr. Food Res.* **2009**, *53*, 751−759.
(3) Do, G. M.; Chot, M. S.; Kim, H. J.; Woo, M. N.; Lee, M. K.; Jeon, S. M. Soy pinitol acts partly as an insulin sensitizer or insulin mediator in 3T3-L1 preadipocytes. *Genes Nutr.* **2008**, *2*, 359−364.
(4) Agarie, S.; Kawaguchi, A.; Kodera, A.; Sunagawa, H.; Kojima, H.; Nose, A.; Nakahara, T. Potential of the common ice plant, *Mesembryanthemum crystallinum* as a new high-functional food as evaluated by polyol accumulation. *Plant Prod. Sci.* **2009**, *12*, 37−46.
(5) Dhanasekaran, M.; Ignacimuthu, S.; Agastian, P. Potential hepatoprotective activity of ononitol monohydrate isolated from *Cassia tora* L. on carbon tetrachloride induced hepatotoxicity in wistar rats. *Phytomedicine* **2009**, *16*, 891−895.
(6) Kim, J. I.; Kim, J. C.; Joo, H. J.; Jung, S. H.; Kim, J. J. Determination of total chiro-inositol content in selected natural materials and evaluation of the antihyperglycemic effect of pinitol isolation from soybean and carob. *Food Sci. Biotechnol.* **2005**, *14*, 441−445.
(7) Adams, P.; Zegeer, A.; Bohnert, H. J.; Jensen, R. G. Anion exchange separation and pulsed amperometric detection of inositols from flower petals. *Anal. Biochem.* **1993**, *214*, 321−324.
(8) Orthen, B.; Popp, M. Cyclitols as cryoprotectants for spinach and chickpea thylakoids. *Environ. Exp. Bot.* **2000**, *44*, 125−132.
(9) Smirnoff, N.; Cumbes, Q. J. Hydroxyl radical scavenging activity of compatible solutes. *Phytochemistry* **1989**, *28*, 1057−1060.
(10) Shen, B.; Jensen, R. G.; Bohnert, H. J. Mannitol protects against oxidation by hydroxyl radicals. *Plant Physiol.* **1997**, *115*, 527−532.
(11) Ichimura, K.; Kohata, K.; Yamaguchi, Y.; Duzono, M.; Ikeda, H.; Koketsu, M. Identification of L-inositol and scyllitol and their distribution in various organ in chrysanthemum. *Biosci., Biotechnol., Biochem.* **2000**, *64*, 865−868.
(12) Richter, A.; Peterbauer, T.; Brereton, I. Structure of galactosylononitol. *J. Nat. Prod.* **1997**, *60*, 749−751.
(13) Ichimura, K.; Kohata, K.; Koketsu, M.; Shimamura, M.; Ito, A. Identification of pinitol as a main sugar constituent and changes in its content during flower bud development in carnation (*Dianthus caryophyllus* L.). *J. Plant Physiol.* **1998**, *152*, 363−367.
(14) Sultana, N.; Hartley, T. G.; Waterman, P. G. Two novel prenylated flavones from the aerial parts of *Melicope micrococca*. *Phytochemistry* **1999**, *50*, 1249−1253.
(15) Vernon, D. M.; Tarczynski, M. C.; Jensen, R. G.; Bohnert, H. J. Cyclitol production in transgenic tobacco. *Plant J.* **1993**, *4*, 199−205.
(16) Cerdan, S.; Hansen, C. A.; Johanson, R.; Inubushi, T.; Williamson, J. R. Nuclear magnetic resonance spectroscopic analysis of *myo*-inositol phosphates including inositol 1,3,4,5-tetrakisphosphate. *J. Biol. Chem.* **1986**, *261*, 14676−14680.
(17) Peterbauer, T.; Brereton, I.; Richter, A. Identification of a digalactosyl ononitol from seeds of adzuki bean (*Vigna angularis*). *Carbohydr. Res.* **2003**, *338*, 2017−2019.
(18) Binder, R. G.; Haddon, W. F. Cyclitols of soybean leaves. *J. Agric. Food Chem.* **1984**, *32*, 685−687.
(19) Ichimura, K.; Kohata, K.; Mukasa, Y.; Yamaguchi, Y.; Goto, R.; Suto, K. Identification of L-bornesitol and changes in its content during flower bud development in sweet pea (*Lathyrus odoratus* L.). *Biosci., Biotechnol., Biochem.* **1999**, *63*, 189−191.
(20) Bain, A. D.; Eaton, D. R.; Hux, R. A.; Tong, J. P. K. An N.M.R. study of the interactions between carboxen and saccharides. *Carbohydr. Res.* **1980**, *84*, 1−12.
(21) Smoum, R.; Rubinstein, A.; Srebnik, M. Combined ^{1}H, ^{13}C and ^{11}B NMR and mass spectral assignments of boronate complexes of D-(+)-glucose, D-(+)-mannose, methyl-α-D-glucopyranoside, methyl-β-D-galactopyranoside and methyl-α-D-mannopyranoside. *Magn. Reson. Chem.* **2003**, *41*, 1015−1020.
(22) Halliwell, B.; Gutteridge, J. M. C. Role of iron in oxygen radical reaction. In *Methods in Enzymology. Vol. 105: Oxygen radicals in Biological Systems*; Packer, L., Ed.; Academic Press: New York, 1984; pp 47−59.
(23) Dittrich, P.; Korax, A. Novel biosynthesis of D-pinitol in *Simmondsia chinensis*. *Phytochemistry* **1984**, *23*, 65−66.
(24) Dittrich, P.; Brandl, A. Revision of the pathway of D-pinitol formation in Leguminose. *Phytochemistry* **1987**, *26*, 1925−1926.
(25) Yao, Y.; Cheng, X. Z.; Ren, G. X. Contents of D-chiro-inositol, vitexin, and isovitexin in various varieties of mung bean and its products. *Agri. Sci. China* **2011**, *10*, 1710−1715.
(26) Yamashita, Y.; Yamada, M.; Hasunuma, T.; Ashida, H.; Yoshida, K. Detection of orally administered inositol stereoisomers in mouse blood plasma and their effects on translocation of glucose transporter 4 in skeletal muscle cells. *J. Agric. Food Chem.* **2013**, *61*, 4850−4854.

DOI: 10.1021/jf5041367
J. Agric. Food Chem. 2015, 63, 2683−2688

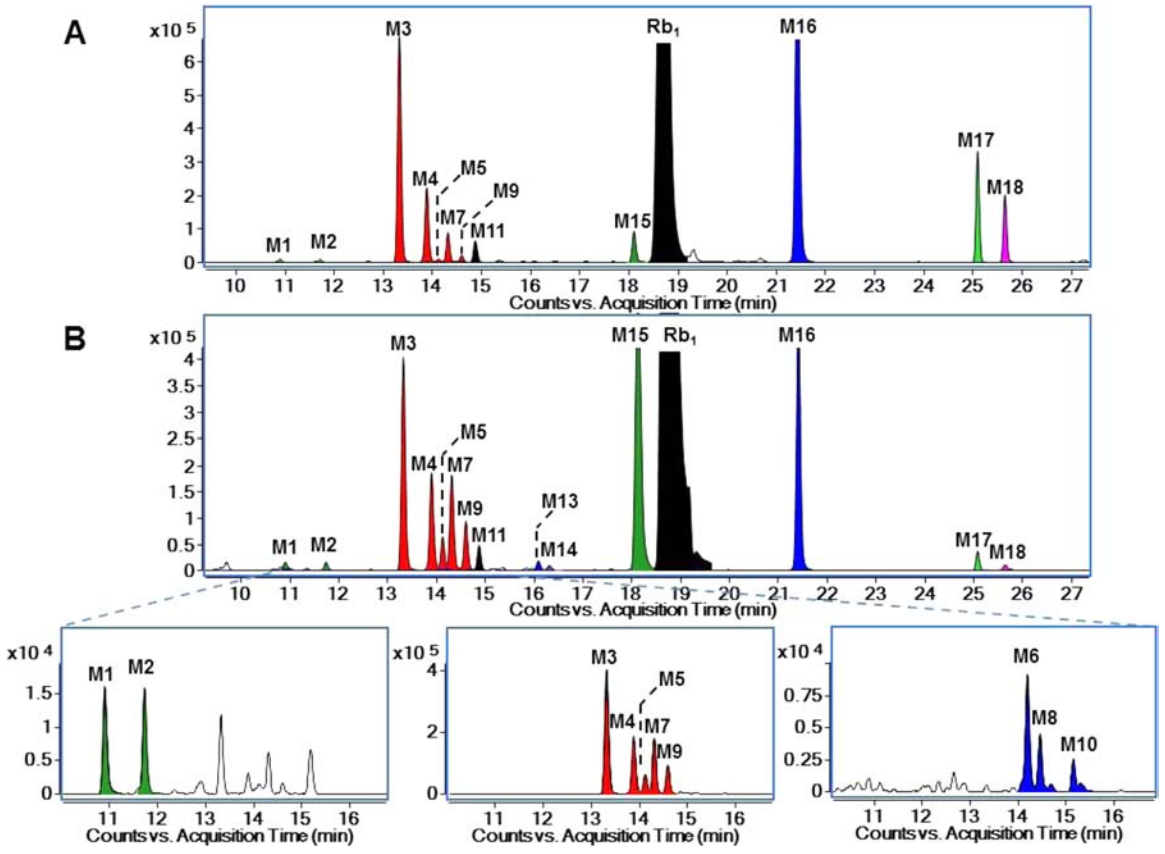

Figure 1. Extracted compound chromatograms (ECC) of metabolites in rat plasma and urine after iv injection of Rb_1 at a dosage of 20 mg/kg: (A) metabolites in plasma sample collected at 5 min after iv injection; (B) metabolites in urine samples collected during 3−6 h after iv dose of Rb_1.

pharmacological effects of the primary ginsenosides as well as their relevant metabolites. However, metabolism of the intact ginsenosides following intravenous administration remains unknown. Consequently, a huge gap between the considerable systemic effects of primary ginsenosides and metabolites reaching circulation system still exist.

In addition to the well-known deglycosylation and dehydration pathways, ginsenosides have been increasingly reported to undergo oxidation.[19−25] Oxygenated metabolites of both intact and deglycosylated ginsenosides have been observed as circulating metabolites.[19,20,22,26,27] Recently, structures of oxygenated metabolites formed in liver microsomes of secondary ginsenosides, that is, Rh_2,[25] PPD,[28] Rh_1, and Rg_2,[29] have been elucidated. However, primary ginsenosides appeared to be metabolized via pathways distinct from that of secondary ginsenosides as they were not metabolized in microsomes. Structures of resulting oxygenated metabolites of primary ginsenosides were still not fully characterized due to technique difficulties, that is, a limitation in determining the exact oxygenated site solely by mass spectrometry, and difficulties in obtaining metabolites in adequate amounts for NMR measurements.

As aforementioned, we herein carried out an extensive in vivo metabolite profiling of ginsenoside Rb_1, the representative PPD-type primary ginsenoside in ginseng, American ginseng, and notoginseng, with a focus on the characterization of its oxygenated metabolites in rat plasma and urine.

MATERIALS AND METHODS

Chemicals and Materials. Ginsenoside Rd and 20(*S*)-Rg_3 (purity ≥ 98%) were purchased from Chengdu Scholar Biotech Co., Ltd. (Chengdu, China). Ginsenoside Rb_1 and F_2 (purity ≥ 98%) were purchased from Chengdu MUST Bio-Technology Co., Ltd. (Chengdu, China). Rose Bengal, triphenylphosphine, Shi Epoxidation Diketal Catalyst (ketone), OXONE, EDTA-Na, and sodium bicarbonate were purchased from Sigma-Aldrich (St. Louis, MO, USA). Liver microsomes, NADPH Regenerating System Solution A (containing 31 mM $NADP^+$, 66 mM glucose-6-phosphate, and 66 mM $MgCl_2$) and Solution B (containing 40 U/mL glucose-6-phosphate dehydrogenase in 5 mM sodium citrate) were purchased from BD Biosciences (San Jose, CA, USA). Saline was purchased from Baxter (Deerfield, IL, USA). HPLC grade methanol (MeOH) and acetonitrile (ACN) were purchased from Anaqua Chemicals Supply Inc., Ltd. (Houston, TX, USA), and distilled water was purified by Milli-Q system (Millipore, Billerica, MA, USA). All other chemicals were of analytical reagent grade.

Animals. Male SD rats (n = 2 for each route of administration) weighing 200−220 g were purchased from the Laboratory Animal Services Center, Chinese University of Hong Kong. All animals were acclimated for more than 1 week under a 12 h light/12 h dark cycle at a room temperature of 22 ± 1 °C. Animal care and treatment procedures were in accordance with the Institutional Guidelines and Animal Ordinance (Department of Health, Hong Kong Special Administrative Region) and approved by the Committee on the Use of Human and Animal Subjects in Teaching and Research of the Hong Kong Baptist University. The rats were fasted overnight but with access to water before the experiment.

UHPLC/TOF MS Analysis of Metabolites. Metabolites in the biological samples of both in vivo and in vitro metabolism experiments were analyzed by using an Agilent 1290 Infinity ultrahigh-performance liquid chromatography (UHPLC) system coupled to an Agilent 6230 accurate-mass time-of-flight (TOF) mass spectrometer (MS) (Agilent, Santa Clara, CA, USA). MS/MS experiments were carried out on an Agilent 1290 Infinity UHPLC system coupled with an Agilent 6550 quadrupole-time-of-flight (Q-TOF) MS.

The chromatography was performed on a Waters Acquity BEH C_{18} column (2.1 × 100 mm, 1.7 μm). The mobile phase consisted of 0.1%

DOI: 10.1021/acs.jafc.5b00710
J. Agric. Food Chem. 2015, 63, 2689−2700

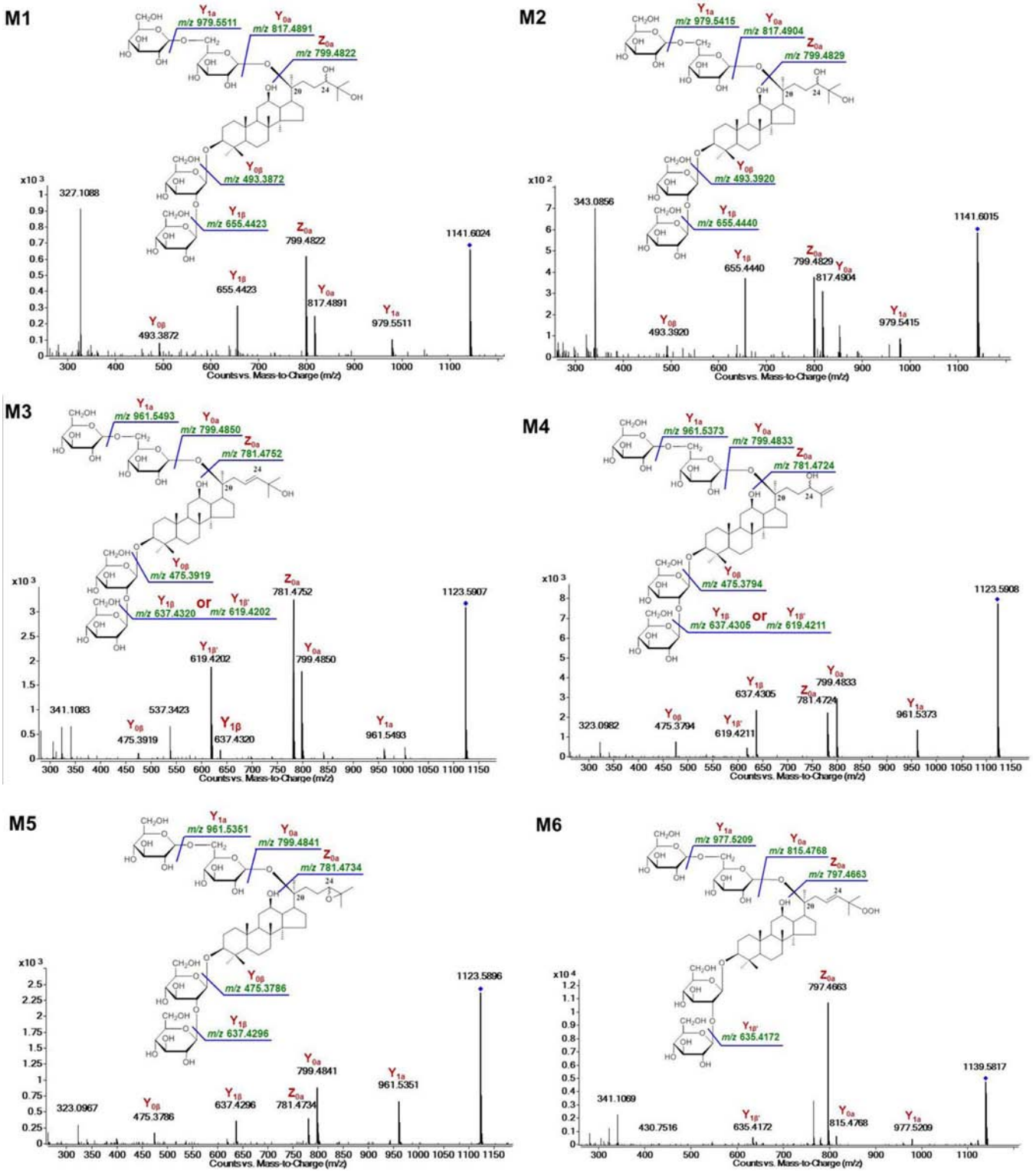

Figure 2. continued

DOI: 10.1021/acs.jafc.5b00710
J. Agric. Food Chem. 2015, 63, 2689−2700

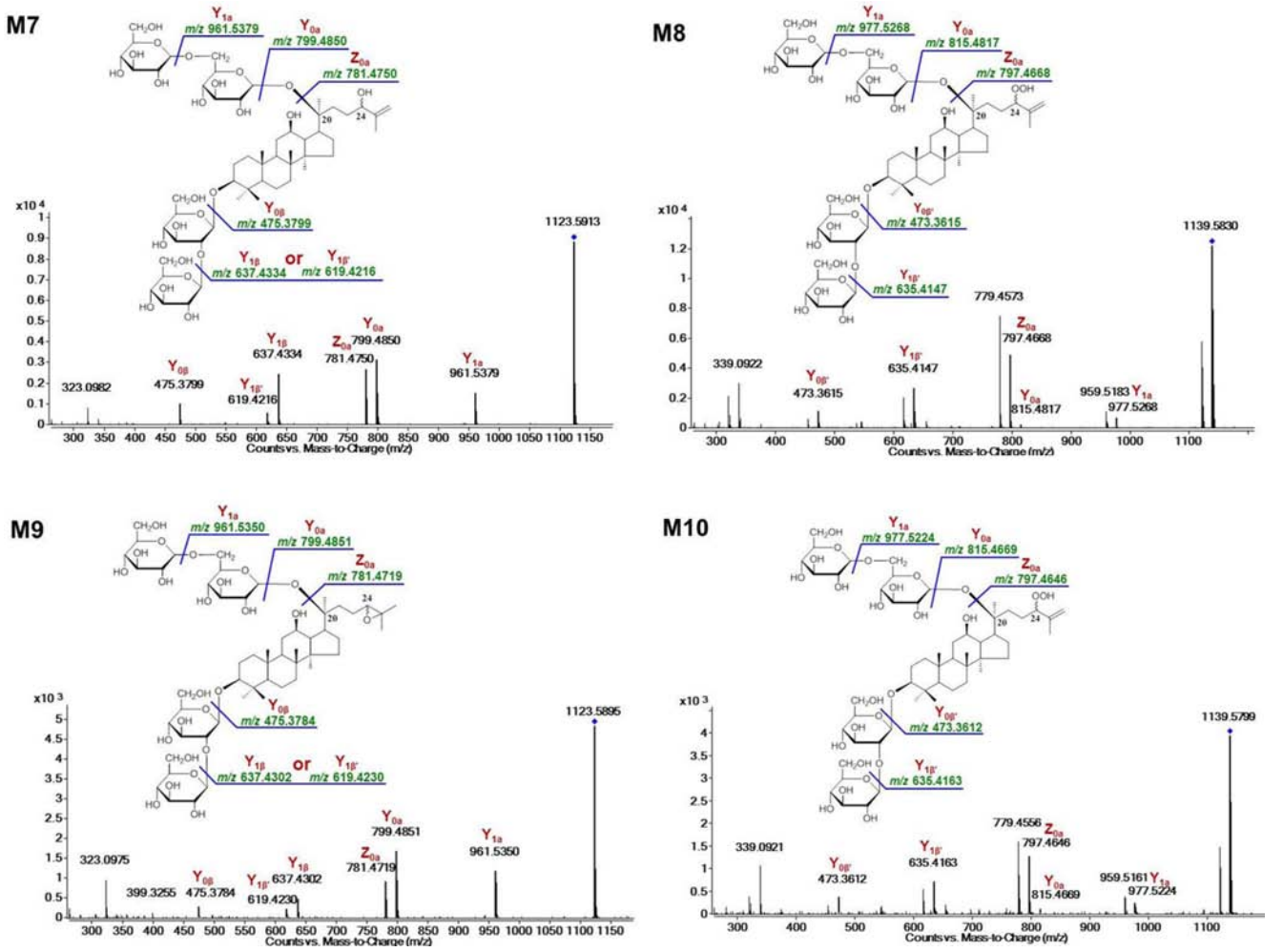

Figure 2. High-resolution MS/MS of urinary **M1**−**M10** obtained on Q-TOF MS.

formic acid in Milli-Q water (A) and ACN containing 0.1% formic acid (B). The optimized UPLC elution condition as follows was employed: from 10 to 40% B at 0−23 min, from 40 to 85% B at 23−27 min, from 85 to 100% B at 27−29 min, and finally maintained at 100% B for 3 min at a flow rate of 0.35 mL/min. The injection volume was 5 μL.

The ESI-MS was performed in the negative mode, and the source parameters were as follows: dry gas (N_2) temperature and flow rate were 325 °C and 11 L/min, respectively; sheath gas (N_2) temperature and flow rate were 350 °C and 11 L/min, respectively; nebulizer, 40 psi; fragmentor voltage, 175 V; skimmer voltage, 65 V. The acquisition mass range was m/z 100−1700, and the MS scan rate was 2 spectra/s. A reference solution was nebulized for continuous calibration in the negative mode using the reference masses of m/z 112.9856 and 966.0007. The targeted MS/MS collision energy (CE) was set at three different values from 20 to 60 eV. All MS and MS/MS data were processed using Agilent MassHunter Qualitative Analysis B.06.00 software.

In Vivo Metabolism of Ginsenoside Rb_1 Following Intravenous Injection and Oral Administration in Rat. Ginsenoside Rb_1 was first dissolved in saline (8 mg/mL), and then a single intravenous (iv) dose of Rb_1 solution (20 mg/kg) was given through the caudal vein. The blood (0.2 mL) was withdrawn via medial canthus of the eye at 0, 5, 15, and 30 min and 1, 2, 3, 4, 5, 6, 7, 24, and 48 h postadministration. One hundred microliters of plasma was collected by centrifuging the blood at 4000 rpm for 5 min, and then 200 μL of ACN was added for protein precipitation and ginsenoside extraction. After centrifugation at 14000 rpm for 5 min, the supernatant was transferred into a new tube and dried by speed vacuum. The residue was reconstituted with 100 μL of 50% MeOH. Each sample was centrifuged at 14000 rpm for 5 min before UPLC/TOF MS analysis. For oral administration, Rb_1 was dissolved in water (2.5 mg/mL) and given at a dose of 50 mg/kg. The blood (0.2 mL) was withdrawn via medial canthus of the eye at 0, 0.5, 1, 1.5, 2, 3, 4, 5, 6, 7, 8, 8.5, 9, 9.5, 10, 24, 27, and 34 h postadministration. Urine samples were collected at time intervals of 0−3, 3−7, 7−10, 10−24, and 24−34 h. For analysis, 1 mL of urine was extracted with 0.5 mL of water-saturated *n*-BuOH three times. The *n*-BuOH layers were then combined and dried by speed vacuum. The resulting residue was reconstituted in 100 μL of 50% MeOH and filtered through a 0.2 μm filter.

Chemical Synthesis of Oxygenated Metabolites. Photosensitized oxygenation was carried out to synthesize the oxygenated products following our protocol described previously.[23] Briefly, a solution of ginsenoside Rb_1 (150 mg) and Rose Bengal (150 mg) in 120 mL of MeOH was stirred and irradiated with a 400 W lamp under an oxygen atmosphere at room temperature for 6 h to synthesize crude dioxygenated Rb_1 (Rb_1 + 2O). Triphenylphosphine (35 mg) was further added to the reaction solution and was stirred at room temperature for 2 h for the production of crude mono-oxygenated Rb_1 (Rb_1 + O). Both solutions were evaporated to a small volume under reduced pressure and then directly subjected to a reverse phase preparative column, respectively (isocatic elution with 35% ACN at the flow rate of 2.5 mL/min) to give individual mono-oxygenated Rb_1 (Rb_1 + O (I), Rb_1 + O (II), and Rb_1 + O (III)) and individual dioxygenated Rb_1 (Rb_1 + 2O (I), Rb_1 + 2O (II), and Rb_1 + 2O (III)).

Epoxidation was performed following the procedures described in the literature with minor modifications in our laboratory.[23] Briefly, a solution of ginsenoside Rb_1 (100 mg) in ACN (10 mL) was mixed with an aqueous EDTA-Na solution (0.4 μM, 10 mL). The mixed

DOI: 10.1021/acs.jafc.5b00710
J. Agric. Food Chem. 2015, 63, 2689−2700

Table 1. Characterized Metabolites in Rat Urine Following Intravenous Injection of Rb_1 at a Dosage of 20 mg/kg ($[M - H]^-$ as Precursor Ion)

metabolite	RT (min)	theor mass (m/z)	measured mass (m/z)	error (ppm)	molecular formula	CID (m/z)
ginsenoside Rb_1	18.8	1107.5957	1107.5984	2.44	$C_{54}H_{92}O_{23}$	945.5415 $[M - Glc - H]^-$, 783.4899 $[M - 2Glc - H]^-$, 621.4332 $[M - 3Glc - H]^-$, 459.3839 $[M - 4Glc - H]^-$
M1 (Rb_1 + O + H_2O)	10.9	1141.6011	1141.6005	−0.53	$C_{54}H_{94}O_{25}$	979.5511 $[M - Glc - H]^-$, 817.4891 $[M - 2Glc - H]^-$, 799.4822 $[M - 2Glc - H_2O - H]^-$, 655.4423 $[M - 3Glc - H]^-$, 493.3872 $[M - 4Glc - H]^-$
M2 (Rb_1 + O + H_2O)	12.1	1141.6011	1141.6026	1.31	$C_{54}H_{94}O_{25}$	979.5415 $[M - Glc - H]^-$, 817.4904 $[M - 2Glc - H]^-$, 799.4829 $[M - 2Glc - H_2O - H]^-$, 655.4440 $[M - 3Glc - H]^-$, 493.3920 $[M - 4Glc - H]^-$
M3 (Rb_1 + O)	13.3	1123.5906	1123.5912	0.53	$C_{54}H_{92}O_{24}$	961.5493 $[M - Glc - H]^-$, 799.4850 $[M - 2Glc - H]^-$, 781.4752 $[M - 2Glc - H_2O - H]^-$, 637.4320 $[M - 3Glc - H]^-$, 619.4202 $[M - 3Glc - H_2O - H]^-$, 475.3919 $[M - 4Glc - H]^-$
M4 (Rb_1 + O)	13.9	1123.5906	1123.5916	0.89	$C_{54}H_{92}O_{24}$	961.5373 $[M - Glc - H]^-$, 799.4833 $[M - 2Glc - H]^-$, 781.4724 $[M - 2Glc - H_2O - H]^-$, 637.4305 $[M - 3Glc - H]^-$, 619.4211 $[M - 3Glc - H_2O - H]^-$, 475.3794 $[M - 4Glc - H]^-$
M5 (Rb_1 + O)	14.1	1123.5906	1123.5923	1.51	$C_{54}H_{92}O_{24}$	961.5351 $[M - Glc - H]^-$, 799.4841 $[M - 2Glc - H]^-$, 781.4734 $[M - 2Glc - H_2O - H]^-$, 637.4296 $[M - 3Glc - H]^-$, 475.3786 $[M - 4Glc - H]^-$
M6 (Rb_1 + 2O)	14.2	1139.5855	1139.5863	0.70	$C_{54}H_{92}O_{25}$	977.5209 $[M - Glc - H]^-$, 815.4768 $[M - 2Glc - H]^-$, 797.4663 $[M - 2Glc - H_2O - H]^-$, 635.4172 $[M - 3Glc - H_2O - H]^-$
M7 (Rb_1 + O)	14.3	1123.5906	1123.5939	2.94	$C_{54}H_{92}O_{24}$	961.5379 $[M - Glc - H]^-$, 799.4850 $[M - 2Glc - H]^-$, 781.4750 $[M - 2Glc - H_2O - H]^-$, 637.4334 $[M - 3Glc - H]^-$, 619.4216 $[M - 3Glc - H_2O - H]^-$, 475.3799 $[M - 4Glc - H]^-$
M8 (Rb_1 + 2O)	14.5	1139.5855	1139.5839	−1.40	$C_{54}H_{92}O_{25}$	977.5268 $[M - Glc - H]^-$, 815.4817 $[M - 2Glc - H]^-$, 797.4668 $[M - 2Glc - H_2O - H]^-$, 635.4147 $[M - 3Glc - H_2O - H]^-$, 473.3615 $[M - 4Glc - H_2O - H]^-$
M9 (Rb_1 + O)	14.6	1123.5906	1123.5937	2.76	$C_{54}H_{92}O_{24}$	961.5350 $[M - Glc - H]^-$, 799.4851 $[M - 2Glc - H]^-$, 781.4719 $[M - 2Glc - H_2O - H]^-$, 637.4302 $[M - 3Glc - H]^-$, 619.4230 $[M - 3Glc - H_2O - H]^-$, 475.3784 $[M - 4Glc - H]^-$
M10 (Rb_1 + 2O)	15.2	1139.5855	1139.5887	2.81	$C_{54}H_{92}O_{25}$	977.5224 $[M - Glc - H]^-$, 815.4669 $[M - 2Glc - H]^-$, 797.4646 $[M - 2Glc - H_2O - H]^-$, 635.4163 $[M - 3Glc - H_2O - H]^-$, 473.3612 $[M - 4Glc - H_2O - H]^-$
M11 (Rb_1+O-2H)	14.9	1121.5749	1121.577	1.87	$C_{54}H_{90}O_{24}$	959.5001 $[M - Glc - H]^-$, 797.4634 $[M - 2Glc - H]^-$, 779.4618 $[M - 2Glc - H_2O - H]^-$, 635.4229 $[M - 3Glc - H]^-$
M12 (Rd + O)	14.9	961.5378	961.5373	−0.52	$C_{48}H_{82}O_{19}$	799.4759 $[M - Glc - H]^-$, 781.4677 $[M - Glc - H_2O - H]^-$, 637.5666 $[M - 2Glc - H]^-$
M13 (Rk_1/Rg_5 + 2O − 2H)	16.1	795.4536	795.453	−0.75	$C_{42}H_{68}O_{14}$	633.4008 $[M - Glc - H]^-$, 615.3908 $[M - Glc - H_2O - H]^-$, 471.3461 $[M - 2Glc - H]^-$, 453.3372 $[M - 2Glc - H_2O - H]^-$
M14 (Rd + O)	16.4	961.5378	961.5369	−0.94	$C_{48}H_{82}O_{19}$	799.4733 $[M - Glc - H]^-$, 637.4408 $[M - 2Glc - H]^-$
M15 (Rb_1 − 2H)	18.1	1105.5800	1105.5805	0.45	$C_{54}H_{90}O_{23}$	943.5252 $[M - Glc - H]^-$, 781.4723 $[M - 2Glc - H]^-$, 619.4136 $[M - 3Glc - H]^-$, 457.3683 $[M - 4Glc - H]^-$
M16 (Rd)	21.5	945.5428	945.5426	−0.21	$C_{48}H_{82}O_{18}$	783.4869 $[M - Glc - H]^-$, 621.4342 $[M - 2Glc - H]^-$, 459.3834 $[M - 3Glc - H]^-$
M17 (F_2)	25.1	783.4900	783.4903	0.38	$C_{42}H_{72}O_{13}$	621.4317 $[M - Glc - H]^-$, 459.3831 $[M - 2Glc - H]^-$
M18 [20(*S*)-Rg_3]	25.7	783.4900	783.4899	−0.13	$C_{42}H_{72}O_{13}$	621.4298 $[M - Glc - H]^-$

DOI: 10.1021/acs.jafc.5b00710
J. Agric. Food Chem. 2015, 63, 2689−2700

Scheme 1. Chemical Synthesis of Mono- and Dioxygenated Derivatives of Ginsenoside Rb_1

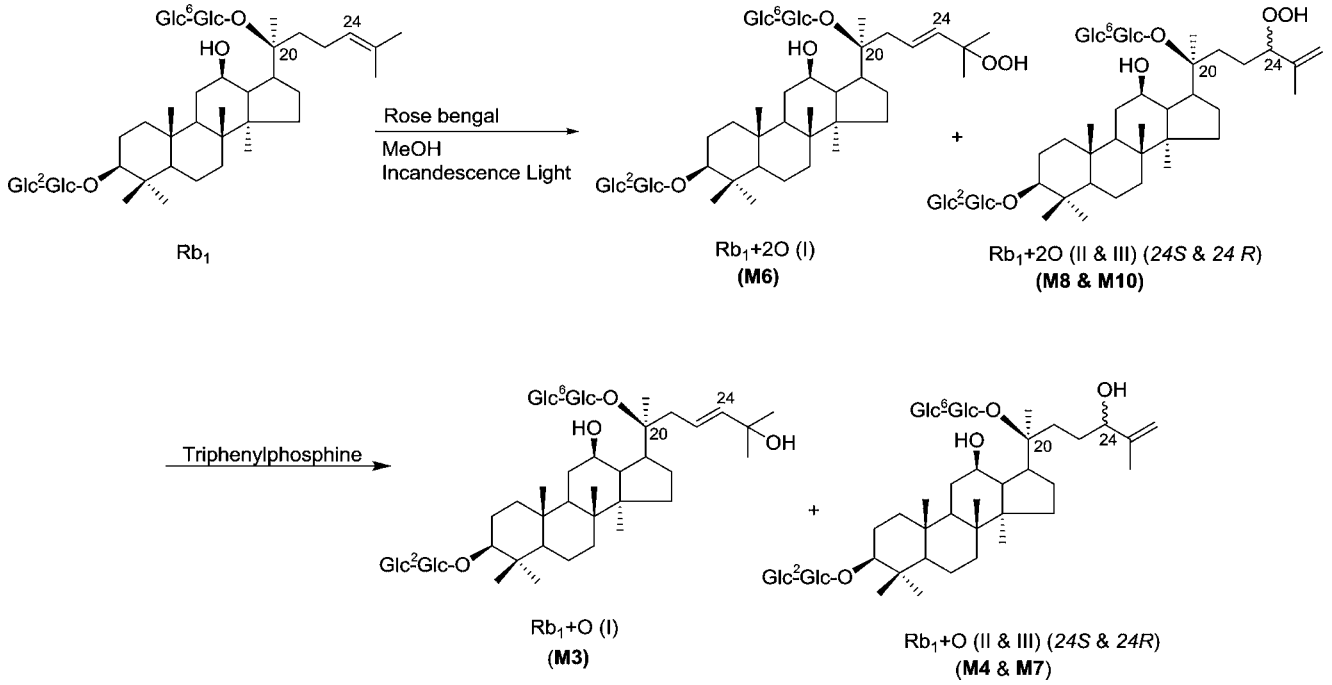

solution was cooled to 0 °C, and then an epoxidation dibetal catalyst solution (ketone, 15 mM in ACN) and a mixture of sodium bicarbonate (67.5 mM) and OXONE (45 mM) were added. The homogeneous solution was stirred for 2 h. Because the epoxide was quite unstable and easily changed to diol (Rb_1 + O + H_2O) as a byproduct, a mixture of Rb_1 epoxides (Rb_1-Epo) and diols (Rb_1 + O + H_2O) appeared in the reaction solution. The reaction solution was reduced in volume by speed vacuum under low temperature and then was directly subjected to a reverse phase preparative column (gradient elution with 10−35% ACN at the flow rate of 2.5 mL/min) to afford individual Rb_1 epoxides (Rb_1-Epo (I) and Rb_1-Epo (II)) and individual Rb_1 diols (Rb_1 + O + H_2O (I) and Rb_1 + O + H_2O (II)).

Chemical structures of the synthesized metabolites were characterized on the basis of the elucidation of NMR data. ^1H and ^{13}C NMR data were measured on a Bruker Ascend 600 NMR spectrometer (600 MHz for ^1H NMR and 150 MHz for ^{13}C NMR).

In Vitro Metabolism of Ginsenoside Rb_1. Metabolism of ginsenoside Rb_1 in liver microsomes and S9 fraction was carried out initially by dissolving Rb_1 in potassium phosphate buffer (pH 7.4), followed by the addition of NADPH Regenerating System Solutions A and B. After prewarming at 37 °C for 5 min, liver microsomes or S9 fraction was added and incubated at 37 °C for 2 h. The reaction was quenched by adding 2-fold ACN for protein precipitation and ginsenoside extraction. After centrifugation at 14000 rpm for 5 min, the supernatant was collected for analysis.

Ginsenoside Rb_1 was spiked in fresh blood, red blood cells, and plasma, respectively. After incubation at 37 °C for 2 h, 100 μL of H_2O was added in the red blood cell sample and incubated at 37 °C for 5 min, whereas plasma was collected from whole blood by centrifugation at 4000 rpm for 5 min. Two-fold ACN was added in the cell lysed sample or plasma for protein precipitation and ginsenoside extraction. After centrifugation at 14000 rpm for 5 min, the supernatant was collected for analysis.

RESULTS

Characterization of Oxygenated Metabolites of Ginsenoside Rb_1 in Rat Urine and Plasma after Intravenous Administration. It has been suggested that oxygenated metabolites of ginsenosides were majorly derived from tissue oxidation.[27] Therefore, oxygenated metabolites of Rb_1 in plasma and urine following iv administration were examined first. All possible metabolites were screened and compared with the profiles of the blank plasma and urine samples collected before administration. As a result, the metabolite profile in plasma samples was found to be generally consistent with that of urine samples (Figure 1A, B), but metabolites in urine samples appeared to be more abundant and diverse (Figure 1B) and therefore were characterized first.

As shown in Figure 1, in total 18 metabolites (**M1**−**M18**) appeared in urine after dosing, among which three groups of peaks corresponding to oxygenated metabolites could be clearly observed at retention times smaller than that of Rb_1 (chromatograms of blank samples are given in the Supporting Information). The first group of the peaks (**M1** and **M2**) (t_R of 10.5−12.5 min) gave $[M - H]^-$ ion peaks at m/z exactly 34 Da more than that of Rb_1, indicating introduction of an O and an H_2O into the molecule of Rb_1, which was confirmed by the molecular formula derived from accurate mass. The MS/MS spectra of **M1** and **M2** showed fragment ions corresponding to the sequential loss of glucose moieties (Figure 2; Table 1). The product ion derived from the loss of all sugar moieties was observed at m/z 493.3872, which was 34 Da greater than corresponding product ion of Rb_1 at m/z 459.3839, indicating that the additional O and H_2O were located on the aglycone moiety. The second group of metabolites (t_R of 13.0−15.0 min) (**M3**, **M4**, **M5**, **M7**, and **M9**) gave $[M - H]^-$ ions that can be assigned as Rb_1 + O on the basis of the accurate mass and isotope abundance, showing that these five metabolites were mono-oxygenated derivatives of Rb_1. Targeted MS/MS experiments of these metabolites gave fragment ions derived from sequential cleavage of glycosidic bonds (Figure 2; Table 1), indicating the introduction of an O atom into the aglycone moiety of these metabolites. The last group of peaks (t_R of 14.0−15.5 min) (**M6**, **M8**, and **M10**) was assigned as dioxygenated metabolites of Rb_1 on the basis of accurate mass and isotope cluster information. MS/MS experiment revealed that the dioxygenation occurred at the aglycone

DOI: 10.1021/acs.jafc.5b00710
J. Agric. Food Chem. 2015, 63, 2689−2700

Scheme 2. Chemical Synthesis of Rb_1 Epoxides and Corresponding Diols

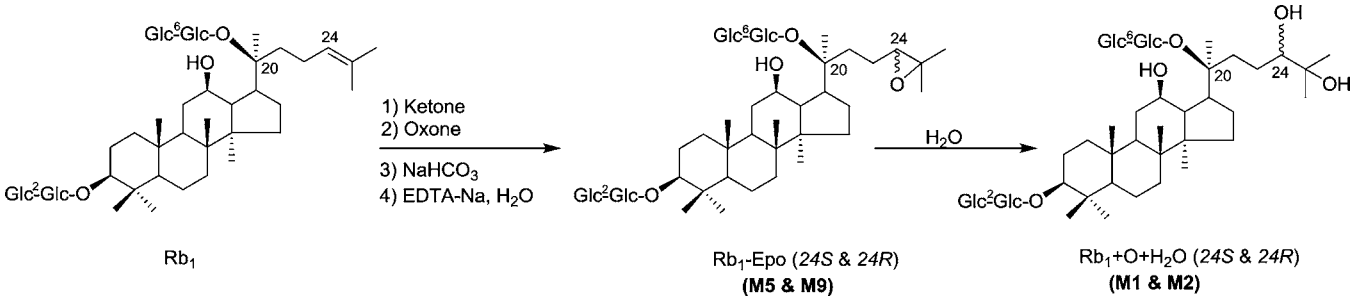

moiety (Figure 2; Table 1). In all of the high-resolution MS/MS spectra of **M1**−**M10** obtained on Q-TOF MS, the sequential fragment resulting from the loss of sugar could be clearly observed (Figure 2).

Although all above oxygenations were suggested to occur on the aglycone part by MS/MS experiments, further structural information related to the exact oxygenation site cannot be obtained solely on the basis of MS/MS experiment. Therefore, possible oxygenated metabolites were chemically synthesized for further characterization. Taking into consideration the chemical characteristic of Rb_1, as well as the possible oxygenation pathway that may lead to the incorporation of an oxygen atom into the molecule, we speculated that Rb_1 may undergo initial oxygenation via either epoxidation or hydroxylation along with displacement of the double bond of the side chain. Therefore, we synthesized epoxides of Rb_1 and photosensitized Rb_1 by using Rb_1 as starting material (Schemes 1 and 2). Chemical structures of these synthesized metabolites were characterized on the basis of spectroscopic data (Supporting Information). They were used as authentic standards for the identification of the above-mentioned oxygenated metabolites (Figure 3).

The synthesized compounds were then employed as standards for the identification of the oxygenated metabolites, which was implemented by comparing retention time, high-resolution MS, and MS/MS pattern of the metabolites with those of synthesized standards. Consequently, **M1** and **M2** were identified as a pair of enantiomers (24α- and 24β-forms) of 3-*O*-[β-D-glucopyranosyl (1→2)-β-D-glucopyranosyl]-20-*O*-[β-D-glucopyranosyl (1→6)-β-D-glucopyranosyl] 3β,12β,20-(*S*),24,25-pentahydroxy-dammarane (quinquenoside L16).[30] The three major mono-oxygenated metabolites (**M3**, **M4**, and **M7**) were identified as 24- and 25-hydroxyl derivatives of Rb_1, that is, 3-*O*-[β-D-glucopyranosyl (1→2)-β-D-glucopyranosyl]-20-*O*-[β-D-glucopyranosyl (1→6)-β-D-glucopyranosyl] 3β,12β,20(*S*),25-tetrahydroxy-dammar-23-ene (notoginsenoside A) (**M3**),[31] 3-*O*-[β-D-glucopyranosyl (1→2)-β-D-glucopyranosyl]-20-*O*-[β-D-glucopyranosyl (1→6)-β-D-glucopyranosyl] 3β,12β,20(*S*)-trihydroxy-24ξ-hydroxydammar-25-ene (ginsenoside V) (**M4** and **M7**),[32] whereas the two minor mono-oxygenated metabolites (**M5** and **M9**) were characterized to be epoxyginsenoside Rb_1 (24α- and 24β-forms).[33,34] The three dioxygenated metabolites (**M6**, **M8**, and **M10**) were identified as 24- and 25-hydroperoxides of Rb_1, that is, 3-*O*-[β-D-glucopyranosyl (1→2)-β-D-glucopyranosyl]-20-*O*-[β-D-glucopyranosyl (1→6)-β-D-glucopyranosyl] 3β,12β,20(*S*)-trihydroxy-25-hydroperoxydammar-23-ene (notoginsenoside K) (**M6**)[35] and 3-*O*-[β-D-glucopyranosyl (1→2)-β-D-glucopyranosyl]-20-*O*-[β-D-glucopyranosyl (1→6)-β-D-glucopyranosyl] 3β,12β,20(*S*)-trihydroxy-24ξ-hydroperoxydammar-25-ene (notoginsenoside C)

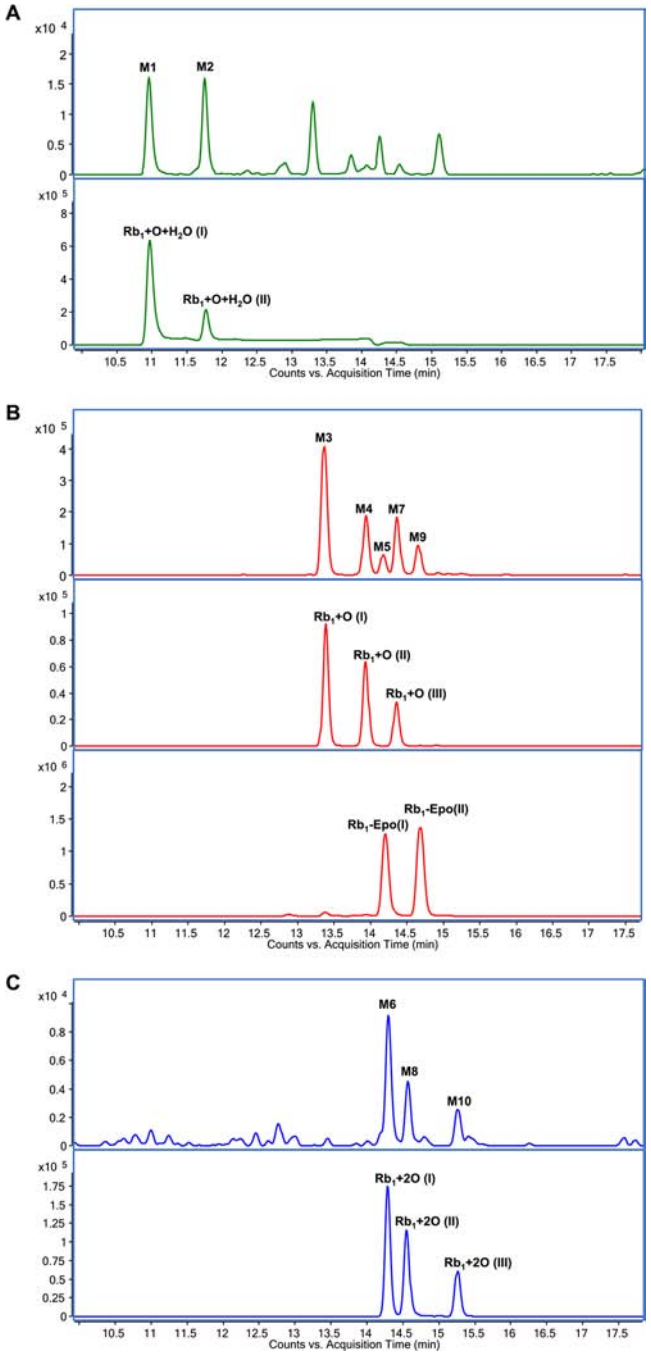

Figure 3. Characterization of oxygenated urinary metabolites **M1**−**M10** (A−C, upper panels) by comparison with synthesized authentic metabolites (A−C, lower panels).

DOI: 10.1021/acs.jafc.5b00710
J. Agric. Food Chem. 2015, 63, 2689−2700

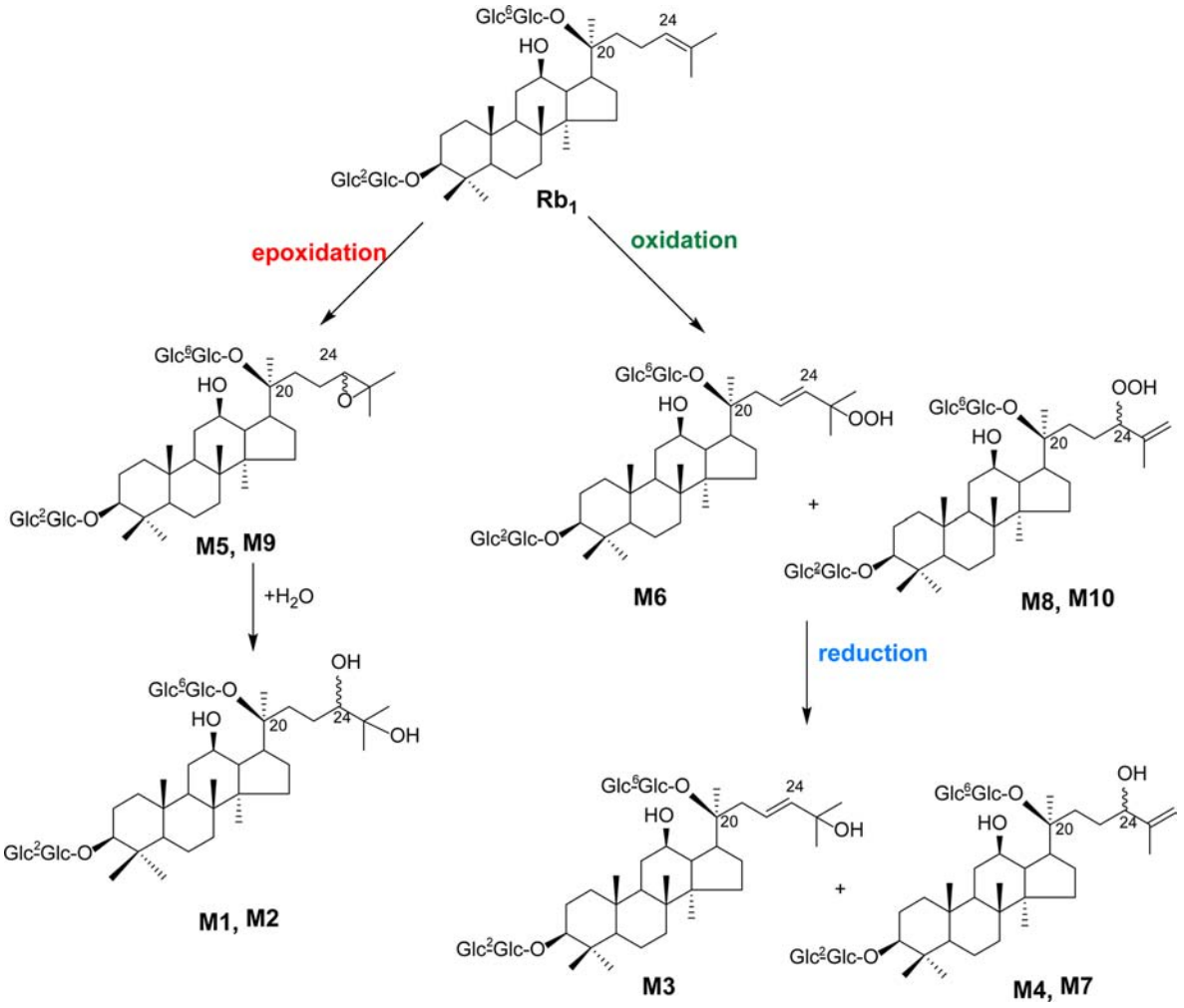

Figure 4. Proposed oxygenation metabolism pathway of ginsenoside Rb_1 in vivo.

(**M8** and **M10**).[31] A metabolism pathway of the major oxygenated metabolites is proposed in Figure 4.

In addition to the major oxygenated metabolites, another eight metabolites (**M11**–**M18**) were observed in rat urine after iv administration of Rb_1 (Figure 1; Table 1). On the basis of the molecular formula derived from accurate mass, **M11** was assigned as dehydrogenation product of mono-oxygenated Rb_1 (Rb_1 + O − 2H). **M12** and **M14** were tentatively identified as mono-oxygenated Rd (Rd + O). **M13** was assigned as Rk_1/Rg_5 + 2O − 2H. **M15** was identified to be the dehydrogenated derivative of Rb_1 (Rb_1 − 2H), whereas **M16**, **M17**, and **M18** were characterized as Rd, F_2, and 20(*S*)-Rg_3 respectively, all of which were deglycosylated products of Rb_1. Characterization of **M16**–**M18** was further confirmed by comparison with authentic ginsenosides, suggesting that deglycosylation is another metabolic pathway of primary ginsenosides in the circulating system (Table 1).

In plasma samples, metabolites **M1** and **M2**, as well as five mono-oxygenated metabolites (**M3**, **M4**, **M5**, **M7**, and **M9**), can be clearly observed. Dehydrogenated metabolites (**M15**) and deglycosylated metabolites (**M16**, **M17**, and **M18**) also appeared in the bloodstream. However, three dioxygenated metabolites (**M6**, **M8**, and **M10**) together with oxygenated metabolites of secondary ginsenoside, that is, **M12** and **M14** (Rd + O) and **M13** (Rk_1/Rg_5 + 2O − 2H), were absent in plasma samples. Because these urinary metabolites possessed increased polarity relative to their parent ginsenosides, their absence in plasma might be due to fast elimination through kidney clearance. By contrast, the relative levels of the deglycosylated metabolites (**M16**–**M18**) in plasma were obviously higher than those in urine, implying that these metabolites were excreted into urine very slowly and thereby accumulated in the bloodstream.

Metabolite Profile in Rat Urine and Plasma after Oral Administration of Rb_1. After oral administration of Rb_1, metabolites in rat plasma and urine were characterized by using a similar approach as that for the iv dose. Metabolites in both plasma and urine after oral administration were significantly less than that observed for iv administration. In plasma, nine metabolites in total were detected (Figure 5A), including three mono-oxygenated metabolites (**M3**, **M4**, and **M7**), two dehydrogenated metabolites (**M11** and **M15**), and two deglycosylated metabolites (**M16** and **M18**), as well as oxygenated Rg_3 (**M19**). Mono-oxygenated Rb_1, **M3**, **M4**, and **M7** were found to be the major metabolites of Rb_1 appearing in the circulating system. The existence of these metabolites in blank plasma and urine samples was examined, and the results suggested that these metabolites were derived from the metabolism of ginsenosides rather than interferences pre-existing in plasma or urine (Supporting Information).

To survey the systemic availability of these metabolites, rat plasma samples collected at different time points were

DOI: 10.1021/acs.jafc.5b00710
J. Agric. Food Chem. 2015, 63, 2689−2700

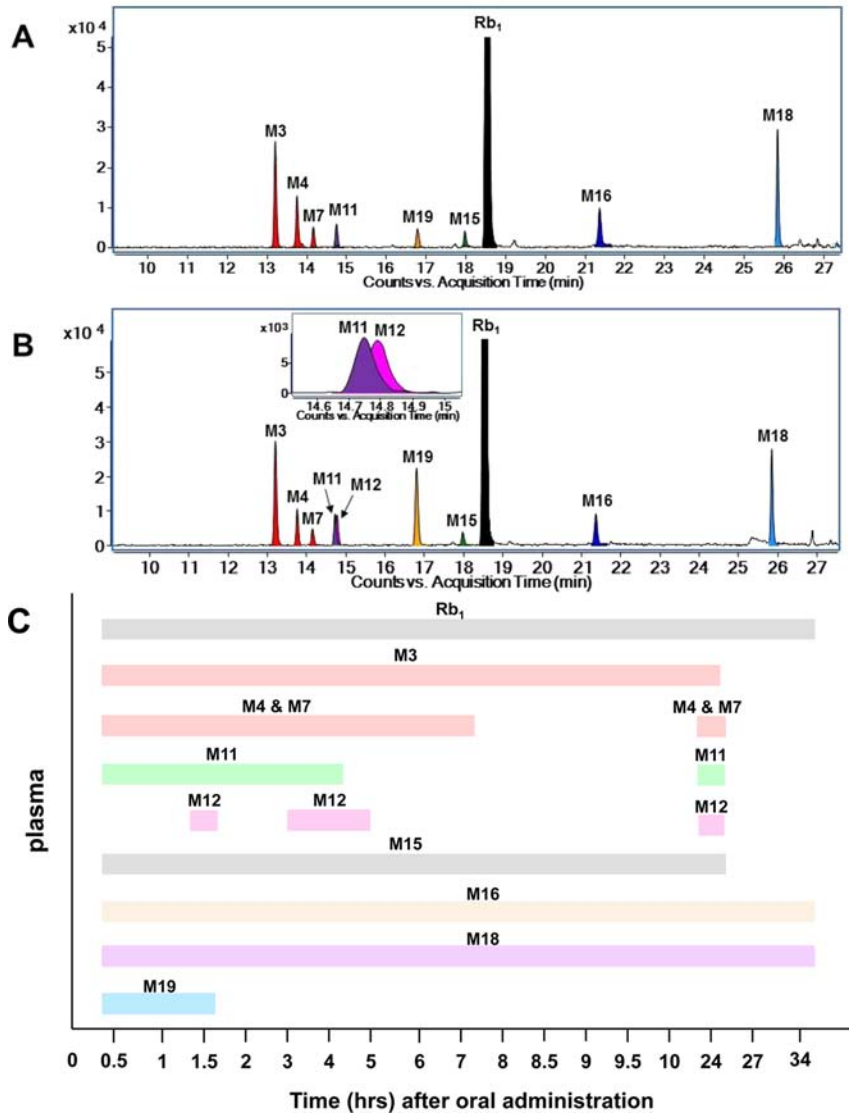

Figure 5. Ginsenoside Rb_1 and its metabolites identified in plasma following oral administration: (A, B) extracted compound chromatograms (ECC) of metabolites identified in plasma collected at 0.5 and 1.5 h after oral dose of Rb_1; (C) appearance of metabolites in rat plasma at different time intervals after oral dose of Rb_1.

examined for all identified metabolites. As shown in Figure 5C, Rb_1, **M3**, **M15**, **M16**, and **M18** were found to be continuously present in the bloodstream for >24 h. However, **M4**, **M7**, **M11**, and **M12** appeared in the plasma at intervals of 0−8 h and after 24 h, whereas the oral administration-specific metabolite **M19** was measured within only 1.5 h after administration. The time duration for the occurrence of the metabolites provided clues for their metabolism site. For instance, the metabolites detected at the early stage, for example, oxygenated Rd (**M12**), might result from oxidation of deglycosylated metabolites that derived from gastric acid decomposition. By contrast, the oxygenated Rd observed at the late stage might result from tissue oxidation of intestinal-decomposed Rb_1.

The plasma metabolites were also excreted into urine (Figure 6A). Twelve metabolites were detected in urine, among which **M1**, **M2**, and **M9** were not found in plasma. The appearance duration of these metabolites in urine showed certain differences. Seven abundant metabolites, **M3**, **M4**, **M7**, **M11**, **M12**, **M15**, **M16**, and **M18**, were detected in urine samples for a long duration (up to 24 h). Less abundant metabolites, **M1**, **M2**, and **M9**, were mainly measured in urine samples within 7 h after oral administration, whereas **M19** appeared in urine only within 3 h after oral dose.

In Vitro Metabolism of Rb_1 in Liver Microsomes, S9 Fraction, and Rat Blood. To get information about the metabolism site of the oxygenated metabolites, in vitro metabolism of Rb_1 in liver microsomes and blood was investigated. Hepatic metabolism is the leading drug disposition pathway because liver is the major site of drug metabolism in which a complex array of phase I, phase II, and phase III transporter systems function in the systemic clearance of xenobiotics. Several studies have revealed the involvement of P450-mediated metabolism in the elimination of secondary ginsenosides and proposed oxygenation as the major metabolic pathway.[19,20,22,36] Therefore, biotransformation of Rb_1 in liver microsomes and S9 fraction was examined. However, neither oxygenated products nor other metabolites were observed during the incubation duration of 2 h. The results were consistent with that observed for the primary PPT-type ginsenosides.[29] Similarly, no metabolites of Rb_1 were detected

DOI: 10.1021/acs.jafc.5b00710
J. Agric. Food Chem. 2015, 63, 2689−2700

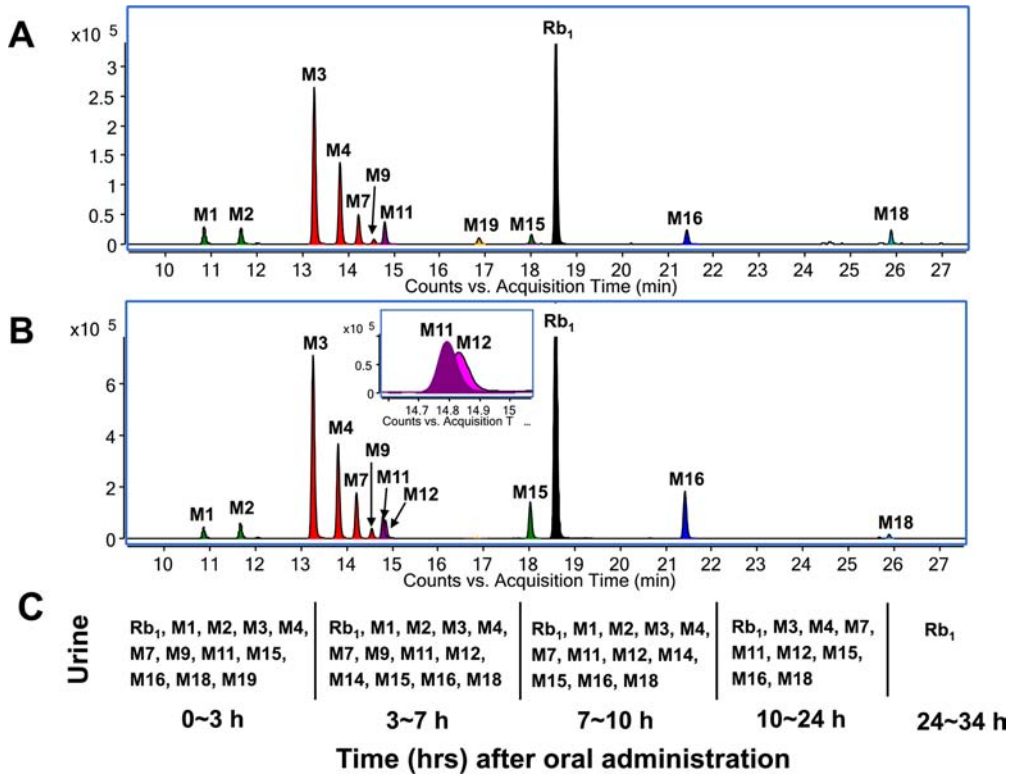

Figure 6. Ginsenoside Rb_1 and its metabolites identified in urine following oral administration: (A, B) extracted compound chromatograms (ECC) of metabolites identified in urine samples collected at 0−3 and 3−7 h after oral dose of Rb_1; (C) appearance of metabolites in rat urine at different time intervals after oral dose of Rb_1.

when it was incubated in fresh blood, red blood cells, and plasma for 2 h, showing that Rb_1 was quite stable in blood. These results suggested that oxygenated metabolites of Rb_1 might result from tissue oxidation as previously suggested.[27]

DISCUSSION

Primary ginsenosides such as Rb_1 and Rg_1, although poorly absorbed after oral administration, were still demonstrated to be relatively abundant ginsenosides reaching the circulation system after oral administration of notoginseng extract, in comparison with secondary ginsenosides such as Rg_3 and Rg_2.[27] In multiple-dose treatment, the primary ginsenosides were found to further accumulate substantially in the systemic circulation, resulting in a considerably higher plasma level.[26] Metabolism of the primary ginsenosides after entering the bloodstream represented one of the essential issues for further evaluation of these intact ginsenosides. Tissue oxygenation has been suggested to be the major metabolism pathway of primary ginsenosides apart from deglycosylation and dehydration in the gastrointestinal tract.[20,24] The resulting mono-oxygenated metabolites were further estimated to account for about 10−15% elimination of intravenously administered Rb_1 in a single iv dose.[27] These results collectively directed the necessity for the characterization of the chemical structures of oxygenated metabolites.

To overcome the technique limitations for structural characterization of metabolites, that is, accumulating adequate amount of metabolites for NMR measurements, we utilized a chemical synthesis approach to obtain chemical standards and unambiguously identified five mono-oxygenated metabolites, three dioxygenated metabolites, and two diol metabolites of Rb_1 in plasma and urine for the first time.

By using such a chemical synthesis approach, we confirmed the generation of two 24,25-epoxides (**M5** and **M9**) of primary ginsenoside as circulating metabolites in plasma and urine. Oxidation of the olefin bond to form epoxide is a well-known oxidation reaction catalyzed by CYP and therefore was proposed to be an important oxidation pathway of ginsenosides in several previous studies.[25,28,29] However, as epoxides are quite reactive due to ring strain, their rearranged products, 20,24-epoxides, are usually observed as the final oxygenated metabolites. Alternatively, the reactive epoxides were captured with nucleophile trapping agents such as GSH to confirm the formation of these bioactive metabolites, whereas the epoxides themselves were normally undetectable. Our study represents the first report of the direct detection of 24,25-epoxides of Rb_1 (**M5** and **M9**) as in vivo metabolites. Accordingly, the diols of Rb_1 (**M1** and **M2**) were identified unambiguously as the in vivo metabolites of Rb_1 for the first time.

Notably, after oral administration, mono-oxygenated metabolites (**M3**, **M4**, and **M7**) represented major metabolites of Rb_1 reaching the circulation system and appearing in the bloodstream once Rb_1 was absorbed. These oxygenated metabolites presented in plasma continuously for 8−24 h after orally taken. Two diol metabolites (**M1** and **M2**) also appeared in urine samples as abundant metabolites. As the sequential metabolites of epoxides (**M5** and **M9**), the appearance of **M1** and **M2** in urine suggested the formation of 24,25-epoxides of Rb_1 in the circulation system. These results concomitantly indicated notable exposure of oxygenated metabolites of Rb_1 after oral administration.

The oxygenated metabolism of ginsenosides with additional hydroxyl or epoxy groups in the side chain may lead to changes in the bioactivity. It has been reported that notoginsenoside H,

DOI: 10.1021/acs.jafc.5b00710
J. Agric. Food Chem. 2015, 63, 2689−2700

a saponin having a side chain the same as that of metabolite **M3**, exhibited immunological adjuvant activity by profoundly increasing the level of IgG in mice sensitized with ovalbumin. Rb_1 epoxide is a patented apoptosis inhibitor and regeneration promoter,[33] implicating its potential bioactivity. On the basis of the mass of the evidence, the mono-oxygenated metabolites of ginsenosides might contribute to the observed pharmacological activity and therapeutic effect of ginsenosides and ginseng product, which needs to be further explored.

Collectively, the structures of 10 oxygenated metabolites in rat urine and plasma after iv administration of Rb_1 were unambiguously characterized. These metabolites were further proved to be major metabolites of ginsenoside Rb_1 appearing in the bloodstream after oral administration. As the major circulating metabolites of ginsenoside Rb_1 after both intravenous injection and oral administration, these metabolites have great potential to be responsible for the observed pharmacological activity and therapeutic effect of ginsenosides. Therefore, exact characterization of the chemical structures of these circulating oxygenated metabolites would shed light on the clarification of possible toxic or pharmacologically active metabolites, thus providing valuable information for explaining the multiple pharmacological activities of ginseng products. The results were also informative for the design of the next generation of drugs to circumvent the undesired metabolic fate of ginsenosides. Moreover, clarification of metabolites reaching the circulation system will lay the foundation for the assessment of pharmacokinetics of ginsenosides and its metabolites. Corresponding results will in turn provide important clues pertaining to various aspects of the disposition of ginsenosides, including first-pass metabolism, elimination half-life, and overall bioavailability.

■ ASSOCIATED CONTENT

Supporting Information

Characterization of **M1**−**M10**. This material is available free of charge via the Internet at http://pubs.acs.org.

■ AUTHOR INFORMATION

Corresponding Authors

*(Z.-H.J.) E-mail: zhjiang@must.edu.mo. Phone: + 853-8897 2777. Fax: + 853-2882 5886;

*(L.L.) E-mail: lliu@must.edu.mo. Phone: +853-8897 2077. Fax: +853-2882 7222.

Funding

This project is sponsored by the Macao Science and Technology Development Fund (066/2011/A3 to J.-R.W.) and the National Institutes of Health, USA (AT005522-03).

Notes

The authors declare no competing financial interest.

■ REFERENCES

(1) Jia, L.; Zhao, Y.; Liang, X. J. Current evaluation of the millennium phytomedicine − ginseng (II): collected chemical entities, modern pharmacology, and clinical applications emanated from traditional Chinese medicine. *Curr. Med. Chem.* **2009**, *16*, 2924−2942.

(2) Ruan, J. Q.; Leong, W. I.; Yan, R.; Wang, Y. T. Characterization of metabolism and in vitro permeability study of notoginsenoside R1 from Radix notoginseng. *J. Agric. Food Chem.* **2010**, *58*, 5770−5776.

(3) He, N. W.; Zhao, Y.; Guo, L.; Shang, J.; Yang, X. B. Antioxidant, antiproliferative, and pro-apoptotic activities of a saponin extract derived from the roots of *Panax notoginseng* (Burk.) F.H. Chen. *J. Med. Food* **2012**, *15*, 350−359.

(4) Wang, J. R.; Yamasaki, Y.; Tanaka, T.; Kouno, I.; Jiang, Z. H. Dammarane-type triterpene saponins from the flowers of *Panax notoginseng*. *Molecules* **2009**, *14*, 2087−2094.

(5) Wang, J. R.; Leung, C. Y.; Ho, H. M.; Chai, S.; Yau, L. F.; Zhao, Z. Z.; Jiang, Z. H. Quantitative comparison of ginsenosides and polyacetylenes in wild and cultivated American ginseng. *Chem. Biodivers.* **2010**, *7*, 975−983.

(6) Xie, C. L.; Wang, W. W.; Xue, X. D.; Zhang, S. F.; Gan, J.; Liu, Z. G. A systematic review and meta-analysis of ginsenoside-Rg1 (G-Rg1) in experimental ischemic stroke. *Sci. Rep.* **2015**, *5*, 7790.

(7) Zhang, Y.; Yu, L.; Cai, W.; Fan, S.; Feng, L.; Ji, G.; Huang, C. Protopanaxatriol, a novel PPARγ antagonist from *Panax ginseng*, alleviates steatosis in mice. *Sci. Rep.* **2014**, *4*, 7375.

(8) Liu, J.-H.; Lee, C.-S.; Leung, K.-M.; Yan, Z.-K.; Shen, B.-H.; Zhao, Z.-Z.; Jiang, Z.-H. Quantification of two polyacetylenes in radix ginseng and roots of related *Panax* species using a gas chromatography-mass spectrometric method. *J. Agric. Food Chem.* **2007**, *55*, 8830−8835.

(9) Dong, H.; Bai, L. P.; Wong, V. K.; Zhou, H.; Wang, J. R.; Liu, Y.; Jiang, Z. H.; Liu, L. The in vitro structure-related anti-cancer activity of ginsenosides and their derivatives. *Molecules* **2011**, *16*, 10619−10630.

(10) Wong, V. K.; Cheung, S. S.; Li, T.; Jiang, Z. H.; Wang, J. R.; Dong, H.; Yi, X. Q.; Zhou, H.; Liu, L. Asian ginseng extract inhibits in vitro and in vivo growth of mouse lewis lung carcinoma via modulation of ERK-p53 and NF-κB signaling. *J. Cell. Biochem.* **2010**, *111*, 899−910.

(11) Kwok, H. H.; Guo, G. L.; Lau, J. K.; Cheng, Y. K.; Wang, J. R.; Jiang, Z. H.; Keung, M. H.; Mak, N. K.; Yue, P. Y.; Wong, R. N. Stereoisomers ginsenosides-20(S)-Rg(3) and -20(R)-Rg(3) differentially induce angiogenesis through peroxisome proliferator-activated receptor-γ. *Biochem. Pharmacol.* **2012**, *83*, 893−902.

(12) Xie, H. T.; Wang, G. J.; Sun, J. G.; Tucker, I.; Zhao, X. C.; Xie, Y. Y.; Li, H.; Jiang, X. L.; Wang, R.; Xu, M. J.; Wang, W. High performance liquid chromatographic-mass spectrometric determination of ginsenoside Rg3 and its metabolites in rat plasma using solid-phase extraction for pharmacokinetic studies. *J. Chromatogr., B* **2005**, *818*, 167−173.

(13) Xie, H. T.; Wang, G. J.; Lv, H.; Sun, R. W.; Jiang, X. L.; Li, H.; Wang, W.; Huang, C. R.; Xu, M. J. Development of a HPLC-MS assay for ginsenoside Rh2, a new anti-tumor substance from natural product and its pharacokinetic study in dogs. *Eur. J. Drug Metab. Pharmacokinet.* **2005**, *30*, 63−67.

(14) Bae, E. A.; Park, S. Y.; Kim, D. H. Constitutive β-glucosidases hydrolyzing ginsenoside Rb1 and Rb2 from human intestinal bacteria. *Biol. Pharm. Bull.* **2000**, *23*, 1481−1485.

(15) Yang, Z.; Wang, J. R.; Niu, T.; Gao, S.; Yin, T.; You, M.; Jiang, Z. H.; Hu, M. Inhibition of P-glycoprotein leads to improved oral bioavailability of compound K, an anticancer metabolite of red ginseng extract produced by gut microflora. *Drug Metab. Dispos.* **2012**, *40*, 1538−1544.

(16) Yang, Z.; Gao, S.; Wang, J.; Yin, T.; Teng, Y.; Wu, B.; You, M.; Jiang, Z.; Hu, M. Enhancement of oral bioavailability of 20(S)-ginsenoside Rh2 through improved understanding of its absorption and efflux mechanisms. *Drug Metab. Dispos.* **2011**, *39*, 1866−1872.

(17) Hasegawa, H. Proof of the mysterious efficacy of ginseng: basic and clinical trials: metabolic activation of ginsenoside: deglycosylation by intestinal bacteria and esterification with fatty acid. *J. Pharmacol. Sci.* **2004**, *95*, 153−157.

(18) Li, X.; Wang, G.; Sun, J.; Hao, H.; Xiong, Y.; Yan, B.; Zheng, Y.; Sheng, L. Pharmacokinetic and absolute bioavailability study of total panax notoginsenoside, a typical multiple constituent traditional chinese medicine (TCM) in rats. *Biol. Pharm. Bull.* **2007**, *30*, 847−851.

(19) Qian, T.; Cai, Z.; Wong, R. N.; Mak, N. K.; Jiang, Z. H. In vivo rat metabolism and pharmacokinetic studies of ginsenoside Rg3. *J. Chromatogr., B* **2005**, *816*, 223−232.

(20) Qian, T.; Jiang, Z. H.; Cai, Z. High-performance liquid chromatography coupled with tandem mass spectrometry applied for metabolic study of ginsenoside Rb1 on rat. *Anal. Biochem.* **2006**, *352*, 87−96.

DOI: 10.1021/acs.jafc.5b00710
J. Agric. Food Chem. 2015, 63, 2689−2700

(21) Lai, L.; Hao, H.; Liu, Y.; Zheng, C.; Wang, Q.; Wang, G.; Chen, X. Characterization of pharmacokinetic profiles and metabolic pathways of 20(S)-ginsenoside Rh1 in vivo and in vitro. *Planta Med.* **2009**, *75*, 797−802.
(22) Qian, T.; Cai, Z.; Wong, R. N.; Jiang, Z. H. Liquid chromatography/mass spectrometric analysis of rat samples for in vivo metabolism and pharmacokinetic studies of ginsenoside Rh2. *Rapid Commun. Mass Spectrom.* **2005**, *19*, 3549−3554.
(23) Wang, J. R.; Yau, L. F.; Zhang, R.; Xia, Y.; Ma, J.; Ho, H. M.; Hu, P.; Hu, M.; Liu, L.; Jiang, Z. H. Transformation of ginsenosides from notoginseng by artificial gastric juice can increase cytotoxicity toward cancer cells. *J. Agric. Food Chem.* **2014**, *62*, 2558−2573.
(24) Wang, X.; Wang, C.; Pu, F.; Lin, P.; Qian, T. Metabolite profiling of ginsenoside Rg after oral administration in rat. *Biomed. Chromatogr.* **2014**, *28*, 1320−1324.
(25) Li, L.; Chen, X.; Zhou, J.; Zhong, D. In vitro studies on the oxidative metabolism of 20(S)-ginsenoside Rh2 in human, monkey, dog, rat, and mouse liver microsomes, and human liver s9. *Drug Metab. Dispos.* **2012**, *40*, 2041−2053.
(26) Hu, Z.; Yang, J.; Cheng, C.; Huang, Y.; Du, F.; Wang, F.; Niu, W.; Xu, F.; Jiang, R.; Gao, X.; Li, C. Combinatorial metabolism notably affects human systemic exposure to ginsenosides from orally administered extract of *Panax notoginseng* roots (Sanqi). *Drug Metab. Dispos.* **2013**, *41*, 1457−1469.
(27) Liu, H.; Yang, J.; Du, F.; Gao, X.; Ma, X.; Huang, Y.; Xu, F.; Niu, W.; Wang, F.; Mao, Y.; Sun, Y.; Lu, T.; Liu, C.; Zhang, B.; Li, C. Absorption and disposition of ginsenosides after oral administration of *Panax notoginseng* extract to rats. *Drug Metab. Dispos.* **2009**, *37*, 2290−2298.
(28) Li, L.; Chen, X.; Li, D.; Zhong, D. Identification of 20(S)-protopanaxadiol metabolites in human liver microsomes and human hepatocytes. *Drug Metab. Dispos.* **2011**, *39*, 472−483.
(29) Hao, H.; Lai, L.; Zheng, C.; Wang, Q.; Yu, G.; Zhou, X.; Wu, L.; Gong, P.; Wang, G. Microsomal cytochrome p450-mediated metabolism of protopanaxatriol ginsenosides: metabolite profile, reaction phenotyping, and structure-metabolism relationship. *Drug Metab. Dispos.* **2010**, *38*, 1731−1739.
(30) Chen, J.; Zhao, R.; Zeng, Y. M.; Meng, H.; Zuo, W. J.; Li, X.; Wang, J. H. Three new triterpenoid saponins from the leaves and stems of *Panax quinquefolium*. *J. Asian Nat. Prod. Res.* **2009**, *11*, 195−201.
(31) Yoshikawa, M.; Murakami, T.; Ueno, T.; Yashiro, K.; Hirokawa, N.; Murakami, N.; Yamahara, J.; Matsuda, H.; Saijoh, R.; Tanaka, O. Bioactive saponins and glycosides. VIII. Notoginseng (1): New dammarane-type triterpene oligoglycosides, notoginsenosides-A, -B, -C, and -D, from the dried root of *Panax notoginseng* (Burk.) F.H. Chen. *Chem. Pharm. Bull.* **1997**, *45*, 1039−1045.
(32) Tu, Y.; Wang, Z.-X.; Shi, Y. An efficient asymmetric epoxidation method for trans-olefins mediated by a fructose-derived ketone. *J. Am. Chem. Soc.* **1996**, *118*, 9806−9807.
(33) Sakanaka, M.; Tanaka, J.; Nakata, K.; Uno, H.; Kuramoto, M. Ginsenoside derivatives as apoptosis inhibitors and regeneration promoters. JP2002249498A, 2002.
(34) Matsuura, H.; Udayama, M.; Dokan, R.; Kasai, R.; Yamasaki, K.; Tanaka, O. Identification and quantification of 20(S)-protopanaxatriol and its 20S,24S-epoxide in human urine with the treatment of alkaline cleavage after the ingestion of Sanchi ginseng, the roots of *Panax notoginseng*. *Nat. Med. (Tokyo, Jpn.)* **2002**, *56*, 34−39.
(35) Yoshikawa, M.; Morikawa, T.; Yashiro, K.; Murakami, T.; Matsuda, H. Bioactive saponins and glycosides. XIX. Notoginseng (3): Immunological adjuvant activity of notoginsenosides and related saponins: structures of notoginsenosides-L, -M, and -N from the roots of *Panax notoginseng* (Burk.) F. H. Chen. *Chem. Pharm. Bull.* **2001**, *49*, 1452−1456.
(36) Lai, L.; Hao, H.; Liu, Y.; Zheng, C.; Wang, Q.; Wang, G.; Chen, X. Characterization of pharmacokinetic profiles and metabolic pathways of 20(S)-ginsenoside Rh1 in vivo and in vitro. *Planta Med.* **2009**, *75*, 797−802.

DOI: 10.1021/acs.jafc.5b00710
J. Agric. Food Chem. 2015, 63, 2689−2700

However, only the influence of germination with water in the dark on the isoflavone contents of chickpeas has been studied. Therefore, in this study, we carried out a quantitative analysis of isoflavone contents and composition in chickpeas and chickpea sprouts by growing them in different conditions, including in light, under ethanol stress, and under salt stress. Employing this analysis, we determined the optimal germination time to maximize isoflavone contents for the purpose of maximizing the nutraceutical benefits of chickpea sprout isoflavone consumption.

MATERIALS AND METHODS

Materials. Chickpeas, 88-1, were provided by the Institute of Food Crops, Xinjiang Academy of Agricultural Sciences in China.

Reagent. Authentic standards of biochanin A and formononetin were purchased from Sigma-Aldrich (Shanghai, China). Acetonitrile, acetic acid, and methanol used were all high-performance liquid chromatography (HPLC)-grade and purchased from Fisher Chemicals (Shanghai, China). NaCl, $NaSO_4$, NaClO, and ethanol were all analytical-grade and purchased from the Beijing Chemical Industry Group (Beijing, China).

Germination of Chickpeas. Chickpea treatments were performed in sterilized sprouting cartridges, which accommodated 300 g of dry chickpeas. The chickpeas were subjected to four different treatments: germination in the dark (GD), germination in the light (GL), germination under ethanol stress (GE), or germination under salt stress (GS) in the dark. The treatment methods and experimental stages are presented in Table 1. In all of the treatments, chickpeas were sequentially subjected to soaking (20 h) and germination stages (12 days). The chickpeas were first surface-sterilized by immersing them in a 1% (w/v) NaClO solution (5 L/kg of chickpeas) for 1 h at room temperature and then rinsed 4 times with distilled pall water (3 L/kg of chickpeas). Then, the sterilized chickpeas were soaked for 20 h at 25 °C in sterilized distilled water in the absence of light, except for the salinity stress chickpeas (GS), which were soaked in a saline solution (1:1 NaCl/$NaSO_4$) of different concentrations (0.01, 0.02, 0.03, and 0.04 mol/L) for 20 h. Subsequently, the soaked chickpeas were put in sterilized plastic cartridges and germinated at 25 °C and 95% relative humidity (RH) in a sprouting machine that was sterilized according to the instructions of the manufacturer in advance. Then, for the experiments with light (GL), a light incubator was placed on top of the machine and used to simulate natural sunlight. The light was applied during the all of the germination stages. In the experiments with ethanol treatments (GE), chickpea sprouts were soaked in solutions of 1, 3, and 5% (v/v) ethanol for 12 h at room temperature for elicitation. All of the experiments were performed in triplicate. Chickpea sprouts in each group were collected on days 2, 4, 6, 8, 10, and 12 and immediately stored at −20 °C.

Table 1. Summary of Different Chickpea Treatments[a]

	stage		
treatment	soaking	germination	ethanol soaking
untreated	–	–	–
GD	√	√ (dark)	–
GL	√	√ (light)	–
GE	√	√ (dark)	√ (1, 3, and 5%)
GS	√ (salt soaking)	√ (dark)	–

[a]GD, germination in the dark; GL, germination in the light. GE, germination under ethanol stress; GS, germination under salt stress; –, treatment mentioned was not performed; and √, treatment mentioned was performed.

Extraction of Isoflavones. Extractions were carried out according to the method previously described, with slight modifications.[19] All samples were dried at 50 °C and milled with a laboratory mill using a 60 mesh screen sieve. A total of 1 g of the ground samples was

Table 2. Changes in Isoflavone Contents during the Germination of Chickpeas in the Dark (mg/g)[a]

	ononin	daidzein	biochanin glucoside	biochanin A glucoside malonylated	formononetin	biochanin A	genistein	pseudobaptigenin	glycitein glucoside acetylated	total
untreated ($\times 10^{-1}$)	nd[b]	0.12 ± 0.01 f	0.08 ± 0.00 e	0.06 ± 0.00 f	0.10 ± 0.01 d	0.18 ± 0.01 e	0.06 ± 0.00 b	nd	nd	0.60 ± 0.03 g
2 days	0.15 ± 0.01 f	0.12 ± 0.01 e	0.43 ± 0.02 e	0.19 ± 0.01 f	0.56 ± 0.03 d	0.61 ± 0.03 e	0.01 ± 0.00 a	nd	0.03 ± 0.00 e	2.69 ± 0.11 f
4 days	0.24 ± 0.01 e	0.19 ± 0.02 d	0.68 ± 0.02 d	0.33 ± 0.04 d	1.11 ± 0.03 c	1.32 ± 0.04 d	0.01 ± 0.00 a	0.05 ± 0.00 e	0.05 ± 0.00 d	3.93 ± 0.16 e
6 days	0.37 ± 0.03 c	0.24 ± 0.02 c	1.23 ± 0.03 b	0.50 ± 0.04 c	1.16 ± 0.03 c	1.61 ± 0.05 c	nd	0.08 ± 0.00 d	0.15 ± 0.01 c	5.34 ± 0.21 d
8 days	0.48 ± 0.02 b	0.29 ± 0.01 b	1.28 ± 0.04 b	0.63 ± 0.04 b	1.28 ± 0.04 b	1.95 ± 0.03 b	nd	0.13 ± 0.01 c	0.17 ± 0.01 b	6.21 ± 0.20 b
10 days	0.50 ± 0.03 a	0.35 ± 0.02 a	1.38 ± 0.03 a	0.75 ± 0.03 a	1.42 ± 0.04 a	2.10 ± 0.05 a	nd	0.14 ± 0.01 b	0.18 ± 0.01 a	6.82 ± 0.22 a
12 days	0.45 ± 0.02 d	0.31 ± 0.03 e	1.39 ± 0.04 c	0.60 ± 0.02 e	1.41 ± 0.05 a	1.99 ± 0.03 b	nd	0.14 ± 0.01 a	0.17 ± 0.01 b	6.46 ± 0.21 c

[a]Data are expressed as the mean ± standard deviation of triplicate samples. Values in the same column that do not share the same letter are significantly different ($p < 0.05$). [b]nd = not detected.

DOI: 10.1021/jf5057524
J. Agric. Food Chem. 2015, 63, 2701−2707

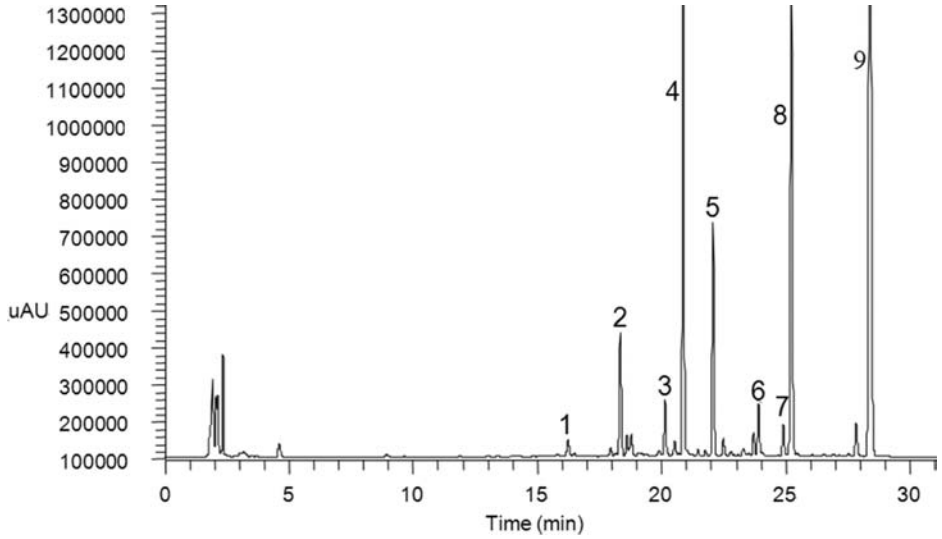

Figure 1. UHPLC−UV profile of 70% aqueous EtOH extracts of germinated chickpeas in the light, with HPLC chromatograms shown at 280 nm. Peaks: 1, glycitein glucoside acetylated; 2, ononin; 3, daidzein; 4, biochanin A glucoside; 5, biochanin A glucoside malonylated; 6, genistein; 7, pseudobaptigenin; 8, formononetin; and 9, biochanin A.

extracted twice and put into 10 mL of 70% ethanol solutions for 3 h at 70 °C. After extraction, the mixture was centrifuged at 3000*g* for 10 min to separate the supernatant. The supernatants were combined and stored at 4 °C for later analysis.

Analysis of Isoflavones. The identification of isoflavones was performed on the basis of ultraviolet (UV) and mass spectrometry (MS) spectra according to Simons et al.[16] and Aisyah et al.[17] The samples were analyzed by ultrahigh-pressure liquid chromatography (UHPLC)−MS. The UHPLC system (San Jose, CA) was equipped with two Shimadzu pumps, a Shimadzu autosampler, and a photodiode array (PDA) detector. Each sample (1 μL) was injected onto a Waters Acquity UPLC BEH shield RP18 column (2.1 × 150 mm, 1.7 mm particle size) with a Waters Acquity UPLC shield RP18 Vanguard pre-column (2.1 × 5 mm, 1.7 mm particle size, Waters, Milford, MA). Water acidified with 0.1% (v/v) acetic acid, eluent A, and acetonitrile (ACN) acidified with 0.1% (v/v) acetic acid, eluent B, were used as solvents at a flow rate of 300 μL/min. The temperature of the column oven was controlled to be 35 °C, and the PDA detector was set to measure a range of 200−400 nm. The elution profile was as follows: 0−5 min, isocratic on 15% (v/v) B; 5−15 min, linear gradient from 15 to 30% (v/v) B; 15−25 min, linear gradient from 30 to 60% (v/v) B; 25−45 min, linear gradient from 60 to 80% (v/v) B; 45−50 min, linear gradient from 80 to 95% (v/v) B; 50−55 min, linear gradient from 95 to 15% (v/v) B; and 55−58 min, isocratic on 15% (v/v) B. A mass spectrometric analysis was performed on a Thermo Scientific LTQ-XL (San Jose, CA) equipped with an electrospray ionization (ESI)−MS probe coupled with reversed-phase (RP)-UHPLC. Nitrogen was used as a sheath and auxiliary gas. Data were obtained in the m/z range of 150−1500. Data-dependent MS^n analysis was performed with a normalized collision energy of 35%. To this end, the system was tuned with biochanin A in both the positive ionization (PI) and negative ionization (NI) modes. For both modes, the ion transfer tube (ITT) temperature was 350 °C and the source voltage was 4.8 kV. Quantification was performed on the basis of the absorption at 280 nm using Xcalibur (version 2.1.0, Thermo Scientific).

For many compounds, no commercial standards were available. The concentrations of individual isoflavonoids were evaluated using the calibration curve of biochanin A (mg/g; 10−0.0001 mg/mL; R^2 = 0.9999).

Statistical Analysis. All values were expressed as the mean ± standard deviation ($\bar{X}$ ± SD). Data were analyzed by one-way analysis of variance (ANOVA), followed by post-hoc Dunnett's t test, using the SAS software. Differences of $p < 0.05$ were considered significant.

RESULTS AND DISCUSSION

Isoflavone Contents in Germinated Chickpea Seeds under Water in the Dark. The variation of isoflavone contents in chickpea seeds and sprouts during germination are shown in Table 2. The contents of formononetin and biochanin A were 0.10 ± 0.01 and 0.18 ± 0.02 mg/10 g, respectively, in the untreated chickpea seeds. During germination, the contents of formononetin and biochanin A increased; the maximum amount was obtained on day 10 (1.42 ± 0.06 and 2.10 ± 0.08 mg/g, respectively). These results suggest that formononetin and biochanin A are principal isoflavones in both chickpea seeds and sprouts and are consistent with results reported by Ma et al.[20] Except for genistein, all of the other isoflavones that we tested increased with treatment and reached their peak content on day 10 ($p < 0.05$). However, genistein showed an opposite tendency and was undetectable after 4 days. Because genistein is formed by the hydrolysis of glycosides through β-glucosidase, the decrease of genistein observed in this study may have resulted from the inhibition of the activity of β-glycosidase during germination.[21] Moreover, the total isoflavone content showed a similar pattern to formononetin and biochanin A from seeds (0.59 ± 0.06 mg/10 g) to 10 day sprouts (6.82 ± 0.33 mg/g). This increase in isoflavone contents may be induced by the metabolic pathways of naringeninchalcone and isoliquiritigenin, the precursors of isoflavonoids commonly found in legumes.[22] However, a slight decrease in the isoflavone contents was observed between days 10 and 12. Terrence et al.[23] reported that the primary soybean leaf tissues underwent a programmed shift from isoflavonoid to flavonoid metabolism 3 days after germination. The decrease observed in this study may be due to a conversion of isoflavonoids to other isoflavones. In addition, the chickpea sprouts contained ononin, pseudobaptigenin, and glycitein glucoside acetylated, which were undetected in the chickpea seeds. Our results showed that the isoflavone composition changed during germination. It has been reported that sprouts grown in the dark have a lower overall nutritional value than sprouts grown under light, because of the lack of photosynthesis in dark conditions.[14] Thus, the following section

DOI: 10.1021/jf5057524
J. Agric. Food Chem. 2015, 63, 2701−2707

investigates the changes of isoflavones in chickpea sprouts germinated in the light.

Isoflavone Contents in Germinated Chickpea Seeds under Water in the Light. We used HPLC−MS to quantify the individual isoflavones of these chickpea sprouts (Figure 1). The isoflavone contents of the chickpea sprouts germinated in the light are listed in Table 3. Exposing the chickpea seedlings to light boosted the accumulation of all of the isoflavones in our experiments, except genistein, which was undetectable after 2 days. The chickpea sprouts germinated on day 8 and had the highest formononetin and biochanin A contents (1.54 ± 0.04 and 2.34 ± 0.04 mg/g, respectively), which were 154 and 130 times higher, respectively, than their contents in untreated chickpea seeds and 1.2 times higher than their contents in the GD group. The same trend was also observed in other isoflavones compared to the GD group, except genistein. These results were consistent with a study by Phommalth et al.,[24] who reported that soybean seeds germinated with light treatments could produce over 1.53 times more isoflavones than when grown under dark conditions. Moreover, the total isoflavone content in chickpea sprouts dramatically increased, from 2.40 ± 0.11 to 4.86 ± 0.14 mg/g during days 2 and 4, and the maximum amount (8.14 ± 0.21 mg/g) of total isoflavones was obtained on day 8. Isoflavones were synthesized in the malonate and phenylpropanoid pathways using three malonyl-CoAs and one coumaroyl-CoA, which are produced during photosynthesis.[14] Light has been thought to increase the amount of malonyl-CoA and coumaroyl-CoA by promoting photosynthesis, thus, in turn, enhance the precursor for isoflavone production commonly found in legumes.[21] Light may influence the phenylalanine ammonia-lyase (PAL), which is reported to be an initial enzyme for synthesizing the isoflavone and result in the biosynthesis of isoflavone compounds[25] apart from the efficiency of photosynthesis.

Isoflavone Content in Germinated Chickpea Seeds in the Ethanol Treatment. The changes of isoflavone contents during germination using ethanol are presented in Table 4. The isoflavone contents of chickpea sprouts significantly increased ($p < 0.05$) compared to the untreated chickpea seeds. The maximum amount of formononetin and biochanin A (1.53 ± 0.05 and 2.21 ± 0.04 mg/g, respectively) in the chickpea sprouts was observed in 3% ethanol-treated chickpea sprouts on day 10. Moreover, the highest total isoflavone content (7.01 ± 0.18 mg/g) was also obtained in the 3% ethanol-treated group. However, in comparison to the GD group, only a slight increase (not significant) in isoflavone contents and slight changes in the composition of isoflavones were observed. Moreover, there was no significant difference among 1% ethanol, 5% ethanol, and GD groups.

Stimulation of the defense response of plants has a large potential to alter the metabolites of the plant, especially when germinated seeds are abruptly exposed to external stresses.[26] In this study, ethanol was used as an external stress to stimulate the defense response of the chickpeas, thus increasing the isoflavone contents. Moreover, ethanol has been reported to induce alcohol dehydrogenase (ADH) activity and could stimulate alcohol fermentation via the action of ADH under aerobic conditions,[27] which, in turn, could induce the conversion of other compounds to other isoflavones.

Isoflavone Contents in Germinated Chickpea Seeds after Salinity Stress Treatment. The isoflavone contents of the chickpea sprouts germinated in saline solutions at the concentrations of 0.01, 0.02, 0.03, and 0.04 mol/L are summarized

Table 3. Changes in Isoflavone Contents during the Germination of Chickpeas in the Light (mg/g)[a]

	ononin	daidzein	biochanin glucoside	biochanin A glucoside malonylated	formononetin	biochanin A	genistein	pseudobaptigenin	glycitein glucoside acetylated	total
untreated ($\times 10^{-1}$)	nd[b]	0.12 ± 0.01 f	0.08 ± 0.00 f	0.06 ± 0.00 f	0.10 ± 0.01 d	0.18 ± 0.01 e	0.06 ± 0.00 b	nd	nd	0.60 ± 0.03 g
2 days	0.35 ± 0.03 f	0.23 ± 0.01 c	0.35 ± 0.02 e	0.20 ± 0.01 e	0.46 ± 0.02 a	0.56 ± 0.02 c	0.01 ± 0.00 a	0.02 ± 0.00 f	0.04 ± 0.00 f	2.40 ± 0.11 f
4 days	0.44 ± 0.02 e	0.28 ± 0.01 e	0.81 ± 0.04 d	0.46 ± 0.02 d	1.05 ± 0.03 d	1.58 ± 0.02 b	nd	0.10 ± 0.00 e	0.07 ± 0.00 e	4.86 ± 0.14 e
6 days	0.64 ± 0.03 d	0.35 ± 0.01 d	1.26 ± 0.05 c	0.73 ± 0.03 c	1.36 ± 0.03 c	1.78 ± 0.04 b	nd	0.15 ± 0.01 d	0.11 ± 0.01 d	6.38 ± 0.21 d
8 days	0.89 ± 0.02 b	0.60 ± 0.01 a	1.45 ± 0.04 a	0.99 ± 0.04 a	1.54 ± 0.04 a	2.34 ± 0.04 a	nd	0.20 ± 0.01 b	0.13 ± 0.01 b	8.14 ± 0.21 a
10 days	0.90 ± 0.01 a	0.61 ± 0.03 a	1.45 ± 0.04 a	0.97 ± 0.05 a	1.50 ± 0.05 b	2.27 ± 0.05 a	nd	0.21 ± 0.02 a	0.14 ± 0.01 a	8.05 ± 0.26 b
12 days	0.85 ± 0.03 c	0.50 ± 0.02 b	1.43 ± 0.04 b	0.99 ± 0.03 b	1.49 ± 0.03 b	2.21 ± 0.04 a	nd	0.18 ± 0.01 c	0.12 ± 0.01 c	7.89 ± 0.21 c

[a]Data are expressed as the mean ± standard deviation of triplicate samples. Values in the same column that do not share the same letter are significantly different ($p < 0.05$). [b]nd = not detected.

DOI: 10.1021/jf5057524
J. Agric. Food Chem. 2015, 63, 2701−2707

Table 4. Changes in Isoflavone Contents during the Germination of Chickpeas Treated with 3% Ethanol (mg/g)[a]

	ononin	daidzein	biochanin glucoside	biochanin A glucoside malonylated	formononetin	biochanin A	genistein	pseudobaptigenin	glycitein glucoside acetylated	total
untreated ($\times 10^{-1}$)	nd[b]	0.12 ± 0.01 f	0.08 ± 0.00 e	0.06 ± 0.00 f	0.10 ± 0.01 d	0.18 ± 0.01 e	0.06 ± 0.00 b	nd	nd	0.60 ± 0.03 g
2 days	0.30 ± 0.01 e	0.10 ± 0.00 e	0.31 ± 0.01 e	0.18 ± 0.01 e	0.56 ± 0.03 d	0.36 ± 0.02 e	0.01 ± 0.00 a	0.02 ± 0.00 e	0.03 ± 0.00 d	1.87 ± 0.08 f
4 days	0.38 ± 0.02 d	0.12 ± 0.01 e	0.41 ± 0.02 d	0.24 ± 0.01 d	0.99 ± 0.02 c	1.16 ± 0.04 d	nd	0.08 ± 0.00 d	0.08 ± 0.00 c	3.46 ± 0.12 e
6 days	0.52 ± 0.02 c	0.14 ± 0.01 d	0.78 ± 0.02 c	0.28 ± 0.01 c	1.21 ± 0.03 b	1.71 ± 0.04 c	nd	0.09 ± 0.00 c	0.13 ± 0.01 b	4.86 ± 0.14 d
8 days	0.67 ± 0.02 b	0.18 ± 0.01 c	1.20 ± 0.04 b	0.39 ± 0.03 b	1.51 ± 0.04 a	1.96 ± 0.03 b	nd	0.15 ± 0.01 b	0.14 ± 0.01 a	6.20 ± 0.19 c
10 days	0.81 ± 0.02 a	0.28 ± 0.02 a	1.33 ± 0.03 a	0.53 ± 0.01 a	1.53 ± 0.05 a	2.21 ± 0.04 a	nd	0.17 ± 0.01 a	0.15 ± 0.00 a	7.01 ± 0.18 a
12 days	0.80 ± 0.03 a	0.26 ± 0.03 b	1.30 ± 0.03 a	0.52 ± 0.02 a	1.48 ± 0.03 a	2.10 ± 0.03 b	nd	0.16 ± 0.01 a	0.15 ± 0.01 a	6.77 ± 0.20 b

[a]Data are expressed as the mean ± standard deviation of triplicate samples. Values in the same column that do not share the same letter are significantly different ($p < 0.05$). [b]nd = not detected.

Table 5. Changes in Isoflavone Contents during the Germination of Chickpeas Treated with 0.03 mol/L Saline Solution (mg/g)[a]

	ononin	daidzein	biochanin glucoside	biochanin A glucoside malonylated	formononetin	biochanin A	genistein	pseudobaptigenin	glycitein glucoside acetylated	total
untreated ($\times 10^{-1}$)	nd[b]	0.12 ± 0.01 e	0.08 ± 0.00 f	0.06 ± 0.00 f	0.10 ± 0.01 e	0.18 ± 0.01 e	0.06 ± 0.00	nd	nd	0.60 ± 0.03 g
2 days	0.29 ± 0.01 f	0.10 ± 0.01 e	0.28 ± 0.01 e	0.13 ± 0.01 e	0.75 ± 0.02 d	0.90 ± 0.02 e	nd	0.03 ± 0.00 e	0.03 ± 0.00 e	2.51 ± 0.08 f
4 days	0.41 ± 0.01 e	0.21 ± 0.01 d	0.77 ± 0.03 e	0.27 ± 0.01 d	0.87 ± 0.02 d	1.06 ± 0.02 d	nd	0.05 ± 0.00 d	0.06 ± 0.00 d	3.70 ± 0.10 e
6 days	0.66 ± 0.01 d	0.24 ± 0.01 c	0.88 ± 0.01 d	0.57 ± 0.01 c	1.10 ± 0.03 c	1.26 ± 0.04 c	nd	0.10 ± 0.01 c	0.10 ± 0.00 c	4.91 ± 0.12 d
8 days	0.91 ± 0.02 b	0.43 ± 0.01 b	1.25 ± 0.03 b	0.61 ± 0.02 b	1.18 ± 0.01 b	1.37 ± 0.05 b	nd	0.17 ± 0.00 b	0.17 ± 0.01 b	6.09 ± 0.15 c
10 days	0.98 ± 0.01 a	0.50 ± 0.01 a	1.33 ± 0.02 a	0.65 ± 0.02 a	1.29 ± 0.03 a	1.77 ± 0.02 a	nd	0.21 ± 0.01 a	0.20 ± 0.01 a	6.93 ± 0.13 a
12 days	0.86 ± 0.02 c	0.45 ± 0.01 b	1.12 ± 0.03 c	0.57 ± 0.02 c	1.28 ± 0.04 a	1.75 ± 0.03 a	nd	0.17 ± 0.00 b	0.19 ± 0.00 a	6.39 ± 0.15 b

[a]Data are expressed as the mean ± standard deviation of triplicate samples. Values in the same column that do not share the same letter are significantly different ($p < 0.05$). [b]nd = not detected.

J. Agric. Food Chem. 2015, 63, 2701−2707
DOI: 10.1021/jf505524

here. In comparison to chickpea sprouts that germinated in 0.01, 0.02, and 0.04 mol/L saline solutions, the isoflavone contents in 0.03 mol/L saline solution were higher, as shown in Table 5. The formononetin content of samples germinated in 0.03 mol/L saline solutions increased to 0.75 ± 0.02 mg/g, and the biochanin A content increased to 0.90 ± 0.02 mg/g on day 2, which was significantly higher ($p < 0.05$) than in untreated chickpea seeds. Genistein was undetected in all of the stages of germination, and ononin, pseudobaptigenin, and glycitein glucoside acetylated were only detected in chickpea sprouts. Moreover, the 0.03 mol/L salt stress significantly enhanced the total isoflavone content, and it reached a peak value (6.93 ± 0.02 mg/g) on day 10.

Salinity can induce osmotic and ionic imbalances inside plant cells, thus affecting plant growth and metabolism.[28] However, our results showed that a low-concentration salt stress could increase the total isoflavone content in chickpea sprouts. Similar results on soybeans have been reported by Abdul et al.,[18] who stated that a low concentration of salt stress exposure on a plant could promote photosynthesis, thus enhancing the accumulation of metabolites in the plant.

In conclusion, in this study, we demonstrated that different stimuli had positive effects on the isoflavone content and composition of chickpea sprouts, and the maximum amount of total isoflavones was obtained on day 10, except for in the GL group, in which the maximum amount was obtained on day 8. On the basis of our results, we suggest that the application of light is the most effective method for producing functional foods with high isoflavone contents, which might help to improve the nutritional quality and health benefits of chickpea sprouts.

AUTHOR INFORMATION

Corresponding Author

*E-mail: renguixing@caas.cn.

Author Contributions

†Yue Gao and Yang Yao contributed equally to this work.

Funding

This work was supported by the Hong Kong, Macao, and Taiwan Science and Technology Cooperation Program of China (2013DFH30050), the Special Fund for Agro-scientific Research in the Public Interest (201403063), the Earmarked Fund for China Agriculture Research System Modern Agro-industry Technology (CYTX-014), and the Science and Technology Innovation Program of the CAAS.

Notes

The authors declare no competing financial interest.

REFERENCES

(1) Viveros, A.; Brenes, A.; Elices, R.; Arija, I.; Canales, R. Nutritional value of raw and autoclaved Kabuli and Desi chickpeas (*Cicer arietinum* L.) for growing chickens. *Br. Poultry Sci.* **2001**, *42*, 242−251.

(2) Singh, U. Nutritional quality of chickpea (*Cicer arietinum* L.): Current status and future research needs. *Plant Foods Hum. Nutr.* **1985**, *35*, 339−351.

(3) Khattak, A. B.; Khattak, G. S. S.; Mahmood, Z.; Bibi, N.; Ihsanullah, I. Study of selected quality and agronomic characteristics and their interrelationship in Kabuli-type chickpea genotypes (*Cicer arietinum* L.). *Int. J. Food Sci. Technol.* **2006**, *41*, 1−5.

(4) Ghavidel, R. A.; Prakash, J. The impact of germination and dehulling on nutrients, antinutrients, in vitro iron and calcium bioavailability and in vitro starch and protein digestibility of some legume seeds. *LWT—Food Sci. Technol.* **2007**, *40*, 1292−1299.

(5) Kuo, Y. H.; Rozan, P.; Lambein, F.; Frias, J.; Vidal-Valverde, C. Effects of different germination conditions on the contents of free protein and non-protein amino acids of commercial legumes. *Food Chem.* **2004**, *86*, 537−545.

(6) Finney, P. L. Effect of germination on cereal and legume nutrient changes and food or feed value: A comprehensive review. In *Mobilization of Reserves in Germination*; Nozzolillo, C., Lea, P. J., Loewus, F. A., Eds.; Springer: New York, 1983; Recent Advances in Phytochemistry, Vol. *17*, Chapter 12, pp 229−305.

(7) Wu, Z.; Song, L.; Feng, S.; Liu, Y.; He, G.; Yioe, Y.; Huang, D. Germination dramatically increases isoflavonoid content and diversity in chickpea (*Cicer arietinum* L.) seeds. *J. Agric. Food Chem.* **2012**, *60*, 8606−8615.

(8) Mao, X.; Zhang, L.; Xia, Q.; Sun, Z.; Zhao, X.; Cai, H.; Tang, Y. Vanadium-enriched chickpea sprout ameliorated hyperglycemia and impaired memory in streptozotocin-induced diabetes rats. *BioMetals* **2008**, *21*, 563−570.

(9) Kolonel, L. N.; Hankin, J. H.; Whittemore, A. S.; Wu, A. H.; Gallagher, R. P.; Wilkens, L. R.; Paffenbarger, R. S. Vegetables, fruits, legumes and prostate cancer: A multiethnic case-control study. *Cancer Epidemiol., Biomarkers Prev.* **2000**, *9*, 795−804.

(10) Zhao, S.; Zhang, L.; Gao, P.; Shao, Z. Isolation and characterisation of the isoflavones from sprouted chickpea seeds. *Food Chem.* **2009**, *114*, 869−873.

(11) Choi, S. B.; Jang, J. S.; Park, S. Estrogen and exercise may enhance beta-cell function and mass via insulin receptor substrate 2 induction in ovariectomized diabetic rats. *Endocrinology* **2005**, *146*, 4786−4794.

(12) Nanri, A.; Mizoue, T.; Takahashi, Y.; Kirii, K.; Inoue, M.; Noda, M.; Tsugane, S. Soy product and isoflavone intakes are associated with a lower risk of type 2 diabetes in overweight Japanese women. *J. Nutr.* **2010**, 109−115.

(13) Lee, S. J.; Ahn, J. K.; Kim, S. H.; Kim, J. T.; Han, S. J.; Jung, M. Y.; Chung, I. M. Variation in isoflavone of soybean cultivars with location and storage duration. *J. Agric. Food Chem.* **2003**, *51*, 3382−3389.

(14) Kim, E. H.; Kim, S. H.; Chung, J. I.; Chi, H. Y.; Kim, J. A.; Chung, I. M. Analysis of phenolic compounds and isoflavones in soybean seeds (*Glycine max* (L.) Merill) and sprouts grown under different conditions. *Eur. Food Res. Technol.* **2006**, *222*, 201−208.

(15) Sharma, R. D. Isoflavone content of Bengalgram (*Cicer arietinum*) at various stages of germination. *J. Plant Foods* **1981**, *3*, 259−264.

(16) Simons, R.; Vincken, J. P.; Roidos, N.; Bovee, T. F. H.; Van Iersel, M.; Verbruggen, M. A.; Gruppen, H. Increasing soy isoflavonoid content and diversity by simultaneous malting and challenging by a fungus to modulate estrogenicity. *J. Agric. Food Chem.* **2011**, *59*, 6748−6758.

(17) Aisyah, S.; Gruppen, H.; Madzora, B.; Vincken, J. P. Modulation of isoflavonoid composition of Rhizopusoryzae elicited soybean (*Glycine max*) seedlings by light and wounding. *J. Agric. Food Chem.* **2013**, *61*, 8657−8667.

(18) Abdul, J. C.; Gopi, R.; Sankar, B.; Manivannan, P.; Kishorekumar, A.; Sridharan, R.; Panneerselvam, R. Studies on germination, seedling vigour, lipid peroxidation and proline metabolism in *Catharanthus roseus* seedlings under salt stress. *S. Afr. J. Bot.* **2007**, *73*, 190−195.

(19) Fu, Y. H.; Zhang, F. C. Changes in isoflavones glucoside and aglycone content of chickpea yoghurt during fermentation by *Lactobacillus bulgaricus* and *Streptococcus thermophilus*. *J. Food Process. Preserv.* **2013**, *37*, 744−750.

(20) Ma, H. R.; Wang, J.; Qi, H. X.; Gao, Y. H.; Pang, L. J.; Yang, Y.; Aisa, H. A. Assessment of the estrogenic activities of chickpea (*Cicer arietinum* L.) sprout isoflavone extract in ovariectomized rats. *Acta Pharmacol. Sin.* **2013**, *34*, 380−386.

(21) Zhu, D.; Hettiarachchy, N. S.; Horax, R.; Chen, P. Isoflavone contents in germinated soybean seeds. *Plant Food Hum. Nutr.* **2005**, *60*, 147−151.

DOI: 10.1021/jf5057524
J. Agric. Food Chem. 2015, 63, 2701−2707

(22) Liu, C. J.; Blount, J. W.; Steele, C. L.; Dixon, R. A. Bottlenecks for metabolic engineering of isoflavone glycoconjugates in *Arabidopsis*. *Proc. Natl. Acad. Sci. U. S. A.* **2002**, *99*, 14578−14583.
(23) Terrence, L. G. Flavonoid and isoflavonoid distribution in developing soybean seedling tissues and in seed and root exudates. *J. Plant Physiol.* **1991**, *95*, 594−603.
(24) Phommalth, S.; Jeong, Y. S.; Kim, Y. H.; Dhakal, K. H.; Hwang, Y. H. Effects of light treatment on isoflavone content of germinated soybean seeds. *J. Agric. Food Chem.* **2008**, *56*, 10123−10128.
(25) Luczkiewicz, M.; Glod, D. Callus cultures of *Genista* plants—In vitro material producing high amounts of isoflavones of phytoestrogenic activity. *Plant Sci.* **2003**, *165*, 1101−1108.
(26) Mishra, A. K.; Sharma, K.; Misra, R. S. Elicitor recognition, signal transduction and induced resistance in plants. *J. Plant Interact.* **2012**, *7*, 95−120.
(27) Miyoshi, K.; Sato, T. The effects of ethanol on the germination of seeds of japonica and indica rice (*Oryza sativa* L.) under anaerobic and aerobic conditions. *Ann. Bot.* **1997**, *79*, 391−395.
(28) Sanchez, D. H.; Siahpoosh, M. R.; Roessner, U.; Udvardi, M.; Kopka, J. Plant metabolomics reveals conserved and divergent metabolic responses to salinity. *Physiol. Plant.* **2008**, *132*, 209−219.

DOI: 10.1021/jf5057524
J. Agric. Food Chem. 2015, 63, 2701−2707

kDa permeate of the heat-treated 10% DH hydrolysate (86.6% protein via Kjeldahl, containing 9.2% ash), the 30 kDa retentate of the control 5% DH hydrolysate (87.5% protein via Kjeldahl, containing 8.7% ash), and their respective whole unfractionated hydrolysates (87.1 and 86.4% protein, respectively).

For fortification of hydrolysate fractions, Fe^{2+} (139 mg of $FeSO_4 \cdot 7H_2O$) was added to 100 mL of 20 g protein L^{-1} solutions (initial concentration) of hydrolysate fractions adjusted to pH 5 with 1 N HCl.

Total Iron Concentration, Ferrous Chelation Determination, and Solid Phase Extraction. Total iron was determined as previously described by O'Loughlin et al.[17] modified from the method of Voillier et al.[21] Briefly, test samples were dissolved in 0.5 M HCl and stored overnight. Test samples (200 μL, 1 g L^{-1}) were diluted with 1.5 mL of dH_2O, and 300 μL of 1.4 M hydroxylamine hydrochloride was subsequently added, whereupon the mixture was vortexed and allowed to stand for 30 min. Ferrozine reagent (200 μL), 0.01 M in 0.1 M ammonium acetate, was added along with 300 μL of 5 M ammonium acetate and the mixture allowed to stand for 3 min. The absorbance was read at 562 nm against a standard curve of $FeSO_4$.

The ferrous chelating capability of the WPI and whole and fractionated hydrolysates was determined using a modification of the method of Decker and Welch[22] as previously described by O'Loughlin et al.[17] Briefly, test samples (1 mL of 1 g L^{-1}) were mixed with 1.35 mL of dH_2O and 50 μL of 2 mM $FeCl_2$. After vortexing, the reaction was initiated with 100 μL of ferrozine, vortexed again, and allowed to stand for 10 min. Samples were read at 562 nm, and EDTA-Na_2 was used as a positive control for the assay. A standard curve for EDTA chelation of iron was prepared for 0.5−100 μM EDTA, giving the following linear relationship:

$$y(A_{562}) = -0.0105x + 1.1476 \ (R^2 = 0.997) \quad (1)$$

The concentration of selected hydrolysates needed to chelate 50% of the ferrous iron (CC_{50}) was determined by assaying and plotting various concentrations of hydrolysates against percentage chelation. Utilizing concentrations of the samples ranging from 0.5 to 10 g L^{-1}, it was possible to determine the concentration of selected samples needed to chelate 50% of the ferrous iron (CC_{50}) under the assay conditions with 2 mM $FeCl_2$.

Solid phase extraction (SPE) was carried out on Phenomenex Strata X cartridges (Phenomenex, Cheshire, UK) using the method of Nongonierma et al.[23] Cartridges were conditioned with methanol followed by washing with Milli-Q water. Samples (5 g protein L^{-1}) were loaded onto the cartridge, where flow-through was extracted under vacuum (≤−381 mmHg). Washes (four times) with Milli-Q water were pooled for analysis. Subsequently, 80% (v/v) acetonitrile (MeCN) was utilized (three times) to elute the bound fraction from the cartridge. Fractions were evaporated on a Büchi Rotavapor R-210 (Büchi Labortechnik AG, Switzerland) and freeze-dried on a Labconco 12 L FreeZone 12 plus freeze drier (Labconco, Kansas City, MO, USA) prior to analysis.

Total and Free Amino Acid Analysis of Hydrolysate Fractions and Iron Solubility of Dispersions. Total and free amino acid analysis was performed as previously described by O'Loughlin et al.[19] A JEOL JLC-500/V Amino Tac amino acid analyzer fitted with a JEOL Na^+ high-performance cation-exchange column (JEOL (UK) Ltd., Herts, UK) was utilized, and deproteination was accomplished with 10% (v v^{-1}) trichloroacetic acid (TCA) followed by centrifugation at 20000*g* for 20 min. The extracted supernatant was analyzed for amino acids through visible adsorption photometry after separation using ion exchange. Ninhydrin derivatization with norvaline was used as an internal standard. For total amino acid analysis samples were heated in 6 M HCl for 23 h under reflux at 105 °C before application to the JLC-500/V analyzer.

For total iron solubility, test samples (10 g L^{-1}) were centrifuged (Eppendorf 5810 R, Eppendorf GmbH, Hamburg, Germany) at 3000*g* for 20 min, whereupon the supernatant was extracted and diluted 1:9 using 0.5 N HCl and stored overnight. Total iron was determined using the previously mentioned methodology.

Attenuated Total Reflectance−Fourier Transform Infrared (ATR-FTIR) Spectroscopy of WPI, Hydrolysates, and Iron-Fortified Dispersions. Secondary structural changes were determined using ATR-FTIR spectroscopy. This was performed utilizing a Bruker Tensor 27 FTIR spectrometer (Bruker Optik GmbH, Ettlingen, Germany) with a thermally controlled BioATR Cell II. Sample solution (25 μL, 10 g L^{-1}) was placed onto the ZnSe crystal, and a total of 180 scans were performed for each sample at a resolution of 4 cm^{-1}. Interferograms were Fourier transformed and analyzed with Bruker OPUS 5.5 software, where both water vapor and CO_2 compensations were performed and data were vector normalized.

Simulated Gastrointestinal Digestion (SGID) of Ferrous-Chelating Fractions. A static two-stage SGID process was performed on the iron-chelating fractions using a modification of the methodology of Walsh et al.[24] The simulated gastric fluid contained pepsin (EC 3.4.23.1, calculated activity of 837 UHb mg^{-1} protein) dispersed in 150 mM NaCl at a concentration of 4 g L^{-1} (final pH 5.5). The simulated pancreatic juice (SPJ) was prepared according to the following protocol: 4.5 g of Corolase PP, 62.5 g of $NaHCO_3$, and 30 g of bile salts per liter of dH_2O modified from the method of Le et al.[25]

Iron-fortified samples (100 mL, 20 g protein L^{-1}) were preincubated at 37 °C for 30 min under stirring (at 140 rpm). The pH of the solution was reduced to 3.5 at 37 °C with 1 N HCl, whereupon a 10 mL solution of simulated gastric fluid was added to give a final E:S of 1:100. The solution was then reduced to a final pH of 2 at 37 °C. Aliquots, 1 mL, were extracted at 1, 10, 30, 60, and 90 min after reaction. After 90 min, the pH was adjusted to pH 7.5 using 0.6 M Na_2HPO_4. SPJ (1:10 v/v of sample) was subsequently added to the solution, which was incubated at 37 °C for 150 min. Enzyme activity was terminated by heating at 80 °C for 20 min.

Chromatographic Characterization of Control and Heated-Treated WPI Solutions. Reversed-phase (C18) HPLC was performed as previously described by O'Loughlin et al.[19] Briefly, a Phenomenex Jupiter C18 column was used (Phenomenex, Cheshire, UK) under gradient elution conditions: solvent B, from 0 to 100% in 30 min, 100% for 5 min, from 100 to 0% in 5 min, and 0% for 5 min at a flow rate of 1 mL min^{-1}, where solvent B was 80% MeCN and 0.1% TFA (v v^{-1}). Solvent A was 0.1% TFA (v v^{-1}).

Size-exclusion chromatography (SEC) described by O'Loughlin et al.[19] utilized a TSK Gel G2000SW, 7.8 mm × 600 mm, column (TosoHaas Bioscience GmbH, Stuttgart, Germany) using an isocratic gradient of 30% (v v^{-1}) MeCN and 0.1% (v v^{-1}) trifluoroacetic acid (TFA) at a flow rate of 0.5 mL min^{-1} over 60 min.

Both C18 and SEC were performed on a Waters 2695 separation module and a Waters 2487 dual-wavelength absorbance detector running on Waters Empower software (Milford, MA, USA).

Statistical Analysis. Statistical analysis was through the use of Minitab 15 software (Minitab Inc., State College, PA, USA). When necessary, data are presented as the mean ± SD for $n = 2$ determinations. The statistical difference of means was determined through the use of a one-way ANOVA followed by a Tukey test.

RESULTS AND DISCUSSION

Amino Acid Content and Ferrous-Chelating Capability of Whey Protein Isolate Hydrolysate Fractions. In a previous investigation by the authors, the ferrous-chelating capabilities of WPI hydrolysates were correlated with their respective average molecular weights (M_w).[17] A total of 22 pilot-scale fractions produced during the study were the subject of further analysis of their iron-chelating characteristics. O'Loughlin et al. showed that a 30 kDa retentate from a 5% DH hydrolysate of unheated control WPI (WPI-C-5DH-30R) possessed a CC_{50} value of 4.500 ± 0.009 g protein L^{-1}.[17] Correspondingly, a 1 kDa permeate of a 10% DH hydrolysate of the prior heat-treated (80 °C, 10 min) WPI (WPI-HT-10DH-1P) possessed a CC_{50} value of 0.846 ± 0.031 g protein L^{-1}. The chelating capability of hydrolysate fractions was shown to increase with a reduction in the average M_w of the fraction.[17]

DOI: 10.1021/jf505817a
J. Agric. Food Chem. 2015, 63, 2708−2714

The WPI-C-5DH-30R fraction possessed 57.5 ± 1.3% of material >30 kDa with the WPI-HT-10DH-1P fraction possessing 80.2 ± 1.1% of material <1 kDa. This altered size distribution of the fractions possessing the greatest and least ferrous-chelating capabilities is shown in Supplementary Figure 1 in the Supporting Information.

During an examination of total and free amino acid concentration of WPI, WPI-C-5DH-30R, and WPI-HT-10DH-1P fractions, there was a significantly ($P < 0.05$) large increase in the total concentration of certain aromatic and basic amino acids in the 1 kDa permeate, especially significantly higher ($P < 0.05$) concentrations of total lysine (Lys), phenylalanine (Phe), and tyrosine (Tyr) and also polar threonine (Thr) compared to the 30 kDa retentate, which possessed higher levels of asparagine/aspartate, glycine (Gly), and leucine (Leu) (Table 1). From Table 1, the concentrations

Table 1. Total Amino Acid Concentration of Whey Protein Isolate (WPI) Hydrolysate Fractions That Demonstrated the Least (WPI Control 5% DH 30 kDa Retentate) and Greatest (WPI Heat-Treated 10% DH 1 kDa Permeate) Ferrous-Chelating Ability for 2 mM $FeCl_2$[a]

amino acid	WPI control (g kg^{-1})	WPI 5-30R[b] (g kg^{-1})	WPI 10-1P[c] (g kg^{-1})
alanine	43.5 ± 1.1a	40.9 ± 1.3b	47.8 ± 1.0c
arginine	16.9 ± 0.8a	16.9 ± 1.2a	22.8 ± 1.5b
aspar(tate) + -agine	92.7 ± 1.3a	92.8 ± 1.0a	83.4 ± 1.7b
cysteine	1.9 ± 1.3a	11.7 ± 1.2b	3.6 ± 1.1a
glutam(ate) + -ine	150.3 ± 1.6a	150.4 ± 1.1a	146.8 ± 1.7b
glycine	15.4 ± 0.9a	15.7 ± 0.7a	12.4 ± 1.2b
histidine	14.0 ± 1.4a	12.4 ± 1.4a	22.9 ± 0.9b
isoleucine	45.5 ± 1.0a	49.7 ± 0.9b	59.6 ± 1.4c
leucine	84.7 ± 1.2a	96.7 ± 1.6b	81.7 ± 1.3c
lysine	87.0 ± 1.5a	73.8 ± 1.7b	91.3 ± 1.1c
methionine sulfone	12.8 ± 1.4a	16.0 ± 1.4b	13.7 ± 1.5a
phenylalanine	24.4 ± 1.1a	21.4 ± 1.2b	33.5 ± 0.8c
proline	50.2 ± 1.9a	45.9 ± 1.5b	52.4 ± 1.2a
serine	41.6 ± 0.7a	41.9 ± 1.3a	34.4 ± 1.6b
threonine	58.5 ± 1.3a	53.8 ± 1.1b	62.4 ± 1.0c
tyrosine	24.1 ± 1.7a	16.3 ± 0.8b	26.7 ± 1.3a
valine	50.2 ± 1.6ab	50.3 ± 1.2a	48.0 ± 0.9b

[a]The same letter across a row indicates no significant difference ($P < 0.05$). [b]30 kDa retentate of hydrolyzed to 5% DH control WPI. [c]1 kDa permeate of hydrolyzed to 10% DH heat-treated (80 °C for 10 min) WPI.

of Asn/Asp, Gly, and Leu in the 30 kDa retentate are similar to those in the control WPI, and therefore they are not considered responsible for the lower chelating capability. There was also a significantly higher histidine (His) concentration in the 1 kDa permeate sample (22.9 ± 0.9 g kg^{-1}) than in the 30 kDa retentate sample (12.4 ± 1.4 g kg^{-1}, Table 1). His is known to play a role in regulating essential trace elements such as iron, and a previous study has demonstrated experimentally that high blood serum levels of iron in humans can be caused by a diet low in His.[26] His is also essential for the binding of ferric (Fe^{3+}) iron to lactoferrin,[27] where the iron-binding active site consists of two tyrosines, a histidine and an aspartate residue.[28] The aromatic amino acids, Phe and Tyr, have been shown previously to provide a negative surface for electrostatic cation interaction, with a buildup of negative charges being present over the face of the benzene ring.[29] This could also be a possible mechanism for interaction with iron cations in the hydrolysate fractions. Whereas previous studies have highlighted Cys playing a central role in facilitating iron chelation,[30] our results demonstrated a greater concentration of Cys residues in the high M_w 30 kDa retentate sample (11.7 ± 1.2 g kg^{-1}), which had a reduced chelating capability, compared to the WPI control and 1 kDa permeate of the 10% DH hydrolysate of heat-treated WPI (1.9 ± 1.3 and 3.6 ± 1.1 g kg^{-1}, respectively; Table 1). Free amino acid analysis of the respective samples was also carried out and demonstrated higher, by up to a factor of 48, concentrations of free arginine (Arg), His, Lys, Phe, and Tyr in the 1 kDa permeate sample (Supplementary Table 1).

Further fractionation of the relatively strong chelating 1 kDa permeate (WPI-HT-10DH-1P) using SPE resulted in a flow-through (relatively more hydrophilic) fraction (Figure 1A) and

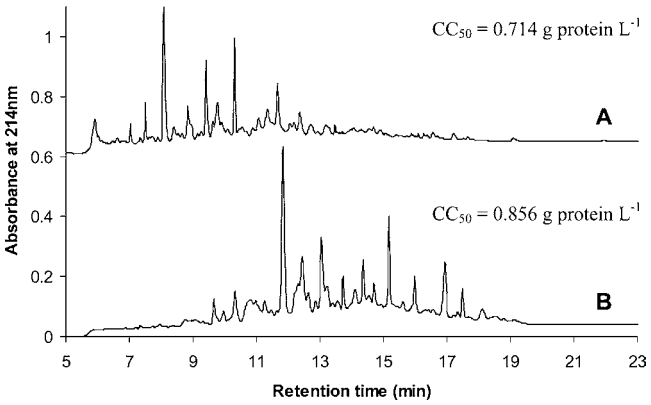

Figure 1. C18 RP-HPLC chromatograms of whey protein isolate (WPI) hydrolysate fraction WPI heat-treated 10% DH−1 kDa permeate subjected to solid-phase extraction (SPE): (A) SPE cartridge flow-through; (B) 80% (v/v) acetonitrile eluate. CC_{50} describes the concentration required to chelate 50% of the Fe^{2+} from 2 mM $FeCl_2$ under assay conditions.

a bound fraction eluted from the matrix using 80% (v/v) MeCN (Figure 1B). Ferrous-chelating capability was higher in the more hydrophilic (CC_{50} = 0.714 g protein L^{-1}) than in the hydrophobic fraction (CC_{50} = 0.856 g protein L^{-1}; Figure 1B). A significantly ($P < 0.05$) higher percentage of hydrophobic amino acids, for example, Ala, Leu, Phe, and Tyr, was present in the bound eluate than in the flow-through fraction containing higher total concentrations of Arg, His, and Lys (Supplementary Table 2). The elevated levels of free His in the fraction may act as monodentate ligands complexing iron through N-containing imidazole side groups. Whereas the concentration through UF/SPE of certain amino acids, for example, His, is concomitant with increased ferrous chelation, the authors postulate that there could also be peptide complexes present that participate in chelation capability in this study.

Through utilization of various concentrations of a known Fe-chelator, EDTA,[31] it was possible to deduce the equivalent concentration of EDTA needed to give the same level of chelation for the 30 kDa retentate and 1 kDa permeate samples. A 1 g L^{-1} solution of the unhydrolyzed unheated WPI, which possessed a ferrous-chelating ability of 9.13 ± 0.21%,[17] was equivalent to 9.22 ± 0.24 μM EDTA as derived from the standard curve. The 1 kDa permeate of the heat-treated 10%

DOI: 10.1021/jf505817a
J. Agric. Food Chem. 2015, 63, 2708−2714

DH WPI hydrolysate possessed a ferrous-chelating capability equivalent to 84.40 ± 1.01 μM EDTA at 1 g L^{-1}. SPE of the 1 kDa permeate sample resulted in a hydrophilic fraction that was equivalent to 93.24 ± 0.87 μM EDTA in ferrous-chelating capability and a hydrophobic fraction with a respective chelating capability of 80.94 ± 0.87 μM EDTA, both at 1 g L^{-1}. The use of EDTA further demonstrates the increased chelation in the lower M_w and hydrophilic fractions and relates this to a known iron chelator. These fractions can offer qualified advantages similar to iron−amino acid chelates, such as ferrous bis-glycinate, which are better tolerated compared to traditional iron supplements and have received approval by EFSA.[32,33]

Fourier Transformed Infrared Spectroscopy of Whey Protein Isolate, Hydrolysates, and Ferrous-Chelating Fractions. FTIR spectroscopy of the 1 kDa permeate solution prior to, and after, iron fortification demonstrated altered structural characteristics (Figure 2). From Figure 2, the FTIR

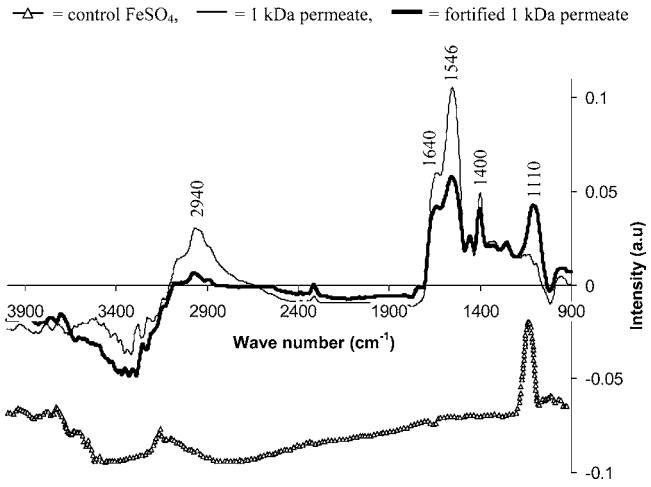

Figure 2. Fourier transformed infrared interferograms of control $FeSO_4$ solution and whey protein isolate hydrolysate fractions of control 1 kDa permeate and iron-fortified 1 kDa permeate.

interferogram of the 1 kDa permeate solution prior to iron fortification exhibits prominent peak intensities at 1640, 1546, and 1400 cm^{-1}. An $FeSO_4$ solution (1.39 g L^{-1} w/v), on the other hand, had a prominent peak intensity at wavenumber 1110 cm^{-1}, which was also identifiable following iron fortification of the 1 kDa permeate along with extensive reductions in peak intensities in the amide I and amide II regions at 1640 and 1546 cm^{-1}, respectively (Figure 2). A corresponding decrease in intensity in the 3100−2700 cm^{-1} region (intensity maximum = 2940 cm^{-1}) of the spectrum of the fortified 1 kDa concurs with a previously reported C−H stretching vibration (ν) of aliphatic CH_2 at 2850−2950 cm^{-1} and C−H ν of aromatic residues at 3050−3080 cm^{-1}.[34,35] An intensification/weakening of vibrations (Figure 2) demonstrates a causative molecular interaction between the ferrous sulfate and the hydrolysate fraction, although whether this is related to Fe−peptide complexing or individual amino acid−Fe interactions is interpretive. The authors postulate that both could be occurring simultaneously. Chaud et al. showed a similar intensity pattern with a ferric−casein hydrolysate complex, attributing chelation to C−O−Fe binding.[12] However, in our case, the concentration of the naturally occurring phenol, Tyr (which could undergo C−O−H substitution), was reduced in the SPE fraction (Supplementary Table 2). Nevertheless, the reduction in aliphatic CH_2 stretching intensity and reduced intensity around amide I (primarily ν C═O) and amide II (N−H deformation) points to, at the very least, altered bond energies.

Iron Solubility and Simulated Gastrointestinal Digestion of Iron-Fortified Whey Protein Isolate Hydrolysate Fractions. The bioavailability of $FeSO_4$ is negatively affected by large changes in intestinal pH; for example, a sudden drop to pH ∼2 under gastric conditions is later corrected to near-neutral pH during subsequent duodenal digestion and absorption.[36−38] This has led to the use of ferric pyrophosphate or NaFe(III)EDTA as more stable replacement additives, the latter having an iron content of 12.5−13.5%.[39] The promising chelating properties of the hydrolysate fractions prompted further investigation of their capacity to solubilize $FeSO_4$ at levels equivalent to higher levels of iron fortification recommended in the diet of pregnant women.[40] Experimentally, this was pursued by examining the solubility of control solutions of $FeSO_4{\cdot}7H_2O$ in Milli-Q water (1.39 g L^{-1} w/v) and fortified (at equivalent level) hydrolysate fractions (10 g L^{-1} w/v) as a function of pH (Figure 3). Dispersion of 1.39 g of

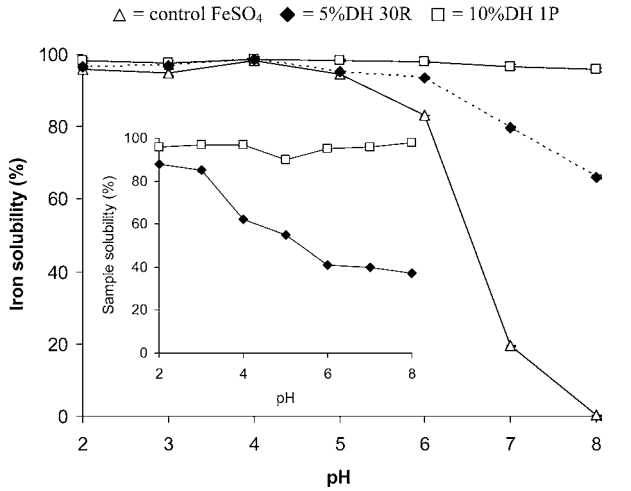

Figure 3. Iron solubility determinations, pH 2−8, for 28 mg of Fe (as $FeSO_4{\cdot}7H_2O$) in control Milli-Q water solutions (100 mL) and hydrolysate dispersions (100 mL, 10 g L^{-1}). WPI control, 5% DH−30 kDa retentate; WPI heat-treated, 10% DH−1 kDa permeate. (Inset) Inherent sample solubility (10 g L^{-1}) over pH 2−8.

$FeSO_4$ L^{-1} in 10 g L^{-1} hydrolysate fractions increased the iron solubility by varying degrees, with those possessing the previously determined lowest and highest CC_{50} values being presented in Figure 3. From Figure 3, the total iron solubility was >95% for all samples (control and fortified hydrolysate fractions) at pH 2−5. Thereafter, total iron solubility declined rapidly in the case of the control (aqueous dispersion), whereas that of the fortified 30 kDa retentate was reduced to 79.6 ± 1.2% at pH 7 and to 66.1 ± 1.0% at pH 8. Only a small (relatively) decrease was observed (to 95.8 ± 1.5% at pH 8) in the iron solubility with the 1 kDa hydrolysate permeate derived from the heat-treated WPI (Figure 3). This fraction was capable of sustaining the highest iron solubility of all fortified samples.

WPI and hydrolysate samples were also analyzed for their inherent solubility over the pH range of 2−8 with the solubility curves for the 30 kDa retentate of the control 5% DH and the 1 kDa permeate of the 10% DH hydrolysate of heat-treated WPI shown in Figure 3 (inset). Generally, the solubility of the 1 kDa

DOI: 10.1021/jf505817a
J. Agric. Food Chem. 2015, 63, 2708−2714

permeate remained high (dropping to 90.2% at pH 5). Conversely, the solubility of the 30 kDa retentate sample was generally poor, dropping to 37.3% at pH 8 from a solubility maximum of 88.2% at pH 2 (Figure 3, inset).

Oral ingestion of fortified hydrolysates may result in exposure to a range of gastrointestinal, luminal, and serum proteinases and peptidases, which may affect iron solubility/bioaccessibility. Initial SGID demonstrated the selective proteolytic digestion of whey proteins (Supplementary Figure 2), with the peptic resistance of β-lg in agreement with previous work.[41,42] Iron-fortified (139 mg of $FeSO_4 \cdot 7H_2O$) samples (20 g L^{-1} protein) were subjected to SGID to ascertain iron solubility during and subsequent to digestion. Figure 4

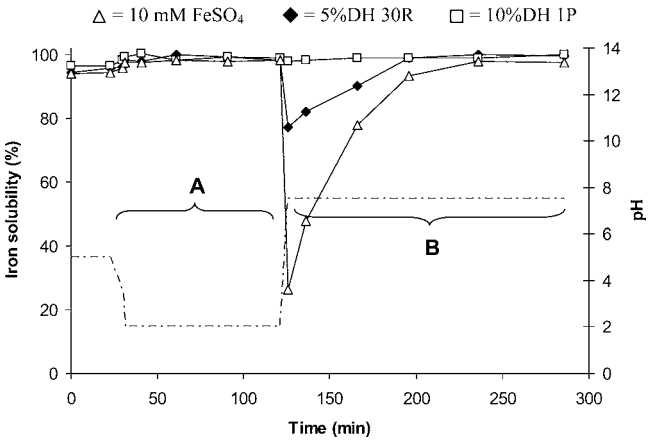

Figure 4. Iron solubility during simulated gastrointestinal digestion of 10 mM $FeSO_4$ control and fortified (2.78 g $FeSO_4$ L^{-1}) whey protein isolate (WPI) hydrolysate dispersions (20 g L^{-1} (initial)): (A) gastric phase; (B) duodenal phase. WPI control, 5% DH−30 kDa retentate; WPI heat-treated, 10% DH−1 kDa permeate.

demonstrates the iron solubility of the 1 kDa permeate and the 30 kDa retentate samples over the course of gastric (marked A in Figure 4) and duodenal (marked B in Figure 4) digestion. From Figure 4, iron solubility remains generally high (≥94.3%) through fortification at pH 5 and subsequent gastric digestion at pH 2 in both samples. However, adjustment of the pH to 7.5 with dibasic sodium phosphate reduced the iron solubility of the 30 kDa retentate sample to 77.1%, although the solubility recovered to approximately 99% after 75 min of simulated duodenal digestion (Figure 4). The authors postulated that this was the result of both the higher ferrous chelating capacity of the 1 kDa sample (CC_{50} = 0.83 ± 0.03 g protein L^{-1}) and also possible chelating capabilities of the constituents of the simulated intestinal fluid. From this, the chelating capacity (expressed as a CC_{50}) of the bile extract was determined to be 1.24 ± 0.10 g L^{-1}, which concurs with the known strong ferrous-chelating capability of porcine bile extract.[43] The iron solubility under SGID of all samples is demonstrated in Supplementary Figure 3.

The SGID of the fortified 1 kDa permeate (Figure 5) reveals relatively minor breakdown following termination of digestion (D, $t_{+286\ min}$) when compared to the undigested sample at time zero (A, t_0). This is corroborated by the statistically insignificant ($P < 0.05$) differences in iron solubility of the samples determined at different reaction time points for gastric (B) and duodenal digestion (C and D, Figure 5). This is in contrast to the 30 kDa retentate sample, where the total iron solubility (TIS) decreased to 77.0 ± 1.2% at pH 7.5 and increased upon

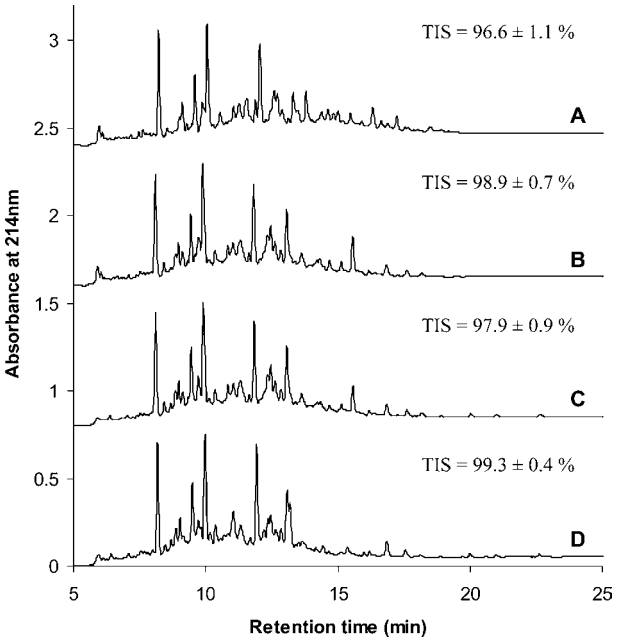

Figure 5. C18 RP-HPLC chromatograms of simulated gastrointestinal digests of the whey protein isolate (WPI) hydrolysate ferrous-chelating fraction, WPI heat-treated, 10% DH−1 kDa permeate: (A) undigested sample at t_0; (B) gastric digest at $t_{+90\ min}$; (C) intestinal digest at $t_{+95\ min}$; (D) intestinal digest at $t_{+286\ min}$. TIS, total iron solubility.

complete simulated digestion, serving to again highlight the relatively poor chelating characteristics of the 30 kDa retentate fraction (Figure 6). Tracking the course of SGID using C18 RP-HPLC (Figure 6) highlighted a reduction in the more hydrophobic material present toward the right of the

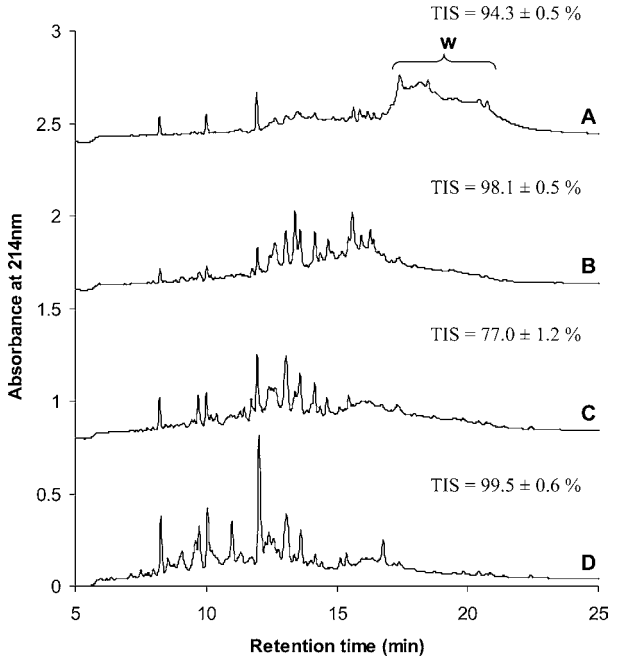

Figure 6. C18 RP-HPLC chromatograms of simulated gastrointestinal digests of the whey protein isolate (WPI) hydrolysate ferrous chelating fraction WPI control, 5% DH−30 kDa retentate: (A) undigested sample at t_0; (B) gastric digest at $t_{+90\ min}$; (C) intestinal digest at $t_{+95\ min}$; (D) intestinal digest at $t_{+286\ min}$. Increased level of hydrophobic proteinaceous material shown at "w".

DOI: 10.1021/jf505817a
J. Agric. Food Chem. 2015, 63, 2708−2714

chromatogram (A, t_0) and a general leftward shift in the chromatograms as digestion occurs with the increasing formation of peptide material in the 30 kDa retentate sample (Figure 6B–D). The high M_w more hydrophobic material present in the 30 kDa retentate sample (marked "w" in Figure 6) is reduced relatively quickly to more hydrophilic, smaller M_w material, upon gastric digestion with pepsin. This is in agreement with previous work on peptic digestion of aggregated/high M_w whey proteins.[44]

This study utilized enzymatic hydrolysis in conjunction with a prior heat treatment to facilitate the production, and subsequent fractionation, of a ferrous-chelating hydrolysate fraction from WPI. The 1 kDa permeate fraction possessed a ferrous-chelating capability equivalent to 84.4 μM EDTA and had a high content of certain aromatic and basic amino acid residues. ATR-FTIR spectroscopy demonstrated that there was a molecular level interaction between the 1 kDa permeate and the ferrous sulfate. Fractionation of the 1 kDa permeate via solid phase extraction yielded a hydrophilic fraction with increased chelation capability, with this fraction having a relatively high content of hydrophilic amino acids, namely, Arg, His, and Lys. The ferrous-chelating 1 kDa permeate fraction was utilized to stabilize iron during SGID, maintaining iron solubility ≥98% throughout digestion. This is exemplified by the 72% increase in the determined solubility of total iron at pH 7.5 subsequent to peptic digestion compared to a $FeSO_4 \cdot 7H_2O$ control solution. It is postulated, therefore, that the 1 kDa hydrolysate fraction is a potential candidate ingredient for formulation into products to enhance iron bioaccessibility. Further investigation into the mechanism of iron chelation by the 1 kDa permeate hydrolysate fraction is warranted.

■ ASSOCIATED CONTENT

Supporting Information

Supplementary Tables 1 and 2 and Supplementary Figures 1–3. This material is available free of charge via the Internet at http://pubs.acs.org.

■ AUTHOR INFORMATION

Corresponding Author

*(A.B.) Phone: +353-25-42222. Fax +353-25-42340. E-mail: andre.brodkorb@teagasc.ie.

Notes

The authors declare no competing financial interest.

■ ACKNOWLEDGMENTS

We acknowledge the help and support offered by Paula O'Connor of Teagasc Food Research Centre, Moorepark, Ireland.

■ REFERENCES

(1) Sharma, S.; Singh, R.; Rana, S. Bioactive peptides: a review. *Int. J. BIO-autom.* **2011**, *15*, 223–250.

(2) O'Connell, J. E.; Fox, P. F. Effect of β-lactoglobulin and precipitation of calcium phosphate on the thermal coagulation of milk. *J. Dairy Res.* **2001**, *68*, 81–94.

(3) Zimmermann, M. B.; Hurrell, R. F. Nutritional iron deficiency. *Lancet* **2007**, *370*, 511–520.

(4) Fox, P. F. Milk: an overview. In *Milk Proteins – from Expression to Food*; Thompson, A., Boland, M., Singh, H., Eds.; Academic Press: New York, 2009; pp 8–43.

(5) Hunt, C. D.; Nielsen, F. H. Nutritional aspects of minerals in bovine and human milks. In *Advanced Dairy Chemistry – Vol .3. Lactose, Water, Salts and Minor Constituents*, 3rd ed.; McSweeney, P. L. H., Fox, P. F., Eds.; Springer Science & Business Media: New York, 2009; pp 416–420.

(6) Fidler, M. C.; Walczyk, T.; Davidsson, L.; Zeder, C.; Sakaguchi, N.; Juneja, L. R.; Hurrell, R. F. A micronised, dispersible ferric pyrophosphate with high relative bioavailability in man. *Br. J. Nutr.* **2004**, *91*, 107–112.

(7) Fritz, J. C.; Pla, G. W.; Roberts, T.; Boehne, J. W.; Hove, E. L. Biological availability in animals of iron from common dietary sources. *J. Agric. Food Chem.* **1970**, *18*, 647–651.

(8) Slivka, A.; Kang, J.; Cohen, G. Hydroxyl radicals and the toxicity of oral iron. *Biochem. Pharmacol.* **1986**, *35*, 553–556.

(9) Ait-Oukhatar, N.; Peres, J. M.; Bouhallab, S.; Neuville, D.; Bureau, F.; Bouvard, G.; Arhan, P.; Bougle, D. Bioavailability of caseinophosphopeptide-bound iron. *J. Lab. Clin. Med.* **2002**, *140*, 290–294.

(10) Bouhallab, S.; Cinga, V.; Aít-Oukhatar, N.; Bureau, F.; Neuville, D.; Arhan, P.; Maubois, J. L.; Bouglé, D. Influence of various phosphopeptides of caseins on iron absorption. *J. Agric. Food Chem.* **2002**, *50*, 7127–7130.

(11) Vegarud, G. E.; Langsrud, T.; Svenning, C. Mineral-binding milk proteins and peptides; occurrence, biochemical and technological characteristics. *Br. J. Nutr.* **2000**, *84*, S91–S98.

(12) Chaud, M. V.; Izumi, C.; Nahaal, Z.; Shuhama, T.; Bianchi, M. d. L. P.; de Freitas, O. Iron derivatives from casein hydrolysates as a potential source in the treatment of iron deficiency. *J. Agric. Food Chem.* **2002**, *50*, 871–877.

(13) Kim, S. B.; Seo, I. S.; Khan, M. A.; Ki, K. S.; Nam, M. S.; Kim, H. S. Separation of iron-binding protein from whey through enzymatic hydrolysis. *Int. Dairy J.* **2007**, *17*, 625–631.

(14) Elias, R. J.; Bridgewater, J. D.; Vachet, R. W.; Waraho, T.; McClements, D. J.; Decker, E. A. Antioxidant mechanisms of enzymatic hydrolysates of β-lactoglobulin in food lipid dispersions. *J. Agric. Food Chem.* **2006**, *54*, 9565–9572.

(15) Zhou, J.; Wang, X.; Ai, T.; Cheng, X.; Guo, H. Y.; Teng, G. X.; Mao, X. Y. Preparation and characterization of β-lactoglobulin hydrolysate-iron complexes. *J. Dairy Sci.* **2012**, *95*, 4230–4236.

(16) Kelleher, S. L.; Chatterton, D.; Nielsen, K.; Lonnerdal, B. Glycomacropeptide and alpha-lactalbumin supplementation of infant formula affects growth and nutritional status in infant rhesus monkeys. *Am. J. Clin. Nutr.* **2003**, *77*, 1261–1268.

(17) O'Loughlin, I. B.; Murray, B. A.; FitzGerald, R. J.; Brodkorb, A.; Kelly, P. M. Pilot-scale production of hydrolysates with altered bio-functionalities based on thermally-denatured whey protein isolate. *Int. Dairy J.* **2014**, *34*, 146–152.

(18) Bouhallab, S.; Oukhatar, N. A.; Mollé, D.; Henry, G.; Maubois, J.-L.; Arhan, P.; Bouglé, D. L. Sensitivity of β-casein phosphopeptide-iron complex to digestive enzymes in ligated segment of rat duodenum. *J. Nutr. Biochem.* **1999**, *10*, 723–727.

(19) O'Loughlin, I. B.; Murray, B. A.; Brodkorb, A.; FitzGerald, R. J.; Robinson, A. A.; Holton, T. A.; Kelly, P. M. Whey protein isolate polydispersity affects enzymatic hydrolysis outcomes. *Food Chem.* **2013**, *141*, 2334–2342.

(20) Mullally, M. M.; O'Callaghan, D. M.; FitzGerald, R. J.; Donnelly, W. J.; Dalton, J. P. Proteolytic and peptidolytic activities in commercial pancreatic protease preparations and their relationship to some whey protein hydrolyzate characteristics. *J. Agric. Food Chem.* **1994**, *42*, 2973–2981.

(21) Viollier, E.; Inglett, P. W.; Hunter, K.; Roychoudhury, A. N.; Van Cappellen, P. The ferrozine method revisited: Fe(II)/Fe(III) determination in natural waters. *Appl. Geochem.* **2000**, *15*, 785–790.

(22) Decker, E. A.; Welch, B. Role of ferritin as a lipid oxidation catalyst in muscle food. *J. Agric. Food Chem.* **1990**, *38*, 674–677.

(23) Nongonierma, A. B.; Schellekens, H.; Dinan, T. G.; Cryan, J. F.; FitzGerald, R. J. Milk protein hydrolysates activate 5-HT2C serotonin receptors: influence of the starting substrate and isolation of bioactive fractions. *Food Funct.* **2013**, *4*, 728–737.

(24) Walsh, D. J.; Bernard, H.; Murray, B. A.; MacDonald, J.; Pentzien, A. K.; Wright, G. A.; Wal, J. M.; Struthers, A. D.; Meisel, H.;

DOI: 10.1021/jf505817a
J. Agric. Food Chem. 2015, 63, 2708–2714

FitzGerald, R. J. In vitro generation and stability of the lactokinin β-lactoglobulin fragment (142−148). *J. Dairy Sci.* **2004**, *87*, 3845−3857.
(25) Le, T. T.; Van de Wiele, T.; Do, T. N. H.; Debyser, G.; Struijs, K.; Devreese, B.; Dewettinck, K.; Van Camp, J. Stability of milk fat globule membrane proteins toward human enzymatic gastrointestinal digestion. *J. Dairy Sci.* **2012**, *95*, 2307−2318.
(26) Cho, E. S.; Anderson, H. L.; Wixom, R. L.; Hanson, K. C.; Krause, G. F. Long-term effects of low histidine intake on men. *J. Nutr.* **1984**, *114*, 369−384.
(27) Nicholson, H.; Anderson, B. F.; Bland, T.; Shewry, S. C.; Tweedie, J. W.; Baker, E. N. Mutagenesis of the histidine ligand in human lactoferrin: iron binding properties and crystal structure of the histidine-253 → methionine mutant. *Biochemistry* **1997**, *36*, 341−346.
(28) Madureira, A. R.; Pereira, C. I.; Gomes, A. M. P.; Pintado, M. E.; Xavier Malcata, F. Bovine whey proteins − overview on their main biological properties. *Food Res. Int.* **2007**, *40*, 1197−1211.
(29) Dougherty, D. A. Cation-π interactions involving aromatic amino acids. *J. Nutr.* **2007**, *137*, 1504S−1508S.
(30) Mulvihill, B.; Kirwan, F. M.; Morrissey, P. A.; Flynn, A. Effect of myofibrillar muscle proteins on the in vitro bioavailability of non-haem iron. *Int. J. Food Sci. Nutr.* **1998**, *49*, 187−192.
(31) Sawyer, D. T. Infrared spectra and correlations for the ethylenediaminetetraacetic acid metal chelates. *Ann. N.Y. Acad. Sci.* **1960**, *88*, 307−321.
(32) Bovell-Benjamin, A. C.; Viteri, F. E.; Allen, L. H. Iron absorption from ferrous bisglycinate and ferric trisglycinate in whole maize is regulated by iron status. *Am. J. Clin. Nutr.* **2000**, *71*, 1563−1569.
(33) European Food Safety Authority.. Opinion: Ferrous bisglycinate as a source of iron for use in the manufacturing of foods and in food supplements. *EFSA J.* **2006**, *299*, 1−17.
(34) Predoi, D. A study on iron oxide nanoparticels coated with dextrin obtained by co-precipitation. *Dig. J. Nanomater. Biostruct.* **2007**, *2* (1), 169−173.
(35) Cheraghipour, E.; Javadpour, S.; Mehdizadeh, A. R. Citrate capped superparamagnetic iron oxide nanoparticles used for hyperthermia therapy. *J. Biomed. Sci. Eng.* **2012**, *5*, 715−719.
(36) Zhu, L.; Glahn, R. P.; Nelson, D.; Miller, D. D. Comparing soluble ferric pyrophosphate to common iron salts and chelates as sources of bioavailable iron in a Caco-2 cell culture model. *J. Agric. Food Chem.* **2009**, *57*, 5014−5019.
(37) Forbes, A. L.; Arnaud, M. J.; Chichester, C. O.; Cook, J. D.; Harrison, B. N.; Hurrell, R. F.; Kahn, S. G.; Morris, E. R.; Tanner, J. T.; Whittaker, P. Comparison of in vitro, animal, and clinical determinations of iron bioavailability: International Nutritional Anemia Consultative Group Task Force report on iron bioavailability. *Am. J. Clin. Nutr.* **1989**, *49*, 225−38.
(38) He, W.-L.; Feng, Y.; Li, X.-L.; Yang, X.-E. Comparison of iron uptake from reduced iron powder and $FeSO_4$ using the Caco-2 cell model: Effects of ascorbic acid, phytic acid, and pH. *J. Agric. Food Chem.* **2008**, *56*, 2637−2642.
(39) European Food Safety Authority.. Scientific opinion on the use of ferric sodium EDTA as a source of iron added for nutritional purposes to foods for the general population (including food supplements) and to foods for particular nutritional uses. *EFSA J.* **2010**, *8*, 1−32.
(40) U.S. National Academies. *Dietary Reference Intakes for Energy, Carbohydrate, Fiber, Fat, Fatty Acids, Cholesterol, Protein, And Amino Acids (Macronutrients)*; National Academies Press: Washington, DC, USA, 2005; pp 1319−1332.
(41) Reddy, I. M.; Kella, N. K. D.; Kinsella, J. E. Structural and conformational basis of the resistance of β-lactoglobulin to peptic and chymotryptic digestion. *J. Agric. Food Chem.* **1988**, *36*, 737−741.
(42) Guo, M. R.; Fox, P. F.; Flynn, A.; Kindstedt, P. S. Susceptibility of β-lactoglobulin and sodium caseinate to proteolysis by pepsin and trypsin. *J. Dairy Sci.* **1995**, *78*, 2336−2344.
(43) Sakata, R.; Oshida, T.; Yu, K. H.; Lin, L. C. In *Assessment of Antioxidative Capacity of Animal Liver and Bile*, 52nd International Congress of Meat Science and Technology, Dublin, 2006; Troy, D., Pearce, R., Byrne, B., Kerry, J., Eds.; Wageningen Academic Publishers: Wageningen, The Netherlands, 2006; pp 703−704.
(44) Peram, M. R.; Loveday, S. M.; Ye, A.; Singh, H. In vitro gastric digestion of heatinduced aggregates of β-lactoglobulin. *J. Dairy Sci.* **2012**, *96*, 63−74.

DOI: 10.1021/jf505817a
J. Agric. Food Chem. 2015, 63, 2708−2714

such as lipid peroxidation. Lutein is dominant in oats, barley, spelt, and durum wheat whereas zeaxanthin is the main component in corn.[23] Carotenoids content, composition, and distribution in cereal grains have been well studied.[20,22,25−28] However, there is limited information on antioxidant potential of carotenoid from cereal grain fractions. Therefore, we hypothesize that carotenoids in aleurone, germ, and endosperm fractions of barley, corn, and wheat can prevent chronic diseases by acting as antioxidants through an oxidative balance mechanism. The main objective of this study was to investigate the antioxidant potential of carotenoid extracts of hand-separated aleurone, germ, and endosperm fractions of barley, corn, and wheat.

MATERIALS AND METHODS

Chemicals and Materials. HPLC grade acetonitrile, hexane, methylbutyl ether (MtBE) 1-butanol, and methanol were acquired from Fisher Scientific (Whitby, ON, Canada). Carotenoid standards, lutein (98.2%), and zeaxanthin (95.8%), were acquired from Chromadex Inc. (Santa Ana, CA), 2,2′-azino-bis(3-ethylbenzothiazoline-6-sulfonic acid) (ABTS; ≥98%), 2,2′azobis (2-amidinopropane)-dihydrochloride (AAPH), 2,2,-diphenyl-1-picrylhydrazyl (DPPH) (95%), and butylated hydroxytoluene (BHT) were acquired from Sigma-Aldrich (St. Louis, MO). The fluorescent dye, 5-(and-6)-chloromethyl-2′,7′-dichlorofluorescin diacetate (CM-H_2DCFDA), was acquired from Invitrogen (Eugene, OR). Fluorescein and trolox (6-hydroxy-2,5,7,8-tramethylchroman-2-carboxylic acid) were acquired from Fisher Acros Organics (Morris Plains, NJ). Dimethyl sulfoxide (DMSO), 3-(4,5-dimethylthiazolyl-2)-2,5-diphenyltetrazolium bromide (MTT), fetal bovine serum (FBS), hybrid-care medium, Caco-2, HT-29, and FHs 74 were acquired from American Type Culture Collection (ATCC) (Manassas, VA). The cell culture medium, Dulbecco's modified Eagle's medium (DMEM), was acquired from Sigma-Aldrich (St. Louis, MO), as were Dulbecco's phosphate buffer solution (PBS), L-glutamine (≥99%), sodium pyruvate (≥99%), epidermal growth factor (EGF), and transferrin human (hTF; ≥98%). Penicillin/streptomycin was acquired from Gibco BRL (Burlington, ON, Canada). Trypsin 0.05% was acquired from Thermo Scientific (Logan, UT). RNeasy mini kit was obtained from Qiagen (Mississauga, ON, Canada). RT^2 First Strand kit and RT^2 Profiler array (PAHS-065Y) were obtained from SABioscience (Mississauga, ON, Canada). The 25 cm^2 polystyrene flask or Transwell and 96-well flat bottom polystyrene microplate were purchased from Corning Incorporated (Ithaca, NY).

Samples. Three cereal grains, barley (regular), corn (flint), and wheat (MSUD8006), as described by Ndolo and Beta[28] were used.

Sample Preparation. The grains were hand dissected to separate the aleurone, germ, and endosperm according to the procedure described by Stewart, Nield, and Lott[29] with further modifications. The grains were brush at the ends, and germs were removed by a sharp scalpel. The degermed grains were soaked in 0.1% (v/v) sodium hypochlorite (NaClO) for 15−20 min to sterilize the surfaces and rinsed using sterile deionized water. The seeds were then placed in 10 cm Petri dishes lined with 2 ashless filters, moistened with 10 mL of sterile deionized water. The Petri dishes were wrapped in aluminum foil and kept at 20 °C for 48 h. The aleurone and endosperm were separated using a scalpel and stored at −20 °C. Samples were freeze-dried thereafter and ground using a multiuse blade grinder, model PCC 770 (Loblaws Inc. MO, Canada) to pass through a 0.5 mm sieve. The ground samples were stored at −20 °C before extraction and analysis.

Extraction of Carotenoids. The extraction method of Cha et al.[30] was further modified for this assay. One-gram samples (aleurone, germ, and endosperm) were extracted in a 100 mL ethanol solution (95%) containing 0.1% (w/v) butylated hydroxytoluene (BHT) at room temperature in the dark. After 3 h of extraction under continuous shaking, the mixtures were filtered through a Whatman no. 1 filter paper. Still at room temperature and in the dark, 120 μL of 100% potassium hydroxide (KOH) was added to 5 mL of the contents for saponification. After saponification for 1 h, 3 mL of hexane was added to partition carotenoids. The mixture was shaken for 1 min and then diluted with 3 mL of water. The mixture was allowed to stand in an amber separatory funnel to clearly separate the two phases. The upper layer containing carotenoids was collected, and the residue was repeatedly extracted until it contained no trace of carotenoids. The carotenoid extracts were concentrated using rotary evaporation.

Preparation of Test Solutions. For biochemical model, the concentrated carotenoid extracts were redissolved in 5 mL methanol/saturated butanol to prepare test solutions. For the in vitro model, stock solutions of carotenoid extracts were prepared by reconstituting concentrated carotenoid extracts in 10% DMSO with PBS. The final concentration of DMSO was less than 1%. The original carotenoid stock solutions were 200 mg/mL which were further diluted to working solutions of 100, 20, 5, 0.5 mg/mL with PBS.

Biochemical Models. *Determination of Total Carotenoid Content (TCC).* The extracted carotenoids were reconstituted with water-saturated butanol and transferred to semimicro quartz cuvette and absorbance measured at 450 nm using Ultrospec 1100 pro, UV/visible spectrophotometer (Biomicron Ltd. Cambridge CB4 QFJ, England). All analysis were conducted in triplicates and expressed as μg xanthophylls equivalent/g sample

$$C = \frac{(5 \times A)}{S \times W\left[\frac{\mu g}{g}\right]} \quad (1)$$

where C = xanthophyll content, μg/g; A = absorbance reading; S = regression coefficient (the number that expresses the relationship which is created based on concentration of xanthophyll working standard solutions in μg/mL and the absorbance); 5 = dilution factor (the factor based on the total extracted volume of 5 mL); and W = sample weight, g.[25]

HPLC Analysis of Carotenoids. Carotenoids were quantified by HPLC, using external calibration of standard mix (lutein and zeaxanthin). Freshly extracted samples were filtered through 0.45 μm nylon disc filter into brown HPLC vial. The quantification of carotenoids was done according to methods from Ndolo and Beta[28] and Abdel-Aal et al.[25] with some modifications. The quantification of carotenoids was performed by an HPLC (Waters 2695) equipment with a photoiodide array detector (PDA) (Waters 996) and autosampler (Waters 717 plus) (Waters, Milford, MA). YMC carotenoid S-3, 3 μm packing, 4.6 × 100 mm column (Waters, Milford, MA) was used. The column was operated at 35 °C, and 20 μL of sample was injected by autosampler and eluted with gradient system consisting of (A) methanol/methyl *tert*-butyl ether/milli-Q water (81:15:4 v/v/v) and (B) methyl *tert*-butyl ether/methanol (90:10 v/v). The flow rate was set at 1 mL/min. The gradient was programmed as follows: 0−9 min, 100−75% A; 10−12 min, 0% A; 12−13 min, 0−100% A; and 13−20 min, 100% A. The separation of carotenoids was detected and measured at 450 nm. Carotenoids in samples were identified based on retention times of standards. Six concentrations in the range of 0.05−5.0 μg/mL per 20 μL were prepared for lutein and zeaxanthin to generate regression equations for quantification.

Estimation of Antioxidant Activity of Carotenoids. *Determination of DPPH Radical Scavenging Activity.* The DPPH method of Brand-William et al.[31] as modified by Li et al.[32] was further modified for this assay. Sixty μM DPPH radical solution was freshly prepared from a stock solution of 300 μM. Extracts (100 μL) were reacted with 3.9 mL of the DPPH radical solution for 30 min. The absorbance at 515 nm was measured against a blank of pure methanol using Ultraspec 1100 pro, UV/visible spectrophotometer (Biomicron Ltd. Cambridge CB4 QFJ, England). The analysis was conducted in quadruplicates. Concentrations ranging from 100 to 800 μmol were used for the trolox standard curve. Antioxidant activity was calculated as a % DPPH radical scavenging activity as

DOI: 10.1021/jf5058606
J. Agric. Food Chem. 2015, 63, 2715−2724

$$\text{DPPH radical scavenging activity}(\%) = \left(1 - \left[\frac{A_{\text{sample}} - A_{\text{Control}}}{A_{\text{control}} - A_{\text{blank}}}\right]\right) \times 100 \quad (2)$$

where $A_{control}$ is the absorbance of DPPH radical in methanol at 0 min and A_{sample} is the absorbance of DPPH radical for the sample extract or standard at 30 min. A calibration curve of % DPPH decolorization obtained from different concentration of trolox was used to quantify the antioxidant capacity of the extracts. Antioxidant capacity was expressed using Trolox equivalents (TE) per gram of dry samples.

Determination of ABTS Radical Scavenging Activity. The ABTS method of Pellegrini et al.[33] was further modified for this assay. Samples of 7 mM of ABTS reagent and 2.45 mM of potassium persulfate solution were mixed and allowed to stand in the dark at room temperature for 16 h before use. Prior to assay, the solution was diluted in methanol to give absorbance at 734 nm of 0.7 ± 0.02. Extracts (100 μL) were reacted with 3.9 mL of the ABTS radical solution for 30 min. The absorbance at 734 nm was measured against a blank of pure methanol using Ultraspec 1100 pro, UV/visible spectrophotometer (Biomicron Ltd. Cambridge CB4 QFJ, England). The analysis was conducted in quadruplicates. Concentrations ranging from 100 to 800 μmol were used for the trolox standard curve. Antioxidant activity was calculated as a % ABTS radical scavenging

$$\text{ABTS radical scavenging activity}(\%) = \left(1 - \left[\frac{A_{\text{sample}} - A_{\text{control}}}{A_{\text{control}} - A_{\text{blank}}}\right]\right) \times 100 \quad (3)$$

where $A_{control}$ is the absorbance of ABTS radical in methanol at 0 min and A_{sample} is the absorbance of ABTS radical for the sample extract or standard at 30 min. A calibration curve of % ABTS decolorization obtained from different concentration of trolox was used to quantify the antioxidant capacity of the fractions extracts. Antioxidant capacity was expressed using Trolox equivalents (TE) per gram of dry samples.

Determination of Oxygen Radical Absorbance Capacity. The determination of oxygen radical absorbance capacity ($ORAC_{FL}$), first developed by Cao et al.,[34] was conducted according to Huang et al.[35] and Li et al.[36] A FLx800 microplate fluorescence reader (Bio-Tek Instruments, Inc., Winooski, VT) was used with fluorescence filters for an excitation wavelength of 485/20 nm and an emission wavelength of 528/20 nm. The plate reader was controlled by KC4 3.0 software (version 29). The instrument was monitored by KC4 3.0 software, version 29. Dilutions of barley, corn, and wheat extracts and trolox standard were done manually. A volume of 300 μL each of buffer solution (blank) and diluted sample solution and trolox standard was transferred to a 96-well flat bottom polystyrene microplate according to their allocated wells. Trolox standards 12.5, 25, 50, and 100 μM were used. The remainder of the procedure was conducted according to Li et al.[36] Antioxidant capacity was calculated based on the method by Huang et al.[37] Regression equation between trolox concentration and the net area under the fluorescence decay curve was constructed. The analysis was conducted in quadruplicates. The formula to obtain the area under curve (AUC) was

$$\text{AUC} = 0.5 + \frac{f_1}{f_0} + \ldots\frac{f_i}{f_0} + \ldots\frac{f_{49}}{f_0} + \ldots 0.5\frac{f_{50}}{f_0} \quad (4)$$

where f_0 = initial fluorescence reading at 0 min and f_i = fluorescence reading at time i min. Relative ORAC value was calculated according to the formula:

$$\text{relative ORAC Value} = \frac{\text{AUC}_{\text{sample}} - \text{AUC}_{\text{blank}}}{\text{AUC}_{\text{Trolox}} - \text{AUC}_{\text{blank}}}\left(\frac{\text{molarity of trolox}}{\text{molarity of sample}}\right) \quad (5)$$

In Vitro Models. *Cell Culture Assay.* Three in vitro models were used in this study: Caco-2, HT-29, and FHs 74 Int. Caco-2 is structurally and functionally similar to human intestinal epithelium, which is the first to come in contact with food. They are regarded as a simple in vitro model for the study of drug transportation and absorption in human intestinal mucosa.[37] HT-29, a cell line with epithelial morphology, is used to study drug transportation, absorption, and secretion by intestinal cells.[38] It was used to verify the data from the Caco-2 cell line. FHs 74 Int is primary human fetal intestine cell culture which does not form confluent, polarized monolayers in culture yet is otherwise genotypically similar to neonatal enterocytes. It has been reported to show mature epithelial-like characteristics.[39]

All 3 cell lines were grown in 25 cm^2 polystyrene flask or Transwell culture chamber. The Caco-2 and HT-29 were maintained in DMEM with D-glucose content supplemented with 10% FBS, penicillin (100 kU/L), streptomycin (100g/L), 200 mM L-glutamine, 100 mM sodium pyruvate, and hTF. FHs 74 Int cells were cultured using Hybri-Care medium with 10% FBS, penicillin (10 kU/L), streptomycin (100g/L), and EGF (40 μg/L). Cells were subcultured after reaching confluence using trypsin (0.05%). Cells were maintained at 37 °C in a 5% CO_2 humidified incubator for optimal growth.

Cytotoxicity Assay. Aleurone, germ, and endosperm fractions of barley, corn, and wheat were tested for their cytotoxicity using the MTT colorimetric assay according to the protocol provided by the manufacturer with some modifications. Caco-2, HT-29, and FHs 74 Int cell suspensions (100 μL) were seeded in a 96 well plate and maintained until confluent (a concentration of 1×10^5/mL) for 72 h. Following cell confluence, media from all wells were aspirated. Then 100 μL of 20, 5, and 0.5 mg/mL sample extract and 100 μL of PBS for control wells were added. Blank well contained PBS only. Cells were treated and left in the incubator for 4 h. MTT reagent (10 μL) was added to all wells including the control wells and left in the incubator for 3 h. After 3 h, dots of purple precipitates were visible under microscope and all 110 μL of treatment solution was then aspirated, and 100 μL of detergent reagent was added to all plates including the control. The plates were swirled gently. The plates were covered with aluminum foil and left in the dark for 15 min at room temperature. After 15 min, plate covers were removed and absorbance measured at 560 nm using Opsys MR 96-well reader (Dynex Technologies, Chantilly, VA). Cytotoxicity level (%) was then calculated by comparing absorbance of samples to that of control. Analysis was done in quadruplicates.

Cytoprotective Activity against AAPH-Induced Oxidation. The cytoprotection of extracts of cereal grain fractions against AAPH-induced oxidation were determined by MTT assay according to Gliwa et al.[40] with some modifications. Caco-2, HT-29, and FHs 74 Int cells suspensions (100 μL) were seeded in 96-well plates and maintained until confluent (a concentration of 1×10^5/mL) for 72 h. Following cell confluence, media from all wells were aspirated, and then 100 μL of 20, 5, and 0.5 mg/mL sample extract was added to appropriate sample wells and 100 μL of PBS was added to control wells. Blank wells contained PBS only. After 2 h of incubation, 10 μL of 3 mM AAPH was added to sample and AAPH positive control wells. Cells were incubated for another 4 h. After that, MTT reagent was added to all except the blank wells, and the plates were incubated for 3 h until the intracellular punctate purple precipitate was visible under the microscope. Detergent reagent was then added to all except the blank wells. The plates were swirled gently. The plates were covered with aluminum foil and left in the dark for 15 min at room temperature. After 15 min, plate covers were removed and the plate was measured for absorbance at 560 nm using Opsys MR 96-well reader (Dynex Technologies, Chantilly, VA). Cytotoxicity level (%) was then calculated by comparing absorbance to that of control.

Intracellular Oxidative Stress. Determination of intracellular oxidative stress was based on the oxidation of CM-H_2DCFDA to yield an intracellular-trapped fluorescent compound. Aleurone, germ, and endosperm fractions of barley, corn, and wheat were then tested for their effect on cellular oxidative status according to Wolfe and Liu[41] with some modifications. Caco-2, HT-29, and FHs 74 Int cell suspensions (100 μL) were seeded in a 96-well plate and maintained until confluent (a concentration of 1×10^5/mL) for 72 h. The media from all wells were aspirated, and 100 μL of 20, 5, and 0.5 mg/mL

DOI: 10.1021/jf5058606
J. Agric. Food Chem. 2015, 63, 2715−2724

sample extract and 100 μL of PBS for control wells were added. The blank well contained PBS only. The cells were treated and left for 1 h. At 30 min of incubation, 100 μL of 10 μM CM-H_2DCFDA solution was added to all wells. The final concentration of CM-H_2DCFDA was then 5 μM. After 1 h of incubation, all 200 μL of treatment solutions was removed and 100 μL of 500 μM AAPH dissolved in PBS was added to all wells except negative control (100 μL of PBS was added instead). The plates were then read immediately by Fluoroskan Ascent FL 96-well plate reader (ThermoLabsystems, Franklin, MA). Temperature was set at 37 °C, emission wavelength at 527 nm, and excitation wavelength at 485 nm, and measurements were taken every 30 min for 2 h. The analysis was done in quadruplicates. The CAA value was calculated by integrating area under the curve (AUC) for each sample and standard using final assay values and their linear regression formula below:

$$\mathrm{AUC} = 1 + \frac{\mathrm{RFU}_1}{\mathrm{RFU}_0} + \frac{\mathrm{RFU}_2}{\mathrm{RFU}_0} + \frac{\mathrm{RFU}_3}{\mathrm{RFU}_0} + \ldots + \frac{\mathrm{RFU}_{120}}{\mathrm{RFU}_0} \quad (6)$$

RFU_0 = relative fluorescence value of time zero

RFU_x = relative fluorescence value of time point

The AUC values were used to determine CAA values according to the formula

$$\text{CAA value} = 100 - \left(\frac{\mathrm{AUC}_{\text{Antioxidant}}}{\mathrm{AUC}_{\text{Control}}}\right) \times 100 \quad (7)$$

Microarray Analysis. RNA of HT-29 cells were isolated using RNeasy mini kit and on-column DNase treatment to eliminate genomic DNA contamination according to manufacturer's instructions. An equal amounts of RNA (500 ng) was reverse transcribed to cDNA using a RT^2 First strand kit according to the manufacturer's instructions. Samples were diluted in quantitative polymerase chain reaction (qPCR) master mix (RT^2 SYBR Green; SABioscience Corp.) according to the supplier's directions and pipetted into 96-well PCR array plates. Real-time PCR for the human oxidative stress and antioxidant defense PCR array (PAHS-065Y) consisting of 84 antioxidant enzymes with 3 RT controls and 3 positive PCR controls, a genomic contamination control, and 5 constitutively expressed housekeeping genes was performed according to the manufacturer's instructions using ABI 7500 standard Real-time PCR system (Applied Biosystems). Three independent replicates of each treatment with or without aleurone, germ, and endosperm fractions of corn were performed and data analyzed using software from the SABioscience Web site.[42]

Statistical Analysis. Data obtained in both the biochemical model and in vitro model assay were analyzed as complete randomized design (CRD)-factorial plus control using the one-way analysis of variance (ANOVA) with GLIMMIX Procedure of SAS, release 9.3 (SAS 2014; SAS Institute). Data obtained from microarray analyses were analyzed using a two-tailed t test assuming equal variance. Sample means were compared using Tukey–Kramer multiple comparison procedure, and data was considered significantly different when $P < 0.05$. All results are presented as mean ± standard error.

RESULTS AND DISCUSSION

Biochemical Models. *Total Carotenoid Content in Aleurone, Endosperm, and Germ of Barley, Corn, and Wheat.* Figure 1 shows total carotenoid content (TCC) expressed as xanthophyll equivalent (mg/kg) in cereal grain fractions. TCC differed significantly among fractions from different cereal grains ($P < 0.001$). TCC was highest in germ fraction of the cereal grains (57.3–60.3 mg/kg) and lower in aleurone and endosperm of barley (28.6 and 28.9 mg/kg, respectively). Corn germ had the highest concentration of carotenoid compared to the other samples ($P < 0.001$). The higher content of TCC in germ could be attributed to the presence of yellow carotenoid pigments. Our results are consistent with studies by Panfili et al.[23] and Ndolo and

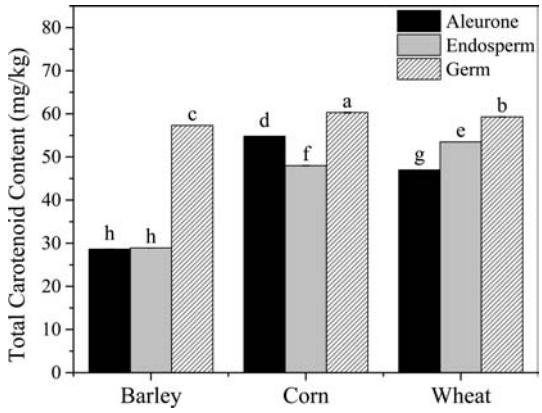

Figure 1. Total carotenoid content (mg/kg) in aleurone, endosperm, and germ fractions of barley, corn, and wheat. Data presented are mean ± standard error ($n = 3$). Different letters indicate significant differences ($p < 0.05$, Tukey–Kramer's multiple range test) among fractions for each cereal.

Table 1. Carotenoid Composition in Aleurone, Endosperm, and Germ Fractions of Barley, Corn, and Wheat (μg/kg) by HPLC[a]

grain fractions	lutein	zeaxanthin
	Barley	
aleurone	112 ± 5.45^c	12 ± 1.54^f
endosperm	nd	nd
germ	1328 ± 3.84^a	15139 ± 4.55^a
	Corn	
aleurone	161 ± 4.48^c	358 ± 2.43^d
endosperm	1369 ± 8.65^a	13671 ± 4.69^b
germ	72 ± 7.69^c	989 ± 6.67^c
	Wheat	
aleurone	72 ± 3.20^c	212 ± 1.82^e
endosperm	155 ± 2.88^c	7 ± 0.70^f
germ	431 ± 3.27^b	215 ± 3.03^e

[a]Values presented are mean ± standard error ($n = 3$). Data in the same column with the same superscript are not significantly different at $p < 0.05$ (Tukey–Kramer's multiple range test).

Table 2. Antioxidant Capacity (μM Trolox Equivalent) per 1 g of Dry Samples[a]

fractions	DPPH	ABTS	ORAC
	Barley		
aleurone	68.0 ± 1.4^b	51.7 ± 0.7^b	27.7 ± 1.8^{bc}
endosperm	4.3 ± 0.6^g	32.0 ± 2.7^d	18.3 ± 1.6^d
germ	76.8 ± 0.2^a	67.6 ± 1.7^a	33.0 ± 3.4^{ab}
	Corn		
aleurone	71.0 ± 0.6^b	47.8 ± 2.1^{bc}	30.5 ± 3.5^{abc}
endosperm	66.2 ± 1.2^b	53.3 ± 3.5^b	33.2 ± 3.5^{ab}
germ	37.1 ± 1.3^e	43.5 ± 2.0^c	37.3 ± 1.2^a
	Wheat		
aleurone	44.4 ± 0.5^d	41.6 ± 1.0^c	24.7 ± 2.1^{cd}
endosperm	25.1 ± 1.1^f	43.9 ± 2.5^c	33.8 ± 3.3^{ab}
germ	50.1 ± 1.1^c	43.3 ± 3.3^c	29.3 ± 1.3^{bc}

[a]Values presented are mean ± standard error ($n = 4$). Data in the same column with the same superscript are not significantly different at $p < 0.05$ (Tukey–Kramer's multiple range test).

DOI: 10.1021/jf5058606
J. Agric. Food Chem. 2015, 63, 2715–2724

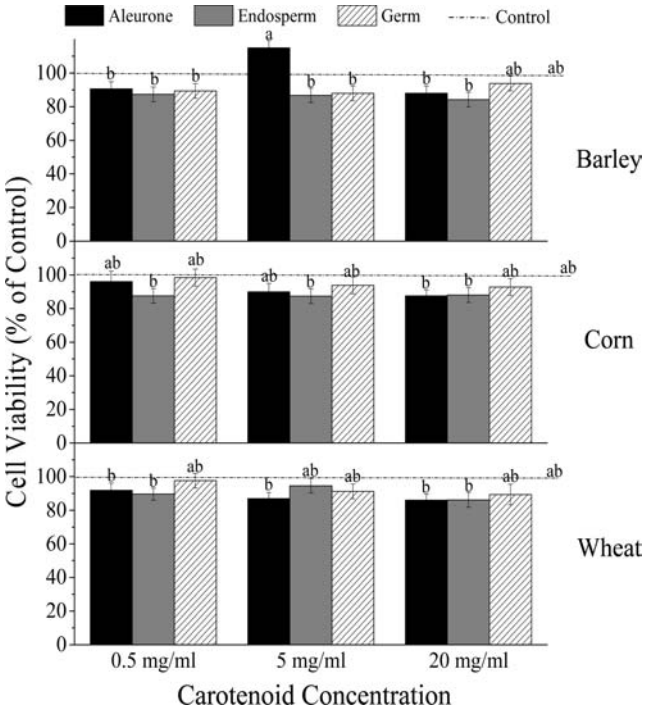

Figure 2. Cytotoxicity of aleurone, germ, and endosperm fractions of barley, corn, and wheat at different concentrations, 0.5, 5, and 20 mg/mL in confluent Caco-2 cell line measured by MTT assay. Different letters indicate significant differences ($p < 0.05$, Tukey–Kramer's multiple range test) among fractions for each cereal.

Table 3. ANOVA Table of Cytotoxicity and Cytoprotective of Aleurone, Germ, and Aleurone Fractions of Barley, Corn, and Wheat As Measured by MTT Assay

	P-value	
	cytotoxicity activity	cytoprotective activity
source	0.65	0.85
fraction	0.02	0.11
source*fraction	0.05	<0.0001
concentration	0.07	0.17
source*concentration	0.35	<0.0001
fraction*concentration	0.12	<0.0001
source*fraction*concentration	0.09	<0.0001

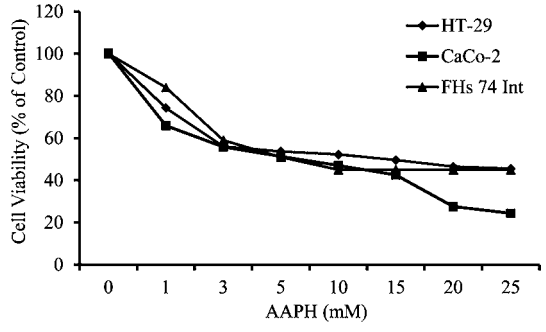

Figure 3. Cytotoxicity of AAPH peroxyl radical generated at 0–25 mM in Caco-2, HT-29, and FHs 74 Int cell measured by MTT assay.

Beta[28] indicating higher carotenoid levels in germs of barley and wheat.

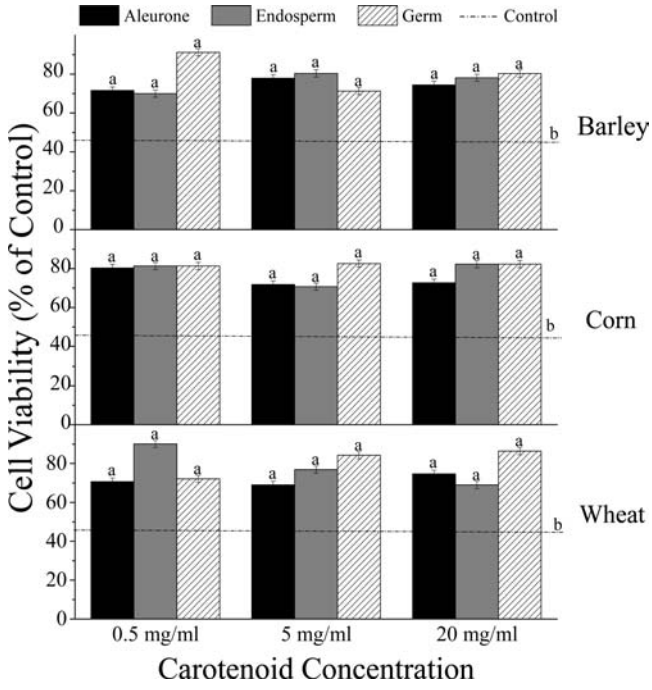

Figure 4. Cytoprotective activity of aleurone, germ, and endosperm fractions of barley, corn, and wheat at different concentrations, 0.5, 5, and 20 mg/mL (mean ± standard error, $n = 4$), in confluent HT-29 cell line against AAPH-induced oxidation. Different letters indicate significant differences ($p < 0.05$, Tukey–Kramer's multiple range test) among fractions for each cereal.

Carotenoids Analysis in Aleurone, Endosperm, and Germ of Barley, Corn, and Wheat. The short method was chosen assuming BHT-ethanol extracted mainly polar carotenoids unlike nonpolar ones, which are found in minimal amount in cereal grains. Carotenoid identification was accomplished by comparing the retention times (t_R) in the sample and those of external standards and the UV–visible absorption spectra from literature. Two peaks were identified for lutein and zeaxanthin, the primary carotenoids found in cereal grains and products.[23,43] Quantitative data were calculated from the linear calibration curves. Lutein levels varied significantly ($P < 0.01$) in all cereal grain fractions. It ranged from nd-1328 μg/kg in barley to 72–431 μg/kg in wheat and 72–1369 μg/kg in corn fractions ($P < 0.01$) (Table 1). The endosperm fraction of corn had higher lutein content (1369 μg/kg) followed by germ fraction of barley (1328 μg/kg) and with no detection in the endosperm of barley. Zeaxanthin levels also varied significantly ($P < 0.01$) in all cereal grain fractions. It ranged from nd-15139 μg/kg in barley to 358–13671 μg/kg in corn and 7–215 μg/kg in wheat. The germ fraction of barley had higher zeaxanthin content (15139 μg/kg) followed by endosperm fraction of corn (13671 μg/kg) and with no detection in the endosperm of barley. Corn fractions had higher levels of zeaxanthin than barley and wheat, and even higher than whole meal as previously shown by Ndolo and Beta.[23] Zeaxanthin has been reported to be concentrated in the germ fraction of wheat[23] and corn endosperm.[44] In the present study, zeaxanthin was also reported as the dominant carotenoid in the aleurone layer in wheat consistent with results reported by Ndolo and Beta.[28] In this study, lutein and zeaxanthin were unevenly distributed in grain fractions and were not detected in the endosperm of barley. Differences in lutein and zeaxanthin levels would be

DOI: 10.1021/jf5058606
J. Agric. Food Chem. 2015, 63, 2715–2724

Table 4. Effect of Aleurone, Germ, and Endosperm Fractions of Corn on Human Oxidative Stress Gene Expression in HT-29 Cell Line[a]

		fold change			*P*-value		
symbol	description	endo	germ	aleu	endo	germ	aleu
CCL5	chemokine (C−C motif) ligand 5	1.01	−2.36	−2.30	0.947	0.120	0.080
BAG2	BCL2-associated athanogene 2	−2.21	0.76	0.79	0.001	0.014	0.034
SLC7A11	solute carrier family 7 (anionic amino acid transporter light chain, xc-system), member 11	−2.06	1.10	1.07	0.003	0.501	0.514
NOX5	NADPH oxidase, EF-hand calcium binding domain 5	2.33	1.22	1.57	0.126	0.375	0.070
MB	myoglobin	2.12	1.78	1.70	0.017	0.022	0.015
NCF1	neutrophil cytosolic factor 1	2.02	2.92	2.63	0.236	0.019	0.034

[a]List of differentially expressed genes. Fold change represents the average of DNA expression level in HT-29 cells treated with aleurone, germ, and endosperm fractions of corn. n = 3 in each condition. endo = endosperm; aleu = aleurone.

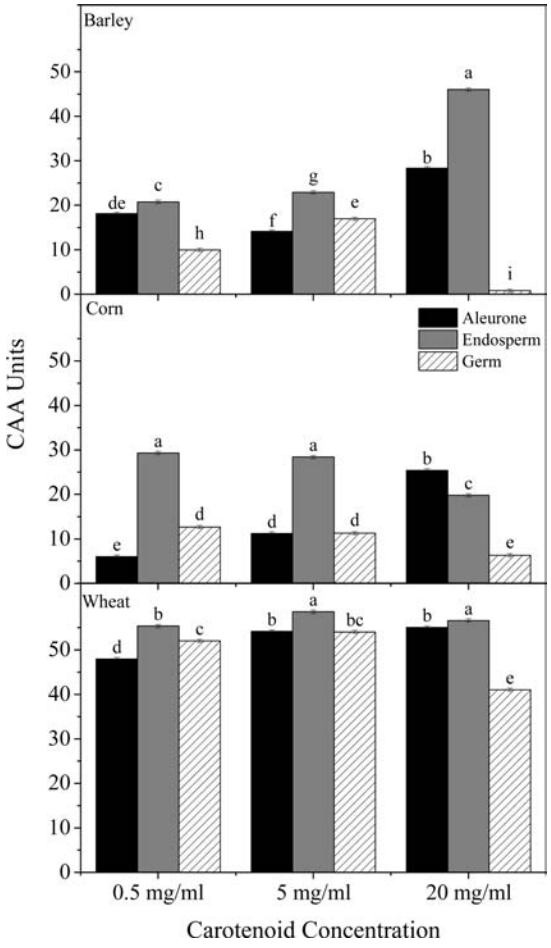

Figure 5. CAA values of aleurone, germ, and endosperm fractions of barley, corn, and wheat at different concentrations, 0.5, 5, and 20 mg/mL (mean ± standard error, n = 8), using Caco-2 cell line. Different letters indicate significant differences (p < 0.05, Tukey-Kramer's multiple range test) among fractions for each cereal.

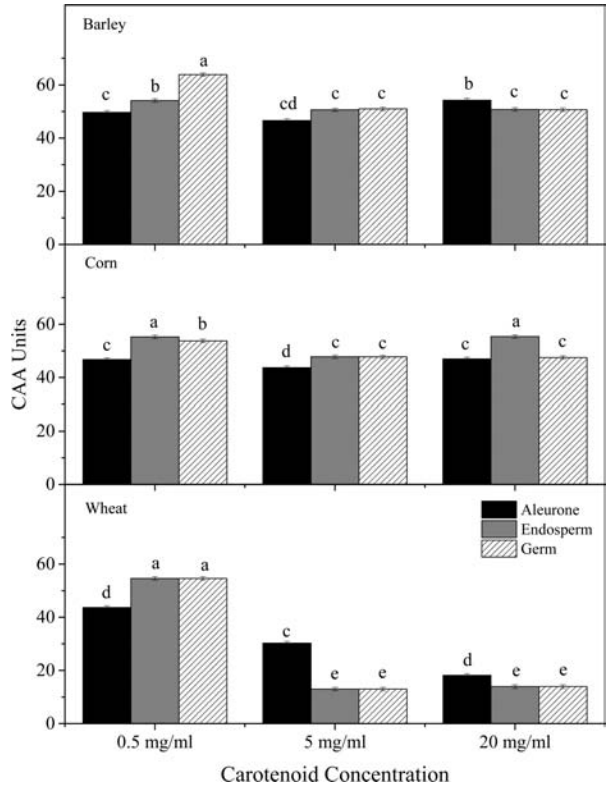

Figure 6. CAA values of aleurone, germ, and endosperm fractions of barley, corn, and wheat at different concentrations, 0.5, 5, and 20 mg/mL (mean ± standard error, n = 8), using FHs 74 Int cell line. Different letters indicate significant differences (p < 0.05, Tukey–Kramer's multiple range test) among fractions for each cereal.

attributable to genetic differences and growing location which affect chemical composition of the cereal grains.[23,44]

DPPH Antioxidant Activity. DPPH scavenging activity is based on discoloration as a result of reduction of DPPH free radical by antioxidant.[31] Our results (Table 2) suggest the better ability to quench DPPH free radicals by the aleurone of corn and barley than of wheat, germ of barley than that of corn and wheat, endosperm of corn than that of barley and wheat (P < 0.01). The antioxidant activity of the fractions ranged from 4.3 to 76.8 for barley, 37.1 to 71.0 for corn, and 25.1 to 50.1 μM trolox equivalent for wheat (Table 2). Barley germ had higher DPPH free radical quenching activity with barley endosperm having the lowest activity (P < 0.01). The low DPPH scavenging activity in the endosperm of barley may be attributed to the low TCC and absence of lutein and zeaxanthin. According to a study by Mortensen and Skibsted[45] on role of carotenoid structure in radical scavenging reaction, zeaxanthin is more reactive than lutein although their order of reactivity shows only slight differences. DPPH scavenging activity in germ fractions ranged from 37.1 μM for wheat to 76.8 μM for barley in aleurone fractions and 44.4 μM for wheat and 71.0 μM for corn.

ABTS+ Antioxidant Activity. ABST+ scavenging activity is based on ABTS+ radical losing its blue-green color when reduced to ABTS at 734 nm.[33] The ABTS scavenging activity ranged from 32.0 to 67.7 for barley, 43.5 to 53.3 for corn, and 41.6 to 43.9 μM trolox equivalent for wheat fractions (Table 2).

DOI: 10.1021/jf5058606
J. Agric. Food Chem. 2015, 63, 2715−2724

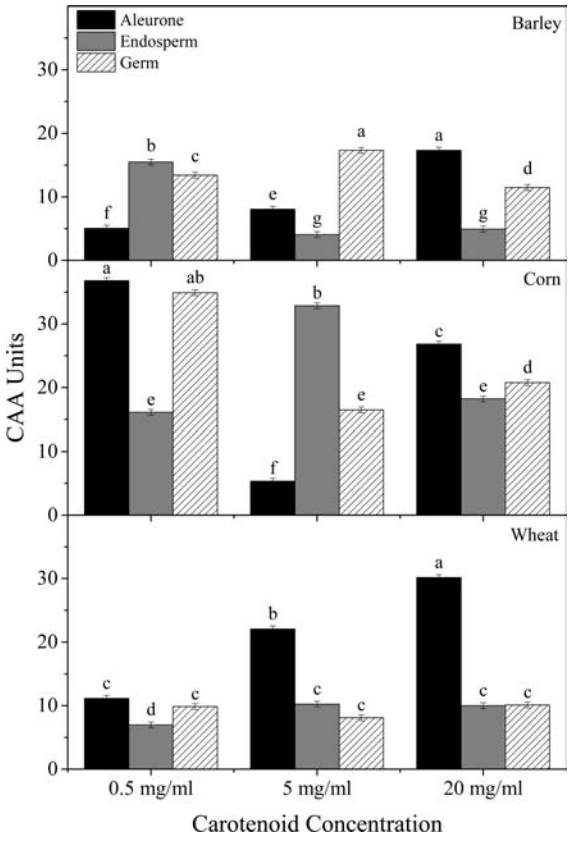

Figure 7. CAA values of aleurone, germ, and endosperm fractions of barley, corn, and wheat at different concentrations, 0.5, 5, and 20 mg/mL (mean ± standard error, n = 8), using HT-29. Different letters indicate significant differences (p < 0.05, Tukey–Kramer's multiple range test) among fractions for each cereal.

Our results suggest that germ of barley had the higher antioxidant activity compared to that of corn and wheat (P < 0.01). Furthermore, the results suggest the better ability to scavenge ABTS free radicals by the aleurone of barley and corn than of wheat, and endosperm of corn than that of wheat and barley. Germ fractions had scavenging activity ranging 43.1 μM for wheat to 67.6 μM for barley; aleurone fractions 41.6 μM for wheat and 51.7 μM for barley; endosperm fractions 32.0 μM for barley and for 53.3 corn (Table 2).

ORAC Values. ORAC assay is based on the principle that antioxidants will prevent peroxyl radicals generated by AAPH from decaying the fluorescence intensity of fluorescein.[34] The ability of a compound to delay the loss of fluorescence intensity over time is a measure of antioxidant capacity. Our results show that ORAC values ranged from 18.3 to 37.3 μmol trolox equivalent (TE)/gram (g) of matter (Table 2). ORAC values were generally low in endosperm (18.3–33.8 μmol TE/g of dry matter) compared to germ and aleurone fractions. Among aleurone fractions, barley had lowest ORAC values. In contrast, ORAC values of germ fractions were highest ranging from 29.3 for wheat and 37.3 μmol TE/g of dry matter for corn. ORAC values were also higher in aleurone fractions, 24.7 for wheat and 30.5 μmol TE/g of dry matter for corn likely due to variation in zeaxanthin levels (Table 1).

In Vitro Models. *Cytotoxicity Assay.* The MTT colorimetric assay evaluated the cytotoxicity of aleurone, germ, and endosperm fractions of barley, corn, and wheat. The cytotoxicity assay was performed to confirm that the sample treatments had minimal negative effect on the viability of the cell line. Compared to the untreated control, extracts were not cytotoxic to Caco-2 (84–115%) (Figure 2; Table 3). Analysis of variance of cytotoxicity data from factorial plus control showed no significant differences between the interactions but showed significant effects between fractions (P < 0.02) which did not pose any toxicity (Figure 2; Table 3). An extract is considered toxic if it is lethal to 50% of the organisms exposed to it in a toxic test. Therefore, our results indicate that different fractions, concentrations, and sources had no negative effect on cell viability. Similar trends were observed with FHs 74 Int and HT-29 cell lines (data not shown). There was no nutrient impact described by the cytotoxicity assay; however, the cytoprotective and intracellular oxidative stress assays further explored antioxidant activity of the sample treatment with different concentrations (0.5, 5, and 20 mg/mL). In order to determine the optimal concentration of AAPH to induce cellular oxidative stress in Caco-2, HT-29, and FHs 74 Int, we constructed dose dependent curves. AAPH concentrations of 0, 1, 3, 5, 10, 15, 20, 25 mM prepared in PBS were incubated with confluent cells in 96-well plates for 4 h. Cell death by AAPH-induced oxidation was determined by MTT assay and expressed as cell viability (%). An escalating concentration of AAPH from 0 to 25 mM resulted in an increasing cell loss in all the cell lines. After 4 h of treatment with AAPH, up to 45–55% loss of cell viability was observed (Figure 3). Different LD_{50} (the concentration of a substance that is lethal to 50% of the organisms exposed to it in a toxic test) obtained from concentration–response curves of the three cell lines indicated Caco-2 cells (LD_{50} = 42.9) are more sensitive than FHs 74 Int (LD_{50} = 37.3) and HT-29 cells (LD_{50} = 22.8) in the presence of AAPH. On basis of the results, 3 mM of AAPH was chosen to stimulate sufficient levels of oxidation in the subsequent study.

Cytoprotective Activity of Aleurone, Endosperm, and Germ Extracts of Barley, Corn and Wheat against AAPH-Induced Cytotoxicity. Based on the cytotoxicity results, 0.5, 5, and 20 mg/mL of aleurone, endosperm, and germ fractions extracts were applied against 3 mM AAPH-induced oxidative damage in Caco-2, HT-29, and FHs 74 Int cells. Analysis of variance of AAPH-induced cytotoxicity data was not significant for the main factors but showed significant effects for all the interactions (P < 0.0001; Figure 4, Table 4). This therefore, indicated different sources, fractions, and concentrations attenuate free radical toxicity differently. The cell viability increased from 45.5% (cell treated with 3 mM of AAPH only) to a maximum of 95.1% (cell pretreated with 0.5, 5, and 20 mg/mL of aleurone, germ, and endosperm extracts followed by 3 mM of AAPH) (Figure 4; Table 4). Similarly, 0.5, 5, and 20 mg/mL of extracts suppressed the AAPH-initiated oxidation damage in Caco-2 and FHs 74 Int cells (data not shown). Elisia and Kitts[46] have previously indicated that AAPH-initiated loss of cell viability in Caco-2 cells is partially attributed to the inductive effect of AAPH on cell apoptosis. AAPH under thermal decomposition produces peroxyl radicals in cultured cell, and this will increase lipid peroxidation, damage cell membrane integrity, and eventually induce cell apoptosis.[47] In this study, all concentrations of cereal grain fractions displayed effective protection in Caco-2, HT-29, and FHs 74 Int cells against AAPH-induced cell loss. Thus, carotenoid extracts from cereal grain fractions may function as free radical cleaner to reduce cellular ROS level and prevent the formation of apoptosis cells caused by AAPH oxidation.

DOI: 10.1021/jf5058606
J. Agric. Food Chem. 2015, 63, 2715–2724

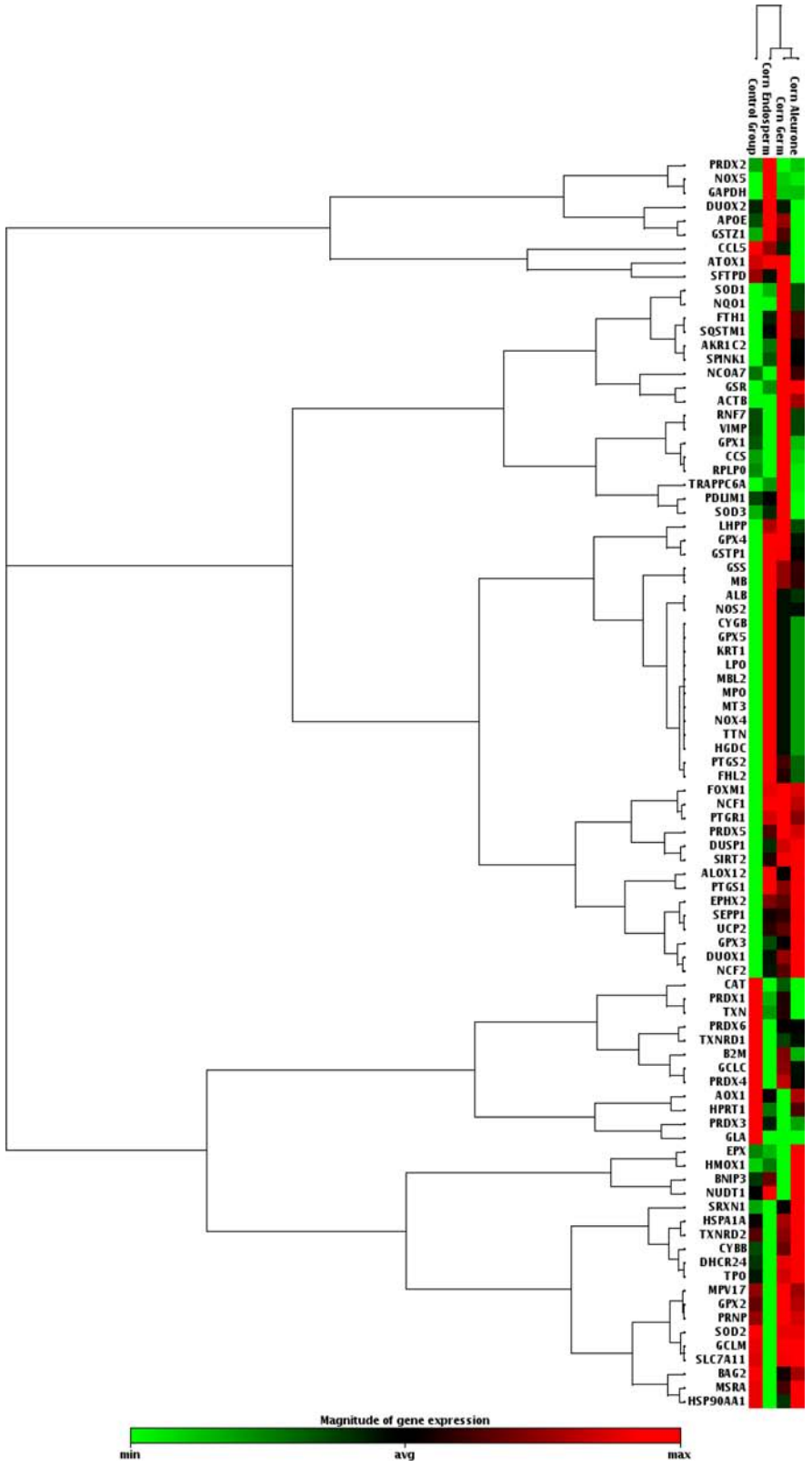

Figure 8. Clustergram or heatmap analysis: The clustergram or heatmap represents expression levels of 84 genes in four conditions (control, endosperm, germ, and aleurone of corn) relative to an average of five housekeeping genes. Each horizontal line in the heatmap represents a single gene, and the columns represent groups. Samples clustered according to the condition. Red represents high expression, while green represents low expression.

Intracellular Oxidative Stress. CM-H_2DCFDA is a fluorogenic dye for measuring hydroxyl, peroxyl, and other ROS activity within the cell. After diffusion into the cell, CM-H_2DCFDA is deacetylated by cellular easterases to a non-fluorescent compound which is later oxidized by ROS into 2′,7′-dichlorofluorescin (DCF). DCF is a highly fluorescent

DOI: 10.1021/jf5058606
J. Agric. Food Chem. 2015, 63, 2715−2724

compound that can be detected by fluorescence spectroscopy with maximum excitation and emission spectra of 495 and 529 nm, respectively. The reaction of sample-treated cell lines against APPH-induced free radical oxidation is shown in Figures 5−7. AAPH induced the oxidation of the dye CM-H_2DCFDA to DCF. The fluorescence intensity of DCF was measured to represent the rate of oxidation. Positive (+) controls showed the fluorescence intensity of the AAPH oxidation over time, while negative (−) controls were cells to which AAPH was not added. They were used to illustrate conditions devoid of any oxidation inducer. Cell lines treated with cereal fractions carotenoid extracts showed the inhibition of oxidation as their fluorescence intensities were higher than the negative control but less than the positive control over time. CAA units were then calculated (eqs 6 and 7) based on the fluorescence intensity of the fraction extracts and AAPH-treated cells. In Caco-2 cell line, CAA ranged from 5.0 to 55.0 CAA units (Figure 5). Wheat fraction always showed the highest antioxidant activity whereas barley fractions showed the lowest CAA units. In FHs 74 Int cell line, CAA ranged from 15.0 to 63.0 CAA units (Figure 6). Barley germ at 0.5 mg/mL showed higher CAA units than wheat which had the lowest. Corn endosperm had highest antioxidant activity while wheat had lowest CAA units. Barley and wheat aleurone fractions at 20 mg/mL showed highest and lowest CAA units, respectively. Using HT-29 cell line, CAA ranged from 5.0 to 37.5 CAA units (Figure 7). Corn fraction always showed the highest antioxidant activity whereas barley fractions showed the lowest CAA units. On the basis of current study, all tested doses inhibited ROS as shown by increase in CAA units ($P < 0.05$).

Aleurone, Endosperm, and Germ Fractions of Corn and Antioxidant Gene Regulation in HT-29 Intestinal Cells. Based on the TCC, lutein and zeaxanthin levels, cytoprotective activity, and CAA results, HT-29 were treated with 20 mg/mL of aleurone, endosperm, and germ fractions of corn to assess abundance of oxidative stress-related genes. Extracted RNA was determined spectrophotometrically at 260/280 nm with NanoDrop ND-1000 (NanoDrop Technologies, Inc.) to be $A_{260/280} = 1.91$. Of the 84 antioxidant pathway genes included in this oxidative stress and antioxidants defense array, the expression of 28 genes was altered by corn aleurone, endosperm, and germ treatments ($P < 0.05$) (Figure 8). However, we only observed twofold upregulation of myoglobin (MB), neutrophil cytosolic factor 1 (NCF1) and NADPH oxidase, EF-hand calcium binding domain 5 (NOX5) and twofold down regulation of chemokine (C−C motif) ligand 5 (CCL5), BCL2-associated athanogene 2 (BAG), and solute carrier family 7 (anionic amino acid transporter light chain, xc- system), member 11 (SLC7A11) in different fractions (Table 4). However, *P*-values did not indicate statistical significance for NOX5 and CCL5 in all fractions, NCF1 in endosperm and SCL7A11 in aleurone and germ. The microarray antioxidant enzymes are enzymes that catalyze the reduction of hydroperoxides and other organic hydroperoxides. The upregulation of 28 genes therefore represents a cell-protective mechanism by which intestinal cells manage oxidative stress elicited by exposure to aleurone, germ, and endosperm fractions.

Generally, lutein and zeaxanthin and TCC were unevenly distributed across the grain fraction. For all cereal grain fractions, the germ had significantly ($P < 0.001$) higher levels of TCC than aleurone and endosperm (corn > wheat > barley). In barley and wheat, lutein and zeaxanthin were concentrated in the germ unlike in corn where they are concentrated in endosperm. DPPH and ABTS showed radical scavenging; ORAC activity showed antioxidant activity. All cereal grain fractions displayed effective protection in Caco-2, HT-29, and FHs 74 Int cells against AAPH-induced cell loss and inhibited ROS as shown by increase in CAA units. Thus, carotenoid extracts from cereal grain fractions may function as free radical cleaner to reduce cellular ROS level and prevent the formation of apoptosis cells caused by AAPH oxidation. On the basis of the current studies, we conclude that carotenoids of aleurone, germ, and endosperm from barley, corn, and wheat improved antioxidant activity and thus have the potential to mitigate oxidative stress. We also showed that antioxidant activity of cereal grain fractions might be through endogenous scavenging and gene expression mechanisms. These findings indicate that corn endosperm, aleurone, and germ of corn, barley, and wheat might be useful functional ingredients in curbing oxidative stress, hence preventing human pathogenesis.

AUTHOR INFORMATION

Corresponding Author

*E-mail: Trust.Beta@umanitoba.ca. Telephone: +1 204- 474-8214. Fax: +1 204-474-7630.

Funding

We are grateful for the financial support provided by the Natural Sciences and Engineering Research Council of Canada (NSERC) through the Discovery Grant program and the Canada Foundation for Innovation (New Opportunities Fund and Leaders Opportunity Fund) for funding the equipment used for this study.

Notes

The authors declare no competing financial interest.

ACKNOWLEDGMENTS

We are thankful for the technical support of Patricia Heritage, Alison Ser, Yang Qui, Babak Sobhi, and Nha Ky Huynh of the Department of Food Science, University of Manitoba.

REFERENCES

(1) Ho, E.; Galougahi, K. K.; Bhindi, R.; Figtree, G. A. Biological markers of oxidative stress: Application to cardiovascular research and practice. *Redox Biol.* **2013**, *1*, 483−491.

(2) Sobha, R. I.; Andallu, B. Oxidative stress and cancer: Role of anti-carcinogenic herbs and species. *Am. J. Phytomed. Clin. Ther.* **2013**, *3*, 351−369.

(3) Young, I. S.; Woodside, J. V. Antioxidant in health and disease. *J. Clin. Pathol.* **2001**, *54*, 176−186.

(4) Nogueira, V.; Hay, N. Molecular pathways: Reactive oxygen species homeostasis in cancer cells and implication for cancer therapy. *Clin. Cancer Res.* **2013**, *19*, 4309−4314.

(5) Leavy, O. Inflammation: Regulating ROS: Nature Review. *Nat. Rev. Immunol.* **2014**, *14*, 357.

(6) Sugamura, K.; Keaney, J. F., Jr. Reactive species in cardiovascular disease. *Free Radical Biol. Med.*. **2011**, *1*, 978−992.

(7) Khandhadia, S.; Lotery, A. Oxidation and age-related macular degeneration: Insights from molecular biology. *Expert Rev. Mol. Med.* **2010**, *12*, e34.

(8) Hancock, J. T.; Desikan, R.; Neill, S. J. Role of reactive oxygen species in cell signalling pathways. *Biochem. Soc. Trans.* **2001**, *29* (Pt2), 345−350.

(9) Krinsky, N. I.; Johnson, E. J. Carotenoid action and their relation to health and diseases. *Mol. Aspects Med.* **2005**, *26*, 456−516.

(10) Tapeiro, H.; Townsend, D. M.; Tew, K. D. The role of carotenoids in the prevention of human pathologies. *Biomed. Pharmacother.* **2004**, *58*, 100−110.

DOI: 10.1021/jf5058606
J. Agric. Food Chem. 2015, 63, 2715−2724

(11) Adom, K. K.; Sorrells, M. E.; Liu, R. H. Phytochemicals and antioxidant activity of milled fractions of different wheat varieties. *J. Agric. Food Chem.* **2005**, *53*, 2297−2306.
(12) Howitt, C. A.; Pogson, B. J. Carotenoid accumulation and function in seeds and non green tissues. *Plant Cell Environ.* **2006**, *29*, 435−445.
(13) Stahl, W.; Sies, H. Antioxidant activity of carotenoids. *Mol. Aspects Med.* **2003**, *24*, 345−351.
(14) Gentili, A.; Caretti, F. Evaluation of method based on liquid chromatography−diode array detector tandem mass spectrometry for a rapid and comprehensive characterization of the fat soluble vitamin and carotenoid profile of selected plant foods. *J. Chromatogr. A* **2011**, *1218*, 684−697.
(15) Leenhardt, F.; Lyan, B.; Rock, E.; Boussard, A.; Potus, J.; Chanliaud, E.; Remesy, C. Genetic variability of carotenoid concentration, and lipoxygenase and peroxidase activities among cultivated wheat species and bread wheat varieties. *Eur. J. Agronom.* **2006**, *25*, 170−176.
(16) Miller, N. J.; Sampson, J.; Candeias, L. P.; Bramley, P. M.; Rice-Evans, C. A. Antioxidant activities of carotenes and xanthophylls. *FEBS Lett.* **1996**, *384*, 240−242.
(17) Palozza, P.; Krinsky, N. I. Antioxidant of carotenoids in vivo and in vitro: An overview. *Methods Enzymol.* **1992**, *213*, 403−420.
(18) Polyakov, N. E.; Kruppa, A. I.; Leshina, T. V.; Konovalova, T. A.; Kispert, L. D. Carotenoids as antioxidants: Spin trapping EPR and optical study. *Free Radic. Biol. Med.* **2001**, *31*, 43−52.
(19) Irakli, M. N.; Samanidou, V. F.; Papadoyannis, I. N. Development and validation of an HPLC method for the simultaneous determination of tocopherols, tocotrienols, and carotenoids in cereals after solid-phase extraction. *J. Sep. Sci.* **2011**, *34*, 1375−1382.
(20) Abdel-Aal, E. S. M.; Young, J. C.; Wood, P. J.; Rabalski, I.; Hucl, P.; Falk, D.; Fregeau-Reid, J. Einkorn: A potential candidate for developing high lutein wheat. *Cereal Chem.* **2002**, *79*, 455−457.
(21) Humphries, J. M.; Khachik, F. Distribution of lutein, zeaxanthin, and related geometrical isomers in fruits, vegetable, wheat, and pasta products. *J. Agric. Food Chem.* **2003**, *51*, 1322−1327.
(22) Hentschel, V.; Kranl, K.; Hollmann, J.; Lindhauer, M. G.; Bohm, V.; Bitsch, R. Spectrophotometric determination of yellow pigment content and evaluation of carotenoids by high-performance liquid chromatography in durum wheat grain. *J. Agric. Food Chem.* **2002**, *50*, 6663−6668.
(23) Panfili, G.; Fratianni, A.; Irano, M. Improved normal-phase high-performance liquid chromatography procedure for the determination of carotenoids in cereals. *J. Agric. Food Chem.* **2004**, *52*, 6373−6377.
(24) Cooke, M. S.; Evans, M. D.; Misty, N.; Lunec, J. Role of dietary antioxidants in the prevention of in vivo oxidative DNA damage. *Nutr. Res. Rev.* **2002**, *15*, 19−41.
(25) Abdel-Aal, E. S. M.; Young, J. C.; Rabalski, I.; Hucl, P.; Fregeau-Reid, J. Identification and quantification of seed carotenoids in selected wheat species. *J. Agric. Food Chem.* **2007**, *55*, 787−794.
(26) Hidalgo, A.; Brandolini, A.; Pompei, C.; Piscozzi, R. Carotenoids and tocols of einkorn wheat (*Triticum monococcum spp. monococcum L.*). *J. Cereal Sci.* **2006**, *44*, 182−93.
(27) Kurilich, A. C.; Juvik, J. A. Simultaneous quantification of carotenoids and tocopherols in corn kernel extracts by HPLC. *J. Liq. Chromatogr. Relat. Technol.*. **1999**, *22*, 2925−2934.
(28) Ndolo, V. U.; Beta, T. Distribution of carotenoids in endosperm, germ, and aleurone fractions of cereal grain kernels. *J. Food Chem.* **2013**, *139*, 663−671.
(29) Stewart, A.; Nield, H.; Lott, J. N. A. An investigation of the mineral-content of barley grains and seedlings. *Plant Physiol.* **1988**, *86*, 93−97.
(30) Cha, K. H.; Koo, S. Y.; Lee, D. U. Antiproliferative effects of carotenoids extracted from *chlorella ellipsoidea* and *chlorella vulgaris* on human colon cancer cells. *J. Agric. Food Chem.* **2008**, *56*, 10521−10526.
(31) Brand-Williams, W.; Cuvelier, M. E.; Berset, C. Use of a free radical method to evaluate antioxidant activity. *Lebnsm.-Wiss. u.-Technol.* **1995**, *28*, 25−30.
(32) Li, W.; Shan, F.; Sun, S.; Corke, H.; Beta, T. Free radical scavenging properties and phenolic content of Chinese black-gained wheat. *J. Food Chem.* **2005**, *53*, 8533−8536.
(33) Pelleggrini, N.; Re, R.; Yang, M.; Rice-Evans, C. Screening of dietary carotenoids and carotenoid-rich fruit extract for antioxidant activities applying 2,2′-azinobis(3-ethylenebenzothiazoline-6-sulfonic acid radical cation decolorization assay. *Methods Enzymol.* **1999**, *229*, 379−389.
(34) Cao, G.; Alessio, H. M.; Cutler, R. G. Oxygen-radical absorbance capacity assay for antioxidants. *Free Radic. Biol. Med.* **1993**, *14*, 303−311.
(35) Huang, D.; Ou, B.; Prior, R. L. The chemistry behind antioxidant capacity assays. *J. Agric. Food Chem.* **2005**, *53*, 1841−1856.
(36) Li, W.; Pickard, M. D.; Beta, T. Effect of thermal processing on antioxidant properties purple wheat bran. *J. Food Chem.* **2007**, *104*, 1080−1086.
(37) Hilgers, A. G.; Conrandi, R. A.; Burton, P. S. Caco-2 cell monolayers as a model for drug transport across the intestinal mucosa. *Pharm. Res.* **1990**, *7*, 902−910.
(38) Lesuffleur, T.; Barbat, A.; Dussaulx, E.; Zweibaum, A. Growth adaptation to methotrexate of HT-29 human colon carcinoma cells is associated with their ability to differentiate into columnar-absorptive and mucus-secreting cells. *Cancer Res.* **1990**, *50*, 6334−43.
(39) Wagner, C. L.; Forsythe, D. W.; Wagner, M. T. The effect of recombinant TGF-alpha, human milk, and human media on gut epithelial proliferation is decreased in the presence of a neutralizing TGF-alpha milk macrophage antibody. *Biol. Neonate* **1998**, *74*, 363−371.
(40) Gliwa, J.; Gunenc, A.; Ames, N.; Willmore, W. G.; Hosseinian, F. S. Antioxidant activity of alkylresorcinols from rye bran and their protective effect on cell viability of PC-12 AC cells. *J. Agric. Food Chem.* **2011**, *59*, 11473−11482.
(41) Wolfe, K. L.; Liu, R. H. Cellular antioxidant activity (CAA) assay for assessing antioxidants, food, and dietary supplements. *J. Agric. Food Chem.* **2007**, *55*, 8896−8907.
(42) RT^2 Profiler PCR array data analysis version 3.5. Available from: http://pcrdataanalysis.sabiosciences.com/pcr/arrayanalysis.php (accessed July 2014).
(43) Fratianni, A.; Irano, M.; Panfili, G.; Acquistucci, R. Estimation of color of durum wheat. Comparison of WSB, HPLC, and reflectance colorimeter measurements. *J. Agric. Food Chem.* **2005**, *53*, 2373−2378.
(44) Kean, E. G.; Hamaker, B. R.; Ferruzzi, M. G. Carotenoid bioaccessibility from whole grain and degermed maize meal products. *J. Agric. Food Chem.* **2008**, *56*, 9918−9926.
(45) Mortensen, A.; Skibsted, L. H. Importance of carotenoid structure in radical-scavenging reactions. *J. Agric. Food Chem.* **1997**, *45*, 2970−2977.
(46) Elisia, I.; Kitts, D. D. Anthocyanins inhibit peroxyl radical-induced apoptosis in Caco-2 cells. *Mol. Cell. Biochem.* **2008**, *312*, 139−145.
(47) Kulkarni, A. P.; Pal, J. K.; Devasagayam, T. P. A. Radiation and free radical exposure and regulation of protein synthesi by heme-regulated eukaryotic initiation factor 2α kinase. *BARC Newsl.* **2008**, *297*, 80−87.

DOI: 10.1021/jf5058606
J. Agric. Food Chem. 2015, 63, 2715−2724

MATERIALS AND METHODS

The net absorption of betaine and choline was studied in three experiments. In the first experiment, pigs were fed a low-fiber Western style diet (WSD)[32] or WSD with added purified betaine, and in the following two experiments, the net absorption of betaine and choline was studied in pigs fed various types of high-fiber breads. The pigs were fed either breads based on whole-grain wheat or wheat aleurone, which they had been adapted to for 4 days,[33] referred to as chronic uptake of betaine, or rye breads with whole rye kernels or milled rye[34] as a single meal, which will be termed acute uptake of betaine.

Animal Model. The pigs for the studies were obtained from the swineherd at Aarhus University, Foulum, Department of Animal Science. The porto-arterial catheterized pig model was used to study the net absorption of betaine and choline. The pigs were surgically fitted with permanent catheters in the portal vein and in the mesenteric artery; in the first experiment, a catheter was furthermore placed in the hepatic vein. An ultrasonic flow probe (Transonic, 20PAU probe, 18/20 mm; Transonic System, Inc., Ithaca, NY, USA) was placed around the portal vein to enable measurement of portal blood flow. The surgical procedure was described in detail by Jørgensen et al.[35] The pigs were allowed to recover from surgery for 5−9 days before entering the experimental period.

The pigs were kept individually in pens with visual and physical contact with neighboring pigs through railings. No bedding was provided, but an elevated plastic grid covering half of the pen allowed the pigs to rest and stay dry. The pigs had ad libitum access to water.

The animal experiments were conducted in compliance with procedures approved by the Danish Animal Experiments Inspectorate, Ministry of Food, Agriculture and Fisheries, Danish Veterinary and Food Administration, in accordance with the Danish Ministry of Justice, Law 1306 of November 23, 2007, concerning experiments with animals and care of experimental animals.

Experimental Design. *Experiment 1: Absorption of Betaine in Pigs Fed a Low-Fiber Diet with or without Betaine Supplementation.* Four female pigs (Duroc × Danish landrace × Yorkshire) with an initial body weight of 59.9 (SEM 2.2) kg surgically fitted with permanent catheters in the mesenteric artery, portal vein, and hepatic vein were included in the experiment. The pigs were fed WSD based on white wheat flour and formulated to be high in saturated fat, protein, and refined carbohydrates and low in dietary fiber (Supporting Information Table S1) for a week prior to blood sampling. After the first sampling, the pigs were fed WSD for an additional 4 days followed by 3 days when they were fed WSD supplemented with betaine (50 mg kg^{-1} body weight) (Betafin S1, Danisco Animal Nutrition, Dupont), and the second blood sampling was conducted after the morning feeding on the fourth day. The chemical composition of the WSD diet is given in Supporting Information Table S1.[32]

Experiment 2: Absorption of Betaine and Choline from Whole-Grain Wheat or Wheat Aleurone, Chronic Intake. Six female pigs (Danish landrace × Yorkshire) with an initial body weight of 56.5 (SEM 1.8) kg surgically fitted with permanent catheters in the mesenteric artery and the portal vein were included in the experiment. The pigs were fed two experimental diets in a cross-over design. Each experimental period lasted 1 week. During dayd 1−3 the pigs were fed a wash-out diet based on white wheat flour (WFL), and on days 4−7 the pigs were fed one of two experimental breads based on either whole-grain wheat (WGW) or wheat aleurone-rich flour (WAF) (Supporting Information, Table S2). On the sampling day the pigs were fed the experimental bread in the morning, and in the evening they were switched to WFL. The ingredients for the experimental breads and their chemical composition are shown in Supporting Information Table S2.[33]

Experiment 3: Absorption of Betaine and Choline from Rye Bread with or without Whole Rye Kernels, Acute Intake. Six female pigs (Duroc × Danish landrace × Yorkshire) with an initial body weight of 60.2 (SEM 3.1) kg surgically fitted with permanent catheters in the mesenteric artery and the portal vein were included in the experiment. The pigs were fed a semisynthetic low-fiber wash-out diet based on wheat flour, whey protein, canola oil, and a vitamin−mineral mixture containing synthetic amino acids (Supporting Information, Table S3), and on experimental days they were fed one of two breads as a single meal prior to collection of blood. The breads were a rye bread with intact kernels (RK) and a dark ground rye bread (GR). The breads are commercially available, produced by Lantmännen Schulstad A/S (Hammerholmen, Hvidovre, Denmark) and sold as Levebrød Multikernerugbrød (multiseed rye bread) (RK) and Mørkt rugbrød (dark rye bread) (GR). The breads were portioned to provide 200 g of available carbohydrate. The chemical composition of the semisynthetic diet and the breads is given in Supporting Information Table S3.[34]

Sample Collection. On sampling days, portal blood flow was measured for 2 min immediately prior to blood sampling. Blood samples were subsequently collected simultaneously from both/all three catheters. The first blood sample was collected 30 or 15 min prior to feeding ($t = 0$) and following samples were collected at 30, 60, 90, 120, and 240 min after feeding. In experiment 2, additional blood samples were collected at 15 and 45 min after feeding. Blood samples were collected in heparinized vacutainers (Greiner Bio-One, Kremsmünster, Austria). Blood was centrifuged (2000*g* for 12 min at 4 °C), and plasma was immediately frozen at −80 °C until analysis.

Solvents and Reagents. HPLC grade acetonitrile and methanol were purchased from VWR − Bie & Berntsen A/S (Herlev, Denmark). Formic acid, betaine, and choline as well as D_9-betaine and D_{11}-choline were purchased from Sigma-Aldrich (St. Louis, MO, USA).

Processing of Plasma and Feed Samples. Choline and betaine in plasma were determined using a modification of the method described by Bruce and co-workers.[36] Plasma was thawed, and aliquots (50 μL) were taken and placed into 2 mL centrifuge tubes. To the aliquots was added 150 μL of internal standard solution (10 μM D_9-betaine and D_9-choline in methanol). After vortexing, the samples were placed at 4 °C for 20 min and centrifuged at 13200*g* for 10 min at 4 °C. The supernatant was pipetted into 200 μL vials for analysis.

Feed (50 mg) was extracted with 5 mL of extraction solution (7.5 μM D_9-betaine and D_9-choline in methanol/water (75:25 v/v)). The mixture was stirred for 5 min and subsequently centrifuged (3000 rpm, 4 °C, 10 min). The supernatant was pipetted into 200 μL vials for analysis.

Analysis of Betaine and Choline by HPLC-ESI-QTOF-MS. Plasma and feed samples were analyzed using a Dionex Ultimate 300 HPLC system (Thermo Scientific Dionex, Sunnyvale, CA, USA) coupled to a MicroTOF-Q quadropole time-of-flight mass spectrometer (Bruker Daltonics, Bremen, Germany). Chromatographic separation was performed on an Ascentis Express HILIC column (2.1 mm × 10 cm, 2.7 μm) (Supelco Analytical, Bellefonte, PA, USA) together with a Ascentis Express HILIC guard column (0.5 cm × 2.1 mm, 2.7 μm) (Supelco Analytical). The column was maintained at 30 °C. Mobile phase A consisted of 5 mM ammonium acetate (adjusted to pH 4 with formic acid), whereas mobile phase B consisted of acetonitrile and 0.025% formic acid. The system equilibrated at 10% A for 5 min before the sample (5 μL) was injected, and the gradient started after 1 min. The gradient increased linearly to 60% A within 5 min and increased linearly from 60 to 90% A within 6 min. The gradient returned to 10% A in 30 s. The total analysis time was 16.5 min, and the flow rate was 100 μL/min.

MS data were acquired in positive electrospray (ESI) mode in a scan range from m/z 50 to 1000 at a sampling rate of 2 Hz. ESI parameters were as follows: capillary, 4.5 kV; nebulizer pressure, 1.8 bar; dry gas flow, 8 L min^{-1}; dry gas temperature, 200 °C. Lithium formate solution (5 mM) was used for automatic calibration and injected at the beginning of each chromatographic run. Blank runs and additional quality control (QC) samples were interspersed between the samples under investigation.

Data were processed using Compass DataAnalysis (version 4.0, Bruker Daltonik GmbH) and Compass QuantAnalysis (version 2.2). The accurate masses of betaine and choline (m/z 118.0860 and 104.1070, respectively) and the internal standards D_9-betaine and D_9-choline (m/z 127.1420 and 113.1630, respectively) were used. Standard curves were prepared from choline and betaine standards with internal standards (7.5 μM D_9-betaine and D_9-choline). The concentrations ranged from 0.39 to 100 μM and from 3.9 to 1000 μM for choline and betaine, respectively, and standard curves were

DOI: 10.1021/jf506024v
J. Agric. Food Chem. 2015, 63, 2725−2733

constructed by linear regression analyses. The regression equations, linear ranges, and correlation coefficients of betaine and choline are summarized in Supporting Information Table S4.

Calculations. The net absorptions (net portal flux) of betaine and choline were calculated using the portal−arterial concentration differences ($c_p - c_a$) and the portal flow measurements using Fick's principle.[30] This was done using the equation

$$q = (c_p - c_a) \times F(dt)$$

where q is the amount of absorbed betaine or choline during the time dt and F is the flow in the portal vein. The concentration of metabolites in the portal vein and mesenteric artery is given by c_p and c_a, respectively. During the postprandial period between t_0 and t_n the quantity absorbed, Q, was calculated as

$$Q = \sum_{t_n}^{t_0} q$$

The enrichment across the gastrointestinal tract was calculated as

$$GI_{enrich} = \frac{c_p - c_a}{c_a} \times 100\%$$

where c_a and c_p denote the concentration of metabolites in the mesenteric artery and the portal vein, respectively.

The net hepatic flux (NHF) of betaine and choline from 0 to 4 h after the first daily meal was determined as

$$NHF = \left(c_h \times \frac{F}{0.85}\right) - (c_p \times F) - \left(c_a \times \left(\frac{F}{0.85} - F\right)\right)$$

where F is the flow in the portal vein, and the total blood flow to the liver was assumed to be 85% from the portal vein and 15% from the hepatic arteries based on the results of Kristensen and co-workers;[31] c_h, c_p, and c_a denote the concentration of metabolites in the hepatic vein, portal vein, and mesenteric artery, respectively.

Furthermore, the hepatic extractions, H_{ex}, of betaine and choline from 0 to 4 h after the first daily meal were determined as

$$H_{ex} = \frac{-NHF}{(c_p \times F) + \left(c_a \times \left(\frac{F}{0.85} - F\right)\right)} \times 100\%$$

Statistics. The effect of the experimental diets within each experiments was analyzed as repeated measurements using the MIXED procedure of Statistical Analysis Software (SAS Institute Inc., Cary, NC, USA) as described by Littell et al.[37] using the model

$$Y_{ijkl} = \mu + \alpha_i + \beta_j + \alpha\beta_{ij} + \gamma_k + \upsilon_l + \tau_{ikl} + \varepsilon_{ijkl}$$

where Y_{ijkl} is the dependent variable, μ is the overall mean, α_i is the effect of diet, β_j is time after feeding, and $\alpha\beta_{ij}$ is the interaction between diet and time. γ_k is the experimental week, and υ_l is the random effect of pig; τ_{ikl} is the random component related to the lth pig fed the ith diet in the kth week, and ε_{ijkl} is the residual error component. The pig and pig × week × diet were included as random components to account for repeated measurements (within pigs and within pigs with sampling days, respectively). Results are presented as least-squares means with their SE. To obtain normality, data on betaine concentrations in the first experiment and in the acute experiment and the net absorption of betaine in the first experiment were logarithm transformed before the statistical analysis. Because confidence intervals on the original scale are not symmetric around the parameter estimates, the 95% confidence intervals rather than SE are presented for those responses. Levels of significance were reported as being significant when $p \leq 0.05$ and as a tendency when $0.05 < p \leq 0.10$.

The relationship between fasting plasma betaine and the betaine concentration in the feed was described by a mechanistic growth model

$$Y = \alpha(1 - \beta\ e^{-cT})$$

where y is the dependent variable (plasma betaine concentration), α the asymptotic value, c the growth rate, β the scale, and T the betaine concentration in the feed. The statistical analysis of the relationship between betaine concentration in the feed and plasma betaine concentration was carried out using JMP, version 11.1.1 (SAS Institute Inc.).

RESULTS

Concentrations of Betaine and Choline in the Experimental Diets. The concentrations of betaine and choline in diets are presented in Table 1. In the diets used in experiment 1 a very low betaine concentration was found in WSD (0.19 mg/g fresh weight). When this diet was supplemented with betaine to provide the pigs with 50 mg betaine/kg body weight, it resulted in a betaine concentration in the diet of 7.59 mg/g fresh weight. In experiment 2, the content of betaine was more than twice as high in WAF (1.75 mg/g fresh weight) as in WGW (0.74 mg/g fresh weight), whereas the betaine concentrations were comparable in the rye breads with or without whole kernels used in experiment 3 (1.53−1.58 mg/g fresh weight). The choline concentration in the experimental diets was less variable (0.05−0.20 mg/g fresh weight), with the lowest concentrations found in the low-fiber diets.

Table 1. Betaine and Choline Concentration in the Experimental Diets and the Intake of Betaine and Choline during the Meal Prior to Sampling

		dietary concentration (mg/g fresh wt)		dietary intake (mg)	
expt	diet[a]	betaine	choline	betaine	choline
1	WSD	0.19 ± 0.01	0.048 ± 0.003	96	24
	WSD + betaine	7.59 ± 0.89	0.046 ± 0.005	3780	23
2	WGW	0.74 ± 0.08	0.150 ± 0.001	760	74
	WAF	1.75 ± 0.27	0.209 ± 0.056	1673	199
3	wash-out	0.30 ± 0.03	0.062 ± 0.003	–[b]	–[b]
	RK	1.53 ± 0.17	0.150 ± 0.021	923	90
	GR	1.58 ± 0.26	0.191 ± 0.031	1013	123

[a]WSD, Western style diet; WGW, whole-grain wheat; WAF, wheat aleurone-rich flour; RK, rye bread with intact kernels; GR, dark ground rye bread. [b]The absorption of betaine and choline was not measured after intake of the wash-out diet.

Net Absorption and Net Hepatic Flux of Betaine and Choline in Pigs Fed a Diet Low in Betaine without and with Added Betaine. The mean betaine concentration was highly elevated in arterial, portal, and hepatic blood of the pigs fed WSD with added betaine compared to WSD without betaine (Table 2). This is also clearly seen in the plasma concentrations during 0−4 h after the first meal of the day (Figure 1a). In pigs fed WSD supplemented with betaine, betaine in the portal vein increased rapidly during the first 30 min post feeding and remained high until 120 min post feeding. Betaine in arterial and hepatic blood was maximal 60 min after feeding and declined thereafter. Betaine concentration was similar at the three sampling sites 180 min post feeding. The net absorption of betaine was 6.21 mmol/h when the pigs were fed WSD supplemented with betaine. This was significantly higher than the net absorption from the WSD diet. The net hepatic flux of betaine was negative (−12.3 mmol/h), indicating that betaine was metabolized in the liver. This

DOI: 10.1021/jf506024v
J. Agric. Food Chem. 2015, 63, 2725−2733

Table 2. Mean Plasma Concentration, Net Portal Absorption, Enrichment across the Gastrointestinal Tract, Net Hepatic Metabolism, and Hepatic Extractions of Betaine and Choline 0−4 h after the First Daily Meal in Pigs Fed either a Western Style Diet (WSD) or WSD Supplemented with Betaine

	diet[a]			p value		
	WSD	WSD + betaine	SE	diet	time	diet × time
mean plasma concentration						
mesenteric artery						
betaine[b] (μM)	137 (97; 193)	983 (699; 1384)		0.0001	0.0001	0.0001
choline (μM)	9.87	8.93	1.00	0.21	0.0001	0.16
portal vein						
betaine[b] (μM)	141 (99; 199)	1064 (753; 1502)		0.0001	0.0001	0.0001
choline (μM)	18.50	16.94	0.86	0.22	0.0001	0.78
hepatic vein						
betaine[b] (μM)	134 (91; 198)	985 (666; 1455)		0.0001	0.0001	0.003
choline (μM)	8.59	7.72	1.32	0.20	0.0004	0.60
net absorption						
betaine[b](mmol/h)	0.70 (0.26; 1.86)	6.21 (2.31; 16.7)		0.004	0.009	0.008
choline (mmol/h)	0.84	0.83	0.10	0.85	0.0001	0.75
enrichment across the GI tract						
betaine (%)	2.82	7.72	1.66	0.02	0.003	0.005
choline (%)	86.8	90.0	15.5	0.83	0.0002	0.70
net hepatic metabolism						
betaine (mmol/h)	−0.29	−12.3	1.8	0.0001	0.10	0.08
choline (mmol/h)	−1.04	−1.08	0.08	0.72	0.0001	0.005
hepatic extraction						
betaine (%)	1.8	9.6	2.2	0.004	0.56	0.12
choline (%)	51	53	6	0.51	0.02	0.21

[a]WSD, Western style diet; WSD + betaine, Western style diet supplemented with betaine. [b]Values are back-transformed least-squares means (lower and upper limits of the 95% confidence interval).

corresponded to a hepatic extraction of 10% of the betaine entering the liver when WSD was supplemented with betaine, whereas only 2% was extracted when a diet low in betaine (WSD) was fed. The mean choline concentration did not differ in arterial, portal, or hepatic blood of pigs fed WSD or WSD supplemented with betaine (Table 2), but the concentration was higher in the portal vein than in the mesenteric artery and hepatic vein (Figure 1b), and the portal concentration peaked 30 min after feeding. The net absorption of choline did not differ between diets. The net hepatic flux of choline was 1 mmol/h, and around 50% of the choline was extracted in the liver irrespective of diet.

Effects of High-Fiber Breads on Plasma Concentrations of Betaine and Choline. Mean betaine concentration was significantly affected by diet and time in both arterial and portal blood when WGW and WAF were fed (Table 3), whereas feeding two types of rye bread once introduced no difference in the mean arterial and portal betaine concentrations. In Figure 2, the betaine concentrations during the first 0−4 h after the first daily meal are shown. When WAF and WGW were fed, a clear difference between the experimental diets is observed (Figure 2a). Pigs fed the WAF diet had higher betaine concentration in both arterial and portal blood during the experimental period than pigs fed WGW. For pigs fed the WAF diet the betaine concentration increased 2 h after feeding, whereas the concentration remained constant in pigs fed WGW. Feeding rye bread without (GR) or with whole kernels (RK) did not result in differences in the betaine concentration in arterial and portal blood during 0−4 h after the first meal of the day (Figure 2b). The betaine concentration increased from 30 to 120 min after ingestion of the first meal of the day, whereafter it reached a plateau.

The mean concentrations of choline in arterial and portal blood did not differ in pigs fed WAF or WGW (Table 3) as also reflected in the plasma choline concentrations during 0−4 h after the first daily meal (Figure 3a). However, the difference between the portal and arterial concentrations was considerable. When consuming rye bread without (GR) or with whole kernels (RK), pigs achieved minor but significant differences in plasma choline concentrations in both arterial and portal blood (Figure 3b).

Absorption across the Gastrointestinal Tract of Betaine and Choline in Pigs Fed High-Fiber Breads. Diet did not influence the net absorption of betaine (Table 4). The net absorption was low and quite variable, and there was no clear effect of the type of experiment, chronic versus acute. The net absorption of choline was not affected by diet, and no difference was observed between the two types of experiment. Although the net absorptions of betaine and choline on a molar basis were similar, the enrichment of betaine across the gastrointestinal tract was very low compared to the enrichment of choline.

Fasting Plasma Betaine in Relation to the Betaine Content in the Feed. The relationship between the fasting plasma betaine in the mesenteric artery and the betaine content in the feed can be explained by a mechanistic growth model

DOI: 10.1021/jf506024v
J. Agric. Food Chem. 2015, 63, 2725−2733

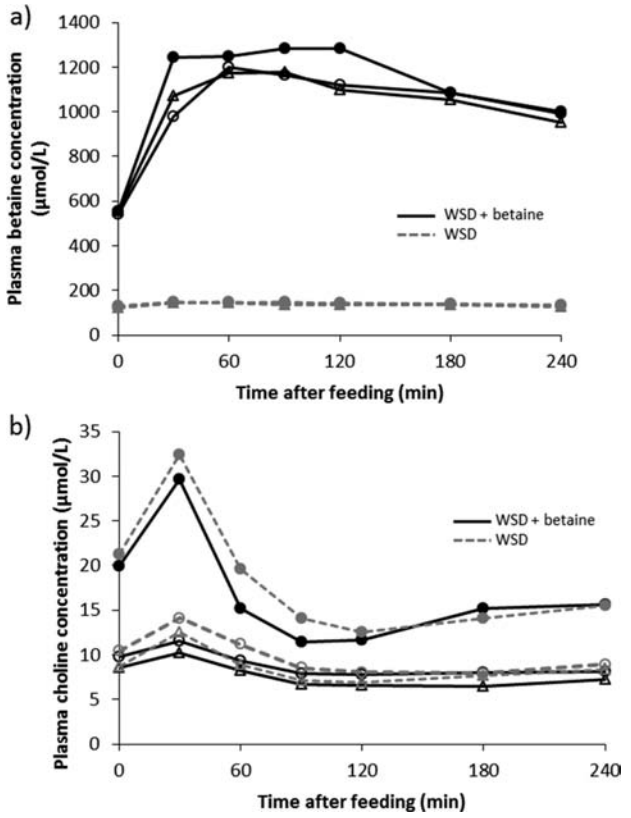

Figure 1. (a) Plasma betaine concentrations (μmol/L) and (b) plasma choline concentrations (μmol/L) in the portal vein (●), the mesenteric artery (○), and the hepatic vein (△) in pigs fed a Western style diet (WSD) or WSD supplemented with betaine (50 mg kg^{-1}) (WSD + betaine). The p values for each sampling point are shown in Table 2.

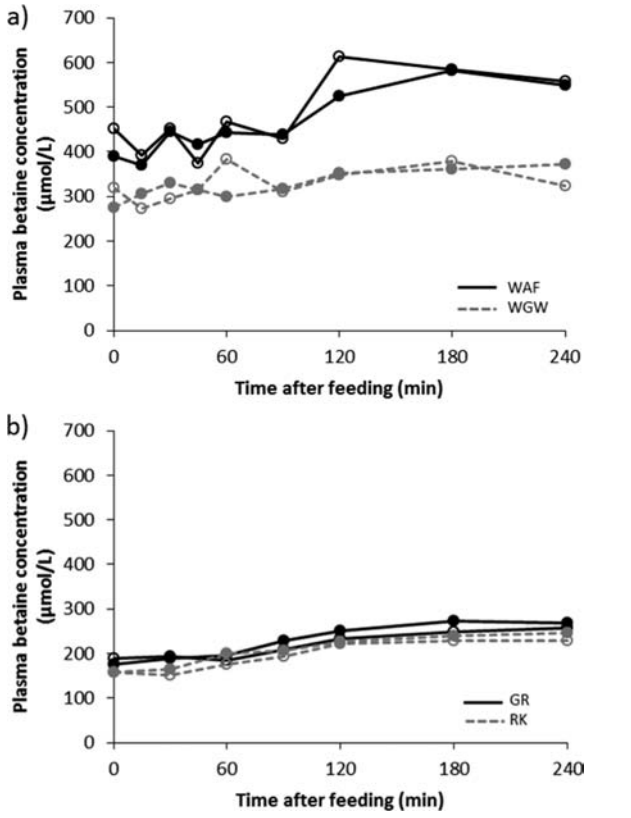

Figure 2. Plasma betaine concentrations (μmol/L) in the portal vein (●) and the mesenteric artery (○) in pigs fed (a) a diet with wheat aleurone flour (WAF) or a diet with whole-grain wheat (WGW) and (b) rye bread with ground rye (GR) or whole rye kernels (RK). The p values for each sampling point are shown in Table 3.

(Figure 4). The model has a growth rate of 0.77 μmol betaine/L plasma/g betaine/kg feed, and the asymptote of the model is 577 μmol/L (R^2 = 0.97).

DISCUSSION

The highest betaine concentration was found in the WAF diet followed by the two rye diets (RK and GR) and the WGW diet, with the lowest levels in the WSD and wash-out diet. These differences reflected the differences in betaine concentration

Table 3. Mean Plasma Concentrations of Betaine and Choline 0−4 h after the First Daily Meal in Pigs Fed Diets Varying in Content or Composition of Dietary Fiber

	diet[a]			p value		
	WGW	WAF	SE	diet	time	diet × time
mesenteric artery						
betaine (μM)	327	481	24.6	<0.0001	<0.0001	0.0009
choline (μM)	20.2	19.5	1.15	0.27	0.01	0.77
portal vein						
betaine (μM)	325	462	20.3	<0.0001	0.0003	0.37
choline (μM)	29.5	28.9	1.27	0.68	0.05	0.54
	diet[a]			p value		
	RK	GR	SE	diet	time	diet × time
mesenteric artery						
betaine[b] (μM)	188 (134; 265)	194 (137; 273)		0.23	<0.0001	0.01
choline (μM)	10.81	12.60	0.95	0.05	0.39	0.25
portal vein						
betaine[b] (μM)	203 (151; 274)	223 (165; 301)		0.14	<0.0001	0.40
choline (μM)	22.71	19.81	1.21	0.01	0.04	0.06

[a]WGW, whole-grain wheat; WAF, wheat aleurone-rich flour; RK, rye bread with intact kernels; GR, dark ground rye bread. [b]Values are back-transformed least-squares means (lower and upper limits of the 95% confidence interval).

DOI: 10.1021/jf506024v
J. Agric. Food Chem. 2015, 63, 2725−2733

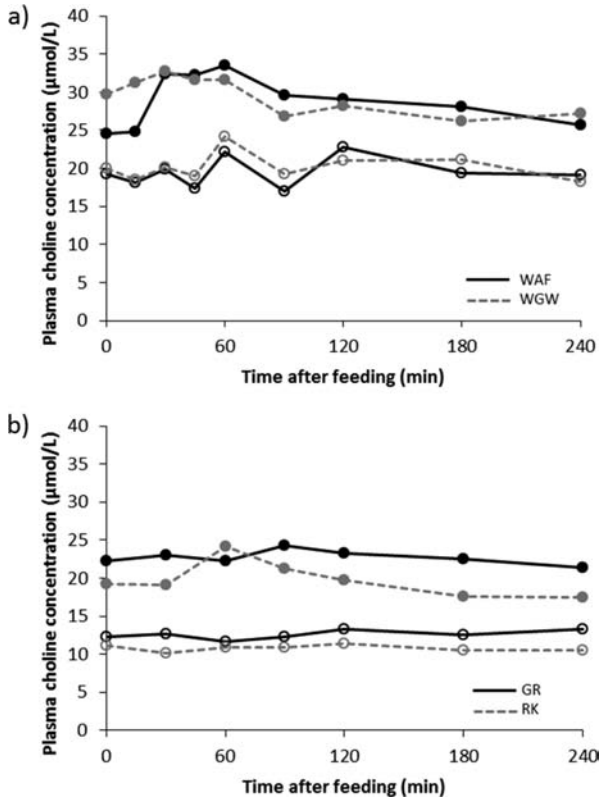

Figure 3. Plasma choline concentrations (μmol/L) in the portal vein (●) and the mesenteric artery (○) in pigs fed (a) a diet with wheat aleurone flour (WAF) or a diet with whole-grain wheat (WGW) and (b) rye bread with ground rye (GR) or whole rye kernels (RK). The p values for each sampling point are shown in Table 3.

between the different tissues of the wheat grain; the betaine concentration is highest in the aleurone tissue and lowest in the endosperm[17] and between cereals with a higher concentration of betaine in rye than in wheat.[15] The two types of rye bread had similar betaine contents, which was not surprising as the main difference between the two bread types was milling or not of the rye kernels.

The choline content of the experimental diets was low and varied less than the betaine content, which reflects that items in high-fiber diets do not belong to groups of ingredients with high choline content, being eggs, red meat, poultry, and milk,[38] and that the choline content of cereal grains is less variable.[15]

The major finding of our study was the distinct difference in absorption patterns when betaine was added as a supplement to a refined Western style diet as compared to when provided from cereals naturally rich in betaine. Thus, when pigs were fed WSD supplemented with betaine (50 mg kg^{-1} body weight), a sharp increase in portal betaine concentration was observed 30 min postprandial. This is in accordance with results obtained in humans following a single oral dose of betaine, where the plasma betaine concentration peaked 60 min after intake.[39] The time difference between the present study and the human study is most likely due to the fact that the blood samples in the present study were taken from the portal vein, where betaine appears immediately after absorption, whereas the samples in the human study were taken in a peripheral vein. In the present study the plasma betaine profile obtained from the mesenteric artery may be compared to peripheral blood samples and the betaine concentration was maximal in the artery 60 min

Table 4. Mean Net Portal Absorption and Enrichment across the Gastrointestinal Tract of Betaine and Choline from the Gastrointestinal Tract from 0 to 4 h after the First Daily Meal in Pigs Fed Diets Varying in Content or Composition of Dietary Fiber

	diet[a]			p value		
	WGW	WAF	SE	diet	time	diet × time
net absorption						
betaine (mmol/h)	−0.97	−4.00	2.07	0.31	0.07	0.05
choline (mmol/h)	1.43	1.49	0.19	0.76	0.002	0.35
	diet[a]			p value		
	RK	GR	SE	diet	time	diet × time
net absorption						
betaine (mmol/h)	1.51	0.92	0.66	0.58	0.11	0.52
choline (mmol/h)	1.16	1.23	0.16	0.58	0.005	0.41
	diet[a]			p value		
	WGW	WAF	SE	diet	time	diet × time
enrichment across the GI tract						
betaine (%)	−0.39	−4.81	3.43	0.36	0.04	0.005
choline (%)	52.0	51.8	8.2	0.98	0.01	0.16
	diet[a]			p value		
	RK	GR	SE	diet	time	diet × time
enrichment across the GI tract						
betaine (%)	7.30	3.97	2.21	0.36	0.19	0.54
choline (%)	84.9	84.8	11.1	0.99	0.03	0.49

[a]WGW, whole-grain wheat; WAF, wheat aleurone-rich flour; RK, rye bread with intact kernels; GR, dark ground rye bread.

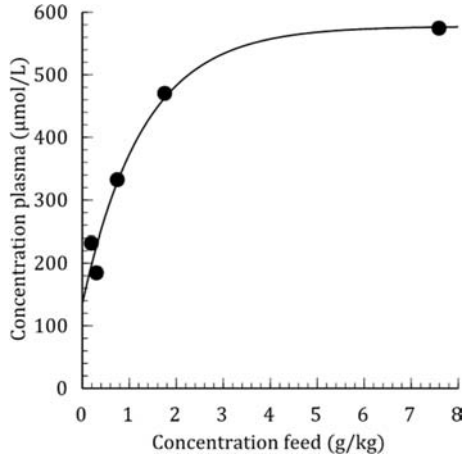

Figure 4. Relationship between fasting plasma betaine in the mesenteric artery (μmol/L) and the betaine content of the feed (μmol/g). Estimated relationship: fasting plasma betain = $577 \times (1 - 0.77 \times e^{(-0.77 \times \text{betain in feed})})$, $R^2 = 0.97$.

postprandial. The plasma betaine observed in pigs fed WSD supplemented with betaine was comparable to what has been observed in humans given the same dose,[39] indicating that pigs and humans have the same capacity to digest and absorb betaine.

DOI: 10.1021/jf506024v
J. Agric. Food Chem. 2015, 63, 2725−2733

In contrast to the rapid absorption of betaine provided as a supplement, betaine embedded in dietary fiber sources is more slowly available as it has to be liberated from the matrix prior to absorption. The postprandial absorption profile in the portal vein was significantly affected by time in all three experiments. The concentration of betaine in the portal vein increased from 60 to 90 min after feeding and peaked 120 min postprandial for pigs fed WAF, GR, and RK. For the WGW and the WSD diets the betaine remained constant after feeding, although at different levels due to the different betaine contents of the diets. The postprandial profiles for diets high in betaine are comparable to those obtained in humans, where it was observed that the betaine concentration increased 120 min after a whole-grain meal and 60 min after a refined-grain meal.[19] The lack of interaction between diet and time in portal vein samples when high-fiber breads were eaten indicated that the accessibility of betaine did not differ between the diets within each experiment. Betaine is a water-soluble compound. It is not known to be bound to any matrix,[14] but it is encapsulated in the aleurone cells. The aleurone cell wall has a rigid structure, which does not allow endogenous enzymes (proteases, carbohydrases) to pass, whereas water-soluble molecules of relatively low molecular weight may pass. Therefore, the cell wall structure of the aleurone cells is responsible for the delayed absorption of betaine in the cereal diets compared to the added betaine. The present study further shows that grinding of rye kernels does not increase the bioavailability of betaine, supporting that the aleurone cell wall is the major hindrance to betaine absorption. Ultrafine grinding or bioprocessing of wheat and rye bran has been shown to increase the antioxidant activity and bioaccessibility of phenolic compounds, presumably due to breakdown of the aleurone layer,[40−42] but whether this increases the bioavailability of betaine as well remains to be investigated.

The plasma betaine concentrations observed in the present experiment after consumption of dietary betaine are generally higher than those observed in humans.[7,19,22,39] The habitual diet of pigs contains a high amount of cereals compared to that of humans, and hence pigs are expected to have a high daily intake of betaine. This has been suggested to lead to the higher plasma concentration of betaine in pigs when compared to humans.[43]

The fasting plasma concentration of betaine reflected the concentration of betaine in the experimental diets in the chronic experiments and in the wash-out diet in the acute experiment. A previous study in pigs showed that when the diet was changed from a low-fiber diet to a high-fiber diet, the fasting betaine level in plasma increased gradually during 3 days,[21] and thus the fasting plasma concentrations observed in this study may be considered to have reached a steady state. In humans it was observed that the fasting betaine concentration was increased 2 days after changing to a high-betaine diet.[7] A chicken study showed that the presence of betaine in the diet increased the Na^+-coupled component of betaine transport and led to a higher capacity of betaine uptake,[44] and hence a higher betaine uptake may be expected when the animals were adapted to the diets. In the present study no clear difference in the absorption profiles was observed when the high-fiber breads were fed in a chronic or an acute experiment, but the betaine concentration after feeding WAF in a chronic experiment was twice as high as when rye bread was fed in an acute experiment, even though the betaine concentrations of the diets were similar, indicating that adaptation to the diet increased the absorption capacity. The observed relationship between fasting plasma betaine concentration and betaine content in the feed indicates that chronic exposure increases the basic circulating level of betaine. However, there is an upper limit on the fasting plasma betaine concentration, probably reflecting a balance between absorption, conversion to other metabolites, and excretion to urine.

Although we found postprandial differences in portal and arterial concentrations and fasting betaine concentrations that were correlated to the dietary levels of betaine, similar betaine concentrations in the portal vein and the mesenteric artery were seen for all but the diet supplemented with betaine. This indicates slow release of betaine from the fiber matrix, giving rise to a low net absorption of betaine from the diets. When betaine was added to the diet, a higher concentration of betaine was observed in the portal vein than in the mesenteric artery during 30−120 min after feeding; however, the net absorption of betaine was still low. The negative net hepatic metabolism shows that betaine was either accumulated or metabolized in the liver. The only known metabolism of betaine is by the zinc metalloenzyme betaine-homocysteine methyltransferase, which is located in the liver and kidneys.[45] This enzyme transfers a methyl group from betaine to homocysteine to produce dimethylglycine and methionine, respectively.[1] In the present study we did not measure the concentration of dimethylglycine in plasma, and consequently we are not able to confirm whether betaine was accumulated or metabolized in the liver. Studies in rats and chicken have shown that when high-betaine diets are fed, betaine is accumulated in the liver,[25,46] and in rats the betaine concentration in liver showed both a plasma-related and a plasma-independent component.[47]

Plasma choline showed a consistent difference between the concentration in the portal vein and the mesenteric artery, disclosing the absorption of choline from the gastrointestinal tract. Measurements of hepatic vein concentrations showed that choline is metabolized in the liver. The major fate of choline is the phosphorylation to phosphocholine, but in the liver it may be oxidized to betaine as well.[48] In the present study, betaine was shown to be metabolized or stored in the liver. This means that if choline was oxidized to betaine, this additional betaine was either immediately stored or metabolized in the liver. The concentration of choline in the hepatic vein was consistently slightly lower than the concentration in the mesenteric artery, indicating that free choline was released from the tissues to the circulation. Different postprandial profiles of choline were observed. When WSD or WSD + betaine was fed, a clear choline peak 30 min after feeding was seen. In contrast, the choline concentration in the portal vein remained constant after feeding with the high-fiber breads. The difference presumably resides in the fat source used in the diets. WSD contained lard, which contains a high amount of choline, whereas the choline content of soybean oil and rapeseed oil used in the studies with bread is low.[38]

In conclusion, using the porto-arterial catheterized pig model the present study showed that free betaine is rapidly absorbed to the portal vein, whereas the absorption of betaine from cereal sources is slower, reflecting a delayed liberation of betaine from the matrix prior to absorption. There was, however, no difference in the rate of absorption from the different cereal sources ,which indicates that the encapsulation of betaine in the aleurone cell layer delays the absorption of betaine from cereal sources. To increase the bioavailability of betaine, the use of ultrafine grinding or bioprocessing (e.g., a

DOI: 10.1021/jf506024v
J. Agric. Food Chem. 2015, 63, 2725−2733

combination of hydrolytic enzymes and yeast fermentation) of bran or aleurone fractions could be considered. Due to a rapid metabolism of betaine, the portal-arterial difference in betaine concentration is very low. The results of the current study indicate that it is preferable to provide betaine as part of a whole-grain diet rather than a concentrate as this ensures slow release of betaine with impact on the circulating levels of betaine and with modest diurnal fluctuation.

■ ASSOCIATED CONTENT

Supporting Information

Ingredients and chemical composition of the experimental diets (Tables S1−S3) and regression equations, linear ranges, and correlation coefficients of betaine and choline for each batch of samples analyzed (Table S4). This material is available free of charge via the Internet at http://pubs.acs.org.

■ AUTHOR INFORMATION

Corresponding Author

*(M.S.H.) E-mail: Mette.Hedemann@anis.au.dk. Phone: +45 87 15 80 78. Fax: +45 87 15 42 49.

Funding

The present study was financially supported by the Nordic Centre of Excellence on Food, Nutrition and Health "Systems biology in controlled dietary interventions and cohort studies" (SYSDIET; 070014) funded by Nordforsk.

Notes

The authors declare no competing financial interest.

■ ACKNOWLEDGMENTS

We thank the technical staff in the Molecular Nutrition and Cell Biology Group and the staff in the intensive barn of he Department of Animal Science for technical assistance. Danisco Animal Nutrition, Dupont, is acknowledged for the delivery of Betafin S1 for the experiment.

■ ABBREVIATIONS USED

GI_{enrich}, enrichment across the gastrointestinal tract; GR, dark ground rye bread; H_{Ex}, hepatic extraction; NHF, net hepatic flux; QC, quality control; RK, rye bread with intact kernels; WAF, wheat aleurone-rich flour; WFL, white wheat flour; WGW, whole-grain wheat; WSD, Western style diet

■ REFERENCES

(1) Craig, S. A. Betaine in human nutrition. *Am. J. Clin. Nutr.* **2004**, *80*, 539−549.

(2) Lever, M.; Slow, S. The clinical significance of betaine, an osmolyte with a key role in methyl group metabolism. *Clin. Biochem.* **2010**, *43*, 732−744.

(3) Ueland, P. M. Choline and betaine in health and disease. *J. Inherit. Metab. Dis.* **2011**, *34*, 3−15.

(4) Ueland, P. M.; Holm, P. I.; Hustad, S. Betaine: a key modulator of one-carbon metabolism and homocysteine status. *Clin. Chem. Lab. Med.* **2005**, *43*, 1069−1075.

(5) Guthikonda, S.; Haynes, W. Homocysteine: role and implications in atherosclerosis. *Curr. Atheroscler. Rep.* **2006**, *8*, 100−106.

(6) Alfthan, G.; Tapani, K.; Nissinen, K.; Saarela, J.; Aro, A. The effect of low doses of betaine on plasma homocysteine in healthy volunteers. *Br. J. Nutr.* **2004**, *92*, 665−669.

(7) Atkinson, W.; Slow, S.; Elmslie, J.; Lever, M.; Chambers, S. T.; George, P. M. Dietary and supplementary betaine: effects on betaine and homocysteine concentrations in males. *Nutr. Metab. Cardiovasc. Dis.* **2009**, *19*, 767−773.

(8) Chiuve, S. E.; Giovannucci, E. L.; Hankinson, S. E.; Zeisel, S. H.; Dougherty, L. W.; Willett, W. C.; Rimm, E. B. The association between betaine and choline intakes and the plasma concentrations of homocysteine in women. *Am. J. Clin. Nutr.* **2007**, *86*, 1073−1081.

(9) Ross, A. B.; Godin, J. P.; Minehira, K.; Kirwan, J. P. Increasing whole grain intake as part of prevention and treatment of nonalcoholic fatty liver disease. *Int. J. Endocrinol.* **2013**, article ID 585876, 13 pages, DOI: 10.1155/2012/585876.

(10) Fardet, A.; Chardigny, J. M. Plant-based foods as a source of lipotropes for human nutrition: a survey of in vivo studies. *Crit. Rev. Food Sci.* **2013**, *53*, 535−590.

(11) Schwab, U.; Torronen, A.; Toppinen, L.; Alfthan, G.; Saarinen, M.; Aro, A.; Uusitupa, M. Betaine supplementation decreases plasma homocysteine concentrations but does not affect body weight, body composition, or resting energy expenditure in human subjects. *Am. J. Clin. Nutr.* **2002**, *76*, 961−967.

(12) Olthof, M. R.; van Vliet, T.; Verhoef, P.; Zock, P. L.; Katan, M. B. Effect of homocysteine-lowering nutrients on blood lipids: results from four randomised, placebo-controlled studies in healthy humans. *PLoS Med.* **2005**, *2*, 446−456.

(13) Zeisel, S. H. Betaine supplementation and blood lipids: fact or artifact? *Nutr. Rev.* **2006**, *64*, 77−79.

(14) Ross, A. B.; Zangger, A.; Guiraud, S. P. Cereal foods are the major source of betaine in the Western diet − analysis of betaine and free choline in cereal foods and updated assessments of betaine intake. *Food Chem.* **2014**, *145*, 859−865.

(15) Corol, D. I.; Ravel, C.; Raksegi, M.; Bedo, Z.; Charmet, G.; Beale, M. H.; Shewry, P. R.; Ward, J. L. Effects of genotype and environment on the contents of betaine, choline, and trigonelline in cereal grains. *J. Agric. Food Chem.* **2012**, *60*, 5471−5481.

(16) 2013 Rye and Health, Statistics and Usage; http://www.ryeandhealth.org/statistics-a-usage (accessed Feb 25, 2015).

(17) Fardet, A. New hypotheses for the health-protective mechanisms of whole-grain cereals: what is beyond fibre? *Nutr. Res. Rev.* **2010**, *23*, 65−134.

(18) Thwaites, D. T.; Anderson, C. M. H. Deciphering the mechanisms of intestinal imino (and amino) acid transport: the redemption of SLC36A1. *Biochim. Biophys. Acta − Biomembr.* **2007**, *1768*, 179−197.

(19) Ross, A. B.; Bruce, S. J.; Blondel-Lubrano, A.; Oguey-Araymon, S.; Beaumont, M.; Bourgeois, A.; Nielsen-Moennoz, C.; Vigo, M.; Fay, L. B.; Kochhar, S.; Bibiloni, R.; Pittet, A. C.; Emady-Azar, S.; Grathwohl, D.; Rezzi, S. A whole-grain cereal-rich diet increases plasma betaine, and tends to decrease total and LDL-cholesterol compared with a refined-grain diet in healthy subjects. *Br. J. Nutr.* **2011**, *105*, 1492−1502.

(20) Price, R. K.; Keaveney, E. M.; Hamill, L. L.; Wallace, J. M. W.; Ward, M.; Ueland, P. M.; McNulty, H.; Strain, J. J.; Parker, M. J.; Welch, R. W. Consumption of wheat aleurone-rich foods increases fasting plasma betaine and modestly decreases fasting homocysteine and LDL-cholesterol in adults. *J. Nutr.* **2010**, *140*, 2153−2157.

(21) Yde, C. C.; Jansen, J. J.; Theil, P. K.; Bertram, H. C.; Knudsen, K. E. B. Different metabolic and absorption patterns of betaine in response to dietary intake of whole-wheat grain, wheat aleurone or rye aleurone in catheterized pigs. *Eur. Food Res. Technol.* **2012**, *235*, 939−949.

(22) Atkinson, W.; Elmslie, J.; Lever, M.; Chambers, S. T.; George, P. M. Dietary and supplementary betaine: acute effects on plasma betaine and homocysteine concentrations under standard and postmethionine load conditions in healthy male subjects. *Am. J. Clin. Nutr.* **2008**, *87*, 577−585.

(23) Bertram, H. C.; Bach Knudsen, K. E.; Serena, A.; Malmendal, A.; Nielsen, N. C.; Frette, X. C.; Andersen, H. J. NMR-based metabonomic studies reveal changes in the biochemical profile of plasma and urine from pigs fed high-fibre rye bread. *Br. J. Nutr.* **2006**, *95*, 955−962.

(24) Bertram, H. C.; Malmendal, A.; Nielsen, N. C.; Straadt, I. C.; Larsen, T.; Bach Knudsen, K. E.; Lærke, H. N. NMR-based metabonomics reveals that plasma betaine increases upon intake of

DOI: 10.1021/jf506024v
J. Agric. Food Chem. 2015, 63, 2725−2733

high-fiber rye buns in hypercholesterolemic pigs. *Mol. Nutr. Food Res.* **2009**, *53*, 1055−1062.
(25) Fardet, A.; Canlet, C.; Gottardi, G.; Lyan, B.; Llorach, R.; Remesy, C.; Mazur, A.; Paris, A.; Scalbert, A. Whole-grain and refined wheat flours show distinct metabolic profiles in rats as assessed by a ^{1}H NMR-based metabonomic approach. *J. Nutr.* **2007**, *137*, 923−929.
(26) Hedemann, M. S.; Damgaard, B. M.; Clausen, T. N.; Larsen, P. F. *Evaluation of the Choline Status in Mink Fed Different Levels and Sources of Choline*; Larsen, P. F., Møller, S. H., Clausen, T., Hammer, A. S., Lassen, T. M., Nielsen, V. H., Tauson, A. H., Jeppesen, L. L., Hansen, S. W., Elnif, J., Malmkvist, J., Eds.; Wageningen Academic Publishers: Wageningen, The Netherlands, 2012; pp 121−127.
(27) Zeisel, S. H.; Mar, M. H.; Howe, J. C.; Holden, J. M. Concentrations of choline-containing compounds and betaine in common foods. *J. Nutr.* **2003**, *133*, 1302−1307.
(28) Tso, P.; Fujimoto, K. The absorption and transport of lipids by the small intestine. *Brain Res. Bull.* **1991**, *27*, 477−482.
(29) Zeisel, S. H.; da Costa, K. A. Choline: an essential nutrient for public health. *Nutr. Rev.* **2009**, *67*, 615−623.
(30) Rerat, A. A.; Vaissade, P.; Vaugelade, P. Absorption kinetics of some carbohydrates in conscious pigs 2. Quantitative aspects. *Br. J. Nutr.* **1984**, *51*, 517−529.
(31) Kristensen, N. B.; Norgaard, J. V.; Wamberg, S.; Engbaek, M.; Fernandez, J. A.; Zacho, H. D.; Poulsen, H. D. Absorption and metabolism of benzoic acid in growing pigs. *J. Anim. Sci.* **2009**, *87*, 2815−2822.
(32) Ingerslev, A. K.; Theil, P. K.; Hedemann, M. S.; Lærke, H. N.; Bach Knudsen, K. E. Resistant starch and arabinoxylan augment SCFA absorption, but affect postprandial glucose and insulin responses differently. *Br. J. Nutr.* **2014**, *111*, 1564−1576.
(33) Theil, P. K.; Jørgensen, H.; Serena, A.; Hendrickson, J.; Bach Knudsen, K. E. Products deriving from microbial fermentation are linked to insulinaemic response in pigs fed breads prepared from whole-wheat grain and wheat and rye ingredients. *Br. J. Nutr.* **2011**, *105*, 373−383.
(34) Christensen, K. L.; Hedemann, M. S.; Lærke, H. N.; Jørgensen, H.; Mutt, S. J.; Herzig, K. H.; Bach Knudsen, K. E. Concentrated arabinoxylan but not concentrated β-glucan in wheat bread has similar effects on postprandial insulin as whole-grain rye in porto-arterial catheterized pigs. *J. Agric. Food Chem.* **2013**, *61*, 7760−7768.
(35) Jørgensen, H.; Serena, A.; Theil, P. K.; Engberg, R. M. Surgical techniques for quantitative nutrient digestion and absorption studies in the pig. *Livest. Sci.* **2010**, *133*, 57−60.
(36) Bruce, S. J.; Guy, P. A.; Rezzi, S.; Ross, A. B. Quantitative measurement of betaine and free choline in plasma, cereals and cereal products by isotope dilution LC-MS/MS. *J. Agric. Food Chem.* **2010**, *58*, 2055−2061.
(37) Littell, R. C.; Milliken, G. A.; Stroup, W. W.; Wolfinger, R. D. *SAS System for Mixed Models*; SAS Institute: Cary, NC, USA, 1996.
(38) *USDA database for the choline content of common foods*, release 2; USDA Agricultural Research Service: Washington, DC, USA, 2008; 37 pp.
(39) Schwahn, B. C.; Hafner, D.; Hohlfeld, T.; Balkenhol, N.; Laryea, M. D.; Wendel, U. Pharmacokinetics of oral betaine in healthy subjects and patients with homocystinuria. *Br. J. Clin. Pharmacol.* **2003**, *55*, 6−13.
(40) Rosa, N. N.; Barron, C.; Gaiani, C.; Dufour, C.; Micard, V. Ultra-fine grinding increases the antioxidant capacity of wheat bran. *J. Cereal Sci.* **2013**, *57*, 84−90.
(41) Anson, N. M.; Selinheimo, E.; Havenaar, R.; Aura, A. M.; Mattila, I.; Lehtinen, P.; Bast, A.; Poutanen, K.; Haenen, G. R. M. M. Bioprocessing of wheat bran improves in vitro bioaccessibility and colonic metabolism of phenolic compounds. *J. Agric. Food Chem.* **2009**, *57*, 6148−6155.
(42) Katina, K.; Laitila, A.; Juvonen, R.; Liukkonen, K. H.; Kariluoto, S.; Piironen, V.; Landberg, R.; Àman, P.; Poutanen, K. Bran fermentation as a means to enhance technological properties and bioactivity of rye. *Food Microbiol.* **2007**, *24*, 175−186.
(43) Nielsen, K. L.; Hartvigsen, M. L.; Hedemann, M. S.; Lærke, H. N.; Hermansen, K.; Bach Knudsen, K. E. Similar metabolic responses in pigs and humans to breads with different contents and compositions of dietary fibers: a metabolomics study. *Am. J. Clin. Nutr.* **2014**, *99*, 941−949.
(44) Kettunen, H.; Peuranen, S.; Tiihonen, K.; Saarinen, M. Intestinal uptake of betaine in vitro and the distribution of methyl groups from betaine, choline, and methionine in the body of broiler chicks. *Comp. Biochem. Physiol. A−Mol. Integr. Physiol.* **2001**, *128*, 269−278.
(45) Sunden, S. L. F.; Renduchintala, M. S.; Park, E. I.; Miklasz, S. D.; Garrow, T. A. Betaine-homocysteine methyltransferase expression in porcine and human tissues and chromosomal localization of the human gene. *Arch. Biochem. Biophys.* **1997**, *345*, 171−174.
(46) Kettunen, H.; Tiihonen, K.; Peuranen, S.; Saarinen, M. T.; Remus, J. C. Dietary betaine accumulates in the liver and intestinal tissue and stabilizes the intestinal epithelial structure in healthy and coccidia-infected broiler chicks. *Comp. Biochem. Physiol. A−Mol. Integr. Physiol.* **2001**, *130*, 759−769.
(47) Slow, S.; Lever, M.; Chambers, S. T.; George, P. M. Plasma dependent and independent accumulation of betaine in male and female rat tissues. *Physiol. Res.* **2009**, *58*, 403−410.
(48) Li, Z.; Vance, D. E. Thematic Review Series: Glycerolipids. Phosphatidylcholine and choline homeostasis. *J. Lipid Res.* **2008**, *49*, 1187−1194.

DOI: 10.1021/jf506024v
J. Agric. Food Chem. 2015, 63, 2725−2733

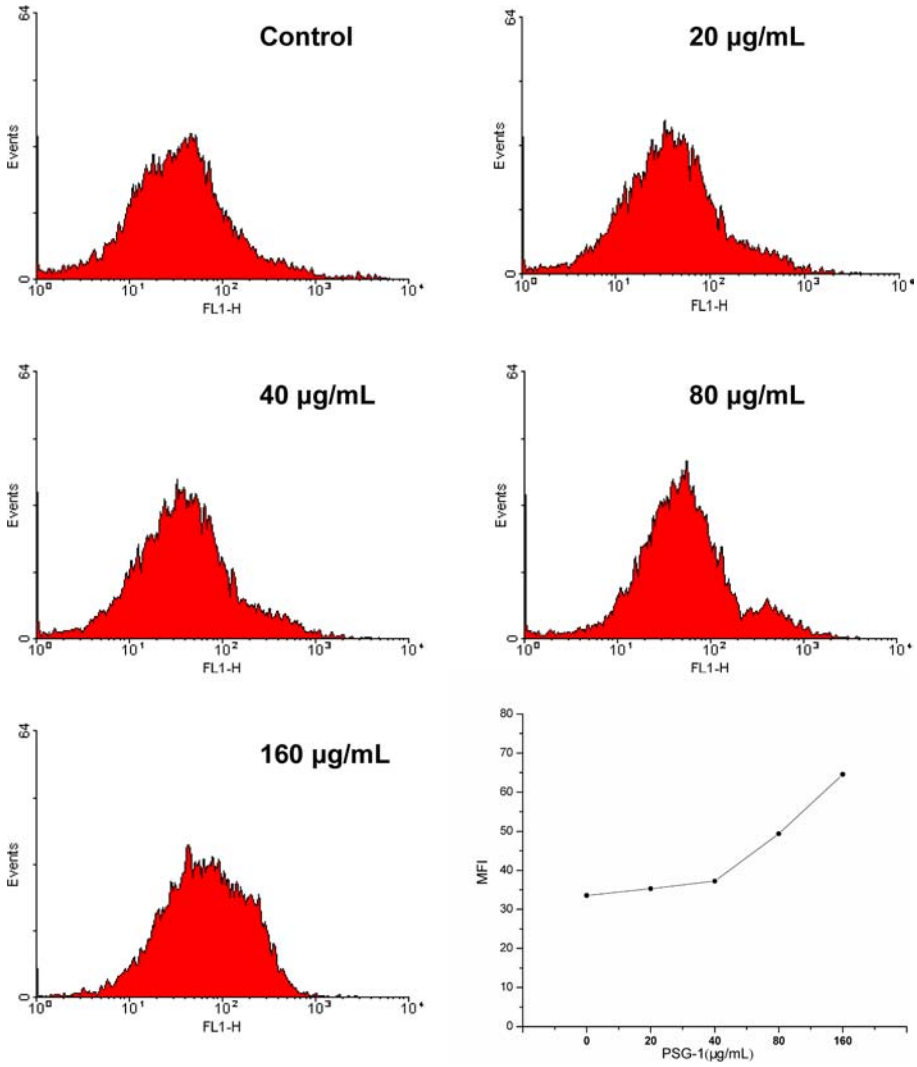

Figure 1. Effect of PSG-1 on the intracellular Ca^{2+} concentration in spleen lymphocytes. Spleen lymphocytes were seeded at a density of 1×10^6 cells/well in the 24 well plate and incubated with PSG-1 (20, 40, 80, and 160 μg/mL) for 48 h. The cells were washed twice with PBS and incubated with the Fluo-3/AM at 37 °C for 60 min. Flow cytometry was performed to measure the fluorescent signal.

Cell culture products were obtained from Life Technologies (Paisley, U.K.).

Preparation of Spleen Lymphocytes. Female BALB/c mice (8 weeks old, 18−20 g) were purchased from Shanghai Slac Laboratory Animal Center, Chinese Academy of Sciences (Shanghai, China). The extirpated spleens were minced into small pieces with scissors in a germ-free condition and then suspended in RPMI 1640 medium. Single-cell suspension was prepared by filtering the suspension through a sterile sieve mesh. The cells were treated with lysis buffer (0.15 M NH_4Cl, 0.01 M $KHCO_3$, and 0.1 mM Na_2EDTA at pH 7.4) to remove red blood cells, followed by washing twice with cold phosphate-buffered saline (PBS). Then, the cells were adjusted to the concentration of 5×10^6 cells/mL in RPMI 1640 medium supplemented with 10% fetal calf serum and incubated for 3 h in Petri dishes. The suspended cells were collected.

Cytokine Measurement by ELISA. Spleen lymphocytes were seeded at a density of 5×10^5 cells/well in the 96 well plate and cultured with various concentrations of PSG-1 for 48 h. The supernatants were harvested, and a level of IL-2 was determined by an ELISA kit according to the instructions of the manufacturer.

Measurement of Intracellular Ca^{2+}. $[Ca^{2+}]_i$ was measured in spleen lymphocyte using a Fluo-3/AM fluorescent probe. Briefly, spleen lymphocytes were seeded at a density of 1×10^6 cells/well in the 24 well plate and stimulated with various concentrations of PSG-1 for 48 h. The cells were collected and washed twice with PBS, followed by incubation with the fluorescent probe Fluo-3/AM at 37 °C for 60 min. After washing twice with PBS, the $[Ca^{2+}]_i$ level, seen as the fluorescent signal, was measured by flow cytometry.

Measurement of CaN Activity. Spleen lymphocytes were seeded at a density of 1×10^6 cells/well in the 24 well plate and stimulated with various concentrations of PSG-1 for 48 h. CaN activity was measured using a CaN activity assay kit according to the instructions of the manufacturer. Briefly, the cells were treated by lysis buffer (reagent B) provided in the kit. The RII phosphopetide was used as the substrate for CaN. The detection of free inorganic phosphate released from RII by CaN was based on the ferrous sulfate method. The optical density at 660 nm was determined for each sample using a microplate reader (Bio-Rad, Hercules, CA). The specific CaN activity was expressed as the fold induction over untreated cells.

Transient Transfection and Luciferase Reporter Assay. Spleen lymphocytes were transiently transfected with pGL4.30-[luc2P/NFAT-RE/Hygro] using FuGENE HD transfection reagent according to the instructions of the manufacturer. Transfected cells were subcultured and seeded at 2×10^5 cells/well in the 24 well plate. The cells were incubated with various concentrations of PSG-1 for 48 h. After incubation, the cells were washed with PBS and extracted in lysis buffer. Luciferase activity was measured using the luciferase assay system according to the instructions of the manufacturer. The specific transactivation was expressed as the fold induction over untreated cells.

DOI: 10.1021/acs.jafc.5b00028
J. Agric. Food Chem. 2015, 63, 2734−2740

Assay of PKC Activity. Spleen lymphocytes were seeded at a density of 2×10^6 cells/well in the 6 well plate and stimulated with various concentrations of PSG-1 for 48 h. Then, the cells were collected and washed twice with PBS. The PKC activity was measured using the PepTag assay for non-radioactive detection of PKC kit according to the instructions of the manufacturer. Briefly, the cells were resuspended and homogenized in 0.5 mL of cold PKC extraction buffer and then centrifuged at 14000*g* for 5 min, and the supernatants were purified on a 1 mL column of DEAE cellulose. The resultant fractions were eluted by PKC extraction buffer and incubated with PKC reaction mixture, followed by agarose gel separation. The bands were quantization by spectrophotometry.

Statistical Analysis. Values are expressed as means ± standard error of the mean (SEM). One-way analysis of variance followed by the Student−Newman−Keuls test was used to determine the statistical significance between various groups. A value of $p < 0.05$ was considered to be statistically significant.

RESULTS

Effect of PSG-1 on the Ca^{2+} Concentration in Spleen Lymphocytes. To examine the effect of PSG-1 on the Ca^{2+} concentration in spleen lymphocytes, flow cytometry was performed to detect the intracellular Ca^{2+} concentration after treatment with various concentrations of PSG-1 (20, 40, 80, and 160 μg/mL). As shown in Figure 1, PSG-1 administration elevated the Ca^{2+} concentration in a dose-dependent manner.

Effect of PSG-1 on CaN Activity in Spleen Lymphocytes. The colorimetric method was used to measure the CaN activity in spleen lymphocytes. It was found that PSG-1 (20, 40, 80, and 160 μg/mL) dose-dependently enhanced CaN activity in spleen lymphocytes (Figure 2).

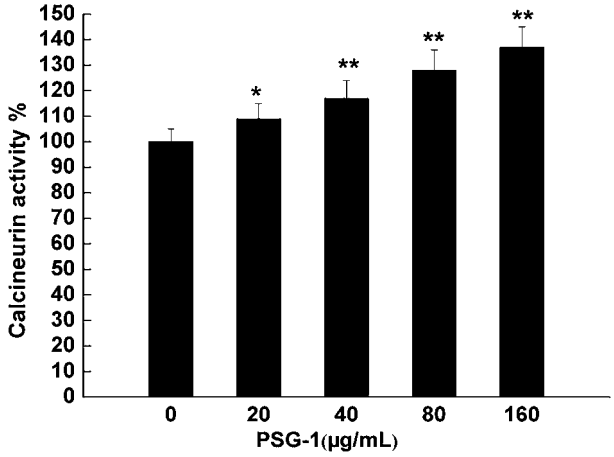

Figure 2. Effect of PSG-1 on CaN activity in spleen lymphocytes. Spleen lymphocytes (2×10^6 cells/well) were seeded in the 6 well plate and cultured with various concentrations of PSG-1 for 48 h. The cells were harvested, and CaN activity was determined by the CaN activity assay kit according to the instructions of the manufacturer. The data are expressed as the mean ± SEM for three separate experiments. (*) $p < 0.05$ and (**) $p < 0.01$ versus the control group.

Effect of PSG-1 on NFAT Transactivation Activity in Spleen Lymphocytes. NFAT is known as an important transcription factor. In the present study, a transient transfection and luciferase reporter assay was used to determine the effect of PSG-1 on NFAT transactivation activity in spleen lymphocytes. As shown in Figure 3, PSG-1 treatment (20, 40, 80, and 160 μg/mL) robustly increased luciferase activity in a dose-dependent manner, which suggested that PSG-1 could enhance NFAT transactivation activity in spleen lymphocytes.

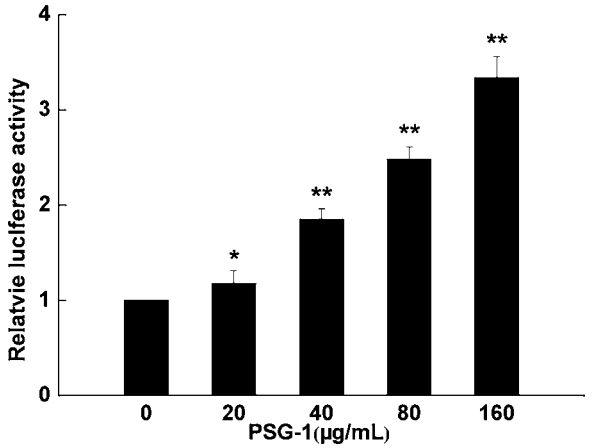

Figure 3. Effect of PSG-1 on NFAT transactivation activity in spleen lymphocytes. Spleen lymphocytes were transiently transfected with pGL4.30[luc2P/NFAT-RE/Hygro] and seeded at 2×10^5 cells/well in the 24 well plate. The cells were stimulated with various concentrations of PSG-1 for 48 h. After incubation, the cells were washed and extracted in lysis buffer. Then, luciferase activity was measured using the luciferase assay system according to the instructions of the manufacturer. The data are expressed as the mean ± SEM for three separate experiments. (*) $p < 0.05$ and (**) $p < 0.01$ versus the control group.

Effect of CaN Inhibitors on NFAT Transactivation Activity Induced by PSG-1 in Spleen Lymphocytes. To determine the role of CaN in PSG-1-mediated activation of NFAT, we used the specific pharmacological antagonists cyclosporin A (CsA) and FK506, which inhibit the activation of CaN. Working concentrations of the inhibitors did not affect the viability of cells (data not shown). Transfected spleen lymphocytes were pre-incubated with various concentrations of CaN inhibitors, CsA (0.25, 0.5, and 1 μM) and FK506 (0.25, 0.5, and 1 μM) for 30 min and then treated with PSG-1 (160 μg/mL) for an additional 48 h. As shown in Figure 4A, luciferase activity was gradually reduced by pretreatment with increasing concentrations of CsA. Similarly, there was a dose-dependent decrease of luciferase activity by the pretreatment of FK506, and PSG-1-induced luciferase activity returned to the basal level when pretreated with 1 μM FK506.

Effect of CaN Inhibitors on IL-2 Production Induced by PSG-1 in Spleen Lymphocytes. To examine the potential role of CaN in the regulation of IL-2 production in PSG-1-stimulated spleen lymphocytes, the cells were pretreated by CsA (0.25, 0.5, and 1 μM) and FK506 (0.25, 0.5, and 1 μM) for 30 min, followed by PSG-1 treatment (160 μg/mL) for 48 h, and then, the IL-2 level was measured by ELISA. As shown in Figure 4B, CsA and FK506 dose-dependently inhibited the PSG-1-induced IL-2 production in spleen lymphocytes.

Effect of PSG-1 on PKC Activity in Spleen Lymphocytes. Furthermore, the effect of PSG-1 on PKC activity was measured. PKC activity was dramatically increased by PSG-1 (20, 40, 80, and 160 μg/mL) in spleen lymphocytes, as compared to the control group (Figure 5).

Effect of the PKC Inhibitor on NFAT Transactivation Activity Induced by PSG-1 in Spleen Lymphocytes. To investigate the role of PKC on NFAT activation induced by PSG-1 in spleen lymphocytes, PKC inhibitor calphostin C (25, 50, and 100 nM) was used to treat the transfected spleen

DOI: 10.1021/acs.jafc.5b00028
J. Agric. Food Chem. 2015, 63, 2734−2740

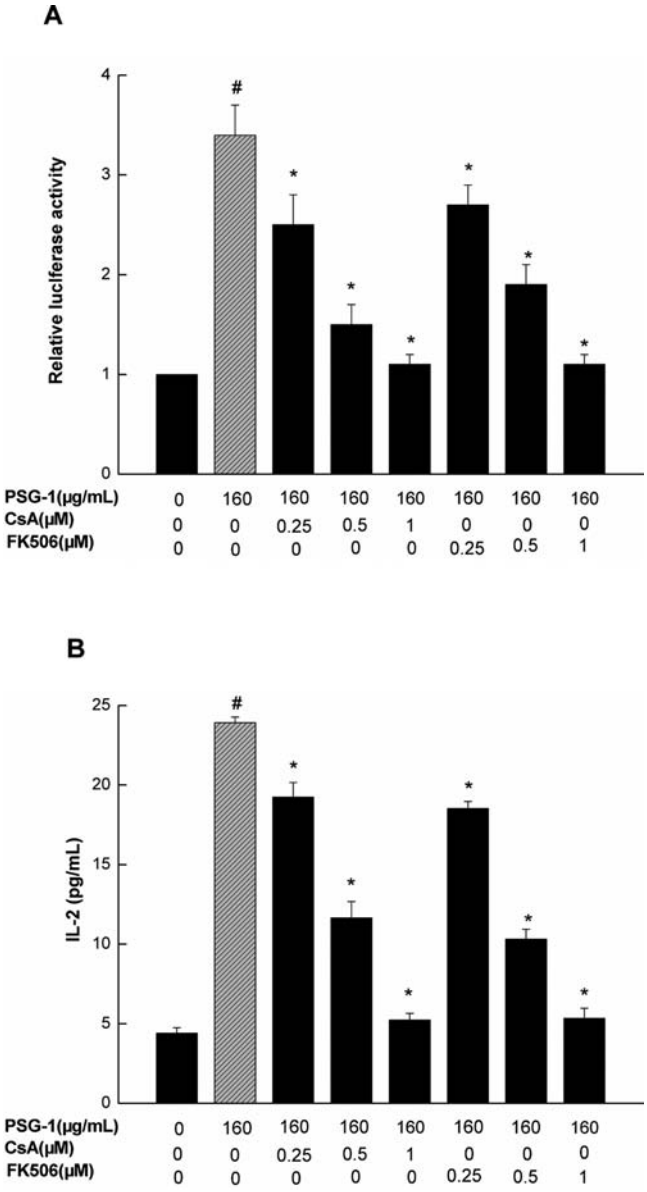

Figure 4. Effect of CaN inhibitors CsA and FK506 on NFAT transactivation activity and IL-2 production induced by PSG-1 in spleen lymphocytes. (A) Transfected spleen lymphocytes were pre-incubated with CsA (0.25, 0.5, and 1 μM) and FK506 (0.25, 0.5, and 1 μM) for 30 min and treated with PSG-1 (160 μg/mL) for an additional 48 h. Then, luciferase activity was measured. (B) Cells were pre-incubated with various concentrations of inhibitors for 30 min, followed by PSG-1 stimulation (160 μg/mL) for an additional 48 h. After incubation, released IL-2 in the supernatant was measured by ELISA. The data are expressed as the mean ± SEM for three separate experiments. (#) $p < 0.05$ versus the control group, and (*) $p < 0.05$ versus the PSG-1 alone group.

lymphocytes for 30 min before PSG-1 treatment (160 μg/mL) for 48 h and then NFAT transactivation activity was measured. As shown in Figure 6A, in comparison to the PSG-1 group, luciferase activities in all three calphostin C groups (25, 50, and 100 nM) were obviously decreased.

Effect of the PKC Inhibitor on IL-2 Production Induced by PSG-1 in Spleen Lymphocytes. The effect of PKC on PSG-1-induced IL-2 production was studied. Prior to the addition of PSG-1 (160 μg/mL), spleen lymphocytes were treated with different concentrations of PKC inhibitor (25, 50, and 100 nM). ELISA was used to measure the IL-2 secretion in the supernatant. As shown in Figure 6B, the production of PSG-1-induced IL-2 was significantly decreased by all inhibitor treatments in a dose-dependent manner ($p < 0.05$). These results demonstrated that the PKC-related signaling pathway was involved in PSG-1-induced IL-2 secretion in spleen lymphocytes.

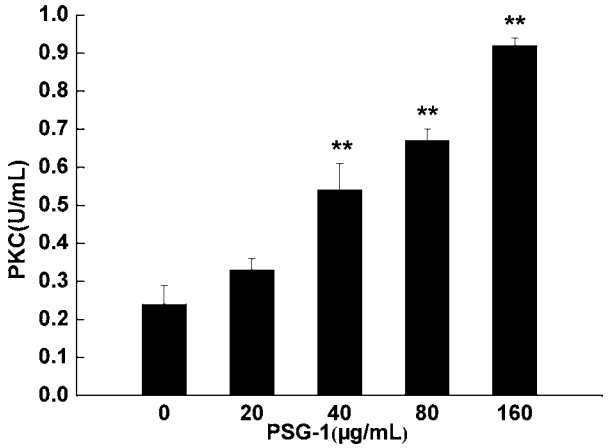

Figure 5. Effect of PSG-1 on PKC activity in spleen lymphocytes. Spleen lymphocytes were seeded at a density of 2×10^6 cells/well in the 6 well plate and stimulated with various concentrations of PSG-1 for 48 h. The cells were collected for measuring PKC activity using the PepTag assay for non-radioactive detection of PKC kit according to the instructions of the manufacturer. The data are expressed as the mean ± SEM for three separate experiments. (*) $p < 0.05$ and (**) $p < 0.01$ versus the control group.

DISCUSSION

Cytokines are intercellular signaling proteins that exert profound effects on the control of homeostasis in the whole organism; thus, monitoring the level of cytokine production is a widely used method to evaluate augmentation activity on immune response. IL-2 is an important cytokine in the cellular and humoral responses. It plays a vital role in regulating functions of all subsets of T cells as well as NK cells, LAK cells, B cells, etc.[28] Our previous study found that PSG-1 significantly increased IL-2 production in spleen lymphocytes, indicating that PSG-1 could activate spleen lymphocytes. To further elucidate the underlying molecular mechanism, we focused on characterizing the signaling pathways involved in the spleen lymphocyte activation by PSG-1.

Ca^{2+} is known as the most widely used intracellular messenger, which encodes a range of cellular information through regulation of Ca^{2+} signals.[2] In response to diverse stimuli, elevation in the concentration of Ca^{2+} in the cytosol triggers many types of events, which play essential roles in lymphocyte activation and maturation.[29] In the present study, flow cytometry analysis using a Fura-3/AM fluorescence probe showed that PSG-1 dramatically increased the intracellular Ca^{2+} level in spleen lymphocytes. CaN is well-known as an unique Ca^{2+}-dependent serine/threonine protein phosphatase, which was originally identified as a calmodulin-binding protein in the brain.[30] It has been reported that CaN activity induced by the increased intracellular Ca^{2+} level played a critical role in diverse biological processes, including lymphocyte function.[31] In our study, we found that CaN activity was noticeably enhanced by PSG-1 treatment, indicating that PSG-1 may activate spleen lymphocytes via the Ca^{2+}/CaN pathway.

DOI: 10.1021/acs.jafc.5b00028
J. Agric. Food Chem. 2015, 63, 2734−2740

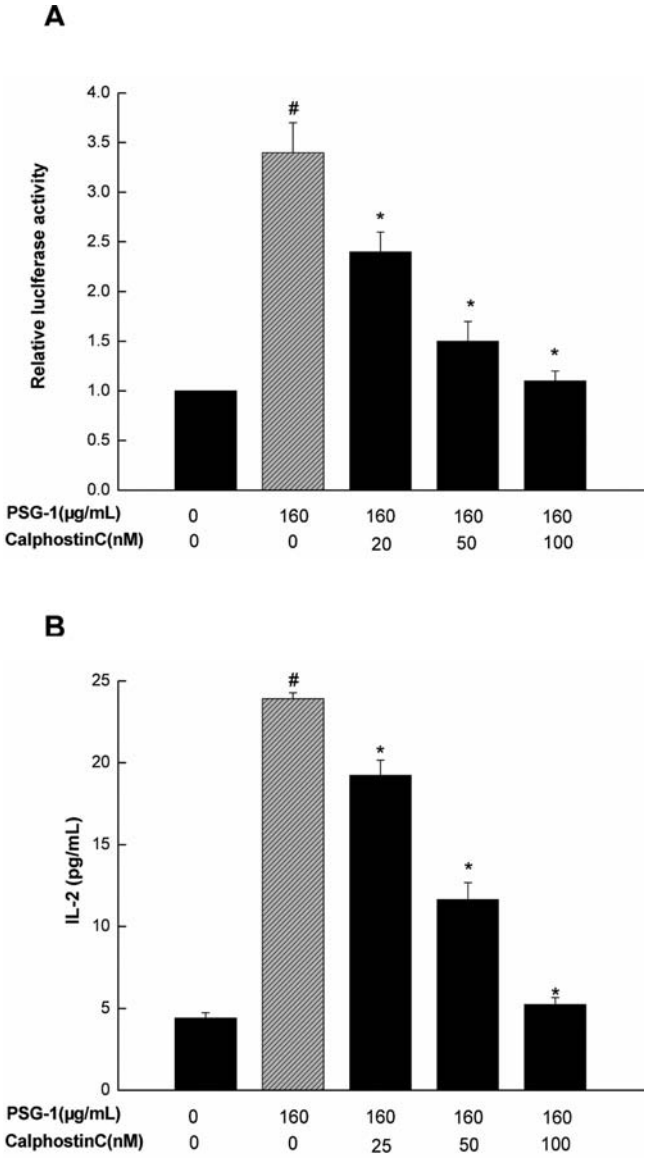

Figure 6. Effect of PKC inhibitor calphostin C on NFAT transactivation activity and IL-2 production induced by PSG-1 in spleen lymphocytes. (A) Calphostin C (25, 50, and 100 nM) was used to treat the transfected spleen lymphocytes for 30 min before PSG-1 treatment (160 μg/mL) for 48 h, and then luciferase activity was measured. (B) Cells were pre-incubated with calphostin C (25, 50, and 100 nM) for 30 min and then stimulated by PSG-1 (160 μg/mL) for 48 h. The supernatant was collected for measuring IL-2 production by ELISA. The data are expressed as the mean ± SEM for three separate experiments. (#) $p < 0.05$ versus the control group, and (*) $p < 0.05$ versus the PSG-1 alone group.

NFAT, a family of four transcription factors first described in lymphocytes, has been found to express in almost all vertebrate cell types.[32] To assess the effect of PSG-1 on NFAT activity in spleen lymphocytes, we performed transient transfection and detected the luciferase activity by the luciferase reporter assay. The data showed that PSG-1 was capable of elevating NFAT activity in a dose-dependent manner. Diverse transcription factors have been reported to be regulated by CaN in many cell types. Among these, NFAT is of special interest and best studied. In resting cells, NFAT resides in the cytoplasm in a phosphorylated form. Upon dephosphorylation by CaN, it subsequently translocates to the nucleus.[33] In this study, we used a pharmacological assay using specific CaN inhibitors (CsA and FK506) to investigate whether NFAT activation by PSG-1 was triggered by CaN. PSG-1-induced NFAT activity was found to be abrogated by the treatment of CsA and FK506. These results suggested that the Ca^{2+}/CaN signaling pathway may act upstream of NFAT activation in PSG-1-stimulated spleen lymphocytes.

It is well-documented that NFAT plays an essential role in immune response via mediating transcription of a number of cytokines. After translocation from the cytoplasm to the nucleus, NFAT subsequently binds to the promoter of cytokines and then stimulates gene expression.[6] To determine the role of the Ca^{2+}/CaN/NFAT pathway in the regulation of PSG-1-induced IL-2 production in spleen lymphocytes, we tested the effect of CaN inhibitors, CsA and FK506, on IL-2 secretion and found that IL-2 production was inhibited by CsA and FK506 in a dose-dependent manner. These results demonstrated that the Ca^{2+}/CaN/NFAT pathway was involved in PSG-1-induced IL-2 secretion in spleen lymphocytes. Taken together, the above results illustrated that PSG-1 may induce spleen lymphocyte activation at least in part via the Ca^{2+}/CaN/NFAT/IL-2 signaling pathway.

PKC, a calcium-dependent kinase, exists in many different cell types.[7] PKC-regulated signaling pathways play significant roles in a wide variety of aspects of immune responses, including development, differentiation, activation, and survival of lymphocytes.[8] Our results showed that PSG-1 significantly enhanced PKC activity in spleen lymphocytes, indicating the involvement of PKC in PSG-1-mediated spleen lymphocyte activation. More and more evidence indicate that PKC signaling also involves the regulation of NFAT activation. In fact, DNA binding by NFAT is quite weak; therefore, it needs a partner for tight association with DNA. Thus, Ca^{2+}/CaN signaling becomes dependent upon coincident PKC signaling for activation of NFAT-dependent transcription.[34,35] To study the putative role of PKC in PSG-1-induced NFAT activation, we tested the effect of the PKC inhibitor on NFAT activity and found that inhibition of PKC by calphostin C diminished PSG-1-induced NFAT activity in a dose-dependent manner, suggesting that the induction of NFAT activity by PSG-1 was dependent upon PKC in spleen lymphocytes. Furthermore, we examined whether PKC was involved in the regulation of IL-2 production induced by PSG-1. Pharmacological dissection using specific PKC inhibitor calphostin C significantly decreased the PSG-1-induced IL-2 production, indicating that PKC was involved in IL-2 production stimulated by PSG-1. On the basis of these results, we concluded that the PKC/NFAT/IL-2 signaling pathway may play an important role in the lymphocyte activation by PSG-1.

In summary, the present study established a signaling pathway, Ca^{2+}/CaN/NFAT/IL-2, by which PSG-1 exerted its effects on the activation of spleen lymphocytes. Moreover, we further demonstrated that the PKC/NFAT/IL-2 signaling pathway cooperatively regulated PSG-1-induced spleen lymphocyte activation. However, because spleen lymphocytes consist of several subgroups, how PSG-1 affects a specific subgroup, such as T cell and B cell, is necessary to be clarified in further studies.

AUTHOR INFORMATION

Corresponding Authors

*Telephone/Fax: +86-791-88304452. E-mail: spnie@ncu.edu.cn.

DOI: 10.1021/acs.jafc.5b00028
J. Agric. Food Chem. 2015, 63, 2734−2740

*Telephone/Fax: +86-791-83969009. E-mail: myxie@ncu.edu.cn.

Funding

The financial support for this study by the National Key Technology Research and Development Program of China (2012BAD33B06), the Key Program of the National Natural Science Foundation of China (31130041), the Program for New Century Excellent Talents in University (NCET-12-0749), the Research Program of State Key Laboratory of Food Science and Technology (SKLF-ZZA-201301), the Project of Science and Technology of Jiangxi Provincial Education Department (KJLD13004), and the Key Project of International Cooperation of Jiangxi Provincial Department of Science and Technology (20141BDH80009) is gratefully acknowledged.

Notes

The authors declare no competing financial interest.

■ ABBREVIATIONS USED

CaN, calcineurin; CsA, cyclosporin A; IL-2, interleukin-2; NFAT, nuclear factor of activated T cells; PKC, protein kinase C

■ REFERENCES

(1) Weiss, A.; Cambier, J. C. Lymphocyte activation. *Curr. Opin. Immunol.* **2004**, *16*, 285−287.
(2) Clapham, D. E. Calcium signaling. *Cell* **2007**, *131*, 1047−1058.
(3) Feske, S. Calcium signalling in lymphocyte activation and disease. *Nat. Rev. Immunol.* **2007**, *7*, 690−702.
(4) Rusnak, F.; Mertz, P. Calcineurin: Form and function. *Physiol. Rev.* **2000**, *80*, 1483−1521.
(5) Rao, A.; Luo, C.; Hogan, P. G. Transcription factors of the NFAT family: Regulation and function. *Annu. Rev. Immunol.* **1997**, *15*, 707−747.
(6) Hogan, P. G.; Chen, L.; Nardone, J.; Rao, A. Transcriptional regulation by calcium, calcineurin, and NFAT. *Genes Dev.* **2003**, *17*, 2205−2232.
(7) Nishizuka, Y. Studies and perspectives of protein kinase C. *Science* **1986**, *233*, 305−312.
(8) Newton, A. C. Protein kinase C: Structure, function, and regulation. *J. Biol. Chem.* **1995**, *270*, 28495−28498.
(9) Kim, H. S.; Kim, Y. J.; Lee, H. K.; Ryu, H. S.; Kim, J. S.; Yoon, M. J.; Kang, J. S.; Hong, J. T.; Kim, Y.; Han, S.-B. Activation of macrophages by polysaccharide isolated from *Paecilomyces cicadae* through toll-like receptor 4. *Food Chem. Toxicol.* **2012**, *50*, 3190−3197.
(10) Kim, H. S.; Shin, B. R.; Lee, H. K.; Park, Y. S.; Liu, Q.; Kim, S. Y.; Lee, M. K.; Hong, J. T.; Kim, Y.; Han, S.-B. Dendritic cell activation by polysaccharide isolated from *Angelica dahurica*. *Food Chem. Toxicol.* **2013**, *55*, 241−247.
(11) Park, M. J.; Ryu, H. S.; Kim, J. S.; Lee, H. K.; Kang, J. S.; Yun, J.; Kim, S. Y.; Lee, M. K.; Hong, J. T.; Kim, Y. *Platycodon grandiflorum* polysaccharide induces dendritic cell maturation via TLR4 signaling. *Food Chem. Toxicol.* **2014**, *72*, 212−220.
(12) Liu, L.; Pan, D.; Zeng, X.; Li, H. Effect of selenium-enriched exopolysaccharide produced by *Lactococcus lactis* subsp. *lactis* on signaling molecules in mouse spleen lymphocytes. *Food Funct.* **2013**, *4*, 1489−1495.
(13) Zhang, S. D.; Yin, Y. X.; Wei, Q. Immunopotentiation on murine spleen lymphocytes induced by polysaccharide fraction of *Panax ginseng* via upregulating calcineurin activity. *APMIS* **2010**, *118*, 288−296.
(14) Gao, Y.; Tang, W.; Gao, H.; Chan, E.; Lan, J.; Li, X.; Zhou, S. Antimicrobial activity of the medicinal mushroom *Ganoderma*. *Food Rev. Int.* **2005**, *21*, 211−229.
(15) Nie, S. P.; Zhang, H.; Li, W. J.; Xie, M. Y. Current development of polysaccharides from *Ganoderma*: Isolation, structure and bioactivities. *Bioact. Carbohydr. Diet. Fibre* **2013**, *1*, 10−20.
(16) Chen, Y.; Xie, M. Y.; Nie, S. P.; Li, C.; Wang, Y. X. Purification, composition analysis and antioxidant activity of a polysaccharide from the fruiting bodies of *Ganoderma atrum*. *Food Chem.* **2008**, *107*, 231−241.
(17) Zhang, H.; Li, W. J.; Nie, S. P.; Chen, Y.; Wang, Y. X.; Xie, M. Y. Structural characterisation of a novel bioactive polysaccharide from *Ganoderma atrum*. *Carbohydr. Polym.* **2012**, *88*, 1047−1054.
(18) Li, W. J.; Nie, S. P.; Chen, Y.; Wang, Y. X.; Li, C.; Xie, M. Y. Enhancement of cyclophosphamide-induced antitumor effect by a novel polysaccharide from *Ganoderma atrum* in sarcoma 180-bearing mice. *J. Agric. Food Chem.* **2011**, *59*, 3707−3716.
(19) Li, W. J.; Chen, Y.; Nie, S. P.; Xie, M. Y.; He, M.; Zhang, S. S.; Zhu, K. X. *Ganoderma atrum* polysaccharide induces anti-tumor activity via the mitochondrial apoptotic pathway related to activation of host immune response. *J. Cell Biochem.* **2011**, *112*, 860−871.
(20) Zhang, S. S.; Nie, S. P.; Huang, D. F.; Huang, J. Q.; Feng, Y. L.; Xie, M. Y. *Ganoderma atrum* polysaccharide evokes antitumor activity via cAMP-PKA mediated apoptotic pathway and down-regulation of Ca^{2+}/PKC signal pathway. *Food Chem. Toxicol.* **2014**, *68*, 239−246.
(21) Zhang, S. S.; Nie, S. P.; Huang, D. F.; Huang, J. Q.; Wang, Y. X.; Xie, M. Y. Polysaccharide from *Ganoderma atrum* evokes antitumor activity via toll-like receptor 4-mediated NF-κB and mitogen-activated protein kinase signaling pathways. *J. Agric. Food Chem.* **2013**, *61*, 3676−3682.
(22) Yu, Q.; Nie, S. P.; Li, W. J.; Zheng, W. Y.; Yin, P. F.; Gong, D. M.; Xie, M. Y. Macrophage immunomodulatory activity of a purified polysaccharide isolated from *Ganoderma atrum*. *Phytother. Res.* **2013**, *27*, 186−191.
(23) Yu, Q.; Nie, S. P.; Wang, J. Q.; Yin, P. F.; Huang, D. F.; Li, W. J.; Xie, M. Y. Toll-like receptor 4-mediated ROS signaling pathway involved in *Ganoderma atrum* polysaccharide-induced tumor necrosis factor-α secretion during macrophage activation. *Food Chem. Toxicol.* **2014**, *66*, 14−22.
(24) Yu, Q.; Nie, S. P.; Wang, J. Q.; Yin, P. F.; Li, W. J.; Xie, M. Y. Polysaccharide from *Ganoderma atrum* induces tumor necrosis factor-α secretion via phosphoinositide 3-kinase/Akt, mitogen-activated protein kinase and nuclear factor-κB signaling pathways in RAW264.7 cells. *Int. Immunopharmacol.* **2012**, *14*, 362−368.
(25) Li, W. J.; Nie, S. P.; Yan, Y.; Zhu, S. B.; Xie, M. Y. The protective effect of *Ganoderma atrum* polysaccharide against anoxia/reoxygenation injury in neonatal rat cardiomyocytes. *Life Sci.* **2009**, *85*, 634−641.
(26) Yu, Q.; Nie, S. P.; Wang, J. Q.; Liu, X. Z.; Yin, P. F.; Huang, D. F.; Li, W. J.; Gong, D. M.; Xie, M. Y. Chemoprotective effects of *Ganoderma atrum* polysaccharide in cyclophosphamide-induced mice. *Int. J. Biol. Macromol.* **2014**, *64*, 395−401.
(27) Zhu, K. X.; Nie, S. P.; Li, C.; Lin, S. L.; Xing, M. M.; Li, W. J.; Gong, D. M.; Xie, M. Y. A newly identified polysaccharide from *Ganoderma atrum* attenuates hyperglycemia and hyperlipidemia. *Int. J. Biol. Macromol.* **2013**, *57*, 142−150.
(28) Serfling, E.; Avots, A.; Neumann, M. The architecture of the interleukin-2 promoter: a reflection of T lymphocyte activation. *Biochim. Biophys. Acta, Gene Struct. Expression* **1995**, *1263*, 181−200.
(29) Oh-hora, M.; Rao, A. Calcium signaling in lymphocytes. *Curr. Opin. Immunol.* **2008**, *20*, 250−258.
(30) Klee, C.; Crouch, T.; Krinks, M. Calcineurin: A calcium-and calmodulin-binding protein of the nervous system. *Proc. Natl. Acad. Sci. U. S. A.* **1979**, *76*, 6270−6273.
(31) Aramburu, J.; Rao, A.; Klee, C. B. Calcineurin: From structure to function. *Curr. Top. Cell. Regul.* **2001**, *36*, 237−295.
(32) Macian, F. NFAT proteins: Key regulators of T-cell development and function. *Nat. Rev. Immunol.* **2005**, *5*, 472−484.
(33) Crabtree, G. R.; Olson, E. N. NFAT signaling: Choreographing the social lives of cells. *Cell* **2002**, *109*, S67−S79.
(34) Crabtree, G. R. Calcium, calcineurin, and the control of transcription. *J. Biol. Chem.* **2001**, *276*, 2313−2316.

DOI: 10.1021/acs.jafc.5b00028
J. Agric. Food Chem. 2015, 63, 2734−2740

(35) Wolfe, S. A.; Zhou, P.; Doetsch, V.; Chen, L.; You, A.; Ho, S. N.; Crabtree, G. R.; Wagner, G.; Verdine, G. L. Unusual Rel-like architecture in the DNA-binding domain of the transcription factor NFATc. *Nature* **1997**, *385*, 172−176.

DOI: 10.1021/acs.jafc.5b00028
J. Agric. Food Chem. 2015, 63, 2734−2740

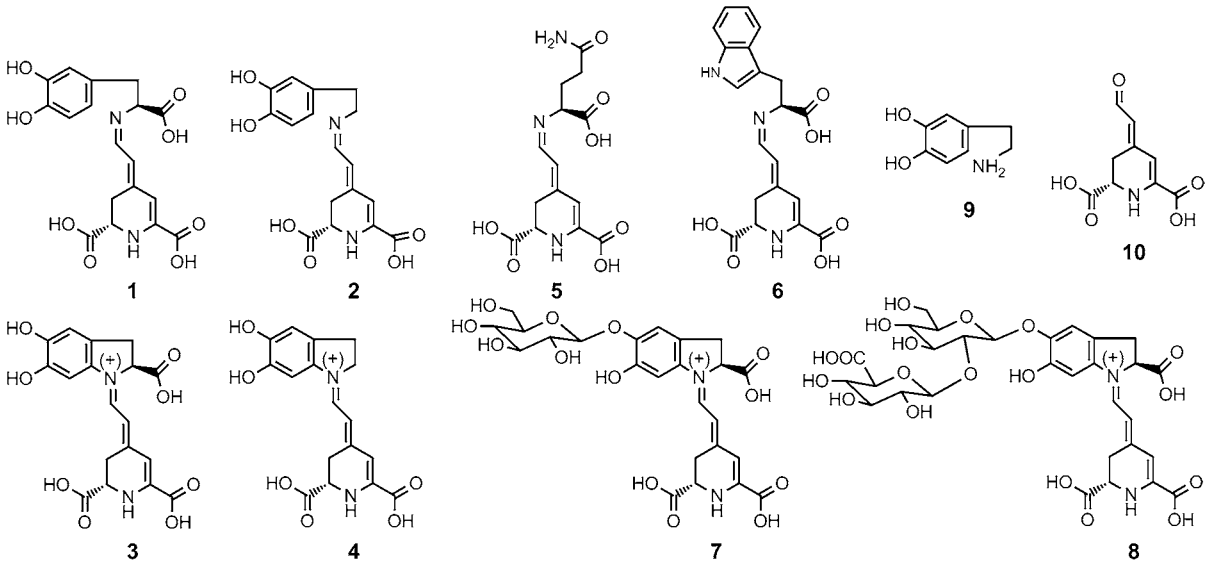

Figure 1. Structures for the dihydroxylated betalains dopaxanthin (1), miraxanthin V (2), betanidin (3), and decarboxy-betanidin (4). Structures for additional pigments obtained in this study are also shown, corresponding to the betaxanthins vulgaxanthin I (5) and tryptophan-betaxanthin (6) and the betacyanins betanin (7) and amaranthin (8). Precursor molecules dopamine (9) and betalamic acid (10) are also shown.

in the sources of betaxanthins and betacyanins may lead to different shades to be used in the coloration of foods and beverages. In this sense, some betalain-containing plants of the Amaranthaceae are consumed cooked or fresh[17,18] and used in traditional medicine to alleviate the symptoms of inflammation.[19,20]

Dihydroxylated betalains have the potential to become bioactive constituents in foods and can be combined to generate tailor-made colors which can be encapsulated to obtain products with a shelf life of months.[21] This study was designed to develop cell cultures of *Celosia argentea* as a model plant of the Amaranthaceae family and to explore the potential of liquid culture in the production of dihydroxylated betalains. The appearance of structurally related molecules is quantitated and discussed in terms of the biosynthetic pathway of betalains.

MATERIALS AND METHODS

Chemicals. Chemicals and reagents were purchased from Sigma (St. Louis, MO). Solvents were from Merck Chemicals Ltd. (Dorset, England). HPLC-grade acetonitrile and methanol were purchased from Labscan Ltd. (Dublin, Ireland). Distilled water was purified using a Milli-Q system (Millipore, Bedford, MA).

Plant Material. *C. argentea* var. *plumosa* plants with violet inflorescences were obtained from Viveros la Generala (Murcia, Spain) and grown at the greenhouse facilities at the University of Murcia (Murcia, Southeastern Spain). Seeds were surface sterilized in commercial liquid detergent 1% for 15 min, followed by 70% ethanol for 30 s, and by 1.8% sodium hypoclorite solution containing 0.2% Tween-20 for 30 min. Seeds were then washed three times with sterile water under aseptic conditions. Sterile seeds were transferred to sterilized tubes (25 × 150 mm) containing 15 mL of semisolid Murashige and Skoog medium (MS).[22] Seedlings were grown up to 2 cm (20 days), and then hypocotyls were removed as explants source. Hypocotyls were transferred to individual tubes ($n = 6$), with 10 mL of MS medium supplemented with different plant growth regulators (PGRs). Environmental conditions consisted of a photoperiod of 16 h under fluorescent light at an irradiance of 50 μmol/m^2/s and temperatures of 23 (day) and 18 °C (night)

Callus Induction. The culture medium used was MS supplemented with 30 g/L sucrose and 2 g/L of the solidifying agent phytagel. To assess response to callus explant induction media were enriched with different concentrations and combinations of PGRs: 6-benzylaminopurine (BAP) (0.0, 4.44, 6.66, 8.88 μM) with 2,4-dichlorophenoxyacetic acid (2,4-D) (0.0, 6.79, 9.05 μM) (Table 1). All

Table 1. Effect of Plant Growth Regulators (PGRs) on Callus Induction from Hypocotyls Explants Obtained from *C. argentea* var. *plumosa* after 30 Days of Culture[a]

PGRs (μM)		
BAP	2,4-D	callus-forming explants (%)
0.00	0.00	0.00[a]
0.00	6.79	0.00[a]
0.00	9.05	0.00[a]
4.44	0.00	0.00[a]
4.44	6.79	0.00[a]
4.44	9.05	33.33[a,b]
6.66	0.00	66.66[b]
6.66	6.79	100.00[b]
6.66	9.05	33.33[a,b]
8.88	0.00	33.33[a,b]
8.88	6.79	100.00[b]
8.88	9.05	100.00[b]

[a]Each value was derived from three independent tubes containing three different explants. Those values sharing the same letter correspond to nonsignificant differences according to the Tukey test ($p < 0.05$).

culture media were adjusted to pH 5.8 with 1 N NaOH and HCl and sterilized by autoclaving at 121 °C for 18 min. The cultures were incubated under a photoperiod of 16 h under fluorescent light at an irradiance of 50 μmol/m^2/s and temperatures of 23 (day) and 18 °C (night). The response of the explants for callus formation at each induction treatment was expressed as the percentage of the number of forming callus hypocotyls explants on the total evaluated, which was recorded at day 30 of culture. Propagation of callus cell lines was done under the same conditions in a MS medium supplemented with 6.66 μM BAP and 6.79 μM 2,4-D. It was selected for proliferation by subcultures on fresh medium with induction every 20 days for 9 subculture cycles. Subculturing and selection gave rise to two callus cell lines with different colors: yellow and red.

Establishment of Cell Suspension Culture and Growth Kinetics. *C. argentea* cell suspension culture was initiated from 3-

DOI: 10.1021/acs.jafc.5b00065
J. Agric. Food Chem. 2015, 63, 2741−2749

week-old red friable callus by transferring 2.5 g to 100 mL Erlenmeyer flasks containing 30 mL of callus induction medium (without phytagel) supplemented with 10 mM ascorbic acid in order to avoid dopamine oxidation and incubated under the same conditions on an orbital shaker at 110 rpm. After subculturing every 15 days during 3 months, the cells were sieved through 200 μm nylon cloth filters in order to obtain a homogeneous and fine cell suspension culture. Then, the culture was maintained during 6 months by subculturing every 15 days using a cell inoculum size of 10% (v/v) in 500 mL Erlenmeyer flasks containing 100 mL of cultured medium. To determine the growth kinetics, 2.5 g of fresh cells harvested after 8 days was inoculated into 100 mL Erlenmeyer flasks containing 30 mL of liquid MS medium supplemented with 3% sucrose (w/v), 10 mM ascorbic acid, BAP 6.66 μM, and 2,4-D 6.79 μM. Aliquots were removed every 3−10 days over a 30 day period from culture flasks and used to determine cell growth, cell morphology, cell viability, and dopamine and betalains content. All experiments were performed in triplicate (n = 3), and the results were expressed as mean values and standard deviations (SD).

Cell Viability. Cell viability was determined by the Evan's blue staining test.[23] A 2 mL amount of samples from each flask was incubated into 0.25% Evan's blue stain for 5 min, and then at least 700 cells were counted. This was repeated twice for each measurement (n = 6).

Preparation of Extracts. Callus samples and cell suspensions of 1, 8, 15, and 30 days of culture were homogenized manually in 10 mM phosphate buffer pH 6.0 containing 10 mM ascorbic acid. The resulting homogenate and samples of the liquid medium of the suspension culture were centrifuged at 14 000g for 15 min. The supernatant of each sample was used for analysis of betalains and dopamine (n = 3) by HPLC. The whole process was carried out at 4 °C. The humidity percentage and dry weight of the cells was obtained with a Kern MLS electronic moisture analyzer (Balingen, Germany).

Standard Betalains. Betanin was obtained from roots of *Beta vulgaris*, dopaxanthin was extracted and purified from yellow flowers of *L. productus*, betanidin was obtained from violet flowers of the same plant, and amaranthin was extracted from *Amaranthus spinosus*.[2,24] Other pigments were obtained by a combined procedure for the release of betalamic acid from purified betanin and condensation with the amine dopamine and the amino acids (*S*)-glutamine and (*S*)-tryptophan, following a previously described method.[25] Betalamic acid was obtained through basic hydrolysis of betanin.[26] All compounds were characterized spectrophotometrically, chromatographically, and by electrospray ionization mass spectrometry (ESI-MS).

Anionic Exchange Chromatography. Anionic exchange chromatography was performed in an Äkta purifier apparatus (Amersham Biosciences, Uppsala, Sweden) using a 25 × 7 mm, 1 mL Q-Sepharose Fast Flow column (cross-linked agarose with quaternary ammonium as exchanger group, 90 μm particle size). Solvents used were sodium phosphate 10 mM, pH 6.0 (solvent A), and 10 mM sodium phosphate, pH 6.0, with 2 M NaCl (solvent B). After sample injection, the elution process was as follows: 0% B from beginning to 3 mL, and then a linear gradient was developed from 0% B to 35% B in 20 mL. In all cases, the flow rate was 1 mL/min, 1 mL fractions were collected, and injection volume was 1 mL. Elutions were followed by UV−vis detection at 280, 480, and 536 nm.

Solid-Phase Extraction. One milliliter C-18 cartridges (Waters, Milford, MA) were conditioned with 5 mL of ethanol followed by 10 mL of purified water. Aqueous solutions of extracted pigments and semisynthetic betalains were injected and bound to the minicolumn. Salts and buffers were washed off by rinsing the column with purified water. Betalains were eluted with ethanol, and the resulting fraction was evaporated to dryness under reduced pressure at room temperature. The residue was redissolved in water for further use or stored at −80 °C.

HPLC-DAD Analysis. A Shimadzu LC-20AD apparatus (Kyoto, Japan) equipped with a SPD-M20A photodiode array detector (PDA) was used for analytical HPLC separations. Reversed phase chromatography was performed with a 250 mm × 4.6 mm i.d., 5 μm, Kromasil 100 C-18 column (Teknokroma, Barcelona, Spain) for identification of betalains.[27] Solvent A was water with 0.05% trifluoroacetic acid (TFA), and solvent B was composed of acetonitrile with 0.05% TFA. A linear gradient was performed for 42 min from 0% B to 65% B. The flow rate was 1 mL/min, operated at 30 °C. Elutions were followed at λ = 270 (dopamine), 405 (betalamic acid), 480 (betaxanthins), and 536 nm (betacyanins). Injection volume was 40 μL. Dopamine and betalains presented the same elution times as the corresponding standards in coelution experiments and superimposable spectra.

Elecrospray Ionization Mass Spectrometry. A VL 1100 apparatus with LC/MSD Trap (Agilent Technologies, Palo Alto, CA) was used for HPLC-ESI-MS analyses. Elution conditions were as described above using the same column (250 mm × 4.6 mm i.d., 5 μm, Kromasil 100 C-18) decreasing the flow rate to 0.8 mL/min. Vaporizer temperature was 350 °C, and voltage was maintained at 3.5 kV. The sheath gas was nitrogen, operated at a pressure of 45 psi. Samples were ionized in positive mode. Ion monitoring mode was full scan in the range m/z 50−1000. The electron multiplier voltage for detection was 1350 V.

UV−Vis Spectroscopy. A V-630 spectrometer (Jasco Corporation, Tokyo, Japan) attached to a Tectron thermostatic bath (JP Selecta, Barcelona, Spain) was used for UV−vis spectroscopy. For quantitation of betalains, pigment concentration was evaluated using molar extinction coefficients of ε = 46 000 (dopaxanthin), 27 000 (betalamic acid), 44 000 (tryptophan-betaxanthin), 46 000 (dopaxanthin), 48 000 (glutamine-betaxanthin and dopamine-betaxanthin), 65 000 (betanin and amaranthin), and 54 000 $M^{-1}\cdot cm^{-1}$ (betanidin).[28−30] All measurements were performed in water at 25 °C.

Microscopy. Brightfield and fluorescence microscopy were performed in a Leica DMRB microscope (Leica Microsystems, Wetzlar, Germany) with incident light beam. In the case of fluorescence imaging, the filtercube I3 (Leica Microsystems) was used limiting excitation to the range λ = 450−490 nm.

Statistical Analysis. Data analysis was carried out by using ANOVA variance parametric analysis and Tuckey range test ($P < 0.05$) using SPSS software, version 8.0 (SPSS, Chicago, IL). In each case, errors associated with the results provided were calculated on the basis of the residual standard deviation.

RESULTS AND DISCUSSION

Establishment of Callus Lines of *C. argentea* var. *plumosa*. All seeds from *C. argentea* var. *plumosa* were geminated on day 10 after sowing, with no sign of microbial contamination. Seedlings were maintained under aseptic conditions for 20 days and then used for callus induction experiments (Figure 2A). Hypocotyls were considered as primary explant sources due to the presence of meristem tissue and the reported endogenous levels of auxins and cytokines.[31,32] Table 1 summarizes the results for callus induction as affected by the presence and concentration of different plant growth regulators. It can be seen that the sole presence of 2,4-dichlorophenoxyacetic acid (2,4-D) was not enough to induce the formation of calli. Such inhibition of the cell growth could be due to the overexpression of genes ARR7 and ARR15 promoted by the auxin as previously reported.[33] The presence of 6-benzylaminopurine (BAP) at a concentration 4.44 μM also yielded negative results if no other regulator was present, in accordance to previous reports with *Celosia cristata*.[34] Treatments with BAP at concentrations 6.66 and 8.88 μM and the combination of 6.66 μM BAP with 9.05 μM 2,4-D generated calli with pale brown color with yields of 33% or 66%. Experiments with the highest concentrations of BAP and 2,4-D showed 100% induction capacity of white-green calli in 30-day cultures.

The medium suplemented with 6.66 μM BAP and 6.79 μM 2,4-D showed the highest cell growth, and the cell mass

DOI: 10.1021/acs.jafc.5b00065
J. Agric. Food Chem. 2015, 63, 2741−2749

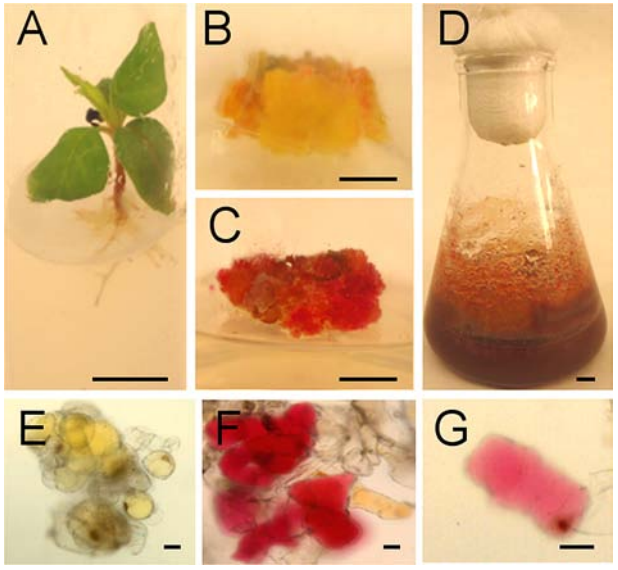

Figure 2. Establishment of in vitro cell lines derived from *C. argentea* var. *plumosa*. (A) Twenty days old seedling used as explants source. (B and C) Macroscopic images showing phenotypic characteristics for yellow and red callus lines, respectively. (D) Suspension culture 15 days after inoculation. (E, F, and G) Brightfield microscopic images of cells present in yellow callus, red callus, and suspension culture, respectively.

presented yellow and red color after 14 days of culture, spreading to the full explants at day 30. The presence of yellow and red colors suggested the presence of betalains. These data are in relation to the observations on the halophytic plant *Suaeda salsa*,[35] on *C. cristata*,[34,36] and on *B. vulgaris* cultures.[37] Due to the presence of red and yellow hues and the culture characteristics, the medium supplemented with 6.66 μM BAP and 6.79 μM 2,4-D was considered for further experimentation. Callus propagation was performed in fresh medium every 20 days for 11 cycles (total cultivation time 7.5 months). As a result of this process two stable and differentially colored lines of *C. argentea* were established: yellow and red (Figure 2B and 2C). Both cell lines obtained were observed under microscopy. The yellow line showed a round shape and yellow pigmentation compatible with the presence of betaxanthins (Figure 2E). The red cell line presented a morphology with round and elongated cells with a major presence of the former (Figure 2F). This phenomenon might be in relation with the cohesive properties of the cell wall reported to occur during plant cell division.[38] Red pigmentation was observed within the line cells compatible with the presence of betacyanins.

Pigment Identification in Yellow and Red Cell Lines. The yellow and red *C. argentea* cell lines obtained were analyzed in terms of the presence of the bioactive pigments betalains. Samples from both lines were extracted and analyzed by HPLC with PDA and ESI-MS/MS detection (Table 2). The yellow line exhibited the major presence of the betaxanthins vulgaxanthin I (**5**), derived from L-glutamine (1.78 mg/g dry weight) and miraxanthin V (**2**), derived from dopamine (1.64 mg/g dry weight) (Table 2). Other betaxanthins detected were those derived from L-dihydroxyphenylalanine (L-DOPA), named dopaxanthin (**1**), and L-tryptophan (**6**). In addition to the yellow pigments, the betacyanins amaranthin (**8**) and betanin (**7**) and the dihydroxylated betanidin (**3**) and decarboxy-betanidin (**4**) were also identified.

Table 2. Production of Betalains, Dopamine, and Betalamic Acid in Cells of the Yellow and Red Callus Lines and in Suspension Cultures of *C. argentea*

compound	R_t (min)	ESI-MS (m/z)	λ_{max} (nm)	infl[a] (mg/g dry weight)	hyp[b] (mg/g dry weight)	yellow line (mg/g dry weight)	red line (mg/g dry weight)	suspension culture			
								1 day (mg/g dry weight)	8 days (mg/g dry weight)	15 days (mg/g dry weight)	30 days (mg/g dry weight)
dopaxanthin (**1**)	11.27	391	472	nd[c]	nd	0.22 ± 0.01	0.34 ± 0.01	0.31 ± 0.01	0.29 ± 0.02	0.16 ± 0.01	0.12 ± 0.01
miraxanthin V (**2**)	12.54	347	460	nd	nd	1.64 ± 0.01	3.04 ± 0.02	1.84 ± 0.07	1.47 ± 0.06	1.49 ± 0.09	0.52 ± 0.02
betanidin (**3**)	11.76	389	542	nd	nd	0.45 ± 0.01	0.74 ± 0.03	2.05 ± 0.04	6.27 ± 0.05	2.46 ± 0.07	0.39 ± 0.04
decarboxy-betanidin (**4**)	13.37	345	539	nd	nd	0.71 ± 0.01	1.32 ± 0.05	2.16 ± 0.05	2.30 ± 0.06	2.21 ± 0.08	0.34 ± 0.01
vulgaxanthin I (**5**)	8.45	340	472	nd	nd	1.78 ± 0.01	2.65 ± 0.01	2.01 ± 0.08	2.01 ± 0.1	0.15 ± 0.04	0.09 ± 0.03
tryptophan-bx (**6**)	10.09	398	472	nd	nd	0.12 ± 0.01	0.11 ± 0.01	0.23 ± 0.02	0.26 ± 0.02	0.01 ± 0.01	0.02 ± 0.01
betanin (**7**)	10.25	551	535	nd	nd	0.62 ± 0.03	0.80 ± 0.01	0.95 ± 0.03	0.75 ± 0.05	0.33 ± 0.03	0.15 ± 0.01
iso-betanin	16.67	551	535	nd	nd	0.94 ± 0.01	1.25 ± 0.01	1.43 ± 0.07	0.67 ± 0.08	0.30 ± 0.07	0.49 ± 0.04
amaranthin (**8**)	9.48	727	535	18.68 ± 0.16	1.52 ± 0.04	1.37 ± 0.01	4.92 ± 0.02	0.62 ± 0.04	0.48 ± 0.02	0.61 ± 0.04	0.2 ± 0.02
iso-amaranthin	9.81	727	535	6.20 ± 0.05	0.60 ± 0.09	0.21 ± 0.01	0.81 ± 0.01	0.65 ± 0.01	0.22 ± 0.05	0.03 ± 0.01	0.01 ± 0.01
dopamine (**9**)	8.60	137	278	nd	nd	17.70 ± 0.05	19.62 ± 0.06	35.28 ± 0.12	42.08 ± 0.15	15.48 ± 0.11	0.94 ± 0.14
betalamic acid (**10**)	12.05	211	405	nd	nd	0.29 ± 0.02	0.46 ± 0.01	0.32 ± 0.06	0.29 ± 0.06	0.13 ± 0.02	0.14 ± 0.03

[a]Inflorescences of the whole plant. [b]Hypocotyls used as explants source. [c]nd: not detected. HPLC retention times, molecular ions as determined by ESI-MS, and PDA maximum wavelengths are shown. Pigment analyses in inflorescences of the whole plant and hypocotyls are shown for comparison.

DOI: 10.1021/acs.jafc.5b00065
J. Agric. Food Chem. 2015, 63, 2741−2749

In the red line, coloration was also due to betalains and the content of betacyanins was higher. In this case the major pigment detected was the violet amaranthin (**8**) (4.92 mg/g dry weight), accompanied by decarboxy-betanidin (**4**) (1.32 mg/g dry weight), betanin (**7**) (0.80 mg/g dry weight), and betanidin (**3**) (0.74 mg/g dry weight). Betaxanthins were also present (Table 2) with dopamine-derived betaxanthin (**2**) being the major yellow pigment (3.04 mg/g dry weight). The joint presence of betacyanins (violet) and betaxanthins (yellow) yields the red color described for the cell mass. Inflorescences of the starting plant material and the hypocotyls used to establish the cell lines were violet. These two samples were also analyzed as a control, and only the presence of amaranthin (**8**) and its isomer iso-amaranthin were found (Table 2). The number of betalains present in the cell cultures indicates that the presence of 6.79 μM 2,4-D and 6.66 μM BAP promotes the biosynthesis of an increased number of betalains compared to the starting plant material. This could be due to the effect of 2,4-D and BAP in the concentrations mentioned on the expression of the key enzymes of the biosynthetic pathway of betalains: 4,5-DOPA-extradiol dioxygenase (DODA), tyrosinase, and cytochrome P450. In this sense, the levels of DODA mRNA and the accumulation of betalains have been previously correlated with the concentration of the growth regulators in in vitro cultures of *S. salsa*.[35]

The presence of betaxanthins in the cells of the yellow *C. argentea* line together with the described fluorescence of these pigments under physiological conditions[39] makes the cells fluorescent in the visible range of the electromagnetic spectrum. Figure 3 shows the pictures derived from the betaxanthins

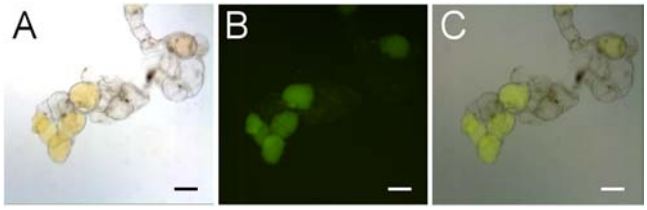

Figure 3. *C. argentea* microscopic images of cells present in the yellow line callus. (A) Brightfield technique. (B) Fluorescence. Only yellow portions of the brightfield image, containing betaxanthins, present light emission in the fluorescence image. (C) Combination of the previous two images.

autofluorescence obtained under a filter system able to irradiate the sample with blue light and to record the emitted light in the green range of the visible spectrum. As can be seen, only the yellow portions of the brightfield image, containing the yellow pigments, present light emission in the fluorescence image. Fluorescence of betaxanthins has previously been used to visualize petal cells[39] and to detect the presence of *Plasmodium falciparum* (malaria) in erythrocytes.[40] However, this is the first time that betalains fluorescence was demonstrated to be of utility in the visualization of plant single cells grown in vitro.

All pigments were identified by comparison with real standards in terms of HPLC retention times, PDA spectra, and electrospray ionization mass spectrometry (ESI-MS) analyses. The mass values determined for the parent ions of all compounds were as expected for the corresponding protonated molecular ions $[M + H]^+$ of the betalains, thus confirming the proposed structures (Table 2). For pigments containing a quaternary ammonium substructure, the mass obtained corresponds to the charged form, as drawn in Figure 1. In all cases a daughter ion corresponding to m/z $[M + H]^+ - 44$ was detected, accounting for loss of a carboxylic group. For betanin (**7**) (R_t 10.25 min), the main daughter ion was m/z 389, corresponding to the mass determined for betanidin (**3**), obtained through cleavage of the glucose unit at the level of the *O*-glucosidic bond (m/z $[M + H]^+ - 162$). Amaranthin (**8**) (R_t 9.48 min) yielded a molecular ion of m/z 727 that was fragmented into m/z 551, corresponding to loss of a glucuronic acid moiety m/z $[M + H]^+ - 176$ (betanin), and into m/z 389, corresponding to an additional loss of glucose m/z $[M + H]^+ - 176-162$ (betanidin). Betanidin (**3**) itself was also present in the extracts derived from both cell lines (R_t 11.76 min). Thus, all the intermediates of the biochemical route of carboxylated betacyanins from betanidin to amaranthin were present. This suggests the transformation of betanidin (**3**) into betanin (**7**) by glucosylation[16] and betanin into amaranthin (**8**) by addition of a glucuronic acid residue. The presence of the intermediates points to the biosynthesis of amaranthin in the callus through this route instead of via cyclo-DOPA glucosylation and glucuronylation and further condensation with betanidin.[41] These intermediates were not present in the starting plant material inflorescences or hypocotyls, where only the final product of the route amaranthin was detected.

The possible presence in the cell cultures of the structural unit of all betalains, betalamic acid (**10**), and the precursor molecule for miraxanthin V, dopamine (**9**), was also investigated. Betalamic acid could be detected in the yellow *C. argentea* cell line at 0.29 mg/g dry weight (Table 2), while in the red line a higher content was detected with 0.46 mg/g dry weight. The presence of betalamic acid (**10**) complements the presence of intermediates of the biosynthetic pathway of betalains. It is an elusive molecule derived from cyclization of the 4,5-seco-DOPA molecule obtained by intramolecular cleavage of the amino acid L-DOPA by the enzyme 4,5-DOPA-extradiol-dioxygenase.[2] Free betalamic acid has previously been found as a natural constituent in fruits of *Opuntia ficus-indica*.[42] Dopamine (**9**) was also detected in the cell lines at significant quantities. Identification was corroborated by comparison with commercial standard (R_t 8.60 min) and ESI-MS. A predominant daughter ion of m/z 137 resulting from loss of the amine group was found in the standard and culture-derived compound. This metabolite was not detected in the plant inflorescences or hypocotyls, but its presence accounts for 17.70 mg/g dry weight in the yellow cell line and 19.63 mg/g dry weight in the red line. In addition to its role as the building block of betalains, betalamic acid itself is a natural pigment with strong antioxidant activity.[26] Dopamine acts as a neurotransmitter, and its deficit has been reported in mental illness such as depression.[5]

The presence of the dihydroxylated betacyanins betanidin (**3**) and decarboxy-betanidin (**4**) and the DOPA and dopamine-derived betaxanthins (**1**, **2**) in the obtained cell cultures is of particular relevance due to their strong antioxidant and free radical scavenging activities.[3,4,43] Furthermore, the tryptophan-derived betaxanthin (**6**) present in both cell lines has recently been identified among all traditional Chinese medicine phytochemicals in a massive in silico screening as a bioactive compound interacting with the age-related enzymes sirtuins.[44] Tryptophan-derived betaxanthin is a lead compound with possible application in drug development for diseases associated with aging.

DOI: 10.1021/acs.jafc.5b00065
J. Agric. Food Chem. 2015, 63, 2741−2749

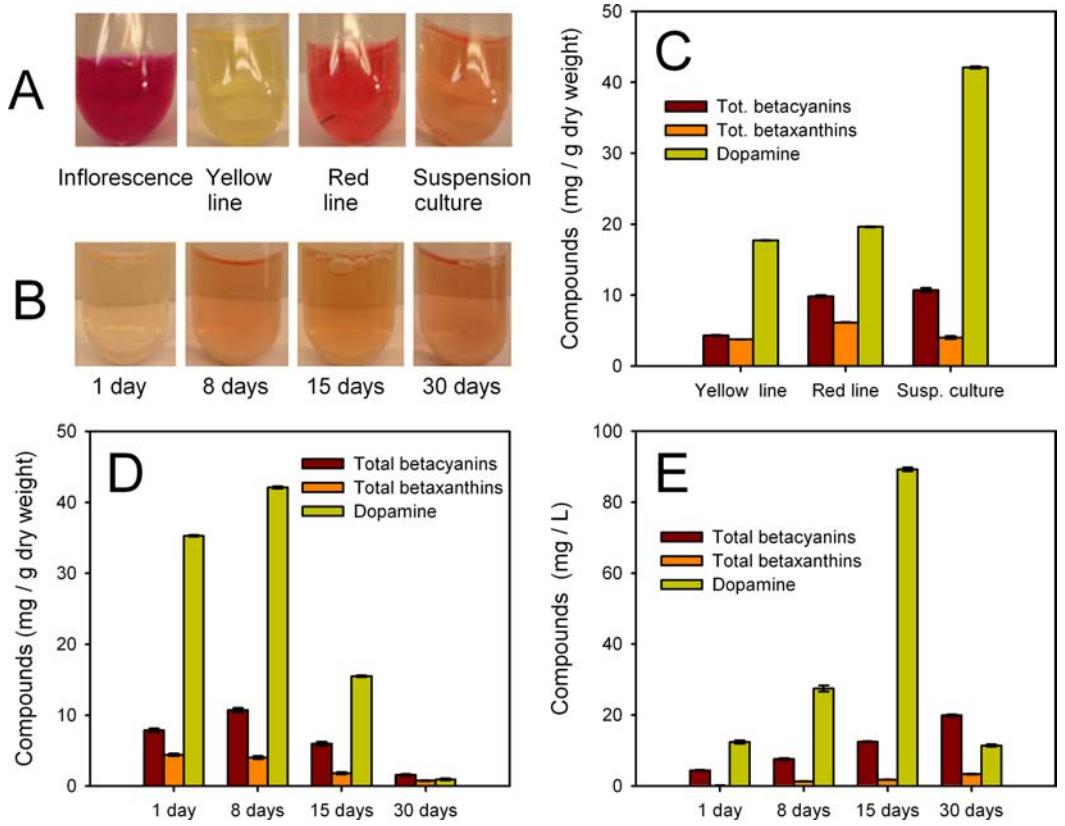

Figure 4. Production of betalains and dopamine by cell lines derived from *C. argentea* var. *plumosa*. (A) Picture showing the pigmentation of cell extracts obtained from plant inflorescences, yellow callus line, red callus line, and suspension culture 8 days after inoculation. (B) Color evolution of the liquid culture medium photographed 1, 8, 15, and 30 days after inoculation. (C) Total pigment content and dopamine presence in extracts obtained from solid and suspension cultures. (D) Time evolution for the production of betalains and dopamine in the cells of the suspension culture at the indicated times after inoculation. (E) Time evolution for the presence of betalains and dopamine in the liquid medium at the indicated times after inoculation.

Suspension Cultures of *C. argentea*. The analyses performed in the cell lines derived from *C. argentea* show that the red line produces higher levels of dopamine, betacyanins, and betaxanthins than the yellow homologue (Figure 4C). Thus, the red cell line was chosen to attempt a suspension culture of *C. argentea* that could be used to produce the identified phytochemicals. The liquid culture was successfully established in MS liquid medium supplemented with 30 g/L sucrose, 6.66 μM BAP, 6.79 μM 2,4-D, and 10 mM ascorbic acid. Figure 2D shows the established culture. The cell growth curve (Figure 5) indicates that a lag phase was present for 4 days, in which biomass reached 3.18 g dry weight/L. After this time, cells entered exponential growth phase. Growth was prolonged up to day 15, and in that time the accumulated biomass was 10.96 g dry weight/L. During this phase, the doubling time of the culture was 6.1 days with a calculated growth rate (μ) of 0.113/day.

During the whole culture time the pH of the suspension was monitored (results not shown) with no significant variation being recorded and a mean pH value of 4.9. This is a convenient pH value to promote the stability of the pigments betalains with special emphasis of those containing the dihydroxylated moiety.[21] The cell shape found in suspension was elongated, showing predominantly red coloration (96%) (Figure 2G). In addition to the red-colored cells, yellow cells were detected in a much lesser extent (4%). This points to the joint presence of betaxanthins and betacyanins in the majority of cells, as detected in the red callus used to start the liquid culture. Cells tended to form aggregates, probably in relation to the cohesive properties of the cell wall and the hydrodynamic stress experienced in suspension culture.[38] Cell viability was also monitored during the process and maintained at 74% during the 30 days of culture period. Viability is well above the limit of 50% considered as positive in plant cell culture,[45] thus confirming the success of the *C. argentea* suspension culture.

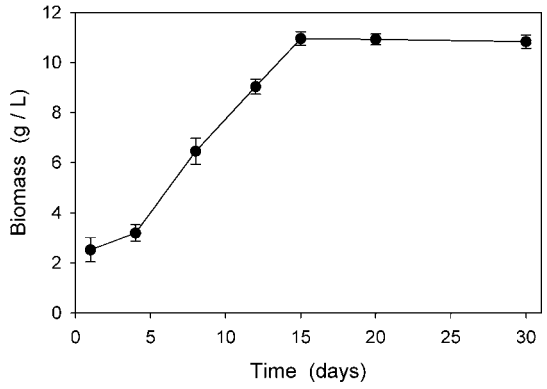

Figure 5. Growth curve for the suspension culture of *C. argentea* obtained in MS liquid medium supplemented with 30 g/L sucrose, 6.66 μM BAP, 6.79 μM 2,4-D, and 10 mM ascorbic acid.

Production of Betalains and Dopamine in Liquid Culture. The presence of betalains and dopamine in *C. argentea* liquid culture was analyzed by HPLC-PDA and ESI-

DOI: 10.1021/acs.jafc.5b00065
J. Agric. Food Chem. 2015, 63, 2741−2749

Table 3. Production of Betalains, Dopamine, and Betalamic Acid in the Liquid Medium of Suspension Cultures of *C. argentea*

compound	1 day (mg/L)	8 days (mg/L)	15 days (mg/L)	30 days (mg/L)
dopaxanthin (**1**)	nd[a]	nd	nd	nd
miraxanthin V (**2**)	0.03 ± 0.01	0.40 ± 0.05	0.50 ± 0.02	1.17 ± 0.04
betanidin (**3**)	0.50 ± 0.04	2.85 ± 0.11	6.75 ± 0.02	13.40 ± 0.04
decarboxy-betanidin (**4**)	1.14 ± 0.05	1.51 ± 0.20	2.47 ± 0.03	4.17 ± 0.09
vulgaxanthin I (**5**)	0.08 ± 0.03	0.88 ± 0.02	1.24 ± 0.03	2.16 ± 0.06
tryptophan-bx (**6**)	nd	nd	nd	nd
betanin (**7**)	nd	nd	nd	nd
iso-betanin	nd	nd	nd	nd
amaranthin (**8**)	2.70 ± 0.07	3.04 ± 0.11	2.99 ± 0.02	2.33 ± 0.08
iso-amaranthin	0.04 ± 0.01	0.12 ± 0.04	0.24 ± 0.03	0.04 ± 0.03
dopamine (**9**)	12.34 ± 0.48	27.42 ± 0.85	89.20 ± 0.51	11.35 ± 0.35
betalamic acid (**10**)	0.88 ± 0.02	0.84 ± 0.01	1.23 ± 0.03	3.63 ± 0.06

[a]nd: Not detected.

MS. Pigments were identified and quantitated both in cells and in liquid medium at different culture times. Cell extracts and media analyses were performed at days 1, 8, 15, and 30 as shown in Tables 2 and 3. Cells exhibited maximum accumulation of total betalains at day 8, corresponding to the exponential growth phase (Figure 4D). Up to 10 pigments were identified corresponding to those present in the calli with a higher content of miraxanthin V (**2**) (1.84 mg/g dry weight), vulgaxanthin I (**5**) (2.01 mg/g dry weight), and betanidin (**3**) (6.27 mg/g dry weight).

This pigment content explains the cell suspension coloration and suggests the possible secretion of pigments into the culture medium. Table 3 shows the results for the analyses of the medium at different culture times. The presence of betalains was detected during all of the process, increasing with incubation time (Figure 4B and 4E). Pigments identified in the culture medium were betalamic acid (**10**), vulgaxanthin I (**5**), miraxanthin V (**2**), amaranthin (**8**), and betanidin (**3**). The total quantity of betalains detected at the end of culture (day 30) was 23.27 mg/L, mainly accounting for the presence of the dihydroxylated betacyanin betanidin (**3**) (13.40 mg/L). Betanidin, which is the betalain with the strongest antioxidant and free radical scavenging activities and also involved in the anti-inflammatory potential of betalain-containing extracts,[46,47] is here the betalain produced in a higher extent.

Cells grown in liquid culture presented a significant increase in the content of dopamine (**9**) in comparison to the levels detected in the cells grown in solid media. After 8 days in liquid culture the levels of dopamine in the cells were 42.08 mg/g dry weight, which is more than double the levels found in the cells grown in solid media (19.62 mg/g dry weight for the red line) (Figure 4C). Plant cells in suspension suffer hydrodynamic forces due to continuous shaking which generates a stress probably involved in the increase of the secondary metabolism.[48,49] Dopamine was also detected to a lesser extent in the culture medium. Figure 4E shows the time evolution of dopamine content. In this case the maximum concentration was achieved after 15 days of culture with a content of 89 mg/L. Although the presence of dopamine in *C. argentea* was known for intact plants,[12] this is the first report on the production of the metabolite in cell culture. In vitro production of dopamine through a plant cell culture was previously only attempted for another plant belonging to the Caryophyllales, *Portulaca oleracea* but using *Agrobacterium rhizogenes* transformation. This achieved a maximum production of dopamine of 0.90 mg/g dry weight after 28 days of culture and chemical elicitation.[50] This value is far from the 42.08 mg/g dry weight obtained here in only 8 days with untransformed cells of *C. argentea*, thus significantly increasing the yield and reducing the culture time.

Cell cultures of *C. argentea* produce four dihydroxylated betalains with the highest antioxidant and free radical scavenging activities, the carboxylated dopaxanthin (**1**) and betanidin (**3**) and the decarboxylated homologues miraxanthin V (**2**) and decarboxy-betanidin (**4**). In addition, they produce tryptophan-betaxanthin (**6**), which has been identified among the bioactive compounds of the traditional Chinese medicine database for their interaction with the age-related enzymes sirtuins. The joint presence of these bioactive betalains together with the production of dopamine (**9**) shows the ability of cell cultures of *C. argentea* to become stable sources of valuable phytochemicals of potential application in the food, pharmaceutical, and cosmetic fields.

AUTHOR INFORMATION

Corresponding Author

*Tel.: +34 868 884786. Fax: +34 868 884147. E-mail: fgandia@um.es.

Funding

This work was supported by "Ministerio de Ciencia e Innovación" (MCINN, FEDER, Spain) (Projects AGL2011-25023 and AGL2014-57431). B.G.-F. holds a fellowship from "Consejo Nacional de Ciencia y Tecnología" and the "Asociación Universitaria Iberoamericana de Postgrado" (CONACYT, Mexico and AUIP, Spain). F G.-H. has a contract with the "Programa Ramón y Cajal" (MCINN, FEDER, Spain).

Notes

The authors declare no competing financial interest.

ACKNOWLEDGMENTS

The authors are grateful to Dr. María Inmaculada García, Dr. María Teresa Castells, and Dr. José Rodríguez (SAI, University of Murcia) for skillful technical assistance in Image Analysis and ESI-MS experiments.

REFERENCES

(1) Gandía-Herrero, F.; Escribano, J.; García-Carmona, F. Biological activities of plant pigments betalains. *Crit. Rev. Food Sci. Nutr.* **2015**, DOI: 10.1080/10408398.2012.740103.

(2) Gandía-Herrero, F.; García-Carmona, F. Biosynthesis of betalains: yellow and violet plant pigments. *Trends Plant Sci.* **2013**, *18*, 334−343.

DOI: 10.1021/acs.jafc.5b00065
J. Agric. Food Chem. 2015, 63, 2741−2749

(3) Gandía-Herrero, F.; Escribano, J.; García-Carmona, F. The role of phenolic hydroxy groups in the free radical scavenging activity of betalains. *J. Nat. Prod.* **2009**, *72*, 1142−1146.
(4) Gliszczyńska-Świgło, A.; Szymusiak, H.; Malinowska, P. Betanin, the main pigment of red beet: Molecular origin of its exceptionally high free radical-scavenging activity. *Food Addit. Contam.* **2006**, *23*, 1079−1087.
(5) Dunlop, B. W.; Nemeroff, C. B. The role of dopamine in the pathophysiology of depression. *Arch. Gen. Psychiatry* **2007**, *64*, 327−337.
(6) Fifel, K.; Cooper, H. M. Loss of dopamine disrupts circadian rhythms in a mouse model of Parkinson's disease. *Neurobiol. Dis.* **2014**, *71*, 359−369.
(7) del Campo, N.; Chamberlain, S. R.; Sahakian, B. J.; Robbins, T. W. The roles of dopamine and noradrenaline in the pathophysiology and treatment of attention-deficit/hyperactivity disorder. *Biol. Psychiatry* **2011**, *69*, E145−E157.
(8) Vasu, T. S.; Cavallazzi, R.; Hirani, A.; Kaplan, G.; Leiby, B.; Marik, P. E. Norepinephrine or dopamine for septic shock: systematic review of randomized clinical trials. *J. Intensive Care Med.* **2012**, *27*, 172−178.
(9) Piattelli, M.; Minale, L.; Nicolaus, R. A. Betaxanthins from *Mirabilis jalapa* L. *Phytochemistry* **1965**, *4*, 817−823.
(10) Kugler, F.; Stintzing, F. C.; Carle, R. Identification of betalains from petioles of differently colored Swiss chard (*Beta vulgaris* L. ssp. *cicla* [L.] alef. cv. bright lights) by high-performance liquid chromatography-electrospray ionization mass spectrometry. *J. Agric. Food Chem.* **2004**, *52*, 2975−2981.
(11) Trezzini, G. F.; Zrÿd, J.-P. Two betalains from *Portulaca grandiflora*. *Phytochemistry* **1991**, *30*, 1897−1899.
(12) Schliemann, W.; Cai, Y.; Degenkolb, T.; Schmidt, J.; Corke, H. Betalains of *Celosia argentea*. *Phytochemistry* **2001**, *58*, 159−165.
(13) Piattelli, M.; Impellizzeri, G. 2-Descarboxybetanidin, a minor betacyanin from *Carpobrothus acinaciformis*. *Phytochemistry* **1970**, *9*, 2553−2556.
(14) Kobayashi, N.; Schmidt, J.; Wray, V.; Schliemann, W. Formation and occurrence of dopamine-derived betacyanins. *Phytochemistry* **2001**, *56*, 429−436.
(15) Impellizzeri, G.; Piattelli, M.; Sciuto, S. A new betaxanthin from *Glottiphyllum longum*. *Phytochemistry* **1973**, *12*, 2293−2294.
(16) Hans, J.; Brandt, W.; Vogt, T. Site-directed mutagenesis and protein 3D-homology modeling suggest a catalytic mechanism for UDP-glucose-dependent betanidin 5-*O*-glucosyltransferase from *Dorotheanthus bellidiformis*. *Plant J.* **2004**, *39*, 319−333.
(17) Amin, I.; Norazaidah, Y.; Hainida, K. I. E. Antioxidant activity and phenolic content of raw and blanched *Amaranthus* species. *Food Chem.* **2006**, *94*, 47−52.
(18) Sang-Uk, C.; Buk-Gu, H.; Yong-Seo, P.; Dong-Kwan, K.; Shela, G. Total phenolics level, antioxidant activities and cytotoxicity of young sprouts of some traditional Korean salad plants. *Plant Foods Hum. Nutr.* **2009**, *64*, 25−31.
(19) Ibrahim, B.; Sowemimo, A.; van Rooyen, A.; Van de Venter, M. Antiinflammatory, analgesic and antioxidant activities of *Cyathula prostrate* (Linn.) Blume (Amaranthaceae). *J. Ethnopharmacol.* **2012**, *141*, 282−289.
(20) Silva, L. R.; Valentão, P.; Faria, J.; Ferreres, F.; Sousa, C.; Gil-Izquierdo, A.; Pinho, B. R.; Andrade, P. B. Phytochemical investigations and biological potential screening with cellular and non-cellular models of globe amaranth (*Gomphrena globosa* L.) inflorescences. *Food Chem.* **2012**, *135*, 756−763.
(21) Gandía-Herrero, F.; Cabanes, J.; Escribano, J.; García-Carmona, F.; Jiménez-Atiénzar, M. Encapsulation of the most potent antioxidant betalains in edible matrixes as powders of different colors. *J. Agric. Food Chem.* **2013**, *61*, 4294−4302.
(22) Murashige, T.; Skoog, F. A revised medium for rapid growth and bioassays with tobacco tissue cultures. *Physiol. Plant.* **1962**, *15*, 473−97.
(23) Rodríguez-Monroy, M.; Galindo, E. Broth rheology, growth and metabolite production of *Beta vulgaris* suspension culture: a comparative study between cultures grown in shake flasks and in stirred tank. *Enzyme Microb. Technol.* **1999**, *24*, 687−693.
(24) Cai, Y.-Z.; Sun, M.; Corke, H. Characterization and application of betalain pigments from plants of the Amaranthaceae. *Trends Food Sci. Technol.* **2005**, *16*, 370−376.
(25) Gandía-Herrero, F.; García-Carmona, F.; Escribano, J. Development of a protocol for the semi-synthesis and purification of betaxanthins. *Phytochem. Anal.* **2006**, *17*, 262−269.
(26) Gandía-Herrero, F.; Escribano, J.; García-Carmona, F. Purification and antiradical properties of the structural unit of betalains. *J. Nat. Prod.* **2012**, *75*, 1030−1036.
(27) Gandía-Herrero, F.; García-Carmona, F.; Escribano, J. A novel method using high-performance liquid chromatography with fluorescence detection for the determination of betaxanthins. *J. Chromatogr. A* **2005**, *1078*, 83−89.
(28) Schwartz, S. J.; von Elbe, J. H. Quantitative determination of individual betacyanin pigments by high-performance liquid chromatography. *J. Agric. Food Chem.* **1980**, *28*, 540−543.
(29) Trezzini, G. F.; Zrÿd, J.-P. Characterization of some natural and semisynthetic betaxanthins. *Phytochemistry* **1991**, *30*, 1901−1904.
(30) Gandía-Herrero, F.; Escribano, J.; García-Carmona, F. Structural implications on color, fluorescence, and antiradical activity in betalains. *Planta* **2010**, *232*, 449−460.
(31) Chapman, E. J.; Greenham K.; Castillejo, C.; Sartor, R.; Bialy, A. Hypocotyl transcriptome reveals auxin regulation of growth-promoting genes through ga-dependent and independent pathways. *PLoS One* **2012**, *7*, 10.1371/journal.pone.0036210.
(32) Abu-Romman, S. The influence of plant growth regulators on callus induction from hypocotyls of cucumber (*Cucumis sativus* L.). *Adv. Environ. Biol.* **2013**, *7*, 339−343.
(33) Ying-Hua, S.; Yu-Bo, L.; Xian-Sheng, Z. Auxin-cytokinin interaction regulates meristem development. *Mol. Plant* **2011**, *4*, 616−625.
(34) Taha, R. M.; Wafa, S. N. Plant regeneration and cellular behaviour studies in *Celosia cristata* grown *in vivo* and *in vitro*. *Sci. World J.* **2012**, DOI: 10.1100/2012/359413.
(35) Zhao, S. Z.; Sun, H. Z.; Gao, Y.; Sui, N.; Wang, B. S. Growth regulator-induced betacyanin accumulation and dopa-4,5-dioxygenase (DODA) gene expression in euhalophyte *Suaeda salsa* calli. *In Vitro Cell. Dev. Biol.: Plant* **2011**, *47*, 391−398.
(36) Jamilah, S. Y.; Azani, S.; Hashimah, E.; Sakinah, A.; Noraini, M.; Normadiha, M. *In vitro* regeneration and acclimatization protocols of selected ornamental plants (*Agapanthus praecox*, *Justicia betonica* and *Celosia cristata*). *Sains Malays.* **2014**, *43*, 715−722.
(37) Akita, T.; Hina, Y.; Nishi, T. Production of betacyanins by a cell suspension culture of table beet (*Beta vulgaris* L.). *Biosci., Biotechnol., Biochem.* **2000**, *64*, 1807−1812.
(38) Trejo-Tapia, G.; Rodríguez-Monroy, M. Cellular aggregation in secondary metabolite production in in vitro plant cell cultures. *Interciencia* **2007**, *32*, 669−674.
(39) Gandía-Herrero, F.; García-Carmona, F.; Escribano, J. Floral fluorescence effect. *Nature* **2005**, *437*, 334−334.
(40) Gonçalves, L. C. P.; Tonelli, R. R.; Bagnaresi, P.; Mortara, R. A.; Ferreira, A. G.; Bastos, E. L. A nature-inspired betalainic probe for live-cell imaging of *Plasmodium*-infected erythrocytes. *PLoS One* **2013**, *8*, e53874.
(41) Sasaki, N.; Abe, Y.; Wada, K.; Koda, T.; Goda, Y.; Adachi, T.; Ozeki, Y. Amaranthin in feather cockscombs is synthesized via glucuronylation at the cyclo-DOPA glucoside step in the betacyanin biosynthetic pathway. *J. Plant Res.* **2005**, *118*, 439−442.
(42) Stintzing, F. C.; Schieber, A.; Carle, R. Amino acid composition and betaxanthin formation in fruits from *Opuntia ficus-indica*. *Planta Med.* **1999**, *65*, 632−635.
(43) Cai, Y.; Sun, M.; Corke, H. Antioxidant activity of betalains from plants of the Amaranthaceae. *J. Agric. Food Chem.* **2003**, *51*, 2288−2294.
(44) Chen, K.-C.; Jian, Y.-R.; Sun, M.-F.; Chang, T.-T.; Lee, C.-C.; Chen, C. Y.-C. Investigation of silent information regulator 1 (Sirt1)

DOI: 10.1021/acs.jafc.5b00065
J. Agric. Food Chem. 2015, 63, 2741−2749

agonists from traditional Chinese medicine. *J. Biomol. Struct. Dyn.* **2013**, *31*, 1207−1218.
(45) Qui, J. A.; Castro-Concha, L. A.; García-Sosa, K.; Peña-Rodríguez, L. M.; Miranda-Ham, M. L. Differential effects of phytotoxic metabolites from *Alternaria tagetica* on *Tagetes erecta* cell cultures. *J. Gen. Plant Pathol.* **2009**, *75*, 331−339.
(46) Vidal, P. J.; López-Nicolás, J. M.; Gandía-Herrero, F.; García-Carmona, F. Inactivation of lipoxygenase and cyclooxygenase by natural betalains and semi-synthetic analogues. *Food Chem.* **2014**, *154*, 246−254.
(47) Martinez, R. M.; Longhi-Balbinot, D. T.; Zarpelon, A. C.; Staurengo-Ferrari, L.; Baracat, M. M.; Georgetti, S. R.; Sassonia, R. C.; Verri, W. A., Jr.; Casagrande, R. Anti-inflammatory activity of betalain-rich dye of *Beta vulgaris*: effect on edema, leukocyte recruitment, superoxide anion and cytokine production. *Arch. Pharmacal Res.* **2014**, DOI: 10.1007/s12272-014-0473-7.
(48) Hua, J.; Erickson, E.; Yiin, T. Y.; Glasgow, L. A review of the effects of shear and interfacial phenomena on cell viability. *Crit. Rev. Biotechnol.* **1993**, *13*, 305−328.
(49) Joshi, J. B.; Elias, C. B.; Patole, M. S. Role of hydrodynamic shear in cultivation of animal, plant and microbial cells. *Chem. Eng. J.* **1996**, *62*, 121−141.
(50) Ahmadi-Moghadam, Y.; Piri, Kh.; Bahramnejad, B.; Ghiasvand, T. Dopamine production in hairy root cultures of *Portulaca oleracea* (purslane) using *Agrobacterium rhizogenes*. *J. Agric. Sci. Technol.* **2014**, *16*, 409−420.

DOI: 10.1021/acs.jafc.5b00065
J. Agric. Food Chem. 2015, 63, 2741−2749

However, the wax composition has been recently correlated also with the antioxidant and anti-inflammatory proprieties.[20,32] The main triterpenoids detected in apple cuticular wax are ursolic, oleanolic, and betulinic acids. Ursolic acid is a ubiquitous triterpenoid in the plant kingdom that was long considered to be biologically inactive, whereas in recent years it has attracted considerable interest because of its pharmacological effects such as the inhibition proliferation of HepG2 human hepatoma cells, MCF-7 human breast cancer cells, and Caco-2 human colon cancer cells.[32]

Only recently, breeding for phytochemicals in horticultural crops has been identified as an important goal in the development of new cultivated lines. The plant's genotype is considered of primal importance in the determination of its phytochemical profile, often surpassing the impact of cultural practices such as irrigation or fertilization. Horticultural crops such as strawberry, apple, tomato, potato, cabbage, broccoli, lettuce, onion, cranberry, and raspberry are currently the subject of breeding programs in which the phytochemical content was considered a key component.[33] The effect of domestication and particularly of breeding on apple bioactive compounds content is still unresolved and is a matter of debate. The inconsistency of recent results[20,22,34] has not yet elucidated the effective impact of breeding activities on the total phytochemical content in apple fruit. We suggest that this open question deserves further investigation since the breeding of the future cultivars should have the roots in a solid knowledge of metabolic phylogenesis, taking into account the composition and relationships among the apples of the past (wild species, old cultivars) and of the present (elite cultivars).

In the present study, a broad apple germplasm collection, composed by both wild and domesticated species, was analyzed to assess the amount of main bioactive compounds of apple fruit, namely, phenolics, triterpenes, and ascorbic acid. The availability of this repertoire of information allowed the study of the largest catalogue of apple bioactive compounds to date presented to the scientific community. It allowed one to discover that apple is a significant dietary source of resveratrols (*trans*- and *cis*-piceid). Moreover, the effect of domestication on the actual concentration of these compounds and their potential role in breeding programs are discussed.

MATERIALS AND METHODS

Plant Material and Fruit Sampling. Metabolic profiling was performed on an apple fruit collection represented by 247 accessions, composed by both wild *Malus* species (97) and *Malus* × *domestica* cultivars (150) (Supporting Information, Table 1). Plant materials were planted in triplicate for each accession and grown at the experimental orchard of the Fondazione Edmund Mach in the Northern part of Italy (Province of Trento). Each plant was maintained following standard agronomical management for pruning, thinning, and pest disease control.

A minimum of five homogeneous apples, harvested at optimal ripening stage as defined by the Extension Service of the Fondazione Edmund Mach, and by fruit color comparison, were collected from each accession and maintained at room temperature (~20 °C) overnight before sampling. The entire collection was assessed for bioactive compound profiling in the first year, while in the second year, only a subset, composed by 23 commercially important accessions, was assessed in order to validate the procedure.

The core of three fruits per sample was removed with an apple corer. Three slices (cortex + skin) of each fruit, taken from opposite sides, were cut in small pieces, ground under liquid nitrogen, and stored in falcon tubes at −80 °C until the analysis.

Phenolic Compound Analysis. Extraction and analysis of phenols were performed according to the UPLC-MS/MS method published by Vrhovsek et al.[26] An aliquot of 2 g of powdered tissues was extracted in sealed glass vials using 4 mL of water/methanol/chloroform solution (20:40:40). After vortexing for 1 min, the samples were mixed using an orbital shaker for 15 min at room temperature and further centrifuged at 1000*g* (4 °C) for 10 min, after which the upper phases, made up of aqueous methanol extract, were collected. Extraction was repeated by adding another 2.4 mL of water/methanol (1:2) to the pellet and chloroform fractions. After the final centrifugation, the upper phases from the two extractions were combined and brought to the volume of 10 mL and filtered with a 0.2 μm PTFE filter prior to liquid chromatography−mass spectrometry analysis. Ultraperformance liquid chromatography was performed employing a Waters Acquity UPLC system (Milford, MA, USA) coupled to a Waters Xevo TQMS (Milford, MA, USA) working in ESI ionization mode. Separation of the phenolic compounds was achieved on a Waters Acquity HSS T3 column 1.8 μm, 100 mm × 2.1 mm (Milford, MA, USA), kept at 40 °C, with two solvents: A (water containing 0.1% formic acid) and B (acetonitrile containing 0.1% formic acid). The flow was 0.4 mL/min, and the gradient profile was 0 min, 5% B; from 0 to 3 min, linear gradient to 20% B; from 3 to 4.3 min, isocratic 20% B; from 4.3 to 9 min, linear gradient to 45% B; from 9 to 11 min, linear gradient to 100% B; from 11 to 13 min, wash at 100% B; and from 13.01 to 15 min, back to the initial conditions of 5% B. From both standard solutions and samples, kept at 6 °C, a volume of 2 μL was injected, after which the needle was rinsed with 600 μL of weak wash solution (water/methanol, 90:10) and 200 μL of strong wash solution (methanol/water, 90:10). Detection was performed by multiple reaction monitoring (MRM) with a Waters Xevo TQMS (Milford, MA, USA) triple quadrupole (QqQ) equipped with an electrospray (ESI) source. Capillary voltage was 3.5 kV in positive mode and −2.5 kV in negative mode; the source was kept at 150 °C; desolvation temperature was 500 °C; cone gas flow, 50 L/h; and desolvation gas flow, 800 L/h. Unit resolution was applied to each quadrupole. Each phenolic compound was analyzed under the optimized MRM conditions (precursor and product ions, quantifier and qualifiers, collision energies, and cone voltages) described by Vrhovsek et al.[26] Data were processed by Waters MassLynx 4.1 and TargetLynx software.

Triterpenoids Analysis. The extraction was performed according to Andre et al.[20] Five milliliters of ethyl acetate and 5 mL of hexane were added to an aliquot of 500 mg of powdered tissues, shaken for 1 h, and centrifuged at 2000*g* for 10 min. The dried extract was dissolved in 1 mL of ethanol and filtrated. Quantification and separation of triterpenoids was carried out with a Waters HPLC system Alliance 2695 Separations Module equipped with a mass spectrometer Micromass ZQ and Waters Empower Pro software. The separation was performed on Phenomenex Luna C18 column, 250 × 2 mm, 5 μm and with a mobile phase consisting of 1% formic acid in water (solvent A) and methanol (solvent B). The column was heated at 35 °C with a flow of 0.3 mL/min under the following conditions: linear gradient from 50 to 85% of B in 5 min, to 90% B in 25 min. The column was washed with 100% B for 5 min and equilibrated with the initial conditions for another 5 min. The injection volume was 20 μL. The conditions of the mass spectrometer were capillary voltage 3000 V, cone voltage 25 V, extractor voltage 10 V, source temperature 125 °C, desolvation temperature 500 °C, cone gas flow (N2) 30 l/h, and desolvation gas flow (N2) 1000 L/h. The scan speed was 0.1 s in SIM mode with detection in negative mode at m/z 455.50. The retention time for the betulinic acid was 21.5 min, 22.7 min for oleanolic acid, and 23.2 min for ursolic acid.

Organic Acids Analysis. An aliquot of 5 g of the edible part of the frozen fruit was homogenized in 50 mL of a solution of metaphosphoric acid (0.6%) in water containing sodium *meta*-bisulfite (1 g/L). Analysis of organic acids was performed as described in Vrhovsek et al.[35] The separation was carried out on a Waters 2690 HPLC system equipped with Waters 2996 DAD (Waters, Milford, MA), and Empower Software (Waters, Milford, MA.) on a reversed-phase column Discovery, RP C18 (Supelco, 250 × 4 mm, 5 μm). The

DOI: 10.1021/acs.jafc.5b00291
J. Agric. Food Chem. 2015, 63, 2750−2759

Table 1. Distribution of the Content of Phenolic, Triterpenoid, and Organic Acid Compounds in the Edible Part of Ripe Fruits from *Malus* Germplasm

	wild *Malus* species				*M.* × *domestica* cvs			
compounds	average[a]	min[a]	max[a]	75th perc.[a]	average[a]	min[a]	max[a]	75th perc.[a]
Hydroxycinnamic Acids								
neochlorogenic acid	1.8	0	21.8	1.9	1.0	0.0	8.8	1.2
cryptochlorogenic acid	13.7	0.2	185.2	11.2	8.0	0.4	92.9	9.7
chlorogenic acid	678.2	10.5	3496.9	1024.3	508.0	40.0	1821.4	673.9
Stilbenes								
trans-piceid	0.6	0	2.4	0.7	0.3	0.0	1.3	0.4
cis-piceid	0.3	0	2.3	0.4	0.1	0.0	1.0	0.2
Dihydrochalcones								
phloridzin	262	4.1	1080.6	332.1	52.8	7.1	310.6	64.8
Flavan-3-ols								
(+)-catechin	24.1	0.2	344.1	23.3	55.7	1.0	300.8	69.7
(−)-epicatechin	212.3	8.9	954.8	299.5	169.8	5.7	669.9	210.3
procyanidin B1	67	0.7	577.4	91.7	114.8	2.2	532.4	153.1
procyanidin B2 + B4	358.3	10.2	1337.6	595.5	261.1	10.8	950.4	311.1
Flavonols								
quercetin-3-Rha	64.4	3.1	413.5	92.5	62.9	0.0	274.5	75.7
isorhamnetin-3-Glc	5.6	0	59.1	6.4	5.5	0.0	63.2	0.0
rutin	12.1	0	57.1	18.5	10.9	0.0	121.3	13.5
isorhamnetin-3-rutinoside	1.2	0	20.4	1.1	3.5	0.0	41.8	0.0
quercetin-3-Glc + quercetin-3-Gal	216.4	26.1	641.7	287.7	133.1	15.3	604.3	166.9
Triterpenoids								
ursolic acid	387.7	55.3	1177.1	489.4	393.2	0.0	997.5	491.1
oleanolic acid	69.8	0	497.8	87.5	55.4	0.0	125.8	75.4
betulinic acid	9.8	0	32	15.9	11.6	0.0	35.7	15.1
Organic Acids								
ascorbic acid	139.5	7.7	685.8	176.7	79.2	11.6	251.2	96.5
malic acid	16478.7	3072.1	37485.9	22636.8	7117.0	1425.0	14791.7	8742.0

[a]μg/g FW.

solvent used was 0.07% phosphoric acid in water. The isocratic separation was carried out at 30 °C in 10 min. After each run, the column was washed for 5 min with 15% acetonitrile in 0.07% phosphoric acid in water and afterward equilibrated for 7 min prior to each analysis. The flow rate was 0.6 mL/min, the injection volume was 20 μL, and the UV−vis signal was set at 243 nm for ascorbic acid and 210 nm for malic acid.

Statistical Analysis. Multivariate statistical analysis was performed on log transformed data using R 3.0.2 internal statistical functions and the external packages "PCA", "gplots", "ape", and "diversitree". Visualization of significant metabolite correlations ($p < 0.01$; $R > 0.50$) was conducted by the generation of a Correlation Analysis Network with Cytoscape.

RESULTS AND DISCUSSION

Total Bioactive Compounds of Apple Species. Total content of bioactive compounds, mainly phenolics, triterpenoids, and ascorbic acid, significantly differed among wild *Malus* species as well as a *M.* × *domestica* cultivars (Table 1).

The overall content of phenols in *M.* × *domestica* ranged between 225 μg/g FW (cv Laimburg Gelber Edelaefer) and 3307 μg/g FW (cv Permein dorato) with the elite market cultivars (Supporting Information, Table 2) in the range between 435 μg/g FW (cv Scilate) and 2450 μg/g FW (cv Renetta Canada). More variation was found between the wild *Malus* species, ranging between 353 μg/g FW (*M.* × *Dawsoniana*) and 6513 μg/g FW (*M. angustifolia*). Distribution of each phenolic compounds in the groups of genotypes assessed in this research is reported in Table 1. In detail, wild *Malus* species were characterized by a higher average content of all phenolic compounds than *M.* × *domestica*, for which the differences between old and elite cultivars were negligible. Remarkably, the dihydrochalcone (phloridzin) content assessed in wild *Malus* species (average of 262 μg/g FW with a maximum of 1081 μg/g FW) was significantly higher when compared with the levels recorded on the *M.* × *domestica* species (average of 52 μg/g FW with a maximum of 310 μg/g FW).

The total content of triterpenoids in *M.* × *domestica* accessions ranged between 6 μg/g FW (cv Spitzlederer) and 1121 μg/g FW (cv Napoleone), with the market elite cultivars between 233 μg/g FW (cv Renetta Canada) and 785 μg/g FW (cv Mutsu). Comparable variation was also found between the wild *Malus* species that ranged between 58 μg/g FW (*M.* × *Hartwigii*) and 1384 μg/g FW (*M. sylvestris*) (Supporting Information, Table 1). Likewise, average content of each triterpenoids (namely, ursolic, oleanolic, and betulinic acids) did not relevantly diverge between *M.* × *domestica* and wild *Malus* accessions. The most abundant triterpenoid, as already reported by Andre et al.[20] and Frighetto et al.,[31] was ursolic acid followed by its isomeric compound oleanolic and betulinic acid (average values, respectively, around 400, 60, and 10 μg/g FW).

Differences in organic acids content between *M.* × *domestica* and wild *Malus* accessions were more noticeable when compared to the other investigated metabolites. In fact, most of the wild *Malus* species had a relevant higher average content of both ascorbic and malic acid (140 and 16319 μg/g FW, respectively). Contrarily, no remarkable differences were discovered between old and elite *M.* × *domestica* cultivars

DOI: 10.1021/acs.jafc.5b00291
J. Agric. Food Chem. 2015, 63, 2750−2759

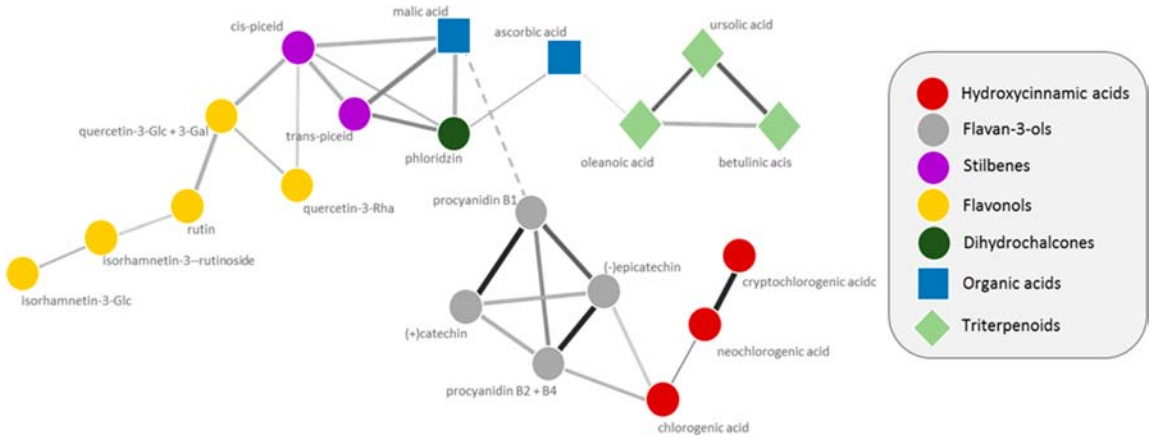

Figure 1. Correlation Analysis Networks (CAN) for the entire bioactive metabolite data set. The network is obtained by determining the significant Pearson correlations ($p < 0.01$) among the metabolites. The color coding of the edges (gradient from light gray to blank) denotes the level of correlation (from 0.5 to 1). Positive and negative correlations are shown, respectively, by solid and dash lines.

(average value of ascorbic and malic acid around 80 μg/g FW and 7000 μg/g FW, respectively).

Correlation network analysis of the investigated metabolites (Figure 1) was mainly assessed to check the accuracy of the used data set rather than to gain knowledge about the metabolic pathways of apple secondary metabolites. The network was created from a significant Pearson correlation data set ($P < 0.01$, Pearson correlation threshold = $\pm$ 0.5), computed among the metabolites detected in all 247 apple accessions present in the collection. The correlation network depicted the robustness and correctness of the data set used in this investigation (*M.* × *domestica* and wild *Malus* species accessions analyzed in two seasons) since compounds belonging to the same chemical family were closely grouped together in accordance with their metabolic pathways.

Phenolic Compounds. Phenolic compound variability assessed within the apple germplasm by principal component analysis (PCA) confirmed the results previously described in Table 1 (Figure 2a). Old and elite *M.* × *domestica* populations

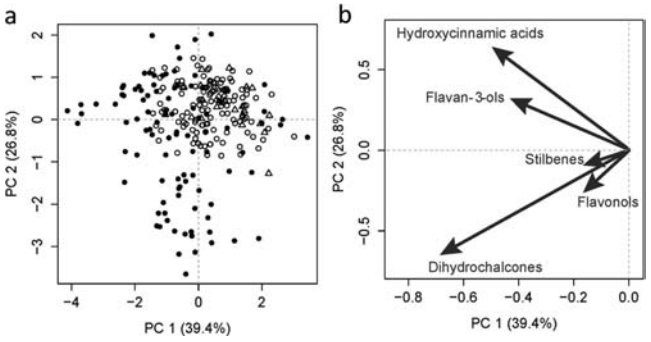

Figure 2. PCA plot (a) and loading projection (b) of the phenolic compounds assessed in the *Malus* germplasm: (●) wild *Malus*, (O) *M.* × *domestica* OLD cvs, and (Δ) *M.* × *domestica* ELITE cvs.

were not noticeably discriminated based on their phenolic content and profile, while a broad collection of wild *Malus* species species (those located in the left and bottom space of Figure 2, panel a) was markedly distinguished mostly according to the second principal component variation (PC2, 26.8%). Most of this variation was due to a generally higher concentration of dihydrochalcones, stilbenes, and flavonols as depicted in the PCA loading plot (Figure 2b). Nevertheless, also the variation of the first principal component (PC1, 39.4%) disclosed a reduced but significant cluster of wild *Malus* accessions characterized by a higher content of hydroxycinnamic acids and flavan-3-ols.

The hydroxycinnamic acid (neochlorogenic acid, cryptochlorogenic acid, and chlorogenic acid) average content assessed on wild *Malus* species was 30% higher than that on *M.* × *domestica* cultivars (Figure 3a and Supporting Information, Figures 1 and 2). Only 16 over the 150 *M.* × *domestica* cultivars showed a content higher than the 75th percentile assessed in wild *Malus* species; among them, Rosa di Caldaro represented the only cultivar with still a marketable value. Among all *Malus* species accessions, *M. brevipes*, *M. angustifolia*, *M.* × *bracteata*, *M. ioensis*, and *M. orthocarpa* were the species with the highest content of hydroxycinnamic acids. Since several unappreciated quality traits, mainly fruit bitterness and astringency[36] and flesh browning after cutting,[37] are commonly related the hydroxycinnamic acids level, the lower content assessed into the "elite" *M.* × *domestica* cultivars (Supporting Information, Figure 1) may be accredited to breeding strategies aimed to reduce these unpleasant features.

Stilbenes, represented by *trans*- and *cis*-piceid, are the phenolic compound class with the lowest concentration detected in *Malus* species fruit. Before the present study, it was only reported in "Golden Delicious" apple,[26] while previously it was considered a "foreign" phytoalexin only reported in transgenic apple transformed with the stilbene synthase gene from grapevine.[38,39] *trans*-Piceid and *cis*-piceid were identified and also quantified for the first time in apple thanks to the very high sensitivity of MS/MS mass spectrometers coupled to a UHPLC separation system. Their identification was furthermore unequivocally confirmed by UHPLC interfaced with two high resolution mass spectrometers (Synapt-QTOF and Orbitrap) by three independent parameters: accurate mass, fragmentation patterns, and retention time (Supporting Information, Figures 3 and 4). Despite their relatively low concentrations, the presence of resveratrol glucosides in apple should lead to not negligible contribution to the dietary intake of resveratrol. From the analysis of the Spanish branch of the EPIC cohort ($n = 40.574$), we know that approximately 32% of the population did not consume resveratrol, while for the remaining group, the most

DOI: 10.1021/acs.jafc.5b00291
J. Agric. Food Chem. 2015, 63, 2750−2759

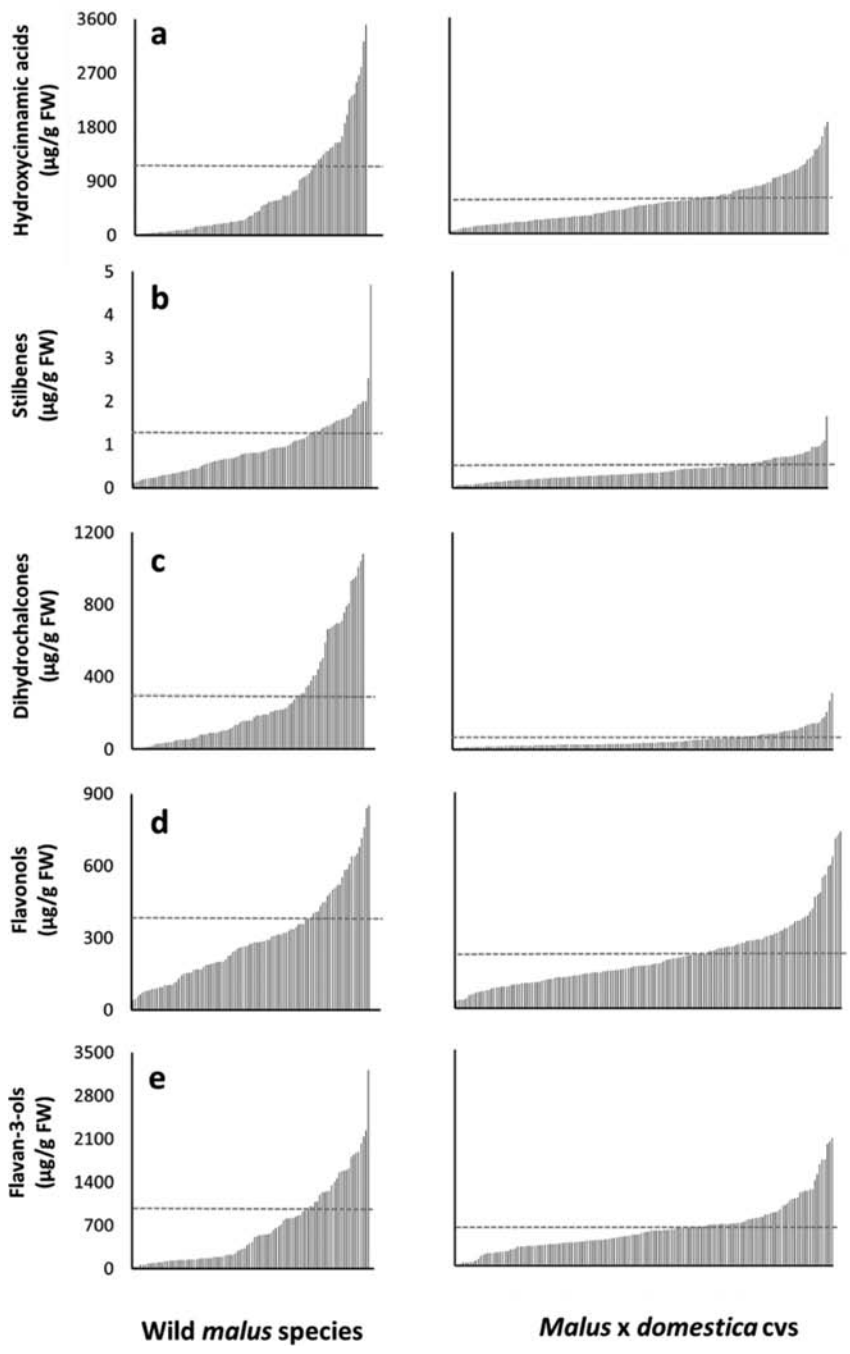

Figure 3. Bar chart plots of phenolic compound content (hydroxycinnamic acids, stilbenes, dihydrochalcones, flavonols, and flavan-3-ols) assessed in the *Malus* germplasm (left column plots, 97 wild *Malus* accessions; right column plots, 150 *M.* × *domestica* cvs). The 75th percentile levels are represented by the dashed line. Distribution density plots of each compound class are reported in Supporting Information, Figure 2.

important sources of resveratrols (piceid + free resveratrols) are wines (98.4%) and grape and grape juices (1.6%), whereas peanuts, pistachios, and berries contributed to less than 0.01%.[40] The average daily intake of resveratrol in the EPIC population was estimated at 137 and 686 μg/day for women and men, respectively. The mean apple consumption per person in the EPIC-Spain study was approximately 90g/day, with 90% of the population being consumers.[40−42] With a mean total content in cultivated apples of 0.4 μg/g FW (Table 1), this would provide 36 μg per day. From the combination of the above data, it appears that apple is the second highest dietary source of resveratrol after wines. The estimated dietary intake of resveratrols is slightly higher, and the percentage of population not exposed to resveratrols is lower than previously reported, after accounting for the presence of resveratrols in apple.

Resveratrol average content in wild *Malus* species was 130% higher than that in *M.* × *domestica*, for which no relevant differences were found between old and elite cultivars (Figure 3b and Supporting Information, Figure 1). Red Field, Geflammter Kardinal, and Renetta Canada had the highest piceide content among the *M.* × *domestica* cultivars while, among the wild *Malus* species, the highest content was detected in *M. sikkimensis* and *M. baccata*.

DOI: 10.1021/acs.jafc.5b00291
J. Agric. Food Chem. 2015, 63, 2750−2759

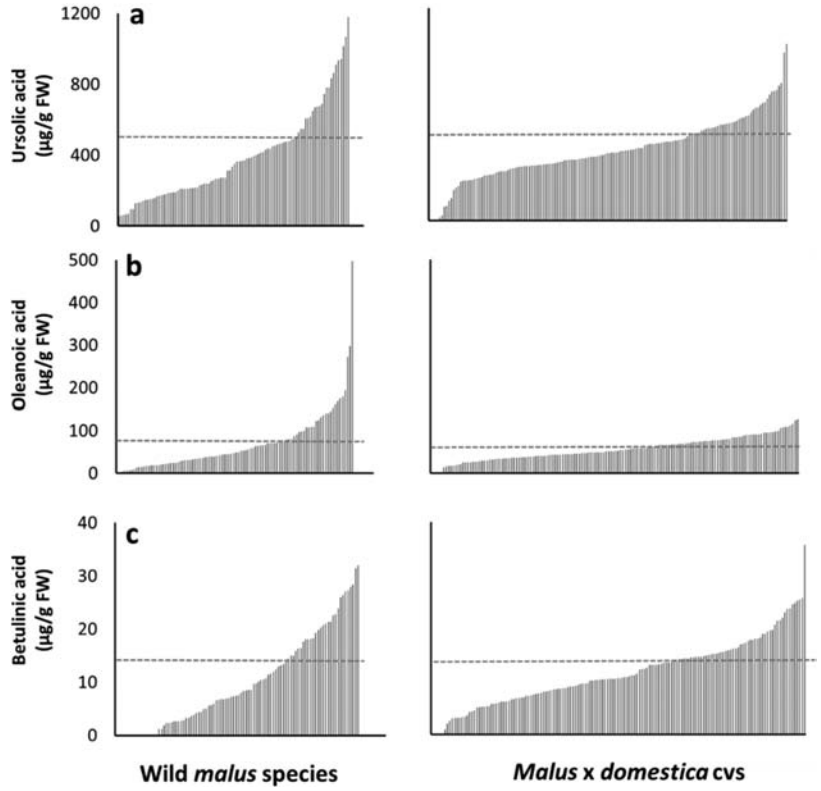

Figure 4. Bar chart plots of triterpenoid compound content (ursolic acids, oleanolic acid, and betulinic acid) assessed in the *Malus* germplasm (left column plots, 97 wild *Malus* accessions; right column plots, 150 *M.* × *domestica* cvs). The 75th percentile levels are represented by the dashed line. Distribution density plots of each compound class are reported in Supporting Information, Figure 2.

The main dihydrochalcone detected in *Malus* species is phlorizin.[20,22,27,35] Phlorizin content evaluated in this experiment significantly varied between *M.* × *domestica* and wild *Malus* accessions (Figure 3c and Supporting Information, Figure 1 and 2). A large number of wild *Malus* species, 25 in total, presented a phloridzine content higher than the maximum level discovered in *M.* × *domestica* cultivars. As a consequence, on the contrary from the other detected secondary metabolites, the distribution of wild *Malus* species based on phloridzin level turned out to be wider and not normally distributed (Supporting Information, Figures 2). Among the *Malus* species *M. ioensis*, *M. angustifolia*, *M. halliana*, *M. yunnanensis*, and *M. honanensis* showed the highest values. No significant differences were found between the old and the elite *M.* × *domestica* cultivars; remarkably, none of them reached the 75th percentile level (332 µg/g FW) recorded on the wild *Malus* species. In accordance with Ehrenkranz et al.,[27] all Renetta accessions (i.e., Renetta grigia, Renetta Canada, and Renetta Canada bianca) were characterized by a high phloridzin content (Supporting Information, Table 2); among the elite cultivars Renetta Canada was, indeed, the one with the highest content (144 µg/g FW).

As depicted by the PCA analysis (Figure 2a,b), fruits of *M.* × *domestica* differed from the ones of wild *Malus* species also due to the generally lower content of flavonols (quercetin-3-rhamnoside, isorhamnetin-3-glucoside, rutin, isorhamnetin-3-rutinoside, quercetin-3-glucoside, and quercetin-3- galactopyranoside; Figure 3d and Supporting Information, Figure 1). However, this separation based on flavonols content was not so distinctive as the discrimination based on hydroxycinnamic acid, stilbene, and dihydrochalcone levels (Figure 3a,b,c). Average value of flavonol content of *M.* × *domestica* cultivars was around 216 µg/g FW, without any relevant differences between elite and old cultivars, while for the wild *Malus* species, it was around 300 µg/g FW. Among the *M.* × *domestica* cultivars, Falchs Guldering, Roter Eiser, and Modì showed the highest flavonol content, whereas the highest among the wild *Malus* species was assessed on *M. halliana*, *M. kansuensis*, *M.* × *hartvigii*, and *M.* × *transitoria*.

Any relevant difference on flavan-3-ol average content (catechin, epicatechin, procyanidin B1, procyanidin B2, and procyanidin B4) was not detected between fruits of *M.* × *domestica* and wild *Malus* (Figure 3e and Supporting Information, Figures 1 and 2). *M. mandshurica*, *M. orientalis*, *M. angustifolia*, and *M. sieversii* were the wild *Malus* acessions with the highest content of flavan-3-ols, while Renetta Baumann, Blancje di Cattino, Lampone, and Aranciata di Cox were the predominant ones among *M.* × *domestica*.

Ordinarily, phenolic content of apple fruit is a relatively unstable trait among seasons due to the high influence of growing and climatic conditions.[24,43] However, repetition of analysis in the second year on a selected minor array of cultivars (23 cultivars, see Supporting Information, Table 1) revealed a reasonable stable total phenolic content with a correlation (R^2) of 0.78 between the two seasons (Supporting Information, Figure 5).

Triterpenoid Compounds. Despite a broad variation in triterpenoid content among wild *Malus* species as well as among *M.* x *domestic*a cultivars (Figure 4 and Supporting Information, Figures 1 and 2) any relevant differences based on triterpenoids (ursolic, oleanolic, and betulinic acids) average content were not discovered (Table 1). Only a minor pool of

DOI: 10.1021/acs.jafc.5b00291
J. Agric. Food Chem. 2015, 63, 2750−2759

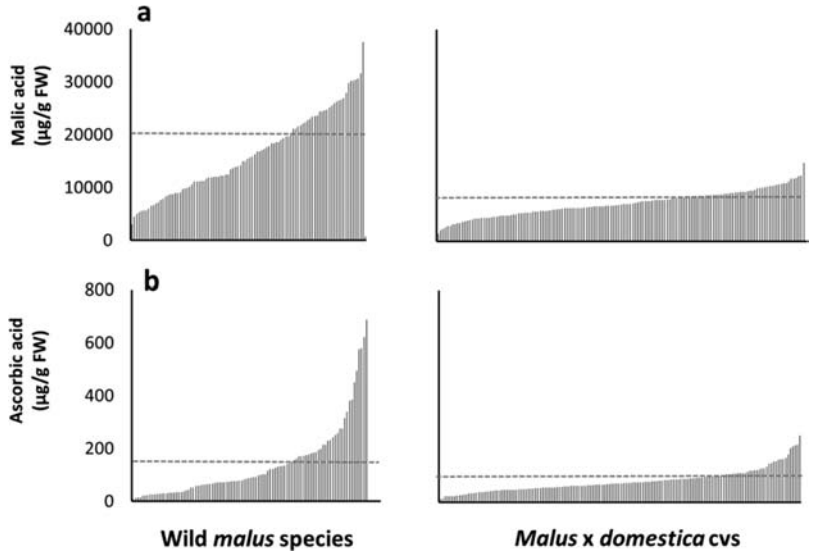

Figure 5. Bar chart plots of organic acid content (malic acid and ascorbic acid) assessed in the *Malus* germplasm (left column plots, 97 wild *Malus* accessions; right column plots, 150 *M.* × *domestica* cvs). The 75th percentile levels are represented by the dashed line. Distribution density plots of each compound class are reported in Supporting Information, Figure 2.

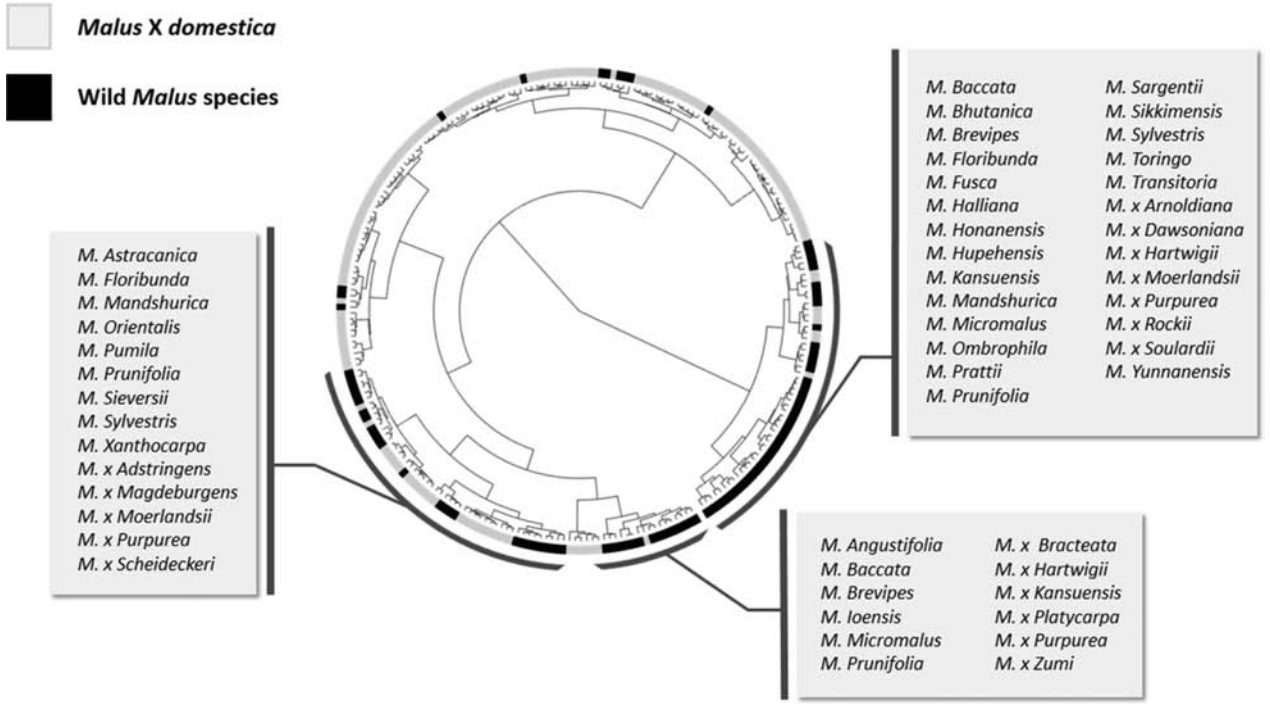

Figure 6. Polar dendrogram based on the cluster analysis performed in the apple germplasm (black, 97 wild *Malus* accessions; light gray, 150 *M.* × *domestica* cvs). Cluster analysis was performed using Ward's method on log transformed data of bioactive compounds content. A high resolution vector form chart is reported in Supporting Information, Figure 6.

wild *Malus* species (*M. ioensis*, *M.* × *soulardii*, and *M. orientalis*) was characterized by a relatively higher content of oleanolic acid (from 4 to 7 times higher fold value with respect to the average content). These irrelevant dissimilarities between *M.* × *domestica* and wild *Malus* accessions may indicate a low pressure of apple domestication and breeding on the expression of this metabolic trait. Up to now, indeed, the content of triterpenoids was not a chief quality trait for apple breeding programs, even though recent studies depicted a possible remarkable role of triterpenoids as functional metabolites for human health.[20,30,32,44] In addition, variation in triterpenoids content, mainly of the fruit skin, ensued to have a possible role in enhancing fruit storability and in inducing resistance to abiotic and biotic stress.[45,46]

Repetition of analysis in the second year on a selected small range of cultivar (n = 23) revealed a correlation (R^2) of 0.50 (Supporting Information, Figure 5). The lower correlation for triterpenoids, in comparison with the other metabolites investigated in this study, may reflect their skin location, which is more exposed to the environment compared to the flesh.

DOI: 10.1021/acs.jafc.5b00291
J. Agric. Food Chem. 2015, 63, 2750−2759

Organic Acids. Malic acid is known to be the most abundant organic acid in apple (Table 1 and Supporting Information, Figures 1 and 2). Differences in malic acid content between *M.* × *domestica* and wild *Malus* species were evident. In fact, most of the wild *Malus* accessions and several old apple cultivars (i.e., Gelber Edelapfel, Tiroler Spitzlederer, or Osnabrücker Renette) were characterized by a significant higher content of malic acid (Figure 5a and Supporting Information, Figures 1 and 2). Considering the fruit acidity level, one of the main quality traits for apple fruit breeding and selection,[47,48] these results confirmed the loss of acidity throughout apple domestication.

Similar results were found also for the ascorbic acid content (Figure 5b, and Supporting Information, Figures 1 and 2). Wild *Malus* species showed a 2-fold higher average value of ascorbic acid than *M.* × *domestica* cultivars. Only 5 over the 150 *M.* × *domestica* cultivars analyzed (cvs Schöner von Nordhausen, Calvilla bianca d'inverno, Renetta Ananas, Gelber Edelapfel, and Zuccalmaglio) had an ascorbic acid content higher than the 75th percentile (176 μg/g FW) assessed in wild *Malus* species. Repetition of analysis in the second year on a selected small range of cultivar (n = 23) revealed a stable total content of ascorbic acid (Supporting Information, Figure 5) with a correlation (R^2) between the two seasons of 0.77. Healthy benefits of apple consumption were generally associated with the high phenolic content rather than the ascorbic acid content since ascorbic content of apples was considered inferior than other commonly consumed fruit and vegetables such as strawberries, oranges, tomato, spinach, or kiwifruit.[34,49−51] Bearing in mind the high average daily intake of apple fruit, these results depicted how inappropriate this generalization is since several *M. domestica* cultivars and in particular a group of wild *Malus* species showed an ascorbic acid content comparable to or even greater than that of other ascorbic acid rich fruits.

Metabolic Phylogenetic Organization of the Genus *Malus*. In the geographical area of apple domestication (Central Asia), more than 40 different species have been characterized.[52] According to the genetic information available to date, the most closely related species to *M.* × *domestica* are represented by *M. asiatica*, *M. baccata*, *M. micromalus*, *M. orientalis*, *M. prunifolia*, *M. siversii*, and *M. sylvestris*. This set of species was included in the final list of 247 accessions considered for this investigation and clustered in a polar dendrogram based on their metabolic content (Figure 6). The grouping performed employing the Ward's algorithm reveals four clades, showing a clear distinction between the several wild *Malus* species (clustered toward the outer edges of the dendrogram) and the *M.* × *domestica* varieties (for the most located in the central portion of the cluster), besides some specific cases. Within the group of the *M.* × *domestica* varieties, three particular *Malus* species were retrieved: *M. sieversii*, *M. pumila*, and *M. floribunda*. It is worth noting that the specific organization of the *Malus* species based on the accumulation of secondary metabolites showed a high consistency with the phylogenetic organization known for apple. *M. sieversii*, which is closely located to the domesticated varieties, was recognized as the closest ancestor to *M.* × *domestica*, especially for fruit quality traits.[53] Genetic analysis carried out during the effort of the "Golden Delicious" genome sequencing confirmed that *M.* × *domestica* derived by *M. sieversii* species.[54] This work also reported that due to the "instant domestication" process occurring in apples, *M. sieversii* and *M.* × *domestica* could be actually considered as a single species, named *M. pumila*. This finding additionally validates the reliability of the metabolic assessment performed here that positioned *M. pumila* within the *M.* × *domestica* group and close to the *M. sieversii* accessions.

Another wild species located within the group of *M.* × *domestica* interesting to note is represented by *M. floribumnda*. This is the most used genetic resource to introgress the *Vf* gene, conferring the natural resistance to scab, the most severe fungal disease in apple.[55,56] This species was in fact largely used in breeding programs, enabling the release of the resistant cultivars available nowadays on the market. One of these varieties, "Ligol", was also included in the set investigated here. The fact that "Ligol" was closely clustered to a *M. floribunda* accession additionally confirms that secondary metabolites play a fundamental role in the control of pathogen attack, favorable for the creation of disease resistant varieties.

In this work, we employed a comprehensive characterization of the several nutraceutical compounds presented in apple fruit, phenols, triterpenoids, and ascorbic acid, by screening a broad collection of wild and domesticated *Malus* species. Results confirmed that the selection pressure of domestication and breeding did not uniformly affect all the phytochemicals contained in apple. For instance, organic acids (malic and ascorbic acids) and some phenolics (stilbenes, hydroxycinnamic acids, and dihydrochalcones) were significantly influenced by selection, while some other relevant flavonoids (flavonols and flavan-3-ols) and triterpenoids (ursolic, oleanolic, and betulinic acids) were not. In our opinion, these results may allow, in the near future, to assist in the selection of *Malus* accessions with specific nutraceutical traits suitable to establish innovative breeding strategies or to patent new functional foods and beverages fundamental to the human diet.

■ ASSOCIATED CONTENT

Supporting Information

The lists of *Malus* accessions analyzed in this research and their phytochemical content; box plots and distribution density plots of each metabolite assessed in wild *Malus* species and *M.* × *domestica* cultivars; metabolite content correlations of analyses repeated in two seasons; high resolution mass spectra of stilbenes obtained with Synapt-QTOF and Orbitrap; and high resolution polar dendrogram based on the cluster analysis performed in the apple germplasm. This material is available free of charge via the Internet at http://pubs.acs.org.

■ AUTHOR INFORMATION

Corresponding Author

*Department of Food Quality and Nutrition, Research and Innovation Centre, Fondazione Edmund Mach (FEM), via E. Mach 1, 38010 San Michele all'Adige, Italy. Tel: +39 0461 615 259. E-mail: fulvio.mattivi@fmach.it.

Funding

This research was funded by the Agroalimentare research AGER project (grant no. 2010-2119) and ADP 2012 (Autonomous province of Trento).

Notes

The authors declare no competing financial interest.

■ ACKNOWLEDGMENTS

We thank Kajetan Trost for the analysis on the Orbitrap mass spectrometer.

DOI: 10.1021/acs.jafc.5b00291
J. Agric. Food Chem. 2015, 63, 2750−2759

REFERENCES

(1) Siró, I.; Kápolna, E.; Kápolna, B.; Lugasi, A. Functional food. Product development, marketing and consumer acceptance—A review. *Appetite* **2008**, *51*, 456−467.

(2) Dillard, C. J.; Bruce German, J. Phytochemicals: Nutraceuticals and human health. *J. Sci. Food Agric.* **2000**, *80*, 1744−1756.

(3) Kaur, C.; Kapoor, H. C. Antioxidants in fruits and vegetables - the millennium's health. *Int. J. Food Sci. Technol.* **2001**, *36*, 703−725.

(4) Boyer, J.; Liu, R. H. Apple phytochemicals and their health benefits. *Nutr. J.* **2004**, *3*, 5.

(5) Gerhauser, C. Cancer chemopreventive potential of apples, apple juice, and apple components. *Planta Med.* **2008**, *74*, 1608−1624.

(6) Hyson, D. A. A comprehensive review of apples and apple components and their relationship to human health. *Adv. Nutr.* **2011**, *2*, 408−420.

(7) Joseph, J.; Cole, G.; Head, E.; Ingram, D. Nutrition, brain aging, and neurodegeneration. *J. Neurosci.* **2009**, *29*, 12795−12801.

(8) Liu, R. H. Potential synergy of phytochemicals in cancer prevention: mechanism of action. *J. Nutr.* **2004**, *134*, 3479S−3485S.

(9) Spencer, J. P. E. The impact of fruit flavonoids on memory and cognition. *Br. J. Nutr.* **2010**, *104*, S40−S47.

(10) Feskanich, D.; Ziegler, R.; Michaud, D.; Giovannucci, E.; Speizer, F.; Willett, W.; Colditz, G. Prospective study of fruit and vegetable consumption and risk of lung cancer among men and women. *J. Natl. Cancer. Inst.* **2000**, *92*, 1812−1823.

(11) Knekt, P.; Jarvinen, R.; Seppanen, R.; Heliovaara, M.; Teppo, L.; Pukkala, E.; Aromaa, A. Dietary flavonoids and the risk of lung cancer and other malignant neoplasms. *Am. J. Epidemiol.* **1997**, *146*, 223−230.

(12) Le Marchand, L.; Murphy, S. P.; Hankin, J. H.; Wilkens, L. R.; Kolonel, L. N. Intake of flavonoids and lung cancer. *J. Natl. Cancer Inst.* **2000**, *92*, 154−160.

(13) Sesso, H.; Gaziano, J. M.; Liu, S.; Buring, J. Flavonoid intake and risk of cardiovascular disease in women. *Am. J. Clin. Nutr.* **2003**, *77*, 1400−1408.

(14) Shaheen, S.; Sterne, J.; Thompson, R.; Songhurst, C.; Margetts, B.; Buerney, P. Dietary antioxidants and asthma in adults- population based case-control study. *Am. J. Respir. Crit. Care Med.* **2001**, *164*, 1823−1828.

(15) Tabak, C.; Arts, I. C. W.; Smit, H. A.; Heederik, D.; Kromhout, D. Chronic obstructive pulmonary disease and intake of cat- echins, flavonols, and flavones: The MORGEN Study. *Am. J. Respir. Crit. Care Med.* **2001**, *164*, 61−64.

(16) Woods, R.; Walters, H.; Raven, J.; Wolfe, R.; Ireland, P.; Thien, F.; Abramson, M. Food and nutrient intakes and asthma risk in young adults. *Am. J. Clin. Nutr.* **2003**, *78*, 414−421.

(17) Knekt, P.; Isotupa, S.; Rissanen, H.; Heliovaara, M.; Jarvinen, R.; Hakkinen, S. H.; Aromaa, A.; Reunanen, A. Quercetin intake and the incidence of cerebrovascular disease. *Eur. J. Clin. Nutr.* **2000**, *54*, 415−417.

(18) Knekt, P.; Kumpulainen, J.; Jarvinen, R.; Rissanen, H.; Heliovaara, M.; Reunanen, A.; Hakulinen, T.; Aromaa, A. Flavonoid intake and risk of chronic diseases. *Am. J. Clin. Nutr.* **2002**, *76*, 560−568.

(19) Koutsos, A.; Lovegrove, J. A. Chapter 12: An Apple a Day Keeps the Doctor Away − Inter-Relationship between Apple Consumption, the Gut Microbiota and Cardiometabolic Disease Risk Reduction, in Diet-Microbe Interactions in the Gut; Tuohy, K., Del RioD., Academic Press: San Diego, CA, 2015; pp 173−194.

(20) Andre, C. M.; Greenwood, J. M.; Walker, E. G.; Rassam, M.; Sullivan, M.; Evers, D.; Perry, N. P.; Laing, W. A. Anti-inflammatory procyanidins and triterpenes in 109 apple varieties. *J. Agric. Food Chem.* **2012**, *60*, 10546−54.

(21) Karaman, S.; Tütem, E.; Başkan, K. S.; Apak, R. Comparison of antioxidant capacity and phenolic composition of peel and flesh of some apple varieties. *J. Sci. Food Agric.* **2013**, *93*, 867−75.

(22) Wojdyło, A.; Oszmiański, J.; Laskowski, P. Polyphenolic compounds and antioxidant activity of new and old apple varieties. *J. Agric. Food Chem.* **2008**, *56*, 6520−30.

(23) Kevers, C.; Pincemail, J. l.; Tabart, J.; Defraigne, J.-O.; Dommes, J. Influence of cultivar, harvest time, storage conditions, and peeling on the antioxidant capacity and phenolic and ascorbic acid contents of apples and pears. *J. Agric. Food Chem.* **2011**, *59*, 6165−6171.

(24) Treutter, D. Biosynthesis of phenolic compounds and its regulation in apple. *Plant Growth Regul.* **2001**, *34*, 71−89.

(25) Vanzani, P.; Rossetto, M.; Rigo, A.; Vrhovsek, U.; Mattivi, F.; D'Amato, E.; Scarpa, M. Major phytochemicals in apple cultivars: contribution to peroxyl radical trapping efficiency. *J. Agric. Food Chem.* **2005**, *53*, 3377−3382.

(26) Vrhovsek, U.; Masuero, D.; Gasperotti, M.; Franceschi, P.; Caputi, L.; Viola, R.; Mattivi, F. A versatile targeted metabolomics method for the rapid quantification of multiple classes of phenolics in fruits and beverages. *J. Agric. Food Chem.* **2012**, *60*, 8831−8840.

(27) Ehrenkranz, J. R.; Lewis, N. G.; Kahn, C. R.; Roth, J. Phlorizin: A review. *Diabetes Metab. Res. Rev.* **2005**, *21*, 31−38.

(28) Rosetti, L.; Shulman, G. I.; Papachristou, D.; DeFronzo, R. A. Correction of hyperglycemia with phlorizin normalizes tissue sensitivity to insulin in diabetic rats. *J. Clin. Invest.* **1987**, *79*, 1510−1515.

(29) Rosetti, L.; Zawalich, W.; DeFronzo, R. A. Effect of chronic hyperglycemia on in vivo insulin secretion in partially pancreatectomized rats. *J. Cin. Invest* **1987**, *80*, 1037−1044.

(30) He, X.; Liu, R. H. Triterpenoids isolated from apple peels have potent antiproliferative activity and may be partially responsible for apple's anticancer activity. *J. Agric. Food Chem.* **2007**, *55*, 4366−4370.

(31) Frighetto, R. T. S.; Welendorf, R. M.; Nigro, E. N.; Frighetto, N.; Siani, A. C. Isolation of ursolic acid from apple peels by high speed counter-current chromatography. *Food Chem.* **2008**, *106*, 767−771.

(32) Ikeda, Y.; Murakami, A.; Ohigashi, H. Ursolic acid: an anti- and pro-inflammatory triterpenoid. *Mol. Nutr. Food Res.* **2008**, *52*, 26−42.

(33) Patil, B. S.; Crosby, K.; Vikram, A.; Byrne, D. Breeding vegetables and fruits to improve human health: A collaborative effort of multidisciplinary scientists, stakeholders and consumers using a systems-based approach. *Acta Hortic.* **2012**, *939*, 19−32.

(34) Lee, S. K.; Kader, A. A. Preharvest and postharvest factors influencing vitamin C content of horticultural crops. *Postharvest Biol. Technol.* **2000**, *20*, 207−220.

(35) Vrhovsek, U.; Rigo, A.; Tonon, D.; Mattivi, F. Quantitation of polyphenols in different apple varieties. *J. Agric. Food Chem.* **2004**, *52*, 6532−6538.

(36) Lea, A. G. H.; Arnold, G. M. The phenolic of ciders: bitterness and astringency. *J. Sci. Food Agric.* **1978**, *29*, 478−483.

(37) Di Guardo, M.; Tadiello, A.; Farneti, B.; Lorenz, G.; Masuero, D.; Vrhovsek, U.; Costa, G.; Velasco, R.; Costa, F. A multidisciplinary approach providing new insight into fruit flesh browning physiology in apple (Malus × domestica Borkh). *PLoS One* **2013**, *8*, e78004 DOI: 10.1371/journal.pone.0078004.

(38) Rühmann, S.; Treutter, D.; Fritsche, S.; Briviba, K.; Szankowski, I. Piceid (resveratrol glucoside) synthesis in stilbene synthase transgenic apple fruit. *J. Agric. Food Chem.* **2006**, *54*, 4633−4640.

(39) Rühmann, S.; Pfeiffer, J.; Brunner, P.; Szankowski, I.; Fischer, T. C.; Forkmann, G.; Treutter, D. Induction of stilbene phytoalexins in grapevine (*Vitis vinifera*) and transgenic stilbene synthase-apple plants (*Malus domestica*) by a culture filtrate of *Aureobasidium pullulans*. *Plant Physiol. Biochem.* **2013**, *72*, 62−71.

(40) Zamora-Ros, R.; Tormo, M. J.; Andres-Lacueva, C.; Lamuela-Raventós, R. M.; et al. Concentrations of resveratrol and derivatives in foods and estimation of dietary intake in a Spanish population: European Prospective Investigation into Cancer and Nutrition (EPIC)-Spain cohort. *Br. J. Nutr.* **2008**, *100*, 188−196.

(41) Zamora-Ros, R.; Andres-Lacueva, C.; Lamuela-Raventós, R. M.; et al. Estimation of dietary sources and flavonoid intake in a Spanish adult population (EPIC-Spain). *J. Am. Diet. Assoc.* **2010**, *110*, 390−398.

(42) Agudo, A.; Slimani, N.; Ocke, M. C.; et al. Consumption of vegetables, fruit and other plant foods in the European Prospective Investigation into Cancer and Nutrition (EPIC) cohorts from 10 European countries. *Public. Health Nutr.* **2002**, *5*, 1179−96.

DOI: 10.1021/acs.jafc.5b00291
J. Agric. Food Chem. 2015, 63, 2750−2759

(43) van der Sluis, A. A.; Dekker, M.; de Jager, A.; Jongen, W. M. F. Activity and concentration of polyphenolic antioxidants in apple: effect of cultivar, harvest year, and storage conditions. *J. Agric. Food Chem.* **2001**, *49*, 3606−3613.
(44) Kondo, M.; MacKinnon, S. L.; Craft, C. C.; Matchett, M. D.; Hurta, R. A. R.; Neto, C. C. Ursolic acid and its esters: occurrence in cranberries and other Vaccinium fruit and effects on matrix metalloproteinase activity in DU145 prostate tumor cells. *J. Sci. Food Agric.* **2011**, *91*, 789−796.
(45) Ju, Z. G.; Bramlage, W. J. Phenolics and lipid-soluble antioxidants in fruit cuticle of apples and their antioxidant activities in model system. *Postharvest Biol. Technol.* **1999**, *16*, 107−118.
(46) Rudell, D. R.; Mattheis, J. P.; Hertog, M. Metabolomic change precedes apple superficial scald symptoms. *J. Agric. Food Chem.* **2009**, *57*, 8459−8466.
(47) Kumar, S.; Volz, R. K.; Alspach, P. A.; Bus, V. G. M. Development of a recurrent apple-breeding programme in New Zealand: a synthesis of results, and a proposed revised breeding strategy. *Euphytica* **2010**, *173*, 207−222.
(48) Visser, T.; Verhaegh, J. J. Inheritance and selection of some fruit characters of apple. I. Inheritance of low and high acidity. *Euphytica* **1978**, *27*, 753−760.
(49) Valente, A.; Albuquerque, T. G. Ascorbic acid content in exotic fruits: a contribution to produce quality data for food composition databases. *Food Res. Int.* **2011**, *44*, 2237−2242.
(50) Szeto, Y. T.; Tomlinson, B.; Benzie, I. F. F. Total antioxidant and ascorbic acid content of fresh fruits and vegetables: implications for dietary planning and food preservation. *Br. J. Nutr.* **2002**, *87*, 55−59.
(51) Leonard, S. S.; Cutler, D.; Ding, M.; Vallyathan, V.; Castranova, V.; Shi, X. Antioxidant properties of fruit and vegetable juices: more to the story than ascorbic acid. *Ann. Clin. Lab. Sci.* **2002**, *32*, 193−200.
(52) Robinson, J. P.; Harris, S. A.; Juniper, B. E. Taxonomy of the genus *Malus* Mill. (Rosaceae) with emphasis on the cultivated apple, *Malus domestica* Borkh. *Plant Syst. Evol.* **2001**, *226*, 35−58.
(53) Forsline, P. L.; Aldwinckle, H. S.; Dickson, E. E.; Luby, J. J.; Hokanson, S. C. Collection, maintenance, characterization, and utilization of wild apples of Central Asia. *Hortic. Rev.* **2003**, *29*, 1−61.
(54) Velasco, R.; Zharkikh, A.; Affourtit, J.; et al. The genome of the domesticated apple (*Malus* × *domestica* Borkh.). *Nat. Genet.* **2010**, *42*, 833−839.
(55) King, G. J.; Tartarini, S.; Brown, L.; Gennari, F.; Sansavini, S. Introgression of the Vf source of scab resistance and distribution of linked marker alleles within the *Malus* gene pool. *Theor. Appl. Genet.* **1999**, *99*, 1039−1046.
(56) Koller, B.; Gianfranceschi, L.; Seglias, N.; McDermott, J.; Gessler, C. DNA markers linked to *Malus floribunda* 821 scab resistance. *Plant Mol. Biol.* **1994**, *26*, 597−602.

DOI: 10.1021/acs.jafc.5b00291
J. Agric. Food Chem. 2015, 63, 2750−2759

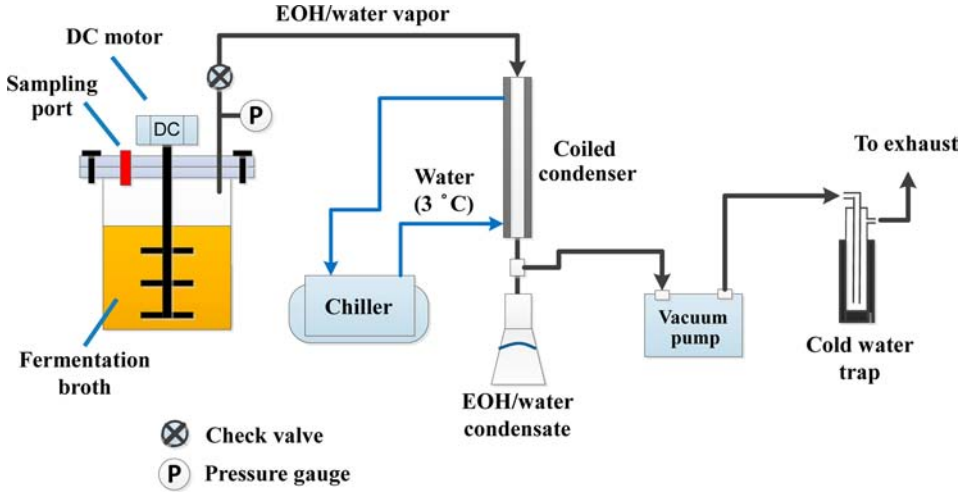

Figure 1. Experimental setup for the food waste fermentation with the vacuum stripping system. The arrows in the figure show flow direction. The vacuum fermentation system consisted of a 3 L water-jacked fermenter, a vacuum pump, a condensation system with a chiller and a coiled condenser, and a cold water trap. During the vacuum application, ethanol and water vapors evaporated from the fermentation broth and condensed in the condensation system. The escaped (uncondensed) ethanol and water vapors were collected in the cold-water trap.

following condensation system with cooling or chilling water. In the vacuum fermentation system, a low ethanol concentration can be maintained in the fermenter during fermentation, thereby eliminating or minimizing yeast ethanol inhibition.[23,27]

The objective of this study was to produce ethanol from food waste at high solids content with vacuum recovery technology. Fermentation of food waste at high solids content results in a very viscous mash and a high glucose concentration (which also inhibits yeast). To overcome this problem, granular starch hydrolyzing enzyme (GSHE) was used to directly digest raw starch in food waste at low temperatures (<48 °C) during simultaneous saccharification and fermentation. GSHE decreases the viscosity of the fermentation broth and reduces the yeast glucose inhibition by gradually breaking down starch to glucose during fermentation.[23,28]

MATERIALS AND METHODS

Design and Characterization of the Vacuum Recovery Process. The vacuum fermentation system was modified on the basis of the system reported by Shihadeh et al.[23] (Figure 1). It consisted of a 3 L jacketed fermenter (Biostat MD, Sartorius BBI Systems, Edgewood, NY), which was sealed and modified for accommodating thermocouples and venting and sampling ports. Slurry (fermentation mixture) was agitated by paddle-type blades driven by an alternating current (AC)/direct current (DC) motor drive (KD P/N 3402-008, Hurst, Princeton, NJ). The vacuum recovery system was connected to the fermenter venting port through a check valve (Figure 1). The evaporated ethanol and water vapor was condensed by passing through a coiled condenser (5977-19, Ace Glass, Vineland, NJ), which was circulated with chilled water at 3 °C from a refrigerated water bath (PolyScience 9106, Cole-Parmer, Vernon Hills, IL). The condensate was collected in a 250 mL conical flask. Vacuum was generated with a dry vacuum pump at 6.7 kPa (28 in Hg gauge) (DryFast model 2044, Welch, Niles, IL). Vacuum pressure was monitored at the fermentation vessel with a pressure gauge (45W1000, Ashcroft, Straford, CT). Vacuum outlet was connected to a cold-water trap (LG-11025, Wilmad Lab Glass, Buena, NJ) chilled with iced water, to collect the escaping ethanol vapors.

To evaluate the vacuum process for ethanol recovery from a dilute solution, the vacuum recovery experiment was conducted at 32 °C using a model ethanol solution in the fermenter. The initial ethanol concentrations in the model solution were 40, 80, and 160 g/L, respectively. Vacuum pressure at 6.7 kPa (28 in Hg gauge) was applied to the ethanol model solution for 1 h, during which the model solution boiled and the vapors were condensed in a 250 mL conical flask. At the completion of each vacuum application, the remaining solution in the fermenter, the condensate in the conical flask, and the solution in the cold water trap were collected and analyzed for volumes and ethanol concentrations.

Experimental Materials and Reagents. The food waste was obtained from a local retail store in Urbana, IL, and mainly contained mashed potatoes, sweet corn, and white bread and was used as a model food waste. The moisture content of the food waste was 64.0%. The composition of the food waste (dry matter basis) was 63.5% starch, 4.3% glucose, 13.9% protein, 4.1% oil, 5.2% neutral detergent fiber, and 3.4% ash. The procedures of the composition measurements are provided in Analytical Procedures and Calculations. The high starch content in the food waste sample was very similar to the sample reported in the previous study.[29] Received food waste was pulverized and mixed using a fruit/vegetable mixer for 3 min, analyzed for moisture content, and stored at 4 °C for the following experiments. For the fermentation slurry preparation, 10 N sulfuric acid (Ricca Chemical, Arlington, TX), solid urea (Fisher Scientific, Waltham, MA), and active dry yeast (Ethanol Red, Fermentis, Lesaffre Yeast, Milwaukee, WI) were used. Enzymes used in the fermentation processes were GHSE (Stargen 002) and protease (GC 212) obtained from Dupont Industrial Biosciences (Palo Alto, CA). Stargen 002 contained *Aspergillus kawachi* α-amylase expressed in *Trichoderma reesei* and a glucoamylase from *Trichoderma reesei* that work synergistically to hydrolyze granular starch substrate to glucose, and it had an activity of ≥570 GSHU/g (where GSHU = granular starch hydrolyzing units). Protease enzyme, GC 212, was obtained by fermentation of a selected strain of *Aspergillus niger* and was able to hydrolyze peptide bonds along a protein chain. It had an activity of 2000 SAPU/g (where SAPU = spectrophotometer acid protease units).

Conventional Fermentation in a Batch Reactor. Fermentation slurry at 35% solid contents (w/w) was prepared by mixing 500 g of dry weight of mixed food waste with a calculated amount of deionized water. The fermentation slurry was then adjusted to pH 4.0 using 10 N sulfuric acid. Experiments were performed in a 3 L fermenter. The slurry was added with 3 mL of GSHE enzyme (Stargen 002), 0.2 mL of protease enzyme (GC 212), 2 mL of urea solution (50%, w/v), and 2 mL of prepared yeast culture. Yeast culture was prepared by dispersing 5 g of active dry yeast and 25 g of deionized water and agitated at 90 rpm at 32 °C for 20 min in an incubator shaker (C24 incubator shaker, New Brunswick, NJ). Fermentation was conducted for 72 h at 32 °C with continuous agitation at 30 rpm. The enzymatic

DOI: 10.1021/jf5054029
J. Agric. Food Chem. 2015, 63, 2760−2766

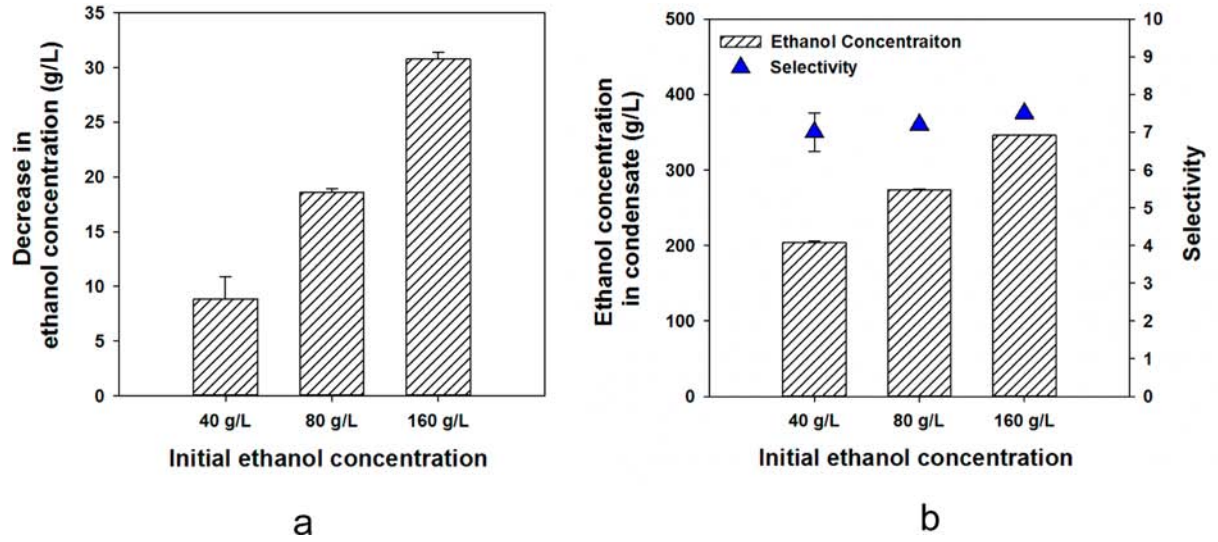

Figure 2. (a) Decrease in ethanol concentrations in the fermenter and (b) ethanol concentrations in the condensate and the vacuum selectivity after 1 h, with vacuum application of the model solution at different initial concentrations.

hydrolysis gradually reduced the slurry viscosity, thus causing an increase in revolutions per minute (rpm) of the agitator higher than 30. Therefore, the agitation rate was checked and manually reset to 30 rpm after each sampling. Fermentation was monitored by taking 1 mL of slurry sample at 4, 8, 12, 24, 36, 48, and 72 h and measuring sugars, ethanol, glycerol, and acid concentrations using high-performance liquid chromatography (HPLC) with at least two determinations. Fermentation was conducted in triplicates.

Vacuum Fermentation. The slurry used for the vacuum fermentation was the same as that used for the conventional fermentation experiments. The developed vacuum recovery system was used (Figure 1). The fermentation was allowed to proceed for 24 h, during which the ethanol concentration approached around 100 g/L and was followed by ethanol recovery by the vacuum stripping (6.7 ± 0.2 kPa), during which broth in the bioreactor boiled at the fermentation temperature, generating ethanol and water vapors. Ethanol and water vapors were then condensed in the coiled condenser at 3 °C and collected in the conical flask. The outlet from the vacuum pump was connected to the cold-water trap, to collect the uncondensed ethanol vapors. Foaming, caused by CO_2 bubbling during the initial vacuum application, was controlled by increasing the agitation rate to 60 rpm and gradually increasing vacuum to the set point. At the completion of each vacuum application, vacuum was stopped and filtered air (filter = 0.2 μm) was introduced gradually to the system until pressure equilibrated to atmosphere. Samples were taken before and after each vacuum application to monitor the immediate effect of vacuum stripping on the ethanol concentration in the fermentation broth. Also, the condensate in the conical flask and the solution in the cold-water trap were collected and analyzed for volumes and ethanol concentrations, to calculate the ethanol yield at each time period. Fermentation was conducted in triplicates.

Analytical Procedures and Calculations. The moisture content of the food waste was determined by drying samples in a forced-draft oven at 135 °C for 2 h.[30] The glucose and starch concentrations in the food waste was measured by the modified dilute acid method.[31] The crude protein, oil, and ash concentrations in the food waste were determined according the AOCS Official and Tentative Methods Ba 4e-93, Am 5-04, and Ba 5a-49, respectively. The neutral detergent fiber concentration in the food waste was determined using the ANKOM$^{200/220}$ fiber analyzer (ANKOM Technology, Macedon, NY).[32] Fermentation samples were analyzed with HPLC (column, Aminex HPX-87H organic acid, Bio-Rad, Hercules, CA; system, Breeze, Waters Corporation, Milford, MA) for glucose, ethanol, glycerol, and acetic acid concentrations. Broth samples were centrifuged for 3 min at 11000*g* (model 5425, Eppendorf, Westbury, NY). Supernatants were filtered through a 0.2 μm filter into a 0.2 mL HPLC vial insert. Ethanol productivity or ethanol production rate was calculated as the produced ethanol (g/L in broth) divided by the fermentation time period. The ethanol yield was defined as total grams of ethanol produced per kilograms of dry food waste.[11,12,33] Ethanol conversion efficiency was calculated by the ratio of actual ethanol yield over theoretical ethanol yield, which was based on the starch and sugar contents in the food waste.[34] Because both ethanol and water in the fermentation broth evaporated during the vacuum application, ethanol selectivity was calculated to measure the preferential removal of ethanol over other components (water in this case). The ethanol selectivity was calculated as

$$\alpha = \frac{y/(1-y)}{x/(1-x)}$$

where x and y are weight fractions of ethanol in fermentation broth and condensate, respectively.

RESULTS AND DISCUSSION

Characterization of Vacuum Technology for Ethanol Recovery. To study the ethanol recovery characteristics under the vacuum application, ethanol recovery experiments were conducted using model ethanol solution at different initial ethanol concentrations (40, 80, and 160 g/L), which covered the possible ethanol concentration range in the food waste fermentation. After 1 h of vacuum application, the ethanol concentration in the model solution decreased by 9−31 g/L, depending upon the initial ethanol concentrations in the model solution. As the initial ethanol concentration in the fermenter increased from 40 to 160 g/L, a greater decrease in the ethanol concentration was observed after the vacuum stripping (Figure 2a). This trend agrees well with the previous studies,[35] which used vacuum technology to remove butanol during fermentation. For a successful application of vacuum stripping to ethanol recovery, the ethanol removal rate should be greater than the ethanol production rate by fermentation, to avoid the ethanol accumulation in the fermentation broth. The ethanol removal rates (9−31 g L^{-1} h^{-1}) in this study were higher than the ethanol production rates (<5 g L^{-1} h^{-1}), as shown in Figure 4. Therefore, the developed vacuum recovery system could be applied to maintain ethanol concentrations in broth at low levels and reduce yeast ethanol inhibition.

DOI: 10.1021/jf5054029
J. Agric. Food Chem. 2015, 63, 2760−2766

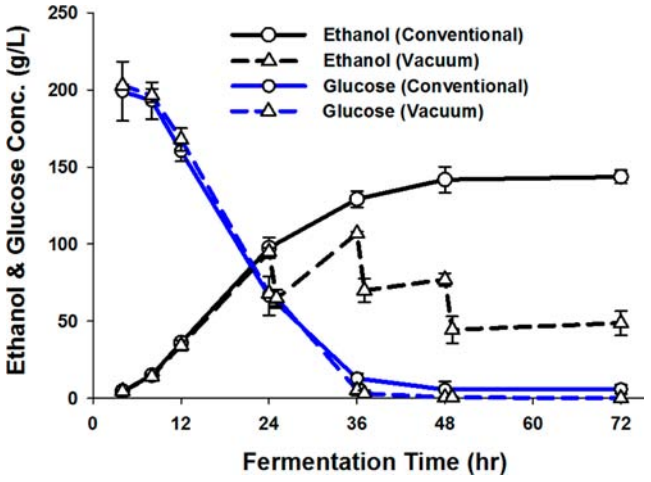

Figure 3. Ethanol and glucose concentrations during SLSF in both conventional and vacuum fermentations.

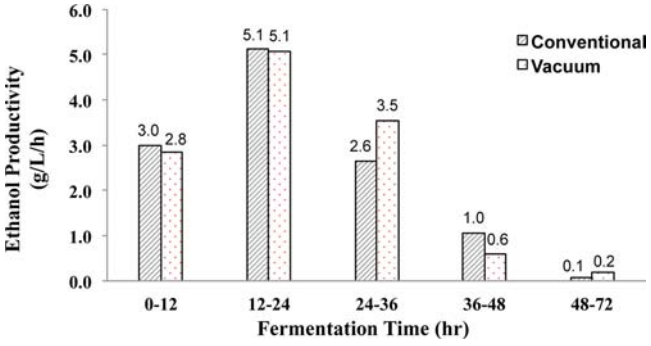

Figure 4. Ethanol productivity in the conventional and vacuum fermentation.

The ethanol concentration in the condensate was found to be much higher than that in the model solution in the fermenter (Figure 2b). The ethanol concentrations in the condensates were 204, 274, and 346 g/L, when the initial ethanol concentrations in the fermenter were 40, 80, and 160 g/L, respectively. This indicates that the vacuum recovery system not only removes ethanol from the fermentation broth but also concentrates it. Selectivity is a variable commonly used to evaluate the ability of a product recovery technology to separate a target product (ethanol in this case) from a mixture. Figure 2b shows that the initial ethanol concentrations in the model solution did not have large effects on the ethanol selectivity. The selectivity was found to be close to 7 for the model solution with all three ethanol concentrations.

Conventional Ethanol Fermentation. The conventional fermentation without vacuum application was conducted in a batch mode. Figure 3 shows the ethanol and glucose concentrations during 72 h of fermentation. The glucose concentration was 199 g/L at 4 h and decreased rapidly during the fermentation process. The ethanol concentration increased to 144 g/L at the end of the fermentation. The residual glucose concentration was 5.7 g/L at 72 h (Table 1), indicating an incomplete fermentation in the batch fermenter. The major reason for fermentation cessation before the exhaustion of glucose was probably due to the high ethanol concentration, which can inhibit yeast.[23,26] Nevertheless, the final ethanol concentration of the batch fermentation was higher than that from the previous studies (Table 2), where the final ethanol concentrations in the broth were between 9 and 82 g/L. The high ethanol concentrations obtained in this study were mainly attributed to the high solids content slurry used for the fermentation and the high starch concentration in the food waste. Higher ethanol concentrations in the fermentation broth can decrease the distillation energy costs, thereby reducing the related capital and operation costs for the conversion of food waste to ethanol.

Table 1. Comparison of Ethanol Fermentation of Food Waste with and without Vacuum Stripping

	residual glucose (g/L)	ethanol yield (g/kg of food waste)	conversion efficiency (%)
conventional fermentation	5.7 ± 2.0	326.5 ± 5.4	85.4 ± 1.4
vacuum fermentation	0.0 ± 0.0	357.5 ± 13.0	93.6 ± 3.4

Table 2. Production of Ethanol from Food Wastes from Different Sources

source of food waste	solid content for fermentation	final ethanol concentration (g/L)	reference
cafeteria	12.1% (w/w)	29.1	15
cafeteria	16.3−19.0% (w/v)	45.0	22
cafeteria	12.9% (w/w)	8.9−55.7	39
dinning room	<20.5% (w/w)	75.9−81.5	29
household	35 and 45% (w/v)	34.9 and 42.8	11
retail store	35% (w/w)	144	this study

Ethanol Fermentation with Vacuum Stripping. To assess the performance of simultaneous ethanol fermentation and recovery by vacuum stripping, the vacuum recovery system for the food waste fermentation was applied. During the 72 h fermentation, vacuum stripping was applied for 1 h at 24, 36, and 48 h, respectively. Figure 3 shows the ethanol and glucose concentrations during fermentation. In the first 24 h, the ethanol concentration increased rapidly to 95 g/L because of sufficient glucose in the fermentation broth. After 1 h of vacuum application, the ethanol concentration decreased to 64 g/L, because of the evaporation of ethanol under the vacuum condition. The ethanol concentration in the fermentation broth decreased by 31, 37, and 33 g/L, when vacuum stripping was applied for 1 h at 24, 36, and 48 h, respectively. Overall, the vacuum stripping successfully removed ethanol and controlled ethanol concentrations below 100 g/L in the fermentation broth, thus reducing yeast ethanol inhibition.

The glucose concentration was 203 g/L in the fermentation broth at 4 h and decreased rapidly to a negligible amount at 36 h (Figure 5). At the end of fermentation (72 h), there was no residual glucose left (Table 1), indicating a complete fermentation in this study. This was mainly due to the reduced ethanol inhibition by controlling the ethanol concentrations at low levels in the broth with the vacuum application. To note, even at 0 g/L glucose concentration, the ethanol concentration was shown to increase slightly between 48 and 72 h. This may be due to glucose being slowly released during the simultaneous liquefaction, saccharification, and fermentation (SLSF) with GSHE enzyme, and yeast used glucose faster than it was released by hydrolysis of the food waste. This phenomenon was also reported in the previous studies when corn or wheat straw was used as the substrate for the simultaneous saccharification and fermentation to produce ethanol or butanol.[23,28,36]

DOI: 10.1021/jf5054029
J. Agric. Food Chem. 2015, 63, 2760−2766

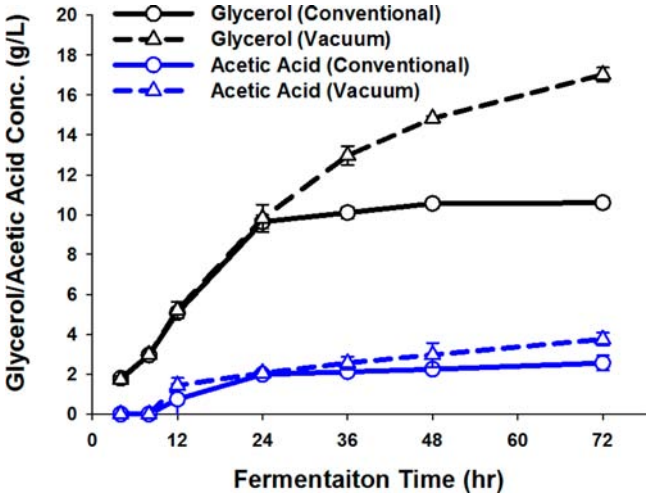

Figure 5. Byproduct (glycerol and acetic acid) concentrations during 72 h of fermentation of the food waste.

Comparison between Ethanol Fermentation with and without Vacuum Stripping. The residual glucose concentration, ethanol yield, and conversion efficiency for both the conventional and vacuum fermentations are presented in Table 1. The ethanol yield for the conventional fermentation was found to be 327 g/kg of food waste (dry matter), while the ethanol yield for the vacuum fermentation was 9% higher at 358 g/kg of food waste. This finding was in agreement with the residual glucose concentrations and the conversion efficiency in Table 1. As discussed above, the residual glucose was zero in the vacuum fermentation but was 5.7 g/L in the conventional fermentation because of yeast ethanol inhibition, which lowered the ethanol yield. The ethanol conversion efficiency for the vacuum fermentation was 93.6%, higher than that for the conventional fermentation efficiency at 85.4%, showing the advantages of applying the vacuum recovery system to the fermentation process. Considering that some sugar was used for yeast growth and that there were other metabolites produced (glycerol, succinic and acetic acids, etc.),[37] the ethanol conversion by vacuum application at 93.6% was quite satisfactory. Overall, the vacuum fermentation showed some advantages over the conventional fermentation for food waste, in terms of the ethanol yield and conversion efficiency.

For the vacuum recovery system, the fermentation design is more complex compared to the conventional fermentation. The energy consumption for vacuum pumps and chilling required for condensation of evaporated ethanol may be high. However, the increase in the ethanol yield and productivity could potentially offset the increased cost of energy for vacuum pumps and chilling. For example, a 9% increase in the ethanol yield in a 50 million gallon capacity ethanol plant (typical size in the U.S.) means an additional 4.5 million gallons of ethanol, which can generate multimillion dollars for the plant. A detailed techno-economic evaluation of vacuum recovery fermentation is warranted to determine its economic viability.

Ethanol productivity for both the conventional and vacuum fermentations at different time periods are shown in Figure 4. The ethanol productivities at 0−12 and 12−24 h time periods were very close between the conventional and vacuum fermentation, because the vacuum stripping was not applied until 24 h. During the time period from 24 to 36 h, the ethanol productivity for the vacuum fermentation (3.5 g L^{-1} h^{-1}) was higher than that for the conventional fermentation (2.6 g L^{-1} h^{-1}), which again was because of the relieved ethanol inhibition by applying the vacuum stripping. During the time period from 36 to 48 h, the ethanol productivity for the vacuum fermentation was 0.6 g L^{-1} h^{-1}, while the ethanol productivity for the conventional fermentation was higher at 1.0 g L^{-1} h^{-1}. This was probably due to the higher amount of glucose left in the conventional fermentation during this time period (Figures 2 and 3). Matsakas et al.[11] summarized various studies on food waste fermentations and showed that the ethanol productivities were between 0.49 and 4.11 g L^{-1} h^{-1}, which was very close to the values showed in Figure 4 in this study.

Glycerol is a byproduct of yeast metabolism, and its production amount was less than ethanol and carbon dioxide during yeast ethanol fermentation. A higher amount of glycerol production usually indicates increased yeast stress.[37] In this study, the glycerol concentrations in the fermentation broth were higher during the vacuum fermentation (17 g/L) than the conventional fermentation (10 g/L) (Figure 5). It was because the removal of ethanol and water from the fermentation broth by vacuum stripping concentrated the glycerol in fermentation broth. A higher glycerol concentration could inhibit yeast metabolism; however, a review of the literature shows that the glycerol inhibition is not significant until it reached 100 g/L.[38] Therefore, the accumulated glycerol by the vacuum recovery system was not a factor in our study. Again, because of the concentration effect, the organic acid (acetic acid) concentrations were higher during the vacuum fermentation than the conventional fermentation (Figure 5). It is noteworthy that no glycerol or acetic acid was found in the condensate.

In conclusion, food waste at high solids content (35%, w/w) was used to produce ethanol with and without the vacuum recovery technology. After 72 h of fermentation, the ethanol concentration in the fermentation broth was 144 g/L for the conventional fermentation. The residual glucose concentration at 72 h was 5.7 g/L, indicating an incomplete fermentation. The conventional fermentation produced 327 g of ethanol from each kilogram of food waste. The vacuum fermentation process integrated with product recovery successfully controlled the ethanol concentration in the fermentation broth below 100 g/L, thereby reducing yeast ethanol inhibition. The vacuum fermentation allowed for complete utilization of glucose in the fermentation broth and produced 358 g of ethanol from each kilogram of food waste. The ethanol conversion efficiency for the vacuum fermentation was 93.6%, higher than that for the conventional fermentation at 85.4%.

AUTHOR INFORMATION

Corresponding Author

*Telephone: 217-333-9510. Fax: 217-244-0323. E-mail: vsingh@illinois.edu.

Notes

The authors declare no competing financial interest.

ACKNOWLEDGMENTS

The authors thank Zhaoqin Wang in the Department of Agricultural and Biological Engineering at the University of Illinois at Urbana−Champaign (Urbana, IL) for her assistance on the preliminary tests of food waste fermentation. Mention of trade names or commercial products in this paper is solely for the purpose of providing scientific information and does not

DOI: 10.1021/jf5054029
J. Agric. Food Chem. 2015, 63, 2760−2766

imply recommendation or endorsement by the USDA. The USDA is an equal opportunity provider and employer.

ABBREVIATIONS USED

GSHE, granular starch hydrolyzing enzyme; SLSF, simultaneous liquefaction, saccharification, and fermentation

REFERENCES

(1) United States Department of Agriculture (USDA). *Bioenergy Statistics*; USDA: Washington, D.C., 2013; www.ers.usda.gov/data-products/us-bioenergy-statitics.aspx#.VCK0tNdFOXd (accessed Sept 22, 2014).

(2) Walker, K.; Vadlani, P.; Madl, R.; Ugorowski, P.; Hohn, K. L. Ethanol fermentation from food processing waste. *Environ. Prog. Sustainable Energy* **2013**, *32*, 1280−1283.

(3) McAloon, A.; Taylor, F.; Yee, W.; Ibsen, K.; Wooley, R. *Determining the Cost of Producing Ethanol from Corn Starch and Lignocellulosic Feedstocks*; National Renewable Energy Laboratory (NREL): Golden, CO, 2000; NREL/TP-580-28893, http://www.nrel.gov/docs/fy01osti/28893.pdf (accessed Sept 22, 2014).

(4) Kwiatkowski, J. R.; McAloon, A. J.; Taylor, F.; Johnston, D. B. Modeling the process and costs of fuel ethanol production by the corn dry-grind process. *Ind. Crops Prod.* **2006**, *23*, 288−296.

(5) Quintero, J.; Montoya, M.; Sánchez, O.; Giraldo, O.; Cardona, C. Fuel ethanol production from sugarcane and corn: Comparative analysis for a Colombian case. *Energy* **2008**, *33*, 385−399.

(6) Lau, M. W.; Dale, B. E. Cellulosic ethanol production from AFEX-treated corn stover using *Saccharomyces cerevisiae* 424A (LNH-ST). *Proc. Natl. Acad. Sci. U. S. A.* **2009**, *106*, 1368−1373.

(7) Kazi, F. K.; Fortman, J. A.; Anex, R. P.; Hsu, D. D.; Aden, A.; Dutta, A.; Kothandaraman, G. Techno-economic comparison of process technologies for biochemical ethanol production from corn stover. *Fuel* **2010**, *89*, S20−S28.

(8) Saha, B. C.; Iten, L. B.; Cotta, M. A.; Wu, Y. V. Dilute acid pretreatment, enzymatic saccharification and fermentation of wheat straw to ethanol. *Process Biochem.* **2005**, *40*, 3693−3700.

(9) Martín, C.; Galbe, M.; Wahlbom, C. F.; Hahn-Hägerdal, B.; Jönsson, L. J. Ethanol production from enzymatic hydrolysates of sugarcane bagasse using recombinant xylose-utilising *Saccharomyces cerevisiae*. *Enzyme Microb. Technol.* **2002**, *31*, 274−282.

(10) Binod, P.; Sindhu, R.; Singhania, R. R.; Vikram, S.; Devi, L.; Nagalakshmi, S.; Kurien, N.; Sukumaran, R. K.; Pandey, A. Bioethanol production from rice straw: An overview. *Bioresour. Technol.* **2010**, *101*, 4767−4774.

(11) Matsakas, L.; Kekos, D.; Loizidou, M.; Christakopoulos, P. Utilization of household food waste for the production of ethanol at high dry material content. *Biotechnol. Biofuels* **2014**, *7*, 1−9.

(12) Humbird, D.; Davis, R.; Tao, L.; Kinchin, C.; Hsu, D.; Aden, A.; Schoen, P.; Lukas, J.; Olthof, B.; Worley, M. *Process Design and Economics for Biochemical Conversion of Lignocellulosic Biomass to Ethanol*; National Renewable Energy Laboratory (NREL): Golden, CO, 2011; NREL/TP-5100-47764, http://www.nrel.gov/docs/fy11osti/47764.pdf (accessed Sept 22, 2014).

(13) Yan, S.; Chen, X.; Wu, J.; Wang, P. Ethanol production from concentrated food waste hydrolysates with yeast cells immobilized on corn stalk. *Appl. Microbiol. Biotechnol.* **2012**, *94*, 829−838.

(14) United States Environmental Protection Agency (U.S. EPA). *Food Waste Basics*; U.S. EPA: Washington, D.C., 2014; www.epa.gov/foodrecovery/ (accessed Sept 22, 2014).

(15) Moon, H. C.; Song, I. S.; Kim, J. C.; Shirai, Y.; Lee, D. H.; Kim, J. K.; Chung, S. O.; Kim, D. H.; Oh, K. K.; Cho, Y. S. Enzymatic hydrolysis of food waste and ethanol fermentation. *Int. J. Energy Res.* **2009**, *33*, 164−172.

(16) Lin, C. S. K.; Pfaltzgraff, L. A.; Herrero-Davila, L.; Mubofu, E. B.; Abderrahim, S.; Clark, J. H.; Koutinas, A. A.; Kopsahelis, N.; Stamatelatou, K.; Dickson, F. Food waste as a valuable resource for the production of chemicals, materials and fuels. Current situation and global perspective. *Energy Environ. Sci.* **2013**, *6*, 426−464.

(17) Uncu, O. N.; Cekmecelioglu, D. Cost-effective approach to ethanol production and optimization by response surface methodology. *Waste Manage.* **2011**, *31*, 636−643.

(18) Kim, J. K.; Oh, B. R.; Chun, Y. N.; Kim, S. W. Effects of temperature and hydraulic retention time on anaerobic digestion of food waste. *J. Biosci. Bioeng.* **2006**, *102*, 328−332.

(19) Lee, D.-Y.; Ebie, Y.; Xu, K.-Q.; Li, Y.-Y.; Inamori, Y. Continuous H_2 and CH_4 production from high-solid food waste in the two-stage thermophilic fermentation process with the recirculation of digester sludge. *Bioresour. Technol.* **2010**, *101*, S42−S47.

(20) Ma, J.; Duong, T. H.; Smits, M.; Verstraete, W.; Carballa, M. Enhanced biomethanation of kitchen waste by different pre-treatments. *Bioresour. Technol.* **2011**, *102*, 592−599.

(21) Nakamura, Y.; Sawada, T. Ethanol production from artificial domestic household waste solubilized by steam explosion. *Biotechnol. Bioprocess Eng.* **2003**, *8*, 205−209.

(22) Kim, J. H.; Lee, J. C.; Pak, D. Feasibility of producing ethanol from food waste. *Waste Manage.* **2011**, *31*, 2121−2125.

(23) Shihadeh, J. K.; Huang, H.; Rausch, K. D.; Tumbleson, M. E.; Singh, V. Design of a vacuum flashing system for high-solids fermentation of corn. *Trans. ASABE* **2013**, *56*, 1441−1447.

(24) Wang, S.; Ingledew, W.; Thomas, K.; Sosulski, K.; Sosulski, F. Optimization of fermentation temperature and mash specific gravity for fuel alcohol production. *Cereal Chem.* **1999**, *76*, 82−86.

(25) da Silva, F. L. H.; Rodrigues, M. I.; Maugeri, F. Dynamic modelling, simulation and optimization of an extractive continuous alcoholic fermentation process. *J. Chem. Technol. Biotechnol.* **1999**, *74*, 176−182.

(26) Shihadeh, J. K.; Huang, H.; Rausch, K. D.; Tumbleson, M. E.; Singh, V. Vacuum stripping of ethanol during high solids fermentation of corn. *Appl. Biochem. Biotechnol.* **2014**, *173*, 486−500.

(27) Mariano, A. P.; Qureshi, N.; Ezeji, T. C. Bioproduction of butanol in bioreactors: New insights from simultaneous in situ butanol recovery to eliminate product toxicity. *Biotechnol. Bioeng.* **2011**, *108*, 1757−1765.

(28) Wang, P.; Singh, V.; Xue, H.; Johnston, D. B.; Rausch, K. D.; Tumbleson, M. Comparison of raw starch hydrolyzing enzyme with conventional liquefaction and saccharification enzymes in dry-grind corn processing. *Cereal Chem.* **2007**, *84*, 10−14.

(29) Yan, S.; Li, J.; Chen, X.; Wu, J.; Wang, P.; Ye, J.; Yao, J. Enzymatical hydrolysis of food waste and ethanol production from the hydrolysate. *Renewable Energy* **2011**, *36*, 1259−1265.

(30) AACC International. Methods 44-19. *Approved Methods of the American Association of Cereal Chemists*, 10th ed.; AACC International: St. Paul, MN, 2000.

(31) Vidal, B. C.; Rausch, K. D.; Tumbleson, M. E.; Singh, V. Determining corn germ and pericarp residual starch by acid hydrolysis. *Cereal Chem.* **2009**, *86*, 133−135.

(32) John Morris Scientific. *Neutral Detergent Fiber in Feeds—Filter Bag Technique*; John Morris Scientific: Sydney, New South Wales, Australia, 2003; http://www.johnmorris.com.au/files/product/attachments/4469/68518_opt2.pdf (accessed Oct 2014).

(33) Dien, B. S.; Sarath, G.; Pedersen, J. F.; Sattler, S. E.; Chen, H.; Funnell-Harris, D. L.; Nichols, N. N.; Cotta, M. A. Improved sugar conversion and ethanol yield for forage sorghum (*Sorghum bicolor* L. Moench) lines with reduced lignin contents. *BioEnergy Res.* **2009**, *2*, 153−164.

(34) Huang, H.; Liu, W.; Singh, V.; Danao, M. C.; Eckhoff, S. R. Effect of corn maturity on dry-grind fermentation characteristics and DDGS composition. *Cereal Chem.* **2012**, *89*, 217−221.

(35) Mariano, A. P.; Qureshi, N.; Filho, R. M.; Ezeji, T. C. Assessment of in situ butanol recovery by vacuum during acetone butanol ethanol (ABE) fermentation. *J. Chem. Technol. Biotechnol.* **2012**, *87*, 334−340.

(36) Qureshi, N.; Saha, B. C.; Hector, R. E.; Hughes, S.; Cotta, M. A. Butanol production from wheat straw by simultaneous saccharification and fermentation using *Clostridium beijerinckii*: Part 1—Batch fermentation. *Biomass Bioenergy* **2008**, *32*, 168−175.

DOI: 10.1021/jf5054029
J. Agric. Food Chem. 2015, 63, 2760−2766

(37) Russell, I. Understand yeast fundamentals. In *Alcohol Textbook: A Reference for the Beverage, Fuel and Industrial Alcohol Industries*, 4th ed.; Jacques, K. A., Lyons, T. P., Kelsall, D. R., Eds.; Nottingham University Press: Nottingham, U.K., 2003; Vol. 9, pp 85−120.
(38) Maiorella, B.; Blanch, H. W.; Wilke, C. R. By-product inhibition effects on ethanolic fermentation by *Saccharomyces cerevisiae*. *Biotechnol. Bioeng.* **1983**, *25*, 103−121.
(39) Kim, J. K.; Oh, B. R.; Shin, H.-J.; Eom, C.-Y.; Kim, S. W. Statistical optimization of enzymatic saccharification and ethanol fermentation using food waste. *Process Biochem.* **2008**, *43*, 1308−1312.

DOI: 10.1021/jf5054029
J. Agric. Food Chem. 2015, 63, 2760−2766

anticancer activities in triggering apoptosis, activating PKC-delta/caspase-3 proteins, and down-regulating the proto-oncogenes in MCF-7 and HeLa cancer cell lines.[27] It is particularly meaningful that PEs could be an important starting material for the synthesis of a promising anti-AIDS drug, prostratin.[28,29]

Similar to the discovery in a recently published paper,[14] our previous published paper disclosed that the total content level of PEs (equivalent to TPA) using the internal standard method at 280 nm is 20 times over that using the external standard method,[15] because the λ_{max} of UV absorbance of TPA is at 242 nm.[14,15] Hence, the purity of PEs is generally regarded as 100% (equivalent to TPA), which is actually below 5%.[16] In this regard, it is very necessary to acquire high-purity PEs to revaluate their toxicity and bioactivity.

At present, continuous liquid−liquid extraction, silica gel column chromatography, and semipreparative HPLC are the conventional strategies for separation and purification of PEs from *J. curcas* seeds.[13−15,17,26] Considering the rapid growth in the jatropha biodiesel industry, the appropriate utilization of PEs (as a byproduct of *J. curcas* seeds) could contribute to enhancing the economic viability and sustainability of the *J. curcas* production chain. It is necessary to establish an effective and rapid method for separating the PEs with a high recovery rate. In this work, PEs were successfully isolated and purified from *J. curcas* seeds by high-speed countercurrent chromatography (HSCCC). In addition, a combined HSCCC and semipreparative HPLC method was established to purify JC1. Furthermore, UPLC−PDA and UPLC−MS were also developed and established to analyze characteristics of the isolated JC1 and the PE-rich crude extracts.

MATERIALS AND METHODS

Materials. Methanol and acetonitrile (HPLC grade) were purchased from Swell Scientific Instruments Co., Ltd. (Chengdu, China). Formic acid (HPLC grade) was purchased from the Chengdu Kelong Reagent Co., Ltd. (Chengdu, China). Water (HPLC grade) was prepared using an ultrapure water system (UPA, Chongqing, China). All of the other reagents used in the present study were of analytical grade. TPA (99%, CAS Registry No. 16561-29-8) was obtained from Sigma-Aldrich (Shanghai, China). *J. curcas* seeds were collected from Xichang (Sichuan, China) in 2013 and were identified by Prof. Tang Lin (Sichuan University).

PE-Rich Crude Extract Preparations. A fine powder of dried *J. curcas* seeds (3.10 kg) was extracted by ethyl acetate (20 L) at room temperature two times (each for 24 h). All the filtrates were combined and concentrated under reduced pressure by a rotary evaporator at 45 °C to gain an oily substance (985.2 g), and 200 g of the oily substance was dissolved with methanol (1000 mL). Subsequently, the mixed solution was frozen at 4 °C for 24 h to produce an upper clarification layer of methanol (PE-rich solution) and a precipitate (168.3 g). The upper methanol layer was concentrated under reduced pressure by rotary evaporation at 55 °C to obtain PE-rich crude extract (23.8 g).

HSCCC Separation Apparatus. A TBE-300C HSCCC (Shanghai Tauto Biotech Co., Ltd., Shanghai, China) is coupled with a set of three multilayer coils and a 20 mL sample loop. The solvents were delivered by a TBP 5002 pump (Shanghai Tauto Biotech Co., Ltd., Shanghai, China). A DC-0506 constant-temperature circulating implement (Shanghai Sunny Hengping Scientific Instrument Co., Ltd., Shanghai, China) was used to control the separation temperature. The UV absorbance of eluent was monitored by a UV-2000 detector (Shanghai Sanotac Scientific Instrument Co., Ltd., Shanghai, China) at the wavelength of 280 nm. The data were collected by an Easy Chrom 1000 workstation (Beijing Qingbohua Ltd., Beijing, China). The temperature of the separation column was maintained at 25 °C. A FB-36/7 air compressor pump was used to force out the stationary phase.

Measurement of Partition Coefficient. Similar to previous studies,[30−34] the optimal two-phase solvent systems are evaluated with partition coefficient (K) and separation factor (α) by HPLC methods. K is defined as A_{upper}/A_{lower} of each analyte, in which, A_{upper} and A_{lower} are the HPLC peak areas of objective compounds in the upper and lower phases, respectively. α is defined as the proportion between the partition coefficients of the two components ($\alpha = K_1/K_2$, $K_1 > K_2$). The HPLC analysis was performed on an Agilent 1200 series system with a C18 column (4.6 × 250 mm, 5.0 μm) at 30 °C. The mobile phase was acetonitrile−water (80:20, v/v) at the flow rate of 0.8 mL/min. The detection wavelength was set at 280 nm. Briefly, a series of two-phase solvent systems (*n*-hexane−ethyl acetate−methanol−water = 1:1:1:1, 3:1:3:1, 2:2:3:1, 3:3:3:1, and 1.5:1.5:1.2:0.5, v/v) was screened as follows: approximately 0.1 mL of primary crude extract sample was placed in a 10 mL test tube, to which was added 2 mL of each phase of the equilibrated two-phase solvent system; the tube was rigorously shaken for 1 min and left to stand at room temperature until equilibrium was obtained. Then, 20 μL of the upper and lower phases was analyzed by HPLC at 280 nm, respectively.

Preparation of Two-Phase Solvent System and Sample Solution. The two-phase solvent system was prepared by adding each solvent to a separatory funnel. After shaking and thoroughly equilibrating at room temperature, the upper phase and lower phase were then separated and degassed ultrasonically for 30 min. The upper phase was used as the stationary phase while the lower phase as the mobile phase. The sample solution for HSCCC separation was prepared by dissolving 2 g of PE-rich crude extract in 20 mL of the lower phase.

HSCCC Separation Procedure. The multilayer coil column was first entirely filled with the stationary phase at a flow rate of 30.0 mL/min. The apparatus was rotated at 800 rpm and then the mobile phase was pumped into the column at a flow rate of 10 mL/min in the head-to-tail elution mode. The mobile phase eluting at the tail outlet indicated that hydrodynamic equilibrium had been reached. Subsequently, 20 mL of sample solution was injected into the column. The peak fractions were collected manually according to the elution profile and evaporated under reduced pressure.

Analysis and Characterization of HSCCC Fractions. PE-rich crude extract sample and each peak fraction obtained from HSCCC were analyzed by HPLC−UV using peak area calculation. The HPLC analyses were performed on an Agilent 1200 series system (Agilent Technologies) equipped with a quaternary pump, a vacuum degasser, an autoinjector, and an ultraviolet detector. The HPLC separation was performed on a C18 column (Ultimate, 4.6 × 250 mm, 4.7 μm, Welch Materials, Inc.) at 30 °C. The ultraviolet detector was set at 280 nm according to the λ_{max} of UV absorbance of PEs. All of the samples were eluted at 0.80 mL/min using an isocratic elution of acetonitrile and water containing 0.2% formic acid (80/20, v/v). Agilent Chemstation version B.04.01 was used for the system control and data acquisition.

Purification and Identification of JC1. A continuous repeated semipreparative HPLC method was applied to further purify the JC1. The separation of JC1 was performed on a reversed-phase C8 semipreparative column (Welchrom-C8, 10 × 250 mm, 5 μm) with an isocratic elution of acetonitrile−water (80:20, v/v) at a flow rate of 2.5 mL/min. The monitoring of the wavelength was set at 280 nm. The purity of JC1 was identified by HPLC. MS spectra of JC1 was measured in the positive mode ($[M + Na]^+$) using a microTOF-QII mass spectrometer (Bruker Daltonics).

UPLC−PDA and UPLC−MS Analysis of Isolated JC1 and PE-Rich Crude Extract. UPLC−PDA analyses were performed on an ACQUITY UPLC H-class system (Waters) equipped with a QSM quaternary solvent manager, an FTN autosampler manager, and an eLambda photodiode array detector. The chromatographic separation was performed on an Acquity UPLC BEH C18 column (1.7 μm, 2.1 × 150 mm, Waters) at 40 °C. All of the samples were eluted at 0.40 mL/min using an isocratic elution of solvent A and B (80/20, v/v), in which solvent A was composed of acetonitrile−water (90/10, v/v) containing 0.1% formic acid and 0.05% ammonium formate and solvent B was water containing 0.1% formic acid and 0.05% ammonium formate. The sample injection volume was 2 μL. The

DOI: 10.1021/jf505655b
J. Agric. Food Chem. 2015, 63, 2767−2772

Table 1. Partition Coefficients (K) and Separation Factors (α) of Compounds in Various Solvent Systems

	partition coefficient (K)					separation factor (α)			
ratio[a]	JC1	JC2	JC3	JC4	JC5	K_2/K_1	K_3/K_2	K_4/K_3	K_5/K_4
1:1:1:1	4.19	25.22	27.21	16.72	46.33	6.02	1.07	1.63	2.77
3:1:3:1	0.07	0.09	0.11	0.12	0.13	1.32	1.18	1.16	1.08
2:2:3:1	0.27	0.29	0.34	0.38	0.34	1.09	1.18	1.11	1.12
3:3:3:1	0.61	0.63	0.79	0.88	0.81	1.02	1.25	1.12	1.09
3:3:2:1	1.93	2.27	2.75	3.05	2.82	1.17	1.21	1.11	1.08
1.5:1.5:1.2:0.5	1.03	1.43	1.80	2.84	1.55	1.40	1.26	1.58	1.83

[a]Ratio of the solvent system *n*-hexane−ethyl acetate−methanol−water.

detection range of the ultraviolet detector was set from 200 to 400 nm. Monitoring of the wavelength was set at 280 nm according to the λ_{max} of the UV absorbance of PEs. Empower software version 3.0 was used for the system control and data acquisition.

UPLC−MS analyses were performed on an ACQUITY UPLC I-Class-Xevo TQD System (Waters) interfaced with a Waters Quattro Premier XE triple quadrupole mass spectrometer equipped with electrospray ionization operated in the positive ionization mode. The chromatographic separation condition of the UPLC−MS analyses was the same as for the UPLC−PDA analyses. The source-dependent parameters maintained for the analytes were as follows: cone gas flow, 50 L/h; desolvation gas flow, 500 L/h; capillary voltage, 3.0 kV, source temperature, 120 °C; desolvation temperature, 500 °C. The optimum values for compound-dependent parameters of cone voltage and collision energy were set at 30 V and 10 eV. Detection of the ions was performed in the multiple-reaction monitoring (MRM) mode, by monitoring the transition pairs (precursor to product ion) of m/z for PEs. Mass Lynx software version 4.1 was used to control all parameters of UPLC and MS.

RESULTS AND DISCUSSION

Selection of the Two-Phase Solvent System. Five main peaks (regarded as JC1−JC5 according to their retention times, which appeared orderly in chromatograms) determined by HPLC were used to select the appropriate two-phase solvent system. The results of the partition coefficients (K) and separation factors (α) of these compounds in various two-solvent systems are listed in Table 1. According to the published papers,[30−34] the appropriate two-phase solvent system requires the following considerations: (1) the equilibrating time should be considerably short enough (<30 s); (2) K should be in a suitable range, usually between 0.2 and 5; and (3) α should be greater than 1.5. After repeated attempts, the two-phase solvent system composed of *n*-hexane−ethyl acetate−methanol−water (1.5:1.5:1.2:0.5, v/v) was considered as optimal for its appropriate K and α values.

Isolation of PEs Fractions by HSCCC. The retention of the stationary phase was 56.7%. Fraction peaks A and B were separated in 30 min with a total mobile elution volume of 300 mL (Figure 2A). Isolated fraction peaks A and B were analyzed by HPLC (Figure 2C.c2,c3). In the HSCCC separation, the expected result is five fractions (Figure 2C.c4). It should be noted that the main PE, JC1, can be isolated fast, and the purity increased from 48.5% to 85.0% (Figure 2C.c3,c4). Compared with the literature,[12−15] the conventional isolation methods of PEs, including liquid−liquid extraction and silica gel column chromatography, are time-consuming, require a large amounts of organic solvents, and typically require numerous steps, resulting in lower recovery and higher cost. In this work, the separation of PEs by HSCCC shows an excellent sample recovery, low cost, and high efficiency.

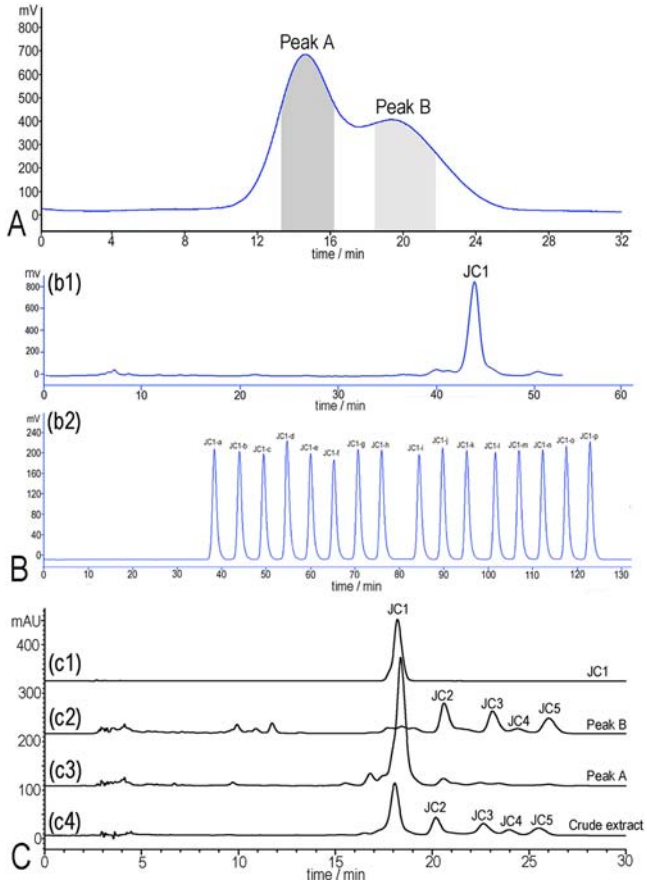

Figure 2. (A) Preparative HSCCC chromatogram of PE-rich crude extract from *J. curcas* seeds. (B) Primary semipreparative HPLC−UV chromatogram of fraction peak A isolated by HSCCC (b1), continuous semipreparative HPLC−UV chromatogram of JC1 using repeating sample injection at an interval of 5 min [the letters a−p (end-label of JC1) represent the continuous repeating sample injection order (b2)]; (C) HPLC−UV chromatograms of JC1 (c1), peak B fraction isolated by HSCCC (c2), peak A fraction isolated by HSCCC (c3), and PEs-rich crude extract (c4).

Purification and Identification of JC1. The semipreparative HPLC chromatogram of peak A is shown in Figure 2B.b1. Subsequently, JC1 was further purified by using continuous semipreparative HPLC through repeating sample injection at an interval of 5 min (Figure 2B.b2). The purity of JC1 measured by HPLC was 99.8% (Figure 2C.c1). The HR−MS spectrum of JC1 is shown in Figure 3C, and the molecular ion peak is 733.3695 m/z ($[M + Na]^+$). According to the papers published over 20 years, JC1 has the highest levels of all the PEs in *J. curcas* seeds.[12−15,17,26] Therefore, it is obvious that the isolated compound in this work is JC1.

DOI: 10.1021/jf505655b
J. Agric. Food Chem. 2015, 63, 2767−2772

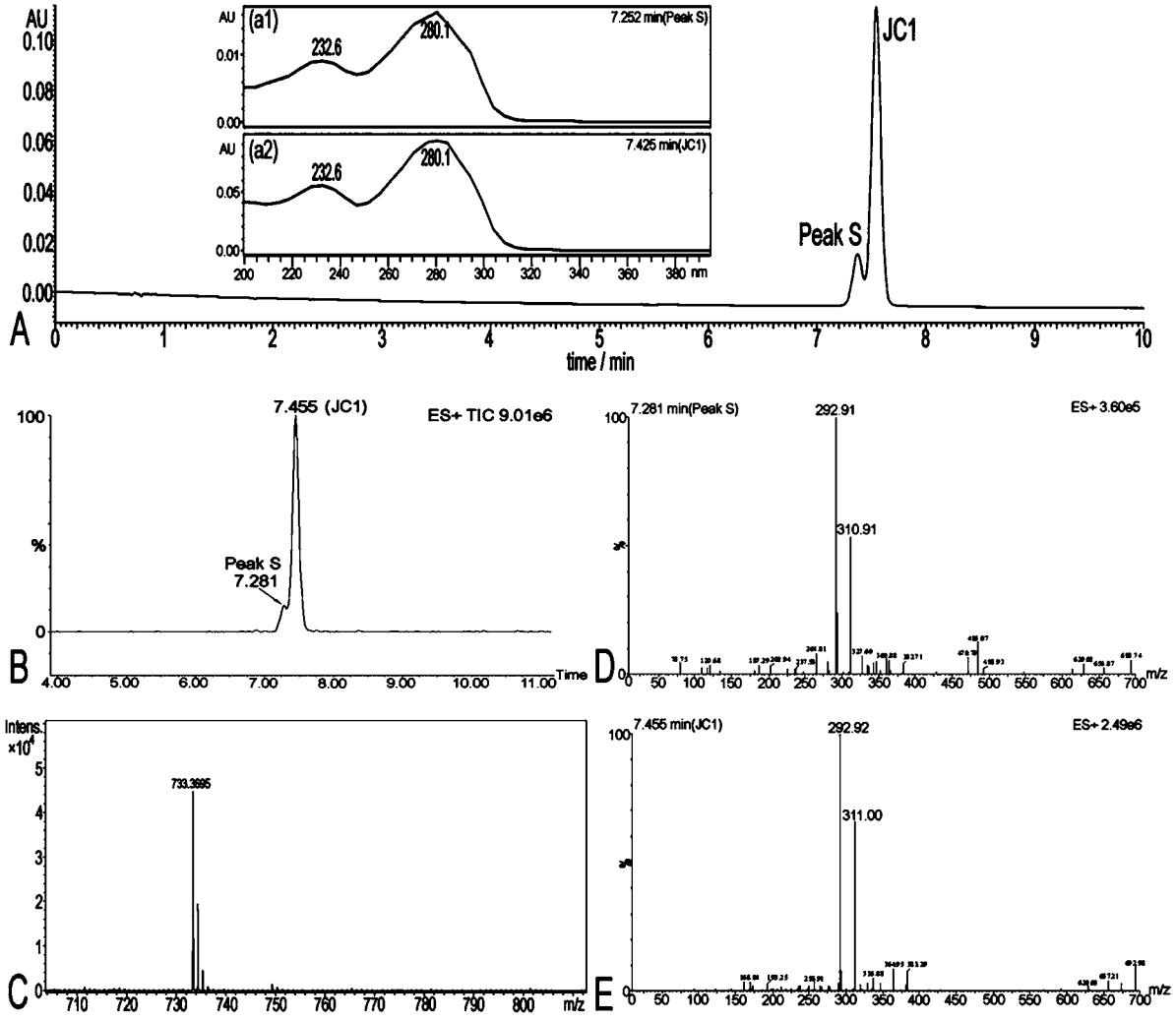

Figure 3. (A) UPLC−UV chromatogram of JC1 and peak S at 280 nm and the UV absorbance spectrogram of peak S (a1) and JC1 (a2). (B) TIC chromatogram of the JC1 and peak S. (C) MS spectrum of the JC1 and peak S. (D) Product ion MS spectrum of peak S. (E) Product ion MS spectrum of JC1.

UPLC−PDA and UPLC−MS Analysis of Isolated JC1 and PE-Rich Crude Extract. It was regrettable that the purity of JC1 was only 87.8% (Figure 3A) by UPLC using the peak area calculation method. It was easily to observe that there is a peak, labeled S, with a UV absorption spectrogram highly similar to that of JC1 (Figure 3A.a1,a2). As we known, the purity of JC1 was usually measured by conventional HPLC using the peak area calculation method in previously published papers.[13−15] The result of UPLC indicated that Peak S (Figure 3A) is difficult to separate from JC1 using conventional HPLC (Figure 2C.c1). Subsequently, UPLC−MS was established and successfully used to identify the characteristics of Peak S. Figure 3B showed the TIC chromatogram of JC1. In the positive ion mass spectra, peak S showed the same quasi-molecular ion peak ($[M + H - H_2O]^+$) at about 693.00 m/z and several similar sequence-specific fragment ions (at about 365.00, 311.00 and 292.90 m/z) as JC1 (Figure 3D,E). The molecular mass of the mother nucleus (12-deoxy-16-hydroxyphorbol, Figure 1) in JC1 is 364.4327, so the fragment ion at about 365.00 m/z was the mother nucleus ion peak ($[M]^+$); moreover, 311.00 and 292.90 m/z were the fragment ions $[M - 3H_2O]^+$ and $[M - 4H_2O]^+$ of the mother nucleus, respectively. Thus, it was easily deduced that peak S is the isomer of JC1.

Furthermore, the sample of JC1 showed only one peak with HPLC but contained another peak (peak S) by UPLC; this cast doubt on the five to seven PE peaks presented by *J. curcas* with the conventional HPLC method.[14−17,35] Thus, it was imperative to establish a high-resolution method to confirm this doubt. In this work, an UPLC−PDA method was developed and applied to analyze the PE-rich crude extract. In our recently published paper, when using a high-resolution C18 column (2.7 μm) instead of the conventional C18 column (4.5 μm), the HPLC−UV chromatogram at 280 nm of PE-rich crude extract showed more than nine peaks, five of which were main ones.[15] The content levels of PEs in *J. curcas* seeds or their related products are always calculated by the total amount equivalent to TPA using an internal standard method.[11,16,35] In this study, TPA was selected as an internal standard to establish the UPLC−PDA method for the PE-rich crude extract. The UPLC−UV chromatograms at 240, 280, and 304 nm of the PE-rich crude extract and TPA are shown in parts A, B, and C of Figure 4, respectively. It was interesting that more than 17 peaks were separated out at 280 nm (Figure 4B). However, similar to previous reports,[14−17] about five to seven peaks were exhibited in the HPLC−UV chromatogram at 280 nm (Figure 2C.c4). It is certified that the λ_{max} of PEs is always at about 280

DOI: 10.1021/jf505655b
J. Agric. Food Chem. 2015, 63, 2767−2772

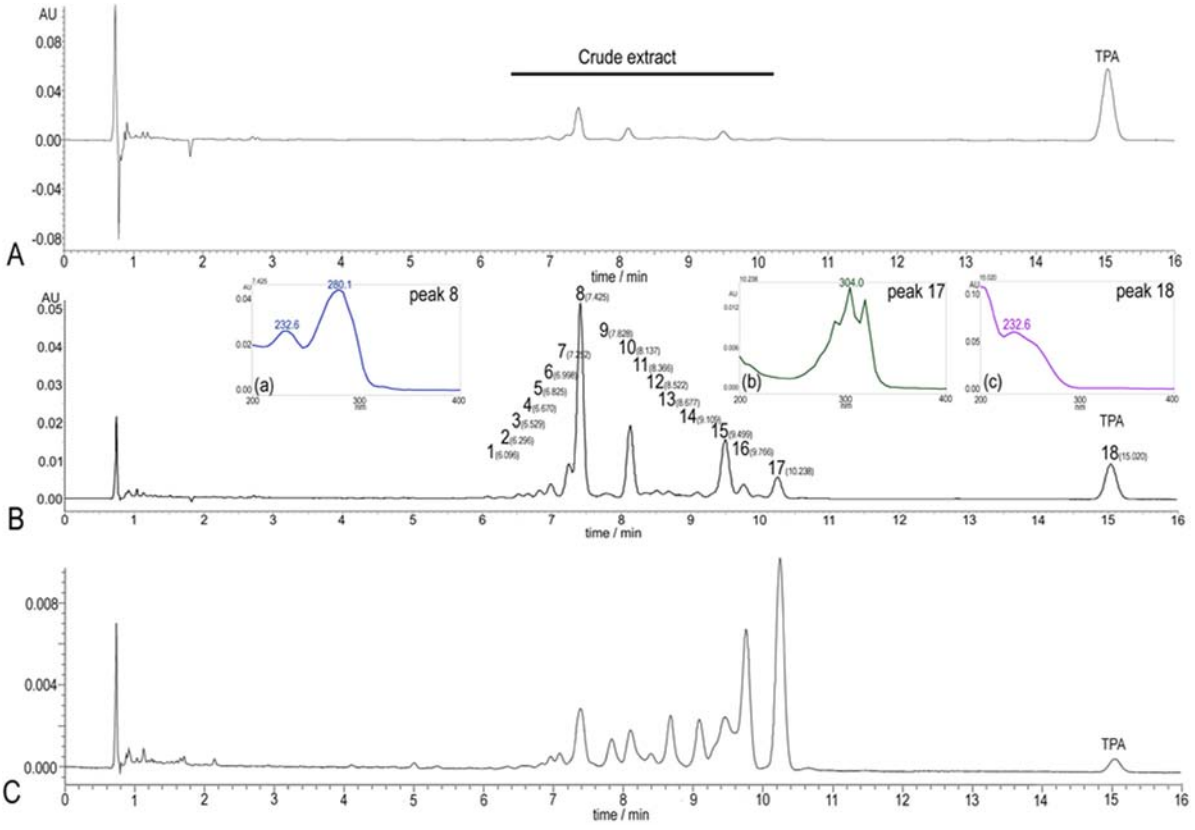

Figure 4. (A) UPLC−UV chromatograms of PE-rich extract and TPA at 240 nm. (B) UPLC−UV chromatograms of PE-rich extract and TPA at 280 nm, UV absorbance spectrogram of peak 8 (a), UV absorbance spectrogram of peak 17 (b), and UV absorbance spectrogram of peak 18 (c). (C) UPLC−UV chromatograms of PE-rich extract and TPA at 304 nm. (TPA is phorbol 12-myristate-13-acetate. "Crude extract" represents the main peaks detected from the PE-rich crude extracts, and 1−18 represent the order in which the peaks were detected during UPLC.)

nm, and the λ_{max} of TPA is at about 242 nm.[14,15] Obviously, the results of the UV absorption spectrogram also demonstrated the λ_{max} of more than 12 peaks was at about 280 nm, including peaks 1−8, 10−12, and 15, all of which were similar to peak 8 (JC1, Figure 4B.a), at the same time, their secondary λ_{max} was at about 232 nm similar to that of TPA (Figure 4B.c). It was easily deduced that there could exist more than 12 homologous compounds of PEs. However, four peaks (λ_{max} at about 304 nm), peaks 13, 14, 16, and 17 (Figure 4B.b), were significantly different from the peak of JC1. It is questionable whether these four peaks (λ_{max} at about 304 nm) are homologues of PEs.

UPLC−MS was used to further certify whether those four peaks are homologues of PEs. The TIC chromatogram of PE-rich crude extract is shown in the Supporting Material (Figure S1). In the positive-ion mass spectra, more than 15 compounds showed the same quasi-molecular ion peaks at about 693.00 ($[M + H - H_2O]^+$) in corresponding mass spectra (Supporting Information, Figure S1) and several similar sequence-specific fragment ions (at about 365.00, 311.00 and 292.90), all of which were similar to those of JC1 (Figure 3E). This indicates that these 15 compounds all contained the same mother nucleus. Therefore, these results indicate that the more than 15 compounds found by UPLC−MS are all homologues of PEs.

In this work, a rapid and efficient HSCCC method was developed and successfully applied to separate the PEs from *J. curcas* seeds. In addition, the combination of HSCCC and semipreparative HPLC was developed and successfully applied to purify the JC1. Meanwhile, the PE-rich crude extract from *J. curcas* was also analyzed by UPLC−PDA and UPLC−MS, and the results indicated there may be more than 15 analogues of PEs in *J. curcas* seeds. This work will enhance the economic viability and sustainability of the *J. curcas* production chain.

■ ASSOCIATED CONTENT

Supporting Information

(A−O) Product ion MS spectrum of peaks 3−17 and (P) UPLC−MS chromatogram in total ion current of PE-rich crude extract (3−17 represent the peaks detected by UPLC−MS in their existing order). This material is available free of charge via the Internet at http://pubs.acs.org.

■ AUTHOR INFORMATION

Corresponding Authors

*F.C.: phone, +86 28 85416957; fax, +86 28 85416957; e-mail, chenfang@scu.edu.cn.

*Z.W.: phone, +86 28 85416957; fax, +86 28 85416957; e-mail, wangzhanguo@scu.edu.cn.

Funding

This work was supported by the National Natural Science Foundation of China (Grant 31170312).

Notes

The authors declare no competing financial interest.

■ ACKNOWLEDGMENTS

We kindly thank Xiaoyu Zhang (Ph.D., College of Life Science, Sichuan Normal University) and Xueran Mei (M.S., College of Life Science, Sichuan Normal University), who provided help with the HSCCC analysis.

DOI: 10.1021/jf505655b
J. Agric. Food Chem. 2015, 63, 2767−2772

ABBREVIATIONS USED

PEs, phorbol esters; TPA, phorbol 12-myristate-13-acetate; JC1−JC6, jatropha factors C_{1-6}; HSCCC, high-speed countercurrent chromatography; UPLC, ultrahigh-pressure liquid chromatography; PDA, photodiode array detection; MS, mass spectrometry; *K*, partition coefficient; α, separation factor; TIC, total ion current

REFERENCES

(1) Sudhakar Johnson, T.; Eswaran, N.; Sujatha, M. Molecular approaches to improvement of *Jatropha curcas* Linn. as a sustainable energy crop. *Plant Cell Rep.* **2011**, *30* (9), 1573−91.

(2) Abdulla, R.; Chan, E. S.; Ravindra, P. Biodiesel production from *Jatropha curcas*: A critical review. *Crit. Rev. Biotechnol.* **2011**, *31* (1), 53−64.

(3) Juan, J. C.; Kartika, D. A.; Wu, T. Y.; Hin, T. Y. Biodiesel production from jatropha oil by catalytic and non-catalytic approaches: An overview. *Bioresour. Technol.* **2011**, *102* (2), 452−60.

(4) King, A. J.; He, W.; Cuevas, J. A.; Freudenberger, M.; Ramiaramanana, D.; Graham, I. A. Potential of *Jatropha curcas* as a source of renewable oil and animal feed. *J. Exp. Bot.* **2009**, *60* (10), 2897−905.

(5) Sharma, S. K.; Singh, H. A review on pharmacological significance of genus *Jatropha* (Euphorbiaceae). *Chin. J. Integr. Med.* **2012**, *18* (11), 868−80.

(6) Devappa, R. K.; Makkar, H. P.; Becker, K. Nutritional, biochemical, and pharmaceutical potential of proteins and peptides from jatropha: Review. *J. Agric. Food Chem.* **2010**, *58* (11), 6543−55.

(7) Thomas, R.; Sah, N. K.; Sharma, P. B. Therapeutic biology of *Jatropha curcas*: A mini review. *Curr. Pharm. Biotechnol.* **2008**, *9* (4), 315−24.

(8) Debnath, M.; Bisen, P. S. *Jatropha curcas* L., a multipurpose stress resistant plant with a potential for ethnomedicine and renewable energy. *Curr. Pharm. Biotechnol.* **2008**, *9* (4), 288−306.

(9) Paulillo, L. C.; Mo, C.; Isaacson, J.; Lessa, L.; Lopes, E.; Romero-Suarez, S.; Brotto, L.; Abreu, E.; Gutheil, W.; Brotto, M. *Jatropha curcas*: from biodiesel generation to medicinal applications. *Recent Pat. Biotechnol.* **2012**, *6* (3), 192−9.

(10) Sabandar, C. W.; Ahmat, N.; Jaafar, F. M.; Sahidin, I. Medicinal property, phytochemistry and pharmacology of several *Jatropha* species (Euphorbiaceae): A review. *Phytochemistry* **2013**, *85*, 7−29.

(11) Devappa, R. K.; Makkar, H. P.; Becker, K. Jatropha toxicity–a review. *J. Toxicol. Environ. Health B Crit. Rev.* **2010**, *13* (6), 476−507.

(12) Hirota, M.; Suttajit, M.; Suguri, H.; Endo, Y.; Shudo, K.; Wongchai, V.; Hecker, E.; Fujiki, H. A new tumor promoter from the seed oil of *Jatropha curcas* L., an intramolecular diester of 12-deoxy-16-hydroxyphorbol. *Cancer Res.* **1988**, *48* (20), 5800−4.

(13) Haas, W.; Sterk, H.; Mittelbach, M. Novel 12-deoxy-16-hydroxyphorbol diesters isolated from the seed oil of *Jatropha curcas*. *J. Nat. Prod.* **2002**, *65* (10), 1434−40.

(14) Roach, J. S.; Devappa, R. K.; Makkar, H. P.; Becker, K. Isolation, stability and bioactivity of *Jatropha curcas* phorbol esters. *Fitoterapia* **2012**, *83* (3), 586−92.

(15) Wang, Z.; Tang, L.; Hu, H.; Guo, Y.; Peng, T.; Yan, F.; Chen, F. Metabolic profiling assisted quality control of phorbolesters in *Jatropha curcas* seed by high-performance liquid chromatography using a fused-core column. *J. Agric. Food Chem.* **2012**, *60* (38), 9567−72.

(16) Li, C. Y.; Devappa, R. K.; Liu, J. X.; Lv, J. M.; Makkar, H. P.; Becker, K. Toxicity of *Jatropha curcas* phorbol esters in mice. *Food Chem. Toxicol.* **2010**, *48* (2), 620−5.

(17) Devappa, R. K.; Roach, J. S.; Makkar, H. P.; Becker, K. Occular and dermal toxicity of *Jatropha curcas* phorbol esters. *Ecotoxicol Environ. Saf.* **2013**, *94*, 172−8.

(18) Oskoueian, E.; Abdullah, N.; Ahmad, S. Phorbol esters isolated from jatropha meal induced apoptosis-mediated inhibition in proliferation of chang and Vero cell lines. *Int. J. Mol. Sci.* **2012**, *13* (11), 13816−29.

(19) Veerabhadrappa, M. B.; Shivakumar, S. B.; Devappa, S. Solid-state fermentation of jatropha seed cake for optimization of lipase, protease and detoxification of anti-nutrients in jatropha seed cake using *Aspergillus versicolor* CJS-98. *J. Biosci. Bioeng.* **2014**, *117* (2), 208−14.

(20) Hidayat, C.; Hastuti, P.; Wardhani, A. K.; Nadia, L. S. Method of phorbol ester degradation in *Jatropha curcas* L. seed cake using rice bran lipase. *J. Biosci. Bioeng.* **2014**, *117* (3), 372−4.

(21) Sadubthummarak, U.; Parkpian, P.; Ruchirawat, M.; Kongchum, M.; Delaune, R. D. Potential treatments to reduce phorbol esters levels in jatropha seed cake for improving the value added product. *J. Environ. Sci. Health B* **2013**, *48* (11), 974−82.

(22) Yunping, B.; Ha, B. T.; Eunice, Y.; Chueng, L. L.; Yan, H. Light induced degradation of phorbol esters. *Ecotoxicol. Environ. Saf.* **2012**, *84*, 268−73.

(23) Kumar, V.; Makkar, H. P.; Amselgruber, W.; Becker, K. Physiological, haematological and histopathological responses in common carp (*Cyprinus carpio* L.) fingerlings fed with differently detoxified *Jatropha curcas* kernel meal. *Food Chem. Toxicol.* **2010**, *48* (8−9), 2063−72.

(24) Wang, X. H.; Ou, L.; Fu, L. L.; Zheng, S.; Lou, J. D.; Gomes-Laranjo, J.; Li, J.; Zhang, C. Detoxification of *Jatropha curcas* kernel cake by a novel *Streptomyces fimicarius* strain. *J. Hazard Mater.* **2013**, *260*, 238−46.

(25) Phengnuam, T.; Suntornsuk, W. Detoxification and anti-nutrients reduction of *Jatropha curcas* seed cake by *Bacillus* fermentation. *J. Biosci. Bioeng.* **2013**, *115* (2), 168−72.

(26) Devappa, R. K.; Rajesh, S. K.; Kumar, V.; Makkar, H. P.; Becker, K. Activities of *Jatropha curcas* phorbol esters in various bioassays. *Ecotoxicol. Environ. Saf.* **2012**, *78*, 57−62.

(27) Oskoueian, E.; Abdullah, N.; Ahmad, S. Phorbol esters from jatropha meal triggered apoptosis, activated PKC-delta, caspase-3 proteins and down-regulated the proto-oncogenes in MCF-7 and HeLa cancer cell lines. *Molecules* **2012**, *17* (9), 10816−30.

(28) Wender, P. A.; Kee, J. M.; Warrington, J. M. Practical synthesis of prostratin, DPP, and their analogs, adjuvant leads against latent HIV. *Science* **2008**, *320* (5876), 649−52.

(29) Devappa, R. K.; Malakar, C. C.; Makkar, H. P.; Becker, K. Pharmaceutical potential of phorbol esters from *Jatropha curcas* oil. *Nat. Prod Res.* **2013**, *27* (16), 1459−62.

(30) Liang, J.; Ito, Y.; Zhang, X.; He, J.; Sun, W. Rapid preparative separation of six bioactive compounds from *Gentiana crassicaulis* Duthie ex Burk. using microwave-assisted extraction coupled with high-speed counter-current chromatography. *J. Sep Sci.* **2013**, *36* (24), 3934−40.

(31) Dai, X.; Huang, Q.; Zhou, B.; Gong, Z.; Liu, Z.; Shi, S. Preparative isolation and purification of seven main antioxidants from *Eucommia ulmoides* Oliv. (Du-zhong) leaves using HSCCC guided by DPPH−HPLC experiment. *Food Chem.* **2013**, *139* (1−4), 563−70.

(32) Regalado, E. L.; Tolle, S.; Pino, J. A.; Winterhalter, P.; Menendez, R.; Morales, A. R.; Rodriguez, J. L. Isolation and identification of phenolic compounds from rum aged in oak barrels by high-speed countercurrent chromatography/high-performance liquid chromatography−diode array detection−electrospray ionization mass spectrometry and screening for antioxidant activity. *J. Chromatogr., Sect. A* **2011**, *1218* (41), 7358−64.

(33) Lopes-Lutz, D.; Mudge, E.; Ippolito, R.; Brown, P.; Schieber, A. Purification of alkylamides from *Echinacea angustifolia* (DC.) Hell. roots by high-speed countercurrent chromatography. *J. Agric. Food Chem.* **2011**, *59* (2), 491−4.

(34) Degenhardt, A.; Engelhardt, U. H.; Lakenbrink, C.; Winterhalter, P. Preparative separation of polyphenols from tea by high-speed countercurrent chromatography. *J. Agric. Food Chem.* **2000**, *48* (8), 3425−30.

(35) Rakshit, K. D.; Darukeshwara, J.; Rathina Raj, K.; Narasimhamurthy, K.; Saibaba, P.; Bhagya, S. Toxicity studies of detoxified jatropha meal (*Jatropha curcas*) in rats. *Food Chem. Toxicol.* **2008**, *46* (12), 3621−5.

DOI: 10.1021/jf505655b
J. Agric. Food Chem. 2015, 63, 2767−2772

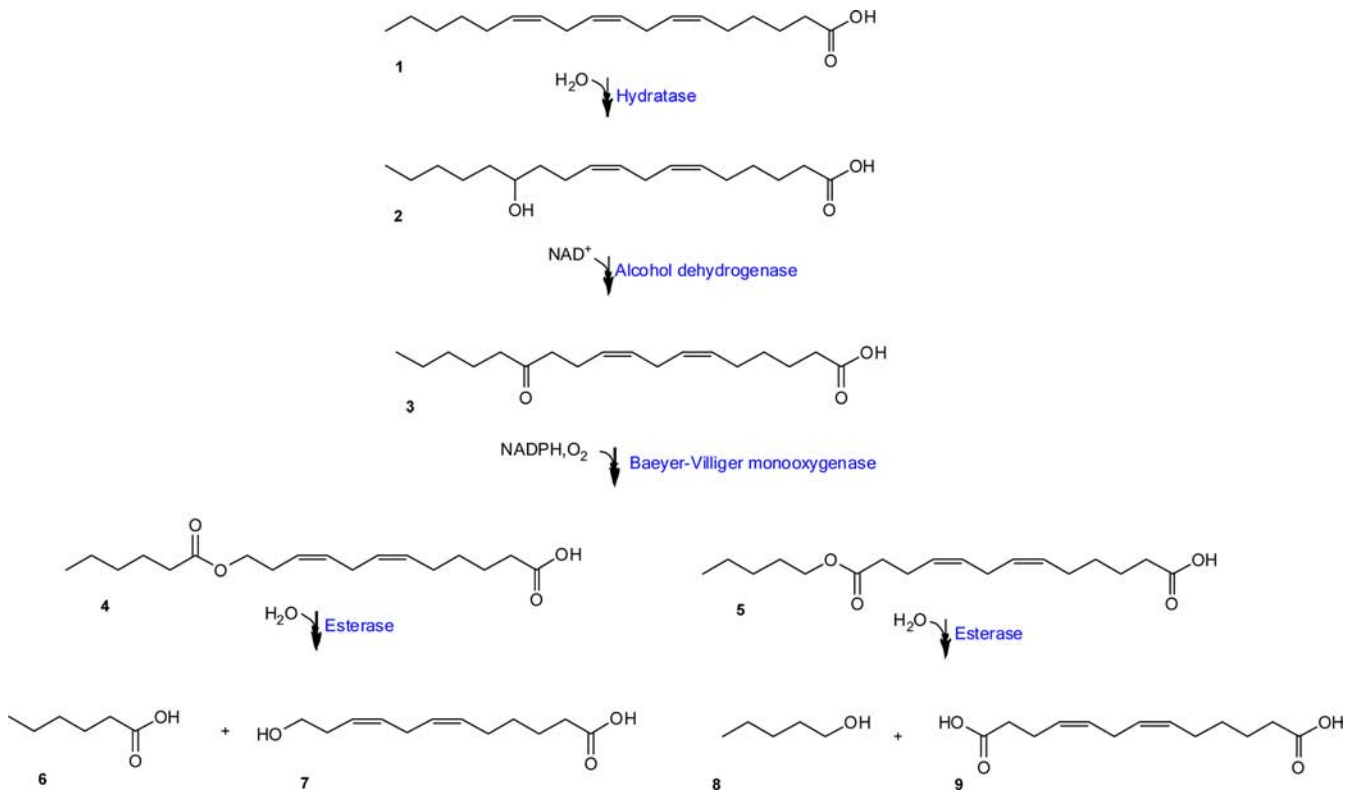

Figure 1. Designed biotransformation pathway 1. γ-Linolenic acid (**1**) was converted into *n*-hexanoic acid (**6**) and (6*Z*,9*Z*)-12-hydroxydodeca-6,9-dienoic acid (**7**) or *n*-pentanol (**8**) and (4*Z*,7*Z*)-trideca-4,7-dienedioic acid (**9**) by the multistep enzyme reactions.

hydratase gene was induced by adding 0.1 mM isopropyl-β-D-thiogalactopyranoside (IPTG) at an optical density (OD_{600}) of 0.5. Afterward, the culture was further incubated at 16 °C for 16 h. The recombinant *E. coli* BL21(DE3), used for hydration of γ-linolenic acid and biotransformation of hydroxy fatty acids, was cultivated in a Riesenberg medium, which was supplemented with 10 g L^{-1} glucose and the appropriate antibiotics for plasmid maintenance (Supporting Information Table S1). The Riesenberg medium consisted of 4 g L^{-1} $(NH_4)_2HPO_4$, 13.5 g L^{-1} KH_2PO_4, 1.7 g L^{-1} citric acid, 1.4 g L^{-1} $MgSO_4$, and 10 mL L^{-1} trace metal solution (10 g L^{-1} $FeSO_4$, 2.25 g L^{-1} $ZnSO_4$, 1.0 g L^{-1} $CuSO_4$, 0.5 g L^{-1} $MnSO_4$, 0.23 g L^{-1} $Na_2B_4O_7$, 2.0 g L^{-1} $CaCl_2$, and 0.1 g L^{-1} $(NH_4)_6Mo_7O_{24}$). *Stenotrophomonas nitritireducens* (Table S1) used for the hydration of the C9 double bond in γ-linolenic acid was cultivated in a nutrient medium as described previously.[23]

Reagents. γ-Linolenic acid (**1**), palmitic acid, *n*-hexanoic acid (**6**), *n*-pentanol (**8**), and ethyl acetate were obtained from Sigma-Aldrich. (6*Z*,9*Z*)-13-Hydroxyoctadeca-6,9-dienoic acid (**2**) and (6*Z*,12*Z*)-10-hydroxyoctadeca-6,12-dienoic acid (**10**) were prepared via hydration of γ-linolenic acid with a linoleate C12 double-bond hydratase or a linoleate C9 double-bond hydratase in our laboratory (see Purification of Hydroxy Fatty Acids below for details). (6*Z*,9*Z*)-12-Hydroxydodeca-6,9-dienoic acid (**7**), (*Z*)-9-hydroxynon-6-enoic acid (**15**), (*Z*)-dec-4-enedioic acid (**17**), and (4*Z*,7*Z*)-trideca-4,7-dienedioic acid (**9**) were synthesized from (6*Z*,9*Z*)-13-hydroxyoctadeca-6,9-dienoic acid (**2**) or (6*Z*,12*Z*)-10-hydroxyoctadeca-6,12-dienoic acid (**10**) via the recombinant *E. coli*-based biocatalysis in our laboratory (see Purification of Unsaturated Carboxylic Acids below for details).

Purification of a Linoleate C12 Double-Bond Hydratase. The linoleate C12 double bond-hydratase of *L. acidophilus* was purified as previously reported.[22] In brief, after cultivation of recombinant *E. coli* ER2566 harboring the linoleate C12 double-bond hydratase gene of *L. acidophilus*, the cell mass was harvested, washed, and resuspended into 50 mM phosphate buffer (pH 8.0) containing 300 mM NaCl, 10 mM imidazole, and 0.1 mM phenylmethanesulfonyl fluoride as a protease inhibitor. The resuspended cells were disrupted, and the supernatant was applied to a His-Trap HP chromatography column (GE Healthcare) equilibrated with 50 mM phosphate buffer (pH 8.0) containing 300 mM NaCl. The active fractions were collected and dialyzed against 50 mM citrate−phosphate buffer (pH 7.0).

Hydration of γ-Linolenic Acid. The enzymatic transformation of γ-linolenic acid into (6*Z*,9*Z*)-13-hydroxyoctadeca-6,9-dienoic acid was performed in 50 mM citrate−phosphate buffer (pH 7.0) containing 10 mM substrate and 2% (v/v) ethanol. In a 15 mL polypropylene tube with a screw cap, 3 mL of reaction mixture was incubated at 35 °C for 6 h with agitation at 200 rpm. The purified hydratases were applied to 3 mg mL^{-1}. One unit (U) of the hydratase activity is defined as 1 μmol of (6*Z*,9*Z*)-13-hydroxyoctadeca-6,9-dienoic acid produced per minute at 35 °C.

The whole-cell transformation of γ-linolenic acid into (6*Z*,9*Z*)-13-hydroxyoctadeca-6,9-dienoic acid was performed in 50 mM Tris-HCl buffer (pH 7.0) containing 38 mM substrate and 0.05% (v/v) Tween 80. In a 15 mL polypropylene tube with a screw cap, 3 mL of reaction mixture was incubated at 35 °C for 24 h with agitation at 200 rpm. The recombinant *E. coli* BL21(DE3) expressing the linoleate C12 double-bond hydratase of *L. acidophilus* NBRC 13951 was added to 14.4 g L^{-1}.

The hydration of γ-linolenic acid into (6*Z*,12*Z*)-10-hydroxyoctadeca-6,12-dienoic acid with *S. nitritireducens* was carried out in 10 mL of 50 mM citrate−phosphate buffer (pH 7.0). γ-Linolenic acid was added to a reaction medium containing 20 g dry cells L^{-1} and 0.05% (v/v) Tween 80. The reaction mixture was incubated at 30 °C and sparged with a gas mixture consisting of 95% N_2 and 5% CO_2 at 0.02 vvm to maintain anaerobic conditions.[23]

Biotransformation of Hydroxy Fatty Acids. The biotransformation of the hydroxy fatty acids with recombinant *E. coli* cells was carried out on the basis of our earlier work.[21] Briefly, the recombinant cells were cultivated in the Riesenberg medium at 30 °C, and the expression of the target genes was induced with 0.1 mM IPTG and/or 2.0 g L^{-1} rhamnose at an OD_{600} of 0.5. Thereafter, the cultivation temperature was reduced to 20 °C to facilitate the soluble expression of the target genes (Supporting Information Figure S4). When the added

DOI: 10.1021/jf5058843
J. Agric. Food Chem. 2015, 63, 2773−2781

glucose was consumed, the recombinant cells were harvested by centrifugation at 3500*g* for 15 min at 4 °C and used as biocatalysts. The biotransformation was initiated by adding 2 mM of a hydroxy fatty acid to 50 mM Tris-HCl buffer (pH 8.0) containing 0.5 g L^{-1} Tween 80 and 7.2 g dry cells L^{-1} of the recombinant *E. coli* BL21(DE3) that expressed the ADH from *Micrococcus luteus*, the esterase from *P. fluorescens* SIK WI, and the BVMO from either *Pseudomonas putida* KT2440 or *Pseudomonas fluorescens* DSM 50106. The biotransformations were conducted in a shaking incubator (35 °C and 200 rpm).

Product Analysis by GC-MS. The concentrations of the remaining fatty acids and accumulating carboxylic acids in the medium (i.e., γ-linolenic acid (**1**), (6*Z*,9*Z*)-13-hydroxyoctadeca-6,9-dienoic acid (**2**), (6*Z*,9*Z*)-12-hydroxydodeca-6,9-dienoic acid (**7**), (*Z*)-9-hydroxynon-6-enoic acid (**15**), (4*Z*,7*Z*)-trideca-4,7-dienedioic acid (**9**), and (*Z*)-dec-4-enedioic acid (**17**)) were determined as described previously.[21] The reaction medium was mixed with an equal volume of ethyl acetate containing 2 or 5 g L^{-1} palmitic acid as an internal standard. The organic phase was harvested after vigorous vortexing and then derivatized with *N*-methyl-*N*-(trimethylsilyl)trifluoroacetamide (MSTFA). The trimethylsilyl (TMS) derivatives were analyzed using a Thermo Ultra Trace GC system connected to an ion trap mass detector (Thermo ITQ1100 GC-ion Trap MS; Thermo Scientific). The derivatives were separated on a nonpolar capillary column (30 m length, 0.25 μm film thickness, HP-5MS; Agilent, Santa Clara, CA, USA). A linear temperature gradient was programmed as follows: 90 °C, 15 °C min^{-1} to 200 °C; 200 °C, 5 °C min^{-1} to 250 °C; 90 °C, 15 °C min^{-1} to 200 °C; and 200 °C, 5 °C min^{-1} to 280 °C. The injection port temperature was 230 °C. Mass spectra were obtained by electron impact ionization at 70 eV. Scan spectra were obtained within the range of m/z 100−600. Selected ion monitoring (SIM) was used for the detection and fragmentation analysis of the reaction products.

Product Analysis by GC. The obtained hydroxy fatty acids were derivatized by using a 3:1 mixture of pyridine and MSTFA. TMS-derivatized hydroxy fatty acids were analyzed by GC (Agilent 6890N) equipped with a flame ionization detector and an SPB-1 capillary column (15 m × 0.32 mm inside diameter, 0.25 μm thickness; Supelco) using palmitic acid as an internal standard.[23] The column temperature increased from 150 to 210 °C at an initial rate of 4 °C min^{-1} and then at rate of 30 °C min^{-1} until 280 °C, and this temperature was maintained at 280 °C for 5 min. The injector and detector temperatures were held at 260 and 250 °C, respectively.

Identification of the Biotransformation Products. The biotransformation products were identified by GC-MS or NMR analyses. (*Z*)-9-Hydroxynon-6-enoic acid (**15**), (4*Z*,7*Z*)-trideca-4,7-dienedioic acid (**9**), and (*Z*)-dec-4-enedioic acid (**17**) were identified by GC-MS analysis and comparison to pure reference compounds (Figures 4 and 7). (6*Z*,9*Z*)-13-Hydroxyoctadeca-6,9-dienoic acid (**2**) and (6*Z*,9*Z*)-12-hydroxydodeca-6,9-dienoic acid (**7**) were identified by GC-MS and NMR analyses (see Figure S3 in the Supporting Information for identification of (6*Z*,9*Z*)-13-hydroxyoctadeca-6,9-dienoic acid and Figure S5 for identification of (6*Z*,9*Z*)-12-hydroxydodeca-6,9-dienoic acid). Identification of compounds **2**, **7**, **9**, **15**, and **17** was further confirmed by the GC-MS analysis of their hydrogenated products, which were obtained by catalytic hydrogenation (Figures 4, 7, and S1B).

Purification of the Biotransformation Products. *Purification of Hydroxy Fatty Acids.* The hydroxy fatty acids (i.e., (6*Z*,9*Z*)-13-hydroxyoctadeca-6,9-dienoic acid (**2**) and (6*Z*,12*Z*)-10-hydroxyoctadeca-6,12-dienoic acid (**10**)) were isolated from the reaction medium by solvent extraction and column chromatography as described previously.[23] In brief, the biotransformation products were isolated by the extraction using two volumes of ethyl acetate two times. After the organic layer was separated from the aqueous phase, the organic extracts were dried with Na_2SO_4 and concentrated by the evaporation in vacuo. The concentrate was purified by the silicic acid column chromatography with methanol gradient (0−5%, v/v) in CH_3Cl (50 mL). Any impurities and the remaining substrate were washed off with CH_3Cl and 1% methanol in CH_3Cl. In the case of (6*Z*,9*Z*)-13-hydroxyoctadeca-6,9-dienoic acid, the concentrate was purified with a semipreparative HPLC system (Agilent) equipped with a Nucleosil C-18 semiprep column as described in a previous study[24] (see Figure S2 in the Supporting Information for purification of (6*Z*,9*Z*)-13-hydroxyoctadeca-6,9-dienoic acid).

Table 1. Products Accessible through the Multistep Biocatalysis

starting material	final product	product yield[a] (%)
γ-linolenic acid (**1**)	(6*Z*,9*Z*)-13-hydroxyoctadeca-6,9-dienoic acid (**2**)	92 ± 2 (60%, 96%)[b]
	(6*Z*,12*Z*)-10-hydroxyoctadeca-6,12-dienoic acid (**10**)	97 ± 4
(6*Z*,9*Z*)-13-hydroxyoctadeca-6,9-dienoic acid (**2**)	(6*Z*,9*Z*)-12-hydroxydodeca-6,9-dienoic acid (**7**)	81 ± 4 (43%, 71%)[b]
	(4*Z*,7*Z*)-trideca-4,7-dienedioic acid (**9**)	34 ± 6[c]
(6*Z*,12*Z*)-10-hydroxyoctadeca-6,12-dienoic acid (**10**)	(*Z*)-9-hydroxynon-6-enoic acid (**15**)	72 ± 7
	(*Z*)-dec-4-enedioic acid (**17**)	73 ± 4

[a]The product yield was calculated on the basis of the substrate depletion and the product concentration, which were determined by GC-MS. All experiments were carried out in triplicate. [b]The numbers in parentheses indicate the isolated yield and purity, respectively. The isolated yields were calculated on the basis of the amount of the products isolated and the amount of the substrates added into the reaction medium. [c]The product yields were low compared to those of the other products because (6*Z*,9*Z*)-12-hydroxydodeca-6,9-dienoic acid (**7**) was coproduced during biotransformation (Figure 3B).

Purification of Unsaturated Carboxylic Acids. The medium-chain, unsaturated carboxylic acids (e.g., 12-hydroxydodeca-6,9-dienoic acid, 9-hydroxynona-6-enoic acid, and 1,10-deca-6-enedioic acid) were isolated from the whole-cell reaction medium as described previously.[21,25] In brief, the biotransformation products were extracted with ethyl acetate three times. The extract was dried over $MgSO_4$ and concentrated via evaporation in vacuo. The impurities (e.g., *n*-alkanoic acids coproduced during biotransformations and long-chain fatty acids originating from the starting materials) were removed by washing with hexane (see Figure S6 in the Supporting Information for purification of (6*Z*,9*Z*)-12-hydroxydodeca-6,9-dienoic acid). (6*Z*,9*Z*)-12-Hydroxydodeca-6,9-dienoic acid was also purified by HPLC (Figure S5).

RESULTS

The fatty acid double-bond hydratases and BVMOs were the key enzymes in our designed biotransformation pathways because the structures of the final products were determined by the regioselectivity of both enzymes (Figures 1 and 5). Thereby, the first step was to select the appropriate enzymes in terms of substrate scope and regioselectivity for the production of the target compounds.

Screening of a γ-Linolenic Acid C12 Double-Bond Hydratase. Recently, a linoleate C12 double-bond hydratase of *L. acidophilus* NBRC 13951 was cloned and characterized.[22] Thereby, the enzyme was first examined for hydration of the C12 double bond in γ-linolenic acid. The enzyme was produced in *E. coli* ER2566 and subjected to purification via His-Trap affinity chromatography. Afterward, the purified enzyme was added to 50 mM citrate−phosphate buffer (pH 7.0) containing 10 mM γ-linolenic acid. A single product was accumulated in the reaction mixture (Figure 2A and Supporting Information Figure S1A). The product (**2**) was purified to a purity of >96% via solvent extraction and column chromatography (Figure S2). The mass spectrum contained peaks at m/z 173 and 369 due to the α-cleavages at both sides of the hydroxy-TMS function at

DOI: 10.1021/jf5058843
J. Agric. Food Chem. 2015, 63, 2773−2781

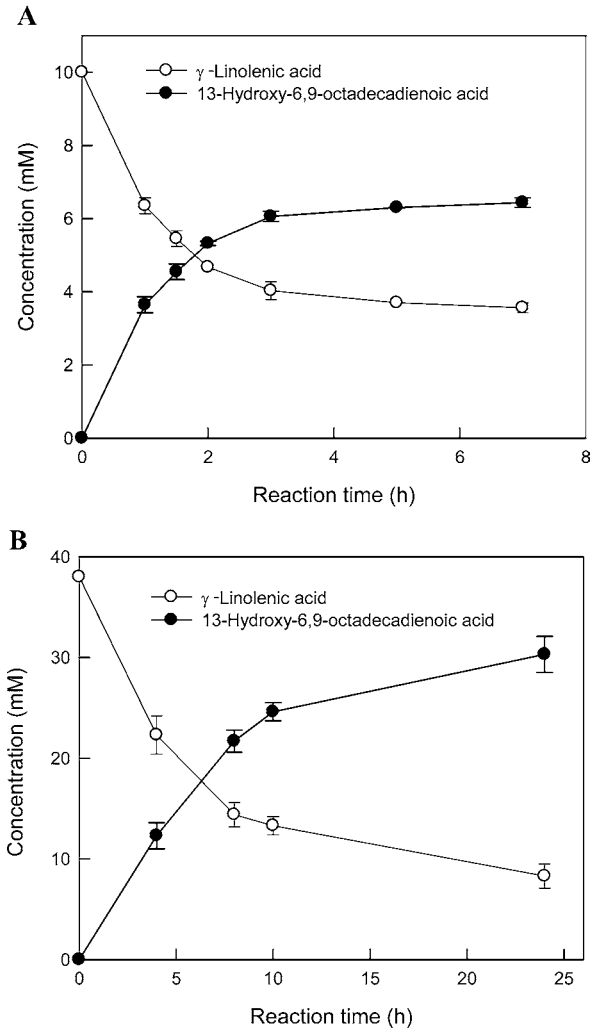

Figure 2. Biotransformation of γ-linolenic acid. γ-Linolenic acid (**1**) was converted into (6*Z*,9*Z*)-13-hydroxyoctadeca-6,9-dienoic acid (**2**) by (A) the isolated linoleate C12 double-bond hydratase of *L. acidiphilus* NBRC 13951 or (B) the recombinant *E. coli* BL21(DE3) expressing the linoleate C12 double-bond hydratase of *L. acidiphilus* NBRC 13951. The experiments were carried out in triplicate, and the error bars indicate the standard deviation.

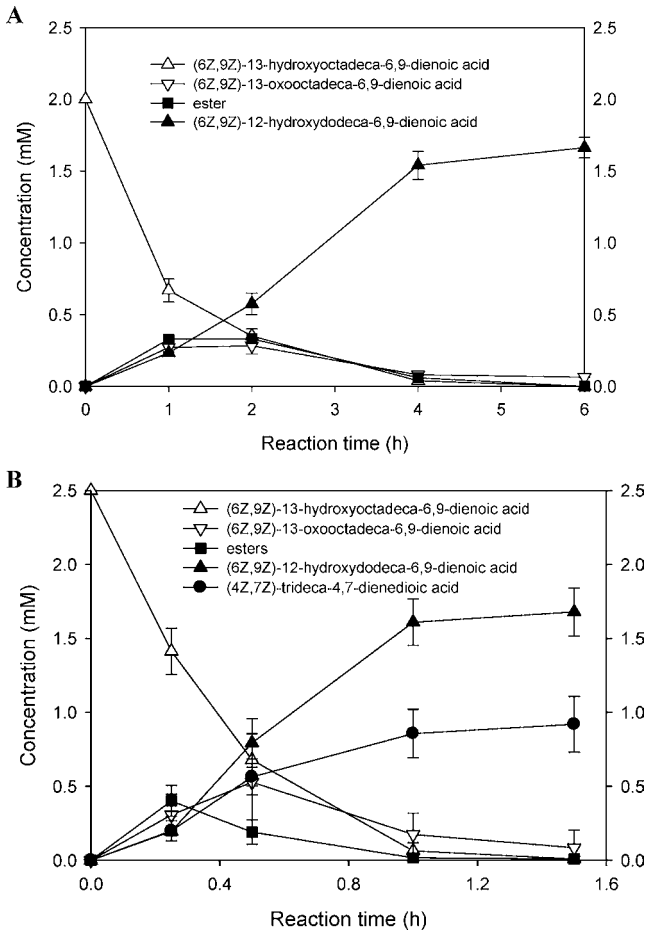

Figure 3. Biotransformation of (6*Z*,9*Z*)-13-hydroxyoctadeca-6,9-dienoic acid. (6*Z*,9*Z*)-13-Hydroxyoctadeca-6,9-dienoic acid (**2**) was converted into (A) (6*Z*,9*Z*)-12-hydroxydodeca-6,9-dienoic acid (**7**) or (B) (6*Z*,9*Z*)-12-hydroxydodeca-6,9-dienoic acid and (4*Z*,7*Z*)-trideca-4,7-dienedioic acid (**9**). The first biotransformation was conducted with the recombinant *E. coli* BL21(DE3) pACYC-ADH, pET-BmoF1, pCOLA-PFE1 expressing the ADH from *M. luteus*, the BVMO from *P. fluorescens* DSM 50106, and the esterase from *P. fluorescens* SIK WI. The second biotransformation was conducted with the recombinant *E. coli* BL21(DE3) pACYC-ADH-BVMO, pCOLA-PFE1, expressing the ADH from *M. luteus*, the BVMO from *Ps. putida* KT2440, and the esterase from *P. fluorescens* SIK WI. The experiments were carried out in triplicate, and the error bars indicate the standard deviation.

C13, whereas the mass spectrum of the hydrogenation product showed peaks at m/z 173 and 373 (Figure S1B). The resonance signals at 3.63 ppm (m, 1H) and four olefinic protons at 5.38 (m, 4H, H-6, H-7, H-9, and H-10) in ^{1}H NMR indicated the existence of a hydroxyl group and a double bond (Figure S3). The observed signal at 71.8 ppm (C-13) of ^{13}C NMR also supported the existence of one hydroxyl group (Figure S3). On the basis of these data, the product was identified as (6*Z*,9*Z*)-13-hydroxyoctadeca-6,9-dienoic acid (**2**). The concentration of (6*Z*,9*Z*)-13-hydroxyoctadeca-6,9-dienoic acid in the reaction medium increased to 6 mM. The hydration rate was increased to 21 U g protein^{-1} at t < 1 h. The isolated yield of the compound was ∼60% with a purity of 96% (Table 1). This result indicated that the linoleate C12 double-bond hydratase also exhibited very high regioselectivity with γ-linolenic acid.

Whole-Cell Production of (6*Z*,9*Z*)-13-Hydroxyoctadeca-6,9-dienoic Acid. The microbial production of (6*Z*,9*Z*)-13-hydroxyoctadeca-6,9-dienoic acid (**2**) from γ-linolenic acid was also investigated. After batch cultivation of recombinant *E. coli* BL21(DE3) expressing the linoleate C12 double-bond hydratase of *L. acidophilus* NBRC 13951, cell harvest via centrifugation, and resuspension into 50 mM Tris-HCl buffer (pH 7.0), γ-linolenic acid was added to a concentration of 38 mM in the reaction medium. γ-Linolenic acid was converted into the target product at a rate of 2.9 μmol g dry cells^{-1} min^{-1} (i.e., 2.9 U g dry cells^{-1}) at t < 10 h, thus resulting in a final product concentration of ∼30 mM (8.9 g L^{-1}) in the reaction medium (Figure 2B). The bioconversion yield, which was calculated on the basis of the substrate depletion and the product concentration determined by GC-MS, reached >95%. The byproduct formation was hardly observed (Supporting Information Figure S1B). These results indicated that the whole-cell biotransformation system was quite efficient in terms of reaction selectivity and rate.

Biotransformation of (6*Z*,9*Z*)-13-Hydroxyoctadeca-6,9-dienoic Acid (2). Hydroxy fatty acids are used as starting materials for the production of diverse secondary metabolites and signaling molecules in living organisms.[12,13] Thus, we

DOI: 10.1021/jf5058843
J. Agric. Food Chem. 2015, 63, 2773−2781

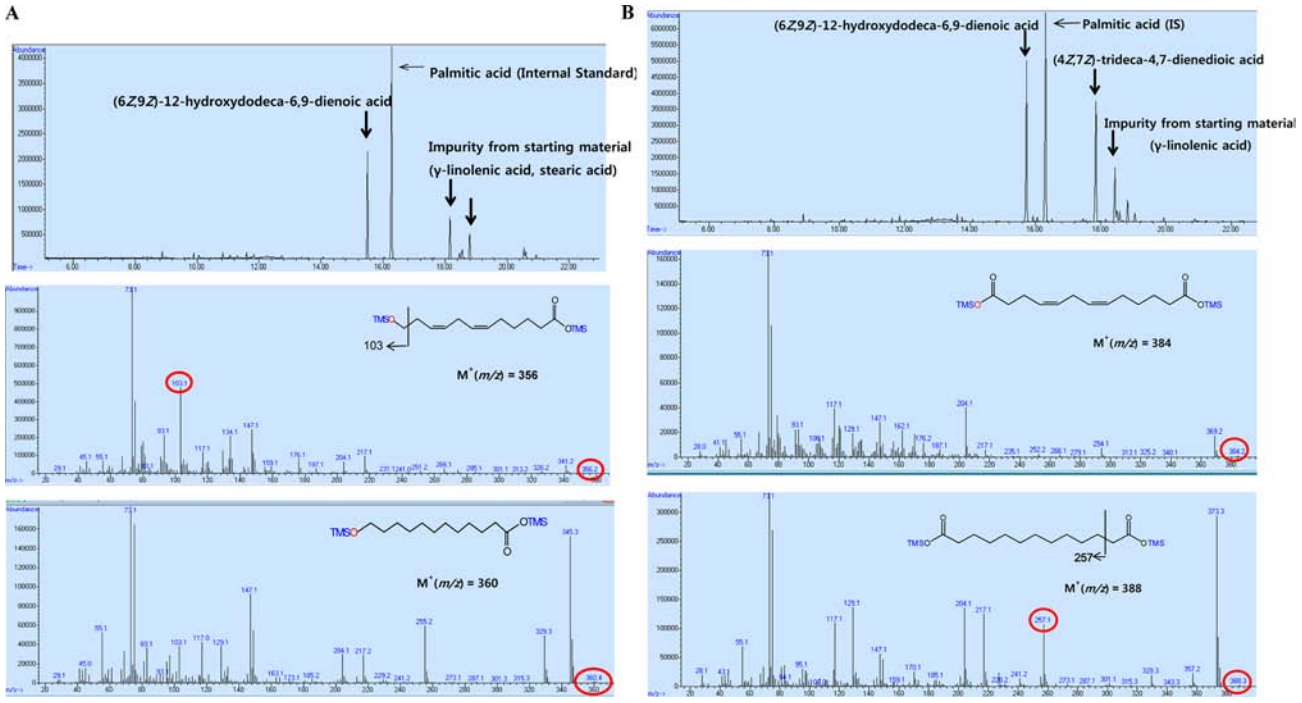

Figure 4. GC-MS analysis of (6*Z*,9*Z*)-13-hydroxyoctadeca-6,9-dienoic acid biotransformation products. (A) GC-MS of the biotransformation products, which were produced with the recombinant *E. coli* BL21(DE3) pACYC-ADH, pET-BmoF1, pCOLA-PFE1. The bottom panel shows the mass spectrum of the hydrogenated product of (6*Z*,9*Z*)-12-hydroxydodeca-6,9-dienoic acid, which is identical to that of the authentic compound 12-hydroxydodecanoic acid. (B) GC-MS of the biotransformation products, which were produced with the recombinant *E. coli* BL21(DE3) pACYC-ADH-BVMO, pCOLA-PFE1. The bottom panel shows the mass spectrum of the hydrogenated product of (4*Z*,7*Z*)-trideca-4,7-dienedioic acid, which is identical to that of the authentic compound tridecane-1,13-dioic acid.

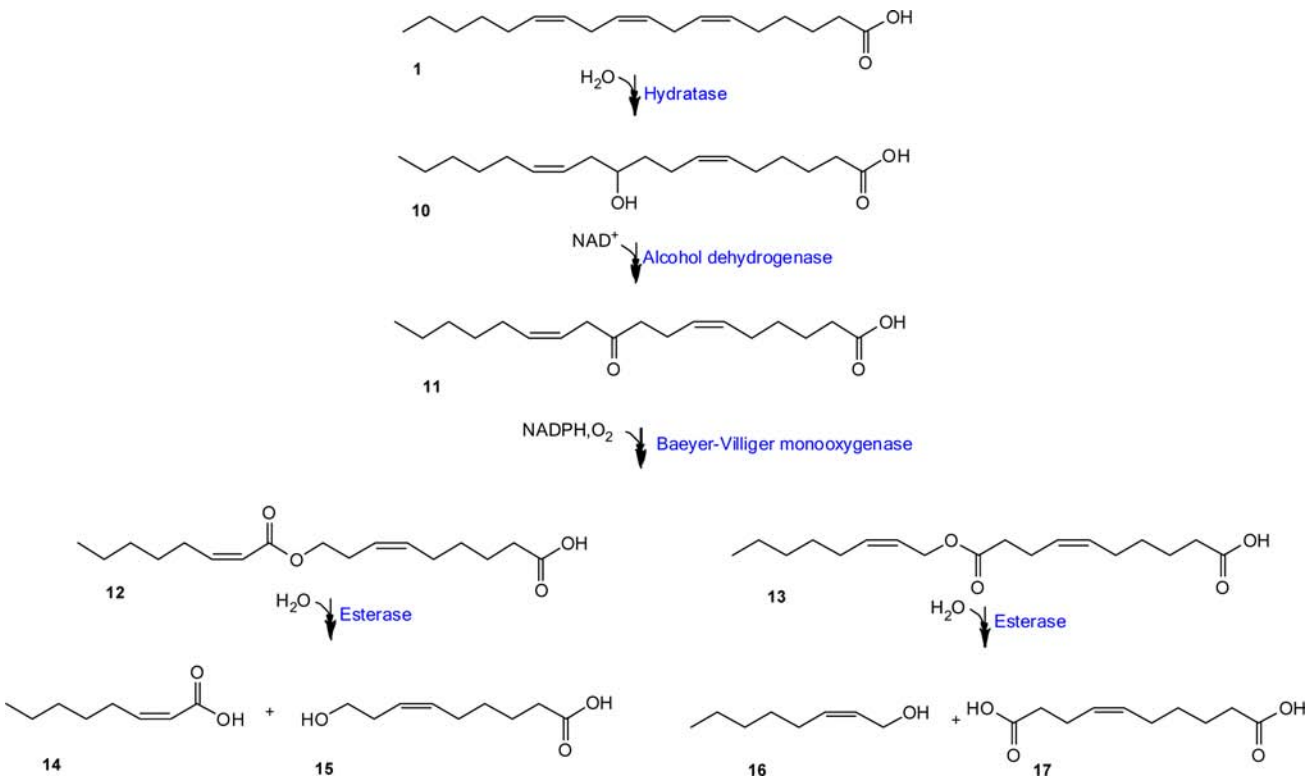

Figure 5. Designed biotransformation pathway 2. γ-Linolenic acid (**1**) is converted into 2-nonenoic acid (**14**) and (*Z*)-9-hydroxynon-6-enoic acid (**15**) or 2-octenol (**16**) and (*Z*)-dec-4-enedioic acid (**17**) by the multistep enzyme reactions.

investigated the biotransformation of (6*Z*,9*Z*)-13-hydroxyoctadeca-6,9-dienoic acid (**2**) into C12 oxylipins (e.g., (6*Z*,9*Z*)-12-hydroxydodeca-6,9-dienoic acid (**7**)). The substrate (**2**) was prepared after the whole-cell reaction of γ-linolenic acid,

DOI: 10.1021/jf5058843
J. Agric. Food Chem. 2015, 63, 2773−2781

isolation via ethyl acetate extraction, and concentration via evaporation in vacuo. The BVMO enzymes, which determine the chemical structure of the final products due to their regioselectivity, were first examined. The BVMOs that are active with long-chain aliphatic ketones[26−29] were chosen as candidates. When the recombinant *E. coli* BL21(DE3) pACYC-ADH, pET-BmoF1, pCOLA-PFE1 expressing an alcohol dehydrogenase (ADH) from *Micrococcus luteus* NCTC2665, a BVMO from *Pseudomonas fluorescens* DSM 50106,[30] and an esterase from *P. fluorescens* SIK WI was added to the reaction medium containing (6*Z*,9*Z*)-13-hydroxyoctadeca-6,9-dienoic acid (**2**), the compound was selectively converted into (6*Z*,9*Z*)-12-hydroxydodeca-6,9-dienoic acid (**7**) and *n*-hexanoic acid (**6**) via (6*Z*,9*Z*)-13-oxooctadeca-6,9-dienoic acid (**3**) and the ester (**4**) (Figures 3A and 4A). (6*Z*,9*Z*)-12-Hydroxydodeca-6,9-dienoic acid (**7**) was identified via GC-MS and NMR analyses after purification (Figures 4A and S5). Notably, the target product (**7**) was produced with a final concentration of 1.6 mM from 2.0 mM of the substrate (6*Z*,9*Z*)-13-hydroxyoctadeca-6,9-dienoic acid.

On the other hand, the addition of the recombinant *E. coli* BL21(DE3) pACYC-ADH-BVMO, pCOLA-PFE1 expressing an ADH from *M. luteus* NCTC2665, a BVMO from *Pseudomonas putida* KT2440,[27] and an esterase from *P. fluorescens* SIK WI resulted in a production of not only (6*Z*,9*Z*)-12-hydroxydodeca-6,9-dienoic acid (**7**) and *n*-hexanoic acid (**6**) but also (4*Z*,7*Z*)-trideca-4,7-dienedioic acid (**9**) and *n*-pentanol (**8**) (Figures 3B and 4B). (4*Z*,7*Z*)-Trideca-4,7-dienedioic acid was identified on the basis of the GC-MS analysis data of the pure compound 1,12-dodec-9-enedioic acid,[31] which has the same functional group in the fatty acid skeleton. It was assumed that the ester compound (**5**) was produced via the formation of the abnormal ester, which was driven by migration of the less-substituted carbon center during BVMO catalysis.[32,33]

Biotransformation of (6*Z*,12*Z*)-10-Hydroxyoctadeca-6,12-dienoic Acid (10). The biotransformation of (6*Z*,12*Z*)-10-hydroxyoctadeca-6,12-dienoic acid (**10**) (Figure 5), which had been produced from γ-linolenic acid by using the hydratase of *S. nitritireducens*[23] (Supporting Information Figure S7), was also carried out using the setup identical to the biotransformation of (6*Z*,9*Z*)-13-hydroxyoctadeca-6,9-dienoic acid (**2**). (*Z*)-9-Hydroxynon-6-enoic acid (**15**) and 2-nonenoic acid (**14**) were produced as the major products by recombinant *E. coli* BL21(DE3) pACYC-ADH-BVMO, pCOLA-PFE1 (Figures 6A and 7A). 9-Hydroxynona-6-enoic acid was identified on the basis of the GC-MS analysis data of the pure compound 12-hydroxyundec-9-enoic acid,[15] which has the same functional group in the fatty acid skeleton. Notably, the BVMO of *P. putida* KT2440 showed quite high selectivity with oxygenation of (6*Z*,12*Z*)-10-oxooctadeca-6,12-dienoic acid (**11**), but it showed low selectivity with (6*Z*,9*Z*)-13-oxooctadeca-6,9-dienoic acid (**3**) (Figure 3B).

The biotransformation of (6*Z*,12*Z*)-10-hydroxyoctadeca-6,12-dienoic acid (**10**) with recombinant *E. coli* BL21(DE3) pACYC-ADH, pET-BmoF1, pCOLA-PFE1 expressing the BVMO from *P. fluorescens* DSM50106 instead of the BVMO from *P. putida* KT2440 resulted in the production of (*Z*)-dec-4-enedioic acid (**17**) and 2-octenol as the major products (Figures 6B and 7B). These results indicated that a variety of plant oxylipins could be produced via combined biocatalysis using fatty acid double-bond hydratases and BVMOs.

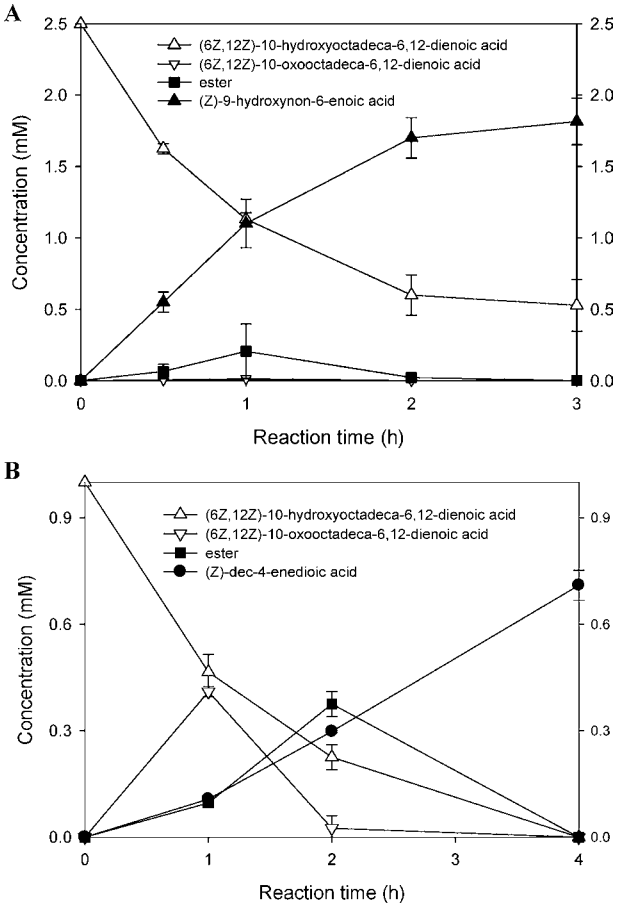

Figure 6. Biotransformation of (6*Z*,12*Z*)-10-hydroxyoctadeca-6,12-dienoic acid. (6*Z*,12*Z*)-10-Hydroxyoctadeca-6,12-dienoic acid (**10**) was converted by (A) the recombinant *E. coli* BL21(DE3) pACYC-ADH-BVMO, pCOLA-PFE1, and (B) the recombinant *E. coli* BL21(DE3) pACYC-ADH, pET-BmoF1, pCOLA-PFE1. The experiments were carried out in triplicate, and the error bars indicate standard deviation.

DISCUSSION

A family of oxygenated unsaturated carboxylic acids (e.g., oxylipins) that play important roles in plant signaling and defense are usually produced via a serial reaction of lipoxygenases and hydroperoxide lyases belonging to CYP74 family.[15] For instance, 12-hydroxydodec-9-enoic acid, 12-oxododec-9-enoic acid, and 1,12-dodec-9-enedioic acid, which were reported to stimulate growth of the roots of plant seedlings, were synthesized from α-linolenic acid by 13-lipoxygenases, hydroperoxide lyases, and alcohol dehydrogenases. 9-Hydroxynonanoic acid and 1,9-nonanedioic acid, which are involved in defense against infection, were produced from α-linolenic acid by 9-lipoxygenases, hydroperoxide lyases, and alcohol dehydrogenases.[15]

Because the oxygenated carboxylic acids have a great potential not only as agrochemicals but also as building blocks and/or additives for the production of plastics (e.g., polyamides and polyesters), resins, hot melt adhesives, powder coatings, corrosion inhibitors, lubricants, plasticizers, greases, and perfumes,[14,18,34,35] their biosyntheses have been extensively investigated. For instance, 9-oxononanoic acid was produced from linoleic acid via an enzymatic two-step reaction catalyzed by the 9*S*-lipoxygenase of *Solanum tuberosum* and the 9/13-hydroperoxide lyase of *Cucumis melo*.[19] Another example was the biotransformation of α-linoleic acid into 3(*Z*)-hexenal

DOI: 10.1021/jf5058843
J. Agric. Food Chem. 2015, 63, 2773−2781

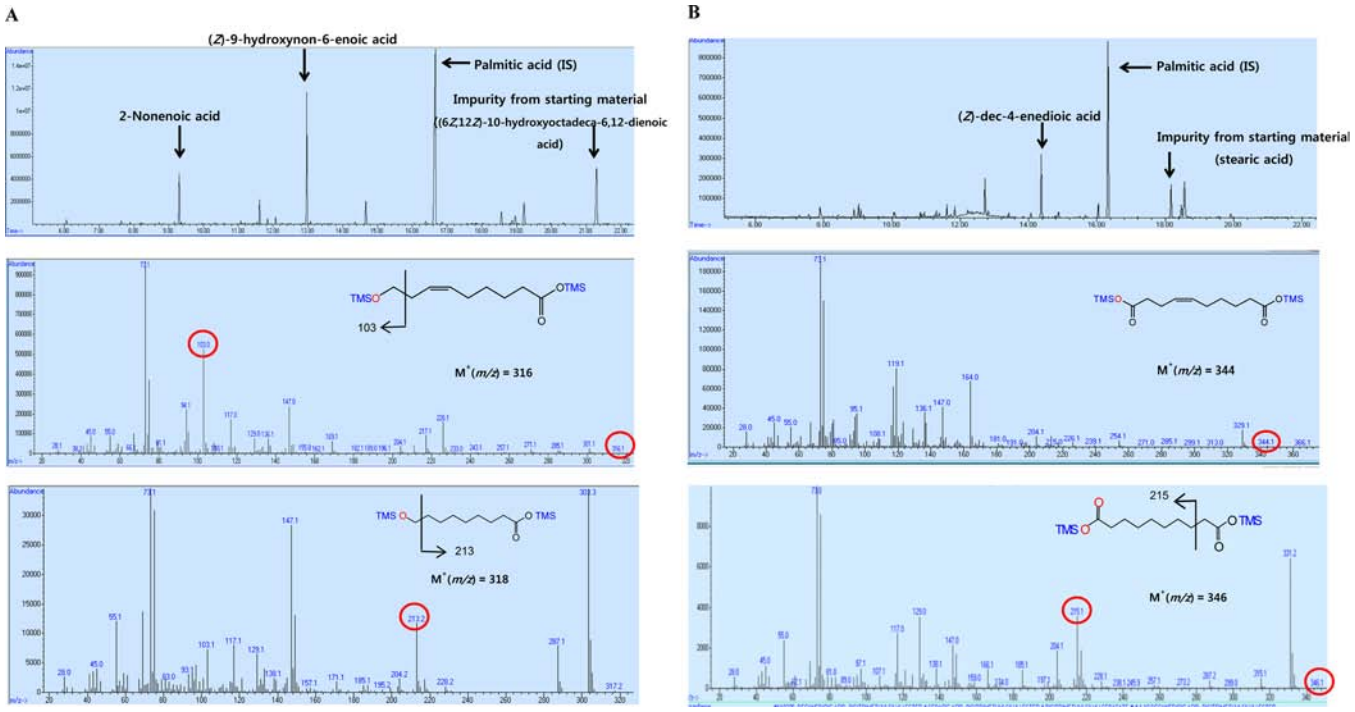

Figure 7. GC-MS analysis of (6*Z*,12*Z*)-10-hydroxyoctadeca-6,12-dienoic acid biotransformation products. (A) GC-MS of the biotransformation products, which were produced with the recombinant *E. coli* BL21(DE3) pACYC-ADH-BVMO, pCOLA-PFE1. The bottom panel shows the mass spectrum of the hydrogenated product of (*Z*)-9-hydroxynon-6-enoic acid, which is identical to that of the authentic compound 9-hydroxynonanoic acid. (B) GC-MS of the biotransformation products, which were produced with the recombinant *E. coli* BL21(DE3) pACYC-ADH, pET-BmoF1, pCOLA-PFE1. The bottom panel shows the mass spectrum of the hydrogenated product of (*Z*)-dec-4-enedioic acid, which is identical to that of the authentic compound decane-1,10-dioic acid.

and 12-oxododec-9-enoic acid by a recombinant *S. cerevisiae* expressing a soybean lipoxygenase and watermelon hydroperoxide lyase.[20] However, the productivity of the biocatalysts appeared to be limited due to the low expression level of the plant enzymes in the microbial cells.

This study herein demonstrated that a variety of the industrially relevant fatty acids and carboxylic acids (i.e., (6*Z*,9*Z*)-13-hydroxyoctadeca-6,9-dienoic acid (**2**), (6*Z*,9*Z*)-12-hydroxydodeca-6,9-dienoic acid (**7**), (*Z*)-9-hydroxynon-6-enoic acid (**15**), (4*Z*,7*Z*)-trideca-4,7-dienedioic acid (**9**), and (*Z*)-dec-4-enedioic acid (**17**)) could be produced from renewable fatty acids (i.e., γ-linolenic acid) by using artificial multistep enzyme reaction pathways (Figures 1 and 5). The synthetic pathways were composed of enzymes originating solely from bacteria, which could be overexpressed easily in functional forms in bacterial cells.

Some of the key enzymes in the biotransformations reported herein are the BVMOs. The regiospecificity of the enzymes was crucial for providing access to the desired reaction products (Figures 1 and 5). The BVMOs (EC 1.4.13.22) catalyzed the insertion of oxygen into the carbon skeletons adjacent to the carbonyl groups.[36−38] The regiochemistry of the reaction was governed by predictable conformational, steric, and electronic effects as the rearrangement process of the tetrahedral peroxo Criegee intermediate proceeded with strict retention of configuration. Common representative substrates were simple cyclic ketones (e.g., cyclobutanone, cyclopentanone, cyclohexanone, and cycloheptanone), chiral cyclic ketones (e.g., 2-methylcyclopentanone and bicyclo[3.2.0]hept-2-en-6-one), and aliphatic ketones (e.g., 2-octanone).[38] Most BVMOs discovered so far showed catalytic activity for the oxygenation of simple cyclic ketones and chiral cyclic ketones, and only a small number of BVMOs including the BVMO from *P. fluorescens* DSM 50106,[30] *P. putida* KT2440,[27,39] *R. jostii* RHA1,[40] *P. veronii* MEK700,[26] *P. cepacia*,[28] and *Mycobacterium tuberculosis*[29] were found to be active with aliphatic ketones.

The present study herein demonstrated that product profiles of the novel biosynthetic pathways (Figures 1 and 5) were dependent on the catalytic activity, but they were especially dependent on the regioselectivity of the BVMOs (Figures 3 and 6). The BVMO originating from *P. fluorescens* DSM 50106 catalyzed the normal ester formation with (6*Z*,9*Z*)-13-oxooctadeca-6,9-dienoic acid (**3**), which was driven by migration of the more-substituted carbon center during BVMO catalysis (Figure 3A). However, the BVMO from *P. putida* KT2440 showed a quite high activity toward the abnormal ester formation[32,33] in the case of (6*Z*,9*Z*)-13-oxooctadeca-6,9-dienoic acid (**3**) (Figure 3B). Notably, the BVMO from *P. fluorescens* DSM 50106 catalyzed the abnormal ester formation of (6*Z*,12*Z*)-10-oxooctadeca-6,12-dienoic acid (**11**), thus resulting in the production of 1,10-dec-6-enedioic acid (Figure 6B). Unfortunately, the BVMOs from *P. fluorescens* DSM 50106 and *P. putida* KT2440 were too unstable to allow for the proper investigation of their kinetic properties and their 3-D structures. As a result, a detailed investigation of their regioselectivity is currently severely hampered.

In summary, we demonstrated that a variety of plant oxylipins (i.e., (6*Z*,9*Z*)-13-hydroxyoctadeca-6,9-dienoic acid (**2**), (6*Z*,9*Z*)-12-hydroxydodeca-6,9-dienoic acid (**7**), (*Z*)-9-hydroxynon-6-enoic acid (**15**), (4*Z*,7*Z*)-trideca-4,7-dienedioic acid (**9**), and (*Z*)-dec-4-enedioic acid (**17**)) could be produced from a renewable fatty acid (i.e., γ-linolenic acid) via the regioselective BVMO-based whole-cell biocatalysis. This study will contribute to the preparation of industrially relevant unsaturated carboxylic acids.

DOI: 10.1021/jf5058843
J. Agric. Food Chem. 2015, 63, 2773−2781

■ ASSOCIATED CONTENT

Supporting Information

Table S1 and Figures S1−S7. This material is available free of charge via the Internet at http://pubs.acs.org.

■ AUTHOR INFORMATION

Corresponding Author

*(J.-B.P.) E-mail: jbpark06@ewha.ac.kr.

Funding

This study was supported by a Marine Biomaterials Research Center grant from the Marine Biotechnology Program funded by the Ministry of Oceans and Fisheries, Korea.

Notes

The authors declare no competing financial interest.

■ REFERENCES

(1) Rodriguez, G. M.; Tashiro, Y.; Atsumi, S. Expanding ester biosynthesis in *Escherichia coli*. *Nat. Chem. Biol.* **2014**, *10*, 259−265.

(2) Bornscheuer, U. T.; Huisman, G. W.; Kazlauskas, R. J.; Lutz, S.; Moore, J. C.; Robins, K. Engineering the third wave of biocatalysis. *Nature* **2012**, *485*, 185−194.

(3) Lee, J. W.; Na, D.; Park, J. M.; Lee, J.; Choi, S.; Lee, S. Y. Systems metabolic engineering of microorganisms for natural and non-natural chemicals. *Nat. Chem. Biol.* **2012**, *8*, 536−546.

(4) Bornscheuer, U. T. Enzymes in lipid modification: past achievements and current trends. *Eur. J. Lipid Sci. Technol.* **2014**, *116*, 1322−1331.

(5) Lin, Y.; Jain, R.; Yan, Y. Microbial production of antioxidant food ingredients via metabolic engineering. *Curr. Opin. Biotechnol.* **2014**, *26*, 71−78.

(6) Zhao, S.; Kumar, R.; Sakai, A.; Vetting, M. W.; Wood, B. M.; Brown, S.; Bonanno, J. B.; Hillerich, B. S.; Seidel, R. D.; Babbitt, P. C.; Almo, S. C.; Sweedler, J. V.; Gerlt, J. A.; Cronan, J. E.; Jacobson, M. P. Discovery of new enzymes and metabolic pathways by using structure and genome context. *Nature* **2013**, *502*, 698−702.

(7) Zhou, J.; Du, G.; Chen, J. Novel fermentation processes for manufacturing plant natural products. *Curr. Opin. Biotechnol.* **2014**, *25*, 17−23.

(8) Paddon, C. J.; Westfall, P. J.; Pitera, D. J.; Benjamin, K.; Fisher, K.; McPhee, D.; Leavell, M. D.; Tai, A.; Main, A.; Eng, D.; Polichuk, D. R.; Teoh, K. H.; Reed, D. W.; Treynor, T.; Lenihan, J.; Fleck, M.; Bajad, S.; Dang, G.; Dengrove, D.; Diola, D.; Dorin, G.; Ellens, K. W.; Fickes, S.; Galazzo, J.; Gaucher, S. P.; Geistlinger, T.; Henry, R.; Hepp, M.; Horning, T.; Iqbal, T.; Jiang, H.; Kizer, L.; Lieu, B.; Melis, D.; Moss, N.; Regentin, R.; Secrest, S.; Tsuruta, H.; Vazquez, R.; Westblade, L. F.; Xu, L.; Yu, M.; Zhang, Y.; Zhao, L.; Lievense, J.; Covello, P. S.; Keasling, J. D.; Reiling, K. K.; Renninger, N. S.; Newman, J. D. High-level semi-synthetic production of the potent antimalarial artemisinin. *Nature* **2013**, *496*, 528−532.

(9) Jetter, R.; Kunst, L. Plant surface lipid biosynthetic pathways and their utility for metabolic engineering of waxes and hydrocarbon biofuels. *Plant J.* **2008**, *54*, 670−683.

(10) Kishimoto, Y.; Radin, N. Occurrence of 2-hydroxy fatty acids in animal tissues. *J. Lipid Res.* **1963**, *4*, 139−143.

(11) Kock, J. L. F.; Strauss, C. J.; Pohl, C. H.; Nigam, S. The distribution of 3-hydroxy oxylipins in fungi. *Prostaglandins Other Lipid Mediat.* **2003**, *71*, 85−96.

(12) Joo, Y. C.; Oh, D. K. Lipoxygenases: potential starting biocatalysts for the synthesis of signaling compounds. *Biotechnol. Adv.* **2012**, *30*, 1524−1532.

(13) Kim, K. R.; Oh, D. K. Production of hydroxy fatty acids by microbial fatty acid-hydroxylation enzymes. *Biotechnol. Adv.* **2013**, *31*, 1473−1485.

(14) Suzuki, Y.; Kurita, O.; Kono, Y.; Hyakutake, H.; Sakurai, A. Strcture of a new antifungal C11-hydroxyfatty acid isolated from leaves of wild rice (*Oryza officinalis*). *Biosci., Biotechnol. Biochem.* **1995**, *59*, 2049−2051.

(15) Mukhtarova, L. S.; Mukhitova, F. K.; Gogolev, Y. V.; Grechkin, A. N. Hydroperoxide lyase cascade in pea seedlings: non-volatile oxylipins and their age and stress dependent alterations. *Phytochemistry* **2011**, *72*, 356−364.

(16) Griehl, W.; Ruestem, D. Nylon-12 preparation, properties and applications. *Ind. Eng. Chem.* **1970**, *62*, 16−22.

(17) Xu, J.; Guo, B. H. *Microbial Succinic Acid, Its Polymer Poly(butylene succinate), and Applications*; Springer: Berlin, Germany, 2010; pp 347−388.

(18) Kroha, K. Industrial biotechnology provides opportunities for commercial production of new long-chain dibasic acids. *INFORM−Champaign* **2004**, *15*, 568−571.

(19) Otte, K. B.; Kirtz, M.; Nestl, B. M.; Hauer, B. Synthesis of 9-oxononanoic acid, a precursor for biopolymers. *ChemSusChem* **2013**, *6*, 2149−2156.

(20) Buchhaupt, M.; Guder, J. C.; Etschmann, M. M. W.; Schrader, J. Synthesis of green note aroma compounds by biotransformation of fatty acids using yeast cells coexpressing lipoxygenase and hydroperoxide lyase. *Appl. Microbiol. Biotechnol.* **2012**, *93*, 159−168.

(21) Song, J. W.; Jeon, E. Y.; Song, D. H.; Jang, H. Y.; Bornscheuer, U. T.; Oh, D. K.; Park, J. B. Multistep enzymatic synthesis of long-chain α,ω-dicarboxylic and ω-hydroxycarboxylic acids from renewable fatty acids and plant oils. *Angew. Chem. Int. Ed.* **2013**, *52*, 2534−2537.

(22) Oh, H. Y.; Kim, S. U.; Song, J. W.; Lee, J. H.; Kang, W. R.; Jo, Y. S.; Kim, K. R.; Bornscheuer, U.; Oh, D. K.; Park, J. B. Biotransformation of linoleic acid into hydroxy fatty acids and carboxylic acids using a linoleate double bond hydratase as key enzyme. *Adv. Synth. Catal.* **2014**, *357*, 408−416.

(23) Yu, I. S.; Yeom, S. J.; Kim, H. J.; Lee, J. K.; Kim, Y. H.; Oh, D. K. Substrate specificity of *Stenotrophomonas nitritireducens* in the hydroxylation of unsaturated fatty acid. *Appl. Microbiol. Biotechnol.* **2008**, *78*, 157−163.

(24) Kim, K.-R.; Seo, M.-H.; Park, J.-B.; Oh, D.-K. Stereospecific production of 9*R*-hydroxy-10*E*,12*Z*-octadecadienoic acid from linoleic acid by recombinant *Escherichia coli* cells expressing 9*R*-lipoxygenase from *Nostoc* sp. SAG 25.82. *J. Mol. Catal. B: Enzym.* **2014**, *104*, 56−63.

(25) Yu, I.-S.; Kim, H.-J.; Oh, D.-K. Conversion of linoleic acid into 10-hydroxy-12(*Z*)-octadecenoic acid by whole cells of *Stenotrophomonas nitritireducens*. *Biotechnol. Prog.* **2008**, *24*, 182−186.

(26) Voelker, A.; Kirschner, A.; Bornscheuer, U. T.; Altenbuchner, J. Functional expression, purification, and characterization of the recombinant Baeyer-Villiger monooxygenase MekA from *Pseudomonas veronii* MEK700. *Appl. Microbiol. Biotechnol.* **2008**, *77*, 1251−1260.

(27) Rehdorf, J.; Kirschner, A.; Bornscheuer, U. T. Cloning, expression and characterization of a Baeyer-Villiger monooxygenase from *Pseudomonas putida* KT2440. *Biotechnol. Lett.* **2007**, *29*, 1393−1398.

(28) Britton, L.; Markovetz, A. A novel ketone monooxygenase from *Pseudomonas cepacia*. Purification and properties. *J. Biol. Chem.* **1977**, *252*, 8561−8566.

(29) Fraaije, M.; Kamerbeek, N.; Heidekamp, A.; Fortin, R.; Janssen, D. The prodrug activator EtaA from *Mycobacterium tuberculosis* is a Baeyer-Villiger monooxygenase. *J. Biol. Chem.* **2004**, *279*, 3354−3360.

(30) Kirschner, A.; Altenbuchner, J.; Bornscheuer, U. T. Cloning, expression, and characterization of a Baeyer-Villiger monooxygenase from *Pseudomonas fluorescens* DSM 50106 in *E. coli*. *Appl. Microbiol. Biotechnol.* **2007**, *73*, 1065−1072.

(31) Cho, J. Y.; Moon, J. H.; Eun, J. B.; Chung, S. J.; Park, K. H. Isolation and characterization of 3(*Z*)-dodecenedioic acid as an antibacterial substance from *Hovenia dulcis* THUNB. *Food Sci. Biotechnol.* **2014**, *13*, 46−50.

(32) Rehdorf, J.; Mihovilovic, M. D.; Bornscheuer, U. T. Exploiting the regioselectivity of Baeyer-Villiger monooxygenases for the formation of β-amino acids and β-amino alcohols. *Angew. Chem. Int. Ed.* **2010**, *49*, 4506−4508.

(33) Noyori, R.; Sato, T.; Kobayashi, H. Remote substituent effects in the Baeyer-Villiger oxidation. I. Through-bond γ substituent effect on the regioselectivity. *Tetrahedron Lett.* **1980**, *21*, 2569−2576.

DOI: 10.1021/jf5058843
J. Agric. Food Chem. 2015, 63, 2773−2781

(34) Kockritz, A.; Martin, A. Synthesis of azelaic acid from vegetable oil-based feedstocks. *Eur. J. Lipid Sci. Technol.* **2011**, *113*, 83−91.
(35) Zhang, F.; Huang, C. H.; Xu, T. W. Production of sebacic acid using two-phase bipolar membrane electrodialysis. *Ind. Eng. Chem. Res.* **2009**, *48*, 7482−7488.
(36) Schmid, R. D.; Urlacher, V. *Modern Biooxidation: Enzymes, Reactions and Applications*; Wiley-VCH: Weinheim, Germany, 2007; pp 77−97.
(37) Orru, R.; Dudek, H. M.; Martinoli, C.; Pazmino, D. E. T.; Royant, A.; Weik, M.; Fraaije, M. W.; Mattevi, A. Snapshots of enzymatic Baeyer-Villiger catalysis; oxygen activation and intermediate stabilization. *J. Biol. Chem.* **2011**, *286*, 29284−29291.
(38) de Gonzalo, G.; Mihovilovic, M. D.; Fraaije, M. W. Recent developments in the application of Baeyer-Villiger monooxygenases as biocatalysts. *ChemBioChem* **2010**, *11*, 2208−2231.
(39) Song, J.-W.; Lee, J.-H.; Bornscheuer, U. T.; Park, J.-B. Microbial synthesis of medium chain α,ω-dicarboxylic acids and ω-amino-carboxylic acids from renewable long chain fatty acids. *Adv. Synth. Catal.* **2014**, *356*, 1782−1786.
(40) Szolkowy, C.; Eltis, L. D.; Bruce, N. C.; Grogan, G. Insights into sequence-activity relationships amongst Baeyer-Villiger monooxygenases as revealed by the intragenomic complement of enzymes from *Rhodococcus jostii* RHA1. *ChemBioChem* **2009**, *10*, 1208−1217.

DOI: 10.1021/jf5058843
J. Agric. Food Chem. 2015, 63, 2773−2781

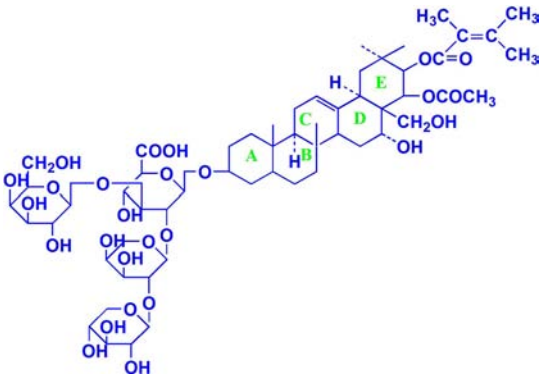

Figure 1. Chemical structural formula of tea saponin.

retardant systems. Using TS in intumescent flame retardant coatings could provide a new idea for the research and development of green flame retardant coatings as well as open up new avenues for its utilization. On the other hand, there could be a potential application and economic prospect of TS-IFRCs because TS has the advantages of being rich, renewable, biodegradable, and environmentally friendly. The coatings were formulated based on TS, APP, and PER. The flame retardant properties of TS-IFRCs were evaluated by limited oxygen index (LOI), smoke density (SDR), and ignition temperature (IT), and the combustion characteristics of TS-IFRCs were tested by cone calorimetry (CONE). Thermal analysis and scanning electron microscopy observations were also conducted.

MATERIALS AND METHODS

Materials. Ammonium polyphosphate (APP, $n > 1000$, industrial) was provided by Zhejiang Longyou Gede Chemical Corp. Alkyd varnish (commercial product), with a medium oil length and solid content of 48.26%, was produced by Hunan Xiangjiang Coating Group. Pentaerythritol (PER, AR) was provided by Kermel Tianjin Chemical Reagent Development Center. Tea saponin (TS, industrial) is a kind of saponin mixture extracted from *C. oleifera* cake, and the content of TS is approximately 60%. Melamine (MEL, CP) was produced by Sinopharm Chemical Reagent Co., Ltd. Three-layer plywood and wood board (Chinese fir) were used as substrates for painting.

Preparation of TS-IFRCs. The TS-IFRCs were prepared by compounding intumescent flame retardants containing APP, PER, and TS (with weight ratios of 15:4:1, 15:7:3, and 15:7:1, respectively) with alkyd varnish; the weight ratio of intumescent flame retardants and alkyd varnish was 3:2. Dispersing agents and other additives were also introduced to improve the overall properties of the coatings. Figure 2 shows the preparation process of TS-IFRCs. In addition, the traditional intumescent flame retardant coatings containing melamine (MEL-IFRC) were selected as a comparison. To make the comparison representative, many screening experiments were also conducted on the basis of previously studied works[26,27] to determine the weight ratio among APP:PER:MEL of MEL-IFRC to be 12:7:1.5 or 24:14:3. In this case, the comparison showed good flame retardancy.

Residue and Expansion Rate Measurement. Residue and expansion rate of the TS-IFRCs with various contents of TS were measured to determine the best formulation of the TS-IFRCs. Liquid flame retardant coatings were poured into the mold and cured at 23 ± 2 °C for 15 days in a ventilated environment. The samples for the test were prepared by cutting cured coatings into pieces of the size of 30 mm × 10 mm × 3 mm (about 1.5 g, accurate to 0.1 mg). Then the samples were placed in an SX-12-10 type box resistance furnace at a constant temperature of 400 °C for 10 min to measure the residue (g carbon/g sample) and expansion rate (mL/g). The residue and expansion rate of coatings were calculated according to the following formulas, respectively.

$$\text{residue} = \frac{\text{wt of carbon residue after heating } (G_2)}{\text{wt of sample } (G_1)}$$

$$\text{expansion rate} = \frac{\text{vol changes before and after heating } (\Delta V)}{\text{wt of sample } (G_1)}$$

Flame Retardancy and Smoke Suppression Tests. The effect of TS on flame retardancy and smoke suppression in the TS-IFRCs was evaluated by means of limiting oxygen index (LOI), ignition temperature (IT), and smoke density measurement (SD). The test samples were prepared in the same way of painting the liquid TS-IFRCs on three-layer plywood twice; the coated plates were dried at 23 ± 2 °C for 15 days in a ventilated environment. The coated weight was about 500 g/m^2, and total thickness of dry film was 1 mm. The LOI tests of the coated plates (140 mm × 6.5 mm × 3 mm) were performed by a JF-3 type oxygen index apparatus (ISO 4589 standard). A JCY-1 material smoke density tester was employed to measure smoke density (coated plates, 30 mm × 30 mm × 3 mm). The ignition temperature was tested on a DW-02 ignition temperature tester (curing coating after crushing and sieving, D = 0.5−1.0 mm).

Analysis of Cone Calorimetry. The combustion behavior of the coated plates (wood boards, 100 mm × 100 mm × 10 mm, coated 500 g/m^2) was investigated by cone calorimetry according to the ISO 5660-1 standard. The test samples were prepared in a similar way as above with regard to painting the liquid TS-IFRCs on wood boards twice; the coated plates were dried at 23 ± 2 °C for 15 days in a ventilated environment. The coated weight was about 500 g/m^2, and total thickness of dry film was 1 mm. The test coated plates were heated after being wrapped in aluminum foil with the upper surface exposed. The measurements were conducted for three replicates per sample under an irradiative heat flow of 50 kW/m^2 horizontally, following the procedure described by Alongi.[9,28] Parameters such as total heat release (THR, kW/m^2), heat release rate (HRR, kW/m^2), effective heat of combustion (EHC, kJ/kg), mass loss rate (MLR, g/s), and total smoke release (TSR, m^2/m^2) were measured. For comparisons, the plates were coated with alkyd varnish and MEL-

Figure 2. Process flow of the preparation of TS-IFRCs.

DOI: 10.1021/jf505898d
J. Agric. Food Chem. 2015, 63, 2782−2788

IFRC with the weight ratio among APP, PER, and MEL of 24:14:3, respectively.

Simultaneous Thermal Analysis of TS-IFRCs. The thermal stability of TS-IFRCs was evaluated by thermogravimetric analyses (TG) and differential scanning calorimetry (DSC) analyses using a NETZSCH STA 449 F3 Jupiter simultaneous thermal analyzer according to the ISO 11357 standard. The measurements were performed for three replicates per sample by placing the samples in open alumina pans (ca. 8.0 ± 0.5 mg) under nitrogen purge (20 cm^3/min) over the whole range of temperature from 40 to 800 °C at a heating rate of 10 °C/min. TG, DTG, and DSC analyses were obtained by using Origin Software 8.0.

Scanning Electron Microscopy (SEM) Observations. SEM observations of the char layer of TS-IFRC sample after being heated at 400 °C for 10 min were performed by a FEI Quanta 450 scanning electron microscope operated at 15 kV and 200× and 1000× levels of magnification.

RESULTS AND DISCUSSION

Thermal Analysis of TS-IFRCs. As seen from the TG-DTG curves in Figure 3a, the thermal degradation process of TS-IFRCs can be broadly divided into three stages. The temperature ranging from 177 to 276 °C is the minor weight loss stage for the total weight loss of 10.4%, which may be caused by the initial thermal decomposition reaction of TS-IFRCs, including the deamination of APP and dehydration of TS to generate noncombustible gas NH_3 and H_2O.[6] In the second stage ranging from 276 to 392 °C, the serious weight loss stage was monitored with a weight loss of 31.6%. At this stage APP, TS, PER, and alkyd resin pyrolyzed severely, and a large amount of gas was generated to form a rich intumescent char layer with catalysis by APP, hindering the decomposition of the TS-IFRCs. The temperature of the third thermal degradation stage was from 392 to 600 °C, and the weight loss was 13.3%. On the other hand, the thermal degradation curves of TS-IFRCs were basically consistent with the curves of MEL-IFRC, whereas the weight loss rate was lower than that of MEL-IFRC; the residue weight of TS-IFRCs during the degradation process was obviously higher than that of MEL-IFRC, and the final weight residual was 39.0%, much higher than the 31.1% of MEL-IFRC and 11.1% of alkyd resin, which indicated that TS combined with other components had a good influence on thermostability. The thermal degradation was weakened, and the carbon residue and thermal stability of the flame retardant coatings were improved effectively.

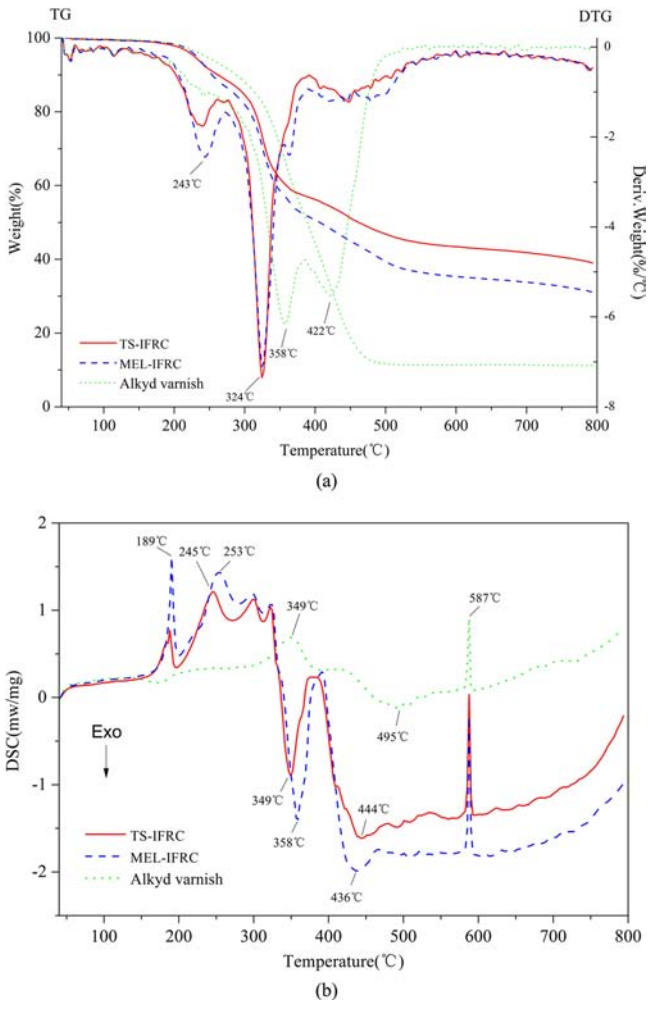

Figure 3. TG-DTG (a) and DSC (b) curves of TS-IFRCs.

DSC curves in Figure 3b revealed that there are mainly two endothermic regions and two exothermic regions during the whole degradation process. At the first endothermic region of the temperature ranging from 160 to 200 °C, there was a sharp endothermic peak at 189 °C, which can be interpreted as the amount of heat needed to be concentrated for the preliminary decomposition of volatile substance released from TS-IFRCs. The temperature ranging from 200 to 320 °C was the second endothermic region, in which there were three small continuous endothermic peaks at temperatures of 245, 300, and 323 °C, respectively. At this region, the TS-IFRCs system continued to absorb heat to concentrate energy for the decomposition of TS-IFRCs and charring, which corresponded to early in the second stage of thermal degradation. Although with the temperature increasing, the flame retardant coating system was decomposed, a lot of heat was released to form the first exothermic region from 330 to 380 °C with a sharp exothermic peak at 349 °C. The second exothermic region was around the temperature of 444 °C, with a wide exothermic peak, owing to the continuous heat released from the decomposition of flame retardant intumescent char layer with the temperature increasing, which corresponds with the third stage of thermal degradation. On the other hand, at the high temperature of 587 °C, it is evident that there was also a sharp endothermic peak, which may be interpreted as a phase change occurring for a sublimation of residue char within a large amount of heat. Compared with the heat release process of the MEL-IFRC, the endothermic peak at 253 °C and the exothermic peak at 358 °C of TS-IFRCs were shifted to the low-temperature area, which was beneficial to the formation of intumescent char layer at low temperature. Furthermore, during the thermal decomposition process, the levels of heat absorption and heat release of TS-IFRCs were larger than those of alkyd resin, but were significantly smaller than those of MEL-IFRC. It was demonstrated that TS-IFRCs had less dependence on heat demand or contribution from outside, which was conducive to slowing the rate of the pyrolysis process and was crucial to the flame retardancy of TS-IFRCs.

From the above, the degradation mechanism can be simply interpreted as APP and PER having nearly no weight loss before 200 °C, whereas TS decomposed with a small weight loss of about 10% at the range from 80 to 190 °C, which mainly eliminated a lot of water vapor to retard oxygen gas and heat. Therefore, we consider this stage as a gas phase flame retardant mechanism before 200 °C. With the decomposition of TS-

DOI: 10.1021/jf505898d
J. Agric. Food Chem. 2015, 63, 2782−2788

IFRCs, APP began to decompose at about 300 °C, eliminating ammonia and water, and interacted with PER to form the char structure, whereas TS involved a key weight loss ranging from 200 to 500 °C, eliminating water and carbon dioxide, which could blow the char formed by APP, PER, and itself to form a uniform and compact intumescent charring layer, which is effective for good thermal and oxygen blockage. We consider this stage as a condensed phase flame retardant mechanism.

Effects of TS on Residue and Expansion Rate of TS-IFRCs. The effects of TS on the performance of TS-IFRCs were studied by fixing the weight ratio of APP and PER in flame retardant systems of TS-IFRCs. The effects of the content of TS on residue and expansion properties of TS-IFRCs are shown in Table 1.

Table 1. Effects of Tea Saponin on Performance of TS-IFRCs

sample[a]	flame retardant coating formulation m(APP):m(PER):m(TS)	residue at 400 °C (g/g)	expansion rate (mL/g)
A_1	alkyd varnish + 40% IFR (12:7:1)	0.477	12
A_2	alkyd varnish + 40% IFR (12:7:3)	0.511	10
A_3	alkyd varnish + 40% IFR (12:7:6)	0.353	9
A_4	alkyd varnish + 40% IFR (12:7:9)	0.332	4
A_5	alkyd varnish + 40% IFR (12:7:12)	0.348	6
B_1	alkyd varnish + 40% IFR (24:14:3)	0.359	8
B_2	alkyd varnish	0.906	3

[a]B_1 refers to melamine comparison, with the flame retardant formula APP:PER:MEL = 24:14:3; B_2 refers to alkyd varnish comparison.

It was shown that TS as blowing agent and carbon source with a different weight ratio in intumescent flame retardant systems can obviously affect the residue and expansion rate of coatings. For A_1 and A_2 with weight ratios of 12:7:1 and 12:7:3 in the TS-IFRC system, the char residues were 0.477 and 0.511 g/g, respectively, higher than the 0.359 g/g of B_2, which contains MEL as blowing agent. The expansion rates of A_1 and A_2 (12 and 10 mL/g, respectively) were also significantly superior to those of alkyd varnishes and MEL-IFRC (B_2 and B_1). The well-developed intumescent char layer could decrease the destruction of gas flow and heat flow and isolate the oxygen, which was effective in retarding the tendency of the fire. However, with the weight ratio of TS increased, the residue and expansion rate of TS-IFRCs decreased. This could possibly be explained by the fact that TS was rich in carbon and hydroxyl groups; as a result, it could promote the formation of char layer during heating and release H_2O, CO_2, and other nonflammable gas to protect the intumescent char layer. However, when the content of TS was too high, as observed in the test, the gas released in the process of thermal decomposition was too much and resulted in the burst of the expanding bubble in char layer, so the quality of the fire retardant char layer was reduced, and, as a result, the effects of flame retardancy and heat insulation were reduced.

Flame Retardant Performance Analysis of TS-IFRCs. As seen from Table 2, when a certain amount of TS was contained in the coatings, the limited oxygen index and ignition temperature were substantially improved: the LOI increased from 24.2 to 43.8%, and the ignition temperature increased from 245 to 310 °C. Compared with the MEL-IFRC plate with a LOI of 38.6%, TS-IFRC plates had some obvious advantages, and the ignition temperature was also slightly higher. It was found that the smoke densities of TS-IFRC plates of different

Table 2. Flame Retardant Performance Indices of TS-IFRCs

sample[a]	LOI (%)	IT (°C)	SDR (g/m^3)
A_1*	43.8 ± 0.06	305 ± 2.9	60.47 ± 2.42
A_2*	38.8 ± 0.12	310 ± 2.9	26.61 ± 1.81
B_1*	38.6 ± 0.06	305 ± 2.9	53.21 ± 2.49
B_2*	38.0 ± 0.12		42.25 ± 2.19
B_3*	24.2 ± 0.12	245 ± 2.9	9.61 ± 0.38

[a]A_1* and A_2* refer to TS-IFRC plates, with the flame retardant formula APP:PER:TS = 15:4:1, 15:7:3, respectively; B_1* refers to MEL-IFRC plate as a comparison, with the flame retardant formula APP:PER:MEL = 24:14:3; B_2* refers to flame retardant coating plate without TS, with the flame retardant formula APP:PER:TS = 12:7:0; B_3* refers to alkyd varnish coating plate as a comparison.

proportions are quite different. When the weight ratio of APP, PER, and TS was 15:7:3 in the TS-IFRCs system, the smoke density with only 26.61 g/m^3 was far lower than those of MEL-IFRC plate and flame retardant coating plate without TS, which greatly reduced the potential danger of the combustion of flame retardant coating plates, whereas when the weight ratio of APP, PER, and TS was 15:4:1, the smoke density was 60.47 g/m^3.

In addition, as seen from SEM micrographs of the outer surface of char layer of TS -IFRC plates at 200× and 1000× magnification, respectively, in Figure 4, at high temperature the

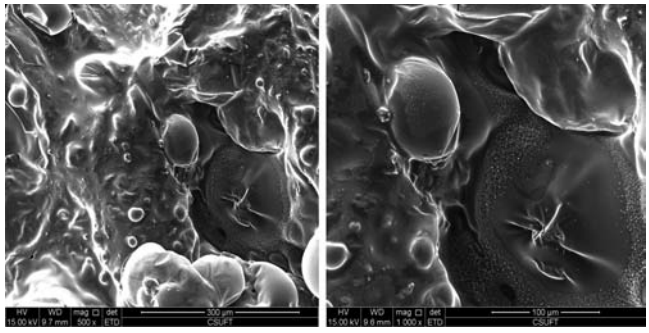

Figure 4. SEM micrographs of intumescent char layer of TS-IFRCs.

surface of flame retardant coating plates formed a well-developed intumescent char layer with a lot of expanding bubbles, and the structure of the intumescent char layer was dense and uniform, which was conductive to decreasing the thermal conductivity coefficient between the intumescent char layer and the substrate; the intumescent char layer effectively prevents oxygen flow and heat flux from eroding into the matrix. It could be explained that TS, being rich in carbon source, can cooperate with PER to play a key role in strengthening the quality of the char layer and preventing the intumescent char layer from being damaged by air flow and heat to decrease the efficiency of flame retardant coatings.

Combustion Performance Analysis of TS-IFRCs. At present, the cone calorimeter test is considered to be an effective way to simulate actual fire burning behavior due to its good correlation with large-scale combustion experiments, which can accurately measure the mass loss rate, heat release rate, smoke production rate, content of toxic gases, and other parameters of materials in the event of burning. Therefore, it was not surprising that the cone calorimeter was increasingly found to be a characterization tool in the research and development of flame retardant materials internationally.[29−32]

Heat release rate (HRR) is an important parameter indicating the spread trends of a fire and the degree of fire

DOI: 10.1021/jf505898d
J. Agric. Food Chem. 2015, 63, 2782−2788

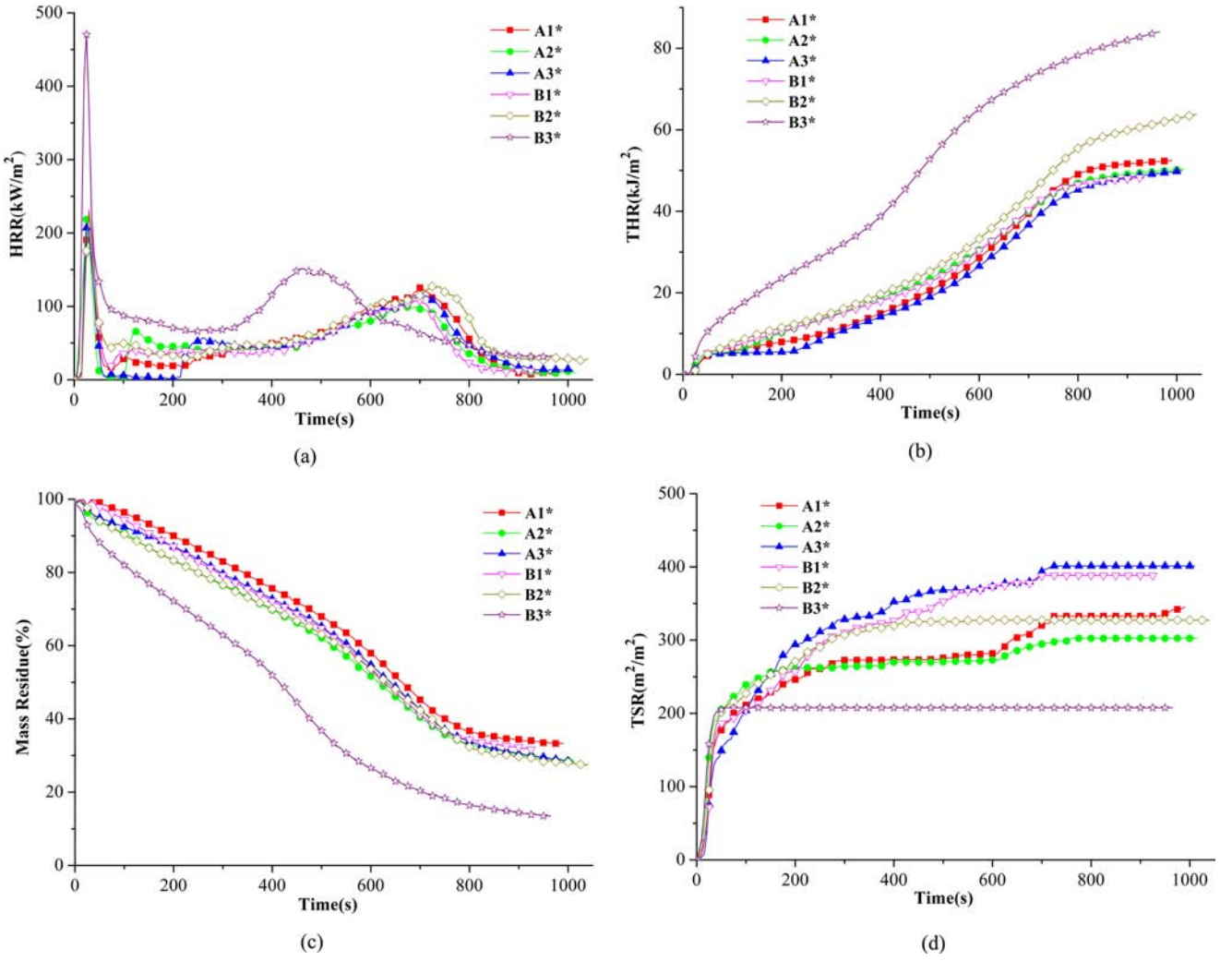

Figure 5. Cone calorimetery test curves of TS-IFRC plates: (a) heat release rate curves; (b) total heat release curves; (c) mass residual curves; (d) total smoke release curves.

hazard. The greater the value of HRR is, the greater the degree of fire risk.[33] The peak heat release rate (pk-HRR), the maximum value of HRR, determines the scale of the fire greatly.[28] The heat release rate curves of different formulations of TS-IFRC plates under the thermal radiation power of 50 kW/m^2 are shown in Figure 5a.

Table 3 and Figure 5a show that the pk-HRR of TS-IFRC plates (190.62 kW/m^2) was significantly lower than that of flame retardant coating plate without TS (227.52 kW/m^2) and MEL-IFRC plate (231.57 kW/m^2). At the same time, the m-HRR of TS-IFRC plates was lower by 25.16 and 6.5% than those of flame retardant coating plate without TS and MEL-IFRC plate, respectively. It was also illustrated that there were two pk-HRR in the combustion process of the flame retardant coating plates. The first pk-HRR came almost at the time of about 25−30 s; subsequently, the HRR of TS-IFRC reduced significantly at a certain degree. Particularly after the first pk-HRR, the A_2* and A_3* plates coated with TS-IFRCs smoldered for 55 and 165 s, respectively, the HRR of which almost decreased to 0, which successfully limited the growth of the fire. Specifically, the HRR of TS-IFRC plates was always obviously lower than those of MEL-IFRC plate and flame retardant coating plate without TS in the entire combustion process, which indicated that the addition of TS can inhibit the HRR of TS-IFRC plates, slow the process of the combustion, and effectively reduce the risk of fire.

From Table 3 and Figure 5b, it is shown that the THR values of TS-IFRC plates were much lower than those of MEL-IFRC plate and the flame retardant coating plate without TS in the entire combustion process. In addition, the THR values of A_3* were reduced by 68.42 and 27.88%, respectively, compared with the alkyd varnish and flame retardant coating plate without TS, which is a key factor to control the scale and spread of the fire.[31]

The mean effective heats of combustion (m-EHC) of the TS-IFRC plates shown in Table 3 were much superior to those of MEL-IFRC plate and flame retardant coating plate without TS. Especially, the values of A_3* being 9.95 KJ/kg decreased by 33.78%, compared with that of the flame retardant coating plate without TS. It could be explained that the addition of the blowing agent (TS) played an extremely important role in making the formation of the intumescent protective char layer rapid, which successfully slowed the accumulation of the heat in the system.

The mass loss of TS-IFRC plates is shown in Table 3 and Figure 5c. The mean mass loss rates (m-MLR) of A_1* and A_3* were slightly higher than those of MEL-IFRC plate and flame retardant coating plate without TS, but the m-MLR of the A_2*

DOI: 10.1021/jf505898d
J. Agric. Food Chem. 2015, 63, 2782−2788

Table 3. Combustion Performance Parameters of Cone Calorimeter Test

sample[a]	pk-HRR (kW/m^2)	m-HRR (kW/m^2)	THR (kJ/m^2)	m-EHC (kJ/kg)	m-MLR (g/s)	TSR (m^2/m^2)	m-SEA (m^2/kg)	m-COY (kg/kg)	m-CO_2Y (kg/kg)
A_1*	190.62 ± 6.23	53.52 ± 2.39	52.45 ± 1.50	10.75 ± 0.36	0.0467 ± 0.0012	337.59 ± 10.15	125.18 ± 6.50	0.0588 ± 0.0013	1.0014 ± 0.0039
A_2*	218.37 ± 5.09	49.81 ± 1.10	50.32 ± 1.33	10.87 ± 0.22	0.0405 ± 0.0005	302.46 ± 7.55	209.89 ± 8.19	0.0782 ± 0.0021	1.0176 ± 0.0017
A_3*	206.94 ± 7.55	49.90 ± 2.05	49.90 ± 1.73	9.95 ± 0.49	0.0442 ± 0.0006	397.36 ± 13.10	145.83 ± 6.24	0.0727 ± 0.0013	0.9145 ± 0.0012
B_1*	231.57 ± 3.61	53.03 ± 1.73	48.29 ± 1.54	10.84 ± 0.36	0.0430 ± 0.0020	363.91 ± 8.02	79.00 ± 4.43	0.0725 ± 0.0022	1.0019 ± 0.0006
B_2*	227.52 ± 8.61	62.34 ± 2.65	63.81 ± 2.65	13.31 ± 0.41	0.0412 ± 0.0014	313.22 ± 7.00	296.08 ± 8.54	0.0668 ± 0.0025	1.0873 ± 0.0019
B_3*	470.62 ± 11.14	87.91 ± 2.18	84.04 ± 2.39	16.05 ± 0.36	0.0484 ± 0.0009	197.37 ± 7.94	436.11 ± 13.37	0.0406 ± 0.0017	1.4594 ± 0.0015

[a]A_1*, A_2*, and A_3* refer to TS-IFRC plates, with the flame retardant formulas APP:PER:TS = 15:4:1, 15:7:3, 15:7:1, respectively; B_1* refers to MEL-IFRC plate as a comparison, with the flame retardant formula APP:PER:MEL = 24:14:3; B_2* refers to flame retardant coating plate without TS as a comparison, with the flame retardant formula APP:PER:TS = 12:7:0; B_3* refers to alkyd varnish coating plate as a comparison. Cone calorimeter test was carried out at a thermal radiation power of 50 kw/m^2.

was much lower than those of any other coatings, only 0.0405 g/s. Figure 5d shows that the mass residue of TS-IFRC plates was relatively higher than that of other coatings throughout the combustion process. At the time of 600 s the mass residue of A_1* was 57.91%, higher than the 53.37% of MEL-IFRC plate and 53.59% of flame retardant coating plate without TS, and much higher than the 26.59% of alkyd varnish coating plate. In addition, after the combustion, the mass residue of A_1* was still the highest at 33.41%, and the mass residues of the other TS-IFRC plates (A_2* and A_3*) were also quite high at 28.17 and 28.61%, respectively.

Furthermore, the properties of smoke release of TS-IFRC plates were studied by analyzing total smoke release (TSR), specific extinction area (SEA), CO yields (COY), and CO_2 yields (CO_2Y) collected by a cone calorimeter. The values of TSR, mean-SEA, mean-COY, and mean-CO_2Y are shown in Table 3, and the total smoke release curve is described in Figure 5d. From Table 3 and Figure 5d, it was concluded that there was a big difference among the TSR values of TS-IFRC plates with different flame retardant formulations; for example, the TSR values of A_1* and A_2* were always lower than the values of MEL-IFRC plate and flame retardant coating plate without TS in the early stage of combustion, but the TSR value of A_3* was the highest. As far as the mean-SEA was concerned, the SEA values of all TS-IFRC plates were decreased significantly, compared with those of flame retardant coating plate without TS and alkyd varnish coating plate, which indicated that TS was conducive to a small SEA value and a low smoke production of TS-IFRC plates during the combustion. In addition, the values of mean-COY and mean-CO_2Y showed that the decrease of CO yields of TS-IFRC plates was not apparent; only the COY value of A_1* was much less than those of the other flame retardant coating plates. The COY values of A_2* and A_3* were similar to that of MEL-IFRC plate, but were much higher than those of flame retardant coating plate without TS and alkyd varnish coating plate. At the same time, the CO_2Y values of TS-IFRC plates were approximate to each other among the flame retardant coating plates, but much lower than that of alkyd varnish coating plate, which can be explained by the incomplete combustion of TS-IFRCs, releasing more CO and less CO_2.

In this study, it was confirmed that the natural product tea saponin (TS) used in a dual role of blowing agent and carbon source in TS-IFRCs can play an important role in improving the flame retardancy, smoke release, and thermostability of TS-IFRCs. When the weight ratio of APP, PER, and TS is 15:4−7:1−3 for a certain addition in TS-IFRCs, the TS-IFRCs exhibited a pretty good flame retardancy, which effectively inhibited the heat release of TS-IFRC plates and reduced heat release rate, effective heat, and smoke release. Absolutely on the basis of this work, the mechanism of action of tea saponin in flame retardant coatings will be the focus of future study.

AUTHOR INFORMATION

Corresponding Author

*(X.-Z.L.) Phone: +86 073185623038. Fax: +86 073185623096. E-mail: rlxz@163.com.

Funding

The work is supported by the National Key Technology R&D Program in the 11th Five year Plan of the People's Republic of China (2009BADB1B0303), the Program of Education and Research of Guandong Province and Ministry of Education (2011B090400333), the Program of Hunan Provincial Innovation Foundation for Postgraduate (CX2012B324), and

DOI: 10.1021/jf505898d
J. Agric. Food Chem. 2015, 63, 2782−2788

the Program of Scientific Innovation Fund for Graduate of Central South University of Forestry and Technology (2010sx05).

Notes

The authors declare no competing financial interest.

■ ACKNOWLEDGMENTS

We acknowledge the support of Wen-Sheng Li, from the College of Chemistry and Chemical Engineering of Hunan University, and Sheng Zhang, from the School of Materials Science and Engineering of Central South University of Forestry and Technology.

■ ABBREVIATIONS USED

TS, tea saponin; APP, ammonium polyphosphate; PER, pentaerythritol; MEL, melamine; TS-IFRCs, tea saponin intumescent flame retardant coatings; MEL-IFRC, intumescent flame retardant coating containing melamine

■ REFERENCES

(1) Yew, M. C.; Ramli Sulong, N. H. Fire-resistive performance of intumescent flame-retardant coatings for steel. *Mater. Design* **2012**, *34*, 719−724.

(2) Gu, J. W.; Zhang, G. C.; Dong, S. L.; Zhang, Q. Y.; Kong, J. Study on preparation and fire-retardant mechanism analysis of intumescent flame-retardant coatings. *Surf. Coat. Technol.* **2007**, *201*, 7835−7841.

(3) Chou, C. S.; Lin, S. H.; Wang, C. I. Preparation and characterization of the intumescent fire retardant coating with a new flame retardant. *Adv. Powder Technol.* **2009**, *20* (2), 169−176.

(4) Carosio, F.; Alongi, J.; Malucelli, G. Layer by layer ammonium polyphosphate-based coatings for flame retardancy of polyester−cotton blends. *Carbohydr. Polym.* **2012**, *88* (4), 1460−1469.

(5) Bourbigot, S.; Le Bras, M.; Duquesne, S.; Rochery, M. Recent advances for intumescent polymers. *Macromol. Mater. Eng.* **2004**, *289* (6), 499−511.

(6) Duquesne, S.; Magnet, S.; Jama, C.; Delobel, R. Intumescent paints:fire protective coatings for metallic substrates. *Surf. Coat. Technol.* **2004**, *180*, 302−307.

(7) Wang, Z. Y.; Han, E. H.; Ke, W. Influence of nano-LDHs on char formation and fire-resistant properties of flame-retardant coating. *Prog. Org. Coat.* **2005**, *53*, 29−37.

(8) Ma, Z. L.; Zhao, M.; Hu, H. F.; Ding, H. T.; Zhang, J. Compatibilization of intumescent flame retardant/polypropylene composites based on α-methacrylic acid grafted polypropylene. *J. Appl. Polym. Sci.* **2002**, *83*, 3128−3132.

(9) Alongi, J.; Poskovic, M.; Frache, A.; Malucelli, G. Cyclodextrin nanosponges as novel green flame retardants for PP, LLDPE and PA6. *Carbohydr. Polym.* **2012**, *88* (4), 1387−1394.

(10) Alongi, J.; Poskovic, M.; Frache, A.; Trotta, F. Novel flame retardants containing cyclodextrin nanosponges and phosphorus compounds to enhance EVA combustion properties. *Polym. Degrad. Stab.* **2010**, *95*, 2093−2100.

(11) Feng, J. X.; Su, S. P.; Zhu, J. An intumescent flame retardant system using β-cyclodextrin as a carbon source in polylactic acid (PLA). *Polym. Adv. Technol.* **2011**, *22*, 1115−1122.

(12) Le Bras, M.; Bourbigot, S.; Le Tallec, Y.; Laureyns, J. Synergy in intumescence-application to β-cyclodextrin carbonisation agent in intumescent additives for fire retardant polyethylene formulations. *Polym. Degrad. Stab.* **1997**, *56*, 11−21.

(13) Alongi, J.; Carletto, R. A.; Blasio, A.; Di Cuttica, F.; Carosio, F.; Bosco, F.; Malucelli, G. Intrinsic intumescent-like flame retardant properties of DNA-treated cotton fabrics. *Carbohydr. Polym.* **2013**, *96* (1), 296−304.

(14) Bosco, F.; Carletto, R. A.; Alongi, J.; Marmo, L.; Blasio, A. Di.; Malucelli, G. Thermal stability and flame resistance of cotton fabrics treated with whey proteins. *Carbohydr. Polym.* **2013**, *94* (1), 372−377.

(15) Alongi, J.; Carletto, R. A.; Bosco, F.; Carosio, F.; Blasio, A.; Di Cuttica, F.; Antonucci, V.; Giordano, M.; Malucelli, G. Caseins and hydrophobins as novel green flame retardants for cotton fabrics. *Polym. Degrad. Stab.* **2014**, *99*, 111−117.

(16) Pan, H. F.; Wang, W.; Pan, Y.; Song, L.; Hu, Y.; Liew, K. M. Formation of self-extinguishing flame retardant biobased coating on cotton fabrics via layer-by-layer assembly of chitin derivatives. *Carbohydr. Polym.* **2015**, *115*, 516−524.

(17) Réti, C.; Casetta, M.; Duquesne, S.; Bourbigot, S.; Delobel, R. Flammability properties of intumescent PLA including starch and lignin. *Polym. Adv. Technol.* **2008**, *19*, 628−635.

(18) Zhou, H.; Wang, C. Z.; Chen, H. X.; Gong, K. Research progress on chemical structure and separation of theasaponin from *Camellia oleifera* Abel. *For. Prod. Chem. Ind.* **2009**, *29* (10), 233−237.

(19) Zhao, P.; Gao, D. F.; Xu, M.; Shi, Z. G.; Wang, D.; Yang, C. R.; Zhang, Y. J. Triterpenoid saponins from the genus *Camellia*. *Chem. Biodivers.* **2011**, *8* (11), 1931−1942.

(20) Yang, F.; Shi, H.; Zhang, X.; Yu, L. L. Two novel anti-inflammatory 21-nordammarane saponins from tetraploid Jiaogulan (*Gynostemma pentaphyllum*). *J. Agric. Food Chem.* **2013**, *61* (51), 12646−12652.

(21) Song, B. L.; Shang, S. B.; Song, Z. Q.; Li, M. H. Preparation of deestered tea saponin and its properties. *Biomass Chem. Eng.* **2011**, *45* (3), 8−10.

(22) Kuo, P. C.; Lin, T. C.; Yang, C. W.; Lin, C. L.; Chen, G. F.; Huang, J. W. *Bioactive saponin from tea seed pomace with inhibitory effects against* Rhizoctonia solani. *J. Agric. Food Chem.* **2010**, *58* (15), 8618−8622.

(23) Li, S. X.; Mu, Y.; Zheng, F. Y. Influence of gastrointestinal digestion and edible plant combination on oral bioavailability of triterpene saponins, using a biomimetic digestion and absorption system and determination by HPLC. *J. Agric. Food Chem.* **2013**, *61* (44), 10599−10603.

(24) Yang, X. P.; Zhang, H. Q. Synergistic interaction of tea saponin with mancozeb against *Pestalotiopsis theae*. *Crop Prot.* **2012**, *40*, 126−131.

(25) Jiang, H. P.; Sun, L. F. Progress on the research fields on the extraction and application of tea saponin. *Jiangxi Chem. Ind.* **2003**, *4*, 52−57.

(26) Gu, J. W.; Zhang, G. C.; Dong, S. L.; Zhang, Q. Y.; Kong, J. Study on preparation and fire-retardant mechanism analysis of intumescent flame-retardant coatings. *Surf. Coat. Technol.* **2007**, *201*, 7835−7841.

(27) Shan, Y. Y.; Jiao, B. X. Exploitation of ultra-thin intumescent fireproof coating for wood structure. *New Chem. Mater.* **2010**, *38* (7), 112−115.

(28) Tata, J.; Alongi, J.; Carosio, F.; Frache, A. Optimization of the procedure to burn textile fabrics by cone calorimeter: Part I. Combustion behavior of polyester. *Fire Mater.* **2011**, *35*, 397−409.

(29) Park, H. S.; Kim, D. W.; Hwang, K. H.; Yong, B. S.; Wu, J. P.; Park, J. W.; Hahm, H. S.; Im, W. B. Preparation and characterization of polyurethane flame-retardant coatings using pyrophosphoric lactone-modified polyesters/isophorone diisocyanate−isocyanurate. *J. Appl. Polym. Sci.* **2001**, *80*, 2316−2327.

(30) Wang, D. Y.; Cai, X. X.; Qu, M. H.; Liu, Y.; Wang, J. S.; Wang, Y. Z. Preparation and flammability of a novel intumescent flame-retardant poly(ethylene-*co*-vinyl acetate) system. *Polym. Degrad. Stab.* **2008**, *80*, 2186−2192.

(31) Schartel, B.; Bartholmai, M.; Knoll, U. Some comments on the use of cone calorimeter data. *Polym. Degrad. Stab.* **2005**, *88*, 540−547.

(32) Lorenzetti, A.; Besco, S.; Hrelja, D.; Roso, M.; Gallo, E.; Schartel, B.; Modesti, M. Phosphinates and layered silicates in charring polymers: the flame retardancy action in polyurethane foams. *Polym. Degrad. Stab.* **2013**, *98*, 2366−2374.

(33) Biswal, M.; Mohanty, S.; Nayak, S. Thermal stability and flammability of banana-fiber-reinforced polypropylene nanocomposites. *J. Appl. Polym. Sci.* **2012**, *125*, 432−443.

DOI: 10.1021/jf505898d
J. Agric. Food Chem. 2015, 63, 2782−2788

bypass this inefficient metabolic step and might result in the enrichment of eggs with amounts of EPA and DHA that today are only achievable by direct supplementation of hens' diet with these VLC n-3 PUFAs. Moreover, because egg FA profiles typically reflect the hens' dietary FA pattern,[12,18] SDA-enriched eggs would theoretically supply additional EPA and DHA via subsequent bioconversion following consumption by humans. In the present study, we fed hens a diet containing high-SDA soybean oil (SBO), which has been engineered through expression of both the Δ6 and Δ15 desaturase enzymes in the soybean plant,[19] and compared it to diets containing conventional SBO (CON), flaxseed oil (FLAX), or fish oil (FISH).

MATERIALS AND METHODS

Animals, Diets, and Management. One-hundred, day-old Hy-Line W-36 chicks, vaccinated against Marek's Disease, were obtained from the Hy-Line hatchery in Elizabethtown, PA. Feeding and lighting programs were conducted in general accordance with breeder recommendations.[20] At 18 wk of age, 80 hens were transferred from floor pens in the pullet rearing facility to individual 30 cm (w) × 43 cm (d) × 36 cm (h) cages with sloping wire floors in the layer facility and were provided 16 h of light daily. A standard corn−soybean meal−based layer mash (MW-121, Wenger Feeds, Rheems, PA) calculated to contain 18.5% crude protein, 2880 kcal metabolizable energy, 4.31% available calcium, and 0.51% available phosphorus, was fed until 33 wk of age, at which time the supplemental dietary fat content of the mash was increased to 5% (animal−vegetable fat blend) in order to acclimate the hens to a higher dietary fat level that was maintained in the experimental diets. At 38 wk of age (d 0 of the study), the 40 best performing hens were selected based on 5-d pre-experimental egg weight and egg production, and 32 birds were allocated (n = 8) to one of four dietary treatments (see below). At that time, the 8 additional hens, with similar average egg production rates and egg weights as the 32 utilized in the feeding trial, were euthanized by electric stunning and exsanguination. Their livers and abdominal fat pads were excised, weighed, and snap-frozen in liquid nitrogen until subsequent analysis for FA content and expression of key genes affecting lipid metabolism (d 0 baseline data).

Diets, differing only in supplemental oil sources, were formulated to meet or exceed the nutritional requirements of W-36 hens[20] and were fed for a period of 28 d. The oil sources were as follows: (1) conventional SBO (CON; Monsanto Company, St. Louis, MO); (2) SDA-enriched SBO from soybean plants engineered to produce oil with significant quantities of SDA (SDA; Monsanto Company, St. Louis, MO); (3) flaxseed oil (FLAX; cold pressed; Jedwards International, Inc., Quincy, MA); (4) fish oil (FISH; refined, deodorized, purified, and molecularly distilled; Jedwards International, Inc., Quincy, MA) (Table 1). Feed and water were provided for ad libitum consumption. Hen body weight was recorded on d 0 and d 28, and individual hen feed intakes and egg weights were recorded daily.

Two of the hens, one from the CON treatment and one from the FLAX treatment, were removed from the study due to a cessation of feed intake and/or egg production on d 19 and d 14, respectively. The former hen had a large mite infestation while the latter hen was subsequently diagnosed with severe chronic active ulcerative stomatitis (inflammation of the mucous membrane of the mouth) with periostial new bone formation of the mandible, which likely caused pain in the beak and mouth. Thus, since the data from these hens were not used in the study, there were 7 hens each in the CON and FLAX diets, and 8 hens each in the SDA and FISH diets.

At the end of the study (d 28), the remaining 30 hens were euthanized by electric stunning and exsanguination. Their livers and abdominal fat pads were excised, weighed, and snap-frozen in liquid nitrogen and stored at −80 °C until subsequent analysis for FA content and expression of key genes affecting lipid metabolism. All animal protocols were approved by the Institutional Animal Care and Use Committee of The Pennsylvania State University (IACUC #37025).

Table 1. Diet Compositions and Nutrient Contents[a]

	diet (%, as-is basis)			
ingredient	CON	SDA	FLAX	FISH
soybean oil	5.00	–	–	–
SDA-enriched soybean oil	–	5.00	–	–
flaxseed oil	–	–	5.00	–
fish oil	–	–	–	5.00
Santoquin 4Q-T[b]	Tr	Tr	Tr	Tr
basal mixture[c]	95.00	95.00	95.00	95.00
analyzed composition[d]				
crude protein	16.3	16.2	16.4	16.8
crude fat	7.42	7.47	7.23	7.68
total fatty acids	6.92	7.24	7.45	7.09
linoleic acid	3.42	2.44	2.24	1.72
total cholesterol	ND[e]	ND	ND	0.035
calculated composition				
metabolizable energy (kcal/kg)	2882	2882	2882	2882
arginine, digestible	0.974	0.974	0.974	0.974
isoleucine, digestible	0.614	0.614	0.614	0.614
lysine, digestible	0.820	0.820	0.820	0.820
methionine, digestible	0.408	0.408	0.408	0.408
methionine + cystine, digestible	0.681	0.681	0.681	0.681
threonine, digestible	0.571	0.571	0.571	0.571
tryptophan, digestible	0.179	0.179	0.179	0.179
valine, digestible	0.711	0.711	0.711	0.711
available phosphorus	0.489	0.489	0.489	0.489

[a]Diets contained 5% supplemental conventional soybean oil (CON), stearidonic acid-enriched soybean oil (SDA), flaxseed oil (FLAX), or fish oil (FISH). [b]Santoquin 4Q-T (Novus International, Inc., St. Charles, MO), a fat-soluble liquid antioxidant feed additive, was added directly to each oil and stirred prior to mixing the oil with the basal. The final content of Santoquin 4Q-T in each diet was calculated to be 62.5 ppm or 0.00625%, and is noted as Tr = trace. [c]The proprietary basal mixture consisted primarily of ground corn, soybean meal, ground wheat, distillers grains with solubles, and wheat middlings, with supplemental vitamins, minerals, essential oils, prebiotic substances, and enzymes. The diet was formulated to meet or exceed the nutrient requirements of the Hy-Line W-36 hen.[20] [d]Mean of two analyses per sample. [e]ND = not detected.

Diet, Egg, and Tissue Analyses. One egg per hen was collected on d 0, d 14, and d 28 of treatment for the determination of component weights and percentages.[21] Diets and lyophilized egg yolks were analyzed for crude protein, crude fat, and total cholesterol contents by the Agricultural Experiment Station Chemical Laboratories at the University of Missouri—Columbia using AOAC International official methods 990.03, 920.39, and 941.09, respectively.[22] Diets, egg yolk, liver, and adipose tissue (abdominal fat pad) samples were acid methylated according to Garcés and Mancha[23] (80 °C for 2 h in reagent containing heptane, methanol, toluene, 2,2-dimethoxypropane, and sulfuric acid at 48.5:32:14:4:1.5, v:v) and yolk FA methyl esters were cholesterol-depleted using an SPE column, as described by Tyburczy et al.[24] Individual FAs were separated and quantified by gas−liquid chromatography using an Agilent 6890A gas chromatograph (Agilent Technologies, Palo Alto, CA) equipped with a fused-silica capillary column (SP2560; 100 m × 25 mm i.d. with 0.2-μm film thickness; Supelco, Inc., Bellefonte, PA) and a flame ionization detector.[25] The oven program was 70 °C for 4 min, 8 °C/min ramp to 110 °C, 5 °C/min ramp to 170 °C for 10 min, and 4 °C/min ramp to 215 °C for 23 min. Inlet and detector temperatures were 250 °C with a 50:1 or 100:1 split ratio. Hydrogen carrier gas flow rate was 1 mL/min. FA concentration and methylation efficiencies were determined using dual external standards (13:0 free FA and 19:0

DOI: 10.1021/jf505185u
J. Agric. Food Chem. 2015, 63, 2789−2797

Table 2. Fatty Acid Contents of the Diets and Oils[a]

	diet (g/kg, as is basis)				oil (% of fatty acids)			
fatty acid[b]	CON	SDA	FLAX	FISH	CON	SDA	FLAX	FISH
12:0	ND[c]	ND	ND	0.1	ND	ND	ND	0.11
14:0	0.1	0.1	0.1	2.5	0.07	0.07	0.02	7.44
16:0	9.6	9.9	7.9	11.2	10.06	10.55	4.97	14.86
16:1	0.7	0.9	0.7	3.0	0.05	ND	0.06	8.69
17:0	0.1	0.1	0.1	0.2	0.11	0.12	0.10	0.46
18:0	2.3	2.4	2.6	2.2	3.83	4.11	4.32	3.10
18:1 c9	13.7	12.4	14.6	10.3	22.02	15.85	21.01	8.26
18:1 c11	1.0	1.0	0.7	1.6	1.50	1.34	0.64	3.31
18:2 n-6	34.2	24.4	22.4	17.2	53.19	22.07	16.48	1.22
18:3 n-6	ND	2.1	ND	0.1	0.31	6.39	0.22	0.41
18:3 n-3	3.7	5.9	21.7	1.7	6.92	13.11	50.86	0.76
18:4 n-3	ND	8.6	ND	0.9	0.05	24.30	ND	2.51
20:0	0.2	0.2	ND	0.2	0.20	0.28	0.21	ND
20:1	0.1	0.2	0.2	0.4	0.21	0.17	0.17	0.10
20:3 n-6	0.2	0.1	ND	0.1	ND	ND	ND	0.15
20:4 n-6	ND	ND	ND	0.4	ND	ND	ND	1.05
20:4 n-3	ND	ND	ND	0.3	ND	ND	ND	0.75
20:5 n-3	ND	ND	ND	5.5	ND	ND	ND	17.24
22:4 n-6	0.2	0.2	0.1	0.2	ND	ND	ND	0.55
22:5 n-3	ND	ND	ND	0.7	ND	ND	ND	2.35
22:6 n-3	ND	ND	ND	3.2	ND	ND	ND	10.93
24:0	0.1	ND	ND	ND	0.06	0.11	ND	0.04
24:1	ND	ND	ND	ND	0.05	0.09	ND	0.09
others	3.0	3.5	3.4	8.9	1.37	1.44	0.94	15.62
total	69.2	72.4	74.5	70.9	100.00	100.00	100.00	100.00
∑n-6	34.8	24.9	22.5	17.7	53.50	28.46	16.70	2.32
∑n-3	3.7	14.9	21.7	12.0	6.97	37.41	50.86	33.78
∑n-6/n-3	9.4	1.7	1.0	1.5	7.67	0.76	0.33	0.07
∑VLC n-3	ND	ND	ND	9.5	ND	ND	ND	30.51

[a]Diets contained 5% supplemental conventional soybean oil (CON), stearidonic acid-enriched soybean oil (SDA), flaxseed oil (FLAX), or fish oil (FISH). [b]SFA = saturated fatty acids; MUFA = monounsaturated fatty acids; PUFA = polyunsaturated fatty acids; vLC n-3 = polyunsaturated n-3 fatty acids greater than 18 carbons. [c]ND = not detected.

methyl ester; Nu-Chek Prep, Inc., Elysian, MN). Peaks were identified based on purified standards (GLC780 and GLC461; Nu-Chek Prep), and 20:4 n-3 was identified using a purified stock (Caymen Chemical Company, Ann Arbor, MI). An equal weight standard (GLC461; Nu-Chek Prep) was used for calculation of recovery factors.

Gene Expression Analysis. Total RNA was extracted from liver tissue by chloroform−phenol extraction followed by column purification with on-column Dnase treatment (Total RNA II Kit with optional Dnase, Omega Bio-Tek, Norcross, GA). The concentration and quality of RNA was determined using an Experion System (Bio-Rad Laboratories, Hercules, CA). cDNA was synthesized from total RNA using random primers (High Capacity cDNA synthesis kit, Life Sciences Advanced Technologies, Inc., St. Petersburg, FL). Expression of long chain FA desaturases (SCD1, FADS1, and FADS2), FA elongases (ELOVL2 and ELOVL5), a lipogenic enzyme (FASN), a cholesterol synthesis enzyme (HMGCR), FA oxidation enzymes (CPT1a and ACOX1), lipogenic transcription factors (SREBP1 and MLX), and two housekeeping genes (BACT and B2M) was determined in quadruplicate by relative quantification SYBR Green Real-Time PCR (PerfeCTa SYBR Green Supermix with ROX, Quanta BioSciences, Gaithersburg, MD) using an 7900 Fast Real-Time PCR System (Applied Biosystems, Grand Island, NY). Gene specific primers (intron spanning when possible) were designed using Primer-BLAST (NCBI; see Supporting Information) and validated for linearity and efficiency. Gene expression was quantified relative to a standard curve of serially diluted cDNA in each plate. The geometric mean of the housekeeping genes[26] was used as a covariant in the statistical analysis and data is reported relative to the control (set to 100).

Statistical Analyses. Data with multiple observations per hen (e.g., feed intake, egg production, body weight, and egg composition) were analyzed as a repeated measures design using Proc Mixed (SAS Institute, Cary, NC). The model included the random effect of bird nested in treatment and the fixed effect of treatment, day, and the interaction of treatment × day. Treatment effects were similar between d 14 and d 28; therefore, only d 28 data are presented. A Protected LSD was used within d 28 when the treatment × day interaction was significant. Data with a single observation per hen were analyzed with a model that included the fixed effect of treatment and means were separated by a Protected LSD when treatment was significant ($P \leq 0.05$). Data was log transformed when necessary and back transformed data are reported. Data points outside of ±3 Studentized residuals were considered outliers and removed from the analysis. This rarely occurred for more than 1 value per variable.

RESULTS

Experimental Diets and Animal Performance. The analyzed fat contents of the four experimental diets agreed well with calculated contents (7.3% fat), on both a crude fat and a sum of FA basis (Tables 1 and 2). The FA profile of the CON diet was representative of the incorporated commercial SBO (6.9% 18:3 n-3 and 7.0% total n-3 FA; Table 2). The high SDA SBO contained 37.4% n-3 FA (13.1% 18:3 n-3 and 24.3% 18:4 n-3) and 6.4% 18:3 n-6 primarily at the expense of 18:1 c9 and linoleic acid (LA; 18:2 n-6; Table 2). The flaxseed oil contained 50.9% 18:3 n-3 and the fish oil contained 30.5% total VLC n-3

DOI: 10.1021/jf505185u
J. Agric. Food Chem. 2015, 63, 2789−2797

Table 3. Yolk Fatty Acid Content and Profile of Eggs from Hens Fed Diets Containing 5% Supplemental Conventional Soybean Oil (CON), Stearidonic Acid-Enriched Soybean Oil (SDA), Flaxseed Oil (FLAX), or Fish Oil (FISH) for 28 d[a]

	diet (mg/yolk)						diet (% of fatty acids)					
fatty acid[b]	CON	SDA	FLAX	FISH	SEM	*P*-value[c]	CON	SDA	FLAX	FISH	SEM	*P*-value[c]
14:0	11 b	12 b	11 b	41 a	2.7	<0.001	0.27 c	0.31 b	0.27 c	0.99 a	0.045	<0.001
14:1	1 b	1 b	2 b	6 a	0.3	<0.001	0.03 b	0.03 b	0.04 b	0.15 a	0.003	<0.001
16:0	989 ab	995 ab	925 b	1099 a	43.8	0.02	23.55 c	24.74 b	21.80 d	26.66 a	0.34	<0.001
16:1	57 ab	51 b	75 ab	142 a	3.9	<0.001	1.35 c	1.26 c	1.76 b	3.43 a	0.064	<0.001
18:0	374 bc	439 a	386 b	345 c	14.0	0.01	8.98 bc	10.61 a	9.09 b	8.38 c	0.23	<0.001
18:1 c9	1416 b	1291 bc	1601 a	1221 c	53.9	<0.010	33.82 b	32.13 c	37.74 a	29.66 d	0.56	<0.001
18:1 c11	58 b	47 c	55 bc	93 a	2.6	<0.001	1.39 b	1.19 d	1.28 c	2.26 a	0.031	<0.001
18:2 n-6	933 a	746 b	625 c	570 c	47.2	<0.001	22.53 a	18.87 b	14.84 c	14.09 c	0.57	<0.001
18:3 n-6	5 b	16 a	3 d	3 b	0.9	<0.001	0.12 b	0.39 a	0.07 d	0.08 c	0.021	<0.001
18:3 n-3	43 c	105 b	283 a	32 d	17.8	<0.001	1.02 c	2.62 b	6.61 a	0.76 d	0.35	<0.001
18:4 n-3	0 c	14 a	2 b	3 b	0.4	<0.001	0.01 c	0.34 a	0.05 b	0.07 b	0.040	<0.001
20:2 n-6	9 a	4 c	5 b	4 c	0.4	<0.001	0.20 a	0.09 c	0.11 b	0.08 c	0.011	<0.001
20:3 n-6	8 b	17 a	7 b	4 c	0.5	<0.001	0.18 b	0.42 a	0.16 c	0.11 d	0.014	<0.001
20:4 n-6	87 a	51 b	46 b	27 c	2.7	<0.001	2.07 a	1.26 b	1.07 c	0.66 d	0.038	<0.001
20:4 n-3	ND[d]	8 a	2 c	3 b	0.5	<0.001	ND	0.21 a	0.04 c	0.06 b	0.013	<0.001
20:5 n-3	1 c	10 b	6 b	56 a	1.3	<0.001	0.01 d	0.23 b	0.14 c	1.36 a	0.10	<0.001
22:4 n-6	8 a	6 bc	5 c	6 b	0.4	<0.01	0.19 a	0.15 b	0.12 c	0.15 b	0.009	<0.001
22:5 n-3	4 d	20 b	11 c	35 a	3.4	<0.001	0.10 d	0.50 b	0.27c	0.88 a	0.075	<0.001
22:6 n-3	46 d	87 b	72 c	211 a	9.9	<0.001	1.10 d	2.18 b	1.77c	5.12 a	0.17	<0.001
others	127	94	109	217			3.08	2.47	2.77	5.05		
total	4178	4012	4232	4117			100.00	100.00	100.00	100.00		
total n-3	94 b	244 b	376 a	340 a	17.2	<0.001	2.25 d	6.11 c	8.91 a	8.23 b	0.25	<0.001
total VLC n-3	51 d	125 b	91 c	305 a	12.5	<0.001	1.21 d	3.13 b	2.22 c	7.39 a	0.25	<0.001

[a]Values are d 28 least-squares means of 7 hens each for the CON and FLAX diets, and of 8 hens each for the SDA and FISH diets. Average d 28 yolk weights of eggs from hens fed the CON, SDA, FLAX, or FISH diets were 15.38, 14.94, 15.11, and 15.18 g, respectively ($P = 0.74$). [b]VLC n-3 = polyunsaturated n-3 fatty acids greater than 18 carbons. [c]Values within a row with different letters are significantly different ($P < 0.05$). [d]ND = not detected

(including 17.2% EPA and 10.9% DHA; Table 2). All diets were sufficiently palatable, and daily intake did not differ between treatment groups, averaging 96.6 g/d (see Supporting Information). Since daily intakes did not differ, the relative differences in FA intakes were therefore similar to the differences in the composition of the experimental oils.

Overall, there was no significant effect of dietary oils on hen performance. When averaged across diets, hens gained 11.3 g of body weight (BW) in 28 d, had a hen-d egg production rate of 90.5%, produced eggs weighing 60.7 g, and consumed 1.77 g feed/g egg mass (see Supporting Information). In addition, there were no significant effects of diet on egg component (yolk, albumen, shell) weights, egg component relative percentages, or yolk cholesterol, crude fat, or crude protein contents, regardless of how they were expressed (mg/g yolk, mg/yolk, or % of yolk dry matter; see Supporting Information).

Yolk Fatty Acid Composition. For egg yolks and tissues, the d 0 FA compositions did not differ from those of the CON diet at 28 d (data not shown). In addition, since the d 14 and d 28 data were not different within a dietary group, only the d 28 data are reported.

Yolk contents of EPA, docosapentaenoic acid (DPA, 22:5 n-3), DHA, and total VLC n-3 PUFAs were greater ($P < 0.001$) in eggs from hens fed FISH compared to the other three diets, while yolk ALA contents were highest ($P < 0.001$) in hens fed FLAX diet (Table 3). In terms of absolute content of VLC n-3 PUFAs, yolks from hens fed the CON, SDA, and FLAX diets contained only 17% (51 mg/305 mg), 41% (125 mg/305 mg), or 30% (91 mg/305 mg), respectively, of the amount in yolks from FISH-fed hens (Table 3).

As compared to the CON and FLAX diets, feeding hens SDA increased ($P < 0.001$) yolk contents of SDA, eicosatetraenoic acid (ETA, C20:4 n-3), EPA, DPA, and DHA, as well as total VLC n-3 PUFAs, on both an absolute and a relative (% of FAs) basis (exception: EPA contents on a mg/yolk basis; SDA value was 67% greater than FLAX value, but NS). Additionally, although the FLAX diet contained more ALA (21.7 g/kg) than the total amount of ALA + SDA in the SDA diet (6.3 g/kg and 8.6 g/kg, respectively; Table 2), the latter were more efficiently desaturated and elongated to VLC n-3 PUFAs than was ALA alone from flaxseed oil. In this regard, laying hens incorporated 0.132 mg, 0.041 mg, or 0.075 mg (estimated; see below) of VLC n-3 PUFAs daily into egg yolk for each milligram of ingested ALA from SBO (CON), ALA from flaxseed oil (FLAX), or SDA, respectively (Table 4). Since the SDA oil also contained ALA, a mathematical calculation was used to estimate the contribution of ALA to egg yolk vLC n-3 PUFA content. Specifically, a conversion value of 0.120 mg VLC n-3 PUFAs/mg ALA ingested was used to estimate the amount of VLC n-3 PUFAs in egg yolks of SDA-fed hens that were derived from ALA. This figure was generated by proportioning the daily ALA intake of the SDA hens (557 mg), as compared to the CON (355 mg) and FLAX hens (2138 mg), to the CON and FLAX ALA conversion values. The estimated amount of yolk VLC n-3 PUFAs derived from ingested ALA were then subtracted from the total VLC n-3 PUFAs in the egg yolks of SDA-fed hens, the difference was divided by the daily SDA intake, and the value was multiplied by hen-day production to generate the daily SDA conversion value (0.075).

DOI: 10.1021/jf505185u
J. Agric. Food Chem. 2015, 63, 2789−2797

Table 4. Estimated in Vivo Conversion of Dietary α-Linolenic Acid (ALA) or Stearidonic Acid (SDA) to Egg Yolk Very Long-Chain n-3 Polyunsaturated Fatty Acids (VLC n-3 PUFAs)

study	diet[a]	substrate	mg VLC n-3 PUFAs incorporated into egg yolk per d per mg intake of n-3 fatty acid substrate[b,c]
present	CON (n = 7)	ALA	0.132 ± 0.025
	FLAX (n = 7)	ALA	0.041 ± 0.006
	SDA (n = 8)	SDA	0.075 ± 0.020
Caston and Leeson (1990)[27]	control		0.078
	10% ground flaxseed	ALA	0.011
	20% ground flaxseed	ALA	0.006
	30% ground flaxseed	ALA	0.003
Cherian and Sim (1991)[28]	control	ALA	0.304
	8% ground flaxseed	ALA	0.054
	16% ground flaxseed	ALA	0.044
Aymond and Van Elswyk (1995)[29]	control	ALA	0.121
	5% whole flaxseed	ALA	0.058
	5% ground flaxseed	ALA	0.052
	15% whole flaxseed	ALA	0.018
	15% ground flaxseed	ALA	0.021

[a]Diets in the present study contained 5% supplemental conventional soybean oil (CON), flaxseed oil (FLAX), or stearidonic acid-enriched soybean oil (SDA). Intakes of VLC n-3 PUFAs for all three treatment groups of the present study were ∼10 mg/hen/d; linoleic acid (18:2 n-6) intakes averaged ∼3400, 2200, and 2400 mg/hen/d for the CON, FLAX, and SDA groups, respectively. [b]Values are means (±SD). In vivo conversion for the present study was estimated as ([mg yolk ETA+EPA+DPA+DHA in eggs laid on d 28] × 28-d hen-d egg production)/(mg ALA intake per d or mg SDA intake per d). In vivo conversion for the three other studies was calculated in a similar manner. A conversion value of 0.120 mg VLC n-3 PUFAs/mg ALA ingested (see text for derivation of this figure) was used to estimate the amount of VLC n-3 PUFAs in egg yolks of SDA-fed hens that were derived from ALA. This amount was subtracted from the total amount of VLC n-3 PUFAs in the yolks of SDA-fed hens in order to determine the amount derived from SDA. ETA = eicosatetraenoic acid; EPA = eicosapentaenoic acid; DPA = docosapentaenoic acid, DHA = docosahexaenoic acid. [c]Caston and Leeson (1990) did not report flaxseed ALA content; it was assumed to be similar to the flaxseed fed by Cherian and Sim (1991). For Caston and Leeson (1991) and Aymond and Van Elswyk (1995), a daily intake of 350 mg of ALA for the control diet was assumed since feed intake data were not reported and diets were corn-based, as in the present study. A daily feed intake of 100 g/hen/d for Cherian and Sim (1991) was assumed since feed intakes were not reported.

The increase in n-3 FAs in all treatments was predominantly offset by a decrease in LA, and small differences in other FAs were observed depending on the specific profile of each oil (e.g., increased 14:0 and decreased 18:1 c9 in FISH). Additionally, feeding FLAX increased yolk 16:1 and 18:1 c9 contents, which may have been reflective of elevated hepatic stearoyl-CoA desaturase activity. Lastly, expression of the Δ6 desaturase in the high SDA soybeans promotes the enhanced synthesis of γ-linoleic acid (GLA; 18:3 n-6) from LA. As a result, GLA levels in the SDA oil were approximately 20-fold higher as compared to the other three oils (Table 2), and hens fed the SDA diet had the highest egg GLA contents (16 mg/yolk vs 5 mg, 3 mg, or 3 mg for the CON, FLAX, and FISH diets, respectively; Table 3). Egg yolks from SDA-fed hens were similarly enriched with 20:3 n-6, the elongation product of GLA (Table 3).

Liver and Adipose Tissue Weights. Liver and abdominal fat pad absolute and relative weights were unaffected by dietary treatment. Averaged across the four dietary treatments, hen BW, liver weight, abdominal fat pad weight, liver weight as % of BW, and abdominal fat pad as a % of BW were 1,636 g, 29.0 g, 82.6 g, 1.77%, and 5.01%, respectively (see Supporting Information).

Liver Fatty Acid Composition. As compared to egg yolk FA profiles (% of FAs; Table 3), liver lipids were relatively richer in stearic acid (18:0), arachidonic acid (20:4 n-6), and DHA, and contained less oleic acid (18:1-c9) and ALA (Table 5). Moreover, relative to the amount of total n-3 FAs, liver lipid (Table 5) was richer in VLC n-3 PUFAs both on an absolute and relative basis, as compared to egg yolk (Table 3) for each treatment group. This was a reflection of the liver's metabolic capacity to desaturate and elongate dietary ALA and SDA and the preference for VLC n-3 FAs in hepatic phospholipid membranes. Additionally, liver tissue fatty acid composition and profile were similar between d 0 (baseline) and the CON treatment at the end of the experiment (d 28; data not shown). As compared to livers from CON hens, livers of birds fed SDA or FLAX contained more than twice the amount of total n-3 FAs (P < 0.001; Table 5). However, livers from SDA-fed hens contained proportionately more VLC n-3 PUFAS, which was a reflection of the more efficient conversion of SDA + ALA vs ALA alone to DTA, EPA, DPA, and DHA (Table 4).

Adipose Tissue Fatty Acid Composition. As compared to yolk FA profiles (% of FAs; Table 3), adipose tissue (abdominal fat pad) had similar contents of 18:1 c9 and ALA, proportionately greater contents of LA and SDA, and lesser amounts of palmitic acid (16:0), 18:0, 20:4 n-6, EPA, DPA, DHA, total n-3 FAs, and VLC n-3 PUFAs (Table 6). Dietary SDA greatly elevated adipose SDA content (1443 mg/100 g tissue; 1.79% of FAs), while EPA, DPA, and DHA were only detected in adipose from hens fed the FISH diet (Table 6). ETA was detected only in adipose tissue from hens fed the SDA and FISH diets, which provided further evidence that dietary SDA was more efficiently converted to VLC n-3 PUFAs than was ALA. As compared to liver (on a mg/100 g fresh tissue basis), adipose contained approximately 12-fold more total FAs and higher total n-3 FAs, but had much lower contents of VLC n-3 PUFAs (Tables 5 and 6). This was most likely a reflection of the relative differences in the contribution of membrane phospholipid and neutral lipids to the total FA content of the two tissues[30] and the low activity of elongase and Δ5 and Δ6 desaturase enzymes in adipose tissue.[31]

DOI: 10.1021/jf505185u
J. Agric. Food Chem. 2015, 63, 2789−2797

Table 5. Fatty Acid Content and Profile of Livers from Hens Fed Diets Containing 5% Supplemental Conventional Soybean Oil (CON), Stearidonic Acid-Enriched Soybean Oil (SDA), Flaxseed Oil (FLAX), or Fish Oil (FISH) for 28 d[a]

	diet (mg/100 g fresh tissue)						diet (% of fatty acids)					
fatty acid[b]	CON	SDA	FLAX	FISH	SEM	*P*-value[c]	CON	SDA	FLAX	FISH	SEM	*P*-value[c]
12:0	16	15	17	18	2.6	0.77	0.20	0.19	0.22	0.21	0.02	0.590
14:0	15 b	19 b	16 b	52 a	4.2	<0.001	0.20 b	0.22 b	0.20 b	0.61 a	0.03	<0.001
14:1	2 b	1 b	1 b	4 a	0.6	<0.01	0.01 b	0.01 b	0.01 b	0.05 a	0.01	<0.001
16:0	1789	1916	1758	2313	202	0.14	23.80 b	24.19 b	22.52 c	27.25 a	0.34	<0.001
16:1	57 b	57 b	78 b	150 a	13.4	<0.001	0.75 bc	0.69 c	0.98 b	1.75 a	0.10	<0.001
18:0	1206	1257	1286	1163	122	0.87	16.15 a	16.10 a	16.45 a	13.67 b	0.24	<0.001
18:1 c9	1628	1718	1992	1,642	209	0.56	21.77 b	21.38 b	25.43 a	19.28 b	0.98	<0.001
18:1 c11	67 b	69 b	69 b	130 a	10.2	<0.001	0.89 b	0.78 c	0.88 b	1.53 a	0.03	<0.001
18:2 n-6	1389	1314	1139	1,003	149	0.19	18.65 a	16.31 b	14.49 b	11.88 c	0.68	<0.001
18:3 n-6	9	8	9	9	3.3	0.75	0.12	0.10	0.12	0.11	0.01	0.40
18:3 n-3	27 c	68 b	201 a	18 c	12.7	<0.001	0.35 c	0.82 b	2.64 a	0.21 d	0.06	<0.001
18:4 n-3	3 b	40 a	3 b	7 b	4.9	<0.001	0.04 b	0.50 a	0.04 b	0.08 b	0.03	<0.001
20:0	8 b	40 a	7 b	8 b	3.3	<0.001	0.12 b	0.48 a	0.10 b	0.10 b	0.02	<0.001
20:2 n-6	27 a	15 b	19 b	15 b	2.3	<0.01	0.36 a	0.19 bc	0.23 b	0.17 c	0.02	<0.001
20:3 n-6	49 bc	110 a	64 b	32 c	8.8	<0.001	0.67 b	1.49 a	0.82 b	0.38 c	0.06	<0.001
20:4 n-6	601 a	409 b	394 b	230 c	48.3	<0.001	8.02 a	5.47 b	5.04 b	2.71 c	0.24	<0.001
20:4 n-3	ND[d]	10 a	4 b	5 b	1.0	<0.001	ND	0.14 a	0.05 b	0.05 b	0.007	<0.001
20:5 n-3	5 c	48 b	44 b	121 a	10.5	<0.001	0.06 c	0.61 b	0.56 b	1.40 a	0.06	<0.001
22:4 n-6	9 b	7 b	7 b	18 a	3.3	0.04	0.11 ab	0.07 b	0.08 b	0.20 a	0.04	<0.05
22:5 n-3	13 c	58 b	40 b	102 a	7.8	<0.001	0.17 d	0.74 b	0.52 c	1.19 a	0.05	<0.001
22:6 n-3	261 c	473 b	406 bc	1068 a	58.6	<0.001	3.48 c	6.20 b	5.23 b	12.63 a	0.44	<0.001
24:0	8 a	9 a	8 a	6 b	0.8	0.02	0.11 ab	0.14 a	0.11 b	0.07 c	0.01	<0.001
24:1	26 a	16 b	17 b	14 b	3.1	0.02	0.35 a	0.20 b	0.22 b	0.16 b	0.03	<0.010
others	274	283	256	365			3.62	2.98	3.06	4.31		
total	7486	7940	7828	8,492			100.00	100.00	100.00	100.00		
total n-3	309 c	697 b	698 b	1321 a	80.2	<0.001	4.10 c	8.93 b	8.94 b	15.41 a	0.55	<0.001
total VLC n-3	279 c	589 b	494 b	1296 a	72.7	<0.001	3.71 c	7.71 b	6.35 b	15.12 a	0.50	<0.001

[a]Values are d 28 least-squares means of 7 hens each for the CON and FLAX diets, and of 8 hens each for the SDA and FISH diets. Average liver weights for hens fed the CON, SDA, FLAX, and FISH diets were 30.4, 27.9, 28.1, and 29.5 g, respectively ($P = 0.48$). [b]VLC n-3 = polyunsaturated n-3 fatty acids greater than 18 carbons. [c]Values within a row with different letters are significantly different ($P < 0.05$). [d]ND = not detected

Hepatic Gene Expression. Expression of SREBP1 was 36% lower in livers of hens fed FISH compared to the CON diet (see Supporting Information). Expression of other genes assayed, including long-chain FA desaturases (SCD1, FADS1, and FADS2), FA elongases (ELOVL2 and ELOVL5), a lipogenic enzyme (FASN), a cholesterol synthesis enzyme (HMGCR), FA oxidation enzymes (CPT1a and ACOX1), and lipogenic transcription factors (SREBP1 and MLX), were not changed by treatment (see Supporting Information). It is noteworthy that HMGCR gene expression was also 43% lower in FISH-fed birds as compared to CON hens, but the difference was not significant ($P = 0.19$).

DISCUSSION

Although the laying hen converted approximately 2-fold more ingested SDA vs ingested ALA from FLAX into egg yolk VLC n-3 PUFAs (Table 4), the absolute amounts of ETA + EPA + DPA + DHA were much less than that in yolks from hens fed the FISH diet (Table 3). We therefore must reject our hypothesis that bypassing the first FADS2 reaction, by feeding laying hens SDA, would enrich eggs with EPA and DHA at levels comparable to those attained by direct dietary supplementation of these VLC n-3 PUFAs. In addition, the current work suggests that, in the chicken, other control points besides the initial Δ6-desaturase (FADS2) reaction (ALA → SDA) exist in the biosynthesis of DHA from ALA, such as steps catalyzed by elongases[17,32] or, depending upon the dietary abundance of ALA, possibly the second Δ6-desaturase reaction[17] (24:5 n-3 → 24:6 n-3; the latter undergoes β-oxidation to yield DHA). It is also conceivable that either the in vivo conversion rate of ALA (or SDA) to DHA, and/or the capacity of the n-3 PUFA biosynthetic pathway, is simply not great enough in the laying hen to allow for the deposition of EPA and DHA into egg yolk at levels equal to those attained by direct dietary supplementation.

The dietary ratio of LA:ALA is another factor that can affect the conversion of ALA to VLC n-3 PUFAs.[33,34] However, LA intakes were similar for the SDA and FLAX groups, averaging approximately 2400 mg/hen/d and 2200 mg/hen/d, respectively, while CON birds ingested approximately 1000 mg/d more LA than the SDA hens but had a greater rate of conversion of ALA (vs SDA) to VLC n-3 PUFAs (0.132 and 0.075, respectively; Table 4).

The in vivo conversion rates of SDA and ALA to VLC n-3 PUFAs observed in the present study were similar to those calculated for hens fed control and flaxseed diets in three previous reports (Table 4).[27−29] In those studies, as the amount of dietary ALA from flaxseed increased, the calculated rate of in vivo conversion to egg yolk VLC n-3 PUFAs decreased. This suggested that high dietary levels of ALA attenuated its hepatic elongation and desaturation and/or enhanced its oxidation or transport to peripheral tissues. Although in the present study it was impossible to know the exact conversion rate of ALA to VLC n-3 PUFAs in the SDA-fed hens, we assumed that it

DOI: 10.1021/jf505185u
J. Agric. Food Chem. 2015, 63, 2789−2797

Table 6. Fatty Acid Content and Profile of Abdominal Fat Pads of Hens Fed Diets Containing 5% Supplemental Conventional Soybean Oil (CON), Stearidonic Acid-Enriched Soybean Oil (SDA), Flaxseed Oil (FLAX), or Fish Oil (FISH) for 28 d[a]

	diet (mg/100 g fresh tissue)						diet (% of fatty acids)					
fatty acid[b]	CON	SDA	FLAX	FISH	SEM	*P*-value[c]	CON	SDA	FLAX	FISH	SEM	*P*-value[c]
12:0	34 bc	33 c	38 b	52 a	1.7	<0.001	0.04 b	0.04 b	0.04 b	0.06 a	0.002	<0.001
14:0	457 b	436 b	493 b	1222 a	35	<0.001	0.55 b	0.54 b	0.55 b	1.46 a	0.025	<0.001
14:1	54 bc	50 c	64 b	83 a	4.0	<0.001	0.07 b	0.06 b	0.07 b	0.10 a	0.005	<0.001
16:0	15590	14850	15620	16390	680	0.42	18.63 ab	18.30 b	17.45 b	19.54 a	0.41	0.01
16:1	1740 bc	1660 c	2140 b	3200 a	163	<0.001	2.08 b	2.07 b	2.39 b	3.83 a	0.18	<0.001
18:0	4380	4360	4580	4130	195	0.430	5.23	5.36	5.12	4.93	0.14	0.17
18:1 c9	30510 ab	28800 b	33190 a	30170 ab	1070	0.050	36.46	35.56	37.07	36.07	0.61	0.34
18:1 c11	1440 b	1400 b	1490 b	1820 a	620	<0.001	1.73 b	1.73 b	1.67 b	2.18 a	0.036	<0.001
18:2 n-6	26340 a	22470 bc	23140 b	20770 c	820	<0.001	30.07 a	27.69 b	25.88 bc	24.91 c	0.71	<0.001
18:3 n-6	181 b	186 b	201 b	249 a	27	<0.001	0.22 b	0.23 b	0.23 b	0.30 a	0.011	<0.001
18:3 n-3	1400 c	2210 b	6140 a	1040 c	221	<0.001	1.67 c	2.72 b	6.88 a	1.24 c	0.26	<0.001
18:4 n-3	24 b	1443 a	44 b	183 b	73	<0.001	0.03 b	1.79 a	0.05 b	0.22 b	0.087	<0.001
20:0	125 b	530 a	101 b	110 b	11	<0.001	0.15 b	0.66 a	0.11 b	0.13 b	0.030	<0.001
20:2 n-6	40 ab	37 b	38 b	46 a	2.3	0.020	0.05 b	0.05 b	0.04 b	0.05 a	0.002	<0.01
20:3 n-6	17 b	30 a	19 b	28 a	2.1	<0.001	0.02 c	0.04 a	0.02 bc	0.03 ab	0.005	<0.01
20:4 n-6	31 b	31 b	26 b	64 a	2.7	<0.001	0.04 bc	0.04 b	0.03 c	0.08 a	0.003	<0.001
20:4 n-3	ND[d]	27 b	ND	58 a	2.8	<0.001	ND	0.03 b	ND	0.07 a	0.00	<0.001
20:5 n-3	ND	ND	ND	523	19	<0.001	ND	ND	ND	0.63 a	0.019	<0.001
22:4 n-6	84	81	82	91	5.5	0.400	0.09	0.10	0.09	0.11	0.007	0.21
22:5 n-3	ND	ND	ND	112	3.8	<0.001	ND	ND	ND	0.13 a	0.004	<0.001
22:6 n-3	ND	ND	ND	307	14	<0.001	ND	ND	ND	0.37 a	0.016	<0.001
others	2190 b	2110 b	2060 b	3030 a	172	<0.001	2.87	2.99	2.31	3.56	0.18	<0.001
total	83600	81040	89460	83610			100.00	100.00	100.00	100.00		
total n-3	1424	3680	6184	2223	245	<0.001	1.72 d	4.56 b	6.95 a	2.66 c	0.29	<0.001
total VLC n-3	ND	ND	ND	1000	38	<0.001	ND	ND	ND	1.20 a	0.04	<0.001

[a]Values are d 28 least-squares means of 7 hens each for the CON and FLAX diets, and of 8 hens each for the SDA and FISH diets. Average abdominal fat pad weights for hens fed the CON, SDA, FLAX, and FISH diets were 82.5 g, 77.8 g. 87.3 g, and 82.6 g, respectively ($P = 0.84$). [b]VLC n-3 = n-3 polyunsaturated fatty acids greater than 18 carbons. [c]Values within a row with different letters are significantly different ($P < 0.05$). [d]ND = not detected

decreased linearly with ALA intake and that there was no inhibition of ALA conversion by SDA. Future work will need to be conducted to assess the latter assumption.

With an average VLC n-3 PUFA content of 305 mg (Table 3), it should be noted that consumption of one egg from the FISH-fed hens would exceed the *2010 Dietary Guidelines for Americans* recommended average daily intake of 250 mg of EPA and DHA,[7] while two eggs from SDA-fed hens would have to be eaten to meet this level. However, because of their cholesterol content, consumption of two eggs per day would not be recommended for "hyper-responders", who exhibit significant increases in circulating low density lipoprotein cholesterol in response to increases in dietary cholesterol, or for persons with elevated plasma low density lipoprotein cholesterol levels, diabetes, and/or cardiovascular disease.[35] Thus, a plant-based dietary supplement capable of enriching eggs with VLC n-3 PUFA levels similar to that attained by feeding hens FISH remains elusive. Feeding fish oil or algae oil remains the most efficient method for maximizing the deposition of VLC n-3 PUFAs in egg yolk[10] or broiler meat,[36] although product oxidative stability or organoleptic properties may not be ideal.

The general lack of effect of dietary SDA on the expression of hepatic lipolytic and lipogenic genes (see Supporting Information) was somewhat surprising, but agreed with a recent report in swine.[37] Another unexpected and novel finding of the present work was that SDA appeared to be more readily incorporated into adipose tissue than into egg yolk. Abdominal fat pads from SDA-fed hens contained 1443 mg SDA and no VLC n-3 PUFAs per 100 g fresh tissue (Table 6). In contrast, only 71 mg (or 9%) of the calculated 761 mg of SDA consumed daily was deposited into egg yolk, either intact (14 mg SDA; Table 3) or in the form of VLC n-3 PUFAs (57 mg). The latter figure was calculated from the estimated in vivo conversion rate of 0.075 mg VLC n-3 PUFAs incorporated into egg yolk per mg SDA intake per d (see Table 4) × 761 mg SDA consumed/hen/d. Thus, most of the consumed SDA, which was assumed to be readily absorbed from the intestine, was likely oxidized and/or transported from the liver to somatic tissues such as adipose. Additionally, of the 125 mg total VLC n-3 PUFAs per yolk of eggs from hens fed the SDA diet (Table 3), by difference 68 mg were presumably derived from the bioconversion of ALA, which agrees well with the calculated amount (67 mg; 0.120 estimated conversion value ×557 mg intake per d). In contrast, FISH-fed hens deposited 305 mg (Table 3), or approximately 33%, of 933 mg of VLC n-3 PUFAs consumed daily directly into egg yolk (933 mg calculated from data in Table 2 and Supporting Information). A small amount of the 305 mg of yolk VLC n-3 PUFAs most likely was derived from the 167 mg of ALA and 88 mg of SDA consumed daily by the hens (calculated from data in Table 2 and Supporting Information).

Another possible reason for the higher SDA content of adipose tissue compared to egg yolk is that deposition into the former was cumulative over 28 d, while a growing ovarian follicle (future egg yolk) accumulates most of its lipids (and

DOI: 10.1021/jf505185u
J. Agric. Food Chem. 2015, 63, 2789−2797

protein) during the final 4−6 d prior to ovulation.[38] Moreover, since the abdominal fat pad represents only a portion of the total body adipose tissue, the absolute amount of SDA deposited ex ovo would be even greater. This raised a question as to how SDA was transported to the abdominal fat pad, since current dogma would predict that most of the absorbed dietary SDA would be esterified into liver triglycerides, packaged into "yolk-targeted" very low density lipoprotein particles,[39] secreted into the bloodstream, and taken up by growing oocytes (future egg yolks) via receptor-mediated endocytosis,[40] thereby preferentially enriching egg yolk. One possibility is that, within the liver, SDA distributes into various intracellular lipid pools and is metabolized differently than other 18-carbon PUFAs, such as GLA, as has been reported in rat hepatocytes.[41] Our findings therefore suggest that, in the chicken, an alternate major pathway for SDA secretion and transport may exist, either via secretion from the liver into the bloodstream as an albumin-bound nonesterified fatty acid or possibly as a component of another recently reported subclass of VLDL particles containing apolipoprotein-VLDL-IV (Apo-IV), which are excluded from oocytic uptake and deliver their lipids to somatic cells.[42] These possibilities await further investigation.

■ ASSOCIATED CONTENT

Supporting Information

Additional tables. This material is available free of charge via the Internet at http://pubs.acs.org

■ AUTHOR INFORMATION

Corresponding Authors

*Phone (814) 863-2102. Fax (814) 865-5691. E-mail: relkin@psu.edu.

*Phone (814) 865-6334. Fax (814) 863-6042. E-mail: kharvatine@psu.edu.

Funding

This study was supported in part by a grant from the Pennsylvania Poultry Industry Egg Research Check-Off Program (R.G.E., K.J.H.).

Notes

The authors declare no competing financial interests.

■ ACKNOWLEDGMENTS

The conventional SBO and the stearidonic acid-enriched SBO were gifts from Monsanto Company, St. Louis, MO.

■ ABBREVIATIONS USED

ALA, α-linolenic acid; Apo-IV, apolipoprotein-VLDL-IV; BW, body weight; CON, conventional soybean oil diet; DHA, docosahexaenoic acid; DPA, docosapentaenoic acid; EPA, eicosapentaenoic acid; ETA, eicosatetraenoic acid; FA, fatty acid; FISH, fish oil diet; FLAX, flaxseed oil diet; GLA, γ-linoleic acid; LA, linoleic acid; OA, oleic acid; PUFA, polyunsaturated fatty acid; SBO, soybean oil; SDA, stearidonic acid; VLC, very long-chain; VLDL, very low density lipoprotein

■ REFERENCES

(1) Flock, M. R.; Harris, W. S.; Kris-Etherton, P. M. Long-chain omega-3 fatty acids: Time to establish a dietary reference intake. *Nutr. Rev.* **2013**, *71*, 692−707.

(2) Spite, M. Deciphering the role of *n*-3 polyunsaturated fatty acid-derived lipid mediators in health and disease. *Proc. Nutr. Soc.* **2013**, *72*, 441−450.

(3) Yashodhara, B. M.; Umakanth, S.; Pappachan, J. M.; Bhat, S. K.; Kamath, R.; Choo, B. H. Omega-3 fatty acids: a comprehensive review of their role in health and disease. *Postgrad. Med. J.* **2009**, *85*, 84−90.

(4) Molloy, C.; Doyle, L. W.; Makrides, M.; Anderson, P. J. Docosahexaenoic acid and visual functioning in preterm infants: A review. *Neuropsychol. Rev.* **2012**, *22*, 425−437.

(5) Harris, W. S. Stearidonic acid as a 'pro-eicosapentaenoic acid'. *Curr. Opin. Lipidol.* **2012**, *23*, 30−34.

(6) Venegas-Calerón, M.; Sayanova, O.; Napier, J. A. An alternative to fish oils: Metabolic engineering of oil-seed crops to produce omega-3 long chain polyunsaturated fatty acids. *Prog. Lipid Res.* **2010**, *49*, 108−119.

(7) U.S. Department of Agriculture; U.S. Department of Health and Human Services. *Dietary Guidelines for Americans, 2010*; Washington, DC, 2010; http://www.health.gov/dietaryguidelines/dga2010/DietaryGuidelines2010.pdf (accessed August 7, 2014).

(8) Nesheim, M. C.; Nestle, M. Advice for fish consumption: Challenging dilemmas. *J. Nutr.* **2014**, *99*, 973−974.

(9) Ryckebosch, E.; Bruneel, C.; Termote-Verhalle, R.; Goiris, K.; Muylaert, K.; Foubert, I. Nutritional evaluation of microalgae oils rich in omega-3 long chain polyunsaturated fatty acids as an alternative to fish oil. *Food Chem.* **2014**, *160*, 393−400.

(10) Fraeye, I.; Bruneel, C.; Lemahieu, C.; Buyse, J.; Muylaert, K.; Foubert, I. Dietary enrichment of eggs with omega-3 fatty acids: A review. *Food Res. Int.* **2012**, *48*, 961−969.

(11) Hargis, P. S.; Van Elswyk, M. E. Manipulating the fatty acid composition of poultry meat and eggs for the health conscious consumer. *World's Poult. Sci. J.* **1993**, *49*, 251−264.

(12) Cruickshank, E. M. Studies in fat metabolism in the fowl. I. The composition of the egg fat and depot fat of the fowl as affected by the ingestion of large amounts of different fats. *Biochem. J.* **1934**, *28*, 965−977.

(13) Navarro, J. G.; Saavedra, J. C.; Borie, F. B.; Caiozzi, M. M. Influence of dietary fish meal on egg fatty acid composition. *J. Sci. Food Agric.* **1972**, *23*, 1287−1292.

(14) Couch, J. R.; Saloma, A. E. Effect of diet on triglyceride structure and composition of egg yolk lipids. *Lipids* **1973**, *8*, 385−392.

(15) Ren, Y.; Perez, T. I.; Zuidhof, M. J.; Renema, R. A.; Wu, J. Oxidative stability of omega-3 polyunsaturated fatty acids enriched eggs. *J. Agric. Food Chem.* **2013**, *61*, 11595−11602.

(16) González-Esquerra, R.; Leeson, S. Alternatives for enrichment of eggs and chicken meat with omega-3 fatty acids. *Can. J. Anim. Sci.* **2001**, *81*, 295−305.

(17) Gregory, M. K.; Gibson, R. A.; Cook-Johnson, R. J.; Cleland, L. G.; James, M. J. Elongase reactions as control points in long-chain polyunsaturated fatty acid synthesis. *PLoS One* **2011**, *6*, e29662.

(18) Kuksis, A. Yolk lipids. *Biochim. Biophys. Acta* **1992**, *1124*, 205−222.

(19) Eckert, H.; LaVallee, B.; Schweiger, B. J.; Kinney, A. J.; Cahoon, E. B.; Clemente, T. Co-expression of the borage Δ^6 desaturase and the *Arabidopsis* Δ^{15} desaturase results in high accumulation of stearidonic acid in the seeds of transgenic soybean. *Planta* **2006**, *224*, 1050−1057.

(20) Hy-Line International. *Hy-Line Variety W-36 Commercial Management Guide*; Hy-Line International: West Des Moines, IA. 2009.

(21) Elkin, R. G.; Yan, Z.; Zhong, Y.; Donkin, S. S.; Buhman, K. K.; Story, J. A.; Turek, J. J.; Porter, R. E., Jr.; Anderson, M.; Homan, R.; Newton, R. S. Select 3-hydroxy-3-methylglutaryl-coenzyme A reductase inhibitors vary in their ability to reduce egg yolk cholesterol levels in laying hens through alteration of hepatic cholesterol biosynthesis and plasma VLDL composition. *J. Nutr.* **1999**, *129*, 1010−1019.

(22) AOAC International. *Official Methods of Analysis of AOAC International*, 17th ed.; AOAC International: Gaithersburg, MD, 2000.

(23) Garcés, R.; Mancha, M. One-step lipid extraction and fatty acid methyl esters preparation from fresh plant tissues. *Anal. Biochem.* **1993**, *211*, 139−143.

(24) Tyburczy, C.; Lock, A. L.; Dwyer, D. A.; Destaillats, F.; Mouloungui, Z.; Candy, L.; Bauman, D. E. Uptake and utilization of

DOI: 10.1021/jf505185u
J. Agric. Food Chem. 2015, 63, 2789−2797

trans octadecenoic acids in lactating dairy cows. *J. Dairy Sci.* **2008**, *91*, 3850−3861.
(25) Rico, D. E.; Harvatine, K. J. Induction of and recovery from milk fat depression occurs progressively in dairy cows switched between diets that differ in fiber and oil concentration. *J. Dairy Sci.* **2013**, *96*, 6621−6630.
(26) Vandesompele, J.; De Preter, K.; Pattyn, F.; Poppe, B.; Van Roy, N.; De Paepe, A.; Speleman, F. Accurate normalization of real-time quantitative RT-PCR data by geometric averaging of multiple internal control genes. *Genome Biol.* **2002**, *3*, research0034.1−0034.11.
(27) Caston, L.; Leeson, S. Research note: Dietary flax and egg composition. *Poult. Sci.* **1990**, *69*, 1617−1620.
(28) Cherian, G.; Sim, J. S. Effect of feeding full fat flax and canola seeds to laying hens on the fatty acid composition of eggs, embryos, and newly hatched chicks. *Poult. Sci.* **1991**, *70*, 917−922.
(29) Aymond, W. M.; Van Elswyk, M. E. Yolk thiobarbituric acid reactive substances and n-3 fatty acids in response to whole and ground flaxseed. *Poult. Sci.* **1995**, *74*, 1388−1394.
(30) Cook, H. W. Fatty acid desaturation and chain elongation in eukaryotes. In *Biochemistry of Lipids, Lipoproteins, and Membranes*; Vance, D. E., Vance, J. E., Eds.; Elsevier: New York, 1996; pp 129−152.
(31) Wang, Y.; Botolin, D.; Christian, B.; Busik, J.; Xu, J.; Jump, D. B. Tissue-specific, nutritional, and developmental regulation of rat fatty acid elongases. *J. Lipid Res.* **2005**, *46*, 706−715.
(32) Gregory, M. K.; Geier, M. S.; Gibson, R. A.; James, M. J. Functional characterization of the chicken fatty acid elongases. *J. Nutr.* **2013**, *143*, 12−16.
(33) Goldberg, E. M.; Ryland, D.; Gibson, R. A.; Aliani, M.; House, J. D. Designer laying hen diets to improve egg fatty acid profile and maintain sensory quality. *Food Sci. Nutr.* **2013**, *1*, 324−335.
(34) Jing, M.; Gakhar, N.; Gibson, R. A.; House, J. D. Dietary and ontogenic regulation of fatty acid desaturase and elongase expression in broiler chickens. *Prostaglandins, Leukotrienes Essent. Fatty Acids* **2013**, *89*, 107−113.
(35) Elkin, R. G. Reducing shell egg cholesterol content. I. Overview, genetic approaches, and nutritional strategies. *World's Poult. Sci. J.* **2006**, *62*, 665−687.
(36) Ribeiro, T.; Lordelo, M. M.; Alves, S. P.; Bessa, R. J. B.; Costa, P.; Lemos, J. P. C.; Ferreira, L. M. A.; Fontes, C. M. G. A.; Prates, J. A. M. Direct supplementation of diet is the most effective way of enriching broiler meat with n-3 long-chain polyunsaturated fatty acids. *Br. Poult. Sci.* **2013**, *54*, 753−765.
(37) Whelan, J.; Gouffon, J.; Zhao, Y. Effects of dietary stearidonic acid on biomarkers of lipid metabolism. *J. Nutr.* **2012**, *142*, 630S−634S.
(38) Johnson, A. L. Reproduction in the female. In *Sturkie's Avian Physiology*, 6th ed.; Scanes, C. G., Ed.; Academic Press: New York, 2015; pp 635−665.
(39) Walzem, R. L.; Hansen, R. J.; Williams, D. L.; Hamilton, R. L. Estrogen induction of VLDLy assembly in egg-laying hens. *J. Nutr.* **1999**, *129*, 467S−472S.
(40) Schneider, W. J. Receptor-mediated mechanisms in ovarian follicle and oocyte development. *Gen. Comp. Endrocrinol.* **2009**, *163*, 18−23.
(41) Voss, A. C.; Sprecher, H. Metabolism of 6,9,12-octadecatrienoic acid and 6,9,12,15-octadecatetraenoic acid by rat hepatocytes. *Biochim. Biophys. Acta* **1988**, *958*, 153−162.
(42) Nikolay, B.; Plieschnig, J. A.; Šubik, D.; Schneider, J. D.; Schneider, W. J.; Hermann, M. A novel estrogen-regulated avian apolipoprotein. *Biochimie* **2013**, *95*, 2445−2453.

DOI: 10.1021/jf505185u
J. Agric. Food Chem. 2015, 63, 2789−2797

fermentation by applying cell wall profiling methods that were optimized for grape berries.[24] Both ripe and overripe grapes were used in order to investigate the impact of cell wall degradation resulting from ripening on these processes. We have applied comprehensive microarray polymer profiling (CoMPP) to monitor the cell wall polysaccharides and proteins directly by virtue of the presence of epitopes. To our knowledge, this is the first study that uses CoMPP to investigate the effect of maceration enzymes on the cell walls of grape berry skin during wine fermentation. CoMPP analysis is a semiquantitative high-throughput profiling technique and consists of the sequential extraction of the pectin (CDTA extract) and hemicellulose (NaOH extract) fractions from cell wall material.[25] These fractions are then printed onto nitrocellulose membranes and probed with monoclonal antibodies (mAbs) as well as carbohydrate-binding modules (CBMs). The data obtained provides an indication of the relative abundance of specific cell wall polysaccharides in a sample. The CoMPP data is supported by monosaccharide compositional analysis (GC-MS) and reflectance spectroscopy (FT-MIR) data. Multivariate data analysis tools were used to identify the components that characterized the differences in cell walls sourced from the different treatments. The combination of methods employed are complementary and produced valuable information on the variation in both the surface polymers as well as the profile of polymer building blocks present at different ripeness levels, winemaking stages, or after different enzyme treatments.

MATERIALS AND METHODS

Vinification of Wine. *Vitis vinifera* cv Pinotage grapes were sourced from vineyards in the Boland region of South Africa during the 2012 and 2013 vintages. Fermentations were done in triplicate in 2012 and quadruplicate in 2013 in polypropylene buckets with 5 kg of destemmed and crushed grapes per bucket (weighed, destemmed, and crushed individually; one bucket is one biological repeat). After the grapes were crushed, sodium metabisulfite was added (30 ppm of SO_2), and the total acid was adjusted to 6.5 g/L. The yeast strain, *Saccharomyces cerevisiae* VIN13 (Anchor Yeast, Johannesburg, South Africa), was rehydrated and inoculated according to the manufacturer's recommendations, and yeast nutrition was supplemented with Fermaid K (Lallemand, Bellville, South Africa). Where applicable, Rapidase Ex Color, -CB, and -Expression (DSM Food Specialties, Heerlen, The Netherlands) were added to the crushed grapes at a dosage of 0.03 g/L. The manufacturer of these enzymes declares that all the mixes have primarily pectinolytic activity but that RapidaseCB has been formulated with enhanced polygalacturonase activity, Rapidase Ex Color has additional hemicellulases for optimum grape skin extraction during maceration, and Rapidase Expression formulations contain arabinases and rhamnogalacturonases (product data sheets, http:\\www.dsm-foodspecialities.com). Fermentations were conducted at 25 °C, and the grape skin caps were punched down twice daily. At the end of alcoholic fermentation, the wines were pressed and transferred to 4.5 L glass bottles fitted with fermentation caps. The pomace was stored at 4 °C until analysis (up to 1 week). Freeze-dried *Oenococcus oeni* Lalvin VP41 (Lallemand, South Africa), supplemented with OPTI-MALO-PLUS (Lallemand), was inoculated in the wine to induce malolactic fermentation (MLF), and the fermentations were incubated at 20 °C. At the end of MLF, the wine was racked off the lees, sulfited (80 ppm of SO_2), stabilized at 4 °C, and then filtered and bottled.

General Oenological Parameters. Three 50 mL samples of the juice were randomly selected from the buckets after the grapes were crushed and analyzed for sugar and acid concentration using Fourier transform infrared (FT-IR) spectroscopy with a WineScan FT120 Basic (FOSS Analytical, Hillerød, Denmark). The same instrument was used to analyze the pH, volatile acidity, total acid, glucose + fructose, and ethanol levels of two 50 mL wine samples from each biological repeat at the end of MLF. The FT-IR scans were done in duplicate per sample (two technical repeats). Wine samples for color analysis were collected three months after the wines had been bottled. The pH of all samples was adjusted to 3.5, and the color characteristics were determined according to Iland et al.[26] using a Specord 50 UV/vis spectrophotometer (Analytik Jena, Jena, Germany). The analysis was done in triplicate.

Pinotage Skin Cell Wall Preparation. For the fresh grape skin samples, the grapes were selected from different harvest crates, from different bunches, and from the top, middle, and bottom of a bunch to mimic the variability that is found in a commercial harvest batch. The berries were frozen and stored at −20 °C before the skins were obtained by manually peeling the grapes with a scalpel and flash-freezing the skins in liquid nitrogen. A group of 21 samples (each 10 g wet weight) was collected in 2012 and kept at −80 °C before freeze-drying (likewise 12 samples in 2013). The fermented grape skin samples (with and without enzyme treatment) were collected at the end of alcoholic fermentation after pressing (at least two samples per biological repeat) and stored at 4 °C before excess pulp was removed from the skins with a scalpel and the skins were freeze-dried. Samples (each 10 g wet weight) were milled and homogenized with a Retsch MM400 mixer mill (Retsch, Haan, Germany) at a frequency of 30 Hz for 30 s, and the resulting powder was used for the isolation of the cell walls using the method described by Ortega-Regules et al.[27] with the following changes. The first acetone step after the buffered phenol extraction was omitted. Furthermore, after the third acetone wash, the alcohol-insoluble residue (AIR) was air-dried, then mixed with a volume of Milli-Q water roughly equal to the pellet size of the AIR, frozen at −80 °C, and then freeze-dried.

Mid-Infrared Spectroscopy. AIR samples isolated from fresh and fermented Pinotage skins (with and without the addition of maceration enzymes) were analyzed by infrared spectroscopy. The samples were placed in direct contact with the diamond window and the spectra between 4000 and 600 cm^{-1} were acquired using a NEXUS 670 (Thermo Scientific, MA, USA) fitted with a Golden Gate Diamond ATR (attenuated total reflectance). A Geon-KBr beam splitter and DTGS/Csl detector were used and each sample was scanned 128 times. The FT-MIR spectra data were filtered with a MSC (multiplicative scatter correction) filter to compensate for light scattering and differences in the effective path length. The spectra for the fingerprint region (1400−800 cm^{-1}, where every polysaccharide has its own unique pattern) as well as wavelengths from 1400 up to 1800 cm^{-1} that conveys information about functional groups[28,29] were compared between treatments. The spectra shown in the Results section represent the average absorbance from at least five AIR samples per treatment. Technical repeats were done once every 10th scan to control for technical reproducibility.

Monosaccharide Analysis of Cell Wall Samples. The monosaccharide composition of the AIR isolated from the grape skins was analyzed according to the method described in ref 30 and used on grape cell walls in ref 24, including a few modifications. Approximately 5 mg of AIR was hydrolyzed to monosaccharides using 2 M TFA and incubated for 2 h at 110 °C.[30] This was followed by derivatization to methoxy sugars at 80 °C for 16 h. After silylation with HMDS/TMCS/pyridine (3:1:9, Sylon HTP kit, Sigma-Aldrich, MO, USA), the derivatives were separated and analyzed in a gas chromatograph instrument (Agilent 6890 N, Agilent Technologies, CA, USA) coupled to an Agilent 5975 MS mass spectrometer detector, using a polar (95% dimethylpolysiloxane) ZB-Semivolatiles Guardian GC column (30 m, 0.25 mm ID, 0.25 μm film thickness). The oven temperature was maintained at 70 °C for 2 min, ramped up at a rate of 1 °C/min to 76 °C, then increased at 8 °C/min to 300 °C, and then held for 5 min. The monosaccharide composition was expressed as the mole percentage contribution of each monosaccharide in relation to the nine monosaccharides present. Error bars in the histograms or the standard deviation in the tables represent the mean of at least three biological samples.

DOI: 10.1021/jf505200m
J. Agric. Food Chem. 2015, 63, 2798−2810

Comprehensive Microarray Polymer Profiling (CoMPP) Analysis of Cell Wall Fractions. The pectin- and hemicellulose-rich fractions of the cell wall samples were sequentially extracted from 10 mg AIR samples using the solvents CDTA (diamino-cyclo-hexane-tetra-acetic acid) and NaOH, respectively, according to a procedure described elsewhere.[24] Arrays printed with the different fractions were probed individually with 26 different mAbs and CBMs as previously described.[25] A mean spot signal was calculated, whereafter it was normalized to the highest signal in the data set (set as 100), and a cutoff value of five was used.

Multivariate and Univariate Statistics. Univariate statistical analyses were done (ANOVA, with $P = 0.05$) under the guidance of the Centre for Statistical Consultation at Stellenbosch University (Prof. Martin Kidd) using Statistica 10 (StatSoft Southern Africa - Analytics, Sandton, South Africa). Multivariate analysis by means of principle component analysis (PCA)[31] and orthogonal projections to latent structures (OPLS) were performed using SIMCA 13 software package (Umetrics AB, Umeå, Sweden).

RESULTS AND DISCUSSION

In this study, we used Pinotage grapes at different ripeness levels as reflected in the glucose + fructose (2012: 227 g/L and 2013: 265 g/L) and total acid (2012: 5.37 g/L and 2013: 4.85 g/L) concentrations of the juice samples (Table S1). According to traditional ripeness criteria discussed in the Supporting Information (section S 1.1), the grapes at 22.7 °B were considered to be at optimum ripeness, whereas those at 26.5 °B are deemed overripe.[32,33] Each year, we compared the cell wall composition of fresh (unfermented) skins with skins that went through an alcoholic fermentation. Additionally, we investigated the cell walls from fermentations supplemented with commercial maceration enzymes and compared them to their no-enzyme-added counterparts to determine the changes caused by enzymatic hydrolysis. To evaluate the influence of ripeness levels, we compared the results from the samples over the two years with each other.

Effect of Ripeness Level in the Fresh Grape Skin Cell Walls. The mole percentage (mol %) ratio of the nine main monosaccharides found in grape skin cell walls of Pinotage is shown in Figure 1 and confirms the abundance (ca. 35 mol %) of galacturonic acid (GalA) as previously shown for grape skin.[14] The profile obtained (ca. 20 mol % Ara, arabinose, 15 mol % Xyl, xylose, and Gal, galactose, and lower than 10 mol % for the other sugars) compared well with other red wine cultivars such as Cabernet Sauvignon, Merlot, and Shiraz.[27,34] However, direct comparisons of monosaccharides levels should be avoided because of the different methods that were used to determine the uronic acids (TMS methyl glycosides or alditol acetates)[30] because this influences the relative molar ratios obtained.

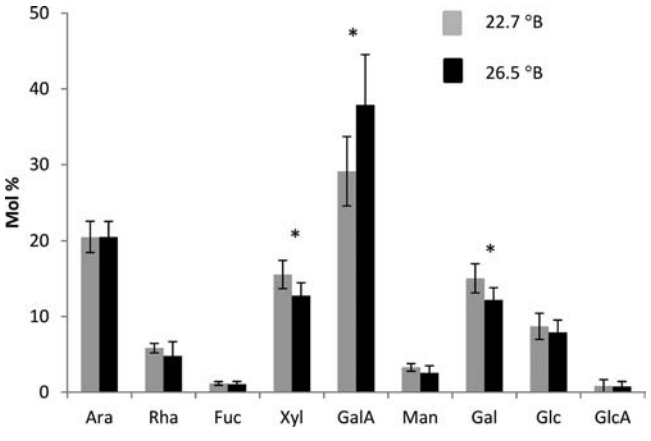

Figure 1. Monosaccharide composition of cell walls from ripe (22.7 °B, 2012) and overripe (26.5 °B, 2013) fresh Pinotage grape skin.The bars represent the average of at least 10 biological repeats. The stars indicate a statistically significant difference for a specific monosaccharide (t test, 95% confidence level) between the two ripeness levels. Ara, arabinose; Rha, rhamnose; Fuc, fucose; Xyl, xylose; GalA, galacturonic acid; Man, mannose; Gal, galactose; Glc, glucose; and GlcA, glucuronic acid.

The abundance of homogalacturonan (HG) in the skin cell walls was confirmed with the CoMPP analysis, as indicated by the signal values in the heat map (Figure 2, CDTA fraction, fresh samples). The cell walls also contained high levels of xyloglucan (mAbs LM15 and LM25) and cellulose (mAb CBM3a), with the latter dissolving along with the hemicellulose fraction (Figure 2, NaOH fraction, fresh samples) which might be a reflection of the known association between the cellulose and hemicellulose network in plant cell walls.[35] Both the pectin and the hemicellulose fraction showed the presence of arabinogalactan proteins (AGPs) and extensins. α-1,5-L-Arabinan and β-1,4-D-galactan, probably linked to rhamnogalaturonan I (RG-I), were found in the hemicellulosic fraction. This corresponded with work done by Zykwinska et al.[36] on alkali extracts from potato and sugar beet cell walls where they observed strong interaction between arabinan or galactan side chains and the cellulose microfibrils surface and were also observe in grape tissue.[24]

Comparing ripe (22.7 °B) with overripe (26.5 °B) Pinotage skin cell walls (Figure 1), the overripe samples had significantly less (95% confidence level) Gal (2.9 mol % decrease) and Xyl (2.8 mol % decrease) but more GalA (8.8 mol % increase). The lower percentage contribution of Gal in the overripe grapes corresponds with what other authors[17,24,34] described as typical changes during fruit and grape berry ripening and is believed to be related to arabinogalactan degradation as fruit softens. The lower mole percentage of Xyl and Gal in the overripe grapes is corroborated by the CoMPP analysis (Figures 2 and 3A,B, fresh samples and PCA plot of NaOH fraction, respectively) where a decrease in xyloglucan (mAbs LM15 and LM25) and β-1,4-D-(galacto)(gluco)mannan (mAb LM21) was observed in the skin cell walls of the riper grapes. This was accompanied by a decrease in cellulose (mAb CBM3a). Similar results were seen by Yakushiji et al.,[37] and Vicens et al.[17] reported a decrease in Xyl with a concurrent decrease in xyloglucan during ripening, confirming that not only pectin polysaccharides depolymerize with fruit ripening, but also hemicelluloses.

There is no consensus yet on the fate of GalA in the grape skin during ripening. According to the data from Ortega-Regules et al.,[34] the uronic acid concentration reaches a peak before grape maturity and then declines (Monastrel and Cabernet Sauvignon grapes), but this was not confirmed for all the cultivars that were tested (Syrah increased and Merlot decreased with ripening). The higher levels of GalA found in our overripe grape skins might be due to mesocarp material that peeled off along with the skin. The higher GalA levels were confirmed with the CoMPP data (Figures 2 and 4A,B, PCA plot and CDTA extract, respectively) where the overripe skins were more abundant in HG epitopes (mAbs LM18, LM19, JIM7, and JIM5) than the ripe skins. Additionally, the overripe skins showed more arabinogalactan proteins (AGPs, mAbs JIM8 and JIM13), which corresponded well with the observed accumulation of structural cell wall proteins during fruit

DOI: 10.1021/jf505200m
J. Agric. Food Chem. 2015, 63, 2798−2810

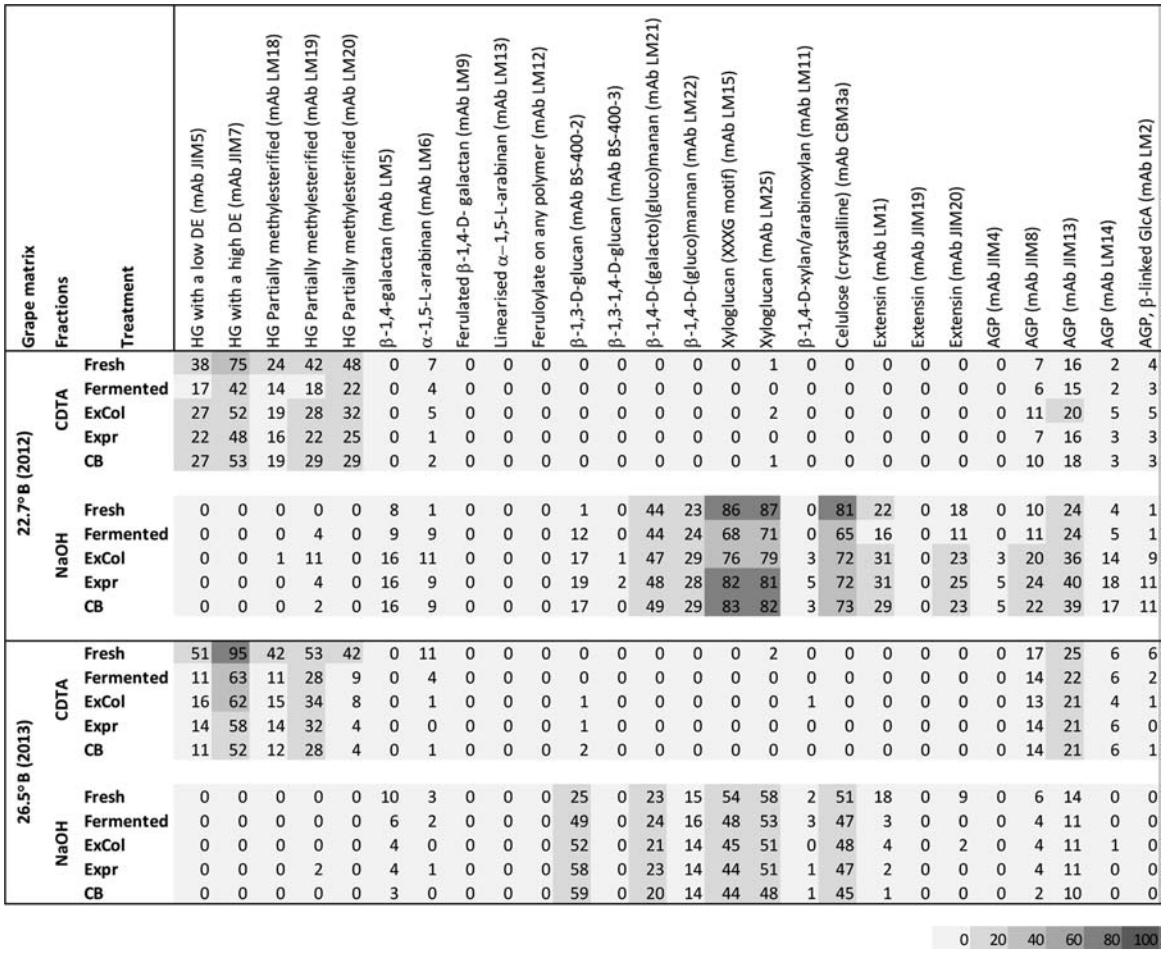

Figure 2. Heat map (CoMPP results) showing the relative abundance of the cell wall polysaccharides found in the pectin (CDTA) and hemicellulose (NaOH) fractions extracted from the cell walls of fresh and fermented (with and without maceration enzyme treatment) grape skins. Fresh = extracts from fresh skin cell walls. Fermented = extracts prepared from the cell walls of skins sampled at the end of alcoholic fermentation (without enzyme addition). ExCol, Expr, and CB = the same as Fermented but with the addition of Rapidase ExColor, Expression, and -CB enzymes, respectively. Values are the average of at least 3 biological repeats.

ripening.[17,38] The overripe samples were more abundant in *β*-1,3-D-glucan (callose, NaOH fraction, Figure 3B, PC2 = 11%), which is typically formed in response to pathogen-induced stress or wounding.[39] The overripe and softer grapes were probably more vulnerable to wounding during the harvest and the peeling of the skins. The separation of the 22.7 °B samples from the 26.5 °B samples is not dominated by the abundance of mAb BS400-2 (callose) as suggested by Figure 3 because the overall pattern of a PCA where we excluded this antibody (results not shown) were unchanged from the PCA in Figure 3.

The PCA plots of the CoMPP data for fresh cell walls sampled from grapes at the two different ripeness levels (Figures 3A and 4A) showed significant heterogeneity between the samples within a harvest. This is indicated in the NaOH fraction (Figure 3) by the different subgroups formed by the 26.5 °B samples (circled) as well as by a strong spread of the 22.7 °B samples along the second component axis, (arrow). Closer examination of the CDTA fraction revealed that certain samples from both ripeness levels clustered together (Figure 4, indicated in a block) because they have an abundance of HG, AGPs, and extensins. These samples thus contained a higher percentage of riper skins than the other samples from their respective ripeness-level groups and demonstrated the heterogeneity found in the grapes harvested for a standard commercial wine fermentation.

Effect of the Maceration Enzymes on the Fermented Grape Skin Cell Walls. During the maceration step of red wine fermentation, the ethanol formed penetrates the berry cell walls and permeabilizes the plasma and the vacuolar membranes of the cells and serves as an extraction solvent for a range of molecules, including high-molecular-weight tannins.[6] Furthermore, pectin solubilization also occurs during fermentation because organic acids such as malate, citrate, and phytic acids present in grape must act as chelating agents, removing the calcium ions that form bridges between HG polymers.[22] Thus, even with no addition of maceration enzymes, cell wall modifications probably occur as a consequence of the fermentation process alone.

The most marked impact of the fermentation process (Figure 5) was an increase in mannose (Man, 2.9 mol % in 2012 and 5.3 mol % in 2013) and glucose (Glc, 8.2 mol % in 2012 and 6.8 mol % in 2013) and a slight decrease in Ara (3.8 mol % in 2012 and 2.7 mol % in 2013). The increase in Glc and Man is probably due to a reduction in pectin polymers, leading to a relative increase in polymers such as cellulose, mannan, and xyloglucan. Although not statistically significant, GalA values showed a decreasing trend (2.8 mol % in 2012 and 5.6 mol % in

DOI: 10.1021/jf505200m
J. Agric. Food Chem. 2015, 63, 2798−2810

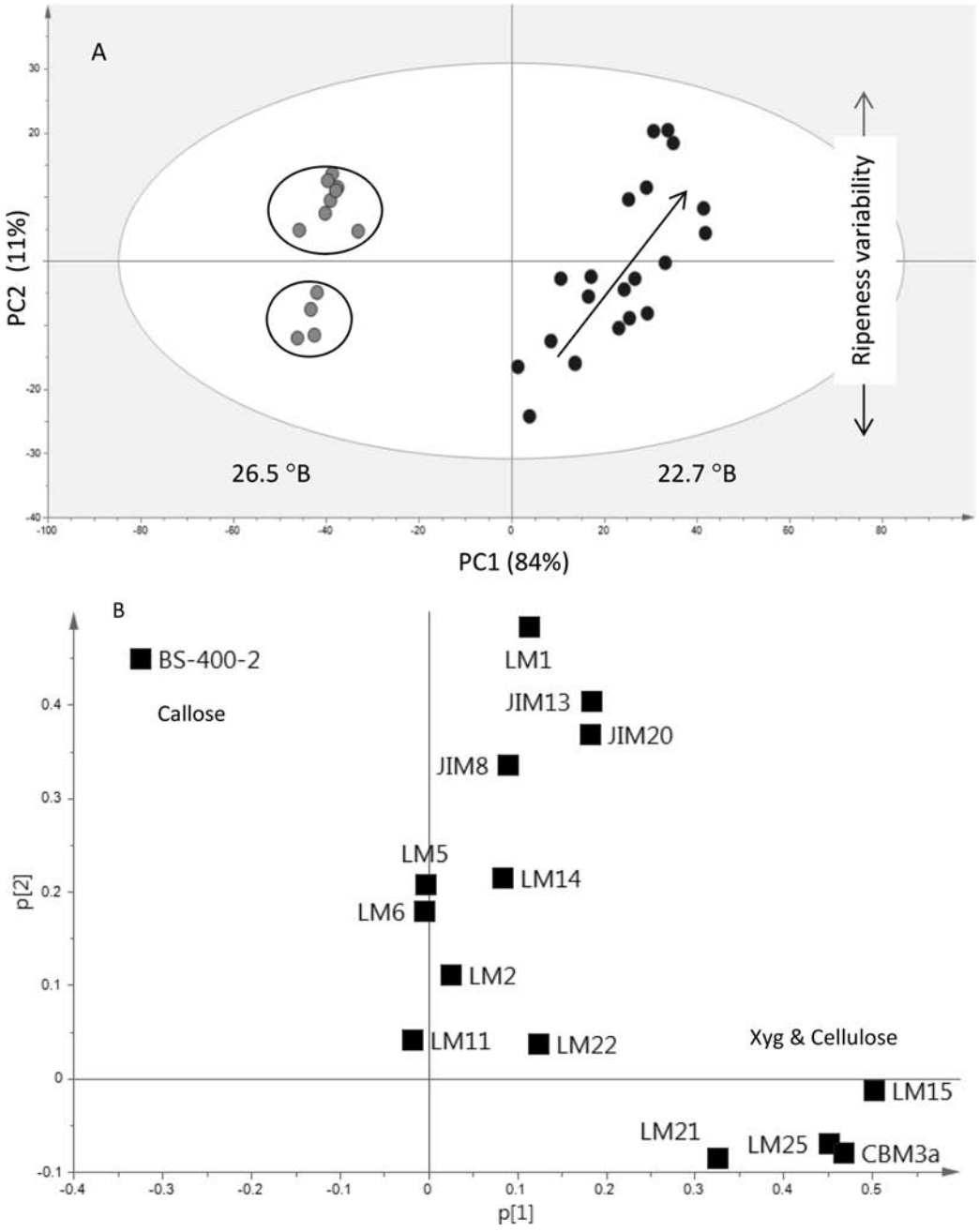

Figure 3. CoMPP results showing a PCA score plot (A) and loading plot (B) of the hemicellulose fraction (NaOH) of cell walls from fresh skins for ripe (22.7 °B, 2012, solid black circles) and overripe (26.5 °B, 2013, solid gray circles) grapes. Subgroups are circled, and the variance in the ripe (22.7 °B) skin data is highlighted with an arrow. Xyg = xyloglucan.

2013; *t* test, 90% significance) as a result of the fermentation. This decrease was also clearly visible in the CoMPP data (Figure S1 A,B). This PCA plot shows the fermented (without enzyme) samples on the left separate from the fresh, unfermented samples on the right. The separation or variance was due to the abundance of HG polymers (labeled by mAbs JIM5, JIM7, LM18, LM19, and LM20) in the fresh samples. A similar analysis with the FT-MIR spectra (Figure 6) also indicated that the fresh skin cell walls had more pectin (high absorbance at 1095 and 1157−1147 cm^{-1}).

Another explanation for the elevated Man concentration (Figure 5) of the fermented samples may be the presence of the wine yeast. A total of 40% of the wine yeast cell wall (dry weight) consists of mannoproteins, and 98% of the sugar in this cell wall component is Man.[40] Yeast cell wall debris that sticks to grape skin fragments could possibly end up in the cell wall extracts and thus inflate the Man values. Similarly, yeast cell wall debris that contains β-1,3-D-glucan[41] might also have contributed to the elevation in Glc concentration seen but a more likely source could be callose (β-1,3-D-glucan) formation in the fermented grape skins. The formation of callose in grape berries that are crushed and punched down during the red wine production process is plausible, and CoMPP analysis confirmed the presence of β-1,3-D-glucan (mAb BS-400-2, specific to callose). It is not known whether this mAb will also label β-1,3-D-glucan in yeast cell walls; however in other results by our group (unpublished), we regularly see a signal for mAb BS-400-2 in grape tissue that did not undergo fermentation.

DOI: 10.1021/jf505200m
J. Agric. Food Chem. 2015, 63, 2798−2810

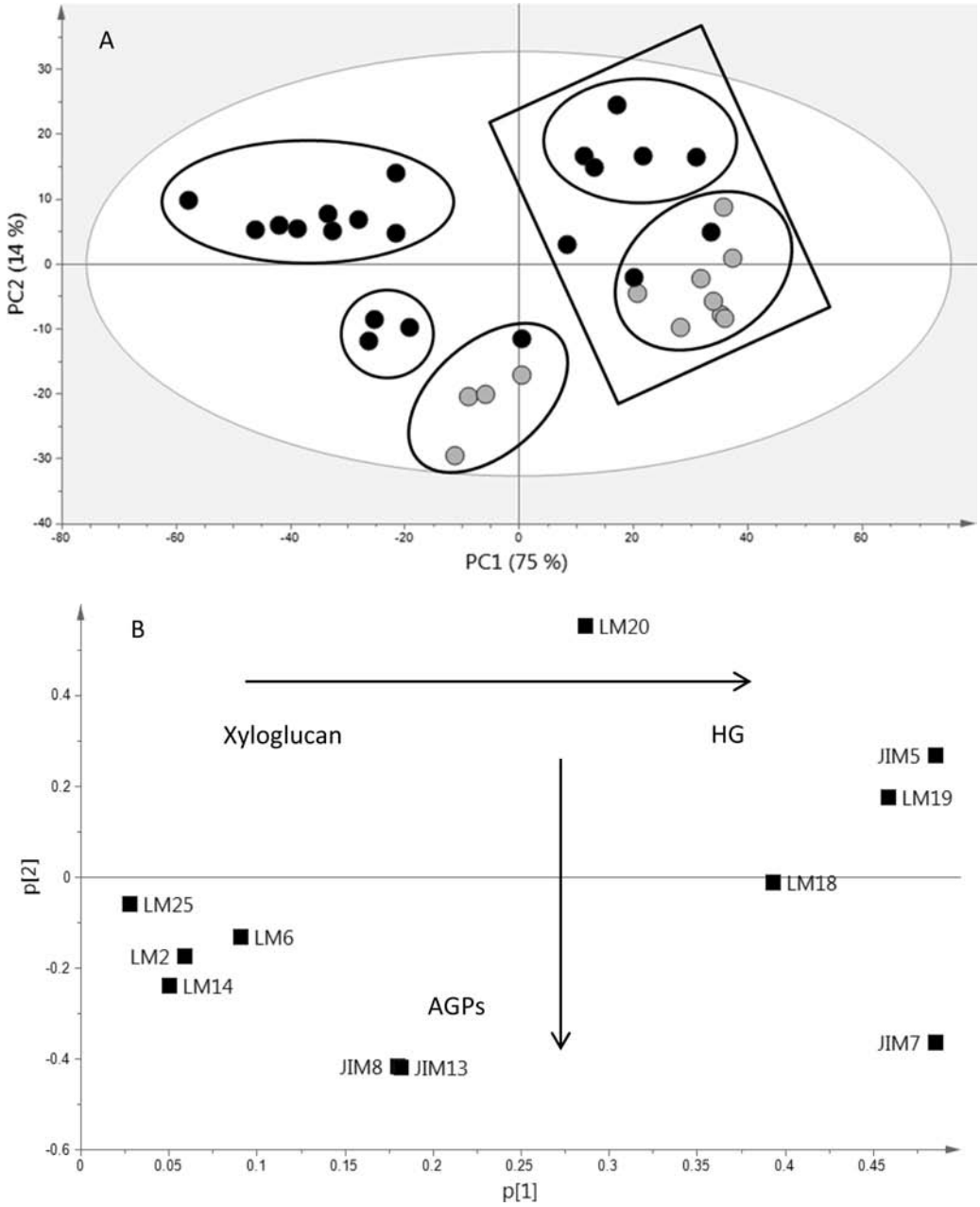

Figure 4. CoMPP results showing a PCA score plot (A) and loading plot (B) of the pectin fraction (CDTA) of cell walls from fresh Pinotage skins at different ripeness levels (22.7 °B, 2012, solid black circles, and 26.5 °B, 2013, solid gray circles). Subgroups are encircled and indicate that the separation of the groups is driven by an abundance in AGPs and HG.

Finally, the decrease in Ara because of the fermentation process may be attributed to the release of AGPs and type II arabinogalactans into the fermenting must. These molecules constitute ca. 40% of the total polysaccharides found in red wine[42,43] and Guadalupe and Ayestarán[44] showed that the Ara concentration increased to more than 150 mg/L at the end of alcoholic fermentation. However, the FT-MIR data (Figure 6) showed that the fermented skin cell walls had more protein (high absorbance at 1650 and 1550 cm^{-1}) than the fresh skins. This seems to be in contrast to the decrease in Ara and the assumed loss of AGPs, but it needs to be considered that the monosaccharide analysis measured the total amount of Ara in the samples, whereas the FT-MIR spectra only evaluated the surface or cell wall proteins exposed after depectination. In general, therefore, we see that the fermentation process caused similar compositional changes in the skin cell walls of grapes, irrespective of the ripeness level of the skins. However, the ripeness might have an influence on the magnitude of the changes observed. This can be seen in Figure 6 at wavelengths 1550 and 1650 cm^{-1}, where the gray dotted line that represents the fermented samples at 26.5 °B showed the largest deviation from the fresh samples.

Color analysis on the wine prepared in this study showed no significant improvement in the color density of the wines produced from enzyme-treated fermentations (Supporting Information, section S 1.2 and Table S1). To supplement this indirect evaluation of the impact of enzymes, we asked whether this implies that the maceration enzymes did not alter the cell walls of the skins. This led to the final investigation of this study where we aimed to determine how typical commercial

DOI: 10.1021/jf505200m
J. Agric. Food Chem. 2015, 63, 2798−2810

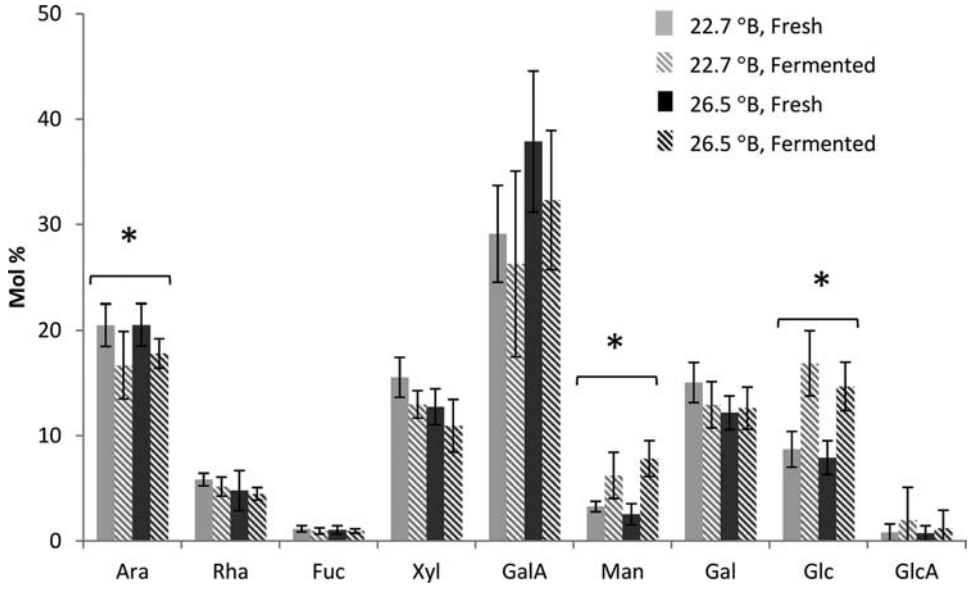

Figure 5. Mole percentage (mol %) changes in the monosaccharide composition of the cell walls extracted from fresh and fermented Pinotage skins in 2012 and 2013. Significant changes (indicated by stars) brought about by the fermentation process include an increase in Man and Glc and a slight decrease in Ara (95% confidence level, ANOVA). The bars represent the average of at least three biological repeats.

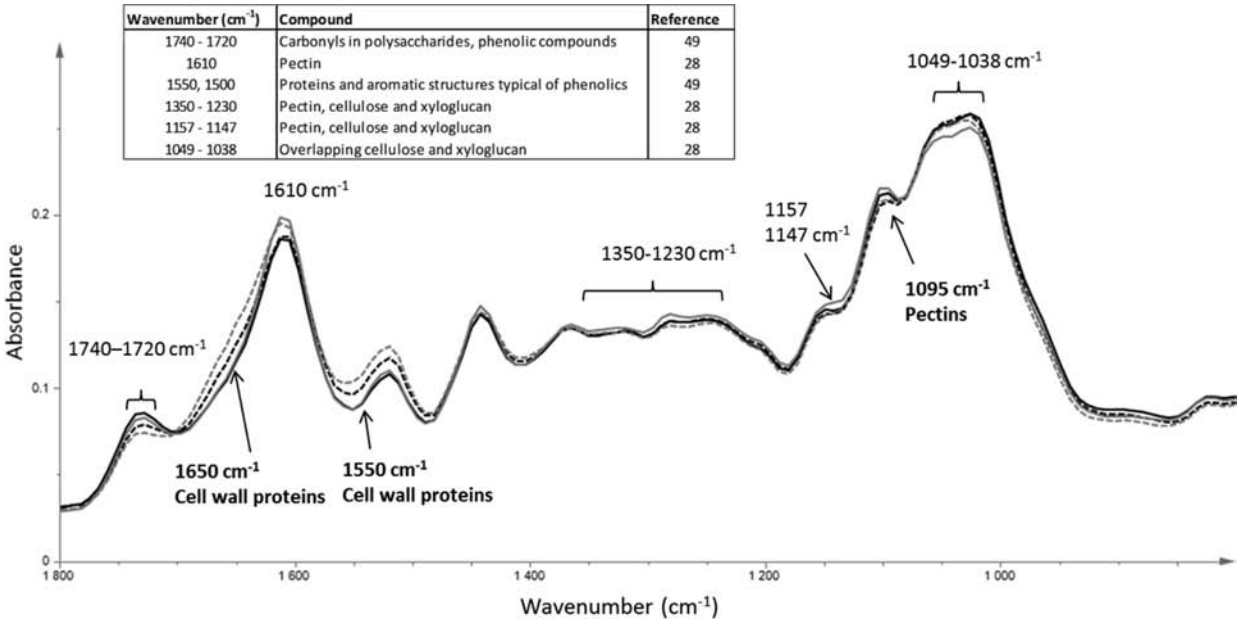

Figure 6. FT-MIR spectra of the fresh versus fermented (without enzymes) cell walls at two ripeness levels. Solid black and dashed black lines, fresh and fermented 22.7 °B 2012, respectively, and solid gray and dashed gray lines, fresh and fermented 26.5 °B 2013, respectively. The areas and peaks that represent typical chemical groups found in plant cell walls are shown on the spectra and in the table. The greatest variations are at wavelengths 1650 and 1550 cm^{-1} where the cell walls isolated from the fresh skins have a lower absorbance than the fermented samples, indicating that they have less cell wall proteins. Another interesting area is the peak at 1095 cm^{-1} that shows that the cell walls isolated from fresh skins have more pectin than the fermented samples. The spectra represent the average absorbance from at least five AIR samples per treatment.

maceration enzymes change the cell walls of grape skins during fermentation. We therefore compared the samples from the enzyme-free fermentations with samples from the enzyme-assisted fermentations. The most dominant changes (Figure 7, 95% confidence level, ANOVA) to the monosaccharide composition of the cell walls brought about by the enzymes were: (1) an increase in Man (avg. of 3.7 mol % in 2012 and 4.8 mol % in 2013) and Glc (no significant increase in 2012 and avg. of 4.7 mol % in 2013) and (2) a decrease in Ara (avg. of 2.3 mol % in 2012 and 2.9 mol % in 2013), Rha (avg. of 0.9 mol % in 2012 and 1.1 mol % in 2013), and GalA (no significant increase in 2012 and an avg. of 9.6 mol % in 2013) composition. As previously discussed, the relative increase of the cellulose, mannan, and xyloglucan monosaccharides (Man and Glc) is a consequence of the degradation of pectin polymers (HG and RG), but this time it was due to the hydrolysis and depectination of the cell wall polysaccharides by the maceration enzymes (enzyme-treated values were compared to control fermentation values). Similarly, the decrease in Ara and Rha is an indication of RG-I, arabinan, and AGP

DOI: 10.1021/jf505200m
J. Agric. Food Chem. 2015, 63, 2798−2810

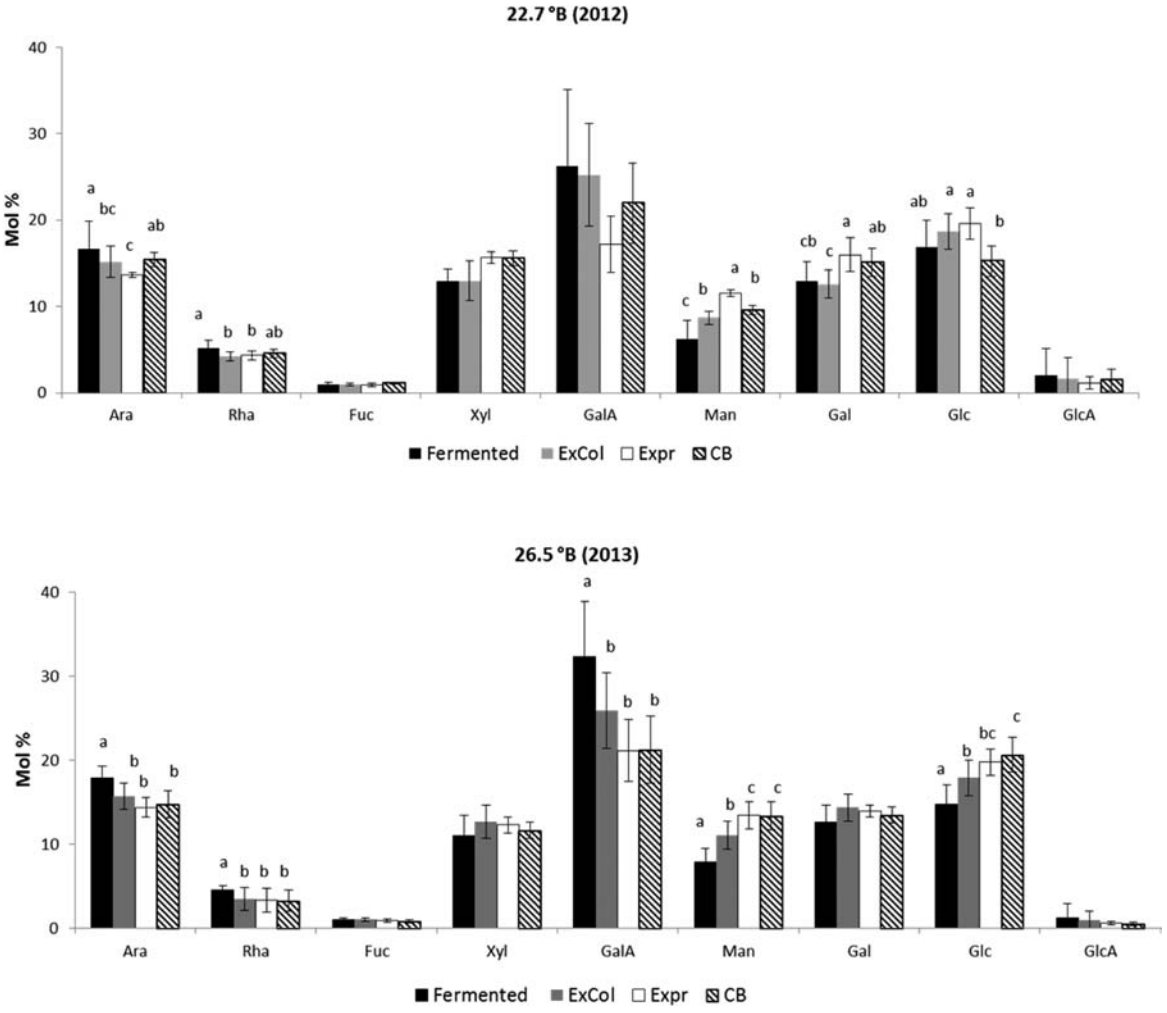

Figure 7. Mole percentage (mol %) changes in the monosaccharide composition of the cell walls from Pinotage skins from fermented (no enzyme addition) and maceration enzyme-treated fermentations at 22.7 and 26.5 °B. Different letters indicate a significant difference between the different treatments for a specific sugar (95% confidence level, ANOVA). "Fermented" stands for cell wall samples from fermentation without enzyme addition. "ExCol", "Expr", and "CB" represent cell wall samples from fermentation with the addition of Rapidase Ex Color, Rapidase Expression, and Rapidase CB, respectively. The values represent the average of three biological repeats.

degradation. We thus see the same type of monosaccharide changes occurring in enzyme-free and enzyme-assisted fermentation, but the enzymes increased the magnitude of the changes. Maceration enzymes might also introduce additional changes to the cell wall such as the proportional decrease in Rha (Figure 7) because a similar decrease was not observed under enzyme-free conditions (Figure 5).

On the polymer level (CoMPP data), one would expect to see that maceration enzyme action lead to a consequential decrease in pectin polymers, reflecting the decrease in GalA and Rha values. We did in fact note a loss of pectin in the FT-MIR spectra (Figure S2) for the enzyme-treated samples. One would expect depectination to be the most prominent change because pectinases are the major enzyme activity present in the maceration enzyme preparations that were used. However, the CoMPP heat map (Figure 2) showed an increase in HG labeling (CDTA fraction, all HG mAbs) of the enzyme-treated skins of 2012 (22.7 °B) compared to that of the control fermentation skins. Considering that the polymers that were identified in the different fractions of the CoMPP analysis were those polymers extracted and dissolved in CDTA and NaOH, respectively, we can speculate that the increase in HG was the result of enzyme hydrolysis that unravelled the cell wall structure. This process allowed more of the HG that is interspersed with the hemicellulose−cellulose scaffold to move out and dissolve in CDTA, leading to higher labeling signals. In the overripe grape skins (26.5 °B) however, the values only increased for mAbs JIM5 and LM19 and only for ExCol treated samples. In general, for the overripe grape skins there was only an initial marked decrease in HG and α-1,5-L-arabinan as a result of the depectination that took place during the standard red wine fermentation (no added enzymes).

In the hemicellulose fraction of the ripe grapes 2012 (Figure 2), there was an increase in the dissolved β-1,4-D-galactan, mannans (slight), xyloglucans (mAbs LM15 and LM25), cellulose (mAb CBM3a), extensins (mAb JIM20), and AGPs (mAbs JIM4, JIM8, JIM13, LM14, and LM2), which can all be ascribed to the hydrolysis actions of the enzymes that enhanced the solubilization of these polymers in the NaOH extract. As with the CDTA fraction, these effects were not repeated in the NaOH fraction of the overripe grapes. This may indicate that the high degree of cell wall degradation that took place because of the natural grape-ripening processes in the overripe grapes led to a nearly complete removal of all easily accessible cell wall

DOI: 10.1021/jf505200m
J. Agric. Food Chem. 2015, 63, 2798−2810

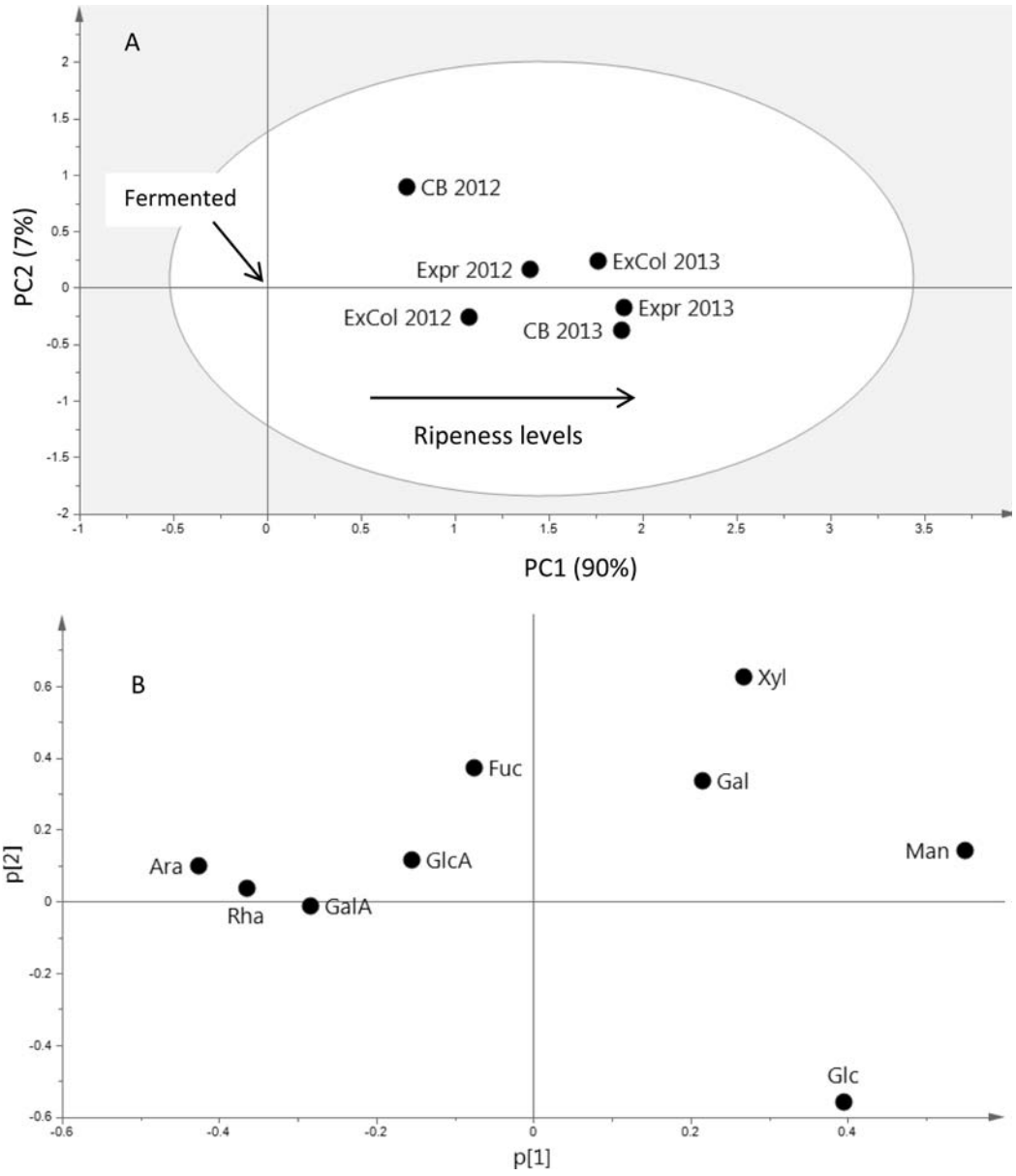

Figure 8. Score (A) and loading (B) plots of a correlation matrix analysis on the monosaccharide composition of enzyme-treated grape skin cell walls compared to samples from the control fermentation (no enzyme addition is represented by the intersection of the axis) at two different ripeness levels.

polymers during fermentation, even in the control fermentation. No significant additional change caused by hydrolysis by the maceration enzymes could be detected in the overripe cell walls. Thus, the maceration enzyme actions quantitatively (monosaccharide data) have a similar effect to that of the natural grape-tissue-ripening enzymes (depectination), but their mode of action might be different. The former seem to contribute to an increase in cell wall porosity, which is not seen with the latter. This might indicate that the plant ripening enzymes act in a block-wise fashion (as seen with plant pectin methyl esterases (pPME),[45,46] whereas the fungal enzymes from commercial maceration preparations act more randomly (as seen with some fungal PMEs).[47] However, the differences observed might just be a factor of the degree of degradation that has taken place. As hydrolysis time increase (as grapes ripen or have a longer incubation with maceration enzymes), the degradation might progress in alternating stages of depolymerization and diffusion of the resulting oligomers into the surrounding matrix (fermenting must) and pore formation.

Orthogonal projections to latent structures (OPLS) models[48] were used to focus more specifically on the difference between each enzyme treatment effect versus its control. The resulting six OPLS models (three treatments/vintage) can be summarized by its correlation loadings. These correlation values of the models were portrayed in principle component analysis (PCA) plots (Figures 8 and 9 for monosaccharides and CoMPP data, respectively). Figure 8 showed that in terms of monosaccharide composition all the enzymes had a similar effect on the cell wall (all are in the same direction, a distance away from the control samples represented by the intersection of the axis). However, the 2013 enzyme-treated samples were further removed along the first component axis (PC1 = 90%) than were the 2012 samples, indicating a greater impact on monosaccharide composition. This impact is partly due to the hydrolysis by

DOI: 10.1021/jf505200m
J. Agric. Food Chem. 2015, 63, 2798−2810

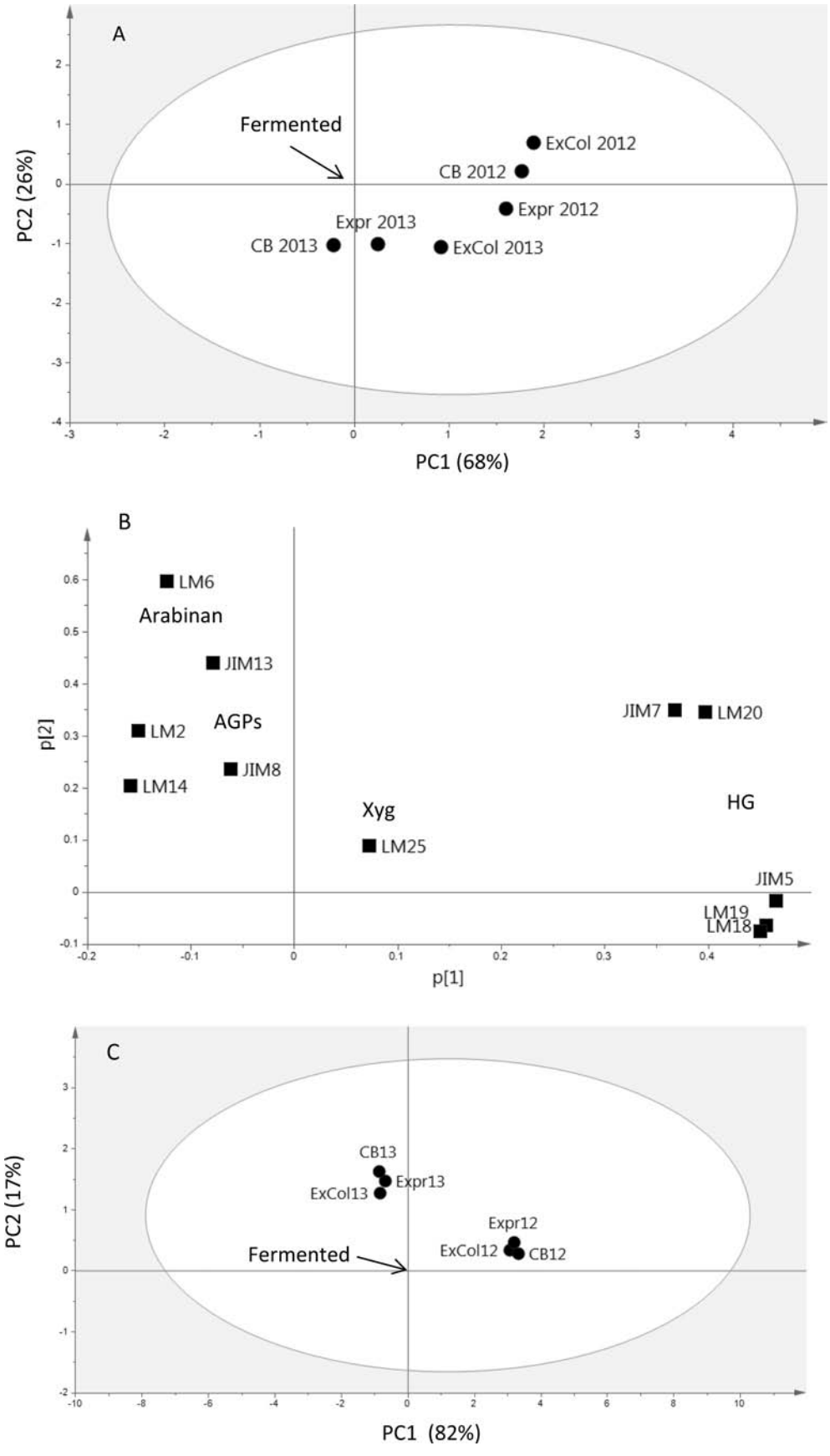

Figure 9. continued

DOI: 10.1021/jf505200m
J. Agric. Food Chem. 2015, 63, 2798−2810

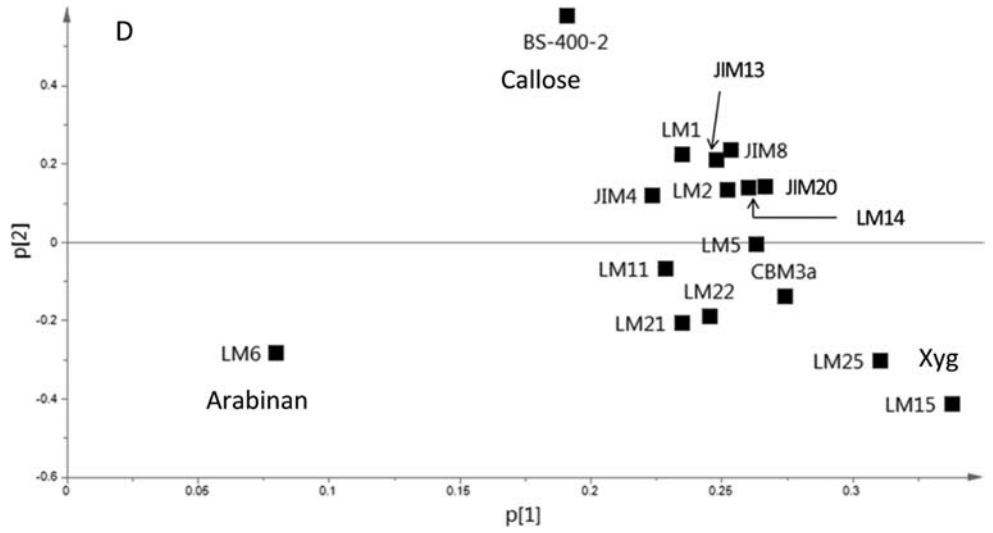

Figure 9. Score (A) and loading (B) plots of a correlation matrix analysis on the CDTA fraction (CoMPP data) of enzyme-treated grape-skin cell walls compared to samples from the control fermentation (no enzyme addition). Score (C) and loading (D) plots of a correlation matrix analysis on the NaOH fraction (CoMPP data) of enzyme-treated grape-skin cell walls compared to samples from the control fermentation (no enzyme addition). The codes for the epitopes are described in Figure 2. Xyg = xyloglucan.

the commercial maceration enzymes, but it is also the result of endogenous cell wall enzymes. The loading plot confirms that the enzyme-treated cell walls have higher proportions of Man and Glc and lower percentages of Ara, Rha, and GalA than the control group. The cell walls treated with Rapidase CB during 2012 are the main contributors to the variance along the second component of the model, and this variance is driven by a relative abundance of Xyl in the samples. According to the manufacturer, Rapidase CB has primarily pectinase activity with enhanced polygalacturonases; thus, this unique behavior could not be connected to a specific enzyme activity present in Rapidase CB.

On a polymer level (CoMPP data), the correlation values obtained from OPLS models on individual enzyme treatments versus the enzyme-free fermentation are shown in the PCA plots of Figure 9. In the analysis of the CDTA fraction (Figure 9A,B), ExCol 2012 and CB 2012 were positively correlated with an abundance in HG (mAbs JIM7 and LM20) in the first component (PC1 = 68%), likewise xyloglucan (mAb LM25), α-1,5-L-arabinan (mAb LM6), and AGPs (mAbs JIM13, LM14, and LM2) in the second component (PC2 = 26%). Expr 2012 had a positive correlation with HG labeled by mAbs LM18, LM19, and JIM5. In 2013, Expr and ExCol showed a positive correlation with an abundance in HG (mAbs LM19, LM18, and JIM5; also seen in the heat map, Figure 2), but CB 2013 did not show the same effect. In the NaOH fraction (Figure 9C,D), all the enzyme treatments in 2012 correlated positively (PC1 = 82%) with the abundance in β-1,4-galactan (mAb LM5), mannan (mAbs LM21 and LM22), xyloglucan, cellulose, and AGP. The opposite was true for all the enzymes in 2013. Thus, the enzyme action in ExCol 2012, CB 2012, Expr 2013, and ExCol 2013 enhanced extraction of HG in the CDTA fraction, although the effect was much stronger in 2012. In the hemicellulose fraction, all the enzymes treatments in 2012 enhanced the extraction of hemicelluloses, cellulose, and AGPs, whereas none of the enzyme treatments in 2013 caused any changes.

Taken together, we saw that all enzyme treatments group together in the same direction for grapes from a specific year, which indicated that they affected the cell walls in a similar fashion. The ripeness level of grapes had a significant effect on the cell walls of the grape tissue as a result of the action of the endogenous enzymes. The maceration enzymes appear to have similar activity profiles to these enzymes, which makes it difficult to distinguishing between the action of the ripening enzymes and the maceration enzymes. However, this could also be due to the limitations of the CoMPP technique.

In conclusion, this study shows that depectination and consequential exposure of the hemicellulose−cellulose framework and proteins of the cell walls in the skin occurs as a consequence of the fermentation (no enzymes) process. With the addition of maceration enzymes, further depectination takes place and, depending on the ripeness level of the grapes, it was possible to infer an unravelling of the cell wall. We were unable to distinguish between the different maceration enzyme preparations in terms of their specific effects on the cell walls. Future work could use samples from the same vineyard at different harvest dates (levels of ripeness) and different concentrations of maceration enzymes to refine the observations made here. Together with the wine color analysis, it is necessary to look at the concentration of polyphenols retained in the grape skin tissue after fermentation and maceration enzyme treatment.

■ ASSOCIATED CONTENT

Supporting Information

A detailed discussion on the ripeness levels of the grapes, the FT-IR analysis of the wine, the results obtained with the wine color analysis, a PCA plot that shows the patterns in the data when comparing fresh and fermented samples, and the FT-MIR spectra for the enzyme-treated cell walls. This material is available free of charge via the Internet at http://pubs.acs.org.

■ AUTHOR INFORMATION

Corresponding Author

*Tel. +27 21 808 3773. Fax +27 21 808 3771. E-mail: mav@sun.ac.za.

DOI: 10.1021/jf505200m
J. Agric. Food Chem. 2015, 63, 2798−2810

Author Contributions

A.J.J.Z. collected the data, interpreted the results, and drafted the manuscript. J.P.M. and M.A.V. designed the study and helped with data interpretation and preparation of the final document. J.U.F. and W.G.T.W. did the CoMPP analysis. J.T. advised on multivariate data analysis.

Funding

Funding for this study was provided by the Wine Industry Network of Expertise and Technology (Winetech), the Technology and Human Resources for Industry Programme (THRIP), the Institute for Wine Biotechnology (IWBT), Stellenbosch University, and the National Research Foundation (NRF).

Notes

The authors declare no competing financial interest.

REFERENCES

(1) Garrido, J.; Borges, F. Wine and grape polyphenols — A chemical perspective. *Food Res. Int.* **2013**, *54*, 1844−1858.

(2) Pinelo, M.; Arnous, A.; Meyer, A. S. Upgrading of grape skins: Significance of plant cell-wall structural components and extraction techniques for phenol release. *Trends Food Sci. Technol.* **2006**, *17*, 579−590.

(3) Gomez, E.; Martinez, A.; Laencina, J. Localization of free and bound aromatic compounds among skin, juice and pulp fractions of some grape varieties. *Vitis* **1994**, *4*, 1−4.

(4) Darriet, P.; Thibon, C.; Dubourdieu, D. Aroma and Aroma Precursors in Grape Berry. In *The Biochemistry of the Grape Berry*; Geros, H., Chaves, M. M., Delrot, S., Eds.; Bentham: Bussum, The Netherlands, 2012; pp 111−136.

(5) Fontes, N.; Corte-Real, M.; Geros, H. New observations on the integrity, structure, and physiology of flesh cells from fully ripened grape berry. *Am. J. Enol. Vitic.* **2011**, *62*, 279−284.

(6) González-Neves, G.; Gil, G.; Ferrer, M.; Charamelo, D.; Balado, J.; Bochicchio, R.; Gatto, G.; Tessore, A. Prediction of the colour and polyphenolic composition of the young red wines from the phenolic potential of the grapes. *Int. J. Food Sci. Technol.* **2010**, *45*, 1843−1851.

(7) Jackson, R. S. *Wine Science: Principles and Applications*; 3rd ed.; Academic Press, Inc.: San Diego, 2008.

(8) Ducasse, M.-A.; Canal-Llauberes, R.-M.; de Lumley, M.; Williams, P.; Souquet, J.-M.; Fulcrand, H.; Doco, T.; Cheynier, V. Effect of macerating enzyme treatment on the polyphenol and polysaccharide composition of red wines. *Food Chem.* **2010**, *118*, 369−376.

(9) Wightman, J. D.; Price, S. F.; Watson, B. T.; Wrolstad, R. Some effects of processing enzymes on anthocyanins and phenolics in Pinot noir and Cabernet Sauvignon wines. *Am. J. Enol. Vitic.* **1997**, *48*, 39−48.

(10) Haight, K.; Gump, B. The use of macerating enzymes in grape juice processing. *Am. J. Enol. Vitic.* **1994**, *45*, 113−116.

(11) Busse-Valverde, N.; Gómez-Plaza, E.; López-Roca, J. M.; Gil-Muñoz, R.; Bautista-Ortín, A. B. The extraction of anthocyanins and proanthocyanidins from grapes to wine during fermentative maceration is affected by the enological technique. *J. Agric. Food Chem.* **2011**, *59*, 5450−5455.

(12) González-Pombo, P.; Fariña, L.; Carrau, F.; Batista-Viera, F.; Brena, B. M. Aroma enhancement in wines using co-immobilized *Aspergillus niger* glycosidases. *Food Chem.* **2014**, *143*, 185−191.

(13) Arnous, A.; Meyer, A. S. Discriminated release of phenolic substances from red wine grape skins (*Vitis vinifera L.*) by multicomponent enzymes treatment. *Biochem. Eng. J.* **2010**, *49*, 68−77.

(14) Arnous, A.; Meyer, A. S. Quantitative prediction of cell wall polysaccharide composition in grape (*Vitis vinifera L.*) and apple (*Malus domestica*) skins from acid hydrolysis monosaccharide profiles. *J. Agric. Food Chem.* **2009**, *57*, 3611−3619.

(15) Romero-Cascales, I.; Ros-García, J. M.; López-Roca, J. M.; Gómez-Plaza, E. The effect of a commercial pectolytic enzyme on grape skin cell wall degradation and colour evolution during the maceration process. *Food Chem.* **2012**, *130*, 626−631.

(16) Hernández-Hierro, J. M.; Quijada-Morín, N.; Martínez-Lapuente, L.; Guadalupe, Z.; Ayestarán, B.; Rivas-Gonzalo, J. C.; Escribano-Bailón, M. T. Relationship between skin cell wall composition and anthocyanin extractability of *Vitis vinifera L.* cv. Tempranillo at different grape ripeness degree. *Food Chem.* **2014**, *146*, 41−47.

(17) Vicens, A.; Fournand, D.; Williams, P.; Sidhoum, L.; Moutounet, M.; Doco, T. Changes in polysaccharide and protein composition of cell walls in grape berry skin (Cv. Shiraz) during ripening and over-ripening. *J. Agric. Food Chem.* **2009**, *57*, 2955−2960.

(18) Brummell, D. A. Review: Cell wall disassembly in ripening fruit. *Funct. Plant Biol.* **2006**, *33*, 103−119.

(19) Bindon, K. A.; Madani, S. H.; Pendleton, P.; Smith, P. A.; Kennedy, J. A. Factors affecting skin tannin extractability in ripening grapes. *J. Agric. Food Chem.* **2014**, *62*, 1130−1141.

(20) Ruiz-Garcia, Y.; Smith, P. A.; Bindon, K. A. Selective extraction of polysaccharide affects the adsorption of proanthocyanidin by grape cell walls. *Carbohydr. Polym.* **2014**, *114*, 102−114.

(21) Hanlin, R. L.; Hrmova, M.; Harbertson, J. F.; Downey, M. O. Review: Condensed tannin and grape cell wall interactions and their impact on tannin extractability into wine. *Aust. J. Grape Wine Res.* **2010**, *16*, 173−188.

(22) Jarvis, M. C. Plant cell walls: Supramolecular assemblies. *Food Hydrocolloids* **2011**, *25*, 257−262.

(23) Fleischer, A.; O'Neill, M.; Ehwald, R. The pore size of non-graminaceous plant cell walls is rapidly decreased by Borate ester cross-linking of the pectic polysaccharide rhamnogalacturonan II. *Plant Physiol.* **1999**, *121*, 829−838.

(24) Moore, J. P.; Fangel, J. U.; Willats, W. G. T.; Vivier, M. A. Pectic-β(1,4)-galactan, extensin and arabinogalactan-protein epitopes differentiate ripening stages in wine and table grape cell walls. *Ann. Bot. (Oxford, U.K.)* **2014**, *114*, 1279−1294.

(25) Moller, I.; Sørensen, I.; Bernal, A. J.; Blaukopf, C.; Lee, K.; Øbro, J.; Pettolino, F.; Roberts, A.; Mikkelsen, J. D.; Knox, J. P.; Bacic, A.; Willats, W. G. T. High-throughput mapping of cell-wall polymers within and between plants using novel microarrays. *Plant J.* **2007**, *50*, 1118−1128.

(26) Iland, P. .; Ewart, A.; Sitters, J.; Markides, A.; Bruer, N. *Techniques for Chemical Analysis and Quality Monitoring during Winemaking*; Patrick Iland Wine Promotions: Campbelltown, South Australia, Australia, 2000.

(27) Ortega-Regules, A.; Ros-García, J. M.; Bautista-Ortín, A. B.; López-Roca, J. M.; Gómez-Plaza, E. Differences in morphology and composition of skin and pulp cell walls from grapes (*Vitis vinifera L.*): technological implications. *Eur. Food Res. Technol.* **2008**, *227*, 223−231.

(28) Szymanska-Chargot, M.; Zdunek, A. Use of FT-IR spectra and PCA to the bulk characterization of cell wall residues of fruits and vegetables along a fraction process. *Food Biophys.* **2013**, *8*, 29−42.

(29) Kačuráková, M.; Capek, P.; Sasinková, V.; Wellner, N.; Ebringerová, A.; Kac, M. FT-IR study of plant cell wall model compounds: pectic polysaccharides and hemicelluloses. *Carbohydr. Polym.* **2000**, *43*, 195−203.

(30) York, W. S.; Darvill, A. G.; L, M. M.; Stevenson, T. T.; Albersheim, P. Isolation and characterization of plant cell walls and cell wall components. *Methods Enzymol.* **1985**, *2*, 3−40.

(31) Jackson, J. E. *A User's Guide to Principal Components*; Wiley Series in Probability and Statistics; John Wiley & Sons, Inc.: Hoboken, NJ, 1991.

(32) Coombe, B. G.; Dundon, R. J.; Short, A. W. S. Indices of sugar-acidity as ripeness criteria for winegrapes. *J. Sci. Food Agric.* **1980**, *31*, 495−502.

(33) Du Plessis, C. Optimum maturity and quality parameters in grapes: a review. *S. Afr. J. Enol. Vitic.* **1984**, *5*, 35−42.

(34) Ortega-Regules, A.; Ros-García, J. M.; Bautista-Ortín, A. B.; Lopez-Roca, J. M.; Gomez-Plaza, E. Changes in skin cell wall

DOI: 10.1021/jf505200m
J. Agric. Food Chem. 2015, 63, 2798−2810

composition during the maturation of four premium wine grape varieties. *J. Sci. Food Agric.* **2008**, *88*, 420−428.
(35) Hayashi, T. Xyloglucans in the primary cell wall. *Annu. Rev. Plant Physiol. Plant Mol. Biol.* **1989**, *40*, 139−168.
(36) Zykwinska, A.; Thibault, J. F.; Ralet, M. C. Organization of pectic arabinan and galactan side chains in association with cellulose microfibrils in primary cell walls and related models envisaged. *J. Exp. Bot.* **2007**, *58*, 1795−1802.
(37) Yakushiji, H.; Sakurai, N.; Morinaga, K. Changes in cell-wall polysaccharides from the mesocarp of grape berries during veraison. *Physiol. Plant.* **2001**, *111*, 188−195.
(38) Huang, X.-M.; Huang, H.-B.; Wang, H.-C. Cell walls of loosening skin in post-veraison grape berries lose structural polysaccharides and calcium while accumulate structural proteins. *Sci. Hortic. (Amsterdam, Neth.)* **2005**, *104*, 249−263.
(39) Albersheim, P.; Darvill, A.; Roberts, K.; Sederoff, R.; Staehelin, A. *Plant Cell Walls: From Chemistry to Biology*. Garland Science: New York, 2010.
(40) Quirós, M.; Morales, P.; Pérez-Través, L.; Barcenilla, J. M.; Gonzalez, R. A new methodology to determine cell wall mannoprotein content and release in wine yeasts. *Food Chem.* **2011**, *125*, 760−766.
(41) Dallies, N.; François, J.; Paquet, V. A new method for quantitative determination of polysaccharides in the yeast cell wall. Application to the cell wall defective mutants of *Saccharomyces cerevisiae*. *Yeast* **1998**, *14*, 1297−1306.
(42) Pellerin, P.; Vidal, S.; Williams, P.; Brillouet, J. M. Characterization of five type II arabinogalactan-protein fractions from red wine of increasing uronic acid content. *Carbohydr. Res.* **1995**, *277*, 135−143.
(43) Vidal, S.; Williams, P.; Doco, T.; Moutounet, M.; Pellerin, P. The polysaccharides of red wine: total fractionation and characterization. *Carbohydr. Polym.* **2003**, *54*, 439−447.
(44) Guadalupe, Z.; Ayestarán, B. Polysaccharide profile and content during the vinification and aging of Tempranillo red wines. *J. Agric. Food Chem.* **2007**, *55*, 10720−10728.
(45) Willats, W. G. T.; Gilmartin, P. M.; Mikkelsen, J. D.; Knox, J. P. Cell wall antibodies without immunization: generation and use of de-esterified homogalacturonan block-specific antibodies from a naive phage display library. *Plant J.* **1999**, *18*, 57−65.
(46) Micheli, F. Pectin methylesterases: cell wall enzymes with important roles in plant physiology. *Trends Plant Sci.* **2001**, *6*, 414−419.
(47) Benen, J. A. E.; Van Alebeek, G. J.; Voragen, A. G. J.; De Vries, R. P.; Visser, J. Pectic esterases. In *Handbook of Food Enzymology*; Whitaker, J. R., Voragen, A. G. J., Wong, D. W. S., Eds.; Marcel Dekker: New York, 2003; pp 849−856.
(48) Trygg, J.; Wold, S. Orthogonal projections to latent structures (O-PLS). *J. Chemom.* **2002**, *16*, 119−128.
(49) Lu, P.; Hsieh, Y.-L. Cellulose isolation and core−shell nanostructures of cellulose nanocrystals from chardonnay grape skins. *Carbohydr. Polym.* **2012**, *87*, 2546−2553.

DOI: 10.1021/jf505200m
J. Agric. Food Chem. 2015, 63, 2798−2810

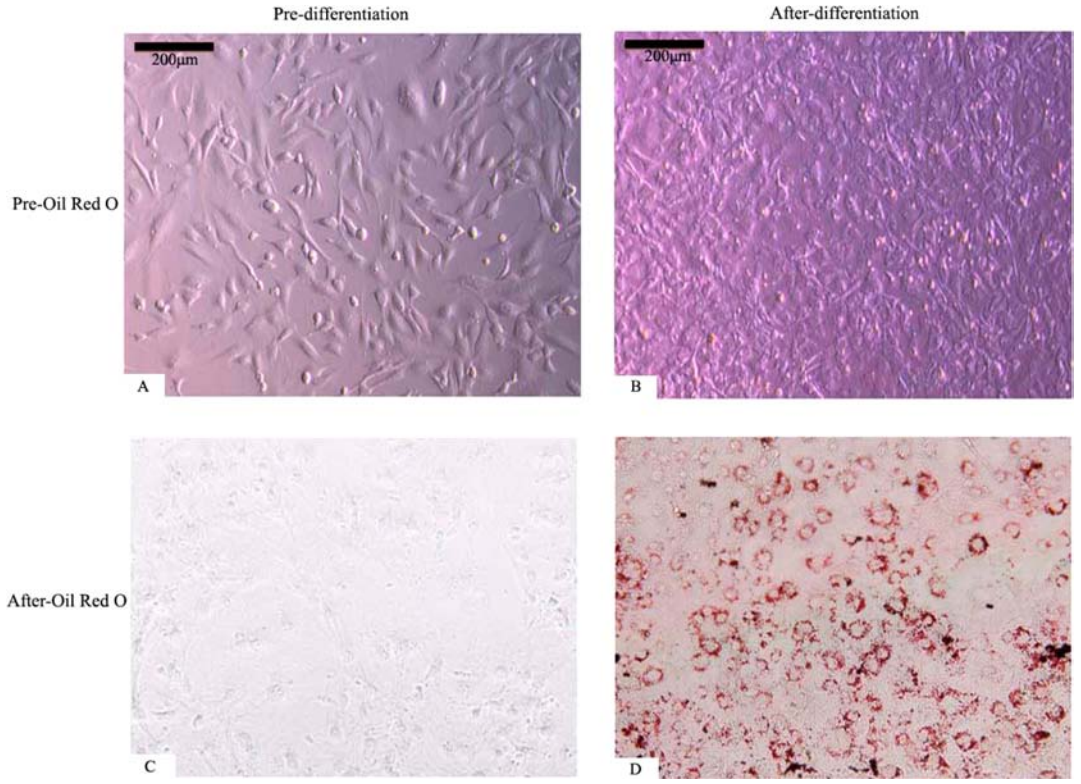

Figure 1. 3T3-L1 cell differentiation detected by Oil Red O staining. Panels A and B show pre-Oil Red O staining, and panels C and D show post-Oil Red O staining. Panels A and C represent undifferentiated cells, and panels B and D represent differentiated cells (magnification, 100×; bar, 200 μm).

Anti-TLR4 and anti-GLUT4 were from Abcam Biochemicals (Hong Kong). Anti-PI-3K and p-NF-κB were obtained from Cell Signaling Technology (Shanghai, China). Anti-TNF-α and anti-β-actin were obtained from Santa Cruz Technology (Carlsbad, CA). Fluorescein (FITC)-AffiniPure donkey anti-rabbit immunoglobulin G (IgG) was from Jackson ImmunoResearch (West Grove, PA). The monoclonal antibody against mouse TLR4/MD-2 (Affymetrix) was obtained from Affymetrix eBioscience (Carlsbad, CA). Mouse IL-6 enzyme-linked immunosorbent assay (ELISA) kits were obtained from Dakewe (Dakewe Biotech Co., Ltd., Beijing, China). Insulin (from bovine pancreas), 3-isobutyl-1-methylxanthine (BioUltra, ≥99%), dexamethasone (purity of ≥97%), lipopolysaccharides from *Escherichia coli* 055:B5, EGCG (purity of ≥95%, from green tea), and routine chemicals were all purchased from Sigma Chemical (Sigma-Aldrich, St. Louis, MO).

Cell Culture and Differentiation. 3T3-L1 fibroblasts were obtained from the American Type Culture Collection (Manassas, VA) and cultured at a 37 °C, 5% CO_2, and 95% humidity. Preadipocytes were induced to differentiate as follows.[22] Cells were maintained in DMEM plus 10% heat-inactivated FCS and 0.5% penicillin−streptomycin (Invitrogen). After 2 days in culture when the cells reached confluence (day 0), they were induced to differentiate by adding medium containing 10% FBS, 1 μM dexamethasone, 0.5 mM 3-isobutyl-1-methylxanthine, and 5 μg/mL insulin for 48 h. Fresh media containing only 5 μg/mL insulin and 10% FBS was added for an additional 48 h. Media was subsequently changed every 48 h. More than 90% of cells expressed the adipocyte phenotype between days 8 and 10 post-differentiation, and they were used for experiments.

Oil Red O Staining of 3T3-L1 Adipocytes. Conversion of 3T3-Ll fibroblasts to adipocytes was monitored by measurement of intracellular lipid accumulation using Oil Red O staining. A 0.5% (w/v) solution of Oil Red O was prepared in 60% isopropanol. After day 8, differentiated 3T3-L1 preadipocytes were washed twice with phosphate-buffered saline (PBS), fixed in 4% paraformaldehyde, then incubated with Oil Red O working solution for 2 h at room temperature, and rinsed to remove unbound dye. Staining was visualized with an Olympus DP70 camera (Olympus, Japan). As shown in Figure 1, differentiated 3T3-L1 cells were positive for fat droplets and lipid storage by Oil Red O. We used the cells for further experiments when more than 90% expressed the adipocyte phenotype between 8 and 10 days post-differentiation.

LPS and EGCG Treatment of Differentiated 3T3-L1 Adipocytes. Fully differentiated adipocytes incubated in serum-free medium and stimulated by adding different concentrations of LPS from *E. coli* for 48 h to elicit an immune response in the absence or presence of 3 h of pretreatment with EGCG. Cells were divided into eight groups, including one control group (blank), while the remaining seven groups were treated with 0.1−1 μg/mL LPS or 1 μg/mL LPS + 10−100 μM EGCG. After treatment, supernatants were collected for ELISA and the adipocytes were collected for detection of inflammation-related proteins (p-NF-κB, IKKβ, and TNF-α) and key insulin signaling protein (PI-3K and GLUT4) levels.

Anti-67LR Treatment. To evaluate the effect of EGCG on TLR4 signaling, we performed blocking experiments in adipocytes. Fully differentiated adipocytes were pretreated with 67LR antibody[35] (10 μg/mL, MLuC5) for 30 min, followed by EGCG (100 μM) for 3 h, and subsequent incubation with LPS (1 μg/mL) for 48 h. IL-6 levels in supernatants of treated and control cells were detected by ELISA, and inflammatory mediators and cytokines, such as TLR4, p-NF-κB p65, and TNF-α, and the key insulin signaling protein GLUT4 were examined by western blotting.

Anti-TLR4 Treatment. Cells were treated with a TLR4-specific antibody (anti-mouse TLR4/MD-2 complex functional-grade purified antibodies, MTS510)[43] to inhibit their response to LPS. Fully differentiated adipocytes were pretreated with MTS510 (5 μg/mL) or PBS for 30 min at 37 °C and subsequently treated with LPS (1 μg/mL) for 48 h. IL-6 levels in supernatants and intracellular p-NF-κB p65, TNF-α, and GLUT4 protein levels were determined by western blotting.

DOI: 10.1021/jf505531w
J. Agric. Food Chem. 2015, 63, 2811−2819

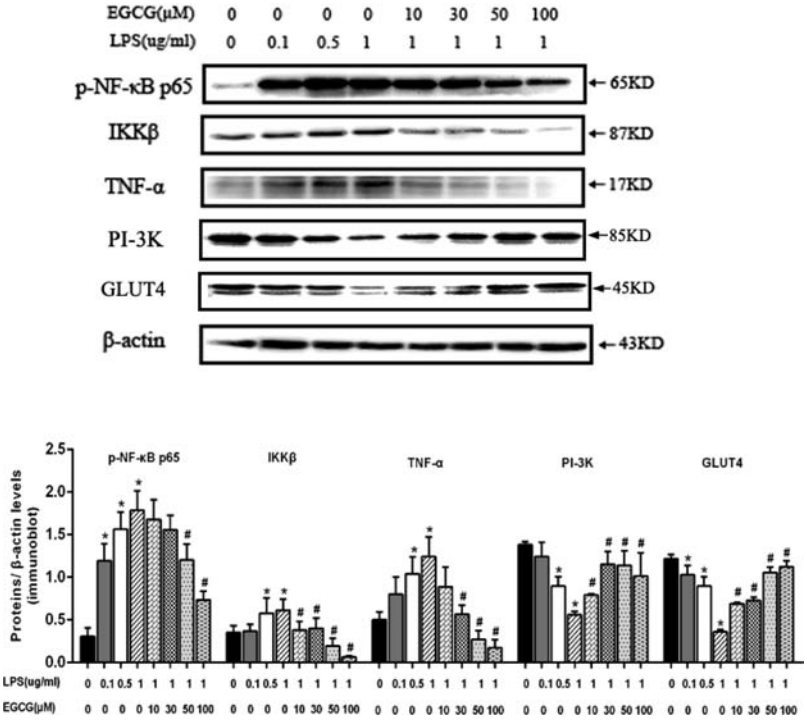

Figure 2. EGCG decreases inflammation-related protein levels and increases the expression of key insulin signaling proteins in adipocytes. Various doses of LPS (0.1, 0.5, and 1 μg/mL) stimulated inflammatory cytokine expression in mature 3T3-L1 adipocytes. Mature 3T3-L1 adipocytes pretreated with EGCG (10, 30, 50, and 100 μM) decreased LPS-stimulated inflammatory-related factor expression (IKKβ, p-NF-κB, and TNF-α) to different degrees. EGCG (10, 30, 50, and 100 μM) increased key insulin signaling protein expression (PI-3K and GLUT4). Results are expressed as the mean ± SD (n = 6). (*) $p < 0.05$ versus the 0 ng/mL LPS + 0 μM EGCG group. (#) $p < 0.05$ versus the 1 μg/mL LPS group.

Cellular ^{3}H-2-Deoxy-D-glucose Uptake Measurements. 3T3-L1 cells were seeded in 24-well plates (1×10^5 cells/well) and induced to differentiate, as described above. On day 9, adipocytes were incubated for 2 h at 37 °C in serum-free medium, and cells were washed twice with 37 °C Krebs Ringer phosphate (KRP) buffer (pH 7.4) and placed in KRP buffer containing insulin (100 nM) for 30 min, followed by the addition of ^{3}H-2-deoxy-D-glucose (2 μCi/mL, Beijing Yuan Zi Gao Ke Corporation, China) for an additional 10 min at 37 °C. Cells were then immediately washed 3 times in ice-cold PBS to terminate the reaction. Lastly, cells were solubilized in 0.5 M NaOH (0.4 mL/well) for 2 h and subjected to scintillation counting for ^{3}H radioactivity as disintegrations per minute. The radioactivity of each sample was normalized to the protein concentration. Counts per minute and per milligram of protein were measured to analyze experimental glucose uptake.

IL-6 Measurements. IL-6 levels in culture supernatants were measured in duplicate by the ELISA (Dakewe Biotech) kit according to the instructions of the manufacturer. The minimum detectable level of each kit was 15.6 pg/mL; the sensitivity was 8 pg/mL; and the coefficient of variation between the plates was <10%.

GLUT4 Immunofluorescence. 3T3-L1 cells were grown and induced to differentiate on glass coverslips, incubated for 2 h in serum-free culture medium, and then stimulated with insulin (100 nM) before EGCG or LPS treatment. Cells were rinsed with PBS, fixed in 4% paraformaldehyde and 0.05% glutaraldehyde for 30 min at room temperature, then blocked in bovine serum albumin, permeabilized with 0.3% Triton X-100 for 1 h, and then incubated with GLUT4 antibody (5 μg/mL) overnight. Primary antibodies were detected with fluorescent secondary antibodies (FITC-AffiniPure donkey anti-rabbit IgG, 1:200) and imaged with a Leica TCS SP5 X camera (Germany).

Immunoblotting Analyses. Mature 3T3-L1 adipocytes were washed 3 times in PBS and lysed (KGP 250 kit, Keygen Biotech, Nanjing, China) on ice. All steps were carried out according to the instructions of the manufacturers. Bound antibodies were detected with horseradish-peroxidase-conjugated anti-IgG with an enhanced chemiluminescence kit (Pierce) protocol and visualized with the Chem Doc XRS with Quantity One software (Bio-Rad). Blots were repeated at least 6 times. The band intensities were quantified using ImageJ analysis software (National Institutes of Health, Bethesda, MD).

Statistical Analyses. All values were expressed as the mean ± standard deviation (SD). Differences between groups were tested for statistical significance using one-way analysis of variance (ANOVA), and when the F value indicated significance, least significant difference (LSD) was used to correct for multiple comparisons. All analyses were performed using SPSS statistics software, version 17.0 (SPSS, Inc., Chicago, IL) on a computer with a Windows operating system. A p value less than 0.05 was considered statistically significant.

RESULTS

EGCG Decreases Inflammation-Related Protein Levels and Increases Insulin Signaling Protein Expression in Adipocytes. We treated mature 3T3-L1 adipocytes with various doses of LPS (0.1, 0.5, and 1 μg/mL) for 48 h to induce inflammation. In comparison to the control group, LPS treatment increased inflammation-related protein levels to different degrees. IKKβ (approximately 1.1-, 1.6-, and 1.7-fold, respectively), p-NF-κB (approximately 3.9-, 5.0-, and 5.8-fold, respectively), and TNF-α (approximately 1.5-, 2.0-, and 2.5-fold, respectively) protein levels significantly increased ($p < 0.05$ versus baseline), while the expression of insulin signaling proteins, such as PI-3K (approximately 89.9, 64.9, and 40.5%, respectively) and GLUT4 (approximately 84.7, 73.7, and 29.6%, respectively), decreased ($p < 0.05$; Figure 2).

Various doses of EGCG (10, 30, 50, and 100 μM) decreased LPS-induced IKKβ, p-NF-κB, and TNF-α expression. EGCG reduced IKKβ (approximately 64.5, 66.8, 31.9, and 10.4%, respectively), p-NF-κB (approximately 89.5, 85.8, 67.5, and 41.2%, respectively), and TNF-α (approximately 71.6, 45.7,

DOI: 10.1021/jf505531w
J. Agric. Food Chem. 2015, 63, 2811−2819

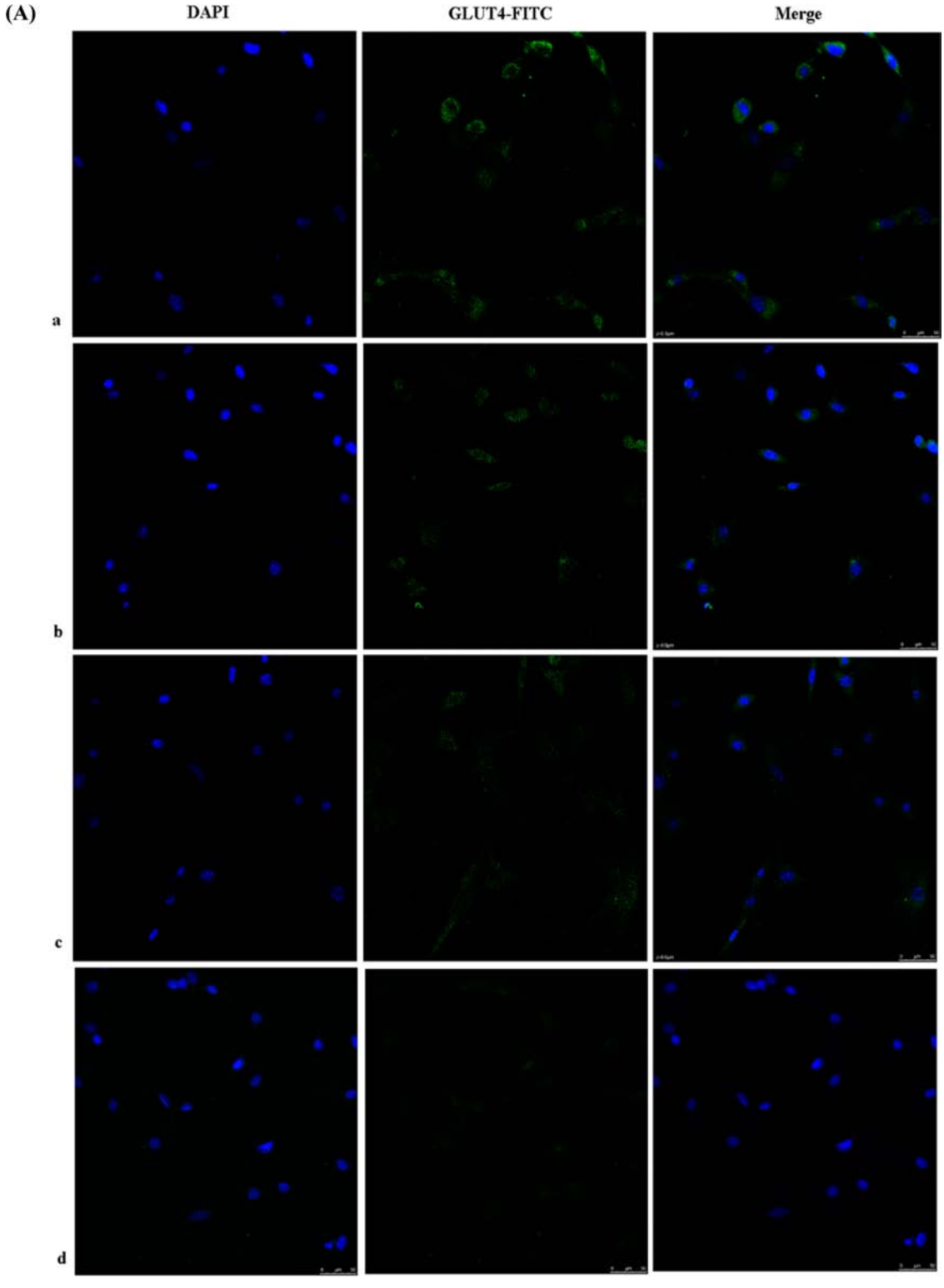

Figure 3. continued

DOI: 10.1021/jf505531w
J. Agric. Food Chem. 2015, 63, 2811−2819

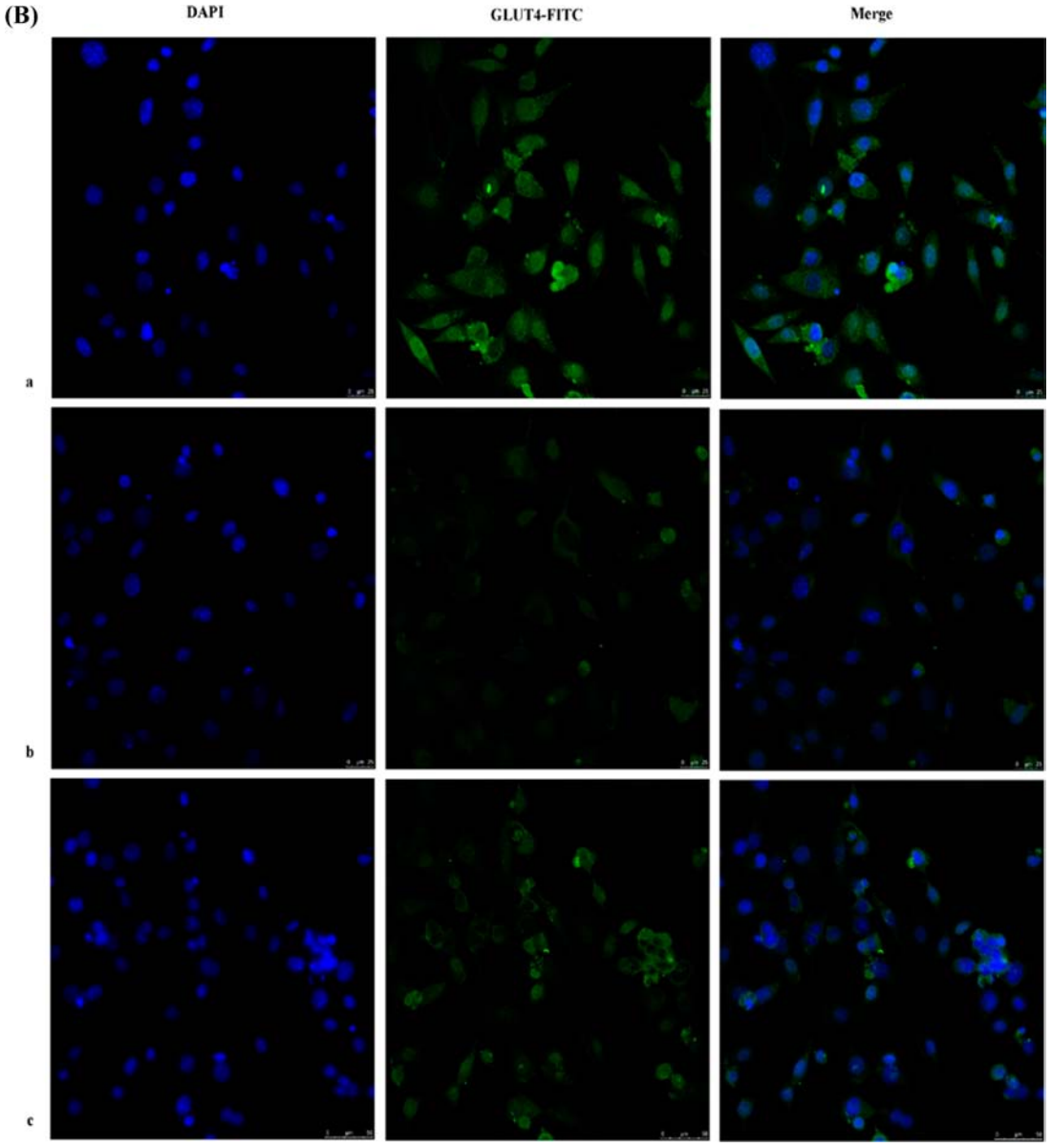

Figure 3. EGCG reversed intracellular GLUT4 expression in LPS-stimulated adipocytes: GLUT4 (FITC, green) and nuclear (DAPI, blue) immunofluorescence, for (A-a) control group, (A-b) 0.1 μg/mL LPS group, (A-c) 0.5 μg/mL LPS group, and (A-d) 1 μg/mL LPS group and (B-a) control group, (B-b) 1 μg/mL LPS group, and (B-c) 100 μM EGCG + 1 μg/mL LPS group (magnification = 400×).

21.9, and 14.0%, respectively) expression and increased PI-3K (approximately by 1.4-, 2.0-, 2.0-, and 1.8-fold, respectively) and GLUT4 (approximately by 1.9-, 2.1-, 2.9-, and 3.1-fold, respectively) levels compared to treatment with 1 μg/mL LPS alone (Figure 2; $p < 0.05$ for each). These data suggest that EGCG decreases LPS-stimulated inflammatory cytokine and insulin signaling protein expression in adipocytes.

EGCG Reverses Intracellular GLUT4 Expression in LPS-Stimulated Adipocytes. We used immunofluorescence labeling to investigate cellular GLUT4 expression. GLUT4 fluorescence intensity demonstrated that LPS treatment decreased GLUT4 levels. As shown in Figures 2 and 3A, various doses of LPS (0.1, 0.5, and 1 μg/mL) dramatically decreased the GLUT4 signal. In contrast, EGCG treatment (100 μM) increased GLUT4 expression compared to LPS (1 μg/mL) treatment alone (Figures 2 and 3B).

67LR Antibody Blocks the Effect of EGCG on LPS-Induced TLR4 Signaling. Upon treatment with the 67LR antibody (10 μg/mL), TLR4 protein levels increased by more than 1.2-fold compared to the EGCG group (Figure 4B; $p < 0.05$). As expected, NF-κB p65 phosphorylation significantly increased (1.4-fold; Figure 4C; $p < 0.05$), as did the downstream protein TNF-α (1.6-fold; Figure 4D; $p < 0.05$). The level of IL-6 increased in the supernatant upon 67LR antibody treatment compared to the EGCG group (1.8-fold; Figure 6A; $p < 0.05$), and there was no difference between the ±EGCG treatment groups in the presence of the 67LR antibody ($p > 0.05$). Furthermore, GLUT4 levels were reduced by approximately 72.4% in the 67LR antibody group compared to the EGCG group (Figure 4E; $p < 0.05$). These data suggest that 67LR antibody blocks the effect of EGCG on LPS-induced TLR4 signaling, resulting in a subsequent series of changes, such as increased inflammatory cytokine expression and decreased GLUT4 levels. However, we did not detect any obvious differences in 67LR expression among the control (blank), EGCG (100 μM EGCG plus 1 μg/mL LPS), and LPS

DOI: 10.1021/jf505531w
J. Agric. Food Chem. 2015, 63, 2811−2819

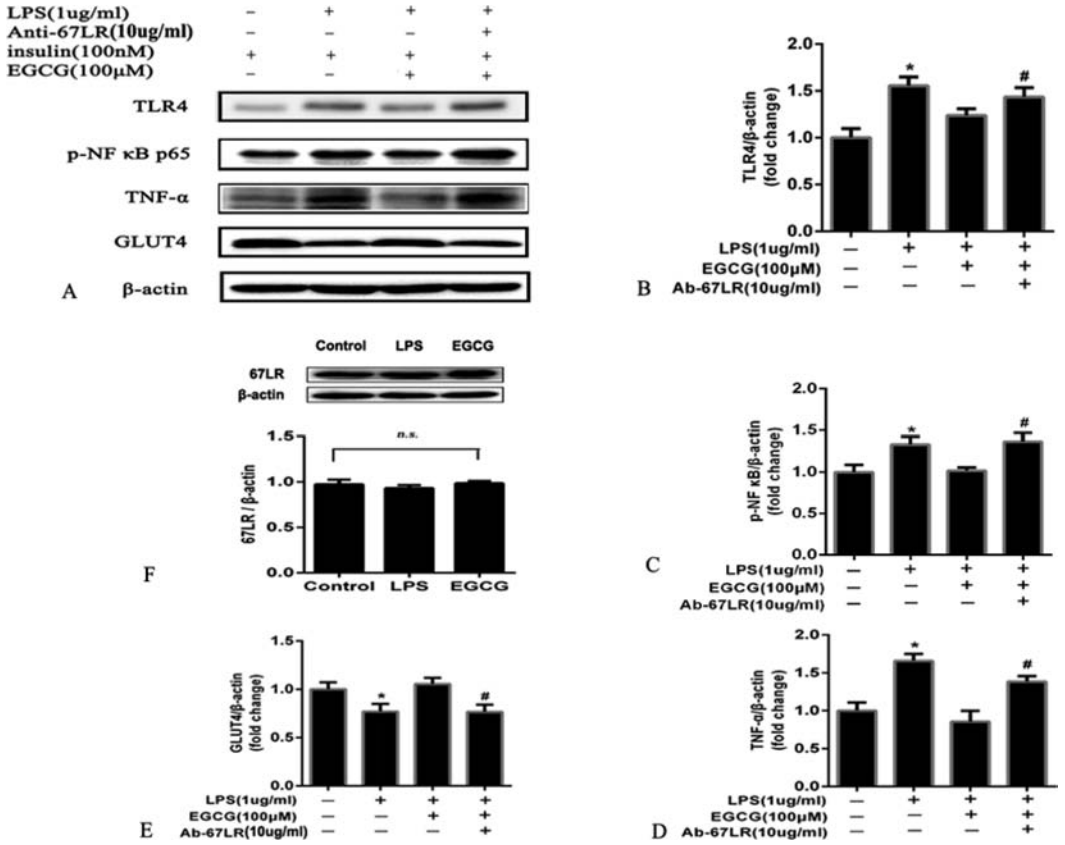

Figure 4. (A–E) 67LR antibody blocks the effects of EGCG on TLR4 signaling and GLUT4 expression in LPS-stimulated adipocytes. (F) EGCG did not affect 67LR expression between the control (blank group), EGCG (100 μM EGCG plus 1 μg/mL LPS), and LPS groups (1 μg/mL LPS). (A–F) Protein levels were determined by western blotting. Bars represent the mean ± SD, and both are expressed as the ratio to the control group (the level of the control group was normalized to 1). (∗) $p < 0.05$, for the LPS group versus the control group; (#) $p < 0.05$, for the 67LR blocker group versus the EGCG group. ns = not significant when the EGCG group was compared to the LPS or control group.

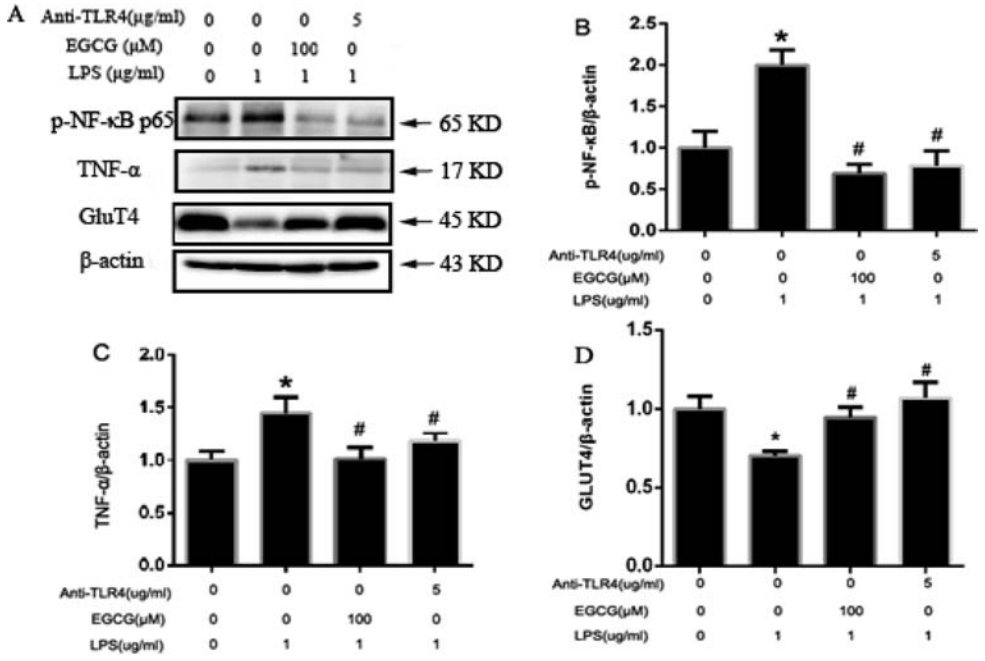

Figure 5. TLR4 mediates LPS-induced inflammation activation and insulin resistance, and EGCG has similar effects to the anti-TLR4 antibody. (A–D) Protein levels determined by western blotting. Bars represent the mean ± SD, expressed as the ratio to the control group (the level of the control group was normalized to 1; $n = 6$ for each group). (∗) $p < 0.05$, for the LPS group versus the control group. (#) $p < 0.05$, for the LPS group versus the EGCG group and TLR4-inhibited group.

DOI: 10.1021/jf505531w
J. Agric. Food Chem. 2015, 63, 2811–2819

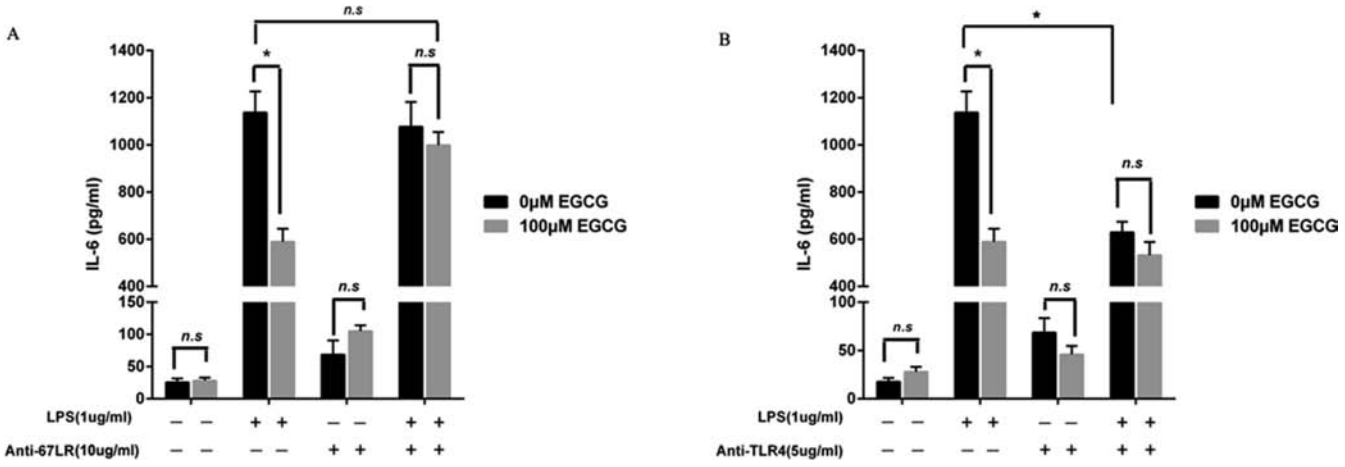

Figure 6. EGCG and the anti-TLR4 antibody inhibit IL-6 production, and an inhibitor of 67LR blocks EGCG effects. IL-6 levels in culture supernatants measured by ELISA. (A and B) IL-6 levels in cell culture supernatants were measured in duplicate. (*) $p < 0.05$. ns = not significant between the two groups. Panel A showed that EGCG inhibits IL-6 production in the context of LPS and does not work effectively with an inhibitor of 67LR. Panel B showed that IL-6 production was blocked with the anti-TLR4 antibody and has similar effect to EGCG.

groups (1 μg/mL LPS) (Figure 4F; $p > 0.05$). We hypothesize that EGCG performs its anti-inflammatory role by regulating 67LR activity or translocation.

TLR4 Mediates LPS-Induced Inflammatory Activation and Insulin Resistance. As shown in Figure 5, the specific TLR4/MD2 inhibitor MTS510 (5 μg/mL) treatment significantly reduced p-NF-κB (67.9% decrease; $p < 0.05$; Figure 5B), TNF-α (21.5% decrease; $p < 0.05$; Figure 5C), and IL-6 (45.5% decrease; $p < 0.05$; Figure 6B) levels after LPS stimulation, although IL-6 levels were still higher than the blank group, perhaps because of the effects of LPS. Meanwhile, MTS510 treatment increased GLUT4 expression by 1.3-fold ($p < 0.05$; Figure 5D) compared to LPS-induced control cells. The above data suggest that TLR4/MD2 inhibition decreased NF-κB activation and upregulated GLUT4 expression and EGCG had similar effects to the anti-TLR4 antibody.

EGCG Upregulates Cellular ^{3}H-2-Deoxy-D-glucose Uptake by Decreasing TLR4 Expression. To determine the effects of TLR4 on glucose transport in inflammation, cellular ^{3}H-2-deoxy-D-glucose uptake contents were measured (Figure 7). We found that insulin-stimulated glucose influxes were significantly greater than untreated control cells ($p < 0.05$). Pretreatment with EGCG (100 μM) for 3 h before 48 h of LPS exposure (1 μg/mL) significantly increased glucose uptake compared to LPS stimulation alone (~1.2-fold; $p < 0.05$), while anti-67LR Ab reversed the trend (about 84.4% of the EGCG group; $p < 0.05$). Anti-TLR4 Ab increased glucose uptake even in the absence of EGCG (about 1.2-fold higher than the LPS group; $p < 0.05$). Our data suggest that TLR4 attenuates insulin-stimulated glucose uptake and EGCG blocks these changes by decreasing TLR4 signaling.

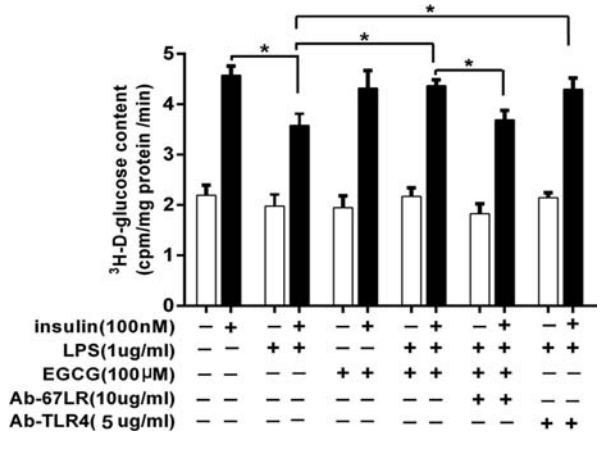

Figure 7. Cellular ^{3}H-2-deoxy-D-glucose uptake. (*) $p < 0.05$.

DISCUSSION

Here, we showed that EGCG suppresses the TLR4 signaling pathway in adipocytes via 67LR. Upon 67LR inhibition, The suppressive effect of EGCG on TLR4 activity was blocked; inflammatory cytokine levels, such as TNF-α and IL-6, increased; and GLUT4 expression decreased. These effects led to attenuated insulin signal transduction and decreased glucose uptake. In contrast, TLR4 inhibition inactivated the inflammation pathway, phenocopying the effect of EGCG and increasing expression of the key insulin signaling protein GLUT4 in LPS-stimulated adipocytes, thus promoting insulin-stimulated glucose uptake. These results suggest that EGCG improves insulin signaling by suppressing TLR4 activity in adipocytes.

Type 2 diabetes and obesity are characterized by low-grade inflammation with increased inflammatory cytokine levels and changes in the gut microbiota.[23] As an important pathogen recognition receptor, high TLR4 levels impair insulin action and negatively regulate insulin signaling.[36,37] Increased TLR4 levels underlie non-infectious chronic inflammation and dysfunction of adipose tissue in obesity.[5,24,25] In our previous study, we found that a high-fat diet increases the TLR4-mediated inflammatory response in the adipose tissue of obese rats.[8] TLR4-deficient mice are partially protected from inflammation and insulin resistance,[26] and inhibition of TLR4 signaling protects against type 2 diabetes in mice.[27,38,39] Studies have shown that the TLR4 ligand LPS activates NF-κB and increases inflammatory biomediator release in 3T3-L1 adipocytes, a process which may be blocked by a TLR4 inhibitor.[12] Importantly, these biomediators also work on insulin target cells and insulin-producing cells, such as adipocytes, pancreatic islet cells, and the hypothalamus, further impairing insulin sensitivity and secretion.[25,28−30] Consistently, our work suggests that LPS activates the TLR4 signaling

DOI: 10.1021/jf505531w
J. Agric. Food Chem. 2015, 63, 2811−2819

pathway, a specific TLR4/MD2 inhibitor partially weakens inflammatory cytokines, such as TNF-α and IL-6, and upregulates insulin signaling protein GLUT4 expression, and TLR4 inhibition has similar effects to EGCG treatment in 3T3-L1 adipocytes.

EGCG is the most abundant polyphenol in tea and has many biological properties.[13−15,17−19] Its metabolites can exist in methylated, glucuronide, and sulfate forms, and the phenolic hydroxyls in their structure determine their antibacterial, anticardiovascular disease, and antitumor activities.[31] Studies have shown that EGCG exclusively binds to 67LR and influences downstream insulin signaling,[17,32,33] and treatment with 67LR antiserum blocks extracellular signal regulated kinase 1/2 (ERK1/2) phosphorylation while increasing insulin receptor-β and insulin receptor substrates 1 and 2 (IRS1 and IRS2) phosphorylation in preadipocytes.[17,32] Our work demonstrated that pretreatment of adipocytes with a 67LR blocking antibody blocked the suppression of the TLR4 signaling pathway of EGCG, activated the NF-κB signal pathway, induced inflammatory cytokine transcription, and decreased GLUT4 expression, leading to a further decrease in cellular ^{3}H-2-deoxy-D-glucose uptake, which is associated with insulin signaling transduction.

Our work demonstrated that 67LR expression did not change upon EGCG treatment. It has yet to be determined whether 67LR membrane localization changes upon EGCG treatment. However, previous research[33] stated that EGCG increases 67LR efficiency by inducing its translocation from the cytoplasm to the membrane. EGCG downregulation of inflammatory signals may be induced by Tollip, which is associated with decreased TLR signaling-mediated NF-κB activation.[34,35] Therefore, it is crucial to further delineate the mechanisms involved to support our findings.

Additionally, TLRs and nucleotide-binding and oligomerization domain (NOD)-like receptors (NLRs) are very remarkable pathogen recognition receptors in obesity and type 2 diabetes characterized by low-grade inflammation.[23,40,41] Both TLRs and NLRs mediate NF-κB activation, leading to inflammatory cytokine production and insulin resistance.[40−42] Therefore, we speculate that EGCG may simultaneously decrease inflammation through the NLR signaling pathway. Therefore, further studies are necessary to target TLR- or NLR-regulated pathways in obesity-related metabolic complications.

Taken together, these data suggest that EGCG affects the TLR4 signaling pathway, reduces chronic low-grade inflammation, and further influences insulin signaling protein expression, while the entire process is blunted by 67LR inhibition, which further strengthens the link between the TLR4-induced inflammatory response and insulin resistance in adipocytes. Our work also provides insight into better prevention of insulin resistance by revealing the possible molecular mechanism and developing targeted therapies to protect against it.

AUTHOR INFORMATION

Corresponding Author

*Telephone: 86-24-83282152. Fax: 86-24-83283294. E-mail: vanilla421@163.com.

Funding

This work was supported by grants from the National Natural Science Foundation of China (Grant 81000327), the Chinese Society of Endocrinology (12030470347), and the General Scientific Research Fund of Liaoning Provincial Education Department (L2013300).

Notes

The authors declare no competing financial interest.

ABBREVIATIONS USED

EGCG, epigallocatechin gallate; TLR4, toll-like receptor 4; LPS, lipopolysaccharide; GLUT4, glucose transporter type 4; 67LR, 67 laminin receptor; FFA, free fatty acid

REFERENCES

(1) Lee, H.; Lee, I. S.; Choue, R. Obesity, inflammation and diet. *Pediatr. Gastroenterol., Hepatol. Nutr.* **2013**, *16*, 143−152.

(2) Brännmark, C.; Nyman, E.; Fagerholm, S.; Bergenholm, L.; Ekstrand, E. M.; Cedersund, G.; Strålfors, P. Insulin signaling in type 2 diabetes: Experimental and modeling analyses reveal mechanisms of insulin resistance in human adipocytes. *J. Biol. Chem.* **2013**, *288*, 9867−9880.

(3) Cao, H. Adipocytokines in obesity and metabolic disease. *J. Endocrinol.* **2014**, *220*, T47−T59.

(4) Charrière, G.; Cousin, B.; Arnaud, E.; André, M.; Bacou, F.; Penicaud, L.; Casteilla, L. Preadipocyte conversion to macrophage. Evidence of plasticity. *J. Biol. Chem.* **2003**, *278*, 9850−9855.

(5) Jialal, I.; Kaur, H.; Devaraj, S. Toll-like receptor status in obesity and metabolic syndrome: A translational perspective. *J. Clin. Endocrinol. Metab.* **2014**, *99*, 39−48.

(6) Eguchi, K.; Manabe, I. Toll-like receptor, lipotoxicity and chronic inflammation: The pathological link between obesity and cardiometabolic disease. *J. Atheroscler. Thromb.* **2014**, *21*, 629−639.

(7) Zu, L.; He, J.; Jiang, H.; Xu, C.; Pu, S.; Xu, G. Bacterial endotoxin stimulates adipose lipolysis via toll-like receptor 4 and extracellular signal-regulated kinase pathway. *J. Biol. Chem.* **2009**, *284*, 5915−5926.

(8) Bao, S.; Cao, Y.; Fan, C.; Fan, Y.; Bai, S.; Teng, W.; Shan, Z. Epigallocatechin gallate improves insulin signaling by decreasing toll-like receptor 4 (TLR4) activity in adipose tissues of high-fat diet rats. *Mol. Nutr. Food Res.* **2014**, *58*, 677−686.

(9) Pal, D.; Dasgupta, S.; Kundu, R.; Maitra, S.; Das, G.; Mukhopadhyay, S.; Ray, S.; Majumdar, S. S.; Bhattacharya, S. Fetuin-A acts as an endogenous ligand of TLR4 to promote lipid-induced insulin resistance. *Nat. Med.* **2012**, *18*, 1279−1285.

(10) Tsukumo, D. M.; Carvalho-Filho, M. A.; Carvalheira, J. B.; Prada, P. O.; Hirabara, S. M.; Schenka, A. A.; Araújo, E. P.; Vassallo, J.; Curi, R.; Velloso, L. A.; Saad, M. J. Loss-of- function mutation in toll-like receptor 4 prevents diet-induced obesity and insulin resistance. *Diabetes* **2007**, *56*, 1986−1998.

(11) Feingold, K. R.; Shigenaga, J. K.; Kazemi, M. R.; McDonald, C. M.; Patzek, S. M.; Cross, A. S.; Moser, A.; Grunfeld, C. Mechanisms of triglyceride accumulation in activated macrophages. *J. Leukocyte Biol.* **2012**, *92*, 829−839.

(12) Cullberg, K. B.; Larsen, J. Ø.; Pedersen, S. B.; Richelsen, B. Effects of LPS and dietary free fatty acids on MCP-1 in 3T3-L1 adipocytes and macrophages in vitro. *Nutr. Diabetes* **2014**, *4*, No. e113.

(13) Kuzuhara, T.; Sei, Y.; Yamaguchi, K.; Suganuma, M.; Fujiki, H. DNA and RNA as new binding targets of green tea catechins. *J. Biol. Chem.* **2006**, *281*, 17446−17456.

(14) Sae-tan, S.; Grove, K. A.; Lambert, J. D. Weight control and prevention of metabolic syndrome by green tea. *Pharmacol. Res.* **2011**, *64*, 146−154.

(15) Tachibana, H.; Koga, K.; Fujimura, Y.; Yamada, K. A receptor for green tea polyphenol EGCG. *Nat. Struct. Mol. Biol.* **2004**, *11*, 380−381.

(16) Mecham, R. P. Receptors for laminin on mammalian cells. *FASEB J.* **1991**, *5*, 2538−2546.

(17) Ku, H. C.; Liu, H. S.; Hung, P. F.; Chen, C. L.; Liu, H. C.; Chang, H. H.; Tsuei, Y. W.; Shih, L. J.; Lin, C. L.; Lin, C. M.; Kao, Y. H. Green tea (−)-epigallocatechin gallate inhibits IGF-I and IGF-II stimulation of 3T3-L1 preadipocyte mitogenesis via the 67-kDa laminin receptor, but not AMP-activated protein kinase pathway. *Mol. Nutr. Food Res.* **2012**, *56*, 580−592.

DOI: 10.1021/jf505531w
J. Agric. Food Chem. 2015, 63, 2811−2819

(18) Klaus, S.; Pultz, S.; Thone-Reineke, C.; Wolfram, S. Epigallocatechin gallate attenuates diet-induced obesity in mice by decreasing energy absorption and increasing fat oxidation. *Int. J. Obes.* **2005**, *29*, 615−623.
(19) Chan, C. Y.; Wei, L.; Castro-Muñozledo, F.; Koo, W. L. (−)-Epigallocatechin-3-gallate blocks 3T3-L1 adipose conversion by inhibition of cell proliferation and suppression of adipose phenotype expression. *Life Sci.* **2011**, *89*, 779−785.
(20) Ueda, M.; Nishiumi, S.; Nagayasu, H.; Fukuda, I.; Yoshida, K.; Ashida, H. Epigallocatechin gallate promotes GLUT4 translocation in skeletal muscle. *Biochem. Biophys. Res. Commun.* **2008**, *377*, 286−290.
(21) Yan, J.; Zhao, Y.; Suo, S.; Liu, Y.; Zhao, B. Green tea catechins ameliorate adipose insulin resistance by improving oxidative stress. *Free. Radical Biol. Med.* **2012**, *52*, 1648−1657.
(22) Tzameli, I.; Fang, H.; Ollero, M.; Shi, H.; Hamm, J. K.; Kievit, P.; Hollenberg, A. N.; Flier, J. S. Regulated production of a peroxisome proliferator-activated receptor-γ ligand during an early phase of adipocyte differentiation in 3T3-L1 adipocytes. *J. Biol. Chem.* **2004**, *279*, 36093−36102.
(23) Raetz, C. R.; Whitfield, C. Lipopolysaccharide endotoxins. *Annu. Rev. Biochem.* **2002**, *71*, 635−700.
(24) Nagai, Y.; Watanabe, Y.; Takatsu, K. The TLR family protein RP105/MD-1 complex: A new player in obesity and adipose tissue inflammation. *Adipocyte* **2013**, *2*, 61−66.
(25) Watanabe, Y.; Nagai, Y.; Takatsu, K. Activation and regulation of the pattern recognition receptors in obesity-induced adipose tissue inflammation and insulin resistance. *Nutrients* **2013**, *5*, 3757−3778.
(26) Shi, H.; Kokoeva, M. V.; Inouye, K.; Tzameli, I.; Yin, H.; Flier, J. S. TLR4 links innate immunity and fatty acid-induced insulin resistance. *J. Clin. Invest.* **2006**, *116*, 3015−3025.
(27) Cha, J. J.; Hyun, Y. Y.; Lee, M. H.; Kim, J. E.; Nam, D. H.; Song, H. K.; Kang, Y. S.; Lee, J. E.; Kim, H. W.; Han, J. Y.; Cha, D. R. Renal protective effects of toll-like receptor 4 signaling blockade in type 2 diabetic mice. *Endocrinology* **2013**, *154*, 2144−2155.
(28) Osborn, O.; Olefsky, J. M. The cellular and signaling networks linking the immune system and metabolism in disease. *Nat. Med.* **2012**, *18*, 363−374.
(29) Ryan, K. K.; Woods, S. C.; Seeley, R. J. Central nervous system mechanisms linking the consumption of palatable high-fat diets to the defense of greater adiposity. *Cell. Metab.* **2012**, *15*, 137−149.
(30) Zhang, W.; Mottillo, E. P.; Zhao, J.; Gartung, A.; VanHecke, G. C.; Lee, J. F.; Maddipati, K. R.; Xu, H.; Ahn, Y. H.; Proia, R. L.; Granneman, J. G.; Lee, M. J. Adipocyte lipolysis stimulated interleukin-6 production requires sphingosine kinase 1 activity. *J. Biol. Chem.* **2014**, DOI: 10.1074/jbc.M114.601096.
(31) Kida, K.; Suzuki, M.; Matsumoto, N.; Nanjo, F.; Hara, Y. Identification of biliary metabolites of (−)-epigallocatechin gallate in rats. *J. Agric. Food Chem.* **2000**, *48*, 4151−4155.
(32) Ku, H. C.; Chang, H. H.; Liu, H. C.; Hsiao, C. H.; Lee, M. J.; Hu, Y. J.; Hung, P. F.; Liu, C. W.; Kao, Y. H. Green tea (−)-epigallocatechin gallate inhibits insulin stimulation of 3T3-L1 preadipocyte mitogenesis via the 67-kDa laminin receptor pathway. *Am. J. Physiol.: Cell. Physiol.* **2009**, *297*, C121−132.
(33) Wang, C. T.; Chang, H. H.; Hsiao, C. H.; Lee, M. J.; Ku, H. C.; Hu, Y. J.; Kao, Y. H. The effects of green tea (−)-epigallocatechin-3-gallate on reactive oxygen species in 3T3-L1 preadipocytes and adipocytes depend on the glutathione and 67 kDa laminin receptor pathways. *Mol. Nutr. Food Res.* **2009**, *53*, 349−360.
(34) Burns, K.; Clatworthy, J.; Martin, L.; Martinon, F.; Plumpton, C.; Maschera, B.; Lewis, A.; Ray, K.; Tschopp, J.; Volpe, F. Tollip, a new component of the IL-1RI pathway, links IRAK to the IL-1 receptor. *Nat. Cell Biol.* **2000**, *2*, 346−351.
(35) Byun, E. B.; Choi, H. G.; Sung, N. Y.; Byun, E. H. Green tea polyphenol epigallocatechin-3-gallate inhibits TLR4 signaling through the 67-kDa laminin receptor on lipopolysaccharide-stimulated dendritic cells. *Biochem. Biophys. Res. Commun.* **2012**, *426*, 480−485.
(36) Arkan, M. C.; Hevener, A. L.; Greten, F. R.; Maeda, S.; Li, Z. W.; Long, J. M.; Wynshaw-Boris, A.; Poli, G.; Olefsky, J.; Karin, M. IKK-β links inflammation to obesity-induced insulin resistance. *Nat. Med.* **2005**, *11*, 191−198.
(37) Uysal, K. T.; Wiesbrock, S. M.; Marino, M. W.; Hotamisligil, G. S. Protection from obesity-induced insulin resistance in mice lacking TNF-α function. *Nature* **1997**, *389*, 610−614.
(38) Saberi, M.; Woods, N. B.; de Luca, C.; Schenk, S.; Lu, J. C.; Bandyopadhyay, G.; Verma, I. M.; Olefsky, J. M. Hematopoietic cell-specific deletion of toll-like receptor 4 ameliorates hepatic and adipose tissue insulin resistance in high-fat-fed mice. *Cell. Metab.* **2009**, *10*, 419−429.
(39) Ueki, K.; Kondo, T.; Kahn, C. R. Suppressor of cytokine signaling 1 (SOCS-1) and SOCS-3 cause insulin resistance through inhibition of tyrosine phosphorylation of insulin receptor substrate proteins by discrete mechanisms. *Mol. Cell. Biol.* **2004**, *24*, 5434−5446.
(40) Tamrakar, A. K.; Schertzer, J. D.; Chiu, T. T.; Foley, K. P.; Bilan, P. J.; Philpott, D. J.; Klip, A. NOD2 activation induces muscle cell-autonomous innate immune responses and insulin resistance. *Endocrinology* **2010**, *151*, 5624−5637.
(41) Prajapati, B.; Jena, P. K.; Rajput, P.; Purandhar, K.; Seshadri, S. Understanding and modulating the toll like receptors (TLRs) and NOD like receptors (NLRs) cross talk in type 2 diabetes. *Curr. Diabetes Rev.* **2014**, *10*, 190−200.
(42) McCormack, W. J.; Parker, A. E.; O'Neill, L. A. Toll-like receptors and NOD-like receptors in rheumatic diseases. *Arthritis Res. Ther.* **2009**, *11*, 243.
(43) Qi, H. Y.; Shelhamer, J. H. Toll-like receptor 4 signaling regulates cytosolic phospholipase A2 activation and lipid generation in lipopolysaccharide-stimulated macrophages. *J. Biol. Chem.* **2005**, *280*, 38969−38975.

DOI: 10.1021/jf505531w
J. Agric. Food Chem. 2015, 63, 2811−2819

integrity of tea catechins, such as encapsulation with liposome[30] or formulation with sucrose or ascorbic acid,[31] is necessary for their bioactivities.

Literature studies have shown that OSA-starch, as an emulsifier, has been used as a carrier material for the controlled release of bioactive compounds with formed micelles in an aqueous environment.[16,17] Therefore, OSA-starch might be prepared as a carrier to protect the structural integrity of tea catechins to improve their bioactivity, and the presence of tea catechins may further improve the slow digestion property of OSA-starch on the basis of a literature report.[23] Thus, the in vivo slow digestion property of OSA-starch in the presence of TPLs, as a novel approach to produce functional carbohydrate materials capable of sustaining glucose release and reducing oxidative stress, was studied in the current investigation to improve the knowledge of functional carbohydrates for improved health.

MATERIALS AND METHODS

Materials. TPLs were obtained from Hetian Biotechnology (Zhejiang, China) with a total tea catechin content of ∼99%, and its composition (EGCG, 66.90%; EGC, 5.88%; ECG, 10.62%; EC, 15.70%) was analyzed using a common HPLC method.[32] Waxy maize starch was obtained from National Starch and Chemical Co. (Bridgewater, NJ, USA). The preparation of OSA-starch and measurement of degree of substitution (DS) were based on a literature report,[13] and the final DS was estimated to be 0.0194. Octenyl succinic anhydride, glucuronidase (G-7896, EC 3.2.1.31, from *Escherichia coli* with 9×10^6U/g solid), and sulfatase (S-9754, EC 3.1.6.1, from abalone entrails with 2.3×10^5U/g solid) were purchased from Sigma Chemical (St. Louis, MO, USA). Diphenyl-(2,4,6-trinitrophenyl)iminoazanium (DPPH) was purchased from Wolsen Bio. Co. (Shanxi, China).

Animals and Treatment. Four-week-old male Kunming mice were purchased from Slac Co. (Shanghai, China) and kept on a 12 h light/dark schedule (lights on from 8:30 a.m. to 8:30 p.m.) in a constant condition (22 ± 1 °C and 60% humidity) with standard chow (Slac Co.) and drinking water provided ad libitum. Experiments were performed 1 week later after overnight fasting. Starch samples (10% w/v in distilled water) with and without TPLs (5%, w/w starch based) were cooked in a boiling water bath for 20 min to gelatinize the starches. After the samples were cooled to room temperature, mice were divided into three groups (20 mice per group) and gavaged with OSA-starch (1000 mg/kg bw, ig) alone or in combination with TPLs (OSAT), and TPLs alone were used as the control (50 mg/kg bw, ig). No chow was provided to mice during the experiment.

Mice were sacrificed at time 0 (as the control without feeding) and 30, 60, and 120 min after gavaging. Blood samples were collected into heparin-containing tubes by eyeball extirpating before cervical dislocation and then centrifuged at 3000*g* for 10 min at 4 °C for plasma insulin analysis. In the meantime, the small intestine tissue (ST) was removed immediately, and luminal contents (LC) was expelled into microcentrifuge tubes with cold saline. ST and LC were snap-frozen and kept at −80 °C for later analysis. All animal experiments were approved by the Institutional Animal Care and Use Committee at Jiangnan University under protocol 20131024-0107.

The samples of ST and LC for the measurement of enzyme activity, TPLs' content, malondialdehyde content, and DPPH scavenging activity were prepared through homogenization of ST and LC by adding ice-cold saline (1:9 (w/v)), which was carried out in a ice bath for a total time period of 30 s (5 s per operation) using a homogenizer (Ultra-Turrax T25, IKA Works Inc., China) at 24000 rpm. The homogenates were centrifuged at 3000*g* for 10 min at 4 °C, and the supernatant was used as the sample for analysis.

Postprandial Glycemic Response Measurement. The postprandial glycemic response was measured by feeding different test diets (TPLs, 50 mg/kg bw; OSA-starch, 1000 mg/kg bw; OSA-starch + 5% TPLs, 1000 mg/kg bw) via gavage. Blood samples were taken from the lateral tail vein at 0 (as the control before gavage), 15, 30, 45, 60, 90, and 120 min after gavage. The blood glucose concentration was measured using a glucose analyzer (Johnson & Johnson, China) and expressed as the mean ± standard error (SE).

α-Amylase and α-Glucosidase Activity Assays. The activity of small intestine α-amylase was examined using the chromogenic GalG2CNP kit according to the specified instruction (Leadman, Bejing, China). Briefly, the supernatants (40 μL) from the homogenates of ST and LC were combined with 200 μL of GalG2CNP (3 mmol/L) suspended in (2-(*N*-morpholino)-ethanesulfonic acid (MES) buffer (100 mmol/L MES in distilled water, pH 6.0), and after incubation at 37 °C for 60 s, the changing rate of OD_{405} monitored within 2 min at 37 °C was used to calculate the activity of α-amylase. For α-glucosidase, 20 mg/mL maltose (1.0 mL) was hydrolyzed by supernatants (0.1 mL) from homogenates of ST and LC in a sodium phosphate buffer (100 mmol/L, $CaCl_2$ 1.0 mmol/L, pH 6.9) at 37 °C for 10 min, and the concentration of glucose was measured using a hexokinase kit (Leadman). The enzyme activities were expressed as percentages compared to the initial values measured before gavaging.

An in vitro experiment was also carried out to test the effect of TPLs on the activity of mucosal α-glucosidase of the small intestine. First, the dose−response effect of TPLs (0−10 μg/mL) on the enzyme activity in the supernatant (0.1 mL) of ST homogenate from fasted mice was studied at 37 °C for 10 min in a sodium phosphate buffer (100 mmol/L, $CaCl_2$ 1.0 mmol/L, pH 6.9) containing 20 mg/mL maltose with a final reaction volume of 2.1 mL. Second, the Michaelis−Menten kinetic model was used to evaluate the kinetic parameters in hydrolysis by measuring the amount of liberated glucose under different substrate (maltose) concentrations (0.02−0.50 mg/mL) in the presence of TPLs (10 μg/mL). A Lineweaver−Burk plot between 1/[substrate] (mg/mL) and 1/[V] (reaction rate, mmol/L/min) was used to determine the action type of TPLs on α-glucosidase.

TPL Concentration Measurement. The content of TPLs in LC and ST was analyzed by HPLC.[33] Briefly, the supernatant from LC or ST homogenate was mixed with 2.5 volumes of sodium phosphate buffer (0.4 mol/L, pH 6.8), hydrolyzed by glucuronidase (250 U/sample) and sulfatase (1 U/sample) at 37 °C for 45 min.[23,34,35] After hydrolysis, the sample was extracted twice with ethyl acetate. The organic phase was dried under vacuum, resuspended in 50% methyl alcohol, and analyzed using an Agilent HPLC 1200 instrument coupled with a GraceSmart reverse-phase C18 column (4.6 × 250 mm, particle size = 5 μm) (Deerfield, IL, USA) and a UV detector (280 nm) at a flow rate of 0.8 mL/min at 30 °C. Solvent A composed of acetonitrile, distilled water, and trifluoroacetic acid (TFA) in a ratio of 10:90:0.05 and solvent B in a ratio of 30:70:0.05 were used as the mobile phase. Beginning with 100% solvent A, a linear gradient mobile phase (decreasing polarity) with solvent B was used until 20 min approaching 100% solvent B. After running for 5 min, the mobile phase was returned to 100% solvent A until 30 min to finish the analysis. The measured result represented the content of total catechins, and samples prepared without glucuronidase/sulfatase were used to quantify the unconjugated fractions of catechins.

Determination of Malondialdehyde (MDA) and DPPH Scavenging Activities. MDA content in the supernatant of ST homogenate was analyzed using the diagnostic kit (Nanjing Jiancheng Bioengineering Institute, Nanjing, China) according to the instruction of the manufacturer, and the results were expressed as nanomoles per milligram of protein. Total protein contents were determined by Coomassie brilliant blue method using bovine serum albumin as the standard. DPPH free radical scavenging activities of ST homogenate was measured as described by Zhong et al. with slight modification.[36,37] DPPH solution in ethanol (0.1 mmol/L) was prepared and used fresh for each test. The DPPH free radical scavenging activities were measured by mixing supernatant from ST homogenate and DPPH solution, and the absorbance at 517 nm was recorded after incubation at room temperature for 30 min. The scavenging rate (%) was calculated with the equation $[1 - (A_1 - A_2)/A_0] \times 100\%$, where A_0 is the absorbance of the control (2 mL of DPPH solution + 1 mL of NaCl (0.9%)), A_1 is the absorbance of the sample (2 mL of DPPH

DOI: 10.1021/jf5059705
J. Agric. Food Chem. 2015, 63, 2820−2829

solution + 1 mL of sample supernatant), and A_2 is the absorbance of blank (1 mL of tissue supernatant + 2 mL of ethanol).

Emulsifying Activity Measurement. The emulsion preparation and emulsifying activity of OSA-starch was measured according to the method proposed by Miao et al. and Meng et al.[7,38] with slight modifications. Starch solutions (1.0% w/w) were prepared by dispersing the samples with/without 5% (w/w, based on starch) TPLs in deionized water at room temperature and heating in a boiling water bath with stirring for 20 min to completely dissolve the samples. Oil-in-water (O/W) emulsions with 5% Arawana soybean salad oil (Yihai Kerry, China) were prepared using a high-speed homogenizer (Ultra-Turrax T25, IKA Works Inc., China) at 24000 rpm for 5 min at room temperature to produce a fine emulsion. For the emulsifying activity, 50 μL of each emulsion was pipetted into 5 mL of 0.1% sodium dodecyl sulfate. After emulsion formation, the absorbance (emulsifying activity, EA) was measured at 500 nm. The emulsion stability (ES) of samples was measured after storage at room temperature for 24 h and calculated as follows:

$$\mathrm{ES} = (\text{height of remaining emulsion layer/total height}) \times 100\%$$

Fourier Transform Infrared Spectral (FT-IR) Analysis. OSA-starch (1.0 g) with or without TPLs (5% w/w based on starch) was mixed in 20 mL of distilled water and cooked in a boiling water bath for 20 min with continuous stirring to completely gelatinize the starch. The samples were freeze-dried after the cooked samples were cooled to room temperature. A Nicolet Nexus 470 Fourier transform infrared spectrometer (Thermo Electron Corp.) equipped with an ATR cell and EZ Omnic software (version 7.0) was used to obtain the spectrograms of the OSA-starch. Accurately weighed samples and KBr (100 times the weight of each sample) were fully milled together to get the infrared information from 4000 to 600 cm^{-1} by accumulating 32 scans per spectra at a resolution of 4 cm^{-1}.

Differential Scanning Calorimetry (DSC). DSC measurements were carried out with a Q20 thermal analyzer (TA Instruments, New Castle, DE, USA). OSA-starch (2 mg) and OSA-starch−TPLs mixture (OSA-starch/TPLs = 20:1) were placed in an aluminum pan with water (2:1, v/w) and held for at least 8 h before analysis. The samples were heated from 30 to 120 °C at a heating rate of 10 °C/min in a nitrogen atmosphere. Thermal transitions for gelatinization were characterized by T_o (onset temperature), T_p (peak temperature), T_c (conclusion temperature), and ΔH (enthalpy of gelatinization).

Scanning Electron Microscopy (SEM) Analysis. To analyze the difference of the microstructure of OSA-starch affected by TPLs, freeze-dried OSA-starch with/without 5% TPLs after gelatinization was used as sample for SEM analysis. Scanning electron micrographs were then obtained with a Quanta 200 scanning electron microscope (FEI Co., Eindhoven, The Netherlands) under a vacuum of 13.33 Pa and an operating voltage of 20 kV.

Dynamic Laser Scattering (DLS) Analysis. A commercial laser light scattering spectrometer (ALV/DLS/SLS-5022F, ALV Co., Langen, Germany) equipped with an ALV-5000/EPP multi-τ digital time correlator covering 125 ns−37 h in delay time and a He−Ne laser (Uniphase, output power ≈ 20 mW at λ = 632.8 nm) was used to measure the hydrodynamic radius of OSA-starch molecules. An OSA-starch solution (0.1 mg/mL) with or without TPLs (5%, OSA-starch weight base) was mixed and used as the sample for analysis. Each sample solution was first passed through a 0.45 μm Millipore syringe filter into a dust-free cell. The dynamic light scattering measurements were obtained at 90°, and CONTIN FIT (ALV Co.) was performed to obtain the hydrodynamic radius distribution of starch molecules.

Viscosity Measurement. OSA-starch (5%) with or without TPLs (5% based on dry weight of starch) was first cocooked at 100 °C for 20 min to completely gelatinize the starch, and then the apparent viscosity (Pa.s) of the samples was measured at 25 °C along the shear rate from 0.1 to 100 s^{-1} using an AR-G2 rheometer (TA Instruments-Waters LLC, Shanghai, China) with a 40 mm diameter steel plate gapped by 1 mm.

Statistical Analysis. Experimental data of in vivo glycemic response, insulin level, and enzyme activity were expressed as means ± SEM, and standard deviation of the mean was used for other experimental results. Statistical analysis was carried out using the one-way analysis of variance (one-way ANOVA) to determine the statistical significance at $p < 0.05$ by Tukey's honest significant difference (HSD) test.

RESULTS AND DISCUSSION

TPLs Modulate the Postprandial Glycemic Response of OSA-Starch. Chemically modified starch has long been used in food applications with different purposes, and nutritionally, most of the chemically modified starches belong to the category of resistant starch. OSA-starch, to our knowledge, is the only one with a substantial fraction of SDS after heat−moisture treatment.[13] However, a human study of its effect on postprandial glycemia showed the glycemic profile is still not good enough to provide a sustained glucose release.[13] Thus, tea polyphenols, which have been shown to inhibit the activity of α-amylase[39,40] and glucose transport of SGLT1,[22] were chosen to further improve the slow digestion property of OSA-starch. The dose of TPLs used in the current study was determined to be 5% (w/w, based on dry weight of OSA-starch) because the lowest digestion rate of OSA-starch was observed at this dosage (data not shown). The OSA-starch was produced according to a literature report,[13] and the degree of substitution of the final OSA-starch was determined to be 0.0194. The successful esterification of waxy corn starch was proved by FTIR analysis (Figure 1) with two new absorption

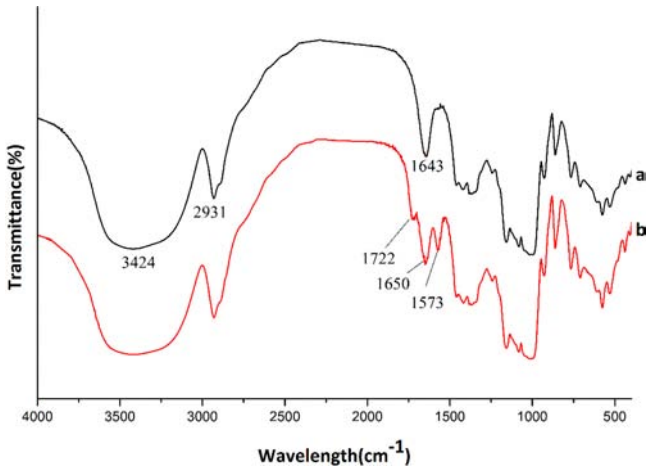

Figure 1. Fourier transform infrared spectrometry of native and OSA starches: (a) waxy starch; (b) OSA-starch. The DS is 0.0194.

bands at 1722 and 1573 cm^{-1} corresponding to the C=O stretching vibration of the ester group and the asymmetric stretching vibration of carboxyl group, respectively.[12]

The postprandial glycemic response to starch reflects the rate of glucose release from starch digestion and glucose absorption in the small intestine. The triggered secretion of insulin also contributes to a reduced blood glucose level by promoting glucose absorption. The addition of TPLs to OSA-starch significantly improved the postprandial glycemic response using Kunming mouse as the animal model. For OSA-starch, the postprandial blood glucose concentration reached a peak value of 4.9 mmol/L above the baseline after gavaging for 15 min. When OSA-starch was cocooked with TPLs (5%, based on starch dry weight, termed OSAT), a significant decrease of postprandial glycemia (from 4.9 to 3.0 mmol/L at the peak from baseline) with a delayed blood glucose peak (from 15 to 30 min) was observed (Figure 2A), although no significant

DOI: 10.1021/jf5059705
J. Agric. Food Chem. 2015, 63, 2820−2829

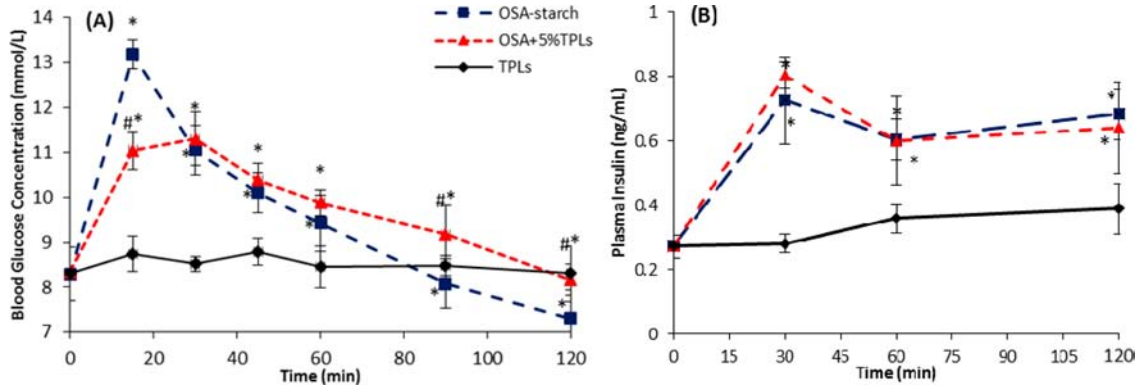

Figure 2. Postprandial glycemic response to OSA-starch affected by the addition of TPLs (A) and insulin levels (B) in mice. Results are shown as means ± SEM (n = 6); (#) $p < 0.05$ compared to OSA starch; (∗) $p < 0.05$ compared to TPLs.

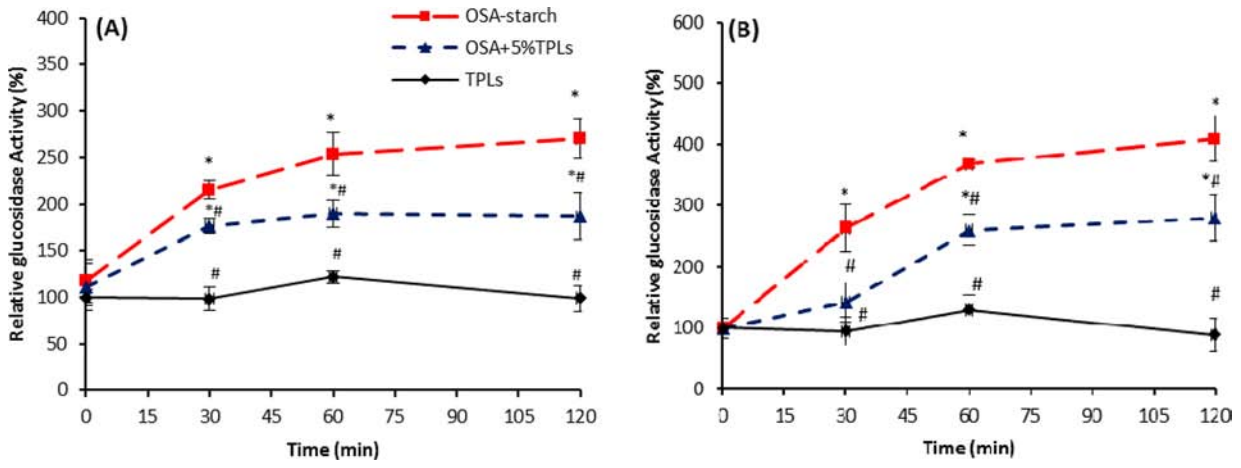

Figure 3. Activities of α-glucosidase in the small intestine tissue (A) and luminal contents (B) of mice after feeding different diets. Results are shown as means ± SEM (n = 6); (#) $p < 0.05$ compared to OSA starch; (∗) $p < 0.05$ compared to TPLs.

difference of the area under the glycemic curves (AUC) was found (1140.8 ± 39.2 for OSA-starch, 1173.2 ± 65.9 min·mmoL/L for OSAT). Compared to regular waxy corn starch with a peak glycemia of ∼7.5 mmol/L from baseline in the same mouse model,[41] the OSA-starch itself is of slow digestion property, and the addition of TPLs to OSA-starch further significantly decreased its postprandial glycemia. However, the addition of TPLs did not significantly affect the secretion of insulin following oral administration of OSA-starch or OSAT (Figure 2B), indicating insulin is not likely responsible for the decreased glycemia. Additionally, our previous study showed an identical postprandial glycemic response profile to glucose whether in the presence or absence of TPLs, indicating that TPLs have a negligible effect on glucose absorption in the small intestine,[22] which is also supported by a study showing that acute administration of EGCG did not inhibit glucose transport across the intestinal wall.[23] Therefore, the decreased postprandial glycemia of OSA-starch in the presence of TPLs is likely due to the reduced digestibility of OSA-starch.

Effect of TPLs on the Activity of α-Glucosidase. Starch is primarily digested by α-amylase and mucosal α-glucosidase in the small intestine. α-Amylase is responsible for cleaving the large strach molecules into maltooligosaccharides and α-limit dextrins, and α-glucosidase is a group of enzymes anchored on the cell membrane to generate monosaccharides for absorption. As shown above, starch digestion is likely the main reason for decreased postprandial glycemia, so the enzyme activities of α-amylase and α-glucosidase in the small intestine were first examined. Because the secretion of digestive enzymes needs the stimuli of food materials, TPLs alone did not show any changes of enzyme activity and can only act as the baseline.

Regarding the influence of TPLs on α-amylase activity, it has been well documented in the literature that TPLs mainly inhibit the activity of α-amylase for carbohydrate digestion based on in vitro studies under the optimum condition of enzyme activity.[39,40,42−44] Indeed, there was a literature report[23] that decreased α-amylase activity was concluded as the reason for decreased postprandial glycemia in a mouse model study using normal corn starch. However, the in vivo activity of α-amylase was not studied, and the conclusion was solely based on an in vitro measurement using commercially sourced α-amylase.[23] In the current study, we did not find significant changes of α-amylase activities in the small intestine (data not shown).

α-Glucosidase inhibitors are commonly prescribed to diabetics to reduce postprandial hyperglycemia induced by the digestion of starchy foods in the small intestine,[45] and TPLs are potent α-glucosidase inhibitors from a literature study on Caco-2 cell cultures.[46] Thus, the activity of small intestine α-glucosidase was examined in both luminal content (LC) and the tissue (ST) of the small intestine. The activities of α-glucosidase in LC and ST were significantly decreased in the OSAT-treated mice compared to that in OSA-starch-treated mice (Figure 3). Considering the regulatory effct of starch molecules on the gene expression of starch-hydrolyzing

DOI: 10.1021/jf5059705
J. Agric. Food Chem. 2015, 63, 2820−2829

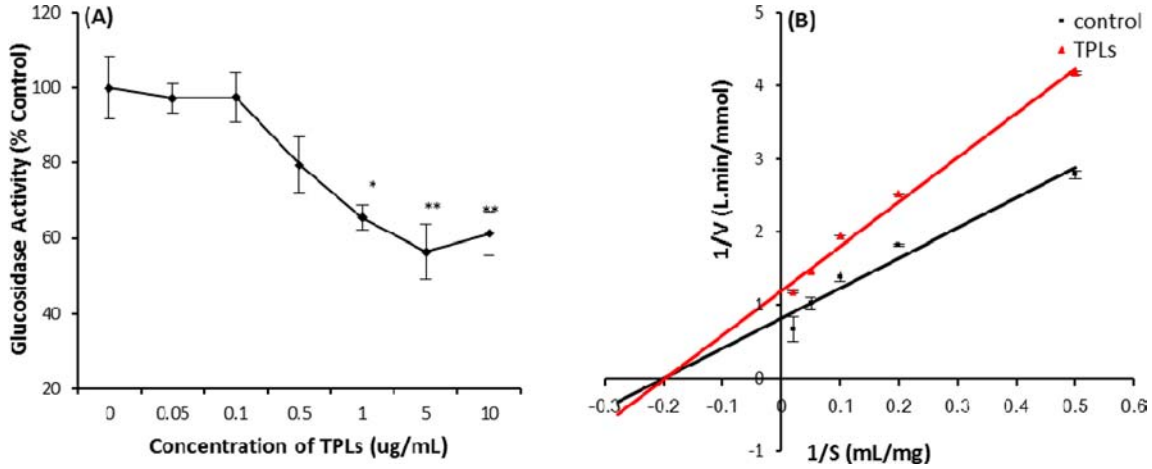

Figure 4. Effect of TPLs on the activity of small intestine α-glycosidase from mice as expressed by a dose-dependent inhibition pattern (A) and its kinetics (B). Results are shown as means ± SD (n = 3); (*) $p < 0.05$; (**) $p < 0.01$ compared to control.

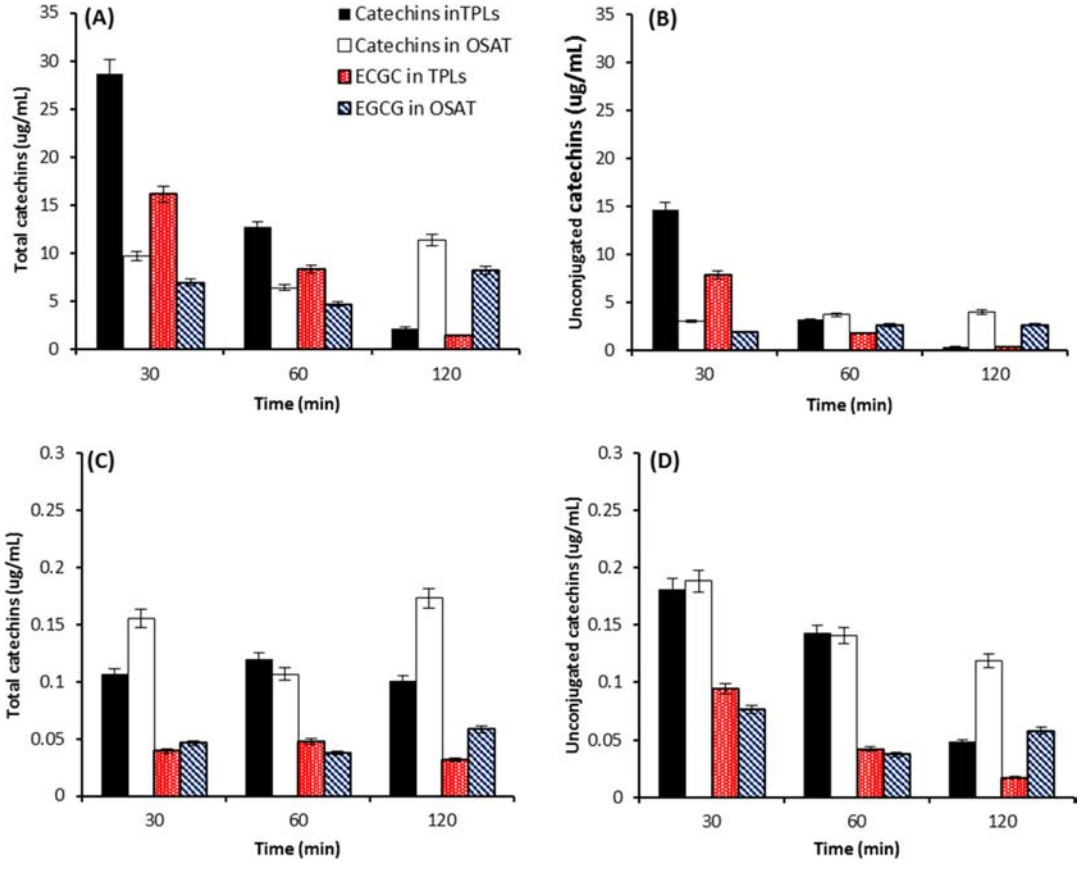

Figure 5. Concentrations of catechins and EGCG in luminal contents (A, B) and the small intestine tissue (C, D) of mice after oral administration of different diets (TPLs alone and OSAT). Results are shown as means ± SEM (n = 6).

enzymes,[47] the decreased activity of α-glucosidase might be due to a decreased gene expression. However, at least 6 h is required for carbohydrate to affect the expression and post-translation modification of mucosal sucrase-isomaltase (one type of α-glucosidase) in a Caco-2 cell model study.[48] Thus, the duration of our in vivo experiment (2 h) is not likely long enough for OSA-starch to affect the expression of small intestine mucosal α-glucosidase, so the decreased activities of α-glucosidase in LC and ST were most likely caused by the inhibiton effect of tea catechins in OSAT during digesiton. Indeed, the in vitro study of the effect of TPLs on the activity α-glucosidase in small intestine homogenate (Figure 4A) showed that its activity was inhibited by TPLs in a dose-dependent manner. Kinetic analysis on homogenate α-glucosidase showed a decreased reaction velocity (from 1.21 to 0.83 mmol/L/min) without affecting the enzyme's affinity for substrate, indicating a noncompetitive inhibition function of TPLs (Figure 4B). Therefore, the decreased activity of α-glucosidase in the presence of TPLs might be the main reason for the reduced and prolonged postprandial glycemia, which is characteristic of slowly digestible starch.[49] A higher enzyme activity of α-glucosidase after feeding OSA-starch alone also

DOI: 10.1021/jf5059705
J. Agric. Food Chem. 2015, 63, 2820−2829

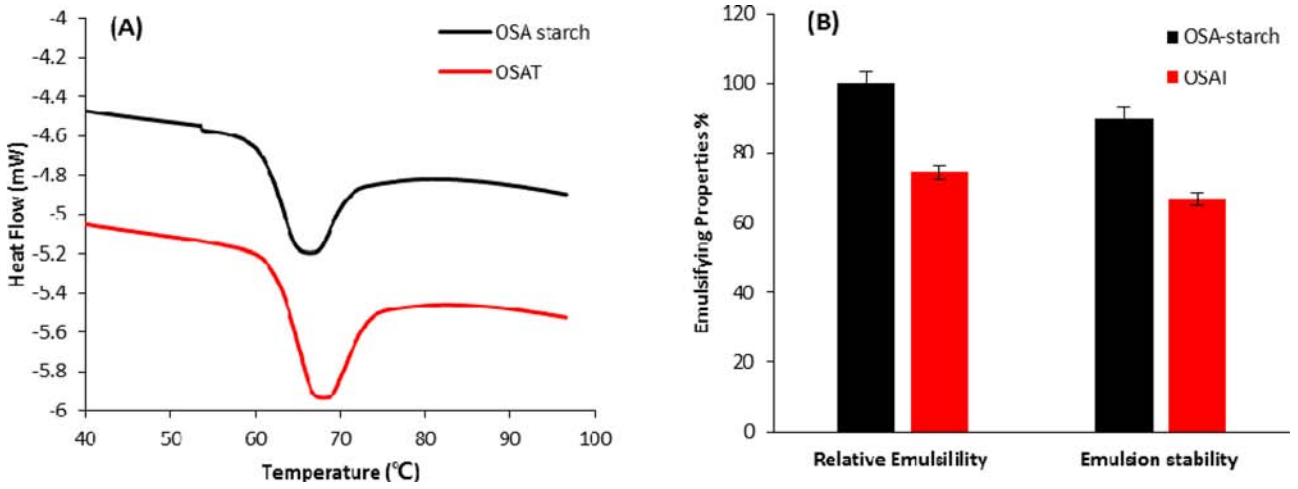

Figure 6. Differential scanning calorimetry profiles (A) and emulsion property (B) of OSA-starch affected by TPLs.

supports the inhibition effect of TPLs on the activity of mucosal α-glucosidase.

Catechin Release from OSAT Sample. Although TPLs can inhibit the activities of digestive enzymes and alleviate postprandial hyperglycemia, their sensitivity to environmental conditions might affect their bioactivity. In the environment of the small intestine, the alkaline pH makes TPLs more susceptible to degradation, leading to a rapid clearance and a loss of bioactivities.[31] The levels of four major catechins in LC after mice were administered OSAT (1000 mg/kg bw, ig) and control of TPLs (50 mg/kg bw, ig) were first analyzed. The results (Figure 5) showed that the concentration of catechins (total and unconjugated) decreased rapidly in LC following administration of the control sample of TPLs and almost undetectable after 120 min, whereas concentration of catechins in the small intestine (ST + LC) of OSAT-treated mice remained relatively stable along the digestion of starch. A lower content of catechins (total and unconjugated forms) was also detected in LC at the early stage of digestion from the OSAT-treated mice. All of these results indicate a sustained release of TPLs from OSAT along the digestion process.

Conjugated forms of tea catechins are formed during the in vivo elimination process through the action of phase II enzymes. Literature reports showed that glucuronidated EGCG is the major conjugated form when EGCG is orally administered to mice,[35] and sulfated and methylated forms are also widely present in the conjugated catechins.[27] The biotransformation of TPLs after absorption is intimately associated with the bioactivities of tea cateahins. A literature report showed methylated EGCGs such as 4″-MeEGCG are much less effective than EGCG to induce the apoptosis of prostate cancer cells of LNCaP,[50] and some glucuronidated forms of EGCG and EGC are less effective in free radical scavenge activity than their unconjugated forms.[51] Thus, we also measured the content of tea catechins in the small intestine tissues, and the results (Figure 5C,D) showed that catechins and EGCG after OSAT treatment were mostly present as the unconjugated forms rather than the conjugated types, indicating the OSAT sample might also have the function to improve the bioactivity of TPLs. However, comparison of the amount of total catechins and unconjugated TPLs showed that the content of total catechins is less than the unconjugated forms, which has also been observed in the literature.[23] The reason is likely due to the complex of biotransformation that makes the used method less effective in detecting all of the conjugated catechins, but the actual reason needs further clarification through a systematic study, which is beyond the scope of this paper.

Complexation between TPLs and OSA-Starch. Decreased postprandial glycemic response in the presence of TPLs has been shown to be associated with the inhibitory funciton of TPLs on small intestinal α-glucosidase in the current study. However, our previous study of the effect of TPLs on the glycemic responses of normal corn and waxy corn starch did not show significant changes.[24] Therefore, it is necessary to understand how TPLs in OSAT sample inhibit α-glucosidase and decrease the postprandial glycemia.

Differential scanning calorimetry records the amount of heat involved in the starch gelatinization. TPLs considerably affected the gelatinization properties of OSA-starch (Figure 6A), and there was a clear shift in the endothermic peak toward a lower temperature with significantly decreased enthalpy (from 11.05 ± 0.25 to 9.32 ± 0.12 J/g). The reason for the decreased gelatinization temperature in the presence of TPLs might be due to a rapid hydration of OSA-starch when its hydrophobicity is decreased through a possible hydrophobic interaction with TPLs. Specifically, the interaction between the aromatic rings of TPLs and hydrocarbon chains of OSA groups[51] that are mostly present in the amorphous regions of starch granules because the crystalline regions in the granules are difficult for chemical regents to penetrate. In the meantime, the H-bond interactions between the hydrophilic group of TPLs with linear segment[33] of amylopectin located in the amorphous region of starch granules might weaken the coupling forces between the crystallites and the amorphous matrix,[52] leading to a lower energy required to gelatinize the starch granules.

OSA-starch, as an amphiphilic derivative of starch, is an effective stabilizer in water in oil emulsions and some oil-in-water systems.[12] As shown in Figure 6B, the emulsifiability of OSA-starch and its stability were decreased significantly after cocooking with TPLs (25.5 and 23.2% declines, respectively), which directly indicates the presence of a hydrophobic interaction between TPLs and OSA-starch leading to a decrease of the hydrophobic property of OSA-starch, and so to a decreased emulsifiability. The above conclusion is supported by a literature report showing that TPLs, especially EGCG, can interact with the lipid layer of emulsions and increase emulsion drop size,[53] and this might reflect the same phenomenon of an

DOI: 10.1021/jf5059705
J. Agric. Food Chem. 2015, 63, 2820−2829

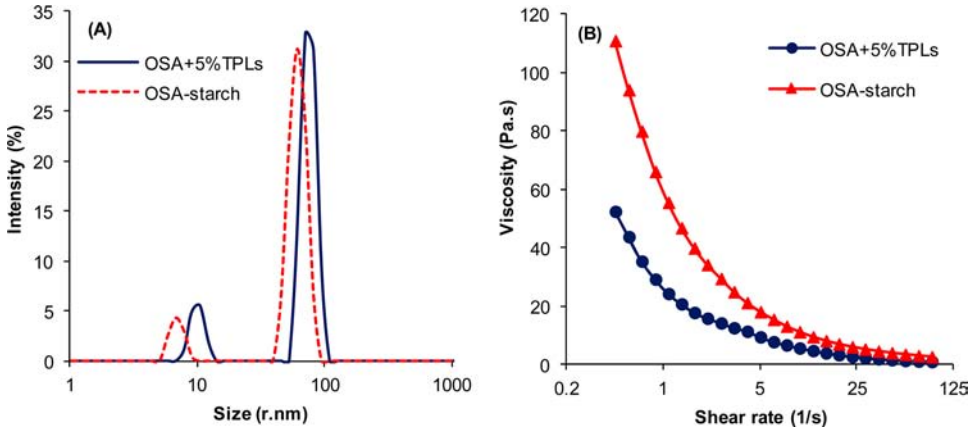

Figure 7. Effect of TPLs on the molecular size distribution (A) and the viscosity of OSA-starch (B).

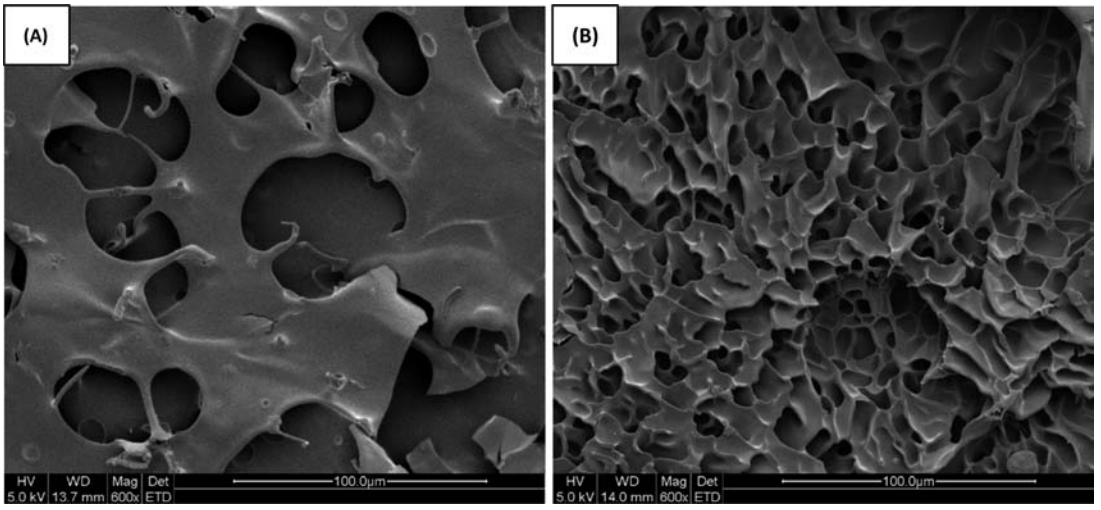

Figure 8. SEM analysis of freeze-dried OSA-starch (A) and OSAT (B). Scale bar = 100 μm.

increase of particle size of OSA-starch molecules (Figure 7A) in which TPLs might bridge more OSA-starch molecules together through hydrophobic interaction. In the meantime, this bridge also changes the conformation or shape of the OSA-starch molecules with a more spherical nature that is less viscous and less shear-thinning (Figure 7B) because shear-thinning behavior is characteristic of linear macromolecules. The influence of TPLs on OSA-starch structure due to hydrophobic interaction was also supported by SEM observation of the freeze-dried samples of OSA-starch and OSAT sample with dramatic difference of macroscopic structures (Figure 8).

All of the above experimental results showed the interaciton between OSA-starch and TPLs, and considering the molecular structure of OSA-starch and the TPLs, there might exist a spherical-like OSA-starch−TPL (OSAT) complex in which the hydrophobic interaction between the OSA group of OSA-starch and aromatic hydrocarbons of TPLs is the major force for their complexation.[54] When the hydrophobic complexation occurs, they might pull the amylopectin molecules together to shorten the distance between these molecules, facilitating the interaction between linear segments of amylopectin through TPLs' bridge function as shown in our previous study,[33] which further tightens the aggregation of OSA-starch molecules in the OSAT complex. When the complex was digested by α-amylase, the TPLs embedded in the complex might not be accessible to α-amylase, so that the activity of α-amylase in the small intestine is not likely affected even though TPLs do have the capability of inhibiting the activity of α-amylase. However, the complex structure might be a barrier to α-amylase, making it less efficient to hydrolyze starch, which also contributes to a reduction of postprandial glycemia. After TPL-containing (through interaction with OSA group) malto-oligosaccharides or α-limited dextrin (substrate of α-glucosidase) are slowly produced by α-amylase, their accessibility to mucosal α-glucosidase might also be affected. A gradual release of TPLs after digestion by α-amylase and α-glucosidase might lead to a high association between TPLs and α-glucosidase due to their closeness in distance, which facilitates the binding of TPLs by α-glucosidase, resulting in activity inhibition. Thus, the OSAT complex causes not only a decreased digestion efficiency by α-amylase and a slow production of substrate for mucosal α-glucosidase but also an inhibition of α-glucosidase activity by a sustained release of tea catechins from the complex, which all together result in a lower and prolonged postprandial glycemia.

Health Implication. Epidemiological studies have associated tea consumption with prevention of chronic and degenerative diseases including cancer,[55] cardiovascular disorder,[56] obesity, and diabetes.[57] However, low bioavailability limits the bioactivities of catechins.[31] In our study, a sustained release of unconjugated catechins from OSAT after acute administration was observed (Figure 5). Catechins, mainly EGCG, were present mostly as the more active unconjugated

DOI: 10.1021/jf5059705
J. Agric. Food Chem. 2015, 63, 2820−2829

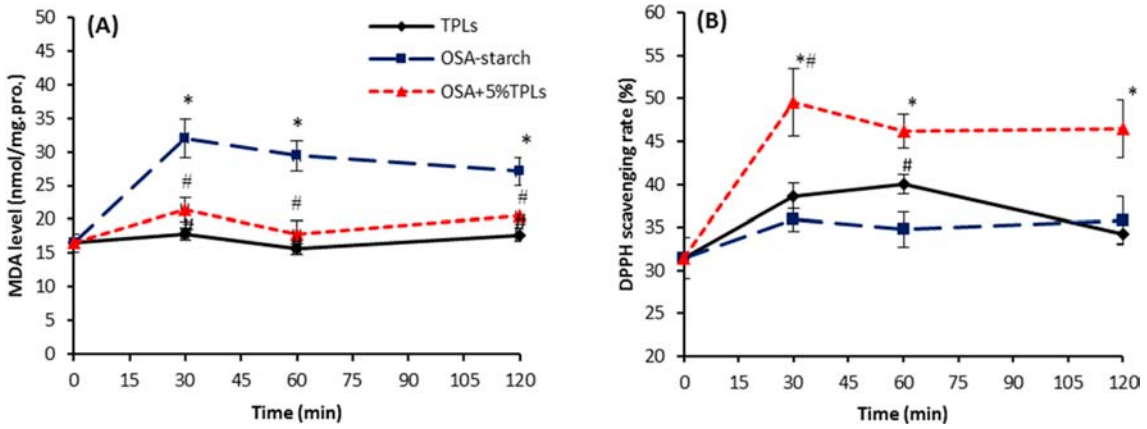

Figure 9. Level of MDA (A) and DPPH radical scavenging activity (B) in the small intestine tissue of mice. Results are shown as means ± SEM (n = 6); (#) $p < 0.05$ compared to OSA starch; (∗) $p < 0.05$ compared to TPLs.

form in ST rather than the conjugated form. In the meantime, the uptake of unconjugated TPLs might also be increased due to a high concentration of unconjugated TPLs in the luminal side of the small intestine and closeness to the absorptive enterocytes.

MDA is a major reactive aldehyde that appears during the peroxidation of fatty acid. Therefore, the content of MDA is widely used as a biomarker of oxidative stress and indicator of tissue damage involving a series of chain reactions.[58] We observed a significant increase of MDA level in intestinal tissue of mice due to the fluctuation of plasma glucose caused by OSA starch (Figure 9A). It has been demonstrated that glucose fluctuation is more deleterious to endothelial function through excessive generation of reactive oxygen species (ROS), resulting in oxidative stress.[59] Our study showed that the content of MDA decreased significantly in mice dosing OSAT (Figure 9A). Additionally, OSAT feeding also showed stronger DPPH scavenging activity than both OSA-starch and TPLs alone in the ST of mice (Figure 9B; $p < 0.05$). Thus, the OSAT complex also has an antioxidative bioactivity.

In conclusion, experimental results on the physicochemical properties of OSAT sample demonstrate the presence of a hydrophobic interaction-induced complexation between OSA-starch and TPLs. This complex not only changes the digestion property of OSA-starch, leading to a slow elevation of postprandial glycemia and possibly a sustained glucose release, but also has the capability to reduce the oxidative stress, which is likely the first study on functional or bioactive starch material to improve health. Although OSA-starch is not a common food ingredient that is generally consumed in large quantity, the complex formed between OSA-starch and TPLs, as the structural basis for TPLs' function, indicates some carbohydrate-coupled delivery systems of TPLs might be developed to efficiently decrease the postprandial glycemia for improved health.

AUTHOR INFORMATION

Corresponding Author

*(G.Z.) Phone: +86 510 8532 8731. Fax: +86 510 8532 9081. E-mail: genyiz@gmail.com.

Funding

The current investigation was supported by the National Natural Science Foundation of China (Project 31471585) and the Ministry of Science and Technology of People's Republic of China Infrastructure Program (Project 2012BAD33B05).

Notes

The authors declare no competing financial interest.

REFERENCES

(1) Ginsberg, H. N. Insulin resistance and cardiovascular disease. *J. Clin. Invest.* **2000**, *106* (4), 453−458.

(2) Zhang, W.; Zhao, S.; Li, Y.; Peng, G.; Han, P. Acute blood glucose fluctuation induces myocardial apoptosis through oxidative stress and nuclear factor-κB activation. *Cardiology* **2013**, *124* (1), 11−17.

(3) Wu, D.; Gong, C. X.; Meng, X.; Yang, Q. L. Correlation between blood glucose fluctuations and activation of oxidative stress in type 1 diabetic children during the acute metabolic disturbance period. *Chin. Med. J. (Engl.)* **2013**, *126* (21), 4019−4022.

(4) Monnier, L.; Mas, E.; Ginet, C.; Michel, F.; Villon, L.; Cristol, J. P.; Colette, C. Activation of oxidative stress by acute glucose fluctuations compared with sustained chronic hyperglycemia in patients with type 2 diabetes. *JAMA, J. Am. Med. Assoc.* **2006**, *295* (14), 1681−1687.

(5) Lehmann, U.; Robin, F. Slowly digestible starch − its structure and health implications: a review. *Trends Food Sci. Technol.* **2007**, *18* (7), 346−355.

(6) Zhang, G.; Ao, Z.; Hamaker, B. R. Slow digestion property of native cereal starches. *Biomacromolecules* **2006**, *7* (11), 3252−3258.

(7) Miao, M.; Li, R.; Jiang, B.; Cui, S. W.; Zhang, T.; Jin, Z. Structure and physicochemical properties of octenyl succinic esters of sugary maize soluble starch and waxy maize starch. *Food Chem.* **2014**, *151*, 154−160.

(8) Liu, Z.; Li, Y.; Cui, F.; Ping, L.; Song, J.; Ravee, Y.; Jin, L.; Xue, Y.; Xu, J.; Li, G.; Wang, Y.; Zheng, Y. Production of octenyl succinic anhydride-modified waxy corn starch and its characterization. *J. Agric. Food Chem.* **2008**, *56* (23), 11499−11506.

(9) Tian, Y. Q.; Zhan, J. L.; Zhao, J. W.; Xie, Z. J.; Xu, X. M.; Jin, Z. Y. Preparation of products rich in slowly digestible starch (SDS) from rice starch by a dual-retrogradation treatment. *Food Hydrocolloids* **2013**, *31* (1), 1−4.

(10) Son Trinh, K.; Joo Lee, C.; Jun Choi, S.; Wha Moon, T. Hydrothermal treatment of water yam starch in a non-granular state: slowly digestible starch content and structural characteristics. *J. Food Sci.* **2012**, *77* (6), C574−C582.

(11) Chung, H. J.; Liu, Q.; Hoover, R. Impact of annealing and heat-moisture treatment on rapidly digestible, slowly digestible and resistant starch levels in native and gelatinized corn, pea and lentil starches. *Carbohydr. Polym.* **2009**, *75* (3), 436−447.

(12) Sweedman, M. C.; Tizzotti, M. J.; Schaefer, C.; Gilbert, R. G. Structure and physicochemical properties of octenyl succinic

DOI: 10.1021/jf5059705
J. Agric. Food Chem. 2015, 63, 2820−2829

anhydride modified starches: a review. *Carbohydr. Polym.* **2013**, *92* (1), 905−920.
(13) He, J. H.; Liu, J.; Zhang, G. Y. Slowly digestible waxy maize starch prepared by octenyl succinic anhydride esterification and heat-moisture treatment: glycemic response and mechanism. *Biomacromolecules* **2008**, *9* (1), 175−184.
(14) Bai, Y.; Shi, Y.-C. Structure and preparation of octenyl succinic esters of granular starch, microporous starch and soluble maltodextrin. *Carbohydr. Polym.* **2011**, *83* (2), 520−527.
(15) Wu, Y.; Lin, Q.; Chen, Z.; Xiao, H. The interaction between tea polyphenols and rice starch during gelatinization. *Food Sci. Technol. Int.* **2011**, *17* (6), 569−577.
(16) Wang, X.; Li, X.; Chen, L.; Xie, F.; Yu, L.; Li, B. Preparation and characterisation of octenyl succinate starch as a delivery carrier for bioactive food components. *Food Chem.* **2011**, *126* (3), 1218−1225.
(17) da Silva, F. C.; da Fonseca, C. R.; de Alencar, S. M.; Thomazini, M.; Balieiro, J. C. D.; Pittia, P.; Fauaro-Trindade, C. S. Assessment of production efficiency, physicochemical properties and storage stability of spray-dried propolis, a natural food additive, using gum Arabic and OSA starch-based carrier systems. *Food Bioprod. Process.* **2013**, *91* (C1), 28−36.
(18) Wolfram, S. Effects of green tea and EGCG on cardiovascular and metabolic health. *J. Am. Coll. Nutr.* **2007**, *26* (4), 373S−388S.
(19) Kao, Y. H.; Chang, H. H.; Lee, M. J.; Chen, C. L. Tea, obesity, and diabetes. *Mol. Nutr. Food Res.* **2006**, *50* (2), 188−210.
(20) Frei, B.; Higdon, J. V. Antioxidant activity of tea polyphenols in vivo: evidence from animal studies. *J. Nutr.* **2003**, *133* (10), 3275S−3284S.
(21) Hara, Y.; Honda, M. The inhibition of α-amylase by tea polyphenols (biological chemistry). *Agric. Biol. Chem.* **1990**, *54* (8), 1939−1945.
(22) Kobayashi, Y.; Suzuki, M.; Satsu, H.; Arai, S.; Hara, Y.; Suzuki, K.; Miyamoto, Y.; Shimizu, M. Green tea polyphenols inhibit the sodium-dependent glucose transporter of intestinal epithelial cells by a competitive mechanism. *J. Agric. Food Chem.* **2000**, *48* (11), 5618−5623.
(23) Forester, S. C.; Gu, Y.; Lambert, J. D. Inhibition of starch digestion by the green tea polyphenol, (−)-epigallocatechin-3-gallate. *Mol. Nutr. Food Res.* **2012**, *56* (11), 1647−1654.
(24) Liu, J.; Wang, M.; Peng, S.; Zhang, G. Effect of green tea catechins on the postprandial glycemic response to starches differing in amylose content. *J. Agric. Food Chem.* **2011**, *59* (9), 4582−4588.
(25) Hu, M. Commentary: Bioavailability of flavonoids and polyphenols: call to arms. *Mol. Pharmaceutics* **2007**, *4* (6), 803−806.
(26) Green, R. J.; Murphy, A. S.; Schulz, B.; Watkins, B. A.; Ferruzzi, M. G. Common tea formulations modulate in vitro digestive recovery of green tea catechins. *Mol. Nutr. Food Res.* **2007**, *51* (9), 1152−1162.
(27) Scalbert, A.; Morand, C.; Manach, C.; Rémésy, C. Absorption and metabolism of polyphenols in the gut and impact. *Biomed. Pharmacother.* **2002**, *56* (6), 276−282.
(28) Neilson, A. P.; Song, B. J.; Sapper, T. N.; Bomser, J. A.; Ferruzzi, M. G. Tea catechin auto-oxidation dimers are accumulated and retained by Caco-2 human intestinal cells. *Nutr. Res. (N.Y.)* **2010**, *30* (5), 327−340.
(29) Appeldoorn, M. M.; Vincken, J. P.; Gruppen, H.; Hollman, P. C. Procyanidin dimers A1, A2, and B2 are absorbed without conjugation or methylation from the small intestine of rats. *J. Nutr.* **2009**, *139* (8), 1469−1473.
(30) Rashidinejad, A.; Birch, E. J.; Sun-Waterhouse, D.; Everett, D. W. Delivery of green tea catechin and epigallocatechin gallate in liposomes incorporated into low-fat hard cheese. *Food Chem.* **2014**, *156*, 176−183.
(31) Peters, C. M.; Green, R. J.; Janle, E. M.; Ferruzzi, M. G. Formulation with ascorbic acid and sucrose modulates catechin bioavailability from green tea. *Food Res. Int.* **2010**, *43* (1), 95−102.
(32) Wang, H.; Provan, G. J.; Helliwell, K. HPLC determination of catechins in tea leaves and tea extracts using relative response factors. *Food Chem.* **2003**, *81* (2), 307−312.
(33) Chai, Y.; Wang, M.; Zhang, G. Interaction between amylose and tea polyphenols modulates the postprandial glycemic response to high-amylose maize starch. *J. Agric. Food Chem.* **2013**, *61* (36), 8608−8615.
(34) Chen, L. S.; Lee, M. J.; Li, H.; Yang, C. S. Absorption, distribution, and elimination of tea polyphenols in rats. *Drug Metab. Dispos.* **1997**, *25* (9), 1045−1050.
(35) Lambert, J. D.; Lee, M.-J.; Lu, H.; Meng, X.; Hong, J. J. J.; Seril, D. N.; Sturgill, M. G.; Yang, C. S. Epigallocatechin-3-gallate is absorbed but extensively glucuronidated following oral administration to mice. *J. Nutr.* **2003**, *133* (12), 4172−4177.
(36) Zhong, K.; Li, X.-J.; Gou, A.-N.; Hunag, Y.-N.; Bu, Q.; Gao, H. Antioxidant and cytoprotective activities of flavonoid glycosides-rich extract from the leaves of *Zanthoxylum bungeanum*. *J. Food Nutr. Res.* **2014**, *2* (7), 349−356.
(37) Dimitrijević, D. S.; Kostić, D. A.; Stojanović, G. S.; Mitić, S. S.; Mitić, M. N.; Đorđević, A. S. Phenolic composition, antioxidant activity, mineral content and antimicrobial activity of fresh fruit extracts of *Morus alba* L. *J. Food Nutr. Res.* **2014**, *1*, 22−30.
(38) Meng, F.; Zheng, L.; Wang, Y.; Liang, Y.; Zhong, G. Preparation and properties of konjac glucomannan octenyl succinate modified by microwave method. *Food Hydrocolloids* **2014**, *38*, 205−210.
(39) Gao, J.; Xu, P.; Wang, Y.; Wang, Y.; Hochstetter, D. Combined effects of green tea extracts, green tea polyphenols or epigallocatechin gallate with acarbose on inhibition against α-amylase and α-glucosidase in vitro. *Molecules* **2013**, *18* (9), 11614−11623.
(40) Yilmazer-Musa, M.; Griffith, A. M.; Michels, A. J.; Schneider, E.; Frei, B. Grape seed and tea extracts and catechin 3-gallates are potent inhibitors of α-amylase and α-glucosidase activity. *J. Agric. Food Chem.* **2012**, *60* (36), 8924−8929.
(41) Liu, J.; Wang, M.; Peng, S.; Zhang, G. Effect of green tea catechins on the postprandial glycemic response to starches differing in amylose content. *J. Agric. Food Chem.* **2011**, *59* (9), 4582−4588.
(42) Hanhineva, K.; Torronen, R.; Bondia-Pons, I.; Pekkinen, J.; Kolehmainen, M.; Mykkanen, H.; Poutanen, K. Impact of dietary polyphenols on carbohydrate metabolism. *Int. J. Mol. Sci.* **2010**, *11* (4), 1365−1402.
(43) Kusano, R.; Andou, H.; Fujieda, M.; Tanaka, T.; Matsuo, Y.; Kouno, I. Polymer-like polyphenols of black tea and their lipase and amylase inhibitory activities. *Chem. Pharm. Bull.* **2008**, *56* (3), 266−272.
(44) He, Q.; Lv, Y.; Yao, K. Effects of tea polyphenols on the activities of α-amylase, pepsin, trypsin and lipase. *Food Chem.* **2007**, *101* (3), 1178−1182.
(45) Bolen, S.; Feldman, L.; Vassy, J.; Wilson, L.; Yeh, H.-C.; Marinopoulos, S.; Wiley, C.; Selvin, E.; Wilson, R.; Bass, E. B.; Brancati, F. L. Systematic review: Comparative effectiveness and safety of oral medications for type 2 diabetes mellitus. *Ann. Intern. Med.* **2007**, *147* (6), 386−399.
(46) Kamiyama, O.; Sanae, F.; Ikeda, K.; Higashi, Y.; Minami, Y.; Asano, N.; Adachi, I.; Kato, A. In vitro inhibition of α-glucosidases and glycogen phosphorylase by catechin gallates in green tea. *Food Chem.* **2010**, *122* (4), 1061−1066.
(47) Shimada, M.; Mochizuki, K.; Goda, T. Methylation of histone H3 at lysine 4 and expression of the maltase-glucoamylase gene are reduced by dietary resistant starch. *J. Nutr. Biochem.* **2013**, *24* (3), 606−612.
(48) Cheng, M.-W.; Chegeni, M.; Kim, K.-H.; Zhang, G.; Benmoussa, M.; Quezada-Calvillo, R.; Nichols, B. L.; Hamaker, B. R. Different sucrose-isomaltase response of Caco-2 cells to glucose and maltose suggests dietary maltose sensing. *J. Clin. Biochem. Nutr.* **2014**, *54* (1), 55.
(49) Zhang, G.; Hamaker, B. R. Slowly digestible starch: concept, mechanism, and proposed extended glycemic index. *Crit. Rev. Food Sci. Nutr.* **2009**, *49* (10), 852−867.
(50) Wang, P.; Aronson, W. J.; Huang, M.; Zhang, Y.; Lee, R.-P.; Heber, D.; Henning, S. M. Green tea polyphenols and metabolites in prostatectomy tissue: implications for cancer prevention. *Cancer Prevention Res.* **2010**, *3* (8), 985−993.

DOI: 10.1021/jf5059705
J. Agric. Food Chem. 2015, 63, 2820−2829

(51) Lu, H.; Meng, X. F.; Li, C.; Sang, S. M.; Patten, C.; Sheng, S. Q.; Hong, J. G.; Bai, N. S.; Winnik, B.; Ho, C. T.; Yang, C. S. Glucuronides of tea catechins: enzymology of biosynthesis and biological activities. *Drug Metab. Dispos.* **2003**, *31* (4), 452−461.
(52) Wu, Y.; Chen, Z. X.; Li, X. X.; Li, M. Effect of tea polyphenols on the retrogradation of rice starch. *Food Res. Int.* **2009**, *42* (2), 221−225.
(53) Shishikura, Y.; Khokhar, S.; Murray, B. S. Effects of tea polyphenols on emulsification of olive oil in a small intestine model system. *J. Agric. Food Chem.* **2006**, *54* (5), 1906−1913.
(54) Polaczek, E.; Starzyk, F.; Malenki, K.; Tomasik, P. Inclusion complexes of starches with hydrocarbons. *Carbohydr. Polym.* **2000**, *43* (3), 291−297.
(55) Yuan, J.-M.; Sun, C.; Butler, L. M. Tea and cancer prevention: epidemiological studies. *Pharmacol. Res.* **2011**, *64* (2), 123−135.
(56) Kuriyama, S. The relation between green tea consumption and cardiovascular disease as evidenced by epidemiological studies. *J. Nutr.* **2008**, *138* (8), 1548S−1553S.
(57) Greenberg, J.; Axen, K.; Schnoll, R.; Boozer, C. Coffee, tea and diabetes: the role of weight loss and caffeine. *Int. J. Obes.* **2005**, *29* (9), 1121−1129.
(58) Lykkesfeldt, J. Malondialdehyde as biomarker of oxidative damage to lipids caused by smoking. *Clin. Chim. Acta* **2007**, *380* (1), 50−58.
(59) Ceriello, A.; Esposito, K.; Piconi, L.; Ihnat, M. A.; Thorpe, J. E.; Testa, R.; Boemi, M.; Giugliano, D. Oscillating glucose is more deleterious to endothelial function and oxidative stress than mean glucose in normal and type 2 diabetic patients. *Diabetes* **2008**, *57* (5), 1349−1354.

DOI: 10.1021/jf5059705
J. Agric. Food Chem. 2015, 63, 2820−2829

Nuclear magnetic resonance (NMR) spectroscopy holds many advantages, such as high reproducibility, fast analysis, minimal preparation, and available databases, which make it useful as a metabolic profiling technique in metabolomics. Therefore, using urine and fecal samples from the study by Soerensen et al.,[10] the aims of the present study were (i) to investigate possible metabolic mechanisms associated with cheese and milk intake by employing untargeted NMR-based metabolomics and (ii) to identify potential metabolites that may explain how the intake of cheese and milk affects blood cholesterol level as reported by Soerensen et al.[10]

MATERIALS AND METHODS

Subjects and Study Design. A total of 15 healthy young men (ages, 18−50 years; body mass index, 20−28 kg/m^2) participated in a crossover intervention study during which they randomly consumed three isocaloric diets, which were either high in semiskimmed milk (1.5% fat) or high in semihard cow's cheese with equal amounts of dairy calcium (1.7 g/day) or a control diet containing butter but no other dairy products for 14 days. Nutrient compositions of the three diets are listed in Table S1 of the Supporting Information. Exclusion criteria of subjects were as follows: chronic illnesses, supplements or medications, excessive physical activity (>10 h/week), milk allergy, lactose intolerance, participation in other studies, or inability to follow the intervention. The intervention periods were separated by a washout period of at least 14 days. During each intervention, 5 days of feces samples (days 10−14) and 24 h urine samples (day 14) were collected and frozen at −80 °C. The detailed study design has previously been described.[10] The trial was approved by the Municipal Ethical Committee of Copenhagen (H-1-2011-004) and registered in the database (NCT01317251, http://www.clinicaltrial.gov).

NMR Measurements. NMR spectra were recorded on a Bruker Avance 600 spectrometer equipped with a 5 mm TXI probe (Bruker BioSpin, Rheinstetten, Germany) operating at a frequency of 600.13 MHz. The main acquisition parameters included 32K data points, a relaxation delay of 2 s, a spectral width of 7288.63 Hz, and an acquisition time per scan of 2.25 s. For urine, samples were thawed, vortexed, and centrifuged at 10000*g* for 5 min, and 500 μL of supernatant was transferred to a 5 mm NMR tube and mixed with 100 μL of a 0.75 M phosphate buffer solution containing 0.5% sodium trimethlysilyl propionate-d_4 (TSP) in D_2O. A standard Bruker "zgpr" pulse program with water presaturation was used to acquire ^{1}H NMR spectra at 25 °C. For fecal extracts, approximately 40 mg of lyophilized fecal powder was weighed into a 1.5 mL Eppendorf tube, and then 300 μL of ice-cold methanol was first added and then mixture vortexed thoroughly and placed on ice for 10 min. Then, ice-cold chloroform and water were consecutively used for extraction acording to the same procedure with methanol. The mixture last was put in a 4 °C refrigerator overnight for separation. On the next day, the mixture was centrifuged at 1400*g* for 30 min at 4 °C, and the upper methanol−water layer as water-soluble extract (WSE) and the lower chloroform layer as lipid extract (LE) were transferred to fresh 1.5 mL Eppendorf tubes, respectively, and then dried by using vacuum centrifugation for around 3 h. The dried sample was stored at −80 °C until NMR analysis. The dried WSE was redissolved in 550 μL of D_2O, 25 μL of H_2O, and 25 μL of D_2O containing 0.05% TSP, and the dried LE was redissolved in 575 μL of $CHCl_3$-*d* and 25 μL of $CHCl_3$-*d* containing 0.05% tetramethylsilane (TMS). Then, the mixture was vortexed thoroughly and transferred to a 5 mm NMR tube immediately. Both the water-soluble and lipid samples were analyzed by using a standard "zgpr" pulse program at 25 °C.

NMR Data Preprocessing. NMR data were processed in the Topspin 3.0 software (Bruker BioSpin) as described in our previous paper.[12] The ^{1}H spectra of urine and feces were referenced to TSP and TMS signals at 0 ppm, respectively. The "icoshift" procedure was applied to align NMR spectra in MATLAB (R2012a, The Mathworks Inc., Natick, MA, USA).[19] The spectral region from 0.0 to 10.0 ppm without the residual water signals from 4.7 to 5.0 ppm for urine, the region between 0.6 and 9.4 ppm excluding the water signals from 4.7 to 5.0 ppm for fecal WSE sample, and the region between 0.4 and 8.1 ppm excluding the chloroform signals from 7.1 to 7.3 ppm for fecal LE sample were subdivided into 0.01 ppm spectral regions (bins) and integrated. Finally, the binned data were normalized to the total signal amplitude of each NMR spectrum to minimize the dilution effect for urine but not for feces.

Multivariate Data and Statistical Analyses. Principal component analysis (PCA) is an unsupervised model that provides visualization of a multivariate data set and thereby enables identification of clusters of different diet groups in the present study. In addition, orthogonal partial least-squares discriminant analysis (OPLS-DA) as a supervised model was used to compare the difference between any two diet groups. The advantage of OPLS-DA is to separate the classification property in the predictive component P[1] and the within-class variation in the orthogonal component O[1], which can achieve better separations and thereby make data interpretation easier.[20] PCA and OPLS-DA were carried out on Pareto-scaled data by using SIMCA 13.0 software (Umetrics, Umeå, Sweden). Pareto scaling keeps the structure of the original spectra and thereby reduces the impact of low-intensity, noisy signals. For OPLS-DA, a leave-one-out cross-validation (LOOCV) method was performed, where R^2Y and Q^2 were calculated as the explained variance in the Y matrix and the predictive capability of the model, respectively. Values of these two parameters close to 1.0 represent an excellent model. Furthermore, the significance of the models was tested by CV-ANOVA in the SIMCA software.[21] The significance of variables for the separation between two groups in OPLS-DA was assessed by the variable importance in the projection (VIP) method, and those variables with VIP scores above 2.0 are considered important and used for further analysis.

The NMR signals (VIP > 2.0) were carefully inspected for the quality of spectral alignment and assigned on the basis of our previous paper for urine[12] and reported data for feces[22] as well as HMDB,[23] as shown in Table S2 in the Supporting Information. In addition, 2D ^{1}H−^{1}H total correlation (TOCSY) and 2D ^{13}C−^{1}H heteronuclear single-quantum coherence (HSQC) experiments were performed on representative samples of urine and feces. All NMR spectra were processed by the Processor module in Chenomx NMR Suite software (version 7.7, Edmonton, Canada) including phase, baseline, and shim correction and saved as the CNX file format. The identified metabolite peak was integrated and quantified using the Profiler module in the software. Each metabolite peak was checked manually to ensure a good fitting, and the data were then output to an Excel file for univariate analysis.

Prior to univariate analysis, all data were evaluated for normal distribution based on the Anderson−Darling test (P value < 0.05) in SAS software (PROC UNIVARIATE procedure, SAS 9.2, SAS Institute Inc., Cary, NC, USA). When non-normality was observed, data were log-transformed and assessed for normal distribution once again. Analysis of variance (ANOVA) was carried out by using a linear mixed effects model (PROC MIXED procedure, SAS 9.2)[12] to evaluate the effect of diet, period, and their interaction for each quantified metabolite. The mixed model included the fixed effects of diet, period, and their interaction, whereas the intercept of model and individuals was used as random effect. Least-squares mean procedure was performed to calculate means and standard errors. Statistical significance was assessed using Student's t test with Bonferroni correction for multiple comparisons, and a Bonferroni-adjusted P value <0.05 was considered statistically significant. In the present study, we analyzed the metabolite profiles in urine and feces samples from the study of Soerensen et al.,[10] wherein they found that total and LDL cholesterol levels in blood were increased with all three diets during intervention. The cholesterol levels increased significantly less in the cheese and milk groups relative to the control group.[10] Dietary effects on cholesterol levels are likely to correlate with changes in the metabolome, and thus a correlation analysis between changes in cholesterol levels and metabolites that were significantly affected by the dietary intervention may help elucidate the underlying metabolic mechanism regulating cholesterol metabolism. Pearson correlation

DOI: 10.1021/jf505878a
J. Agric. Food Chem. 2015, 63, 2830−2839

coefficients (R) were calculated to explore the relationship between each metabolite and total or LDL cholesterol in SAS 9.2 (PROC CORR procedure, SAS 9.2) and considered statistically significant when a P value was <0.05.

RESULTS

Multivariate Analysis of Data from the Intervention with Cheese and Milk. High-resolution ^{1}H NMR spectra were obtained on the urine and fecal samples (Figure 1) that

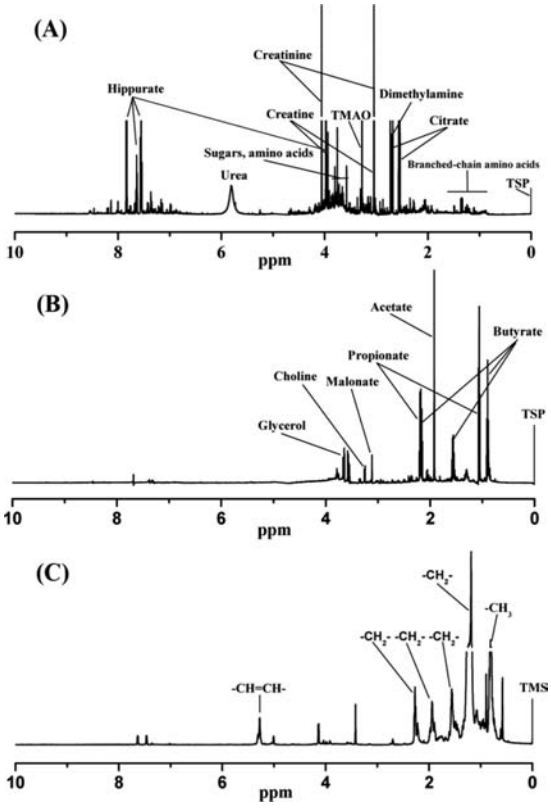

Figure 1. Representative 600 MHz ^{1}H NMR spectra of (A) urine, (B) feces water-soluble extract, and (C) feces lipid extract from a healthy young man.

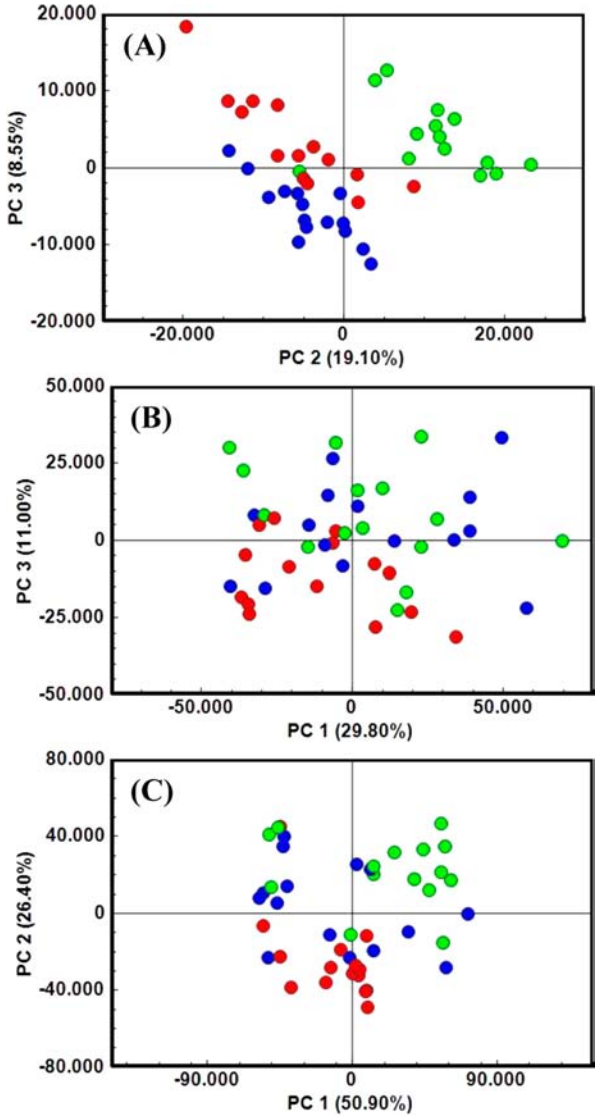

Figure 2. PCA scores plots from NMR-based metabolomics of (A) urine, (B) feces water-soluble extract (WSE), and (C) feces lipid extract (LE) during the human intervention study with cheese (blue), milk (green), and a control diet (red).

enabled the detection and assignment of a number of metabolites including a range of amino acids, organic acids, and fatty acids. Figure 2 illustrates PCA scores plots based on metabolite profiles of urine and feces samples collected after the interventions with cheese, milk, and control. A clear separation among groups can be observed from the urinary (Figure 2A) and fecal LE (Figure 2C) metabolomes. In addition, from the fecal WSE metabolome (Figure 2B), a slight separation between the control group and the dairy groups is evident along PC3.

OPLS-DA models resulted in satisfactory model performances using one predictive component and one orthogonal component (components = 1 + 1; A, milk versus control, R^2Y = 0.95, Q^2 = 0.86, CV-ANOVA = 6.02e−010; B, cheese versus control, R^2Y = 0.91, Q^2 = 0.78, CV-ANOVA = 1.14e−007; C, cheese versus milk, R^2Y = 0.96, Q^2 = 0.90, CV-ANOVA = 1.12e−011), achieving clear separations between any dietary groups based on the urinary metabolome (Figure 3). The corresponding loading in Figure 3A shows that milk intake increased urinary excretion of citrate, creatine, creatinine, and urea, but decreased prolinebetaine, TMAO, and hippurate levels in urine, when compared with the control diet. Figure 3B reveals that the differentiation of cheese intake from the control group could be ascribed to an increase in urinary prolinebetaine and urea excretion and a decrease in the levels of creatine, creatinine, choline, TMAO, and tyrosine. In addition, inspection of the loading plot from Figure 3C revealed that cheese consumption increased prolinebetaine and hippurate levels in urine and reduced urinary citrate, creatine, creatinine, and urea relative to milk intake.

Figure 4 shows that OPLS-DA model parameters based on the fecal WSE metabolome between the milk and control groups (components = 1 + 1, R^2Y = 0.87, Q^2 = 0.79, CV-ANOVA = 2.89e−008) were higher than for the other two models (cheese versus control, components = 1 + 2, R^2Y = 0.72, Q^2 = 0.36, CV-ANOVA = 0.04; cheese versus milk, components = 1 + 1, R^2Y = 0.73, Q^2 = 0.50, CV-ANOVA = 0.001). The corresponding loadings reveal that both cheese and milk groups had an increased level of fecal short-chain fatty acids (SCFAs), acetate, butyrate, and propionate, and a

DOI: 10.1021/jf505878a
J. Agric. Food Chem. 2015, 63, 2830−2839

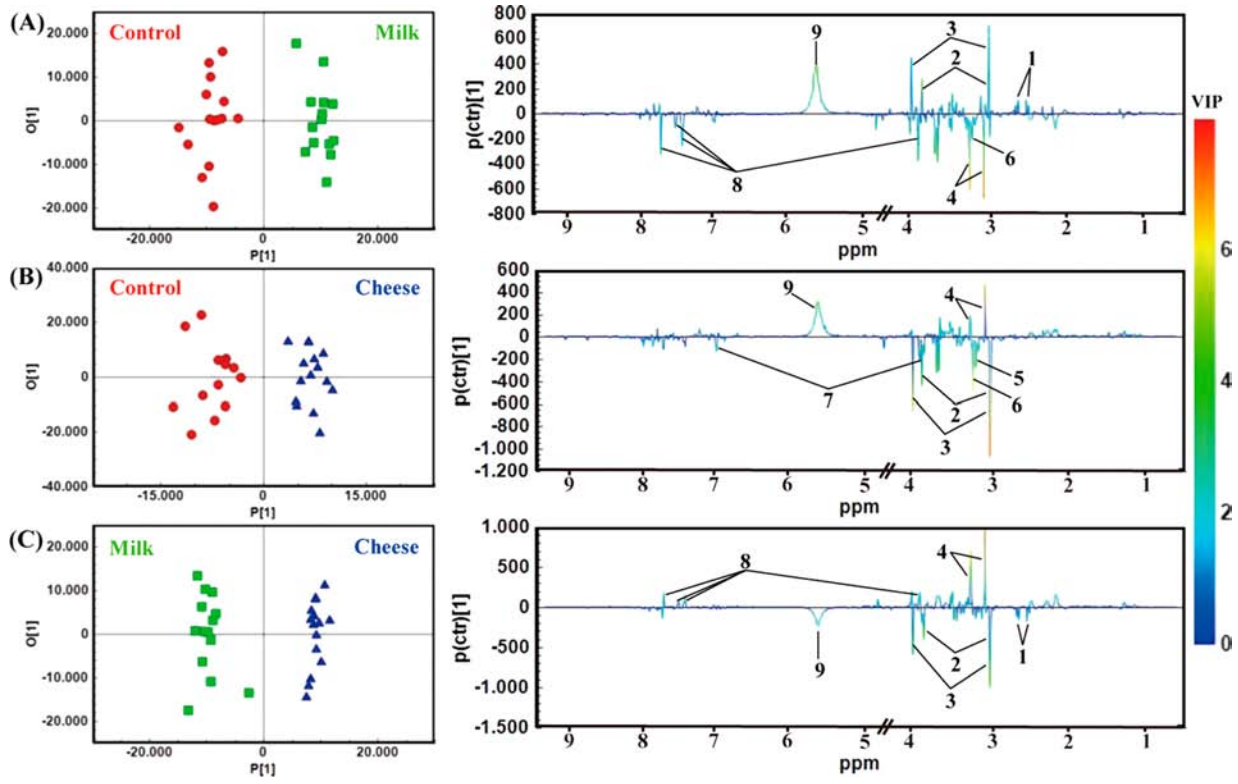

Figure 3. OPLS-DA scores and loadings plots obtained from NMR-based urine metabolomics during the human intervention study with cheese, milk, and a control diet: (A) milk versus control, components = 1 + 1, R^2Y = 0.95, Q^2 = 0.86, CV-ANOVA = 6.02e−010; (B) cheese versus control, components = 1 + 1, R^2Y = 0.91, Q^2 = 0.78, CV-ANOVA = 1.14e−007; (C) cheese versus milk, components = 1 + 1, R^2Y = 0.96, Q^2 = 0.90, CV-ANOVA = 1.12e−011. The loadings are colored according to VIP values. The numbers represent the assignment of metabolites: 1, citrate (2.54 and 2.68 ppm); 2, creatine (3.04 and 3.92 ppm); 3, creatinine (3.05 and 4.06 ppm); 4, prolinebetaine (3.11 and 3.30 ppm); 5, choline (3.23 ppm); 6, trimethylamine *N*-oxide (3.27 ppm); 7, tyrosine (3.94 and 6.68 ppm); 8, hippurate (3.97, 7.55, 7.64, and 7.84 ppm); 9, urea (5.80 ppm).

reduction in the levels of malonate and choline compared with the control group. In addition, milk intake was associated with a higher fecal excretion of glycerol than the control group (Figure 4A). Compared with the milk group, cheese intake increased fecal butyrate, propionate, and malonate concentrations and decreased fecal acetate and glycerol (Figure 4C).

For the lipophilic fecal metabolites, according to OPLS-DA results in Figure 5, a separation of all intervention groups could be obtained; however, the differentiation between the milk and control groups (components = 1 + 1, R^2Y = 0.82, Q^2 = 0.78, CV-ANOVA = 1.34e−007) was stronger as compared with the differentiation between the cheese and control groups (components = 1 + 2, R^2Y = 0.76, Q^2 = 0.45, CV-ANOVA = 0.03) and between the cheese and milk groups (components = 1 + 1, R^2Y = 0.44, Q^2 = 0.31, CV-ANOVA = 0.05). Inspection of the loadings from Figure 5A,B shows that cheese and milk intake in general increased fecal lipid excretion relative to the control diet as all lipid signals was positively associated with the dairy diets compared with control. The OPLS-DA loadings also show that the methylene ($-CH_2-$) peak at 1.22 ppm had the highest contribution to the discrimination between interventions. The OPLS-DA model between milk and cheese indicated also a higher lipid excretion for the milk group than for the cheese group (Figure 5C).

Mixed Linear Model Analysis of Identified Metabolite. Metabolites identified to be important in the discrimination of the dietary interventions from multivariate data analysis were quantified, and Table 1 lists the change of metabolites between different dietary interventions and Bonferroni-adjusted *P* values based on a linear mixed-effects model. Urinary prolinebetaine and tyrosine levels were significantly higher in the cheese group relative to the other two groups, whereas a significant reduction was obtained in urinary creatine and creatinine excretion. Compared with the control group, cheese intake significantly decreased urinary choline level. Fecal butyrate level tended to be increased significantly after cheese consumption relative to intake of the other two diets (Bonferroni-adjusted *P* value = 0.06). In the milk group, urinary citrate and fecal glycerol were significantly increased as compared with the other two groups, whereas a significant reduction was observed in the level of hippurate in urine and malonate in feces (Table 1). Relative to the control group, milk intake increased urinary urea excretion significantly, whereas no significant difference was observed after cheese intake. Fecal acetate and choline levels tended to be significantly increased and decreased in the milk group compared with the control group (Bonferroni-adjusted *P* value = 0.06), respectively. Furthermore, compared with the control group, both cheese and milk consumptions had significantly lower levels of urinary TMAO, but significantly higher fecal lipid excretion.

Correlation Analysis between Identified Metabolite and Cholesterol. Figure 6 shows the correlation coefficients obtained between the 10 significant metabolites in urine or feces and diet-induced increases in total and LDL cholesterol levels. The corresponding biplots based on correlation analyses are illustrated in Figure S1 in the Supporting Information. Weak but significant negative correlations between fecal butyrate, propionate, and lipid levels and the increase in total

DOI: 10.1021/jf505878a
J. Agric. Food Chem. 2015, 63, 2830−2839

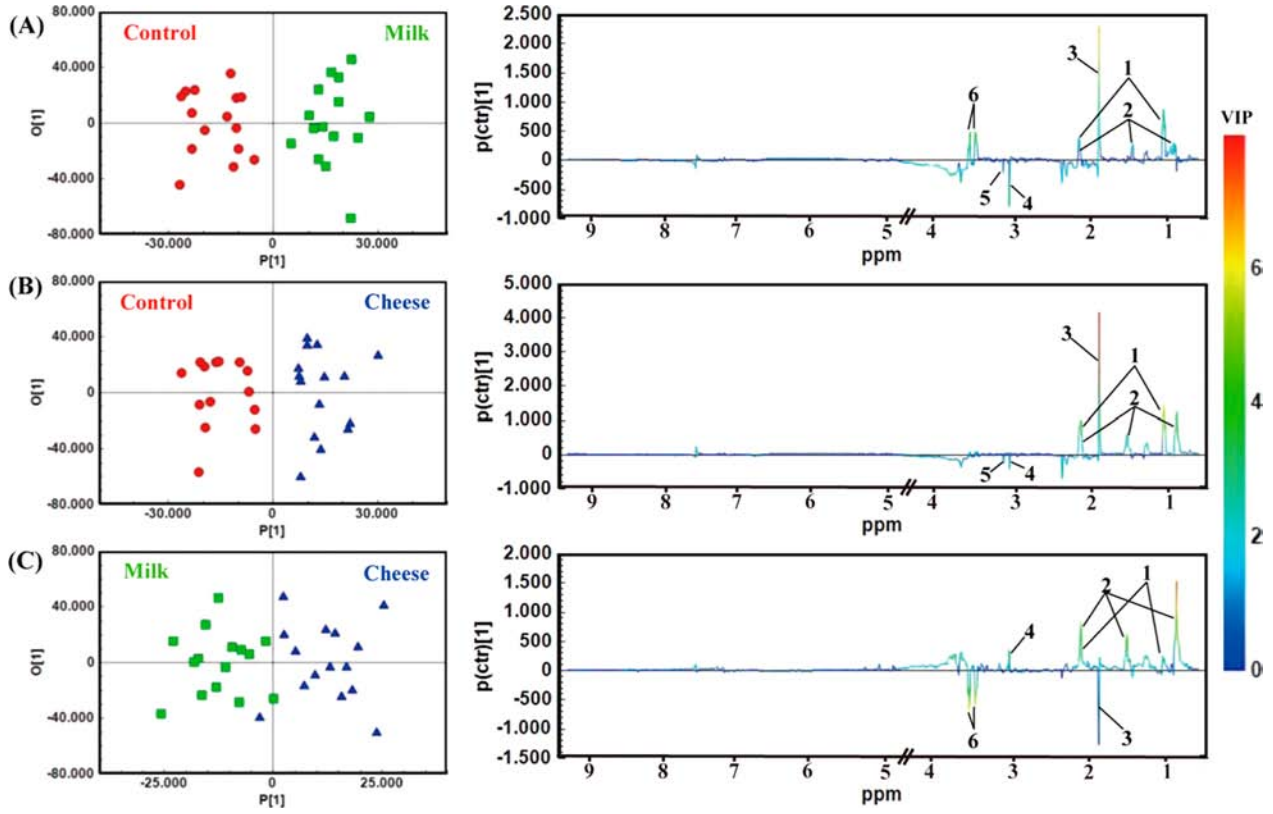

Figure 4. OPLS-DA scores and loadings plots obtained from NMR-based metabolomics of feces water-soluble extract (WSE) during the human intervention study with cheese, milk, and a control diet: (A) milk versus control, components = 1 + 1, $R^2Y = 0.87$, $Q^2 = 0.79$, CV-ANOVA = 2.89e−008; (B) cheese versus control, components = 1 + 2, $R^2Y = 0.72$, $Q^2 = 0.36$, CV-ANOVA = 0.04; (C) cheese versus milk, components = 1 + 1, $R^2Y = 0.73$, $Q^2 = 0.50$, CV-ANOVA = 0.001. The loadings are colored according to VIP values. The numbers represent the assignment of metabolites: 1, propionate (1.05 and 2.16 ppm); 2, butyrate (0.90, 1.56, and 2.20 ppm); 3, acetate (1.92 ppm); 4, malonate (3.11 ppm); 5, choline (3.20 ppm); 6, glycerol (3.56, 3.65, and 3.77 ppm).

cholesterol were identified (Figure 6). A similar result was observed for LDL cholesterol (Figure 6). In addition, urinary citrate concentration was weakly, but significantly, positively correlated with the increase in LDL cholesterol. The results of the correlation analyses could suggest that microbial and lipid metabolism may play a role in the effect of cheese and milk consumption on cholesterol level as shown in Figure 7.

DISCUSSION

In the present study, we found that the urine metabolome could clearly discriminate between intake of cheese and milk, and metabolites responsible for the discrimination could easily be identified by NMR-based metabolomics. Relative to the milk group, a significantly lower urinary excretion of citrate, creatine, and creatinine in the cheese group suggests that cheese consumption affects TCA and urea cycles (Figure 7). In fact, a cheese-induced lowering of urinary citrate is consistent with previous findings showing a lower urinary excretion of TCA intermediates after casein intake (the main protein fraction in cheese) than after whey intake in a murine model.[17] Lillefosse et al.[17] speculated that a lower metabolic acidosis and higher levels of organic acids (citrate, cisaconitic acid, and citramalic acid) and amino acids (alanine, aspartate/aspargine, threonine, and trytophane) after whey intake might be responsible for an enhanced urinary TCA intermediate excretion compared with casein intake. Compared with the control, we found that intake of milk but not cheese significantly increased urinary excretion of urea, which is the major outcome of protein catabolism.[12] Because cheese mainly consists of casein and milk contains approximately 80% casein and 20% whey, this finding might be attributed to the fact that whey and casein have been characterized as "fast" and "slow" proteins, respectively, on the basis of their digestion and absorption rates.[24] Moreover, the urea cycle is an energy-consuming pathway. A cheese-induced change in these metabolites could imply an effect on energy utilization. However, additional metabolites need to be identified for the detailed metabolic pathway analysis of metabolic effects associated with cheese intake.

Furthermore, it is worth noting that urinary prolinebetaine and tyrosine excretions were significantly increased in the cheese group compared with the other two groups. A high prolinebetaine content has been reported in some types of cheese, such as brie (≈185 μg/g) and blue (≈48 μg/g) cheeses.[25] The level of free tyrosine in cheese is significantly increased during cheese ripening.[26] Thus, urinary prolinebetaine and tyrosine may possibly be assigned as exposure markers of cheese consumption. This would have an interesting potential because identification of dietary biomarkers receives a lot of attention in relation to compliance in both intervention and large cohort studies. However, it remains to be further explored if they are sufficiently specific for cheese intake to be useful markers.

In addition, the microbiota-related metabolite hippurate was significantly higher in the cheese group than in the milk group, suggesting that a stimulation of gut bacteria activity after intake of cheese was different from the stimulation achieved with milk

DOI: 10.1021/jf505878a
J. Agric. Food Chem. 2015, 63, 2830−2839

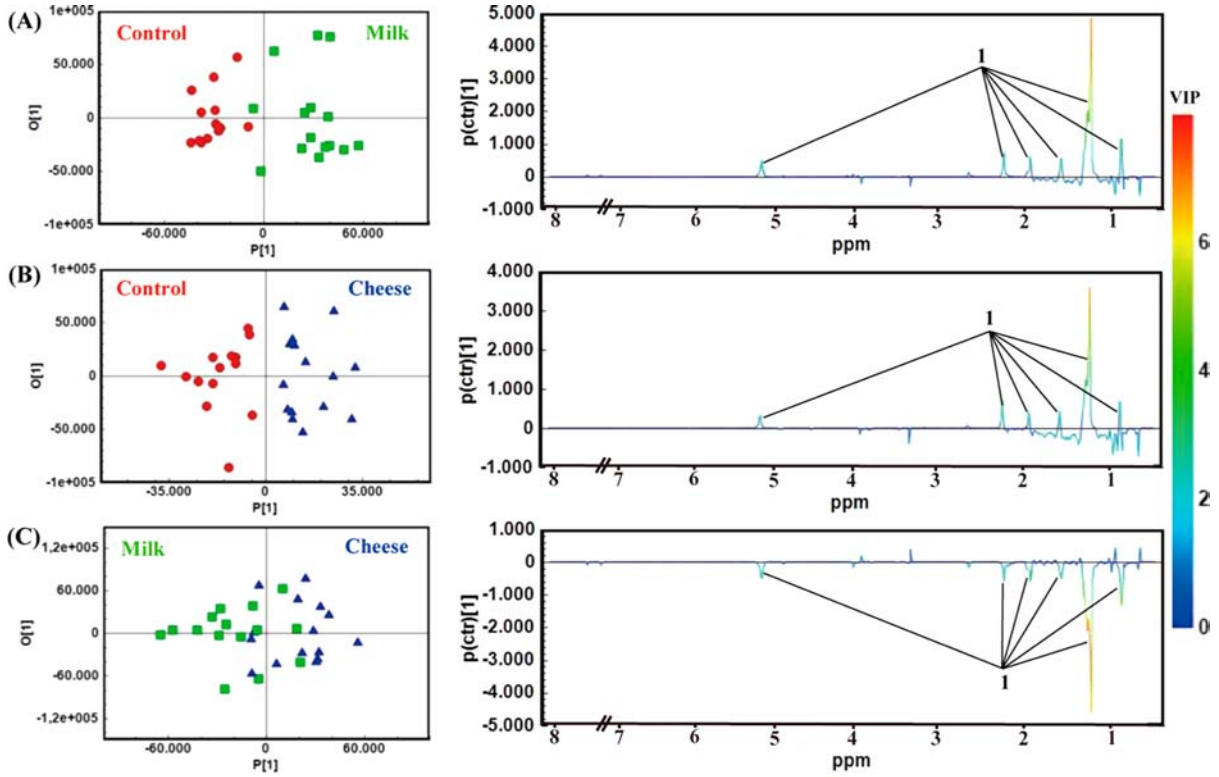

Figure 5. OPLS-DA scores and loadings plots obtained from NMR-based metabolomics of feces lipid extract (LE) during the human intervention with cheese, milk, and a control diet: (A) milk versus control, components = 1 + 1, $R^2Y = 0.82$, $Q^2 = 0.78$, CV-ANOVA = 1.34e−007; (B) cheese versus control, components = 1 + 2, $R^2Y = 0.76$, $Q^2 = 0.45$, CV-ANOVA = 0.03; (C) cheese versus milk, components = 1 + 1, $R^2Y = 0.44$, $Q^2 = 0.31$, CV-ANOVA = 0.05. The loadings are colored according to VIP values. The numbers represent the assignment of metabolites: 1, lipid (0.80, 1.22, 1.55, 1.95, 2.27, and 5.27 ppm).

Table 1. Mixed Linear Model Analysis of Metabolites Identified by Multivariate Analysis

		diet[a]			Bonferroni-adjusted *P* value		
no.	metabolite	cheese	control	milk	cheese vs control	milk vs control	cheese vs milk
				Urine			
1	citrate	0.62 ± 0.05	0.63 ± 0.05	0.73 ± 0.04	–[b]	0.02	0.009
2	creatine	0.41 ± 0.01	0.62 ± 0.01	0.64 ± 0.01	0.02	–	0.009
3	creatinine	3.59 ± 0.13	3.82 ± 0.14	3.90 ± 0.13	0.06	–	0.009
4	prolinebetaine	1.09 ± 0.04	0.90 ± 0.04	0.27 ± 0.04	0.002	<0.0001	<0.0001
5	choline	0.27 ± 0.03	0.38 ± 0.03	0.34 ± 0.03	0.009	–	–
6	TMAO	1.13 ± 0.05	1.36 ± 0.04	1.14 ± 0.05	0.003	0.004	–
7	tyrosine	0.39 ± 0.02	0.26 ± 0.02	0.25 ± 0.02	<0.0001	–	<0.0001
8	hippurate	0.89 ± 0.09	0.88 ± 0.09	0.68 ± 0.09	–	0.002	0.001
9	urea	26.93 ± 0.96	24.46 ± 0.95	29.11 ± 0.96	–	0.002	–
				Feces Water-Soluble Extract			
1	propionate	1.14 ± 0.08	0.87 ± 0.08	1.05 ± 0.07	0.001	0.03	–
2	butyrate	0.94 ± 0.05	0.82 ± 0.05	0.82 ± 0.05	0.06	–	0.06
3	acetate	7.14 ± 0.44	6.33 ± 0.43	7.40 ± 0.44	–	0.06	–
4	malonate	0.18 ± 0.03	0.23 ± 0.03	0.12 ± 0.03	0.02	<0.0001	0.006
5	choline	0.08 ± 0.02	0.14 ± 0.03	0.07 ± 0.03	–	0.06	–
6	glycerol	0.26 ± 0.02	0.23 ± 0.02	0.34 ± 0.02	–	0.0009	0.02
				Feces Lipid Extract			
1	lipid	8.37 ± 0.97	5.14 ± 0.95	9.95 ± 0.97	0.03	0.003	–

[a]Values are presented as the mean ± SE (mM, $n = 15$). [b]Nonsignificant.

intake.[4] Another interesting finding is that urinary TMAO excretion was significantly reduced after cheese and milk consumption. TMAO is a well-known metabolite produced from the metabolization of choline. Many animal-based foods, such as egg, milk, red meat, poultry, and fish, are principal dietary sources of choline, which thereby increases TMAO production and excretion. In this study, relative to the control group, a decrease in choline was also found in urine samples in the cheese and milk groups, which resulted in a concomitant lowering of the TMAO level (Figure 7). Yet, the formation of

DOI: 10.1021/jf505878a
J. Agric. Food Chem. 2015, 63, 2830−2839

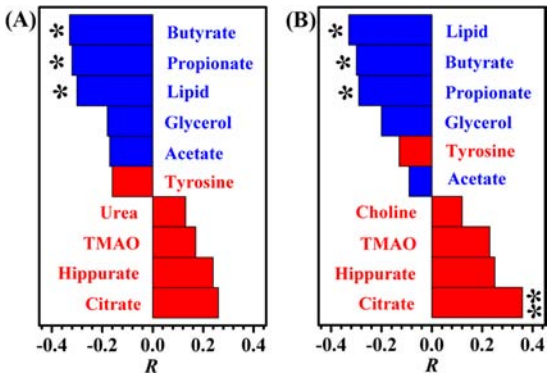

Figure 6. Top 10 metabolites correlated with the diet-induced increases in (A) total and (B) LDL cholesterol based on Pearson correlation coefficients. Red and blue bars represent urinary and fecal metabolites, respectively. (∗) $P < 0.05$; (∗∗) $P < 0.01$.

TMAO is dependent on the metabolism of specific gut microbiota.[27] Thus, our results may suggest that cheese and milk can beneficially modify the gut microbiota to decrease TMAO production; however, this hypothesis needs to be further tested in future studies. Wang et al.[28] identified TMAO as a possible marker of CVD in serum samples from human CVD patients. Consequently, a lowering of TMAO may also be involved in the mechanisms contributing to a beneficial effect of dairy products in relation to the risk of CVD and CHD.

On the fecal metabolome, diet-induced differences were also evident. SCFAs including acetate, butyrate, and propionate were identified as potential contributors to the diet-induced differences. SCFAs are reported to be present in milk[29] and, particularly, in cheese,[30] and therefore the fecal SCFAs could be a direct effect of differences in the intake of SCFAs. However, it is also likely that the change of fecal SCFAs was ascribed to a diet-induced effect on the gut microbiota. Many studies have reported the impact of diet on the gut microbiota.[31,32] In fact, the present results indicate that dairy consumption, especially cheese, can beneficially modify the gut microbiota to increase SCFA levels. This finding is consistent with the result of St-Onge et al.,[4] in which they reported that fermented dairy products cause an increase in the content of gut microbiota that ferment indigestible carbohydrates to produce SCFAs. The C_3 dicarboxylic acid, malonate, is also produced by the gut bacteria at lower concentration. Thus, cheese intake significantly increased fecal malonate level relative to milk intake but significantly reduced it as compared with intake of the control

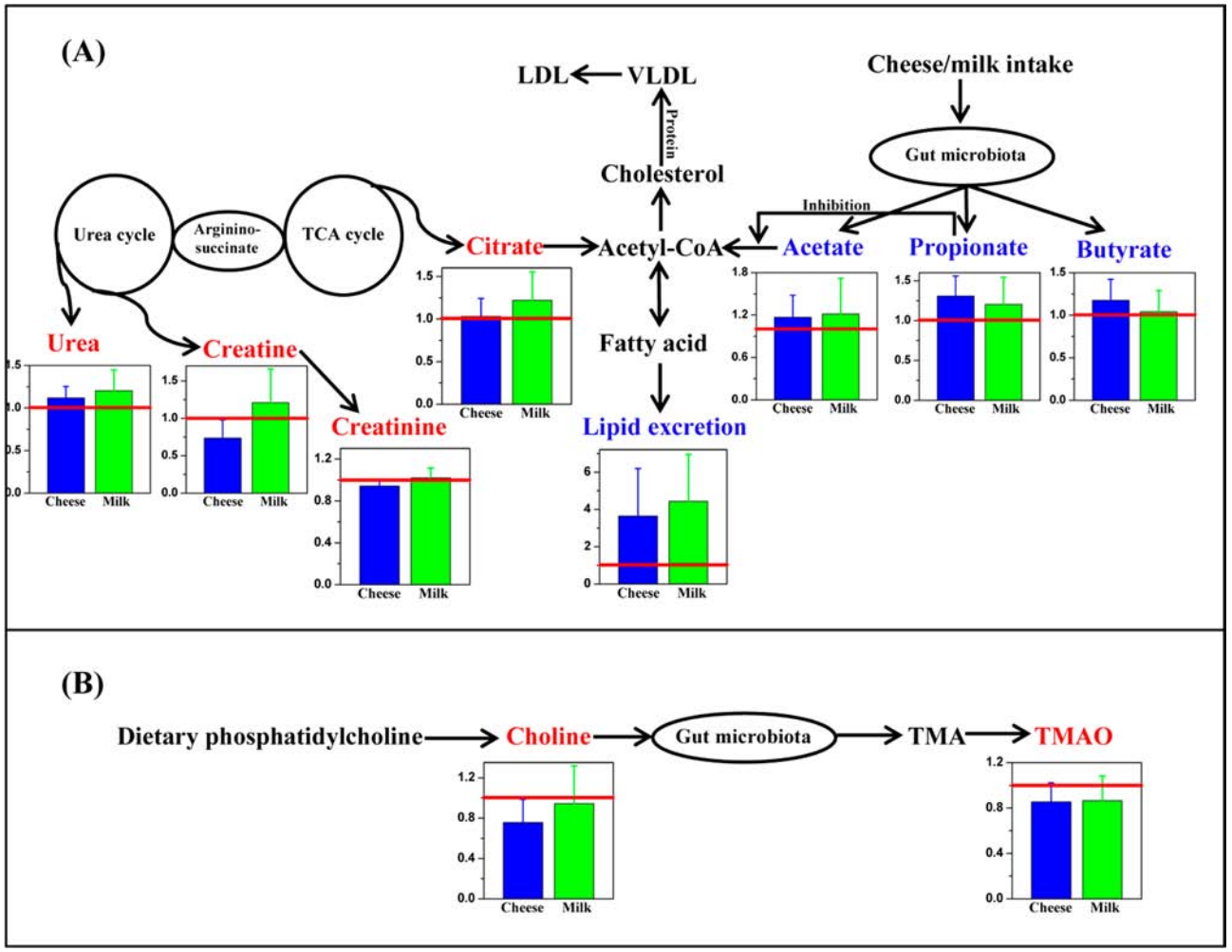

Figure 7. Schematic metabolic pathways explaining the effects of cheese and milk on microbial and lipid metabolism: (A) lipid metabolism and SCFAs; (B) TMAO production. Bar charts show the fold change of metabolite levels in the cheese and milk groups relative to the control group, respectively (mean ± SE), and the red line represents a fold change cutoff of 1.0. Red and blue text represents urinary and fecal metabolites, respectively.

DOI: 10.1021/jf505878a
J. Agric. Food Chem. 2015, 63, 2830−2839

diet, suggesting a distinct stimulation of gut bacteria activity after the intake of cheese.[4]

Metabolomics analysis of the lipophilic extracts showed a higher lipid excretion for the dairy diets compared with control, which is probably attributed to a higher content of calcium in dairy products.[33,34] A meta-analysis also revealed that increasing dairy calcium intake by 1241 (800−1600) mg/day resulted in an increase in fecal fat excretion of approximately 5.2 (1.6−8.8) g/day.[35] The lipid excretion was higher for milk than for cheese. A higher fecal glycerol excretion in the milk group was also identified from the fecal water extracts, likewise revealing higher lipid excretion after milk intake compared with cheese intake. The results are consistent with the findings of Soerensen et al.[10]

^{1}H NMR spectroscopy enables detection of saturated and unsaturated fat and has even been applied for the determination of specific fatty acids in cheese.[36] In the present study, OPLS-DA models showed a contribution from all lipid signals to the discriminations of the groups, whereas the contribution from the methylene signal was dominating. This could possibly be a result of longer fatty acid chains giving rise to a stronger methylene signal, which would imply an effect of the intervention on both the amount and composition of the lipids excreted in the feces. However, the fact that the contribution from the methylene signal was dominating in the loading should most likely be ascribed to the fact that this signal has the highest signal intensity.

Overall, the present results clearly document that metabolomics as a postgenomic technique has great promise in the exploration of the metabolic effects associated with specific diets.[37] Recently Hjerpsted et al.[38] used an untargeted LC-MS metabolomics approach to investigate differences between cheese and butter intake in a comparable crossover design. Even though the untargeted LC-MS metabolomics approach identified a substantially higher number of metabolites than the NMR-based methodology applied here, a much stronger separation and thus diet-induced effect was demonstrated in the present study. This should most likely be ascribed to the fact that the study by Hjerpsted et al.[38] included subjects in an age range between 22 and 70 years and both genders were represented, whereas all of the subjects in the present study were young men. We have previously demonstrated a strong gender and age effect on the metabolome,[39] which likely will mask a diet effect in an intervention study. In addition, sample collection,[40] storage,[41] preparation,[41] and analysis[42] may also affect metabolomics results.

Soerensen et al.[10] previously reported that all three diets in the current intervention study resulted in an increase in total and LDL cholesterol. However, the increases were lower for the cheese and milk intake compared with the control group. Here we employed correlation analyses to elucidate the associations between perturbations identified in the urinary and fecal metabolome and the concomitant changes observed in total and LDL cholesterol. The correlation analyses revealed that citrate in urine and butyrate, propionate, and total lipid in feces were weakly but significantly correlated to the increases in total and LDL cholesterol. Even though no causal relationship could be proved, these findings imply that microbial and lipid metabolism may be involved in diet-induced effects on cholesterol metabolism (Figure 7). SCFAs have been reported to play a key role in the regulation of lipid metabolism.[43] Acetate is a precursor of cholesterol synthesis, whereas propionate may decrease cholesterol by inhibiting the formation of acetyl-CoA from acetate.[44] We also found that there was a significant negative relationship between fecal butyrate excretion and the diet-induced increase in cholesterol level including total and LDL cholesterol. A possible reason for this is that butyrate, like propionate, can inhibit cholesterol synthesis and in turn reduce intestinal fat absorption and circulating lipoprotein levels as demonstrated in Caco-2 cells.[45] In addition, a significant negative relationship between fecal lipid excretion and the increases in total and LDL cholesterol, which is in accordance with the findings of Soerensen et al.,[10] suggests that the increase in fecal lipid excretion reduced available substrates for cholesterol formation and in turn decreased blood cholesterol level (Figure 7). Citrate is an intermediate in the TCA cycle and is converted to acetyl-CoA for cholesterol synthesis through ATP-citrate lyase.[46] Therefore, a decrease in citrate after cheese intake may also be responsible for reducing the increases in total and LDL cholesterol.

Niemann−Pick C2 (NPC-2) protein as a cholesterol-binding protein plays an important role in regulating intracellular transport and homeostasis of cholesterol.[47] Nielsen et al.[48] reported that NPC-2-deficient mice increased visceral cholesterol level compared with wild-type mice, whereas a lowering effect was found after NPC-2 protein treatment. However, no difference was observed in blood cholesterol.[48] Interestingly, NPC-2 protein, also called EPV20, was obtained at approximately 2.5 mg/L in bovine milk.[49] Thus, it could be of great interest to investigate the effect of NPC-2 protein in dairy products on the regulation of cholesterol metabolism.

In conclusion, using an NMR-based metabolomics approach in a human intervention study, the present study demonstrated strong effects of dairy product intake on the urine and fecal metabolome. Furthermore, it was demonstrated that cheese consumption was associated with a different metabolic response compared with milk consumption. Our results lead us to suggest that cheese consumption is associated with an increased level of SCFAs in the gut, possibly induced by stimulation of beneficial gut microbiota, as well as an increased extent of lipid excretion with resultant beneficial effects on cholesterol metabolism. In addition, a reduced TMAO production may also contribute to potential beneficial effects of cheese intake on the risk of CVD. Overall, this metabolomics study suggests that cheese could be an important piece in the French paradox puzzle. However, further studies are needed to explore the exact metabolic mechanisms linking cheese consumption, stimulation of the gut microflora, and cholesterol metabolism.

■ ASSOCIATED CONTENT

Ⓢ Supporting Information

Figure S1 and Tables S1 and S2. This material is available free of charge via the Internet at http://pubs.acs.org.

■ AUTHOR INFORMATION

Corresponding Author

*(H.C.B.) Phone: (+45) 8715 8353. E-mail: hannec.bertram@food.au.dk.

Funding

The study was supported by The Danish Council for Strategic Research, Arla Foods, and the Danish Dairy Research Foundation in the project "FIAF - Milk in regulating lipid metabolism and overweight. Uncovering milk's ability to

DOI: 10.1021/jf505878a
J. Agric. Food Chem. 2015, 63, 2830−2839

increase expression and activity of fasting-induced adipose factor" (10-093539).

Notes

The authors declare no competing financial interest.

REFERENCES

(1) U.S. Department of Agriculture and U.S. Department of Health and Human Services. *Dietary Guidelines for Americans*, 7th ed.; U.S. Government Printing Office: Washington, DC, USA, 2010.

(2) Artaud-Wild, S. M.; Connor, S. L.; Sexton, G.; Connor, W. E. Differences in coronary mortality can be explained by differences in cholesterol and saturated fat intakes in 40 countries but not in France and Finland. A paradox. *Circulation* **1993**, *88* (6), 2771−2779.

(3) Soedamah-Muthu, S. S.; Ding, E. L.; Al-Delaimy, W. K.; Hu, F. B.; Engberink, M. F.; Willett, W. C.; Geleijnse, J. M. Milk and dairy consumption and incidence of cardiovascular diseases and all-cause mortality: dose-response meta-analysis of prospective cohort studies. *Am. J. Clin. Nutr.* **2011**, *93* (1), 158−171.

(4) St-Onge, M. P.; Farnworth, E. R.; Jones, P. J. Consumption of fermented and nonfermented dairy products: effects on cholesterol concentrations and metabolism. *Am. J. Clin. Nutr.* **2000**, *71* (3), 674−681.

(5) Nestel, P. J.; Chronopulos, A.; Cehun, M. Dairy fat in cheese raises LDL cholesterol less than that in butter in mildly hypercholesterolaemic subjects. *Eur. J. Clin. Nutr.* **2005**, *59* (9), 1059−1063.

(6) Hjerpsted, J.; Leedo, E.; Tholstrup, T. Cheese intake in large amounts lowers LDL-cholesterol concentrations compared with butter intake of equal fat content. *Am. J. Clin. Nutr.* **2011**, *94* (6), 1479−1484.

(7) Welland, D. Make room for cheese − if incorporated wisely, it can be part of a healthful diet. *Today's Dietitian* **2011**, *13* (2), 16.

(8) Petyaev, I. M.; Bashmakov, Y. K. Could cheese be the missing piece in the French paradox puzzle? *Med. Hypoth.* **2012**, *79* (6), 746−749.

(9) Astrup, A. A changing view on saturated fatty acids and dairy: from enemy to friend. *Am. J. Clin. Nutr.* **2014**, *100* (6), 1407−1408.

(10) Soerensen, K. V.; Thorning, T. K.; Astrup, A.; Kristensen, M.; Lorenzen, J. K. Effect of dairy calcium from cheese and milk on fecal fat excretion, blood lipids, and appetite in young men. *Am. J. Clin. Nutr.* **2014**, *99* (5), 984−991.

(11) Andersen, M. B. S.; Rinnan, Å.; Manach, C.; Poulsen, S. K.; Pujos-Guillot, E.; Larsen, T. M.; Astrup, A.; Dragsted, L. O. Untargeted metabolomics as a screening tool for estimating compliance to a dietary pattern. *J. Proteome Res.* **2014**, *13* (3), 1405−1418.

(12) Zheng, H.; Yde, C. C.; Dalsgaard, T. K.; Arnberg, K.; Mølgaard, C.; Michaelsen, K. F.; Larnkjær, A.; Bertram, H. C. Nuclear magnetic resonance-based metabolomics reveals that dairy protein fractions affect urinary urea excretion differently in overweight adolescents. *Eur. Food Res. Technol.* **2015**, *240* (3), 489−497.

(13) Hodgson, A. B.; Randell, R. K.; Mahabir-Jagessar-T, K.; Lotito, S.; Mulder, T.; Mela, D. J.; Jeukendrup, A. E.; Jacobs, D. M. Acute effects of green tea extract intake on exogenous and endogenous metabolites in human plasma. *J. Agric. Food Chem.* **2014**, *62* (5), 1198−1208.

(14) Boto-Ordóñez, M.; Urpi-Sarda, M.; Queipo-Ortuño, M. I.; Corella, D.; Tinahones, F. J.; Estruch, R.; Andres-Lacueva, C. Microbial metabolomic fingerprinting in urine after regular dealcoholized red wine consumption in humans. *J. Agric. Food Chem.* **2013**, *61* (38), 9166−9175.

(15) Llorach, R.; Garrido, I.; Monagas, M.; Urpi-Sarda, M.; Tulipani, S.; Bartolome, B.; Andres-Lacueva, C. Metabolomics study of human urinary metabolome modifications after intake of almond (*Prunus dulcis* (Mill.) DA Webb) skin polyphenols. *J. Proteome Res.* **2010**, *9* (11), 5859−5867.

(16) Medina, S.; Domínguez-Perles, R.; Ferreres, F.; Tomás-Barberán, F. A.; Gil-Izquierdo, Á. The effects of the intake of plant foods on the human metabolome. *Trends Anal. Chem.* **2013**, *52*, 88−99.

(17) Lillefosse, H. H.; Clausen, M. R.; Yde, C. C.; Ditlev, D. B.; Zhang, X.; Du, Z. Y.; Bertram, H. C.; Madsen, L.; Kristiansen, K.; Liaset, B. Urinary loss of tricarboxylic acid cycle intermediates as revealed by metabolomics studies: an underlying mechanism to reduce lipid accretion by whey protein ingestion? *J. Proteome Res.* **2014**, *13* (5), 2560−2570.

(18) Yde, C. C.; Clausen, M. R.; Ditlev, D. B.; Lillefosse, H.; Madsen, L.; Kristiansen, K.; Liaset, B.; Bertram, H. C. Multi-block PCA and multi-compartmental study of the metabolic responses to intake of hydrolysed versus intact casein in C57BL/6J mice by NMR-based metabolomics. *Metabolomics* **2014**, *10*, 938−949.

(19) Savorani, F.; Tomasi, G.; Engelsen, S. B. *i*coshift: a versatile tool for the rapid alignment of 1D NMR spectra. *J. Magn. Reson.* **2010**, *202* (2), 190−202.

(20) Bylesjö, M.; Rantalainen, M.; Cloarec, O.; Nicholson, J. K.; Holmes, E.; Trygg, J. OPLS discriminant analysis: combining the strengths of PLS-DA and SIMCA classification. *J. Chemom.* **2006**, *20*, 341−351.

(21) Eriksson, L.; Trygg, J.; Wold, S. CV-ANOVA for significance testing of PLS and OPLS models. *J. Chemom.* **2008**, *22*, 594−600.

(22) Le Gall, G.; Noor, S. O.; Ridgway, K.; Scovell, L.; Jamieson, C.; Johnson, I. T.; Colquhoun, I. J.; Kemsley, E. K.; Narbad, A. Metabolomics of fecal extracts detects altered metabolic activity of gut microbiota in ulcerative colitis and irritable bowel syndrome. *J. Proteome Res.* **2011**, *10* (9), 4208−4218.

(23) Wishart, D. S.; Jewison, T.; Guo, A. C.; Wilson, M.; Knox, C.; Liu, Y.; Djoumbou, Y.; Mandal, R.; Aziat, F.; Dong, E.; Bouatra, S.; Sinelnikov, I.; Arndt, D.; Xia, J.; Liu, P.; Yallou, F.; Bjorndahl, T.; Perez-Pineiro, R.; Eisner, R.; Allen, F.; Neveu, V.; Greiner, R.; Scalbert, A. HMDB 3.0 − the human metabolome database in 2013. *Nucleic Acids Res.* **2012**, *41* (D1), D801−D807.

(24) Frühbeck, G. Protein metabolism: slow and fast dietary proteins. *Nature* **1998**, *391* (6670), 843−845.

(25) Slow, S.; Donaggio, M.; Cressey, P. J.; Lever, M.; George, P. M.; Chambers, S. T. The betaine content of New Zealand foods and estimated intake in the New Zealand diet. *J. Food Compos. Anal.* **2005**, *18* (6), 473−485.

(26) Le Boucher, C.; Courant, F.; Jeanson, S.; Chereau, S.; Maillard, M. B.; Royer, A. L.; Thierry, A.; Dervilly-Pinel, G.; Le Bizec, B.; Lortal, S. First mass spectrometry metabolic fingerprinting of bacterial metabolism in a model cheese. *Food Chem.* **2013**, *141* (2), 1032−1040.

(27) Tang, W. W.; Wang, Z.; Levison, B. S.; Koeth, R. A.; Britt, E. B.; Fu, X.; Wu, Y.; Hazen, S. L. Intestinal microbial metabolism of phosphatidylcholine and cardiovascular risk. *New Engl. J. Med.* **2013**, *368* (17), 1575−1584.

(28) Wang, Z.; Klipfell, E.; Bennett, B. J.; Koeth, R.; Levison, B. S.; DuGar, B.; Feldstein, A. E.; Britt, E. B.; Fu, X.; Chung, Y.-M.; Wu, Y.; Schauer, P.; Smith, J. D.; Allayee, H.; Tang, W. H. W.; DiDonato, J. A.; Lusis, A. J.; Hazen, S. L. Gut flora metabolism of phosphatidylcholine promotes cardiovascular disease. *Nature* **2011**, *472* (7341), 57−63.

(29) Fox, P. F.; McSweeney, P. L. H. *Dairy Chemistry and Biochemistry*; Blackie Academic & Professional: London, UK, 1998.

(30) Belitz, H. D; Grosch, W.; Schieberle, P. Milk and dairy products. In *Food Chemistry*, 4th ed.; Belitz, H. D, Grosch, W., Schieberle, P., Eds.; Springer-Verlag: Berlin, Germany, 2004; pp 505−549.

(31) Scott, K. P.; Gratz, S. W.; Sheridan, P. O.; Flint, H. J.; Duncan, S. H. The influence of diet on the gut microbiota. *Pharmacol. Res.* **2013**, *69* (1), 52−60.

(32) Flint, H. J.; Duncan, S. H.; Scott, K. P.; Louis, P. Links between diet, gut microbiota composition and gut metabolism. *Proc. Nutr. Soc.* **2014**, 1−10.

(33) Bendsen, N. T.; Hother, A. L.; Jensen, S. K.; Lorenzen, J. K.; Astrup, A. Effect of dairy calcium on fecal fat excretion: a randomized crossover trial. *Int. J. Obes.* **2008**, *32* (12), 1816−1824.

(34) Lorenzen, J. K.; Astrup, A. Dairy calcium intake modifies responsiveness of fat metabolism and blood lipids to a high-fat diet. *Br. J. Nutr.* **2011**, *105* (12), 1823−1831.

(35) Christensen, R.; Lorenzen, J. K.; Svith, C. R.; Bartels, E. M.; Melanson, E. L.; Saris, W. H.; Tremblay, A.; Astrup, A. Effect of

DOI: 10.1021/jf505878a
J. Agric. Food Chem. 2015, 63, 2830−2839

calcium from dairy and dietary supplements on faecal fat excretion: a meta-analysis of randomized controlled trials. *Obes. Rev.* **2009**, *10* (4), 475−486.
(36) Prema, D.; Pilfold, J. L.; Krauchi, J.; Church, J. S.; Donkor, K. K.; Cinel, B. Rapid determination of total conjugated linoleic acid content in select Canadian cheeses by ^{1}H NMR spectroscopy. *J. Agric. Food Chem.* **2013**, *61* (41), 9915−9921.
(37) Llorach, R.; Garcia-Aloy, M.; Tulipani, S.; Vazquez-Fresno, R.; Andres-Lacueva, C. Nutrimetabolomic strategies to develop new biomarkers of intake and health effects. *J. Agric. Food Chem.* **2012**, *60* (36), 8797−8808.
(38) Hjerpsted, J. B.; Ritz, C.; Schou, S. S.; Tholstrup, T.; Dragsted, L. O. Effect of cheese and butter intake on metabolites in urine using an untargeted metabolomics approach. *Metabolomics* **2014**, *10* (6), 1176−1185.
(39) Zheng, H.; Yde, C. C.; Arnberg, K.; Mølgaard, C.; Michaelsen, K. F.; Larnkjær, A.; Bertram, H. C. NMR-based metabolomic profiling of overweight adolescents: an elucidation of the effects of inter-/intraindividual differences, gender, and pubertal development. *BioMed. Res. Int.* **2014**, *2014*, No. article ID 537157.
(40) Rasmussen, L. G.; Savorani, F.; Larsen, T. M.; Dragsted, L. O.; Astrup, A.; Engelsen, S. B. Standardization of factors that influence human urine metabolomics. *Metabolomics* **2011**, *7* (1), 71−83.
(41) Lauridsen, M.; Hansen, S. H.; Jaroszewski, J. W.; Cornett, C. Human urine as test material in ^{1}H NMR-based metabonomics: recommendations for sample preparation and storage. *Anal. Chem.* **2007**, *79* (3), 1181−1186.
(42) Teahan, O.; Gamble, S.; Holmes, E.; Waxman, J.; Nicholson, J. K.; Bevan, C.; Keun, H. C. Impact of analytical bias in metabonomic studies of human blood serum and plasma. *Anal. Chem.* **2006**, *78* (13), 4307−4318.
(43) Tremaroli, V.; Bäckhed, F. Functional interactions between the gut microbiota and host metabolism. *Nature* **2012**, *489* (7415), 242−249.
(44) Wolever, T. M.; Fernandes, J.; Rao, A. V. Serum acetate: propionate ratio is related to serum cholesterol in men but not women. *J. Nutr.* **1996**, *126* (11), 2790−2797.
(45) Marcil, V.; Delvin, E.; Garofalo, C.; Levy, E. Butyrate impairs lipid transport by inhibiting microsomal triglyceride transfer protein in Caco-2 cells. *J. Nutr.* **2003**, *133* (7), 2180−2183.
(46) Chypre, M.; Zaidi, N.; Smans, K. ATP-citrate lyase: a mini-review. *Biochem. Biophys. Res. Commun.* **2012**, *422* (1), 1−4.
(47) Vanier, M. T.; Millat, G. Structure and function of the NPC2 protein. *Biochim. Biophys. Acta (BBA)−Mol. Cell Biol. Lipids* **2004**, *1685* (1), 14−21.
(48) Nielsen, G. K.; Dagnaes-Hansen, F.; Holm, I. E.; Meaney, S.; Symula, D.; Andersen, N. T.; Heegaard, C. W. Protein replacement therapy partially corrects the cholesterol-storage phenotype in a mouse model of Niemann-Pick type C2 disease. *PLoS One* **2011**, *6* (11), No. e27287.
(49) Larsen, L. B.; Ravn, P.; Boisen, A.; Berglund, L.; Petersen, T. E. Primary structure of EPV20, a secretory glycoprotein containing a previously uncharacterized type of domain. *Eur. J. Biochem.* **1997**, *243*, 437−441.

DOI: 10.1021/jf505878a
J. Agric. Food Chem. 2015, 63, 2830−2839

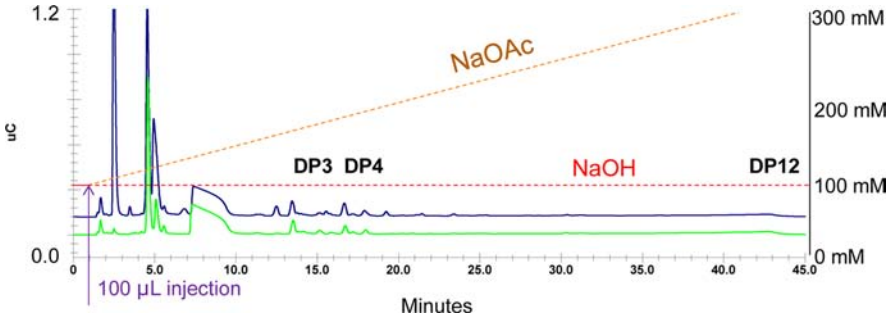

Figure 1. Gradient separation on a Thermo Scientific (previously Dionex) CarboPac PA1 column of oligosaccharides in fresh (green line) and deteriorated (blue line) sugar cane juice (samples were standardized to the same Brix value). DP, degree of polymerization. See the text for full IC-IPAD method conditions.

strong alkaline mobile phase also catalyzes the mutarotation of reducing sugars such as glucose and fructose very efficiently, and at room temperature the α- and β-anomers elute together in one sharp peak.[3] This is an added advantage of IC-IPAD over both gas and liquid cation-exchange chromatography with RI detection, with which double peaks of the reducing sugars are often obtained.[3]

The high-resolving power of IC-IPAD and its ability to determine oligosaccharides of higher degrees of polymerization has allowed the "fingerprinting" of numerous products manufactured from sugar crops. This includes sugar cane and sugar beet used in the global manufacture of sugar, as well as sweet sorghum, which is increasingly being used as a sugar feedstock for the manufacture of biofuels and bioproducts. The fingerprinting capability of a NaOH/NaOAc gradient IC method utilizing a Thermo Scientific (previously Dionex) CarboPac PA1 strong anion-exchange column, combined with the sensitivity of the IPAD has allowed its application to numerous industrial problems associated with these sugar crops, which are discussed herein.

MATERIALS AND METHODS

Chemicals and Reagents. HPLC grade sodium hydroxide and sodium acetate were obtained from Thermo Scientific Dionex (Sunnyvale, CA, USA). Deionized water (with resistivity of 18 MΩ) was used to prepare eluents and samples. Standard sugars, oligosaccharides, and mannitol were of analytical grade. 1-Kestose, 1,1-nystose, and 1,1,1-fructofuranosylnystose were from Meiji Seika Kaisha, Ltd. (Tokyo, Japan). Theanderose (6-*O*-α-D-glucosylsucrose) was from Wako Chemicals (Richmond, VA, USA) and kindly purified by Dr. Greg Cote of USDA-ARS-NCAUR. Dextran was T2000 (2,000,000 Da) from Amersham Biosciences AB (Uppsala, Sweden). Dextranase was obtained from BioCat, Inc. (Troy, VA, USA), and pullanase (Promozyme D2 manufactured by Novozymes (Franklinton, NC, USA)) was obtained from Brenntag Southwest (Houston, TX, USA). Distiller's yeast in dried form (*Saccharomyces cerevisiae*; Crosby & Baker Ltd., Westport, MA, USA) was donated by Delta BioRenewables LLC (Memphis, TN, USA). Absolute ethanol was from Aaper (USA).

IC-IPAD Oligosaccharide Chromatograms. Carbohydrates (mainly oligosaccharides up to 12 dp), including sugar alcohols and ethanol, were separated on a Dionex (now Thermo Scientific, Sunnyvale, CA, USA) BioLC or Dx500 instrument, using a strong NaOH/NaOAc gradient over 40 min.[14] The compounds were separated on Thermo Scientific CarboPac PA1 analytical anion-exchange (250 × 4 mm) and guard columns (50 × 4 mm) at 30 °C or, unless otherwise stated, using a Dionex LC25 Chromatography Oven. The CarboPac PA1 column was designed for the rapid analysis of mono- and oligosaccharides, in particular, linear homopolymers.[13] The CarboPac PA1 column contains 10 μm substrate of polystyrene (2% cross-linked with divinylbenzene) agglomerated with MicroBead quaternary ammonium fuctionalized latex (5% cross-linked). Flow rate = 1.0 mL/min. Injection volume = 25 μL. Eluent conditions were as follows: carbonate-free 100 mM NaOH (isocratic (0.0−1.1 min; inject 1.0 min), a gradient of 0−300 mM NaOAc in 100 mM NaOH (1.1−40.0 min), and return to 100 mM NaOH (40.1−45.0 min) to re-equilibrate the column to the starting conditions prior to injection). The re-equilibration is needed for good retention time reproducibility. The eluents were prepared by diluting a 50% w/w NaOH solution with 18 MΩ deionized water and then degassing them with ultrahigh-purity helium for 20 min. Once the eluents were prepared, they were kept blanketed under helium (20 kPa) at all times. The samples were diluted 1 g/25 mL in deionized water, unless otherwise stated, and filtered through a 0.45 μm PVDF filter to remove particulates. IPAD detection was with either a Dionex PED-2 or Dionex ED50 detector; both detectors were equipped with Au working and Ag/AgCl reference electrodes. The PED-2 detector operated with the following working electrode pulse potentials and durations: E_1 = +0.05 V (t_0 = 0.00 s), E_2 = 0.05 V (t_1 = 0.42 s), E_3 = +0.75 V (t_3 = 0.43 s), E_4 = +0.75 V (t_4 = 0.60 s), E_5 = −0.60 V (t_5 = 0.61 s), and E_6 = −0.60 V (t_6 = 0.96 s). The ED50 detector operated as follows: E_1 = +0.10 V (t_0 = 0.00 s), E_2 = 0.10 V (t_1 = 0.20 s), E_3 = +0.10 V (t_3 = 0.40 s), E_4 = +2.00 V (t_4 = 0.41 s), E_5 = −2.00 V (t_5 = 0.42 s), E_6 = +0.60 V (t_6 = 0.43 s), E_7 = −0.10 V (t_7 = 0.44 s), and E_8 = −0.10 V (t_8 = 0.50 s). A refrigerated Spectra-Physics SP8880 or Dionex AS refrigerated autoinjector/autosampler was used to prevent degradation of sugars in samples while waiting for injection onto the column. Dionex Peaknet or Chromeleon chromatography software was used to accumulate multiple samples and check standards.[15] Oligosaccharides, mannitol, and ethanol were identified by comparing retention times with standards and by spiking with standards.

A representative chromatogram with the gradient method conditions overlaid is shown in Figure 1. To maintain baseline stability, the sodium hydroxide was kept constant during the sodium acetate gradient, because acetate has no buffering capacity at high pH.[11]

Brix (Percent Refractometric Dry Substance). Brix value was measured using an Index Instruments (Kissimmee, FL, USA) TCR 15-30 temperature-controlled refractometer accurate to ±0.01 Brix, and results were expressed as an average of triplicates.

RESULTS AND DISCUSSION

Deterioration of Juices from Sugar Crops. IC oligosaccharide fingerprint profiles have been used to investigate the deterioration of juices extracted from sugar cane (*Saccharum officinarum*) and sweet sorghum (*Sorghum bicolor*) during storage, as well as from freeze-deteriorated sugar cane.[16−18] The typical progression of deterioration in sugar cane juice during storage at ∼25 °C is illustrated in Figure 2. By overloading the column with high concentrations of glucose, fructose, and sucrose present in the juice, the presence of oligosaccharides and other related deterioration compounds

DOI: 10.1021/jf506370s
J. Agric. Food Chem. 2015, 63, 2841−2851

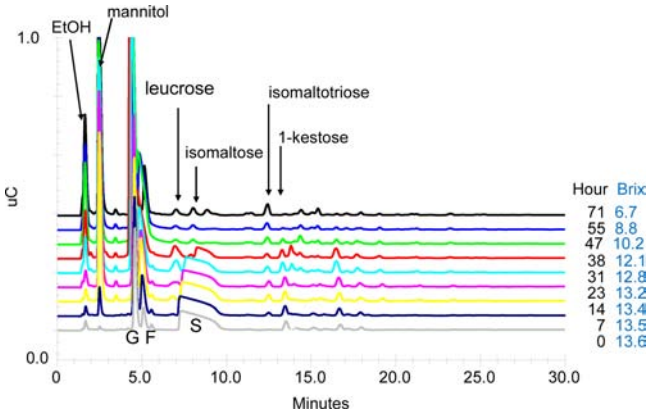

Figure 2. Changes in IC-IPAD profiles and Brix value on the deterioration of sugar cane juice during storage time. S, sucrose; G, glucose; F, fructose. The chromatograms were obtained on a Dionex BioLC system with a PED-2 detector at room temperature (~25 °C). See Materials and Methods for full details. Reprinted with permission from ref 16. Copyright 2002 Elsevier.

was detectable (Figure 2). This highlights another marked advantage of this IC-IPAD method in that the anion-exchange CarboPac PA1 column can tolerate high concentrations of samples (up to 20 °Brix[15]), yet still detect low levels of oligosaccharides and other compounds of interest. The very large sucrose peak is not quantitated at this high concentration but is completely separated from these other low-level oligosaccharides, permitting their quantitation. Moreover, extensive column washings between runs are not required.[15]

Oligosaccharides form on the deterioration of sugar crops, with the main oligosaccharides produced being glycosyl acceptor (secondary) products produced from the action of dextransucrase by *Leuconostoc mesenteroides* bacteria.[16,19] Examples of *Leuconostoc* oligosaccharides are leucrose, isomaltose, and isomaltotriose (Figure 2). Other oligosaccharides formed on sugar cane deterioration include kestoses (GF_2 trisaccharides), which can form from invertase activity. However, kestoses are also primary oligosaccharides that occur naturally in the sugar cane plant, particularly in the leaves and top part of the stalk.[14] Early in our sugar crop deterioration research, we discovered that mannitol was a major degradation marker of sugar cane deterioration[16] and later found it in sweet sorghum deterioration.[20] Mannitol is also formed by *Leuconostoc* lactic acid bacteria via a metabolic pathway separate from that for dextran biosynthesis. Fructose is reduced to mannitol by the enzyme mannitol dehydrogenase in that pathway.[21] As illustrated in Figure 2, mannitol is a very sensitive indicator of sugar cane deterioration and is even more sensitive than dextran as a deterioration marker.[22] Steinmetz et al.[23] had also reported that mannitol was even a better marker of sugar beet deterioration than dextran. Mannitol (a sugar alcohol) is a reduced carbohydrate that is a weaker acid than its nonreduced counterpart mannose and, therefore, it is poorly retained on the CarboPac PA1 column, which explains its early elution (Figure 2). Ethanol is also formed during the

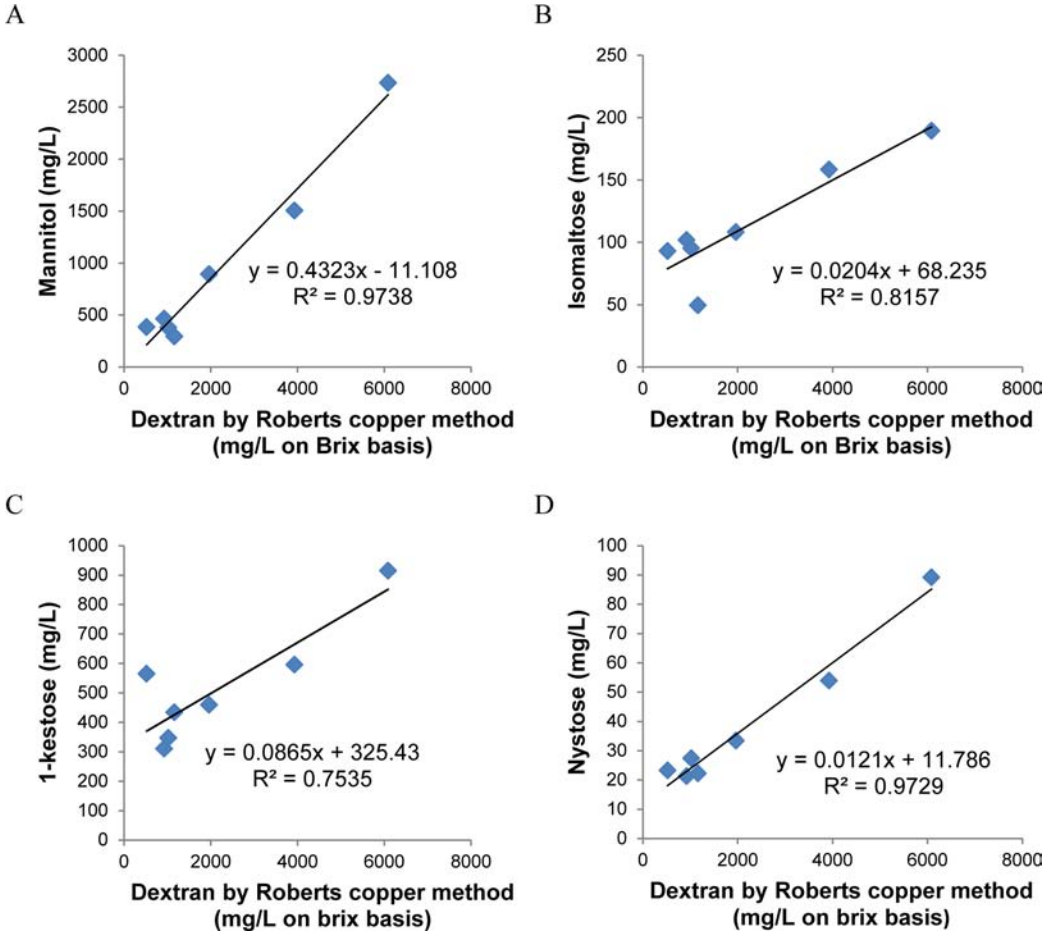

Figure 3. Dextran concentration correlations with (A) mannitol, (B) isomaltose, (C) 1-kestose, and (D) nystose determined in sugar cane juice.

DOI: 10.1021/jf506370s
J. Agric. Food Chem. 2015, 63, 2841−2851

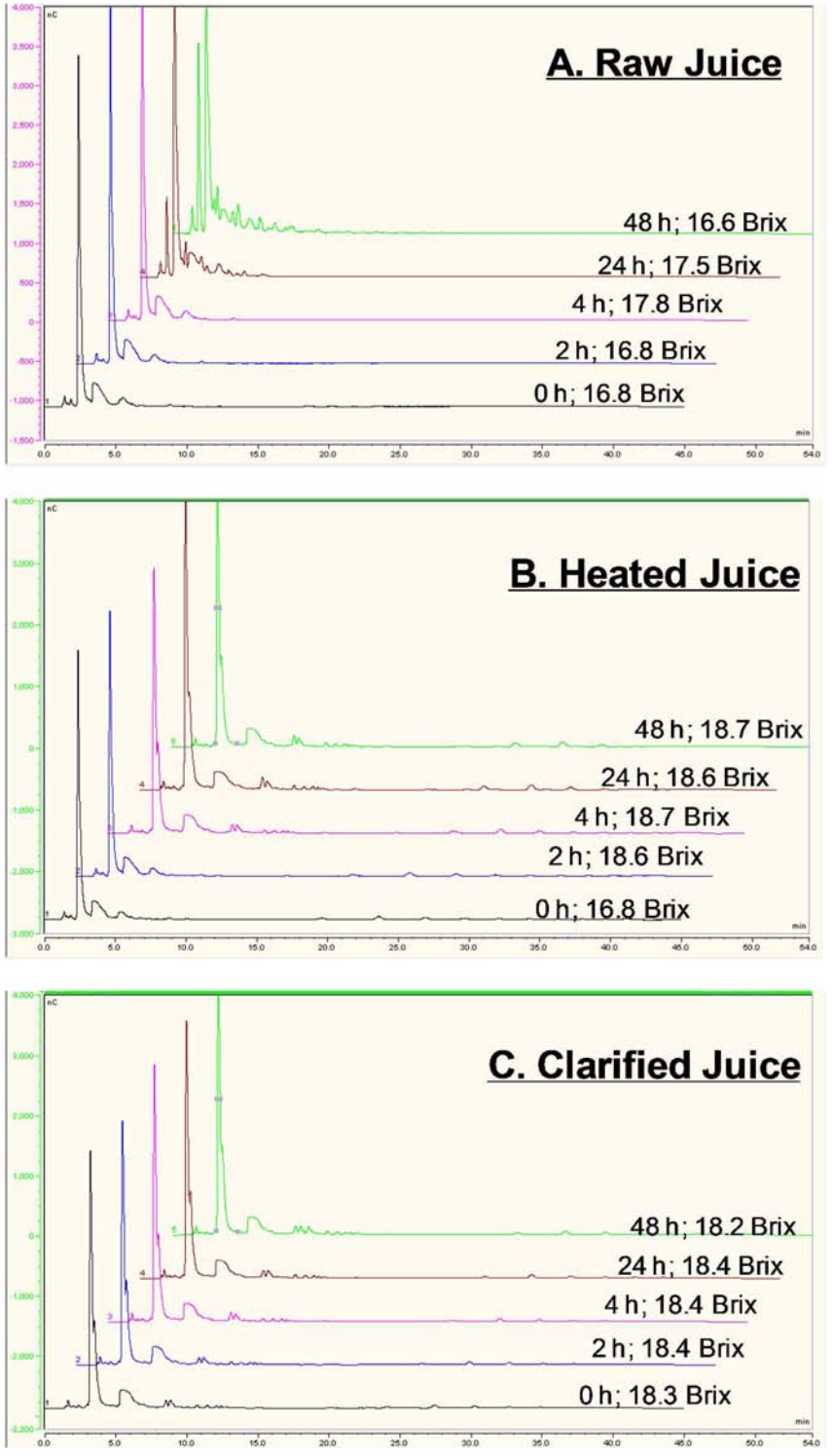

Figure 4. IC-IPAD fingerprint oligosaccharide chromatograms of stored juice extracted from KN Morris sweet sorghum cultivar (November 2013): (A) raw juice; (B) heated juice; (C) clarified juice. Times of storage and Brix values of the juices are denoted on the overlaid chromatograms. Reprinted with permission from ref 20. Copyright 2014 Elsevier.

Leuconostoc deterioration of sugar cane but is only a minor metabolite of *Leuconostoc* compared to dextran and mannitol.[16] Similarly to mannitol, ethanol elutes very early due to its weak interaction with the stationary phase in the column. Detection of ethanol by PAD using a gold working electrode is also less sensitive than for mannitol.[16]

In sugar cane juice collected from a Brazilian factory, there was a strong correlation between the mannitol concentration and the dextran concentration when the latter was measured accurately by the Roberts copper method[24] (Figure 3A). Other microorganism and plant metabolites, including isomaltose, 1-kestose, and nystose, were also shown to strongly correlate with the dextran concentration (Figure 3B–D). However, as concluded in previous research,[16,22] mannitol was shown to be the most sensitive deterioration indicator (Figure 3A).

DOI: 10.1021/jf506370s
J. Agric. Food Chem. 2015, 63, 2841−2851

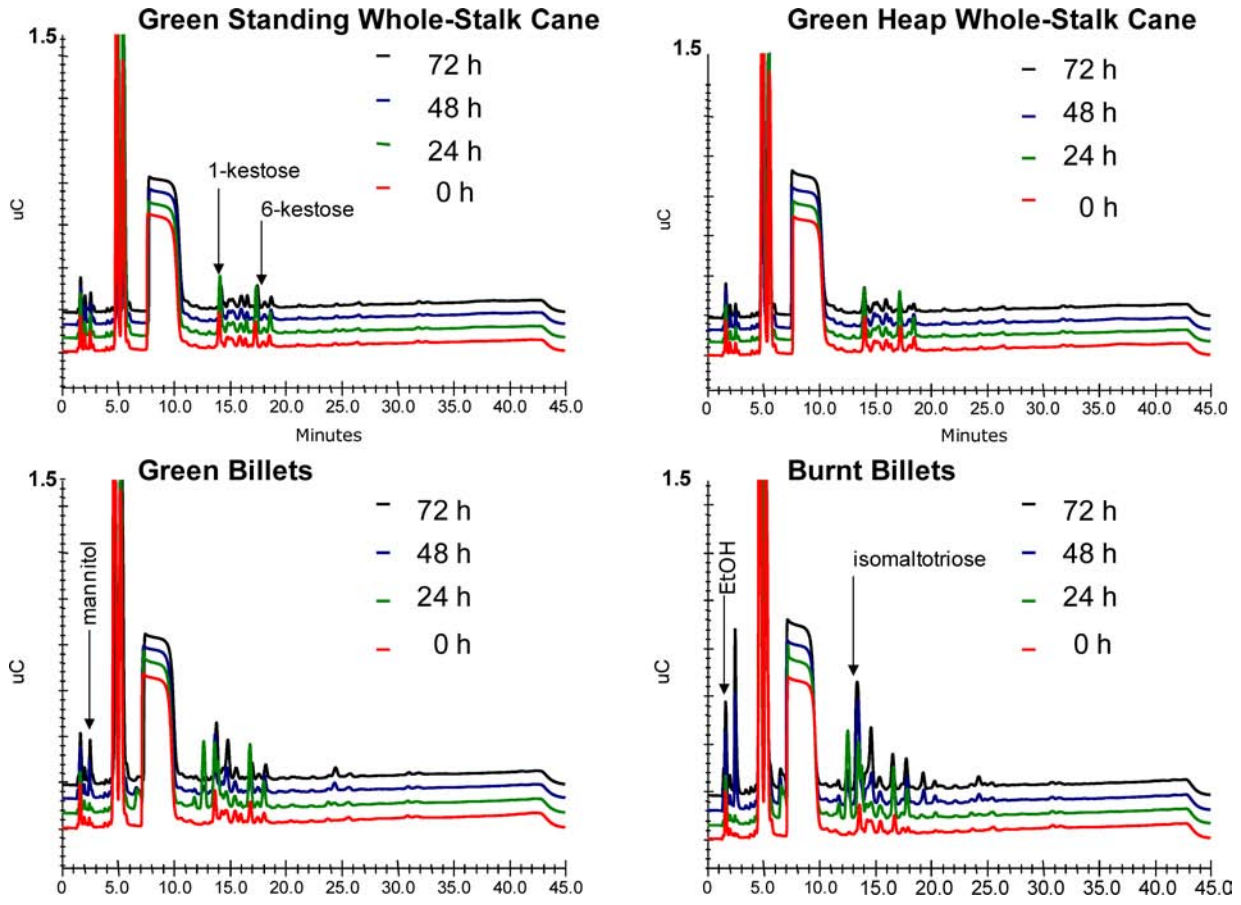

Figure 5. Example IC-IPAD oligosaccharide fingerprint profiles to illustrate the effect of sugar cane harvest method and cut-to-crush delays on deterioration (Brix value was standardized in the samples). The chromatograms were obtained on a Dionex BioLC system with a PED-2 detector at ~25 °C. Adapted from ref 14.

More recently, the IC-IPAD has been used to successfully confirm bacterial count results in a study to stabilize and preserve sweet sorghum juices.[20] Sweet sorghum is similar to sugar cane in that it has a juicy stalk that is rich in sugars. The effects of heat pasteurization (80 °C; 30 min) and clarification (80 °C; limed to pH 6.5; addition of 5 ppm of polyanionic flocculant; settling for 30 min) to juice from sweet sorghum cultivar KN Morris, which was then stored for up to 48 h at 25 °C, are illustrated in Figure 4 oligosaccharide fingerprint profiles. Treated juices were compared to the susceptible raw juice (not treated) (Figure 4). No formation of deterioration products was detected in KN Morris clarified juices stored from 0 to 48 h, although a slight amount of oligosaccharides after the sucrose peak was detected in the 24 and 48 h heated juice samples (Figure 4). This agreed with the lactic acid microbial data, with no detectable growth in the amount of total and lactic acid bacteria in the clarified juice across the 48 h storage period.[20] In comparison, deterioration products were found in the 24 h stored raw juice, which was worse after 48 h of storage (Figure 4). This was no surprise, as before storage the raw juice contained 2.8×10^8 total bacteria/mL, which increased ~5-fold during the 48 h storage period.[20] In contrast, total bacteria in the 0 h heated and clarified juices were approximately 4-log less than in the 0 h raw juice, and no lactic acid bacteria were detected in the clarified juice at 0 h.[20] Lactic acid formation was slightly worse in KN Morris heated than in clarified juice, but this was still considerably lower than in the raw juice.[20] Thus, the IC fingerprint profiles confirmed the bacterial growth results as well as the fact that the clarification process destroyed or removed all lactic acid bacteria, although other bacteria remained at $\sim 10^3$ cfu/mL levels.

Overall, it was shown that the IC-IPAD fingerprint profiles are extremely sensitive, being able to detect as low as 10^2 cfu/mL lactic acid bacterial growth.[20] Additionally, the effect of heat pasteurization was very similar to the whole clarification process, which confirmed that heat was the major contributor to juice stabilization.

Optimization of Sugar Cane Harvesting Methods and Cut-to-Crush Times. The IC-IPAD profile method has also been used to determine the formation of oligosaccharides and other deterioration products caused by various sugar cane harvest and storage treatments, and example chromatograms are illustrated in Figure 5. The changing oligosaccharide profiles allowed for a much more sensitive elucidation of the different deterioration reactions contributing to overall sugar cane deterioration than typical deterioration analyses, those being pH and titratable acidity.[14] Using the IC-IPAD method it was possible to show that at 0 h there were no marked differences in oligosaccharide profiles for harvest treatments, which reflected the freshness of all of the samples and indicated that, initially, when the field cane is cut, freshness is more important than harvest method.[25] This result had considerable consequences for the factory in that as long as billeted cane is transported to the factory quickly on the day it is harvested, deterioration problems should be no worse than encountered in fresh-cut whole stalks (soldier harvested). There were, however, marked

DOI: 10.1021/jf506370s
J. Agric. Food Chem. 2015, 63, 2841−2851

differences in the formation of oligosaccharides and other deterioration products on cut-to-crush/delay time (Figure 5). For the whole-stalk treatments shown in Figure 5, no significant formation of either *Leuconostoc* oligosaccharides and mannitol or kestose oligosaccharides occurred during storage. 1-Kestose (1^F-*O*-*β*-fructofuranosylsucrose) was the most abundant isomer, followed by 6-kestose (6^F-*O*-*β*-fructofuranosylsucrose) and neo-kestose (1^G-*O*-*β*-fructofuranosylsucrose), and separate peaks for 1- and 6-kestose isomers are shown in Figure 5. In strong contrast, deterioration products formed within 24 h during the storage of both green and burnt billeted cane, with greater deterioration occurring in burnt than green billets (Figure 5).

Figure 6 illustrates a correlation between the sum of oligosaccharide concentrations related to sugar cane deterioration (isomaltose, palatinose, isomaltotriose, 1-kestose, nystose, and 1^F-fructofuranosylnystose) and cut-to-crush time in a Brazilian sugar factory that had problems with delivered sugar cane from two different fields. The results were compared with relatively fresh sugar cane delivered to the factory with a cut-to-crush time of <24 h. As the problem sugar cane loads were extremely deteriorated, it was possible to observe (Figure 6) that the longer the cut-to-crush time, the higher the oligosaccharide concentrations. As expected, the mannitol concentration was also higher as the cut-to-crush time increased (results not shown).

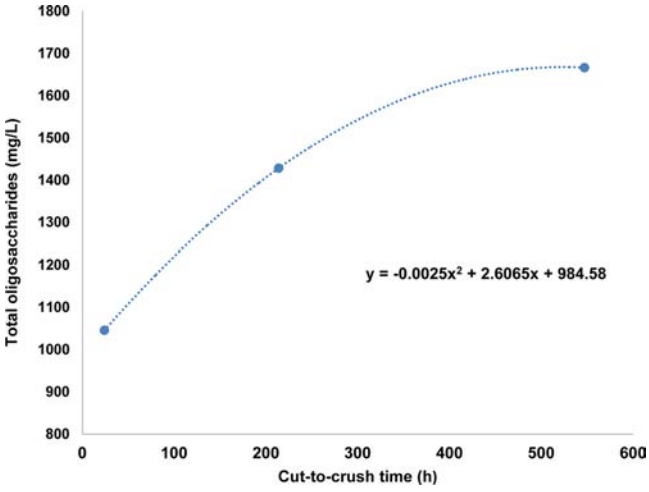

Figure 6. Correlation between sum of oligosaccharides concentration (isomaltose + palatinose + isomaltotriose + 1-kestose + nystose + 1^F-fructofuranosylnystose) with sugar cane cut-to-crush time.

Differentiation between White Refined Sugar from Sugar Cane and Sugar Beets. Approximately 11 years ago, there were reports of illegal trading in Serbia and Montenegro, whereby the origin of white refined sugar could not be certified[26,27] Other countries have also most likely suffered from illegal intermixing of (less expensive to produce) cane white sugar (CWS) with beet white sugar (BWS). For the purpose of international sugar trade, we were requested by industry to develop a new analytical screening method that (1) was capable of distinguishing between CWS and BWS and (2) could measure the percentage of CWS in a CWS/BWS mixture. Moreover, if methods are readily available to differentiate CWS/BWS mixtures, then illegal traders may reconsider their practices. In addition, from an economic standpoint, detection of adulteration is essential to avoid unfair competition that can create a destabilized market and disrupt the regional economy. The detection of adulteration of refined sugars is also of interest to sugar and food manufacturers, consumers, and regulators because of issues of legal compliance. Manufacturers need to ensure that correctly labeled refined sugar is available to the consumer and/or buyer. Consumers also have an interest in ensuring the food they purchase is authentic.

Although raffinose (*O*-*α*-D-Gal*p*-(1→6)-*O*-*α*-D-Glu*p*-(1→2)-*β*-D-Fru*f*) and theanderose (*O*-*α*-D-Glc*p*-(1→6)-*O*-*α*-D-Glu*p*-(1→2)-*β*-D-Fru*f*) had both been advocated as differential markers, raffinose is present in both BWS and CWS (although to a much lesser extent in CWS) and pure theanderose was not commercially available; also, small IC peaks had been found in BWS samples with the same retention time as theanderose. Although some highly sophisticated methods exist to differentiate the source of white sugar, such as isotope ratio mass spectrometry (IRMS) and deuterium NMR, these were considered only to be reference techniques[28] because the equipment is expensive and not readily available. A general analytical screening method was needed to detect a wide range of compounds in the same run. Suspect samples could then be detected and evaluated by more sophisticated techniques as just described.

Because IC-IPAD had (i) become a preferred technique for the routine monitoring of sugars in sugar industry products, (ii) been used to detect simple types of adulteration such as the addition of sucrose to honey,[29] and (iii) a very high sensitivity that offered the great advantage of detecting very low levels of adulterant compounds, we investigated its use to differentiate between beet (BWS) and cane white (CWS) refined sugar.[30] By overloading the CarboPac PA1 column with ∼7.0 Brix blind BWS/CWS samples and running the IC-IPAD NaOH/NaOAc 45 min gradient method, low raffinose combined with numerous characteristic cane marker peaks was successfully used to detect 20% CWS adulteration, which is illustrated in Figure 7. In general, IC profiles of CWS samples had more peaks of 2−12 dp than BWS samples. Increasing the Brix levels to 10.0 allowed detection of 10% CWS adulteration.[30]

Chromatography libraries of CWS, BWS, and BWS/CWS samples for direct comparisons would aid adulterant detection, as would pattern recognition chemometric techniques.[31] The use of an internal standard would greatly help in the standardization of chromatographic patterns and be necessary for chemometric analysis. The use of column ovens and refrigerated autosamplers also aids in the stabilization of retention times. Overall, at the least, the use of IC profiles can be used as a screening method before the further verification and quantitation with more sophisticated techniques.

Verification of the Activities of Carbohydrate Enzymes. Dextran (*α*-1→6-*α*-D-glucan) is a detrimental glucose polysaccharide that is found in deteriorated sugar cane, sugar beet, and sweet sorghum products. In the sugar industry, dextranase (EC 3.2.1.11; *α*-D-1,6-glucan-6-glucanohydrolase) is applied to hydrolyze high molecular weight (HMW) dextran into more manageable lower MW poly- and oligosaccharides. The goal is to improve viscosity and throughput rates in sugar cane and sugar beet factories (in sugar cane factories crystal elongation is also reduced). Most dextranases currently available are manufactured from *Chaetomium gracile* or *erraticum* fungi[32] and are generally recognized as safe (GRAS). One of the greatest sources of confusion for factory or refinery personnel is that it is not possible to compare the activities of commercial dextranases because suppliers/vendors

DOI: 10.1021/jf506370s
J. Agric. Food Chem. 2015, 63, 2841−2851

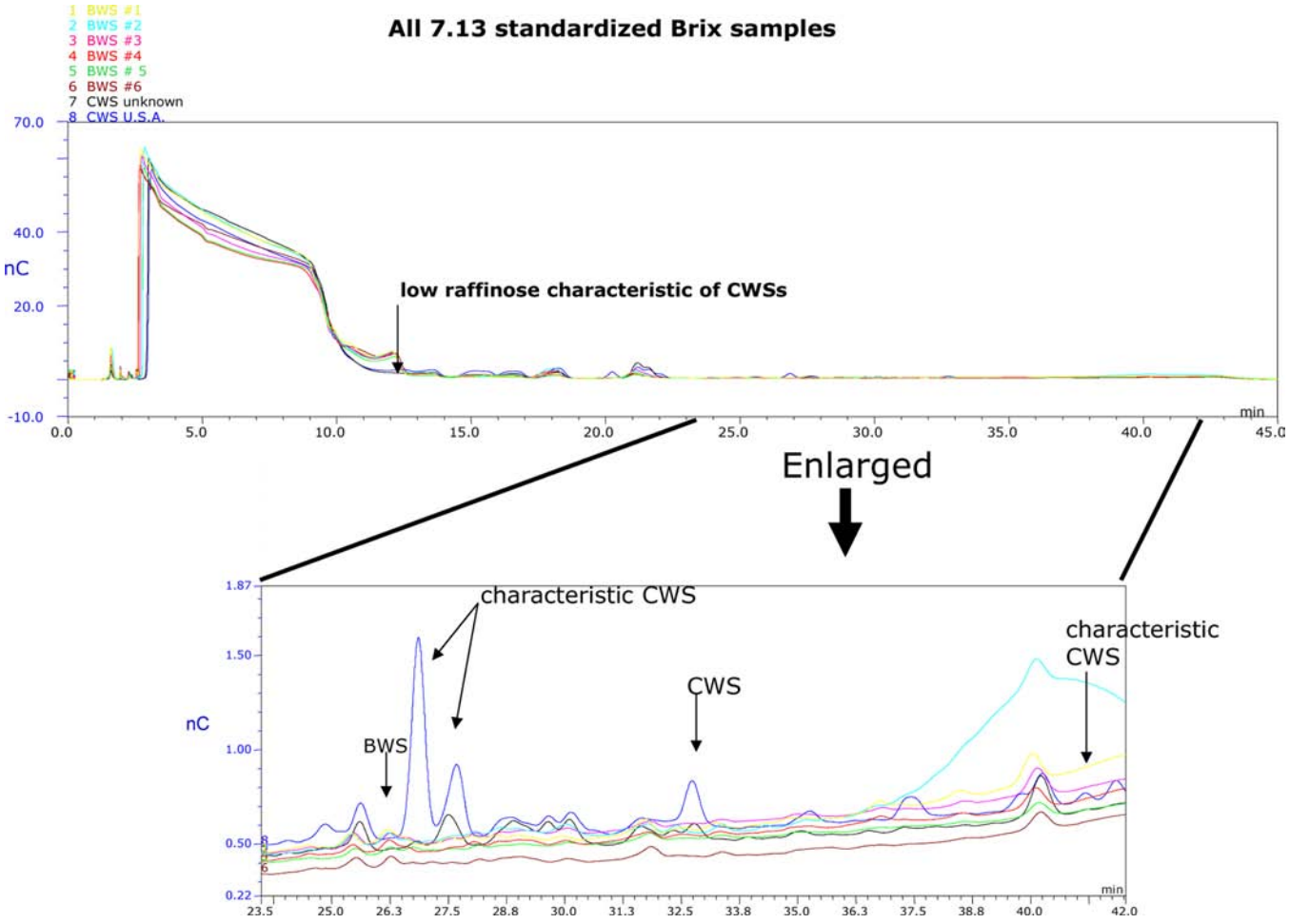

Figure 7. Comparison of six beet white sugars (BWS) of European origin to two cane white sugars (CWS) using IC-IPAD profiles. All samples were adjusted to 7.13 Brix. The chromatograms were obtained on a Dionex BioLC system with a PED-2 detector at ~25 °C. Reprinted with permission from ref 30. Copyright 2005 Verlag Dr. Albert Bartens.

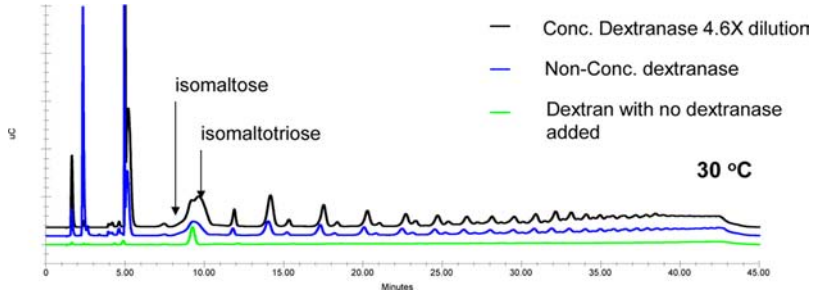

Figure 8. IC-IPAD oligosaccharides profiles used to accurately verify the relative activities of different commercial dextranases used in the sugar industry to hydrolyze dextran. The nonconcentrated dextranase had an activity of ~5500 DU/mL. The initial activity of the concentrated dextranase was 52000 DU/mL but was diluted 4.6-fold to make the dextranases equal in price based on DU/mL/$US. Reprinted with permission from ref 32. Copyright 2005 Elsevier.

use different methods, and activities are quoted in different units. This problem is exacerbated by the dextranase market being very dynamic with activities and prices changing regularly.[32] For these reasons, an easy, inexpensive method based on ferricyanide reduction of free sugars and simple thiosulfate titration of a starch−iodine complex was developed by Eggleston and Monge[32] to measure dextranase activities at the industrial site. Even more importantly, it allowed the calculation of activities per unit cost. The developed industrial method was confirmed as accurate by using IC-IPAD profiles of dextran/dextranase mixtures, which are illustrated in Figure 8. Dextranase hydrolyzed HMW dextran into a series of isomaltogoligosaccharides, with isomaltose, isomaltotriose, and glucose being the major breakdown products. The IC-IPAD method was even able to detect isomaltooligosaccharide isomers (Figure 8). The greater the activity of the dextranase, the greater the number and heights of the oligosaccharide peaks that occurred on the fingerprint chromatograms (Figure 8). The concentrated dextranase (52000 DU/mL) had approximately 8−10-fold differences in activity relative to non-

DOI: 10.1021/jf506370s
J. Agric. Food Chem. 2015, 63, 2841−2851

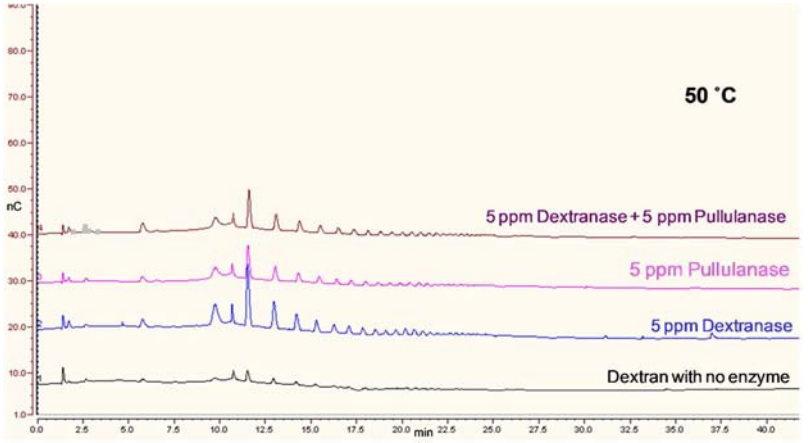

Figure 9. IC-IPAD oligosaccharide profiles used to demonstrate that pullulanase hydrolyzes HMW dextran (2000 ppm) very similarly to dextranase, after 3 min at 50 °C. The concentrated dextranase was 52000 DU/mL.[33] The pullulanase (Promozyme D2) was 1350 NPUN/g activity.[34] The enzymes (5 ppm), individually or combined, were added to the dextran solution (200 mL) in an Erhlenmeyer flask placed in a 50 °C water bath with slight shaking. Samples were removed after 3 min and then boiled immediately for 2.5 min to denature the enzyme(s). The resulting sample was diluted 1 g/25 mL deionized water, filtered through a 0.45 μm filter, and injected onto the CarboPac PA1 column. ED50 detector settings and Chromeleon software were utilized (see Materials and Methods).

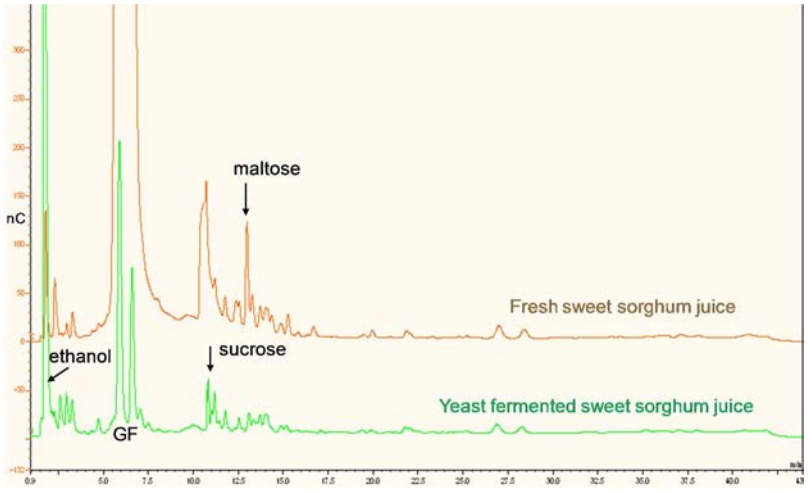

Figure 10. IC-IPAD oligosaccharide profiles used to demonstrate the use of distiller's yeast (*S. cerevisiae*) to metabolize glucose, fructose, sucrose, and maltose in juice from sweet sorghum cultivar Top 76-6 (1:10 w/w) for the production of bioethanol. Fermentations were undertaken at 35 °C with no shaking for 14 h.

concentrated dextranases, but only ~4.6-fold difference in price per pound. IC-IPAD profiles were successfully used to show that, even when the concentrated dextranase was diluted to the economical equivalent to the nonconcentrated dextranase, it still produced a greater number and height of breakdown peak products (Figure 8). As for the sugar cane harvest method research (see previous section), when trying to persuade industrial customers to adopt or change a technology, the visual chromatograms containing numerous peaks often proved more effective as evidence than numerical data results alone.

We also used the IC profiles to show that pullulanase (EC 3.2.1.41; pullulan-6-glucan hydrolase) debranching enzyme can also break down HMW dextran (Figure 9). Although pullulanase is available as an industrial enzyme (it is often used as a processing aid in the production of ethanol and sweeteners from starch in grains, because it specifically hydrolyzes glucose molecules linked by $\alpha 1 \rightarrow 6$ bonds), it may be more expensive than dextranase. Sometimes, however, dextranase has not always been easily or readily available, because the market for this enzyme is very small.[33] When there is an emergency with regard to dextran at a sugar factory, for example, after a sugar cane or sugar beet freeze, and dextranase is not readily available, then more readily available pullulanase may be useful. The optimum pH and temperature conditions for the pullanase, pH 4.5−5.4 and 60 °C,[34] roughly coincide with the recommended best practice for dextranase in juices (pH 5.4 and 50 °C[33]). Pullanase may also be useful to break down sarkaran polysaccharide (pullulan), which has been reported in dry areas of the world where sugar cane is vulnerable to fungal deterioration.[35] Brunt[3] reported the use of a NaOH (100 mM)/NaOAc (500 mM) CarboPac PA1 gradient method over 90 min to characterize the side-chain length binomial distribution of amylopectins after enzymatic debranching. Torto et al.[36] used an online microdialysis system coupled with IC-IPAD to characterize the enzymatic mannanase hydrolysates of ivory nut mannan.

Selection of Yeasts for Bioethanol Fermentations. Most conventional fermentation processes of sugar cane juices

DOI: 10.1021/jf506370s
J. Agric. Food Chem. 2015, 63, 2841−2851

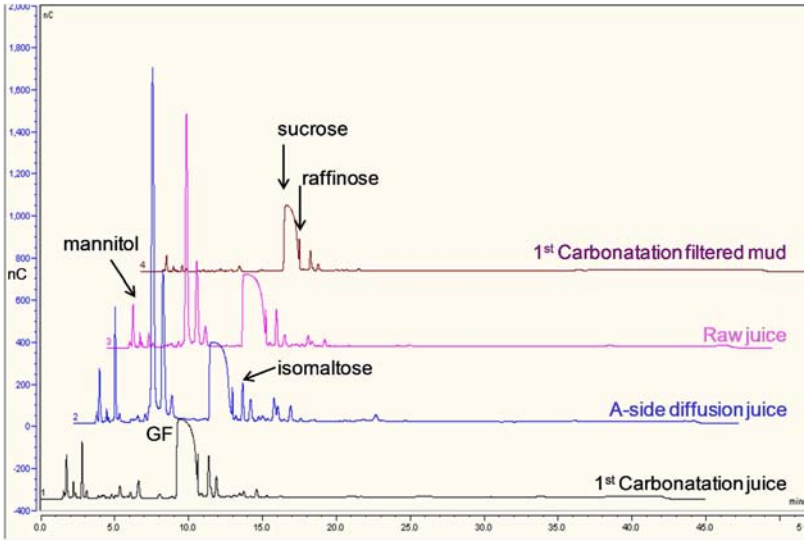

Figure 11. IC-IPAD oligosaccharide profiles of various products from a U.S. sugar beet factory (February 2014) to diagnose processing problems. The factory had been suffering from multiple sugar beet processing problems including freeze−thaw cycles of the sugar beets on storage and low-purity sugar beets.

have used yeasts such as *S. cerevisiae* and its derived mutants. Basso et al.[37] reported results from a yeast selection program consisting of 12 years of cumulative research data aimed at selecting *S. cerevisiae* strains suitable for fermenting sugar cane substrates (juice or molasses) into fuel ethanol in Brazil. A great yeast diversity exists with respect to fermentation characteristics, those being high yield, reduced glycerol and foam formation, maintenance of high viability during recycling, high transfer ability into industrial fermenters, and tolerance to inhibitor compounds and high concentrations of end-product.[37,38] Another important and associated issue for industrial fermentations includes the control of contaminating microorganisms,[39] for example, by the application of sulfuric acid or antibiotics, to maximize fermentation yields. Amorim et al.[40] of Fermentec Ltda., Piracicaba, Brazil, have selected yeast strains particularly for Brazilian bioethanol processing needs and have evaluated different yeasts for sweet sorghum and corn fermentations (H. Amorim, Fermentec Ltda., personal communication). With increased interest in the production of fuel ethanol and other biofuels and bioproducts from sweet sorghum and other biomass crops, there is now a need to select yeasts that can utilize maltose and other maltooligosaccharides from starch to augment fermentation yields.[41] This is because starch occurs in much greater amounts in sweet sorghum than in sugar cane, being particularly rich in the seed heads but also found in relatively large amounts in other tissues.[41]

Figure 10 displays how we have used IC-IPAD fingerprint profiles to simultaneously (i) screen yeast for their ability to utilize maltose in a sweet sorghum juice, (ii) check that bacterial contamination has not occurred in the fermentation broth, particularly from *Leuconostoc* and *Lactobacillus* bacteria, and (iii) qualitatively monitor the production of ethanol and consumption of glucose, fructose, and sucrose. Hanko and Rohrer[42] previously reported the use of IC-IPAD to determine carbohydrates, sugar alcohols, and glycols in cell cultures and fermentation broths. By using IC-IPAD profiles, it was found that baker's yeast was not able to utilize maltose, but distiller's yeast could (results not shown).

Isolation of Microbial Infections and Processing Problems at Sugar Beet Factories. We are frequently asked to solve acute processing problems in a multiple array of factories, refineries, and distilleries that are part of the sugar industry or connected to it. The IC-IPAD profile method is always the first diagnostic tool we apply to "problem" samples, because of the breadth of visual data gained from one chromatogram and the method's high sensitivity and selectivity. Examples of the use of IC-IPAD profiles as a diagnostic tool applied on problem sugar beet factory samples are illustrated in Figure 11. This factory had been suffering from multiple sugar beet processing problems including (i) freeze−thaw cycles of the stored sugar beets, (ii) low purity and relatively high fiber sugar beets, and (iii) bacterial infections causing substandard lime mud filtration during the carbonatation clarification process (Greg Golovanoff, Amalgamated Sugar, Boise, ID, USA, personal communication). Sugar beet juices, in comparison to sugar cane and sweet sorghum juices, contain very little glucose and fructose, which is illustrated in the first carbonatation juice and filtered mud. By using the IC-IPAD method we were able to isolate a lactic acid bacterial infection in the A-side of a tower diffuser (method used to extract juice from sugar beet juice) as compared to none in the B-side (results not shown). The high amounts of glucose and fructose in the raw juice sample also suggested that unwanted inversion reactions had occurred in the stored beet or in production of cossettes (Figure 11). Using this data, the factory personnel were able to mitigate this problem in the future by reconfiguring steam lines to the diffusers to allow the use of heat cycling for the practical reduction of reduce bacterial infections (Greg Golovanoff, personal communication).

It must be noted that anion-exchange columns other than the CarboPac PA1 have been developed that have greater resolution and require a lower sodium acetate concentration to elute the higher dp oligosaccharides as well as lower volume of eluent.[14] Also, Clarke et al.,[43] by utilizing a PAD waveform with six potentials, have allowed the detection of amino acids and amino sugars, which may be particularly more abundant in sugar beets.

DOI: 10.1021/jf506370s
J. Agric. Food Chem. 2015, 63, 2841−2851

AUTHOR INFORMATION

Corresponding Author

*(G.E.) Phone: (504) 286-4446. Fax: (504) 286-4367. E-mail: gillian.eggleston@ars.usda.gov.

Notes

Mention of trade names or commercial products in this paper is solely for the purpose of providing specific information and does not imply recommendation or endorsement by the U.S. Department of Agriculture.

The authors declare no competing financial interest.

ACKNOWLEDGMENTS

We thank Greg Golovanoff (Amalgamated Sugar, Boise, ID, USA) and John Vercellotti (V-Laboratories, Inc., Covington, LA, USA) for useful comments and Mary An Godshall (Sugar Processing Research Institute, New Orleans, LA, USA), who invited us to present the information herein at the 2014 New Orleans Carbohydrate Symposium.

ABBREVIATIONS USED

IC-IPAD, ion chromatography with integrated pulsed amperometric detection; HPAEC, high-performance anion-exchange chromatography; dp, degree of polymerization; HMW, high molecular weight; Da, dalton; G, glucose; F, fructose; cfu, colony-forming units; CWS, cane white sugar; BWS, beet white sugar; DU, dextranase units; GRAS, generally recognized as safe

REFERENCES

(1) Hughes, S.; Johnson, D. C. High-performance liquid chromatographic separation with triple-pulse amperometric detection of carbohydrates in beverages. *J. Agric. Food Chem.* **1982**, *30*, 712−714.

(2) Rocklin, R. D.; Pohl, C. A. Determination of carbohydrates by anion exchange chromatography with pulsed amperometric detection. *J. Liq. Chromatogr.* **1983**, *6*, 1577−1590.

(3) Brunt, K. Liquid chromatography of carbohydrates in human food and animal feeding stuffs. *Adv. Food Anal.* **2014**, May, 10−17.

(4) Lee, Y. C. Carbohydrate analyses with high-performance anion-exchange chromatography. *J. Chromatogr., A* **1996**, *720*, 137−149.

(5) Rohrer, J. Chapter 2. High performance anion exchange chromatography with pulsed amperometric detection (HPAE-PAD) for the determination of oligosaccharides in food and agricultural products. In *Oligosaccharides in Food and Agriculture*; ACS Symposium Series 849; Eggleston, G., Cote. G. L., Eds.; American Chemical Society: Washington, DC, USA, 2003; pp 16−31.

(6) Cataldi, T. R. I.; Campa, C.; De Benedetto, G. E. Carbohydrate analysis by high-performance anion-exchange chromatography with pulsed amperometric detection: the potential is still growing. *Fresenius' J. Anal. Chem.* **2000**, *368*, 739−758.

(7) Corradini, C.; Cavazza, A.; Bignardi, C. High-performance anion-exchange chromatography coupled with pulsed amperometric detection as a powerful tool to evaluate carbohydrates of food interest: principles and applications. *Int. J. Carbohydr. Chem.* **2012**, 1−13.

(8) Basumallik, L.; Rohrer, J. Determination of hydroxymethylfurfural in honey and biomass. *Thermo Scientific Dionex Appl. Note Update 270* **2011**, 1−6.

(9) Koizumi, K.; Kubota, Y.; Tanimoto, T.; Okada, Y. High-performance anion-exchange chromatography of homogenous D-gluco-oligosaccharides and polysaccharides polymerization degree 50 with pulsed amperometric detection. *J. Chromatogr.* **1989**, *464*, 365−373.

(10) Hanashiro, I.; Abe, J.; Hizukuri, S. A periodic distribution of the chain length of amylopectin as revealed by high-performance anion-exchange chromatography. *Carbohydr. Res.* **1996**, *283*, 151−159.

(11) Determination of plant-derived neutral oligo-and polysaccharides. *Thermo Scientific Appl. Note 67* **1993**, 1−11.

(12) Rocklin, R. D.; Clarke, A. P.; Weitzhandler, M. Improved long-term reproducibility for pulsed amperometric detection of carbohydrates via a new quadruple-potential waveform. *Anal. Chem.* **1998**, *70*, 1496−1501.

(13) Determination of plant-derived neutral oligo- and polysaccharides using the CarboPac PA200. *Thermo Scientific Appl. Note Update 150* **2005**, 1−6.

(14) Eggleston, G.; Grisham, M. Chapter 16. Oligosaccharides in cane and their formation on cane deterioration. In *Oligosaccharides in Food and Agriculture*; ACS Symposium Series 849; Eggleston, G., Cote, G. L., Eds.; American Chemical Society: Washington, DC, USA, 2003; pp 211−232.

(15) Eggleston, G.; Clarke, M. A. Applications of HPAE-PAD in the sugar industry. *Semin. Food Anal.* **1997**, *2*, 119−127.

(16) Eggleston, G. Deterioration of cane juice − sources and indicators. *Food Chem.* **2002**, *78*, 99−107.

(17) Eggleston, G.; Legendre, B. L. Mannitol and oligosaccharides as new criteria for determining cold tolerance in sugarcane varieties. *Food Chem.* **2003**, *80*, 451−461.

(18) Eggleston, G.; Legendre, B. L.; Tew, T. Indicators of freeze damaged sugarcane varieties which can predict processing problems. *Food Chem.* **2004**, *87*, 119−133.

(19) Robyt, J. F.; Eklund, S. H. Stereochemistry involved in the mechanism of action of dextransucrase in the synthesis of dextran and the formation of acceptor products. *Bioorg. Chem.* **1982**, *11*, 115−132.

(20) Eggleston, G.; DeLucca, A.; Sklanka, S.; Dalley, C.; St. Cyr, E.; Powell, R. Investigation of the stabilization and preservation of sweet sorghum juices. *Ind. Crops Prod.* **2015**, *64*, 258−270.

(21) Soetart, W. Synthesis of D-mannitol and L-sorbose by microbial hydrogenation and dehydrogenation of monosaccharides. Ph.D. thesis, University of Ghent, Belgium, 1991.

(22) Eggleston, G.; Huet, J. M. The measurement of mannitol in sugar beet factories to monitor deterioration and processing problems. *Zuckerindustrie (Berlin, Ger.)* **2012**, *137*, 33−39.

(23) Steinmetz, K.; Buczys, R.; Buchholz, K. The quality of frost-damaged sugar beet. *Zuckerindustrie (Berlin, Ger.)* **1998**, *123*, 933−942.

(24) AOAC Official Method 988.12. Chapter 44.1.30. Dextran in raw cane sugar. Roberts copper method. *Official Methods of the AOAC*; 1995; pp 13−14.

(25) Eggleston, G.; Legendre, B. L.; Richard, C. Effect of harvest method and storage time on cane deterioration. II: Oligosaccharide formation. *Int. Sugar J.* **2001**, *103*, 495−504.

(26) EU news. EU suspends sugar imports from Serbia. *Zuckerindustrie (Berlin, Ger.)* **2003**, *128*, 400.

(27) Sugar industry news. *Int. Sugar J.* **2004**, *106*, 114.

(28) Cordella, C.; Antinelli, J.-F.; Aurieres, C.; Faucon, J.-P.; Cabrol-Bass, D.; Sbirazzuoli, N. Use of differential scanning calorimetry (DSC) as a new technique for detection of aldulterated honeys. 1. Study of adulteration effect on honey thermal behavior. *J. Agric. Food Chem.* **2002**, *50*, 203−208.

(29) Hammond, D. A. Synergy between liquid chromatography-pulsed amperometric detection and capillary-gas chromatographic methods for the detection of juice adulteration. *J. AOAC Int.* **2001**, *83*, 964−975.

(30) Eggleston, G.; Pollach, G.; Triche, R. The use of ion chromatography profiles as screening tool to differentiate cane white sugar from beet white sugar. *Zuckerindustrie (Berlin, Ger.)* **2005**, *130*, 611−616.

(31) Kowalski, B. R.; Bender, C. F. Pattern recognition a powerful approach to interpreting chemical data. *J. Am. Chem. Soc.* **1972**, *94*, 5632−5639.

(32) Eggleston, G.; Monge, A. Optimization of sugarcane factory application of commercial dextranases. *Process. Biochem. (Oxford, U.K.)* **2005**, *40*, 1881−1894.

(33) Eggleston, G.; Monge, A.; Montes, B.; Stewart, D. Chapter 6. Overcoming practical problems of enzyme applications in industrial processes: dextranases in the sugar industry. In *Industrial Application of*

DOI: 10.1021/jf506370s
J. Agric. Food Chem. 2015, 63, 2841−2851

Enzymes on Carbohydrate Based Materials; ACS Symposium Series 972; Eggleston, G., Vercellotti, J. R., Eds.; American Chemical Society: Washington, DC, 2007; pp 73−87.
(34) Starch information sheet. Promozyme® D2; Novoyzmes publication, Bagsvaerd, Denmark, 2012.
(35) Morel du Boil, P. G.; Wienese, S.; Schoones, B. The cause of sarkaran in sugarcane. *Proc. S. Afr. Sugar Cane Technol. Assoc.* **2005**, *79*, 48−62.
(36) Torto, N.; Marko-Varga, G.; Gorton, L.; Stalbrand, H.; Tjerneld, F. Online quantitation of enzymatic mannan hydrolysates in small-volume bioreactors by microdialysis sampling and column liquid chromatography-integrated pulsed electrochemical detection. *J. Chromatogr., A* **1996**, *725*, 165−175.
(37) Basso, L. C.; Amorim, H. V.; Oliveira, A. J.; Lopes, M. L. Yeast selection for fuel ethanol production in Brazil. *FEMS Yeast Res.* **2008**, *8*, 1155−1163.
(38) Klinke, H. B.; Thomsen, A. B.; Ahring, B. K. Inhibition of ethanol-producing yeast and bacteria by degradation products produced during pre-treatment of biomass. *Appl. Microbiol. Biotechnol.* **2004**, *66*, 10−26.
(39) Beckner, M.; Ivey, M. L.; Phister, T. G. Microbial contamination of fuel ethanol fermentations. *Lett. Appl. Microbiol.* **2011**, *53*, 387−394.
(40) Amorim, H. V.; Lopes, M. L.; de Castro Oliveira, J. V.; Buckeridge, M. S.; Goldman, G. H. Scientific challenges of bioethanol production in Brazil. *Appl. Microbiol. Biotechnol.* **2011**, *91*, 1267−1275.
(41) Eggleston, G.; Cole, M.; Andrzejewski, B. New commercially viable processing technologies for the production of sugar feedstocks from sweet sorghum (*Sorghum bicolor* L. Moench) for biofuel and bioproducts manufacture. *Sugar Technol.* **2013**, *15* (3), 232−249.
(42) Hanko, V. P.; Rohrer, J. S. Determination of carbohydrates, sugar alcohols, and glycols in cell cultures and fermentation broths using high performance anion exchange chromatograms with pulsed amperometric detection. *Anal. Biochem.* **2000**, *283*, 192−199.
(43) Clarke, A. P.; Jandik, P.; Rocklin, R. D.; Liu, Y.; Avdalovic, N. An integrated amperometry waveform for the direct, sensitive direction of amino acids and amino sugars following anion-exchange chromatography. *Anal. Chem.* **1999**, *71*, 2774−2781.

DOI: 10.1021/jf506370s
J. Agric. Food Chem. 2015, 63, 2841−2851

were rarely studied in cultivation experiments. One study analyzing the influence of fertilization on the leaf glucosinolates of *Tropaeolum majus* L. showed that sulfur fertilization increased benzyl glucosinolate content, whereas nitrogen fertilization had no significant influence.[17] *M. oleifera* contained in all plant parts (below- and above-ground) very high levels of aromatic glucosinolates, which is a characteristic that makes this plant unique. In addition to some other trees in the families of Akaniaceae, Bretschneideraceae, or Gyrostemonaceae,[18] *M. oleifera* has in all plant parts considerable quantities of glucosinolates. Our knowledge of the glucosinolate content in tree species is only rudimentary compared to the numerous studies that have been conducted on the influence of nitrogen and/or sulfur fertilization on brassicaceous leafy plants.

Several studies have been undertaken about nitrogen and sulfur fertilization and their influence on phenolics in Brassicaceae.[19−22] Li and colleagues[20] as well as other authors[21,22] found an improving influence of sulfur fertilization on phenolic compounds in different *Brassica* species. Based on the findings of the aforementioned studies, the influence of sulfur fertilization on the content and composition of phenolic acids and flavonoids was analyzed using *M. oleifera* ecotypes.

Because of the fact that one characteristic of *M. oleifera* is drought tolerance and that harvest takes place all year round, the influence of water deficiency on the polyglycosylated aromatic glucosinolates was also analyzed. Because *M. oleifera* is not an annual plant like other herbaceous species containing glucosinolate, results are difficult to predict. Analysis of other studies showed enhancing or decreasing effects depending on the extent of water stress (e.g., refs 23 and 24) and plant species (e.g., refs 25 and 26). On the basis of different previous studies, which show increasing phenolic content after drought stress,[27,28] a change in the content and composition of phenolics in *M. oleifera* leaves is conceivable. Therefore, the corresponding analyses were included in the present study.

Because studies on accumulation of secondary metabolites under varying conditions are rare or nonexistent for *M. oleifera*, effects of sulfur fertilization and drought stress on plant growth and levels of secondary metabolites in the leaves of different *M. oleifera* ecotypes were investigated. The results will generate information providing insights into the optimal cultivation conditions for *M. oleifera* ecotypes. The overarching aim of the study was to find differences in *M. oleifera* ecotypes in growth and secondary metabolite content to determine the most suitable ecotype for leaf and secondary metabolite production. The goal was to identify an optimal cultivation variant with the best plant-growth performance and the highest secondary metabolite content. The results provided information about how to achieve a high yield in biomass as well as potentially health-promoting ingredients in the cultivation of *M. oleifera*.

MATERIALS AND METHODS

Cultivation Experiments in Großbeeren. After a prescreening using 13 different ecotypes of *Moringa oleifera* Lam., seeds of the six best-germinating and -growing ecotypes were selected for the experiments. The *M. oleifera* ecotypes were precultivated in a greenhouse at the Leibniz-Institute of Vegetable and Ornamental Crops in Großbeeren (Germany). Seeds from four ecotypes adapted to different climatic conditions were obtained from AVRDC - The World Vegetable Center (Taiwan): TOT4880 (origin USA, ecotype 1); TOT5028 and TOT7277 (origin Thailand, ecotypes 2 and 3); TOT7267 (origin India, ecotype 4). Seeds from the other two ecotypes were collected in the Philippines and Taiwan (ecotypes 5 and 6). Seedlings (8 weeks old) were planted in grid patterns at 0.5 m apart in a 1 m deep enclosed greenhouse bed. Drip irrigation and a nebulization system were used to humidify soil and air. In 2010, the mean temperature during the vegetation period (from June to October) in the greenhouse was 19.5 °C (2011: 18.6 °C and 2012: 19.5 °C) and varied during this period between a maximum temperature of 23.5 °C in July and a minimum temperature of 16.3 °C in October (2011: 20.5 °C in August and 14.6 °C in October; 2012: 22.3 °C in July and 15.7 °C in October). The ventilation temperature was set to 19 °C. Biomass production, height, and total glucosinolate content were determined to analyze ecotype differences. Plant samples were taken in August 2010 (first harvest, H1), November 2010 (second harvest, H2), July 2011 (third harvest, H3), October 2011 (fourth harvest, H4), and August 2012 (fifth harvest, H5). The leaf/stem ratio of well-established plants was analyzed from plant material at the second harvest, November 2010. By this time, the plants had grown into completely developed trees.

Furthermore, the influence of different growing variants on the growth and secondary metabolite content (glucosinolates, phenolic acids, and flavonoids) of the six *M. oleifera* ecotypes was analyzed in November 2010 (second harvest) and in July 2011 (third harvest) (normal variant, sulfur variant, water-deficiency variant; Supporting Information, Table 1). Per variant and ecotype 5 plants were cultivated. Each growing variant was located in a closed bed surrounded with concrete, separating the variants from one another. All beds were fertilized (basic fertilization) with 7.04 g/m^2 nitrogen (372 g of calcium ammonium nitrate per parcel, twice a year), 2.56 g/m^2 phosphorus (Superphospate, 465 g of phosphorus pentoxide per parcel), and 5.76 g/m^2 potassium (Patentkali, 330 g of potassium oxide per parcel) once a year at the end of April/beginning of May. The plants of the sulfur variant received an additional 0.704 g/m^2 sulfur annually (56 g of potassium sulfate per parcel). To reach low to moderate water deficiency in one bed, the irrigation and the nebulization system for the whole cabin was switched off in defined periods (August−November 2010 and June−September 2011). In the cultivation beds containing the normal and sulfur variant, a continuous soil water tension of approximately 50−100 hPa was maintained. In the bed with the water-deficiency variant, a higher soil water tension was determined (second harvest: 380 hPa, third harvest: 175 hPa; Supporting Information, Figure 1). At the second harvest, the upper limit of the field capacity (FC) was exceeded (FC ranged between 63−316 hPa, therefore pF 1.8−2.5). The water content of the sandy soil was at this time <2%. At the third point of harvest, the soil water tension was in the range of field capacity. Tensiometers used had a measurement range between 0 and 1.000 hPa. A rewetting of the dry bed from December 2010 to May 2011 was necessary to prevent plants from death. Wilting and chlorosis of leaves have been recognized.

Leaves from the top of the plants (upper 20 cm, youngest leaves) were used for the analysis of glucosinolates, flavonoids, and phenolic acids (secondary metabolites). In this way, it was possible to guarantee that leaf material of the same age was used for analysis. The glucosinolate content of older and middle-aged leaves was determined additionally to get an idea of the allocation of the glucosinolate over the whole plant. After each sampling, the whole plantation was pruned back to a height of 60−70 cm. Because of space limitations in the

DOI: 10.1021/jf506174v
J. Agric. Food Chem. 2015, 63, 2852−2861

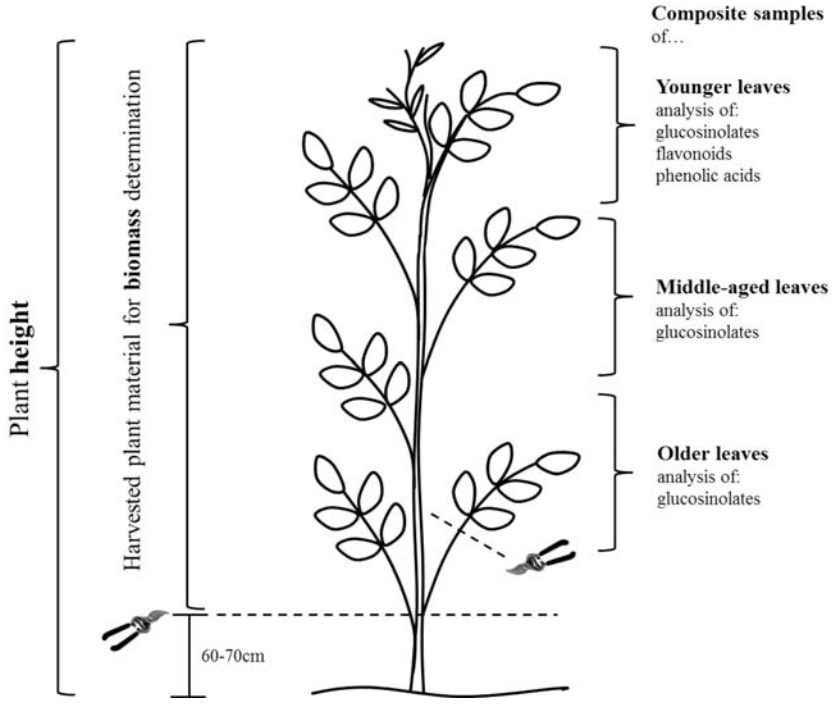

Figure 1. Sampling of plant material of *Moringa oleifera*.

greenhouse, a doubled pruning of the plants was required. The biomass was determined at each harvest by weighing the freshly cut plant material (leaves and stem of each plant, which exceeded the 60−70 cm). As an example, for the first harvest, the glucosinolate profit per plant was calculated to show ecotype variability (Supporting Information, Table 2).

For all cultivation variants, samples from five different plants per ecotype were taken according to Figure 1. Therefore, the analysis was performed in five replications.

Determination of Glucosinolates. Leaf material for glucosinolate analysis was shock-frozen in liquid nitrogen and kept at −20 °C until freeze-drying. The content and composition of *M. oleifera* glucosinolates were determined using a method for extraction of intact glucosinolates described in detail by Förster et al.[29] Briefly, a methanolic extraction (70%) was performed in three steps with 20 mg of pulverized leaf material (Retsch Mixer Mill MM 301, fineness about 5 μm, manufacturer specifications). The combined supernatant was concentrated (vacuum concentrator, Thermo Scientific Savent SPD111 V Concentrator; vacuum pump, Vacuumbrand PC 3000 series, SVC3000) and precipitated with barium acetate (0.4 M). After precipitation (30 min), samples were centrifuged (16 000 g, Thermo Scientific, Heraeus Megafuge 11R Centrifuge for 10 min), decanted, and filled up to 2 mL with ultrapure water. In each HPLC vial, 1 mL of filtered sample (Costar SpinX tubes) was transferred. The remaining amount of each sample was incubated with 0.05 U myrosinase (thioglucosidase, Sigma-Aldrich) for 8 h at 37 °C to hydrolyze glucosinolates to their corresponding breakdown products. Hydrolyzed samples were filtered (Costar SpinX tube) and transferred to HPLC sample vials for analysis. The internal standard, 2-propenyl glucosinolate, was added at the first extraction step.

Extracts were qualitatively and quantitatively analyzed on a Merck Hitachi HPLC system. A volume of 10 μL of sample was injected (LaChrom L-7200 auto sampler) and separated on a 4.6 × 250 mm SB-C18 column (Zorbax 5 μm, Agilent) using a gradient program described by Förster et al.[29] Two solvents were used for the HPLC analysis: solvent A, 100% 0.1 M ammonium acetate, and solvent B, 40% acetonitrile/0.1 M ammonium acetate. Detection was performed at 229 nm using a photodiode array detector (LaChrom L-7455), and components were identified from the retention time and quantified against internal standard. The peak area remaining after myrosinase treatment of the intact glucosinolate extract was subtracted from the peak area of the glucosinolate of the intact glucosinolate extract without myrosinase treatment. Interfering/coeluting ballast compounds were excluded from the calculation by using myrosinase (described in detail by Förster et al.).[29] Relative response factors (RF) were used according to Förster et al.[29] and were therefore generated from fractionated standards.

Determination of Flavonoids and Phenolic Acids. Flavonoids and phenolic acids in *M. oleifera* leaves were analyzed using a slightly modified HPLC method described by Mewis et al.[30] A total of 20 of mg lyophilized, powdered leaf material was extracted in 300 μL of 70% methanol (pH 4, acetic acid) for 15 min in ice water using sonification (Bandelin Sonorex Super AG 102H). The pellet was re-extracted twice with 300 μL of the extraction solvent for 10 min. After each extraction step, the samples were centrifuged for 5 min at 16 000 g (Thermo Scientific, Heraeus Megafuge 11R Centrifuge), and the supernatants were combined. Supernatants were concentrated (vacuum concentrator, Thermo Scientific Savent SPD111 V Concentrator; vacuum pump, Vacuumbrand PC 3000 series, SVC3000) to near dryness, dissolved in 50% methanol, and filled up to 1 mL. The samples were centrifuged for 2 min, filtered (Costar SpinX tubes), and transferred to HPLC vials. 4-Methoxycinnamic acid (1 mmol/L, Sigma-Aldrich) was used as internal standard.

Extracts were qualitatively and quantitatively analyzed on a HPLC−MS/MS system (Agilent 1100 Series, Waldbronn,

DOI: 10.1021/jf506174v
J. Agric. Food Chem. 2015, 63, 2852−2861

Table 1. Biomass, Height, and Total Glucosinolate Content of Six Different *Moringa oleifera* Ecotypes at Five Harvest Times[a]

harvest	ecotype E1	E2	E3	E4	E5	E6	$\bar{x}$
			Biomass (g fw)				
H1	$104_{(B)}$	$253_{(B)}$	122	331	154	94	**$176_{(B)}$**
H2	$416_{(AB)}$	$270_{(B)}$	269	353	228	257	**$272_{(B)}$**
H3	$883_{(ab,A)}$	$1137_{(a,A)}$	$385_{(b)}$	$626_{(ab)}$	$286_{(b)}$	$301_{(b)}$	**$603_{(A)}$**
H4	$443_{(AB)}$	$340_{(B)}$	161	463	175	178	**$293_{(B)}$**
H5	$769_{(AB)}$	$468_{(AB)}$	661	844	451	437	**$605_{(A)}$**
$\bar{x}$	**523**	**494**	**320**	**523**	**259**	**253**	
			Height (cm)				
H1	$140_{(B)}$	$135_{(AB)}$	111	176	151	117	**$138_{(B)}$**
H2	$166_{(AB)}$	$122_{(B)}$	163	195	151	164	**$155_{(B)}$**
H3	$215_{(ab,AB)}$	$216_{(ab,A)}$	$183_{(b)}$	$260_{(a)}$	$164_{(ab)}$	$176_{(ab)}$	**$187_{(A)}$**
H4	$153_{(ab,B)}$	$145_{(ab,AB)}$	$103_{(b)}$	$201_{(a)}$	$101_{(b)}$	$102_{(b)}$	**$134_{(B)}$**
H5	$226_{(A)}$	$171_{(AB)}$	172	219	162	171	**$187_{(A)}$**
$\bar{x}$	**$175_{(ab)}$**	**$153_{(bc)}$**	**$138_{(c)}$**	**$206_{(a)}$**	**$146_{(bc)}$**	**$144_{(bc)}$**	
			GS[z] (μmol/g dw)				
H1	$148_{(B)}$	$155_{(B)}$	$101_{(B)}$	$144_{(B)}$	$129_{(B)}$	$110_{(B)}$	**$131_{(C)}$**
H2	$348_{(a,A)}$	$267_{(ab,A)}$	$237_{(b,A)}$	$285_{(ab,A)}$	$274_{(ab,A)}$	$266_{(ab,A)}$	**$276_{(A)}$**
H3	$194_{(B)}$	$202_{(AB)}$	$180_{(AB)}$	$214_{(AB)}$	$141_{(AB)}$	$119_{(B)}$	**$175_{(B)}$**
H4	$200_{(a,B)}$	$194_{(a,AB)}$	$68_{(b,C)}$	$217_{(a,AB)}$	$169_{(a,AB)}$	$244_{(a,A)}$	**$182_{(B)}$**
H5	$281_{(ab,A)}$	$281_{(ab,A)}$	$201_{(b,A)}$	$303_{(ab,A)}$	$319_{(a,A)}$	$272_{(ab,A)}$	**$276_{(A)}$**
$\bar{x}$	**$234_{(a)}$**	**$220_{(a)}$**	**$157_{(b)}$**	**$229_{(a)}$**	**$206_{(a)}$**	**$202_{(a)}$**	

[a]Significant differences were determined using Tukey's HSD test, $p < 0.05$ (capital letters: significant differences between the harvests; lower case letters: significant differences between the ecotypes); z = glucosinolate content.

Germany). A volume of 10 μL of extract was injected and separated using a 150 × 2.1 mm C16 column (AcclaimPA, 3 μm, Dionex) with the following gradient program: 0−1 min, 0.5% B; 1−10 min, 0.5−40% B; 10−12 min, 40% B; 12−18 min, 40−80% B; 18−20 min, 80% B; 20−24 min, 80−100% B; 24−30 min, 100% B; 30−34 min, 100−0.5% B; and 34−39 min, 0.5% B at a flow rate of 0.4 mL/min. Two solvents were used for analysis: solvent A, H_2O (0.5% formic acid), and solvent B, 40% acetonitrile. The oven temperature was 35 °C. Detection was carried out at 290, 320, and 370 nm on a photodiode array detector. Because all components showed a good signal at 290 nm, the compounds were quantified against internal standard 4-methoxycinnamic acid detected at this wavelength. Compounds were identified as deprotonated molecular ions and characteristic mass fragment ions by HPLC-DAD-ESI-MS.[2] Commercially available standards of single compounds were used as references. Relative response factors (RF) were used to correct for absorbance differences between the reference standard 4-methoxycinnamic acid (RF = 1): RF = 1.16 for chlorogenic acid (Sigma-Aldrich) and an isomer of chlorogenic acid, RF = 1.06 for neochlorogenic acid (Sigma-Aldrich), RF = 1 for the two isomers of *p*-coumaroyl quinic acid and an isomer of feruloyl quinic acid (commercial standard not available), RF = 1.51 for vitexin (Fluka) and isovitexin, RF = 1.53 for quercetin 3-*O*-glucoside (Carl Roth GmbH), RF = 1.4 for kaempferol 3-*O*-glucoside (Carl Roth GmbH), RF = 1.84 for quercetin 3-*O*-(6″-malonylglucoside) (Sigma-Aldrich) and kaempferol 3-*O*-(6″-malonylglucoside) (commercial standard not available).

Statistical Analysis. Data were analyzed for significant differences using analysis of variance (ANOVA) following the mean comparison test, Tukey's HSD, with SigmaPlot 12.0. Cross dependence was analyzed by using the two-way ANOVA. The p-value was fixed at $p < 0.05$; any exceptions are mentioned in the text.

RESULTS

Ecotype Differences. *Biomass, Height, and Glucosinolate Content.* In addition to the growth parameters, ecotype differences in secondary metabolites were analyzed by focusing on the glucosinolates that were considered to have health-promoting effects. The data were collected at five different harvest points (Table 1). A very high variability among ecotype replicates in biomass production, height, and glucosinolate content can be noticed. Significant differences were hard to identify. When considering all points of harvest, ecotypes 1, 2, and 4 had the highest biomass. Ecotypes 2, 3, 5, and 6 were significantly smaller than ecotype 4 (Table 1). On average across all ecotypes at each point of harvest, the biomass production and plant height were significantly higher at the third and fifth points of harvest in comparison to the other points of harvest. Considering the glucosinolate levels, ecotype 3 contained significantly lower glucosinolate content than the other ecotypes (Table 1). Ecotype 1 showed the highest glucosinolate content overall. The mean glucosinolate content of all analyzed ecotypes was significantly lower at the first point of harvest. At the second and fifth points of harvest, the ecotypes showed a significantly higher glucosinolate content in comparison to the other points of harvest. No significant interaction between the point of harvest and the ecotype was found for the biomass production, plant height, and glucosinolate content (two-way ANOVA, $p < 0.05$). Taking height, biomass, and glucosinolate content of the five harvest points into consideration, ecotypes 1 and 4 were found to be the best performers in terms of biomass production and glucosinolate amounts in leaves. Not surprisingly, we detected a correlation between height and biomass. With an elimination of extreme values, a polynomial dependency ($y = 0.0153x^2 - 0.7184x$, $R^2 = 0.80$) was found. In contrast, no correlation was found between biomass/height and glucosinolate content. Also,

DOI: 10.1021/jf506174v
J. Agric. Food Chem. 2015, 63, 2852−2861

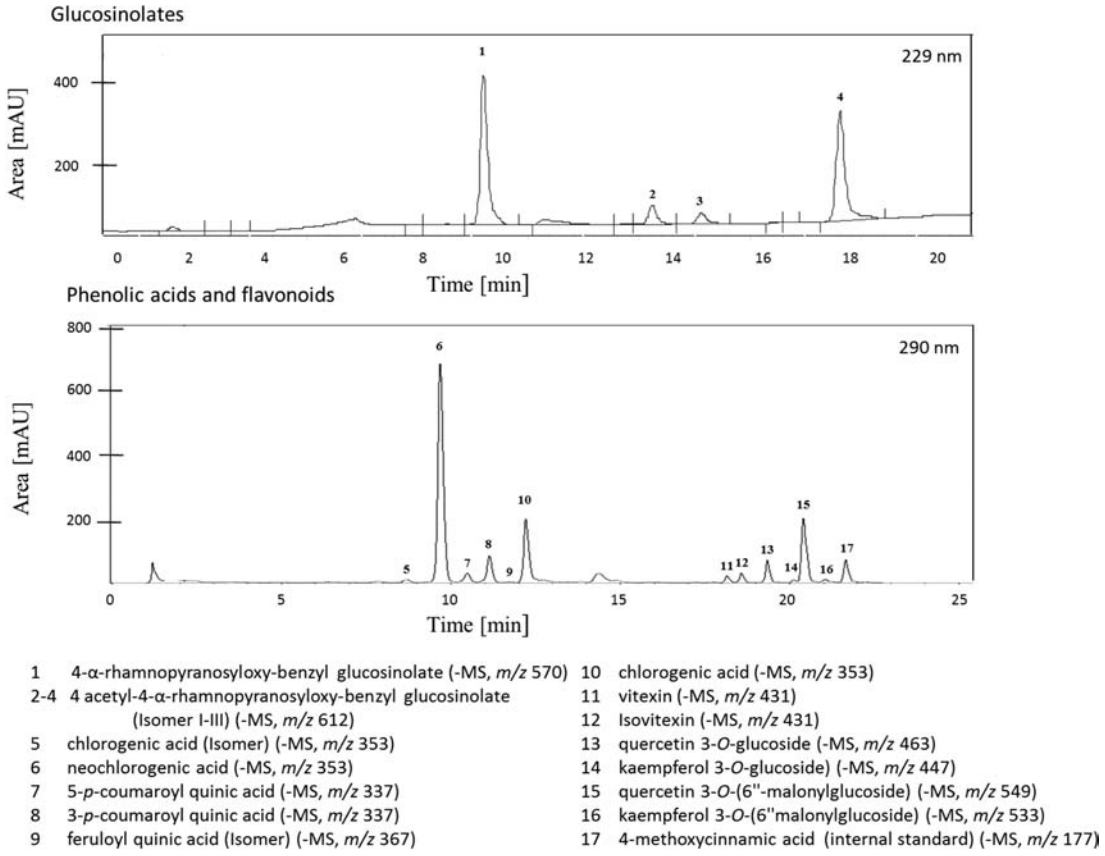

Figure 2. Chromatograms of *Moringa oleifera* glucosinolates, flavonoids, and phenolic acids.

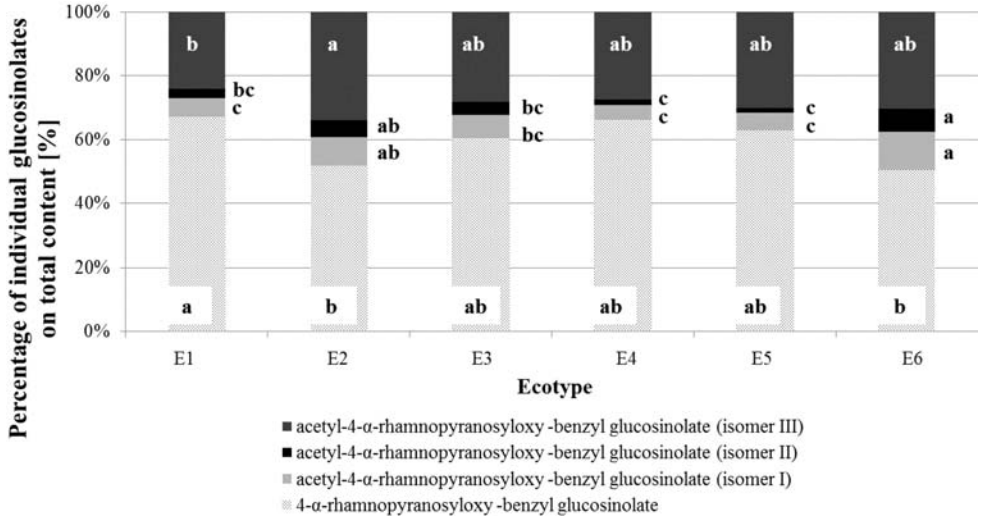

Figure 3. Percentage of single *Moringa oleifera* glucosinolates on the total glucosinolate content in leaves at the third point of harvest (different letters indicate significant differences between the different ecotypes within each glucosinolate, Tukey's HSD test, $p < 0.05$).

the leaf−stem ratio did not differ between the six *M. oleifera* ecotypes. A total of 60% of the tree biomass harvested was formed by the leaves (Supporting Information, Table 2).

Glucosinolate Profile. *M. oleifera* ecotypes differed in their total glucosinolate content depending on the date of harvest. In all six ecotypes, four *Moringa* glucosinolates were identified: 4-α-rhamnopyranosyloxy-benzyl glucosinolate (Rhamno-Benzyl-GS) and three isomeric acetyl-4-α-rhamnopyranosyloxy-benzyl glucosinolates (Ac-Isomer-GSs I−III, Figure 2). As an exception in individual plants of ecotypes 5 and 6, only one glucosinolate, Rhamno-Benzyl-GS, was found. Furthermore, the six *M. oleifera* ecotypes exhibited differences in their glucosinolate composition. The percentage of individual glucosinolates relative to the total glucosinolate content was determined (Figure 3, exemplary presentation based on data from the third harvest, plants from ecotypes 5 and 6 with only Rhamno-Benzyl-GS were excluded from the calculation). Ecotype 1 displayed a consistently higher percentage of Rhamno-Benzyl-GS and a lower percentage of Ac-Isomer-GS III. A low percentage of Rhamno-Benzyl-GS and a high

DOI: 10.1021/jf506174v
J. Agric. Food Chem. 2015, 63, 2852−2861

Table 2. Content of Phenolic Acids and Flavonoids in Six *Moringa oleifera* Ecotypes at the Third Point of Harvest[a]

		ecotype					
		E1	E2	E3	E4	E5	E6
phenolic acids (μmol/g dw)	chlorogenic acid (isomer)	0.19(a)	0.23(a)	0.15(a)	0.22(a)	0.23(a)	0.22(a)
	neochlorogenic acid	8.80(a)	10.39(a)	6.56(a)	10.45(a)	11.28(a)	11.00(a)
	5-*p*-coumaroyl quinic acid	0.74(ab)	0.46(b)	0.57(ab)	1.05(a)	1.01(a)	0.81(ab)
	3-*p*-coumaroyl quinic acid	1.77(a)	1.10(a)	1.23(a)	2.61(a)	2.32(a)	1.81(a)
	feruloyl quinic acid (isomer)	0.30(a)	0.16(a)	0.18(a)	0.28(a)	0.18(a)	0.14(a)
	chlorogenic acid	1.27(b)	1.34(b)	1.17(b)	1.26(b)	2.06(a)	2.10(a)
	∑(phenolic acids)	**11.06(ab)**	**13.67(ab)**	**9.86(b)**	**15.86(ab)**	**17.08(a)**	**16.08(ab)**
flavonoids (μmol/g dw)	vitexin	0.12(a)	0.00(a)	0.00(a)	0.13(a)	0.10(a)	0.06(a)
	isovitexin	0.22(a)	0.00(b)	0.00(b)	0.13(ab)	0.17(ab)	0.13(ab)
	quercetin 3-*O*-glucoside	1.24(a)	0.95(a)	0.63(a)	1.89(a)	1.58(a)	1.19(a)
	kaempferol 3-O-glucoside	0.32(a)	0.24(a)	0.09(a)	0.11(a)	0.38(a)	0.39(a)
	quercetin 3-*O*-(6″-malonylglucoside)	4.47(a)	3.61(a)	2.50(a)	6.56(a)	3.78(a)	3.03(a)
	kaempferol 3-*O*-(6″-malonylglucoside)	1.91(a)	1.90(a)	1.25(a)	1.90(a)	1.34(a)	1.43(a)
	∑(flavonoids)	**8.28(a)**	**6.70(a)**	**4.47(a)**	**10.73(a)**	**7.35(a)**	**6.23(a)**
	∑(phenolic acid+flavonoids)	**19.34(a)**	**20.37(a)**	**14.33(a)**	**26.59(a)**	**24.43(a)**	**22.31(a)**

[a]Significant differences within each phenolic acid or flavonoid between the ecotypes, Tukey's-HSD-test, $p < 0.05$.

percentage of the three Ac-Isomer-GSs were found for ecotypes 2 and 6. Ac-Isomer-GS I was found at consistently low content levels in ecotypes 4 and 5, likewise Ac-Isomer-GS II in ecotypes 1, 4, and 5. Furthermore, the glucosinolate composition of younger and older leaves of the different *M. oleifera* ecotypes was compared, but no significant differences were observed (detailed data not shown).

Phenolic Acid and Flavonoid Profile. In *M. oleifera* leaves, the following phenolic compounds were identified: an isomer of chlorogenic acid, neochlorogenic acid, two isomers of *p*-coumaroyl quinic acid, an isomer of feruloyl quinic acid, chlorogenic acid, vitexin, isovitexin, quercetin 3-*O*-glucoside, kaempferol 3-*O*-glucoside, quercetin 3-*O*-(6″-malonylglucoside), and kaempferol 3-*O*-(6″-malonylglucoside) (Figure 2). The main phenolic acid was identified as neochlorogenic acid, and the main flavonoid was quercetin 3-*O*-(6″-malonylglucoside). The total phenolic acid content in the leaves differed significantly between the six *M. oleifera* ecotypes (Table 2). Ecotype 5 had a significantly higher phenolic acid content than ecotype 3 (one-way ANOVA, Tukey's HSD test, $p < 0.05$). The phenolic acid content ranged between 9.86 and 17.08 μmol/g dry weights (dw), and the flavonoid content ranged between 4.47 and 10.73 μmol/g dw. Significant differences between single phenolic acids and flavonoids were identified (Table 2). Vitexin and isovitexin were found in all plants of the *M. oleifera* ecotype 5, whereas these secondary metabolites were not present in detectable levels in the plants of ecotypes 2 and 3. No correlation was found between plant height and the phenolic acid/flavonoid content ($R^2 < 0.06$). In summary, ecotypes 4 and 5 had the highest contents of flavonoids and phenolic acids.

Influence of Water Deficiency and Sulfur Fertilization on Biomass, Height, and Secondary Metabolite Content of *M. oleifera* Ecotypes. The influence of water deficiency and sulfur fertilization on biomass accumulation, plant height, and the secondary metabolite profile (glucosinolate, phenolic acids, and flavonoids) was analyzed in six *M. oleifera* ecotypes. Contrary to the results of the second point of harvest (plants were exposed to drought stress, Supporting Information, Figure 2), plants showed stronger reactions at the beginning of a repeated water limitation (third point of harvest, Figure 4). Therefore, the results of the third point of harvest are presented in more detail in the present work. At the third point of harvest, the plants in the normal cultivation variant were significantly taller and had a higher biomass than plants grown under water limitation (Figure 4, Tukey's HSD test, $p < 0.05$). The glucosinolate content was overall significantly higher in the water-deficiency variant in comparison to the normal variant (Tukey's HSD test, $p < 0.05$). Cultivation conditions had different impacts on biomass accumulation, plant height, and glucosinolate content of the six ecotypes (Figure 4). No statistically significant correlation between the cultivation variant and the ecotype was found for the glucosinolate content, biomass, and plant height (two-way ANOVA, $p < 0.05$). Although no influence of the cultivation variant on the flavonoid content was identified for the single ecotypes, statistical differences in the phenolic acid content were found (Figure 5, ecotypes 1 and 4). With regard to the sum of phenolic acids and flavonoids, ecotypes 1 and 2 had significantly higher levels in the sulfur variant in comparison to the normal variant. Ecotypes 3 and 4 had significant higher levels in the drought variant in comparison to the normal variant (Tukey's HSD test, $p < 0.05$). A statistically significant interaction between the cultivation variant and ecotype was identified (two-way ANOVA, $p < 0.01$). In general, the effect of the cultivation variant on the plant biomass and content of glucosinolates, phenolic acids, and flavonoids strongly depended on the ecotype.

DISCUSSION

M. oleifera ecotypes are characterized by phenotypic differences, such as the shape of leaves, the production of leaf biomass, the plant height, and the secondary metabolite profile, as reported in other studies.[3,12,31] Therefore, the intensive cultivation of *M. oleifera* ecotypes should be associated with a high yield of leaf biomass and secondary metabolites. Differences in the secondary metabolite content and composition have not been the basis for selecting ecotypes for intensive cultivation until today, although the health-promoting effects of chemical compounds of *M. oleifera* are commonly described next to its nutritional value.[2,9] The six different *M. oleifera* ecotypes used in this study showed morphological (height and biomass) and chemical (glucosinolates, phenolic acids, and flavonoids)

DOI: 10.1021/jf506174v
J. Agric. Food Chem. 2015, 63, 2852−2861

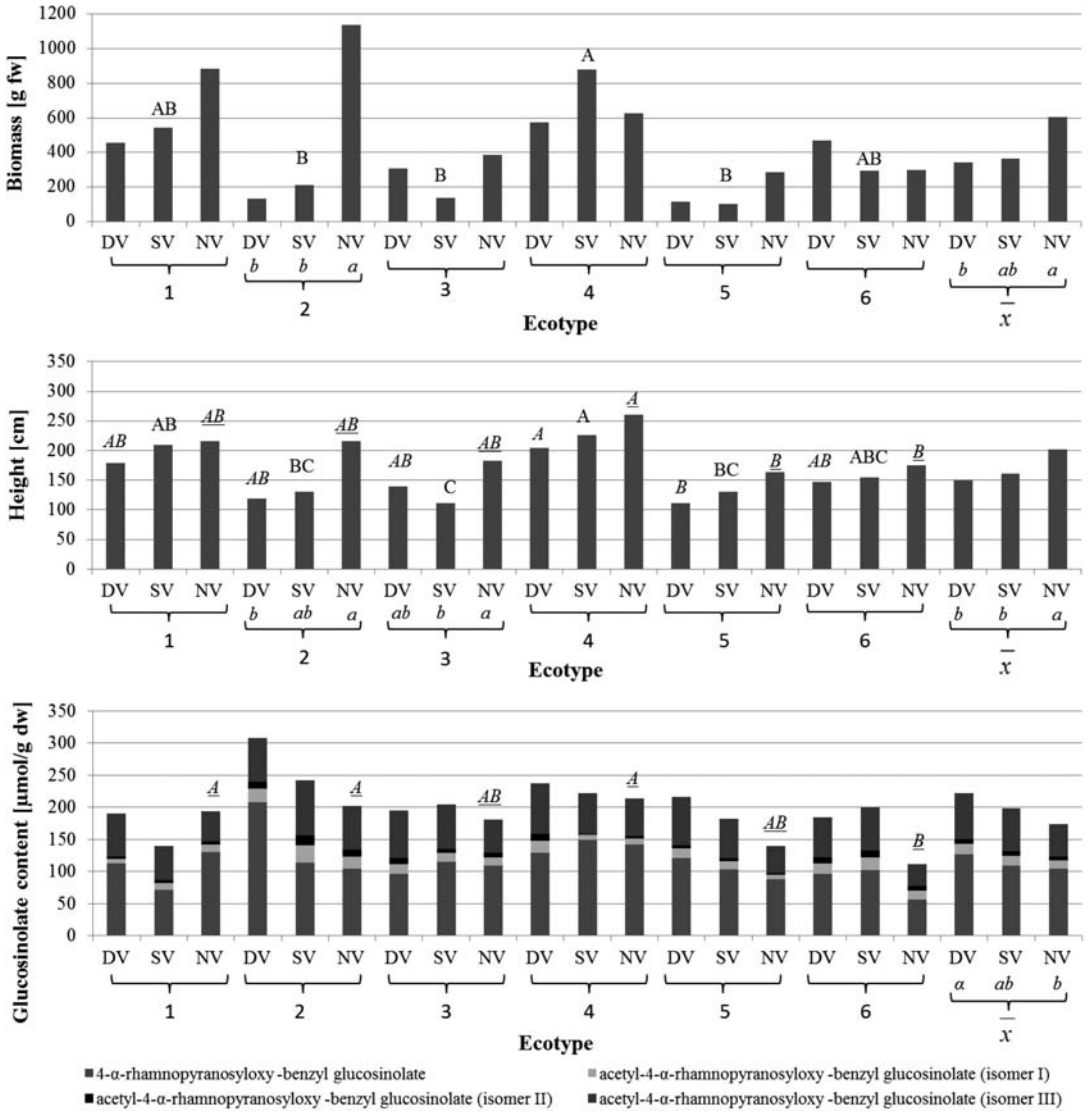

Figure 4. Influence of cultivation variants on biomass, height, and glucosinolate content of six *Moringa oleifera* ecotypes at the third point of harvest (lower case letters = significant differences between the cultivation variants within each ecotype; capital letters = significant differences between the different ecotypes within one cultivation variant; Tukey's HSD test, $p < 0.05$; DV = water-deficiency variant; SV = sulfur variant; NV = normal variant).

phenotypic differences under similar cultivation conditions. Ecotypes 1 and 4 were identified as having the highest yields of biomass and glucosinolate content (Table 1), and ecotypes 4 and 5 were identified as having the highest yields of phenolic acids and flavonoids, followed by ecotypes 1 and 6 (Table 2). It is most likely that the diverse characteristics in the phenotype (growth characteristics and chemical profile) found in our analysis are fixed genetically because the ecotypes arise from germplasm collection and were cultivated and analyzed in a similar manner. To exclude the effects of the environment on the analyzed parameter, seeds were sown and planted at the same time so that each plant was of the same age and at the same developmental stage. Interestingly, most trees of ecotypes 5 and 6 in the present study contained only one glucosinolate, Rhamno-Benzyl-GS, with none of the three Ac-Isomer GSs. This observation was not described by other authors. Shockey et al.[32] reported that acyl-activating enzymes are present in all living organisms. According to these authors, *Arabidopsis thaliana* L. possesses an acyl-activating enzyme superfamily containing 63 different genes. It is conceivable that different enzyme activity in the plants could lead to a lack of acetylated glucosinolates in some plants of the *M. oleifera* ecotypes.

As described by Brown et al.[33] for *A. thaliana*, we found higher glucosinolate contents in the younger leaves of *M. oleifera* than in the older leaves, whereas no differences in glucosinolate composition were determined (Supporting Information, Table 2). This could be explained by glucosinolate concentration dropping and stabilizing during leaf expansion.[33]

Consistent with findings of several authors in different glucosinolate containing plant species,[31,34] the glucosinolate content of the *M. oleifera* plants tended to increase as the plant matured. Although the glucosinolate content increased for all ecotypes at approximately 50−100%, the biomass accumulation increased at different degrees depending on the ecotype. Analysis using different *Salix* clones, a tree species that is very similar in its growth characteristics and high content of secondary metabolites (salicylates) to *M. oleifera*, showed that the amount of shoots and the biomass increased in trees of three different species from the first to the second year after planting.[35] On the one hand, this increase can be attributed to

DOI: 10.1021/jf506174v
J. Agric. Food Chem. 2015, 63, 2852−2861

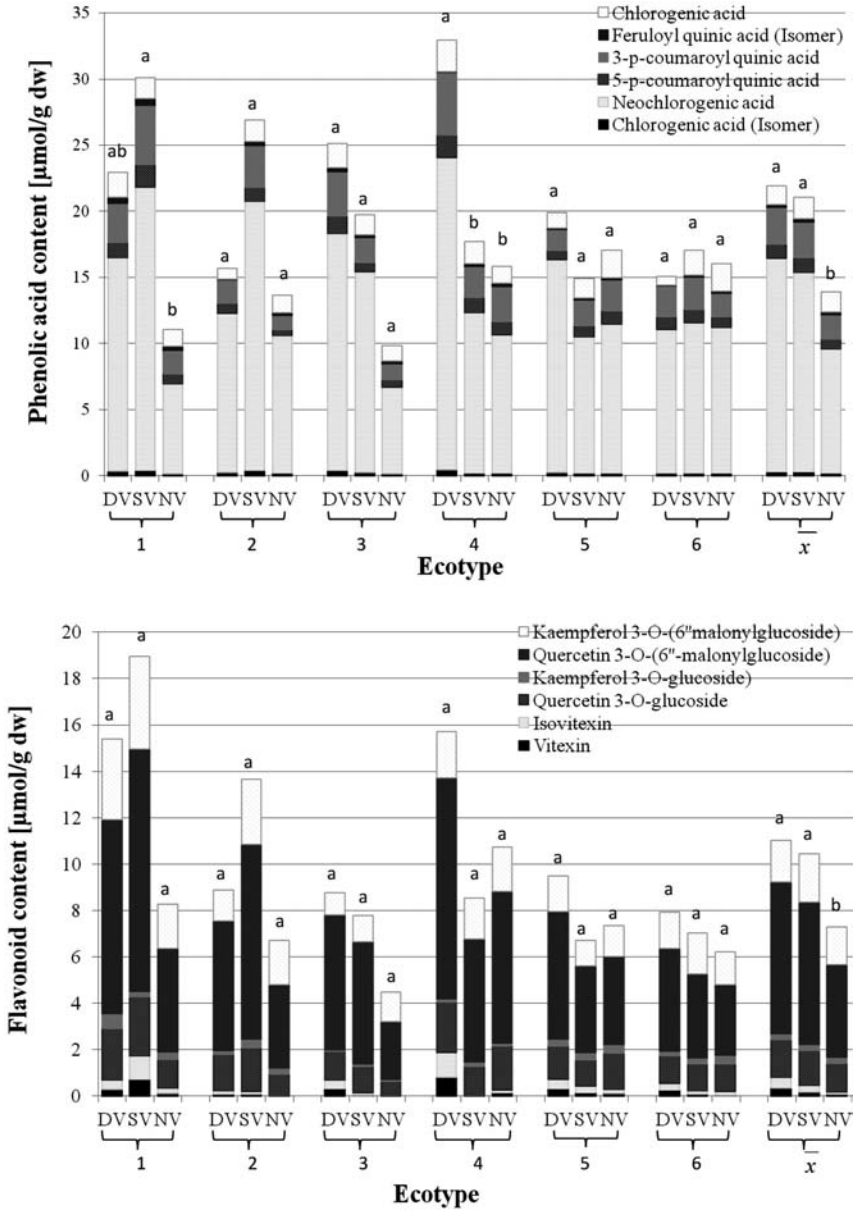

Figure 5. Phenolic acid and flavonoid content of six *Moringa oleifera* ecotypes in different cultivation variants at the third point of harvest (lower case letters = significant differences in total contents between the cultivation variants within each ecotype; Tukey's HSD test, $p < 0.05$; DV = water deficiency variant; SV = sulfur variant; NV = normal variant).

different environmental conditions at the harvests (temperature, day length, and solar radiation). On the other hand, the plant became better adapted over time (root penetration in the rhizosphere and access to existing water and nutrition sources). The ecotypes seem to be able to adapt to the set environmental conditions at a different speed and degree because of a variable increase in biomass accumulation over the five harvest points. A possible influence of plant age on phenolic acids and flavonoids will not be discussed at this point because these secondary metabolites were only determined at the second and third point of harvest.

Different authors have described the influence of nitrogen and sulfur fertilization[15,16,36] and different water regimes[23] on the glucosinolate content and growth of plants. Our analysis did not show a consistent result of either sulfur fertilization or water deficiency on growth and secondary metabolite accumulation in *M. oleifera*. Under water limitation (second point of harvest) ecotypes showed no differences in biomass accumulation and glucosinolate content (Supporting Information, Figure 2). With repeated moderate water limitation (third point of harvest, soil water tension did not exceed the range of the field capacity; Supporting Information, Table 3), biomass and plant height were reduced; on average across all ecotypes, the glucosinolate content increased in comparison to the normal variant (Figure 4). The content of phenolic acids (more so than flavonoids) at the third point of harvest was significant lower in the normal cultivation variant in comparison to the sulfur variant and under water limitation (Figure 5). Growth and glucosinolate content were not significantly influenced by sulfur fertilization. Additional sulfur input could not be identified in soil analyses two months after fertilization, indicating a complete sulfur uptake of plants. For further studies, more frequent and higher sulfur fertilization is recommended. Clearly, all effects are strongly ecotype-depend-

DOI: 10.1021/jf506174v
J. Agric. Food Chem. 2015, 63, 2852−2861

ent. To our knowledge, there are no studies available about the influence of sulfur and water deficiency on the growth and secondary metabolite content of *M. oleifera*. *M. oleifera* seems to be an intermediate between annual brassicaceous plants that contain glucosinolate and fast-growing tree species; this makes a comparison of the growth as well as secondary metabolite development of *M. oleifera* with other plants described in the literature very difficult. Furthermore, this rapidly growing tree is cut back several times a year,[1] which makes it even more difficult to compare growth parameters with other trees. Regular pruning, as also performed with the trees in the present study, promotes a compact and dense habitus, and the trees were much more strongly branched, resulting in an increased biomass accumulation. Clearly, the results of the present study showed that different cultivation variants influenced the morphological and chemical phenotype of single *M. oleifera* ecotypes differently.

A trade-off between biomass accumulation and secondary metabolite production, for example, as observed in the fast-growing tree species *Salix sericea* Marsh by Nichols-Orians et al.,[37] was not generally the case for the *M. oleifera* ecotypes investigated here. Ecotypes 1, 2, and 4 each had a biomass twice as high as those of ecotypes 5 and 6. At the same time, the glucosinolate content of ecotypes 1, 2, and 4−6 was not significantly different (Table 1). These findings are not in agreement with the trade-off between growth and defense over a resource-availability gradient, as stated in the growth-differentiation-balance hypothesis. However, on average across all ecotypes, the biomass accumulation was significantly higher in the normal cultivation variant in comparison to plants grown under drought stress at the third point of harvest. We found the opposite pattern for the glucosinolate content. These findings confirm results from Zhang et al.[24] or Schreiner et al.[38] that determined increased glucosinolate contents under moderate drought stress in *Brassica carinata* A. Braun and *Brassica rapa* L. ssp. *rapa*, whereas other authors found contradictory results (e.g., ref 39). The content of phenolic acids and flavonoids was not dependent on the biomass and plant height of *M. oleifera*.

Observed phenotypic differences under the same environmental conditions as in the present study can be attributed to plant genetics. The effects of sulfur and water deficiency (different cultivation variants) on six *M. oleifera* ecotypes, as a tree containing glucosinolate, had not previously been the subject of investigation. The phenotype of *M. oleifera* plants depended on the analyzed environmental factors (water deficiency and sulfur supply). This demonstrates that the plant genetics determine biomass production, growth, and content of phytochemicals, although environmental factors can modulate these parameters.[31] The presented results showed that no general cultivation recommendations can be made. The optimal cultivation of *M. oleifera* seems to be highly dependent on the ecotype. Nevertheless, potential suitable ecotypes, meeting the criteria of an optimal leaf yield (high biomass) with high levels of nutritional and health-promoting properties (glucosinolate, phenolic acid, and flavonoid content) in addition to a capability to withstand water limitation could be identified within the present study: Ecotypes 1 (TOT4880, origin USA) and 4 (TOT7267, origin India). Because of an enormous suggestibility of growth and secondary metabolites by the environment, findings should be proved in field trials in *M. oleifera* cultivation areas.

■ ASSOCIATED CONTENT

Ⓢ Supporting Information

Supporting Information Figure 1: Soil water tension in the bed of the *Moringa oleifera* ecotypes of normal cultivation and the water deficiency variant from September 2010 until August 2011; Supporting Information Figure 2: Influence of cultivation variants on biomass, height, and glucosinolate content of six *M. oleifera* ecotypes at the second point of harvest (lower case letters = significant differences between the cultivation variants within each ecotype; capital letters = significant differences between the different ecotypes within one cultivation variant; Tukey's HSD test, $p < 0.05$; DV = water deficiency variant; SV = sulfur variant; NV = normal variant); Supporting Information Table 1: Growing Parameters in the Three Different Growing Variants of *M. oleifera*; Supporting Information Table 2: Calculated Glucosinolate Profit of Harvested Leaf Material of Six Ecotypes of *M. oleifera* (first point of harvest); and Supporting Information Table 3: Temperature, Humidity, and Water Content of the Air in the Greenhouse at the Second and Third Point of Harvest. This material is available free of charge via the Internet at http://pubs.acs.org.

■ AUTHOR INFORMATION

Corresponding Author

*Tel.: +49 (0)30 2093 46430. Fax +49 (0)30 2093 46440. E-mail nadjafoerster@gmx.net.

Funding

We thank the Konrad-Adenauer-Stiftung e.V. and the Caroline von Humboldt Foundation, Humboldt-Universität zu Berlin, for supporting this work.

Notes

The authors declare no competing financial interest.

■ ACKNOWLEDGMENTS

We thank Andreas Ebert from AVRDC - The World Vegetable Center (Shanhua, Tainan, Taiwan) for providing seed material from *Moringa oleifera*.

■ ABBREVIATIONS USED

Ac-Isomer-GS I−III, acetyl-4-α-rhamnopyranosyloxy-benzyl glucosinolates I−III (tree isomers); dw, dry weight; fw, fresh weight; Rhamno-Benzyl-GS, 4-α-rhamnopyranosyloxy-benzyl glucosinolate

■ REFERENCES

(1) Fuglie, L. J.; Sreeja, K. V. Cultivation of *Moringa*. In *Miracle Tree: The Multiple Attributes of Moringa*; Fuglie, I. J., Ed.; CTA and CWS: Dakar, Senegal, 2001; pp 153−158.

(2) Ferreira, P. M. P.; Farias, D. F.; Oliveira, J. T. d. A.; Carvalho, A. d. F. U. *Moringa oleifera*: bioactive compounds and nutritional potential. *Rev. Nutr.* **2008**, *21*, 431−437.

(3) Palada, M. C.; Chang, L. C. Suggested cultural practices for Moringa, AVRDC publication no. 03−545. An International Cooperators' Guide prepared for AVRDC - The World Vegetable Center: Shanhua, Tainan, Taiwan, March 2003.

(4) Olivier, C. Intensive *Moringa oleifera* cultivation in the north of Senegal. http://www.moringanews.org/documents/Leafproduction.doc (accessed January 28, 2014).

(5) Gamatie, M. *Moringa oleifera* management systems in the river Niger valley: The case of Sarando area. *Development Potential of Moringa Products: Proceedings of a Workshop in Dar es Salaam, Tanzania*, 2001. http://www.docstoc.com/docs/97576483/Moringa-

DOI: 10.1021/jf506174v
J. Agric. Food Chem. 2015, 63, 2852−2861

oleifera-management-systems-in-the-river-Niger-valley-the (accessed January 28, 2014).
(6) Palada, M. C. *Moringa* (*Moringa oleifera* Lam.): A versatile tree crop with horticultural potential in the subtropical United States. *Hortscience.* **1995**, *31*, 794−797.
(7) Radovich, T. Farm and forestry, production and marketing profile for Moringa (*Moringa oleifera*). Technical report prepared for *Specialty Crops for Pacific Island Agroforestry*; Permanent Agriculture Resources: Hōlualoa, Hawai'i. http://www.agroforestry.net/scps/Moringa_specialty_crop.pdf (accessed January 28, 2014).
(8) Saha, P.; Jena, R. C.; Sahoo, B.; Sahoo, K.; Lenka, A.; Adansonia, A. Sufficing neutraceutical rich multipurpose leafy vegetable on earth: Moringa. *Odisha Rev.* **2012**, *October*, 72−80.
(9) Fahey, J. W. *Moringa oleifera*: A review of the medical evidence for its nutritional, therapeutic, and prophylactic properties. Part 1. *Trees for Life Journal* **2005**, *1*, http://www.tfljournal.org/article.php/20051201124931586 (accessed January 28, 2014).
(10) Bellostas, N.; Sørensen, J. C.; Nikiema, A.; Sørensen, H.; Pasternak, D.; Kumar, S. Glucosinolates in leaves of *Moringa* species grown and disseminated in Niger. *Afr. J. Agric. Res.* **2010**, *5*, 1336−1340.
(11) Thurber, M. D.; Fahey, J. W. Adoption of *Moringa oleifera* to combat under-nutrition viewed through the lens of the "Diffusion of Innovations" theory. *Ecol. Food Nutr.* **2009**, *48*, 212−225.
(12) Bennett, R. N.; Mellon, F. A.; Foidl, N.; Pratt, J. H.; Dupont, M. S.; Perkins, L.; Kroon, P. A. Profiling glucosinolates and phenolics in vegetative and reproductive tissues of the multi-purpose trees *Moringa oleifera* L. (Horseradish Tree) and *Moringa stenopetala* L. *J. Agric. Food Chem.* **2003**, *51*, 3546−3553.
(13) Siddhuraju, P.; Becker, K. Antioxidant properties of various solvent extracts of total phenolic constituents from three different agroclimatic origins of drumstick tree (*Moringa oleifera* Lam.) leaves. *J. Agric. Food Chem.* **2003**, *51*, 2144−2155.
(14) Dai, J.; Mumper, R. J. Plant phenolics: Extraction, analysis and their antioxidant and anticancer properties. *Molecules.* **2010**, *15*, 7313−7352.
(15) Ahmad, G.; Jan, A.; Arif, M.; Jan, M. T.; Khattak, R. A. Influence of nitrogen and sulfur fertilization on quality of canola (*Brassica napus* L.) under rainfed conditions. *J. Zhejiang Univ., Sci., B* **2007**, *8*, 731−737.
(16) Aires, A.; Rosa, E.; Carvalho, R. Effect of nitrogen and sulfur fertilization on glucosinolates in the leaves and roots of broccoli sprouts (*Brassica oleracea* var. *italica*). *J. Sci. Food Agric.* **2006**, *86*, 1512−1516.
(17) Bloem, E.; Haneklaus, S.; Schnug, E. Comparative effects of sulfur and nitrogen fertilization and post-harvest processing parameters on the glucotropaeolin content of *Tropaeolum majus* L. *J. Sci. Food Agric.* **2007**, *87*, 1576−1585.
(18) Mithen, R.; Bennett, R.; Marquez, J. Glucosinolate biochemical diversity and innovation in the Brassicales. *Phytochemistry* **2010**, *71*, 2074−2086.
(19) Sousa, C.; Pereira, D. M.; Pereira, J. A.; Bento, A.; Rodrigues, M. A.; Dopico-Garcia, S.; Valentão, P.; Lopes, G.; Ferreres, F.; Seabra, R. M.; Andrade, P. B. Multivariate analysis of Tronchuda cabbage (*Brassica oleracea* L. var. *costata* DC) phenolics: Influence of fertilizers. *J. Agr. Food Chem.* **2008**, *56*, 2231−2239.
(20) Li, J.; Zhu, Z.; Gerendás, J. Effects of nitrogen and sulfur on total phenolics and antioxidant activity in two genotypes of leaf mustard. *J. Plant Nutr.* **2008**, *31*, 1542−1655.
(21) Vallejo, F.; Tomás-Barberán, F. A.; García-Viguera, C. Effects of climatic and sulphur fertilizsation conditions, on phenolic compounds and vitamin C, in the inflorescences of eight broccoli cultivars. *Eur. Food Res. Technol.* **2003**, *216*, 395−401.
(22) De Pascale, S.; Maggio, A.; Pernice, R.; Fogliano, V.; Barbieri, G. Sulphur fertilization may improve the nutritional value of *Brassica rapa* L. subsp. *sylvestris*. *Eur. J. Agron.* **2007**, *26*, 418−424.
(23) Khan, M. A. M.; Ulrichs, C.; Mewis, I. Influence of water stress on the glucosinolate profile of *Brassica oleracea* var. *italica* and the performance of *Brevicoryne brassicae* and *Myzus persicae*. *Entomol. Exp. Appl.* **2010**, *137*, 1−8.
(24) Zhang, H.; Schonhof, I.; Krumbein, A.; Gutezeit, B.; Li, L.; Stüztel, H.; Schreiner, M. Water supply and growing season influence glucosinolate concentration and composition in turnip root (*Brassica rapa* ssp. *rapifera* L.). *J. Plant Nutr. Soil Sci.* **2008**, *171*, 255−265.
(25) Halkier, B. A.; Gershenzon, J. Biology and Biochemistry of Glucosinolates. *Annu. Rev. Plant Biol.* **2006**, *57*, 303−333.
(26) van Dam, N. M.; Tytgat, T. O. G.; Kirkegaard, J. A. Root and shoot glucosinolates: a comparison of their diversity, function and interactions in natural and managed ecosystems. *Phytochem. Rev.* **2009**, *8*, 151−186.
(27) de Abreu, I. N.; Mazzafera, P. Effect of water and temperature stress on the content of active constituents of *Hypericum brasiliense* Choisy. *Plant Physiol. Biochem.* **2005**, *43*, 241−248.
(28) Hernández, I.; Alegre, L.; Munné-Bosch, S. Drought-induced changes in flavonoids and other low molecular weight antioxidants in *Cistus clusii* grown under Mediterranean field conditions. *Tree Physiol.* **2004**, *24*, 1303−1311.
(29) Förster, N.; Ulrichs, C.; Schreiner, M.; Müller, C. T.; Mewis, I. Development of a reliable extraction and quantification method for glucosinolates in *Moringa oleifera*. *Food Chem.* **2015**, *166*, 456−64.
(30) Mewis, I.; Smetanska, I. M.; Müller, C.; Ulrichs, C. Specific poly phenolic compounds in cell culture of *Vitis vinifera* L. cv. Gamay Fréaux. *Appl. Biochem. Biotechnol.* **2011**, *164*, 148−161.
(31) Doerr, B.; Wade, K. L.; Stephenson, K. K.; Reed, S. B.; Fahey, J. W. Cultivar effect on *Moringa oleifera* glucosinolate content and taste: A pilot study. *Ecol. Food Nutr.* **2009**, *48*, 100−211.
(32) Shockey, J. M.; Fulda, M. S.; Browse, J. Arabidopsis contains a large superfamily of acyl-activating enzymes. Phylogenetic and biochemical analysis reveals a new class of acyl-coenzyme a synthetases. *Plant Physiol.* **2003**, *132*, 1065−1076.
(33) Brown, P. D.; Tokuhisa, J. G.; Reichelt, M.; Gershenzon, J. Variation of glucosinolates accumulation among different organs and developmental stages of *Arabidopsis thaliana*. *Phytochem.* **2003**, *62*, 471−481.
(34) Farnham, M. W.; Wilson, P. E.; Stephenson, K. K.; Fahey, J. W. Genetic and environmental effects on glucosinolate content and chemoprotective potency of broccoli. *Plant Breeding.* **2004**, *123*, 60−65.
(35) Förster, N. *Eignung unterschiedlicher salicylathaltiger Salix-Klone für die Arzneimittelindustrie*; Berliner ökophysiologische und phytomedizinische Schriften, Vol. 7; Der Andere Verlag: Tönning, Lübeck, und Marburg, Germany, 2010; pp 103−105.
(36) Omirou, M. D.; Papadopoulou, K. K.; Papastylianou, I.; Constantinou, M.; Karpouzas, D. G.; Asimakopoulos, I.; Ehaliotis, C. Impact of nitrogen and sulfur fertilization on the composition of glucosinolates in relation to sulfur assimilation in different plant organs in broccoli. *J. Agric. Food Chem.* **2009**, *57*, 9406−9417.
(37) Nichols-Orians, C. M.; Fritz, R. S.; Clausen, T. P. The genetic basis for variation in the concentration of phenolic glycosides in *Salix sericea*: Clonal variation and sex-based differences. *Biochem Syst. Ecol.* **1993**, *21*, 535−542.
(38) Schreiner, M.; Beyene, B.; Krumbein, A.; Stützel, H. Ontogenetic changes of 2-propenyl and 3-indolylmethyl glucosinolates in *Brassica carinata* leaves as affected by water supply. *J. Agric. Food Chem.* **2009**, *57*, 7259−7263.
(39) Gutbrodt, B.; Mody, K.; Dorn, S. Drought changes plant chemistry and causes contrasting responses in lepidopteran herbivores. *Oikos* **2011**, *120*, 1732−1740.

DOI: 10.1021/jf506174v
J. Agric. Food Chem. 2015, 63, 2852−2861

amino acids. In addition to the most abundant 7S β-conglycinin and the 11S glycinin, soybeans also accumulate a few other proteins that contain higher concentrations of methionine and cysteine. Earlier studies have demonstrated low-level accumulation of a methionine-rich protein in soybean seeds.[7,8] This 2S albumin protein contains 8.6% methionine and has been proposed as a candidate protein for overexpression in transgenic soybean seeds to elevate the methionine content.[9] Other potential proteins for overexpression in soybean include the Bowman−Birk inhibitor (BBI) and the BBI-related family of isoinhibitors. These protease inhibitors are rich in cysteine and are mainly responsible for the overall sulfur-containing amino acids of soybean seed.[10−12]

Leginsulin, a peptide consisting of 37 amino acids, belongs to the cysteine-knot family[13] and is homologous to pea (*Pisum sativum* L.) albumin (PA1b).[14] Soybean leginsulin is synthesized as a precursor polypeptide that is subjected to post-translational processing to give rise to 6 and 4 kDa peptides.[15−17] The 4 kDa peptide that is rich in cysteine residues is coined "leginsulin". We have previously shown that this peptide is preferentially soluble in 50% isopropanol and that the accumulation of this cysteine-rich peptide is drastically higher in Asian than in North American soybean accessions.[18] Furthermore, it was demonstrated that the soybean genome contains two leginsulin genes, which are differentially expressed in the embryonic axis and the cotyledons.[18] Because North American soybean cultivars accumulate low levels of leginsulin, we hypothesized that overexpression of this cysteine-rich peptide in North American soybean cultivars would improve their overall cysteine content. In this study, we crossed PI 427138, an Asian soybean accession, with an experimental North American line, resulting in lines that exhibited significantly higher protein content with improved protein quality. However, the amount of sulfur-containing amino acids was not increased.

MATERIALS AND METHODS

Reagents. Acrylamide, bis-acrylamide, ammonium persulfate, *N*,*N*,*N*′,*N*′-tetramethylethylenediamine (TEMED), and Coomassie Brilliant Blue G-250 and R-250 were obtained from BioRad Laboratories, Inc. (Hercules, CA, USA). Protease inhibitor cocktail (Plant ProteaseArrest) was obtained from G-Biosciences (St. Louis, MO, USA). IPG strips were obtained from GE Healthcare (Piscataway, NJ, USA). Urea, thiourea, and β-mercaptoethanol were obtained from Fisher Scientific (Pittsburgh, PA, USA). Dithiothreitol (DTT), iodoacetamide, EDTA, and 2-hydroxyethyl disulfide (2-HED) were obtained from Sigma-Aldrich (St. Louis, MO, USA).

Plant Material. During the course of identification of soybean lines exhibiting high BBI activity, we serendipitously identified PI 427138 as a soybean line accumulating high amounts of leginsulin. In 2007, LD00-3309 was crossed with PI 427138 in Urbana, IL, USA. LD00-3309 is an early-maturity group IV cultivar developed at the University of Illinois and was selected because it was one of the highest yielding, publicly developed cultivars available at the time.[19] In 2008, two F1 plants were grown, and the seeds from each plant were harvested separately. In 2009, approximately 500 seeds were planted from each F1 plant. The F2 populations confirmed that each putative F1 plant was the product of cross-pollination with segregation for flower and pubescence color as expected, and 285 plants were harvested and threshed individually. In 2010, seeds from each harvested F2 plant were planted in rows 1.2 m long. Between 1 and 5 single plants were harvested from 66 rows selected for agronomic appearance for a total of 172 plants. In 2011, 27 of the F4 plant rows had a homogeneous appearance and acceptable agronomic characteristics and were bulk harvested.

Seeds from 40 F4 lines with acceptable agronomic characteristics were selected for characterization. Fifty percent isopropanol soluble proteins were isolated from these 40 F4 plants and examined for the accumulation of leginsulin. Examination of Coomassie-stained gels revealed that 15 plants accumulated high amounts of leginsulin (Supplemental Figure 1). We also measured the sulfur content of the soybean seeds from 40 plants by inductively coupled plasma−mass spectrometry. The sulfur content of these plants ranged from 3000 to 4000 ppm (Supplemental Figure 2). Seeds from the 40 plants were advanced another generation, and seeds from lines having a homogeneous appearance and acceptable agronomic characteristics were bulk harvested. From these F5 plants, we selected two lines (Leg-3 and Leg-7) that accumulated high amounts of leginsulin and high sulfur content for further characterization. Another line (Leg-8) that had high sulfur content but failed to accumulate leginsulin was also selected for further analysis.

Small plots of the three experimental lines plus the two parents were planted in two replications at Bellflower, Ivesdale, and Urbana, IL, USA, and Bradford, MO, USA, and on two soil types at Portageville, MO, USA. Seeds were harvested from all plots for analysis.

Nitrogen Content. Fifteen seeds per line from each field plot were ground to a fine powder and used for total nitrogen/protein analysis. Nitrogen content was measured using a LECO truSpec model FP-428 nitrogen analyzer (St. Joseph, MI, USA). A 200 mg sample of seed powder was combusted at 900 °C in a chamber in the presence of oxygen, leading to the release of carbon dioxide, water, and nitrogen. The gases were then passed over a potassium hydroxide aqueous solution, eliminating carbon dioxide and water. A column containing a thermal conductivity detector was then used to separate the nitrogen from any residual carbon dioxide and water, and the remaining nitrogen content was measured. The instrument was calibrated using ultrapure EDTA of known nitrogen content. The protein content of the seeds was inferred from its nitrogen content using a protein correction factor of 6.25. Three separate biological replicates were evaluated per line, and results were compared using standard deviation of the mean.[20]

Oil Content. The oil content of 10−15 seeds per line was determined using an Oxford Instruments America MQC Oilseeds Analyzer with a 26 mm probe (Concord, MA, USA). A 15-point calibration curve was built using data obtained from both pure soybean oil and soybean seeds of known oil contents (11−21%) as determined by the University of Missouri Experiment Station Chemical Laboratories (AOCS Official Method Ca 5b-71). Three separate biological replicates were evaluated per line, and results were compared using standard deviation of the mean. JMP version 9 software (SAS Institute Inc., Cary, NC, USA) was used to perform one-way analysis of variance (ANOVA) tests.[20]

Sulfur Content. Inductively coupled plasma−mass spectrometry was performed as previously described.[21] Individually weighed dry seeds were digested overnight with 2.5 mL of concentrated HNO_3 at room temperature before the samples were heated to 105 °C over 2 h and then cooled to room temperature over 2 h. Following this step, the samples were diluted with ultrapure water and transferred to 96-well autosampler plates. A PerkinElmer Elan DRC-e inductively coupled plasma mass spectrometer (Waltham, MA, USA) with an Apex Desolvation Nebulizer, a FAST sampling valve, and an Elemental Scientific SC4 DX autosampler (Omaha, NE, USA) was used for the analysis of sulfur. A liquid reference material composed of pooled samples of soybean digests was run every ninth sample to correct for ICP-MS run-to-run variation and within-run drift. All samples were normalized to the recorded dry weights.

Amino Acid Analysis. Amino acid analysis was performed at the Donald Danforth Plant Science Center Proteomics and Mass Spectrometry Facility. For the determination of the total amino acid content, the seed powder was first subjected to hydrolysis with 6 N HCl. For the quantification of methionine and cysteine, duplicate samples were first subjected to an initial oxidation step using performic acid prior to acid hydrolysis. Amino acids were quantified using the manufacturer's instructions for sample preparation in the Waters AccQ-Tag Ultra Kit and quantified on a Waters Acquity UPLC system

DOI: 10.1021/jf505202z
J. Agric. Food Chem. 2015, 63, 2862−2869

(Milford, MA, USA). Samples were run in quadruplicate and subjected to appropriate statistical analysis. Cysteine and methionine quantities are reported as cysteic acid and methionine sulfone.

1-D Electrophoresis. For 1-D electrophoretic analysis, dried mature seeds were ground into a fine powder, and 10 mg was placed into a tube for extraction using 1 mL of sodium dodecyl sulfate (SDS) sample buffer (60 mM Tris-HCl, pH 6.8, 2% SDS (w/v), 10% glycerol (v/v), and 5% 2-mercaptoethanol (v/v)) followed by boiling for 5 min. The clarified supernatant was resolved with 15% gels run using a Hoeffer SE 250 mini-Vertical electrophoresis apparatus (GE Healthcare). Separation was achieved with a constant 20 mA/gel and a typical run time of 1.2 h. Gels were removed from the cassette and placed immediately in Coomassie Blue R-250 solution.

Western Blot Analysis. Western blot analysis was performed as described earlier.[18] Briefly, total seed proteins or 50% isopropanol extracted proteins were first resolved on a 15% SDS-PAGE gels. Subsequently, the proteins were transferred to a 0.45 μm nitrocellulose membrane. After blocking with TBS (10 mM Tris-HCl, pH 7.5, 500 mM NaCl) containing 5% nonfat dry milk, the nitrocellulose membranes were incubated overnight with either lunasin or synthesized BBi peptide (N-CVDITDFCYEPCKPSEDDK) antibodies that had been diluted 1:5000 in TBST (TBS with 3% nonfat dry milk containing 0.2% Tween 20). Following three washings with TBST, the membranes were incubated with goat anti-rabbit IgG–horseradish peroxidase conjugate. Proteins reacting specifically with the antibodies were detected using the Pierce SuperSignal West Pico kit's instruction (Rockford, IL, USA).

2-D Electrophoresis. Sample preparation for 2-D electrophoretic analysis was carried out as previously described.[22] For isoelectric focusing, 300 μg of protein sample was loaded per strip using overnight in-gel rehydration. Linear gradient, 13 cm IPG strips (GE Healthcare) were brought to a rehydration volume of 250 μL with 7 M urea, 2 M thiourea, 1% CHAPS, 2% C7BzO, 5% glycerol, and 2.2% 2-HED. Strips were then passively rehydrated with the entire rehydration solution containing protein sample at 23 °C for 15 h prior to focusing. Prior to the second dimension, IEF strips were equilibrated with 5% SDS in a urea-based solution (0.05 M Tris-Cl, pH 8.8, 6 M urea, 30% glycerol, and 0.1% bromophenol blue) containing 2% DTT for 20 min and again but with 2.5% iodoacetamide for 20 min. IEF strips were placed carefully onto a Hoeffer SE600 (GE Healthcare) 16%T vertical second-dimension and secured into place with a warm 1% agarose SDS-PAGE running buffer solution (0.2% SDS). Gels were run at an initial 10 mA/gel for 1 h followed by 5 W/gel for the remainder of the run (elimination of dye front; approximately 4 h). After electrophoresis, the gels were immediately removed and fixed in 5:4:1 methanol/water/acetic acid for 30 min, followed by two brief rinses in water, and stained in a Coomassie G-250 solution overnight.

Image Acquisition and Analysis. 2-D Coomassie-stained gels were destained with multiple changes of ultrapure H_2O to remove background. Individual gels of PI 427138 and LD00-3309 were scanned separately using an Epson V700 Perfection scanner controlled through Adobe Photoshop. Images were analyzed using Decodon Delta2D v3.6 (Greifswald, Germany) to provide normalized percent spot volume data using a technique known as differential gel imaging. Essentially, each gel image was imported into Delta2D individually and overlaid to provide a combined fusion image in gray scale, whereas the individual images of each were assigned either a blue (PI 427138) or an orange (LD00-3309) color. Differences in color between the two samples indicate a higher or lower amount of that particular protein in that sample. Delta2D parameters were set to maximize spot detection (using *global* image warping and *exact* spot matching) and minimize background detection.

RESULTS

PI 427138 Accumulates High Amounts of Leginsulin. BBI and the BBI-related family of isoinhibitors are rich in cysteine and are mainly responsible for the overall sulfur-containing amino acids of soybean seed.[10−12] During the course of screening a diverse array of soybean accessions from the USDA Soybean Germplasm Collection for the identification of soybean lines with high and low contents of Bowman–Birk protease inhibitor, we serendipitously observed that soybean PI 427138 accumulated high amounts of a 4 kDa protein. We have previously shown that Asian soybean accessions accumulate higher amounts of a 4 kDa protein than the genetic base of U.S. cultivars.[18] On the basis of Western blot analysis and mass spectrometry, this protein was identified as leginsulin.[18] Even though this protein accumulates in higher amounts in Asian soybean accessions, its contribution to overall protein content of the seed is only minimal. To confirm the identity of the 4 kDa protein that is enriched in PI 427138, we performed Western blot analysis using antibodies raised against the leginsulin peptide. The antibodies reacted strongly against the 4 kDa peptide, indicating that this protein is leginsulin (Figure 1).

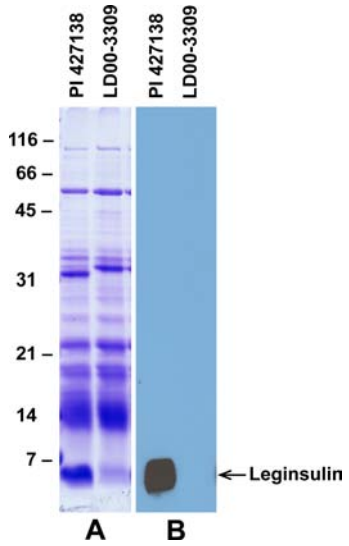

Figure 1. Accumulation of leginsulin in soybean seeds. Isopropanol (50%) soluble proteins were extracted from PI 427138 (lane 1) and LD00-3309 (lane 2), a high-yielding North American soybean cultivar, and analyzed by SDS-PAGE. Separated proteins were detected by staining the gel with Coomassie Blue (panel A) or electrophoretically transferred to a nitrocellulose membrane and reacted with leginsulin specific antibodies that were diluted 1:5000 in TBS containing 3% dry milk powder. Immunoreactive proteins were identified using anti-rabbit IgG–horseradish peroxidase conjugate followed by chemiluminescent detection (panel B). The arrow points to the 4 kDa immunoreactive peptide preferentially accumulating in PI 427138. The 4 kDa protein band in the stained gel is a mixture of the proteins, whereas the immunoreactive band shown in panel B is a single protein. The positions and sizes of the molecular weight markers in kilodaltons are shown on the left side of the figure. The same amount of protein used in panel A was used for the Western blot analysis (panel B). Also, note the size polymorphism of a prominent polypeptide (32–33 kDa) between PI 427138 and LD00-3309; however, the basis of this polymorphism is unknown (panel A).

Information on the country of origin, phenotypic data, and seed composition of PI 427138 was obtained from the USDA Germplasm Resources Information Network (GRIN) database (http://www.ars-grin.gov/cgi-bin/npgs/acc/search.pl?accid=PI+427138+). PI 427138 originated from South Korea, belongs to maturity group 0, and accumulates 48% protein and 14% oil. Earlier we reported the biochemical characterization of several high-protein soybean accessions.[23] By high-resolution two-

DOI: 10.1021/jf505202z
J. Agric. Food Chem. 2015, 63, 2862−2869

dimensional gel electrophoretic analysis, it was demonstrated that the 11S globulins (glycinin) were mainly responsible for the increased protein content of these high-protein soybean accessions. Because PI 427138 is also a high-protein accession, we wanted to examine its protein composition. For this purpose we performed high-resolution two-dimensional gel electrophoretic analysis of seed proteins of PI 427138 and compared it with LD00-3309, a high-yielding, publicly developed cultivar that contains 38% protein.[19] To monitor proteome differences between PI 427138 and LD00-3309, total seed proteins resolved by 2-DE were analyzed using Delta2D image analysis software (Figure 2). Delta2D parameters were set to maximize

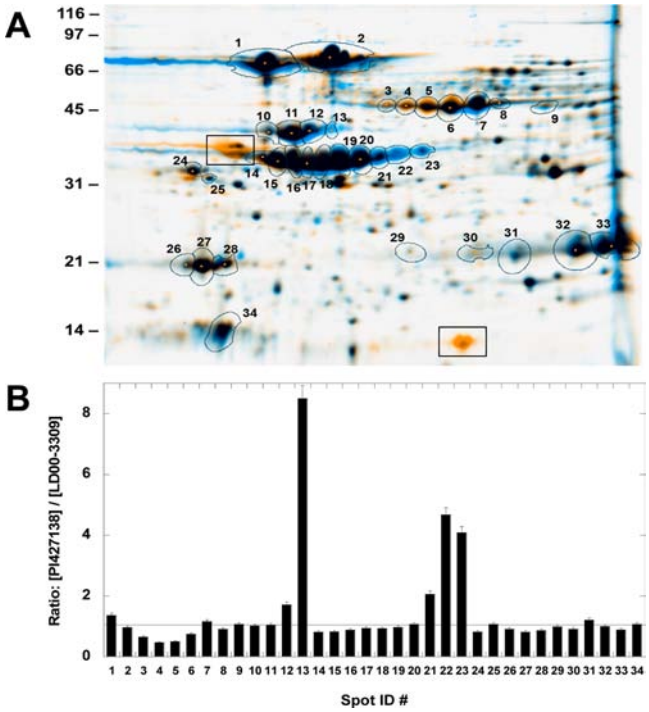

Figure 2. 2-DE comparison of total seed proteins extracted from PI 427138 and LD00-3309. Equal volumes of identically extracted seed proteins were separated using 2-DE. The Coomassie-stained gel images were analyzed using Delta2D software. Panel A shows the fusion of the two independently derived images. Gel images of PI 427138 and LD00-3309 were imported separately into Delta2D and overlaid to provide a combined fusion image. The blue color denotes those protein spots that were found to be higher in percent spot volume in PI 427138 compared with LD00-3309, whereas the orange color denotes those proteins that were found to be lower in percent spot volume. IEF separation was from pH 4 to 7, and molecular weight markers are designated in kDa. Panel B shows the ratios of percent volume [PI 427138]/[LD00-3309] of 34 spots generated from percent spot volume data collected using Delta2D image analysis software. The identities of the 34 proteins spots are shown in Supplemental Table 1. Leginsulin is not detected in these gels due to their low abundance in the total seed protein fraction.

spot detection (using global image warping and exact spot matching). A total of 34 protein spots identified previously by matrix-assisted laser desorption time of flight (MALDI-TOF) mass spectrometry as the major seed storage proteins of soybean were compared (Supplemental Table 1).[23] A comparison of the spot percent volume ratio differences clearly indicated that spots 12 (glycinin A3B4), 13 (glycinin A3B4), 21 (glycinin A1aBx precursor), 22 (proglycinin A1ab1b), and 23 (proglycinin A1ab1b) accumulated at higher amounts in PI 427138 (Figure 2). The preferential accumulation of the 11S globulins appears to the major contributing factor for the higher protein content of PI 427138.

Characterization Soybean Lines Derived from PI 427138 × LD00-3309 Crosses. The influence of environment on the seed composition traits of soybean LD00-3309, PI 427138, Leg-3, Leg-7, and Leg-8 were evaluated by growing these soybean lines at six locations, three in Illinois and three in Missouri. Total seed protein and oil content were determined with a LECO truSpec model FP-428 nitrogen analyzer and near-infrared (NIR) spectroscopy, respectively. The protein content of LD00-3309 seeds obtained from the six locations ranged from 36 to 39% (Figure 3A), whereas their oil content ranged from 19 to 21% (Figure 3B). In contrast, the protein content of PI 427138 seeds ranged from 45 to 51% (Figure 3A) and their oil content ranged from 11 to 13% (Figure 3B). The protein content of Leg-3, Leg-7, and Leg-8 ranged from 42 to 47%, which was significantly higher than that of LD00-3309, indicating the high-protein trait from PI 427138 had been successfully introgressed into these three lines (Figure 3A). The seed oil content of these soybean lines, which ranged from 14 to 17%, was intermediate when compared with the values obtained for the parents (Figure 3B). In general, soybeans grown in Columbia, MO, USA, had the highest protein content, whereas plants grown in Portageville, MO, USA, had the highest seed oil content.

The protein composition of leginsulin introgressed lines (Leg-3 and Leg-7) was also examined by 2-D gel electrophoresis (Figure 4). An examination of the Coomassie Blue stained gel revealed that PI 427138 accumulated higher amounts of 11S globulins when compared to LD00-3309. PI 427138 also failed to accumulate the Gy4 subunits. Interestingly, no substantial difference in the β-conglycinin content was observed between these two lines (Figure 4). The leginsulin introgressed lines (Leg-3 and Leg-7) also exhibited higher 11S glycinin content and, like PI 427138, lacked the Gy4 subunits (Figure 4).

Leginsulin Introgressed Lines Accumulate Lower Amounts of Bowman–Birk Protease Inhibitor. We also investigated the effect of growing location on the accumulation of leginsulin in soybean seeds. Isopropanol (50%) soluble proteins isolated from seeds grown at six locations were analyzed by SDS-PAGE (Figure 5A). A prominent 4 kDa protein was detected readily in leginsulin introgressed lines from all six locations. Western blot analysis using leginsulin antibodies confirmed the identity of this 4 kDa protein as leginsulin (Figure 5B). Previous studies have shown that the introduction of sulfur-rich proteins in soybean is often accomplished at the expense of native sulfur-rich proteins.[24] Bowman–Birk protease inhibitors are rich in cysteine and are the major contributors to the overall sulfur amino acid content of the seed. To investigate the effect of introgression of leginsulin on the accumulation of BBI, we performed Western blot analysis using antibodies raised against BBI. This analysis revealed a reduction in the accumulation of BBI in the leginsulin introgressed lines (Figure 5C). LD00-3309, which does not accumulate leginsulin, contained relatively high amounts of BBI (Figure 5C). These results suggest that accumulation of leginsulin in Leg-3 and Leg-7 occurs at the expense of BBI.

Leginsulin Introgressed Lines Contain Relatively Higher Amounts of Elemental Sulfur but the Concen-

DOI: 10.1021/jf505202z
J. Agric. Food Chem. 2015, 63, 2862–2869

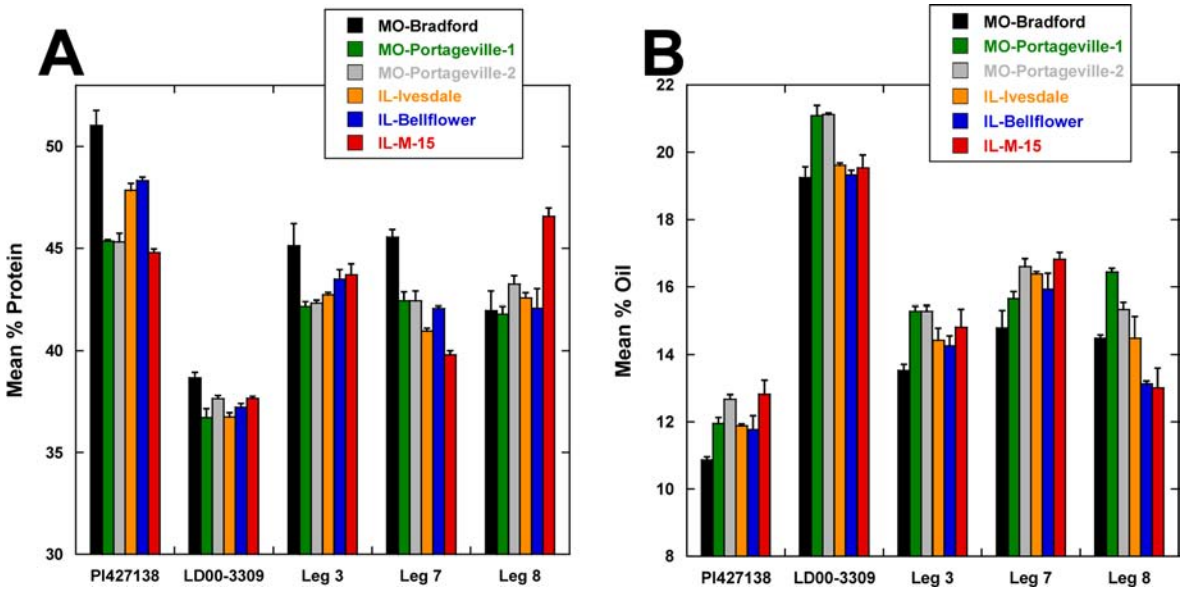

Figure 3. Mean protein and oil concentrations of soybean seeds grown in six different locations. Soybeans LD00-3309, PI 427138, Leg-3, Leg-7, and Leg-8 were grown at six locations (three in Illinois and three in Missouri). Seed protein and oil contents were determined with a LECO truSpec model FP-428 nitrogen analyzer and near-infrared (NIR) spectroscopy, respectively. Three separate biological replicates were evaluated per line. Error bars indicate the standard deviation of the mean.

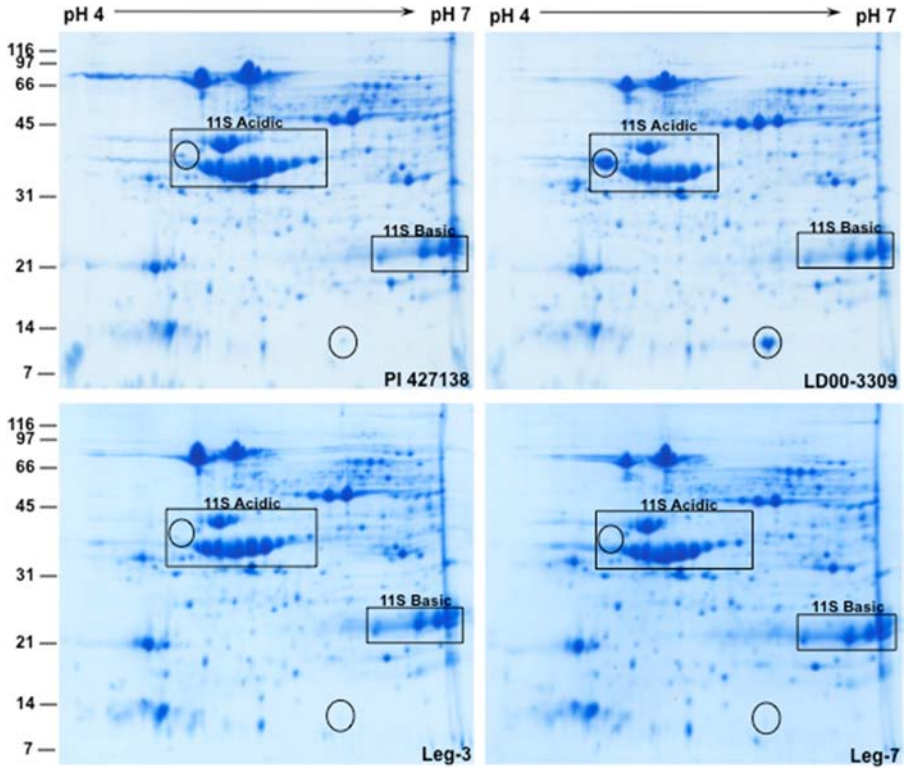

Figure 4. Comparison of the storage proteins of leginsulin introgressed soybean lines by 2-D gel electrophoresis. Total seed proteins isolated from the parents (PI 427138 and LD00-3309) and leginsulin introgressed lines (Leg-3 and Leg-7) were first separated by isoelectric focusing using a pH gradient from 4 to 7 and then by SDS-PAGE on a 13% gel. The rectangles in each panel represent the acidic and basic subunits of glycinin. The circles represent the Gy4 subunits, which are missing in PI 427138, Leg-3, and Leg-7. The gels were stained with Colloidal Coomassie Blue G-250. The positions and sizes of the molecular weight markers in kilodaltons are shown on the left side of the figure. Leginsulin is not detected in these gels due to their low abundance in the total seed protein fraction.

tration of Sulfur-Containing Amino Acids Remains Unchanged. The sulfur content of soybean seeds grown at six different locations was determined by inductively coupled plasma− mass spectrometry (Figure 6). Regardless of the location, LD00-3309 had the lowest amount of sulfur, which ranged from 3000 to 3600 ppm, whereas PI 427138 had the highest amount in most locations, ranging from 4000 to 4780 ppm (Figure 6). The sulfur content averaged from the six

DOI: 10.1021/jf505202z
J. Agric. Food Chem. 2015, 63, 2862−2869

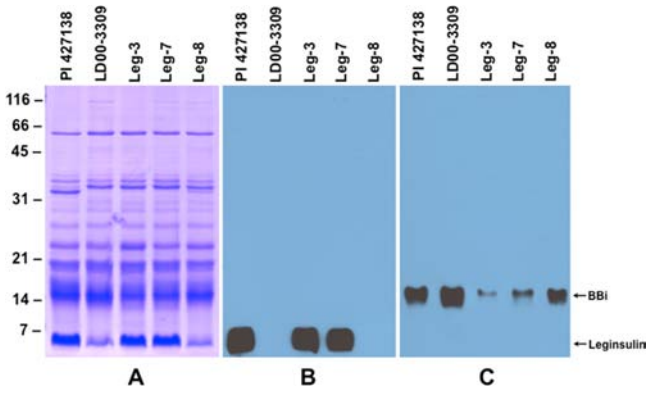

Figure 5. Leginsulin and Bowman–Birk protease inhibitor accumulation in soybean seeds. Fifty percent isopropanol soluble proteins isolated from the parents (PI 427138 and LD00-3309) and the resulting offspring (Leg-3, Leg-7, and Leg-8) were separated by SDS-PAGE on a 15% gel. Resolved proteins were detected by staining the gel with Coomassie Blue (panel A) or electrophoretically transferred to a nitrocellulose membrane and probed with leginsulin (panel B) or Bowman–Birk protease inhibitor (panel C) specific antibodies that were diluted 1:5000 in TBS containing 3% dry milk powder. Immunoreactive proteins were identified using anti-rabbit IgG–horseradish peroxidase conjugate followed by chemiluminescent detection.

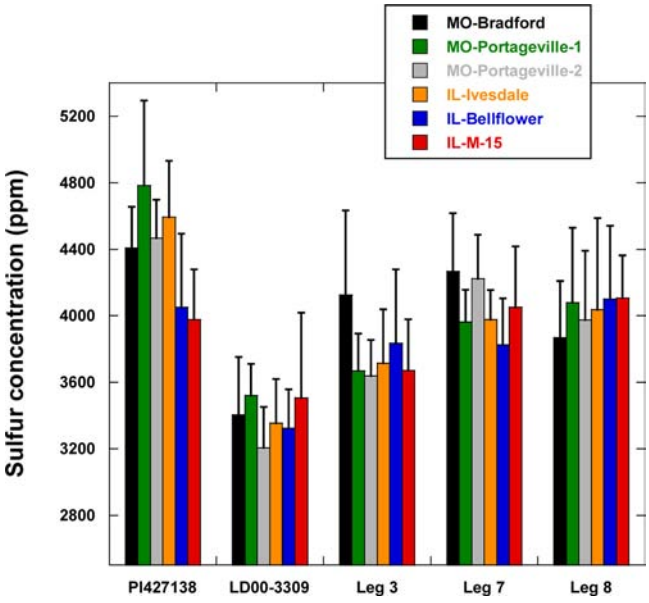

Figure 6. Elemental sulfur content of soybean seeds grown at six different locations. Soybeans LD00-3309, PI 427138, Leg-3, Leg-7, and Leg-8 were grown at six locations (three in Illinois and three in Missouri). Sulfur was determined by inductively coupled plasma–mass spectrometry. The error bars indicate the standard deviation of the mean.

locations for Leg-3, Leg-7, and Leg-8 were 3774, 4057, and 4027 ppm, respectively. These values are significantly higher than values obtained for LD00-3309. These results indicate that the high-sulfur trait from PI 427138 has been partially transferred to Leg-3, Leg-7, and Leg-8. It is also evident that growing location had only a minimal effect on sulfur accumulation in the seeds with a similar trend observed at all six locations (Figure 6).

The two soybean lines used as parents in this study, LD00-3309 and PI 427138, differ significantly in their sulfur contents. LD00-3309 averaged from the six locations had 3380 ± 264 ppm of sulfur, whereas PI 427138 had 4499 ± 113 ppm of sulfur. We were interested to examine if the differences seen in the sulfur content are also reflected in the concentration of sulfur-containing amino acids, cysteine and methionine. For this purpose we determined the amino acid content of soybean seeds of LD00-3309, PI 42713, Leg-3, Leg-7, and Leg-8. Interestingly the overall concentrations of cysteine and methionine were equivalent in all of these soybean lines (Table 1).

DISCUSSION

In this study we have successfully introgressed leginsulin from PI 427138 into a North American experimental line. Previously we have shown that leginsulin is encoded by two closely related genes (Gm13 g26330 (leginsulin 1) and Gm13 g26340 (leginsulin 2)). These two genes are located on chromosome 13 and are 5.9 kB apart.[18] Accumulation of leginsulin is drastically lower in most North American soybean cultivars than in Asian accessions.[18] Northern blot analysis has revealed that leginsulin accumulates only in the cotyledons but not in the embryonic axis in the North American soybean cultivars. In contrast, leginsulin mRNA was abundantly expressed in both the cotyledons and the embryonic axis of Asian soybean accessions. Thus, it appears the expression of leginsulin in both cotyledons and the embryonic axis may be responsible for the higher accumulation of leginsulin in Asian soybean accessions.[18]

Leginsulin, a peptide composed of 37 amino acids, is rich in cysteine residues. Our objective was to improve the overall sulfur amino acid content into adapted experimental lines by introgression of leginsulin. However, this goal was elusive because amino acid analysis revealed that the overall sulfur amino acid content (cysteine + methionine) remained unchanged (Table 1). Accumulation of Bowman–Birk protease inhibitor, another cysteine-rich protein, is reduced in leginsulin introgressed soybean lines Leg-3 and Leg-8, indicating that there is a limitation in the availability of cysteine in developing soybean seeds. Introgression of sulfur-rich proteins results in siphoning the limited cysteine pool from native sulfur-rich proteins such as Bowman–Birk protease inhibitor. Previous studies have shown the expression of Brazil nut 2S albumin, a methionine-rich protein, in transgenic soybean resulted in the reduction of Kunitz trypsin inhibitor.[24] Thus, it appears that introduction of sulfur-rich proteins into soybean alone will not be sufficient for improving the sulfur amino acid content. Metabolic engineering of sulfur assimilatory pathway will be critical for improving the availability of cysteine and methionine in developing soybean seeds.[25] Recent studies have demonstrated that such an approach can be used successfully to elevate the sulfur amino acid content of soybean seeds.[26,27]

Numerous high-protein plant introductions exist in the USDA Germplasm Collection. These plant introductions are currently being exploited as a source of high-protein alleles. The USDA ARS Soybean Genetics and Genomics Database (SoyBase) lists several potential protein QTLs located in different genomic regions. In addition, recent studies have identified new QTLs that could be used by breeders to develop high-protein lines.[28−30] We have transferred the high-protein trait of PI 427138 into Leg-3, Leg-7, and Leg-8, resulting in a substantial increase in the overall protein content. The increase

DOI: 10.1021/jf505202z
J. Agric. Food Chem. 2015, 63, 2862−2869

Table 1. Total Hydrolyzed Amino Acid Composition of Parental Seeds and Leginsulin Introgressed Crosses[a]

	mol %				
amino acid	PI 427138	LD00-3309	Leg-3	Leg-7	Leg-8
CyA	1.52 ± 0.21	1.49 ± 0.07	1.51 ± 0.01	1.45 ± 0.01	1.56 ± 0.05
His	2.16 ± 0.01	2.26 ± 0.01	2.15 ± 0.00	2.14 ± 0.02	2.24 ± 0.06
Ser	4.28 ± 0.30	5.15 ± 0.74	4.19 ± 0.17	5.27 ± 1.21	4.17 ± 0.35
Arg	6.19 ± 0.44	5.59 ± 0.01	5.87 ± 0.04	6.13 ± 0.35	5.91 ± 0.59
Gly	7.67 ± 0.06	7.56 ± 0.02	7.58 ± 0.12	7.37 ± 0.04	7.82 ± 0.18
Asp	11.63 ± 0.14	11.86 ± 0.09	11.92 ± 0.27	11.80 ± 0.11	11.85 ± 0.23
MetS	2.00 ± 0.11	1.98 ± 0.04	2.00 ± 0.04	1.94 ± 0.05	2.15 ± 0.01
Glu	16.81 ± 0.13	15.99 ± 0.16	16.55 ± 0.11	16.64 ± 0.51	16.17 ± 0.48
Thr	3.68 ± 0.12	4.07 ± 0.23	3.67 ± 0.05	3.96 ± 0.40	3.80 ± 0.25
Ala	6.23 ± 0.01	6.21 ± 0.04	6.29 ± 0.12	6.09 ± 0.01	6.38 ± 0.08
Pro	5.90 ± 0.07	5.78 ± 0.05	5.91 ± 0.01	5.91 ± 0.09	5.79 ± 0.06
Lys	5.97 ± 0.04	6.04 ± 0.05	6.16 ± 0.08	5.99 ± 0.05	6.18 ± 0.02
Tyr	2.46 ± 0.03	2.62 ± 0.00	2.18 ± 0.46	2.38 ± 0.06	2.30 ± 0.14
Val	6.24 ± 0.04	6.22 ± 0.16	6.29 ± 0.06	5.88 ± 0.45	6.27 ± 0.06
Ile	5.15 ± 0.06	5.10 ± 0.21	5.31 ± 0.01	4.99 ± 0.42	5.27 ± 0.11
Leu	7.58 ± 0.04	7.77 ± 0.11	7.82 ± 0.04	7.58 ± 0.20	7.69 ± 0.09

[a]Dry seed powder from triplicate samples was analyzed by HPLC to measure the total hydrolyzed amino acids from the parents (PI 427138 and LD00-3309) and the resulting offspring (Leg-3, Leg-7, and Leg-8). Cysteine is reported as cysteic acid (CyA), and methionine is reported as methionine sulfone (MetS). Results are the mean of three samples (n = 3), reported along with standard error (SE) of the mean.

in the protein content is, however, accompanied by a reduction in the oil content. It is well established that there is a negative correlation between seed protein and oil content.[31−35] Typically an increase of 2% protein results in a 1% decrease in oil content.[36] It has been proposed that this inverse correlation is associated with either a pair of tightly linked QTLs for protein and oil or by one pleiotropic QTL, the two alleles of which have inverse effects on both oil and protein contents.[28] Recent studies have identified new oil QTLs that have no major impact on seed protein content.[28−30] These oil-related QTLs could be exploited to increase the oil content of Leg-3, Leg-7, and Leg-8 without lowering the protein content.

Our study has identified PI 427138 as a *Gy*4 mutant. 2-D gel electrophoresis analysis of the total seed proteins from PI 427138 reveals the absence of the A5, A4, and B3 glycinin subunits, the product of the Gy4 gene. Leg-3, Leg-7, and Leg-8 generated in this study were also found to lack A5, A4, and B3 glycinin subunits (Figure 4). Tofu, a food product made of soy milk, is widely consumed in Asian countries. It is well-known that the tofu firmness, texture, and volume can be influenced by the absence of specific glycinin polypeptides.[37−39] For this reason *Gy*4 null lines such as 'Enrei' and 'Raiden' are commonly utilized in breeding programs to develop high-quality tofu cultivars. Thus, the soybean experimental lines Leg-3, Leg-7, and Leg-8 could be valuable breeding material for the production of high-quality tofu. It is not known if there is any correlation between the concentration of sulfur-containing amino acids and tofu quality. The 7S β-conglycinin is relatively low in sulfur amino acids, and its absence has been shown to alter tofu quality.[37] Additional studies are required to establish a correlation or lack thereof between the sulfur amino acid content of soybean seed proteins and tofu quality.

■ ASSOCIATED CONTENT

Supporting Information

Supplemental Table 1 and Supplemental Figures 1 and 2. This material is available free of charge via the Internet at http://pubs.acs.org.

■ AUTHOR INFORMATION

Corresponding Author

*(H.B.K.) Mail: Plant Genetics Research Unit, USDA-ARS, 108 Curtis Hall, University of Missouri, Columbia, MO 65211, USA. E-mail: Hari.Krishnan@ars.usda.gov.

Notes

The authors declare no competing financial interest.

■ ACKNOWLEDGMENTS

We thank Dr. M. S. Pathan for growing soybeans at University of Missouri Fisher Delta Research Center, Portageville, MO, USA. Product names are necessary to report factually on available data; however, the University of Missouri and the USDA neither guarantee nor warrant the standard of product, and the use of the name by the University of Missouri and the USDA implies no approval of the product to the exclusion of others that may be suitable.

■ REFERENCES

(1) Imsande, J. Selection of soybean mutants with increased concentrations of seed methionine and cysteine. *Crop Sci.* **2001**, *41*, 510−515.

(2) Krishnan, H. B. Engineering soybean for enhanced sulfur amino acid content. *Crop Sci.* **2005**, *45*, 454−461.

(3) Townsend, J. A.; Thomas, L. A. Factors which influence the *Agrobacterium*-mediated transformation of soybean. *J. Cell Biochem. Suppl.* **1994**, *18A*, 78.

(4) Nordlee, J. A.; Taylor, S. L.; Townsend, J. A.; Thomas, L. A.; Bush, R. K. Identification of a Brazil-nut allergen in transgenic soybeans. *N. Engl. J. Med.* **1996**, *334*, 688−692.

(5) Dinkins, R. D.; Reddy, R.; Curtis, A.; Meurer, C. A.; Yan, B.; Trick, H.; Thhibaud-Nissen, F.; Finer, J. J.; Parrott, W. A.; Collins, G. B. Increased sulfur amino acids in soybean plants overexpressing the maize 15 kD zein protein. *In Vitro Cell Dev. Biol. Plant* **2001**, *37*, 742−747.

(6) Kim, W. S.; Krishnan, H. B. Expression of an 11 kDa methionine rich delta-zein in transgenic soybean results in the formation of two types of novel protein bodies in transitional cells situated between the vascular tissue and storage parenchyma cells. *Plant Biotechnol. J.* **2004**, *2*, 199−210.

DOI: 10.1021/jf505202z
J. Agric. Food Chem. 2015, 63, 2862−2869

(7) Kho, C. J.; de Lumen, B. O. Identification and isolation of methionine-cysteine rich proteins in soybean seeds. *Plant Foods Hum. Nutr.* **1988**, *38*, 287−296.
(8) George, A. A.; de Lumen, B. O. A novel methionine-rich protein in soybean seed: identification, amino acid composition, and N-terminal sequence. *J. Agric. Food Chem.* **1991**, *39*, 224−227.
(9) de Lumen, B. O.; Galvez, A. F.; Revilleza, M. J.; Krenz, D. C. Molecular strategies to improve the nutritional quality of legume proteins. *Adv. Exp. Med. Biol.* **1999**, *464*, 117−126.
(10) Birk, Y. The Bowman-Birk inhibitor. *Int. J. Pept. Protein Res.* **1985**, *25*, 113−131.
(11) Clarke, E. J.; Wiseman, J. Developments in plant breeding for improved nutritional quality of soya beans II. Anti-nutritional factors. *J. Agric. Sci.* **2000**, *134*, 125−136.
(12) Livingstone, D.; Beilinson, V.; Kalyaeva, M.; Schmidt, M. A.; Herman, E. M.; Nielsen, N. C. Reduction of protease inhibitor activity by expression of a mutant Bowman-Birk gene in soybean seed. *Plant Mol. Biol.* **2007**, *64*, 397−408.
(13) Nishizawa, N. K.; Mor, S.; Watanabe, Y.; Hirano, H. Ultrastuructural localization of the basic 7S globulin in soybean (*Glycine max*) cotyledons. *Plant Cell Physiol.* **1994**, *35*, 1079−1085.
(14) Rahioui, I.; Laugier, C.; Balmand, S.; Da Silva, P.; Rahbe, Y.; Gressent, F. Toxicity, binding and internalization of the pea-A1b entomotoxin in Sf9 cells. *Biochimie* **2007**, *89*, 1539−1543.
(15) Watanabe, Y.; Hirano, H. Nucleotide sequence of the basic 7S globulin gene from soybean. *Plant Physiol.* **1994**, *105*, 1019−1020.
(16) Hanada, K.; Nishiuchi, Y.; Hirano, H. Amino acid residues on the surface of soybean 4-kDa peptide involved in the interaction with its binding protein. *Eur. J. Biochem.* **2003**, *270*, 2583−2592.
(17) Hirano, H. 4-kDa peptide. In *Handbook of Biologically Active Peptides*; Kastin, A. J., Ed.; Academic Press: Burlington, MA, USA, 2006; pp 1−4.
(18) Kim, W.-S.; Jang, S.; Krishnan, H. B. Accumulation of leginsulin, a hormone-like bioactive peptide, is drastically higher in Asian than in North American soybean accessions. *Crop Sci.* **2012**, *52*, 262−271.
(19) Diers, B. W.; Cary, T. R.; Thomas, D. J.; Nickell, C. D. Registration of 'LD00-3309' soybean. *Crop Sci.* **2006**, *46*, 1384.
(20) Samuels, M. L.; Witmer, J. A. *Statistics for the Life Sciences*, 2nd ed.; Prentice-Hall: London, UK, 1999.
(21) Krishnan, H. B.; Jang, S.; Baxter, I.; Wiebold, W. J. Growing location has a pronounced effect on the accumulation of cancer chemopreventive agent Bowman-Birk Inhibitor in soybean seeds. *Crop Sci.* **2012**, *52*, 1788−1794.
(22) Krishnan, H. B.; Oehrle, N. W.; Natarajan, S. S. A rapid and simple procedure for the depletion of abundant storage proteins from legume seeds to advance proteome analysis: a case study using *Glycine max*. *Proteomics* **2009**, *9*, 3174−3188.
(23) Krishnan, H. B.; Nelson, R. L. Proteomic analysis of high protein soybean (*Glycine max*) accessions demonstrates the contribution of novel glycinin subunits. *J. Agric. Food Chem.* **2011**, *59*, 2432−2439.
(24) Streit, L. G.; Beach, L.; Register, J. C.; Jung, R., III; Fehr, W. R. Association of the Brazil nut protein gene and Kunitz trypsin inhibitor alleles with soybean protease inhibitor activity and agronomic traits. *Crop Sci.* **2001**, *41*, 1757−1760.
(25) Jez, J. M.; Krishnan, H. B. Sulfur assimilation and cysteine biosynthesis in soybean seeds: towards engineering sulfur amino acid content. In *Modification of Seed Composition to Promote Health and Nutrition*; Krishnan, H. B., Ed.; ASA-CSSA-SSSA Publishing: Madison, WI, USA, 2009; pp 249−261.
(26) Kim, W. S.; Chronis, D.; Juergens, M.; Schroeder, A. C.; Hyun, S. W.; Jez, J. M.; Krishnan, H. B. Transgenic soybean plants overexpressing *O*-acetylserine sulfhydrylase accumulate enhanced levels of cysteine and Bowman-Birk protease inhibitor in seeds. *Planta* **2012**, *235*, 13−23.
(27) Song, S.; Hou, W.; Godo, I.; Wu, C.; Yu, Y.; Matityahu, I.; Hacham, Y.; Sun, S.; Han, T.; Amir, R. Soybean seeds expressing feedback-insensitive cystathionine-y-synthase exhibit a higher content of methionine. *J. Exp. Bot.* **2013**, *64*, 1917−1926.
(28) Sun, Y.-K. *Identification of Soybean Seed Oil QTLs with Little or No Impact on Seed Protein*. M.S. thesis, Student Research in Agronomy and Horticulture, University of Nebraska, Dec 2011.
(29) Eskandari, M.; Cober, E. R.; Rajcan, I. Genetic control of soybean seed oil: II. QTL and genes that increase oil concentration without decreasing protein or with increased seed yield. *Theor. Appl. Genet.* **2013**, *126*, 1677−1687.
(30) Hwang, E.-Y.; Song, Q.; Jia, G.; Specht, J. E.; Hyten, D. L.; Costa, J.; Cregan, P. B. A genome-wide association study of seed protein and oil content in soybean. *BMC Genomics* **2014**, *15*, 1.
(31) Thorne, J. C.; Fehr, W. R. Incorporation of high-protein, exotic germplasm into soybean populations by 2- and 3-way crosses. *Crop Sci.* **1970**, *10*, 652−655.
(32) Brim, C. A.; Burton, J. W. Recurrent selection in soybeans. II. Selection for increased percent protein in seeds. *Crop Sci.* **1979**, *19*, 494−498.
(33) Hartwig, E. E.; Kilen, T. C. Yield and composition of soybean seed from parents with different protein, similar yield. *Crop Sci.* **1991**, *31*, 290−292.
(34) Helms, T. C.; Orf, J. H. Protein, oil, and yield of soybean lines selected for increased protein. *Crop Sci.* **1998**, *38*, 707−711.
(35) Cober, E. R.; Voldeng, H. D. Developing high-protein, high-yield soybean populations and lines. *Crop Sci.* **2000**, *40*, 39−42.
(36) Schwender, J.; Ohlrogge, J. B.; Shachar Hill, Y. A flux model of glycolysis and the oxidative pentosephosphate pathway in developing *Brassica napus* embryos. *J. Biol. Chem.* **2003**, *278*, 29442−29453.
(37) Poysa, V.; Woodrow, L.; Yu, K. Effect of soy protein subunit composition on tofu quality. *Food Res. Int.* **2006**, *39*, 309−317.
(38) Kim, W. S.; Ho, H. J.; Nelson, R. L.; Krishnan, H. B. Identification of several gy4 nulls from the USDA soybean germplasm collection provides new genetic resources for the development of high-quality tofu cultivars. *J. Agric. Food Chem.* **2008**, *56*, 11320−11326.
(39) Kim, W. S.; Gillman, J. D.; Krishnan, H. B. Identification of a plant introduction soybean line with genetic lesions affecting two distinct glycinin subunits and evaluation of impacts on protein content and composition. *Mol. Breed.* **2013**, *32*, 291−298.

DOI: 10.1021/jf505202z
J. Agric. Food Chem. 2015, 63, 2862−2869

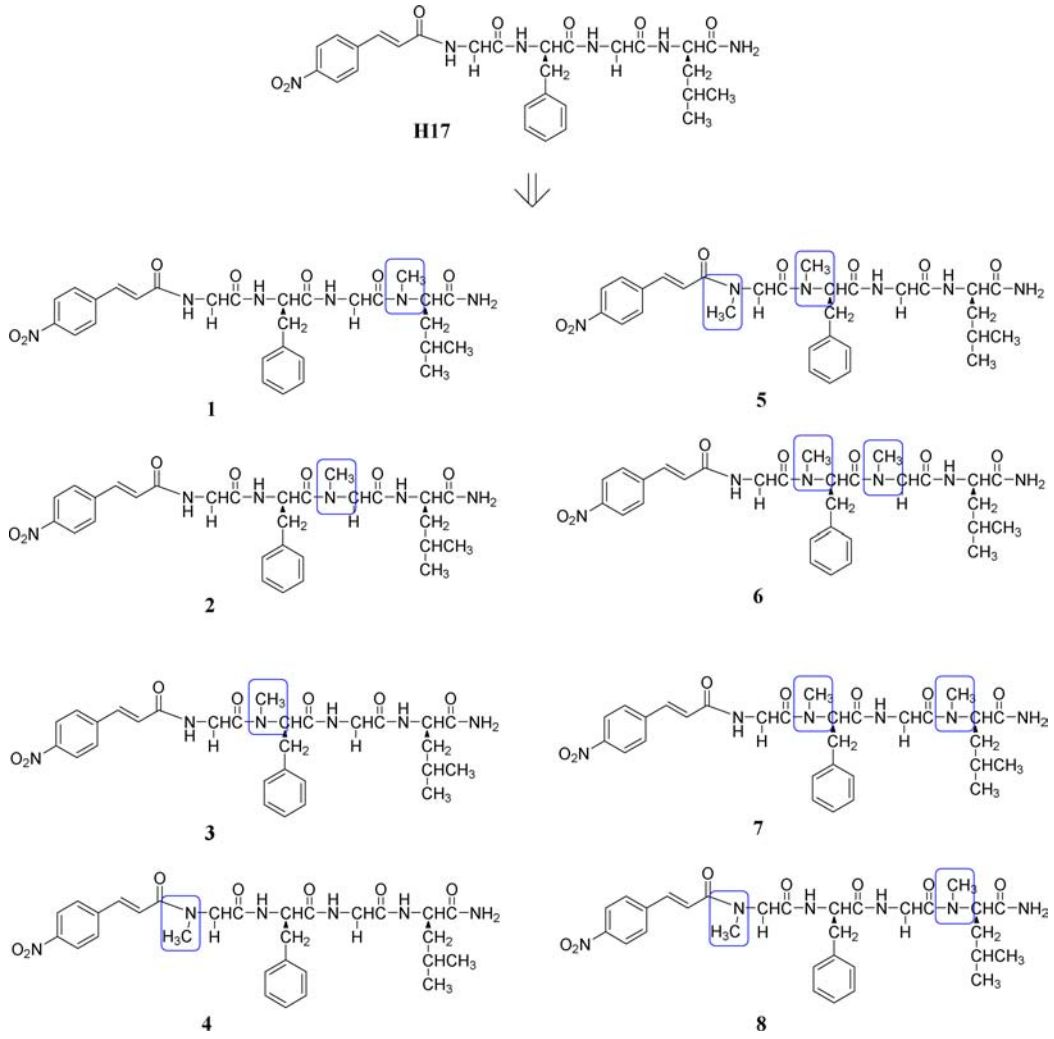

Figure 1. Structures of N-methylated AST analogues **1**−**8**.

MATERIALS AND METHODS

Chemistry. Protected N^{α}-Fmoc-amino acids, N^{α}-Fmoc-[*N*-Me]-amino acids, Rink amide-AM resin (0.68 mmol/g), 1-hydrozybenzotriazole anhydrous (HBTU), *O*-benzotriazole-*N*,*N*,*N*′,*N*′-tetramethyluroniumhexafluorophosphate (HOBt), *N*,*N*-diisopropylethylamine (DIEA), trifluoroacetic acid (TFA), and *N*,*N*′-diisoprophlcarbodiimide (Dic) were purchased from GL Biochem, Ltd. (Shanghai, China). *N*,*N*-Dimethylformanide (DMF), dichloromethane (CH_2Cl_2), and acetonitrile were purchased from DIMA Technology, Inc. (Beijing, China) and were of high-performance liquid chromatography (HPLC)-grade or better. (*E*)-3-(4-nitrophenyl)-acrylic acid (NAA) and other reagents for chemical synthesis were purchased from Alfa Aesar (Shanghai, China).

All N-methylated analogues were synthesized by solid-phase peptide synthetic techniques.[21−23] The analogues were prepared using a N^{α}-Fmoc-protection scheme with Rink amide-AM resin. Individual N^{α}-Fmoc-amino acids were coupled via HBTU, HOBt, and DIEA in DMF for 3 h. Removal of the N^{α}-Fmoc group was accomplished with 20% piperidine in CH_2Cl_2 for 20 min. The resin was then washed in turn with DMF, MeOH, and CH_2Cl_2 (2× each) and dried under reduced pressure. The peptides were then cleaved from the resin using TFA containing 5% phenol, 2.5% thioanisole, and 5% water for 2.5 h. The peptides were then washed with anhydrous ethyl ether and lyophilized.

Crude peptides were dissolved in a mixture of aqueous 0.1% TFA and acetonitrile (exact ratio depending upon the solubility of the peptide) and then purified by preparative reversed-phase HPLC with a flow rate of 10 mL/min using acetonitrile/water (50:50, v/v). Ultraviolet (UV) detection was at 225 nM. Peptide fractions determined to be pure by analytical HPLC were combined, concentrated under reduced pressure, and lyophilized.

Preparation of Analogue 1. N^{α}-Me-Leu-Rink amide-AM resin (0.5 mmol) was prepared as described in the general procedure. N^{α}-Fmoc-Gly (3 mmol, 6 equiv) and Dic (1.5 mmol, 3 equiv) were mixed in CH_2Cl_2 (5 mL) for 30 min at 0 °C, and then N^{α}-Me-Leu-Rink amide-AM resin and DIEA (3 mmol, 6 equiv) were added. The reaction mixture was shaken for 2 h, and the procedure was repeated. After removal of the N^{α}-Fmoc group, N^{α}-Fmoc-Phe, N^{α}-Fmoc-Gly, and (*E*)-3-(4-nitrophenyl)-acrylic acid were coupled to the resin with HBTU, HOBt, and DIEA in DMF. The crude analogue **1** was purified by reversed-phase HPLC with a flow rate of 10 mL/min using acetonitrile/water (50:50, v/v) to yield 100 mg of peptide; HPLC t_R, 10.5 min; HRMS, *m*/*z* 603.2537 $[M + Na]^+$ (calcd $[M + Na]^+$, 603.2538).

Preparation of Analogue 2. N^{α}-Me-Gly-Leu-Rink amide-AM resin (0.5 mmol) was prepared as described in the general procedure. N^{α}-Fmoc-Phe (3 mmol, 6 equiv) and Dic (1.5 mmol, 3 equiv) were mixed in CH_2Cl_2 (5 mL) for 30 min at 0 °C, and then N^{α}-Me-Gly-Leu-Rink amide-AM resin and DIEA (3 mmol, 6 equiv) were added. The reaction mixture was shaken for 2 h. After removal of the N^{α}-Fmoc group, N^{α}-Fmoc-Gly and (*E*)-3-(4-nitrophenyl)-acrylic acid were coupled to the resin with HBTU, HOBt, and DIEA in DMF. The crude analogue **2** was purified by reversed-phase HPLC with a flow rate of 10 mL/min using acetonitrile/water (50:50, v/v) to yield 97 mg of peptide; HPLC t_R, 8.7 min; HRMS, *m*/*z* 603.2541 $[M + Na]^+$ (calcd $[M + Na]^+$, 603.2538).

DOI: 10.1021/acs.jafc.5b00882
J. Agric. Food Chem. 2015, 63, 2870−2876

Preparation of Analogue 3. N^{α}-Me-Phe-Gly-Leu-Rink amide-AM resin (0.5 mmol) was prepared as described in the general procedure. N^{α}-Fmoc-Gly (3 mmol, 6 equiv) and Dic (1.5 mmol, 3 equiv) were mixed in CH_2Cl_2 (5 mL) for 30 min at 0 °C, and then N^{α}-Me-Phe-Gly-Leu-Rink amide-AM resin and DIEA (3 mmol, 6 equiv) were added. The reaction mixture was shaken for 2 h. After removal of the N^{α}-Fmoc group, (*E*)-3-(4-nitrophenyl)-acrylic acid was coupled to the resin with HBTU, HOBt, and DIEA in DMF. The crude analogue **2** was purified by reversed-phase HPLC with a flow rate of 10 mL/min using acetonitrile/water (50:50, v/v) to yield 104 mg of peptide; HPLC t_R, 11.2 min; HRMS, *m/z* 581.2715 $[M + H]^+$ (calcd $[M + H]^+$, 581.2718).

Preparation of Analogue 4. N^{α}-Me-Gly-Phe-Gly-Leu-Rink amide-AM resin (0.5 mmol) was prepared as described in the general procedure. (*E*)-3-(4-Nitrophenyl)-acrylic acid (3 mmol, 6 equiv) and Dic (1.5 mmol, 3 equiv) were mixed in CH_2Cl_2 (5 mL) for 30 min at 0 °C, and then N^{a}-Me-Gly-Phe-Gly-Leu-Rink amide-AM resin and DIEA (3 mmol, 6 equiv) were added. The reaction mixture was shaken for 2 h. The crude analogue **2** was purified by reversed-phase HPLC with a flow rate of 10 mL/min using acetonitrile/water (50:50, v/v) to yield 89 mg of peptide; HPLC t_R, 8.8 min; HRMS, *m/z* 603.2540 $[M + Na]^+$ (calcd $[M + Na]^+$, 603.2538).

Preparation of Analogue 5. N^{α}-Me-Phe-Gly-Leu-Rink amide-AM resin (0.5 mmol) was prepared as described in the general procedure. N^{α}-Fmoc-*N*-Me-Gly (3 mmol, 6 equiv) and Dic (1.5 mmol, 3 equiv) were mixed in CH_2Cl_2 (5 mL) for 30 min at 0 °C, and then N^{α}-Me-Phe-Gly-Leu-Rink amide-AM resin and DIEA (3 mmol, 6 equiv) were added. The reaction mixture was shaken for 2 h. After removal of the N^{a}-Fmoc group, (*E*)-3-(4-nitrophenyl)-acrylic acid (3 mmol, 6 equiv) and Dic (1.5 mmol, 3 equiv) were mixed in CH_2Cl_2 (5 mL) for 30 min at 0 °C and then N^{α}-Me-Gly-*N*-Me-Phe-Gly-Leu-Rink amide-AM resin and DIEA (3 mmol, 6 equiv) were added. The reaction mixture was shaken for 2 h, and the procedure was repeated. The crude analogue **5** was purified by reversed-phase HPLC with a flow rate of 10 mL/min using acetonitrile/water (50:50, v/v) to yield 85 mg; HPLC t_R, 8.7 min; HRMS, *m/z* 595.2874 $[M + H]^+$ (calcd $[M + H]^+$, 595.2875).

Preparation of Analogue 6. N^{α}-Me-Gly-Leu-Rink amide-AM resin (0.5 mmol) was prepared as described in the general procedure. N^{α}-Fmoc-*N*-Me-Phe (3 mmol, 6 equiv) and Dic (1.5 mmol, 3 equiv) were mixed in CH_2Cl_2 (5 mL) for 30 min at 0 °C, and then N^{α}-Me-Gly-Leu-Rink amide-AM resin and DIEA (3 mmol, 6 equiv) were added. The reaction mixture was shaken for 2 h. After removal of the N^{α}-Fmoc group, N^{α}-Fmoc-Gly was coupled to the resin using the same method as N^{α}-Fmoc-*N*-Me-Phe. (*E*)-3-(4-Nitrophenyl)-acrylic acid was coupled to the resin with HBTU, HOBt, and DIEA in DMF. The crude analogue **6** was purified by reversed-phase HPLC with a flow rate of 10 mL/min using acetonitrile/water (50:50, v/v) to yield 58 mg of peptide; HPLC t_R, 10.9 min; HRMS, *m/z* 617.2694 $[M + Na]^+$ (calcd $[M + Na]^+$, 617.2694).

Preparation of Analogue 7. N^{α}-Me-Leu-Rink amide-AM resin (0.5 mmol) was prepared as described in the general procedure. N^{α}-Fmoc-Gly (3 mmol, 6 equiv) and Dic (1.5 mmol, 3 equiv) were mixed in CH_2Cl_2 (5 mL) for 30 min at 0 °C, and then N^{α}-Me-Leu-Rink amide-AM resin and DIEA (3 mmol, 6 equiv) were added. The reaction mixture was shaken for 2 h. After removal of the N^{α}-Fmoc group, N^{α}-Fmoc-*N*-Me-Phe, N^{α}-Fmoc-Gly, and (*E*)-3-(4-nitrophenyl)-acrylic acid were coupled to the resin with HBTU, HOBt, and DIEA in DMF. The crude analogue **7** was purified by reversed-phase HPLC with a flow rate of 10 mL/min using acetonitrile/water (50:50, v/v) to yield 67 mg of peptide; HPLC t_R, 12.3 min; HRMS, *m/z* 617.2698 $[M + Na]^+$ (calcd $[M + Na]^+$, 617.2694).

Preparation of Analogue 8. N^{α}-Me-Leu-Rink amide-AM resin (0.5 mmol) was prepared as described in the general procedure. N^{α}-Fmoc-Gly (3 mmol, 6 equiv) and Dic (1.5 mmol, 3 equiv) were mixed in CH_2Cl_2 (5 mL) for 30 min at 0 °C, and then N^{a}-Me-Leu-Rink amide-AM resin and DIEA (3 mmol, 6 equiv) were added. The reaction mixture was shaken for 2 h. After removal of the N^{α}-Fmoc group, N^{α}-Fmoc-Phe and N^{α}-Fmoc-*N*-Me-Gly were coupled to the resin with HBTU, HOBt, and DIEA in DMF. (*E*)-3-(4-Nitrophenyl)-acrylic acid was coupled to the resin using Dic. The crude analogue **8** was purified by reversed-phase HPLC with a flow rate of 10 mL/min using acetonitrile/water (50:50, v/v) to afford 63 mg of peptide; HPLC t_R, 7.9 min; HRMS, *m/z* 617.2692 $[M + Na]^+$ (calcd $[M + Na]^+$, 617.2694).

Biological Assay *in Vitro*. All radiochemical assays for JH biosynthesis were performed using individual CA from day 7 mated females. Compounds were dissolved in medium 199 with Hank's salts, without L-methionine (custom formulation) (GIBCO, Grand Island, NY) for assay as described previously.[24−26] Compounds were used in the bioassay on the same day of sample preparation. The solutions were discarded at the end of each day. Rates of JH release were determined using the modified *in vitro* radiochemical assay.[26] This assay measures the incorporation of radiolabeled methionine into JH III in the final step of biosynthesis by CA maintained *in vitro*. CA were incubated for 3 h in 100 μL of medium 199 (GIBCO, 1.3 mM Ca^{2+}, 2% Ficoll, methionine-free) containing [^{14}C-*S*-methyl]-L-methionine (40 μM, specific radioactivity of 1.48−2.03 GBq/mmol) (Amersham Pharmacia Biotech, Inc., Piscataway, NJ). Samples were extracted, and JH release was determined. Each data point on the dose−response figures represents replicate incubations of 10−17 experimental CA compared to control CA (i.e., no analogue added).

NMR Experiments. All spectra of analogues **1**−**4** were obtained using a Bruker AMX 400 spectrometer (Bruker, Beijing, China) located at Beijing Nuclear Magnetic Resonance Center, Peking University, with tetramethylsilane (TMS) as the internal standard. The probe temperature was 298 K. The analogues were dissolved in 6 mM DMSO-d_6 in a standard 5 mm NMR tube. Peaks were assigned using total correlation spectroscopy (TOCSY) spectra. TOCSY spectra were recorded with 640 points in F2 and 256 points in F1. Proton distances were calculated using the two-spin approximation from nuclear Overhauser enhancement spectroscopy (NOESY). The mixing times in TOCSY and NOESY spectra were 50 and 500 ms, respectively.[13,27,28]

Molecular Modeling. All molecular modeling calculations were performed using Sybyl 7.3 (Tripos, Inc., St. Louis, MO) running on a Silicon Graphics Fuel Visual workstation (Silicon Graphics, Inc., Milpitas, CA). Distance ranges of 1.8−2.7, 1.8−3.3, and 1.8−5.0 Å were assigned for strong, medium, and weak nuclear Overhauser enhancement (NOE) interactions, respectively. The dihedral angles of θ (H−N−C_α−H_α) and θ (H_α−C_α−C_β−H_β) were calculated according the value of $^3J_{N\alpha}$ and $^3J_{\alpha\beta}$.[29,30] The energy minimization of four analogues (analogues **1**−**4**) used the minimized module of Sybyl. The force field was Merck Molecular Force Field 94 (MMFF94) with an 8.0 Å cutoff for non-bonded interactions, and the atomic point charges were also calculated by MMFF94. The minimizations were implemented with the descent method for the first 100 steps, followed by the Broyden Fletcher Goldfarb Shanno (BFGS) method until the root mean square (RMS) of the gradient was less than 0.005 kcal mol^{-1} $Å^{-1}$.[28] Then, these sample minimization procedures were selected to study their conformations using the method of the rotating-frame Overhauser enhancement (ROE)-restrained simulated annealing (SA) calculations. The ROE-derived distance constraints were applied as a biharmonic constraining function, and force constants for upper and lower boundaries were initially set to 20 kcal mol^{-1} $Å^{-2}$. The atomic velocities were applied following a Boltzmann distribution about the center of mass to obtain a starting temperature of 100 K.

RESULTS AND DISCUSSION

Chemistry. Several methods for N-methylation of amino acids are known in the literature.[23,31−33] Following the Fmoc strategy in peptide synthesis, methods of symmetrical anhydrides and esterification are favorable because it results in N-methylated Fmoc-protected amino acids in good overall yields without racemization.

To permit N-protected amino acids and (*E*)-3-(4-nitrophenyl)-acrylic acid coupling to HBTU, their symmetrical anhydrides were used if amino acids or (*E*)-3-(4-nitrophenyl)-

DOI: 10.1021/acs.jafc.5b00882
J. Agric. Food Chem. 2015, 63, 2870−2876

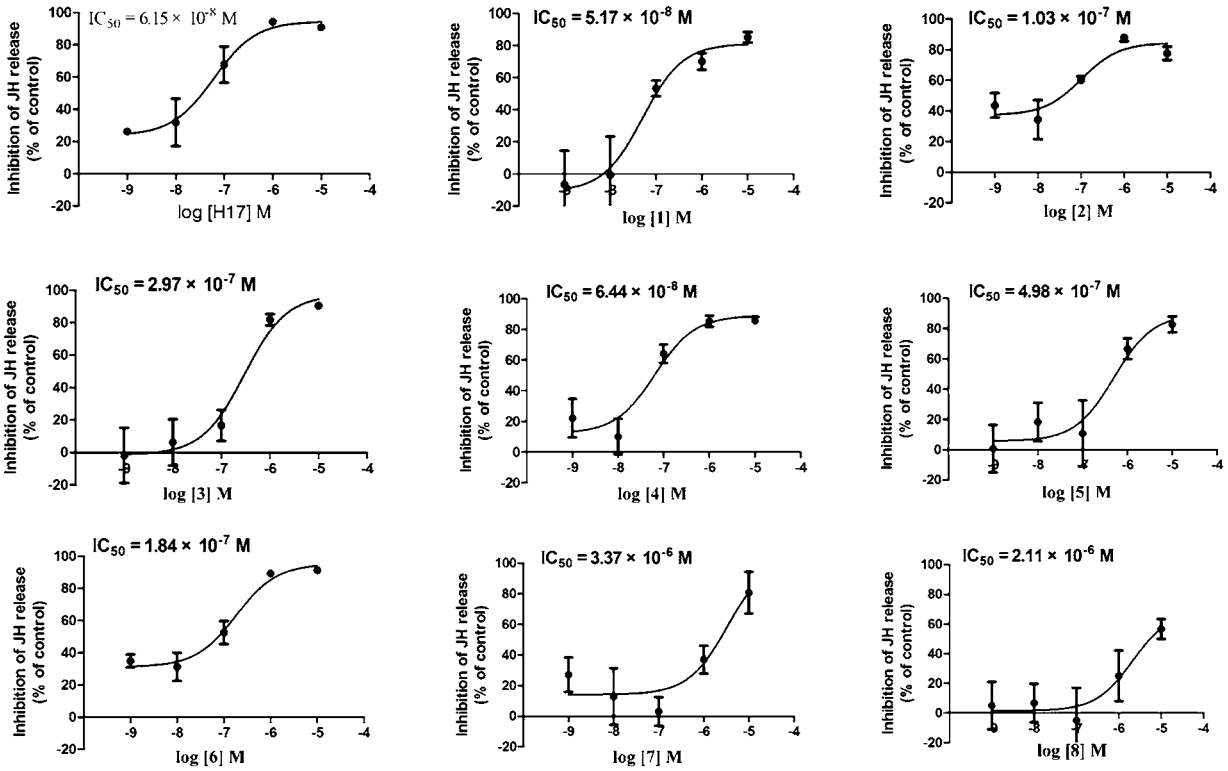

Figure 2. Dose−response curves for analogues **1**−**8** and H17 with respect to inhibition of JH release by CA of day 7 mated female *D. punctata in vitro*. The IC_{50} is the concentration of analogue required to achieve 50% inhibition relative to maximal inhibition of JH production achievable. Each point represents the mean ± standard error of the mean (SEM); N = 10−20.

Table 1. NMR Assignment for AST Analogues

analogue	residue	Hα (ppm)	Hβ (ppm)	N−H (ppm)	other (ppm)
1	NAA[1] [a]	6.92	7.54		7.83 Hγ, 8.26 Hδ
	Gly[2]	3.75, 3.87		8.40	
	Phe[3]	4.64	2.75, 3.05	8.21	7.22 Hγ, 7.15 Hδ, 7.19 Hε
	Gly[4]	4.06		8.26	
	N-Me-Leu[5]	4.98	1.61		1.38 Hγ, 0.86 Hδ, 2.84 *N*-CH_3, 7.08, 7.29 NH_2
2	NAA[1] [a]	6.90	7.54		7.84 Hγ, 8.20 Hδ
	Gly[2]	3.75		8.42	
	Phe[3]	4.93	2.81, 2.96	8.36	7.25 Hγ, 7.16 Hδ, 7.20 Hε
	N-Me-Gly[4]	3.87			2.76 *N*-CH_3
	Leu[5]	4.22, 4.32	1.43, 1.48	7.89	1.57 Hγ, 0.85 Hδ, 7.05, 7.35 NH_2
3	NAA[1] [a]	7.05	7.56		7.85 Hγ, 8.23 Hδ
	Gly[2]	3.89		8.28	
	N-Me-Phe[3]	4.85	2.96, 3.26		7.30 Hγ, 7.21 Hδ, 7.26 Hε, 2.78 *N*-CH_3
	Gly[4]	3.56, 3.72		8.14	
	Leu[5]	4.27	1.49	7.82	1.57 Hγ, 0.84 Hδ, 7.17, 7.48 NH_2
4	NAA[1] [a]	7.41	7.52		7.93 Hγ, 8.26 Hδ
	N-Me-Gly[2]	4.10			2.70 *N*-CH_3
	Phe[3]	4.56	2.77, 3.05	8.43	7.26 Hγ, 7.16 Hδ, 7.22 Hε
	Gly[4]	3.75		8.32	
	Leu[5]	4.21	1.47	8.01	1.55 Hγ, 0.85 Hδ, 7.01, 7.31 NH_2

[a]NAA = (*E*)-3-(4-nitrophenyl)-acrylic acyl group.

acrylic acid were coupled to the N^{α}-Me-amino acid-Rink amide-AM resin. If incomplete incorporation of the acylating agent was indicated, the amino acid was recoupled until a negative Kaiser test[30,34] was obtained. After coupling of (*E*)-3-(4-nitrophenyl)-acrylic acid, the peptide mimics were cleaved from the resin and then the crude peptide mimics were extracted into aqueous solution, concentrated under reduced pressure, and lyophilized. Purification by reversed-phase high-performance liquid chromatography (RP-HPLC) yielded peptides that were >98% pure.

Biological Data *in Vitro*. The ability of N-methylated AST analogues to inhibit biosynthesis of JH by the CA of *D. punctata* was evaluated by measuring the incorporation of radiolabeled methionine into JH III. As shown in Figure 2, analogues **1** and

DOI: 10.1021/acs.jafc.5b00882
J. Agric. Food Chem. 2015, 63, 2870−2876

4 in which C-terminal Leu^5 and Gly^2 were modified into N-methylated Leu and N-methylated Gly, respectively, exhibited activity similar to H17 ($IC_{50} = 6.15 \times 10^{-8}$ M *in vitro* and $IC_{50} = 1.2 \times 10^{-8}$ M *in vitro*[19]). These results demonstrated that analogues **1** and **4** have a significant effect *in vitro* when compared to the pentapeptide ($IC_{50} = 1.3 \times 10^{-7}$ M).[18] Single N-methylation of Phe^3 and Gly^4 produced about 2- and 4-fold lower activity than H17 but still showed significant potency with IC_{50} values of 1.03×10^{-7} and 2.97×10^{-7} M, respectively. A comparison of the activities elicited by single N-methylation mimics with double N-methylation mimics (to give analogues **5**−**8**) suggested that the introduction of a double N-methylation could decrease activity. Analogue **5**, containing both N-methylated Gly^2 and N-methylated Phe, was less active, with an IC_{50} value of 4.98×10^{-7} M. Analogue **6**, containing both N-methylated Phe and N-methylated Gly^4, was less active than analogue **2** but still showed activity, with an IC_{50} of 1.84×10^{-7} M. Analogue **7**, which contains N-methylated Phe and N-methylated Leu, and Analogue **8**, which contains N-methylated Gly^2 and N-methylated Leu, were found to have the lowest activity, with IC_{50} values of 3.37×10^{-6} and 2.11×10^{-6} M, respectively.

NMR Studies. Conformational investigations of analogues **1**−**4** were performed using standard one-dimensional (1D) and two-dimensional (2D) NMR spectroscopy in DMSO-d_6 at 298 K. A complete assignment of the protons was obtained (Table 1). The aliphatic spin systems and amide protons, besides the amide protons of the first residues, were observed using TOCSY experiments. The protons of Phe and (*E*)-3-(4-nitrophenyl)-acrylic acid as well as the prochiral methylene protons of Gly^2 and Gly^4 were identified by corresponding $^3J_{\alpha\beta}$ coupling constants and NOE correlations to their respective aromatic protons. Hα of the (*E*)-3-(4-nitrophenyl)-acrylic acyl group in analogues **1**−**3** appeared near 7 ppm, and in analogue **4**, it appeared as 7.4 ppm. For analogue **1**, *N*-CH_3 appeared as a singlet at 2.84 ppm and Hα of *N*-Me-Leu^5 appeared near 4.98 ppm. For analogue **2**, *N*-CH_3 appeared as a singlet at 2.76 ppm and Hα of *N*-Me-Gly^4 appeared near 3.87 ppm. For analogue **3**, *N*-CH_3 appeared as a singlet at 2.78 ppm and Hα of *N*-Me-Gly^4 appeared near 4.85 ppm. For analogue **4**, *N*-CH_3 appeared as a singlet at 2.70 ppm and Hα of *N*-Me-Gly^4 appeared near 4.11 ppm.

Important NOE correlations for analogue **1** included strong interactions between Gly^4 Hα and Leu^5 Hα and (*E*)-3-(4-nitrophenyl)-acrylic acyl group Hγ and Phe^3 N−H, a medium interaction between (*E*)-3-(4-nitrophenyl)-acrylic acyl group Hβ and Phe^3 Hγ, and a weak interaction between (*E*)-3-(4-nitrophenyl)-acrylic acyl group Hα and Gly^2 N−H. For analogue **2**, strong interactions were observed for (*E*)-3-(4-nitrophenyl)-acrylic acyl group Hδ and Leu^5 N−H and (*E*)-3-(4-nitrophenyl)-acrylic acyl group Hα and Leu^5 CO−NH_2, a medium interaction was observed for (*E*)-3-(4-nitrophenyl)-acrylic acyl group Hβ and Leu^5 N−H, and a weak interaction was observed for (*E*)-3-(4-nitrophenyl)-acrylic acyl group Hγ and Leu^5 CO−NH_2. For analogue **3**, an interaction was observed for (*E*)-3-(4-nitrophenyl)-acrylic acyl group Hβ and Leu^5 CO−NH_2, a medium interaction was observed for (*E*)-3-(4-nitrophenyl)-acrylic acyl group Hγ and Gly^4 N−H, and a weak interaction was observed for (*E*)-3-(4-nitrophenyl)-acrylic acyl group Hγ and Leu^5 N−H. Finally, for analogue **4**, a medium interaction occurred between (*E*)-3-(4-nitrophenyl)-acrylic acyl group Hδ and Leu^5 N−H, and a weak interaction occurred between (*E*)-3-(4-nitrophenyl)-acrylic acyl group Hα and Phe^3 Hδ.

Molecular Modeling. Because of conformational flexibility, restrained molecular dynamics was applied, to determine conformation in the case of peptides. The 10 lowest energy structures found for the four analogues are shown in Figure 3.

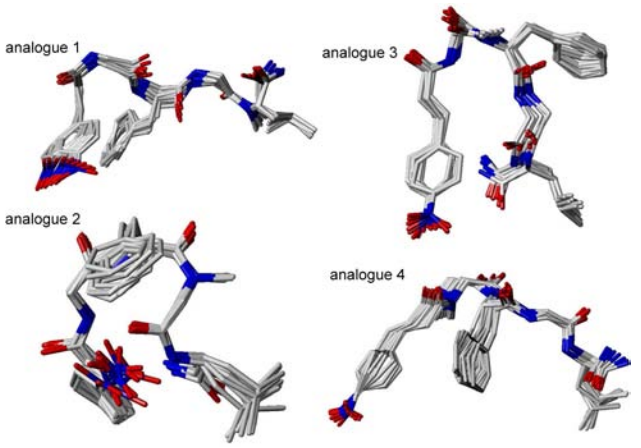

Figure 3. Backbone atom superposition of the low-energy structures obtained for analogues **1**−**4** by simulated annealing. Only backbone atoms are shown for clarity.

Torsion angles and distance between Cα of different residues of the lowest energy structure are summarized in Tables 2 and 3, respectively. The different turn conformations were assigned by comparing the average Φ (i + 1), Ψ (i + 1), Φ (i + 2), and Ψ (i + 2) values with standard values, allowing for a ±30° deviation from standard values.[35] Analogue **2** showed a type IV β-turn around Gly^2-Phe^3-Gly^4-Leu^5, and analogue **3** formed a type IV β-turn around NAA^1-Gly^2-Phe^3-Gly^4. As shown in Table 3, the distances of Cα(NAA^1)−Cα(Leu^5) of analogues **1** and **4** were 9.17 and 11.39 Å, respectively, and the distances of Cα(NAA^1)−Cα(Leu^5) for analogues **2** and **3** were 5.00 and 4.56 Å, respectively. Analogues **1** and **4** did not form a classic turn because the Cα(NAA^1)−Cα(Gly^4) and Cα(Gly^2)−Cα(Leu^5) distances were larger than 7.0 Å, the upper limit for turns.[35] It seems that the conformation of analogues **1** and **4** was flexible and linear.[36,37]

In previous studies, the β-turn at the end of the C terminus was predicted in ASTs and AST mimics.[11,13,28,38−40] We also found that analogues **2** and **3**, which demonstrated significant activity, formed a type IV β-turn. However, analogues **1** and **4**, which exhibited more activity, showed a flexible linear conformation. Banerjee et al.[15] observed that Dippu-AST 5 did not form a β-turn at the end of its C-terminal motif, using sodium dodecyl sulfate and water as solvent, but rather showed a γ-turn.[15] Therefore, we suggest that this kind of flexible linear conformation is a very important and indispensable structural element in AST mimics, and it may be directly involved in the recognition of the AST receptors. However, these ASTs and AST mimics are flexible, which are free to form any number of conformations under different conditions, such as β-turns, helical turns, or other conformations. Particularly, the flexible conformation does not eliminate the fact that the actual active conformation may be a β-turn, so that more data are required to confirm this hypothesis.

In summary, eight AST analogues were synthesized using N-methylation scanning, in an effort to understand the

DOI: 10.1021/acs.jafc.5b00882
J. Agric. Food Chem. 2015, 63, 2870−2876

Table 2. Torsion Angles of the Lowest Energy Structure of Four Analogues by Simulated Annealing

	Gly[2]		Phe[3]		Gly[4]		Leu[5]	
analogue	Φ (deg)	Ψ (deg)	Φ (deg)	Ψ (deg)	Φ (deg)	Ψ (deg)	Φ (deg)	Ψ (deg)
1	110	−32	11	−78	122	−72	−99	−86
2	175	−45	−129	−54	86	88	−121	37
3	67	24	−134	95	113	93	−158	147
4	136	−71	−146	−51	−155	117	88	−130

Table 3. Average Distance (Å) between Cα of NAA[1] and Cα of Leu[5], between Cα of NAA[1] and Cα of Gly[4], and between Cα of Gly[2] and Cα of Leu[5] in Analogues 1−4 of the Lowest Energy Conformation

analogue	Cα(NAA[1] [a])−Cα(Leu[5]) distance (Å)	Cα(NAA[1] [a])−Cα(Gly[4]) distance (Å)	Cα(Gly[2])−Cα(Leu[5]) distance (Å)
1	9.17	7.82	7.84
2	5.00	6.09	6.44
3	4.56	4.79	7.38
4	11.39	8.00	9.13

[a]NAA = (*E*)-3-(4-nitrophenyl)-acrylic acyl group.

conformation of novel AST analogues and their ability to inhibit JH biosynthesis. The activity of analogues **1** and **4** proved roughly equivalent to that of the lead H17, with IC_{50} values of 5.17×10^{-8} and 6.44×10^{-8} M, respectively. Single N-methylation mimics (analogues **1**−**4**) showed higher activity than double N-methylation mimics (analogues **5**−**8**). We further investigated the conformational properties of single N-methylation mimics (analogues **1**−**4**) by 1D and 2D ^{1}H NMR and molecular modeling. Evaluating the torsion angles and distances between Cα of different residues, we found that analogues **1** and **4**, which formed a flexible linear conformation, exhibited more activity than analogues **2** and **3** containing a type IV β-turn. On the basis of our present study, these results provide evidence that the flexible linear conformation may be an indispensable structural element in AST mimics and may be involved in the interaction with the AST receptors.

AUTHOR INFORMATION

Corresponding Author

*Telephone: 86-10-62732223. E-mail: yangxl@cau.edu.cn.

Author Contributions

Yong Xie, Xinling Yang, and Stephen S. Tobe designed experiments. Yong Xie, Chuanliang Zhang, Xiaoqing Wu, and Xile Deng synthesized AST mimics. Yong Xie finished biological assay and NMR studies. Li Zhang investigated the molecular modeling. Yong Xie, Xinling Yang, and Stephen S. Tobe wrote the paper.

Funding

Financial support was provided by the National Natural Science Foundation of China (21372257 and 21132003), the National Basic Research Program of China (973 Program) (2010CB126104 and 2010CB126105), and the Natural Sciences and Engineering Research Council of Canada.

Notes

The authors declare no competing financial interest.

REFERENCES

(1) Woodhead, A. P.; Stay, B.; Seidel, S. L.; Khan, M. A.; Tobe, S. S. Primary structure of four allatostatins: Neuropeptide inhibitors of juvenile hormone synthesis. *Proc. Natl. Acad. Sci. U. S. A.* **1989**, *86*, 5997−6001.

(2) Pratt, G. E.; Farnsworth, D. E.; Siegel, N. R.; Fok, K. F.; Feyereisen, R. Identification of an allatostatin from adult *Diploptera punctata*. *Biochem. Biophys. Res. Commun.* **1989**, *163*, 1243−1247.

(3) Pratt, G. E.; Farnsworth, D. E.; Fok, K. F.; Siegel, N. R.; McCormack, A. L.; Shabanowitz, J.; Hunt, D. F.; Feyereisen, R. Identity of a second type of allatostatin from cockroach brains: An octadecapeptide amide with a tyrosine-rich address sequence. *Proc. Natl. Acad. Sci. U. S. A.* **1991**, *88*, 2412−2416.

(4) Stay, B.; Tobe, S. S.; Bendena, W. G. Allatostatins: Identification, primary structures, functions and distribution. *Adv. Insect Physiol.* **1994**, *25*, 267−337.

(5) Yagi, K. J.; Elliott, K. L.; Teesch, L.; Tobe, S. S.; Stay, B. Isolation of cockroach Phe-Gly-Leu-amide allatostatins from the termite *Reticulitermes flavipes* and their effect on juvenile hormone synthesis. *J. Insect Physiol.* **2008**, *54*, 939−948.

(6) Yagi, K. J.; Kwok, R.; Chan, K. K.; Setter, R. R.; Myles, T. G.; Tobe, S. S. Phe-Gly-Leu-amide allatostatin in the termite *Reticulitermes flavipes*: Content in brain and corpus allatum and effect on juvenile hormone synthesis. *J. Insect Physiol.* **2005**, *51*, 357−365.

(7) Lorenz, M. W.; Kellner, R.; Hoffmann, K. H. Identification of two allatostatins from the cricket, *Gryllus bimaculatus* de Geer (Ensifera, Gryllidae): Additional members of a family of neuropeptides inhibiting juvenile hormone biosynthesis. *Regul. Pept.* **1995**, *57*, 227−236.

(8) Stay, B. A review of the role of neurosecretion in the control of juvenile hormone synthesis: A tribute to Berta Scharrer. *Insect Biochem. Mol. Biol.* **2000**, *30*, 653−662.

(9) Bendena, W. G.; Donly, B. C.; Tobe, S. S. Allatostatins: A growing family of neuropeptides with structural and functional diversity. *Ann. N. Y. Acad. Sci.* **1999**, *897*, 311−329.

(10) Stay, B.; Woodhead, A. P.; Joshi, S.; Tobe, S. S. Allatostatins. Neuropeptide inhibitors of juvenile hormone synthesis in brain and corpora allata of the cockroach *Diploptera punctata*. *ACS Symp. Ser.* **1991**, *453*, 164−176.

(11) Hayes, T. K.; Guan, X. C.; Johnson, V.; Strey, A.; Tobe, S. S. Structure−activity studies of allatostatin 4 on the inhibition of juvenile hormone biosynthesis by corpora allata: The importance of individual side chains and stereochemistry. *Peptides* **1994**, *15*, 1165−1171.

(12) Piulachs, M. D.; Vilaplana, L.; Bartolome, J. M.; Carreno, C.; Martin, D.; Rosario, G. M.; Herranz, R.; Garcia-Lopez, M. T.; Andreu, D.; Belles, X. Ketomethylene and methyleneamino pseudopeptide analogs of insect allatostatins inhibit juvenile hormone and vitellogenin production in the cockroach *Blattella germanica*. *Insect Biochem. Mol. Biol.* **1997**, *27*, 851−858.

(13) Nachman, R. J.; Moyna, G.; Williams, H. J.; Tobe, S. S.; Scott, A. I. Synthesis, biological activity, and conformational studies of insect allatostatin neuropeptide analogs incorporating turn-promoting moieties. *Bioorg. Med. Chem.* **1998**, *6*, 1379−1388.

(14) Nachman, R. J.; Garside, C. S.; Tobe, S. S. Hemolymph and tissue-bound peptidase-resistant analogs of the insect allatostatins. *Peptides* **1999**, *20*, 23−29.

DOI: 10.1021/acs.jafc.5b00882
J. Agric. Food Chem. 2015, 63, 2870−2876

(15) Banerjee, M.; Meyerowitz, E.; Huang, C.; Mohanty, S. Probing the conformation and dynamics of allatostatin neuropeptides: A structural model for functional differences. *Peptides* **2008**, *29*, 375−385.
(16) Xie, Y.; Kai, Z. P.; Tobe, S. S.; Deng, X. L.; Ling, Y.; Wu, X. Q.; Huang, J.; Zhang, L.; Yang, X. L. Design, synthesis and biological activity of peptidomimetic analogs of insect allatostatins. *Peptides* **2011**, *32*, 581−586.
(17) Kai, Z. P.; Xie, Y.; Huang, J.; Tobe, S. S.; Zhang, J. R.; Ling, Y.; Zhang, L.; Zhao, Y. C.; Yang, X. L. Peptidomimetics in the discovery of new insect growth regulators: Studies on the structure−activity relationships of the core pentapeptide region of allatostatins. *J. Agric. Food Chem.* **2011**, *59*, 2478−2485.
(18) Kai, Z. P.; Huang, J.; Xie, Y.; Tobe, S. S.; Ling, Y.; Zhang, L.; Zhao, Y. C.; Yang, X. L. Synthesis, biological activity, and hologram quantitative structure−activity relationships of novel allatostatin analogues. *J. Agric. Food Chem.* **2009**, *58*, 2652−2658.
(19) Kai, Z. P.; Huang, J.; Tobe, S. S.; Yang, X. L. A potential insect growth regulator: Synthesis and bioactivity of an allatostatin mimic. *Peptides* **2009**, *30*, 1249−1253.
(20) Xie, Y.; Zhang, L.; Wu, X. Q.; Zhang, C. L.; Yang, X. L.; Tobe, S. S. Probing the active conformation of FGLamide allatostatin analogs with N-terminal modifications using NMR spectroscopy and molecular modeling. *Peptides* **2014**, DOI: 10.1016/j.peptides.2014.1006.1015.
(21) Carpino, L. A. The 9-fluorenylmethyloxycarbonyl family of base-sensitive amino-protecting groups. *Acc. Chem. Res.* **1987**, *20*, 401−407.
(22) Brown, E. G.; Nuss, J. M. Alkylation of Rink's amide linker on polystyrene resin: A reductive amination approach to modified amine-linkers for the solid phase synthesis of N-substituted amide derivatives. *Tetrahedron Lett.* **1997**, *38*, 8457−8460.
(23) Carpino, L. A.; Han, G. Y. The 9-fluorenylmethoxycarbonyl function, a new base-sensitive amino-protecting group. *J. Am. Chem. Soc.* **1970**, *92*, 5748.
(24) Tobe, S. S.; Pratt, G. E. Influence of substrate concentrations on the rate of insect juvenile hormone biosynthesis by corpora allata of the desert locust in vitro. *Biochem. J.* **1974**, *144*, 107−113.
(25) Feyereisen, R.; Tobe, S. S. A rapid partition assay for routine analysis of juvenile hormone release by insect corpora allata. *Anal. Biochem.* **1981**, *111*, 372−375.
(26) Tobe, S. S.; Clarke, N. The effect of L-methionine concentration on juvenile hormone biosynthesis by corpora allata of the cockroach *Diploptera punctata*. *Insect Biochem.* **1985**, *15*, 175−179.
(27) Dechantsreiter, M. A.; Planker, E.; Mathae, B.; Lohof, E.; Hoelzemann, G.; Jonczyk, A.; Goodman, S. L.; Kessler, H. *N*-methylated cyclic RGD peptides as highly active and selective $\alpha_v\beta_3$ integrin antagonists. *J. Med. Chem.* **1999**, *42*, 3033−3040.
(28) Kai, Z. P.; Ling, Y.; Liu, W. J.; Zhao, F.; Yang, X. L. The study of solution conformation of allatostatins by 2-D NMR and molecular modeling. *Biochim. Biophys. Acta, Proteins Proteomics* **2006**, *1764*, 70−75.
(29) Cung, M. T.; Marraud, M.; Neel, J. Experimental calibration of a Karplus relationship in order to study the conformations of peptides by nuclear magnetic resonance. *Macromolecules* **1974**, *7*, 606−613.
(30) Kaiser, E. T.; Kezdy, F. J. Amphiphilic secondary structure: design of peptide hormones. *Science* **1984**, *223*, 249−255.
(31) McDermott, J. R.; Benoiton, N. L. *N*-methylamino acids in peptide synthesis. II. New synthesis of *N*-benzyloxycarbonyl-*N*-methylamino acids. *Can. J. Chem.* **1973**, *51*, 1915−1919.
(32) Cheung, S. T.; Benoiton, N. L. *N*-Methylamino acids in peptide synthesis. VII. Studies on the enantiomeric purity of *N*-methylamino acids prepared by various procedures. *Can. J. Chem.* **1977**, *55*, 916−921.
(33) Freidinger, R. M.; Hinkle, J. S.; Perlow, D. S. Synthesis of 9-fluorenylmethyloxycarbonyl-protected *N*-alkyl amino acids by reduction of oxazolidinones. *J. Org. Chem.* **1983**, *48*, 77−781.
(34) Bozzoli, A.; Kazmierski, W.; Kennedy, G.; Pasquarello, A.; Pecunioso, A. A solid-phase approach to analogues of the antibiotic mureidomycin. *Bioorg. Med. Chem. Lett.* **2000**, *10*, 2759−2763.
(35) Chou, K. C. Prediction of tight turns and their types in proteins. *Anal. Biochem.* **2000**, *286*, 1−16.
(36) Anderson, C. Y.; Kellogg, G. E.; Freer, R. J. C5aR ligand peptide 3D QSAR study performed with an applied linear conformation. *J. Pept. Res.* **1997**, *49*, 476−483.
(37) Seebach, D.; Brenner, M.; Rueping, M.; Jaun, B. γ2-, γ3-, and γ2,3,4-amino acids, coupling to γ-hexapeptides: CD spectra, NMR solution and X-ray crystal structures of γ-peptides. *Chem.—Eur. J.* **2002**, *8*, 573−584.
(38) Yang, H.; Lim, Y. Solution structure determination of four *Diploptera punctata* allatostatins by NMR spectroscopy and molecular modeling. *Bull. Korean Chem. Soc.* **2005**, *26*, 845−848.
(39) Yang, H.; Young, J.; Lee, E.; Lim, Y. Structure in solution of *Diploptera punctata* allatostatin-2. *Agric. Chem. Biotechnol.* **2006**, *49*, 186−188.
(40) Marris, G. C.; Weavevr, R.; Olieff, S. M.; Mosson, H. J.; Edwards, J. P. Insect growth regulators: A slow start but outlook is promising. *Int. Pest Control* **1997**, *39*, 44−45.

DOI: 10.1021/acs.jafc.5b00882
J. Agric. Food Chem. 2015, 63, 2870−2876

Table 1. Optimized Extraction Times and Temperatures for Target Compounds in Grape Samples[a]

compound	optimized time	optimized temperature	predicted response	relative peak size (RPS)	inverse RPS[b]	inverse RPS × OPT time	inverse RPS × OPT temperature
2-isobutyl-3-methoxypyrazine	70.0	70.0	23479	0.018	53	3724	3724
2-isoproyl-3-methoxypyrazine	69.0	67.0	9706	0.008	129	8880	8622
3-octanone	70.0	70.0	79560	0.063	16	1099	1099
fenchone	65.5	45.5	1168575	0.935	1.1	70	48
1-octen-3-one	64.5	69.5	57264	0.045	22	1406	1516
fenchol	64	51.5	622317	0.498	2	128	103
1-octen-3-ol	64.5	59.5	1249123	1.000	1	64	59
trans-2-octen-1-ol	50.5	49.5	41463	0.033	30	1521	1491
2-methylisoborneol	69.5	52.5	3965	0.003	315	21895	16539
2,4,6-trichoroanisole	70.0	70.0	4360	0.003	286	20054	20054
geosmin	66.0	70.0	5283	0.004	236	15605	16550
2,4,6-tribromoanisole	56.6	70.0	6995	0.005	178	10107	12500
pentachloroanisole	63.0	70.0	1701	0.001	734	46263	51404
sum					2004	130820	133714
weighted mean extraction temperature and time					65.3 min	66.7 °C	

[a]Determined from the midpoint of the calibration curve. [b]Rounding errors account for minor differences of expressed values.

limits of quantitation well below the reported sensory threshold for these compounds. However, when multiple analyte responses require optimization, the most favorable handling conditions for individual analytes becomes increasingly convoluted. This method has also allowed for the first reported investigation of compounds that contribute to the off-flavors found in wines made from ripe rot (*Colletotrichum acutatum*)-affected grapes.

MATERIALS AND METHODS

Chemicals. Analytical-grade chemicals and reagents for the preparation of standard solutions for GC−MS analysis were used without further purification. 2-Isobutyl-3-methoxypyrazine, 2-isopropyl-3-methoxypyrazine, 3-octanone, 1-octen-3-one, *trans*-2-octen-1-ol, 1-octen-3-ol, 2-methylisoborneol, 2,4,6-trichoroanisole, geosmin, 2,4,6-tribromoanisole, methyl isobutyl ketone, 2-octanol, and geosmin-d_3 were obtained from Sigma-Aldrich (St. Louis, MO). Fenchone and fenchol were obtained from Fulka (Buchs, Switzerland). 2-Methyl-d_3-isoborneol, 2,4,6-trichloroanisole-d_5, 2,4,6-tribromoanisole-d_5, and pentachloroanisole-d_3 were obtained from CDN Isotopes (Pointe-Claire, Quebec, Canada). Ethanol (VWR Prolabo, Fontenay Sous Bois, France), L-(+) tartaric acid (Sigma, Steinheim, Germany), and potassium hydrogen tartrate (BHD Chemicals, Ltd., Poole, U.K.) were used for preparation of model wine base solutions. Deionized water was obtained from a Milli-Q mixed bed resin system (18 MΩ/cm, 25 °C).

Instrumentation. An Agilent 7890A gas chromatograph, equipped with a Gerstel multipurpose sampler with automated SPME capability and Peltier cooled sample tray, interfaced to an Agilent 5975C triple axis mass detector, was used for confirmation of compound identity, method development, and final sample analysis. MSD Chemstation E.02.00.493 (Agilent Technologies, Ltd.) and NIST MS Search 2.0, version 2008, were used to control the instrument and for mass spectra assessment. Prepared samples were placed into the Peltier cooler tray set at 8 °C until analysis, whereupon vials were transferred to a heater block with a 2 min pre-incubation time before insertion of the SPME fiber. A fused silica capillary column (DB-Waxetr, 60 m × 0.25 mm inner diameter, 0.25 μm film thickness, Agilent Technologies, Santa Clara, CA) was used for compound separation by GC. The injector block was fitted with a 2 mm internal diameter borosilicate liner (SGE), and the injector temperature set to 260 °C in splitless mode. Fibers were inserted into the injector for 1 min, withdrawn, and injected into a second injector set at 270 °C with a 50:1 split for 10 min with a 15 mL/min purge flow to clean the fiber, prior to the next sample analysis. The oven temperature program commenced at 40 °C for 3 min, increased to 115 °C at a rate of 5 °C/min, increased to 166 °C at a rate of 3 °C/min, a final increase to 210 °C at a rate of 10 °C/min, and held for 12 min. The total run time was 51.4 min. The flow rate of ultra-high-purity helium gas was constant at 3 mL/min. The MS source, quadrupole, and transfer line temperatures were set to 230, 150, and 275 °C, respectively.

Compound Identification and Elution Profiles. Solutions of all listed compounds were prepared at the approximate midpoint of the calibration range, in a model wine consisting of tartaric acid (0.008 M), potassium hydrogen tartrate (0.011 M), and ethanol (3.0%, v/v). These solutions were used to confirm compound elution times and ion profiles. Samples (10 mL) were transferred to the heater block set at 50 °C with an agitation rate of 250 revolutions per minute (rpm) and equilibrated for 1 min. A divinylbenzene/carboxen/polydimethylsiloxane (DVB/CAR/PDMS) SPME fiber, which is reported to possess a high level of sensitivity for the compounds of interest,[15] had been preconditioned according to the instructions of the manufacturers and was then inserted into the headspace for 20 min at 50 °C, before the insertion into the GC injector. Mass spectral data was collected in both selective ion monitoring (SIM) at ionization voltage of 70 eV and scan mode (m/z 35−350). Final elution profiles were confirmed by matching mass spectral data with the National Institute of Standards and Technology (NIST) mass spectral search program (version 2.0) MS library (version 8.0) and the determination of Kovat's retention indices (RIs). RIs were checked for each compound using a commercial mixture of *n*-alkanes (Sigma, Steinheim, Germany), an identical oven ramp profile, and gas flow rates as used for the final analyses.

Preparation of Wine Base (WB) and Grape Base (GB) Solutions. A WB solution was prepared by diluting commercial Chardonnay wine (Charles Sturt University Winery 2009) with ultrapure water 1:4 to achieve an ethanol concentration of 3% (v/v) and adjusting the pH to 7.0 by the addition of sodium hydroxide (1 M). A GB solution was prepared by homogenizing Thompson seedless grapes (approximately 2 kg) with an ultra-Turax T25 (Jane & Kunkel Ika-labtechnik) for 2 min. This was diluted 1:5 with ultrapure water to achieve a carbohydrate concentration of 2.5% (w/v), and pH was adjusted to 7.0. Prior to the use of WB and GB for further method development, the absence of the compounds of interest was confirmed by HS-SPME−GC−MS using SIM mode, with all conditions as previously mentioned.

Optimization of Sample Extraction Conditions. Optimization of extraction time and temperature was determined using a Box−Behnken experiment designed with a three-level factorial design as previously described.[13,16] Compounds were tested in WB or GB with salt at approximately the one-tenth point of the calibration curve. SPME extraction was performed using a DVB/CAR/PDMS fiber. Temperature conditions of 30, 50, and 70 °C with extraction times of 30, 50, and 70 min were examined in a randomized order, with the central condition

DOI: 10.1021/jf505444r
J. Agric. Food Chem. 2015, 63, 2877−2885

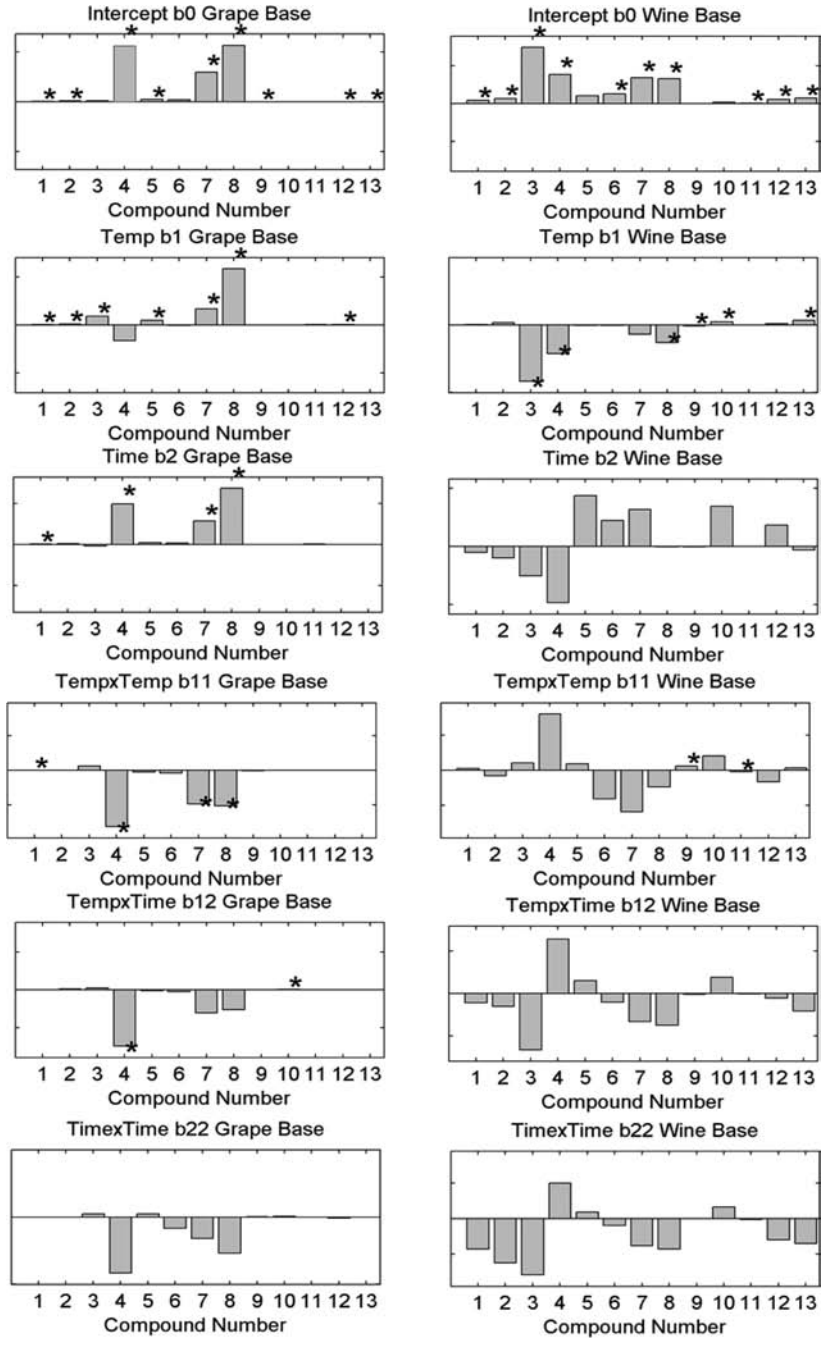

Figure 1. Response surface modeling of quantification ion counts to determine the optimized experimental conditions was undertaken in accordance with eq 1 for each analyte of interest. An asterisk above the coefficient indicates a significant term in the regression model ($p < 0.05$). Compound numbers: (**1**) 2-isopropyl-3-methoxypyrazine, (**2**) 2-isobutyl-3-methoxypyrazine, (**3**) 3-octanone, (**4**) fenchone, (**5**) 1-octen-3-one, (**6**) *trans*-2-octen-1-ol, (**7**) fenchol, (**8**) 1-octen-3-ol, (**9**) methylisoborneol, (**10**) 2,4,6-trichloroanisole, (**11**) geosmin, (**12**) 2,4,6-tribromoanisole, and (**13**) pentachloroanisole.

repeated 3 times to determine the extraction repeatability. Thus, the experimental design was constructed with independent variables at levels (−1, 0, and 1) for temperature (30, 50, and 70 °C) and time (30, 50, and 70 min). Compound quantitation ion results for each compound were exported to MATLAB R2007a (The Mathworks, Natick, MA), and extraction conditions were modeled using response surface methodology. The predicted maximum quantitation ion response at optimized conditions for each compound was determined from the response surface model using a full quadratic model to account for constant, linear, and squared terms[17]

$$Y = b_0 + b_1X_1 + b_2X_2 + b_{12}X_1X_2 + b_{11}X_1^2 + b_{22}X_2^2 + \varepsilon \qquad (1)$$

where Y is the predicted response for each compound, X_1 is the extraction temperature, X_2 is the extraction time, b_0 is the constant term, b_1 and b_2 are the coefficients for the linear terms, b_{12} is the coefficient for the interactions, b_{11} and b_{22} are the coefficients for the squared terms or variables (time and temperature) for each compound model, and ε is the residual. The coefficients were calculated using regression analysis, and the significance of each variable was determined using a two-tailed t test. The coefficients b_n and indication of their significance are shown in Figure 1.

The response surface curve of geosmin for the extraction conditions is shown in Figure 2. A modified desirability method for the optimization of multiple response variables was used, in which the importance of

DOI: 10.1021/jf505444r
J. Agric. Food Chem. 2015, 63, 2877−2885

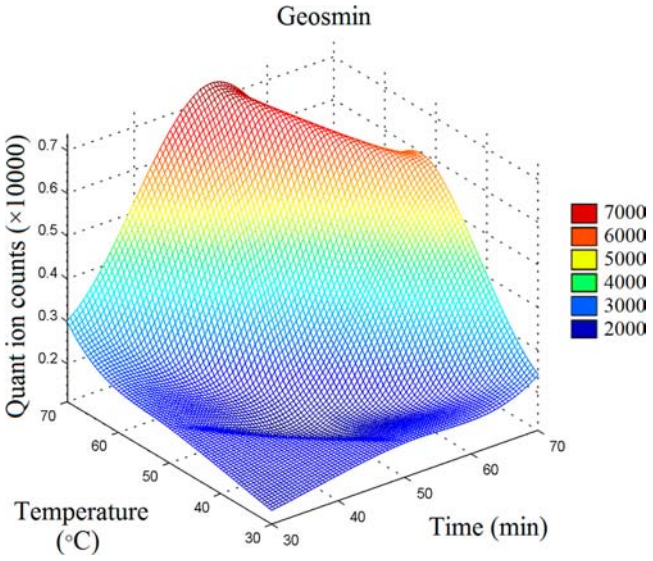

Figure 2. Response surface curve in WB for geosmin of varying sample incubation temperatures and fiber exposure time.

specific responses were down-weighted.[14] Briefly, relative peak size (RPS) coefficients for each compound were calculated from the inverse of the largest predicted maximum quantitation ion peak divided by each target compound peak area in the compound list (Tables 1 and 2). Weighted mean extraction times and temperatures were then calculated from the product of inverse RPS and optimized time or optimized temperature for the compounds. This enabled a comparison of the relative extraction and detection efficiencies for all compounds and assisted in minimizing the loss of analytical sensitivity for specific compounds that give low peak areas compared to compounds with large peak areas.

Effect of Salting on Extraction Efficiency. Duplicate samples were prepared in either a WB or GB with or without salt. Samples were spiked with compounds to produce a concentration of one-tenth of the maximum calibration point. The effects of salting on the ionic strength were determined by placing 3.0 g of NaCl into each 20 mL sample vial prior to introducing 10 mL of sample. SPME extraction was conducted at final SPME optimized extraction conditions [for GB, 65 °C for 67 min (Table 1) and, for WB, 44 °C for 65 min (Table 2)] using a DVB/CAR/PDMS fiber with quantitation ions counted in SIM mode. Quantitation ion counts for target compounds in WB or GB solution with or without the salt are presented in Figure 3.

Calibration Curves. Calibration solutions were prepared in either WB or GB by diluting a mix of the pure compounds to seven concentrations over the analytical range (Table 3) and internal standard (IS), as designated in Table 4, and saturated with NaCl (30%). Triplicate analysis was conducted for each calibration level in both WB and GB, and SPME extraction was conducted as previously mentioned.

Limit of Detection (LOD) and Limit of Quantitation (LOQ). WB and GB spiked with low levels of target compounds were used to establish the LOD and LOQ of the overall method. The LOD (concentration for signal/noise = 3) and the LOQ (concentration for signal/noise = 10) were manually calculated from the ratio of the peak heights to the average noise before and after each peak. These data are listed in Table 3.

Recovery Experiments in Red and White Wine and Grapes. Recovery experiments were conducted in triplicate in wines (diluted 1:4) and grape homogenates (diluted 1:5) adjusted to a pH of 7.0 using 1 M NaOH. Compounds were spiked in these solutions at approximately one-fifth and one-tenth of the calibration curve. NaCl (3.0 g) was placed into each 20 mL sample vial prior to introducing 10 mL of sample. Compound recoveries are reported as a percentage of the spiked quantity determined from the calibration curves for each analyte.[18]

Repeatability and Reproducibility. To evaluate repeatability, five white wines (Chardonnay) and five homogenate Thompson seedless grape samples were spiked with a concentrated mix of target compounds, as described above. To evaluate reproducibility spiked, samples were prepared and analyzed over a period of 5 days with results expressed as the coefficient of variation (% CV).[18]

Analysis of Healthy and Infected Grape and Wine Samples. *Healthy and Infected Grape Samples.* Bunches of Shiraz grapes were collected from a vineyard in the Riverina, New South Wales, Australia, during the 2012 vintage. Fruit was handpicked and sorted into two separate batches according to a visual assessment for the presence of obvious fungal bunch rots. On the basis of a visual examination, gray mold or *B. cinerea*[19] was the predominant bunch rot disease in these grapes. Cabernet Sauvignon bunches were similarly collected from a commercial vineyard located in the Hunter Valley, New South Wales, Australia, during the 2013 vintage and sorted into two batches according to the presence or absence of obvious mold growth. On the basis of a visual examination, ripe rot or *C. acutatum*[20] was the predominant bunch rot disease in these grapes. Triplicate samples from each batch of grapes were prepared the same as GB samples.

Wine Made from Grapes Affected with Bunch Rot Molds. Grapes were obtained from a single block of Semillon vines located in the Riverina, New South Wales, Australia, during the 2011 vintage.

Table 2. Optimized Extraction Times and Temperatures for Target Compounds in Wine[a]

compound	optimized time	optimized temperature	predicted response	relative peak size (RPS)	inverse RPS[b]	inverse RPS × OPT time	inverse RPS × OPT temperature
2-isobutyl-3-methoxypyrazine	70	70	13035	0.188	3	180	180
2-isoproyl-3-methoxypyrazine	70	70	18217	0.054	18	1290	1290
3-octanone	70	70	92474	0.275	4	254	254
fenchone	30	30	1335750	1.000	1.0	30	30
1-octen-3-one	70	70	66676	0.199	5	352	352
fenchol	70	70	247942	0.738	1.3	95	95
1-octen-3-ol	37	30	1301970	0.899	1.1	41	33
trans-2-octen-1-ol	70	70	208108	0.619	2	112	112
2-methylisoborneol	70	70	15421	0.046	22	1524	1524
2,4,6-trichoroanisole	30	70	5791	0.017	58	1739	4058
geosmin	70	70	20984	0.062	16	1120	1120
2,4,6-tribromoanisole	31	46	8835	0.026	38	1178	1748
pentachloroanisole	30	70	8954	0.0267	37	1125	2624
sum					205	9040	13419
weighted mean extraction temperature and time					43.9 min	65.2 °C	

[a]Determined from the midpoint of the calibration curve. [b]Rounding errors account for minor differences of expressed values.

DOI: 10.1021/jf505444r
J. Agric. Food Chem. 2015, 63, 2877−2885

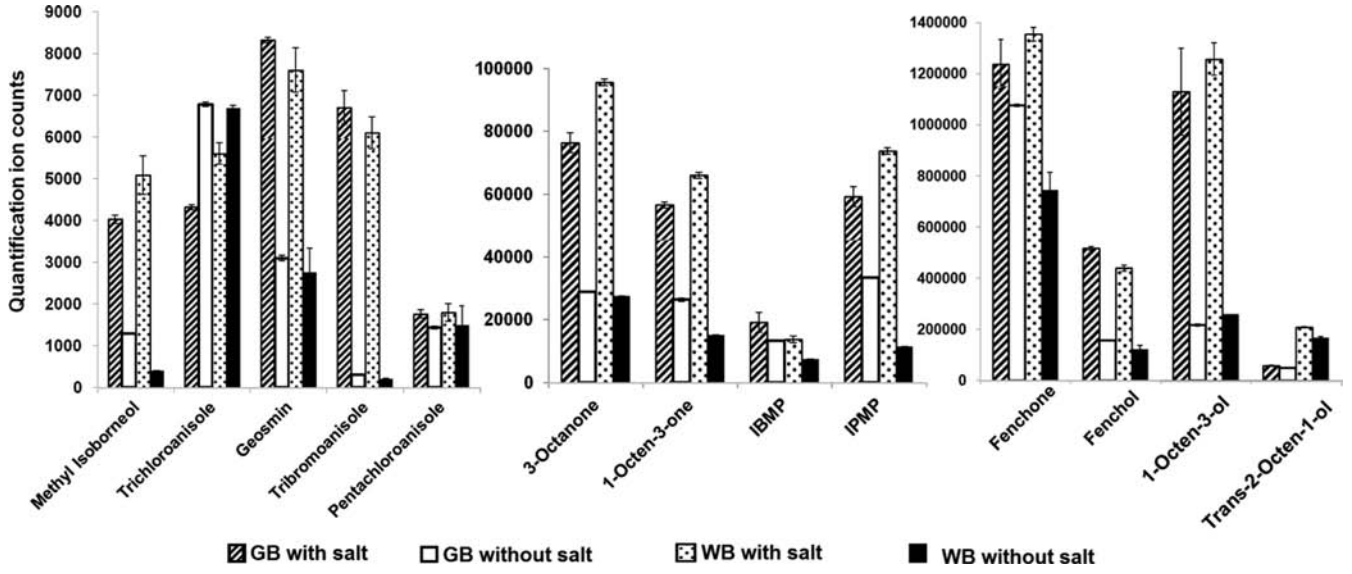

Figure 3. Effects of salting in WB or GB solution on the quantitation ion counts for all target compounds. The WB or GB solution was spiked at a concentration at one-tenth of the maximum calibration point. GB, grape base; WB, wine base.

Table 3. Details of Target Compound Identification, Calibration Curves, and Method Evaluations

number	compound	IS	quantitation ion[a] *m/z*	qualifier ion *m/z* (%)	calibration range (ng/L)	sample type[b]	r^2	LOD (ng/L)	LOQ (ng/L)	repeatability (% CV)	reproducibility (% CV)
1	2-isobutyl-3-methoxypyrazine	IS1	124	151 (20)	4.4−282	WB	0.996	0.2	0.6	7.4	8.7
				94 (21)		GB	0.994	0.1	0.3	9.7	8.9
2	2-isoproyl-3-methoxypyrazine	IS1	137	152 (31)	2.8−179	WB	0.986	0.1	0.3	6.8	8.1
				124 (41)		GB	0.995	0.05	0.2	5.1	7.2
3	3-octanone	IS2	57	72 (73)	20−4010	WB	0.998	10	20	9.6	10.2
				71 (63)		GB	0.988	7	20	11	9.8
				99 (75)							
4	fenchone	IS2	81	69 (44)	33−26760	WB	0.993	1	4	9.8	4.9
				152 (17)		GB	0.981	1	4	9.6	5.7
5	1-octen-3-one	IS2	55	70 (95)	2−980	WB	0.999	0.3	1	7.1	8.8
				83 (16)		GB	0.981	0.3	0.8	8.7	8.6
				97 (25)							
6	*trans*-2-octen-1-ol	IS3	57	68 (31)	3−2480	GB	0.993	1	3	9.8	4.9
				55 (46)		WB	0.991	1	3	9.6	5.7
7	fenchol	IS3	81	80 (61)	34−6905	WB	0.993	1	3	6.4	6.4
				121 (14)		GB	0.997	1	3	8.1	6.7
8	1-octen-3-ol	IS3	57	72 (18)	35−7000	WB	0.997	1.5	3.5	5	8.0
				85 (11)		GB	0.996	1.5	3.5	9.4	6.1
				99 (6)							
9	2-methylisoborneol	IS4	107	135(12)	3.1- 200	WB	0.992	3.1	6.2	4.3	3.6
				95 (5)		GB	0.996	3.1	6.2	8.6	6.7
10	2,4,6-trichoroanisole	IS5	195	210 (67)	0.58−37.3	WB	0.998	0. 10	0. 30	8.5	7.14
				212 (65)		GB	0.994	0.10	0. 30	11.1	5.5
11	geosmin	IS6	112	111 (24)	1.25- 80	WB	0.955	1.00	2.5	5.2	5.17
				125 (17)		GB	0.997	0.42	1.5	7.4	8.7
12	2,4,6-tribromoanisole	IS7	346	344 (98)	0.82−52.5	WB	0.997	0. 2	0.8	9.7	8.9
				329 (73)		GB	0.997	0.1	0.3	8.7	1.9
13	pentachloroanisole	IS8	280	265 (95)	3.47−55.5	WB	0.919	0.12	0.4	7.9	8.04
				237 (92)		GB	0.991	0.5	1.8	10.3	10.9
				267 (81)							

[a]As a proportion of the quantitation ion. [b]WB, wine base; GB, grape base.

Whole bunches were randomly selected along vine rows from both sides of the vine and sorted into two groups based on the visible level of infection. The control group had no perceived infection (i.e., clean fruit or 0% bunch infected), while the second treatment had high level infection (up to 45−50% of the bunch infected). These treatments were juiced and fermented separately to finished wine.[21] A further experimental wine made from Cabernet Sauvignon grapes that investigated the effect of ripe rot in an earlier study[22] was also used in this investigation.

Three commercially made wines were selected for analysis. These wines were a 2003 Semillon wine from the Hunter Valley, New South Wales, Australia, a 1978 Cabernet Sauvignon wine, and a 1987 vintage

DOI: 10.1021/jf505444r
J. Agric. Food Chem. 2015, 63, 2877−2885

Table 4. Details of IS Identification and Concentration

number	compound	retention time (min)	quantitation ion[a] m/z	qualifier ion m/z (%)	concentration (ng/L)
IS1	2-isobutyl-3-methoxy-d_3-pyrazine	24.0	127	154 (15)	25
IS2	methyl isobutyl ketone	9.5	58	85 (96)	97
				100 (88)	
IS3	2-octanol	21.3	45	55 (36)	60.2
				56 (12)	
				70 (10)	
IS4	2-methyl-d_3-isoborneol	26.0	110	138 (24)	100
				55 (10)	
IS5	2,4,6-trichloroanisole-d_5	33.9	215	217 (94)	20
IS6	geosmin-d_3	34.4	115	129 (12)	30
				128 (18)	
IS7	2,4,6-tribromoanisole-d_5	44.6	349	347 (36)	20
IS8	pentachloroanisole-d_3	46.2	283	285 (57)	20

[a]As a proportion of the quantitation ion.

Table 5. Recovery of Two Different Addition Concentrations of Compounds of Interest in Wine and Grape Juice

	recovery (%)[a]			recovery (%)[b]		
compound	red wine	white wine	grape	red wine	white wine	grape
2-isobutyl-3-methoxypyrazine	104	125	116	125	116	89
2-isoproyl-3-methoxypyrazine	87	108	96	111	99	111
3-octanone	103	108	120	108	113	121
fenchone	83	92	100	105	92	115
1-octen-3-one	100	83	101	94	90	98
trans-2-octen-1-ol	97	97	92	123	107	95
fenchol	103	95	104	131	117	104
1-octen-3-ol	100	95	95	118	108	96
2-methylisoborneol	99	103	104	100	104	102
2,4,6-trichoroanisole	118	95	107	94	106	105
geosmin	99	102	100	116	106	104
2,4,6-tribromoanisole	99	100	113	100	98	101
pentachloroanisole	97	91	115	115	104	108

[a]Recoveries of one-tenth addition of the maximum calibrate. [b]Recoveries of one-fifth addition of the maximum calibrate.

wine made from *Botrytis* Muscat of Alexandria grapes from the Riverina, New South Wales, Australia. Triplicate samples from each batch of wine were prepared the same as WB samples for the quantitation of the compounds of interest.

RESULTS AND DISCUSSION

Optimization. Optimization of sample treatment parameters is arguably the most important aspect of method development for sensitive, accurate, and precise quantitation of volatile compounds.[23,24] Optimized sample handling parameters were determined using response surface modeling and a desirability function, in which the importance of sample conditions for compounds with a high signal response relative to those with a low signal, is down-weighted by the calculation of a relative response factor.[14] Weighted mean extraction times and temperatures were calculated from the product of inverse RPS and optimized time or optimized temperature for the compounds of interest (Tables 1 and 2 for WB and GB, respectively). This approach for HS-SPME optimization enabled lower limits of quantitation to be achieved than previously reported for the compounds of interest.[25]

Response surface modeling to determine the optimized experimental conditions was undertaken in accordance with eq 1 for each analyte of interest. Consequently, for each analyte and solvent system (WB or GB), there exists six b coefficients that correspond to the fitted response when linear, squared, and interaction terms are modeled for a two-factor (time and temperature) model. The magnitude of each b coefficient is dependent upon the analyte signal, and the significance for each coefficient can be determined using a t test. Inspection of the t test values for the b coefficients for each compound in WB infers that an optimized sample incubation temperature is a more important factor than fiber exposure time to achieve maximum analytical sensitivity (Figure 1). In GB, fiber exposure time and sample incubation temperature are both important factors to optimize for the analysis of some compounds. The diminished importance of fiber exposure time for optimizing WB analysis may reflect a modified polarity of the solvent base because of the presence of ethanol, which has increased the volatility of the analytes and, hence, headspace concentration. Consequently, equilibrium between the WB headspace concentration and binding of these compounds onto the fiber, once exposed to the sample, occurs more rapidly than in GB. The analysis of alcoholic beverages can be challenging for HS-SPME analysis because the competitive adsorption between ethanol and other interesting volatile compounds onto the SPME fiber may cause loss of analytical sensitivity. This is due to the relative concentration of ethanol far exceeding that of other compounds leading to fiber saturation.[26] Dilution of samples to a lower ethanol concentration limits competitive binding of ethanol to the fiber, allowing for a lower detection limit for interesting compounds to be achieved.[27]

DOI: 10.1021/jf505444r
J. Agric. Food Chem. 2015, 63, 2877−2885

Table 6. Sensory Threshold and LOD of Target Compounds in the Wine Matrix

target compound	sensory threshold in wine (ng/L)	odor	LOD (ng/L) present study	LOD (ng/L) previously reported
2-isobutyl-3-methoxypyrazine	1−16[31]	vegetal, green pepper	0.1	3.1[25]
2-isoproyl-3-methoxypyrazine	2[31]	muddy	0.2	3.1[25]
3-octanone			10	NR[a]
fenchone		muddy	1	1.8[25]
1-octen-3-one	70[25] and 15	fungus	0.3	0.75[32]
trans-2-octen-1-ol	NR		1	NR
fenchol		muddy	1	1.6[25]
1-octen-3-ol	40000[25]	fungus	1.5	1[25]
2-methylisoborneol	55[25]	muddy	3.1	5.1
2,4,6-trichoroanisole	3[25]	mold	0.1	0.05,[33] 0.1,[34] 2,[35] 0.8,[36] and 0.3[25]
geosmin	50[25]	muddy	1	0.5[35] and 1.5[25]
2,4,6-tribromoanisole	2−5[25]	mold	0.2	0.09,[33] 0.1,[34] and 0.2[25]
pentachloroanisole	10000[25]	dust	0.12	0.5[25]

[a]NR = not reported.

The incorporation of high ionic strength solutes into the sample matrix is frequently employed for the analysis of volatile compounds with HS-SPME methods,[28,23] with sodium chloride or sodium sulfate most commonly used. An increased ionic strength sample matrix often results in higher analyte signal responses with HS-SPME methods. This is because an increased volatility of specific compounds arises from the altered solubility of polar compounds.[29] Partition coefficients for the gaseous phase are therefore improved, and consequently, greater analyte quantities are absorbed by the SPME fiber. This phenomenon was observed for all compounds of interest in the present investigation (Figure 3).

Calibration Curves and Method Evaluation. Calibration curves prepared in a diluted wine or grape homogenate matrix were constructed from the mean quantitation ion count of three replicate analyses, using a mix of naturally occurring and deuterated analogues as ISs. Good correlation coefficients (r^2 > 0.981) for all compounds (Table 3) and recovery experiments (Table 5) indicate that matrix interferences were relatively minor. Recovery values expressed as the coefficient of variation ranged from 83 to 131 in WB and from 89 to 121 in GB and indicate that the wine matrix had a greater impact upon the analysis than the grape base. This is not unexpected because, even with dilution, the ethanol concentration in wine was still relatively high compared to the analyte concentration. Additionally, the wine matrix is comprised of a significantly greater number of volatile compounds arising from yeast metabolism, which may lead to competitive interactions on the fiber surface and contribute to the matrix effect. Recovery values for spiked red wine also indicate possible interactions of the matrix with analytes to a greater extent than in the white wine (Table 5). It is possible that the greater concentration of phenolic compounds in red wine may have caused interference with recovery. However, values from two spiked additions were acceptable for analytical use (Table 5).

The limits of detection and quantitation for all analytes (Table 3) are lower than levels previously reported for wine and grape samples.[30] These values for are remarkably lower than those found in the literature (Table 6) and, in any case, are well below the reported sensory threshold of these components in wine. To the authors knowledge, no prior single GC−MS method has been developed that enable rapid and sensitive analysis of the diverse compounds elicited from mold growth that impart earthy taint aromas in one single GC−MS run. Our approach demonstrates the value of using optimization of multiple response factors by weighting specific variables according to a global desirability function.

Analysis of Healthy and Infected Grape and Wine Samples. The method has been applied to the analysis of infected grapes and wines. The growth of *C. acutatum* and *B. cinerea* on grapes is clearly associated with elevated levels of 2-methylisoborneol, geosmin, and 1-octen-3-one (Table 7). These compounds are also present in wine made from grapes infected with these fungal pathogens and are reported above in sensory thresholds. Previously reported levels of geosmin in grapes infected with *B. cinerea* support our findings for the production of these compounds in grapes infected with this mold.[5−8]

As shown in Table 7, geosmin was measured at levels higher than the reported sensory perception threshold in Semillon wine made from grapes infected with *B. cinerea*. Similarly, in Cabernet Sauvignon wines made from grapes infected with *C. acutatum*, 2-methylisoborneol levels were higher than the sensory perception threshold. It appears that 2-methylisoborneol contributes to the off-flavors found in wines made from ripe-rot-affected grapes, while geosmin has a greater role in contributing to the off-flavors found in wines made from gray-mold-affected grapes. While previous studies have examined off-flavors found in wine made from grape infected with gray mold (*B. cinerea*) and *Penicillium* rots[8] and sour rot,[11] as far as we are aware, this is the first study that has attempted to identify the chemical nature of the off-flavors found in wine made from grapes affected with ripe rot (*C. acutatum*).

Dilution of wines to an approximate ethanol concentration of 3% (v/v), increasing ionic strength in SPME fiber exposure, and sample extraction conditions have enabled a sensitive HS-SPME method to be devised. This method is also suitable for grape samples and has excellent analytical reproducibility and repeatability for volatile fungal metabolites. It has been validated across a large range of analytical levels and has a higher sensitivity than previously reported. The methods described enabled the determination of off-flavors in wine and grapes at nanograms per liter levels and achieve a linear, specific, accurate, and repeatable method in a single run. The levels of detection are below the reported olfactory thresholds of perception.[25] The method had good recoveries (83−131%), with acceptable repeatability and reproducibility. The developed method requires little or no sample preparation, is easily automated and reliable, and has no requirement for solvent extraction. Because of its simplicity, the method is suitable for the analysis of fungal off-flavor

DOI: 10.1021/jf505444r
J. Agric. Food Chem. 2015, 63, 2877−2885

Table 7. Off-Flavor Compounds in Bunch-Rot-Affected Grape and Wine Samples and Commercial Wines[a]

sample/ treatments	2-isobutyl-3-methoxypyrazine	2-isopropyl-3-methoxypyrazine	3-octanone	fenchone	1-octen-3-one	*trans*-2-octen-1-ol	fenchol	1-octen-3-ol	2-methylisoborneol	2,4,6-trichloroanisole	geosmin	2,4,6-tribromoanisole	pentachloroanisole
							Grape						
Sh/Con	ND	ND	BLQ	BLQ	ND	400 ± 10 a	BLQ	935 ± 10 a	ND	ND	12 ± 0 a	ND	ND
Sh/Gray	ND	ND	BLQ	BLQ	2567 ± 48	425 ± 21 a	BLQ	5647 ± 74 b	127 ± 13	ND	118 ± 10 b	ND	ND
Cab/Con	2 ± 0 a	1 ± 0 a	BLQ	BLQ	ND	185 ± 10 a	BLQ	1087 ± 2 a	ND	ND	7 ± 0 a	ND	ND
Cab/Ripe	2 ± 0 a	1 ± 0 a	BLQ	BLQ	1190 ± 46	195 ± 13 a	BLQ	5735 ± 52 b	156 ± 27	ND	24 ± 1 b	ND	ND
							Experimental Wine						
Semi/Con	ND	ND	ND	ND	1 ± 1 a	ND	ND	1186 ± 24 a	ND	BLQ	9 ± 1 a	ND	ND
Semi/Gray	ND	ND	121 ± 31	ND	112 ± 8 b	ND	ND	1416 ± 14 b	ND	BLQ	51 ± 5 b	ND	ND
Cab/Con	1 ± 0 a	ND	ND	ND	ND	140 ± 1 a	ND	ND	ND	ND	5 ± 1 a	ND	ND
Cab/Ripe	1 ± 0 a	ND	ND	ND	38 ± 13	138 ± 4 a	ND	166 ± 12	53 ± 8	ND	27 ± 3 b	ND	ND
							Commercial Wine						
Muscat	ND	ND	ND	1657 ± 132	ND	ND	2542 ± 235	ND	ND	ND	75 ± 21	ND	ND
Semi	1 ± 0	BLQ	BLQ	ND	BLQ	15 ± 2	ND	ND	17 ± 1	BLQ	ND	BLQ	ND
Cab	4 ± 1	BLQ	ND	ND	BLQ	17 ± 3	ND	13 ± 4	87 ± 18	ND	ND	ND	21 ± 2

[a]Samples: Sh, Shiraz; Semi, Semillon; and Cab, Cabernet Sauvignon. Treatment: Con, control; Gray, gray mold (*B. cinerea* affected); and Ripe, ripe rot (*C. acutatum* affected). ND, not detected; BLQ, below limit of quantitation. Mean ± standard deviation of triplicate determinations are reported. Mean values within grape and experimental wine sample columns (healthy and infected) followed by different letters (a and b) are significantly different at $p < 0.05$.

compounds in wine and grapes and may have applicability for the analysis of other fruit and beverage products impacted by fungal growth.

■ ASSOCIATED CONTENT

Ⓢ Supporting Information

Response surface curves for all of the target compounds in WB (Figure S1) and GB (Figure S2) for varying sample incubation temperatures and fiber exposure times. This material is available free of charge via the Internet at http://pubs.acs.org.

■ AUTHOR INFORMATION

Corresponding Author

*Telephone: +61-2-6933-4047. E-mail: nsadoughi@csu.edu.au.

Notes

The authors declare no competing financial interest.

■ ACKNOWLEDGMENTS

Kyra Boissery is thanked for collection of berry samples and production of Semillon wine affected with *B. cinerea*. Navideh Sadoughi was a recipient of a Charles Sturt University International Postgraduate Research Scholarship (IPRS).

■ ABBREVIATIONS USED

WB, wine base; GB, grape base; IS, internal standard; LOD, limit of detection; LOQ, limit of quantification; CV, coefficient of variation

■ REFERENCES

(1) Steel, C. C.; Blackman, J. W.; Schmidtke, L. M. Grapevine bunch rots: Impacts on wine composition, quality, and potential procedures for the removal of wine faults. *J. Agric. Food Chem.* **2013**, *61*, 5189−5206.

(2) Peña-Neira, A.; Fernández de Simón, B.; García-Vallejo, M. C.; Hernández, T.; Cadahía, E.; Suarez, J. A. Presence of cork-taint responsible compounds in wines and their cork stoppers. *Eur. Food Res. Technol.* **2000**, *211*, 257−261.

(3) Chatonnet, P.; Bonnet, S.; Boutou, S.; Labadie, M.-D. Identification and responsibility of 2,4,6-tribromoanisole in musty, corked odors in wine. *J. Agric. Food Chem.* **2004**, *52*, 1255−1262.

(4) Buser, H. R.; Zanier, C.; Tanner, H. Identification of 2,4,6-trichloroanisole as a potent compound causing cork taint in wine. *J. Agric. Food Chem.* **1982**, *30*, 359−362.

(5) La Guerche, S.; Chamont, S.; Blancard, D.; Dubourdieu, D.; Darriet, P. Origin of (−)-geosmin on grapes: On the complementary action of two fungi, *Botrytis cinerea* and *Penicillium expansum*. *Antonie van Leeuwenhoek* **2005**, *88*, 131−139.

(6) Morales-Valle, H.; Silva, L. C.; Paterson, R. R.; Oliveira, J. M.; Venancio, A.; Lima, N. Microextraction and gas chromatography/mass spectrometry for improved analysis of geosmin and other fungal "off" volatiles in grape juice. *J. Microbiol. Methods* **2010**, *83*, 48−52.

(7) Bañeras, L.; Trias, R.; Godayol, A.; Cerdán, L.; Nawrath, T.; Schulz, S.; Anticó, E. Mass spectrometry identification of alkyl-substituted pyrazines produced by *Pseudomonas* spp. isolates obtained from wine corks. *Food Chem.* **2013**, *138*, 2382−2389.

(8) La Guerche, S.; Dauphin, B.; Pons, M.; Blancard, D.; Darriet, P. Characterization of some mushroom and earthy off-odors microbially induced by the development of rot on grapes. *J. Agric. Food Chem.* **2006**, *54*, 9193−9200.

(9) Martins, J.; Esteves, C.; Limpo-Faria, A.; Barros, P.; Ribeiro, N.; Simões, T.; Correia, M.; Delerue-Matos, C. Analysis of six fungicides and one acaricide in still and fortified wines using solid-phase micro-extraction−gas chromatography/tandem mass spectrometry. *Food Chem.* **2012**, *132*, 630−636.

(10) Antalick, G.; Perello, M.-C.; de Revel, G. Development, validation and application of a specific method for the quantitative determination

DOI: 10.1021/jf505444r
J. Agric. Food Chem. 2015, 63, 2877−2885

of wine esters by headspace-solid-phase microextraction−gas chromatography−mass spectrometry. *Food Chem.* **2010**, *121*, 1236−1245.
(11) Barata, A.; Campo, E.; Malfeito-Ferreira, M.; Loureiro, V. l.; Cacho, J.; Ferreira, V. Analytical and sensorial characterization of the aroma of wines produced with sour rotten grapes using GC−O and GC−MS: Identification of key aroma compounds. *J. Agric. Food Chem.* **2011**, *59*, 2543−2553.
(12) Aberl, A.; Coelhan, M. Determination of sulfur dioxide in wine using headspace gas chromatography and electron capture detection. *Food Addit. Contam.* **2012**, *30*, 226−233.
(13) Ryan, D.; Watkins, P.; Smith, J.; Allen, M.; Marriott, P. Analysis of methoxypyrazines in wine using headspace solid phase microextraction with isotope dilution and comprehensive two-dimensional gas chromatography. *J. Sep. Sci.* **2005**, *28*, 1075−1082.
(14) Derringer, G.; Suich, R. Simultaneous optimization of several response variables. *J. Qual. Technol.* **1980**, *12*, 214−219.
(15) Ezquerro, O.; Tena, M. T. Determination of odour-causing volatile organic compounds in cork stoppers by multiple headspace solid-phase microextraction. *J. Chromatogr. A* **2005**, *1068*, 201−208.
(16) Rebiere, L.; Clark, A. C.; Schmidtke, L. M.; Prenzler, P. D.; Scollary, G. R. A robust method for quantification of volatile compounds within and between vintages using headspace-solid-phase microextraction coupled with GC−MS—Application on Semillon wines. *Anal. Chim. Acta* **2010**, *660*, 149−157.
(17) Leardi, R. Experimental design in chemistry: A tutorial. *Anal. Chim. Acta* **2009**, *652*, 161−172.
(18) Lizarraga, E.; Irigoyen, A.; Belsue, V.; Gonzalez-Penas, E. Determination of chloroanisole compounds in red wine by headspace solid-phase microextraction and gas chromatography−mass spectrometry. *J. Chromatogr. A* **2004**, *1052*, 145−149.
(19) Elmer, P. G.; Michailides, T. Epidemiology of *Botrytis cinerea* in orchard and vine crops. In *Botrytis: Biology, Pathology and Control*; Elad, Y., Williamson, B., Tudzynski, P., Delen, N., Eds.; Springer: Dordrecht, Netherlands, 2007; pp 243−272.
(20) Whitelaw-Weckert, M. A.; Curtin, S. J.; Huang, R.; Steel, C. C.; Blanchard, C. L.; Roffey, P. E. Phylogenetic relationships and pathogenicity of *Colletotrichum acutatum* isolates from grape in subtropical Australia. *Plant Pathol.* **2007**, *56*, 448−463.
(21) Boissery, K. Effect of bunch rot on the berry microflora and composition of semillon wine. Honors Thesis, Charles Sturt University, Wagga Wagga, Australia, 2011.
(22) Meunier, M.; Steel, C. C. Effect of *Colletotrichum acutatum* ripe rot on the composition and sensory attributes of cabernet sauvignon grapes and wine. *Aust. J. Grape Wine Res.* **2009**, *15*, 223−227.
(23) Rocha, S.; Ramalheira, V.; Barros, A.; Delgadillo, I.; Coimbra, M. A. Headspace solid phase microextraction (SPME) analysis of flavor compounds in wines. Effect of the matrix volatile composition in the relative response factors in a wine model. *J. Agric. Food Chem.* **2001**, *49*, 5142−5151.
(24) Alpendurada, D. F. M. Solid-phase microextraction: A promising technique for sample preparation in environmental analysis. *J. Chromatogr. A* **2000**, *889*, 3−14.
(25) Boutou, S.; Chatonnet, P. Rapid headspace solid-phase microextraction/gas chromatographic/mass spectrometric assay for the quantitative determination of some of the main odorants causing off-flavours in wine. *J. Chromatogr. A* **2007**, *1141*, 1−9.
(26) Khio, S. W.; Cheong, M. W.; Zhou, W.; Curran, P.; Yu, B. Characterization of the volatility of flavor compounds in alcoholic beverages through headspace solid-phase microextraction (HS-SPME) and mathematical modeling. *J. Food Sci.* **2012**, *77*, C61−C70.
(27) Stackler, B.; Christensen, E. N. Quantitative determination of ethanol in wine by gas chromatography. *Am. J. Enol. Vitic.* **1974**, *25*, 202−207.
(28) Howard, K. L.; Mike, J. H.; Riesen, R. Validation of a solid-phase microextraction method for headspace analysis of wine aroma components. *Am. J. Enol. Vitic.* **2005**, *56*, 37−45.
(29) Fries, E. Determination of benzothiazole in untreated wastewater using polar-phase stir bar sorptive extraction and gas chromatography−mass spectrometry. *Anal. Chim. Acta* **2011**, *689*, 65−68.
(30) Cortada, C.; Vidal, L.; Canals, A. Determination of geosmin and 2-methylisoborneol in water and wine samples by ultrasound-assisted dispersive liquid−liquid microextraction coupled to gas chromatography−mass spectrometry. *J. Chromatogr. A* **2011**, *1218*, 17−22.
(31) Allen, M. S.; Lacey, M. J.; Harris, R. L. N.; Brown, W. V. Contribution of methoxypyrazines to sauvignon blanc wine aroma. *Am. J. Enol. Vitic.* **1991**, *42*, 109−112.
(32) Culleré, L.; Cacho, J.; Ferreira, V. Validation of an analytical method for the solid phase extraction, in cartridge derivatization and subsequent gas chromatographic−ion trap tandem mass spectrometric determination of 1-octen-3-one in wines at ng L^{-1} level. *Anal. Chim. Acta* **2006**, *563*, 51−57.
(33) Schmarr, H.-G.; Koschinski, S.; Sang, W.; Slabizki, P. Trace level analysis of corky off-flavor compounds: Development of a new analytical method based on solid phase extraction and analysis by multidimensional gas chromatography with mass spectrometric detection. *J. Chromatogr. A* **2012**, *1226*, 96−102.
(34) Slabizki, P.; Schmarr, H.-G. Analysis of corky off-flavour compounds at ultra trace level with multidimensional gas chromatography−electron capture detection. *J. Chromatogr. A* **2013**, *1271*, 181−184.
(35) Weingart, G.; Schwartz, H.; Eder, R.; Sontag, G. Determination of geosmin and 2,4,6-trichloroanisole in white and red Austrian wines by headspace SPME−GC/MS and comparison with sensory analysis. *Eur. Food Res. Technol.* **2010**, *231*, 771−779.
(36) Özhan, D.; Anli, R. E.; Vural, N.; Bayram, M. Determination of chloroanisoles and chlorophenols in cork and wine by using HS-SPME and GC−ECD detection. *J. Inst. Brew.* **2009**, *115*, 71−77.

DOI: 10.1021/jf505444r
J. Agric. Food Chem. 2015, 63, 2877−2885

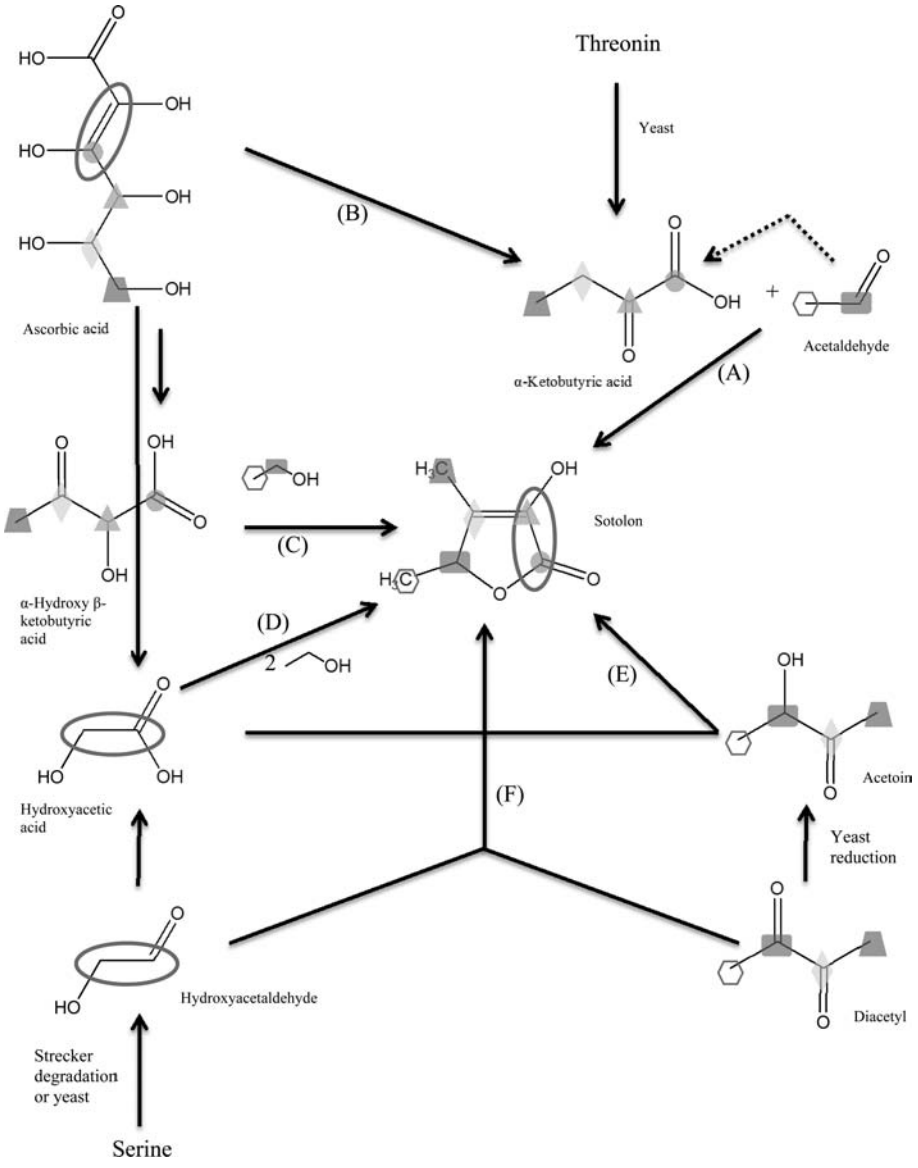

Figure 1. Potential synthesis pathways for sotolon in beverages.

Table 1. Chemical and Sensorial Characteristics of the Selected Special Beers

type	beer	alcohol (% vol)	original extract (g/100g)	real extract (g/100g)	pH	bitterness (BU)	color (EBC)	sensorial characteristics	particularities
blond	BL1	8.5	16.3	4.2	4.4	29	14.5	lemon, banana, apple, spicy, phenols	unfiltrated, bottle refermentation
	BL2	7.5	14.9	3.7	4.5	24	15.5	orange, pineapple, spicy, phenols	organic beer (organic version of BL1), unfiltrated, bottle refermentation
	BL3	6.3	14.4	4.6	4.2	15	12.5	butter, apple, hop, green	centrifuged, flash pasteurization, ascorbic acid addition
	BL4	7.5	16.8	5.1	4.5	21	16.5	butter, sulfur, hop	high gravity brewing, unfiltrated, bottle refermentation, flash pasteurization, ascorbic acid addition
	BL5	6.3	14.4	4.6	4.2	15	12.5	butter, apple, hop, green	BL3 without ascorbic acid
dry hopped trappist	TR1	6.2	13.3	3.2	4.1	29	26	hop, phenols, citrus, cheese	dry hopping, unfiltrated, bottle refermentation (with *Brettanomyces*)
amber	AM1	12.0	20.8	5.5	4.4	18	11	alcohol, banana, cheese, phenols	caramel malt, filtrated, ascorbic acid and sulfites addition
brown	BR1	8.0	19.8	6.2	4.7	16	11	malt, sulfur, green	chocolate malt (7%), light filtration, bottle refermentation

DOI: 10.1021/jf505953u
J. Agric. Food Chem. 2015, 63, 2886−2892

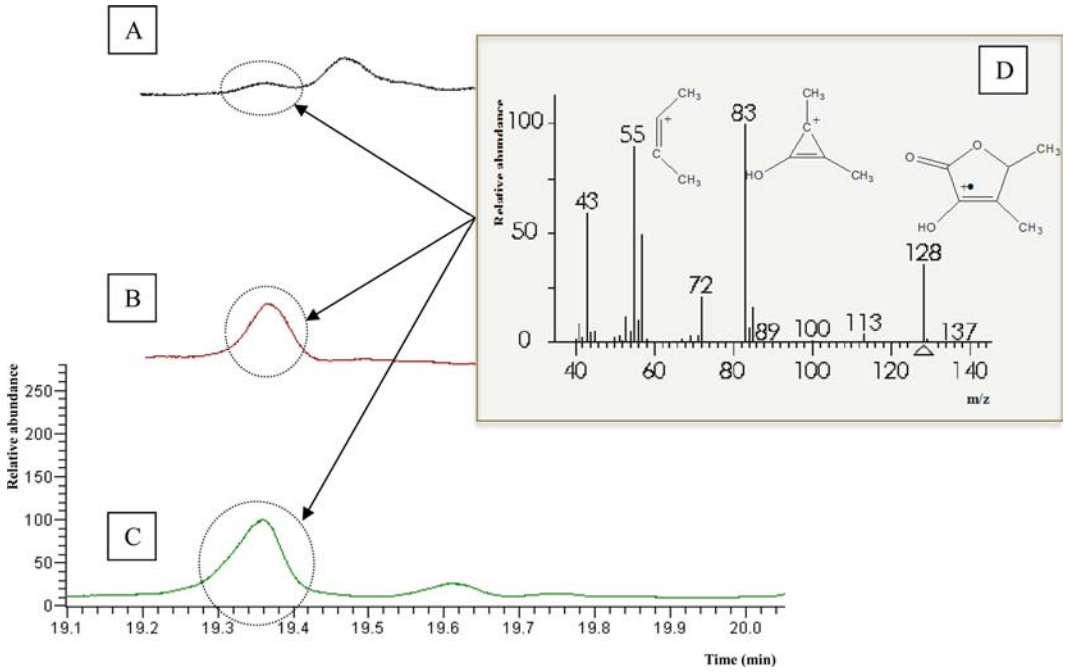

Figure 2. MS (SIM) chromatogram of fresh (A), 18-month-aged (B), and 24-month-aged (C) BL3 beer, and TIC mass spectrum of sotolon after 24 months (D).

No scientific paper describes how sotolon might be involved in the Madeira off-flavor found in aged beers, especially when strongly oxidized. Callemien et al.[6] detected the presence of sotolon in an aged lager beer. The aim of the present work was to compare the concentration of sotolon in fresh and aged samples of different commercial specialty beers. A specific lactone extraction procedure was applied, and the extracts were analyzed by GC-MS (gas chromatography-mass spectrometry). Beers or model media spiked with different hypothetical precursors and subjected to different beer storage conditions were compared in order to evidence which key factors should be controlled by brewers.

MATERIALS AND METHODS

Chemicals. Diethyl ether (99.9%), nonadecane (99.9%), hydrogen peroxide (30%), iron(II) chloride (98%), sotolon (99%), L-ascorbic acid (>99%), acetoin (>96%), diacetyl (97%), acetaldehyde (≥98%), and glycolaldehyde (hydroxyacetaldehyde dimer) were purchased from Sigma-Aldrich (Bornem, Belgium). Methanol (99.9%), acetone, and absolute ethanol were obtained from Analar Normapur (Fontenay-sous-bois, France). Anhydrous sodium sulfate (99%) was obtained from Merck (Darmstadt, Germany). Hydrochloric acid (36%) was purchased from Fisher Scientific (Tournai, Belgium). Sodium hydroxide was purchased from VWR international (Radnor, PA). Dichloromethane (99.9%) from Romil (Cambridge, U.K.) was distilled before use. Milli-Q water was used (Millipore, Bedford, MA). Amberlite XAD 2 resin (Supelco, Bellefonte, PA) (with a pore size of 9 nm and a specific area of 330 m^2/g) was sequentially washed with methanol and diethyl ether (each for 4 h) in a Soxhlet and stored in methanol at 4 °C.

Beer Samples. Seven commercial top-fermented beers (BL1, BL2, BL3, BL4, AM1, BR1, and TR1) were kindly supplied by Belgian brewers and stored in the dark at 20 °C for 2 years (Table 1) for natural aging. An analog of BL3 without ascorbic acid (BL5) was produced by a brewer for some spiking and accelerated aging experiments.

XAD 2 Procedure for Sotolon Extraction.[14] Amberlite XAD 2 resin (2 g) was thoroughly rinsed with Milli-Q water (approximately 400 mL), and the mixture was poured into a 250 mL Schott flask containing 50 mL of degassed beer adjusted at pH 11.5 by addition of 4 M NaOH. Beer alkalinization was done to increase lactone polarity, thus avoiding its adsorption onto the resin. Samples were shaken in the dark for 2 h and then poured onto a glass XAD column for separation. Beer percolating from the XAD 2 resin was recovered. Then, resin was washed with 50 mL of water, which was collected and mixed to the first eluate. This mixture was extracted three times with 40 mL of dichloromethane (10 min, 1000 rpm) after adjusting the pH to 3 to allow lactone cyclization. The organic phases were finally pooled and dried with anhydrous sodium sulfate. Then 0.5 mL of nonadecane stock solution (20 mg/L) was added as EST (external standard) before concentration to 0.5 mL in a Kuderna–Danish apparatus at 45 °C (total concentration factor = 100, final EST concentration = 20 mg/L). The final extract was stored at −80 °C for further analysis. A recovery factor of 89% was calculated for sotolon by the standard addition method in BL3.

Gas Chromatography Connected to Mass Spectrometry (GC-MS). Electronic impact mass spectra were recorded at 70 eV on a ThermoFinnigan (Waltham, MA) Trace MS simple quadrupole mass spectrometer connected to a ThermoFinnigan Trace GC 2000 gas chromatograph equipped with a split/splitless injector (splitless time = 0.5 min) and a polar FFAP-CB column (Varian, CP7485, 25 m × 0.32 mm i.d., 0.3 μm film thickness). The carrier gas was helium, and the pressure was set at 50 kPa (100 kPa were applied on the CP-Sil5-CB MS column, 50 m × 0.32 mm, 1.2 μm film thickness, that we used for RI (retention index) checking on a second chromatographic phase). The injection volume was 1 μL. The oven temperature was programmed to rise from 36 to 85 °C at 20 °C/min, then to 145 °C at 1 °C/min, and finally to 250 °C at 3 °C/min. Sotolon was quantified by standard addition with an EST (spiking to beer of 0.5, 1, 7, 15, and 20 μg/L), as recently described by Collin et al.[23] The SIM mode (single-ion monitoring mode) was used with m/z = 83 and 128. Spectral recording was automatic throughout separation (Xcalibur software, NIST database).

Gas Chromatography Connected to Olfactometric Detection (GC-O). A 1 μL amount of each extract was analyzed with a Chrompack CP9001 (Santa Clara, CA) gas chromatograph equipped with a split/splitless injector maintained at 250 °C (the split vent was opened 0.5 min postinjection) and connected to a GC-O port (Chrompack), also at 250 °C. The sotolon odor was checked with a polar FFAP-CB capillary column (Varian, CP7485, 25 m × 0.32 mm

DOI: 10.1021/jf505953u
J. Agric. Food Chem. 2015, 63, 2886−2892

i.d., 0.3 μm film thickness) and the CP-Sil5-CB MS column (50 m × 0.32 mm, 1.2 μm film thickness). The carrier gas was nitrogen, and the pressure was set at 30 (FFAP-CB) or 60 kPa (CP-Sil5-CB). The oven temperature program was the same as that described for GC-MS. The effluent was diluted with a large volume of air (20 mL/min) prehumidified with an aqueous copper(II) sulfate solution.

Beer Standard Analysis. Alcohol and extract determination were done with an Anton Paar (Graz, Austria) density meter DMA 4500M. Color, pH, and bitterness analyses were performed according to EBC analytical procedures.[24]

Sensory Analyses. Ten trained panelists scored 6 aging attributes on a scale of 1−5: cardboard, Madeira, nutty, bread, cooked fruit, and honey. A score of 0 meant the panelist did not detect the aroma, whereas a score of 5 meant the aroma was strongly perceived.

Determination of Sotolon Flavor Threshold in Beer. Determination of the flavor threshold of sotolon was performed with the ASTM method (Ascending Concentration Series Method of Limits), as recommended by the European Brewery Convention (method 13.9).[24] Sotolon was added to fresh beer (reference beer = fresh BL3) at six different levels of concentrations (from 0.5 to 20 μg/L). The panel was composed of 10 nontrained university students and 10 trained experts. Each assessor received 6 sequences of 3-Alternate Forced Choice (3-AFC) tests. For each sequence, sotolon was spiked into one test sample, the other two containing reference beer without any addition. The "best estimated threshold" (BET) of a panelist corresponds to the geometric mean of the highest concentration missed and the next highest adjacent concentration tested. The group best estimated threshold (group BET) was calculated as the geometric mean of the individual best estimated thresholds.

Investigation of Sotolon Pathways. *Pathway A.* BL3 bottles were spiked with 100 mg/L acetaldehyde and aged in the dark at 40 °C for 10 or 30 days. Pathways E/F: diacetyl 40 μg/L, acetoin 400 μg/L, serine 10 mg/L, and/or glycolaldehyde 40 μg/L were added to a sterilized phosphate buffer (pH = 4.5) containing 5% v/v ethanol. Samples were stored in the dark at 40 or 60 °C for 30 days. Pathways B/C/D: Oxygenated and control samples consisted in fresh BL5 exposed or not to sterile oxygen (final concentration = 6 mg/L in the "oxygen" sample) without any other spiking. Ascorbic acid was added at 880 mg/L final concentration, with or without 555 mg/L SO_2, to 200 mL of fresh BL5 in a glass flask exposed to oxygen by bubbling 6 mg/L sterile oxygen. A combination of iron at 1 mg/L and hydrogen peroxide at 1 g/L was also spiked as pro-oxidants to a BL5 sample exposed in the same way to 6 mg/L oxygen. Samples were stored for 30 days in the dark at 40 °C.

Statistical Analyses. Analyses were carried out in duplicate, and comparisons of means were performed with the Student−Newman−Keuls test with SAS software version 9.2 (SAS Institute, Inc., Carry, NC). Values sharing no common letter are significantly different ($p < 0.05$).

RESULTS AND DISCUSSION

Identification and Quantitation of Sotolon in Aged Beers. As depicted in Figure 2 and Table 2, only traces of sotolon (<1 μg/L) were found in fresh beer samples. In contrast, the lactone-specific extraction enabled us to quantify it in all special beers after 6, 12, 18, and 24 months of natural aging, whatever the type of beer (blond, amber, trappist, or brown, with or without bottle refermentation or ascorbic acid addition; Table 1). Identification was confirmed by mass spectrometry (coincidence of the main m/z with the commercial reference and the NIST library entry), the retention indices on two capillary columns (RI = 2213 on FFAP-CB and 1068 on CP-Sil5-CB), and odors (curry, walnut). For the 7 beers analyzed, the amount of sotolon already reached 4.6−14.2 μg/L after 6 months and continued to increase thereafter up to 42.1 μg/L in the ascorbic-acid-protected beer BL3 after 2 years. These values are well above the 2 μg/L sensory threshold previously assessed in hydro-alcoholic solution.[15] They also exceed after 12 months the 8 μg/L sensory threshold that a jury of 20 panelists here determined in BL3 (already after 6 months for BL2, BL3, and BL4). The Madeira attribute was also scored (together with five other aging descriptors) in all beers over the first year of storage by a jury of trained panelists (data given for BL3 in Figure 3). The Madeira character was set above 2 in all 6- and 12-months-aged beers and under 1 in fresh beers.

Table 2. Sotolon Concentration (μg/L) in Top-Fermentation Beers Stored at 20 °C[a]

	BL1	BL2	BL3	BL4	TR1	AM1	BR1
fresh	nq	nq	nq	nq	nq	nq	nq
6 months	6.4	14.2	9.5	11.6	7.8	4.6	6.8
12 months	8.9	17.0	9.0	10.1	12.0	9.4	13.7
18 months	10.9	36.2	27.1	20.8	16.2	14.7	13.0
24 months	8.9	24.3	42.1	37.5	29.1	12.1	16.5

[a]GC-MS (SIM mode) Data. nq = detected but not quantifiable (<1μg/L). Means of duplicates (CV < 5%).

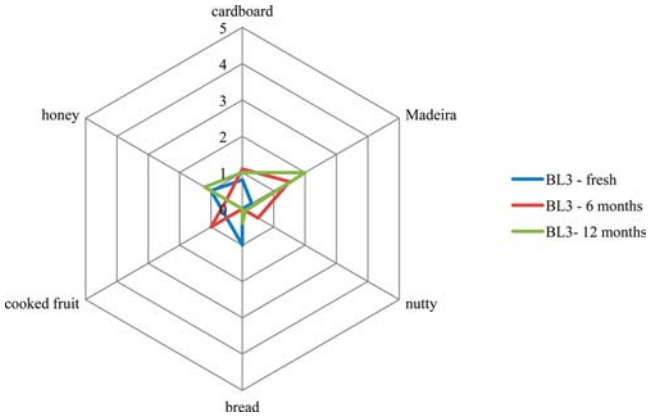

Figure 3. Aging off-flavors in BL3 through natural aging.

As depicted in Figure 4 for BL3, 30 days at 40 °C treatment revealed to produce sotolon (9 μg/L) in a range close to what we observed after 6 months of natural aging. Such accelerated aging was therefore applied to assess in a short time which synthesis pathways could occur in beer. As BL3 contained

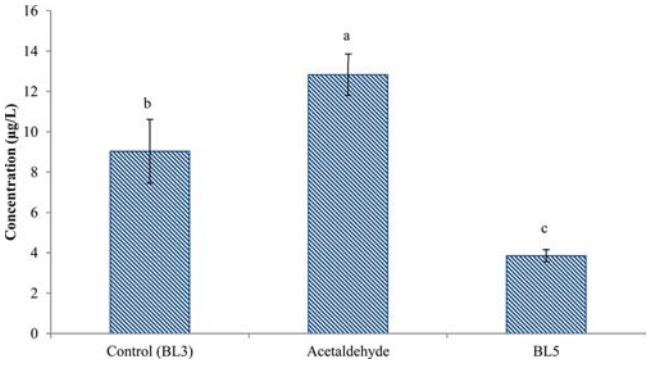

Figure 4. Sotolon concentration (μg/L) in a control beer (BL3, containing ascorbic acid), in the same beer spiked with 100 mg/L acetaldehyde, and in BL5 (devoided of ascorbic acid) after 30 days at 40 °C. Values sharing no common letters are significantly different ($p < 0.05$).

DOI: 10.1021/jf505953u
J. Agric. Food Chem. 2015, 63, 2886−2892

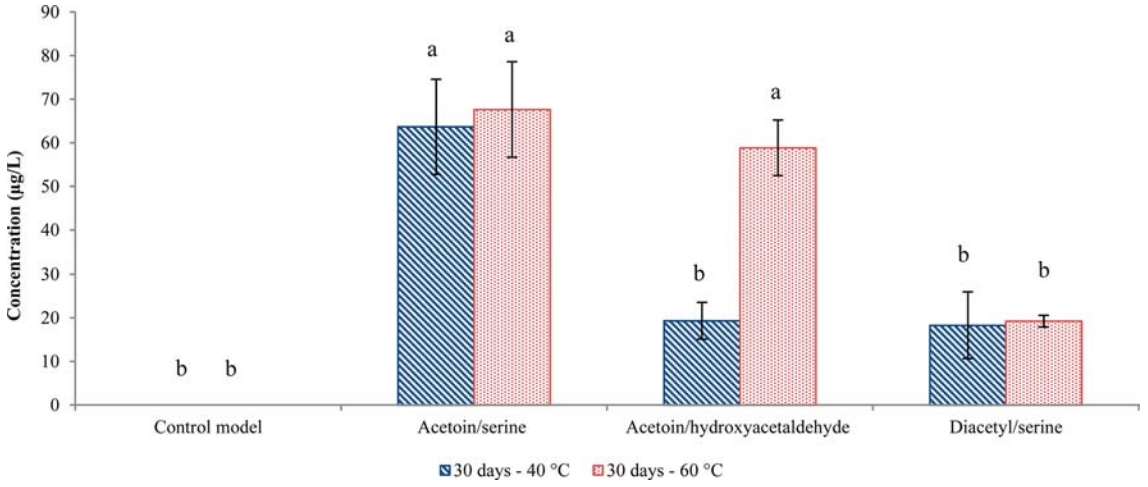

Figure 5. Sotolon concentration (μg/L) in a model beer medium (control model), and the same solution spiked with acetoin, serine, diacetyl, and/or hydroxyacetaldehyde after 30 days at 40 or 60 °C. Values sharing no common letters are significantly different ($p < 0.05$).

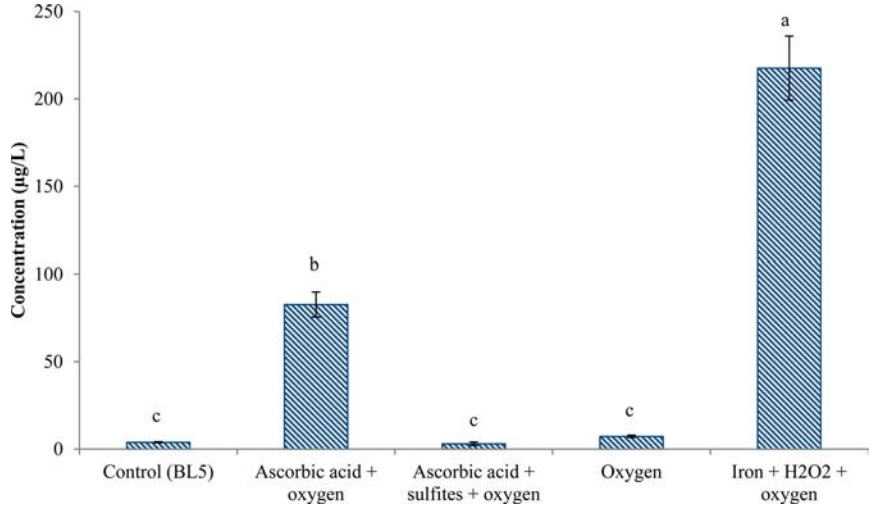

Figure 6. Sotolon concentration (μg/L) in a control beer (BL5, devoided of ascorbic acid) and the same BL5 beer spiked with 8 mg/L oxygen, with 880 mg/L ascorbic acid and 8 mg/L oxygen, a combination of 880 mg/L ascorbic acid, 6 mg/L oxygen, and 555 mg/L sulfites, or pro-oxidant species (Fe^{2+} (1 mg/L) + H_2O_2 (1 g/L)) after 30 days at 40 °C. Values sharing no common letters are significantly different ($p < 0.05$).

ascorbic acid, a pilot version without ascorbic acid addition at bottling (BL5) was requested of the manufacturer. This beer was used for all experiments where oxidation could play a key role. As shown by its accelerated aging (30 days at 40 °C), the absence of ascorbic acid already allowed minimizing the content of sotolon (4 μg/L in BL5 instead of 9 in BL3).

Potential Pathways for Sotolon Formation in Beer. *Pathway A.* Many researchers have demonstrated the key role of acetaldehyde in the appearance of sotolon in beverages.[19−25] Therefore, fresh BL3 was spiked with 100 mg/L acetaldehyde (usual concentration in fresh ales = 3.8−33.8 mg/L[26]) in the absence of oxygen, and samples were aged for 30 days at 40 °C. As depicted in Figure 4, sotolon was found to be significantly produced from added acetaldehyde (12.8 μg/L versus 8 in the control).

Pathways E/F. Diacetyl has been mentioned in the literature as a possible precursor of sotolon when combined with hydroxyacetaldehyde under quite harsh conditions[22] (usual diacetyl concentration in ale = 60−300 mg/L[27]). Its reduced form, acetoin, is another well-known constituent of beer (usual acetoin concentration in ale = 10−200 mg/L[27]) which could react with serine-derived compounds such as hydroxyacetic acid by aldol condensation (usual serine concentration in beer = 2−12 mg/L[28]). The compounds diacetyl, acetoin, glycolaldehyde (the commercial dimer of hydroxyacetaldehyde), and serine were mixed in different combinations in a beer model solution before aging for 30 days at 40 or 60 °C. As depicted in Figure 5, only acetoin proved able to generate large amounts of sotolon. The highest concentrations (63−67 μg/L) were obtained after addition of acetoin in the presence of serine. Hydroxyacetaldehyde together with acetoin led to lower amounts of sotolon at 40 °C (19.3 μg/L after 30 days) but reached 59 μg/L at 60 °C, probably because glycolaldehyde must dissociate to hydroxyacetaldehyde before it can react. In the case of diacetyl together with serine, both temperatures led to only 12−14 μg/L, suggesting that it is probably a minor pathway in natural beer aging. Transferred to beer, these results could mean that the efficiency of the reduction of diacetyl to acetoin by yeast could impact the Madeira off-flavor.

Pathways B/C/D. In the brewing industry, ascorbic acid is sometimes used as antioxidant at the bottling step in association (e.g., AM1) or not (e.g., BL3) with sulfites. As

DOI: 10.1021/jf505953u
J. Agric. Food Chem. 2015, 63, 2886−2892

illustrated in Figure 1 from the literature (pathways B–D), degradation of ascorbic acid can generate different species, possibly involved in sotolon synthesis. Ascorbic acid can also act as a pro-oxidant in beer.[28] Spiking of BL5 with 880 mg/L ascorbic acid (much higher amount than the industrial spiking of BL3 = 30 mg/L) and 6 mg/L oxygen led to sotolon concentrations up to 82.7 μg/L after 30 days at 40 °C, whereas the same beer, when untreated (control = no ascorbic acid and <0.05 mg/L oxygen), did not even reach the 8 μg/L flavor threshold of the lactone in beer (Figure 6). As expected, mixing 555 mg/L sulfites with ascorbic acid annihilated the latter's negative effect. In beer, sulfites arise either through the action of yeast or through exogenous addition at the bottling step.

BL5 was also aged for 30 days at 40 °C in absence of ascorbic acid, under a bottleneck saturated with 6 mg/L oxygen. Only 7.3 μg/L sotolon was measured here, suggesting that beer polyphenols are able to minimize its effect. In comparison, spiking of hydrogen peroxide and iron (well known for the Fenton reaction) dramatically increased sotolon concentration (up to 217 μg/L). Ethanol most probably acts as a quencher of hydroxyl radicals, as mentioned by Andersen et al.,[29] leading to the formation of acetaldehyde involved himself in sotolon synthesis (Pathway A).

In conclusion, prevention of oxidation is required to decrease the Madeira off-flavor brought to the beer by sotolon. Yet addition of ascorbic acid at bottling should be avoided, at least if not combined with sulfites, because of the role of ascorbic acid either as a reagent (precursor of α-ketobutyric acid, α-hydroxy-β-ketobutyric acid, or hydroxyacetic acid) or as a pro-oxidant (for acetaldehyde production). Despite a very low oxygen content in such beers, refermented beers seem not to be fully protected against the Madeira off-flavor, probably because of additional pathways, including the biochemical deamination of threonine and serine by yeast, followed by combination with either acetaldehyde or acetoin.

AUTHOR INFORMATION

Corresponding Author

*Tel.: +32 10 47 29 13. Fax: +32 10 47 21 78. E-mail: sonia.collin@uclouvain.be.

Notes

The authors declare no competing financial interest.

ACKNOWLEDGMENTS

The authors thank the CONSALIM project for kind collaboration.

REFERENCES

(1) Noël, S.; Liégeois, C.; Lermusieau, G.; Bodart, E.; Badot, C.; Collin, S. Release of deuterated nonenal during beer ageing from labeled precursors synthetized in the boiling kettle. *J. Agric. Food Chem.* **1999**, *47*, 4323–4326.

(2) Liégeois, C.; Meurens, N.; Badot, C.; Collin, S. Release of deuterated (E)-2-nonenal during beer ageing from labeled precursors synthetized before boiling. *J. Agric. Food Chem.* **2002**, *50*, 7634–7638.

(3) Gijs, L.; Chevance, F.; Jerkovic, V.; Collin, S. How low pH can intensify beta-damascenone and dimethyl trisulfide production through beer aging. *J. Agric. Food Chem.* **2002**, *50*, 5612–5616.

(4) Chevance, F.; Guyot-Declerck, C.; Dupont, J.; Collin, S. Investigation of the beta-damascenone level in fresh and aged commercial beers. *J. Agric. Food Chem.* **2002**, *50*, 3818–3821.

(5) Vanderhaegen, B.; Neven, H.; Daenen, L.; Verstrepen, K. J.; Verachtert, H.; Derdelinckx, G. Furfuryl ethyl ether: important aging flavor and a new marker for the storage conditions of beer. *J. Agric. Food Chem.* **2004**, *52*, 1661–8.

(6) Callemien, D.; Dasnoy, S.; Collin, S. Identification of a stale-beer-like odorant in extracts of naturally aged beer. *J. Agric. Food Chem.* **2006**, *54*, 1409–1413.

(7) Scholtes, C.; Nizet, S.; Collin, S. Guaiacol and 4-methylphenol as specific markers of torrefied malts. Fate of volatile phenols in special beers through aging. *J. Agric. Food Chem.* **2014**, *62*, 9522–9528.

(8) Tran, T. T. H.; Gros, J.; Bailly, S.; Nizet, S.; Collin, S. Fate of 2-sulphanylethyl acetate and 3-sulphanylpropyl acetate through beer aging. *J. Inst. Brew.* **2012**, *118*, 198–204.

(9) Clapperton, J. F. Ribes Flavour in Beer. *J. Inst. Brew.* **1976**, *82*, 175–176.

(10) Tran, T. T. H.; Nizet, S.; Gros, J.; Collin, S. Occurence of the ribes odorant 3-sulphanyl-3-methylbutyl formate and its analogues in beer. *Flavours Fragrances J.* **2013**, *28*, 174–179.

(11) Dalgliesh, C. E. Flavour stability. *Proc. Congr.-Eur. Brew. Conv* **1977**, 623–659.

(12) Pons, A.; Lavigne, V.; Landais, Y.; Darriet, P.; Dubourdieu, D. Distribution and organoleptic impact of sotolon enantiomers in dry white wines. *J. Agric. Food Chem.* **2008**, *56*, 1606–1610.

(13) Cutzach, I.; Chatonnet, P.; Dubourdieu, D. Rôle du sotolon dans l'arôme des vins doux naturels, influence des conditions d'élevage et de vieillissement. *J. Int. Sci. Vigne Vin* **1998**, *32*, 223–233.

(14) Scholtes, C.; Nizet, S.; Collin, S. Occurrence of sotolon, abhexon and theaspirane-derived molecules in gueuze beers. Chemical similarities with "Yellow wines". *J. Inst. Brew.* **2012**, *118*, 223–229.

(15) Lavigne-Cruège, V.; Dubourdieu, D. Role of glutathione on development of aroma defects in dry white wines. *13th International Enology Symposium*, Montpellier, 2002.

(16) Cantarelli, C. Etude de la madérisation et de sa prévention dans les vins blancs. *Deuxième Symposium*; Institute d'Œnologie, Bordeaux Cognac, 1967; Vol. *2*, pp392– 407.

(17) Sulser, H.; Depizzol, J.; Büchi, W. A probable flavoring principle in vegetable-protein hydrolysates. *J. Food Sci.* **1967**, *32*, 611–615.

(18) Takahashi, K.; Tadenuma, M.; Sato, S. 3-Hydroxy-4,5-dimethyl-2(5H)-furanone, a burnt flavoring compound from aged sake. *Agric. Biol. Chem.* **1976**, *40*, 325–330.

(19) Pisarnitsky, A. K.; Bezzubov, A. A.; Egorov, I. A. Nonenzymatic formation of 4, 5-dimethyl-3-hydroxy-2(5H)-furanone in foodstuffs. *Prikl. Biokhim. Mikrobiol.* **1987**, 642–646.

(20) König, T.; Gutsche, B.; Hartl, M.; Hübscher, R.; Schreier, P.; Schwab, W. 3-Hydroxy-4,5-dimethyl-2(5H)-furanone (sotolon) causing an off-flavor: elucidation of its formation pathways during storage of citrus soft drinks. *J. Agric. Food Chem.* **1999**, *47*, 3288–3291.

(21) Silva Ferreira, A. C.; Barbe, J. C.; Bertrand, A. 3-Hydroxy-4,5-dimethyl-2(5H)-furanone: A key odorant of the typical aroma of oxidative aged port wine. *J. Agric. Food Chem.* **2003**, *51*, 4356–4363.

(22) Hofmann, T.; Schieberle, P. Studies on intermediates generating the flavour compounds 2-methyl-3-furanthiol, 2-acetyl-2-thiazoline and sotolon by Maillard-type reactions. *Flavour Science: Recent Developments*; The Royal Society of Chemistry: London, 1996, pp 182–187.

(23) Collin, S.; Nizet, S.; Claeys Bouuaert, T.; Despature, P.-M. Main odorant in Jura flor-sherry wines. Relative contributions of sotolon, abhexon, and theaspirane-derived compounds. *J. Agric. Food Chem.* **2012**, *60*, 380–387.

(24) European Brewery Convention. *Analytica EBC*; Getränke-Fachverlag: Nürnberg, Germany, 2006.

(25) Pons, A.; Lavigne, V.; Landais, Y.; Darriet, P.; Dubourdieu, D. Identification of a sotolon pathway in dry white wines. *J. Agric. Food Chem.* **2010**, *58*, 7273–7279.

(26) Otter, G. E.; Taylor, L. Estimation and occurrence of acetaldehyde in beer. *J. Inst. Brew.* **1971**, *77*, 467–472.

(27) Harrison, G. A. F.; Byrne, W. J.; Collins, E. The determination of diacetyl and 2,3-pentanedione in beer head space by gas chromatography. *J. Inst. Brew.* **1965**, *71*, 336–341.

(28) Moll, M. *Bières & Coolers*; Tech & Doc–Lavoisier: Paris, France, 1991.

DOI: 10.1021/jf505953u
J. Agric. Food Chem. 2015, 63, 2886–2892

(29) Andersen, M. L.; Outtrup, H.; Skibsted, L. H. Potential antioxidants in beer assessed by ESR spin trapping. *J. Agric. Food Chem.* **2000**, *48*, 3106−3111.

DOI: 10.1021/jf505953u
J. Agric. Food Chem. 2015, 63, 2886−2892

be the most effective glycerophospholipid with regard to the reduction of viscosity while having less of an effect on reducing the chocolate yield value. PE, on the other hand, is said to be more effective in reducing the chocolate yield value than the viscosity.[17−19] Therefore, when sunflower lecithin is replaced with soybean lecithin, it is important to keep in mind that sunflower lecithin has slightly more PC and less PE.

With regard to the analysis of lecithin's glycerophospholipids, various methods have been used such as thin layer chromatography (TLC), high-performance thin-layer chromatography (HPTLC), gas chromatography (GC), and high-performance liquid chromatography (HPLC).[1,20] GC was usually used for the identification of the individual fatty acids,[1] wheras TLC, HPTLC, and HPLC methods were applied to separate and identify glycerophospholipid classes (assignment of headgroups by normal phase chromatography) or the fatty acid species (reversed phase (RP) chromatography, silver ion chromatography).[6,21] HPLC was the most applied method because of its speed, resolution, high sensitivity, and specificity[22,23] as well as hyphenation with MS. For the MS analysis soft ionization methods such as fast atom bombardment (FAB), nowadays rarely used, or electrospray ionization (ESI) and matrix-assisted laser desorption ionization (MALDI) were preferred because they allowed a direct analysis of the glycerophospholipid species.[24] In recent studies, HPTLC separation was combined with MALDI−time of flight mass spectrometry (TOFMS).[25−28] Recently, sialylated and sulfated glycosphingolipids as well as a total lipid extract of bovine brain were investigated by HPTLC-MS.[29] Two different direct elution techniques (contactless surface sampling versus the elution head-based approach) were compared. Although it was mentioned that in the bovine brain glycerophospholipids such as PE, PI, and phosphotidylserine (PS) were detected, no further details were given.

Hence, the aim of this study was to investigate the interchangeability of soybean and sunflower lecithin with regard to changes in the rheology of different chocolate masses. Occurring changes in rheology were compared with glycerophospholipid differences of the lecithin samples. The glycerophospholipid pattern and content of the different lecithin samples used in chocolate production were analyzed by HPTLC-FLD and further characterized by HPTLC-ESI$^+$-MS and HPTLC-FLD-ESI$^+$-MS. LODs and LOQs were determined for seven glycerophospholipids by the three analytical techniques for the first time. HPTLC-MALDI-TOFMS was employed for confirmation.

MATERIALS AND METHODS

Materials and Reagents. Two sunflower lecithin samples from different suppliers (SN1 and SN2) and one soybean lecithin sample (SJ) were obtained from Stollwerck (Cologne, Germany). The standards PE 34:1, PC 34:1, lyso-phosphatidylcholine (LPC 18:0), lyso-phosphatidylethanolamine (LPE 18:0), phosphatidylserine (PS 36:4), and phosphatidic acid (PA 36:4) were all purchased from Avanti Polar Lipids (Alabasta, AL, USA), except PE 32:0, which was bought from Sigma-Aldrich (Steinheim, Germany). For HPTLC-FLD and HPTLC-ESI$^+$-MS as well as HPTLC-FLD-ESI$^+$-MS, HPTLC plates silica gel 60 F_{254} (20 × 10 cm), and for HPTLC-MALDI-TOFMS, HPTLC foils silica gel 60 F_{254} (20 × 20 cm) were used (all Merck, Darmstadt, Germany). 2,5-Dihydroxybenzoic acid (DHB) was also provided by Merck. Chloroform (>99.5%, stabilized with 1% ethanol), isopropyl acetate (>99.0%), acetonitrile (≥99.9%), trifluoroacetic acid (≥98.0%), ammonium phosphate (≥99.0%), and primuline (≥50%, as sodium salt) were purchased from Sigma-Aldrich (Steinheim, Germany). Ammonia (25%, w/w) and methanol (gradient grade) were obtained from VWR (Darmstadt, Germany) and acetone (HPLC grade) from Carl Roth (Karlsruhe, Germany). Chocolate masses and lecithin samples were obtained from Stollwerck.

Standard Solutions. The solvent used for the preparation of standard solutions was a mixture of chloroform and methanol (1:1, v/v). About 0.5−1.0 mg of each glycerophospholipid standard was dissolved in 10 mL of solvent mixture (50−100 ng/μL). The standard solutions were stored in the dark at −20 °C. For limit of detection (LOD)/limit of quantification (LOQ) studies, the standard solutions were diluted 1:10 (5−10 ng/μL). Standard mixtures were generated via overspraying of the individual solutions onto the same starting zone.

Lecithin Sample Preparation. About 50 mg of the different lecithin samples were extracted with a mixture of methanol and isopropyl acetate (2:3, v/v). After centrifugation at 2300*g* for 10 min, the supernatant was removed and stored in the dark at −20 °C.

Sample Application. For quantitation, the solutions were sprayed with the Automatic TLC Sampler 4 (ATS4, CAMAG, Muttenz, Switzerland) as 8 mm bands allowing up to 20 tracks to be applied on one HPTLC plate of 20 × 10 cm (distance from lower edge 8 mm, distance from left edge 15 mm, automatic distance between bands). For calibration, 3.0−12.0 μL of the standard solutions was sprayed on the HPTLC plate (140−1200 ng/band), and sample volumes ranged between 4.0 and 12.0 μL. For LOD/LOQ determinations by HPTLC-ESI$^+$-MS and HPTLC-FLD-ESI$^+$-MS, 4 mm bands were applied to fit the dimensions of the oval elution head (4 × 2 mm). To determine the maximum sample application volume possible, volumes of the lecithin sample SN2 ranging between 60.0 and 320.0 μL were applied as rectangles (8 × 3 mm) on a cut HPTLC plate (smartCUT Plate Cutter, CAMAG). For HPTLC-MALDI-TOFMS, bands of 4 mm length were applied on HPTLC foils, later cut to the size of 5 × 7.5 cm (distances from lower and side edge as before, distance between bands 8 mm). The sample extracts (10 μL) and standard solutions of PC 34:1 and PE 34:1 (1 μg/band) were applied.

Chromatography. Development was performed on HPTLC plates or foils silica gel 60 F_{254} with a mixture of chloroform/methanol/water/ammonia (25%) (30:17:2:1, v/v/v/v)[20] in the Automatic Developing Chamber (ADC2, CAMAG). Before development, the chamber was saturated for 20 min and the relative humidity was adjusted to 33% by a saturated magnesium chloride-6-hydrate solution for 3 min. The migration distance was 65 mm (from the lower edge of the plate). After application of the starting zones and after development, the plate was automatically dried for 0.5 and 2 min, respectively.

Derivatization. For visualization of the glycerophospholipids, the developed plates were dipped into a primuline solution (100 mg of primuline in 200 mL of acetone/water 4:1, v/v) at a speed of 3 cm/s and an immersion time of 1 s using a TLC Chromatogram Immersion Device (CAMAG). The plate was dried in a stream of warm air (hair dryer at 30 cm distance from the plate) for 2 min.

Densitometry and Documentation. The densitometric evaluation via fluorescence measurement at UV 366/>400 nm (mercury lamp, measurement slit size 6.0 mm × 0.2 mm, scanning speed 20 mm/s, K400 optical filter) was performed using a TLC Scanner 4 (CAMAG). Plate images were documented at 366 nm by a TLC Visualizer (CAMAG). All CAMAG instrumentation used so far as well as data obtained was processed with winCATS, version 1.4.6.2002 (CAMAG).

Mass Spectrometry. The derivatized, at 366 nm, blue fluorescent glycerophospholipid bands (4 mm band length applied) were marked at UV 366 nm illumination with a soft pencil and directly eluted via the oval elution head (4 × 2 mm) of the TLC-MS Interface (CAMAG) using 100% methanol at a flow rate of 0.1 mL/min (pump of the HP 1100 ChemStation, Agilent, Waldbronn, Germany). In the tubing to the MS a C18 guard cartridge (SecurityGuard cartridge, Phenomex, Torrance, CA, USA) was integrated. A single-quadrupole MS (mass resolution of 1 unit) equipped with an ESI ion source was employed (ExpressIon CMS, Advion, Ithaca, NY, USA). For positive ionization, the capillary voltage was set to 170 V, the ESI voltage to

DOI: 10.1021/jf506332f
J. Agric. Food Chem. 2015, 63, 2893−2901

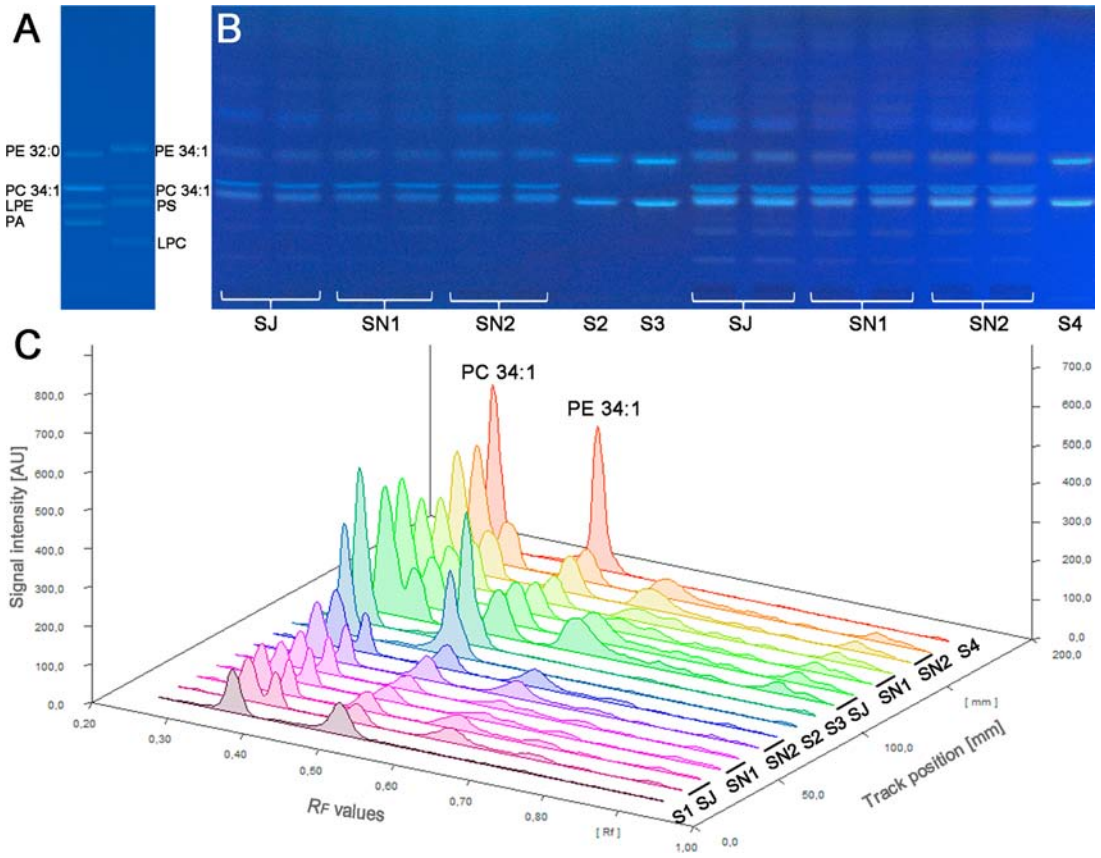

Figure 1. HPTLC chromatograms of (A) all glycerophospholipid standards available (tracks 1 and 2) and (B) PC 34:1 and PE 34:1 with different volumes applied (S2−S4) beside samples of soy lecithin (SJ) and sunflower lecithins (SN1 and SN2) as well as (C) an HPTLC 3 D densitogram.

3500 V, and the source voltage to 25 V. The nebulizer gas pressure was 60 psi, the temperatures of the capillary and the source gas were set to 250 °C, and the dissolvation gas flow rate was 4 L/min. The mass spectra were recorded in the full scan mode (total ion current (TIC) chronogram) m/z 100−1000 using a detection gain of 1100. Data processing for MS measurement was carried out with Mass Express 1.1.22.15, and evaluation was done with Data Express 1.1.22.15 (both Advion). A plate background at a migration distance comparable to the analyte zone was subtracted from the analyte spectrum. For LOD/LOQ determination by HPTLC-FLD-ESI$^+$-MS, the x,y-coordinate for elution was obtained after fluorescence measurement at UV 366/>400 nm, as such a low substance amount was not visible in the UV 366 nm image. For HPTLC-ESI$^+$-MS of nonderivatized zones, the x,y-coordinate for elution was received by extrapolation from the respective derivatized band on a cut plate strip (y-coordinate) and from the respective starting zone (x-coordinate).

For HPTLC-MALDI-TOFMS,[28,30] the HPTLC foil was homogeneously coated with a DHB solution (8 g in 40 mL of a mixture of acetonitrile and 10 mM aqueous ammonium phosphate solution with 0.1% trifluoroacetic acid 9:1, v/v). Therefore, the foil was dipped into the DHB solution at a speed of 4.5 cm/s and an immersion time of 1 s using the TLC Chromatogram Immersion Device (CAMAG). For the first 90 s the solvent was allowed to evaporate in the air, followed by 90 s of drying with a hair dryer. All steps were repeated, but the last drying step was extended to 4 min. The foil's reverse side was cleaned with a tissue, and the foil was cut to a size of 5 × 7.5 cm using a scissors. The cut foil part was mounted into a TLC-MALDI adapter target (Bruker Daltonics, Bremen, Germany). The HPTLC-MALDI-TOF mass spectra were acquired in the positive mode on an Ultraflex 1 TOF/TOFMS (Bruker Daltonics), which had a mass accuracy of about 75 ppm.

Rheological Measurements of the Chocolate Masses. Three different chocolate masses (dark, milk, and white) were manufactured without emulsifiers. Of the regular soybean lecithin sample SJ the original concentration according to the recipe (original-%) was added, whereas for the sunflower samples SN1 and SN2 three different concentrations (original-% as well as ±0.1%) were added to each of the three base chocolates by a defined manual mixing process.[31] The rheology of the chocolate samples was measured at 40 °C with a RheolabQC viscosimeter (Anton Paar, Graz, Austria) using a DIN cup and bob geometry. After a defined conditioning step including 30 s of preshearing at 5 s^{-1}, the viscosity measurements were carried out with increasing shear rates from 2 to 100 s^{-1} and recording of 29 data points. The rheological parameters viscosity and yield value were taken by fitting the Casson equation to the data.[32,33] Each analysis was executed in triplicate (n = 3).

Statistical Analysis. Statistical analysis was done with Microsoft Excel, version Office Standard 2010. The respective means, standard deviations, and relative standard deviations were calculated. The two-sample t test (independent, two-sided, P = 95, 99, 99.9%) was applied to test the different lecithins for significant differences in the PC and PE contents.

RESULTS AND DISCUSSION

The HPTLC-FLD method allowed a satisfying separation of seven glycerophospholipid standard substances (available in our institute), which were divided in two mixtures (Figure 1A). The standard compound PC 34:1 showed a hR_F value of 30, whereas both of the PE standards (PE 32:0 and PE 34:1) had higher hR_F values (hR_F = 41 and 43).

Comparison of the Lecithin Fingerprints. The separation of the lecithin samples' glycerophospholipids showed equally good results (Figure 1B). The brilliance of the blue fluorescence increased with the concentration. The lecithins from both plants had a comparable glycerophospholipid pattern, with PC (hR_F = 31) and PE (hR_F = 43) as the main

DOI: 10.1021/jf506332f
J. Agric. Food Chem. 2015, 63, 2893−2901

glycerophospholipids. Other glycerophospholipid bands visible in the samples (hR_F = 12, 21, 36, 54, and 84) could not definitively be assigned to any standard compound available in our institute. Thus, the glycerophospholipid zones found were subjected to a subsequent characterization by MS (see Characterization by HPTLC-FLD-ESI+-MS). As PC and PE were identified to have the highest influence on rheology,[17−19] quantitation was focused on these two compounds.

Quantitation of PC and PE in the Lecithin Samples. With regard to the quantitative analysis of PC and PE in soybean and sunflower lecithins, the calibration was performed in the ranges of 140−550 ng/band for PC 34:1 and 300−900 ng/band for PE 34:1 (Figure 1C). If required, the working ranges can be expanded; however, they were sufficiently wide for the given analysis. The mean repeatabilities (%RSD, n = 2, instant repetition within a laboratory) for both compounds in the lecithin matrix were mostly ≤5.0%, whereas the intermediate precisions (%RSD, n = 2, repetitions within a laboratory over several weeks) were mostly ≤10.0% (Supporting Information Table S1). After statistical analysis, the mean PC and PE contents were found to be different in soybean and sunflower lecithins (Figure 2). Both sunflower lecithin samples

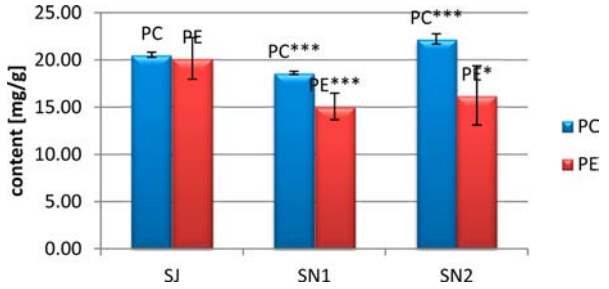

Figure 2. PC 34:1 and PE 34:1 contents (mean ± standard deviation) of one soybean (SJ) and two sunflower (SN1 and SN2) lecithin samples. (*) Statistically, (**) significantly, and (***) highly significantly different compared to SJ (P = 95, 99, 99.9%).

showed significantly lower values for PE than the soybean lecithin, currently used for chocolate production. For both soybean and sunflower lecithin samples, the mean PC content was about 20 ± 2 mg/g (2.0%), whereas the results for PE showed a wider content range between 14 and 22 mg/g (1.4−2.2%). This was reflected in the ratios PC/PE. The soybean lecithin sample (SJ) had a PC/PE ratio of 1.0. In contrast, the two sunflower samples (SN1 and SN2) showed higher ratios of 1.2 and 1.3, respectively (Table S1). According to the independent, two-sided t test, there were differences in the glycerophospholipid content between SJ and either SN1 (calculated t value t_1 = 10.36 for PC and t_1 = 4.76 for PE) or SN2 (calculated t value t_2 = 5.55 for PC and t_2 = 2.52 for PE) (Figure 2).

Selection of the Ionization Mode of HPTLC-FLD-ESI-MS. For HPTLC-FLD-ESI-MS, the derivatized, blue fluorescent zones of interest were eluted via the TLC-MS Interface as described.[30] The derivatization reaction with the primuline reagent was based on a physisorption (only interaction with the analyte due to van der Waals forces), and during the MS measurement the primuline molecule was separated from the glycerophospholipid molecule. The primuline was observed in the negative ionization mode as a desodiated molecule at m/z 452 $[M-Na]^-$ (S/N 24 in the extracted ion current (EIC) chronogram). As the primuline substance bought was only 50% pure, an additional ion at m/z 319 was observed as base peak (S/N 50 in EIC chronogram). This ion was assumedly assigned as the desodiated fragment of primuline, named 2-(4-aminophenyl)-6-methyl-1,3-benzothiazole-7-sulfonate $[M-C_7H_3NS-Na]^-$). Because the primuline forms negative ions, the phospholipid measurement was performed in the positive ionization mode. Thus, the derivatization reagent did not impair the glycerophospholipid mass signal and eased its interpretation. Using a single-quadrupole MS, the glycerophospholipid bands in the standard mixture were clearly detected at 400 ng/band (S/N 110 and S/N 310 for the base peaks $[M+Na]^+$ of PE 34:1/32:0 and PC 34:1, respectively). Thus, the positive ionization mode was found to be a good compromise, although the negative ionization might be more sensitive for some glycerophospholipids.

Characterization by HPTLC-FLD-ESI$^+$-MS. The preliminary assignment of the head groups (PC and PE) of the unknown glycerophospholipid bands in the lecithin samples was based on the hR_F values. For characterization of their fatty acyl residues, the ESI^+ mass spectra of the glycerophospholipid bands found were recorded. For comparison, the mass spectra of the PC and PE standards were recorded, too. The identities of the standards PE 32:0 and PE 34:1 as well as PC 34:1 were confirmed due to their characteristic sodium adducts $[M+Na]^+$ and $[M+2Na-H]^+$(Supporting Information Figure S1).

The mass spectra of the respective glycerophospholipid bands preliminarily assigned as PC in the lecithin samples SJ, SN1, and SN2 (12.0 μL applied, Figure 3) showed a mass signal pattern comparable to the PC standard. Two molecular species with mass signals at m/z 782 $[PC1]^+$ and m/z 758 $[PC2]^+$ were evident. This suggested the presence of PC 36:4 (PC1) and PC 34:2 (PC2). These results corresponded with the literature, in which *sn*-1,2-dilinoleoyl-PC and *sn*-1-palmitoyl-2-linoleoyl-PC were reported in soybean lecithin.[27] The respective sodium adducts were observed at m/z 804 $[PC1+Na]^+$ and m/z 780 $[PC2+Na]^+$. Furthermore, the mass signal at m/z 564 was explained by fragmentation (fatty acid elimination), that is, elimination, of linoleic acid $[PC1-C18:2]^+$ and palmitic acid $[PC2-C16:0]^+$, respectively.

With regard to the PE preliminarily assigned bands in the lecithin samples, all mass spectra showed a mass signal pattern (Figure 4) comparable to that of the PE standard. According to Stübinger et al.,[27] the mass signals were assigned as PE 36:4 (PE1) and PE 34:2 (PE2). The obtained mass signals showed predominantly adducts, that is, the respective sodium adducts at m/z 762 $[PC1+Na]^+$ and m/z 738 $[PC2+Na]^+$ as well as the disodium adducts at m/z 784 $[PC1+2Na-H]^+$ and m/z 760 $[PC2+2Na - H]^+$.

It can be concluded that the PE and PC present in the lecithin samples were most likely esterified with palmitic and linoleic acid. The latter is the main fatty acid in soybean and sunflower oil.[13,38] In oils derived from plants, the unsaturated fatty acid (here, linoleic acid) is predominately located at the *sn*-2-position of the glycerophospholipid.[3,27] For an unequivocal identification of the fatty acyl residues, additional MS/MS measurements and also measurements in the negative mode could be helpful, especially for samples in which the glycerophopholids and their fatty acyl pattern are not yet described in such detail. For the purpose of the current study, however, the simple identification in the positive ionization mode with a single-quadrupole MS and comparison with data from the literature were sufficient.

DOI: 10.1021/jf506332f
J. Agric. Food Chem. 2015, 63, 2893−2901

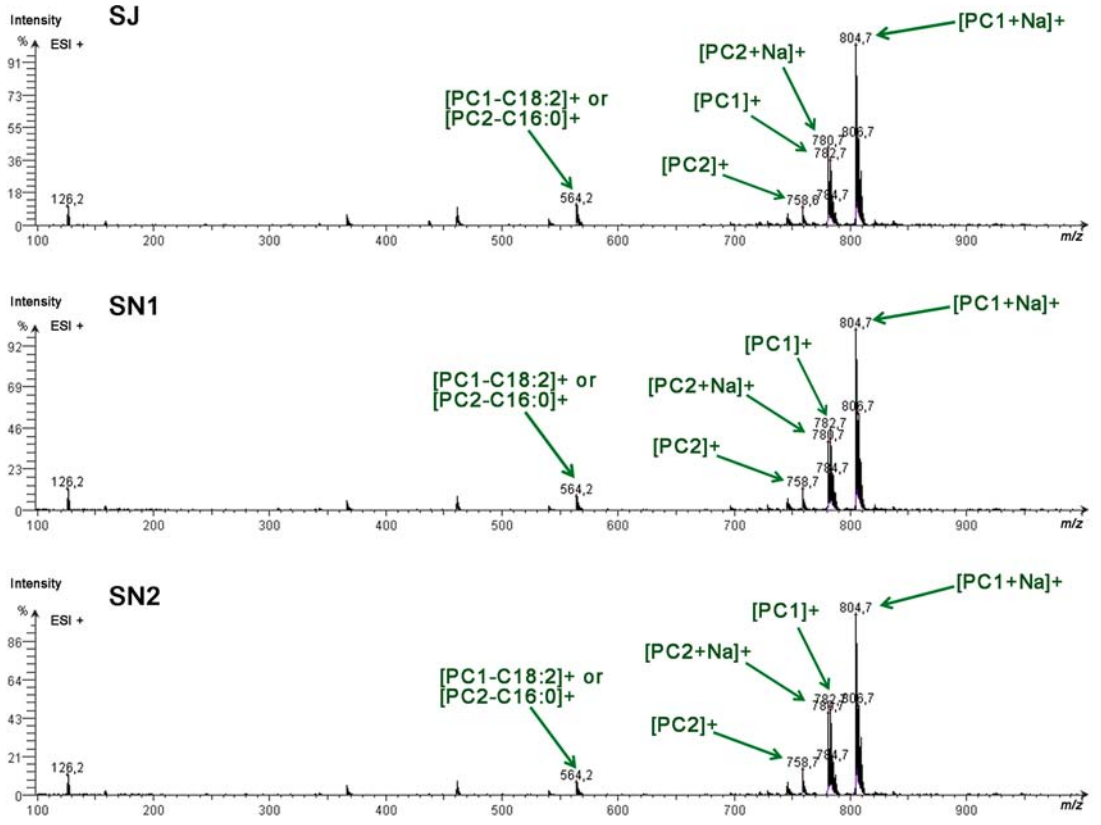

Figure 3. HPTLC-FLD-ESI$^+$-MS: recorded mass spectrum of unknown zones at hR_F 31 in the lecithin samples (SJ, SN1, and SN2, application volume 12 μL) and confirmation of the preliminary assignment as PC, specified as PC 36:4 (PC1) and PC 34:2 (PC2).

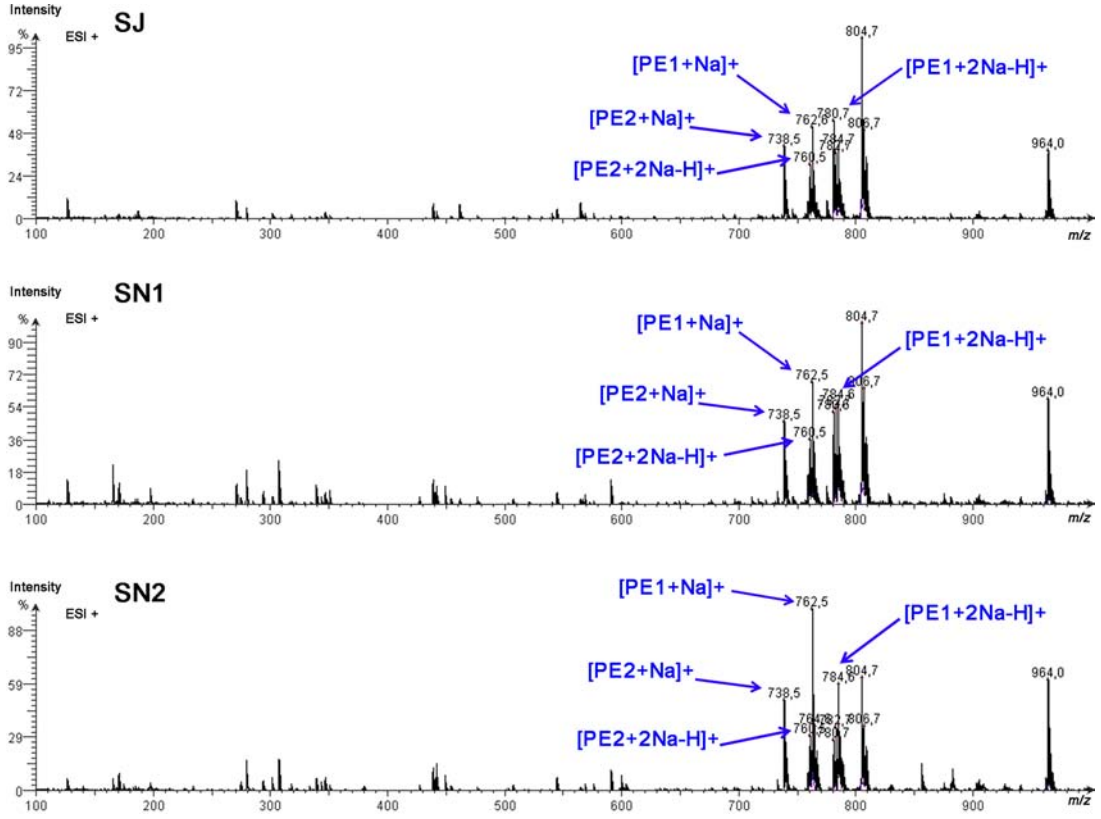

Figure 4. HPTLC-FLD-ESI$^+$-MS: recorded mass spectrum of unknown zones at hR_F 42 in the lecithin samples (SJ, SN1, and SN2, application volume 12 μL) and confirmation of the preliminary assignment as PE, specified as PE 36:4 (PE1) and PE 34:2 (PE2).

DOI: 10.1021/jf506332f
J. Agric. Food Chem. 2015, 63, 2893−2901

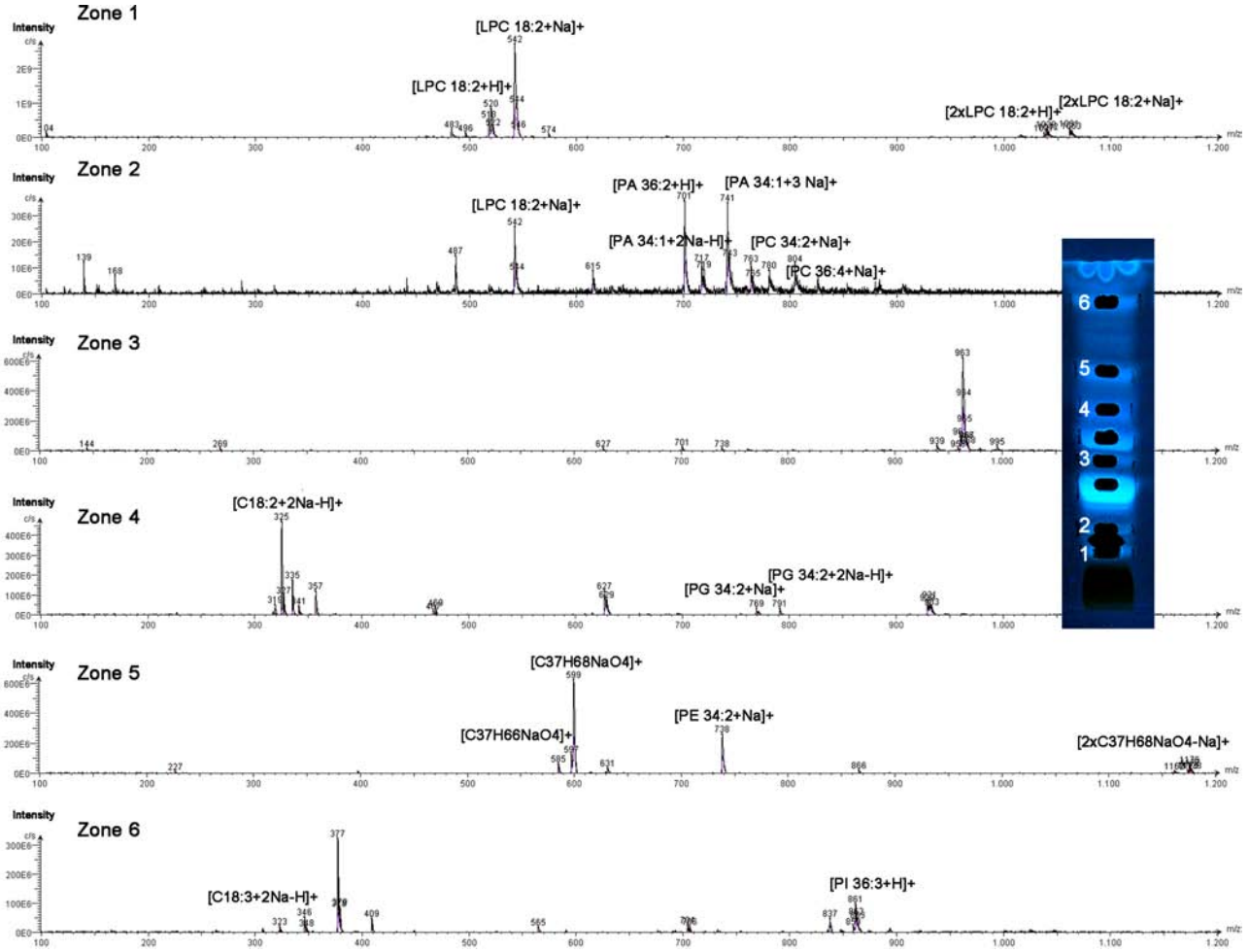

Figure 5. HPTLC-FLD-ESI$^+$-MS of six lower concentrated glycerophospholipid zones of the sunflower sample SN2 (zones 1−6, application volume 60 μL).

Additionally, mass spectra were recorded from the SN2 sample's lower concentrated fluorescent zones, clearly visible on the plate at higher application volumes (Supporting Information Figure S2). Several unknown minor glycerophospholipid zones were tentatively assigned, for example, LPC 18:2, PA 34:1, and 36:2, phosphatidylglycerol (PG) 34:2, and PI 36:3 (Figure 5).[39] However, the zone 3 (hR_F 36) just above PC could not be assigned unambiguously. Although the signal at m/z 963 would be consistent with both a triacylglycerol ($C_{63}H_{110}O_6$) and PI (43:1) or PI (44:8), the zone's position on the plate seemed to be implausible for a triacylglycerol, and the fatty acyl pattern of PI fits to neither soybean nor sunflower lecithins. Whereas for a final identification high-resolution MS would be the logical next step, this still demonstrated that mass spectra were obtainable also from minor glycerophospholipids and that it is a matter of the application volume in HPTLC to obtain clear mass signals (here, 60 μL applied).

Mean LODs and LOQs of Seven Glycerophospholipids via HPTLC-FLD, HPTLC-ESI$^+$-MS, and HPTLC-FLD-ESI$^+$-MS. So far, no literature has reported LOD and LOQ values for glycerophospholipids via HPTLC-FLD, HPTLC-ESI$^+$-MS, and HPTLC-FLD-ESI$^+$-MS, so it was unclear how sensitive potential phospholipids in samples could be detected. Thus, LOD and LOQ values[34] were studied for three modes of detection, that is, via HPTLC-FLD, HPTLC-ESI$^+$-MS, and HPTLC-FLD-ESI$^+$-MS. In HPTLC, the application volume applied influences the calculation of the LOD/LOQ. As the spray-on application (as aerosol) includes a concentration step, the selected application volume determines the LOD/LOQ obtained. The rule is the higher the application volume, the lower the LOD. Thus, for the calculation of the LOD and LOQ, increased sample volumes (between 60 and 320 μL) were applied to get an impression of how the matrix influences the separation and how high a maximal application volume can be. Even at the highest investigated sample volume of 320 μL, the phospholipid zones were still clearly distinguishable (Supporting Information Figure S2). Therefore, it was possible to apply at least 320 μL to achieve low LODs. Thus, the highest experimentally proven sample volume (320 μL) was taken into account for the calculation of the LOD and LOQ values. However, it is important to keep in mind that for the LOD and LOQ analyses by HPTLC-ESI$^+$-MS and HPTLC-FLD-ESI$^+$-MS, 4 mm instead of 8 mm bands were applied to ensure that the glycerophospholipid zones were eluted as completely as possible. Therefore, by halving the application band, the maximum application volume that was experimentally proven (320 μL) was also halved to be 160 μL. The mean LODs (S/N 3) of HPTLC-FLD-ESI$^+$-MS were 60 and 45 mg/kg for PE 34:1 and PE 32:0, respectively. For PC 34:1, the mean LOD was 15 mg/kg. Mean LODs and LOQs of the seven glycerophospholipids investigated were mostly comparable, although slightly higher for most of the nonderivatized bands

DOI: 10.1021/jf506332f
J. Agric. Food Chem. 2015, 63, 2893−2901

Table 1. Mean LOD and LOQ Values[a] (n = 3) of Glycerophospholipids for HPTLC-FLD after Derivatization with Primuline and for HPTLC-ESI$^+$-MS with and without Derivatization (Each via Peak Height (H) and Area (A) for a Given Application Volume of 320 μL on an 8 mm Band or 160 μL on a 4 mm Band)

	FLD		ESI$^+$-MS[b]				
	derivatized (mg/kg)		signal ion	SIM	derivatized (mg/kg)		nonderivatized (mg/kg)
	LOD	LOQ			LOD	LOQ	LOD
	H/A	H/A	base peak	m/z	H/A	H/A	H/A
PA 36:4	8/<8	25/25	$[M + 2Na + H]^+$	741.6	90/90	310/310	140/140
LPE 18:0	8/8	30/40	$[M + Na]^+$	504.5	45/45	400/600	45/45
PC 34:1	15/15	70/70	$[M + Na]^+$	782.7	15/15	45/45	45/45
PE 34:1	15/15	45/40	$[M + Na]^+$	740.8	60/60	230/230	110/110
LPC 18:0	25/25	45/45	$[M + Na]^+$	546.5	60/60	370/370	10/10
PS 36:4	8/8	45/30	$[M + Na + H]^+$	806.7	310/310	700/700	280/208
PE 32:0	40/40	120/110	$[M + Na]^+$	714.8	45/45	210/210	60/60

[a]Calculated according to ICH using S/N 3 and 10. [b]Only a 50% aliquot of the 8 mm band was covered by the TLC-MS Interface elution head of 4 × 2 mm.

Table 2. Mean Rheological Values (n = 3) of Dark, Milk, and White Chocolates Using Soybean (SJ) and Sunflower Lecithins (SN1, SN2)

		lecithin samples in chocolate mass		
type of chocolate	Casson parameter	SJ	SN1	SN2
dark (0.54%)[a]	yield value (Pa)	19.40 ± 0.67	19.09 ± 1.27	19.89 ± 0.41
	viscosity (Pa·s)	4.28 ± 0.05	4.46 ± 0.04[b]	4.24 ± 0.07
milk (0.58%)[a]	yield value (Pa)	9.25 ± 0.36	9.63 ± 0.10	10.35 ± 0.28[b]
	viscosity (Pa·s)	1.87 ± 0.02	1.87 ± 0.02	1.87 ± 0.02
white (0.50%)[a]	yield value (Pa)	6.18 ± 0.24	6.33 ± 0.33	5.75 ± 0.17
	viscosity (Pa·s)	1.68 ± 0.02	1.71 ± 0.01	1.64 ± 0.03

[a]Lecithin content that is added according to the recipe (original-%). [b]Statistically different compared to SJ (p < 0.05).

(Table 1). Reasons for this could be that properly targeting the nonderivatized zones was more difficult or that the derivatization reagent helped to promote the ionization of some glycerophospholipids. Also, to achieve better LOD and LOQ values, especially for PS 36:4 and LPE 18:0, optimizing the ionization parameters for these substances would be an important next step. LOD and LOQ (experimentally obtained in ng/band as listed in Table S2 in the Supporting Information) were calculated as milligrams per kilogram on the basis of the experimentally proven application volume (160 μL applied as 4 mm bands); if necessary, lower LOD and LOQ values could also be achieved by a more complex sample preparation to reduce the matrix influence and allow the application of even higher application volumes.

Comparison with HPTLC-MALDI-TOFMS. The manually cut foil was fixed in the TLC-MALDI adapter target (Supporting Information Figure S3A). The mass signals obtained by HPTLC-FLD-ESI$^+$-MS were confirmed by HPTLC-MALDI-TOFMS, exemplarily shown for PC 34:1 (Figure S3B). However, in some HPTLC-MALDI-TOFMS spectra the signals were shifted by about $\Delta m/z$ = 1 if compared to those obtained by HPTLC-FLD-ESI$^+$-MS. In this case, the shift was also evident for the mass signals of the DHB matrix, resulting in mass signals at m/z 552 and 728 instead of m/z 551 $[3DHB - 3H + 4Na]^+$ and m/z 727 $[4DHB - 4H + 5Na]^+$. This shift may have been caused by irregularities of the HPTLC surface after repeated immersion in the DHB matrix solution, but more likely by an uneven aluminum foil carrier, due to the necessity of cutting the 20 × 20 cm plate to fit the dimensions of the TLC-MALDI adapter target.[40] In a further study, precut HPTLC foils, silica gel 60 F_{254} MS-grade, for MALDI (5 × 7.5 cm) solved this problem. This demonstrated how important it is to fix an even foil with a plane and smooth rear in the TLC-MALDI adapter target.

Comparison with Other Methods and Benefit of the HPTLC Method. For the HPLC-MS/MS method published by Lee et al.[35] (phospholipids in soybean cultivars) and for the SPE-HPLC-ELSD method published by Narváez et al.[36] (phospholipids in the subcutaneous fat of Iberian pig) the glycerophospholipid LOD/LOQ values were in the low micrograms per kilogram range. For a recently published RP-HPLC-UV method[37] (fatty acid composition of soybean PC), the values were in the low milligrams per liter range. Although some of these methods may be more sensitive, one has to keep in mind that the sample preparation was more complex and time-consuming (e.g., additional SPE step) or more powerful MS analyzers (e.g., MS/MS) were used. Thus, a direct method comparison is often not feasible or leads to wrong conclusions.

HPTLC-FLD-ESI$^+$-MS proved to be well suited for the investigation of glycerophospholipids in crude lecithin extracts from soybean and sunflower seeds. The lecithin sample preparation was kept simple (only dissolving the sample). The method allowed the visual comparison of the phospholipid patterns of different samples separated next to each other on one plate. Although it is fast and cost-effective and has a high matrix tolerance, the separation on silica gel layers also allowed the separation according to the headgroup, making this method complementary to RP18-HPLC methods. Additionally, the

DOI: 10.1021/jf506332f
J. Agric. Food Chem. 2015, 63, 2893−2901

hyphenation with MS allowed the investigation of the glycerophospholipids' fatty acyl pattern. It was proven that the derivatization reagent did not impair the detectability by MS (only slight differences), and quantitation by fluorescence measurement as well as documentation can be performed before the mass spectra are recorded. In favor of this method are also relatively low LOD and LOQ values. The present study clearly demonstrated that the hyphenated HPTLC-FLD-ESI$^+$-MS method is highly suited for the analysis of incoming lecithin samples and their quality control with regard to the lecithin pattern and content.

Rheology of Respective Chocolate Samples Prepared. The interchangeability of soybean and sunflower lecithins in chocolate masses was investigated next. Two sunflower lecithin samples (SN1 and SN2) were compared to soybean lecithins (SJ) in three different chocolate masses (dark, milk, and white) regarding a potential diverse influence on the rheology of the chocolate. The rheology of the respective chocolates (lecithin samples added according to the original recipe) showed overall comparable results using sunflower or soybean lecithins (Table 2). Similar flow parameters were detected by using SN1 or SJ in milk and white chocolate. However, SN1 led to slightly higher values in the viscosity of dark chocolate than SJ. The sunflower lecithin SN2 showed similar functionality as SJ regarding the rheology of dark and white chocolates. Nevertheless, the yield value of milk chocolate using SN2 was slightly increased compared to the use of SJ (Table 2). In white chocolate, no significant differences in the flow parameters could be detected. It was found that the differences between the flow parameters of chocolates containing sunflower lecithin instead of soybean lecithin were marginal. To a certain extent, there were slight differences in the rheological characteristics of dark and milk chocolates. A reduction or increase of the sunflower lecithin content (original content (%) ± 0.1%) led to significant and sometimes highly significant differences compared to the original content of SJ.[41]

Comparison of the Glycerophospholipid Content with the Rheological Result. Additionally, the differences in the PC and PE contents of sunflower and soybean lecithins were studied regarding a potential causal correlation to the measured rheological parameters. Previous studies using enriched lecithin samples revealed PC as the most effective glycerophospholipid in reducing chocolate viscosity and PE in decreasing the yield value.[17−19] Thus, a regression analysis was done for the respective glycerophospholipid content of the lecithin sample and the rheological result of the prepared chocolate mass (original concentration). Nevertheless, a correlation between the PE content of the lecithins and the yield value could not be found for any of the chocolates prepared in this study. In addition, neither the 10% lower (SN1) nor the 10% higher (SN2) PC content with regard to SJ (Table S1 in the Supporting Information) had a divergent effect on the viscosity of dark or milk chocolate. However, a negative correlation (r = −0.99) between the PC content and the viscosity of white chocolate was found for the studied samples. Further investigations with a higher number of samples and different concentrations of lecithin have to verify this initial result. In summary, the content differences for PC (18.4−22.2 mg/g) or PE (13.8−22.3 mg/g) in the lecithin samples seem to be too marginal to be the reason for the slight differences in the rheology of milk or dark chocolate by using sunflower or soybean lecithin. Nevertheless, a correlation between viscosity and PC content was indicated for white chocolate. It can be concluded, on the basis of these initial results, that the soybean lecithin can be substituted by one of the sunflower lecithins investigated. However, this conclusion might not be generalized due to potential natural variances in the single glycerophospholipid contents of the lecithins.

■ ASSOCIATED CONTENT

Supporting Information

Tables S1 and S2 and Figures S1−S3. This material is available free of charge via the Internet at http://pubs.acs.org.

■ AUTHOR INFORMATION

Corresponding Author

*(G.E.M.) Phone: +49-641-99-39141. Fax: +49-641-99-39149. E-mail: gertrud.morlock@ernaehrung.uni-giessen.de.

Author Contributions

S.K. wrote the initial manuscript, but some parts were contributed by L.B., and all were revised by G.E.M. L.B. performed the PE and PC quantitation in the lecithin samples as well as the rheological tests of the produced chocolate masses. S.K. performed all of the mass spectrometric investigations and evaluations. The statistical tests were calculated by both. All experiments were supervised by G.E.M.

Notes

The authors declare no competing financial interest.

■ ACKNOWLEDGMENTS

We thank Stollwerck, Cologne, Germany, for providing the lecithin samples, chocolate masses, and instrumental equipment for the rheological analysis; Prof. Dr. Lochnit, Department of Biochemistry, Justus Liebig University Giessen, Germany, for recording the HPTLC-MALDI-TOFMS spectra; and Bruker Daltonics, Bremen, Germany, for the TLC-MALDI adapter target.

■ REFERENCES

(1) Peterson, B. L.; Cummings, B. S. A review of chromatographic methods for the assessment of phospholipids in biological samples. *Biomed. Chromatogr.* **2006**, *20*, 227−243.

(2) Parsons, J. G.; Keeney, P. G.; Patton, S. Identification and quantitative analysis of phospholipids in cocoa beans. *J. Food Sci.* **1969**, *34*, 497−499.

(3) Pardun, H. Pflanzenlecithine − wertvolle Hilfs− und Wirkstoffe? *Fat Sci. Technol.* **1989**, *91*, 45−58.

(4) Pulfer, M.; Murphy, R. C. Electrospray mass spectrometry of phospholipids. *Mass Spectrom. Rev.* **2003**, *22*, 332−364.

(5) Schiller, J.; Süß, R.; Arnhold, J.; Fuchs, B.; Leßig, J.; Müller, M.; Petković, M.; Spalteholz, H.; Zschörnig, O.; Arnold, K. Matrix-assisted laser desorption and ionization time-of-flight (MALDI-TOF) mass spectrometry in lipid and phospholipid research. *Prog. Lipid Res.* **2004**, *43*, 449−488.

(6) Singleton, J. A.; Ruan, M.; Sanford, J. H.; Haney, C. A.; Stikeleather, L. F. Separation and characterization of peanut phospholipid molecular species using high-performance liquid chromatography and fast atom bombardment mass spectrometry. *J. Am. Oil Chem. Soc.* **1999**, *76*, 49−56.

(7) Weyland, M.; Hartel, R. Emulsifiers in confectionery. In *Food Emulsifiers and Their Applications*, 2nd ed.; Hasenhuettl, G. L., Hartel, R. W., Eds.; Springer: New York, 2008; pp 285−305.

(8) Ziegleder, G., Danzl, W., Eds. Fließverhalten von Schokoladenmassen. Kakaobutter und Milchfett als Fließmittel. *Deutsche Molkerei Zeitung* **2012**, *12*, 32−34.

(9) Schantz, B.; Linke, L.; Setrdle, A.; Köhler, P. Wirkung handelsüblicher Emulgatoren auf die rheologischen Eigenschaften

DOI: 10.1021/jf506332f
J. Agric. Food Chem. 2015, 63, 2893−2901

flüssiger Schokoladenmassen, Teil I. Die theoretischen Grundlagen der Untersuchung. *ZSW* **2001**, *54*, 30−32.
(10) Herman, E. M. Genetically modified soybeans and food allergies. *J. Exp. Bot.* **2003**, *54*, 1317−1319.
(11) Burks, A., Jr.; Brooks, J.; Sampson, H. Allergenicity of major component proteins of soybean determined by enzyme-linked immunosorbent assay (ELISA) and immunoblotting in children with atopic dermatitis and positive soy challenges. *J. Allergy Clin. Immunol.* **1988**, *81*, 1135−1142.
(12) van Nieuwenhuyzen, W.; Tomás, M. C. Update on vegetable lecithin and phospholipid technologies. *Eur. J. Lipid Sci. Technol.* **2008**, *110*, 472−486.
(13) Szuhaj, B. F. Lecithins. In *Bailey's Industrial Oil and Fat Products*, 6th ed.; Bailey, A. E., Shahidi, F., Eds.; Wiley: Hoboken, NJ, USA, 2005; pp 361−456.
(14) Schantz, B.; Linke, L.; Rohm, H. Effects of different emulsifiers on rheological and physical properties of chocolate. Presented at the 3rd International Symposium on Food Rheology and Structure; http://www.isfrs.ethz.ch/proc/2003_proc/329_333.pdf (last accessed Dec 28, 2014).
(15) Stroppa, V. L. Z.; Ribeiro, A. P. B.; Luccas, V.; Grimaldi, R., Gonçalves, L. A. G.; Kieckbusch, T. G. Influence of soy lecithin and PGRP levels in chocolate crystallization behavior. http://www.icef11.org/content/papers/epf/EPF1081.pdf (last accessed Dec 28, 2014).
(16) Bergenstahl, B. Physiochemical aspects of an emulsifier functionality. In *Food Emulsifiers and Their Applications*, 2nd ed.; Hasenhuettl, G. L., Hartel, R. W., Eds.; Springer: New York, 2008; pp 173−194.
(17) Büschelberger, H.-G. Lecithins. In *Emulsifiers in Food Technology*; Whitehurst, R. J., Ed.; Blackwell Publishing: Oxford, UK, 2004; pp 18−23.
(18) van Nieuwenhuyzen, W.; Szuhaj, B. F. Effects of lecithins and proteins on the stability of emulsions. *Fett/Lipid* **1998**, *100*, 282−291.
(19) Beckett, S. T., Ed. *Industrial Chocolate Manufacture and Use*, 4th ed.; Blackwell Publishing: Oxford, UK, 2009.
(20) Handloser, D.; Widmer, V.; Reich, E. Separation of phospholipids by HPTLC − an investigation of important parameters. *J. Liq. Chromatogr. Relat. Technol.* **2008**, *31*, 1857−1870.
(21) Andrikopoulos, N. K. Chromatographic and spectroscopic methods in the analysis of triacylglycerol species and regiospecific isomers of oils and fats. *Crit. Rev. Food Sci. Nutr.* **2002**, *42*, 473−505.
(22) Guan, Z.; Grünler, J.; Piao, S.; Sindelar, P. J. Separation and quantitation of phospholipids and their ether analogues by high-performance liquid chromatography. *Anal. Biochem.* **2001**, *297*, 137−143.
(23) Lima, E. S.; Abdalla, D. High-performance liquid chromatography of fatty acids in biological samples. *Anal. Chim. Acta* **2002**, *465*, 81−91.
(24) Myher, J. J.; Kuksis, A. General strategies in chromatographic analysis of lipids. *J. Chromatogr., B: Biomed. Sci. Appl.* **1995**, *671*, 3−33.
(25) Sommerer, D.; Süß, R.; Hammerschmidt, S.; Wirtz, H.; Arnold, K.; Schiller, J. Analysis of the phospholipid composition of bronchoalveolar lavage (BAL) fluid from man and minipig by MALDI-TOF mass spectrometry in combination with TLC. *J. Pharm. Biomed. Anal.* **2004**, *35*, 199−206.
(26) Fuchs, B.; Schiller, J.; Süß, R.; Zscharnack, M.; Bader, A.; Müller, P.; Schürenberg, M.; Becker, M.; Suckau, D. Analysis of stem cell lipids by offline HPTLC-MALDI-TOF MS. *Anal. Bioanal. Chem.* **2008**, *392*, 849−860.
(27) Stübiger, G.; Pittenauer, E.; Belgacem, O.; Rehulka, P.; Widhalm, K.; Allmaier, G. Analysis of human plasma lipids and soybean lecithin by means of high-performance thin-layer chromatography and matrix-assisted laser desorption/ionization mass spectrometry. *Rapid Commun. Mass Spectrom.* **2009**, *23*, 2711−2723.
(28) Schürenberg, M.; Fuchs, B.; Bischoff, A.; Süß, R.; Anders, U.; Suckau, D.; Morlock, G.; Schiller, J. *High resolution lipid profiling and identification by hyphenated HPTLC-MALDI-TOF/TOF*; Application Note MT-101; Bruker Daltonik: Germany, 2010.
(29) Park, H.; Zhou, Y.; Costello, C. E. Direct analysis of sialylated or sulfated glycosphingolipids and other polar and neutral lipids using TLC-MS interfaces. *J. Lipid Res.* **2014**, *55*, 773−781.
(30) Morlock, G. High-performance thin-layer chromatography mass-spectrometry for analysis of small molecules. In *Mass Spectrometry Handbook*; Lee, M. S., Ed.; Wiley: Hoboken, NJ, USA, 2012; pp 1181−1206.
(31) Schantz, B.; Linke, L.; Setrdle, A.; Köhler, P. Wirkung handelsüblicher Emulgatoren auf die rheologischen Eigenschaften flüssiger Schokoladenmassen, Teil II. Die experimentelle Untersuchung. *ZSW* **2001**, *54*, 36−38.
(32) Afoakwa, E. O.; Paterson, A.; Fowler, M.; Vieira, J. Comparison of rheological models for determining dark chocolate viscosity. *Int. J. Food Sci. Technol.* **2009**, *44*, 162−167.
(33) Wells, M. Controlling the rheology of chocolate and fillings. In *Science and Technology of Enrobed and Filled Chocolate, Confectionery and Bakery Products*, 1st ed.; Talbot, G., Ed.; Woodhead Publishing: Cambridge, UK, 2009.
(34) International Conference on Harmonisation of Technical Requirements for Registration of Pharmaceuticals for Human Use ICH Harmonised Tripartite Guideline. Validation of Analytical Procedures Text and Methodology Q2(R1), 2005.
(35) Lee, S. J.; Choi, J. Y.; Park, S.; Chung, J. I.; Jin, J. S.; Lee, S. J.; Sung, N.-J.; Bae, D. W.; Shin, S. C. Determination of phospholipids in soybean (*Glycine max* (L.) Merr) cultivars by liquid chromatography−tandem mass spectrometry. *J. Food Compos. Anal.* **2010**, *23*, 314−318.
(36) Narváez-Rivas, M.; Gallardo, E.; Ríos, J. J.; León-Camacho, M. A new high-performance liquid chromatographic method with evaporative light scattering detector for the analysis of phospholipids. Application to Iberian pig subcutaneous fat. *J. Chromatogr., A* **2011**, *1218*, 3453−3458.
(37) Jangle, R. D.; Galge, R. V.; Patil, V. V.; Thorat, B. N. Selective HPLC method development for soy phosphatidylcholine fatty acids and its mass spectrometry. *Indian J. Pharm. Sci.* **2013**, *75*, 339−345.
(38) Lendrath, G.; Bonekamp-Nasner, A.; Kraus, L. Analytische Möglichkeiten zur qualitativen und quantitativen Bestimmung der Phospholipide in Lecithinen unterschiedlicher Herkunft. *Fat Sci. Technol.* **1991**, *93*, 53−61.
(39) Furse, S.; Liddell, S.; Ortori, C. A.; Williams, H.; Neylon, D. C.; Scott, D. J.; Barrett, D. A.; Gray, D. A. The lipidome and proteome of oil bodies from *Helianthus annuus* (common sunflower). *J. Chem. Biol.* **2013**, *6*, 63−76.
(40) Russel, D. H.; Edmondson, R. D. High-resolution mass spectrometry and accurate mass measurement with emphasis on the characterization of peptides and proteins by martix-assisted laser desorption/ionization time-of-flight mass spectrometry. *J. Mass Spectrom.* **1997**, 263−276.
(41) Bürmann, L. *Austausch von Sojalecithinen gegen Sonnenblumenlecithine in Schokoladenmassen*. Master's thesis, Justus Liebig University Giessen, Germany, 2013.

DOI: 10.1021/jf506332f
J. Agric. Food Chem. 2015, 63, 2893−2901

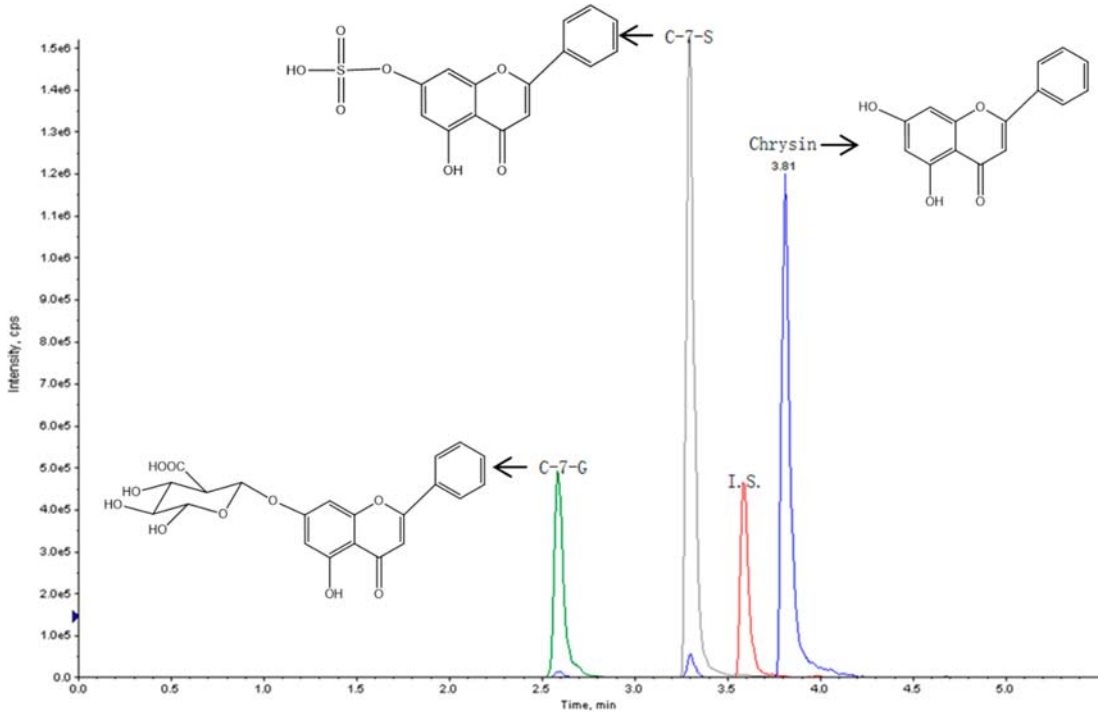

Figure 1. MS/MS chromatograms for chrysin, C-7-O-glucuronide (C-7- G), C-7-O-sulfate (C-7-S), and formononetin (I.S.) in a blood sample.

exposure level of chrysin and its metabolites in Bcrp1 (−/−) mice would be observed. Finally, human Caco-2 cells were used as in vitro tool to explore the disposition mechanisms of chrysin phase II conjugates in intestinal epithelial cells.

MATERIALS AND METHODS

Chemicals. Chrysin was purchased from INDOFINE Chemical Company (Hillsborough, NJ). Formononetin was purchased from LC Laboratory (Woburn, MA). Solid phase extraction (C18) columns were purchased from J.T. Baker (Phillipsburg, NJ). Ora-Plus oral suspending vehicle was obtained from Paddock Laboratories Inc. (Minneapolis, MN). Ko143 was purchased from Cayman Chemical (Ann Arbor, MI). Hanks' balanced salt solution (powder form) was purchased from Sigma−Aldrich (St. Louis, MO). All other materials (typically analytical grade or better) were used as received.

Biosynthesis of Chrysin Glucuronide and Sulfate. Chrysin glucuronide/sulfate was obtained from FVB mouse intestine perfusate samples and used for method development and validation. The intestinal surgical procedures, approved by the University of Houston's Institutional Animal Care and Use Committee, were described in previous publications.[18,19] Briefly, the mouse intestine was perfused with 20 μM of chrysin at the flow rate of 0.191 mL/min, and the perfusate sample was applied to a C18 solid phase extraction column. After washing out the salt, acetonitrile was used to elute chrysin and its conjugates, and the concentrations of these conjugates were determined using UPLC. This solution was then used as the stock solutions of chrysin and its metabolites, and it was stored in acetonitrile at −80 °C.

Instruments and Conditions. *UPLC.* A UPLC system, Waters AcQuity with diode-arrayed detector (DAD) was performed to determine the concentrations of stock solution of chrysin conjugates. The UPLC conditions for analyzing chrysin, its conjugates, and formononetin (I.S.) in aqueous samples were the following: column, AcQuity UPLC BEH C18 column (50 mm × 2.1 mm I.D., 1.7 μm, Waters, Milford, MA, U.S.A.); mobile phase A, 100% aqueous buffer (2.5 mM ammonium acetate, pH7.4); mobile phase B, 100% acetonitrile; gradient: 0−0.5 min, 5% B, 0.5−1 min, 15% B, 1−2 min, 15−25% B, 2−3 min, 25−50% B, 3−3.5 min, 50−85% B, 3.5−4 min, 85−95%, 4−4.3 min, 95% B, 4.3−4.5 min, 95−5% B, 4.5−5.5 min, 95% B; flow rate, 0.45 mL/min; column temperature, 45 °C; sample temperature, 20 °C; and injection volume, 10 μL.

LC-MS/MS. A Waters Ultra Performance Liquid Chromatography (UPLC) system coupled with an ESI-triple quadrupole mass spectrometer (QTRAP5500; AB Sciex, Foster City, California) was used for the analysis in plasma medium by MRM (Multiple Reaction Monitoring) method in the negative ion mode. The instrument dependent parameters for mass spectrum were set as follows: ionspray voltage, −4.5 kV; ion source temperature, 600 °C; gas1, 20 psi; gas2, 30 psi; curtain gas, 10 psi. Unit mass resolution was set in both mass-resolving quadruples Q1 and Q3. Compound-dependent parameters were summarized in Table 1.

Table 1. Compound-Dependent Parameters in UPLC-MS Analysis

analyte	Q1 (m/z)	Q3 (m/z)	DP (V)	CE (V)	CXP (V)	dwell time (ms)
chrysin	252.9	142.9	−160	−36	−11	100
C-7-G	428.9	252.9	−160	−36	−11	100
G-7-S	332.9	252.9	−100	−36	−11	100
formononetin	267.0	252.0	−235	−29	−15	100

Determination of Concentrations of Chrysin Conjugates. The concentrations for conjugated metabolites were determined by using a chrysin standard curve and conversion factors of molar extinction coefficients. Conversion factor (K) was determined using a previously published method.[20] Briefly, it was determined by comparing the UV absorption peak area change of chrysin after glucuronide and sulfate was hydrolyzed by β-glucuronidases or sulfatase with the corresponding peak area change in glucuronide or sulfate. Concentrations of metabolites were calculated using the following equations:

$$K = \Delta PA_{metabolites}/\Delta PA_{chrysin} \quad \text{(eq 1)}$$

$$C_G = C/K_G \quad \text{(eq 2)}$$

$$C_S = C/K_S \quad \text{(eq 3)}$$

DOI: 10.1021/jf5056979
J. Agric. Food Chem. 2015, 63, 2902−2910

where K is the coefficient factor, $\Delta PA_{metabolites}$ is the change in peak area of conjugated metabolites (glucuronide or sulfate), and $\Delta PA_{chrysin}$ is the change in peak area of parent chrysin. C, C_G, and C_S are concentrations of chrysin, chrysin glucuronide, and chrysin sulfate, respectively, and K_G and K_S were conversion factors for glucuronide and sulfate, respectively.

Method Validation. *Calibration Curve, LLOQ, and LOD.* Calibration curve was prepared in the same way as described in Pharmacokinetic Studies. The linearity of each calibration curve was determined by plotting the peak area ratio of chrysin, chrysin glucuronide, and chrysin sulfate to I.S. Weighted least-squares linear regression method ($1/x^2$) was applied to determine the slope and correlation coefficient of linear regression equation. The lower limit of quantitation (LLOQ) was determined on the basis of a signal-to-noise ratio of 10:1. The limit of detection (LOD) was determined on the basis of a signal-to-noise ratio of 3:1.

Precision and Accuracy. The "intraday" and "interday" precision and accuracy of the method were determined with three different concentrations of QC samples on the same day or on three different days.

$$\text{Precision} = \frac{\text{standard deviation of measured concentration}}{\text{mean of measured concentration}} \times 100\% \quad \text{(eq 4)}$$

$$\text{Accuracy} = \frac{\text{mean of measured concentration}}{\text{nominated concentration}} \times 100\% \quad \text{(eq 5)}$$

Extraction Recovery and Matrix Effect. The extraction recovery of chrysin and its metabolites were determined by comparing the peak areas obtained from blank blood spiked with analytes before the extraction with those from samples to which analytes were added after the extraction. The matrix effect was assayed to compare the peak areas of blank blood extracts spikes with analytes with those of the standard solutions dried and reconstituted.

$$\text{Extraction recovery} = \frac{\text{pre-extraction spike}}{\text{post-extraction spike}} \times 100\% \quad \text{(eq 6)}$$

$$\text{Matrix effect} = \frac{\text{post-extraction spike}}{\text{matrix-free spike}} \times 100\% \quad \text{(eq 7)}$$

Stability. Short-term (25 °C for 4 h), long-term (−80 °C for 3 days), and three freeze−thaw cycle stabilities were determined.

Pharmacokinetic Studies. *Animals.* Male FVB wild-type mice (25−30 g, 10−12 weeks old) were from Harlan Laboratory (Indianapolis, IN). Male FVB Bcrp knockout mice (25−30 g, 10−12 weeks old) were purchased from Taconic Farm, Inc. (Hudson, NY). All the animals were kept in an environmentally controlled room (temperature: 25 ± 2 °C, humidity: 50 ± 5%, 12 h dark−light cycle) for at least 1 week before any experiments.

Experimental Design. The animal protocols used in this paper were approved by the University of Houston's Institutional Animal Care and Use Committee. Animals were fasted overnight with free access to water before the day of experiment. An oral gavage of chrysin dispersed in oral suspension vehicle was given to mice at a dose of 20 mg/kg. After a mouse was anesthetized with isoflurane gas, its tail was snipped near the tip of the tail to allow the collection of blood samples. Blood samples (about 10 μL) were collected in heparinized tubes at 15, 30, 60, 120, 240, 360, 480, and 1440 min. The blood samples were stored at −80 °C until analysis.

Blood Sample Preparation. The blood sample (10 μL) was spiked with 10 μL of HBSS buffer and 100 μL of I.S. (formononetin in acetonitrile, 4 nM). The mixture was vortexed for 1 min. After centrifugation at 15 000 rpm for 15 min, the supernatant was transferred to a new tube and evaporated to dryness under air. The residue was reconstituted in 50 μL of 30% acetonitrile aqueous solution and centrifuged at 15 000 rpm for 15 min. Ten microliters of supernatant were injected into the UPLC-MS/MS system for quantitative analysis.

Preparation of Standard and Quality Control Samples. Calibration standard samples were prepared in HBSS buffer by diluting the perfusate stock solution prepared in previous section to the following analyte concentrations: 0.78, 1.56, 3.13, 6.25, 12.5, 25, 50, 100, 200, 400, 800, 1600, 3200 nM for chrysin; 0.85, 1.70, 3.41, 6.82, 13.63, 27.27, 54.53, 109.06, 218.13, 436.25, 872.5, 1745, 3490 nM for chrysin glucuronide; 0.50, 1.01, 2.01, 4.02, 8.05, 16.09, 32.19, 64.38, 128.75, 257.50, 515, 1030, 2060 nM for chrysin sulfate. The quality control samples for each compound were prepared at three different concentrations in the same way as the blood samples for calibration, and QC samples were stored at −80 °C until analysis.

Cell Culture and Transcellular Transport Study. Caco-2 cells have been routinely cultured in our laboratory. The culture conditions were the same as those described previously.[21,22] Briefly, porous polycarbonate cell culture inserts (3 μm) from Corning Life Sciences (Lowell, MA) were used to seed the cells at a seeding density of 60 000 cells/cm^2. Cell monolayers were ready for experiments from 19 to 22 days after seeding. Transepithelial electrical resistance values of the cell monolayers were measured before experiments. The protocol for performing transport experiments was the same as described previously.[23] Loading solution (2.5 mL) containing 5 μM of chrysin with or without 5 μM of Ko143 in HBSS was added to the apical side of the cell monolayers for BCRP inhibition studies. Blank HBSS (2.5 mL) was loaded onto the basolateral side. Samples (0.4 mL) were taken at different times (0, 1, 2, 3, and 4 h) from both sides. The same volume of loading solution was added immediately to replace the volume lost.

Chrysin and its metabolites were determined in both apical and basolateral side by UPLC-MS/MS. Rate of transport was calculated as described before.[23] The following equation (eq 8) was used to obtain both apical and basolateral excretion rates.

$$\text{Rate of transport} = \frac{dC}{dt} \times V \quad \text{(eq 8)}$$

dC/dt: rates of change in concentration of transported chrysin/metabolites as a function of time. V: volume of the chamber.

The percentage of basolateral excretion was calculated by the following equation:

$$\%\ \text{basolateral excretion} = \frac{\text{basolateral excretion rate}}{\text{basolateral excretion rate} + \text{apical excretion rate}} \times 100\% \quad \text{(eq 9)}$$

Intracellular concentrations of chrysin and its conjugates were also determined at the end of experiment using the same protocol as described in a previous study.[23] The fraction of dose metabolized (f_{met}) was calculated using the following equation (eq 10).

$$f_{met} = \frac{\sum \text{metabolites}}{\sum \text{metabolites} + \sum \text{parent compound}} \quad \text{(eq 10)}$$

Data Analysis. Chrysin and its metabolites' pharmacokinetic parameters were calculated by the noncompartmental method, using Win-Nonlin 3.3 (Pharsight Corporation, Mountain View, California). Data were presented as means ± S.D., if not specified otherwise. Student's t test was used to analyze data. The level of significance was set at $p < 0.05$.

RESULTS

Conversion Factors of Chrysin Metabolites. We performed the hydrolysis studies at three different concentrations to calculate average K values. The conversion factor K is 1.6 for chrysin glucuronide and 0.91 for chrysin sulfate. These conversion factors were used to calculate the concentration of chrysin glucuronide/sulfate in the perfusate stock solution.

Identification of Chrysin Metabolites. In previous studies,[7] UV spectroscopy coupled with moderate alkalization, which was reported to be a sensitive diagnostic approach to identify the site of substitutions for flavonoid molecules,[24] had been used to determine the molecular position of the conjugation for chrysin, and it had been demonstrated that the

DOI: 10.1021/jf5056979
J. Agric. Food Chem. 2015, 63, 2902−2910

site of conjugation was the 7-position for both glucuronide and sulfate (Figure 1).

UPLC Analysis. Two metabolite peaks that have UV absorbance profile similar to parent chrysin were detected in mouse perfusate (Supplemental Figure S1). After incubating perfusate sample with β-glucuronidases (without sulfatase) or sulfatase (without glucuronidase), the peaks corresponding to chrysin glucuronide or chrysin sulfate disappeared, whereas the peak for parent chrysin increased (data not shown).

Chromatography and Mass Spectrometry. A sensitive and reliable method to quantify chrysin and its two metabolites' concentrations was established in this study. This method enabled us to determine the plasma concentration of chrysin and its metabolites in mouse after oral administration. Because of the fact that the blood volume we can take from a mouse is very limited and at the same time mice are often used as animal model in different studies, this method will be very useful in these situations. Typical chromatograms of spiked chrysin and its two metabolites in blank blood sample are shown in Figure 1. The retention time of C-7-G, C-7-S, chrysin, and formononetin (I.S.) were 2.60, 3.32, 3.84, 3.59 min, respectively.

Chrysin and its two metabolites were further confirmed by mass spectrometer. The MS2 full scan mass chromatograms are shown in Figure 2a–c. Chrysin glucuronide has ion $[M - H]^-$ at m/z 429, which is consistent with a glucuronic acid moiety (176 amu) added to the molecular ion of chrysin of m/z 253. Chrysin sulfate has an $[M - H]^-$ ion of m/z 333, which is 80 Da higher (addition of one sulfuric acid) than that of parent chrysin (m/z 253). In addition, the MS2 full scan showed that the ion $[M - H]^-$ of m/z 429 and 333 can produce fragment ion m/z 253, which also confirmed the presence of glucuronide and sulfate.

Method Validation. *Linearity and Sensitivity.* The method validation was conducted in blank mouse blood. The standard curves were linear in the concentration range of 3.13–3200 nM for chrysin, 3.41–3490 nM for chrysin glucuronide (C-7-G), 0.5–2060 nM for chrysin sulfate (C-7-S). The lower limit of quantitation (LLOQ) was 1.48 nM for chrysin, 1.70 nM for C-7-G, and 0.5 nM for C-7-S. The limit of detection (LOD) was 1.25, 0.68, and 0.05 nM for chrysin, C-7-G, and C-7-S respectively.

Accuracy and Precision. Accuracy, intraday, and interday precision were determined by measuring six replicates of QC samples at three concentration levels in mouse blood. The precision and accuracy are shown in Table 2. These results demonstrated that the precision and accuracy values were in the acceptance range (<15%).

Recovery, Matrix Effect, and Stability. The mean extraction recoveries determined using three replicates of QC samples at three concentration levels in mouse blood are shown in Table 2. Acetonitrile was used to extract chrysin and its metabolites. The recoveries were not less than 85.3% for all the analytes at three different concentrations.

The results showed that the relative peak areas of the analytes after spiking blood samples at three concentration levels were similar to aqueous standard solutions, indicating that there was no measurable matrix effect or recovery problem that interfered with the quantification of all analytes in blood. The results were also reported in Table 2.

Stabilities of chrysin and its metabolites in blood were evaluated by analyzing triplicates of QC samples at three different concentrations following storage at 25 °C for 4 h, at −80 °C for 3 days, and after going through three freeze–thaw cycles (−80 and 25 °C). All the samples showed 85–115% recoveries after various stability tests.

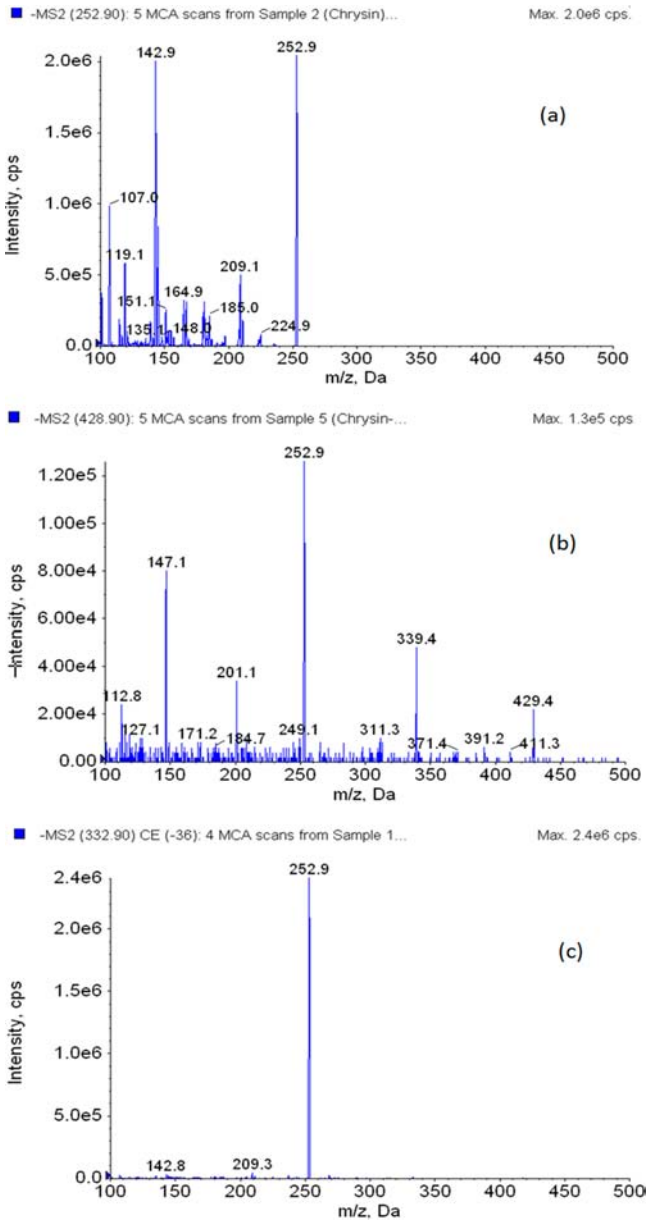

Figure 2. MS2 full scan for chrysin (a), C-7-G (b), and C-7-S (c). The results showed the molecular ion 429 $[M - H]^-$ and its MS2 fragment 253 $[M - H]^-$ for C-7-G and molecular ion 333 $[M - H]^-$ and its MS2 fragment at m/z 253$[M - H]^-$ for C-7-S.

Pharmacokinetic Studies of Chrysin in Wild-Type and Bcrp1 (−/−) Mice. The validated analytical method was employed to study the pharmacokinetic behaviors of chrysin in FVB wild-type and Bcrp1 (−/−) mice. The mean plasma concentration–time curves of chrysin and its two metabolites after p.o. administration (20 mg/kg dose) in FVB wild-type and Bcrp1 (−/−) mice are shown in Figure 3.

Chrysin and its metabolites' pharmacokinetic parameters were calculated by the noncompartmental method, using Win-Nonlin 3.3. The results are shown in Table 3. After 20 mg/kg oral administration, chrysin reached a maximum concentration (C_{max}) of 0.01 ± 0.01 μM at approximately 4 h in wild-type mice and 0.02 ± 0.01 μM at 3.31 h in Bcrp1 (−/−) mice. C-7-G and C-7-S were detected as major metabolites. In wild-type mice, the T_{max} of glucuronide and sulfate were 7.0 and 6.5 h, and the C_{max} of these two metabolites were 0.16 and 0.13 μM,

DOI: 10.1021/jf5056979
J. Agric. Food Chem. 2015, 63, 2902–2910

Table 2. Extraction Recovery, Intraday and Interday Precision, and Matrix Effects for Chrysin and Its Metabolites Using the MRM Method

			intraday (n = 6)		interday (n = 6)		
analyte	concn (nM)	extraction recovery(n = 3) average ± SD (%)	accuracy (bias, %)	precision (CV, %)	accuracy (bias, %)	precision (CV, %)	matrix effect (%)
chrysin	12.5	90.1 ± 13.3	114.6	13.5	110.7	11.3	111
	100	91.6 ± 3.3	106.7	12.6	102.2	9.9	116.6
	1600	92.6 ± 4.1	100.5	4.9	93.3	11.7	108
C-7-G	13.63	85.3 ± 9.7	98.7	10.4	101.6	10.4	107.9
	109.06	85.3 ± 7.7	100.6	13.5	94.5	9.5	105.8
	1745	85.3 ± 1.8	100.8	8.6	93	9.9	109.9
C-7-S	8.05	88.8 ± 6.7	110.6	6.6	110.5	8	109
	64.38	89.5 ± 8.5	109.2	11.1	105.4	8.3	114.3
	1030	98.5 ± 1.4	91.7	8.5	89.1	6.5	114.7

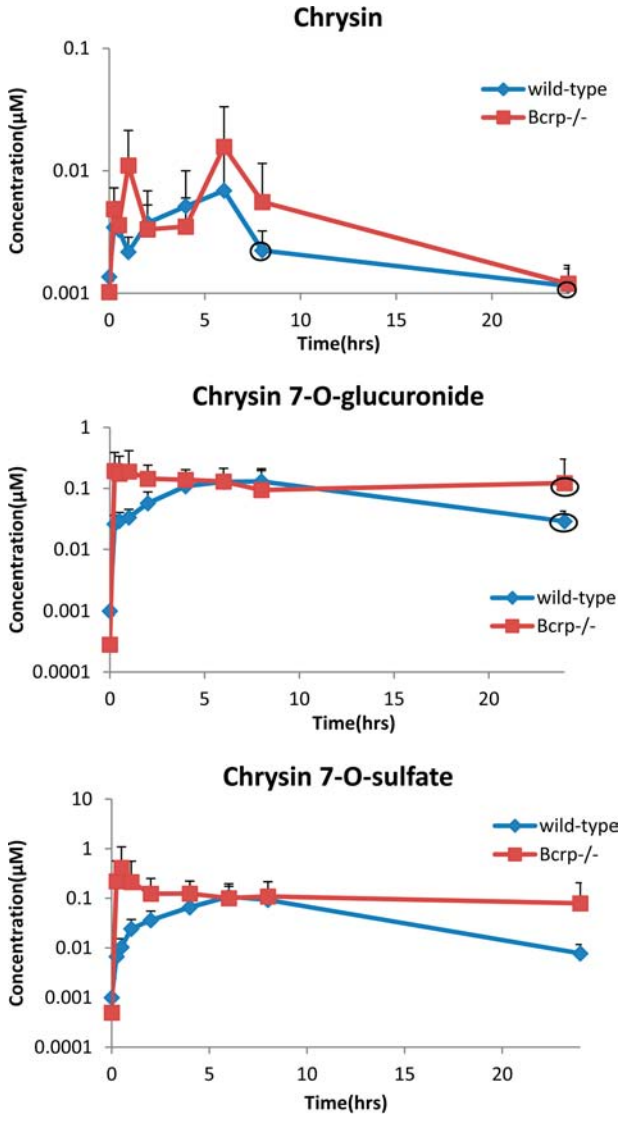

Figure 3. Blood concentrations of chrysin, C-7-G, and C-7-S after oral administration of 20 mg/kg chrysin in FVB wild-type and Bcrp−/− mice. Each point is the average of four determinations, and the bars are standard deviations of the mean. The circled points represented data points where concentrations for some mouse blood samples fell below the quantitation limit.

Table 3. Pharmacokinetics Parameters of Chrysin, Chrysin-7-O-G, and Chrysin-7−O-S after Oral Administration of 20 mg/kg Chrysin in Mice (n = 4)

	parameters	T_{max} (h)	C_{max} (μm)	AUC_{0-t} (h μM)
chrysin	wild-type mouse	4.00 ± 1.36	0.01 ± 0.01	0.06 ± 0.03
	Bcrp −/− mouse	3.31 ± 3.12	0.02 ± 0.01	0.11 ± 0.08
C-7-G	wild-type mouse	7.00 ± 1.15	0.16 ± 0.04	2.00 ± 0.82
	Bcrp −/− mouse	1.81 ± 1.63 **	0.22 ± 0.21	2.83 ± 3.03
G-7-S	wild-type mouse	6.50 ± 1.00	0.13 ± 0.04	1.32 ± 0.42
	Bcrp −/− mouse	3.25 ± 3.57	0.43 ± 0.67	2.62 ± 3.13

respectively. In Bcrp1 (−/−) mice, C_{max} was slightly higher for both metabolites and was reached at shorter T_{max}. For chrysin glucuronide, T_{max} was significantly shorter (p < 0.01) in Bcrp1 (−/−) mice, whereas the difference in T_{max} of chrysin sulfate in two species was not statistically significant because of large variations among mice. The AUC_{0-24h} of chrysin, chrysin glucuronide, and chrysin sulfate were summarized in Figure 4. In Bcrp-deficient mice, the AUC values of parent compound and its metabolites were higher (~2 folds) than the AUC values in wild-type mice. However, the differences were not statistically significant because of high standard deviation.

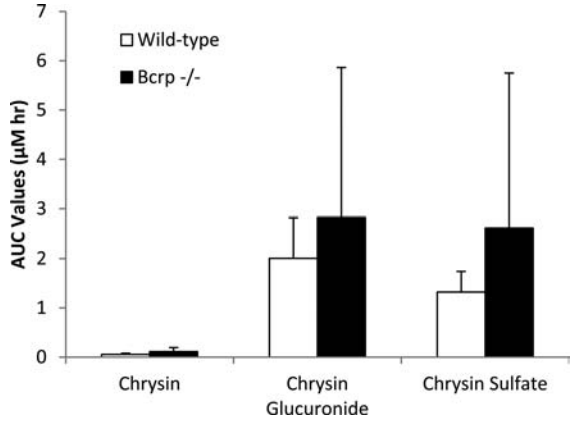

Figure 4. AUC values of chrysin and its conjugates in wild-type and Bcrp (−/−) mice (n = 4) after oral administration of chrysin at 20 mg/kg.

DOI: 10.1021/jf5056979
J. Agric. Food Chem. 2015, 63, 2902−2910

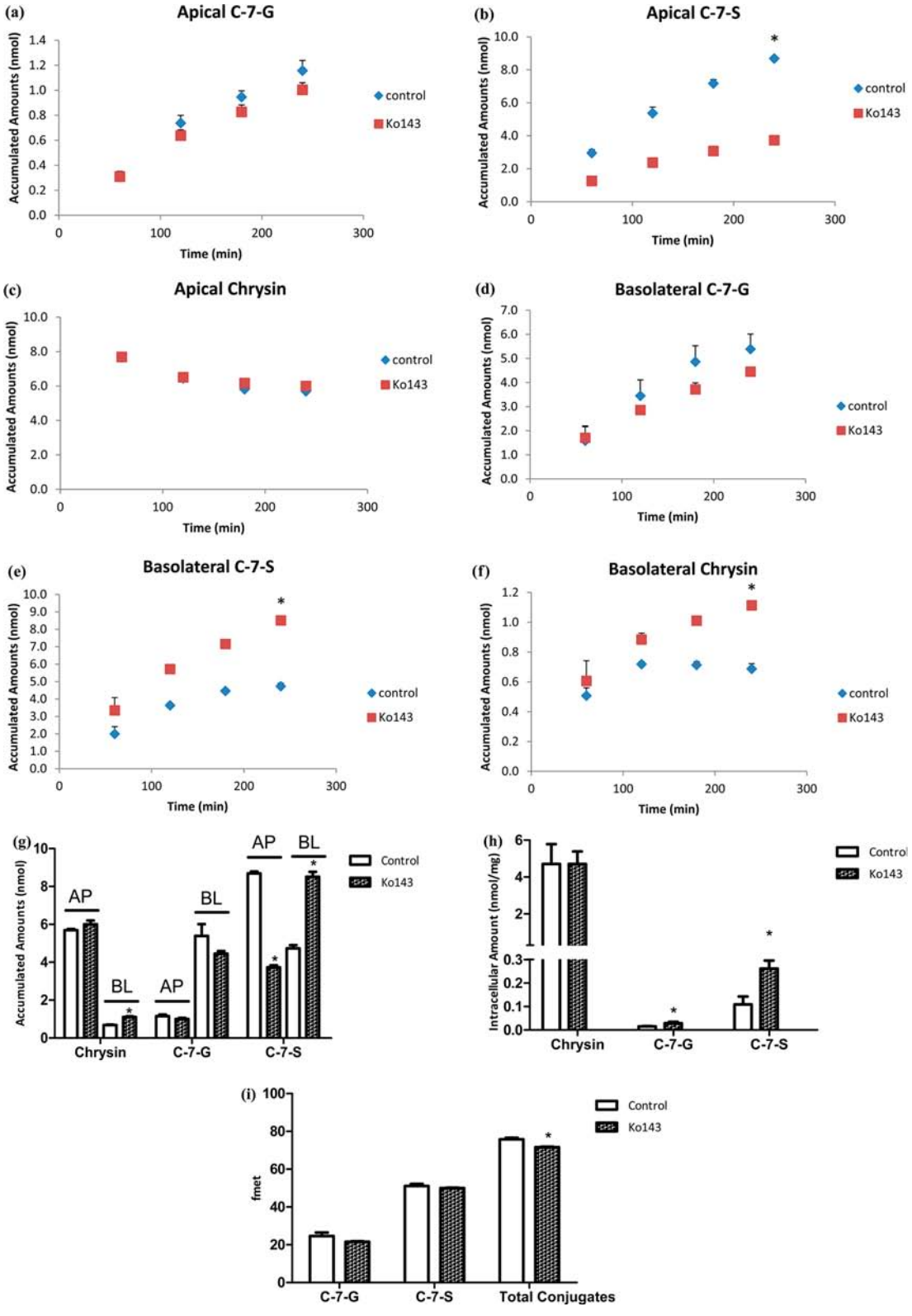

Figure 5. Excretion of chrysin and its conjugates in Caco-2 cells. The apical (a–c) and basolateral (d–f) excretion of chrysin, chrysin glucuronide (C-7-G), and sulfate (C-7-S) was shown at different time points. The accumulated amounts of compounds at the end of experiment (4 h) with or without treatment were summarized (g). The intracellular amount of chrysin and its metabolites were determined and normalized with total protein amount in each well (h). f_{met} of chrysin glucuronide, chrysin sulfate, and total conjugates in Caco-2 cells was also calculated (i).

Role of BCRP in the Excretion of Chrysin Glucuronides and Sulfates in Caco-2 Cells. To show how BCRP inhibition by Ko143 affected polarized excretion of chrysin conjugates in enterocytes, studies using 5 μM of chrysin in the presence or absence of 5 μM of Ko143 were conducted using the Caco-2 cell membrane. With Ko143 treatment, there was no significant alteration in the apical excretion of chrysin glucuronide. However, the apical excretion of chrysin sulfate decreased

DOI: 10.1021/jf5056979
J. Agric. Food Chem. 2015, 63, 2902–2910

significantly (>2-fold) in the presence of Ko143 treatment. Meanwhile, a similar amount of chrysin aglycone was found in apical side with or without the inhibitor (Figure 5a−c, g).

With respect to basolateral excretion, no significant change was found for chrysin glucuronide in the presence of Ko143. As for chrysin sulfate, a significant increase in basolateral excretion of chrysin sulfate was observed. It was found that the percentage of basolateral excretion of chrysin sulfate increased from 35% (control) to 70% (Ko143 treatment), whereas the percentage of basolateral excretion of chrysin glucuronide remained about the same (80%) (Figure 5d−f, g; Supplemental Figure S2). Our results suggested that the excretion pathway of chrysin sulfate was substantially changed when BCRP was inhibited, resulting in more basolateral excretion. It was also found that with Ko143 treatment, the transport of chrysin from apical to basolateral side significantly increased after 1 h (Figure 5).

Intracellular concentrations of chrysin and its conjugates were also determined at the end of experiments and normalized with total protein amount in each well (Figure 5h). Our data showed that the intracellular amount of chrysin glucuronide and sulfate increased significantly (~2-fold) in the presence of Ko143, whereas the amount of chrysin inside cells remained the same.

To determine if Ko143 had any impact on phase II metabolism of chrysin in Caco-2 cells, f_{met} values of glucuronide and sulfate were calculated as a measurement of phase II enzyme activities in cells. It was found that f_{met} of glucuronide and sulfate did not change much after Ko143 treatment, and the decrease in f_{met} of total conjugates (glucuronide plus sulfate) was statistically significant, although the extent of difference was small due to extensive phase II chrysin metabolism (Figure 5i).

DISCUSSION

BCRP was initially discovered in multidrug resistant breast cancer cell lines and recognized as an efflux pump which renders cancer cells resistant to diverse chemotherapeutic agents. Besides chemotherapeutic drugs, more and more drugs from other therapeutic classes and other compounds (e.g., dietary flavonoids and their conjugated metabolites) are recognized as BCRP substrates.[17] BCRP is also expressed in normal human tissues including the small intestine, liver, placenta, and brain endothelium. In recent studies, it has been shown that BCRP in small intestine can efflux glucuronide and sulfate conjugates into intestinal lumen. For example, Adachi et al. (2004) have demonstrated that BCRP plays an important role in extruding conjugates of 4-methylumbelliferone and E3040 back into the lumen in rat and mouse.[13] In another study, experiments in ABCG2-expressing membrane vesicles showed that BCRP transports estrone 3-sulfate.[16] In our previous studies, the bioavailability of genistein (an isoflavone) was found to increase moderately in Bcrp knockout mice, but the disposition of genistein conjugates was also altered substantially (often AUC changes more than 10−20-fold) in the Bcrp1 knockout mice.[23] In other published studies, it has been demonstrated that genistein's phase II metabolites (glucuronides and sulfates) can serve as the reservoir for parent compound in vivo because of enteric/enterohepatic recycling and enzymatic hydrolysis.[25,26] Therefore, we thought it would be of great value to reveal the mechanism for the distribution of phase II conjugates of another flavonoid, and in this study, we investigated the impact of BCRP on phase II disposition of chrysin.

As expected, we also observed that the pharmacokinetic profile of chrysin was different in Bcrp1 (−/−) mice when compared to the control FVB mice. For example, in the knockout mice, blood concentrations of chrysin and its metabolites were higher than concentrations in wild-type mice, and the peak blood concentrations of metabolites were achieved sooner. For chrysin glucuronide, a significantly shorter T_{max} (Figure 3, Table 3) was observed in the knockout mice. We also observed a different apparent slope of terminal phase for the metabolites in Bcrp1 (−/−) mice. Blood concentrations of chrysin metabolites decreased at a slower rate after 8 h in Bcrp-deficient mice. Because the fitting goodness (R^2) in the terminal phase was less than 0.8 using noncompartmental model method, the elimination rate constant (k) values could not be reliably determined and therefore were not reported. However, the AUC values of chrysin and its metabolites in Bcrp1 (−/−) mice were not significantly different ($P > 0.05$) from the AUC values observed in wild-type mice, which indicated BCRP might not be a critical efflux transporter for phase II disposition of chrysin in vivo, or other transporters such as MRP2 were overexpressed as a compensation for the knockout of BCRP. To determine if MRP2 is overexpressed in Bcrp1 (−/−) mice, protein quantification or PCR assays need to be performed for intestine and liver in WT and Bcrp1 (−/−) mice.

Moreover, we performed in vitro studies in Caco-2 cells to further investigate the role of BCRP in the intestine. Cells were treated in the presence or absence of Ko143 as a specific BCRP inhibitor. Because about 70% of chrysin was metabolized into conjugates by the end of experiment (Figure 5i), the accumulated amount excreted in apical or basolateral side versus time was not linear at the later sampling time as shown in Figure 5. In the presence of Ko143, the basolateral excretion of chrysin sulfate significantly increased (Figure 5), indicating that BCRP was an important transporter to efflux chrysin sulfate into the lumen. However, significant impact of BCRP on systemic exposure of chrysin conjugates was not observed in our in vivo studies (Figure 4). The discrepancy could be explained by the possibility that certain amount of chrysin conjugates can be excreted into the bile instead of entering the systemic circulation. Furthermore, this explanation is supported by the fact that chrysin metabolites were found at high concentrations in bile when chrysin was dosed in rat.[10] Inhibition of BCRP did not change the amount of chrysin aglycone in apical side but slightly increased (<2-fold) the accumulated amount in basolateral side (Figure 5g). There could be two explanations for this observation: 1. Chrysin itself is a substrate for BCRP, and the inhibition of BCRP can affect the distribution of chrysin. However, we also noticed that the intracellular amount of chrysin did not change with Ko143 treatment (Figure 5h). Therefore, we believe that this should not be the major reason. 2. The metabolism of chrysin was inhibited in the presence of Ko143, more chrysin left enterocytes intact as a result, and this explanation is in agreement with our observations in f_{met} (Figure 5i). Zhang et al. reported that chrysin was an inhibitor of BCRP in BCRP-overexpressing human breast cancer cells (MCF-7) and large cell lung carcinoma cells (NCI-H460)[27] and Ebert et al. showed that chrysin could induce the expression of BCRP in Caco-2 cells and enhance the transport of benzo[a]pyrene-3-sulfate,[15] there was no report to show that this compound is a good substrate of BCRP. Hence, we believe that BCRP plays a more important role in the disposition of chrysin phase II conjugates (i.e., glucuronides and sulfates).

Besides BCRP, other ABC transporters can also be involved in the transport of chrysin conjugates. Walle et al. (1999) have shown that the treatment of anion transport inhibitor MK-571 can reduce the apical excretion of chrysin glucuronide and sulfate in Caco-2 cells, suggesting chrysin conjugates can be effluxed by

DOI: 10.1021/jf5056979
J. Agric. Food Chem. 2015, 63, 2902−2910

MRP2.[11] They found that the inhibition of MRP2 could result in 71% and 20% inhibition of the efflux of chrysin glucuronide and chrysin sulfate, respectively. However, MK-571 is known to inhibit activities of UGT but not SULT enzymes.[22] In contrast, our studies in Caco-2 cells showed that the efflux of chrysin sulfate could be inhibited more efficiently by BCRP inhibitor. Therefore, it is reasonable to conclude that BCRP has more impact on the transport of chrysin sulfate whereas transport of chrysin glucuronide may be more influenced by other efflux transporters such as MRP2. To our knowledge, the role of other transporters in disposition of chrysin conjugates is still not clear. MRP1 and MRP3 may also be involved. As a dietary supplement in humans, the recommended dose of chrysin supplements is 500−2000 mg/day.[28] Therefore, high concentrations of chrysin could be found in the intestine and large amount of conjugates could interact with transporters on the cell membrane, which could result in chrysin-drug interactions in vivo.

Taken together, our studies have shown that although there was an alteration in the pharmacokinetic profile (with shorter T_{max}) of chrysin conjugate, the in vivo disposition of chrysin (a flavone) was not as sensitive to Bcrp1 knockout as we had expected and very different from our earlier study using genistein in the same animal model. In our in vitro studies, inhibition of BCRP showed greater inhibitory effect on the efflux of chrysin sulfate than that of chrysin glucuronide. The use of a sensitive and reliable UPLC-MS/MS method for the simultaneous determination of chrysin, chrysin 7-O-glucuronide, and chrysin-7-O-sulfate in mice was the enabling factor for us to determine their pharmacokinetics in expensive knockout mice. This is because only 10 μL of blood is required for each time point, which means that the animals did not have to be sacrificed for the study. Hence, it is highly significant that we were able to develop and validate the LC-MS/MS method for analyzing chrysin and its conjugates.

In conclusion, a sensitive and reliable UPLC-MS/MS method for determination of chrysin and its phase II metabolites in blood was developed and validated. This method was successfully applied for pharmacokinetic studies in mice. The impact of BCRP on phase II disposition of chrysin and its metabolites in Bcrp-deficient mice was different from those observed using genistein, and our in vitro data showed inhibition of BCRP reduced the efflux of chrysin sulfate significantly. Our data suggested that impact of efflux transporters on phase II disposition may be dependent on the structure of aglycone and/or its conjugates, and deserve further investigation.

■ ASSOCIATED CONTENT

Supporting Information

Supplemental data as referenced in the text. This material is available free of charge via the Internet at http://pubs.acs.org.

■ AUTHOR INFORMATION

Corresponding Author

*E-mail: mhu@uh.edu. Tel.: (713) 795-8320. Fax: (713) 795-8305.

Notes

The authors declare no competing financial interest.

■ REFERENCES

(1) Williams, C. A.; Harborne, J. B.; Newman, M.; Greenham, J.; Eagles, J. Chrysin and other leaf exudate flavonoids in the genus Pelargonium. *Phytochemistry* **1997**, *46*, 1349−1353.

(2) Barbaric, M.; Miskovic, K.; Bojic, M.; Loncar, M. B.; Smolcic-Bubalo, A.; Debeljak, Z.; Medic-Saric, M. Chemical composition of the ethanolic propolis extracts and its effect on HeLa cells. *J. Ethnopharmacol.* **2011**, *135*, 772−778.

(3) Pichichero, E.; Cicconi, R.; Mattei, M.; Muzi, M. G.; Canini, A. Acacia honey and chrysin reduce proliferation of melanoma cells through alterations in cell cycle progression. *Int. J. Oncol.* **2010**, *37*, 973−981.

(4) Lapidot, T.; Walker, M. D.; Kanner, J. Antioxidant and prooxidant effects of phenolics on pancreatic beta-cells in vitro. *J. Agric. Food Chem.* **2002**, *50*, 7220−7225.

(5) Woo, K. J.; Jeong, Y. J.; Inoue, H.; Park, J. W.; Kwon, T. K. Chrysin suppresses lipopolysaccharide-induced cyclooxygenase-2 expression through the inhibition of nuclear factor for IL-6 (NF-IL6) DNA-binding activity. *FEBS Lett.* **2005**, *579*, 705−711.

(6) Cardenas, M.; Marder, M.; Blank, V. C.; Roguin, L. P. Antitumor activity of some natural flavonoids and synthetic derivatives on various human and murine cancer cell lines. *Bioorg. Med. Chem.* **2006**, *14*, 2966−2971.

(7) Machala, M.; Kubinova, R.; Horavova, P.; Suchy, V. Chemoprotective potentials of homoisoflavonoids and chalcones of Dracaena cinnabari: modulations of drug-metabolizing enzymes and antioxidant activity. *Phytother. Res.* **2001**, *15*, 114−118.

(8) Wu, N. L.; Fang, J. Y.; Chen, M.; Wu, C. J.; Huang, C. C.; Hung, C. F. Chrysin protects epidermal keratinocytes from UVA- and UVB-induced damage. *J. Agric. Food Chem.* **2011**, *59*, 8391−8400.

(9) Galijatovic, A.; Otake, Y.; Walle, U. K.; Walle, T. Extensive metabolism of the flavonoid chrysin by human Caco-2 and Hep G2 cells. *Xenobiotica* **1999**, *29*, 1241−1256.

(10) Walle, T.; Otake, Y.; Brubaker, J. A.; Walle, U. K.; Halushka, P. V. Disposition and metabolism of the flavonoid chrysin in normal volunteers. *Br. J. Clin. Pharmacol.* **2001**, *51*, 143−146.

(11) Walle, U. K.; Galijatovic, A.; Walle, T. Transport of the flavonoid chrysin and its conjugated metabolites by the human intestinal cell line Caco-2. *Biochem. Pharmacol.* **1999**, *58*, 431−438.

(12) Jia, X.; Chen, J.; Lin, H.; Hu, M. Disposition of flavonoids via enteric recycling: enzyme-transporter coupling affects metabolism of biochanin A and formononetin and excretion of their phase II conjugates. *J. Pharmacol. Exp. Ther.* **2004**, *310*, 1103−1113.

(13) Adachi, Y.; Suzuki, H.; Schinkel, A. H.; Sugiyama, Y. Role of breast cancer resistance protein (Bcrp1/Abcg2) in the extrusion of glucuronide and sulfate conjugates from enterocytes to intestinal lumen. *Mol. Pharmacol.* **2005**, *67*, 923−928.

(14) Alvarez, A. I.; Vallejo, F.; Barrera, B.; Merino, G.; Prieto, J. G.; Tomas-Barberan, F.; Espin, J. C. Bioavailability of the glucuronide and sulfate conjugates of genistein and daidzein in breast cancer resistance protein 1 knockout mice. *Drug Metab. Dispos.* **2011**, *39*, 2008−2012.

(15) Ebert, B.; Seidel, A.; Lampen, A. Identification of BCRP as transporter of benzo[a]pyrene conjugates metabolically formed in Caco-2 cells and its induction by Ah-receptor agonists. *Carcinogenesis* **2005**, *26*, 1754−1763.

(16) Suzuki, M.; Suzuki, H.; Sugimoto, Y.; Sugiyama, Y. ABCG2 transports sulfated conjugates of steroids and xenobiotics. *J. Biol. Chem.* **2003**, *278*, 22644−22649.

(17) Doyle, L.; Ross, D. D. Multidrug resistance mediated by the breast cancer resistance protein BCRP (ABCG2). *Oncogene* **2003**, *22*, 7340−7358.

(18) Liu, Y.; Hu, M. Absorption and metabolism of flavonoids in the caco-2 cell culture model and a perused rat intestinal model. *Drug Metab. Dispos.* **2002**, *30*, 370−377.

(19) Jeong, E. J.; Jia, X.; Hu, M. Disposition of formononetin via enteric recycling: metabolism and excretion in mouse intestinal perfusion and Caco-2 cell models. *Mol. Pharmaceutics* **2005**, *2*, 319−328.

(20) Tang, L.; Singh, R.; Liu, Z.; Hu, M. Structure and concentration changes affect characterization of UGT isoform-specific metabolism of isoflavones. *Mol. Pharmaceutics* **2009**, *6*, 1466−1482.

(21) Hu, M.; Chen, J.; Tran, D.; Zhu, Y.; Leonardo, G. The Caco-2 cell monolayers as an intestinal metabolism model: metabolism of dipeptide Phe-Pro. *J. Drug Targeting* **1994**, *2*, 79−89.

DOI: 10.1021/jf5056979
J. Agric. Food Chem. 2015, 63, 2902−2910

(22) Hu, M.; Chen, J.; Lin, H. Metabolism of flavonoids via enteric recycling: mechanistic studies of disposition of apigenin in the Caco-2 cell culture model. *J. Pharmacol. Exp. Ther.* **2003**, *307*, 314−321.
(23) Yang, Z.; Zhu, W.; Gao, S.; Yin, T.; Jiang, W.; Hu, M. Breast cancer resistance protein (ABCG2) determines distribution of genistein phase II metabolites: reevaluation of the roles of ABCG2 in the disposition of genistein. *Drug Metab. Dispos.* **2012**, *40*, 1883−1893.
(24) Seiffert, W.; Limbach, H. H.; Zanker, V.; Mantsch, H. UV-spectra and electronic structures of monoamino-acridinium cations. *Histochemie* **1970**, *23*, 220−243.
(25) Chen, J.; Lin, H.; Hu, M. Metabolism of flavonoids via enteric recycling: role of intestinal disposition. *J. Pharmacol. Exp. Ther.* **2003**, *304*, 1228−1235.
(26) Sfakianos, J.; Coward, L.; Kirk, M.; Barnes, S. Intestinal uptake and biliary excretion of the isoflavone genistein in rats. *J. Nutr.* **1997**, *127*, 1260−1268.
(27) Zhang, S.; Yang, X.; Morris, M. E. Flavonoids are inhibitors of breast cancer resistance protein (ABCG2)-mediated transport. *Mol. Pharmacol.* **2004**, *65*, 1208−1216.
(28) Herbs MD, Your Natural Health Partner. http://examine.com/supplements/Chrysin/.

DOI: 10.1021/jf5056979
J. Agric. Food Chem. 2015, 63, 2902−2910

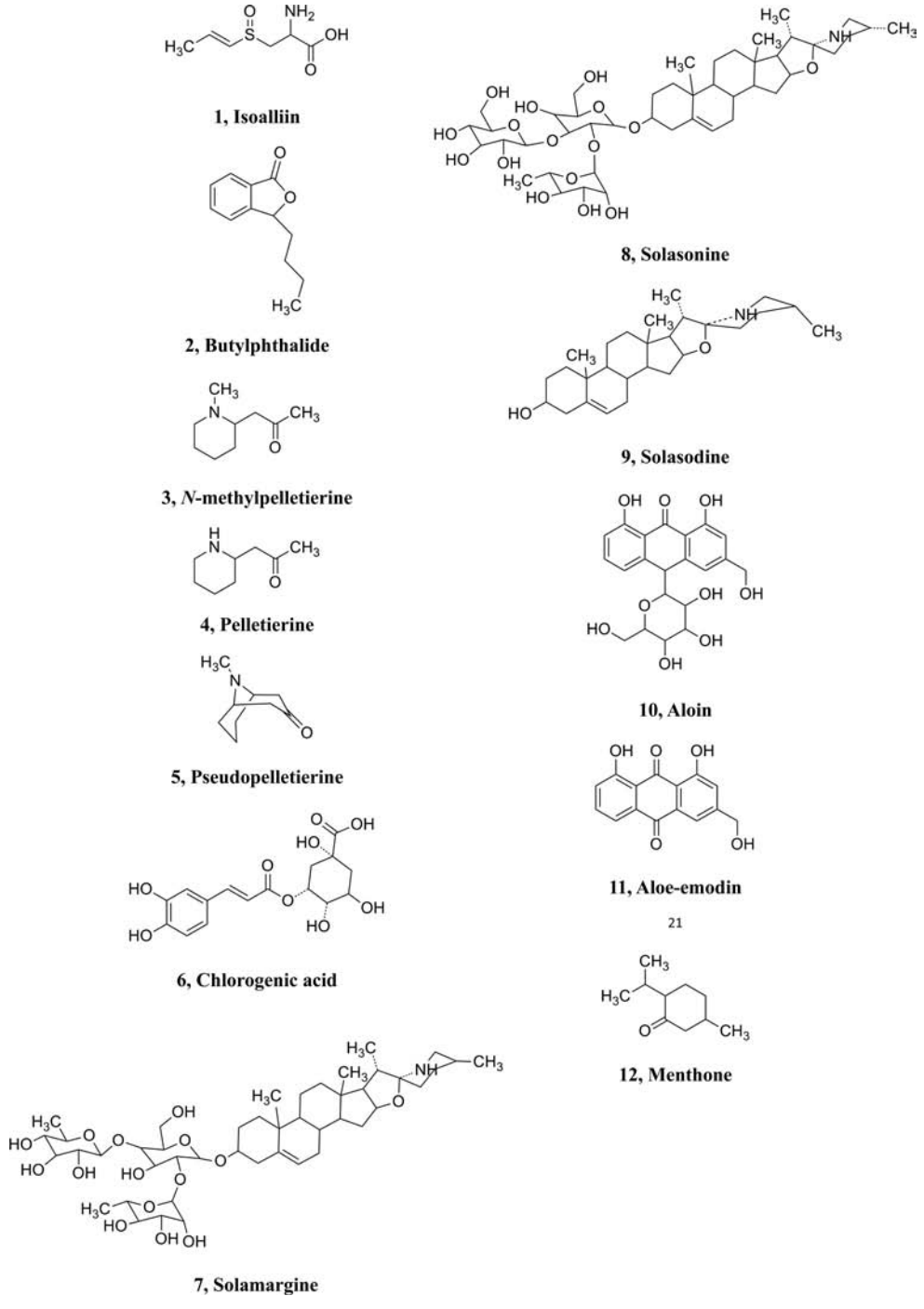

Figure 2. Chemical structures of compounds **1**−**12**.

Fabrication of in Vivo Nanospray Ion Source. The in vivo nanospray device was similar to that used in our previous study.[17] A quartz capillary (50 μm i.d., 148 μm o.d.) of 20 mm length was partially inserted into a specific region of the plant selected for sampling. A high dc voltage (3.5 kV, positive or negative) was applied to the plant via a needle close to the capillary to generate a spray of charged droplets carrying bioactive molecules toward the inlet of the mass spectrometer (Figure 1). The formation of charged droplets relies on the tissue fluid of fresh plants and eliminates the need for any auxiliary solvent. The sample was placed on an electrically insulated platform, in front of the MS inlet. The length of capillary outside the plant was 10 mm, and the distance between the end of the capillary and the MS inlet was 30 mm, to prevent electrical discharge.

HR-MS Analyses. Full-scan, selected ion monitoring (SIM) and MS/MS experiments were performed using a Q Exactive mass spectrometer (Thermo Scientific, Bremen, Germany). Mass spectra were processed using the instrument software Xcalibur 2.1 (Thermo Scientific), and both positive and negative ion spectra were recorded. Software Mass Frontier 7.0 SR1 was used to offer theoretical fragments and fragmentation mechanisms of compounds for the prediction of fragmentation patterns. The system was operated with a capillary temperature of 320 °C, an S-lens RF level of 50%, and a mass resolution of 70000.

In this work, the accurate mass measurements of precursor ions and fragment ions were accomplished by HR-MS. Full-scan/SIM was used to provide an accurate mass and possible elemental composition of the target ions. Further fragmentation and structural elucidation of the

DOI: 10.1021/jf505749n
J. Agric. Food Chem. 2015, 63, 2911−2918

selected precursor ions was performed by MS/MS. The mass tolerances of the parent and fragment ions were below 3 and 5 ppm, respectively.

RESULTS AND DISCUSSION

Vegetables. Isoalliin, **1**, in onion and butylphthalide, **2**, in celery were identified and confirmed. Onion has long been cultivated for its flavor and health benefits, which are both due to the unique sulfur chemistry and biochemistry of members of this genus.[18,19] Isoalliin, the main alkylated cysteine sulfoxide in onion, is the main source of its bioactive compounds.[20] Upon mechanical damage, isoalliin degrades into *trans*-1-allyl-methyl thiosulfate ($C_4H_8OS_2$), the main pharmacologically bioactive component in onion.[19] The chemical structures of all the identified bioactive ingredients may be found in Figure 2.

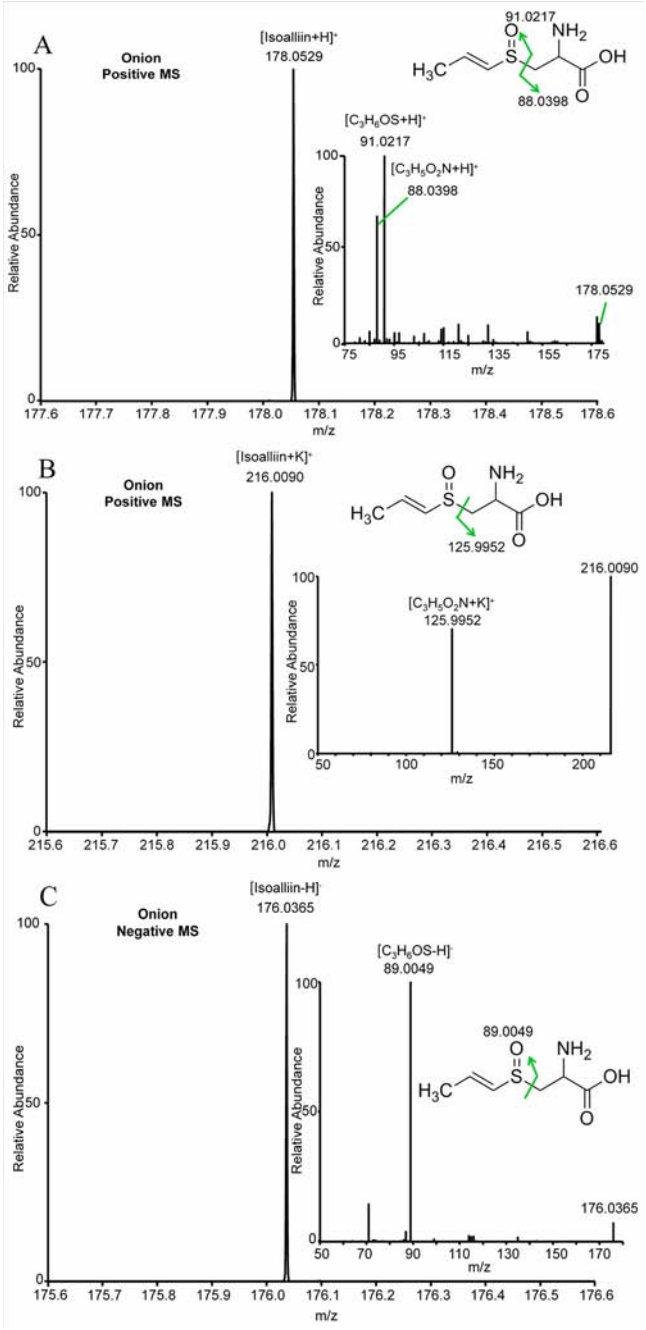

Figure 3. Mass spectra of isoalliin in onion: (A) protonated isoalliin and its fragment ions (inset); (B) potassium adducts of isoalliin and its fragment ions (inset); (C) deprotonated isoalliin and its fragment ions (inset).

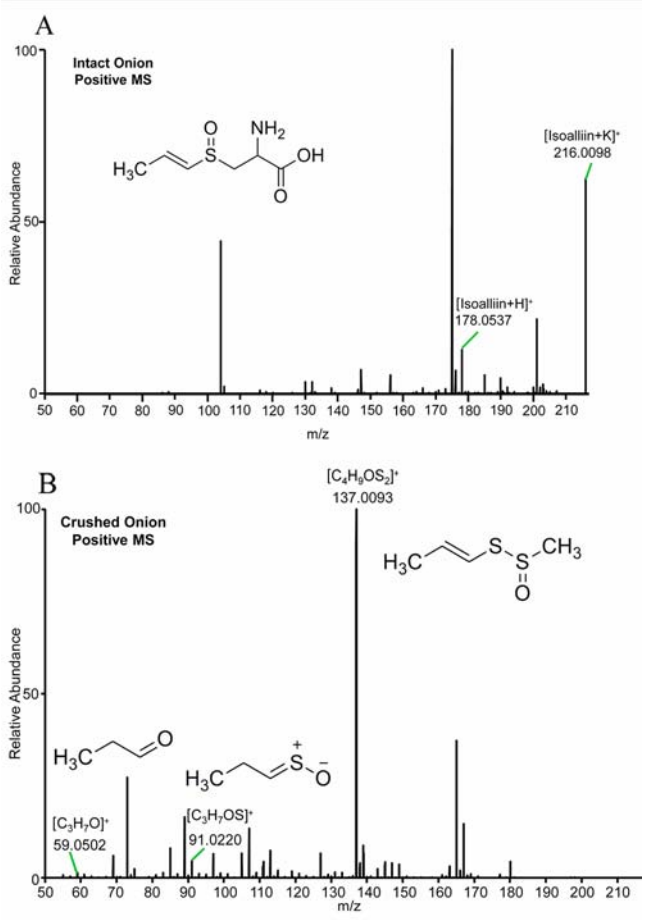

Figure 4. Mass spectra of isoalliin in different conditions: (A) intact onion observed by in vivo nanospray; (B) crushed onion observed in conventional nanospray.

Full-scan/SIM and MS/MS were performed in both positive and negative ion modes. In the positive ion mode, protonated isoalliin, m/z 178.0529 (Figure 3A) and the potassium adduct of isoalliin, m/z 216.0090 $[\text{isoalliin} + K]^+$ (Figure 3B), are observed in SIM mode. In the MS/MS spectrum of $[\text{isoalliin} + H]^+$, the two highest abundance ions are m/z 91.0217 $[C_3H_6OS + H]^+$ and m/z 88.0398 $[C_3H_5O_2N + H]^+$ (Figure 3A inset). The same fragmentation is observed in the MS/MS spectrum of $[\text{isoalliin} + K]^+$, which shows a base peak with m/z 125.9952 $[C_3H_5O_2N + K]^+$ (Figure 3B inset). In the negative ion mode, deprotonated isoalliin, m/z 176.0365 $[\text{isoalliin} - H]^-$ (Figure 3C) in SIM mode, and a product ion with m/z 89.0049 $[C_3H_6OS - H]^-$ in MS/MS (Figure 3C inset) are detected. All MS/MS fragmentation patterns are identical to those reported in the literature.[21−23]

Isoalliin, the major bioactive ingredient in onion, is also a labile compound. We studied the full-scan spectra of intact onion recorded by our in vivo nanospray and compared the results to those obtained from crushed onion using conventional nanospray. The results are shown in Figure 4. Only the protonated product and the potassium adduct of isoalliin were detected using in vivo nanospray ionization, and no degradation products were detected (Figure 4A). In contrast, in conven-

DOI: 10.1021/jf505749n
J. Agric. Food Chem. 2015, 63, 2911−2918

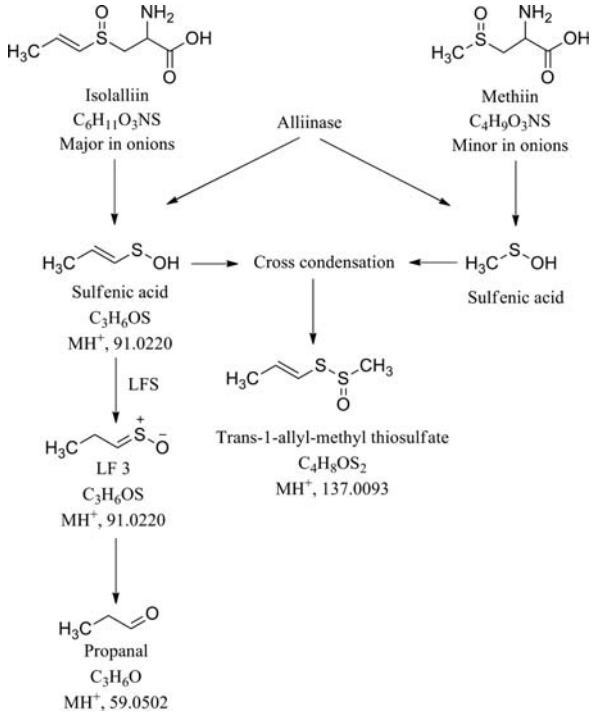

Figure 5. Biochemical degradation process of isoalliin in crushed onion.[19−23]

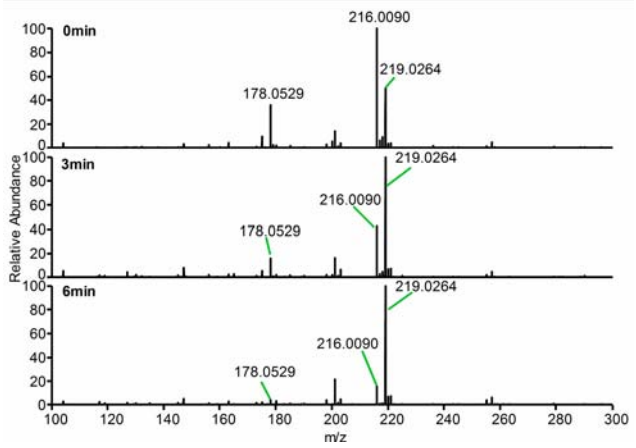

Figure 6. MS spectra of isoalliin in injured onion at multiple sampling time points.

tional nanospray ionization, only degradation products of isoalliin, including protonated *trans*-1-allyl-methyl thiosulfate, lachrymatory constituent LF3, and propanal, were observed (Figure 4B). These results indicate that in vivo nanospray HR-MS is suitable for the rapid in situ detection of labile ingredients in plants.

Isoalliin and methiin are the major and minor bioactive ingredients, respectively, in onion.[20] When onion tissue is damaged, isoalliin is released from the cells, and the exposed isoalliin will rapidly degrade to lachrymatory constituent LF3 (C_3H_6OS) and further to propanal (C_3H_6O) by the catalytic action of alliinase and lachrymatory factor synthase (LFS).[19] By the catalysis of alliinase, isoalliin and methiin are also transformed into sulfenic acids, which further cross-condense into *trans*-1-allyl-methyl thiosulfate ($C_4H_8OS_2$).[20] This degradation process of isoalliin in crushed onion is shown in Figure 5.

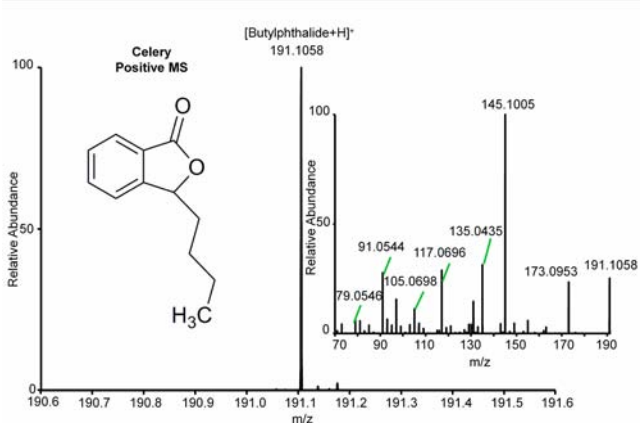

Figure 7. Mass spectra of butylphthalide and its fragment ions (inset) in celery.

The in vivo nanospray method was also used to track the changes of isoalliin concentration in onion at multiple sampling time points after punching, and the MS spectra are shown in Figure 6. The potassium adduct of glucose (m/z 219.0264 [glucose + K]$^+$) was used as a reference. The relative abundance of [isoalliin + H]$^+$ and [isoalliin + K]$^+$ reduced gradually over time, and the results show that the method is also suitable for continuously monitoring the change in concentration of labile ingredients in injured plant tissue.

The outer diameter of the capillary is about 148 μm; therefore, it could be used to analyze biomolecules in a microregion of the plant. We used in vivo nanospray to detect compounds located in three different microregions of the onion (top, middle, and bottom) using a scan region of m/z 150−250. Three main compounds were detected: protonated arginine (m/z 175.1191), potassium adducts of isoalliin, and glucose (m/z 216.0090 and 219.0264, respectively). However, there was a big difference in the relative abundance of these three ions in the different parts of the onion. In the top regions of the onion, glucose (relative abundance 100%) was the most abundant, followed by isoalliin (26%), and finally arginine (12%). In the middle region, too, glucose (100%) exhibited the highest signal intensity, followed by arginine (58%) and then by isoalliin (1%). In the bottom region of the onion, arginine (100%) was the most abundant, followed by glucose (32%) and finally by isoalliin (16%).

Celery is rich in volatile oils. Butylphthalide, **2**, is a typical volatile oil and shows antitumor, antioxidant, anti-inflammatory, and sedative properties.[24,25] In the positive ion mode mass spectrum of celery, protonated butylphthalide, m/z 191.1058 (Figure 7), was detected. The MS/MS experiment was performed on the [M + H]$^+$ ion of butylphthalide, and the spectrum exhibited peaks mainly at m/z 173.0953, 145.1005, 135.0435, 117.0696, 105.0698, 91.0544, and 79.0546 (Figure 7 inset). The m/z values of the fragment ions are in agreement with those reported in the literature.[26,27] This fragmentation can be partly explained by the loss of various neutral species. It is proposed that the peaks at m/z 173.0953, 145.1005, 135.0435, and 117.0696 can be attributed to the loss of 18 (− H_2O), 46 (− H_2O, − CO), 56 (− C_4H_8), and 74 (− H_2O, − C_4H_8) Da, respectively.

Fruits. The identification and structural elucidation of bioactive ingredients in fresh fruits were also accomplished,

DOI: 10.1021/jf505749n
J. Agric. Food Chem. 2015, 63, 2911−2918

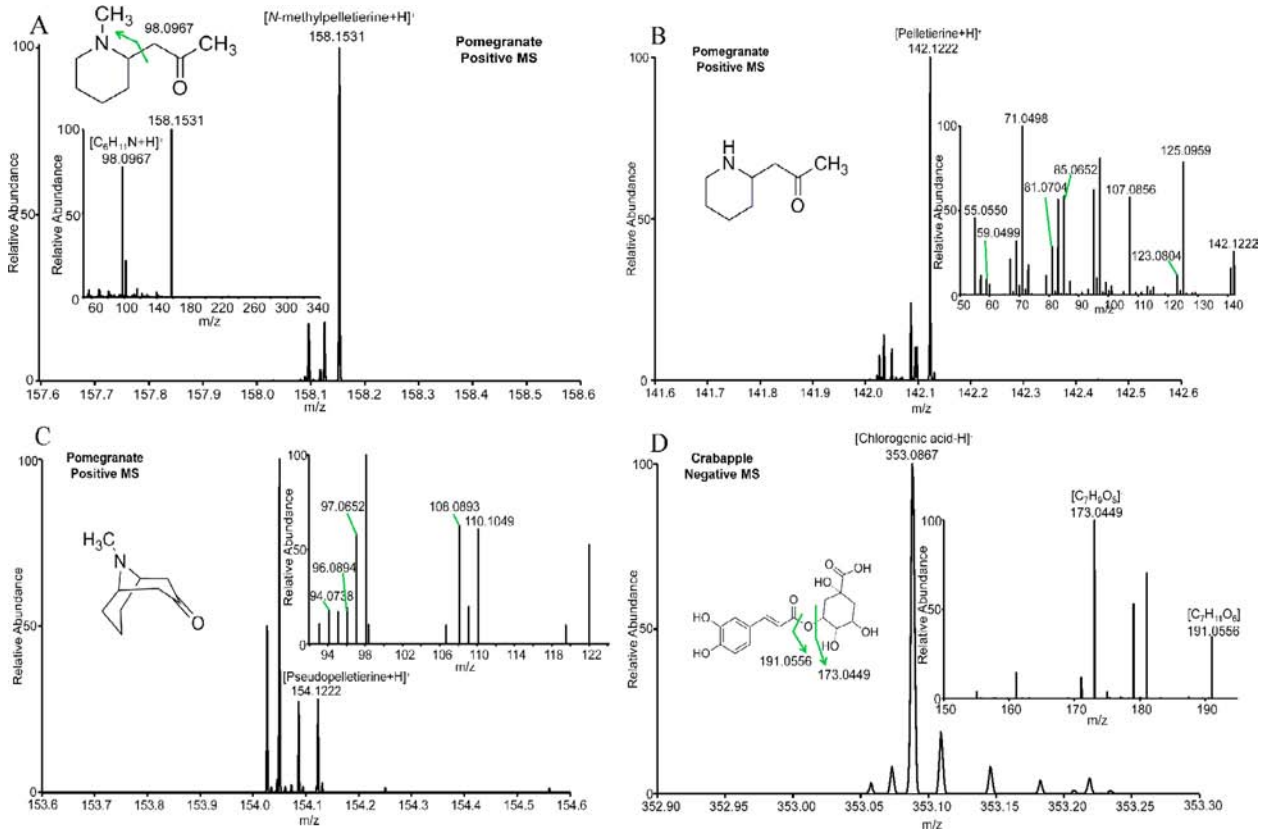

Figure 8. Mass spectra of bioactive ingredients in fruits: (A) protonated *N*-methylpelletierine and MS/MS (inset) in pomegranate; (B) protonated pelletierine and its fragment ions (inset) in pomegranate; (C) protonated pseudopelletierine and its fragment ions (inset) in pomegranate; (D) deprotonated chlorogenic acid and its fragment ions (inset) in crabapple.

including the piperidine alkaloids *N*-methylpelletierine, **3**, pelletierine, **4**, and pseudopelletierine, **5**, in pomegranate, and chlorogenic acid, **6**, in crabapple (Figure 2).

Pomegranate has medicinal and nutritional value due to various bioactive ingredients, such as piperidine alkaloids, which have antibacterial and anti-inflammatory effects.[28,29] In the positive ion mode mass spectra of pomegranate berry, protonated *N*-methylpelletierine, m/z 158.1531 (Figure 8A), pelletierine, m/z 142.1222 (Figure 8B), and pseudopelletierine, m/z 154.1222 (Figure 8C), were detected. Structural confirmation of the three ions was conducted in the MS/MS mode. In the MS/MS spectrum of *N*-methylpelletierine, we observed a prominent product ion at m/z 98.0967 ($[C_6H_{11}N + H]^+$). The fragmentation pattern and MS/MS spectrum have been labeled (Figure 8A inset). The result is in agreement with previously published research.[30] The MS/MS spectra of protonated pelletierine and pseudopelletierine are also shown in the insets in panels B and C, respectively, of Figure 8. The product ions indicated by the green line in the spectra are consistent with theoretical fragmentation patterns of protonated pelletierine and pseudopelletierine obtained by Mass Frontier. The results confirmed the presence of pelletierine and pseudopelletierine.

Phenolic acids are known to play an important role in plants' resistance to pathogens and herbivores, allelopathy, oxidative stress, and plant growth regulation.[31] Furthermore, they have been shown to have beneficial effects on human health.[32] Chlorogenic acid has antioxidant and antineoplastic properties and is found in a wide range of fruits.[33,34] Here, negative ion mode was selected for the analysis of chlorogenic acid in crabapple, and the mass spectrum of deprotonated chlorogenic acid (m/z 353.0867 [chlorogenic acid − H]$^-$) was obtained (Figure 8D). The MS/MS experiment was performed on deprotonated chlorogenic acid for structural elucidation (Figure 8D inset). The two product ions (m/z 173.0449 and 191.0556) were produced by cleavage at two different locations across the ester bond and are indicated by the green arrows in Figure 8D. The fragmentation patterns are in agreement with those reported in the literature.[35,36]

Medicinal Plants. Medicinal plants, including nightshade, aloe, and mint, have also been analyzed by our in vivo nanospray HR-MS technique. We have detected solamargine, **7**, solasonine, **8**, and solasodine, **9**, in berry of nightshade; aloin, **10**, and aloe-emodin, **11**, in aloe; and menthone, **12**, in mint (Figure 2).

The unripe berry of nightshade has both neural and cardiovascular pharmacological effects, and glycosides, including solasodine, solasonine, and solamargine, are the major contributors to this effect.[37,38] In the positive ion mode mass spectrum of unripe nightshade berry, protonated solasonine and solamargine, m/z 884.4965 and 868.5025, respectively (Figure 9A), and solasodine, m/z 414.3353 (Figure 9D), were detected. The MS/MS experiment was performed on the [M + H]$^+$ of these three ions. The fragmentation of the [M + H]$^+$ of solamargine is illustrated in Figure 9B. The initial loss from the precursor ion (from m/z 868.5025 to 850.4911) corresponds to M + H -18 (loss of water). The subsequent fragmentations yielding the product ions m/z 722.4431 (M + H − 146), m/z 704.4341 (M + H − 18 − 146), and m/z 558.3768 (M + H − 18 − 146 − 146) correspond to the consecutive loss of

DOI: 10.1021/jf505749n
J. Agric. Food Chem. 2015, 63, 2911−2918

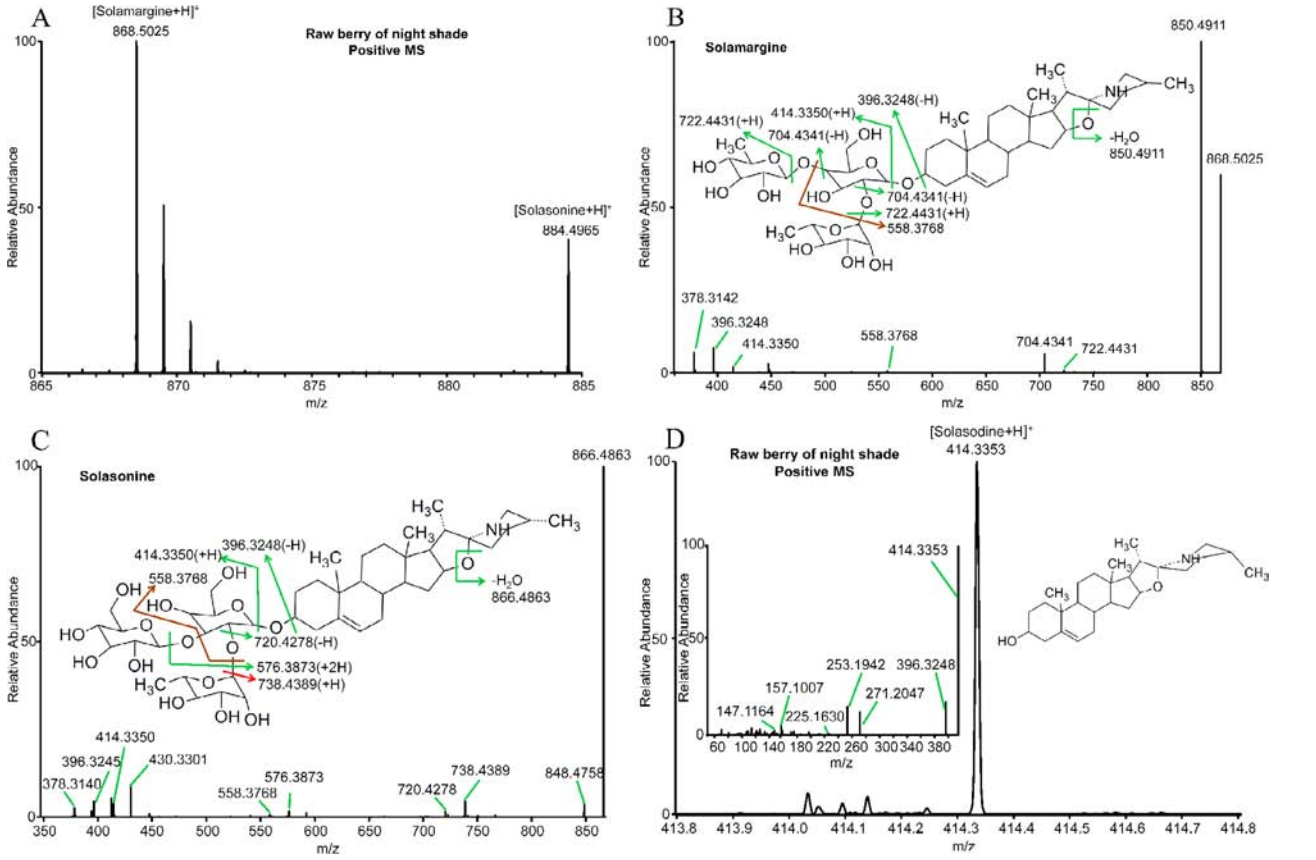

Figure 9. Positive mode mass spectra of alkaloids in raw unripe nightshade berry: (A) protonated solasonine and solamargine; (B) MS/MS of solamargine; (C) MS/MS spectrum of solasonine; (D) protonated solasodine and its MS/MS spectrum (inset).

rhamnosyl groups (164 − 18 → 146). The subsequent fragmentation to m/z 396.3248 (M + H − 18 − 146 − 146 − 162) corresponds to the loss of a glucosyl group (180 − 18 → 162). The final fragmentation to m/z 378.3142 (M + H − 18 − 146 − 146 − 162 − 18) corresponds to the loss of water. The detailed fragmentation process is shown in Figure 9B. This spectrum is identical to spectra reported in the literature.[39,40] Almost the same fragmentation pattern is observed with solasonine, as shown in Figure 9C. The inset in Figure 9D illustrates the MS/MS and fragmentation pattern of $[\text{solasodine} + \text{H}]^+$ in the positive ion mode and shows a rapid loss of water (M + H − 18) from the structure to yield the 396.3248 product ion. This spectrum is in accordance with other reports in the literature.[41] There is a huge difference in the content of bioactive compounds between raw unripe nightshade berry and raw ripe nightshade berry. In raw unripe nightshade berry, protonated solamargine, solasonine, and solasodine were all detected. However, in ripe berry, solasodine was not detected, and the signal of protonated solamargine decreased substantially, whereas only a small change in signal occurred for protonated solasonine.

Aloin and aloe-emodin, the two main bioactive components in aloe, have the strongest antibacterial activity of the anthraquinones.[42] The negative ion mode was selected for the detection of aloin and aloe-emodin (Figure 10A,B), because it resulted in the best sensitivity. The corresponding $[\text{M} - \text{H}]^-$ ion was selected as the precursor ion for each analyte. The most abundant product ion observed for aloin was at m/z 297.0768, which corresponds to the loss of $[\text{C}_4\text{H}_8\text{O}_4]^-$ from the precursor ion (Figure 10A inset). The main product ion observed for aloe-emodin was m/z 240.0425, which corresponds to the loss of $[\text{CHO}]^-$ from the precursor ion (Figure 10B inset). The above results are in accordance with those reported in the literature.[43,44]

Mint is one of the main raw materials for the production of toothpaste and chewing gum,and is also a medicinal plant. Menthone is the major bioactive ingredient in mint, giving it its intense flavor and strong analgesic effect.[45] Protonated menthone, m/z 155.1425 (Figure 10C), was observed in the positive ion mode spectra. The product ions in the MS/MS spectrum (Figure 10C inset) are consistent with the theoretical fragmentation pattern derived from Mass Frontier.

The above results demonstrate that in vivo nanospray HR-MS is a good method for the rapid detection and identification of bioactive compounds in microregions of plants. Because many of the bioactive molecules in plants are labile, this method has great potential for obtaining information on labile compounds and their biochemical reaction intermediates, so as to elucidate the degradation principle. In the future, we plan to apply this method for the study of easily degradable chemicals in plants. However, it is important to note that because the in vivo nanospray uses tissue fluid in plants to generate charged droplets during electrospray ionization, the method is viable for detecting polar molecules in fresh plants rich in water. Although the inner diameter of the capillary tip used in this study is 50 um, a capillary with a much smaller inner diameter can be used to enhance the signal intensity. In addition, the device, which is small and convenient to carry, can be combined with a portable mass spectrometer for rapid field analysis and will be beneficial for the full application of the methodology.

DOI: 10.1021/jf505749n
J. Agric. Food Chem. 2015, 63, 2911−2918

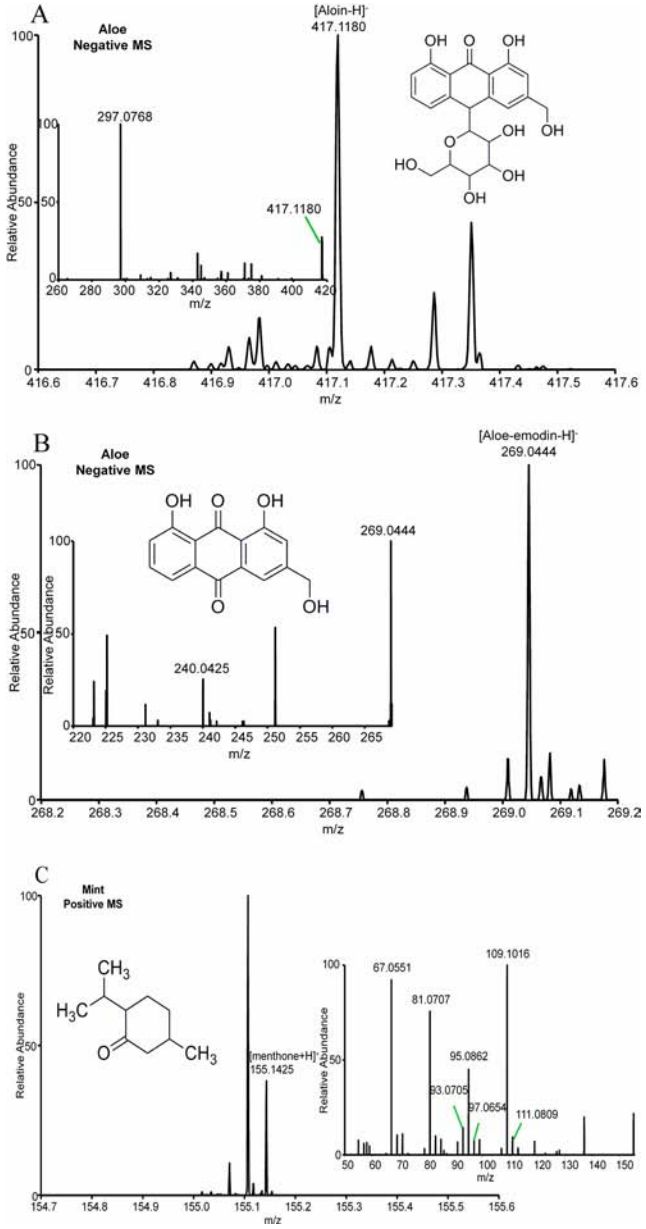

Figure 10. Mass spectra of bioactive ingredients: (A) deprotonated aloin in aloe and its production ion spectrum (inset); (B) deprotonated aloe-emodin in aloe and its production ion spectrum (inset); (C) protonated menthone in mint and its production ion spectrum (inset).

■ ASSOCIATED CONTENT

Supporting Information

Figures S1–S6. This material is available free of charge via the Internet at http://pubs.acs.org.

■ AUTHOR INFORMATION

Corresponding Author

*(Y.P.) E-mail: ye.peng@cug.edu.cn.

Funding

The project is supported by the fundamental research funds for the central universities, China University of Geosciences (Wuhan), and NSFC (No. 21305130).

Notes

The authors declare no competing financial interest.

■ ABBREVIATIONS USED

HR-MS, high-resolution mass spectrometry; MS/MS, tandem mass spectrometry; SIM, selected ion monitoring

■ REFERENCES

(1) Pieterse, C. M. J.; Leon-Reyes, A.; Van der Ent, S.; Van Wees, S. C. M. Networking by small-molecule hormones in plant immunity. *Nat. Chem. Biol.* **2009**, *5*, 308–316.

(2) Raskin, I.; Ribnicky, D. M.; Komarnytsky, S.; Ilic, N.; Poulev, A.; Borisjuk, N.; Brinker, A.; Moreno, D. A.; Ripoll, C.; Yakoby, N.; O'Neal, J. M.; Cornwell, T.; Pastor, I.; Fridlender, B. Plants and human health in the twenty-first century. *Trends Biotechnol.* **2002**, *20*, 522–531.

(3) Palombo, E. A. Phytochemicals from traditional medicinal plants used in the treatment of diarrhoea: modes of action and effects on intestinal function. *Phytother. Res.* **2006**, *20*, 717–724.

(4) Pieterse, C. M.; Dicke, M. Plant interactions with microbes and insects: from molecular mechanisms to ecology. *Trends Plant Sci.* **2007**, *12*, 564–569.

(5) Ibanez, M.; Sancho, J. V.; Bijlsma, L.; van Nuijs, A. L. N.; Covaci, A.; Hernández, F. Comprehensive analytical strategies based on high-resolution time-of-flight mass spectrometry to identify new psychoactive substances. *TrAC, Trends Anal. Chem.* **2014**, *57*, 107–117.

(6) Schymanski, E. L.; Jeon, J.; Gulde, R.; Fenner, K.; Ruff, M.; Singer, H. P.; Hollender, J. Identifying small molecules via high resolution mass spectrometry: communicating confidence. *Environ. Sci. Technol.* **2014**, *48*, 2097–2098.

(7) Schymanski, E. L.; Singer, H. P.; Longree, P.; Loos, M.; Ruff, M.; Stravs, M. A.; Vidal, C. R.; Hollender, J. Strategies to characterize polar organic contamination in wastewater: exploring the capability of high resolution mass spectrometry. *Environ. Sci. Technol.* **2014**, *48*, 1811–1818.

(8) Lacina, O.; Urbanova, J.; Poustka, J.; Hajslova, J. Identification/quantification of multiple pesticide residues in food plants by ultra-high-performance liquid chromatography-time-of-flight mass spectrometry. *J. Chromatogr., A* **2010**, *1217*, 648–659.

(9) Cajka, T.; Hajslova, J.; Lacina, O.; Mastovska, K.; Lehotay, S. J. Rapid analysis of multiple pesticide residues in fruit-based baby food using programmed temperature vaporiser injection–low-pressure gas chromatography–high-resolution time-of-flight mass spectrometry. *J. Chromatogr., A* **2008**, *1186*, 281–294.

(10) Berchtold, C.; Meier, L.; Steinhoff, R.; Zenobi, R. A new strategy based on real-time secondary electrospray ionization and high-resolution mass spectrometry to discriminate endogenous and exogenous compounds in exhaled breath. *Metabolomics* **2014**, *10*, 291–301.

(11) El-Aneed, A.; Cohen, A.; Banoub, J. Mass spectrometry, review of the basics: electrospray, MALDI, and commonly used mass analyzers. *Appl. Spectrosc. Rev.* **2009**, *44*, 210–230.

(12) Alberici, R. M.; Simas, R. C.; Sanvido, G. B.; Romão, W.; Lalli, P. M.; Benassi, M.; Cunha, I. B. S.; Eberlin, M. N. Ambient mass spectrometry: bringing MS into the "real world". *Anal. Bioanal. Chem.* **2010**, *398*, 265–294.

(13) Harris, G. A.; Galhena, A. S.; Fernandez, F. M. Ambient sampling/ionization mass spectrometry: applications and current trends. *Anal. Chem.* **2011**, *83*, 4508–4538.

(14) Jackson, A. U.; Tata, A.; Wu, C.; Perry, R. H.; Haas, G.; West, L.; Cooks, R. G. Direct analysis of stevia leaves for diterpene glycosides by desorption electrospray ionization mass spectrometry. *Analyst* **2009**, *134*, 867–874.

(15) Zhang, J. I.; Li, X.; Ouyang, Z.; Cooks, R. G. Direct analysis of steviol glycosides from stevia leaves by ambient ionization mass spectrometry performed on whole leaves. *Analyst* **2012**, *137*, 3091–3098.

(16) Liu, J.; Wang, H.; Cooks, R.; Ouyang, G. Z. Leaf spray: direct chemical analysis of plant material and living plants by mass spectrometry. *Anal. Chem.* **2011**, *83*, 7608–7613.

DOI: 10.1021/jf505749n
J. Agric. Food Chem. 2015, 63, 2911–2918

(17) Peng, Y.; Zhang, S.; Wen, F.; Ma, X.; Yang, C.; Zhang, X. In vivo nanoelectrospray for the localization of bioactive molecules in plants by mass spectrometry. *Anal. Chem.* **2012**, *84*, 3058−3062.
(18) Donaldson, M. S. Nutrition and cancer: a review of the evidence for an anti-cancer diet. *Nutr. J.* **2004**, *3*, 19.
(19) Joyce, N. I.; Eady, C. C.; Silcock, P.; Perry, N. B.; Klink, J. W. Fast phenotyping of LFS-silenced (tearless) onions by desorption electrospray ionization mass spectrometry (DESI-MS). *J. Agric. Food Chem.* **2013**, *61*, 1449−1456.
(20) Edwards, S. J.; Musker, D.; Collin, H. A.; Britton, G. The analysis of *S*-alk(en)yl-L-cysteine sulfoxides (flavor precursors) from species of *Allium* by high performance liquid chromatography. *Phytochem. Anal.* **1994**, *5*, 4−9.
(21) Block, E.; Dane, A. J.; Thomas, S.; Cody, R. B. Applications of direct analysis in real time mass spectrometry (DART-MS) in *Allium* chemistry. 2-Propenesulfenic and 2-propenesulfinic acids, diallyl trisulfane s-oxide, and other reactive sulfur compounds from crushed garlic and other *Alliums*. *J. Agric. Food Chem.* **2010**, *58*, 4617−4625.
(22) Corzo-Martínez, M. C.; Corzo, N.; Villamiel, M. Biological properties of onions and garlic. *Trends Food Sci. Technol.* **2007**, *18*, 609−625.
(23) Lanzotti, V. The analysis of onion and garlic. *J. Chromatogr., A* **2006**, *1112*, 3−22.
(24) Lin, L. Z.; Lu, S.; Harnly, J. M. Detection and quantification of glycosylated flavonoid malonates in celery, Chinese celery, and celery seed by LC-DAD-ESI/MS. *J. Agric. Food Chem.* **2007**, *55*, 1321−1326.
(25) Zhou, K.; Zhao, F.; Liu, Z.; Zhuang, Y.; Chen, L.; Qiu, F. Triterpenoids and flavonoids from celery (*Apium graveolens*). *J. Nat. Prod.* **2009**, *72*, 1563−1567.
(26) Teng, J.; Chen, H.; Li, D.; Luo, A. Identification and characterization of supercritical fluid extracts of *Rhizoma Chuanxiong* by high performance liquid chromatography ion trap mass spectrometry. *Front. Chem. China* **2006**, *4*, 454−458.
(27) Zhang, X.; Xiao, H.; Xu, Q.; Li, X.; Wang, J.; Liang, X. Characterization of phthalides in *Ligusticum chuanxiong* by liquid chromatographic−atmospheric pressure chemical ionization−mass spectrometry. *J. Chromatogr. Sci.* **2003**, *41*, 428−433.
(28) Szőke, É.; Lemberkovics, É.; Kursinszki, L. Alkaloids derived from lysine: piperidine alkaloids. In *Handbook of Natural Products*; Ramawat, K. G., Mérillon, J.-M., Eds.; Springer Verlag: Berlin, Germany, 2013; pp 303−341.
(29) Zhang, L.; Gao, Y.; Zhang, Y.; Liu, J.; Yu, J. Changes in bioactive compounds and antioxidant activities in pomegranate leaves. *Sci. Hortic.* **2010**, *123*, 543−546.
(30) Schneider, M. J.; Brendze, S.; Montali, J. A. Alkaloids of *Picea breweriana*. *Phytochemistry* **1995**, *39*, 1387−1390.
(31) Gruz, J.; Novák, O.; Strnad, M. Rapid analysis of phenolic acids in beverages by UPLC−MS/MS. *Food Chem.* **2008**, *111*, 789−794.
(32) Bazzano, L. A.; He, J.; Ogden, L. G.; Loria, C. M.; Vupputuri, S.; Myers, L.; Whelton, P. K. Fruit and vegetable intake and risk of cardiovascular disease in US adults: the first national health and nutrition examination survey epidemiologic follow-up study. *Am. J. Clin. Nutr.* **2002**, *76*, 93−99.
(33) Ong, K. W.; Hsu, A.; Tan, B. K. H. Anti-diabetic and anti-lipidemic effects of chlorogenic acid are mediated by AMPK activation. *Biochem. Pharmacol.* **2013**, *85*, 1341−1351.
(34) Cho, A. S.; Jeon, S. M.; Kim, M. J.; Yeo, J.; Seo, K.; Choi, M. S.; Lee, M. K. Chlorogenic acid exhibits anti-obesity property and improves lipid metabolism in high-fat diet-induced-obese mice. *Food Chem. Toxicol.* **2010**, *48*, 937−943.
(35) Fang, N. B.; Yu, S. G.; Prior, R. L. LC/MS/MS characterization of phenolic constituents in dried plums. *J. Agric. Food Chem.* **2002**, *50*, 3579−3585.
(36) Ye, J. X.; Wei, W.; Quan, L. H.; Liu, C. Y.; Chang, Q.; Liao, Y. H. An LC−MS/MS method for the simultaneous determination of chlorogenic acid, forsythiaside A and baicalin in rat plasma and its application to pharmacokinetic study of Shuang-huang-lian in rats. *J. Pharm. Biomed. Anal.* **2010**, *52*, 625−630.
(37) Parmar, S.; Gangwal, A.; Sheth, N. *Solanum xanthocarpum* (yellow berried nightshade): a review. *Pharm. Lett.* **2010**, *2*, 373−383.
(38) Müller, J. L. Love potions and the ointment of witches: historical aspects of the nightshade alkaloids. *Clin. Toxicol.* **1998**, *36*, 617−627.
(39) Sanchez-Mata, M. C.; Yokoyama, W. E.; Hong, Y. J.; Prohens, J. α-Solasonine and α-solamargine contents of Gboma (*Solanum macrocarpon* L.) and Scarlet (*Solanum aethiopicum* L.) eggplants. *J. Agric. Food Chem.* **2010**, *58*, 5502−5508.
(40) Munafo, J. P., Jr.; Gianfagua, T. J. Quantitative analysis of steroidal glycosides in different organs of Easter lily (*Lilium longiflorum* Thunb.) by LC-MS/MS. *J. Agric. Food Chem.* **2011**, *59*, 995−1004.
(41) Smith, C. R.; Zentz, G. A.; Kindscher, K.; Chapman, J. M. Detection of solamargine in asadero cheese by LC-ESI-MS. http://dobyobktvl6u3.cloudfront.net/media/filer_private/2012/01/06/detectionofsolamargineinasaderocheesebylc-esi-ms.pdf (accessed Feb 22, 2015).
(42) Nidiry, E. S. J.; Ganeshan, G.; Lokesha, A. N. Antifungal activity of some extractives and constituents of *Aloe vera*. *Res. J. Med. Plant.* **2011**, *5*, 196−200.
(43) Wang, P. G.; Zhou, W. L.; Wamer, W. G.; Krynitsky, A. J.; Rader, J. I. Simultaneous determination of aloin A and aloe emodin in products containing *Aloe vera* by ultra-performance liquid chromatography with tandem mass spectrometry. *Anal. Methods* **2012**, *4*, 3612−3619.
(44) Wu, X. F.; Ding, W. J.; Zhong, J. S.; Wan, J. Z.; Xie, Z. Y. Simultaneous qualitative and quantitative determination of phenolic compounds in *Aloe barbadensis* Mill by liquid chromatography−mass spectrometry-ion trap-time-of-flight and high performance liquid chromatography-diode array detector. *J. Pharm. Biomed. Anal.* **2013**, *80*, 94−106.
(45) Farco, A.; Grundmann, J. O. Menthol − pharmacology of an important naturally medicinal. *Mini-Rev. Med. Chem.* **2013**, *13*, 124−131.

DOI: 10.1021/jf505749n
J. Agric. Food Chem. 2015, 63, 2911−2918

disease diagnosis, drug discovery, and the evaluation of drug efficacy and toxicity.[19−23] Such an approach may shed new light on the holistic therapeutic efficacies and synergistic effects of traditional herbal medicines.[24,25] NMR- and MS-based metabolomics have been employed to measure variations in the properties of ginseng in the context of plant age, cultivation conditions, origin, and processing[26−30] and to evaluate the effects of ginseng on diabetes, excessive fatigue, and myocardial infarction in animal models.[31−33]

As both hyperlipidemia and obesity are disorders of lipid metabolism, characterized by abnormal lipid levels, more attention must be paid to the effects of ginseng on lipid metabolism. However, only very limited data on lipidomic biomarkers reflecting the pharmacological effects of ginseng are available.[34] In the present study, we used mass spectrometry (MS)-based serum lipid profiling and conventional serum chemical analysis to explore the biochemical abnormalities in obese mice fed HFD and determined the pharmacological effects of compound K-reinforced ginsenosides (CK) in such mice. MS-based lipidomics yielded global profiles of endogenous lipids including lysophopholipids, phospholipids, and triacylglycerols, all of which are metabolites closely associated with metabolic diseases. We subjected the data to multivariate statistical analysis to define lipid metabolites contributing to discrimination among mice fed a normal diet (ND), an HFD, and an HFD plus CK.

MATERIALS AND METHODS

Chemicals and Reagents. Methanol and water were purchased from Merck (LC-MS grade, Darmstadt, Germany). Ammonium acetate, chloroform, methyl-*tert*-butyl ether (MTBE), and triglycerides (TG) mixture standard (8:0/8:0/8:0, 10:0/10:0/10:0, and 12:0/12:0/12:0) were purchased from Sigma-Aldrich (St. Louis, MO, USA). Phosphatidylcholine (PC 18:2/16:0 and PC 18:2/18:2), phosphatidylethanolamine (PE 16:0/18:1), phosphatidylglycerol (PG 16:0/18:1), phosphatidylinositol (PI 16:0/18:1), lysophosphatidylcholine (LPC 16:0 and LPC 18:0), lysophosphatidylethanolamine (LPE 16:0), lysophosphatidylglycerol (LPG 16:0), and lysophosphatidylinositol (LPI 18:1) were purchased from Avanti Polar Lipids (Alabaster, AL, USA).

Preparation of Compound K-Reinforced Ginsenosides. Four-year-old Korean ginseng (*P. ginseng* C.A. Meyer) roots were cultivated in and collected from farms in Geumsan, Chungcheongnam-do, Korea. The CK fraction was prepared via enzymatic conversion and column fractionation as described in our patent application (WO 2013/109062 A1). Briefly, dried roots of ginseng were extracted three times with boiling water at 80 °C for 4 h and the extracts filtered and concentrated to obtain a crude extract (60 °Brix). The extract was next diluted with water (to 7 °Brix) and adjusted to pH 4.3 with citric acid; an enzyme powder containing pectinase (Cytolase PCL5; DSM Food Specialties, Servian, France) was next added to 2% (w/v) to bioconvert the ginsenosides at 56 °C for 72 h. The reaction mixture was then heat-treated at 95 °C for 30 min to eliminate enzyme activity and the ginsenoside fraction next isolated via adsorption column chromatography using Diaion HP-20 resin (Samyang, Seoul, Korea). The loaded column was washed with water to remove non-ginsenosides and the ginsenosides fraction eluted with 90% (v/v) ethanol. The eluted sample was evaporated under vacuum and freeze-dried to obtain the CK powder. HPLC revealed that compound K constituted ∼12% of total ginsenosides of the CK fraction, but compound K was not detectable in the crude extract.

Animal Study. Five-week-old male C57BL/6J mice purchased from Central Laboratory Animal Inc. (Seoul, Korea) were housed in standard plastic cages with free access to water and food in a room under constant temperature (21 ± 2.0 °C) and relative humidity (50 ± 5%) with a 12 h light/12 h dark cycle. The mice were acclimatized to the laboratory environment for 1 week and were next randomly divided into three groups (eight mice per group): (1) ND; (2) HFD; (3) HFC plus CK at 400 mg/kg (HFD+CK). The ND (3.1 kcal/g; 18% of calories from fat) was the "2018S Teklad Global 18% Protein Rodent Diet" and the HFD (5.1 kcal/g; 60% of calories from fat) the "TD.06414 Teklad Adjusted Calories Diet"; both chows were purchased from Harlan Laboratories (Madison, WI, USA). The mice were allowed free access to either diet for a total of 16 weeks. CK was given orally six times per week for the last 8 weeks. Body weights were measured once weekly.

Histological Examination and Triglycerides in Liver Tissue. Slices of liver tissue were frozen immediately in OCT compound (Fisher Scientific, Waltham, MA, USA) and subjected to Oil Red O staining. For the triglyceride assay, total lipids were extracted according to the Folch method from liver tissue.[35] Briefly, frozen liver (50-mg amounts) was weighed and homogenized in 1 mL of chloroform/methanol (2:1, v/v). The homogenate was centrifuged at 12000 rpm to recover the liquid phase. Water (0.2 mL) was added and the mixture centrifuged at 4000 rpm; the lower lipid-containing phase was retained. Triglycerides content was measured via a colorimetric assay, using a kit from Asian Biochemicals.

Serum Assay. Mouse blood extracted via cardiac puncture was allowed to clot for 30 min at room temperature and then centrifuged for 10 min at 12000 rpm at 4 °C to collect serum. Serum total cholesterol, low-density lipoprotein cholesterol (LDL-c), and triglycerides (TG) were analyzed using BS-400, an automatic blood chemistry analyzer (Mindray, Shenzhen, China).

Sample Preparation. Serum lipids were extracted using the Matyash method with some modifications.[16,36] In brief, 225 μL of ice-cold methanol was added to 10 μL of serum, and the mixture vortexed for 10 s. Next, 750 μL of ice-cold MTBE was added, and phase separation was induced by the addition of 187.5 μL of distilled water. After centrifugation (14000*g*, 4 °C), the supernatant was collected and completely dried prior to lipid profiling. Dried samples were stored at −70 °C prior to analysis.

Direct Infusion MS Analysis. Each dried lipid extract was reconstituted in 100 μL of chloroform/methanol (1:9, v/v) and diluted 5-fold with chloroform/methanol (1:9, v/v) containing 7.5 mM ammonium acetate. The lipid solution was infused into a Thermo LTQ XL ion trap mass spectrometer (Thermo Fisher Scientific, West Palm Beach, FL, USA) using a chip-based nanoelectrospray infusion system (TriVersa NanoMate, Advion Biosciences, Ithaca, NY). The ion source was controlled with the aid of Chipsoft software (version 8.3.1, Advion Biosciences, Ithaca, NY, USA). The ionization voltage was 1.4 kV in the positive mode and the backpressure, 0.4 psi. The temperature of the ion transfer capillary was 200 °C and the tube voltage, 100 V. For lipid profiling, 5 μL of each sample was randomly loaded onto a 96-well plate of the TriVersa Nanomate ion source, to avoid analytical bias. A standard mixture of TG, PC, and LPC and a quality control (QC) sample (a pooled sample) were loaded at the beginning, middle, and end of each batch. Each 96-well plate was sealed with Thermowell aluminum sealing tape (Corning, Corning, NY, USA) and next placed on a Nanomate cooling plate (4 °C) to prevent evaporation of the solvent. The mass spectrum of each sample was acquired in the profile mode over 2 min. Data collection featured a full scan (scan range m/z 400−1000) and a data-dependent MS/MS scan of abundant ions. Standard spectra were obtained in low-resolution mode using a 30 eV collision-induced dissociation (CID) voltage to achieve specific MS/MS fragmentation. All spectra were recorded with the aid of the Thermo Xcalibur software (version 2.1, Thermo Fisher Scientific, Waltham, MA, USA).

Data Processing. Nominal ion mass spectra data files from the ion trap mass spectrometer (".raw" files) were directly loaded into the Genedata Expressionist MSX module (Genedata AG, Basel, Switzerland). The default processing parameters were applied unless otherwise specified. The spectral data were first averaged between 0.5 and 1.0 min and simplified by subtracting background noise. After subtraction, all data points below a threshold intensity of 300 were clipped to zero. The spectral set was next aligned in the m/z direction via nonlinear transformation, mapping the original m/z data set onto a common universal data set. Next, spectrum peak detection was used to

DOI: 10.1021/jf506216p
J. Agric. Food Chem. 2015, 63, 2919−2929

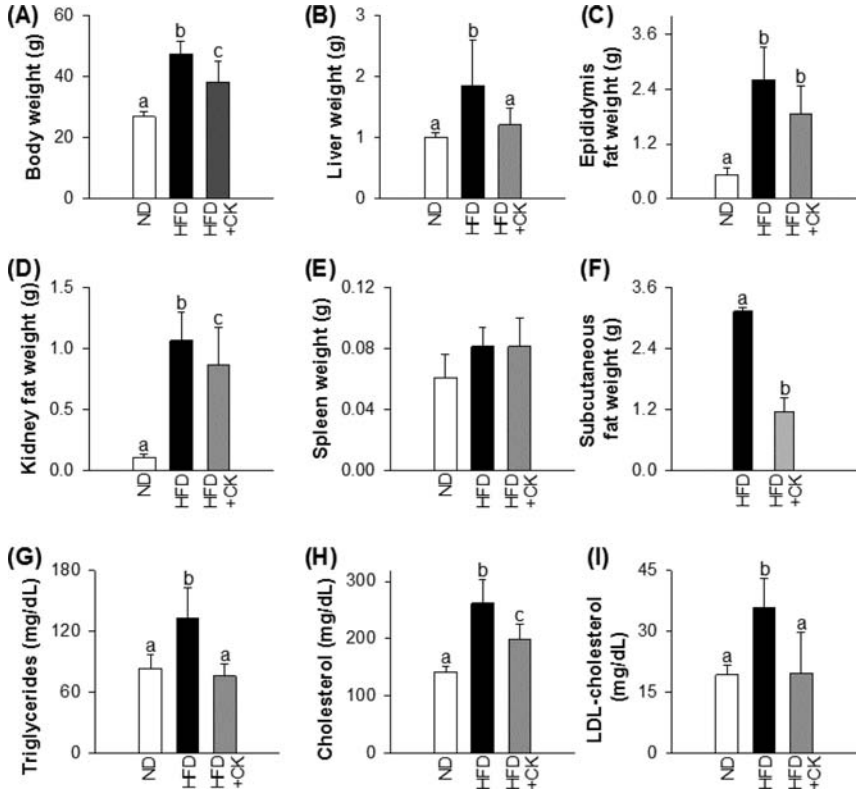

Figure 1. Characteristics of mice fed a normal diet (ND, n = 7), a high-fat diet (HFD, n = 7), or a high-fat diet + compound K-reinforced ginsenosides (HFD+CK, n = 7): (A) body weight; (B) liver weight; (C) epididymis fat weight; (D) kidney fat weight; (E) spleen fat weight; (F) subcutaneous fat weight; (G) triglycerides level; (H) cholesterol level; (I) LDL-cholesterol level. Different letters indicate significant differences by analysis of variance (ANOVA; $p < 0.05$).

define peaks on the temporarily averaged spectrum; the following parameters were used: smoothing window, three points; method, curvature-based peak detection; peak refinement threshold, 5%; consistency filter threshold, 0.8; and signal/noise threshold, 1. Peaks thus detected were grouped into isotopic clusters of individual peaks via spectrum isotope clustering activity, using the following parameters: minimum charge, 1; maximum charge, 2; maximum missing peaks, 1; first allowed gap position, 3; ionization, protonation; and m/z tolerance, 0.1 Da. Data on all detected peaks, including m/z and intensity values, were exported as Excel files. To normalize spectral data, the average of the sum of intensities of QC samples was divided by the sum of the intensities of each sample spectrum, and next each value (-fold) was multiplied by the peak intensity of each lipid species in that sample. The resulting Excel data were exported to SMICA P+ software (version 13.0, Umetrics, Umea, Sweden). In addition, serum lipids were identified by comparison with the MS/MS fragmentation patterns of commercially available standards or using the LIPID MAPS Lipidomics Gateway (http://www.lipidmaps.org), the Human Metabolome Database (HMDB; http://www.hmdb.com), and/or our in-house lipid library (LipidBlast).[37]

Statistical Analysis. Principal component analysis (PCA) was performed, featuring mean centering and Pareto scaling, to explore the extent of differences among the three groups (ND, HFD, and HFD +CK). Hotelling's$T2$ test was used to exclude outliers from the 95% confidence region.[34] Partial least-squares discriminant analysis (PLS-DA) and orthogonal partial least-squares discriminant analysis (OPLS-DA, which affords clearer separations than does PCA, by considering the nature of each group) were performed using the same scaling mode that was used in PCA. The level of fitness and predictability were next examined by determining R^2Y and Q^2Y values, respectively. Generally, R^2Y varies between 0 and 1, where 1 indicates a model with a perfect fit, whereas a Q^2Y value >0.5 is considered to reflect good predictive capability.[38] The reliability of PLS-DA modeling was rigorously validated via permutation testing (n = 999). All of the variables in the model were selected by the value of variable importance in the projection (VIP) value (>0.7) and p value (<0.05) using SIMCA-P+ software and Stastistica 7 (StatSoft Inc., Tulsa, OK, USA). An S-plot showing the combined covariance $p(1)$ and correlation $p(\mathrm{corr})$ values from the OPLS-DA model was created to allow us to identify metabolites contributing to discrimination.[34] In addition, statistical comparisons of body weights, liver weights, epididymis fat weights, kidney fat weights, spleen weights, subcutaneous fat weights, triglyceride levels, and cholesterol levels were performed using Duncan's multiple-range test.

RESULTS AND DISCUSSION

Animal Characteristics. The characteristics of mice fed a normal diet, a high-fat diet, and a high-fat diet plus compound K-reinforced ginsenosides are shown in Figure 1. The body weight (47.3 ± 4.2 g), liver weight (1.84 ± 0.74 g), and subcutaneous fat weight (3.12 ± 0.08 g) of mice fed an HFD were significantly greater than those of mice fed ND, but the weight gains were ameliorated in mice fed an HFD+CK (Figure 1A–F). These results show that an HFD triggered obesity in

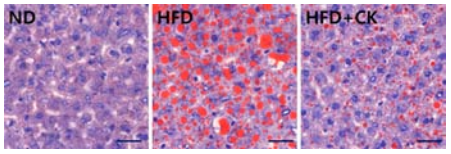

Figure 2. Histology of fatty liver sections. Liver tissues were stained with Oil-Red O [normal diet (ND), high-fat diet (HFD), and high-fat diet + compound K-reinforced ginsenosides (HFD+CK)]. The bar represents 30 μm.

DOI: 10.1021/jf506216p
J. Agric. Food Chem. 2015, 63, 2919−2929

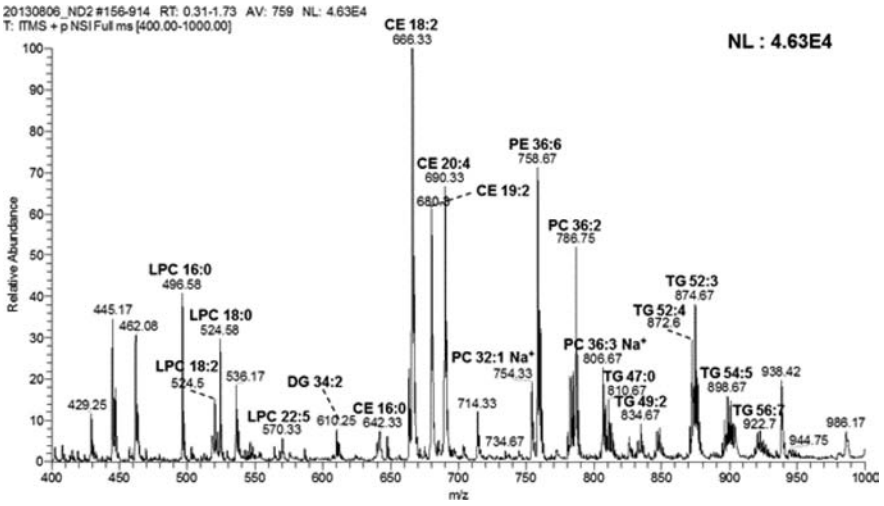

Figure 3. Analysis of phospholipids and triacylglycerols in mouse serum by direct infusion into a nanoelectrospray ionization−tandem mass spectrometry (ESI-MS/MS) operating in the positive mode. LPC, lysophosphatidylcholine; DG, diacylglycerol; CE, cholesteryl ester; PE, phosphatidylethanolamine; PC, phosphatidylcholine; TG, triacylglycerol; *m/z*, mass-to-charge ratio; NL, normalized intensity level.

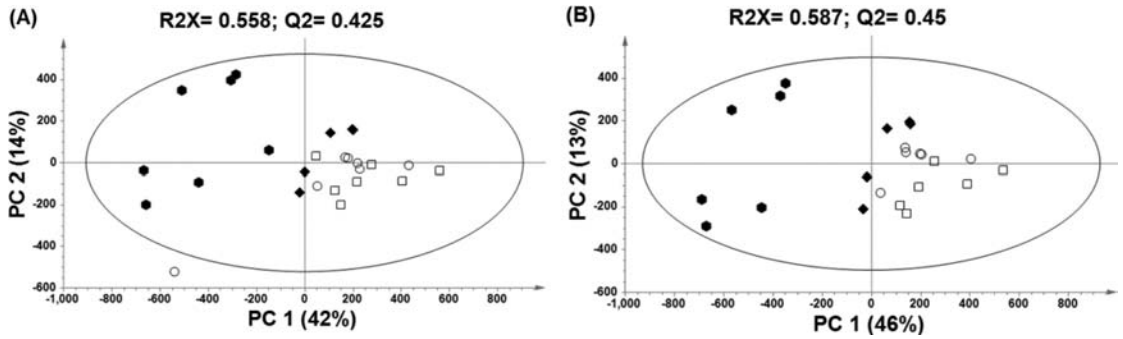

Figure 4. (A) Principal component analysis (PCA) score plots (PC1 vs PC2) based on direct infusion nanoelectrospray−mass spectrometry data of mice serum samples from three groups [normal diet (ND, ●), high-fat diet (HFD, □), high-fat diet + compound K-reinforced ginsenosides(HFD +CK, ○), and quality control (QC, ◆)]. On the score plot, each point represents an individual sample. The center and margin of the eclipse indicate the mean and standard deviation, respectively. (B) The PCA score plot (R^2X, 0.587; Q^2, 0.45) of serum samples obtained from the three groups without outliers.

Table 1. Validation Parameters of the Partial Least-Squares Discrimination Analysis (PLS-DA) Models That Were We Developed, Using "Variable Importance in the Projection" (VIP) Cutoff Values, Employing 999 Permutations

VIP cutoff value	total no. of compounds	R^2Y	Q^2Y	R^2Y intercept	Q^2Y intercept
none	250	0.94369	0.88459	0.425	−0.342
0.7	65	0.94125	0.88907	0.338	−0.348
0.8	54	0.93837	0.88345	0.327	−0.35
0.9	47	0.94008	0.88236	0.325	−0.361

mice and that CK exerted an antiobesity effect. In line with this observation, when CK was fed to obese mice that consumed an HFD, serum levels of triglycerides ($p < 0.01$), cholesterols ($p < 0.01$), and LDL-cholesterols ($p < 0.01$) returned to the levels seen in ND-fed mice (Figure 1G−I). The sterol regulatory element-binding proteins-1c gene (*SREBP-1c*) plays a major role in regulating cholesterol and fatty acid synthesis.[39] Kim et al. reported that compound K attenuated expression of *SREBP-1c* as well as genes encoding fatty acid synthase and stearoyl-CoA desaturase (SCD1), well-known targets of SREBP-1c.[16] RT-PCR (data not shown here) also revealed that *SREBP-1c* expression was significantly suppressed in mice given HFD +CK. Thus, compound K-reinforced ginsenosides restored normal clinical biochemistry in our obesity model. Fatty livers were histologically apparent in mice fed a HFD, whereas in the CK group, fat droplet numbers were significantly reduced in liver tissues, as revealed by Oil Red O staining (Figure 2). In line with these observations, the liver triglyceride contents (ND, HFD, and HFD+CK) were 28.3 ± 5.0, 75.6 ± 12.8, and 34.3 ± 4.6 mg/g, respectively. These results suggest that compound K-reinforced ginsenosides could decrease the extent of fatty liver.

Lipid Identification. Representative pooled samples of mouse sera were used to identify lipids therein. In the positive ion mode, 132 lipids [11 cholesteryl esters (CE), 6 diacylglycerols (DG), 24 LPC, 19 PC, 6 PE, and 66 TG] were detected (Figure 3). LPC, LPE, PC, and PE were present as $[M + H]^+$ or $[M + Na]^+$ adducts, whereas DG and TG were detected as $[M + NH_4]^+$. Serum lipids were identified on the basis of pseudomolecular ion masses ($[M + H]^+$, $[M + Na]^+$, or $[M + NH_4]^+$); MS/MS product ion analysis; and/or comparison with authentic standards or information in databases including the LIPID MAPS Lipidomics Gateway (http://www.lipidmaps.org), the Human Metabolome Database (HMDB; http://www.hmdb.com), and our in-house lipid library (LipidBlast).[37] Specific diagnostic ions were also used to

DOI: 10.1021/jf506216p
J. Agric. Food Chem. 2015, 63, 2919−2929

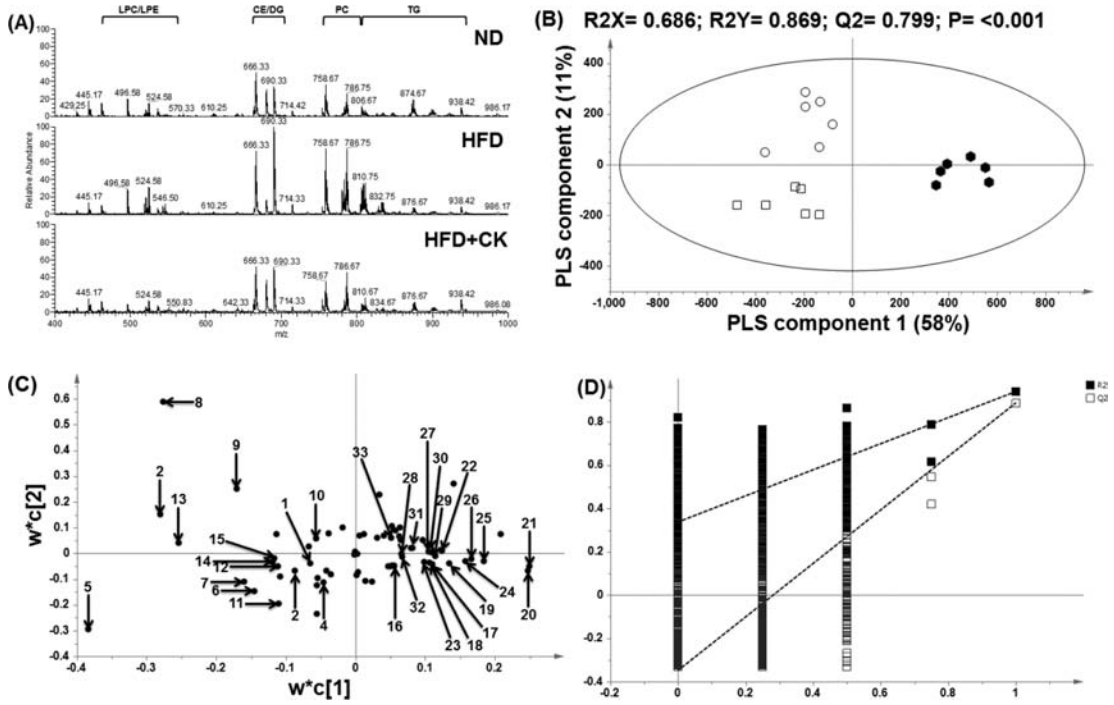

Figure 5. (A) Direct infusion nanoelectrospray−mass spectrometry profiles of serum lipids of mice fed a normal diet (ND, ⬢), a high-fat diet (HFD, □), and a high-fat diet + compound K-reinforced ginsenosides (HFD+CK, ○). (B) Partial least-squares discriminant analysis score plots (R^2X, 0.686, Q^2, 0.799). (C) Loading plots. (D) Permutation test. Identified metabolites were marked with numbers on the loading plot, and in the metabolites list, the predictive vectors are as given in Tables 1 and 2.

Table 2. Identification of Mouse Serum Metabolites Analyzed via Direct Infusion Nanoelectrospray−Mass Spectrometry[a]

no.	identified ion (m/z)	metabolite[b]	adduct	p value[c]	VIP value	no.	identified ion (m/z)	metabolite[b]	adduct	p value[c]	VIP value
1	522.5	LPC 18:1	M + H	0.0196	0.840	18	848.7	TG 50:2	M + NH_4	<0.001	1.195
2	524.5	LPC 18:0	M + Na	<0.001	3.332	19	870.6	TG 52:5	M + NH_4	<0.001	1.489
3	544.5	LPC 20:4	M + H	<0.001	1.172	20	872.6	TG 52:4	M + NH_4	<0.001	2.736
4	568.5	LPC 22:6	M + H	<0.001	1.272	21	874.7	TG 52:3	M + NH_4	<0.001	2.712
5	690.2	CE 20:4	M + NH_4	<0.001	5.146	22	876.7	TG 52:2	M + NH_4	0.0052	1.323
6	692.4	CE 20:3	M + NH_4	<0.001	2.195	23	894.6	TG 54:7	M + NH_4	<0.001	1.105
7	782.7	PC 34:1	M + Na	<0.001	2.081	24	896.6	TG 54:6	M + NH_4	<0.001	1.726
8	786.7	PC 36:2	M + H	<0.001	6.662	25	898.7	TG 54:5	M + NH_4	<0.001	2.002
9	788.7	PC 36:1	M + H	<0.001	3.111	26	900.7	TG 54:4	M + NH_4	<0.001	1.792
10	790.7	TG 46:3	M + NH_4	<0.001	0.832	27	902.7	TG 54:3	M + NH_4	<0.001	1.117
11	806.6	PC 36:3	M + Na	0.0018	2.367	28	918.6	TG 56:9	M + NH_4	<0.001	0.702
12	808.7	TG 47:1	M + NH_4	0.0464	1.309	29	920.6	TG 56:8	M + NH_4	<0.001	1.220
13	810.7	TG 47:0	M + NH_4	<0.001	2.726	30	922.7	TG 56:7	M + NH_4	<0.001	1.168
14	812.7	TG 48:6	M + NH_4	0.0014	1.358	31	924.7	TG 56:6	M + NH_4	<0.001	0.886
15	834.7	TG 49:2	M + NH_4	<0.001	1.266	32	926.7	TG 56:5	M + NH_4	<0.001	0.720
16	844.5	TG 50:4	M + NH_4	<0.001	0.764	33	946.7	TG 58:9	M + NH_4	<0.001	0.835
17	846.7	TG 50:3	M + NH_4	<0.001	1.245						

[a]Variables were selected on the basis of VIP (variable importance in the projection) value (>0.7) and p value (<0.05) upon PLS-DA modeling. [b]LPC, lysophosphatidylcholine; PC, phosphatidylcholine; CE, cholesteryl ester; TG, triacylglycerol. [c]p values were analyzed by ANOVA.

identify each lipid class. For example, LPC and CE species were identified by ion fragments at m/z 184 and 369, corresponding to phosphocholine (Figure S1) and [cholesterol − H_2O] (Figure S2), respectively. In addition, PC species were identified via the loss of choline (−59) and phosphocholine (−184) from protonated pseudomolecular ions of their MS/MS spectra (Figure S3), whereas CE species were identified by the loss of a C_4H_8 (56 amu) and a C_8H_{16} (112 amu) moiety from the side chain of cholesterol (Figure S2); this is a characteristic CE fragment pattern.[40] In addition, acyl chain information on LPC, PC, and TG species was obtained via the loss of fatty acyl chains from pseudomolecular ions. Ions of m/z 524.6, 786.6, and 900.8 in the positive ion mode serve as examples illustrating the identification process for LPC, PC, and TG species, respectively. The product ion mass spectrum of m/z 524.6 (Figure S1) revealed a major fragment ion at m/z 506 attributable to loss of a water molecule from the protonated molecular ion and two minor peaks at m/z 258 and 240 attributable to loss of the stearoyl group (C18:0) and the stearoyl group and a water molecule, respectively. The peak at m/z524.6 was identified as LPC 18:0. The MS/MS spectrum of m/z 786.6 (Figure S3) yielded characteristic fragment ions at

DOI: 10.1021/jf506216p
J. Agric. Food Chem. 2015, 63, 2919−2929

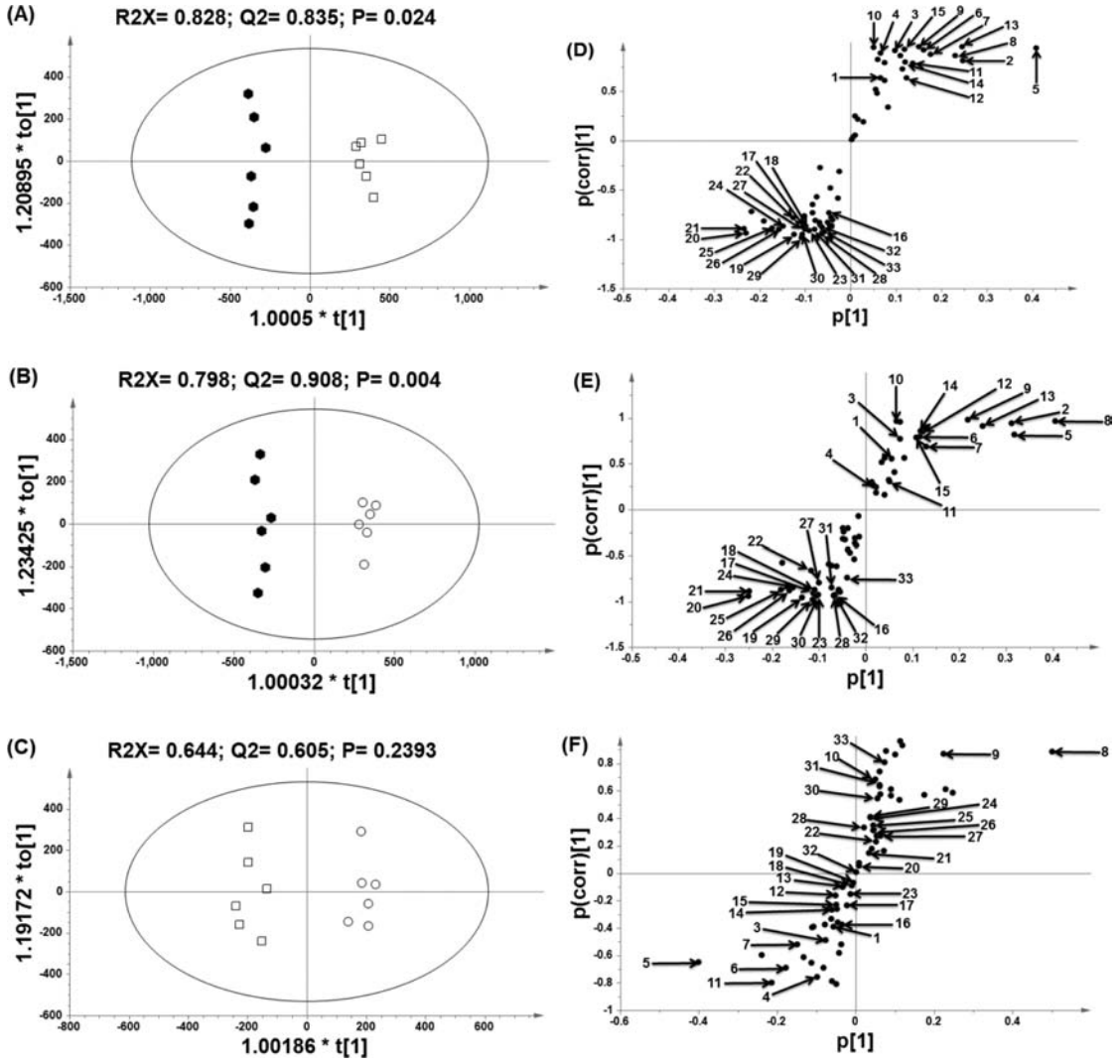

Figure 6. OPLS-DA scores plots of serum lipids of mice fed (A) a normal diet (●) and a high-fat diet (□), (B) a normal diet and a high-fat diet + compound K-reinforced ginsenosides (○), or (C) a high-fat diet and a high-fat diet + compound K-reinforced ginsenosides, and the S-plots associated with the OPLS-DA score plots (D−F) of serum metabolite profiles derived via direct infusion nanoelectrospray−mass spectrometry. The numbers for the metabolites are as given in Table 2.

m/*z* 524 and 520 caused by loss of a linoleoyl group (C18:2) and a stearoyl group (C18:0), respectively. The spectrum also yielded fragment ions at *m*/*z* 506 and 502 caused by loss of water molecules from ions of *m*/*z* 514 and 520, respectively. On the basis of these findings, the peak at 786.6 was identified as PC 36:2 (18:0/18:2). The MS/MS spectrum of *m*/*z* 900.8 (Figure S4) contained a major fragment ion at *m*/*z* 883.7 caused by loss of an ammonia molecule from the ammonium adduct ion and three peaks at *m*/*z* 627.5, 601.5, and 577.5 caused by loss of the pamitoyl (C16:0), oleoyl (C18:1), and meadoyl (C20:3) moieties, respectively. The peak at *m*/*z* 900.8 was identified as TG 54:4 (16:0/18:1/20:3).

Multivariate Statistical Analysis of Serum Metabolite Levels. To validate our model, a QC sample was prepared by mixing equal volumes of serum from all samples studied. System stability was evaluated by analyzing fresh QC samples after groups of eight serum samples were run. Of the 250 ions detected, the number of ions with CV values <30% was >95%, suggesting that the analytical system was stable.[41] These results indicate the excellent stability and reproducibility of the mass spectrometric analysis. To normalize the spectra, the average of the sum of QC sample intensities was divided by the sum of sample spectrum intensities, and, next, each value (fold) was multiplied by the intensity of each lipid species in that sample. After normalization, outliers were selected with the aid of Hotelling's *T*2 test (Figure 4A).[34] If outliers were present outside the ellipse, representing the 95% confidence region of the PCA score plot (these were thus strong outliers), the analysis was repeated after deleting such outliers (Figure 4B) to remove factors irrelevant in the identification of metabolites.[42] PLS-DA is a form of PLS regression employing categorical response variables and is a powerful tool enabling predictions to be made with a minimum probability of error when many variables are in play.[43] In a PLS-DA model, VIP reflects the influence of every *X* variable on *Y*, and, generally, a cutoff VIP value of about 0.7−0.8 is considered significant when *Y* is to be explained.[44] To select metabolites playing key roles in the differentiation of each group, we ran PLS-DA models built using variables chosen by reference to various VIP cutoff values with the aid of permutation test parameters. Such parameters, in the context of the various VIP cutoff values, are listed in Table 1. The highest R^2Y and Q^2Y values were observed when

DOI: 10.1021/jf506216p
J. Agric. Food Chem. 2015, 63, 2919−2929

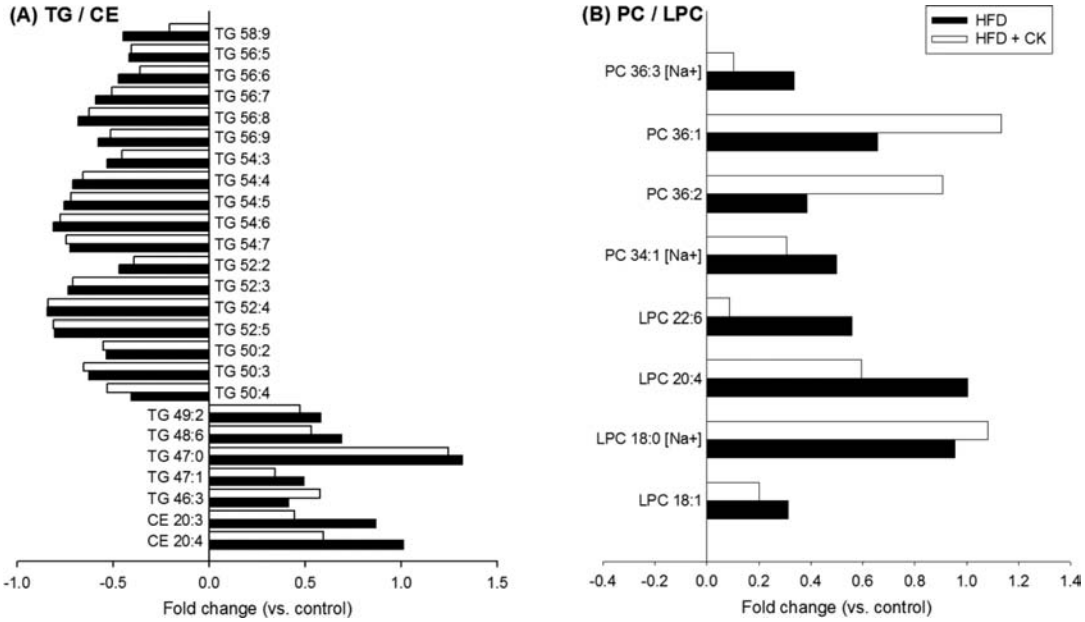

Figure 7. Quantitative fold changes in serum lipid metabolite levels in the high-fat diet (HFD, $n = 7$) and the high-fat diet + compound K-reinforced ginsenosides (HFD+CK, $n = 7$) groups, by reference to those in the normal diet [CE (cholesteryl ester), LPC (lysophosphatidylcholine), PC (phosphatidylcholine), and TG (triacylglycerol)].

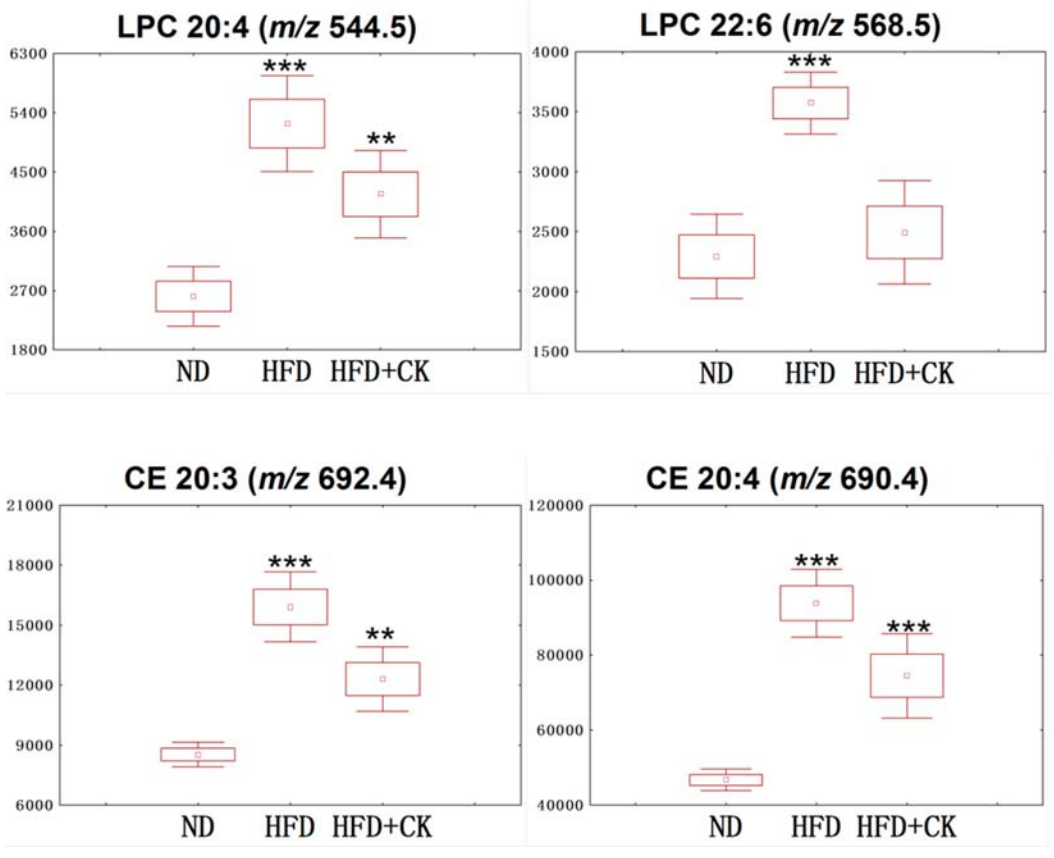

Figure 8. Box-and-whisker plots showing compounds, the levels of which differed significantly among the normal diet (ND, $n = 7$), high-fat diet (HFD, $n = 7$), and high-fat diet + compound K-reinforced ginsenosides (HFD+CK, $n = 7$) groups. The *Y*-axis indicates the mass peak intensity. Statistical analyses of each biomarker candidates in HFD and HFD+CK groups, compared to the ND group, were conducted via analysis of variance [(**) $p < 0.01$, (***) $p < 0.001$].

the PLS-DA model was constructed using metabolites (65 lipid species) with VIP values >0.7 (Table 1). Therefore, the PLS-DA model may be optimized to allow differentiation among the three groups.

DOI: 10.1021/jf506216p
J. Agric. Food Chem. 2015, 63, 2919−2929

Table 3. Correlation between Serum Lipid Biomarker Candidates and Animal Characteristic Data[a]

parameter	CE 20:3	CE 20:4	LPC 20:4	LPC 22:6
liver wt (g)	0.75***	0.80***	0.60**	0.61**
kidney fat wt (g)	0.89***	0.92***	0.79***	0.62**
epididymis fat wt (g)	0.78***	0.72***	0.76***	0.63**
cholesterol in serum (mg/dL)	0.94***	0.94***	0.93***	0.85***
triglyceride in serum (mg/dL)	0.54*	0.61**	0.61**	0.70**
LDL-cholesterol (mg/dL)	0.77***	0.74***	0.57*	0.62**

[a]Different letters indicate significant differences by analysis of variance [ANOVA; (*) $p < 0.05$, (**)$p < 0.01$, and (***) $p < 0.001$].

The metabolite profiles of the sera of mice fed ND, HFD, and HFD+CK, as determined via direct infusion nano-electrospray−ion trap mass spectrometry, were statistically evaluated using a PLS-DA. Figure 5A shows typical direct infusion mass spectra of sera from the ND, HFD, and HFD +CK groups. The HFD-fed groups (HFD and HFD+CK) could be clearly distinguished from the ND group on the first two-component PLS-DA scores plot generated using Pareto scaling (Figure 5B). The metabolite profile of the HFD+CK-fed group differed from that of the HFD group, indicating that CK rectified disturbances in metabolism induced by HFD. The significant differences evident between the two groups ($p < 0.001$) indicated that the metabolic patterns were distinct. We obtained good-quality parameters using the PLS-DA model, which were validated by 7-fold cross-validation ($p < 0.001$) [fitness (R^2X) = 0.686 and R^2Y = 0.869]; predictability (Q^2 = 0.799); and permutation values (the R^2 and Q^2 intercepts = 0.338 and −0.348, respectively), indicating that the PLS-DA model was not overfitted and could be regarded as a predictable model (Figure 5B,D). A PLS-DA loadings plot for all groups was generated using Pareto scaling to identify metabolites contributing to the observed discrimination (Figure 5C). This plot revealed that metabolites located distant from the intersection of $w*c[1]$ and $w*c[2]$ principally explained the observed discrimination. Metabolites in the positive $w*c[1]$ increased in level in mice on the HFD, whereas the opposite was true for those in the negative $w*c[1]$. Major metabolites were identified on the basis of p values and VIP values (Table 2) and numbered on the loadings plot (Figure 5C).

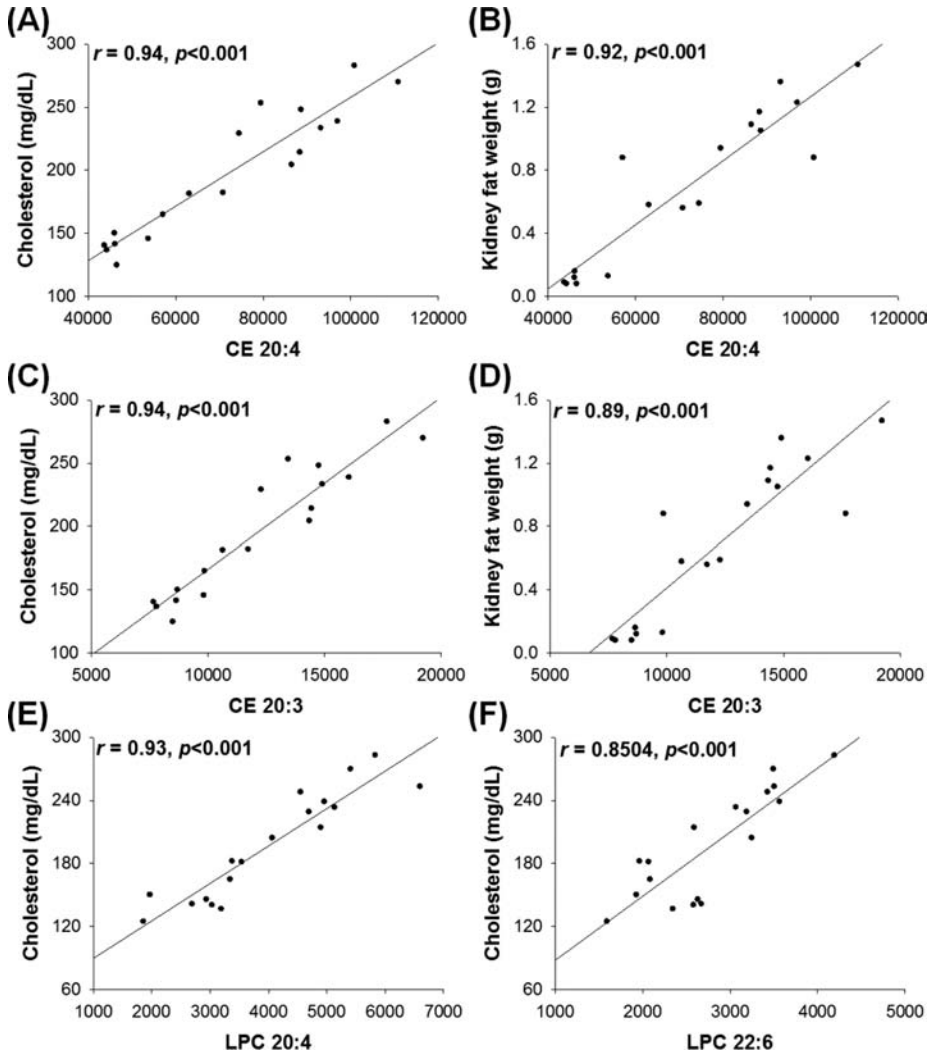

Figure 9. Correlation analysis between serum lipid biomarker candidates and animal characteristic data (kidney fat weight or serum cholesterol level): (A) CE 20:4 versus serum cholesterol; (B) CE 20:4 versus kidney fat weight; (C) CE 20:3 versus serum cholesterol; (D) CE 20:3 versus kidney fat weight; (E) LPC 20:4 versus serum cholesterol; (F) LPC 22:6 versus serum cholesterol.

DOI: 10.1021/jf506216p
J. Agric. Food Chem. 2015, 63, 2919−2929

To explore the differences between pairs of groups by treatment, discriminations afforded by the models between the ND and HFD groups, the ND and HFD+CK groups, and the HFD and HFD+CK groups were visualized on OPLS-DA scores plots (Figure 6A−C). All groups of samples were significantly separated from each other. To identify metabolites contributing to such discrimination, S-plots of all models were generated using Pareto scaling (Figure 6D−F); this revealed the metabolites responsible for separations between groups. Numbered metabolites in the plots were identified (Table 2). The farther the distance of a metabolite from the origin, the greater the potential thereof as a biomarker candidate;[41] these metabolites were responsible for the observed differences in ND versus HFD, ND versus HFD+CK, and HFD versus HFD +CK.

Effect of a High-Fat Diet on Mice. Of the 250 metabolites detected by direct infusion mass spectrometry, the levels of 65 exhibiting "variable importance in the projection" (VIP) values of >0.7 and that were very relevant in explaining the differences between the three groups were statistically analyzed using a nonparametric *t* test. Of the 65 metabolites, 33 (all LPC, CE, PC, and TG) exhibited statistically significant differences ($p < 0.05$) between the HFD and HFD+CK groups (Table 2). Of these, LPC 18:0, CE 20:3, CE 20:4, PC 34:1, PC 36:1, PC 36:2, PC 36:3, TG 47:0, TG 52:3, TG 52:4, and TG 54:5 had VIP values >2.0 and were the principal metabolites contributing to discrimination among the three groups (Table 2). The levels of TGs of higher carbon number (>50) were significantly decreased by the HFD group, whereas the levels of TGs of lower carbon number (<50) and CEs (CE 20:3 and CE20:4) were increased (Figure 7A). Similar observations were reported by Rhee et al.[45] The cited authors also found that triacylglycerols of lower carbon number and reduced double bond content (TG 44:1, TG 46:1, TG 48:0, and TG 50:0) were associated with an increased risk of diabetes, whereas TGs of higher carbon number and greater double-bond content (TG 56:9, TG 58:10, and TG 60:12) were associated with a decreased risk of the disease.[45] DeMarco et al. also reported recently that triacylglycerol composition changed to feature more saturated fatty acyl chains of lower carbon number in obese male *db*/*db* mice 15 weeks of age.[46]

In our present study, the TG 47:0 content increased with a VIP value of 2.726, whereas those of TG52:3, 52:4, 52:5, 54:4, 54:5, and 54:6 decreased with VIP values of 2.712, 2.736, 1.489, 1.792, 2.002, and 1.726, respectively (Table 2). It has been reported that diabetes- and obesity-induced changes in hepatic lipid compositions correlated with changes in the levels of fatty acid elongase and desaturase.[47−49] For example, insulin is known to increase the expression levels of various fatty acid desaturases in animals.[47] In addition, HFD significantly suppressed expression of fatty acid elongase-5 (Elovl-5) (a key enzyme of polyunsaturated fatty acid synthesis) by inhibiting the expression of nuclear sterol-regulatory element binding protein-1 (SREBP-1).[48] In addition, deletion of Elovl-5 triggered fatty liver development in mice by activating SREBP-1c.[50] On the basis of these findings, we suggest that the carbon number and double-bond values of TGs may serve as very useful markers of metabolic diseases including obesity and diabetes mellitus. However, further study is needed.

Of the PCs and LPCs, four PCs (PC 34:1, PC 36:1, PC 36:2, and PC 36:3) and four LPCs (LPC 18:0, LPC 18:1, LPC 20:4, and LPC 22:6) were significantly increased in level in the HFD group (Figure 7B). Changes in LPC levels caused by HFD have been reported. For example, the levels of LPC 18:0,[18,51] 20:4,[51,52] and 22:6[51] in serum and LPC 20:4[18] in the liver were significantly higher in mice fed HFD, similar to our findings. In addition, overweight/obese males also had higher levels of LPC 14:0 and LPC 18:0 than did lean subjects.[38] Obese cotwins had higher concentrations of LPC 18:0, LPC 18:1, and LPC 20:4 than did nonobese cotwins.[53]

Effect of Compound K-Reinforced Ginsenosides in Mice. In the present study, we identified four biomarker candidates that might explain the effects of compound K-reinforced ginsenosides on mice fed an HFD. The compounds are shown in Figure 8 (box-and-whisker plots). As shown in Figure 8, the levels of four compounds (LPC 20:4, LPC 22:6, CE 20:3, and CE 20:4) were significantly increased in mice fed an HFD. Of these compounds, the levels of the cholesterol esters (CE 20:3 and CE 20:4) were lower in the HFD+CK group than in the HFD group (Figure 8). The biosynthesis of cholesteryl esters is regulated by stearoyl-CoA desaturase (SCD1), which increases lipogenesis and the synthesis of such esters.[54,55] SCD-1-deficient mice had reduced levels of cholesteryl esters despite high activity of acyl-CoA:cholesterol acyltransferase (ACAT), which catalyzes the synthesis of such esters.[54] Compound K attenuated expression of the gene encoding the sterol regulatory element-binding protein 1c (SREBP-1c), thus indirectly suppressing the SCD1 gene, the well-known target of SREBP-1c in insulin-resistant HepG2 human hepatoma cells.[16] Therefore, the fall in cholesteryl ester levels in the HFD+CK group (compared to the HFD group) may be attributable to down-regulation of *SREBP-1c* by compound K.

LPCs are major components of "atherogenic factor" and important biomarkers of the effects of HFD.[51] LPCs, major lipid constituents of oxidized LDL, are generated via hydrolysis of the lipid components of oxidized LDL by lipoprotein-associated phospholipase A2.[51,56] The levels of LPCs, including LPC 20:4 and LPC 22:6, increased on ingestion of an HFD but were significantly reduced in mouse serum if the diet contained compound K. Especially, the LPC 22:6 level did not differ significantly from normal controls under such circumstances (Figure 8). Earlier studies found that LDL oxidation was inhibited by ginsenosides Rb1 and Rg1.[57] Therefore, our work highlights the fact that the reduced LPC 20:4 and LPC 22:6 levels in the HFD+CK group may be attributable to an effect of compound K, a metabolite of ginsenoside Rb1.

These biomarker candidates were significantly correlated with the animal characteristic data ($p < 0.05$, Table 3). Especially, the levels of CE 20:3 and CE 20:4 were highly correlated with kidney fat weight ($r > 0.89$, $p < 0.001$), and those of CE 20:3, CE 20:4, LPC 20:4, and LPC 22:6 were significantly correlated with serum cholesterol levels ($r > 0.85$, $p < 0.001$) (Figure 9). Therefore, these metabolites may serve as valuable "biomarker candidates" indicating consumption of an HFD and can be used to measure the efficacy of a compound K-containing diet or medication used to treat obesity. Together, our findings suggest that diets containing compound K might help to control lipid metabolism when such diets are basically HFD.

■ ASSOCIATED CONTENT

Ⓢ Supporting Information

Figures S1−S4. This material is available free of charge via the Internet at http://pubs.acs.org.

DOI: 10.1021/jf506216p
J. Agric. Food Chem. 2015, 63, 2919−2929

AUTHOR INFORMATION

Corresponding Authors

*(K.-H.L.) Phone: +82-53-950-8567. Fax: +82-53-950-8557. E-mail: dstlkh@knu.ac.kr

*(H.S.) Phone: +82-31-8041-0619. Fax: +82-31-8041-0629. E-mail: hshin@kpu.ac.kr.

Funding

This study was supported by a grant from the Bio & Medical Technology Development Program of the National Research Foundation (NRF) funded by the Ministry of Science, ICT & Future Planning (Grants NRF-2013M3A9B6046416 and NRF-2014M3A9C4066459) and also by a grant from the High Value-added Food Technology Development Program of the Korea Institute of Planning & Evaluation for Technology (IPET) funded by the Ministry of Agriculture, Food and Rural Affairs (Grant 311043-03-3-HD110).

Notes

The authors declare no competing financial interest.

ABBREVIATIONS USED

AMPK, AMP-activated protein kinase; B&W plot, box-and-whisker plots; CE, cholesteryl ester; CV, coefficient of variation; DG, diacylglycerol; HFD, high-fat diet; HFD+CK, high-fat diet + compound K-reinforced ginsenosides; LPC, lysophosphatidylcholine; *m/z*, mass-to-charge ratio; ND, normal diet; NL, normalized intensity level; OPLS-DA, orthogonal partial least-squares discriminant analysis; PC, phosphatidylcholine; PCA, principal component analysis; PE, phosphatidylethanolamine; PL, phospholipid; PLS-DA, partial least-squares discriminant analysis; SCD1, stearoyl-CoA desaturase; SREBP-1c, sterol regulatory element-binding proteins-1c; TG, triacylglycerol

REFERENCES

(1) Vogler, B. K.; Pittler, M. H.; Ernst, E. The efficacy of ginseng. A systematic review of randomised clinical trials. *Eur. J. Clin. Pharmacol.* **1999**, *55*, 567−575.

(2) Helms, S. Cancer prevention and therapeutics: *Panax ginseng*. *Altern. Med. Rev. J. Clini. Ther.* **2004**, *9*, 259−274.

(3) Park, J. D.; Rhee, D. K.; Lee, Y. H. Biological activities and chemistry of saponins from *Panax ginseng* C. A. Meyer. *Phytochem. Rev.* **2005**, *4*, 159−175.

(4) Kim, Y. O.; Lee, H. Y.; Won, H.; Nah, S. S.; Lee, H. Y.; Kim, H. K.; Kwon, J. T.; Kim, H. J. Influence of Panax ginseng on the offspring of adult rats exposed to prenatal stress. *Int. J. Mol. Med.* **2015**, *35*, 103−109.

(5) Woods, S. C.; Seeley, R. J.; Rushing, P. A.; D'Alessio, D.; Tso, P. A controlled high-fat diet induces an obese syndrome in rats. *J. Nutr.* **2003**, *133*, 1081−1087.

(6) Vinaixa, M.; Rodriguez, M. A.; Rull, A.; Beltran, R.; Blade, C.; Brezmes, J.; Canellas, N.; Joven, J.; Correig, X. Metabolomic assessment of the effect of dietary cholesterol in the progressive development of fatty liver disease. *J. Proteome Res.* **2010**, *9*, 2527−2538.

(7) Miao, H.; Chen, H.; Zhang, X.; Yin, L.; Chen, D. Q.; Cheng, X. L.; Bai, X.; Wei, F. Urinary metabolomics on the biochemical profiles in diet-induced hyperlipidemia rat using ultraperformance liquid chromatography coupled with quadrupole time-of-flight SYNAPT high-definition mass spectrometry. *J. Anal. Methods Chem.* **2014**, *2014*, 184162.

(8) Oh, J.; Lee, S. R.; Hwang, K. T.; Ji, G. E. The anti-obesity effects of the dietary combination of fermented red ginseng with levan in high fat diet mouse model. *Phytother. Res.* **2014**, *28*, 617−622.

(9) Shitara, Y.; Sugiyama, Y. Pharmacokinetic and pharmacodynamic alterations of 3-hydroxy-3-methylglutaryl coenzyme A (HMG-CoA) reductase inhibitors: drug-drug interactions and interindividual differences in transporter and metabolic enzyme functions. *Pharmacol. Ther.* **2006**, *112*, 71−105.

(10) Yen, M.; Ewald, M. B. Toxicity of weight loss agents. *J. Med. Toxicol.: Off. J. Am. Coll. Med. Toxicol.* **2012**, *8*, 145−152.

(11) Lee, M. R.; Kim, B. C.; Kim, R.; Oh, H. I.; Kim, H. K.; Choi, K. J.; Sung, C. K. Anti-obesity effects of black ginseng extract in high fat diet-fed mice. *J. Ginseng Res.* **2013**, *37*, 308−349.

(12) Kim, J. H.; Hahm, D. H.; Yang, D. C.; Kim, J. H.; Lee, H. J.; Shim, I. Effect of crude saponin of Korean red ginseng on high-fat diet-induced obesity in the rat. *J. Pharmacol. Sci.* **2005**, *97*, 124−131.

(13) Hwang, J. T.; Lee, M. S.; Kim, H. J.; Sung, M. J.; Kim, H. Y.; Kim, M. S.; Kwon, D. Y. Antiobesity effect of ginsenoside Rg3 involves the AMPK and PPAR-gamma signal pathways. *Phytother. Res.* **2009**, *23*, 262−266.

(14) Kwak, Y. S.; Kyung, J. S.; Kim, J. S.; Cho, J. Y.; Rhee, M. H. Anti-hyperlipidemic effects of red ginseng acidic polysaccharide from Korean red ginseng. *Biol. Pharm. Bull.* **2010**, *33*, 468−472.

(15) Han, G. C.; Ko, S. K.; Sung, J. H.; Chung, S. H. Compound K enhances insulin secretion with beneficial metabolic effects in db/db mice. *J. Agric. Food Chem.* **2007**, *55*, 10641−10648.

(16) Kim, D. Y.; Yuan, H. D.; Chung, I. K.; Chung, S. H. Compound K, intestinal metabolite of ginsenoside, attenuates hepatic lipid accumulation via AMPK activation in human hepatoma cells. *J. Agric. Food Chem.* **2009**, *57*, 1532−1537.

(17) Park, D.; Yoon, M. Compound K, a novel ginsenoside metabolite, inhibits adipocyte differentiation in 3T3-L1 cells: involvement of angiogenesis and MMPs. *Biochem. Biophys. Res. Commun.* **2012**, *422*, 263−267.

(18) Kim, H. J.; Kim, J. H.; Noh, S.; Hur, H. J.; Sung, M. J.; Hwang, J. T.; Park, J. H.; Yang, H. J.; Kim, M. S.; Kwon, D. Y.; Yoon, S. H. Metabolomic analysis of livers and serum from high-fat diet induced obese mice. *J. Proteome Res.* **2011**, *10*, 722−731.

(19) Song, I. S.; Lee, D. Y.; Shin, M. H.; Kim, H.; Ahn, Y. G.; Park, I.; Kim, K. H.; Kind, T.; Shin, J. G.; Fiehn, O.; Liu, K. H. Pharmacogenetics meets metabolomics: discovery of tryptophan as a new endogenous OCT2 substrate related to metformin disposition. *PLoS One* **2012**, *7*, No. e36637.

(20) Sreekumar, A.; Poisson, L. M.; Rajendiran, T. M.; Khan, A. P.; Cao, Q.; Yu, J.; Laxman, B.; Mehra, R.; Lonigro, R. J.; Li, Y.; Nyati, M. K.; Ahsan, A.; Kalyana-Sundaram, S.; Han, B.; Cao, X.; Byun, J.; Omenn, G. S.; Ghosh, D.; Pennathur, S.; Alexander, D. C.; Berger, A.; Shuster, J. R.; Wei, J. T.; Varambally, S.; Beecher, C.; Chinnaiyan, A. M. Metabolomic profiles delineate potential role for sarcosine in prostate cancer progression. *Nature* **2009**, *457*, 910−914.

(21) Yore, M. M.; Syed, I.; Moraes-Vieira, P. M.; Zhang, T.; Herman, M. A.; Homan, E. A.; Patel, R. T.; Lee, J.; Chen, S.; Peroni, O. D.; Dhaneshwar, A. S.; Hammarstedt, A.; Smith, U.; McGraw, T. E.; Saghatelian, A.; Kahn, B. B. Discovery of a class of endogenous mammalian lipids with anti-diabetic and anti-inflammatory effects. *Cell* **2014**, *159*, 318−332.

(22) Clayton, T. A.; Lindon, J. C.; Cloarec, O.; Antti, H.; Charuel, C.; Hanton, G.; Provost, J. P.; Le Net, J. L.; Baker, D.; Walley, R. J.; Everett, J. R.; Nicholson, J. K. Pharmaco-metabonomic phenotyping and personalized drug treatment. *Nature* **2006**, *440*, 1073−1077.

(23) Suzuki, M.; Nishiumi, S.; Matsubara, A.; Azuma, T.; Yoshida, M. Metabolome analysis for discovering biomarkers of gastroenterological cancer. *J. Chromatogr., B: Anal. Technol. Biomed. Life Sci.* **2014**, *966*, 59−69.

(24) Yuliana, N. D.; Khatib, A.; Choi, Y. H.; Verpoorte, R. Metabolomics for bioactivity assessment of natural products. *Phytother. Res.* **2011**, *25*, 157−169.

(25) Zhang, A.; Sun, H.; Wang, Z.; Sun, W.; Wang, P.; Wang, X. Metabolomics: towards understanding traditional Chinese medicine. *Planta Med.* **2010**, *76*, 2026−2035.

(26) Kim, N.; Kim, K.; Lee, D.; Shin, Y. S.; Bang, K. H.; Cha, S. W.; Lee, J. W.; Choi, H. K.; Hwang, B. Y.; Lee, D. Nontargeted metabolomics approach for age differentiation and structure

DOI: 10.1021/jf506216p
J. Agric. Food Chem. 2015, 63, 2919−2929

interpretation of age-dependent key constituents in hairy roots of *Panax ginseng*. *J. Nat. Prod.* **2012**, *75*, 1777−1784.
(27) Park, H. E.; Lee, S. Y.; Hyun, S. H.; Kim da, Y.; Marriott, P. J.; Choi, H. K. Gas chromatography/mass spectrometry-based metabolic profiling and differentiation of ginseng roots according to cultivation age using variable selection. *J. AOAC Int.* **2013**, *96*, 1266−1272.
(28) Park, H. W.; In, G.; Kim, J. H.; Cho, B. G.; Han, G. H.; Chang, I. M. Metabolomic approach for discrimination of processed ginseng genus (*Panax ginseng* and *Panax quinquefolius*) using UPLC-QTOF MS. *J. Ginseng Res.* **2014**, *38*, 59−65.
(29) Song, H. H.; Moon, J. Y.; Ryu, H. W.; Noh, B. S.; Kim, J. H.; Lee, H. K.; Oh, S. R. Discrimination of white ginseng origins using multivariate statistical analysis of data sets. *J. Ginseng Res.* **2014**, *38*, 187−193.
(30) Lee, D. Y.; Kim, J. K.; Shrestha, S.; Seo, K. H.; Lee, Y. H.; Noh, H. J.; Kim, G. S.; Kim, Y. B.; Kim, S. Y.; Baek, N. I. Quality evaluation of *Panax ginseng* roots using a rapid resolution LC-QTOF/MS-based metabolomics approach. *Molecules* **2013**, *18*, 14849−14861.
(31) Niu, J.; Pi, Z. F.; Yue, H.; Yang, H.; Wang, Y.; Yu, Q.; Liu, S. Y. Effect of 20(*S*)-ginsenoside Rg3 on streptozotocin-induced experimental type 2 diabetic rats: a urinary metabonomics study by rapid-resolution liquid chromatography/mass spectrometry. *Rapid Commun. Mass Spectrom.* **2012**, *26*, 2683−2689.
(32) Dai, W.; Zhang, F.; Jia, Z.; Wei, C.; Gao, P.; Lu, X.; Wu, Y.; Xu, G. [Evaluation of the effect of the traditional Chinese medicine tongxinluo or ginseng on excess fatigue rats studied by metabonomics approach based on liquid chromatography-mass spectrometry]. *Zhongguo Hua Xue Hui* **2011**, *29*, 1049−1054.
(33) Liang, X.; Chen, X.; Liang, Q.; Zhang, H.; Hu, P.; Wang, Y.; Luo, G. Metabonomic study of Chinese medicine Shuanglong formula as an effective treatment for myocardial infarction in rats. *J. Proteome Res.* **2011**, *10*, 790−799.
(34) Kim, H. J.; Cho, C. W.; Hwang, J. T.; Son, N.; Choi, J. H.; Shim, G. S.; Han, C. K. LC-MS-based metabolomic analysis of serum and livers from red ginseng-fed rats. *J. Ginseng Res.* **2013**, *37*, 371−378.
(35) Folch, J.; Lees, M.; Sloane Stanley, G. H. A simple method for the isolation and purification of total lipides from animal tissues. *J. Biol. Chem.* **1957**, *226*, 497−509.
(36) Matyash, V.; Liebisch, G.; Kurzchalia, T. V.; Shevchenko, A.; Schwudke, D. Lipid extraction by methyl-*tert*-butyl ether for high-throughput lipidomics. *J. Lipid Res.* **2008**, *49*, 1137−1146.
(37) Kind, T.; Liu, K. H.; Lee, D. Y.; DeFelice, B.; Meissen, J. K.; Fiehn, O. LipidBlast in silico tandem mass spectrometry database for lipid identification. *Nat. Methods* **2013**, *10*, 755−758.
(38) Kim, J. Y.; Park, J. Y.; Kim, O. Y.; Ham, B. M.; Kim, H. J.; Kwon, D. Y.; Jang, Y.; Lee, J. H. Metabolic profiling of plasma in overweight/obese and lean men using ultra performance liquid chromatography and Q-TOF mass spectrometry (UPLC-Q-TOF MS). *J. Proteome Res.* **2010**, *9*, 4368−4375.
(39) Brown, M. S.; Goldstein, J. L. The SREBP pathway: regulation of cholesterol metabolism by proteolysis of a membrane-bound transcription factor. *Cell* **1997**, *89*, 331−340.
(40) Butovich, I. A. Cholesteryl esters as a depot for very long chain fatty acids in human meibum. *J. Lipid Res.* **2009**, *50*, 501−513.
(41) Niu, J.; Pi, Z.; Yue, H.; Wang, Y.; Yu, Q.; Liu, S. Effect of ginseng polysaccharide on the urinary excretion of type 2 diabetic rats studied by liquid chromatography-mass spectrometry. *J. Chromatogr., B: Anal. Technol. Biomed. Life Sci.* **2012**, *907*, 7−12.
(42) Sun, L. W.; Zhang, H. Y.; Wu, L.; Shu, S.; Xia, C.; Xu, C.; Zheng, J. S. (1)H-Nuclear magnetic resonance-based plasma metabolic profiling of dairy cows with clinical and subclinical ketosis. *J. Dairy Sci.* **2014**, *97*, 1552−1562.
(43) Perez-Enciso, M.; Tenenhaus, M. Prediction of clinical outcome with microarray data: a partial least squares discriminant analysis (PLS-DA) approach. *Hum. Genet.* **2003**, *112*, 581−592.
(44) Eriksson, L.; Andersson, P. L.; Johansson, E.; Tysklind, M. Megavariate analysis of environmental QSAR data. Part I − A basic framework founded on principal component analysis (PCA), partial least squares (PLS), and statistical molecular design (SMD). *Mol. Diversity* **2006**, *10*, 169−186.
(45) Rhee, E. P.; Cheng, S.; Larson, M. G.; Walford, G. A.; Lewis, G. D.; McCabe, E.; Yang, E.; Farrell, L.; Fox, C. S.; O'Donnell, C. J.; Carr, S. A.; Vasan, R. S.; Florez, J. C.; Clish, C. B.; Wang, T. J.; Gerszten, R. E. Lipid profiling identifies a triacylglycerol signature of insulin resistance and improves diabetes prediction in humans. *J. Clin. Invest.* **2011**, *121*, 1402−1411.
(46) Demarco, V. G.; Ford, D. A.; Henriksen, E. J.; Aroor, A. R.; Johnson, M. S.; Habibi, J.; Ma, L.; Yang, M.; Albert, C. J.; Lally, J. W.; Ford, C. A.; Prasannarong, M.; Hayden, M. R.; Whaley-Connell, A. T.; Sowers, J. R. Obesity-related alterations in cardiac lipid profile and nondipping blood pressure pattern during transition to diastolic dysfunction in male db/db mice. *Endocrinology* **2013**, *154*, 159−171.
(47) Guillou, H.; Zadravec, D.; Martin, P. G.; Jacobsson, A. The key roles of elongases and desaturases in mammalian fatty acid metabolism: insights from transgenic mice. *Prog. Lipid Res.* **2010**, *49*, 186−199.
(48) Wang, Y.; Botolin, D.; Xu, J.; Christian, B.; Mitchell, E.; Jayaprakasam, B.; Nair, M. G.; Peters, J. M.; Busik, J. V.; Olson, L. K.; Jump, D. B. Regulation of hepatic fatty acid elongase and desaturase expression in diabetes and obesity. *J. Lipid Res.* **2006**, *47*, 2028−2041.
(49) Naudi, A.; Jove, M.; Ayala, V.; Portero-Otin, M.; Barja, G.; Pamplona, R. Membrane lipid unsaturation as physiological adaptation to animal longevity. *Front. Physiol.* **2013**, *4*, 372.
(50) Moon, Y. A.; Hammer, R. E.; Horton, J. D. Deletion of ELOVL5 leads to fatty liver through activation of SREBP-1c in mice. *J. Lipid Res.* **2009**, *50*, 412−423.
(51) Kim, J.; Choi, J. N.; Choi, J. H.; Cha, Y. S.; Muthaiya, M. J.; Lee, C. H. Effect of fermented soybean product (Cheonggukjang) intake on metabolic parameters in mice fed a high-fat diet. *Mol. Nutr. Food Res.* **2013**, *57*, 1886−1891.
(52) Barber, M. N.; Risis, S.; Yang, C.; Meikle, P. J.; Staples, M.; Febbraio, M. A.; Bruce, C. R. Plasma lysophosphatidylcholine levels are reduced in obesity and type 2 diabetes. *PLoS One* **2012**, *7*, No. e41456.
(53) Pietilainen, K. H.; Sysi-Aho, M.; Rissanen, A.; Seppanen-Laakso, T.; Yki-Jarvinen, H.; Kaprio, J.; Oresic, M. Acquired obesity is associated with changes in the serum lipidomic profile independent of genetic effects − a monozygotic twin study. *PLoS One* **2007**, *2*, No. e218.
(54) Miyazaki, M.; Kim, Y. C.; Gray-Keller, M. P.; Attie, A. D.; Ntambi, J. M. The biosynthesis of hepatic cholesterol esters and triglycerides is impaired in mice with a disruption of the gene for stearoyl-CoA desaturase 1. *J. Biol. Chem.* **2000**, *275*, 30132−30138.
(55) Paton, C. M.; Ntambi, J. M. Biochemical and physiological function of stearoyl-CoA desaturase. *Am. J. Physiol. Endocrinol. Metab.* **2009**, *297*, E28−E37.
(56) Murugesan, G.; Fox, P. L. Role of lysophosphatidylcholine in the inhibition of endothelial cell motility by oxidized low density lipoprotein. *J. Clin. Invest.* **1996**, *97*, 2736−2744.
(57) Seo, C. S.; Kim, O. S.; Kim, Y.; Shin, H. K. Simultaneous quantification and inhibitory effect on LDL oxidation of the traditional Korean medicine, Leejung-tang. *BMC Complement. Altern. Med.* **2014**, *14*, 3.

DOI: 10.1021/jf506216p
J. Agric. Food Chem. 2015, 63, 2919−2929

to a classic luminol−H_2O_2 system, the Lum-AgNP−H_2O_2 CL system is a relatively slow process and dynamically tunable according to adjusting various reaction conditions, such as pH and the H_2O_2 concentration.[14] A single experimental operation can obtain triple-channel information containing CL intensity, the time for CL emissions to appear (T_a), and the time to reach the CL peak value (T_p).[14]

It has been demonstrated that various pesticides can influence the luminol CL system with different degrees.[15] Additionally, some pesticides have a strong affinity for AgNPs.[16] Thus, the addition of different pesticides will cause distinct CL responses. On these bases, we develop a simple and sensitive CL sensor array based on the utilization of triple-channel properties of the Lum-AgNP−H_2O_2 CL system for the discrimination of organophosphate and carbamate pesticides for the first time. The developed sensor array allows for the differentiation of five organophosphate and carbamate pesticides (Figure 1) with detection limits of 24 μg/mL.

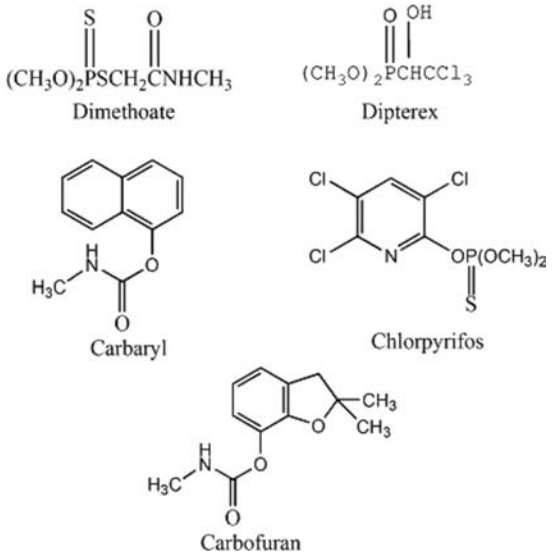

Figure 1. Chemical structures of five selected pesticides.

Moreover, the triple-channel properties are easily simultaneously detected via a single experiment, thereby greatly simplifying the operation procedure.

EXPERIMENTAL SECTION

Chemicals and Materials. Silver nitrate, absolute ethanol, sodium hydroxide, and hydrogen peroxide were purchased from Sinopharm Chemical Reagent Co., Ltd. (Shanghai, China). Luminol was obtained from Sigma-Aldrich. Dimethoate, dipterex, carbaryl, chlorpyrifos, and carbofuran (Figure 1) were supplied by J&K Scientific, Ltd. (Shanghai, China). All of the reagents are used as received without further purification. Ultrapure water (18.2 MΩ cm^{-1}) was produced from a Millipore Milli-Q system and used throughout the experiment.

Instrumentations. All of the CL measurements were carried out on an ultraweak luminescence analyzer (BPCL, China) with a fixed voltage of −700 V. The morphology of the as-prepared Lum-AgNPs was investigated using JEM-2100F field emission transmission electron microscopy (TEM) operating at 200 kV.

Synthesis of Lum-AgNPs. Lum-AgNPs were synthesized by the published protocol.[14] Typically, a mixture solution of $AgNO_3$ aqueous solution (4 mL, 5 mM) and absolute ethanol (10 mL) was heated to 60 °C under vigorous stirring and a luminol solution (0.5 mL, 10 mM) dissolved in 0.1 M NaOH aqueous solution was rapidly added. The solution was heated at 60 °C with vigorous stirring for another 2 h. Then, the mixture solution was allowed to cool to room temperature. The Lum-AgNPs were separated from the mixture via centrifugation and washed with ultrapure water. The collected Lum-AgNPs were dispersed into 30 mL of ultrapure water and stored at 4 °C before use.

Analyte Pesticide Response. The stock solutions of five organophosphate and carbamate pesticides were prepared in toluene. For each pesticide detection, the as-prepared Lum-AgNPs (100 μL) were added to pesticide solutions (10 μL) with a final concentration of 24 μg/mL and incubated for 10 min at room temperature, followed by successive injection of H_2O_2 solution (300 μL, 10 mM), and the CL emission was simultaneously measured. Five replicates were tested for each pesticide to give a 3 channel (T_a, T_p, and CL intensity) × 5 pesticide × 5 replicate data matrix. To identify randomly selected pesticide samples, similar procedures were also carried out.

Data Analysis. The CL patterns were processed using a classical principal component analysis (PCA) in MATLAB (version 7.0). After the analysis, three principal components were generated, which represented linear combinations of the response matrices obtained from the raw data matrix [3 channels (T_a, T_p, and CL intensity) × 5 pesticides × 5 replicates]. The first two most significant principal components were employed to produce a two-dimensional plot. The identification of unknown samples, which were randomly prepared by three separate researchers, was made by estimating Mahalanobis distance close to known group centroids from the training matrix.

RESULTS AND DISCUSSION

Principle of the CL Sensor Array Based on the Lum-AgNP−H_2O_2 System. The CL sensor array is based on the triple-channel properties (T_a, T_p, and CL intensity) of the Lum-AgNP−H_2O_2 CL system (Figure 2). Lum-AgNPs were prepared via a previously reported method,[14] which were characterized by TEM, as shown in Figure S1 of the Supporting Information.

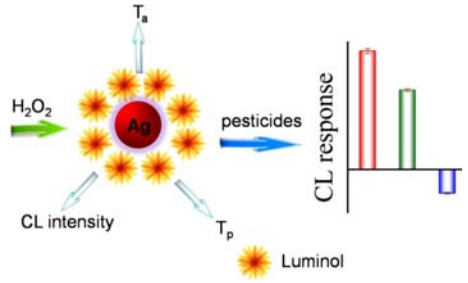

Figure 2. Schematic diagram of the principle of the CL sensor array based on the triple-channel properties of the Lum-AgNP−H_2O_2 CL system.

As expected, the Lum-AgNPs can react with H_2O_2, producing a slow CL kinetic process, as shown in Figure 3. When 0.3 mL of 10 mM H_2O_2 was injected into 0.1 mL of Lum-AgNP solution, the CL emission did not emerge immediately, which was completely different from the traditional luminol-based CL systems. After 9 s, CL emission gradually appeared and the corresponding intensity increased with the increase of time and reached its maximum at 276 s. Thus, a single experiment could obtain triple-channel properties (T_a, T_p, and CL intensity) from this CL system.

The mechanism of this CL system contains the following three processes:[14] (1) Lum-AgNPs were partially dissolved by H_2O_2 to form Ag^+ ions, producing $HO^•$ radicals, which were adsorbed on the surface of AgNPs. (2) The formed $HO^•$ radicals reacted with H_2O_2 and luminol, generating superoxide anion and luminol radical, respectively. (3) Further reaction between the superoxide anion radical and luminol radical

DOI: 10.1021/acs.jafc.5b00671
J. Agric. Food Chem. 2015, 63, 2930−2934

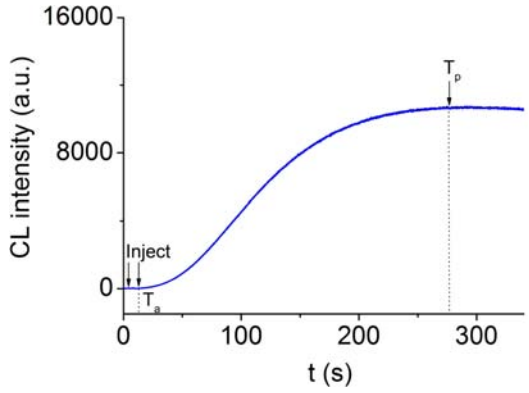

Figure 3. CL kinetic curve of the Lum-AgNP–H_2O_2 system. Reaction conditions: 0.1 mL of Lum-AgNP solution and 0.3 mL of 10 mM H_2O_2 aqueous solution.

generated excited-state 3-aminophthalate anions, resulting in a CL emission. The concentration of H_2O_2 and luminol on the surface of AgNPs was low. Moreover, the CL reaction occurred under static conditions rather than stirring (see the Experimental Section). Therefore, the CL emission was controlled by the diffusion process of H_2O_2. On the initial stage, no CL emission was observed because of the lack of adequate H_2O_2 around the Lum-AgNPs. With the reaction proceeding, the amount of H_2O_2 around the Lum-AgNPs increased, leading to the increase of $HO^•$ radicals and appearance of CL emission (T_a). When the consumption and diffusion of H_2O_2 reached a state of equilibrium around the Lum-AgNPs, the CL intensity attained its maximum, corresponding to T_p. The diffusion process of H_2O_2 was demonstrated by investigating the effect of the H_2O_2 concentration on T_a and T_p. As shown in Figure S2 of the Supporting Information, with the decrease of the H_2O_2 concentration, T_a and T_p became longer. Besides, with the decrease of the AgNP concentration, T_a and T_p also became longer, which further confirmed the presence of the diffusion process (see Figure S3 of the Supporting Information). The dissolution of AgNPs to form Ag^+ ions was confirmed by inductively coupled plasma–atomic emission spectroscopy. The supernatant prepared by centrifugation of the CL reaction solution was found to possess Ag element, whose content was 13.05 μg/mL, which was evidently over that of the control sample (2.03 μg/mL). Furthermore, the effect of various radical scavengers on the CL system was investigated (see Table S1 of the Supporting Information), which demonstrated the presence of various radicals in the CL emission process.

On the other hand, as seen from Figure 1, the structures of organophosphate and carbamate pesticides contain sulfur, phosphorus, or nitrogen groups, which are easy to adsorb on the surface of AgNPs via covalent interaction.[16] Additionally, the reducing group of −OH or −NH− in pesticides reacted readily with the oxygen-containing intermediate radicals.[17] The differential interactions between the Lum-AgNP–H_2O_2 CL system and various pesticides generate distinct CL responses related to each specific pesticide.

Fingerprints of Pesticides Generated via the Triple-Channel Properties (T_a, T_p, and CL Intensity) of the Lum-AgNP–H_2O_2 System. As a proof-of-concept system, five organophosphate and carbamate pesticides with different molecular structures, including dimethoate (Dim), dipterex (Dip), carbaryl (Car), chlorpyrifos (Chl), and carbofuran (Cbf), were chosen as the sensing targets, as shown in Figure 1. As illustrated in Figure S4 of the Supporting Information, the presence of analyte pesticides (24 μg/mL) caused a variety of CL responses. This result confirmed that different pesticides would influence the CL kinetic process of the Lum-AgNP–H_2O_2 system with different degrees, leading to distinct response patterns. To better investigate the effect of various analyte pesticides on the CL sensor array, the signal change rate ($\Delta I/I_0$) for each pesticide as the fingerprint was calculated, as shown in Figure 4. Car and Chr are observed to significantly increase

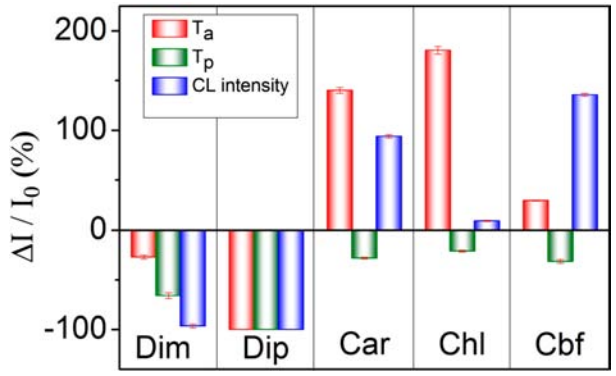

Figure 4. Fingerprints of five selected pesticides based on the CL response patterns ($\Delta I/I_0$) at 24 μg/mL analyte concentration. $\Delta I = I - I_0$, where I and I_0 are the values of T_a, T_p, or CL intensity in the presence and absence of various pesticides, respectively.

T_a by 140.2 and 180.5%, respectively, while Dim and Dip decreased T_a by 27 and 100%, respectively. Cbf made a mild impact on T_a, and the signal was increased by 29.9%.

The effect of analyte pesticides on T_p of the sensor array was also studied (olive-colored column diagram in Figure 4). All of the pesticides decreased T_p with different degrees. Car, Chl, and Cbf decreased T_p by 28.1, 21.1, and 32%, respectively. However, Dim and Dip decreased T_p more effectively, because they decreased the signal by 65.9 and 100%. The influence of various pesticides on CL intensity was further investigated (blue-colored column diagram in Figure 4). Dim and Dip were found to apparently decrease the CL intensity by 96.5 and 100%, while Chl slightly enhanced the CL intensity by 9.4%. Besides, Cbf and Car evidently enhanced the CL intensity by 135.7 and 93.9%.

The distinct CL responses after adding different pesticides could be explained as follows. The presence of a reductive hydroxyl group (−OH) and amino group (−NH−) for Dip and Dim could consume the oxidants in the CL system, such as H_2O_2, $HO^•$ radicals,[17] and superoxide anion radical, leading to the decrease of the CL intensity and increase of T_a and T_p. It was reported that Chl, Car, and Cbf could react with oxidants, such as H_2O_2, to form unstable intermediates, which accelerated the oxidation of luminol,[18−20] leading to the increase of the CL intensity and T_a and decrease of T_p. Owing to the difference of molecular structures for Chl, Car, and Cbf, the corresponding triple-channel information (T_a, T_p, and CL intensity) was not all exactly the same.

CL Sensor Array for Discrimination of Pesticides. These differential CL responses, like "fingerprints", were further subjected to PCA; PCA converts the patterns of the training matrix (3 channels × 5 pesticides × 5 replicates) to canonical scores, as shown in Figure 5. The first two most significant principal components contain 87.5 and 9.8% of the variation,

DOI: 10.1021/acs.jafc.5b00671
J. Agric. Food Chem. 2015, 63, 2930−2934

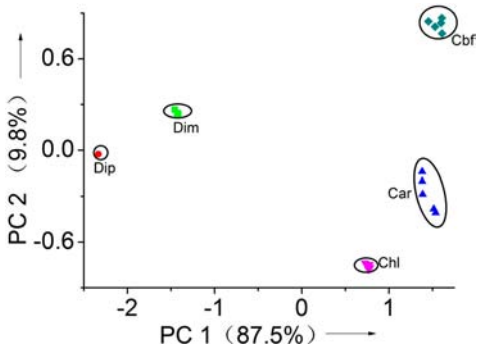

Figure 5. Canonical score plot of the two primary principle components for the discrimination of five selected pesticides (24 μg/mL).

respectively, which occupies 97.3% of total variation. At a pesticide concentration of 24 μg/mL, PCA verifies that the canonical response patterns of the pesticides to the triple-channel properties of the Lum-AgNP−H_2O_2 CL system were classified into five separate groups that corresponded to each pesticide. Moreover, the five repeated measurements of each pesticide were in a narrow distribution in the PCA plots. These results indicated that the five organophosphate and carbamate pesticides at concentrations of no less than 24 μg/mL could be effectively distinguished.

The performance of the CL sensor array was further tested by the discrimination of unknown samples. The identification accuracy of 20 unknown samples at the 24 μg/mL level was found to be 95% (see Table S3 of the Supporting Information). It meant that the CL sensor array could identify pesticides as low as 24 μg/mL.

For a sensor array, another challenge is to discriminate different pesticides at different concentration levels. To elucidate the application potential of the CL sensor array, we performed experiments with Chl, Car, and Cbf at three different concentrations (1, 5, and 10 μg/mL). As shown in Figure 6, various concentrations of three pesticides were able to

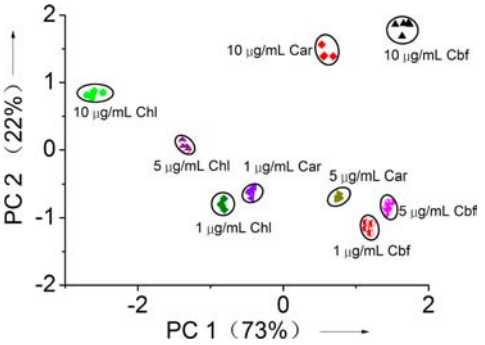

Figure 6. PCA score plot for the discrimination of Chl, Car, and Cbf at three different concentrations (1, 5, and 10 μg/mL).

be discriminated from each other in the PCA score plot. In addition, the CL responses from different concentrations of one pesticide produced patterns around a center; thus, each pesticide could be differentiated.

In summary, we have demonstrated that various analyte pesticides could influence T_a, T_p, and light intensity of the Lum-AgNP−H_2O_2 CL system simultaneously. The signal changes in such triple-channel properties of this CL system resulted in distinct patterns related to each pesticide, which were able to be incorporated into a novel pesticide sensor array with a single sensing unit. Benefiting from the high sensitivity and simple operation of CL technology, several organophosphate and carbamate pesticides, such as dimethoate, dipterex, carbaryl, chlorpyrifos, and carbofuran, have been recognized and discriminate with a high sensitivity.

To the best of our knowledge, this work is the first case of recognition and discrimination of organophosphate and carbamate pesticides in aqueous solution by virtue of a nanoparticle-based CL sensor array that is fabricated by a simple Lum-AgNP−H_2O_2 CL system with triple-channel information. In view of the simple preparation method and available surface modification technique of Lum-AgNPs as well as ready dynamically tunable CL process of this system, we believe that the present study opens a new avenue for the development of simple and facile high-throughput assays for the identification of organophosphate and carbamate pesticides, which may hold great potential application in environmental protection and food safety. In our future work, we will further improve the discrimination ability of the nanoparticle-based CL sensor array to extend its application for recognition of other pesticides.

■ ASSOCIATED CONTENT

Ⓢ Supporting Information

TEM image of Lum-AgNPs (Figure S1), effect of the H_2O_2 concentration on (a) T_a and (b) T_p of this CL system (Figure S2), effect of different addition amounts of Lum-AgNPs on this CL system: (a) 50 μL, (b) 100 μL, and (c) 150 μL (Figure S3), CL kinetic curve of the Lum-AgNP−H_2O_2 system in the absence (first curve) and presence of various pesticides (Figure S4), effects of radical scavengers on CL of the Lum-AgNP−H_2O_2 system (Table S1), training matrix of the response patterns against pesticides at 24 μg/mL (Table S2), and detection and identification of unknown pesticides at 24 μg/mL (Table S3). This material is available free of charge via the Internet at http://pubs.acs.org.

■ AUTHOR INFORMATION

Corresponding Author

*E-mail: yhe2014@126.com.

Funding

This work was supported by the Foundation of Science and Technology Department of Sichuan Province (Grant 2015JY0053) and the Doctoral Program of Southwest University of Science and Technology (Grant 14zx7165).

Notes

The authors declare no competing financial interest.

■ REFERENCES

(1) Kim, G. Y.; Shim, J.; Kang, M. S.; Moon, S. H. Optimized coverage of gold nanoparticles at tyrosinase electrode for measurement of a pesticide in various water samples. *J. Hazard. Mater.* **2008**, *156* (1−3), 141−147.

(2) Liu, D.; Chen, W.; Wei, J.; Li, X.; Wang, Z.; Jiang, X. A highly sensitive, dual-readout assay based on gold nanoparticles for organophosphorus and carbamate pesticides. *Anal. Chem.* **2012**, *84* (9), 4185−4191.

(3) Zhang, K.; Mei, Q.; Guan, G.; Liu, B.; Wang, S.; Zhang, Z. Ligand replacement-induced fluorescence switch of quantum dots for ultrasensitive detection of organophosphorothioate pesticides. *Anal. Chem.* **2010**, *82* (22), 9579−9586.

DOI: 10.1021/acs.jafc.5b00671
J. Agric. Food Chem. 2015, 63, 2930−2934

(4) Liu, S.; Zheng, Z.; Li, X. Advances in pesticide biosensors: Current status, challenges, and future perspectives. *Anal. Bioanal. Chem.* **2013**, *405* (1), 63−90.
(5) (a) Gong, J.; Wang, X.; Li, X.; Wang, K. Highly sensitive visible light activated photoelectrochemical biosensing of organophosphate pesticide using biofunctional crossed bismuth oxyiodide flake arrays. *Biosens. Bioelectron.* **2012**, *38* (1), 43−49. (b) Liang, M.; Fan, K.; Pan, Y.; Jiang, H.; Wang, F.; Yang, D.; Lu, D.; Feng, J.; Zhao, J.; Yang, L.; Yan, X. Fe_3O_4 magnetic nanoparticle peroxidase mimetic-based colorimetric assay for the rapid detection of organophosphorus pesticide and nerve agent. *Anal. Chem.* **2013**, *85* (1), 308−312.
(6) Wang, Y.; Zhang, S.; Du, D.; Shao, Y.; Li, Z.; Wang, J.; Engelhard, M. H.; Li, J.; Lin, Y. Self assembly of acetylcholinesterase on a gold nanoparticles−graphene nanosheet hybrid for organophosphate pesticide detection using polyelectrolyte as a linker. *J. Mater. Chem.* **2011**, *21* (14), 5319−5325.
(7) Li, Z.; Wang, Y.; Ni, Y.; Kokot, S. Unmodified silver nanoparticles for rapid analysis of the organophosphorus pesticide, dipterex, often found in different waters. *Sens. Actuators, B* **2014**, *193*, 205−211.
(8) Zhang, K.; Yu, T.; Liu, F.; Sun, M.; Yu, H.; Liu, B.; Zhang, Z.; Jiang, H.; Wang, S. Selective fluorescence turn-on and ratiometric detection of organophosphate using dual-emitting Mn-doped ZnS nanocrystal probe. *Anal. Chem.* **2014**, *86* (23), 11727−11733.
(9) Chauhan, N.; Pundir, C. S. An amperometric acetylcholinesterase sensor based on Fe_3O_4 nanoparticle/multi-walled carbon nanotube-modified ITO-coated glass plate for the detection of pesticides. *Electrochim. Acta* **2012**, *67*, 79−86.
(10) Liu, Y.; Bonizzoni, M. A supramolecular sensing array for qualitative and quantitative analysis of organophosphates in water. *J. Am. Chem. Soc.* **2014**, *136* (40), 14223−14229.
(11) Guan, G.; Yang, L.; Mei, Q.; Zhang, K.; Zhang, Z.; Han, M. Y. Chemiluminescence switching on peroxidase-like Fe_3O_4 nanoparticles for selective detection and simultaneous determination of various pesticides. *Anal. Chem.* **2012**, *84* (21), 9492−9497.
(12) Wang, S.; Ge, L.; Li, L.; Yan, M.; Ge, S.; Yu, J. Molecularly imprinted polymer grafted paper-based multi-disk micro-disk plate for chemiluminescence detection of pesticide. *Biosens. Bioelectron.* **2013**, *50*, 262−268.
(13) He, Y.; Liu, D.; He, X.; Cui, H. One-pot synthesis of luminol functionalized silver nanoparticles with chemiluminescence activity for ultrasensitive DNA sensing. *Chem. Commun.* **2011**, *47* (38), 10692−10694.
(14) He, Y.; He, X.; Liu, X.; Gao, L.; Cui, H. Dynamically tunable chemiluminescence of luminol functionalized silver nanoparticles and its application to protein sensing arrays. *Anal. Chem.* **2014**, *86*, 12166−12171.
(15) (a) Wang, J.; Zhang, C.; Wang, H.; Yang, F.; Zhang, X. Development of a luminol-based chemiluminescence flow-injection method for the determination of dichlorvos pesticide. *Talanta* **2001**, *54* (6), 1185−1193. (b) Pérez-Ruiz, T.; Martínez-Lozano, C.; García, M. D. Determination of *N*-methylcarbamate pesticides in environmental samples by an automated solid-phase extraction and liquid chromatographic method based on post-column photolysis and chemiluminescence detection. *J. Chromatogr. A* **2007**, *1164* (1), 174−180.
(16) Bootharaju, M.; Pradeep, T. Understanding the degradation pathway of the pesticide, chlorpyrifos by noble metal nanoparticles. *Langmuir* **2012**, *28* (5), 2671−2679.
(17) Zhang, Z. F.; Cui, H.; Lai, C. Z.; Liu, L. J. Gold nanoparticle-catalyzed luminol chemiluminescence and its analytical applications. *Anal. Chem.* **2005**, *77* (10), 3324−3329.
(18) Huertas-Pérez, J. F.; Gámiz-Gracia, L.; García-Campaña, A. M.; González-Casado, A.; Vidal, J. L. M. Chemiluminescence determination of carbofuran at trace levels in lettuce and waters by flow-injection analysis. *Talanta* **2005**, *65* (4), 980−985.
(19) Gámiz-Gracia, L.; Cuadros-Rodríguez, L.; Soto-Chinchilla, J. J.; Huertas-Pérez, J. F.; González-Casado, A.; García-Campaña, A. M. Establishment of signal-recovery functions for calculation of recovery factor. Application to monitoring of contaminant residues in vegetables by chemiluminescence detection. *Anal. Bioanal. Chem.* **2006**, *384* (1), 295−301.
(20) Xie, C.; Li, H.; Li, S.; Gao, S. Surface molecular imprinting for chemiluminescence detection of the organophosphate pesticide chlorpyrifos. *Microchim. Acta* **2011**, *174*, 311−320.

DOI: 10.1021/acs.jafc.5b00671
J. Agric. Food Chem. 2015, 63, 2930−2934

polyphenols extracted from frozen and freeze-dried blueberry powder. We have also evaluated the ability of these polyphenols to inhibit α-glucosidase, a key enzyme in the human stomach responsible for catabolizing maltose, a disaccharide, that contributes to postprandial increase in blood glucose.

MATERIALS AND METHODS

Blueberries. Frozen wild blueberries (low-bush) obtained from the local supermarket were divided in two batches: (1) kept as frozen blueberries and (2) used for making blueberry freeze-dried powder. Blueberries were freeze-dried (at −45 ± 5 °C and 100 Pa/1 mbar) in a freeze-dryer (Thermo Savant, USA) for 72 h (2% moisture content on dry basis), milled with a blender, and stored in airtight containers at −20 °C until further analysis. Blueberries from the same lot were used for all experiments.

Chemicals and Reagents. All chemicals and solvents were purchased from Fisher Scientific (Ottawa, ON, Canada) or Sigma-Aldrich (Oakville, ON, Canada). Dulbecco's Modified Eagle's Medium (DMEM), fetal bovine serum (FBS), L-glutamine, trypsin−EDTA, sulforhodamine B (SRB), acetic acid, and Tris base were purchased from Sigma-Aldrich (Oakville, ON, Canada). Cyanidin- and delphinidin-3-glucosides were purchased from Chromadex (Irvine, CA) and malvidin-3-glucoside from extrasynthese (Genay, Cedex, France). Human epithelial colorectal adenocarcinoma cell line HT-29 and human normal epithelial colon cell line CRL-1790 were obtained from the American Type Culture Collection (Rockville, MD). Minimal Essential Medium Eagle (MEME) was purchased from Hyclone (Thermoscientific, Canada). Phosphate-buffered saline (PBS) 10x, penicillin−streptomycin solution, and trypan blue were from Gibco (Bethesda, MD).

Polyphenol Extraction. Methanol and water were used as extraction solvents. Methanolic extraction enabled a more efficient way of extracting phenolic components, and water, on the other hand, simulated the state where anthocyanins are extracted and liberated after consumption as food. One part of frozen blueberries was homogenized with two parts of solvent (50 g of blueberries in 100 mL of solvent) using a shear homogenizer (Brinkman Instruments, Westbury, NY) fitted with a Polytron PTA 10 probe for 5 min. The homogenates were centrifuged (Beckman J2-21, Missisauga, ON) at 27 000*g* for 20 min; the supernatants were collected and stored in amber tubes at −20 °C for further analysis.

Separation of Free and Bound Polyphenols. Blueberry extracts from the aqueous and methanolic crude extracts (10 mL) were transferred into a dialysis membrane reservoir (6−8 kDa cutoff, Spectrapor, Spectrum Laboratories, Houston, TX) previously soaked and rinsed with distilled water. Dialysis was carried out in 500 mL of distilled water at 4 °C for 24 h. The dialyzed (complexed polyphenols) and the dialyzate (free polyphenols) were collected and used for various analyzes.[12]

Total Polyphenol Content. Total polyphenol contents of the samples were estimated according to the Folin−Ciocalteau method.[13] An aliquot of extract was mixed with 50% (v/v) of ethanol in water, to a final volume of 100 μL. Reaction mixture was prepared by adding 500 μL of distilled water, 50 μL of Folin Ciocalteau reagent (2 N), and 100 μL of 5% (w/v) sodium carbonate solution to the sample, vortexed, and incubated in the dark for 1 h. Samples were mixed thoroughly after incubation, and the absorbance was measured at λ_{max} = 725 nm using a Beckman Coulter DU 800 spectrophotometer (Beckman Coulter Inc., IN). A standard curve was generated using gallic acid with concentrations ranging from 0 to 200 μg/mL. Polyphenol concentrations were expressed as weight of gallic acid equivalent per gram fresh weight of fruit. Dry weight of a known amount of polyphenols was determined after freeze-drying. While expressing polyphenol content of blueberries from dry powder, the value was expressed as fresh weight equivalent.

Solid-Phase Extraction. Solid-phase extraction (SPE) with Sep-Pak C18 (Waters Corporation, MA) cartridge was used to purify polyphenols.[14] The columns were washed with water and polyphenols eluted with 100% methanol. All samples were adjusted to 1 mg/mL of polyphenols with methanol, filtered with 0.45 μm nylon filters, and subjected to LC-MS analyses.

Identification of Individual Polyphenols by LC- ESI- MS. Chromatographic analysis of anthocyanins isolated from the crude extracts, the dialyzed extracts, and the dialyzate fractions was performed on an Agilent 1100 series LC-MS. Separation was carried out using an X-Terra MS C-18 (5 μm, 150 × 3.0 mm, Waters Corporation, MA). Anthocyanins were eluted with a gradient of mobile phases formed by mixing methanol (phase A) and 2.0% (v/v) formic acid (phase B) at a flow rate of 0.8 mL/min. The gradient used was as follows: 0−2 min, 93% B; 2−30 min, 80% B; 30−45 min, 70% B; 45−50 min; 65% B, 50−60 min, 50% B; 60−65 min, 20% B; 65−70 min, 93% B. Detection was carried out both at 520 and 260 nm. Electrospray ionization (ESI) was performed with an API-ES mass spectrometer. Nitrogen was used as the nebulizing and drying gas, 12 L/min at 350 °C, ion spray voltage, 4000 V, and fragmentor voltage, 80 V. Electrospray ionization mass spectra were scanned from m/z 100 to 1000. Spectra were acquired in the positive ion mode for anthocyanins and negative ion mode for phenolics and flavonoids. A sample injection volume of 20 μL (20 μg) was used for all samples. Chemical identification of the compounds was achieved by matching the molecular ions (m/z) and daughter ions obtained by LC-ESI-MS with spectral data (www.metabolomics.jp).

Relative amounts of individual phenolic components were calculated as follows. The sum of all peak areas was taken as 100% resulting from the separation of 20 μg of phenolics sample. Individual peak areas corresponding to specific components were also calculated. From these values, (individual peak area/total peak area) × 20, the relative content of specific peaks in micrograms was obtained. From these values, mg phenolics content per gram fresh weight of fruit could be calculated knowing the fresh weight of the sample and its polyphenol content.

Antioxidant Assays. Total antioxidant activity of blueberry crude extracts and dialyzed fractions was measured by using 2,2-diphenyl-1-picrylhydrazyl (DPPH) radical (Molyneux),[16] superoxide scavenging,[17] and hydroxyl radical scavenging[18] assays according to standard methods.

α-Glucosidase Inhibition. α-Glucosidase inhibitory activity was measured as described.[19] Blueberry polyphenol samples were diluted with water to a sample volume of 50 μL to obtain concentrations of 10, 25, 50, and 100 μg/mL of polyphenols, and water of equal volume was used as a control. Reaction was initiated by the addition of 100 μL of 0.1 M sodium phosphate buffer (pH 6.9) containing α-glucosidase solution (1.0 U/mL) to the samples followed by incubation at 25 °C for 10 min. After the reaction, 50 μL of 5 mM *p*-nitrophenyl-α-D-glucopyranoside solution [prepared in 0.1 M sodium phosphate buffer (pH 6.9)] was added to the reaction mixture (final volume = 200 μL) and incubated at 25 °C for 5 min. After incubation, distilled water (800 μL) was added to the reaction mixture and the absorbance was recorded at λ_{max} = 405 nm (A). Inhibition of the enzyme activity was expressed as percentage inhibition and calculated as α-glucosidase inhibition (%) = (A control − A sample)/(A control) × 100.

Fruit Matrix Isolation and Estimation of Pectin Content. Polyphenols were removed from whole blueberries (50 g) by soaking (5×) in 50% v/v ethanol (100 mL) and (2×) in distilled water (100 mL) for 1 h each. The fruits were homogenized in water as described in Polyphenol Extraction. To verify the absence of polyphenols, samples were dialyzed overnight, and Folin−Ciocalteau assay was performed on the extracts. Samples containing the fruit matrix were stored at −20 °C until further analysis. Pectin content in the fruit matrix and crude extracts was estimated according to Taylor.[15] Briefly, 200 μL of samples, 3 mL of concentrated sulfuric acid, and 100 μL of 0.1% (w/v) carbazole reagent (made up in 100% ethanol) were mixed, incubated in a water bath at 60 °C for 1 h, and cooled to room temperature, and absorbance was measured at 530 nm against a water blank. A stock solution of pectin from apples was used at concentrations in the range of 0−200 μg/mL to generate a standard curve.

Cell Proliferation Assay. HT-29 cells were cultured in 25 cm^2 flasks with Dulbecco's Modified Eagle's (DMEM) medium supple-

DOI: 10.1021/acs.jafc.5b00016
J. Agric. Food Chem. 2015, 63, 2935−2946

Table 1. Total Polyphenol and Anthocyanin Content of Different Blueberry Extracts

sample	solvent	polyphenol (mg GAE/g fruit fresh weight)[a]		
		crude extract	dialyzed extract	dialyzate
frozen blueberries	water	1.66 ± 0.03[a]	0.57 ± 0.02[a]	0.79 ± 0.02[a]
frozen blueberries	methanol	3.20 ± 0.07[b]	0.97 ± 0.01[b]	2.21 ± 0.09[b]
blueberry freeze-dried powder	water	2.00 ± 0.15[a]	0.72 ± 0.01[a]	1.21 ± 0.01[a]
blueberry freeze-dried powder	methanol	3.63 ± 0.19[b]	0.80 ± 0.02[b]	2.82 ± 0.04[b]

[a]The data represent the mean ± SEM from three independent analyses. Means with different superscript letters are statistically significant ($p < 0.05$).

mented with 10% (v/v) FBS, 200 mM L-glutamine, and 1% (v/v) penicillin−streptomycin. CRL-1790 cells were cultured in Eagle's minimal essential medium (EMEM) contained in 25 cm^2 flasks and supplemented with FBS, penicillin−streptomycin, and L-glutamine as described above. Both cell lines were incubated at 37 °C in a humidified chamber including 5% CO_2. Cells were incubated with blueberry extracts for 24 and 48 h. HT-29 cells seeded at 2.0×10^3 cells/well and CRL-1790 seeded at 1.0×10^3 cells/well in 96-well plates were incubated for 24 h to attach to the surface and achieve log phase growth at the time of treatment (time 0). Stock solutions were prepared containing 1 mg/mL of polyphenols dissolved in water and diluted in growth media to obtain concentrations of 10, 25, 50, 75, and 100 μg/mL of media for each sample and immediately tested for antiproliferative activity. Negative control cells were supplied with growth media, and blank wells contained growth media only. The medium was changed every 24 h. Cell proliferation assay was carried out according to a modification of procedure used by Vichai and Kirtikara.[20] After 24 and 48 h of treatment, cells were stained with sulforhodamine dye (0.4% dissolved in 1% acetic acid, 50 μL per well), and the optical density of each well was measured at 570 nm using a Synergy HT Multi Detection Microplate Reader (Bio-Tek Instruments, Winooski, VT), and KC4 version 3.03 Power Report Bio-Tek software was used to analyze the data.

Statistical Analysis. Statistical analyses were conducted by using Graph Pad Prism software, version 4. Results with multiple means were compared by using one-way analyses of variance (ANOVA), which was followed by Tukey's test to evaluate the level of significance. Significantly different means ($p < 0.05$) are denoted by different letters.

RESULTS

Polyphenol Composition of Blueberry Extracts. Total polyphenol content from different preparations of blueberries ranged from 1.6 to 3.6 mg GAE/g frozen fruit (Table 1). Polyphenol content of methanol extracts of frozen blueberries and freeze-dried blueberries were much higher than that obtained after water extraction, suggesting the presence of significant amounts of bound polyphenols that are not extractable with water. Dialyzed fraction and dialyzate of methanol extracts also possessed increased levels of polyphenols as compared to those from water extracts. Further experiments were largely carried out using polyphenols obtained after water extraction of frozen blueberries, as this was also similar to the levels obtained after water extraction of freeze-dried blueberries. Occasional comparisons have also been made with polyphenols obtained from methanol extracts.

Identification and Quantification of Phenolic Compounds. Polyphenols from the original extract (crude extract), dialyzed extract, and dialyzate of blueberry homogenates were analyzed to compare their composition. Major phenolic components identified in the water extracts from frozen blueberries are given in Table 2. These components were also isolated after methanol extraction and dialysis of the extracts which were similar as in water extract but generally higher in amounts (data not shown). Chlorogenic acid was the major phenolic acid in blueberry extracts. Glucosides, galactosides, and arabinosides of major aglycones including delphinidin, cyanidin, petunidin, peonidin, and malvidin were observed. Glycosylated flavonoids such as quercetin arabinoside (xyloside) and syringetin galactoside (glucoside) were also identified. Acetoylated anthocyanins of delphinidin, and malvidin glucosides, were major components among anthocyanins.

Table 2. Major Polyphenols Identified in Blueberry Extracts by HPLC-MS-ESI

peak[a]	t_R[b] (min)	major ions[c]	compound[d]
1	15.75	353, 336, 288, 180	chlorogenic acid
2	22.00	465, 302, 148	delphinidin 3-*O*-galactoside
3	24.91	465, 302, 148	delphinidin 3-*O*-glucoside
4	26.91	435, 302, 132	delphinidin 3-*O*-arabinoside
5	28.70	449, 287,148	cyanidin 3-*O*-glucoside
6	30.27	479, 316, 148	petunidin 3-*O*-galactoside
7	33.30	463, 301, 148	peonidin 3-*O*-galactoside
8	35.05	449, 316, 132	petunidin 3-*O*-arabinoside
9	36.77	493, 331, 148	malvidin 3-*O*- galactoside
10	39.03	433, 301, 132	peonidin 3-*O*-arabinoside
11	40.56	493, 331, 148	malvidin 3-*O*-glucoside
12	45.15	463, 331, 132	malvidin 3-*O*-arabinoside
13	47.44	507, 367, 302, 204, 148	delphinidin 6-acetoyl,3-*O*-glucoside
14	49.06	535, 367, 302, 204, 148	malvidin 6-acetoyl,3-*O*-glucoside
15	52.98	435, 303, 229, 153	quercetin 3-*O*-arabinoside/xyloside
16	55.54	507, 347, 331, 315, 287, 153	syringetin 3-*O*-galactoside/glucoside

[a]Peaks were recorded at 260 nm, the absorbance maximum of phenolic moiety in polyphenols. [b]Retention time for individual component is denoted as t_R. [c]Mass spectra for anthocyanins were obtained in the positive ion mode, and those for phenolics and flavonoids in the negative ion mode. [d]Compounds were identified by comparing the mass spectra to authentic standards that are available at www.metabolomics.jp.

HPLC profiles of polyphenols purified from water extracts, dialyzed extract, and the dialyzate of frozen blueberries revealed the presence of 16 major phenolic compounds (Figure 1). The content of individual phenolic/flavonoid components and anthocyanins in these samples is shown in Table 3 and Table 4, respectively. Chlorogenic acid was the major phenolic acid component in blueberries, approaching nearly 50% of the total phenolic components in the aqueous crude extract and the dialyzate. Quercetin arabinoside (xyloside) was the major flavonoid glucoside, present in both crude extract and dialyzate. In addition, flavonoids such as myricetin, quercetin arabinoside, and syringetin galactoside (glucoside) were also present in aqueous crude extracts. Several other phenolic components such as isorhamnetin, 4-*O*-feruloylquinic acid, and myricetin

DOI: 10.1021/acs.jafc.5b00016
J. Agric. Food Chem. 2015, 63, 2935−2946

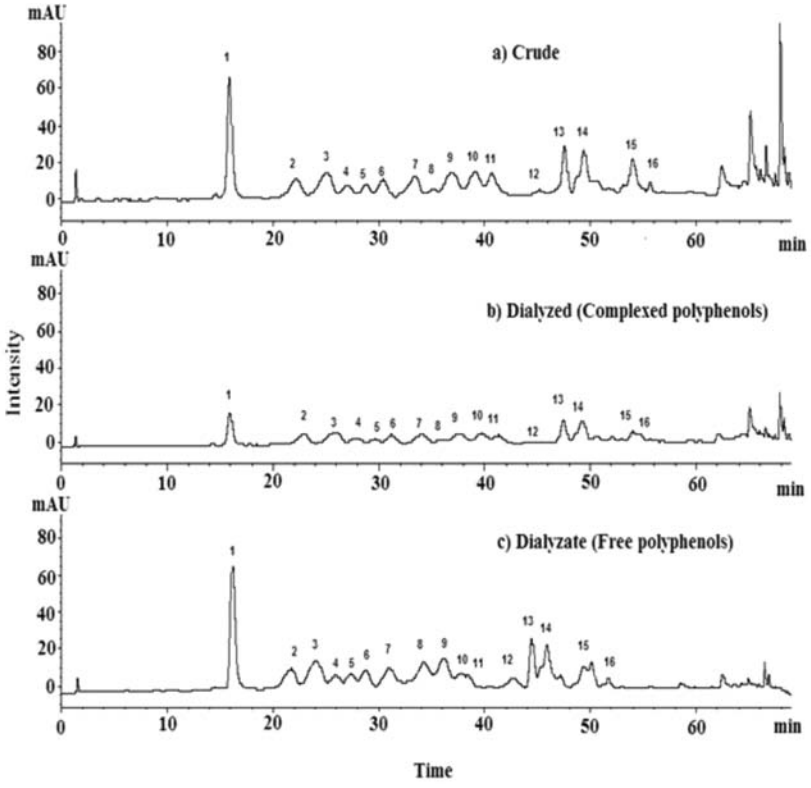

Figure 1. HPLC profile of blueberry polyphenols, detected at 260 nm. (a) Crude extract, (b) dialyzed fraction, (c) dialyzate fraction. Polyphenols from berries were extracted with water and subjected to purification using sep-pak C_{18} columns before analysis. Identification of the peaks denoted by numbers is given in Table 2

Table 3. Flavonoid and Phenolic Acid Composition (mg/g Fresh Weight) of Crude Extract, Dialyzed Extract, and Dialyzate Fraction Obtained from Frozen Blueberries Extracted with Water[a]

phenolic component	crude extract	dialyzed extract	dialyzate
isorhamnetin	0.028 ± 0.003[a]	Tr[b]	Tr
myricetin	0.024 ± 0.001[a]	0.009 ± 0.000[b]	0.010 ± 0.002[b]
chlorogenic acid	0.216 ± 0.010[a]	0.031 ± 0.014[b]	0.190 ± 0.026[a]
4-*O*-feruloylquinic acid	0.041 ± 0.008[a]	0.062 ± 0.006[b]	Tr
quercetin- 3-*O*-arabinoside/ xyloside	0.091 ± 0.021[a]	0.036 ± 0.006[b,c]	0.054 ± 0.005[c]
syringetin 3-*O*-galactoside/ glucoside	0.020 ± 0.006[a]	Tr	0.050 ± 0.004[b]
total	0.420 ± 0.040[a]	0.128 ± 0.015[b]	0.304 ± 0.037[c]

[a]The values given are mean ± SEM from three independent analyzes. Means with different superscript letters in the same row are statistically significant ($p < 0.05$). [b]Tr = traces.

were detected in very low amounts (mass spectral identification). Aqueous dialyzed fraction contained less than 10% of the polyphenols present in the original crude extract, having most of the components typically present in the crude extract and the dialyzate.

Antioxidant Activity. Antioxidant activities of free and complexed blueberry polyphenols isolated from frozen- and freeze-dried blueberries were evaluated to observe if freeze-drying affected complex formation with the food matrix, and this in turn affected the antioxidant activity of polyphenols. The specific quenching values per 10 μg polyphenols were calculated from the linear phase of the activity curve (Table 5). Maximal levels of DPPH radical scavenging and hydroxyl radical scavenging were observed in the free polyphenol fraction obtained after dialysis of frozen blueberry extracts, and these values were nearly twice as high as in the crude extract. The highest level of superoxide scavenging was observed in the dialyzed fraction (polyphenols bound to the matrix) of frozen blueberry extracts. Dialyzate of the frozen blueberry extract was as efficient as the standards in DPPH scavenging and far reduced in hydroxyl radical scavenging. For freeze-dried blueberries, dialyzed extract showed the highest DPPH scavenging and superoxide scavenging activities. But the dialyzate of the freeze-dried berries showed the maximum level of hydroxyl radical activity (Table 5).

α-Glucosidase Inhibition. Polyphenols isolated from water and methanol extracts of blueberries (crude extracts, dialyzed extract, and dialyzate) from both frozen fruits and freeze-dried powder were evaluated for their potential to inhibit α-glucosidase, a key sugar catabolizing enzyme in the stomach responsible for the liberation of sugars from disaccharides such as maltose, produced during the digestion of starch. As shown in Figure 2, the specific inhibition of α-glucosidase by the crude extract, the dialyzed extract, and dialyzate was highly variable, with the dialyzed extracts showing the most efficient inhibition and the dialyzate showing the least inhibition. The crude extracts of polyphenols in methanol showed levels of glucosidase inhibition higher than those of water extracts from both frozen and freeze-dried blueberries. A similar pattern was observed while using the dialyzed extract, but with effectiveness nearly twice as high as that observed in the crude extracts with maximal inhibition observed between 80% and 100%. Interestingly, the dialyzed methanol extract was

DOI: 10.1021/acs.jafc.5b00016
J. Agric. Food Chem. 2015, 63, 2935−2946

Table 4. Composition of Anthocyanins (mg/g Fresh Weight) of Crude Extract, Dialyzed Extract and Dialyzate Fraction Obtained from Frozen Blueberry Fruits Extracted with Water[a]

anthocyanin component	crude extract	dialyzed extract	dialyzate
delphinidin 3-*O*-galactoside	0.007 ± 0.001[a]	Tr[b]	0.009 ± 0.001[a]
delphinidin 3-*O*-glucoside	0.015 ± 0.003[a]	Tr	0.011 ± 0.003[a]
delphinidin 3-*O*-arabinoside	Tr	Tr	Tr
cyanidin 3-*O*-glucoside	0.016 ± 0.003[a]	Tr	Tr
petunidin 3-*O*-galactoside	0.012 ± 0.003[a,b]	Tr	0.014 ± 0.003[b]
peonidin 3-*O*-galactoside	0.019 ± 0.004[a]	Tr	0.010 ± 0.003[b]
petunidin 3-*O*-arabinoside	Tr	Tr	0.055 ± 0.005[a]
malvinidin 3-*O*-galactoside	0.077 ± 0.011[a]	Tr	0.061 ± 0.012[a,b]
peonidin 3-*O*-arabinoside	Tr	Tr	0.017 ± 0.005[a]
malvidin 3-*O*-glucoside	0.072 ± 0.007[a]	Tr	Tr
malvidin 3-*O*-arabinoside	0.024 ± 0.004[a]	Tr	Tr
delphinidin 6-acetoyl-3-*O*-glucoside	0.095 ± 0.014[a]	0.029 ± 0.008[b]	0.101 ± 0.022[a]
malvidin 6-acetoyl-3-*O*-glucoside	0.116 ± 0.010[a]	0.054 ± 0.018[b,c]	0.101 ± 0.036[c]
total	0.453 ± 0.056[a]	0.083 ± 0.025[b]	0.379 ± 0.089[a]

[a]The values given are mean ± SEM from three independent analyzes. Means with different superscript letters in the same row are statistically significant ($p < 0.05$). [b]Tr = traces.

Table 5. In Vitro Antioxidant Activities of Crude Water Extract, Dialyzed Extract, and Dialyzate from Frozen and Freeze-Dried Wild Blueberries[a]

samples	specific scavenging (% reduction per 10 μg of polyphenols)		
	DPPH radical	superoxide radical	hydroxyl radical
Frozen Blueberries			
crude extract	17.61 ± 0.56[b]	30.78 ± 9.17[a]	11.17 ± 3.48[b]
dialyzed extract	24.66 ± 2.10[b]	46.06 ± 2.49[a]	13.53 ± 4.44[b]
dialyzate	33.12 ± 4.30[aA]	7.80 ± 1.99[bA]	25.90 ± 2.60[aA]
vitamin C	40.90 ± 3.23	21.62 ± 1.57	–
trolox	33.57 ± 2.60	22.18 ± 2.90	79.30 ± 1.34
Freeze-Dried Blueberries			
crude extract	21.73 ± 0.96[a]	23.11 ± 5.62[a]	11.54 ± 3.20[b]
dialyzed extract	22.63 ± 6.38[a]	35.55 ± 8.0[a]	6.85 ± 2.03[b]
dialyzate	11.40 ± 3.80[aB]	28.84 ± 6.99[aB]	40.43 ± 1.26[aB]
vitamin C	40.90 ± 3.23	21.62 ± 1.57	–
trolox	33.57 ± 2.60	22.18 ± 2.90	79.30 ± 1.34

[a]Data are representative of 3 independent assays, and expressed as mean ± SEM. Means with different superscript letters in the same column are statistically significant ($p < 0.05$).

twice as effective as the dialyzed water extract from frozen blueberries at 20 μg/mL level. The dialyzate from extracts of both frozen and freeze-dried blueberries comprising free polyphenols showed the least amount of α-glucosidase inhibition (<10%; Figure 2). Neither gallic acid (data not shown) nor catechin inhibited α-glucosidase activity more than 20% at 100 μg/mL.

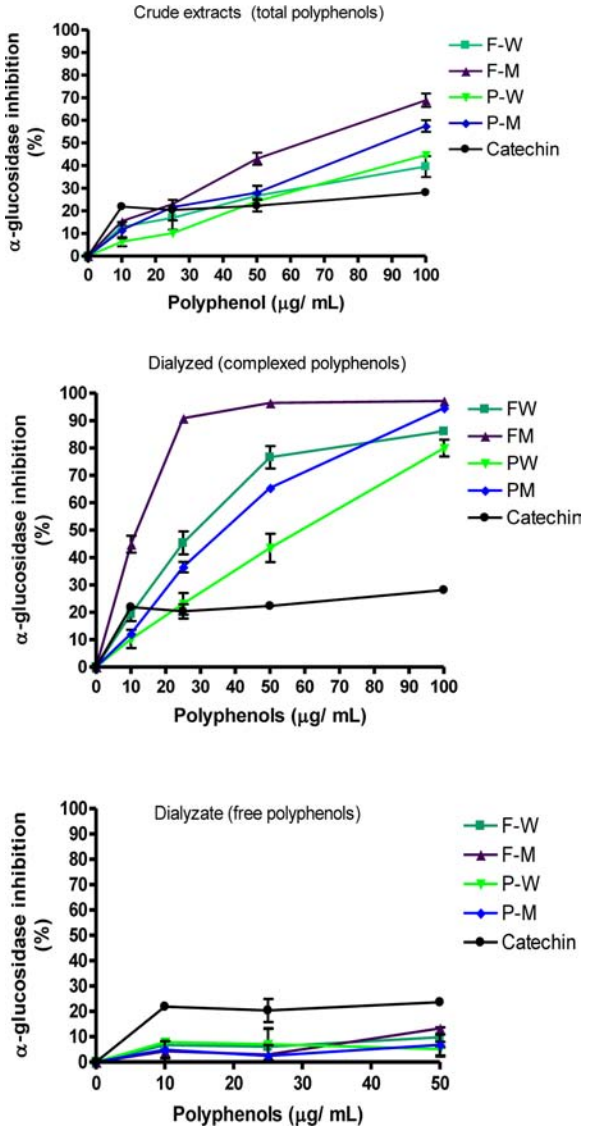

Figure 2. Percent inhibition of α-glucosidase activity of polyphenols isolated from blueberry extract, dialyzed extract, and dialyzate fractions. Frozen blueberries and freeze-dried blueberries were extracted with water or methanol, and the polyphenols were subjected to dialysis against water and purified using sep-pak C_{18} columns. Inhibition of α-glucosidase activity was performed in the presence of increasing levels of polyphenols. The activity curves are denoted as follows: dark green square, frozen blueberries extracted with water; purple triangle, frozen blueberries extracted with methanol; light green triangle, freeze-dried powder extracted with water; blue diamond, freeze-dried powder extracted with methanol. Catechin was used as a standard: black circle. The results shown are mean ± SEM from three independent experiments.

Antiproliferative Activity. Colon cancer (HT-29) and normal colon (CRL-1790) cells were incubated in the presence or absence of free and complexed blueberry polyphenols (dialyzed and dialyzate fractions) at concentrations ranging from 0 to 100 μg total polyphenols/mL medium, and proliferation was evaluated using the SRB binding assay relative to an untreated control (only medium without polyphenols) (Figure 3). Results clearly indicated that all samples exhibited significant inhibitory activities on the growth of both HT-29

DOI: 10.1021/acs.jafc.5b00016
J. Agric. Food Chem. 2015, 63, 2935−2946

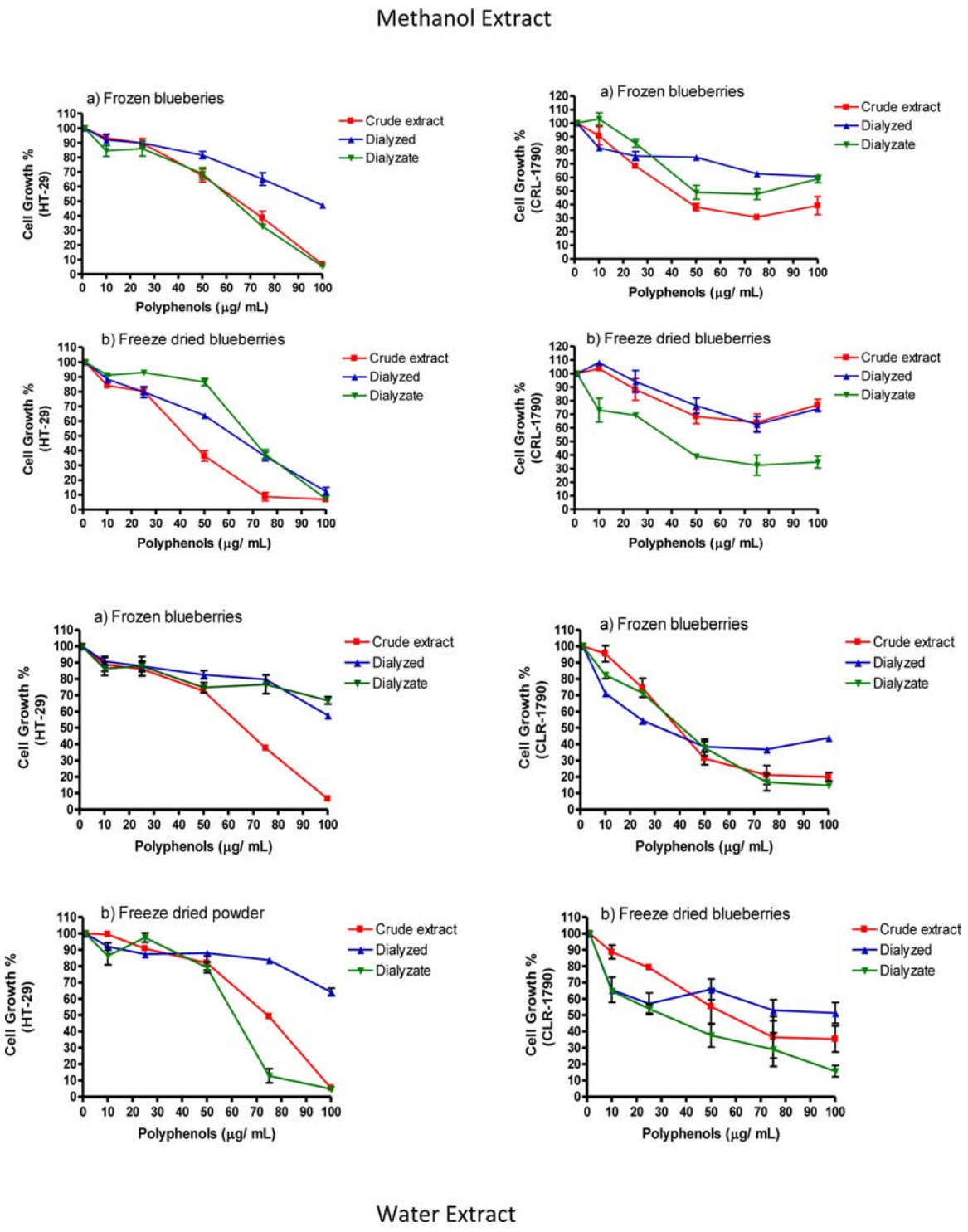

Figure 3. Antiproliferative activity of various fractions isolated from blueberries. Frozen blueberries and freeze-dried blueberries were extracted with methanol (top four panels) or water (bottom four panels). Activities of polyphenols isolated from crude extract, dialyzed extract, and dialyzate were evaluated using a colorectal cancer cell line HT 29 and a normal colon cell line CRL 1790. The data represent the mean ± SEM of results from four independent experiments.

and CRL-1790 cells in a dose-dependent manner but generally at relatively high concentrations (>50 μg/mL). Methanol-extracted and purified polyphenols, dialyzed extract, and dialyzate from frozen blueberries showed a similar degree of antiproliferative action on HT-29 cells as compared to similar extracts from freeze-dried blueberries (Figure 3). Inhibitory properties of these extracts were slightly reduced in CRL 1790 cells. Antiproliferative activity of polyphenols obtained after water extraction and purification of frozen blueberries and freeze-dried blueberries was much higher against HT 29 cells, while that of the dialyzed extract was marginal (~30% inhibition). Dialyzate from freeze-dried blueberries showed much higher antiproliferative activity against HT-29 cells. Polyphenols isolated from the aqueous extracts of frozen

DOI: 10.1021/acs.jafc.5b00016
J. Agric. Food Chem. 2015, 63, 2935−2946

blueberries and freeze-dried blueberries, as well as their dialyzed extracts and dialyzates, showed a relatively higher antiproliferative activity against CRL 1790 cells at concentration ranges lower than 50 μg/mL.

Pectin Content of Blueberry Extracts. To further understand the potential nature of polyphenol food matrix interactions, levels of pectin, the major cell wall component in ripe fruit, were analyzed in different berry fractions (Figure 4).

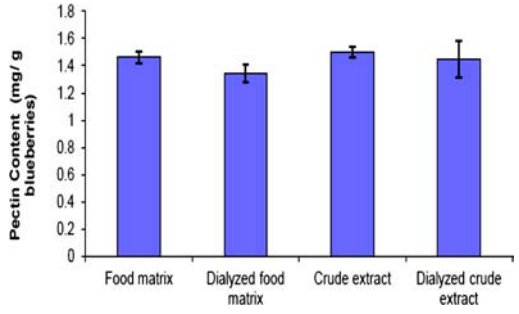

Figure 4. Pectin contents of different blueberry food matrixes. A set of blueberry fruit (50 g) was bleached with ethanol to remove the polyphenols completely, and the resulting fruit were subjected to homogenization in water, removal of debris by centrifugation, and dialysis. These fractions are denoted as food matrix and dialyzed food matrix. A separate set (50 g) was subjected to water extraction, removal of debris, centrifugation, and dialysis. Pectin content was estimated by a colorimetric method. The data are from three separate analyses and expressed as mean ± SEM.

There were no significant differences in pectin content between crude extracts and dialyzed extracts of decolorized fruits and the original blueberry extracts and dialyzed extracts. The average pectin content in all samples was approximately 1.5 mg/g frozen weight of blueberries.

To evaluate the ability of purified carbohydrate-rich matrixes to complex with polyphenols, varying concentrations of pectin and cellulose were mixed with 1 mg gallic acid equivalent of free polyphenols. To confirm that these polyphenols could form complexes with pectin and cellulose after mixing, the mixtures were dialyzed overnight. Table 6 shows the proportion of polyphenols complexed with pectin−cellulose and those that are free and recovered in the dialyzate fraction after dialysis. A fixed amount of polyphenols (1.3 mg) was mixed with different solutions: 0.5% w/v pectin, 0.5% w/v cellulose, and 0.5% w/v pectin−cellulose, and total polyphenols were quantified. During dialysis, over 90% of the polyphenols leaked out of the bag when polyphenols were alone or mixed with cellulose. When mixed with pectin or pectin and cellulose, there was some retention of the polyphenols within the dialysis bag, indicating a weak binding between pectin and polyphenols, but this was far lower than what was observed in the dialyzed extract of blueberries (Table 1).

Antioxidant Activity in Mixed Complexes. The ability of fruit matrix (i.e., pectin, cellulose, and pectin + cellulose) to scavenge DPPH radicals was assessed in comparison to the dialyzed and dialyzate fractions obtained from blueberry homogenate. Fruit matrix alone (obtained after the extraction of the polyphenols) was tested after mixing with equivalent levels of polyphenols that were present in the original blueberry homogenate. Blueberry dialyzed extract containing polyphenols showed a dose-dependent increase in DPPH scavenging ability (Figure 5). Dialyzate from blueberry extract containing free polyphenols showed almost 90% scavenging of DPPH radicals at the highest concentration tested, followed by complexed polyphenols obtained from dialyzed extract of blueberries. Natural food matrix isolated from ethanol-bleached blueberries before and after dialysis showed a very low scavenging ability of DPPH at ∼10%. Different solutions containing food matrixes made of pectin or cellulose showed ∼5% inhibition. When complexed as in the dialyzed extract, the matrix tends to reduce the antioxidant capacity of polyphenols in the range of 10−20% (Figure 5).

Antiproliferative Activity in Mixed Complexes. Antiproliferative activities of blueberry polyphenols and different food matrixes were evaluated using colon cancer cell line HT-29. As shown in Figure 6, free polyphenols at the highest concentration (100 μg/mL) inhibited approximately 80% of the growth of HT-29 cells. By contrast, when the same amount of polyphenols was naturally complexed with the blueberry fruit matrix, there was only 50% inhibition. Samples containing 100 μg/mL of the fruit matrix, or the dialyzed food matrix, showed only 10% and 30% inhibition of cell growth after 24 and 48 h incubation periods, respectively. In another experiment, when the dialyzate containing free polyphenols or purified polyphenols was mixed with pectin, cellulose, or a mixture of pectin and cellulose and incubated with HT 29 cells, antiproliferative action was nearly similar for 24 h incubation, but during prolonged incubation for 48 h, polyphenol−pectin mixture tended to show a higher degree of antiproliferative activity, suggesting that during long-term incubation in media, pectin may complex with proteins, resulting in enhanced bioavailability of polyphenols and an increase in antiproliferative activity (Figure 7). These aspects need further investigation.

DISCUSSION

Public interest in blueberries as a functional food has increased in recent years because of its health benefits. Blueberry is commonly consumed fresh, frozen, and as a powder. Simple and acylated anthocyanins have been found in some low bush cultivars.[21,22] Overall, the profile of polyphenols in this study is consistent with those reported previously in the literatur-

Table 6. Effect of Dialysis on the Retention of Polyphenols by Pectin (0.5%), Cellulose (0.5%), and a Mixture of Pectin and Cellulose (0.25% each)[a]

	original extract		dialyzed extract		dialyzate	
sample	phenolic content (mg)	recovery (%)	phenolic content (mg)	recovery (%)	phenolic content (mg)	recovery (%)
polyphenols alone	1.3 ± 0.05	100	0.10 ± 0.003	7.7	1.20 ± 0.02	92
pectin−polyphenol	1.3 ± 0.03	100	0.10 ± 0.002	7.7	1.13 ± 0.09	86
cellulose−polyphenol	1.3 ± 0.06	100	0.10 ± 0.006	7.7	1.18 ± 0.18	91
pectin−cellulose−polyphenol	1.3 ± 0.04	100	0.08 ± 0.001	6.2	1.16 ± 0.02	89

[a]Data presented are mean ± SEM from three separate analyzes. The values in columns are not significantly different from one another at $P < 0.5$.

DOI: 10.1021/acs.jafc.5b00016
J. Agric. Food Chem. 2015, 63, 2935−2946

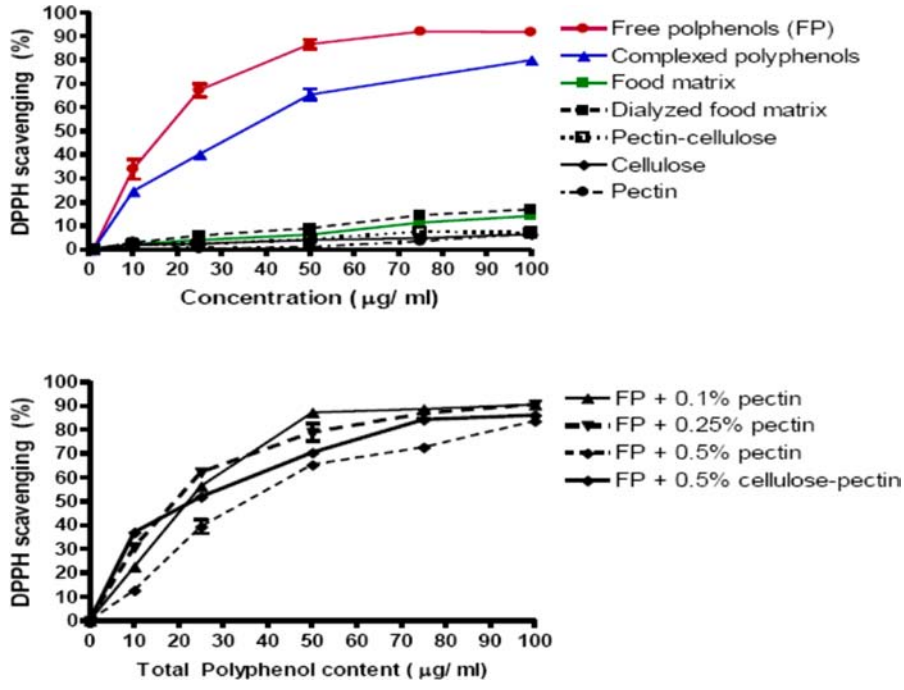

Figure 5. A comparison of DPPH radical scavenging activities of isolated bleached blueberry fruit matrix, pectin, and cellulose (each at 100 μg/mL) alone, with the dialyzed extract (complexed polyphenols) and with the dialyzate (free polyphenols) of water extracted blueberries (top panel). The concentrations indicated (x-axis) are for both polyphenols (as estimated by Folin's reagent) and the matrix (weight). The bottom panel shows the effect of pectin and a combination of cellulose and pectin (100 μg/mL) on the DPPH-radical scavenging activity of free polyphenols isolated from blueberries. The data represent mean ± SEM from three separate experiments.

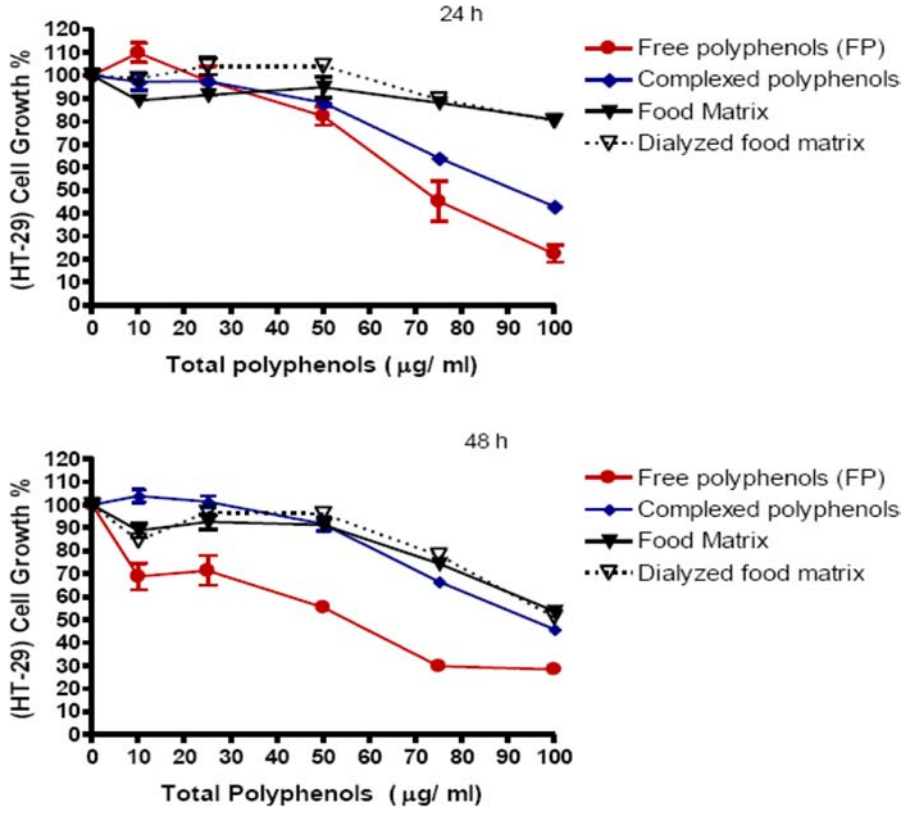

Figure 6. Effect of food matrix (100 μg/mL) isolated from blueberries on antiproliferative activity of free polyphenols (dialyzate) and complexed polyphenols (dialyzed extract) monitored at 24 h after treatment (top panel) and 48 h after treatment (bottom panel) using HT 29 colorectal cancer cells. The data are mean ± SEM from three independent experiments.

DOI: 10.1021/acs.jafc.5b00016
J. Agric. Food Chem. 2015, 63, 2935−2946

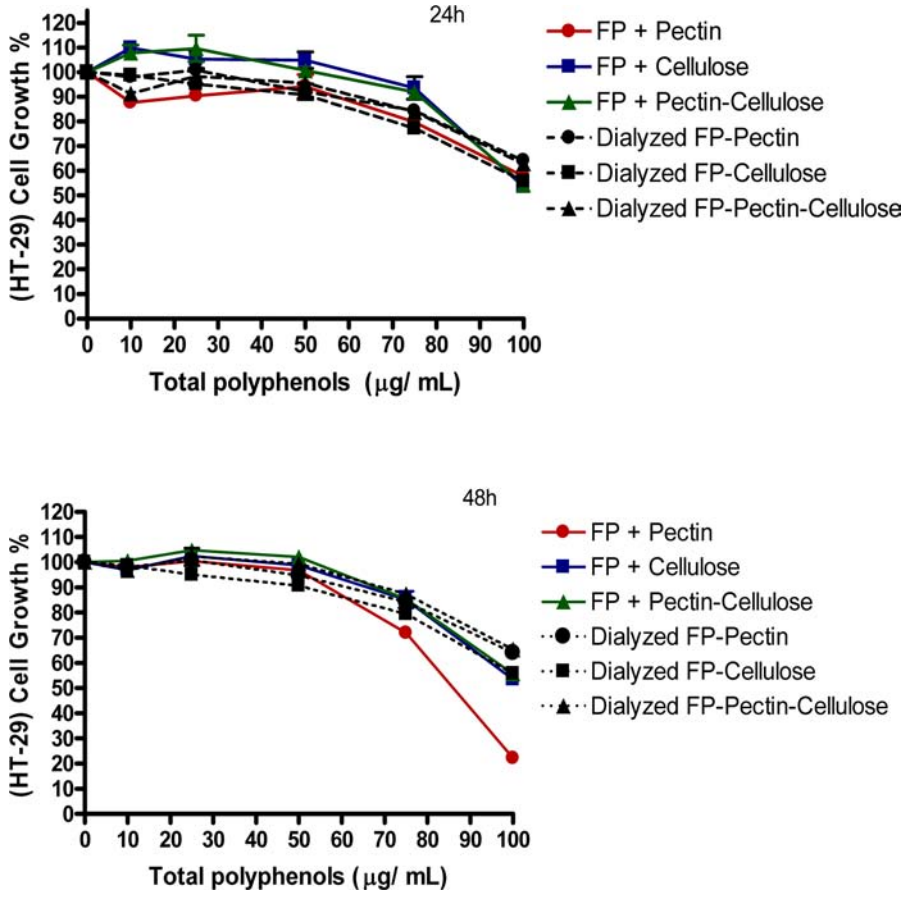

Figure 7. Antiproliferative activity of free polyphenols (dialyzate) in combination with various mixtures of polyphenols, pectin, and cellulose (100 μg/mL) evaluated using HT 29 cells. Antiproliferative activity was monitored at 24 h (top panel) and 48 h (bottom panel). The data are mean ± SEM from three independent experiments.

e.[23−26]Organic acids are also helpful in the stabilization of ascorbic acid and anthocyanins in frozen and processed berries.[27]

Blueberries are rich in phenolic acids such as benzoic acid and cinnamic acid derivatives. Benzoic acid derivatives include vanillic acid, syringic acid, gallic acid, protocatechuic acid, *m*-hydroxybenzoic acid, *p*-hydroxybenzoic acid and ellagic acid. Major cinnamic acid derivatives include chlorogenic acid, caffeic acid, ferulic acid, quinic acid and coumaric acid.[23] Polyphenols in blueberries are naturally esterified with other phenolic acids or sugars, suggesting that they are frequently found as glucosides such as quercetin glucoside, myricetin glucoside, and kaempferol glucoside.[28] In our study, chlorogenic acid was the major component identified, and other phenolic acids were nondetectable or occurred as minor components eluting before chlorogenic acid.[10] Flavonoid derivatives of quercetin, rhamnetin, syringetin, and myricetin were also identified.

In blueberry skin and flesh, delphinidin, cyanidin, petunidin, peonidin, and malvidin monoglycosides (glycosides, galactosides and arabinosides) are the main anthocyanins. Because of the diversity in the glycosylation and acylation pattern, more than 25 anthocyanins have been identified in blueberries. The distribution of anthocyanins in five different blueberry genotypes have been reported,[29] where delphinidin was the most abundant anthocyanin (27−40%), followed by malvidin (22−33%), petunidin (19−26%), cyanidin (6−14%), and peonidin (1−5%). Nearly equal distribution of anthocyanins was observed in blueberry fruits analyzed in this study.

Anthocyanins are rarely ingested on their own but as a component of fruits or vegetables or in meals containing other simple and macromolecular food components. Studies carried out by Mazza and co-workers[30] have shown that there are significant differences in the absorption rates of anthocyanins when consumed either alone or with high fat meals.[30,31] In a study[32] on red grape juice, a synergistic enhancement in intestinal anthocyanin absorption by glucose was observed, as compared to that from red wine. It has also been shown that isolated polyphenols from grape juice are more effective in arresting the growth of tumor in mice than those isolated from red wine, when provided through gavage.[33] Although it is generally believed that the food matrix may not affect the functionality of polyphenols, molecular interactions between polyphenols and other components present in the food matrix ultimately may alter their antioxidant function and bioefficacy.[12,34,35] For instance, 34−40% of polyphenols in red wine seem to be complexed to dietary fiber.[35] In another study, nearly 25% of polyphenols present in grape juice concentrate were found to be complexed with carbohydrates.[12] Thus, food-matrix interactions may play a major role in the functionality of polyphenols.

In this study, we analyzed the potential modulatory role of food matrix in polyphenol function. During ripening, the structural matrixes such as cellulose and pectin undergo degradation. As the compartmentalization of ripening tissue decreases, the polyphenols that are normally confined to vacuoles may leak out and form complexes with cellular

DOI: 10.1021/acs.jafc.5b00016
J. Agric. Food Chem. 2015, 63, 2935−2946

macromolecules. Thus, it was interesting to see if food matrix isolated from ripe fruits or those reconstituted by components such as cellulose and pectin had any influence in polyphenol functionality, such as its antioxidant function or anticancer properties. These interactions may have an impact on the delivery and absorption of polyphenols in vivo. Our results show that nearly 28% of the polyphenols in blueberry crude extracts are naturally complexed with the food matrix. These results are in agreement with previous studies[12] demonstrating that approximately 25% of nondialyzable polyphenols in grapes were bound to carbohydrates and lipids.

The present study suggests that food matrix alone, as well as the synthesized food matrixes used in the experiments, did not have a considerable antioxidant activity. When free polyphenols were mixed with different concentrations of pectin or/and cellulose, their scavenging capacity of the DPPH radical was similar to that of free polyphenols. As well, isolated matrix devoid of polyphenols by itself showed minimal antioxidant or antiproliferative activity. When polyphenols are mixed with high amounts of pectin or cellulose, antioxidant activity of polyphenols does not decrease. However, when the dialyzed extract containing naturally complexed polyphenols was mixed with food matrix, it showed a lower antioxidant activity and antiproliferative activity as compared to that of free polyphenols. This may be due to complex formations involving key hydroxyl groups of the polyphenols with polygalacturonic acid moieties of pectin that make polyphenols less amenable to scavenge free radicals.

Despite the fact that there are numerous reports of inhibition of cancer cell growth and proliferation in vitro by purified anthocyanin-rich extracts or crude extracts, very few studies have been conducted to delineate potential influences of food matrix on the biological activity of components studied. In this study, the antiproliferative action of free polyphenols, complexed polyphenols, and food matrix was compared separately.[36,37] It is of great interest to understand the effect of the food matrix on the biological activity of polyphenols to develop processing techniques that take advantage of such interactions and lead to the production of high quality and value-added products. Although, blueberry food matrix did not show a considerable effect on antiproliferative activity, there was a significant decrease in the inhibitory activity when polyphenols were naturally complexed with the blueberry food matrix. By contrast, various mixtures containing free polyphenols and the synthetic food matrixes did not have the same effect as polyphenols complexed with matrix during extraction. These results suggest that strong interactions between polyphenols and fruit matrixes may affect the bioavailability and efficacy of polyphenols in several ways.

Besides having high in vitro antioxidant activity, different fruit extracts have been studied for their ability to inhibit α-glucosidase, a key enzyme involved in the digestion of starch into sugars. Inhibition of the activity of carbohydrate-hydrolyzing enzymes has the potential to lower sugar absorption and consequently may provide an additional tool for the management of blood sugar levels by preventing postprandial hyperglycemia, thus controlling the onset of type II diabetes.[38,39] Efficacy of the polyphenols in binding with proteins and subsequent enzymatic inhibition could be attributed to the fact that polyphenols are multidentate ligands, capable of binding simultaneously (via different hydroxyl groups) to more than one site of the protein (enzyme).[40] In contrast to the reduction observed in antioxidant and antiproliferative activities, the dialyzed extract containing complexed polyphenols showed the highest inhibitory activity toward α-glucosidase. It has been previously hypothesized[41] that the inhibitory effectiveness of berry fruit extracts against α-glucosidase was related to their anthocyanin content. The results from this study suggest that the complexed polyphenols or their interactions with other components of the food matrix enhance their ability to inhibit α-glucosidase activity. In vivo studies with healthy human volunteers demonstrated that freeze-dried wild blueberry powder increased the serum antioxidant status.[42] Whole blueberry freeze-dried powder also reduced the insulin resistance in adipose tissue and increased the function of β cells in male C57BL mice fed high fat diets, suggesting that processed fruits are equally effective in providing health benefits.[42,43] Thus, polyphenols, whether free or complexed with fruit matrixes, can thus provide multiple protective roles in the human body.

Apart from the phenolic components, flavonoids, and anthocyanins, blueberries are a rich source of procyanidins which are dimers, trimers, and polymers of flavan-3-ols, catechin, and epicatechin.[44] These components have not been analyzed in the present study. Because of their complex structure, procyanidins are ideally suited to form molecular complexes with pectin and other cell wall polymers. It is also highly likely that the health benefits observed in blueberries may in part be due to their procyanidin content.[44]

In conclusion, interactions between polyphenols and food matrix can play an important role in the bioactivity of blueberries. Although complex formation did not reduce the antioxidant and α-glucosidase activities of blueberry polyphenols, it slightly reduced the antiproliferative activity. These results suggest that different fractions of polyphenols obtained in frozen or freeze-dried blueberry products may provide multiple effects such as antioxidant activity, regulation of glucose homeostasis, and antiproliferative functions to different extents depending on their complexed or free state. The presence of a food matrix may positively affect the stability of polyphenols in the gastrointestinal tract, as well as the extent of absorption and their metabolism in vivo. A better understanding of which compounds form complexes with the polyphenols is needed, as well as their stability in the gastrointestinal tract to obtain relevant information about the bioavailability and metabolism of phenolic compounds in blueberries.

AUTHOR INFORMATION

Corresponding Author

*Phone: 519-824-4120 x54856. E-mail: gpaliyat@uoguelph.ca.

Funding

We are grateful to the Ontario Ministry of Agriculture, Food and Rural Affairs for the financial assistance to conduct this research. We also thank CONACYT, Mexico, for providing a scholarship to Julieta C. Betanzo.

Notes

The authors declare no competing financial interest.

REFERENCES

(1) Strik, B. Berry crops: Worldwide area and production systems. In *Berry fruit: Value-added products for health promotion*; Zhao, Y., Ed.; CRC Press: Boca Raton, FL, 2007; pp 3 − 50.

(2) Papadopoulou, A.; Frazier, R. A. Characterization of protein-polyphenol interactions. *Trends Food Sci. Technol.* **2004**, *15*, 186−190.

DOI: 10.1021/acs.jafc.5b00016
J. Agric. Food Chem. 2015, 63, 2935−2946

(3) Williamson, G.; Manach, C. Bioavailability and bioefficacy of polyphenols in humans. II. Review of 93 intervention studies. *Am. J. Clin. Nutr.* **2005**, *81*, 243S−255S.
(4) Wang, L. S.; Stoner, G. D. Anthocyanins and their role in cancer prevention. *Cancer Lett.* **2008**, *269*, 281−290.
(5) Jacob, J. K.; Tiwari, K.; Correa-Betanzo, J.; Misran, A.; Chandrasekaran, R.; Paliyath, G. Biochemical basis for functional ingredient design from fruits. *Annu. Rev. Food Sci. Technol.* **2012**, *3*, 79−104.
(6) Prior, R. L.; Martin, A.; Cao, G.; Sofic, E.; McEwan, J.; O'Brien, C.; Lischner, N.; Ehlenfeldt, M.; Krewer, G.; Mainland, C. M. Antioxidant capacity as influenced by total phenolics and anthocyanin content, maturity and variety of *Vaccinium* species. *J. Agric. Food Chem.* **1998**, *46*, 2686−2693.
(7) Kyle, J. A. M.; Duthie, G. G. Flavonoids in foods. In *Flavonoids: Chemistry, Biochemistry and Applications*; Andersen, O. M., Markham, K. R., Eds.; CRC Press, Taylor and Francis: Boca Raton, FL, 2006; pp 219−261.
(8) Andersen, O. M.; Jordheim, M. The anthocyanins. In *Flavonoids: Chemistry, Biochemistry and Applications*; Andersen, O. M., Markham, K. R., Eds.; CRC Press, Taylor and Francis: Boca Raton, FL, 2006; pp 471−551.
(9) Turgeon, S. L.; Rioux, L. E. Food matrix impact on macronutrients nutritional properties. *Food Hydrocolloids* **2011**, *25*, 1915−1924.
(10) Correa-Betanzo, J.; Allen-Vercoe, E.; McDonald, J.; Schroeter, K.; Corredig, M.; Paliyath, G. Stability and biological activity of wild blueberry (*Vaccinium angustifolium*) polyphenols during simulated in vitro gastrointestinal digestion. *Food Chem.* **2014**, *165*, 522−531.
(11) Aguilera, J. M.; Stanley, D. W.; Baker, K. W. New dimensions in microstructure of food products. *Trends Food Sci. Technol.* **2000**, *11*, 3−9.
(12) Jacob, J. K.; Paliyath, G. Physicochemical characteristics of nanovesicle−carbohydrate complexes in grape juice concentrate. *J. Agric. Food Chem.* **2008**, *56*, 1305−1315.
(13) Singleton, V. L.; Orthofer, R.; Lamuela-Raventos, R. M. Analysis of total phenols and other oxidation substrates and antioxidants by means of Folin−Ciocalteu reagent. *Methods Enzymol.* **1999**, *299*, 52−57.
(14) Jacob, J. K.; Hakimudin, F.; Paliyath, G.; Fischer, H. Antioxidant and antiproliferative activity of polyphenols in novel high-polyphenol grape lines. *Food Res. Int.* **2008**, *41*, 419−428.
(15) Taylor, K. A. C. C. A colorimetric method for the quantitation of galacturonic acid. *Appl. Biochem. Biotechnol.* **1993**, *43*, 51−54.
(16) Molyneux, P. The use of stable free radical diphenyl picrylhydrazyl (DPPH) for estimating antioxidant activity. *J. Sci. Technol.* **2004**, *26*, 211−219.
(17) Madamanchi, N. R.; Donahue, J. L.; Cramer, C. L.; Alscher, R. G.; Pedersen, K. Differential response of Cu, Zn superoxide dismutase in two pea cultivars during a short-term exposure to sulfur dioxide. *Plant Mol. Biol.* **1994**, *26*, 95−103.
(18) Halliwell, B.; Gutteridge, J. M. C.; Aruoma, O. I. The deoxyribose method: A simple "test-tube" assay for determination of rate constants for reactions of hydroxyl radicals. *Anal. Biochem.* **1987**, *165*, 215−219.
(19) Kwon, Y.; Apostolidis, E.; Shetty, K. 2008. Inhibitory potential of wine and tea against α-amylase and α-glucosidase for management of hyperglycemia linked to type 2 diabetes. *J. Food Biochem.* **2008**, *32*, 15−31.
(20) Vichai, V.; Kirtikara, K. Sulforhodamine B colorimetric assay for antiproliferative activity screening. *Nat. Protocols* **2006**, *1*, 1112−1117.
(21) Gao, L.; Mazza, G. Quantitation and distribution of simple and acylated anthocyanins and other phenolics in blueberries. *J. Food Sci.* **1994**, *59*, 1057−1059.
(22) Wu, X.; Prior, R. L. Systemic identification and characterization of anthocyanins by HPLC-ESI-MS/MS in common foods in the United States: Fruits and berries. *J. Agric. Food Chem.* **2005**, *53*, 2589−2599.
(23) Su, Z. Anthocyanins and flavonoids of *Vaccinium* L. *Pharm. Crops* **2012**, *3*, 7−37.
(24) Sellappan, S.; Akoh, C. C.; Krewer, G. Phenolic compounds and antioxidant capacity of Georgia-grown blueberries and blackberries. *J. Agric. Food Chem.* **2002**, *50*, 2432−2438.
(25) You, Q.; Wang, B.; Chen, F.; Huang, Z.; Wang, X.; Luo, P. G. Comparison of anthocyanins and phenolics in organically and conventionally grown blueberries in selected cultivars. *Food Chem.* **2011**, *125*, 201−208.
(26) Wang, S. Y.; Chen, H.; Camp, M. J.; Ehlenfeldt, M. K. Flavonoid constituents and their contribution to antioxidant activity in cultivars and hybrids of rabbiteye blueberry (*Vaccinium ashei* Reade). *Food Chem.* **2012**, *132*, 855−864.
(27) Viljakainen, S.; Visti, A.; Laakso, S. Concentrations of organic acids and soluble sugars in juices from Nordic berries. *Acta Agric. Scand.* **2002**, *52*, 101−109.
(28) Häkkinen, S. H.; Heinonen, I. M.; Karenlampi, S. O.; Mykkanen, H.M.; Ruus-Kanen, J.; Torronen, A. R. Screening of selected flavonoids and phenolic acids in 19 berries. *J. Food Res. Int.* **1999**, *32*, 345−353.
(29) Cho, M. J.; Howard, L.; Prior, R.; Clark, J. Flavonoid glycosides and antioxidant capacity of various blackberry, blueberry and red grape genotypes determined by high-performance liquid chromatography/mass spectrometry. *J. Sci. Food Agric.* **2004**, *84*, 1771−1782.
(30) Mazza, G.; Kay, C. D.; Cottrell, T.; Holub, B. J. Absorption of anthocyanins from blueberries and serum antioxidant status in human subjects. *J. Agric. Food Chem.* **2002**, *50*, 7731−7737.
(31) Kay, C. D.; Mazza, G.; Holub, B. J.; Wang, J. Anthocyanin metabolites in human urine and serum. *Br. J. Nutr.* **2004**, *91*, 933−942.
(32) Bitsch, R.; Netzel, M.; Frank, T.; Strass, G.; Bitsch, I. Bioavailability and biokinetics of anthocyanins from red grape juice and red wine. *J. Biomed. Biotechnol.* **2004**, *5*, 293−298.
(33) Hakimuddin, F.; Tiwari, K.; Paliyath, G.; Meckling, K. Grape and wine polyphenols down-regulate the expression of signal transduction genes and inhibit the growth of estrogen receptor-negative MDA-MB231 tumors in nu/nu mouse xenografts. *Nutr. Res. (N. Y., NY, U. S.)* **2008**, *28*, 702−713.
(34) Rice-Evans, C. A.; Miller, N. J. Antioxidant activities of flavonoids as bioactive components of food. *Biochem. Biochem. Soc. Trans.* **1996**, *24*, 790−795.
(35) Saura-Calixto, F.; Serrano, J.; Goñi, I. Intake and bioaccessibility of total polyphenols in a whole diet. *Food Chem.* **2007**, *101*, 492−501.
(36) Seeram, N. P.; Adams, L. S.; Zhang, Y.; Lee, R.; Sand, D.; Scheuller, H. S.; Heber, D. Blackberry, black raspberry, blueberry, cranberry, red raspberry, and strawberry extracts inhibit growth and stimulate apoptosis of human cancer cells in vitro. *J. Agric. Food Chem.* **2006**, *54*, 9329−9339.
(37) Zhao, C.; Giusti, M. M.; Malik, M.; Moyer, M. P.; Magnuson, B. Effects of commercial anthocyanin-rich extracts on colonic cancer and nontumorigenic colonic cell growth. *J. Agric. Food Chem.* **2004**, *52*, 6122−6128.
(38) Shetty, K. Biosynthesis of rosmarinic acid and applications in medicine. *J. Herbs Spices Med. Plants* **2001**, *8*, 161−181.
(39) Grace, M. H.; Ribnicky, D. M.; Kuhn, P.; Poulev, A.; Logendra, S.; Yousef, G. G.; Raskin, I.; Lila, M. A. Hypoglycemic activity of a novel anthocyanin-rich formulation from lowbush blueberry, *Vaccinium angustifolium* Aiton. *Phytomedicine* **2009**, *16*, 406−415.
(40) Freitas, V.; Carvalho, E.; Mateus, N. Study of carbohydrate influence on protein-tannin aggregation by nephelometry. *Food Chem.* **2003**, *81*, 503−509.
(41) Kay, C. D.; Holub, B. J. The effect of wild blueberry (*Vaccinium angustifolium*) consumption on postprandial serum antioxidant status in human subjects. *Br. J. Nutr.* **2002**, *88*, 389−397.
(42) DeFuria, J.; Bennett, G.; Strissel, K. J.; Perfield, J. W.; Milbury, P. E.; Greenberg, A. S.; Obin, M. S. Dietary blueberry attenuates whole-body insulin resistance in high fat-fed mice by reducing adipocyte death and its inflammatory sequel. *J. Nutr.* **2009**, *139*, 1510−1516.

DOI: 10.1021/acs.jafc.5b00016
J. Agric. Food Chem. 2015, 63, 2935−2946

(43) Prior, R. L.; Wilkes, S. E.; Rogers, T. R.; Khanal, R. C.; Wu, X.; Howard, L. R. Purified blueberry anthocyanins and blueberry juice alter development of obesity in mice fed an obesogenic high-fat diet. *J. Agric. Food Chem.* **2010**, *58*, 3970−3976.
(44) Prior, R. L.; Lazarus, S. A.; Cao, G.; Muccitelli, H.; Hammerstone, J. F. Identification of procyanidins and anthocyanins in blueberries and cranberries (*Vaccinium Spp.*) using high-performance liquid chromatography/mass spectrometry. *J. Agr. Food Chem.* **2001**, *49*, 1270−1276.

DOI: 10.1021/acs.jafc.5b00016
J. Agric. Food Chem. 2015, 63, 2935−2946

Excess production of free radicals is associated with oxidative damage to biomolecules, including lipids, proteins, and DNA, eventually leading to many chronic diseases, such as atherosclerosis, cancer, and other degenerative diseases in humans.[15] Plant-based dietary polyphenols and flavonoids have been used to estimate antioxidant activity in vitro, and have been associated with the prevention of cancer, type 2 diabetes, and cardiovascular diseases.[16−18] However, there is little information on the polyphenol and flavonoid levels or the potential cancer-prevention activity of horseradish roots. Because these phytochemicals and bioactivities have been associated with reduced disease incidence, quantitation of horseradish root polyphenol and antioxidant activity will be useful information.

The objectives of this study were to determine the variation of AITC formation and corresponding nitrile formation from several horseradish accessions, including accessions from the Li and Kushad study.[2] Another objective of this study was to evaluate the potential cancer-prevention properties of horseradish roots by assessing QR-inducing bioactivity, as well as antioxidant activity, using two different commercial grades (U.S. Fancy vs U.S. No. 1) in four different genotypes of horseradish. As a result, significant variation of AITC and CETP formation was observed among genotypes and grades. To our knowledge, this is the first detection and measurement of CETP from horseradish. There were significant correlations between sinigrin and AITC as well as AITC and QR bioactivity that can be useful information for horseradish quality. U.S. Fancy grade showed significantly higher sinigrin and AITC concentrations than U.S. No. 1, whereas U.S. No. 1 showed significantly higher CETP and total phenolic concentrations than U.S. Fancy.

MATERIALS AND METHODS

Chemicals. Benzyl GS was purchased from POS Pilot Plant Corp (Saskatoon, SK, Canada). DEAE Sephadex A-25 resin was purchased from GE Healthcare (Piscataway, NJ, USA). Lead acetate, barium acetate, AITC, benzyl isothiocyanate (BITC), 2-penethyl isothiocyanate (PEITC), 2-phenylpropionitrile (PPNT), benzyl cyanide, alpha-minimum essential medium (α-MEM) high-performance liquid chromatography (HPLC)-grade acetonitrile, ACS-grade hexane, 2,2′-azino-bis(3-ethylbenzothiazoline-6-sulfonic acid (ABTS), Folin-Ciocalteu, potassium persulfate, 2,4,6-tripyridyl-s-triazine, $FeCl_3 \cdot 6H_2O$, and Trolox were purchased from Sigma (St. Louis, MO, USA).

Cultivation of Horseradish. Six accessions of horseradish were selected for this study: IL196, IL706, IL785, IL813, IL1091, and IL1573. Horseradish accessions IL813 and IL196 previously showed high sinigrin content, whereas IL1573 showed comparatively low levels.[2] In addition, IL785 and IL1091 accessions were selected as new high root sinigrin-containing horseradish accessions as well as IL706 with low levels. These accessions are part of a germplasm collection housed at the Vegetable Research Farm, University of Illinois, Urbana−Champaign, IL. Vegetative propagation of two plants in three replications of each accession were established in a completely randomized block design on the Vegetable Research Farm on April 4, 2012 from root cuttings (sets) approximately 35−40 cm long and 1.0−1.5 cm in diameter. Sets were hand-planted in rows, spaced at 90 cm between rows and 56 cm within each row. The ends of the sets that would send up a shoot were planted facing the same direction (for ease of harvest) in furrows, then hilled-over into ridges approximately 18 cm high and 30 cm wide. According to the U.S. Department of Agriculture standard, horseradish roots are classified U.S. Fancy, U.S. No. 1, and U.S. No. 2 on the basis of diameter of horseradish and length of root.[19] Specifically, in order to meet U.S. Fancy grade, the roots "shall be not less than 20.32 cm in length when the diameter is 3.81 cm or more". For U.S. No. 1 grade, the roots "shall be not less than 15.24 cm in length when the diameter is 3.18 cm or more". For U.S. No. 2 grade, the roots "shall be not less than 10.16 cm in length and not less than 1.27 cm in diameter". The two primary horseradish roots harvested from each three field replications of each accession (n = 6) that met the U.S. Fancy grade standard,[19] were cleaned with tap water, and dried with paper towels. Two primary main roots from U.S. Fancy grade plants were pooled for each three field replications for four accessions, and an additional two root samples from the same plants that met the U.S. No. 1 requirements were collected in this manner. Because U.S. No. 2 grade root is not commercially preferred, replicated samples were collected from only one accession that has low sinigrin concentration for better correlation analysis. Harvest was done on October 20, 2013. Samples were frozen in liquid nitrogen and stored at −20 °C prior to freeze-drying (less than a week). Freeze-dried tissues were ground into a fine powder using a coffee grinder and stored at −20 °C prior to analyses (less than a month).

Determination of GS Concentrations. Extraction and quantitation of GS using HPLC was carried out using a protocol described by Brown et al.[20] with some modifications. Freeze-dried, powdered horseradish (0.2 g) and 2 mL of 70% methanol were placed in 10 mL centrifuge tubes (Nalgene, Rochester, NY) and heated on a heating block at 95 °C for 10 min. After cooling on ice for 5 min, 0.5 mL of benzyl GS (1 mM) was added as internal standard (POS Pilot Plant Corp, Saskatoon, SK, Canada), mixed, and centrifuged at 3000 g for 15 min at 4 °C using a Beckman L7-65 Ultracentrifuge (Beckman Coulter, Brea, CA). The supernatant was saved and the pellet was re-extracted with 2 mL of 70% methanol at 95 °C for 10 min, and the two extracts were combined. A subsample (1 mL) from each pooled extract was transferred into a 2 mL microcentrifuge tube (Fisher Scientific, Waltham, MA). Protein in the extract was precipitated with 0.15 mL of a 1:1 mixture of 1 M lead acetate and 1 M barium acetate. After centrifugation at 12 000 g for 1 min using an Eppendorf 5415 benchtop centrifuge (Hamburg, Germany), each sample was then loaded onto a column containing DEAE Sephadex A-25 resin for desulfation with arylsulfatase (*Helix pomatia* Type-1, Sigma-Aldrich, St. Louis, MO) for 18 h. The desulfated GS samples were eluted off the column using 2 mL of distilled water. A 100 μL sample of each was filtered through a 0.2 μm nylon filter and injected into an HPLC system under the previously reported conditions.[21] For individual GS quantitation (sinigrin, gluconasturtiin, gluconapin glucobrassicin, and 4-methoxy glucobrassicin), relative response factors was used as previously published.[21] The concentration of GS was expressed as micromole per gram dry weight.

Measurement of GS Hydrolysis Products. Freeze-dried horseradish tissue (50 mg) was suspended in 1 mL of distilled water and 1 mL of hexane in a 2 mL microcentrifuge tube (Fisher Scientific, Waltham, MA). Hydrolysis products were generated naturally by endogenous myrosinase in the absence of light at room temperature for 24 h. The samples were then centrifuged at 12 000 g for 2 min using a Eppendorf 5415 benchtop centrifuge (Hamburg, Germany), and the supernatant was collected for analysis using a Hewlett-Packard HP 5890 Series-I gas chromatography (GC) system equipped with a single flame-ionization detector (Agilent Technologies, Santa Clara, CA), an Agilent model 7683B series autosampler, and a 30 m × 0.32 mm J&W HP-5 capillary column (Agilent Technologies). A 1 μL sample of the hexane extract was injected onto the GC. After an initial temperature hold at 40 °C for 2 min, the oven temperature was increased by 10 °C/min to 260 °C and held for 10 min.[8] Injector and detector temperatures were set at 200 and 280 °C, respectively. The flow rate of the helium carrier gas was set at 25 mL/min. Results were quantitated on the basis of external standards of AITC, BITC, PEITC, PPNT, and benzyl cyanide. 1-Cyano 2,3-epithiopropane (CETP) was quantitated on the basis of effective carbon number concept.[22] Each peak from the horseradish sample extracts was further identified using a 6890N GC coupled to an HP-5973N MS Detector, according to a previously published study.[11] The concentration of GS hydrolysis products were expressed as micromole per gram dry weight. Samples were assayed in triplicate.

Quinone Reductase Activity. Freeze-dried powdered horseradish root (75 mg) was suspended in 1.5 mL of water in the dark for 24 h at

DOI: 10.1021/jf505591z
J. Agric. Food Chem. 2015, 63, 2947−2955

Table 1. Glucosinolate Concentration (μmol/g DW) of Different Accession Numbers and USDA Grades of Horseradish Roots

accession	grade	sinigrin	gluconasturtiin	glucobrassicin	total[a]
IL706	U.S. Fancy	41.0 ± 1.2	4.81 ± 0.26	0.52 ± 0.04	46.4 ± 1.4
IL1091	U.S. Fancy	80.3 ± 3.2	5.82 ± 0.14	1.31 ± 0.11	87.5 ± 3.6
IL196	U.S. Fancy[b]	60.9 ± 2.1	10.0 ± 0.24	0.41 ± 0.07	71.4 ± 2.4
IL196	U.S. No. 1	44.9 ± 4.5	14.5 ± 0.20	0.27 ± 0.05	61.9 ± 4.8
IL1573	U.S. Fancy[b]	55.1 ± 2.4	9.42 ± 0.25	0.16 ± 0.06	64.7 ± 2.7
IL1573	U.S. No. 1	32.4 ± 2.1	9.33 ± 0.05	0.00 ± 0.00	42.4 ± 2.4
IL813	U.S. Fancy[b]	54.4 ± 2.3	9.91 ± 0.04	0.31 ± 0.06	64.6 ± 2.4
IL813	U.S. No. 1	26.1 ± 2.2	5.35 ± 0.06	0.00 ± 0.00	31.8 ± 2.4
IL785	U.S. Fancy[b]	73.2 ± 3.2	3.77 ± 0.07	2.07 ± 0.10	79.1 ± 3.5
IL785	U.S. No. 1	48.9 ± 4.1	9.56 ± 0.24	0.32 ± 0.05	59.1 ± 4.2
IL785	U.S. No. 2	42.0 ± 3.2	10.3 ± 0.33	0.25 ± 0.05	53.5 ± 3.4
mean	U.S. Fancy (n = 6)	60.8 ± 14.1	7.91 ± 2.81	0.80 ± 0.74	70.0 ± 14.1
mean	U.S. Fancy marked (n = 4)[b]	60.9 ± 10.6	8.28 ± 3.01	0.74 ± 0.89	70.0 ± 6.9
mean	U.S. No. 1 (n = 4)	38.1 ± 8.7	9.67 ± 3.75	0.15 ± 0.17	48.8 ± 14.2
P value[c]	U.S. Fancy vs U.S. No. 1[b]	0.003	0.591	0.464	0.021
$F_{5,12}$; CV[d]	U.S. Fancy (n = 6)	110[e]; 23.2	662[e]; 35.5	652[e]; 92.5	103[e]; 20.1
$F_{3,8}$; CV[d]	U.S. Fancy marked (n = 4)[b]	39.4[e]; 17.4	969[e]; 36.4	1062[e]; 120	355[e]; 9.9
$F_{3,8}$; CV[d]	U.S. No. 1 (n = 4)	32.5[e]; 22.8	1834[e]; 38.8	1836[e]; 113	55.5[e]; 29.1

[a]Includes gluconapin and 4-methoxyglucobrassicin. [b]Selected U.S. Fancy accession for comparing with corresponding U.S. No. 1. [c]Calculated by paired t test. All data are expressed as mean ± SD, n = 3. [d]For $F_{x,y}$, x and y indicate degree of freedom of numerator and the denominator, respectively, for F test; CV, coefficient of variation (%). [e]Highly significant variance by F test at ≤ 0.01.

room temperature in a sealed 2 mL microcentrifuge tube (Fisher Scientific, Waltham, MA) to allow for GS hydrolysis by endogenous myrosinase. GS hydrolysis extracts were then centrifuged at 12 000 g for 5 min using an Eppendorf 5415 benchtop centrifuge (Hamburg, Germany), and the supernatant was used for the QR assay. Hepa1c1c7 murine hepatoma cells (ATCC, Manassas, VA) were grown in α-MEM, enriched with 10% fetal bovine serum, and maintained at 37 °C in ambient air enriched with 5% CO_2. The cells were divided every 3 days with a split ratio of 7. Cells with 80−90% confluence were plated into 96-well plates (Costar 3595, Corning Inc., Corning, NY), 1×10^4 cells per well, and incubated for 24 h in antibiotic-enriched media (100 units/mL penicillin and 100 μg/mL streptomycin). The QR-induction activities of different samples were determined by means of the protocol described by Prochaska and Santamaria.[23] Samples were assayed in triplicate.

Estimation of Myrosinase Activity Using Glucose Appearance. Total myrosinase activity was measured by using the glucose release assay.[24] Briefly, freeze-dried plant material (50 mg) was weighed in duplicate (for adjusting background glucose) into 2 mL tubes and 1 mL of sinigrin (10 mM) was added to each tube. After 10 s of vigorous vortexing, one of the paired samples was put directly into a heating block (95 °C) for 10 min to inactivate the myrosinase enzyme (zero time blank). The second sample was incubated at 40 °C for 30 min and then inactivated as outlined above. After inactivation, samples were cooled on ice for 5 min and then centrifuged at 16 000 g for 2 min using an Eppendorf 5415 benchtop centrifuge (Hamburg, Germany). The supernatants were diluted 96-fold with water and aliquots of 30 μL were added in a 96 well plate, followed by adding 200 μL of an ABTS-glucose solution (2.7 mM ABTS, 10 000 units peroxidase, and 4000 units glucose oxidase). The mixtures were incubated for 20 min and their absorbances were measured at 630 nm in a μQuant plate reader (Bio-Tek instruments, Winooski, VT). Glucose standards were also prepared similarly, as described above, and their absorbance was used to develop a standard curve (7.8−250 μg/mL). One unit was defined as 1 μmol glucose release per min. Samples were assayed in triplicate.

Determination of Nitrile and Epithionitrile Formation from Different GSs. Freeze-dried horseradish root (75 mg) was suspended in 0.75 mL of 1 mM benzyl GS. After 20 s vigorous vortexing, 0.75 mL of hexane was added and incubated for 20 min in the absence of light. The mixture was vigorously vortexed for 10 s and then centrifuged at 16 000 g for 1 min using an Eppendorf 5415 benchtop centrifuge (Hamburg, Germany). The supernatant was transferred to GC vials and injected onto the GC as described above. Nitrile formation (simple nitrile PPNT from gluconasturtiin and epithionitrile CEPT from sinigrin) is presented as percentage formed relative to total hydrolysis products of individual endogenous and exogenous GS, as previously described.[9] Samples were assayed in triplicate.

Determination of Total Polyphenol Content. Analysis of total polyphenol content (TPC) was conducted as previously described.[25] The extraction procedure was identical to that described above for the QR activity measurement. The assay conditions were as follows: a 10 μL sample was added to 0.2 N Folin-Ciocalteu's phenol reagent (100 μL) in 96 well plates. After 3 min, 90 μL of 7.5% sodium carbonate solution was added to the mixture and subsequently incubated at room temperature for 1 h. The absorbance of the mixture was measured at 630 nm using a BioTek EL 808 microplate reader (Biotek Instruments Inc., Power Wave XS, Winooski, VT). Total polyphenol content was calculated on the basis of a standard curve using gallic acid (concentration range = 31.25−500 μg/mL). Results are expressed in milligram gallic acid equivalents (GAE) per gram of dried horseradish. Samples were assayed in triplicate.

Determination of ABTS Radical Scavenging Activity and Ferric Reducing/Antioxidant Power Activity. The ABTS assay was conducted as previously described.[25] Briefly, 7 mM ABTS ammonium salt was dissolved in a 2.45 mM potassium persulfate solution. The mixture was then allowed to stand at room temperature for 12−16 h for full color development (dark blue). The solution was then diluted with potassium phosphate buffer (pH 7.4) until absorbance reached 1.0 ± 0.02 at 630 nm using a BioTek EL 808 microplate reader (Biotek Instruments Inc., Power Wave XS, Winooski, VT). Subsequently, 190 μL of this solution was mixed with 10 μL of the sample. The absorbance was recorded at room temperature after 6 min. Results are expressed as percent of radical-scavenging activity compared to controls as extraction solvent. Samples were evaluated in triplicate.

The ferric reducing/antioxidant power (FRAP) reagent, freshly prepared and kept at room temperature, contained 2.5 mL of a 10 mM 2,4,6-tripyridyl-s-triazine solution in 40 mM HCl plus 2.5 mL of 20 mM $FeCl_3 \cdot 6H_2O$ and 25 mL of 300 mM acetate buffer (pH 3.6).[25] The FRAP reagent (190 μL) was mixed with 10 μL of sample, and absorbance was measured at 593 nm after 4 min using a BioTek EL 808 microplate reader. The FRAP values were calculated from a standard curve of Trolox concentrations ranging from 62.5 to 500 μmols.

DOI: 10.1021/jf505591z
J. Agric. Food Chem. 2015, 63, 2947−2955

Table 2. Hydrolysis Products of GS from Different Genotypes and USDA Grades of Horseradish

		sinigrin hydrolysis (μmol/g DW)		gluconasturtiin hydrolysis (μmol/g DW)	
accession	grade	AITC	CETP	PEITC	PPNT
IL706	U.S. Fancy	37.4 ± 5.3	0.00 ± 0.00	4.30 ± 0.48	0.10 ± 0.18
IL1091	U.S. Fancy	44.8 ± 3.1	11.4 ± 0.19	4.30 ± 0.28	0.40 ± 0.18
IL196	U.S. Fancy[a]	44.7 ± 4.4	5.8 ± 0.22	13.4 ± 0.64	0.70 ± 0.04
IL196	U.S. No. 1	18.5 ± 2.1	10.3 ± 0.30	10.9 ± 0.68	2.30 ± 0.08
IL1573	U.S. Fancy[a]	38.2 ± 1.9	0.00 ± 0.00	7.30 ± 0.53	0.10 ± 0.13
IL1573	U.S. No. 1	20.7 ± 3.0	2.8 ± 0.20	8.80 ± 0.55	0.50 ± 0.13
IL813	U.S. Fancy[a]	41.9 ± 6.5	3.3 ± 0.28	7.70 ± 0.84	0.40 ± 0.24
IL813	U.S. No. 1	3.9 ± 0.1	10.1 ± 0.37	3.50 ± 0.57	5.20 ± 0.17
IL785	U.S. Fancy[a]	47.1 ± 6.2	1.09 ± 0.33	3.90 ± 0.20	0.10 ± 0.10
IL785	U.S. No. 1	34.8 ± 3.3	4.6 ± 0.22	7.70 ± 0.60	0.40 ± 0.20
IL785	U.S. No. 2	14.8 ± 1.8	10.0 ± 0.35	8.10 ± 0.46	2.10 ± 0.16
mean	U.S. Fancy	42.4 ± 3.9	3.73 ± 4.35	6.82 ± 3.62	0.30 ± 0.26
mean	U.S. Fancy marked[a]	43.0 ± 12.7	2.75 ± 2.44	8.10 ± 3.11	0.32 ± 0.31
mean	U.S. No. 1 (n = 4)	19.5 ± 3.8	6.95 ± 3.82	7.73 ± 3.94	2.09 ± 2.22
P value[b]	U.S. Fancy vs U.S. No. 1[a]	0.013	0.022	0.860	0.192
$F_{5,12}$; CV[c]	U.S. Fancy (n = 6)	5.53^{NS}; 9.2	280**; 117	135**; 53.1	0.919^{NS}; 86.7
$F_{3,8}$; CV[c]	U.S. Fancy marked (n = 4)[b]	7.0*; 29.5	875**; 88.7	648**; 38.4	2.2**; 96.9
$F_{3,8}$; CV[c]	U.S. No. 1 (n = 4)	71.0**; 19.5	334**; 55.0	80.2**; 51.0	665**; 106

[a]Selected U.S. Fancy accession for comparing corresponding U.S. No. 1. [b]Calculated by paired t test. All data are expressed as mean ± SD, n = 3. [c]For $F_{x,y}$, x and y indicate degree of freedom of numerator and the denominator, respectively, for F test; CV, coefficient of variation (%). Superscripted NS, *, and ** indicate non-significant, significant, and highly significant variance by F test at > 0.05, ≤ 0.05, and ≤ 0.01, respectively.

Statistical Analysis. Horseradish accessions were considered a fixed factor with blocks a random factor. Analysis of variance (ANOVA), Student's t test, paired t test, F test, and Pearson's correlation coefficient analysis were conducted using JMP 10 (SAS institute Inc., Cary, NC). All sample analyses were conducted in triplicate. The results are presented as means ± SD. Coefficients of variation (CV) are presented in the tables.

RESULTS AND DISCUSSION

Concentration of GS in Different Accessions and Grades of Horseradish Root. There is significant variation in sinigrin concentration among the U.S. Fancy horseradish accession extracts ($F_{5,12}$ = 110, P < 0.001); the lowest sinigrin concentration was found in accession IL706 extract (41.0 μmol/g dry weight, DW), whereas the highest was found in IL1091 (80.3 μmol/g DW, Table 1). Among the accessions of U.S. Fancy grade, the maximum to minimum ratio is approximately 2-fold, suggesting that genotype plays a major role in determining sinigrin concentration. Gluconasturtiin concentrations from six U.S. Fancy grade accession root extracts ranged from 3.77 to 10.0 μmol/g DW. Average glucobrassicin concentrations from six U.S. Fancy accession root extracts ranged from 0.16 to 2.07 μmol/g DW, which is a 13-fold difference in minimum to maximum values. Aside from these, the only other GS found was gluconapin in trace amounts (less than 0.05 μmol/g DW). According to a previous study using 168 Nordic horseradish accessions,[26] sinigrin levels varied between 10 and 45 μmol/g DW, gluconasturtiin between 1.3 and 7.4 μmol/g DW, and glucobrassicin between 0.1 and 2.6 μmol/g DW. A recent paper reported that sulfate supply was closely related with GS accumulation in horseradish.[27] The different GS concentration between US Midwest horseradish and Nordic horseradish accessions may be related to different weather and/or soil conditions as well as genetic backgrounds, which require further research. Another study[28] detected 11 different GS levels from horseradish roots using LC electrospray ionization hybrid linear ion trap with Fourier transform ion cyclotron resonance mass spectrometry and infrared multiphoton dissociation, but we only identified five GS by HPLC, as also reported in previous studies.[2,26]

Horseradish root diameter (grades) was another source of variation in sinigrin concentration. Partitioning variance component analysis based on ANOVA estimated that differences among root diameters accounted for 44% of sinigrin variation displayed in Table 1. Selected accessions of horseradish of U.S. Fancy grade (IL196, IL1573, IL813, and IL785) contained an average of 60.9 μmol/g DW of sinigrin, whereas corresponding U.S. No. 1 grade samples contained 38.1 μmol/g DW of sinigrin. Across the four accessions tested, the U.S. Fancy grade root extracts exhibited significantly greater sinigrin concentrations than the U.S. No. 1 grade roots extracts, on the basis of a paired t test (P = 0.003, Table 1). Previous research also reported that the total amount of GS as well as sinigrin was higher in the shoulder zone than in the middle and tip zones of horseradish roots.[26] 4-Methoxyglucobrassicin was not present in the U.S. Fancy grade, whereas the U.S. No. 1 and U.S. No. 2 grade root extracts had measurable concentrations of this compound (0.24−2.21 μmol/g DW; data not shown).

Variation in Content of GS Hydrolysis Products among Horseradish Accessions and Grades. Generation of isothiocyanate (AITC) or epithionitrile (CETP) concentrations from sinigrin varied among the horseradish accessions. The average of AITC concentration from the six U.S. Fancy grade horseradish root extracts was 42.4 μmol/g DW and ranged from 37.4 to 47.1 μmol/g DW. Even though sinigrin showed about a 2-fold ratio between maximum to minimum concentrations, the variation in AITC (CV = 9.2%) was smaller than that of its precursor GS (CV = 23.2%). The reduced variation in AITC may be related its volatility. The average CETP concentration from root extracts of the six U.S. Fancy grade horseradish accessions was 3.73 μmol/g DW and ranged from 0 to 11.4 μmol/g DW. PEITC showed significant variation with a 3.4-fold difference between minimum to maximum values (3.9 and 13.4 μmol/g DW, respectively, $F_{5,12}$

DOI: 10.1021/jf505591z
J. Agric. Food Chem. 2015, 63, 2947−2955

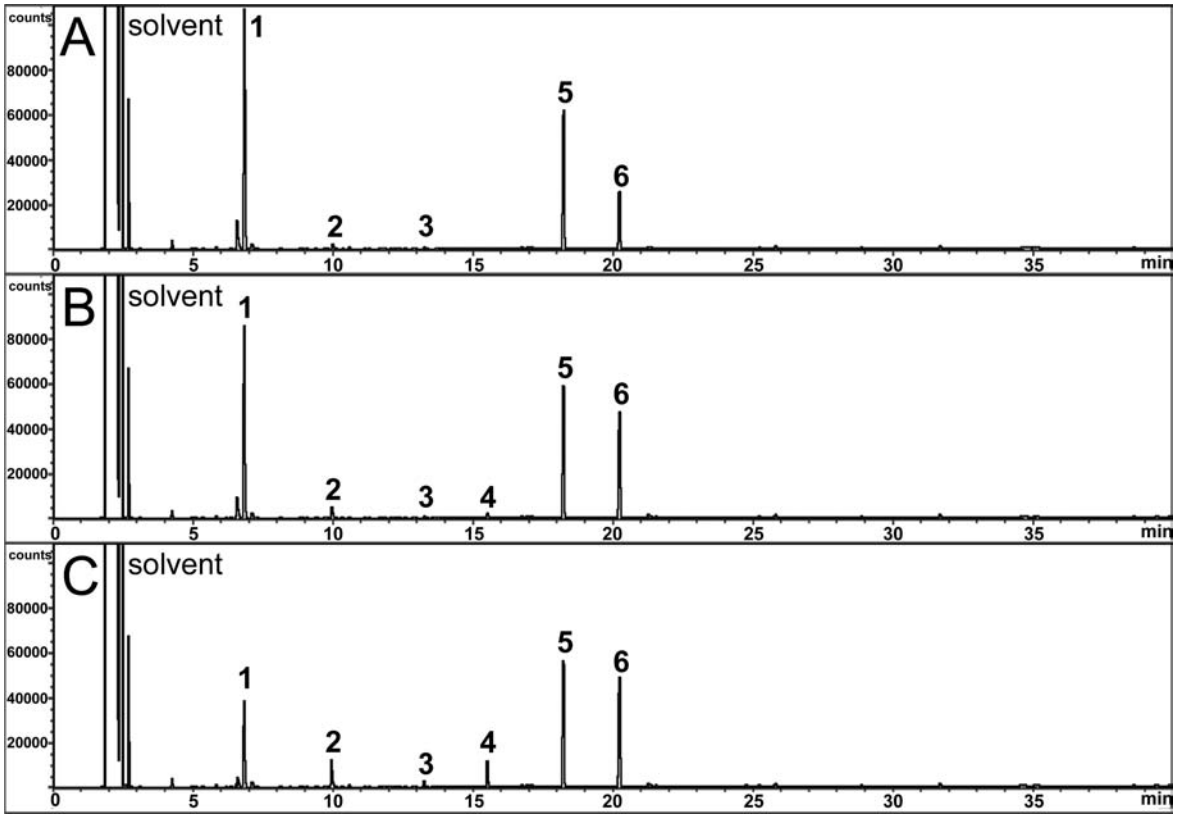

Figure 1. Gas chromatograms of different USDA grades of horseradish accession IL785. (A) U.S. Fancy, (B) U.S. No. 1, and (C) U.S. No. 2. Peaks: 1, AITC; 2, CETP; 3, BZCN; 4, PPNT; 5, BZITC; and 6, PEITC.

= 135, $P < 0.001$). Regardless of genotypes, PPNT concentrations were less than 1.0 μmol/g DW. Allyl cyanide was not detected because of its extreme volatility and loss during sample preparation.[12]

Horseradish root diameter (grade) was another source of variation in AITC and CETP concentrations. Selected horseradish accessions of U.S. Fancy grade (IL196, IL1573, IL813, and IL785) contained 43.0 μmol/g DW of AITC, whereas corresponding U.S. No. 1 grade roots generated only 19.5 μmol/g DW of AITC, which was significantly lower than U.S. Fancy on the basis of a paired t test ($P = 0.013$, Table 2). These same accessions of U.S. Fancy grade contained 2.75 μmol/g DW of CETP, whereas their corresponding U.S. No. 1 grade roots contained significantly greater amounts, averaging 6.95 μmol/g DW ($P = 0.022$, Table 2). In general, AITC levels fell and CETP levels rose in the lower root grades including U.S. No. 1 and U.S. No. 2, compared to the corresponding levels in U.S. Fancy grade roots. PEITC and PPNT concentrations were not significantly different between U.S. Fancy and U.S. No. 1 grades, although PPNT levels rose in the lower grades (Table 2 and Figure 1). Horseradish accession IL785 is good example how phytochemical composition changes depending on the grade. Past reports suggest that horseradish roots contain about 79% AITC and 18% PEITC, whereas wasabi, another GS-rich plant root, contains 95% AITC.[29] Thus, the PEITC in horseradish provides a distinct flavor difference compared to wasabi.[29] Most horseradish roots produced AITC as the major hydrolysis product (Table 2). However, U.S. No. 1 grade roots of accession IL813 produced more CETP and PPNT than AITC and PEITC (Table 2). The U.S. Fancy grade root of accession IL785 produced a greater proportion of AITC than U.S. No. 1 or U.S. No. 2 grades (Table 2 and Figure 1). It has been reported that horseradish produces only AITC and no CETP because of a lack of ESP in horseradish.[11,12] However, this study reports on the presence of CETP (the epithionitrile form of sinigrin) in certain horseradish accessions, suggesting that there may be ESP activity in horseradish or the activity of some other cofactors, including ascorbic acid and metal ions, to form nitriles.[7] Reduction in CETP levels as root grade improves suggests that less ESP or other myrosinase cofactors may be present in larger, more mature roots.

According to previous research, AITC has about a 300-fold stronger odor than CETP.[30] AITC-rich horseradish is therefore suitable material for the food industry, for example, high-quality horseradish sauce. In addition to the flavor of AITC, the compound has potential cancer-prevention bioactivity, which can be quantitated by its capacity for the induction of QR. In contrast, CETP has comparatively reduced QR-inducing activity.[5,31] AITC may be a good dietary anticarcinogen, because bioavailability of AITC is extremely high, with nearly 90% absorption of an oral dose.[14] In addition AITC, even at high doses, exhibits a relatively low degree of cytotoxicity and genotoxicity in animal studies.[14] Significant variation in AITC levels across the accessions was observed within the U.S. No. 1 grade samples ($F_{3,8} = 71.0$, $P < 0.001$; Table 2): U.S. No. 1 grade IL785 accession has about a 9-fold-higher AITC concentration than the IL813 accession. These chemical analyses indicate that the USDA grading system is a good indicator for pungency.

Averaged AITC and PEITC concentrations determined that the genotype and root grade described 66 and 17%,

DOI: 10.1021/jf505591z
J. Agric. Food Chem. 2015, 63, 2947−2955

Table 3. Quinone Reductase Inducing Activity, Myrosinase Activity, and ESP Activities on Individual GS of Different Genotype and USDA Grades of Horseradish

				Percent of nitrile formation to individual GS[c]		
accession	grade	QR[a]	myrosinase (U/g)[b]	sinigrin	gluconasturtiin	benzyl GS
IL706	U.S. Fancy	1.37 ± 0.10	0.25 ± 0.18	0.0 ± 0.0	1.4 ± 0.4	0.40 ± 0.10
IL1091	U.S. Fancy	1.29 ± 0.09	1.72 ± 0.18	20.2 ± 1.1	7.3 ± 0.4	0.90 ± 0.10
IL196	U.S. Fancy[d]	1.35 ± 0.05	0.55 ± 0.04	11.5 ± 2.1	4.2 ± 0.9	0.70 ± 0.10
IL196	U.S. No. 1	1.33 ± 0.03	0.53 ± 0.08	35.8 ± 3.2	14.3 ± 1.0	0.90 ± 0.10
IL1573	U.S. Fancy[d]	1.32 ± 0.04	0.51 ± 0.13	0.0 ± 0.0	1.4 ± 0.2	0.40 ± 0.10
IL1573	U.S. No. 1	1.14 ± 0.03	0.16 ± 0.13	11.9 ± 1.7	4.6 ± 0.5	0.50 ± 0.20
IL813	U.S. Fancy[d]	1.37 ± 0.08	1.13 ± 0.24	7.3 ± 1.8	3.6 ± 0.8	0.50 ± 0.20
IL813	U.S. No. 1	1.05 ± 0.07	0.82 ± 0.17	71.9 ± 1.0	54.2 ± 1.3	4.40 ± 0.20
IL785	U.S. Fancy[d]	1.30 ± 0.06	0.53 ± 0.10	3.8 ± 1.4	1.3 ± 0.4	0.40 ± 0.10
IL785	U.S. No. 1	1.25 ± 0.02	0.75 ± 0.20	11.8 ± 2.1	3.9 ± 0.7	0.60 ± 0.10
IL785	U.S. No. 2	1.26 ± 0.05	0.88 ± 0.16	40.3 ± 2.5	17.4 ± 1.1	1.80 ± 0.10
Mean	U.S. Fancy	1.33 ± 0.04	0.78 ± 0.54	7.1 ± 7.8	3.2 ± 2.4	0.55 ± 0.21
Mean	U.S. Fancy[d] marked	1.34 ± 0.03	0.68 ± 0.30	5.7 ± 4.9	2.6 ± 1.5	0.50 ± 0.14
Mean	U.S. No. 1 (n = 4)	1.19 ± 0.12	0.57 ± 0.30	32.9 ± 28.4	19.3 ± 23.8	1.60 ± 1.87
P value[e]	U.S. Fancy vs U.S. No. 1[d]	0.129	0.453	0.126	0.243	0.324
$F_{5,12}$; CV[f]	U.S. Fancy (n = 6)	0.685[NS]; 3.0	35.2**; 69.2	100**; 110	51.3**; 75.0	8.61**; 38.2
$F_{3,8}$; CV[f]	U.S. Fancy marked (n = 4)[d]	9.94**; 2.2	38.5**; 44.1	83.8**; 86.0	61.2**; 57.7	24.0**; 28.0
$F_{3,8}$; CV[f]	U.S. No. 1 (n = 4)	25.5**; 10.1	11.5**; 52.6	521**; 86.3	5088**; 123	421**; 117

[a]Sample extract activity divided by the nontreated control cells. [b]Unit defined as 1 μmole glucose release per min. Analysis was done in triplicates. [c]Amount of products are expressed as a percentage of nitrile form over the total amount of hydrolysis products measured [CETP /(AITC+CETP) and PPNT/(PEITC+PPNT) for sinigrin and gluconasturtiin, respectively]. Exogenous benzyl glucosinolate was used for determination of nitrile formation (%) [benzyl cyanide/(benzyl cyanide + benzyl isothiocyanate). [d]Selected U.S. Fancy accession for comparing corresponding U.S. No. 1. [e]Calculated by paired t test. All data are expressed as mean ± SD, n = 3. [f]$F_{x,y}$, where x and y indicate degree of freedom of numerator and the denominator, respectively, for F test; CV, coefficient of variation (%). Superscripted NS, *, and ** indicate non-significant, significant, and highly significant variance by F test at > 0.05, ≤ 0.05, and ≤ 0.01, respectively.

respectively, of the total variation (as calculated from Table 2), which is comparable to a previous study that reported these variables accounted for 64−82% and 4−18% of the variation, respectively.[32] However, this study reported a broader range of AITC and PEITC concentrations.

Quinone Reductase, Myrosinase, and Nitrile/Epithionitrile Formation (%) of Different Accessions and Grades of Horseradish. The QR-inducing activity of the U.S. Fancy grade horseradish did not correlate with the variation in phytochemical concentrations (Table 3). The mean value of QR-inducing activity from extracts of all six of the U.S. Fancy grades evaluated (expressed as induction ratio relative to the control) was 1.33 ± 0.04. QR-inducing activity ranged from 1.29 to 1.37, which was small compared to the variation in sinigrin and AITC. Variation of myrosinase activity in U.S. Fancy horseradish ranged from 0.25 to 1.72 U/g. Nitrile generation from sinigrin (0.0−20.2%) was greater than from gluconasturtiin (1.3−7.3%) and benzyl GS (0.4−0.9%). There was no epithionitrile formation in accessions IL706 and IL1573. These accessions could be good resources for a high-AITC-producing horseradish-breeding program.

QR-inducing activity of horseradish roots varied among grades. In general, QR-inducing activity in the U.S. Fancy grade roots of accessions IL196, IL1573, IL813, and IL785 (mean = 1.34, Table 3) were not significantly higher than those from U.S. No. 1 grade roots of the same accessions (mean = 1.19, P = 0.129, Table 3). However, U.S. Fancy grade roots of accessions IL1573 and IL813 have significantly higher QR-inducing activity than those of U.S. No. 1 grade roots of the same accessions, suggesting more research is needed to confirm the interaction between accessions and grades. QR-inducing activity of U.S. No. 1 grade roots ranged from 1.05 to 1.33. Myrosinase activity in U.S. Fancy and U.S. No. 1 grade roots were similar (0.68 U/g, n = 4 and 0.57 U/g, n = 4, respectively; Table 3) and not significantly different. The average of percent epithionitrile formation (expressed as percent nitriles formed over total hydrolysis products) for endogenous sinigrin from the selected four U.S. Fancy grade accessions was 5.7% (mean of all U.S. Fancy grade roots = 7.1%), whereas the corresponding percent epithionitrile formation across the U.S. No. 1 grade root samples was 32.9%. Thus, U.S. No. 1 grade horseradish roots had about 4.6-fold higher percent epithionitrile formation than the U.S. Fancy grade horseradish.

Average percent nitrile formation relative to endogenous gluconasturtiin from the selected four U.S. Fancy grade horseradish accessions was 2.6% (mean of all U.S. Fancy = 3.2%), whereas the corresponding percent nitrile formation across the U.S. No. 1 grade samples was 19.3% (t-test P = 0.243, Table 3). U.S. No. 1 grade horseradish had about 7-fold higher nitrile formation levels than the U.S. Fancy grade (Table 3). Average percent nitrile formation for exogenous benzylglucosinolate from selected four U.S. Fancy grade horseradish accessions was 0.50% (mean of all U.S. Fancy = 0.55%), which is less than the percent nitrile formation across U.S. No. 1 grade samples (1.60%, t-test P = 0.324; Table 3). Thus, U.S. No. 1 grade horseradish had about a 3-fold greater percent nitrile formation than the U.S. Fancy grade horseradish. The low percent nitrile formation from benzyl GS compared to the two other substrates has previously been reported.[9] This indicates that ESP or another myrosinase cofactor activity may be different for different GS and/or for endogenous and exogenous GS. The variation of nitrile/epithionitrile formation observed here for different accessions and grades of horseradish root could be due to differences in ESP abundance or to

DOI: 10.1021/jf505591z
J. Agric. Food Chem. 2015, 63, 2947−2955

different levels of cofactors such as ferrous or magnesium metal ions or other protein cofactors.[9]

Total Phenolic Content and Antioxidant Activity in Different Accessions and Grades of Horseradish. Total phenolic content of horseradish roots varied among accessions and grades. Total phenolics present in U.S. Fancy grade horseradish ranged from 2.83 to 5.48 mg/g DW (Table 4).

Table 4. Total Phenolic Content, ABTS, and FRAP Antioxidant Activity from Different Genotype and USDA Grades of Horseradish

accession	grade	total phenolics (mg/g)[a]	ABTS (mmol/g)[b]	FRAP (mmol/g)[b]
IL706	U.S. Fancy	2.83 ± 0.10	19.7 ± 0.8	20.5 ± 0.5
IL1091	U.S. Fancy	4.46 ± 0.15	31.4 ± 0.8	34.1 ± 0.6
IL196	U.S. Fancy[c]	3.87 ± 0.09	28.1 ± 0.2	30.3 ± 1.3
IL196	U.S. No. 1	5.48 ± 0.09	30.1 ± 0.4	34.9 ± 1.3
IL1573	U.S. Fancy[c]	3.80 ± 0.12	24.1 ± 0.7	26.8 ± 1.6
IL1573	U.S. No. 1	4.75 ± 0.07	24.3 ± 0.3	28.2 ± 0.4
IL813	U.S. Fancy[c]	3.25 ± 0.29	20.6 ± 0.7	22.5 ± 0.7
IL813	U.S. No. 1	4.65 ± 0.11	32.0 ± 0.5	35.3 ± 0.1
IL785	U.S. Fancy[c]	3.66 ± 0.21	22.4 ± 0.5	25.2 ± 0.3
IL785	U.S. No. 1	3.64 ± 0.05	20.5 ± 0.8	24.1 ± 0.4
IL785	U.S. No. 2	5.20 ± 0.13	21.6 ± 0.4	26.3 ± 0.6
mean	U.S. Fancy	3.67 ± 0.58	24.4 ± 4.6	26.6 ± 5.0
mean	U.S. Fancy marked[c]	3.68 ± 0.26	23.8 ± 3.3	26.2 ± 3.3
mean	U.S. No. 1 (n = 4)	4.63 ± 0.79	26.7 ± 5.3	30.6 ± 5.4
P value[d]	U.S. Fancy vs U.S. No. 1[c]	0.073	0.392	0.240
$F_{5,12}$; CV[e]	U.S. Fancy (n = 6)	30.6[f]; 15.8	145[f]; 18.9	83.3[f]; 18.8
$F_{3,8}$; CV[e]	U.S. Fancy marked (n = 4)[c]	28.1[f]; 7.1	551[f]; 13.9	93.0[f]; 12.6
$F_{3,8}$; CV[e]	U.S. No. 1 (n = 4)	248[f]; 17.1	294[f]; 19.9	175[f]; 17.6

[a]Value expressed as gallic acid equivalent concentration. [b]Value expressed as Trolox equivalent concentration. [c]Selected U.S. Fancy accession for comparing corresponding U.S. No. 1. [d]Calculated by paired t test. All data are expressed as mean ± SD, n = 3. [e]$F_{x,y}$, where x and y indicate degree of freedom of numerator and the denominator, respectively, for F test; CV, coefficient of variation (%). ** [f]Highly significant variance by F test at ≤ 0.01.

ABTS and FRAP antioxidant activities showed significant variations in U.S. Fancy grade horseradish, ranging from 19.7 to 31.4 mmol/g DW ($F_{5,12}$ = 145) and from 20.5 to 34.1 mmol/g DW ($F_{5,12}$ = 83.3), respectively (Table 4).

Within the same accession, U.S. No.1 grade horseradish roots have higher concentrations (4.63 mg/g DW) of total phenolics compared to the U.S. Fancy grade roots (3.68 mg/g DW), implying that total phenolic accumulation may be related to diameter and length of horseradish roots. Smaller diameter roots have greater levels of total phenolics (and less sinigrin and total GS, as shown in Table 1) than thicker roots, but the trend was not significant in a paired t test (P = 0.073, Table 4).

Correlations between Phytochemicals and Bioactivities in Different Accession and Grades of Horseradish Roots. As expected, there were significant correlations between sinigrin and AITC (r = 0.834, P = 0.001) and between gluconasturtiin and PEITC (r = 0.830, P = 0.002; Table 5). Similarly, AITC also significantly correlated to QR activity (r = 0.727, P = 0.011; Table 5). It is reported that AITC is relatively volatile and has low solubility in water (1.3 mg/mL) compared to sulforaphane (8.0 mg/mL).[33] Although AITC was successfully extracted by adding hexane to water and measured by GC, there would be some AITC loss after treatments in cell media and incubation at 37 °C for 24 h for the QR assay. This probably attributed to the relatively small QR-inducing difference between U.S. Fancy and U.S. No. 1, even though there was a significant AITC concentration difference between U.S. Fancy and U.S. No. 1 (Tables 2 and 3). AITC has high bioavailability when orally consumed.[14] Considering the significant correlation between AITC and QR activity, the difference in QR activity between U.S. Fancy and U.S. No. 1 maybe underestimated because of the volatility of active compounds and the attributes of the QR assay system. This also indicates that a reliable QR assay system needs to be be established for volatile compounds. Similarly, PEITC has been reported to induce QR activity[34] and was detected in our study when measured immediately after hydrolysis; the lack of correlation between PEITC and QR may also have been due to evaporation of this volatile compound (solubility in water = 0.051 mg/mL)[33] during the 24 h cell treatment. Previous studies have reported that PEITC was not detected following hydrolysis of watercress and broccoli.[34,35] Interestingly, QR activity was negatively correlated with concentrations of two different nitriles (sinigrin-dependent epithionitrile formation, r = −0.682 and P = 0.021; gluconasturtiin-dependent simple nitrile formation, r = −0.742 and P = 0.009). AITC was also significantly negatively correlated with epithionitrile formation

Table 5. Correlations between Phytochemicals and Bioactivities of Different Genotype and USDA Grades of Horseradish[a]

		2	3	4	5	6	7	8	9	10	11
1	sinigrin	−0.224	**0.834**	−0.069	0.511	0.569	−0.110	−0.177	−0.258	−0.495	−0.546
2	gluconasturtiin		−0.255	**0.830**	−0.111	0.211	−0.184	−0.086	0.474	0.076	−0.116
3	AITC			0.009	0.180	**0.727**	−0.224	−0.106	**-0.689**	**-0.836**	**-0.792**
4	PEITC				−0.265	0.292	−0.120	0.057	0.269	−0.120	−0.272
5	myrosinase					0.051	−0.081	−0.398	0.117	0.240	0.161
6	QR						−0.426	−0.121	−0.466	**-0.682**	**-0.742**
7	ABTS							**0.974**	0.596	0.155	0.101
8	FRAP								**0.750**	−0.137	−0.178
9	TPC									**0.682**	0.480
10	epithionitrile formation (sinigrin)										**0.952**
11	nitrile formation (gluconasturtiin)										1.000

[a]The numbers in the first row, from 2 to 11, correspond to the phytochemicals and bioactivities listed in the left column. Pearson's correlation was calculated on the basis of P = 0.05. Bold values are significantly correlated at P = 0.05.

DOI: 10.1021/jf505591z
J. Agric. Food Chem. 2015, 63, 2947−2955

(from sinigrin) and simple nitrile formation (from gluconasturtiin, Table 5). Our data show that higher grades of horseradish accumulate more sinigrin and tend to have lower ESP or other myrosinase cofactor activity than lower grades (Table 1 and 3), which may explain why epithionitrile formation correlates negatively with AITC concentrations.

There were significant and positive correlations between TPC and FRAP (r = 0.750, P = 0.008) as well as between FRAP and ABTS (r = 0.974, P < 0.001). These correlations are explained by the fact that these two different antioxidant assays and TPC measurement are based on the electron-transfer reaction mechanism.[25,36] Thus, three different methods measuring the same event should result in correlations, otherwise one of the methods is not valid. There were significant correlations between TPC and epithionitrile formation (from singirin, r = 0.682, P = 0.021) as well as between TPC and AITC (r = −0.689, P = 0.019). This relationship between TPC and epithionitrile formation requires further investigation to determine if TPC impacts on GS hydrolysis.

In conclusion, this study has examined for the first time the variation in health-promoting properties of different accessions and grades of horseradish roots and measured induction of QR as well as estimates of AITC and nitrile formation. U.S. Fancy showed significantly higher sinigrin and AITC concentrations than U.S. No. 1, whereas U.S. No. 1 showed significantly higher CETP, the epithionitrile hydrolysis product of sinigrin, and significantly higher total phenolic concentrations than U.S. Fancy. The present results suggest that higher grades of horseradish roots display better quality, with higher sinigrin and AITC that is responsible for chemopreventive bioactivity.

AUTHOR INFORMATION

Corresponding Author

*Tel: 217-244-5691; Email: kushad@illinois.edu.

Present Address

M.M.K.: Department of Crop Science, University of Illinois at Urbana−Champaign, 1019 Plant Sciences Lab, 1201 South Dorner Drive, Urbana, Illinois 61801.

Notes

The authors declare no competing financial interest.

ABBREVIATIONS USED

GS, glucosinolate; AITC, allyl isothiocyanate; PEITC, phenethyl isothiocyanate; ESP, epithionitrile specifier protein; BZITC, benzyl isothiocyanate; CETP, 1-cyano 2,3-epithiopropane; PPNT, 2-phenylpropionitrile; TPC, total phenolic content; ABTS, 2,2′-azino-bis(3-ethylbenzothiazoline-6-sulfonic acid); FRAP, ferric reducing/antioxidant power

REFERENCES

(1) Walters, S. A.; Wahle, E. A. Horseradish Production in Illinois. *HortTechnology.* **2010**, *20*, 267−276.

(2) Li, X.; Kushad, M. M. Correlation of glucosinolate content to myrosinase activity in horseradish (*Armoracia rusticana*). *J. Agric. Food Chem.* **2004**, *52*, 6950−5.

(3) Agrawal, A.; Kurashige, N. A role for isothiocyanates in plant resistance against the specialist herbivore *Pieris rapae*. *J. Chem. Ecol.* **2003**, *29*, 1403−1415.

(4) Prestera, T.; Zhang, Y.; Spencer, S. R.; Wilczak, C. A.; Talalay, P. The electrophile counterattack response: Protection against neoplasia and toxicity. *Adv. Enzyme Regul.* **1993**, *33*, 281−296.

(5) Talalay, P.; Fahey, J. W.; Holtzclaw, W. D.; Prestera, T.; Zhang, Y. Chemoprotection against cancer by phase 2 enzyme induction. *Toxicol. Lett.* **1995**, *82*−*83*, 173−9.

(6) Cuendet, M.; Oteham, C. P.; Moon, R. C.; Pezzuto, J. M. Quinone reductase induction as a biomarker for cancer chemoprevention. *J. Nat. Prod.* **2006**, *69*, 460−463.

(7) Dosz, E. B.; Jeffery, E. H. Commercially produced frozen broccoli lacks the ability to form sulforaphane. *J. Funct. Foods* **2013**, *5*, 987−990.

(8) Bones, A. M.; Rossiter, J. T. The myrosinase-glucosinolate system, its organisation and biochemistry. *Acta Fac. Rerum Nat. Univ. Comenianae, Physiol. Plant.* **1996**, *97*, 194−208.

(9) Burow, M.; Markert, J.; Gershenzon, J.; Wittstock, U. Comparative biochemical characterization of nitrile-forming proteins from plants and insects that alter myrosinase-catalysed hydrolysis of glucosinolates. *FEBS J.* **2006**, *273*, 2432−2446.

(10) Matusheski, N. V.; Swarup, R.; Juvik, J. A.; Mithen, R.; Bennett, M.; Jeffery, E. H. Epithiospecifier protein from broccoli (*Brassica oleracea* L. *ssp. italica*) inhibits formation of the anticancer agent sulforaphane. *J. Agric. Food Chem.* **2006**, *54*, 2069−76.

(11) Kyung, K. H.; Fleming, H. P.; Young, C. T.; Haney, C. A. 1-Cyano-2,3-Epithiopropane as the primary sinigrin hydrolysis product of fresh cabbage. *J. Food Sci.* **1995**, *60*, 157−159.

(12) Petroski, R. J.; Tookey, H. L. Interactions of thioglucoside glucohydrolase and epithiospecifier protein of cruciferous plants to form 1-cyanoepithioalkanes. *Phytochem.* **1982**, *21*, 1903−1905.

(13) Munday, C. M. Selective induction of phase II enzymes in the urinary bladder of rats by allyl isothiocyanate, a compound derived from brassica vegetables. *Nutr. Cancer* **2002**, *44*, 52−59.

(14) Zhang, Y. Allyl isothiocyanate as a cancer chemopreventive phytochemical. *Mol. Nutr. Food Res.* **2010**, *54*, 127−135.

(15) Valko, M.; Izakovic, M.; Mazur, M.; Rhodes, C. J.; Telser, J. Role of oxygen radicals in DNA damage and cancer incidence. *Mol. Cell. Biochem.* **2004**, *266*, 37−56.

(16) Moon, Y. J.; Wang, X.; Morris, M. E. Dietary flavonoids: Effects on xenobiotic and carcinogen metabolism. *Toxicol. In Vitro* **2006**, *20*, 187−210.

(17) Poulsen, H. E.; Prieme, H.; Loft, S. Role of oxidative DNA damage in cancer initiation and promotion. *Eur. J. Cancer Prev.* **1998**, *7*, 9−16.

(18) van Dam, R. M.; Naidoo, N.; Landberg, R. Dietary flavonoids and the development of type 2 diabetes and cardiovascular diseases: review of recent findings. *Curr. Opin. Lipidol.* **2013**, *24*, 25−33.

(19) United States Department of Agriculture, Agricultural Marketing Service, Fruit and Vegetable Division, Fresh Products Branch *United States Standards for Grades for Horseradish Roots*; United States Department of Agriculture: Washington, DC, 1936. http://www.ams.usda.gov/AMSv1.0/getfile?dDocName=STELPRDC5050272 (accessed on May 2014).

(20) Brown, A. F.; Yousef, G. G.; Jeffery, E. H.; Klein, B. P.; Wallig, M. A.; Kushad, M. M.; Juvik, J. A. Glucosinolate profiles in broccoli: Variation in levels and implications in breeding for cancer chemoprotection. *J. Am. Soc. Hortic. Sci.* **2002**, *127*, 807−813.

(21) Ku, K. M.; Jeffery, E. H.; Juvik, J. A. Exogenous methyl jasmonate treatment increases glucosinolate biosynthesis and quinone reductase activity in kale leaf tissue. *PLoS One.* **2014**, *9*, e103407.

(22) Scanlon, J. T.; Willis, D. E. Calculation of flame ionization detector relative response factors using the effective carbon number concept. *J. Chromatogr. Sci.* **1985**, *23*, 333−340.

(23) Prochaska, H. J.; Santamaria, A. B. Direct measurement of NAD(P)H:quinone reductase from cells cultured in microtiter wells: a screening assay for anticarcinogenic enzyme inducers. *Anal. Biochem.* **1988**, *169*, 328−36.

(24) Dosz, E. B.; Ku, K. M.; Juvik, J. A.; Jeffery, E. H. Total myrosinase activity estimates in brassica vegetable produce. *J. Agric. Food Chem.* **2014**, *62*, 8094−100.

(25) Ku, K. M.; Choi, J. N.; Kim, J.; Kim, J. K.; Yoo, L. G.; Lee, S. J.; Hong, Y. S.; Lee, C. H. Metabolomics analysis reveals the

DOI: 10.1021/jf505591z
J. Agric. Food Chem. 2015, 63, 2947−2955

compositional differences of shade grown tea (*Camellia sinensis* L.). *J. Agric. Food Chem.* **2010**, *58*, 418−26.
(26) Wedelsbäck Bladh, K.; Olsson Kerstin, M.; Yndgaard, F. Evaluation of glucosinolates in Nordic horseradish (*Armoracia Rusticana*). *Bot. Lith.* **2013**, *19*, 48−56.
(27) Alnsour, M.; Kleinwächter, M.; Böhme, J.; Selmar, D. Sulfate determines the glucosinolate concentration of horseradish in vitro plants (*Armoracia rusticana* Gaertn., Mey. & Scherb.). *J. Sci. Food Agric.* **2013**, *93*, 918−923.
(28) Agneta, R.; Rivelli, A. R.; Ventrella, E.; Lelario, F.; Sarli, G.; Bufo, S. A. Investigation of glucosinolate profile and qualitative aspects in sprouts and roots of horseradish (*Armoracia rusticana*) using LC-ESI-hybrid linear ion trap with Fourier transform ion cyclotron resonance mass spectrometry and infrared multiphoton dissociation. *J. Agric. Food Chem.* **2012**, *60*, 7474−82.
(29) Sultana, T.; Savage, G.; McNeil, D.; Porter, N.; Clark, B. Comparison of flavour compounds in wasabi and horseradish. *J. Food, Agric. Environ.* **2003**, *1*, 117−121.
(30) Chin, H. W.; Zeng, Q.; Lindsay, R. C. Occurrence and flavor properties of sinigrin hydrolysis products in fresh cabbage. *J. Food Sci.* **1996**, *61*, 101−104.
(31) Kelleher, M. O.; McMahon, M.; Eggleston, I. M.; Dixon, M. J.; Taguchi, K.; Yamamoto, M.; Hayes, J. D. 1-Cyano-2,3-epithiopropane is a novel plant-derived chemopreventive agent which induces cytoprotective genes that afford resistance against the genotoxic α,β-unsaturated aldehyde acrolein. *Carcinogenesis.* **2009**, *30*, 1754−1762.
(32) Tomsone, L.; Kruma, Z.; Galoburda, R.; Talou, T. Composition of volatile compounds of horseradish roots (*Armoracia rusticana* L.) depending on the genotype. *Proc. Latv. Univ. Agric.* **2013**, *29*, 1.
(33) Wilson, E. A.; Ennahar, S.; Marchioni, E.; Bergaentzlé, M.; Bindler, F. Improvement in determination of isothiocyanates using high-temperature reversed-phase HPLC. *J. Sep. Sci.* **2012**, *35*, 2026−2031.
(34) Rose, P.; Faulkner, K.; Williamson, G.; Mithen, R. 7-Methylsulfinylheptyl and 8-methylsulfinyloctyl isothiocyanates from watercress are potent inducers of phase II enzymes. *Carcinogenesis* **2000**, *21*, 1983−8.
(35) Ku, K. M.; Jeffery, E. H.; Juvik, J. A. Influence of seasonal variation and methyl jasmonate mediated induction of glucosinolate biosynthesis on quinone reductase activity in broccoli florets. *J. Agric. Food Chem.* **2013**, *61*, 9623−31.
(36) Huang, D.; Ou, B.; Prior, R. L. The chemistry behind antioxidant capacity assays. *J. Agric. Food Chem.* **2005**, *53*, 1841−56.

DOI: 10.1021/jf505591z
J. Agric. Food Chem. 2015, 63, 2947−2955

Table 1. Parameters of the TIM-1 System When Simulating Digestive Conditions of a Healthy Adult after Intake of a High-Fat Semisolid Meal ("Fed State")[a]

compartment	starting content/secretions/filtration fluid	volume (mL)	pH (min/pH)	$t_{1/2}/\beta$
stomach	starting content:	310	0/5.5	70/2
	• 10 g of gastric juice (pH 2), 10400 U of pepsin, and 400 U of lipase in GES		10/5.0	
			20/4.2	
	secretions:		40/2.8	
	• 1040 U/mL of pepsin and 40 U/mL of lipase in GES circulating at 0.5 mL/min		60/2.1	
			90/1.8	
	• water or HCl (1 M) circulating at 0.5 mL/min		120/1.7	
			300/1.7	
duodenum	starting content:	60	6.3	160/1.6
	• 15 g of a pancreatin solution (21%), 30 g of fresh bile, 1 mL of trypsin solution (2 mg/mL), and 15 g of SIES (pH 7)			
	secretions:			
	• pancreatin solution (21%) circulating at 0.25 mL/min			
	• fresh bile circulating at 0.50 mL/min			
	• SIES[b] or $NaHCO_3$ (1 M) circulating at 0.25 mL/min			
	• SIES circulating at 3.2 mL/min			
jejunum	starting content:	160	6.5	160/1.6
	• 40 g of SIES, 80 g of fresh bile, and 40 g of pancreatin solution (21%)			
	secretions:			
	• $NaHCO_3$ (1 M) if necessary			
	• SIES containing 10% of fresh bile circulating at 3.2 mL/min			
	filtration fluid:			
	• SIES circulating at 4.5 mL/min			
ileum	starting content:	160	7.4	160/1.6
	• 160 g of SIES			
	secretions:			
	• $NaHCO_3$ (1 M) if necessary			
	• SIES circulating at 3.0 mL/min			
	filtration fluid:			
	• SIES circulating at 4.5 mL/min			

[a]Gastric and ileal deliveries are modeled with a power exponential formula: $f = 1 - 2^{-(t/t1/2)\beta}$, where f represents the fraction of meal delivered; t, the time of delivery; $t^{1/2}$, the half-time of delivery; and β, the coefficient describing the shape of the curve. [b]SIES, small intestine electrolyte solution.

digestive stability and bioaccessibility of egg carotenoids is poorly understood. Therefore, the objectives of this study were to determine the effect of cooking and digestion on the stability and bioaccessibility of carotenoids and to characterize the carotenoid profile in digested eggs using TIM-1.

MATERIALS AND METHODS

Chemicals. Pepsin (3200 U/mg, P6887, from porcine gastric mucosa), trypsin (7500 U/mg, T9201, from bovine pancreas), and pancreatin (4xUSP, P1750, from porcine pancreas), lutein (xanthophyll from marigold), zeaxanthin, canthaxanthin, and butylated hydroxytoluene (BHT) were obtained from Sigma-Aldrich (Oakville, ON, Canada). β-Apo-8′-carotenoic acid ethyl ester was obtained from CaroteNature (Lupsingen, Switzerland). (*Z*)-Isomers were obtained by iodine-catalyzed photoisomerization of the (all-*E*)-carotenoids.[24] Lipase (150 units/mg, from *Rhizopus oryzae* DF 15) was obtained from Amano Enzyme USA Co. The electrolyte solutions used for the digestion of proteins were gastric electrolyte solution (GES) containing NaCl (4.8 g/L), KCl (2.2 g/L), $CaCl_2$ (0.3 g/L), and $NaHCO_3$ (1.25 g/L) and small intestinal electrolyte solution (SIES) containing NaCl (5.0 g/L), KCl (0.6 g/L), and $CaCl_2$ (0.3 g/L). Fresh pig bile was collected from Olymel slaughterhouse (Vallée-Jonction, QC, Canada), aliquoted for individual TIM experiments and stored at −20 °C until use. Bile bladder had a minimal size of 8 cm in length. HPLC grade solvents (methanol, ethyl acetate, petroleum ether, and *tert*-butyl methyl ether) were purchased from Fisher Scientific (Ottawa, ON, Canada).

Sample Preparation. Fresh eggs (n = 180) were obtained from the Poultry Research Centre of University of Alberta (Edmonton, AB, Canada). Eggs were divided into three groups of 60 each and subjected to boiling, frying, and scrambling. Boiled and fried eggs were prepared using the same cooking conditions that were reported previously.[24] Briefly, shell eggs were boiled in a boiling water bath for 10 min, cooled under running tap water, and peeled, and the yolks were separated from the whites. A nonstick frying pan (model SK200TY nonstick frying pan, Black & and Decker Canada Inc., Brockville, ON, Canada) preheated to 205 °C was used to prepare fried eggs. Whole eggs were fried for 6 min (3 min each side), and the yolks were separated from the whites. To prepare scrambled eggs, yolks were separated and combined and stirred on a preheated (205 °C) model SK200TY nonstick frying pan (Black & Decker Canada Inc.) by stirring yolks for 1 min. Each sample of cooked egg yolks was divided into two subgroups. Samples were vacuum packed, covered with aluminum foil to protect carotenoids from light exposure, and frozen immediately at −20 °C. The next day, all samples were shipped in a Styrofoam box along with dry ice to the Institute of Nutrition and Functional Foods (INAF) at Laval University (Quebec City, QC, Canada), where they were stored at −80 °C until subjected to digestion.

DOI: 10.1021/jf505615w
J. Agric. Food Chem. 2015, 63, 2956−2962

TIM-1 Dynamic Gastrointestinal Model. TIM-1, which has been previously described in detail[8] and commercialized by TNO Nutrition and Food Research (Zeist, The Netherlands), was used for this study. In brief, the computer-controlled system consists of four compartments made of a glass outer wall and a flexible inner wall to represent the stomach, duodenum, jejunum, and ileum. These compartments are connected by peristaltic valve pumps, which facilitate the passage of a constant volume of chyme during each open-and-close cycle. The space between the two walls is filled with water at 37 °C to mimic body temperature. Changing the water pressure enables peristaltic movements and churning of chyme by alternated compression and relaxation of the inner walls. Previously formulated solutions to mimic salivary, gastric, biliary, and pancreatic secretions are introduced into the system via a computer-controlled pumping system. Two hollow-fiber membranes are connected to the jejunum and ileum to simulate the absorption of nutrients/drug and water from chyme. The volume in each compartment and pH, which is regulated using hydrochloric acid and/or sodium bicarbonate, are continuously monitored and controlled.

Digestion of Samples with TIM-1. Approximately 200 g of cooked egg sample was homogenized with 200 g of distilled water to prepare the "meal" using a hand-held blender model CSB-79C (Cuisinart, Woodbridge, ON, Canadae) for 12 s. A sample of 100 g from the meal was taken out as a control, and the rest (300 g) was immediately fed into the gastric compartment of the TIM-1 system. The digestion was carried out using predetermined parameters of TIM-1 modified from Speranza et al.[25] and adapted to reproduce the digestion of a semisolid meal in a healthy human adult (Table 1). The jejunal and ileal compartments were connected to specific hollow-filter membranes (MiniKros module M80S-300-01P, Spectrum Laboratories Inc., Rancho Dominguez, CA, USA) that separate the micellar phase from the fat phase to determine bioaccessibility of lipophilic products.[26,27] The mixed micelles that contain the bioaccessible lipophilic fraction are able to pass through these membranes, whereas the undigested fat is retained. These bioaccessible fractions are collected in separate pouches kept on ice. After the passage of the chyme throughout the system, the residual digestion mixture is discharged as the effluent, which was kept on ice during the experiment. The digestion was carried out under subdued light to prevent photodegradation of carotenoids. All solutions/secretions used during the digestion were purged with nitrogen, and continuous nitrogen flow to the jejunal, ileal, and effluent compartments was maintained to minimize carotenoid oxidation and to reproduce the in vivo luminal conditions. Duplicated digestions were carried out for each cooked egg sample. A blank digestion was also performed using the same parameters with 200 g of distilled water in place of egg sample to estimate the carotenoids from digestive secretions and bile found in each sample.

Sampling Location and Time. During the total digestion time of 300 min, samples were obtained from different compartments as follows: 8 g of stomach chyme at 120 min and 8 g samples from duodenal, jejunal, and ileal chyme at 150 min were taken out. Jejunal filtrate, ileal filtrate, and effluent were collected from 0 to 150 min and from 150 to 300 min into separate pouches kept on ice. The residual chyme samples in duodenal, jejunal, and ileal compartments at the end of the digestion were also collected. Samples were weighed, aliquoted, and immediately transferred to a −80 °C freezer in airtight containers. All samples were freeze-dried and transported to the University of Alberta (Canada) with ice packs, where they were stored at −20 °C until analysis.

Analysis of Carotenoids in Digested Samples. Carotenoids in each sample were extracted as described previously with modifications.[28] Briefly, 500 mg of sample was accurately weighed into a microcentrifuge tube and extracted twice with 0.5 mL of a ternary solvent mixture consisting of methanol/ethyl acetate/petroleum ether (1:1:1 v/v/v) containing 0.1% BHT. The supernatants were combined in microcentrifuge tubes, evaporated under nitrogen, and reconstituted in 0.5 mL of acetone. The acetone extracts were kept at −80 °C for ∼1 h, and then the samples were vacuum filtered using a sintered glass funnel in a freezer compartment at −20 °C to remove the crystallized lipids.[24,46] The crystallized white color lipids were retained in the funnel; the filtrates containing carotenoids were centrifuged at 16500*g* for 30 s, and the supernatants were immediately transferred to a separate microcentrifuge tube, evaporated under nitrogen, and reconstituted in 200 μL of methanol. The extracts were filtered through a 0.45 μm nylon syringe filter and analyzed by HPLC using a Waters 600 HPLC system (Waters, Millford, MA, USA) equipped with a 2702 thermoautosampler, a binary gradient pump, and a 2998 photodiode array detector. The separation of carotenoids was performed on a C_{30} reversed-phase column (YMC 250 mm × 4.6 mm, i.d. = 5 μm) operated at room temperature (22 °C) using the conditions reported before.[24] Duplicate analyses were performed. To protect carotenoids from light- and oxygen-induced degradation, dim light conditions were used during sample handling, extraction, and analysis, and solvents used were purged with nitrogen. Identification of *trans* and *cis* isomers of lutein and zeaxanthin standards were performed on the basis of our previous study.[24] Carotenoids in the samples were identified on the basis of their UV spectra, retention time, and order of elution compared to the standard compounds and quantified using seven-point standard calibration curves.

Calculations and Statistical Analysis. The recovery of carotenoid compounds (separately for lutein and zeaxanthin) in each cooked egg sample was calculated as a percentage of the total amount of carotenoid compounds in the initial meal fed into the system using following equation:

$$\begin{aligned}&\text{recovery of carotenoids (\%)}\\&= (\text{total amount in jejunal filtrate} + \text{ileal filtrate} + \text{effluent}\\&\quad + \text{chyme residue at 300 min})/(\text{total amount fed into the system}\\&\quad - \text{amount detected during blank digestion}) \times 100\end{aligned}$$

All data were analyzed by analysis of variance (ANOVA) followed by Tukey's multiple-range test using Statistical Analysis System software (SAS version 9.3, SAS Institute Inc., Cary, NC, USA). Significance of differences was defined at the 5% level ($p < 0.05$).

RESULTS AND DISCUSSION

Carotenoid Profile of Eggs. The main carotenoid isomers found in undigested egg yolk were all-*E*-lutein, all-*E*-zeaxanthin, 13′-*Z*-lutein, and 13-*Z*-zeaxanthin. The other carotenoids usually found in eggs, such as all-*E*-canthaxanthin and all-*E*-β-apo-8′ carotenoic acid ethyl ester, were found in only trace amounts (Figure 1). The eggs used in this study did not use synthetic carotenoids as poultry feed additives. This might explain their absence in eggs as the egg carotenoid profile is

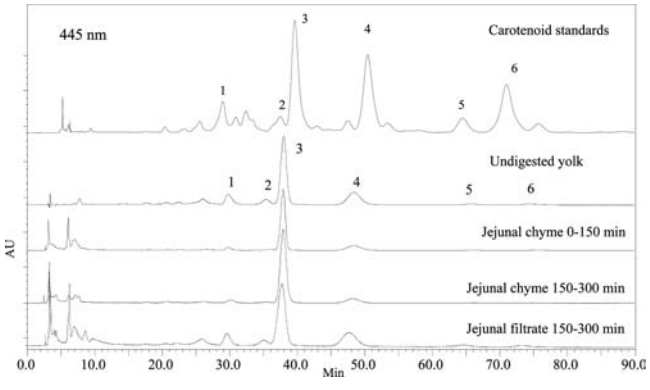

Figure 1. Representative HPLC chromatograms of carotenoid standards, egg yolk carotenoids from meal, and different intestinal compartments during digestion. Peaks: (1) 13′-*Z*-lutein; (2) 13-*Z*-zeaxanthin; (3) all-*E*-lutein; (4) all-*E*-zeaxanthin; (5) all-*E*-cantha-xanthin; (6) all-*E*-β-apo-8′-carotenoic acid ethyl ester.

DOI: 10.1021/jf505615w
J. Agric. Food Chem. 2015, 63, 2956−2962

highly dependent on hens' diet.[28] The qualitative HPLC chromatographic profile of the egg carotenoid isomers remained unchanged during the digestion as no new isomer formation was observed (Figure 1). 13′-*Z*-Lutein and 13-*Z*-zeaxanthin were found in most of the samples, but were below the limit of quantitation in the duodenal, jejunal, and ileal chyme. Thus, the total recovery of these *cis* isomers could not be calculated. Coinciding with previous results,[29,30] no significant *trans*−*cis* isomerization of carotenoids was observed during the digestion due to the high recovery of *trans*-lutein and -zeaxanthin as well as the total quantity of *cis* isomers in filtrates and effluent being much lower than the amounts in the meal. Therefore, in this study we mainly focused on all-*E*-lutein and all-*E*-zeaxanthin levels in the gut during the digestion; unless mentioned otherwise, lutein and zeaxanthin represent the *trans* form of the respective carotenoid.

Digestive Stability of Carotenoids and Distribution in TIM-1 Compartments during Digestion. Only trace amounts of endogenous lutein and zeaxanthin from bile and/or other intestinal secretions were observed in the samples from the blank digestion, which were below the quantitative limits of HPLC. Hence, the distribution and recovery of carotenoids were calculated as a percentage of carotenoid content present in eggs fed into the TIM-1. Overall, both lutein and zeaxanthin were stable at 300 min of the digestion, with average recoveries of 90 and 88% calculated for all-*E*-lutein and all-*E*-zeaxanthin, respectively. At half time of the digestion (150 min), approximately 37% of lutein, irrespective of the type of sample, exited the small intestine (indicated as "effluent") without absorption (Figure 2A). Around 16 and 8% of lutein were passed through the hollow fiber membrane as bioaccessible lutein into the jejunal and ileal filtrates, respectively. Most of the remaining lutein was still in the jejunal and ileal compartments, whereas only about 2% was present in the duodenum. No lutein was detected in the stomach samples even at 120 min through digestion, and by 150 min the stomach was completely free from meal. All-*E*-zeaxanthin had distribution profiles similar to those of lutein at 150 min; however, a comparatively higher proportion (∼50%) in scrambled eggs was found in effluent as nonbioaccessible zeaxanthin (Figure 2). The average recovery of zeaxanthin from fried eggs at 150 min was 69.7%, much lower than those of boiled and scrambled samples (Figure 2B). This is because the zeaxanthin contents in duodenal, jejunal, and ileal chyme samples at 150 min from one of the two fried egg digestions were below the quantifiable limits of HPLC. Consequently, the calculated recovery at 150 min was lower than the true recovery of zeaxanthin. However, this does not influence the digestive stability calculations at 300 min, as we have collected all of the chyme remaining in the intestinal compartments and had enough samples for quantification (see the equation under Materials and Methods). At the end of the digestion (at 300 min), almost 50% of the total lutein was found in effluent followed by 30% in jejunal filtrates. Around 10% of lutein was in ileal filtrate, whereas only a small amount remained in duodenal, jejunal, and ileal compartments. A similar distribution pattern was observed with zeaxanthin except that a higher amount (∼63%) was found in the effluent in scrambled eggs (Figure 2B), apparently the reason for comparatively lower bioaccessibility (Figure 3), which is discussed below. Even

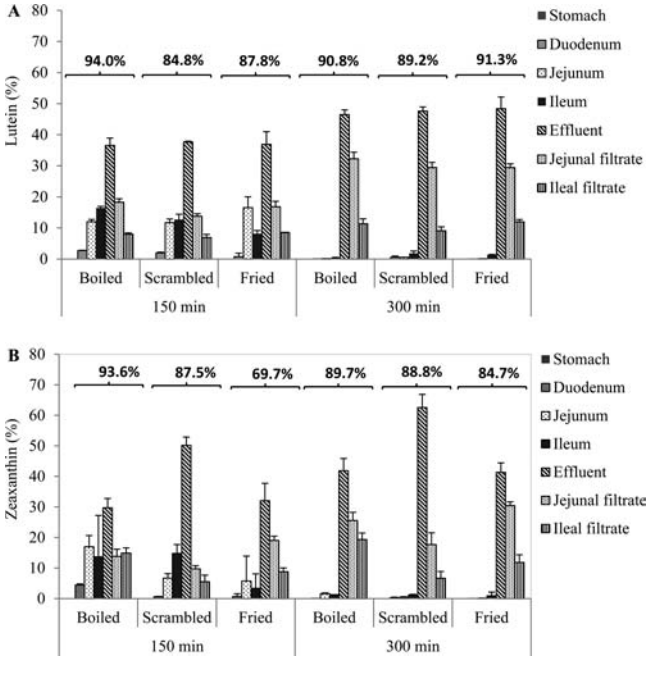

Figure 2. Total recovery (indicated on top of the bars) and distribution of all-*E*-lutein (A) and all-*E*-zeaxanthin (B) in the gut during digestion (as a % of the feeding). Data are the average of two measurements.

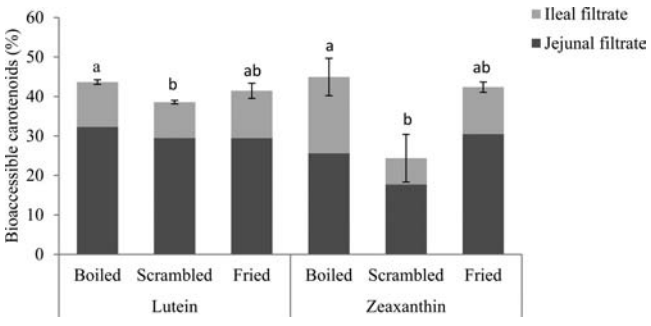

Figure 3. Cumulative carotenoids in jejunal and ileal filtrates (bioaccessible carotenoids) as a percentage of the feeding at the end of the digestion (n = 2; different letters (a, b) denote significant difference (p < 0.05)).

though no studies are available regarding the gut distribution and/or stability of lutein and zeaxanthin from egg yolk, these carotenoids have been reported as highly stable during gastrointestinal digestion regardless of the food source. Blanquet et al.[20] used TIM-1 to compare the digestive stability of xanthophylls and carotenes and found that lutein and zeaxanthin were stable throughout the digestion and the digestive stability of xanthophylls is higher than that of carotenes. Studies that used other in vitro digestion methods also showed a higher digestive stability (>80%) of lutein and zeaxanthin derived from different food sources.[9,10,19,29]

Bioaccessibility of Carotenoids from Cooked Eggs. Bioaccessibility of carotenoids was the total amount of ileal and jejunal filtrates expressed as a percentage of the total carotenoids present in starting meal. According to Etcheverry et al.,[31] there are principally four in vitro methods for measuring bioaccessibility and/or bioavailability: solubility, dialyzability, or a gastrointestinal model (e.g.,TIM) for bioaccessibility and cell culture for bioavailability. There exist no in vitro digestion models that have the capability to mimic

DOI: 10.1021/jf505615w
J. Agric. Food Chem. 2015, 63, 2956−2962

perfectly the complex environment of the GI tract. However, TIM-1 is the only in vitro digestion model with the capacity to simulate the dynamic conditions of the stomach and small intestine during digestion.[32] As shown in Figure 1, the isomeric profiles of carotenoids were similar in both nonbioaccessible (jejunal chyme, 0−150 and 150−300 min) and bioaccessible samples (jejunal filtrate, 150−300 min), indicating both *trans* and *cis* isomers of carotenoids passed through the hollow fiber membranes into the bioaccessible filtrates. In boiled, fried, and scrambled eggs, the bioaccessibility of lutein was 44, 41, and 39%, whereas that of zeaxanthin was 45, 42, and 24%, respectively (Figure 3). Total bioaccessible carotenoids were higher in the jejunal filtrate than in the ileal filtrate. A similar trend was observed in recent studies using TIM-1 to study the effect of fat on blueberry anthocyanins[33] and β-carotene bioaccessibility.[21] Although we did not find any study on lutein bioaccessibility using TIM-1, there are many other papers on lutein bioaccessibility using other in vitro digestion models. Garrett et al.[9] developed an in vitro digestion model and found the lutein bioavailability (solubility assay + cells culture) in a standard baby food to be 25−40%, which is consistent with our results. Using the same model, O'Connell et al. demonstrated that lutein from fruits including orange, kiwi, grapefruit, and honeydew melon (100−109%) is more bioaccessible compared to that from dark green vegetables, spinach (19%), and broccoli (38%).[11] However, Chitchumroonchokchai et al.[10] found a much higher lutein micellarization (53%) in microwave-cooked spinach using solubility assay coupling with Caco-2 cells, presumably due to the disruption of cell walls. Bioaccessibility of lutein from pure durum wheat pasta amounted to 71%, whereas from egg pasta it was 57%,[34] which seems contradictory to the fact of high bioavailability of egg lutein. It was speculated that egg lutein was incorporated into the complex mixture of proteins and starch during pasta processing, leading to low bioaccessibility. Lutein-fortified whole, semiskimmed, and skimmed milk showed bioaccessible levels of 46.5, 45.8, and 19.7%, whereas in whole, semiskimmed, and skimmed yogurts, it was 47.5, 38.3, and 17.8%, respectively;[35] these data are comparable to bioaccessibility levels observed in our study.

The bioaccessibility of both lutein and zeaxanthin was affected by the type of cooking (Figure 3). Lutein and zeaxanthin from scrambled eggs yielded significantly lower bioaccessibility compared to boiled eggs, but were not different from fried eggs. The exact reason for this difference is not clear, but presumably the chemical and structural changes of proteins and lipoproteins in egg yolk occurring during different cooking conditions may have influenced the micellarization efficiency, that is, the transfer of carotenoids to the filtrates. Textural differences between the cooked eggs can be a considerable factor on micellarization as boiled eggs are easily blended with water compared to fried and scrambled eggs. Particle size, food processing, and food preparation[16−19] have been reported as influencing factors on carotenoid bioaccessibility. Panozzo et al.[18] showed bioaccessibility of carotenoids from tomato pulp was affected by homogenization in two main ways: (a) decreased particle size, which enables release of carotenoids; and (b) increased consistency due to the formation of a fiber network, which entraps the carotenoids. Similarly, the industrially extracted orange juice resulted in smaller particle sizes and increased the relative bioaccessibility compared to hand extraction.[16] The composition and degree of saturation of fatty acids are also considered important factors on carotenoid bioaccessibility and bioavailability.[36−38] Gleize et al.[38] observed that saturated and monounsaturated short-chain fatty acids (MUFA) lead to the formation of small micelles and higher bioaccessibility of lutein and zeaxanthin compared to the long-chain polyunsaturated fatty acids (PUFA). The significant inverse relationship between micelle size and bioaccessibility was attributed to increased specific surface area with smaller micelles. They hypothesized that due to the polar nature, xanthophylls located at the micelle surface and, therefore, increased surface area increases amount of xanthophylls that can be incorporated into the micelles. Different cooking methods resulted in diverse fatty acid profiles in egg yolk.[39,43] The amount of PUFA reported in scrambled eggs is significantly higher compared to boiled eggs, which may lead to the formation of larger micelles and lower bioaccessibility. This can also explain our observations on bioaccessibility of carotenoid from eggs after different cooking methods. Lutein and zeaxanthin differ only by the position of one double bond. This minor structural difference may influence how these two compounds incorporated into the micelles and their respective bioaccessibility. It has been shown that the orientations of lutein and zeaxanthin in a phospholipid bilayer are different. Zeaxanthin adopts an orientation spanning the membranes from outer polar headgroup layer to the other polar headgroup layer, whereas lutein can have two different orientations; one way of orientation is similar to that of zeaxanthin, whereas the other is arranged horizontally to the membrane.[48] In a similar way, lutein and zeaxanthin may have different orientation patterns in mixed micelles during digestion, which might contribute to their differences in bioaccessibility.

TIM-1 is so far considered the digestive model simulating the in vivo conditions of human gut and very useful in predicting the fate of nutrients and pharmaceuticals, optimizing the oral formulations for clinical studies and also allowing the simulation of the digestion of infants, young adults, seniors, and patients with impaired gastrointestinal conditions.[40] However, the data obtained through in vitro digestion models on the bioaccessibility of carotenoids may not directly be applied as bioavailability in humans and should be interpreted with caution. On the basis of previously published studies, Reboul et al.[19] made a comparison between the bioaccessibilities of carotenoids obtained using in vitro digestive models and bioavailability values measured in healthy subjects. They found that there is a significant relationship ($r = 0.98$, $p < 0.0001$) between bioaccessibility ratios measured in vitro and the mean bioavailability ratios. In contrast, Granado et al.[41] showed that the bioaccessibility of carotenoids and vitamin E from broccoli under in vitro conditions does not fully explain the changes they observed in healthy individuals. Another paper stated that, although the micellarization efficiencies of lutein from human milk and infant formula were similar, accumulation efficiency of human milk lutein was 4.5 times higher by Caco-2 human intestinal cells.[42]

In summary, we studied the effect of different domestic cooking methods on the stability and bioaccessibility of carotenoids from egg yolk. In alignment with the previous findings, lutein and zeaxanthin were stable during the in vitro digestion. Digestive stability was not affected by the different types of cooking, whereas scrambling resulted in significantly lower bioaccessibility compared to boiled eggs in both lutein and zeaxanthin. To the best of our knowledge, this is the first study to investigate the bioaccessibility of egg yolk carotenoids affected by the cooking methods. The results presented here provide detailed information on digestive stability and

DOI: 10.1021/jf505615w
J. Agric. Food Chem. 2015, 63, 2956−2962

bioaccessibility of egg carotenoids under various thermal processing conditions and may be useful in estimating the bioavailable carotenoids from eggs and egg-containing foods.

AUTHOR INFORMATION

Corresponding Author

*(J.W.) Phone: (780) 492-6885. Fax: (780) 492-4265. E-mail: jwu3@ualberta.ca.

Funding

This research was funded by grants from Egg Farmers of Canada (EFC), Alberta Egg Producers (AEP), the Agriculture and Food Council, which is responsible for delivering Agriculture and Agri-Food Canada's Advancing Canadian Agriculture and Agri-Food (ACAAF) Program in Alberta, Food for Health Initiative (Vitamin Fund) of the Faculty of Agricultural, Life and Environmental Science of the University of Alberta, Burnbrae Farms Limited, Poultry Industry Council, and Natural Sciences and Engineering Research Council (NSERC) of Canada to J. Wu.

Notes

The authors declare no competing financial interest.

REFERENCES

(1) Krinsky, N.; Landrum, J.; Bone, R. Biologic mechanisms of the protective role of lutein and zeaxanthin in the eye. *Annu. Rev. Nutr.* **2003**, *23*, 171−201.

(2) Chung, H.-Y.; Rasmussen, H. M.; Johnson, E. J. Lutein bioavailability is higher from lutein-enriched eggs than from supplements and spinach in men. *J. Nutr.* **2004**, *134*, 1887−1893.

(3) Handelman, G. J.; Nightingale, Z. D.; Lichtenstein, A. H.; Schaefer, E. J.; Blumberg, J. B. Lutein and zeaxanthin concentrations in plasma after dietary supplementation with egg yolk. *Am. J. Clin. Nutr.* **1999**, *70*, 247−251.

(4) Surai, P. F.; MacPherson, A.; Speake, B. K.; Sparks, N. H. C. Designer egg evaluation in a controlled trial. *Eur. J. Clin. Nutr.* **2000**, *54*, 298−305.

(5) Faulks, R. M.; Southon, S. Challenges to understanding and measuring carotenoid bioavailability. *Biochim. Biophys. Acta* **2005**, *1740*, 95−100.

(6) Faulks, R. M.; Hart, D. J.; Brett, G. M.; Dainty, J. R.; Southon, S. Kinetics of gastro-intestinal transit and carotenoid absorption and disposal in ileostomy volunteers fed spinach meals. *Eur. J. Nutr.* **2004**, *43*, 15−22.

(7) Hur, S. J.; Lim, B. O.; Decker, E. A.; McClements, D. J. *In vitro* human digestion models for food applications. *Food Chem.* **2011**, *125*, 1−12.

(8) Minekus, M.; Marteau, P.; Havenaar, R.; Huis in't Veld, J. H. H. Multicompartmental dynamic computer-controlled model simulating the stomach and small intestine. *ATLA, Altern. Lab. Anim.* **1995**, *23*, 197−209.

(9) Garrett, D. A.; Failla, M. L.; Sarama, R. J. Development of an in vitro digestion method to assess carotenoid bioavailability from meals. *J. Agric. Food Chem.* **1999**, *47*, 4301−4309.

(10) Chitchumroonchokchai, C.; Schwartz, S. J.; Failla, M. L. Assessment of lutein bioavailability from meals and a supplement using simulated digestion and Caco-2 human intestinal cells. *J. Nutr.* **2004**, *134*, 2280−2286.

(11) O'Connell, O. F.; Ryan, L.; O'Brien, N. M. Xanthophyll carotenoids are more bioaccessible from fruits than dark green vegetables. *Nutr. Res. (N.Y.)* **2007**, *27*, 258−264.

(12) Granado-Lorencio, F. *In vitro* bioaccessibility of carotenoids and tocopherols from fruits and vegetables. *Food Chem.* **2007**, *102*, 641−648.

(13) van het Hof, K. H.; Brouwer, I. A.; West, C. E.; Haddeman, E.; Steegers-Theunissen, R. P.; van Dusseldorp, M.; Weststrate, J. A.; Eskes, T. K. A. B.; Hautvast, J. G. A. J. Bioavailability of lutein from vegetables is 5 times higher than that of β-carotene. *Am. J. Clin. Nutr.* **1999**, *70*, 261−268.

(14) Tyssandier, V.; Reboul, E.; Dumas, J.-F.; Bouteloup-Demange, C.; Armand, M.; Marcand, J.; Sallas, M.; Borel, P. Processing of vegetable-borne carotenoids in the human stomach and duodenum. *Am. J. Physiol. Gastrointest. Liver Physiol.* **2003**, *284*, G913−G923.

(15) Schweiggert, R. M.; Kopec, R. E.; Villalobos-Gutierrez, M. G.; Hogel, J.; Qusada, S.; Esquivel, P.; Schwarz, S. J.; Carle, R. Carotenoids are more bioavailable from papaya than from tomato and carrot in humans: a randomised cross-over study. *Br. J. Nutr.* **2013**, *111*, 490−498.

(16) Stinco, C. M.; Fernández-Vázquez, R.; Escudero-Gilete, M. L.; Heredia, F. J.; Meléndez-Martínez, A. J.; Vicario, I. M. Effect of orange juice's processing on the color, particle size, and bioaccessibility of carotenoids. *J. Agric. Food Chem.* **2012**, *60*, 1447−1455.

(17) Moelants, K. R. N.; Lemmens, L.; Vandebroeck, M.; Van Buggenhout, S.; Van Loey, A. M.; Hendrickx, M. E. Relation between particle size and carotenoid bioaccessibility in carrot-and tomato-derived suspensions. *J. Agric. Food Chem.* **2012**, *60*, 11995−12003.

(18) Panozzo, A.; Lemmens, L.; Van Loey, A.; Manzocco, L.; Nicoli, M. C.; Hendrickx, M. Microstructure and bioaccessibility of different carotenoid species as affected by high pressure homogenisation: a case study on differently coloured tomatoes. *Food Chem.* **2013**, *141*, 4094−4100.

(19) Reboul, E.; Richelle, M.; Perrot, E.; Desmoulins-Malezet, C.; Pirisi, V.; Borel, P. Bioaccessibility of carotenoids and vitamin E from their main dietary sources. *J. Agric. Food Chem.* **2006**, *54*, 8749−8755.

(20) Blanquet-Diot, S.; Soufi, M.; Rambeau, M.; Rock, E.; Alric, M. Digestive stability of xanthophylls exceeds that of carotenes as studied in a dynamic *in vitro* gastrointestinal system. *J. Nutr.* **2009**, *139*, 876−883.

(21) Van Loo-Bouwman, C. A.; Naber, T. H. J.; Minekus, M.; van Breemen, R. B.; Hulshof, P. J. M.; Schaafsma, G. Food matrix effects on bioaccessibility of β-carotene can be measured in an in vitro gastrointestinal model. *J. Agric. Food Chem.* **2014**, *62*, 950−955.

(22) Deat, E.; Blanquet-Diot, S.; Jarrige, J.-F.; Denis, S.; Beyssac, E.; Alric, M. Combining the dynamic TNO-gastrointestinal tract system with a Caco-2 cell culture model: application to the assessment of lycopene and α-tocopherol bioavailability from a whole food. *J. Agric. Food Chem.* **2009**, *57*, 11314−11320.

(23) Richelle, M.; Sanchez, B.; Tavazzi, I.; Lambelet, P.; Bortlik, K.; Williamson, G. Lycopene isomerisation takes place within enterocytes during absorption in human subjects. *Br. J. Nutr.* **2010**, *103*, 1800−1807.

(24) Nimalaratne, C.; Lopes-Lutz, D.; Schieber, A.; Wu, J. Effect of domestic cooking methods on egg yolk xanthophylls. *J. Agric. Food Chem.* **2012**, *60*, 12547−12552.

(25) Speranza, A.; Corradini, M. G.; Hartman, T. G.; Ribnicky, D.; Oren, A.; Rogers, M. A. Influence of emulsifier structure on lipid bioaccessibility in oil-water nanoemulsions. *J. Agric. Food Chem.* **2013**, *61*, 6505−6515.

(26) Minekus, M.; Jelier, M.; Xiao, J.-Z.; Kondo, S.; Iwatsuki, K.; Kokubo, S.; Bos, M.; Dunnewind, B.; Havenaar, R. Effect of partially hydrolyzed guar gum (PHGG) on the bioaccessibility of fat and cholesterol. *Biosci., Biotechnol., Biochem.* **2005**, *69*, 932−938.

(27) Reis, P. M.; Raab, T. W.; Chuat, J. Y.; Leser, M. E.; Miller, R.; Watzke, H. J.; Holmberg, K. Influence of surfactants on lipase fat digestion in a model gastro-intestinal system. *Food Biophys.* **2008**, *3*, 370−381.

(28) Schlatterer, J.; Breithaupt, D. E. Xanthophylls in commercial egg yolks: quantification and identification by HPLC and LC-(APCI)MS using a C_{30} phase. *J. Agric. Food Chem.* **2006**, *54*, 2267−2273.

(29) Granado-Lorencio, F.; Olmedilla-Alonso, B.; Herrero-Barbudo, C.; Pérez-Sacristán, B.; Blanco-Navarro, I.; Blázquez-García, S. Comparative in vitro bioaccessibility of carotenoids from relevant contributors to carotenoid intake. *J. Agric. Food Chem.* **2007**, *55*, 6387−6394.

(30) Granado-Lorencio, F.; López-López, I.; Herrero-Barbudo, C.; Blanco-Navarro, I.; Cofrades, S.; Pérez-Sacristán, B.; Delgado-Pando,

DOI: 10.1021/jf505615w
J. Agric. Food Chem. 2015, 63, 2956−2962

G.; Jiménez-Colmenero, F. Lutein-enriched frankfurter-type products: physicochemical characteristics and lutein *in vitro* bioaccessibility. *Food Chem.* **2010**, *120*, 741−748.
(31) Etcheverry, P.; Grusak, M. A.; Fleige, L. E. Application of *in vitro* bioaccessibility and bioavailability methods for calcium, carotenoids, folate, iron, magnesium, polyphenols, zinc, and vitamins B(6), B(12), D, and E. *Front. Physiol.* **2012**, *3*, 317.
(32) Kostewicz, E. S.; Abrahamsson, B.; Brewster, M.; Brouwers, J.; Butler, J.; Carlert, S.; Dickinson, P. A.; Dressman, J.; Holm, R.; Klein, S.; Mann, J.; McAllister, M.; Minekus, M.; Muenster, U.; Müllertz, A.; Verwei, M.; Vertzoni, M.; Weitschies, W.; Augustijns, P. *In vitro* models for the prediction of *in vivo* performance of oral dosage forms. *Eur. J. Pharm. Sci.* **2014**, *57*, 342−366.
(33) Ribnicky, D. M.; Roopchand, D. E.; Oren, A.; Grace, M.; Poulev, A.; Lila, M. A.; Havenaar, R.; Raskin, I. Effects of a high fat meal matrix and protein complexation on the bioaccessibility of blueberry anthocyanins using the TNO gastrointestinal model (TIM-1). *Food Chem.* **2014**, *142*, 349−357.
(34) Werner, S.; Böhm, V. Bioaccessibility of carotenoids and vitamin E from pasta: evaluation of an in vitro digestion model. *J. Agric. Food Chem.* **2011**, *59*, 1163−1170.
(35) Xavier, A. A. O.; Mercadante, A. Z.; Garrido-Fernández, J.; Pérez-Gálvez, A. Fat content affects bioaccessibility and efficiency of enzymatic hydrolysis of lutein esters added to milk and yogurt. *Food Res. Int.* **2014**, *65*, 171−176.
(36) Nidhi, B.; Baskaran, V. Influence of vegetable oils on micellization of lutein in a simulated digestion model. *J. Am. Oil Chem. Soc.* **2010**, *88*, 367−372.
(37) Goltz, S. R.; Campbell, W. W.; Chitchumroonchokchai, C.; Failla, M. L.; Ferruzzi, M. G. Meal triacylglycerol profile modulates postprandial absorption of carotenoids in humans. *Mol. Nutr. Food Res.* **2012**, *56*, 866−877.
(38) Gleize, B.; Tourniaire, F.; Depezay, L.; Bott, R.; Nowicki, M.; Albino, L.; Lairon, D.; Kesse-Guyot, E.; Galan, P.; Hercberg, S.; Borel, P. Effect of type of TAG fatty acids on lutein and zeaxanthin bioavailability. *Br. J. Nutr.* **2013**, *110*, 1−10.
(39) Cortinas, L.; Galobart, J.; Barroeta, A. C.; Baucells, M. D.; Grashorn, M. A. Change in α-tocopherol contents, lipid oxidation and fatty acid profile in eggs enriched with linolenic acid or very long-chain ω-3 polyunsaturated fatty acids after different processing methods. *J. Sci. Food Agric.* **2003**, *83*, 820−829.
(40) Guerra, A.; Etienne-Mesmin, L.; Livrelli, V.; Denis, S.; Blanquet-Diot, S.; Alric, M. Relevance and challenges in modeling human gastric and small intestinal digestion. *Trends Biotechnol.* **2012**, *30*, 591−600.
(41) Granado, F.; Olmedilla, B.; Herrero, C.; Pérez-Sacristán, B.; Blanco, I.; Blázquez, S. Bioavailability of carotenoids and tocopherols from broccoli: *in vivo* and *in vitro* assessment. *Exp. Biol. Med.* **2006**, *231*, 1733−1738.
(42) Lipkie, T. E.; Banavara, D.; Shah, B.; Morrow, A. L.; McMahon, R. J.; Jouni, Z. E.; Ferruzzi, M. G. Caco-2 accumulation of lutein is greater from human milk than from infant formula despite similar bioaccessibility. *Mol. Nutr. Food Res.* **2014**, *58*, 2014−2022.
(43) U.S. Department of Agriculture: National Nutrient Database for standard reference, release 27; available at http://ndb.nal.usda.gov/ndb/ (accessed Sept 25, 2014).
(44) Klein, R. J.; Zeiss, C.; Chew, E. Y.; Tsai, J. Y.; Sackler, R. S.; Haynes, C.; et al. Complement factor H polymorphism in age-related macular degeneration. *Science* **2005**, *308*, 385−389.
(45) Coleman, H. R.; Chan, C. C.; Ferris, F. L., III; Chew, E. Y. Age-related macular degeneration. *Lancet* **2008**, *372*, 1835−1845.
(46) Rodriguez-Amaya, D. B. Food carotenoids: analysis, composition and alterations during storage and processing of foods. *Forum Nutr.* **2003**, *56*, 35−37.
(47) Ryan, L.; O'Connell, O.; O'Sullivan, L.; Aherne, S. A.; O'Brien, N. M. Micellarisation of carotenoids from raw and cooked vegetables. *Plant Food Hum. Nutr.* **2008**, *63*, 127−133.
(48) Britton, G. Functions of intact carotenoids. In *Carotenoids*; Britton, G., Liaaen-Jensen, S., Pfander, H., Eds.; Birkhäuser Verlag: Basel, Switzerland, 2008; Vol. 4, pp 189−212.

DOI: 10.1021/jf505615w
J. Agric. Food Chem. 2015, 63, 2956−2962

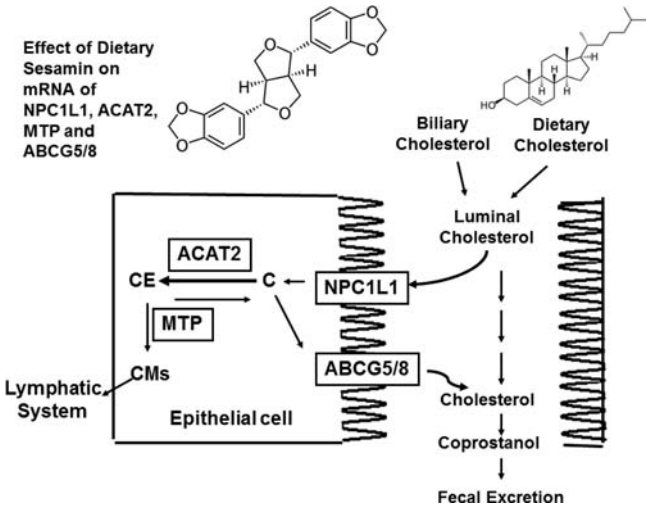

Figure 1. Structure of sesamin and cholesterol absorption pathway. Dietary and biliary cholesterol (C) is transported into enterocytes by Niemann−Pick C1 like 1 transporter (NPC1L1). Acyl-CoA:cholesterol acyltransferase 2 (ACAT2) esterifies cholesterol to form cholesteryl ester (CE), which is then packed into chylomicrons (CMs) by microsomal triacylglycerols transport protein (MTP). CMs containing CE are then transferred into blood through the lymphatic system. ATP binding cassette transporters (ABCG5 and ABCG8) return the unabsorbed cholesterol to the lumen of intestine. Cholesterol in the large intestine is converted to coprostanol and other derivatives by bacteria.

into enterocytes.[16] Second, intestinal acyl-CoA:cholesterol acyltransferase 2 (ACAT2) subsequently converts the free cholesterol to cholesteryl ester (CE) followed by the action of microsomal triacylglycerol transport protein (MTP), which packs CE into chylomicrons (CM).[17] Third, CM are transferred into blood through the lymphatic system. Finally, ATP-binding cassette transporter subfamily G members 5 and 8 (ABCG5 and ABCG8) return the unabsorbed free cholesterol left in the enterocytes to the lumen for excretion.[18,19] Although some research has addressed the effect of sesamin on plasma cholesterol, no study to date has investigated the effect of dietary sesamin on gene expression of intestinal NPC1L1, ACAT2, MTP, ABCG5, and ABCG8 (Figure 1).

A systematic investigation concerning the effect of sesamin on cholesterol metabolism is also lacking. Cholesterol homeostasis is partially regulated by two different transcription factors, namely, sterol regulatory element-binding protein 2 (SREBP-2) and liver X receptor alpha (LXRα).[20,21] SREBP-2 controls the gene expressions of LDL receptor and HMG-CoA reductase. LDL receptor is responsible for the removal of LDL-C from circulation, whereas HMG-CoA reductase is a rate-limiting enzyme in the cholesterol synthesis pathway. LXRα is a sensor of cholesterol concentration in the liver and governs the gene expression of hepatic cholesterol-7α-hydroxylase (CYP7A1), a key enzyme in bile acid synthesis. The excess cholesterol in the liver is partially removed by being converted to bile acids. To date, there is no study that has examined the effect of dietary sesamin on gene expression of these transcript factors, enzymes, or receptor involved in maintaining cholesterol homeostasis.

The present study was therefore designed to (i) investigate if dietary sesamin could reduce plasma TC in a dose-dependent manner and (ii) examine the interaction of dietary sesamin with the gene expressions of hepatic SREBP-2, LXRα, HMG-CoA reductase, LDL receptor, and CYP7A1 as well as intestinal NPC1L1, ACAT2, MTP, and ABCG5 and ABCG8.

MATERIALS AND METHODS

Chemicals and Diet Ingredients. Sesamin with a purity of 93% was purchased from KEB Biotechnology (Beijing, China). Casein, mineral mix, and vitamin mix were purchased from Harlan Teklad (Madison, WI, USA). Cholesterol and DL-methionine were purchased from Sigma-Aldrich (St. Louis, MO, USA). Lard was obtained from Hop Hing Oils & Fats Ltd. (Hong Kong, China).

Preparation of Diets. The three diets were prepared with some modification of AIN-93 Purified Diet for Laboratory Rodents. The control diet (CON) was prepared by mixing the following ingredients (g): cornstarch, 508; casein, 242; lard, 50; sucrose, 119; mineral mix, 40, vitamin mix, 20; DL-methionine, 1; cholesterol, 1. The two experimental diets were formulated by adding 0.2% (SL) or 0.5% (SH) sesamin into the control diet, respectively. The total cholesterol content in the three diets was actually 1.05 mg/kg as lard contained 90 mg cholesterol/100 g. The rationale for adding cholesterol at 0.1% was because such a level could induce a rise in plasma TC to reach >6.2 mM, which is similar to human hypercholesterolemia.[22]

Hamsters. Male Golden Syrian hamsters (n = 30) were divided into three groups (n = 10 each) and fed one of the three diets formulated above. Hamsters were housed in an animal room at 23 °C with 12/12 h light/dark cycles. The fresh diets were given daily, and body weight was recorded twice a week. The hamsters were fed ad libitum. At weeks 0, 3 and 6, about 100 μL of blood from each hamster was taken from the retro-orbital sinus under inhalational anesthesia of isoflurane after overnight fasting. At the end of week 6, all of the hamsters were killed with the liver being removed for the mRNA analyses of SREPB-2, LXRα, LDL receptor, HMG-CoA reductase, and CYP7A1. The first 40 cm of the small intestine was kept for the

Table 1. Quantitative Real-Time PCR Primers Used To Measure the mRNA Levels of Genes Involved in Cholesterol Absorption and Homeostasis in Hamster Liver and Intestine

gene	accession no.	forward primer 5′ 3′	reverse primer 5′ 3′	TaqMan probe 5′
		TaqMan		
GAPDH	DQ403055	GAACATCATCCCTGCATCCA	CCAGTGAGCTTCCCGTTCA	CTTGCCCACAGCCTTGGCAGC
CYP7A1	L04690	GGTAGTGTGCTGTTGTATATGGGTTA	ACAGCCCAGGTATGGAATCAAC	CACCTGCTTTCCTTCTCC
HMGR	X00494	CGAAGGGTTTGCAGTGATAAAGGA	GCCATAGTCACATGAAGCTTCTGTA	ACGTGCGAATCTGCT
LDL-R	M94387	GCCGGGACTGGTCAGATG	ACAGCCACCATTGTTGTCCA	GCACTCATTGGTCCTGCAGTCCTT
SREBP-2	U12330	GGACTTGGTCATGGGAACAGATG	TGTAATCAATGGCCTTCCTCAGAAC	CCAAGATGCACAAATC
		SYBRGreen		
NPC1L1		CCTGACCTTTATAGAACTCACCACAGA	GGGCCAAAATGCTCGTCAT	
ABCG5		TGATTGGCAGCTATAATTTTGGG	GTTGGGCTGCGATGGAAA	
ABCG8		TGCTGGCCATCATAGGGAG	TCCTGATTTCATCTTGCCACC	
ACAT2		CCGAGATGCTTCGATTTGGA	GTGCGGTAGTAGTTGGAGAAGGA	
MTP		GTCAGGAAGCTGTGTCAGAATG	CTCCTTTTTCTCTGGCTTTTCA	

DOI: 10.1021/jf5063606
J. Agric. Food Chem. 2015, 63, 2963−2969

mRNA analyses of NPC1L1, ACAT-2, MTP, ABCG5, and ABCG8. All samples were stored in a −80 °C freezer prior to analysis. All of the feces from each hamster at weeks 1, 3, and 6 were pooled, freeze-dried, ground, and saved for neutral and acidic sterol analyses. The whole experimental procedure was approved by the Animal Experimental Ethical Committee, The Chinese University of Hong Kong.

Analysis of Plasma Lipoproteins. Plasma TC, high-density lipoprotein cholesterol (HDL-C), non-HDL-C, and TG were measured using the commercial enzymatic kits from Infinity (Waltham, MA, USA) and Stanbio Laboratories (Boerne, TX, USA), respectively.[23]

Analysis of Cholesterol in the Liver. Cholesterol in the liver was analyzed as previously described.[22,24] In brief, the total lipids were extracted from 300 mg of sample using a solvent of chloroform/methanol (2:1, v/v) with 5α-cholestane being added as an internal standard. The extract was then subjected to cold saponification at room temperature. Nonsaponifiable materials were extracted into hexane followed by TMS derivatization. The cholesterol TMS-ether derivative was analyzed in a SAC-5 column in a Shimadzu GC-14B equipped with a FID detector (Shimadzu, Tokyo, Japan).

Table 2. Food Consumption, Body Weight, and Organ Weights in Male Golden Syrian Hamsters Fed the Control (CON) or One of the Two Experimental Diets Containing 0.2% Sesamin (SL) or 0.5% Sesamin (SH), Respectively[a]

	CON	SL	SH
food intake (g)	9.9 ± 0.7	9.9 ± 1.2	10.0 ± 1.1
body wt (g)			
initial	110 ± 7	109 ± 9	110 ± 9
final	122 ± 8	125 ± 9	122 ± 9
absolute organ wt (g)			
liver	6.0 ± 0.6	6.3 ± 0.8	6.4 ± 0.7
kidney	1.1 ± 0.1	1.1 ± 0.2	1.1 ± 0.2
heart	0.4 ± 0.1	0.4 ± 0.1	0.4 ± 0.1
testis	3.0 ± 1.0	3.3 ± 0.7	2.3 ± 1.4
epididymal fat pad	1.9 ± 0.6	2.0 ± 0.5	1.9 ± 0.4
perirenal fat pad	1.1 ± 0.2	1.3 ± 0.5	1.1 ± 0.3

[a]Data are expressed as the mean ± SD; n = 10 each group.

Determination of Fecal Cholesterol, Coprostanol, and Other Neutral and Acidic Sterols. Fecal cholesterol, coprostanol, other neutral and acidic sterols were determined as previously described.[22−24] 5α-Cholestane and hyodeoxycholic acid were added into the fecal samples as internal standards to quantify the amount of total neutral and acidic sterols, respectively. In brief, the dried fecal samples were hydrolyzed and extracted with cyclohexane. Neutral sterols in cyclohexane extract were dried and converted into their corresponding TMS derivatives. Acidic sterols in the bottom aqueous layer left after cyclohexane extraction were saponified, extracted, and similarly converted to their corresponding TMS derivatives. Both neutral and acidic sterol TMS derivatives were then subjected to the GC analysis.

Real-Time PCR Analysis of Intestinal NPC1L1, ACAT2, ABCG5, ABCG8, and MTP and Hepatic SREBP-2, LXRα, CYP7A1, HMG-CoA Reductase, and LDL Receptor. mRNA for each target gene was quantified as previously described.[22−25] In brief, the total RNA in the intestine or the liver was extracted followed by transcription to complementary DNA (cDNA) using a high-capacity cDNA reverse transcription kit (Invitrogen, Carlsbad, CA, USA). Reverse transcription was then carried out followed by the real-time PCR analysis on a Fast Real-time PCR System 7500 (Applied Biosystems, Foster City, CA, USA). The expression of NPC1L1, ACAT-2, ABCG5, ABCG8, and MTP was normalized with cyclophilin, whereas that of hepatic SREBP-2, LXRα, CYP7A1, HMG-CoA reductase, and LDL receptor was normalized with GAPDH. Each primer and TaqMan probe (Table 1) was obtained from Applied Biosystems. Real-time PCR was performed using a TaqMan Fast Universal PCR Master Mix. Data were analyzed using Sequence Detection Software version 1.3.1.21.

Statistical Analysis. One-way analysis of variance (ANOVA) followed by post hoc LSD test was used to statistically evaluate differences in lipoproteins, gene expression of transcription factors, sterol transporters, and enzymes involved in the cholesterol metabolism among the three groups. A simple linear regression analysis was carried out to assess the dose-dependent activity of sesamin using SPSS (PASW Statistics for Windows, version 18.0, Chicago, IL, USA).

RESULTS

Food Intake and Body and Organ Weights. No differences in food intake and body weight were seen among the three groups (Table 2). The weights of kidney, heart, and

Table 3. Changes in Plasma Total Cholesterol (TC), Triacylglycerols (TG), High-Density Lipoprotein Cholesterol (HDL-C), and Non-HDL-Cholesterol (Non-HDL-C) in Hamsters Fed the Control (CON) and the Two Experimental Diets Containing 0.2% Sesamin (SL) or 0.5% Sesamin (SH), Respectively, for 3 and 6 Weeks[a]

	CON	SL	SH	P value
week 0				
TC (mmol/L)	2.88 ± 0.43	2.96 ± 0.34	2.94 ± 0.43	0.76
TG (mmol/L)	2.75 ± 0.52	2.81 ± 0.59	2.63 ± 0.34	0.57
HDL-C (mmol/L)	1.49 ± 0.18	1.53 ± 0.19	1.50 ± 0.09	0.93
non-HDL-C(mmol/L)	1.39 ± 0.35	1.43 ± 0.29	1.44 ± 0.38	0.75
non-HDL-C:HDL-C	0.94 ± 0.23	0.94 ± 0.22	0.96 ± 0.24	0.83
week 3				
TC (mmol/L)	6.63 ± 0.49a	5.98 ± 0.55b	5.37 ± 0.59b	0.01
TG (mmol/L)	4.25 ± 0.99	3.72 ± 0.51	3.80 ± 0.67	0.24
HDL-C (mmol/L)	2.57 ± 0.22a	2.46 ± 0.20a	2.19 ± 0.24b	0.01
non-HDL-C(mmol/L)	4.06 ± 0.44a	3.52 ± 0.40b	3.17 ± 0.57b	0.01
non-HDL-C:HDL-C	1.59 ± 0.22	1.42 ± 0.13	1.40 ± 0.25	0.07
week 6				
TC (mmol/L)	6.62 ± 0.40a	5.32 ± 0.63b	5.00 ± 0.44b	0.01
TG (mmol/L)	5.13 ± 1.32	4.51 ± 0.78	4.31 ± 1.31	0.22
HDL-C (mmol/L)	2.69 ± 0.51a	2.36 ± 0.24b	2.19 ± 0.08b	0.01
non-HDL-C(mmol/L)	3.97 ± 0.60a	2.96 ± 0.55b	2.70 ± 0.41b	0.01
non-HDL-C:HDL-C	1.57 ± 0.47a	1.26 ± 0.23b	1.21 ± 0.18b	0.01
liver cholesterol (μmol/g)	128 ± 15a	105 ± 20b	99 ± 24b	0.01

[a]Mean values within a row with unlike letters are significantly different (P < 0.05).

DOI: 10.1021/jf5063606
J. Agric. Food Chem. 2015, 63, 2963−2969

Table 4. Changes in Fecal Neutral and Acidic Sterols in Hamsters Fed the Control (CON) and the Two Experimental Diets Containing 0.2% Sesamin (SL) or 0.5% Sesamin (SH), Respectively, at Weeks 1, 3, and 6[a]

	CON	SL	SH	P value
Week 1				
neutral sterols (μmol/day)				
coprostanol	1.10 ± 0.33	1.13 ± 0.21	1.46 ± 0.47	0.21
coprostanone	0.05 ± 0.03	0.11 ± 0.09	0.17 ± 0.10	0.07
cholesterol	0.32 ± 0.17	0.39 ± 0.06	0.39 ± 0.06	0.41
dihydrocholesterol	0.29 ± 0.13	0.44 ± 0.06	0.51 ± 0.20	0.08
campesterol	0.03 ± 0.01	0.04 ± 0.00	0.05 ± 0.01	0.15
stigmasterol	0.02 ± 0.01	0.01 ± 0.00	0.02 ± 0.01	0.87
sitosterol	0.02 ± 0.01	0.01 ± 0.02	0.03 ± 0.01	0.26
total	1.82 ± 0.61	2.13 ± 0.19	2.62 ± 0.70	0.08
acidic sterols (μmol/day)				
lithocholic acid	4.27 ± 1.98	4.62 ± 1.21	5.26 ± 1.69	0.53
deoxycholic acid	1.48 ± 0.46	1.56 ± 0.21	1.93 ± 0.86	0.39
chenodeoxycholic acid + cholic acid	0.17 ± 0.05b	0.14 ± 0.06b	0.26 ± 0.02a	0.02
ursocholic acid	0.64 ± 0.22	0.69 ± 0.15	0.52 ± 0.10	0.13
total	6.55 ± 2.19	7.01 ± 1.42	7.97 ± 2.14	0.29
Week 3				
neutral sterols (μmol/day)				
coprostanol	1.52 ± 0.43	1.82 ± 0.65	2.16 ± 1.29	0.35
coprostanone	0.06 ± 0.01	0.08 ± 0.01	0.08 ± 0.03	0.28
cholesterol	0.58 ± 0.29b	0.81 ± 0.17b	1.37 ± 0.42a	0.01
dihydrocholesterol	0.34 ± 0.08c	0.69 ± 0.23b	0.82 ± 0.21a	0.01
campesterol	0.02 ± 0.01	0.01 ± 0.01	0.01 ± 0.00	0.48
stigmasterol	0.04 ± 0.00	0.03 ± 0.01	0.04 ± 0.01	0.67
sitosterol	0.05 ± 0.01	0.06 ± 0.01	0.06 ± 0.02	0.39
total	2.61 ± 0.28c	3.51 ± 0.63ab	4.53 ± 1.40a	0.02
acidic sterols (μmol/day)				
lithocholic acid	2.49 ± 0.37b	2.88 ± 0.41ab	4.24 ± 0.61a	0.01
deoxycholic acid	1.27 ± 0.01	2.16 ± 0.58	2.02 ± 0.37	0.09
chenodeoxycholic acid + cholic acid	0.26 ± 0.12	0.42 ± 0.15	0.33 ± 0.10	0.63
ursocholic acid	0.91 ± 0.49	0.93 ± 0.22	0.80 ± 0.33	0.65
total	4.94 ± 0.75b	6.40 ± 1.22ab	7.39 ± 0.77a	0.02
Week 6				
neutral sterols (μmol/day)				
coprostanol	0.93 ± 0.16b	1.52 ± 0.97ab	2.20 ± 0.28a	0.01
coprostanone	0.08 ± 0.01b	0.11 ± 0.03ab	0.12 ± 0.02a	0.03
cholesterol	1.04 ± 0.35b	1.75 ± 0.36ab	2.25 ± 0.94a	0.01
dihydrocholesterol	0.54 ± 0.16b	0.76 ± 0.46ab	1.09 ± 0.39a	0.04
campesterol	0.01 ± 0.00	0.01 ± 0.01	0.01 ± 0.00	0.25
stigmasterol	0.04 ± 0.01b	0.08 ± 0.03ab	0.09 ± 0.04a	0.02
sitosterol	0.03 ± 0.01b	0.07 ± 0.02a	0.07 ± 0.02a	0.01
total	2.65 ± 0.57b	4.30 ± 1.65ab	5.84 ± 1.27a	0.01
acidic sterols (μmol/day)				
lithocholic acid	2.62 ± 1.09b	3.71 ± 1.01ab	4.31 ± 1.54a	0.05
deoxycholic acid	1.74 ± 0.73	2.55 ± 0.99	2.33 ± 0.51	0.32
chenodeoxycholic acid + cholic acid	0.20 ± 0.04b	0.32 ± 0.14ab	0.43 ± 0.18a	0.03
ursocholic acid	0.50 ± 0.17	0.50 ± 0.31	0.50 ± 0.16	0.98
total	5.08 ± 1.23b	7.09 ± 1.36a	7.56 ± 1.27a	0.01

[a]Mean values within a row with unlike letters are significantly different, $P < 0.05$.

perirenal and epididymal adipose tissues were similar among the three groups.

Plasma TC, LDL, TG, and Liver Cholesterol. The three groups of hamsters had similar levels of plasma TC, HDL-C, non-HDL-C, and TG at week 0. When the experiment reached the end of weeks 3 and 6, SL and SH hamsters had decreased plasma TC, non-HDL-C, and TG in a dose-dependent manner (Table 3). At week 6, SL and SH groups had plasma TC reduced by 20 and 25%, respectively, compared with the control hamsters at the end of week 6. The amount of cholesterol in the liver decreased significantly in both SL and SH groups (Table 3). Results demonstrated that the control hamsters had liver cholesterol of 128.0 μmol/g, whereas SL and SH hamsters had liver cholesterol of 105.0 and 99.4 μmol/g, equivalent to 16 and 22% reductions, respectively.

Fecal Neutral Sterols. Microbial hydrogenation and bioconversion of cholesterol in the large intestine produce several derivatives, namely, coprostanol, coprostanone, and

DOI: 10.1021/jf5063606
J. Agric. Food Chem. 2015, 63, 2963−2969

dihydrocholesterol, whereas stigmasterol and β-sitosterol are of dietary origin. At week 1, no differences in individual and total fecal neutral sterols were seen among the three groups (Table 4). At week 3, SL and SH groups had increased fecal excretion of cholesterol, dihydrocholesterol, and total neutral sterols in a dose-dependent manner. At week 6, addition of sesamin into the diet dose-dependently increased the fecal excretion of cholesterol, coprostanol, coprostanone, and dihydrocholesterol. Compared with the control hamsters, SL and SH groups had increased excretion of fecal total neutral sterols by 62 and 120%, respectively (Table 4).

Fecal Acidic Sterols. Fecal bile acids are divided into primary and secondary bile acids. The primary bile acids are cholic acid and chenodeoxycholic acids, whereas the secondary bile acids are deoxycholic, lithocholic, and ursocholic acids. In week 1, no differences in the excretion of total bile acids were seen among the three groups. At week 3, the excretion of total bile acids and secondary bile acids lithocholic and deoxycholic acids was significantly increased in SL and SH groups in a dose-dependent manner (Table 4). At week 6, addition of sesamin into the diet dose-dependently increased the excretion of total fecal bile acids by 40 and 49% in the SL and SH groups, respectively.

Real-Time PCR mRNA of Intestinal NPC1L1, ACAT2, MTP, ABCG5, and ABCG8. RT-PCR analysis demonstrated that addition of sesamin into diets had significant effects on gene expression of transporters, enzymes, and protein involved in cholesterol absorption. As shown in Figure 2, dietary sesamin dose-dependently down-regulated the mRNA of intestinal NPC1L1, ACAT2, MTP, ABCG5, and ABCG8. For mRNA NPC1L1, it was down-regulated in SL and SH groups by 22.3 and 51.5%, respectively, compared with the control. Similarly, mRNA ACAT2 was decreased by 24.5 and 53.3%, whereas mRNA MTP was down-regulated by 24.4 and 50.1% in SL and SH groups, respectively, compared with the control. mRNA ABCG5 and ABCG8 were also decreased by 13.1−13.5 and 26.1−49.5%, respectively, compared with the control values.

Real-Time PCR mRNA Analysis of Hepatic SREBP2, LDL Receptor, HMG-CoA Reductase, LXRα, and CYP7A1. RT-PCR analysis found the addition of sesamin in the diet had no effect on mRNA of LDL receptor and SREBP2 (Figure 3). Dietary sesamin at 0.2 and 0.5% significantly up-regulated the mRNA of CYP7A1 by 55.3 and 71.3%, respectively, compared with the control value. In contrast, sesamin at 0.2 and 0.5% in diets significantly down-regulated mRNA HMG-CoA reductase by 46.8−49.4% and mRNA LXRα by 60.1−62.6%, respectively, compared with the control values.

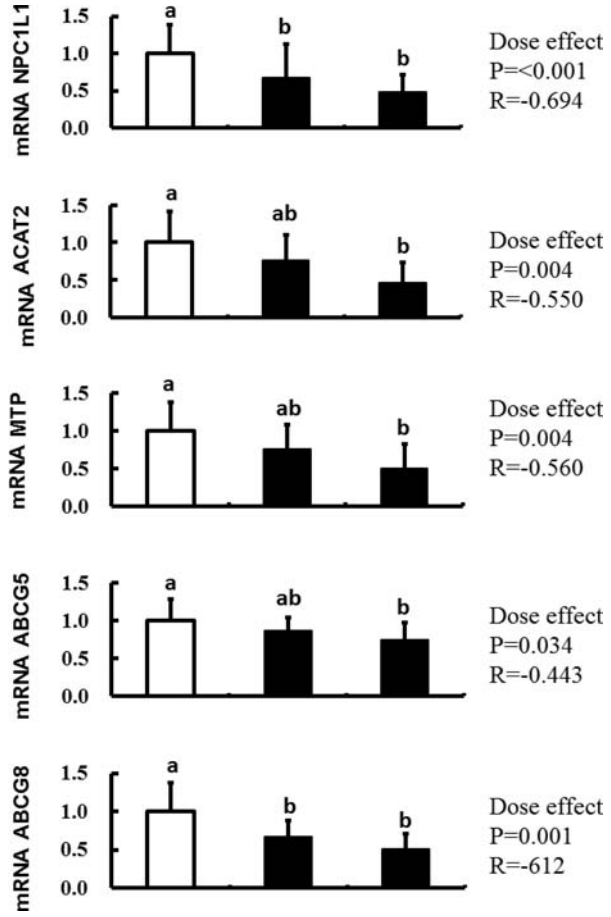

Figure 2. mRNA levels of intestinal Niemann−Pick C1 like 1 protein (NPC1L1), acyl coenzyme A:cholesterol acyltransferase 2 (ACAT2), microsomal triacylglycerol transport protein (MTP), and ATP binding cassette transporters subfamily G members 5 and 8 (ABCG5 and ABCG8) in hamsters fed the control diet (CON) or one of the two experimental diets with the addition of 0.2% sesamin (SL) or 0.5% sesamin (SH). Data were normalized with cyclophilin. Values are expressed as means ± SD (n = 10) with those for the control group being arbitrarily taken as 1. Means with different letters (a, b) differ significantly, $P < 0.05$. R is the coefficient of correlation for the regression analysis on the dose-dependent effect of sesamin on target genes.

DISCUSSION

We chose sesamin as a representative lignan and investigated its effect on plasma TC using hamsters as a hypercholesterolemia model. It was found that dietary sesamin was capable of modulating favorably the plasma lipoprotein profile with the following observations. First, dietary sesamin at 0.2 and 0.5% could decrease plasma TC by 20−25% in a dose-dependent manner (Table 3). Second, dietary sesamin decreased both non-HDL-C and HDL-C; however, it decreased non-HDL-C more than HDL-C, thus favorably reducing the ratio of non-HDL-C to HDL-C. The rationale for adding sesamin into diets at 0.2 and 0.5% was that such doses were comparable to the recommended intake for other cholesterol-lowering nutraceuticals such as plant sterols. It is generally recommended to take 2 g of plant sterols per day to decrease plasma LDL-C by about 10% for humans.[26] This translates to a dose of 1 g plant sterols/1000 kcal in the diet provided that humans daily consume about 2000 kcal energy. In the present study, 0.2−0.5% sesamin added in diets was equivalent to 0.5−1.2 g/1000 kcal, which was close to the recommended intake for plant sterols.

We proposed two underlying mechanisms by which dietary sesamin decreased plasma TC. The first mechanism was that dietary sesamin reduced plasma TC concentration by down-regulating the gene expression of transporters and enzymes involved in cholesterol absorption pathway in the intestine. The proposed mechanism was supported by the results from RT-PCR analysis with the following evidence. First, dietary sesamin dose-dependently down-regulated mRNA of intestinal NPC1L1, ACAT-2, MTP, ABCG5, and ABCG8 (Figure 2), all of which are essential for cholesterol absorption. Second, such down-regulation on these genes was accompanied by 62−120% greater excretion of neutral sterols (Table 4), proving that dietary sesamin inhibited cholesterol absorption. To the best of

DOI: 10.1021/jf5063606
J. Agric. Food Chem. 2015, 63, 2963−2969

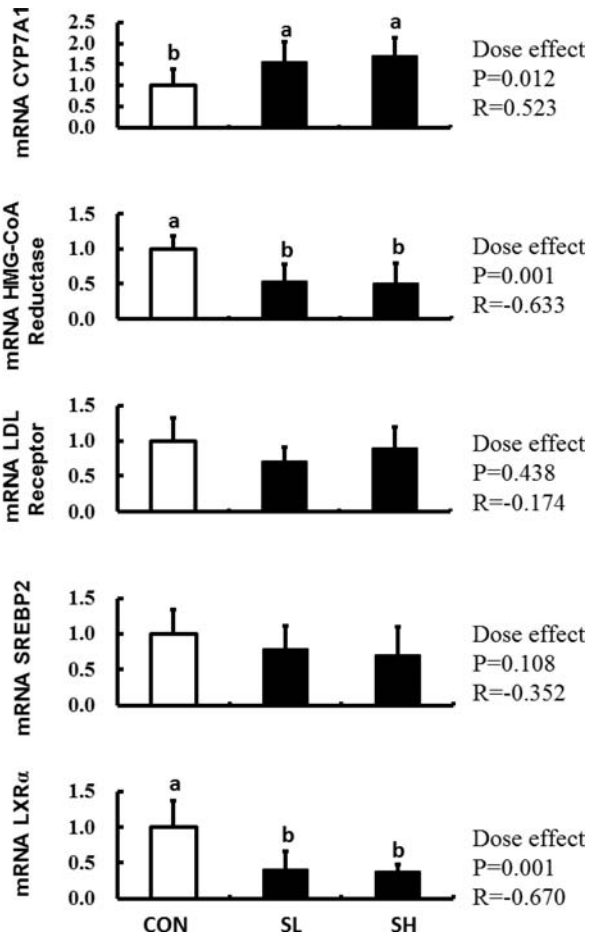

Figure 3. mRNA levels of hepatic sterol regulatory element-binding protein-2 (SREBP-2), liver X receptor-alpha (LXRα), 3-hydroxy-3-methylglutaryl-CoA (HMG-CoA) reductase, LDL receptor (LDLR), and cholesterol-7α-hydroxylase (CYP7A1) in hamsters fed the control diet (CON) or one of two experimental diets with the addition of 0.2% sesamin (SL) or 0.5% sesamin (SH). Data were normalized with GAPDH. Values are expressed as means ± SD (n = 10) with those for the control group being arbitrarily taken as 1. Means with different letters (a, b) differ significantly, $P < 0.05$. R is the coefficient of correlation for the regression analysis on the dose-dependent effect of sesamin on target genes.

our knowledge, this is the first study to demonstrate that the cholesterol-lowering activity of dietary sesamin was mediated by down-regulation on the gene expression of intestinal NPC1L1, ACAT2, MTP, ABCG5, and ABCG8.

The second mechanism was that sesamin could modulate the cholesterol homeostasis in a way favoring the reduction of plasma TC. The present study clearly demonstrated that dietary sesamin down-regulated mRNA HMG-CoA reductase in a dose-dependent manner, suggesting dietary sesamin inhibited cholesterol biosynthesis in the liver (Figure 3). The present results also demonstrated that sesamin had a trend of down-regulating mRNA SREBP-2 in the liver, although such an effect was statistically insignificant. It is known that the expression of HMG-CoA reductase is under the control of SREBP-2, which is activated at a lower cholesterol level. Therefore, down-regulation of HMG-CoA reductase was expected in response to reduction of liver cholesterol and mRNA SREBP-2. The most important observation was that dietary sesamin dose-dependently up-regulated the mRNA CYP7A1, indicating dietary sesamin promoted the biosynthesis of bile acids and deceased the liver cholesterol concentration. This was supported by a 40−49% increase in the excretion of fecal bile acids in hamsters given diets with the addition of 0.2 or 0.5% sesamin. It is worth noting that dietary sesamin could down-regulate the mRNA of LXRα by 60.1−62.6% in the liver. It is known that LXRα acts as a cholesterol concentration sensor in the liver. When cellular oxysterols accumulate as a result of increasing concentrations of cholesterol in the liver, LXRα is up-regulated to induce the transcription of genes that protect cells from cholesterol overload and then activate the bile acid synthesis.[27] In the present study, such down-regulation of mRNA LXRα was expected because dietary sesamin decreased the cholesterol concentration in the liver by 16−22%. The discrepancy between down-regulation of mRNA LXRα and up-regulation of mRNA CYP7A1 was probably due to changes in other nuclear receptors such as farnesoid X receptor (FXR), which can also regulate the gene expression of CYP7A1.[27,28] We plan to investigate the issue in our future research.

In summary, dietary sesamin could favorably modulate plasma lipoprotein profile by decreasing plasma TC, non-HDL-C, and the non-HDL-C/HDL-C ratio. Dietary sesamin-induced reduction in plasma TC was accompanied by greater excretion of both total fecal neutral and acidic sterols. It was concluded that the cholesterol-lowering activity of dietary sesamin was mediated by up-regulation of hepatic mRNA CYP7A1 and down-regulation of intestinal mRNA NPC1L1, ACAT2, MTP, ABCG5, and ABCG8 as well as down-regulation of hepatic mRNA HMG-CoA reductase.

AUTHOR INFORMATION

Corresponding Author

*(Z.-Y.C.) Fax: (852) 2603-7246. Phone: (852) 3943-6382. E-mail: zhenyuchen@cuhk.edu.hk.

Funding

This project was supported by a grant from the Hong Kong Research Grant Council (CUHK462813).

Notes

The authors declare no competing financial interest.

REFERENCES

(1) Peterson, J.; Dwyer, J.; Adlercreutz, H.; Scalbert, A.; Jacques, P.; McCullough, M. L. Dietary lignans: physiology and potential for cardiovascular disease risk reduction. *Nutr. Rev.* **2010**, *68* (10), 571−603.

(2) Penalvo, J. L.; Haajanen, K. M.; Botting, N.; Adlercreutz, H. Quantification of lignans in food using isotope dilution gas chromatography/mass spectrometry. *J. Agric. Food Chem.* **2005**, *53*, 9342−9347.

(3) Penalvo, J. L.; Heinonen, S. M.; Aura, A. M.; Adlercreutz, H. Dietary sesamin is converted to enterolactone in humans. *J. Nutr.* **2005**, *135*, 1056−1062.

(4) Pan, A.; Yu, D.; Demark-Wahnefried, W.; Franco, O. H.; Lin, X. Meta-analysis of the effects of flaxseed interventions on blood lipids. *Am. J. Clin. Nutr.* **2009**, *90*, 288−297.

(5) Hirata, F.; Fujita, K.; Ishikura, Y.; Hosoda, K.; Ishikawa, T.; Nakamura, H. Hypocholesterolemic effect of sesame lignan in humans. *Atherosclerosis* **1996**, *122*, 135−136.

(6) Wu, W. H.; Kang, Y. P.; Wang, N. H.; Jou, H. J.; Wang, T. A. Sesame ingestion affects sex hormones, antioxidant status, and blood lipids in postmenopausal women. *J. Nutr.* **2006**, *136*, 1270−1275.

(7) Rogi, T.; Tomimori, N.; Ono, Y.; Kiso, Y. The mechanism underlying the synergetic hypocholesterolemic effect of sesamin and

DOI: 10.1021/jf5063606
J. Agric. Food Chem. 2015, 63, 2963−2969

α-tocopherol in rats fed a high-cholesterol diet. *J. Pharmacol. Sci.* **2011**, *115*, 408−416.
(8) Ide, T.; Ashakumary, L.; Takahashi, Y.; Kushiro, M.; Fukuda, N.; Sugano, M. Sesamin, a sesame lignan, decreases fatty acid synthesis in rat liver accompanying the down-regulation of sterol regulatory element binding protein-1. *Biochim. Biophys. Acta* **2001**, *1534* (1), 1−13.
(9) Hirose, N.; Inoue, T.; Nishihara, K.; Sugano, M.; Akimoto, K.; Shimizu, S.; Yamada, H. Inhibition of cholesterol absorption and synthesis in rats by sesamin. *J. Lipid Res.* **1991**, *32* (4), 629−638.
(10) Ide, T.; Hong, D. D.; Ranasinghe, P.; Takahashi, Y.; Kushiro, M.; Sugano, M. Interaction of dietary fat types and sesamin on hepatic fatty acid oxidation in rats. *Biochim. Biophys. Acta* **2004**, *1682* (1−3), 80−91.
(11) Ide, T. Combined effect of sesamin and soybean phospholipid on hepatic fatty acid metabolism in rats. *J. Clin. Biochem. Nutr.* **2014**, *54* (3), 210−218.
(12) Grundy, S. M. Absorption and metabolism of dietary cholesterol. *Annu. Rev. Nutr.* **1983**, *3*, 71−96.
(13) Grundy, S. M.; Metzger, A. L. A physiological method for estimation of hepatic secretion of biliary lipids in man. *Gastroenterology* **1972**, *62*, 1200−1217.
(14) Howles, P. N.; Carter, C. P.; Hui, D. Y. Dietary free and esterified cholesterol absorption in cholesterol esterase (bile salt-stimulated lipase) gene-targeted mice. *J. Biol. Chem.* **1996**, *271*, 7196−7202.
(15) Grober, J.; Lucas, S.; Sorhede-Winsell, M.; Zaghini, I.; Mairal, A.; Contreras, J. A.; Besnard, P.; Holm, C.; Langin, D. Hormone-sensitive lipase is a cholesterol esterase of the intestinal mucosa. *J. Biol. Chem.* **2003**, *278*, 6510−6515.
(16) Davis, H. R., Jr.; Zhu, L. J.; Hoos, L. M.; Tetzloff, G.; Maguire, M.; Liu, J.; Yao, X.; Iyer, S. P.; Lam, M. H.; Lund, E. G.; Detmers, P. A.; Graziano, M. P.; Altmann, S. W. Niemann-Pick C1 Like 1 (NPC1L1) is the intestinal phytosterol and cholesterol transporter and a key modulator of whole-body cholesterol homeostasis. *J. Biol. Chem.* **2004**, *279*, 33586−33592.
(17) Atzel, A.; Wetterau, J. R. Mechanism of microsomal triglyceride transfer protein catalyzed lipid transport. *Biochemistry* **1993**, *32*, 10444−10450.
(18) Lee, M. H.; Lu, K.; Hazard, S.; Yu, H.; Shulenin, S.; Hidaka, H.; Kojima, H.; Allikmets, R.; Sakuma, N.; Pegoraro, R.; Srivastava, A. K.; Salen, G.; Dean, M.; Patel, S. B. Identification of a gene, ABCG5, important in the regulation of dietary cholesterol absorption. *Nat. Genet.* **2001**, *27*, 79−83.
(19) Berge, K. E.; Tian, H.; Graf, G. A.; Yu, L.; Grishin, N. V.; Schultz, J.; Kwiterovich, P.; Shan, B.; Barnes, R.; Hobbs, H. H. Accumulation of dietary cholesterol in sitosterolemia caused by mutations in adjacent ABC transporters. *Science* **2000**, *290*, 1771−1775.
(20) Eberlé, D.; Hegarty, B.; Bossard, P.; Ferré, P.; Foufelle, F. SREBP transcription factors: master regulators of lipid homeostasis. *Biochimie* **2004**, *86* (11), 839−848.
(21) Gupta, S.; Pandak, W. M.; Hylemon, P. B. LXR alpha is the dominant regulator of CYP7A1 transcription. *Biochem. Biophys. Res. Commun.* **2002**, *26*, 338−343.
(22) Zhang, Z. S.; Wang, H.; Jiao, R.; Peng, C.; Wong, Y. M.; Yeung, V. S. Y.; Huang, Y.; Chen, Z. Y. Choosing hamsters but not rats as a model for studying plasma cholesterol-lowering activity of functional foods. *Mol. Nutr. Food Res.* **2009**, *53*, 921−930.
(23) Lei, L.; Liu, Y.; Wang, X.; Jiao, R.; Ma, K. Y.; Li, Y. M.; Wang, L.; Man, S. W.; Sang, S.; Huang, Y.; Chen, Z. Y. Plasma cholesterol-lowering activity of gingerols- and shogaols-riched extract is mediated by increasing sterol excretion. *J. Agric. Food Chem.* **2014**, *62*, 10515−10521.
(24) Jiao, R.; Guan, L.; Yang, N.; Peng, C.; Liang, Y.; Ma, K. Y.; Huang, Y.; Chen, Z. Y. Frequent cholesterol intake up-regulates intestinal NPC1L1, ACAT2, and MTP. *J. Agric. Food Chem.* **2010**, *58*, 5851−5857.
(25) Lei, L.; Wang, X.; Huang, W.; Liu, Y.; Zheng, F.; Ma, K. Y.; Li, Y. M.; Wang, L.; Man, S. W.; Zhang, C.; Chen, Z. Y. Cholesterol side chain analogs but not its ether analogs possess cholesterol-lowering activity. *Food Funct.* **2015**, *6*, 630−634.
(26) National Cholesterol Education Program, National Heart, Lung, and Blood Institute, National Institutes of Health, NIH. *Publication 02-5215*; U.S. GPO: Washington, DC, USA, Sept 2002.
(27) Zhao, C.; Dahlman-Wright, K. Liver X receptor in cholesterol metabolism. *J. Endocrinol.* **2010**, *204*, 233−240.
(28) Fu, Z. D.; Cui, J. Y.; Klaassen, C. D. Atorvastatin induces bile acid-synthetic enzyme Cyp7a1 by suppressing FXR signaling in both liver and intestine in mice. *J. Lipid Res.* **2014**, *55*, 2576−2586.

DOI: 10.1021/jf5063606
J. Agric. Food Chem. 2015, 63, 2963−2969

isolation and analysis were of analytical grade and used without further purification.

Fractionation and Purification of Hemicellulosic Polysaccharides. The ground powders were suspended in a 95% ethanol solution and heated to 75 °C for 2 h to remove small molecular components. After centrifugation at 4500*g* for 10 min at 4 °C, the obtained residues were suspended in a 15-fold volume of distilled water (DD H_2O, w/v) and kept at 80 °C for 2 h to remove the water-soluble polysaccharides and proteins. Each step was repeated three times. The water-insoluble residue was extracted four times by a 20-fold volume of 1 M NaOH at ambient temperature with continuous stirring for 12 h. The alkali extract was neutralized with HCl solution and precipitated with a 4-fold volume of 95% ethanol (v/v) and washed three times with 75% ethanol, followed by lyophilization to obtain the crude hemicellulosic polysaccharides of alfalfa stem.

The crude polysaccharides were subjected to further fractionation by membrane ultrafiltration (Minimate TFF system, Pall Corp., Port Washington, NY, USA) with a molecular weight (MW) cutoff of 10 kDa to obtain the cold alkali-extractable polysaccharide molecules of alfalfa stem (ACAP) with MW larger than 10 kDa. ACAP was further purified by gel filtration on a Sephacryl S-400 Superfine column (80 × 1.6 cm i.d., Amersham Pharmacia Biotech, Uppsala, Sweden) eluted with DD H_2O at 1.0 mL/min. The collected fraction was freeze-dried prior to further analyses.

Molecular Weight and Size. A particle size analyzer (Zetasizer Nano-ZS90, Malvern Instruments Ltd., Malvern, Worcs, UK) was used to determine the molecular weight and size of ACAP. In brief, the purified ACAP was dissolved in DD H_2O and heated at 80 °C for 2 h to avoid aggregation. The dispersed solution was diluted to 1.00, 0.75, 0.50, 0.25, and 0.10 mg/mL. The laser light scattering was measured for these samples using a static light scattering (SLS) to obtain the Debye plot, which was used to calculate the weight-averaged molecular weight (M_w) according to the Rayleigh equation (eq 1).[15] To avoid the interactions of molecules, 0.05 mol/L NaOH solution was prepared to dissolve ACAP molecules for size determination using the SLS method. The molecular size was obtained at the concentration of 0.25 mg/mL.

$$\frac{KC}{R_\theta} = \left(\frac{1}{M_w} + 2A_2C\right) \times P(\theta) \quad (1)$$

In the equation, K, M_w, A_2, and C represent optical constant, sample molecular weight, second virial coefficient, and sample concentration, respectively. The Rayleigh ratio (R_θ) indicates the ratio of scattered light to incident light of the sample, whereas $P(\theta)$ means the angular dependence of the sample scattering intensity. $P(\theta)$ reduces to 1 when the particles are much smaller than the wavelength of incident light. The M_w (Da or g/mol) was then determined from the intercept at zero concentration ($C \rightarrow 0$) according to $KC/R_\theta = 1/M_w$.

Chemical Composition Analysis. The total carbohydrate and uronic acid contents were determined using the phenol−sulfuric acid[16] and *m*-hydroxydiphenylsulfuric acid methods,[17] respectively. The protein content was analyzed by bicinchoninic acid protein assay (BCA) as described previously.[18]

The compositions of neutral sugars and uronic acids of ACAP were determined by PMP-HPLC method.[19] ACAP (10 mg) was hydrolyzed with 200 μL of 4 M trifluoroacetic acid (TFA) at 110 °C for 2 h. TFA in the reaction mixture was removed under nitrogen stream with the addition of 200 μL of methanol and repeated three times. The hydrolysates were dissolved in 50 μL of 0.3 M NaOH solution and reacted at 70 °C for 100 min with the addition of 50 μL of 0.5 M 1-phenyl-3-methyl-5-pyrazolone (PMP) solution in methanol. After cooling to room temperature, the mixture was neutralized with 0.3 M HCl, followed by the addition of DD H_2O to the final volume of 1 mL. An equal volume of dichloromethane was added, vortex-mixed, and repeated three times to remove the residual PMP. The sugar standard was prepared by mixing a solution of L-rhamnose (Rha), L-fucose (Fuc), L-arabinose (Ara), D-xylose (Xyl), D-mannose (Man), D-galactose (Gal), D-glucose (Glc), D-glucouronic acid (Glc*p*A), and D-galactouronic acid (Gal*p*A). The mixed standard also went through the above procedures except for hyrolyzation with TFA. The obtained upper layer solution was filtered through a 0.45 μm Millipore filter and subjected to HPLC analysis at 250 nm with an Inersil ODS-3 column (100 mm × 2.1 mm i.d., 2 μm, GL Sciences Inc., Tokyo, Japan). The chromatographic separation was carried out at 30 °C under the elution conditions of 0.1 M phosphate buffer (pH 6.7)/acetonitrile at a ratio of 80:20 (v/v).

Linkage Analysis by Methylation. For the existence of uronic acid, ACAP was first reduced using $NaBD_4$[20] and then methylated using methyl iodide (CH_3I) in a NaOH−DMSO dry slurry as reported previously,[21] followed by hydrolysis with 4 M TFA for 2 h at 121 °C. Samples were reduced with 0.1 mL of 10 mg/mL $NaBD_4$ and then acetylated by 100 μL of acetic anhydride. Afterward, the obtained partially methylated alditol acetate (PMAA) mixtures were examined using an Agilent 7890A-5975C GC-MS system (Agilent Technology, Santa Clara, CA, USA) equipped with a HP-5 capillary column (30 m × 0.32 mm i.d., 0.25 μm film). The GC conditions were as follows: initial temperature, 50 °C, increased at 30 °C/min to 150 °C, increased at 3 °C/min to 220 °C, and finally increased to 300 °C at 30 °C/min and held for 10 min; injector temperature, 250 °C; interface temperature, 280 °C. The MS conditions were as follows: ion source temperature, 300 °C; ionization energy, 70 eV; detector voltage, 1.5 kV; mass range, 50−550. Glycosidic linkages of ACAP were determined by comparing the GC-MS results of the PMAAs with mass spectrum patterns from the online database.[22] The molar ratios of individual linkage residues were calculated on the basis of the peak areas and response factors for individual sugars in the TIC as described previously.[23]

Spectroscopic Analysis. The Fourier transform infrared (FT-IR) spectrum of ACAP was recorded using a FT-IR spectrometer (Nicolet 6700, Thermo Fisher, USA) in the range of 4000−400 cm^{-1} using the KBr disk method.

One- and two-dimensional measurements (including ^1H NMR, ^{13}C NMR, DEPT 135, HH COSY, TOCSY, and HSQC) of ACAP were recorded on a 600 MHz NMR spectrometer (Bruker Avance III HD) with a 5 mm TCl CryoProbe ($^{13}C/^1H/^{15}N$) at 25 °C using D_2O as the solvent at a final concentration of 40 mg/mL.

Microscopic Analysis. To observe the microstructure of ACAP, sodium dodecyl sulfate (SDS) was selected as a surfactant to disperse the polysaccharide in aqueous solution as described previously.[24,25] ACAP aqueous solution was prepared at a concentration of 1 mg/mL, followed by the addition of an equal volume of SDS solution (1 mg/mL). The mixture was then heated at 80 °C for 2 h with constant stirring and diluted with DD H_2O to a final concentration of 5 μg/mL. A droplet of ACAP solution was deposited on the carbon film specimen (200 mesh, Beijing Zhongjingkeyi Technology, Beijing, China). Transmission electron microscopy (TEM, Tecnai G2 Spirit BIOTWIN, FEI, USA) with an accelerating voltage of 120 kV was applied to visualize the molecular morphology of the ACAP samples after they were dried at ambient temperature and humidity.

Isoconversional Thermal Characteristics. A simultaneous thermal analyzer (SDT-Q600, TA Instruments, USA) was used to determine the thermodynamic characteristics of the ACAP. ACAP samples (5 mg for each) were treated at three different heating rates (including 5, 10, and 20 °C/min from 50 to 600 °C) under a nitrogen atmosphere at a flow rate of 100 cm^3/ min. The obtained data were then analyzed by the isoconversional Flynn−Wall−Ozawa (FWO) method (eq 2) as previous studies reported.[26,27]

$$\log \beta = \log \frac{AE_a}{Rg(\alpha)} - 2.315 - 0.4567\frac{E_a}{RT} \quad (2)$$

$g(\alpha) = \int_0^\alpha d\alpha/f(\alpha)$; β is the heating rate; R is the general gas constant; A stands for the pre-exponential factor; E_a is the apparent activation energy; and T is the temperature at the conversion α. This model-free approach was applied to obtain a plot of log β versus $1/T$ at different conversion rates for calculation of $-E_a/R$ as the slope.

Following the calculation of an average E_a value, ln$A$ was obtained by the compensation effect relationship as eq 3. The compensation parameters of a and b could be obtained from a plot of ln$A$ versus E_a from a model-fitting approach using Coats−Redfern eq 4 with T' being the average experimental temperature. In addition, the experimental ln A could be calculated according to eq 3.

DOI: 10.1021/acs.jafc.5b00063
J. Agric. Food Chem. 2015, 63, 2970−2978

$$\ln A = aE_a + b \quad (3)$$

$$\ln \frac{g(\alpha)}{T^2} = \ln\left[\left(\frac{AR}{\beta E_a}\right)\left(1 - \frac{2RT'}{E_a}\right)\right] - \frac{E_a}{RT} \quad (4)$$

The thermal analysis data were analyzed using Universal Analysis 2000 software (version 4.5A, TA Instruments, USA) and MS Excel 2013.

Anti-inflammatory Activity Determination. To analyze the anti-inflammatory effect of ACAP, RAW 264.7 mouse macrophage cells were selected to detect the inhibition of IL-1β, IL-6, and COX-2 gene expressions. The aqueous ACAP solution was prepared at two treatment concentrations of 10 and 50 μg/mL. RAW 264.7 cells were cultured in 6-well plates for 24 h to reach an 80% confluence before the addition of ACAP-containing media. After further incubation for 24 h, LPS was pipetted into the medium at a final concentration of 10 ng/mL and incubated for another 4 h at 37 °C under 5% CO_2. The macrophage cells were collected and washed for RNA isolation and real-time PCR analysis according to previously described laboratory procedures.[28,29] In general, total RNA was isolated using the TRIzol reagent, followed by the reverse transcription cDNA using a IScript Advanced cDNA Synthesis kit. Real-time PCR was carried out on an ABI 7900HT Fast Real-Time PCR System (Applied Biosystems, Foster City, CA, USA) using the following PCR conditions: 50 °C for 2 min, 95 °C for 10 min, and 46 cycles of amplification at 95 °C for 15 s and 60 °C for 1 min.

Statistical Analysis. Significant differences between means were evaluated by one-way ANOVA followed by Tukey's multiple-comparison test to identify differences in means using SPSS for Windows (version rel. 18.0, SPSS Inc., Chicago, IL, USA). Statistical significance was declared at $P < 0.05$.

RESULTS AND DISCUSSION

Preparation of ACAP. After successive extractions with 95% ethanol and hot water, the crude cold alkali-soluble fraction was obtained, and the yield was found to be 8.47% on a per alfalfa stem dry weight basis. The composition analysis indicated that ACAP was composed of approximately 95.42% (w/w) of total carbohydrate, which contained about 9.38% uronic acid, whereas no protein was detected in the crude ACAP.

After sequential purification by ultrafiltration and gel permeation chromatography, a single fraction was obtained and designated ACAP (Figure S1 in the Supporting Information). The PMP-HPLC analysis showed that ACAP was composed of xylose, glucouronic acid, and arabinose in a molar ratio of 23:3:1. The M_w of ACAP was calculated to be 7.94×10^3 kDa (or 7.94×10^6 g/mol), whereas A_2 was calculated to be 2.45×10^{-4} from the gradient of the Debye plot (Figure S2 in the Supporting Information). The value of A_2 (>0) indicated that the aqueous solution of ACAP was a stable system. The radius of gyration (R_g) was determined to be 58 ± 6 nm for ACAP. The SLS method was applied to determine the molecular weight of ACAP because the commonly used size exclusion chromatographic analysis is not suitable for weight determination of branched polysaccharides.

Glycosidic Linkages of ACAP. ACAP was composed of a terminal arabinose (T-L-Ara*f*), 1,3,4-D-xylose (Xyl*p*), 1,2,4-D-Xyl*p*, 1,4-D-Xyl*p*, and a terminal glucouronic acid (T-D-Glc*p*A) in a molar ratio of 1:1.1:3.2:20.6:3.1, according to the PMAA analysis (Table 1). The ratio between terminal units (T-L-Ara*f* and T-D-Glc*p*A) and the branching points (1,3,4-D-Xyl*p* and 1,2,4-D-Xyl*p*) was 0.95, indicating that the number of terminal units was approximately equal to the number of branching points in ACAP. These results indicated that ACAP might contain a →1)-D-Xyl*p*-(4→ backbone with T-L-Ara*f* and T-D-Glc*p*A residues at the *O*-2 or *O*-3 site to form the side chains. Additionally, the degree of branching (DB) value of ACAP was calculated as 29% following the equation DB = (NT + NB)/ (NT + NB + NL) as described by Hawker and others,[30] where NT, NB, and NL are the numbers of the terminal residues, branch residues, and linear residues, respectively.

Table 1. Molar Ratio of Glycosidic Linkages in ACAP by Methylation Analysis

retention time (min)	PMAA[a]	mass fragments (*m*/*z*)	linkage type	molar ratio
10.632	1,4-*O*-Ac2-2,3,5-*O*-Me3-D-arabinitol	87, 101, 117, 129, 161	T-L-Ara*f*	1.0
13.015	1,4,5-*O*-Ac3-2,3-*O*-Me2-D-xylitol	87, 101, 117, 129, 189	1,4-L-Xyl*p*	20.6
13.314	1,2,4,5-*O*-Ac4-3-*O*-Me-D-xylitol	87, 129, 189	1,2,4-D-Xyl*p*	3.2
13.637	1,3,4,5-*O*-Ac4-2-*O*-Me-D-xylitol	85, 99, 117, 127, 159, 201, 261	1,3,4-D-Xyl*p*	1.1
22.046	1,5-*O*-Ac2-2,3,4,6-*O*-Me4-6-deuterio-D-glucitol	87, 101, 117, 129, 146, 161, 206	T-D-Glc*p*A	3.1

[a]Ac, acetyl; Me, methyl.

FT-IR Spectrum. As shown in Figure S3 in the Supporting Information, most of the absorption bands could be assigned according to previous literature.[31,32] The signals at 3431 and 2925 cm^{-1} originated from the stretching vibrations of OH and CH_2, respectively. The strong absorption at 1635 cm^{-1} was attributed to the H−O−H angle vibration of water, because hemicellulosic polymers was usually reported to contain bound water. The absorptions at 1465, 1383, 1248, 1158, 1044, 989, and 897 cm^{-1} were the characteristic peaks of hemicelluloses. Among them, the two weak signals at 1158 cm^{-1} (the C−O−C vibration) and 989 cm^{-1} represented small amounts of arabinosyl side chains, which were only attached at positions of the xylopyranosyl backbone according to a previous study.[33] Moreover, the strong peak at 1044 cm^{-1} (the C−O, C−C stretching, or C−OH bending vibration) was a typical absorbance of xylopyranosyl units in hemicellulose, whereas the signal at 897 cm^{-1} was attributed to β-glycosidic linkages between monosaccharide units.[34−36] In addition, the signal at 1420 cm^{-1} was from the symmetric stretching vibration of glucuronic acid groups in side chains.

Structural Characterization by NMR Analysis. The attributions of structural residues with different substitution patterns in the polysaccharide were determined by quantitative ^{1}H NMR (Figure 1A) and ^{13}C NMR (Figure 1B) spectra, along with HSQC spectrum (Figure 1C) and single-bond (COSY) and multiple-bond (TOCSY) proton−proton correlations and HMBC spectra (Figure S4 in the Supporting Information). In the HSQC spectrum (Figure 1C), the anomeric region of ^{1}H is from 4.3 to 5.5 ppm, whereas the corresponding ^{13}C is in the range of 90−110 ppm. The obtained assignments were confirmed according to the previous reports on hemicellulosic heteroxylan and summarized in Table 2. Consistent with the result of linkage analysis, β-1→4-linked xylopranosyl units were characterized to be dominant in ACAP by five primary peaks at 101.6 (4.38), 72.6 (3.17), 73.6 (3.45), 72.7 (3.68), and 62.9 (4.01 and 3.28) ppm, which were assigned to C1 (H1), C2 (H2), C3 (H3), C4 (H4), and C5 (H5) of the β-D-Xyl*p* units, respectively. In addition, weak signals of α-4-*O*-MeGlc*p*A and T-α-L-Ara*f* were identified to be in the side chains of β-D-Xyl*p* backbone from the present spectra (Table 2). The results of linkage analysis, FT-IR

DOI: 10.1021/acs.jafc.5b00063
J. Agric. Food Chem. 2015, 63, 2970−2978

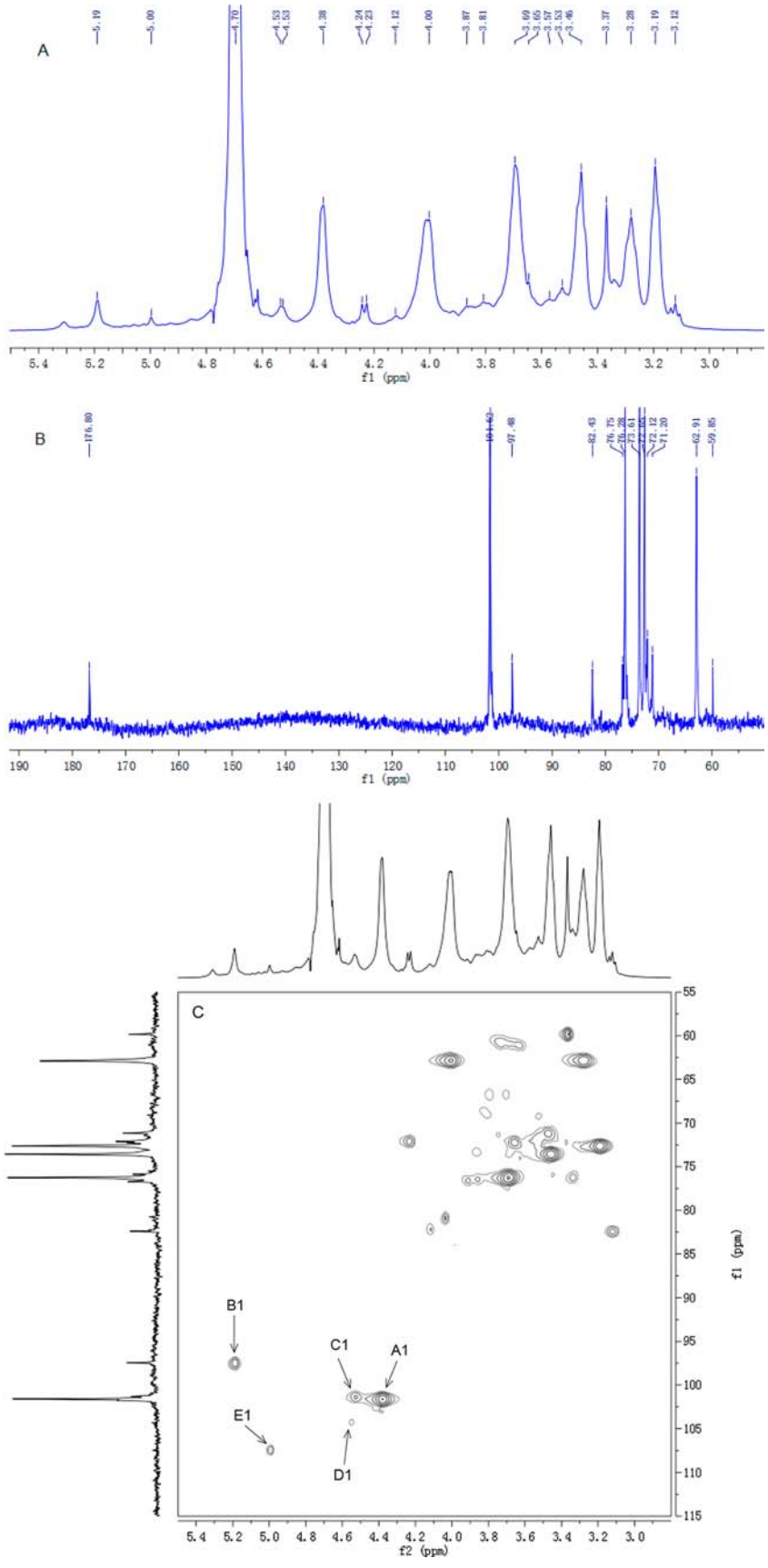

Figure 1. ^{1}H NMR (A), ^{13}C NMR (B), and HSQC (C) spectra (D_2O, 25 °C) for ACAP. A1 means the correlation between C1 and H1 of residue A. Order of residues A, B, C, D, and E was consistent with Table 2.

DOI: 10.1021/acs.jafc.5b00063
J. Agric. Food Chem. 2015, 63, 2970−2978

Table 2. ^{1}H and ^{13}C NMR Chemical Shifts of ACAP Recorded in D_2O at 25 °C

			chemical shift, δ							
no.[a]	residue		1	2	3	4	5		OMe	COOH
A	β-1,4-D-Xyl*p*	H	4.38	3.18	3.45	3.68	4.01	3.28		
		C	101.62	72.64	73.57	76.28	62.85			
B	α-4-*O*-MeGlc*p*A	H	5.19	3.48	3.18	3.12	4.23		3.38	
		C	97.49	71.21	71.54	82.42	72.11		59.83	176.88
C	β-1,2,4-D-Xyl*p*	H	4.53	3.34	3.52	3.86	3.70			
		C	101.36	76.24	72.10	76.47	66.75			
D	β-1,3,4-D-Xyl*p*	H	4.54	3.55	3.36	4.38				
		C	104.30	72.08	76.24	77.45				
E	T-α-L-Ara*f*	H	4.99	4.03	3.99	4.12	3.63			
		C	107.43	80.90	83.91	82.22	61.09			

[a]Residues A, B, C, D, and E were designated according to the decreasing order of proton peak intensity.

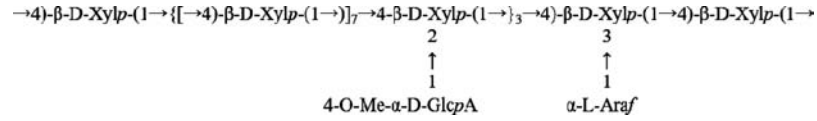

Figure 2. Proposed partial structure of the ACAP repeating unit.

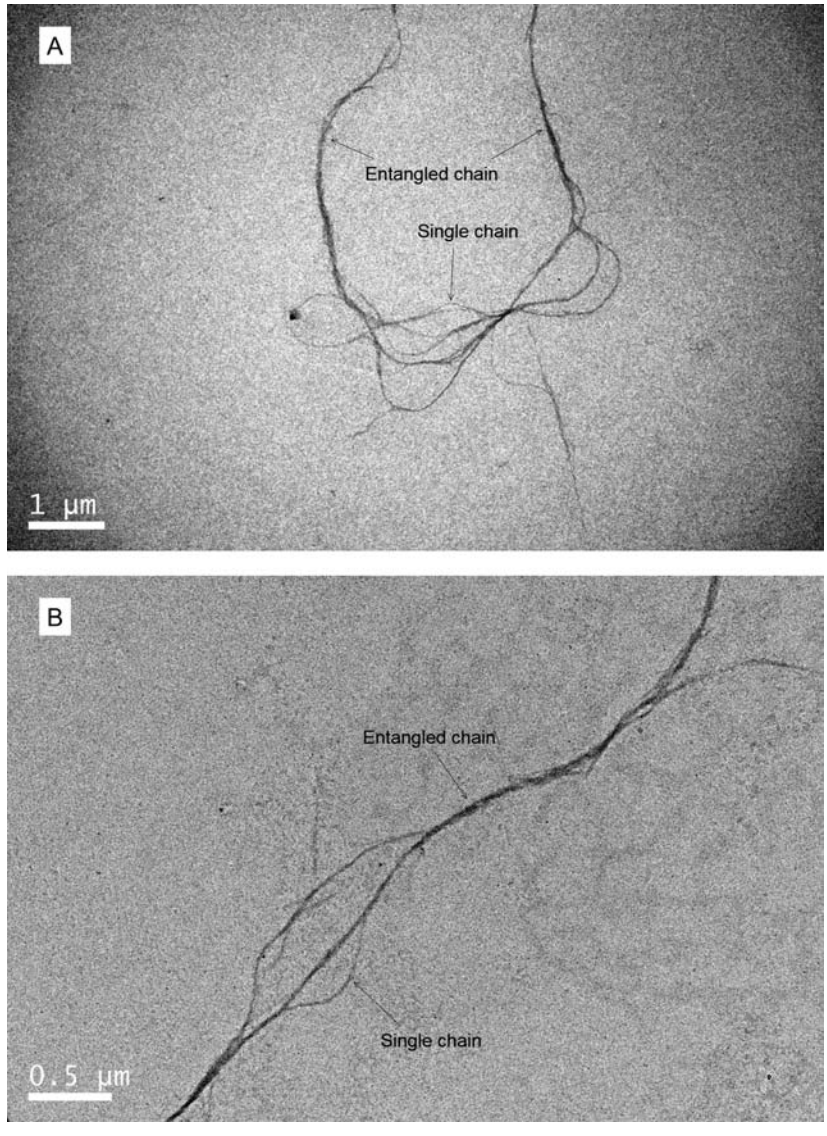

Figure 3. TEM images of ACAP in sodium dodecyl sulfate solution.

DOI: 10.1021/acs.jafc.5b00063
J. Agric. Food Chem. 2015, 63, 2970−2978

spectrum, and NMR analysis also indicated that ACAP contained no $-OCH_3$ group, which was different from other hemicellulosic heteroxylans. According to previous studies, hemicellulosic xylan often contains large amounts of $-OCH_3$ groups on the *O*-2 and/or *O*-3 sites of the xylan backbone. This difference might be explained by the fact that the alkali extraction procedure might result in the hydrolysis of potential $-OCH_3$ groups in ACAP. Additionally, the above result indicated that T-D-Glc*p*A existed in the ACAP molecule as the form of *α*-4-*O*-MeGlc*p*A. According to the present results and previous literature on the structure of hemicellulosic xylan,[37−39] the primary structure of ACAP could be deduced as a *β*-1→4-D-Xyl*p* backbone with small amounts of *α*-4-*O*-MeGlc*p*A and T-*α*-L-Ara*f* in the side chains on the *O*-2 and *O*-3 sites, respectively (Figure 2).

Microscopic Morphology of ACAP. Morphological information is important to illustrate the fine structure of macromolecules intuitively. In the present study, TEM analysis was conducted to further observe the microstructure of ACAP. As shown in Figure 3, both single chain and entangled chain were observed in ACAP molecules under the experimental conditions. Similar to the triple-helical conformation of lentinan, ACAP molecules trended to form entangled chains, which contained even more than three single chains as shown in Figure 3A. Moreover, the approximately linear structure with minor branches from Figure 3B was consistent with the above results of methylation and NMR analysis.

Thermal Decomposition Analysis. The applicability of polysaccharide is also largely dependent on its thermal behavior. Thermal degradation characteristics of ACAP were determined from the curves of thermal gravity, differential thermal gravity, and second-time derivatives (TG, DTG, and D^2TG) in the temperature range of 50−600 °C. As shown in Figure 4A, two steps of weight loss occurred in the thermogravimetric analysis. The major decomposition of polysaccharide structure occurred at 200−350 °C, because about 70% of the weight was lost within this temperature range. In addition, minor weight loss (∼7%) occurred in the 50−150 °C range due to the loss of trapped water. Therefore, the weight at 150 °C was defined as 100% dry weight for the next degradation analysis of ACAP.

Three different heating rates were applied to identify the thermal degradation parameters of ACAP in the 150−600 °C range (Figure 4B) and deduced to a β value of 0 for each of the three temperatures (Figure 4C). The degradation characteristics are summarized in Table 3, where the parameters T_o, T_p, and T_s represent the onset, maximum, and shift decomposition temperatures, respectively, whereas WL_o, WL_p, and WL_s indicate the corresponding weight loss percentage parameters. As indicated in Table 3, the maximum degradation rate was observed at 278.6 °C (T_p) with a weight loss of 21.81% on a dry weight basis (WL_p), whereas ACAP experienced a rapid degradation in a narrow temperature range from the transition of T_p to T_s.

The apparent activation energy (E_a) and pre-exponential factor *A* were obtained by the isoconversional FWO method (Figure 5) at a conversion range from 0.3 to 0.7 with a 0.1 increment. The average E_a value was calculated as 220.0 kJ/mol, whereas the experimental ln *A* was obtained by the compensation effect relationship as eq 3 (Table S1 in the Supporting Information). The compensation parameters of *a* and *b* were obtained from a plot of ln *A* versus E_a (Figure S5 in the Supporting Information) using the Coats−Redfern equation (eq 4) (Table S2 in the Supporting Information).

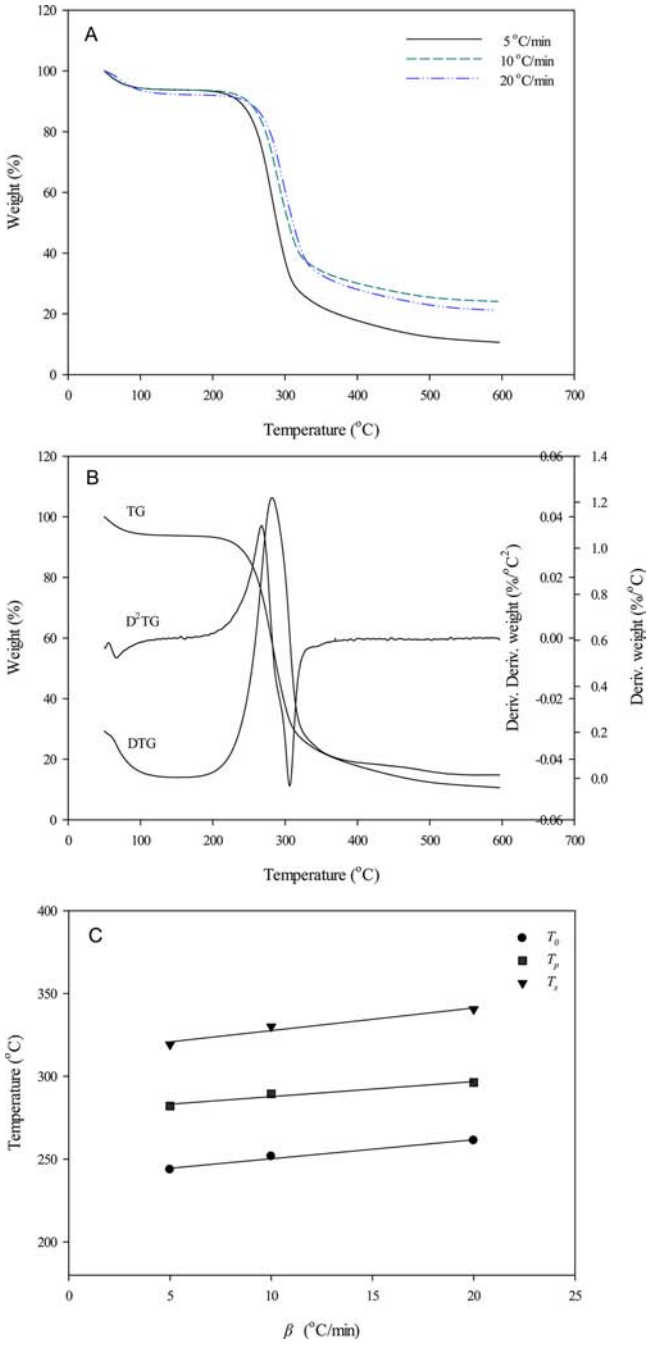

Figure 4. Thermal decomposition analysis of ACAP: (A) TG curves of ACAP at different heating rates; (B) determination of thermal decomposition parameters of ACAP at a heating rate of 5 °C/min; and (C) thermal degradation parameters of ACAP at different heating rates.

Compared with the single-heating rate method, the isoconversional method provides more accurate values of E_a and *A*.[40] Therefore, the obtained thermal kinetic parameters had greater practical value to comprehend and predict the thermal degradation process of ACAP. The thermal analysis has been widely performed on cellulose and hemicellulose to obtain the degradation characteristics.[41,42]

The pyrolysis range of ACAP (238.8−314.0 °C) was found to be consistent with a previous study of several isolated natural polysaccharides, the major weight loss of which occurred in the range of 225−325 °C.[41] In this temperature range (238.8−314.0

DOI: 10.1021/acs.jafc.5b00063
J. Agric. Food Chem. 2015, 63, 2970−2978

Table 3. Degradation Characteristics of ACAP[a]

$T_{o\ \beta\to0}$ (°C)	WL_o (%)	$T_{p\ \beta\to0}$ (°C)	WL_p (%)	$T_{s\ \beta\to0}$ (°C)	WL_s (%)	$T_s - T_o$ (°C)	$WL_s - WL_o$ (%)
238.8	2.88	278.6	21.81	314.0	57.24	75.2	54.37

[a]Data are means. *T*, temperature; WL, weight loss; subscript o, onset; subscript p, DTG peak; subscript s, shift; subscript $\beta\to0$, extrapolated values to the heating rate of 0 °C/min.

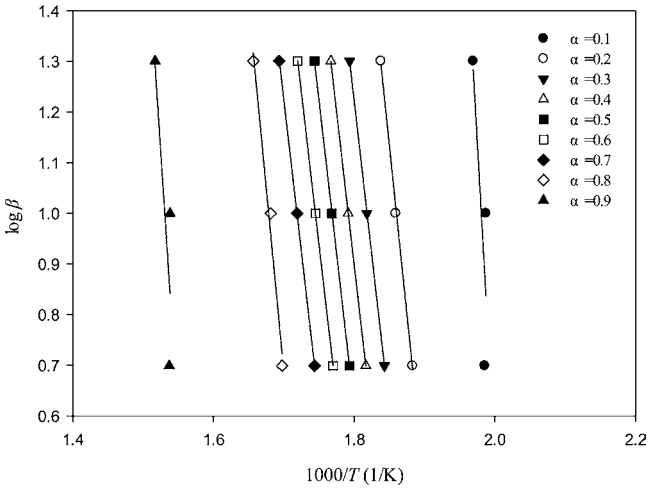

Figure 5. Typical isoconversional plot of Flynn–Wall–Ozawa (FWO) method at different conversion rates.

°C), most of the ACAP (54.37%, Table 3) decomposed to volatiles, including CO, CO_2, CH_4, CH_3COOH, and HCOOH, according to the literature.[31,43] Moreover, the E_a value of ACAP was determined to be 220.0 kJ/mol, which indicated the good thermal stability of this hemicellulosic heteroxylan. Among these thermal parameters, E_a might indicate a minimum energy requirement to initiate the degradation reaction, with a lower E_a value associated with a lower thermal degradation temperature. These thermal kinetic parameters, including the experimental E_a and A, may also be important for thermal stability evaluation and shelf life prediction of the related polysaccharide products. In other words, the thermal kinetic parameters of ACAP might be important for determining its future applications.

Anti-inflammation Effects of ACAP. ACAP was able to suppress the LPS-induced mRNA expressions of IL-1β, IL-6, and COX-2 genes in the cultured RAW 264.7 macrophage cells under the experimental conditions (Figure 6). The suppression was dose-dependent for IL-1β and IL-6 mRNA expressions, but not for COX-2 gene expression. As shown in Figure 6A, 73.98% of IL-1β mRNA expression was suppressed by ACAP at the final treatment concentration of 50 μg/mL, whereas the IL-1β mRNA expression was reduced to 56.80% at 10 μg/mL. ACAP at 10 μg/mL reduced the LPS-induced IL-6 mRNA expressions and showed a stronger inhibition effect by 49.38% compared to that at 50 μg/mL by 31.79% (Figure 6B), suggesting that concentration or dosage may be critical for a desired level of inhibition on IL-6 mRNA expression. Moreover, its inhibitory effects on COX-2 mRNA expression were 20.86 and 26.18% at 50 and 10 μg/mL final treatment concentrations (Figure 6C), respectively. These results suggested that ACAP might be further developed as a potential functional food ingredient to reduce the risk of inflammation related chronic human diseases.

Hemicelluloses have attracted more and more interest for their environmentally friendly and biosafety properties. Nowadays, hemicellulose has been extensively developed as an important

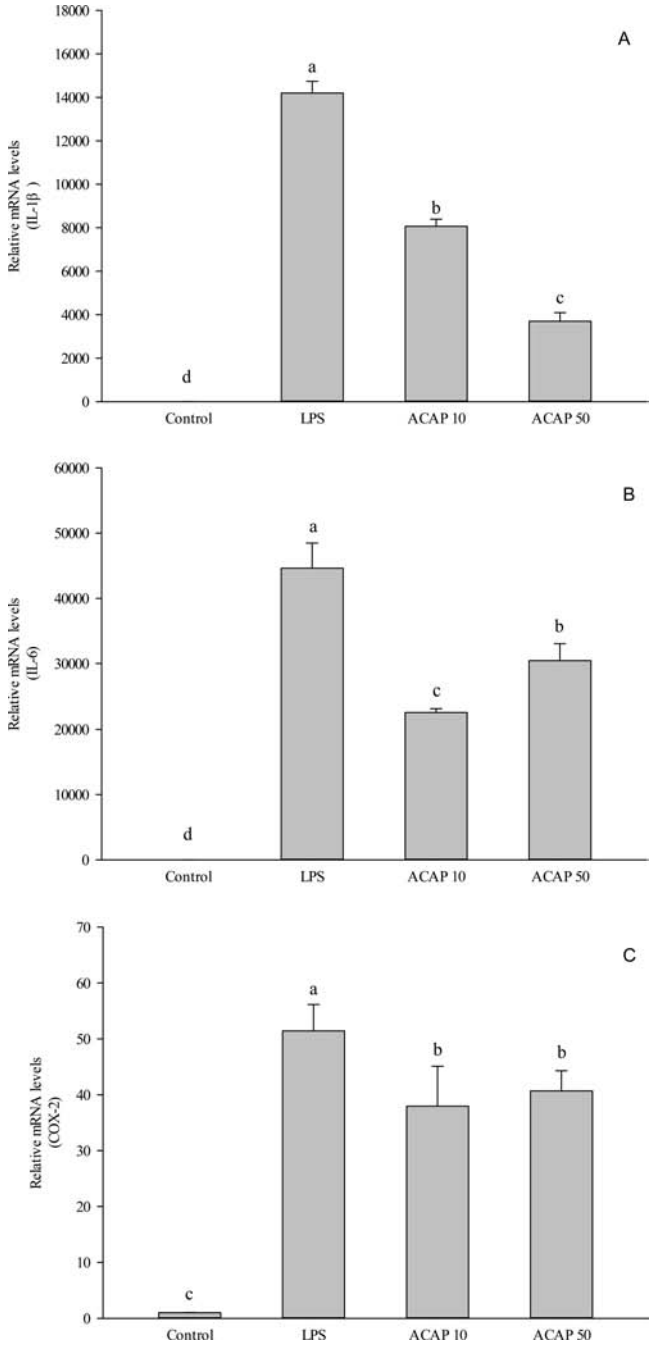

Figure 6. Effects of ACAP on (A) IL-1β, (B) IL-6, and (C) COX-2 mRNA expressions in LPS-stimulated RAW 264.7 cells. LPS stands for lipopolysaccharide at final concentration of 10 ng/mL; ACAP 10 and ACAP 50 stand for the final treatment concentrations of ACAP at 10 and 50 μg/mL, respectively. The vertical bars represent the standard deviation (n = 3) of each data point. Different letters (a–d) represent significant differences ($P < 0.05$).

biomass in several important fields, including materials, energy, medical, and food industries.[37,44,45] Alfalfa stem contains

DOI: 10.1021/acs.jafc.5b00063
J. Agric. Food Chem. 2015, 63, 2970–2978

abundant hemicellulosic polysaccharides, but little is known about their chemical structures and functionalities at the molecular level. The structural study of alfalfa polysaccharides remained at the level of the 1960s, which only revealed the monosaccharide composition and partial glycosidic linkages[3,4] without detailed structural features due to the restriction of prevailing technique and equipment. Elucidation of the structure, pyrolysis features, and anti-inflammatory bioactivity will facilitate the further application of hemicellulosic polysaccharides from alfalfa stem.

In summary, a new hemicellulosic polysaccharide (ACAP) was purified from the cold alkali extract of alfalfa stem and characterized as a heteroxylan, with a molecular weight of 7.94 × 10^3 kDa and a radius of 58 nm. ACAP contained a β-1→4-linked D-Xyl*p* backbone with 29% short side chains of 4-*O*-MeGlc*p*A and T-L-Ara*f* units at the *O*-2 and *O*-3 branching points, respectively, and had entangled chains. ACAP showed excellent thermal stability with a key decomposition in 238.8−314.0 °C (the extrapolated temperatures) and apparent activation energy E_a and pre-exponential factor *A* values of 220.0 kJ/mol and 2.81 × 10^{24}/s, respectively. The thermal characteristic parameters provided a simplified approach to evaluate the thermal decomposition behavior of ACAP in food or industrial applications. In addition, ACAP significantly inhibited the mRNA expressions of the pro-inflammatory cytokine genes, especially for IL-1β, suggesting its potential anti-inflammatory effect. These results suggested the potential application of ACAP in functional foods and dietary supplement products.

■ ASSOCIATED CONTENT

Supporting Information

Tables S1 and S2 and Figures S1−S5. This material is available free of charge via the Internet at http://pubs.acs.org.

■ AUTHOR INFORMATION

Corresponding Author

*(L.Y.) Phone: (301) 405-0761. E-mail: lyu5@umd.edu.

Funding

This project was supported by a General Grant from the China Postdoctoral Science Foundation (Grant 2014M561476), a special fund for Agro-scientific Research in the Public Interest (Grant 201203069), a National High Technology Research and Development Program of China (Grants 2013AA102202 and 2013AA102207), SJTU 985-III disciplines platform and talent fund (Grants TS0414115001 and TS0320215001), and a grant from Wilmar (Shanghai) Biotechnology Research & Development Center Co., Ltd.

Notes

The authors declare no competing financial interest.

■ REFERENCES

(1) Hu, Y. G.; Cash, D. Global status and development trends of alfalfa. In *Alfalfa Management Guide for Ningxia*; Cash, D., Ed.; Beijing, China, 2009; pp 1−3.

(2) Lamb, J. F. S.; Jung, H. J. G.; Sheaffer, C. C.; Samac, D. A. Alfalfa leaf protein and stem cell wall polysaccharide yields under hay and biomass management systems. *Crop Sci.* **2007**, *47*, 1407−1415.

(3) Aspinall, G. O.; McGrath, D. Hemicelluloses of lucerne. *J. Chem. Soc. C* **1966**, 2133−2139.

(4) Aspinall, G. O.; Fanshawe, R. S. Pectic substances from lucerne (*Medicago sativa*). Part I. Pectic acid. *J. Chem. Soc.* **1961**, 4215−4125.

(5) Myhre, D. V.; Smith, F. Alfalfa hemicellulose, constitution of the hemicellulose of alfalfa (*Medicago sativa*). Hydrolysis of hemicellulose and identification of neutral and acidic components. *J. Agric. Food Chem.* **1960**, *8*, 359−364.

(6) Dong, X. F.; Gao, W. W.; Su, J. L.; Tong, J. M.; Zhang, Q. Effects of dietary polysavone (alfalfa extract) and chlortetracycline supplementation on antioxidation and meat quality in broiler chickens. *Br. Poult. Sci.* **2011**, *52*, 302−309.

(7) Dong, X. F.; Gao, W. W.; Tong, J. M.; Jia, H. Q.; Sa, R. N.; Zhang, Q. Effect of polysavone (alfalfa extract) on abdominal fat deposition and immunity in broiler chickens. *Poult. Sci.* **2007**, *86*, 1955−1959.

(8) Wang, S. P.; Dong, X. F.; Tong, J. M. Optimization of enzyme-assisted extraction of polysaccharides from alfalfa and its antioxidant activity. *Int. J. Biol. Macromol.* **2013**, *62*, 387−396.

(9) Liu, H. W.; Dong, X. F.; Tong, J. M.; Zhang, Q. Alfalfa polysaccharides improve the growth performance and antioxidant status of heat-stressed rabbits. *Livest. Sci.* **2010**, *131*, 88−93.

(10) Deng, W.; Dong, X. F.; Tong, J. M.; Xie, T. H.; Zhang, Q. Effects of an aqueous alfalfa extract on production performance, egg quality and lipid metabolism of laying hens. *J. Anim. Physiol. Anim. Nutr.* **2012**, *96*, 85−94.

(11) Wang, S. P.; Dong, X. F.; Ma, H.; Cui, Y. M.; Tong, J. M. Purification, characterisation and protective effects of polysaccharides from alfalfa on hepatocytes. *Carbohydr. Polym.* **2014**, *112*, 608−614.

(12) Hill, M. J. Bacterial fermentation of complex carbohydrate in the human colon. *Eur. J. Cancer Prev.* **1995**, *4*, 353−358.

(13) Takenaka, S.; Itoyama, Y. Rice bran hemicellulose increases the peripheral blood lymphocytes in rats. *Life Sci.* **1993**, *52*, 9−12.

(14) Ebringerová, A.; Hromádková, Z.; Heinze, T. Hemicellulose. In *Advances in Polymer Science*; Heinze, T., Ed.; Springer: Berlin, Germany, 2005; Vol. 186, pp 1−67.

(15) Dollinger, G.; Cunico, B.; Kunitani, M.; Johnson, D.; Jones, R. Practical on-line determination of biopolymer molecular weights by high-performance liquid chromatography with classical light-scattering detection. *J. Chromatogr., A* **1992**, *592*, 215−228.

(16) DuBois, M.; Gilles, K. A.; Hamilton, J. K.; Rebers, P. A.; Smith, F. Colorimetric method for determination of sugars and related substances. *Anal. Chem.* **1956**, *28*, 350−356.

(17) Blumenkrantz, N.; Asboe-Hansen, G. New method for quantitative determination of uronic acids. *Anal. Biochem.* **1973**, *54*, 484−489.

(18) Hill, H. D.; Straka, J. G. Protein determination using bicinchoninic acid in the presence of sulfhydryl reagents. *Anal. Biochem.* **1988**, *170*, 203−208.

(19) Yan, W.; Niu, Y. G.; Lv, J. L.; Xie, Z. H.; Jin, L.; Yao, W. B.; Gao, X. D.; Yu, L. L. L. Characterization of a heteropolysaccharide isolated from diploid *Gynostemma pentaphyllum* Makino. *Carbohydr. Polym.* **2013**, *92*, 2111−2117.

(20) Pettolino, F. A.; Walsh, C.; Fincher, G. B.; Bacic, A. Determining the polysaccharide composition of plant cell walls. *Nat. Protoc.* **2012**, *7*, 1590−1607.

(21) Kim, J. S.; Reuhs, B. L.; Michon, F.; Kaiser, R. E.; Arumugham, R. G. Addition of glycerol for improved methylation linkage analysis of polysaccharides. *Carbohydr. Res.* **2006**, *341*, 1061−1064.

(22) CCRC. http://www.ccrc.uga.edu/specdb/ms/pmaa/pframe.html (accessed Aug 30, 2014).

(23) Rezanka, T.; Sigler, K. Structural analysis of a polysaccharide from *Chlorella kessleri* by means of gas chromatography-mass spectrometry of its saccharide alditols. *Folia Microbiol. (Praha)* **2007**, *52*, 246−252.

(24) Chen, L.; Cheung, P. C. K. Mushroom dietary fiber from the fruiting body of *Pleurotus tuber-regium*: fractionation and structural elucidation of nondigestible cell wall components. *J. Agric. Food Chem.* **2014**, *62*, 2891−2899.

(25) Chen, L.; Zhang, B. B.; Chen, J. L.; Cheung, P. C. K. Cell wall structure of mushroom sclerotium (*Pleurotus tuber-regium*): Part 2. Fine structure of a novel alkali-soluble hyper-branched cell wall polysaccharide. *Food Hydrocolloids* **2014**, *38*, 48−55.

(26) Flynn, J. H.; Wall, L. A. General treatment of the thermogravimetry of polymers. *J. Res. Natl. Bur. Stand.* **1966**, *70*, 487−523.

DOI: 10.1021/acs.jafc.5b00063
J. Agric. Food Chem. 2015, 63, 2970−2978

(27) Ozawa, T. A new method of analyzing thermogravimetric data. *Bull. Chem. Soc. Jpn.* **1965**, *38*, 1881−1886.
(28) Zhang, X. W.; Shang, P. P.; Qin, F.; Zhou, Q.; Gao, B. Y.; Huang, H. Q.; Yang, H. S.; Shi, H. M.; Yu, L. L. L. Chemical composition and antioxidative and anti-inflammatory properties of ten commercial mung bean samples. *LWT−Food Sci. Technol.* **2013**, *54*, 171−178.
(29) Huang, H. Q.; Cheng, Z. H.; Shi, H. M.; Xin, W. B.; Wang, T. T. Y.; Yu, L. L. L. Isolation and characterization of two flavonoids, engeletin and astilbin, from the leaves of *Engelhardia roxburghiana* and their potential anti-inflammatory properties. *J. Agric. Food Chem.* **2011**, *59*, 4562−4569.
(30) Hawker, C. J.; Lee, R.; Frechet, J. M. J. One-step synthesis of hyperbranched dendritic polyesters. *J. Am. Chem. Soc.* **1991**, *113*, 4583−4588.
(31) Sun, S. N.; Cao, X. F.; Xu, F.; Sun, R. C.; Jones, G. L.; Baird, M. Structure and thermal property of alkaline hemicelluloses from steam exploded *Phyllostachys pubescens*. *Carbohydr. Polym.* **2014**, *101*, 1191−1197.
(32) Kačuráková, M.; Belton, P. S.; Wilson, R. H.; Hirsch, J.; Ebringerová, A. Hydration properties of xylan-type structures: an FTIR study of xylooligosaccharides. *J. Sci. Food Agric.* **1998**, *77*, 38−44.
(33) Kačuráková, M.; Ebringerova, A.; Hirsch, J.; Hromadkova, Z. Infrared study of arabinoxylans. *J. Sci. Food Agric.* **1994**, *66*, 423−427.
(34) Jiang, H.; Chen, Q. Q.; Ge, J. H.; Zhang, Y. Efficient extraction and characterization of polymeric hemicelluloses from hybrid poplar. *Carbohydr. Polym.* **2014**, *101*, 1005−1012.
(35) Kacurakova, M.; Capek, P.; Sasinkova, V.; Wellner, N.; Ebringerova, A. FT-IR study of plant cell wall model compounds: pectic polysaccharides and hemicelluloses. *Carbohydr. Polym.* **2000**, *43*, 195−203.
(36) Ebringerova, A.; Hromadkova, Z.; Alföldi, J.; Berth, G. Structural and solution properties of corn cob heteroxylans. *Carbohydr. Polym.* **1992**, *19*, 99−105.
(37) Capek, P.; Matulová, M. An arabino(glucurono)xylan isolated from immunomodulatory active hemicellulose fraction of *Salvia officinalis* L. *Int. J. Biol. Macromol.* **2013**, *59*, 396−401.
(38) Sun, S. L.; Wen, J. L.; Ma, M. G.; Sun, R. C. Successive alkali extraction and structural characterization of hemicelluloses from sweet sorghum stem. *Carbohydr. Polym.* **2013**, *92*, 2224−2231.
(39) Peng, Y. Y.; Wu, S. B. The structural and thermal characteristics of wheat straw hemicellulose. *J. Anal. Appl. Pyrol.* **2010**, *88*, 134−139.
(40) Vyazovkin, S. Model-free kinetics. Staying free of multiplying entities without necessity. *J. Therm. Anal. Calorim.* **2006**, *83*, 45−51.
(41) Iqbal, M. S.; Massey, S.; Akbar, J.; Ashraf, C. M.; Masih, R. Thermal analysis of some natural polysaccharide materials by isoconversional method. *Food Chem.* **2013**, *140*, 178−182.
(42) Yao, F.; Wu, Q. L.; Lei, Y.; Guo, W. H.; Xu, Y. J. Thermal decomposition kinetics of natural fibers: activation energy with dynamic thermogravimetric analysis. *Polym. Degrad. Stab.* **2008**, *93*, 90−98.
(43) Maschio, G.; Koufopanos, C.; Lucchesi, A. Pyrolysis, a promising route for biomass utilization. *Bioresour. Technol.* **1992**, *42*, 219−231.
(44) Ragauskas, A. J.; Williams, C. K.; Davison, B. H.; Britovsek, G.; Cairney, J.; Eckert, C. A.; Frederick, W. J.; Hallett, J. P.; Leak, D. J.; Liotta, C. L. The path forward for biofuels and biomaterials. *Science* **2006**, *311*, 484−489.
(45) Pan, X. J.; Arato, C.; Gilkes, N.; Gregg, D.; Mabee, W.; Pye, K.; Xiao, Z. Z.; Zhang, X.; Saddler, J. Biorefining of softwoods using ethanol organosolv pulping: preliminary evaluation of process streams for manufacture of fuel-grade ethanol and co-products. *Biotechnol. Bioeng.* **2005**, *90*, 473−481.

DOI: 10.1021/acs.jafc.5b00063
J. Agric. Food Chem. 2015, 63, 2970−2978

known as the lipogenic transcription factors.[18] Therefore, we hypothesized that chitosan might inhibit lipogenesis-related protein/gene expressions induced by obesity through an AMPK-regulated signaling pathway. In the present study, high-fat (HF) diet-fed rats were used as an in vivo obesity model to clarify the mode of action and the possible mechanism of chitosan in lipid responses and lipid-related metabolic changes.

MATERIALS AND METHODS

Materials. High molecular weight (HMW) chitosan was purchased from Taiwan Tanabe Seiyaku Co. (Taipei, Taiwan). Chitosan was prepared by processing crab shell, which involves demineralization, deprotienization, and deacetylation. The measurements of average molecular weight (MW) and degree of deacetylation (DD) of chitosan were determined by high-performance liquid chromatography and Fourier transform infrared spectroscopy, respectively. The detection of viscosity was performed on chitosan dissolved in 0.1 N HCl solution by a viscometer (CV20, Haake Mess-Technik GmbH Co., Karlsruhe, Germany). The DD of chitosan was about 89.8%, and the average MW and viscosity of chitosan were about 560 kDa and 33 cP, respectively. Cellulose was obtained from Sigma Chemical Co. (St. Louis, MO, USA).

Animals and Diets. Male, 6-week-old Sprague−Dawley rats were purchased from BioLASCO Taiwan Co., Ltd. (Taipei, Taiwan). Rats were fed a chow diet (Rodent Laboratory Chow, Ralston Purina, St. Louis, MO, USA) for 1 week, and then the animals were randomly divided into two groups: a control group that received standard rodent diet with 5% cellulose (ND) and a HF group that received a HF diet with 5% cellulose. After 4 weeks of acclimation, the rats that received a HF diet were further randomly divided into four groups: (1) HF-diet-fed rats with 5% cellulose, (2) HF-diet-fed rats with 3% HMW chitosan (HF diet+3%CS), (3) HF-diet-fed rats with 5% HMW chitosan (HF+5%CS), and (4) HF-diet-fed rats with 7% HMW chitosan (HF+7%CS). Each group contained eight animals. The compositions of the experimental diets given to test animals are shown in Table 1. Rats were housed in individual stainless steel cages in a room kept at 23 ± 1 °C and 40−60% relative humidity with a 12 h light and dark cycle (lighting from 8:00 a.m. to 8:00 p.m.). The body weight was measured every week. After the 7 week feeding study, the animals were sacrificed. This study was approved by the Animal House Management Committee of the National Taiwan Ocean University (permission no. ACUC98045). The animals were maintained in accordance with the guidelines for the care and use of laboratory animals as issued by the Animal Center of the National Science Council.

Table 1. Composition (Percent) of Experimental Diets[a]

ingredient	ND	HF	HF+3%CS	HF+5%CS	HF+7%CS
casein	20	20	20	20	20
lard	3	15	15	15	15
soybean oil	2	2	2	2	2
vitamin mixture[b]	1	1	1	1	1
mineral mixture[c]	4	4	4	4	4
cholesterol		0.5	0.5	0.5	0.5
choline chloride	0.2	0.2	0.2	0.2	0.2
cholic acid		0.2	0.2	0.2	0.2
corn starch	65.8	53.1	53.1	53.1	51.1
cellulose	5	5	2		
chitosan[d]			3	5	7

[a]ND, normal control diet; HF, high-fat diet; HF+3%CS, HF + 3% chitosan; HF+5%CS, HF + 5% chitosan; HF+7%CS, HF + 7% chitosan. [b]AIN-93 vitamin mixture. [c]AIN-93 mineral mixture. [d]The average molecular weight and viscosity of chitosan were about 5.6 × 10^5 Da and 33 mPa·s, respectively. The degree of deacetylation was about 89.8%.

Collection of Feces and Tissue Samples. At the end of the experimental period, animals were fasted for 12 h prior to being sacrificed by exsanguination via the abdominal aorta while under carbon dioxide anesthesia. The liver and epididymal and perirenal white adipose tissues from each animal were excised, dried, weighed, flash-frozen, and stored at −80 °C until biopsy. Feces were collected for three consecutive days before euthanasia and stored at −80 °C until lipid content analysis was performed.

Triglyceride (TG) and Total Cholesterol (TC) Determination. The levels of hepatic and fecal TG and TC were measured as described previously by Carlson and Glodfarb.[19] Briefly, 0.2 g of liver or feces was mixed with 4 mL of chloroform/methanol (2:1, v/v). The chloroform layer was collected and concentrated in a Speed Vac Sc 110 rotary evaporator (Savant, Farmingdale, NY, USA). After the addition of Triton X-100, the sample was assayed with TG enzymatic kits (Audit Diagnostics, Cork, Ireland) and TC enzymatic kits (Audit Diagnostics) according to the manufacturer's instructions.

Determination of Hepatic Lipid Metabolism Enzymes. Hepatic fatty acid synthase (FAS) and acetyl-CoA carboxylase (ACC) were assayed as described previously by Nepokroeff et al.[20] and Mohan and Kekwick,[21] respectively. HMGCR reductase was determined as described previously by Edwards et al.[22] The enzyme activities were determined by the rate of nanomoles of NADPH increased.

Lipolysis Rate Measurement. Adipose tissue (0.2 g) was minced into small pieces and placed in 2 mL of 25 mM *N*-tris-(hydroxymethyl)methyl-2-aminoethanesulfonic acid buffer containing 1 μM isoproterenol and incubated at 37 °C. Isoproterenol produced a dose-dependent increase in lipolysis. There was a time-dependent increase in lipolysis. After 1, 2, and 3 h of incubation, 0.2 mL of medium was used to measure the levels of glycerol by a commercial reagent (RANDOX GY105, Amtrim, UK), and then the absorbance at 520 nm was recorded using a spectrophotometer. The lipolysis rate was indicated by micromoles of glycerol released per gram of tissue per hour.

Lipoprotein Lipase (LPL) Activity. LPL activity in adipose tissue was measured as described previously by Kusunoki et al.[23] Adipose tissue (0.1 g) was minced into small pieces and placed in Krebs−Ringer bicarbonate buffer (pH 7.4) in the presence of heparin (10 units/mL) for 60 min at 37 °C. The heparin solution was mixed with an equal volume of 2 mM *p*-nitrophenyl butyrate (pNPB). Absorbance at 400 nm was recorded following a 10 min incubation using a spectrophotometer. LPL activity was recorded as the amount of *p*-nitrophenol product formed over the 10 min incubation.

Histological Examination. Epididymal white adipose tissue was fixed with 10% formalin and paraffin embedded. Standard sections of 5 μm were mounted on glass slides and stained with hematoxylin and eosin (H&E). The sections were observed and photographed with an Olympus BX51 light microscope (Olympus, Tokyo, Japan). Three H&E sections of each group were selected, and three random fields of each section were used to measure adipocyte area by ImageJ software, which is represented as the average adipocyte area.

Western Blot Analysis. Total protein containing 50−100 μg was separated on 10% sodium dodecyl sulfate (SDS)−polyacrylamide minigels and transferred to polyvinylidene difluoride membranes (Millipore, Billerica, MA, USA). After blocking, blots were incubated with antibodies for phosphorylated AMPKα (p-AMPKα), AMPKα (Cell Signaling Technology, Danvers, MA, USA), microsomal triglyceride transfer protein (MTTP), angiopoietin-like 4 (Angptl4), GAPDH, PPAR-γ, β-actin (Santa Cruz Biotechnology, Santa Cruz, CA, USA), apolipoprotein E (ApoE) (Bioss Antibodies, Woburn, MA, USA), and SREBP1c (Proteintech Group, Chicago, IL, USA) in phosphate-buffered saline (PBS)/Tween-20 for 1 h, followed by two washings in PBS/Tween-20, and then incubated with horseradish peroxidase-conjugated goat anti-mouse or anti-rabbit IgG for 30 min. Moreover, GAPDH served as a control for sample loading and integrity. The antibody-reactive bands were revealed by the enhanced

DOI: 10.1021/acs.jafc.5b00198
J. Agric. Food Chem. 2015, 63, 2979−2988

Table 2. Primer Sequences

gene	forward (5′ to 3′)	reverse (5′ to 3′)	length (bp)
FABP4	CCTTTGTGGGGACCTGGAAA	TGACCGGATGACGACCAAGT	152
FAS	CTTGGGTGCCGATTACAACC	GCCCTCCCGTACACTCACTC	163
FATP1	GTGCGACAGATTGGCGAGTT	GCGTGAGGATACGGCTGTTG	106
HMGCR	TGTGGGAACGGTGACACTTA	CTTCAAATTTTGGGCACTCA	101
GAPDH	CTGGAGAAACCTGCCAAGTATGAT	TTCTTACTCCTTGGAGGCCATGTA	250

chemiluminescence kit (BioRad Laboratories, Redmond, WA, USA) and were exposed to Kodak radiographic film.

Quantitative Reverse Transcription Polymerase Chain Reaction (qRT-PCR) Analysis. Total RNA was extracted from the liver and epididymal fat tissues using Trizol (Invitrogen, Carslbad, CA, USA) and was reverse-transcribed to cDNA using a MMLV High Performance Reverse Transcriptase kit as recommended by the manufacturer (Epicentre, Madison, WI, USA). The sequences of the designed primers are shown in Table 2. GAPDH was used as an internal control. The resultant cDNA was stored at −20 °C until commencement of the qRT-PCR procedures. For qRT-PCR, the reaction was done on StepOne Real-Time PCR Systems (Applied Biosystems, Life Technologies, Grand Island, NY, USA) to check the expression using Maxima SYBR Green/ROX qPCR Master Mix (Thermo Scientific, Waltham, MA, USA). Relative quantification of gene expression was performed by using the comparative threshold cycle method (ΔΔCT), in which the expression level of each target gene was normalized to the levels of GAPDH. Data output was expressed as fold changes of mRNA expression levels, given by $2^{-\Delta\Delta CT}$.

Statistical Evaluation. Results are given as mean ± standard deviation (SD) values. The significant difference from the respective controls for each experimental test condition was assessed by one-way analysis of variance (ANOVA) and two-tailed Student's *t* test. The statistical software SPSS for Windows version 10.0.7C (SPSS, Chicago, IL, USA) was used.

RESULTS

Effects of Chitosan on Lipid Responses and Lipid-Related Metabolic Changes in HF-Diet-Fed Rats. During the obesity induction period (first 4 weeks), the body weights of HF-diet-fed rats were significantly higher than those of ND-fed rats, and supplementation of 7% chitosan could efficiently decrease the increased body weights in HF-diet-fed rats throughout the rest of the 7 weeks (HF+7%CS vs HF, a decrease of 9.13%, $p < 0.05$) (Figure 1 and Table 3). In addition, rats fed a HF diet supplemented with chitosan (3, 5, and 7%) had lower liver weights, and a significant reduction (HF+7%CS vs HF, a decrease of 18.18%, $p < 0.05$) in adipose tissue weights was exhibited only in the HF diet + 7% chitosan group (Table 3). There were no significant changes in plasma TC levels of all tested groups. The plasma TG of HF-diet-fed rats exhibited a decreased level as compared to the ND group, which could be significantly reversed by chitosan (3, 5, and 7%) supplementation (Table 3).

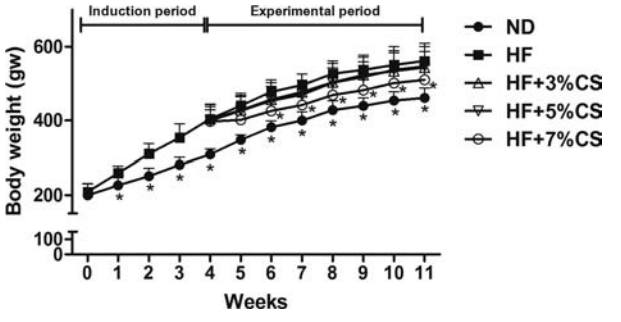

Figure 1. Effects of chitosan on body weights of HF-diet-fed rats. The changes of body weights in rats fed the HF diet in the presence or absence of chitosan (3−7%) during induction period (weeks 0−4) and experimental period (weeks 4−11) are shown. Results are expressed as the mean ± SD for each group ($n = 8$). (*) $p < 0.05$ as compared with the HF-diet group.

The effects of chitosan on adipose tissue characteristics are shown in Figures 2 and 3. Rats fed the HF diet showed a significant increase (29.74%, $p < 0.05$) in cell size of epididymal adipose tissues, and supplementation of 5 and 7% chitosan could significantly suppress hypertrophic adipocyte formation (adipose cell size: HF, 36.45 ± 3.03 μm^2; HF+5%CS, 29.5 ± 2.67 μm^2; HF+7%CS, 21.25 ± 1.85 μm^2) (Figure 2B). Moreover, the TG level (Figure 3A) and the LPL activity (Figure 3B) in epididymal fat of HF-diet-fed rats were elevated, and the rate of lipolysis (Figure 3C) was contrarily diminished. Supplementation of 7% chitosan in the diet significantly raised the lipolysis rate and decreased the accumulation of TG and the LPL activity.

We next tested the levels of TG and TC in the livers and feces. As shown in Figure 4 and Table 4, the livers/feces of the HF-diet-fed rats supplemented with chitosan (3, 5, and 7%) contained significantly less/more TC than the HF-diet-fed control rats. The TG levels were also decreased by 27.68% ($p < 0.05$) in the livers of the HF+7%CS group and increased in the feces of chitosan-supplemented groups (HF+CS7% vs HF, an increase of 46.88%, $p < 0.05$). Furthermore, the increased hepatic enzyme activities of lipid biosynthesis (acetyl-CoA carboxylase, fatty acid synthase, and HMG-CoA reductase) in HF-diet-fed rats could also be efficiently ameliorated by chitosan (7%) supplementation (Figure 4).

We next examined protein expressions of Angptl4, MTTP, and ApoE, which are known to be involved in TG metabolism.[24−26] The inhibitions of Angptl4, MTTP, and ApoE protein expressions were observed in the plasma and liver of HF-diet-fed rats, which could be significantly reversed by chitosan supplementation (Figure 5).

Effects of Chitosan on Lipogenesis-Related Factors in Livers and Adipose Tissues of HF-Diet-Fed Rats. AMPK is known to play an important role in regulating lipid metabolism of the liver and adipose tissue.[15−17] We next investigated the effects of chitosan on AMPK-regulated lipogenesis-associated protein/gene expressions in HF-diet-fed rats. We found that the suppression of AMPK phosphorylation in livers (Figure 6) and adipose tissues (Figure 7) of HF-diet-fed rats could be significantly reversed by chitosan supplementation in a dose-dependent manner (HF+CS3, 5, and 7% vs HF, increases of 3.39-, 3.67-, and 4.98-fold in livers, respectively, $p < 0.05$ for all groups; increases of 0.5-, 1.3-, and 1.5-fold in adipose tissues, respectively, $p < 0.05$ for HF+5%CS and HF+7%CS). Supplementation of 7% chitosan in the diet could also significantly attenuate the HF-diet-increased protein expressions of PPARγ (Figures 6 and 7) and SREBP1c (Figures 6 and 7) in livers (HF+CS7% vs HF, decreases of 80 and 25% in

DOI: 10.1021/acs.jafc.5b00198
J. Agric. Food Chem. 2015, 63, 2979−2988

Table 3. Effects of Chitosan on Liver and Adipose Tissue Weights and Plasma Lipid Profile in Sprague−Dawley Rats Fed the Different Experimental Diets for 7 Weeks[a]

	diet				
	ND	HF	HF+3%CS	HF+5%CS	HF+7%CS
relative liver wt (g/100 g BW)	2.5 ± 0.1*	5.3 ± 0.5	4.6 ± 0.5*	4.6 ± 0.5*	3.8 ± 0.3*
rel adipose tissue wt[b] (g/100 g BW)	5.0 ± 1.0	4.4 ± 0.8	4.7 ± 1.2	3.7 ± 0.4	3.6 ± 0.8*
triglyceride (mg/dL)	152.7 ± 33.1*	88.5 ± 28.0	126.1 ± 37.6*	124.0 ± 30.3*	132.1 ± 40.8*
total cholesterol (mg/dL)	92.0 ± 22.2	93.7 ± 12.2	98.8 ± 14.5	96.8 ± 18.1	90.9 ± 26.9

[a]Results are expressed as the mean ± SD for each group (n = 8). (*) $p < 0.05$ versus HF. [b]The adipose tissue weight is the sum of epididymal and perirenal white adipose tissue weight.

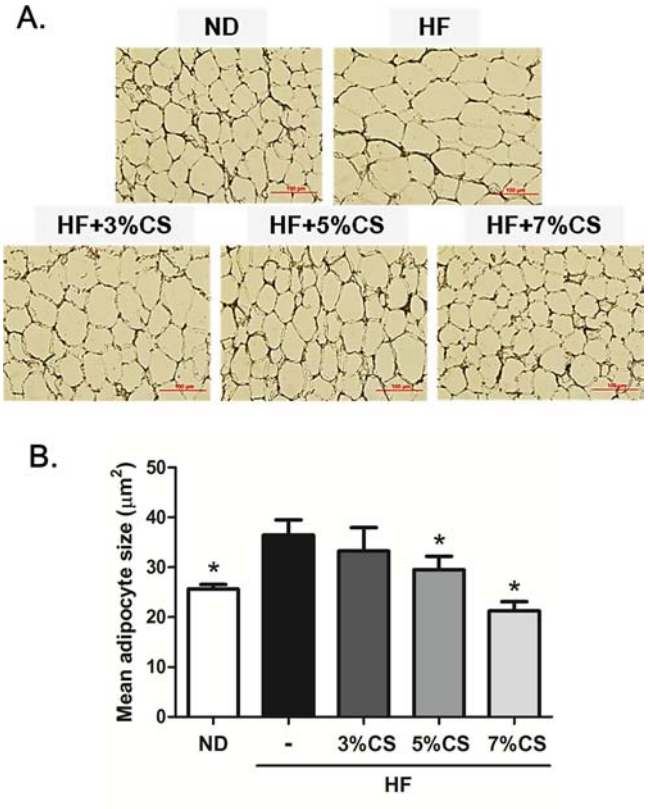

Figure 2. Effects of chitosan on adipocyte morphology of HF-diet-fed rats: (A) histological morphology of adipocytes; (B) mean adipocyte size. Histological analysis of epididymal white adipose tissues isolated from rats fed different experimental diets for 7 weeks is shown. Tissue sections were stained with H&E. Results are expressed as the mean ± SD for each group (n = 3). Scale bar = 100 μm. (*) $p < 0.05$ as compared with HF diet alone group.

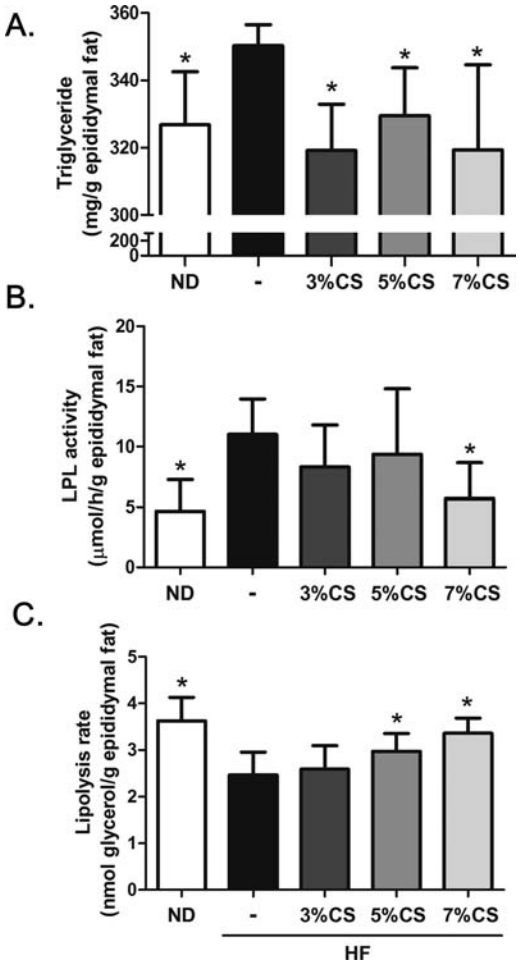

Figure 3. Effects of chitosan on adipose tissue characteristics of HF-diet-fed rats: levels of triglyceride (A), lipoprotein lipase (LPL) activity (B), and lipolysis rate (C) in epididymal white adipose tissues of Sprague−Dawley rats fed different experimental diets for 7 weeks. Results are expressed as the mean ± SD for each group (n = 8). (*) $p < 0.05$ as compared with HF diet alone group.

PPARγ and SREBP1c expressions, respectively, $p < 0.05$) and adipose tissues (HF+CS7% vs HF, decreases of 41 and 74% in PPARγ and SREBP1c expressions, respectively, $p < 0.05$).

Further investigations were carried out to determine the effect of chitosan on lipogenesis-associated gene expressions in livers or epididymal adipose tissues, such as *FAS*, *HMGCR*, *FATP1*, and *FABP4*. As shown in Figure 8, supplementation of 7% chitosan in the diet significantly inhibited the gene expressions in livers (*FAS* and *HMGCR*) (HF+CS7% vs HF, decreases of 67 and 62% in *FAS* and *HMGCR* expressions, respectively, $p < 0.05$; Figure 8A) and in adipose tissues (*FATP1* and *FABP4*) (HF+CS7% vs HF, decreases of 78 and 68% in *FATP1* and *FABP4* expressions, respectively, $p < 0.05$; Figure 8B) of HF diet-fed rats.

DISCUSSION

Chitosan is used as a dietary supplement against obesity because synthetic compounds exhibit some harmful side effects, including dry mouth, constipation, and insomnia.[18,27] Sumiyoshi and Kimura have indicated that low molecular weight chitosan prevents increases in body weights, white adipose tissue weights, and accumulation of liver lipids and enhances the fecal fat excretion in mice fed a HF diet.[28] Liu and colleagues have also shown that chitosan and its two derivatives, *O*-carboxymethyl chitosan and *N*-[(2-hydroxy-3-

DOI: 10.1021/acs.jafc.5b00198
J. Agric. Food Chem. 2015, 63, 2979−2988

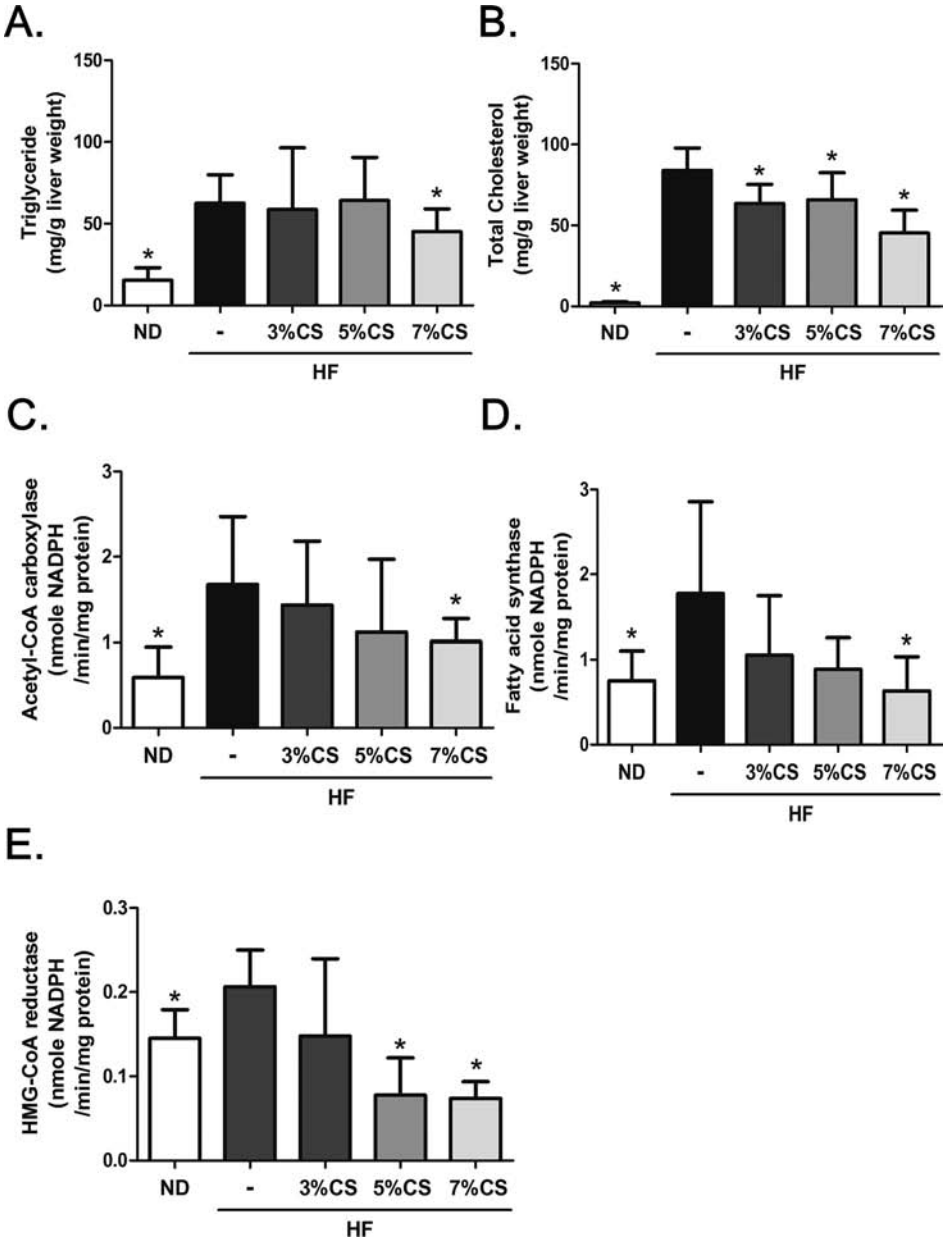

Figure 4. Effects of chitosan on hepatic lipid profile and enzyme activity of lipid biosynthesis in HF-diet-fed rats rats: levels of triglyceride (A), total cholesterol (B), acetyl-CoA carboxylase (C), fatty acid synthase (D), and HMG-CoA reductase (E) in livers of Sprague−Dawley rats fed different experimental diets for 7 weeks. Results are expressed as the mean ± SD for each group (n = 8). (∗) $p < 0.05$ as compared with HF diet alone group.

Table 4. Changes of Fecal Weight, Triglyceride, and Total Cholesterol Concentration in Rats Fed the Different Experimental Diets for 7 Weeks[a]

	diet				
	ND	HF	HF+3%CS	HF+5%CS	HF+7%CS
feces wet wt (g/day)	1.6 ± 0.2*	1.9 ± 0.3	2.1 ± 0.3	2.4 ± 0.3*	2.7 ± 0.7*
feces dry wt (g/day)	1.5 ± 0.2	1.6 ± 0.2	1.8 ± 0.2	2.0 ± 0.2*	2.3 ± 0.5*
triglyceride (mg/g feces)	1.8 ± 0.6*	3.2 ± 1.2	4.9 ± 0.7*	5.2 ± 1.1*	4.7 ± 0.6*
triglyceride (mg/day)	2.6 ± 1.3*	5.0 ± 2.0	8.7 ± 2.0*	10.3 ± 2.9*	10.9 ± 3.2*
total cholesterol (mg/g feces)	3.4 ± 0.7*	14.1 ± 2.7	21.8 ± 2.8*	22.9 ± 2.7*	21.7 ± 1.5*
total cholesterol (mg/day)	4.9 ± 1.2*	22.3 ± 4.5	38.3 ± 5.3*	45.0 ± 8.0*	50.2 ± 12.4*

[a]Results are expressed as the mean ± SD for each group (n = 8). (*) $p < 0.05$ versus HF.

N,*N*-dimethylhexadecylammonium)-propyl] chitosan chloride, decrease the body weights and the levels of TG and free fatty acids and increase fecal lipid excretion in a murine over-nutrition-induced obesity.[29] In the current study, we have shown similar effects of HMW chitosan as the aforementioned studies on the body weight and the level of TG in livers and

DOI: 10.1021/acs.jafc.5b00198
J. Agric. Food Chem. 2015, 63, 2979−2988

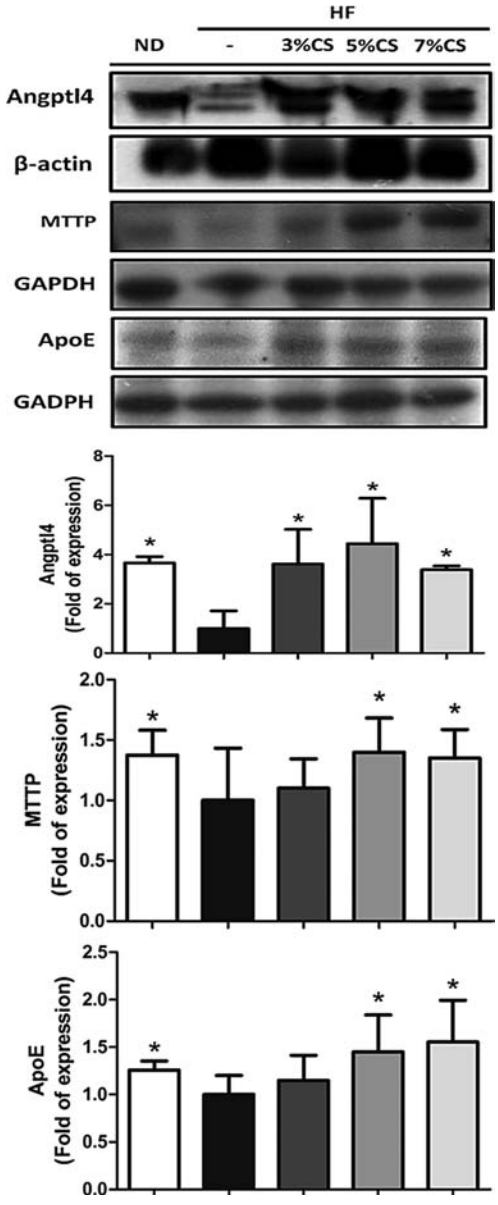

Figure 5. Effects of chitosan on angiopoietin-like protein 4 (Angptl4) expression in the plasma and microsomal triglyceride transfer protein (MTTP) and apolipoprotein E (ApoE) protein expressions in the liver of HF-diet-fed rats. Protein expressions of Angplt4, MTTP, and ApoE were measured by Western blotting. Densitometric analysis for protein levels corrected to each internal control is shown. Results are expressed as the mean ± SD for each group (n = 4−6). (∗) $p < 0.05$ as compared with HF diet alone group.

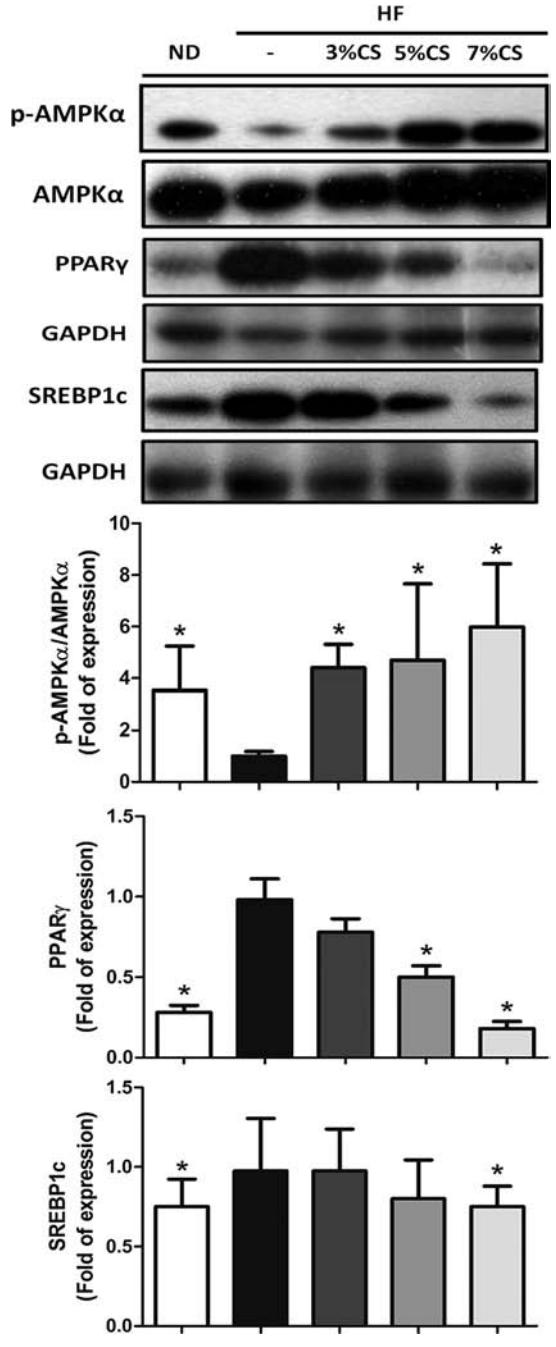

Figure 6. Effects of chitosan on hepatic protein expressions of lipid metabolism of HF-diet-fed rats. Protein expressions of p-AMPKα, PPARγ, and SREBP1c were measured by Western blotting. Densitometric analysis for protein levels corrected to each internal control is shown. Results are expressed as the mean ± SD for each group (n = 4−6). (∗) $p < 0.05$ as compared with the HF diet alone group.

feces of HF-diet-fed rats. Although the association between chitosan and obesity has been well established, the detailed mechanism that links chitosan to lipid-related metabolic changes remains unclear.

Obesity develops due to an imbalance of lipid metabolism. Lipoprotein lipase and lipolysis rate are known to play important roles in TG metabolism. Lipoprotein lipase is an enzyme that hydrolyzes triglycerides of triglyceride-rich lipoproteins (such as very-low-density lipoprotein, VLDL) into nonesterified fatty acids and glycerol.[30] Lipolysis in the adipose tissue is modulated in a stepwise process by adipose triglyceride lipase (ATGL), hormone-sensitive lipase (HSL), and monoacylglycerol lipase (MAGL). The regulation is that ATGL initiates lipolysis by cleaving the fatty acids (FA) from triacylglycerol and then HSL and MAGL react on diacylglycerol and monoacylglycerol to release two additional FAs and one glycerol.[31] However, previous studies have shown that the HF diet dysregulates lipolysis and lipid metabolism, increasing LPL activities and decreasing lipolysis rates in visceral and subcutaneous adipocytes, which may promote adipocyte enlargement by facilitating TG accumulation in adipocytes.[23,32] The results of the present study were in agreement with those

DOI: 10.1021/acs.jafc.5b00198
J. Agric. Food Chem. 2015, 63, 2979−2988

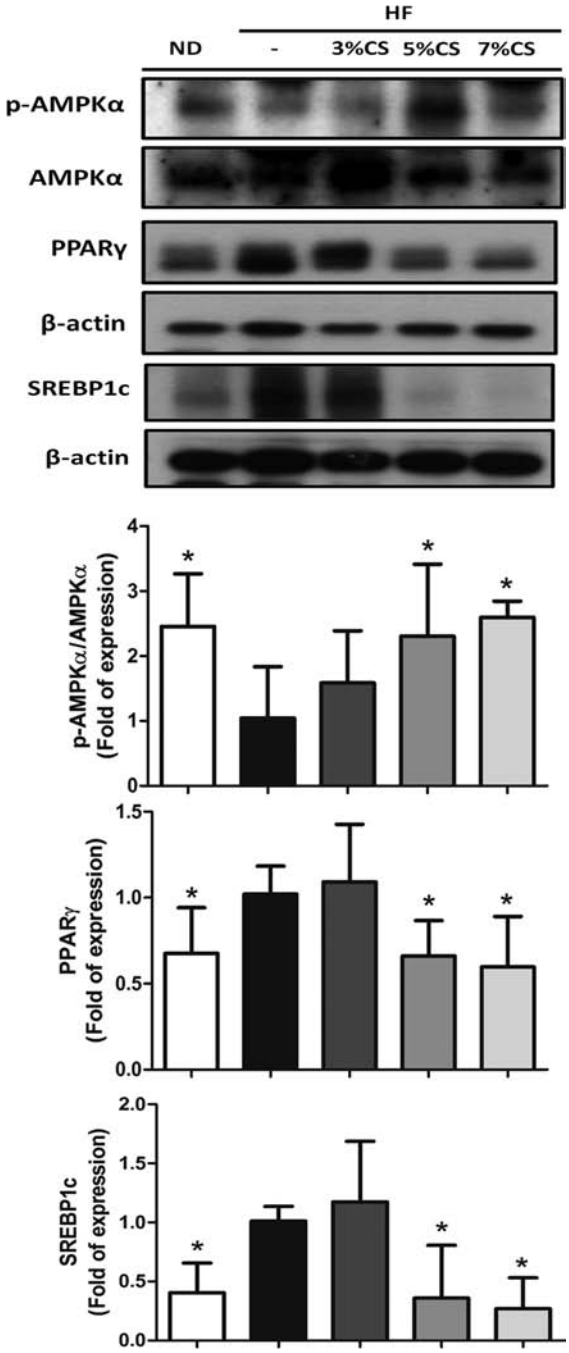

Figure 7. Effects of chitosan on adipose protein expressions of lipid metabolism of HF-diet-fed rats. Protein expressions of p-AMPKα, PPARγ, and SREBP1c were measured by Western blotting. Densitometric analysis for protein levels corrected to each internal control is shown. Results are expressed as the mean ± SD for each group (n = 4–6). (*) $p < 0.05$ as compared with the HF diet alone group.

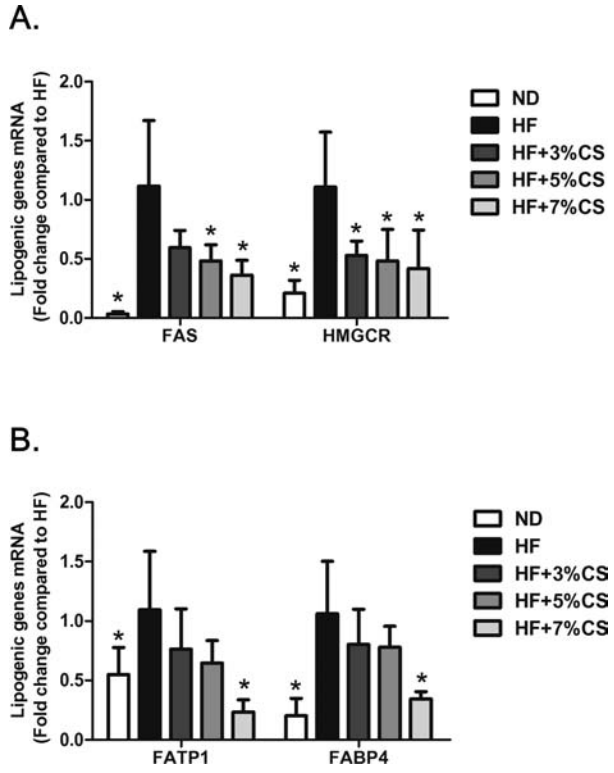

Figure 8. Effects of chitosan on lipogenesis-associated gene expressions in livers and epididymal white adipose tissues of HF-diet-fed rats. Gene expressions of livers (*FAS* and *HMGCR*) (A) and epididymal white adipose tissues (*FATP1* and *FABP4*) (B) were determined by qRT-PCR. Results are expressed as the mean ± SD for each group (n = 6). (*) $p < 0.05$ as compared with the HF diet alone group.

in the foregoing research that HF diet feeding suppressed the rate of lipolysis and elevated LPL activities, which may induce FA entry into adipose tissue, resulting in adipocyte enlargement. In addition, supplementation of 5 and 7% chitosan in the diet significantly reversed the dysregulation of lipid metabolism in HF-diet-fed rats.

In the present study, we found a paradoxically decreased plasma TG in HF-diet-fed rats. A decreased plasma TG has also been reported in HF-diet-fed mice, which may be owing to reduction of dietary carbohydrate.[33,34] Meugnier et al. have also found a significant decreased circulating TG level of lean men with fat overfeeding.[35] We further found that Angptl4, characterized as a suppressor of LPL in the plasma,[36] MTTP, which functioned as a transporter of TG in the liver,[37] and ApoE, acting as a VLDL-TG secretion enhancer in the liver,[38] were down-regulated by HF diet feeding, indicating it might result in TG accumulation in the liver. Administration of chitosan-supplemented diet (5 and 7%) could significantly reverse this phenomenon to the baseline level. These findings suggest that supplementation of chitosan in the diet may improve the altered lipid homeostasis induced by HF diet.

AMPK is a major regulator of cellular energy homeostasis (glucose and lipid metabolism) in the target tissues (liver, adipose tissue, and muscle).[39] AMPK can also phosphorylate and inactivate acetyl-CoA carboxylase (ACC) and HMGCR in the liver, which are the rate-limiting enzymes of fatty acid and sterol synthesis, respectively.[40] Additionally, AMPK is capable of down-regulating lipogenic transcription factor SREBPs, which regulates the lipogenesis-associated genes, including *FATP*, *FABP*, *FAS*, *ACC*, and *HMGCR*.[41,42] Moreover, PPARγ is known to be a key positive regulator of adipogenesis and TG storage in adipocyte. It has been demonstrated that AMPK exerts antiadiposity activity through the suppression of PPARγ in adipose tissue.[43] In the present study, we found that HF diet feeding inactivated the protein expression of AMPK and promoted the protein expressions of PPARγ and SREBP and the lipogenesis-associated gene expressions in the liver and adipose tissue. The significant increase of lipogenic tran-

DOI: 10.1021/acs.jafc.5b00198
J. Agric. Food Chem. 2015, 63, 2979–2988

scription factors and lipogenesis-associated genes results in promoting lipid synthesis in the liver and the abnormal accumulation of fat in the liver, which may refer to the fatty liver. Recent studies have suggested that the derivatives of chitin and chitosan (carboxymethyl chitin and chitosan oligosaccharides) exert the antiobesity effect on blocking lipid accumulation and inhibition of adipocyte differentiation via AMPK activation in 3T3-L1 adipocytes.[44,45] We further found that administration of a chitosan-supplemented diet, especially supplementation of 7% chitosan, was resistant to HF-diet-induced obesity and fat accumulation in the liver accompanying AMPK activation and suppressive expression of lipogenic transcription factors and lipogenesis-associated genes. On the other hand, leptin is an adipocyte-secreted hormone in proportion to white adipose mass. Obesity is known to be characterized by leptin resistance. Leptin is capable of stimulating the fatty acid oxidation via AMPK activation, which prevents lipid accumulation in nonadipose tissues.[43] Our previous study has found that chitosan can induce leptin secretion, which triggers the inhibition of liver gluconeogenesis via AMPK activation in streptozotocin-induced diabetic rats.[14] Therefore, chitosan reversed the inhibition of HF diet on AMPK activity through the induction of leptin secretion. In general, it would be reasonable to assume that AMPK is necessary for inhibition of lipogenic transcription factors and downstream target lipogenic genes in the liver and adipose tissue. Chitosan can serve as an antiobesity functional food for control of lipid accumulation in the liver and the adipose tissue via AMPK activation.

In the present study, we found that the abdominal (epididymal and perinephrial) adipose tissue weights and blood TC levels were not changed, but TG exhibited a decreased level in HF-diet-fed (15% lard + 0.5% cholesterol) rats for 11 weeks as compared to the ND-fed rats. Takeuchi et al. have shown that the weights of abdominal (epididymal, perinephrial, and mesenteric) adipose tissue in rats are not affected by feeding a lard fat-containing (20% lard) diet for 12 weeks as compared with dietary vegetable oils.[46] Bronkowska et al. have found that the blood level of TC, but not TG, in rats fed a lard-containing diet (15% lard + 1% cholesterol) for 28 days is higher than in rats receiving the diet containing vegetable oil.[47] However, Li et al. have shown that the blood TG contents in rats fed a HF diet (10% lard + 1% cholesterol) are higher than those of rats receiving ND on day 6, but the TG contents drop to a statistically significant level lower than ND-fed rats on day 42.[48] Moreover, Águila et al. have found that the serum TC levels are not changed, but serum TG levels are significantly decreased in rats long-term (45 weeks) fed a HF diet (29% lipids—lard + egg yolk) as compared with rats fed a soybean oil-containing diet.[49] These previous and our findings indicate that the different experimental conditions or parameters for HF diet may affect the changes in blood lipid profile in experimental animals.

During obesity, there is an increase in adipocyte size by abnormal TG accumulation, which is not only associated with FA biosynthesis but also with the regulation of FA fluxes, including fatty acid transport proteins (FATPs) and fatty acid binding proteins (FABPs).[3,50] The putative mechanism of lipogenesis in adipocytes during obesity is that excess insulin activated LPL located on the cell surface of vascular endothelium, and activated LPL removes FA from chylomicron and VLDL into adipocytes through fatty acid transporters, such as FABP and FATP. FA is subsequently esterified into triglycerides, leading to adipocyte hypertrophy.[51] FATP1, the first member of FA transport proteins, is mostly expressed in adipose tissue and also present in muscle. It is reported that mice with whole body deletion of FATP1 (*fatp1*−/−) are protected from HF-diet-induced obesity and insulin resistance.[52] Once FAs have crossed the membrane, they are transported by FATPs and bound by cytoplasmic FABPs. FABP4 is highly expressed in adipose tissue and also one of the most abundant proteins in mature adipocytes.[53] Several studies have shown that deficiency of FABP4 expression protects mice from dietary or genetic obesity-induced metabolic syndrome, such as hypercholesterolemia, insulin resistance, and atherosclerosis.[54−56] In the present study, we found that supplementation of chitosan in the diet significantly decreased the mRNA expression of *FATP1* and *FABP4* in epididymal adipose tissues and alleviated the levels of TG in epididymal adipose tissues. It is therefore plausible that chitosan attenuated adipocyte hypertrophy via inhibiting FA synthesis and uptake. On the basis of evidence presented in this study, we conclude that a postulated mechanism for the lipid regulation of chitosan is that chitosan activates AMPK phosphorylation and sequentially suppresses downstream expression of lipogenic transcription factors and lipogenesis-associated genes, which can attenuate TG accumulation and lipid biosynthesis in the liver and adipose tissues.

AUTHOR INFORMATION

Corresponding Authors

*(S.-H.L.) Mail: Institute of Toxicology, College of Medicine, National Taiwan University, No. 1, Section 1, Jen-Ai Road, Taipei 10051, Taiwan. Phone: 886-2-23123456, ext. 88605. Fax: 886-2-23410217. E-mail: shinghwaliu@ntu.edu.tw.

*(M.-T.C.) Phone: +886-2-24622192, ext. 5117/5118. Fax: +886-2-24634203. E-mail: a0071@mail.ntou.edu.tw.

Funding

This study was supported by a grant from the National Science Council of Taiwan (NSC103-2313-B-019-001-MY3).

Notes

The authors declare no competing financial interest.

ABBREVIATIONS USED

ACC, acetyl-CoA carboxylase; AMPK, AMP-activated protein kinase; CS, chitosan; FA, fatty acid; FABPs, fatty-acid-binding proteins; FAS, fatty acid synthase; FATPs, fatty acid transport proteins; HF, high fat; HMW, high molecular weight; HMG-CoA, 3-hydroxy-3-methylglutaryl coenzyme A; HMGCR, HMG-CoA reductase; LPL, lipoprotein lipase; ND, standard rodent diet with 5% cellulose; PPARγ, peroxisome proliferator-activated receptor-gamma; SREBPs, sterol regulatory element binding proteins; TC, total cholesterol; TG, triglyceride

REFERENCES

(1) World Health Organization (WHO). Obesity and overweight, 2014; http://www.who.int/mediacentre/factsheets/fs311/en/.

(2) Mokdad, A. H.; Ford, E. S.; Bowman, B. A.; Dietz, W. H.; Vinicor, F.; Bales, V. S.; Marks, J. S. Prevalence of obesity, diabetes, and obesity-related health risk factors, 2001. *JAMA, J. Am. Med. Assoc.* **2003**, *289* (1), 76−79.

(3) Ouchi, N.; Parker, J. L.; Lugus, J. J.; Walsh, K. Adipokines in inflammation and metabolic disease. *Nat. Rev. Immunol.* **2011**, *11* (2), 85−97.

(4) Jung, U. J.; Choi, M. S. Obesity and its metabolic complications: the role of adipokines and the relationship between obesity,

DOI: 10.1021/acs.jafc.5b00198
J. Agric. Food Chem. 2015, 63, 2979−2988

inflammation, insulin resistance, dyslipidemia and nonalcoholic fatty liver disease. *Int. J. Mol. Sci.* **2014**, *15* (4), 6184−223.
(5) Grummer, R. R. Etiology of lipid-related metabolic disorders in periparturient dairy cows. *J. Dairy Sci.* **1993**, *76* (12), 3882−3896.
(6) Rahman, A.; Kumar, S. G.; Yun, J. W. Proteome analysis in adipose tissue of ob/ob mice in response to chitosan oligosaccharides treatment. *Biotechnol. Bioprocess. Eng.* **2010**, *15*, 559−571.
(7) Lai, Y. S.; Chen, W. C.; Ho, C. T.; Lu, K. H.; Lin, S. H.; Tseng, H. C.; Lin, S. Y.; Sheen, L. Y. Garlic essential oil protects against obesity-triggered nonalcoholic fatty liver disease through modulation of lipid metabolism and oxidative stress. *J. Agric. Food Chem.* **2014**, *62* (25), 5897−5906.
(8) Deuchi, K.; Kanauchi, O.; Imasato, Y.; Kobayashi, E. Effect of the viscosity or deacetylation degree of chitosan on fecal fat excreted from rats fed on a high fat diet. *Biosci., Biotechnol., Biochem.* **1995**, *59*, 781−785.
(9) Chen, J. K.; Yeh, C. H.; Wang, L. C.; Liou, T. H.; Shen, C. R.; Liu, C. L. Chitosan, the marine functional food, is a potent adsorbent of humic acid. *Mar. Drugs* **2011**, *9* (12), 2488−2498.
(10) Shahidi, F.; Abuzaytoun, R. Chitin, chitosan, and co-products: chemistry, production, applications, and health effects. *Adv. Food Nutr. Res.* **2005**, *49*, 93−135.
(11) Yao, H. T.; Chiang, M. T. Effect of chitosan on plasma lipids, hepatic lipids, and fecal bile acid in hamsters. *J. Food Drug Anal.* **2006**, *14*, 183−189.
(12) Gallaher, D. D.; Gallaher, C. M.; Mahrt, G. J.; Carr, T. P.; Hollingshead, C. H.; Hesslink, R., Jr.; Wise, J. A glucomannan and chitosan fiber supplement decreases plasma cholesterol and increases cholesterol excretion in overweight normocholesterolemic humans. *J. Am. Coll. Nutr.* **2002**, *21* (5), 428−433.
(13) Hsieh, Y. L.; Yao, H. T.; Cheng, R. S.; Chiang, M. T. Chitosan reduces plasma adipocytokines and lipid accumulation in liver and adipose tissues and ameliorates insulin resistance in diabetic rats. *J. Med. Food* **2012**, *15* (5), 453−460.
(14) Liu, S. H.; Chang, Y. H.; Chiang, M. T. Chitosan reduces gluconeogenesis and increases glucose uptake in skeletal muscle in streptozotocin-induced diabetic rats. *J. Agric. Food Chem.* **2010**, *58* (9), 5795−800.
(15) Yuan, H. D.; Piao, G. C. An active part of *Artemisia sacrorum* Ledeb inhibits adipogenesis via the AMPK signaling pathway in 3T3-L1 adipocytes. *Int. J. Mol. Med.* **2011**, *27* (4), 531−536.
(16) Lim, C. T.; Kola, B.; Korbonits, M. AMPK as a mediator of hormonal signalling. *J. Mol. Endocrinol.* **2010**, *44* (2), 87−97.
(17) Jeong, K. J.; Kim, G. W.; Chung, S. H. AMP-activated protein kinase: an emerging target for ginseng. *J. Ginseng Res.* **2014**, *38* (2), 83−88.
(18) Bray, G. A. A concise review on the therapeutics of obesity. *Nutrition* **2000**, *16* (10), 953−960.
(19) Carlson, S. E.; Goldfarb, S. A sensitive enzymatic method for determination of free and esterified tissue cholesterol. *Clin. Chim. Acta* **1977**, *79* (3), 575−582.
(20) Nepokroeff, C. M.; Lakshmanan, M. R.; Porter, J. W. Fatty-acid synthase from rat liver. *Methods Enzymol.* **1975**, *35*, 37−44.
(21) Mohan, S. B.; Kekwick, R. G. Acetyl-coenzyme A carboxylase from avocado (*Persea americana*) plastids and spinach (*Spinacia oleracea*) chloroplasts. *Biochem. J.* **1980**, *187* (3), 667−676.
(22) Edwards, P. A.; Lemongello, D.; Kane, J.; Shechter, I.; Fogelman, A. M. Properties of purified rat hepatic 3-hydroxy-3-methylglutaryl coenzyme A reductase and regulation of enzyme activity. *J. Biol. Chem.* **1980**, *255* (8), 3715−3725.
(23) Kusunoki, M.; Hara, T.; Tsutsumi, K.; Nakamura, T.; Miyata, T.; Sakakibara, F.; Sakamoto, S.; Ogawa, H.; Nakaya, Y.; Storlien, L. H. The lipoprotein lipase activator, NO-1886, suppresses fat accumulation and insulin resistance in rats fed a high-fat diet. *Diabetologia* **2000**, *43* (7), 875−880.
(24) Shindo, N.; Fujisawa, T.; Sugimoto, K.; Nojima, K.; Oze-Fukai, A.; Yoshikawa, Y.; Wang, X.; Yasuda, O.; Ikegami, H.; Rakugi, H. Involvement of microsomal triglyceride transfer protein in non-alcoholic steatohepatitis in novel spontaneous mouse model. *J. Hepatol.* **2010**, *52* (6), 903−912.
(25) Oike, Y.; Akao, M.; Kubota, Y.; Suda, T. Angiopoietin-like proteins: potential new targets for metabolic syndrome therapy. *Trends Mol. Med.* **2005**, *11* (10), 473−479.
(26) Maugeais, C.; Tietge, U. J.; Tsukamoto, K.; Glick, J. M.; Rader, D. J. Hepatic apolipoprotein E expression promotes very low density lipoprotein-apolipoprotein B production in vivo in mice. *J. Lipid Res.* **2000**, *41* (10), 1673−1679.
(27) Walsh, A. M.; Sweeney, T.; Bahar, B.; O'Doherty, J. V. Multi-functional roles of chitosan as a potential protective agent against obesity. *PLoS One* **2013**, *8* (1), No. e53828.
(28) Sumiyoshi, M.; Kimura, Y. Low molecular weight chitosan inhibits obesity induced by feeding a high-fat diet long-term in mice. *J. Pharm. Pharmacol.* **2006**, *58* (2), 201−207.
(29) Liu, X.; Zhi, X.; Liu, Y.; Wu, B.; Sun, Z.; Shen, J. Effect of chitosan, *O*-carboxymethyl chitosan, and *N*-[(2-hydroxy-3-*N*,*N*-dimethylhexadecyl ammonium)propyl] chitosan chloride on over-weight and insulin resistance in a murine diet-induced obesity. *J. Agric. Food Chem.* **2012**, *60* (13), 3471−3476.
(30) Roberts, C. K.; Barnard, R. J.; Liang, K. H.; Vaziri, N. D. Effect of diet on adipose tissue and skeletal muscle VLDL receptor and LPL: implications for obesity and hyperlipidemia. *Atherosclerosis* **2002**, *161* (1), 133−141.
(31) Lafontan, M.; Langin, D. Lipolysis and lipid mobilization in human adipose tissue. *Prog. Lipid Res.* **2009**, *48* (5), 275−297.
(32) Gaidhu, M. P.; Anthony, N. M.; Patel, P.; Hawke, T. J.; Ceddia, R. B. Dysregulation of lipolysis and lipid metabolism in visceral and subcutaneous adipocytes by high-fat diet: role of ATGL, HSL, and AMPK. *Am. J. Physiol. Cell Physiol.* **2010**, *298* (4), C961−C971.
(33) Guo, J.; Jou, W.; Gavrilova, O.; Hall, K. D. Persistent diet-induced obesity in male C57BL/6 mice resulting from temporary obesigenic diets. *PLoS One* **2009**, *4* (4), No. e5370.
(34) Biddinger, S. B.; Almind, K.; Miyazaki, M.; Kokkotou, E.; Ntambi, J. M.; Kahn, C. R. Effects of diet and genetic background on sterol regulatory element-binding protein-1c, stearoyl-CoA desaturase 1, and the development of the metabolic syndrome. *Diabetes* **2005**, *54* (5), 1314−1323.
(35) Meugnier, E.; Bossu, C.; Oliel, M.; Jeanne, S.; Michaut, A.; Sothier, M.; Brozek, J.; Rome, S.; Laville, M.; Vidal, H. Changes in gene expression in skeletal muscle in response to fat overfeeding in lean men. *Obesity (Silver Spring)* **2007**, *15* (11), 2583−2594.
(36) Shan, L.; Yu, X. C.; Liu, Z.; Hu, Y.; Sturgis, L. T.; Miranda, M. L.; Liu, Q. The angiopoietin-like proteins ANGPTL3 and ANGPTL4 inhibit lipoprotein lipase activity through distinct mechanisms. *J. Biol. Chem.* **2009**, *284* (3), 1419−1424.
(37) Jamil, H.; Gordon, D. A.; Eustice, D. C.; Brooks, C. M.; Dickson, J. K., Jr.; Chen, Y.; Ricci, B.; Chu, C. H.; Harrity, T. W.; Ciosek, C. P., Jr.; Biller, S. A.; Gregg, R. E.; Wetterau, J. R. An inhibitor of the microsomal triglyceride transfer protein inhibits apoB secretion from HepG2 cells. *Proc. Natl. Acad. Sci. U.S.A.* **1996**, *93* (21), 11991−11995.
(38) Kuipers, F.; Jong, M. C.; Lin, Y.; Eck, M.; Havinga, R.; Bloks, V.; Verkade, H. J.; Hofker, M. H.; Moshage, H.; Berkel, T. J.; Vonk, R. J.; Havekes, L. M. Impaired secretion of very low density lipoprotein-triglycerides by apolipoprotein E-deficient mouse hepatocytes. *J. Clin. Invest.* **1997**, *100* (11), 2915−2922.
(39) Hardie, D. G. The AMP-activated protein kinase pathway − new players upstream and downstream. *J. Cell Sci.* **2004**, *117* (Pt 23), 5479−5487.
(40) Clarke, P. R.; Hardie, D. G. Regulation of HMG-CoA reductase: identification of the site phosphorylated by the AMP-activated protein kinase in vitro and in intact rat liver. *EMBO J.* **1990**, *9* (8), 2439−2446.
(41) Srivastava, R. A.; Pinkosky, S. L.; Filippov, S.; Hanselman, J. C.; Cramer, C. T.; Newton, R. S. AMP-activated protein kinase: an emerging drug target to regulate imbalances in lipid and carbohydrate metabolism to treat cardio-metabolic diseases. *J. Lipid Res.* **2012**, *53* (12), 2490−2514.

DOI: 10.1021/acs.jafc.5b00198
J. Agric. Food Chem. 2015, 63, 2979−2988

(42) Oikari, S.; Ahtialansaari, T.; Heinonen, M. V.; Mauriala, T.; Auriola, S.; Kiehne, K.; Fölsch, U. R.; Jänne, J.; Alhonen, L.; Herzig, K. H. Downregulation of PPARs and SREBP by acyl-CoA-binding protein overexpression in transgenic rats. *Pfluegers Arch.* **2008**, *456* (2), 369−377.
(43) Sugden, M. C.; Warlow, M. P.; Holness, M. J. The involvement of PPARs in the causes, consequences and mechanisms for correction of cardiac lipotoxicity and oxidative stress. *Curr. Mol. Pharmacol.* **2012**, *5*, 224−240.
(44) Kong, C. S.; Kim, J. A.; Bak, S. S.; Byun, H. G.; Kim, S. K. Anti-obesity effect of carboxymethyl chitin by AMPK and aquaporin-7 pathways in 3T3-L1 adipocytes. *J. Nutr. Biochem.* **2011**, *22* (3), 276−281.
(45) Rahman, A.; Kumar, S. G.; Kim, S. W.; Hwang, H. J.; Baek, Y. M.; Lee, S. H.; Hwang, H. S.; Shon, Y. H.; Nam, K. S.; Yun, J. W. Proteomic analysis for inhibitory effect of chitosan oligosaccharides on 3T3-L1 adipocyte differentiation. *Proteomics* **2008**, *8* (3), 569−581.
(46) Takeuchi, H.; Matsuo, T.; Tokuyama, K.; Shimomura, Y.; Suzuki, M. Diet-induced thermogenesis is lower in rats fed a lard diet than in those fed a high oleic acid safflower oil diet, a safflower oil diet or a linseed oil diet. *J. Nutr.* **1995**, *125* (4), 920−925.
(47) Bronkowska, M.; Orzeł, D.; Łoźna, K.; Styczyńska, M.; Biernat, J.; Gryszkin, A.; Zieba, T.; Kapelko, M. Effect of resistant starch RS4 added to the high-fat diets on selected biochemical parameters in Wistar rats. *Rocz. Panstw. Zakl. Hig.* **2013**, *64* (1), 19−24.
(48) Li, N.; Chen, Z.; Mao, X.; Yu, J.; Zhao, R. Effects of lipid regulation using raw and processed radix polygoni multiflori in rats fed a high-fat diet. *Evidence-Based Complement. Alternat. Med.* **2012**, *2012*, 329171.
(49) Aguila, M. B.; Loureiro, C. C.; Pinheiro, A. D. R.; Mandarim-De-Lacerda, C. A. Lipid metabolism in rats fed diets containing different types of lipids. *Arq. Bras. Cardiol.* **2002**, *78* (1), 25−38.
(50) Westerbacka, J.; Kolak, M.; Kiviluoto, T.; Arkkila, P.; Sirén, J.; Hamsten, A.; Fisher, R. M.; Yki-Järvinen, H. Genes involved in fatty acid partitioning and binding, lipolysis, monocyte/macrophage recruitment, and inflammation are overexpressed in the human fatty liver of insulin-resistant subjects. *Diabetes* **2007**, *56* (11), 2759−2765.
(51) Maeda, N.; Funahashi, T.; Shimomura, I. Metabolic impact of adipose and hepatic glycerol channels aquaporin 7 and aquaporin 9. *Nat. Clin. Pract. Endocrinol. Metab.* **2008**, *4* (11), 627−634.
(52) Wu, Q.; Ortegon, A. M.; Tsang, B.; Doege, H.; Feingold, K. R.; Stahl, A. FATP1 is an insulin-sensitive fatty acid transporter involved in diet-induced obesity. *Mol. Cell. Biol.* **2006**, *26* (9), 3455−3467.
(53) Maeda, K.; Cao, H.; Kono, K.; Gorgun, C. Z.; Furuhashi, M.; Uysal, K. T.; Cao, Q.; Atsumi, G.; Malone, H.; Krishnan, B.; Minokoshi, Y.; Kahn, B. B.; Parker, R. A.; Hotamisligil, G. S. Adipocyte/macrophage fatty acid binding proteins control integrated metabolic responses in obesity and diabetes. *Cell Metab.* **2005**, *1* (2), 107−119.
(54) Hotamisligil, G. S.; Johnson, R. S.; Distel, R. J.; Ellis, R.; Papaioannou, V. E.; Spiegelman, B. M. Uncoupling of obesity from insulin resistance through a targeted mutation in aP2, the adipocyte fatty acid binding protein. *Science* **1996**, *274* (5291), 1377−1379.
(55) Boord, J. B.; Maeda, K.; Makowski, L.; Babaev, V. R.; Fazio, S.; Linton, M. F.; Hotamisligil, G. S. Adipocyte fatty acid-binding protein, aP2, alters late atherosclerotic lesion formation in severe hypercholesterolemia. *Arterioscler. Thromb. Vasc. Biol.* **2002**, *22* (10), 1686−1691.
(56) Perrella, M. A.; Pellacani, A.; Layne, M. D.; Patel, A.; Zhao, D.; Schreiber, B. M.; Storch, J.; Feinberg, M. W.; Hsieh, C. M.; Haber, E.; Lee, M. E. Absence of adipocyte fatty acid binding protein prevents the development of accelerated atherosclerosis in hypercholesterolemic mice. *FASEB J.* **2001**, *15* (10), 1774−1776.

DOI: 10.1021/acs.jafc.5b00198
J. Agric. Food Chem. 2015, 63, 2979−2988

inflammatory[15,16] and anticarcinogenic properties.[17] In this context, the consumption of fruit pomaces or extracts produced from them ensures exhaustive utilization of the biological potential of the harvested fruits.

The main component of strawberry ellagitannins is dimeric GOG type agrimoniin built of two monomeric units of α-1-*O*-galloyl-2,3:4,6-bis-HHDP-D-glucose that are linked by two residues of gallic acid with a C−O−C bond.[10,18] In turn, raspberries contain sanguiin-H-6 and lambertianin-C,[19] the monomeric units that are linked with a sanguiinsorboyl group.[18] This difference in the structure of ellagitannins may affect the physiological effect of polyphenols of Rosaceae family fruits as well as byproducts of fruit processing and seeds used for oil production. It is a novel product so far little recognized in terms of composition and physiological properties.

In the context of the above overview of the literature, the goal of this study was to enrich knowledge about the chemical composition of interesting and rich in dietary fiber ellagitannins, byproducts of fat carbon dioxide supercritical extraction of strawberry and raspberry seeds, and to identify the local and systemic physiological effects of such products on intestinal functions, blood glucose level, and selected blood markers of lipid metabolism of experimental rats.

MATERIALS AND METHODS

Recovery of Seeds and Their Defatting Using SFE. Strawberry and raspberry seeds after removal of oils by CO_2 supercritical extraction constituted research material. Seeds were separated from industrial residues of juice production. Seeds (300 g) were crushed in a roller crusher in a CO_2 atmosphere to the particle size of 0.4−0.6 mm and immediately placed in a supercritical extractor. The plant (NCSI) was composed of the extractor with 1 dm^3 volume, two separators with separation capacity up to 500 bar (S_1) and up to 100 bar (S_2), circulating pump, condenser, and CO_2 tank. The following conditions were used: extraction pressure, 200, 250 bar; I grade separation level pressure, 53 bar; temperature of the inlet, T_w, 40 °C; mass of raw material, 300 g; flow rate, Q_{CO_2}, 6.0−7.0 kg (one cycle duration = 180−210 min).

Analyses of Preparations. *Basic Composition.* AOAC methods[20] were used: dry matter and ash, 940.26; protein, 920.152; crude fat, 930.09; TDF, 985.29; IDF, 991.42.

Polyphenols. Extraction of polyphenols was carried out according to the method in ref 1 using 70% acetone. To 500 mg of the material was added 4 mL of a solvent, which was mixed, sonified for 15 min, and centrifuged at 800 rad/s, and the solution was decanted. The procedure was repeated twice. The solutions were combined, and the acetone was evaporated by the use of a vacuum rotary evaporator. Residue was dissolved in 2 mL of 70% glycerol and analyzed with HPLC.

Sum of Ellagitannins (ET). The released ellagic acid (EA) was computed from the difference between the contents of total and free EA. The total ET, expressed per monomer α-1-*O*-galloyl-2,3:4,6-bis-HHDP-D-glucose, was calculated by multiplying the content of released EA by a conversion factor of 1.55, which takes into account the molar content of EA in α-1-*O*-galloyl-2,3:4,6-bis-HHDP-D-glucose, a monomer unit of agrimoniin.[1] Half a milliliter of a 70% glycerin solution and 0.075 mL of trifluoroacetic acid (Fluka) were added to 0.15 g of the sample. The components were mixed and kept at a temperature of 95 °C for 18 h. After hydrolysis, the samples were filled to 5 mL with methanol, filtered through syringe Teflon filters with a pore size of 0.45 μm (Millipore, Bedford, MA, USA), and analyzed with HPLC.

Polyphenol HPLC Analysis. A Smartline (Knauer, Berlin, Germany) chromatograph with a PDA detector was used. A Phenomenex Gemini 5u C18 110a (250 × 4.60 mm; 5 μm) column was kept at 35 °C. Eluent A contained 0.05% phosphoric acid in water, and eluent B contained 0.05% phosphoric acid in 80% (v/v) acetonitrile in water. Flow rate was 1.25 mL/min. Gradient was as follows: 0−5 min, 4% B; 5−12.5 min, 4−15% B; 12.5−42.5 min, 15−40% B; 42.5−51.8 min, 40−50% B; 51.8−53.4 min, 50−55% B; and 53.4−55 min, 4% B. The volume of injection was 20 μL. Detection conditions were as follows: 280 nm (agrimoniin, sanguiin-H-6, and lambertianin-C); 360 nm (ellagic acid, quercetin and kaempferol glycosides, quercetin, and kaempferol); 520 nm (anthocyanins). Standards used were ellagic acid, quercetin-3-*O*-glucoside, kaempferol-3-*O*-glucoside, quercetin, kaempferol, pelargonidin-3-*O*-glucoside, cyanidin-3-*O*-glucoside, kaempferol-3-*O*-β-D-(6″-*E*-*p*-coumaroyl)-glucopyranoside (Extrasynthese, Genay, France), agrimoniin, sanguiin-H-6, and lambertianin-C (see below).

Extraction and Purification of Agrimoniin, Sanguiin-H-6, and Lambertianin-C. The extraction of agrimoniin was carried out from strawberry pomace and that of sanguiin-H-6 and lambertianin-C from raspberry pomace before the separation of seeds, with 70% acetone. One hundred grams of pomace was treated with the solvent at a 1:14 weight ratio and left to macerate for 24 h. The solution was filtered through a filter paper, and acetone was evaporated by vacuum. The solution was loaded onto an Amberlite XAD-1600N column (8 cm × 2 cm), which was rinsed with 25 mL of water and eluted with 50 mL of 60% ethanol. Purified 10 mL fractions were collected. Isolation of ETs was carried by the use of a Knauer chromatograph, composed of two pumps (Knauer K-501), a Phenomenex Luna 10u C18 100a (250 × 21, 20 mm; 10 μm) (Torrance, CA, USA) column, a UV−vis detector, and a Foxy R1 Teledyne ISCO (Lincoln, NE, USA) fraction collector.[7] The flow rate was 15 mL/min. Eluent A was 0.1% formic acid in water, and eluent B was 80% methanol. Gradient was as follows: 0−3 min, 20% B; 3−20 min, 20−35% B; 20−45 min, 35−70% B; 45−50 min, 70% B; 50−55 min, 70−20% B; and 55−60 min, 20% B. The volume of injection was 500 μL. Detection parameter was 280 nm. Agrimoniin, sanguiin-H-6, and lambertianin-C peaks were collected from 10 separations, then combined; methanol was removed by distillation, and the preparations were freeze-dried. The purity of agrimoniin at 280 nm was 96%, that of sanguiin-H-6, 92.5%, and that of lambertianin-C, 92.1%.

The molecular masses of agrimoniin, sanguiin-H-6, and lambertianin-C were confirmed by ESI-MS/MS detector. Water solution of the substance was directly injected into the MS detector (lCQ DECa, Thermo-Finnigan). The negative ion mode was used. The source parameters were as follows: ion spray voltage, 3.00 kV; capillary temperature, 325 °C; sheath gas and auxiliary gas, 30 and 10 units/min, respectively. To generate MS/MS data, the precursor ions were fragmented by helium gas collision in the ion trap by optimizing the collision energy to obtain an intensity of the precursor ion close to 10% of the relative scale of the spectrum.[18]

The main pseudomolecular ion [M − H] of agrimoniin H-6 was observed at 1869 (m/z), and the analysis of decomposition showed the presence of 1567, 1265, 935, 633, and 301 (m/z) fragment ions. The main pseudomolecular ion [M − H] of sanguiin-H-6 was observed at 1869 (m/z), and the analysis of decomposition showed the presence of 1235, 935, 933, 633, and 301 (m/z) fragment ions. The main pseudomolecular ion [M − H] of lambertianin-C was observed at 1401 $[M - 2H]^2$ (m/z), and the analysis of decomposition showed the presence of 1869, 1567, 1265, 1103, 933, 631, and 301 (m/z) fragment ions.

Proanthocyanidins and Free Catechins. Proanthocyanidin degradation in an acidic environment with an overdose of phloroglucinol was performed as in ref 21. To 20 mg of a sample was added 800 μL of a methanol solution containing phloroglucinol (75 g/L) and ascorbic acid (15 g/L). Phloroglucinolysis was started by adding 400 μL of 0.2 mol/L hydrochloric acid in methanol and was carried out for 30 min at the temperature of 50 °C and then stopped by adding 600 μL of a 40 mmol/L sodium acetate solution in an ice bath. The samples were centrifuged for 5 min at 500 rad/s and diluted with a 40 mmol/L sodium acetate solution. A Knauer Smartline chromatograph with a fluorescence detector (FD) RF-10AXL (Shimadzu, Tokyo, Japan) and a Phenomenex Gemini 5u C18 110a (250 × 4.60 mm; 5 μm) column was used. The gradient was as follows: 0−10 min, 4−7% B; 10−27 min, 7−30% B; 27−29 min, 30−70% B; 29−34 min, 70% B; 34−35 min, 70−4% B; and 35−40 min, 4% B. Phase A consisted of a 2.5%

DOI: 10.1021/acs.jafc.5b00648
J. Agric. Food Chem. 2015, 63, 2989−2996

water solution (v/v) of acetic acid, and phase B consisted of 80% (v/v) acetonitrile in water. The flow rate was 1 mL/min, and the temperature was 25 °C. The identification was conducted on the basis of the retention times of standards of (−)-epicatechin, (+)-catechin, (−)-epicatechin-phloroglucinol, and (+)-catechin-phloroglucinol. Quantitative analyses of released flavonols, namely, (+)-catechin and (−)-epicatechin, and phloroglucinol adducts were conducted on the basis of chromatograms recorded with the FD set at 278 nm excitation wavelength and 360 nm emission wavelength.

The mean degree of polymerization was determined on the basis of the molar ratio of all flavan-3-ol units, that is, adducts of phloroglucinol and terminal units to the sum of terminal units, which included (+)-catechin and (−)-epicatechin.

All of the analyses were performed in duplicate.

In Vivo Experiments. *Animals and Diets.* Experiments were conducted on 24 Wistar strain rats following the protocol approved by the Local Ethical Commission for Experiments on Animals in Olsztyn (permission no. 71/2012). The animals were maintained under standard conditions: temperature of 21−22 °C, relative air humidity of 50−70%, intensive ventilation of rooms (15×/h), and 12 h lighting. Individual body weights and food intakes were recorded. The experiment, conducted on three experimental groups (eight males each), lasted for 4 weeks from week 4 of age. All animals were housed individually in metabolic cages with free access to water and the experimental diets. Diets contained similar levels of protein, fat, minerals, and vitamins and a similar content of fiber. All of the diets were isocaloric.

Experimental diets were prepared as modified semisynthetic AIN-G93G diet[22] and differed only in the addition of defatted seeds of strawberries (strawberry) or raspberries (raspberry), introduced instead of a respective content of maize starch. The analyzed preparations were introduced into the diet at the same dose of 6%. The preparations introduced dietary fiber (4%), a small quantity of protein (<1%) and polyphenols (0.1%). A 1% addition of cellulose as an additional source of dietary fiber was administered to diets, whereas in the control diet cellulose content was 5%. The compositions of the experimental diets are summarized in Table 1. All diets contained 3% of fructooligosaccharides (FOS) added to reduce the potential negative effect of polyphenols on fermentative functions of the intestines.[23]

Table 1. Composition (Percent) of Diets

	diet[a]		
	control	strawberry	raspberry
casein	14.8	14.8	14.8
DL-methionine	0.2	0.2	0.2
cellulose	5.0	1.0	1.0
FOS	3.0	3.0	3.0
soybean oil	8.0	8.0	8.0
cholesterol	0.5	0.5	0.5
minerals	3.5	3.5	3.5
vitamins	1.0	1.0	1.0
defatted strawberry seeds		6	
defatted raspberry seeds			6.0
maize starch	64.0	61.7	61.5

[a]Experimental diets: strawberry, diet with defatted strawberry seeds; raspberry, diet with defatted raspberry seeds.

Analytical Procedures. Individual feed consumption and body weight gains of rats were determined. After 4 weeks of experiment, animals were weighed and anesthetized with sodium pentobarbitone. Blood samples were taken from the caudal vein. Serum was prepared by centrifugation at 300 rad/s for 15 min at 4 °C and stored at −40 °C. The concentrations of triacylglycerol (TG), total cholesterol (TC), high-density lipoprotein cholesterol (HDL-C), and glucose in the serum were determined with commercial diagnostic kits Alpha Diagnostics (Warsaw, Poland) and Pointe Scientific (Warsaw, Poland). The atherogenic index (AI) of a diet was calculated for each animal according to the formula AI = log(TG/HDL). The rats were then sacrificed by cervical dislocation. After laparotomy, the small intestine, cecum, and colon, including the contents, were taken from each rat. As soon as possible the small intestine, cecal, and colonic pH values were directly measured using a microelectrode and pH/ION meter (model 301, Hanna Instruments, Vila do Conde, Portugal). The small intestine was weighed with the contents. Samples of cecal and colonic digesta were then stored at −70 °C. The cecum and the colon were flushed clean with ice-cold saline, blotted on filter paper, and weighed. In cecal digesta samples, ammonia was extracted and trapped in a solution of boric acid in Conway dishes.[12] The activity of bacterial enzymes (α- and β-glucosidase, α- and β-galactosidase, and β-glucuronidase) in the cecum was measured by the rate of *p*- or *o*-nitrophenol release from their nitrophenylglucosides, according to the method described elsewhere.[23] The enzymatic activity was expressed as micromoles of product formed per an hour per gram of digesta. Cecal digesta samples were subjected to SCFA analysis, using GC (Shimadzu GC-2010, Kyoto, Japan). The samples (0.2 g) were mixed with 0.2 mL of formic acid, diluted with deionized water, and centrifuged at 800 rad/s for 10 min. The supernatant was loaded onto a capillary column (SGE BP21, 30 m × 0.53 mm) using an on-column injector. The initial oven temperature was 85 °C and was raised to 180 °C at 8 °C/min and held there for 3 min. The temperatures of flame ionization detector and the injection port were 180 and 85 °C, respectively. The volume of injection was 1 μL.

Dry Matter. The dry matter of small intestinal and cecal digesta was determined at 105 °C for 4 h.

Free Ellagic Acid and Metabolites in Cecal Digesta. Extraction of free ellagic acid and metabolites (urolithin-A and nasutin) was carried by the use of methanol and formic acid 99:1 (v/v) solution. To 500 mg of cecal digesta was added 2 mL of the solvent, which was mixed, sonified for 15 min, and centrifuged (800 rad/s). The procedure was repeated twice with 1.5 mL of the solvent. The extracts were combined and filled to 5 mL. For HPLC parameters, see Polyphenol HPLC Analysis. Detection was performed at 280 nm. Urolithin-A, a standard for the determination of EA metabolites, was used as described in ref 24. Nasutin-A and urolithin-A were the main EA metabolites of cecum digesta.[24]

Ellagic Acid Bound with Cecal Digesta. The content of ellagic acid bound with cecal digesta was determined by direct hydrolysis of ET adducts with proteins of digesta, extraction of released EA with methanol, and its analysis with HPLC. Half a milliliter of a 70% glycerin solution and 0.075 mL of trifluoroacetic acid (Fluka) were added to 0.15 g of cecal digesta. Next, the components were mixed and kept at a temperature of 95 °C for 18 h. After hydrolysis, the samples were filled to 5 mL with 100% methanol. The solution was centrifuged (900 rad/s) and analyzed with HPLC (see Polyphenol HPLC Analysis).

Statistics. Statistics were performed using a one-way ANOVA and Duncan's multiple-range tests at a significance level of $P \leq 0.05$ using STATISTICA 6.0 (StatSoft Corp., Kraków, Poland) software.

RESULTS

Chemical Composition of Strawberry and Raspberry Seeds. The main component of defatted seeds of strawberry and raspberry was the polysaccharide fraction, determined as total dietary fiber (Table 2). Compared to strawberry seeds, raspberry seeds contained less crude protein (10.4 vs 15.6%), less crude ash (1.8 vs 3.6%), more TDF (73.7 vs 68.6%) mainly in the insoluble form; and less total polyphenols (2.41 vs 1.75%).

The main components of the seed polyphenols were ellagitannins (ET), 0.97 and 1.76% in strawberry and raspberry seeds, respectively (Table 2). The contributions of ET in total polyphenols were 55 and 81%, respectively. Seeds were characterized by a significant content of proanthocyanidins, that is, 0.64% in strawberry and 0.37% in raspberry seeds. The

DOI: 10.1021/acs.jafc.5b00648
J. Agric. Food Chem. 2015, 63, 2989−2996

Table 2. Chemical Composition (Percent) of Preparations

	preparation[a]	
	strawberry	raspberry
dry matter	95.30	95.80
ash	3.61	1.81
protein	15.62	10.42
fat	0.41	0.20
carbohydrates,[b] including	73.90	81.33
TDF	68.61	73.71
SDF	1.40	6.10
low molecular	5.31	7.32
total polyphenols,[3] including	1.75	2.15
free ellagic acid	0.06	0.05
total ellagitannins (ET total)[c], including	0.97	1.76
lambertianin-C[d]	0.00	0.59
sanguiin-H-6[d]	0.00	0.86
agrimoniin[d]	0.43	0.01
monomeric ET[e]	0.53	0.31
content of monomeric ET/ET total, %	54.64	17.61
anthocyanins	0.01	0.02
flavonols	0.13	0.00
proanthocyanidins (DP[f], %)	0.64 (4.01)	0.37 (2.20)

[a]Strawberry, defatted strawberry seeds; raspberry, defatted raspberry seeds. [b]Carbohydrates = dry matter − (ash + protein + fat + polyphenolics). [c]ET as ellagic acid released in hydrolysis × 1.55. [d]ET determined by HPLC. [e]Monomeric ET = ET total − (lambertianin-C + sanguiin-H-6 + agrimoniin). [f]DP, degree of polymerization.

degree of polymerization of these compounds reached 4 and 2, respectively. Contents of the remaining groups of polyphenols, flavonols and anthocyanins, were relatively low. The compared preparations differed in the composition of ellagitannins; in strawberry seeds the only non-monomer was dimeric agrimoniin, whereas in raspberry seeds non-monomers were sanguiin-H6 (dimer) and lambertianin-C (trimer). In addition, the monomeric ellagitannins represented 55% of strawberry seeds ET and barely 18% of raspberry seeds ET.

Diet Intake and Parameters of Rat Growth and Development. Dietary inclusion of seed preparations did not affect the final body weight of rats (Table 3). Diet intake was not affected by dietary treatments (data not shown). Compared to group C, in the animals from the strawberry and raspberry groups, analyses showed a lower mass of the small intestine with digesta ($P = 0.028$), lower mass of cecal digesta ($P = 0.004$), and higher dry matter content of cecal digesta ($P < 0.001$). No significant differences were demonstrated between the analyzed groups in pH value of the intestinal digesta.

Ellagitannin Metabolites in Intestinal Digesta. The cecal digesta of rats from the strawberry and raspberry groups were characterized by various contents of ellagic acid and ellagitannin metabolites (Table 4). In both groups, the main ET metabolite was nasutin (54 and 39 μg/g digesta in, respectively, in the strawberry and raspberry groups), followed by urolithin A (35 and 9 μg/g digesta, respectively). The sum of these ET metabolites in cecal digesta of rats from the strawberry group was almost 2-fold higher than in the raspberry group, but still the contribution of urolithin A in the sum of metabolites in the strawberry group reached 39%, whereas in the raspberry group, 19%. In addition, cecal digesta of rats were found to contain bound ellagic acid, that is, 1.31 and 2.35 mg/g in the strawberry and raspberry groups, respectively.

Table 4. Content of Ellagic Acid (EA) Metabolites in Cecal Digesta

	group[a]		
content in intestinal digesta	strawberry	raspberry	P value
urolithin-A, μg/g	35.01 ± 10.12a	9.11 ± 14.04b	0.020
nasutin, μg/g	54.03 ± 25.11	39.04 ± 20.12	0.291
sum of EA metabolites			
μg/g intestinal digesta	89.04 ± 18.13a	48.11 ± 17.01b	0.013
μg/total mass of intestinal digesta	73.11 ± 18.21	38.11 ± 17.04	0.191
bound EA mg/g	1.31 ± 0.18b	2.35 ± 0.46a	0.021

[a]Experimental diets: strawberry, diet with defatted strawberry seeds; raspberry, diet with defatted raspberry seeds. Values in rows with different letters are different at $\alpha < 0.05$.

Fermentation Processes in the Cecum of Rats. The applied dietary interventions had various effects upon the enzymatic activity of microflora of rat cecum (Table 5). Compared with the control group, a significant increase was determined in the activity of α-glucosidase in cecal digesta of rats from the strawberry and raspberry groups ($P = 0.078$), whereas no difference was demonstrated in the activity of β-glucosidase. Activities of α-galactosidase and β-glucuronidase were significantly higher in the strawberry group (both $P = 0.001$), and β-galactosidase activity was higher in both strawberry and raspberry groups than in the control group (C).

Compared to group C, a higher concentration of acetate was determined in cecal digesta of rats from the raspberry group (P

Table 3. Body Weight of Rats and Parameters of Gastrointestinal Tract Functions

	group[a]			
	control	strawberry	raspberry	P value
body wt, g	330.01 ± 3.75	322.02 ± 3.72	329.11 ± 3.25	0.160
small intestine				
whole mass, g/100 g BW	2.26 ± 0.04a	2.16 ± 0.03b	2.17 ± 0.02b	0.028
pH	6.37 ± 0.09	6.33 ± 0.11	6.32 ± 0.09	0.744
cecum				
tissue, g/100 g BW	0.27 ± 0.01	0.25 ± 0.01	0.26 ± 0.01	0.094
digesta, g/100 g BW	1.11 ± 0.09a	0.82 ± 0.05b	0.79 ± 0.06b	0.004
DM of digesta, %	23.10 ± 0.64b	26.51 ± 0.55a	27.11 ± 0.36a	0.001
pH of digesta	6.50 ± 0.09	6.59 ± 0.07	6.39 ± 0.08	0.118

[a]Experimental diets: strawberry, diet with defatted strawberry seeds; raspberry, diet with defatted raspberry seeds. Values in rows with different letters are different at $\alpha < 0.05$.

DOI: 10.1021/acs.jafc.5b00648
J. Agric. Food Chem. 2015, 63, 2989−2996

Table 5. Concentration of Ammonia, Bacterial Enzyme Activity, Short-Chain Fatty Acid (SCFA) Concentration, SCFA Profile, and SCFA Pool in Cecal Digesta

	group[a]			
	control	strawberry	raspberry	*P* value
enzyme activity (μmol/h/g)				
α-glucosidase	15.60 ± 0.96	19.60 ± 1.85	17.00 ± 1.42	0.078
β-glucosidase	3.88 ± 0.58	5.42 ± 0.73	4.72 ± 0.70	0.141
α-galactosidase	8.34 ± 0.58b	16.50 ± 1.26a	10.90 ± 0.80b	0.001
β-galactosidase	28.00 ± 2.61b	45.70 ± 2.68a	38.50 ± 4.26a	0.001
β-glucuronidase	8.48 ± 1.04b	19.40 ± 2.65a	8.55 ± 0.99b	0.001
SCFA concentration (μmol/g)				
acetic	91.51 ± 6.42b	101.04 ± 6.52b	130.03 ± 8.23a	0.001
propionic	14.92 ± 0.61b	21.11 ± 1.83a	26.84 ± 2.80a	0.001
isobutyric	1.12 ± 0.20	1.18 ± 0.17	1.60 ± 0.28	0.162
butyric	16.30 ± 1.80b	29.40 ± 3.00a	35.10 ± 4.60a	0.001
isovaleric	1.08 ± 0.11	1.59 ± 0.25	1.03 ± 0.22	0.072
valeric	1.36 ± 0.10b	2.06 ± 0.21a	1.62 ± 0.16ab	0.007
PSCFA	3.56 ± 0.32	4.84 ± 0.48	4.25 ± 0.54	0.075
total SCFA	126.04 ± 8.21c	156.00 ± 10.51b	196.01 ± 11.40a	0.001
SCFA pool (μmol/100 g BW)	137.00 ± 7.41	126.00 ± 9.21	158.00 ± 19.81	0.124
SCFA profile (% of total)				
acetic	72.30 ± 0.95a	66.20 ± 1.03b	66.60 ± 2.43b	0.004
propionic	12.00 ± 0.64	12.90 ± 0.65	13.50 ± 0.97	0.190
butyric	12.80 ± 0.72b	18.60 ± 1.34a	17.80 ± 1.79a	0.008
ammonia, mg/g of digesta	0.21 ± 0.01ab	0.23 ± 0.02a	0.18 ± 0.01b	0.018

[a]Experimental diet: strawberry, diet with defatted strawberry seeds; raspberry, diet with defatted raspberry seeds. Values in rows with different letters are different at $\alpha<0.05$.

Table 6. Blood Plasma Markers

	group[a]			
	control	strawberry	raspberry	*P* value
glucose, mmol/L	13.10 ± 0.30b	14.50 ± 0.41ab	15.60 ± 0.77a	0.005
TG, mmol/L	1.95 ± 0.08a	2.01 ± 0.06a	1.55 ± 0.05b	<0.001
total cholesterol, mmol/L	2.54 ± 0.07ab	2.63 ± 0.11a	2.31 ± 0.06b	0.013
HDL-cholesterol, mmol/L	0.97 ± 0.03	1.01 ± 0.03	0.95 ± 0.02	0.134
HDL-TC, % of TC	38.20 ± 1.21	38.70 ± 1.75	41.20 ± 1.35	0.175
lg (TG/HDL)	0.70 ± 0.05a	0.69 ± 0.04a	0.49 ± 0.04b	0.007

[a]Experimental diets: strawberry, diet with defatted strawberry seeds; raspberry, diet with defatted raspberry seeds. Values in rows with different letters are different at $\alpha < 0.05$.

= 0.001) as well as higher concentrations of propionate and butyrate in the strawberry and raspberry groups (both P = 0.001). In terms of total SCFA concentration in cecal digesta, the order of groups was as follows: raspberry > strawberry > C, P = 0.001. Both groups administered diets with seeds showed decreased percentages of acetate (P = 0.004) and an increased contribution of butyrate (P = 0.008) in total SCFA, compared to group C.

Ammonia content in cecal digesta was significantly lower in the raspberry group than in the strawberry group (P = 0.018) and numerically higher compared to group C.

Biochemical Blood Markers. The study demonstrated various effects of the applied dietary interventions on the levels of the analyzed biochemical blood markers (Table 6). Fruit seeds content in the diet increased blood glucose level; however, a statistically significant (P = 0.005) difference was found only between raspberry and C groups. In the raspberry group lower concentrations of triacylglycerols and total cholesterol (P = 0.001 and P = 0.013, respectively) and a lower value of atherogenic index (P = 0.007) were shown.

DISCUSSION

Results of ample investigations proved that dietary fiber intake from vegetables and fruits is one of the key elements in prophylactics of human health, as implicated in reducing the risk of many diseases such as diarrhea, diabetes, obesity, ischemic heart disease, and colon cancers.[25] It results from a complex chemical structure of dietary fiber, its specific intestinal fermentation, and a wide spectrum of physiological effects.[26] An additional fact is that dietary fiber occurs in complexes with polyphenols, metabolized in the lower section of the gastrointestinal tract by gut microflora.[27] This release of polyphenols in the colon is believed to be a factor determining a lower incidence of chronic diseases in persons preferring consumption of food products made of whole cereal grains.[28] Moreover, the interaction between the gut flora and polyphenols is two-way: on the one hand, the ingested compounds modify the qualitative composition of the flora; on the other hand, 90−95% of the total intake of polyphenols (5−10% in ingested in the small intestine) reaches the colon, where they are metabolized by the colonic microbiota.[5] For

DOI: 10.1021/acs.jafc.5b00648
J. Agric. Food Chem. 2015, 63, 2989−2996

these reasons, a key element in the evaluation of the physiological properties of components rich in fiber−polyphenolic complexes is the assessment of the physiological response of the gastrointestinal tract and, most of all, the gut ecosystem.[23]

In the reported experiment, the main component of defatted seeds of strawberry and raspberry was the polysaccharide fraction, determined as total dietary fiber. The total protein content of the seeds was relatively low (10−15%). Compared with raspberry seeds, the strawberry seeds contained more crude protein and crude ash and less total dietary fiber, 15.6 vs 10.4% and 68.6 vs 73.7%, respectively, including soluble fiber (1.4 vs 6.1%). Similar results were obtained in earlier analyses of the chemical composition of strawberry, raspberry, and blackberry.[12,14] The higher crude ash content determined in strawberry seeds could be due to greater contamination of strawberry pomace with sand, as shown in the study.[10]

In the discussed experiment, the content of total polyphenols in raspberry seeds was significantly higher than in strawberry seeds (2.15 vs 1.75%). Compared to raspberry seeds, strawberry ellagitannins were characterized by a high concentration of monomers (56 vs 17% of total polyphenols) and the occurrence of agrimoniin only, whereas in raspberry seeds the ellagitannins were constituted mainly by sanguiin-H6 and lambertianin-C. The differences noted in contents of polyphenols in seeds corresponded to these determined in fresh fruits of raspberry and strawberry.[7,29] Results of earlier investigations have demonstrated that the main components of the polyphenolic fraction of strawberry and raspberry seeds are ellagitannins and proanthocyanidins[1,8,18,30] and that contents of anthocyanins and flavonols are negligible compared to the values assayed in fruits of these species.[6,8,16]

In the presented experiment, the content of strawberry and raspberry seeds in diet had no influence on feed intake and body weight gains of rats, but reduced the bulk of digesta in the small intestine and the cecum. This was, probably, due to the physiological effect of the dietary fiber of the seeds, which substituted for 4% of cellulose in the control diet. Studies of other authors demonstrate that insoluble dietary fiber accelerates gut peristalsis,[26] whereas soluble dietary fiber increases viscosity and delays transit of digesta.[31] One of the effects of increasing dietary fiber content in a diet may be increased hydration of digesta.[32,33] This was, however, not observed in our experiment in digesta with the content of fruit seeds. The concentration of dry matter was even increased; however, dry matter content in cecal digesta of the rats from strawberry and raspberry groups was lower than in the control diet in which cellulose was the component of the dietary fiber fraction.

The use of strawberry and raspberry seeds as substitutes for cellulose and part of the maize starch in the diet evoked tangible enhancement of α-glucosidase activity and a statistically significant increase in the activity of β-galactosidase, as well as, only in the case of strawberry seeds, a significant increase in α-galactosidase and β-glucuronidase activities. Consequently, an increase in SCFA concentration was observed in both experimental groups compared to the control group. Strawberry and raspberry seeds did not increase the concentration of acids with a branched chain (isobutyric and isovaleric). This was consistent with no effect of the content of fruit seeds in the diet on increasing ammonia concentration in cecal digesta. In the raspberry group, the concentration of ammonia in cecal digesta of rats was even lower than in the control group. Results of the presented experiment were in agreement with results obtained in other studies in which rats were administered diets with 10% content of defatted seeds of black currant, which resulted in enhanced glycolytic activity of intestinal microflora confirmed by increased SCFA production in cecal digesta.[13] This indicates that dietary fiber contained in strawberry and raspberry seeds was a distinctly better substrate than cellulose in fermentation processes proceeding in the cecum of rats. This is also confirmed by the reported increased production of propionate and, most of all, a significant increase in the content of butyrate in total SCFAs. It is known that SCFAs are rapidly absorbed and metabolized by various tissues, including liver (propionate and partly acetate), muscle (acetate), and intestinal epithelium (butyrate).[34] In this context, the higher production of butyrate in cecal digesta of experimental rats was a significant outcome of the presented experiment, because butyric acid is more effective in inducing the proliferation of intestinal epithelial cells than acetic acid.[35] Similar concentrations of isobutyric and isovaleric acids in intestinal digesta of the rats indicate that the contribution of strawberry and raspberry seeds in diet does not enhance bacterial proteolytic degradation, which results in the production of acid with a branched chain.[36]

Results of the previous study indicate that dietary polyphenols may reach any segment of the gastrointestinal tract in measurable quantities and modify the functioning of its ecosystem.[37] In the case of ellagitannins only trace amounts of these substances are absorbed in the stomach and small intestine;[38] however, the majority of these substances are metabolized by the intestinal microbiota.[39] According to this, the use of strawberry and raspberry seeds in diets caused the presence of metabolites of ellagic acid and ellagitannin, that is, urolithin and nasutin, in cecal digesta.

In the gastrointestinal tract of humans and some experimental animals, mainly urolithins were metabolites of ellagitannins.[27] In selected animals, such as beavers and pigs, dehydroxyellagic acid derivative, referred to as nasutin, was determined as an ET metabolite.[39] Also in cecal digesta of the rats from our experiment, the main metabolite of ellagitannin was nasutin (respectively 61 and 81% of total ET metabolites in the strawberry and raspberry groups), and urolithin A occurred in a lower quantity. A surprising outcome of the presented experiment was the fact that administration of the raspberry diet with a higher content of ellagitannins than in the strawberry group (1.76 vs 0.97%), resulted in lower concentrations of ET metabolites in cecal digesta (48 vs 89 μg/g). This indicates that strawberry ellagitannins, with a high contribution of monomers and dimer, agrimoniin, were more easily metabolized by cecal microbiota. The ETs contained in raspberry seeds were degraded, to a greater extent, to nasutin; however, the total content of nasutin and urolitin A in intestinal digesta was tangibly lower. A significantly higher ratio of ellagic acid to ET metabolites in cecal digesta was observed in the raspberry group.

In the presented experiment, the above-indicated differences in the content and composition of ET metabolites could differentiate selected parameters of the functioning of cecal ecosystem of rats, including the activity of microflora and SCFA production.

The comparison of results achieved in the strawberry and raspberry groups demonstrated that the increased content of ET metabolites in cecal digesta modified the effect of dietary fiber from fruits on fermentation processes. One of the effects

DOI: 10.1021/acs.jafc.5b00648
J. Agric. Food Chem. 2015, 63, 2989−2996

was both beneficial enhancement of the glycolytic activity of α-galactosidase as well as an unfavorable increase of β-glucuronidase activity. The enhanced activity of β-glucuronidase is claimed to result from the increased count of unfavorable microflora, such as *Escherichia coli* and *Clostridium*, in intestinal digesta.[40] Results of other experiments demonstrate that the increase of β-glucuronidase activity may result from dietary inclusion of pectins, dietary fiber with beneficial physiological properties.[32,41] Some experiments showed that strawberry polyphenols in rats' diet resulted in reduced activity of β-glucuronidase.[21]

The content of strawberry seeds, unlike that of raspberry seeds, did not increase the total SCFA production in the cecum of rats, and even negligibly lowered the SCFA pool, compared to the control diet. Such a result ought to be linked with a higher content of ET metabolites in cecal digesta, thus suppressing the glycolytic activity of microflora. The enhanced enzymatic activity in the cecum of rats fed the diet with raspberry seeds corresponded with a higher blood level of glucose in this group of rats.

In our experiment, raspberry seeds containing 1.8% of ellagitannins affected the blood lipid profile, especially the content of triglycerides, which corresponded with a decreased atherogenicity index in blood (0.49 vs 0.70). This was confirmed in results of other investigations, which demonstrated the positive effect of ellagitannins on the level and composition of blood lipids.[42,43] In the case of strawberry seeds, with a lower content of ellagitannins (1.0%), analyses did not show any statistically significant effect on the lipid profile in blood.

The results of the presented experiment demonstrate that ellagitannins of strawberry seeds are mainly composed of monomers (54% of total ETs) and a dimer, agrimoniin, whereas raspberry seeds characterized by a higher content of ET polymers (83% of total ET) were mainly constituted by a dimer, sanguiin-H6, and a trimer, lambertianin-C. The lower content and less polymerized structure of strawberry ellagitannins, applied in rat diets, resulted in a higher concentration of metabolites in the cecum, which reduced SCFA synthesis but did not affect the blood lipid profile. Raspberry seeds were a better metabolized substrate in fermentation processes in the cecum of rats, resulting in enhanced production of SCFA and a higher content of butyrate as well as promoting reduced serum atherogenic index compared to control dietary treatment. Defatted strawberry and raspberry seeds were found to be an interesting source of dietary fiber and ellagitannins.

AUTHOR INFORMATION

Corresponding Authors

*(M.K.) Phone: +48 42 6312779. Fax: +48 42 6367488. E-mail: monika.kosmala@p.lodz.pl.

*(J.J.) Phone: +48 89 5234673. Fax: +48 89 5240124. E-mail: j.juskiewicz@pan.olsztyn.pl.

Funding

This research was supported in part by the National Science Centre Poland (Grant DEC-2012/05/B/NZ9/03402).

Notes

The authors declare no competing financial interest.

REFERENCES

(1) Klimczak, E.; Rozpara, E.; Król, B. Distribution of ellagitannins in juice, flesh, and achenes as additional criterion for optimal utilization of strawberries. *Food Sci. Technol. Qual.* **2011**, *6*, 142−154.

(2) Bobinaitė, R.; Viškelis, P.; Šarkinas, A.; Venskutonis, P. R. Phytochemical composition, antioxidant and antimicrobial properties of raspberry fruit, pulp, and marc extracts. *CyTA−J. Food* **2013**, *11*, 334−342.

(3) Volák, J.; Stodola, J. In *Rośliny Lecznicze [Medical Plants]*; Państwowe Wydawnictwo Rolnicze i Leśne: Warsaw, Poland, 1987.

(4) Giampieri, F.; Tulipani, S.; Alvarez-Suarez, J.; Quiles, J. L.; Mezzetti, B.; Battino, M. The strawberry: composition, nutritional quality, and impact on human health. *Nutrition* **2012**, *28*, 9−19.

(5) Chiva-Blanch, G.; Visioli, F. Polyphenols and health: moving beyond antioxidants. *J. Berry Res.* **2012**, *2*, 63−71.

(6) Alvarez-Suarez, J. M.; Giampieri, F.; Tulipani, S.; Casoli, T.; Di Stefano, G.; González-Paramás, A. M.; Santos-Buelga, C.; Busco, F.; Quiles, J. L.; Cordero, M. D.; Bompadre, S.; Mezzetti, B.; Battino, M. One-month strawberry-rich anthocyanin supplementation ameliorates cardiovascular risk, oxidative stress markers and platelet activation in humans. *J. Nutr. Biochem.* **2014**, *25*, 289−294.

(7) Gasperotti, M.; Masuero, D.; Vrhovsek, U.; Guella, G.; Mattivi, F. Profiling and accurate quantification of *Rubus* ellagitannins and ellagic acid conjugates using direct UPLC-Q-TOF HDMS and HPLC-DAD analysis. *J. Agric. Food Chem.* **2010**, *58*, 4602−4616.

(8) Aaby, K.; Skrede, G.; Wrolstad, R. E. Phenolic composition and antioxidant activities in flesh and achenes of strawberries (*Fragaria ananassa*). *J. Agric. Food Chem.* **2005**, *53*, 4032−4040.

(9) Oomah, B. D.; Ladet, S.; Godfrey, D. V.; Liang, J.; Girard, B. Characteristics of raspberry (*Rubus idaeus* L.) seed oil. *Food Chem.* **2000**, *69*, 187−193.

(10) Sójka, M.; Klimczak, E.; Macierzyński, J.; Kołodziejczyk, K. Nutrient and polyphenolic composition of industrial strawberry press cake. *Eur. Food Res. Technol.* **2013**, *237*, 995−1007.

(11) Dimić, E. B.; Vujasinović, V. B.; Radočaj, O. F.; Pastor, O. P. Characteristics of blackberry and raspberry seeds and oils. *APTEFF* **2012**, *43*, 1−342 DOI: 10.2298/APT1243001D.

(12) Bushman, B. S.; Phillips, B.; Isbell, T.; Ou, B.; Crane, J. M.; Knapp, S. J. Chemical composition of caneberry (*Rubus* spp.) seeds and oils and their antioxidant potential. *J. Agric. Food Chem.* **2004**, *52*, 7982−7987.

(13) Jurgoński, A.; Juśkiewicz, J.; Sójka, M.; Król, B.; Rój, E.; Zduńczyk, Z. Black currant seeds after supercritical carbon dioxide extraction as a potential dietary supplement. *Rocz. Panstw. Zakl. Hig.* **2008**, *59*, 421−427.

(14) Korus, J.; Juszczak, L.; Ziobro, R.; Witczak, M.; Grzelak, K.; Sójka, M. Defatted strawberry and blackcurrant seeds as functional ingredient of gluten-free bread. *J. Texture Stud.* **2012**, *43*, 29−39.

(15) Giménez, J. A.; González-Sarrías, A.; Larrosa, M.; Tomás-Barberán, F. A.; Espín, J. C.; García-Conesa, M. T. Ellagitannin metabolites urolithins A glucuronide and its aglycone urolithin A ameliorate TNF-α-induced inflammation and associated molecular markers in human aortic endothelial cells. *Mol. Nutr. Food Res.* **2012**, *56*, 784−796.

(16) Jean-Gilles, D.; Li, L.; Ma, H.; Yuan, T.; Chichester, C. O.; Seeram, N. P. Anti-inflammatory effects of polyphenolic-enriched red raspberry extract in an antigen-induced arthritis rat model. *J. Agric. Food Chem.* **2012**, *60*, 5755−5762.

(17) Seeram, N. P.; Aronson, W. J.; Zhang, Y.; Henning, S. M.; Moro, A.; Lee, R.-P.; Sartippour, M.; Harris, D. M.; Rettig, M.; Suchard, M. A.; Pantuck, A. J.; Belldegrun, A.; Heber, D. Pomegranate ellagitannin-derived metabolites inhibit prostate cancer growth and localize to the mouse prostate gland. *J. Agric. Food Chem.* **2007**, *55*, 7732−7737.

(18) Vrhovsek, U.; Guella, G.; Gasperotti, M.; Pojer, E.; Zancato, M.; Mattivi, F. Clarifying the identity of the main ellagitannins in the fruit of the strawberry *Fragaria vesca* and *Fragaria ananassa* Duch. *J. Agric. Food Chem.* **2012**, *60*, 2507−2516.

(19) Lee, J.; Dossett, M.; Finn, C. E. Rubus fruit phenolic research: the good, the bad, and the confusing. *Food Chem.* **2012**, *130*, 785−796.

DOI: 10.1021/acs.jafc.5b00648
J. Agric. Food Chem. 2015, 63, 2989−2996

(20) Horwitz, W.; Latimer, G. W. In *Official Methods of Analysis of AOAC International*, 18th ed.; AOAC International: Rockville, MD, USA, 2007.
(21) Kosmala, M.; Zduńczyk, Z.; Kołodziejczyk, K.; Klimczak, E.; Juskiewicz, J.; Zduńczyk, P. Chemical composition of polyphenols extracted from strawberry pomace and their effect on physiological properties of diets supplemented with different types of dietary fiber in rats. *Eur. J. Nutr.* **2014**, *53*, 521−532.
(22) Reeves, P. AIN-93 purified diets for laboratory rodents: final report of the American Institute of Nutrition ad hoc writing committee on the reformation of the AIN-76A rodent diet. *J. Nutr.* **1993**, *123*, 1939−1951.
(23) Juśkiewicz, J.; Zduńczyk, Z.; Żary-Sikorska, E.; Król, B.; Milala, J.; Jurgoński, A. Effect of the dietary polyphenolic fraction of chicory root, peel, seed and leaf extracts on caecal fermentation and blood parameters in rats fed diets containing prebiotic fructans. *Br. J. Nutr.* **2011**, *105*, 710−720.
(24) Fotschki, B.; Milala, J.; Karlińska, E.; Zduńczyk, Z.; Juśkiewicz, J. The chemical composition and modulatory effect of an ellagitannin-rich strawberry extract on the physiological effects of dietary fructooligosaccharides in rats. *J. Agric. Food Chem.* **2014**, *62*, 5871−5880.
(25) Kaczmarczyk, M. M.; Miller, M. J.; Freund, G. G. The health benefits of dietary fiber: beyond the usual suspects of type 2 diabetes mellitus, cardiovascular disease and colon cancer. *Metab., Clin. Exp.* **2012**, *61*, 1058−1066.
(26) Brownlee, I. A. The physiological roles of dietary fibre. *Food Hydrocolloids* **2011**, *25*, 238−250.
(27) Cerdá, B.; Tomás-Barberán, F. A.; Espín, J. C. Metabolism of antioxidant and chemopreventive ellagitannins from strawberries, raspberries, walnuts and oak-aged wine in humans: identification of biomarkers and individual variability. *J. Agric. Food Chem.* **2005**, *53*, 227−235.
(28) Kern, S. M.; Bennett, R. N.; Mellon, F. A.; Kroon, P. A.; Garcia-Conesa, M. T. Absorption of hydroxycinnamates in human after high-bran cereal consumption. *J. Agric. Food Chem.* **2003**, *51*, 6050−6055.
(29) Larrosa, M.; García-Conesa, M. T.; Espín, J. C.; Tomás-Barberán, F. A. Ellagitannins, ellagic acid and vascular health. *Mol. Aspects Med.* **2010**, *31*, 513−539.
(30) Goďevac, D.; Tešević, V.; Vajs, V.; Milosavljević, S.; Stanković, M. Antioxidant properties of raspberry seed extracts on micronucleus distribution in peripheral blood lymphocytes. *Food Chem. Toxicol.* **2009**, *47*, 2853−2859.
(31) Li, C.; Uppal, M. Canadian Diabetes Association National Nutrition Committee clinical update on dietary fibre in diabetes: food sources to physiological effects. *Can. J. Diabetes* **2010**, *34*, 355−361.
(32) Ohkami, H.; Tazawa, K.; Yamashita, I.; Shimizu, T.; Murai, K.; Kobashi, K.; Fujimaki, M. Effects of apple pectin on fecal bacterial enzymes in azoxymethane-induced rat colon carcinogenesis. *Jpn. J. Cancer Res.* **1995**, *86*, 523−529.
(33) Kosmala, M.; Kołodziejczyk, K.; Zduńczyk, Z.; Juśkiewicz, J.; Boros, D. Chemical composition of natural and polyphenol-free apple pomace and the effect of this dietary ingredient on intestinal fermentation and serum lipid parameters in rats. *J. Agric. Food Chem.* **2011**, *59*, 9177−9185.
(34) Priebe, M. G.; Vonk, R. J.; Sun, X.; He, T.; Harmsen, H. J. M.; Welling, G. W. The physiology of colonic metabolism: possibilities for intervention with pre- and probiotics. *Eur. J. Nutr.* **2002**, *41* (Suppl.I), I/2−I/10.
(35) Williams, B. A.; Verstegen, M. W. A.; Tamminga, S. Fermentation in the large intestine of single-stomached animals and its relationship to animal health. *Nutr. Res. Rev.* **2001**, *14*, 207−227.
(36) Swanson, K. S.; Grieshop, C. M.; Flickinger, E. A.; Bauer, L. L.; Chow, J.; Wolf, B. W.; Garleb, K. A.; Fahey, G. C., Jr. Fructooligosaccharides and *Lactobacillus acidophilus* modify gut microbial populations, total tract nutrient digestibilities and fecal protein catabolite concentrations in healthy adults dogs. *J. Nutr.* **2002**, *132*, 3721−3731.
(37) Manach, C.; Williamson, G.; Morand, C.; Scalbert, A.; Rémésy, C. Bioavailability and bioefficacy of polyphenols in humans. I. Review of 97 bioavailability studies. *Am. J. Clin. Nutr.* **2005**, *81* (1 Suppl.), 230S−242S.
(38) Espin, J. C.; Gonzalez-Barrio, R.; Cerda, B.; Lopez-Bote, C.; Rey, A. I.; Tomas-Barberan, F. A. Iberian pig as a model to clarify obscure points in the bioavailability and metabolism of ellagitannins in humans. *J. Agric. Food Chem.* **2007**, *55*, 10476−10485.
(39) González-Barrio, R.; Truchado, P.; Ito, H.; Espín, J. C.; Tomás-Barberan, F. A. UV and MS identification of urolithins and nasutins, the bioavailable metabolites of ellagitannins and ellagic acid in different mammals. *J. Agric. Food Chem.* **2011**, *59*, 1152−1162.
(40) Klewicka, E.; Zduńczyk, Z.; Juskiewicz, J. Effect of lactobacillus fermented beetroot juice on composition and activity of cecal microflora in rats. *Eur. Food Res. Technol.* **2009**, *229*, 153−157.
(41) Licht, T. R.; Hansen, M.; Bergström, A.; Poulsen, M.; Krath, B. N.; Markowski, J.; Dragsted, L. O.; Wilcks, A. Effects of apples and specific apple components on cecal environment of conventional rats: role of apple pectin. *BMC Microbiol.* **2010**, *10*, 1−11.
(42) Basu, A.; Wilkinson, M.; Penugonda, K.; Simmons, B.; Betts, N. M.; Lyons, T. J. Freeze-dried strawberry powder improves lipid profile and lipid peroxidation in women with metabolic syndrome: baseline and post intervention effects. *Nutr. J.* **2009**, *8*, DOI: 10.1186/1475-2891-8-43.
(43) Jaroslawska, J.; Juskiewicz, J.; Wroblewska, M.; Jurgowski, A.; Krol, B.; Zdunczyk, Z. Polyphenol-rich strawberry pomace reduces serum and liver lipids and alters gastrointestinal metabolite formation in fructose-fed rats. *J. Nutr.* **2011**, *141*, 1777−1783.

DOI: 10.1021/acs.jafc.5b00648
J. Agric. Food Chem. 2015, 63, 2989−2996

Proteolytic and carbohydrate-degrading enzymes have been shown to enhance protein extractability from rapeseed press cake.[21] We have also previously shown that hydrolysis of the embryonic cell walls (consisting of pectin, arabinogalactan, arabinan, xyloglucan, xylan, and cellulose) with a commercial pectinase preparation can increase protein recovery from cold-pressed rapeseed press cake by 73%.[8] However, the effect of solid content on protein recovery during combined enzymatic treatment and aqueous extraction has not been previously reported.

In the current study, we aimed to increase the total solid content during pectinase treatment of cold-pressed, SC-CO_2-defatted rapeseed press cake to limit water consumption in the production of a rapeseed protein concentrate. Another aim was to investigate the impact of extraction pH and isoelectric precipitation on protein recovery as well as on the solution behavior of the protein concentrates.

MATERIALS AND METHODS

Materials and Enzymes. Rapeseed press cake (6.8% moisture) was obtained from Kankaisten Öljykasvit Oy (Turenki, Finland). The press cake had been produced by cold pressing of oil from *Brassica rapa* L. seeds at 50−60 °C, pelletizing, and air-drying. A commercial pectinase preparation, Pectinex Ultra SP-L, was obtained from Novozymes A/S (Bagsvaerd, Denmark). It had a total protein content of 61 mg/mL and contained 2876 nkat of polygalacturonase (pectinase, assayed using polygalacturonic acid as a substrate), 135 nkat of endo-β-glucanase (assayed using β-glucan as a substrate), 22 nkat of endoglucanase (cellulase, assayed using hydroxyethyl cellulose as a substrate), and 7 nkat of endo-1,4-β-xylanase activity (assayed using glucuronoxylan as a substrate) per total protein, as measured at 30 °C and pH 5.5.[8]

Pretreatment. Rapeseed press cake was ground at 1000 rpm using an SM 300 cutting mill (Retsch GmbH, Düsseldorf, Germany) and defatted by SC-CO_2 extraction in a Nova Swiss extraction vessel (Nova Werke Ag, Effretikon, Switzerland) equipped with a Chematur Ecoplanning compressor (Chematur Engineering Ltd., Pori, Finland). The vessel was operated for approximately 5 h under 300 bar of pressure at 40 °C. The defatted press cake was dry-milled twice at 17 800 rpm using a 100 UPZ-II Fine Impact mill (Hosokawa Alpine Ag, Ausburg, Germany). The defatted press cake contained 39% crude protein, 2% crude fat, 24% carbohydrates, and 8% ash on dry matter basis, as measured by using the methods described in Rommi et al.[8]

Enzymatic Treatment, Protein Extraction, and Isoelectric Precipitation. The defatted and milled rapeseed press cake was treated with Pectinex Ultra SP-L at an enzyme dosage of 5 mg total protein/g dry substrate (Figure 1). The treatment was performed at 40 and 20% (w/v) solid content in water without pH adjustment at the natural pH of the substrate (pH 5.8−6.0). Reference treatments were carried out similarly but without enzyme addition. All treatments were performed in duplicate. After 2 h of enzyme or reference treatment at 40 °C in a closed 500 mL stirred tank reactor with 40 rpm mixing, the reaction suspension was thoroughly mixed and aliquoted into 50 mL extraction tubes. Water was added to obtain 10 and 20% (w/v) solid content. The subsequent water or alkaline extraction and precipitation steps were performed in duplicate for each replicate enzyme treatment or reference treatment (N = 4). Water extraction was performed without pH adjustment at pH 5.5−6.0. After agitation at 320 rpm and 30 °C for 1 h, the suspension was centrifuged for 15 min at 3220g and 4 °C. Both the liquid fractions (supernatant) and the residual solids (pellet) were freeze-dried and weighed before further analysis. The lyophilized liquid fraction from water extraction will be referred to as "water extract", "pH6 E" throughout the text.

For alkaline extraction, the pH of the initial aliquoted suspensions (10 or 20% solid content) was adjusted to 10 using 10 M NaOH. The suspensions were stirred at 320 rpm for 1 h at 30 °C and centrifuged for 15 min at 3220g. The residual solids were directly freeze-dried and weighed for further analysis. The liquid fractions (supernatant) from

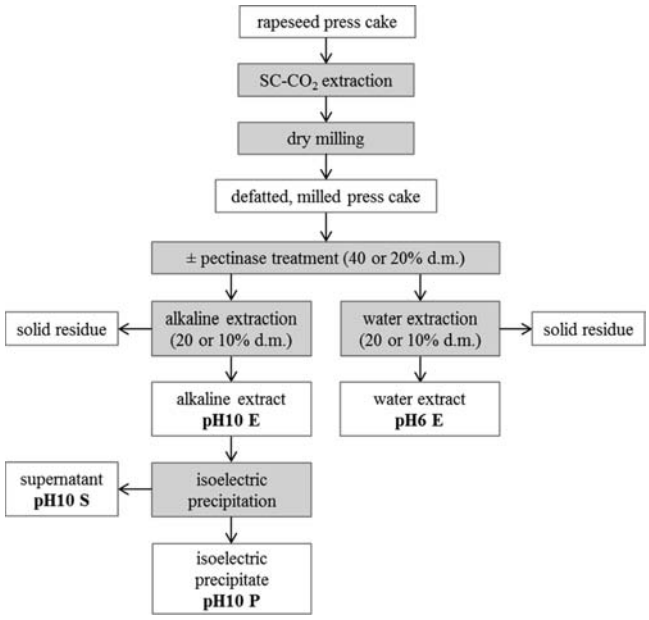

Figure 1. Pretreatment, enzymatic treatment, protein extraction, and protein precipitation schemes performed for rapeseed press cake. Pectinase treatment was performed at 40 or 20% total solid content (dm), and protein extractions were performed at 20 or 10% total solid content. Respective extraction and precipitation steps were performed after reference treatments of the defatted, milled press cake without enzyme addition. The isoelectric precipitates (pH10 P), water extracts (pH6 E), and extraction residues were obtained after centrifugation and freeze-dried before further analysis. Samples of the alkaline (pH10 E) and water extracts (pH6 E) and supernatants after precipitation (pH10 S) were stored at −20 °C.

alkaline extraction (referred to as "pH10 E") were subjected to isoelectric precipitation by adjusting the pH to 4 with 1 M HCl, mixing for 10 min, and centrifugation at 3220g for 20 min. The precipitate was recovered and freeze-dried without washing. The lyophilized precipitate will be referred to as "isoelectric precipitate", "pH10 P", throughout the text. All lyophilized samples as well as samples of unlyophilized water and alkali extracts (pH6 E and pH10 E) and supernatants remaining after isoelectric precipitation (referred to as "pH10 S") were stored at −20 °C until carbohydrate and protein analysis. Protein extraction yield was determined as the percentage of total nitrogen removed from the solids. The yield of protein precipitation was expressed as the percentage of total nitrogen or alkali-extracted nitrogen that was recovered in the precipitate. Extraction and precipitation yields were calculated as the average of four replicate experiments.

Protein Composition. Protein composition of the water and alkali extracts, isoelectric precipitates, and supernatants after isoelectric precipitation was analyzed by SDS-PAGE in reducing conditions using a Criterion TGX, Stain-Free Precast 18% gel (Bio-Rad, Hercules, CA, USA) and Precision Plus Protein standards (Bio-Rad). Water and alkali extracts and supernatants after isoelectric precipitation were diluted in 0.15% NaCl solution, mixed with loading buffer (0.1 M Tris-HCl, pH 6.8, 20% (v/v) glycerol, 4% (w/v) SDS, 10% (v/v) β-mercaptoethanol, 0.02% (w/v) bromophenol blue), and heated at 98 °C for 5 min. Isoelectric precipitates were dissolved in the loading buffer by heating at 98 °C for 10 min. Samples (20−30 μg of protein/lane) were loaded onto the precast gel and subjected to electrophoresis at a constant voltage of 250 V. The gel was imaged using Criterion Stain Free Imager with UV-induced fluorescence detection of tryptophan residues and examined with Image Lab software (Bio-Rad). Cruciferin and napin polypeptides were identified on the basis of correspondence of their known molecular weights with the band molecular weights. Protein concentration in the residual solids, isoelectric precipitates (pH10 P), and lyophilized water extracts

DOI: 10.1021/acs.jafc.5b01077
J. Agric. Food Chem. 2015, 63, 2997−3003

(pH6 E) was determined as the total nitrogen content (N × 6.25) analyzed in duplicate by Kjeldahl, according to the method by Kane.[22]

Carbohydrate Composition. Free monosaccharide and sucrose concentrations in the water and alkali extracts were determined by high-performance anion-exchange chromatography with pulse amperometric detection (HPAEC-PAD) using an ICS-3000 ion chromatography system equipped with a CarboPac PA1 column (Dionex, Sunnyvale, CA, USA) after filtration of the samples through a 0.45 μm syringe filter.[23] Total carbohydrate concentration was determined in duplicate by secondary hydrolysis of the extracts in 4% sulfuric acid for 1 h at 120 °C and analysis of the resulting monosaccharides by HPAEC-PAD after filtration of the hydrolysates through a 0.45 μm syringe filter.[23,24] Polysaccharide concentration was obtained by subtracting the free monosaccharides and sucrose from the total carbohydrates. To determine the total carbohydrate content of the isoelectric precipitates, the precipitates were hydrolyzed in triplicate with 70% sulfuric acid for 1 h at 30 °C followed by hydrolysis with 4% sulfuric acid for 50 min at 120 °C.[24] The released monosaccharides were analyzed by HPAEC-PAD as described above.[23]

Ash Content. The ash content of the lyophilized water extracts and isoelectric precipitates was determined in duplicate by combustion for 23 h at 550 °C in an N 11 muffle furnace (Nabertherm GmbH, Lilienthal, Germany) and weighing of the incombustible residue.

Solubility, Particle Size, and ζ-Potential. The amount of soluble protein in the lyophilized water extracts and isoelectric precipitates was determined at pH 4 and 8. The samples were dispersed in water to 2% (w/w) protein concentration on the basis of their total nitrogen content. The pH was adjusted to 4 and 8 using HCl or NaOH. The dispersions were stirred with a magnetic stirrer at 300 rpm and 40 °C for 2 h, after which they were centrifuged for 15 min at 10000*g*. The protein concentration of the supernatant was measured using a DC Protein Assay Kit (Bio-Rad) to determine the proportion of soluble protein in relation to the total nitrogen content of the dispersion.

Particle size distribution and ζ-potential of the supernatants were analyzed using Zetasizer nano ZS (Malvern Instruments, Malvern, UK). Two replicates with three consecutive measurements at 25 °C were performed. The samples were diluted 1:100 in MQ water and filtered through a 0.2 μm membrane (Millex Syringe Filter Unit, Millipore, Cork, Ireland). Disposable cuvettes and disposable folded capillary cells were used for particle size and ζ-potential measurements, respectively. Before the particle size measurement, the diluted and filtered samples were equilibrated in cuvettes for 2 h at 25 °C. For the intensity-based distribution of the particle sizes, the "general purpose" (non-negative least-squares analysis) algorithm in the Zetasizer Software was used. Volume size distributions were derived from the intensity distributions using the Mie theory by the software (refractive index $(RI)_{protein}$ = 1.450, RI_{water} = 1.330).

Statistical Analysis. Statistical analysis of the yield of extracted and precipitated protein from four replicate experiments was carried out by general linear model multivariate analysis using SPSS Statistics software (version 22, IBM, Armonk, NY, USA). The level of significance was set at $p < 0.05$ and assessed by Tukey's test.

RESULTS AND DISCUSSION

Effect of Total Solid Content, Enzymatic Treatment, and Extraction pH on Protein Extractability. The impact of solid content and pH on enzyme-aided recovery of protein from defatted rapeseed press cake was studied. Pectinase treatment was carried out at 20 and 40% total solid content to understand the influence of substrate concentration on the hydrolysis efficiency and subsequent protein release. As previously reported for nondefatted rapeseed press cake,[8] enzymatic treatment of the defatted press cake improved the protein recovery at pH 6 ($p \leq 0.05$ at 10% solid content, Tukey's test) (Figure 2). However, in alkaline extraction the preceding pectinase treatment did not have a clear benefit. Pectinase treatment at either 20 or 40% solid content resulted in similar protein extraction yields at 10% solid content, pH 6

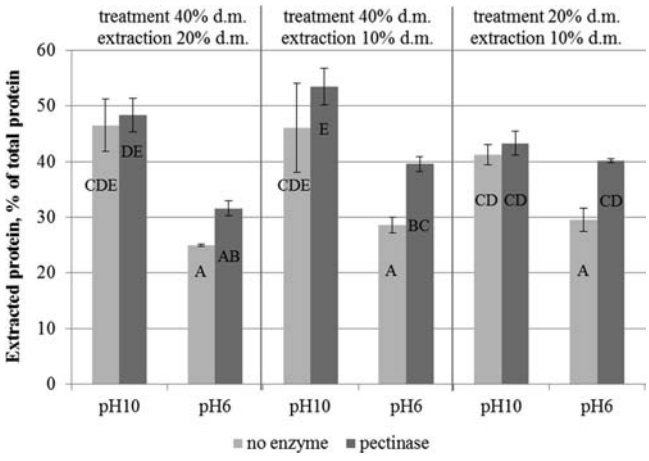

Figure 2. Yield of extracted proteins from defatted rapeseed press cake after pectinase treatment or reference treatment (no enzyme) at 40 and 20% solid content (dm) followed by alkaline (pH 10) or water extraction (pH 6) at 20 and 10% solid content. The yield was calculated on the basis of the loss of total nitrogen from the residual solids after extraction. Error bars represent standard deviations of two parallel extractions performed after each of the two replicate enzyme or reference treatments ($N = 4$). The sample points were categorized into subsets (A–E) on the basis of Tukey's test ($p < 0.05$).

(Figure 2, bars 8 and 12), indicating that the increase of solid content did not affect the hydrolysis efficiency. Interestingly, protein recovery in alkaline conditions seemed to increase when the enzyme or reference treatment was performed at higher solid content. Specifically after pectinase treatment at 40% solid content, alkaline extraction at 10% solid content was significantly improved ($p < 0.05$ Tukey's test) (Figure 2, bars 6 and 10). Although the enzyme itself did not clearly influence alkaline extraction, mixing at high solid content may have facilitated the release of additional protein that was extractable at pH 10.

Solid content of the extraction step (10 or 20%) did not significantly affect the protein yield (Figure 2), although at pH 6, somewhat less protein was extracted at 20% than at 10% solid content. The protein recovery was most probably limited by insufficient phase separation at increased solid content: after centrifugation of the 20% dm suspensions, a larger relative amount of liquid remained associated with the residual solids. Therefore, the residual solids presumably contained solubilized protein, which was not recovered in the extract. Protein recovery at low water content could be facilitated by more effective centrifugation practices that reduce the entrapment of soluble components in the sediment.

Overall, 41–53% of the total protein in the defatted rapeseed press cake was recovered in the alkaline extracts (pH10 E) and 25–40% in the water extracts (pH6 E) (Figure 2). In accordance with previous studies, protein recovery could be improved using either pectinase treatment or alkaline conditions.[8,16] When the extraction step was carried out at 10% solid content, enzyme-aided extraction at pH 6 resulted in the same protein yield as nonenzymatic alkaline extraction (Figure 2). This suggests that by facilitating protein recovery, pectinase treatment could allow protein extraction to be carried out without the use of alkali. However, enzyme-aided extraction at pH 6 was applicable only at relatively low (10%) solid content, whereas at 20% solid content, alkaline conditions

DOI: 10.1021/acs.jafc.5b01077
J. Agric. Food Chem. 2015, 63, 2997–3003

could more effectively improve protein recovery than pectinase treatment.

The highest protein yield (53% of total protein) was obtained by enzymatic treatment of the defatted press cake for 2 h at 40% solid content and subsequent alkaline extraction for 1 h at 10% solid content (Figure 2). A similar amount of protein was previously recovered during 48 h of pectinase treatment of a nondefatted rapeseed press cake at 10% solid content, pH 6.[8] At the highest, >80% of the total protein had been extracted at pH 11−12, ca. 5% solid content[19] and upon enzymatic hydrolysis of the proteins into peptides.[21] The effect of enzymatic hydrolysis was less profound than in the previous study,[8] in which pectinase treatment increased protein extractability by 73% in comparison to the reference treatment. In the present study, the enzymatic hydrolysis may have been less extensive due to reduced enzyme dosage and treatment time. According to protein patterns visualized by reducing SDS-PAGE, no selective extraction of the major rapeseed proteins occurred (Figure 3, lanes 2−5).

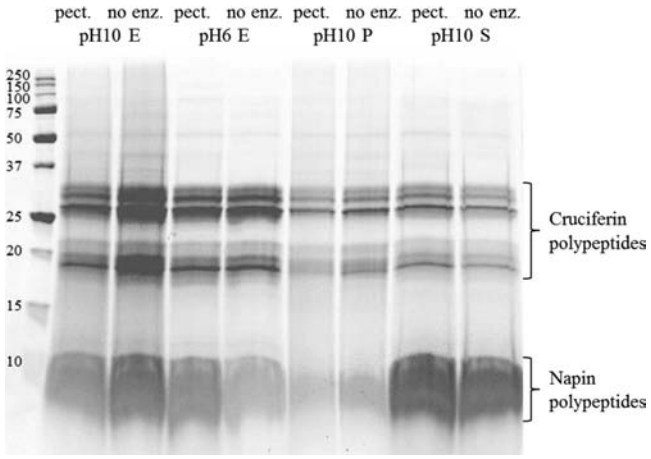

Figure 3. Protein patterns of the alkaline (pH10 E) and water extracts (pH6 E), isoelectric precipitates (pH10 P), and supernatants after isoelectric precipitation (pH10 S), as analyzed by SDS-PAGE in reducing conditions. The fractions were obtained after pectinase or reference (no enzyme) treatment of defatted rapeseed press cake at 40% solid content followed by extraction at 20% solid content and isoelectric precipitation of proteins from the alkaline extracts.

Effect of Enzymatic Treatment and Total Solid Content on Protein Precipitation. Precipitation of alkali-extracted proteins was carried out at pH 4, at which cruciferin (p*I* 4−7) was expected to have very low solubility.[25,26] However, upon acidification to pH 4, only 35−64% of the total extracted protein precipitated (Table 1). An expected factor for the limited precipitation yield was that napin, which constitutes 20% of rapeseed proteins, was positively charged and not prone to precipitation at pH 4. This was also shown in the SDS-PAGE patterns of the precipitates and the supernatants after isoelectric precipitation (Figure 3, lanes 5−8), where the precipitates (pH10 P) contained mainly cruciferin polypeptides and the supernatants (pH10 S) were enriched with napin polypeptides. Interference from nonprotein compounds in the extracts is another factor that probably contributed to the low protein precipitation yield. Anionic carbohydrates and proteins are known to interact through electrostatic interactions, and depending on the charge state of the proteins, either repulsion or formation of soluble or insoluble complexes can occur.[27] Isoelectric precipitation of cruciferin at pH 4 could have therefore been hindered by the formation of soluble complexes between negatively charged pectic carbohydrates and cruciferin, which, on the basis of its p*I* range (4−7), is suggested to have possessed a weak positive charge at pH 4.[5] The proposed cationic state of cruciferin is in accordance with a previous study on the surface charge of cruciferin-rich protein isolates as a function of pH.[28]

Proteins in the alkaline extracts were significantly less prone to precipitation after enzymatic treatment ($p < 0.05$ Tukey's test) (Table 1, precipitated protein/extracted protein). These extracts most probably contained partially hydrolyzed pectin with lower molecular weight, higher surface charge, and lower degree of esterification due to the pectin esterase activity of Pectinex.[29,30] Because the strength of pectin−protein complexes is affected by pectin molecular mass and degree of esterification,[31] the low-molecular-weight hydrolysis products of pectin may have formed stronger interactions with cruciferin at pH 4, limiting its aggregation and precipitation (Table 1).

Composition of Water Extracts and Isoelectric Precipitates. Water extracts and isoelectric precipitates (one representative from each of the four replicate samples) from extraction at 20% total solid content were characterized for chemical composition and solution behavior. In the water extracts (pH6 E), 16−29% of the total dry mass was recovered, comprising 38−47% protein and 48−52% carbohydrates (Table 2). By contrast, only 17−18% of the total dry mass was recovered in the isoelectric precipitates (pH10 P). In comparison to the extracts, the precipitates had a slightly higher protein content of 57−66% and contained 11−13% of carbohydrates and 5−6% of ash on dry matter basis. The composition is similar to that reported by Karaca et al.[18] The presence of carbohydrates and ash most probably results from

Table 1. Protein Yield in the Isoelectric Precipitates (pH10 P) Obtained after Pectinase and Reference (No Enzyme) Treatment of Defatted Rapeseed Press Cake Followed by Alkaline Extraction and Isoelectric Precipitation[a]

sample (pH10 P)	solid content in treatment (%)	solid content in extraction (%)	precipitated protein/total protein (%)	precipitated protein/extracted protein (%)
no enzyme	40	20	29.7 ± 3.2 (C)	63.9 ± 1.4 (E)
pectinase	40	20	25.6 ± 3.0 (BC)	53.1 ± 5.5 (CD)
no enzyme	40	10	28.0 ± 6.7 (BC)	60.3 ± 4.4 (DE)
pectinase	40	10	22.7 ± 2.5 (ABC)	42.4 ± 3.0 (AB)
no enzyme	20	10	20.3 ± 0.6 (AB)	49.4 ± 2.7 (BC)
pectinase	20	10	15.1 ± 1.3 (A)	34.9 ± 4.2 (A)

[a]Yields were calculated as the proportion of total or alkali-extracted nitrogen that was recovered in the precipitates. ± values represent standard deviations of two parallel extractions performed after each of the two replicate enzyme or reference treatments ($N = 4$). The sample points were categorized into subsets (A−E) on the basis of Tukey's test ($p < 0.05$).

DOI: 10.1021/acs.jafc.5b01077
J. Agric. Food Chem. 2015, 63, 2997−3003

Table 2. Protein, Carbohydrate, and Ash Concentrations of Rapeseed Isoelectric Precipitates (pH10 P) and Water Extracts (pH6 E)[a]

sample	protein (% dm)	total carbohydrates (% dm)	ash (% dm)
no enzyme pH10 P	65.6	10.7	10.1
pectinase pH10 P	57.3	13.1	10.1
no enzyme pH6 E	47.3	47.6	6.0
pectinase pH6 E	37.8	51.7	7.7

[a]The precipitates were obtained after pectinase or reference treatment (no enzyme) of rapeseed press cake at 40% solid content, followed by alkaline extraction at 20% solid content and isoelectric precipitation. The water extracts were obtained after extraction of protein from the pectinase and reference-treated samples without pH adjustment. The concentrations represent an average result from two parallel analyses.

the fact that the precipitates were not washed after centrifugation to prevent redissolution of proteins. The undefined 18−24% of dm was expected to include phenolic compounds such as condensed tannins and phenolic acids, which are strongly coextracted with rapeseed proteins in alkaline conditions.[32]

On the basis of the protein patterns visualized by SDS-PAGE, the isoelectric precipitates seemed more enriched in cruciferin, whereas no clear difference was observed in the intensities of the cruciferin and napin bands in the water extracts. After pectinase treatment, the majority of the extracted neutral carbohydrates were in the form of monosaccharides (mainly glucose, fructose, arabinose, and galactose), whereas without enzymatic treatment, mainly polysaccharides were present in the water extracts (data not shown). This is consistent with the results of our earlier study in which the pectinase and glucanase activities in Pectinex Ultra SP-L partially hydrolyzed rapeseed carbohydrates into monosaccharides and uronic acids.[8]

Solution Behavior of Water Extracts and Isoelectric Precipitates. Solubility of proteins in the isoelectric precipitates (pH10 P) and water extracts (pH6 E) was determined at pH 4 and 8. As expected, the solubility was pH-dependent: at pH 4, which is close to the p*I* range of cruciferin, only 6−13% of the protein among different samples was soluble, whereas at pH 8 the protein solubility varied between 20 and 41% (Table 3). The isoelectric precipitates generally contained less soluble protein in comparison to the water extracts. Similar solubility differences between rapeseed protein extracts and isoelectric precipitates were also reported by Karaca et al.[18] and Yoshie-Stark et al.[26] Lower protein solubility in the precipitates at pH 4 can be partially explained by the higher proportion of cruciferin in these samples, because the solubility of cruciferin was expected to be highly reduced at pH 4. In addition, it has been suggested that the lower solubility of oilseed isoelectric precipitates regardless of pH is related to possible partial denaturation of the protein during their production.[33] In the current study, SDS-PAGE analysis in nonreducing conditions (data not shown) revealed faint, smeared bands in the high molecular weight region of the isoelectric precipitates, indicating formation of non-native disulfide bonds as a result of partial polypeptide unfolding. Proteins are known to be prone to partial denaturation in alkaline conditions, and thus partial unfolding may have occurred during the alkaline extraction.[34] Because high protein solubility is usually associated with better technological functionality,[17] minimal processing in mild conditions can be favorable for the production of rapeseed protein ingredients for food and cosmetics applications.

Table 3. Solubility and ζ-Potential of the Supernatants Obtained after Dispersing the Isoelectric Precipitates and Dried Water Extracts in Water at pH 4 and 8[a]

	soluble protein/total protein (%)		zeta potential (mV)	
sample	pH 4	pH 8	pH 4	pH 8
no enzyme pH10 P	6.2 ± 0.1	25.1 ± 0.2	8.7 ± 0.2	−21.9 ± 1.9
pectinase pH10 P	6.4 ± 0.1	19.8 ± 0.1	10.2 ± 0.2	−21.3 ± 2.4
no enzyme pH6 E	13.4 ± 0.0	40.7 ± 0.1	−1.6 ± 0.6	−6.4 ± 0.5
pectinase pH6 E	10.2 ± 0.0	39.1 ± 0.1	−5.7 ± 0.6	−11.4 ± 0.3

[a]The isoelectric precipitates (pH10 P) were obtained after pectinase or reference treatment (no enzyme) of rapeseed press cake at 40% solid content followed by alkaline extraction at 20% solid content and isoelectric precipitation. The water extracts (pH6 E) were obtained after extraction of proteins from the pectinase and reference-treated samples without pH adjustment. ± values represent standard deviations of two parallel analyses for solubility and at least three parallel analyses for zeta potential.

The soluble fractions obtained from the protein dispersions were further characterized by ζ-potential (describing the net charge of the particles in the media) and particle size measurements to obtain insights on their dispersion stability. At acidic pH, ζ-potential values for the water extracts (pH6 E) obtained after pectinase and reference treatment were around −6 and −2 mV, respectively (Table 3). Isoelectric precipitates (pH10 P), on the other hand, attained positive ζ-potential values around +9 mV at pH 4, supporting the fact that cruciferin most probably possessed a weak positive charge at this pH. The proximity of the ζ-potentials to zero was in accordance with the low solubility of both products at pH 4. At pH 8, ζ-potentials of the water extracts were −11 and −6 mV with and without pectinase treatment, respectively, whereas isoelectric precipitates attained a higher negative charge around −21 mV. The net charge of isoelectric precipitates was not influenced by enzymatic treatment, whereas in the water extracts, the more negative charge of the enzymatically treated samples may be related to the de-esterification and depolymeration of pectin by the pectin esterase and polygalacturonase activities of Pectinex[29,30] and the resultant exposure of polar groups.[31]

Higher surface charge of proteins is generally associated with improved solubility.[35] However, the isoelectric precipitates, which attained stronger net charges, showed lower protein solubility than the water extracts, which attained net charges closer to zero (Table 3). This inverse relationship between solubility and net charge was more clearly seen at pH 8. Similar results were obtained by Karaca et al. when comparing rapeseed protein isolates prepared by isoelectric precipitation and salt extraction.[18] The low solubility of isoelectric precipitates may be related to partial denaturation during alkaline extraction, as indicated by the smears in nonreducing SDS-PAGE. Furthermore, soluble carbohydrates (Table 2) most probably contributed to the improved protein solubility of the water extracts. As previously discussed, protein solubility in the water extracts may have been increased by the formation of soluble complexes between oppositely charged proteins and pectic carbohydrates.[36] Similar mechanisms are well documented in

DOI: 10.1021/acs.jafc.5b01077
J. Agric. Food Chem. 2015, 63, 2997−3003

milk[37] and soy protein systems,[38] where attachment of pectin on protein particles rendered electrostatic and steric stabilization against sedimentation.

Particle size distribution in the supernatants of the protein dispersions was determined at pH 8, at which at least 20% of the protein was soluble. The water extract (pH6 E) samples contained mainly particles of 10 nm in diameter (constituting 15−20% of the sample volume), whereas the dominant particle size in the isoelectric precipitate (pH10 P) samples was remarkably higher and closer to 50 nm (Figure 4). Changes in

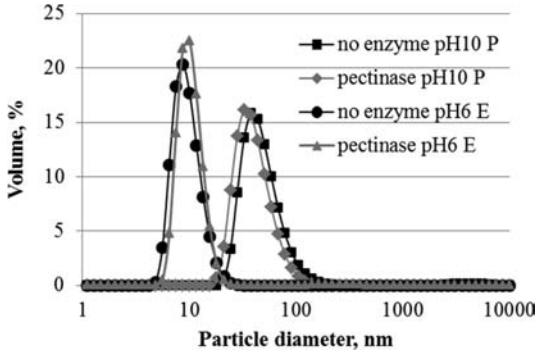

Figure 4. Volume-based particle size distribution in the supernatants obtained after dispersing the isoelectric precipitates and dried water extracts in water at pH 8. The isoelectric precipitates (pH10 P) were obtained after pectinase or reference (no enzyme) treatment of defatted rapeseed press cake at 40% solid content followed by alkaline extraction at 20% solid content and isoelectric precipitation. The water extracts (pH6 E) were obtained after extraction of proteins from the pectinase and reference-treated samples without pH adjustment.

particle size during storage were also monitored by carrying out measurements for the diluted, filtered samples, which were stored in the cuvettes at 25 °C for 24 h. A gradual increase in particle size of the isoelectric precipitate samples was observed, whereas absolutely no change occurred in the particle size distribution of the water extract samples (data not shown). The results support the proposed electrostatic and steric stabilization of protein particles by anionic carbohydrates in the water extracts.

The volume-based mean diameter of the protein particles in the water extract samples was around 10 nm, which corresponds to the reported size of rapeseed globulins measured by small-angle X-ray scattering.[39] By contrast, larger mean diameter in the isoelectric precipitate samples suggests that the precipitates contained aggregates of several monomers formed either via physical or chemical interactions. The formation of disulfide-linked soluble aggregates in the isoelectric precipitates was likewise observed by nonreducing SDS-PAGE (data not shown). Limited dispersion stability in the precipitate samples may have resulted from both partial protein denaturation and reduced concentration of stabilizing pectic carbohydrates. Additionally, it should be noted that apart from charged carbohydrates, other components in the water extracts and isoelectric precipitates may also have influenced the dispersion stability. Although not analyzed in this study, the aqueous extracts from rapeseed press cake commonly contain phytates and phenolics, which interact and form insoluble complexes with proteins.[18,32] Pectin has been reported to solubilize protein−phenolic aggregates, which may have further contributed to the better dispersion stability of the crude water extracts in comparison to the isoelectric precipitates.[31]

Our results suggest that alkaline extraction and isoelectric precipitation, which are commonly used to recover protein from rapeseed press cake, could be replaced by enzyme-aided aqueous extraction without pH adjustment in dilute conditions. Enzymatic hydrolysis of carbohydrates improved the recovery of protein extracts at pH 6 but did not introduce improvements in alkaline extraction. By contrast, enzyme treatment hindered the recovery of protein from alkaline extracts by isoelectric precipitation. Pectinase treatment was feasible also at high (40%) total solid content, which could open up possibilities for water-lean fractionation technologies. However, extraction of rapeseed protein at increased solid content is suggested to require the use of alkali due to the limited efficiency of water extraction in these conditions. Crude water extracts from pH 6 extraction had better protein solubility and dispersion stability than isoelectric precipitates from alkaline extraction. Different solution properties of these fractions are proposed to be caused by stabilizing electrostatic interactions of proteins and anionic pectic carbohydrates in the water extracts and partial denaturation of proteins in the isoelectric precipitates.

AUTHOR INFORMATION

Corresponding Author

*(K.R.) Phone: +358 20 722 4514. Fax: +358 20 722 7071. E-mail: katariina.rommi@vtt.fi.

Funding

The research leading to these results has received funding from the European Community's Seventh Framework Programme FP7/2007-2013 under Grant Agreement 289170-APROPOS. In addition, we gratefully acknowledge funding from the Academy of Finland to Kaisa Poutanen.

Notes

The authors declare no competing financial interest.

ACKNOWLEDGMENTS

We thank Kankaisten Öljykasvit Oy for the rapeseed press cake, Tuija Kössö for the mechanical pretreatment and supercritical carbon dioxide extraction, and Atte Mikkelson for the carbohydrate analyses. We asknowledge with gratitude the experimental work performed by Mariitta Svanberg, Nina Vihersola, and Heljä Heikkinen at VTT Technical Research Centre of Finland.

REFERENCES

(1) Newkirk, R. W.; Classen, H. L.; Edney, M. J. Effects of prepress-solvent extraction on the nutritional value of canola meal for broiler chickens. *Anim. Feed Sci. Technol.* **2003**, *104*, 111−119.

(2) Bell, J. M.; Keith, M. O. A survey of variation in the chemical composition of commercial canola meal produced in western Canadian crushing plants. *Can. J. Anim. Sci.* **1991**, *71*, 469−480.

(3) Höglund, A.; Rödin, J.; Larsson, E.; Rask, L. Distribution of napin and cruciferin in developing rape seed embryos. *Plant Physiol.* **1992**, *98*, 509−515.

(4) Bérot, S.; Compoint, J. P.; Larré, C.; Malabat, C.; Guéguen, J. Large scale purification of rapeseed proteins (*Brassica napus* L.). *J. Chromatogr., B* **2005**, *818*, 35−42.

(5) Wu, J.; Muir, A. D. Comparative structural, emulsifying, and biological properties of 2 major canola proteins, cruciferin and napin. *J. Food Sci.* **2008**, *73*, 210−216.

(6) Sawada, M. M.; Venâncio, L. L.; Toda, T. A.; Rodrigues, C. E. C. Effects of different alcoholic extraction conditions on soybean oil yield, fatty acid composition and protein solubility of defatted meal. *Food Res. Int.* **2014**, *62*, 662−670.

DOI: 10.1021/acs.jafc.5b01077
J. Agric. Food Chem. 2015, 63, 2997−3003

(7) Salleh, M. R. B. M.; Maruyama, N.; Adachi, M.; Hontani, N.; Saka, S.; Kato, N.; Ohkawa, Y.; Utsumi, S. Comparison of protein chemical and physicochemical properties of rapeseed cruciferin with those of soybean glycinin. *J. Agric. Food Chem.* **2002**, *50*, 7380−7385.
(8) Rommi, K.; Hakala, T. K.; Holopainen, U.; Nordlund, E.; Poutanen, K.; Lantto, R. Effect of enzyme-aided cell wall disintegration on protein extractability from intact and dehulled rapeseed (*Brassica rapa* L. and *Brassica napus* L.) press cakes. *J. Agric. Food Chem.* **2014**, *62*, 7989−7997.
(9) Schöne, F.; Kirchheim, U.; Schumann, W.; Lüdke, H. Apparent digestibility of high-fat rapeseed press cake in growing pigs and effects on feed intake, growth and weight of thyroid and liver. *Anim. Feed Sci. Technol.* **1996**, *62*, 97−110.
(10) Manamperi, W. a R.; Wiesenborn, D. P.; Chang, S. K. C.; Pryor, S. W. Effects of protein separation conditions on the functional and thermal properties of canola protein isolates. *J. Food Sci.* **2011**, *76*, 266−273.
(11) Moure, A.; Sineiro, J.; Domínguez, H.; Parajó, J. C. Functionality of oilseed protein products: a review. *Food Res. Int.* **2006**, *39*, 945−963.
(12) Catchpole, O. J.; Tallon, S. J.; Grey, J. B.; Fletcher, K.; Fletcher, A. J. Extraction of lipids from a specialist dairy stream. *J. Supercrit. Fluids* **2008**, *45*, 314−321.
(13) Sun, M.; Xu, L.; Saldaña, M. D. A.; Temelli, F. Comparison of canola meals obtained with conventional methods and supercritical CO_2 with and without ethanol. *J. Am. Oil Chem. Soc.* **2008**, *85*, 667−675.
(14) Kaukonen, O.; Sontag-Strohm, T.; Salovaara, H.; Lampi, A.-M.; Sibakov, J.; Loponen, J. Foaming of differently processed oats: role of nonpolar lipids and tryptophanin proteins. *Cereal Chem.* **2011**, *88*, 239−244.
(15) Konak, Ü. İ.; Ercili-Cura, D.; Sibakov, J.; Sontag-Strohm, T.; Certel, M.; Loponen, J. CO_2-defatted oats: solubility, emulsification and foaming properties. *J. Cereal Sci.* **2014**, *88*, 37−41.
(16) Ghodsvali, A.; Khodaparast, M. H. H.; Vosoughi, M.; Diosady, L. L. Preparation of canola protein materials using membrane technology and evaluation of meals functional properties. *Food Res. Int.* **2005**, *38*, 223−231.
(17) Aluko, R. E.; McIntosh, T. Polypeptide profile and functional properties of defatted meals and protein isolates of canola seeds. *J. Sci. Food Agric.* **2001**, *81*, 391−396.
(18) Karaca, A. C.; Low, N.; Nickerson, M. Emulsifying properties of canola and flaxseed protein isolates produced by isoelectric precipitation and salt extraction. *Food Res. Int.* **2011**, *44*, 2991−2998.
(19) Klockeman, D. M.; Toledo, R.; Sims, K. A. Isolation and characterization of defatted canola meal protein. *J. Agric. Food Chem.* **1997**, *45*, 3867−3870.
(20) Tang, Q. N. Protein concentrates and isolates, and processes for the production thereof. Protein concentrates and isolates, and processes for the production thereof. US 2010/0136173 A1, 2010.
(21) Niu, Y. X.; Li, W.; Zhu, J.; Huang, Q.; Jiang, M.; Huang, F. Aqueous enzymatic extraction of rapeseed oil and protein from dehulled cold-pressed double-low rapeseed cake. *Int. J. Food Eng.* **2012**, *8*, 1−14.
(22) Kane, P. F. $CuSO_4$-TiO_2 as Kjeldahl digestion catalyst in manual determination of crude protein in animal feeds. *J. Assoc. Off. Anal. Chem.* **1986**, *69*, 664−666.
(23) Tenkanen, M.; Siika-Aho, M. An *alpha*-glucuronidase of *Schizophyllum commune* acting on polymeric xylan. *J. Biotechnol.* **2000**, *78*, 149−161.
(24) Sluiter, A.; Hames, B.; Ruiz, R.; Scarlata, C.; Sluiter, J.; Templeton, D.; Crocker, D. Determination of structural carbohydrates and lignins in biomass. In *Laboratory Analytical Procedure (LAP)*; National Renewable Energy Laboratory: Golden, CO, USA, 2008; 18 pp.
(25) Wanasundara, J. P. D.; Abeysekara, S. J.; McIntosh, T. C.; Falk, K. C. Solubility differences of major storage proteins of Brassicaceae oilseeds. *J. Am. Oil Chem. Soc.* **2012**, *89*, 869−881.
(26) Yoshie-Stark, Y.; Wada, Y.; Wäsche, A. Chemical composition, functional properties, and bioactivities of rapeseed protein isolates. *Food Chem.* **2008**, *107*, 32−39.
(27) Klassen, D. R.; Elmer, C. M.; Nickerson, M. T. Associative phase separation involving canola protein isolate with both sulphated and carboxylated polysaccharides. *Food Chem.* **2011**, *126*, 1094−1101.
(28) Cheung, L.; Wanasundara, J.; Nickerson, M. T. The effect of pH and NaCl levels on the physicochemical and emulsifying properties of a cruciferin protein isolate. *Food Biophys.* **2014**, *9*, 105−113.
(29) Mikeš, O.; Sedláčková, J.; Rexová-Benková, L.; Omelková, J. High-performance liquid chromatography of pectic enzymes. *J. Chromatogr., A* **1981**, *207*, 99−114.
(30) Gonzalez, S. L.; Rosso, N. D. Determination of pectin methylesterase activity in commercial pectinases and study of the inactivation kinetics through two potentiometric procedures. *Cienc. Tecnol. Aliment.* **2011**, *31*, 412−417.
(31) Zhao, G.-Y.; Diao, H.-J.; Zong, W. Nature of pectin-protein-catechin interactions in model systems: pectin-protein-catechin interactions. *Food Sci. Technol. Int.* **2013**, *19*, 153−165.
(32) Xu, L.; Diosady, L. L. Interactions between canola proteins and phenolic compounds in aqueous media. *Food Res. Int.* **2000**, *33*, 725−731.
(33) Krause, J.-P.; Schultz, M.; Dudek, S. Effect of extraction conditions on composition, surface activity and rheological properties of protein isolates from flaxseed (*Linum usitativissimum* L). *J. Sci. Food Agric.* **2002**, *82*, 970−976.
(34) Ma, C.-Y.; Harwalkar, V. R.; Paquet, A. Physicochemical properties of alkali-treated oat globulin. *J. Agric. Food Chem.* **1990**, *38*, 1707−1711.
(35) Kramer, R. M.; Shende, V. R.; Motl, N.; Pace, C. N.; Scholtz, J. M. Toward a molecular understanding of protein solubility: increased negative surface charge correlates with increased solubility. *Biophys. J.* **2012**, *102*, 1907−1915.
(36) Stone, A. K.; Teymurova, A.; Dang, Q.; Abeysekara, S.; Karalash, A.; Nickerson, M. T. Formation and functional attributes of electrostatic complexes involving napin protein isolate and anionic polysaccharides. *Eur. Food Res. Technol.* **2014**, *238*, 773−780.
(37) Tromp, R. H.; de Kruif, C. G.; van Eijk, M.; Rolin, C. On the mechanism of stabilisation of acidified milk drinks by pectin. *Food Hydrocolloids* **2004**, *18*, 565−572.
(38) Tran, T.; Rousseau, D. Stabilization of acidic soy protein-based dispersions and emulsions by soy soluble polysaccharides. *Food Hydrocolloids* **2013**, *30*, 382−392.
(39) Plietz, P.; Damaschun, G.; Müller, J. J.; Schwenke, K.-D. The structure of 11-S globulins from sunflower and rape seed: a small-angle X-ray scattering study. *Eur. J. Biochem.* **1983**, *130*, 315−320.

DOI: 10.1021/acs.jafc.5b01077
J. Agric. Food Chem. 2015, 63, 2997−3003

In general, studies are focused on the effect of bentonite fining on fermentative and varietal aroma compounds in finished wines.[15,18] Moreover, very few works have studied the effects on aroma compounds of the use of bentonite in musts,[19,20] and only two previous works have considered bentonite addition during fermentation for a Macabeo wine.[20,21] In this way, bentonite fining may affect both the production and the loss of fermentative compounds. The relationship between grape varieties, protein content, and protein stability has been briefly described up to now. The relationship of varieties such as Sauvignon Blanc[22] and Macabeo[23] and protein stability has been largely described, but for other varieties like Albariño, there is no information available.

To avoid the risk of haze in bottled wine, bentonite treatment is often done to remove unstable proteins and protect the wine. However, this is a nonselective treatment, with the result that some of the proteins associated with the good characteristics of the wine are removed as well. This fact makes oenologists especially concerned when applying bentonite for protein stability.

The main objective of this work was to determine the best time for treatment with bentonite in a white wine of the Albariño variety both from the standpoint of protein stability and the preservation of aromas, minimizing the bentonite dose.

MATERIALS AND METHODS

Fermentation Process. The winemaking of Albariño wines was performed on a pilot scale in the "Estación Experimental de Viticultura y Enoloxía de Ribadumia EGEVA—INGACAL" (Pontevedra, SPAIN) between September and October of 2012. Grapes berries used came from the same vineyard (Ribadumia, Pontevedra; D.O. Rías Baixas, Subzone Salnés, Spain), the soil of which has a granitic rock origin, and vines were planted on 2001 on a V trellis conduction system, at a density of 4.000 pl/Ha, over 196−17 Castel rootstock. Albariño grapes were hand harvested in plastic trails of 20 kg, received 8 g/hL of potassium metabisulphite and 6.67 g/hL of ascorbic acid before the pressing of whole clusters in a pneumatic press (Bucher, Vaslin X pro), and then distributed to the different tanks according to each treatment.

Each tank contained the free run juice or juice obtained at low pressures ($\leq$1.0 kg/cm^2) and treated with 5 g/100 kg of grapes of pectolytic extractive enzymes (Lafazym press, Laffort, Bordeaux, France). Juice clarification was done at low temperatures (18 °C for 48 h), except for the tank clarified also with bentonite as part of the treatments in the study.

The volume of the fermentation stainless steel tanks was 30 L, filled up to the recommended height (85% of the tank volume), and the process was carried out in triplicate. Temperature and density controls were carried out on a daily basis according to the center protocols for this variety in the same way as every addition or treatment was usually made. Fermentation was carried out with the commercial yeast IOC-18-2007 (Institut Oenologique de Champagne, Reims, France) in a dose of 30 g/hL. In addition, during fermentation, two different nutrients were used: 15 g/hL of Nutriferm (Enartis, Vilafranca del Penedès, Spain) and 10 g/hL Helper (Oenofrance, Bordeaux, France). Fermentation was carried out around 18 °C until dry wines were obtained.

Once alcoholic fermentation finished, 6.5 g/hL of potassium metabisulphite was added in order to keep 3.5 g/hL of free sulfur dioxide and the wines were kept at 12 °C the first 2 days and later at 8 °C until tartaric and protein stabilization treatments were applied. Tartaric stabilization treatment was done during 9 days at −6 °C in a cold chamber. Before bottling, wines were filtered with a cellulose plates filter AF-110, checking before that free sulfur dioxide was between 3.0−3.5 g/hL.

Bentonite Treatments. A dose of 40 g/hL bentonite was decided together with the oenological center, considering the stabilizing treatment done in previous years. The bentonite used was natural sodium granular bentonite (Microcol-Alpha, Laffort; Bordeaux, France). The bentonite treatments were performed to grape juice before alcoholic fermentation and removing this bentonite by settling before starting fermentation, at the beginning of alcoholic fermentation, in the middle of alcoholic fermentation, and at the end of alcoholic fermentation. An untreated fermentation without application of bentonite was used as a control.

Protein Analysis by Bradford's Method. Total protein concentration was measured by Bradford's method using Coomassie brilliant blue reagent. Under acidic conditions, the red form of the dye is converted into its bluer form upon binding to protein. This change was assayed at 595 nm on a spectrophotometer (Cecil CE2021, Cambridge, England) after 5 min of incubation.[24] The anionic (bound) form of the dye has a maximum absorption spectrum historically held to be at 595 nm. The cationic (unbound) forms are green or red. Binding of the dye to the protein stabilizes the blue anionic form. The increase of absorbance at 595 nm is proportional to the amount of bound dye and thus to the concentration of protein present in the sample. The protein content was expressed as mg/L of bovine serum albumin (BSA; Sigma, cat. no. A-3803, Madrid, Spain). Unlike other protein assays, the Bradford protein assay is less susceptible to interference by various chemicals that may be present in protein samples. All analyses were done in triplicate.

Fast Protein Liquid Chromatography (FPLC). Samples of 200 mL of each must, wine, or sample obtained during fermentation were centrifuged at 4000*g* for 5 min at 4 °C. Aliquots of 45 mL of the supernatant were immediately dialyzed for 72 h in three dialysis tubes (SIGMA, dialysis tubing−cellulose membrane, D-9652, Madrid, Spain) to remove salts and other low molecular weight compounds. The dialyzed samples were lyophilized and kept at −20 °C. The lyophilized samples were resuspended in freshly obtained pure deionized water (15 × 106 W/cm) until the protein concentration was about 0.5 mg/mL, expressed as BSA. The samples were centrifuged 12000*g* for 2 min at 4 °C and frozen again. On the day of the analysis, they were lyophilized again and resuspended in 0.6 mL of 0.3 M ammonium acetate solution (pH 6.80) to obtain a protein concentration of 0.25 μg/μL. The samples were centrifuged (5 min at 12000*g*, 4 °C), and the supernatants were used directly for FPLC analysis.[25] Analyses were carried out with a Superdex 75 PC 3.2/30 column on an FPLC system (Smart System, Pharmacia, Uppsala, Sweden). The samples (50 μL) were injected and eluted with a 0.3 M ammonium acetate solution (pH 6.80) at a flow rate of 40 μL/min. The column eluents were continuously monitored at 280 nm using a μPeak Monitor (Pharmacia, Uppsala, Sweden).

Determination of Bentonite Dose. The treatment with bentonite included a preliminary test that use a variety of different dose (5−100 g/hL) so that the most appropriate dose could be determined. For every treatment a heat stability test was applied.

Heat Stability Test. A wine sample of 20 mL was filtered through a cellulose nitrate membrane with a pore size of 0.45 μm (Whatman, catalogue no. 7184009, England) and heated for 2 h at 80 °C in a bath equipped with a digital control immersion thermostat (Digiterm 100 model). It was then incubated for 2 h at 4 °C. Finally, the turbidity was measured by nephelometry (Turbiquant 1000 IR turbidimeter) and expressed in nephelometric turbidity units (NTU). The difference in turbidity between the initial wine and the wine after the thermal test was proportional to protein instability. The wines were considered stable if this difference did not exceed 2 NTU.[4] All analyses were carried out in triplicate.

Chemical Analysis of Musts and Wines. Basic parameters of wines (alcohol content, residual sugars, pH, titratable and volatile acidity, tartaric, malic, and lactic acids) were determined by Fourier transform infrared spectrometry (FTIR) using a Bacchus II analyzer (TDI, Barcelona, Spain) calibrated according to the official methods for wine analysis (EC Regulation 479/2008). The spectra were obtained in triplicate and averaged for each sample. In addition, density, total dry matter, and free and total sulfur dioxide were determined using methods of the OIV (June 2012).

DOI: 10.1021/acs.jafc.5b00993
J. Agric. Food Chem. 2015, 63, 3004−3011

Table 1. Chemical Analysis of White Wines Obtained after Bentonite Treatment at a Pilot Scale of the Albariño Grape Variety (Average ± Standard Deviation)

wine (dosing time)	alcohol content (% v/v)[a]	volatile acidity (g acetic acid/L)[a]	total acidity (g tartaric acid/L)[a]	pH[a]	residual sugar (g/L)[a]
must clarification	14.01 ± 0.28 a	0.29 ± 0.01 a	6.82 ± 0.14 c	3.20 ± 0.03 a	3.15 ± 0.03 c
beginning of fermentation	14.22 ± 0.28 a	0.31 ± 0.02 a	7.27 ± 0.15 a	3.11 ± 0.03 b	3.72 ± 0.04 a
middle of fermentation	13.93 ± 0.26 a	0.31 ± 0.02 a	6.92 ± 0.14 bc	3.11 ± 0.03 b	3.74 ± 0.04 a
end of fermentation	13.93 ± 0.28 a	0.29 ± 0.01 a	7.19 ± 0.14 ab	3.10 ± 0.03 b	3.39 ± 0.03 b
control	14.03 ± 0.28 a	0.29 ± 0.01 a	7.34 ± 0.15 a	3.09 ± 0.03 b	3.49 ± 0.03 b

[a]Different letters indicate a significant difference ($p \leq 0.05$) for different wine treatments.

Table 2. Protein Content, Stability, Bentonite Stabilizing Dose, Bentonite Total Dose, and Protein Profile by FLPC of Musts and Wines Treated with Bentonite at Different Vinification Stages for Albariño Wines

dosing time	sample	protein content (mg BSA/L)	F1 protein content (mg BSA/L)	F2 protein content (mg BSA/L)[a]	F3 protein content (mg BSA/L)[a]	bentonite stabilizing dose (g/hL)	bentonite total treatment (g/hL)
must	free run juice (with enzyme)	40.8 ± 0.6	0.5 ± 0.0	5.4 ± 0.4	23.3 ± 0.3	40	80
	clarified must (with bentonite)	35.1 ± 0.4	0.0 ± 0.0	2.2 ± 0.3	14.2 ± 1.4		
	dry wine	32.7 ± 0.1	0.0 ± 0.0	1.9 ± 0.0	11.1 ± 0.3		
	stable wine	28.5 ± 0.6	0.0 ± 0.0	0.4 ± 0.0	3.0 ± 0.0		
beginning of fermentation	clarified must (with enzyme)	39.6 ± 0.5	0.6 ± 0.1	5.8 ± 0.1	26.3 ± 0.4	10	50
	pretreatment	38.7 ± 0.6	0.6 ± 0.1	8.0 ± 0.5	28.4 ± 2.9		
	24 h post-treatment	30.1 ± 1.0	0.6 ± 0.2	4.3 ± 0.4	19.7 ± 4.0		
	dry wine	31.5 ± 0.2	0.0 ± 0.0	1.0 ± 0.4	4.9 ± 0.9		
	stable wine	26.4 ± 0.2	0.0 ± 0.0	1.1 ± 0.2	4.5 ± 0.1		
middle of fermentation	clarified must (with enzyme)	39.6 ± 0.5	0.6 ± 0.1	5.8 ± 0.1	26.3 ± 0.4	0	40
	pretreatment	38.8 ± 0.5	1.0 ± 0.1	9.1 ± 0.2	32.8 ± 0.4		
	24 h post-treatment	26.2 ± 0.4	0.2 ± 0.1	4.2 ± 0.2	23.0 ± 0.1		
	dry wine	29.5 ± 0.1	0.0 ± 0.0	1.8 ± 0.0	6.1 ± 0.1		
	stable wine	26.9 ± 0.3	0.0 ± 0.0	0.7 ± 0.1	5.7 ± 0.0		
end of fermentation	clarified must (with enzyme)	39.6 ± 0.5	0.6 ± 0.1	5.8 ± 0.1	26.3 ± 0.4	0	40
	pretreatment	36.9 ± 0.4	1.1 ± 0.1	4.8 ± 0.7	25.3 ± 0.4		
	24 h post-treatment	28.0 ± 0.2	0.1 ± 0.0	2.4 ± 0.0	15.1 ± 2.1		
	dry wine	31.0 ± 0.2	0.1 ± 0.0	1.4 ± 0.1	5.1 ± 0.6		
	stable wine	26.5 ± 0.3	0.0 ± 0.0	0.7 ± 0.1	4.8 ± 0.0		
control	clarified must (with enzyme)	39.6 ± 0.5	0.6 ± 0.1	5.8 ± 0.1	26.3 ± 0.4	70	70
	dry wine	38.7 ± 0.4	0.5 ± 0.1	2.1 ± 0.6	17.0 ± 1.5		
	stable wine	26.9 ± 0.4	0.0 ± 0.0	3.0 ± 0.8	5.7 ± 0.7		

[a]Protein fractions: F1 (>100 kDa), F2 (60−40 kDa, invertase and β-glucanases), and F3 (20−30 kDa, chitinases and thaumatin like protein TLP).

Wine Sensory Analysis. A test of preference was performed with a panel of 24 untrained tasters (14 male, 10 female). Fourteen tasters had some previous tasting experience against 10 that did not have any, but none of them were professional tasters. They were asked to choose between the five different wines obtained from the four treatments and the control and to sort from the highest to the lowest preference at nose and palate. The objective was to select the best samples to contrast it with their analytical information.

Wines were tasted by the panel 5 months after being bottled. The tasting was done in the tasting laboratory of the Enology Faculty of Rovira i Virgili University (Tarragona, Spain), which has the right conditions for the wine service and tasting. Before the sensorial analysis, wine panelists tasted different wines to make sure that they understood the purpose of the tasting.

The results were analyzed using the test of Friedman, performing a global comparison of each series and then a comparison of pairs to determine the differences found by the tasters.

Aroma Profile. Because of the wide range of contents that present the volatile compounds of wines, the approach for the aroma compounds analysis was based according to groups of compounds with contents in similar order of magnitude. Thus, three analytical methodologies were used. Major volatile compounds (methanol, higher alcohols, acetaldehyde, ethyl acetate, ethyl lactate, 1-hexanol, γ-butyrolactone, and 2-phenylethanol) were determined by gas chromatography−flame ionization detection (GC−FID) using a

DOI: 10.1021/acs.jafc.5b00993
J. Agric. Food Chem. 2015, 63, 3004−3011

method of direct injection described in Blanco et al.[26] The quantification was carried out by interpolation into calibration curves obtained with model wines spiked at different levels with the pure commercial aroma compounds. For determination of minor alcohols, volatile fatty acids, ethyl esters of fatty acids, and acetates of higher alcohols, a liquid−liquid extraction (with diethyl ether−hexane (1:1 v/v)) was carried out previous to the injection in a GC−FID system according with the method described in Blanco et al.[26] For the quantification, model wines spiked at different levels with the pure commercial aroma compounds were extracted to build the calibration graphs.

For the analysis of terpenols, a solid phase extraction (SPE) was carried out according with the method described in López-Vázquez et al. with some modifications.[27] A sample of 50 mL of wine diluted with 50 mL of distilled water (spiked with 0.132 mg/L of 4-decanol as internal standard) was percolated through an Isolute ENV+ SPE cartridge (1 g). The free aroma components were eluted with 30 mL of dichloromethane; the eluate was dried with sodium sulfate and concentrated to 1.5 mL on a Vigreux column, stored at −10 °C, and immediately prior to GC analysis, further concentrated to 100 μL under a gentle nitrogen stream. The chromatographic analysis were conducted using Agilent 6890 gas chromatograph with a mass spectrometric detector (MSD) model 5973N (Agilent Technologies). The capillary column was a HP-Innowax (Agilent) (30 m × 0.25 mm i.d. and 0.25 μm of phase thickness) and the column oven program was 35 °C (2 min), at 30 °C/min to 60 °C (0.5 min), at 2 °C/min to 160 °C (10 min), and at 3 °C/min to 230 °C (10 min). Injector temperature was 250 °C, and the injection (2 μL) was in split mode 1:5. The carrier gas was helium at 1 mL/min. The mass spectrometer was operated in the electron ionization mode at a voltage of 70 eV. The temperatures of source, quadrupole, and transfer-line were 230, 150, and 220 °C, respectively. The acquisition mass range was 30−300 amu. The identification was carried out by comparison with the spectra of Nist Mass Library (rev 05) and with those obtained from the injection of the pure commercial compounds (when available). The quantification were carried out by the internal standard method, so the concentrations was expressed in μg/L equivalent of 4-decanol. Quantification ions (m/z) were the following: terpinene (105), linalool (71), hotrienol (71), α-terpineol (59), citronellol (69), nerol (69), geraniol (69), 3,7-dimethyl-1-octen-3,7-diol (71), *E*-3,7-dimethyl-1,5-octadien-3,7-diol (82), *E*-3,7-dimethyl-1,5-octadien-3,6-diol (71), and 4-decanol (55). Linear retention indexes were calculated by injection of the standards of aliphatic alkanes for each analytical method.

For theoretical estimation of the sensory importance of each compound, the odor activity values (OAV) were calculated using the formula OAV = (concentration of compound)/(odor threshold) (expressed in units of aroma [ua]) and odor thresholds published in the literature.[28−35]

Statistical Analysis. All the statistical analyses were performed with the SPSS statistical package (version 17.0, SPSS Inc., Chicago, IL, USA). One-way analysis of variance (ANOVA) was applied to the data for scale and treatment effect and Principal component analysis (PCA) was applied to compounds with odor activity value higher than 1 ua.

RESULTS AND DISCUSSION

Fermentation Kinetics and Chemical Analysis of Wines. The main characteristics of initial must used for all the experiments were: density of 1101 ± 11 kg/m^3, total acidity of 8.63 ± 0.09 g tartaric acid/L, potential alcoholic degree of 14.08 ± 0.14% v/v, and pH of 3.30 ± 0.03. Alcoholic fermentation followed a similar tendency in all fermentations, except for the must clarified with bentonite that had a faster evolution in the first 2−5 days, favored by the presence of bentonite not removed by racking.[36,37] Fermentations lasted 14 ± 2 days within a temperature range of 17 ± 2 °C.

In Table 1 are shown the main analytical parameters for each wine once stabilized and bottled. Differences in analytical values were due to the time of sampling and the analytical methods used for each case but did not represent a significant difference among the final wines from a practical point of view.

Table 3. Statistical Analysis of Preference Tests (Nose and Palate)[a]

samples compared	nose Ra − Rb[b]	palate Ra − Rb[b]
must/beginning	2.0 ns	4.0 ns
must/middle	35.0 s	4.0 ns
must/end	15.0 ns	26.0 s
must/control	3.0 ns	4.0 ns
beginning/middle	33.0 s	8.0 ns
beginning/end	13.0 ns	30.0 s
beginning/control	1.0 ns	8.0 ns
middle/end	20.0 ns	22.0 s
middle/control	32.0 s	0.0 ns
end/control	12.0 ns	22.0 s

[a]ns, not significant difference; s,: significant difference. [b]Ra − Rb: difference between ranges. Critical value Ra − Rb = 21.5 (p = 0.05).

Protein Content Evolution and Stability. The protein content, stability, bentonite stabilizing dose, bentonite total dose, and protein profile of samples obtained from the initial grape juice until the finished wine in the whole process is presented in Table 2 for each treatment and the control. Of the five wines obtained, the two treated at the end of fermentation were stable, while the other three were unstable. Unstable wines needed an additional bentonite dose of 40 and 10 g/hL for the wine obtained with the must clarified with bentonite and the wine treated at the beginning of fermentation, respectively. The control wine needed a dose of 70 g/hL for its stabilization. From these data, it can be concluded that wines treated during fermentation need less bentonite for their stabilization. Similar results were obtained by Lira et al.[20,21] and Pocock et al.,[10] for Macabeo and Sauvignon Blanc wines, respectively.

Analysis of the protein profile (Table 2) showed the presence of three fractions: F1 (>100 kDa), F2 (60−40 kDa, invertase and β-glucanases), and F3 (20−30 kDa, chitinases and thaumatin like protein TLP).[7,25,38] Fractions F1 and F2 had a lower protein concentration than F3. Fraction F1 showed a high sensitivity to bentonite treatment, as independently of the dosage during fermentation, its diminution was almost complete.

The concentration of fraction F2 in free run juice and initial musts clarified with enzymes was in the range of 5.4−5.8 mg BSA/L. Must clarified with bentonite showed a 60% decrease in fraction F2, which remained stable until the end of the fermentation and was further diminished with the additional treatment of bentonite. In wines treated at the beginning and in the middle of fermentation, there was an increase of the concentration of F2 before the treatment, probably due to yeast action, up to values between 8−9 mg BSA/L.[39] In the wine treated at the end of fermentation, there was a decrease in F2 compared with the initial content, similar to the control dry wine. The fermentation had a longer action time and followed the normal evolution with an increase of the protein content due to yeast lysis and the later diminution as an effect of the hydrolysis.[38] The final effect of bentonite dosage during fermentation led to a decrease of F2 fraction of around 50−60%, and as bentonite remained in the medium, the F2 fraction continued to decrease, as observed in dry wines.

The main fraction was F3, with an initial content in the free run juice of 23.3 ± 0.3 mg BSA/L and a content of 26.3 ± 0.4

DOI: 10.1021/acs.jafc.5b00993
J. Agric. Food Chem. 2015, 63, 3004−3011

Table 4. Volatile Compounds Analyzed in Final Wines (mg/L except Where Indicated Otherwise) and Odor Activity (OAV) Values for Compounds with OAV > 1 (Presented in Brackets)

		must clarification		beginning of fermentation		middle of fermentation		end of fermentation		control	
compd (odor threshold)	retention index calculated	average [OAV]	SD	average [OAV]	SD	average [OAV]	SD	average [OAV]	SD	average [OAV]	SD
Alcohols											
1-propanol (500[c])	1036	40.1	2.2	50.5	1.7	52.9	0.6	54.0	0.9	50.7	0.8
isobutanol (40[g])	1100	19.4	0.7	19.1	1.2	20.0	0.5	18.5	0.2	19.5	0.3
1-butanol (150[g])	1153	1.56	0.01	1.28	0.02	1.64	0.01	1.66	0.00	1.89	0.02
(2+3)-methyl-1-butanol (65[f])	1220	213 [3.28]	2	220 [3.39]	0	218 [3.36]	1	217 [3.34]	1	226 [3.47]	1
1-hexanol (8[i])	1364	2.47	0.00	1.02	0.00	2.42	0.01	1.84	0.00	1.72	0.01
t-3-hexen-1-ol (1[f])	1374	0.013	0.005	0.010	0.002	0.013	0.001	0.018	0.005	0.020	0.007
c-3-hexen-1-ol (0.4[i])	1395	0.064	0.002	0.082	0.003	0.089	0.007	0.121	0.002	0.154	0.002
benzyl alcohol (200[g])	1893	2.25	0.04	2.204	0.03	4.52	0.05	2.38	0.00	2.66	0.25
2-phenylethyl alcohol (14[i])	1935	32.4 [2.31]	1.1	27.3 [1.95]	1.8	32.8 [2.34]	1.3	28.0 [2.00]	1.1	29.0 [2.07]	0.7
total alcohols		861 [5.59]	6	384 [5.34]	5	394 [5.70]	1	377 [5.34]	4	385 [5.54]	3
Esters											
ethyl butyrate (0.02[g])	1046	0.456 [22.8]	0.015	0.600 [30.0]	0.018	0.597 [29.8]	0.022	0.694 [34.7]	0.061	0.888 [44.4]	0.036
ethyl hexanoate (0.014[g])	1255	0.836 [59.7]	0.002	1.21 [86.3]	0.00	1.24 [88.4]	0.00	1.22 [87.5]	0.00	1.11 [78.9]	0.00
ethyl octanoate (0.005[g])	1447	1.34 [268]	0.00	1.84 [368]	0.00	1.92 [384]	0.00	1.89 [378]	0.00	1.68 [336]	0.00
ethyl decanoate (0.2[g])	1649	0.413 [2.06]	0.035	0.523 [2.62]	0.000	0.564 [2.82]	0.001	0.543 [2.72]	0.000	0.560 [2.80]	0.001
ethyl lactate (154[h])	1354	14.5	0.6	16.8	1.2	17.7	0.5	15.8	0.4	16.0	0.5
isoamyl acetate (0.03[g])	1131	1.01 [33.5]	0.00	1.66 [55.5]	0.02	1.72 [57.4]	0.01	1.80 [60.0]	0.01	1.59 [52.9]	0.01
hexyl acetate (1.5[g])	1257	0.022	0.001	0.056	0.000	0.065	0.000	0.057	0.000	0.047	0.000
ethyl acetate (12.3[c])	885	50.6 [4.12]	1.3	67.2 [5.47]	1.4	64.9 [5.28]	0.5	67.0 [5.44]	0.9	66.1 [5.37]	0.8
total esters		69.2 [390]	1.9	89.9 [548]	0.2	88.7 [568]	0.9	89.0 [568]	1.4	88.0 [520]	0.3
Acids											
isobutyric acid (2.3[e])	1584	1.33	0.36	1.14	0.05	1.29	0.06	1.68	0.01	1.04	0.03
butyric acid (0.173[e])	1648	0.026	0.002	0.020	0.001	0.080	0.006	0.165	0.191	0.384 [2.01]	0.233
isovaleric acid (0.033[e])	1686	1.64 [49.7]	0.05	1.98 [59.9]	0.02	2.04 [61.8]	0.03	2.97 [90.1]	0.01	4.34 [131.6]	0.01
hexanoic acid (0.42[e])	1863	5.15 [12.3]	0.03	6.75 [16.1]	0.00	7.05 [16.8]	0.02	7.90 [18.8]	0.02	7.73 [18.4]	0.02
octanoic acid (0.5[e])	2070	7.17 [14.3]	0.02	9.41 [18.8]	0.00	9.73 [19.5]	0.01	9.04 [18.1]	0.00	7.80 [15.6]	0.02
decanoic acid (1[e])	2286	2.19 [2.19]	0.05	2.57 [2.57]	0.01	2.65 [2.65]	0.01	2.56 [2.56]	0.01	2.29 [2.29]	0.01
total acids		17.5 [78.5]	0.3	21.9 [97.4]	0.0	22.8 [101]	0.2	24.3 [130]	0.2	23.5 [170]	0.2
Carbonyl Compounds											
acetaldehyde (0.5[h])	714	36.8 [73.6]	1.1	22.2 [44.4]	0.8	22.2 [44.3]	0.3	20.9 [41.8]	0.5	19.2 [38.5]	1.6
γ-butyrolactone (35[h])	1642	39.7 [1.13]	0.8	56.4 [1.61]	0.3	55.2 [1.58]	0.2	41.4 [1.47]	0.7	49.2 [1.41]	0.4
total carbonyl compds		76.5 [74.7]	0.3	78.6 [46.0]	0.4	77.4 [45.9]	0.1	72.3 [43.3]	0.2	68.4 [39.9]	2.1
Terpenes[a]											
terpinene[a] (1500[d])	1174	0.141	0.005	0.259	0.009	0.316	0.011	0.61	0.022	0.043	0.002
linalool[a] (25[h])	1541	10.1	0.3	8.36	0.24	8.33	0.24	8.70	0.25	6.70	0.20
hotrienol[a] (110[j])	1605	181 [1.65]	9	201 [1.83]	10	130 [1.18]	6	122 [1.11]	6	149 [1.35]	7
α-terpineol[a] (250[h])	1691	8.11	0.06	8.26	0.06	9.56	0.07	8.8	0.06	9.17	0.07
citronellol[a] (100[h])	1760	1.01	0.05	1.35	0.07	1.65	0.08	2.57	0.13	1.77	0.09
nerol[a] (500[f])	1793	4.36	0.32	5.39	0.40	3.46	0.26	3.87	0.29	5.27	0.39
geraniol[a] (20[h])	1847	4.92	0.37	10.3	0.8	9.14	0.68	11.3	0.8	10.5	0.8
3,7-dimethyl-1-octen-3,7-diol[a,b]	1967	6.69	0.15	12	0.3	13.2	0.3	11.5	0.2	9.38	0.20

DOI: 10.1021/acs.jafc.5b00993
J. Agric. Food Chem. 2015, 63, 3004−3011

Table 4. continued

compd (odor threshold)	retention index calculated	must clarification		beginning of fermentation		middle of fermentation		end of fermentation		control	
		average [OAV]	SD	average [OAV]	SD	average [OAV]	SD	average [OAV]	SD	average [OAV]	SD
Terpenes[a]											
E-3,7-dimethyl-1,5-octadien-3,7-diol[a,b]	1935	59.6	1.3	85.3	1.9	122	3	278	6	228	5
E-3,7-dimethyl-1,7-octadien-3,6-diol[a,b]	2121	2.49	0.05	8.27	0.18	5.83	0.13	6.72	0.15	4.36	0.10
total terpenes[a]		279 [1.65]	16	340 [1.83]	19	303 [1.18]	15	454 [1.11]	20	424 [1.35]	20

[a]Expressed in μg/L equivalent of 4-decanol. [b]Tentative identification (not commercial pure compound available). [c]Odor thresholds from ref 28. [d]Odor thresholds from ref 29. [e]Odor thresholds from ref 30. [f]Odor thresholds from ref 31. [g]Odor thresholds from ref 32. [h]Odor thresholds from ref 33. [i]Odor thresholds from ref 34. [j]Odor thresholds from ref 35.

Table 5. Principal Components Analysis Results for the Volatile Compound (with Odor Activity Values (OAV) >1) of Musts and Wines Treated with Bentonite at Different Vinification Stages, for Albariño Wines

	PC1	PC2	PC3
eigenvalue	10.00	3.13	1.34
variance explained (%)	66.7	20.9	8.9
octanoic acid	0.991	−0.113	0.024
decanoic acid	0.988	−0.121	0.092
ethyl octanote	0.962	0.243	0.121
γ-butyrolactone	0.951	0.202	−0.147
ethyl hexanoate	0.946	0.319	0.061
isoamyl acetate	0.880	0.448	0.121
ethyl acetate	0.803	0.591	−0.750
ethyl decanoate	0.730	0.617	0.236
ethyl butyrate	0.116	0.987	0.106
isovaleric acid	−0.099	0.980	0.168
(2+3)-methyl-1-butanol	0.170	0.897	−0.168
hexanoic acid	0.581	0.758	0.236
ethanal	−0.702	−0.709	−0.044
hotrienol	−0.286	−0.300	−0.886
2-phenylethyl alcohol	−0.336	−0.550	0.599

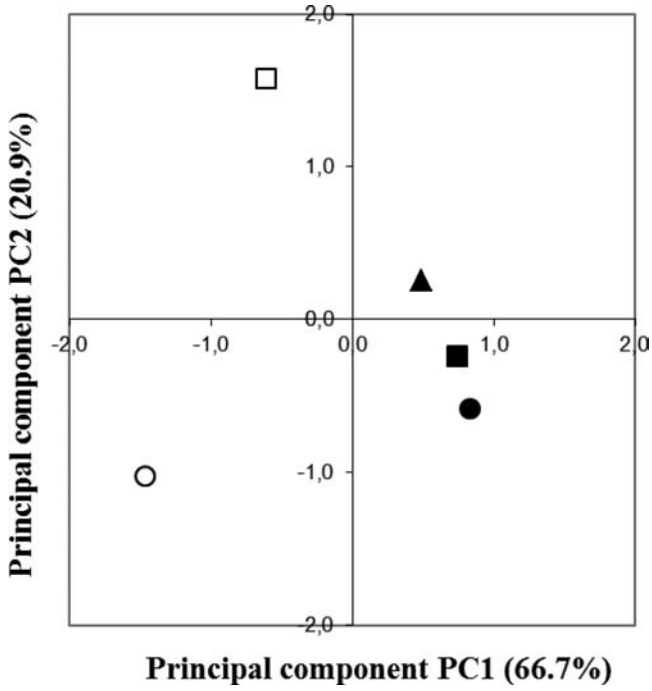

Figure 1. Principal component analysis of musts and wines treated with bentonite at different vinification stages, for Albariño wines. (○) Must clarification, (■) beginning fermentation, (●) middle fermentation, (▲) end fermentation, (□) control. Numbers in figure indicate the order in the sensory preference test.

mg BSA/L in musts clarified with enzymes. The diminution of this fraction in the must clarified with bentonite was until 14.2 ± 1.4 mg BSA/L 24 h after applying the treatment. At the end of fermentation, the content of the F3 fraction was 11.1 ± 0.3 mg BSA/L, representing unstable wines. The additional stabilizing treatment with bentonite reduced this concentration to 3.0 ± 0.0 mg BSA/L. The wines treated with bentonite during fermentation showed a diminution of the F3 fraction of 30−40% after 24 h of treatment, similar to the F2 fraction that decreased after the addition of bentonite, by around 50%. In these wines, the content of fraction F3 decreased until the end of fermentation to values in a range of 4.9−6.1 mg BSA/L, representing stable wines, except the wine treated at the beginning of fermentation, which needed an additional dose of 10 g/hL of bentonite. In the control wine, the content of the F3 fraction in dry wine was 17.0 ± 1.5 mg BSA/L, which decreased to 5.7 ± 0.7 mg BSA/L after the stabilizing treatment with bentonite. The results obtained suggest that the F3 fraction would be involved in protein stability.[3,7]

Sensory Evaluation. The tasting panel evaluated the Albariño wines obtained from the four treatments and the control in nose and palate, ranking them according to their preferences in nose and palate separately. Statistical analysis of results between pairs of wines (for $p < 0.05$) are presented in Table 3. As can be seen, in the case of nose sensory data, a clear preference of tasters for the wine treated in the middle of fermentation were observed, with a significant difference versus each of the other wines except with the wine treated at the end of fermentation, which was ranked in second place. The other three wines had similar values and, according to the tasters, there was no difference. On palate, the comparative analysis of the wines resulted in a clear preference for the wine treated at the end of fermentation over the other four wines, which did not have significant differences for the panel.

Aroma Compounds. The results of the volatile composition analysis of wines are presented in Table 4. In addition, in order to estimate the sensory importance of each compound and the differences between treatments, the odor activity values (OAVs) are also presented in Table 4 (in brackets) for compounds with OAV > 1 ua. As can be seen, treatments with bentonite at different stages of fermentation, in general, affected the production of volatile fermentative compounds. The effect of the treatments on the contents of esters and acids was remarkable and probably affected the wine aroma because most

DOI: 10.1021/acs.jafc.5b00993
J. Agric. Food Chem. 2015, 63, 3004−3011

of them are in contents higher than their odor thresholds. In addition to the possible loss of volatile compounds due to adsorption on bentonite, the effects on the production of fermentative compounds could be related to the variation in nitrogen composition and other nutrients[3,40] of musts and wines removed by the bentonite. In the case of varietal compounds, is it remarkable that the total terpenes amounts were highest in control and wines treated at the end of fermentation, while the lowest content was observed for clarified must. These effects could be related to the adsorption on bentonite of bound terpenes (glycoside forms). In addition, the release of free terpenes from the glycoside forms during fermentation could be influenced by the bentonite treatments affecting the interaction of yeast and the specific glycosides.[16] Among all terpenes analyzed, it can be observed that studied wines contain high amounts of hotrienol and *E*-3,7-dimethyl-1,5-octadien-3,7-diol, characteristic of this variety, with respect to other Galician varieties[41] and that only hotrienol showed contents higher than its odor thresholds, however, some less aromatic terpenes, such as *E*-3,7-dimethyl-1,5-octadien-3,7-diol, could transform into other more aromatic terpenes during wine aging.[42]

To obtain more information on the volatile composition analysis and with the aim of focus the discussion on the compounds with sensory importance, a principal component analysis (PCA) was carried out considering only the compounds with odor activity value higher than 1 ua. PCA selected three principal components with eigenvalue higher than 1. Table 5 shows the loading of each variable for the three PC, as well as the eigenvalue for each factor.

It was observed that more than 87% of the variation of the values could be explained by the two first principal components. The plot of the different wine samples in the plane defined by the first two PCs is shown in Figure 1. As can be seen, the PC1 (66.7%) showed a clear separation of the treated wines during fermentation (with positive PC1 values) of the control (negative values of PC1 over −0.6) and of the wine obtained from clarified musts (PC1 values over −1.5). On the other hand, the PC2 (20.9%) also allow separation of the samples treated during fermentation (situated between −06 and 0.25 values for PC2) and the control (values of PC2 of 1.6) and musts clarified wines (values of PC2 over −1). As can be seen in Table 5, the PC1 is mainly associated and positively correlated with seven compounds: two acids (octanoic and decanoic acids), five esters (ethyl esters of decanoic, octanoic, and hexanoic acids, and ethyl and isoamyl acetates), and the γ-butyrolactone. According with the results of sensory preference test (Wine Sensory Analysis section) and the position of the treated samples during fermentation (preferred by tasters) and the wine worst ranked (must clarified) in the plot (Figure 1), it could be concluded that the sensory quality of these wines is related, at least in part, with the concentration of these seven compounds. On the basis on the bibliography, acids, ethyl esters, and acetates have an important influence on the fruity and freshness character of wine aroma.[28] On the other hand, PC2 is mainly positively associate with two acids (isovaleric and hexanoic acids), ethyl butyrate, and isoamyl alcohols and negatively correlated with ethanal. In this case, probably the influence of these compounds on the "preference test" was less important, and it did not show a clear separation of the better and worst wines ranked.

In summary, the addition of bentonite during alcoholic fermentation, and especially in the middle or at the end, reduced the total dose required for protein stabilization of Albariño wines and maintained the sensory characteristics of this variety. For practical purposes, the oenological parameters of the fermentations were not affected by any of the treatments. With regard to the sensory quality of wine, the results obtained from aroma analysis allow us to conclude that the wines with higher aroma intensity and quality will be the ones treated with bentonite in the middle or at the end of fermentation. These results were corroborated by the sensory analysis in which the wines treated in the middle and at the end of fermentation were preferred by tasters. In addition, both wines were stable and did not need any extra dose of bentonite, so they were the wines with a less aggressive stabilizing treatment. Nevertheless, further work must be carried out in the future with other varieties and on an industrial winemaking scale to adjust, improve, and adapt this technique.

AUTHOR INFORMATION

Corresponding Author

*Phone: +34 977 558503. E-mail: francisco.lopez@urv.cat.

Funding

J.J.R.B. thanks the fellowship of the program "Beatriu de Pinós" with the support of the Secretariat d'Universitats i Recerca del Departament d'Economia i Coneixement de la Generalitat de Catalunya and the European Union.

Notes

The authors declare no competing financial interest.

REFERENCES

(1) Bayly, F. C.; Berg, H. W. Grape and wine proteins of white wine varietals. *Am. J. Enol. Vitic.* **1967**, *18*, 18−32.

(2) Hsu, J. C.; Heatherbell, D. A.; Flores, J. H.; Watson, B. T. Heat-unstable proteins in grape juice and wine. II. Characterization and removal by ultrafiltration. *Am. J. Enol. Vitic.* **1987**, *38*, 17−22.

(3) Waters, E. J.; Alexander, G.; Muhlack, R.; Pocock, K. F.; Colby, C.; O'Neill, B. K.; Høj, P. B.; Jones, P. Preventing protein haze in bottled white wine. *Aus. J. Grape Wine Res.* **2005**, *11*, 215−225.

(4) Moine-Ledoux, V.; Dubourdieu, D. An invertase fragment responsible for improving the protein stability of dry white wines. *J. Sci. Food Agric.* **1999**, *79*, 537−543.

(5) Dupin, I. V. S.; McKinnon, B. M.; Ryan, C.; Boulay, M.; Markides, A. J.; Jones, G. P.; Williams, P. J.; Waters, E. J. *S. cerevisiae* mannoproteins that protect wine from protein haze: their release during fermentation and lees contact and a proposal for their mechanism of action. *J. Agric. Food Chem.* **2000**, *48*, 3098−3105.

(6) Dizy, M.; Bisson, L. F. Proteolytic activity of yeast stains during grape juice fermentation. *Am. J. Enol. Vitic.* **2000**, *51*, 155−167.

(7) Vincenzi, S.; Marangon, M.; Tolin, S.; Curioni, A. Protein evolution during the early stages of white winemaking and its relations with wine stability. *Aust. J. Grape Wine Res.* **2011**, *17*, 20−27.

(8) Chalier, P.; Angot, B.; Delteil, D.; Doco, T.; Gunata, Z. Interactions between aroma compounds and whole mannoprotein isolated from *Saccharomyces cerevisiae* strains. *Food Chem.* **2007**, *100*, 22−30.

(9) Waters, E. J.; Wallace, W.; Williams, P. J. Heat haze characteristics of fractionated wine proteins. *Am. J. Enol. Vitic.* **1991**, *101*, 365−369.

(10) Pocock, K. F.; Salazar, F. N.; Waters, E. J. The effect of bentonite fining at different stages of white winemaking on protein stability. *Aust. J. Grape Wine Res.* **2011**, *17*, 280−284.

(11) Salazar, F. N.; de Bruijn, J. P. F.; Seminario, L.; Güell, C.; López, F. Improvement of wine crossflow microfiltration by a new hybrid process. *J. Food Eng.* **2007**, *79*, 1329−1336.

(12) Miller, G. C.; Amon, J. M.; Gibson, R. L.; Simpson, R. F. Loss of wine aroma attributable to protein stabilization with bentonite or ultrafiltration. *Aust. Grape Grower Winemaker* **1985**, *256*, 46−50.

DOI: 10.1021/acs.jafc.5b00993
J. Agric. Food Chem. 2015, 63, 3004−3011

(13) Voilley, A.; Lamer, C.; Dubois, P.; Feuillat, M. Influence of macromolecules and treatments on the behavior of aroma compounds in a model wine. *J. Agric. Food Chem.* **1990**, *38*, 251−258.
(14) Chagas, R.; Monteiro, S.; Ferreira, R. B. Assessment of potential effects of common fining agents used for white wine protein stabilization. *Am. J. Enol. Vitic.* **2012**, *63*, 574−578.
(15) Sanborn, M.; Edwards, C. G.; Ross, C. F. Impact of fining on chemical and sensory properties of Washington state chardonnay and gewürztraminer wines. *Am. J. Enol. Vitic.* **2010**, *61*, 31−41.
(16) Moio, L.; Ugliano, M.; Gambuti, A.; Genovese, A.; Piombino, P. Influence of clarification treatment on concentrations of selected free varietal aroma compounds and glycoconjugates in falanghina (*Vitis vinifera* L.) must and wine. *Am. J. Enol. Vitic.* **2004**, *55*, 7−12.
(17) Armada, L.; Falqué, E. Repercussion of the clarification treatment agents before the alcoholic fermentation on volatile composition of white wines. *Eur. Food Res. Technol.* **2007**, *225*, 553−558.
(18) Lambri, M.; Dordoni, R.; Silva, S.; De Faveri, D. M. Effect of bentonite fining on odor-active compounds in two different white wine styles. *Am. J. Enol. Vitic.* **2010**, *61*, 225−233.
(19) Lambri, M.; Dordoni, R.; Silva, S.; De Faveri, D. M. Comparing the impact of bentonite addition for both must clarification and wine fining on the chemical profile of wine from chambave muscat grapes. *Int. J. Food Sci. Technol.* **2012**, *47*, 1−12.
(20) Lira, E.; Salazar, F. N.; Rodríguez-Bencomo, J. J.; Vincenzi, S.; Curioni, A.; López, F. Effect of using bentonite during fermentation on protein stabilization and sensory properties of white wine. *Int. J. Food Sci. Technol.* **2014**, *49*, 1070−1078.
(21) Lira, E.; Salazar, F. N.; Vincenzi, S.; Curioni, A.; López, F. Effect of bentonite fining during fermentation on protein content in macabeu wines: comparison of pilot and industrial scale experiments. *J. Int. Sci. Vigne Vin* **2013**, *47*, 221−226.
(22) Esteruelas, M.; Poinsaut, P.; Sieczkowski, N.; Manteau, S.; Fort, M. F.; Canals, J. M.; Zamora, F. Characterization of natural haze protein in sauvignon white wine. *Food Chem.* **2009**, *113*, 28−35.
(23) Salazar, F. N.; Achaerandio, I.; Labbé, M. A.; Güell, C.; López, F. Comparative study of protein stabilization in white wine using zirconia and bentonite: physicochemical and wine sensory analysis. *J. Agric. Food Chem.* **2006**, *54*, 9955−9958.
(24) Bradford, M. A rapid and sensitive method for the quantification of microgram quantities of proteins utilizing the principle of protein−dye binding. *Anal. Biochem.* **1976**, *72*, 248−254.
(25) Canals, J. M.; Arola, L.; Zamora, F. Protein fraction analysis of white wine by FPLC. *Am. J. Enol. Vitic.* **1998**, *49*, 383−388.
(26) Blanco, P.; Mirás-Avalos, J. M.; Pereira, E.; Orriols, I. Fermentative aroma compounds and sensory profiles of godello and albariño wines as influenced by *Saccharomyces cerevisiae* yeast strains. *J. Sci. Food Agric.* **2013**, *93*, 2849−2857.
(27) López-Vázquez, C.; Bollaín, M. H.; Moser, S.; Orriols, I. Characterization and differentiation of monovarietal grape pomace distillate from native varieties of Galicia. *J. Agric. Food Chem.* **2010**, *58*, 9657−9665.
(28) Etievant, P. Wine. In *Volatile Compounds in Foods and Beverages*; Maarse, H., Ed.; Marcel Dekker: New York, 1991; pp 483−546.
(29) Clutton, D. W.; Evans, M. B. The flavour constituents of gin. *J. Chromatogr.* **1978**, *167*, 409−419.
(30) Culleré, L.; Escudero, A.; Cacho, J.; Ferreira, V. Gas chromatography−olfactometry and chemical quantitative study of the aroma of six premium quality Spanish aged red wines. *J. Agric. Food Chem.* **2004**, *52*, 1653−1660.
(31) Moyano, L.; Zea, L.; Moreno, J.; Medina, M. Analytical study of aromatic series in sherry wines subjected to biological aging. *J. Agric. Food Chem.* **2002**, *50*, 7356−7361.
(32) Aznar, M.; López, R.; Cacho, J.; Ferreira, V. Prediction of aged red aroma properties from aroma chemical composition. Partial least-squares regression models. *J. Agric. Food Chem.* **2003**, *51*, 2700−2707.
(33) Campo, E.; Ferreira, V.; Escudero, A.; Marqués, J. C.; Cacho, J. Quantitative gas chromatography−olfactometry and chemical quantitative study of the aroma of four Madeira wines. *Anal. Chim. Acta* **2006**, *563*, 180−187.
(34) Escudero, A.; Gogorza, B.; Melus, M. A.; Ortín, N.; Cacho, J.; Ferreira, V. Characterization of the aroma of a wine from macabeo. Key role played by compounds with low odor activity values. *J. Agric. Food Chem.* **2004**, *52*, 3516−3524.
(35) Ribéreau-Gayon, P.; Glories, Y.; Maujean, A.; Dubourdieu, D. *Handbook of Enology. Vol. 2: The Chemistry of Wine Stabilization and Treatments*; John Wiley & Sons Inc.: New York, 2006; pp 272−299.
(36) Casalta, E.; Aguera, E.; Picou, C.; Rodríguez-Bencomo, J. J.; Salmon, J. M.; Sablayrolles, J. M. A comparison of laboratory and pilot-scale fermentations in winemaking conditions. *Appl. Microbiol. Biotechnol.* **2010**, *87*, 1665−1673.
(37) Ferrando, M.; Güell, C.; López, F. Industrial wine making: comparison of must clarification treatments. *J. Agric. Food Chem.* **1998**, *46*, 1523−1528.
(38) Vincenzi, S.; Curioni, A. Anomalous electrophoretic behavior of a chitinase isoform from grape berries and wine in glycol chitin containing SDS-PAGE gels. *Electrophoresis* **2005**, *26*, 60−63.
(39) Sauvage, F. X.; Bach, B.; Moutounet, M.; Vernhet, A. Proteins in white wines: thermosensitivity and differential adsorption by bentonite. *Food Chem.* **2010**, *118*, 26−34.
(40) Ugliano, M.; Fedrizzi, B.; Siebert, T.; Travis, B.; Magno, F.; Versini, G.; Henschke, P. A. Effect of nitrogen supplementation and *Saccharomyces* species on hydrogen sulfide and other volatile sulfur compounds in shiraz fermentation and wine. *J. Agric. Food Chem.* **2009**, *57*, 4948−4955.
(41) Versini, G.; Orriols, I.; Dalla Serra, A. Aroma components of Galician albariño, loureira and godello wines. *Vitis* **1994**, *33*, 165−170.
(42) Williams, P. I.; Strauss, C. R.; Wilson, B. Hydroxylated linalool derivatives as precursors of volatile monoterpenes of muscat grapes. *J. Agric. Food Chem.* **1980**, *28*, 766−771.

DOI: 10.1021/acs.jafc.5b00993
J. Agric. Food Chem. 2015, 63, 3004−3011

Table 1. Identification of Phenolic Compounds in Thorny and Thornless Fruits[a]

peak	t_R	UV λ_{max} (nm)	$[M-H]^-/[M+H]^+$ (m/z)[b]	MS/MS (m/z)[b]	proposed formula	exact mass	measured mass	tentative identification	Δm (ppm)
1	2.40	325	353.0880	191.0552 $[M-caff-H]^-$	$C_{16}H_{18}O_9$	354.3087	354.0959	neochlorogenic acid[c,d]	0.21
2	3.73	314	325.0949	163.0778 $[M-hex-H]^-$	$C_{15}H_{18}O_8$	326.2986	326.1028	*p*-coumaric acid hexoside[d]	0.20
3	4.12	515	449.1083	287.0557 $[M-hex+H]^+$	$C_{21}H_{20}O_{11}$	448.3769	448.1004	cyanidin 3-*O*-galactoside[d]	0.28
4	4.79	515	449.1063	287.0536 $[M-hex+H]^+$	$C_{21}H_{20}O_{11}$	448.3769	448.0984	cyanidin 3-*O*-glucoside	0.28
5	5.12	246	$[1401.0981]^{-2}$	935.0669 [gall/bisHHDP/glc − H]$^-$, 633.0727 [gall/HHPD/glc − H]$^-$, 469.0005 [sanguisorbic acid dilactone − H]$^-$, 300.9999 [EA − H]$^-$	$C_{123}H_{80}O_{78}$	2805.9045	1402.106	lambertanin C	1.01
6	5.14	516	419.0987	287.0571 $[M-pent+H]^+$	$C_{20}H_{18}O_{10}$	418.3509	418.0908	cyanidin 3-*O*-arabinoside[d]	0.26
7	5.15	512	494.8155	348.8967 $[M-rha+H]^+$, 287.0502 $[M-Meth-Meth+H]^+$	$C_{23}H_{25}O_{12}$	493.4374	493.8076	cyanidin dimethoxyrhamnoside[c]	0.37
8	5.17	517	595.1713	287.0571 $[M-rha-hex+H]^+$	$C_{27}H_{30}O_{15}$	594.5181	594.1634	cyanidin 3-*O*-rutinoside[d]	0.35
9	5.61	246	1869.1028	935.0878 [gall/bis-HHDP/glc − H]$^-$, 633.0853 [gall/HHPD/glc − H]$^-$, 469.0005 [sanguisorbic acid dilactone − H]$^-$, 300.9999 [EA − H]$^-$	$C_{82}H_{53}O_{52}$	1871.2750	1870.1107	sanguiin H-6	1.16
10	5.82	245	1103.0897	935.0878 [gall/bis-HHDP/glc − H], 633.1234 [gall/HHPD/glc − H]$^-$,469.0005 [sanguisorbic acid dilactone -H]$^-$, 300.9999 [EA − H]$^-$	$C_{48}H_{32}O_{31}$	1104.7491	1104.0976	sanguiin H-2	0.65
11	6.13	516	419.0980	287.0536 $[M-xyl+H]^+$	$C_{20}H_{18}O_{10}$	418.3509	418.0901	cyanidin 3-*O*-xyloside	0.26
12	6.35	254/357	433.0415	300.9999 $[M-pent-H]^-$, 229.0137 $[M-pent-O-CO-CO-H]^-$	$C_{19}H_{14}O_{12}$	434.3073	434.0494	ellagic acid pentoside	0.26
13	6.45	253/361	491.0434	315.0113 $[M-glcA-H]^-$, 300.9999 $[M-glcA-O-H]^-$, 257.0208 $[M-glcA-O-CO-H]^-$, 229.0137 $[M-glcA-O-CO-CO-H]^-$	$C_{21}H_{16}O_{14}$	492.3433	492.0513	methylellagic acid glucuronide 1	0.29
14	6.57	518	535.1084	287.0536 $[M-mal-hex+H]^+$	$C_{24}H_{22}O_{14}$	534.4231	534.1005	cyanidin 3-*O*-(6-*O*-malonyl-β-D)-glucoside	0.32
15	6.60	254/364	489.1042	300.9999 $[M-Ac-Me-pent-H]^-$, 257.0208 $[M-Ac-Me-pent-O-CO-H]^-$, 229.0137 $[M-Ac-Me-pent-O-CO-CO-H]^-$	$C_{22}H_{18}O_{14}$	490.3705	490.1121	ellagic acid acetyl methylpentosid[c]	0.26
16	6.63	253/362	300.9999	285.0425 $[M-O-H]^-$, 257.0208 $[M-O-CO-H]^-$, 229.0137 $[M-O-CO-CO-H]^-$	$C_{14}H_6O_8$	302.1926	302.0078	ellagic acid[d]	0.18
17	6.96	256/354	609.1483	301.0277 $[M-rha-hex-H]^-$, 178.9938 $[M-rha-hex-C_7H_8O_2-H]^-$, 151.0042 $[M-rha-hex-C_7H_8O_2-CO-H]^-$	$C_{27}H_{30}O_{16}$	610.5175	610.1562	quercetin 3-*O*-rutinoside[d]	0.36
18	7.07	518	593.1520	287.0571 $[M-diox-hex+H]^+$	$C_{25}H_{20}O_{17}$	592.4161	592.1441	cyanidin 3-*O*-dioxalylglucoside	0.27
19	7.11	256/354	463.0879	301.0359 $[M-hex-H]^-$, 178.9965 $[M-hex-C_7H_8O_2-H]^-$, 151.0017 $[M-hex-C_7H_8O_2-CO-H]^-$	$C_{21}H_{20}O_{12}$	464.3763	464.0958	quercetin 3-*O*-galactoside[d]	0.28
20	7.26	257/354	477.0665	301.0354 $[M-glcA-H]^-$, 178.9965 $[M-glcA-C_7H_8O_2-H]^-$, 151.0042 $[M-glcA-C_7H_8O_2-CO-H]^-$	$C_{21}H_{18}O_{13}$	478.3598	478.0744	quercetin glucuronide[d]	0.29
21	7.38	256/354	463.0879	301.0277 $[M-hex-H]^-$, 178.9920 $[M-hex-C_7H_8O_2-H]^-$, 151.0042 $[M-hex-C_7H_8O_2-CO-H]^-$	$C_{21}H_{20}O_{12}$	464.3763	464.0958	quercetin 3-*O*-glucoside[d]	0.28
22	7.82	256/354	505.0979	301.0354 $[M-Ac-hex-H]^-$, 178.9938 $[M-Ac-hex-C_7H_8O_2-H]^-$, 151.0042 $[M-Ac-hex-C_7H_8O_2-CO-H]^-$	$C_{23}H_{22}O_{13}$	506.1060	506.1058	quercetin 3-*O*-acetylhexoside 1[c]	0.00
23	7.94	256/348	433.0735	301.0354 $[M-pent-H]^-$, 178.9938 $[M-pent-C_7H_8O_2-H]^-$, 151.0042 $[M-pent-C_7H_8O_2-CO-H]^-$	$C_{20}H_{18}O_{11}$	434.3503	434.0814	quercetin pentoside	0.27
24	7.99	256/354	505.0979	301.0354 $[M-Ac-hex-H]^-$, 178.9938 $[M-Ac-hex-C_7H_8O_2-H]^-$, 151.0042 $[M-Ac-hex-C_7H_8O_2-CO-H]^-$	$C_{23}H_{22}O_{13}$	506.1060	506.1058	quercetin 3-*O*-acetylhexoside 2[c]	0.00
25	8.34	253/360	447.0570	315.0113 $[M-pent-H]^-$, 300.9999 $[M-pent-Meth-H]^-$	$C_{20}H_{16}O_{12}$	448.3338	448.0649	methylellagic acid pentoside	0.27
26	8.51	265/347	447.0959	285.0394 $[M-hex-H]^-$	$C_{21}H_{20}O_{11}$	448.3769	448.1038	kaempferol glucoside[d]	0.27

J. Agric. Food Chem. 2015, 63, 3012−3021

DOI: 10.1021/jf5039794

Table 1. continued

peak	t_R	UV λ_{max} (nm)	$[M - H]^-/[M + H]^+$ $(m/z)^b$	MS/MS $(m/z)^b$	proposed formula	exact mass	measured mass	tentative identification	Δm (ppm)
27	8.59	253/360	447.0570	300.9999 [M − Me − pent − H]$^-$, 257.0208 [M − Me − pent − O − CO − CO − H]$^-$, 229.0137 [M − Me − pent − O − CO − CO − H]$^-$	$C_{20}H_{16}O_{12}$	448.3338	448.0649	ellagic acid methylpentoside	0.27
28	8.70	253/360	491.1976	315.0113 [M − glcA − H]$^-$, 300.9999 [M − glcA − O − H]$^-$, 257.0208 [M − glcA − O − CO − H]$^-$, 229.0137 [M − glcA − O − CO − CO − H]$^-$	$C_{21}H_{16}O_{14}$	492.3433	492.2055	methylellagic acid glucuronide 2	0.14
29	8.81	256/354	505.0979	301.0354 [M − Ac − hex − H]$^-$, 178.9938 [M − Ac − hex − $C_7H_8O_2$−H]$^-$, 151.0042 [M − Ac − hex − $C_7H_8O_2$ − CO − H]$^-$	$C_{23}H_{22}O_{13}$	506.1060	506.1058	quercetin 3-*O*-acetylhexoside 3[c]	0.00
30	8.94	252/369	489.1042	447.0959 [M − Ac − H]$^-$, 315.0149 [M − Ac − pent − H]$^-$, 300.9999 [M − Ac − pent − Me − H]$^-$	$C_{20}H_{16}O_{12}$	490.3705	490.1121	methylellagic acid acetylpentoside 1[c]	0.26
31	9.37	265/347	489.1059	285.0394 [M − Ac − hex − H]$^-$	$C_{23}H_{22}O_{12}$	490.4136	490.1138	kaempferol acetylgalactoside[c]	0.30
32	9.91	256/354	507.2253	361.1638 [M − rha − H]$^-$,301.0277 [M − Meth − Meth − H]$^-$	$C_{23}H_{24}O_{13}$	508.4289	508.2332	quercetin dimethoxyrhamnoside[c]	0.20
33	10.26	265/347	489.1059	285.0394 [M − Ac − hex − H]$^-$	$C_{23}H_{22}O_{12}$	490.4136	490.1138	kaempferol acetylglucoside[c]	0.30
34	10.30	252/369	489.1042	447.0959 [M − Ac − H]$^-$, 315.0149 [M − Ac − pent − H]$^-$, 300.9999 [M − Ac − pent − Me − H]$^-$	$C_{20}H_{16}O_{12}$	490.3705	490.1121	methylellagic acid acetylpentoside 2[c]	0.26
35	11.10	255/373	301.0354	178.9938 [M − glcA − $C_7H_8O_2$ − H]$^-$, 151.0042 [M − glcA − $C_7H_8O_2$ − CO − H]$^-$	$C_{15}H_{10}O_7$	302.2357	302.0433	quercetin[d]	0.19

[a]Abbreviations: t_R, retention time; Ac, acetyl; caff, caffeoyl; diox, dioxallyl; EA, ellagic acid; gall, galloyl; glc, glucose; glcA, glucuronic acid; he, hexoside; HHDP, hexahydroxydiphenic acid; Me, methyl; meth, methoxy; mal, malonyl; pent, pentoside; rha, rhamnoside; xyl, xyloside. [b]Experimental data. [c]Chemicals identified for the first time in *Rubus fruticosus* L. [d]Identification confirmed by commercial standards.

were purchased from Extrasynthese (Lyon, France). Formic acid and methanol were purchased from Sigma-Aldrich (Steinheim, Germany). Acetonitrile was from Merck (Darmstadt, Germany).

Plant Material. Blackberry fruits (*Rubus fruticosus* L.) of five thorny cultivars ('Darrow', 'Gazda', 'Leśniczanka', 'Early Wilson', and 'Zagroda') and nine thornless cultivars ('Black Beauty', 'Black Satin', 'Chester Thornless', 'Hull Thornless', 'Loch Ness', 'Orkan', 'Smoothstern', 'Tayberry', and 'Thornfree') were used for this study. Fruits were collected from the Research Station for Cultivar Testing in Masłowice and hand-harvested at the stage of consumption (full color) during the growing season of July−August 2012. Before analysis, fruits were cleaned, frozen with liquid nitrogen, and stored overnight at −20 °C.

Extraction of Polyphenols for Quantitative and Qualitative Analysis. Frozen fruits of blackberries were homogenized. A 5 g portion of homogenate was extracted twice with 80% aqueous methanol (v/v) acidified with 1% HCl (ultrasound bath, 10 min). Combined solution was then filtered through a Schott funnel with Whatman no. 1 filter paper, and filtrates were collected into 50 mL flasks. Each sample was prepared three times in order to have three technical replicates. For HPLC/UPLC-MS analysis, portions of extracts (2 mL) were centrifuged at 19000*g* for 15 min at 4 °C, and the supernatant was filtered through a Hydrophilic PTFE 0.22 μm membrane (Millex Samplicity Filter, Merck) and used for analysis.

UPLC-MS/MS Analysis of Polyphenols. Identification of blackberry polyphenols was carried out by using an ACQUITY Ultra Performance LC system (UPLC) with binary solvent manager (Waters Corp., Milford, MA, USA) and a Micromass Q-Tof Micro mass spectrometer (Waters, Manchester, UK) equipped with an electrospray ionization (ESI) source operating in negative and positive modes. Separations of individual polyphenols were carried out using a UPLC BEH C18 column (1.7 mm, 2.1 mm × 50 mm, Waters Corp., Milford, MA, USA) at 30 °C. The elution solvents were aqueous 0.1% formic acid (A) and 100% acetonitrile (B). Samples (10 μL) were eluted according to the linear gradient described previously by Kolniak-Ostek et al.[16] Analysis was carried out using full scan, data-dependent MS scanning from m/z 100 to 2500. The effluent was led directly to an electrospray source with a source block temperature of 130 °C, desolvation temperature of 350 °C, capillary voltage of 2.5 kV, and cone voltage of 30 V. Nitrogen was used as desolvation gas at a flow rate of 300 L/h.

HPLC-PDA Analysis of Polyphenol. The contents of anthocyanins, flavonols, ellagitannins, and phenolic acids were calculated on the basis of assays by HPLC-PDA described previously by Sokół-Łętowska et al.[17] The compounds were monitored at 254 nm (ellagitannins and ellagic acid derivatives), 320 nm (hydroxycinnamic acids), 360 nm (flavonols), and 520 nm (anthocyanins). The amounts of anthocyanins, flavonols, ellagitannins, including ellagic acid derivatives, and hydroxycinnamic acids were calculated as an external standard of regression equations, determined experimentally and converted into cyanidin 3-*O*-glucoside (anthocyanins), quercetin (flavonols), chlorogenic acid (hydroxycinnamic acids), and ellagic acid (ellagitannins and ellagic acid derivatives).

Statistical Analysis. Results were presented as the mean ± standard deviation of three technical replications. All statistical analyses were performed with Statistica version 10.0 (StatSoft, Tulsa, OK, USA). One-way analysis of variance (ANOVA) by Duncan's test was used to compare the mean values. Differences were considered to be significant at $p < 0.05$. Principal component analysis (PCA) was performed using XLSTAT on mean values of 14 samples (thorny and thornless blackberries) and 5 variables (anthocyanins, ellagic acid derivatives, ellagitannins, flavonols and hydroxycinnamic acids).

RESULTS AND DISCUSSION

Qualitative Analysis of Polyphenols. *General.* Table 1 lists the 35 compounds identified through UPLC-MS/MS (with PDA and Q/TOF detectors) experiments along with their retention times (t_R), UV−vis spectral profiles at 200−600 nm, and comparison with standard reference compounds, when available. Molecules that were certainly or putatively identified in negative ion mode belong to the compound groups of flavonols,

DOI: 10.1021/jf5039794
J. Agric. Food Chem. 2015, 63, 3012−3021

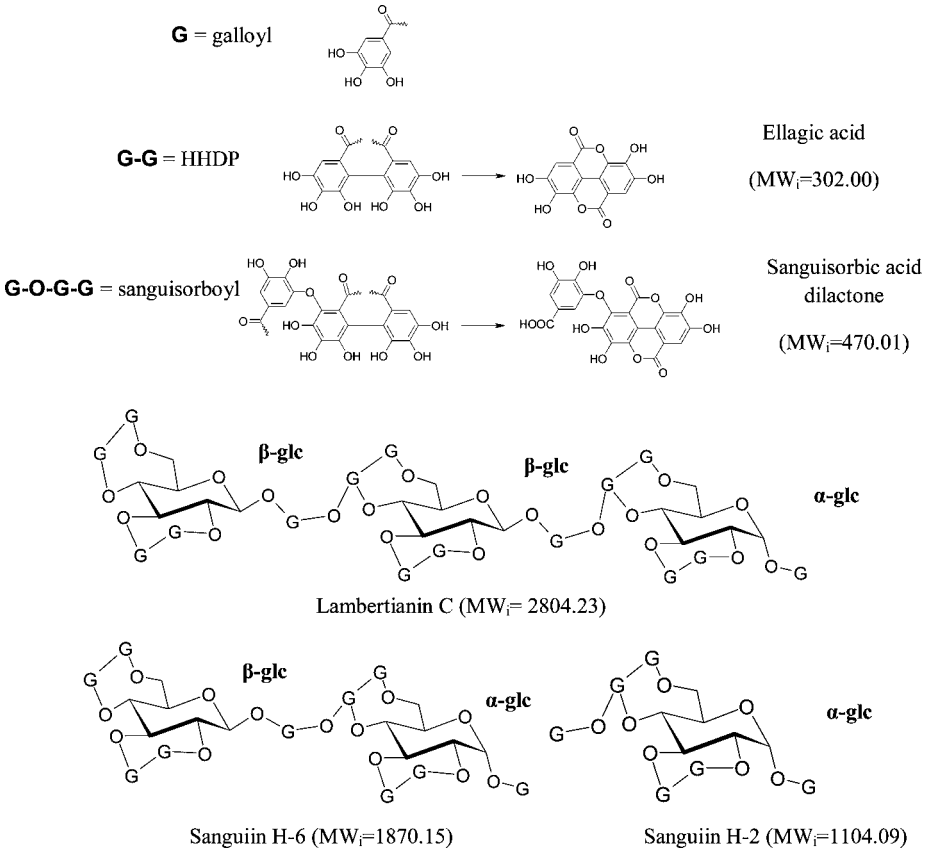

Figure 1. Structures of identified ellagitannins.

ellagitannins, ellagic acid derivatives, and hydroxycinnamic acids. Positive ionization was used for the identifiction of anthocyanins.

Seven anthocyanins (peaks 3, 4, 6, 8, 11, 14, and 18), seven flavonols (17, 19, 20, 21, 23, 26, and 35), three ellagitannins (5, 9, and 10), six ellagic acid derivatives (12, 13, 16, 25, 27, and 28), and one hydroxycinnamic acid (peak 2) were reported previously in blackberry fruits.[13,18−20] The following compounds, one phenolic acid (peak 1), one anthocyanin (peak 7), six flavonols (22, 24, 29, 31, 32, and 33), and three ellagic acid derivatives (15, 30, and 34) were identified for the first time in blackberries.

Anthocyanins. The analysis in the TOF-MS revealed the presence of eight anthocyanins in the investigated cultivars of blackberries, using positive ionization mode (Table 1). As previously stated, the identification of anthocyanins was performed by using the complementary information on chromatographic behavior and mass fragmentation, together with UV−vis profile and retention time. The MS/MS fragmentation demonstrated that the pseudomolecular cations of identified anthocyanins (peaks 3, 4, 6, 7, 8, 11, 14, and 18) were the precursors of cyanidin ($[M + H]^+$ at m/z 287.0557), indicative of cyanidin -glycosides. Peaks 3 and 4, with identical pseudomolecular cation (m/z 449.1183) and mass spectrometric fragmentation patterns, were identified as cyanidin 3-*O*-galactoside and cyanidin 3-*O*-glucoside on the basis of their retention times and UV−vis absorption spectra, compared with those of corresponding authentic standards. According to Long-Ze and Harnly,[21] the elution order of phenolic compounds for C18 columns is invariant. Glycosylated flavonoids with a monosaccharide at the same position elute in the order galactoside, glucoside, xyloside, arabinopyranoside, arabinofuranoside, rhamnoside, and then glucuronide. Peak 8, with m/z at 595.1713, was identified as cyanidin 3-*O*-rutinoside and peak 7, with m/z at 494.8155, as cyanidin dimethoxyrhamnoside. Peaks 6 and 11, with identical psudomolecular cation (m/z 419.0987) and mass spectrometric fragmentation patterns, were identified as cyanidin 3-*O*-arabinoside and cyanidin 3-*O*-xyloside on the basis of their retention times and UV−vis absorption spectra, compared with those of corresponding authentic standards. Peak 14, with $[M + H]^+$ at m/z at 535.1084, was identified as cyanidin 3-*O*-(6-*O*-malonyl-*β*-D)-glucoside, whereas peak 18, with $[M + H]^+$ at m/z at 593.1520, was identified as cyanidin 3-*O*-dioxalylglucoside.

Flavonols. The examination of the chromatograms in TOF-MS mode revealed the presence of quercetin (peak 35, m/z 301.0354). The MS/MS fragmentation showed further dissociation of the main fragment and produced the typical ion cluster of quercetin with large abundance of m/z 178.9938 and 151.0042.[22] Examination of the chromatograms in TOF-MS mode of thorny and thornless blackberries also revealed the presence of 10 quercetin glycosides (peaks 17, 19−24, 29, and 32).

Peak 17 had a pseudomolecular ion at m/z 609.1483 that fragmented in m/z 301.0354, owing to the loss of rhamnose (146 Da) and glucose (162 Da) residues. This compound was therefore tentatively identified as quercetin 3-*O*-rutinoside (rutin) on the basis of its retention time and UV−vis spectra, compared with those of corresponding authentic standards. Peaks 19 and 21, with identical pseudomolecular anions at m/z 463.0879 that fragmented in m/z 301.0359 owing to the loss of a hexose residue (162 Da), were identified as quercetin 3-*O*-galactoside (hyperoside) and quercetin 3-*O*-glucoside (isoquercitrin) on the basis of their retention times, UV−vis spectral profiles, and accurate standards. Peak 20 showed an $[M - H]^-$ at m/z 477.0665, which produced fragments at m/z 301.0354,

DOI: 10.1021/jf5039794
J. Agric. Food Chem. 2015, 63, 3012−3021

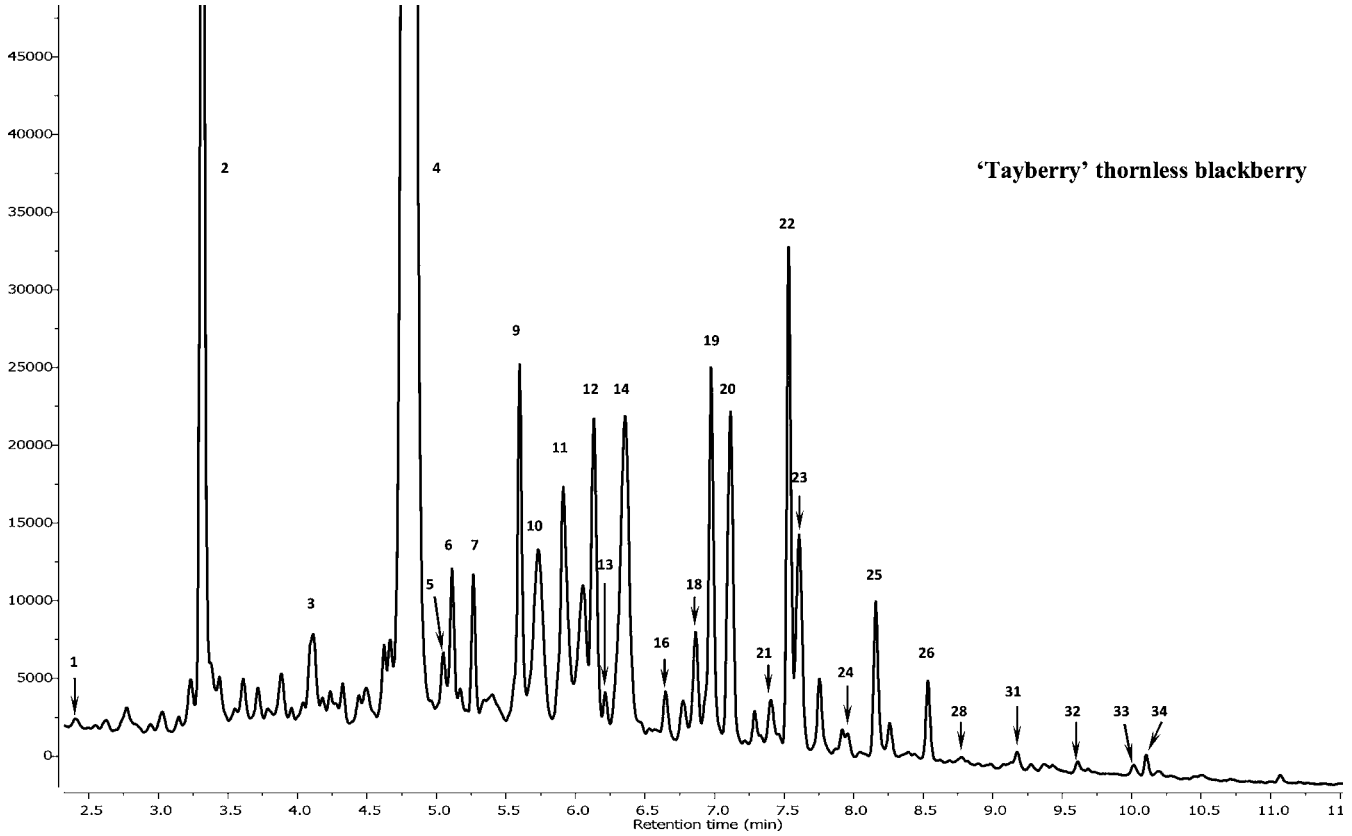

Figure 2. Segment from 2.25 to 11.25 min of LC-DAD chromatogram at 280 nm of 'Tayberry' thornless blackberry. Peak number identities are displayed in Table 1.

corresponding to the loss of a glucuronic acid residue (176 Da), and at 178.9938 and 151.0042, which are characteristic for quercetin. This pattern of fragmentation is in agreement with quercetin glucuronide, which was previously reported in *Rubus* species.[22] Peaks 23 (m/z 433.0735) and 32 (m/z 507.2253) were characterized as quercetin pentoside and quercetin dimethoxyrhamnoside, on the basis of their fragmentation pattern, with a loss of pentose (132 Da) and rhamnose (146 Da), respectively. Peaks 22, 24, and 29, with an identical pseudomolecular anion (m/z 505.0979) and mass spectrometric fragmentation patterns, were identified as quercetin acetylhexosides.

Peak 26 had a pseudomolecular ion at m/z 447.0959, which fragmented to m/z 285.0394, owing to the sugar moiety (162 Da) and corresponding formation of the aglycone.[23] This fragmentation was in agreement with those elsewhere and was attributed to kaempferol glucoside.[24] Peaks 31 and 33 have pseudomolecular ions at m/z 489.1059 and are fragmented at 285.0394, owing to the loss of the acetylhexose unit (204 Da). These compounds may be identified as kaempferol acetylgalactoside and acetylglucoside.

Ellagitannins. High MW ellagitannins based on galloyl-bis-HHDP-glucose units, such as sanguiins and lambetianins, have been commonly found in different kinds of berries, including blackberries.[18,19] The structures of identified ellagitannin are shown in Figure 1. The analysis in the TOF-MS revealed the presence of sanguiin H-6, a dimeric ellagitannin (peak 9, m/z 1869.1028). The MS/MS fragmentation gave an ion with $[M - H]^-$ at m/z at 935.0878, owing to the loss of galloyl-bis-HHDP-glucose (935 Da), a fragment with m/z at 633.0853, corresponding to the galloyl-HHDP-glucose structure, a fragment with m/z at 469.0005, corresponding to sanguisorbic acid dilactone, which is formed from the liberated sanguisorboyl group (Figure 1), and a fragment with m/z at 300.9999, corresponding to ellagic acid. Peak 5 had an $[M - 2H]^{-2}$ at m/z 1401.0981 and was identified as trimer lambertianin C. The MS/MS fragmentation gave an ion with $[M - H]^-$ at m/z at 935.0669, owing the loss of galloyl-HHDP-glucose (466 Da), and fragments with m/z at 633.0727, 469.0005, and 300.9999, corresponding to galloyl-HHDP-glucose, sanguisorbic acid dilactone, and ellagic acid, respectively. Peak 10 had a $[M - H]^-$ ion at m/z 1103.0897 and a principal MS/MS fragment at m/z 934.5746 derived from the loss of a gallic acid unit (169 Da) and was identified as monomeric sanguiin H-2. The MS/MS fragmentation also gave fragments with m/z at 633.1234, 469.0005, and 300.9999, as described above.

Ellagic Acid and Its Derivatives. The examination of the UPLC chromatograms in TOF-MS mode of thorny and thornless blackberries revealed the presence of free ellagic acid (peak 16, m/z 300.9999), MS/MS fragments at m/z 285.0425, 257.0208, and 229.0137, which are characteristic for ellagic acid,[25] and eight ellagic acid derivatives (peaks 12, 13, 15, 25, 27, 28, 30, and 34). Peak 12 has a pseudomolecular ion at m/z 433.0415 and MS/MS fragments at m/z 300.9999 and 229.0137; this dissociation pattern was previously observed by Simirgiotis and Schmeda-Hirschann[26] in *Fragaria chiloensis* berries and attributed to an ellagic acid pentoside. The TOF-MS analysis revealed the presence of ellagic acid acetylmethylpentoside (peak 15, m/z 489.1042). The MS/MS mass spectrum showed peaks at m/z 300.9999, corresponding to the loss of acetyl (42 Da) and methylpentoside (146 Da); 257.0208, corresponding to the loss of carbon oxide (28 Da); and 229.0137, corresponding to the loss of the second carbon

DOI: 10.1021/jf5039794
J. Agric. Food Chem. 2015, 63, 3012−3021

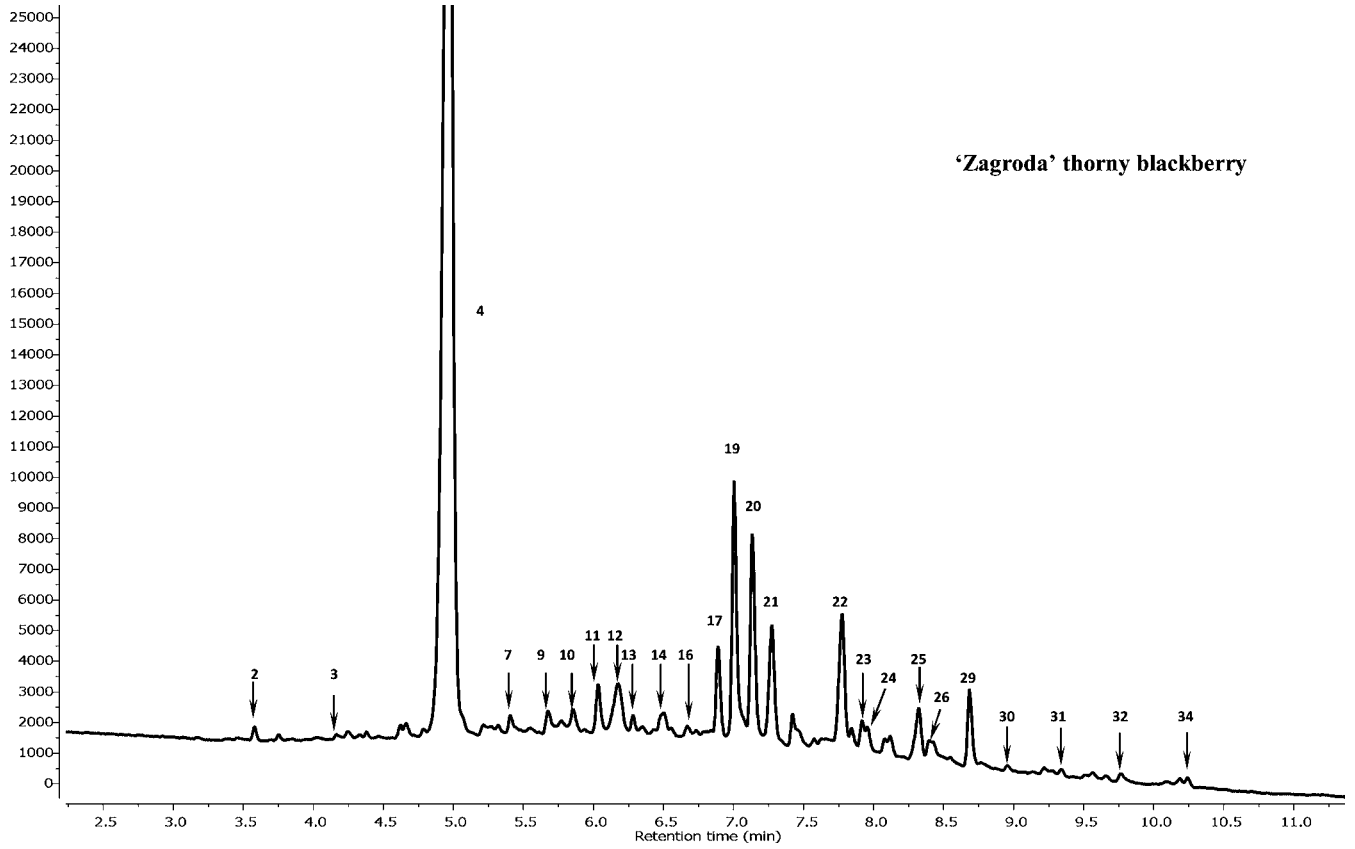

Figure 3. Segment from 2.25 to 11.25 min of LC-DAD chromatogram at 280 nm of 'Zagroda' thorny blackberry. Peak number identities are displayed in Table 1.

monoxide (28 Da). Peak 25, which showed $[M - H]^-$ at m/z 447.0570 and fragmentation with MS/MS ions at m/z 315.0113, owing to the loss of a pentose residue (132 Da) and m/z 300.9999 (further loss of methyl), can be attributed to methylellagic acid pentoside. Peak 27 had an $[M - H]^-$ at m/z 447.0570 that fragmented in the MS/MS at m/z 300.9999, corresponding to the loss of rhamnose residue (146 Da); 257.0208, owing to the loss of carbon oxide (28 Da); and 229.0137, corresponding to the loss of the second carbon monoxide (28 Da). This compound was identified as ellagic acid methylpentoside.[19] The analysis in the TOF-MS revealed the presence of two methylellagic acid glucuronide isomers (peak 13 with m/z at 491.0434 and peak 28 with m/z at 491.1976). The MS/MS mass spectrum showed peaks at m/z 315.0113 and 300.9999, corresponding to the loss of glucuronide (176 Da) and methyl (15 Da). Peaks 30 and 34 were identified as methylellagic acid acetylpentosides.[19] They had a pseudomolecular ion at m/z 489.1042 and produced MS/MS fragments at m/z 447.0959, corresponding to the loss of acetyl (42 Da); 315.0149, owing to the loss of pentose (132 Da); and 300.9999, corresponding to the loss of methyl (15 Da).

Hydroxycinnamic Acids and Others. Two hydroxycinnamic acids were identified by monitoring precursor and product ion scans and their retention times and UV−vis absorption spectra, by comparing them with those of corresponding authentic standards. Hydroxycinnamic acid (peak 1) yielded $[M - H]^-$ at m/z 353.0880, which was fragmented to generate m/z at 191.0552 (quinate ion). This component was identified as neochlorogenic acid by comparing it with the retention times and UV−vis profile of authentic standards of chlorogenic, cryptochlorogenic, and neochlorogenic acids. Hydroxycinnamic acid (peak 2) was identified as the *p*-coumaric acid hexoside by comparing it with the retention times and UV−vis profile of authentic standards of *p*-coumaric acid. Its MS/MS produced an $[M - H]^-$ of m/z 325.0949, which fragmented to 163.2778, corresponding to the loss of hexose residue (162 Da).

Quantitative Analysis of Polyphenols. *General.* Figures 2 and 3 show the LC-DAD chromatograms of thornless blackberries 'Tayberry' and thorny blackberries 'Zagroda'. Tables 2 and 3 show the contents of individual phenolic compounds of thorny and thornless blackberries. The amounts of anthocyanins, flavonols, ellagitannins, ellagic acid derivatives, and hydroxycinnamic acids were converted into cyanidin 3-*O*-glucoside (anthocyanins), quercetin (flavonols), chlorogenic acid (hydroxycinnamic acids), and ellagic acid (ellagitannins and ellagic acid derivatives). The qualitative compositions were similar for all cultivars but were quantitatively very different (Tables 2 and 3).

Anthocyanins. In thorny blackberries, the dominant compound among anthocyanins was cyanidin 3-*O*-glucoside (mean = 73.85 mg/100 g fresh weight). The highest amount of this compound (122.54 mg/100 g FW) has been found in 'Zagroda', whereas the lowest (25.15 mg/100 g FW) was reported in the 'Gazda' variety. The 'Zagroda' variety was also characterized by the highest contents of cyanidin methylpentoside, 3-*O*-arabinoside, 3-*O*-xyloside, and 3-*O*-(6-*O*-malonyl-*β*-D)-glucoside (11.00, 0.41, 6.37, and 3.34 mg/100 g FW, respectively). Cyanidin 3-*O*-rutinoside has been found only in 'Early Wilson' blackberries (4.66 mg/100 g FW) and cyanidin 3-*O*-dioxalylglucoside only in the 'Leśniczanka' variety.

DOI: 10.1021/jf5039794
J. Agric. Food Chem. 2015, 63, 3012−3021

Table 2. Phenolic Compound Contents of Thorny Blackberries (mg/100 g FW)[a,b]

peak	compound[c]	'Darrow'	'Early Wilson'	'Gazda'	'Leśniczanka'	'Zagroda'	mean
1	Cy 3-glc	88.78 ± 0.41h	55.17 ± 0.98j	25.15 ± 1.30k	81.59 ± 1.82i	122.54 ± 1.32f	74.65
2	Cy diMeth-rham	8.51 ± 0.04f	3.89 ± 0.49h	1.67 ± 0.31i	7.42 ± 0.05g	11.00 ± 0.23d	6.50
3	Cy 3-rut		4.66 ± 0.32b				0.93
4	Cy 3-ara		0.08 ± 0.00efg		0.05 ± 0.00g	0.41 ± 0.04a	0.11
5	Cy 3-xyl				3.06 ± 0.09i	6.37 ± 0.08e	1.89
6	Cy 3-mal-glc	2.04 ± 0.01h	0.96 ± 0.08k	1.15 ± 0.09j	1.48 ± 0.04i	3.34 ± 0.04e	1.79
7	Cy 3-diox-glc				3.03 ± 0.04g		0.61
8	lambertianin C	2.70 ± 0.11j	3.27 ± 0.19i	2.37 ± 0.01j	3.11 ± 0.28i	4.56 ± 0.09g	3.20
9	sanguiin H-6	1.17 ± 0.14j	1.00 ± 0.14j	2.56 ± 0.14h	2.21 ± 0.14i	4.82 ± 0.14e	2.35
10	sanguiin H-2	0.05 ± 0.01f	0.03 ± 0.00f	0.17 ± 0.02de	0.13 ± 0.04e	0.29 ± 0.01c	0.13
11	EA pent		0.19 ± 0.01c			0.76 ± 0.02a	0.19
12	MeEA glcA	0.32 ± 0.01bcd		0.15 ± 0.00fg	0.22 ± 0.01ef	0.19 ± 0.05efg	0.18
13	EA Ac-Me-pent		0.10 ± 0.00c				0.02
14	EA	1.36 ± 0.03fg	2.21 ± 0.37c	2.30 ± 0.01bc	2.71 ± 0.28b	0.66 ± 0.03h	1.85
15	MeEA pent		0.16 ± 0.03f	0.67 ± 0.02a	0.18 ± 0.01ef	0.51 ± 0.04b	0.30
16	EA Me-pent		0.22 ± 0.00a	0.10 ± 0.01c	0.08 ± 0.00d		0.08
17	MeEA Ac-pent	0.24 ± 0.00c	0.39 ± 0.00b	0.52 ± 0.03a	0.37 ± 0.01b		0.30
18	NChA					0.95 ± 0.05c	0.19
19	*p*-cum hex					0.47 ± 0.02a	0.09
20	Q 3-rut	0.46 ± 0.02b	0.32 ± 0.00c			0.59 ± 0.04a	0.27
21	Q 3-gal	1.56 ± 0.04b	0.72 ± 0.09e	2.56 ± 0.01a	0.91 ± 0.10d	1.49 ± 0.03b	1.45
22	Q glcA + Q 3-glc	0.90 ± 0.06d	1.22 ± 0.05c	1.67 ± 0.06b	1.58 ± 0.03b	1.79 ± 0.02a	1.43
23	Q 3-Ac-hex	0.95 ± 0.03fg	0.69 ± 0.00i	1.73 ± 0.09b	1.86 ± 0.00a	1.11 ± 0.08e	1.27
24	Q pent	0.36 ± 0.00e	0.26 ± 0.03f	0.56 ± 0.02e	1.01 ± 0.04a		0.44

[a]Abbreviations: Cy 3-glc, cyanidin 3-*O*-glucoside; Cy diMeth-rham, cyanidin dimethoxyrhamnoside; Cy 3-rut, cyanidin 3-*O*-rutinoside; Cy 3-ara, cyanidin 3-*O*-arabinoside; Cy 3-xyl, cyanidin 3-*O*-xyloside; Cy 3-mal-glc, cyanidin 3-*O*-(6-*O*-malonyl-*β*-D)-glucoside; Cy 3-diox-glc, cyanidin 3-*O*-dioxalylglucoside; EAd, ellagic acid derivative; EA pent, ellagic acid pentoside; MeEA glcA, methylellagic acid glucuronide; EA Ac-Me-pent, ellagic acid acetylmethylpentoside; MeEApen, methylellagic acid pentoside; EA Me-pent, ellagic acid methylpentoside; MeEA Ac-pent, methylellagic acid acetylpentoside; EA, ellagic acid; NChA, neochlorogenic acid; p-cum hex, *p*-coumaric acid hexoside; Q 3-rut, quercetin 3-*O*-rutinoside; Q 3-gal, quercetin 3-*O*-galactoside; Q glcA, quercetin glucuronide; Q 3-glc, quercetin 3-*O*-glucoside; Q 3-Ac-hex, quercetin 3-*O*-acetyl-hexoside; Q pent, quercetin pentoside. [b]Values are means ± standard deviation, $n = 3$. Mean values within a row with different letters are significantly different at $p < 0.05$. [c]Amounts of anthocyanins, flavonols, ellagitannins, including ellagic acid derivatives, and hydroxycinnamic acids were converted into cyanidin 3-*O*-glucoside (anthocyanins), quercetin (flavonols), chlorogenic acid (hydroxycinnamic acids), and ellagic acid (ellagitannins and ellagic acid derivatives).

The dominant compound among anthocyanins in thornless blackberries was cyanidin 3-*O*-glucoside (mean = 134.77 mg/100 g FW). The highest amount of this compound (188.77 mg/100 g FW) was found in 'Loch Ness' fruits, whereas the lowest (80.76 mg/100 g FW) was in 'Hull Thornless'. Simultaneously, cyanidin 3-*O*-rutinoside (11.14 mg/100 g FW) has been found only in 'Hull Thornless' blackberries.

The analysis revealed statistically significant differences in the anthocyanin concentrations of thorny and thornless blackberries. The sum of those compounds of individual thornless varieties was higher by 47% in comparison to thorny ones.

Flavonols. In thorny blackberries, the dominant compound among flavonols was quercetin 3-*O*-galactoside (mean = 1.64 mg/100 g FW). The highest amount of this compound was found in 'Gazda' fruits (2.56 mg/100 g FW), whereas the lowest (0.72 mg/100 g FW) was reported in the 'Early Wilson' variety. The 'Zagroda' variety was characterized by the highest contents of quercetin 3-*O*-rutinoside and glucuronide (0.59 and 1.79 mg/100 g FW) simultaneously; quercetin 3-*O*-pentoside was not found in those fruits.

In thornless fruits, the dominant compound among flavonols was quercetin 3-*O*-acetyl-hexoside (1.13 mg/100 g FW). The highest concentration of this compound has been determined in the 'Chester Thornless' variety (1.60 mg/100 g FW), whereas the lowest (0.66 mg/100 g FW) was in 'Hull Thornless' blackberries. Quercetin 3-*O*-rutinoside has been found only in 'Smoothstern' and 'Orkan' fruits (0.14 and 0.18 mg/100 g FW, respectively). The analysis shows that the concentrations of flavonols in thorny and thornless blackberries were significantly different. In thornless blackberries the sum of flavonols of individual varieties was lower by 86% in comparison to thorny ones.

Ellagitannins. In thorny blackberries, the dominant compound was lambertianin C (mean = 3.47 mg/100 g FW). The highest amount of this compound (4.56 mg/100 g FW) has been found in 'Zagroda', whereas the lowest (2.37 mg/100 g FW) is in 'Gazda' blackberries. The 'Zagroda' variety was characterized by the highest content of all ellagitannins. The amounts of sangiuiins H-6 and H-2 in those fruits were 4.82 and 0.29 mg/100 g FW, respectively. The lowest concentration of ellagitannins has been found in 'Early Wilson' blackberries. The amounts of sanguiins H-6 and H-2 in those varieties were 1.00 and 0.03 mg/100 g FW, respectively.

In thornless blackberries, similar to in thorny ones, lambertianin C was dominant (mean = 6.30 mg/100 g FW). The highest amount of this compound (8.65 mg/100 g FW) was found in 'Thornfree', whereas the lowest (3.95 mg/100 g FW) was in 'Hull Thornless' blackberries. The 'Thornfree' variety was also characterized by the highest concentration of other ellagitannins. The amounts of sanguiins H-6 and H-2 in those fruits were 7.58 and 0.47 mg/100 g FW, respectively. The lowest amounts of sanguiin H-6 (2.48 mg/100 FW) and

DOI: 10.1021/jf5039794
J. Agric. Food Chem. 2015, 63, 3012−3021

Table 3. Phenolic Compound Contents of Thornless Blackberries (mg/100 g FW)[a,b]

peak	compound[c]	'Black Beauty'	'Black Satin'	'Chester Thornless'	'Hull Thornless'	'Loch Ness'	'Orkan'	'Smoothstem'	'Tayberry'	'Thornfree'	mean
1	Cy 3-glc	147.65 ± 0.37d	138.94 ± 0.46e	166.89 ± 2.45b	80.76 ± 1.52i	188.77 ± 6.83a	113.26 ± 2.29g	151.07 ± 2.23c	143.97 ± 1.54d	113.91 ± 0.48g	138.36
2	Cy diMeth-rham	12.40 ± 0.05c	12.21 ± 0.02c	14.83 ± 0.22a	7.04 ± 0.11g	13.54 ± 0.83b	9.87 ± 0.27e	13.20 ± 0.14b	12.27 ± 0.07c	9.98 ± 0.00e	11.70
3	Cy 3-rut					11.14 ± 0.26a					1.24
4	Cy 3-ara	0.07 ± 0.00fg	0.33 ± 0.01c	0.09 ± 0.00ef	0.24 ± 0.02d	0.25 ± 0.01d	0.11 ± 0.00ef	0.11 ± 0.01e	0.37 ± 0.02b	0.31 ± 0.02c	0.21
5	Cy 3-xyl	5.00 ± 0.00g	8.47 ± 0.03b	5.88 ± 0.12f	7.24 ± 0.16c	6.41 ± 0.18de	4.69 ± 0.10h	6.63 ± 0.09d	8.98 ± 0.19a	6.99 ± 0.03c	6.70
6	Cy 3-mal-glc	4.37 ± 0.01c	2.58 ± 0.01g	4.19 ± 0.08d	3.35 ± 0.05e		4.90 ± 0.18b	5.80 ± 0.10a	2.18 ± 0.03h	2.75 ± 0.00f	3.35
7	Cy 3-diox-glc	9.97 ± 0.04c	12.99 ± 0.01b	8.46 ± 0.06e	6.76 ± 0.09f		9.59 ± 0.05d	9.74 ± 0.04d	10.07 ± 0.14c	13.52 ± 0.02a	9.01
8	lambertianin C	7.40 ± 0.16c	6.99 ± 0.07d	5.93 ± 0.13f	3.95 ± 0.03h	4.43 ± 0.36g	7.88 ± 0.07b	6.40 ± 0.10e	4.21 ± 0.14gh	8.65 ± 0.03a	6.20
9	sanguiin H-6	3.29 ± 0.10g	6.52 ± 0.16b	2.48 ± 0.04h	2.56 ± 0.01h	2.63 ± 0.14h	5.24 ± 0.04d	4.51 ± 0.01f	5.59 ± 0.06c	7.58 ± 0.08a	4.49
10	sanguiin H-2	0.19 ± 0.00d	0.43 ± 0.02ab	0.12 ± 0.03e	0.13 ± 0.01e	0.17 ± 0.06de	0.31 ± 0.01c	0.27 ± 0.00c	0.38 ± 0.00b	0.47 ± 0.03a	0.27
11	EA pent					0.45 ± 0.04b					0.05
12	MeEA glcA	0.44 ± 0.13a	0.16 ± 0.00fg	0.27 ± 0.01cde	0.11 ± 0.00g		0.35 ± 0.00abc	0.37 ± 0.01ab	0.22 ± 0.02def	0.23 ± 0.00def	0.24
13	EA Ac-Me-pent		0.16 ± 0.00b						0.22 ± 0.02a	0.23 ± 0.00a	0.07
14	EA	2.14 ± 0.11 cd	1.21 ± 0.01g	1.49 ± 0.44efg	4.02 ± 0.23a	1.81 ± 0.36def	1.69 ± 0.02defg	1.35 ± 0.01fg	1.18 ± 0.02g	1.90 ± 0.24cde	1.87
15	MeEA pent	0.18 ± 0.02ef	0.19 ± 0.00ef	0.18 ± 0.01ef	0.18 ± 0.01ef	0.16 ± 0.00f	0.24 ± 0.00 cd	0.24 ± 0.00 cd	0.28 ± 0.04c	0.21 ± 0.00df	0.21
16	EA Me-pent				0.17 ± 0.00b	0.16 ± 0.00b					0.04
17	MeEA Ac-pent				0.23 ± 0.03c						0.03
18	NChA	1.55 ± 0.02a	1.01 ± 0.03bc	0.57 ± 0.02e		0.20 ± 0.01f			0.74 ± 0.04d	1.08 ± 0.07b	0.57
19	*p*-cum hex	0.19 ± 0.01c	0.33 ± 0.03b						0.25 ± 0.03c	0.38 ± 0.00b	0.13
20	Q 3-rut						0.18 ± 0.00d	0.14 ± 0.01d			0.04
21	Q 3-gal	0.52 ± 0.02fg	0.25 ± 0.00h	0.62 ± 0.11ef		1.12 ± 0.01c	0.61 ± 0.00fg	0.49 ± 0.00g	0.22 ± 0.00h	0.11 ± 0.01i	0.44
22	Q glcA + Q 3-glc	0.75 ± 0.02e		0.75 ± 0.13e		0.60 ± 0.05f	0.46 ± 0.01g	0.39 ± 0.01gh	0.28 ± 0.01h		0.36
23	Q 3-Ac-hex	1.34 ± 0.04d	0.87 ± 0.00g	1.60 ± 0.06c	0.66 ± 0.03i	0.67 ± 0.01i	0.78 ± 0.00h	1.01 ± 0.00f	0.91 ± 0.00g	0.73 ± 0.01hi	0.95
24	Q pent	0.45 ± 0.01d	0.46 ± 0.00d	0.71 ± 0.02b	0.16 ± 0.02g		0.23 ± 0.01f	0.29 ± 0.02ef	0.29 ± 0.08ef	0.23 ± 0.01f	0.31

[a]Abbreviations: Cy 3-glc, cyanidin 3-*O*-glucoside; Cy diMeth-rham, cyanidin dimethoxyrhamnoside; Cy 3-rut, cyanidin 3-*O*-rutinoside; Cy 3-ara, cyanidin 3-*O*-arabinoside; Cy 3-xyl, cyanidin 3-*O*-xyloside; Cy 3-mal-glc, cyanidin 3-*O*-(6-*O*-malonyl-*β*-D)-glucoside; Cy 3-diox-glc, cyanidin 3-*O*-dioxalylglucoside; EAd, ellagic acid derivative; EA pent, ellagic acid pentoside; MeEA glcA, methylellagic acid glucuronide; EA Ac-Me-pent, ellagic acid acetylmethylpentoside; MeEApen, methylellagic acid pentoside; EA Me-pent, ellagic acid methylpentoside; MeEA Ac-pent, methylellagic acid acetylpentoside; EA, ellagic acid; NChA, neochlorogenic acid; p-cum hex, *p*-coumaric acid hexoside; Q 3-rut, quercetin 3-*O*-rutinoside; Q 3-gal, quercetin 3-*O*-galactoside; Q glcA, quercetin glucuronide; Q 3-glc, quercetin 3-O-glucoside; Q 3-Ac-hex, quercetin 3-*O*-acetyl-hexoside; Q pent, quercetin pentoside. [b]Values are means ± standard deviation, $n = 3$. Mean values within a row with different letters are significantly different at $p < 0.05$. [c]Amounts of anthocyanins, flavonols, ellagitannins, including ellagic acid derivatives, and hydroxycinnamic acids were converted into cyanidin 3-*O*-glucoside (anthocyanins), quercetin (flavonols), chlorogenic acid (hydroxycinnamic acids), and ellagic acid (ellagitannins and ellagic acid derivatives).

J. Agric. Food Chem. 2015, 63, 3012−3021
DOI: 10.1021/jf5039794

sanguiin H-2 (0.12 mg/100 g FW) were found in 'Chester Thornless' variety. The analysis revealed statistically significant differences in the total ellagitannins concentration of thorny and thornless blackberries. The sum of those compounds of individual thornless varieties was higher by 44% in comparison to thorny ones.

Ellagic Acid and Its Derivatives. In thorny blackberries, the dominant compound among ellagic acid derivatives was ellagic acid (mean = 1.69 mg/100 g FW). The highest amount of ellagic acid (2.71 mg/100 g FW) was determined in 'Leśniczanka', whereas the lowest (0.66 mg/100 g FW) was in 'Zagroda' variety. 'Early Wilson' variety was characterized by the greatest diversity of ellagic acid derivatives. Ellagic acid acetyl methylpentoside (0.10 mg/100 g FW) was found in only those fruits. Ellagic acid pentoside was found only in 'Zagroda' and 'Early Wilson' varieties (0.76 and 0.19 mg/100 g FW, respectively).

In thornless blackberries, ellagic acid was also the dominant compound (mean = 2.60 mg/100 g FW). The highest content of this compound (4.02 mg/100 g FW) was found in 'Hull Thornless' blackberries, whereas the lowest (1.18 mg/100 g FW) was in the 'Tayberry' variety. Ellagic acid pentoside was found only in 'Loch Ness' variety (0.45 mg/100 g FW), whereas methylellagic acid acetylpentoside 2 was found only in 'Hull Thornless' (0.23 mg/100 g FW). The analysis revealed statistically significant differences in the sum of ellagic acid derivatives of thorny and thornless blackberries. The sum of those compounds of individual thornless varieties was higher by 27% in comparison to thorny ones.

Hydroxycinnamic Acids. In thorny blackberries, hydroxycinnamic acids were found only in the 'Zagroda' variety. The amount of neochlorogenic acid was 0.95 mg/100 g FW, and that of *p*-coumaric acid hexoside acid was 0.47 mg/100 g FW.

In thornless blackberries, the highest amount of neochlorogenic acid has been determined in 'Black Beauty' fruits (1.55 mg/100 g FW). The highest amount of *p*-coumaric acid hexoside (0.38 mg/100 g FW) was found in the 'Thornfree' variety. In 'Hull Thornless', 'Smoothstern', and 'Orcan' blackberries, no hydroxycinnamic acids were found. The analysis shows that the concentrations of the sum of hydroxycinnamic acids in thorny and thornless blackberries were significantly different. In thornless blackberries, the sum of hydroxycinnamic acids of individual varieties was lower by 21% in comparison to thorny ones.

The concentrations of ellagic acid derivatives (mean = 2.92 mg/100 g FW in thorny and 2.49 mg/100 g FW in thornless blackberries) were quite similar to those reported by other authors. Siriwoharn and Wrolstad[9] reported that blackberries had ellagic acid derivative contents varying from 1.64 to 3.62 mg/100 g FW, whereas Gancel et al.[27] reported 7.57 mg of ellagic acid in 100 g FW of highland blackberry. Hager et al.[5] reported that ellagitannins content in blackberries varied from 2.06 to 9.78 mg/100 g FW, whereas Siriwohran et al.[7] reported anthocyanins content varying from 131 to 256 mg/100 g FW, which was higher than our research (mean = 86.47 mg/100 g FW in thorny and 171.23 mg/100 g FW in thornless blackberries) and similar to values of Gancel et al.,[27] who reported 126.3 mg/100 g FW for cyanidin 3-*O*-glucoside and 11.73 mg/100 g FW for cyanidin 3-*O*-malonylglucoside in highland blackberry. Bilyk and Sapers[28] reported a mean of 1.55 mg/100 g FW of flavonols, which was lower than in our research (5.70 mg/100 g FW in thorny and 2.09 mg/100 g FW in thornless blackberries), whereas Heinonen et al.[29] and Siriwoharn and Wrolstad[9] described higher concentrations of these compounds: 8.3 mg/100 g FW and 11.6−17.8 mg/100 g, respectively. Sellappan et al.[12] reported that blackberries and blueberries had hydroxycinnamic acid contents varying from 0.40 to 2.08 mg/100 g FW, which was quite similar to our results (1.42 mg/100 g FW in thorny and 0.7 mg/100 g FW in thornless blackberries).

According to Wang and Lin[30] and Jiao and Wang,[31] the levels of phenolics are influenced by maturity and there is pronounced variation among cultivars. The results of the present study demonstrate that the proportion and content of anthocyanins, flavonols, ellagitannins, and phenolic acids varied greatly among cultivars and types of blackberries. The large standard deviation in some of the results underscores the difficulty in obtaining evenly matured fruit samples for analysis. Thornlessness has long been a priority in almost all blackberry breeding programs and remains a major goal today; the second one is pest and disease resistance.[32]

In plants, flavonoids play an important role in biological processes. Polyphenols, which can be acquired in tissues under stress, are key components of active and potent defense mechanisms against pests and pathogens.[33] In many works[34−36] there is a strong correlation between a high phenolic concentration and resistance against herbivores including insect pests.

The higher concentration of polyphenols in thornless blackberries may be the result of development of cultivars resistant to pests and diseases. At the same time, thornless blackberries could develop new strategies of physiological defense by the production of larger amounts of flavonoids, including tannins. Tannins are derivatives with a bitter taste and toxic properties that can discourage or deter animals from feeding. The incorporation of novel resistance to pests and diseases is regarded as essential for the development of cultivars suitable for processing.

In conclusion, total phenolic and total anthocyanin contents varied greatly among cultivars. The 'Loch Ness' and 'Chester Thornless' cultivars contained the highest total anthocyanin and total phenolic contents among the 14 cultivars studied. 'Gazda' berries had the highest flavonol concentrations, whereas 'Thornfree' and 'Hull Thornless' selections were highest in ellagitannins and ellagic acid derivatives, respectively. Thorny and thornless blackberries are a good source of antioxidants that can be used in foods and nutritional supplement formulations.

■ ASSOCIATED CONTENT

Supporting Information

Representative MS spectra for all group of compounds, comparison table, and PCA of the polyphenolic content of thorny and thornless blackberries. This material is available free of charge via the Internet at http://pubs.acs.org.

■ AUTHOR INFORMATION

Corresponding Author

*(J.K.-O.) Phone/fax: +48 71 3207 706. E-mail: joanna.kolniak-ostek@up.wroc.pl.

Funding

This work was financially supported by Wroclaw Centre of Biotechnology, program The Leading National Research Centre (KNOW) for years 2014−2018.

Notes

The authors declare no competing financial interest.

DOI: 10.1021/jf5039794
J. Agric. Food Chem. 2015, 63, 3012−3021

REFERENCES

(1) Dey, P. M.; Harborne, J. B. *Methods in Plant Biochemistry. Vol. 1. Plant Phenolics, Tannins*; Academic Press: London, UK, **1993**; pp 389−419.

(2) Okuda, T.; Yoshida, T.; Hatano, T. Classification of oligomeric hydrolysable tannins and specificity of their occurrence in plant. *Phytochemistry* **1993**, *32*, 507−521.

(3) Okuda, T.; Yoshida, T.; Hatano, T. Correlation of oxidative transformations of hydrolyzable tannins and plant evolution. *Phytochemistry* **2000**, *55*, 513−529.

(4) Tanaka, T.; Tachibana, H.; Nonaka, G.; Nischioka, I.; Hsu, F. L.; Kohda, H.; Tanaka, O. *Chem. Pharm. Bull.* **1993**, *41* (7), 1214−1220.

(5) Hager, T. J.; Howard, L. R.; Liyange, R.; Lay, J. O.; Prior, L. R. Ellagitannin composition of blackberry as determined by HPLCESI-MS and MALDI-TOF-MS. *J. Agric. Food Chem.* **2008**, *56*, 661−669.

(6) Parr, A. J.; Bolwell, G. P. Phenols in the plant and in human. The potential for possible nutritional enhancement of the diet by modifying the phenols content or profile. *J. Sci. Food Agric.* **2000**, *80*, 985−1012.

(7) Siriwoharn, T.; Wrolstad, R. E.; Finn, C. E.; Pereira, C. B. Influence of cultivar, maturity, and sampling on blackberry (*Rubus* L. hybrids) anthocyanins, polyphenolics, and antioxidant properties. *J. Agric. Food Chem.* **2004**, *52*, 8021−8030.

(8) Hancock, J. F. *Temperate Fruit Crop Breeding*; Springer Science + Business Media: Berlin, Germany, 2008

(9) Siriwoharn, T.; Wrolstad, R. E. Characterization of phenolics in Marion and Evergreen blackberries. *J. Food Sci.* **2004**, *69*, 233−240.

(10) Häkkinen, S. H.; Kärenlampi, S. O.; Heinonen, M.; Mykkänen, H. M.; Törrönen, A. R. Content of the flavonols quercetin, myricetin, and kaempferol in 25 edible berries. *J. Agric. Food Chem.* **1999**, *47*, 2274−2279.

(11) Benvenuti, S.; Pellati, F.; Melegari, M.; Bertelli, D. Polyphenols, anthocyanins, ascorbic acid, and radical scavenging activity of *Rubus*, *Ribes*, and *Aronia*. *J. Food Sci.* **2004**, *69* (3), 164−169.

(12) Sellappan, S.; Akoh, C. C.; Krewer, G. Phenolic compounds and antioxidant capacity of Georgia-grown blueberries and blackberries. *J. Agric. Food Chem.* **2002**, *50* (8), 2432−2438.

(13) Fan-Chiang, H. J.; Wrolstad, R. E. Anthocyanin pigment composition of blackberries. *J. Food Sci.* **2005**, *70*, 198−202.

(14) Seeram, N. P.; Momin, R. A.; Nair, M. G.; Bourquin, L. D. Cyclooxygenase inhibitory and antioxidant cyanidin glycosides in cherries and berries. *Phytomedicine* **2001**, *8*, 362−369.

(15) Seeram, N. P. Berry fruits: compositional elements, biochemical activities, and the impact of their intake on human health, performance, and disease. *J. Agric. Food Chem.* **2008**, *56*, 627.

(16) Kolniak-Ostek, J.; Oszmiański, J.; Wojdyło, A. Effect of L-ascorbic acid addition on quality, polyphenolic compounds and antioxidant capacity of cloudy apple juices. *Eur. Food Res. Technol.* **2013**, *236* (5), 777−798.

(17) Sokół-Łętowska, A.; Kucharska, A. Z.; Wińska, K.; Szumny, A.; Nawirska-Olszańska, A.; Mizgier, P.; Wyspiańska, D. Composition and antioxidant activity of red fruit liqueurs. *Food Chem.* **2014**, *157* (0), 533−539.

(18) Mertz, C.; Cheynier, V.; Gánata, Z.; Brat, P. Analysis of phenolic compounds in two blackberry species (*Rubus glaucus* and *Rubus adenotrichus*) by high-performance liquid chromatography with diode array detection and electrospray ion trap mass spectrometry. *J. Agric. Food Chem.* **2007**, *55*, 8616−8624.

(19) James Hutton Institute. The sustainable improvement of European berry production, quality and nutritional value in a changing environment: strawberries, currants, blackberries, blueberries and raspberries. Fruit quality characterization and determination; Aberdeen, Scotland, **2010**; FP7-KBBE-2010-4 265942.

(20) Kaume, L.; Howard, L. R.; Devareddy, L. The blackberry fruit: a review on its composition and chemistry, metabolism and bioavailability, and health benefits. *J. Agric. Food Chem.* **2012**, *60* (23), 5716−5727.

(21) Long-Ze, L.; Harnly, J. M. LC-MS profiling and quantification of food phenolic components using a standard analytical approach for all plants. In *Food Science and Technology: New Research*; Greco, L. V., Bruno, M. N., Eds.; Nova Science Publishers: New York, **2008**; 60 pp.

(22) Määttä-Riihinen, K. R.; Kamal-Eldin, A.; Törrönen, A. R. Identification and quantification of phenolic compounds in berries of *Fragaria* and *Rubus* species (family Rosaceae). *J. Agric. Food Chem.* **2004**, *52*, 61−78.

(23) Hvattum, E.; Ekeberg, D. Study of the collision-induced radical cleavage of flavonoid glycosides using negative electrospray ionization tandem quadrupole mass spectrometry. *J. Mass Spectrom.* **2003**, *38*, 43.

(24) Simirgiotis, M. J.; Theoduloz, C.; Caligari, P. D. S.; Schmeda-Hirschmann, G. Comparison of phenolic composition and antioxidant properties of two native Chilean and one domestic strawberry genotypes. *Food Chem.* **2009**, *113*, 377.

(25) Del Bubba, M.; Checchini, L.; Chiuminatto, U.; Doumett, S.; Fibbi, D.; Giordan, E. Liquid chromatographic/electrospray ionization tandem mass spectrometric study of polyphenolic composition of four cultivars of *Fragaria vesca* L. berries and their comparative evaluation. *J. Mass Spectrom.* **2012**, *47* (9), 1207−1220.

(26) Simirgiotis, M. J.; Schmeda-Hirschann, G. Determination of phenolic composition and antioxidant activity in fruits, rhizomes and leaves of the white strawberry (*Fragaria chiloensis* spp. Chiloensis form chiloensis) usng HPLC-DAD-ESI-MS and free radical quenching techniques. *J. Food Compos. Anal.* **2010**, *23*, 545−553.

(27) Gancel, A. L.; Feneuil, A.; Acosta, O.; Mercedes Pérez, A.; Vaillant, F. Impact of industrial processing and storage on major polyphenols and the antioxidant capacity of tropical highland blackberry (*Rubus adenotrichus*). *Food Res. Int.* **2011**, *44* (7), 2243−2251.

(28) Bilyk, A.; Sapers, G. M. Varietal differences in the quercetin, kaempferol, and myricetin contents of highbush blueberry, cranberry, and thornless blackberry fruits. *J. Agric. Food Chem.* **1986**, *34*, 585−588.

(29) Heinonen, I. M.; Meyer, A. S.; Frankel, E. N. Antioxidant activity of berry phenolics on human low-density lipoprotein and liposome oxidation. *J. Agric. Food Chem.* **1998**, *46*, 4107−4112.

(30) Wang, S. Y.; Lin, H. S. Antioxidant activity in fruit and leaves of blackberry, raspberry, and strawberry varies with cultivar and development stage. *J. Agric. Food Chem.* **2000**, *48*, 140−146.

(31) Jiao, H.; Wang, S. Y. Correlation of antioxidant capacities to oxygen radical scavenging enzyme activities in blackberry. *J. Agric. Food Chem.* **2000**, *48*, 5672−5676.

(32) Clark, J. R.; Finn, C. E. Trends in blackberry breeding. *Acta Hortic.* **2008**, *777*, 41−48.

(33) Feucht, W. The localization of phenols at the cellular and tissue level. *Acta Hortic.* **1994**, *381*, 803−815.

(34) Bennett, R. N.; Wallsgrove, R. M. Secondary metabolites in plant defense mechanisms. *New Phytol.* **1994**, *127*, 617−633.

(35) Grayer, R. J.; Kimmins, F. M.; Padgham, D. E.; Harborne, J. B.; Ranga, D. V. Condensed tannins levels and resistance of groundnuts against *Aphis craccivora*. *Phytochemistry* **1992**, *31*, 3795−3780.

(36) Michalek, S.; Mayr, U.; Treutter, D.; Lux-Endrich, A.; Gutmann, M.; Feucht, W.; Geibel, M. Role of flavan-3-ols in resistance of apple trees to *Venturia inaequalis*. *Acta Hortic.* **1999**, *484*, 535−539.

DOI: 10.1021/jf5039794
J. Agric. Food Chem. 2015, 63, 3012−3021

corresponding volatiles, can be further transformed in the mouth. This leads to a long-lasting hoppy aroma.[21] This source of hoppy note must be viewed as part of the hop flavoring potential.

Besides free and bound terpenoids, polyfunctional thiols have recently been referred to as important hop-derived flavoring compounds in beer, especially when dual-purpose hop varieties are used. Forty-one volatile polyfunctional thiols have been reported in hop, most of them having a 3-carbon distance between the thiol and the oxygenated functions.[8] Rhubarb/grapefruit-like 3-sulfanyl-4-methylpentan-1-ol (3S4MPol) and blackcurrant-like 4-sulfanyl-4-methylpentan-2-one (4S4M2Pone) constitute key compounds of the "Sauvignon-like" notes imparted to beer by Nelson Sauvin hop.[14] Floral-like 3-sulfanyl-2-ethylpropyl acetate (3S2EPrA) and citrus/peach-like 3-sulfanyloctanal (3SOal) distinguish Tomahawk from all other thiol-rich varieties. Most low-bitter varieties, including Saaz, appear to be greatly lacking in polyfunctional thiols. Yet blackcurrant-like 4S4M2Pone and grapefruit-like 3-sulfanylhexan-1-ol (3SHol) have been described as key aroma compounds participating in the Muscat-like flavor perceived in Cascade (4.5−8% α-acids) hopped beer.[8,13,15,22]

Whatever the cultivar, the thiol content of the final beer reaches much higher values than expected from the hop content. S-cysteine conjugates, recently evidenced for the first time in hop,[23,24] are partly responsible for the increases in thiol content from hop to wort and beer. The β-lyase activity of yeast, causing specific cleavage of the thiol from its conjugate, converts nonvolatile precursors to odorant thiols. The commercial apotryptophanase from *Escherichia coli* has been widely used to investigate cysteine- and cysteinylglycine adducts in plants[24−27] (free amine required for the enzyme activity-glutathione adducts not quantified by this assay[27]). Depending on the hop variety, the S-cysteine conjugate fraction represents a bound potential 23−126 times as high as the fraction of corresponding volatiles.[24] The rate of conversion by the action of yeast remains low during the main fermentation.[28−30] The late stage of bottle refermentation[20] and dry hopping during maturation constitute additional chances for yeast to convert these intact S-conjugates.[19] The nutrient-depleted conditions encountered after fermentation are thought to favor this yeast activity.[19,30,31]

Chemical information concerning the aromatic potential of other new dual-purpose varieties remains scarce. The aim of the present work was therefore to quantify free terpenoids and both free and bound polyfunctional thiols in five selected cultivars: Amarillo, Citra, Hallertau Blanc, Mosaic, and Sorachi Ace. The aromatic profiles of these cultivars were compared with those previously obtained for the dual-purpose varieties Tomahawk and Nelson Sauvin and for the low-bitter aromatic reference Saaz.[8,24]

EXPERIMENTAL PROCEDURES

Chemicals. Ammonia (28%) was from VWR (Leuven, Belgium). *p*-Hydroxymercuribenzoic acid (*p*HMB), 37% HCl, S-benzyl-L-cysteine (IST for apotryptophanase assays), apotryptophanase, pyridoxal-5-phosphate, ethylenediaminetetraacetic acid, the Amberlite IR-120 resin, carvone (IST for Likens Nikerson extractions), myrcene, linalool, geraniol, β-caryophyllene, α-humulene, β-farnesene, undecan-2-one, 3-sulfanylpropyl acetate (**1**)*, 3-sulfanylpropan-1-ol (**14**)*, 3-sulfanyl-3-methylbutan-1-ol (**17**)*, 2-sulfanylethan-1-ol (**36**)*, 2-sulfanylethyl acetate (**38**)*, and 2-acetylthiophene (EST for free thiol extractions) were purchased from Sigma-Aldrich (Bornem, Belgium). An asterisk means that numbering of compounds is conserved from refs 8 and 24. 4-Methoxy-2-methylbutan-2-thiol (IST for free thiol extractions), 3-sulfanylhexyl acetate (**11**)*, 3-sulfanylhexan-1-ol (**23**)*, and 3-methyl-2-buten-1-thiol (**37**)* were obtained from Oxford Chemicals (Oxford, U.K.). 4-Sulfanyl-4-methylpentan-2-one (**29**)* was from Frutarom (Hartlepool, U.K.). Dichloromethane (99.9%) obtained from VWR (Leuven, Belgium) was distilled before use. Milli-Q water was used (Millipore, Bedford, MA, U.S.A.). NaOH and sodium sulfate (99%) were supplied by Janssen (Geel, Belgium). A strongly basic Dowex resin 1 × 2, Cl^- form (Sigma-Aldrich, Bornem, Belgium) was stored in hydrogen chloride (0.1 M). Anhydrous sodium sulfate was obtained from Merck (Darmstadt, Germany), and tris(hydroxymethyl)-aminomethane (Tris) was obtained from USB (Cleveland, Ohio, U.S.A.). Formic acid was provided by Fischer (Loughborough, U.K.). Polyvinylpyrrolidone was supplied by Spindal (Gretz-Armainvilliers, France).

Reference Compounds Synthesized in Our Laboratory. 3-Sulfanyl-2-ethylpropyl acetate (**10**)* was synthesized prior to this work (reagents and complete procedure described in ref 32). 1-Sulfanylpentan-3-ol (**19**)* and 3-sulfanylpentan-1-ol (**21**)* were obtained with the reagents and procedure disclosed in ref 33. 3-Sulfanylheptanal (**33**) and 3-sulfanyloctanal (**35**)* were obtained according to the procedure described in ref 34. 3-Sulfanyl-4-methylpentan-1-ol (**26**)* was synthesized according to ref 35.

Hop Samples. Amarillo, Citra, Mosaic, and Sorachi Ace bred in the U.S.A. were provided by Yakima Chief (Louvain-la-Neuve, Belgium). Hallertau Blanc hop came from Hopsteiner (Germany). Their α-acid contents were given by the suppliers.

Extraction of Terpenoids and Other Non-Sulfur Hop Oils by the Likens Nickerson Method. Steam distillation−solvent extraction was carried out in a microextractor (Alltech 8910) according to ref 36. Hop pellets (0.5 g) were milled and mixed with 50 mL of deoxygenated ultrapure water and 1.5 mL of a carvone solution at 20 mg/L (internal standard) in flask A. Dichloromethane and ultrapure, deoxygenated water (1.5 mL each) were introduced into the liquid/liquid extraction area. Dichloromethane (1.5 mL) was introduced into the organic-phase vessel (B). A few clean grains of carborundum were added into flasks A and B. Prior to the procedure, the entire system was purged with nitrogen (2−3 mL/min) for 5 min. Flask A was then heated in a 140 °C oil bath, and flask B was heated in a 70 °C water bath. The vapors were condensed by means of a coldfinger maintained at −10 °C by a cryostat. The entire steam distillation−solvent extraction procedure was carried out under a 2 mL/min nitrogen flow. The steam distillation was stopped after 45 min. The dichloromethane extract was then concentrated to 0.5 mL at 45 °C with a Kuderna−Danish concentrator. The method allows most of the terpenic compounds to be recovered with factors >92% and variation coefficients <6%.[36]

Extraction of Free Polyfunctional Thiols by *p*HMB. Polyfunctional thiols were extracted from hop according to ref 8, adapted from ref 37 (dichloromethane liquid/solid extraction of 15 g of hop, extraction of the resulting organic phase with a *p*HMB solution, loading of bound thiols onto a strong anion-exchange resin, release of free thiols by exchange with washed cysteine [4 × 50 mL of dichloromethane for washing 640 mg of cysteine], final extraction with dichloromethane, and concentration to 250 μL in a Kuderna−Danish apparatus and to 70 μL in a Dufton column). 4-Methoxy-2-methylbutane-2-thiol was added as internal standard (IST, at 33.5 μg/kg), and 2-acetylthiophene was added as external standard (EST, 1 mL at 200 μg/L added before concentration).

Extraction of Cysteine-S-conjugates from Hop and Release of the Corresponding Free Thiols by the Apotryptophanase Assay. The extraction was conducted on the hop according to the procedure of ref 24 adapted from ref 27. Milled pellets (100 g) spiked with 1 mL of 1600 mg/L S-benzyl-L-cysteine were extracted with 1 L of hydroalcoholic solution ($EtOH/H_2O/HCOOH$ = 49.5:49.5:1, v/v/v) for 2 h. After centrifugation for 30 min at 1200*g*, the polyphenols present in the supernatant were partially removed by addition of 30 g of polyvinylpyrrolidone and stirring for 30 min. After a second centrifugation, the extract was purified on the IR-120 (H+) cation-exchange resin (100 g) conditioned with 100 mL of 6% HCl followed by 1 L of ultrapure water. After washing with 500 mL of water, sequential fractions were recovered by eluting with aqueous ammonia solutions (100 mL each) at the following concentrations: 0.3, 0.6, 0.9, 1.2, 1.5, 1.8,

DOI: 10.1021/jf5058556
J. Agric. Food Chem. 2015, 63, 3022−3030

Table 1. Terpenoids (Top Part) and Other Non-Sulfur Hop Oil Constituents (Bottom Part) Determined by GC-MS (Concentrations in mg/kg of Hop, IST Equivalents for Compounds Carrying the IST Superscript), after Likens Nickerson Extraction (Mean of Duplicates, CV < 6%);[36] Values within a Row with Different Letters Are Significantly Different ($p < 0.05$) According to the Student−Newman−Keuls Test

substance			Amarillo	Citra	Hallertau Blanc	Mosaic	Sorachi Ace		
			α-acid content (% w/w)						
retention index CP-Sil 5 CB	name	odor (GC-O)	9.3	13.9	8.4	11.7	12.3	previously reported cultivars[8a]	identification reliability (3 main m/z ions given in parentheses)
982	myrcene	lime	2225.4 d	3945.2 b	3273.6 c	2370.0 d	4654 a	T c, NS e, S f	I^+ (41, 93, 69)
1086	linalool	floral	109.2 c	18.6 e	18.6 e	58.0 d	57.9 d	T b, NS a, S e	I^+ (71, 93, 41)
1212	β-citronellol	lemon	10.6 c	7.8 d	13.0 b	10.0 c	33.3 a	T e, NS e, S e	I^+ (41, 69, 55)
1236	geraniol	floral	105.1 b	68.9 d	16.6 f	83.2 c	18.9 f	T a, NS e, S f	I^+ (69, 41, 68)
1313	methylgeranate[b IST]	greenery	1.7 e	0.3 e	1.6 e	0.9 e	1.0 e	T a, NS c, S d	I^+ (69, 41, 114)
1435	β-caryophyllene	spicy	753.3 d	828.0 d	745.0 d	365.8 e	36.1 f	T a, NS b, S e	I^+ (41, 93, 69)
1469	α-humulene[b]	resin	1273.1 ab	1320.1 ab	1187.6 b	884.4 c	1328 a,b	T a, NS c, S ab	I^+ (93, 41, 121)
1475	bergamotene[b IST]	tea	1.7 c	3.1 c	1.9 c	1.4 c	1.2 c	T c, NS c, S a	I^+ (119, 93, 41)
1486	β-farnesene[b]	woody	102.8 c	32.3 c	47.1 c	152.6 c	2101.0 a	T c, NS c, S b	I^+ (93, 41, 69)
1499	α-amorphene[b IST]	woody	5.9 ef	8.4 e	14.6 d	3.9 ef	1.9 f	T a, NS b, S e	I^+ (105, 161, 94)
1548	α-selinene[b IST]	woody	35.8 cd	11.6 d	37.3 c,d	18.4 d	126.7 b	T a, NS b, S cd	I^+ (189, 93, 107)
1538	β-selinene[b IST]	herbs	17.7 ef	6.4 f	36.9 de	7.7 f	77.0 c	T a, NS b, S e	I^+ (41, 105, 204)
1074	3-methylbutyl-isobutyrate[b]	sweet	69 d	111.9 c	180.7 a	125.7 bc	12.9 e	T a, NS b, S e	I^+ (43, 71, 70)
1279	undecan-2-one[b]	citrus	48.8 e	113.1 b	29.9 f	236.9 a	72 d	T f,g, NS cd, S c	I^+ (43, 58, 71)
	total		4760.1 cd	6475.7 b	5604.4 c	4318.9 d	8521.9 a	T a, NS c,d, S e	

[a]Data issued from ref 8; letters after T, NS, or S indicate the statistical group for the reported concentrations in Tomahawk, Nelson Sauvin, and Saaz. I^+, compound identified by mass spectrometry (full scan monitoring) and coincidence with the retention index. [b]Compounds previously selected for discriminating Cascade, Challenger, Hallertau Mittelfrueh, Lublin, Mount Hood, Northdown, Northern Brewer, Nugget, Saaz, Styrian Golding, and Target.[5,7]

and 2.1 M. The 1.2 and 1.5 M fractions were pooled, vacuum-evaporated, and lyophilized. The dried 1.2−1.5 M fraction (~100 mg) was suspended in 2 mL of potassium phosphate buffer (100 mM, pH 7.7) containing pyridoxal 5-phosphate (0.1 mM) and ethylenediaminetetraacetic acid (1 mM). Five hundred microliters of a solution containing the commercial apotryptophanase from *Escherichia coli* (75−150 units/mg), freshly prepared (1 mg in 0.5 mL of buffer), were added. The incubation was kept at 28 °C for 30 min. A control without enzyme was conducted in parallel. The mixture was then stirred with 5 mL of bidistilled dichloromethane for 30 min. The organic phase was dried over sodium sulfate prior to concentration to 500 μL in a Kuderna−Danish apparatus and to 70 μL in a Dufton column.

Gas Chromatography Hyphenated to Olfactometric and Flame Ionization Detectors (GC-O and GC-FID). Two μL of extract (Likens Nikerson, *p*HMB free thiols or enzymatically released thiols) was analyzed with a Chrompack CP9001 gas chromatograph equipped with a splitless injector maintained at 250 °C; the split vent was opened 0.5 min postinjection. Compounds were analyzed with a wall-coated open tubular (WCOT) apolar CP-Sil 5 CB (50 m × 0.32 mm i.d., 1.2 μm film thickness) column or a polar FFAP (25 m × 0.32 mm i.d., 0.3 μm film thickness) capillary column. The carrier gas was nitrogen, and the pressure was set at 50 kPa (CP-Sil 5 CB) or 30 kPa (FFAP). The oven temperature was programmed to rise from 36 to 85 °C at 20 °C/min, then to 145 °C at 1 °C/min, and finally to 220 °C at 3 °C/min and held for 30 min. The column was connected to an FID detector (set at 250 °C with inlet of 21 mL/min H_2 and 210 mL/min air) and a GC-O port (Chrompack) maintained at 250 °C. The GC-O effluent was diluted with a large volume of air (20 mL/min) prehumidified with an aqueous copper(II) sulfate solution. All extracts were analyzed immediately after extraction by two trained panelists.

Quantitation of Terpenoids and Other Non-Sulfur Hop Constituents. For commercially available compounds, FID calibration curves (with areas relative to carvone (IST)) were used. For commercially unavailable compounds, quantitations are given in IST equivalents (response coefficient relative to the IST set at 1; values carrying an IST superscript in Table 1).

Gas Chromatography Hyphenated to a Pulsed-Flame Photometric Detector (GC-PFPD) and an Electronic Impact Mass Spectrometer (GC-MS). Two μL of extract (Likens Nikerson, *p*HMB free thiols or enzymatically released thiols) were analyzed with an Agilent 6890N gas chromatograph. The injections were carried out in the splitless mode at 250 °C, the split being turned on after 0.5 min. The oven temperature program and the columns were the same as described for GC-FID and GC-O. The carrier gas was helium, and the pressure was set at 100 kPa (CP-Sil 5 CB) or 45 kPa (FFAP). The column was connected to a mass spectrometer (m/z = 40−380 recorded at 70 eV) and a PFPD port (O.I. Analytical PFPD, model 5380). The following parameters were selected for the PFPD detector: temperature, 220 °C; voltage, 590 V; gate width, 18 ms; gate delay, 6 ms; trigger level, 400 mV; pulse frequency, 3.33 Hz. PFPD and MS chromatograms were simultaneously recorded throughout elution; ChemStation software was used. Identifications were done as previously described in ref 8.

Quantitation of Thiols (A) in *p*HMB Extracts. The following general equation was used for compound A quantitation: concentration of A (in μg/kg) = IST concentration (in μg/kg) × (A molecular weight/IST molecular weight) × (A area/IST area) × (IST molar response coefficient/A molar response coefficient) × (IST recovery factor/A recovery factor).

The IST-relative recovery factor was set at 1 for all compounds (experimental values from 0.8 to 1.2, previously determined by standard addition) except for 2-sulfanylethan-1-ol (bad recovery at the second dichloromethane extraction; approximate concentrations given by applying a ratio of 0.1 assessed by standard addition). For commercially available thiols, complete calibration curves relative to the IST were used (use of the experimental response coefficient ratio in the above equation). For commercially unavailable compounds (values carrying an

DOI: 10.1021/jf5058556
J. Agric. Food Chem. 2015, 63, 3022−3030

Table 2. Amounts of Polyfunctional Thiols Determined by GC-PFPD in Hop (μg/kg, IST Equivalents for Compounds Carrying the IST Superscript); Mean of Duplicates; Values within a Row with Different Letters Are Significantly Different ($p < 0.05$) According to the Student−Newman−Keuls Test[a]

	retention index		substance			Amarillo	Citra	Hallertau Blanc	Mosaic	Sorachi Ace		
						α-acid content (% w/w)						
no.	FFAP	CP-Sil 5 CB	name	acronym	odor (GC-O)	9.3	13.9	8.4	11.7	12.3	previously reported cultivars[b]	identification reliability (3 main m/z ions given in parentheses)
37	1112	810	3-methyl-2-buten-1-thiol	MBT	coffee, skunky	nd c	nd c	nd c	nd c	nd c	T a, NS b, S c	I^+ (69, 53, 102)
29	1380	918	4-sulfanyl-4-methylpentan-2-one	4S4M2Pone	catty, black currant	3 c	d	nd c	30 b	83 a	T c, NS c, S c	I^+ (132, 75, 55)
38	1452	887	2-sulfanylethyl acetate	2SEA	toasted, grilled	d	867 a	d	8 b	nd b	T b, NS b, S b	I^+ (43, 60, 61)
36	1532	722	2-sulfanylethan-1-ol	2SEol	grilled	d	362 a	d	d	d	T b, NS b, S b	I^+ (47, 60, 78)
1	1578	1007	3-sulfanylpropyl acetate	3SPrA	grilled	nd b	7 a	nd b	nd b	nd b	T b, NS b, S b	I^+ (74, 43, 47)
14	1623	849	3-sulfanylpropan-1-ol	3SProl	popcorn	nd a	d	d	d	nd a	T a, NS a, S a	I^+ (57, 58, 45)
17	1654	933	3-sulfanyl-3-methylbutan-1-ol	3S3MBol	sulfur, soup	d	d	d	d	d	T a, NS a, S a	I^+ (86, 69, 75)
33	1655	1113	3-sulfanylheptanal^{IST}	3SHptal	lemon, candy	nd c	nd c	nd c	nd c	nd c	T a, NS b, S c	
10	1657	1147	3-sulfanyl-2-ethylpropyl acetate^{IST}	3S2EPrA	floral, vinegar	nd c	nd c	nd c	nd c	nd c	T a, NS b, S c	I^+ (102, 60, 69)
11	1717	998	3-sulfanylhexyl acetate	3SHA	passionfruit, grapefruit	5 bc	27 a	4 bc	8 b	nd c	T c, NS c, S c	I^-
19	1722	970	1-sulfanylpentan-3-ol^{IST}	1S3Pol	nettle	11 b	5 c	9 b	30 a	nd c	T c, NS c, S c	I
21	1760	1009	3-sulfanylpentan-1-ol	3SPol	citrus	10 a	6 b	d	d	nd c	T c, NS c, S c	I^+ (86, 69, 57)
35	1765	1214	3-sulfanyloctanal^{IST}	3SOal	citrus, peach	nd c	nd c	nd c	nd c	nd c	T b, NS a, S c	I^+ (131, 83, 109)
26	1815	1186	3-sulfanyl-4-methylpentan-1-ol^{IST}	3S4MPol	grapefruit	25 cd	10 de	109 a	46 b	nd e	T d,e, NS bc, S e	I^+ (100, 55, 73)
23	1858	1095	3-sulfanylhexan-1-ol	3SHol	grapefruit/ rhubarb	d	12 a	d	d	nd c	T a, NS b, S c	I^+ (57, 41, 61)
			total			54 b	1296 a	122 b	122 b	83 b	T b, NS b, S b	

[a]d, detected under the quantitation limit (0.1 μg/kg) or unresolved. nd, not detected (<0.03 μg/kg). [b]Data issued from ref 8; letters after T, NS, or S indicate the statistical group for the reported concentrations in Tomahawk, Nelson Sauvin, and Saaz. I, compound identified by coincidence with the GC-PFPD retention indexes and odor descriptor of the pure or synthesized compound on two capillary columns (CP-Sil 5 CB and FFAP); I^+, additional confirmation by mass spectrometry (full scan monitoring); I^-, compound tentatively identified by coincidence with the GC-O retention indexes and odors of pure or synthesized compound on two capillary columns (CP-Sil 5 CB and FFAP).

J. Agric. Food Chem. 2015, 63, 3022−3030
DOI: 10.1021/jf505855b

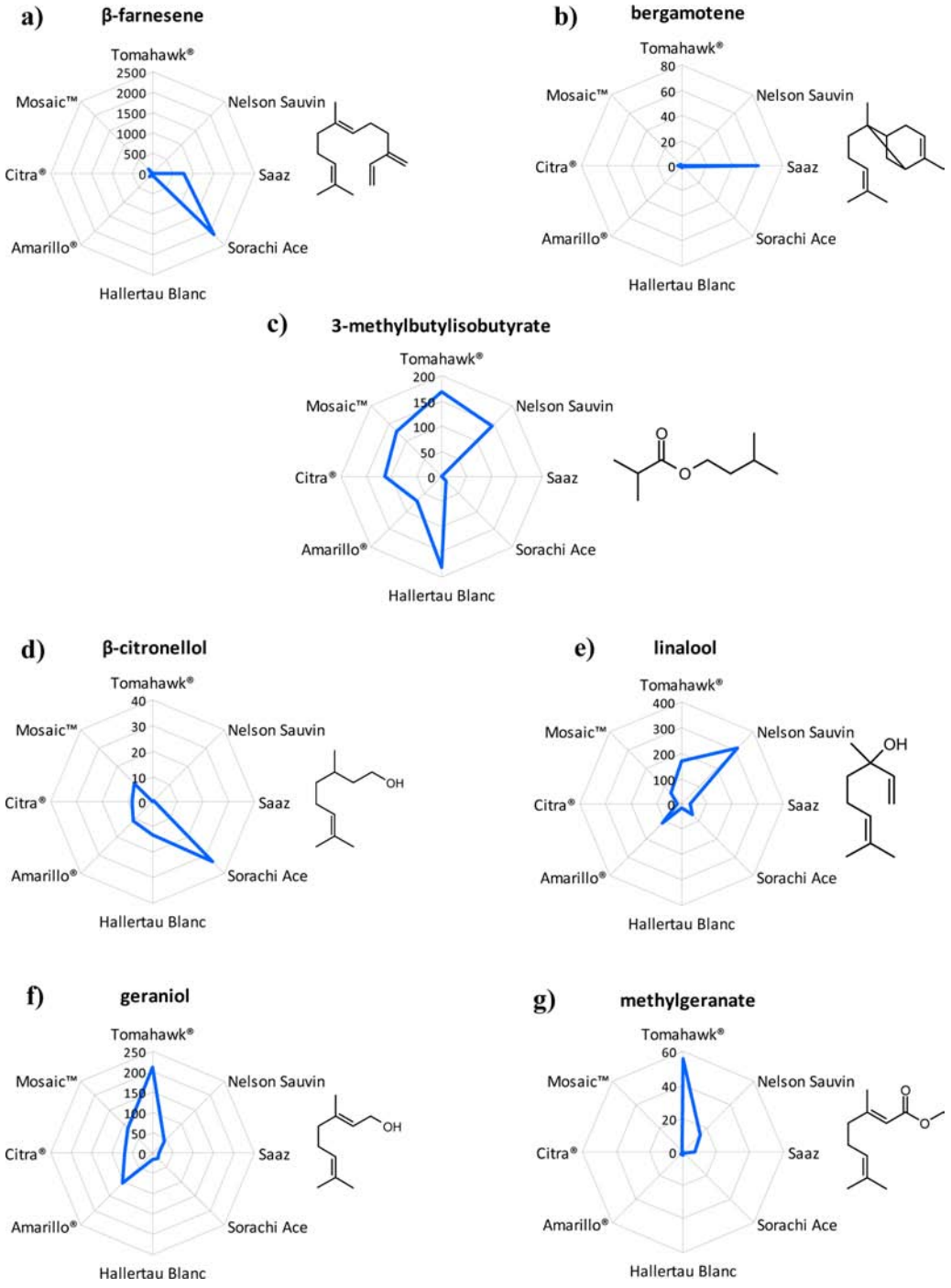

Figure 1. Spider diagrams and corresponding chemical structures of discriminant nonsulfur constituents in seven dual-purpose hop varieties, as compared to Saaz. Concentrations in mg/kg of hop.

IST superscript in Table 2), the good equimolarity of the PFPD detector enabled us to set the IST-relative molar response coefficients at 1. The variation coefficients for thiols (extraction and analysis) were below 15%.

Quantitation of Free Thiols (X) Released by Enzymatic Treatment. For free thiol quantitation, the following equation was used:[24] concentration of X (in μg/kg) = concentration of bound IST (in μg/kg) × (molecular weight of free IST/molecular weight of bound IST) × (peak area of X/peak area of free IST) × (mass response coefficient of free IST/mass response coefficient of X).

The same bound-to-free thiol conversion rates were used for all compounds.[24] For commercially unavailable compounds, the mass response coefficient of X was assessed as the molar response coefficient of free IST × (molecular weight of X/molecular weight of free IST)

Statistical Analyses. All analyses were carried out in duplicate. Multiple comparisons of means were performed by means of Student−Newman−Keuls tests, with SAS software version 9.2 (SAS Institute, Inc., Cary, NC, U.S.A.). Values that do not share a letter indicating significance are significantly different ($p < 0.05$).

RESULTS AND DISCUSSION

To extend the data provided by Gros et al.,[8] the terpenoid profiles of five new dual-purpose hops were determined (Figure 1

DOI: 10.1021/jf5058556
J. Agric. Food Chem. 2015, 63, 3022−3030

and Table 1). GC-MS analyses of hop Likens Nickerson extracts showed much diversity.

The most unexpected result was the concentration of β-farnesene (2101 mg/kg) in the Sorachi Ace variety, despite its high α-acid content (12.3%) (Figure 1a). Amarillo (9.3% α-acids) and Mosaic (11.7% α-acids) also contained concentrations of β-farnesene (152.6 and 102.8 mg/kg, respectively) very close to those usually found in the finest aromatic varieties Lublin, Saaz, and Styrian Golding (discrimination level for these aromatic hop set at 150 mg/kg for fresh samples).[5] On the other hand, bergamotene, claimed to be the second discriminating sesquiterpene of aromatic varieties (>10 mg/kg),[7] was found only at trace levels in all dual-purpose varieties (1.4−3.1 mg/kg).

As expected for bitter varieties, 3-methylbutylisobutyrate derived from α-acid lateral chain degradation was found at much higher levels (69−181 mg/kg) in Amarillo, Citra, Hallertau Blanc, and Mosaic than in Saaz (Figure 1c). Surprisingly, a low concentration was found in Sorachi Ace (13 mg/kg).

The concentration of β-citronellol was above 7 mg/kg in the five dual-purpose hops investigated here, while values under 1.2 mg/kg have been reported for Nelson Sauvin and Tomahawk (Figure 1d). Taking into account a dilution factor of ∼500 between hop and beer (hopping rate generally ∼200 g/hL) and a flavor threshold of 8 μg/L,[14] we can assume an impact of this citrus-like terpenoid in the flavor of derived beers. On the other hand, the two other monoterpenic alcohols linalool (Figure 1e) and geraniol (Figure 1f) remain good discriminating compounds for Nelson Sauvin and Tomahawk, respectively (18−109 mg/kg linalool in the five hops investigated here versus 312 mg/kg in Nelson Sauvin; 16−105 mg/kg geraniol versus 211 mg/kg in Tomahawk, where more methylgeranate was also found, together with α- and β-selinene and α-amorphene). The fruity Mosaic variety was characterized by the presence of 237 mg/kg of undecan-2-one (<113 in all other varieties).

Polyfunctional thiols were selectively extracted from hops with an organomercuric reagent (*p*HMB). Identifications were achieved on two capillary columns (polar FFAP and apolar CP-Sil 5 CB) by the coincidence of retention times at the selective pulsed flame photometric detector (PFPD) and odors at the olfactometric port (GC-O). The selective PFPD enabled us to quantify 9 thiols (some peaks previously found in other hop extracts were here undetected or unsufficiently resolved; see Table 2 and Figure 2). As previously evidenced for Nelson Sauvin and Tomahawk,[8,13,35] each variety investigated here exhibited a unique thiol profile.

2-Sulfanylethyl acetate (no. 38, 2SEA, toasted, Figure 3a), 3-sulfanylpropyl acetate (no. 1, 3SPrA, grilled), and 2-sulfanylethan-1-ol (no. 36, 2SEol, grilled, Figure 3b) were found in the Citra variety at levels never encountered in other hops (see also Figure 2b and Table 2). 2SEA and 2SEol explain 95% of the exceptionally high total amount of polyfunctional thiols found in Citra (1296 μg/kg). Also worth stressing is the presence in the Citra variety of a very pleasant discriminating compound, 3-sulfanylhexyl acetate (no. 11, 3SHA, passionfruit, grapefruit, 27 μg/kg, Figure 3c). By comparison with its threshold of 0.005 μg/L in beer[38] and taking into account a dilution ratio of ∼500 from hop to beer, 3SHA should have an impact in the flavor of Citra-hopped beers. This is probably not the case for the empyreumatic odorants discussed earlier (867 μg/kg / 500 L/kg = 1.7 μg/L of 2SEA for a threshold of 40 μg/L).[39]

Although relatively poor in other polyfunctional thiols (total = 122 μg/kg), the Hallertau Blanc cultivar proved much richer in 3-sulfanyl-4-methylpentan-1-ol (no. 26, 3S4MPol, grapefruit, rhubarb, Figure 3d), although 3S4MPol was previously claimed to be specific to the Nelson Sauvin. Here we found it at

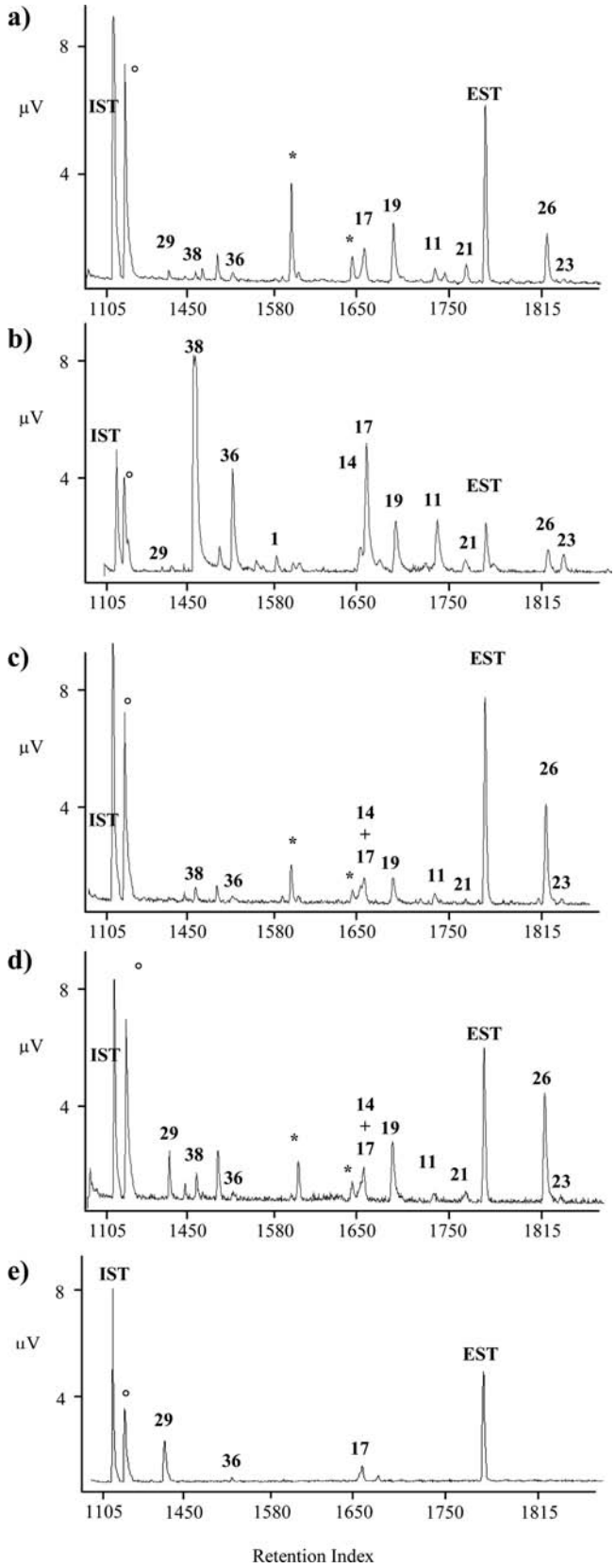

Figure 2. GC-PFPD chromatograms (FFAP column) of pHMB extracts obtained from Amarillo (a), Citra (b), Hallertau Blanc (c), Mosaic (d), and Sorachi Ace (e). °Impurity, *unknown.

DOI: 10.1021/jf5058556
J. Agric. Food Chem. 2015, 63, 3022−3030

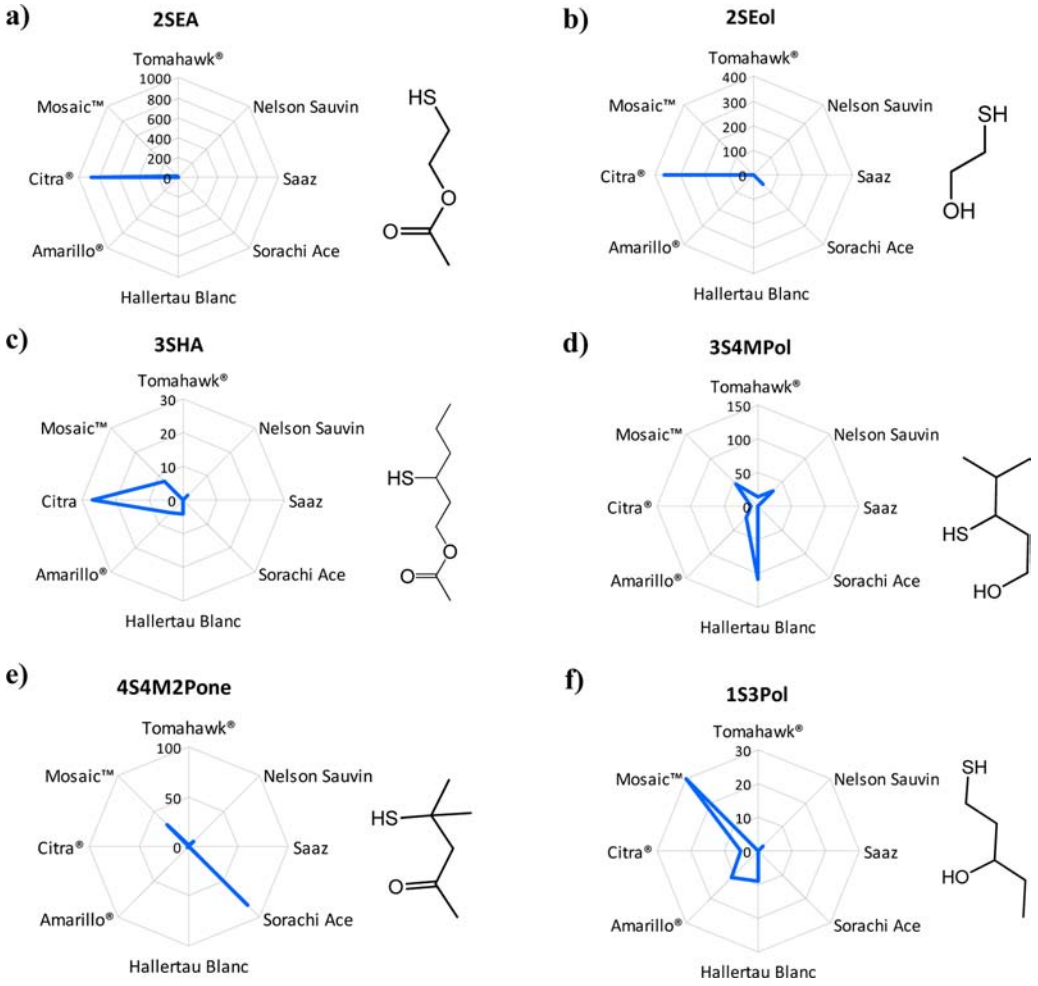

Figure 3. Spider diagrams and corresponding chemical structures of discriminant free polyfunctional thiols in seven dual-purpose hop varieties, as compared to Saaz. Concentrations in μg/kg of hop.

Table 3. Amounts of Thiols (μg/kg, IST Equivalents for Compounds Carrying the IST Superscript) Released from Purified Hop Extract by Apotryptophanase[a,b]

	retention index		substance								
no.	FFAP	CP-Sil 5 CB	name	acronym	odor (GC-O)	Amarillo	Citra	Hallertau Blanc	Mosaic	Sorachi Ace	previously reported cultivars[24c]
37	1112	810	3-methyl-2-buten-1-thiol	MBT	coffee, skunky	nd b	414 a	nd b	453 a	418 a	T a, NS a, S b
29	1380	918	4-sulfanyl-4-methylpentan-2-one	4S4M2Pone	catty, black currant	nd c	nd c	nd c	nd c	nd c	T b, NS a, S c
36	1532	722	2-sulfanylethan-1-ol	2SEol	grilled, gas	2499 a	2525 a	655 b	985 b	2087 a	T c, NS c, S c
14	1623	849	3-sulfanylpropan-1-ol	3SProl	popcorn	nd c	nd c	nd c	nd c	nd c	T a, NS b, S c
17	1654	933	3-sulfanyl-3-methylbutan-1-ol	3S3MBol	sulfur, soup	127 a	d	nd c	109 a	d	T c, NS c, S c
21	1760	1009	3-sulfanylpentan-1-ol	3SPol	catty, citrus	391 b	nd e	70 d	nd e	130 c	T d, NS a, S e
26	1815	1186	3-sulfanyl-4-methylpentan-1-ol^{IST}	3S4MPol	grapefruit	nd b	nd b	39 a	nd b	nd b	T b, NS b, S b
23	1858	1095	3-sulfanylhexan-1-ol	3SHol	grapefruit	413 c	616 b	188 c,d	47 d	1158 a	T cd, NS cd, S cd
			total			3430 a	3555 a	952 b,c	1594 b	3793 a	T bc, NS bc, S c

[a]Concentration determined by GC-PFPD. Mean of duplicates. Values within a row with different letters are significantly different ($p < 0.05$) according to the Student−Newman−Keuls test. [b]nd, not detected (<8 μg/kg). d, detected but unresolved. [c]Data issued from ref 24; letters after T, NS, or S indicate statistical group for the reported concentrations in Tomahawk, Nelson Sauvin, and Saaz.

concentrations up to 109 μg/kg (IST equivalents), compared to 25−46 μg/kg in Mosaic, Nelson Sauvin, and Amarillo and 10−13 μg/kg in Citra and Tomahawk. This compound was not detected at all in the Sorachi Ace variety.

DOI: 10.1021/jf5058556
J. Agric. Food Chem. 2015, 63, 3022−3030

4-Sulfanyl-4-methylpentan-2-one (no. 29, 4S4M2Pone, catty, Figure 3e), another proposed marker of the Nelson Sauvin cultivar (7 μg/kg), was found at amounts 4-fold higher (30 μg/kg) in Mosaic and 11-fold higher (83 μg/kg) in Sorachi Ace. 1-Sulfanylpentan-3-ol (no. 19, 1S3Pol, nettle, Figure 3f) was found at the highest level in Mosaic (30 μg/kg, IST equivalents).

3-Sulfanyl-2-ethylpropyl acetate (no. 10, 3S2EPrA, floral, vinegar) and 3-sulfanyloctanal (no. 35, 3SOal, citrus, peach) remained undetected in all five new dual-purpose varieties investigated here, whereas they were previously identified as markers of Tomahawk and Nelson Sauvin.

S-cysteine conjugates of our five varieties were purified and subjected to apotryptophanase treatment (Table 3). Quantitations were done in IST equivalents, assuming that benzylthiol was released from its S-cysteine conjugate in the same way as all free amine hidden hop thiols.[24] Eight different adducts were identified, including two never before reported (2SEol and 3S4MPol).

The Sorachi Ace, Citra, and Amarillo varieties contained 1158, 616, and 413 μg/kg of hidden 3SHol, respectively. These values should be compared to the 1641 μg/kg previously found by Gros et al. in Cascade,[24] the hop variety where they identified the first S-cysteine conjugate by high-performance liquid chromatography (HPLC)/MS/MS. No obvious relation seems to exist between free and bound 3SHol. The following ratios of free to bound 3SHol were calculated: 1.9% for Citra, 4.3% for Tomahawk, and 7.1% for Cascade. For the Sorachi Ace variety, the free thiol was undetectable.

3-Sulfanyl-3-methylbutan-1-ol (3S3MBol) was also found to be released (127 μg/kg from Amarillo and 109 μg/kg from Mosaic). The thiol S-cysteine conjugate of 3S3MBol, known as felinine, has never been evidenced before in hop but was recently identified in cat urine.[40]

Never reported before, the 3-sulfanyl-4-methylpentan-1-ol S-conjugate was found in the Hallertau Blanc cultivar. Unlike the others, it occurred at lower concentration than the corresponding free thiol (39 and 109 μg/kg, respectively).

Already discriminant in its free form for the Citra variety, 2-sulfanylethan-1-ol also proved to be enzymatically released in a high amount (2.5 mg/kg) from the Citra bound extract (free/bound ratio = 14%). A strong impact of the hop variety on the amount of 2SEol generated during beer fermentation has recently been reported.[23] From this first evidence of the presence of 2SEol S-conjugate, we can suspect that its cleavage might be an additional 2SEol synthesis pathway occurring during beer fermentation, together with Ehrlich degradation of cysteine.[39,41]

In conclusion, although much diversity was found among the investigated dual-purpose hops, all proved to contain an exceptional citrus-like potential. In Sorachi Ace, β-citronellol is probably the main compound responsible for such notes, while in others, polyfunctional thiols such as 3SHA (Citra) or 3S4MPol (Hallertau Blanc, Mosaic) could play a key role. Complementary investigations are now needed to assess which molecules involved in the citrus note must be preferred in beer, especially for increasing its flavor stability. The free/bound ratio of discriminating polyfunctional thiols also should be determined for successive harvest years.

AUTHOR INFORMATION

Corresponding Author

*E-mail: sonia.collin@uclouvain.be. Fax: +32-10-47 21 78.

Funding

The authors thank the Inbev-Baillet Latour Foundation and the Barth Haas Grant 2013 for their support.

Notes

The authors declare no competing financial interest.

ACKNOWLEDGMENTS

Thanks are due to the hop suppliers Yakima Chief and Hopsteiner.

ABBREVIATIONS USED

*p*HMB, *p*-hydroxymercuribenzoic acid; PFPD, pulse flame photometric detector; RI, retention index; IST, internal standard; EST, external standard

REFERENCES

(1) Beatson, R.; Alspach, P. Developments in the New Zealand hop breeding programme. *Master. Brew. Assoc. Am.* **2002**.

(2) Gros, J.; Kankolongo Cibaka, M. L.; Collin, S. Revue sur les étonnantes analogies et les différences relevées entre un cône de houblon et une baie de raisin. Partie I: Pratiques culturales, anatomie et sélection de nouvelles variétés. *Cerevisia* **2013**, *38*, 61−70.

(3) Deinzer, M.; Yang, X. *Hop aroma: Character impact compounds found in beer, methods of formation of individual compounds*; EBC Monograph XXII; Symposium on Hops, Zoeterwoude, The Netherlands; Verlag Hans Carl: Nurnberg, Germany, 1994; pp 81−197.

(4) De Keukeleire, D.; De Cooman, L.; Everaert, E.; Sandra, P.; Vindevogel, J.; Szucs, R. Novel methodology for unambiguous identification of hop varieties. *Institute of Brewing 23rd Convention*, Australia and New Zealand Section; Winetitles - Hyde Park Press: Adelaide, Australia, 1994; pp 129−132.

(5) Perpète, P.; Mélotte, L.; Dupire, S.; Collin, S. Varietal discrimination of hop pellets. I. Comparison of fresh samples. *J. Am. Soc. Brew. Chem.* **1998**, *56*, 104−108.

(6) Eri, S.; Khoo, B. K.; Lech, J.; Hartman, T. G. Direct thermal desorption-gas chromatography and gas chromatography−mass spectrometry profiling of hop (*Humulus lupulus* L.) essential oils in support of varietal characterization. *J. Agric. Food Chem.* **2000**, *48*, 1140−1149.

(7) Lermusieau, G.; Collin, S. Varietal discrimination of hop pellets. II. Comparison between fresh and aged samples. *J. Am. Soc. Brew. Chem.* **2001**, *59*, 39−43.

(8) Gros, J.; Nizet, S.; Collin, S. Occurrence of odorant polyfunctional thiols in the super alpha Tomahawk hop cultivar. Comparison with the thiol-rich Nelson Sauvin bitter variety. *J. Agric. Food Chem.* **2011**, *59*, 8853−8865.

(9) Takoi, K.; Itoga, Y.; Koie, K.; Kosugi, T.; Shimase, M.; Katayama, Y.; Nakayama, Y.; Watari, J. The contribution of geraniol metabolism to the citrus flavour of beer: Synergy of geraniol and β-citronellol under coexistence with excess Linalool. *J. Inst. Brew.* **2010**, *116*, 251−260.

(10) Siebert, K. J. Sensory analysis of hop oil−derived compounds in beer; flavor. Effects of individual compounds. Quality control. *Eur. Brew. Conv.* Monograph XXII, Symposium on Hops. **1994**, 198−212.

(11) Kishimoto, T.; Wanikawa, A.; Kagami, N.; Kawatsura, K. Analysis of hop-derived terpenoids in beer and evaluation of their behavior using the stir bar−sorptive extraction method with GC-MS. *J. Agric. Food Chem.* **2005**, *53*, 4701−4707.

(12) Peppard, T. L.; Ramus, S. A.; Witt, C. A.; Siebert, K. J. Correlation of sensory and instrumental data in elucidation the effect of varietal differences on hop flavour in beer. *J. Am. Soc. Brew. Chem.* **1989**, *47*, 18−26.

(13) Kishimoto, T.; Wanikawa, A.; Kono, K.; Shibata, K. Comparison of the odor-active compounds in unhopped beer and beers hopped with different hop varieties. *J. Agric. Food Chem.* **2006**, *54*, 8855−8861.

(14) Takoi, K.; Koie, K.; Itoga, Y.; Katayama, Y.; Shimase, M.; Nakayama, Y.; Watari, J. Biotransformation of hop-derived monoterpene alcohols by lager yeast and their contribution to the flavor of hopped beer. *J. Agric. Food Chem.* **2010**, *58*, 5050−5058.

DOI: 10.1021/jf5058556
J. Agric. Food Chem. 2015, 63, 3022−3030

(15) Steinhaus, M.; Schieberle, P. Transfer of potent hop odorants linalool, geraniol and 4-methyl-4-sulfanyl-2-pentanone from hops to beer. Proc. 31st Congr. Eur. Brew. Conv., Venice, 2007.
(16) Biendl, M.; Kollmannsberger, H.; Nitz, S. Occurrence of glycosidically bound flavour compounds in different hop products. Proc. 29th Congr. Eur. Brew. Conv., Dublin, 2003.
(17) Kollmannsberger, H.; Biendl, M.; Nitz, S. Occurrence of glycosidically bound flavour compounds in hops, hop products and beer. *Monatsschr. Brauwiss.* **2006**, *5/6*, 83−89.
(18) Goldstein, H.; Ting, P.; Schulze, W. G.; Murakami, A. A.; Lusk, L. T.; Young, V. D. Methods of making and using purified kettle hop flavorants. U.S. Patent No. 5972411, 1999.
(19) Collin, S.; Nizet, S.; Gros, J. Le houblonnage à cru des bières spéciales belges est bien plus qu'une simple dissolution des composés aromatiques du houblon. *Cerevisia* **2012**, *36*, 119−124.
(20) Nizet, S.; Gros, J.; Peeters, F.; Chaumont, S.; Robiette, R.; Collin, S. First evidence of the production of odorant polyfunctional thiols by bottle refermentation. *J. Am. Soc. Brew. Chem.* **2013**, *71*, 15−22.
(21) Fujita, T.; Nakayama, M. Perilloside a, a monoterpene glucoside from Perilla frutescens. *Phytochemistry* **1992**, *31*, 3265−3267.
(22) Steinhaus, M.; Wilhelm, W.; Schieberle, P. Comparison of the most odor-active volatiles in different hop varieties by application of a comparative aroma extract dilution analysis. *Eur. Food Res. Technol.* **2007**, *226*, 45−55.
(23) Gros, J.; Peeters, F.; Collin, S. Occurrence of odorant polyfunctional thiols in beers hopped with different cultivars. First evidence of an S-cysteine conjugate in hop (*Humulus lupulus* L.). *J. Agric. Food Chem.* **2012**, *60*, 7805−7816.
(24) Gros, J.; Tran, T. T. H.; Collin, S. Enzymatic release of odourant polyfunctional thiols from cysteine conjugates in hop. *J. Inst. Brew.* **2013**, *119*, 221−227.
(25) Peyrot des Gachons, C.; Tominaga, T.; Dubourdieu, D. Measuring the aromatic potential of *Vitis vinifera* L. Cv. Sauvignon Blanc grapes by assaying S-cysteine conjugates, precursors of the volatile thiols responsible for their varietal aroma. *J. Agric. Food Chem.* **2000**, *48*, 3387−3391.
(26) Starkenmann, C.; Niclass, Y. New cysteine-S-conjugate precursors of volatile sulfur compounds in bell peppers (*Capsicum annuum* L. cultivar). *J. Agric. Food Chem.* **2011**, *59*, 3358−3365.
(27) Starkenmann, C.; Niclass, Y.; Troccaz, M. Non volatile S-alk(en)ylthio-l-cysteine derivatives in fresh onion (*Allium cepa* L. cultivar). *J. Agric. Food Chem.* **2011**, *59*, 9457−9465.
(28) Fretz, C. B.; Rouvinez, V.; Känel, S.; Luisier, J. L.; Amado, R. Use of an experimental design model to determine the impact of different fermentation parameters on the development of flavour compounds in wine. *Vitis* **2006**, *45*, 37−43.
(29) Murat, M. L.; Masneuf, I.; Darriet, P.; Lavigne, V.; Tominaga, T.; Dubourdieu, D. Effect of *Saccharomyces cerevisiae* yeast strains on the liberation of volatile thiols in Sauvignon Blanc wine. *Am. J. Enol. Vitic.* **2001**, *52*, 136−139.
(30) Subileau, M.; Schneider, R.; Salmon, J. M.; Degryse, E. Nitrogen catabolite repression modulates the production of aromatic thiols characteristic of Sauvignon Blanc at the level of precursor transport. *FEMS Yeast Res.* **2008**, *8*, 771−780.
(31) Thibon, C.; Marullo, P.; Claisse, O.; Cullin, C.; Dubourdieu, D.; Tominaga, T. Nitrogen catabolic repression controls the release of volatile thiols by *Saccharomyces cerevisiae* during wine fermentation. *FEMS Yeast Res.* **2008**, *8*, 1076−1086.
(32) Vermeulen, C.; Collin, S. Combinatorial synthesis and sensorial properties of 21 mercapto esters. *J. Agric. Food Chem.* **2003**, *51*, 3618−3622.
(33) Vermeulen, C.; Guyot-Declerck, C.; Collin, S. Combinatorial synthesis and sensorial properties of mercapto primary alcohols and analogues. *J. Agric. Food Chem.* **2003**, *51*, 3623−3628.
(34) Vermeulen, C.; Collin, S. Synthesis and sensorial properties of mercaptoaldehydes. *J. Agric. Food Chem.* **2002**, *50*, 5654−5659.
(35) Takoi, K.; Degueil, M.; Shinkaruk, S.; Thibon, C.; Maeda, K.; Ito, K.; Bennetau, B.; Dubourdieu, D.; Tominaga, T. Identification and characteristics of new volatile thiols derived from the hop (*Humulus lupulus* L.) cultivar Nelson Sauvin. *J. Agric. Food Chem.* **2009**, *57*, 2493−2502.
(36) Bouseta, A.; Collin, S. Optimized Likens−Nickerson methodology for quantifying honey flavors. *J. Agric. Food Chem.* **1995**, *43*, 1890−1897.
(37) Tominaga, T.; Murat, M. L.; Dubourdieu, D. Development of a method for analysing the volatile thiols involved in the characteristic aroma of wines made from *Vitis vinifera* L. cv. Sauvignon Blanc. *J. Agric. Food Chem.* **1998**, *46*, 1044−1048.
(38) Kishimoto, T.; Morimoto, M.; Kobayashi, M.; Yako, N.; Iida, A.; Wanikawa, A. Behaviors of 3-mercaptohexan-1-ol and 3-mercaptohexyl acetate during brewing processes. *J. Am. Soc. Brew. Chem* **2008**, *66*, 192−196.
(39) Tran, T. T. H.; Gros, J.; Bailly, S.; Nizet, S.; Collin, S. Fate of 2-sulphanylethyl acetate and 3-sulphanylpropyl acetate through beer aging. *J. Inst. Brew.* **2012**, *118*, 198−204.
(40) Starkenmann, C.; Niclass, Y.; Cayeux, I.; Brauchli, R.; Gagnon, A.-C. Odorant volatile sulfur compounds in cat urine: Occurrence of (±)-3,7-dimethyloct-3-sulfanyl-6-en-1-ol and its cysteine conjugate precursor. *Flavour Fragrance J.* **2015**, *30*, 91−100.
(41) Vermeulen, C.; Lejeune, I.; Tran, T. T. H.; Collin, S. Occurrence of polyfunctional thiols in fresh lager beers. *J. Agric. Food. Chem.* **2006**, *54*, 5061−5068.

DOI: 10.1021/jf5058556
J. Agric. Food Chem. 2015, 63, 3022−3030

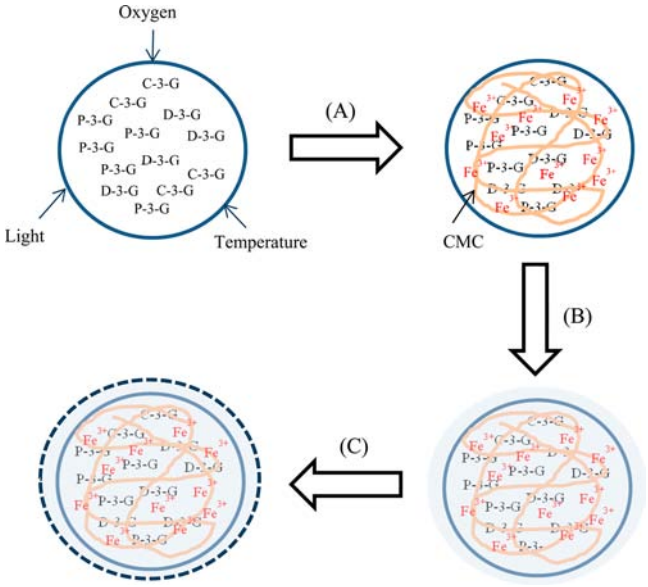

Figure 1. Diagram of the research hypothesis: (A) polysaccharide (CMC)−metal ($FeCl_3$)−anthocyanin complex, (B) CNF coating containing $CaCl_2$ and/or MC, and (C) SA treatment to form a second layer coating (LBL coating system).

than 50. The aqueous suspensions/slurries of the fibrous nanocellulose are capable of forming highly water-resistant and thermomechanical coatings/films because of the strong and percolated inter-/intrafibrillar networks through hydrogen bonds.[16] However, CNF coating/film can be disintegrated in aqueous media because of the competitive interaction with water through hydrogen bonds,[17] which would displace CNF coatings from the surface of fruits in the aqueous system. To enhance the attachment of CNF coating onto the fruit surface and hydrophobicity against water, CNF was modified by calcium chloride ($CaCl_2$) and/or methyl cellulose (MC). Fruits coated by CNF containing $CaCl_2$ and then subjected to SA solution can form Ca^{2+} cross-linked alginic acid hydrogel onto the CNF layer because Ca^{2+} is gradually released from CNF structures, thus generating a water-insoluble semi-permeable LBL coating on the fruit surface. It was also expected that, by incorporating MC into CNF, CNF coating can be less impacted by water because of less hydrophilic blocks of the methoxyl groups.[18] Therefore, the LBL coating system established with CNF as the first layer and SA-based hydrogel as the second layer would not only provide close adhesion between CNF and the fruit surface but also improve the protection of fruit anthocyanins from leaching and coating swelling when subjected to heating in aqueous media.

Therefore, the specific objective of this study was to investigate the retention mechanisms of combined MA or PMA complexation and CNF/SA LBL coating on anthocyanin pigments and the developed technologies on the physicochemical properties of the fruits using blueberries as a model system. To investigate the efficiency and stability of MA and PMA complexation, percent polymeric color (PPC) and monomeric anthocyanin content were evaluated for fresh sample, complexed sample, and complexed sample subjected to the thermal process at 93 °C for 7 min (simulated canning conditions for acidified food). The microstructure of coated fruits and the simulated LBL coating system were also investigated using a stereoscope microscope and/or a scanning electron microscope (SEM) to demonstrate protection mechanisms. Results from this study would provide a new understanding on the anthocyanin retention mechanism in thermally processed whole fruits for improving the existing technologies and developing new value-added colorful fruit products.

MATERIALS AND METHODS

Materials. CNF was obtained from University of Maine Process Development Center (Orono, ME) and prepared from bleached pulp. The following chemical reagents were used for the experiments: Folin−Ciocalteu's (FC) phenol reagent (MP Biomedicals, LLC, Santa Ana, CA), gallic acid (Sigma-Aldrich Co., LLC, St. Louis, MO), acetic acid (Avantor Performance Materials International, Inc., Center Valley, PA), L-ascorbic acid (Avantor Performance Materials International, Inc., Center Valley, PA), 2,2-diphenyl-1-picrylhydrazyl (DPPH) (95%) (Alfa Aesar, Ward Hill, MA), hydrochloric acid (HCl) (EMD Chemicals, Inc., Gibbstown, NJ), sodium acetate (EMD Chemicals, Inc. Gibbstown, NJ), potassium chloride (KCl) (EMD Chemicals, Inc., Gibbstown, NJ), sodium carbonate (EMD Chemicals, Inc., Gibbstown, NJ), and trifluoroacetic acid (EMD Chemicals, Inc., Gibbstown, NJ). Analytical-grade methanol, ethanol, and acetone were used for the extraction of anthocyanins. CMC, MC, and SA were obtained from Sigma-Aldrich (St. Louis, MO), Hercules, Inc. (Wilmington, DE), and TIC Gums, Inc. (White Marsh, MD), respectively.

Sample Preparation. The sample preparation procedures from complexation to LBL coating are illustrated in Figure 1.[15] Fresh blueberries (California Giant, Inc., Watsonville, CA, and Hurst Berry Farm, McMinnville, OR) were soaked in Environne (Consumer Health Research, Inc., Roseburg, OR) for 10 min to wash out the remaining substances (pesticides and waxes) on fruit surfaces and dried at ambient temperature. Two different complexations were applied at ambient conditions: (1) Fe^{3+}−anthocyanin and (2) CMC−Fe^{3+}−anthocyanin. For Fe^{3+}−anthocyanin complexation,[6] blueberries were soaked in 1% $FeCl_3$ solution for 30 min and then dried under an air-flow fan. For CMC−Fe^{3+}−anthocyanin complexation, fruits were soaked in 1% $FeCl_3$ solution for 30 min, followed by soaking in 0.1% CMC at pH 6.5 phosphate buffer for another 30 min, and then dried under an air-flow fan.

Two different CNF coating formulations were prepared: (1) 0.75% CNF containing 0.5% $CaCl_2$ and (2) 0.75% CNF containing 0.5% $CaCl_2$ and 0.5% MC in distilled water (w/w). Coating formulations were sprayed onto fruit surfaces using an air-spray gun (25−30 psi) and dried at ambient temperature under an air-flow fan. To apply SA-based hydrogel coating onto the CNF coating layer further, coated fruits were put into 0.5% SA bath for 5 min and then transferred to a 3% $CaCl_2$ bath for 5 min to form reverse and basic spherifications, respectively. After the prepared fruit samples were washed by distilled water to remove the residual $CaCl_2$ compounds, they were put into glass jars containing 15% sucrose solution with pH 4.0 (adjusted by 1% formic acid) and then thermally processed at a 93 °C water bath (Precision, Winchester, VA) for 7 min to stimulate canning process conditions for berry fruits. The hot jars were cooled in a cold-water bath to reach ambient temperature and stored at the ambient conditions for 2 days before analysis. Anthocyanins, total phenolic content (TPC), PPC, color, total soluble solid, pH, texture property of fruits, and total monomeric anthocyanin (TMA), PPC, and TPC of the packing solutions were all analyzed.

Extraction of Phenolic Compounds from Fruits. Samples were extracted using 60% methanol at a 1:10 (sample/methanol) ratio for 20 min using a sonication unit (B-200H, Branson, Danbury, CT) in 50 mL centrifuge tubes (VWR International, LLC, Radnor, PA) based on the optimized extraction conditions developed from our laboratory (data not shown). The obtained extracts were centrifuged (International Equipment Co., Boston, MA) at 10000*g* at 4 °C for 10 min and filtrated through the Whatman No. 1 filter paper. Methanol was evaporated with a vacuum rotary evaporator (Brinkmann Instruments, Westbury, NY) at 40 °C, and resulting extracts were redissolved in citric buffer (pH 3.5) in a 25 mL volumetric flask. The extracts were

DOI: 10.1021/acs.jafc.5b00616
J. Agric. Food Chem. 2015, 63, 3031−3038

stored in a −80 °C freezer (VWR International LLC, Radnor, PA) until further analysis on TPC, TMA, and PPC.

Analysis of Monomeric Anthocyanins, TPC, and PPC of Fruit and Packing Solution. The TMA content was determined using the pH-differential method[19] and expressed as milligrams of Cy-3-glu per 100 g of fresh fruits with a molecular weight of 449.2 g/mol and a molar absorptivity of 26 900. TPC was measured using the FC-reagent-based colorimetric assay as described by Singleton and Rossi.[20] The phenolic content was calculated as gallic acid equivalent (GAE) and reported as milligrams per 100 g of fresh fruits.

PPC of the fruits was determined using the method by Cao et al.[21] Briefly, 0.2 mL of 0.2 g/mL potassium metabisulfite was added to 2.8 mL of diluted sample (bleached sample), whereas 0.2 mL of distilled water was also added to 2.8 mL of diluted sample (control sample). After equilibration for 30 min at ambient conditions, the absorbance of the bleached and control sample was evaluated at a wavelength of 420 nm, $\lambda_{vis\text{-}max}$, and 700 nm, respectively, using an ultraviolet/visible (UV/vis) spectrophotometer (Shimadzu, Japan). The color density of the control sample and the polymeric color of the thermally processed sample were calculated using the following equation:

$$\text{color density or polymeric color} = [(A_{420\ nm} - A_{700\ nm}) + (A_{\lambda_{vis\text{-}max}} - A_{700\ nm})] \times \text{dilution factor}$$

PPC was further calculated as (polymeric color/color density) × 100%.

With consideration of the possible leaching of anthocyanin pigments from fruits into packing solution during thermal process and storage, TPC, TMA, and PPC of packing solutions were also analyzed using the same methods described above.

Physicochemical Properties of Blueberries. Color and total soluble solid content (TSS, °Brix) of fruits were measured using a colorimeter (HunterLab LabScan XE spectrophotometer, Reston, VA) and a refractometer (Brix RA-250 HE, Kyoto Electronics Manufacturing Co., Ltd., Kyoto, Japan), respectively.[22] Fruit pH and titratable acidity (TA) were determined using the methods from Fisk et al.[22] Briefly, five berries were randomly collected, weighed, mixed with distilled water at 1:9 (w/w) ratio, and blended for 1 min using a homogenizer (Osterizer, Jarden Corp., Mexico). The mixture was filtered through qualitative filter paper to remove insoluble materials. The filtrate was titrated with a standardized 0.1 N aqueous NaOH solution up to an end point of pH 8.2 using a pH meter (Corning 125, Corning Science Products, Tewksbury, MA). TA values were calculated on the basis of the assumption that citric acid was the predominant acid in blueberries. Firmness was measured using a texture analyzer (TA.XT2, Stable Micro Systems, Inc., U.K.),[23,24] where individual fruit was compressed for a total deformation of 3 mm between two parallel plates at a speed of 0.5 mm/s. The stem−calyx axis of blueberries was placed in parallel onto the compression plates. The firmness index was calculated as the slope of force/deformation curves between 0.5 and 2.5 mm of displacements and represented as N/mm. Three berries were randomly chosen from the processed fruits for texture analysis.

To investigate the effect of complexation and coating on fruit weight after thermal treatment and storage, the weight change (%) of fruits was calculated as the weight of processed fruits subtracted from the initial weight of fresh fruits divided by the initial fruit weight and multiplied by 100.

Microscopic Analysis. To evaluate adhesion of coatings onto the fruit surface, images on the cross-sections of non-coated and coated fruits (CNF/$CaCl_2$ and CNF/$CaCl_2$/MC coatings) before the thermal process were taken using a stereomicroscope (Leica Microsystems AG, Heerbrugg, Switzerland) equipped with an extended digital camera (QImaging, Surrey, British Columbia, Canada).

The morphology of CNF film incorporated with $CaCl_2$ and/or MC was analyzed using the AmRay 3300 field emission (FE)-SEM (AmRay, Bedford, MA). To investigate the LBL coating system, CNF/$CaCl_2$ and CNF/$CaCl_2$/MC films were treated at 0.5% SA bath for 10 min, dried at 50 °C for 24 h, and then stored in a desiccator for 1 day. Prepared film pieces were mounted on aluminum stubs with the cross-section oriented up and coated by a gold−palladium alloy sputter coater (Edwards model S150B sputter coater, BOC Edwards Vacuum, Ltd., West Sussex, U.K.) to improve the interface conductivity. Digital images were collected at an accelerating voltage of 5 kV.

To quantify the amount of $CaCl_2$ released from the CNF/$CaCl_2$ and CNF/$CaCl_2$/MC films, Ca and Cl contents in the films before and after the films were soaked in water were measured using energy-dispersive X-ray analysis (EDXA). The result would show the reactions of $CaCl_2$ released from CNF with SA to help interpret the adhesion of a SA-based second layer of hydrogel coating on the CNF coating based on the cross-linking between Ca^{2+} and alginic acid within the short reaction time.

Experimental Design and Statistical Analysis. A randomized factorial design with two treatment factors was applied in this study. Factor A [complexation type (CT)] had three levels: non-complexation, Fe^{3+}−anthocyanin complexation, and CMC−Fe^{3+}−anthocyanin complexation. Factor B [coating formulation (CF)] included three types: non-coated, coated by 0.75% CNF containing 0.5% $CaCl_2$, and coated by 0.75% CNF containing 0.5% $CaCl_2$ and 0.5% MC. Replication was also considered as the main effect because of the large variations among individual fruits. Non-complexed and non-coated blueberries subjected to the same thermal process and fresh blueberries without any treatment were considered as controls. About 25−30 individual fruits were treated for each replication, and all experiments were performed in duplicate. The results were analyzed for statistical significance via multi-way analysis of variance (ANOVA), with post-hoc testing using least significant difference (LSD) by means of statistical software (SAS, version 9.2, SAS Institute, Cary, NC). Results were considered to be significantly different at $p < 0.05$.

RESULTS AND DISCUSSION

Effect of Complexation and CNF/SA LBL Coatings. Fruit samples subjected to different complexation and/or CNF/SA LBL coating, followed by thermal process and storage at the ambient conditions for 2 days, are illustrated in Figure 2.

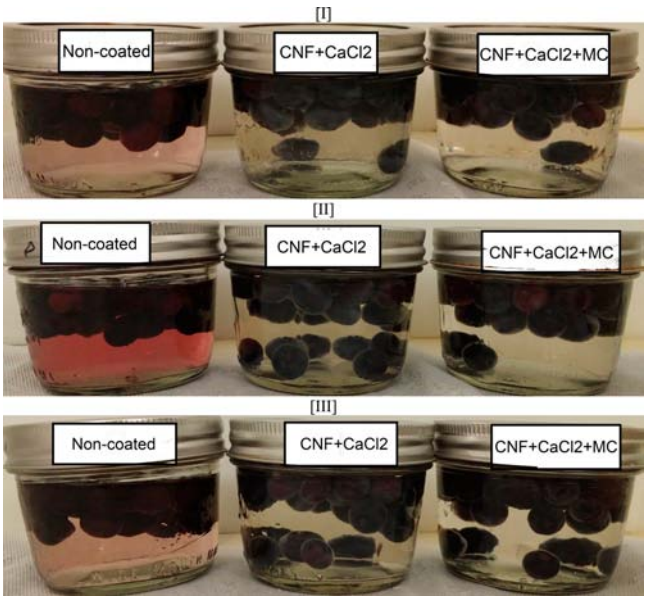

Figure 2. Illustration of pretreated samples after subjected to the thermal process at 93 °C for 7 min and stored at the ambient conditions for 2 days. Second layer coating with SA was applied on all samples with CNF coating. (I) Non-complexation, (II) Fe^{3+}−anthocyanin complexation, and (III) CMC−Fe^{3+}−anthocyanin complexation. The label on the jar indicates different types of coating treatment. MC is methyl cellulose.

DOI: 10.1021/acs.jafc.5b00616
J. Agric. Food Chem. 2015, 63, 3031−3038

Table 1. ANOVA (p = 0.05) for Analyzing the Significance of Each Treatment Factor, Including Replication, CT, and CF, and the Interactive Effect between TC and CF in Thermally Processed Blueberries Stored at the Ambient Conditions for 2 Days

		p value									
	df	weight change	firmness index	chroma	ΔE	pH	TA[a]	TSS[b]	TPC[c]	TMA[d]	PPC[e]
Main Effects											
replications	1	0.0665	0.7927	0.0007	0.0001	0.5685	0.0008	0.7523	0.4929	0.0025	0.0413
CT	2	0.3639	0.2168	0.2720	0.6170	0.9521	0.9914	0.0446	0.6564	0.3817	0.0805
CF	2	<0.0001	0.0032	0.7468	0.0969	0.5294	0.1381	0.0037	0.1748	0.2126	0.7920
Interaction Effects											
CT × CF	4	0.1375	0.2138	0.1558	0.3576	0.9969	0.6738	0.7146	0.9254	0.5951	0.2157
model	9	<0.0001	0.0297	0.0218	0.0058	0.9819	0.0362	0.0314	0.6731	0.0646	0.1282
error	8										
corrected	1										
total	7										

[a]TA = titratable acidity. [b]TSS = total soluble solid. [c]TPC = total phenolic content. [d]TMA = total monomeric anthocyanin. [e]PPC = percent polymeric color.

Table 2. Effect of Complexations and CNF Coating Treatments on Weight Change (%), Firmness Index (N/mm), and TSS (°Brix) of Thermally Processed Blueberries Stored at the Ambient Conditions for 2 Days[a]

CT	CF[b]	weight change[c] (%)	firmness index (N/mm)	TSS (°Brix)
non-complexation	non-coated	−1.95 a	65.30 cde	12.22 bcd
	$CNF/CaCl_2$	13.00 a	79.19 abcd	14.29 ab
	$CNF/CaCl_2$/MC[d]	11.37 a	109.75 a	14.54 ab
$FeCl_3$ complexation	non-coated	−2.69 b	38.08 e	11.90 cd
	$CNF/CaCl_2$	13.56 a	90.24 abc	14.30 ab
	CNF + $CaCl_2$+MC	13.93 a	97.79 ab	15.76 a
$FeCl_3$ + CMC complexation	non-coated	−0.51 b	51.98 de	10.32 d
	$CNF/CaCl_2$	10.87 a	81.73 abcd	13.25 bc
	$CNF/CaCl_2$/MC	10.71 a	71.37 bcd	12.96 bc

[a]Means followed by the same letter in a column were not significantly different (p > 0.05). [b]All coated fruits were also subjected to SA second layer coatings. [c]Weight change (%) was calculated as the weight of processed fruits subtracted with the initial weight of fresh fruits divided by the initial fruit weight and multiplied by 100. [d]MC = methyl cellulose.

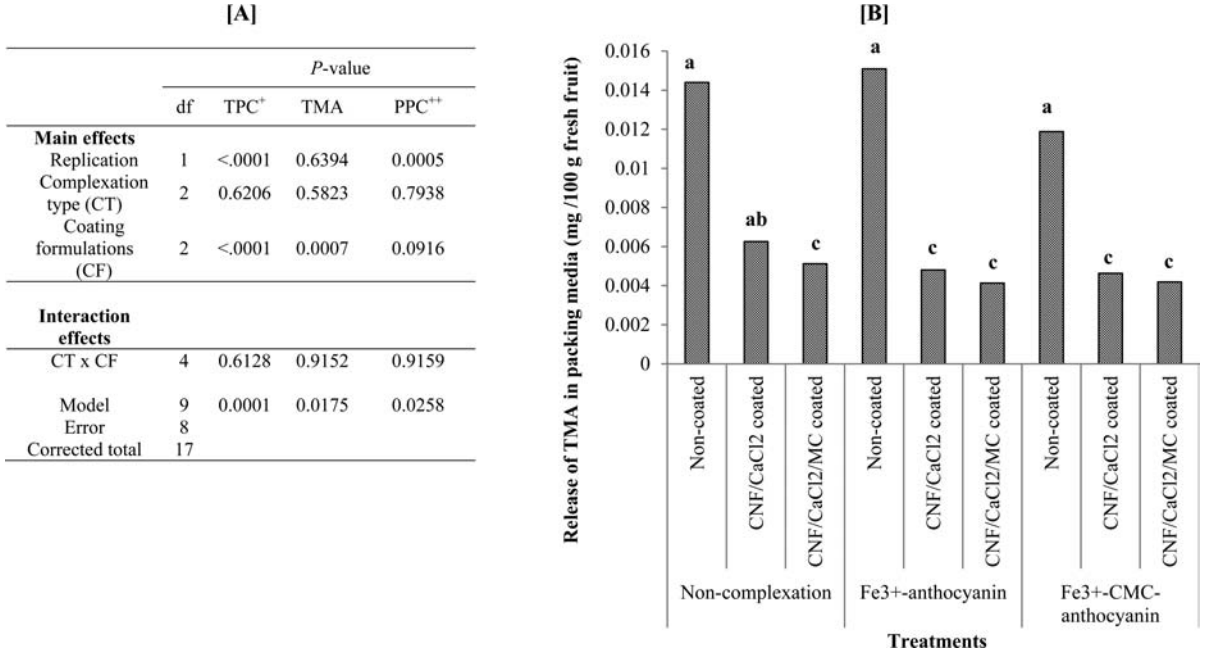

Figure 3. ANOVA results (p = 0.05) for analyzing (A) independence or interactions among treatment factors and (B) amount of released TMA (milligrams of Cy-3-glu/100 g of fresh fruit) in the packing media from thermally processed blueberries subjected to different treatments and stored at the ambient conditions for 2 days. Second layer SA coating was applied on all samples coated by CNF. TPC, total phenolic content; PPC, percent polymeric color.

DOI: 10.1021/acs.jafc.5b00616
J. Agric. Food Chem. 2015, 63, 3031−3038

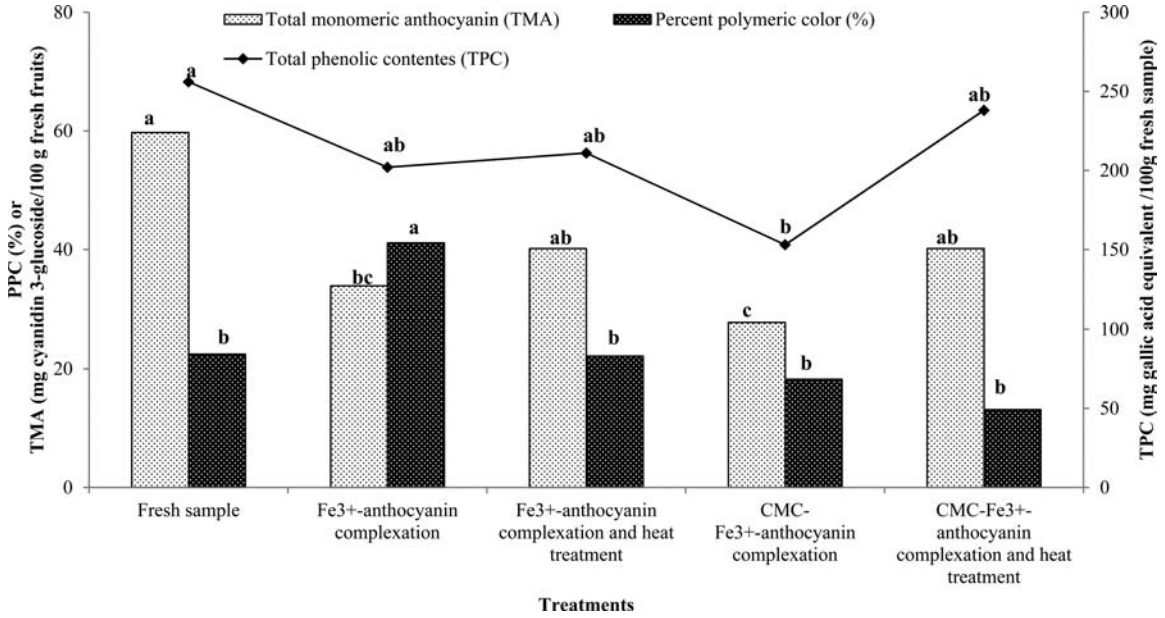

Figure 4. TMA (milligrams of Cy-3-glu/100 g of fresh fruits), TPC (milligrams of GAE/100 g of fresh sample), and PPC (polymeric color/color density × 100) of fresh fruits, fruit subjected to complexation, and complexation and then heat treatment at 93 °C for 7 min. The same letter placed above each column and line within the measurement were not significantly different ($p > 0.05$).

For non-coated fruits, it was observed that anthocyanin pigments were leached from fruits into the packing media, regardless of complexation types (non-coated of I, II, and III in Figure 2). Moreover, Fe^{3+}−anthocyanin complexation (II in Figure 2) resulted in more pigment leaching than both non-complexation (I) and Fe^{3+}−CMC−anthocyanin complexation (III). It was previously reported that heating causes dissociation of the co-pigmented anthocyanins,[25] and Fe^{3+}−anthocyanin complex is dissociated in acidic media.[26] Hence, thermally processed fruit packing in the acidic media (pH of 4.0 in this study) could exert the dissociation of the Fe^{3+}−anthocyanin complex, leading to pigment loss with a similar rate to that of the control (non-complexation) or even worse. It was found that fruits subjected to CMC−Fe^{3+}−anthocyanin complexation had less pigment leach than fruits subjected to Fe^{3+}−anthocyanin complexation (III in Figure 2), which was similar to the previous study that anthocyanin−metal chelates interacting with polysaccharides enhanced the anthocyanin stability in comparison to anthocyanin−metal chelates.[27] Nonetheless, both Fe^{3+}−anthocyanin and CMC−Fe^{3+}−anthocyanin complexation did not prevent leaching of anthocyanin pigments into the aqueous media because both were dissociated and/or degraded by heat and acid.

The effect of each treatment factor and their interactions on the anthocyanin retention and physicochemical properties of fruits are reported in Table 1. Color, TA, TMA, and PPC of processed fruits were significantly ($p < 0.05$) affected by the replication factor because of large variations among individual fruits. Weight change (%), firmness index (N/mm), and TTS of fruits were significantly affected by CF. For these three measurements, post-hoc testing using LSD was conducted and is reported in Table 2. The weight of CNF/SA LBL coated fruits were significantly ($p < 0.05$) increased (10.7−14.0% increase) after thermal treatment and storage, whereas those of non-coated fruits lost weight (0.5−2.7% decrease). The weight loss in non-coated fruits could be due to the hydrolyzation of pectin in fruit skin and soluble solids and pigment leaching into packing solution during thermal treatment and storage. The weight gain in CNF/SA LBL coated fruits might be contributed by the weight of both hydrogel type of SA coating and CNF coating. This CNF/SA LBL coating system also significantly ($p < 0.05$) improved the firmness index and TSS of fruits in comparison to those of non-coated fruits.

ANOVA of TPC, TMA, and PPC of the packing solution along with post-hoc testing results of TMA are presented in Figure 3. CF showed a significant ($p < 0.05$) effect on TPC and TMA. Because of the significant ($p < 0.05$) effect of the replication factor on TPC, post-hoc testing was only conducted for TMA (Figure 3B). CNF/SA LBL coatings significantly ($p < 0.05$) prevented TMA leaching from fruits into the packing media in comparison to non-coated fruits. These results demonstrated that the CNF/SA LBL coating system was successful in retaining anthocyanin pigments in thermally processed fruits packing in aqueous media.

Stability of Fe^{3+}−Anthocyanin and Fe^{3+}−CMC−Anthocyanin Complexes. To investigate the stability of complexation (Fe^{3+}−anthocyanin and Fe^{3+}−CMC−anthocyanin) on the thermally processed blueberries packed in aqueous media, TMA, TPC, and PPC of fresh fruits, fruit subjected to complexation, and complexation plus heat treatment at 93 °C for 7 min were quantified (Figure 4). Fe^{3+}−anthocyanin complexation induced the polymerization of anthocyanin compounds, leading to a significantly increase in PPC (41.13%) compared to that of the fresh sample (22.49%). This might be explained as a metal-chelation-formed ligand (Fe^{3+}−anthocyanin), which binds with other anthocyanins, resulting in polymerization of anthocyanins. Consistently, Fe^{3+}−anthocyanin complexation resulted in significantly lower TMA (38.89 mg of Cy-3-glu/100 g of fresh fruits) of fruit in comparison to that of the fresh sample (59.73 mg of Cy-3-glu/100 g of fresh fruits). After the thermal process, however, PPC of fruits subjected to Fe^{3+}−anthocyanin complexation was significantly reduced (22.15%), reaching a similar level to that of the fresh sample (22.49%). These results indicated that the thermal process dissociated the polymerized Fe^{3+}−anthocyanin complex in fruits packing in the aqueous media, consistent with

DOI: 10.1021/acs.jafc.5b00616
J. Agric. Food Chem. 2015, 63, 3031−3038

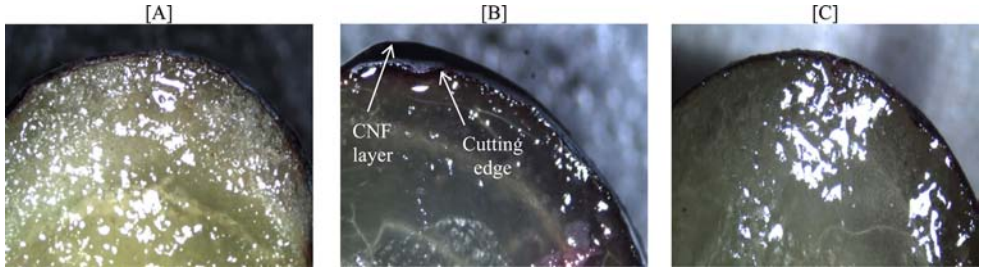

Figure 5. Stereomicroscopic images on the cross-sections of fresh or coated blueberries before the thermal process to illustrate the effect of MC-modified CNF on adhesion properties between CNF and the fruit surface: (A) fresh fruit, (B) CNF coating containing $CaCl_2$, and (C) MC-modified CNF containing $CaCl_2$.

the previous report that the metal−anthocyanin complex was dissociated by the heating process.[25] CMC−Fe^{3+}−anthocyanin complexation was not able to induce further polymerization (PPC of 18.26%) in comparison to Fe^{3+}−anthocyanin complexation (PPC of 41.13%), even without the thermal treatment. This result might be related to the stability of Fe^{3+}−anthocyanin complexation in aqueous media. While the fruits subjected to Fe^{3+}−anthocyanin complexation were soaked in CMC solution, the complex was dissociated before associating with CMC. This result was inconsistent with previous studies reporting the stabilization effect of PMA complexation.[27,28] However, the pigment leaching of fruits treated by CMC−Fe^{3+}−anthocyanin complexation was less than that from Fe^{3+}−anthocyanin complexation treatment (Figure 2), which might be more related to the cation (Fe^{3+}) bridges between fruit pectin and anionic CMC. Hence, the complexation was not successful to achieve the objective of enhancing anthocyanin stability in thermally treated blueberries because of the lack of stability under heat and during storage in aqueous media. Therefore, more studies to improve the heat stability of polysaccharide−metal ion−anthocyanin complexation in aqueous media are necessary.

Pigment Retention Mechanisms of CNF/SA LBL Coatings. From ANOVA results for fruits and packing media (Table 1 and Figure 3), CF only showed the significant effect on weight change (%), firmness index (N/mm), and TTS of fruits and TPC and TMA of packing media. To investigate retention mechanisms of different types of CNF-based coatings and to demonstrate the principal of the CNF/SA based LBL coating system, a stereomicroscope and SEM were illustrated in Figures 5 and 6, respectively. Stereomicroscopic images on the cross-sections of non-coated, CNF/$CaCl_2$-coated, and MC-modified CNF/$CaCl_2$-coated fruits without the thermal process are illustrated to demonstrate the adhesion of CNF coating onto the hydrophobic fruit surface as the first layer of the LBL system (Figure 5). Blueberries have a visible, white- or bluish-colored epicuticular wax layer on the surface, which limits the diffusion of hydrophilic coating materials.[29] Although the washing process was applied to remove the wax layer on the fruit surface in this study, some white substances still visibly remained after washing (data not shown). It was observed that MC-modified CNF/$CaCl_2$ coating improved the adhesion of the coating onto the fruit surface (Figure 5C) because of the modified CNF surface by less hydrophilic methoxyl groups of MC.[30] Two strategies have been commonly applied for enhancing adhesion of coating solutions onto the fruit surface.[31] One was to apply surface-active agents, such as emulsifiers and other amphiphilic chemicals, to reduce the surface tension of the coating solution and decrease the solid

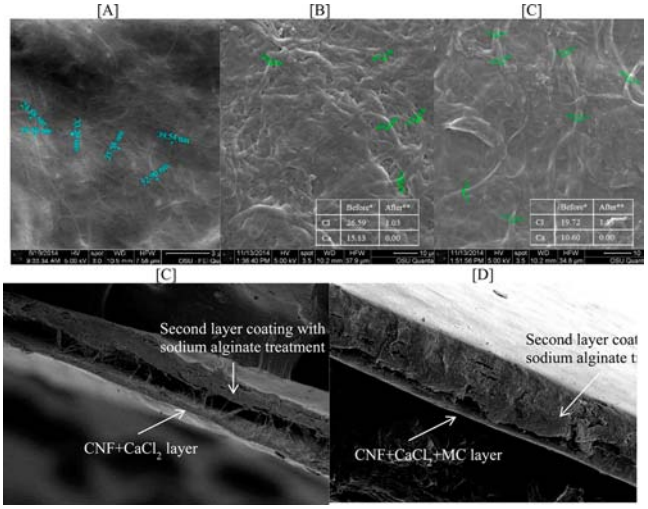

Figure 6. SEM images of different types of CNF films and LBL coating system. Panels A, B, and C illustrate the morphology of CNF, CNF/$CaCl_2$, or CNF/$CaCl_2$/MC films, respectively. Tables in panels B and C show the change of calcium contents in films before and after soaking in water for 10 min at the ambient temperature using EDXA. Panels C and D are the simulated LBL coating system after SA treatment for CNF/$CaCl_2$ and CNF/$CaCl_2$/MC coating, respectively.

surface energy.[32] Another approach was by means of chemical modifications of biopolymers, introducing hydrophobic groups into their structures.[31] MC-modified surface characteristics of CNF coating became more hydrophobic, thus enhancing the adhesion between CNF coating and the hydrophobic fruit surface. A previous study demonstrated that hydrophobization of chitosan successfully enhanced compatibility with the strawberry surface.[33]

SEM analysis illustrated the CNF morphology incorporating with $CaCl_2$ and/or MC to demonstrate anthocyanin-retaining mechanisms of the simulated CNF/SA LBL coating system (Figure 6). EDXA evaluated released $CaCl_2$ contents of CNF films after soaking in water and supported the principal of forming a hydrogel SA layer with released Ca^{2+} as the cross-linking agent onto the CNF layer. The cross-sectioned sample of the simulated CNF/SA LBL film was prepared to demonstrate the development of the hydrogel SA layer onto CNF and the effect of MC-modified CNF on the interaction with the fruit surface and SA layer. It was confirmed that $CaCl_2$ crystals were assimilated on the CNF film matrix (Figure 6B) and MC-modified CNF/$CaCl_2$ film made the surface more homogeneous (Figure 6C) in comparison to CNF and CNF/$CaCl_2$ films (panels A and B of Figure 6). CNF/$CaCl_2$ coating subjected to SA was able to form an impermeable layer of Ca^{2+}

DOI: 10.1021/acs.jafc.5b00616
J. Agric. Food Chem. 2015, 63, 3031−3038

cross-linked alginic acid onto CNF because Ca^{2+} was rapidly released from the CNF structure. MC-modified CNF/$CaCl_2$ induced closer attachment with SA hydrogel than CNF/$CaCl_2$ (panels C and D of Figure 6) because of the presence of Ca^{2+} as a cross-linking agent between MC and SA. A previous study also showed the cross-linking between SA and MC through Ca^{2+}, which was successfully applied in the microencapsulation technology.[34] Hence, $CaCl_2$- and MC-incorporated CNF was able to develop a versatile CNF/SA LBL system and to improve the association with both the fruit surface and SA hydrogel layer, thus preventing leaching of anthocyanin pigments and fruit damage from thermally processed fruit.

This study was the first demonstrating the efficacy of CNF/SA LBL coating for preventing leaching of heat-sensitive and water-soluble anthocyanin pigments from thermally processed whole fruits. The developed coating technology can be used for protecting overall quality and bioactive compounds in various types of anthocyanin-rich fruits while processing and storing in the aqueous system. More studies on the potential structure changes of anthocyanins when subjected to developed treatments, long-term stability of the pigments at ambient storage conditions in aqueous media, sensory attributes through both trained and consumer sensory panels, and evaluations on other types of anthocyanin-rich fruits, such as cherries, plumbs, and red-colored pears, are under way.

AUTHOR INFORMATION

Corresponding Author

*Telephone: 541-737-9151. Fax: 541-737-1877. E-mail: yanyun.zhao@oregonstate.edu.

Funding

The authors are grateful for the financial support of the Oregon State University Venture Development Fund on this project.

Notes

The authors declare no competing financial interest.

ACKNOWLEDGMENTS

The authors thank the Process Development Center at the University of Maine for providing CNF.

REFERENCES

(1) Routray, W.; Orsat, V. Blueberries and their anthocyanins: Factors affecting biosynthesis and properties. *Compr. Rev. Food Sci. Food Saf.* **2011**, *10*, 303−320.

(2) Lohachoompol, V.; Srzednicki, G.; Craske, J. The change of total anthocyanins in blueberries and their antioxidant effect after drying and freezing. *J. Biomed. Biotechnol.* **2004**, *2004*, 248−252.

(3) Rein, M. Copigmentation reactions and color stability of berry anthocyanins. Academic Dissertation, University of Hesinki, Hesinki, Finland, 2005.

(4) Wrolstad, R. E. *Anthocyanins*; Marcel Dekker, Inc.: New York, 2000.

(5) Sadilova, E.; Stintzing, F. C.; Carle, R. Thermal degradation of acylated and nonacylated anthocyanins. *J. Food Sci.* **2006**, *71*, C504−C512.

(6) Tachibana, N.; Kimura, Y.; Ohno, T. Examination of molecular mechanism for the enhanced thermal stability of anthocyanins by metal cations and polysaccharides. *Food Chem.* **2014**, *143*, 452−458.

(7) Takeda, K. Blue metal complex pigments involved in blue flower color. *Proc. Jpn. Acad., Ser. B* **2006**, *82*, 142−154.

(8) Elhabiri, M.; Figueiredo, P.; Toki, K.; Figueiredo, P.; Toki, K.; Saito, N.; Brouillard, R.; Figueiredo, P.; Toki, N.; Saito, N.; Brouillard, R. Anthocyanin−aluminium and −gallium complexes in aqueous solution. *J. Chem. Soc., Perkin Trans.* **1997**, *2*, 355−362.

(9) Shiono, M.; Matsugaki, N.; Takeda, K. Phytochemistry: Structure of the blue cornflower pigment. *Nature* **2005**, *436*, 791−791.

(10) Buchweitz, M.; Carle, R.; Kammerer, D. R. Bathochromic and stabilising effects of sugar beet pectin and an isolated pectic fraction on anthocyanins exhibiting pyrogallol and catechol moieties. *Food Chem.* **2012**, *135*, 3010−3019.

(11) Ngo, T.; Zhao, Y. Stabilization of anthocyanins on thermally processed red D'Anjou pears through complexation and polymerization. *LWT—Food Sci. Technol.* **2009**, *42*, 1144−1152.

(12) Ngo, T.; Zhao, Y. Formation of zinc−chlorophyll-derivative complexes in thermally processed green pears (*Pyrus communis* L.). *J. Food Sci.* **2007**, *72*, C397−C404.

(13) Ngo, T.; Zhao, Y. Retaining green pigments on thermally processed peels-on green pears. *J. Food Sci.* **2005**, *70*, C568−C574.

(14) Brouillard, R.; Figueiredo, P.; Elhabiri, M.; Dangles, O. Molecular interactions of phenolic compounds in relation to the color of fruit and vegetables. *Proc. Phytochem. Soc. Eur.* **1997**, *41*, 29−49.

(15) Zhao, Y.; Simonsen, J.; Cavender, G.; Jung, J.; Fuchigami, L. H. Nano-cellulose coatings to prevent damage in foodstuffs. U.S. Patent 20140272013 A1, 2014.

(16) Aulin, C.; Gällstedt, M.; Lindström, T. Oxygen and oil barrier properties of microfibrillated cellulose films and coatings. *Cellulose* **2010**, *17*, 559−574.

(17) Dagnon, K. L.; Shanmuganathan, K.; Weder, C.; Rowan, S. J. Water-triggered modulus changes of cellulose nanofiber nanocomposites with hydrophobic polymer matrices. *Macromolecules* **2012**, *45*, 4707−4715.

(18) Viera, R. G. P.; Filho, G. R.; de Assunção, R. M. N.; Meireles, S.; Meireles, C. S.; Vieira, J. G.; de Oliveira, G. S. Synthesis and characterization of methylcellulose from sugar cane bagasse cellulose. *Carbohydr. Polym.* **2007**, *67*, 182−189.

(19) Lee, J.; Durst, R. W.; Wrolstad, R. E. Determination of total monomeric anthocyanin pigment content of fruit juices, beverages, natural colorants, and wines by the pH differential method: Collaborative study. *J. AOAC Int.* **2005**, *88*, 1269−1278.

(20) Singleton, V. L.; Rossi, J. A. Colorimetry of total phenolics with phosphomolybdic−phosphotungstic acid reagents. *Am. J. Enol. Vitic.* **1965**, *16*, 144−158.

(21) Cao, X.; Zhang, Y.; Zhang, F.; Wang, Y.; Yi, J.; Liao, X. Effects of high hydrostatic pressure on enzymes, phenolic compounds, anthocyanins, polymeric color and color of strawberry pulps. *J. Sci. Food Agric.* **2011**, *91*, 877−885.

(22) Fisk, C. L.; Silver, A. M.; Strik, B. C.; Zhao, Y. Postharvest quality of hardy kiwifruit (*Actinidia arguta* 'Ananasnaya') associated with packaging and storage conditions. *Postharvest Biol. Technol.* **2008**, *47*, 338−345.

(23) Slaughter, D. C.; Rohrbach, R. P. Developing a blueberry firmness standard. *Trans. ASAE* **1985**, *28*, 986−992.

(24) Leiva-Valenzuela, G. A.; Lu, R.; Aguilera, J. M. Prediction of firmness and soluble solids content of blueberries using hyperspectral reflectance imaging. *J. Food Eng.* **2013**, *115*, 91−98.

(25) Welch, C. R.; Wu, Q.; Simon, J. E. Recent advances in anthocyanin analysis and characterization. *Curr. Anal. Chem.* **2008**, *4*, 75−101.

(26) Castañeda-Ovando, A.; Andrés Galán-Vidal, C.; Contreras-López, E.; Páez-Hernández, M. E. Purification of anthocyanins with *o*-dihydroxy arrangement by sorption in cationic resins charged with Fe(III). *J. Chem.* **2014**, *2014*, 9.

(27) Buchweitz, M.; Nagel, A.; Carle, R.; Kammerer, D. R. Characterisation of sugar beet pectin fractions providing enhanced stability of anthocyanin-based natural blue food colourants. *Food Chem.* **2012**, *132*, 1971−1979.

(28) Lewis, C. E.; Walker, J. R. L.; Lancaster, J. E. Effect of polysaccharides on the colour of anthocyanins. *Food Chem.* **1995**, *54*, 315−319.

(29) Velásquez, P.; Skurtys, O.; Enrione, J.; Osorio, F. Evaluation of surface free energy of various fruit epicarps using acid−base and Zisman approaches. *Food Biophys.* **2011**, *6*, 349−358.

DOI: 10.1021/acs.jafc.5b00616
J. Agric. Food Chem. 2015, 63, 3031−3038

(30) Vargas, M.; Pastor, C.; Chiralt, A.; McClements, D. J.; González-Martínez, C. Recent advances in edible coatings for fresh and minimally processed fruits. *Crit. Rev. Food Sci. Nutr.* **2008**, *48*, 496−511.
(31) Cordeiro de Azeredo, H. M., Edible coatings. In *Advances in Fruit Processing Technologies*; Rodrigues, S., Fernandes, F. A. N., Eds.; CRC Press: Boca Raton, FL, 2012; Chapter 14, pp 345−362.
(32) Han, J. H.; Gennadios, A. Edible films and coating: A review. In *Innovations in Food Packaging*; Han, J. H., Ed.; Elsevier: Amsterdam, Netherlands, 2005.
(33) Vu, K. D.; Hollingsworth, R. G.; Leroux, E.; Salmieri, S.; Lacroix, M. Development of edible bioactive coating based on modified chitosan for increasing the shelf life of strawberries. *Food Res. Int.* **2011**, *44*, 198−203.
(34) Pal, D.; Nayak, A. Development, optimization, and anti-diabetic activity of gliclazide-loaded alginate−methyl cellulose mucoadhesive microcapsules. *AAPS PharmSciTech* **2011**, *12*, 1431−1441.

DOI: 10.1021/acs.jafc.5b00616
J. Agric. Food Chem. 2015, 63, 3031−3038

FED 53 ripening cabinet (Binder, Tuttlingen, Germany) for a period of 9 days. During the first 24 h the units were kept at 22 °C and the relative humidity of 95%. Within 48 h, storage conditions were gradually reduced to 89% humidity and 17 °C. Models were stored at 12 °C the remaining days. Sampling was carried out at different ripening days: 0 (24 h after batter meat preparation and just before stuffing into casings), 1, 3, 5, 7, and 9 days. A total of three units of each batch were collected for each of the studied times. Physicochemical analyses were performed at each sampling time and, in any case, before freezing. Then sausages were vacuum packaged and stored at −20 °C until further analyses.

Physicochemical Analysis. Water activity (a_w), pH, and dry matter (DM) were determined in triplicate samples of each of the considered products and ripening times. Water activity (a_w) was measured using a Decagon CX1 hygrometer (Decagon Devices Inc., Pullman, WA, USA) at 25 °C. The pH was determined in a homogenate of the sample with distilled water (1:10 w/v). DM was determined by drying the sample at 110 °C to constant weight, and the results were expressed as a percentage.[18]

NMR Analyses. Sausage models were thawed prior to NMR analysis. To carry out thawing, samples were kept at room temperature for approximately 6 h. Sausage behavior was similar in both SMS and SMS+P, and syneresis or exudate loss was never observed. Samples (approximately 4 cm long and 1 cm in diameter, weight approximately 5 g) were placed in a cylindrical glass tube (5 cm long by 14 mm diameter). Before measurement, the sausage samples were thermostated to 25 °C in a water bath for 15−20 min. Proton NMR T_2 relaxation measurements were performed on a Maran Benchtop Pulsed NMR Analyzer (Resonance Instruments, Witney, UK) operating at 23.2 MHz and equipped with an 18 mm variable-temperature probe where the cylindrical glass tubes were placed. A total of six replicates of each product and ripening time were analyzed at 25 °C. Transverse relaxation time, T_2, was measured using the Carr−Purcell−Meiboom−Gill sequence (CPMG)[19,20] with a τ value (time between 90 °C pulse and 180 °C pulse) of 150 μs. Data from 4096 echoes were acquired as 16 scan repetitions. The repetition time between two succeeding scans was 2 s. The obtained T_2 data were analyzed using algorithm[21] and carried out in MatLab (The Mathworks Inc., Natick, MA, USA) using in-house scripts. Distributed exponential fittings are shown in a plot of relaxation amplitude versus relaxation time, over a predefined range of characteristic relaxation times.

Measurement of Proteolysis. Degree of proteolysis was estimated by measurement of free amino terminal groups using the fluorescamine assay described earlier.[22] One hundred milligrams of each sample was solubilized in 1 mL of phosphate-buffered saline (0.05 M phosphate buffer, 0.14 M NaCl, pH 6.7). To 500 μL of 1.67 M (24%) trichloroacetic acid in water was added an equal volume of solubilized sample, and the mixture was held for 20 min on ice to allow precipitation of intact proteins. The precipitated mixture was centrifuged (17000*g* for 20 min) and then filtered through a no. 41 filter paper (Whatman PLC, Brentford, UK). A 12.5 μL aliquot of this filtrate was mixed with 1 mL of 100 mM borate buffer and 500 μL of 719 μM fluorescamine in acetone, and 250 μL was then transferred to each well in a microtiter plate. Fluorescence of the samples was measured, 18 min after the addition of the fluorescamine, at an excitation wavelength of 390 nm and an emission wavelength of 480 nm using a model Synergy 2 Multi-Mode microplate reader (Holm & Halby, Brøndby, Denmark). Quantitation was achieved by calculating leucine equivalents using an external leucine standard curve prepared as follows: a 0.1 M leucine stock solution was made (327.5 mg of leucine in 25 mL of 1 mM HCl), and from the stock solution six different concentrations were made (0.00050−0.0030 M leucine) and mixed with 10 mL of 1 mM HCl and analyzed as the sausage samples.

SDS-PAGE. Myofibrillar proteins were extracted by homogenization of 1 g of sausage in 5 mL of a solution containing 7 M urea, 2 M thiourea, and 400 mM Tris-base. The homogenate was centrifuged for 20 min at 10000*g* at 4 °C, and the supernatant containing myofibrillar proteins was separated. The protein concentration of the myofibrillar protein extracts were determined by using the Bradford assay.[23] The protein concentration was adjusted with water to give a final concentration of 2 mg/mL and diluted 1:1 with SDS-PAGE sample buffer [2% SDS, 20% glycerol, 20 mM Tris-Cl, pH 6.8, 2 mM ethylenediaminetetraacetic acid (EDTA), 160 mM dithiothreitol (DTT), and 0.1 mg/mL bromphenol blue] to give a final concentration of 1 mg/mL. The samples were heated at 100 °C for 5 min prior to electrophoresis. SDS-PAGE was carried out under reducing conditions,[24] using Criterion TGX (any kDa) precast ready-made gels (Bio-Rad Laboratories, Hercules, CA, USA). The amount of protein solution injected into the electrophoresis gels was 20 μL in each lane. After electrophoresis, the gels were covered with fixative solution (40% methanol, 10% acetic acid) and then stained using Coomassie Brilliant Blue R-250. The molecular weights of the products of proteolysis were estimated by reference to the relative motilities of standard proteins.

Statistical Analysis. Statistical analysis was carried out using Statgraphics, ver. 5.1. Plus. The analyses were conducted across the two manufactured batches (SMS and SMS+P) and six different ripening times (0, 1, 3, 5, 7, and 9 days), so 18 individual units per treatment were analyzed. Data are presented as mean and standard deviation (SD). One-way ANOVA was performed. Bartlett's test was used to test the null hypothesis that the standard deviations of data (within each of the model systems) were the same. Duncan's test for multiple mean comparisons procedure was used to determine which means are significantly different from others (at 95% of confidence level).

RESULTS AND DISCUSSION

Physicochemical Parameters. DM, pH, and a_w mean values and standard deviations for SMS and SMS+P are shown in Figure 1. The products showed significant differences ($P < 0.05$) for the three physicochemical parameters studied throughout all stages of the manufacturing process. As expected, results showed that the lowest DM content ($P < 0.05$) could be attributed to the samples collected on day 0 (28.11 ± 0.31% for SMS and 27.16 ± 0.30% for SMS+P). As ripening progressed, a steady and considerable increase in DM was observed, and the highest value was reached at day 9 (56.12 ± 0.98% for SMS and 51.66 ± 0.62% for SMS+P). There were also significant differences ($P < 0.05$) in pH, so the highest value was detected at day 0 (5.64 ± 0.04 for SMS and 5.84 ± 0.03 for SMS+P). Lactic acid production due to the fermentation of sugars by lactic acid bacteria led to the lowest pH values at day 3 (around 5.00). From day 5, a slight increase in pH was observed in both batches. This may be due to production of free amino acids and ammonia as a result of enzymatic activity.[2,25] With the increase in DM, previously mentioned, a_w decreased constantly (from 0.960 ± 0.001 in SMS and 0.953 ± 0.001 in SMS+P to 0.911 ± 0.001 and 0.903 ± 0.001, respectively), which results in a microbial stabilization of the transformed product. The measured parameters are within the normal range previously described for dry fermented sausages,[26,27] taking into account that the products manufactured for this study had a shorter ripening time (9 days) compared to commercial brands (around 20−28 days), which explains that higher DM values have not been reached at the end of the process.

NMR Studies on Sausage Model Systems. *Water Mobility and Distribution throughout Sausage Model Manufacturing.* Distributed exponential analysis of the NMR T_2 relaxation data revealed the presence of three different water populations in SMS (Figure 2A): a minor component, with relaxation times around 1−10 ms (T_{2b}), a major component around 30−70 ms (T_{21}), and a slower relaxing component (T_{22}) around 100−300 ms. Chopping results in disintegration

DOI: 10.1021/acs.jafc.5b00660
J. Agric. Food Chem. 2015, 63, 3039−3045

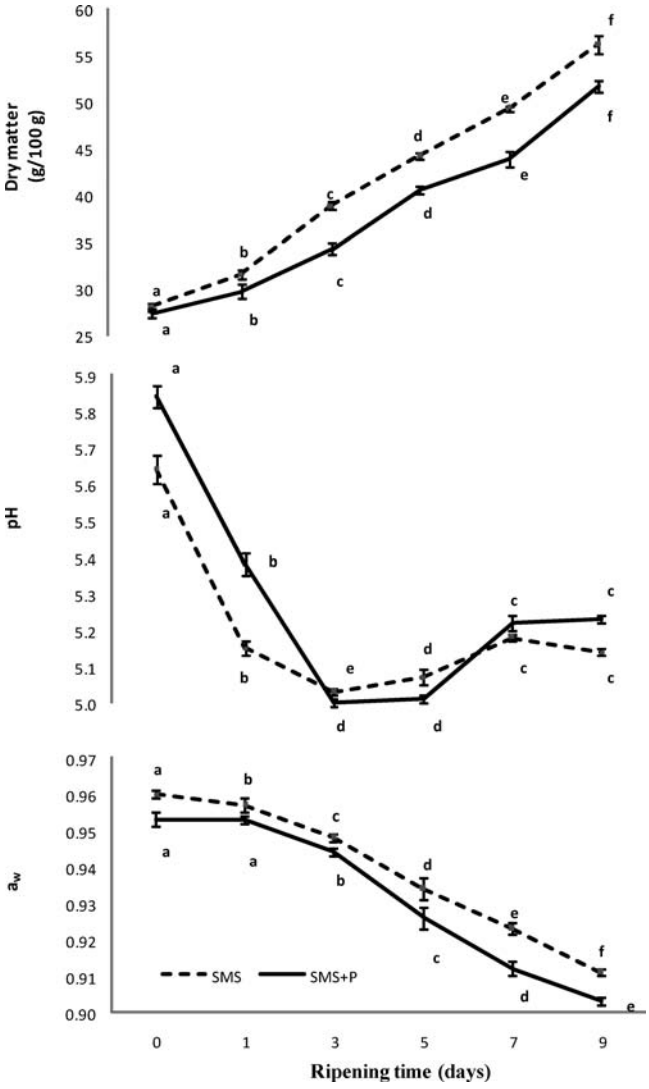

Figure 1. Physicochemical parameters obtained for sausage model systems (SMS) and models with protease (SMS+P) at different ripening times (mean value and standard deviation of six replicates). Values with different letters within the same line are statistically different ($P < 0.05$).

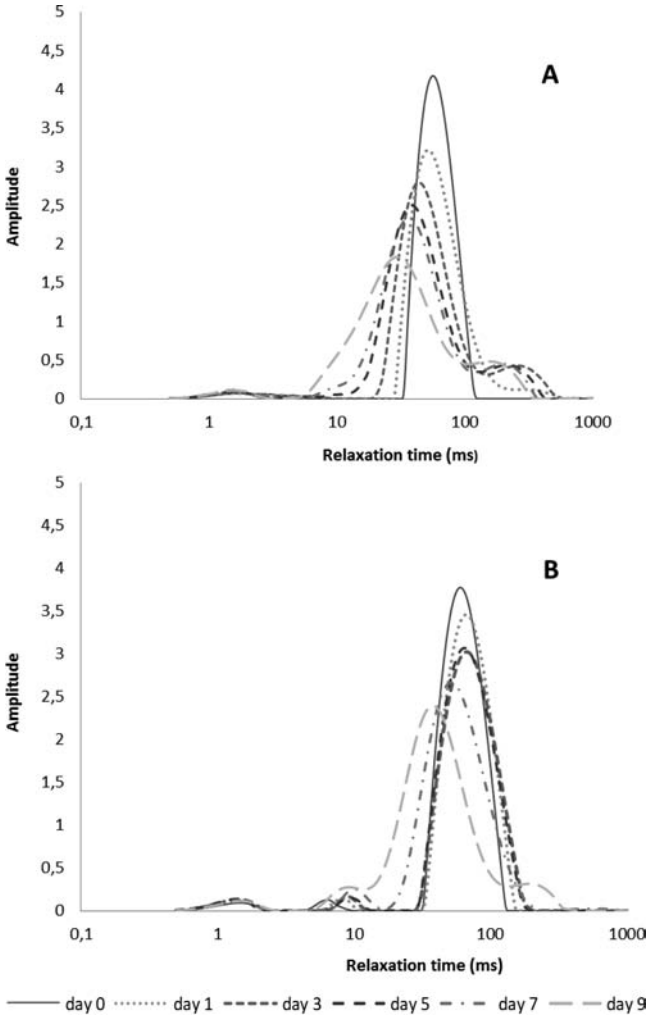

Figure 2. Distributed NMR T_2 relaxation times obtained on sausage models on days 0, 1, 3, 5, 7, and 9 after production: (A) sausage models systems (SMS); (B) sausage models with proteases (SMS+P). Each curve represents a mean of six measurements.

of the overall structure with maintenance of intact myofilaments. It has been previously proved[12] that disruption of the macroscopic structure of fresh meat did not change the relaxation pattern in meat, so water assignments for minced meat are comparable to those obtained in fresh meat. It has been suggested that T_{2b} represents water closely associated with macromolecules and/or protons in plasticized macromolecular structures; T_{21} reflects water located within highly organized protein structures, and T_{22} represents more mobile water located in extramyofibrillar spaces.[12,28,29] The T_{22} population was not present at day 0, but it was detected on all of the consecutive ripening days analyzed, which suggests that it may be related to protein aggregation. Intensive chopping and a high concentration of NaCl result in the swelling of myofibrils and the dissolving process of proteins, so water is mainly associated with myofibrillar proteins. After a certain period of adaptation, the growth of lactic acid bacteria results in the formation of lactic acid,[2] and the pH decrease brings the myofibrillar proteins gradually closer to their isoelectric point and their water-binding capacity decreases.[30] Consequently, the amount of immobilized water entrapped by myofibrillar proteins is reduced; meanwhile, protein chains are approaching each other, creating aggregates. Once inside the ripening cabinet, water release from the interior of the sausage takes place partially by diffusion, due to the moisture difference between the sausages and the environment,[31] which leads to the appearance of the T_{22} population, related to this mobile extramyofibrillar water fraction. The drying process of meat resulted in a shift toward faster relaxation times for both populations, T_{21} and T_{22}. This shift may be explained, mainly, by the fact that the viscous protein system is transformed from the "sol-state" into the colloidal viscous "gel-state"[31] that leads to the constitution of an irreversible protein network that holds water in a less mobile state.[32] The existence of different water fractions and their changes during the drying process in sausage models found in the present work is in good agreement with data obtained in a previous study on fermented meat[14] except for the absence of the T_{22} component at day 0. This difference could be due to the existence of a resting period at cooling temperature (4 °C, approximately) before stuffing into casings and the absence of starter added culture in the present work, which may have a significant effect on preserving protein structure from coagulation or aggregation, because, as

DOI: 10.1021/acs.jafc.5b00660
J. Agric. Food Chem. 2015, 63, 3039−3045

Table 1. Mean Relaxation Time and Relative Area for the T_2 Relaxation Populations T_{21} and T_{22} Obtained for Sausage Model Systems (SMS) and Models with Proteases (SMS+P) on Days 0, 1, 3, 5, 7, and 9 after Production[a]

	T_{21}		T_{22}	
sample/ripening time (days)	relative area	relaxation time	relative area	relaxation time
SMS/0	96.3 ± 0.3 a,α	56.7 ± 0.9 a,β		
SMS/1	93.7 ± 0.3 b,β	52.4 ± 1.3 b,β	3.2 ± 0.4 c	228.9 ± 71.1 a
SMS/3	84.4 ± 0.5 c,β	44.4 ± 1.2 c,β	12.4 ± 0.5 a	260.5 ± 12.0 a
SMS/5	85.0 ± 0.9 c,β	38.3 ± 1.2 d,β	11.7 ± 0.7 b	215.8 ± 8.0 a
SMS/7	85.6 ± 0.6 c,β	37.1 ± 1.4 d,β	11.5 ± 0.3 b	202.7 ± 7.0 b
SMS/9	84.3 ± 0.7 c,β	30.0 ± 1.4 e,β	12.8 ± 0.2 a,α	149.1 ± 21.3 c,β
SMS+P/0	95.7 ± 0.2 a,β	60.4 ± 1.1 b,α		
SMS+P/1	94.8 ± 0.5 b,α	66.5 ± 1.1 a,α		
SMS+P/3	94.7 ± 0.3 b,α	67.3 ± 2.9 a,α		
SMS+P/5	94.5 ± 0.6 b,α	64.7 ± 2.5 a,α		
SMS+P/7	92.5 ± 1.2 c,α	51.8 ± 2.5 c,α		
SMS+P/9	89.5 ± 1.9 d,α	37.9 ± 2.1 d,α	7.8 ± 1.8 β	190.8 ± 40.5 α

[a]Mean values and standard deviation of six replicates. Values with different letters (a–d) in the same column for the same model system indicate significant differences ($P < 0.05$): differences between ripening times Values with different letters (α, β) in the same column for the same ripening time indicate significant differences ($P < 0.05$): differences between batches.

mentioned above, the temperature and the pH descent are key factors in promoting the structural changes in the protein matrix.

Effect of Proteases on Sausage Models Structure. Figure 2B shows distributed T_2 relaxation times obtained on SMS+P. T_{2b1}, T_{2b2}, and T_{21} populations were identified for all ripening times. Previous studies[14,33] have related the addition of salt to the appearance of a T_{2b2} population (5–10 ms), absent in fresh meat, and also identified in this batch throughout the entire manufacturing process. The presence of this new population could be associated with a different distribution of salt in both batches. For the SMS batch, it was possible to distinguish the T_{2b2} component only on days 0, 1, and 3 of production, although it was not a clear peak and appeared almost merged with T_{2b1}. In this batch, ripening took place on a conventional basis, which means that the myofibrils were able to swell and retain water, and the added salt was easily absorbed or incorporated into protein structure as ripening progressed. The proteins dissolved as a result of the mincing and the addition of salt produce filament-shaped aggregates that interact and contribute to the stability of the gel.[2] However, in SMS+P models, protein breakdown prevented an efficient absorption of salt by myofibrils in such a way that it together with water constituted an independent compartment with faster relaxation time, different from the major myofibrillar protein component (T_{21}) that could be clearly identified during the entire process. The presence of the T_{2b2} population suggests that the protein matrix did not present a strong and well-organized structure. The T_{22} component was not present in SMS+P samples until day 9, which constitutes an important difference compared to T_2 distributions in SMS. The absence of the T_{22} component suggests a nonaggregation behavior of the proteins. Partial denaturation of protein is required as an initial step to achieve the ordered protein–protein interaction and aggregation;[34] however, the hydrolysis induced by proteases prevents the proper establishment of the protein network and severely affects final texture resulting in a softening of the product, as previously reported.[4,5] Consequently, T_{2b2} and T_{22} populations are both related to the absence of a strong and firm protein matrix. Proteolysis can also produce an extensive unfolding of the protein inducing the formation of a network with large cavities where the T_{22} can be related to the mobile water in the cavities. Distributed T_2 relaxation times in SMS+P compared to that obtained for SMS showed how the structural integrity was changed by the introduction of proteases. In fact, the ripening-induced shift of T_{21} and T_{22} populations in SMS+P is not as noticeable as it is in SMS, suggesting that water immobilization is not taking place until day 7, as affected by protein degradation.

Time constants and relative areas (corresponding to the proportion of protons represented by the specific T_2 population) of the two main components (T_{21} and T_{22}) for SMS and SMS+P are shown in Table 1. Significant differences were detected by comparison between T_{21} relaxation times corresponding to SMS and SMS+P throughout ripening time, so that SMS+P consistently maintained higher T_{21} values over time. These findings can be related to the fact that the water content was also higher in SMS+P than SMS for the same studied stage, ranging from 71.9 ± 0.3 to 43.9 ± 0.9 g of water/100 g of sample in SMS and from 72.8 ± 0.3 to 48.3 ± 0.6 g of water/100 g sample in SMS+P. The drying process resulted in a decrease of the relative areas of both populations, although the decrease was more progressive in SMS and values were higher in SMS+P, especially from day 3 on.

Proteolysis in Model Samples As Measured by Increase in Free Amino Groups. Proteolysis was quantified by assaying for protein breakdown products through determination of free amino terminals (N-terminal + lysine side chains, as well as other amines that may be present). Although the concentration of free amino groups increased for both batches over time (Figure 3), higher values were found for SMS+P (concentration varied from 657.83 ± 1.54 to 1487.09 ± 5.06 mg Leu equiv/DM at days 0 and 9, respectively) than for SMS (values from 290.35 ± 3.71 to 487.78 ± 0.93 mg Leu equiv/DM, respectively), showing that the proteolysis was more prominent in the protease-added batch, SMS+P. This finding is in agreement with previous works[4,5] in which the nitrogen fractions achieved higher values in protease-added batches than those of the control. Significant differences were found over time for both batches regarding free amino group concentration, although the lower increase occurred toward the end of the process for SMS+P, during days 7 and 9 (5.5%),

DOI: 10.1021/acs.jafc.5b00660
J. Agric. Food Chem. 2015, 63, 3039–3045

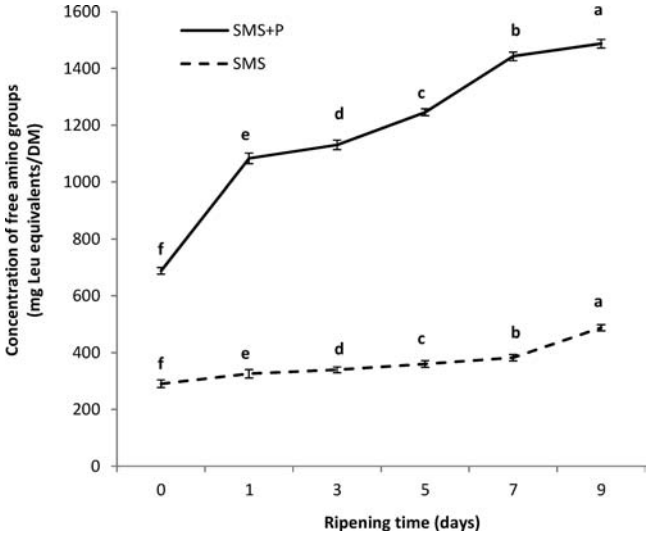

Figure 3. Concentration of free amino groups (mean values and standard deviation; expressed as mg leucine equiv/DM) quantified in SMS+P and SMS samples over time. Values with different letters within the same line are statistically different ($P < 0.05$).

suggesting a trend to stabilization, because the protease activity was higher between days 0 and 3 of production. During the fermentation and ripening of dry fermented sausages, a large number of biochemical reactions associated with the degradation of myofibrillar and sarcoplasmic proteins take place.[4,5] These biochemical reactions are promoted by muscle endopeptidases (calpains I and II and cathepsins B, D, H, and L).[35] For batch SMS, therefore, the increase of free amino groups corresponds to a natural proteolysis process conducted by endogenous enzymes, so the protein degradation was lower during the whole process and, finally, the proteolysis rate increased during days 7 and 9, when the greatest increase in the concentration was found (53.5%). SMS+P samples experienced a substantial degradation from the moment of the addition of the enzymes (day 0), resulting in low-molecular-weight compounds. Meanwhile, SMS samples experienced a lower extent of proteolysis, and it was possible to distinguish high-molecular-weight compounds, almost during the whole process. The considerably lower degree of protein degradation in SMS samples could explain why different free amino group concentrations were obtained. On the other hand, as proteolysis contributes to a weakening of the myofibrillar network and the subsequent generation of peptides and free amino acids that contribute to flavor development,[36] the formation of a large amount of free amino groups is inconsistent with the emergence of the T_{22} component, because this fact is opposed to the establishment of an organized and compact meat matrix. However, a moderate production of amino groups combined with appropriate dehydration conditions allow the development of a high structured meat gel in which T_2 distributed data could be characterized by the presence of the T_{22} population during almost the whole process.

SDS-PAGE. As the contribution from myofibrillar proteins is the most important parameter for the development of desirable gel characteristics in processed meat products,[3,37] SDS-PAGE of myofibrillar proteins was performed to elucidate the differences in protein degradation pattern between SMS and SMS+P. Some bands were identified on the basis of their molecular weights, determined by comparison with standards in the stained gel (Figure 4). Heavy myosin chain (MHC) (220 kDa), α-actinin (94 kDa), actin (45 kDa), troponin-T (37 kDa), tropomyosin (35 kDa), myosin light chains (MLC) 1, 2, and 3 (25, 18, and 15 kDa, respectively), troponin I (24 kDa), and troponin C (20 kDa) were present in all SMS samples.[38] As ripening progressed, a degradation of myofibrillar proteins was evident. The intensity of MHC and actin bands decreased over time; troponin T and tropomyosin degradation was also noticeable. MLC 1 and troponin I bands were not so intense from day 3 on, and MLC 2 and 3 were especially affected by proteolysis because they disappeared completely after 3 days of ripening. New polypeptides of smaller size (≈12 kDa) also accumulated from day 1 on. These findings are in agreement with previous studies on fermented sausages,[15,16,39] although in the present study the pattern of proteolysis was not that intense due to the fact that sausages were ripened for a shorter period

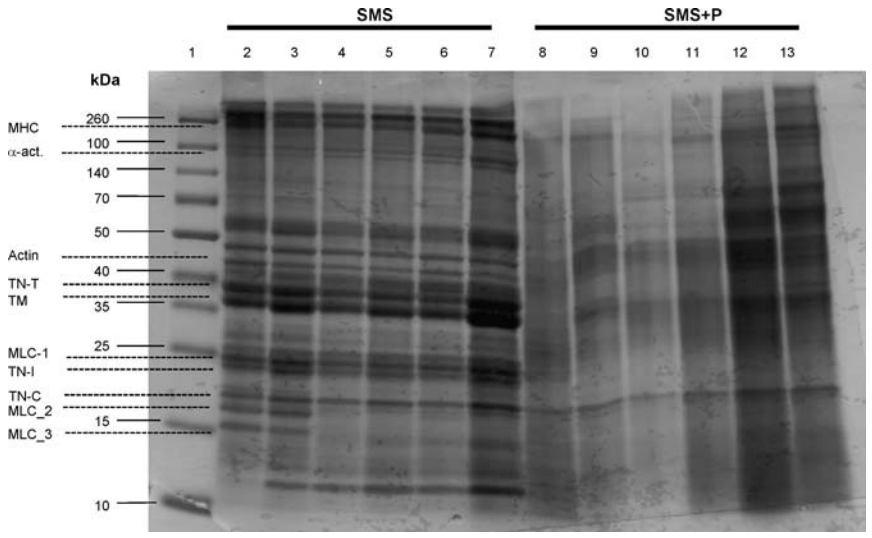

Figure 4. SDS-PAGE electrophoretograms of myofibrilar proteins throughout the ripening of sausages. Lanes: 1, protein standards; 2−7, sausage model systems (SMS), days 0, 1, 3, 5, 7, and 9; 8−13, models with proteases (SMS+P), days 0, 1, 3, 5, 7, and 9. MHC, heavy myosin chain; α-act., α-actinin; TN-T, troponin-T; TM, tropomyosin; MLC 1, 2, 3, myosin light chains 1, 2, and 3; TN-I, troponin I; TN-C, troponin C.

DOI: 10.1021/acs.jafc.5b00660
J. Agric. Food Chem. 2015, 63, 3039−3045

of time. Throughout fermentation, the combination of salt, temperature (20−26 °C), and the decline in pH provokes insolubilization of sarcoplasmic and myofibrillar proteins. Insolubilization progresses during ripening due to advanced dehydration.[2,41] A decrease in the solubility of myofibrillar proteins was observed, because the bands were much more intensely stained at the end of ripening than at day 0. The loss in myofibrillar protein solubility has been previously described by other researchers.[15,40] A dramatically different protein band pattern was observed for SMS+P, where high-molecular-weight compounds cannot be distinguished as a result of the proteolysis to which samples have been subjected. However, protein insolubilization during drying was clearly evident. These results, together with proteolysis measurements (Figure 3), prove that protein denaturation on SMS+P was very intense from day 0; consequently, the molecular weight of the protein chains is too low, and they solubilize completely before aggregating. The solubility of myofibrillar proteins in SMS+P decreased with ripening time due to the dehydration process and the increase in salt concentration, which leads to the aggregation of protein chains and the formation of higher molecular weight compounds, so the bands on days 7 and 9 were more intensely stained than on previous days. With regard to T_2 distributions, the stronger protein chain association at day 9 compared with earlier stages by reducing the pore size of the matrix due to the water loss, together with the extensive unfolding suffered by proteins, could be associated with the appearance of T_{22} population, suggesting that some degree of aggregation is needed for the presence of the water population T_{22} in dried sausages. The fact that the T_{2b2} population was also present in the final stages supports the hypothesis that a true coagulation is not taking place and the structural modification is not complete and, further, related to the dehydration taking place during ripening.

In conclusion, the present study revealed that (i) changes in water mobility and distribution during the manufacture of sausage model systems were detectable by means of LF-NMR relaxation, where ripening produced a shift toward faster relaxation times related to the reduction of the intrinsic pore size of the meat matrix; and (ii) the distribution of water in sausage models was significantly affected by the addition of proteases to the meat batter, supporting the role of myofibrillar proteins in meat coagulation and suggesting that some aggregation degree is needed for the presence of a T_{22} population in fermented sausages. Finally, the extinction of the T_{22} population in meat systems could be associated with a high enzymatic proteolysis degree and, consequently, the presence of great amounts of free amino groups.

AUTHOR INFORMATION

Corresponding Author

*(H.C.B.) Phone: +45 87 158 353. E-mail: HanneC.Bertram@food.au.dk.

Funding

The present work received financial support from Project AGL2010-19158 funded by the Spanish Ministry of Economy and Competitivity − General Directorate of Scientific Research, and A.B.G.G. was awarded a grant (BES-2011-047485) from the same institution. H.C.B. acknowledges the Danish Research Council FTP for financial support through Project "Advances in food and nutrition research through implementation of metabolomics technologies (274-09-0107)".

Notes

The authors declare no competing financial interest.

ACKNOWLEDGMENTS

We thank Hanne Søndergaard Møller, Department of Food Science, Aarhus University, for technical assistance.

REFERENCES

(1) Trout, G. R. Techniques for measuring water-binding capacity in muscle foods − a review of methodology. *Meat Sci.* **1988**, *23*, 235−252.

(2) Ordóñez, J. A.; Hierro, E. M.; Bruna, J. M.; Hoz, L. Changes in the components of dry-fermented sausages during ripening. *Crit. Rev. Food Sci.* **1999**, *34*, 329−367.

(3) Tornberg, E. Effects of heat on meat proteins-Implications on structure and quality of meat products. *Meat Sci.* **2005**, *70*, 493−508.

(4) Díaz, O.; Fernández, M.; García de Fernando, D. G.; de la Hoz, L.; Ordóñez, J. A. Proteolysis in dry fermented sausages: the effect of selected exogenous proteases. *Meat Sci.* **1997**, *46*, 115−128.

(5) Díaz, O.; Fernández, M.; García de Fernando, G. D.; De la Hoz, L.; Ordóñez, J. A. Effect of the addition of Pronase E on the proteolysis in dry fermented sausages. *Meat Sci.* **1993**, *34*, 205−216.

(6) Fernández, M.; Ordóñez, J. A.; Bruna, J. M.; Herrans, B.; de la Hoz, L. Acelerated ripening of dry fermented sausages. *Food Sci. Technol.* **2000**, *11*, 201−209.

(7) Capitani, D.; Mannina, L.; Proietti, N.; Sobolev, A. P.; Tomassini, A.; Miccheli, A.; DiCocco, M. E.; Capuani, G.; DeSalvador, F. R.; Delfini, M. Metabolic profiling and outer pericarp water starte in Zespri CI.GI and Hayward Kiwifruits. *J. Agric. Food Chem.* **2013**, *61*, 1727−1740.

(8) Li, T.; Rui, S.; Li, W.; Chen, X. H.; Jiang, M.; Dong, M. S. Water distribution in tofu and application of T_2 relaxation measurements in determination of tofu's water holding capacity. *J. Agric. Food Chem.* **2014**, *62*, 8594−8601.

(9) Hager, A. S.; Bosmans, G. M.; Delcour, J. A. Physical and molecular changes during the storage of gluten-free rice and oat bread. *J. Agric. Food Chem.* **2014**, *62*, 5682−5689.

(10) Greiff, K.; Fuentes, A.; Aursand, I. G.; Erikson, U.; Masot, R.; Alcaniz, M.; Barat, J. M. Innovative non-destructive measurements of water activity and the content of salts in low-salt hake minces. *J. Agric. Food Chem.* **2014**, *62*, 2496−2505.

(11) Bertram, H. C.; Dønstrup, S.; Karlsson, A. H.; Andersen, H. J. Continuous distribution analysis of T_2 relaxation in meat- An approach in the determination of water holding capacity. *Meat Sci.* **2001**, *60*, 279−285.

(12) Bertram, H. C.; Karlsson, A. H.; Rasmussen, M.; Pedersen, O. D.; Andersen, H. J. Origin of multiexponential T_2 relaxation in muscle myowater. *J. Agric. Food Chem.* **2001**, *49*, 3092−3100.

(13) Bertram, H. C.; Andersen, H. J. Applications of NMR in meat science. *Annu. Rep. NMR Spectrosc.* **2004**, *53*, 158−202.

(14) Møller, S.; Gunvig, A.; Bertram, H. C. Effect of starter culture and fermentation temperature on water mobility and distribution in fermented sausages and correlation to microbial safety studied by nuclear magnetic resonance relaxometry. *Meat Sci.* **2010**, *86*, 462−467.

(15) García de Fernando, D. G.; Fox, P. F. Study of proteolysis during the ripening of a dry fermented pork sausage. *Meat Sci.* **1991**, *30*, 367−383.

(16) Hughes, M. C.; Kerry, J. P.; Arendt, E. K.; Kenneallu, P. M.; McSweeney, P. L.; O'Neill, H. Characterization of proteolysis during the ripening of semi-dry fermented sausages. *Meat Sci.* **2002**, *62*, 205−2016.

(17) Ohashi, K.; Negishi, H. Hydrolysis of pork myofibrillar proteins during fermentation using starter cultures of *Lactobacillus bulgaricus* and *Streptococcus thermophilus*. *Food Sci. Technol. Res.* **2014**, *20*, 679−685.

(18) *Official Methods of Analysis of the Association of Official Analytical Chemists*, 18th ed., 1st rev.; AOAC International: Gaithersburg, MD, USA, 2006.

DOI: 10.1021/acs.jafc.5b00660
J. Agric. Food Chem. 2015, 63, 3039−3045

(19) Carr, H. Y.; Purcell, E. M. Effects of diffusion on free precession in nuclear magnetic resonance experiments. *Am. J. Physiol.* **1954**, *94*, 630−638.
(20) Meiboom, S.; Gill, D. Modified spin-echo method for measuring nuclear times. *Rev. Sci. Instrum.* **1958**, *29*, 688−691.
(21) Butler, J. P.; Reeds, J. A.; Dawson, S. V. Estimating solutions of 1st kind integral equations with nonnegative constraints and optimal smoothing. *SIAM J. Numer. Anal.* **1981**, *18*, 381−397.
(22) Jansson, T.; Clausen, M. R.; Sundekilde, U.; Eggers, N.; Nyegaard, S.; Larsen, L.; Ray, C.; Sundgren, A.; Andersen, H. J.; Bertram, H. C. Lactose-hydrolyzed milk is more prone to chemical changes during storage than conventional UHT milk. *J. Agric. Food Chem.* **2014**, *62*, 7886−7896.
(23) Bradford, M. M. A rapid and sensitive method for the quantitation of microgram quantities of protein utilizing the principle of protein-dye binding. *Anal. Biochem.* **1976**, *72*, 248−254.
(24) Laemmli, U. K. Cleavage of structural proteins during the assembly of the head of bacteriophage T4. *Nature* **1970**, *227*, 680−685.
(25) Lücke, F. K. Fermented sausages. In *Microbiology of Fermented Foods*; Wood, B. J. B., Ed.; Blackie Academic and Professional: New York, 1998; pp 441−483.
(26) Ordóñez, J. A.; Hoz, L. Embutidos crudos curados. Tipos. Fenomenos madurativos. Alteraciones. In *Enciclopedia de la Carne y los Productos Cárnicos*; Martin and Macias: Cáceres, Spain, 2001; Vol. II, pp 1063−1090.
(27) Herrero, A. M.; Ordóñez, J. A.; Romero de Ávila, M. D.; Herranz, B.; de la Hoz, L.; Cambero, M. I. Breaking strength of dry fermented sausages and their correlation with texture profile analysis (TPA) and physico-chemical characteristics. *Meat Sci.* **2007**, *77*, 331−338.
(28) Bertram, H. C.; Purslow, P. P.; Andersen, H. J. Relationship between meat structure, water mobility, and distribution: a low-field nuclear magnetic resonance study. *J. Agric. Food Chem.* **2002**, *50*, 824−829.
(29) Venturi, L.; Rocculi, P.; Cavani, C.; Placucci, G.; Rosa, M. D.; Cremonini, M. A. Water absorption of freeze-dried meat at different water activities: a multianalytical approach using sorption isotherm, differential scanning calorimetry, and nuclear magnetic resonance. *J. Agric. Food Chem.* **2007**, *55*, 10572−10578.
(30) Albarracín, W.; Sánchez, I. C.; Grau, R.; Barat, J. M. Salt in food processing; usage and reduction: a review. *Int. J. Food Sci. Technol.* **2009**, *46*, 1329−1336.
(31) Katsaras, K. Microstructure of fermented sausage. *Meat Sci.* **1992**, *31*, 121−134.
(32) Sun, X. D.; Holley, R. A. Factors influencing gel formation by myofibrillar proteins in muscle foods. *Compr. Rev. Food Sci. Food Saf.* **2010**, *10*, 33−51.
(33) Andersen, R. H.; Andersen, H. J.; Bertram, H. C. Curing-induced water mobility and distribution within intra- and extra-miofibrilar spaces of three pork qualities. *Int. J. Food Sci. Technol.* **2007**, *42*, 1059−1066.
(34) Barbut, S. Importance of fat emulsification and protein matrix characteristics in meat batter stability. *J. Muscle Foods* **1995**, *6*, 161−177.
(35) Toldrá, F. Biochemical proteolysis basis for improved processing of dry-cured meats. In *Advanced Technologies for Meat Processing*; Nollet, L. M. L., Toldrá, F., Eds.; CRC Press: Boca Raton, FL, USA, 2006; pp 329−354.
(36) Toldrá, F. The role of muscle enzymes in dry-cured mat products with different drying conditions. *Trends Food Sci. Technol.* **2004**, *17*, 164−168.
(37) Andersson, K.; Andersson, A.; Tornberg, E. Microstructure as related to the water-holding, textural and sensory properties of emulsion sausages. In *Food Colloids − Proteins, Lipids and Polysaccharides*; Dickinson, D., Bergenstahl, B., Eds.; Royal Society of Chemistry: Cambridge, UK, 1997; pp 29−42.
(38) Porcio, M. A.; Pearson, A. M. Improved resolution of myofibrillar proteins with sodium dodecyl sulfate-polyacrilamide gel electrophoresis. *Biochim. Biophys. Acta* **1977**, *490*, 27−34.
(39) Roseiro, L. C.; Santos, C.; Sol, M.; Borges, M. J.; Anjos, M.; Goncalves, H.; Carvalho, A. S. Proteolysis in Painho de Portalegre dry fermented sausage in relation to ripening time and salt content. *Meat Sci.* **2008**, *79*, 784−794.
(40) Astiasarán, I.; Villanueva, R.; Bello, J. Analysis of proteolysis and protein insolubility during the manufacture of some varieties of dry sausage. *Meat Sci.* **1990**, *28*, 111−117.
(41) Wardlaw, F. B.; Skelley, G. C.; Johnson, M. G.; Acton, J. C. Changes in meat components during fermentation, heat processing and drying of a summer sausage. *J. Food Sci.* **1973**, *38*, 1228−1231.

DOI: 10.1021/acs.jafc.5b00660
J. Agric. Food Chem. 2015, 63, 3039−3045

Table 1. Fiber and Proximate Composition of Kernels from Glyphosate-Tolerant and CRW-Protected Sweet Corn MON 88017 and Insect-Protected Sweet Corn MON 89034

component[a]	MON 88017 mean[b] (range)[b]	MON 89034 mean[b] (range)[b]	control mean[b] (range)[b]	reference range[b]
ADF	3.64[c]	3.55[c]	3.03	
	(2.02−5.16)	(2.64−5.27)	(1.90−4.43)	1.43−5.27
NDF	4.98[c]	4.11	3.80	
	(3.35−7.10)	(2.60−6.13)	(1.82−6.43)	0−9.23
TDF	8.88[c]	7.89	7.56	
	(6.83−11.45)	(6.65−10.39)	(5.49−9.73)	5.80−15.30
ash	2.77	2.88[c]	2.68	
	(2.42−3.39)	(2.43−3.25)	(1.90−3.34)	2.14−4.17
carbohydrates	81.55[c]	81.52[c]	82.20	
	(79.48−83.90)	(79.11−83.33)	(79.46−84.51)	77.14−85.86
moisture	73.00	73.45	73.00	
	(70.50−77.90)	(70.80−76.90)	(70.30−77.60)	66.50−83.70
protein	12.13	12.12	12.14	
	(10.85−13.85)	(11.06−14.52)	(10.71−13.97)	9.27−16.16
total fat	3.52[c]	3.49[c]	3.00	
	(2.26−5.38)	(1.98−4.90)	(1.72−4.40)	0.86−5.40

[a]Percent dry weight (moisture = % fresh weight, carbohydrates by calculation). [b]Least-squares mean and range (minimum and maximum replicate values) across all sites. [c]Statistically different ($p < 0.05$) from control.

Diabrotica sp.), as well as the 5-enolpyruvylshikimate-3-phosphate synthase protein from *Agrobacterium* sp. strain CP4 (CP4 EPSPS) that confers tolerance to glyphosate. MON 89034 expresses the *Bt* Cry1A.105 and Cry2Ab2 proteins that protect against feeding damage caused by the European corn borer (*Ostrinia nubilalis*) and other select lepidopteran insect pests.

MON 88017 and MON 89034 traits were introgressed into the conventional sweet corn variety Temptation, which served as the control in this study. Harvested fresh sweet corn kernels were collected from MON 88017, MON 89034, the conventional control, and reference sweet corn hybrids grown in a 2010 U.S. field production. The field trials were conducted at five replicated sites representative of major commercial sweet corn production areas. These sites were Jefferson County, Iowa; Clinton County, Indiana; Ottawa County, Michigan; Freeborn County, Minnesota; and Miami County, Ohio.

At each site, starting seeds were planted in a randomized complete block design with four blocks each for MON 88017, MON 89034, the conventional control, and reference sweet corn hybrids. A total of 17 reference hybrids were included in the study and distributed across the five sites (see the Supporting Information for details of site distribution of reference hybrids). Normal agronomic practices were followed for each growing region, including the application of registered non-glyphosate-containing maintenance pesticides. Glyphosate was applied to MON 88017 sweet corn. Fresh ear samples were collected at the R3 growth stage from approximately 20 plants from each plot by removing pollination bags from collected ears and placing all nonshucked ears into an appropriately labeled sample container. Samples were then transferred to dry ice within 30 min after collection and shipped to Monsanto in St. Louis on the day of harvest. Fresh sweet corn kernels were removed from husked, desilked whole ears, and after samples were processed, stored in a −80 °C freezer prior to compositional analysis.

Compositional Analyses. Compositional analyses included proximates (ash, carbohydrates by calculation, moisture, protein, and fat), acid detergent fiber (ADF), neutral detergent fiber (NDF), total dietary fiber (TDF), 18 amino acids, fatty acids (C8−C22), sugars (raffinose, glucose, fructose, sucrose, and maltose), vitamins [β-carotene (referred to as vitamin A), B_1 (thiamin), B_2 (riboflavin), B_3 (niacin), B_6 (pyridoxine), B_9 (folic acid), C, and E (α- and γ-tocopherol)], other carotenoids (lutein and zeaxanthin), and minerals (calcium, copper, iron, magnesium, manganese, phosphorus, potassium, sodium, and zinc). The antinutrient phytic acid was also measured, as well as the secondary metabolites furfural (2-furaldehyde), ferulic acid, and *p*-coumaric acid. Compositional analyses were conducted by Covance Laboratories Inc. in Madison, WI, USA. Samples were analyzed in a randomized order to minimize assay bias. Methods for all components, with the exception of vitamin C and carotenoids, have been previously described.[10] Measurement of vitamin C followed AOAC International Method 967.22.[11] Briefly, vitamin C in each sample was extracted, oxidized, and mixed with *o*-phenylenediamine to produce a fluorophor having an activation maximum at approximately 350 nm and a fluorescence maximum at 430 nm. Fluorescence was proportional to concentration. Development of the fluorescence compound with the vitamin was prevented by forming a boric acid−dehydroascorbic acid complex prior to addition of the *o*-phenylenediamine solution. Any remaining fluorescence was due to extraneous material and served as the blank. The limit of quantitation for the vitamin C method was 1.00 mg/100 g. Carotenoid measurements followed AOAC International Method 967.22[12] (for β-carotene) and AOAC International Method 2005.07[13] (for lutein and zeaxanthin). Briefly, samples were blended with alcohol, filtered, and extracted with hexane. The extracts were evaporated, reconstituted with mobile phase, and analyzed on a reverse-phase HPLC system equipped with UV detection. Individual carotenoids were determined by comparison to known standards. The limit of quantitation for the carotenoid method was 0.0200 mg/100 g. Measurement of the sugars followed the same methodology used in raffinose determinations described previously.[10] Samples for sugar analysis were extracted with deionized water, and the extract was treated with hydroxylamine hydrochloride solution in pyridine, containing phenyl-β-D-glucoside as an internal standard. The resulting oximes were converted to silyl derivatives by treatment with hexamethyldisilazane and trifluoroacetic acid and analyzed by gas chromatography using a flame ionization detector. The limit of quantitation for the sugar method was 0.0500%.

Prior to the compositional study, the stabilities of vitamin C, sugars, and carotenoids after sweet corn harvest were evaluated in the conventional sweet corn (Temptation) stored at three storage conditions: at 5 °C and −20 °C for up to 45 days and at −70 °C for up to 200 days. On the basis of these results, it was determined that the best storage condition for the samples was in freezers set to maintain at least −70 °C (see the Supporting Information).

Statistical Analysis of Composition Data. In all, 77 different analytical components were measured. Across all samples, components with >50% of observations below the assay's limit of quantitation (LOQ) were excluded from summaries and statistical analysis. The following 22 components were excluded: caprylic acid, capric acid, lauric acid, myristic acid, myristoleic acid, pentadecanoic acid, pentadecenoic acid, palmitoleic acid, heptadecanoic acid, heptadecenoic acid, γ-linolenic acid, eicosadienoic acid, eicosatrienoic acid,

DOI: 10.1021/jf505687s
J. Agric. Food Chem. 2015, 63, 3046−3052

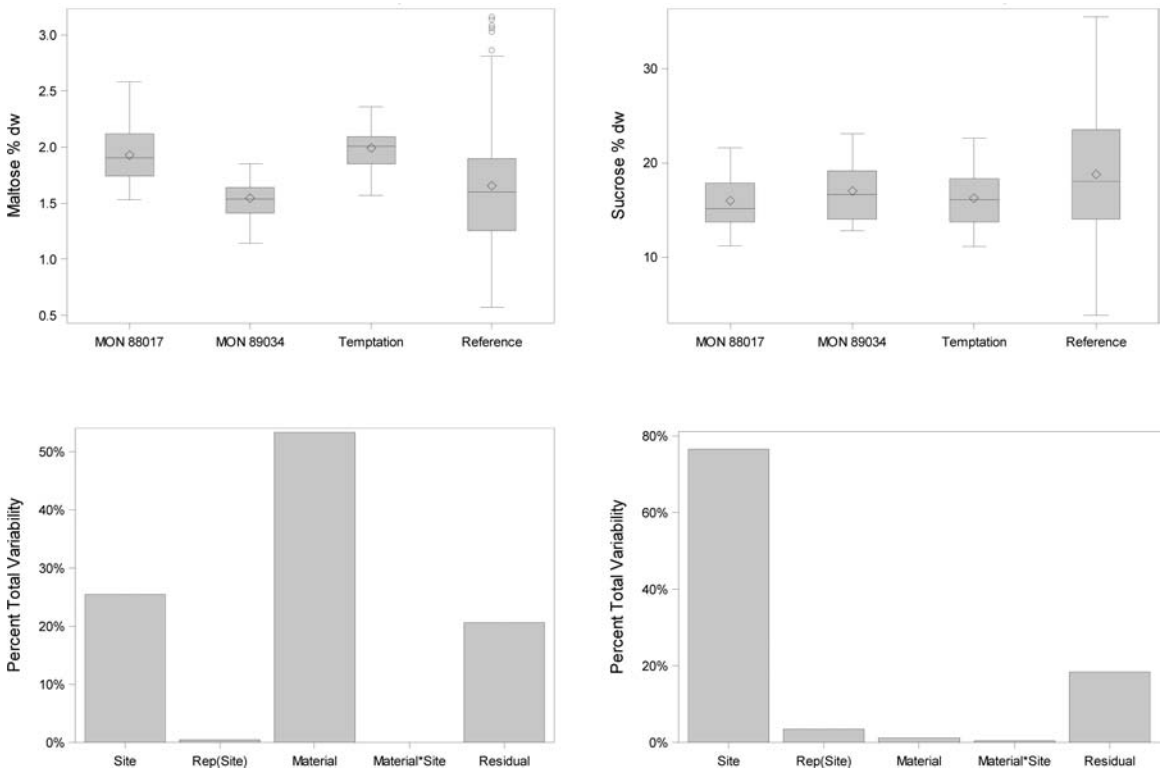

Figure 1. Box plots for maltose (top left) and sucrose (top right) and results of variance components analysis for maltose (bottom left) and sucrose (bottom right). For the box plots, the "whiskers" extend to the minimum and maximum values, the box indicates the 25th and 75th percentiles of the data, the middle line indicates the median, and the diamond indicates the mean.

arachidonic acid, sodium, β-carotene (referred to as vitamin A), furfural (2-furaldehyde), phytic acid, *p*-coumaric acid, raffinose, α-tocopherol, and γ-tocopherol. For components with individual measurements below the assay's LOQ, where fewer than 50% of the values were below the LOQ, a value equal to half the quantitation limit was assigned prior to statistical analyses. Outliers were investigated using PRESS residuals. Analytical components with values outside the ±6 studentized PRESS residual range were considered for removal as outliers. A single copper value was outside the ±6 studentized PRESS residual range and was removed. The outlier test procedure was reapplied to all remaining copper values; no additional result had a PRESS residual value outside the ±6 range.

The data analysis and output for this compositional assessment were generated using SAS software, versions 9.2 and 9.3 of the SAS System for Windows (SAS, 2002−2010). The replicated sites were assessed as a combination of all sites (the combined-site analysis). All component levels were statistically modeled using a mixed model analysis of variance. In particular, data were analyzed using the model

$$Y_{ijk} = U + T_i + S_j + B(S)_{jk} + ST_{ij} + e_{ijk}$$

where Y_{ijk} = unique individual observation, U = overall mean, T_i = fixed effect of material i, S_j = random effect of site j, $B(S)_{jk}$ = random effect of block k within site j, ST_{ij} = random effect of the interaction between site i and material j, and e_{ijk} = residual error. For each analytical component, the mean of MON 88017 and MON 89034 sweet corns was compared with the conventional control. Significant differences were determined at the 5% level.

A variance components analysis was also conducted by fitting the above model with a single modification; to compare the sources of variability, T_i was modeled as a random effect. The restricted maximum likelihood (REML) method was used to calculate covariance parameter estimates from the MIXED procedure in SAS. Bar charts and box plots were generated.

RESULTS AND DISCUSSION

Means and ranges of observed values for MON 88017, MON 89034, control, and reference sweet corn hybrids are presented in Tables 1−4 and Supplementary Tables 1 and 2 in the Supporting Information. Results of the combined-site analysis included 21 significant differences ($p < 0.05$) between the test materials and the conventional control. These encompassed 11 analytes in the assessment of MON 88017 sweet corn (ADF, NDF, TDF, carbohydrates by calculation, total fat, stearic acid, calcium, copper, iron, manganese, and zinc) and 10 analytes in the assessment of MON 89034 sweet corn (ADF, ash, carbohydrates by calculation, total fat, maltose, vitamin B_1, vitamin C, zeaxanthin, stearic acid, and arachidic acid). None of these 21 significant differences were considered compositionally meaningful as they were characterized by small magnitudes of difference and were much smaller than natural variation known to be associated with crop composition.[14−16] Graphical options to display the compositional data in this assessment were also pursued.[17] This is shown as box plots of selected analytes including maltose and sucrose (Figure 1), lutein and zeaxanthin (Figure 2), and vitamin C (Figure 3) and bar graphs of the fatty acid composition data (Figure 4). Results of variance components analysis on selected analytes are also shown graphically: sucrose and maltose (Figure 1), lutein and zeaxanthin (Supplementary Figure 2), vitamin C (Figure 3), and fructose and glucose (Supplementary Figure 1).

Proximate and Fiber Composition. There were a total of five significant differences ($p < 0.05$) between mean values of MON 88017 sweet corn and control components and four differences between MON 89034 sweet corn and the control (Table 1). In general, fat and fiber levels were higher in both MON 88017 and MON 89034 sweet corn hybrids when

DOI: 10.1021/jf505687s
J. Agric. Food Chem. 2015, 63, 3046−3052

Table 2. Sugar Composition of Kernels from Glyphosate-Tolerant and CRW-Protected Sweet Corn MON 88017 and Insect-Protected Sweet Corn MON 89034

component[a]	MON 88017 mean[b] (range)[b]	MON 89034 mean[b] (range)[b]	control mean[b] (range)[b]	reference range[b]	literature range
fructose	1.70 (1.02–3.15)	1.55 (0.81–3.42)	1.62 (0.90–2.92)	0.37–5.57	1.15–3.51[d] 0.81–4.15[e]
glucose	2.00 (1.27–3.63)	1.74 (1.05–3.56)	1.80 (1.32–2.99)	0.85–6.89	1.57–4.98[d] 1.40–4.86[e]
maltose	1.93 (1.53–2.58)	1.54[c] (1.14–1.85)	1.99 (1.57–2.36)	0.57–3.16	
sucrose	15.90 (11.22–21.51)	16.93 (12.74–23.03)	16.20 (11.05–22.55)	3.78–35.48	16.86–40.5[d] 9.68–37.1[e]

[a]Percent dry weight. [b]Least-squares mean and range (minimum and maximum replicate values) across all sites. [c]Statistically different ($p < 0.05$) from control. [d]Reference 18. [e]Reference 19.

Table 3. Vitamin and Carotenoid Composition of Kernels from Glyphosate-Tolerant and CRW-Protected Sweet Corn MON 88017 and Insect-Protected Sweet corn MON 89034

component[a]	MON 88017 mean[b] (range)[b]	MON 89034 mean[b] (range)[b]	control mean[b] (range)[b]	reference range[b]	literature range
vitamins					
B_1 (thiamin)	2.91[c] (1.78–4.88)	3.42 (2.53–4.62)	3.51 (2.51–4.50)	1.38–5.17	
B_2 (riboflavin)	5.23 (2.82–7.98)	4.82 (3.28–7.43)	4.93 (2.92–7.90)	3.11–11.22	
B_3 (niacin)	66.38 (56.41–74.79)	66.62 (56.16–78.52)	66.14 (56.32–75.45)	40.48–101.99	
B_6 (pyridoxine)	10.01 (6.56–12.31)	10.06 (8.46–12.34)	9.86 (8.82–12.84)	6.50–15.15	
B_9 (folic acid)	3.45 (2.68–4.64)	3.65 (2.61–5.81)	3.53 (2.75–4.31)	1.96–5.70	
C	324.47 (267.86–391.67)	368.40[c] (283.90–528.14)	331.88 (270.85–397.94)	183.77–730.06	283–470[d]
carotenoids					
lutein	0.63 (0.50–0.90)	0.59 (0.45–0.83)	0.61 (0.35–0.94)	0.036–1.62	0.59[e] 0.01–1.83[e]
zeaxanthin	0.47 (0.40–0.59)	0.55[c] (0.42–0.68)	0.46 (0.31–0.53)	0.058–1.26	0.28[e] 0.01–0.81[e]

[a]Vitamins in mg/kg dry weight; Carotenoids in mg/100 g dry weight. [b]Least-squares mean and range (minimum and maximum replicate values) across all sites. [c]Statistically different ($p < 0.05$) from control. [d]Reference 22. [e]Reference 21

compared to the sweet corn control. The increase in fiber was somewhat more pronounced in MON 88017 sweet corn, for which the TDF value was 8.88% dwt, whereas corresponding values for MON 89034 sweet corn and the control were 7.89 and 7.56% dwt, respectively. Fat values for MON 88017 and MON 89034 were 3.52 and 3.49% dwt, respectively, whereas the corresponding control value was 3.00% dwt. These differences were considerably less than the range of variation associated with the in-study reference sweet corn hybrids (Table 2).

Sugar Composition. Table 2 summarizes data from the analysis of sugar (fructose, glucose, maltose, and sucrose) levels in MON 88017 and MON 89034 sweet corns. No differences were observed between MON 88017 sweet corn and the conventional sweet corn control, and only one significant difference (maltose, $p < 0.05$) was observed between MON 89034 sweet corn and the control. The mean maltose value for MON 89034 sweet corn was 1.54% dwt, and the corresponding value for the conventional sweet corn control was 1.99% dwt, a difference of 0.45% dwt. This difference was considerably less than the range of variation (2.59% dwt) associated with the reference sweet corn hybrids (0.57–3.16% dwt, Table 2). Box plots for sucrose and maltose (Figure 1) highlighted the lack of significant impact on sugar composition. Consistent with these findings, variance components analysis showed that for maltose the MON 88017 and MON 89034 sweet corn materials contributed in part to the small amount of variation observed between the biotech and control comparator, and that for sucrose (Figure 1) and fructose and glucose (Supplementary Figure 1) variation is predominately due to location with negligible contribution from the biotech materials.

Characteristics of high-quality sweet corn are tenderness and sweetness,[18] and cultivars with greater sugar concentrations at harvest maturity have been shown to improve eating quality and consumer acceptance.[19,20] The data from this compositional assessment of MON 88017 and MON 89034 sweet corns have demonstrated sugar values consistent with the values reported in the literature[21,22] and that the biotech traits do not meaningfully affect sugar composition.

DOI: 10.1021/jf505687s
J. Agric. Food Chem. 2015, 63, 3046–3052

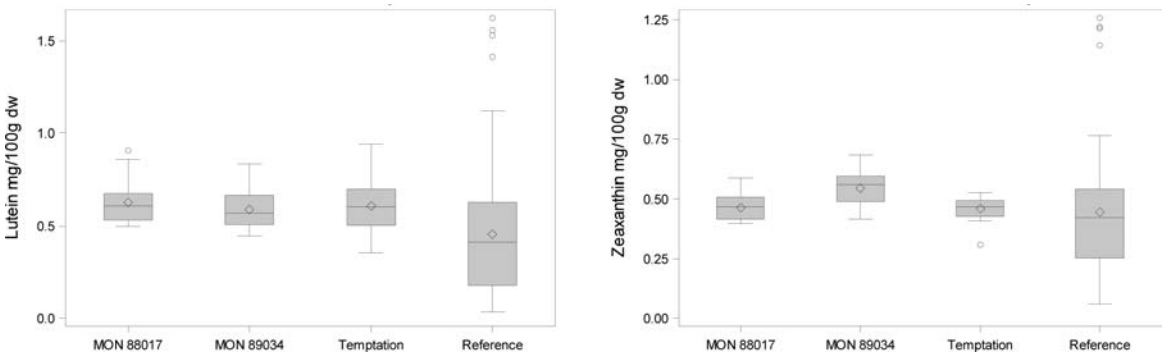

Figure 2. Box plots for lutein (left) and zeaxanthin (right). For the box plots, the "whiskers" extend to the minimum and maximum values, the box indicates the 25th and 75th percentiles of the data, the middle line indicates the median, and the diamond indicates the mean.

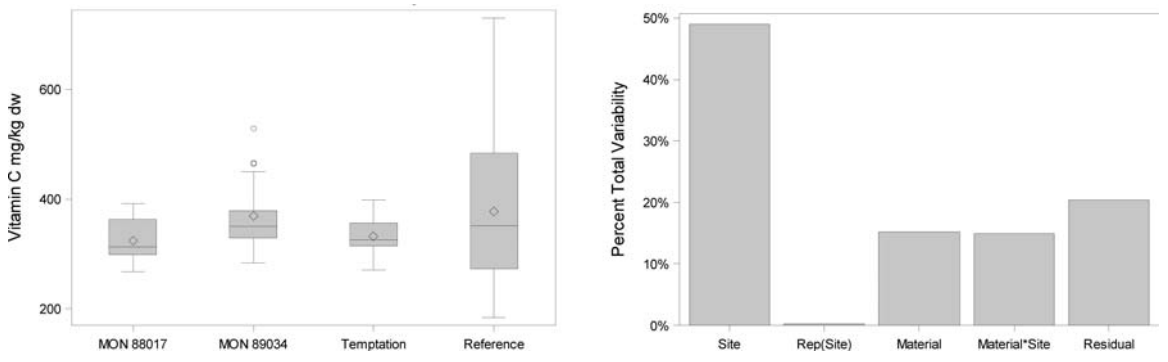

Figure 3. Box plot (left) and results of variance components analysis (right) for vitamin C. For the box plots, the "whiskers" extend to the minimum and maximum values, the box indicates the 25th and 75th percentiles of the data, the middle line indicates the median, and the diamond indicates the mean.

Table 4. Fatty Acid Composition of Kernels from Glyphosate-Tolerant and CRW-Protected Sweet Corn MON 88017 and Insect-Protected Sweet Corn MON 89034

component[a]	MON 88017 mean[b] (range)[b]	MON 89034 mean[b] (range)[b]	control mean[b] (range)[b]	reference range[b]
palmitic	11.39 (10.40–13.05)	11.35 (9.87–13.85)	11.44 (10.32–13.84)	10.55–18.67
stearic	2.18[c] (1.83–2.52)	2.05[c] (1.66–2.51)	2.26 (1.88–2.64)	1.71–4.40
oleic	40.61 (37.18–43.03)	40.38 (36.82–46.36)	39.76 (35.66–42.45)	27.13–48.59
linoleic	43.36 (41.04–46.70)	43.84 (37.86–47.26)	44.10 (41.92–47.23)	34.57–50.49
linolenic	1.12 (0.83–1.69)	1.10 (0.85–1.53)	1.13 (0.87–1.46)	0.85–2.59
arachidic	0.65 (0.56–0.77)	0.62[c] (0.53–0.75)	0.66 (0.58–0.77)	0.63–0.98
eicosenoic	0.44 (0.41–0.49)	0.43 (0.23–0.48)	0.43 (0.25–0.47)	0.21–0.69
behenic	0.26 (0.14–0.40)	0.24 (0.13–0.40)	0.24 (0.14–0.36)	0.83–6.86

[a]Percent total fatty acid. [b]Least-squares mean and range (minimum and maximum replicate values) across all sites. [c]Statistically different ($p < 0.05$) from control.

Vitamin and Carotenoid Composition. Vitamin (B_1, B_2, B_3, B_6, B_9, and C) and carotenoid (lutein and zeaxanthin) compositional analysis results are presented in Table 3. One significant difference ($p < 0.05$) was found for MON 88017 sweet corn in vitamin or carotenoid composition when compared with conventional control; the combined site mean value of vitamin B_1 (thiamine) in MON 88017 sweet corn was 2.91 mg/kg dwt and the corresponding value for the conventional sweet corn control was 3.51 mg/kg dwt, a difference of 0.6 mg/kg. This difference was considerably less than the range of variation (3.79 mg/kg) associated with the reference sweet corn hybrids (1.38–5.17 mg/kg dwt; Table 3). Two significant differences were observed between MON 89034 sweet corn and the conventional sweet corn control (vitamin C and zeaxanthin). Mean values for vitamin C and zeaxanthin in MON 89034 sweet corn were 368.4 mg/kg dwt

DOI: 10.1021/jf505687s
J. Agric. Food Chem. 2015, 63, 3046–3052

and 0.55 mg/100 g dwt, respectively. Corresponding values for vitamin C and zeaxanthin in the conventional sweet corn control were 331.88 mg/kg dwt and 0.46 mg/100 g dwt, respectively. Again, mean differences between the biotech and conventional comparators are of small magnitude and considerably less than the range of variation associated with the reference sweet corn hybrids (Table 3). Similar to the sugars, box plots for the carotenoids, lutein and zeaxanthin (Figure 2) highlight the lack of impact the biotech traits have on key sweet corn components. Results from variance components analysis of the carotenoids are presented in Supplementary Figure 2. The data presented in the supplementary figure demonstrate that MON 88017 and MON 89034 sweet corns have carotenoid values consistent with those reported in the literature[23,24] and that the biotech traits do not significantly affect carotenoid composition. This conclusion extends to the B and C vitamins[25] and is exemplified for vitamin C in Figure 3.

Fatty Acid Composition. Table 4 summarizes fatty acid composition data for MON 89034 and MON 88017 sweet corns. With the exception of stearic acid and arachidic acid, there were no differences ($p > 0.05$) in the mean levels of fatty acid components in MON 89034 sweet corn and the conventional sweet corn control and, with the exception of stearic acid, no significant differences were observed between MON 88017 sweet corn and its control. In those three instances when a significant difference was observed, the relative magnitude difference, with respect to the control, was small (<10%), and overall there was no change in the fatty acid profile. This is demonstrated in graphical form in Figure 4.

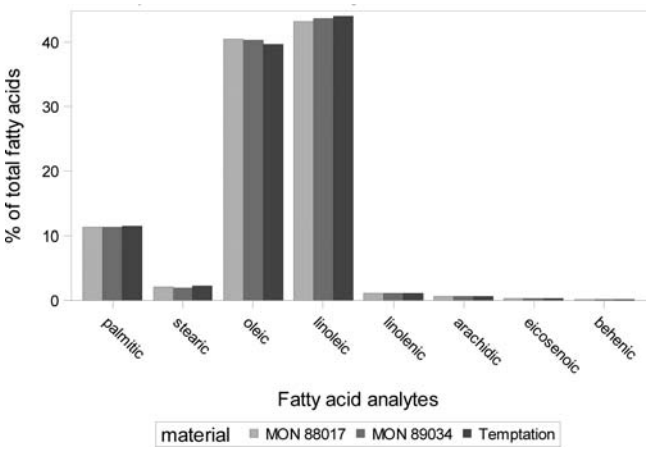

Figure 4. Clustered bar chart of fatty acids (expressed as perecentage of total fatty acids) for MON 88017, MON 89034, and control sweet corns.

Amino Acid Composition. Results from the amino acid analysis are presented in Supplementary Table 1. Consistent with the lack of differences ($p < 0.05$) observed in mean protein levels (Table 1) between both MON 89034 and MON 88017 sweet corns and the conventional sweet corn control, no significant differences were observed in amino acid levels.

Mineral Composition. The results for minerals (calcium, copper, iron, magnesium, manganese, phosphorus, potassium, and zinc) are presented in Supplementary Table 2. There were no significant differences ($p > 0.05$) between MON 89034 sweet corn and the sweet corn control, whereas for MON 88017 sweet corn, five differences ($p < 0.05$) were observed. In those latter instances, magnitudes of differences, with respect to the control, were small, particularly in the context of the extensive variability in mineral composition associated with maize.[14−16] These results established that the biotech traits have no meaningful impact on mineral composition.

Conclusion. Farmers in the United States have benefited from advancements in breeding and biotechnology for over a decade. Studies have consistently shown that these benefits have been accompanied by no loss in nutritional quality.[14−16] In the case of sweet corn, the benefits conferred by biotech traits include reductions in pesticide applications and fuel use.[3] As would be expected from results on field corn, levels of key nutritional components in MON 89034 and MON 88017 sweet corns were equivalent to those of a near-isogenic conventional sweet corn comparator. This conclusion especially extended to components such as sugars that are important determinants of sweet corn quality. Overall, the results of this study were consistent with a 20 year history of observed equivalence between GM and non-GM crops[15] and increasing understanding at the molecular level as to why such equivalence is expected.[26] In fact, it could be noted that the few statistically significant differences observed in this study are most likely due not to the GM traits but are associated with the effects of residual genetic variation between any near-isogenic comparators.[14] In summary, the benefits from biotech traits experienced in corn developed for feed use can also be incorporated into sweet corn while maintaining the high nutritional quality expected in sweet corn for food use.

■ ASSOCIATED CONTENT

Ⓢ Supporting Information

Growing locations of reference hybrids, Supplementary Tables 1 and 2, Supplementary Figures 1−10, and stability assessments of vitamin C, sugars, and carotenoids. This material is available free of charge via the Internet at http://pubs.acs.org.

■ AUTHOR INFORMATION

Corresponding Author

*(G.G.H.) E-mail: george.g.harrigan@monsanto.com.

Notes

The authors declare no competing financial interest.

■ ACKNOWLEDGMENTS

We thank the Monsanto Agronomy and Sample Management groups for the generation and preparation of the samples used in this assessment and the Monsanto Product Characterization group for the molecular analysis of the seed. We are also grateful to Ron Schneider, Monsanto Regulatory Affairs, for constructive and insightful comments.

■ REFERENCES

(1) International Service for the Acquisition of Agri-Biotech Applications (ISAAA). ISAAA Brief 46-2013: Top Ten Facts; http://www.isaaa.org/resources/publications/briefs/46/topfacts/default.asp (accessed June 2014).

(2) Chin, M. L.; Field, L.; Schmidt, J.; Scritchfield, R.; Toner, C. *Food Biotechnology: A Communicator's Guide to Improving Understanding*, 3rd ed.; International Food Information Council Foundation: Washington, DC, USA, April 2013.

(3) James, C. *Global Status of Commercialized Biotech/GM Crops: 2013*; ISAAA Brief 46; ISAAA: Ithaca, NY, USA, 2013.

(4) Chen, H.; Lin, Y. Promise and issues of genetically modified crops. *Curr. Opin. Plant Biol.* **2013**, *16* (2), 255−260.

DOI: 10.1021/jf505687s
J. Agric. Food Chem. 2015, 63, 3046−3052

(5) Medley, T. *APHIS/USDA Petition 92-204-01 for Determination of Nonregulated Status for ZW-20 Squash*; Animal and Plant Health Inspection Service (APHIS); U.S. Department of Agriculture: Washington, DC, USA, Dec 1994; http://www.aphis.usda.gov/biotechnology/petitions_table_pending.shtml (accessed June 2014).
(6) Gonsalves, D.; Gonsalves, C.; Ferreira, S.; Pitz, K.; Fitch, M.; Manshardt, R.; Slightom, J. *Transgenic Virus Resistant Papaya: From Hope to Reality for Controlling Papaya Ringspot Virus in Hawaii*; APSnet Feature Story; American Phytopathological Society: St. Paul, MN, USA, July 2004; http://oregonstate.edu/instruct/bi430-fs430/Documents-2004/3B-BIOTECH%20METH/Gonsalves-papaya-story-AmPhytopSoc2004.pdf (accessed May 2014).
(7) Brookes, G.; Barfoot, P. *GM Crops: Global Socio-economic and Environmental Impacts 1996−2012*; PG Economics: Dorchester, UK, 2014.
(8) Shelton, A.; Olmstead, D.; Burkness, E.; Hutchinson, W.; Dively, G.; Welty, C.; Sparks, A. Multi-state trials of Bt sweet corn varieties for control of the corn earworm (*Lepidoptera: Noctuidae*). *J. Econ. Entomol.* **2013**, *106*, 2151−2159.
(9) Shelton, A. M. Genetically engineered vegetables expressing proteins from *Bacillus thruringiensis* for insect resistance: successes, disappointments, challenges and ways to move forward. *GM Crops Food* **2012**, *3*, 175−183.
(10) Drury, S. M.; Reynolds, T. L.; Ridley, W. P.; Bogdanova, N.; Riordan, S.; Nemeth, M. A.; Sorbet, S.; Trujillo, W. A.; Breeze, M. L. Composition of forage and grain from second-generation insect-protected corn MON 89034 is equivalent to that of conventional corn (*Zea mays* L.). *J. Agric. Food Chem.* **2008**, *56*, 4623−4630.
(11) AOAC. AOAC International Method 967.22. In *Official Methods of Analysis of the AOAC International*, 18th ed.; Association of Official Analytical Chemists International: Gaithersburg, MD, USA, 2011.
(12) AOAC. AOAC International Method 941.15. In *Official Methods of Analysis of the AOAC International*, 18th ed.; Association of Official Analytical Chemists International: Gaithersburg, MD, USA, 2011.
(13) AOAC. AOAC International Method 2005.07. In *Official Methods of Analysis of the AOAC International*, 18th ed.; Association of Official Analytical Chemists International: Gaithersburg, MD, USA, 2011.
(14) Harrigan, G.; Venkatesh, T.; Cook, K.; Liu, B.; Perez, T.; Willse, A.; Tichich, R.; Feng, P. Compositional differences between near-isogenic GM and conventional maize hybrids are associated with back-crossing practices in conventional breeding. *Plant Biotechnol. J.* **2015**, *13*, 210−212.
(15) Herman, R. A.; Price, R. D. Unintended compositional changes in genetically modified (GM) crops: 20 years of research. *J. Agric. Food Chem.* **2013**, *61*, 11695−11701.
(16) Harrigan, G. G.; Lundry, D.; Drury, S.; Ridley, W. P.; Riordan, S. G.; Nemeth, M. A. Natural variation in crop composition and the impact of biotechnology. *Nat. Biotechnol.* **2010**, *28*, 402−404.
(17) Harrigan, G. G.; Harrison, J. M. Assessing compositional variability through graphical analysis and Bayesian statistical approaches; case studies on transgenic crops. *Biotechnol. Genet. Eng. Rev.* **2012**, *28*, 15−32.
(18) Carey, E. E.; Dickinson, D. B.; Rhodes, A. M. Sugar characteristics of sweet corn populations from a sugary enhancer breeding program. *Euphytica* **1984**, *33*, 609−622.
(19) Showalter, R.; Miller, L. Consumer preference for high-sugar sweet corn varieties. *Proc. Fla. State Hortic. Soc.* **1962**, *75*, 278.
(20) Azanza, F.; Klein, B.; Juvik, J. Sensory characterization of sweet corn lines differing in physical and chemical composition. *J. Food Sci.* **1996**, *61*, 253−257.
(21) Reyes, F.; Varseveld, G.; Kuhn, M. Sugar composition and flavor quality of high sugar (shrunken) and normal sweet corn. *J. Food Sci.* **1982**, *47*, 753−755.
(22) Wong, A. D.; Juvik, J. A.; Breeden, D. C.; Swiader, J. M. Shrunkern 2 sweet corn yield and the chemical compoennts of quality. *J. Am. Soc. Hortic. Sci.* **1994**, *119*, 747−755.
(23) Scott, C. E.; Eldridge, A. L. Comparison of carotenoid content in fresh, frozen and canned corn. *J. Food Compos. Anal.* **2005**, *18*, 551−559.
(24) Ibrahim, K.; Juvik, J. Feasibility for improving phytonutrient content in vegetable crops using conventional breeding strategies: case study with carotenoids and tocopherols in sweet corn and broccoli. *J. Agric. Food Chem.* **2009**, *57*, 4636−4644.
(25) OECD. *Consensus Document on Compositional Considerations for New Varieties of Maize (Zea mays): Key Food and Feed Nutrients, Anti-nutrients and Secondary Plant Metabolites*; OECD ENV/JM/MONO; Organisation of Economic Co-Operation and Development: Paris, France, 2002; p 25.
(26) Schnell, J.; Steele, M.; Bean, J.; Neuspiel, M.; Girard, C.; Dormann, N.; Pearson, C.; Savoie, A.; Bourbonniere, L.; MacDonald, P. A comparative analysis of insertional effects in genetically engineered plants: considerations for pre-market assessments. *Transgenic Res.* **2015**, *24*, 1−17.

DOI: 10.1021/jf505687s
J. Agric. Food Chem. 2015, 63, 3046−3052

to characterize the antimicrobial components of commercial *Leuconostoc*/radish root filtrates.

MATERIALS AND METHODS

Materials. *Leuconostoc*/radish root ferment filtrate (LRRFF) was obtained from retail stores in Lincolnton, NC and Olga, WA, via their Web sites. The samples were produced by Active Micro Technologies (Lincolnton, NC), and were marketed as Leucidal Liquid. Lot numbers were given as FSS130415, FSS111019-1, and 29283P-5139. *Raphanus sativus* (daikon/winter radish) was purchased at Planet Organic Market (Edmonton, Canada). Strong anion exchange resin AG 1-X8 (chloride form, 50−100 mesh) was purchased from Bio-Rad (Hercules, CA). Before use, the resin was pretreated with 6 M HCl for 20 min then washed with deionized water until pH 7.

Chemicals. Salicylic acid was purchased from Sigma-Aldrich (St. Louis, MO). Didecyldimethylammonium chloride was purchased from Lonza Inc. (Basel, Switzerland). High-performance liquid chromatography (HPLC)-grade methanol and acetonitrile were purchased from Caledon Laboratory Chemicals (Georgetown, Canada) and filtered through a 0.22 μm membrane before use. All other solvents were of American Chemical Society (ACS) grade and purchased from Fisher Scientific (Hampton, NH). Deionized water was obtained from a Milli-Q reagent water system (Millipore Co., Milford, MA). Protease XIV was obtained from Sigma-Aldrich (St. Louis, MO) and used according to the manufacturer's instructions.

Instrumental Analysis. Analytical high-performance liquid chromatography was done on a Varian ProStar equipped with model 210 pump heads, a model 325 dual wavelength detector, and a 1 mL Rheodyne 7725i manual injector. The analytical column was a 5 μm, 4.6 × 250 mm Vydac C18 (Torrance, CA). The HPLC mobile phase consisted of (A) methanol and (B) water, each containing 0.1% trifluorocetic acid (TFA). A gradient HPLC method was used, consisting of 5 min hold at 5% A; 50 min increase of A from 5 to 90%; 4 min hold at 90% A; 3 min decrease from 90 to 5% A; and 3 min hold at 5% A, with a flow rate of 1 mL/min and ultraviolet (UV) detection at 220 nm.

Nuclear magnetic resonance (NMR) spectra were recorded from samples in $CDCl_3$ on a Varian Unity 500 MHz or Varian Inova 600 MHz spectrometer at ambient temperature. Chemical shifts (δ) are reported in parts per million (ppm) relative to tetramethylsilane and are corrected to the solvent residue peak (7.26 ppm).

High-resolution electrospray ionization (ESI) mass spectra were acquired by flow injection analysis using an Agilent 6220 oaTOF instrument (Santa Clara, CA) equipped with a dual sprayer electrospray ionization source (the second sprayer providing a reference mass solution) and an Agilent 1200 Series isocratic pump, or by direct insertion probe electron impact (EI) ionization using a Kratos MS-50G instrument (Manchester, UK). The carrier solvent for flow injection analysis and mass spectral conditions was methanol. Mass correction of spectra was performed for every individual spectrum, using peaks at m/z 121.0509 and 922.0098 in the positive mode and m/z 226.9785 and 1033.9881 in the negative mode. Data analysis was performed using the Agilent Mass Hunter Qualitative Anaslysis software version B.03.01.

Radiocarbon dating was performed by the Research Laboratory for Archaeology and the History of Art at University of Oxford, England, U.K.[31]

Antimicrobial Activity by Spot-on-Lawn Assay. The assay was performed in a laminar flow hood. Soft agar (0.75% w/v agar) (10 mL) was inoculated with an overnight culture of the desired indicator strain (100 μL, 1% inoculation) and poured over a hard agar (1.5% w/v agar) plate of the same medium. Once the agar solidified, an aliquot of the sample (10 μL) was spotted on the plate and allowed to dry. The plate was incubated overnight at a temperature suitable for the growth of the indicator strain (30 or 37 °C). A clear zone in the bacterial lawn at the site of sample addition indicated antimicrobial activity. Indicator strains were *Escherichia coli* DH5α, *E. coli* ATCC 25922, *Lactococcus lactis* subsp. *cremonis* HP, and *Staphylococcus aureus* ATCC 6538.

Fractionation of *Leuconostoc*/Radish Root Ferment Filtrate by Hydrophobic Interaction Resin. Amberlite XAD-16 resin (40 g) was swelled by gentle stirring in isopropanol (IPA) for 30 min, followed by three rinses with deionized H_2O. To this resin was added a 1:1 mixture of LRRFF (100 mL from the 1100 mL bottle purchased from Formulator Sample Shop) and deionized H_2O (100 mL). The resulting slurry was gently shaken for 20 min then loaded into a 2.5 × 50 cm fritted column. The flow through was collected, and the column was washed with three bed-volumes of deionized H_2O, then two bed-volumes each of 20% IPA, 40% IPA, 60% IPA, 80% IPA, and finally 80% IPA containing 0.1% TFA. All solutions were collected, concentrated to remove isopropanol, and evaluated for biological activity using a spot-on-lawn assay.

Extractive Analysis of LRRFF. A 50 mL portion of *Leuconostoc*/radish root ferment filtrate was mixed with 40 mL of deionized water and extracted with 4 × 70 mL of ethyl acetate (EtOAc). The organic extracts were combined and dried over Na_2SO_4 and then concentrated in vacuo. The resulting white residue was analyzed by NMR spectrometry, HPLC, and elemental analysis. This residue could be further purified by dissolving in approximately 20 mL of EtOAc and extracting into water with 5% NaOH (3 × 70 mL). After the aqueous layers were combined and acidified with 6 M HCl to pH 2, a white solid (salicylic acid) crystallized from the solution. This solid was recrystallized from water, then dissolved in a 1:1 mixture of methanol (MeOH) and water for the spot-on-lawn activity assay.

A second compound (didecyldimethylammonium salt) was isolated as follows: LRRFF (50 mL) was mixed with 5% NaOH (20 mL) to a pH of 9−10 and then extracted with dichloromethane (4 × 70 mL). The organic extracts were pooled, dried with Na_2SO_4, and the solvent was removed in vacuo. The resulting residue was resuspended in a 1:1 mixture of MeOH:H_2O (2 mL) and then combined with a slurry of AG 1-X8 anion exchange resin (2 g, Cl^- form). This mixture was incubated at room temperature for 20 min with occasional swirling, followed by gravity filtration to remove the resin. The flow-through was collected, concentrated to dryness in vacuo, and subjected to NMR analysis.

Characterization Data. *Salicylic Acid.* FTIR (neat, cm^{-1}, ν): 3236, 3004, 2858, 2598, 1669, 1612, 1444. ^{1}H NMR (600 MHz, $CDCl_3$, δ): 7.94 (m, 1H, Ph-H), 7.56 (m, 1H, Ph-H), 7.03 (m, 1H, Ph-H), 6.95 (m, 1H, Ph-H). ^{13}C NMR (125.7 MHz, $CDCl_3$, δ): 174.7, 162.2, 137.0, 130.9, 119.6, 117.9, 111.3. Anal. Calcd. for $C_7H_6O_3$: C, 60.99; H, 4.45, Found: C, 60.87; H, 4.39; EI-HRMS m/z calcd for $C_7H_6O_3$: 138.03169 [M^+]. Found: 138.03116.

Didecyldimethylammonium Chloride. ^{1}H NMR (600 MHz, $CDCl_3$, δ): 3.51 (m, 4H, $(C\underline{H}_2)_2$-N), 3.40 (s, 6H, $(C\underline{H}_3)_2$-N), 1.70 (br. s, 4H, $(C\underline{H}_2CH_2)_2$-N), 1.35 (m, 28H, $(CH_3(C\underline{H}_2)_7$-$CH_2CH_2)_2$-N), 0.88 (t, 6H, $C\underline{H}_3CH_2$. ^{13}C NMR (125.7 MHz, $CDCl_3$, δ): 63.9, 51.6, 31.8, 29.7, 29.4, 29.4, 29.2, 26.4, 22.9, 22.7, 14.1. ESI-HRMS m/z calcd. for $C_{22}H_{48}N$: 326.3781 [$M + H^+$]. Found: 326.3784.

RESULTS AND DISCUSSION

In a spot-on-lawn assay, the commercial LRRFF inhibited the growth of *E. coli* DH5α, *E. coli* 25922, and *L. lactis* subsp. *cremonis* HP (Table 1). Antimicrobial activity was retained following treatment with Protease Type XIV or exposure to 100 °C for 60 min, conditions under which peptides typically degrade. Fractionating the liquid with Amberlite XAD-16 localized activity against both *E. coli* and *L. lactis* strains to the 60% isopropanol and 80% isopropanol, 0.1% TFA fractions. Trifluoroacetic acid was included in the final wash to protonate any potential amines which might otherwise be too hydrophobic to elute from the XAD-16 resin.

When the XAD-16 fractions were left at room temperature overnight, a white needle-like solid precipitated from the 60% IPA and 80% IPA with 0.1% TFA fractions. This solid was collected and characterized by Fourier transform infrared (FTIR), NMR, elemental analysis, and mass spectrometry (EI) analysis. The solid was found to have a mass of 138 g/mol,

DOI: 10.1021/jf5063588
J. Agric. Food Chem. 2015, 63, 3053−3058

Table 1. Results of Spot-on-Lawn Assays of *Leuconostoc*/Radish Root Ferment Filtrate against Indicator Organisms[a]

entry	sample	*E. coli* DH5α	*E. coli* 25922	*L. lactis* subsp. *cremonis* HP
1	*Leuconostoc*/radish root ferment filtrate	+	++	++
2	following Protease treatment	n/a	++	++
3	following heating to 100 °C for 60 min	n/a	++	++
4	flowthrough	+	n/a	++
5	wash (0% IPA)	−	n/a	−
6	20% IPA	−	n/a	−
7	40% IPA	−	n/a	−
8	60% IPA	+	n/a	++
9	80% IPA with 0.1% TFA	+	n/a	++

[a]Entries 4−9 represent various stages of Amberlite XAD-16 fractionation tested as 10 μL aliquots. ++ means that the sample was active; + means the sample was weakly active; − means the sample was inactive; n/a means the sample was not tested against that organism.

consistent with a molecular formula of $C_7H_6O_3$. The mass, FTIR, ^{1}H NMR, and ^{13}C NMR data and chromatographic behavior were in accord with that of salicylic acid, with a minor alkyl impurity visible by ^{1}H NMR (Figure 1).

Salicylic acid is a natural product, produced by both lactic acid bacteria and plants, and is present in fermented radish brine.[21,32,33] It inhibits the growth of some Gram-negative bacteria and fungi but is not generally active against Gram-positive bacteria.[33−38] This was confirmed with a spot-on-lawn assay using commercial salicylic acid, dissolved in 1:1 MeOH:H_2O, which inhibited the growth of *E. coli* DH5α and not *L. lactis* subsp. *cremonis* HP. The solid which was isolated from LRRFF following XAD-16 fractionation was active against both organisms (Figure 2). High-resolution ESI-MS analysis of the solid showed only one signal in the positive mode, with a m/z value of 326.3776. This corresponded to a chemical formula of $C_{22}H_{48}N^+$, suggesting that at least part of the salicylate had a saturated alkyl amine counterion. This was verified via direct extraction of LRRFF with ethyl acetate, followed by washing with sodium hydroxide and acidification with hydrochloric acid. Upon acidification, salicylic acid precipitated out of solution and was collected via filtration. This sample was identical to a commercial sample by HPLC and did not inhibit the growth of *L. lactis* subsp. *cremonis* HP (Figures 2 and 3, Table 2). MS analysis no longer showed a peak at 326.3776 in the positive mode.

To determine the structure of the substance responsible for the activity against *L. lactis*, we concentrated the base-washed ethyl acetate layer and examined the resulting solid by ^{1}H NMR. While generally consistent with didecyldimethylammonium bromide, the spectra contained a small salicylate impurity. To remove this, the mixture was dissolved in water and passed through a column of anion exchange resin AG 1-X8 (Cl^-). Once the sample was concentrated to dryness and reconstituted in $CDCl_3$, NMR analysis showed no trace of salicylate (Figure 4), and all of the ^{1}H and ^{13}C NMR spectra were identical to that of didecyldimethylammonium bromide.[39] In mass spectral analyses, the molecular formula of the positive ion obtained from didecyldimethylammonium bromide matched that obtained by high-resolution mass spectrometry (HRMS), and tandem mass spectrometry analysis of our sample showed only one fragmentation peak, with a molecular formula of $C_{12}H_{28}N^+$. This corresponds to loss of $C_{10}H_{20}$, one of the two decyl chains.

Didecyldimethylammonium chloride is known to inhibit the growth of several Gram-positive bacteria, including *Staphylococcus aureus*.[40,41] Both the isolated salt and a commercial

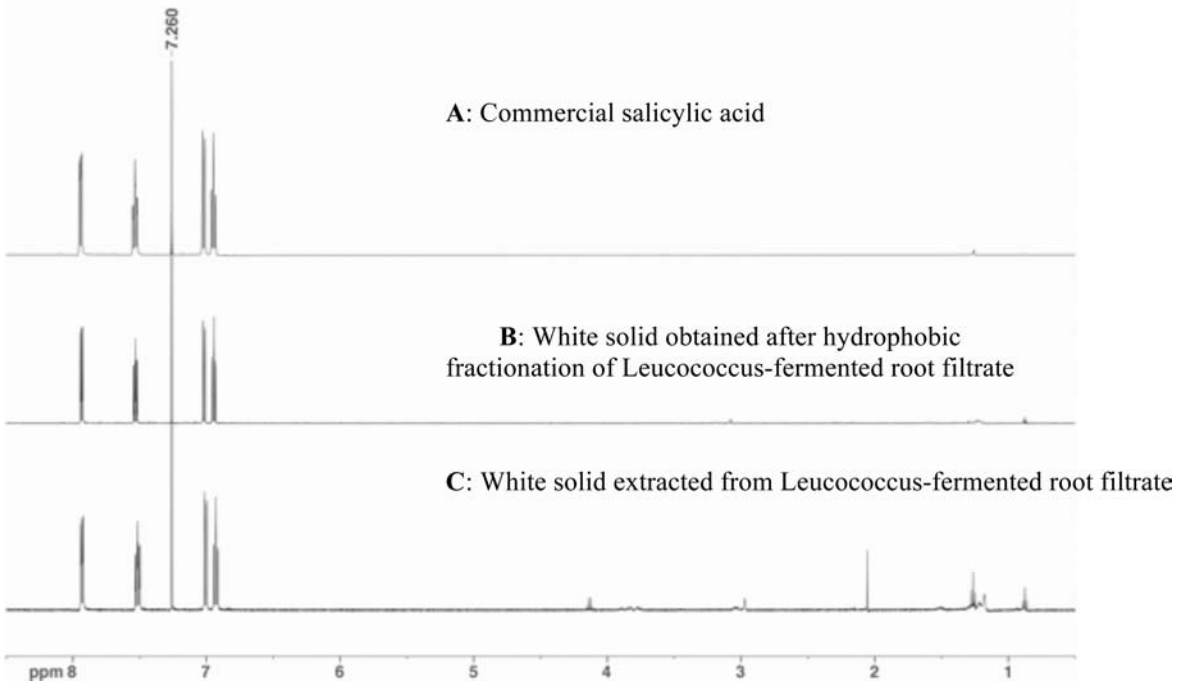

Figure 1. ^{1}H NMR spectra of (A) commercial salicylic acid, (B) the white solid obtained after fractionation using Amberlite XAD-16 resin, and (C) the white solid obtained from EtOAc extraction of *Leuconostoc*/radish root ferment filtrate. The solvent peak of deuterated chloroform appears at 7.26 ppm.

DOI: 10.1021/jf5063588
J. Agric. Food Chem. 2015, 63, 3053−3058

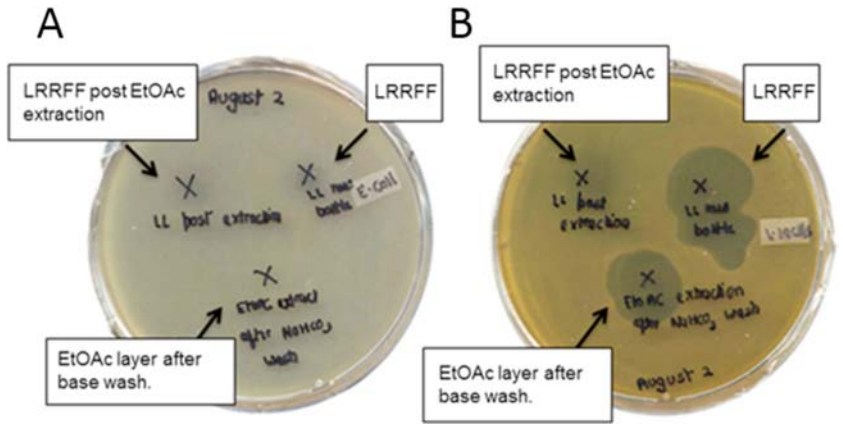

Figure 2. Spot-on-lawn activity test results of *Leuconostoc*/radish root ferment filtrate (LRRFF) pre- and post- EtOAc extraction, EtOAc extract after base wash. Indicator strains are (A) *E. coli* DH5α and (B) *L. lactis* subsp. *cremonis* HP.

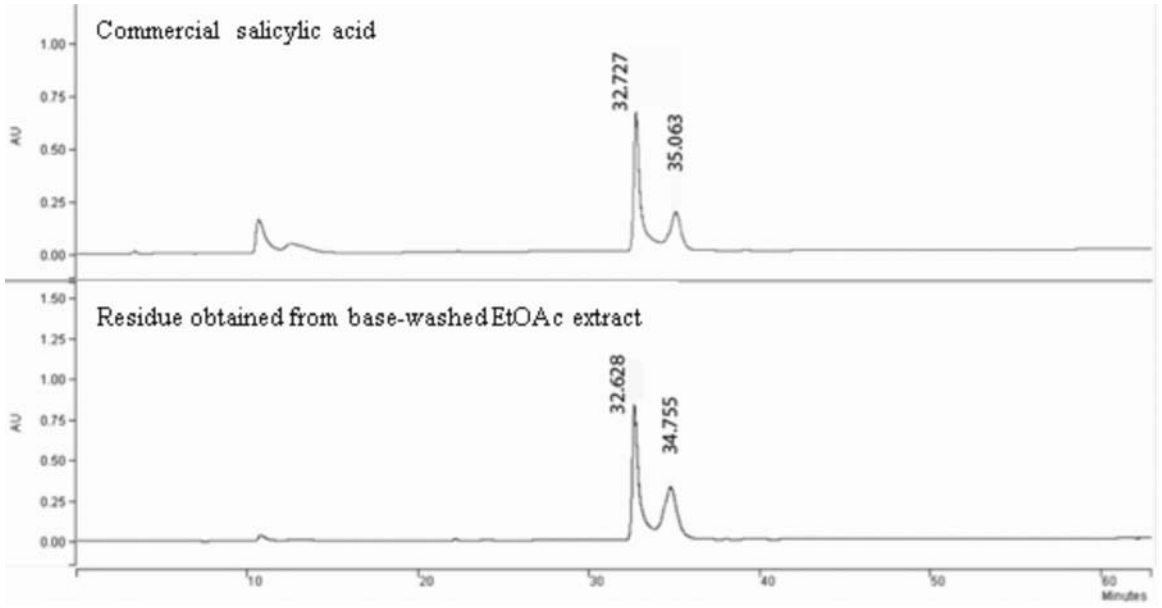

Figure 3. HPLC traces of commercial salicylic acid (top panel) and the residue obtained from base-washed EtOAc extract (bottom panel).

Table 2. Antimicrobial Activity of the Isolated Solid or Residue from *Leuconostoc*/Radish Root Ferment Filtrate[a]

entry	sample (dissolved in MeOH:H_2O/1:1)	*E. coli* DH5α	*L. lactis* subsp. *cremonis* HP
1	MeOH:H_2O/1:1	−	−
2	commercial salicylic acid	+	−
3	solid obtained from fractionation by 60%, 80% IPA on XAD resin	+	++
4	solid obtained by EtOAc extract	+	++
5	residue obtained after the base wash of EtOAc extract	−	++

[a]Samples were dissolved at 1 mg/mL concentration and a 10 μL aliquot was tested. ++ means that the sample was active; + means the sample was weakly active; − means the sample was inactive.

sample strongly inhibited the growth of *S. aureus* ATCC 6538 and *L. lactis* subsp. *cremonis* HP at 8 μg/mL in our spot-on-lawn assay.

To estimate the amount of salicylic and didecyldimethylammonium salt in commercial LRRFF, 50 mL aliquots were drawn from three different samples obtained from two different suppliers. The results were performed without duplication, and are summarized in Table 3. We also blended a 150 g sample of daikon/winter radish (*Raphanus sativus*), and extracted the resulting aqueous mixture with EtOAc, but were unable to detect salicylic acid or didecyldimethylammonium salts by mass spectrometry. While salicylic acid is one of the organic acids produced by lactic acid bacteria and is known to occur in fermented radish brine,[2,33] to date didecyldimethylammonium salts have been produced only through anthropogenic chemical synthesis.[42]

To determine the origin of the salicylic acid and didecyldimethylammonium salts we isolated from LRRFF, samples were submitted for carbon dating. On the basis of the amount of ^{14}C present, these compounds were dated to 52 000 ± 2 900 and 21 140 ± 100 years old, respectively. This clearly indicates that the salicylic acid and the didecyldimethylammonium chloride are largely derived from petroleum-based precursors and that neither is the product of a recent fermentation of plant material. The didecyldimethylammonium salts, which are used as detergent biocides and wood preservatives, have toxicity to aquatic organisms and can also affect human health.[40,42,43] They are known to enhance permeability of salicylic acid through

DOI: 10.1021/jf5063588
J. Agric. Food Chem. 2015, 63, 3053−3058

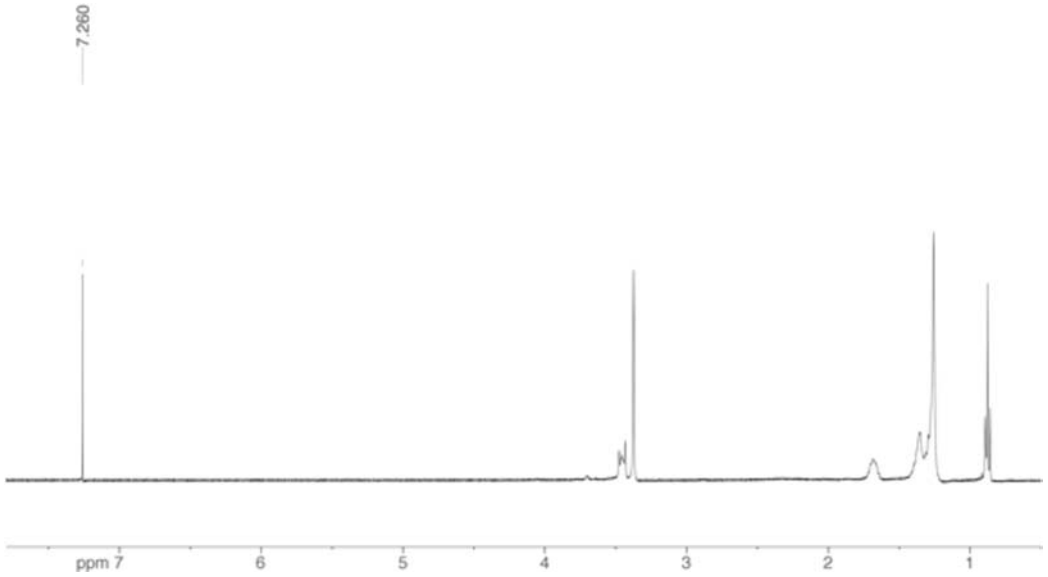

Figure 4. ^{1}H NMR spectrum of didecyl dimethyl chloride obtained after ion-exchange chromatography. The residual solvent peak of deuterated chloroform appears at 7.26 ppm.

Table 3. Amount of Purified Salicylic Acid and Didecyldimethylammonium Salts Obtained from *Leuconostoc*/Radish Root Ferment Filtrate Purchased from Two Companies

sample	1		2
batch	batch 1 (8 oz)	batch 2 (1 kg)	batch 3 (8 oz)
isolated and purified salicylic acid (g/50 mL)	0.31	0.12	0.19
didecyldimethylammonium salts as chloride (mg/50 mL)	8	16	10

animal skin,[44] and can cause skin allergenic effects, asthma, and lung problems, as well as eye irritation.[45−48] In Europe, the acceptable daily intake of didecyldimethylammonium chloride has been set to 0.1 mg/kg body weight per day.[49] As indicated in Table 3, a 50 mL batch of LRRFF would exceed this level for an adult human male.

In summary, the antimicrobial activity of commercial *Leuconostoc*/radish root ferment filtrates (LRRFF) are attributed to salicylic acid and didecyldimethylammonium salts. Moreover, these two compounds are too deficient in ^{14}C to be the product of recent fermentation, suggesting that they are derived from petroleum feedstock. We were unable to detect antimicrobial peptides in any sample of fermented radish root filtrate.

AUTHOR INFORMATION

Corresponding Author

*Tel: + 780 492 5475. Fax: + 780 492 8231. E-mail: John.Vederas@ualberta.ca.

Funding

This work was supported by the Natural Sciences and Engineering Research Council of Canada (NSERC), Griffith Laboratories Limited, Alberta Innovates Health Solutions, and the Canada Research Chair in Bioorganic and Medicinal Chemistry.

Notes

The authors declare the following competing financial interest(s): Griffith Laboratories produces and markets food ingredient systems for enhancement of food safety and flavor.

ACKNOWLEDGMENTS

We thank Dr. Randy Whittal (University of Alberta) for assistance with mass spectrometric analysis.

REFERENCES

(1) Ross, R. P.; Morgan, S.; Hill, C. Preservation and fermentation: Past, present and future. *Int. J. Food Microbiol.* **2002**, *79*, 3−16.

(2) Kim, Y.-S.; Zheng, Z.-B.; Shin, D.-H. Growth inhibitory effects of kimchi (Korean traditional fermented vegetable product) against *Bacillus cereus, Listeria monocytogenes*, and *Staphylococcus aureus*. *J. Food Prot.* **2008**, *71*, 325−332.

(3) Stoyanova, L. G.; Ustyugova, E. A.; Netrusov, A. I. Antibacterial metabolites of lactic acid bacteria: Their diversity and properties. *Appl. Biochem. Microbiol.* **2012**, *48*, 229−243.

(4) Cotter, P. D.; Hill, C.; Ross, R. P. Bacteriocins: Developing innate immunity for food. *Nat. Rev. Microbiol.* **2005**, *3*, 777−788.

(5) De Vuyst, L.; Leroy, F. Bacteriocins from lactic acid bacteria: Production, purification, and food applications. *J. Mol. Microbiol. Biotechnol.* **2007**, *13*, 194−199.

(6) Dalié, D. K. D.; Deschamps, A. M.; Richard-Forget, F. Lactic acid bacteria − Potential for control of mould growth and mycotoxins: A Review. *Food Control* **2010**, *21*, 370−380.

(7) Arnison, P. G.; Bibb, M. J.; Bierbaum, G.; Bowers, A. A.; Bugni, T. S.; Bulaj, G.; Camarero, J. A.; Campopiano, D. J.; Challis, G. L.; Clardy, J.; et al. Ribosomally synthesized and post-translationally modified peptide natural products: Overview and recommendations for a universal nomenclature. *Nat. Prod. Rep.* **2013**, *30*, 108−160.

(8) Delves-Broughton, J.; Blackburn, P.; Evans, R. J.; Hugenholtz, J. Applications of the bacteriocin, nisin. *Antonie Van Leeuwenhoek* **1996**, *69*, 193−202.

(9) Lee, W. A.; Keupp, G. M.; Brieva, H.; Warren, M. R. Compositions containing extracts from radish. US Patent 2010/0129305 A1, May 27, 2010.

(10) Lee, H. J.; Joo, Y. J.; Park, C. S.; Kim, S. H.; Hwang, I. K.; Ahn, J. S.; Mheen, T. I. Purification and characterization of a bacteriocin produced by *Lactococcus lactis* subsp. lactis H-559 isolated from kimchi. *J. Biosci. Bioeng.* **1999**, *88*, 153−159.

DOI: 10.1021/jf5063588
J. Agric. Food Chem. 2015, 63, 3053−3058

(11) Lee, J.-H.; Kim, M.; Jeong, D.-W.; Kim, M.; Kim, J. H.; Chang, H. C.; Chung, D. K.; Kim, H.-Y.; Kim, K. H.; Lee, H. J. Identification of bacteriocin-producing *Lactobacillus paraplantarum* first isolated from kimchi. *J. Microbiol. Biotechnol.* **2005**, *15*, 428−433.
(12) Chang, J. Y.; Lee, H. J.; Chang, H. C. Identification of the agent from *Lactobacillus plantarum* KFRI464 that enhances bacteriocin production by *Leuconostoc citreum* GJ7. *J. Appl. Microbiol.* **2007**, *103*, 2504−2515.
(13) Lundov, M. D.; Moesby, L.; Zachariae, C.; Johansen, J. D. Contamination versus preservation of cosmetics: A review on legislation, usage, infections, and contact allergy. *Contact Dermatitis* **2009**, *60*, 70−78.
(14) Bosund, I.; Erichsen, I.; Molin, N. The bacteriostatic action of benzoic and salicylic Acids. *Physiol. Plant.* **1960**, *13*, 800−811.
(15) Madan, R. K.; Levitt, J. A review of toxicity from topical salicylic acid preparations. *J. Am. Acad. Dermatol.* **2014**, *70*, 788−792.
(16) Shelton, R. S.; Van Campen, M. G. Quaternary ammonium salts as germicides. I. Non-acylated quaternary ammonium salts derived from aliphatic amines. *J. Am. Chem. Soc.* **1946**, *68*, 753−755.
(17) Chaplin, C. E. Observations on quaternary ammonium disinfectants. *Can. J. Bot.* **1951**, *29*, 373−382.
(18) Takasaki, A.; Hashida, T.; Fujiwara, S.; Kato, K.; Nishihara, T. Bactericidal action of a quaternary ammonium disinfectant, didecyldimethyl ammonium chloride, against *Staphylococcus aureus*. *Jpn. J. Toxicol. Environ. Health* **1994**, *40*, 344−350.
(19) Buffet-Bataillon, S.; Tattevin, P.; Bonnaure-Mallet, M.; Jolivet-Gougeon, A. Emergence of resistance to antibacterial agents: The role of quaternary ammonium compounds—a critical review. *Int. J. Antimicrob. Agents* **2012**, *39*, 381−389.
(20) Kuca, K.; Marek, J.; Stodulka, P.; Musilek, K.; Hanusova, P.; Hrabinova, M.; Jun, D. Preparation of benzalkonium salts differing in the length of a side alkyl chain. *Molecules* **2007**, *12*, 2341−2347.
(21) Duthie, G. G.; Wood, A. D. Natural salicylates: Foods, functions and disease prevention. *Food Funct.* **2011**, *2*, 515−520.
(22) Negi, P. S. Plant extracts for the control of bacterial growth: Efficacy, stability and safety issues for food application. *Int. J. Food Microbiol.* **2012**, *156*, 7−17.
(23) Karre, L.; Lopez, K.; Getty, K. J. K. Natural antioxidants in meat and poultry products. *Meat Sci.* **2013**, *94*, 220−227.
(24) Juneja, V. K.; Dwivedi, H. P.; Yan, X. Novel natural food antimicrobials. *Annu. Rev. Food Sci. Technol.* **2012**, *3*, 381−403.
(25) Takeoka, T.; Dao, L.; Wong, R. Y.; Lundin, R.; Mahoney, N. Identification of benzethonium chloride in commercial grapefruit seed extracts. *J. Agric. Food. Chem.* **2001**, *49*, 3316−3320.
(26) Pawlowska, A. M.; Zannini, E.; Coffey, A.; Arendt, E. K. "Green preservatives": Combating fungi in the food and feed industry by applying antifungal lactic acid bacteria. *Adv. Food Nutr. Res.* **2012**, *66*, 217−238.
(27) Lohans, C. T.; Vederas, J. C. Structural characterization of thioether-bridged bacteriocins. *J. Antibiot.* **2014**, *67*, 23−30.
(28) Lohans, C. T.; Huang, Z.; van Belkum, M. J.; Giroud, M.; Sit, C. S.; Steels, E. M.; Zhang, J.; Whittal, R. M.; McMullen, L. M.; Vederas, J. C. Structural characterization of the highly cyclized lantibiotic paenicidin A via a partial desulfurization/reduction strategy. *J. Am. Chem. Soc.* **2012**, *134*, 19540−19543.
(29) Lohans, C. T.; van Belkum, M. J.; Cochrane, S. A.; Huang, Z.; Sit, C. S.; McMullen, L. M.; Vederas, J. C. Biochemical, structural, and genetic characterization of tridecaptin A_1, an antagonist of *Campylobacter jejuni*. *ChemBioChem* **2014**, *15*, 243−249.
(30) Lohans, C. T.; van Belkum, M. J.; Li, J.; Vederas, J. C. Characterization of bacterial antimicrobial peptides active against *Campylobacter jejuni*. *Can. J. Chem.* DOI: 10.1139/cjc-2014-0411.
(31) Ramsey, C. B.; Higham, T. F. G.; Owen, D. C.; Pike, A. W. G.; Hedges, R. E. M. Radiocarbon dates from the Oxford ams System: Archaeometry datelist 31. *Archaeometry* **2002**, *44*, 1−150.
(32) Broberg, A.; Jacobsson, K.; Ström, K.; Schnürer. Metabolite profiles of lactic acid bacteria in grass silage. *J. Appl. Environ. Microbiol.* **2007**, *73*, 5547−5552.
(33) Jing, P.; Song, L.-H.; Shen, S.-Q.; Zhao, S.-J.; Pang, J.; Qian, B.-J. Characterization of phytochemicals and antioxidant activities of red radish brines during lactic acid fermentation. *Molecules* **2014**, *19*, 9675−9688.
(34) Amborabé, B.-E.; Fleurat-Lessard, P.; Chollet, J.-F.; Roblin, G. Antifungal effects of salicylic acid and other benzoic acid derivatives towards *Eutypa lata*: structure−activity relationship. *Plant Physiol. Biochem.* **2002**, *40*, 1051−1060.
(35) Gershon, H.; Parmegiani, R. Antimicrobial activity of 8-quinolinols, salicylic acids, hydroxynaphthoic acids, and salts of selected quinolinols with selected hydroxy-acids. *Appl. Microbiol.* **1962**, *10*, 348−353.
(36) Martín, J. A.; Solla, A.; Witzell, J.; Gil, L.; García-Vallejo, M. C. Antifungal effect and reduction of *Ulmus minor* symptoms to *Ophiostoma novo-ulmi* by carvacrol and salicylic acid. *Eur. J. Plant Pathol.* **2010**, *127*, 21−32.
(37) Qi, P.-F.; Johnston, A.; Balcerzak, M.; Rocheleau, H.; Harris, L. J.; Long, X.-Y.; Wei, Y.-M.; Zheng, Y.-L.; Ouellet, T. Effect of salicylic acid on *Fusarium graminearum*, the major causal agent of fusarium head blight in wheat. *Fungal Biol.* **2012**, *116*, 413−426.
(38) Vlot, A. C.; Dempsey, D. A.; Klessig, D. F. Salicylic acid, a multifaceted hormone to combat disease. *Annu. Rev. Phytopathol.* **2009**, *47*, 177−206.
(39) Spectral Database for Organic Compounds (SDBS), entry 19599: Didecyldimethylammonium bromide (accessed February, 2015). http://sdbs.db.aist.go.jp/ .
(40) GESTIS Database on Hazardous Substances, entry 612-131-00-6: Didecyldimethylammonium chloride (accessed February, 2015). http://gestis-en.itrust.de/.
(41) Ioannou, C. J.; Hanlon, G. W.; Denyer, S. P. Action of disinfectant quaternary ammonium compounds against *Staphylococcus aureus*. *Antimicrob. Agents Chemother.* **2007**, *51*, 296−306.
(42) Henderson, N. D. *A Review of the Environmental Impact and Toxic Effects of DDAC*; Environmental Protection Division, BC Environment Ministry of Environment, Lands and Parks, Victoria, British Columbia, 1992.
(43) Bailey, H. C.; Elphick, J. R.; Potter, A.; Chao, E.; Zak, B. Acute toxicity of the antisapstain chemicals DDAC and IPBC, alone and in combination, to rainbow trout (*Oncorhynchus mykiss*). *Water Res.* **1999**, *33*, 2410−2414.
(44) Kitagawa, S.; Kasamaki, M. Enhancement effects of double-chained cationic surfactants of n-dimethyldialkylammoniums on permeability of salicylate through guinea pig dorsal skin. *Chem. Pharm. Bull.* **2002**, *50*, 1370−1372.
(45) Oropeza, A. R.; Friis, U. F.; Johansen, J. D. Occupational contact urticaria caused by didecyl dimethyl ammonium chloride. *Contact Dermatitis* **2011**, *64*, 297−298.
(46) Geier, J.; Lessmann, H.; Krautheim, A.; Fuchs, T. Airborne allergic contact dermatitis caused by didecyldimethylammonium chloride in a geriatric nurse. *Contact Dermatitis* **2013**, *68*, 123−125.
(47) Ohnuma, A.; Yoshida, T.; Tajima, H.; Fukuyama, T.; Hayashi, K.; Yamaguchi, S.; Ohtsuka, R.; Sasaki, J.; Fukumori, J.; Tomita, M.; Kojima, S.; Takahasji, N.; Takeuchi, Y.; Kuwahara, M.; Takeda, M.; Kosaka, T.; Nakashima, N.; Harada, T. Didecyldimethylammonium chloride induces pulmonary inflammation and fibrosis in mice. *Exp. Toxicol. Pathol.* **2010**, *62*, 643−651.
(48) Kwon, J.-T; Kim, H.-M.; Kim, P.; Choi, K. Didecyldimethylammonium chloride induces oxidative stress and inhibits cell growth in lung epithelial cells. *Mol. Cell Toxicol.* **2014**, *10*, 41−45.
(49) Bertuzzi, T.; Pietri, A. Determination of benzalkonium homologues and didecyldimethylammonium in powdered and liquid milk for infants by hydrophilic interaction liquid chromatography-mass spectrometry. *Food Anal. Methods* **2014**, *7*, 1278−1254 and references therein.

DOI: 10.1021/jf5063588
J. Agric. Food Chem. 2015, 63, 3053−3058

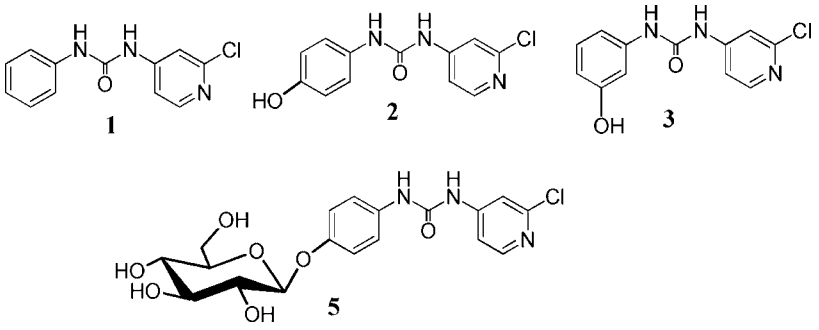

Figure 1. Structures of the primary compounds.

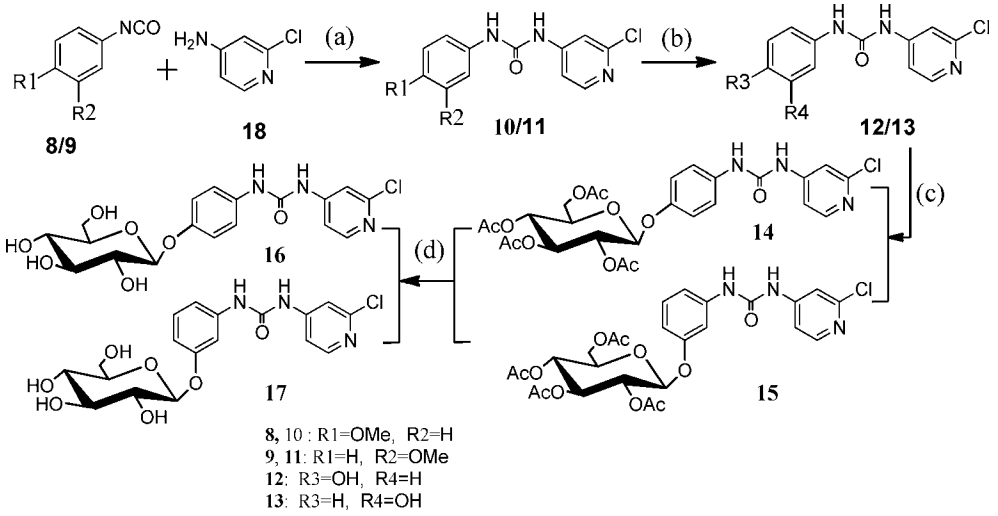

Figure 2. Synthetic route to forchlorfenuron metabolites. Reagents and conditions: (a) 80 °C, 8 h; (b) BBr_3, CH_2Cl_2, −30 °C, 24 h; (c) TBAB, K_2CO_3, $CHCl_3$, 50 °C, 12 h; (d) $NH_3{\cdot}H_2O$, CH_3OH, rt, 12 h.

and in turn, to identify these metabolites by the synthesis standard as well as to assess safety of forchlorfenuron and its metabolites.

MATERIAL AND METHODS

General. Forchlorfenuron (purity >99%), high performance liquid chromatography (HPLC) grade methanol, and acetonitrile were provided by Sigma-Aldrich (St Louis, Missouri). Formic acid and ethyl acetate used were of analytical grade (Sigma-Aldrich, St Louis, Missouri). HPLC-grade water was obtained by Milli-Q-Plus ultrapure water system from Millipore (Milford, MA). Nuclear magnetic resonance spectra were recorded on an AVANCE III, 500 MHz spectrometer (Bruker, Fällanden, Switzerland). Melting points were recorded on an MP420 automelting-point system (Jinan Hai-neng Co., China). Optical density (OD) was read on iMark microplate reader (Bio-Rad, Richmond, CA). Commercial solvents and reagents were of analytical grade (Sigma-Aldrich, St Louis, Missouri).

Plant Material. The trial was carried out between 2012 and 2013, in Xi'an city, Shaanxi province, China, in a 7-year-old Hayward kiwifruit orchard. The vines were spaced 5 m × 4 m and trained to the T-bar trellis system. These experiments were designed according to the standard operating procedures on pesticide registration residue field trials, issued by the Institute for the Control of Agrochemicals, Ministry of Agriculture, China.[27] Twenty kiwifruit vines were selected, with uniform vegetative and reproductive characteristics. Fifteen days after full bloom, all initial fruits of 15 vines were dipped for 5 s in aqueous forchlorfenuron solution (50 mg/kg), while the fruit of the other five vines were dipped in water only as a control set. After 90 days, representative forchlorfenuron-treated samples and the control samples were randomly collected.

Sample Preparation. A brief description of the extraction procedure used is as follows: forchlorfenuron-treated samples were processed in a blender. A 300 g, thoroughly homogenized sample was placed in a 1000 mL glass beaker then mixed thoroughly with 300 mL of ethyl acetate, 120 g of anhydrous magnesium sulfate, and 30 g of anhydrous sodium acetate, using ultrasonic-assisted extraction for 40 min. The homogenate was allowed to settle, and the supernatant was paper-filtered into a 1000 mL rotary evaporation flask. The solid residue was washed twice with 60 mL of ethyl acetate. A rotary evaporator, set at 40 °C and 250 mbar, was used to evaporate the extract to less than 5 mL. Once reduced, extract was transferred to a graduated conical tube (15 mL) and evaporated at 50 °C. The sample was reconstituted in 2 mL of methanol and filtered through a 0.22 μm microporous membrane and stored at −20 °C until used.[28−30]

Chromatographic Conditions. Liquid chromatography experiments were conducted on a HPLC system, consisting of an LC-20AD binary pump, DGU-14A degasser, SIL-20AD autosampler, and CTO-20AC column oven (Shimadzu, Kyoto, Japan). Chromatographic separation was achieved in a Shim-pack XR ODS column (75 mm × 3.0 mm i.d, 2.2 μm Shimadzu). The mobile phase (delivered at 0.2 mL/min) consisted of solvent A (acetonitrile) and B (0.1% formic acid in water). Elutions were performed with under the following conditions: linear gradient 95−30% B from 0 to 5 min, 30−0% B from 5 to10 min, retained for 1 min, then quickly returned to initial 95% B and maintained for 20 min for column equilibration.

MS^n analyses were conducted on an LC-IT-TOF-MS (Shimadzu, Kyoto, Japan) equipped with an electrospray ionization (ESI) source, under the following optimized operating conditions: positive ion mode, detector voltage at 1.6 kV, curved desolvation line (CDL) temperature at 200 °C, heat block temperature at 200 °C, nebulizing gas flow of 1.5 L/min, drying gas (N_2) pressure of 100 kPa, and scan

DOI: 10.1021/acs.jafc.5b01100
J. Agric. Food Chem. 2015, 63, 3059−3066

ranges of m/z 100−1000 for MS^1, m/z 100−800 for MS^2, and m/z 100−800 for MS^3. Metabolite analyses were performed by MetID solution, version 1.1. Finally, the Composition Formula Predictor software (Shimadzu) was used to provide chemical formulas for forchlorfenuron and its metabolites.

Assay for Cytotoxicity. Forchlorfenuron and three metabolites were evaluated for reproductive cytotoxicity by sulforhodamine B (SRB) assay, using Chinese hamster ovary (CHO) cells.[31,32] CHO cells were provided by the College of Life Sciences, Northwest A&F University. CHO cells were cultured in high-glucose DMEM medium, containing 10% (v/v) fetal bovine serum (FBS), penicillin (100 KU/L), and streptomycin (100 μg/mL), at 37 °C, in a 5% CO_2 atmosphere with 95% (v/v) humidity. Forchlorfenuron and its kiwifruit metabolites were dissolved in DMSO then diluted in culture media to the required concentration. The DMSO content of the final concentration was below 0.1%(v/v).[33]

Exponentially growing cells (2.5×10^4) were seeded in a 96-well flat microtiter plate for 24 h, at a volume of 100 μL per well. After 24 h, cells were then incubated for an additional 48 h with various concentrations of the compounds under the same conditions. Next, cells were fixed with 10% trichloroacetic acid and incubated for 60 min at 4 °C. The supernatant was discarded, then the plates were washed 5 times with distilled water and air-dried. Using 0.4% SRB solution dissolved in 1% acetic acid, the cell layer was strained, then the plates were incubated for 20 min at room temperature. After staining, unbound dye was recovered and residual dye was removed by washing 5 times with 1% acetic acid before allowing plates to air-dry. The stained cells was solubilized in 10 mM unbuffered Tris base and optical density (OD) was measured at 560 nm.[33]

Synthesis of the Reference Standards. The general synthetic routes of the reference standards are outlined in Figure 2. The compounds **10**,[34] **11**,[35] and **13**[36,37] have been previously mentioned in research literature.

Synthesis of 1-(2-chloropyridin-4-pyridinyl)-3-(4-methoxyphenyl)-urea (**10**). To a solution of 4-amino-2-chloropyridine (2.38 g, 18.52 mmol) in toluene (103 mL) was added 4-methoxyphenyl isocyanate (2.30 g, 15.43 mmol) at room temperature. The reaction mixture was stirred at 80 °C for 8 h. To prevent reaction between 4-methoxyphenyl isocyanate and water, the synthesis of **10** was conducted under anhydrous conditions. The resulting precipitate was collected by filtration, washed with toluene, and dried in vacuo to yield the title compound as a colorless solid (3.70 g, 13.33 mmol, 86% yield in this step);[38] mp 166−168 °C. ^{1}H NMR (500 MHz, acetone-d_6) δ 8.62 (s, 1H, NH), 8.16 (s, 1H, NH), 8.13 (d, J = 5.6 Hz, 1H, −HC═N−), 7.71 (d, J = 1.7 Hz, 1H, HC═CCl), 7.41 (d, J = 9.0 Hz, 2H, Ar−H), 7.35 (dd, J = 5.6, 1.8 Hz, 1H, −HC-C═N−), 6.87 (d, J = 9.0 Hz, 2H, Ar−H), 3.76 (s, 3H, $-CH_3$). ^{13}C NMR (125 MHz, acetone-d_6) δ, 157.0, (CH_3O−C), 153.0 (−C-C═CCl), 152.6 (−C═O), 150.7 (C═N), 150.4 (−CCl), 132.7 (Ar−C), 122.2 (Ar−C), 114.9 (Ar−C), 112.7 (−C═CCl), 112.6 (−C-C═N), 55.7 ($-CH_3$).

Synthesis of 1-(2-chloropyridin-4-pyridinyl)-3-(3-methoxyphenyl) urea (**11**). The synthesis of procedure of **11** was similar to that of **10**, with the exception that 3-methoxyphenyl isocyanate was used as the starting material instead of 4-methoxyphenyl isocyanate, a colorless solid, yield 85%, mp 160−162 °C. ^{1}H NMR (500 MHz, acetone-d_6) δ 8.66 (s, 1H, NH), 8.34 (s, 1H, NH), 8.16 (d, J = 5.6 Hz, 1H, −HC═N−), 7.73 (s, 1H, HC═CCl), 7.37 (d, J = 4.3 Hz, 1H, −HC-C═N−), 7.27 (s, 1H, Ar−H), 7.19 (t, J = 8.1 Hz, 1H, Ar−H), 7.01 (d, J = 7.9 Hz, 1H, Ar−H), 6.62 (dd, J = 8.2, 1.6 Hz, 1H, Ar−H), 3.78 (s, 3H, −CH3). ^{13}C NMR (125 MHz, acetone-d_6) δ, 161.3 (CH_3O−C), 152.7 (−C-C═CCl), 152.6 (−C═O), 150.8 (−C═N), 150.2 (C−Cl), 141.2 (Ar−C), 130.5 (Ar−C), 112.8 (Ar−C), 112.7 (Ar−C), 112.2 (C═CCl), 109.3 (−C-C═N), 106.0 (Ar−C), 55.6 ($-CH_3$).

Synthesis of 4-hydroxyphenyl-forchlorfenuron (**12**). BBr_3 (6.76 g, 27.01 mmol) was dropwise added to a solution of **10** (3.00 g, 10.80 mmol) in dry CH_2Cl_2 (50 mL) at −30 °C. The reaction mixture was gradually warmed to room temperature and stirred for 24 h, when reaction was terminated by the dropwise addition of methanol, with further stirring for 20 min. The solvent was then concentrated until dry.[39−41] Two pre-experiment demethylations with HBr, BBr_3 were performed, where we found the reaction of HBr demethylation has disadvantages such as many impurities and low productivity. We therefore chose the BBr_3 demethylation reaction. The reaction mixture was evaporated to dryness. The crude product was purified by silica gel column chromatography (chloroform:methanol, 9:1), to obtain **12** (2.17g, 76%) as a colorless solid; mp 214−216 °C. ^{1}H NMR (500 MHz, MeOD) δ, 8.04 (d, J = 5.8 Hz, 1H, −HC═N−), 7.58 (d, J = 1.9 Hz, 1H, HC═CCl), 7.24 (dd, J = 5.8, 2.0 Hz, 1H, −HC-C═N−), 7.20−7.05 (m, 2H, Ar−H), 6.89−6.63 (m, 2H, Ar−H). ^{13}C NMR (125 MHz, MeOD) δ, 153.5 (−C-C═CCl), 152.9 (HO-C), 151.5 (−C═O), 149.5 (−C═N), 148.9 (−CCl), 129.4 (−Ar-C), 122.2 (−Ar-C), 115.3 (−Ar-C), 112.0 (−C═CCl), 111.5 (−C-C═N).

Synthesis of 3-hydroxyphenyl-forchlorfenuron (**13**). The synthesis procedure of **13** was similar to that of **12**, with the exception that **11** was used as the starting material instead of **10**. **13** was a colorless solid, yield 73%, mp 213−215 °C. ^{1}H NMR (500 MHz, MeOD) δ, 8.03 (d, J = 5.8 Hz, 1H, −HC═N−), 7.59 (d, J = 1.8 Hz, 1H, HC═CCl), 7.24 (dd, J = 5.8, 1.9 Hz, 1H, −HC-C═N−), 7.01 (t, J = 8.1 Hz, 1H, Ar−H), 6.96 (t, J = 2.1 Hz, 1H, Ar−H), 6.78−6.68 (m, 1H, Ar−H), 6.45−6.35 (m, 1H, Ar−H). ^{13}C NMR (125 MHz, MeOD) δ, 159.3 (HO-C), 154.0 (−C-C═CCl), 153.0 (−C═O), 151.3 (−C═N), 151.0 (C−Cl), 141.0 (Ar−C), 131.0 (Ar−C), 113.3(Ar−C), 113.1 (Ar−C), 111.8 (C═CCl), 111.7 (−C-C═N), 108.0 (Ar−C).

Synthesis of forchlorfenuron-4-*O*-β-D-acetylglucoside (**14**). A mixture of **12** (1.00 g, 3.79 mmol), tetrabutylammonium bromide (0.20 g, 0.63 mmol), and 2,3,4,6-tetra-*O*-acetyl-α-D-glucopyranosyl bromide (2.34 g, 5.7 mmol) in $CHCl_3$(80 mL) was added to 0.25 mol/L K_2CO_3 (15 mL, 2.5 mmol), the mixture was stirred for 12 h at 50 °C, the organic phase was separated, and the aqueous phase was extracted with $CHCl_3$.[42] The organic extracts were combined, washed with brine, and dried over anhydrous $MgSO_4$. The residue obtained was purified by silica gel column chromatography (chloroform/methanol, 5:1) and dried in vacuo to give the title compound as a yellow solid 0.86 g, yield 38%.

Synthesis of forchlorfenuron-3-*O*-β-D-acetylglucoside (**15**). The synthesis procedure of **15** was similar to that of **14**, with the exception that **13** was used as the starting material instead of **12**. The resulting **15** compound was a yellow solid, with a yield of 30%.

Synthesis of forchlorfenuron-4-*O*-β-D-glucoside (**16**). **14** (0.30 g, 0.5 mmol) was added to a solution of 30% $NH_3 \cdot H_2O$ (10 mL) in CH_3OH (40 mL) with stirring for 12 h at room temperature, after which the solvent was removed under reduced pressure. Using ethyl acetate/methanol (3:1) as eluent, chromatography of the residue was performed on silica gel, providing 0.15 g of colorless solid, a yield of 71%,[42] mp 207−209 °C. ^{1}H NMR (500 MHz, MeOD) δ, 8.12 (d, J = 5.8 Hz, 1H, −HC═N−), 7.70 (d, J = 1.8 Hz, 1H, HC═CCl), 7.39−7.36 (m, 2H, Ar−H), 7.35 (dd, J = 5.8, 1.9 Hz, 1H, −HC-C═N−), 7.12−7.07 (m, 2H, Ar−H), 4.88 (d, J = 7.4 Hz, 1H, O−CH-O), 3.93 (dd, J = 12.0, 1.9 Hz, 1H, $-CH_2OH$), 3.73 (dd, J = 12.0, 5.3 Hz, 1H, $-CH_2OH$), 3.52−347 (m, 2H, $-CH_2C\underline{H}OH-$, $-CH_2CHC\underline{H}OH$), 3.45 (m, 1H, $-CH_2CHCHC\underline{H}OH$), 3.44−3.39 (m, 1H, −OOHC-C<u>H</u>OH). ^{13}C NMR (125 MHz, MeOD) δ, 155.6 (−C-C═CCl), 154.3 (HO-C), 152.9 (−C═O), 151.4 (−C═N), 150.9 (−CCl), 134.3 (Ar−C), 122.5 (Ar−C), 118.5 (Ar−C), 113.3 (−C═CCl), 113.2 (−C-C═N), 102.9 (O−C−O), 78.3 ($-CH_2\underline{C}HOH-$), 78.1 ($-CH_2CH\underline{C}HOH$), 75.1 ($-CH_2CHCH\underline{C}HOH$), 71.5 (−OOHC-<u>C</u>HOH), 62.7 (CH_2).

Synthesis of forchlorfenuron-3-*O*-β-D-glucoside (**17**) was performed similar to the procedure for **16**, and synthesis of **17** proceeded, with the exception that **15** was used as the starting material instead of **14**. Although the yields for steps (c) and (d) were lower than that reported previously,[42,43] we obtain our target products, **16** and **17**. Compound **17** was a colorless solid, yield 69%; mp 210−211 °C. ^{1}H NMR (500 MHz, DMSO) δ, 9.54 (s, 1H, −NH), 9.15 (s, 1H, −NH), 8.17 (d, J = 5.6 Hz, 1H, −HC═N−), 7.64 (s, 1H, HC═CCl), 7.33 (d, J = 5.4 Hz, 1H, −HC-C═N−), 7.23 (s, 1H, Ar−H), 7.20 (t, J = 8.2 Hz, 1H, Ar−H), 7.06 (d, J = 8.0 Hz, 1H, Ar−H), 6.72 (d, J = 8.2 Hz, 1H, Ar−H), 5.34 (s, 1H, −OH), 5.09 (S, 1H, −OH), 5.02 (S, 1H, −OH), 4.82 (d, J = 7.4 Hz, 1H, O-CH-O), 4.55 (s, 1H, −OH), 3.69 (d, J = 11.4 Hz, 1H, $-CH_2OH$), 3.53−3.43 (m, 1H, $-CH_2OH$),

DOI: 10.1021/acs.jafc.5b01100
J. Agric. Food Chem. 2015, 63, 3059−3066

3.16−3.30 (m, 4H, $-CH_2CHOH-$, $-CH_2CHCHOH$, $-CH_2CHCHCHOH$, $-OOHCCHOH$). ^{13}C NMR (125 MHz, DMSO) δ, 157.9 (HO-C), 151.9 (−C-C═CCl), 150.9 (−C═O), 150.0 (−C═N), 149.2 (C−Cl), 139.9 (Ar−C), 129.5 (Ar−C), 112.3 (Ar−C), 111.9 (Ar−C), 111.3 (C═CCl), 110.2 (−C-C═N), 107.1 (Ar−C), 100.5 (O−C−O), 77.05 ($-CH_2CHOH-$), 76.61 ($-CH_2CHCHOH$), 73.22 ($-CH_2CHCHCHOH$), 69.59 (−OOHC-CHOH), 60.60 (CH_2).

RESULTS AND DISCUSSION

On the basis of the published findings,[23−26] the proposed strategy for identifying and assessing the safety of forchlorfenuron metabolites involves four procedural steps: Forchlorfenuron metabolites detected by total ion current (TIC) were recorded, searching for evident differences between peaks of the blanks and those of treated samples by MetID solution software. Obtained MS^1 and MS^n spectra of differences in peaks were used to deduce forchlorfenuron metabolites. The standard substances were synthesized, and comparison between synthetic standard substances and forchlorfenuron metabolites was performed. Safety of forchlorfenuron and its metabolites were assessed.

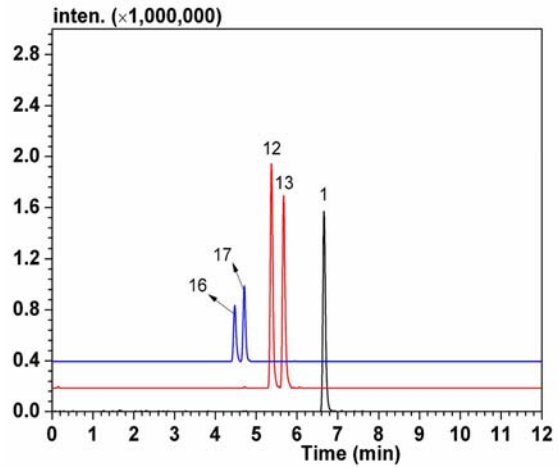

Figure 3. Extracted ion chromatograms of the synthetic standards.

Fragmentations of Forchlorfenuron. For the fragmentation pattern study, 200 μg/mL forchlorfenuron and four synthetic standard substances of its metabolites (**12**, **13**, **16**, **17**), prepared in methanol, were used. Extraction chromatograms of 20 μg/mL forchlorfenuron and four synthetic standard substances (**12**, **13**, **16**, **17**) appear in Figure 3. The proposed fragmentation patterns are illustrated in Figure 4. Figure 5 presents accurate mass measurements of the protonated molecules and fragment ions of forchlorfenuron and four synthetic metabolites. Table 1 shows data for forchlorfenuron and synthetic metabolites by LC-ESI-IT/TOF-MS analysis in positive ion mode.

Analysis of Metabolites. The treated sample and the control sample were analyzed by LC-ESI-IT-TOF/MS. In a search of possible metabolites, targeted data analysis was carried out with the aid of MetID solution software. The biotransformation reactions of forchlorfenuron follow typical patterns of hydroxylation and glycosylation. Aside from the parent compound, there are six peaks which can be found as potential metabolites derived from oxidation and glycosylation. Extraction chromatograms of the treated sample and the control sample are depicted in Figure 6, while Figure 7 shows mass spectra of **2**−**7** in positive ion mode. MS^n of metabolite data from forchlorfenuron in positive ion mode, by LC-ESI-IT-TOF/MS analysis, are presented in Table 2.

Metabolite 2 (Figure 7, Table 2), eluting at 5.193 min, shows the predominant protonated molecule ion $[M + H]^+$ at m/z

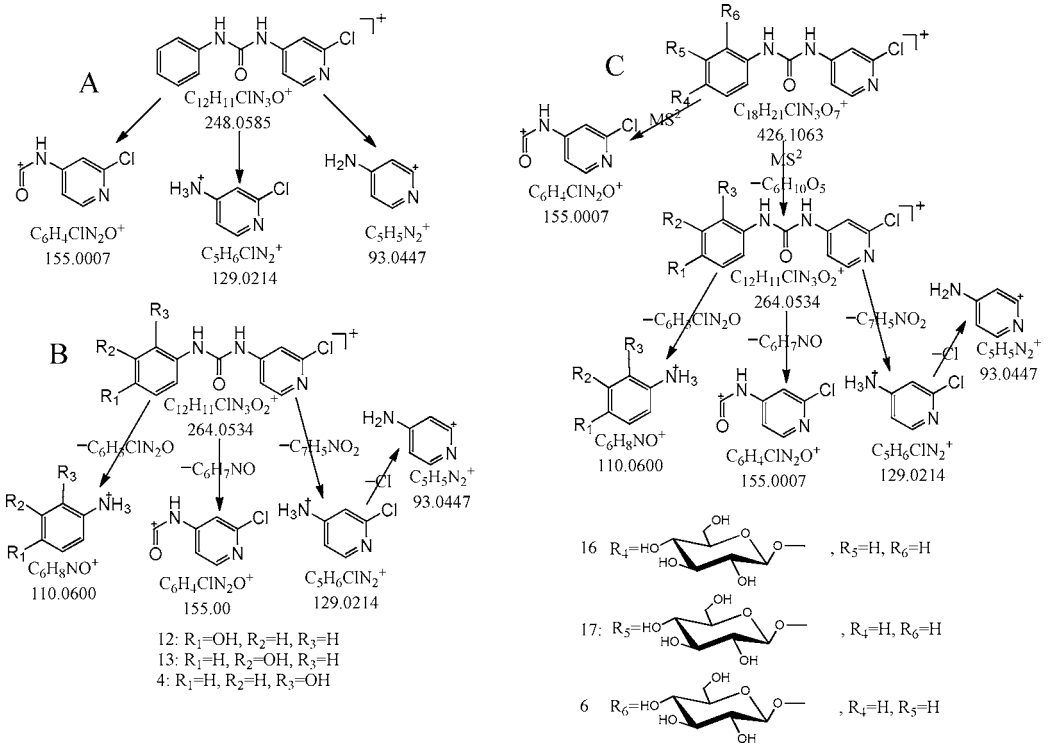

Figure 4. Fragmentation pattern of the synthetic standards and metabolite.

DOI: 10.1021/acs.jafc.5b01100
J. Agric. Food Chem. 2015, 63, 3059−3066

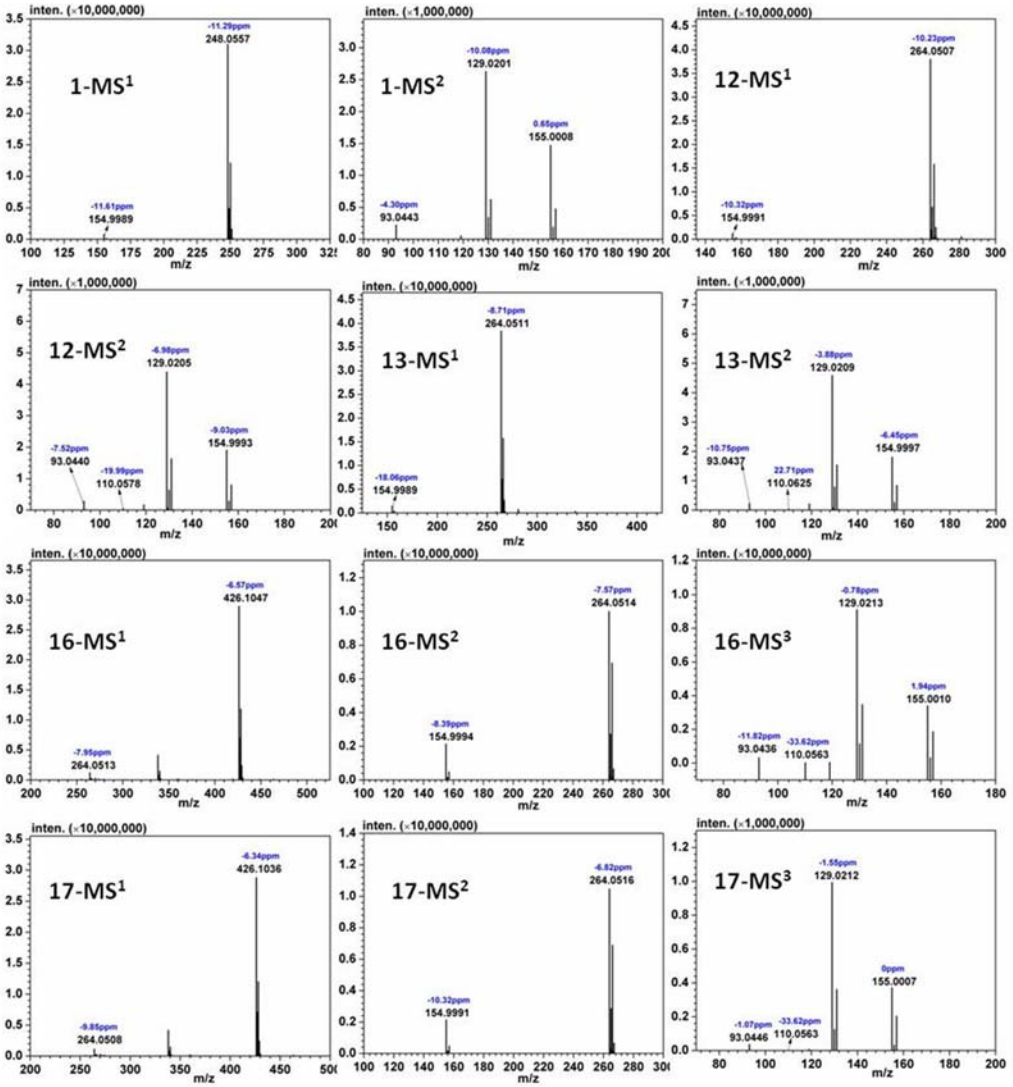

Figure 5. Mass spectra of the synthetic standards in positive ion mode.

Table 1. MS^n Data for the Synthetic Standards in Positive Ion Mode[a]

SS	RT (min)	theoretical value (m/z)	elemental compositions	MS^n	$[M + H]^+$ (m/z)	error (ppm)
12	5.37	264.0534	$C_{12}H_{10}ClN_3O_2$	**12**-MS^1	264.0507	−10.23
				12-MS^2	154.9993, 129.0205, 110.0578, 93.0440	
13	5.67	264.0534	$C_{12}H_{10}ClN_3O_2$	**13**- MS^1	264.0511	−8.71
				13- MS^2	154.9997, 129.0209, 110.0625, 93.0437	
16	4.47	426.1063	$C_{18}H_{20}ClN_3O_7$	**16**- MS^1	426.1035	−6.57
				16-MS^2	***264.05143***, 154.9994	
				16-MS^3	155.0010, 129.0213, 110.0563, 93.0436	
17	4.71	426.1063	$C_{18}H_{20}ClN_3O_7$	**17**- MS^1	426.1036	−6.34
				17-MS^2	***264.0516***, 154.9991	
				17-MS^3	155.0007, 129.0212, 110.0563, 93.0446	
1	6.66	248.0585	$C_{12}H_{10}ClN_3O$	**1**- MS^1	248.0557	−11.29
				1-MS^2	155.0008, 129.0201, 93.0443	

[a]SS = synthetic standards. RT = retention time.

264.0552, with a ^{37}Cl isotope signal at m/z 266.0581. **2** yields two main MS^2 ions at m/z 155.0009 (error, 1.29 ppm) and 129.0230 (error, 12.40 ppm). The fragment ion at m/z 129.0230 yields an MS^3 ion at m/z 93.0430 (error, −18.27 ppm). **2** calculates as $C_{12}H_{10}ClN_3O_2$ according to the accurate mass by Formula Predictor software. The protonated molecule at m/z 264.0552 is 15.9967 Da higher than the protonated molecule of forchlorfenuron (m/z 248.0585), corresponding to addition of oxygen. To deduce the site of hydroxylation on **2** (m/z 264.0552), we compared the MS^n data of **2** with the corresponding data for forchlorfenuron. The MS^2 ions of **2** at m/z 155.0007 and 129.0230 form through neutral loss of

DOI: 10.1021/acs.jafc.5b01100
J. Agric. Food Chem. 2015, 63, 3059−3066

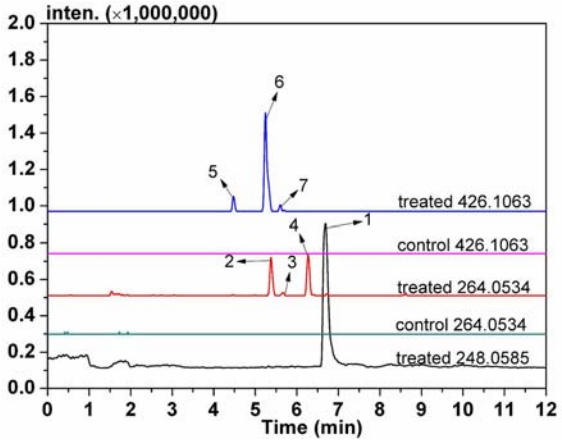

Figure 6. Extracted ion chromatograms of the treated and control samples.

C_6H_7NO and $C_7H_5NO_2$; therefore, the most likely hydroxylation position is located on the benzene ring. On the basis of the results of the above analysis, standards (**12**, **13**) of possible metabolites were synthesized. As can be seen in Figure 4 (Figure 7, Table 1), **2** shares with **12** the common MS^1 ion at m/z 264.0534, MS^2 ions at m/z 155.0007/129.0214 and the MS^3 ions at m/z 93.0447. We conclude that **2** and **12** share the same fragment pathway. The retention time for **2** and **10** corresponded. Therefore, **2** is identified as **12**.

Metabolite 3, (Figure 7, Table 2), eluting at 5.667 min, shows the predominant protonated quasimolecular ion [M +

Table 2. MS^n Data of CPPU Metabolites in Positive Ion Mode[a]

SS	RT (min)	elemental compositions	MS^n	$[M + H]^+$ (m/z)	error (ppm)
2	5.37	$C_{12}H_{10}ClN_3O_2$	**2**-MS^1	264.0552	6.82
			2-MS^2	155.0009, ***129.023***	
			2-MS^3	93.0430	
3	5.67	$C_{12}H_{10}ClN_3O_2$	**3**-MS^1	264.0528	−2.27
4	6.24	$C_{12}H_{10}ClN_3O_2$	**4**-MS^1	264.0514	−7.57
			4-MS^2	155.0002, 129.0213	
5	4.47	$C_{18}H_{20}ClN_3O_7$	**5**-MS^1	426.1065	0.47
6	5.22	$C_{18}H_{20}ClN_3O_7$	**6**-MS^1	426.1063	0
			6-MS^2	264.0535	
			6-MS^3	154.9978, 129.0227	
7	5.62	$C_{18}H_{20}ClN_3O_7$	**7**-MS^1	426.0971	−21.59
1	6.68	$C_{12}H_{10}ClN_3O$	**1**-MS^1	248.0580	−2.02
			1-MS^2	154.9998, 129.0204, 93.0414	

[a]SS = synthetic standards. RT = retention time.

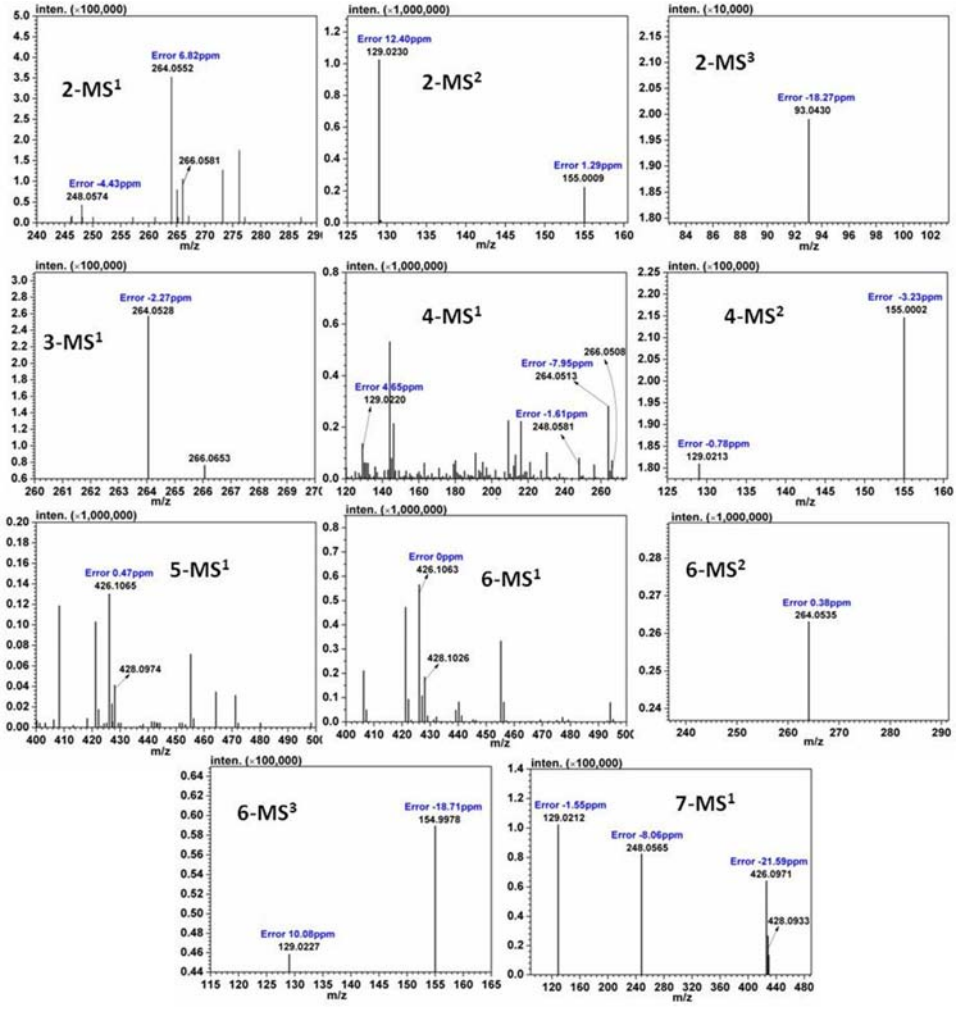

Figure 7. Mass spectra of **2**−**7** in positive ion mode.

DOI: 10.1021/acs.jafc.5b01100
J. Agric. Food Chem. 2015, 63, 3059−3066

$H]^+$ at m/z 264.0528, with a ^{37}Cl isotope signal at m/z 266.0653. According to the accurate mass by the Formula Predictor software, **3** calculates as $C_{12}H_{10}ClN_3O_2$. Thus, **3** is identified as **13**.

Metabolite 4 (Figure 7, Table 2), eluting at 6.240 min, shows the predominant protonated molecule ion $[M + H]^+$ at m/z 264.0513, with a ^{37}Cl isotope signal at m/z 266.0508. **4** yields two main MS^2 ions at m/z 155.0002 (error, −3.23 ppm) and 129.0213 (error, −0.78 ppm). Using the accurate mass by the Formula Predictor software, **4** calculates as $C_{12}H_{10}ClN_3O_2$. The protonated molecule at m/z 264.0513 is 15.9928 Da higher than the protonated molecule of forchlorfenuron (m/z 248.0585). On the basis of the analysis result for **2**, the most likely hydroxylation position for **4** is at the benzene ring. Because **2** and **3** are respectively 4-hydroxyphenyl-forchlorfenuron and 3-hydroxyphenyl-forchlorfenuron, **4** is therefore identified as 2-hydroxyphenyl-forchlorfenuron (Figure 5B).

Metabolite **5** (Figure 7, Table 2) shows the protonated molecular ion $[M + H]^+$ at m/z 426.1065, with a ^{37}Cl isotope signal at m/z 428.0974, retention time 4.468 min. In comparison with the protonated molecule of **2** (**3**, **4**), **5** represents an increase of 162.0531 Da ($C_6H_{10}O_5$). **5** calculates as $C_{18}H_{20}ClN_3O_{7,}$ according to the accurate mass by Formula Predictor software. Thus, we deduce that **5** is a glycosylated metabolite of **2**, **3**, or **4**. Comparing the data of **5** and the standard substances (**16**, **17**), the retention time difference for **5** and **16** is 0.002 min, while the retention error for **5** and **17** is 0.242 min. Therefore, **5** is identified as **16**.

Metabolite **6** (Figure 7, Table 2), shows the protonated molecular ion $[M + H]^+$ at m/z 426.1063 (a ^{37}Cl isotope signal at m/z 428.1026) with mass error of 0 ppm and representing an increase of 162.0529 Da ($C_6H_{10}O_5$), compared to the spectra of MS^2 at m/z 264.0535. The fragment ion at m/z 264.0535 (error, −0.38 ppm) leads to two MS^3 product ions at m/z 154.9978 (error, −18.71 ppm) and 129.0227 (error, 10.08 ppm). in MS^1, a fragment ion at m/z 110.0606 (error, 5.45 ppm) was generated. **6** calculates to be $C_{18}H_{20}ClN_3O_7$, and thus the glycosylated metabolite of **2**, **3**, or **4**. As can be seen in Table 1, Table 2, the retention time error is 0.507 min between **6** and **17**. From the above, we may deduce that **6** is an isomer of **16** or **17**, which are respectively forchlorfenuron-4-*O*-*β*-D-glucoside and forchlorfenuron-3-*O*-*β*-D-glucoside. Therefore, **6** is identified as forchlorfenuron-2-*O*-*β*-D-glucoside (Figure 5C).

Eluted at 5.62 min, a possible metabolite (Figure 7, Table 2) at m/z 426.0971 (error, −21.59 ppm) and a ^{37}Cl isotope signal at m/z 428.0933, exhibits the protonated molecular ion $[M + H]^+$. MS^1 for **7** reveals the protonated fragment ions at m/z 248.0565 (error, −8.06 ppm) and 129.0212 (error, −1.55 ppm). Our observations included only the MS^1 data for **7**, however, and lack MS^n for **7**. Thus, **7** is not presumed to be a metabolite of forchlorfenuron.

Cytotoxicity. Cytotoxic action is expressed as the value of 50% inhibition concentration. Results of the in vitro studies demonstrate IC_{50} values of **1** and **2** are, respectively, 12.1 ± 2.1 and 36.2 ± 1.6 μM. Cytotoxicity of **1** is higher than **2**, while **3** and **5** exhibit no activity in CHO. Hydroxylation reduced cytotoxicity of forchlorfenuron, whereas glycosylation resulted in loss of cytotoxicity. Therefore, for increasing yield and quality of kiwifruit, we ought to use modern biological techniques to breed new varieties instead of dipping in solution of plant growth regulator.

■ ASSOCIATED CONTENT

Supporting Information

^1H, ^{13}C NMR spectra of **10**−**13**, **16**, and **17**. This material is available free of charge via the Internet at http://pubs.acs.org.

■ AUTHOR INFORMATION

Corresponding Authors

*For T.Y.: phone, +86-29-87092492; fax, +86-29-87092492; E-mail, yuetl305@nwsuaf.edu.cn.

*For K.G.: E-mail, jdgkq@nwsuaf.edu.cn.

Funding

The research was supported by the China State "12th Five-Year Plan" Scientific and Technological Support Schemes (2012BAK17B06, 2012BAD31B01)

Notes

The authors declare no competing financial interest.

■ REFERENCES

(1) Kim, J. G.; Takami, Y.; Mizugami, T.; Beppu, K.; Fukuda, T.; Kataoka, I. CPPU application on size and quality of hardy kiwifruit. *Sci. Hortic.* **2006**, *110*, 219−222.

(2) Patterson, K. J.; Mason, K. A.; Gould, K. S. Effects of CPPU (*n*-(2-chloro-4-pyridyl)-*n*-phenylurea) on fruit-growth, maturity, and storage quality of kiwifruit. *N. Z. J. Crop Hortic. Sci.* **1993**, *21*, 253−261.

(3) Lewis, D. H.; Burge, G. K.; Hopping, M. E.; Jameson, P. E. Cytokinins and fruit development in the kiwifruit *(Actinidia deliciosa)*. II. Effects of reduced pollination and CPPU application. *Physiol. Plant.* **1996**, *98*, 187−195.

(4) Famiani, F.; Proietti, P.; Pilli, M.; Battistelli, A.; Moscatello, S. Effects of application of thidiazuron (TDZ), gibberellic acid (GA(3)), and 2,4-dichlorophenoxyacetic acid (2,4-D) on fruit size and quality of *Actinidia deliciosa* 'Hayward'. *N. Z. J. Crop Hortic. Sci.* **2007**, *35*, 341−347.

(5) Cruz-Castillo, J. G.; Woolley, D. J.; Lawes, G. S. Kiwifruit size and CPPU response are influenced by the time of anthesis. *Sci. Hortic.* **2002**, *95*, 23−30.

(6) Chen, W. J.; Jiao, B. N.; Su, X. S.; Zhao, Q. Y.; Qin, D. M.; Wang, C. Q. Dissipation and residue of forchlorfenuron in citrus fruits. *Bull. Environ. Contam. Toxicol.* **2013**, *90*, 756−760.

(7) Suárez-Pantaleón, C.; Mercader, J. V.; Agulló, C.; Abad-Somovilla, A.; Abad-Fuentes, A. Forchlorfenuron-mimicking haptens: from immunogen design to antibody characterization by hierarchical clustering analysis. *Org. Biomol. Chem.* **2011**, *9*, 4863−4872.

(8) Suárez-Pantaleón, C.; Mercader, J. V.; Agullo, C.; Abad-Somovilla, A.; Abad-Fuentes, A. Hapten synthesis and polyclonal antibody-based immunoassay development for the analysis of forchlorfenuron in kiwifruit. *J. Agric. Food Chem.* **2010**, *58*, 8502−8511.

(9) Kobayashi, M.; Takano, I.; Tamura, Y.; Tomizawa, S.; Tateishi, Y.; Sakai, N.; Kamijo, K.; Ibe, A.; Nagayama, T. Clean-up method of forchlorfenuron in agricultural products for HPLC analysis. *J. Food Hyg. Soc. Jpn.* **2007**, *48*, 148−152.

(10) Sharma, D.; Awasthi, M. D. Behaviour of forchlorfenuron residues in grape, soil and water. *Chemosphere.* **2003**, *50*, 589−594.

(11) Valverde, A.; Aguilera, A.; Ferrar, C.; Camacho, F.; Cammarano, A. Analysis of forchlorfenuron in vegetables by LC/TOF-MS after extraction with the buffered QuEChERS method. *J. Agric. Food Chem.* **2010**, *58*, 2818−2823.

(12) Valverde, A.; Piedra, L.; Aguilera, A.; Boulaid, M.; Camacho, F. Analysis and residue levels of forchlorfenuron (CPPU) in watermelons. *J. Environ. Sci. Health, Part B* **2007**, *42*, 801−807.

(13) Trevor H. *Public release summary on evaluation of the new active forchlorfenuron in the product sitofex 10EC plant growth regulator*; Australian Pesticides and Veterinary Medicines Authority: Symonston, Australia, 2005.

DOI: 10.1021/acs.jafc.5b01100
J. Agric. Food Chem. 2015, 63, 3059−3066

(14) Field, J. A.; Reed, R. L.; Sawyer, T. E.; Martinez, M. Diuron and its metabolites in surface water and ground water by solid phase extraction and in-vial elution. *J. Agric. Food Chem.* **1997**, *45*, 3897−3902.
(15) Tixier, C.; Sancelme, M.; Ait-Aissa, S.; Widehem, P.; Bonnemoy, F.; Cuer, A.; Truffaut, N.; Veschambre, H. Biotransformation of phenylurea herbicides by a soil bacterial strain, Arthrobacter sp N2: structure, ecotoxicity and fate of diuron metabolite with soil fungi. *Chemosphere* **2002**, *46*, 519−526.
(16) Khadrani, A.; Seigle-Murandi, F.; Steiman, R.; Vroumsia, T. Degradation of three phenylurea herbicides (chlortoluron, isoproturon and diuron) by micromycetes isolated from soil. *Chemosphere* **1999**, *38*, 3041−3050.
(17) Amine-Khodja, A.; Boulkamh, A.; Boule, P. Photochemical behaviour of phenylurea herbicides. *Photochem. Photobiol. Sci.* **2004**, *3*, 145−156.
(18) Cui, G.; Niu, Y. R.; Wang, H.; Dong, J.; Yuki, H.; Chen, S. Z. Rapid isolation and identification of active antioxidant ingredients from Gongju using HPLC-DAD-ESI-MS^n and postcolumn derivatization. *J. Agric. Food Chem.* **2012**, *60*, 5407−5413.
(19) Xu, J.; Duan, J. J.; Xue, C. H.; Feng, T. Y.; Dong, P.; Sugawara, T.; Hirata, T. Analysis and comparison of glucocerebroside species from three edible sea cucumbers using liquid chromatography-ion trap-time-of-flight mass spectrometry. *J. Agric. Food Chem.* **2011**, *59*, 12246−12253.
(20) Barnes, J. S.; Schug, K. A. Oxidative Degradation of quercetin with hydrogen peroxide using continuous-flow kinetic electrospray-ion trap-time-of-flight mass spectrometry. *J. Agric. Food Chem.* **2014**, *62*, 4322−4331.
(21) Grace, M. H.; Warlick, C. W.; Neff, S. A.; Lila, M. A. Efficient preparative isolation and identification of walnut bioactive components using high-speed counter-current chromatography and LC-ESI-IT-TOF-MS. *Food Chem.* **2014**, *158*, 229−238.
(22) Liu, Z. Y. An introduction to hybrid ion trap/time-of-flight mass spectrometry coupled with liquid chromatography applied to drug metabolism studies. *J. Mass Spectrom.* **2012**, *47*, 1627−1642.
(23) Liang, Y.; Hao, H. P.; Xie, L.; Kang, A.; Xie, T.; Zheng, X. A.; Dai, C.; Hao, K.; Sheng, L. S.; Wang, G. J. Development of a systematic approach to identify metabolites for herbal homologs based on liquid chromatography hybrid ion trap time-of-flight mass spectrometry: gender-related difference in metabolism of schisandra lignans in rats. *Drug Metab. Dispos.* **2010**, *38*, 1747−1759.
(24) Liang, Y.; Xiao, W.; Dai, C.; Xie, L.; Ding, G.; Wang, G. J.; Meng, Z. Q.; Zhang, J.; Kang, A.; Xie, T.; Liu, Y. N.; Zhou, Y. Y.; Liu, W. J.; Zhao, L.; Xu, J. Structural identification of the metabolites for strictosamide in rats bile by an ion trap-tof mass spectrometer and mass defect filter technique. *J. Chromatogr., B: Anal. Technol. Biomed. Life Sci.* **2011**, *879*, 1819−1822.
(25) Li, H.; Wan, L. R.; Hashi, Y.; Chen, S. Z. Fragmentation study of a 8-*C*-glycosyl isoflavone, puerarin, using electrospray ion trap time-of-flight mass spectrometry at high resolution. *Rapid Commun. Mass Spectrom.* **2007**, *21*, 2497−2504.
(26) Song, M. T.; Wang, T. J.; Li, Q.; Zhao, L. S.; Fang, H. J.; Li, D. X.; Bi, K. S. Identification and dynamic analysis of the purine alkaloids in rat plasma after oral administration of green tea by liquid chromatography hybrid ion trap time-of-flight mass spectrometry. *J. Chromatogr., B: Anal. Technol. Biomed. Life Sci.* **2012**, *903*, 23−29.
(27) Wang, Y. H. *Standard Operating Procedures on Pesticide Registration Residue Field Trials*; Standards Press of China: Beijing, 2007.
(28) Shi, X. M.; Jin, F.; Huang, Y. T.; Du, X. W.; Li, C. M.; Wang, M.; Shao, H.; Jin, M. J.; Wang, J. Simultaneous determination of five plant growth regulators in fruits by modified quick, easy, cheap, effective, rugged, and safe (QuEChERS) extraction and liquid chromatography−tandem mass spectrometry. *J. Agric. Food Chem.* **2012**, *60*, 60−65.
(29) Xu, Y.; Shou, L. F.; Wu, Y. L. Simultaneous determination of flonicamid and its metabolites in vegetables using QuEChERS and reverse-phase liquid chromatography−tandem mass spectrometry. *J. Chromatogr., A* **2011**, *1218*, 6663−6666.
(30) Wong, J.; Hao, C. Y.; Zhang, K.; Yang, P.; Banerjee, K.; Hayward, D.; Iftakhar, I.; Schreiber, A.; Tech, K.; Sack, C.; Smoker, M.; Chen, X. R.; Utture, S. C.; Oulkar, D. P. Development and interlaboratory validation of a QuEChERS-based liquid chromatography−tandem mass spectrometry method for multiresidue pesticide analysis. *J. Agric. Food Chem.* **2010**, *58*, 5897−5903.
(31) Federico, C.; Motta, S.; Palmieri, C.; Pappalardo, M.; Librando, V.; Saccone, S. Phenylurea herbicides induce cytogenetic effects in Chinese hamster cell lines. *Mutat. Res., Genet. Toxicol. Environ. Mutagen.* **2011**, *721*, 89−94.
(32) Nikoloff, N.; Soloneski, S.; Larramendy, M. L. Genotoxic and cytotoxic evaluation of the herbicide flurochloridone on Chinese hamster ovary (CHO-K1) cells. *Toxicol. in Vitro* **2012**, *26*, 157−163.
(33) Dong, S.; Tang, J. J.; Zhang, C. C.; Tian, J. M.; Guo, J. T.; Zhang, Q.; Li, H.; Gao, J. M. Semisynthesis and in vitro cytotoxic evaluation of new analogues of 1-*O*-acetylbritannilactone, a sesquiterpene from *Inula britannica*. *Eur. J. Med. Chem.* **2014**, *80*, 71−82.
(34) Henrie, R. N.; Green, C. M.; Yeager, W. H.; Ball, T. F., III. Activity optimization of pyridinyl *N*-oxide urea cytokinin mimics. *J. Agric. Food Chem.* **1988**, *36*, 626−633.
(35) Isogai, Y. Cytokinin activities of *N*-phenyl-*N*′-(4-pyridyl) ureas. In *Metabolism and Molecular Activities of Cytokinins*; Guern, J., Peaud-Lenoel, C., Eds.; Springer: Berlin, Heidelberg, 1981; pp 115−128.
(36) Isogai, Y.; Kawachi, E.; Takahashi, S.; Shudo, K.; Okamoto, T. Shoot formation effect of ureas, pyrimidines and related compounds on tobacco pith disk cultured in vitro. *Tokyo Daigaku, Kyoyo-Gakubu* **1980**, *30* (2), 151−166.
(37) Shudo K., Okamoto T., Isogai Y., et al. *N*-(2-Chloro-4-pyridyl) ureas. U.S. Patent 4,193,788. 1980.
(38) Takami, A.; Iwakubo, M.; Okada, Y.; Kawata, T.; Odai, H.; Takahashi, N.; Shindo, K.; Kimura, K.; Tagami, Y.; Miyake, M.; Fukushima, K.; Inagaki, M.; Amano, M.; Kaibuchi, K.; Iijima, H. Design and synthesis of Rho kinase inhibitors (I). *Bioorg. Med. Chem.* **2004**, *12*, 2115−2137.
(39) Parraga, J.; Cabedo, N.; Andujar, S.; Piqueras, L.; Moreno, L.; Galan, A.; Angelina, E.; Enriz, R. D.; Ivorra, M. D.; Sanz, M. J.; Cortes, D. 2,3,9-and 2,3,11-Trisubstituted tetrahydroprotoberberines as D-2 dopaminergic ligands. *Eur. J. Med. Chem.* **2013**, *68*, 150−166.
(40) Mikula, H.; Skrinjar, P.; Sohr, B.; Ellmer, D.; Hametner, C.; Frohlich, J. Total synthesis of masked Alternaria mycotoxins-sulfates and glucosides of alternariol (AOH) and alternariol-9-methyl ether (AME). *Tetrahedron* **2013**, *69*, 10322−10330.
(41) Parhi, A. K.; Xiang, A.; Bauman, J. D.; Patel, D.; Vijayan, R. S. K.; Das, K.; Arnold, E.; LaVoie, E. J. Phenyl substituted 3-hydroxypyridin-2(1*H*)-ones: inhibitors of influenza A endonuclease. *Bioorg. Med. Chem.* **2013**, *21*, 6435−6446.
(42) Liu, J.; Chen, L.; Cai, S.; Wang, Q. Semisynthesis of apigenin and acacetin-7-*O*-*β*-D-glycosides from naringin and their cytotoxic activities. *Carbohydr. Res.* **2012**, *357*, 41−46.
(43) Ho, K.-L.; Murphy, M. B.; Wan, Y.; Fong, B. M.-W.; Tam, S.; Giesy, J. P.; Leung, K. S.-Y.; Lam, M. H.-W. Synthesis and characterization of bromophenol glucuronide and sulfate conjugates for their direct LC-MS/MS quantification in human urine as potential exposure markers for polybrominated diphenyl ethers. *Anal. Chem.* **2012**, *84*, 9881−9888.

DOI: 10.1021/acs.jafc.5b01100
J. Agric. Food Chem. 2015, 63, 3059−3066

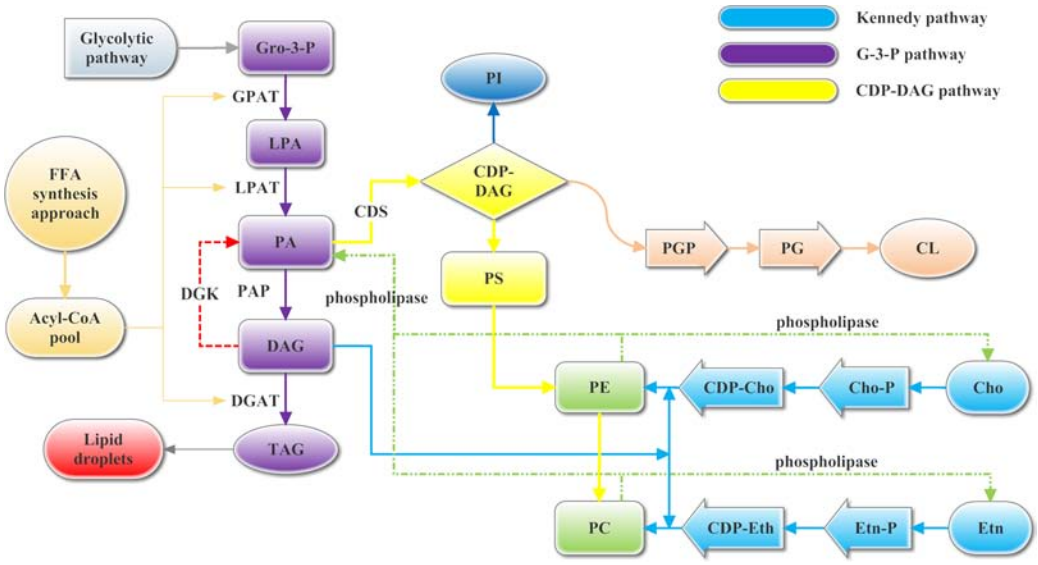

Figure 1. Lipid metabolism includes the TAG and phospholipid assembly process in the microorganism. Pink represents de novo synthesis of free fatty acids, which provides acyl-CoA for three times acylation reaction in TAG synthesis; purple represents the G3P pathway; the red imaginary line represents the reverse reaction of DAG formation; yellow represents the CDP-DAG pathway; blue represents the Kennedy pathway; the green imaginary line represents the degradation of PE and PC catalyzed by phospholipase. See text for additional details.

However, before we begin rational genetic manipulation of genes in TAG formation pathway or competing pathways, we need to have a better comprehensive understanding of how TAG biosynthesis is regulated in different oleaginous microorganisms. This review primarily focuses on PAP, DGAT, and a reverse reaction enzyme (diacylglycerol kinase) involved in the G3P pathway for TAG accumulation and other related pathways that also have an influence on TAG formation.

OLEAGINOUS MICROORGANISMS

Numerous studies have looked at the process of lipid anabolism and catabolism in yeast or microalgae.[6−9] It was speculated that, among the oleaginous microbial species, microalgae and yeast maybe the most promising ones for biodiesel production. Microalgae are considered to be among the best oleaginous organisms to displace fossil diesel.[10] However, the identification and cultivation of ideal algal strains that are excellent in high levels of both biomass productivity and TAG content is still an ongoing and laborious process.[1] Common oleaginous microalgae include green algae (*Chlorophyceae*) and diatoms (*Bacillariophyceae*), such as *Chlorella*, *Dunaliella*, and *Cylindrotheca*.[10−12] Researchers also show great interest in oleaginous yeast, their genes, regulatory factors, and enzyme and functional motifs in lipid synthesis or degradation. Budding yeast *Saccharomyces cerevisiae*, fission yeast *Schizosaccharomyces pombe*, and an unconventional yeast *Yarrowia lipolytica* are the species that have been widely studied among yeast. Actinomycete is one of the few oleaginous groups in bacteria that are suitable for volume production of biofuel. Common oleaginous actinomycetes include *Mycobacterium*, *Nocardia*, *Rhodococcus*, and *Streptomyces*.[13]

TAG BIOSYNTHESIS

Triglyceride (TAG, triacylglycerol, or triacylglyceride) consists of glycerol and fatty acids. In TAG formation, the upstream part that mainly focuses on generating acyl-CoA is the fatty acid synthesis approach, and the downstream is the G3P pathway.

In fact, the processes of TAG synthesis in higher plants and microalgae are very similar. Glyceraldehyde-3-phosphate (GAP) is catalyzed by glyceraldehyde-3-phosphate dehydrogenase (GAPDH, EC 1.2.1.12) to form 1,3-diphosphoglycerate; GAPDH is a highly conserved enzyme across the phylogenetic scale but also plays a multifunctional role in critical cell activities, and it uses NADH or NADPH or both as its cofactors.[14] Finally, through the remaining steps in the glycolytic pathway, pyruvate is formed. Afterward, with the help of the citrate−pyruvate cycle, citrate (an intermediate product of TCA cycle) eventually splits into oxaloacetic acid (OOA) and acetyl-CoA. The next step is the formation of malonyl-CoA, catalyzed by acetyl-CoA carboxylic enzyme (ACC, EC 6.4.1.2), whose substrate is acetyl-CoA. Then, malonyl-CoA:ACP transacylase (MAT) catalyzes the newly produced malonyl-CoA to form malonyl-acyl-carrier protein (malonyl-ACP); the malonyl part will participate in the elongation of long chain fatty acids with the help of β-ketoacyl-ACP synthase (KAS, EC 2.3.1.41), and, after several times of C2 (malonyl) addition, long chain fatty acids are formed. This is the simplified description about the process of fatty acid synthesis.

The TAG synthesis approach mainly takes place in endoplasmic reticulum (ER). As can be seen in Figure 1, in this approach, acyl-CoAs are sequentially added onto the sn-1, sn-2, and sn-3 positions of a G3P molecule. G3P is derived from dihydroxyacetone phosphate (DHAP), and this dehydrogenation reaction is catalyzed by glycerol-3-phosphate dehydrogenase (G3PDH, EC 1.1.1.8), a key enzyme in the pathway of glycerol synthesis,[15,16] which is encoded by *GPD1* and necessary for the process of growth under osmotic stress in *Saccharomyces cerevisiae*.[17] In *Dunaliella*, long-term osmotic response (starts under the osmotic stress within 12−24 h) is involved in related gene expression and protein generation,[18,19] indicating that *GPD1* expression and G3DPH accumulation may be influence by long-term response.

The enzyme catalyzing the first acylation step is acyl-CoA:glycerol-*sn*-3-phosphate acyltransferase (GPAT, EC

DOI: 10.1021/jf505975k
J. Agric. Food Chem. 2015, 63, 3067−3077

Table 1. Four Enzymes Exhibiting Phosphatidic Acid Phosphatase Activity in Yeast

gene	enzyme	enzyme cofactor	substrate	catalytic motif	involved in de novo TAG synthesis or not	location
PAH1	Pah1p	Mg^{2+}	specific for PA	DXDX (T/V)	yes	cytoplasm and ER
APP1	App1p	Mg^{2+}, while Mn^{2+} can serve as substitute	PA, LPA, DGPP	DXDXT	no	cytoplasm
DPP1	Dpp1p	Mg^{2+} not required	PA, LPA, DGPP, SBP, IP	KX_6RP, PSGH, and SRX_5HX_3D	no	vacuole
LPP1	Lpp1p	Mg^{2+} not required	PA, LPA, DGPP, SBP, IP	KX_6RP, PSGH, and SRX_5HX_3D	no	Golgi

Table 2. Genes That Are Referred to in This Article[a]

gene	microorganism	strain	enzyme	reference
PAH1 (*SMP2*)	yeast	*S. cerevisiae*	Pah1p (PAP)	26−28
DGK1	yeast	*S. cerevisiae*	Dgk1p	47,49,96
APP1	yeast	*S. cerevisiae*	App1p (PAP)	29,40,97,98
DPP1	yeast	*S. cerevisiae*	Dpp1p (PAP)	41,42,44,99
LPP1	yeast	*S. cerevisiae*	Lpp1p (PAP)	43,44,100
LPPα and *LPPβ*	bacteria	*S. coelicolor*	Lpp*α* and Lpp*β* (PAP)	13
CDS1	yeast	*S. cerevisiae*	CDS	23,93
MrDGAT2A and *MrDGAT2B*	fungus	*M. ramanniana*	MrDGAT2	57
DGA1	yeast	*S. cerevisiae*	*Sc*DGAT2	66
ARE1 and *ARE2*	yeast	*S. cerevisiae*	sterol acyltransferases	69
LRO1	yeast	*S. cerevisiae*	PDAT	74
ATFA	bacteria	*A. calcoaceticus*	WS/DGAT	84

[a]PDAT: phosphatidylcholine:diacylglycerol acyltransferase. WS/DGAT: wax ester synthase/acyl-CoA:diacylglycerol acyltransferase. *S. cerevisiae*: *Saccharomyces cerevisiae*. *S. coelicolor*: *Streptomyces coelicolor*. *M. ramanniana*: *Mortierella ramanniana*. *A. calcoaceticus*: *Acinetobacter calcoaceticu*.

2.3.1.15); it consumes an acyl-CoA and a G3P molecule to form lysophosphatidate (LPA). Once LPA has formed, lysophosphatidate acyltransferase (LPAT, EC 2.3.1.51) expends another acyl-CoA to form phosphatidate (PA). Then, phosphatidic acid phosphatase (PAP) releases the phosphate from PA to produce diacylglycerol (DAG), the immediate precursor of TAG. Finally, diacylglycerol acyltransferase (DGAT), an important determinant in the accumulation of TAGs, employs a third acyl-CoA as acyl donor, and utilizes DAG to form TAG. It is generally accepted that DAGs, zymolyte of the last step of the G3P pathway, are produced by endoplasmic reticulum (ER)-specific acyltransferases, but a recent study has suggested that the *Chlamydomonas reinhardtii*, a unicellular microalga, employs diacylglycerol (DAG) only from the chloroplast for the accumulation of TAGs.[20]

G3P PATHWAY

Reports about genetic engineering aimed at GPAT, LPAT, PAP, DGAT, or multiple gene transformation are quite few, but in terms of contemporary research, most of them are involved in plants (oil seeds). However, as stated above, oleaginous microorganisms have shown their huge advantages (compared to oil seeds) such as less necessity for a good environment (wasted water), short life cycle, high percentage of oil, and convenience for scaling up. Obviously, oleaginous microorganisms have a promising future for biodiesel production. Hence, it makes sense to introduce recent research about enzymes in the G3P pathway in an oleaginous microbial cell.

G3P produced by the glycolytic pathway is the origin and source of the G3P pathway. LPA is mainly derived from its precursor G3P via acylation reaction with the help of GPAT. However, in yeast, the DHAP pathway can generate LPA as well. Then LPA is engaged to the synthesis of PA, a crucial crossroad in lipid metabolism; this step is catalyzed by LPAT and needs acyl-CoA provided by the FA synthesis pathway to cooperate with this acyltransferase. Among the three acyltransferase in the TAG synthesis approach, LPAT was the first one to be cloned from plants (in *Limnanthes douglasii* and *Cocos nucifera*, both 1995).[21,22]

The PA substrate pool is utilized by two competing pathways (Figure 1) in addition to the G3P pathway, and the metabolic flux of PA into these three pathways has a huge influence on TAG biosynthesis. One is the CDP-DAG pathway, an important phospholipid biosynthesis approach based on glycerophosphate and involved in regulating the nuclear membrane biogenesis;[23] the other is the Kennedy pathway for the de novo biosynthesis of phosphatidylethanolamine (PE) and phosphatidylcholine (PC).[24]

Compared to PAP and DGAT, GPAT and LPAT are not good candidates for metabolic engineering. Comparatively less work has been done on the role of GPATs and LPATs in lipid biosynthesis. This review focuses on PAP and DGAT, two key rate-limiting enzymes in the G3P pathway, to introduce the progresses of their genetic and metabolic engineering for TAG accumulation in oleaginous microorganisms.

PAP in Microorganisms. Phosphatidate (PA) is an intermediate product of the G3P pathway; it is employed by phosphatidic acid phosphatase (PAP) to form DAG and P_i. In essence, the process is a step of dephosphorylation. The function studies of PAP in the accumulation of TAGs are mainly involved in yeast and bacteria. It has been proved that PAP plays a major role in lipid metabolism regulation.[13,25]

Yeast Pah1p. *PAH1* (alias: *SMP2*[26,27]) gene (Table 2), first named by Gil-Soo Han et al.,[28] encoded Pah1p in yeast *Saccharomyces cerevisiae*. *PAH1*-encoded Mg^{2+}-dependent phosphatidate phosphatase (PAP1, Pah1p, specific for PA), containing the DXDX (T/V) catalytic motif in the haloacid dehalogenase (HAD)-like structural domain, is an enzyme

DOI: 10.1021/jf505975k
J. Agric. Food Chem. 2015, 63, 3067−3077

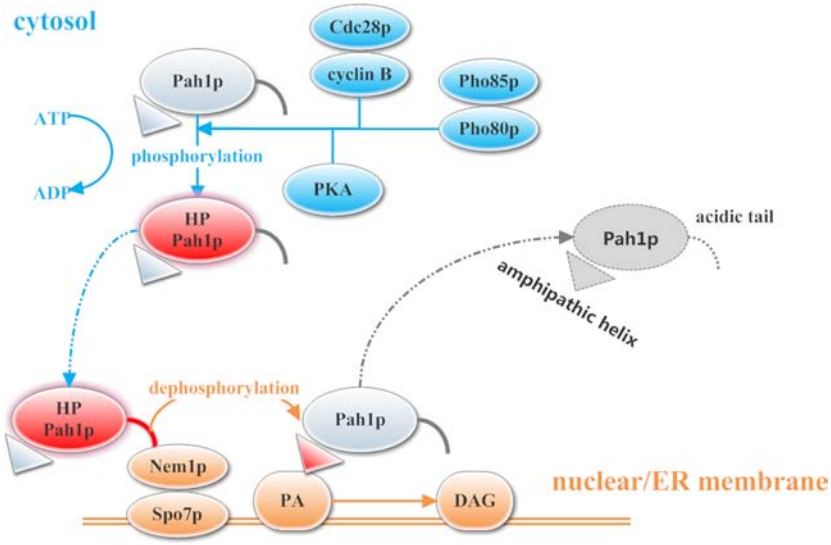

Figure 2. Action mechanism of DAG formation catalyzed by Pah1p.[30] Red represents one of the key components of the Pah1p (amphipathic helix or acidic tail) that is functioning in a specific time. Pho85p-Pho80p,[28] Cdc28p-cyclin B,[29] and protein kinase A (PKA)[27] are involved in the phosphorylation process of Pah1p in cytosol. Then highly phosphorylated Pah1p experiences a series of dephosphorylation by Nem1p-Spo7p in the surface nuclear/ER membrane surface, and a C-terminal acidic tail contributes to the combination of Pah1p and Nem1p-Spo7p.[31,34] Subsequently, Pah1p tethered onto the nuclear/endoplasmic reticulum (ER) membrane and touched PA with the help of a functional amino-terminal amphipathic helix.[35] HP Pah1p: highly phosphorylated Pah1p. For more details, see text.

located in cytoplasm and ER, and its enzyme cofactor is Mg^{2+} ions.[28,29] Within the catalytic motif of DXDX (T/V), there are some conserved Asp residues (398−402) that are found to be essential for the catalytic function of Pah1p. Mutational analysis revealed that the activity of the D398E and D400E mutant enzyme is less than 0.1% compared to wild-type enzyme.[25]

Pah1p serves as a substrate of several protein kinases in phosphorylation reaction; it is an ATP-consuming process.[30,31] Three protein kinases are involved in the process: Pho85p-Pho80p,[32] Cdc28p-cyclin B,[33] and protein kinase A (PKA),[31] and have respectively seven (Ser-110, Ser-114, Ser-168, Ser-602, Thr-723, Ser-744, Ser-748), three (Ser-602, Thr-723, Ser-744), and five (Ser-10, Ser-677, Ser-773, Ser-774, Ser-788) target phosphorylation sites. As shown in Figure 2, highly phosphorylated Pah1p then undergoes multisite dephosphorylation in the nuclear/ER membrane. Nem1p-Spo7p transmembrane phosphatase complex, encoded by *NEM1* and *SPO7* and localized to the nuclear/ER membrane,[32,34] is essential for the dephosphorylation of Smp2p, namely, Pah1p,[27,35] and thus regulates ER membrane flow and nuclear growth.[27,34] A C-terminal acidic tail of the yeast Pah1p has been confirmed to mediate the interaction between Nem1p-Spo7p protein phosphatase complex and Pah1p, and thus affect the membrane recruitment and the expression of *INO1* gene that encodes inositol-1-phosphate synthase (EC 5.5.1.4), which catalyzes glucose-6-phosphate to inositol-1-phosphate and was first purified by Donahue and Henry from *S. cerevisiae*.[36−38] Subsequently, Pah1p tethers onto the nuclear/endoplasmic reticulum (ER) membrane by a functional amino-terminal amphipathic helix, which has been shown to be responsible for the recruitment of dephosphorylated Pah1p and plays an indispensable role in both TAG assembly and phospholipid biosynthesis.[39]

It is suggested that Pah1p is the veritable enzyme that is involved in the process of de novo lipid synthesis in *S. cerevisiae*. App1p, Dpp1p, and Lpp1p (for more details, see Other PAP Enzymes in Yeast and Bacteria) actually have no impact on de novo TAG assembly in ER (Table 1).[28] Inositol is one of the important factors in mediating phospholipid synthesis. It could combine with the phosphatidyl moiety of CDP-DAG to form phosphatidylinositol (PI), as well as affect transcription regulation of the genes in phospholipid biosynthesis.[35] *PAH1* expression is induced throughout its growth cycle, and can be stimulated by inositol supplementation in the stationary phase.

Other PAP Enzymes in Yeast and Bacteria. Three other enzymes (App1p, Dpp1p, Lpp1p, see Table 2) exhibit PAP activity in yeast as well, but the characteristics and function of each are not all the same (Table 1).[29,40] App1p is a cytosolic enzyme that has been well studied by Chae et al.;[29,40] it is a Mg^{2+}-dependent phosphatidate phosphatase. Lysophosphatidate (LPA) and DAG pyrophosphate (DGPP) can also be dephosphorylated by App1p apart from PA. Unlike the sole status of Mg^{2+} in Pah1p, Mn^{2+} can partly substitute the role of Mg^{2+} in App1p. Its PAP activity can be influenced by the DXDXT motif to a large extent, but this conserved domain has low-level similarity to the haloacid dehalogenase (HAD)-like domain.[29,40] A ten times increase in PAP activity has been found in the *pah1*Δ*dpp1*Δ*lpp1*Δ triple mutant by overexpression *APP1* gene.[29] Of the 20 mutants deleting genes that encode potential enzymes involved in the phospholipid formation process, only *app1*Δ manifests a 30% reduction of PAP activity compared to the wild strain of yeast *S. cerevisiae*.[29] A 34-fold disparity of turnover number (k_{cat} = 406 $s^{-1}$for App1p and k_{cat} = 12 s^{-1} for Pah1p) in PAP activity between App1p and Pah1p may explain why App1p exhibits high PAP activity despite its being a low abundant protein in yeast.[28,40]

DPP1 and *LPP1* are the genes that encode diacylglycerol pyrophosphate phosphatase and lipid phosphate phosphatase, respectively. In *S. cerevisiae*, studies about *DPP1* were earlier than *LPP1*, and *DPP1* was first characterized by Wu et al.,[41] whereas *LPP1* was first named, isolated, and characterized by Toke et al.[42,43]

Dpp1p and Lpp1p were identified by Faulkner et al.,[44] and they have some common attributes. For instance, they are

DOI: 10.1021/jf505975k
J. Agric. Food Chem. 2015, 63, 3067−3077

Mg^{2+}-independent enzymes containing six transmembrane regions, their PAP activities are subject to a three-domain catalytic motif (KX_6RP, PSGH, and SRX_5HX_3D), and their substrates are the same.[25,42,43] They also catalyze the dephosphorylation of sphingoid base phosphate and isoprenoid phosphate.[28,29,40] However, positions of the two enzymes are different: Dpp1p is located in the vacuole, and Lpp1p is in Golgi. Studies have shown that, in yeast, *dpp1*Δ *lpp1*Δ mutations exhibit no obvious influence on TAG formation in ER, and App1p also is not involved in de novo lipid synthesis. However, Pah1p indeed participates or even plays a key role in the synthesis of TAG in ER.[28,40,45]

In eukaryotes, genes encoding for the Mg^{2+}-dependent phosphatidate phosphatase are highly conserved, whereas in bacteria, there are no homologues for PAP-encoded genes.[13] In *Streptomyces coelicolor*, *LPPα* and *LPPβ* (Table 2) are decisive PAP enzymes for TAG biosynthesis; they belong to the PAP2 (Mg^{2+}-independent enzymes) family.[13] Overexpression of *LPPα* and *LPPβ* resulted in a rise of cellular TAG (15.7% and 29.9%, respectively). Heterogeneous expression of PAPs derived from *S. coelicolor* in *Escherichia coli* or yeast also aroused a severalfold increase of cellular DAG level.[13]

Summary of PAPs from Horizontal Perspective. The dephosphorylation reaction catalyzed by PAP exists widely in plants and microorganisms. We have listed different enzymes above that exhibit PAP activity; now it will be safe to conclude that in terms of TAG formation, although App1p (or Lpp1p and Dpp1p) and Pah1p have similarity in cofactor, substrate, and catalytic motif, Pah1p is the only one that is involved in de novo synthesis of TAG. But in some bacteria such as *S. coelicolor*, lipid phosphate phosphatase indeed controls the dephosphorylation reaction for DAG formation. The mechanism of DAG formation (Figure 2) may become a new field of improving the efficiency of Pah1p; perhaps further effort should be spent on enhancing the function of highly phosphorylated Pah1p, the functional amino-terminal amphipathic helix, and the C-terminal acidic tail or other keypoints in this complicated process.

Dgk1p: The Counter Reaction Enzyme of DAG Formation. PA is a key regulator of lipid synthesis because it is the intersection of the G3P pathway (for TAG formation), the CDP-DAG pathway (for PS, PE, and PC formation), and the Kennedy pathway (for PC and PE formation). Besides LPAT and phospholipase, diacylglycerol kinase (Dgk1p, EC 2.7.1.107 Table 2), an ER-associated enzyme, also takes part in the mobilization of TAG for membrane phospholipid biosynthesis.[46] In plants, animals, and bacteria, Dgk1p uses ATP as phosphate donor, whereas in yeast, CTP substitutes the place of ATP and forms PA and CDP.[47] Dgk1p catalyzes the reverse reaction of DAG synthesis from PA; it is a crucial step that is necessary for phospholipid synthesis and membrane expansion in yeast.[48] The *DGK1*-encoded CTP-dependent diacylglycerol kinase in budding yeast *Saccharomyces cerevisiae* was characterized by Han et al. for the first time.[47,49] Point mutations of four conserved residues in the CTP transferase domain, a crucial portion in Dgk1p in that it is the actual performer to incorporate CTP when it comes to reactivity, resulted in an inactivation of diacylglycerol kinase activity.[47] In addition, a *dgk1*Δ strain (*DGK1*(D177A)) also lost its Dgk1p activity after undergoing alanine mutation on one of the residues in the CTP transferase domain.[49] Therefore, the CTP transferase domain maybe a good candidate for regulating TAG biosynthesis and membrane expansion. Furthermore, CDP-DAG has been proved to have inhibitory activity for CTP-dependent DAG kinase activity, and this CDP-DAG-caused inhibition is considered to contribute to the accumulation of DAG and TAG.[47] Qiu revealed that the Reb1p-binding site mutations could weaken the conversion from TAG to phospholipids, indicating that the newly discovered transcription factor Reb1p has a certain influence on *DGK1* expression and Dgk1p activity.[46]

Researchers also have revealed that Dgk1p and Pah1p counteract each other to a great degree, which is the reason that DAG and PA are kept balanced, and thus influences the level of TAG and phospholipid. Based on the analysis, we can conclude that yeast *DGK1* expression and DAG kinase activity affect membrane growth, lipid droplet formation, and cellular growth.[46]

DGAT and Other TAG Synthetase in Microorganisms. DGAT is the rate-limiting enzyme that catalyzes the last step of the G3P pathway.[50] At least four classes of DGAT have been identified in plants and microorganisms: they are DGAT1, DGAT2, DGAT3, and wax ester synthase/acyl-CoA:diacylglycerol acyltransferase (WS/DGAT, EC 2.3.1.75). It is worth mentioning that another important TAG synthetase, named phosphatidylcholine:diacylglycerol acyltransferase (PDAT, EC 2.3.1.158), is also responsible for the biosynthesis of TAG. Although these enzymes catalyze the same reaction, they belong to different gene families and have different functions.

DGAT1 and DGAT2. DGAT1 is similar to the acyl-CoA:cholesterol acyltransferase (ACAT, EC 2.3.1.26) family in gene sequence. Both ACAT and DGAT1 are subject to the membrane-bound *O*-acyltransferase (MBOAT) protein superfamily, which contains six or more transmembrane domains, including KSR block, PTR block, QP block, LWLFFEFDRFYWWNWWNPPFSHP block, LQL block, and NGQPY block.[51−54] A mouse DGAT1 gene was cloned by Cases and Zheng for the first time.[55] Soon after, DGAT1 gene was cloned from the model organism *Arabidopsis thaliana*.[56] DGAT2 belongs to the monoacylglycerol transferase (MGAT, EC 2.3.1.22) family (Table 2); it was first found in the oleaginous fungus *Mortierella ramanniana*.[57] Then the acyltransferase was cloned and characterized in other organisms like mouse and yeast.[58,59] There are six conserved motifs in DGAT2: PH block, PR block, GGE block, RGFA block, VPFG block, and G block.[51]

The DGAT1 and DGAT2 gene family consists of members of microorganisms, plants, and animals. They catalyze the same enzymatic reaction, and have similar relatively conserved residues that contribute to TAG synthesis.[51] Both DGAT1 and DGAT2 are ER membrane-bound proteins. However, the two enzymes are situated in different and specific domains of ER. The identity between type 1 and type 2 DGAT gene sequences is low, and they also have substrate discrimination.[60,61] It is suggested that the two types of DGATs play different roles in oleaginous plants or microorganisms in spite of their convergent evolution; discrepant biochemical characteristics may responsible for the divergence of the two types of DGATs.[1]

One or two decades ago, studies on *Arabidopsis thaliana* had shown that DGAT1 plays an extremely important role in TAG biosynthesis via mutation experiment.[62,63] DGAT1 mutants exhibited a 20−40% decrease on oil content in *Arabidopsis* seed.[64] DGAT2 plays a dominant role in TAG accumulation in *Ricinus communis* or yeast.[65−67] In developing castor bean seeds, DGAT2 showed much higher level than that in leaves, whereas

DOI: 10.1021/jf505975k
J. Agric. Food Chem. 2015, 63, 3067−3077

DGAT1 is indifferent to this organ diversity, and the same situation happened in tung tree.[61,65] Sequence analysis of deduced amino acids of DGAT2 has shown that *Mortierella ramanniana*, a fungus, has close homology to DGAT2 in plants or animals.[65] When only expressing DGAT2 encoded by *DGA1* (Table 2) in yeast (open reading frame YOR245c), TAG level in the mutant type reached 87% of the wild type.[66] It is demonstrated that none of the two types of enzymes is redundant in tung tree in that they have no overlap regions in ER. However, DGAT2 often participates in the synthesis of trieleostearin, a kind of unusual fatty acid which is the major ingredient of tung oil.[61] Other studies also support the conclusion that DGAT2 is preferential to take part in the synthesis of unusual fatty acids (UFA).[65,67,68] DGAT2 is in favor of 18:1-OH DAG (DAG which contains hydroxy fatty acids) compared to 18:1- or 18:2-DAG in castor bean or in yeast, and thus improves the content of hydroxy fatty acids (belongs to UFA).[67]

Compared to DGAT1, DGAT2 and PDAT are more likely to assemble epoxy and hydroxy fatty acids onto the sn-3 position in TAG formation.[68] In yeast, the *ARE1* and *ARE2*-encoded acyltransferases (Table 2), which are mainly responsible for sterol biosynthesis (thus contribute to storage lipid synthesis), also exhibit feeble DGAT activity, and influence TAG accumulation to a slight degree.[69] Coexpression of DGAT and *LPPα* or *LPPβ* derived from *Streptomyces coelicolor* in *E. coli* gains the ability to create an entire pathway for de novo TAG biosynthesis.[13]

PDAT. PDAT is an acyltransferase catalyzing the last step in the G3P pathway. It is acyl-CoA-independent, and its activity has been found in both yeast and plant microsomes.[70,71] In the wild type and the mutants of *Streptomyces coelicolor*, PDAT activity has also been reported.[72] As shown in Figure 3, PDAT employs phospholipids as acyl-donor, whereas DGAT utilizes acyl-CoA (Figure 3). PDAT is thought to be related to the accumulation of unusual fatty acids, including hydroxylated fatty acid and epoxidated fatty acid.[50,70] In eukaryotic cells, PDAT influences the ingredients of cell membrane lipid.[73]

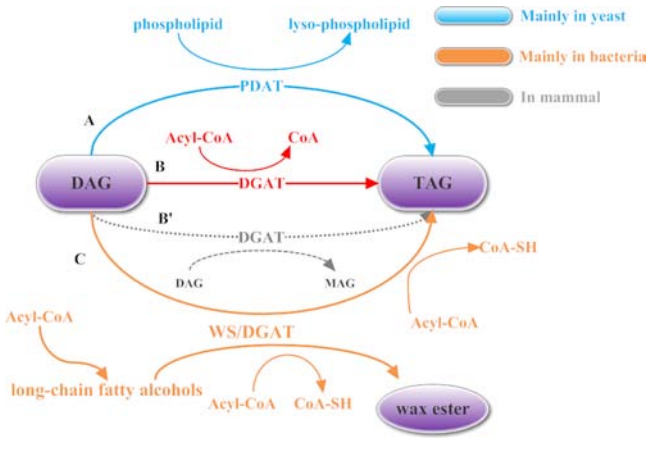

Figure 3. DGATs that are involved in the last step of TAG assembly. (A) PDAT uses phospholipid as acyl-donor to form TAG, meanwhile, PDAT is the only acyl-CoA-independent DGAT enzyme. (B) DGAT employs acyl-CoA as acyl-donor for the accumulation of TAG, and that is the most common way in this acylation reaction. (B′) To our knowledge, it is a special way that only exists in mammals. (C) Bifunctional WS/DGAT consumes acyl-CoA to synthesis wax ester (WE) and TAGs simultaneously.

LRO1, a gene encoding PDAT in yeast,[74] is suggested to incorporate with *DAG1* (encode DGAT2) for the last acylation reaction step in the G3P pathway (Table 2). However, the ways that Lro1p and Dga1p perform their functions are different. The fatty acid that previously belonged to the sn-2 position of PE or PC is utilized by *LRO1* to form TAG, whereas Dga1p uses the fatty acid derived from acyl-CoA.[75] A mutant of *S. cerevisiae* which only induces *LRO1* has nearly 40% of the wild type TAG level, indicating that *LRO1*-encoded PDAT plays the non-negligible role in TAG accumulation.[66] When the carbon source for the oleaginous yeast *Yarrowia lipolytica* is oleic acid, TAG synthesis is much faster in the *DGA1*-defective mutants than in wild type or lro1Δ mutant. Further experiment indicated that two other triacylglycerol synthases (except Dga1p and Lro1p) existing in *Y. lipolytica* play a major role when oleic acid serves as carbon source.[6]

An in vivo experiment in developing *Arabidopsis* pollen and seed revealed that PDAT and DGAT1 have complementary functions.[64] Obvious change did not take place in over-expressing AtPDAT mutants or in T-DNA insertion mutants of PDAT in *Arabidopsis*,[71,76] and the loss of TAG content in null mutants of DGAT1 is 20 to 40% compared to the wild type;[64] the reason is that PDAT partly makes up for the absence of DGAT1. By and large, the simultaneous absence of DGAT1 and PDAT is fatal, but not fatal for budding yeast (e.g., *S. cerevisiae*) in that lipid storage is not imperative for yeast.[66] However, in the fission yeast *Schizosaccharomyces pombe*, the absence of TAG assembly can cause apoptosis when it comes into the stationary phase.[77]

At least three aspects affect the efficiency of PDAT in TAG formation. First, sn-2 acyl group of PC, acyl groups with more double bonds, or more epoxy and hydroxyl groups have higher PDAT activity.[71] Second, it depends on the growth phase. In exponential growth phase PDAT does better for TAG accumulation compared to the late period of logarithmic phase.[65] Finally, PDATs in different species exhibit different activity, although several former examples have demonstrated that the function of PDAT cannot be ignored; some studies in oil palm or olive calli revealed that PDAT may be not that important.[65,71,76,78]

WS/DGAT. WS/DGAT is a membrane-related bifunctional enzyme catalyzing the last acyl transfer reaction of the G3P pathway. In the process, wax ester (WE) and TAGs, both of which are crucial storage lipids and biodiesel in some prokaryotes, are incorporated synchronously (Figure 3).[79] The broad range substrates of WS/DGAT are long-chain fatty alcohols and fatty acid CoA thioesters including linear and cyclic alkyl alcohols, mono- and diacylglycerols, and sterols,[80−82] which indicated that WS/DGAT has a boundless potential in producing fatty acid ethyl esters (FAEEs), fatty acid isoamyl esters, fatty alcohols, and waxes via its prokaryotic or even eukaryotic expression hosts.[83] The *ATFA*-encoded WS/DGAT (Table 2) was found in *Acinetobacter calcoaceticu* (a Gram-negative bacterium) strain ADP1 for the first time, and its function in mediating WE and TAG (to a smaller extent) formation was proved by an experiment on the *ATFA*-knockout mutant which showed an obvious reduction of storage lipids.[81,84] Nearly every member in bacterial WS/DGATs has a highly conserved motif: HHXXXDG motif, which may be responsible for the combination with fatty acyl-CoA or play a catalytic activity role in the acylation reaction.[82]

As mentioned above, in budding yeast *S. cerevisiae*, four genes are responsible for the synthesis of storage lipids: *DGA1*, *LRO1*,

DOI: 10.1021/jf505975k
J. Agric. Food Chem. 2015, 63, 3067−3077

ARE1, and *ARE2*. Heterologous expression of WS/DGAT from *A. calcoaceticus* ADP1 in the quadruple mutant (*DGA1*, *LRO1*, *ARE1*, and *ARE2*) strain *S. cerevisiae* H1246, which is defective in TAG synthesis and steryl ester accumulation, exhibited a restoration of TAG assembly and also produced FAEEs (an advanced biodiesel feedstock)[85] as well as fatty acid isoamyl esters.[81] Through coexpression of the WS/DGAT gene from *Acinetobacter baylyi* strain ADP1with ethanol production genes from *Zymomonas mobilis* in recombinant *E. coli* and fed-batch fermentation, the consistency of FAEE has reached 1.28 g/L.[79] In the engineered *E. coli*, expression of several genes including the gene encoding wax-ester synthase led to a decent production of nearly 400 mg/L of FAEEs in 2 days from the economic raw material glucose.[86] A recently discovered WS2 derived from *Marinobacter hydrocarbonoclasticus* has proved to have greater wax synthase activity for ethanol but does not exhibit DGAT activity.[83] A novel DGAT-like protein which has high similarity with the *Acinetobacter calcoaceticus* WS/DGAT has been cloned by Cui et al. from the diatom *Phaeodactylum tricornutum*.[87] Heterologous expression in strain *S. cerevisiae* H1246, ptDGAT3 exhibited its preference to incorporate C_{18} fatty acids into TAGs.

DGAT3. In peanut, castor bean, and *Arabidopsis thaliana*, another DAG acyltransferase named DGAT3 has been found and soon became a hot research point.[88−90] The third type of DGAT is a cytosolic enzyme without membrane-bound regions. Unlike the conventional DGATs, DGAT3 is a soluble enzyme. It shares more similarity with WS/DGAT (13%) compared to DGAT1 or DGAT2 (10%).[88] Expression of the peanut (*Arachis hypogaea*) *ahDGAT* gene in *E. coli* led to the biosynthesis of TAG.[88] In a recent study, three DGAT genes were identified and isolated from peanut (*Arachis hypogaea*), and their activity was proved by heterologous expression in the quadruple mutant (*DGA1*, *LRO1*, *ARE1*, and *ARE2*) strain *S. cerevisiae* H1246.[91]

In *Arabidopsis thaliana*, the soluble DGAT3 plays an important role in a putative cytosolic pathway for TAG synthsis. In various developmental stages, the *Arabidopsis thaliana* DGAT3, which is encoded by *At1g48300*, always maintains a high expression level. This fact suggests that ahDGAT3 has a management function in mediating the metabolic flux between the cytosolic acyl-CoA pool and TAG.[92] The ahDGAT3 shows a preference for 18:3 and 18:2 (to a lesser degree) other than 20:1 acyl-CoA, while a larger percentage of acyl-CoA pool is 20:1 acyl-CoA.[92] *DCR* (*At5g23940*), the gene in *Arabidopsis thaliana* that encodes a soluble DAG acyltransferase, has a typical HX_4D motif (N-terminal) and the VX_2GF motif binding to the lipid body.[90] Overexpression of *At5g23940* in *S. cerevisiae* H1246 led to the formation of TAG.[90]

Summary of TAG Synthetases from Horizontal Perspective. Although these TAG synthetases catalyze the same acylation reaction, they have different characteristics. DGAT1 widely exists in plants and microorganisms. In various developmental stages or in different organs, DGAT1 always maintains a relatively high expression level, whereas DGAT2, PDAT, and DGAT3 may be more sensitive. In addition, DGAT2 and PDAT preferentially participate in the synthesis of UFA. To be more specific, DGAT2 and PDAT are more likely to incorporate epoxy and hydroxy fatty acids to the sn-3 position. WS/DGAT is the only bifunctional enzyme in these TAG synthetases, found only in microorganisms. In yeast, the *ARE1* and *ARE2*-encoded acyltransferases which exhibit feeble DGAT activity can play an auxiliary role of DGAT and PDAT for the conversion from DAG to TAG.

The CDP-DAG Pathway and the Kennedy Pathway for Phospholipids. The conversion from PA to CDP-DAG is catalyzed by CDP-DAG synthase (EC 2.7.7.41), which is encoded by *CDS1* and utilizes PA as its phospholipid substrate.[23,47,93] Once formed, CDP-DAG divides into three ways, one for PI formation, one for phosphatidylglycerol (PG) and cardiolipin (CL) formation, and the last one being the CDP-DAG pathway for phosphatidylserine (PS), PE, and PC formation (Figure 1.). The CDP-DAG pathway is required in many microorganisms including bacteria, yeast, and microalgae because of its pivotal role in generating phospholipids and interactive function with DAG synthesis. In microalgae, PI and PG can only be derived from the CDP-DAG pathway, whereas both the CDP-DAG pathway and the Kennedy pathway can generate PE and PC.[94]

The CDP-DAG pathway and the TAG synthesis pathway are in metabolic interlock (MI) with each other.[95] More specifically, PA will convert to DAG if excess accumulation of CDP-DAG occurs; the reverse is also true.[95]

The Kennedy pathway is another important metabolic process for PE and PC formation. It shares with the G3P pathway the same way from G3P to DAG, and the two pathways then start to go their separate ways (Figure 1). Obviously, the diversion of DAG inevitably leads to a decrease in TAG concentration. However, like the MI effect between the CDP-DAG pathway and the TAG synthesis approach, there is an intercommunication between the Kennedy pathway and the TAG synthesis approach as well. To be specific, once DAG level is sufficient, the two branches (CDP-choline branch and CDP-ethanolamine branch) then have a chance of synthesizing PE and PC, and the two phospholipids can in turn be catalyzed by phospholipase for the accumulation of PA, choline, and ethanolamine (Figure 1).

In conclusion, the free fatty acid synthesis approach plays a significant role in de novo synthesis of TAG. This approach persistently provides acyl-CoA for the G3P pathway, the latter part of TAG biosynthesis. Of the four enzymes (GPAT, LPAT, PAP, and DGAT) that are involved in the G3P pathway, PAP and DGAT largely affect the accumulation of TAG or other lipids like FAEE and WE. Via genetic engineering and metabolic engineering, the operating force of PAPs and DGATs in ultimate production of TAG has been amplified dramatically.

PA is a crucial intermediate product in the G3P pathway and the CDP-DAG pathway. Naturally, we can promote the TAG synthesis approach and repress the CDP-DAG pathway by regulating genes that encoded diacylglycerol kinase, PAP and CDP-DAG synthase, or even overexpression of more genes (multigene approach). In addition, the degradation of phospholipids is beneficial to the accumulation of PA as well, thus forming more TAGs by the rational use of the metabolic interlock between the CDP-DAG pathway and the TAG synthesis pathway. DAG is another critical point; by mediating diacylglycerol kinase, DGAT, and enzymes involved in the Kennedy pathway, we can also enhance the G3P pathway.

PAP is well studied in yeast. For the aim of improving TAG yield, *PAH1* seems to be the most suitable PAP gene in yeast to be modified. In bacteria, *LPPα* and *LPPβ* may enjoy similar status like *PAH1* in yeast. In bacteria and yeast, the ER-associated diacylglycerol kinase influences the level of PA and

DOI: 10.1021/jf505975k
J. Agric. Food Chem. 2015, 63, 3067−3077

DAG to a large extent, indicating that inhibition of this enzyme may benefit TAG accumulation in bacteria or yeast.

Among the four classes of DGAT, WS/DGAT becomes a new concern. The reason is that, except for TAGs, WS/DGAT can generate another important biodiesel feedstock: FAEEs. Hence, bacteria that contain WS/DGAT will be a hot area of biodiesel production research.

To summarize, PA and DAG are the central hubs of the three pathways in lipid metabolism, therefore, the enzymes that can regulate PAP and DAG (PAP, DGAT, diacylglycerol kinase, CDP-DAG synthase, and phospholipase) are all suitable candidates for mediating the conversion between TAG and phospholipids, and thus affect TAG concentration.

AUTHOR INFORMATION

Corresponding Author

*E-mail: jgjiang@scut.edu.cn. Phone: +86-20-87113849. Fax: +86-20-87113843.

Funding

This project was supported by National Natural Foundation of China (Grant 31171631).

Notes

The authors declare no competing financial interest.

ABBREVIATIONS USED

ACC, acetyl-CoA carboxylic enzyme; ACP, acyl-carrier protein; APP, actin patch protein; ASP, Aquatic Species Program; CDP-Cho, CDP-choline; CDP-DAG, CDP-diacylglycerol; CDP-Etn, CDP-ethanolamine; CDS, CDP-DAG synthase; Cho, choline; Cho-P, choline phosphate; CL, cardiolipin; DAG, diacylglycerol; DGAT, diacylglycerol acyltransferase; DGK, diacylglycerol kinase; DGPP, DAG pyrophosphate; DHAP, dihydroxyacetone phosphate; DPP, diacylglycerol pyrophosphate phosphatase; ER, endoplasmic reticulum; Etn, ethanolamine; Etn-P, ethanolamine phosphate; FAEEs, fatty acid ethyl esters; FFA, free fatty acids; G3PDH, glycerol-3-phosphate dehydrogenase; GAPDH, glyceraldehyde-3-phosphate dehydrogenase; GPAT, glycerol-3-phosphate acyltransferase; Gro-3-P, glycerol-3-phosphate; HAD, haloacid dehalogenase; IP, isoprenoid phosphate; KAS, β-ketoacyl-ACP synthase; LPA, lysophosphatidate; LPAT, lysophosphatidate acyltransferase; LPP, lipid phosphate phosphatase; MAT, malonyl-CoA:ACP transacylase; OOA, oxaloacetic acid; PA, phosphatidic acid; PAP, phosphatidic acid phosphatase; PC, phosphatidylcholine; PE, phosphatidylethanolamine; PG, phosphatidylglycerol; PGP, phosphatidylglycerol phosphate; PI, phosphatidylinositol; PKA, protein kinase A; PS, phosphatidylserine; SBP, sphingoid base phosphate; SCO, single cell oils; TAG, triacylglycerols

REFERENCES

(1) Chen, J. E.; Smith, A. G. A look at diacylglycerol acyltransferases (DGATs) in algae. *J. Biotechnol.* **2012**, *162*, 28−39.

(2) Liang, M. H.; Jiang, J. G. Advancing oleaginous microorganisms to produce lipid via metabolic engineering technology. *Prog. Lipid Res.* **2013**, *52*, 395−408.

(3) Xu, H.; Miao, X.; Wu, Q. High quality biodiesel production from a microalga *Chlorella protothecoides* by heterotrophic growth in fermenters. *J. Biotechnol.* **2006**, *126*, 499−507.

(4) Wen, Z. Y.; Chen, F. Optimization of nitrogen sources for heterotrophic production of eicosapentaenoic acid by the diatom *Nitzschia laevis*. *Enzyme Microb. Technol.* **2001**, *29*, 341−347.

(5) Qv, X. Y.; Zhou, Q. F.; Jiang, J. G. Ultrasound-enhanced and microwave-assisted extraction of lipid from *Dunaliella tertiolecta* and fatty acid profile analysis. *J. Sep. Sci.* **2014**, *37*, 2991−2999.

(6) Athenstaedt, K. YALI0E32769g (*DGA1*) and YALI0E16797g (*LRO1*) encode major triacylglycerol synthases of the oleaginous yeast *Yarrowia lipolytica*. *Biochim. Biophys. Acta, Mol. Cell Biol. Lipids* **2011**, *1811*, 587−596.

(7) Sasser, T.; Qiu, Q. S.; Karunakaran, S.; Padolina, M.; Reyes, A.; Flood, B.; Smith, S.; Gonzales, C.; Fratti, R. A. Yeast lipin 1 orthologue Pah1p regulates vacuole homeostasis and membrane fusion. *J. Biol. Chem.* **2011**, *287*, 2221−2236.

(8) Deng, X. D.; Gu, B.; Li, Y. J.; Hu, X. W.; Guo, J. C.; Fei, X. W. The roles of acyl-CoA: diacylglycerol acyltransferase 2 genes in the biosynthesis of triacylglycerols by the green algae *Chlamydomonas reinhardtii*. *Mol. Plant* **2012**, *5*, 945−7.

(9) Gong, Y.; Zhang, J.; Guo, X.; Wan, X.; Liang, Z.; Hu, C. J.; Jiang, M. Identification and characterization of PtDGAT2B, an acyltransferase of the DGAT2 acyl-Coenzyme A: Diacylglycerol acyltransferase family in the diatom *Phaeodactylum tricornutum*. *FEBS Lett.* **2013**, *587*, 481−487.

(10) Hu, Q.; Sommerfeld, M.; Jarvis, E.; Ghirardi, M.; Posewitz, M.; Seibert, M.; Darzins, A. Microalgal triacylglycerols as feedstocks for biofuel production: perspectives and advances. *Plant J.* **2008**, *54*, 621−639.

(11) Qv, X. Y.; Guo, Y. Y.; Jiang, J. G. Assessment of the effects of nutrients on biomass and lipid accumulation in *Dunaliella tertiolecta* using a response surface methodology. *RSC Adv.* **2014**, *4*, 42202−42210.

(12) Cheng, K. C.; Ren, M.; Ogden, K. L. Statistical optimization of culture media for growth and lipid production of *Chlorella protothecoides* UTEX 250. *Bioresour. Technol.* **2013**, *128*, 44−8.

(13) Comba, S. Identification and physiological characterization of phosphatidic acid phosphatase enzymes involved in triacylglycerol biosynthesis in *Streptomyces coelicolor*. *Microb. Cell Fact.* **2013**, *12*.

(14) Lao, Y. M.; Lu, Y.; Jiang, J. G.; Luo, L. X. Six regulatory elements lying in the promoter region imply the functional diversity of chloroplast GAPDH in *Duanliella bardawil*. *J. Agric. Food Chem.* **2012**, *60*, 9211−9220.

(15) Chen, H.; Lao, Y. M.; Jiang, J. G. Effects of salinities on the gene expression of a (NAD+)-dependent glycerol-3-phosphate dehydrogenase in *Dunaliella salina*. *Sci. Total Environ.* **2011**, *409*, 1291−7.

(16) Chen, H.; Lu, Y.; Jiang, J. G. Comparative analysis on the key enzymes of the glycerol cycle metabolic pathway in *Dunaliella salina* under osmotic stresses. *PLoS One* **2012**, *7*, e37578.

(17) Albertyn, J.; Hohmann, S.; Thevelein, J. M. *GPD1*, which encodes glycerol-3-phosphate dehydrogenase, is essential for growth under osmotic stress in *Saccharomyces cerevisiae*, and its expression is regulated by the high-osmolarity glycerol response pathway. *Mol. Cell. Biol.* **1994**, *14*, 4135−4144.

(18) Chen, H.; Jiang, J. G. Osmotic Responses of *Dunaliella* to the Changes of Salinity. *J. Cell. Physiol.* **2009**, *219*, 251−258.

(19) Lao, Y. M.; Xiao, L.; Luo, L. X.; Jiang, J. G. Hypoosmotic expression of *Dunaliella bardawil* zeta-carotene desaturase is attributed to a hypoosmolarity-responsive element different from other key carotenogenic genes. *Plant Physiol.* **2014**, *165*, 359−72.

(20) Fan, J.; Andre, C.; Xu, C. A chloroplast pathway for the de novo biosynthesis of triacylglycerol in *Chlamydomonas reinhardtii*. *FEBS Lett.* **2011**, *585*, 1985−1991.

(21) Brown, A. P.; Brough, C. L.; Kroon, J. T.; Slabas, A. R. Identification of a cDNA that encodes a 1-acyl-sn-glycerol-3-phosphate acyltransferase from *Limnanthes douglasii*. *Plant Mol. Biol.* **1995**, *29*, 267−78.

(22) Knutzon, D. S.; Lardizabal, K. D.; Nelsen, J. S.; Bleibaum, J. L.; Davies, H. M.; Metz, J. G. Cloning of a coconut endosperm cDNA encoding a 1-acyl-sn-glycerol-3-phosphate acyltransferase that accepts medium-chain-length substrates. *Plant Physiol.* **1995**, *109*, 999−1006.

(23) Shen, H.; Heacock, P. N.; Clancey, C. J.; Dowhan, W. The *CDS1* gene encoding CDP-diacylglycerol synthase in *Saccharomyces cerevisiae* is essential for cell growth. *J. Biol. Chem.* **1996**, *271*, 789−795.

DOI: 10.1021/jf505975k
J. Agric. Food Chem. 2015, 63, 3067−3077

(24) Kennedy, E. P.; Weiss, S. B. The function of cytidine coenzymes in the biosynthesis of phospholipids. *J. Biol. Chem.* **1956**, *222*, 193−214.
(25) Han, G. S.; Siniossoglou, S.; Carman, G. M. The cellular functions of the yeast lipin homolog Pah1p are dependent on its phosphatidate phosphatase activity. *J. Biol. Chem.* **2007**, *282*, 37026−37035.
(26) Irie, K.; Takase, M.; Araki, H.; Oshima, Y. A gene, *SMP2*, involved in plasmid maintenance and respiration in *Saccharomyces cerevisiae* encodes a highly charged protein. *Mol. Gen. Genet.* **1993**, *236*, 283−8.
(27) Santos Rosa, H.; Leung, J.; Grimsey, N.; Peak Chew, S.; Siniossoglou, S. The yeast lipin *SMP2* couples phospholipid biosynthesis to nuclear membrane growth. *EMBO J.* **2005**, *24*, 1931−1941.
(28) Han, G. S. The *Saccharomyces cerevisiae* lipin homolog is a Mg2+-dependent phosphatidate phosphatase enzyme. *J. Biol. Chem.* **2006**, *281*, 9210−9218.
(29) Chae, M.; Han, G. S.; Carman, G. M. The *Saccharomyces cerevisiae* actin patch protein App1p is a phosphatidate phosphatase enzyme. *J. Biol. Chem.* **2012**, *287*, 40186−40196.
(30) Choi, H. S.; Su, W. M.; Han, G. S.; Plote, D.; Xu, Z.; Carman, G. M. Pho85p-Pho80p phosphorylation of yeast Pah1p phosphatidate phosphatase regulates its activity, location, abundance, and function in lipid metabolism. *J. Biol. Chem.* **2012**, *287*, 11290−11301.
(31) Su, W. M.; Han, G. S.; Casciano, J.; Carman, G. M. Protein kinase A-mediated phosphorylation of Pah1p phosphatidate phosphatase functions in conjunction with the Pho85p-Pho80p and Cdc28p-Cyclin B kinases to regulate lipid synthesis in yeast. *J. Biol. Chem.* **2012**, *287*, 33364−33376.
(32) O'Hara, L.; Han, G. S.; Peak Chew, S.; Grimsey, N.; Carman, G. M.; Siniossoglou, S. Control of phospholipid synthesis by phosphorylation of the yeast lipin Pah1p/Smp2p Mg2+-dependent phosphatidate phosphatase. *J. Biol. Chem.* **2006**, *281*, 34537−34548.
(33) Choi, H. S.; Su, W. M.; Morgan, J. M.; Han, G. S.; Xu, Z.; Karanasios, E.; Siniossoglou, S.; Carman, G. M. Phosphorylation of phosphatidate phosphatase regulates its membrane association and physiological functions in *Saccharomyces cerevisiae*: identification of ser602, thr723, and ser744 as the sites phosphorylated by CDC28 (*CDK1*)-encoded cyclin-dependent kinase. *J. Biol. Chem.* **2011**, *286*, 1486−1498.
(34) Siniossoglou, S.; Santos Rosa, H.; Rappsilber, J.; Mann, M.; Hurt, E. A novel complex of membrane proteins required for formation of a spherical nucleus. *EMBO J.* **1998**, *17*, 6449−6464.
(35) Pascual, F. S. C. A., Carman GM. *PAH1*-encoded phosphatidate phosphatase plays a role in the growth phase-and inositol-mediated regulation of lipid synthesis in *Saccharomyces cerevisiae*. *J. Biol. Chem.* **2013**, *288*, 35781−35792.
(36) Donahue, T. F.; Henry, S. A. Myo-inositol-1-phosphate synthase. Characteristics of the enzyme and identification of its structural gene in yeast. *J. Biol. Chem.* **1981**, *256*, 7077−7085.
(37) Shirra, M. K. The *Snf1* protein kinase and *Sit4* protein phosphatase have opposing functions in regulating TATA-binding protein association with the *Saccharomyces cerevisiae INO1* promoter. *Genetics* **2005**, *169*, 1957−1972.
(38) Karanasios, E.; Barbosa, A. D.; Sembongi, H.; Mari, M.; Han, G. S.; Reggiori, F.; Carman, G. M.; Siniossoglou, S. Regulation of lipid droplet and membrane biogenesis by the acidic tail of the phosphatidate phosphatase Pah1p. *Mol. Biol. Cell* **2013**, *24*, 2124−2133.
(39) Karanasios, E.; Han, G. S.; Xu, Z.; Carman, G. M.; Siniossoglou, S. A phosphorylation-regulated amphipathic helix controls the membrane translocation and function of the yeast phosphatidate phosphatase. *Proc. Natl. Acad. Sci. U.S.A.* **2010**, *107*, 17539−17544.
(40) Chae, M.; Carman, G. M. Characterization of the yeast actin patch protein App1p phosphatidate phosphatase. *J. Biol. Chem.* **2013**, *288*, 6427−6437.
(41) Wu, W. I.; Liu, Y.; Riedel, B.; Wissing, J. B.; Fischl, A. S.; Carman, G. M. Purification and characterization of diacylglycerol pyrophosphate phosphatase from *Saccharomyces cerevisiae*. *J. Biol. Chem.* **1996**, *271*, 1868−1876.
(42) Toke, D. A.; Bennett, W. L.; Dillon, D. A.; Wu, W. I.; Chen, X. M.; Ostrander, D. B.; Oshiro, J.; Cremesti, A.; Voelker, D. R.; Fischl, A. S.; Carman, G. M. Isolation and characterization of the *Saccharomyces cerevisiae DPP1* gene encoding diacylglycerol pyrophosphate phosphatase. *J. Biol. Chem.* **1998**, *273*, 3278−3284.
(43) Toke, D. A.; Bennett, W. L.; Oshiro, J.; Wu, W. I.; Voelker, D. R.; Carman, G. M. Isolation and characterization of the *Saccharomyces cerevisiae LPP1* gene encoding a Mg2+-independent phosphatidate phosphatase. *J. Biol. Chem.* **1998**, *273*, 14331−14338.
(44) Faulkner, A.; Chen, X.; Rush, J.; Horazdovsky, B.; Waechter, C. J.; Carman, G. M.; Sternweis, P. C. The *LPP1* and *DPP1* gene products account for most of the isoprenoid phosphate phosphatase activities in *Saccharomyces cerevisiae*. *J. Biol. Chem.* **1999**, *274*, 14831−14837.
(45) Fakas, S.; Qiu, Y.; Dixon, J. L.; Han, G. S.; Ruggles, K. V.; Garbarino, J.; Sturley, S. L.; Carman, G. M. Phosphatidate phosphatase activity plays key role in protection against fatty acid-induced toxicity in yeast. *J. Biol. Chem.* **2011**, *286*, 29074−29085.
(46) Qiu, Y.; Fakas, S.; Han, G. S.; Barbosa, A. D.; Siniossoglou, S.; Carman, G. M. Transcription factor Reb1p regulates *DGK1*-encoded diacylglycerol kinase and lipid metabolism in *Saccharomyces cerevisiae*. *J. Biol. Chem.* **2013**, *288*, 29124−29133.
(47) Han, G. S.; O'Hara, L.; Siniossoglou, S.; Carman, G. M. Characterization of the yeast *DGK1*-encoded CTP-dependent diacylglycerol kinase. *J. Biol. Chem.* **2008**, *283*, 20443−20453.
(48) Fakas, S.; Konstantinou, C.; Carman, G. M. *DGK1*-encoded diacylglycerol kinase activity is required for phospholipid synthesis during growth resumption from stationary phase in *Saccharomyces cerevisiae*. *J. Biol. Chem.* **2010**, *286*, 1464−1474.
(49) Han, G. S.; O'Hara, L.; Carman, G. M.; Siniossoglou, S. An unconventional diacylglycerol kinase that regulates phospholipid synthesis and nuclear membrane growth. *J. Biol. Chem.* **2008**, *283*, 20433−20442.
(50) Bennett, M.; Peng, Z.; Li, L.; Yang, L.; Zhang, B.; Chen, G.; Bi, Y. Overexpression of peanut diacylglycerol acyltransferase 2 in *Escherichia coli*. *PLoS One* **2013**, *8*, e61363.
(51) Cao, H. Structure-function analysis of diacylglycerol acyltransferase sequences from 70 organisms. *BMC Res. Notes* **2011**, *4*, 249.
(52) Li, M.; Zhao, M.; Wu, H.; Wu, W.; Xu, Y. Cloning, characterization and functional analysis of two type 1diacylglycerol acyltransferases (DGAT1s) from *Tetraena mongolica*. *J. Integr. Plant Biol.* **2013**, *55*, 490−503.
(53) Turchetto Zolet, A. C.; Maraschin, F. S.; de Morais, G. L.; Cagliari, A.; Andrade, C. M. B.; Margis Pinheiro, M.; Margis, R. Evolutionary view of acyl-CoA diacylglycerol acyltransferase (DGAT), a key enzyme in neutral lipid biosynthesis. *BMC Evol. Biol.* **2011**, *11*, 263.
(54) Hofmann, K. A superfamily of membrane-bound *O*-acyltransferases with implications for wnt signaling. *Trends Biochem. Sci.* **2000**, *25*, 111−2.
(55) Cases, S.; Zheng, Y. W. Identification of a gene encoding an acyl CoA:diacylglycerol acyltransferase, a key enzyme in triacylglycerol synthesis. *Proc. Natl. Acad. Sci. U.S.A.* **1998**, *95*, 13018−13023.
(56) Hobbs, D. H.; Lu, C. F.; Hills, M. J. Cloning of a cDNA encoding diacylglycerol acyltransferase from *Arabidopsis thaliana* and its functional expression. *FEBS Lett.* **1999**, *452*, 145−149.
(57) Lardizabal, K. D. DGAT2 is a new diacylglycerol acyltransferase gene family - purification, cloning, and expression in insect cells of two polypeptides from *Mortierella ramanniana* with diacylglycerol acyltransferase activity. *J. Biol. Chem.* **2001**, *276*, 38862−38869.
(58) Cases, S. Cloning of DGAT2, a second mammalian diacylglycerol acyltransferase, and related family members. *J. Biol. Chem.* **2001**, *276*, 38870−38876.
(59) Sorger, D.; Daum, G. Synthesis of triacylglycerols by the acyl-coenzyme A:diacyl-glycerol acyltransferase Dga1p in lipid particles of the yeast *Saccharomyces cerevisiae*. *J. Bacteriol.* **2002**, *184*, 519−524.

DOI: 10.1021/jf505975k
J. Agric. Food Chem. 2015, 63, 3067−3077

(60) Seethala, R.; Peterson, T.; Dong, J.; Chu, C.-H.; Chen, L.; Golla, R.; Ma, Z.; Panemangalore, R.; Lawrence, R. M.; Cheng, D. A simple homogeneous scintillation proximity assay for acyl-coenzyme A:diacylglycerol acyltransferase. *Anal. Biochem.* **2008**, *383*, 144−150.
(61) Shockey, J. M. Tung tree DGAT1 and DGAT2 have nonredundant functions in triacylglycerol biosynthesis and are localized to different subdomains of the endoplasmic reticulum. *Plant Cell* **2006**, *18*, 2294−2313.
(62) Katavic, V.; Reed, D. W.; Taylor, D. C.; Giblin, E. M.; Barton, D. L.; Zou, J.; Mackenzie, S. L.; Covello, P. S.; Kunst, L. Alteration of seed fatty acid composition by an ethyl methanesulfonate-induced mutation in *Arabidopsis thaliana* affecting diacylglycerol acyltransferase activity. *Plant Physiol.* **1995**, *108*, 399−409.
(63) Zou, J.; Wei, Y.; Jako, C.; Kumar, A.; Selvaraj, G.; Taylor, D. C. The *Arabidopsis thaliana* TAG1 mutant has a mutation in a diacylglycerol acyltransferase gene. *Plant J.* **1999**, *19*, 645−53.
(64) Zhang, M.; Fan, J.; Taylor, D. C.; Ohlrogge, J. B. DGAT1 and PDAT1 acyltransferases have overlapping functions in *Arabidopsis* triacylglycerol biosynthesis and are essential for normal pollen and seed development. *Plant Cell* **2009**, *21*, 3885−3901.
(65) Kroon, J. T. M.; Wei, W.; Simon, W. J.; Slabas, A. R. Identification and functional expression of a type 2 acyl-CoA:diacylglycerol acyltransferase (DGAT2) in developing castor bean seeds which has high homology to the major triglyceride biosynthetic enzyme of fungi and animals. *Phytochemistry* **2006**, *67*, 2541−2549.
(66) Sandager, L. Storage lipid synthesis is non-essential in yeast. *J. Biol. Chem.* **2001**, *277*, 6478−6482.
(67) Burgal, J.; Shockey, J.; Lu, C.; Dyer, J.; Larson, T.; Graham, I.; Browse, J. Metabolic engineering of hydroxy fatty acid production in plants: *Rc*DGAT2 drives dramatic increases in ricinoleate levels in seed oil. *Plant Biotechnol. J.* **2008**, *6*, 819−831.
(68) Li, R.; Yu, K.; Hildebrand, D. F. DGAT1, DGAT2 and PDAT expression in seeds and other tissues of epoxy and hydroxy fatty acid accumulating plants. *Lipids* **2010**, *45*, 145−157.
(69) Zweytick, D.; Leitner, E.; Kohlwein, S. D.; Yu, C. J.; Rothblatt, J.; Daum, G. Contribution of Are1p and Are2p to steryl ester synthesis in the yeast *Saccharomyces cerevisiae*. *Eur. J. Biochem.* **2000**, *267*, 1075−1082.
(70) Dahlqvist, A.; Stahl, U.; Lenman, M.; Banas, A.; Lee, M.; Sandager, L.; Ronne, H.; Stymne, S. Phospholipid:diacylglycerol acyltransferase: An enzyme that catalyzes the acyl-CoA-independent formation of triacylglycerol in yeast and plants. *Proc. Natl. Acad. Sci. U.S.A.* **2000**, *97*, 6487−6492.
(71) Stahl, U. Cloning and functional characterization of a phospholipid:diacylglycerol acyltransferase from *Arabidopsis*. *Plant Physiol.* **2004**, *135*, 1324−1335.
(72) Arabolaza, A.; Rodriguez, E.; Altabe, S.; Alvarez, H.; Gramajo, H. Multiple pathways for triacylglycerol biosynthesis in *Streptomyces coelicolor*. *Appl. Environ. Microbiol.* **2008**, *74*, 2573−2582.
(73) Li, R.; Yu, K.; Wu, Y.; Tateno, M.; Hatanaka, T.; Hildebrand, D. F. *Vernonia* DGATs can complement the disrupted oil and protein metabolism in epoxygenase-expressing soybean seeds. *Metab. Eng.* **2012**, *14*, 29−38.
(74) Oelkers, P. A lecithin cholesterol acyltransferase-like gene mediates diacylglycerol esterification in yeast. *J. Biol. Chem.* **2000**, *275*, 15609−15612.
(75) Voynova, N. S.; Vionnet, C.; Ejsing, C. S.; Conzelmann, A. A novel pathway of ceramide metabolism in *Saccharomyces cerevisiae*. *Biochem. J.* **2012**, *447*, 103−114.
(76) Mhaske, V.; Beldjilali, K.; Ohlrogge, J.; Pollard, M. Isolation and characterization of an *Arabidopsis thaliana* knockout line for phospholipid: diacylglycerol transacylase gene (At5g13640). *Plant Physiol. Biochem.* **2005**, *43*, 413−417.
(77) Zhang, Q. *Schizosaccharomyces pombe* cells deficient in triacylglycerols synthesis undergo apoptosis upon entry into the stationary phase. *J. Biol. Chem.* **2003**, *278*, 47145−47155.
(78) Ramli, U. S.; Salas, J. J.; Quant, P. A.; Harwood, J. L. Metabolic control analysis reveals an important role for diacylglycerol acyltransferase in olive but not in oil palm lipid accumulation. *FEBS J.* **2005**, *272*, 5764−70.
(79) Kalscheuer, R. Microdiesel: *Escherichia coli* engineered for fuel production. *Microbiology* **2006**, *152*, 2529−2536.
(80) Uthoff, S.; Stoveken, T.; Weber, N.; Vosmann, K.; Klein, E.; Kalscheuer, R.; Steinbuchel, A. Thio wax ester biosynthesis utilizing the unspecific bifunctional wax ester synthase/acyl coenzyme A:Diacylglycerol acyltransferase of *Acinetobacter* sp. Strain ADP1. *Appl. Environ. Microbiol.* **2005**, *71*, 790−796.
(81) Kalscheuer, R.; Luftmann, H.; Steinbuchel, A. Synthesis of novel lipids in *Saccharomyces cerevisiae* by heterologous expression of an unspecific bacterial acyltransferase. *Appl. Environ. Microbiol.* **2004**, *70*, 7119−7125.
(82) Waltermann, M.; Stoveken, T.; Steinbuchel, A. Key enzymes for biosynthesis of neutral lipid storage compounds in prokaryotes: properties, function and occurrence of wax ester synthases/acyl-CoA:diacylglycerol acyltransferases. *Biochimie* **2007**, *89*, 230−242.
(83) Colin, V. L.; Rodriguez, A.; Cristobal, H. A. The role of synthetic biology in the design of microbial cell factories for biofuel production. *J. Biomed. Biotechnol.* **2011**, *2011*, 1−9.
(84) Kalscheuer, R. A novel bifunctional wax ester synthase/acyl-CoA:diacylglycerol acyltransferase mediates wax ester and triacylglycerol biosynthesis in *Acinetobacter calcoaceticus ADP1*. *J. Biol. Chem.* **2002**, *278*, 8075−8082.
(85) Valle Rodriguez, J. O.; Shi, S.; Siewers, V.; Nielsen, J. Metabolic engineering of *Saccharomyces cerevisiae* for production of fatty acid ethyl esters, an advanced biofuel, by eliminating non-essential fatty acid utilization pathways. *Appl. Energy* **2014**, *115*, 226−232.
(86) Steen, E. J.; Kang, Y.; Bokinsky, G.; Hu, Z.; Schirmer, A.; McClure, A.; del Cardayre, S. B.; Keasling, J. D. Microbial production of fatty-acid-derived fuels and chemicals from plant biomass. *Nature* **2010**, *463*, 559−562.
(87) Cui, Y. L.; Zheng, G. T.; Li, X. Q.; Lin, H. Z.; Jiang, P.; Qin, S. Cloning and characterization of a novel diacylglycerol acyltransferase from the diatom *Phaeodactylum tricornutum*. *J. Appl. Phycol.* **2013**, *25*, 1509−1512.
(88) Saha, S.; Enugutti, B.; Rajakumari, S.; Rajasekharan, R. Cytosolic triacylglycerol biosynthetic pathway in oilseeds. Molecular cloning and expression of peanut cytosolic diacylglycerol acyltransferase. *Plant Physiol.* **2006**, *141*, 1533−1543.
(89) Trenz, T.; Turchetto-Zolet, A.; Margis, M.; Margis, R.; Maraschin, F. Functional characterization of castor bean (*Ricinus communis*) DGAT3 and DAcT enzymes in *Arabidopsis thaliana*. *BMC Proc.* **2014**, *8*, P117.
(90) Rani, S. H.; Krishna, T. H. A.; Saha, S.; Negi, A. S.; Rajasekharan, R. Defective in cuticular ridges (*DCR*) of *Arabidopsis thaliana*, a gene associated with surface cutin formation, encodes a soluble diacylglycerol acyltransferase. *J. Biol. Chem.* **2010**, *285*, 38337−38347.
(91) Chi, X.; Hu, R.; Zhang, X.; Chen, M.; Chen, N.; Pan, L.; Wang, T.; Wang, M.; Yang, Z.; Wang, Q.; Yu, S. Cloning and functional analysis of three diacylglycerol acyltransferase genes from peanut (*Arachis hypogaea L.*). *PLoS One* **2014**, *9*, e105834.
(92) Hernandez, M. L.; Whitehead, L.; He, Z.; Gazda, V.; Gilday, A.; Kozhevnikova, E.; Vaistij, F. E.; Larson, T. R.; Graham, I. A. A cytosolic acyltransferase contributes to triacylglycerol synthesis in sucrose-rescued *Arabidopsis* seed oil catabolism mutants. *Plant Physiol.* **2012**, *160*, 215−25.
(93) Kelley, M. J.; Carman, G. M. Purification and characterization of CDP-diacylglycerol synthase from *Saccharomyces cerevisiae*. *J. Biol. Chem.* **1987**, *262*, 14563−14570.
(94) Wang, Y.; Lu, S.; Wang, J.; Ma, Q.; Yang, J.; Li, X.; Yuan, Y. J. Phospholipid metabolism in an industry microalga *Chlorella sorokiniana*: the impact of inoculum sizes. *PLoS One* **2013**, *8*, e70827.
(95) Kosa, M.; Ragauskas, A. J. Lipids from heterotrophic microbes: advances in metabolism research. *Trends Biotechnol.* **2011**, *29*, 53−61.
(96) Kosodo, Y.; Imai, K.; Hirata, A.; Noda, Y.; Takatsuki, A.; Adachi, H.; Yoda, K. Multicopy suppressors of the sly1 temperature-sensitive

DOI: 10.1021/jf505975k
J. Agric. Food Chem. 2015, 63, 3067−3077

mutation in the ER-Golgi vesicular transport in *Saccharomyces cerevisiae*. *Yeast* **2001**, *18*, 1003−1014.
(97) Bon, E.; Recordon Navarro, P.; Durrens, P.; Iwase, M.; Toh, E. A.; Aigle, M. A network of proteins around Rvs167p and Rvs161p, two proteins related to the yeast actin cytoskeleton. *Yeast* **2000**, *16*, 1229−1241.
(98) Drees, B. L.; Sundin, B.; Brazeau, E. A protein interaction map for cell polarity development. *J. Cell Biol.* **2001**, *154*, 549−571.
(99) Han, G. S.; Johnston, C. N.; Chen, X. M.; Athenstaedt, K.; Daum, G.; Carman, G. M. Regulation of the *Saccharomyces cerevisiae DPP1*-encoded diacylglycerol pyrophosphate phosphatase by zinc. *J. Biol. Chem.* **2001**, *276*, 10126−10133.
(100) Furneisen, J. M.; Carman, G. M. Enzymological properties of the *LPP1*-encoded lipid phosphatase from *Saccharomyces cerevisiae*. *Biochim. Biophys. Acta, Mol. Cell Biol. Lipids* **2000**, *1484*, 71−82.

DOI: 10.1021/jf505975k
J. Agric. Food Chem. 2015, 63, 3067−3077

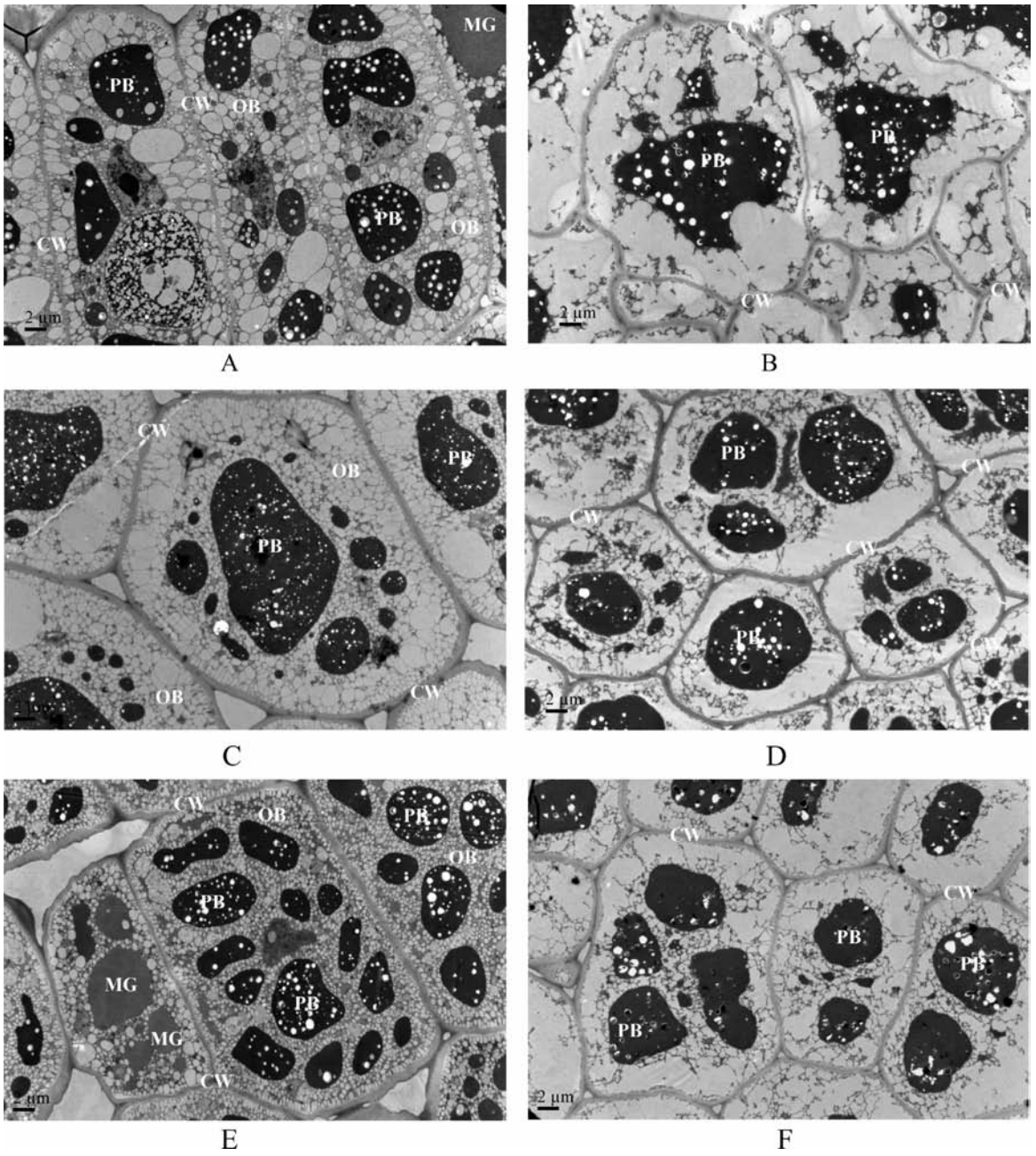

Figure 1. Transmission electron microscopy of two types of *Brassica napus* rapeseed and *Brassica juncea* mustard without or with microwave treatment: (A) *B. napus* rapeseed (intermediate-glucosinolate; as-is); (B) *B. napus* rapeseed (intermediate-glucosinolate) microwaved for 5 min; (C) *B. napus* rapeseed (low-glucosinolate; as-is); (D) *B. napus* rapeseed (low-glucosinolate) microwaved for 5 min; (E) *B. juncea* mustard (high-glucosinolate; as-is); (F) *B. juncea* mustard (high glucosinolate) microwaved for 5 min. CW, cell wall; PB, protein bodies; MG, myrosin cells; OB, oil bodies. Magnification: ×4000.

Crops Research Institute, Chinese Academy of Agricultural Sciences, Hubei Province, People's Republic of China. *Brassica juncea* mustard (high-glucosinolate; ∼130 μmol/g, fat-free basis; moisture content = 11.0%) was provided by the Institute of Economic Crops, Xinjiang Academy of Agricultural Sciences, Xinjiang Province, People's Republic of China. All seeds were produced in 2012.

Sample Preparation and Treatments. The seed samples (400 g each) were subjected to microwave irradiation (MarsX, CEM, Matthews, NC, USA) at a frequency of 2450 MHz at a medium power of 800 W for 1, 2, 3, 4, 5, and 6 min. All microwave-treated samples were allowed to cool to room temperature for 60 min. The samples without or with microwave heating were expeller-pressed using an oil expeller at a feeding rate of 3 kg h^{-1} and barrel temperature of no more than 90 °C (KOMET CA59G, IBG Monforts Oekotec GmbH & Co. KG, Germany).

Microscopy Analysis. The seed samples were fixed with 2.5% glutaraldehyde in phosphate buffer (pH 7.0) for 4 h, washed three times with phosphate buffer, postfixed with 1% of OsO_4 in phosphate buffer (pH 7.0) for 1 h, and washed three times in the phosphate buffer. The samples were then dehydrated in the progressive ethanol solutions of 50, 70, 80, 90, 95, and 100% for about 15−20 min at each solution, embedded in acetone and Spurr resin. Sections 70−90 nm in size were cut from the embedded tissue using a microtome (Ultracut E, Reichert-Jung, Vienna, Austria), double stained with uranyl acetate and lead citrate, and then were examined under a transmission electron microscope (H-7650, Hitachi Instrument, Tokyo, Japan).

DOI: 10.1021/jf504872x
J. Agric. Food Chem. 2015, 63, 3078−3084

Chemical Analyses. The samples were ground and were adjusted to the same moisture content by exposure to room humidity for 7 days at 25 °C.[11] The samples were then defatted with hexane for 6 h and air-dried. Oil content and neutral detergent fiber (NDF) were analyzed according to AOAC (1990) method 920.39 and Van Soest et al.,[12] respectively.

Glucosinolate analysis was performed as described by Slominski and Campbell.[13] Briefly, 100 mg of high-glucosinolate or 300 mg of low-glucosinolate samples was weighed into 15 mL centrifuge tubes. Two milliliters of methanol, 1.0 mL of benzyl glucosinolate (internal standards, 0.5 mM), and 0.1 mL of lead−barium acetate were added to the tubes, extracted for 3 h at room temperature, and then centrifuged. Two milliliters of supernatant was transferred to a DEAE-Sephadex column, which was washed successively with 1 mL each of 67% methanol, water, and pyridine acetate. Purified sulfatase solution was then added to the column, and the contents were incubated at room temperature overnight. The resulting desulfated glucosinolates were eluted with 2 mL of 60% methanol and evaporated under nitrogen. The dry residue was trimethylsilylated by adding 0.2 mL of a mixture of anhydrous acetone/*N*,*O*-bis(trimethylsilyl)acetamide (BSA)/trimethylchlorosilane (TMCS)/1-methylimidazole (2:1:0.1:0.05 v/v) and incubated for 30 min at room temperature. The trimethylsilyl derivatives of desulfoglucosinolates were separated by gas−liquid chromatography using a glass column (1.2 m × 2 mm i.d.) packed with 2% OV-7 on Chromosob W (HP) (100−120 mesh) with helium gas at a flow rate of 40 mL/min. The oven temperature was kept at 200 °C for 4 min and then increased at 5 °C min^{-1} to 275 °C. Injection port and detector temperatures were 280 and 300 °C, respectively.

Myrosinase activity was determined by difference between total sample glucosinolate content and the glucosinolates remaining following incubation of the sample with distilled water (autolysis) at 40 °C for a defined period of time. Glucosinolate analysis was conducted as described above. One unit of myrosinase activity was defined as the amount of enzyme that catalyzes the hydrolysis of 1 μmol of glucosinolate per 1 min.

The analyses of moisture content, oil content, NDF, and glucosinolate content were run in triplicate, wheereas those for myrosinase activity were run in duplicate.

Statistical Analysis. All of the statistical analysis was conducted by the SAS program (version 9.1, SAS Institute Inc., Cary, NC, USA). Means were separated by Tukey's honestly significant difference. All statements of significance were based on $P \leq 0.05$.

RESULTS AND DISCUSSION

Effect of Microwave Treatment on Microstructure of the Seed. The effect of microwave heating (400 g, 800 W) on the microstructure of the seed samples is shown in Figure 1. The microstructure of the intact (unheated) seed revealed well-defined pattern of protein bodies and intact myrosin cells amid oil bodies with smooth cell walls. In high-glucosinolate *B. juncea* (E) and intermediate-glucosinolate *B. napus* (A) myrosin cells were quite visible, whereas there were almost no visible myrosin cells in the seed of low-glucosinolate rapeseed (C). The microstructure of all samples changed significantly after 5 min of microwave heating (see images F, B, and D) with the oil bodies and myrosin cells almost disappearing. The microscopy images clearly demonstrate that microwave treatment disrupts the membranes of oil bodies as well as other intracellular organelles.

Most of the biological membranes of rapeseed are composed of phospholipids and proteins (i.e., oleosins) with the oil bodies covered by a single-layer membrane. Eighty percent of this layer is filled with phospholipids, and the other 20% is occupied by oleosins. Phospholipids constitute a polar headgroup and a nonpolar fatty acid region.[14] It has been reported that the composition of phospholipids in the oil bodies would account for 60% of phosphatidylcholine, 6% of phosphatidylethanolamine, 14% of phosphatidylinositol, and 20% of phosphatidylserine. According to Valentov et al.,[15] microwave treatment could improve the content of phospholipids in the crude oil by more than twice, which would be a consequence of the membrane rupture. A strong relationship between oil bodies' stability and oil extractability has been reported,[16] indicating that the oil from the microwave-treated rapeseed should be easier to extract.

Myrosin cells are the subcellular compartments associated with enzyme myrosinase. Normally, glucosinolates are located in vacuoles and are separated from the myrosin cells.[17] The presence of the glucosinolate−myrosinase system is characteristic of the Brassicaceae family, and it serves as a defense system against biotic and abiotic stressors.[18] Disruption of the tissue induced by mechanical damage, infection, or pest attack brings glucosinolates into contact with myrosinase,[19] resulting in their hydrolysis to biologically active and often toxic breakdown products, including isothiocyanates, goitrin, and nitriles. After microwave treatment, it appeared evident that the structure of myrosin cells was effectively damaged, indicating the potential for myrosinase to come into contact with glucosinolates.

In Figure 1 images A, C, and E, the cells of rapeseed were well coherent, and the shape was smooth, whereas in the microwave-treated samples (i.e., images B, D, and F) the cell walls became folded. This phenomenon may be ascribed to the water loss of the cells, as documented by Niu et al.[20] As illustrated in Figure 2, there was a significant decline in moisture content of *B. napus* rapeseed and *B. juncea* mustard.

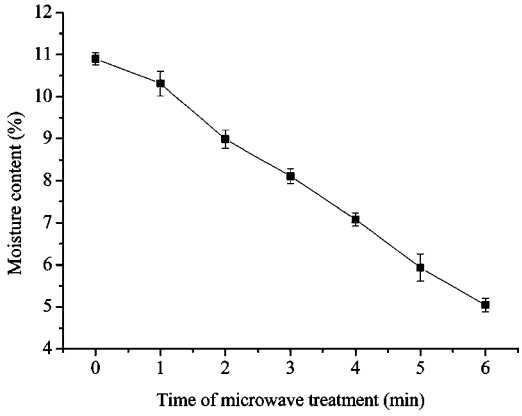

Figure 2. Effect of time of microwave heating on mean moisture content of *B. napus* rapeseed and *B. juncea* mustard.

Effect of Microwave Treatment on Oil Content of Expeller Meal. The effect of time of microwave heating on the oil content of seed and expeller meal of two types of *B. napus* rapeseed and *B. juncea* mustard is shown in Table 1. The oil contents of *B. napus* rapeseed (intermediate- and low-glucosinolate) and *B. juncea* mustard were similar. After expeller-pressing, however, the oil content of expeller meal decreased significantly with increased time of microwave heating. After 6 min of microwave heating, the oil content of intermediate- and low-glucosinolate *B. napus* rapeseed and of *B. juncea* mustard expeller meal decreased from 26.6, 22.6, and 29.8 to 13.5, 11.3, and 14.1%, respectively. Overall, the microwave treatment decreased the oil content of expeller meal by 49−53% with an oil extraction rate of 79−83%.

The oil contents of expeller meals are in agreement with the changes in microstructure of microwave-treated seed showing

DOI: 10.1021/jf504872x
J. Agric. Food Chem. 2015, 63, 3078−3084

Table 1. Effect of Time of Microwave Heating on Oil Content of Seed and Expeller Meal of Two Types of *Brassica napus* Rapeseed and *Brassica juncea* Mustard (Percent, As-Is Basis)

		time of microwave heating					
sample	untreated	1 min	2 min	3 min	4 min	5 min	6 min
B. napus rapeseed (intermediate-glucosinolate)							
seed	44.9 ± 0.3a[a]	45.0 ± 0.4a	44.2 ± 0.5a	44.4 ± 0.7a	44.9 ± 0.9a	44.0 ± 0.2a	43.7 ± 0.6a
expeller meal	26.6 ± 0.8a	23.6 ± 0.9b	20.6 ± 0.2c	18.0 ± 0.3d	16.7 ± 1.0e	15.3 ± 0.6f	13.5 ± 0.3g
B. napus rapeseed (low-glucosinolate)							
seed	42.6 ± 0.3a	42.0 ± 0.8a	42.5 ± 0.1a	41.3 ± 0.2a	41.5 ± 0.2a	42.5 ± 0.6a	42.4 ± 0.4a
expeller meal	22.6 ± 0.5a	22.9 ± 0.3a	19.4 ± 1.0b	17.4 ± 0.7c	15.2 ± 0.9d	14.2 ± 0.5d	11.3 ± 0.9e
B. juncea mustard (high-glucosinolate)							
seed	44.4 ± 0.4a	44.1 ± 0.2a	44.1 ± 0.2a	44.0 ± 0.2a	43.4 ± 0.1a	43.2 ± 0.2a	43.1 ± 0.2a
expeller meal	29.8 ± 0.4a	27.3 ± 0.5b	22.4 ± 0.1c	18.8 ± 0.3d	15.9 ± 0.7e	14.4 ± 0.6f	14.1 ± 0.3g

[a]Mean ± SD. Values within rows with the same letter (a–g) are not significantly different ($P \leq 0.05$).

Table 2. Effect of Time of Microwave Heating on Neutral Detergent Fiber (NDF) Content of Seed and Expeller Meal of Two Types of *Brassica napus* Rapeseed and *Brassica juncea* Mustard (Percent, As-Is, Fat-Free Basis)

		time of microwave heating					
sample	untreated	1 min	2 min	3 min	4 min	5 min	6 min
B. napus rapeseed (intermediate-glucosinolate)							
seed	23.7 ± 0.1a[a]	23.8 ± 0.5a	24.1 ± 0.4a	23.8 ± 0.7a	24.3 ± 0.5a	23.9 ± 0.5a	24.6 ± 0.7a
expeller meal	22.7 ± 0.4b	24.1 ± 0.7b	23.7 ± 0.1b	23.1 ± 0.4b	23.2 ± 0.2b	24.7 ± 0.2b	29.2 ± 2.2a
B. napus rapeseed (low-glucosinolate)							
seed	22.0 ± 0.5a	22.4 ± 1.0a	23.0 ± 0.2a	22.4 ± 0.4a	22.4 ± 0.4a	22.2 ± 0.9a	22.1 ± 0.7a
expeller meal	23.6 ± 0.3a	24.8 ± 0.4a	23.0 ± 0.1a	24.1 ± 1.7a	25.1 ± 1.7a	25.9 ± 1.3a	25.6 ± 1.4a
B. juncea mustard (high-glucosinolate)							
seed	17.5 ± 1.3a	18.1 ± 0.5a	17.5 ± 1.3a	18.6 ± 1.5a	18.3 ± 0.5a	18.0 ± 0.8a	19.6 ± 1.0a
expeller meal	17.4 ± 1.0a	16.8 ± 0.2a	18.9 ± 2.2a	17.3 ± 1.3a	16.8 ± 0.3a	18.8 ± 2.8a	17.6 ± 0.8a

[a]Mean ± SD. Values within rows with the same letter (a, b) are not significantly different ($P \leq 0.05$).

Table 3. Effect of Time of Microwave Heating on Myrosinase Activity of Seed of Two Types of *Brassica napus* Rapeseed and *Brassica juncea* Mustard (Units per Minute, As-Is, Fat-Free Basis)

		time of microwave heating					
sample	untreated	1 min	2 min	3 min	4 min	5 min	6 min
B. napus rapeseed (intermediate-glucosinolate)	32.7 ± 0.9a[a]	27.6 ± 1.5b	22.8 ± 1.5c	16.8 ± 0.6d	5.6 ± 0.6e	3.6 ± 0.8f	nd[b]
B. napus rapeseed (low-glucosinolate)	11.6 ± 0.4b	14.9 ± 0.1a	13.6 ± 0.2a	8.0 ± 0.5c	5.5 ± 0.4d	5.2 ± 0.2d	4.2 ± 0.4d
B. juncea mustard (high-glucosinolate)	49.2 ± 2.5a	26.2 ± 4.2b	26.9 ± 1.7b	11.2 ± 1.7c	nd	nd	nd

[a]Mean ± SD. Values within rows with the same letter (a–f) are not significantly different ($P \leq 0.05$). [b]Not detected.

the broken membranes of oil bodies, which, in turn, facilitated higher efficacy of oil extraction during expeller-pressing. The oil extraction rate by expeller-pressing after 6 min of microwave heating used in the current study was similar to the conditioning of the seed at 80 °C for 30 min, flaking of the seed, and then expeller-pressing.[21] In another study, similar results were achieved when the seed was subjected to 40 min of heat treatment with the temperature increased to 80 °C and then heat treatment at 80 °C for 30 min followed by 40 min of flaking to 0.3 mm thickness and expeller pressing under a barrel temperature of 105–110 °C.[1] According to Grageola et al.[22] expeller-pressing recovers around 75% of oil from canola seed. This indicates that the microwave treatment could be an effective method of increasing the efficacy of oil extraction by expeller pressing and would facilitate oil extraction down to the industry standards of 8–10% of residual oil. which, in turn, would prevent the need for double pressing.

Effect of Microwave Treatment on NDF Content of Expeller Meal. The effect of time of microwave heating on NDF content of seed and expeller meal is shown in Table 2. The contents of NDF in the seed and expeller meal of two types of *B. napus* rapeseed and *B. juncea* mustard were different, with *B. juncea* showing significantly less fiber than *B. napus*. This is due to the fact that *B. juncea* mustard is yellow-seeded, whereas *B. napus* rapeseed is black-seeded. The yellow seed coat color is a visual marker of lower polyphenol (i.e., proanthocyanidin) content and a thinner seed hull. As a result, black-seeded rapeseed contains more fiber than its yellow-seeded *B. napus* counterparts or *B. juncea* mustard.[23] After microwave heating for 6 min, the NDF contents of all seed samples were similar, so there was no significant effect of heat treatment on fiber content. In the expeller meals, however, the NDF content of intermediate-glucosinolate *B. napus* rapeseed increased from 24.1 to 29.2% after 6 min of microwave heating, whereas in low-glucosinolate *B. napus* rapeseed and *B. juncea* mustard no significant changes were observed. It is well-known that heat treatment of oilseeds during processing may lead to losses of digestible amino acids due to the formation of Maillard reaction products. This highly indigestible fraction, often referred to as a neutral detergent insoluble crude protein

DOI: 10.1021/jf504872x
J. Agric. Food Chem. 2015, 63, 3078–3084

Table 4. Effect of Time of Microwave Heating on Total Glucosinolate Content of Seed and Expeller Meal of Two Types of *Brassica napus* Rapeseed and *Brassica juncea* Mustard (Micromoles per Gram, As-Is, Fat-Free Basis)

		time of microwave heating					
sample	untreated	1 min	2 min	3 min	4 min	5 min	6 min
B. napus rapeseed (intermediate-glucosinolate)							
seed	58.4 ± 6.2a[a,b]	53.9 ± 3.0ab	54.4 ± 1.7ab	54.4 ± 3.1ab	51.2 ± 3.7abc	46.8 ± 2.8bc	43.0 ± 3.4c
expeller meal	12.2 ± 0.1ef	11.6 ± 0.5f	16.4 ± 2.7e	28.9 ± 2.1d	44.9 ± 2.9b	53.5 ± 3.7a	38.7 ± 2.0c
B. napus rapeseed (low-glucosinolate)							
seed	18.3 ± 2.7ab[b]	18.3 ± 1.4ab	20.8 ± 2.3a	17.4 ± 0.9ab	15.1 ± 0.5bc	13.9 ± 1.0bc	11.6 ± 1.7c
expeller meal	7.7 ± 0.1e	8.0 ± 0.3de	9.3 ± 0.3cd	11.2 ± 0.3ab	11.9 ± 0.6a	10.2 ± 1.5bc	7.7 ± 0.1e
B. juncea mustard (high-glucosinolate)							
seed	134.9 ± 2.1a[c]	137.3 ± 17.6a	135.7 ± 1.9a	146.4 ± 16.2a	135.4 ± 4.8a	131.0 ± 3.9a	135.9 ± 5.1a
expeller meal	20.8 ± 1.5e	29.8 ± 3.0e	67.1 ± 5.4d	106.5 ± 9.1c	150.5 ± 9.9a	134.4 ± 2.9b	132.1 ± 9.5b

[a]Mean ± SD. Values within rows with the same letter (a–f) are not significantly different ($P \leq 0.05$). [b]Includes gluconapin (3-butenyl), glucobrassicanapin (4-pentenyl), progoitrin (2-hydroxy-3-butenyl), gluconapoleiferin (2-hydroxy-4-pentenyl), glucobrassicin (3-indolylmethyl), and 4-hydroxyglucobrassicin (4-hydroxy-3-indolylmethyl). [c]Includes sinigrin (2-propenyl), gluconapin (3-butenyl), progoitrin (2-hydroxy-3-butenyl), gluconapoleiferin (2-hydroxy-4-pentenyl), and 4-hydroxyglucobrassicin (4-hydroxy-3-indolylmethyl).

(NDICP), would contribute to the increase in the NDF content of heat-treated products and would significantly affect the nutritive value of rapeseed/canola meal.[24] In the current study, expeller pressing of intermediate-glucosinolate *B. napus* rapeseed microwave heated for 6 min resulted in some protein damage as documented by the increase in NDF content which, in turn, could lead to reduced protein and amino acid digestibilities. Therefore, extending the time of microwave treatment could further contribute to protein damage and the increase in NDICP content of expeller meal.

Effect of Microwave Treatment on Myrosinase Activity of the Seed. As illustrated in Table 3, there was a significant decline in myrosinase (thioglucoside glucohydrolase, EC 3.2.3.1) activity with increased time of microwave heating for two types of *B. napus* and *B. juncea* seed. This is in agreement with a study by Verkerk and Dekker,[25] who demonstrated that myrosinase in microwave-treated cabbage almost completely lost its hydrolytic capacity, despite the fact that the stability of myrosinase is strongly dependent on the water content,[26] which was most likely much higher in cabbage than in the seed samples used in the current study (i.e., 10%). When compared with *B. napus* intermediate-glucosinolate rapeseed and *B. juncea* mustard, the myrosinase activity in *B. napus* low-glucosinolate rapeseed was relatively low, although the enzyme per se appeared to be more heat-stable with some activity still being present after 6 min of microwave treatment.

Among other reasons, application of heat treatment in any crushing operation of rapeseed is essential for an effective inactivation of myrosinase enzyme. In the presence of moisture and following rupture of the seed, this enzyme would hydrolyze glucosinolates to unstable aglucones, which would then break down to yield a range of products, including isothiocyanates, goitrin, nitriles, and thiocyanates, that interfere with the function of the thyroid gland and would adversely affect growth performance of monogastric animals.[24] Therefore, it is critical that myrosinase is effectively inactivated by heat treatment prior to seed expelling.

Effect of Microwave Treatment on Glucosinolate Content of Seed and Expeller Meal. The effect of time of microwave heating on total glucosinolate content in seed and expeller meal is shown in Table 4. The total glucosinolate content of *B. napus* seed samples decreased after 4 min of microwave heating. It is of interest to note that in the seed of *B. juncea* mustard the total glucosinolate content did not change during microwave heating. The glucosinolate content of the corresponding expeller meals was much lower and reflected the hydrolysis of glucosinolates by myrosinase during the expelling process. However, their contents increased with increased time of microwave heating and, thus, myrosinase inactivation and then decreased due to excessive time of microwave heating, which coincided with the decrease in glucosinolate content in the seed samples for 5–6 min. More specifically, the glucosinolate content of expeller meal of *B. juncea* mustard and intermediate-glucosinolate *B. napus* rapeseed increased significantly during microwave heating for 4 and 5 min, respectively, and then decreased. Somewhat similar changes, although not significant, were observed for low-glucosinolate *B. napus* rapeseed.

According to their structure, glucosinolates can be divided into aliphatic glucosinolates, including sinigrin, gluconapin, glucobrassicanapin, and progoitrin, and indole glucosinolates, including glucobrassicin and 4-hydroxyglucobrassicin. In different *Brassica* species the compositions of glucosinolates are different. The major glucosinolates of *B. napus* rapeseed are gluconapin, progoitrin, and 4-hydroxyglucobrassicin, whereas sinigrin and gluconapin are the predominant glucosinolates of *B. juncea* mustard.

It is well-known that heat treatment and myrosinase activity are the factors that affect the glucosinolate content during processing.[27] It has also been shown that indole glucosinolates are more susceptible to thermal degradation than aliphatic glucosinolates.[27−30] As a result, the decrease in total glucosinolate content due to microwave heating observed in the current study was more pronounced for two types of *B. napus* rapeseed than for *B. juncea* mustard.

The effect of time of microwave heating on the major glucosinolate contents in the seed and expeller meal samples of two types of *B. napus* rapeseed and *B. juncea* mustard are shown in Figures 3, 4, and 5. When compared to the seed samples, the aliphatic glucosinolates gluconapin and progoitrin contents of the corresponding expeller meal samples of intermediate-glucosinolate *B. napus* rapeseed (Figure 3) increased significantly after 3 min, which was directly related to myrosinase inactivation and thus lack of glucosinolate autolysis. The decrease after 6 min of microwave treatment was a consequence of extended microwave heating. The indole glucosinolate hydroxyglucobrassicin content of expeller meal demonstrated a less clear pattern, probably due to its

DOI: 10.1021/jf504872x
J. Agric. Food Chem. 2015, 63, 3078−3084

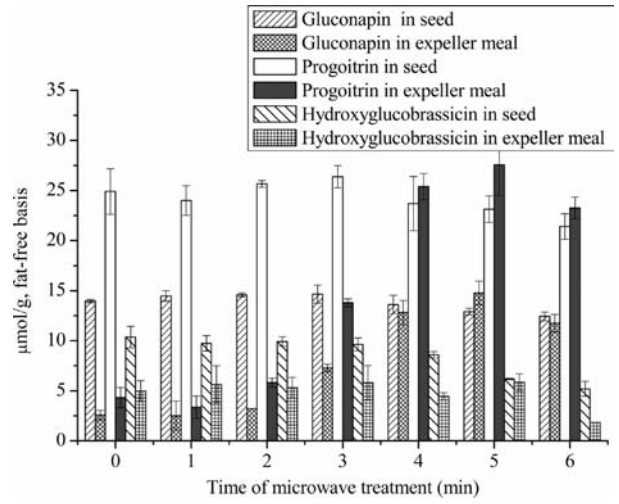

Figure 3. Effect of time of microwave heating on major glucosinolate of *B. napus* intermediate-glucosinolate rapeseed and expeller meal.

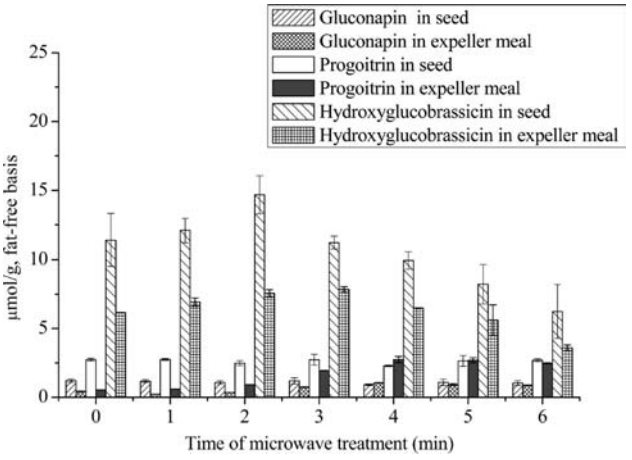

Figure 4. Effect of time of microwave heating on major glucosinolate of *B. napus* low-glucosinolate rapeseed and expeller meal.

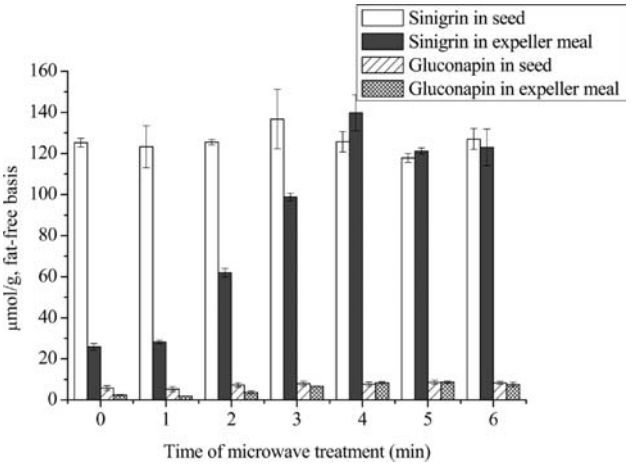

Figure 5. Effect of time of microwave heating on major glucosinolate of *B. juncea* high-glucosinolate mustard seed and expeller meal.

pronounced thermal decomposition in the seed during 5 or 6 min of microwave heating. The glucosinolate content of the seed and expeller meal samples of low-glucosinolate *B. napus* rapeseed (Figure 4) showed a similar pattern with the indole glucosinolate hydroxyglucobrassicin showing a significant thermal decomposition after 4, 5, and 6 min. Overall, the content of hydroxyglucobrassicin in the seed of intermediate- and low-glucosinolate *B. napus* rapeseed decreased by 50 and 53%, respectively, after 6 min of microwave heating. As aliphatic glucosinolates are less sensitive to heat treatment, sinigrin and gluconapin contents of *B. juncea* mustard seed showed no significant differences with increased time of microwave heating (Figure 5). However, their content after 4, 5, and 6 min of microwave treatment reached the level of that of the seed, which was a consequence of complete myrosinase inactivation.

There was a strong negative relationship between myrosinase activity in the seed (Table 3) and the total glucosinalate content in the corresponding expeller meals (Table 4) with intermediate-glucosinolate *B. napus* rapeseed and *B. juncea* mustard showing R^2 values of −0.92 and −0.92, respectively.

In a study on the effect of microwave treatment on the glucosinolate content of canola seed, Ebrahimi et al.[9] reported that the glucosinolate content after 2, 4, and 6 min of microwave heating decreased by 42, 55, and 59%, respectively, which was significantly higher than that observed in the current study. The main reason for the difference could be related to the processing method used. In their study, canola seed was dried at 55 °C for 48 h, after which time water was added to increase the moisture content to 25%. It is very probable that drying of the seed inactivated the myrosinase activity, whereas the heat produced during microwave treatment under high moisture conditions facilitated glucosinalate degradation.

In conclusion, it would appear evident that microwave heating of 2 W kg^{-1} for 6 min could be an effective method of producing expeller meal without toxic glucosinolate breakdown products while at the same time increasing the yield of oil during the expelling process.

AUTHOR INFORMATION

Corresponding Author

*(B.A.S.) Phone: (204) 474-8291. Fax: (204) 474-7628. E-mail: Bogdan.Slominski@umanitoba.ca.

Funding

Funding of this study was provided by the National Natural Science Foundation of China (Grant 31201461) and the Canola Council of Canada.

Notes

The authors declare no competing financial interest.

ACKNOWLEDGMENTS

We acknowledge Ruibao Zhou, He'nan University of Technology, and Junying Li, Zhejiang University, for their assistance in microstructure analysis and Zirong Guo, Mianyang Academy of Agricultural Sciences, Sichuan, for providing the samples.

ABBREVIATIONS USED

NDF, neutral detergent fiber; BSA, *N,O*-bis(trimethylsilyl)-acetamide; TMCS, trimethylchlorosilane; NDICP, neutral detergent insoluble crude protein

REFERENCES

(1) Prior, E. M.; Vadke, V. S.; Sosulski, F. W. Effect of heat treatments on canola press oils. I. Non-triglyceride components. *J. Am. Oil Chem. Soc.* **1991**, *68*, 401−406.

DOI: 10.1021/jf504872x
J. Agric. Food Chem. 2015, 63, 3078−3084

(2) Azadmard-Damirchi, S.; Habibi-Nodeh, F.; Hesari, J.; Nemati, M.; Achachlouei, B. F. Effect of pretreatment with microwaves on oxidative stability and nutraceuticals content of oil from rapeseed. *Food Chem.* **2010**, *121*, 1211−1215.
(3) Lanzani, A.; Petrini, M. C.; Cozzoli, O.; Gallavresi, P.; Carola, C.; Jacini, G. On the use of enzymes for vegetable-oil extraction. A preliminary report. *Riv. Ital. Sostanze Grasse* **1975**, *L11*, 226−229.
(4) Oberndorfer, C.; Pawelzik, E.; Lückea, W. Prospects for the application of dielectric heating processes in the pre-treatment of oilseeds. *Eur. J. Lipid Sci. Technol.* **2000**, *102*, 487−493.
(5) Szydlowska-Czerniak, A.; Trokowski, K.; Karlovits, G.; Szlyk, E. Determination of antioxidant capacity, phenolic acids, and fatty acid composition of rapeseed varieties. *J. Agric. Food Chem.* **2010**, *58*, 7502−7509.
(6) Zhou, Q.; Yang, M.; Huang, F.; Zheng, C.; Deng, Q. Effect of pretreatment with dehulling and microwaving on the flavor characteristics of cold-pressed rapeseed oil by GC-MS-PCA and electronic nose discrimination. *J. Food Sci.* **2013**, *78*, C961−C970.
(7) Ponne, C. T.; Moller, A. C.; Tijskens, M. M.; Bartels, P. V.; Meijer, M. M. T. Influence of microwave and steam heating on lipase activity and microstucture of rapeseed (*Barassica napus*). *J. Agric. Food Chem.* **1996**, *44*, 2818−2824.
(8) Sadeghi, A. A.; Shawrang, P. Effects of microwave irradiation on ruminal degradability and *in vitro* digestibility of canola meal. *Anim. Feed Sci. Technol.* **2006**, *127*, 45−54.
(9) Ebrahimi, S. R.; Nikkhah, A.; Sadeghi, A. A. Changes in nutritive value and digestion kinetics of canola seed due to microwave irradiation. *Asian−Aust. J. Anim. Sci.* **2010**, *23*, 347−354.
(10) Wiesenborn, D.; Doddapaneni, R.; Tostenson, K.; Kangas, N. Cooking indices to predict screw-press performance for crambe seed. *J. Am. Oil Chem. Soc.* **2001**, *78*, 467−471.
(11) Tao, K. J. Factors causing variations in the conductivity test for soybean seeds. *J. Seed Technol.* **1978**, *3*, 10−18.
(12) Van Soest, P. J.; Robertson, J. B.; Lewis, B. A. Methods for dietary fiber, neutral detergent fiber and nonstarch polysaccharides in relation to animal nutrition. *J. Dairy Sci.* **1991**, *74*, 3583−3597.
(13) Slominski, B. A.; Campbell, L. D. Gas chromatographic determination of indole glucosinolates − a re-examination. *J. Sci. Food Agric.* **1987**, *40*, 131−143.
(14) Deleu, M.; Vaca-Medina, G.; Fabre, J.-F.; Roïz, J.; Valentin, R.; Mouloungui, Z. Interfacial properties of oleosins and phospholipids from rapeseed for the stability of oil bodies in aqueous medium. *Colloid Surf. B* **2010**, *80*, 125−132.
(15) Valentová, O.; Novotná, Z.; Svoboda, Z.; Schwarz, W.; Káš, J. Microwave heating and γ-irradiation treatment of rapeseed (*Brassica napus*). *J. Food Lipids* **2000**, *7*, 237−245.
(16) Jolivet, P.; Deruyffelaere, C.; Boulard, C.; Quinsac, A.; Savoire, R.; Nesi, N.; Chardot, T. Deciphering the structural organization of the oil bodies in the *Brassica napus* seed as a means to improve the oil extraction yield. *Ind. Crops Prod.* **2013**, *44*, 549−557.
(17) Bones, A. M.; Rossiter, J. T. The myrosinase-glucosinolate system, its organization and biochemistry. *Physiol. Plant.* **1996**, *97*, 194−208.
(18) Ahuja, I.; Borgen, B. H.; Hansen, M.; Honne, B. I.; Muller, C.; Rohloff, J.; Rossiter, J. T.; Bones, A. M. Oilseed rape seeds with ablated defence cells of the glucosinolate-myrosinase system. Production and characteristics of double haploid *MINELESS* plants of *Brassica napus* L. *J. Exp. Bot.* **2011**, *62*, 4975−4993.
(19) Chen, S.; Andreasson, E. Update on glucosinolate metabolism and transport. *Plant Physiol. Biochem.* **2001**, *39*, 743−758.
(20) Niu, Y.; Jiang, M.; Wan, C.; Yang, M.; Hu, S. Effect of microwave treatment on sinapic acid derivatives in rapeseed and rapeseed meal. *J. Am. Oil Chem. Soc.* **2013**, *90*, 307−313.
(21) Kraljic, K.; Skevin, D.; Pospisil, M.; Obranovic, M.; Nederal, S.; Bosolt, T. Quality of rapeseed oil produced by conditioning seeds at modest temperatures. *J. Am. Oil Chem. Soc.* **2013**, *90*, 589−599.
(22) Grageola, F.; Landero, J. L.; Beltranena, E.; Cervantes, M.; Araiza, A.; Zijlstra, R. T. Energy and amino acid digestibility of expeller-pressed canola meal and cold-pressed canola cake in ileal-cannulated finishing pigs. *Anim. Feed Sci. Technol.* **2013**, *186*, 169−176.
(23) Slominski, B. A.; Jia, W.; Rogiewicz, A.; Nyachoti, C. M.; Hickling, D. Low-fiber canola. Part 1. Chemical and nutritive composition of the meal. *J. Agric. Food Chem.* **2012**, *60*, 12225−12230.
(24) Khajali, F.; Slominski, B. A. Factors that affect the nutritive value of canola meal for poultry. *Poult. Sci.* **2012**, *91*, 2564−2575.
(25) Verkerk, R.; Dekker, M. Glucosinolates and myrosinase activity in red cabbage (*Brassica oleracea* L. var. *capitata* f. *rubra* DC.) after various microwave treatments. *J. Agric. Food Chem.* **2004**, *52*, 7318−7323.
(26) Oliviero, T.; Verkerk, R.; Van Boekel, M. A. J. S.; Dekker, M. Effect of water content and temperature on inactivation kinetics of myrosinase in broccoli (*Brassica oleracea* var. *italica*). *Food Chem.* **2014**, *163*, 197−201.
(27) Campbell, L. D.; Slominski, B. A. Extent of thermal decomposition of indole glucosinolates during the processing of canola seed. *J. Am. Oil Chem. Soc.* **1990**, *67*, 73−75.
(28) Slominski, B. A.; Campbell, L. D. Formation of indole glucosinolate breakdown products in autolyzed, steamed and cooked *Brassica* vegetables. *J. Agric. Food Chem.* **1989**, *37*, 1297−1299.
(29) Jensen, S. K.; Liu, Y.G.; Eggum, B. O. The effect of heat treatment on glucosinolates and nutritive value of rapeseed meal in rat. *Anim. Feed Sci. Technol.* **1995**, *53*, 17−28.
(30) Oliviero, T.; Verkerk, R.; Van Boekel, M. A. J. S.; Dekker, M. Effect of water content and temperature on glucosinolate degradation kinetics in broccoli (*Brassica oleracea* var. *italica*). *Food Chem.* **2012**, *132*, 2037−2045.

DOI: 10.1021/jf504872x
J. Agric. Food Chem. 2015, 63, 3078−3084

Table 1. Characteristics of Grain Shape, Grain Weight, and Head Rice Percentage According to Ripening Temperature[a]

		grain size characteristics of milled rice					
cultivar	ripening temperature (°C)	length (mm)	width (mm)	thickness (mm)	length/width	1000-grain weight (g)	head rice (%)
Ilpum	22/14	4.81c	3.01a	2.09b	1.60b	21.7a	62.5b
	25/17	5.12a	3.04a	2.20a	1.69a	21.5a	82.0a
	28/20	4.90b	2.97ab	2.22a	1.65a	20.3b	83.9a
	31/23	4.79c	2.90b	2.03b	1.65a	20.1c	71.0b
Chucheong	22/14	4.84a	2.80b	2.09ab	1.73a	19.8a	77.7c
	25/17	4.78a	2.92a	2.12ab	1.64c	19.8a	80.1c
	28/20	4.70b	2.81b	2.06b	1.68bc	19.5b	88.7a
	31/23	4.81a	2.84b	2.14a	1.69ab	18.9c	84.8b

[a]Values with the same letter in a column are not significantly different according to a Duncan's multiple-range test ($p < 0.05$).

The 24 h temperature regimens for day/night during the grain-filling period were 22/14, 25/17, 28/20, and 31/23 °C, changed at 1 h intervals. This 8 °C gap between day and night during the grain-filling period was based on the climate data (30 year average) of 1971−2000 from the Korea Meteorological Administration. The relative humidity in the room was maintained at 70 ± 5%.

Rice samples were harvested at an accumulated temperature of 1000 °C from heading, the panicle exsertion. Harvested grain samples were dried to achieve 15% moisture content. The rough rice was dehulled and milled using a rice sheller (Kiya ST-50; Yanmar Co., Ltd., Osaka, Japan) and miller (Pearlest; Kett Electric Laboratory, Tokyo, Japan). Milled rice was kept in sealed bags under refrigeration (4 °C) until analysis.

Ripening and Physicochemical Characteristics. Grain size characteristics (e.g., length, width, and thickness) were measured from 10 head rice kernels using a Mitutoyo Digimatic Caliper (CD-15CP; Mitutoyo Corp., Kawasaki, Japan). A 1000-grain weight from each sample was determined randomly in triplicate and weighed separately. The head rice of the milled rice was assessed by using a standard consisting of a kernel or a piece of kernel with its length equal to or greater than three-fourths of the average length of the unbroken kernel and kernels with half or less opaque like the color of chalk and brittle.

The amylose contents were tested by two methods, iodine and concanavalin A, to confirm the results. The iodine test was performed according to the method of Juliano,[9] and the concanavalin A method was performed by using an amylose/amylopectin assay kit (Megazyme International Ltd. Co., Wicklow, Ireland).[10] Protein content was determined by using the Kjeldahl method with the conversion factor for nitrogen to protein of 5.95.[11] Hardness was determined with 10 head rice kernels using a TA-XT2 texture analyzer (Stable Micro Systems Ltd., Godalming, Surrey, UK) with a 2 mm probe following the method of Song et al.[12]

Amylopectin Fine Structure. The molecular structure of amylopectin were determined by using HPSEC-MALLS-RI (high-performance size-exclusion chromatography on a system equipped with multiangle laser-light scattering and refractive index detectors) following Patindol's method.[13] The weight-average molecular weight (M_w), z-average radius of gyration (R_z), and polydispersity (ratio of weight-average and number-average molar masses: M_w/M_n) were determined using HPSEC-MALLS-RI (Wyatt Technology, Santa Barbara, CA, USA), and the density ($\rho = M_w/R_z^3$) and specific volume for gyration (SVg = 2.522 R_z^3/M_w) were calculated from these values.[13]

Amylopectin chain length distribution was determined by high-performance anion-exchange chromatography (HPAEC) with a pulsed-amperometric detector as performed by Nishi et al. with a slight modification.[14] The milled rice was ground with a mortar and pestle, and then 5−7 mg of the resulting powder was suspended in 5 mL of methanol and allowed to dissolve for 1 day. The homogenate was centrifuged at 2500g for 5 min. The pelleted polyglucan was washed twice with 5 mL of 90% (v/v) methanol, suspended in 5 mL of distilled water, and then boiled for 3 h. Then, 50 μL of 600 mM sodium acetate buffer (pH 4.4) and 10 μL of 2% (w/v) NaN_3 was added to an aliquot (1 mL) of gelatinized polyglucan. Hydrolysis was achieved by the addition of 0.5 μL of isoamylase from *Pseudomonas amyloderamosa* (Sigma I2758, 1,250,000 units) and incubation at 37 °C with shaking at 150 rpm for 24 h. The homogenate was centrifuged at 15000 rpm for 5 min, and then a 1 mL aliquot was filtered through a 0.2 μm syringe filter (PTFE). The HPAEC system (ICS-3000; Dionex Corp., Sunnyvale, CA, USA) components were an ICS 3000 dual pump, an EO1 eluent organizer, a gold electrode with an AgCl reference electrode, and an ED electrochemical detector. Samples were analyzed with a CarboPac PA1 column (2 × 250 mm) with a CarboPac PA1 guard column (2 × 50 mm). Samples (50 μL) were eluted by a 60 min linear gradient from 100 to 475 mM sodium acetate in 150 mM sodium hydroxide at a flow rate of 0.250 mL/min. Peak area ratios (%) were calculated using Dionex Chromeleon (version 6.80).

Gelatinization and Pasting Properties. The gelatinization properties of rice starch were analyzed using a differential scanning calorimeter (DSC) (TA Q1000; TA Instruments, New Castle, DE, USA) following the method of Song et al.[15] Rice starch (20 mg) was weighed into aluminum sample pans (TA Instruments) and mixed with 40 μL of distilled water. The pans were sealed and allowed to reach equilibrium for 1 h. Thermal curves were obtained from 30 to 150 °C with a heating rate of 10 °C/min. All DSC analyses were conducted in triplicate. The pasting properties of rice flour were determined in triplicate with a Rapid Visco Analyzer (RVA; Newport Scientific model 3D, Warriewood, NSW, Australia) following AACC method 61-02.

X-ray Diffraction. The crystallinity of the rice starch was analyzed according to the method of Han et al.[16] Amorphous starch was used to generate a background pattern, as used by Cairns et al.[17] X-ray diffraction patterns were obtained using a Philips PW3710 diffractometer with a step width of 0.010° in the 2θ range of 3−38°. Approximately 0.5−1 g of rice flour was firmly packed into an aluminum sample holder. X-ray data were collected at a rate of 3 s/step, and there were 3501 steps. Cu Kα (λ = 1.5418 Å) radiation was used from a generator operating at 40 kV and 25 mA. Data were analyzed with Philips PC-APD (version 3.6) software.

Cooking Properties. Cooking properties were evaluated according to Chun's method in triplicate.[18] First, 8 g of rice grains in a stainless steel mesh container was washed to eliminate surface residue. The container was fixed in a 300 mL tall beaker with 160 mL of distilled water using a glass rod, and these grains were cooked in an electric rice cooker (CR-3020 V; Cuckoo Electronics Co. Ltd., Yangsan, Republic of Korea). After 20 min for equilibrium, the water absorption ratio (w/w) and expansion volume of the cooked rice were measured. The eluate was filtered and dried at 105 °C, and the soluble solid was weighed from it. The pH and iodine index were also measured from filtrate of eluate with 2% iodine solution and using absorbance at 600 nm, respectively. The shape of cooked rice kernels (length, width, and thickness) was measured 40 times using a Mitutoyo Digimatic Caliper.

Sensory Evaluation. The sensory properties of cooked rice were evaluated by six trained panels in triplicate.[19] A modified preference

DOI: 10.1021/jf504870p
J. Agric. Food Chem. 2015, 63, 3085−3093

Table 2. Physicochemical Properties of Milled Rice According to Ripening Temperature[a]

cultivar	ripening temperature (°C)	amylose (%)		protein (%)	hardness (g)
		iodine	concanavalin A		
Ilpum	22/14	17.3a	19.1b	6.66b	4433b
	25/17	16.4b	20.6a	6.86b	5470b
	28/20	15.0c	16.6c	6.90b	4504b
	31/23	14.8c	14.6d	7.86a	8249a
Chucheong	22/14	17.4a	22.8a	6.30c	4585b
	25/17	16.5b	19.8b	6.79b	4131b
	28/20	15.7c	18.9c	7.54a	4946ab
	31/23	14.7d	15.2d	7.55a	5705a

[a]Values with the same letter in a column are not significantly different according to a Duncan's multiple-range test ($p < 0.05$).

test was used involved scoring the cooked rice quality on a 7-point hedonic scales from −3 to +3. The sensory evaluation test provided information on appearance, aroma, taste, hardness, stickiness, and overall quality of cooked rice.[20]

Statistical Analysis. Data were processed with Statistical Analysis System software (version 9.1.; SAS Institute Inc., Cary, NC, USA). The data were statistically analyzed using Duncan's multiple-range test at a probability level of 0.05. Homogeneity of variance was calculated with Levene's test. General linear model analysis and correlation analysis with Pearson's correlation coefficient were also performed. Quantification analysis was conducted to evaluate the relative importance of various factors for the textural properties of the cooked rice by using the SAS PROC REG program, with PCORR2 in the model.[21] The squared partial correlation coefficients of PCORR2 measure the marginal contribution of one explanatory variable when all others are already included in multiple linear regression models.

RESULTS AND DISCUSSION

Grain Characteristics. The weight, shape, appearance, and hardness of the rice grains changed according to the ripening temperature (Table 1). The 1000-grain weight ranged from 20.1 to 21.7 g for Ilpum (IP) and from 18.9 to 19.8 g for Chucheong (CC). Even though the grains of CC weighed less than those of IP in each ripening temperature state, the higher the ripening temperature of the rice, the lower the 1000-grain weight of the rice kernels, with significant differences for both cultivars. These results are consistent with previous studies stating that a high temperature at the grain-filling stage decreases grain weight.[5,22]

The decreased grain weight in response to a higher ripening temperature is caused by various factors. The decrease in weight seemed to be related to the sink size or kernel shape. The grain size of milled rice depended on cultivar and temperature. Grains grown at a high ripening temperature tend to be shorter and thinner.[23] Likewise, the grain shape (i.e., grain length, width, and thickness) of IP was stable until 28/20 °C, but showed a significant reduction in shape at the highest ripening temperature (31/23 °C). On the other hand, the grain size of CC did not noticeably change with ripening temperature, meaning that ripening temperature affected the grain size of IP more than that of CC. Testing the interaction effects (cultivar × ripening temperature) using general linear model analysis revealed a significant interaction effect for length and thickness ($p < 0.001$) and grain width ($p < 0.1$). This result also means that there is an interaction effect of both cultivar and ripening temperature on grain size properties. The grain weight is also positively associated with the grain-filling duration and negatively with the grain-filling rate in rice cultivars during ripening.[24] Thus, a high ripening temperature slightly increases the grain-filling rate and decreases the grain-filling duration, decreasing the grain weight.[22,25]

The head rice yield, considering not only the shape but also the appearance of the grain tissue, was decreased in both cultivars when the grain-filling temperature was higher or lower than 28/20 °C. There is more non-head rice (i.e., chalky, immature, and dead rice) when the grain-filling temperature is higher or lower than the optimum temperature.[25] Low temperature causes spikelet sterility, a delay of grain filling, and reductions in yield.[6,26,27] The head rice percentage were lowest at 22/14 °C, peaked at 28/20 °C, and re-decreased at 31/23 °C in both IP and CC cultivars. Non-head rice is one of the primary issues in the rice market due to its undesirability to consumers. The palatability of cooked rice is decreased by an increased chalky rice proportion in sensory evaluation tests, even at just a 5% blend of non-head to head rice.[28]

A high ripening temperature reduces cereal yield by increasing imperfect or empty grains.[29] Here, head rice percentage decreased at 31/23 °C ripening temperature in both IP and CC cultivars. IP showed a steeper decrease in head rice than CC at 31/23 °C. The optimum temperature for these cultivars for producing head rice during grain filling has previously been reported: IP and CC show the highest yield and grain filling near 28/20 °C, and IP has a slightly lower optimum temperature (0.6 °C lower) than CC.[30]

Starch Compositions, Structures, and Crystallinities. With regard to starch composition, amylose content and short amylopectin chains decreased and intermediate amylopectin chains increased with an increased grain-filling temperature (Table 2; Figure 1). The amylose contents of IP and CC grown at the high ripening temperature were clearly decreased in both analyses. As previously reported, the high-temperature-ripened grain showed decreased levels of amylose,[7,8,31] which might be due to the repressed expression of granule-bound starch synthase I (*GBSSI*) at high temperatures, through which the amylose in endosperm of rice grain is synthesized.[5,32,33]

In the amylopectin chain length profile, the degree of polymerization (DP) for the peak chain length distribution of amylopectin was equal (at 11) in both cultivars. The proportion of short chains clearly reduced as the ripening temperature increased, ranging from DP 5 to 12 for IP and from DP 5 to 13 for CC. On the other hand, the relative amounts of amylopectin intermediate chains, DP 20−30 for IP and DP 18−33 for CC, increased when the ripening temperature increased. However, the longer chains above DP 30 or 33 were unaffected by the maturation temperature in both cultivars. A similar tendency was reported in wheat,[34] in which amylopectin branch chains were classified into three groups as the maturation temperature

DOI: 10.1021/jf504870p
J. Agric. Food Chem. 2015, 63, 3085−3093

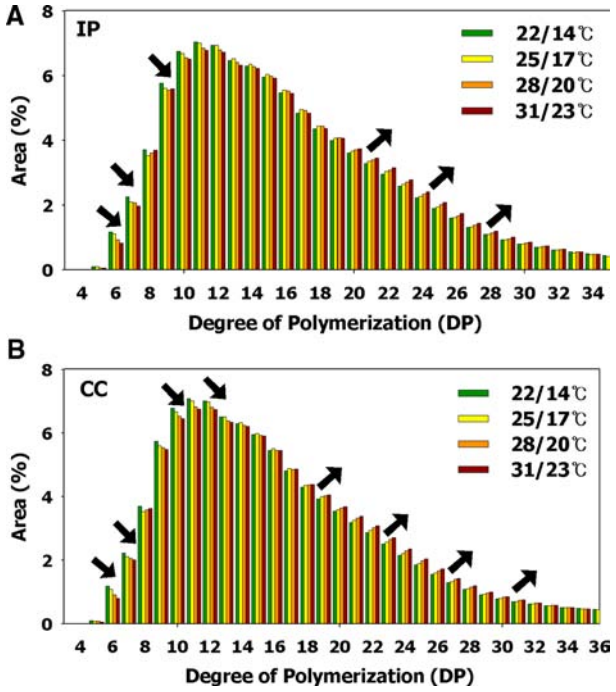

Figure 1. HPAEC determination of changes in the amylopectin chain length distribution according to ripening temperature: (IP) degree of polymerization of the branched amylopectin of Ilpum; (CC) degree of polymerization of the branched amylopectin of Chucheong.

increased: amylopectin branch chains with DP 6−12 decreased, the proportion of DP 13−34 increased, and those of DP ≥ 35 showed no significant difference. The high-temperature-ripened rice grain was also reported to contain intermediate and long-chain-enriched amylopectin, which might be due to the repressed expression of branching enzymes, especially the branching enzyme IIb.[5,6]

HPSEC-MALLS-RI analysis of the molecular structure of amylopectin revealed a different tendency in response to ripening temperature (Table 3). Amylopectin showed the highest density (ρ) at the optimal temperature for grain filling, suggesting that amylopectin had the highest compactness. The M_w of amylopectin ranged from 1.64×10^8 to 2.20×10^8 g/mol and from 1.52×10^8 to 2.02×10^8 g/mol for IP and CC, respectively, similar to Patindol's results for rice amylopectin.[13]

The polydispersity (M_w/M_n), an indication of the narrowness of the distribution,[13] of amylopectin grown at higher ripening temperatures (28/20, 31/23 °C) had lower values of 1.15−1.42 and 1.20−1.24 for IP and CC than the polydispersity at a lower ripening temperature (22/14, 25/17 °C; 1.83−1.96 and 1.66−1.99 for IP and CC, respectively). These lower polydispersity values meant that amylopectin molecules of rice ripened at a high temperature had a more homogeneous mass distribution than those of rice ripened at a low temperature. On the other hand, amylopectin molecules had the smallest specific volume for gyration (SVg) value when ripened at 28/20 °C, 0.16 and 0.19 for IP and CC, respectively. The specific volume for gyration, the theoretical gyration volume per unit of molar mass, is significantly reduced by branching.[35] The R_z, the theoretical probability of finding a molecule at a given distance from the center, showed a similar tendency to SVg. These results revealed that the amylopectin molecule was more highly branched at 28/20 °C than at other ripening temperatures. Similarly, the density (ρ) had the largest values at 28/20 °C, 15.4 and 13.0 g/mol/nm^3 for IP and CC, respectively. These results suggest that the appropriate ripening temperature may be around 28/20 °C for amylopectin branches and compactness compared with SVg, R_z, and ρ at lower or higher ripening temperatures.

X-ray powder diffraction pattern analysis of the crystallinity of rice flour also showed that the highest compactness and largest crystalline region were at the optimum temperature (28/20 °C; Table 4). X-ray diffraction provides data on the relative amounts of crystallites and amorphous phases for elucidating the crystal structures of the crystallites of the starch granules. By integrating the X-ray scattering intensity separately over the peak and the background, a number is obtained and interpreted as the "X-ray crystallinity".[36] The crystallinities for

Table 4. X-ray Diffraction Pattern Analysis of the Crystallinity of Rice Flour According to Ripening Temperature

cultivar	ripening temperature (°C)	crystallinity (%)
Ilpum	22/14	19.7
	25/17	21.2
	28/20	21.6
	31/23	21.5
Chucheong	22/14	20.5
	25/17	21.2
	28/20	25.2
	31/23	24.3

Table 3. HPSEC-MALLS-RI Determination of the Molecular Characteristics of Amylopectin According to Ripening Temperature

cultivar	ripening temperature (°C)	M_w[a] (10^8 g/mol)	R_z[b] (nm)	M_w/M_n[c]	ρ[d] (g/mol/nm^3)	SVg[e] (nm^3/g)
Ilpum	22/14	1.96 (0.07)[f]	278 (15)	1.83 (0.01)	9.1	0.28
	25/17	2.20 (0.07)	330 (32)	1.96 (0.05)	6.1	0.41
	28/20	1.64 (0.05)	220 (9)	1.42 (0.03)	15.4	0.16
	31/23	1.90 (0.13)	239 (11)	1.15 (0.04)	13.9	0.18
Chucheong	22/14	1.52 (0.05)	289 (3)	1.66 (0.04)	6.3	0.40
	25/17	1.86 (0.10)	269 (9)	1.99 (0.05)	9.5	0.26
	28/20	1.58 (0.03)	230 (8)	1.20 (0.09)	13.0	0.19
	31/23	2.02 (0.11)	275 (9)	1.24 (0.05)	9.7	0.26

[a]Weight-average molecular weight. [b]z-average radius of gyration. [c]Polydispersity. [d]Density (ρ) = M_w/R_z^3. [e]Specific volume for gyration (SVg) = 2.522 R_z^3/M_w. [f]Standard deviation.

DOI: 10.1021/jf504870p
J. Agric. Food Chem. 2015, 63, 3085−3093

Table 5. Gelatinization Properties of Rice Starch According to Ripening Temperature[a]

cultivar	ripening temperature (°C)	T_o (°C)	T_p (°C)	ΔH (J/g)	T_c (°C)	ΔT (°C)
Ilpum	22/14	68.5b	74.8d	4.18c	86.6d	18.1d
	25/17	70.1a	77.0c	5.58b	89.8c	19.8c
	28/20	70.7a	79.7b	6.11b	92.1b	21.4b
	31/23	70.8a	81.3a	7.32a	94.2a	23.6a
Chucheong	22/14	67.7c	74.8d	4.69b	88.0d	20.2b
	25/17	68.3c	76.7c	6.56c	90.3c	21.7ab
	28/20	70.6b	79.5b	6.16b	92.3b	21.7ab
	31/23	71.5a	81.6a	8.26a	94.9a	23.4a

[a] T_o, onset temperature; T_p, peak temperature; T_c, completion temperature; ΔH, gelatinization enthalpy; $\Delta T = T_c - T_o$. Values with the same letter in a column are not different significantly according to a Duncan's multiple-range test ($p < 0.05$).

IP and CC ranged from 19.7 to 21.6% and from 20.5 to 25.2%, respectively. In all ripening conditions, CC had a higher degree of crystallinity than IP. The crystallinity, related to the double helices of amylopectin in X-ray diffraction analysis,[37] was greater at high ripening temperatures (28/20, 31/23 °C) than at a low ripening temperature (21/14, 25/17 °C) in both cultivars. The largest crystalline regions were at 28/20 °C, with values of 21.6 and 25.2% for IP and CC, respectively. The crystallinity of rice flour was slightly decreased, by 0.1% for IP and by 0.9% for CC, from 28/20 to 31/23 °C.

In this study, amylopectin intermediate chains, which construct double helices, increased under elevated temperature conditions (Figure 1). In addition, the samples had a higher proportion of crystalline regions when ripened at high temperatures of 28/20 and 31/23 °C in both cultivars. The increase in crystallinity with an increased ripening temperature was likely due to the increased amount of amylopectin intermediate chains. However, this increase could not explain the reduced crystallinity at 31/23 °C. Instead of the amylopectin chain length distribution from a previous study,[38] the crystallinity of rice flour was highly correlated with the head rice percentage, with a correlation coefficient of 0.790 ($p < 0.05$). As stated above, the head rice percentage of both cultivars was highest at 28/20 °C. Therefore, one likely reason for the decreased crystallinity was the increased chalky rice at high ripening temperatures. The amylopectin chain length distribution and DSC properties were determined with only head rice to reduce the error due to the differences between head rice and chalky rice,[39] but the crystallinity was measured using rice flour, which included chalky rice. Chalky rice has less starch accumulation in the tissue. In addition, crystallinity is related to the density of the packing arrangement,[40] as also shown here by the decreased head rice percentage and reduced packing density (based on SVg, R_z, and ρ values) at 31/23 °C in Table 3. These results revealed that the crystallinity of rice flour was related to the head rice percentage, as well as the amylopectin chain length distribution, and confirmed the decreases in head rice yield, the compactness of amylopectin molecular structure, and the crystallinity of rice flour at a high grain-filling temperature above the optimal temperature.

Gelatinization and Pasting Properties. The gelatinization properties of rice are closely related to the eating quality.[41] In this study, the gelatinization properties of starch markedly changed as the ripening temperature changed (Tables 5), supporting our findings that rice starch grown at a high temperature would require a higher cooking temperature and longer cooking time.

The rice starch matured at a high temperature had consistently higher gelatinization temperatures (e.g., T_o, T_p, and T_c) and enthalpies, and the gelatinization temperatures increased with an increased ripening temperature. The gelatinization starting (onset) temperature, T_o, increased by 2.3 °C, from 68.5 to 70.8 °C, for IP and by 3.8 °C, from 67.7 to 71.5 °C, for CC. The peak temperature (T_p), completion temperature (T_c), and gelatinization enthalpy (ΔH) also significantly increased with increases in the ripening temperature in both cultivars, reflecting differences in the amylopectin crystalline order. These findings are consistent with those of a previous study, which suggested that the DSC characteristics of rice correlated with the environmental temperature.[8] Our results confirmed that a higher ripening temperature increased the gelatinization temperatures of rice starch.

Previous reports found that a longer chain length of an individual double helix of amylopectin increases the stability of the amylopectin double helix in gelatinization conditions.[42] In addition, the gelatinization enthalpy mainly reflects a loss of the double-helical order of amylopectin.[38] The formation of the double-helical structure that leads to crystallization requires a chain length of at least 10 for pure malto-oligosaccharides.[42] Therefore, more long amylopectin chains (DP > 10) forming double helices due to a higher ripening temperature would lead to more stable gelatinization.

The temperature range of gelatinization (ΔT) of starch also tended to widen in response to ripening temperature increases. This increased range would mean that the starch of rice grown in a high ripening temperature condition would require more energy in terms of cooking time and temperature than that grown in a low ripening temperature condition. This trend was more obvious for IP starch than for CC starch. In the IP cultivar, the ΔT of the starch showed a significant tendency to increase from 18.1 to 23.6 °C under elevated ripening temperature conditions. On the other hand, the ΔT of CC starch also increased, but the increase was not statistically significant.

The ΔT is a function of both the proportion of amylopectin short chains and their DP.[1] The ΔT of starch was reported to positively correlate with the amount of DP 6−9 in amylopectin due to an increase in the relative crystallinity in comparison with other rice varieties.[43] However, here, the ΔT increased with an increase in the crystallinity at a high ripening temperature, despite a reduction in the amount of DP 6−9 in amylopectin (Tables 4 and 5; Figure 1). The increase in the ΔT was mainly due to an increase in the T_c. Moreover, a negative correlation between the ΔT and short chains of amylopectin was identified ($r = -0.841$; $p < 0.01$). It seems that the ΔT is

DOI: 10.1021/jf504870p
J. Agric. Food Chem. 2015, 63, 3085−3093

Table 6. Pasting Properties of Rice Flour According to Ripening Temperature[a]

cultivar	ripening temperature (°C)	peak viscosity (RVU)	trough viscosity (RVU)	final viscosity (RVU)	breakdown (RVU)	setback (RVU)
Ilpum	22/14	147.8c	102.3d	198.6d	45.4ab	50.9a
	25/17	152.0b	109.6c	202.3c	42.4b	50.3a
	28/20	180.6a	131.0b	217.5a	49.6a	36.9b
	31/23	181.6a	135.0a	210.0b	46.6ab	28.4c
Chucheong	22/14	130.4d	84.6d	174.2c	45.8c	43.8a
	25/17	138.4c	88.5c	177.3c	49.9b	38.8b
	28/20	170.3b	116.3b	203.4b	54.0a	33.1c
	31/23	183.3a	133.3a	212.3a	49.9b	29.1d

[a]Values with the same letter in a column are not significantly different according to a Duncan's multiple-range test ($p < 0.05$).

Table 7. Pearson Correlation Coefficients between Parameters Describing the Starch Structure and Pasting Properties of Rice Flour According to Ripening Temperature

factor	peak viscosity	trough viscosity	final viscosity	breakdown	setback
ripening temperature	0.912**[a]	0.883**	0.716*	–[c]	−0.888**
amylose	−0.912**	−0.909**	−0.803*	–	0.731*
DP 5−12	−0.898**	−0.838**	−0.713*	–	0.861**
DP 13−24	0.700[b]	0.748*	0.793*	–	–
DP 25−36	0.863**	0.805*	–	–	−0.943**
DP 37−60	–	–	–	0.802*	–
protein	0.833*	0.803*	–	–	−0.805*

[a]* and **, significant at $p < 0.05$ and $p < 0.01$, respectively. [b]Significant at $p < 0.10$. [c]No correlation.

related to the packing density, which is related to crystallinity, and not directly with the amount of short chains of amylopectin.

Amylography using the RVA is a commonly used pasting property test that predicts the texture of cooked rice. With regard to the pasting properties of rice flour, the viscosity increased with an increased ripening temperature in both cultivars (Table 6). Peak and trough viscosities were clearly increased and setback was decreased with increasing ripening temperature. The CC cultivar had a higher increase in peak viscosity, with 52.9 RVA units (RVUs) compared with the 33.8 RVUs of IP. The trough viscosity of CC also increased to 48.7 RVUs compared with the 32.7 RVUs of IP. The breakdown displayed maximum values of 49.6 RVUs for IP and 54.0 RVUs for CC at 28/20 °C, with no statistically significant difference of IP. Setback was markedly decreased with an increase in the ripening temperature. However, the decreased amount of the CC cultivar was lower than that of the IP (14.7 vs 22.5 RVUs, respectively), with a different trend from above. These results concur with a report stating that a lower peak viscosity and higher setback are seen in rice with a higher amylose content (from the coldest growing season) than in rice with a lower amylose content.[7]

Pasting properties are affected by amylose content and by the branch chain length distribution of amylopectin.[44] The amylose content is generally thought to be a critical determinant of starch pasting properties because amylose suppresses starch swelling. The amylose helix has an internal hydrophobic tube,[45] providing a space for hydrophobic complexing agents such as lipids.[46] Amylose−lipid complexes restrict granule swelling,[47] which consequently affects pasting.[48] Hence, the apparent amylose content was negatively correlated with flour swelling volume[49] and stickiness[50] and was positively correlated with the hardness[50] of cooked rice. However, the correlation between amylose content and pasting properties is variable,[50] because amylopectin structure also affects pasting properties.[51] The amylopectin fine structure has been reported to be related to the breakdown of swollen granules and viscosity, with a negative correlation with long chains and a positive correlation with short chains.[52]

We confirmed the negative correlation between amylose content and peak ($r = -0.912$, $p < 0.01$) and trough ($r = -0.909$, $p < 0.01$) viscosities (Table 7). Thus, rice flour made from rice ripened at higher temperatures swelled more easily and resisted shear more readily than that of rice grown at low temperatures. On the other hand, the breakdown had a slightly different tendency with maximal values at 28/20 °C in both cultivars, showing that the capacity of starch granules to rupture after cooking was higher near the optimum temperature for grain weight, especially in the CC cultivar. Breakdown has also been reported to be positively correlated with the stickiness of cooked rice.[53] Setback also has a positive correlation with cohesiveness of mass in cooked rice, a sensory textural attribute.[54] Here, the lower amylose content at higher ripening temperatures is related to decreased setback ($r = 0.731$, $p < 0.05$). Those values in the breakdown and setback, together with the lower amylose content mentioned above, showed that cooked rice grown at high ripening temperatures may have lower hardness and cohesiveness and higher stickiness. However, in this study, these results were not confirmed by analysis of the textural properties of the cooked rice using a texture analyzer (data not shown). The higher protein content in rice grown at higher ripening temperatures may explain the texture differences, because protein content correlates with cooked rice texture. Protein is also involved in providing structural support to the rice kernel during cooking, thereby restricting starch granule swelling. Thus, treatment with protease, an enzyme that cleaves protein, significantly decreases cooked rice firmness.[55] In addition, protein influences the stickiness of cooked rice, with increased stickiness after protein disruption.[56] We concluded that these contradictory roles of protein in the texture of cooked rice offset the predicted effects

DOI: 10.1021/jf504870p
J. Agric. Food Chem. 2015, 63, 3085−3093

Table 8. Comparison of Cooking Properties of Rice According to Ripening Temperature[a]

cultivar	ripening temperature (°C)	water absorption ratio	expansion volume (cm^3)	pH	iodine index	soluble solid (mg)
Ilpum	22/14	2.67b	34.85a	6.81a	0.14a	5.16a
	25/17	2.69b	34.65a	6.79a	0.13ab	5.07a
	28/20	2.69b	33.95a	6.72b	0.11bc	5.00a
	31/23	2.84a	35.37a	6.66c	0.10c	5.16a
Chucheong	22/14	2.67c	34.77a	6.79a	0.16a	6.41a
	25/17	2.71c	35.76a	6.75b	0.16a	6.08a
	28/20	3.00b	34.95a	6.73b	0.12b	4.83b
	31/23	3.15a	37.33a	6.76ab	0.12b	5.58ab

[a]Values with the same letter in a column of the same cultivar are not significantly different according to a Duncan's multiple-range test ($p < 0.05$).

Table 9. Sensory Evaluation of the Eating Quality of Cooked Rice According to Ripening Temperature[a]

cultivar	ripening temperature (°C)	appearance	flavor	taste	stickiness	hardness	palatability
Ilpum	22/14	0.46a	0.08a	0.08ab	0.25a	0.46a	0.25a
	25/17	0.42a	−0.04a	0.29a	0.83a	0.29a	0.17a
	28/20	0.04ab	0.13a	0.17a	0.33a	0.29a	0.08a
	31/23	−0.17b	−0.25a	−0.33b	0.38a	0.00a	−0.13a
Chucheong	22/14	0.54ab	−0.13a	0.21a	0.21a	0.25a	0.17a
	25/17	0.88a	0.08a	0.38a	0.50a	0.67a	0.54a
	28/20	0.00b	−0.08a	0.13a	0.50a	0.25a	0.21a
	31/23	0.42ab	−0.29a	0.17a	0.29a	0.38a	0.13a

[a]Values with the same letter in a column of the same cultivar are not significantly different according to a Duncan's multiple range test ($p < 0.05$). Evaluation score: from −3 (bad) to +3 (good).

Table 10. Relative Importance of Starch Properties and Protein Content for the Palatability of Cooked Rice through Quantification Analysis

	amylopectin					
	DP 6−12	DP 13−24	DP 25−36	DP 37−60	amylose	protein
palatability (%)	9.2[a]	6.9	29.4	1.4	27.6	25.6

[a]Squared partial correlation coefficients (%) through quantification analysis.

of a low amylose content on the pasting properties discussed above at high ripening temperatures.

Furthermore, the setback value reflects the degree of retrogradation of starch paste and shows that starch grown at high ripening temperatures had less retrogradation. However, the short amylopectin chain of DP 6−9 has the opposite effect on retrogradation, showing a negative correlation.[57] Thus, the retrogradation did not appear to be affected by an increased ripening temperature, shown by the percentage retrogradation, calculated by the $\Delta H_{\text{retrograded starch}}/\Delta H_{\text{gelatinization}}$ in the rice starch tested (data not shown).[44]

Cooking Properties and Palatability. The cooking properties of the rice were predicted to be best at the optimum temperature according to water absorbability and a low iodine index and soluble solid value (Table 8). The water absorption ratio was significantly higher at 31/23 °C in both cultivars. Water absorbability is highly related to the gelatinization and eating quality of rice.[58] This high water absorption following a high ripening temperature is related to the starch granular structure and low amylose content. The rigidity of the starch granular structure is in proportion to its amylose content and in inverse proportion to the degree of granular swelling.[59] In other words, a high temperature during grain filling caused a loose starch granular structure due to low amylose content, increasing water absorbability.

The starch−iodine blue value of the residual liquid after cooking has been negatively correlated with eating quality.[60] Here, the iodine index was significantly lower at a high ripening temperature than at a low temperature. This low iodine index may be due to the low amylose content of the samples. However, the amylose content did not seem to be affected by the leaching of starch exudates. Despite the low amylose content, the amount of leaching of starch exudates was decreased during the cooking of rice grown at a high ripening temperature, although high levels of amylose reduced the amount of starch exudates leaching into the solution, because amylose suppresses starch swelling.[49] Enriched long amylopectin may be related, because lower levels of soluble solid were seen in both cultivars at 28/20 °C, the optimum temperature for amylopectin density.

Finally, we performed a sensory evaluation of the palatability of the cooked rice. Palatability showed a nonsignificant tendency to decrease in response to an increase in the ripening temperature (Table 9). The relative importance or contribution of starch components and protein content for the palatability of cooked rice was analyzed using the quantification method type I[61] (Table 10). The amylopectin chains of DP 25−36 showed the greatest effect on palatability at 29.4% among the rice samples grown with various ripening temperatures. In addition, the amylopectin chains of DP 25−36 had a high effect on the gelatinization properties of rice starch, as discussed above.

DOI: 10.1021/jf504870p
J. Agric. Food Chem. 2015, 63, 3085−3093

However, the amylose and protein contents also had high relative importances of 27.6 and 25.6%, respectively. Therefore, we could conclude that palatability was mostly related to the following chemical properties: amylopectin, amylose, and protein content. Of amylopectin chains, the DP 25−36 chains had the greatest relative importance on eating quality, because of their effect on starch gelatinization.

AUTHOR INFORMATION

Corresponding Author

*(A.C.) Phone: +82-31-695-0603. Fax: +82-31-695-4085. E-mail: areum@korea.kr.

Funding

This work was carried out with the support of "Cooperative Research Program for Agriculture Science & Technology Development (Project title: Identification of useful grain quality characteristics in rice mutants using reverse and forward genetics, Project No. PJ00923907)", Rural Development Administration, Republic of Korea.

Notes

The authors declare no competing financial interest.

ACKNOWLEDGMENTS

We appreciate Y.-J. Wang for MALLS analysis.

ABBREVIATIONS USED

IP, Ilpum; CC, Chucheong; HPSEC-MALLS-RI, high-performance size exclusion chromatography with multiangle laser-light scattering and refractive index detectors; HPAEC, high-performance anion-exchange chromatography; DSC, differential scanning calorimeter; GBSSI, granule-bound starch synthase I; RVA, Rapid Visco Analyzer; DP, degree of polymerization; M_w, weight-average molecular weight; R_z, z-average radius of gyration; M_n, number-average molar mass; ρ, density; SVg, specific volume for gyration; T_o, onset temperature; T_p, peak temperature; T_c, completion temperature; ΔH, gelatinization enthalpy

REFERENCES

(1) BeMiller, J. N. *Carbohydrate Chemistry for Food Scientists*; American Association of Cereal Chemists (AACC): St. Paul, MN, USA, 2007.

(2) Hizukuri, S. Polymodal distribution of the chain lengths of amylopectins, and its significance. *Carbohydr. Res.* **1986**, *147*, 342−347.

(3) Reddy, K. R.; Ali, S. Z.; Bhattacharya, K. R. The fine structure of rice-starch amylopectin and its relation to the texture of cooked rice. *Carbohydr. Polym.* **1993**, *22*, 267−275.

(4) Huang, J. R.; Schols, H. A.; van Soest, J. J. G.; Jin, Z. Y.; Sulmann, E.; Voragen, A. G. J. Physicochemical properties and amylopectin chain profiles of cowpea, chickpea and yellow pea starches. *Food Chem.* **2007**, *101*, 1338−1345.

(5) Yamakawa, H.; Hirose, T.; Kuroda, M.; Yamaguchi, T. Comprehensive expression profiling of rice grain filling-related genes under high temperature using DNA microarray. *Plant Physiol.* **2007**, *144*, 258−277.

(6) Jiang, H. W.; Dian, W. M.; Wu, P. Effect of high temperature on fine structure of amylopectin in rice endosperm by reducing the activity of the starch branching enzyme. *Phytochemistry* **2003**, *63*, 53−59.

(7) Dang, J. M. C.; Copeland, L. Genotype and environmental influences on pasting properties of rice flour. *Cereal Chem.* **2004**, *81*, 486−489.

(8) Asaoka, M.; Okuno, K.; Sugimoto, Y.; Kawakami, J.; Fuwa, H. Effect of environmental temperature during development of rice plants on some properties of endosperm starch. *Starch/Staerke* **1984**, *36*, 189−193.

(9) Juliano, B. O. A simplified assay for milled-rice amylose. *Cereal Sci. Today* **1971**, *16*, 334−340, 360.

(10) Gibson, T. S.; Solah, V. A.; McCleary, B. V. A procedure to measure amylose in cereal starches and flours with concanavalin A. *J. Cereal Sci.* **1997**, *25*, 111−119.

(11) *Official Methods of Analysis of AOAC International*; Association of Analytical Communities: Arlington, VA, USA, 1995.

(12) Song, J.; Lee, C. K.; Youn, J. T.; Kim, S. L.; Kim, D. S.; Kim, J. H.; Jeong, E. G.; Suh, S. J. Relationship among alkali digestive value, amylopectin fine structure and physical properties of cooked rice. *Korean J. Crop Sci.* **2008**, *53*, 320−325.

(13) Patindol, J. A.; Gonzalez, B. C.; Wang, Y. J.; McClung, A. M. Starch fine structure and physicochemical properties of specialty rice for canning. *J. Cereal Sci.* **2007**, *45*, 209−218.

(14) Nishi, A.; Nakamura, Y.; Tanaka, N.; Satoh, H. Biochemical and genetic analysis of the effects of amylose-extender mutation in rice endosperm. *Plant Physiol.* **2001**, *127*, 459−472.

(15) Song, J.; Kim, J. H.; Kim, D. S.; Lee, C. K.; Youn, J. T.; Kim, S. L.; Suh, S. J. Physicochemical properties of starches in japonica rices of differenct amylose content. *Korean J. Crop Sci.* **2008**, *53*, 285−291.

(16) Han, X. Z.; Ao, Z.; Janaswamy, S.; Jane, J. L.; Chandrasekaran, R.; Hamaker, B. R. Development of a low glycemic maize starch: preparation and characterization. *Biomacromolecules* **2006**, *7*, 1162−1168.

(17) Cairns, P.; Bogracheva, T. Y.; Ring, S. G.; Hedley, C. L.; Morris, V. J. Determination of the polymorphic composition of smooth pea starch. *Carbohydr. Polym.* **1997**, *32*, 275−282.

(18) Chun, A.; Song, J.; Kim, K. J.; Kim, J. H.; Son, J. R.; Oh, Y. J. Sensory and quality evaluation of aseptic-packaged cooked rice by cultivar. *Korean J. Crop Sci.* **2007**, *52*, 439−446.

(19) Chun, A.; Jeong, E. G.; Choi, Y. H.; Kim, K. J.; Lee, J. S. Grain quality of imported steamed-rice. *Korean J. Crop Sci.* **2006**, *51*, 7−11.

(20) Kwak, H. S.; Kim, H.-G.; Kim, H. S.; Ahn, Y. S.; Jung, K.; Jeong, H.-Y.; Kim, T. H. Sensory characteristics and consumer acceptance of frozen cooked rice by a rapid freezing process compared to homemade and aseptic packaged cooked rice. *Prev. Nutr. Food Sci.* **2013**, *18*, 67−75.

(21) Yim, S. B.; Seo, Y. S.; Kim, C. Y.; Kim, K. Y. A study on geological factors affecting behavior of sedimentary rock tunnel using quantification method type I. *J. Eng. Geol.* **2007**, *17*, 263−270.

(22) Morita, S. Prospect for developing measures to prevent high-temperature damage to rice grain ripening. *Jpn. J. Crop Sci.* **2008**, *77*, 1−12.

(23) Tashiro, T.; Wardlaw, I. F. The effect of high-temperature on kernel dimensions and the type and occurrence of kernel damage in rice. *Aust. J. Agric. Res.* **1991**, *42*, 485−496.

(24) Yang, W. H.; Park, T. S.; Kwak, K. S.; Choi, K. J.; Oh, M. H. Association of duration and rate of grain filling with grain yield in temperate japonica rice (*Oryza sativa* L.). *Korean J. Crop Sci.* **2007**, *52*, 112.

(25) Kim, K. C. Studies on the effect of temperature during the reduction division and the grain filling stage in rice plants: II. Effect of air temperature at the grain filling stage in indica-japonica crosses. *Korean J. Crop Sci.* **1983**, *28*, 58−75.

(26) Matsuo, T.; Kumazawa, K.; Ishii, R.; Ishihara, K.; Hirata, H. *Science of the Rice Plant. Vol. 2. Physiology*; Food and Agriculture Policy Research Center: Tokyo, Japan, 1995.

(27) Nahar, K.; Hasanuzzaman, M.; Majumder, R. R. Effect of low temperature stress in transplanted Aman rice varieties mediated by different transplanting dates. *Acad. J. Plant Sci.* **2009**, *2*, 132−138.

(28) Chun, A.; Song, J.; Kim, K. J.; Lee, H. J. Quality of head and chalky rice and deterioration of eating quality by chalky rice. *J. Crop Sci. Biotechnol.* **2009**, *12*, 239−244.

DOI: 10.1021/jf504870p
J. Agric. Food Chem. 2015, 63, 3085−3093

(29) Zakaria, S.; Matsuda, T.; Tajima, S.; Nitta, Y. Effect of high temperature at ripening stage on the reserve accumulation in seed in some rice cultivars. *Plant Prod. Sci.* **2002**, *5*, 160−168.
(30) Kim, D. S.; Shin, J. C.; Choi, K. J.; Lee, C. K.; Kim, J. K. Varietal characteristics of kernel growth of rice influenced by different temperature regimes during grain filling. *Korean J. Crop Sci.* **2003**, *48*, 397−401.
(31) Aboubacar, A.; Moldenhauer, K. A. K.; McClung, A. M.; Beighley, D. H.; Hamaker, B. R. Effect of growth location in the United States on amylose content, amylopectin fine structure, and thermal properties of starches of long grain rice cultivars. *Cereal Chem.* **2006**, *83*, 93−98.
(32) Ahmed, N.; Tetlow, I. J.; Nawaz, S.; Iqbal, A.; Mubin, M.; Nawaz Ul Rehman, M. S.; Butt, A.; Lightfoot, D. A.; Maekawa, M. Effect of high temperature on grain filling period, yield, amylose content and activity of starch biosynthesis enzymes in endosperm of basmati rice. *J. Sci. Food Agric.* **2014**, DOI: 10.1002/jsfa.6941 (accessed Dec 26, 2014).
(33) Pandey, M. K.; Rani, N. S.; Madhav, M. S.; Sundaram, R. M.; Varaprasad, G. S.; Sivaranjani, A. K.; Bohra, A.; Kumar, G. R.; Kumar, A. Different isoforms of starch-synthesizing enzymes controlling amylose and amylopectin content in rice (*Oryza sativa* L.). *Biotechnol. Adv.* **2012**, *30*, 1697−1706.
(34) Matsuki, J.; Yasui, T.; Kohyama, K.; Sasaki, T. Effects of environmental temperature on structure and gelatinization properties of wheat starch. *Cereal Chem.* **2003**, *80*, 476−480.
(35) You, S.; Lim, S. T. Molecular characterization of corn starch using an aqueous HPSEC-MALLS-RI system under various dissolution and analytical conditions. *Cereal Chem.* **2000**, *77*, 303−308.
(36) Whistler, R. L.; Bemiller, J. N.; Paschall, E. F. *Starch: Chemistry and Technology*, 2nd ed.; Academic Press: New York, 1984.
(37) Ball, S.; Guan, H. P.; James, M.; Myers, A.; Keeling, P.; Mouille, G.; Buléon, A.; Colonna, P.; Preiss, J. From glycogen to amylopectin: a model for the biogenesis of the plant starch granule. *Cell* **1996**, *86*, 349−352.
(38) Cooke, D.; Gidley, M. J. Loss of crystalline and molecular order during starch gelatinization − origin of the enthalpic transition. *Carbohydr. Res.* **1992**, *227*, 103−112.
(39) Patindol, J.; Wang, Y. J. Fine structures and physicochemical properties of starches from chalky and translucent rice kernels. *J. Agric. Food Chem.* **2003**, *51*, 2777−2784.
(40) Thomas, D. J.; Atwell, W. A. *Starches: Practical Guides for the Food Industry*; Eagan Press: St. Paul, MN, USA, 1999; p 19.
(41) Ohtsubo, K.; Toyoshima, H.; Okadome, H. Quality assay of rice using traditional and novel tools. *Cereal Foods World* **1998**, *43*, 203−206.
(42) Gidley, M. J.; Bulpin, P. V. Crystallisation of malto-oligosaccharides as models of the crystalline forms of starch: minimum chain-length requirement for the formation of double helices. *Carbohydr. Res.* **1987**, *161*, 291−300.
(43) Vandeputte, G. E.; Vermeylen, R.; Geeroms, J.; Delcour, J. A. Rice starches. I. Structural aspects provide insight into crystallinity characteristics and gelatinisation behaviour of granular starch. *J. Cereal Sci.* **2003**, *38*, 43−52.
(44) Jane, J.; Chen, Y. Y.; Lee, L. F.; McPherson, A. E.; Wong, K. S.; Radosavljevic, M.; Kasemsuwan, T. Effects of amylopectin branch chain length and amylose content on the gelatinization and pasting properties of starch. *Cereal Chem.* **1999**, *76*, 629−637.
(45) Morrison, W. R.; Law, R. V.; Snape, C. E. Evidence for inclusion complexes of lipids with V-amylose in maize, rice and oat starches. *J. Cereal Sci.* **1993**, *18*, 107−109.
(46) Godet, M. C.; Tran, V.; Delage, M. M.; Bulén, A. Molecular modelling of the specific interactions involved in the amylose complexation by fatty acids. *Int. J. Biol. Macromol.* **1993**, *15*, 11−16.
(47) Biliaderis, C. G.; Tonogai, J. R. Influence of lipids on the thermal and mechanical properties of concentrated starch gels. *J. Agric. Food Chem.* **1991**, *39*, 833−840.
(48) Kaur, K.; Singh, N. Amylose-lipid complex formation during cooking of rice flour. *Food Chem.* **2000**, *71*, 511−517.
(49) Bhattacharya, M.; Zee, S. Y.; Corke, H. Physicochemical properties related to quality of rice noodles. *Cereal Chem.* **1999**, *76*, 861−867.
(50) Juliano, B. O. *Rice: Chemistry and Technology*, 2nd ed.; American Association of Cereal Chemists: St. Paul, MN, USA, 1985.
(51) Park, I. M.; Ibáñez, A. M.; Zhong, F.; Shoemaker, C. F. Gelatinization and pasting properties of waxy and non-waxy rice starches. *Starch/Staerke* **2007**, *59*, 388−396.
(52) Han, X. Z.; Hamaker, B. R. Amylopectin fine structure and rice starch paste breakdown. *J. Cereal Sci.* **2001**, *34*, 279−284.
(53) Chung, W. K.; Meullenet, J. F. Prediction of cooked rice texture in long-grain rice using Rapid Visco Analyser data. In *B. R. Wells Rice Research Studies 2004*; Norman, R. J., Meullenet, J. F., Moldenhauer, K. A. K., Eds.; Arkansas Agricultural Experiment Station: Fayetteville, AR, USA, 2005; pp 371−379.
(54) Champagne, E. T.; Bett, K. L.; Vinyard, B. T.; McClung, A. M.; Barton, F. E.; Moldenhauer, K.; Linscombe, S.; McKenzie, K. Correlation between cooked rice texture and Rapid Visco Analyser measurements. *Cereal Chem.* **1999**, *76*, 764−771.
(55) Saleh, M. I.; Meullenet, J. F. Effect of protein disruption using proteolytic treatment on cooked rice texture properties. *J. Texture Stud.* **2007**, *38*, 423−437.
(56) Hamaker, B. R.; Griffin, V. K.; Moldenhauer, K. A. K. Potential influence of a starch granule-associated protein on cooked rice stickiness. *J. Food Sci.* **1991**, *56*, 1327−1329.
(57) Vandeputte, G. E.; Derycke, V.; Geeroms, J.; Delcour, J. A. Rice starches. II. Structural aspects provide insight into swelling and pasting properties. *J. Cereal Sci.* **2003**, *38*, 53−59.
(58) Choi, H. C.; Chi, J. H.; Cho, S. Y. Varietal difference in water absorption characteristics of milled rice, and its relation to the other grain quality components. *Korean J. Crop Sci.* **1999**, *44*, 288−295.
(59) Lii, C. Y.; Tsai, M. L.; Tseng, K. H. Effect of amylose content on the rheological property of rice starch. *Cereal Chem.* **1996**, *73*, 415−420.
(60) Chikubu, S.; Watanabe, S. Establishment of palatability estimation formula of rice by multiple regression analysis. *J. Jpn. Soc. Starch Sci.* **1985**, *32*, 51−60.
(61) Huh, M. H. *Quantification Method I·II·III·IV*; Seoul, Korea, 1998.

DOI: 10.1021/jf504870p
J. Agric. Food Chem. 2015, 63, 3085−3093

Scheme 1. Parallel Adsorbent Column Tester (PACT)

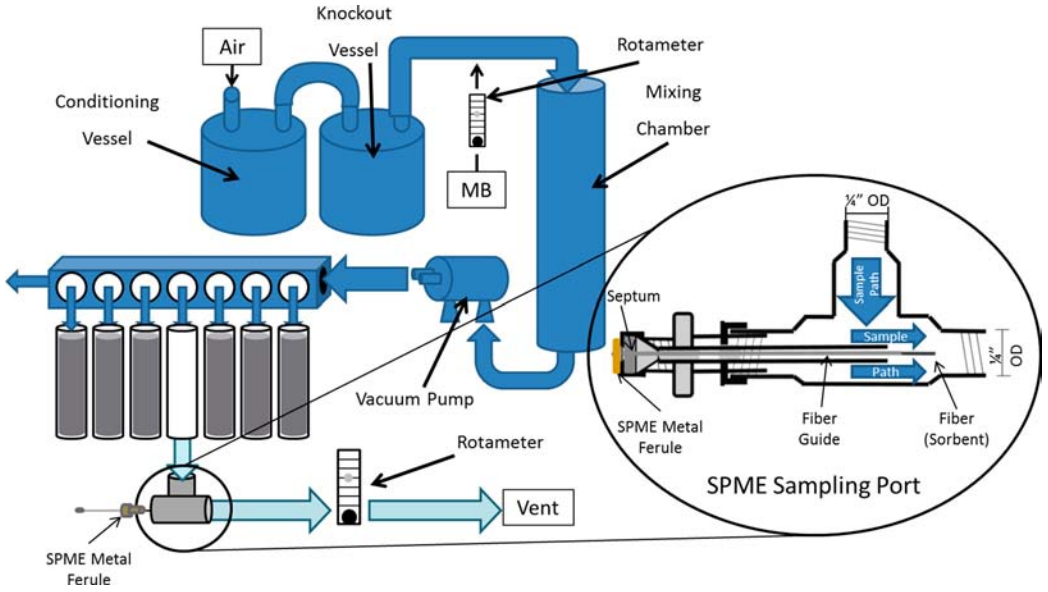

Results are presented and discussed relative to activated carbon derived from coconut shell, the type of sorbent used in several commercial systems that remove MB from effluent during chamber ventilation.

MATERIALS AND METHODS

Chemicals. A 50-lb (23 kg) cylinder of compressed MB, Meth-o-gas 100 (>99.5% purity), was obtained from Cardinal Professional Products (Woodland, CA, USA). Respective 300-lb (136 kg) cylinders of compressed ultra high purity nitrogen (>99.9% purity) and carbon dioxide (>99.3% purity) gases were used for the carbon preparation and were received from the Fresno, California USA Airgas distributor. When air was used for carbon preparation, it was supplied by a compressor that pushed air (60 psi) serially through an Altech L21 charcoal filter and a Drierite-filled moisture trap. Commercially marketed activated carbon derived from coconut shell source, Westates Vocarb 48C (WEST-AC), was purchased from Siemens Industry, Inc. (Alpharetta, GA, USA) and was stored at ambient conditions in an airtight jar until use. Deionized (DI) water was produced with a Millipore Elix 10/Gradient A10 water purification system to a specification of 18 MΩ resistivity.

SPME Quantification: Modeling TWA versus DFE. The PACT was used to evaluate, in parallel, gram-scale quantities of materials for capture performance as a function of conditions typical of ventilation effluent from chamber fumigations: effluent flows (ca. 0−225 mL min^{-1}), volumes (≥ 6.75 L), durations (≥ 30 min), and [MB]s (ca. 3−16000 ppmv). Over the range of these conditions, solid-phase microextraction (SPME) fibers have the potential to be more effective than established methods for MB quantification (e.g., colorimetric tubes, gas-sampling, IR detection, electrochemical detection). Two passive sampling techniques involving SPME, direct fiber exposure (DFE) "instantaneous grabs" as well as "diffusive" time-weighted averaging (TWA),[16−20] were comparatively evaluated for potential to quantify MB in the flowing air of the PACT system as well as in headspace of a static system for comparison.

With DFE sampling, the SPME fiber was directly exposed to the sample matrix (i.e., air−MB mixtures). When the sample volume is much larger (>10×) than the volume of the SPME fiber and the analyte concentration in the sample is less than that required to saturate the fiber (vide infra), the amount of analyte (e.g., MB) collected on the fiber can be predicted by[16,17]

$$m_{eq} = K_{fs} v_f C_0 \quad (1)$$

where m_{eq} is the mass of MB sorbed onto fiber at equilibrium, v_f is the volume of the fiber, and C_0 is the initial concentration of MB. The distribution of MB between the fiber and sample, K_{fs} (unitless), is expressed as the ratio

$$K_{fs} = [MB]_{fiber}/[MB]_{sample} \quad (2)$$

where $[MB]_{fiber}$ is the concentration of MB in the fiber, and $[MB]_{sample}$ is the concentration of MB in the sample matrix.

At equilibrium, the rate of MB sorption and desorption are equal in magnitude where

$$d[MB]_{fiber}/dt = d[MB]_{sample}/dt = 0 \text{ and } K_{fs} = \text{constant} \quad (3)$$

K_{fs} varies for each type of fiber coating (and anlyte) and as a function of many factors including total concentration of analyte (MB), matrix interferences, thickness of the coating, temperature, humidity, etc.

With TWA sampling, the SPME fiber was exposed to the sample matrix while "retracted" in the fiber guide, which served as a physicomechanical constraint on the diffusive flux of MB from the sample matrix toward the fiber. The use of SPME fibers in concert with TWA sampling to quantify an analyte has been rigorously discussed.[16−22] The translational rate of MB diffusion, *SR*, is approximated by

$$SR = A/z \times D \quad (4)$$

where A is the cross-sectional area of the fiber guide, z is the distance that the fiber is retracted into the fiber guide, and D is the diffusion coefficient for MB. The mass of MB sorbed to the fiber, m, is calculated using

$$m = \bar{C} \times SR \times t \quad (5)$$

where $\bar{C}$ is the time-weighted average concentration of MB over the span of time, t, the fiber assembly is exposed to the sample matrix. Variation in m is only linear (i.e., eq 5 will be valid) for times < $t_{50,v}$ which is the time required for sorption of 0.5 m_{eq} (vide infra).

SPME Quantification: TWA versus DFE Protocols. To sample MB-containing airstreams in the PACT system, each SPME sampling port (vide infra) was outfitted with a Carboxen/PDMS Stable Flex SPME fiber assembly (#57335-U, Sigma-Aldrich (Milwaukee, WI), 23 gauge, $A = 1.464 \times 10^{-3} cm^2$ (eq 4), 85-μm thick coating on a 170-μm OD fiber, length = 10 mm, $v_f = 0.549$ μL (eq 1)). Autosampler SPME fiber assemblies, such as the ones employed in this study, were chosen because one can manually adjust the position of the fiber on the z-axis (z value) without the need for a fiber holder. DFE and TWA sampling was conducted at a temperature in the range of 25−30 °C with t = 5

DOI: 10.1021/jf505193e
J. Agric. Food Chem. 2015, 63, 3094−3103

min and t = 0.5−30 min, respectively, while z was consistent across the respective sampling techniques. For TWA sampling, a fiber holder (#57330-U, Sigma-Aldrich) was used to standardize a fully retracted "zero position" for z, ∼31 mm from metal ferule to the screw hub of the fiber assembly. For DFE sampling, z = 17 mm based on using a piece of plastic (length = 14 mm, diameter = 6.3 mm) to standardize the distance between the metal ferule and the screw hub of the fiber assembly.

To sample MB-containing headspace in static systems, serial dilutions of MB (Meth-o-gas 100, Great Lakes Chemical Corporation, >99.5% purity) in air were prepared in volumetric 1200−1300 mL glass gas flasks (1-L Erlenmeyer flask fitted with two ports). Flasks had ∼200 mL of air withdrawn using a gastight syringe (B-D Yale, # Z 3876), predetermined amounts of MB were introduced (<200 mL), and then normal atmospheric pressure (NAP) was (re)established at a temperature of 25−30 °C. A 10 mL "headspace" vial (#SU860099, Sigma-Aldrich) was fitted with a screw cap (PTFE/silicone septa (#SU860101, Sigma-Aldrich) that was then pierced by two needles with Leur-lock connectors (Ranfac, #6515430440). The inlet needle was positioned in the center of the septum, just above the bottom of the vial, and the vent needle was positioned at the edge of the septum, penetrating just below its inner surface. Headspace was then purged from the vial over the span of ∼10 s with 50 mL of a MB dilution from a gas flask. After the needles were removed, the fiber guide from the fiber assembly described above was inserted through the hole made by the inlet needle. To control the depth of the fiber from the septa following penetration, the fiber guide (and fiber) was inserted concentrically through a 1/4 in. OD tube reducer to 1/8 in. tube fitting (#B-200-R-4, L = 1.42 in, Swagelok, Northern California, Fremont, CA) so that the metal ferule of the fiber assembly was supported by the fitting, which buttressed against the septa of the vial. Values of t and z for DFE and TWA sampling were as described above.

Gas Chromatography. An Agilent 6890 gas chromatograph (GC) was used with a split−splitless inlet at 250 °C, a 100:1 split ratio activated at 0.01 min, and a 0.75 mm ID SPME injection sleeve inlet liner (#2−6375,05, Sigma-Aldrich, Bellefonte, PA). The inlet was also equipped with a 250-μL loop on a gas-sampling valve (GSV) held at 110 °C. The analytical column was a 30 m (L) × 250 μm (ID) DB-5 with 0.25 μm film thickness held isothermally at 150 °C for 3 min and 1.8 mL min^{-1} He carrier flow. The flame ionization (FID) detector was at 275 °C with respective flows of 30 mL min^{-1} H_2, 400 mL min^{-1} air, and 30 mL min^{-1} N_2 makeup. Retention time was used for chemical verification of MB and hexane.

After sampling MB in either the static or flowing systems, the fiber was retracted to "zero position" (if necessary), and the fiber guide was capped by burying it into a septum (#6514, Grace, Deerfield, IL) to prevent the loss of MB (vide infra) until just before GC-FID analysis. The SPME fiber assembly was loaded into a SPME fiber holder (#57330-U, Sigma-Aldrich), the fiber guide was injected 2 in. into the inlet, and the fiber was desorbed for 1 min. Alternatively, GSV injections were conducted for comparison as noted below.

Sorbent Preparation. Pits from two species of tree fruits, *Prunus domestica* (prunes) and Prunus persica (peaches), as well as shells from two species of tree nuts, *Juglans sp.* (walnuts) and *Prunus amygdalus* (almonds), were obtained as end-products of key California USA horticultural production and used as carbon sources. Sorbents from respective carbon sources were prepared, as detailed below, using different methods following the general sequence of pyrolysis, activation, and then quenching. During pyrolysis, the carbon source was heated under an inert gas atmosphere to form char, a carbonaceous derivative material with a "rudimentary porous structure" relatively void of noncarbon heteroatoms.[15] A single type of carbon source served as starting material and was loaded into a 2 in × 2.25 in × 22 in (5.1 cm × 5.7 cm × 55.9 cm, inner diameter (ID) × outer diameter (OD) × length (L)) mullite working tube (Carbolite, MVO66325-N-18) to fill the heated-zone of a 13 in (33.0 cm) tube furnace (Thermolyne, 21100). The mass of the carbon source loaded into the working tube was measured gravimetrically. The contents of the tube were flushed with nitrogen gas at ∼900 mL min^{-1} for 1 h with the temperature controller set to 75 °C. The furnace temperature controller was increased to 700 °C, which resulted in ramp rate of ∼25 °C min^{-1}, and held isothermal for 1 h. The furnace temperature controller was increased to 800 °C, and the char was then "activated" to form a sorbent, as described in detail below, by introducing either carbon dioxide or steam into the tube to remove residual material, such as tars, from the pore spaces. Sorbent was "quenched" using various procedures during the return to temperature <50 °C. When preparation was completed, the mass of the carbon sorbent was measured gravimetrically. Sorbents were ground using a hand mill equipped with tooth auger and fine plates (Lehman Mills, Quaker City Mill #1171295), sized to a 20/40 mesh with brass sieves (McMaster-Carr, 3286K14 and 3286K16), and stored at ambient conditions in an airtight jar until use.

CO_2 Activation with Nitrogen Quenching. To activate the char, carbon dioxide was flushed through the tube furnace at ∼900 mL min^{-1} following pyrolysis and just before the furnace temperature controller was set to 800 °C. After 1 h, the carbon dioxide was replaced with nitrogen, and the temperature controller was turned off to initiate a gradual decrease of the CO_2-activated nitrogen-quenched carbon (CO2A-NQ) to <50 °C.

Steam Activation with Nitrogen Quenching. Steam was directed through high temperature silicone rubber tubing (McMaster-Carr, 5236K871) into the char-containing tube for 1 h following pyrolysis and just before the furnace temperature controller was set to 800 °C. Steam was generated by sparging nitrogen through a 1000 mL round-bottom flask containing ∼800 mL of boiling DI water. The feed rate of steam, 4.73 ± 0.34 g min^{-1}, was determined by measuring the mass of water before and after the 1-h process in triplicate trials. Quenching was as above to yield steam-activated nitrogen-quenched carbon (SA-NQ).

CO_2 Activation with Air Quenching. Following CO_2 activation, the furnace temperature controller was lowered to 300 °C, and air (ca. 20−40 RH) was directed through the furnace tube at ∼900 mL min^{-1} for 1 h. The air was then replaced with nitrogen gas, and the CO_2-activated air-quenched carbon (CO2A-AQ) was allowed to cool to <50 °C before being processed for use as described above.

CO_2 Activation with Water Quenching. Following CO_2 activation, the furnace temperature controller was lowered to 300 °C, and the entire contents was transferred using heat-resistant gloves to a 32 oz (946 mL) Mason jar filled with approximately 1 mL of water for every 2 g of raw material. The carbon−water mixture was allowed to cool to <50 °C, the water was decanted, and the CO_2-activated water-quenched carbon (CO2A-WQ) was dried in an oven at 110 °C overnight before being ground, sized, and stored for use as above.

PACT System and Sorbent Evaluation. The PACT was constructed based on modification to the bench scale adsorbent column apparatus as described by Leesch et al.,[7] which was about a 3,500:1 scaled-down model of a chamber ventilation system (Scheme 1). PACT diverts a single source of flowing air into seven channels. Briefly, air is pulled with an oil-free vacuum pump through 1 in. Tygon tubing connecting two vessels and a mixing chamber in series. The first vessel (conditioning) was filled with either water, to humidify, or silica gel, to dry, the airstream. To increase the humidity from ∼25 to ∼70%, silica gel was removed from the conditioning vessel and replaced with water to a depth of ∼10 cm. The second vessel (knockout) allowed any water droplets to fall out of the airstream and contained a HOBO datalogger (Onset, #U10−003) to monitor temperature and %RH. Next, the airstream was combined with MB (Meth-o-gas 100 Great Lakes Chemical Corporation, >99.5% purity) as metered by a rotameter (Key Instruments, #10410_R5) before entering into a mixing chamber comprised of a 3 in (ID) × 39 in (L) schedule 40 poly(vinyl chloride) pipe. The MB-containing airstream was then routed through the vacuum pump; the pressure of the airstream entering and exiting the pump was monitored with respective Magnehelic gauges (Dwyer Insruments, Cat. No. 2020C). Exhaust from the pump was directed through a stainless-steel manifold with seven channels as well as an outlet that was tuned to balance pressure. Unless otherwise noted, the total flow of MB and air into the manifold was 50 SCFH (∼23,502 mL min^{-1}).

DOI: 10.1021/jf505193e
J. Agric. Food Chem. 2015, 63, 3094−3103

Each channel was outfitted with a quick-connect fitting (McMaster-Carr, #s 51545K23 and 51545K79) to a 1/2 in (OD) × 6 in (L) stainless-steel column with a bed volume (for sorbent materials) of ∼12 mL. Flow from the column exited through 1/4 in. Swagelok tee and was directed to the outlet at 90° (see inlay of Scheme 1). The branch opposite the outlet was fitted with a Teflon 1/8−1/4 in (OD) tube reducer (Swagelok, #T-200-R-4), which was bored so that a 1/8 in (OD) × 56 mm (L) piece of stainless-steel tubing spanned into the central cavity of the tee. The fiber guide was inserted through a septum (Grace-Davison, #6514) and into the stainless-steel tubing (to protect the fiber) so that the tip of the fiber guide was flush with the end of the tubing. This alignment enabled the fiber to access the airstream coaxially within the outlet branch of the tee. The outlet flow from each SPME sampling port was metered to 224 mL min^{-1}, unless otherwise noted, with a rotameter (Lab-crest # FP 1/8−041-G-6/443U381U10).

Prior to each experiment where carbon performance was evaluated, six (of seven) stainless-steel columns were loaded with sorbent material to a 11.4 cm bed depth, the ends of each column were capped with circular 40-mesh stainless steel strainer cloth (1/8 in OD), all columns were placed in the working tube (vide infra), and the furnace temperature controller was set to 300 °C with a nitrogen gas flow of ∼900 mL min^{-1} for 2 h. The seventh column contained no sorbent. After the heating period, all columns were stored in an airtight jar containing ∼5 g of drierite until being fitted onto the seven-channeled manifold of the PACT apparatus. SPME fiber assemblies, with the fibers retracted into the fiber guide for TWA sampling with z = 10 mm,[16] were inserted into the sampling ports, and all airflows were metered as described above.

To simulate chamber effluent consistent with ventilation of a postharvest MB fumigation,[7,8] [MB] in the airstream of the PACT apparatus was temporally modulated from the start of a dose (when t = 0): 16,210 ppmv for 3 min, 4,870 ppmv for 13 min, and 0 ppmv for the remaining 14 min (30 min total). For a single test, dosing was repeated serially ($Dose_n$, where n = 1, 2, 3, etc.) at ∼60 min intervals. After each dose, the mass of the MB cylinder was gravimetrically measured. Additionally, each column was gravimetrically measured, and each Carboxen/PDMS Stable Flex SPME fiber assembly (#57335-U, Sigma-Aldrich (Milwaukee, WI)) was removed from the sampling ports of the PACT apparatus for analysis of MB with GC coupled to FID (vide supra). A "breakthrough" threshold was reached when [MB] exiting a column exceeded 500 ppmv (∼13 mg escaping the column over the 30 min dosing period).[7] If breakthrough (BT) was observed on the same column for two consecutive doses, the column was replaced with an empty column. Dosing continued until all columns containing sorbent were removed from the PACT apparatus.

The capacity of an activated carbon sorbent to sorb MB was calculated as the percentage of the total mass of MB sorbed ($m_{MB,sorbed}$) by the column over consecutive doses, including the first dose where BT was observed ($Dose_n$, where n = 1,2,3,4...first BT), relative to the mass of carbon sorbent measured just before testing, m_{AC}, in the form

$$\%\ \text{Capacity}_{MB} = m_{MB,sorbed}/m_{AC} \times 100 \tag{6}$$

where $m_{MB,sorbed}$ is calculated by

$$m_{MB,sorbed} = m_{entering} - m_{exiting} \tag{7}$$

and $m_{entering}$ is the total mass of MB entering the column containing no carbon sorbent (e.g., column attached to the seventh channel of manifold), and $m_{exiting}$ is the total mass of MB exiting a carbon containing-column as calculated by

$$m_{entering} = \sum_{Dose_1}^{Dose_{BT}} \bar{C} \times 0.224\ \text{LPM} \times 30\ \text{min} \tag{8}$$

or

$$m_{exiting} = \sum_{Dose_1}^{Dose_{BT}} \bar{C} \times 0.224\ \text{LPM} \times 30\ \text{min} \tag{9}$$

where $\bar{C}$ is the time-weighted average [MB] in mg L^{-1} (vide infra), 0.224 LPM (L min^{-1}) is the flow rate through the column, and 30 min is the duration of a dose.

RESULTS AND DISCUSSION

SPME Calibration and Response Factors. Seven individual fibers were each arbitrarily assigned a number, one through seven. For each fiber, a total of 17 analyses were conducted on the PACT system, nine using TWA sampling (n = 9) and eight using DFE sampling (n = 8). A response factor, RF, was calculated for each fiber, with Fiber 7 serving as reference for comparison:

$$RF_{FiberX} = \sum_{i=1}^{n} \left(\frac{Area_{FiberX,i}}{Area_{Fiber7,i}} \right) / n \tag{10}$$

Respective analyses (JMP, Version 9. SAS Institute Inc.) for TWA and DFE sampling indicated that the RFs of individual fibers were significantly different from the grand mean of all RFs (ANOVA: TWA, $F_{5,48}$ = 3.751, p < 0.01; DFE, $F_{5,17.532}$ = 39.764, p < 0.0001). For TWA sampling, the RFs of Fibers 3 and 4 were distinct from that of Fiber 6, while Fibers 1, 2, and 5 did not differ from Fibers 3 and 4, nor Fiber 6 (Tukey-Kramer HSD, α = 0.05). For the DFE sampling, the RFs of Fibers 1 and 4 were each different from the RFs of all other fibers, and the RFs of Fibers 2 and 6 were different from each other (Tukey-Kramer HSD, α = 0.05). t tests of individual fibers indicated that RFs associated with DFE sampling were significantly (P < 0.01) more extreme than respective RFs from TWA sampling ($RF_{DFE} < RF_{TWA} < 1.000$ or $1.000 < RF_{TWA} < RF_{DFE}$). These results support the conclusion that quantitative analyses with SPME using TWA and DFE sampling should differentiate, at least for MB, between each fiber and sampling technique (i.e., each fiber and sampling technique should be considered unique).

Accordingly, the RFs respective to each fiber and sampling technique (DFE and TWA) were used for the quantification of MB. Following each GC analysis, the integral of the MB peak area, *Area*, was adjusted using

$$Area_{Adj} = Area/RF \tag{11}$$

The RF-adjusted areas, $Area_{Adj}$, (i.e., detector response) were then plotted on the y-axis versus an x-axis of m, m_{eq}, [MB], or the concentration−time "CT" product (i.e., [MB] × t). Linear least-squares analyses of the respective correlations were used for calibration and quantification.

The RF of each fiber was tracked chronologically for performance or loss of function. Over the course of this study, only accidents (e.g., nicks, dents, etc.) that physically damaged the fiber changed the RF. Future studies will evaluate the potential "drift" in RF values over relatively long experimental time courses or operational periods.

DFE Sampling. The distribution of MB between the fiber and sample matrix, K_{fs}, reached equilibrium (i.e., K_{fs} was constant, eq 1 is valid) at t < 2 and t < 5 min when airstreams in PACT and static headspace, respectively, were sampled with DFE. The time required for equilibrium (disadvantageously) impacts quantification of MB from static headspace with t < 5 min as well as from flowing systems where concentration changes are occurring when t < 2 and resolution of this change is required, such as when quantifying MB in ventilation effluent from postharvest chamber fumigations. The time required for equilibrium can (advantageously) concentrate MB from flowing

DOI: 10.1021/jf505193e
J. Agric. Food Chem. 2015, 63, 3094−3103

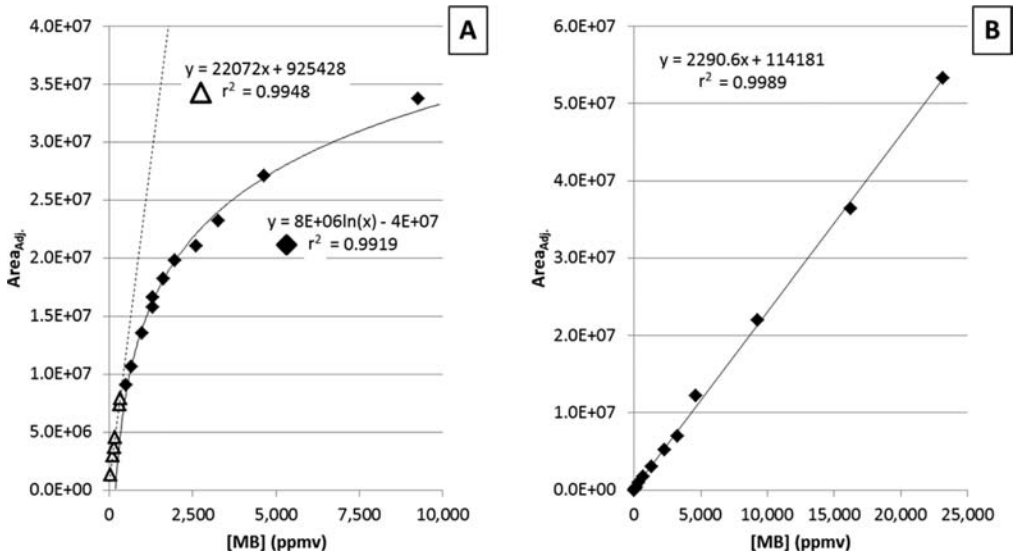

Figure 1. (A) A calibration curve for DFE sampling of methyl bromide concentrations ([MB]) (32−9542 ppmv) in the static headspace of vials with t = 5 min shows a linear response up to ∼300 ppmv (triangles, dashed line) and logarithmic response at higher concentrations (diamonds, solid line). (B) A calibration prepared from GSV injections shows that GC-FID detector response remains linear at [MB]s exceeding 20,000 ppmv.

airstreams or static headspace, which thereby increases the limit or the dynamic range of detection. For example, when [MB] of 504 ppmv in static headspace was sampled with DFE when t = 5 min, nearly 10× more MB was detected (m = ∼4096 ng) in subsequent GC-FID analyses as compared to a 250-μL GSV injection of the same headspace concentration (m = ∼490 ng). The ability of DFE (with t = 5 min) to concentrate MB from static headspace was not linear over [MB]s of 31.8−9542 ppmv (Figure 1A). The detector response (GC-FID) was linear at relatively low concentrations, but above [MB] of ∼300 ppmv, the response was logarithmic possibly due to a lack of, or modification to, sorption sites on the fiber as critically discussed by Ouyang and Pawliszyn.[17] Figure 1, panel B shows a calibration plot made from GSV injections over the same detector response range; the correlation was linear throughout, which indicates that the logarithmic response at higher [MB] with DFE (Figure 1A) was not a detector artifact. It is critical to note the consequence of this nonlinear phenomenon when using DFE sampling to quantify (or predict) K_{fs} for a particular fiber. Figure 2 provides further support for these observations and shows an exponential decrease in K_{fs} (unitless) based on DFE sampling, with $t \geq 5$ min, of the airstream in the PACT system as well as in static headspace of vials. K_{fs} values derived from eq 1 versus eq 2 were consistent (slope = 0.995, r^2 = 1) and ranged from ∼10−8000 over the relevant [MB]s with the ∼300ppmv estimated upper limit of the linear response corresponding to an experimentally measured K_{fs} of 5196 (Figure S1, Supporting Information). Note that much of the robust modeling associated with SPME-based air sampling stems from analyte-fiber pairings exhibiting at least an order of magnitude greater K_{fs}values. As related to this study and the relatively low distribution of MB between the Carboxen/PDMS fiber and sample, the works of Górecki et al.[21] and Koziel et al.[22] offer theoretical insight to possibly explain observations; as K_{fs} for a given analyte and fiber decreases, the overall response across an equivalent (subsaturation) concentration regime shows less curvature (more linearity) (i.e., less pronounced linear-, kinetic-, and equilibrium regimes). Future studies will probe the mechanism and develop novel theories for SPME sampling of fumigants with Carboxen-based fiber types and

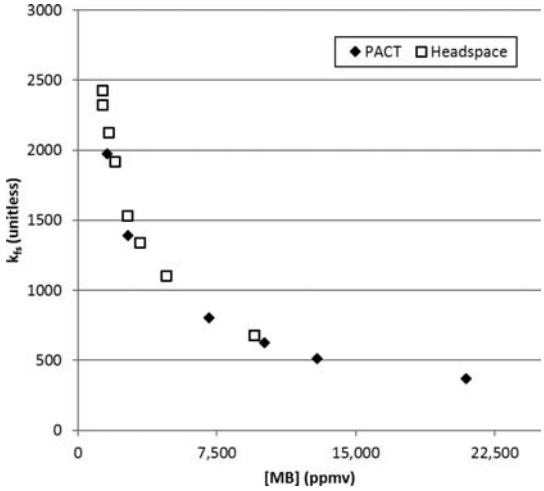

Figure 2. K_{fs} values calculated for DFE sampling of MB concentrations, with $t \geq 5$ min, in flowing (PACT,◆) and static (headspace,□) systems.

specifically address the influences of relatively low K_{fs} values on the maintenance of "zero-sink" conditions; however, such investigations are outside the scope of this manuscript, in which experimental results are described in relation to existing SPME models.

TWA Sampling. With TWA sampling, the time required for equilibrium between MB and the fibers (i.e., K_{fs} is constant, eq 1 is valid) occurs over considerably longer time scales than for DFE. With reference to the example above in static headspace, TWA sampling [MB] of 504 ppmv with t = 30 min yielded a value of m equivalent to that of a 250-μL GSV injection and ∼10-fold less than DFE with t = 5 min. Relative to DFE sampling, the longer amount of time required by TWA sampling for equilibrium can be used (advantageously) to quantify MB in ventilation effluent from postharvest chamber fumigations, as it allows for a linear detector response of [MB] values in the range of ∼20−5000 ppmv when t = 30 min (equivalent to "CT" products in the range of ∼500−150,000 ppmv min).

DOI: 10.1021/jf505193e
J. Agric. Food Chem. 2015, 63, 3094−3103

As noted in the work of Ouyang and Pawliszyn,[17] the temporal interval(s) of TWA sampling should occur when $t < t_{50,x}$, which was calculated and tabulated (Figure 3) for six

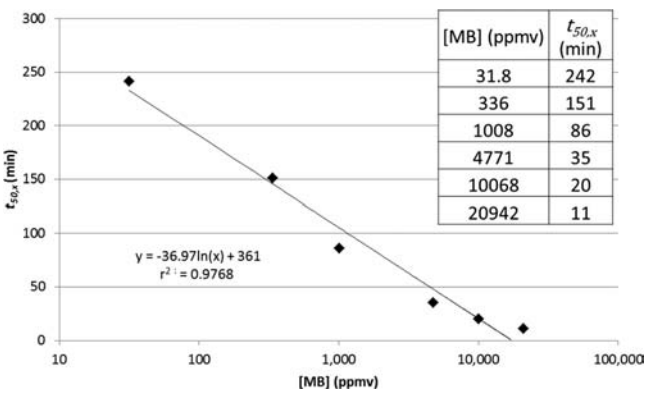

Figure 3. Approximate $t_{50,x}$ values calculated using eq 8 with m_{eq} values determined by DFE sampling of [MB] in static headspace with a t = 5 min.

different fumigation-relevant [MB]s using a modification to eq 5:

$$t_{50,x} = \frac{0.5m_{eq}}{C_x SR} \quad (12)$$

where m_{eq} is measured experimentally by DFE sampling with t = 5 min at a given concentration, C_x. Twenty-two separate measurements using TWA sampling of either static headspace or the PACT system at fixed [MB] were used to calculate SR, (1.416 ± 0.09) × 10^{-4} cm^3/s ($\bar{x}$ ± s), a lower value than calculated by solving eq 4 using D = 0.114 cm^2 s^{-1}.[23] The suggestion that the value of SR be derived from measurement, rather than literature reference, is consistent with the work of Ouyang et al.,[24] which linked this discrepancy, at least in part, to an instrument-specific difference in the amount of analyte entering the GC inlet versus that transferred onto the analytical column.

Calibration from Flowing Systems. Several approaches to detector calibration can be utilized if the temporal interval(s) of TWA sampling occur when $t < t_{50,x}$. Figure S2A of the Supporting Information shows the adjusted GC-FID detector response $Area_{Adj}$ versus "CT" products from TWA sampling of MB flows in the PACT system. Different [MB] values were sampled with t = 10 min (diamonds), and constant [MB] was sampled while varying t (squares) (each point represents the response from one fiber). Note the utility of the later calibration approach for use with TWA sampling of the PACT system at fixed [MB], as the entire range of relevant "CT" products can be obtained by varying the span of time, t, that the fiber assembly is exposed to airstream; as described above, this approach was used to calibrate FID detector response relative to PACT airstreams metered to ∼2500 or 11,000 ppmv over exposure (i.e., sampling) times of 0.75, 1.5, 3.0, 6.0, 10, and 15 min, which encompass $\bar{C}$ values in the range of ∼60−6000 ppmv when t = 30 min (Figure S3, Supporting Information).

Calibration from Static Systems. If SR is known, the relationship between m and $\bar{C}$ can be calculated using eq 5, which thereby allows detector response from TWA sampling to be calibrated based on measurements of MB in static headspace. Calibration in static headspace can accommodate a wider range of [MB]s than what may be achieved in flowing systems, which can be operationally restricted by the physics of mass-flow controllers or rotameter(s). For example, MB flows in the PACT system were metered to either 1562 or 10,068 ppmv (theoretical), and six channels (n = 6) were sampled using the TWA technique with t in the range of 0.5−15 min. Figure S2B of the Supporting Information shows the agreement between theoretical [MB]s and those detected based on calibrations derived from sampling static headspace using either GSV injections of MB dilutions (white) or TWA sampling of different [MB]s with t = 5 min (gray).

Advantage of Using TWA versus DFE Sampling with PACT. The effect of the airstream flow rate on the quantification of MB in the PACT system was evaluated. Airflows of 75 mL min^{-1} or 224 mL min^{-1} were establish as the outlet flow from each channel of the PACT system with [MB]s metered to 5092 ppmv or 548 ppmv for TWA and DFE sampling, respectively. For both sampling approaches, a t test showed no difference at the 99% confidence interval between MB quantification at either flow rate (TWA, t test: t_4 = 0.7436, $P > |t|$ = 0.5023; DFE, t test: t_6 = 0.6214, $P > |t|$ = 0.5680).

However, if the simulated ventilation of a postharvest chamber fumigation (vide supra) is sampled using the TWA technique with a t of 30 min, an average [MB] of 3434 ± 211 ppmv (n = 35, $\bar{x}$ ± s) (5 replicate analyses of 7 samplings) was obtained, which agrees well with a calculated $\bar{C}$ of 3731 ppmv MB. It is interesting to note the accuracy of TWA sampling for MB quantification in the PACT system despite changes in concentration over the sampling interval, a period where no MB is released, and a relatively short exposure to the highest [MB]. This result is in marked contrast to DFE "instantaneous grab" sampling in the PACT system with a single fiber (i.e., without temporally exchanging fiber assemblies) and t = 30 min, where m would be based overwhelmingly on the [MB] in the minutes preceding the conclusion of the simulated ventilation, rather than the total amount of MB in the effluent over that time.

TWA Sampling of PACT: Handling, Parametrics, Interferents, and Limits of Detection. Desorption of MB from the SPME fiber over the time that lapsed between sample acquisition and analyses was evaluated. With respect to TWA sampling of the airstream in the PACT system, the fiber guide was capped by burying it into a septum (to seal the tip of the fiber guide) immediately following acquisition for a "hold" time of 0, 30, 60, or 195 min. Alternatively, the fiber guide was analyzed without being buried in a septum after "hold" times of 0 or 60 min. Figure S4 of the Supporting Information shows a linear least-squares analysis of the data (solid line = with septa: r^2 = 0.2074, $F_{1,46}$ = 12.0366, P = 0.0011; dashed line = without septa: r^2 = 0.8026, $F_{1,26}$ = 105.707, P < 0.0001); burying the fiber into the septum resulted in minimal MB loss over ∼30 min (solid line), with just 0.089% loss per minute. Without burying the fiber into a septum, a statistically significant loss (95% confidence interval) of MB occurred after ∼11 min (solid red vertical line), consistent with a 0.4% loss of MB per minute.

Experiments were conducted to address the possibility that a nontarget compound, or interferent, could compete for sorption sites on the fiber and impact the quantification of MB using TWA sampling. The PACT system was metered to a [MB] of about 725 ± 53.13 ppmv ($\bar{x}$ ± 95% CI) with either ∼25% "dry" or ∼75% RH " wet" airstreams, and six channels (n = 6) were sampled for 15 min using the TWA approach. Three independent replicate analyses were performed for each

DOI: 10.1021/jf505193e
J. Agric. Food Chem. 2015, 63, 3094−3103

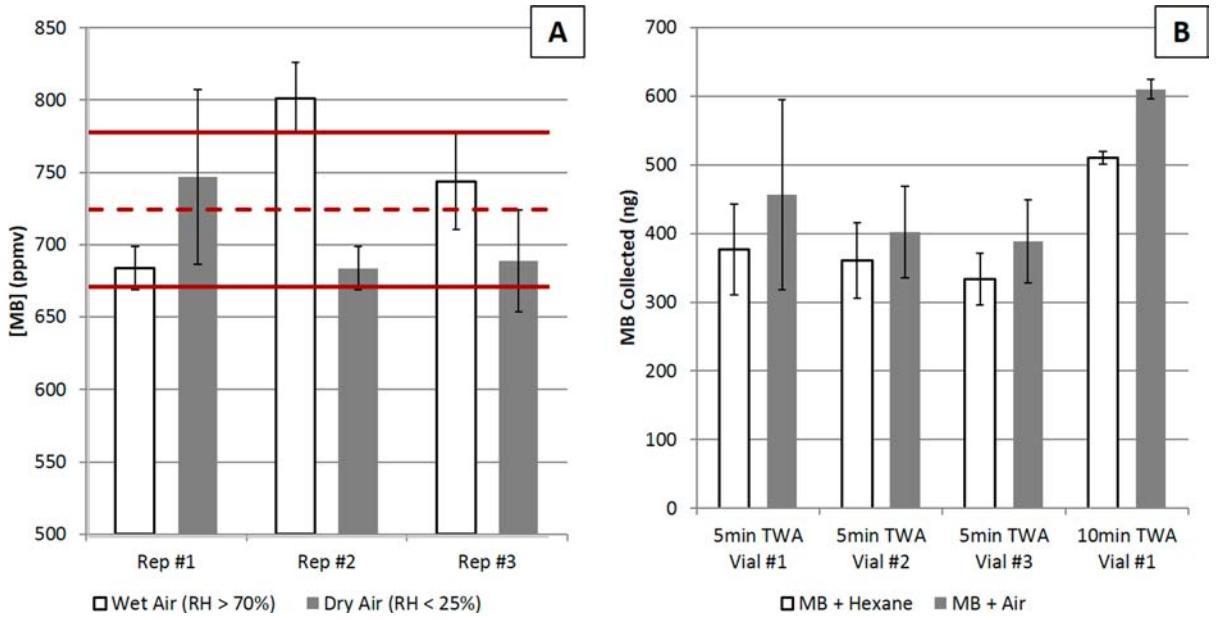

Figure 4. Effects of interferents with values reported as $\bar{x} \pm s$: (A) TWA sampling of [MB] from either humid (≥70% relative humidity (RH)) or dry (≤25% RH) airstreams (dashed red line indicates the theoretical concentration, solid red lines the 95% confidence intervals), (B) mass of MB on fiber (m) via TWA sampling of static headspace with or without hexane.

condition, and the [MB] was calculated from a calibration curve based on response under dry conditions. When mean [MB]s for each of the six analyses were adjusted for model uncertainty, there was no significant difference between wet and dry conditions (Figure 4A).

Hexane, which has a higher vapor pressure relative to H_20,[25] was selected as a surrogate volatile organic carbon (VOC) interferent to MB quantification. A [MB] of about 1040 ppmv was established in the static headspace of eight vials, and then 1 mL aliquots of the headspace were removed. Four of the vials then received 1 mL aliquots of air, while the other four were fortified with 1 mL aliquots of ~170,000 ppmv hexane in air. Three vials, both with and without hexane fortifications, were sampled with t = 5 min using the TWA technique, while the remaining two vials were with t = 10 min (Figure 4B). On the basis of triplicate analyses, a consistently lower (357 ± 22 ng) ($\bar{x} \pm s$), but not statistically distinct, amount of MB was detected in the hexane-fortified vials relative to the control (416 ± 36 ng) with t = 5 min (t test: $t_{16} = -1.7304$, $P < t = 0.0514$). Interference was more pronounced with t = 10 min, as ~20% less MB (510 ± 9 ng) (n = 3, $\bar{x} \pm s$) was detected in the hexane-fortified vial relative to the control (610 ± 14 ng MB) (t test: $t_4 = -10.337$, $P > |t| = 0.0005$). This result suggests that with longer sampling times, compounds with physiochemical properties similar to hexane may affect TWA sampling of MB in the PACT system.

SPME is a sampling technique, not a method of analysis; the ability to resolve the signal for MB from any interferents and background depends on the method of analysis used. As with interference, the limit of detection (LOD)[26] is dependent on the instrument and parameters used for analysis. For TWA sampling of MB in the PACT system, determining a LOD was complicated by physical limitations of the rotameters, which could not be metered below [MB] of ~1100 ppmv. At this lower limit of [MB], the LOD was 14.7 ng MB based on seven replicate (n = 7) TWA samplings with t = 30 s and subsequent GC-FID detection, which corresponds to an average $\bar{C}$ of 14.9 ppmv over the 30 min timespan (t = 30 min) of the simulated ventilation.

Quantifying Sorbed MB on PACT: TWA versus Gravimetric Methodology. In addition to measuring $m_{entering}$ via TWA sampling of a column containing no sorbent, the mass of MB lost from the cylinder was tracked to provide an analogous estimate, $m_{entering-grav}$, in the form

$$m_{entering-grav} = (m_{cyl\text{-}f} - m_{cyl\text{-}i}) \times flow_{PACT}/flow_{column} \quad (6a)$$

where $m_{cyl\text{-}f}$ and $m_{cyl\text{-}i}$ are respectively the final and initial mass of the cylinder and $flow_{PACT}$ and $flow_{column}$ are the total PACT flow into the manifold (~23,502 mL min^{-1}) and an individual column (~224 mL min^{-1}), respectively.

Figure 5 shows the relationship between the quantification of MB across eight serial doses (Dose$_n$, where n = 1, 2, 3, ...8) of the PACT apparatus using gravimetric- versus TWA SPME-based methodologies. Note the agreement between the slope of the line obtained from a least-squares analysis (m = 0.75) and

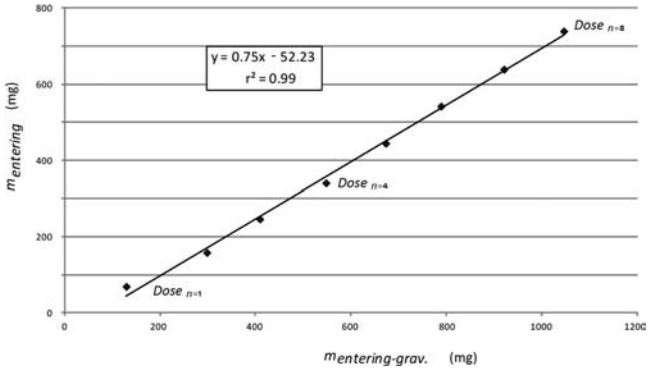

Figure 5. Relationship between the quantification of MB across eight serial doses to the PACT apparatus (Dose$_n$,where n = 1, 2, 3, ...8) using gravimetric measurement ($m_{entering-grav}$)) of MB loss from the source cylinder versus SPME-based TWA sampling of a column containing no sorbent ($m_{entering}$).

DOI: 10.1021/jf505193e
J. Agric. Food Chem. 2015, 63, 3094−3103

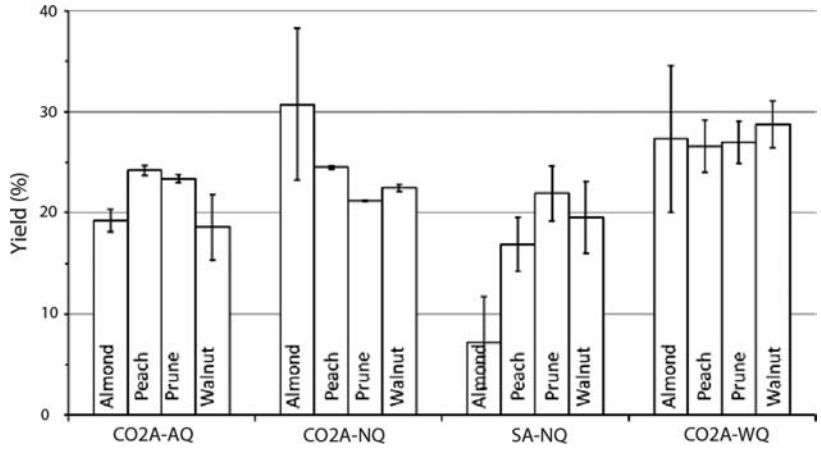

Figure 6. Yields (n = 4, bar height = $\bar{x}$, error bars = ± s) of each type of preparation (CO_2-activated air-quenched (CO2A-AQ), CO_2-activated nitrogen-quenched (CO2A-NQ), steam-activated nitrogen-quenched (SA-NQ), and CO_2-activated water-quenched (CO2A-WQ)) for each source of activated carbon sorbent (almond shell, peach pit, prune pit, and walnut shell) were estimated as a percentage of the mass of material after quenching relative to the mass of starting material loaded into the tube furnace prior to pyrolysis.

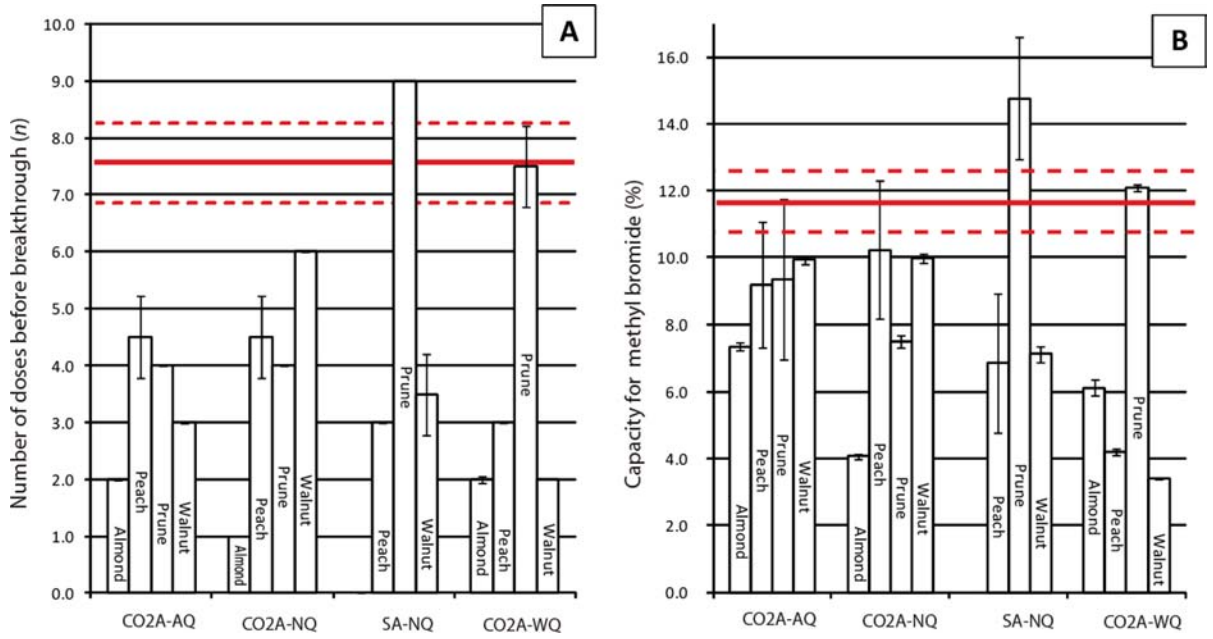

Figure 7. Number of doses needed to first observe breakthrough (A) and the capacity (%) to sorb MB (B) were used as measures of sorbent performance and evaluated for each type of preparation (CO_2-activated air-quenched (CO2A-AQ), CO_2-activated (CO2A-NQ), steam-activated (SA-NQ), and CO_2-activated water-quenched (CO2A-WQ)) and each source of activated carbon (almond shell, peach pit, prune pit, and walnut shell), where bar height = $\bar{x}$, error bars = ± s, and n = 2. Commercially marketed activated carbon, Westates Vocarb 48C (WEST-AC) served as a benchmark of comparison (n = 18) with results shown ±95% confidence intervals (dashed red lines).

the average ratio, 0.737 ± 0.055 (ave. ± stdev., $\bar{x} \pm s$, n = 8), of MB concentrations measured by TWA SPME, $m_{entering}$, relative to gravimetric methodology, $m_{entering-grav}$. We have interpreted this difference to be a result of MB losses to the system forward of the SPME sampling ports. This result identifies that TWA SPME measurements of $m_{entering}$ should be used, whenever possible, to quantify MB in airstreams of the PACT apparatus. Additionally, this result supports the conclusion that MB loss due to system was consistent across trials and that experiments involving the PACT apparatus be conducted in facilities with sufficient ventilation (e.g., fume hoods) to minimize MB inhalation exposure to individuals conducting the tests.

Commercially Sourced Activated Carbon Sorbent "Benchmark". WEST-AC, derived from coconut shell, served as a commercially marketed "benchmark" of comparison for the various preparations of activated carbon sorbents from tree fruit pits and tree nut shells. WEST-AC, randomly selected from one of four different commercial batches, was loaded into two columns of the PACT apparatus, and nine replicate tests were conducted to evaluate, as measures of performance, the capacity for MB (%) and the number of doses needed to first observe BT. One-way ANOVAs were not significant (capacity: $F_{(17, 0.006)}$ = 2.273; P = 0.1215, BT: $F_{(17, 0.004)}$ = 2.531; P = 0.1562), which indicates that the overall average capacity, 10.9 ± 1.8% ($\bar{x} \pm s$), as well as the average number of doses applied before BT, 7 ± 1 ($\bar{x} \pm s$), could be used to estimate the performance of WEST-AC irrespective of the batch.

DOI: 10.1021/jf505193e
J. Agric. Food Chem. 2015, 63, 3094−3103

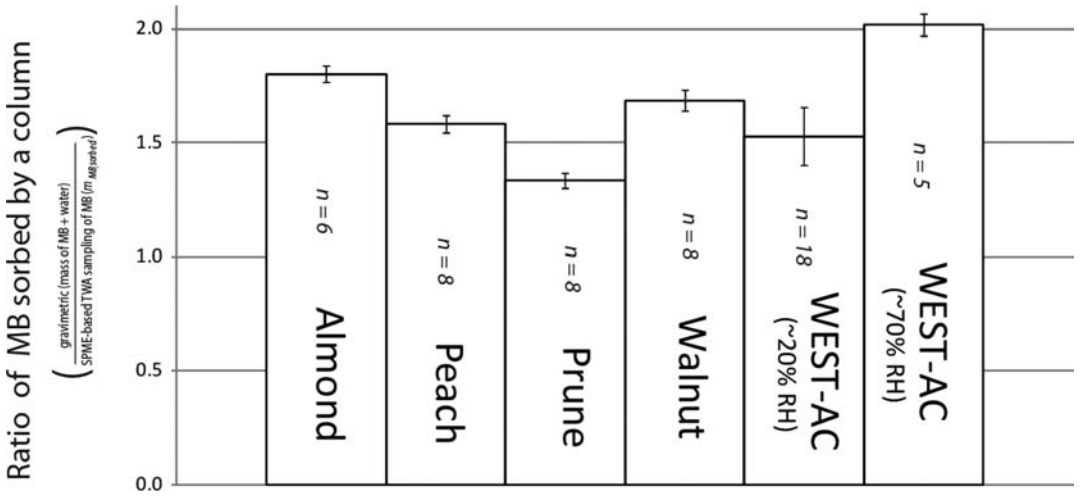

Figure 8. Results from PACT testing of all activated carbon preparations were grouped by type of carbon source. The grand mean of the mass of MB (and water) sorbed by a particular column based on gravimetric measurement was normalized relative to that detected by SPME-based TWA sampling, $m_{MB,sorbed}$. Results suggest the discrepancy between the ability of carbon source types to sorb MB was related to the source-specific competitive sorption of water vapor.

Tree Fruit Pit and Tree Nut Shell Activated Carbon Sorbents. The average yields across all preparations and sources of activated carbon sorbent, ranged from 7−31% (w/w) and were estimated as the fractional percentage of the mass after quenching relative to the mass of starting material loaded into the working tube prior to pyrolysis (Figure 6). A one-way ANOVA was significant ($F_{(15,\ 0.0476)} = 5.262$; $P = 0.015$), which indicated that the overall average yield across all preparations and carbon sources, 22 ± 6% ($\bar{x} \pm rsd$), was not an accurate indicator of all yields. Means comparison testing only showed significant difference between yields for CO2A-WQ and SA-NQ preparations, independent of source carbon type (Tukey-Kramer HSD, $\alpha = 0.05$). The yield of activated carbon sorbent prepared by SA-NQ from almond shells was <10%, far below any other preparations, which suggests an unlikely prospect of its commercial use to remove MB in ventilation effluent from postharvest chamber fumigations.

The performance of each type of preparation and source on the PACT tests, expressed as both the number of doses needed to first observe BT (Figure 7A) as well as the corresponding capacity for MB (%) (Figure 7B), were evaluated relative to results for WEST-AC. Activated carbons from prune pits prepared by CO2A-WQ as well as SA-NQ resulted in the greatest number of doses needed to first observe BT, ∼7.5, and the highest corresponding capacity, ∼12−14%. CO2A-AQ and CO2A-NQ preparations of activated carbon from prune pits as well as all preparations of activated carbons from peach pits and walnut shells reached BT in ∼3−6 doses and had capacities ranging from 4−7%. Regardless of preparation, activated carbons derived from almond shells performed relatively worse, as is clearly demonstrated by fewer number of doses needed to first observe BT.

In an attempt to correlate the performance of activated carbon derived from peach pits, prune pits, almond shells, and walnut shells to the type of carbon source, data were analyzed to indirectly probe the competitive sorption of water vapor and its potential influence on the sorption of MB. Results from PACT testing of preparations were grouped by type of carbon source, and the grand mean of the mass of MB (and water) sorbed by a particular column at BT based on gravimetric measurement was normalized relative to that detected by TWA SPME sampling, $m_{MB,sorbed}$ (Figure 8). Given the finding that TWA-SPME quantification, and thus $m_{MB,sorbed}$, is unaffected across a range of ∼20−80% RH (see Figure 4A), a likely explanation for the discrepancy in performance was the preferential sorption of water vapor by carbon source types. It is critical to note that activated carbons derived from prune pits had the lowest ratio (of water sorbed relative to MB sorbed), and those derived from almond shells had the highest ratio. A one-way ANOVA was significant ($F_{(14,\ 0.835)} = 3.983$; $P = 0.038$), which indicated that the overall average ratio across carbon sources, 1.45 ± 0.2% ($\bar{x} \pm sd$), was not a representative estimate for each carbon source. Subsequent means comparison testing only showed significant difference between prune- and almond-derived activated carbon sorbents (Tukey-Kramer HSD, $\alpha = 0.05$).

The interpretation that the performance of activated carbon derived from almond shells, peach pits, prune pits, and walnut shells was related to the source-specific competitive sorption of water vapor was further supported by an experiment conducted with WEST-AC. The relative humidity in the PACT system was increased from ∼25−70%, WEST-AC was loaded into five columns, and eight tests were conducted that evaluated, as above, the grand mean of the mass of MB sorbed by a particular column based on gravimetric measurement normalized relative to that detected by SPME-based TWA sampling, $m_{MB,sorbed}$ (see Figure 8). The ratio resulting from the PACT testing at ∼70% RH was significantly higher at the 99% confidence interval than that obtained with ∼20% RH (t test: $t_{21} = 2.0796$, $P > |t| = 0.0003$).

It is interesting to note the selectivity of each activated carbon source for water vapor as related to the MB removal from the airstreams of the PACT apparatus. Data suggest that the two preparations of activated carbon from prune pits that used water vapor for either activation, SA-NQ, or quenching, CO2A-WQ, imparted a surface modification that decreased the potential for competitive sorption and ultimately resulted in more MB removal from the airstream per mass of activated carbon sorbent. Future studies will focus on scaling, from gram- to kilogram-scale, the production of prune pit-derived activated carbon prepared by SA-NQ and CO2A-WQ. If the preparations are effectively scaled, as assayed by performance on the PACT

DOI: 10.1021/jf505193e
J. Agric. Food Chem. 2015, 63, 3094−3103

apparatus, the logical extension would be to conduct confirmatory trials in which ventilation effluent following a commercial postharvest chamber fumigation was directed through a columnar bed of the respective prune pit-derived activated carbons, with subsequent evaluation of MB removal performance.

■ ASSOCIATED CONTENT

Supporting Information

K_{fs} values derived from eqs 1 and 2 plotted against each other; calibration of airstreams prepared by TWA sampling of the PACT system; TWA sampling of the PACT flowing system with instrument response calibrated from TWA sampling of static headspace and GSV injections of MB dilutions in static headspace; calibration associated with TWA sampling of the PACT system at fixed [MB] and varying the span of time, t, that the fiber assembly is exposed to airstream; [MB] detected relative to that expected with or without burying the SPME fiber into a septum for varying durations prior to GC-FID analysis. This material is available free of charge via the Internet at http://pubs.acs.org.

■ AUTHOR INFORMATION

Corresponding Author

*E-mail: spencer.walse@ars.usda.gov. Phone: 559-596-2750. Fax: 559-596-2721.

Notes

The authors declare no competing financial interest.

■ ACKNOWLEDGMENTS

This research was funded by the USDA-Agricultural Research Service as well as the USDA-Foreign Agricultural Service and the California Dried Plum Board under the Technical Assistance for Specialty Crops program, Agreement No. 2010-19. Mention of trade names or commercial products in this publication is solely for the purpose of providing specific information and does not imply recommendation or endorsement by the U.S. Department of Agriculture. USDA is an equal opportunity provider and employer.

■ REFERENCES

(1) Johnson, J. A.; Walse, S. S.; Gerik, J. S. Status of alternatives for methyl bromide in the United States. *Outlooks Pest Manage.* **2012**, *23*, 53−58.

(2) Bell, C. H.; Price, N.; Chakrabarti, B. *The Methyl Bromide Issue*; John Wiley and Sons: Hoboken, NJ, 1997.

(3) Lary, D. J. Gas phase atmospheric bromine photochemistry. *J. Geophys. Res.: Atmos.* **1996**, *101*, 1505−1516.

(4) Solomon, S. Progress towards a quantitative understanding of Antarctic ozone depletion. *Nature* **1990**, *347*, 347−354.

(5) Yung, Y. L.; Pinto, J. P.; Watson, R. T.; Sander, S. P. Bromine and ozone perturbations in the lower stratosphere. *J. Atmos. Sci.* **1980**, *37*, 339−353.

(6) Thompson, J. *Proceedings of Annual International Research Conference on Methyl Bromide Alternatives and Emissions Reductions*; U.S. EPA: San Diego, CA, USA, 2013; pp 1−2. http://www.mbao.org/2013/Proceedings/51ThompsonJ.pdf (accessed October 2014).

(7) Leesch, J. G.; Knapp, G. F.; Mackey, B. E. Methyl bromide adsorption on activated carbon to control emissions from commodity fumigations. *J. Stored Prod. Res.* **2000**, *36*, 65−74.

(8) Synder, J. D.; Leesch, J. G. Methyl bromide recovery on activated carbon with repeated adsorption and electrothermal regeneration. *Ind. Eng. Chem. Res.* **2001**, *40*, 2925−2933.

(9) Knapp, G. F. *Proceedings of Annual International Research Conference on Methyl Bromide Alternatives and Emissions Reductions*; U.S. EPA: San Diego, CA, USA, 1995. http://www.mbao.org/1995airc/002.pdf (accessed October 2014).

(10) Gan, J.; Yates, S. R. Recapturing and decomposing methyl bromide in fumigation effluents. *J. Hazard. Mater.* **1998**, *57*, 249−258.

(11) Gañán, J.; González, J. F.; González-García, C. M.; Ramiro, A.; Sabio, E.; Román, S. Carbon dioxide-activated carbons from almond tree pruning: Preparation and characterization. *Appl. Surf. Sci.* **2006**, *252*, 5993−5998.

(12) Heschel, W.; Klose, E. On the suitability of agricultural by-products for the manufacture of granular activated carbon. *Fuel* **1995**, *74*, 1786−1791.

(13) Kazemipour, M.; Ansari, M.; Tajrobehkar, S.; Majdzadeh, M.; Kermani, H. R. Removal of lead, cadmium, zinc, and copper from industrial wastewater by carbon developed from walnut, hazelnut, almond, pistachio shell, and apricot stone. *J. Hazard. Mater.* **2008**, *150*, 322−327.

(14) Klassen, T. K.; Ledbetter, C. A.; Uchimiya, M.; Lima, I. M. Activated biochar removes 100% dibromochloropropane from from field well water. *Environ. Chem. Lett.* **2013**, *11* (3), 271−275.

(15) Rodríguez-Reinoso, F. *Encyclopedia of Materials: Science and Technology*, 2nd ed.; Buschow, J. K. H., Cahn, R. W., Flemings, M. C., Ilschner, B., Kramer, E. J., Mahajan, S., Veyssiere, P., Eds.; Elsevier: Oxford, 2001; pp 22−34.

(16) Ouyang, G.; Pawliszyn, J. SPME in environmental analysis. *Anal. Bioanal. Chem.* **2006**, *386*, 1059−1073.

(17) Ouyang, G.; Pawliszyn, J. A critical review in calibration methods for solid-phase microextraction. *Anal. Chim. Acta* **2008**, *627*, 184−197.

(18) Koziel, J.; Jia, M.; Khaled, A.; Noah, J.; Pawliszyn, J. Field air analysis with SPME device. *Anal. Chim. Acta* **1999**, *400*, 153−162.

(19) Ouyang, G.; Pawliszyn, J. Time-weighted average sampling of volatile and semi-volatile airborne organic compounds by the solid-phase microextraction device. *J. Chromatogr. A* **2000**, *892*, 455−467.

(20) Martos, P. A.; Pawliszyn, J. Time-weighted average sampling with solid-phase microextraction device: Implications for enhanced personal exposure monitoring to airborne pollutnats. *Anal. Chem.* **1999**, *71*, 1513−1520.

(21) Górecki, T.; Yu, X.; Pawliszyn, J. Theory of analyte extraction by selected porous polymer SPME fibers. *Analyst* **1999**, *124*, 643−649.

(22) Koziel, J.; Jia, M.; Pawliszyn, J. Air sampling with porous solid-pahse microextraction fibers. *Anal. Chem.* **2000**, *72*, 5178−5186.

(23) *Contaminant Fate and Transport: Methyl Bromide*; USDA-ARS: Washington, DC, 2005. http://www.ars.usda.gov/Research/docs.htm?docid=10408 (accessed February 2015).

(24) Ouyang, G.; Chen, Y.; Setkova, L.; Pawliszyn, J. Calibration of solid-phase microextraction for quantitative analysis by gas chromatography. *J. Chromatogr. A* **2005**, *1097*, 9−16.

(25) O'Neil, M. J. *The Merck Index: An Encyclopedia of Chemicals, Drugs, and Biologicals*; Merck: Whitehouse Station, NJ, 2001.

(26) Armbruster, D. A.; Pry, T. Limit of blank, limit of detection, and limit of quantitation. *Clin. Biochem. Rev.* **2008**, *29*, S49.

DOI: 10.1021/jf505193e
J. Agric. Food Chem. 2015, 63, 3094−3103

Table 1. MS/MS Parameters for the 11 Regulated Mycotoxins of AFB_1, AFB_2, AFG_1, AFG_2, OTA, FB_1, FB_2, HT-2, T2, DON, and ZEA[a]

	precursor ion	Q1 (m/z)	Q3 (m/z)	DP (V)	EP (V)	CE (V)	CXP (V)	RT (min)
AFB_1	$[AFB_1+H]^+$	313.1	241.0	55	10	49	10	6.2
			285.0			37		
AFB_2	$[AFB_2+H]^+$	315.2	287.2	60	10	37	10	6.0
			259.0			43		
AFG_1	$[AFG_1+H]^+$	329.1	243.1	54	10	37	10	5.8
			115.1			89		
AFG_2	$[AFG_2+H]^+$	331.1	313.0	60	10	41	10	5.5
			115.1			81		
OTA	$[OTA+H]^+$	404.0	239.0	30	10	27	10	8.1
			102.0			93		
FB_1	$[FB_1+H]^+$	722.5	334.4	91	10	57	10	6.8
			704.4			43		
FB_2	$[FB_2+H]^+$	706.5	336.3	96	10	51	4	7.7
			688.4			41	10	
HT-2	$[HT\text{-}2+NH_4]^+$	442.2	263.1	50	10	21	19	6.7
			215.0			27	20	
T-2	$[T\text{-}2+NH_4]^+$	484.3	215.2	60	10	29	18	7.2
			185.1			31	11	
DON	$[DON+CH_3COO]^-$	355.1	295.2	−30	−10	−15	−17	4.0
			265.0			−21	−16	
ZEA	$[ZEA\text{-}H]^-$	317.0	273.0	−70	−10	−25	−10	8.0
			175.1			−30		
^{13}C-AFB_1	$[^{13}C\text{-}AFB_1+H]^+$	330.2	300.9	120	10	33	24	6.2
^{13}C-AFB_2	$[^{13}C\text{-}AFB_2+H]^+$	332.0	273.2	82	10	42	18	6.0
^{13}C-AFG_1	$[^{13}C\text{-}AFG_1+H]^+$	346.1	257.0	92	10	38	20	5.8
^{13}C-AFG_2	$[^{13}C\text{-}AFG_2+H]^+$	348.0	330.1	60	10	33	10	5.5
^{13}C-OTA	$[^{13}C\text{-}OTA+H]^+$	424.0	250.1	100	10	34	12	8.1
^{13}C-FB_1	$[^{13}C\text{-}FB_1+H]^+$	756.5	374.4	70	10	37	10	6.8
^{13}C-FB_2	$[^{13}C\text{-}FB_2+H]^+$	740.5	358.3	90	10	47	13	7.7
^{13}C-HT-2	$[^{13}C\text{-}HT\text{-}2+NH_4]^+$	464.2	278.4	50	10	18.5	13	6.7
^{13}C-T-2	$[^{13}C\text{-}T\text{-}2+NH_4]^+$	508.3	322.1	60	10	29	18	7.2
^{13}C-DON	$[^{13}C\text{-}DON+CH_3COO]^-$	370.2	310.2	−30	−10	−12.7	−17	4.0
^{13}C-ZEA	$[^{13}C\text{-}ZEA\text{-}H]^-$	335.0	290.0	−70	−10	−25	−10	8.0

[a]Q1, first quadrupole; Q3, third quadrupole; DP, declustering potential; EP, entrance potential; CE, collision energy; CXP, collision cell exit potential; RT, retention time.

Table 2. Purity (%) of Individual Mycotoxins and Their Respective Stable Carbon Isotopically Labelled Standards (ISTD) and Calibration Levels (μg/L)

	purity of standard (%)	purity of ^{13}C ISTD (%)	S1 (μg/L)	S2 (μg/L)	S3 (μg/L)	S4 (μg/L)	S5 (μg/L)	S6 (μg/L)
AFB_1	98.0	99.0	0.199	0.498	0.996	1.99	3.98	5.97
AFB_2	98.0	99.0	0.198	0.495	0.99	1.98	3.96	5.94
AFG_1	98.0	99.0	0.265	0.5	1.32	2.64	5.28	7.92
AFG_2	98.0	99.0	0.185	0.463	0.925	1.85	3.70	5.55
OTA	98.0	98.7	0.504	1.26	2.52	5.04	10.1	15.1
FB_1	97.6	97.8	25	62.5	125	250	500	750
FB_2	98.0	98.7	20.8	51.9	104	208	416	624
HT-2	98.8	98.9	5	10	25	50	100	150
T-2	99.7	98.8	5	10	25	50	100	150
DON	99.4	99.5	5	10	25	50	100	150
ZEA	99.0	99.2	5	10	25	50	100	150

AFG_1, AFG_2), ochratoxin (OTA), fumonisins (FB_1, FB_2) HT-2 and T-2, and their respective stable carbon-labeled isotopes (^{13}C-AFB_1, ^{13}C-AFB_2, ^{13}C-AFG_1, ^{13}C-AFG_2, ^{13}C-OTA, ^{13}C-FB_1, ^{13}C-FB_2, ^{13}C-HT-2 and ^{13}C-T-2). Negative polarity was applied for the analyses of deoxynivalenol (DON) and zearalenone (ZEA), and their stable carbon-labeled isotopes (^{13}C-DON and ^{13}C-ZEA). Electrospray voltages were set to 5.5 kV for positive ionization polarity and −4.5 kV for negative ionization polarity. The source temperature and nitrogen gas flows (GS1 and GS2) were set to 500 °C and 40 psi, respectively. A summary of precursor ions, their respective retention times, and MS conditions is listed in Table 1.

Materials and Reagents. Acetonitrile (MeCN) and MeOH were of HPLC grade from Labscan (a brand from

DOI: 10.1021/acs.jafc.5b00471
J. Agric. Food Chem. 2015, 63, 3104−3113

Sigma-Aldrich). HPLC grade NH_4-formate, acetic acid, and benzene were purchased from Sigma-Aldrich (St. Louis, MO, U.S.A.). Water was purified by passing through a Purelab Option-Q water purification system (a brand from Elga, U.K.). Analytical standards of aflatoxins, OTA, and fumonisins were purchased from Sigma-Aldrich, whereas HT-2, T-2, DON, and ZEA were purchased from Biopure (Tulln, Austria). Stable carbon isotopic standards of all 11 mycotoxins were purchased from Biopure (Tulln, Austria). Purity of the standards and their respective ^{13}C-labeled isotopes is summarized in Table 2. Stock preparation of Aflatoxins and OTA was reproduced from previous work.[10] Briefly, an individual stock solution of aflatoxins was prepared by dissolving in benzene (to extend the shelf life of aflatoxins). For OTA, methanol was selected as solvent of choice. Stock solutions of FB_1 and FB_2 were prepared in 50% MeOH and then diluted using mobile phase B. Next, individual stock solution of HT-2, T-2, DON, and ZEA was prepared in MeCN. From these individual stock solutions, mixed calibrants of all 11 analytes were freshly prepared, by dilution, using mobile phase B at six concentration levels as shown in Table 2. For aflatoxins, an additional drying step (under a gentle stream of nitrogen gas) was required to remove benzene prior to preparation of mixed calibrants. ^{13}C-AFB_1, ^{13}C-AFB_2, ^{13}C-AFG_1, ^{13}C-AFG_2, ^{13}C-OTA, ^{13}C-FB_1, ^{13}C-FB_2, ^{13}C-HT-2, ^{13}C-T-2, ^{13}C-DON, and ^{13}C-ZEA were applied for spiking experiments and commercial sample screening. Concentrations ranged from 1 μg/L for ^{13}C-AFG_2 to 20 μg/L for ^{13}C-FB_2. All chemicals were used without further purification.

Sample Preparation and Extraction. Rice samples from 9 Asian countries were investigated in this work, as follows: P.R. China (6 samples, white rice), India (31 samples, parboiled rice and basmati rice,), Japan (26 samples, white rice and brown rice), Malaysia (6 samples, white rice and brown rice), Myanmar (2 samples, broken rice), Pakistan (15 samples, basmati rice), Taiwan (10 samples, white rice), Thailand (79 samples, white rice, brown rice and red rice) and Vietnam (15 samples, white rice and brown rice) were purchased from a local distributor in Singapore. An aggregate sample of 1 kg (minimum) was required for retail sampling (European Union Commission Regulation 401/2006). White rice, brown rice, red rice, and basmati rice were randomly selected from the pool of 190 rice varieties and tested for mycotoxins before the selected sample was used for the matrix effect assessment, recovery, and individual analyte stability study.

Before performing extraction, an individual rice sample (approximately 1 kg) was milled using Ultra Centrifugal Mill ZM 200 from Retsch (a brand from Haan, Germany), which was fitted with a ring sieve with an aperture size of 0.5 mm. For a sample size of 1 kg, three batches of milling were required because the miller has a capacity limit of 400 g for rice samples. A household blender was then used to blend the milled samples. To ensure minimum carry over between rice samples' preparation, potato starch powder was applied to both the miller and the household blender, and then discarded.

Sample extraction was developed with the intention of ease of execution and low cost of operation for a routine laboratory. Rice extraction was performed by applying a modified sample extraction protocol reported by Sulyok et al.[11] and Varga et al.[12] for maize analysis. A 1 g sample weight was used to determine matrix effects and recovery. Single extraction using an equal volume of MeCN and purified water containing 1% acetic acid was applied. Briefly, 4 mL ($v1$) of extraction solvent was added to a 1 g (w) sample in a 50 mL taper tube and shaken for 30 min. Then, the mixture was centrifuged at 8000 rpm (3226g) for 6 min at room temperature. Next, 1:1 dilution ($v2$) using mobile phase B was performed. Individual isotopic standards were added to the diluted supernatant and shaken vigorously by hand, and the samples were then purified using a 0.2 μm PTFE syringe filter before they were transferred into 1.5 mL HPLC amber vial with deactivated inserts. Finally, 10 μL of purified supernatant was injected into the LC-MS/MS for analysis. By applying this sample purification protocol for method validation and commercial sample screening, a solute to solvent ratio of 1:8 can be achieved. For commercial rice samples screening, a scaled-up extraction protocol was applied to a 25 g sample weight portion.

Data Processing for LC-MS/MS. The data were analyzed using the quantitation wizard built into Analyst software 1.6.0 for windows (AB Sciex, Foster City, CA, U.S.A.). Transition ions representing individual analytes were summarized in Table 1. The most abundant transition ion of each isotope was used to perform quantitative analysis.

Evaluation of Matrix Effect and Detection Limit. The intention of performing matrix effect assessment is to examine ion signal enhancement/suppression due to coextractants originating from the rice matrix over a practicable concentration range. A 1 g rice sample was first extracted, followed by spiking at six concentration levels. Isotopic dilution was not applied. The application of the post-extraction spiking strategy identified ion signal enhancement/suppression due to matrix interference and distinguished them from effects due to recovery. Spiking levels (A, in μg/kg) were determined as

$$A = [(\text{spiking concentration}/w)] \times v1 \times 2 \quad \text{(eq A.1)}$$

Six levels of spiking concentration were generated by applying eq A.1, as summarized in Table 2 (n = 3). Matrix effect (ME) was evaluated as[13]

$$\text{ME} = (\text{peak area of matrix-matched}/\text{peak area of matrix-free}) \times 100 \quad \text{(eq A.2)}$$

Linearity was assessed using a residual plot and statistical test for goodness-of-fit. Limits of detection (LOD) and limits of quantitation (LOQ) were determined as (2.33 × standard deviation)/gradient of slope and LOD + (1.64 × standard deviation)/gradient of slope, respectively.[14]

Recovery, Intraday, Interday Repeatability and Stability Studies. Fumonisins are known to suffer from poor recovery in maize based on reports published previously.[11,12] Losses can occur during sample preparation and during storage. In this study, we examined the fate of all 11 analytes (including fumonisins) in rice through spiking experiments, and by using normal and deactivated glass inserts for storage. Briefly, 1 g aliquots (n = 6) of rice samples were spiked at three concentration levels (standard 2, 3, and 5) and extracted using protocols described in the section Sample Preparation and Extraction. Matrix-free calibration curves at six concentration levels (Table 2) were freshly prepared for recovery study. Isotopic dilution was applied. Recovery (extraction efficiency, R) was assessed as

$$R = [(\text{mean measured concentration}_{\text{standard2,3,5}}) / (\text{spiked concentration}_{\text{standard2,3,5}})] \times 100 \quad \text{(eq A.3)}$$

using the respective calibration curves of individual mycotoxin.

For analyte stability study, two sets of matrix-free calibrants were required. The first set of calibrants was used for recovery

DOI: 10.1021/acs.jafc.5b00471
J. Agric. Food Chem. 2015, 63, 3104−3113

Table 3. Summary Table of Mycotoxins' Surveys Reported Recently

country	matrix	mycotoxin	sample size	ref
Austria	rice (basmati, whole grain, long grain short grain, puffed)	AFB_1, B_2, G_1, G_2	81	(Reiter et al., 2010)
Brazil	rice and its processing fractions	total aflatoxin, OTA, ZEA, DON, citreoviridin	230	(Almeida et al., 2012)
Canada	rice (white, brown, red, black, basmati, jasmine)	AFB_1, AFB_2, OTA, FB_1, FB_2, FB_3	200	(Bansal et al., 2011)
Egypt	rice, maize	AFB_1, AFB_2, AFG_1, AFG_2, total aflatoxin, FB_1, FB_2	40	(Madbouly et al., 2012)
India (Review)	rice	aflatoxins	-	(Reddy et al., 2008)
Iran	rice	T-2	140	(Riazipour et al., 2009)
Malaysia (Review)	cereals, nuts, spices	aflatoxins, OTA, tricothecenes, ZEA, fumonisins	-	(Afsah-Hejri et al., 2013)
Nepal	rice	fumonisin, beauvericin, gibberellic acid, moniliformin, tricothecenes	48	(Desjardins et al., 2000)
Nigeria	rice	AFB_1, AFB_2, AFG_1, AFG_2, OTA, ZEA, DON, FB_1, FB_2, FB_3, patulin, T-2	21	(Makun et al., 2011)
Pakistan	rice (white, brown, sella)	AFB_1, AFB_2, AFG_1, AFG_2	519	(Firdous et al., 2012)
Pakistan	basmati rice	AFB_1, AFB_2, AFG_1, AFG_2	2047	(Asghar et al., 2013)
Sweden	rice (basmati, brown, jasmine)	AFB_1, AFB_2, AFG_1, AFG_2, OTA	99	(Fredlund et al., 2009)
Turkey	rice	total aflatoxin, AFB_1, OTA	100	(Aydin et al., 2011)
United Kingdoms	rice and rice products (long grain, easy cook, basmati, specialty, brown, short grain, flaked, ground)	aflatoxins, fumonisins, OTA, sterigmatocystin, tricothecenes, ZEA	100	(FSA, 2002)
Vietnam	rice	AFB_1, citrinin, OTA	100	(Nguyen et al., 2007)

experiments. The same set of sample vials used for recovery experiments were measured 1 month later using freshly prepared calibrants. Sample vials were stored at 4 °C when not in use. This way, information related to individual analyte stability in solution and in matrix can be obtained.

In addition, effects of acetic acid on recovery for all analytes including fumonisins in selected white rice were investigated. This study was motivated by a report on degradation of fumonisins in various samples of Thai white rice.[15] For this purpose, spiking experiments (at standard 2 concentration) were conducted in triplicates for each composition of acetic acid (extraction solvent containing 0.1% and 1% acetic acid, respectively) by applying the protocols described in the section Sample Preparation and Extraction. To distinguish losses due to degradation from losses due to extraction inefficacy, single concentration calibrant (standard 2) was prepared in supernatant. Measurements were performed 12 h later to simulate degradation in matrix reported previously.[15] Isotopic dilution was then applied. Recovery for individual analytes was calculated using eq A.3.

Screening of Commercial Samples. A total of 190 rice samples were screened for aflatoxins, OTA, fumonisins, HT-2 and T-2 toxins, DON, and ZEA. Duplicate testing was performed on suspect samples. An average of the two values was reported. Owing to a lack of reference materials containing all 11 mycotoxins in rice, compensation for recovery for individual analyte was made by spiking.

Statistical Analysis. Two-tailed Student's *t*-test was applied to identify significant differences between two sets of experimental data at 95% confidence level,[16] where applicable. To determine the correlation between mycotoxins contamination and rice species, Pearson Correlation (r) was calculated for results obtained described in the section Screening of Commercial Samples by assigning rice species (count) as (X) and mycotoxins positive samples as (Y).

RESULTS AND DISCUSSION

MS Method, Mobile Phase Selection, and Chromatography. Applying MS for multimyotoxins detection in rice is not new.[17,18] Common to these publications, aflatoxins, fumonisins, deoxynivalenol, zearalenone, ochratoxin A, T-2 and HT-2 toxins in rice were examined using analyte-specific sample purification columns. In this study, we applied a simple dilute-and-shoot workflow to determine aflatoxin B_1 (AFB_1), B_2 (AFB_2), G_1 (AFG_1) and G_2 (AFG_2), deoxynivalenol (DON), fumonisins (FB_1 and FB_2), T-2 and HT-2 toxins, ochratoxin A (OTA), and zearalenone (ZEA) in rice. Our choice of mycotoxins is based on mycotoxins' occurrence reports published previously, as shown in Table 3.[19−33]

For MS method selection, we applied scheduled MRM because only targeted analytes at their respective retention time were monitored. The application of scheduled MRM provided the benefit of decreasing the number of concurrent MRMs monitored at the same time.[34] This way, we were able to achieve reproducible peak symmetry and optimum data quality by adhering to the guideline of 10 to 15 data points per peak even when concurrent polarity switching was applied for the entirety of our experiment.[35] In our work published previously, MS^3 was applied as an accurate tool to identify and quantify aflatoxins and OTA in chilli matrices because it exhibited superior resilience to ion ratio distortion for AFG_2 and OTA.[10] In this study, however, the application of scheduled MRM was fit-for-purpose for quantification of multimycotoxins in rice because ion ratio distortion was absent.

DOI: 10.1021/acs.jafc.5b00471
J. Agric. Food Chem. 2015, 63, 3104−3113

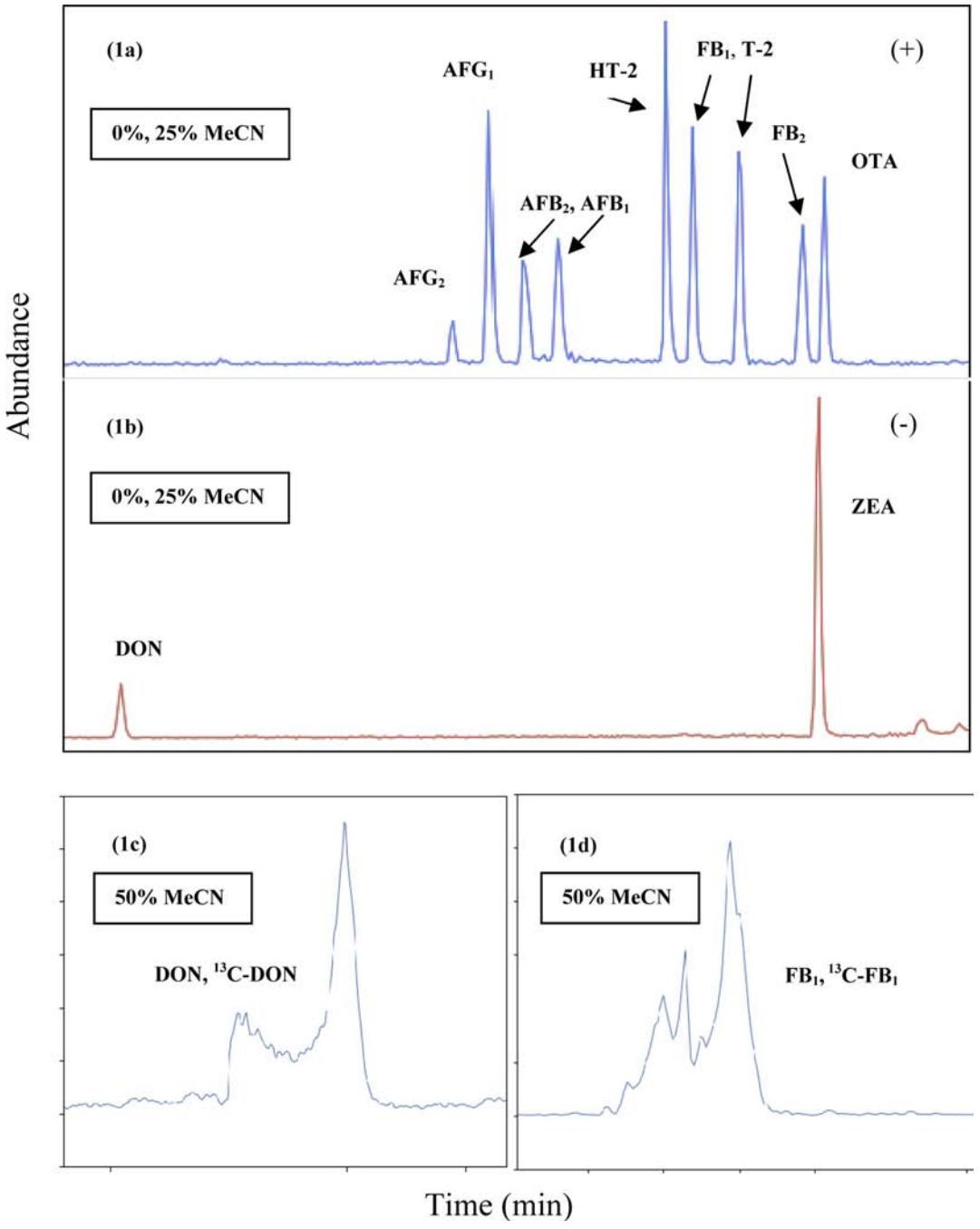

Figure 1. LC-MS/MS separation and detection showing current polarity switching for concentration **S1** (1a) total ion chromatograms of AFG_2, AFG_1, AFB_2, AFB_1, HT-2, FB_1, T-2, FB_2, and OTA. (1b) Total ion chromatograms of DON and ZEA prepared in mobile phase B and 25% MeCN. (1c) and (1d) show distorted ion chromatograms of DON and FB_1 (as well as their respective isotopes) at 50% MeCN strength.

For mobile phases selection, we considered the ionization efficacy of aflatoxins and HT-2 toxin in acetonitrile and methanol individually. For aflatoxins, we reported previously that the addition of 1 mM ammonium formate to both the extraction solvent and mobile phase would yield a combined ion signal improvement of 3 orders of magnitude based on triplicate measurements[10] using triple stage mass spectrometry (MS^3). Under MRM mode, adding 1 mM ammonium formate to the extraction solvent provided insignificant ion signal enhancement for aflatoxins. The addition of ammonium formate to both mobile phases A and B alone enabled measurements for sub μg/L (~0.01 μg/L) concentrations of AFB_1, AFB_2, AFG_1, and AFG_2 to be made. In order to improve the ionization efficiency of NH_4-adduct for HT-2 toxin under positive polarity,[10] we chose methanol over acetonitrile as mobile phase A. Experimentally, LOD for HT-2 from 50 μg/kg to 2.3 μg/kg in white rice. Similarly, the addition of 0.1% acetic acid converted DON into its acetate adduct for MRM quantitation.[36] The transitions monitored for DON in this study is different from those reported previously[12] because the QTRAP 5500 did not generate useful fragmentation pattern for $[DON + H]^+$. We attribute the difference in fragmentation reaction for $[DON + H]^+$ to be collision-cell-specific. Selection of methanol and water as mobile phases of choice (containing 1

DOI: 10.1021/acs.jafc.5b00471
J. Agric. Food Chem. 2015, 63, 3104−3113

Table 4. Matrix Effect (%) Determined at Six Concentration Levels for the 11 Regulated Mycotoxins of AFB_1, AFB_2, AFG_1, AFG_2, OTA, FB_1, FB_2, HT-2, T2, DON, and ZEA in White Rice, Brown Rice, Red Rice, and Basmati Rice[a]

	average matrix effect (%)											
	AFB_1	AFB_2	AFG_1	AFG_2	OTA	FB_1	FB_2	HT-2	T2	DON	ZEA	rice
S1	77	63	81	91	123	197	1959	96	104	79	102	white
	97	98	68	50	268	250	5730	131	312	138	264	brown
	77	72	90	73	172	259	2476	115	141	59	152	red
	83	71	73	69	113	214	1831	90	92	70	95	basmati
S2	45	44	41	49	58	157	1172	72	76	84	72	white
	40	56	66	58	147	180	741	128	146	131	125	brown
	65	63	71	60	110	219	1770	104	114	62	126	red
	65	74	75	79	89	160	1290	86	90	89	89	basmati
S3	51	48	51	57	88	140	471	76	83	76	103	white
	45	46	60	48	123	191	701	112	128	113	118	brown
	84	74	89	76	147	198	729	118	138	109	151	red
	66	67	81	82	101	155	550	98	100	85	110	basmati
S4	62	62	70	66	107	167	402	102	100	86	120	white
	51	53	67	60	156	225	550	138	155	122	147	brown
	97	86	95	85	179	219	545	140	143	112	182	red
	77	69	88	94	135	170	425	113	120	114	146	basmati
S5	50	52	51	54	92	139	300	82	88	85	105	white
	47	46	57	50	129	170	268	111	122	116	111	brown
	80	79	83	76	160	182	409	121	137	98	148	red
	52	55	59	65	106	127	382	84	92	76	106	basmati
S6	62	63	64	64	107	150	299	84	102	95	120	white
	64	68	77	69	176	190	188	130	150	112	139	brown
	98	97	94	92	186	197	447	133	149	110	168	red
	49	43	45	55	75	100	429	58	72	57	79	basmati

[a]Average matrix effect (%) = (peak area of matrix-matched/peak area of matrix-free) × 100.

mM ammonium formate and 0.1% acetic acid) would provide the optimum chemical environment needed to examine individual analyte on our proposed LC column.

There were challenges related to peak shape reproducibility when we performed rice extraction without applying dilution using mobile phase B. Briefly, we found the peak shapes for both DON and FB_1, as well as their respective isotopes were severely distorted. Performing 1:1 dilution (25% MeCN) using mobile phase B preserved peak shape integrity for both DON and FB_1. Figure 1a,b showed the total ion chromatogram representing individual mycotoxins when prepared in water dominant mobile phase B (respective isotopically labeled peaks not shown) and 25% MeCN. Figure 1c,d showed distorted peaks for DON and FB_1 in extraction solvent (50% MeCN) without 1:1 dilution. Although peak shape integrity is easily dismissed by some researchers as cosmetic imperfection due to poor chromatographic skills, we observed significant variation for precision (RSD > 50%) at three spiking concentrations in rice for both DON and FB_1. Clearly, adopting good chromatographic separation practices provided data confidence through repeatability assessment.

Evaluation of Matrix Effect. Matrix effect or the occurrence of ion-suppression or enhancement in quantitative analysis using LC-ESI-MS/MS was reported previously.[37] It has a significant impact on method integrity by giving inaccurate and unreliable results, thereby affecting reproducibility, linearity, and recovery values. Thus, matrix effect was evaluated at six concentration levels using both matrix-free and matrix-matched calibration curves to assess analyte performance without internal standards.

A summary of matrix effect on LC-MS/MS using MRM is tabulated in Table 4. In particular, fumonisins showed severe ion signal enhancement effect in all rice matrices at all six concentration levels, ranging from 100 to 5730%. Ion signal suppression for aflatoxins ranged from 40% to 97%. For OTA, T2 and HT2 toxins, DON, and ZEA, effect of ion signal enhancement or suppression were observed. Mechanisms such as competition for available charges and access to droplet surface for gas phase emission,[37] among others, could explain the wide ranging matrix effect results shown in Table 4. Although matrix effect in some rice was reported previously,[38] there was no mention of significant variation in matrix effect for fumonisins in white rice, brown rice, red rice, and basmati rice. Application of *dilute-and-shoot* strategy alone was insufficient to compensate for matrix effect. Isotopic dilution was therefore applied.

Evaluation of Recovery, Linearity, Intraday, Interday Repeatability and Stability. We investigated the recovery performance of all analytes in white rice, brown rice, red rice, and basmati rice. From Table 5A, we found there is no evidence to show mycotoxins can degrade in white rice extract from Thailand/China. However, we did observe recovery losses for all analytes when 0.1% acetic acid was applied to the initial extraction solvent (Table 5B) for some rice samples from Thailand/China. From Table 5C, the presence of 1% acetic acid in the extraction solvent provided significant recovery improvement ($p < 0.05$) for all analytes (including fumonisins) in white rice samples from China/Thailand. Although the use of 1% acetic acid for extraction of mycotoxins was reported previously,[11,38] the data reveal the reason it is used.

Our recovery study aimed to assess method accuracy, precision, and repeatability by performing spiking using rice blanks ($n = 6$) made at three concentration levels. Recoveries were evaluated using matrix-free calibration curves with internal

DOI: 10.1021/acs.jafc.5b00471
J. Agric. Food Chem. 2015, 63, 3104−3113

Table 5. Recovery for AFB_1, AFB_2, AFG_1, AFG_2, OTA, FB_1, FB_2, HT-2, T2, DON, and ZEA in White Rice Extract (Thailand/China) with 0.1% Acetic Acid (A); Effect of Acetic Acid Composition (in Extraction Solvent) on Recovery for AFB_1, AFB_2, AFG_1, AFG_2, OTA, FB_1, FB_2, HT-2, T2, DON, and ZEA in White Rice from Thailand/China (B, C)[a]

	mean recoveries (%, $RSD_{n=3}$)		
	(A)	(B)	(C)
analytes	0.1% acetic acid[b]	0.1% acetic acid[c]	1.0% acetic acid[c]
AFB_1	115 (2)	82 (4)	110* (9)
AFB_2	91 (9)	43 (6)	88* (3)
AFG_1	110 (8)	51 (9)	94* (4)
AFG_2	108 (3)	55 (5)	87* (10)
OTA	110 (9)	48 (5)	86* (8)
T2	107 (7)	58 (2)	99* (5)
HT2	102 (3)	78 (9)	102* (8)
FB_1	109 (6)	57 (2)	94* (1)
FB_2	96 (2)	46 (9)	82* (4)
DON	94 (7)	63 (5)	102* (8)
ZEA	97 (9)	46 (9)	103* (10)

[a]Experiments for recovery were performed at S2 spiking concentration in triplicates, with isotopic dilution. [b]Measurements were performed 12 h later to simulate "degradation" in rice extract. [c]Measurements were performed immediately after extraction. *Indicates significantly different from values obtained at 0.1% acetic acid[b] composition, ($p < 0.05$) at 95% confidence interval.

standards added. Mean recoveries, intraday and interday relative standard deviation (RSD) values were calculated and shown in Table 6. RSD values were less than 15% for all analytes.

From Table 6, satisfactory recovery values ranged from 70% to 120% were achieved for all analytes in all rice matrices. The application of single extraction protocol containing 1% acetic acid provided recovery advantage for fumonisins in all rice matrices without the need to apply double extraction protocols to address fumonisins' losses such as in maize.[12] The sample extraction protocol presented in this study is also suitable for maize analysis (based on FAPAS 04223 Proficiency Test) because it produced a satisfactory z-score value of <0.7 for all analytes. Method precision and accuracy fulfils the performance criteria for aflatoxins, OTA, fumonisins, T-2 and HT-2 toxins, DON, and ZEA in foodstuffs.[14]

For the same set of sample vials (1 month old) containing spiked solution of aflatoxins, OTA, fumonisins, T-2 and HT-2 toxins, DON, and ZEA, recovery values were greater than 150% for all analytes except for fumonisins. When the same set of sample vials were determined using a set of freshly prepared calibrants, significant losses of more than 50% was reported for most analytes except fumonisins. Fumonisins did not undergo significant degradation ($p < 0.05$, $n = 3$) when prepared in mobile phase B. Clearly, all analytes except fumonisins underwent significant degradation when prepared in mobile phase B.

For fumonisins, it was necessary to use deactivated inserts because normal glass inserts resulted in significant ($p < 0.05$, $n = 3$) random losses when prepared in mobile phase B. The application of deactivated inserts provided lower uncertainty range for fumonisins. The combined uncertainty in rice using deactivated inserts and normal inserts were 12% and 82%, respectively. The application of deactivated inserts would provide significant improvement for method accuracy for fumonisins, which represented the major contributing factor toward uncertainty calculation. Therefore, we can conclude that deactivated inserts improved measurement uncertainty by providing greater accuracy in the determination of fumonisins in rice.

Hence, we recommend fresh preparation of mycotoxin calibrants and store in deactivated inserts, when prepared in water-enriched solvent system such as mobile phase B. Therefore, for the first time, information related to aflatoxins, OTA, fumonisins, T-2 and HT-2 toxins, DON and ZEA stability in rice matrix and in solution has been made available.

Coefficient of determination values obtained were between 0.9991 and 0.9998 for all analytes examined. LOD and LOQ values for individual mycotoxins are summarized in Table 6. Measurement uncertainty ($k = 2$) values were calculated[39] and reported for rice samples tested positive for mycotoxins.

Screening Commercial Rice Samples for Multimycotoxins. Screening commercial rice samples for multimycotoxins would provide occurrence data in the supply chain to support prospective maximum regulatory limits revision.

A survey involving 190 rice samples from nine countries was conducted of which six rice samples were tested positive for mycotoxins. This constituted a mere 3.2% compared to contamination figures published previously (Table 3). One possible reason for the difference in mycotoxin-contaminated rice values presented in this study and those reported previously in Table 3 could be due to sampling strategy. A summary of samples tested positive for mycotoxins is shown in Table 7. Information related to contamination levels, mycotoxins, source of production, and types of rice were provided. Table 7 provided no evidence for co-occurrence of mycotoxins. The results showed that AFB_1 concentration levels ranged from 1.1 to 3.2 (±0.1 to 0.2) μg/kg, which was below the EU maximum limits of 5 μg/kg[7]. From a wide variety of rice species analyzed, basmati rice samples have the highest risk of contamination from AFB_1 based on occurrence. Basmati rice produced by Pakistan represent four out of six rice samples tested positive for AFB_1, as shown in Table 7. A sample of Indian parboiled rice for use by diabetic patients was positive for AFB_1 at 1.7 ± 0.1 μg/kg. Only one sample of broken rice produced by Myanmar was positive for OTA at 46.6 ± 4.2 μg/kg. All rice samples were negative for AFB_2, AFG_1, FB_1, FB_2, DON, T2, HT-2, and ZEA. Our rice survey identified Pakistan as a major aflatoxin-contaminated rice producer in the supply chain. This observation is consistent with data reported previously by RASFF in 2008, which identified Pakistan as the major aflatoxin-contaminated rice producer.

There are parallels in rice contamination profiles between our report and those published previously.[19,21,30] Common to these survey outcomes, AFB_1 represented the single major contaminant in all basmati rice samples examined. Indeed, Reiter et al.[21] showed that 22 out of 24 basmati varieties which were positive for AFB_1 in Sweden were produced by Pakistan and India. In yet another series of similar rice profiling exercises conducted previously,[30,32] basmati rice samples of localized Pakistan produce represented the host crops for AFB_1 contamination. The prevalence of AFB_1 in rice samples produced by localized Pakistan farmers[10] explained the need for increased level of official controls on imports for basmati rice from Pakistan.[40] Indeed, a study conducted by Asghar et al.[29] over a period of 6 years revealed a persistent AFB_1 fingerprint (1.2 μg/kg) in the supply chain. The level detected

DOI: 10.1021/acs.jafc.5b00471
J. Agric. Food Chem. 2015, 63, 3104−3113

Table 6. Limits of Detection (LOD) and Limits of Quantitation (LOQ), Mean Recovery Values (%) for All Spiking Experiments Made in Rice Blanks at Concentration Levels of S2, S3, and S5, and Coefficient of Determination Values Based on Individual Mycotoxin Calibration Curves

				mean recovery (%, $RSD_{Intraday}$, $RSD_{Interday}$)			
	LOD[a] (μg/kg)	LOQ[a] (μg/kg)	coefficient of determination	S2	S3	S5	rice
AFB_1	0.2	0.3	0.9998	104 (3,3)	108 (3,5)	104 (2,7)	white
	0.3	0.4		102 (3,7)	104 (6,6)	103 (2,4)	brown
	0.3	0.4		80 (10,9)	79 (9,8)	81 (11,9)	red
	0.1	0.2		109 (9,6)	107 (9,8)	108 (3,6)	basmati
AFB_2	0.2	0.3	0.9994	97 (8,9)	102 (9,8)	102 (5,11)	white
	0.1	0.2		110 (2,3)	103 (7,5)	94 (3,3)	brown
	0.2	0.3		79 (10,10)	81 (9,8)	77 (12,8)	red
	0.1	0.3		105 (3,4)	99 (5,6)	98 (7,7)	basmati
AFG_1	0.2	0.3	0.9993	101 (1,3)	87 (4,4)	87 (1,3)	white
	0.1	0.2		109 (2,3)	108 (4,4)	104 (2,3)	brown
	0.2	0.4		85 (7,7)	84 (7,6)	82 (9, 8)	red
	0.1	0.2		110 (6,7)	100 (4,5)	108 (4,9)	basmati
AFG_2	0.1	0.2	0.9991	103 (1,7)	101 (6,7)	93 (2,6)	white
	0.2	0.4		100 (3,4)	105 (6,8)	97 (6,4)	brown
	0.1	0.2		86 (6, 7)	81 (6,12)	83 (7,11)	red
	0.3	0.5		100 (4,6)	102 (6,8)	99 (3,3)	basmati
OTA	0.2	0.4	0.9997	90 (3,6)	86 (4,5)	95 (8,10)	white
	0.2	0.4		97 (2,6)	101 (5,4)	108 (3,3)	brown
	2.4	4.1		77 (3,5)	75 (5, 5)	70 (4,4)	red
	0.2	0.4		94 (5,4)	98 (9,8)	103 (2,2)	basmati
FB_1	14.0	24.0	0.9994	78 (5,7)	80 (9,11)	80 (9,13)	white
	4.0	7.0		96 (7,10)	101 (3,11)	112 (5,7)	brown
	6.0	11.0		80 (9,9)	78 (5,7)	71 (6,6)	red
	3.0	5.0		97 (8,7)	100 (5,6)	107 (5,8)	basmati
FB_2	7.0	12.0	0.9993	87 (5,5)	100 (5,7)	100 (4,5)	white
	3.0	5.0		114 (5,6)	120 (4,6)	120 (3,3)	brown
	5.0	9.0		88 (8,8)	86 (7,7)	81 (3,3)	red
	3.0	5.0		105 (6,6)	111 (5,5)	118 (3,3)	basmati
HT-2	2.3	3.9	0.9992	93 (3,6)	106 (2,10)	105 (6,9)	white
	11.0	18.0		92 (9,10)	102 (3,5)	102 (3,4)	brown
	9.0	17.0		88 (6,7)	87 (4, 5)	81 (6,8)	red
	10.0	18.0		96 (4,4)	96 (3,5)	105 (5,5)	basmati
T-2	2.4	4.0	0.9997	101 (10,14)	104 (12,12)	109 (7,7)	white
	4.0	8.0		100 (5,6)	103 (3,3)	102 (5,4)	brown
	5.0	10.0		90 (4,5)	88 (8,10)	82 (4,7)	red
	3.7	6.4		101 (5,4)	99 (4,4)	107 (4,3)	basmati
DON	10.0	18.0	0.9994	110 (4,5)	103 (3,4)	93 (2,3)	white
	15.0	25.0		109 (13,15)	97 (13,12)	104 (13,10)	brown
	18.0	31.0		84 (8,10)	91 (9,12)	94 (7, 9)	red
	16.0	27.0		101 (12,10)	96 (14,12)	97 (12,14)	basmati
ZEA	2.1	3.6	0.9997	110 (6,5)	111 (2,4)	104 (4,4)	white
	8.0	13.0		99 (4,8)	97 (4,5)	103 (3,4)	brown
	7.0	13.0		87 (8,8)	85 (4, 6)	82 (7,7)	red
	10.0	17.0		101 (9,10)	98 (9,7)	94 (3,3)	basmati

[a]Three independent sets of matrix-matched calibrants prepared at six concentration levels were used to calculate LOD and LOQ values. LOD and LOQ were calculated as (2.33 × standard deviation)/gradient of slope and LOD + (1.64 × standard deviation)/gradient of slope, respectively (EU, 2006a). Values for LOD and LOQ were rounded to one decimal place.

is below the 5.0 ug/kg limit recommended by European Commission.[7] Even though there was only a single OTA positive sample from Myanmar in our survey, this preliminary data may be useful for prospective food safety efforts with focus on multimycotoxins control in Asian rice. To date, no complete information related to mycotoxins in rice is available from Myanmar, albeit Nguyuen et al.[33] presented some preliminary data on Vietnamese rice and reported some values for AFB_1, citrinin, and OTA contamination. The reason for this paucity of data on mycotoxins contamination in rice from Myanmar and Vietnam remains unclear. Based on our study, there is insufficient evidence to show that a correlation exists between mycotoxins contamination and rice species ($r = 0$).

In brief, a comprehensive paper describing analytical method validation, its application as an analytical tool, and its impact on food safety in Asia was presented for regulated mycotoxins in Asian rice. These mycotoxins are, namely, aflatoxins, OTA, fumonisins, T-2 and HT-2 toxins, DON, and ZEA. Method

DOI: 10.1021/acs.jafc.5b00471
J. Agric. Food Chem. 2015, 63, 3104−3113

Table 7. Summary of Rice Samples (n = 190) Tested Positive for Mycotoxins, Including Information Related to Country of Origin, Types of Mycotoxins, and Contamination Levels

sample no.	type of rice	country of origin	concentration (μg/kg)	
			AFB_1	OTA
16	fragrant basmati rice	Pakistan	2.0 ± 0.1	nd
21	broken rice	Myanmar	nd	46.5 ± 4.2
170	basmati rice	Pakistan	3.2 ± 0.2	nd
176	basmati rice	Pakistan	1.1 ± 0.1	nd
182	parboiled rice for diabetics	India	1.7 ± 0.1	nd
188	premium basmati rice	Pakistan	1.7 ± 0.1	nd

nd = not detected.

accuracy, precision, sensitivity, repeatability, robustness, and individual analyte stability were examined and found to be highly satisfactory. Random fumonisins' losses in solution was also identified and suitably counteracted using deactivated inserts. Significant ($p < 0.05$) degradation of all analytes except for fumonisins in mobile phase B was reported for the first time. Spiked recoveries performed at three concentration levels using single extraction (measured over 2 days) provided satisfactory mean recovery range from 70% to 120% for all analytes, including some white rice from Thailand and China. The application of 1% acetic acid (to the extraction solvent) addressed recovery losses for all analytes, including fumonisins in white rice from Thailand/China. Incidence of staple rice crop tested positive for mycotoxins was reported to be 3.2%. Rice from Pakistan represented 67% of naturally AFB_1 contaminated samples. Unlike spices,[10] there is no evidence to suspect regulated mycotoxins can co-occur in Asian rice. Likewise, there is insufficient evidence to show *Fusarium graminearum* can occur in Asian rice.

AUTHOR INFORMATION

Corresponding Author

*E-mail: Jeff_lim@hsa.gov.sg. Tel.: +65 6213 0756. Fax: +65 6213 0749.

Notes

The authors declare no competing financial interest.

REFERENCES

(1) Zain, M. E. Impact of mycotoxins on humans and animals. *J. Saudi Chem. Soc.* **2011**, *15*, 129−144.

(2) Food and Agriculture Organisation of the United Nations (FAO). Worldwide regulations for mycotoxins 1995. A compendium. *FAO Food Nutr. Pap.* **1997**, *64*, 1−43.

(3) Bennett, J. W.; Klich, M. Mycotoxins. *Clin. Microbiol. Rev.* **2003**, *16*, 497−516.

(4) International Agency for Research on Cancer (IARC). Some Naturally Occurring Substances: Food Items and Constituents, Heterocyclic Aromatic Amines and Mycotoxins. *IARC Monogr. Eval. Carcinog. Risks Hum.* **1993**, *56*, 245−395.

(5) Food and Agriculture Organization of the United Nations (FAO) *Worldwide regulations for mycotoxins in food and feed in 2003*; FAO: Rome, Italy, 2004

(6) Food and Agriculture Organisation of the United Nations (FAO). *FAO Rice Market Monitor November 2013*; FAO: Rome, Italy, 2013; Vol. *16*, pp 1−38.

(7) European Commission. No. 1881/2006 of 19 December 2006 setting maximum levels for certain contaminants in foodstuffs. *Off. J. Eur. Communities: Legis.* **2006b**, *L364*, 1−16.

(8) Tanaka, K.; Kobayashi, H.; Nagata, T.; Manabe, M. Natural occurrence of trichothecenes on lodged and water-damaged domestic rice in Japan. *J. Food Hyg. Soc. Jpn.* **2004**, *45*, 63−66.

(9) Tanaka, K.; Sago, Y.; Zheng, Y.; Nakagawa, H.; Kushiro, M. Mycotoxins in rice. *Int. J. Food Microbiol.* **2007**, *119*, 59−66.

(10) Khui, K. W.; Lim, C. W.; Lee, L. M.; Yap, W. K.; Chan, S. H. Triple-stage mass spectrometry as the go-to physico-chemical tool for the accurate assessment of multi-mycotoxins in processed chilli of Asian origin. *World Mycotoxin J.* **2014**, accepted.

(11) Sulyok, M.; Krska, R.; Schuhmacher, R. A liquid chromatography/tandem mass spectrometric multi-mycotoxin method for the quantification of 87 analytes and its application to semi-quantitative screening of moldy food samples. *Anal. Bioanal. Chem.* **2007**, *389*, 1505−1523.

(12) Varga, E.; Glauner, T.; Koppen, R.; Mayer, K.; Sulyok, M.; Schuhmacher, R.; Krska, R.; Berthiller, F. Stable isotope dilution assay for the accurate determination of mycotoxins in maize by UHPLC-MS/MS. *Anal. Bioanal. Chem.* **2012**, *402*, 2675−2686.

(13) Chen, Y. H.; Lim, C. W.; Chan, S. H. Evaluation of triple stage mass spectrometry as a robust and accurate diagnostic tool for determination of free cordycepin in designer egg. *Food Chem.* **2014**, *150*, 213−219.

(14) European Commission. No. 401/2006 Laying down the methods of sampling and analysis for the official control of the levels of mycotoxins in foodstuffs. *Off. J. Eur. Communities: Legis.* **2006a**, *L 70*, 1−12.

(15) Kim, E. K.; Scott, P. M.; Lau, B. P.Y.; Lewis, D. A. Extraction of fumonisins B_1 and B_2 from white rice flour and their stability in white rice flour, cornstarch, cornmeal, and glucose. *J. Agric. Food Chem.* **2002**, *50*, 3614−3620.

(16) McCluskey, A.; Lalkhen, A. G. Statistics IV: Interpreting the results of statistical tests. *Continuing Education in Anaesthesia Critical Care & Pain* **2007**, *7*, 208−212.

(17) Tang, Y. Y.; Lin, H. Y.; Chen, Y. C.; Su, W. T.; Wang, S. C.; Chiueh, L. C.; Shin, Y. C. Development of a Quantitative Multi-Mycotoxin Method in Rice, Maize, Wheat and Peanut Using UPLC-MS/MS. *Food Anal. Methods* **2013**, *6*, 727−736.

(18) Liao, C. D.; Wong, J. W.; Zhang, K.; Hayward, D. G.; Lee, N. S.; Trucksess, M. W. Multi-mycotoxin Analysis of Finished Grain and Nut Products Using High-Performance Liquid Chromatography-Triple-Quadrupole Mass Spectrometry. *J. Agric. Food Chem.* **2013**, *61*, 4771−4782.

(19) Reiter, E. V.; Vouk, F.; Böhm, J.; Razzazi-Fazeli, E. Aflatoxins in rice − A limited survey of products marketed in Austria. *Food Control* **2010**, *21*, 988−991.

(20) Almeida, M. I.; Almeida, N. G.; Carvalho, K. L.; Goncalves, G. A. A.; Silva, C. N.; Santos, E. A.; Garcia, J. C.; Vargas, E. A. Co-occurrence of aflatoxins B-1, B-2, G(1) and G(2), ochratoxin A, zearalenone, deoxynivalenol, and citreoviridin in rice in Brazil. *Food Addit. Contam., Part A* **2012**, *29*, 694−703.

(21) Bansal, J.; Pantazopoulos, P.; Tam, J.; Cavlovic, P.; Kwong, K.; Turcotte, A. M.; Lau, B. P. Y.; Scott, P. M. Surveys of rice sold in Canada for aflatoxins, ochratoxin A and fumonisins. *Food Addit. Contam., Part A* **2011**, *28*, 767−774.

(22) Madbouly, A. K.; Ibrahim, M. I. M.; Sehab, A. F.; Abdel-Wahhab, M. A. Co-occurrence of mycoflora, aflatoxins and fumonisins in maize and rice seeds from markets of different districts in Cairo, Egypt. *Food Addit. Contam., Part B* **2012**, *5*, 112−120.

(23) Reddy, K. R. N.; Reddy, C. S.; Abbas, H. K.; Abel, C. A.; Muralidharan, K. Mycotoxigenic fungi, mycotoxins, and management of rice grains. *Toxin Rev.* **2008**, *27*, 287−317.

(24) Riazipour, M.; Fooladi, A. A. I.; Razzaghi-Abyaneh, M. Natural Occurrence of T-2 Toxin in Domestic and Imported Rice. *Iran. J. Public Health* **2009**, *38*, 111−116.

(25) Afsah-Hejri, L.; Jinap, S.; Hajeb, P.; Radu, S.; Shakibazadeh, S. 2013. A Review on Mycotoxins in Food and Feed: Malaysia Case Study. *Compr. Rev. Food Sci. Food Saf.* **2013**, *12*, 629−651.

(26) Desjardins, A. E.; Manandhar, H. K.; Plattner, R. D.; Manandhar, G. G.; Poling, S. M.; Maragos, C. M. Fusarium species

DOI: 10.1021/acs.jafc.5b00471
J. Agric. Food Chem. 2015, 63, 3104−3113

from nepalese rice and production of mycotoxins and gibberellic acid by selected species. *Appl. Environ. Microbiol.* **2000**, *66*, 1020−1025.
(27) Makun, H. A.; Dutton, M. F.; Njobeh, P. B.; Mwanza, M.; Kabiru, A. Y. Natural multi-occurrence of mycotoxins in rice from Niger State, Nigeria. *Mycotoxin Res.* **2011**, *27*, 97−104.
(28) Firdous, S.; Ejaz, N.; Aman, T.; Khan, N. Occurrence of aflatoxins in export-quality Pakistani rice. *Food Addit. Contam., Part B* **2012**, *5*, 121−125.
(29) Asghar, M. A.; Iqbal, J.; Ahmed, A.; Shamsuddin, Z. A.; Khan, M. A. Incidence of aflatoxins in export quality basmati rice collected from different areas of Pakistan. *Sci. Technol. Dev.* **2013**, *32*, 110−119.
(30) Fredlund, E.; Thim, A. M.; Gidlund, A.; Brostedt, S.; Nyberg, M.; Olsen, M. Moulds and mycotoxins in rice from the Swedish retail market. *Food Addit. Contam., Part A* **2009**, *26*, 527−533.
(31) Aydin, A.; Aksu, H.; Gunsen, U. Mycotoxin levels and incidence of mould in Turkish rice. *Environ. Monit. Assess.* **2011**, *178*, 271−280.
(32) Food Standards Authority (FSA). Survey of Retail Rice for a Range of Mycotoxins 2002. Available at: http://multimedia.food.gov.uk/multimedia/pdfs/22rice.pdf (accessed February 6 2014).
(33) Nguyen, M. T.; Tozovanu, M.; Tran, T. L.; Pfohl-Leszkowicz, A. Occurrence of aflatoxin B_1, citrinin and ochratoxin A in rice in five provinces of the central region of Vietnam. *Food Chem.* **2007**, *105*, 42−47.
(34) Hunter, C.; Simons, B. The Scheduled MRM Algorithm Enables Intelligent Use of Retention Time During Multiple Reaction Monitoring. (**n.d.**) Available at: http://www.absciex.com/Documents/Downloads/Literature/mass-spectrometry-ScheduledMRM-0921010.pdf (accessed February 5, 2014).
(35) Schreiber, A.; Pace, N. Intelligent Use of Retention Time during Multiple Reaction Monitoring for Faster and Extended Compound Screening with Higher Sensitivity and Better Reproducibility. (**n.d**). Available at: http://www.absciex.com/Documents/Downloads/Literature/mass-spectrometry-Multiple-Reaction-1282310.pdf (accessed February 20, 2014).
(36) Lim, C. W.; Tai, S. H.; Lee, L. M.; Chan, S. H. Analytical method for the accurate determination of tricothecenes in grains using LC-MS/MS: a comparison between MRM transition and MS^3 quantitation. *Anal. Bioanal. Chem.* **2012**, *403*, 2801−2806.
(37) Trufelli, H.; Palma, P.; Famiglini, G.; Cappiello, A. An overview of matrix effects in liquid chromatography−mass spectrometry. *Mass Spectrom. Rev.* **2011**, *30*, 491−509.
(38) Sulyok, M.; Krska, R.; Schuhmacher, R. Application of a liquid-chromatography-tandem mass spectrometric multi-mycotoxin method to different raw cereals and evaluation of matrix effects. *Food Addit. Contam.* **2007**, *24*, 1184−1195.
(39) Pantazopoulos, P. Uncertainty estimate for: Procedure ONT-FCL-0024 determination of ochratoxin A in wine and grape juice by high performance liquid chromatography with fluorescence detection. Food Laboratory Division, Ontario Region, 2001; pp 17−22.
(40) European Commission.. No 669/2009 of 24 July 2009 implementing Regulation (EC) No 882/2004 of the European Parliament and of the Council as regards the increased level of official controls of certain feed and food of non-animal origin and amending Decision 2006/504/EC. *Off. J. Eur. Communities: Legis.* **2009**, *L194*, 11−21.

DOI: 10.1021/acs.jafc.5b00471
J. Agric. Food Chem. 2015, 63, 3104−3113

salts and lecithin) which generate micelles that may enhance the dissolution rate and solubility of lipophilic resveratrol-loaded lipid nanoparticles.[36,37] Hence, a monolithic C18 column, consisting of micro- and mesopores,[38,39] was selected with regard to its suitability for bioanalysis,[40] avoiding further sample treatment.

MATERIALS AND METHODS

Chemicals. *trans*-Resveratrol was purchased from Sigma-Aldrich (St. Louis, MO, USA). Acetonitrile and acetic acid (LiChrosolv HPLC grade) were obtained from Merck (Darmstadt, Germany). Water from an arium water purification system (resistivity > 18 MΩ cm, Sartorius, Goettingen, Germany) was used for the preparation of all solutions. Acetic acid aqueous solution (2% (v/v)) was filtered through a 0.22 μm Millipore-type GVWP filter. Prior to use, the mobile phase was degassed in an ultrasonic bath for 15 min. The transport medium HBSS was purchased from Gibco (Paisley, UK), whereas FaSSIF and FeSSIF were prepared by using SIF instant powder (Phares Drug Delivery AG, Muttenz, Switzerland) according to the instructions of the manufacturer. Table S2 summarizes the compositions of HBSS, FaSSIF, and FeSSIF media.

For the nanoparticle synthesis, cetyl palmitate was kindly supplied by Gattefossé (Nanterre, France), polysorbate 60 (Tween 60) was provided by Merck, and miglyol-812 was from Acofarma (Madrid, Spain). For cell culturing, the Caco-2 cell line purchased from the American Type Culture Collection (ATCC, Wesel, Germany) between passages 35 and 55 was maintained in Dulbecco's modified Eagle medium (DMEM) supplemented with 10% fetal bovine serum, 1% fungizone (amphotericin B, 250 μg mL^{-1}), and 1% Pen Strep (penicillin, streptomycin), all obtained from Gibco.

Equipment and Chromatographic Conditions. The samples were injected (50 μL) into a reversed-phase monolithic column (Chromolith RP-18e, 100 mm × 4.6 mm i.d., Merck), connected to a Jasco (Easton, MD, USA) HPLC system (pump PU-2089, autosampler AS-2057, and LC-Net II/ADC controller) coupled to a fluorometric detector (Jasco FP-2020, λ_{exc} = 330 nm, λ_{em} = 374 nm). Chromatographic separation was achieved by isocratic mode consisting of 80:20 (v/v) aqueous solution (acetic acid 2%, v/v) and acetonitrile at a flow rate of 1.0 mL min^{-1}.

Standard Solutions and Quality Control Samples. Stock solutions of *trans*-resveratrol were daily prepared in mobile phase, HBSS, FaSSIF, and FeSSIF at 10 μmol L^{-1}. Standard solutions were accurately prepared by dilution in the same transport media to final concentrations of 0.020, 0.050, 0.100, 0.150, 0.200, 0.400, 0.700, 1.00, 1.50, and 2.00 μmol L^{-1}. The standard solutions were divided in two calibration curves for each transport media, the low-level calibration curve between 0.020 and 0.200 μmol L^{-1} and the high-level calibration curve between 0.200 and 2.00 μmol L^{-1}.

The quality control (QC) samples at three different levels (low, middle, and high) were prepared at concentrations of 0.020, 0.200, and 1.50 μmol L^{-1} for each transport medium, within three batches of five samples each. The standards containing 0.020 and 0.200 μmol L^{-1} were interpolated in the low-level calibration curve, whereas the 1.50 μmol L^{-1} standard was interpolated in the high-level calibration curve.

Acetonitrile was added to all standard solutions and samples immediately after preparation or collection to attain a 20% (v/v) concentration (100 μL of standard or sample +25 μL of acetonitrile:-acetic acid (92:8, v/v)) to match the mobile phase composition, avoiding peak broadening effects.

Validation of HPLC Method. The chromatographic method developed was validated for selectivity, concentration range, detection and quantification limits, accuracy, precision, and stability according to the ICH guidelines on bioanalytical method validation.[11] Selectivity concerns the ability to differentiate the analyte of interest (*trans*-resveratrol) from endogenous components in the matrix or in the sample and was assessed by analyzing six different samples of blank HBSS, FaSSIF, and FeSSIF, which were evaluated for interference. To evaluate linearity, calibration curves were acquired in triplicate, on three consecutive days, by plotting the integrated peak area of *trans*-resveratrol in all three media against the nominal concentration of six standard solutions, for each low-level and high-level calibration curve. Linear regression analysis was performed using the least-squares method. The detection limit (DL) and the quantification limit (QL) of the developed HPLC method were determined by the signal to-noise ratio. The DL and QL were the concentrations of *trans*-resveratrol generated by a peak 3 times and 10 times, respectively, higher than the baseline noise. Precision and accuracy were estimated by analyzing five replicates of the three different QC levels (0.020, 0.200, and 1.50 μmol L^{-1} of *trans*-resveratrol) for each matrix. Repeatability and reproducibility were assessed by analyzing five replicates of the three QC levels on three different runs within the same day (intraday) and on three different days (interday), respectively. Stability studies were performed by maintaining the samples inside the autosampler of the HPLC instrument at 4 °C for 24 h, at room temperature for 24 h, and after three freeze−thaw cycles, by thawing at room temperature for 2 h and freezing again for 24 h. Five replicates of each QC sample were analyzed for each storage condition in all matrices.

Application to in Vitro Intestinal Permeability Studies. The developed method was targeted to application in studies of intestinal permeability of *trans*-resveratrol carried inside lipid nanoparticles (SLNs and NLCs), after oral administration. Resveratrol-loaded lipid nanoparticles were prepared by a modified hot homogenization technique and characterized as described elsewhere.[10] The results showed spherical and uniform nanoparticles with a smooth surface, a *Z*-average of 150−250 nm, a highly negative zeta potential of −30 mV, and a resveratrol entrapment efficiency of 70%.[10] The recovery of resveratrol from lipid nanoparticles corresponded to 93%, and it was determined using 4.0 mL of a 1.25 mg mL^{-1} suspension of *trans*-resveratrol-loaded nanoparticles, where 1.0 mL of acetonitrile was added to promote the disruption of the lipid matrix and the release of *trans*-resveratrol. Next, *trans*-resveratrol was quantified by direct spectrophotometric detection at 306 nm, using standards prepared in 20% (v/v) acetonitrile/water, after subtraction of signal scattering by blank nanoparticles. In vitro intestinal permeability assays were performed using Caco-2 monolayers in transwell devices that mimic the intestinal barrier.[41] Three different transport media were used to mimic intestinal fluids: HBSS as the control medium, FaSSIF as the fasted state medium, and FeSSIF as the fed state medium. Resveratrol-loaded lipid nanoparticles were incubated during 4 h in the apical side of the intestinal barrier, and aliquots of 100 μL were withdrawn at regular intervals of 30 min from the basolateral side for quantification to determine the intestinal permeability in all three media. Sample treatment was minimal, involving the addition of 25 μL of acetonitrile/acetic acid (92:8, v/v) solution to 100 μL of sample to promote the disruption of the lipid matrix and the release of *trans*-resveratrol to be quantified by HPLC and also to avoid band broadening effects due to differences from mobile phase composition.

Statistical Analysis. Statistical analyses were performed using SPSS software (v 18.0; IBM, Armonk, NY, USA). Permeability measurements were repeated at least six times, and data were expressed as the mean ± SD. Data were analyzed using one-way analysis of variance (one-way ANOVA), followed by Bonferroni, Tukey, and Dunnett post hoc tests. A p value <0.05 was considered statistically significant.

RESULTS AND DISCUSSION

Study of Chromatographic Conditions. Considering the method application to studies of intestinal permeability of *trans*-resveratrol inside lipid nanoparticles, the main goal to be achieved in the development of this chromatographic method was low detection and quantification limits. Furthermore, because there was a constraint in the available sample volume, it was also important to develop a method that needed minimal sample treatment. Therefore, a monolithic column coupled to fluorescence detection was chosen to meet these needs.

In this work, the development of a simplified HPLC method with isocratic elution was aimed for. The choice of the organic

DOI: 10.1021/acs.jafc.5b00390
J. Agric. Food Chem. 2015, 63, 3114−3120

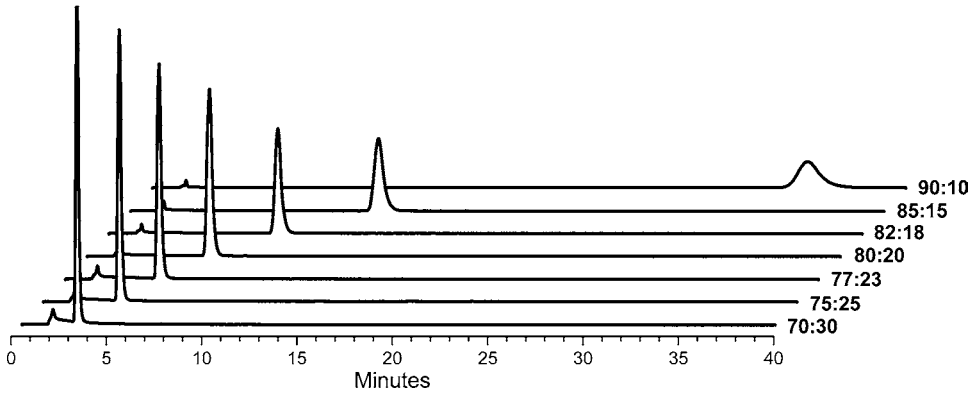

Figure 1. Chromatograms of *trans*-resveratrol (10 μmol L^{-1}) using different mobile phase compositions containing acetic acid (2%, v/v)/acetonitrile.

phase was based on the ability to break nanoparticles for the release of the compound to be quantified. Therefore, acetonitrile was selected as the organic phase once it could destroy the matrix of the nanoparticles. The aqueous phase chosen was acetic acid 2% (v/v) as described elsewhere.[30] Hence, the mobile phase composition was studied to decrease the retention time of *trans*-resveratrol, to provide resolution from sample matrix, and to determine the best acetonitrile concentration that enabled the disruption of the lipid matrix of nanoparticles, releasing the compound to be quantified. Different ratios of organic phase (acetonitrile) and aqueous phase (acetic acid 2%, v/v) were tested as depicted in Figure 1.

Table 1 summarizes the properties of chromatographic peak retention time, area, height, and symmetry of *trans*-resveratrol.

Table 1. Values of Retention Time, Area, Height, and Symmetry Factor for Each Chromatogram of *trans*-Resveratrol (10 μmol L^{-1}) Using Different Mobile Phase Compositions (Acetic Acid (2%)/Acetonitrile)

mobile phase composition (acetic acid (2%)/ACN (v/v))	t_R (min)	area	height	symmetry factor[a]
90:10	34.4	6870310	83486	1.34
85:15	13.0	7896145	231309	1.32
82:18	8.9	7951473	334921	1.33
80:20	6.5	10616719	533260	1.22
77:23	4.9	10813149	685258	1.26
75:25	4.0	11376163	866610	1.30
70:30	2.9	11661639	1008455	1.34

[a]Calculated as the ratio between W and $2f$, where W is the peak width at 5% of the peak height and f is the distance between the maximum and the leading edge of the peak.

As expected, when the volume of the organic phase decreases, the retention time of the compound increases, and a reduction of the peak area due to peak broadening for longer retention times or possible lack of total nanoparticle disruption is visible. It is also important to note that the mobile phase with only 10% (v/v) of organic phase produced a retention time more than twice higher than that found for 15% (v/v). In addition, from previous experiments with similar types of nanoparticles, at least 20% (v/v) of acetonitrile is required to cause total disruption of the lipid matrix and to promote the release of the compound for correct quantification. In fact, the results obtained are in agreement with this observation as the increase in peak area was 33% when acetonitrile was increased from 18 to 20% (v/v), whereas only a 2% enhancement in peak area was observed when acetonitrile was increased from 20 to 23% (v/v). Therefore, a mobile phase composed of 20% of acetonitrile and 80% of acetic acid (2%, v/v) was selected. This composition permitted the elution of *trans*-resveratrol with a good compromise between the *trans*-resveratrol retention time and the peak symmetry factor, allowing a sharp peak separation. Using this isocratic condition, *trans*-resveratrol was eluted with a retention time of 6.5 min and with the lowest peak symmetry factor of 1.22, which reflects a reduced peak tailing in these conditions (Table 1).

The injection volume was also tested to increase the sensitivity of the developed method. Injection volumes of 50 and 100 μL were tested, providing a signal area enhancement of ca. 2 as expected. The injection volume chosen was 50 μL as the volume collected during the permeability assay should be <100 μL. Hence, improved sensitivity can be attained if required by increasing the sample volume.

Method Validation. The validation of the analytical HPLC method was carried out after evaluation of selectivity, linearity, detection and quantification limits, accuracy, precision, and stability as proposed by ICH guidelines on bioanalytical method validation.[11]

Selectivity is the ability to differentiate the analyte of interest from endogenous components in the matrix or in the sample and was assessed by analyzing six different samples of blank matrices HBSS, FaSSIF, and FeSSIF (Figure S2). No interfering peaks from endogenous substances were observed at the retention time of *trans*-resveratrol. A good separation was obtained under the described conditions, and *trans*-resveratrol was eluted at 6.5 min, with any potentially interfering compound washed from the column together with the solvent. Therefore, the method was shown to be selective for the intended application.

The linearity of response was established by analyzing standard solutions in two ranges of concentrations for mobile phase and for each transport medium (HBSS, FaSSIF, and FeSSIF), the low-level calibration curve (n = 5) between 0.020 and 0.200 μmol L^{-1}, and the high-level calibration curve (n = 6) between 0.200 and 2.00 μmol L^{-1}. Calibration curves were acquired in triplicate, on three consecutive days, with relative standard deviations (RSD) for slope <8.6%. As shown in Table 2, the calibration curves for *trans*-resveratrol indicated good linearity for all matrices in the proposed range, with correlation coefficients for all linear regressions >0.99. When the calibration slopes obtained using each cell culture media were

DOI: 10.1021/acs.jafc.5b00390
J. Agric. Food Chem. 2015, 63, 3114−3120

Table 2. Regression Analysis of Low-Level and High-Level Calibration Curves, Detection Limit (DL), and Quantification Limit (QL) for *trans*-Resveratrol in Mobile Phase, HBSS, FaSSIF, and FeSSIF

matrix	range (μmol L^{-1})	slope	intercept	correlation coefficient (r^2)	DL (nmol L^{-1})	QL (nmol L^{-1})
mobile phase	0.020−0.200[a]	1657688	11313	0.998	1	2
	0.200−2.00[b]	2100408	−128538	0.998		
HBSS	0.020−0.200[a]	543619	2775	0.997	3	6
	0.200−2.00[b]	906961	−67586	0.999		
FaSSIF	0.020−0.200[a]	922636	−4028	0.997	2	3
	0.200−2.00[b]	1042299	−7286	0.998		
FeSSIF	0.020−0.200[a]	1131404	−12660	0.998	3	5
	0.200−2.00[b]	1182890	35020	0.998		

[a]Low-level calibration curve. [b]High-level calibration curve.

Table 3. Accuracy and Precision Analysis of QC Samples of *trans*-Resveratrol in HBSS, FaSSIF, and FeSSIF Media

		intraday (repeatability) measured concentration			interday (reproducibility) measured concentration		
matrix	nominal concentration (μmol L^{-1})	mean (μmol L^{-1})	accuracy (%)	precision (%)	mean (μmol L^{-1})	accuracy (%)	precision (%)
HBSS	0.020[a]	0.020 ± 0.001	99.9	4.2	0.019 ± 0.001	93.4	5.4
	0.200[a]	0.219 ± 0.004	109.7	1.9	0.215 ± 0.006	107.7	2.8
	1.50[b]	1.46 ± 0.05	97.6	3.7	1.52 ± 0.05	101.2	3.2
FaSSIF	0.020[a]	0.020 ± 0.001	101.4	3.6	0.021 ± 0.001	104.5	2.6
	0.200[a]	0.194 ± 0.006	96.8	3.2	0.192 ± 0.005	95.8	2.5
	1.50[b]	1.34 ± 0.05	89.3	3.8	1.57 ± 0.01	104.5	0.1
FeSSIF	0.020[a]	0.024 ± 0.001	120.1	2.4	0.026 ± 0.001	120.5	2.3
	0.200[a]	0.206 ± 0.012	102.8	5.8	0.204 ± 0.003	101.7	1.3
	1.50[b]	1.33 ± 0.05	85.0	3.9	1.32 ± 0.06	88.2	4.4

[a]Quality control concentrations interpolated in low-level calibration curve (n = 5). [b]Quality control concentrations interpolated in high-level calibration curve (n = 5).

compared, values were between 33 and 68% of those found for mobile phase (Table 2). This decrease in sensitivity may account for fluorescence quenching effects reported for complex media, where interactions with solvent molecules (for instance, formation−disruption of hydrogen bonds with solvent molecules)[42] or ions (for instance, quenching of phenolics emission due to the deprotonation of the phenolic group promoted in the excited state by phosphate ions)[43] may occur. The decrease in sensitivity was more pronounced for HBSS media, followed by FaSSIF and FeSSIF. In these last two media, despite the increased amount of salts when compared to HBSS (Table S2), sodium taurocholate and lecithin were also present, promoting hydrophobic interactions with resveratrol and decreasing its exposure to hydrogen bonding with solvent.

Furthermore, the slope values obtained for the low-level calibration curves are lower than those of the high-level calibration curves, and this effect is more pronounced for HBSS and for standards prepared in mobile phase, where the slope values for low-level standards are 60 and 79% of those found for high-level standards prepared in the same solvent, respectively. This decrease in sensitivity is almost absent in FeSSIF medium, where low-level slope value accounts for 96% of the high-level counterpart. These results might be also due to the quenching effects described above for interaction of resveratrol with solvent molecules and ions present in the medium. These effects would be more pronounced for low concentrations of resveratrol (low-level standards), where the protection from hydrophobic interactions with emulsifier agents would also be more pronounced. Considering that FeSSIF has 5 times more sodium taurocholate and lecithin (Table S2) than FaSSIF, this might explain that the slope ratio between low and high levels for FaSSIF (0.855) increased for FeSSIF (0.956). Hence, considering the matrix effects found, further calibrations and quantifications were undertaken using standards containing the target matrix.

Sensitivity was investigated by determining the DL and QL of the developed HPLC method through the signal to-noise ratio. The DL and QL were the concentrations of *trans*-resveratrol generated by peaks 3 times and 10 times higher than the baseline noise, respectively. Because matrix effects were observed and calibration curves were performed for mobile phase and for each transport medium (HBSS, FaSSIF, and FeSSIF), a set of DL and QL values was also determined for each matrix (Table 2). DL and QL values decrease in all matrices when compared to the mobile phase, probably due to the composition of the studied matrices (Table S2). In the case of HBSS, the composition is very rich in salts of chlorides, sulfates, and phosphates that are known to promote the fluorescence quenching phenomenon. FaSSIF and FeSSIF are very rich in bile salts and micelles of phospholipids, which may also promote events of fluorescence quenching, lowering the sensitivity of the method in these media, even though the minimum detectable concentration of *trans*-resveratrol achieved, for a 50 μL injection volume, was 1−3 nmol L^{-1}

DOI: 10.1021/acs.jafc.5b00390
J. Agric. Food Chem. 2015, 63, 3114−3120

Table 4. Stability of QC Samples of *trans*-Resveratrol at Different Experimental Conditions in HBSS, FaSSIF, and FeSSIF Media

		measured concentration								
		24 h in the autosampler at 4 °C			24 h at room temperature			three freeze−thaw cycles		
matrix	nominal concentration (μmol L^{-1})[a]	mean (μmol L^{-1})	precision (%)	recovery (%)	mean (μmol L^{-1})	precision (%)	recovery (%)	mean (μmol L^{-1})	precision (%)	recovery (%)
HBSS	0.020[a]	0.022 ± 0.001	2.2	101.3	0.002 ± 0.001	24.1	11.9	0.002 ± 0.001	11.2	12.2
	0.200[a]	0.206 ± 0.005	2.6	103.1	0.080 ± 0.002	2.8	40.0	0.080 ± 0.002	2.8	40.0
	1.50[b]	1.35 ± 0.04	2.9	92.3	0.87 ± 0.02	2.6	58.2	0.87 ± 0.05	5.8	57.7
FaSSIF	0.020[a]	0.020 ± 0.001	4.8	101.7	0.017 ± 0.001	5.0	89.6	0.022 ± 0.001	3.3	108.5
	0.200[a]	0.190 ± 0.007	3.5	98.0	0.151 ± 0.016	10.7	77.4	0.201 ± 0.011	5.6	100.6
	1.50[b]	1.62 ± 0.13	7.8	108.2	1.65 ± 0.15	9.3	105.1	1.07 ± 0.06	5.4	71.3
FeSSIF	0.020[a]	0.027 ± 0.001	2.2	105.8	0.021 ± 0.001	3.0	105.9	0.025 ± 0.001	3.9	96.4
	0.200[a]	0.190 ± 0.006	2.9	95.1	0.121 ± 0.001	0.9	78.1	0.180 ± 0.005	2.8	90.1
	1.50[b]	1.24 ± 0.01	1.2	89.3	1.07 ± 0.08	7.2	82.0	1.21 ± 0.12	9.9	94.9

[a]Quality control concentrations interpolated in low-level calibration curve (n = 5). [b]Quality control concentrations interpolated in high-level calibration curve (n = 5).

and the limit of quantification was 2−6 nmol L^{-1}. Hence, the proposed method allows the quantification of 23−69 pg of *trans*-resveratrol. Therefore, the sensitivity of the method developed is very high, and the values for DL and QL are substantially lower than those found in previous studies (Table S1), which can be considered an advantage compared with the other methods, being particularly adequate to the measurement of *trans*-resveratrol at very low concentrations, carried inside lipid nanoparticles after intestinal permeability studies.

The accuracy of the analytical method was determined by the percentage of recoveries of five replicates of QC samples, whereas precision was obtained by determination of the RSD. The intraday precision and accuracy were determined on the same day by analyzing QC samples (n = 5) on three different runs for all transport media, and the interday precision and accuracy were assayed on three consecutive days for QC samples (n = 5) in each matrix. The method was shown to be accurate and precise as depicted in Table 3. Intraday and interday precisions of the method were lower than 5.8 and 5.4%, respectively, for all of the matrices studied, which was within the acceptable limits of the guidelines for bioanalytical method validation, considered to be <15%. The accuracy of the method for all of the matrices was also good with the deviation between the nominal concentration and the calculated concentration for *trans*-resveratrol within the limit of 20% for the lowest QC sample and below 15% for all other QC samples. Accordingly, the intraday accuracy was found to be between 85.0 and 120.1% of the nominal *trans*-resveratrol concentrations and the interday accuracy between 88.2 and 120.5% of the nominal values in all matrices. This precision and accuracy evaluation indicates that the HPLC method developed for quantification of *trans*-resveratrol inside lipid nanoparticles from mimetic intestinal fluids is highly reproducible and robust.

Evaluation of stability was carried out in all matrices by analyzing five replicates of each QC sample after three storage conditions: inside the autosampler of the HPLC instrument (at 4 °C) for 24 h; at room temperature for 24 h; and after three freeze−thaw cycles, comprising at least 24 h at −18 °C before defrost. According to ICH guidelines, samples were considered to be stable when the mean concentration of *trans*-resveratrol after the storage period was within ±15% of the initial concentration of freshly prepared samples.

As shown in Table 4, the results suggested that *trans*-resveratrol was stable in all matrices after 24 h in the autosampler at 4 °C with mean recoveries of *trans*-resveratrol >89.3% and precision values <7.8% for all transport media. However, *trans*-resveratrol was not stable after 24 h at room temperature and after three freeze−thaw cycles, mainly in HBSS medium for which recoveries were <58.2% and with poor precision (RSD up to 24.1%). On the other hand, FaSSIF and FeSSIF media seem to protect *trans*-resveratrol against degradation because recoveries were higher (between 71.3 and 108.5%). These media mimic intestinal juices because they contain natural surfactants (bile salts and lecithin) that can also have effects on *trans*-resveratrol protection against oxidation and degradation.[36,37] However, the results for recoveries of *trans*-resveratrol in these two mimetic intestinal fluids are still below acceptable levels for ICH guidelines, at room temperature and at freeze−thaw conditions tested. Therefore, *trans*-resveratrol is only stable after 24 h at 4 °C for all three media, and its storage at room temperature or its utilization after three freeze−thaw cycles is not recommended.

Application to in Vitro Intestinal Permeability Studies. The proposed HPLC method was applied in studies of in vitro intestinal permeability of *trans*-resveratrol inside lipid nanoparticles, by using Caco-2 cell monolayers. The use of these nanodelivery systems can be an important tool to increase the protection, to enhance the absorption, and thereby to improve the bioavailability of *trans*-resveratrol inside the organism, after oral administration as a food additive. The representative intestinal permeability profile for resveratrol-loaded NLCs in HBSS, FaSSIF, and FeSSIF media is illustrated in Figure 2, as a relevant application of this method.

Values between 0.05 ± 0.01 and 1.8 ± 0.3 μmol L^{-1} were found along the experimental time frame, showing the suitability of the proposed method to assess the minimum amount of *trans*-resveratrol assessed, present in the first aliquot, taken after 30 min. These preliminary results suggest that FaSSIF and FeSSIF media increase *trans*-resveratrol permeability inside lipid nanoparticles, after 4 h of incubation, when compared to the control medium HBSS (2-fold higher for FaSSIF and 2.5-fold higher for FeSSIF; $p < 0.05$).

Comparison with Other Methods. The comparison between the developed method and methods described in the literature for *trans*-resveratrol quantification (Table S1)

DOI: 10.1021/acs.jafc.5b00390
J. Agric. Food Chem. 2015, 63, 3114−3120

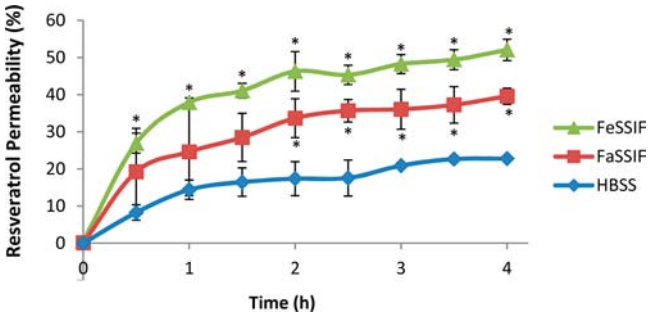

Figure 2. *trans*-Resveratrol permeability (%) across Caco-2 cell monolayers loaded in lipid nanoparticles (NLCs), using different media (HBSS, FaSSIF, and FeSSIF). All data represent the mean ± SD ($n > 6$). (*) Statistically significant differences in relation to HBSS medium ($p < 0.05$).

suggested that the proposed method is suitable for measuring *trans*-resveratrol carried by lipid nanoparticles in intestinal fluid matrices, when generally the other methods are suitable mostly for quantifying *trans*-resveratrol at higher levels, targeted to wines, grapes, and plasma. In fact, the present method revealed an extended range of the linear zone (0.020−2.00 μmol L^{-1}), the lower level of quantification of which was matched only by the method proposed by Das and Ng.[27] Nevertheless, this method presented a higher detection limit and required extensive sample preparation by liquid−liquid extraction. In the proposed method, the only sample treatment necessary is the addition of acetonitrile for nanoparticle disruption and release of *trans*-resveratrol, showing the suitability of monolithic columns for application to complex samples. Moreover, the detection (1−3 nmol L^{-1}) and quantification (2−6 nmol L^{-1}) limits were the lowest obtained so far to the best of our knowledge, as confirmed by the information in Table S1, where the lowest values are 2−10 nmol L^{-1}.[12,25,27]

In general, the proposed method provides a simple chromatographic procedure with minimal sample treatment, good peak resolution, reduced run time, and low cost, allowing the analysis of a large number of samples and avoiding possible degradation of *trans*-resveratrol due to long run times. The isocratic elution also allowed the simplification of the technique. In fact, the estimated cost per run concerning mobile phase consumption is ca. 0.017 euro. These are, undoubtedly, clear advantages of the proposed method, which enables the performance of pharmacokinetic studies concerning *trans*-resveratrol to enhance its bioavailability after oral administration as a nutraceutical.

■ ASSOCIATED CONTENT

Supporting Information

Figures S1 and S2 and Tables S1 and S2. This material is available free of charge via the Internet at http://pubs.acs.org.

■ AUTHOR INFORMATION

Corresponding Author

*(M.A.S.) Phone: +351 220428676. Fax: +351 226093483. E-mail: msegundo@ff.up.pt.

Funding

A.R.N. acknowledges FCT (Fundação para a Ciência e a Tecnologia) for financial support through a Ph.D. grant (SFRH/BD/73379/2010). This work received financial support from the European Union (FEDER funds through COMPETE) and National Funds (FCT, Fundação para a Ciência e Tecnologia) through Project Pest-C/EQB/LA0006/2013. The work also received financial support from the European Union (FEDER funds) within the framework of QREN/ON2 through Projects NORTE-07-0124-FEDER-000067, NORTE-07-0162-FEDER-000088, and NORTE-07-0162-FEDER-000124.

Notes

The authors declare no competing financial interest.

■ REFERENCES

(1) Burns, J.; Yokota, T.; Ashihara, H.; Lean, M. E. J.; Crozier, A. Plant foods and herbal sources of resveratrol. *J. Agric. Food Chem.* **2002**, *50*, 3337−3340.

(2) Roldan, A.; Palacios, V.; Caro, I.; Perez, L. Evolution of resveratrol and piceid contents during the industrial winemaking process of sherry wine. *J. Agric. Food Chem.* **2010**, *58*, 4268−4273.

(3) Bertelli, A. A. A.; Das, D. K. Grapes, wines, resveratrol, and heart health. *J. Cardiovasc. Pharmacol.* **2009**, *54*, 468−476.

(4) Neves, A. R.; Lucio, M.; Lima, J. L.; Reis, S. Resveratrol in medicinal chemistry: a critical review of its pharmacokinetics, drug-delivery, and membrane interactions. *Curr. Med. Chem.* **2012**, *19*, 1663−1681.

(5) Trela, B. C.; Waterhouse, A. L. Resveratrol: isomeric molar absorptivities and stability. *J. Agric. Food Chem.* **1996**, *44*, 1253−1257.

(6) Stervbo, U.; Vang, O.; Bonnesen, C. A review of the content of the putative chemopreventive phytoalexin resveratrol in red wine. *Food Chem.* **2007**, *101*, 449−457.

(7) Walle, T.; Hsieh, F.; DeLegge, M. H.; Oatis, J. E., Jr.; Walle, U. K. High absorption but very low bioavailability of oral resveratrol in humans. *Drug Metab. Dispos.* **2004**, *32*, 1377−1382.

(8) Francioso, A.; Mastromarino, P.; Masci, A.; d'Erme, M.; Mosca, L. Chemistry, stability and bioavailability of resveratrol. *Med. Chem.* **2014**, *10*, 237−245.

(9) Davidov-Pardo, G.; McClements, D. J. Resveratrol encapsulation: designing delivery systems to overcome solubility, stability and bioavailability issues. *Trends Food Sci. Technol.* **2014**, *38*, 88−103.

(10) Neves, A. R.; Lucio, M.; Martins, S.; Lima, J. L.; Reis, S. Novel resveratrol nanodelivery systems based on lipid nanoparticles to enhance its oral bioavailability. *Int. J. Nanomed.* **2013**, *8*, 177−187.

(11) ICH guideline Q2(R1): Validation of Analytical Procedures: Text and Methodology, 2005.

(12) Viñas, P.; López-Erroz, C.; Marín-Hernández, J. J.; Hernández-Córdoba, M. Determination of phenols in wines by liquid chromatography with photodiode array and fluorescence detection. *J. Chromatogr., A* **2000**, *871*, 85−93.

(13) Souto, A. A.; Carneiro, M. C.; Seferin, M.; Senna, M. J. H.; Conz, A.; Gobbi, K. Determination of *trans*-resveratrol concentrations in Brazilian red wines by HPLC. *J. Food Compos. Anal.* **2001**, *14*, 441−445.

(14) Dominguez, C.; Guillen, D. A.; Barroso, C. G. Automated solid-phase extraction for sample preparation followed by high-performance liquid chromatography with diode array and mass spectrometric detection for the analysis of resveratrol derivatives in wine. *J. Chromatogr., A* **2001**, *918*, 303−310.

(15) Careri, M.; Corradini, C.; Elviri, L.; Nicoletti, I.; Zagnoni, I. Direct HPLC analysis of quercetin and trans-resveratrol in red wine, grape, and winemaking byproducts. *J. Agric. Food Chem.* **2003**, *51*, 5226−5231.

(16) Kolouchova-Hanzlikova, I.; Melzoch, K.; Filip, V.; Smidrkal, J. Rapid method for resveratrol determination by HPLC with electrochemical and UV detections in wines. *Food Chem.* **2004**, *87*, 151−158.

(17) Ratola, N.; Faria, J. L.; Alves, A. Analysis and quantification of *trans*-resveratrol in wines from Alentejo region (Portugal). *Food Technol. Biotechnol.* **2004**, *42*, 125−130.

(18) Katsagonis, A.; Atta-Politou, J.; Koupparis, M. A. HPLC method with UV detection for the determination of *trans*-resveratrol in plasma. *J. Liq. Chromatogr. Relat. Technol.* **2005**, *28*, 1393−1405.

DOI: 10.1021/acs.jafc.5b00390
J. Agric. Food Chem. 2015, 63, 3114−3120

(19) Tokusoglu, O.; Unal, M. K.; Yemis, F. Determination of the phytoalexin resveratrol (3,5,4′-trihydroxystilbene) in peanuts and pistachios by high-performance liquid chromatographic diode array (HPLC-DAD) and gas chromatography-mass spectrometry (GC-MS). *J. Agric. Food Chem.* **2005**, *53*, 5003−5009.
(20) Mark, L.; Nikfardjam, M. S. P.; Avar, P.; Ohmacht, R. A validated HPLC method for the quantitative analysis of *trans*-resveratrol and *trans*-piceid in Hungarian wines. *J. Chromatogr. Sci.* **2005**, *43*, 445−449.
(21) Vian, M. A.; Tomao, V.; Gallet, S.; Coulomb, P. O.; Lacombe, J. M. Simple and rapid method for *cis*- and *trans*-resveratrol and piceid isomers determination in wine by high-performance liquid chromatography using Chromolith columns. *J. Chromatogr., A* **2005**, *1085*, 224−229.
(22) Chen, X.; He, H.; Wang, G.; Yang, B.; Ren, W.; Ma, L.; Yu, Q. Stereospecific determination of *cis*- and *trans*-resveratrol in rat plasma by HPLC: application to pharmacokinetic studies. *Biomed. Chromatogr.* **2007**, *21*, 257−265.
(23) Huang, H.; Zhang, J.; Chen, G.; Lu, Z.; Wang, X.; Sha, N.; Shao, B.; Li, P.; Guo, D.-a. High performance liquid chromatographic method for the determination and pharmacokinetic studies of oxyresveratrol and resveratrol in rat plasma after oral administration of Smilax china extract. *Biomed. Chromatogr.* **2008**, *22*, 421−427.
(24) Brizzi, A.; Brizzi, V.; Corradini, D. Identification and quantification of *trans*-resveratrol in dietary supplements by a rapid and straightforward RP-HPLC method. *J. Liq. Chromatogr. Relat. Technol.* **2008**, *31*, 2089−2100.
(25) Emilia Juan, M.; Maijo, M.; Planas, J. M. Quantification of *trans*-resveratrol and its metabolites in rat plasma and tissues by HPLC. *J. Pharm. Biomed. Anal.* **2010**, *51*, 391−398.
(26) Paulo, L.; Domingues, F.; Queiroz, J. A.; Gallardo, E. Development and validation of an analytical method for the determination of *trans*- and *cis*-resveratrol in wine: analysis of its contents in 186 Portuguese red wines. *J. Agric. Food Chem.* **2011**, *59*, 2157−2168.
(27) Das, S.; Ng, K.-Y. Quantification of *trans*-resveratrol in rat plasma by a simple and sensitive high performance liquid chromatography method and its application in pre-clinical study. *J. Liq. Chromatogr. Relat. Technol.* **2011**, *34*, 1399−1414.
(28) Porgali, E.; Buyuktuncel, E. Determination of phenolic composition and antioxidant capacity of native red wines by high performance liquid chromatography and spectrophotometric methods. *Food Res. Int.* **2012**, *45*, 145−154.
(29) Singh, G.; Pai, R. S.; Pandit, V. Development and validation of a HPLC method for the determination of *trans*-resveratrol in spiked human plasma. *J. Adv. Pharm. Technol. Res.* **2012**, *3*, 130−135.
(30) Nour, V.; Trandafir, I.; Muntean, C. Ultraviolet irradiation of trans-resveratrol and HPLC determination of *trans*-resveratrol and *cis*-resveratrol in Romanian red wines. *J. Chromatogr. Sci.* **2012**, *50*, 920−927.
(31) Ji, M.; Li, Q.; Ji, H.; Lou, H. Investigation of the distribution and season regularity of resveratrol in *Vitis amurensis* via HPLC-DAD-MS/MS. *Food Chem.* **2014**, *142*, 61−65.
(32) Sanchez, J. B. J.; Corral, E. C.; Delgado, M. J. S.; Orea, J. M.; Urena, A. G. Analysis of *trans*-resveratrol by laser ionization mass spectrometry and HPLC with fluorescence detection − comparison between both techniques. *J. Chromatogr., A* **2005**, *1074*, 133−138.
(33) Lopez, R.; Dugo, P.; Mondello, L. Determination of *trans*-resveratrol in wine by micro-HPLC with fluorescence detection. *J. Sep. Sci.* **2007**, *30*, 669−672.
(34) Basavaraj, S.; Benson, H. A. E.; Brown, D. H.; Chen, Y. Application of solvent influenced fluorescence-quenching and enhancement to develop a highly sensitive HPLC methodology for analysis of resveratrol-peg conjugates. *Curr. Pharm. Anal.* **2013**, *9*, 199−207.
(35) Vlase, L.; Kiss, B.; Leucuta, S. E.; Gocan, S. A rapid method for determination of resveratrol in wines by HPLC-MS. *J. Liq. Chromatogr. Relat. Technol.* **2009**, *32*, 2105−2121.
(36) Schwebel, H. J.; van Hoogevest, P.; Leigh, M. L.; Kuentz, M. The apparent solubilizing capacity of simulated intestinal fluids for poorly water-soluble drugs. *Pharm. Dev. Technol.* **2011**, *16*, 278−286.
(37) Frank, K. J.; Westedt, U.; Rosenblatt, K. M.; Holig, P.; Rosenberg, J.; Magerlein, M.; Brandl, M.; Fricker, G. Impact of FaSSIF on the solubility and dissolution-/permeation rate of a poorly water-soluble compound. *Eur. J. Pharm. Sci.* **2012**, *47*, 16−20.
(38) Guiochon, G. Monolithic columns in high-performance liquid chromatography. *J. Chromatogr., A* **2007**, *1168*, 101−168.
(39) Unger, K. K.; Skudas, R.; Schulte, M. M. Particle packed columns and monolithic columns in high-performance liquid chromatography-comparison and critical appraisal. *J. Chromatogr., A* **2008**, *1184*, 393−415.
(40) Saunders, K. C.; Ghanem, A.; Hon, W. B.; Hilder, E. F.; Haddad, P. R. Separation and sample pre-treatment in bioanalysis using monolithic phases: a review. *Anal. Chim. Acta* **2009**, *652*, 22−31.
(41) Willenberg, I.; Michael, M.; Wonik, J.; Bartel, L. C.; Empl, M. T.; Schebb, N. H. Investigation of the absorption of resveratrol oligomers in the Caco-2 cellular model of intestinal absorption. *Food Chem.* **2015**, *167*, 245−250.
(42) Demchenko, A. P. *Introduction to Fluorescence Sensing*; Springer: Berlin, Germany, 2009.
(43) Alev-Behmoaras, T.; Toulme, J.-J.; Hélène, C. Quenching of tyrosine fluorescence by phosphate ions: a model study for protein-nucleic acid complexes. *Photochem. Photobiol.* **1979**, *30*, 533−539.

DOI: 10.1021/acs.jafc.5b00390
J. Agric. Food Chem. 2015, 63, 3114−3120

Table 1. Oligonucleotide Sequences

oligonucleotide name	sequence (5′ → 3′)
	PCR Primers
SNP2	
forward 2 PCR I	GCAACTCAAATGAATGAATCATGAT
reverse 2 PCR I	CTAACTCGATGGCCGTTTTCTAA
forward 2 PCR II	GAAAATAACCTGCATTTTCG
reverse 2 PCR II	TATTGCTTGTTGGGTAGAAG
SNP3	
forward 3 PCR I	TTCACAGGTAAAATTCTTCTTTCC
reverse 3 PCR I	AACCCTCAGCTGTGCAATCTG
forward 3 PCR II	TCATTCATGGCATTTATTCTTC
reverse 3 PCR II	CTGGGCAATCCTCTAACACC
SNP4	
forward 4 PCR I	TGTTGGTGAACCACTGGATG
reverse 4 PCR I	CAGCAACAAAATCCAGGAAG
forward 4 PCR II	AGGCGATTGTACGATGCTG
reverse 4 PCR II	TCCCTTTCCGAAAACAACAG
	Extension Primers
tag2A	TTACCTTTATACCTTTCTTTTTAC**CCGTAACTCATT**AAGACATATAGCACGTATACCT
tag2B	TACACTTTCTTTCTTTCTTTCTTT**CCGTAACTCATT**AAGACATATAGCACGTATACCG
tag3A	CTTTATCAATACATACTACAATCA**CCGTAACTCATT**TTCTTCTATTCTCAGTTTTTCTAG
tag3B	CAATTTCATCATTCATTCATTTCA**CCGTAACTCATT**TTCTTCTATTCTCAGTTTTTCTAA
tag4A	TCATCAATCAATCTTTTTCACTTT**CCGTAACTCATT**CAACCAAACTAATCAAATTAAAAG
tag4B	ATACTACATCATAATCAAACATCA**CCGTAACTCATT**CAACCAAACTAATCAAATTAAAAA
	Antitags
anti-tag2A	GTAAAAAGAAAGGTATAAAGGTAA
anti-tag2B	AAAGAAAGAAAGAAAGAAAGTGTA
anti-tag3A	TGATTGTAGTATGTATTGATAAAG
anti-tag3B	TGAAATGAATGAATGATGAAATTG
anti-tag4A	AAAGTGAAAAAGATTGATTGATGA
anti-tag4B	TGATGTTTGATTATGATGTAGTAT
	Synthetic Targets
target2A	CTGCATTTTCGGGCCATCTTCGGCGACCCAGAAGTAATC**A**GGTATACGTGCTATATGTCTT
target2B	CTGCATTTTCGGGCCATCTTCGGCGACCCAGAAGTAATC**C**GGTATACGTGCTATATGTCTT
target3A	ACAAAAAGGAAATTGTAAACCAATTAACATGGAAGT**C**TAGAAAAACTGAGAATAGAAGAA
target3B	ACAAAAAGGAAATTGTAAACCAATTAACATGGAAGT**T**TAGAAAAACTGAGAATAGAAGAA
target4A	ATGCTGTTAATGTCATCCTTTCATTACAGGTATTGAAG**C**TTTTAATTTGATTAGTTTGGTTG
target4B	ATGCTGTTAATGTCATCCTTTCATTACAGGTATTGAAG**T**TTTTAATTTGATTAGTTTGGTTG

fragment length polymorphisms (AFLP).[22,23] The above methods are based on the comparison of the patterns of DNA fragments separated by gel electrophoresis or capillary electrophoresis in automated systems. More recently, single-nucleotide polymorphisms (SNPs) have emerged as new genetic markers with unique advantages for varietal discrimination.[24−27] The progress in automated sequencing technology has facilitated greatly the discovery of characteristic SNPs for olive cultivars.[28,29] The main advantages of SNPs over other genetic markers are as follows:[12,29] (a) SNPs enable pinpointing very similar cultivars because the differentiation is based on a single-nucleotide change rather than a whole DNA sequence. (b) SNP genotyping can be accomplished even with short amplified DNA sequences (e.g., 100 bp). This is particularly important in cases when the integrity of the DNA may be affected during the extraction process and storage of olive oil. (c) SNPs constitute the most abundant genetic markers. (d) They are mainly biallelic and stably inherited. Therefore, the trend is that SNP genotyping will replace the classical genetic markers for cultivar identification. The methods reported so far for SNP genotyping of olive oil DNA include capillary electrophoresis of restriction enzyme-digested DNA fragments[25,26] and DNA-microarray analysis of ligation reaction products.[24] It should be noted, however, that microarrays are suitable for parallel genotyping of thousands of SNPs in one sample; that is, the SNP-throughput per sample is high but the sample-throughput is low.

The proposed method for SNP genotyping is based on a suspension of fluorescent microspheres and, in comparison with the above methods, offers the following advantages. (i) It allows for high sample throughput; that is, compared to microarrays, the method is best suited for genotyping of a small number of useful SNPs in a large number of samples. (ii) The suspension of microspheres provides flexibility and convenience in modification and/or expansion of the assay by just replacing sets of microspheres or adding more sets of microspheres in the suspension. (iii) The microspheres offer rapid solution kinetics.

Previous studies have employed suspensions of fluorescent microspheres for the detection and/or quantification of PCR-amplified DNA fragments from food samples.[30,31] However, to our knowledge, this is the first report of SNP genotyping assays for food authenticity testing using this technological platform.

The aim of the present work is the development of a high sample throughput method for the identification of olive

DOI: 10.1021/jf5054657
J. Agric. Food Chem. 2015, 63, 3121−3128

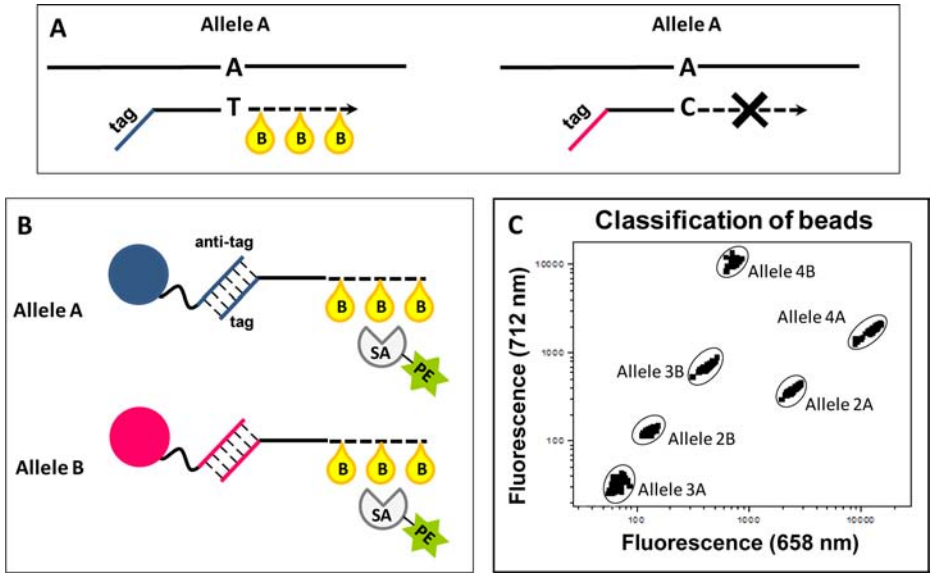

Figure 1. (A) Allele-specific primer extension reaction. Each allele-specific primer consists of a segment complementary to the target sequence, a tag sequence at the 5′ end, and a 12 nt spacer. The two allele-specific primers differ only at the 3′ end nucleotide. Extension by DNA polymerase occurs only when the primer anneals to the corresponding allele. (B) Hybridization assay on spectrally encoded fluorescent microspheres. The extension reaction products are captured on the surface of the microspheres through hybridization with the immobilized antitag sequences. The added streptavidin−phycoerythrin conjugate binds only to the extended primers that contain biotin moieties. The fluorescence of phycoerythrin of each microsphere is measured by flow cytometry. (C) Classification of the fluorescent microspheres by flow cytometry. The classification is based on the fluorescence intensities of the two dyes used for the staining of the microspheres. Each cluster represents a set of microspheres. The dots inside the cluster are data from at least 100 microspheres.

cultivars based on the simultaneous genotyping of single-nucleotide polymorphisms.

MATERIALS AND METHODS

Apparatus and Reagents. PCR and primer extension reactions were performed in the MJ Research PTC-0150 thermal cycler (Watertown, MA, USA). The digital camera, Kodak DC 120, and the Gel Analyzer software for DNA documentation were purchased from Kodak (Rochester, NY). The ultrasonic cleaner from Branson Ultrasonics (Danbury, CT, USA) was used for resuspension of the microspheres. The Luminex 100 IS flow cytometer (Luminex, Austin, TX, USA) was used for the analysis of the microspheres. Fluorescent carboxylated microspheres (5.6 μm) were purchased from Luminex. Amplitaq Gold DNA polymerase was from Applied Biosystems (Foster City, CA, USA), and Vent (exo-) DNA polymerase was from New England Biolabs (Beverly, MA, USA). Ultrapure 2′-deoxyribonucleoside 5′-triphosphates (dNTPs) were purchased from Invitrogen (Carlsbad, CA, USA). KAPA 2G Fast multiplex PCR kit was from Kapa Biosystems (Woburn, MA, USA). Biotin-11-dUTP was from Applichem (Darmstadt, Germany). Streptavidin-R-phycoerythrin conjugate (SA-PE) was purchased from Molecular Probes (Eugene, OR, USA). The primers and probes used in this study were synthesized by VBC-Biotech (Vienna, Austria). The sequences of the oligonucleotides used throughout this work are listed in Table 1. All other common reagents were from Sigma (St. Louis, MO, USA).

Experimental Outline. The method includes the following steps: (i) DNA isolation; (ii) PCR amplification of three DNA segments that contain the three SNPs (SNP2, SNP3, and SNP4); (iii) multiplex genotyping reaction based on the extension of six allele-specific primers; (iv) multiplex hybridization assay of the genotyping reaction products on spectrally encoded fluorescent microspheres (Figure 1).

Samples and DNA Extraction. The Koroneiki and Chondrolia monovarietal extra virgin olive oil samples were provided by Anatoli S.A. Chania, Crete, and Makedoniki Elaiourgia S.A. Kalives, Chalkidiki, respectively. The monovarietal olive oil samples of Adramytini, Valanolia, and Kalamon were extracted from fruits of the respective cultivars in the pilot olive mill of the Institute of Subtropical Plants and Olive, NAGREF, Chania, Crete. The samples were stored in the dark at room temperature for several months before use. Genomic DNA was extracted from young leaves of five Greek olive varieties (Adramytini, Chondrolia Chalkidikis, Kalamon, Koroneiki, and Valanolia) according to the method Saghai-Maroof et al.[32] as modified by Angiolillo et al.[33] Monovarietal olive oil samples (500 μL) were used to extract genomic DNA according to the CTAB/hexane/chloroform protocol.[34]

DNA Amplification Protocol A. DNA isolated from olive leaves and oil was subjected to two consecutive rounds of amplification (PCR I and PCR II). PCR I was carried out in a total volume of 50 μL containing 15 mM Tris-HCl, pH 8.0, 50 mM KCl, 2.5 mM $MgCl_2$, 200 μM of each dNTP, 0.3 μM of each primer, 1.25 U of Amplitaq Gold DNA polymerase, and 2 μL of genomic DNA or PCR I product. The cycling conditions for PCR I and PCR II for SNP2, SNP3, and SNP4[25] were as follows: 10 min at 95 °C followed by 35 cycles (40 cycles for PCR I of olive oil) at 95 °C for 30 s, 50 °C (60 °C for PCR I for SNP2) for 30 s, and 72 °C for 30 s. At the end of the cycling, the mixture was held at 72 °C for 10 min. A 2 μL aliquot from PCR I of olive oil was used directly in PCR II. The products of PCR I from leaves were first diluted 200 times, and a 2 μL aliquot was used as DNA template for PCR II. The PCR II primers (nested primers) were as previously reported.[25] The cycling conditions for PCR II were exactly the same as for PCR I. The PCR II products were confirmed and quantified by 2% agarose gel electrophoresis and ethidium bromide staining. The PCR I products were 501, 224, and 239 bp for SNP2, SNP3, and SNP4, respectively, whereas the PCR II products were 112, 105, and 137 bp for SNP2, SNP3, and SNP4, respectively.

DNA Amplification Protocol B (Multiplex PCR). The multiplex PCR was performed in a final volume of 25 μL containing 12.5 μL of Kapa 2G fast multiplex PCR mix, 0.2 μM of each of the PCR II primers for the three SNPs, and 2 μL of the isolated DNA. The multiplex PCR conditions were as follows: an initial step at 95 °C for 3 min followed by 35 cycles of 95 °C for 15 s, 50 °C for 30 s, and 72 °C for 30 s. A final step at 72 °C for 10 min was included. An aliquot of 5 μL of the PCR products was then subjected to a multiplex primer extension reaction, and an aliquot of 10 μL of the primer extension products was subjected to a multiple hybridization assay (see below).

DOI: 10.1021/jf5054657
J. Agric. Food Chem. 2015, 63, 3121−3128

Allele-Specific Primer Extension Reaction. Each allele-specific primer contained (a) at the 5′ end, a unique 24 bp oligonucleotide sequence (tag) complementary to the antitag sequence that was attached to the surface of a specific set of fluorescent microspheres; (b) a 12 bp common spacer; and (c) an allele-specific sequence 17−24 bp (Figure 1). Extension reactions were performed in the presence of a mixture of six primers specific for the six alleles of all three SNPs (SNP2, SNP3, and SNP4). The extension reaction was carried out in a total volume of 20 μL containing 20 mM Tris-HCl, 10 mM $(NH_4)_2SO_4$, 10 mM KCl, 0.1% Triton X-100, pH 8.8, 1.5 U Vent (exo-) DNA polymerase, 400 fmol of amplified DNA, 2 pmol of each primer, 2 mM $MgSO_4$, 10 μM of each dATP, dCTP, and dGTP, and 10 μM biotin-dUTP. The extension reactions were performed in the thermal cycler as follows: 95 °C for 5 min and 40 cycles of 95 °C for 15 s, 58 °C for 15 s, and 72 °C for 15 s.

Multiplex Hybridization Assay on Spectrally Distinct Microspheres. The extension reaction products (10 μL) were analyzed by a multianalyte hybridization assay, performed in a total volume of 55 μL (Figure 1). A suspension of six sets of spectrally encoded microspheres was prepared for the assay, each set consisting of 5000 identical microspheres. Each microsphere was stained with precise amounts of two fluorescent dyes, thus creating a built-in fluorescent signature. Also, antitag oligonucleotides were attached on the surface of each microsphere for molecular recognition of the allele-specific extension products. All of the microspheres were suspended in the hybridization buffer (100 mM Tris-HCl, pH 8.0, 200 mM NaCl, and 0.8 mL/L Triton X-100) and preheated at 37 °C. The extension reaction products were denatured for 3 min at 95 °C, placed immediately on ice for 2 min, and subsequently added to the above mixture and incubated for 1 h at 37 °C. The microspheres were then pelleted by centrifugation at 10000*g* for 1 min and washed once with 50 μL of hybridization buffer followed by resuspension in 80 μL of hybridization buffer containing 250 ng of streptavidin−phycoerythrin conjugate (SA-PE). The mixture was incubated for 20 min at room temperature, and the microspheres were analyzed by flow cytometry without prior washing. During the flow cytometric detection process, each microsphere was irradiated by two laser beams, 635 and 532 nm. The 635 nm beam was used for the excitation of the two fluorescent dyes within the microsphere and the ratio of the fluorescence intensities at 658 and 712 nm provided the classification of the microsphere. The 532 nm laser beam was used for the excitation of the reporter molecule, phycoerythrin, and the fluorescence intensity was related to the presence of a specific allele in the sample. At least 100 microspheres of each set were analyzed by the flow cytometer, and the median fluorescence value was calculated (Figure 1).

Genotype Assignment. The genotype of a sample, for SNP2, SNP3, and SNP4, was determined as follows: The fluorescence intensity obtained from each set of microspheres was first normalized to scale of 0−100, that is, it was expressed as a percentage of the maximum fluorescence value of the set. Then, for each SNP, the allelic fraction $R = 100F_A/(F_A + F_B)$ was calculated (as a percentage), where F_A and F_B are the normalized fluorescence values for alleles A and B of the SNP, respectively. In the presence of allele A only, the value of R is expected to be close to 100, whereas in the absence of allele A (only allele B present), the value of R would be close to 0. If both alleles, A and B, of the SNP are present, then R is about 50.

RESULTS AND DISCUSSION

The olive oil cultivar identification is based on the genotyping of three SNPs, namely, SNP2, SNP3, and SNP4, that are located in the plant's genome, giving a unique genotype fingerprint for each variety.[25] The SNP database of the five Greek olive cultivars is presented in Table 2.[25] The principle of the method is illustrated in Figure 1. The method is performed on a suspension of spectrally encoded microspheres in a high sample throughput and cost-effective format. We used sets of microspheres stained with precise amounts of two spectrally distinct fluorophores, thus providing unique "fluorescence signatures" for 100 different sets, which in turn permit the rapid simultaneous genotyping of up to 50 SNPs. Allele discrimination was accomplished through primer extension reaction. The extension reaction products were captured from the suspension of the microspheres and reacted with a streptavidin−phycoerythrin conjugate. The microspheres were then analyzed, within seconds, by a flow cytometer. Each microsphere "fluorescence signature" corresponds to a specific allele, whereas the signal of the phycoerythrin reporter denotes the presence of this allele in the sample. The suspension of microspheres allows solution kinetics and great assay flexibility.

Table 2. SNP Database of the Five Greek Olive Cultivars[a]

SNP	Adramytini	Chondrolia	Kalamon	Koroneiki	Valanolia
SNP2	A/A	A/C	A/A	A/C	A/C
SNP3	A/G	A/G	G/G	A/G	G/G
SNP4	C/C	C/C	C/C	C/T	C/C

[a]A, adenine; C, cytosine; G, guanine; T, thymine.

Biotin-dUTP was incorporated during the extension, and hence the reaction products were labeled with biotin. The products were heat-denatured and allowed to hybridize with a mixture of six sets of microspheres, each set carrying a characteristic antitag sequence. The hybrids were detected with a streptavidin−phycoerythrin conjugate. The fluorescence of the microspheres was finally measured by a flow cytometer.

As a model, the proposed method was applied to the authentication of five olive varieties: Adramytini, Chondrolia Chalkidikis, Kalamon, Koroneiki, and Valanolia.

The PCR amplification yielded fragments with sizes of 112, 105, and 137 bp for SNP2, SNP3, and SNP4, respectively. The PCR products were subjected to the extension reaction in the presence of six allele-specific primers (two primers per SNP).

Several parameters were evaluated for the optimization of the allele-specific primer extension reaction. The concentration of primers was tested in the range from 0.05 to 0.1 μM. The concentrations of dATP, dGTP, and dCTP were studied in the range of 2.5−25 μM of each, and the concentration of biotin-dUTP was tested in the range of 1.25−10 μM. The annealing temperature of the reaction was performed at 50−58 °C, and the reaction was carried out for 20−40 cycles. The optimized conditions are reported under Materials and Methods. Finally, the effect of the PCR product purification prior to the PEXT reaction was tested. Several PCR products were treated with exonuclease I and alkaline phosphatase, which hydrolyze the primers and the dNTPs, respectively. The treated PCR products were subjected to extension reaction in parallel with untreated products. The untreated products performed the same with treated ones. Optimization studies for hybridization assays on fluorescent microspheres included the effect of the number of microspheres (500−10000) on the signal of the assay, the hybridization time (30−120 min), the amount of streptavidin−phycoerythrin conjugate (100−500 ng), and the incubation time for the conjugate (10−30 min). Finally, the volume of the extension reaction mixture used for the multiplex hybridization assay was optimized, and 10 μL of the product was sufficient to obtain a high fluorescence signal.

Synthetic DNA Controls for Olive Varieties. The method was initially evaluated by using synthetic DNA controls representative of each variety. A synthetic control was a mixture of single-stranded DNA target sequences (60-mers), each corresponding to an allele (two targets per SNP). The sequences of the synthetic targets are listed in Table 1.

DOI: 10.1021/jf5054657
J. Agric. Food Chem. 2015, 63, 3121−3128

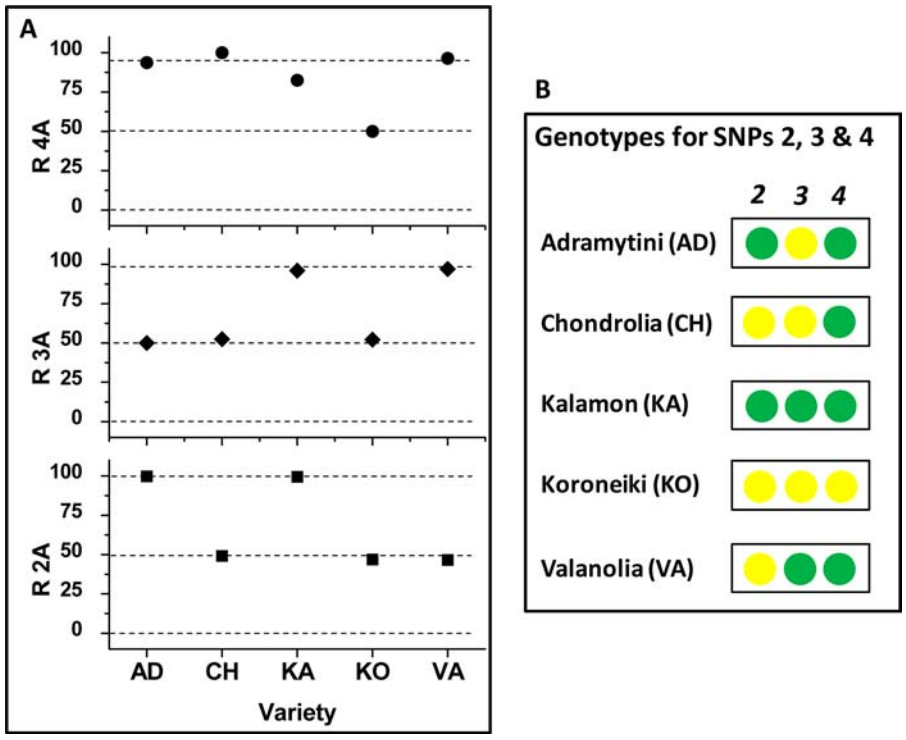

Figure 2. (A) Genotyping results for synthetic controls that represent the five Greek olive varieties, namely, Adramytini (AD), Chondrolia Chalkidikis (CH), Kalamon (KA), Koroneiki (KO), and Valanolia (VA). For each SNP, an allelic fraction *R* (expressed as a percentage) close to 100 corresponds to the presence of the allele A only, whereas an *R* value close to 50 indicates the presence of both alleles A and B. R 2A, allelic fraction (percentage) of allele A of SNP2; R 3A, allelic fraction (percentage) of allele A of SNP3; R 4A, allelic fraction (percentage) of allele A of SNP4. (B) Color code for the genotypes of the five olive varieties as assigned by the combination of the three SNPs. For each SNP, the green circle shows the presence of allele A only, whereas the yellow circle indicates the presence of both alleles (A and B).

Mixtures of the synthetic targets of the three SNPs were prepared, according to the known genotype of each olive variety. Given that the two alleles of each SNP are denoted with the letters A and B, the known genotypes of the five olive varieties for SNP2−SNP3−SNP4 are as follows:[25] Adramytini (AD), AA−AB−AA; Chondrolia Chalkidikis (CH), AB−AB−AA; Kalamon (KA), AA−AA−AA; Koroneiki (KO), AB−AB−AB; Valanolia (VA,: AB−AA−AA. Thus, the combination of the three genotypes provided a unique varietal code.

We produced synthetic controls that represent the five olive varieties: Adramytini, Chondrolia Chalkidikis, Kalamon, Koroneiki, and Valanolia. The synthetic controls contained 200 fmol/μL of each allele in the case of a "homozygote" control of the specific SNP and 100 fmol/μL of each allele in the case of a "heterozygote" control. A 1 μL aliquot of each synthetic control was subjected to a multiple extension reaction using a mixture of six extension primers, specific for the SNP2, SNP3, and SNP4 alleles. The extension products were subjected to a multiplex hybridization assay with the six sets of microspheres. The genotyping results for the synthetic controls are presented as plots of the allelic fraction *R* versus the olive variety that corresponds to each synthetic control (Figure 2). A color-code presentation of the SNP2, SNP3, and SNP4 genotypes for the five olive varieties is shown in Figure 2. It is demonstrated that the combination of the three genotypes gives a unique identification code for each variety.

Genotyping of Olive Leaves and Olive Oil. The proposed method was applied to the genotyping of DNA samples isolated from leaves and oil of the five olive varieties. The olive leaves and fruits used for olive oil production of Adramytini, Valanolia, and Kalamon were collected from the same olive trees. Adramytini and Valanolia samples were harvested from olive groves on the island of Lesvos and Kalamon samples from an olive grove in Chalkidiki. The Koroneiki leaf sample was harvested from the experimental olive grove at MAICh. The Chondrolia leaf and fruit samples were harvested from an olive grove in the Chalkidiki area. The fruits were then transferred for olive oil extraction to the Makedoniki Elaiourgia Co. (Greece). The leaf and olive oil DNA samples of all cultivars were characterized accordingly.[25] Following PCR, an amount of 400 fmol of amplified DNA was subjected to the multiplex primer extension reaction in the presence of the six allele-specific primers. A volume of 10 μL of the extension products, after heat denaturation for 3 min at 95 °C, was hybridized to a mixture of the six sets of microspheres. The results of the genotyping of the leaf samples are presented in Figure 3. Similarly, the proposed method was applied to the genotyping of DNA isolated from various olive oil samples, and the results are presented in Figure 4. We observe that, for each olive variety, the genotypes obtained from the leaf samples and from olive oil samples coincide with those of the synthetic controls.

All-Multiplex Method. An all-multiplex method was developed comprising (a) multiplex PCR amplification, (b) multiplex extension reaction, and (c) multiplex hybridization assay. The multiplex PCR of all three SNP segments in a single round of amplification was accomplished by using the Kapa 2G fast DNA polymerase. The genotyping results, presented in Figure 5, show the agreement of the all-multiplex protocol with the single-PCR approach.

Reproducibility. The reproducibility of the method was assessed by analyzing DNA samples from Valanolia, Kalamon,

DOI: 10.1021/jf5054657
J. Agric. Food Chem. 2015, 63, 3121−3128

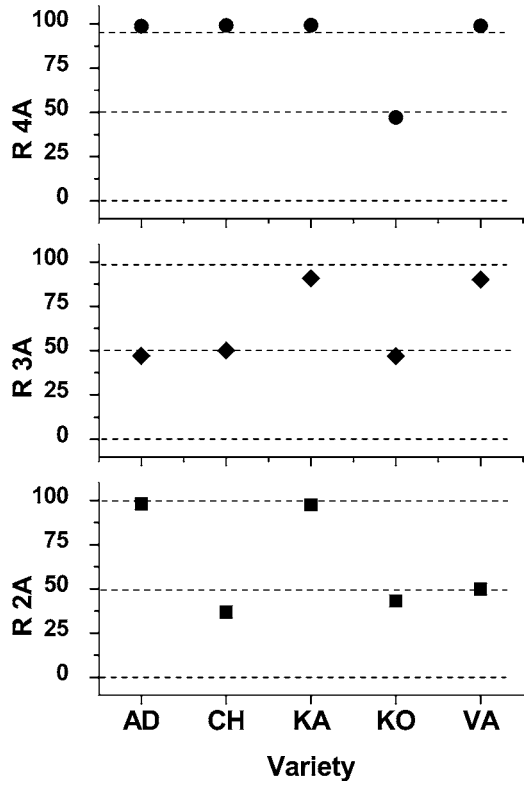

Figure 3. Genotyping results obtained from leaf samples of the five olive varieties, Adramytini (AD), Chondrolia Chalkidikis (CH), Kalamon (KA), Koroneiki (KO), and Valanolia (VA). For each SNP, an allelic fraction *R* close to 100 corresponds to the presence of allele A only, whereas an *R* value close to 50 indicates the presence of both alleles A and B.

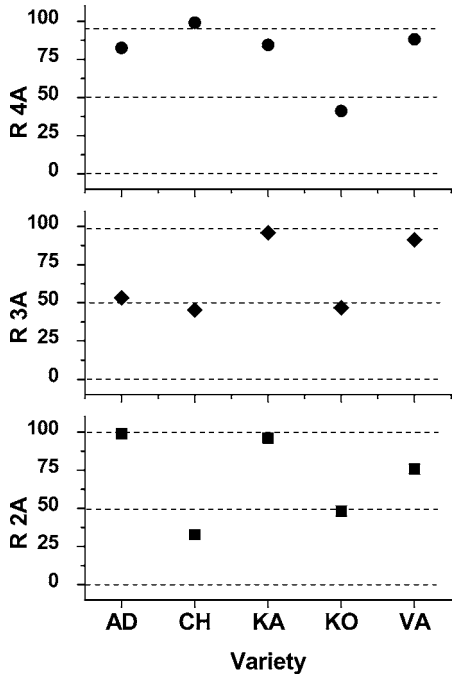

Figure 4. Genotyping results obtained from olive oil samples of the five olive cultivars, Adramytini (AD), Chondrolia Chalkidikis (CH), Kalamon (KA), Koroneiki (KO), and Valanolia (VA). For each SNP, an allelic fraction *R* close to 100 corresponds to the presence of allele A only, whereas an *R* value close to 50 indicates the presence of both alleles A and B.

and Koroneiki. The analyses were performed in triplicate, and the mean allelic fractions along with their coefficient of variation (%CV) were calculated for each SNP. The results are presented in Table 3. In all cases the reproducibility of the allelic fraction was very good for all three SNPs and genotypes.

The proposed method can be easily expanded to include more olive varieties because there are 100 sets of commercially available and spectrally distinguishable fluorescent microspheres carrying antitag sequences. Given that each set corresponds to an allele, the potential of the present method extends to the multiplex genotyping of 50 biallelic SNPs. Furthermore, the flexibility of the proposed method arises from the fact that the suspension of microspheres is not a fixed array (as in the case of planar arrays), but it can be easily adapted to specific laboratory needs because it is convenient to select and mix only those microsphere sets that are relevant to the SNP panel that is used for the interrogation of a particular olive oil sample. Moreover, the PCR products are introduced directly (without prior purification) to a single-tube multiplex primer extension reaction followed by a single-tube multiplex hybridization of all extension products on the microspheres and flow cytometric analysis. The flow cytometric detection is completed within 30 s. The method is accurate because the results obtained from the five olive cultivars are in full agreement with previous studies[25] that established the genotypes of the five olive varieties for SNP 2, SNP3, and SNP4. Moreover, for each cultivar, DNA isolated from leaf samples gave identical genotypes with DNA isolated from olive oil.

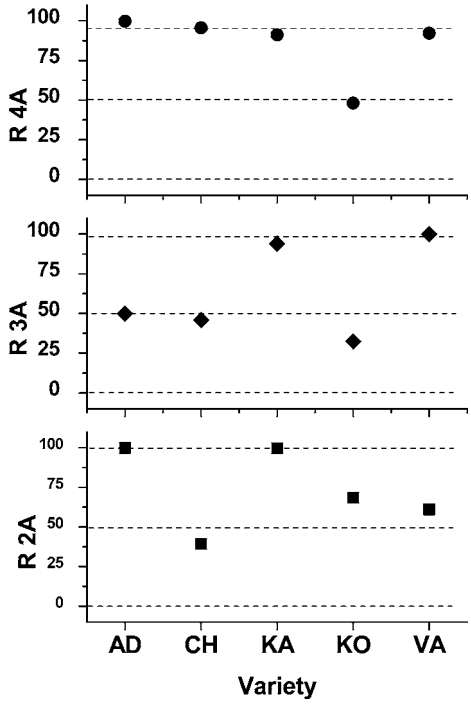

Figure 5. Genotyping results of the all-multiplex method for the five cultivars, Adramytini (AD), Chondrolia Chalkidikis (CH), Kalamon (KA), Koroneiki (KO), and Valanolia (VA). For each SNP, an allelic fraction *R* close to 100 corresponds to the presence of allele A only, whereas an *R* value close to 50 indicates the presence of both alleles A and B.

In our opinion, the proposed high sample throughput assay will contribute significantly to the traceability and authenticity

DOI: 10.1021/jf5054657
J. Agric. Food Chem. 2015, 63, 3121−3128

Table 3. Reproducibility Study

	Valanolia			Kalamon			Koroneiki		
SNP	genotype	allelic fraction (mean)	%CV (n = 3)	genotype	allelic fraction (mean)	%CV (n = 3)	genotype	allelic fraction (mean)	%CV (n = 3)
SNP2	AB	51.9	5.2	AA	94.2	2.5	AB	48.5	4.4
SNP3	AA	98.7	0.4	AA	99.8	0.4	AB	52.3	4.0
SNP4	AA	99.8	0.1	AA	99.7	0.1	AB	49.8	1.4

of olive oil samples. It is expected to be particularly useful in an industrial context and in laboratories involved in official control, that is, laboratories that require methods offering high sample throughput.

AUTHOR INFORMATION

Corresponding Author

*(T.K.C.) Phone: (+30)2610 962951. E-mail: tchrist@upatras.gr.

Present Address

⊥(C.B.) INRA, UMR 1318, Institut Jean-Pierre Bourgin, RD10, F-78000 Versailles, France.

Notes

The authors declare no competing financial interest.

REFERENCES

(1) Loukas, M.; Krimbas, C. B. History of olive cultivars based on genetic distances. *J. Hortic. Sci.* **1983**, *58*, 121−127.

(2) Stefanoudaki, E.; Kotsifaki, F.; Koutsaftakis, A. Sensory and chemical profiles of three European olive varieties (*Olea europaea* L); an approach for the characterisation and authentication of the extracted oils. *Sci. Food Agric.* **2000**, *80*, 381−389.

(3) Casale, M.; Oliveri, P.; Casolino, C.; Sinelli, N.; Zunin, P.; Armanino, C.; Forina, M.; Lanteri, S. Characterisation of PDO olive oil Chianti Classico by non-selective (UV-visible, NIR and MIR spectroscopy) and selective (fatty acid composition). *Anal. Chim. Acta* **2012**, *712*, 56−63.

(4) European Council Regulation No. 510/2006 of 20 March 2006.

(5) Sinelli, N.; Casale, M.; Di Egidio, V.; Oliveri, P.; Bassi, D.; Tura, D.; Casiraghi, E. Varietal discrimination of extra virgin olive oils by near and mid infrared spectroscopy. *Food Res. Int.* **2010**, *43*, 2126−2131.

(6) Vergara-Barberan, M.; Lerma-Garcia, M. J.; Herrero-Martinez, J. M.; Simo-Alfonso, E. F. Use of protein profiles established by CZE to predict the cultivar of olive leaves and pulps. *Electrophoresis* **2014**, *35*, 1652−1659.

(7) Dais, P.; Hatzakis, E. Quality assessment and authentication of virgin olive oil by NMR spectroscopy: a critical review. *Anal. Chim. Acta* **2013**, *765*, 1−27.

(8) Casas, J. S.; Gordillo, C. D.; Bueno, E. O.; Exposito, J. M.; Mendoza, M. F.; Hierro, T. A.; Gonzalez, L. G.; Cano, M. M. Characteristics of virgin olive oils from the olive zone of Extremadura (Spain), and an approximation to their varietal origin. *J. Am. Oil Chem. Soc.* **2009**, *86*, 933−940.

(9) Laddomada, B.; Colella, G.; Tufariello, M.; Durante, M.; Angiuli, M.; Salvetti, G.; Mita, G. Application of a simplified calorimetric assay for the evaluation of extra virgin olive oil quality. *Food Res. Int.* **2013**, *54*, 2062−2068.

(10) Dias, L. G.; Fernandes, A.; Veloso, A. C.; Machado, A. A.; Pereira, J. A.; Peres, A. M. Single-cultivar extra virgin olive oil classification using a potentiometric electronic tongue. *Food Chem.* **2014**, *160*, 321−329.

(11) Montealegre, C.; Alegre, M. L. M.; Garcıa-Ruiz, C. Traceability markers to the botanical origin in olive oils. *J. Agric. Food Chem.* **2010**, *58*, 28−38.

(12) Bracci, T.; Busconi, M.; Fogher, C.; Sebastiani, L. Molecular studies in olive (*Olea europaea* L.): overview on DNA markers applications and recent advances in genome analysis. *Plant Cell Rep.* **2011**, *30*, 449−462.

(13) Agrimonti, C.; Vietina, M.; Pafundo, S.; Marmiroli, N. The use of food genomics to ensure the traceability of olive oil. *Trends Food Sci. Technol.* **2011**, *22*, 237−244.

(14) Pasqualone, A.; Montemurro, C.; Summo, C.; Sabetta, W.; Caponio, F.; Blanco, A. Effectiveness of microsatellite DNA markers in checking the identity of protected designation of origin extra virgin olive oil. *J. Agric. Food Chem.* **2007**, *55*, 3857−3862.

(15) Martins-Lopes, P.; Gomes, S.; Santos, E.; Guedes-Pinto, H. DNA markers for Portuguese olive oil fingerprinting. *J. Agric. Food Chem.* **2008**, *56*, 11786−11791.

(16) Ben-Ayed, R.; Grati-Kamoun, N.; Sans-Grout, C.; Moreau, F.; Rebai, A. Characterization and authenticity of virgin olive oil (*Olea europaea* L.) cultivars by microsatellite markers. *Eur. Food Res. Technol.* **2012**, *234*, 263−271.

(17) Sanz-Cortés, F.; Badenes, M. L.; Paz, S.; Iniguez, A.; Llacer, G. Molecular characterization of olive cultivars using RAPD markers. *J. Am. Soc. Hortic. Sci.* **2001**, *126*, 7−12.

(18) Besnard, G.; Breton, C.; Baradat, P.; Khadari, B.; Bervillé, A. Cultivar identification in olive based on RAPD markers. *J. Am. Soc. Hortic. Sci.* **2001**, *126*, 668−675.

(19) Pasqualone, A.; Caponio, F.; Blanco, A. Inter-simple sequence repeat DNA markers for identification of drupes from different *Olea europaea* L. cultivars. *Eur. Food Res. Technol.* **2001**, *213*, 240−243.

(20) Gemas, V. J. V.; Almadanim, M. C.; Tenreiro, R.; Martins, A.; Fevereiro, P. Genetic diversity in the olive tree (*Olea europaea* L. subsp. *europaea*) cultivated in Portugal revealed by RAPD and ISSR markers. *Genet. Resour. Crop Evol.* **2004**, *51*, 501−511.

(21) Pafundo, S.; Agrimonti, C.; Maestri, E.; Marmiroli, N. Applicability of SCAR markers to food genomics: olive oil traceability. *J. Agric. Food Chem.* **2007**, *55*, 6052−6059.

(22) Pafundo, S.; Agrimonti, C.; Marmiroli, N. Traceability of plant contribution in olive oil by amplified fragment length polymorphisms. *J. Agric. Food Chem.* **2005**, *53*, 6995−7002.

(23) Montemurro, C.; Pasqualone, A.; Simeone, R.; Sabetta, W.; Blanco, A. AFLP molecular markers to identify virgin olive oils from single Italian cultivars. *Eur. Food Res. Technol.* **2008**, *226*, 1439−1444.

(24) Consolandi, C.; Palmieri, L.; Severgnini, M.; Maestri, E.; Marmiroli, N.; Agrimonti, C.; Baldoni, L.; Donini, P.; DeBellis, G.; Castiglioni, B. A procedure for olive oil traceability and authenticity: DNA extraction, multiplex PCR and LDR-universal array analysis. *Eur. Food Res. Technol.* **2008**, *229*, 375−382.

(25) Bazakos, C.; Dulger, A. O.; Uncu, A. T.; Spaniolas, S.; Spano, T.; Kalaitzis, P. A SNP-based PCR−RFLP capillary electrophoresis analysis for the identification of the varietal origin of olive oils. *Food Chem.* **2012**, *134*, 2411−2418.

(26) Perez-Jimenez, M.; Besnard, G.; Dorado, G.; Hernandez, P. Varietal tracing of virgin olive oils based on plastid DNA variation profiling. *PLoS One* **2013**, *8*, No. e70507.

(27) Brookes, A. J. The essence of SNPs. *Gene* **1999**, *234*, 77−186.

(28) Gut, I. G. Automation in genotyping of single nucleotide polymorphisms. *Hum. Mutat.* **2001**, *17*, 475−492.

(29) Consolandi, C.; Palmieri, L.; Doveri, S.; Maestri, E.; Marmiroli, N.; Reale, S.; Lee, D.; Baldoni, L.; Tosti, N.; Severgnini, M.; de Bellis, G.; Castiglioni, B. Olive variety identification by ligation detection in a universal array format. *J. Biotechnol.* **2007**, *129*, 565−574.

(30) Kalogianni, D. P.; Elenis, D. S.; Christopoulos, T. K.; Ioannou, P. C. Multiplex quantitative competitive polymerase chain reaction

DOI: 10.1021/jf5054657
J. Agric. Food Chem. 2015, 63, 3121−3128

based on a multianalyte hybridization assay performed on spectrally encoded microspheres. *Anal. Chem.* **2007**, *79*, 6655−6661.
(31) Li, Y.; Wu, Y.; Han, J.; Wang, B.; Ge, Y.; Chen, Y. Species-specific identification of seven vegetable oils based on suspension bead array. *J. Agric. Food Chem.* **2012**, *60*, 2362−2367.
(32) Saghai-Maroof, M. A.; Soliman, K. M.; Jorgensen, R. A.; Allard, R. W. Ribosomal DNA spacer length polymorphisms in barley: Mendelian inheritance, chromosomal location and population dynamics. *Proc. Natl. Acad. Sci. U.S.A.* **1984**, *81*, 8014−8018.
(33) Angiolillo, A.; Mencuccini, M.; Baldoni, L. Olive genetic diversity assessed using amplified fragment length polymorphisms. *Theor. Appl. Genet.* **1999**, *98*, 411−421.
(34) Gimenez, M. J.; Piston, F.; Martın, A.; Atienza, S. G. Application of real-time PCR on the development of molecular markers and to evaluate critical aspects for olive oil authentication. *Food Chem.* **2010**, *118*, 482−487.

DOI: 10.1021/jf5054657
J. Agric. Food Chem. 2015, 63, 3121−3128

with advantageous, low-cost ultrahigh performance LC−MS/MS (UPLC−MS/MS). This method combined the advantages of IAC specificity with the speed and sensitivity of UPLC−MS/MS instrumentation. Further, the optimized method was applied to the detection of TTX in real samples.

MATERIALS AND METHODS

Chemicals and Materials. TTX was purchased from Tocris Cookson (Bristol, UK) (purity ≥99.6%). HPLC grade acetonitrile, methanol, formic acid, glacial acetic acid, and ammonium acetate were purchased from Sigma-Aldrich (St. Louis, MO, USA). Ultrapure water was produced by a Millipore Milli-Q system (Millipore, Bedford, MA, USA). All other chemicals and solvents were of analytical grade and were obtained from Shanghai Chemical Reagent Co. (Shanghai, China).

Standard Solutions and Buffers. TTX standard stock solution (100 μg mL^{-1}) was prepared by dissolving TTX (5 mg) in ultrapure water (50 mL) containing formic acid/acetonitrile (0.1%, 5:5, v/v). The working standard solution of TTX was prepared by appropriate dilution of the stock solution using ultrapure water containing 0.1% formic acid/acetonitrile (5:5, v/v) and stored at 4 °C. Phosphate buffered saline (PBS, pH 7.4) was prepared by dissolving $KH_2PO_4 \cdot 2H_2O$ (1.09 g), $Na_2HPO_4 \cdot 12H_2O$ (6.45 g), and NaCl (4.25 g) in ultrapure water (500 mL).

Preparation of Immunoaffinity Column. Cynogen bromide (CNBr)-activated Sepharose 4B powder (0.5 g) was added to hydrochloric acid (HCl, 1 M, 100 mL) and poured into a sintered glass funnel (40−60 mm). The gel was washed with the coupling buffer (0.1 mol L^{-1} NaHCO3, 0.5 mol L^{-1} NaCl, pH 8.3, 100 mL). Subsequently, the gel (1.5 mL) was mixed with TTX monoclonal antibody (mAb, 10 mg mL^{-1}, 1.5 mL); the mixture was transferred into a stoppered flask and incubated on a shaker (120 rpm) at room temperature for 2 h. The resulting solution was collected to calculate the coupling efficiency and determine the antibody amount by Bradford protein assay method. The mixture was then washed with coupling buffer (30 mL) to remove the uncombined MAbs. The unreacted active groups on the sorbents were capped with the blocking buffer (0.1 mol L^{-1} Tris-HCl, pH 8.0) for 2 h at room temperature following which the column was washed with PBS (100 mL, 0.01 mol L^{-1}, pH 7.3) and stored in PBS (0.01 mol L^{-1}, pH 7.3) containing ethylmercurithiosalicylic acid (0.05%, w/v) at 2−8 °C.

Determination of Column Capacity. A relatively large amount (6000 ng) of TTX was dissolved in PBS (25 mL) containing 20% methanol. The solutions were then transferred into the IAC column (preconditioned with 10 mL of PBS) with the flow rate of 1 mL min^{-1}. The saturated column was washed with water (8 mL). Finally, methanol (4 mL) containing 0.1% acetic acid was used to elute the analytes. The eluate was evaporated to dryness under a stream of nitrogen at 60 °C. The so-obtained residue was redissolved in methanol (1 mL). Further, the solution was filtered through a 0.22 μm PTFE filter, and 10 μL of the solution was injected into the UPLC system.

Sample Preparation for IAC. Muscle tissue homogenate (2 g, ± 0.01 g) was weighted into a 50 mL polypropylene centrifuge tube. Acetic acid (0.1%) in methanol (10 mL) was added to the sample and vortexed for 2 min and then ultrasonicated for 15 min. After centrifugation at 6000 × g for 50 min, 5 mL of the supernatant was decanted into a clean tube. The supernatant was diluted with PBS (20 mL, pH 7.4), and the pH was adjusted to 7−8 using 1 M NaOH solution.

The IAC column was preconditioned with PBS (10 mL) prior to the analyte loading. Subsequently, the analyte solution was loaded onto the IAC at a flow rate of about 9 mL/min by gravity. The analyte was washed with water (8 mL) and eluted with 1% acetic acid in methanol (4 mL). The elute was completely dried under a stream of nitrogen at 60 °C. The residue was redissolved in LC mobile phase (1 mL, 95% A mix with 5% B) and filtered through a 0.22 μm PTFE filter into an autosampler vial for analysis. The columns, after elution, were immediately regenerated by PBS (50 mL) and stored in PBS (containing 0.01% sodium azide) at 4 °C for the subsequent use.

LC−MS/MS Equipment and Parameters. The TTX analysis was carried out on an ACQUITY UPLC system (Waters, Milford, MA,USA) coupled with Quattro Premier XE Micromass triple−quadrupole mass spectrometer (Waters, Manchester, UK). The UPLC separation was performed on an ACQUITY UPLC BEH Amide column (50 mm × 2.1 mm I.D., 1.7 mm particle size) at 40 °C. The injection volume was 10 μL. Acetonitrile (A) and 5 mmol L^{-1} ammonium acetate in ultrapure water containing 0.1% formic acid (v/v) (B) were used as the mobile phases, and the flow rate was 0.3 mL min^{-1} throughout the analysis. The solvent gradient was increased linearly from 5−80% B in 1.5 min, kept constant for 1.5 min, and then returned to 5% B after 0.5 min, and held at this level for 1.5 min so that the system could re-equilibrate prior to the next injection.

The mass spectrometer was operated in electrospray positive mode with the capillary voltage set at 3.0 kV. The source temperature was set at 110 °C, desolvation temperature at 350 °C, and cone gas flow at 50 L h^{-1} with desolvation gas flow at 600 L h^{-1}. Data acquisition was in multiple reactions monitoring mode (MRM). The cone voltage and collision energy were optimized for TTX by standard infusion. The precursor/product ions monitored were 320.0 > 302.0 (cone voltage 45 V, collision energy 25 eV) and 320.0 > 161.8 (cone voltage 45 V, collision energy 35 eV). The precursor/product ion m/z 320.0 > 302.0 was used for quantification in MRM mode.

Calculations of Results. Data acquisition was acquired and processed using MassLynx 4.1 and QuanLynx software. The concentrations of TTX in samples (ng g^{-1}) were calculated directly from the area responses using a linear six-point calibration produced from 0.3−20 ng mL^{-1} TTX standard solutions. If the concentration of analyte exceeds the linear range, the sample solution should be diluted with mobile phase appropriately, then injected into the UPLC−MS/MS system.

RESULTS AND DISCUSSION

Preparation of IAC Column. The antibody plays an important role in the potential use of the immunosorbent whether the IAC is used for a single analyte or for class-selective purposes. In this study, TTX−BSA (bovine serum albumin) conjugate was synthesized, and mAb against TTX was successfully produced using the hybridoma method.[30] CNBr-activated Sepharose 4B was employed as a coupling matrix because it is water insoluble; however, it is hydrophilic and could be easily activated. To obtain the best binding capacity, several amounts of antibodies (3−15 mg mL^{-1} gel) were separately conjugated to Sepharose 4B, and the corresponding capacities were measured. Coupling efficiency of different amount of mAb combined with CNBr-activated Sepharose 4B (1 mL) are shown in Figure 2. The result showed that 6 mg of the mAb saturated in 1 mL gel exhibited a good coupling efficiency of about 97.4%. An excessive amount of antibody (>6 mg) might introduce steric hindrance to antigen/antibody recognition and thus lead to the reduction of column capacity.

Optimization of IAC Conditions. Appropriate elution solvents are important not only for the efficient uncoupling of the captured analyte off the IAC, but also in preserving the column reusability.[31] In this study, loading, washing, and elution conditions were developed and optimized. It is universally acknowledged that the bond between the antigen/hapten and the antibody is due to electrostatic forces, Vander Waals forces, hydrogen bonds, and hydrophobic interactions.[32] To elute the antigen from the antibody−antigen complex in the IAC, the column environment was required to be changed. In this study, pure methanol and acetonitrile were tested to elute the analyte; however, the results were not satisfying with the recoveries of only 65.6 and 75.2%, respectively. Moreover, a

DOI: 10.1021/acs.jafc.5b00045
J. Agric. Food Chem. 2015, 63, 3129−3134

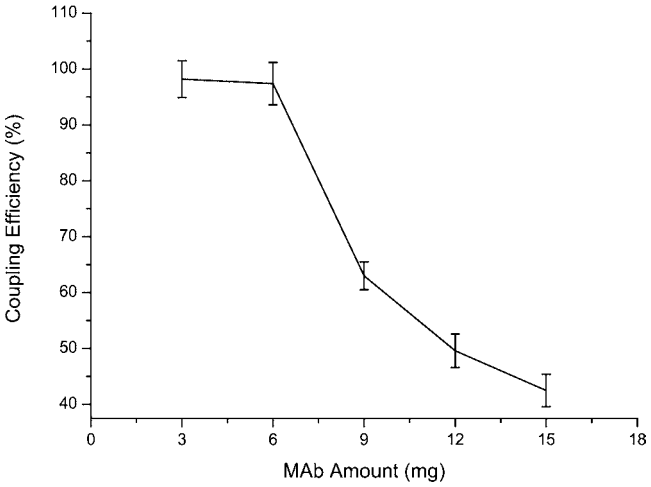

Figure 2. Coupling efficiency of different amount of mAb combined with CNBr-activated Sepharose 4B (1 mL).

large amount of solvent was required for elution, and the process was time-consuming. According to the literature,[29] the acidic solvents could enhance the strength of the eluent solution in IAC elution procedure. Therefore, acidic methanol and acetonitrile were tested to elute the analyte, with the volumes for elution measured to be about 1−5 mL. The recoveries corresponding to different elution conditions are listed in Table 1. The result shows that 5 mL of acidic methanol

Table 1. Recoveries of TTX (400 ng) at Different Elution Conditions

	recovery in various fractions (%)[a]			
elution fraction[a]	methanol	acetonitrile	1% acetic acid in methanol	1% acetic acid in acetonitrile
fraction 1 (1 mL)	34.8	21.5	89.8	68.7
fraction 2 (1 mL)	17.8	13.1	5.3	7.5
fraction 3 (1 mL)	10.0	10.2	2.4	5.4
fraction 4 (1 mL)	7.0	11.4	0.6	2.7
fraction 5 (1 mL)	5.6	9.4	0.3	2.3
total recovery[b]	75.2	65.6	98.4	86.6

[a]New IAC column was preconditioned with PBS (10 mL), the analyte solution containing 400 ng of TTX was loaded, then the column washed with water (8 mL) and eluted with each elution summarized in the table. [b]Total recovery is the sum of fraction 1 to fraction 5.

leads to the best recovery of 98.4% in less time, which thus indicates that organic solvents with low pH could disrupt these bonds and efficiently elute the antigen from the IAC column. Therefore, 5 mL of 1% acetic acid in methanol was selected as the optimized elution condition.

Column Capacity and Reusability. In this study, the capacity was evaluated and presented as nanograms of analyte relative to IAC bed volume (ng mL^{-1}). The column capacity of new IAC column was found to be 1106 ng mL^{-1}, which was sufficient for TTX determination and suitable for marine organisms. The reusability of IAC depended on the concentration and activity of the immobilized antibodies and chemical stability of the support. The reusability of IAC was evaluated in 10 days at 1 day intervals. Each time after using, the IAC was stored in PBS at 4 °C. The column capacity curve is shown in Figure 3. The column capacity decreases with

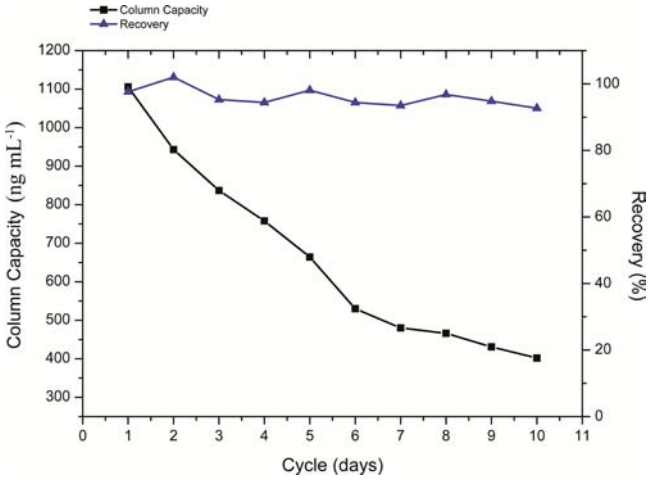

Figure 3. Capacity and recovery variation curves of the IAC column during ten cycles.

increasing cycles of usage, in particular, during the fifth and the sixth runs. In China, the official test method for TTX in aquatic products is HPLC method with a measure range 50−500 ng g^{-1}; and a HPLC−MS/MS confirmation is needed. When the UPLC−MS/MS method described in this paper used for confirming of TTX, the IAC column has the potential to reuse for five times with column capacity above 500 ng mL^{-1} to meet the HPLC method measure range.

Optimization of UPLC−MS/MS Conditions. The optimization of the electrospray ionization (ESI) interface parameters was highly desirable for obtaining the maximum abundance of the molecular ions of the analyte. Acquisition parameters were determined by direct infusion of standard solution (5.0 μg mL^{-1}) into the mass spectrometer at a flow rate of 10 μL min^{-1}. ESI probe temperature was set at the minimum acceptable value (110 °C), and capillary voltage was kept at 3.0 kV. The predominant peak in the primary ESI spectra of TTX corresponded to the $[M + H]^+$ ion at m/z 320.0. Then, dissociation with argon was induced, and different collision energies were tested to find the most abundant product ion. Figure 4 shows the product ion spectra of the [M

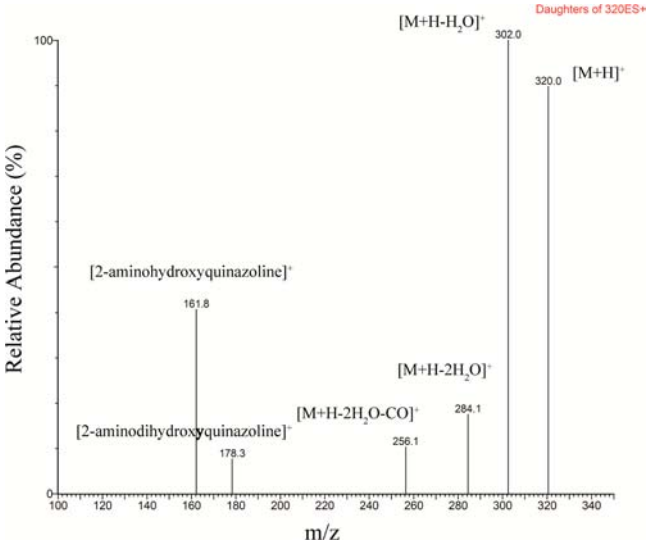

Figure 4. MS/MS fragmentation spectra of TTX.

DOI: 10.1021/acs.jafc.5b00045
J. Agric. Food Chem. 2015, 63, 3129−3134

+ H]$^+$ ion of TTX. The major fragment ions at m/z 302.0, 161.8, 284.1, 256.1, and 178.3 are observed. The daughter ion m/z 302.0 (CE 25 eV), with the highest relative abundance, was selected for quantification in MRM mode. The fragmentation pathways of TTX have been studied and reported in the literature.[8] On the basis of the product ion spectra of TTX (Figure 4), the ions at m/z 302.0, 284.1, and 256.1 are assigned to [M+H−H_2O]$^+$, [M+H−2H_2O]$^+$, and [M +H−2H2O−CO]$^+$, respectively. Notably, the ion at m/z 256.1 fragmentation pathway mentioned previously was different from that reported by Cho et al.[23] The other ions at m/z 178.3 and m/z 161.8 were derived probably from [2-amino-dihydroquinazoline]$^+$ and [2-aminodihydroxyquinazoline]$^+$, respectively, with sequential elimination of water molecules.

Chromatographic conditions were optimized to obtain maximum sensitivity and best peak shape. The Acquity UPLC BEH C18, Acquity UPLC BEH HILIC, and Acquity UPLC BEH Amide columns were tested for the separation of TTX. Lack of retention was observed with reverse-phase chromatography on BEH C18 column. As expected, TTX was not retained on this stationary phase because of its high polarity. Although TTX was retained in BEH HILIC column and the column provided several advantages[24] in chromatographic separation, asymmetric peak was observed in this study. UPLC BEH Amide column enabled the use of a wide range of pH values of the mobile phase, and the presence of amide group also favored both partitioning and hydrogen bonding separation mechanism, which facilitated the separation of high polarity analyte. The results revealed that BEH Amide column provided the best resolution and peak shape for the studied analyte in the shortest time of 5 min. Consequently, following the optimization of the gradient profile, the Acquity UPLC BEH Amide column was selected as the proper column for chromatographic separation. Typical LC−MS/MS chromatograms of blank sample, standard solution, spiked sample, and naturally contaminated TTX sample are shown in Figure 5.

Method Validation. The proposed method was validated by assessment of its specificity, linearity, limit of detection (LOD), limit of quantification (LOQ), recovery, and intra- and inter-day precision. The specificity of the method was determined by comparing the chromatograms of blank sample with standard-spiked sample. The TTX was detected without apparent interference from endogenous components of all marine organisms. Good linearity was obtained at concentrations of standard solutions ranging from 0.3−20 ng mL^{-1} for calibrating TTX in marine organisms, as demonstrated by the high correlation coefficient (r^2) value above 0.9984. The LOD and LOQ for TTX in marine organisms, which were defined as signal/noise ratios of 3:1 and 10:1, respectively, were determined to be 0.1 and 0.3 ng g^{-1}. To date, there are few methods available for the detection of TTX with LOD from 0.32−100 ng g^{-1}.[21−23] However, in this study, the method was found to be more sensitive. Precision and accuracy were assessed from replicated experiments (n = 6) using new IAC columns at three different concentrations, namely, 0.3, 1.5, and 5 ng mL^{-1}. The values corresponding to the results for intra- and inter-day precision and accuracy are listed in Table 2. The recoveries of TTX from fortified samples ranged from 86.5−103.6% with intraday RSDs of 3.40−7.22% and interday RSDs of 4.74−9.88%.

Application to Real Samples. One-hundred marine organisms samples (no. 1−100) including puffer fish, shrimps, crabs, clam, and horseshoe crab collected from Zhoushan local market were analyzed for the presence of TTX. All the samples were processed according to the IAC method described above, and the results are listed in Table 3. Nine samples were found to contain TTX at concentrations ranging from 2.22−590 ng g^{-1}. The result shows that some puffer fish (*Lagocephalus gloveri*) and horseshoe crab (*Carcinoscorpins rotundicauda*) contain a certain amount of TTX; however, it is virtually absent in horseshoe crab (*Tachpleus tridentatus*). These results were consistent with the previously published study.[33] One of the 20 manila clams (*Ruditapes philippinarum*) was found to contain TTX with a low value of 2.22 ng g^{-1}. Although several studies[22] have reported that bivalves such as *Paphies australis* were found to contain TTX, TTX positive *Ruditapes*

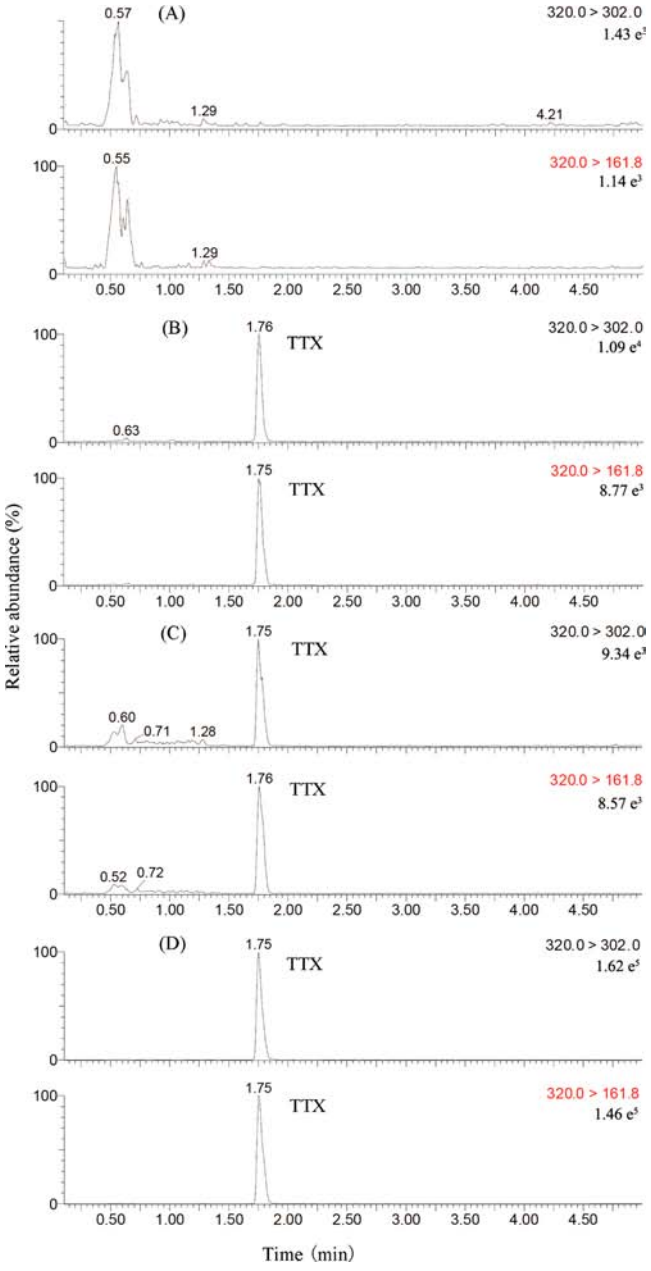

Figure 5. MRM chromatogram of TTX: (A) blank puffer fish sample, (B) 1.0 ng mL^{-1} of standard solution, (C) spiked puffer fish sample at concentration of 1.0 ng g^{-1}, and (D) naturally contaminated TTX puffer fish sample (24.8 ng g^{-1}).

DOI: 10.1021/acs.jafc.5b00045
J. Agric. Food Chem. 2015, 63, 3129−3134

Table 2. Recovery, Intra- and Inter-Day Precision of TTX in Marine Organisms[a]

species	added (ng g^{-1})	average recovery (%, n = 6)	intraday RSD (%, n = 6)	interday RSD (%, n = 6)
shrimps (*Penaeus orientalis*)	0.3	101.8	7.22	5.33
	1.5	96.7	5.42	4.74
	5.0	103.6	3.94	6.07
puffer fish (*Lagocephalus gloveri*)	0.3	86.5	6.31	6.74
	1.5	89.1	4.82	9.88
	5.0	94.7	3.40	6.03
horseshoe crab (*Tachpleus tridentatus*)	0.3	92.0	5.36	4.86
	1.5	96.9	5.95	5.15
	5.0	94.4	4.54	6.63

[a]TTX was determined according to section Sample Preparation for IAC using new IAC columns.

Table 3. Presence of TTX in Marine Organisms (Analysis of 100 Samples)

species	sample number	positive sample code	concentration of TTX (ng g^{-1})
puffer fish (*Lagocephalus gloveri*)	1–20	3	128
		4	103
		14	590
		17	146
		18	61.6
shrimps (*Solenocera melantho*, *Penaeus orientalis*)	21–40		ND[a]
crabs (*Portunus trituberculatus*)	41–60		ND
manila clams (*Ruditapes philippinarum*)	61–80	67	2.22
horseshoe crab (*Carcinoscorpins rotundicauda*)	81–90	83	162
		88	101
		90	24.8
horseshoe crab (*Tachpleus tridentatus*)	90–100		ND

[a]ND indicates "not detected".

philippinarum found in this study has never been mentioned before.

AUTHOR INFORMATION

Corresponding Author

*Tel.: +86-580-2299898. Fax: +86-580-2299882. E-mail: guoyuanming@msn.com.

Notes

The authors declare no competing financial interest.

ACKNOWLEDGMENTS

This work was supported by the National Natural Science Foundation of China (No.81470148) and National Key Technology R&D Program during the "12th Five-Year Plan" (2012BAD29B06). The authors would like to thank Jian Wang and Lili Lun for their valuable technical assistance.

REFERENCES

(1) Chowdhury, F. R.; Ahasan, H. A.; Al Mamun, A.; Rashid, A. K.; Al Mahboob, A. Puffer fish (Tetrodotoxin) Poisoning: An Analysis and Outcome of Six Cases. *Trop. Doct.* **2007**, *37*, 263–264.

(2) Chau, R.; Kalaitzis, J. A.; Neilan, B. A. On the Origins and Biosynthesis of Tetrodotoxin. *Aquat. Toxicol.* **2011**, *104*, 61–72.

(3) Tsuda, K.; Ikuma, S.; Kawamura, M.; Tachikawa, R.; Sakai, K. Tetrodotoxin. VII. On the Structure of Tetrodotoxin and Its Derivatives. *Chem. Pharm. Bull. (Tokyo)* **1964**, *12*, 1357–1374.

(4) Noguchi, T.; Jeon, J. K.; Arakawa, O.; Sugita, H.; Deguchi, Y.; Shida, Y.; Hashimoto, K. Occurrence of Tetrodotoxin and Anhydrotetrodotoxin in *Vibrio sp.* Isolated from the Intestines of a Xanthid Crab, *Atergatis floridus*. *J. Biochem.* **1986**, *99*, 311–314.

(5) Wood, S. A.; Casas, M.; Taylor, D. I.; McNabb, P.; Salvitti, L.; Ogilvie, S.; Cary, S. C. Depuration of Tetrodotoxin and Changes in Bacterial Communities in *Pleurobranchea maculata* Adults and Egg Masses Maintained in Captivity. *J. Chem. Ecol.* **2012**, *38*, 1342–1350.

(6) McNabb, P.; Selwood, A. I.; Munday, R.; Wood, S. A.; Taylor, D. I.; Mackenzie, L. A.; van Ginkel, R.; Rhodes, L. L.; Cornelisen, C.; Heasman, K.; Holland, P. T.; King, C. Detection of Tetrodotoxin from the Grey Side-Gilled Sea Slug, *Pleurobranchea maculata*, and Associated Dog Neurotoxicosis on Beaches Adjacent to the Hauraki Gulf, Auckland, New Zealand. *Toxicon* **2010**, *56*, 466–473.

(7) Lin, S. J.; Hwang, D. F. Possible Source of Tetrodotoxin in the Starfish *Astropecten scoparius*. *Toxicon* **2001**, *39*, 573–579.

(8) Bane, V.; Lehane, M.; Dikshit, M.; O'Riordan, A.; Furey, A. Tetrodotoxin: Chemistry, Toxicity, Source, Distribution, and Detection. *Toxins (Basel)* **2014**, *6*, 693–755.

(9) Williams, B. L.; Hanifin, C. T.; Brodie, E. D., Jr.; Caldwell, R. L. Ontogeny of Tetrodotoxin Levels in Blue-Ringed Octopuses: Maternal Investment and Apparent Independent Production in Offspring of *Hapalochlaena lunulata*. *J. Chem. Ecol.* **2011**, *37*, 10–17.

(10) Pratheepa, V.; Vasconcelos, V. Microbial Diversity Associated with Tetrodotoxin Production in Marine Organisms. *Environ. Toxicol. Pharmacol.* **2013**, *36*, 1046–1054.

(11) Nzoughet, J. K.; Campbell, K.; Barnes, P.; Cooper, K. M.; Chevallier, O. P.; Elliott, C. T. Comparison of Sample Preparation Methods, Validation of a UPLC–MS/MS Procedure for the Quantification of Tetrodotoxin Present in Marine Gastropods and Analysis of Pufferfish. *Food Chem.* **2013**, *136*, 1584–1589.

(12) Yang, C. C.; Han, K. C.; Lin, T. J.; Tsai, W. J.; Deng, J. F. An Outbreak of Tetrodotoxin Poisoning Following Gastropod Mollusc Consumption. *Hum. Exp. Toxicol.* **1995**, *14*, 446–450.

(13) Botana, L. M. *Seafood and Freshwater Toxins: Pharmacology, Physiology, and Detection*, 2nd ed.; CRC Press: Boca Raton, FL, 2008; Vol. *xvii*, p 941.

(14) Katikou, P.; Georgantelis, D.; Sinouris, N.; Petsi, A.; Fotaras, T. First Report on Toxicity Assessment of the Lessepsian Migrant Pufferfish *Lagocephalus sceleratus* (Gmelin, 1789) from European Waters (Aegean Sea, Greece). *Toxicon* **2009**, *54*, 50–55.

(15) Wu, Z.; Yang, Y.; Xie, L.; Xia, G.; Hu, J.; Wang, S.; Zhang, R. Toxicity and Distribution of Tetrodotoxin-Producing Bacteria in Puffer Fish *Fugu rubripes* Collected from the Bohai Sea of China. *Toxicon* **2005**, *46*, 471–476.

(16) Hwang, D. F.; Cheng, C. A.; Tsai, H. T.; Shih, D.; Ko, H. C.; Yang, R. Z.; Jeng, S. S. Identification of Tetrodotoxin and Paralytic Shellfish Toxins in Marine Gastropods Implicated in Food Poisoning. *Fish. Sci.* **1995**, *61*, 675–679.

(17) Tao, J.; Wei, W. J.; Nan, L.; Lei, L. H.; Hui, H. C.; Fen, G. X.; Jun, L. Y.; Jing, Z.; Rong, J. Development of Competitive Indirect ELISA for the Detection of Tetrodotoxin and a Survey of the Distribution of Tetrodotoxin in the Tissues of Wild Puffer Fish in the Waters of South-East China. *Food Addit. Contam., Part A* **2010**, *27*, 1589–1597.

(18) Zhou, Y.; Li, Y.; Lu, S.; Ren, H.; Li, Z.; Zhang, Y.; Pan, F.; Liu, W.; Zhang, J.; Liu, Z. Gold Nanoparticle Probe-Based Immunoassay as a New Tool for Tetrodotoxin Detection in Puffer Fish Tissues. *Sens. Actuators, B* **2010**, *146*, 368–372.

(19) O'Leary, M. A.; Schneider, J. J.; Isbister, G. K. Use of High Performance Liquid Chromatography To Measure Tetrodotoxin in Serum and Urine of Poisoned Patients. *Toxicon* **2004**, *44*, 549–553.

(20) Chen, X. W.; Liu, H. X.; Jin, Y. B.; Li, S. F.; Bi, X.; Chung, S.; Zhang, S. S.; Jiang, Y. Y. Separation, Identification, and Quantification of Tetrodotoxin and Its Analogs by LC–MS without Calibration of Individual Analogs. *Toxicon* **2011**, *57*, 938–943.

DOI: 10.1021/acs.jafc.5b00045
J. Agric. Food Chem. 2015, 63, 3129–3134

(21) Rodríguez, P.; Alfonso, A.; Otero, P.; Katikou, P.; Georgantelis, D.; Botana, L. M. Liquid Chromatography−mass Spectrometry Method To Detect Tetrodotoxin and Its Analogues in the Puffer Fish *Lagocephalus sceleratus* (Gmelin, 1789) from European Waters. *Food Chem.* **2012**, *132*, 1103−1111.
(22) McNabb, P. S.; Taylor, D. I.; Ogilvie, S. C.; Wilkinson, L.; Anderson, A.; Hamon, D.; Wood, S. A.; Peake, B. M. First Detection of Tetrodotoxin in the Bivalve *Paphies australis* by Liquid Chromatography Coupled to Triple Quadrupole Mass Spectrometry with and without Precolumn Reaction. *J. AOAC Int.* **2014**, *97*, 325−333.
(23) Cho, H. E.; Ahn, S. Y.; Son, I. S.; In, S.; Hong, R. S.; Kim, D. W.; Woo, S. H.; Moon, D. C.; Kim, S. Determination and Validation of Tetrodotoxin in Human Whole Blood Using Hydrophilic Interaction Liquid Chromatography Tandem Mass Spectroscopy and Its Application. *Forensic Sci. Int.* **2012**, *217*, 76−80.
(24) Fong, B. M.; Tam, S.; Tsui, S. H.; Leung, K. S. Development and Validation of a High-Throughput Double Solid Phase Extraction−Liquid Chromatography−Tandem Mass Spectrometry Method for the Determination of Tetrodotoxin in Human Urine and Plasma. *Talanta* **2011**, *83*, 1030−1036.
(25) Taylor, A. D.; Vaisocherová, H.; Deeds, J.; DeGrasse, S.; Jiang, S. Tetrodotoxin Detection by a Surface Plasmon Resonance Sensor in Pufferfish Matrices and Urine. *J. Sens.* **2011**, *2011*, 1−10.
(26) Tsai, Y. H.; Ho, P. H.; Hwang, C. C.; Hwang, P. A.; Cheng, C. A.; Hwang, D. F. Tetrodotoxin in Several Species of Xanthid Crabs in Southern Taiwan. *Food Chem.* **2006**, *95*, 205−212.
(27) Vaclavikova, M.; MacMahon, S.; Zhang, K.; Begley, T. H. Application of Single Immunoaffinity Clean-up for Simultaneous Determination of Regulated Mycotoxins in Cereals and Nuts. *Talanta* **2013**, *117*, 345−351.
(28) Senyuva, H. Z.; Gilbert, J. Immunoaffinity Column Clean-up Techniques in Food Analysis: A Review. *J. Chromatogr. B Analyt. Technol. Biomed. Life Sci.* **2010**, *878*, 115−132.
(29) Tsikas, D. Quantitative analysis of biomarkers, drugs and toxins in biological samples by immunoaffinity chromatography coupled to mass spectrometry or tandem mass spectrometry: A focused review of recent applications. *J. Chromatogr. B: Anal. Technol. Biomed. Life Sci.* **2010**, *878*, 133−148.
(30) Erlanger, B. F.; Borek, F.; Beiser, S. M.; Lieberman, S. Steroid−protein Conjugates. Ii. Preparation and Characterization of Conjugates of Bovine Serum Albumin with Progesterone, Deoxycorticosterone, and Estrone. *J. Biol. Chem.* **1959**, *234*, 1090−1094.
(31) Zhao, S.; Li, X.; Ra, Y.; Li, C.; Jiang, H.; Li, J.; Qu, Z.; Zhang, S.; He, F.; Wan, Y.; Feng, C.; Zheng, Z.; Shen, J. Developing and Optimizing an Immunoaffinity Cleanup Technique for Determination of Quinolones from Chicken Muscle. *J. Agric. Food Chem.* **2009**, *57*, 365−371.
(32) Delaunay, N.; Pichon, V.; Hennion, M. C. Immunoaffinity Solid-Phase Extraction for the Trace-Analysis of Low-Molecular-Mass Analytes in Complex Sample Matrices. *J. Chromatogr. B: Biomed. Sci. Appl.* **2000**, *745*, 15−37.
(33) Ngy, L.; Yu, C. F.; Takatani, T.; Arakawa, O. Toxicity Assessment for the Horseshoe Crab *Carcinoscorpius rotundicauda* Collected from Cambodia. *Toxicon* **2007**, *49*, 843−847.

DOI: 10.1021/acs.jafc.5b00045
J. Agric. Food Chem. 2015, 63, 3129−3134

Table 1. Composition of Multivitamin Preparations Found by qNMR and Recovery Values Respecting Labelling Information [mg/g][a]

sample		A	B1	B3	B5	B6	B9	C	E
S1 (tablet)		0.85	3.95	12.0	3.3	2.4	<LOD	38.5	9.0
S2 (caplet)		<LOD	3.7	17.5	4.9	1.0	0.25	58.0	17.0
S3 (capsule)		<LOD	4.3	73.0	14.5	5.4	<LOD	152	13.0
S4 (effervescent tablet)		<LOD	0.70	5.	1.7	1.1	0.10	29.5	3.2
S5 (effervescent tablet)		<LOD	0.20	2.9	1.2	0.3	<LOD	12.5	2.5
S6 (tablet)		0.15	1.4	12	3.3	1.1	<LOD	80.5	9.0
S7(effervescent tablet)		*b*	0.20	2.7	1.3	0.30	0.1	17.0	2.9
S8 (effervescent tablet)		*b*	0.25	3.4	1.4	0.35	0.10	16.0	3.2
S9 (tablet)		0.15	1.1	12.0	3.8	0.80	<LOD	48.0	9.0
S10 (ampule with vitamin B12)		*b*							
S11 (effervescent tablet)		*b*	0.15	2.8	1.0	0.20	0.05	13.5	2.3
S12 (lozenge tablet)		*b*	0.35	4.7	2.75	0.40	0.10	26.5	3.9
S13 (effervescent tablet)		*b*	0.30	4.7	1.8	0.35	0.10	19.0	1.9
recovery [%]	average	85	101	103	94	90	132	89	108
	minimum	119	132	114	121	126	171	126	134
	maximum	51	80	87	63	67	86	55	77

[a]Vitamin B2 was not detected due to its low solubility in methanol; vitamin B7 was not quantified due to spectral overlap; vitamins B12, D3, and K were not detected by NMR (below LOD). [b]Not detected by NMR and is not labeled by the manufacturer.

Apart from active ingredients (vitamins), a number of accompanying substances (sweeteners, acidifiers, and antioxidant agents) can be found in multivitamin preparations. The methods for their simultaneous quantification in this matrix were not reported so far. However, the nuclear magnetic resonance (NMR) method exists, for example, for quantification of some sweeteners in carbonated soft drinks or coenzyme Q10 in dietary supplements.[20,21]

Therefore, development of a fast, reliable, and precise analytical method for the determination of the majority of fat- and water-soluble vitamins as well as accompanying substances without a need for time-consuming sample preparation is desirable. In this study, a method based on NMR spectroscopy was proposed, which provides spectral information about all mixture constituents and opportunities to quantitative analysis using an internal standard. Previous studies have shown that NMR can successfully solve the task of multicomponent analysis of food and medicinal products; however, it has never been applied to multivitamin preparations.[22−24]

MATERIALS AND METHODS

Samples and Chemicals. A total of 16 different products were investigated. The samples including effervescent tablets (n = 6), tablets (n = 4), capsules (n = 1), caplets (n = 1), and ampules (n = 1) were randomly selected from local supermarkets in Cologne, Germany. Furthermore, three liquid multivitamin drinks based on orange juice concentrate and multivitamin direct juice were examined. The information about the samples is summarized in Table 1.

The deuterated solvents of 99.8% purity (methanol, chloroform, water, and dimethyl sulfoxide) were purchased from Euriso-top (Saarbrücken, Germany). The certified reference standards of retinol palmitate (vitamin A, >85%), nicotinamide (vitamin B3, >99.5%), and ascorbic acid (vitamin C, 99%) were obtained from Fluka Chemie; cobalamin (vitamin B12, >98%), cholecalciferol (vitamin D3, >98%), and α-tocopherol (vitamin E, >96%) were purchased from Sigma-Aldrich (Steinheim, Germany).

Thymol (99.5%), mannitol (99%), saccharin (>98%), and citric acid (99%) were provided by Sigma-Aldrich; cyclamate (99.8%) and butylhydroxytoluene (>99%) by Supelco (Bellefonte, Pennsylvania, USA); maleic acid and acesulfame K (>99%) by Fluka Chemie (Buchs, Switzerland); and phosphonoacetic acid (98.8%) by Alfa Aesar (Karlsruhe, Germany). The purity of all chemicals is shown in parentheses.

Sample Preparation. The content of investigated tablets and the capsules was first pulverized. For the standard sample preparation, 200 mg of the sample was weighed and mixed with 1 mL of thymol solution (1 mg/mL in MeOD). The resulting solution was centrifuged (2 min at 2000 rpm). The extract was carefully removed and placed in a separate flask. Two additional successive extractions with pure MeOD were conducted, and the liquid phases from each extraction step were combined with the first part. The resulting mixture was centrifuged, and an aliquot was then transferred in the NMR tube for direct measurements.

Stock solutions were prepared by weighing approximately 5 mg of reference compounds and dissolving this amount in 1 mL of MeOD. For spiking experiments, 10−20 μL of each standard solution was separately added to the methanol extract prepared according to the standard scheme.

To investigate the stability of ascorbic acid in solution, the methanol extract of sample S4 was measured 10 times with 5 h intervals while staying in the autosampler. Additionally, reference ascorbic acid solution (30 mg/mL in MeOD) was measured before and after staying in a drying oven at 70 °C for 24 h to accelerate the degradation reaction.

To model the composition of sample S4, the defined amounts of vitamins B3, C, and E were directly weighed and mixed with 200 μL of aliquot of each of the separately prepared stock solutions of vitamins A, B1, B5, B6, B7, B9, B12, D3, E, and K. Afterward, thymol solution in methanol (1 mg/mL) was added to the mixture. The composition of this artificial mixture corresponds to that of sample S4 except for the presence of accompanying compounds.

NMR Measurements. NMR measurements were performed on Bruker Avance III 500/600 MHz spectrometers (Bruker Biospin, Rheinstetten, Germany) with BBO Prodigy cryo/QNP cryo probes equipped with Bruker Automatic Sample Changer (B-ACS 120). ^{1}H NMR spectra were recorded using a standard 1D pulse sequence with 30° flip angle. One hundred twenty-eight scans and 4 prior dummy scans of 131k points were acquired with a spectral width of 24.0258 ppm, a receiver gain of 9, and an acquisition time of 5.4525952 s. The relaxation delay was 1.0 s, which was sufficient for accurate quantification of vitamins. The data were acquired automatically under the control of ICON-NMR (Bruker Biospin, Rheinstetten, Germany). All NMR spectra were phased, baseline-corrected, and manually integrated using Topspin 3.1 (Bruker Biospin, Rheinstetten, Germany).

DOI: 10.1021/acs.jafc.5b00087
J. Agric. Food Chem. 2015, 63, 3135−3143

Quantification and Validation Studies. The NMR signals of vitamins in the samples were assigned using spectra of reference compounds and spiked solutions. Baseline-separated peaks (i.e., peaks not overlapped or interfered with by a matrix) of each substance were selected for integration.

For quantification, the well-known equation was utilized, which includes molar weight, integral, number of protons of reference compound (thymol) and analytes (vitamins), and purity and concentration of the reference compound.[25] The quantity of targeted substances is calculated by integrating a particular signal of interest and signal of thymol at δ 6.57 ppm, which corresponds to two protons.

Validation was performed for vitamins and not for accompanying substances. The limits of detection (LODs) and the limits of quantification (LOQs) were defined as signals with signal-to-noise ratios (SNRs) of 3 and 6, respectively. The average values were calculated using six separately prepared sample extracts (sample S4). SNR of 1D spectra was calculated according to the formula SNR = maxval/(2·noise), where maxval is the highest spectral intensity in the spectral region. The noise is computed from the data points in the defined frequency range. The limits of noise and signal regions were located close to each other and were set manually for each spectrum. The noise regions were approximately 0.2 ppm wide, where no real matrix signal was observable.

To assess repeatability, six separate standard sample preparations were performed for one sample and measured within a short period of time. To estimate linearity, the standard extraction procedure was conducted three times for the sample weight of 140 mg (70%), 200 mg (100%), and 260 mg (130%). The recovery rates were ascertained by adding standard solutions at four different concentrations (0%, 37.5%, 75%, 112.5%, and 150% of the labeled content for each vitamin) to a real sample (S4). The recovery rates were additionally estimated using the artificial mixture of all vitamins, whose concentrations exactly coincide with the labeling information for sample S4.

RESULTS AND DISCUSSION

Rationale of NMR Analysis of Vitamins. To be competitive with existing chromatographic methods, a new NMR method has to be characterized by simple sample preparation and fast acquisition time, and, therefore, be suitable for routine analysis with high throughput. However, as many fat- and water-soluble vitamins as possible should be simultaneously analyzed. For the method development, an effervescent tablet (sample S4) was used, which can be considered as a representative sample for our data set because it contains both fat- and water-soluble vitamins (Table 1).

Table 2. NMR Integration Regions Used for Quantification and Validation Studies (δ, Multiplicity, Number of Protons)[a]

compound	main signal	alternative signal[b]
vitamin A	1.02 (s, 1)	1.90 (s, 3)
vitamin B1	5.50 (s, 3)	8.15 (s, 3)
vitamin B3	8.30 (tt, 1)	
vitamin B5	0.91 (s, 6)	
vitamin B6	4.67 (s, 2)	8.04 (s, 1)
vitamin B7	2.31 (t, 2)	
vitamin B9	6.73 (d, 2)	
vitamin B12	0.45 (s, 3)	
vitamin C	4.79 (s, 1)	
vitamin D3	0.55 (s, 6)	
vitamin E	2.31 (s, 3)	
vitamin K	0.81 (d, 6)	
citric acid	2.80−2.74 (AB, 2)	
mannitol	3.84−3.76 (m, 2)	
saccharin	8.10−7.90 (m, 4)	
sodium cyclamate	1.78−1.68 (m, 2)	
butylhydroxytoluene (BHT)	6.93−6.91 (s, 2)	
steviol glycoside[c]	4.68−4.65 (d, 1)	

[a]Related to the main signal for quantification and standard sample preparation. [b]Used for quantification in the case of overlap of the main signal. [c]The sum of steviol glycosides was calculated.

Selection of Solvent, Internal Standard, and Optimization of the Extraction Procedure. The most important requirement for the solvent utilized in the NMR method is the complete solubility of the investigated analytes in it. In our case, most of vitamins regardless of their physical properties have to be extracted by the optimal solvent without heating of the samples. The NMR signals of extracted compounds selected for quantification should be stable and not overlap with each other.

During the method optimization, different deuterated solvents (pure D_2O, MeOD, $CDCl_3$, and DMSO) and their mixtures (DMSO-$CDCl_3$ (1:4), MeOD/D_2O (1:1), MeOD/D_2O (3:1), MeOD/DMSO (1:1), and D_2O/MeOD/$CDCl_3$ (1:1:2)) were tested. It was observed that the majority of vitamins can be extracted using ternary mixture D_2O/MeOD/$CDCl_3$. The advantage of this solvent mixture is that the signals of water- and fat-soluble vitamins were separately observed in polar and nonpolar phases after centrifugation (except vitamin B3, which was found in both phases). Therefore, the matrix effect can be minimized. However, we decided to utilize MeOD as a solvent for routine analysis due to better phase separation, lower extraction, and acquisition time.

During optimization, the sample weight was varied between 100 mg and 250 mg using methanol as a solvent for extraction. We have found that 200 mg is the optimum value because the smaller initial sample weight did not provide the required sensitivity for quantification, while bigger ones led to the saturation of the sample solutions.

For the development of quantitative procedure, 100% extraction of all compounds has to be ensured. The second methanol extraction resulted in an additional yield of approximately 14% of vitamins compared to that of the first extraction step. Additionally, the precipitation resulted after three successive extractions of sample S4 mixed with MeOD and was analyzed. In this experiment, signals of vitamins had approximately the same height as ^{13}C satellites of niacin after the three-step extraction. It means that the addition uncertainty resulting from the extraction procedure is about 1%. Therefore, three successive extractions were considered to be enough to achieve almost complete extraction of vitamins.

In qNMR, it is important to select an appropriate reference compound (internal standard) for calculating the concentration of all analytes. Among the main requirements for the choice of a particular compound are low costs and high purity, together with its stability and inertness. It should also be nonvolatile, nonhygroscopic, and soluble in the selected NMR solvent. The signal of an ideal internal standard should not overlap with other signals and preferably be a singlet with low relaxation time.[25,26] A number of internal standards were tested during our preliminary experiments. Phosphonoacetic acid was rejected because its signals overlap with those of citric acid present in multivitamin preparations in the δ 2.84−2.79 ppm range. Maleic acid that shows an undisturbed singlet at δ 6.33 ppm was also found unsuitable for quantification purposes because after its addition to an authentic sample, several new signals in the δ 6.45−6.05 ppm range appeared in the spectrum due to an unknown reaction. Thymol was chosen as an

DOI: 10.1021/acs.jafc.5b00087
J. Agric. Food Chem. 2015, 63, 3135−3143

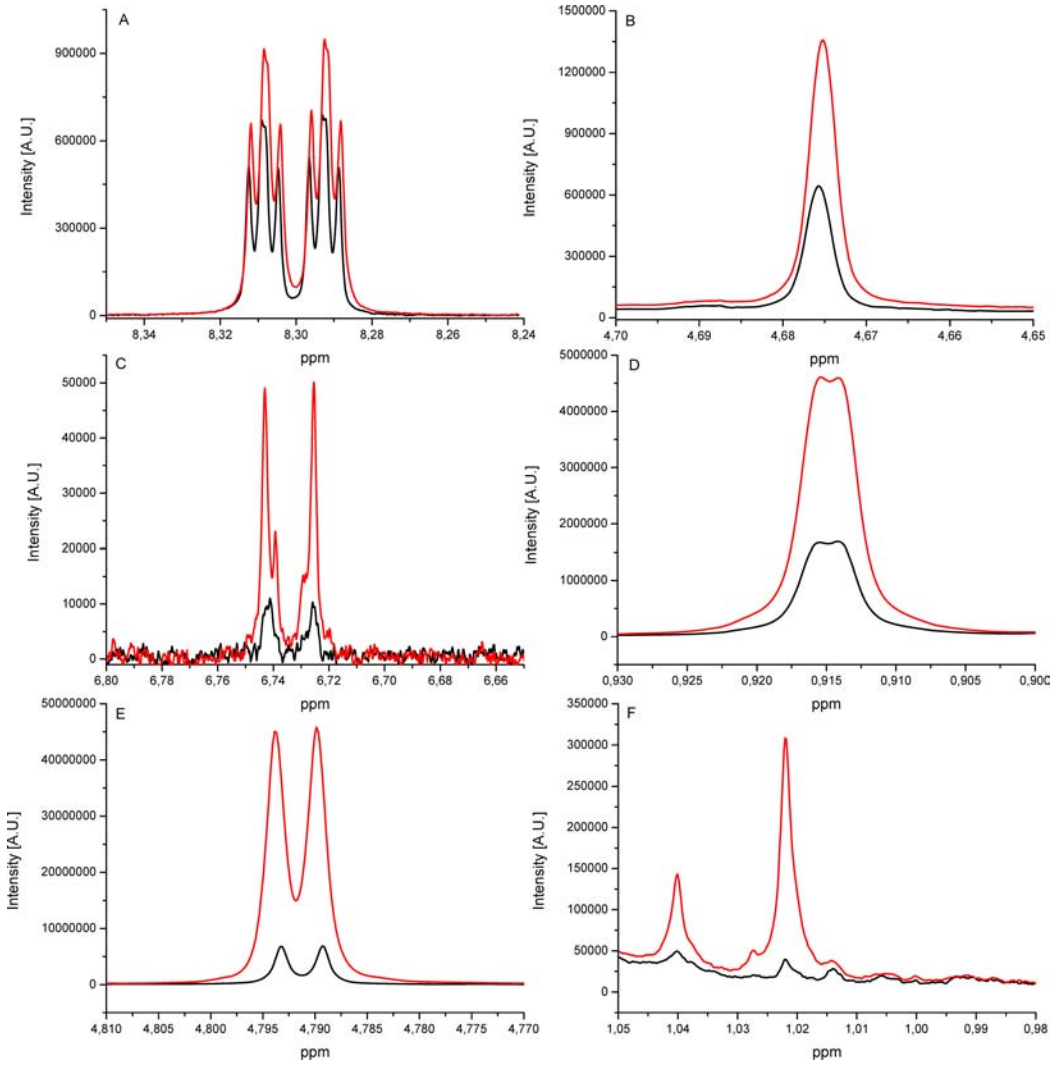

Figure 1. NMR resonances of vitamins B3 (A), B6 (B), B9 (C), B5 (D), C (E), and A (F) in multivitamin preparation (S4) and its spiked solutions. Spiked amounts were 100 μg for all vitamins except vitamin A (50 μg) and vitamin C (undefined amount).

appropriate internal standard for quantification. This compound has a signal at δ 6.57 ppm derived from two protons of the molecule.

NMR Ranges for the Quantification of Vitamins and Accompanying Substances. The NMR peaks together with their multiplicity and the number of protons selected for quantification for each analyte are given in Table 2. For vitamins A, B1, and B6, alternative peaks were defined for their quantification in case of the overlap of the main signal. Figures 1 and 2 showed some examples of the defined NMR regions for vitamins. It can be concluded that vitamins B5, B12, D3, and K1 have signals in the δ 0.81−0.45 ppm region, which is particularly suitable for identification and quantification by NMR spectroscopy due to the absence of other signals. However, the contents of vitamins K1 and D3 were too low in our samples to be detected by NMR (Figure 2). Other substances showed suitable signals in the δ 6.0−1.0 ppm region (A, B1, B6, C, and E). Vitamins B3 and B9 can be differentiated in the low-field NMR region. Unfortunately, it was only possible to provide qualitative analysis of vitamin B7 in multivitamin preparations due to signal overlap (Figure 2). The NMR analysis of only vitamin B2 was impossible because of its insolubility in methanol.

Alternatively to the qNMR approach, multivariate calibration methods, e.g., partial least-squares (PLS) regression could be used to improve quantification results because several peaks of each substance (including those with spectral overlap) can be simultaneously evaluated. However, this will require time-consuming reference analysis of all studied vitamins. In our case, the specific undisturbed signal was identified for each analyte of interest; therefore, direct NMR quantification was preferable in this case (Table 2).

Apart from vitamins, a number of accompanying substances were detected in NMR spectra of multivitamin preparations. The identification of citric acid, mannitol, saccharin, sodium cyclamate, and the sum of steviol glycosides and butylhydroxytoluene was performed using its specific signals (Table 2). As these substances are contained in relatively high concentrations in multivitamin preparations and show undisturbed NMR signals (Figure 3), their quantification was also possible based on the qNMR approach (Table 3).

Validation Studies. Table 4 provides validation results for the investigated vitamins. In particular, the LODs were found between 9.0 mg/kg for vitamin A and 77.0 mg/kg for vitamin B3. LOQ values varied between 18.0 mg/kg and 153.5 mg/kg. Intermediate LOQ values were found for vitamin B6 (34.5 mg/

DOI: 10.1021/acs.jafc.5b00087
J. Agric. Food Chem. 2015, 63, 3135−3143

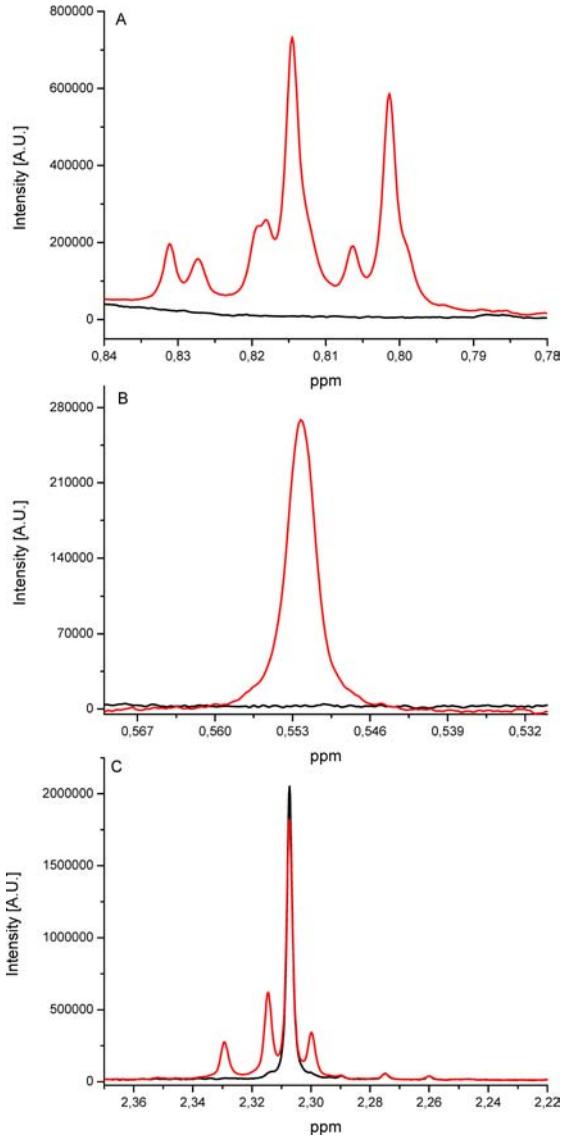

Figure 2. NMR resonances of vitamins K (A), D (B), and B7 (C) in multivitamin preparation (S4) and its spiked solutions. Spiked amounts were 100 μg in all cases.

kg) and vitamin C (93.5 mg/kg). All values were calculated for the 200 mg sample weight. The reference values for the daily vitamin requirement provided by the US Food and Drug Administration are shown in Table 4 for comparison.[27] Taking into account the vitamin contents in multivitamin preparations, we observed that LOD/LOQ values are sufficient to quantify major vitamins by NMR (Table 4).

Validation of the NMR method was further conducted by repeated sample preparation of sample S4 (n = 6, intraday validation). The concentrations obtained by the qNMR method were summarized, and repeatability values expressed as CVs were calculated. Table 4 showed that CVs ranged between 0.9% for vitamin B3 and 12% for vitamin A. The relatively high CV of 12% for vitamin A is due to spectral overlap that leads to impossibility of obtaining a baseline-separated signal. The comparably high CV value for vitamin B9 (6.4%) can be explained by its small concentration in the sample. In other cases (except vitamins A and B9), the repeatability never exceeded 6%, which also showed the reliable quantification of the developed qNMR method (Table 4). The EU legislation allows tolerances for vitamins in foods from minus 50% up to plus 35%; therefore, even the highest errors are acceptable.[28] It should be noted that, in general, better repeatability can be achieved with a concentrated sample solution, where a better SNR can be obtained. However, an authentic sample (S4) was used to estimate practically meaningful validation characteristics.

Furthermore, linear ranges were established for three different sample weights (140 mg, 200 mg, and 260 mg) using in-house calibration curves (concentration versus integral value related to the IS integral) for all investigated substances. The standard deviations for three different sample weights showed that the best repeatability between 1.5% and 5.3% was obtained for the 200 mg sample weight for the majority of vitamins (E, C, B1, and B5). On the contrary, comparable but better values were found for the higher sample weight (260 mg) for vitamins A and B3 and for the smallest sample weight (140 mg) for vitamin B6. These results also confirmed our choice of 200 mg as the optimum sample weight. The ^{1}H NMR spectra showed linearity in the defined concentration ranges (70−140%). The regression coefficients of the calibration curves varied between 0.962 and 0.997 for vitamins B1 and B3, respectively. The worst correlation coefficient (R = 0.918) was obtained for vitamin A due to spectral overlap and the low intensities leading to the big uncertainties in integrals values for this compound. Additionally, spiking solutions at four different concentrations (0%, 37.5%, 75%, 112.5%, and 125% of the labeled amount for each vitamin) were used to ascertain the vitamin content in an authentic sample.

The contents of vitamins B1 and B9 in the spiked sample were found to be 0.83 mg/g and 1.1 mg/g using the standard addition approach, which correspond to the recovery values of 96% and 92%, respectively, with respect to the declared amounts. However, worse recoveries were found for vitamin A (0.06 mg/g was found; 250% recovery), B9 (0.21 mg/g was found; 135% recovery), and B5 (2.73 mg/g was found; 142% recovery) probably due to incomplete solubility of reference compounds in methanol, low SNR, or erroneous labeling information.

Furthermore, qNMR analysis was performed for the artificial vitamin mixture, whose composition coincides with that of sample S4. Acceptable recovery rates were found for vitamins B1 (88%), B3 (100%), B5 (89%), B6 (96%), B9 (86%), and C (93%). The insufficient recoveries for vitamin A (38%), E (61%), and K (32%) can be explained by difficulties in weighing the viscous reference substances.

Stability of Ascorbic Acid in Multivitamin Preparations. It was observed that ascorbic acid was not stable in samples prepared according to our standard procedure. Its main peak at δ 4.76 ppm selected for quantification gradually degrades within 100 h (Figure 4A). The same effect was monitored for the ascorbic acid signals at δ 3.91 ppm, δ 3.67 ppm, and δ 3.32 ppm. At the same time, several multiples appeared in the range of δ 4.5−4.0 ppm (Figure 4B).

It is known that equilibrium exists in solutions between ascorbic acid and its first oxidation product, dehydroascorbic acid (DHAA), which undergoes hydrolysis with the formation of 2,3-diketogulonic acid.[29−31] Some additional products can be formed by further reactions in complex matrixes such as fruit juice or wine.[30,31] In our case, linear dependency was observed between the integral values of the ascorbic acid signal at δ 4.76 ppm and the DHAA peak at δ 4.50 ppm with the correlation coefficient of −0.97. The equilibrium is achieved in solution

DOI: 10.1021/acs.jafc.5b00087
J. Agric. Food Chem. 2015, 63, 3135−3143

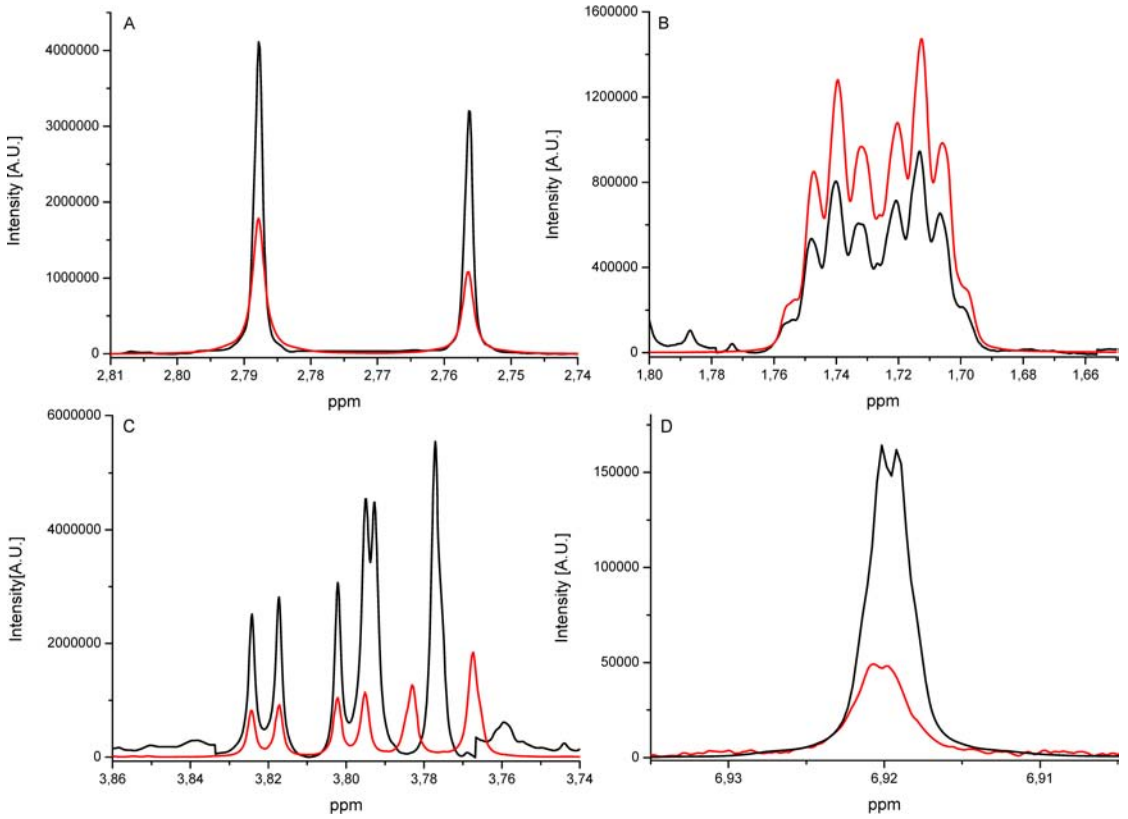

Figure 3. NMR resonances of citric acid (A), cyclamate (B), mannitol (C), and BHT (D) in multivitamin preparation S4 (black) and standard solutions (red).

Table 3. Contents of Accompanying Substances in Investigated Multivitamin Preparations and Amounts Found by qNMR [mg/g]

sample	citric acid	mannitol	saccharin	cyclamate	BHT	steviol glycoside[b]
S1 (tablet)	*a*					
S2 (caplet)	*a*					
S3 (capsule)	*a*	*a*	*a*	*a*	0.20	*a*
S4 (effervescent tablet)	485	16.0	0.70	8.5	0.05	*a*
S5 (effervescent tablet)	510	*a*	0.75	4.0	*a*	*a*
S6 (tablet)	*a*	*a*	*a*	*a*	0.05	*a*
S7(effervescent tablet)	510	*a*	*a*	*a*	*a*	5.0
S8 (effervescent tablet)	540	*a*	1.3	2.8	*a*	*a*
S9 (tablet)	*a*	*a*	*a*	*a*	0.05	*a*
S10 (ampule with vitamin B12)	*a*	22.0	*a*	*a*	*a*	*a*
S11 (effervescent tablet)	505	*a*	*a*	*a*	*a*	4.4
S12 (lozenge tablet)	70	*a*	*a*	*a*	*a*	*a*
S13 (effervescent tablet)	405	*a*	0.35	2.0	*a*	*a*

[a]Not detected by NMR and is not labeled by the manufacturer. [b]The sum of steviol glycosides was calculated.

after 100 h after sample preparation, and afterward, no changes in integral values were observed. The time course of the degradation reaction can be observed in NMR spectra of an authentic sample. The peak at δ 4.76 ppm belongs to ascorbic acid, whereas the signals in the 4.5−4.0 ppm region can be explained by the presence of different degradation products of ascorbic acid such as DHAA and 2,3-diketogulonic acid (Figure 4B). DHAA has been also previously detected in herbal formulations by ^{1}H NMR.[32] This compound showed resonances at δ 4.58 ppm, δ 4.43 ppm, δ 4.21 ppm, and δ 4.05 ppm in the CD_3CN:D_2O mixture, which is in good agreement with our results (Figure 4B).

The existing equilibrium of ascorbic acid in the multivitamin preparation is complicated due to the presence of other matrix compounds. Indeed, it was shown that the metal ions (e.g., Cu, Fe) present in multivitamin preparations can act as catalysts.[29,31] However, ascorbic acid solution can be stabilized in the presence of citric acid used as an acidifier in our samples.[29] Unambiguous assignment of all substances existing in solution requires the use of 2D NMR experiments, which was not a primary goal of this study.

Clearly, the appearance of degradation products of ascorbic acid influences the accuracy of its quantification. Because of the complexity of the matrix, we did not try to stabilize solutions similar to what has been recently done for acrolein in alcoholic

DOI: 10.1021/acs.jafc.5b00087
J. Agric. Food Chem. 2015, 63, 3135−3143

Table 4. Validation Results for Selected Vitamins Using NMR[a]

vitamin	LOD [mg/kg]	LOQ [mg/kg]	CV [%]	reference daily intake [mg][27]
A	9.0	18.0	12	1.5
B1	47.5	95.0	5.6	1.5
B3	77.0	153	0.9	20
B5	23.0	46.0	4.2	5.0
B6	17.5	34.5	5.6	2.0
B9	71.0	143	6.4	0.4
C	46.5	93.5	1.8	60
E	22.5	45.0	2.0	15

[a]Related to the main signal for quantification (see Table 2) and standard sample preparation with three successive extractions.

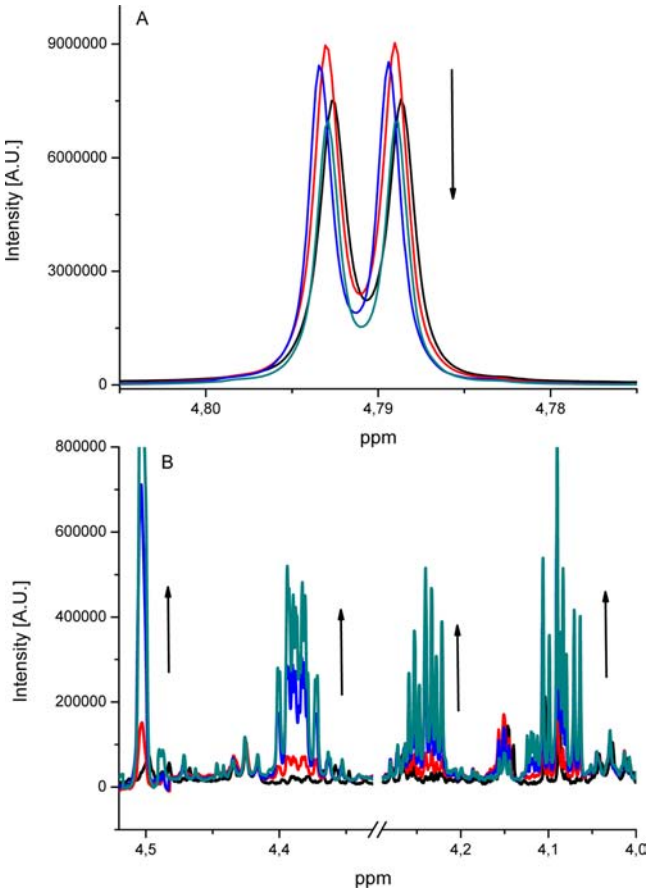

Figure 4. Signals of ascorbic acid (A) and its degradation products (B) in the NMR spectrum of the sample S4 while placed in an NMR autosampler for 100 h (four points at 0, 2, 15, 100 h are shown). The arrows show the direction of intensity change during the reaction.

beverages.[33] The multivitamin preparations have to be measured directly after extraction, where the percentage of degradated ascorbic acid is negligible.

Application to Authentic Samples. The final goal of each method development is its applicability to the broad range of matrixes. Therefore, our data set included different kinds of multivitamin preparations, namely, tablets, capsules, caplets, effervescent tablets, and liquid samples (Table 1). Contrary to tablets and capsules that usually contain high doses of both water- and fat-soluble vitamins, effervescent tablets are characterized by smaller amounts of water-soluble vitamins in the absence of fat-soluble vitamins. These products, however,

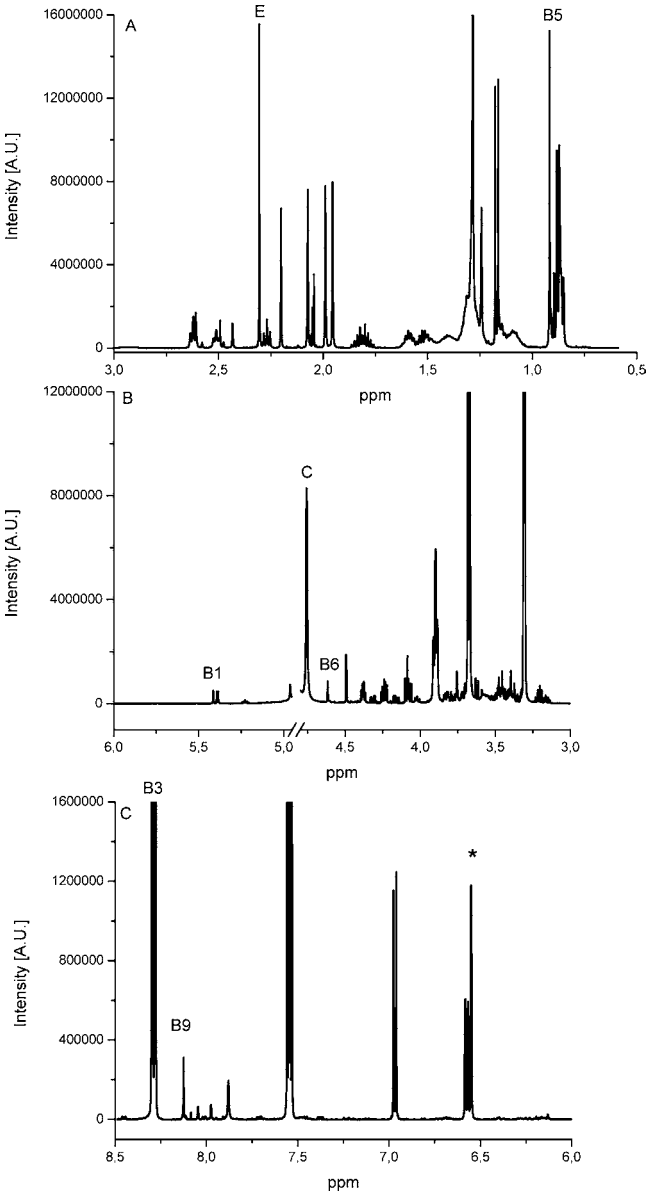

Figure 5. Detailed NMR spectrum of sample S2. The peaks of each individual vitamin and internal standard (*) used for quantification are depicted on the spectrum. The calculated vitamin contents can be found in Table 1

are rich in accompanying substances such as sweeteners. Another matrix studied was liquid samples, e.g., fruit juices enriched with vitamins and syrups containing sweeteners, stabilizers, preservatives, thickening agents, and oils. The method development for these kinds of samples was complicated by their viscosity and high liquid content, which result in difficulties in weighing and in the appearance of a broad water signal in ^{1}H NMR spectra. Actually, another sample preparation procedure has to be developed for this group of matrixes.

The NMR results for 13 investigated samples are summarized in Table 1 for vitamins and in Table 3 accompanying substances. As an example, Figure 5 shows the detailed NMR spectra of an authentic sample (S2). First, it can be seen that NMR provided reliable qualitative analysis of all vitamins. For example, vitamin A was not detected in six samples, which was in agreement with the labeling information.

DOI: 10.1021/acs.jafc.5b00087
J. Agric. Food Chem. 2015, 63, 3135−3143

However, in some samples NMR was not able to detect vitamins A and B9 due to small concentrations of these substance (LOD values are listed in Table 4).

The results of quantitative analysis showed a broad variation of vitamin content in the investigated samples ranging from 0.30 mg/g to 42.5 mg/g on average for vitamins A and C, respectively (Table 1). Furthermore, the NMR concentrations were compared with the information provided on the label by the manufacturer. Good average recovery rates were found for vitamins B1 (101%), B3 (103%), B5 (94%), B6 (90%), C (93%), and E (108%). That means that NMR is a reliable analytical tool for quantification of these compounds in multivitamin preparations. Worse recoveries for vitamins A (85%) and B9 (132%) can be explained by their small concentrations (near the LODs) in the products studied, which result in large uncertainties in integral values. The errors were, however, acceptable in accordance with the official guideline for food products.[28]

Vitamin B12 was found in sample S10 (ampule with vitamin B12), and its concentration was in very good agreement with the labeled content (87.5 mg/kg compared to 100 mg/kg provided on the label), which shows that NMR is suitable for the analysis of B12-rich multivitamin preparations. In other samples, vitamin B12, however, cannot be detected due to its small content in comparison with that of other vitamins.

It should be mentioned that the observed deviations cannot lead to a conclusion of inapplicability of NMR for the analysis of these vitamins. Indeed, the labeling information cannot be considered as real reference data. The deviations between declared and found values can be a result of the sample inhomogeneity or erroneous labeling information. The reference analysis should be conducted to make comprehensive evaluation of the accuracy of the NMR method.

Selected accompanying compounds were also quantified in the multivitamin preparations (Table 3). Citric acid was detected in 7 of 13 samples (the content varied between 70 mg/g and 540 mg/g), saccharin (0.35−1.25 mg/g), sodium cyclamate (2.0−2.80 mg/g), and BHT (0.05−0.20 mg/g) in four samples. Steviol glycosides and mannitol were found only in two investigated multivitamin preparations (Table 3). In all other samples, investigated accompanying compounds were not detected, and this was in accordance with the labeling information (Table 3).

Comparison with Previous Studies and Future Perspective. This study is the first to show the feasibility of qNMR for simultaneous analysis of 12 essential vitamins (except B2) and accompanying substances (citric acid, mannitol, saccharin, cyclamate, steviol glycoside, and BHT) in complex multivitamin preparations. This includes effervescent tablets, coated tablets, caplets, and capsules. Juices and syrups, however, cannot be analyzed by the present method due to their specific physical properties. The total analysis time including sample preparation, measurements, spectra evaluation requires approximately 1 h and, therefore, can be used as an alternative to existing HPLC methods.

Regarding quantification analysis, it is possible to reliably determine 5 of 13 vitamins, namely, B1, B3, B5, B6, and E. Although ascorbic acid is the most abundant compound in the studied products, its determination sometimes leads to incorrect values due to degradation reactions (mainly, oxidation) taking place in solution. Accordingly, for more accurate quantification, NMR measurements have to be conducted directly after sample preparation. Vitamins A, B9, B12, D3, and K are usually present in multivitamin preparations in low quantities; therefore, their quantitative analysis can be accompanied by relatively high uncertainty. A number of accompanying substances can be additionally quantified from the same NMR spectrum.

Previous studies on vitamins using NMR spectroscopy were restricted to qualitative analysis and signal assignments of separate vitamin molecules. For example, 1D and 2D NMR were applied to distinguish among α-, β-, γ-, δ- tocopherols (vitamin E) and to estimate the purity of reference materials using benzoic acid as an internal standard.[34] Multinuclear solid-state NMR methods (^{59}Co, ^{13}C, ^{15}N, and ^{31}P NMR) were applied for structural and dynamic analysis of different polymorphs of cyanocobalamin (vitamin B12).[35] Another solid state NMR study was devoted to the characterization of four vitamin D compounds.[36] Vaysse et al. using ^{1}H NMR have identified different vitamins (B-group, C, and E) as accompanying ingredients in herbal medicines or dietary supplements marketed as natural slimming products.[32] The authors, however, did not perform quantitative analysis of vitamins.[32]

Further research should be conducted toward more precise NMR method validation including comparison with the results of a reference method and additional spiking experiments to establish the correction factors for quantitation of some vitamins. Finally, some efforts can be made to improve the LOD values by using solvent evaporation at low temperatures and dimmed light in order to preserve unstable vitamins.

AUTHOR INFORMATION

Corresponding Author

*Tel: +49 02236 969470. Fax: +49 02236 9694711. E-mail: diehl@spectralservice.de.

Notes

The authors declare no competing financial interest.

REFERENCES

(1) Petroczi, A.; Taylor, G.; Naughton, D. P. Mission impossible? Regulatory and enforcement issues to ensure safety of dietary supplements. *Food Chem. Toxicol.* **2011**, *49*, 393−402.

(2) Chatzimichalakis, P. F.; Samanidou, V. F.; Papadoyannis, I. N. Development of a validated liquid chromatography method for the simultaneous determination of eight fat-soluble vitamins in biological fluids after solid-phase extraction. *J. Chromatogr., B* **2004**, *805*, 289−296.

(3) Cuerq, C.; Peretti, N.; Chikh, K.; Mialon, A.; Guillaumont, M.; Drai, J.; Blond, E. Overview of the in vitro stability of commonly measured vitamins and carotenoids in whole blood. *Ann. Clin. Biochem.* **2015**, *52*, 259−269.

(4) Loitsch, S. M.; Reuter, K. C.; Oremek, G. M.; Wetzstein, R.; Stangl, K.; Armbruster, F. P.; Dschietzig, T. B.; Stein, J. Comparison of a new microbiological assay with a standard high-performance liquid chromatographic method for determination of vitamin B6 in serum. *Clin Lab.* **2014**, *60*, 1035−1041.

(5) Blake, C. J. Analytical procedures for water-soluble vitamins in foods and dietary supplements: a review. *Anal. Bioanal. Chem.* **2007**, *389*, 63−76.

(6) Márquez-Sillero, I.; Cárdenas, S.; Valcárcel, M. Determination of water-soluble vitamins in infant milk and dietary supplement using a liquid chromatography on-line coupled to a corona-charged aerosol detector. *J. Chromatogr., A* **2013**, *1313*, 253−258.

(7) Jin, P.; Xia, L.; Li, Z.; Che, N.; Zou, D.; Hu, X. Rapid determination of thiamine, riboflavin, niacinamide, pantothenic acid, pyridoxine, folic acid and ascorbic acid in vitamins with minerals

DOI: 10.1021/acs.jafc.5b00087
J. Agric. Food Chem. 2015, 63, 3135−3143

tablets by high-performance liquid chromatography with diode array detector. *J. Pharm. Biomed. Anal.* **2012**, *70*, 151−157.
(8) Maráková, K.; Piestanský, J.; Havránek, E.; Mikus, P. Simultaneous analysis of vitamins B in pharmaceuticals and dietary supplements by capillary electrophoresis hyphenated with triple quadrupole mass spectrometry. *Pharmazie* **2014**, *69*, 663−668.
(9) Mohamed, A. M.; Mohamed, H. A.; Abdel-Latif, N. M.; Mohamed, M. R. Spectrofluorimetric determination of some water-soluble vitamins. *J. AOAC Int.* **2011**, *94*, 1758−1769.
(10) Shabangi, M.; Sutton, J. A. Separation of thiamin and its phosphate esters by capillary zone electrophoresis and its application to the analysis of water-soluble vitamins. *J. Pharm. Biomed. Anal.* **2005**, *38*, 66−71.
(11) Serni, E.; Audino, V.; Del Carlo, S.; Manera, C.; Saccomanni, G.; Macchia, M. Determination of water-soluble vitamins in multivitamin dietary supplements and in artichokes by micellar electrokinetic chromatography. *Nat. Prod. Res.* **2013**, *27*, 2212−2215.
(12) Chatzimichalakis, P. F.; Samanidou, V. F.; Papadoyannis, I. N. Development of a validated liquid chromatography method for the simultaneous determination of eight fat-soluble vitamins in biological fluids after solid-phase extraction. *J. Chromatogr., B* **2004**, *805*, 289−296.
(13) Olędzka, I.; Kowalski, P.; Bałuch, A.; Bączek, T.; Paradziej-Łukowicz, J.; Taciak, M.; Pastuszewska, B. Quantification of the level of fat-soluble vitamins in feed based on the novel microemulsion electrokinetic chromatography (MEEKC) method. *J. Sci. Food Agric.* **2014**, *94*, 544−551.
(14) Turne, C.; King, J. W.; Mathiasson, L. Supercritical fluid extraction and chromatography for fat-soluble vitamin analysis. *J. Chromatogr., A* **2001**, *936*, 215−237.
(15) Tayade, A. B.; Dhar, P.; Kumar, J.; Sharma, M.; Chaurasia, O. P.; Srivastava, R. B. Sequential determination of fat- and water-soluble vitamins in *Rhodiola imbricata* root from trans-Himalaya with rapid resolution liquid chromatography/tandem mass spectrometry. *Anal. Chim. Acta* **2013**, *789*, 65−73.
(16) Yamada, H.; Kitagawa, S.; Ohtani, H. Simultaneous separation of water- and fat-soluble vitamins in isocratic pressure-assisted capillary electrochromatography using a methacrylate-based monolithic column. *J. Sep. Sci.* **2013**, *36*, 1980−1985.
(17) Monakhova, Y. B.; Mushtakova, S. P.; Kolesnikova, S. S.; Astakhov, S. A. Chemometrics-assisted spectrophotometric method for simultaneous determination of vitamins in complex mixtures. *Anal. Bioanal. Chem.* **2010**, *397*, 1297−1306.
(18) Mohamed, A. M.; Mohamed, H. A.; Mohamed, N. A.; El-Zahery, M. R. Chemometric methods for the simultaneous determination of some water-soluble vitamins. *J. AOAC Int.* **2011**, *94*, 467−481.
(19) Taguchi, K.; Fukusaki, E.; Bamba, T. Simultaneous analysis for water- and fat-soluble vitamins by a novel single chromatography technique unifying supercritical fluid chromatography and liquid chromatography. *J. Chromatogr., A* **2014**, *1362*, 270−277.
(20) Maes, P.; Monakhova, Y. B.; Kuballa, T.; Reusch, H.; Lachenmeier, D. W. Qualitative and quantitative control of carbonated cola beverages using ^{1}H NMR spectroscopy. *J. Agric. Food Chem.* **2012**, *60*, 2778−2784.
(21) Monakhova, Y. B.; Ruge, I.; Kuballa, T.; Lerch, C.; Lachenmeier, D. W. Rapid determination of coenzyme Q10 in food supplements using ^{1}H NMR spectroscopy. *Int. J. Vitam. Nutr. Res.* **2013**, *83*, 67−72.
(22) Holzgrabe, U. Quantitative NMR spectroscopy in pharmaceutical applications. *Prog. Nucl. Magn. Reson. Spectrosc.* **2010**, *56*, 229−240.
(23) Monakhova, Y. B.; Schütz, B.; Schäfer, H.; Spraul, M.; Kuballa, T.; Hahn, H.; Lachenmeier, D. W. Validation studies for multi-component quantitative NMR analysis: the example of apple fruit juice. *Accredit. Qual. Assur.* **2014**, *19*, 17−29.
(24) Skiera, C.; Steliopoulos, P.; Kuballa, T.; Diehl, B.; Holzgrabe, U. Determination of free fatty acids in pharmaceutical lipids by 1H NMR and comparison with the classical acid value. *J. Pharm. Biomed. Anal.* **2014**, *93*, 43−50.
(25) Bharti, S. K.; Roy, R. Quantitative 1H NMR spectroscopy. *Trends Anal. Chem.* **2012**, *35*, 5−27.
(26) Cullen, C. H.; Ray, G. J.; Szabo, C. M. A comparison of quantitative nuclear magnetic resonance methods: internal, external, and electronic referencing. *Magn. Reson. Chem.* **2013**, *51*, 705−713.
(27) U.S. Food and Drug Administration. Guidance for Industry: A Food Labeling Guide (14. Appendix F: Calculate the Percent Daily Value for the Appropriate Nutrients), 2013. http://www.fda.gov/Food/GuidanceRegulation/GuidanceDocumentsRegulatoryInformation/LabelingNutrition/ucm064928.htm.
(28) European Commission. *Guidance Document for Competent Authorities for the Control of Compliance with EU Legislation*; 2012.
(29) Golubitskii, G. B.; Budko, E. V.; Basova, E. M.; Kostarnoi, A. V.; Ivanov, V. M. Stability of ascorbic acid in aqueous and aqueous−organic solutions for quantitative determination. *J. Anal. Chem.* **2007**, *62*, 742−747.
(30) Hsu, H. Y.; Tsai, Y. C.; Fu, C. C.; Wu, J. S. Degradation of ascorbic acid in ethanolic solutions. *J. Agric. Food Chem.* **2012**, *60*, 10696−10701.
(31) Bradshaw, M. P.; Barril, C.; Clark, A. C.; Prenzler, P. D.; Scollary, G. R. Ascorbic acid: a review of its chemistry and reactivity in relation to a wine environment. *Crit. Rev. Food Sci. Nutr.* **2011**, *51*, 479−498.
(32) Vaysse, J.; Balayssac, S.; Gilard, V.; Desoubdzanne, D.; Malet-Martino, M.; Martino, R. Analysis of adulterated herbal medicines and dietary supplements marketed for weight loss by DOSY 1H-NMR. *Food Addit. Contam.* **2010**, *27*, 903−916.
(33) Kächele, M.; Monakhova, Y. B.; Kuballa, T.; Lachenmeier, D. W. NMR investigation of acrolein stability in hydroalcoholic solution as a foundation for the valid HS-SPME/GC-MS quantification of the unsaturated aldehyde in beverages. *Anal. Chim. Acta* **2014**, *820*, 112−118.
(34) Baker, J. K.; Myers, C. W. One-dimentional and two-dimentional 1H- and 13C-Nuclear magnetic resonance (NMR) analysis of vitamin E raw materials or analytical reference standards. *Pharm. Res.* **1991**, *8*, 763−770.
(35) Medek, A.; Frydman, L. A multinuclear solid-state NMR analysis of vitamin B12 in its different polymorphic forms. *J. Am. Chem. Soc.* **2000**, *122*, 684−691.
(36) Mousavi, M.; Yu, S. S.; Tzou, D. M. A ^{13}C solid-state NMR analysis of vitamin D compounds. *Solid State Nucl. Magn. Reson.* **2009**, *36*, 24−31.

DOI: 10.1021/acs.jafc.5b00087
J. Agric. Food Chem. 2015, 63, 3135−3143

based safety and efficacy data have not been published, and established methods for the detection and characterization of nanomaterials within these products have not been well documented in the literature.

To date, several detection and separation techniques have been reported by researchers to address these needs, specifically for SiO_2 or TiO_2 nanomaterials in food products.[2,9,31−35] Lozano et al.[34] documented an ion beam technique, particle-induced X-ray emission (PIXE), for the quantification of SiO_2 nanoparticles dispersed in water, coffee, and milk. This technique offers fast measurements, minimal sample preparation, and parts per million (ppm) levels of sensitivity. Dekkers et al.[35] described the presence of nanoscale SiO_2 (known as food additive E551) in several food products (e.g., sugar, noodle, soup, seasoning mix) and discussed the potential risks of the intake of nanoscale SiO_2 through the food chain. Chen et al.[2] applied a centrifugation method to separate TiO_2 nanoparticles in sugar-coated chewing gum and described several characterization techniques for TiO_2 nanostructures. Although centrifugation is a relatively simple and cost-effective method to isolate nanomaterials without altering particle size or shape, the potential for many other interfering compounds and/or particles remaining with the target nanostructures is of concern. Other methods with high efficiency are still needed to separate nanometer particles, especially for nanoscale SiO_2 and TiO_2 in foods, including dietary supplements.

In this study we describe a simple and unique method to separate and characterize SiO_2 and TiO_2 nanomaterials in dietary supplements marketed specifically for women. A total of 12 dietary supplements claiming the inclusion of SiO_2 and TiO_2, but not providing any information related to particle size in their products, were purchased through various retailers. SiO_2 and TiO_2 nanostructures were selectively separated from the products using a simple acid digestion and centrifugation step, in which other metallic particles were dissolved during the process. The resulting nanostructures were characterized using multiple techniques including dynamic light scattering (DLS), field emission scanning electron microscopy (FESEM), transmission electron microscopy (TEM), energy dispersive spectroscopy (EDS), and X-ray diffraction (XRD). Nanometer-sized SiO_2 and TiO_2 particles were detected in 11 products, and many of those particles were aggregated. The methods that were developed can be utilized to detect and characterize the physicochemical properties of these nanoparticles within other consumer products.

EXPERIMENTAL PROCEDURES

Materials and Reagents. SiO_2 (amorphous, 20−60 nm in diameter) and TiO_2 (rutile, 10−30 nm) nanoparticles were purchased from Skyspring Nanomaterials, Inc. (Houston, TX, USA), to use as reference materials. TiO_2 nanopowder (anatase, diameter < 25 nm) was purchased from Sigma-Aldrich (St. Louis, MO, USA). Polystyrene (PS) standard nanoparticles, 50 and 500 nm in diameter, were purchased from Thermo Fisher Scientific Inc. (Waltham, MA, USA). Nitric acid (HNO_3, Optima 67−70%), hydrogen peroxide (H_2O_2, 30%), and ethanol (C_2H_6O) were purchased from Fisher Scientific (Houston, TX, USA). Type I ultrapure water (18 MΩ·cm) was available through a Thermo Scientific Barnstead Nanopure System (Waltham, MA, USA).

Detection and Characterization of SiO_2 and TiO_2 Particles. *Isolation of SiO_2 and TiO_2 Particles.* To separate SiO_2 and TiO_2 particles from complex matrices, a digestion solution consisting of 10 mL of hydrogen peroxide and 0.5 mL of nitric acid was prepared in a 15 mL conical tube. Approximately 100 mg of each dietary supplement and 3 mL of the digestion solution were mixed and heated in a sand bath at 120 °C. When the sample volume was reduced to 2 mL, the solution was allowed to cool to room temperature. The sample was then transferred into a 2 mL centrifuge tube and ultrasonicated for 1 min (Branson 2510, Danbury, CT, USA). The white particles were centrifuged at approximately 10000*g* for 20 min (Eppendorf Centrifuge 5430R, Hauppauge, NY, USA). The supernatant was carefully removed and the precipitate was resuspended in 2 mL of ethanol. The extraction processes were repeated twice with the isolated particles being redispersed in ethanol or ultrapure water.

Dynamic Light Scattering. For particle size and size distribution analysis, DLS measurements were carried out using a ZetaPALS from Brookhaven Instruments Corp. (Holtsville, NY, USA), with particle sizing software version 5.23. All particles were diluted with ultrapure water and ultrasonicated for 3 min. The instrument was operated at a laser wavelength of 658 nm and a temperature of 23 °C. The data collection period was set at 2 min and replicated five times (total elapsed time = 10 min).

Table 1. Dietary Supplements Investigated[a]

sample	formulation	market claim	labeling of SiO_2 or TiO_2 as ingredient
DS-1	solid/tablet	sexual health formula for women	TiO_2
		supports energy production	
DS-2	solid/tablet	support hormonal balance	SiO_2
DS-3	solid/capsule	maximum strength enhancement	SiO_2
DS-4	liquid/soft gel	passion and pleasure boost	TiO_2
DS-5	solid/capsule	menopause support	TiO_2
DS-6	solid/capsule	enhances fertility and desire	SiO_2
DS-7	solid/capsule	female fertility support	SiO_2
DS-8	solid/capsule	balances yeast and bacteria to maintain feminine health	TiO_2
DS-9	solid/tablet	menopause support	SiO_2
DS-10	solid/capsule	urinary tract health	SiO_2, TiO_2
DS-11	solid/capsule	urinary tract support	SiO_2
DS-12	solid/capsule	pleasure enhancer for women	SiO_2, TiO_2

[a]The dietary supplements (DS) were given arbitrary numbers and reviewed for (a) physical condition, (b) intent of use, and (c) indications of contents containing SiO_2 or TiO_2 based on product labeling.

Table 2. Particle Size and Size Distribution Measured by Dynamic Light Scattering (DLS)[a]

	particle size			
sample	number-based mean diameter (nm)	intensity-based mean diameter (nm)	size distribution (nm)	polydispersity index (*P*)
DS-1	308	557	260−1255	0.20
DS-2	282	2146	236−3590	0.38
DS-3	100	4275	87−7288	0.40
DS-4	142	500	121−834	0.30
DS-5	328	542	202−705	0.20
DS-6	344	2701	281−4019	0.43
DS-7	441	2736	237−4617	0.37
DS-8	156	869	136−1418	0.38
DS-9	254	2496	213−3680	0.45
DS-10	146	350	120−416	0.10
DS-11	47	4905	41−6840	0.41
DS-12	57	403	53−533	0.29

[a]The dietary supplements (DS) were given arbitrary numbers. A solution of nitric acid and hydrogen peroxide was used to dissolve the various components of the products at high temperature, leaving only SiO_2 and TiO_2. The particles sizes were characterized by DLS following suspension and ultrasonication in ultrapure water.

DOI: 10.1021/acs.jafc.5b00392
J. Agric. Food Chem. 2015, 63, 3144−3152

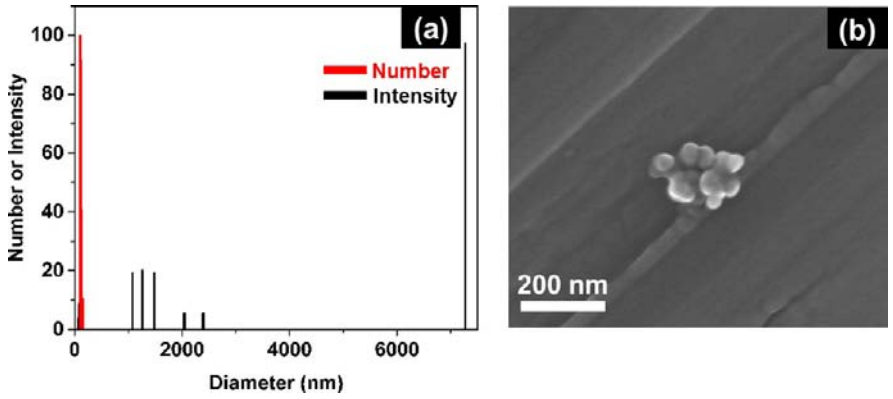

Figure 1. (a) Number- and intensity-based hydrodynamic particle size of sample DS-3 analyzed by DLS and (b) representative FESEM image of sample DS-3.

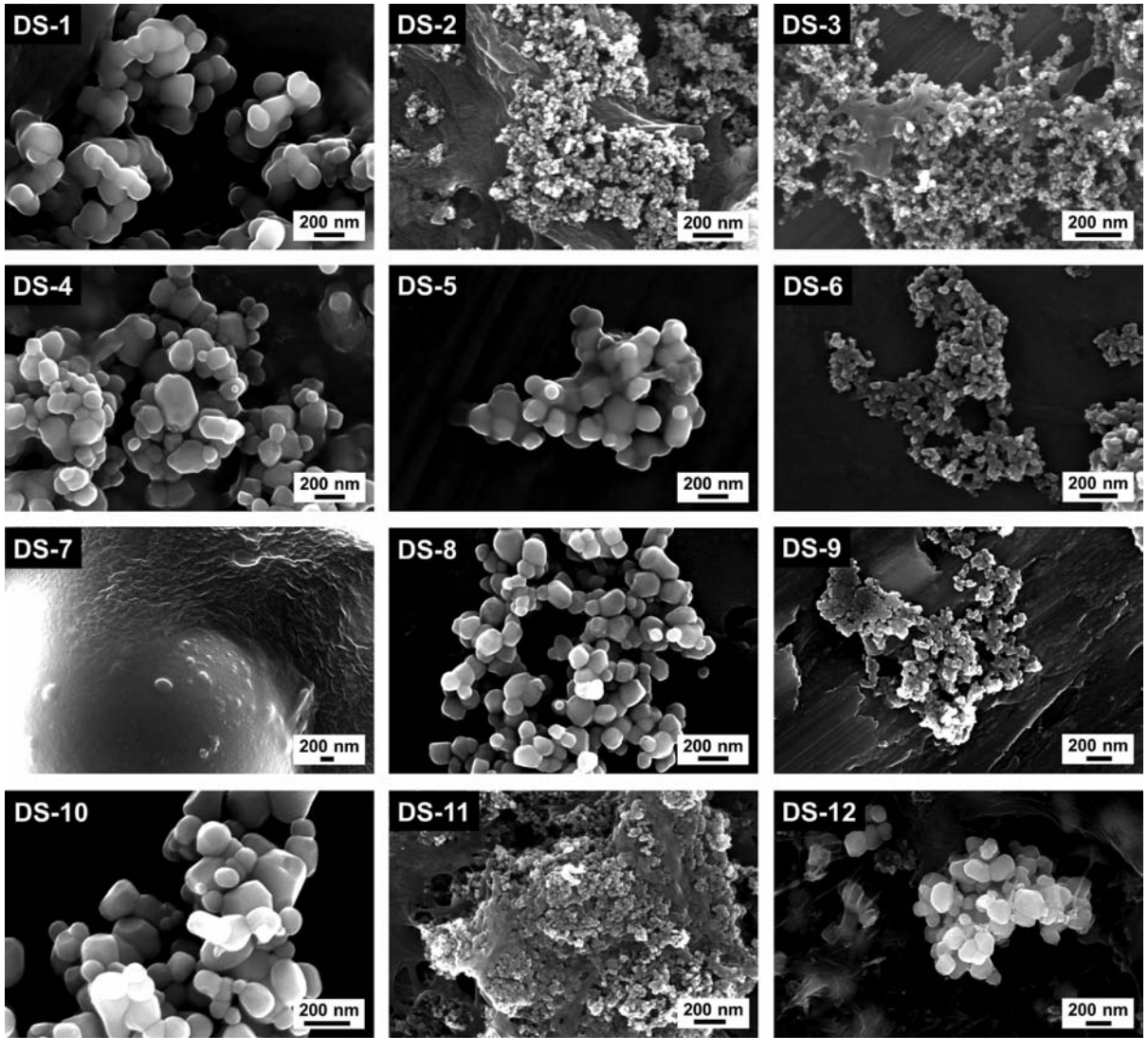

Figure 2. FESEM images of SiO_2 and TiO_2 particles separated from each product labeled DS-1—DS-12. The dietary supplements were digested and SiO_2 and TiO_2 particles isolated, suspended in ethanol, and placed on FESEM platform for analysis.

Field Emission Scanning Electron Microscopy. The shape and morphology of the nanostructures were characterized by a Zeiss-Merlin FESEM (Thornwood, NY, USA) under high-vacuum conditions. Before characterization, the particles were dispersed in ethanol, ultrasonicated for 1 min (Branson 2510), and directly placed on a standard Zeiss sample holder. The dispersion was allowed to evaporate to dryness and a very thin layer (approximately 4 nm) of Au/Pd was sputtered onto the sample using a Denton Vacuum Desk V (Moorestown, NJ, USA). The presence of Si and Ti in the SiO_2 and TiO_2 particles, respectively, was confirmed using an EDAX Apollo XL (EDAX Inc., Mahwah, NJ, USA) energy dispersive X-ray spectroscopy (EDS) while the sample was irradiated in the FESEM.

DOI: 10.1021/acs.jafc.5b00392
J. Agric. Food Chem. 2015, 63, 3144−3152

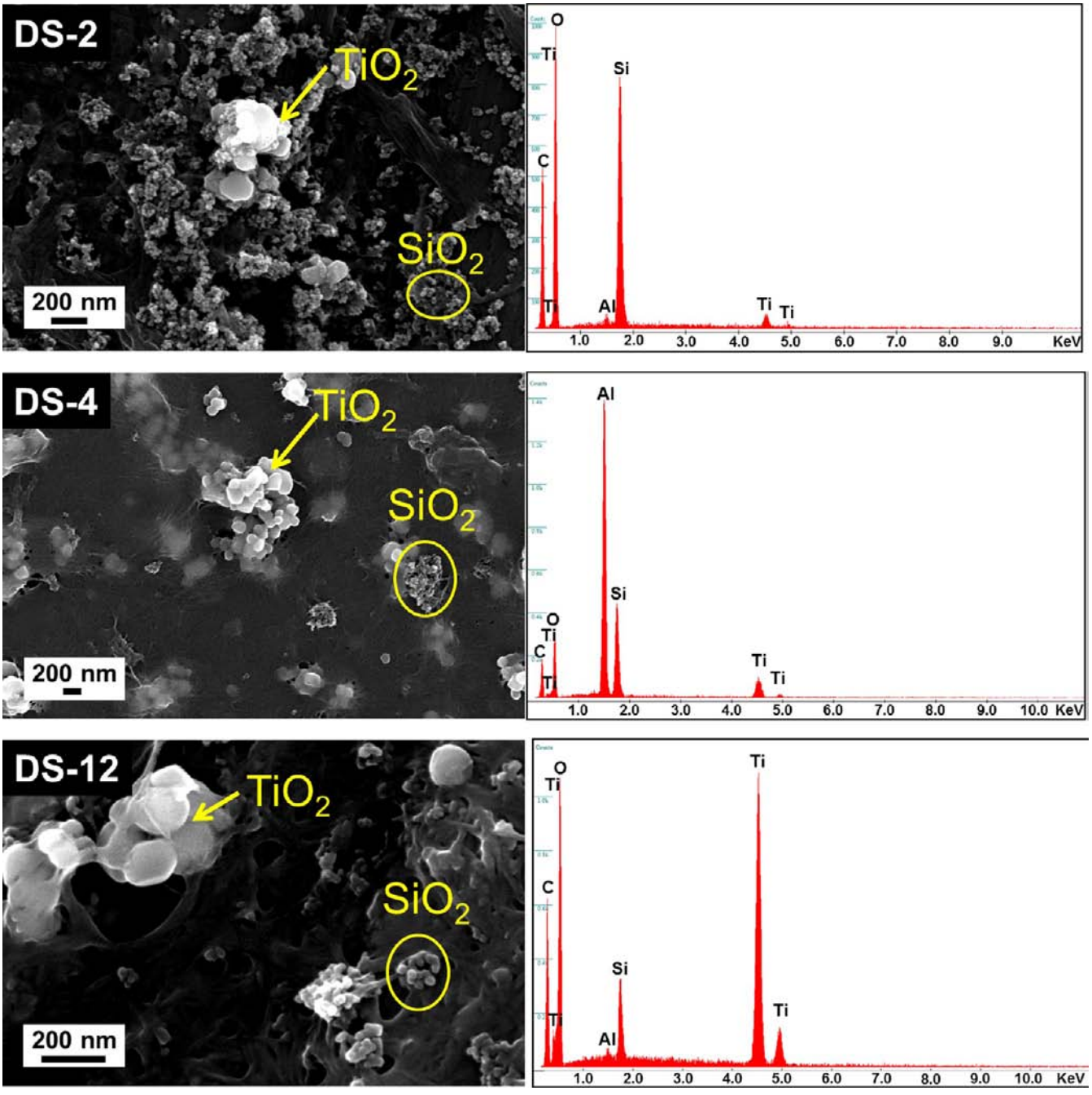

Figure 3. FESEM images and EDS spectra of SiO_2 and TiO_2 nanoparticles in DS-2, DS-4, and DS-12. Al peaks are associated background signal of the sample holder.

Transmission Electron Microscopy. TEM samples were prepared by adding 5−10 μL of the specimen dispersed in ethanol on 300-mesh carbon coated copper grids purchased from Electron Microscopy Sciences (Hatfield, PA, USA), and the samples were allowed to dry at room temperature. TEM images were acquired using a JEOL 2100 TEM (Peabody, MA, USA) operated at an acceleration voltage of 80 kV. Particle shape, size, and size distribution were characterized using multiple images of each sample with the reported statistics based on a minimum of 500 particles. The elemental composition of the nanostructures was determined by an EDS detector (EDAX Genesis 2000).

X-ray Diffraction (XRD). The crystalline structure of the particles, separated from dietary supplements, was determined using a Bruker AXS (Madison, WI, USA) XRD D2 Phaser operated at 30 kV and 10 mA at 24 °C. Samples placed onto the zero diffraction silicon sample holder (MTI Corp., Richmond, CA, USA) were dried overnight at room temperature. XRD patterns were obtained from 20° to 80° (2θ) using a Lynxeye detector and Cu Kα (λ = 1.541 Å) radiation.

RESULTS AND DISCUSSION

Twelve dietary supplements (arbitrarily assigned DS-1−DS-12) were randomly selected and procured from national retailers. A list of the products can be found in Table 1 including the corresponding formulation type, market claim, and labeling information on the inclusion of SiO_2 and/or TiO_2. None of the supplements included in this paper contained labeling that specifically indicated the presence or absence of nanosized materials as dietary ingredients, preservatives, or colorants.

The products selected for analysis contain a variety of active ingredients and excipients (e.g., vitamins, botanicals or herbs,

DOI: 10.1021/acs.jafc.5b00392
J. Agric. Food Chem. 2015, 63, 3144−3152

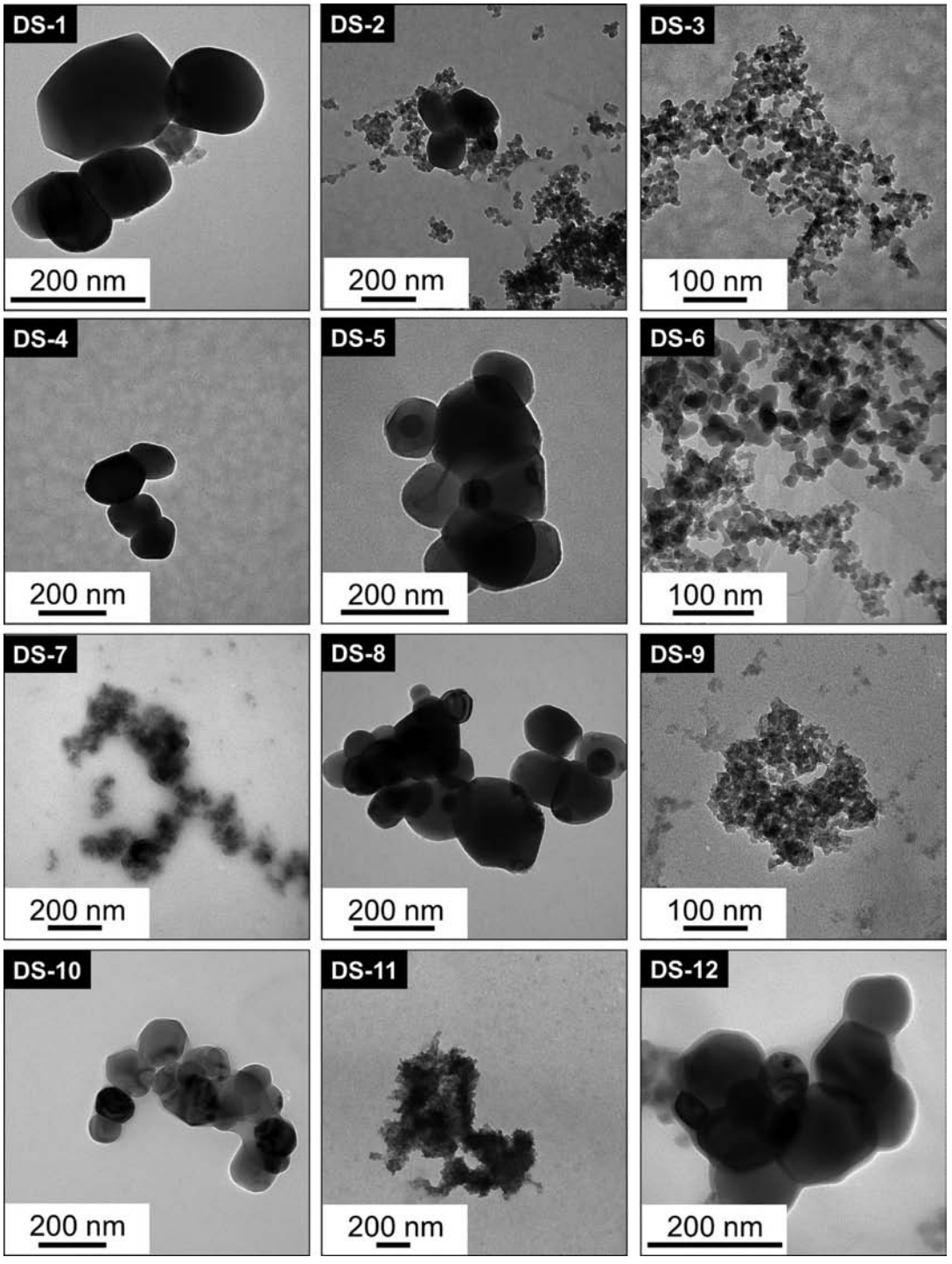

Figure 4. TEM images of SiO_2 and TiO_2 particles in DS-1−DS-12.

amino acids, dietary substances), which are problematic for the isolation of the SiO_2 and TiO_2 nanostructures. To overcome this obstacle, a combination of acid digestion and centrifugation was adopted from Weir et al.[36] and used to isolate SiO_2 and TiO_2 simultaneously. A solution of nitric acid and hydrogen peroxide was used to dissolve or decompose the various components of the products at high temperature, leaving only SiO_2 and TiO_2. It has been well documented that SiO_2 and TiO_2 are not dissolved without the presence of HF.[37] The remaining particles were rinsed three times with ethanol (collection by centrifugation) and suspended in ethanol or ultrapure water. This simple and facile method was able to isolate the metal oxide particles while not altering the particle size and morphology of the separated materials (see Supporting Information Figures SI1 and SI2).[38] The average size, morphology, size distribution, and crystal structure of the isolated particles were further characterized using multiple techniques as described below.

DLS is a technique that is commonly used to measure particle size or particle size distributions due to its rapid and simple operation. The particle size can be analyzed and reported on the basis of the number or intensity average with multimodal size distribution. A summary of the particle size analysis is shown in

DOI: 10.1021/acs.jafc.5b00392
J. Agric. Food Chem. 2015, 63, 3144−3152

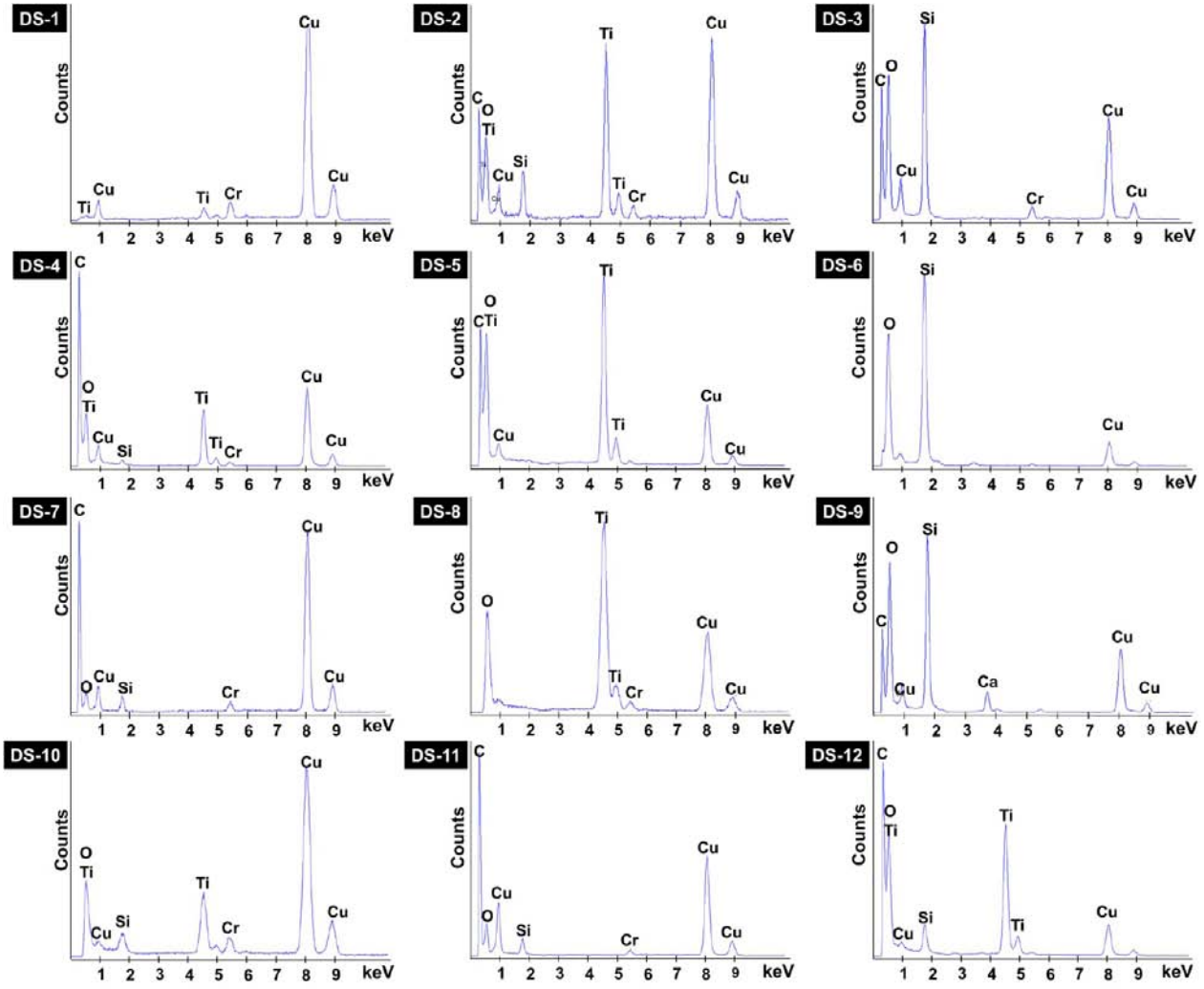

Figure 5. EDS spectra of particles in TEM images (Figure 2). The C, Cr, and Cu peaks are associated with background signal of the sample holder.

Table 2. The size of the nanoparticles isolated from the dietary supplements was very polydisperse. This is indicated by the differences in the modes of analysis of the DLS data (number versus intensity) and a high polydispersity index (P) as shown in Table 2. The smallest particle sizes of three samples including DS-3, DS-11, and DS-12 were below 100 nm. As shown in Figure 1, the actual size of the nanoparticles was closer to the number-based particle size in DLS. In this case, the hydrodynamic particle size calculated by intensity-based mode is highly dependent on the larger particles because the intensity (I) of light scattered is proportional to d^6 and $1/\lambda^4$ from the Rayleigh approximation, where d is a particle diameter and λ is a laser wavelength.[39,40] For instance, as shown in Supporting Information Figure SI3, the particles have a narrow size distribution showing very close numbers in both number- and intensity-based modes. However, when the particles with 50 and 500 nm in diameter were mixed, large different mean diameters were observed in the two modes and the P value was also >0.3. This occurred because the intensity of the 500 nm particles would be 10^6 times higher than that of the 50 nm particles.[40] Larger particles exhibit a greater instrumental response compared to smaller particles, and the signal corresponding to the smaller particles can be masked. It is important to note that when the value of the polydispersity index is >0.3, the size information obtained by DLS calculations is not always accurate.[40,41] In addition, the shape of the particles can also play a role in the experimental determination of the hydrodynamic size, as the principles of DLS are based on the Stokes−Einstein relationship, which has two fundamental assumptions: (1) the particle shape is spherical and (2) the particles are in Brownian motion.[39] As shown in Figures 2−4, the SiO_2 and TiO_2 particles were not spherical, with many single particles being barrel-shaped, and many primary particles aggregated into small clusters.

To characterize the morphology and size of separated particles from each product, microscopic imaging techniques were adopted. Nanometer-scale particles were found in a total of 11 products, with the exception of DS-7. Although DLS data for DS-7 indicated that nanometer-scale materials were present, advanced imaging via FESEM and TEM could not locate particles in this size domain. FESEM images in Figure 2 showed both spherically shaped and irregularly shaped nanoparticles with various particle sizes. By using the X-ray emission spectra from FESEM-EDS, it was determined that the isolated particles were consistent with the presence of Si and Ti. The samples containing TiO_2 (DS-1, DS-2, DS-4, DS-5, DS-8, DS-10, and DS-12) showed 50−200 nm sized individual particles; however, several of those particles were found within aggregates. Unlike TiO_2 particles, the sizes of individual SiO_2 particles in DS-2, DS-3, DS-4, DS-6, DS-9, DS-11, and DS-12 were <100 nm, but they were likewise found in a state of aggregation. Clusters of SiO_2 nanoparticles showed size ranges of several nanometers to micrometers.

DOI: 10.1021/acs.jafc.5b00392
J. Agric. Food Chem. 2015, 63, 3144−3152

FESEM images suggest that individual SiO_2 nanoparticles are much smaller than TiO_2 nanoparticles. The degree of aggregation supports the large polydispersity observed in products containing SiO_2 as compared to other products (Table 2). Figure 3 shows that both SiO_2 and TiO_2 nanoparticles could be found within the same samples, as was the case in DS-2, DS-4, and DS-12. TEM images (Figure 4) were consistent with the morphology and size information obtained using FESEM. The TiO_2 particles separated from products DS-1, DS-2, DS-4, DS-5, DS-8, DS-10, and DS-12 were found to have at least one dimension below 100 nm in size and a round shape. An analysis of the size showed that 94% of the TiO_2 particles showed size ranges between 50 and 200 nm, and 99% of SiO_2 nanoparticles found in DS-2, DS-3, DS-4, DS-6, DS-9, DS-11, and DS-12 were <100 nm in diameter and present in large aggregates. As can be seen in Figures 2 and 4, no nanosized structures were found in DS-7.

In Figure 5, EDS analysis showed the presence of elements (i.e., Si, Ti, and O peaks indicating SiO_2 or TiO_2) in the specific area corresponding to TEM images in Figure 4. The C, Cr, and Cu peaks were from the sample grid and instrument. Taken together, the FESEM, TEM, and EDS data demonstrated that the particles isolated from 11 products consist of nanosized SiO_2 and/or TiO_2.

To assess the crystal structure of the isolated particles, XRD was used in conjunction with the reference data file, Joint Committee on Powder Diffraction Standards (JCPDS) card. XRD data presented in Figure 6 reveal that SiO_2 nanoparticles exhibit a 2θ broad peak from 20° to 25° corresponding to amorphous SiO_2 (broad peaks near 55−70° are from the sample holder). TiO_2 particles show diffraction peaks at 2θ = 25.3°, 36.9°, 37.8°, 38.5°, and 48.1°, which can be indexed to the (101), (103), (004), (112), and (200) planes. The diffraction peak positions are consistent with the standard diffraction pattern of anatase TiO_2 (JCPDS card no. 21-1272).[42] In the cases of DS-2 and DS-4, both SiO_2 and TiO_2 peaks were detected even though the labeling on product DS-2 discloses only SiO_2 and the labeling on product DS-4 discloses only TiO_2. These results suggest that the isolated particles were a mixture of amorphous SiO_2 and anatase TiO_2 particles. Furthermore, DS-12 showed both amorphous SiO_2 and anatase TiO_2 peaks as claimed.

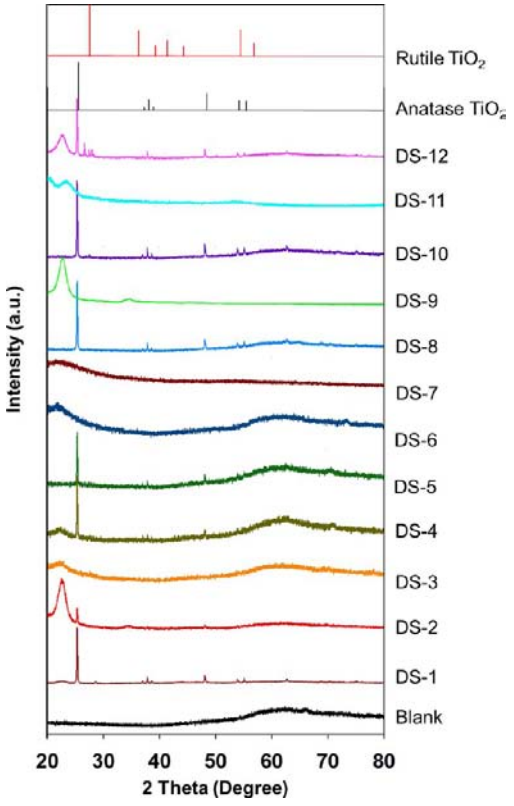

Figure 6. XRD analysis of samples DS-1−DS-12. Reference patterns for anatase (JCPDS no. 21-1272) and rutile (JCPDS no. 21-1276) TiO_2 peaks are provided along with the pattern observed from the zero diffraction silicon XRD sample holder.

A comparison between experimentally determined data and product labeling showed that unexpected TiO_2 and SiO_2 nanoparticles were detected in DS-2 and DS-4, respectively. DS-10 claims the inclusion of both SiO_2 and TiO_2, but only anatase TiO_2 was detected. All TiO_2 nanoparticles detected and characterized in this study were found in the anatase phase, which is reported to be more toxic than the rutile phase.[43,44] The concentrations of Si and Ti in each product were experimentally determined by inductively coupled plasma−mass spectrometry (ICP-MS) and can be seen in Supporting Information Table SI1.

Herein we developed a simple and high-temperature acid digestion method to isolate SiO_2 and TiO_2 nanomaterials in commercially available dietary supplements. The isolated SiO_2 and TiO_2 particles were characterized using several complementary techniques. The analytical data demonstrated that 11 of the 12 dietary supplements contained nanometer-scale SiO_2 and/or TiO_2 particles. Interestingly, the properties of TiO_2 nanomaterials detected in this study are very close to those identified in several different commercial products, for example, foods,[2] cosmetics,[45] textiles,[46] or personal care products[36] recently reported in the literature. It is important to note that all of those products did not indicate the presence of nanomaterials on their labels. A recent survey released by "As you Sow" concluded that most manufacturers are uncertain whether nanomaterials are used within their products.[47] Although this is a small number of studies to represent a global market, it is possible that large amounts of SiO_2 and TiO_2 nanomaterials are included in various commercial products without proper labeling.

We expect that the developed methodologies can be applied to properly isolate and characterize the physicochemical properties of SiO_2 and TiO_2 nanoparticles within consumer products and can assist in the critical assessment of public health risk and science-based regulation of products using nanotechnology-based ingredients.

■ ASSOCIATED CONTENT

Ⓢ Supporting Information

Additional figures depicting TEM images of commercial SiO_2 and TiO_2 nanoparticles, DLS data of polystyrene (PS) standard nanoparticles, and experimentally determined Si and Ti contents per capsule/tablet by ICP-MS. This material is available free of charge via the Internet at http://pubs.acs.org.

■ AUTHOR INFORMATION

Corresponding Authors

*(J.-H.L.) E-mail: Jin.Lim@fda.hhs.gov. Phone: (870) 543-4660. Fax: (870) 543-4041.
*(S.W.L.) E-mail: Sean.Linder@fda.hhs.gov. Phone: (870) 543-4667. Fax: (870) 543-4041.

DOI: 10.1021/acs.jafc.5b00392
J. Agric. Food Chem. 2015, 63, 3144−3152

Funding

This work was graciously supported by the FDA Office of Women's Health. This project was supported in part by an appointment to the Research Participation Program at the Office of Regulatory Affairs/Arkansas Regional Laboratory, U.S. Food and Drug Administration, administered by the Oak Ridge Institute for Science and Education through an interagency agreement between the U.S. Department of Energy and FDA. The views expressed in this paper are those of the authors and should not be interpreted as the official opinion or policy of the U.S. Food and Drug Administration, Department of Health and Human Services, or any other agency or component of the U.S. government. The mention of trade names, commercial products, or organizations is for clarification of the methods used and should not be interpreted as an endorsement of a product or manufacturer.

Notes

The authors declare no competing financial interest.

■ ACKNOWLEDGMENTS

This work was conducted using the *Nanotechnology Core Facility (NanoCore)* located on the U.S. Food and Drug Administration's Jefferson Laboratories campus (Jefferson, AR, USA), which houses the FDA National Center for Toxicological Research and the FDA Office of Regulatory Affairs Arkansas Regional Laboratory. We gratefully thank Yvonne Jones for assistance in performing TEM.

■ ABBREVIATIONS USED

PIXE, particle-induced X-ray emission; ppm, parts per million; PS, polystyrene; DLS, dynamic light scattering; *P*, polydispersity index; FESEM, field emission scanning electron microscopy; TEM, transmission electron microscopy; EDS, energy dispersive X-ray spectroscopy; XRD, X-ray diffraction; JCPDS, Joint Committee on Powder Diffraction Standards; ICP-MS, inductively coupled plasma-mass spectrometry; FDA, U.S. Food and Drug Administration

■ REFERENCES

(1) Bradley, E.; Castle, L.; Chaudhry, Q. Applications of nanomaterials in food packaging with a consideration of opportunities for developing countries. *Trends Food Sci. Technol.* **2011**, *22*, 604−610.

(2) Chen, X.-X.; Cheng, B.; Yang, Y.-X.; Cao, A.; Liu, J.-H.; Du, L.-J.; Liu, Y.; Zhao, Y.; Wang, H. Characterization and preliminary toxicity assay of nano-titanium dioxide additive in sugar-coated chewing gum. *Small* **2012**, *9*, 1765−1774.

(3) Napierska, D.; Thomassen, L. C.J.; Lison, D.; Martens, J. A.; Hoet, P. H. The nanosilica hazard: another variable entity. *Part. Fibre Toxicol.* **2010**, *7*, 1−32.

(4) Yang, Y.; Doudrick, K.; Bi, X.; Hristovski, K.; Herckes, P.; Westerhoff, P.; Kaegi, R. Characterization of food-grade titanium dioxide: the presence of nanosized particles. *Environ. Sci. Technol.* **2014**, *48*, 6391−6400.

(5) Lim, J.-H.; Rotaru, A.; Min, S.-G.; Malkinski, L.; Wiley, J. B. Synthesis of mild-hard AAO templates for studying magnetic interactions between metal nanowires. *J. Mater. Chem.* **2010**, *20*, 9246−9252.

(6) Jung, J.-S.; Lim, J.-H.; Choi, K.-H.; Oh, S.-L.; Kim, Y.-R.; Lee, S.-H.; Smith, D. A.; Stokes, K. L.; Malkinski, L.; O'Connor, C. J. $CoFe_2O_4$ nanostructures with high coercivity. *J. Appl. Phys.* **2005**, *97*, 10F306-1−10F306-3.

(7) Nel, A.; Xia, T.; Mädler, L.; Li, N. Toxic potential of materials at the nanolevel. *Science* **2006**, *311*, 622−627.

(8) Cushena, M.; Kerryb, J.; Morrisc, M.; Cruz-Romerob, M.; Cummins, E. Nanotechnologies in the food industry − recent developments, risks and regulation. *Trends Food Sci. Technol.* **2012**, *24*, 30−46.

(9) Blasco, C.; Picó, Y. Determining nanomaterials in food. *Trends Anal. Chem.* **2011**, *30*, 84−98.

(10) Sadrieh, N.; Wokovich, A. M.; Gopee, N. V.; Zheng, J.; Haines, D.; Parmiter, D.; Siitonen, P. H.; Cozart, C. R.; Patri, A. K.; McNeil, S. E.; Howard, P. C.; Doub, W. H.; Buhse, L. F. Lack of significant dermal penetration of titanium dioxide from sunscreen formulations containing nano- and submicron-size TiO_2 particles. *Toxicol. Sci.* **2010**, *115*, 156−166.

(11) Karlsson, H. L.; Gustafsson, J.; Cronholm, P.; Möller, L. Size-dependent toxicity of metal oxide particles-A comparison between nano- and micrometer size. *Toxicol. Lett.* **2009**, *188*, 112−118.

(12) Tyner, K. M.; Wokovich, A. M.; Doub, W. H.; Buches, L. F.; Sung, L. P.; Watson, S. S.; Sadrieh, N. Comparing methods for detecting and characterizing metal oxide nanoparticles in unmodified commercial sunscreens. *Nanomedicine* **2009**, *4*, 145−159.

(13) Auffan, M.; Rose, J.; Bottero, J.-Y.; Lowry, G. V.; Jolivet, J.-P.; Wiesner, M. R. Towards a definition of inorganic nanoparticles from an environmental, health and safety perspective. *Nat. Nanotechnol.* **2009**, *4*, 634−641.

(14) Mastronardi, M. L.; Hennrich, F.; Henderson, E. J.; Maier-Flaig, F.; Blum, C.; Reichenbach, J.; Lemmer, U.; Kübel, C.; Wang, D.; Kappes, M. K.; Ozin, G. A. Preparation of monodisperse silicon nanocrystals using density gradient ultracentrifugation. *J. Am. Chem. Soc.* **2011**, *133*, 11928.

(15) Hagendorfer, H.; Kaegi, R.; Parlinska, M.; Sinnet, B.; Ludwig, C.; Ulrich, A. Characterization of silver nanoparticle products using asymmetric flow field fractionation with a multidetector approach − a comparison to transmission electron microscopy and batch dynamic light scattering. *Anal. Chem.* **2012**, *84*, 2678−2685.

(16) Nischwitz, V.; Goenaga-Infante, H. Improved sample preparation and quality control for the characterisation of titanium dioxide nanoparticles in sunscreens using flow field flow fractionation on-line with inductively coupled plasma mass spectrometry. *J. Anal. At. Spectrom.* **2012**, *27*, 1084−1092.

(17) Soto-Alvaredo, J.; Montes-Bayón, M.; Bettmer, J. Speciation of silver nanoparticles and silver(I) by reversed-phase liquid chromatography coupled to ICPMS. *Anal. Chem.* **2013**, *85*, 1316.

(18) Bailey, R. L.; Gahche, J. J.; Lentino, C. V.; Dwyer, J. T.; Engel, J. S.; Thomas, P. R.; Betz, J. M.; Sempos, C. T.; Picciano, M. F. Dietary supplement use in the United States 2003−2006. *J. Nutr.* **2011**, *141*, 261−266.

(19) Bailey, R. L.; Gache, J. J.; Miller, P. E.; Thomas, P. R.; Dwyer, J. T. Why US adults use dietary supplements. *JAMA Intern. Med.* **2013**, *173*, 355−361.

(20) Timbo, B. B.; Ross, M. P.; McCarthy, P. V.; Lin, C. J. Dietary supplements in a national survey: prevalence of use and reports of adverse events. *J. Am. Diet. Assoc.* **2006**, *106*, 1966−1974.

(21) Qato, D. M.; Alexander, G. C.; Conti, R. M.; Johnson, M.; Schumm, P.; Lindau, S. T. Use of prescription and over-the-counter medications and dietary supplements among older Adults in the United States. *JAMA, J. Am. Med. Assoc.* **2008**, *300*, 2867−2878.

(22) Raiten, D. J.; Picciano, M. F.; Coates, P. M. Dietary supplement use in women: current status and future directions − introduction and conference summary. *J. Nutr.* **2003**, *133*, 1957S−1960S.

(23) Albanese, A.; Tang, P. S.; Chan, W. C.W. The effect of nanoparticle size, shape, and surface chemistry on biological systems. *Annu. Rev. Biomed. Eng.* **2012**, *14*, 1−16.

(24) Chen, J.; Saeki, F.; Wiley, B. J.; Cang, H.; Cobb, M. J.; Li, Z. Y.; Au, L.; Zhang, H.; Kimmey, M. B.; Li, X.; Xia, Y. Gold nanocages: bioconjugation and their potential use as optical imaging contrast agents. *Nano Lett.* **2005**, *5*, 473−477.

(25) Su, S.; Wu, W.; Gao, J.; Lu, J.; Fan, C. Nanomaterials-based sensors for applications in environmental monitoring. *J. Mater. Chem.* **2012**, *22*, 18101−18110.

(26) Cho, K.; Wang, X.; Nie, S.; Chen, Z.; Shin, D. M. Therapeutic nanoparticles for drug delivery in cancer. *Clin. Cancer Res.* **2008**, *14*, 1310−1316.

DOI: 10.1021/acs.jafc.5b00392
J. Agric. Food Chem. 2015, 63, 3144−3152

(27) Sánchez-Pomales, G.; Mudalige, T. K.; Lim, J.-H.; Linder, S. W. Rapid determination of silver in nanobased liquid dietary supplements using a portable X-ray fluorescence analyzer. *J. Agric. Food Chem.* **2013**, *61*, 7250−7257.
(28) IFST information statement − Nanotechnology, Dec 2013, Institute of Food Science and Technology, http://ifst2.pseltd.com/documents/misc/Nanotechnologydec2013.pdf (accessed Nov 18, 2014).
(29) Peters, R.; Bemmel, G.; Herrera Raivera, Z.; Helsper, H. P. F. G.; Marvin, H. J. P.; Weigel, S.; Tromp, P. C.; Oomen, A. G.; Rietveld, A. G.; Bouwmen, H. Characterization of titanium dioxide nanoparticles in food products: analytical methods to define nanoparticles. *J. Agric. Food Chem.* **2014**, *62*, 6285−6293.
(30) Heroul, J.; Nischwitz, V.; Bartczak, D.; Goenaga Infante, H. The potential of asymmetric flow field-flow fractionation hyphenated to multiple detectors for the quantification and size estimation of silica nanoparticles in a food matrix. *Anal. Bioanal. Chem.* **2014**, *406*, 3919−3927.
(31) Peters, R.; Kramer, E.; Oomen, A. G.; Herrera Rivera, Z. E.; Oegema, G.; Tromp, P. C.; Fokkink, R.; Rietveld, A.; Marvin, H. J. P.; Weigel, S.; Peijnenburg, A. A. C. M.; Bouwmeester, H. Presence of nano-sized silica during in vitro digestion of foods containing silica as a food additive. *ACS Nano* **2012**, *6*, 2441−2451.
(32) Kammer, F.; Legros, S.; Hofmann, T.; Larsen, E. H.; Loeschner, K. Separation and characterization of nanoparticles in complex food and environmental samples by field-flow fractionation. *Trends Anal. Chem.* **2011**, *30*, 425−436.
(33) Dudkiewicz, A.; Tiede, K.; Loescher, K.; Jensen, L. H. S.; Jensen, E.; Wierzbicki, R.; Boxall, A. B. A.; Molhave, K. Characterization of nanomaterials in food by electron microscopy. *Trends Anal. Chem.* **2011**, *30*, 28−43.
(34) Lozano, O.; Mejia, J.; Tabarrant, T.; Masereel, B.; Dogné, J. M.; Toussanint, O.; Lucas, S. Quantification of nanoparticles in aquous food matrices using particle-induced X-ray emission. *Anal. Bioanal. Chem.* **2012**, *403*, 2835−2841.
(35) Dekkers, S.; Krystek, P.; Peters, R. J.; Lankveld, D. P.; Bokkers, B. G.; van Hoeven-Arentzen, P. H.; Bouwmeester, H.; Oomen, A. G. Presence and risks of nanosilica in food products. *Nanotoxicology* **2011**, *5*, 393−405.
(36) Weir, A.; Westerhoff, P.; Fabricius, L.; Hristovski, K.; Goetz, N. Titanium dioxide nanoparticles in food and personal care products. *Environ. Sci. Technol.* **2012**, *46*, 2242−2250.
(37) Wet chemical etching; chemical and physical mechanisms-revised 11/25/2005, MicroChemicals, http://www.microchemicals.de/secret/etching.pdf (accessed Oct 31, 2014).
(38) Regonini, D.; Jaroenworaluck, A.; Stevens, R.; Bowen, C. R. Effect of heat treatment on the properties and structure of TiO_2 nanotubes: phase composition and chemical composition. *Surf. Interface Anal.* **2010**, *42*, 139−144.
(39) Hassellöv, M.; Readman, J. W.; Ranville, J. F.; Tiede, K. Nanoparticle analysis and characterization methodologies in environmental risk assessment of engineered nanoparticles. *Ecotoxicology* **2008**, *17*, 344−361.
(40) Dynamic light scattering technical note, MRK656-01, Malvern Instruments Ltd., http://www3.nd.edu/~rroeder/ame60647/slides/dls.pdf (accessed Nov 18, 2014).
(41) Nanocomposix's guide to dynamic light scattering measurements and analysis, Guidelines for dynamic light scattering measurements, Sept 2012, V1.3, nanoComposix, http://nanocomposix.com/sites/default/files/nanoComposix%20Guidelines%20for%20DLS%20Measurements%20and%20Analysis.pdf (assessed Nov 18, 2014).
(42) Reyes-Coronado, D.; Rodríguez-Gattorno, G.; Espinosa-Pesqueira, M. E.; Cab, C.; de Coss, R.; Oskam, G. Phase-pure TiO_2 nanoparticles: anatase, brookite and rutile. *Nanotechnology* **2008**, *19*, 145605−145614.
(43) Braydich-Stolle, L. K.; Schaeublin, N. M.; Murdock, R. C.; Jiang, J.; Biswas, P.; Schlager, J. J.; Hussain, S. M. Crystal structure mediates mode of cell death in TiO_2 nanotoxicity. *J. Nanopart. Res.* **2009**, *11*, 1361−1374.
(44) Yeo, M.-K.; Kang, M. The biological toxicities of two crystalline phases and differential sizes of TiO_2 nanoparticles during zebrafish embryogenesis development. *Mol. Cell Toxicol.* **2012**, *8*, 317−326.
(45) Contado, C.; Pagnoni, A. TiO_2 nano-and micro-particles in commercial foundation creams: field flow-fractionation techniques together with ICP-AES and SQW voltammetry for their characterization. *Anal. Methods* **2010**, *2*, 1112−1124.
(46) Winder, L.; Lorenz, C.; Goets, N.; Hungerbühler, K.; Amberg, M.; Heuberger, M.; Nowack, B. Release of titanium dioxide form textiles during washing. *Environ. Sci. Technol.* **2012**, *46*, 8181−8188.
(47) Nanomaterials in Foods, As you sow, http://www.asyousow.org/health_safety/gmosnano.shtml (accessed Nov 18, 2014).

DOI: 10.1021/acs.jafc.5b00392
J. Agric. Food Chem. 2015, 63, 3144−3152

separation mechanism in CE is different from those in liquid chromatography, it is considered as an orthogonal analysis and provides complementary information.[19]

For online detection of species after separation, the detection method must possess sufficient sensitivity and be able to interface with the separation system. Among all of the techniques that have been applied for elemental analysis, atomic spectrometry has played a crucial role in the determination of the arsenic concentration in a variety of samples.[8−10] Earlier development works involved the use of atomic emission spectrometry (AES) or atomic absorption spectrometry (AAS) coupled with liquid chromatography for arsenic speciation.[20,21] In recent years, with the continuous improvement in sensitivity, inductively coupled plasma mass spectrometry (ICPMS) has become the most popular detector for elemental analysis. It offers several advantages over other atomic spectroscopy techniques, including improved detection limits, minimization of interferences with the application of reaction/collision cell gases, capability to easily interface with other instruments, and the simultaneous monitoring of multiple isotopes. It has been demonstrated to be an essential tool in the routine analysis of arsenic species.[14,15,22,23]

CE interfaced with ICPMS has been widely used in the speciation of elements in various matrices. Although there have been reports about speciation of selenium, arsenic, and other elemental species in wastewater, soil, and seafood matrices using CE,[23−27] quantitation of common arsenic species in rice products using CE still remains relatively unexplored. In this study, we report the development of a hyphenated analytical technique consisting of CE and ICPMS for arsenic speciation in a rice matrix. An enzyme-assisted water-phase microwave digestion procedure was tested and used for the extraction. Multiple conditions that would affect the separation or detection of rice samples were evaluated. The optimized conditions were used for analysis of locally purchased rice samples. The precision and accuracy of this method was validated by analyzing rice standard reference materials and comparing the results to certified values.

EXPERIMENTAL SECTION

Materials and Chemicals. Methylarsonic acid monosodium salt (MMA, 98.5%) was purchased from Crescent Chemicals (Islandia, NY). Dimethylarsinic acid (DMA, 98%) was purchased from Strem Chemicals (Newburyport, MA), and *o*-arsanilic acid (*o*-ASA, 98%) was purchased from Pfaltz & Bauer (Waterbury, CT). National Institute of Standards and Technology (NIST)-traceable arsenite [As(III)] and arsenate [As(V)] stock solutions (1000 mg L^{-1}) were purchased from Spex Certiprep (Metuchen, NJ). All chemicals that were used to prepare calibration standards were assayed using ICPMS to verify the arsenic concentration. The enzyme, α-amylase from *Bacillus subtilis* [165 000 bacterial amylase units (BAU)/g], was purchased from MP Biomedicals (Carlsbad, CA). TraceSELECT sodium carbonate (≥99.9999% metal basis), TraceSELECT sodium hydroxide monohydrate (≥99.9995% metal basis), and TraceSELECT 2-propanol (≥99.9%) were purchased from Sigma-Aldrich (St. Louis, MO). Potassium hydroxide pellets (>85%) and nitric acid (68−70%, OPTIMA ultrapure grade) were purchased from Fisher Scientific (Waltham, MA). All chemicals were used as received without further purification. Deionized water (>18 MΩ cm^{-1}) from a Milli-Q reference system (Millipore, Billerica, MA) was used throughout the experiments. Individual stock solutions (1000 ng g^{-1}) of DMA, MMA, *o*-ASA, As(III), and As(V) were prepared with Milli-Q water and stored at 4 °C in the dark. The As concentrations of the stock solutions were analyzed by ICPMS. Multi-analyte calibration standards were prepared fresh on the day of use by diluting DMA, MMA, *o*-ASA, As(III), and As(V) stock solutions with Milli-Q water. For the rice flour standard reference materials, SRM 1568b was purchased from NIST (Gaithersburg, MD) and CRM 7503-a [prepared by the National Metrology Institute of Japan (NMIJ)] was purchased from Waco Chemicals US (Richmond, VA). Rice (polished long grain rice) and rice cereal (single-grain infant cereal) were acquired from a local market.

Instrumentation. CE was performed on a 7100 CE system (Agilent Technology, Santa Clara, CA). A 60 cm long coated fused-silica capillary (Molex, Phoenix, AZ) with a 100 μm inner diameter and a 360 μm outer diameter was used for sample introduction. The separation of five arsenic species was carried out under basic condition through the use of Na_2CO_3 (8 mM, pH 11) buffer. A new capillary was initialized by flushing 1 M KOH at 950 mbar for 30 min and running buffer (8 mM Na_2CO_3, pH 11) for 30 min, followed by rinsing with water for 5 min. The capillary was conditioned with 0.1 M KOH and running buffer for 15 min prior the analysis. Before each run, the capillary was equilibrated with 0.1 M KOH for 3 min and running buffer for 3 min. After each run, the capillary was rinsed with water for 1 min. Samples were hydrodynamically injected at 15 mbar for 8 s, followed by an injection of running buffer at 15 mbar for 5 s. The temperature of the cartridge was set at 21 °C (ambient temperature), and the applied voltage for the separation was 20 kV. The coupling of CE with ICPMS (Agilent 7700x, Agilent Technology, Santa Clara, CA) was performed by directly connecting the outlet of the capillary to a Mira Mist CE nebulizer (Burgener Research, Inc., Mississauga, Ontario, Canada). A solution containing 1% HNO_3 (v/v) and 10% 2-propanol (v/v) was used as the makeup solution. Alcohol was added to the makeup solution to lower the liquid surface tension and facilitate the formation of an aerosol. Additionally, alcohol was used as a carbon source to enhance the signal intensity and overcome matrix effects.[28] A final concentration of 10% 2-propanol was chosen for the analysis. Although a higher alcohol concentration can be used,[29] carbon deposits on the sampling cone can occur and affect system stability. The peristaltic pump speed was set at 0.06 rpm using a 0.5 mm inner diameter tube. This configuration gives a flow rate of 15 μL min^{-1}, with no visual droplets formulating inside the spay chamber, suggesting an approximate 100% sample delivery efficiency. The pH value of the running buffer was adjusted by adding 0.1 M NaOH or 0.1 M HNO_3 solutions and was measured with an Orion Star A214 pH meter (Thermo Scientific, Waltham, MA). The ICPMS was tuned daily under reaction gas (H_2) mode. The polyatomic interference of $ArCl^+$ is eliminated by hydrogen gas through a proton-transfer process.[30] The mass isotopes of m/z 75 and 77 were monitored for arsenic and the interference. Detailed operation conditions are listed in Table 1. The viscosity of the rice extract was measured on a VISCOlab

Table 1. CE−ICPMS Operating Parameters

	CE Parameters
capillary	polymer-coated fused-silica capillary, 100 μm inner diameter, 360 μm outer diameter, and 60 cm length
running electrolyte	8 mM Na_2CO_3, pH 11.0
voltage	20 kV
temperature	21 °C
sample injection	15 mbar, 8 s, hydrodynamic
	ICPMS Parameters
RF power	1500 W
sample depth	8.0 mm
plasma gas	15.0 L min^{-1}
carrier gas	0.9 L min^{-1}
makeup gas	0.45 L min^{-1}
collision/reaction gas	H_2, 2 mL/min
monitored isotope (m/z)	75 (As^+), 77 ($ArCl^+$)
dwell time	0.4 s (^{75}As), 0.1 s (^{77}Se)
nebulizer	Mira Mist CE

DOI: 10.1021/acs.jafc.5b00446
J. Agric. Food Chem. 2015, 63, 3153−3160

5000 viscometer with temperature control (Cambridge Viscosity, Medford, MA). The measurement of viscosity was performed in triplicate.

Sample Preparation. Rice flour of NIST SRM 1568b and CRM 7503-a were received as fine powder and used directly for the extraction. Rice and rice cereal were first ground with an 8000 M mixer/mill (SPEX SamplePrep, Metuchen, NJ) and sieved using 0.1 mm mesh size. Rice powders were oven-dried at 90 °C for 2 h to determine the residual moisture content. An enzyme-assisted water-phase microwave extraction was used for sample extraction. Typically, in a 15 mL glass tube, 0.2 g of rice powder and 0.1 g of 0.5% (w/w) α-amylase solution were diluted with water to a total weight of 2 g, which gave a final enzyme concentration of 0.05% (w/w). The tube was capped and put in a Discover SP microwave digestion system (CEM, Matthews, NC) at 80 °C for 1 h and 90 °C for 2 h with stirring. No pressure was generated inside the tube during the extraction. A method blank, which contains only 0.05% α-amylase, was also included in each extraction batch as a control to verify the absence of arsenic species. The extracted mixture was centrifuged, and any remaining solids were removed. An aliquot of 30 μL of *o*-ASA (50 ng g^{-1}) was added to the 270 μL of rice extract for a final concentration of 5.0 ng g^{-1} of *o*-ASA. Each sample was prepared in triplicate. All of the standards and samples were prepared gravimetrically.

RESULTS AND DISCUSSION

Optimization of the Separation Condition. The target arsenic species in this study are DMA, MMA, As(III), and As(V). In addition, *o*-ASA, which is not present in the rice, was also added for this analysis. It served as an internal standard and mobility marker for the other four analytes of interests. The five arsenic species were separated with the use of CE and then directly delivered to ICPMS for detection.

Several factors that may affect the separation efficiency were evaluated. Separation conditions were first investigated at various buffer concentrations (i.e., 3−10 mM). The results suggested that a buffer solution with a concentration as low as 3 mM can be used to obtain acceptable resolution among the five tested arsenic species. From Figure 1a, baseline separations were achieved in all assayed conditions with enhanced peak resolution as the buffer concentration increased. Higher buffer concentrations led to stronger ionic strengths, which can suppress the electron double layer on the inner surface of the capillary, reducing electroosmotic flow (EOF) and resulting in longer migration times. Furthermore, a concentrated buffer solution largely increases the electric current in the capillary and results in larger variations because of Joule heating.[19] After the resolution and analysis duration of each run were balanced, 8 mM Na_2CO_3 was selected as the running buffer for all of the measurements. Similar to the buffer concentration, the applied voltage had a strong effect on the EOF, which affected the migration speed of all analytes. However, it only exhibited a limited contribution to the peak separation. As shown in Figure 1b, voltages as low as 8 kV could resolve all of the species of interest. Because the magnitude of EOF generated from the low voltage is relatively small, the migration of the analytes is slow, leading to a longer elution time. Increasing the applied voltage was effective in shortening the analysis time without compromising the resolution. A voltage of 20 kV was found to be an optimum value. Although higher voltages can further reduce the analysis time, these voltages caused a significant loss in peak resolution. This is especially true for DMA and As(III). Furthermore, higher voltages also generate strong currents that can lead to an undesired heating effect, especially for capillaries with a large inner diameter. In other buffer systems, similar

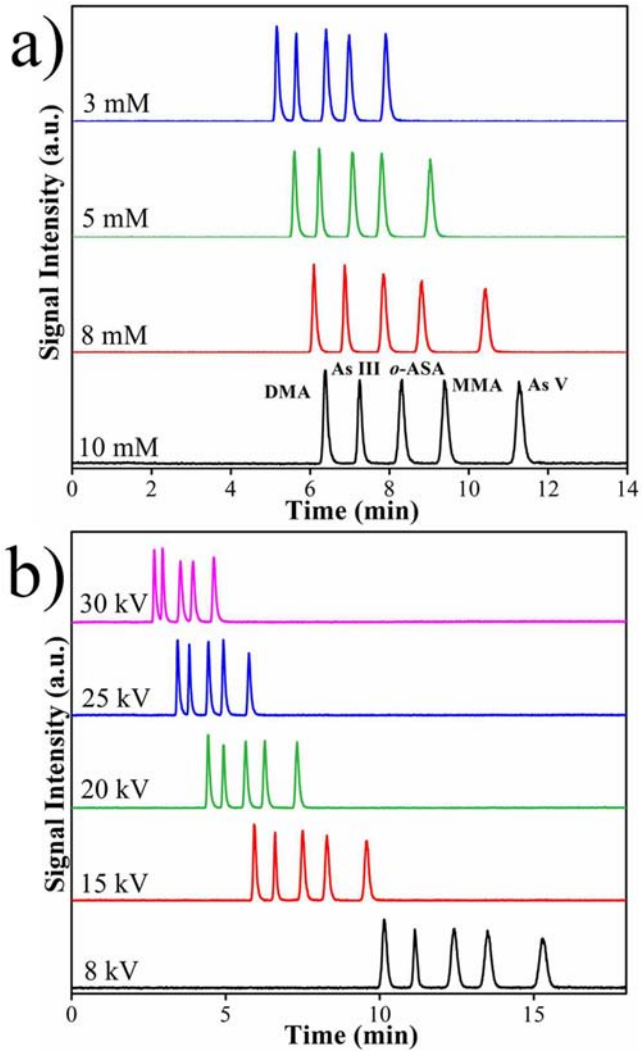

Figure 1. (a) Separation of five arsenic species under different buffer concentrations (voltage, 15 kV), and (b) effect of the applied voltage on the migration of arsenic species (buffer concentration, 5 mM). Other conditions: buffer, Na_2CO_3, pH, 11.

effects of the buffer concentration and voltage on the migration of arsenic species have been observed.[26,27]

The effects of pH on the separation of arsenic species were also evaluated. A basic condition with positive polarity was selected for CE separation to take advantage of the strong EOF toward the cathode. From Table 2, the acid dissociation constants (pK_a) of five As species ranged from 0.7 to 9.2. To maintain the magnitude of the EOF and avoid repeatability problems commonly encountered at weak basic conditions, moderate to strong basic conditions are favorable.[31] Because As(V) is eluted last, its migration ultimately determines the duration of the analysis. It was found that higher pH conditions

Table 2. Acid Dissociation Constants of As Species[31,35]

As species	formula	pK_a
As(V)	$O{=}As(OH)_3$	2.3, 6.8, 11.6
As(III)	$O{=}As(OH)$	9.2
DMA	$(CH_3)_2AsO(OH)$	6.2
MMA	$CH_3AsO(OH)_2$	3.6, 8.2
o-ASA	$H_2NC_6H_4AsO(OH)_2$	0.7, 3.8, 8.9

DOI: 10.1021/acs.jafc.5b00446
J. Agric. Food Chem. 2015, 63, 3153−3160

generated a faster EOF, increasing the migration speed of As(V), therefore reducing its overall retention time. Special attention was paid to DMA and As(III) for the accurate determination of their identities. In an earlier study, Liu and co-workers studied the migration behavior of multiple arsenic species in HBO_3 and NaH_2PO_4 buffers at different pH conditions. They found that, as the pH values of the buffer solution increased from 8.5 to 9.8, the elution time of As(III) also increased, whereas the elution time of DMA was almost unaffected.[26] We have observed a similar trend in our study. Furthermore, we discovered (Figure 2a) that, when the pH

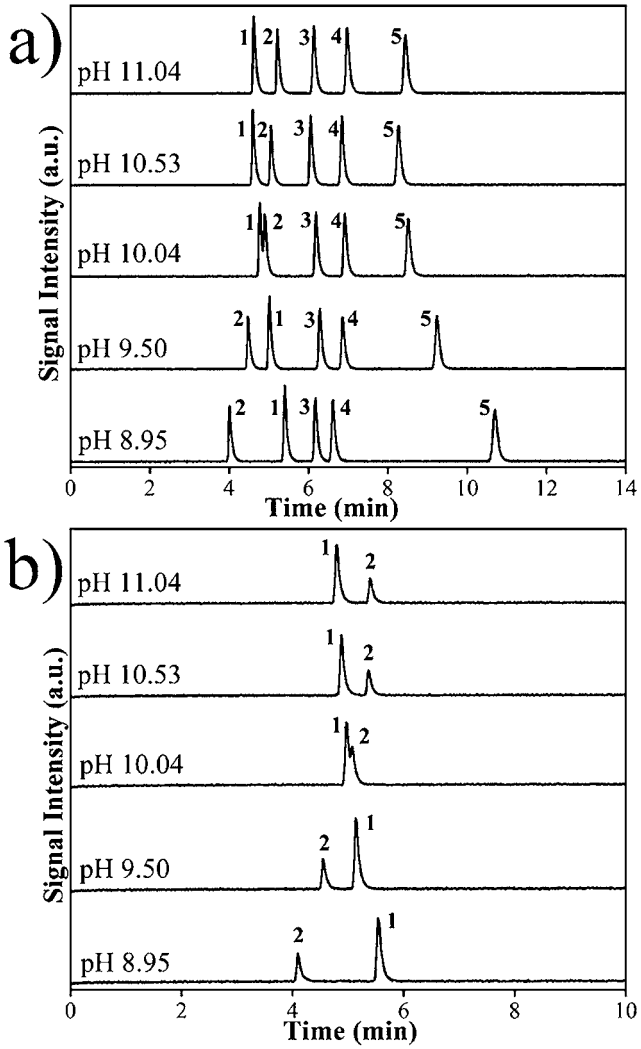

Figure 2. (a) Effect of the pH value on the migration of five arsenic species [1, DMA; 2, As(III); 3, *o*-ASA; 4, MMA; and 5, As(V)] and (b) electropherogram of a mixture containing 10 ng g^{-1} of DMA and 5 ng g^{-1} of As(III).

value of the running buffer increased beyond 10, the elution order of the peaks for DMA and As(III) reversed. The separation between As(III) and DMA first became less resolved at a pH of approximately 10 and then recovered at higher pH conditions. Because As(III) has a pK_a value of 9.2, it gradually acquired a negative charge when the pH was adjusted from 8.9 to 11. However, because DMA remained negatively charged throughout the entire range, its electrophoretic mobility was surpassed by that of As(III) at around pH 10 and the peaks of the two species were resolved at higher pH conditions. To verify the peak position of DMA and As(III), we analyzed a sample containing 10 ng g^{-1} of DMA and 5 ng g^{-1} of As(III) within the same pH range. It is clearly shown in Figure 2b that the elution time of As(III) and DMA continually changed as the pH increased.

Both injection pressure and time are factors that determine the injection plug length, which directly affects the precision of the method. Different combinations of pressure and time were tested to find the optimal conditions (see Table S-1 of the Supporting Information). All of the measurements with injection pressures above 30 mbar resulted in relative standard deviations (RSD %) higher than 10%. It is very clear that high injection pressures combined with relatively short injection times resulted in poor repeatability. A high applied pressure usually requires a much longer injection time to equilibrate the vacuum level change inside the capillary.[32] However, this would increase the plug length and enlarge the variation.[19] When a low pressure with a moderate injection time was applied, the precision was significantly improved. With an injection pressure of 15 mbar, the RSD % was reduced to an average of 5%. After both injection volume and precision of the method were considered, an applied pressure of 15 mbar with 8 s of injection time was chosen for the analysis. Additionally, in our study, the application of an internal standard mixed with sample effectively negated the variance caused by inconsistent injection volumes.

Analytical Performance. Figure 3 is a typical electropherogram of the separation of five arsenic compounds under

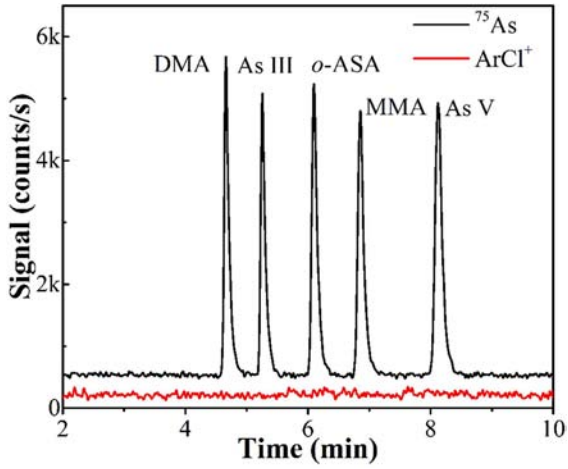

Figure 3. Electropherogram of a standard solution containing 5 ng g^{-1} of five arsenic species. m/z 77 was selected to monitor $ArCl^+$ (^{40}Ar and ^{37}Cl) interference.

optimized conditions (as presented in Table 1) at a level of 5 ng g^{-1}. Baseline separation was achieved for all species in less than 10 min. Hydrogen gas (H_2) was used as the reaction gas to eliminate the polyatomic interference of $ArCl^+$. A baseline was observed for m/z 77 ($^{40}Ar^{37}Cl^+$) during the assay, demonstrating the absence of interference. A calibration range of 0.5−20 ng g^{-1} was analyzed, and a linear relationship between the concentration and peak area was plotted. From previous studies, most of the rice samples surveyed have less than 200 ng g^{-1} of each arsenic species.[6,13,14] Because the extraction procedure usually involves a dilution factor of 10−20, our calibration range is sufficient to analyze most of the rice

DOI: 10.1021/acs.jafc.5b00446
J. Agric. Food Chem. 2015, 63, 3153−3160

products on the market. To further evaluate the method linearity, a standard spike (50 ng g^{-1}) at approximate 2.5 times the highest calibrator was analyzed. The results (see Table S-2 of the Supporting Information) suggested that acceptable recoveries were reached for all analytes. As listed in Table 3, the

Table 3. Analytical Performance of CE−ICPMS

			RSD %[a]			
compound	linear range (ng g^{-1})	R^2	migration time	peak area	LOD (ng g^{-1})[b]	LOQ (ng g^{-1})
DMA	0.5−20	0.998	0.82	2.62	0.27	0.87
MMA	0.5−20	0.999	1.08	2.08	0.16	0.52
As(III)	0.5−20	0.999	0.75	2.62	0.15	0.47
As(V)	0.5−20	0.997	1.23	2.91	0.24	0.75

[a]Sample concentration = 5 ng g^{-1} (n = 7). [b]Instrument detection limit.

RSD % (n = 7) for migration time ranged from 0.75 to 1.23% for four arsenic species. After adjustment for the signal variation, the RSD % of the peak area was between 2.08 and 2.91%, demonstrating satisfactory repeatability for this method. The limit of detection (LOD, 3σ criteria) was determined to be 0.27, 0.16, 0.15, and 0.24 ng g^{-1} for DMA, MMA, As(III), and As(V), respectively (Table 3).

Analysis of the Arsenic Concentration in Rice and Rice Cereal. The sample extraction procedure was performed prior to analysis to isolate arsenic species from the matrix. Previous studies have suggested several possible methods to extract common arsenic species from rice and rice products with acceptable confidence. Among these methods, nitric acid-assisted extraction has received a considerable amount of attention and was used in HPLC−ICPMS for arsenic speciation by many groups.[12,13,15] However, because the speciation in CE−ICPMS was carried out under basic pH conditions, injections of sample extracts from acid digestion negatively affect the results. Heat-assisted aqueous extraction is another effective alternative to fully extract arsenic from rice samples.[11] A common problem in this methodology is that large amounts of starch remain in the solution, which cannot be separated by simple centrifugation or filtration. Loss of resolution, peak broadening, and column deterioration because of carbohydrates was observed in previous studies.[11,14] Some methodologies have demonstrated that low-temperature extraction with enzymes or the addition of enzymes post-extraction can be effective in removing biological matrices, such as proteins and starch, in rice.[14,33,34] To simplify the procedure, we focused our efforts on a direct enzyme-assisted microwave digestion for the extraction process. It is known that thermally stable α-amylase is able to catalyze the hydrolysis of starches and break them down to smaller sugar molecules. The addition of this type of enzyme during the extraction should reduce matrix effects. To compare the extraction efficiency, rice samples were microwave-extracted with and without the addition of α-amylase during preparation. The analysis (see Figure S-1 of the Supporting Information) exhibited significantly higher signal responses for all arsenic species when the enzyme was added during the extraction. The migration of arsenic species was faster for samples extracted with the enzyme, which can also be attributed to the lower viscosity. The extracts were also digested with nitric acid and analyzed using ICPMS for total arsenic concentration to compare the results from the two different extraction methods. Upon evaluation of the analytical results, it was concluded that the two different extraction methods provide equivalent results.

We believe that the differences in signal response of samples prepared from two methods were primarily attributed to the viscosity of the extraction solution. In CE, the injection volume (V_{inj}) can be calculated by

$$V_{inj} = \frac{\Delta P d^4 \pi t_{inj}}{128 \eta L} \quad (1)$$

where ΔP is the pressure difference across the capillary, d is the capillary inner diameter, t_{inj} is the injection time, η is the buffer viscosity, and L is the total capillary length. When the viscosity of the sample solution increases, it will result in a decrease in total injection volume and a lower signal response. We have measured the viscosity of sample solutions from the extraction procedures with and without the addition of α-amylase. The results show that the viscosity is 7.5 ± 0.1 mPa s (T = 23.3 °C) in samples (rice 1) extracted with only water. If α-amylase is introduced into the extraction procedure, the viscosity dropped to 1.3 ± 0.1 mPa s (T = 23.3 °C). Additionally, a similar signal loss was also observed for o-ASA in samples extracted without the enzyme, and in both cases, the signal ratios of o-ASA to analytes of interest were the same. Because o-ASA was added as an internal standard post-extraction to both samples, the results support the conclusion that the signal difference is from sample viscosity rather than the extraction efficiency.

Under optimized conditions, common arsenic species in rice were successfully separated and detected by the CE−ICPMS methodology (Figure 4). Increased migration times were observed in the capillary column during analysis. We believe that this can be attributed to the dissolved sugar molecules left in the sample solution, which affected the movement of the analytes in the capillary. In addition to the four analytes of interest in this study, a trace amount of unknown arsenic species produced unidentified peaks. Rice and rice cereal (denoted as rice 1 and rice 2) acquired from a local market were analyzed. The rice powder was divided into two portions. One portion was digested with nitric acid for a total arsenic measurement. The second portion was first treated with the enzyme-assisted microwave digestion, and the supernatant was further analyzed by the CE−ICPMS method. From Table 4, the summation of the four arsenic species in the rice samples generated a quantitative value very close to the total arsenic amount. The recoveries were 96.2 and 92.2% for rice 1 and rice 2, respectively. Previous studies have suggested the possible existence of tetramethylarsonium and other trace amounts of arsenic species in rice grain.[13] These species may contribute up to 10% of the total arsenic amount, but in our case, the intensity of unknown peaks were insignificant. To assess the reliability of this method, two rice standard reference materials (NIST SRM 1568b and NMIJ CRM 7503-a) were assayed. The analytical results were compared to certified values. As summarized in Table 4, the quantitative values of organic arsenic and the sum value of inorganic arsenic were within 5% of the certified values of the two reference materials. Small differences between the quantitative and certified values for As(III) and As(V) were observed in rice flour CRM 7503-a reference materials. We believed that these differences were due to a well-documented interspecies conversion that may occur during the extraction process.[8,11]

DOI: 10.1021/acs.jafc.5b00446
J. Agric. Food Chem. 2015, 63, 3153−3160

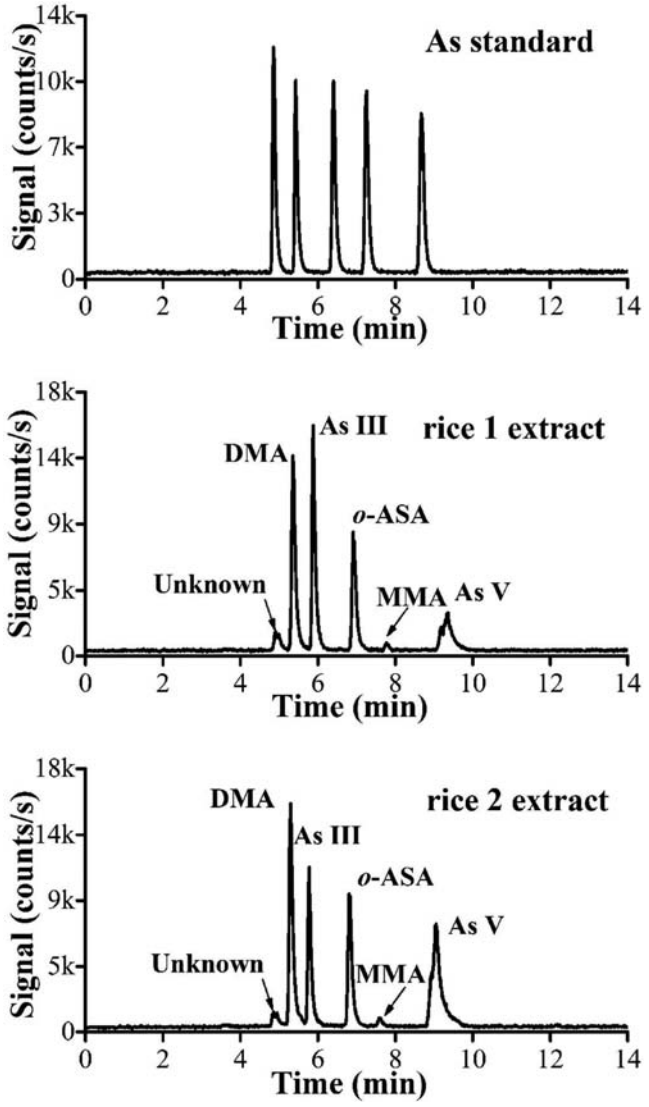

Figure 4. Electropherogram of arsenic standards and rice extracts with post extraction addition of *o*-AsA.

This study demonstrated a robust and reliable analytical method using CE−ICPMS, for the determination of common arsenic species, including DMA, MMA, As(III) and As(V), in rice and rice cereal by providing better separation efficiency over several liquid chromatography methods. An arsenic-containing compound *o*-ASA was used as an internal standard to compensate for signal drift and variance caused by the CE injection. Under a basic buffer condition of moderate concentration with a pH value around 11 and applied voltage of 20 kV, CE−ICPMS analysis can be completed within 10 min with excellent repeatability. The detection limits were determined to be lower than 0.3 ng g^{-1}, with a linear range from 0.5 to 20 ng g^{-1}. The linearity up to 50 ng g^{-1} was also demonstrated. The enzyme α-amylase was deemed necessary to achieve sufficient digestion and signal response. Rice samples purchased from a local market were successfully analyzed by this method, and the summed quantitative value of each arsenic species was consistent with the total arsenic quantitative concentration determined by standard ICPMS measurements. This methodology was further validated through the analysis of two rice standard reference materials. The quantitative results of DMA, MMA, and inorganic arsenic were well-matched with the certified values.

■ ASSOCIATED CONTENT

Supporting Information

Relative standard deviation (n = 5) of the peak area of arsenic species under different injection conditions (Table S-1), recovery values for As spikes at 2−3 times the highest calibration concentration (Table S-2), and electropherogram of the rice sample prepared by water-phase extraction and enzyme-assisted extraction (Figure S-1). This material is available free of charge via the Internet at http://pubs.acs.org.

■ AUTHOR INFORMATION

Corresponding Authors

*Telephone: +1-870-543-4665. Fax: +1-870-543-4041. E-mail: thilak.mudalige@fda.hhs.gov.

*Telephone: +1-870-543-4667. Fax: +1-870-543-4041. E-mail: sean.linder@fda.hhs.gov.

Funding

This project was supported in part by an appointment to the Research Participation Program at the Office of Regulatory Affairs/Arkansas Regional Laboratory, FDA, administered by the Oak Ridge Institute for Science and Education through an interagency agreement between the U.S. Department of Energy and the FDA. The views expressed in this document are those of the authors and should not be interpreted as the official opinion or policy of the FDA, Department of Health and Human Services, or any other agency or component of the U.S. government. The mention of trades names, commercial products, or organizations is for clarification of the methods

Table 4. Analytical Results of the Arsenic Concentration (ng g^{-1}) in Rice Samples and Rice Standard Reference Materials SRM 1568b and CRM 7503-a

sample[a]	DMA	MMA	As(III)	As(V)	inAs sum[b]	sum[c]	total[d]
SRM 1568b							
certified values	180 ± 12	11.6 ± 3.5			92 ± 10	284	285 ± 14
measured values	186.49 ± 3.10	11.62 ± 0.48	55.42 ± 1.90	40.92 ± 6.78	96.32 ± 5.71	294.45 ± 6.97	
CRM 7503-a							
certified values	13.3 ± 0.9		71.1 ± 2.9	13.0 ± 0.9	84 ± 3.8	97	98 ± 7
measured values	12.94 ± 1.15	<LOD	62.10 ± 1.73	19.27 ± 1.10	81.37 ± 0.92	94.31 ± 1.05	
rice 1	86.13 ± 1.64	<LOD	97.99 ± 2.38	37.51 ± 1.24	135.51 ± 3.52	221.63 ± 5.05	230.94 ± 1.21
rice 2	76.47 ± 3.55	<LOD	54.21 ± 5.61	84.75 ± 3.57	138.96 ± 2.04	215.43 ± 5.59	234.38 ± 3.82

[a] n = 3. [b] Combined value of As(III) and As(V). [c] Combined value of four arsenic species: DMA, MMA, As(III), and As(V). [d] Total arsenic concentrations in rice 1 and rice 2 were determined by ICPMS after a microwave acid digestion.

DOI: 10.1021/acs.jafc.5b00446
J. Agric. Food Chem. 2015, 63, 3153−3160

used and should not be interpreted as an endorsement of a product or manufacturer.

Notes

The authors declare no competing financial interest.

■ ACKNOWLEDGMENTS

These studies were conducted using the Nanotechnology Core Facility (NanoCore) located on the FDA's Jefferson Laboratories campus (Jefferson, AR), which houses the FDA National Center for Toxicological Research and the FDA Office of Regulatory Affairs Arkansas Regional Laboratory. The authors thank Ivan Quevedo, Jin-Hee Lim, Patrick Sisco, Yasith Nanayakkara, Douglas Heitkemper, Madhavi Mantha, Sean Conklin, and Gregory Noonan for their valuable comments on draft manuscript.

■ REFERENCES

(1) European Food Safety Authority (EFSA).. Scientific opinion on arsenic in food. EFSA Panel on Contaminants in the Food Chain (CONTAM). *EFSA J.* **2009**, *7*, 1531−1550.

(2) Williams, P. N.; Villada, A.; Deacon, C.; Raab, A.; Figuerola, J.; Green, A. J.; Feldmann, J.; Meharg, A. A. Greatly enhanced arsenic shoot assimilation in rice leads to elevated grain levels compared to wheat and barley. *Environ. Sci. Technol.* **2007**, *41*, 6854−6859.

(3) Pizarro, I.; Gómez, M.; Palacios, M.; Cámara, C. Evaluation of stability of arsenic species in rice. *Anal. Bioanal. Chem.* **2003**, *376*, 102−109.

(4) Codex Alimentarius Commission. *The Report of the Eighth Session of the Codex Committee on Contaminants in Foods*; Codex Alimentarius Commission: Rome, Italy, 2014.

(5) United States Food and Drug Administration (FDA). *FDA Statement on Testing and Analysis of Arsenic in Rice and Rice Products*; FDA: Silver Spring, MD, 2013.

(6) United States Food and Drug Administration (FDA). *Analytical Results from Inorganic Arsenic in Rice and Rice Products Sampling*; FDA: Silver Spring, MD, 2013.

(7) The International Agency for Research on Cancer (IRAC).. Some drinking-water disinfectants and contaminants, including arsenic. *IARC Monogr. Eval. Carcinog. Risks Hum.* **2004**, *84*, 1−477.

(8) Tyson, J. The determination of arsenic compounds: A critical review. *ISRN Anal. Chem.* **2013**, *2013*, 24.

(9) Clough, R.; Drennan-Harris, L. R.; Harrington, C. F.; Hill, S. J.; Tyson, J. F. Atomic spectrometry update. Elemental speciation. *J. Anal. At. Spectrom.* **2012**, *27*, 1185−1224.

(10) Francesconi, K. A.; Kuehnelt, D. Determination of arsenic species: A critical review of methods and applications, 2000−2003. *Analyst* **2004**, *129*, 373−395.

(11) Narukawa, T.; Chiba, K. Heat-assisted aqueous extraction of rice flour for arsenic speciation analysis. *J. Agric. Food. Chem.* **2010**, *58*, 8183−8188.

(12) Maher, W.; Foster, S.; Krikowa, F.; Donner, E.; Lombi, E. Measurement of inorganic arsenic species in rice after nitric acid extraction by HPLC−ICPMS: Verification using XANES. *Environ. Sci. Technol.* **2013**, *47*, 5821−5827.

(13) Huang, J. H.; Fecher, P.; Ilgen, G.; Hu, K. N.; Yang, J. Speciation of arsenite and arsenate in rice grain—Verification of nitric acid based extraction method and mass sample survey. *Food Chem.* **2012**, *130*, 453−459.

(14) Nookabkaew, S.; Rangkadilok, N.; Mahidol, C.; Promsuk, G.; Satayavivad, J. Determination of arsenic species in rice from Thailand and other Asian countries using simple extraction and HPLC−ICP−MS analysis. *J. Agric. Food. Chem.* **2013**, *61*, 6991−6998.

(15) Kubachka, K. M.; Shockey, N. V.; Hanley, T. A.; Conklin, S. D.; Heitkemper, D. T. *Elemental Analysis Manual: Section 4.11: Arsenic Speciation in Rice and Rice Products Using High Performance Liquid Chromatography−Inductively Coupled Plasma−Mass Spectrometric Determination. Version 1.1*; United States Food and Drug Administration (FDA): Silver Spring, MD, 2012.

(16) Křížek, T.; Doubnerová, V.; Ryšlavá, H.; Coufal, P.; Bosáková, Z. Offline and online capillary electrophoresis enzyme assays of *β*-*N*-acetylhexosaminidase. *Anal. Bioanal. Chem.* **2013**, *405*, 2425−2434.

(17) Albrecht, J. C.; Lin, J. S.; Barron, A. E. A 265-base DNA sequencing read by capillary electrophoresis with no separation matrix. *Anal. Chem.* **2010**, *83*, 509−515.

(18) Al Azzam, K. M.; Saad, B.; Aboul-Enein, H. Y. Simultaneous determination of atenolol, chlorthalidone and amiloride in pharmaceutical preparations by capillary zone electrophoresis with ultraviolet detection. *Biomed. Chromatogr.* **2010**, *24*, 977−981.

(19) Lauer, H. H.; Rozing, G. P. *High Performance Capillary Electrophoresis*; Agilent Technologies, Inc.: Santa Clara, CA, 2010.

(20) Chausseau, M.; Roussel, C.; Gilon, N.; Mermet, J. M. Optimization of HPLC−ICP−AES for the determination of arsenic species. *Fresenius' J. Anal. Chem.* **2000**, *366*, 476−480.

(21) Karthikeyan, S.; Hirata, S. Simultaneous determination of arsenic(III) and arsenic(V) by flow injection−inductively coupled plasma−atomic emission spectrometry (ICP−AES) with ultrasonic nebulization. *Anal. Bioanal. Chem.* **2003**, *375*, 139−144.

(22) Kohlmeyer, U.; Jantzen, E.; Kuballa, J.; Jakubik, S. Benefits of high resolution IC−ICP−MS for the routine analysis of inorganic and organic arsenic species in food products of marine and terrestrial origin. *Anal. Bioanal. Chem.* **2003**, *377*, 6−13.

(23) Koellensperger, G.; Nurmi, J.; Hann, S.; Stingeder, G.; Fitz, W. J.; Wenzel, W. W. CE−ICP−SFMS and HPIC−ICP−SFMS for arsenic speciation in soil solution and soil water extracts. *J. Anal. At. Spectrom.* **2002**, *17*, 1042−1047.

(24) Li, B.-H. Rapid speciation analysis of mercury by short column capillary electrophoresis on-line coupled with inductively coupled plasma mass spectrometry. *Anal. Methods* **2011**, *3*, 116−121.

(25) Yang, G.; Xu, J.; Zheng, J.; Xu, X.; Wang, W.; Xu, L.; Chen, G.; Fu, F. Speciation analysis of arsenic in *Mya arenaria* Linnaeus and shrimp with capillary electrophoresis−inductively coupled plasma mass spectrometry. *Talanta* **2009**, *78*, 471−476.

(26) Liu, L.; He, B.; Yun, Z.; Sun, J.; Jiang, G. Speciation analysis of arsenic compounds by capillary electrophoresis on-line coupled with inductively coupled plasma mass spectrometry using a novel interface. *J. Chromatogr. A* **2013**, *1304*, 227−233.

(27) Liu, L.; Yun, Z.; He, B.; Jiang, G. Efficient interface for online coupling of capillary electrophoresis with inductively coupled plasma−mass spectrometry and its application in simultaneous speciation analysis of arsenic and selenium. *Anal. Chem.* **2014**, *86*, 8167−8175.

(28) Larsen, E. H.; Sturup, S. Carbon-enhanced inductively coupled plasma mass spectrometric detection of arsenic and selenium and its application to arsenic speciation. *J. Anal. At. Spectrom.* **1994**, *9*, 1099−1105.

(29) Baba, K.; Arao, T.; Maejima, Y.; Watanabe, E.; Eun, H.; Ishizaka, M. Arsenic speciation in rice and soil containing related compounds of chemical warfare agents. *Anal. Chem.* **2008**, *80*, 5768−5775.

(30) Feldmann, I.; Jakubowski, N.; Thomas, C.; Stuewer, D. Application of a hexapole collision and reaction cell in ICP−MS Part II: Analytical figures of merit and first applications. *Fresenius' J. Anal. Chem.* **1999**, *365*, 422−428.

(31) Rosal, C. G.; Momplaisir, G.-M.; Heithmar, E. M. Roxarsone and transformation products in chicken manure: Determination by capillary electrophoresis−inductively coupled plasma−mass spectrometry. *Electrophoresis* **2005**, *26*, 1606−1614.

(32) Mayer, B. X. How to increase precision in capillary electrophoresis. *J. Chromatogr. A* **2001**, *907*, 21−37.

(33) Diaz Huerta, V.; Hinojosa Reyes, L.; Marchante-Gayon, J. M.; Fernandez Sanchez, M. L.; Sanz-Medel, A. Total determination and quantitative speciation analysis of selenium in yeast and wheat flour by isotope dilution analysis ICP−MS. *J. Anal. At. Spectrom.* **2003**, *18*, 1243−1247.

(34) Guzmán Mar, J. L.; Hinojosa Reyes, L.; Mizanur Rahman, G. M.; Kingston, H. M. S. Simultaneous extraction of arsenic and selenium species from rice products by microwave-assisted enzymatic

DOI: 10.1021/acs.jafc.5b00446
J. Agric. Food Chem. 2015, 63, 3153−3160

extraction and analysis by ion chromatography−inductively coupled plasma−mass spectrometry. *J. Agric. Food. Chem.* **2009**, *57*, 3005−3013.
(35) Buckingham, J. *Dictionary of Organic Compounds*; CRC Press: Boca Raton, FL, 1987; Vol. *8*.

DOI: 10.1021/acs.jafc.5b00446
J. Agric. Food Chem. 2015, 63, 3153−3160

with fluorescence detection (UPLC-FLD) method for the analysis of nitro-PAHs. The method involves Fe/H^+-induced reduction of the nitro-PAHs to amino-PAHs that are intensely fluorescent for the indirect analysis of nitro-PAHs by UPLC-FLD (Figure 1). Derivatization conditions such as the reaction

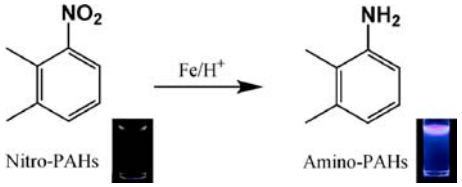

Figure 1. Fe/H^+-induced nitro-reduction of nonfluorescing nitro-PAHs forms fluorescent amino-PAHs for UPLC-FLD analysis.

temperature, reaction time, and amount of acid in the reaction medium were optimized for the highest reaction yield of the amino-PAH derivatives for the sensitive determination of nitro-PAHs by UPLC-FLD. Our developed method offering superior sensitivity was validated and applied in quantifying nitro-PAHs in different foodstuffs.

MATERIALS AND METHODS

Chemicals and Reagents. All chemicals and reagents of the highest purity available were used without further purification unless otherwise stated. 1-Nitronaphthalene (1-NN, 99%), 2-nitrofluorene (2-NF, 98%), and 1-nitropyrene (1-NP, 99%) were obtained from Sigma (St. Louis, MO, USA). Meat products were obtained from local supermarkets. HPLC grade acetonitrile was purchased from Tedia (Fairfield, OH, USA). *n*-Hexane and dichloromethane (DCM) were obtained from Mallinckrodt (St. Louis, MO, USA). Water was produced by a Milli-Q Ultrapure water system with the water outlet operating at 18.2 MΩ (Billerica, MA, USA).

Instrumentation. UPLC-FLD analysis was performed on an Agilent 1260 Infinity LC system (Palo Alto, CA, USA) equipped with a diode array and a FLD detector. High mass accuracy mass spectrometric and collision-induced dissociation (CID) mass spectrometric analyses were performed on a hybrid quadrupole time-of-flight mass spectrometer with a standard electrospray ionization interface (Xevo G2 Q-TOF, Waters, Milford, MA, USA) in positive ionization mode.

Sample Preparation. *Extraction.* Meat products were cut into small slices, lyophilized, and ground using a mortar and pestle. Prior to analysis, approximately 1 g of the powdered meat samples was accurately weighed and extracted with 20 mL of DCM by sonication. After 30 min of ultrasonication at room temperature, the samples were filtered through PTFE filter papers (20 μm, Whatman) to separate the meat powder from the sample extracts. The filtrates after evaporation of DCM were resuspended in 1 mL of *n*-hexane and loaded onto silica SPE columns for sample cleanup.

SPE Purification. The sample extracts were loaded onto Waters silica Sep-Pak SPE cartridges, which were conditioned with 10 mL of DCM followed by 10 mL of *n*-hexane for sample cleanup. After loading the sample, the columns were eluted with 2 mL of *n*-hexane and 6 mL of *n*-hexane/DCM (75:25, v/v). The eluates were collected and evaporated to dryness under nitrogen. The residue was dissolved in 1.5 mL of acetonitrile and centrifuged at 13800 rpm for 5 min prior to Fe/H^+ treatment.

Fe/H^+ Treatment. To 100 μL of the concentrated extracts were added 900 μL of acidified methanol (15% acetic acid, v/v) and 10 mg of iron powder. The sample mixture after vortex mixing was incubated at 60 °C for 40 min with periodic mixing. The Fe/H^+-treated samples after being cooled to room temperature were centrifuged at 13800 rpm for 10 min before the supernatant was transferred to an HPLC vial for UPLC-FLD analysis.

Determination of Derivatization Efficiency. The efficiency of reducing the nitro-PAHs to their corresponding amino-PAHs under the developed condition was evaluated by UPLC-UV analysis (254 nm) of nitro-PAHs under the same LC conditions as described above. Specifically, a standard solution mixture of nitro-PAHs at 40 μg/mL was prepared and analyzed before and after the Fe/H^+ treatment. According to the relative peak areas of nitro-PAHs, reaction efficiency was calculated.

UPLC-FLD Analysis. Ten microliters of the Fe/H^+-treated sample extract was injected on an Agilent Eclipse Plus C18 column (100 mm × 3.0 mm, 1.8 μm) thermostated at 40 °C for chromatographic separation. The column was eluted with a binary solvent system, with solvent A being water and solvent B being acetonitrile. Gradient elution at a constant flow rate of 0.5 mL/min was adopted, with the solvent gradient as follows: 30% B programmed linearly to 100% B in 10 min and held for another 5 min before reconditioning. The UPLC was coupled to a programmable FLD with the FLD time-programmed at excitation/emission wavelengths ($\lambda_{ex}/\lambda_{em}$) as follows: 0−6.3 min, λ_{ex} 240 and λ_{em} 430 nm; 6.3−7.6 min, λ_{ex} 280 and λ_{em} 370 nm; 7.6−15 min, λ_{ex} 240 and λ_{em} 435 nm.

Calibration and Method Validation. A stock solution mixture of 1-NN, 2-NF, and 1-NP at 460, 375, and 412.5 mg/L, respectively, was prepared in methanol and stored at −20 °C until diluted and Fe/H^+ treated for UPLC-FLD analysis. The working standard solutions of 1-NN (0.05−4.6 μg/mL), 2-NF (0.04−3.75 μg/mL), and 1-NP (0.04−4.13 μg/mL) were prepared by diluting the nitro-PAH stock solution mixture with methanol, derivatized, and UPLC-FLD analyzed as described above. Calibration curves were established by plotting the peak areas of the amino-PAHs against the nitro-PAHs concentrations in the calibration standard solutions.

The optimized method was also validated for analytical sensitivity, precision, and accuracy. The limit of detection (LOD) was established as the amount of nitro-PAH that generated a response 3 times the standard deviation of the analytical signal from replicated analyses (n = 7) of 1-NN, 2-NF, and 1-NP at 0.05, 0.04, and 0.04 μg/mL, respectively.[16,20] The method precision was evaluated by analyzing ham extracts spiked with nitro-PAHs at three concentrations (1-NN, 11.5, 115, and 460 μg/L; 2-NF, 9.4, 93.8, and 375 μg/L; 1-NP, 10.3, 103.1, and 412.5 μg/L), on the same day (n = 5) and over five separate days in a month. The method accuracy was determined by spiking nitro-PAHs at the three stated concentrations to ham sample matrix, SPE enriched, reduced by Fe/H^+ treatment, and analyzed using the UPLC-FLD method described above.

RESULTS AND DISCUSSION

Preparation and Characterization of the Nitro-reduction Product of Nitro-PAHs. The analysis of carcinogenic nitro-PAHs is challenging due to their low concentrations and the presence of complex matrices of food and environmental samples. The molecular fluorescence of nitro-PAHs, although rigid polycyclic compounds, is not observed due to the presence of the fluorescence-inhibiting nitro group.[6,16,17] Therefore, the analysis of nitro-PAHs by fluorescence detection, one of the most sensitive analytical methods, is hampered.[6] Few reports on the use of fluorescence in detecting nitro-PAHs in meat samples were reported in the literature. We report in this study the development of a simple and robust method converting nitro-PAHs to amino-PAHs facilitating their analysis by UPLC-FLD (Figure 1).

The commonly identified food- and environment-contaminating nitro-PAHs, namely, 1-NN, 2-NF, and 1-NP, were targeted in this study.[12] Upon treatment with powdered iron in an acidic medium, the nitro-PAHs were reduced to their corresponding amino-PAHs. The reduction products were characterized by fluorescence spectrophotometry. Depicted in Figure 2 are the fluorescence excitation and emission spectra of the amino-PAHs. Due to the very much differentiated

DOI: 10.1021/acs.jafc.5b00523
J. Agric. Food Chem. 2015, 63, 3161−3167

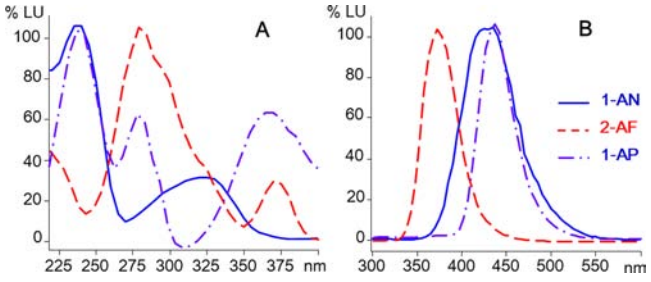

Figure 2. Fluorescence excitation (A) and emission (B) spectra of the amino-PAHs formed by reduction of nitro-PAHs.

fluorescence excitation (λ_{ex}) and emission maximum (λ_{em}) wavelength of the target analytes, a programmed compound-dependent fluorescence detection method was adopted in this study for the sensitive and selective quantification of nitro-PAHs in food samples (see Materials and Methods).

The resultant amino-PAHs were also analyzed by high mass accuracy mass spectrometry and collision-induced dissociation (CID) mass spectrometry. High mass accuracy mass spectrometric analysis of the HPLC eluate collected at 5.75, 6.97, and 8.38 min showed $[M + H]^+$ ion peaks at 144.0810, 182.0971, and 218.0971, respectively (Supporting Information Figure S1), which correlated closely with that of the theoretical m/z values for 1-aminonaphthalene (144.0808), 2-aminofluorene (182.0964), and 1-aminopyrene (218.0964). Product ion scan MS/MS analyses of the pseudomolecular ions produced a major fragment ion of m/z value 17 Da less than their corresponding parent ions, originating from the neutral loss of the exocyclic amino group. Both findings lead to a common conclusion that the fluorescing products were amino-PAHs.

Optimization of Fe/H$^+$-Induced Nitro-reduction Parameters. The heterogeneous reducing agent of iron powder in an acidic medium was adopted for this study to reduce the nonfluorescent nitro-PAHs to amino-PAHs, which strongly fluoresce for UPLC-FLD analysis (Figure 1). Factors affecting the nitro-reduction process were optimized for the highest yield of the amino-PAHs. Specifically, the concentration of acetic acid, the reaction time, and the reaction temperature were investigated for the highest analytical signal in UPLC-FLD analysis.

With the reduction medium containing a fixed acetic acid content (15%, v/v), the effects of various reaction temperatures (from 25 to 70 °C) and reaction times (from 0 to 120 min) in different reactions were investigated. It was found in UPLC-FLD analyses that 40 min of heating (Figure 3A) at 60 °C (Figure 3B) is the most efficient condition for producing the fluorescing amino-PAHs. Further increases in reaction time and reaction temperature were found to have a negative impact on the analytical signal. We postulated that the predominance of the inadvertent amino-oxidation process over nitro-reduction reaction in the adverse heating condition reduced the population of the fluorescing amino-PAHs, thus their detector response in the UPLC-FLD analyses.

We then investigated the effect of different acetic acid contents (from 1 to 25%, v/v) on the reduction yield. Our results showed that 15% acetic acid in methanol (v/v) gave the best detector response (Figure 3C). Under the above developed nitro-reduction conditions, the reduction yields of amino-PAHs were found to be >97% (Figure 4), indicating the Fe/H$^+$-induced nitro-reduction process is highly efficient. Depicted in Figure 3 are the relative peak areas from analyzing

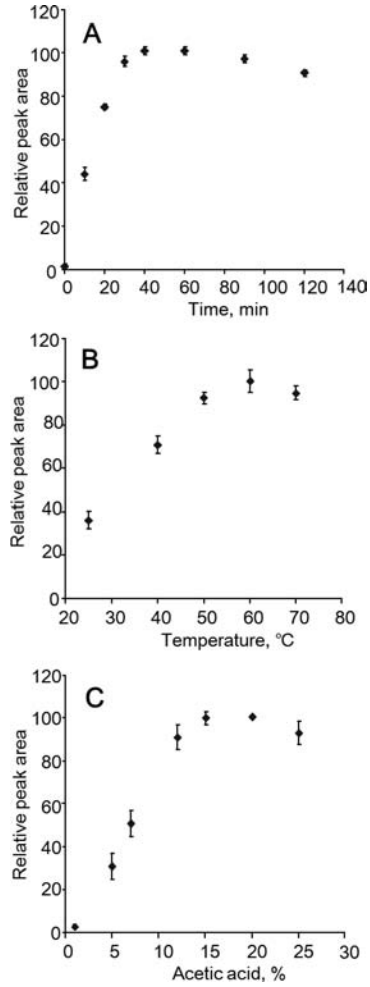

Figure 3. Influence of (A, 60 °C) reaction time, (B, 40 min) reaction temperature, and (C) acetic acid content on the reaction efficiency of the Fe/H$^+$-induced nitro-reduction of nitro-PAHs. The data represent the mean ± SD of three independent experiments with 1-NN at 4.6 μg/mL.

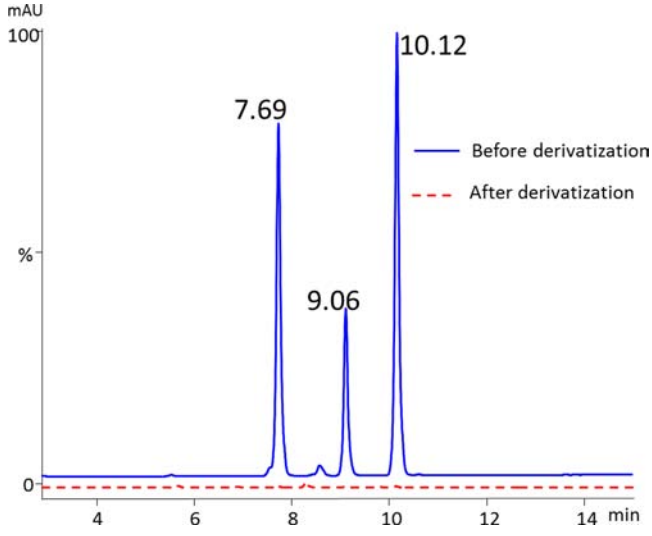

Figure 4. UPLC-UV analysis of underivatized and Fe/H$^+$-treated nitro-PAHs. 1-NN, 2-NF, and 1-NP were eluted at retention times of 7.69, 9.06, and 10.12 min, respectively.

DOI: 10.1021/acs.jafc.5b00523
J. Agric. Food Chem. 2015, 63, 3161−3167

the reaction mixtures in the different derivatization conditions. The optimized derivatization parameters of heating at 60 °C for 40 min in 15% acetic acid (v/v) were selected and used in all subsequent studies quantifying nitro-PAHs in meat products.

Calibration, Recovery, and Method Validation. Calibration curves were established by derivatizing and UPLC-FLD analyzing standard solution mixtures of nitro-PAHs in triplicate reactions using the optimized method described above. The concentrations of individual nitro-PAHs ranged from 0.04 to 4.6 μg/mL. The peak areas of amino-PAHs increased linearly over the tested concentration range, with coefficients of determination (R^2) >0.9994, indicating that the nitro-reduction step is highly quantitative. Table 1 summarizes the calibration slopes, intercepts, and coefficients of determination for the nitro-PAHs. Depicted in Figure 5A is a typical chromatogram obtained from analyzing the standard mixture.

Table 1. Linear Regression Parameters of the Calibration Curves and Limit of Detection (LOD) of the Developed UPLC-FLD Method

	1-NN	2-NF	1-NP
linear range (μg/mL)	0.05−4.60	0.04−3.75	0.04−4.13
slope[a]	1009.6 ± 89.8	1384.5 ± 68.6	1902.9 ± 146.9
intercept[a]	−58.4 ± 5.4	−37.5 ± 4.4	−73.3 ± 8.3
R^2	0.9994	0.9996	0.9997
LOD (μg/L)	5.9	5.1	3.1
LOD[b] (μg/kg)	0.59	0.51	0.31
LOQ[c] (μg/kg)	1.97	1.70	1.03

[a]The data represent the mean ± SD for three independent experiments. [b]The LOD is the sample extract based on 1 g of sample. [c]Limit of quantitation, S/N = 10.

The recovery of the method, as determined by spiking nitro-PAHs at three concentrations (1-NN, 11.5, 115, and 460 μg/L; 2-NF, 9.4, 93.8, and 375 μg/L; 1-NP, 10.3, 103.1, and 412.5 μg/L) to a ham sample matrix, SPE purified, Fe/H^+ treated, and UPLC-analyzed using the method described above were found to be 78.1 ± 4.8, 84.3 ± 2.8, and 78.5 ± 2.2%, respectively. Measurements of 1-NN, 2-NF, and 1-NP were thus corrected by factors of 1.28, 1.19, and 1.27 to achieve their respective concentrations in the meat samples.

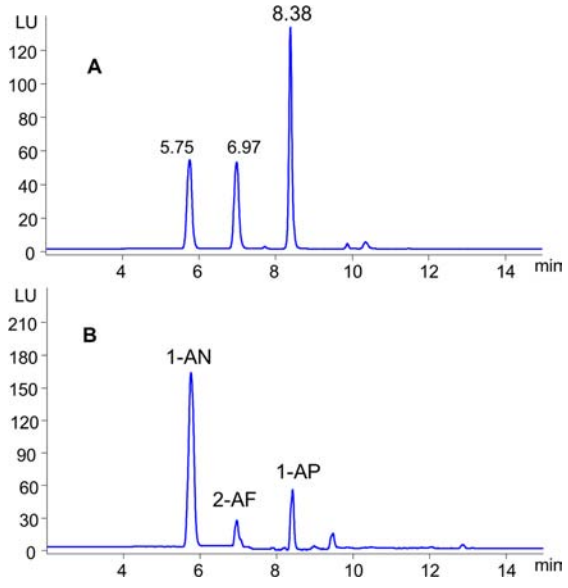

Figure 5. Typical chromatograms obtained from UPLC-FLD analyses of Fe/H^+-treated (A) standard mixture (1-NN, 0.5 μg/mL; 2-NF, 0.4 μg/mL; and 1-NP, 0.4 μg/mL) and (B) fresh chicken sample extract. The chromatographic retention times of 1-AN, 2-AF, and 1-AP were 5.75, 6.97, and 8.38 min, respectively.

The intraday precision of the analytical method for determining nitro-PAHs at low, medium, and high concentrations revealed relative standard deviation (RSD) of <6.4% for within-day analyses (n = 5). Over a period of 1 month, the RSD for individual nitro-PAHs measurements ranged from 7.5 to 12.8% (n = 5). The data of reproducibility and accuracy shown in Table 2 demonstrate good performance of UPLC-FLD method for the quantitative analysis of nitro-PAHs in the complex matrix of food products. The high reproducibility of the method allowed the analysis to be performed without the use of an internal standard.

Table 2. Validation Parameters of the Developed Method for the Determination of 1-NN, 2-NF, and 1-NP in Meat Samples

		accuracy		precision[a]	
	concn spiked (μg/kg)	concn found (μg/kg)	recovery (%)	intraday (% RSD)	interday (% RSD)
1-NN	11.5	8.9 ± 0.9	77.7 ± 7.8	6.3	12.8
	115	87.8 ± 3.7	76.3 ± 3.2	4.7	11.0
	460	369.1 ± 15.7	80.2 ± 3.4	5.5	8.8
2-NF	9.4	8.3 ± 0.4	88.7 ± 4.2	6.4	7.5
	93.8	68.6 ± 1.9	73.1 ± 2.0	5.9	10.9
	375	341.4 ± 8.2	91.0 ± 2.2	2.6	10.4
1-NP	10.3	8.3 ± 0.3	80.8 ± 2.6	4.9	7.6
	103.1	75.7 ± 0.4	73.4 ± 0.4	6.0	10.1
	412.5	339.9 ± 14.9	81.3 ± 3.6	2.2	11.9

[a]n = 5.

Determination of Nitro-PAHs in Meat Products. The developed method combining precolumn nitro-reduction and UPLC-FLD analysis was applied to the quantification of 1-NN, 2-NF, and 1-NP in meat products. Twenty frozen meat samples (Table 3) including chicken, pork, beef, ham, salmon, etc., were randomly selected from supermarkets in Hong Kong. These samples were processed and tested for the presence of nitro-PAHs using the newly developed method. Figure 5B shows a typical chromatogram obtained from UPLC-FLD analysis of fresh chicken sample using the developed method.

Interestingly, our results revealed that 1-NN was the most commonly identified nitro-PAH in the collected meat products (Table 3). Among the tested samples, 1-NN was detected at its highest levels in fresh chicken (158.1 ± 40.5 μg/kg) and smoked salmon (161.7 ± 29.5 μg/kg) samples. On the contrary, 2-NF was reported to be the most commonly identified nitro-PAHs by Schlemitz and Pfannhauser.[12] It is our belief that the choice of samples may explain the bulk of the observed discrepancy. Whereas a combination of fresh and cured meat products was chosen in this study, most of the food commodities chosen by Schlemits and Pfannhauser were heat-treated foods.[12]

Furthermore, our results showed significantly higher levels of nitro-PAHs in most of the food products than those tested by

DOI: 10.1021/acs.jafc.5b00523
J. Agric. Food Chem. 2015, 63, 3161−3167

Table 3. Determination of Nitro-PAHs in Meat Samples by the Developed UPLC-FLD Method[a]

		1-NN[b] (μg/kg)	2-NF[b] (μg/kg)	1-NP[b] (μg/kg)	total (μg/kg)
1	fresh chicken	158.1 ± 40.5	18.8 ± 6.7	18.5 ± 2.7	195.4
	boiled chicken	22.5 ± 4.8	15.6 ± 1.3	5.1 ± 0.8	43.2
	grilled chicken	ND[c]	ND	ND	ND
2	fresh pork	2.8 ± 0.3	<LOQ	1.4 ± 0.4	4.2
	boiled pork	<LOQ[d]	<LOQ	2.0 ± 0.1	2.0
	grilled pork	<LOQ	ND	ND	<LOQ
3	fresh beef	2.3 ± 0.4	ND	ND	2.3
	boiled beef	2.6 ± 0.6	ND	ND	2.6
	grilled beef	2.1 ± 0.4	ND	ND	2.1
4	ham	<LOQ	ND	ND	<LOQ
	boiled ham	3.5 ± 0.3	<LOQ	ND	3.5
	grilled ham	29.2 ± 5.9	ND	<LOQ	29.2
5	red sausage	6.4 ± 1.1	10.6 ± 2.6	21.5 ± 5.6	38.5
6	chicken sausage	<LOQ	ND	<LOQ	<LOQ
7	pork sausage	6.2 ± 0.1	ND	ND	6.2
8	sausage	7.6 ± 1.6	241.7 ± 48.8	<LOQ	249.3
9	short sausage	ND	ND	ND	ND
10	sweet sausage	ND	ND	ND	ND
11	ground chicken	<LOQ	69.2 ± 4.8	<LOQ	69.2
12	hamburger meat	<LOQ	ND	ND	<LOQ
13	smoked bacon	<LOQ	ND	<LOQ	<LOQ
14	smoked salmon	161.7 ± 29.5	ND	ND	161.7
15	smoked duck breast	2.6 ± 0.3	ND	<LOQ	2.6
16	canned pork	<LOQ	ND	ND	<LOQ
17	canned beef	2.2 ± 0.5	<LOQ	<LOQ	2.2
18	BBQ chicken	12.3 ± 4.5	ND	ND	12.3
19	BBQ pork	5.3 ± 0.3	ND	ND	5.3
20	BBQ beef	7.6 ± 1.2	ND	ND	7.6

[a]The data represent the mean ± SD for three independent determinations. [b]Sample extracts were 10-fold diluted before the UPLC-FLD analysis. [c]Not detected. [d]Limit of quantitation, S/N = 10.

Schlemitz and Pfannhauser.[12] The difference is partly attributed to the different choices of samples, as described above. Food processing by heat treatment may cause thermal decomposition of nitro-PAHs and therefore lead to lower nitro-PAH content. The other potential cause for the observed discrepancy includes differences in the sample preparation methods that were used. Whereas Schlemitz and Pfannhauser extracted nitro-PAHs from the food sample with acetonitrile at 98 °C,[12] a milder condition of ultrasonication at room temperature was employed in our study. As will be discussed in detail shortly, high-temperature food processing may reduce the nitro-PAH content in fresh meat products.

1-NP, being one of the most mutagenic compounds and marker molecules for diesel exhaust,[21−23] was detected in a few of the tested samples. UPLC-FLD analysis identified 1-NP at concentrations dramatically lower than that of 1-NN. This result is in fairly good agreement with the results of Schlemitz and Pfannhauser, who reported low microgram per kilogram levels of 1-NP in selected meat products.[12] The trend of nitro-PAHs levels is also in line with the reported levels of 1-NN, 2-NF, and 1-NP in the ambient environment in selected locations around the world. It was reported that 1-NN and 2-NF were detected at levels significantly higher than that of 1-NP in both urban and suburban areas.[24] Therefore, results from this study may provide evidence linking environmental pollution to nitro-PAHs in meat products.

Effect of Thermal Processing on Nitro-PAH Contents in Food Products. Our results also revealed high-temperature food processing to have pronounced, but dramatically differentiated, effects on the levels of nitro-PAHs in fresh and cured food commodities. As elucidated from studies in fresh chicken samples (sample 1), heat treatment produced a temperature-dependent decrease in the levels of 1-NN, 2-NF, and 1-NP in the chicken samples. Potential reasons for the observed decline in nitro-PAH levels include dissolvation of nitro-PAHs in the cooking water/oil or thermal decomposition of nitro-PAHs during the cooking process.

On the contrary, ham cooked by boiling in water or stir-frying was observed to have a pronounced effect in elevating the level of 1-NN (sample 4). A temperature-dependent increase in 1-NN concentration was observed in ham cooked in boiling water (100 °C) and in corn oil (250 °C). With ham being a cured meat product containing higher levels of nitrate and nitrite salts (>100 mg/kg) than fresh meats,[25,26] it is possible that nitro-PAHs are formed by reacting nitrate/nitrite with PAHs in the meat and that the nitro-PAH formation outweighed the thermal decomposition/dissolvation. Therefore, elevated nitro-PAH content was observed in the cooked ham samples.

DOI: 10.1021/acs.jafc.5b00523
J. Agric. Food Chem. 2015, 63, 3161−3167

In summary, we have developed a sensitive and selective UPLC-FLD method for the determination of nitro-PAHs in meat products. The combination of precolumn nitro-reduction and UPLC-FLD analysis allows confident determination of 1-NN, 2-NF, and 1-NP at sub parts per billion levels. The method after validating for accuracy and precision was applied for the determination of nitro-PAHs in fresh and cured meat products. High levels of nitro-PAHs were detected in fresh chicken (195.4 μg/kg) and smoked salmon (161.7 μg/kg). For the first time, our study revealed that high-temperature food processing has a pronounced, but differentiated, effect on nitro-PAHs in fresh and cured meats.

■ ASSOCIATED CONTENT

Supporting Information

High-accuracy MS spectra of 1-aminonaphthalene, 2-aminofluorene, and 1-aminopyrene that were formed from Fe/H^+-induced nitro-reduction of 1-nitronaphthalene, 2-nitrofluorene, and 1-nitropyrene, respectively. This material is available free of charge via the Internet at http://pubs.acs.org.

■ AUTHOR INFORMATION

Corresponding Author

*(W.C.) Phone: +852-2358-7370. Fax: +852-2358-1594. E-mail: chanwan@ust.hk.

Funding

W.C. expresses his sincere thanks to The Hong Kong University of Science and Technology for supporting this research (Grant R9310).

Notes

The authors declare no competing financial interest.

■ ACKNOWLEDGMENTS

We extend thanks to Prof. Jianzhen Yu (Department of Chemistry, The Hong Kong University of Science and Technology) for providing the fluorescence detector for this research. We also extend thanks to AB Sciex for providing the UPLC for this study.

■ REFERENCES

(1) Pham, C. T.; Kameda, T.; Toriba, A.; Hayakawa, K. Polycyclic aromatic hydrocarbons and nitropolycyclic aromatic hydrocarbons in particulates emitted by motorcycles. *Environ. Pollut.* **2013**, *183*, 175−183.

(2) Rosenkranz, H. S. Mutagenic nitroarenes, diesel emissions, particulate-induced mutations and cancer: an essay on cancer-causation by a moving target. *Mutat. Res.* **1996**, *367*, 65−72.

(3) Heeb, N. V.; Schmid, P.; Kohler, M.; Gujer, E.; Zennegg, M.; Wenger, D.; Wichser, A.; Ulrich, A.; Gfeller, U.; Honegger, P.; Zeyer, K.; Emmenegger, L.; Petermann, J. L.; Czerwinski, J.; Mosimann, T.; Kasper, M.; Mayer, A. Secondary effects of catalytic diesel particulate filters: conversion of PAHs versus formation of nitro-PAHs. *Environ. Sci. Technol.* **2008**, *42*, 3773−3779.

(4) Durant, J. L.; Busby, W. F., Jr.; Lafleur, A. L.; Penman, B. W.; Crespi, C. L. Human cell mutagenicity of oxygenated, nitrated and unsubstituted polycyclic aromatic hydrocarbons associated with urban aerosols. *Mutat. Res.* **1996**, *371*, 123−157.

(5) Sasaki, J.; Arey, J.; Harger, W. P. Formation of mutagens from the photooxidations of 2−4-ring PAH. *Environ. Sci. Technol.* **1995**, *29*, 1324−1335.

(6) Zielinska, B.; Samy, S. Analysis of nitrated polycyclic aromatic hydrocarbons. *Anal. Bioanal. Chem.* **2006**, *386*, 883−890.

(7) Tsapakis, M.; Stephanou, E. G. Diurnal cycle of PAHs, nitro-PAHs, and oxy-PAHs in a high oxidation capacity marine background atmosphere. *Environ. Sci. Technol.* **2007**, *41*, 8011−8017.

(8) Schauer, C.; Niessner, R.; Poschl, U. Analysis of nitrated polycyclic aromatic hydrocarbons by liquid chromatography with fluorescence and mass spectrometry detection: air particulate matter, soot, and reaction product studies. *Anal. Bioanal. Chem.* **2004**, *378*, 725−736.

(9) Jinhui, X.; Lee, F. S. Analysis of nitrated polynuclear aromatic hydrocarbons. *Chemosphere* **2001**, *42*, 245−250.

(10) Bamford, H. A.; Bezabeh, D. Z.; Schantz, S.; Wise, S. A.; Baker, J. E. Determination and comparison of nitrated-polycyclic aromatic hydrocarbons measured in air and diesel particulate reference materials. *Chemosphere* **2003**, *50*, 575−587.

(11) Albinet, A.; Leoz-Garziandia, E.; Budzinski, H.; Viilenave, E. Polycyclic aromatic hydrocarbons (PAHs), nitrated PAHs and oxygenated PAHs in ambient air of the Marseilles area (South of France): concentrations and sources. *Sci. Total Environ.* **2007**, *384*, 280−292.

(12) Schlemitz, S.; Pfannhauser, W. Analysis of nitro-PAHs in food matrices by on-line reduction and high performance liquid chromatography. *Food Addit. Contam.* **1996**, *13*, 969−977.

(13) Schlemitz, S.; Pfannhauser, W. Monitoring of nitropolycyclic aromatic hydrocarbons in food using gas chromatography. *Z. Lebensm. Unters. Forsch.* **1996**, *203*, 61−64.

(14) Dennis, M. J.; Massey, R. C.; McWeeny, D. J.; Knowles, M. E. Estimation of nitropolycyclic aromatic hydrocarbons in foods. *Food Addit. Contam.* **1984**, *1*, 29−37.

(15) Dotter, R. N.; Smith, C. H.; Young, M. K.; Kelly, P. B.; Jones, A. D.; McCauley, E. M.; Chang, D. P. Laser desorption/ionization time-of-flight mass spectrometry of nitrated polycyclic aromatic hydrocarbons. *Anal. Chem.* **1996**, *68*, 2319−2324.

(16) Chan, W.; Lee, K. C.; Liu, N.; Cai, Z. A sensitivity enhanced high-performance liquid chromatography fluorescence method for the detection of nephrotoxic and carcinogenic aristolochic acid in herbal medicines. *J. Chromatogr., A* **2007**, *1164*, 113−119.

(17) Wang, Y.; Chan, W. Determination of aristolochic acids by high-performance liquid chromatography with fluorescence detection. *J. Agric. Food Chem.* **2014**, *62*, 5859−5864.

(18) Hayakawa, K. Chromatographic methods for carcinogenic/mutagenic nitropolycyclic aromatic hydrocarbons. *Biomed. Chromatogr.* **2000**, *14*, 397−405.

(19) Al-Kindy, S. M.; Miller, J. N. High-performance liquid chromatography determination of nitrated polycyclic aromatic hydrocarbons by indirect fluorescence detection. *Biomed. Chromatogr.* **2009**, *23*, 166−169.

(20) Leung, E. M.; Chan, W. A novel reversed-phase HPLC method for the determination of urinary creatinine by pre-column derivatization with ethyl chloroformate: comparative studies with the standard Jaffe and isotope-dilution mass spectrometric assays. *Anal. Bioanal. Chem.* **2014**, *406*, 1807−1812.

(21) Purohit, V.; Basu, A. K. Mutagenicity of nitroaromatic compounds. *Chem. Res. Toxicol.* **2000**, *13*, 673−692.

(22) Zwirner-Baier, I.; Neumann, H. G. Polycyclic nitroarenes (nitro-PAHs) as biomarkers of exposure to diesel exhaust. *Mutat. Res.* **1999**, *441*, 135−144.

(23) Roy, A. K.; Upadhyaya, P.; Fu, P. P.; el-Bayoumy, K. Identification of the major metabolites and DNA adducts formed from 2-nitropyrene in vitro. *Carcinogenesis* **1991**, *12*, 475−479.

(24) Bamford, H. A.; Baker, J. E. Nitro-polycyclic aromatic hydrocarbon concentrations and sources in urban and suburban atmospheres of the Mid-Atlantic region. *Atmos. Environ.* **2003**, *37*, 2077−2091.

(25) De Gonzalez, M. T. N.; Osburn, W. N.; Hardin, M. D.; Longnecker, M.; Garg, H. K.; Bryan, N. S.; Keeton, J. T. Survey of residual nitrite and nitrate in conventional and organic/natural/uncured/indirectly cured meats available at retail in the United States. *J. Agric. Food Chem.* **2012**, *60*, 3981−3990.

DOI: 10.1021/acs.jafc.5b00523
J. Agric. Food Chem. 2015, 63, 3161−3167

(26) Yalcin, S.; Yalcin, S. S. Nitrate and nitrite content of meat products. *Arch. Dis. Child.* **1998**, *79*, 198−198.

DOI: 10.1021/acs.jafc.5b00523
J. Agric. Food Chem. 2015, 63, 3161−3167

by Chung et al.,[8] the mechanism underlying D-psicose's hypolipidemic action is less clear at present.

Commercial production of D-psicose is now available, which makes it feasible to do in vivo research.[24] Because D-psicose does not stay in the body and is excreted in the urine as D-psicose,[9] animals may have a fluctuation of serum D-psicose level throughout a 24 h feeding−fasting cycle. This suggested that timing of collecting serum and tissues from rats fed D-psicose for subsequent analysis would be important observations to find the relationship between D-psicose and lipid metabolism. Thus, rats fed the 3% D-psicose diet for 4 weeks were sacrificed without fasting every 6 h over a period of 24 h, and changes in serum lipid and glucose levels, liver lipid levels, liver enzyme activity, and gene expression of proteins related to lipid and glucose metabolism were quantified in experiment 1. Effects of D-psicose on 24 h energy expenditure were evaluated in experiment 2.

MATERIALS AND METHODS

Chemicals. D-Psicose was provided by Matsutani Chemical Industry Co., Ltd. (Itami, Japan). The purity of D-psicose was 97.5%. Other reagents were of analytical grade and used without further purification.

Experiment 1 (24 h Continuous Measurement of Serum and Liver Lipid Levels). *Animal Experiments.* Four-week-old Sprague−Dawley (SD) rats were purchased from Japan SLC (Shizuoka, Japan) and individually housed in stainless steel cages under controlled atmospheric conditions (temperature, 22 ± 1 °C; humidity, 55 ± 5%; light cycle, 8:00 a.m.−8:00 p.m.), and fed a commercial pellet diet (CE-2, Clea Japan, Tokyo, Japan) for a week. Animal studies were carried out under the Guidelines for Animal Experiments of University of Nagasaki (Nagasaki, Japan), and Law no. 105 and Notification no. 6 of the government of Japan. After a week's acclimation, rats were then assigned to two groups, 24 animals per group. The control group was fed a modified AIN-93G diet with corn starch as a major source of carbohydrate. For the animals fed the D-psicose diet, 3% D-psicose replaced the same amount of corn starch in the control diet (Table 1).

Table 1. Nutrient Composition (Percent) in the Diets

	control	D-psicose
casein[a]	20.0	20.0
α-corn starch	13.2	13.2
soybean oil	7.0	7.0
sucrose	10.0	10.0
cellulose	5.0	5.0
mineral mix AIN-93G[b]	3.5	3.5
vitamin mix AIN-93G[b]	1.0	1.0
tert-butylhydroquinone	0.0014	0.0014
choline bitartrate	0.25	0.25
L-cystine	0.30	0.30
D-psicose		3.0
β-corn starch	39.75	36.75
total (%)	100.0	100.0

[a]Purchased from Wako Pure Chemical Industries (Osaka, Japan). [b]Purchased from Oriental Yeast (Tokyo, Japan).

Animals were provided diets ad libitum for 4 weeks. Subsequently, five to six animals on each dietary regimen were decapitated every 6 h, beginning at 9:00 a.m. and followed at 3:00 p.m., 9:00 p.m., and 3:00 a.m. without fasting. Blood was collected with decapitation, and serum was obtained after centrifugation at 1500*g* for 15 min. Liver, soleus muscle, and adipose tissue (mesenteric, perirenal, and epididymal) were dissected and stored at −80 °C prior to further analysis for tissue lipid, enzyme activity, or gene expression. Interscapular brown adipose tissue was also removed for the measurement of enzyme activity. The small intestine was collected, flushed with ice-cold saline, and divided into two segments designated jejunum and ileum, respectively. Serum and liver lipid levels were measured. The activity of liver enzymes involved in lipid metabolism was also measured.

Serum and Tissue Biochemical Analyses. Serum glucose and lipid levels were assayed enzymatically using commercial kits (Glu CII-Test, Cholesterol E-Test, Triglyceride E-Test, Phospholipid C-Test, NEFA C-Test; Wako Pure Chemical Industries, Osaka, Japan). Serum insulin and leptin levels were measured by enzyme-linked immunosorbent assay (ELISA) kits (Morinaga Institute of Biological Science, Yokohama, Japan). Liver was weighed and a fraction removed, and lipids were extracted according to the method of Folch et al.[25] Cholesterol, phospholipid, and triglyceride levels in the liver were enzymatically measured with the kits used for serum lipids.

Liver Enzyme Activity. To determine how D-psicose alters lipid metabolism, the activity of lipid metabolism-related enzymes in the liver and brown adipose tissue was measured. A small aliquot of the excised liver was homogenized in 6 volumes of 0.25 M sucrose solution containing 10 mM Tris-HCl and 1 mM EDTA (pH 7.4) to obtain aliquots for isolated liver subcellular fractions. After sedimentation of the nuclei fraction, the supernatant was centrifuged to sediment mitochondria at 12000*g* for 10 min. Then, the supernatant was again centrifuged at 100000*g* for 60 min to precipitate microsomes, and the remaining supernatant was used as cytosol fraction. The mitochondrial and microsomal pellets were resuspended in the same 0.25 M sucrose solution. Activities of cytosol fatty acid synthase (FAS),[26] glucose-6-phosphate dehydrogenase (G6PDH),[27] and malic enzyme (ME)[28] in the liver were measured. Microsomal phosphatidate phosphohydrolase (PAP)[29] and mitochondrial carnitine palmitoyltransferase (CPT)[30] were also determined. Interscapular brown adipose tissue was collected and homogenized as described above, and mitochondrial CPT activity was measured. Protein was assayed according to the method of Lowry et al.[31]

Analysis of Gene Expression by Real-Time Quantitative PCR. To further determine how D-psicose affects lipid metabolism at the molecular level, gene expression of enzymes and proteins involved in lipid metabolism as listed in Table 2 was analyzed. Total RNA was extracted from a subsample of liver, jejunum, soleus muscle, and mesenteric adipose tissue using RNA extraction reagent (RNAiso Plus, Takara Bio, Shiga, Japan) according to the manufacturer's instructions. Total RNA (1 μg) was reverse-transcribed to synthesize cDNA with a reverse-transcription kit (PrimeScript RT Master Mix, Takara Bio). Real-time PCR was performed on a 7300 Real-Time PCR system (Applied Biosystems, Foster City, CA, USA) using the manufacturer's standard protocol. The PCR reaction mixture was prepared using THUNDERBIRD SYBR qPCR Mix (Toyobo, Osaka, Japan). The mRNA (mRNA) levels, measured relative to 36B4 mRNA levels used as an internal control,[32] were determined using the $2^{-\Delta\Delta Ct}$ method. Primers were designed using Primer Express Software for Real-Time PCR (Applied Biosystems), and the forward and reverse primers used are listed in Table 2.

Experiment 2 (Measurement of 24 h Energy Expenditure). *Animals.* Four-week-old male SD rats weighing about 100 g were individually housed and fed the commercial pellet diet. After a week's acclimation period, one group (eight rats) was fed the control diet and the test group (eight rats) was fed the 3% D-psicose diet ad libitum for 4 weeks as in experiment 1.

Measurement of 24 h Energy Expenditure. At 9 weeks of age and with an approximate weight of 400 g, rats fed each diet were individually housed in a metabolic chamber and maintained on the control or D-psicose diet ad libitum through subsequent measurements. Energy expenditure and oxidation of carbohydrate and fat were measured over a 24 h period by a combined gas analyzer and mass spectrometer (model ARCO-200 Series, ArcoSystem, Chiba, Japan). Room air was pumped through the chamber at a rate of 1.0 L/min. Measurement of oxygen and carbon dioxide started at 9:00 a.m. and were continuous at 5 min intervals over 24 h. The oxidation of carbohydrate and fat was calculated with a multiprocess monitor

DOI: 10.1021/jf502535p
J. Agric. Food Chem. 2015, 63, 3168−3176

Table 2. Primer Sequences of Genes for Real-Time PCR

	forward primer	reverse primer
36B4	5′-GGTGTTTGACAATGGCAGCAT-3′	5′-ATTGCGGACACCCTCTAGGA-3′
SREBP-lc	5′-CATCGACTACATCCGCTTCTTACA-3′	5′-GTCTTTCAGTGATTTGCTTTTGTGA-3′
FAS	5′-TGCTCCCAGCTGCAGGC-3′	5′-GCCCGGTAGCTCTGGGTGTA-3′
ACC	5′-CGTTCGCCATAACCAAGTAGAGT-3′	5′-AAAAAGTTTGGGAGGACATCGA-3′
MTP	5′-CGACGGTGACGATGATCAACT-3′	5′-TGACCCGCATTTTCGACATT-3′
PPARα	5′-AAGAGAATCCACGAAGCCTACCT-3′	5′-TGACAAAAGGCGGATTGTT G-3′
PPARγ	5′-ATCTTAACTGTCGGATCCACAAAAA-3′	5′-AACCTGATGGCATTGTGAGACAT-3′
GK	5′-TTCCTTGACAAGCATCAGATGAA-3′	5′-TGAGGAGGATGCCCTTGTCT-3′
LXR	5′-TGCATGCCTATGTCTCCATCA-3′	5′-GAATGGACGCTGCTCAAAGTC-3′
HMG-CoA R	5′-TGCAGAGAAAGGTGCGAAGTT-3 ′	5′-CGTCTCCATGAGGGTTTCCA-3′
LDLR	5′-GATCCCCAACCTGAAGAATGTG-3′	5′-CACGGCGCTGTAGATCTTTCTC-3′
CPT	5′-AACCTCGGACCCAAATTGC-3′	5′-GGCCCCGCAGGTAGATATATT-3′
GLUT4	5′-GCTTTGTGGCCTTCTTTGAG-3′	5′-CAGGAGGACGGCAAATAGAA-3′
LPL	5′-GGAAATGATGTGGCCAGGTT-3′	5′-GCAGCATGGGCTCCAAGA-3′
HSL	5′-CGATTGTGGAAAGATGTCAGGAT-3′	5′-TGAGAATGCCGAGGCTGTATC-3′
CD36	5′-CGAAGGCTTGAATCCTAACGAA-3 ′	5′-GTTGACCTGCAGTCGTTTTGC-3′
NPC1L1	5′-CGGATACTTCCTTCAACTGCTTAAA-3′	5′-GCGGATCATTCAGGAACCA-3′
SR-B1	5′-ACCCTGACCCAAAGGAGCAT-3′	5′-TTGATGTACAGACTCAGCTGCATCT-3′

Table 3. Effect of the 4 Week Administration of the 3% D-Psicose Diet on Body Weight, Food Intake, and Tissue Weight in Rats[a]

					two-way ANOVA		
	9:00 a.m.	3:00 p.m.	9:00 p.m.	3:00 a.m.	group	time	interaction
final BW (g)							
control	447 ± 14	446 ± 12	439 ± 14	447 ± 16	$p < 0.05$	NS[b]	NS
D-psicose	421 ± 10	418 ± 11	412 ± 11	417 ± 14			
food intake (g/day)							
control	26.4 ± 1.0	26.1 ± 0.9	26.7 ± 1.2	27.7 ± 1.2	NS	NS	NS
D-psicose	24.8 ± 0.6	25.7 ± 0.8	25.6 ± 1.1	25.4 ± 0.8			
liver weight (g/100 g BW)							
control	4.54 ± 0.30	4.15 ± 0.17	3.86 ± 0.25	4.00 ± 0.11	NS	$p < 0.05$	NS
D-psicose	4.62 ± 0.14	4.30 ± 0.23	4.23 ± 0.14	4.40 ± 0.09			
total white adipose tissue weigh (g/100 g BW) (mesenteric, perirenal, and epididymal)							
control	4.88 ± 0.28	4.21 ± 0.35	4.71 ± 0.49	4.87 ± 0.55	NS	NS	NS
D-psicose	4.00 ± 0.34	4.12 ± 0.22	4.36 ± 0.46	3.85 ± 0.42			

[a]Data are the mean ± SE (n = 5−6). [b]NS, not significant.

system (ARCO 2000 MM, ArcoSystem) as described by Ishihara et al.[33]

Statistical Analysis. All of the values are expressed as means ± SE. In experiment 1, two-way ANOVA was used to analyze time course changes (dietary group × time). When a significant effect of dietary groups and interactions was found, an independent t test was carried out at each point. In experiment 2, an independent t test was performed. Values were considered to be significantly different when the p value was <0.05.

RESULTS

Experiment 1 (24 h Continuous Measurement of Serum and Liver Lipid). Body weight, food intake, and organ weights of the rats in experiment 1 are reported in Table 3. Feeding D-psicose significantly decreased body weight, but not food intake. As reported in Figure 2, the D-psicose diet significantly reduced serum total cholesterol level at 3:00 a.m. without significant differences in serum triglyceride and nonesterified fatty acid levels. No difference was observed for serum glucose level between the two diets, whereas serum insulin level was significantly decreased in the D-psicose-fed rats compared to the control-fed animals at 3:00 a.m. and 9:00 a.m. ($p < 0.05$ at both time points). The level of serum leptin was also affected by D-psicose and significantly lowered at 3:00 p.m. ($p < 0.05$). Feeding D-psicose lowered liver triglyceride level and increased liver cholesterol levels as compared to the control-fed animals, but these consistent observations were not significantly different (Figure 3).

Activities of specific liver enzymes involved in lipid homeostasis at 6 h intervals over 24 h are illustrated in Figure 4. The activity of FAS was not modulated by the diets. In contrast, feeding the D-psicose diet constantly reduced activities of G6PDH and ME over a 24 h period compared to the control diet, with a significant difference at 9:00 a.m. ($p < 0.05$). No effect of the diets was seen on PAP activity. The activity of CPT in liver was marginally increased in the D-psicose group compared to the control group at 9:00 p.m. ($p = 0.06$) and at 3:00 a.m. ($p = 0.09$). The activity of the CPT in brown adipose tissue was not modified by dietary treatment. No significant interaction between diet and time to sacrifice was found for any enzyme activities.

To see the effects of D-psicose on lipid homeostasis at the molecular level, gene expression of proteins involved in lipid and glucose metabolism was measured, and results are reported as shown in Figures 5−8. In the liver (Figure 5), mRNA of

DOI: 10.1021/jf502535p
J. Agric. Food Chem. 2015, 63, 3168−3176

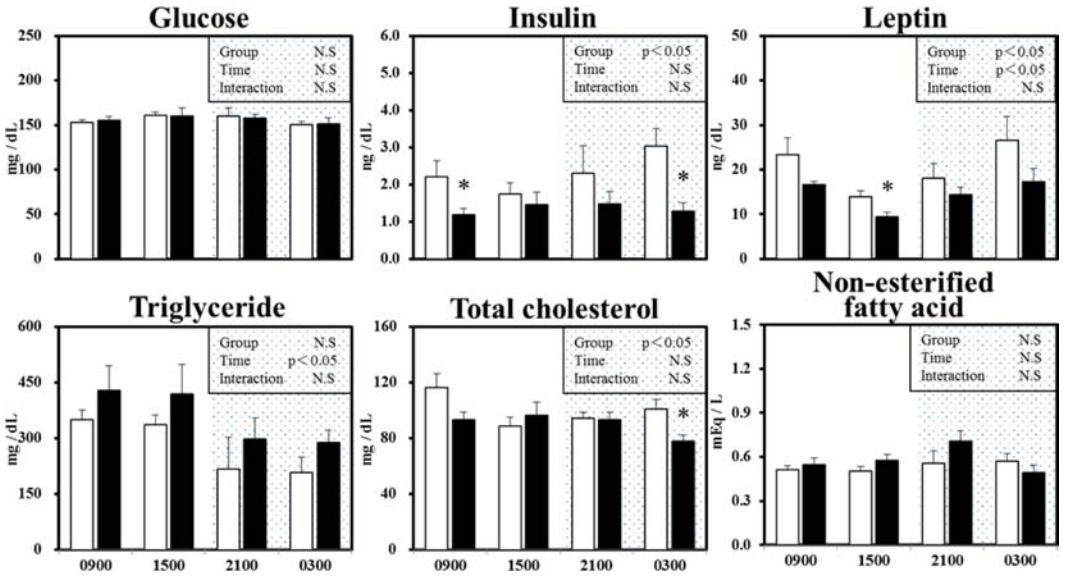

Figure 2. Effect of the 4 week administration of the 3% D-psicose diet on serum levels of lipids, glucose, insulin and leptin in rats: (white bars) control; (black bars) D-psicose. Data are the mean ± SE (n = 5–6). (*) Significant difference at $p < 0.05$, using independent t test.

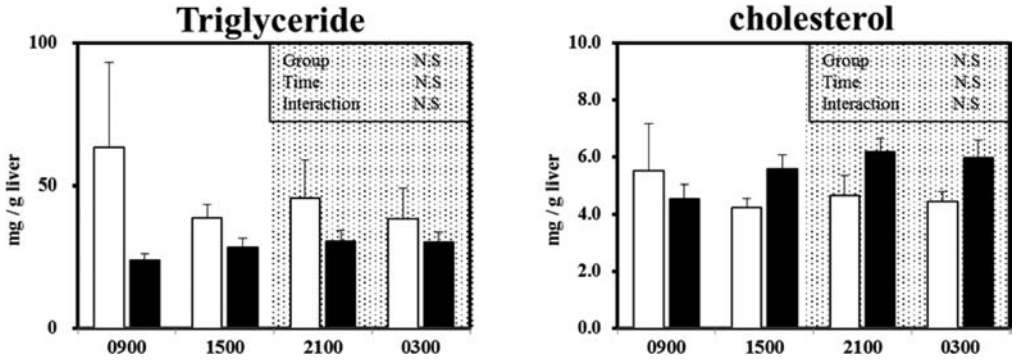

Figure 3. Effect of the 4 week administration of the 3% D-psicose diet on the levels of liver lipids: (white bars) control; (black bars) D-psicose. Data are the mean ± SE (n = 5–6).

peroxisome proliferator-activated receptor α(PPARα), a regulator of fatty acid oxidation,[34] was significantly higher in rats fed the D-psicose diet compared to rats fed the control diet ($p < 0.05$). In soleus muscle (Figure 6) and adipose tissue (Figure 7), gene expression of proteins involved in lipid metabolism was not modified by the diets. From the examination of the tissue from the jejunum, mRNA expression was generally lowered by the D-psicose diet. A significant interaction between type of carbohydrate and time to sacrifice was found for mRNA of fatty acid translocase (CD36) and scavenger receptor B1 (SR-B1) (Figure 8). Gene expression of CD36 was significantly down-regulated by the D-psicose diet compared to the control diet at 9:00 a.m. ($p < 0.05$). mRNA of microsomal triglyceride transfer protein (MTP), essential for the assembly/secretion of chylomicrons,[35] was significantly down-regulated by the D-psicose diet compared to the control diet.

Experiment 2 (Measurement of 24 h Energy Expenditure). Hour-by-hour profiles of 24 h energy expenditure and oxidation of fat and carbohydrate are illustrated in Figure 9. When rats were housed in metabolic cages after feeding diets for 4 weeks, final body weights (426 ± 6 vs 389 ± 3 g, $p < 0.05$) and food intake (25.7 ± 0.4 vs 23.8 ± 0.2 g/day, $p < 0.05$) were significantly lower in the rats fed D-psicose compared to the rats fed the control diet. When expressed per kilogram of body weight, total energy expenditure in rats fed the D-psicose diet was significantly higher during a late light period. Following the consumption of the D-psicose diet for 4 weeks, fat oxidation was significantly enhanced during the dark period. Conversely, carbohydrate oxidation was significantly reduced in rats fed the D-psicose diet during the dark period compared to rats fed the control diet (Figure 9).

DISCUSSION

With the intense interest and study of fructose's lipogenic properties,[5,6] it is of interest and potential benefit to determine how D-psicose, an epimer of D-fructose, affects lipid homeostasis. In the current study, we fed 3% D-psicose in a modified AIN-93G diet to SD rats for 4 weeks and measured lipid levels and related parameters every 6 h over a 24 h period and compared with data obtained from rats fed the control AIN-93G diet.

In agreement with previous studies,[16,18,22,23] body weight and food intake were significantly lower in rats fed the D-psicose diet compared to rats fed the control diet in experiment 2. It therefore appears that although D-psicose provides no calories,[11] rats fed the 3% D-psicose diet did not increase

DOI: 10.1021/jf502535p
J. Agric. Food Chem. 2015, 63, 3168–3176

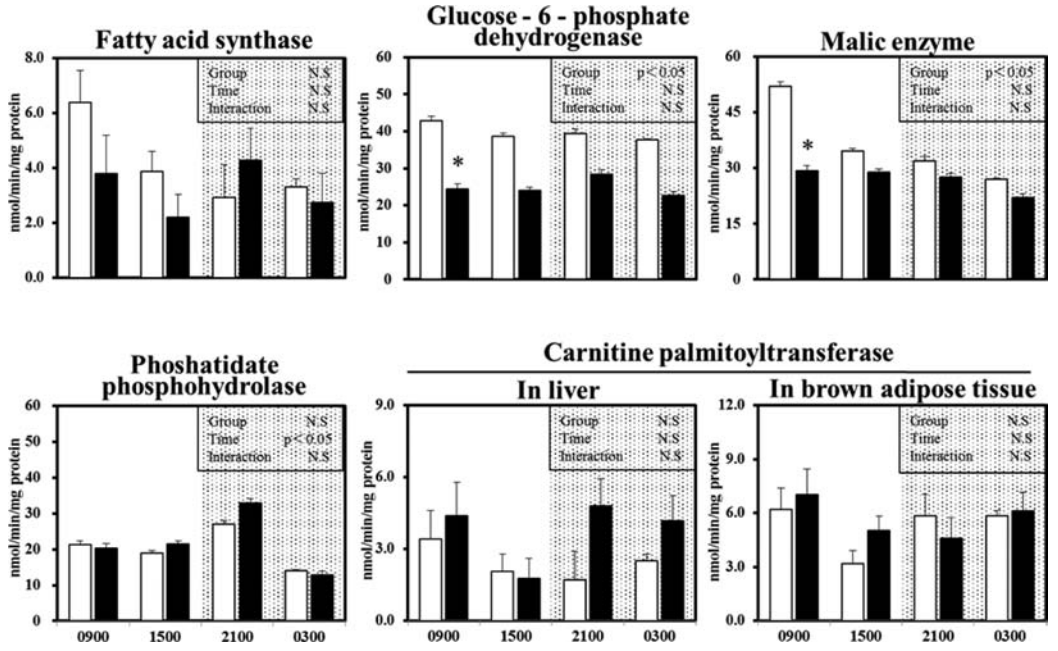

Figure 4. Effect of the 4 week administration of the 3% D-psicose diet on activities of enzymes related to lipid metabolism in liver and brown adipose tissue: (white bars) control; (black bars) D-psicose. Data are the mean ± SE (n = 5−6). (∗) Significant difference at $p < 0.05$, using independent t test.

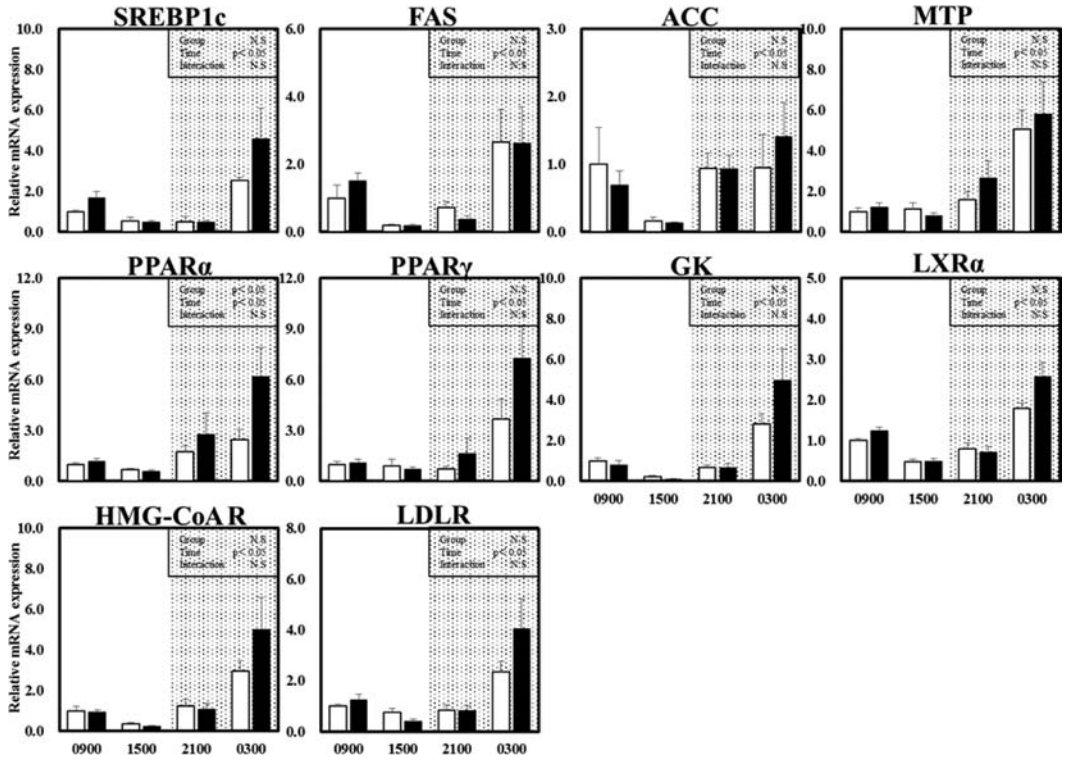

Figure 5. Effect of the 4 week administration of the 3% D-psicose diet on mRNA expression in liver: (white bars) control; (black bars) D-psicose. Data are the mean ± SE (n = 5−6) expressed relative to the control at 9:00 a.m., which was set at 1.0.

food intake to compensate for the displaced energy, resulting in reduced body weight. The level of serum leptin, a modulator of food intake,[36] was significantly decreased by D-psicose, whereas food intake was not elevated. The decreased level of serum leptin was also confirmed in Otsuka Long-Evans Tokushima Fatty (OLETF) rats supplemented with D-psicose in their drinking water and male Wistar rats fed a D-psicose-containing mixture of sugars.[15,21] Because several studies observed D-psicose-induced lower food intake,[21−23] further detailed studies are warranted to clarify the relationship among D-psicose, hormone levels, and food intake. These studies are especially important in the event that D-psicose would be used for foods to treat and help manage weight gain and blood glucose level by providing food with fewer calories. Serum levels of insulin

DOI: 10.1021/jf502535p
J. Agric. Food Chem. 2015, 63, 3168−3176

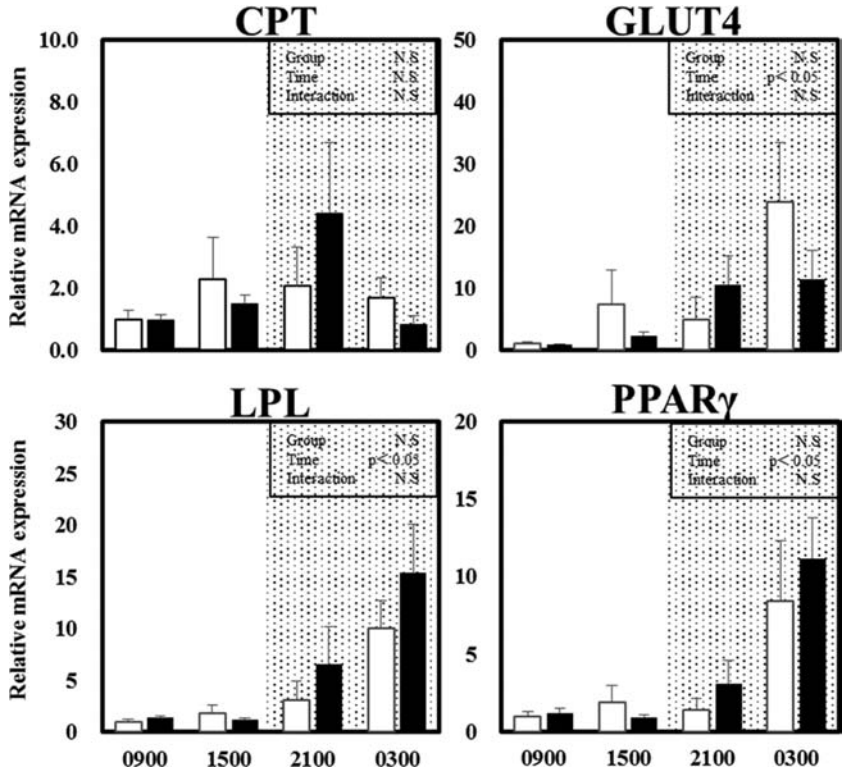

Figure 6. Effect of the 4 week administration of the 3% D-psicose diet on mRNA expression in skeletal muscle: (white bars) control; (black bars) D-psicose. Data are the mean ± SE (n = 5−6) expressed relative to the control at 9:00 a.m., which was set at 1.0.

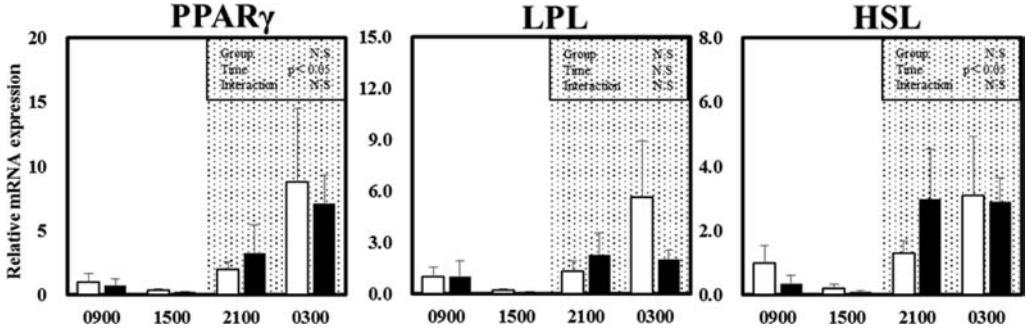

Figure 7. Effect of the 4 week administration of the 3% D-psicose diet on mRNA expression in white adipose tissue: (white bars) control; (black bars) D-psicose. Data are the mean ± SE (n = 5−6) expressed relative to the control at 9:00 a.m., which was set at 1.0.

and leptin were significantly diminished by D-psicose as compared to the control. However, no difference was found in serum glucose levels (Figure 2), which is different from studies showing that D-psicose reduced plasma glucose levels in *db*/*db* mice, rats meal-fed D-psicose, and Wistar rats fed D-psicose and a mixture of other sugars.[13,18,21] This is partly attributed to the fact that the rats used in our study were not fasted upon termination. In addition, it is possible that the level of D-psicose in the 3% D-psicose diet is not high enough to provide an inhibitory action of D-psicose on α-glucosidase, and corn starch as a major carbohydrate in the diet is not a good substrate for α-glucosidase. However, effects of difference in model animals, species, and experimental conditions on serum glucose could not be ruled out. Irrespective of these reported differences, this finding is of interest in terms of managing weight gain with dietary treatment because both insulin and leptin in blood are directly correlated with the degree of adiposity.[37] Furthermore, D-psicose diminished serum leptin and adipose tissue weight in OLETF rats and male Wistar rats.[15,21]

With regard to lipid homeostasis, the activities of lipogenic enzymes such as G6PDH and ME, but not FAS, were significantly and constantly diminished by feeding the D-psicose diet compared to the control diet (Figure 4). These results confirmed the study done by Matsuo et al. in which rats fed D-psicose had decreased activity of lipogenic enzymes compared to rats fed glucose or fructose.[20] Hepatic CPT, an enzyme that catalyzes a rate-limiting step in fatty acid oxidation,[38] was marginally elevated by D-psicose during the dark period (p = 0.06 at 9:00 p.m.) (Figure 4). Given that D-psicose reduces liver levels of triglyceride[13,16] and adipose tissue weight,[15−18,22,23] these results probably imply that the combined effects of lowered fatty acid synthesis and enhanced fatty acid oxidation in the liver at least partly contribute to decreased liver triglyceride and adipose tissue weight in rats fed the D-psicose diet. This hypothesis may also support the results observed in

DOI: 10.1021/jf502535p
J. Agric. Food Chem. 2015, 63, 3168−3176

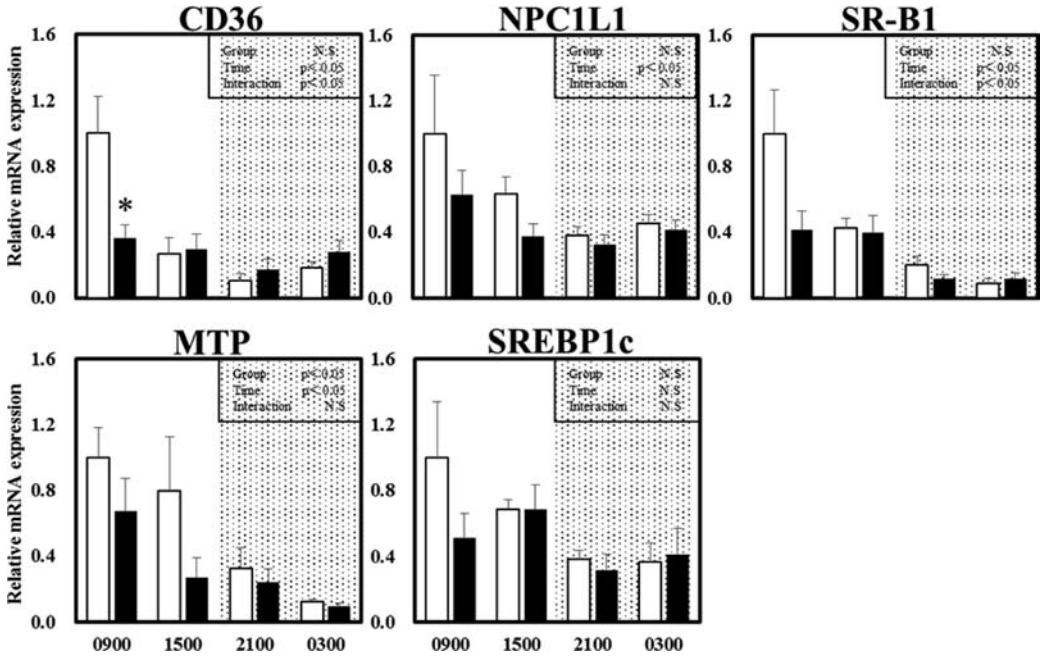

Figure 8. Effect of the 4 week administration of the 3% D-psicose diet on mRNA expression in jejunum: (white bars) control; (black bars) D-psicose. Data are the mean ± SE (n = 5−6) expressed relative to the control at 9:00 a.m., which was set at 1.0. (∗) Significant difference at $p < 0.05$, using independent t test.

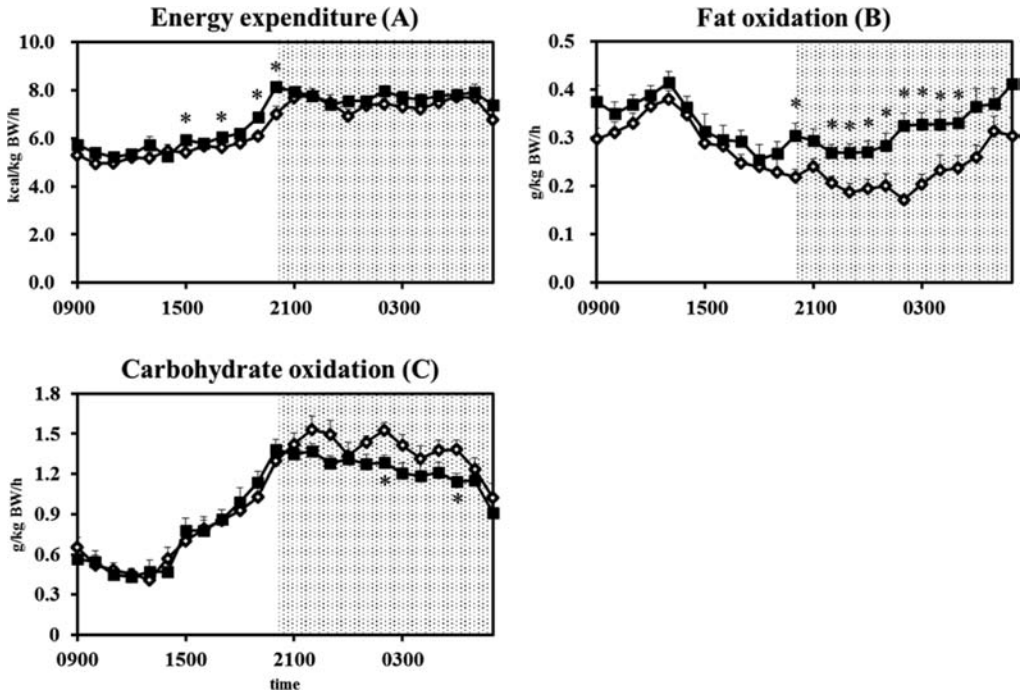

Figure 9. Effect of the 4 week administration of the 3% D-psicose diet on (A) energy expenditure, (B) fat oxidation, and (C) carbohydrate oxidation: (◇) control; (■) D-psicose. Data are the mean ± SE (n = 8). (∗) Significant difference at $p < 0.05$, using independent t test.

24 h energy expenditure; D-psicose enhanced energy expenditure in the light period and fat oxidation during the dark period (Figure 9). Because D-psicose is chemically similar to, but structurally different from, fructose, it is of interest to note that the effect of D-psicose on 24 h energy expenditure and fat oxidation in the present study was totally different from the previous report showing that fructose-sweetened beverages diminished energy expenditure and fat oxidation in overweight and obese subjects.[39] This is probably because D-psicose decreases insulin levels and the resultant lowered insulin levels do not impair lipid homeostasis, given that insulin plays an important role in lipid metabolism in the liver.[40] We observed that D-psicose constantly gave lower liver triglyceride levels over 24 h without a significant difference, whereas Baek et al. showed that D-psicose significantly decreases liver lipids in *db/db* mice.[13] This difference may be due to the type of animals and diet composition. Because our current study demonstrated that a D-psicose diet exhibited lower lipogenic enzyme activities

DOI: 10.1021/jf502535p
J. Agric. Food Chem. 2015, 63, 3168−3176

(Figure 4), further studies to confirm the hypolipidemic action of D-psicose are needed using hyperlipidemic animals and high-fat and/or high-fructose diets.

To gain insight into D-psicose-induced hypolipidemic action at the molecular level, gene expression of proteins and enzymes related to lipid metabolism was analyzed as depicted in Figures 5−8. In the liver, the qualitative response of individual mRNA in response to D-psicose was similar; gene expression was up-regulated at 3:00 a.m. and 9:00 a.m. mRNA expression of PPARα, a key transcriptional modulator of fatty acid oxidation, was up-regulated by D-psicose, probably supporting the observations that liver CPT activity tended to be higher during the dark period. These observations correspond with the observed results that D-psicose significantly increased fat oxidation during the dark period as shown in Figure 9. This substantiates results from the recent study in which the 5% D-psicose diet enhanced energy expenditure during the dark period.[23] However, these authors did not determine if fatty acid oxidation is at least partly responsible for enhanced energy expenditure at enzymatic and molecular levels. Our data on enzyme activity and gene expression of lipid metabolism-related proteins seem to suggest the underlying mechanism of D-psicose-induced hypolipidemic action.

It is of interest to note that D-psicose affects gene expression of intestinal proteins involved in lipid transfer such as CD36, SR-B1, and MTP (Figure 8), all of which are associated with lipid absorption in the small intestine.[35] Although D-psicose inhibits intestinal α-glucosidase in vitro, probably resulting in a decrease in glucose absorption in the small intestine,[12] to our knowledge, no studies have thus far shown an involvement of D-psicose in intestinal events. In addition to altered enzymatic activities in the liver, D-psicose may modulate lipid handling at the small intestinal level, subsequently contributing hypolipidemic action. Given that diabetes patients and genetically diabetic obese rats have increased intestinal lipid transport,[41,42] D-psicose may be a promising food ingredient to maintain and control blood glucose level under conditions where glucose metabolism is compromised. Further studies are warranted to determine how the small intestine has a role in lipid metabolism in D-psicose-fed rats.

Taken together, our results suggest that D-psicose favorably alters lipid metabolism partly through decreased fatty acid synthesis and increased fatty acid oxidation, thereby enhancing energy expenditure. Additional studies are needed to unravel the precise molecular mechanism underlying the effects of D-psicose on antiobesity and antihyperlipidemic actions. In summary, D-psicose appears to be a unique sugar that could offer beneficial effects to help control body weight and maintain healthy blood lipid and glucose level in many individuals and especially in obese people with insulin resistance.

AUTHOR INFORMATION

Corresponding Author

*(Y.N.) Phone: +81-95-813-5470. Fax: +81-95-813-5470. E-mail: y-nagata@sun.ac.jp.

Notes

The authors declare no competing financial interest.

ABBREVIATIONS USED

ACC, acetyl coenzyme A carboxylase:; ANOVA, analysis of variance; BW, body weight; ChREBP, carbohydrate responsive element-binding protein; CD36, fatty acid translocase; CPT, carnitine palmitoyltransferase; ELISA, enzyme-linked immunosorbent assay; FAS, fatty acid synthase; GK, glucokinase; GLP-1, glucagon-like peptide-1; GLUT 4, glucose transporter 4; G6PDH, glucose-6-phosphate dehydrogenase; HMG CoA R, 3-hydroxyl-3-methylglutaryl-coenzyme A reductase; HSL, hormone sensitive lipase; LDLR, low-density lipoprotein receptor; LPL, lipoprotein lipase; LXR, liver X receptor; ME, malic enzyme; mRNA, messenger ribonucleic acid; MTP, microsomal triglyceride transfer protein; NPC1L1, Niemann−Pick C1-like 1; OLETF, Otsuka Long-Evans Tokushima Fatty; PAP, phosphatidate phosphohydrolase; PPARα, peroxisome proliferator-activated receptor α; PPARγ, peroxisome proliferator-activated receptor γ; SREBP-1c, sterol regulatory element binding protein-1c; SD, Sprague−Dawley; SR-B1, scavenger receptor B1

REFERENCES

(1) Villareal, D. T.; Apovian, C. M.; Kushner, R. F.; Klein, S. Obesity in older adults: technical review and position statement of the American Society for Nutrition and NAASO, The Obesity Society. *Am. J. Clin. Nutr.* **2005**, *82*, 923−934.

(2) Haslam, D. W.; James, W. P. Obesity. *Lancet* **2005**, *366*, 1197−1209.

(3) Malik, V. S.; Schulze, M. B.; Hu, F. B. Intake of sugar-sweetened beverages and weight gain: a systematic review. *Am. J. Clin. Nutr.* **2006**, *84*, 274−288.

(4) Schulze, M. B.; Manson, J. E.; Ludwig, D. S.; Colditz, G. A.; Stampfer, M. J.; Willett, W. C.; Hu, F. B. Sugar-sweetened beverages, weight gain, and incidence of type 2 diabetes in young and middle-aged women. *JAMA, J. Am. Med. Assoc.* **2004**, *292*, 927−934.

(5) Aeberli, I.; Murer, S. B.; Hochuli, M.; Tappy, L.; Gerber, P. A.; Spinas, G. A.; Sze, L.; Berneis, K. Moderate amounts of fructose consumption impair insulin sensitivity in healthy young men. *Diabetes Care* **2013**, *36*, 150−156.

(6) Rutledge, A. C.; Adeli, K. Fructose and the metabolic syndrome: pathophysiology and molecular mechanisms. *Nutr. Rev.* **2007**, *65*, S13−S23.

(7) Elliott, S. S.; Keim, N. L.; Stern, J. S.; Teff, K.; Havel, P. Fructose, weight gain, and the insulin resistance syndrome. *Am. J. Clin. Nutr.* **2002**, *76*, 911−922.

(8) Chung, M.; Oh, D.; Lee, K. W. Hypoglycemic health benefits of D-psicose. *J. Agric. Food Chem.* **2012**, *60*, 863−869.

(9) Whistler, R. L.; Singh, P. P.; Lake, W. C. D-Psicose metabolism in the rat. *Carbohydr. Res.* **1974**, *34*, 200−202.

(10) Iida, T.; Hayashi, N.; Yamada, T.; Yoshikawa, Y.; Miyazato, S.; Kishimoto, Y.; Okuma, K.; Tokuda, M.; Izumori, K. Failure of D-psicose absorbed in the small intestine to metabolize into energy and its low large intestinal fermentability in humans. *Metabolism* **2010**, *59*, 206−214.

(11) Matsuo, T.; Suzuki, H.; Hashiguchi, M.; Izumori, K. D-Psicose is a rare sugar that provides no energy to growing rats. *J. Nutr. Sci. Vitaminol.* **2002**, *48*, 77−80.

(12) Matsuo, T.; Izumori, K. D-Psicose inhibits intestinal α-glucosidase and suppresses the glycemic response after ingestion of carbohydrates in rats. *J. Clin. Biochem. Nutr.* **2009**, *45*, 202−206.

(13) Baek, S. H.; Park, S. J.; Lee, H. G. D-Psicose, a sweet monosaccharide, ameliorate hyperglycemia, and dyslipidemia in C57BL/6J *db/db* mice. *J. Food Sci.* **2010**, *75*, H49−H53.

(14) Iida, T.; Kishimoto, Y.; Yoshikawa, Y.; Hayashi, N.; Okuma, K.; Tohi, M.; Yagi, K.; Matsuo, T.; Izumori, K. Acute-D-psicose administration decreases the glycemic responses to an oral maltodextrin tolerance test in normal adults. *J. Nutr. Sci. Vitaminol.* **2008**, *54*, 511−514.

(15) Hossain, A.; Yamaguchi, F.; Matsunaga, T.; Hirata, Y.; Kamitori, K.; Dong, Y.; Sui, L.; Tsukamoto, I.; Ueno, M.; Tokuda, M. Rare sugar D-psicose protects pancreas β-islets and thus improves insulin

DOI: 10.1021/jf502535p
J. Agric. Food Chem. 2015, 63, 3168−3176

resistance in OLETF rats. *Biochem. Biophys. Res. Commun.* **2012**, *425*, 717−723.
(16) Hossain, M. A.; Kitagaki, S.; Nakano, D.; Nishiyama, A.; Funamoto, Y.; Matsunaga, T.; Tsukamoto, I.; Yamaguchi, F.; Kamitori, K.; Dong, Y.; Hirata, Y.; Murao, K.; Toyoda, Y.; Tokuda, M. Rare sugar D-psicose improves insulin sensitivity and glucose tolerance in type 2 diabetes Otsuka Long-Evans Tokushima Fatty (OLETF) rats. *Biochem. Biophys. Res. Commun.* **2011**, *405*, 7−17.
(17) Chung, Y.; Lee, J.; Kim, D. Y.; Hwang, S.; Hong, Y.; Kim, S.; Lee, S. J.; Park, C. H. Dietary D-psicose reduced visceral fat mass in high-fat diet-induced obese rats. *J. Food Sci.* **2012**, *77*, H53−58.
(18) Matsuo, T.; Izumori, K. Effects of dietary D-psicose on diurnal variation in plasma glucose and insulin concentrations of rats. *Biosci., Biotechonol., Biochem.* **2006**, *70*, 2081−2085.
(19) Yagi, K.; Matsuo, T. The study on long-term toxicity of D-psicose in rats. *J. Clin. Biochem. Nutr.* **2009**, *45*, 271−277.
(20) Matsuo, T.; Baba, Y.; Hashiguchi, M.; Takeshita, K.; Izumori, K.; Suzuki, H. Dietary D-psicose, a C-3 epimer of D-fructose, suppresses the activity of hepatic lipogenic enzymes in rats. *Asia Pac. J. Clin. Nutr.* **2001**, *10*, 233−237.
(21) Iida, T.; Yamada, T.; Hayashi, N.; Okuma, K.; Izumori, K.; Ishii, R.; Matsuo, T. Reduction of abdominal fat accumulation in rats by 8-week ingestion of a newly developed sweetener made from high fructose corn syrup. *Food Chem.* **2013**, *138*, 781−785.
(22) Ochiai, M.; Nakanishi, Y.; Yamada, T.; Iida, T.; Matsuo, T. Inhibition by dietary D-psicose of body fat accumulation in adult rats fed a high-sucrose diet. *Biosci., Biotechnol., Biochem.* **2013**, *77*, 1123−1126.
(23) Ochiai, M.; Onishi, K.; Yamada, T.; Iida, T.; Matsuo, T. D-Psicose increases energy expenditure and decreases body fat accumulation in rats fed a high-sucrose diet. *Int. J. Food Sci. Nutr.* **2014**, *65*, 245−250.
(24) Mu, W.; Zhang, W.; Feng, Y.; Jiang, B.; Zhou, L. Recent advances on applications and biotechnological production of D-psicose. *Appl. Microbiol. Biotechnol.* **2012**, *94*, 1461−1467.
(25) Folch, J.; Lees, M.; Sloane-Stanley, G. H. A simple method for the isolation and purification of total lipids from animal tissues. *J. Biol. Chem.* **1957**, *226*, 497−509.
(26) Kelley, D. S.; Nelson, G. J.; Hunt, J. E. Effect of prior nutritional status on the activity of lipogenic enzymes in primary monolayer cultures of rat hepatocytes. *Biochem. J.* **1986**, *235*, 87−90.
(27) Kelley, D. S.; Kletzien, R. F. Ethanol modulation of the hormonal and nutritional regulation of glucose 6-phosphate dehydrogenase activity in primary cultures of rat hepatocytes. *Biochem. J.* **1984**, *217*, 543−549.
(28) Ochoa, S. Malic enzyme: malic enzymes from pigeon and wheat germ. In *Methods in Enzymology*; Colowick, S. P., Kaplan, N. O., Eds.; Academic Press: New York, 1955; Vol. 1, pp 739−753.
(29) Walton, P. A.; Possmayer, F. Mg^{2+}-dependent phosphatidate phosphohydrolase of rat lung: development of an assay employing a defined chemical substrate which reflects the phosphohydrolase activity measured using membrane-bound substrate. *Anal. Biochem.* **1985**, *151*, 479−486.
(30) Markwell, M. A.; McGroarty, E. J.; Bieber, L. L.; Tolbert, N. E. The subcellular distribution of carnitine acyltransferases in mammalian liver and kidney. *J. Biol. Chem.* **1973**, *248*, 3426−3432.
(31) Lowry, O. H.; Rosebrogh, N. J.; Farr, A. L.; Randall, R. J. Protein measurement with Folin phenol reagent. *J. Biol. Chem.* **1951**, *193*, 265−275.
(32) Akimine, R.; Yamamoto, T.; Watanabe, M.; Yamazaki, N.; Kataoka, M.; Ishikawa, M.; Ooie, T.; Baba, Y.; Shinohara, Y. Usefulness of the 5′ region of the cDNA encoding acidic ribosomal phosphoprotein P0 conserved among rats, mice, and humans as a standard probe for gene expression analysis in different tissues and animal species. *J. Biochem. Biophys. Methods* **2007**, *70*, 481−486.
(33) Ishihara, K.; Oyaizu, S.; Fukuchi, Y.; Mizunoya, W.; Segawa, K.; Takahashi, M.; Mita, Y.; Fukuya, Y.; Fushiki, T.; Yasumoto, K. A soybean peptide isolate diet promotes postprandial carbohydrate oxidation and energy expenditure in type II diabetic mice. *J. Nutr.* **2003**, *133*, 752−757.
(34) Fruchart, J. Peroxisome proliferator-activated receptor-alpha (PPARα): at the crossroads of obesity, diabetes and cardiovascular disease. *Atherosclerosis* **2009**, *205*, 1−8.
(35) Iqbal, J.; Hussain, M. M. Intestinal lipid absorption. *Am. J. Physiol.* **2009**, *296*, E1183−E1194.
(36) Friedman, J. M.; Halaas, J. L. Leptin and the regulation of body weight in mammals. *Nature* **1998**, *395*, 763−770.
(37) Woods, S. C.; Seeley, R. J.; Rushing, P. A.; D'Alessio, D.; Tso, P. A controlled high-fat diet induces an obese syndrome in rats. *J. Nutr.* **2003**, *133*, 1081−1087.
(38) McGarry, J. D.; Foster, D. W. Regulation of hepatic fatty acid oxidation and ketone body production. *Annu. Rev. Biochem.* **1980**, *49*, 395−420.
(39) Cox, C. L.; Stanhope, K. L.; Schwarz, J. M.; Graham, J. L.; Hatcher, B.; Griffen, S. C.; Bremer, A. A.; Berglund, L.; McGahan, J. P.; Havel, P. J.; Keim, N. L. Consumption of fructose-sweetened beverages for 10 weeks reduces net fat oxidation and energy expenditure in overweight/obese men and women. *Eur. J. Clin. Nutr.* **2012**, *66*, 201−208.
(40) Savage, D. B.; Semple, R. K. Recent insights into fatty liver, metabolic dyslipidaemia and their links to insulin resistance. *Curr. Opin. Lipidol.* **2010**, *21*, 329−336.
(41) Schaefer, E. J.; Cupples, L. A.; McNamara, L. R.; Ordoval, J. M.; Shah, P. K.; Wilson, P. W. F.; Nakajima, K. Elevated remnant-like particle cholesterol and triglyceride levels in diabetic men and women in the Framingham Offspring Study. *Diabetes Care* **2002**, *25*, 989−994.
(42) Hayashi, H.; Sato, Y.; Kanai, S.; Ichikawa, M.; Funakoshi, A.; Miyasaka, K. Increased lymphatic lipid transport in genetically diabetic obese rats. *Am. J. Physiol.* **2002**, *282*, G69−G76.

DOI: 10.1021/jf502535p
J. Agric. Food Chem. 2015, 63, 3168−3176

Table 1. Summary of Optimum Hydrolysis Conditions, Characteristics, and Enzyme Sources

enzyme	optimum conditions[a] pH	optimum conditions[a] temperature (°C)	characteristics	brand/source
Alcalase	8.0	50	endopeptidase	Sigma-Aldrich/*Bacillus lichenifarmis*
Flavourzyme	7.0	50	endoprotease and exopeptidase	Sigma-Aldrich/*Aspergillus oryzae*
Cellulase	4.5	50	cellulase	Sigma-Aldrich/*Aspergillus niger*
Viscozyme L	4.5	50	multienzyme complex of carbohydrases: arabanase, cellulase, β-glucanase, hemicellulase, and xylanase	Sigma-Aldrich/*Aspergillus* sp.

[a]Information based on Wang et al.[13] and Heo et al.;[25] pH values of *S. muticum*, *O. pinnatifida*, and *C. tomentosum* water solutions before extraction were 5.6, 4.3, and 6.6, respectively.

assisted extraction (UAE), an alternative energy input-assisted extraction method, is based on sound wave migration, which generates cavitations that grow and collapse, leading to disruption of cells and their walls.[13] UAE and EAE have been reported as alternative approaches with great potential to extract bioactive substances from marine algae.[14]

Considering the limitations of water-based extraction (low selectivity and low extraction yields), yet wishing to target efficient food compatible methods, the main objective of this study was to obtain extracts rich in bioactive compounds using alternative water-based approaches such as EAE and UAE on representative red, brown, and green species of the Central West Portuguese coast, some of which are less studied such as *Osmundea pinnatifida* and *Codium tomentosum*. Hence, this study was based on three steps: (i) performance of different extraction modes and evaluation of respective yield, (ii) chemical characterization of each extract obtained from each of the three different seaweeds, and (iii) evaluation of the biological potential of the extracts in terms of antioxidant, antidiabetic, and prebiotic activities.

Seaweeds such as *Sargassum* species (Phaeophyceae, brown algae) have been found to be good sources of dietary fiber and of phenolic compounds and carotenoids with antioxidant activity, all of which play important roles in the prevention of intestinal and neurodegenerative diseases, respectively.[15−17] Several other compounds able to scavenge and/or neutralize oxidative compounds (antioxidant activity) have been isolated from other seaweeds including phenolic compounds, sulfated polysaccharides, or proteins.[18,19] Prebiotics are defined as nondigestible compounds mainly of carbohydrate nature that selectively enhance the activity and viability of beneficial bacteria in the intestine by providing these with fermentable substrates that lead to the production of short-chain fatty acids.[20] They have been associated with several health benefits in the large intestine such as modulation of beneficial gut bacteria, hypocholesterolemic effect, reduction of cancer and obesity risks, or increase of the bioavailability and uptake of some minerals (Ca and Mg).[20] Inhibitory compounds of α-glucosidase or α-amylase with antidiabetic activity are of much interest because by acting as competitive inhibitors of the enzymes they inhibit the hydrolysis of oligo-, tri-, and disaccharides to glucose and other monosaccharides in the small intestine and thereby delay postprandial glucose absorption, lowering blood glucose.[21] Inhibition of the carbohydrate-hydrolyzing enzymes has been reported for different extracts of red and green seaweeds.[22]

To our knowledge this is the first study applying water-based extraction through combined EAE and UAE technologies in *Sargassum muticum*, *O. pinnatifida*, and *C. tomentosum* seaweeds, and there are no papers regarding the prebiotic and antidiabetic potential of water-based enzyme-assisted extracts for these studied species.

MATERIALS AND METHODS

Chemicals. Ethyl acetate, hydrogen peroxide, boric acid, barium chloride dihydrate, sodium salicylate, sodium carbonate decahydrate, L-(+)-ascorbic acid, potassium peroxodisulfate ($K_2S_2O_8$), Folin−Ciocalteu, and MRS broth were purchased from Scharlau (Sentmenat, Spain). Ethanol, Kjeldahl catalyst, trichloroacetic acid, sodium dihydrogen phosphate 1-hydrate, and ethylenediaminetetraacetic acid disodium salt (EDTA) were purchased from Panreac (Barcelona, Spain). Phenol, 2,2-diphenyl-1-picrylhydrazyl (DPPH), α-glucosidase, Alcalase, Flavourzyme, Cellulase, Viscozyme L, 4-nitrophenyl-α-D-glucopyranoside, acarbose, and catechol were purchased from Sigma-Aldrich (St. Louis, MO, USA), and ferrous sulfate heptahydrate was purchased from Sigma-Aldrich (Sintra, Portugal). Sulfuric acid was purchased from Fisher Chemical (Leicestershire, UK), and hydrogen chloride and sodium sulfate were obtained from Pronalab (Lisbon, Portugal). 2,2′-Azinobis(3-ethylbenzothiazoline-6-sulfonic acid) diammonium salt (ABTS) was purchased from Fluka (Germany), and L-cysteine hydrochloride monohydrate and MRS agar were obtained from Merck (Gernsheim, Germany). D-(+)-Glucose monohydrate and disodium hydrogen phosphate-7-hydrate were purchased from Riedel-de Häen (Germany) and riboflavin and L-methionine from Acrōs Organics (Geel, Belgium); nitroblue tetrazolium (NBT) was purchased from Fisher Scientific (Erembodegem-Aalst, Belgium).

Specimens of Seaweeds. Specimens of the red alga (Rhodophyta, Florideophyceae) *O. pinnatifida* (Ceramiales) Rhodomelaceae family, the brown alga (Heterokontophyta, Phaeophyceae) *S. muticum* (Fucales) Sargassaceae family, and the green alga (Chlorophyta, Ulvophyceae) *C. tomentosum* (Bryopsidales) Codiaceae family were harvested in April 2012 from Buarcos bay (Figueira da Foz, Portugal). The classification of seaweeds was based on *AlgaeBase*.[23] The seaweeds were first washed with running tap water and then with deionized water and then dried in an oven at 60 °C. The dried samples of seaweeds were milled to <1.0 mm particle size.

Ultrasound- and Enzyme-Assisted Extractions. In this study UAE and EAE as well as hot water extraction (HWE) were performed on the three different seaweeds (*S. muticum*, *O. pinnatifida*, and *C. tomentosum*). Two carbohydrate-degrading enzymes (Viscozyme L, Cellulase) and two proteases (Alcalase, Flavourzyme) were tested for EAE. All extraction procedures were conducted in triplicate.

For HWE, 2 g of dried seaweed was dispersed in 50 mL of deionized water and incubated in an agitated water bath at 50 °C for 24 h in darkness. The aqueous solution (4% dw) was then centrifuged at 5000*g* for 10 min at 4 °C (centrifuge Medifriger BL-S, JP Selecta, Spain), and the supernatant was filtered with a glass filter funnel (porosity 1) and the extract frozen at −80 °C until lyophilization.

UAE and EAE were performed according to the methods of Huang et al.[24] and Wang et al.,[9] respectively, with modifications. The UAE extracts were prepared on the basis of the HWE procedure except that after 24 h at 50 °C, an ultrasound extraction was carried out in a water bath ultrasonicator (Ultrasonik 57H Ney, 400 W, 50/60 Hz) for 60 min (sonicate for 10 min and pause for 2 min) at 50 °C. The resultant

DOI: 10.1021/jf504220e
J. Agric. Food Chem. 2015, 63, 3177−3188

aqueous solution was then centrifuged, filtered, and frozen according to HWE procedures.

For the EAE extracts, the same amount of seaweed (2 g) was dispersed in 50 mL and incubated in an agitated water bath for 10 min. After adjustment of the pH to specific enzyme optimum conditions (Table 1), 100 mg of enzyme was added and incubated for enzymatic hydrolysis for 24 h at 50 °C. The enzymatic reaction was stopped by heating the sample at 90−100 °C for 10 min followed by immediate cooling in an ice bath. The enzymatic aqueous solutions were then centrifuged, filtered, and frozen according to HWE procedures.

The pH of all extracts was adjusted to pH 7.0 with 1 M HCl and/or NaOH before freezing. The frozen extracts were lyophilized, weighed, and stored in desiccators in the dark at room temperature. The extraction yield was calculated as weight percentage of lyophilized extract to the dried seaweed submitted to extraction.

Proximate Characterization of Extracts. The total nitrogen content in the extracts was determined according to the Kjeldahl method adapted from US ISO 5983-1. Total sugars content was determined by the phenol−H_2SO_4 method[25] with modifications using glucose (0−200 μg/mL) as a standard. The content of sulfate groups was determined by turbidity through the barium chloride−gelatin method.[26]

Total phenolic content was determined by the colorimetric method of Folin−Ciocalteu,[27] using catechol (0−75 mg/L) as standard and expressed as micrograms of catechol equivalent per gram of lyophilized seaweed extract. Extraction was carried out with 0.1 g of lyophilized seaweed extract in 10 mL of ethyl acetate after 30 min of sonication. The extract was filtered with anhydrous sodium sulfate and brought to dryness with a rotary evaporator (Laborato 4000, Heidolph). The residue was redissolved in 5 mL of Milli-Q water and the content of total polyphenols of 2 mL was determined by colorimetry at 720 nm.

Determination of Antioxidant Activity of Extracts. Total Antioxidant Capacity. The total antioxidant capacity of extracts' solutions was measured according to method described by Gião et al.[28] This method is able to quantify both water- and lipid-soluble antioxidants, as pure compounds or in crude extracts via direct production of the $ABTS^{\bullet+}$ chromophore (blue/green) by reaction of ABTS and potassium persulfate. To 2 mL of diluted $ABTS^{\bullet+}$ solution was added 120 μL of extract solution (2 mg lyophilized solids/mL), and the absorbance at 734 nm was measured (A_{sample}). Three replicates were performed. Using ascorbic acid as standard (0−100 μg/mL), the results were expressed as equivalent concentration of ascorbic acid ($\mu g_{ascorbic\ acid\ equiv}$/mL). The percentage of scavenging activity was also determined using the following formula:

$$\text{scavenging}\,\% = \left(\frac{A_{ABTS^{\bullet+}} - A_{sample}}{A_{ABTS^{\bullet+}}}\right) \times 100$$

For each sample the initial absorbance of 2 mL of diluted $ABTS^{\bullet+}$ was measured ($A_{ABTS^{\bullet+}}$).

DPPH Free Radical Scavenging Activity. The DPPH free radical scavenging activity was measured according to the method described by Suresh et al.[29] An aliquot (0.1 mL) of each extract (2 mg of lyophilized solids/mL) was added to 3.0 mL of a 0.1 mM ethanolic DPPH solution, and the absorbance was measured at 517 nm after incubation for 30 min at 30 °C in the dark (A_{sample}). Three replicates were performed. Using catechol as standard (0−50 μg/mL), the results were expressed as equivalent concentration of catechol ($\mu g_{catechol\ acid\ equiv}$/mL), whereas the percentage of scavenging activity was also calculated using the following formula:

$$\text{scavenging}\,\% = \left(1 - \frac{A_{sample} - A_{blank}}{A_{control}}\right) \times 100$$

For each sample, the absorbance of 3 mL of DPPH plus 0.1 mL of ethanol was measured as control ($A_{control}$), whereas the absorbance of 3 mL of ethanol plus 0.1 mL of extract was measured as the blank (A_{blank}).

Hydroxyl Radical Scavenging Activity. Hydroxyl radical ($OH^{\bullet}$) scavenging activity was measured according to the method described by Sudha et al.[30] based on that of Smirnoff and Cumbes.[31] An aliquot (1 mL) of each extract (2 mg of lyophilized solids/mL) was added to 2 mL of reaction mixture containing 1 mL of 1.5 mM $FeSO_4$, 0.7 mL of 6 mM hydrogen peroxide, and 0.3 mL of 20 mM sodium salicylate. After incubation for 1 h at 37 °C, the absorbance of the hydroxylated salicylate complex was measured at 562 nm (A_{sample}). Three replicates were performed. Using ascorbic acid as standard (0−100 μg/mL), results were expressed as equivalent concentration of ascorbic acid equivalent ($\mu g_{ascorbic\ acid\ equiv}$/mL) whereas the percentage of scavenging activity of hydroxyl radical was also calculated using the following formula:

$$\text{scavenging}\,\% = \left(1 - \frac{A_{sample} - A_{blank}}{A_{control}}\right) \times 100$$

For each sample, the absorbance of 2 mL of reaction mixture plus 1 mL of deionized water was measured as the control ($A_{control}$), whereas 2 mL of reaction mixture, with sodium salicylate substituted by water plus 1 mL of extract, was measured as blank ($A_{control}$).

Superoxide Radical Scavenging Activity. Superoxide anion radical ($O_2^{\bullet-}$) scavenging activity was based on the capacity of the extract to inhibit the photochemical reduction of NBT in the riboflavin−light−NBT system according to the method described by Fiorentino et al.[32] An aliquot (0.1 mL) of each extract (0.2 mg lyophilized solids/mL) was added to 3 mL of reaction mixture containing 50 mM sodium phosphate buffer (pH 7.8), 13 mM methionine, 2 μM riboflavin, 100 μM EDTA, and 75 μM NBT. After 20 min of illumination (fluorescent lamp), the absorbance was measured at 560 nm (A_{sample}). Three replicates were performed. Using gallic acid as standard (0−15 μg/mL), results were expressed as equivalent concentration of gallic acid equivalent ($\mu g_{gallic\ acid\ equiv}$/mL), whereas the percentage of scavenging activity of hydroxyl radical was also calculated using the following formula:

$$\text{scavenging}\,\% = \left(1 - \frac{A_{sample} - A_{blank}}{A_{control}}\right) \times 100$$

For each sample, the absorbance of 3 mL of reaction mixture plus 0.1 mL of deionized water was measured as control ($A_{control}$), whereas the absorbance of 3 mL of reaction mixture plus 0.1 mL of extract without light incidence throughout the 20 min was measured as the blank (A_{blank}).

Determination of Prebiotic Potential of Seaweed Extracts. The evaluation of potential prebiotic activity of seaweed extracts was performed by enumeration of viable cells of two probiotic strains, namely, *Lactobacillus acidophilus* La-5 and *Bifidobacterium animalis* BB-12, in MRS broth without conventional carbon source and supplemented with seaweed extracts (6%) throughout 48 h at 37 °C. The probiotic cultures of *B. animalis* BB-12 and *L. acidophilus* La-5 were obtained as freeze-dried cultures from CHR-Hansen (Denmark). Growth of both probiotic bacteria were also evaluated in MRS broth with glucose (6%), with fructooligosaccharides (FOS) (6%) as well as without glucose. All media were sterilized at 110 °C for 10 min and, after cooling, were added with filter-sterilized 0.5 g/L L-cysteine-HCl and were inoculated with a 24 h probiotic culture (2%). Two replicates of inoculated media were incubated at 37 °C under agitation and sampled at 0, 4, 8, 12, 24, and 48 h. At each sampling time, decimal dilutions using sterile 0.1% (w/v) peptone water were plated with 20 μL aliquots, in duplicate, on MRS agar containing 0.5 g/L L-cysteine-HCl. The viable cells were enumerated according to the Miles and Mishra method[33] after incubation at 37 °C for 48 h under aerobic conditions for La-5 and under anaerobic conditions for BB-12 with GENbox.

Determination of α-Glucosidase Inhibitory Activity. The α-glucosidase inhibitory activity was determined in 96-well plates according to the method described by Kwon et al.[34] The extracts (50 μL), at the concentration of 10 mg lyophilized solids/mL, were mixed with 100 μL of 0.1 M phosphate buffer (pH 6.9) containing α-glucosidase solution (1.0 U/mL) and pre-incubated at 25 °C for 10 min. Then, 50 μL of 5 mM *p*-nitrophenyl-α-D-glucopyranoside

DOI: 10.1021/jf504220e
J. Agric. Food Chem. 2015, 63, 3177−3188

solution in 0.1 M phosphate buffer (pH 6.9) was added to each well at 5 s intervals. The reaction mixtures were incubated at 25 °C for 5 min, and the absorbance readings were recorded at 405 nm by a multiscan microplate fluorometer (FLUOstar optima, BMG Labtech, Offeuburg, Germany) and compared to a control, which had 50 μL of buffer solution in place of the extract. Acarbose (Sigma) was used as positive control at the concentration of 10 mg/mL. The α-glucosidase inhibitory activity was expressed as inhibition (%) and was calculated as

$$\%\ \text{inhibition} = \left(\frac{\Delta\text{Abs}_{\text{control}} - \Delta\text{Abs}_{\text{sample}}}{\Delta\text{Abs}_{\text{control}}}\right) \times 100$$

where $\Delta\text{Abs}_{\text{control}}$ is the variation of absorbance of the control and $\Delta\text{Abs}_{\text{sample}}$ is the variation of absorbance of the samples.

Statistical Analysis. Data are expressed as the mean plus standard deviation of replicates. Two-way analysis of variance (ANOVA) was performed for each parameter analyzed, except for prebiotic activity, with SigmaStat (Systat Software, Chicago, IL, USA) to assess if seaweed species and extraction method were a significant source of variation, at a significance level of $p = 0.05$. Subsequently, and because significant differences and significant interactions were recorded, one-way (ANOVA) was carried out for each seaweed species to assess whether each extraction method was a significant source of variation for the parameters analyzed, at a significance level of $p = 0.05$. The Holm−Sidak method was used for pairwise comparisons at a significance level of $p = 0.05$.

In terms of prebiotic activity, for each probiotic bacterium, a three-way analysis of variance (ANOVA) was carried out with SigmaStat (Systat Software) to assess whether the seaweed species, extract, and incubation time at 37 °C were significant sources of variation at a significance level of $p = 0.05$. Because significant differences were observed for each factor (seaweed species, extract, and incubation time) as well as significant interactions, one-way ANOVAs were carried out for each seaweed species to observe if the carbon source (glucose, FOS, or extract) was statistically significant for the number of viable cells of *L. acidophilus* La-5 or *B. animalis* BB12, after 24 or 48 h of incubation, respectively. One-way ANOVAS were also performed to evaluate statistical significance of the viable cells after 24 and 48 h, in comparison to values at 0 h.

RESULTS AND DISCUSSION

Extraction Yield. The extraction yields achieved for each of the different aqueous extractions of the three seaweeds are displayed in Figure 1. Both seaweed species and extraction method were shown to have a significant effect on extraction yield ($p < 0.05$). In general, in terms of species, higher extraction yields were observed for *C. tomentosum* (green algae), followed by *O. pinnatifida* (red algae) and *S. muticum* (brown algae) extracts. Interestingly, an inverse correlation between the organic matter of the seaweed and the respective extraction yields was observed; 67, 58, and 55% of organic matter were reported for *S. muticum*, *O. pinnatifida*, and *C. tomentosum*, respectively.[35] According to Wijesinghe and Jeon,[11] the amount, diversity, and complexity of polysaccharides in the seaweeds' cell wall could reduce the extraction efficiency especially with classical extraction methods. In terms of extraction method, EAE extracts were shown to be the most effective. The extraction efficiency of compounds from seaweeds is limited due to the presence of complex cell walls and, therefore, the degradation of their structure is a fundamental step for the release of compounds from seaweeds. Hydrolytic enzymes have been reported to improve the extraction yield in seaweeds,[9] an effect that was corroborated with the results reported herein for all three seaweed types studied.

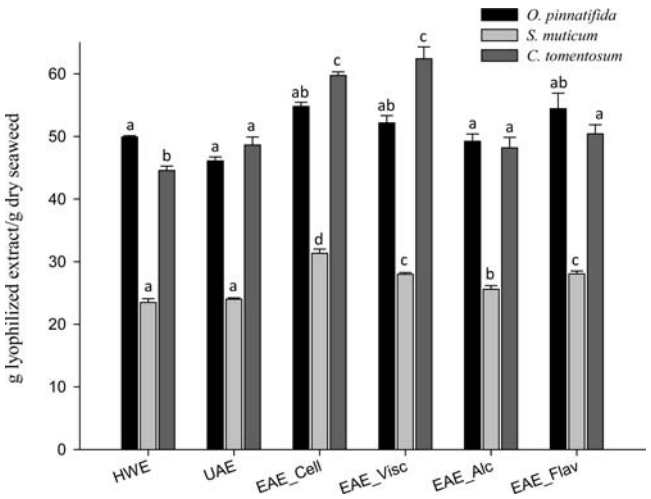

Figure 1. Extraction yields of *O. pinnatifida*, *S. muticum*, and *C. tomentosum* extracts obtained by hot water extraction (HWE), ultrasound-assisted extraction (UAE), and enzyme-assisted extraction (EAE) with Cellulase (Cell), Viscozyme L (Visc), Alcalase (Alc), and Flavourzyme (Flav) at 50 °C. Different letters indicate significant differences ($p < 0.05$) between extracts for each seaweed.

In general, higher extraction yields were observed when assisted by both types of enzymes (carbohydrases and proteases) than in hot water-based extracts or ultrasound-assisted extracts, especially in the case of *S. muticum* and *C. tomentosum*. Higher yields were also reported by Hardouin et al.[12] for *S. muticum* extracts obtained with proteases and carbohydrases than with hot water. To our best of knowledge, there are no studies involving EAE of functional ingredients from *O. pinnatifida* or *C. tomentosum*, which hinders any further comparison besides that achieved within this study. Cellulase and Viscozyme L were responsible for the statistically significant highest extraction yields (60−62%) in *C. tomentosum* (Figure 1, $p < 0.05$), whereas no statistical differences were found in extraction by both proteases (Alcalase and Flavourzyme) or by ultrasound procedures (49−50%, $p > 0.05$) in comparison to HWE. Apparently, cellulase and the multicarbohydrase complex actions of Viscozyme on *C. tomentosum* cell wall polysaccharides were responsible for higher solid content in lyophilized extracts. Extraction yields with Cellulase and Viscozyme L were of similar magnitude to those observed by Wang et al.[9] with red algae *Palmaria palmata*, which were around 60%. Complex polysaccharides such as alginates, agar, carrageenans, and α- and β-D-mannans are practically nondigested by human gastrointestinal enzymes, whereas microorganism-derived enzymes such as some types of carbohydrases are able to degrade complex polysaccharides, converting water-insoluble seaweeds into water-soluble materials collected in water-based extracts.[7]

Similar tendencies such as those for *C. tomentosum* but with lower extraction yield values were observed for *S. muticum* (Figure 1). Cellulase was responsible for the statistically significant highest extraction yield of 31.3% ($p < 0.05$). This value is in the range of extract yield (30−40%) reported by Plaza et al.[36] with subcritical water extraction (SWE) at 100 and 200 °C and by Hardouin et al.[12] with EAE (cellulase) for *S. muticum*, respectively. Although SWE is known for its speed, high yields, and the use of reduced amount of solvents, EAE with Cellulase may also provide several advantages given the enzyme versatility and robustness; furthermore, similar

DOI: 10.1021/jf504220e
J. Agric. Food Chem. 2015, 63, 3177−3188

Table 2. Contents of Nitrogen, Sugars, Sulfated Sugars, and Total Phenolics in the Different Extracts of *S. muticum*, *O. pinnatifida*, and *C. tomentosum* Seaweeds[a]

seaweed	extraction method	nitrogen (mg/g_{lyoph})	sugars ($mg_{glucose\ equiv}/g_{lyoph\ extract}$)	sulfated sugars ($Mg_{Na_2S_4\ acid\ equiv}/g_{lyoph\ extract}$)	total phenolic content ($\mu g_{catechol\ equiv}/g_{lyoph\ extract}$)
S. muticum	HWE	24.6 ± 3.58b	40.6 ± 2.45b	9.5 ± 0.36c	275.8 ± 4.98b
	UAE	24.4 ± 0.33b	37.8 ± 0. 16b	10.1 ± 0.27c	235.0 ± 5.57a
	EAE_CelL	22.1 ± 0.43ab	87.3 ± 4.82c	5.9 ± 0.40a	261.9 ± 29.42ab
	EAE_Visc	25.1 ± 0.62b	29.9 ± 1.95a	7.6 ± 0.61b	300.3 ± 11.67b
	EAE_Alc	29.6 ± 0.01bc	30.7 ± 0.39a	7.5 ± 0.50b	289.7 ± 18.46b
	EAE_Flav	25.4 ± 0.74b	34.7 ± 2.37ab	9.7 ± 0.77c	200.5 ± 7.40a
O. pinnatifida	HWE	12.7 ± 0.50b	73.9 ± 5.15b	41.4 ± l.30b	118.6 ± 5.98a
	UAE	10.3 ± 0.02a	83.2 ± 6.56b	42.8 ± l.64b	103.7 ± l.67a
	EAE_CelL	11.7 ± 0.50ab	102.2 ± 5.34c	41.4 ± 1.81b	112.4 ± 0.27a
	EAE_Visc	12.5 ± 0.53b	71.3 ± 6.48b	59.8 ± l.20d	109.2 ± 2.17a
	EAE_Alc	15.5 ± l.04c	59.5 ± 3.06ab	38.6 ± 1.25ab	106.0 ± 2.92a
	EAE_Flav	19.4 ± 0.14d	76.0 ± 5.16b	46.0 ± l.97bc	123.1 ± 21.89a
C. tomentosum	HWE	17.7 ± 0.19b	62.9 ± 2.38b	11.7 ± 0.20c	107.6 ± 3.13a
	UAE	19.0 ± 0.54b	69.3 ± 5.73b	11.7 ± 0.25c	141.1 ± 9.79b
	EAE_CelL	13.1 ± 0.07a	102.93 ± 5.68c	10.5 ± 0.29b	108.2 ± 5.94a
	EAE_Visc	13.8 ± 1.37a	156.7 ± 4.55d	12.1 ± 0.16c	125.6 ± 8.56ab
	EAE_Alc	22.2 ± 0.36c	40.9 ± 2.17a	9.9 ± 0.25b	121.8 ± 7.64ab
	EAE_Flav	24.1 ± 0.4c	56.8 ± 0.47ab	9.3 ± 0.33a	159.0 ± 11.25b

[a]For each seaweed, different letters indicate significant differences ($p < 0.05$) between methods of extraction.

extraction efficiency of targeted compounds and bioactivity properties is achieved using conventional equipment.

No statistically significant differences ($p > 0.05$) were found between *S. muticum* extracts obtained from Viscozyme (28.0%) and Flavourzyme (28.1%) and between extracts obtained from UAE (24.0%) and HWE (22.5%) methods. Alcalase action resulted in the lowest extraction yield (25.6%) within the EAE methods applied.

In *O. pinnatifida*, Cellulase and Flavourzyme were responsible for the statistically significant highest extraction yields (54−55%, $p < 0.05$), whereas no statistically significant differences ($p > 0.05$) were found between extracts obtained from Alcalase (49.2%), UAE (49.1%), and HWE (49.9%) treatments. The hydrolytic action of the endoprotease and exopeptidase in the Flavourzyme enzymatic complex from *Aspergillus oryzae* (Table 1) on peptide bonds of *O. pinnatifida* proteins could be responsible, at least in part, for the higher extraction yield given its highest protein content (23.8%) in comparison to *S. muticum* and *C. tomentosum* (16.9−18.8%, respectively).[35] According to Cian et al.,[37] proteolysis promoted by Flavourzyme in *Porphyra columbina* (red seaweed) residual cake enhanced extraction of peptides.

UAE is considered an emerging potential technology being considered an efficient alternative to traditional extraction techniques that has been successfully used in the plant extraction field.[38] However, in the present study UAE was not responsible for higher extraction efficiency than HWE for *O. pinnatifida* and *S. muticum*, yet in the case of *C. tomentosum* it enabled a slightly higher, and statistically significant, value (48.6%) than HWE (44.6%). Because UAE was applied to water extracts after 24 h at 50 °C, an improved yield extract was expected, resulting from ultrasound waves due to the implosion of cavitation bubbles. In addition, it has been reported that UAE should be carefully used because unstable compounds such as carotenoids could be degraded.[39] Lee et al.[40] evaluated the potential use of UAE in water and methanolic extracts of *Ecklonia cava* (brown alga) and reported slightly higher extraction yield values after 6 and 12 h at 30 °C in an ultrasonic bath with 200 W (31.3−34.3%) than after 24 h in a shaking incubator at room temperature (28.7%).

Proximate Characterization of the Extracts. In general, and as expected, enzymatic extracts resulting from proteases action presented higher nitrogen content (Table 2); Alcalase and Flavourzyme were responsible for higher content in *S. muticum* (25−30 $mg/g_{lyoph\ extract}$; $p < 0.05$), *O. pinnatifida* (15−19 $mg/g_{lyoph\ extract}$; $p < 0.05$), and *C. tomentosum* (22−24 $mg/g_{lyoph\ extract}$; $p < 0.05$). Indeed, proteases appeared as the most effective enzyme for protein recovery and accessibility.

In terms of sugars, EAE extracts obtained from carbohydrase action presented higher content of sugars; Cellulase was responsible for higher content in *S. muticum* (87 $mg_{glucose\ equiv}/g_{lyoph\ extract}$; $p < 0.05$) and in *O. pinnatifida* (102 $mg_{glucose\ equiv}/g_{lyoph\ extract}$; $p < 0.05$), whereas higher values were obtained by Viscozyme action in *C. tomentosum* (157 $mg_{glucose\ equiv}/g_{lyoph\ extract}$; $p < 0.05$).

The different yields of nitrogen and sugar contents in the extracts for the three species (Table 2) did not correlate with the seaweeds proximate composition in terms of total protein and total sugars content. For both parameters, an inverse correlation between their content in the enzymatic extracts and the seaweed composition was observed: a statistically significant higher value of protein content was observed for *O. pinnatifida* (23.8 $g/100\ g_{dry\ seaweed}$) and the lowest for *S. muticum* (16.9 $g/100\ g_{dry\ seaweed}$); in terms of total sugars *S. muticum* was characterized by a higher content in sugar (49.3 $g/100\ g_{dry\ seaweed}$) than *O. pinnatifida* and *C. tomentosum*, with similar contents of 32−33 $g/100\ g_{dry\ seaweed}$.[35]

No statistically differences were observed for both nitrogen and sugar contents in the extracts obtained with HWE and UAE for the three seaweeds except for *O. pinnatifida*, for which the nitrogen content was higher in the HWE extract than in the UAE counterpart ($p < 0.05$). These results may indicate that

DOI: 10.1021/jf504220e
J. Agric. Food Chem. 2015, 63, 3177−3188

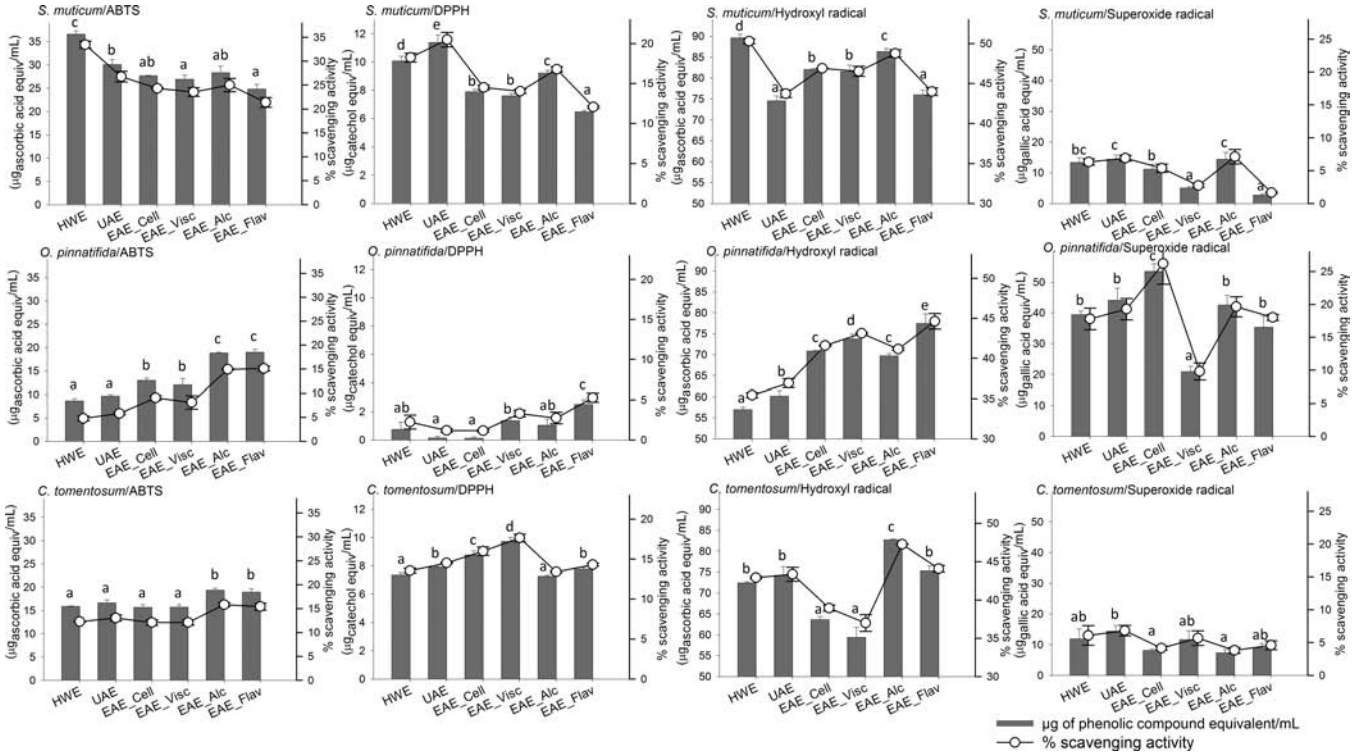

Figure 2. Total antioxidant capacity, DPPH free radical, hydroxyl radical, and superoxide radical scavenging activities of *S. muticum*, *O. pinnatifida*, and *C. tomentosum* extracts obtained by hot water extraction (HWE), ultrasound-assisted extraction (UAE), and enzyme-assisted extraction (EAE) with Cellulase (Cell), Viscozyme L (Visc), Alcalase (Alc), and Flavourzyme (Flav) at 50 °C. Different letters indicate significant differences ($p < 0.05$) between extracts for each seaweed.

the mechanical action resulting from ultrasound waves under the extraction time and temperature conditions used did not promote the release of extra proteins or polysaccharides from the intracellular or wall contents of seaweeds.

Variable content in sulfate groups, which was significantly different for each seaweed species and extraction method ($p < 0.05$), is observable in Table 2. Previous studies with FTIR-ATR analysis showed that in the brown algae *S. muticum*, alginates and fucoidans were the main polysaccharides, whereas *O. pinnatifida* was mostly an agar producer; sulfate esters of sulfated polysaccharides were observed in the spectrum of *C. tomentosum*.[35] Therefore, the sulfated content in each extract was in part related to the nature and amount of sulfated polysaccharide in each seaweed species as well as the extraction efficiency.

High content of sulfate groups was observed in *O. pinnatifida* extracts (39−60 $\mu g_{Na_2SO_4\ acid\ equiv}/g_{lyoph\ extract}$) probably from agar, a less sulfated polysaccharide than carrageenans, also characteristic in some red seaweeds. A significantly higher content was obtained with EAE using Viscozyme. According to Domozych,[10] red algae possess complex composite cell walls, which are made of cellulose, xylan, or mannan fibrils as well as an extensive matrix of polysaccharides such as agar and carrageenan.

For *S. muticum* extracts, enzymatic activity did not result in higher content of sulfate groups except for extraction performed with Flavourzyme, in accordance with data reported by Hardouin et al.[12] for this seaweed. Hot water and UAE extracts were revealed to be more suitable to obtain extracts richer in the sulfate groups. These probably result from fucoidans. The presence of sulfated ester groups (S═O), a characteristic component in fucoidan and other sulfate polysaccharides, was assigned by FTIR-ATR for *S. muticum*.[35] According to Ale and Meyer,[41] fucoidans cover several different structural fucose-containing sulfated polysaccharides, comprising many different types of fucose-rich polysaccharides, including sulfated fucogalacturonans found in *Sargassum* sp., for example. The lower content of sulfated groups in *S. muticum* in comparison to *O. pinnatifida* could be related to the presence of alginates (a nonsulfated polysaccharide), also evidenced by FTIR-ATR analysis. *S. muticum*, an original species from Japan now found in the Atlantic Ocean and in the Mediterranean Sea, has been reported to possess, when dry, 10−18% alginates.[42] A slightly higher content in sulfated groups, in comparison to *S. muticum*, was observed in *C. tomentosum* extracts. These could be related to the presence of sulfated xyloarabinogalactans such as sulfated arabinan and sulfated arabinogalactan, which have been identified in *C. tomentosum*[43] or other sulfated polysaccharides.[35] Extracts that resulted from EAE with Cellulase and Viscozyme, as well as from HWE and UAE, were those with higher content in sulfated groups.

Total phenolic content varied significantly according to extraction mode and seaweed type ($p < 0.05$). Higher values for total phenolic content were found for *S. muticum* extracts, which ranged between 201 and 301 $\mu g_{catechol\ equivalent}/g_{lyoph\ extract}$ (Table 2). Once again, no direct correlation was observed between total phenolic content in each seaweed and those in the respective aqueous extracts. Significant differences in total phenolic content were observed between the three seaweed species, namely, 460, 250, and 169 $\mu g_{catechol\ equivalent}/g_{dry\ seaweed}$ for *C. tomentosum*, *S. muticum*, and *O. pinnatifida*, respectively.[35] This observation might suggest that none of the extraction modes were sufficiently efficient to extract all phenolics in *C. tomentosum* and *O. pinnatifida*. It has been

DOI: 10.1021/jf504220e
J. Agric. Food Chem. 2015, 63, 3177−3188

reported that organic solvents such as ethanol are more efficient for polyphenol extraction than water.[19]

Variable efficiency of phenolic compound extraction was observed by the different extraction modes for each seaweed species. For *S. muticum* statistically higher values were obtained by HWE and by Viscozyme and Alcalase EAE (Table 2). For *C. tomentosum*, UAE and Flavourzyme EAE were responsible for higher efficiency, whereas for *O. pinnatifida* no statistical difference were observed for the different extracts. No information on effects of water-based extraction mode on phenolic compounds was found in the literature. For example, higher content in total phenols values was reported by Plaza et al.[36] in *S. muticum* extracts obtained by SWE water extracts at 100 and 200 °C ranging between 10.7 and 58.67 $mg_{gallic\ acid}/g_{extract}$, respectively, but no explanation is given for the increment in total phenols except that with a higher extraction temperature a higher mass transfer occurs, which increases extraction yield. Water and ethanolic extracts of 16 species collected at the Danish coast were screened for extraction yield and respective total phenolic content by Farvin and Jacobsen.[19] For all species, water extracts showed higher yield, but in terms of phenolic content this was dependent on the species. In general, the ethanolic extracts had higher content of total phenolics except for four species including *S. muticum*.[19] No explanation is yet available for the higher extractability of phenolic compounds by water in some species such as in *S. muticum*. In turn, for *O. pinnatifida*, methanolic extraction rendered a higher extraction yield and higher polyphenol content than by aqueous extraction.[44] According to Budhiyanti et al.[45] phenolic content varied from 0.006 to 0.65 and from 6.72 to 21.99 $g_{phloroglucinol\ equiv}/100\ g_{dried\ extract}$ for cytoplasmic and membrane-bound extracts from *Sargassum* sp., respectively. These data show that the phenolic contents are extremely variable among species of *Sargassum* and cell structure.

Antioxidant Activity. Figure 2 presents data for total antioxidant capacity and for DPPH free radical as well as hydroxyl and superoxide radical scavenging activities of the different extracts for each seaweed, evaluated both as micrograms of phenolic compound equivalent and as percent of scavenging activity. Because the diverse expression of results for the different antioxidant capacity evaluation methodologies found in the literature makes comparison between studies difficult,[46] the authors think that the perception of the relative proportion between phenolic content (μg/mL) of extract and the corresponding value in terms of percentage of scavenging activity makes the interpretation more objective and more valuable (Figure 2). The four different antioxidant evaluations varied significantly among seaweed species and among extraction modes ($p < 0.05$). Maximum total antioxidant capacities as well as DPPH free radical and hydroxyl radical scavenging activities were observed in the extracts of *S. muticum* followed by *C. tomentosum* (Figure 2). In *O. pinnatifida* extracts, lower total antioxidant capacity and DPPH free radical scavenging activity were observed in comparison to any of the two other seaweeds, but higher scavenging capacity for reactive oxygen species such as $HO^{\bullet}$ and in particular of radical $O_2^{\bullet -}$ were achieved. Heo et al.[18] also reported variable scavenging activities in brown seaweed extracts obtained by carbohydrases or proteases in terms of DPPH free, hydroxyl, and superoxide radicals. According to Freitas et al.[46] no single assay seems to be able to accurately reflect the mechanism of action of all radicals and antioxidants, especially in complex systems. For example, some antioxidants may not be efficient quenchers of peroxyl radicals but be only singlet-oxygen scavengers.[47]

The statistically significant difference between the seaweed extracts ($p < 0.05$) could be, at least in part, attributed to the higher amount of total phenolic compounds and proteinaceous compounds found in *S. muticum* (Table 2). The radical scavenging activity of phenolic compounds is, however, dependent on the phenolic structure and number and location of hydroxyl groups,[48] and therefore the radical scavenging potential of the extracts is dependent on qualitative and quantitative phenolic combination. Our results are in accordance with those published by Yangthong et al.,[49] who reported higher phenolic content and antioxidant activity for brown seaweeds than for red and green seaweeds. Polysaccharides in brown algae such as those with high content of uronic acid and alginates with low molecular weight have also been reported as good antioxidant potential.[50]

The antioxidant potential of *S. muticum* water extracts was higher in HWE especially in terms of total antioxidant capacity ($p < 0.05$) with 33.5% scavenging activity (corresponding to 37 $\mu g_{ascorbic\ acid\ equiv}$/mL) and hydroxyl radical scavenging activity ($p < 0.05$) with 50.3% scavenging activity (corresponding to 90 $\mu g_{ascorbic\ acid\ equiv}$/mL), respectively. Maximum DPPH free radical scavenging activity was observed for UAE with 20% scavenging activity (corresponding to 11 $\mu g_{catechol\ equiv}$/mL). In terms of antioxidant activity no increase was observed in the *S. muticum* extracts obtained from EAE. Higher values of free and hydroxyl scavenging activity were reported by Je et al.[16] in EAE extracts with Alcalase and Viscozyme from brown seaweed *Undaria pinnatifida*, but no hydroxyl scavenging activity from EAE extracts with Flavourzyme was reported. Hydroxyl scavenging activity of *S. muticum* extracts produced with Flavourzyme was 42%, one of the lowest values together with those obtained for UAE extracts (Figure 2). In *O. pinnatifida*, EAE extracts had, in general, higher scavenging potential than HWE or UAE. In terms of total antioxidant capacity, protease-assisted extracts with 19% scavenging activity (corresponding to 15−16 $\mu g_{ascorbic\ acid\ equiv}$/mL) presented statistically significant higher values ($p < 0.05$) than the other extraction methods. According to Cian et al.,[37] the low molecular weight peptides and polyphenols released during proteolysis were responsible for the DPPH radical scavenging activity of red seaweed *Porphyra columbina*. No radical scavenging activity toward ABTS was reported by Jiménez-Escrig et al.[44] for aqueous extracts of *O. pinnatifida*. For the hydroxyl radical, EAE extracts were capable of 42−45% scavenging activity (corresponding to 70−79 $\mu g_{ascorbic\ acid\ equiv}$/mL) (Figure 2). *O. pinnatifida* EAE extracts from Cellulase had a statistically significant ($p < 0.05$) higher superoxide scavenger potential with 28% scavenging activity (corresponding to 54 $\mu g_{gallic\ acid\ equiv}$/mL) than the other extracts.

The extraction procedures did not affect the total antioxidant capacity displayed by *C. tomentosum* extracts except for those obtained by protease EAE, where results were higher and statistically different (Figure 2). In terms of superoxide radical scavenging activity only slight differences were observed between the different *C. tomentosum* extracts. However, Cellulase and Viscozyme extracts of *C. tomentosum*, which had higher sugar content, had statistically significant ($p < 0.05$) higher DPPH free radical scavenger activity with 16−18% (corresponding to 9−10 $\mu g_{catechol\ acid\ equiv}$/mL). Valentão et al.[51] also reported a weak concentration-dependent antioxidant capacity for *C. tomentosum* aqueous lyophilized extracts (10% of

DOI: 10.1021/jf504220e
J. Agric. Food Chem. 2015, 63, 3177−3188

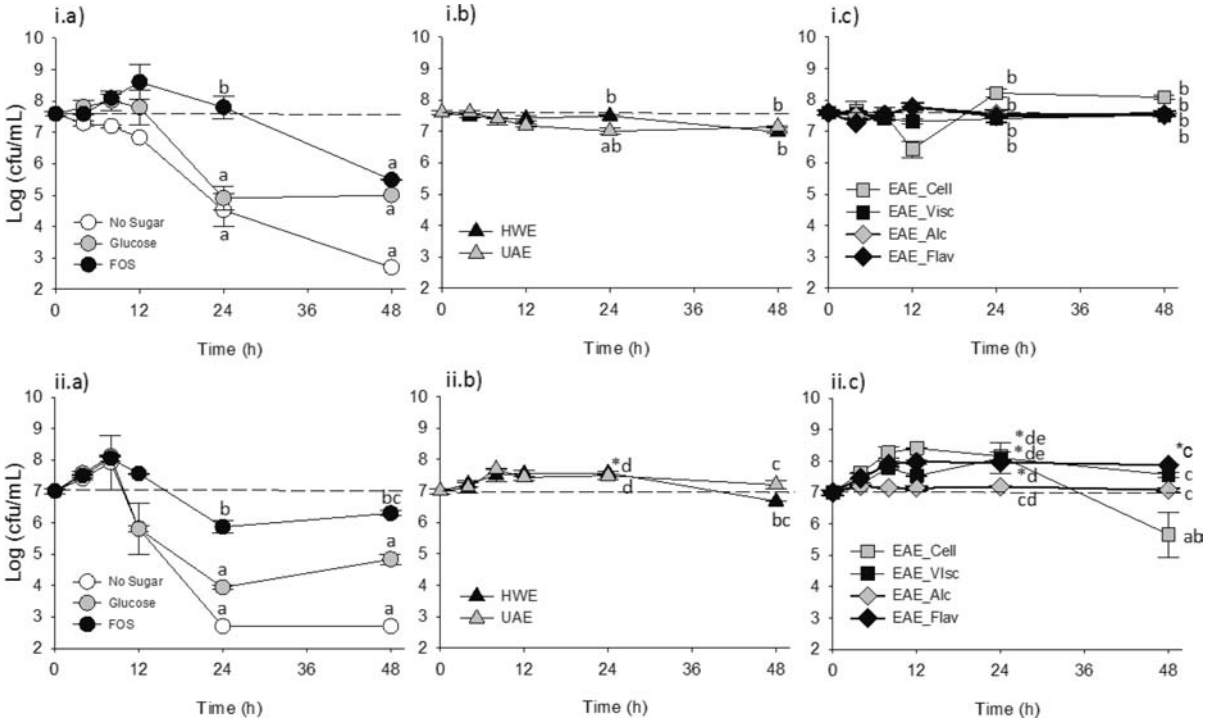

Figure 3. Mean and standard deviation of cell counts of *B. animalis* BB-12 (i) and *L. acidophilus* La-5 (ii) throughout 48 h of incubation at 37 °C in the presence or absence of sugars (a) or *S. muticum* extracts: hot water extraction (HWE) and ultrasound-assisted extraction (UAE) (b); enzyme-assisted extraction (EAE) with Cellulase (Cell), Viscozyme L (Visc), Alcalase (Alc), and Flavourzyme (Flav) (c). Different letters indicate significant differences ($p < 0.05$) for the viable cells after 24 or 48 h of incubation at 37 °C in the presence or absence of sugars or *S. muticum* extracts, and ∗ indicates significant differences ($p < 0.05$) in comparison to values at 0 h.

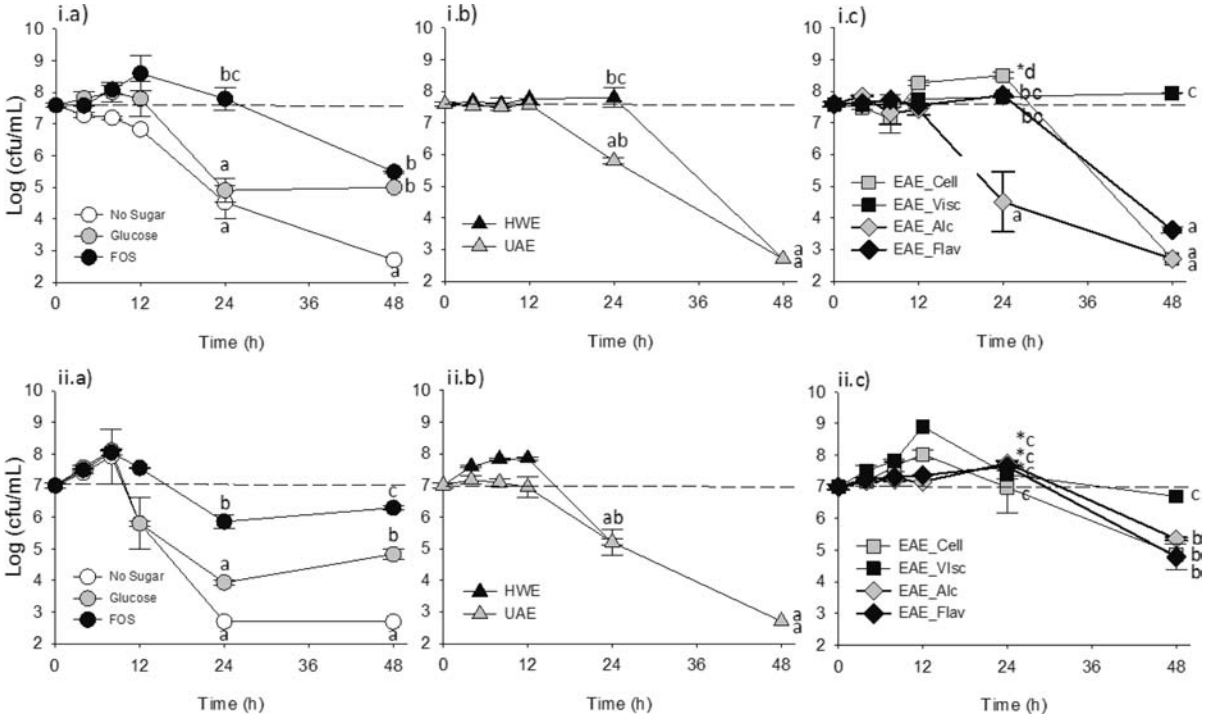

Figure 4. Mean and standard deviation of cell counts of *B. animalis* BB-12 (i) and *L. acidophilus* La-5 (ii) throughout 48 h of incubation at 37 °C in the presence or absence of sugars (a) or *O. pinnatifida* extracts: hot water extraction (HWE) and ultrasound-assisted extraction (UAE) (b); enzyme-assisted extraction (EAE) with Cellulase (Cell), Viscozyme L (Visc), Alcalase (Alc), and Flavourzyme (Flav) (c). Different letters indicate significant differences ($p < 0.05$) for the viable cells after 24 or 48 h of incubation at 37 °C in the presence or absence of sugars or *O. pinnatifida* extracts, and ∗ indicates significant differences ($p < 0.05$) in comparison to values at 0 h.

DOI: 10.1021/jf504220e
J. Agric. Food Chem. 2015, 63, 3177−3188

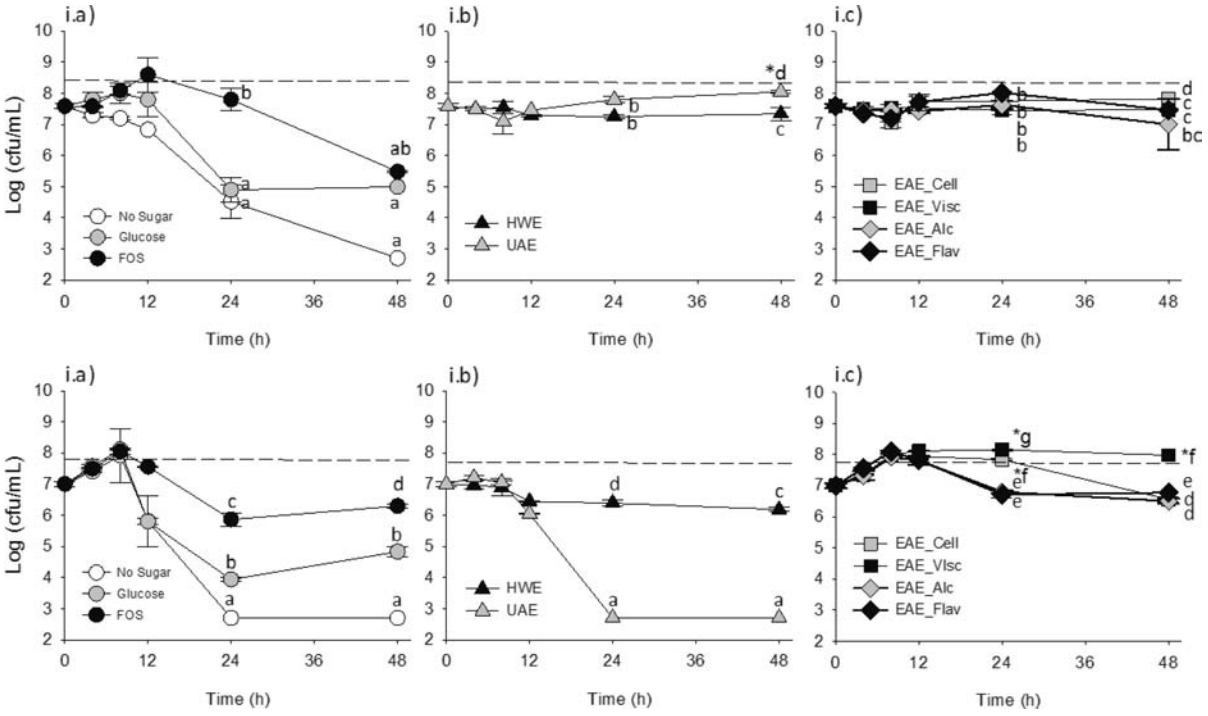

Figure 5. Mean and standard deviation of cell counts of *B. animalis* BB-12 (i) and *L. acidophilus* La-5 (ii) throughout 48 h of incubation at 37 °C in the presence or absence of sugars (a) or *C. tomentosum* extracts: hot water extraction (HWE) and ultrasound-assisted extraction (UAE) (b); enzyme-assisted extraction (EAE) with Cellulase (Cell), Viscozyme L (Visc), Alcalase (Alc), and Flavourzyme (Flav) (c). Different letters indicate significant differences ($p < 0.05$) for the viable cells after 24 or 48 h of incubation at 37 °C in the presence or absence of sugars or *C. tomentosum* extracts, and ∗ indicates significant differences ($p < 0.05$) in comparison to values at 0 h.

DPPH free radical scavenging activity with 794 μg/mL extract). In terms of the hydroxyl radical, Alcalase and Flavourzyme extracts were able to inhibit >44% of scavenging activity corresponding to 76−83 $g_{\text{ascorbic acid equiv}}$/mL, which may indicate that such bioactivity is related not only to total phenolic content but also to proteinaceous compounds (Table 2). Nevertheless, given the statistically significant difference between Alcalase and Flavourzyme scavenging capacities and their respective phenolic and nitrogen contents shown in Table 2, it seems that not only the content but also the nature of the compounds is important to eventually justify the antioxidant properties. For example, Heo et al.[18] reported that enzymatic extracts of brown algae *Ecklonia cava* with Alcalase did not possess DPPH free radical scavenging activity, although they contained as much phenolic compounds as other extracts with free radical scavenging activity. In turn, Farvin and Jacobsen[19] reported some extracts with good antioxidant effects but with low total phenolic content, indicating that other compounds were coextracted in water extracts such as sulfate polysaccharides, proteins, or peptides. However, not much antioxidant potential was observed in crude sulfated polysaccharides from *Sargassum plagiophyllum* (2 mg/mL) for free radical (11.2%), hydroxyl (11.2%), or superoxide (0%) radical scavenging activities.[29]

In summary, the different extracts, with 2 mg lyophilized extract/mL, from *S. muticum*, *O. pinnatifida*, and *C. tomentosum* did not exhibit high total antioxidant capacity or DPPH free radical scavenging activity but more prominent effects on hydroxyl radical scavenging activity (35−50%). Extracts from *O. pinnatifida* with 0.2 mg lyophilized extract/mL, namely, HWE, UAE, and EAE with Cellulase and Alcalase, exhibited moderate effects on superoxide radical scavenging activity (18−26%).

Prebiotic Potential of Seaweed Extracts. Recently, some research has been done in identifying potential prebiotic compounds in marine resources, namely, in seaweeds, given their rich profile in polysaccharides present in the cell walls;[52] nonetheless, to our best of knowledge, no information is available regarding the prebiotic potential of the three seaweed species targeted in our study. Hence, the potential prebiotic effect of seaweed water-based extracts was evaluated by using pure cultures of representative beneficial bacteria including strains of lactobacilli and bifidobacteria (usual target genera for prebiotics) in parallel with well-established prebiotics, such as FOS, for comparison purposes. Both probiotic strains were also grown under the same conditions but in the absence of sugar (negative control) as well as in the presence of glucose or FOS at similar concentrations (positive controls) (Figures 3−5). Seaweed species, extraction mode, and incubation time were revealed to be significant factors for both probiotic strains viability ($p < 0.05$). Because significant differences were observed for each factor as well as significant interactions, one-way ANOVAs were carried out for each seaweed species to observe if the carbon source (glucose, FOS, or extract) was statistically significant for the viable cell numbers of *L. acidophilus* La-5 or *B. animalis* BB12, after 24 or 48 h of incubation, respectively. With regard to *L. acidophilus* La-5, significantly higher values ($p < 0.05$) of viable cell numbers were observed for the majority of culture media enriched with seaweed water-based extracts after 24 h of incubation in comparison to growth in media with glucose or FOS. In addition, some significant increases ($p < 0.05$) in viable cell numbers in comparison to those at 0 h were observed such as

DOI: 10.1021/jf504220e
J. Agric. Food Chem. 2015, 63, 3177−3188

in media containing HWE and EAE with Viscozyme, Cellulase, and Flavorzyme extracts of *S. muticum*, and EAE with Viscozyme and Alcalase extracts of *O. pinnatifida* as well as EAE with Viscozyme and Cellulase extracts of *C. tomentosum* (Figures 3ii,a–c, 4ii,a–c, and 5ii,a–c). Despite the enhanced growth by 24 h of incubation, after 48 h of incubation lower viable cell numbers were observed, in particular for *O. pinnatifida* extracts (Figure 4ii,b–c); end-product formation or substrate depletion could justify this decrease in viable cell numbers.

In terms of seaweed extracts' impact on *B. animalis* BB-12, it was found that, in general, they have a lower prebiotic potential (Figures 3i,a–c, 4i,a–c, and 5i,a–c). Nonetheless viable cell numbers of *B. animalis* BB-12 in all *S. muticum* and *C. tomentosum* extracts after 48 h of incubation were significantly higher than those obtained with prebiotic FOS and glucose ($p < 0.05$) (Figures 3i,a–c and 5i,a–c).

Although of preliminary nature, these results show that the majority of the extracts obtained from the three seaweeds possess carbon sources that can be metabolized by *L. acidophilus* La-5 and *B. animalis* BB-12. A more promising prebiotic potential was observed for *S. muticum* and *C. tomentosum* extracts, especially for those obtained by enzymatic action. Because a lower potential was observed in extracts of *O. pinnatifida*, this could be related to the largest amount of sulfated sugars observed in these extracts. Red seaweed *O. pinnatifida* has been mostly characterized as an agar producer, and it is known that microorganisms are not able to hydrolyze and metabolize this polysaccharide, which is used as a solidifying agent of culture media. On the other hand, it should not be totally overlooked because it was shown recently that some low molecular weight polysaccharide fractions derived from seaweed agar and alginate by acid hydrolysis or degradation with hydrogen peroxide were fermented by gut microbiota, namely, bifidobacterial populations, exhibiting potential to be used as a novel source of prebiotics.[53]

Enzymatic extracts, especially those obtained with carbohydrases (Viscozyme and Cellulase), probably possess polysaccharides and oligosaccharides derived from hydrocolloids present in each type of seaweed that can act as sources of soluble fibers exerting a prebiotic effect. According to Wu et al.[54] *Bifidobacterium longum* BCRC 11847 could utilize polysaccharide extracts of red seaweed *Gracilaria* sp. extracted with Cellulase R-10 and Macerozyme R-10 and display an increase in pH-lowering ability. Zaporozhets et al.[52] recently reviewed the prebiotic potential of polysaccharides and extracts from seaweeds. In that review the authors included their research group studies' results on the prebiotic potential of fucoidan and alginic acid derived from brown seaweed *Fucus evanescens* in vitro and in vivo with mice. These authors confirmed that fucoidan and alginic acid were used instead of lactose with a 3–5.8-fold increase in biomass of *Bifidobacterium* in comparison to the control.

Given the promising reported results obtained in terms of growth promotion of *L. acidophilus* La-5 and *B. animalis* BB-12 and considering the prebiotic potential of polysaccharides and seaweed extracts reported in the literature concerning other seaweed species, further in vitro (nondigestibility and selective fermentation capacity) and in vivo studies must be performed with the enzymatic extracts assisted by Cellulase of *S. muticum* and *C. tomentosum* as well as in UAE extracts of *C. tomentosum*. The identification of polysaccharide (and associated molecular weight) and oligosaccharide fractions in the extracts derived from the enzymatic action will also be determinant to understand and correlate with the prebiotic activity.

α-Glucosidase Inhibitory Activity. The α-glucosidase inhibitory activity, expressed as percent of inhibition, by *S. muticum*, *O. pinnatifida*, and *C. tomentosum* water-based extracts is displayed in Figure 6. Extraction mode and seaweed species

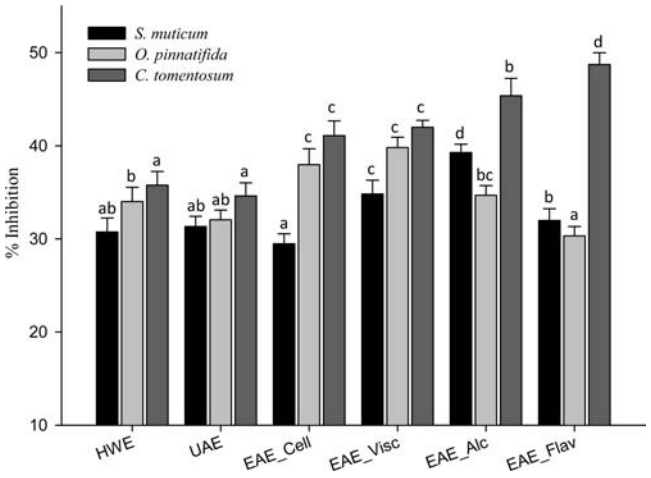

Figure 6. α-Glucosidase inhibitory activity, expressed as percent of inhibition, of *S. muticum*, *O. pinnatifida*, and *C. tomentosum* extracts obtained by hot water extraction (HWE), ultrasound-assisted extraction (UAE), and enzyme-assisted extraction (EAE) with Cellulase (Cell), Viscozyme L (Visc), Alcalase (Alc), and Flavourzyme (Flav) at 50 °C. Different letters indicate significant differences ($p < 0.05$) between extracts for each seaweed.

were both statistically significant factors ($p < 0.05$). Extracts obtained by enzymatic action possess higher inhibition activity especially for *O. pinnatifida*, with 38–40% inhibition in the extracts obtained by Cellullase and Viscozyme, and for *C. tomentosum* with 45–49% inhibition in the extracts obtained by Alcalase and Flavourzyme. To our knowledge there are no reports on potential antidiabetic activity of water-based enzymatic seaweed extracts, in particular for the studied species, and therefore no direct comparisons with other works with only other seaweed species and other extraction modes are possible. For example, Senthil et al.[22] reported that ethyl acetate extracts of red seaweeds of *Chondrococcus harnmanni* and *Padina gymnospora* (81 and 94%, respectively) possesses high levels of α-amylase inhibitory activity. Lower values of α-glucosidase inhibitory activity were observed for *S. muticum* extracts with a maximum of inhibition in the extracts obtained with Alcalase (39%). This is an interesting observation because the *S. muticum* extract showed the highest protein content among all other extracts (Table 2). Other research works have studied the role of seaweed polysaccharides, from other *Sargassum* species, or of phenolic compounds on the inhibition activity of α-amylase and α-glucosidase but less on the role of protein or peptides for the same purpose. For example, Hardoko et al.[55] reported inhibitory activity on α-glucosidase by laminaran and fucoidan fractions from two brown seaweeds (*Sargassum duplicatum* and *Turbinaria decurens*) but not by the alginate fraction. According to Motshakeri et al.,[56] 35–36% blood glucose reduction was observed in type 2 diabetic rats after 22 days of feeding with 300 mg/kg body weight ethanolic or water extracts of *Sargassum polycystum*. In the present study, EAE extracts from *O. pinnatifida* and *C. tomentosum* showed promising inhibitory

DOI: 10.1021/jf504220e
J. Agric. Food Chem. 2015, 63, 3177–3188

potential against α-glucosidase and, although further in vivo studies are required to test for effective hypoglycaemic activity, these may prove to be important strategies in the prevention (functional food) or management (oral therapeutic agent) of blood glucose level in type 2 diabetic and borderline patients.

In conclusion, this study demonstrates once more that edible seaweeds such as *S. muticum* (brown alga), *O. pinnatifida* (red alga), and *C. tomentosum* (green alga) are natural sources of compounds with important biological interest. In the present study, water-based crude extracts were obtained from efficient methods that are also food grade compatible and sustainable. Enzyme-assisted extraction was revealed to be a promising tool to obtain extracts with attractive biological properties. According to the general results achieved, it becomes difficult to pinpoint the most efficient extraction method with the highest biological potential because it depends on several factors: (i) seaweed species; (ii) extraction mode considering the duality extraction yield versus chemical/biological properties; and (iii) the type of analysis made. From this perspective, *S. muticum* EAE presented interesting antioxidant and prebiotic potentials, *O. pinnatifida* enzyme-assisted free radical scavenging activity given its high sulfated sugar content, and *C. tomentosum* EAE a promising α-glucosidase inhibitory activity and consequently attractive antidiabetic potential. In general, it can be pointed out that the enzyme-assisted extraction seems to be one of the best options in terms of food compatible extraction method with higher yield rates, and through the selection of a specific enzyme some biological properties may be favored over other properties. It is our opinion that, for future studies with these seaweeds in terms of functional food development, the selection of the most efficient extraction mode will need to be coupled to the best results in terms of biological properties according to the intended purpose associated with the identification of polysaccharides, peptides, and phenolic compounds.

AUTHOR INFORMATION

Corresponding Author

*(D.R.) Phone: (+351) 232 910 117. Fax: (+351) 232 910 193. E-mail: dinarodrigues@ua.pt.

Funding

This work was supported by the Portuguese Science Foundation (FCT − Fundação para a Ciência e Tecnologia) through individual research grant references SFRH/BPD/73781/2010 and SFRH/BD/77647/2011 under QREN − POPH funds, cofinanced by the European Social Fund and Portuguese National Funds from MCTES and projects PEst-C/MAR/LA0017/2013 and PEst-OE/EQB/LA0016/2013 supported by European Funds through COMPETE and by National Funds through the FCT.

Notes

The authors declare no competing financial interest.

REFERENCES

(1) Holdt, S. L.; Kraan, S. Bioactive compounds in seaweed: functional food applications and legislation. *J. Appl. Phycol.* **2011**, *23*, 543−597.

(2) Ibañez, E.; Cifuentes, A. Benefits of using algae as natural sources of functional ingredients. *J. Sci. Food Agric.* **2013**, *93*, 703−709.

(3) Pangestuti, R.; Kim, S.-K. Biological activities and health benefit effects of natural pigments derived from marine algae. *J. Funct. Foods* **2011**, *3*, 255−266.

(4) El Gamal, A. A. Biological importance of marine algae. *Saudi Pharm. J.* **2010**, *18*, 1−25.

(5) Jeon, Y.-J.; Wijesinghe, W. A. J. P.; Kim, S.-K. Biotechnology and applied phycology. In *Handbook of Marine Macroalgae*; Kim, S.-K., Ed.; Wiley-Blackwell: Chichester, UK, 2012; online ISBN 978-0-470-97918-1.

(6) Herrero, M.; Cifuentes, A.; Ibañez, E. Sub- and supercritical fluid extraction of functional ingredients from different natural sources: plants, food-by-products, algae and microalgae. *Food Chem.* **2006**, *98*, 136−148.

(7) Heo, S.-J.; Jeon, Y.-J.; Lee, J.; Kim, H. T.; Lee, K.-W. Antioxidant effect of enzymatic hydrolyzate from a kelp, *Ecklonia cava*. *Algae* **2003**, *18*, 341−347.

(8) Gil-Chávez, G. J.; Villa, J. A.; Ayala-Zavala, J. F.; Heredia, J. B.; Sepulveda, D.; Yahia, E. M.; González-Aguilar, G. A. Technologies for extraction and production of bioactive compounds to be used as nutraceuticals and food ingredients: an overview. *Compr. Rev. Food Sci. Food Saf.* **2013**, *12*, 5−23.

(9) Wang, T.; Jónsdóttir, R.; Kristinsson, H. G.; Hreggvidsson, G. O.; Jónsson, J. O.; Thorkelsson, G.; Ólafsdóttir, G. Enzyme-enhanced extraction of antioxidant ingredients from red algae *Palmaria palmate*. *LWT−Food Sci. Technol.* **2010**, *43*, 1387−1393.

(10) Domozych, D. S. Algal cell walls. In *eLS*; Wiley: Chichester, UK, 2011. http://www.els.net [DOI: 10.1002/9780470015902.a0000315.pub3].

(11) Wijesinghe, W. A. J. P.; Jeon, Y.-J. Enzyme-assistant extraction (EAE) of bioactive components: a useful approach for recovery of industrially important metabolites from seaweeds: a review. *Fitoterapia* **2012**, *83*, 6−12.

(12) Hardouin, K.; Burlot, A.-S.; Umami, A.; Tanniou, A.; Stiger-Pouvreau, V.; Widowati, I.; Bedoux, G.; Bourgougnon, N. Biochemical and antiviral activities of enzymatic hydrolysates from different invasive French seaweeds. *J. Appl. Phycol.* **2014**, *26*, 1029−1042.

(13) Hahn, T.; Lang, S.; Ulber, R.; Muffler, K. Novel procedures for the extraction of fucoidan from brown algae. *Process Biochem.* **2012**, *47*, 1691−1698.

(14) Kadam, S. U.; Tiwari, B. K.; O'Donnell, C. P. Application of novel extraction technologies for bioactives from marine algae. *J. Agric. Food Chem.* **2013**, *61*, 4667−4675.

(15) Chandini, S. K.; Ganesan, P.; Bhaskar, N. *In vitro* antioxidant activities of three selected brown seaweeds of India. *Food Chem.* **2008**, *107*, 707−713.

(16) Je, J.-Y.; Park, P.-J.; Kim, E.-K.; Park, J.-S.; Yoon, H.-D.; Kim, K.-R.; Ahn, C.-B. Antioxidant activity of enzymatic extracts from the brown seaweed *Undaria pinnatifida* by electron spin resonance spectroscopy. *LWT−Food Sci. Technol.* **2009**, *42*, 874−878.

(17) Tanniou, A.; Vandanjon, L.; Incera, M.; Leon, E. S.; Husa, V.; Le Grand, J.; Nicolas, J.-L.; Poupart, N.; Kervarec, N.; Engelen, A.; Walsh, R.; Guerard, F.; Bourgougnon, N.; Stiger-Pouvreau, V. Assessment of the spatial variability of phenolic contents and associated bioactivities in the invasive alga *Sargassum muticum* samples along it European range from Norway to Portugal. *J. Appl. Phycol.* **2014**, *26*, 1215−1230.

(18) Heo, S.-J.; Park, E.-J.; Lee, K.-W.; Jeon, Y.-J. Antioxidant activities of enzymatic extracts from brown seaweeds. *Bioresour. Technol.* **2005**, *96*, 1613−1623.

(19) Farvin, K. H. S.; Jacobsen, C. Phenolic compounds and antioxidant activities of selected species of seaweeds from Danish coast. *Food Chem.* **2013**, *138*, 1670−1681.

(20) Al-Sheraji, S. H.; Ismail, A.; Manap, M. Y.; Mustafa, S.; Yusof, R. M.; Hassan, F. A. Prebiotics as functional foods: a review. *J. Funct. Foods* **2013**, *5*, 1542−1553.

(21) Ali, H.; Houghton, P. J.; Soumyanath, A. α-Amylase inhibitory activity of some Malaysian plants used to treat diabetes; with particular reference to *Phyllanthus amarus*. *J. Ethnopharmacol.* **2006**, *107*, 449−455.

(22) Senthil, S. L.; Kumar, T. V.; Geetharamani, D.; Maruthupandi, T. Screening of seaweeds collected from southeast coastal area of India for α-amylase inhibitory activity, antioxidant and biocompatibility. *Int. J. Pharm. Pharm. Sci.* **2013**, *5*, 240−244.

DOI: 10.1021/jf504220e
J. Agric. Food Chem. 2015, 63, 3177−3188

(23) Guiry, M. D.; Guiry, G. M. *AlgaeBase*; National University of Ireland: Galway, 2013; http://www.algaebase.org (accessed June 6, 2013).
(24) Huang, S.-Q.; Li, J.-W.; Wang, Z.; Pan, H.-X.; Chen, J. X.; Ning, Z.-X. Optimization of alkaline extraction of polysaccharides from *Ganoderma lucidum* and their effect on immune function in mice. *Molecules* **2010**, *15*, 3694−3708.
(25) Dubois, M.; Gilles, K. A.; Hamilton, J. K.; Rebers, R. A.; Smith, F. Colorimetric method for determination of sugars and related substances. *Anal. Chem.* **1956**, *28*, 350−356.
(26) Dodgson, K. S. Determination of inorganic sulphate in studies on the enzymic and non-enzymic hydrolysis of carbohydrate and other sulphate esters. *Biochem. J.* **1961**, *78*, 312−319.
(27) Mulinacci, N.; Romani, A.; Galardi, C.; Pinelli, P.; Giaccherini, C.; Vincieri, F. F. Polyphenolic content in olive oil waste waters and related olive samples. *J. Agric. Food Chem.* **2001**, *49*, 3509−3514.
(28) Gião, M. S.; González-Sanjosé, M. L.; Rivero-Pérez, M. D.; Pereira, C. I.; Pintado, M. E.; Malcata, F. X. Infusions of Portuguese medicinal plants: dependence of final antioxidant capacity and phenol content on extraction features. *J. Sci. Food Agric.* **2007**, *87*, 2638−2647.
(29) Suresh, V.; Senthilkumar, N.; Thangam, R.; Rajkumarc, M.; Anbazhagana, C.; Rengasamy, R.; Gunasekaran, P.; Kannan, S.; Palani, P. Separation, purification and preliminary characterization of sulfated polysaccharides from *Sargassum plagiophyllum* and its in vitro anticancer and antioxidant activity. *Process Biochem.* **2013**, *48*, 364−373.
(30) Sudha, G.; Priya, M. S.; Shree, R. I.; Vadivukkarasi, S. *In vitro* free radical scavenging activity of raw pepino fruit (*Solanum muricatum* Aiton). *Int. J. Curr. Pharm. Res.* **2011**, *3*, 137−140.
(31) Smirnoff, N.; Cumbes, Q. J. Hydroxyl radical scavenging activity of compatible solutes. *Phytochemistry* **1989**, *28*, 1057−1060.
(32) Fiorentino, A.; D'Abrosca, B.; Pacifico, S.; Golino, A.; Mastellone, C.; Oriano, P.; Monaco, P. Reactive oxygen species scavenging activity of flavone glycosides from *Melilotus neapolitana*. *Molecules* **2007**, *12*, 263−270.
(33) Miles, A. A.; Misra, S. S. The estimation of the bactericidal power of the blood. *J. Hyg.* **1938**, *38*, 732−749.
(34) Kwon, Y.-I.; Apostolidis, E.; Shetty, K. In vitro studies of eggplant (*Solanum melongena*) phenolics as inhibitors of key enzymes relevant for type 2 diabetes and hypertension. *Bioresour. Technol.* **2008**, *99*, 2981−2988.
(35) Rodrigues, D.; Freitas, A. C.; Pereira, L.; Rocha-Santos, T. A. P.; Vasconcelos, M. W.; Roriz, M.; Rodríguez-Alcalá, L. M.; Gomes, A. M. P.; Duarte, A. C. Chemical composition of red, brown and green macroalgae from Buarcos bay in Central West Coast of Portugal. *Food Chem.* **2014**, DOI: 10.1016/j.foodchem.2015.03.057.
(36) Plaza, M.; Amigo-Benavent, M.; del Castillo, M. D.; Ibáñez, E.; Herrero, M. Facts about the formation of new antioxidants in natural samples after subcritical water extraction. *Food Res. Int.* **2010**, *43*, 2341−2348.
(37) Cian, R. E.; Alaiz, M.; Vioque, J.; Drago, S. R. Enzyme proteolysis enhanced extraction of ACE inhibitory and antioxidant compounds (peptides and polyphenols) from *Porphyra columbina* residual cake. *J. Appl. Phycol.* **2013**, *25*, 1197−1206.
(38) Chemat, F.; Zill-e-Huma; Khan, M. K. Applications of ultrasound in food technology: processing, preservation and extraction. *Ultrason. Sonochem.* **2011**, *18*, 813−835.
(39) Zhao, L.; Zhao, G.; Chen, F.; Wang, Z.; Wu, J.; Hu, X. Different effects of microwave and ultrasound on the stability of (all-*E*)-astaxanthin. *J. Agric. Food Chem.* **2006**, *54*, 8346−8351.
(40) Lee, S.-H.; Kang, M.-C.; Moon, S.-H.; Jeon, B.-T.; Jeon, Y.-J. Potential use of ultrasound in antioxidant extraction from *Ecklonia cava*. *Algae* **2013**, *28*, 371−378.
(41) Ale, M. T.; Meyer, A. S. Fucoidans from brown seaweeds: an update on structures, extraction techniques and use of enzymes as tools for structural elucidation. *RSC Adv.* **2013**, *3*, 8131−8141.
(42) Guiry, M. D. The seaweed site: information on marine algae. http://www.seaweed.ie/uses_general/alginates.php (accessed April 10, 2014).
(43) Shanmugan, M.; Mody, K. H. Heparinoid-active sulphated polysaccharides from marine algae as potential blood anticoagulant agents. *Curr. Sci.* **2000**, *79*, 1672−1683.
(44) Jiménez-Escrig, A.; Gómez-Ordóñez, E.; Rupérez, P. Brown and red seaweeds as potential sources of antioxidant nutraceuticals. *J. Appl. Phycol.* **2012**, *24*, 1123−1132.
(45) Budhiyanti, S. A.; Raharjo, S.; Marseno, D. W.; Lelana, I. Y. B. Antioxidant activity of brown algae *Sargassum* species extract from the coastline of Java Island. *Am. J. Agric. Biol. Sci.* **2012**, *7*, 337−346.
(46) Freitas, A. C.; Andrade, J. C.; Silva, F. M.; Rocha-Santos, T. A. P.; Duarte, A.; Gomes, A. M. Antioxidative peptides: trends and perspectives for future research. *Curr. Med. Chem.* **2013**, *20*, 4575−4594.
(47) Karadag, A.; Ozcelik, B.; Saner, S. Review of methods to determine antioxidant capacities. *Food Anal. Methods* **2009**, *2*, 41−60.
(48) Balboa, E. M.; Conde, E.; Moure, A.; Falque, E.; Dominguez, H. In vitro antioxidant properties of crude extracts and compounds from brown algae. *Food Chem.* **2013**, *138*, 1764−1785.
(49) Yangthong, M.; Hutadilok-Towatana, N.; Phromkunthong, W. Antioxidant activities of four edible seaweeds from the southern coast of Thailand. *Plant Foods Hum. Nutr.* **2009**, *64*, 218−223.
(50) Zhao, X.; Li, B.; Xue, C.; Sun, L. Effect of molecular weight on the antioxidant property of low molecular weight alginate from *Laminaria japonica*. *J. Appl. Phycol.* **2012**, *24*, 295−300.
(51) Valentão, P.; Trindade, P.; Gomes, D.; de Pinho, P. G.; Mouga, T.; Andrade, P. B. *Codium tomentosum* and *Plocamium cartilagineum*: chemistry and antioxidant potential. *Food Chem.* **2010**, *119*, 1359−1368.
(52) Zaporozhets, T. S.; Besedova, N. N.; Kuznetsova, T. A.; Zvyagintseva, T. N.; Makarenkova, I. D.; Kryzhanovsky, S. P.; Melnikov, V. G. The prebiotic potential of polysaccharides and extracts from seaweeds. *Russ. J. Mar. Biol.* **2014**, *40*, 1−9.
(53) Ramnani, P.; Chitarrari, R.; Tuohy, K.; Grant, J.; Hotchkiss, S.; Philp, K.; Campbell, R.; Gill, C.; Rowland, I. In vitro fermentation and prebiotic potential of novel low molecular weight polysaccharides derived from agar and alginate seaweeds. *Anaerobe* **2012**, *18*, 1−6.
(54) Wu, S.-C.; Kang, S.-K.; Kazlowski, B.; Wu, C.-J.; Pan, C.-L. Antivirus and prebiotic properties of seaweed-oligosaccharides lysates derived from agarase AS-II. *J. Fish. Soc. Taiwan* **2012**, *39*, 11−21.
(55) Hardoko; Siratantri, T.; Eveline; Yogabuana, M.; Olivia, S. Na in vitro of antidiabetic activity of *Sargassum duplicatum* and *Turbinaria decurens* seaweed. *Int. J. Pharm. Sci. Invent.* **2014**, *3*, 13−18.
(56) Motshakeri, M.; Ebhrahimi, M.; Goh, Y. M.; Othman, H. H.; Hair-Bejo, M.; Mohamed, S. Effects of brown seaweed (*Sargassum polycystum*) extracts on kidney, liver, and pancreas of type 2 diabetic rat model. *Evidence-Based Complement. Altern. Med.* **2014**, 1−11.

NOTE ADDED AFTER ASAP PUBLICATION

This paper was published ASAP on March 18, 2015, without an update to reference 35. The corrected version was reposted on March 23, 2015.

DOI: 10.1021/jf504220e
J. Agric. Food Chem. 2015, 63, 3177−3188

highly differ in their phenolics profile, 'Amari' and 'Hallawi',[13] in order to obtain fractions of diverse composition. The isolated fractions were analyzed for their composition, ferric-reducing power, free radical scavenging capacity, inhibition of copper ion-induced LDL oxidation, and enhancement of HDL-mediated cholesterol efflux from macrophages. Date fruit phenolics' structure–activity relationships were examined by comparing the nature and magnitude of activities manifested by the two phenolics' subgroups, as well as different compositions within each subgroup.

MATERIALS AND METHODS

Chemicals. Caffeic acid, catechin, catechin gallate, chlorogenic acid, *o*-coumaric acid, *p*-coumaric acid, epicatechin, epicatechin gallate, epigallocatechin, epigallocatechin gallate, ferulic acid, gallic acid, gallocatechin, gallocatechin gallate, hydrocaffeic acid, phenyl acetate, pyrogallol, protocatechuic acid, sinapic acid, syringic acid, vanillic acid, tannic acid, and Folin-Ciocalteau reagent were all purchased from Sigma-Aldrich Co., Israel. Ellagic acid, 2-hydroxybenzoic (salicylic) acid, 3-hydroxybenzoic acid, 4-hydroxybenzoic acid, kaempferol-3-glucoside, procyanidin B2, and quercetin-3-β-glucoside were acquired from Fluka, France. 2.2′-Azobis-2-amidinopropane hydrochloride (AAPH) was from Wako, Japan. Acetonitrile HPLC grade was purchased from Merck, Germany, and phosphoric acid from Frutarum, Israel. [^{3}H]-Labeled cholesterol was acquired from Amersham Biosciences, Inc., USA. Dulbecco's modified Eagle's medium (DMEM) and fetal calf serum (FCS) were purchased from Biological Industries, Beit Haemek, Israel.

Date Fruit. Commercial ready-to-eat tree-ripened semidry fruits ("tamr" stage) of two date varieties, 'Amari' and 'Hallawi', were obtained shortly after harvest from Hadiklaim, Israel Date Growers Cooperative Ltd., and stored at −20 °C until processing.

Date Crude Phenolics Extract Preparation. Pitted 'Amari' or 'Hallawi' fruits were ground with a Kenwood MG600 meat grinder (Kenwood Ariete, Italy) and homogenized in cold 70% acetone solution containing 0.5% acetic acid at a fruit to solvent ratio of 1:3 (w/v) using a mortar and pestle. The homogenate was kept at 4 °C overnight and shaken on ice for an additional 2 h. The procured slurry was centrifuged at 12000*g* for 10 min at 4 °C (Sorvall Instruments RC5C), and the clear supernatant was collected and stored at −20 °C in light-protected vessels.

Date Phenolics Subgroup Fractionation. The crude phenolics extracts were fractionated into phenolic acids and flavonols subgroups by solid-phase extraction (SPE) on a C18 column, following Oszmianski et al.,[24] with some modification. Two extraction columns [Bakerbond spe octadecyl (C18) disposable extraction columns, sorbent weight 1000 mg, column size 6 mL, J.T. Baker] were preconditioned with 5 mL of methanol. One column was equilibrated to neutral pH with 10 mL of double-distilled water (DDW), pH 7.0, and the other, to acidic pH with 10 mL of DDW, pH 2.0. The crude acetone extracts were diluted 20-fold with DDW and adjusted to pH 7.0 with 1 N NaOH. A total of 10 mL of the diluted extract was loaded onto the pH 7.0 column. The effluent containing the ionized phenolic acids and other polar components was saved. The column was then washed with 10 mL of DDW pH 7.0, and the two effluents were combined.

Phenolic Acids' Isolation. The combined effluents were adjusted to pH 2.0 with 1 N HCl and loaded onto the acidified column. The phenolic acids were then eluted with a total of 3 mL methanol; the latter were collected sequentially in aliquots of 0.8, 1.0, and 1.2 mL. The second aliquot of eluent was dried in a miVac Duo concentrator (Genevac Limited, UK) at 45 °C and kept at −20 °C.

Flavonols' Isolation. After the removal of the polar compounds, the pH 7.0 column was adjusted to pH 2.0 by passing 10 mL of DDW at pH 2.0 and washed with 3 mL of 16% acetonitrile at pH 2.0. The flavonols were then eluted with a total of 3 mL methanol; the latter were collected sequentially in aliquots of 0.8, 1.0, and 1.2 mL. The second aliquot of eluent was dried as described before and kept at −20 °C.

Total Phenolics Content. The dried isolated fractions were each dissolved in 1.0 mL of 50% ethanol. The resulting solutions were diluted 5- and 10-fold with DDW and assayed for total phenolics content with Folin-Ciocalteau 2 N phenol reagent, following Singleton and Rossi.[25] Aliquots of 100 μL were added to 900 μL of reaction solution consisting of 200 μL of freshly prepared 10-fold diluted Folin-Ciocalteau reagent, 100 μL of 20% Na_2CO_3, and 600 μL of DDW. Calibration curves were constructed with gallic acid (0–0.8 μmol mL^{-1}). The absorbance at 765 nm was measured after 1 h incubation, and the results are expressed in terms of gallic acid equivalents (GAE). Each measurement was done in triplicate.

RP-HPLC Analysis of Isolated Phenolics Fractions. Phenolics analysis by RP-HPLC was carried out as described earlier.[13] The dissolved isolated fractions were filtered through a 0.45 μm PTFE filter and analyzed with a LaChrom Merck Hitachi HPLC system, consisting of pump L7100, column oven L7350, and mixer-degasser L-7614, coupled with a diode array detector with a 3D feature (multi-wavelength detector, Jasco MD-2010 Plus), interface (Jasco LC-Net II/ADC), and scientific software (EZChrom Elite Client/Server version 3.1.6 build 3.1.6.2433) that provides real-time data acquisition and postrun data manipulation and integration capabilities. Aliquots of 20 μL were injected by a manual injector (Rheodyne, Rohnert Park, CA, USA) and loaded onto a PurospherStar RP-18 end-capped column (250 × 4 mm LichroCART cartridge, 5 μm particle size) with an end-capped Lichrospher100 RP-18 guard column (4 × 4 mm LichroCART cartridge, 5 μm particle size). The binary mobile phase consisted of 0.1% phosphoric acid, pH 2.4 (solution A), and acetonitrile (solution B) and was delivered at a flow rate of 1 mL min^{-1}. Elution was carried out with the following stepwise gradient outline: 1 to 10 min, 5% to 15% solution B; 10 to 30 min, 15% to 30% solution B; 30 to 40 min, 30% to 100% solution B. The column was then washed and equilibrated by 10 min postruns with 100% and 5% B, respectively. The oven temperature was set at 40 °C, and the pressure was 158 atm. Acetonitrile was HPLC grade (LiChrosolv Merck, Germany); column-filtered water was further distilled by a Corning Megapure System, MP-6A, and passed through a 0.20 μm nylon membrane. Phosphoric acid was of analytical grade.

Phenolics classification and tentative identification were performed by the system software on the basis of UV/vis absorbance spectra and the retention times of the chromatograms peaks, and the system phenolics library constructed from authentic standards.

Individual phenolic compounds were quantified from the corresponding chromatogram peak areas calculated by the software in three repetitive runs, and calibration curves constructed with authentic standards of caffeic, coumaric, ferulic, and salicylic acid and kaempferol-3-glucoside. A cutoff area of 100000 mV min was applied to discern between significant and nonsignificant peaks. The concentrations of the various hydroxybenzoic acids, hydroxycinnamic acids, and flavonols were expressed in terms of nmol equivalents of the corresponding standards mL^{-1}.

Ferric-Reducing Antioxidant Power (FRAP). The dissolved isolated fractions were diluted 5- and 10-fold with DDW and assayed for ferric-reducing ability by the colorimetric test originally developed to assess the ferric-reducing antioxidant power of plasma.[26] A 50 μL aliquot was added to 950 μL of reaction solution freshly prepared by mixing 50 mL of 300 mmol L^{-1} acetate buffer, 5 mL of 10 mmol L^{-1} 2,4,6-tripyridyl-*s*-triazine (TPTZ), and 5 mL of 20 mmol L^{-1} ferric chloride. Absorbance at 593 nm was measured after 4 min incubation in a 37 °C water bath. Vitamin C was used for the calibration curve (0–0.6 μmol mL^{-1}), and the results were expressed in terms of vitamin C equivalents (VCE). Each measurement was done in triplicate.

Free Radical Scavenging Capacity. The radical-generating compound 1,1-diphenyl-2-picryl-hydrazyl (DPPH) was employed to assess the capacity of the isolated fractions to scavenge free radicals.[27] Aliquots of 50 μL of the isolated fractions at a concentration of 0.5 mmol L^{-1} GAE in 50% ethanol were mixed with 1 mL of 0.1 mmol L^{-1} DPPH in ethanol, and the optical density (OD) at 517 nm was

DOI: 10.1021/jf506094r
J. Agric. Food Chem. 2015, 63, 3189–3195

Table 1. Yield and Antioxidant Properties of Phenolic Acid and Flavonol Fractions Isolated from 'Amari' and 'Hallawi' Date Fruits[a]

			yield	ferric reducing power	free radical scavenging capacity
date variety	phenolics subgroup	fraction label	(μmol GAE per g fruit)	(VCE/GAE, mole ratio)	(% $OD_{517\ nm}$ loss)
'Amari'	phenolic acids	PhA 1	4.27 ± 0.62	0.81 ± 0.02 b	14 ± 1 b
'Hallawi'		PhA 2	0.38 ± 0.09	0.80 ± 0.01 b	22 ± 3 a
'Amari'	flavonols	Fl 1	1.37 ± 0.15	0.88 ± 0.01 a	8 ± 1 c
'Hallawi'		Fl 2	0.43 ± 0.11	0.87 ± 0.03 a	9 ± 2 c

[a]Abbreviations: GAE, gallic acid equivalents; VCE, vitamin C equivalents; $OD_{517\ nm}$, optical density at 517 nm.Values are mean ± SD (n = 3). Values within a column with different letters are significantly different at a 95% confidence interval (Tukey–Kramer *post hoc*).

monitored continuously for 5 min at room temperature. For the control, 50 μL of 50% ethanol was added to the DPPH solution. The free radical scavenging capacity in terms of percentage loss of OD at 517 nm was calculated using the following equation:

$$\text{Free radical scavenging capacity} = \left[1 - \frac{\text{sample OD at 517 nm}}{\text{control OD at 517 nm}}\right] \times 100$$

where the sample and control OD at 517 nm correspond to the measurements after 5 min incubation in the presence and absence of the isolated phenolic fraction, respectively.

LDL and HDL Preparation. Fresh plasma was derived from three healthy normolipidemic volunteers (Rambam Hospital Helsinki Committee number 30572-10-RBM). These volunteers received a Mediterranean diet, but they did not consume any additional antioxidants. The plasma samples were inactivated (30 min at 56 °C) and then pooled together. The LDL and HDL fractions were isolated from the pooled plasma sample by discontinuous density gradient ultracentrifugation.[28] The LDL was separated at d = 1.063 g mL^{-1}, and the HDL at d = 1.210 g mL^{-1}. Both lipoproteins were dialyzed against 150 mmol L^{-1} NaCl and 1 mmol L^{-1} Na_2EDTA (pH 7.4) at 4 °C and then sterilized by filtration (0.45 μm), kept under nitrogen in the dark at 4 °C, and used within 2 weeks. The LDL and HDL protein concentration was determined with the Folin phenol reagent.[29]

Copper Ion-Induced LDL Oxidation. Prior to oxidation, the LDL was dialyzed overnight against EDTA-free, phosphate-buffered saline (PBS) solution, pH 7.4, at 4 °C. LDL (100 μg of protein mL^{-1}) was preincubated for 30 min at room temperature with increasing volume concentrations (0–25 μL mL^{-1}) of the isolated phenolics fractions. Then, 5 μmol L^{-1} of $CuSO_4$ was added and the tubes were incubated for 1.5 h at 37 °C. At the end of the incubation, the extent of LDL oxidation was determined by measuring the generated amount of thiobarbituric acid reactive substances (TBARS) and of lipid peroxides. The TBARS assay was performed at 532 nm, using malondialdehyde (MDA) for the standard curve.[30] The lipid peroxide assay, which analyzes lipid peroxide formation by their capacity to convert iodide to iodine, was measured spectrophotometrically at 365 nm.[31] The measurements were repeated three times.

HDL-Mediated Cholesterol Efflux from Macrophages. J774 A.1 murine macrophage cells were purchased from the American Tissue Culture Collection (ATCC, Rockville, MD, USA). Cells were grown in DMEM containing 5% FCS. The macrophages (1 mL of 10^6 cells mL^{-1}) were preincubated at 37 °C for 20 h with 10 to 170 μM GAE of the isolated phenolics fractions. Control cells were incubated with an equivalent volume of 50% ethanol. The cells were then washed and incubated with [^{3}H]cholesterol (2 μCi mL^{-1}) at 37 °C for 1 h, followed by a cell wash in ice-cold PBS three times, and further incubation in the absence (basal cholesterol efflux rate) or presence of HDL (100 μg protein mL^{-1}) for 3 h at 37 °C. Cellular and medium [^{3}H]-labels were quantified and HDL-mediated cholesterol efflux was calculated as the ratio of [^{3}H]-label in the medium/([^{3}H]-label in the medium + [^{3}H]-label in the cells).[32] HDL-mediated cholesterol efflux data were corrected for the nonspecific loss of cholesterol (basal cholesterol efflux rate). The experiments were repeated three times.

Statistical Analysis. The results are reported as means ± their respective standard deviations (SD) of three measurements (n = 3). Statistical analysis of the data was performed with IBM SPSS Statistics, version 17.0. Conformity of all data sets to a normal distribution and homogeneity of variances was established by the Shapiro–Wilk's and Levene's tests, respectively. One-way ANOVA and Tukey–Kramer *post hoc* means comparison test were employed to verify significant differences (p < 0.05, 0.01, or 0.001) in comparison to the control or among fractions. Correlations between fraction capacities were tested with the correlation analysis tool of Microsoft Excel 2010 and are reported in terms of the correlation coefficient, r.

RESULTS AND DISCUSSION

Composition of Isolated Date Phenolics Subgroup Fractions. To obtain variable compositions of phenolic acid and flavonol fractions, we employed fruits of two date varieties, 'Amari' and 'Hallawi', that largely differ in their phenolics composition.[13] Crude phenolics extracts were prepared with acidified 70% acetone, which was found to be more efficient than 50% ethanol in recovering antiatherogenic capacities from dates.[13]

Fractionation of the crude extracts of 'Amari' and 'Hallawi' fruits, carried out as described under Materials and Methods, yielded two fractions of phenolic acids, PhA 1 and PhA 2, and two of flavonols, Fl 1 and Fl 2. Fractions PhA 1 and Fl 1 were derived from 'Amari', and PhA 2 and Fl 2 from 'Hallawi' fruits. The yields of the isolated fractions are presented in Table 1, in terms of μmol GAE per g fruit. The yield of 'Amari'-derived fractions was considerably larger than that of the fractions isolated from 'Hallawi', by approximately 10- and 3.5-fold for phenolic acids and flavonols, respectively. This is consistent with the higher content of soluble phenolics present in 'Amari' compared to 'Hallawi' dates.[13] By and large, the recovery of the various phenolics through the fractionation process was low. Optimization of the process conditions, e.g., the weight ratio of phenolics to solid phase and the flow rate during phenolics loading onto and elution from the column, is likely to improve the yield.

The isolated phenolics fractions were analyzed by RP-HPLC to classify and tentatively identify, as well as quantify, the phenolic constituents. Figure 1 presents the concentrations of the major phenolic acids in PhA 1 and PhA 2, in order of ascending retention time (t_R). Altogether, eight prominent peaks of phenolic acids were detected in the two fractions. The peaks at t_R values of 9.7, 10.1, 11.4, 11.7, and 12.5 min corresponded to caffeic acid derivatives, and their concentrations are expressed as nmol caffeic acid mL^{-1}. The compounds associated with a t_R 14.9, 16.7, and 27.4 min were coumaric and ferulic acid and a salicylic acid derivative, respectively, and their concentrations are expressed accordingly in nmol mL^{-1} equivalents of coumaric, ferulic, and salicylic acid. Seven and five phenolic acids constituted PhA 1 and PhA 2, respectively. The major hydroxycinnamic acid in both fractions

DOI: 10.1021/jf506094r
J. Agric. Food Chem. 2015, 63, 3189–3195

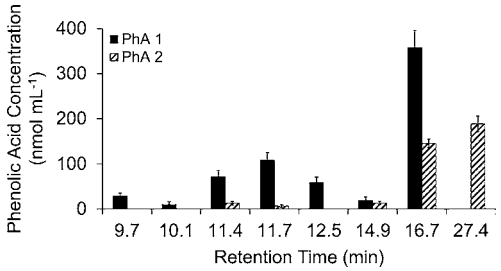

Figure 1. Composition of phenolic acid fractions isolated from date fruits. Fraction composition was analyzed by RP-HPLC. Chromatogram peak concentrations in nmol mL^{-1} are presented in order of ascending retention times. Results are the mean ± SD (n = 3).

was ferulic acid, comprising approximately 55 and 40 mol % of the total phenolic acid concentration in PhA 1 and PhA 2, respectively. This is consistent with our earlier findings on ferulic acid being the most abundant hydroxycinnamic acid in the fruits of nine date varieties, including 'Amari' and 'Hallawi'.[13] The other major phenolic acids in PhA 1 were derivatives of caffeic acid; most prominent were those detected at a t_R of 11.4, 11.7, and 12.5 min, consisting 11, 17, and 9 mol % of the total phenolic acid concentration, respectively. On the other hand, in PhA 2 the most abundant phenolic acid was a salicylic acid derivative that accounted for approximately 51 mol % of the total phenolic acid concentration. Notably, this hydroxybenzoic acid was absent in PhA 1. Small amounts of caffeic acid derivatives at a t_R of 11.4 and 11.7 min were also present in PhA 2. Both fractions contained comparable small amounts of coumaric acid, accounting for merely 3−4 mol % of the total phenolic acid concentration.

In summary, the two isolated fractions of date phenolic acids contained ferulic acid as a major component and comparable small amounts of coumaric acid, but differed considerably in the composition of the complementary set of phenolic acids; that of PhA 1 consisted mostly of caffeic acid derivatives, whereas that of PhA 2 comprised mostly a salicylic acid derivative. In this respect, PhA 1 relates to date varieties such as 'Amari', 'Deglet Noor', and 'Medjool', which are rich in caffeic acid derivatives and poor in salicylic acid derivatives, whereas PhA 2 relates to varieties such as 'Deri', 'Hadrawi', 'Hallawi', and 'Zahidi', which are relatively low in caffeic acid derivatives and have significant amounts of the salicylic acid derivative.[13]

Figure 2 illustrates the concentrations of the major flavonols in Fl 1 and Fl 2, in order of ascending t_R. Altogether, seven prominent peaks of flavonols were evident in the two fractions. On the basis of the authentic standard library all seven flavonols were tentatively classified as kaempferol derivatives; their

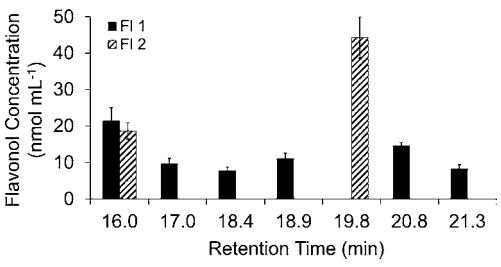

Figure 2. Composition of flavonol fractions isolated from date fruits. Fraction composition was analyzed by RP-HPLC. Chromatogram peak concentrations in nmol mL^{-1} are presented in order of ascending retention times. Results are the mean ± SD (n = 3).

concentrations in the figure are expressed in nmol mL^{-1} kaempferol-3-glucoside equivalents. Six and two peaks constituted Fl 1 and Fl 2, respectively. Both fractions shared a principal component at a t_R of 16.0 min, amounting to approximately 30 mol % of the total flavonol concentration. The other flavonols in Fl 1, corresponding to t_R values of 17.0, 18.4, 18.9, 20.8, and 21.3 min, accounted for approximately 13, 11, 15, 20, and 11 mol % of the total flavonols, respectively. The other flavonol in Fl 2, at a t_R of 19.8 min, was the most abundant in this fraction and was absent in Fl 1.

In summary, the two isolated fractions of date flavonols considerably differed in composition; in addition to one prominent flavonol shared by the two fractions, Fl 1 consisted of significant amounts of five other flavonols, whereas Fl 2 contained a single unique flavonol as the major component.

Antioxidant and Antiatherogenic Properties of Isolated Date Phenolics Subgroup Fractions. *Ferric Ion Reducing Power.* The ferric-reducing activity of the isolated fractions relative to vitamin C is shown in Table 1 in terms of the mole ratio of VCE to GAE. All the fractions exhibited considerable capacities to reduce ferric ions, which on average were 80% to 88% that of vitamin C. Under the FRAP assay conditions, the flavonol fractions were slightly, yet significantly, better reductants, exceeding the reducing power of the phenolic acid fractions by approximately 10%.

Free Radical Scavenging Capacity. The capacity of the isolated fractions to scavenge free radicals is presented in Table 1. All the fractions demonstrated the ability to neutralize free radicals, however, with different potencies. At an equivalent concentration of phenolic hydroxyls (24 μmol GAE L^{-1} in the final reaction mixture) and after 5 min exposure, the phenolic acid fractions exhibited significantly higher efficiencies compared to the flavonol fractions. PhA 2 was significantly the most potent fraction, decreasing DPPH concentration by 22%; PhA 1 followed, with a radical scavenging capacity of 14%. The two flavonol fractions had comparable lower potencies, measuring approximately 39% and 61% of the radical scavenging capacities exhibited by PhA 1 and PhA 2, respectively.

The antioxidant and antiradical capacity of phenolic molecules relate to their molecular structure, most significantly, the number and position of hydroxyl groups, extent of double-bond conjugation, and the nature and position of substituents.[21,22] Negative correlation was obtained between the FRAP and DPPH assays (r = −0.906). It should be noted, however, that the equivalent mole concentration of phenolic hydroxyls of the various fractions employed in our DPPH assay did not correspond to an equivalent mole concentration of phenolic compounds, due to the variable number of hydroxyls per molecule among the phenolics composing the fractions. This may have influenced the order of radical scavenging potencies of the phenolics fractions as presented in Table 1, since the reaction rate is affected by reactant mole concentration.

Date Phenolics' Effect on LDL Oxidation. LDL oxidation is an important process in the initiation of atherosclerosis development. We therefore studied the effect of the isolated date phenolics fractions on the susceptibility of LDL to oxidation. The extent of copper ion-induced LDL oxidation was measured in the presence of increasing concentrations of the isolated fractions. All the fractions considerably and dose-dependently inhibited LDL oxidation, as determined by the TBARS and lipid peroxide assays (Figure 3). By both assays, the potency to protect LDL from oxidation significantly

DOI: 10.1021/jf506094r
J. Agric. Food Chem. 2015, 63, 3189−3195

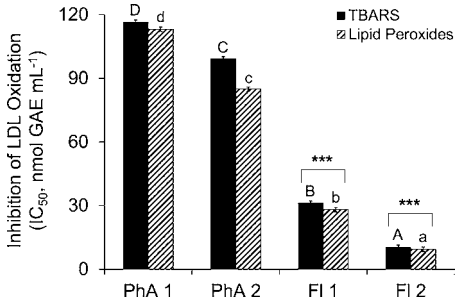

Figure 3. Effect of phenolic acid and flavonol fractions isolated from date fruits on copper ion-induced LDL oxidation. LDL (100 μg protein mL^{-1}) was incubated with increasing concentrations (0–25 μL mL^{-1}) of the isolated date phenolics fractions in the presence of 5 μmol L^{-1} $CuSO_4$. The extent of LDL oxidation was determined by the TBARS and lipid peroxides assays. The phenolics concentrations needed to achieve 50% inhibition (IC_{50}) are shown in terms of nmol GAE mL^{-1}. Results are the mean ± SD (n = 3). Bars labeled with different uppercase (TBARS assay) or lowercase (lipid peroxide assay) letters are significantly different at $p < 0.01$; *** indicates significant differences at $p < 0.001$ compared to PhA 1 and PhA 2 (Tukey–Kramer *post hoc*).

differed ($p < 0.01$) among the four fractions. Moreover, the data sets obtained by the two assays exhibited a strong positive correlation (r = 0.995), strengthening the validity of the assay. The flavonol fractions were significantly more potent than the phenolic acid fractions ($p < 0.001$), requiring considerably lower phenolics concentrations to obtain 50% inhibition (IC_{50}). Fl 2 was the most efficient inhibitor of LDL oxidation, followed by Fl 1, with IC_{50} values of 10 and 31 nmol GAE mL^{-1} by the TBARS assay and 9 and 28 nmol GAE mL^{-1} by the lipid peroxides assay, respectively. PhA 1 was the least effective inhibitor, while PhA 2 was somewhat better, as implied by their IC_{50} values of 116 and 99 nmol GAE mL^{-1} by the TBARS assay and 113 and 85 nmol GAE mL^{-1} by the lipid peroxides assay, respectively.

The competence of phenolic compounds to inhibit copper ion-mediated LDL oxidation depends on their abilities to chelate or oxidize copper ions, act as hydrogen-donating antioxidants, delocalize electrons, and partition between the aqueous medium and the lipophilic microenvironment within the LDL particle, all of which are governed by their molecular structure.[21,22,33−35] Flavonols were found to be especially effective inhibitors of LDL oxidation compared to other flavonoids.[36] Flavonols are superior to simple phenolic acids in electron delocalization capability due to the large number of conjugated double bonds. A quantum-mechanical investigation of the quercetin radical has revealed extended electronic delocalization between adjacent rings, as well as cross-conjugation occurring at the C ring.[37] Moreover, the amphipathic nature of flavonols is more pronounced, especially in that phenolic acids are completely ionized at the physiological pH of 7.4. Consistent with all the above, our study demonstrated that the isolated date flavonol fractions were better inhibitors of LDL oxidation by 3- to 10-fold over the phenolic acid fractions.

Date Phenolics' Effect on HDL-Mediated Cholesterol Efflux. Reverse cholesterol transport (RCT) is a major mechanism for the attenuation of atherosclerosis development. Macrophage cholesterol efflux is the first and potentially most critical step in macrophage RCT. We therefore explored the effect of the isolated date phenolic acid and flavonol fractions on cholesterol removal from J774A.1 macrophage cells. The extent of HDL-mediated cholesterol efflux from macrophages that were preincubated with the date phenolics fractions was compared to that measured in control cells that were pretreated with an equivalent volume of 50% ethanol. The results are shown in Figure 4, in terms of percent change over control cells

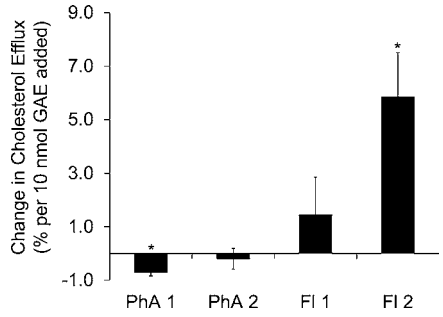

Figure 4. Effect of phenolic acid and flavonol fractions isolated from date fruits on HDL-mediated cholesterol efflux from macrophages. J774A.1 macrophages (1 mL of 10^6 cells mL^{-1}) were preincubated at 37 °C for 20 h with 20 to 170 μM GAE of the isolated phenolics fractions. After a cell wash the cells were labeled with [^{3}H]-cholesterol and the extent of HDL (100 μg protein mL^{-1})-mediated cholesterol efflux from the cells was determined. Phenolics fraction effect is presented in terms of percent change over the control in cholesterol efflux per 10 nmol of GAE added. Results are the mean ± SD (n = 3). * denotes significant difference at $p < 0.05$ (one-way ANOVA) between fraction-treated and control cells.

in the extent of cholesterol efflux per 10 nmol of GAE added. The two subgroups of date phenolics demonstrated markedly different effects on cholesterol removal from the macrophages. Pretreatment of the cells with PhA 1 slightly, yet significantly, inhibited the efflux by approximately 1%; PhA 2 had practically no effect. On the other hand, preincubation with the flavonol fractions increased the magnitude of cholesterol efflux from the cells, especially with Fl 2, which significantly enhanced cholesterol removal by approximately 6%.

A major factor in phenolics' effect on cellular processes is their mode of interaction with the membrane bilayer, i.e., the partition of less polar compounds in the hydrophobic interior of the membrane and the formation of hydrogen bonds between phospholipid polar head groups and the more hydrophilic phenolics at the membrane/water interface.[38] The relatively polar phenolic acids (ionized at a slightly alkaline pH) may cause cell membrane depolarization; a greater depolarization was reported to be induced by hydroxycinnamic acids than the corresponding hydroxybenzoic acids.[39] PhA 1 consists of mostly hydroxycinnamates, whereas PhA 2 accommodates equal proportions of hydroxycinnamates and hydroxybenzoates. PhA 1 is therefore likely to cause a more extensive membrane depolarization (i.e., increased membrane ion permeability) than PhA 2. Such a disturbance in membrane integrity may interfere with the macrophage cellular functions, leading eventually to the adverse effect of PhA 1 on cholesterol efflux. The positive effect exhibited by the flavonol fractions on cholesterol removal from macrophages may pertain to their more profound amphipathic nature that enables protection of the cell membrane from oxidation by free radicals generated both extra- and intracellularly. In this context, it is noteworthy that Fl 1, the less potent enhancer of cholesterol efflux, had a higher proportion of components with shorter t_R (≤18.9 min) compared to Fl 2 and is therefore likely to consist of somewhat

DOI: 10.1021/jf506094r
J. Agric. Food Chem. 2015, 63, 3189−3195

more polar flavonols. The date flavonols may interact with the macrophage plasma membrane and modify it in ways that consequently augment HDL binding to and cholesterol removal from the cells. Moreover, their interaction with the membrane and/or internalization may initiate signaling pathways implicated in the expression of transporters involved in serum-mediated cholesterol efflux from macrophage foam cells. Under a similar experimental setup, pretreatment of macrophages with 20 μM quercetin increased HDL binding to and cholesterol efflux from the cells by 27% and 50%, respectively, compared to control cells.[40] Moreover, the cellular levels of mRNA for the ATP-binding cassette A1 (ABCA1) transporter, a mediator of macrophage cholesterol efflux, and the nuclear factor PPARα, which induces ABCA1 expression in macrophages, increased by 42% and 77%, respectively.[40]

Taken together, our current study demonstrates that both phenolic acids and flavonols of date fruits have activities that affect processes pertinent to atherosclerosis development. However, the nature and potencies of the activities exhibited by the two phenolics subgroups varied considerably. The date phenolic acids were efficient reductants and free radical scavengers, whereas the flavonols were superior inhibitors of LDL oxidation and, in addition, stimulated cholesterol efflux from macrophages. Furthermore, different phenolics' compositions of the same subgroup, i.e., more subtle molecular structure differences, displayed variable levels of activities, as is evident from the performance disparities comparing PhA 1 to PhA 2, and Fl 1 to Fl 2. All in all, the results are consistent with the strong structure−function relationships established for phenolic compounds[21,22,33−36] and support our interpretation that the large differences in the antiatherogenic potency of phenolics extracts from a diverse collection of date varieties were inflicted by the substantial varietal divergence in phenolics composition.[13]

We have recently shown that regular consumption of 'Medjool' and 'Hallawi' dates by healthy human subjects had beneficial antiatherogenic effects.[9] The two date varieties differed in both the range and magnitude of the favorable effects and the fruit phenolics' composition, suggesting a possible role for phenolic compounds in the fruit's health traits. Identifying the antiatherogenic bioactives in dates is necessary to establish the fruit's health value and to utilize dates in nutritional approaches directed at cardiovascular heath preservation. Our present study identifies date flavonols as potentially efficient antiatherogenic biochemicals. The *in vitro* biological assays employed nano- to low micromolar concentrations of the isolated date flavonols, well in the range of blood phenolic concentrations.[41] Thus, the present findings may be relevant to the *in vivo* antiatherogenic capacities of date fruits; the latter may comprise flavonol action in concert and/or synergy with other fruit components, e.g., other phenolics and nutritional fibers. In this context, we have recently demonstrated that consumption of the combination of pomegranate together with date fruit and date seed polyphenols had the most beneficial anti-atherogenic effects, as shown in mice serum, macrophages, and aortas.[42] We are currently exploring the identity and *in vitro* activities of flavonol constituents from a diverse collection of date varieties. However, to establish causal relationships between date fruit flavonol composition and antiatherogenic benefits, *in vivo* studies with the purified flavonols are needed.

AUTHOR INFORMATION

Corresponding Author

*Tel: +972-8-6355747. Tel: +972-8-6355730. E-mail: hamutalborochov@rd.ardom.co.il.

Funding

Financial support was obtained from the Date Palm Growers' Desk of Israel Plants Production and Marketing Board, the Jewish National Fund (KKL), and the JCA Charitable Foundation. Date fruit for this research were provided by HADIKLAIM, Israel Date Growers' Cooperative Ltd.

Notes

The authors declare no competing financial interest.

ABBREVIATIONS USED

AAPH,2,2′-azobis-2-amidinopropane hydrochloride; ABCA1,ATP-binding cassette A1; DDW,double-distilled water; DMEM,Dulbecco's modified Eagle's medium; DPPH,1,1-diphenyl-2-picryl-hydrazyl; FCS,fetal calf serum; FRAP,ferric-reducing antioxidant power; FW,fresh weight; GAE,gallic acid equivalents; HDL,high-density lipoprotein; LDL,low-density lipoprotein; MDA,malondialdehyde; OD,optical density; PBS,phosphate-buffered saline; PPARα,peroxisome proliferator-activated receptor alpha; RCT,reverse cholesterol transport; RP-HPLC,reversed phase high-performance liquid chromatography; SD,standard deviation; TBARS,thiobarbituric acid reactive substances; VCE,vitamin C equivalents

REFERENCES

(1) Barreveld, W. H. Date palm products. *Food and Agriculture Organization of the United Nations*; Agricultural Services Bulletin No. 101, FAO: Rome, Italy, 1993.

(2) Vayalil, P. K. Date fruits (*Phoenix dactylifera* Linn): an emerging medicinal food. *Crit. Rev. Food Sci. Nutr.* **2012**, *52*, 249−271.

(3) Puri, A.; Sahai, R.; Singh, K. L.; Saxena, R. P.; Tanton, J. S.; Saxena, K. C. Immunostimulant activity of dry fruits and plant materials used in Indian traditional medical system for mothers after child birth and invalids. *J. Ethnopharmacol.* **2000**, *71*, 89−92.

(4) Sallal, A.-K; Ashkenani, A. Effect of date extract on growth and spore germination of *Bacillus subtilis*. *Microbios* **1989**, *59*, 203−210.

(5) Shraideh, Z. A.; Abu-El-Teen, K. H.; Sallal, A.-K. Ultrastructural effects of date extract on Candida albicans. *Mycopathologia* **1998**, *142*, 119−123.

(6) Vayalil, P. K. Antioxidant and antimutagenic properties of aqueous extract of date fruit (*Phoenix dactylifera* L. *Arecaceae*). *J. Agric. Food Chem.* **2002**, *50*, 610−617.

(7) Mansouri, A.; Embarek, G.; Kokkalouc, E.; Kefalas, P. Phenolic profile and antioxidant activity of the Algerian ripe date palm fruit (*Phoenix dactylifera*). *Food Chem.* **2005**, *89*, 411−420.

(8) Al-Farsi, M.; Alasalvar, C.; Morris, A.; Baron, M.; Shahidi, F. Comparison of antioxidant activity, anthocyanins, carotenoids, and phenolics of three native fresh and sun-dried date (*Phoenix dactylifera* L.) varieties grown in Oman. *J. Agric. Food Chem.* **2005**, *53*, 7592−7599.

(9) Rock, W.; Rosenblat, M.; Borochov-Neori, H.; Volkova, N.; Judeinstein, S.; Elias, M.; Aviram, M. Effects of date (*Phoenix dactylifera* L., Medjool or Hallawi variety) consumption by healthy subjects on serum glucose and lipid levels and on serum oxidative status: a pilot study. *J. Agric. Food Chem.* **2009**, *57*, 8010−8017.

(10) Amoros, A.; Pretel, M. T.; Almansa, M. S.; Botella, M. A.; Zapata, P. J.; Serrano, M. Antioxidant and nutritional properties of date fruit from Elche Grove as affected by maturation and phenotypic variability of date palm. *Food Sci. Technol. Int.* **2009**, *15*, 65−72.

(11) Regnault-Roger, C.; Hadidane, R.; Biard, J. F.; Boukef, K. High performance liquid and thin-layer chromatographic determination of

DOI: 10.1021/jf506094r
J. Agric. Food Chem. 2015, 63, 3189−3195

phenolic acids in palm (*Phoenix dactilifera*) products. *Food Chem.* **1987**, *25*, 61−67.
(12) Hong, Y. J.; Tomas-Barberan, F. A.; Kader, A. A.; Mitchell, A. E. The flavonoid glycosides and procyanidin composition of Deglet Noor dates (*Phoenix dactylifera*). *J. Agric. Food Chem.* **2006**, *54*, 2405−2411.
(13) Borochov-Neori, H.; Judeinstein, S.; Greenberg, A.; Volkova, N.; Rosenblat, M.; Aviram, M. Date (*Phoenix dactylifera* L.) fruit soluble phenolics composition and anti-atherogenic properties in nine Israeli varieties. *J. Agric. Food Chem.* **2013**, *61*, 4278−4286.
(14) Lusis, A. J. Atherosclerosis. *Nature* **2000**, *404*, 233−241.
(15) Schulze, P. C.; Lee, R. T. Oxidative stress and atherosclerosis. *Curr. Arterioscler. Rep.* **2005**, *7*, 242−248.
(16) Aviram, M.; Kaplan, M.; Rosenblat, M.; Fuhrman, B. Dietary antioxidants and paraoxonases against LDL oxidation and atherosclerosis development. *Handb. Exp. Pharmacol.* **2005**, *170*, 263−300.
(17) Geleijnse, J. M.; Hollman, P. Ch. Flavonoids and cardiovascular health: which compounds, what mechanisms? *Am. J. Clin. Nutr.* **2008**, *88*, 12−13.
(18) Hertog, M. G.; Kromhout, D.; Aravanis, C.; Blackburn, H.; Buzina, R.; Fidanza, F.; Giampaoli, S.; Jansen, A.; Menotti, A.; Nedeljkovic, S.; Pekkarinen, M.; Simic, B. S.; Toshima, H.; Feskens, E. J. M.; Hollman, P. C. H.; Katan, M. B. Flavonoid intake and long-term risk of coronary heart disease and cancer in the seven countries study. *Arch. Int. Med.* **1995**, *155*, 381−386.
(19) Aviram, M.; Rosenblat, M.; Gaitini, D.; Nitecki, S.; Hoffman, A.; Dornfeld, L.; Volkova, N.; Presser, D.; Attias, J.; Liker, H.; Hayek, T. Pomegranate juice consumption for 3 years by patients with carotid artery stenosis reduces common carotid intima-media thickness, blood pressure and LDL oxidation. *Clin. Nutr.* **2004**, *23*, 423−433.
(20) Borochov-Neori, H.; Judeinstein, S.; Greenberg, A.; Fuhrman, B.; Attias, J.; Volkova, N.; Hayek, T.; Aviram, M. Phenolic antioxidants and antiatherogenic effects of Marula (Sclerocarrya birrea Subsp. caffra) fruit juice in healthy humans. *J. Agric. Food Chem.* **2008**, *56*, 9884−9891.
(21) Rice-Evans, C. A.; Miller, N. J.; Paganga, G. Structure-antioxidant activity relationships of flavonoids and phenolic acids. *Free Radical Biol. Med.* **1996**, *20*, 933−956.
(22) Brown, J. E.; Khodr, H.; Hider, R. C.; Rice-Evans, C. A. Structural dependence of flavonoid interactions with Cu^{2+} ions: implications for their antioxidant properties. *Biochem. J.* **1998**, *330*, 1173−1178.
(23) Mrabet, A.; Rodríguez-Arcos, R.; Guillén-Bejarano, R.; Chaira, N.; Ferchichi, A.; Jiménez-Araujo, A. Dietary fiber from Tunisian common date cultivars (*Phoenix dactylifera* L.): chemical composition, functional properties, and antioxidant capacity. *J. Agric. Food Chem.* **2012**, *60*, 3658−3664.
(24) Oszmianski, J.; Ramos, T.; Bourzeix, M. Fractionation of phenolic compounds in red wine. *Am. J. Enol. Vitic.* **1988**, *39*, 259−262.
(25) Singleton, V. L.; Rossi, J. A. Colorimetry of total phenolics with phosphomolybdic phosphotungstic acid reagents. *Am. J. Enol. Vitic.* **1965**, *16*, 144−158.
(26) Benzie, I. F. F.; Straino, J. J. The ferric reducing ability of plasma (FRAP) as a measure of "antioxidant power": the FRAP assay. *Anal. Biochem.* **1996**, *239*, 70−76.
(27) Malterud, K. M.; Farbort, T. L.; Huse, A. C. E.; Sund, R. B. Antioxidant and radical scavenging effects of arthraquinones and anthorones. *Pharmacology* **1993**, *47*, 77−85.
(28) Aviram, M. Plasma lipoprotein separation by discontinuous density gradient ultracentrifugation in hyperlipoproteinemic patients. *Biochem. Med.* **1983**, *30*, 111−118.
(29) Lowry, O. H.; Rosebrough, N. J.; Farr, A. L.; Randall, R. J. Protein measurement with the Folin phenol reagent. *J. Biol. Chem.* **1951**, *193*, 265−275.
(30) Buege, J. A.; Aust, S. D. Microsomal lipid peroxidation. *Methods Enzymol.* **1978**, *52*, 302−310.
(31) El-Saadani, M.; Esterbauer, N.; El-Sayed, M.; Goher, M.; Nassar, A. Y.; Jurgens, G. Spectrophotometric assay for lipid peroxides in serum lipoproteins using commercially available reagent. *J. Lipid Res.* **1989**, *30*, 627−630.
(32) Gu, X.; Kozarsky, K.; Krieger, M. Scavenger receptor class B, type I-mediated [^{3}H] cholesterol efflux to high and low density lipoproteins is dependent on lipoprotein binding to the receptor. *J. Biol. Chem.* **2000**, *275*, 29993−30001.
(33) Cheng, J.-C.; Dai, F.; Zhou, B.; Yang, L.; Liu, Z.-L. Antioxidant activity of hydroxycinnamic acid derivatives in human low density lipoprotein: mechanism and structure−activity relationship. *Food Chem.* **2007**, *104*, 132−139.
(34) Laranjinha, J. Caffeic acid and related antioxidant compounds: biochemical and cellular effects. In *Handbook of Antioxidants*, 2nd ed.; Cadenas, E.; Packer, L., Eds.; Marcel Dekker, Inc.: New York, NY, 2001; pp 279−302.
(35) Fuhrman, B.; Aviram, M. Polyphenols and flavonoids protect LDL against atherogenic modifications. In *Handbook of Antioxidants*, 2nd ed.; Cadenas, E.; Packer, L., Eds.; Marcel Dekker, Inc.: New York, NY, 2001; pp 303−336.
(36) Vaya, J.; Mahmood, S.; Goldblum, A.; Aviram, M.; Volkova, N.; Shaalan, A.; Musa, R.; Tamir, S. Inhibition of LDL oxidation by flavonoids in relation to their structure and calculated enthalpy. *Phytochemistry* **2003**, *62*, 89−99.
(37) Russo, N.; Toscano, M.; Uccella, N. Semiempirical molecular modeling into quercetin reactive site: structural, conformation, and electronic features. *J. Agric. Food Chem.* **2000**, *48*, 3232−3237.
(38) Hendrich, A. B. Flavonoid-membrane interactions: possible consequences for biological effects of some polyphenolic compounds. *Acta Pharmacol. Sin.* **2006**, *27*, 27−40.
(39) Glass, A. D. M.; Dunlop, J. Influence of phenolic acids on ion uptake. IV. Depolarization of membrane potentials. *Plant Physiol.* **1974**, *54*, 855−858.
(40) Rosenblat, M.; Volkova, N.; Khatib, S.; Mahmood, S.; Vaya, J.; Aviram, M. Reduced glutathione (GSH) increases quercetin stimulatory effects on HDL- or apoA1-mediated cholesterol efflux from J774A.1 macrophages. *Free Radical Res.* **2014**, *48*, 1462−1472.
(41) Manach, C.; Scalbert, A.; Morand, C.; Rémésy, C.; Jiménez, L. Polyphenols: food sources and bioavailability. *Am. J. Clin. Nutr.* **2004**, *79*, 727−747.
(42) Rosenblat, M.; Volkova, N.; Borochov-Neori, H.; Judeinstein, S.; Aviram, M. Anti-atherogenic properties of date *vs.* pomegranate polyphenols *in-vitro* and *in-vivo* in atherosclerotic mice: the benefits of the combination. *Food Funct.* **2015**, DOI: 10.1039/c4fo00998c.

DOI: 10.1021/jf506094r
J. Agric. Food Chem. 2015, 63, 3189−3195

other triterpenic acids such as AA and GA might benefit survival and function of human bronchial epithelial cells.

Both 16HBE and BEAS-2B cells are normal human bronchial epithelial cell lines, and have been widely used in bronchial disease related research.[3,18] Hydrogen peroxide, an oxidant in cigarette smoke extract, could cause apoptotic and oxidative injury in those bronchial epithelial cells.[19,20] Thus, 16HBE and BEAS-2B cells were used in this present study to investigate the protective activities of AA, GA, and OA at two doses, 4 and 8 μmol/L, against hydrogen peroxide induced apoptotic, oxidative, and inflammatory stress. The impact of these triterpenic acids upon the activity and protein expression of associated factors including COX-2, NADPH oxidase, MAPK, and NF-κB was evaluated.

MATERIALS AND METHODS

Materials. AA, GA, and OA (95%) and rhodamine123 (Rh123) were bought commercially (Sigma-Aldrich Chemical Co., Milwaukee, WI, USA). 16HBE and BEAS-2B cells were purchased from American Type Culture Collection (Rockville, MD, USA). Medium, antibiotics, chemicals, and plates used for cell culture were obtained from Difco Laboratory (Detroit, MI, USA).

Experimental Design and Cell Culture. Our preliminary data indicated that 12, 24, 36, and 48 h of incubation resulted in approximately 21.7, 48.6, 72.9, and 96.3% incorporation of test compound into test cells. Thus, 48 h of incubation was used for the present study. In addition, the improvement upon cell viability of test compounds at 0.5, 1, 2, 4, and 8 μmol/L against H_2O_2 was also examined in a preliminary test, and results showed that these compounds at 0.5, 1, or 2 μmol/L did not significantly improve cell viability. Thus, these compounds at 4 and 8 μmol/L were further used. Dimethyl sulfoxide (DMSO) was used to prepare stock solution for three triterpenic acids, and stock solution was further diluted by bronchial epithelial growth medium (BEGM). The final concentration of DMSO in cell culture was lower than 0.5%, which did not impact any measurements. 16HBE and BEAS-2B cells were routinely cultured in BEGM containing 2.5 mM L-glutamine, 10% fetal calf serum, 100 units/mL streptomycin, and 100 units/mL penicillin (pH 7.4) under 5% CO_2 and 95% air at 37 °C. Culture medium was renewed every 72 h, and cells were subcultured every 7 days. Cell number (10^5/mL) was adjusted by a phosphate buffer saline (PBS) with pH at 7.2 for experiments and measurements. After aspiration, cells were pretreated by test compound at 4 or 8 μmol/L at 37 °C for 48 h, followed by washing twice with PBS. The concentration of test compound in PBS was measured using a HPLC method described by Yin et al.[12] The compound left in cells was considered as incorporated. Results showed that 48 h of incubation resulted in 97.1 ± 1.3 and 95.8 ± 0.9% incorporation into 16HBE and BEAS-2B cells, respectively. Cells were then treated with 100 μM H_2O_2 for 4 h at 37 °C. Control groups had no test compound and were without H_2O_2 treatment.

Cell Viability Assay. Cell viabiliaty was examined by 3-(4,5-dimethylthiazol-2-yl)-2,5-diphenyltetrazolium bromide (MTT).[21] Cells (10^5/mL) were treated by test compound for 48 h and then H_2O_2 treatment for 4 h. MTT at 0.25 mg of MTT/mL was added into the medium, followed by incubating at 37 °C for 3 h. MTT formazan product was quantified by a Bio-Rad microplate reader (Hercules, CA, USA) to measure the absorbance at 570 nm, with a reference wavelength at 630 nm. Cell viability was shown as a percent of control groups.

Determination of DNA Fragmentation. DNA fragmentation was determined by using a cell death detection kit purchased from Roche Molecular Biochemicals (Mannheim, Germany). Cells were mixed with 5 mL of lysis buffer containing HEPES (10 mM, pH 7.9), KCl (10 mM), $MgCl_2$ (1.5 mM), EDTA (0.1 mM), PMSF (1 mM), DTT (1 mM), and Nonidet P-40 (0.6%) for 30 min, followed by centrifugation for 10 min at 200×*g*. Supernatant at 20 μL was added on a plate precoated with streptavidin, followed by adding 80 μL of immunoreagent and incubating at 25 °C for 2 h. PBS was used to wash twice. After adding substrate solution, the mixture was incubated for a further 15 min. The absorbance at 405 nm, with 490 nm as a reference wavelength, was measured by a microplate reader. DNA fragmentation was determined as the enrichment factor by using the following equation: absorbance of sample (cells with test compound and/or H_2O_2) ÷ absorbance of control (cells without H_2O_2 and test compound).

Mitochondrial Membrane Potential (MMP) Assay. MMP was assayed by a Beckman-FC500 flow cytometer (Beckman Coulter, Fullerton, CA, USA) and Rh123, a fluorescent dye.[22] After centrifugation for 5 min at 1200×*g*, cells were resuspended in BEGM medium, and further mixed with Rh123 at 100 μg/L. After incubating at 37 °C for 45 min, the collected cells were washed twice by PBS. Mean fluorescence intensity (MFI) was then analyzed by flow cytometry.

Preparation of Mitochondrial Fractions. Cells were lysed first, followed by centrifugation at 4 °C and 200×*g* for 10 min. The supernatant was collected for further centrifugation at 4 °C and 10 000×*g* for 20 min to get a mitochondrial pellet. PBS was used to resuspend this mitochondrial pellet, and the protein concentration of this fraction was measured by a kit purchased from Pierce Biotechnology Inc. (Rockford, IL, USA). Bovine serum albumin was used as a standard.

Assay of Na^+-K^+-ATPase Activity. Na^+-K^+-ATPase activity was assayed by monitoring the released inorganic phosphate (Pi) from ATP.[23] The cell mitochondrial fraction was mixed with 30 mM Tris−HCl buffer (pH 7.4) containing 100 mM NaCl and 20 mM KCl. ATP at 2 mM was added to initiate this assay. After 15 min of incubation at 37 °C, the assay was stopped by adding 15% trichloroacetic acid. The absorbance at 640 nm was measured to determine the Pi level. The value of a sample was shown as a percent of that of the control groups.

Measurement of Caspase Activity. Fluorometric assay kits (Upstate, Lake Placid, NY, USA) were obtained to meaure caspase-3 or -8 activity according to the manufacturer instructions. The interassay CV was 4.5−6.1%, and the intra-assay CV was 4.2−4.9%. Cells were first lysed in 25 mL of lysis buffer, followed by incubating on ice for 10 min. Cell lysates at 50 μL were then added into 25 mL of reaction buffer and further mixed with 5 mL of fluorogenic substrates which were specific for either caspase-3 or -8. After incubating at 37 °C for 60 min, a Hitachi F-4500 fluorophotometer (Tokyo, Japan) was applied to determine fluorescence, in which excitation and emission were set at 400 and 505 nm, respectively. The value was expressed as a percent of the control groups.

Analyses for ROS, 8-Hydroxydeoxyguanosine (8-OHdG), and Glutathione (GSH) Levels. ROS level was measured by $DCFH_2$-DA, a dye. After they were washed and resuspended in medium, cells were mixed with $DCFH_2$-DA at 50 μmol/L for 30 min. PBS was used to wash and suspend cells, followed by centrifugation at 4 °C and 412×*g* for 10 min. Collected cells were dissolved by adding 1% Triton X-100. A fluorescence microplate reader was used to measure the fluorescence change, in which excitation and emission were set at 485 and 530 nm, respectively. The result was shown as relative fluorescence unit (RFU)/mg of protein, in which RFU was the change in fluorescence between 5 min and time 0. A DNA Extractor WB kit purchased from Wako Pure Chemical Industries Ltd. (Tokyo, Japan) was used to extract the DNA fraction. The obtained DNA at 1 mg/mL was dissolved in water. An ELISA assay kit for 8-OHdG bought from OXIS Health Products Inc. (Portland, OR, USA) was used to determine the oxidative injury of DNA. The detection limit of 8-OHdG was 10 pg/mg of protein. A colorimetric GSH kit purchased from OxisResearch (Portland, OR, USA) was used to measure GSH concentration (ng/mg of protein), and its detection limit was 10 ng/mg of protein.

Measurements for Tumor Necrosis Factor (TNF)-α, Interleukin (IL)-6, and PGE_2. After cells were homogenized and centrifuged, the TNF-α or IL-6 level (pg/mg of protein) in supernatant was assayed by cytoscreen immunoassay kits obtained from BioSource International (Camarillo, CA, USA). The detection limit of TNF-α and IL-6 was 10 and 5 pg/mg of protein, respectively. The PGE_2 level (pg/mg of protein) was measured by a PGE_2 EIA kit

DOI: 10.1021/acs.jafc.5b00102
J. Agric. Food Chem. 2015, 63, 3196−3204

purchased from Cayman Chemical Co. (Ann Arbor, MI, USA), and its detection limit was 10 pg/mg of protein.

Cytosolic or Nuclear Fraction Preparation. Cells were treated with cold buffer containing 1.5 mM $MgCl_2$, 10 mM KCl, 10 mM HEPES (pH 7.9), 0.5 mM DTT, 0.5 mM PMSF, 1 mg/mL aprotinin, and 1 mg/mL leupeptin for 15 min. After centrifugation for 1 min at 4 °C and 14 000×*g*, the cytosolic fraction was obtained. The nuclear pellet was then resuspended in buffer containing 1.5 mM $MgCl_2$, 450 mM NaCl, 20 mM HEPES (pH 7.9), 25% glycerol, 0.5 mM DTT, 0.5 mM PMSF, 0.2 mM EDTA, 1 mg/mL aprotinin, and 1 mg/mL leupeptin for 30 min. After centrifugation for 15 min at 4 °C and 14 000×*g*, the nuclear fraction was obtained.

Western Blot Analyses. PBS was used to wash the plate twice. Cells were then scraped and suspended in lysis buffer. Reagents purchased from Bio-Rad Laboratories Inc. (Hercules, CA, USA) were used to assay protein content. A 40 μg protein sample was used for gel electrophoresis containing 10% SDS−polyacrylamide, followed by applying to a Millipore nitrocellulose membrane (Bedford, MA, USA) for 60 min. After being treated by a solution of 5% nonfat milk for 60 min to block binding from nonspecific antibody, the membrane was then reacted with monoclonal antibodies against Bcl-2, cleaved caspase-3, or Bax (1:2000); $p47^{phox}$, $gp91^{phox}$, or COX-2 (1:1000); NF-κB p65, NF-κB p50, or MAPK (1:500) at 4 °C overnight. These antibodies were bought from Boehringer-Mannheim (Indianapolis, IN, USA). The sample was further treated with horseradish peroxidase conjugated antibody at 25 °C for 3.5 h. Glyceraldehyde-3-phosphate dehydrogenase (GAPDH) was a control for loading, and the obtained bands were processed by an ATTO image analyzer (Tokyo, Japan). Densitometric analysis was processed to quantify the blot, and data were normalized against GAPDH.

Statistical Analysis. A Shapiro−Wilk test was used to assess normality of data. Nine preparations were used to examine the effects of treatments (n = 9). Statistical analysis was undertaken by one-way ANOVA. Post-hoc comparisons were processed by Dunnett's t test. A difference of $P < 0.05$ was considered to be significant.

RESULTS

Effects of AA, GA, or OA upon Cell Viability. Without H_2O_2 treatment, three triterpenic acids at two doses did not change 16HBE and BEAS-2B cell viability (Figure 1, $P > 0.05$).

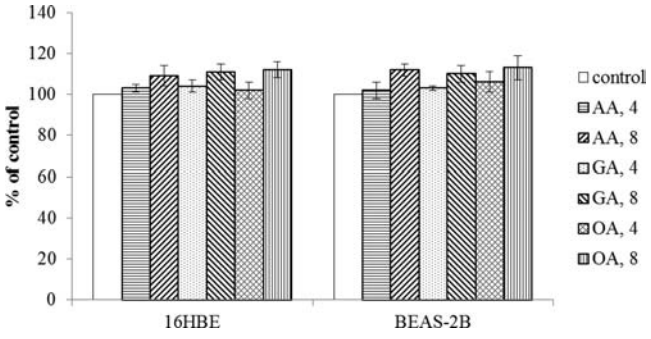

Figure 1. Effects of AA, GA, and OA upon the growth of 16HBE and BEAS-2B cells, without H_2O_2 treatment. Cells were pretreated with test compound at 4 or 8 μmol/L for 48 h. Control groups were cells that contained no test compound. Data are mean ± SD (n = 9).

H_2O_2 treatment decreased survival and raised DNA fragmentation of test cells (Figure 2, $P < 0.05$). AA, GA, or OA pretreatments enhanced cell survival and lowered fragmentation of DNA in those cells ($P < 0.05$). H_2O_2 treatment downregulated Bcl-2 expression and enhanced Bax and cleaved caspase-3 expression in test cells (Figure 3, $P < 0.05$). AA treatments retained Bcl-2 expression, but GA and OA only at high dose preserved protein expression of Bcl-2 ($P < 0.05$). Three triterpenic acids lowered cleaved caspase-3 expression

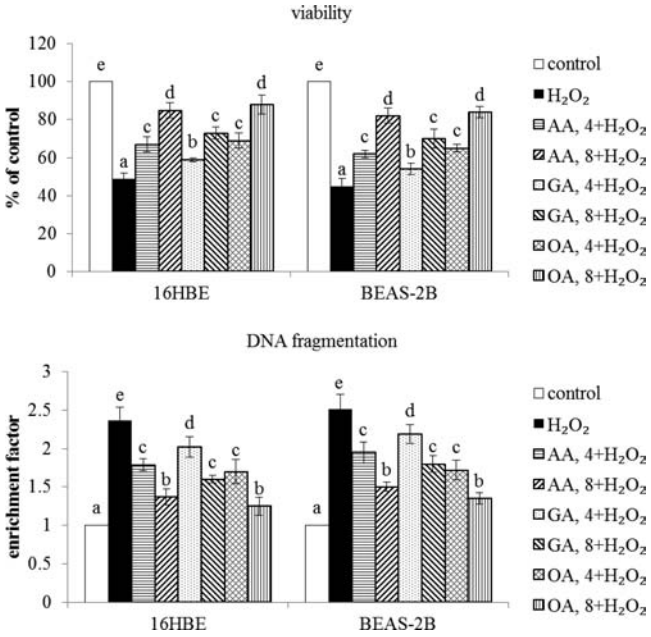

Figure 2. Effects of AA, GA, and OA upon viability and DNA fragmentation determined as the enrichment factor in 16HBE and BEAS-2B cells. Cells were pretreated with test compound at 4 or 8 μmol/L for 48 h and followed by adding 100 μM H_2O_2 to induce cell damage. Control groups were cells that contained no test compound, and without H_2O_2 treatment. Data are mean ± SD (n = 9). a−e: Mean values among bars without a common letter differ, $P < 0.05$.

dose-dependently. Three test compounds did not change the protein expression of Bax in test cells ($P > 0.05$).

Influence of AA, GA, or OA on Mitochondrial Stability. H_2O_2 treatment lowered Na^+-K^+-ATPase activity or MMP in two cell lines (Table 1, $P < 0.05$). AA, GA, or OA maintained Na^+-K^+-ATPase activity or MMP dose-dependently ($P < 0.05$). H_2O_2 treatment raised the activity of caspase-3 and caspase-8 in 16HBE and BEAS-2B cells (Figure 4, $P < 0.05$). AA, GA, or OA decreased caspase-3 activity in both cell lines dose-dependently but only at high dose significantly reduced caspase-8 activity in test cells ($P < 0.05$).

Impact of AA, GA, or OA upon Oxidative and Inflammatory Factors. H_2O_2 treatment significantly increased ROS and 8-OHdG production, and reduced the GSH level in 16HBE and BEAS-2B cells (Table 2). AA, GA, or OA treatments dose-dependently lowered the ROS and 8-OHdG levels; also reserved GSH level of test cells ($P < 0.05$). H_2O_2 treatment significantly increased TNF-α, IL-6, or PGE_2 levels (Table 3). AA, GA, or OA treatments decreased TNF-α, IL-6, and PGE_2 generation dose-dependently ($P < 0.05$).

Effects of AA, GA, or OA on NADPH Oxidase, COX-2, NF-κB, and MAPK Expression. H_2O_2 treatment promoted protein expression of $p47^{phox}$, $gp91^{phox}$, and COX-2 as well as cytosolic and nuclear NF-κB of 16HBE and BEAS-2B cells (Figure 5, $P < 0.05$). AA, GA, or OA treatments downregulated protein expression of $p47^{phox}$, COX-2, and cytosolic or nuclear NF-κB p65 ($P < 0.05$), but these agents decreased $gp91^{phox}$ expression only at high dose ($P < 0.05$). Three triterpenic acids failed to affect NF-κB p50 expression of test cells ($P > 0.05$). H_2O_2 treatment upregulated MAPK expression in 16HBE and BEAS-2B cells (Figure 6, $P < 0.05$). AA, GA, or OA treatments significantly downregulated p-p38 expression and decreased

DOI: 10.1021/acs.jafc.5b00102
J. Agric. Food Chem. 2015, 63, 3196−3204

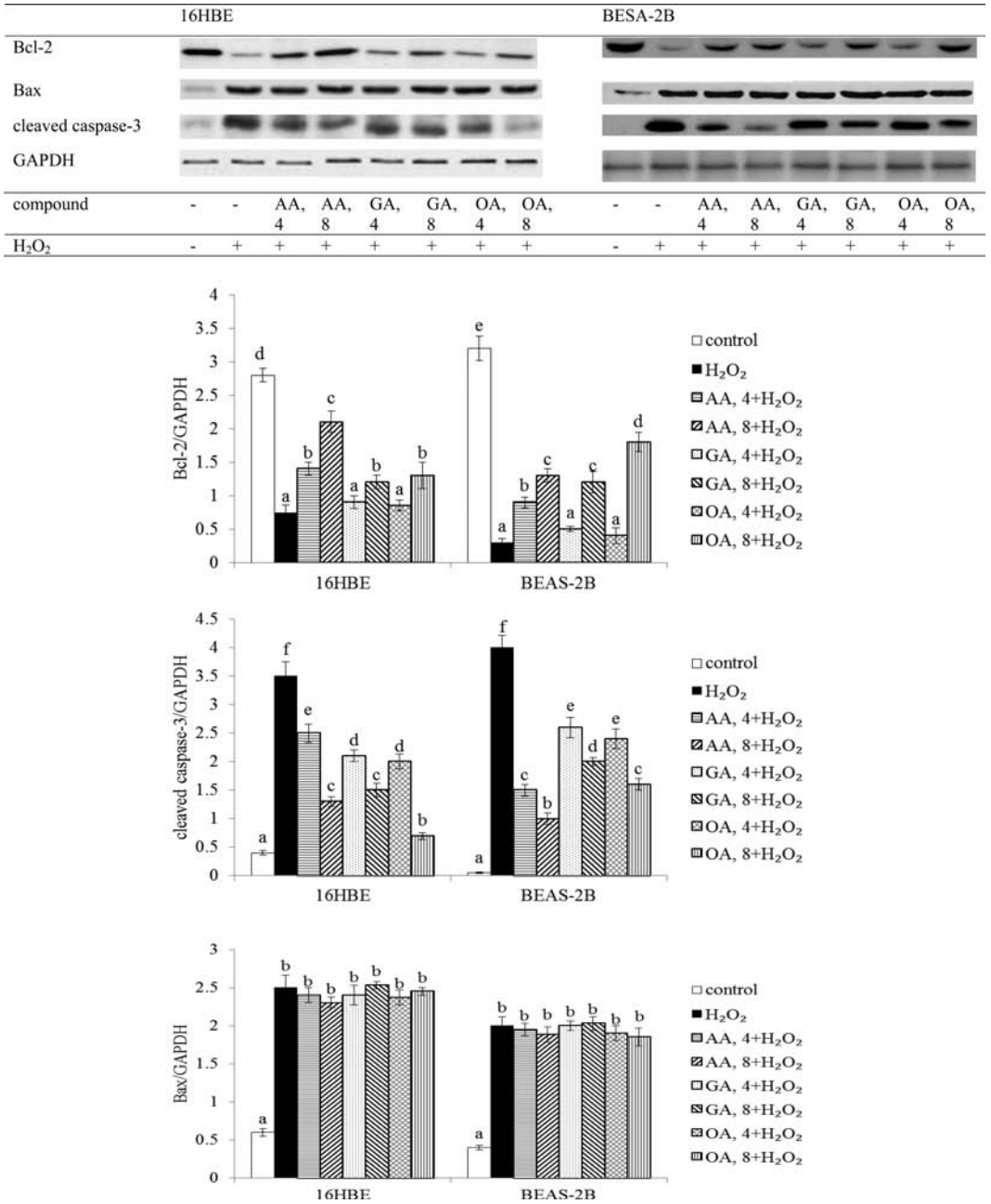

Figure 3. Effects of AA, GA, or OA upon Bcl-2, Bax, and cleaved caspase-3 expression in 16HBE and BEAS-2B cells. Cells were pretreated with test compound at 4 or 8 μmol/L for 48 h and followed by adding 100 μM H_2O_2 to induce cell damage. Control groups were cells that contained no test compound, and without H_2O_2 treatment. Data are mean ± SD (n = 9). a–f: Mean values among bars without a common letter differ, $P < 0.05$.

protein expression of p-JNK only at high dose in test cells ($P < 0.05$).

DISCUSSION

Cigarette smoke or particulate matter could stimulate the release of hydrogen peroxide in airway epithelial cells, which contributes to apoptotic, oxidative, and inflammatory stress in those cells.[24,25] In our present study, pretreatments from three triterpenic acids, AA, GA, and OA, markedly protected two human bronchial epithelial cell lines (16HBE and BEAS-2B cells) against hydrogen peroxide induced oxidative and inflammatory injury, which in turn enhanced cell survival. In addition, we found that these compounds were able to mediate protein expression of NADPH oxidase, COX-2, NF-κB, and MAPK in these bronchial epithelial cells. Furthermore, these triterpenic acid treatments alone, without hydrogen peroxide, did not affect the growth of these test cells. These findings implied that these triterpenic acids might be safe and benefit respiratory epithelium stability and functions.

Bcl-2, Bax, and cleaved caspase-3 are involved in mitochondrial apoptotic regulation. Bcl-2 is an antiapoptotic factor; Bax and cleaved caspase-3 are proapoptotic factors. Hydrogen peroxide triggered a mitochondria-mediated apoptotic pathway via decreasing Bcl-2 expression, and enhancing the expression of cleaved caspase-3 and Bax. However, triterpenic acid pretreatments effectively downregulated protein expression of cleaved caspase-3 and also mildly retained the expression of Bcl-2 of two cell lines, which consequently mitigated hydrogen

DOI: 10.1021/acs.jafc.5b00102
J. Agric. Food Chem. 2015, 63, 3196–3204

Table 1. Effects of AA, GA, or OA upon the Level of Mitochondrial Membrane Potential, Determined as MFI, and Na^+-K^+-ATPase Activity in 16HBE and BEAS-2B Cells[a]

	MFI	Na^+-K^+-ATPase activity
	16HBE	
control	100f	100f
H_2O_2	37 ± 2a	47 ± 4a
AA, 4 + H_2O_2	76 ± 4d	67 ± 3c
AA, 8 + H_2O_2	84 ± 5e	79 ± 5d
GA, 4 + H_2O_2	52 ± 3b	57 ± 4b
GA, 8 + H_2O_2	72 ± 3d	70 ± 5c
OA, 4 + H_2O_2	65 ± 4c	72 ± 2c
OA, 8 + H_2O_2	80 ± 2e	84 ± 5e
	BEAS-2B	
control	100e	100f
H_2O_2	34 ± 3a	41 ± 4a
AA, 4 + H_2O_2	69 ± 5c	65 ± 4c
AA, 8 + H_2O_2	78 ± 6d	83 ± 5e
GA, 4 + H_2O_2	48 ± 4b	50 ± 2b
GA, 8 + H_2O_2	62 ± 3c	63 ± 4c
OA, 4 + H_2O_2	68 ± 5c	71 ± 3d
OA, 8 + H_2O_2	79 ± 3d	81 ± 5e

[a]Cells were pre-treated with test compound at 4 or 8 μmol/L for 48 h and followed by adding 100 μM H_2O_2 to induce cell damage. Control groups were cells that contained no test compound, and without H_2O_2 treatment. Data are mean ± SD (n = 9). a–f: Mean values in a column without a common letter differ, $P < 0.05$.

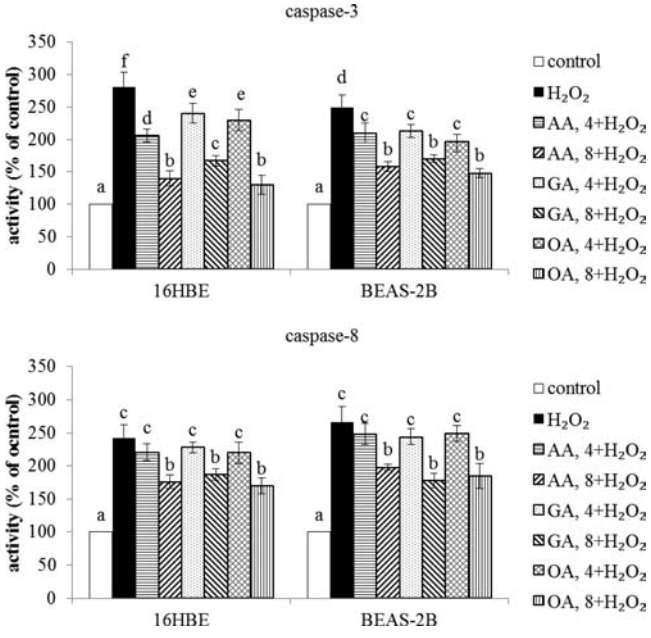

Figure 4. Effects of AA, GA, and OA upon activity of caspase-3 and caspase-8 in 16HBE and BEAS-2B cells. Cells were pretreated with test compound at 4 or 8 μmol/L for 48 h and followed by adding 100 μM H_2O_2 to induce cell damage. Control groups were cells that contained no test compound, and without H_2O_2 treatment. Data are mean ± SD (n = 9). a–f: Mean values among bars without a common letter differ, $P < 0.05$.

Table 2. Effects of AA, GA, or OA upon the Level of ROS (RFU/mg of Protein), 8-OHdG (pg/mg of Protein), and GSH (ng/mg of Protein) in 16HBE and BEAS-2B Cells[a]

	ROS	8-OHdG	GSH
	16HBE		
control	0.13 ± 0.07a	29 ± 5a	106 ± 6e
H_2O_2	2.08 ± 0.22f	187 ± 19e	43 ± 3a
AA, 4 + H_2O_2	1.15 ± 0.14c	133 ± 14d	64 ± 4b
AA, 8 + H_2O_2	0.59 ± 0.09b	82 ± 4b	90 ± 5d
GA, 4 + H_2O_2	1.57 ± 0.18e	148 ± 18d	56 ± 4b
GA, 8 + H_2O_2	0.98 ± 0.11c	113 ± 11c	75 ± 5c
OA, 4 + H_2O_2	1.27 ± 0.15d	142 ± 13d	62 ± 3b
OA, 8 + H_2O_2	0.66 ± 0.10b	88 ± 8b	84 ± 4d
	BEAS-2B		
control	0.15 ± 0.04a	25 ± 6a	109 ± 4f
H_2O_2	2.14 ± 0.25e	195 ± 2e	46 ± 2a
AA, 4 + H_2O_2	1.32 ± 0.16c	141 ± 16c	69 ± 5c
AA, 8 + H_2O_2	0.61 ± 0.09b	86 ± 9b	90 ± 6e
GA, 4 + H_2O_2	1.69 ± 0.17d	160 ± 13d	57 ± 2b
GA, 8 + H_2O_2	1.13 ± 0.12c	123 ± 11c	81 ± 3d
OA, 4 + H_2O_2	1.24 ± 0.14c	137 ± 15c	79 ± 4d
OA, 8 + H_2O_2	0.79 ± 0.08b	74 ± 7b	92 ± 5e

[a]Cells were pre-treated with test compound at 4 or 8 μmol/L for 48 h and followed by adding 100 μM H_2O_2 to induce cell damage. Control groups were cells that contained no test compound, and without H_2O_2 treatment. Data are mean ± SD (n = 9). a–f: Mean values in a column without a common letter differ, $P < 0.05$.

Table 3. Effects of AA, GA, or OA upon the Level (pg/mg of Protein) of IL-6, TNF-α, and PGE_2 in 16HBE and BEAS-2B Cells[a]

	IL-6	TNF-α	PGE_2
	16HBE		
control	14 ± 2a	19 ± 4a	23 ± 3a
H_2O_2	127 ± 5e	149 ± 8e	136 ± 5d
AA, 4 + H_2O_2	76 ± 4c	111 ± 7d	95 ± 2c
AA, 8 + H_2O_2	42 ± 3b	80 ± 3c	71 ± 4b
GA, 4 + H_2O_2	93 ± 5d	114 ± 6d	92 ± 4c
GA, 8 + H_2O_2	69 ± 3c	82 ± 5c	66 ± 3b
OA, 4 + H_2O_2	88 ± 4d	102 ± 4d	90 ± 5c
OA, 8 + H_2O_2	65 ± 3c	56 ± 5b	68 ± 2b
	BEAS-2B		
control	15 ± 3a	20 ± 3a	21 ± 4a
H_2O_2	137 ± 6d	162 ± 6f	167 ± 9e
AA, 4 + H_2O_2	85 ± 2c	104 ± 5e	99 ± 6d
AA, 8 + H_2O_2	58 ± 3b	67 ± 4c	64 ± 3b
GA, 4 + H_2O_2	89 ± 5c	88 ± 6d	94 ± 5d
GA, 8 + H_2O_2	66 ± 4b	46 ± 3b	61 ± 4b
OA, 4 + H_2O_2	81 ± 3c	101 ± 2e	78 ± 2c
OA, 8 + H_2O_2	60 ± 2b	69 ± 4c	53 ± 3b

[a]Cells were pre-treated with test compound at 4 or 8 μmol/L for 48 h and followed by adding 100 μM H_2O_2 to induce cell damage. Control groups were cells that contained no test compound, and without H_2O_2 treatment. Data are mean ± SD (n = 9). a–f: Mean values in a column without a common letter differ, $P < 0.05$.

peroxide elicited mitochondria-mediated apoptotic stress. Na^+-K^+-ATPase plays a critical role in maintaining ion homeostasis of mitochondrial membrane. Abnormality of this enzyme disturbs ion homeostasis and causes mitochondrial malfunctions.[26] Thus, the reduction in Na^+-K^+-ATPase activity or mitochondrial membrane potential in cells from hydrogen peroxide treatment indicated that mitochondrial structure and functions in those cells had been impaired, which in turn contributed to apoptotic insult. However, three triterpenic acid pretreatments markedly maintained the activity of Na^+-K^+-ATPase and the potential of the mitochondrial membrane in

DOI: 10.1021/acs.jafc.5b00102
J. Agric. Food Chem. 2015, 63, 3196–3204

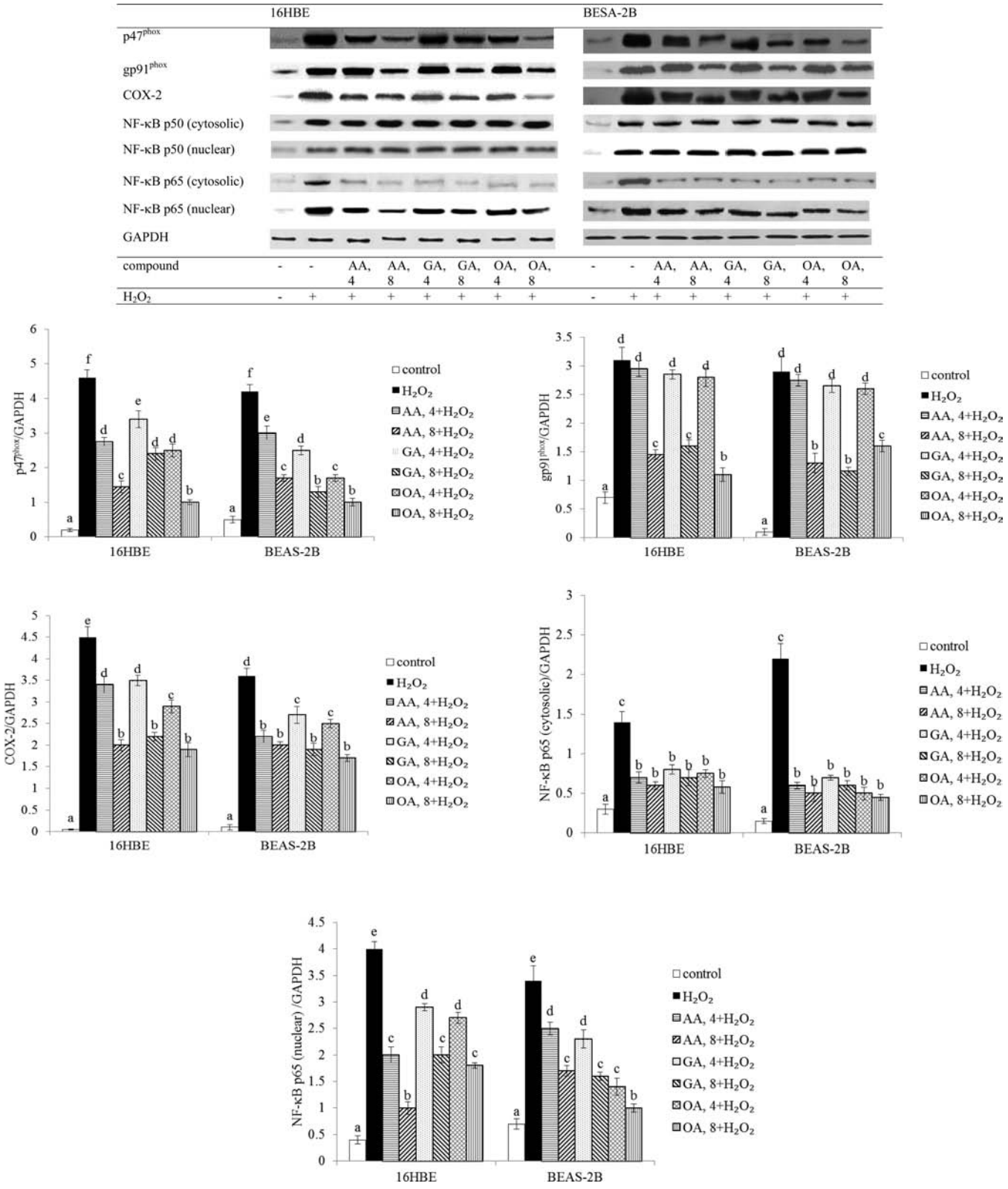

Figure 5. Effects of AA, GA, or OA upon protein expression of $p47^{phox}$, $gp91^{phox}$, COX-2, and NF-κB in 16HBE and BEAS-2B cells. Cells were pretreated with test compound at 4 or 8 μmol/L for 48 h and followed by adding 100 μM H_2O_2 to induce cell damage. Control groups were cells that contained no test compound, and without H_2O_2 treatment. Data are mean ± SD (n = 9). a–f: Mean values among bars without a common letter differ, $P < 0.05$.

those cells. These results suggested that these compounds could enhance mitochondrial stability for those cells. Furthermore, our data revealed that these triterpenic acids alleviated hydrogen peroxide induced DNA fragmentation and 8-OHdG formation, indicators of DNA oxidative stress. These findings suggested that these compounds might penetrate these

DOI: 10.1021/acs.jafc.5b00102
J. Agric. Food Chem. 2015, 63, 3196–3204

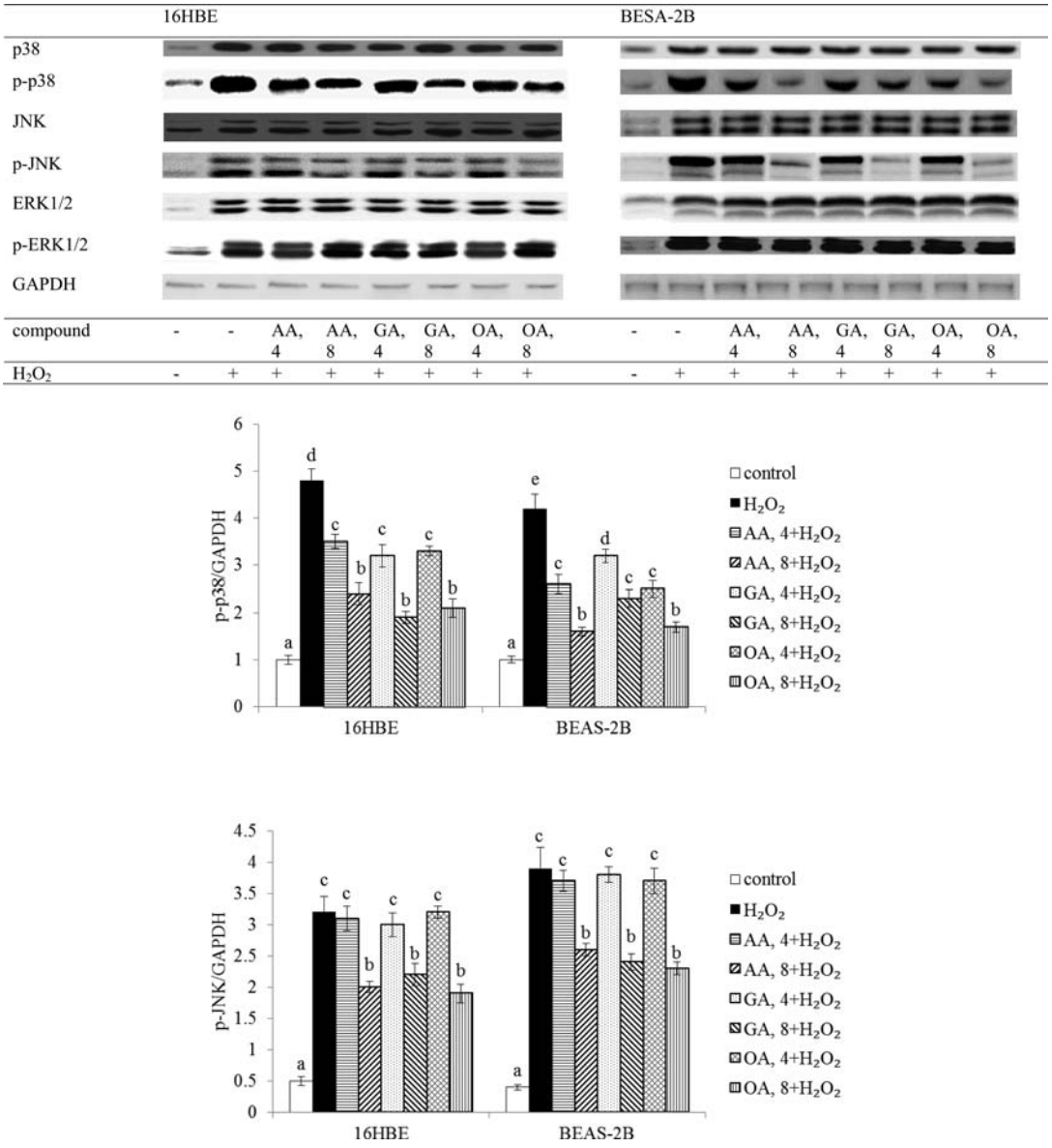

Figure 6. Effects of AA, GA, or OA upon protein expression of MAPK in 16HBE and BEAS-2B cells. Cells were pretreated with test compound at 4 or 8 μmol/L for 48 h and followed by adding 100 μM H_2O_2 to induce cell damage. Control groups were cells that contained no test compound, and without H_2O_2 treatment. Data are mean ± SD (n = 9). a−e: Mean values among bars without a common letter differ, $P < 0.05$.

bronchial epithelial cells to protect DNA, and counteract apoptotic stress from hydrogen peroxide. On the other hand, loss in the membrane potential of mitochondria activates caspase-3 and caspase-8.[27] Both caspase-3 and caspase-8 are apoptotic executors because they could cause cell morphological changes and/or nuclear protein cleavage.[21] Thus, the increased activity of caspase-3 or caspase-8 in 16HBE and BEAS-2B cells from hydrogen peroxide treatment was partially due to mitochondrial membrane potential change. Since test triterpenic acids already maintained the membrane potential of mitochondria in those cells, it was reasonable to observe the lower caspase activities. These results support that these compounds could protect 16HBE and BEAS-2B cells against apoptosis by stabilizing the mitochondrial membrane and caspases.

Hydrogen peroxide evoked oxidative and inflammatory stress in two cell lines in our present study, which was evidenced by overproduction of ROS, 8-OHdG, IL-6, and TNF-α. It is documented that three triterpenic acids could exhibit antioxidative and antiinflammatory activities.[28−30] Thus, the observed less generation of oxidative and inflammatory factors in triterpenic acid-treated cells seems acceptable. NADPH oxidase is an important regulator responsible for ROS generation within the progression of respiratory system disorders.[31,32] Our data indicated that these triterpenic acids substantially suppressed protein expression of $p47^{phox}$ and $gp91^{phox}$, a cytosolic and a membrane component of NADPH oxidase, which subsequently decreased ROS production in hydrogen peroxide treated cells. Apparently, these triterpenic acids could execute their antioxidative action through mediating NADPH oxidase. It is known that ROS could activate NF-κB and MAPK signaling pathways, which further exacerbates the formation of proinflammatory mediators.[33,34] In this present study, triterpenic acid pretreatments at two doses markedly downregulated protein expression of NF-κB p65 and p-p38 and limited JNK phosphorylation at high dose. These results could

DOI: 10.1021/acs.jafc.5b00102
J. Agric. Food Chem. 2015, 63, 3196−3204

be explained as being due to the fact that these agents already reduced ROS production. The other possibility was that these triterpenic acids directly regulated NF-κB and/or MAPK expression. Thus, the lower release of inflammatory cytokines, IL-6 and TNF-α, in triterpenic acid treated cells could be explained, since these two pathways were already declined. In addition, COX-2 is responsible for PGE_2 synthesis and PGE_2 is another key proinflammatory mediator. It has been indicated that COX-2 and its derived prostanoids such as PGE_2 are involved in cigarette smoking associated lung cancer progression.[35] We found that three triterpenic acids markedly suppressed COX-2 protein expression, which in turn decreased PGE_2 formation, and finally diminished inflammatory stress in those cells. These findings revealed that these compounds could protect 16HBE and BEAS-2B cells against hydrogen peroxide induced oxidative and inflammatory injury via declining NF-κB, MAPK, and COX-2 pathways.

It is interesting to find that OA was greater than other test compounds in suppressing NF-κB p65 expression in 16HBE cells but AA was more effective than others in lowering cleaved caspase-3 expression in BEAS-2B cells. Although AA, GA, and OA have similar structures, their protective effects for these two bronchial epithelial cell lines were not identical. These three triterpenic acids are compounds naturally present in herbs, vegetables, and fruits.[12] They are also used as food supplement ingredients.[36] Humans could obtain these natural triterpenic acids through consuming certain edible plants. Thus, these agents seem safe for application. Our previous animal study indicated that dietary AA and OA could be absorbed and accumulated in organs such as liver.[12] The bioavailability of these agents certainly benefits their application. Thus, using these compounds for respiratory protection might be feasible; even so, further in vivo study is needed in order to prove the safety and efficiency of these compounds for airway disease prevention or alleviation.

In conclusion, asiatic acid, glycyrrhizic acid, or oleanolic acid at 4 or 8 μmol/L protected human bronchial 16HBE and BEAS-2B cells against hydrogen peroxide induced oxidative and inflammatory injury via enhancing mitochondrial stability, decreasing ROS and PGE_2 production, and suppressing protein expression of NAPDH oxidase, COX-2, NF-κB p65, and p-p38. These results support that these triterpenic acids or foods rich in these agents could benefit bronchial epithelial cells, and might prevent the development of airway disorders.

AUTHOR INFORMATION

Corresponding Author

*Address: Department of Nutrition, China Medical University, 91, Hsueh-shih Rd, Taichung City, Taiwan. Phone: 886-4-22053366, ext. 7510. Fax: 886-4-22062891. E-mail: mcyin@mail.cmu.edu.tw.

Funding

This study was partially supported by a grant from Ministry of Science and Technology, Taipei City, Taiwan (NSC 102-2313-B-039-002-MY3).

Notes

The authors declare no competing financial interest.

REFERENCES

(1) Goldkorn, T.; Filosto, S. Lung injury and cancer: Mechanistic insights into ceramide and EGFR signaling under cigarette smoke. *Am. J. Respir. Cell Mol. Biol.* **2010**, *43*, 259−268.

(2) Tesfaigzi, Y. Roles of apoptosis in airway epithelia. *Am. J. Respir. Cell Mol. Biol.* **2006**, *34*, 537−547.

(3) Shi, Y.; Wang, F.; He, J.; Yadav, S.; Wang, H. Titanium dioxide nanoparticles cause apoptosis in BEAS-2B cells through the caspase 8/t-Bid-independent mitochondrial pathway. *Toxicol. Lett.* **2010**, *196*, 21−27.

(4) Domej, W.; Oettl, K.; Renner, W. Oxidative stress and free radicals in COPD - implications and relevance for treatment. *Int. J. Chronic Obstruct. Pulm. Dis.* **2014**, *9*, 1207−1224.

(5) Mukherjee, B.; Bindhani, B.; Saha, H.; Ray, M. R. Increased oxidative DNA damage and decreased expression of base excision repair proteins in airway epithelial cells of women who cook with biomass fuels. *Environ. Toxicol. Pharmacol.* **2014**, *38*, 341−352.

(6) Cho, I. H.; Gong, J. H.; Kang, M. K.; Lee, E. J.; Park, J. H.; Park, S. J.; Kang, Y. H. Astragalin inhibits airway eotaxin-1 induction and epithelial apoptosis through modulating oxidative stress-responsive MAPK signaling. *BMC Pulm. Med.* **2014**, *14*, 122.

(7) Geiszt, M.; Witta, J.; Baffi, J.; Lekstrom, K.; Leto, T. L. Dual oxidases represent novel hydrogen peroxide sources supporting mucosal surface host defense. *FASEB J.* **2003**, *17*, 1502−1504.

(8) Ahn, E. K.; Yoon, H. K.; Jee, B. K.; Ko, H. J.; Lee, K. H.; Kim, H. J.; Lim, Y. COX-2 expression and inflammatory effects by diesel exhaust particles in vitro and in vivo. *Toxicol. Lett.* **2008**, *176*, 178−187.

(9) Park, G. Y.; Hu, N.; Wang, X.; Sadikot, R. T.; Yull, F. E.; Joo, M.; Peebles, R. S., Jr.; Blackwell, T. S.; Christman, J. W. Conditional regulation of cyclooxygenase-2 in tracheobronchial epithelial cells modulates pulmonary immunity. *Clin. Exp. Immunol.* **2007**, *150*, 245−254.

(10) Yang, J.; Li, Q.; Zhou, X. D.; Kolosov, V. P.; Perelman, J. M. Naringenin attenuates mucous hypersecretion by modulating reactive oxygen species production and inhibiting NF-κB activity via EGFR-PI3K-Akt/ERK MAPKinase signaling in human airway epithelial cells. *Mol. Cell. Biochem.* **2011**, *351*, 29−40.

(11) Antognelli, C.; Gambelunghe, A.; Talesa, V. N.; Muzi, G. Reactive oxygen species induce apoptosis in bronchial epithelial BEAS-2B cells by inhibiting the antiglycation glyoxalase I defence: involvement of superoxide anion, hydrogen peroxide and NF-κB. *Apoptosis* **2014**, *19*, 102−116.

(12) Yin, M. C.; Lin, M. C.; Mong, M. C.; Lin, C. Y. Bioavailability, distribution, and antioxidative effects of selected triterpenes in mice. *J. Agric. Food Chem.* **2012**, *60*, 7697−7701.

(13) Kao, T. C.; Wu, C. H.; Yen, G. C. Bioactivity and potential health benefits of licorice. *J. Agric. Food Chem.* **2014**, *62*, 542−553.

(14) Raphael, T. J.; Kuttan, G. Effect of naturally occurring triterpenoids glycyrrhizic acid, ursolic acid, oleanolic acid and nomilin on the immune system. *Phytomedicine* **2003**, *10*, 483−489.

(15) Asl, M. N.; Hosseinzadeh, H. Review of pharmacological effects of Glycyrrhiza sp. and its bioactive compounds. *Phytother. Res.* **2008**, *22*, 709−724.

(16) Ramachandran, V.; Saravanan, R. Efficacy of asiatic acid, a pentacyclic triterpene on attenuating the key enzymes activities of carbohydrate metabolism in streptozotocin-induced diabetic rats. *Phytomedicine* **2013**, *20*, 230−236.

(17) Wächter, G. A.; Valcic, S.; Flagg, M. L.; Franzblau, S. G.; Montenegro, G.; Suarez, E.; Timmermann, B. N. Antitubercular activity of pentacyclic triterpenoids from plants of Argentina and Chile. *Phytomedicine* **1999**, *6*, 341−345.

(18) Liu, W.; Tan, X.; Shu, L.; Sun, H.; Song, J.; Jin, P.; Yu, S.; Sun, M.; Jia, X. Ursolic acid inhibits cigarette smoke extract-induced human bronchial epithelial cell injury and prevents development of lung cancer. *Molecules* **2012**, *17*, 9104−9115.

(19) Kastner, P. E.; Casset, A.; Pons, F. Formaldehyde interferes with airway epithelium integrity and functions in a dose- and time-dependent manner. *Toxicol. Lett.* **2011**, *200*, 109−116.

(20) Deng, Z.; Zhou, J. J.; Sun, S. Y.; Zhao, X.; Sun, Y.; Pu, X. P. Procaterol but not dexamethasone protects 16HBE cells from H_2O_2-induced oxidative stress. *J. Pharmacol. Sci.* **2014**, *125*, 39−50.

DOI: 10.1021/acs.jafc.5b00102
J. Agric. Food Chem. 2015, 63, 3196−3204

(21) Sharifi, A. M.; Eslami, H.; Larijani, B.; Davoodi, J. Involvement of caspase-8, −9, and −3 in high glucose-induced apoptosis in PC12 cells. *Neurosci. Lett.* **2009**, *459*, 47−51.
(22) Musa, M. A.; Badisa, V. L.; Latinwo, L. M. Cytotoxic activity of N, N′-Bis (2-hydroxybenzyl) ethylenediamine derivatives in human cancer cell lines. *Anticancer Res.* **2014**, *34*, 1601−1607.
(23) Torlinska, T.; Grochowalska, A. Age-related changes of Na^+, K^+-ATPase, Ca^{2+}-ATPase and Mg^{2+}-ATPase activities in rat brain synaptosomes. *J. Physiol. Pharmacol.* **2004**, *55*, 457−465.
(24) Yi, S.; Zhang, F.; Qu, F.; Ding, W. Water-insoluble fraction of airborne particulate matter (PM10) induces oxidative stress in human lung epithelial A549 cells. *Environ. Toxicol.* **2014**, *29*, 226−233.
(25) Downs, C. A.; Montgomery, D. W.; Merkle, C. J. Age-related differences in cigarette smoke extract-induced H2O2 production by lung endothelial cells. *Microvasc. Res.* **2011**, *82*, 311−317.
(26) Liu, N.; Li, Y.; Su, S.; Wang, N.; Wang, H.; Li, J. Inhibition of cell migration by ouabain in the A549 human lung cancer cell line. *Oncol. Lett.* **2013**, *6*, 475−479.
(27) Xiao, H.; Rawal, M.; Hahm, E. R.; Singh, S. V. Benzo[a]pyrene-7,8-diol-9,10-epoxide causes caspase-mediated apoptosis in H460 human lung cancer cell line. *Cell Cycle* **2007**, *6*, 2826−2834.
(28) Chan, C. Y.; Mong, M. C.; Liu, W. H.; Huang, C. Y.; Yin, M. C. Three pentacyclic triterpenes protect H9c2 cardiomyoblast cells against high-glucose-induced injury. *Free Radical Res.* **2014**, *48*, 402−411.
(29) Kao, T. C.; Wu, C. H.; Yen, G. C. Glycyrrhizic acid and 18β-glycyrrhetinic acid recover glucocorticoid resistance via PI3K-induced AP1, CRE and NFAT activation. *Phytomedicine* **2013**, *20*, 295−302.
(30) Wang, X.; Liu, R.; Zhang, W.; Zhang, X.; Liao, N.; Wang, Z.; Li, W.; Qin, X.; Hai, C. Oleanolic acid improves hepatic insulin resistance via antioxidant, hypolipidemic and anti-inflammatory effects. *Mol. Cell. Endocrinol.* **2013**, *376*, 70−80.
(31) Griffith, B.; Pendyala, S.; Hecker, L.; Lee, P. J.; Natarajan, V.; Thannickal, V. J. NOX enzymes and pulmonary disease. *Antioxid. Redox Signaling* **2009**, *11*, 2505−2516.
(32) Dergham, M.; Lepers, C.; Verdin, A.; Billet, S.; Cazier, F.; Courcot, D.; Shirali, P. Garçon, G. Prooxidant and proinflammatory potency of air pollution particulate matter ($PM_{2.5\text{-}0.3}$) produced in rural, urban, or industrial surroundings in human bronchial epithelial cells (BEAS-2B). *Chem. Res. Toxicol.* **2012**, *25*, 904−919.
(33) Yao, H.; Yang, S. R.; Kode, A.; Rajendrasozhan, S.; Caito, S.; Adenuga, D.; Henry, R.; Edirisinghe, I.; Rahman, I. Redox regulation of lung inflammation: role of NADPH oxidase and NF-kappaB signalling. *Biochem. Soc. Trans.* **2007**, *35*, 1151−1155.
(34) Park, W. H. Effects of antioxidants and MAPK inhibitors on cell death and reactive oxygen species levels in H2O2-treated human pulmonary fibroblasts. *Oncol. Lett.* **2013**, *5*, 1633−1638.
(35) Huang, R. Y.; Chen, G. G. Cigarette smoking, cyclooxygenase-2 pathway and cancer. *Biochim. Biophys. Acta* **2011**, *1815*, 158−169.
(36) Caligiani, A.; Malavasi, G.; Palla, G.; Marseglia, A.; Tognolini, M.; Bruni, R. A simple GC-MS method for the screening of betulinic, corosolic, maslinic, oleanolic and ursolic acid contents in commercial botanicals used as food supplement ingredients. *Food Chem.* **2013**, *136*, 735−741.

DOI: 10.1021/acs.jafc.5b00102
J. Agric. Food Chem. 2015, 63, 3196−3204

Table 1. Experimental Design for the Extraction of Anthocyanin from Corn DDGS[a]

	independent variables						dependent (Y)		
	coded			actual			anthocyanin concentration (μg C3G/g DDGS)		
trt	x_1	x_2	x_3	x_1	x_2	x_3	C-PC	GC-PC	GC-DC
1	−1	−1	−1	0	30	4	174.3 ± 6.4h	385.2 ± 34.0ghi	534.4 ± 63.0jkl
2	−1	−1	0	0	30	22	185.4 ± 12.8gh	577.2 ± 76.9abcdefg	859.2 ± 33.9fg
3	−1	−1	+1	0	30	40	196.7 ± 28.0fgh	422.2 ± 22.2efghi	702.2 ± 12.8ghij
4	−1	0	−1	0	40	4	202.5 ± 8.6efgh	330.1 ± 34.2i	740.7 ± 51.3fghi
5	−1	0	0	0	40	22	201.3 ± 22.5efgh	312.9 ± 17.0i	580.9 ± 8.5jkl
6	−1	0	+1	0	40	40	237.1 ± 25.7bcdefgh	325.9 ± 0.0i	900.5 ± 17.1ef
7	−1	+1	−1	0	50	4	203.9 ± 18.5efgh	317.8 ± 92.3i	1038.0 ± 52.4de
8	−1	+1	0	0	50	22	252.6 ± 10.7abcdefg	444.6 ± 18.5defghi	850.3 ± 73.9fg
9	−1	+1	+1	0	50	40	216.5 ± 10.7defgh	530.8 ± 93.2bcdefgh	898.5 ± 76.9ef
10	0	−1	−1	12.5	30	4	226.4 ± 25.7bcdefgh	361.4 ± 89.4hi	1086.6 ± 58.7cd
11	0	−1	0	12.5	30	22	207.4 ± 25.7defgh	460.0 ± 46.3defghi	1096.2 ± 25.7cd
12	0	−1	+1	12.5	30	40	185.2 ± 23.1gh	481.3 ± 89.8cdefghi	1079.3 ± 12.8cd
13	0	0	−1	12.5	40	4	207.8 ± 0.0defgh	424.6 ± 17.1efghi	1105.7 ± 45.2cd
14	0	0	0	12.5	40	22	**321.0 ± 37.3a**	662.9 ± 120.0abc	1326.0 ± 95.4b
15	0	0	+1	12.5	40	40	197.5 ± 22.6fgh	404.8 ± 34.2fghi	**1573.4 ± 84.0a**
16	0	+1	−1	12.5	50	4	222.2 ± 32.1cdefgh	394.2 ± 21.3ghi	1248.1 ± 77.2bc
17	0	+1	0	12.5	50	22	259.2 ± 18.5abcdef	667.8 ± 64.3abc	1355.5 ± 56.5b
18	0	+1	+1	12.5	50	40	296.3 ± 18.5ab	580.1 ± 77.1abcdefg	1378.5 ± 56.4b
19	+1	−1	−1	25	30	4	222.2 ± 19.2cdefgh	593.7 ± 46.4abcdef	686.5 ± 12.9ghijk
20	+1	−1	0	25	30	22	259.2 ± 6.4abcdef	**741.4 ± 12.8a**	742.2 ± 34.0fghi
21	+1	−1	+1	25	30	40	270.9 ± 46.3abcde	534.4 ± 66.8cdefgh	668.0 ± 73.0hijk
22	+1	0	−1	25	40	4	236.4 ± 0.0bcdefgh	687.6 ± 22.7ab	470.0 ± 87.0l
23	+1	0	0	25	40	22	227.3 ± 22.6bcdefgh	606.2 ± 76.8abcde	509.6 ± 17.1kl
24	+1	0	+1	25	40	40	275.9 ± 30.8abcd	541.9 ± 45.1bcdefgh	841.1 ± 37.4fgh
25	+1	+1	−1	25	50	4	296.9 ± 0.0ab	596.6 ± 91.9abcdef	791.7 ± 46.7fgh
26	+1	+1	0	25	50	22	296.4 ± 32.1ab	637.5 ± 39.2abcd	525.7 ± 38.6jkl
27	+1	+1	+1	25	50	40	290.7 ± 28.3abc	714.3 ± 56.5ab	853.5 ± 66.9fg

[a]Extraction was performed using different ethanol concentrations ranging from 0 to 25%, at 4, 22, and 40 °C and liquid solid ratio of 30:1, 40:1, and 50:1 mL/g DDGS. Anthocyanin concentration was measured using the pH differential method. Optimum anthocyanin concentration recorded at 12.5% ethanol, 40:1 liquid-to-solid ratio, and 22 °C extraction. Means followed by different letters are significantly different from each other. DDGS, dried distillers grains with solubles; C-PC, conventional-purple corn; GC-PC, granular starch hydrolysis-purple corn; GC-DC, granular starch hydrolysis-dark corn.

ingredient, DDGS from colored corn can be used as a starting material for anthocyanin pigment extraction.

To our knowledge, extraction of anthocyanins from DDGS generated by ethanol fermentation from colored corn cultivars has not been previously reported. For this purpose, the use of an effective tool such as response surface methodology (RSM) is valuable in the extraction of bioactive compounds when responses are influenced by many factors and their interactions. RSM is a group of mathematical and statistical techniques used in the development of a functional relationship between a response of interest (also known as dependent variable) and a number of associated control variables (also known as independent or input variables).[19] RSM has been successfully used in the extraction of flavonoids in medicinal plants and mangiferin from mango leaves.[20,21] Therefore, the objectives of this study were to determine optimum parameters for the extraction of anthocyanins from purple and dark corn DDGS and determine the effect of DDGS processing methods and corn cultivars on anthocyanin and polyphenol concentrations and their identification in extracts from DDGS.

MATERIALS AND METHODS

Materials. Proprietary purple (PC) and dark corn (DC) varieties in development were obtained from a private company. Chemicals used for extraction were all ACS grade and purchased from Sigma-Aldrich (St. Louis, MO) and Fisher Scientific (Pittsburgh, PA). All solvents for chromatographic techniques were of high-performance liquid chromatography (HPLC)-grade or better.

Preparation of DDGS. DDGS was prepared using two different processes, conventional (C) and granular starch hydrolysis (GC), as previously reported.[22] Briefly, in the conventional process, cleaned corn samples (50 g, dry basis) were ground in a hammer mill (model MHM4, Glen Mills, Clifton, NJ) at 500 rpm using a 0.5 mm sieve. Ground corn acclimated at room temperature was mixed with deionized water to obtain a mash of 30% dry solids content. The pH was adjusted to 5.7 using 10 N sulfuric acid. Liquefaction was conducted by adding 0.013 mL of α-amylase (Spezyme CL, Dupont Industrial Biosciences, Palo Alto, CA) and agitating the mash for 1.5 h at 85 °C. The slurry was cooled to 32 °C, and pH was adjusted to 4.0. Simultaneous saccharification and fermentation was conducted for 72 h with addition of 0.025 mL of glucoamylase (Distillase SSF, Dupont Industrial Biosciences, Palo Alto, CA), 1 mL of yeast inoculum, and 0.5 mL of 50% urea. For the conventional process, purple corn (C-PC) was used to generate the DDGS. In the GC process, 0.15 mL of granular starch hydrolyzing enzyme (Stargen 001, Dupont Industrial Biosciences, Palo Alto, CA) containing α-amylase from *Aspergillus kawachi* and a glucoamylase from *Aspergillus niger* was added to the mash (30% dry solids content) along with 0.02 mL of protease (GC212, Dupont Industrial Biosciences). For the GC process, both purple (GC-PC) and dark (GC-DC) corns were used to produce DDGS. After fermentation, the mash from both processes was heated at 90 °C for 3 h to evaporate ethanol. DDGS was recovered by drying in a convection oven at 49 °C for 72 h.

DOI: 10.1021/acs.jafc.5b00128
J. Agric. Food Chem. 2015, 63, 3205−3218

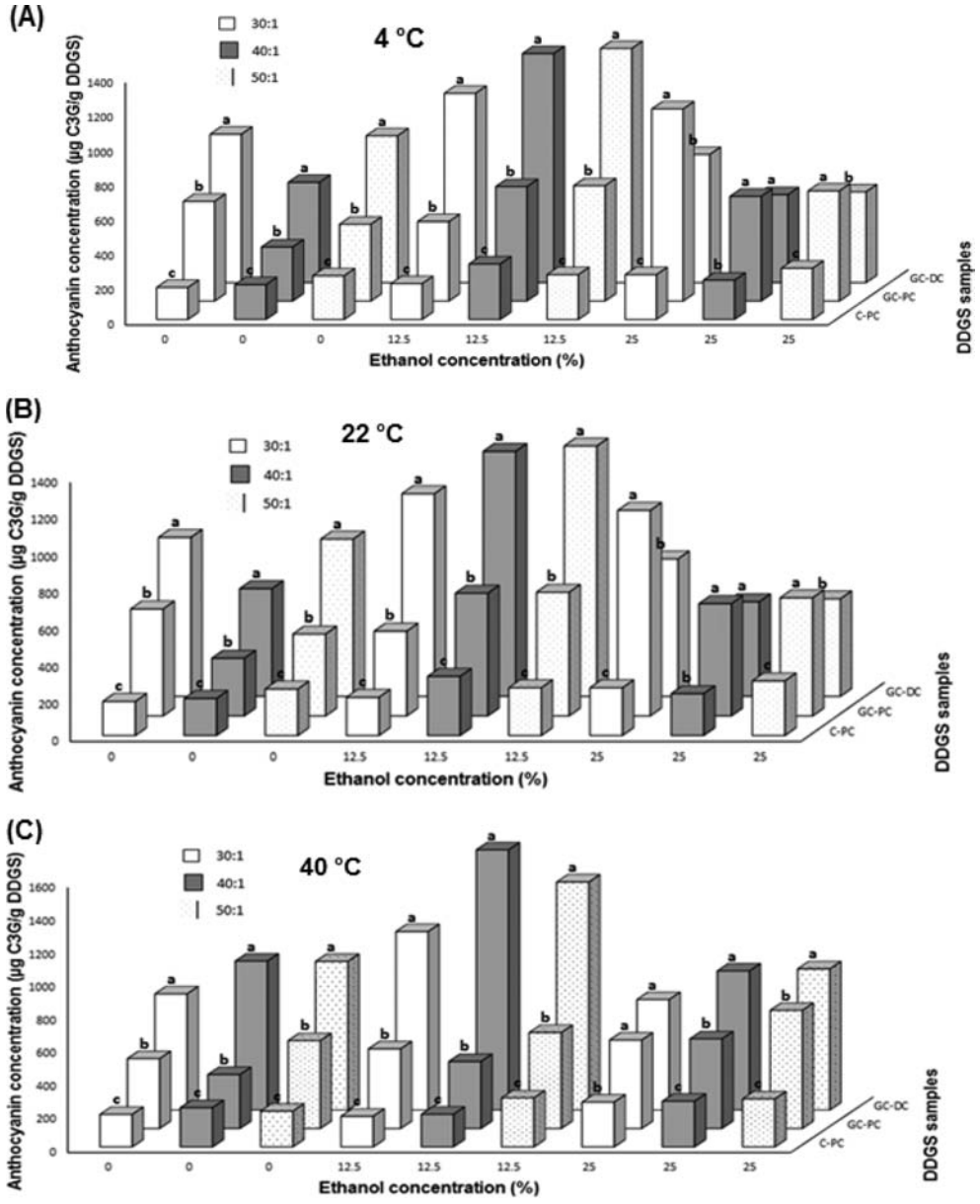

Figure 1. Anthocyanin concentrations of DDGS extracts derived from different corn cultivars and processing methods. In general, dark corn DDGS (GC-DC) had anthocyanin concentration higher than that of purple corn (GC-PC) and DDGS obtained by granular starch hydrolysis process (GC-PC) had anthocyanin concentration higher than that of DDGS obtained by conventional method (C-PC). Bars followed by different letters within the same ethanol concentration and liquid-to-solid ratio were statistically different from each other ($P < 0.05$). (A) 4 °C, (B) 22 °C, and (C) 40 °C extraction ($N = 3$).

Extraction of Anthocyanin from DDGS Samples. Anthocyanins were extracted from DDGS samples using 2% formic acid in water (pH 2.0) with different concentrations of ethanol ranging from 0 to 25%. Extraction was performed by stirring (600 rpm) at room temperature for 2 h, 40 °C for 2 h, and at 4 °C for 24 h. Liquid−solid ratios of 30:1, 40:1 and, 50:1 were used for the extraction of anthocyanin from DDGS. After extraction, the mixture was filtered using Whatman no. 4 filter paper. All extracts were immediately analyzed for total monomeric anthocyanin, total polyphenol, and total flavonoid concentrations.

Measurement of Total Monomeric Anthocyanin Concentration. Total monomeric anthocyanin was determined by a pH differential method as previously reported.[23] Samples were diluted to a factor of 1:20 using two buffers (pH 1.0, 0.25 M KCl buffer and pH 4.5, 0.40 M sodium acetate buffer). Samples of 200 μL of diluted solutions at each pH were transferred to a 96-well plate, and the absorbance was read at 520 and 700 nm using a Synergy 2 multiwell plate reader (Biotek, Winooski, VT). The total monomeric anthocyanin concentration was calculated as cyanidin-3-glucoside (C3G) equivalents per liter as below:

$$\text{total monomeric anthocyanins (mg/L)} = \frac{A \cdot \text{MW} \cdot D \cdot 1000}{\varepsilon \cdot \text{PL} \cdot 0.45}$$

Where $A = (A_{520} - A_{700})$ at $\text{pH}_{1.0} - (A_{520} - A_{700})$ at $\text{pH}_{4.5}$; MW = 449.2 g/mol for C3G; D, dilution factor; PL, constant path length (1 cm); $\varepsilon = 26\,900$ L/(mol cm), which is the molar extinction coefficient for C3G, 1000 conversion factor from grams to milligrams, and 0.45 as the conversion factor from the established method[23] to the plate reader method. Milligrams per liter of extract was then expressed as micrograms of C3G equivalents per gram of DDGS.

Measurement of Total Polyphenol Concentration. Total polyphenol was measured using the Folin−Ciocalteu method adapted to a microassay.[24] Samples were diluted to a factor of 1:10 and 1:20 with deionized water. To a 96-well plate were added 50 μL of diluted samples, standard or blank (deionized water); 50 μL of 1N Folin−Ciocalteu's phenol reagent was added. After 5 min, 100 μL of 20% Na_2CO_3 was added, and the mixture was allowed to stand for another 10 min. The absorbance was read at 690 nm using a Synergy multiwall plate reader

DOI: 10.1021/acs.jafc.5b00128
J. Agric. Food Chem. 2015, 63, 3205−3218

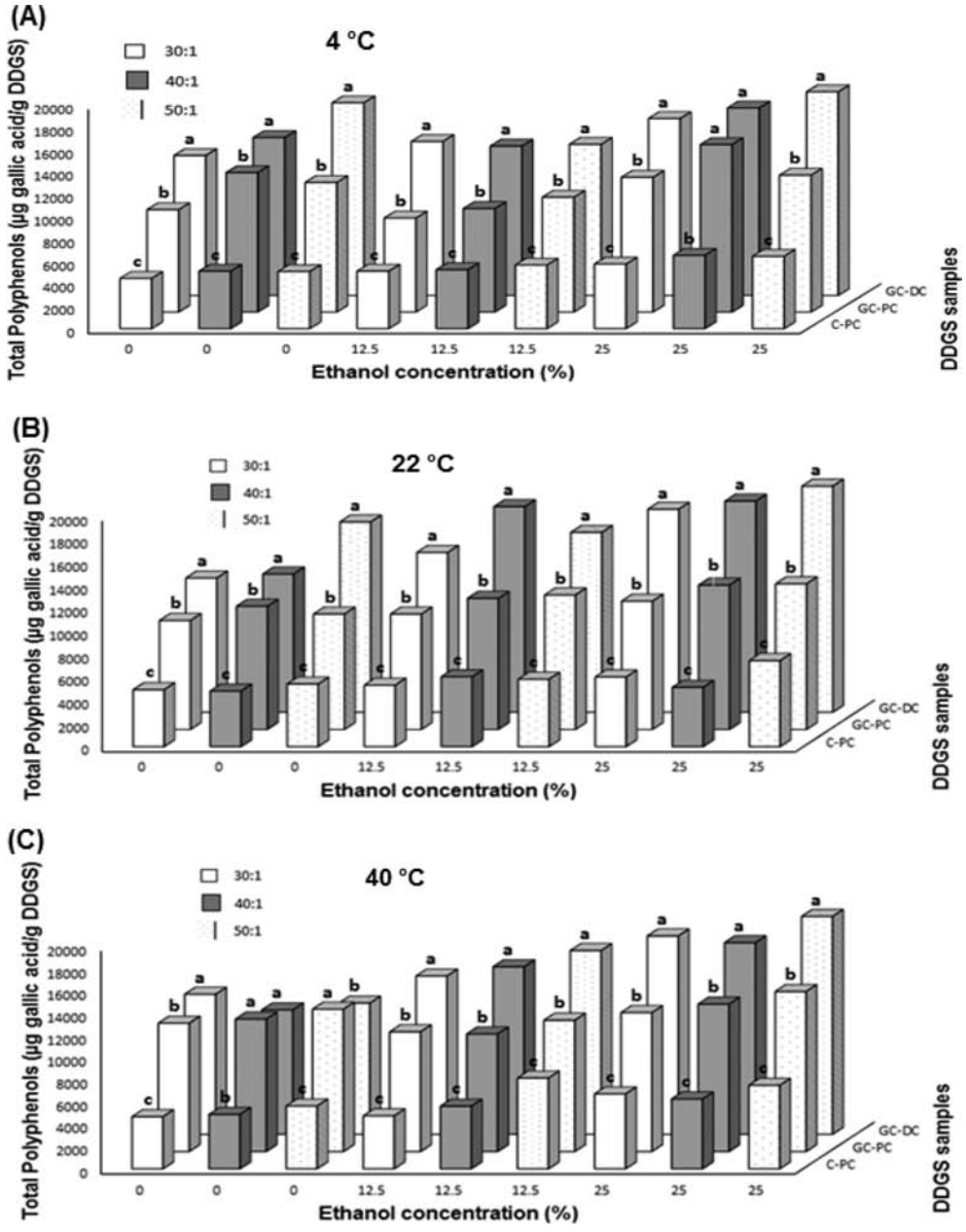

Figure 2. Polyphenol concentrations of DDGS extracts derived from different corn cultivars and processing methods. In general, dark corn DDGS (GC-DC) had polyphenol concentration higher than that of purple corn (GC-PC) and DDGS obtained by granular starch hydrolysis (GC-PC) had polyphenol concentration higher than that of DDGS obtained by conventional method (C-PC). Bars followed by different letters within the same ethanol concentration and liquid-to-solid ratio were statistically different from each other ($P < 0.05$). (A) 4 °C, (B) 22 °C, and (C) 40 °C extraction ($N = 3$).

(Biotek, Winooski, VT), and the results were expressed as micrograms of gallic acid per gram of DDGS.

Measurement of Total Flavonoid Concentration. Total flavonoid concentration was measured using the absorbance at 400 nm method as reported previously.[25] Briefly, 50 μL of diluted samples (1:20), standards, and blank (methanol) were added to a 96-well plate. After which, 180 μL of methanol and 20 μL of 1% aminoethylborinate in methanol were added. After the samples were shaken gently, the absorbance was read at 400 nm using an ELX 808 microplate reader (Biotek, Winooski, VT). Results were expressed as micrograms of rutin per gram of DDGS.

HPLC/MS-MS Analysis. DDGS extract from GC-PC was concentrated 10× by evaporation using a Centrivap Concentrator (Labconco, Kansas City, MO) at 45 °C for 6−8 h. Concentrated samples were analyzed by an HPLC system (Waters, Milford, MA) equipped with a photodiode array detector, MassLynx software, and a C18 3 μ analytical column, 250 mm × 4.6 mm, at 30 °C using previously reported conditions.[26] The mobile phase was a linear gradient of 2% formic acid (v/v) in water and methanol starting at 0% methanol, increasing to 25% methanol in 10 min, and to 50% methanol in 30 min; flow rate was 0.5 mL/min, and the injection volume was 20 μL. Chromatograms were generated at 280, 320, 360, and 520 nm wavelengths. For MS/MS analysis, an electrospray ionization-time-of-flight system (Bruker Daltoniks, Billerica, MA) was used with the following conditions: Survey ion mode, ES mode; polarity, positive; scan range, 50−950 m/z; source temperature, 114 °C; desolvation temperature, 248 °C; cone gas flow, 964 L/h; and desolvation gas flow, 1175 L/h.

Colorimetric Measurements. Color was measured using a Lovibond Tintometer PFX990 (The Tintometer Limited, England) instrument. The instrument was calibrated, and the following parameters were used: L^*, a^*, and b^*; observer/illuminant, 10° and D65 and path length, 1 cm. Briefly, 2−3 mL of extracts acclimated at room

DOI: 10.1021/acs.jafc.5b00128
J. Agric. Food Chem. 2015, 63, 3205−3218

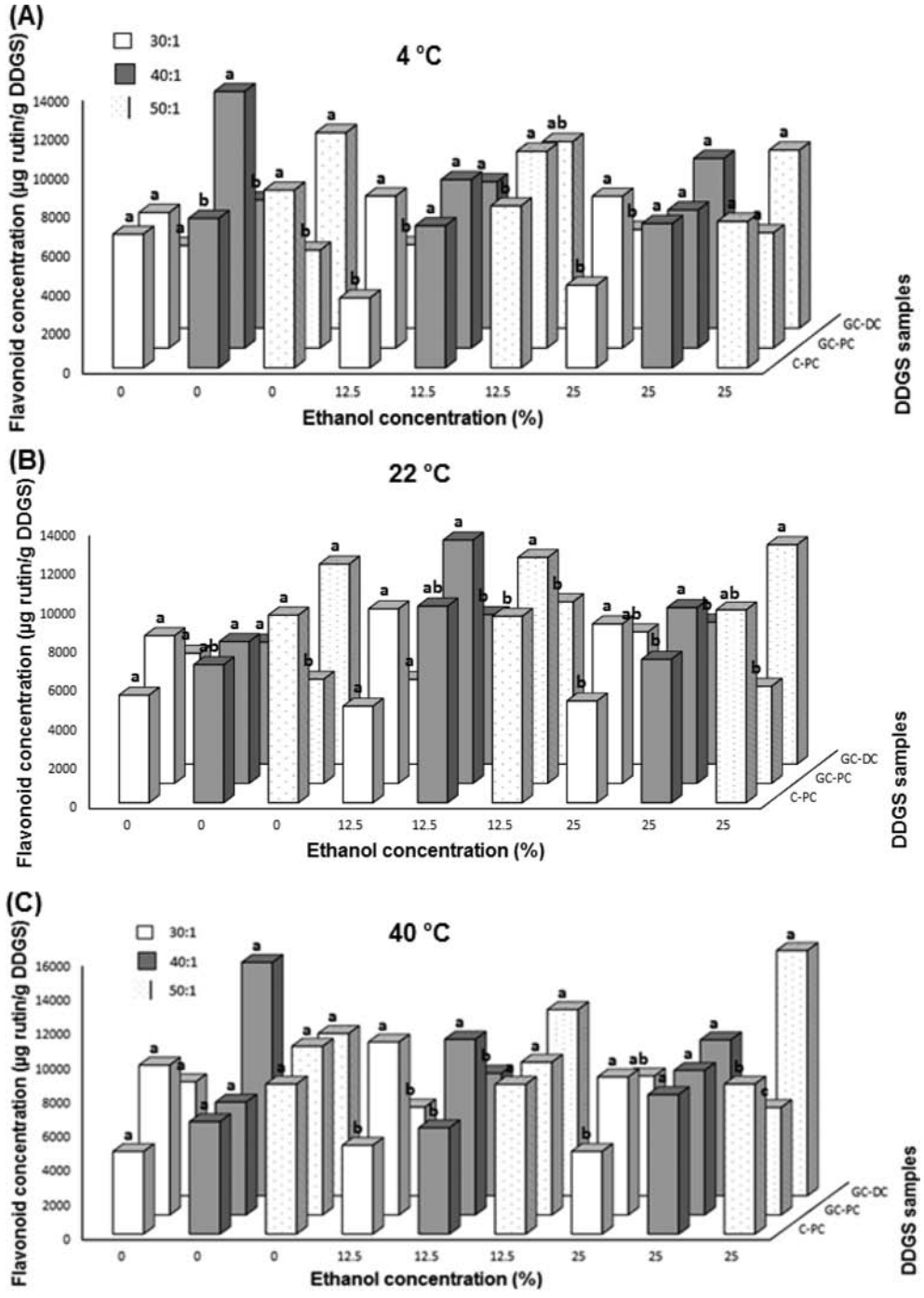

Figure 3. Flavonoid concentrations of DDGS extracts derived from different corn cultivars and processing methods. In general, no effect of corn cultivar and DDGS processing method on flavonoid concentrations of DDGS extracts was detected. Bars followed by different letters within the same ethanol concentration and liquid-to-solid ratio were statistically different from each other ($P < 0.05$). (A) 4 °C, (B) 22 °C, and (C) 40 °C extraction ($N = 3$).

temperature was placed in a disposable ultraviolet−visible cuvette, and the color parameters L^*, a^*, and b^* were measured and recorded. Color squares were generated by converting L^*, a^*, and b^* values to R, G, and B values using http://colormine.org/convert/rgb-to-lab and Microsoft Power Point Software.[26]

Response Surface Methodology. RSM was used to optimize the extraction of anthocyanin from DDGS using functional relationships between the dependent variable and the independent variables as previously reported.[19] Ethanol concentration (x_1), liquid-to-solid ratio (x_2), and extraction temperature (x_3) were chosen for independent variables. The range and center point values with actual and coded values of variables used for the optimization of anthocyanin extraction from purple corn DDGS were for coded levels −1, 0, +1, for ethanol concentration (x_1, %), 0, 12.5, and 25; for liquid-to-solid ratio (x_2, mL/g), 30:1, 40:1 and 50:1; and for extraction temperature (x_3, °C), 4, 22 and 40.

Anthocyanin concentration and a^*-value (measure of redness) were selected as the responses for the combination of the independent variables, as presented in Table 1. The variables were coded according to the following equation:

$$x = (x_i - x_0)/\Delta x$$

where x is the coded value, x_i the corresponding actual value, x_0 the actual value at the center of the domain, and Δx the increment of x_i

DOI: 10.1021/acs.jafc.5b00128
J. Agric. Food Chem. 2015, 63, 3205−3218

Table 2. Tristimulus Color Parameters of DDGS Extracts from Corn Cultivars Produced by Different Methods

	C-PC			GC-PC			GC-DC		
trt[a]	*L**	*a**	*b**	*L**	*a**	*b**	*L**	*a**	*b**
1	67.2 ± 1.3defgh	23.7 ± 0.4ghij	19.3 ± 0.2ef	57.0 ± 1.1efgh	32.6 ± 0.5ghi	32.6 ± 0.3bcd	48.3 ± 1.1abcd	45.5 ± 0.9ef	29.9 ± 0.4defg
2	63.0 ± 1.5fghi	25.4 ± 0.5defghi	24.7 ± 0.4b	67.9 ± 0.9abcde	42.5 ± 0.5cdef	22.2 ± 0.1cdefg	66.7 ± 1.0a	32.8 ± 0.4g	16.0 ± 0.0lm
3	31.4 ± 0.3k	18.0 ± 0.2j	20.1 ± 0.2e	36.3 ± 14.0j	25.4 ± 7.3ijk	17.5 ± 5.3ghijk	51.9 ± 1.9abcd	29.8 ± 0.8g	17.6 ± 0.4l
4	57.0 ± 2.4ij	18.9 ± 0.6j	17.9 ± 0.4g	65.4 ± 2.9bcdef	24.0 ± 1.4jk	17.7 ± 0.4fghijk	40.7 ± 3.9d	30.8 ± 2.5g	24.3 ± 2.1jk
5	72.1 ± 0.1abcde	21.4 ± 0.0hij	16.2 ± 0.0i	60.1 ± 2.1cdefgh	9.1 ± 0.4l	18.5 ± 0.7defghijk	56.1 ± 2.5abc	28.9 ± 2.7g	21.7 ± 2.0k
6	69.5 ± 0.6bcdefg	22.4 ± 0.1fghij	17.8 ± 0.1gh	38.8 ± 5.1ij	18.7 ± 2.1k	15.0 ± 0.1ijkl	65.9 ± 1.4ab	11.3 ± 0.3h	14.3 ± 0.6mn
7	68.7 ± 0.1cdefgh	18.0 ± 0.0j	19.5 ± 0.1ef	62.6 ± 0.0cdefg	26.2 ± 0.0jik	15.3 ± 0.0hijkl	56.6 ± 0.6abc	45.9 ± 0.4e	26.6 ± 0.1hij
8	71.0 ± 5.6abcde	18.1 ± 1.3j	13.4 ± 0.6k	72.8 ± 0.1abc	30.9 ± 2.2hij	16.1 ± 1.1hijkl	66.1 ± 0.9ab	41.3 ± 0.6f	23.6 ± 0.3jk
9	76.6 ± 0.3ab	20.0 ± 0.1ij	13.0 ± 0.0k	59.2 ± 5.9cdefgh	25.8 ± 4.5jik	19.9 ± 3.3defghi	72.8 ± 0.8abc	9.8 ± 0.1h	11.9 ± 0.2n
10	71.9 ± 0.0abcde	27.9 ± 0.0bcdefg	16.5 ± 0.0i	70.6 ± 1.5abcde	42.1 ± 0.7cdef	18.2 ± 0.3efghijk	51.7 ± 0.2abcd	54.9 ± 0.1b	32.4 ± 0.0cde
11	61.3 ± 0.8hi	27.6 ± 0.3bcdefgh	22.6 ± 0.2c	50.8 ± 0.2ghi	51.7 ± 0.3ab	28.5 ± 0.1ab	47.6 ± 0.7abcd	54.4 ± 0.7b	35.0 ± 0.4bc
12	66.1 ± 0.3efgh	7.0 ± 0.1bcdefgh	20.1 ± 0.0e	50.7 ± 0.9ghi	42.7 ± 0.5cdef	29.2 ± 0.1a	40.9 ± 1.1cd	49.7 ± 0.9cde	34.4 ± 0.4bc
13	74.4 ± 0.1abcd	22.8 ± 0.0efghij	14.8 ± 0.0j	75.9 ± 0.9ab	38.5 ± 0.1efgh	14.2 ± 0.0jklm	52.8 ± 0.3abcd	52.3 ± 0.2bc	30.2 ± 0.0defg
14	61.4 ± 0.4hi	23.8 ± 0.1efghij	21.7 ± 0.1d	65.7 ± 0.1bcdef	42.2 ± 0.2cdef	21.8 ± 0.1defg	46.6 ± 0.9bcd	51.5 ± 1.0bc	31.2 ± 0.6de
15	64.8 ± 0.1efghi	23.4 ± 0.0efghij	21.1 ± 0.0d	68.4 ± 1.8abcde	42.7 ± 0.7cdef	19.8 ± 0.6defghi	43.6 ± 0.6cd	48.7 ± 0.3cde	31.3 ± 0.0de
16	74.4 ± 1.3abcd	19.7 ± 0.3ij	13.5 ± 0.0k	80.1 ± 0.6a	35.6 ± 0.2fgh	11.8 ± 0.1l	55.5 ± 3.2abc	50.5 ± 2.7bcd	24.7 ± 1.5ij
17	70.5 ± 0.1bcdef	22.1 ± 0.0fghij	17.5 ± 0.0gh	73.2 ± 0.4abc	40.0 ± 0.2efg	16.5 ± 0.1hijkl	49.2 ± 1.1abcd	49.5 ± 0.8cde	28.2 ± 0.5fgh
18	51.5 ± 0.1j	25.2 ± 0.0cdefghi	26.7 ± 0.0a	59.6 ± 2.0cdefgh	35.7 ± 0.9fgh	19.2 ± 0.6defghij	50.5 ± 0.7abcd	50.6 ± 0.6bcd	27.4 ± 0.2ghi
19	71.7 ± 0.2abcde	36.8 ± 0.2ab	15.0 ± 0.0j	61.1 ± 1.0cdefgh	52.1 ± 0.6a	23.0 ± 0.1cdef	46.1 ± 0.6cd	59.6 ± 0.5a	35.9 ± 0.2b
20	62.0 ± 0.0ghi	35.0 ± 1.5a	21.6 ± 0.0d	52.6 ± 0.0ghij	40.4 ± 0.2defg	27.3 ± 0.1abc	44.3. ± 0.4cd	60.2 ± 0.5a	40.5 ± 0.3a
21	49.5 ± 0.3j	33.3 ± 0.1ab	25.9 ± 0.0a	48.3 ± 1.7hij	46.6 ± 1.1abcde	27.3 ± 0.0abc	34.0 ± 0.5d	49.2 ± 0.5cde	34.7 ± 0.3bc
22	76.5 ± 0.2abc	31.6 ± 0.1abc	10.6 ± 0.1l	64.1 ± 0.3bcdefg	49.7 ± 0.2abc	20.3 ± 0.0defgh	51.8 ± 1.3bcd	52.0 ± 1.0bc	32.6 ± 0.3cd
23	68.3 ± 0.2defgh	30.7 ± 0.1abcd	16.6 ± 0.1i	64.8 ± 0.0bcdefg	49.5 ± 0.0abc	20.1 ± 0.0defghi	44.5 ± 0.1cd	46.8 ± 0.1de	29.4 ± 0.1efgh
24	65.4 ± 0.1efgh	28.9 ± 0.0abcde	19.0 ± 0.0f	58.0 ± 0.7defgh	48.3 ± 0.3abcd	23.2 ± 0.4cde	54.1 ± 0.0abc	60.2 ± 0.1a	28.1 ± 0.0fgh
25	78.8 ± 0.1a	27.3 ± 0.0bcdefgh	8.7 ± 0.1m	71.3 ± 0.5abcd	45.3 ± 0.3abcde	13.6 ± 0.1kl	54.0 ± 0.0abc	60.0 ± 0.0a	28.0 ± 0.0fgh
26	52.1 ± 2.3j	23.2 ± 0.7efghij	17.0 ± 0.5hi	65.4 ± 6.3bcdef	44.2 ± 3.0bcde	17.7 ± 1.5ghijk	48.9 ± 0.0cd	52.0 ± 0.1bc	30.5 ± 0.2def
27	67.2 ± 0.0ghi	28.4 ± 0.0bcdef	16.5 ± 0.0i	63.1 ± 0.5bcdefg	44.3 ± 0.2abcde	19.0 ± 0.2defghij	48.4 ± 2.9abcd	45.6 ± 2.2ef	26.6 ± 1.3hij

[a]The conditions for each treatment are presented in Table 1.

DOI: 10.1021/acs.jafc.5b00128
J. Agric. Food Chem. 2015, 63, 3205−3218

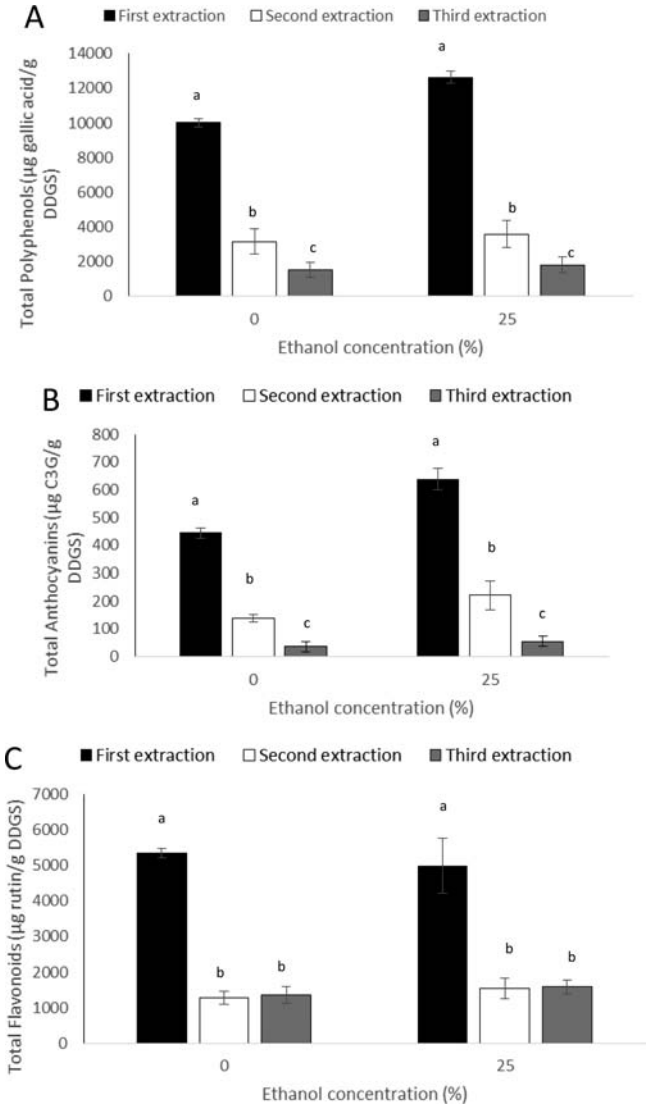

Figure 4. Effect of multiple extractions on total polyphenols (A), total anthocyanins (B), and total flavonoids (C) of purple corn DDGS extracts using 2% formic acid acidified 0% ethanol and 25% ethanol. Bars with different letters within ethanol concentration were significantly different from each other ($N = 3$).

corresponding to a variation of 1 unit of x. The polynomial second degree equation is described by the following equation:

$$y = b_0 + \sum_{i=1}^{3} b_i x_i + \sum_{i=1}^{3} b_{ii} x_i^2 + \sum_{i=1}^{2} \sum_{j=i+1}^{3} b_{ij} x_i x_j$$

Statistical Analysis. All analyses were done in 2−3 independent replicates. The data obtained were analyzed using one-way ANOVA to compare experimental to control values using SAS version 9.4 (Cary, NC); statistical differences among independent variables were determined using the Proc GLM procedure and Tukey posthoc test ($P < 0.05$). RSM analysis was performed using the Proc Rsreg procedure. Correlation among parameters measured was performed using the GraphPad Prism software (Version 5.02; GraphPad Software, Inc.; San Diego, CA).

RESULTS

Total Anthocyanin Concentrations of Corn DDGS Extracts. Figure 1 shows the concentrations of total monomeric anthocyanin in corn DDGS extracts. In the C-PC samples, anthocyanin concentration ranged from 174.3 μg C3G equivalents/g DDGS (for 0% ethanol extract, 30:1 liquid-to-solid ratio, 4 °C) to 321.0 μg C3G equivalents/g DDGS (for 12.5% ethanol extract, 40:1 liquid-to-solid ratio, and 22 °C extraction conditions). In the GC-PC samples, the highest anthocyanin concentration of 714.3 μg C3G equivalent/g DDGS was observed when extracted with 25% ethanol extract, 50:1 liquid-to-solid ratio, and 40 °C. The lowest anthocyanin concentration of 312.9 μg C3G equivalent/g DDGS was attained at 0% ethanol, 40:1 liquid-to-solid ratio, and 4 °C. In the GC-DC samples, the total anthocyanin concentration ranged from 509.6 μg C3G equivalent/g DDGS (25% ethanol, 40:1 liquid-to-solid ratio, and 22 °C) to 1573.4 μg C3G equivalent/g DDGS (12.5% ethanol, 40:1 liquid-to-solid ratio, and 40 °C). As shown in Figure 1, considering the effect of corn cultivar (GC-PC vs GC-DC), dark corn DDGS gave anthocyanin concentrations higher than that of purple corn DDGS. On the other hand, the GC process of obtaining DDGS from corn showed total anthocyanin concentrations higher than that of the conventional method of DDGS production (C-PC vs GC-PC).

Table 3. Identification of Anthocyanins and Condensed Forms in 2% Formic Acid Water Extract of DDGS from Purple Corn Cultivars Obtained by Granular Starch Hydrolysis Processing Method

	GC-PC			
peak	Rt (min)	M^+	MS/MS fragments	possible identity[a]
1	17.87	823	605, 274, 214	catechin-(4,8)-cyanidin-3-malonylglucoside
2	18.42	899	575, 737, 423, 329, 287	catechin-(4,8)-cyanidin-3,5-diglucoside
3	21.42	317	229	isorhamnetin (presumed)
4	28.03	449	287, 288	cyanidin-3-glucoside
5	31.42	433	271	pelargonidin-3-glucoside
6	34.12	463	301	peonidin-3-glucoside
7	35.13	535	287, 288	cyanidin-3-(6″-malonyl) glucoside
8	38.35	549	301	peonidin-3-(6″-malonyl) glucoside
9	41.12	641	449	cyanidin-disuccinylglucoside (presumed)

[a]Identification of the major peaks was done using the database service massbank.jp.

Total Polyphenol Concentrations of Corn DDGS Extracts. The total polyphenol concentrations of different DDGS extracts are shown in Figure 2. In C-PC samples, the highest polyphenol concentration (8154.1 μg gallic acid equivalent/g DDGS) was obtained at extraction conditions of 25% ethanol, 50:1 liquid-to solid ratio, and 40 °C, while the lowest polyphenol concentrations (4489.6 μg gallic acid equivalent/g DDGS) was attained at 0% ethanol, 30:1 liquid-to-solid ratio, and 4 °C extraction conditions. The total polyphenol concentrations for GC-PC samples ranged from 8405.3 to 14975.7 μg gallic acid equivalent/g DDGS for extraction conditions of 12.5% ethanol, 30:1 liquid-to-solid ratio, 4 °C, and 25% ethanol, 40:1 liquid-to-solid ratio, and 4 °C, respectively. GC-DC sample had a total polyphenol concentration from 11178.8 μg gallic acid equivalent/g DDGS (0 ethanol, 40:1 liquid-to-solid ratio, and 40 °C) to 19603.7 μg gallic acid equivalent/g DDGS (25% ethanol, 50:1 liquid-to-solid ratio, and 40 °C). As can be observed in Figure 2, polyphenol concentrations were higher in DDGS extracts obtained from dark corn cultivar than from purple corn cultivar (GC-DC vs GC-PC) while DDGS obtained by GC process had

DOI: 10.1021/acs.jafc.5b00128
J. Agric. Food Chem. 2015, 63, 3205−3218

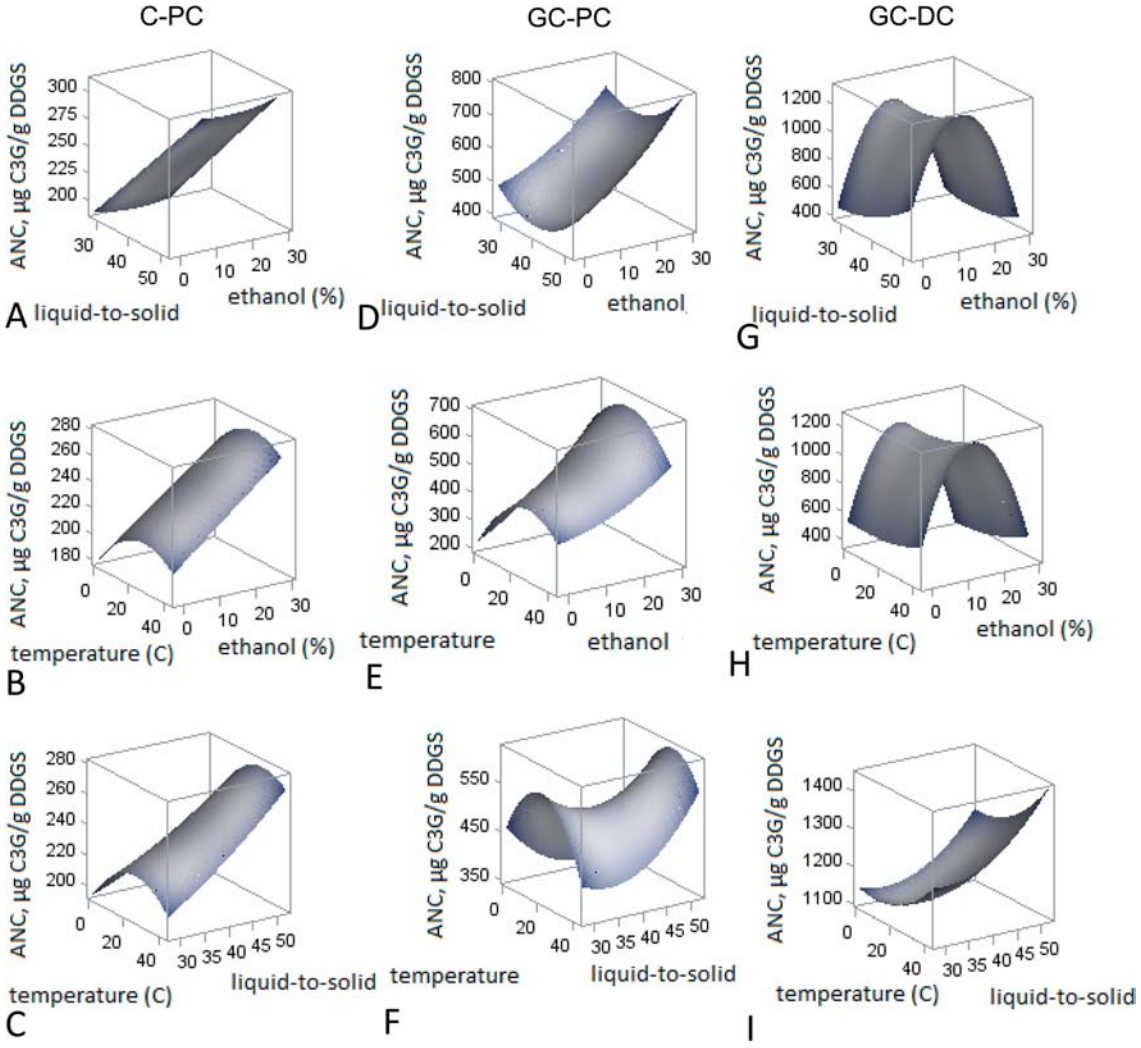

Figure 5. Response surface methodology for the extraction of anthocyanin of DDGS obtained from different cultivars of corn and different processing methods of DDGS as affected by ethanol concentration, liquid-to-solid ratio, and extraction temperature.

polyphenol concentration higher than that of DDGS obtained by the conventional method (GC-PC vs C-PC).

Total Flavonoid Concentrations of Corn DDGS Extracts. The total flavonoid concentrations from DDGS extracts are presented in Figure 3. The highest flavonoid concentrations for C-PC, GC-PC, and GC-DC samples were 10098.7, 13158.8, and 14348.0 μg rutin/g DDGS, respectively. These concentrations were obtained at extraction conditions of 12.5% ethanol, 40:1 liquid-to-solid ratio, and 22 °C for C-PC; 0% ethanol, 40:1 liquid-to-solid ratio, and 4 °C for GC-PC; and 25% ethanol, 50:1 liquid-to-solid ratio, and 40 °C for GC-DC. Unlike total anthocyanin and total polyphenol concentrations, there was no distinct effect of corn cultivar and DDGS processing method on total flavonoid concentrations of DDGS samples.

Effect of Multiple Extractions on Total Anthocyanin, Total Polyphenol, and Total Flavonoid Concentrations of DDGS Extracts from GC-PC. Panels A, B, and C of Figure 4 show the total polyphenol, total anthocyanins, and total flavonoid concentrations, respectively, after a three-step sequential extraction using 2% formic acid acidified 0% ethanol and 25% ethanol extracting solvents. All first extracts generated statistically higher concentrations of anthocyanin, polyphenols, and flavonoids as compared to those of the second and third extracts. In addition, the first extract accounted for 63.6, 63.8, and 66.9% of the cumulated polyphenols, anthocyanins, and flavonoid concentrations for 0% ethanol extracts, respectively. For 25% ethanol extracts, the first extract accounted for 70.1, 69.7, and 61.4% of the cumulated polyphenols, anthocyanins, and flavonoid concentrations, respectively.

Optimization of Anthocyanin Concentration and *a-Value of DDGS Extracts.** The concentration of anthocyanins and *a*-value from DDGS extracts were further optimized using the RSM approach. The coded and actual values of the three variables, namely, ethanol concentration, liquid-to-solid ratio, and extraction temperature, were selected to optimize the yield. In Table 1, the treatments together with coded and actual values are presented. The actual anthocyanin concentration for DDGS samples was recorded in the dependent yield variable as measured in the procedures described in Materials and Methods. A total of 27 treatments were recorded and used to model the equation using the RSM method. Multiple regression analysis of anthocyanin concentration from C-PC sample showed that the test variables were related to anthocyanin concentration by the following second-degree polynomial equation:

$$Y = 162 + 1.75x_1 - 0.54x_2 + 1.51x_3 + 0.01x_1x_2 + 0.005x_1x_3 + 0.02x_2x_3 + 0.0001{x_1}^2 + 0.03{x_2}^2 - 0.04{x_3}^2$$

DOI: 10.1021/acs.jafc.5b00128
J. Agric. Food Chem. 2015, 63, 3205−3218

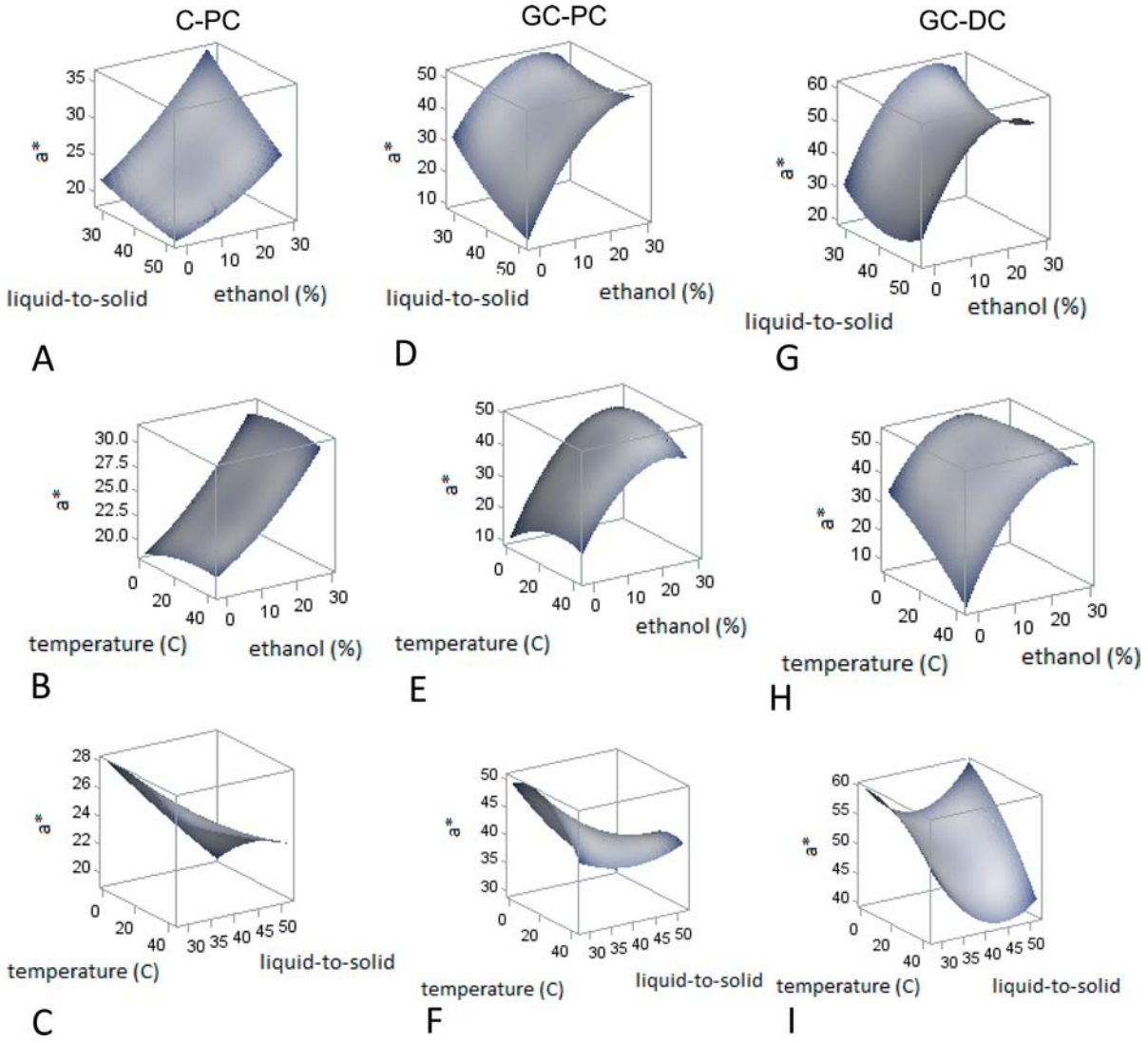

Figure 6. Response surface methodology for a^* color parameter from DDGS extracts from different cultivars of corn and different processing methods of DDGS as affected by ethanol concentration, liquid-to-solid ratio, and extraction temperature.

When multiple regression analysis was applied, anthocyanin concentration and the test variables were related by the following second-degree polynomial equation for GC-PC:

$$Y = 1175 + 2.14x_1 - 43.17x_2 + 7.72x_3 + 0.14x_1x_2 - 0.12x_1x_3 + 0.19x_2x_3 + 0.16{x_1}^2 + 0.49{x_2}^2 - 0.28{x_3}^2$$

For GC-DC, anthocyanin concentration was related by the following second-degree polynomial equation:

$$Y = 1046 + 83.77x_1 - 25.03x_2 - 4.30x_3 - 0.27x_1x_2 + 0.06x_1x_3 + 0.06x_2x_3 - 3.14{x_1}^2 + 0.43{x_2}^2 - 0.10{x_3}^2$$

In the preceding equations, Y pertains to anthocyanin concentration, x_1 to ethanol concentration, and x_2 to liquid-to-solid ratio; x_3 is the extraction temperature. The total model was highly significant ($P < 0.0001$) for all 3 DDGS samples. For the C-PC sample, ethanol concentration and liquid-to-solid ratio were highly significant with P-values of <0.0001 and 0.0002, respectively. All test variables were significant for the GC-PC sample, indicating that ethanol concentration ($P < 0.0001$), liquid-to-solid ratio ($P < 0.0089$), and temperature of extraction ($P < 0.0001$) affected anthocyanin concentrations of GC-PC extracts. On the other hand, only ethanol concentration and liquid-to-solid ratio affected anthocyanin concentrations of GC-DC extracts with P-values of <0.0001 and 0.0041, respectively. Figure 5 shows the three-dimensional response surface plots. As shown in Figure 5, an increase in ethanol concentration (x_1) led to an increase in the concentration of anthocyanin extracted for C-PC (Figure 5A,B) and GC-PC (Figure 5D,E) samples. On the other hand, an initial increase in ethanol concentration to 12.5% led to a peak anthocyanin concentration for the GC-DC sample, and a reduction of anthocyanin concentration was observed with an additional increase in ethanol concentration (Figure 5G,H). In the case of liquid-to-solid ratio (x_2) and extraction temperature (x_3), there was an initial increase in anthocyanin concentration which then decreased with an increase in liquid-to-solid ratio and extraction temperature (Figure 5C,F,I). The optimal conditions when fixed as given by the SAS Rsreg procedure were 12.5% ethanol, 40:1 liquid-to-solid ratio, and 22 °C for C-PC; 12.3% ethanol, 39.9:1 liquid-to-solid ratio, and 22 °C for GC-PC; and 12.5% ethanol, 40:1 liquid-to-solid ratio, and 22 °C for the GC-DC sample.

DOI: 10.1021/acs.jafc.5b00128
J. Agric. Food Chem. 2015, 63, 3205−3218

Trt	x1	x2	x3	CPC	GC-PC	GC-DC
1	0	30	4			
2	0	30	22			
3	0	30	40			
4	0	40	4			
5	0	40	22			
6	0	40	40			
7	0	50	4			
8	0	50	22			
9	0	50	40			
10	12.5	30	4			
11	12.5	30	22			
12	12.5	30	40			
13	12.5	40	4			
14	12.5	40	22			
15	12.5	40	40			
16	12.5	50	4			
17	12.5	50	22			
18	12.5	50	40			
19	25	30	4			
20	25	30	22			
21	25	30	40			
22	25	40	4			
23	25	40	22			
24	25	40	40			
25	25	50	4			
26	25	50	22			
27	25	50	40			

Figure 7. Color squares of DDGS extracts from different corn cultivars obtained by different processing methods. The conditions for each treatment were x_1, ethanol concentration (%); x_2, liquid-to-solid ratio (mL/g); x_3, extraction temperature (°C).

Regarding a^*-value, a measure of the redness of the DDGS extract, multiple regression analysis showed that the a^*-value was related with the test variables for C-PC as follows:

$$Y = 32 + 0.62x_1 - 0.37x_2 - 0.11x_3 - 0.01x_1x_2 - 0.001x_1x_3 + 0.01x_2x_3 + 0.01{x_1}^2 + 0.001{x_2}^2 - 0.001{x_3}^2$$

For GC-PC, the relationship was as follows:

$$Y = 90 + 1.07x_1 - 2.52x_2 - 0.18x_3 + 0.03x_1x_2 - 0.01x_1x_3 + 0.01x_2x_3 - 0.04{x_1}^2 + 0.02{x_2}^2 - 0.01{x_3}^2$$

Finally, for GC-DC, the analysis revealed

$$Y = 105 + 1.93x_1 - 3.34x_2 + 0.02x_3 - 0.0002x_1x_2 - 0.02x_1x_3 - 0.01x_2x_3 - 0.06{x_1}^2 + 0.04{x_2}^2 - 0.005{x_3}^2$$

Figure 6 presents the surface response for a^*-value parameter as affected by ethanol concentration, liquid-to-solid ratio, and temperature of extraction. Ethanol concentration significantly affected a^*-value for 3 DDGS samples, and surface response showed that an increase in ethanol concentration led to an increase in a^*-value of the extract. Liquid-to-solid ratio also significantly affected a^*-value for 3 DDGS, and surface response showed that increase in liquid-to-solid ratio resulted in reduction in a^*-value parameter (Figure 5A,B,D,E,G,H). Temperature of extraction significantly affected a^*-value for GC-PC and GC-DC samples, with an initial increase leading to an increased a^*-value and further decrease leading to a reduction in a^*-value, as shown in the surface response (Figure 6F,I).

Table 2 and Figure 7 show the color measurements and color squares of the extracts, respectively, from 3 DDGS samples with 27 treatments. In general, GC-DC extracts show higher red intensity in the color squares as compared to that of GC-PC and C-PC extracts (Figure 7), which is further validated by higher a^*-value color parameters (Table 2).

HPLC/MS-MS Analysis of Purple Corn Anthocyanin Extracts. Figure 8 presents the HPLC chromatograms at 520 nm, total ion chromatogram, and representative time-of-flight MS/MS ions for the 2% formic acid aqueous extract (0% ethanol)

DOI: 10.1021/acs.jafc.5b00128
J. Agric. Food Chem. 2015, 63, 3205−3218

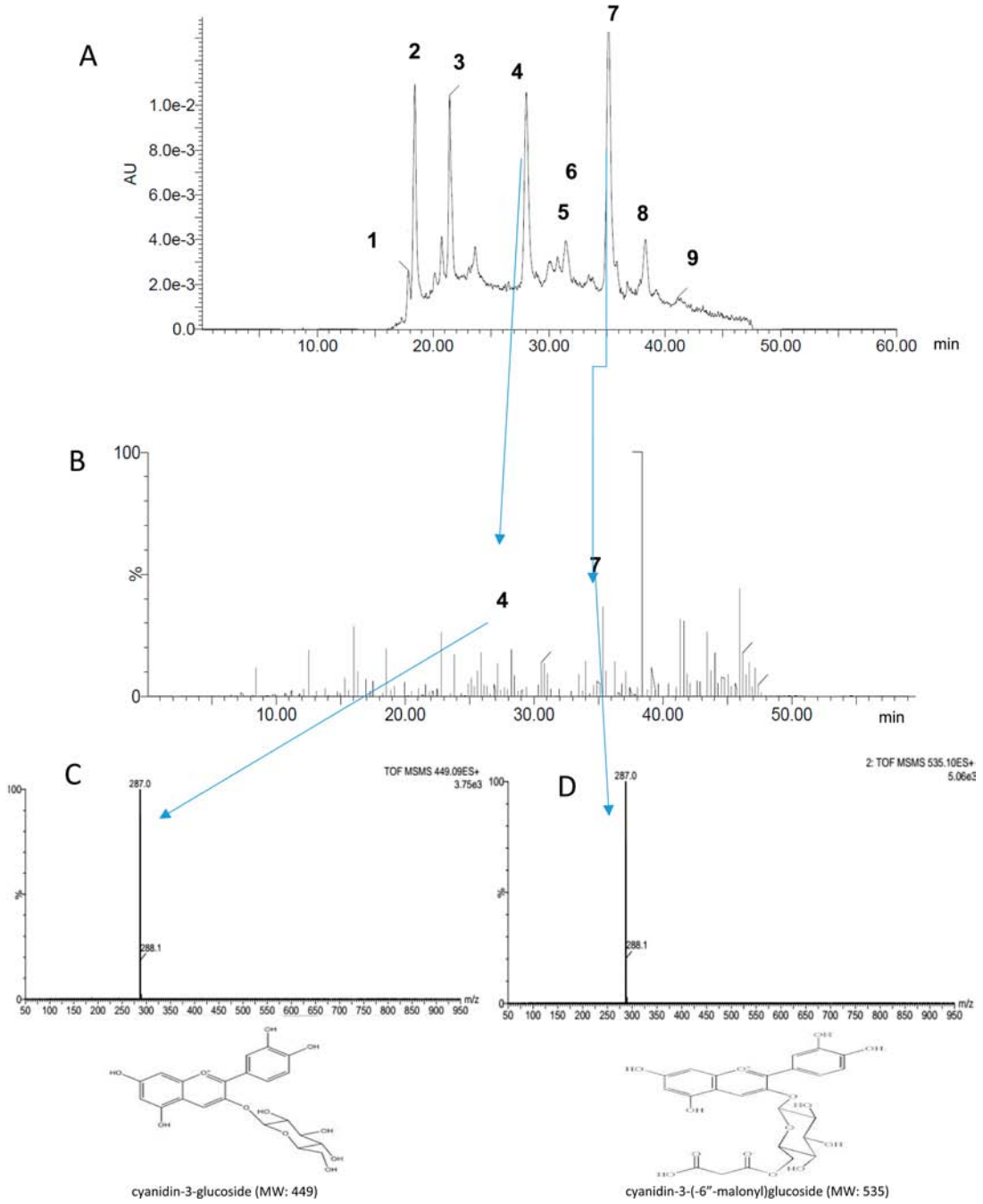

Figure 8. Anthocyanin profile of DDGS purple corn extract prepared by granular starch hydrolysis process (GC-PC).

from purple corn DDGS. The HPLC chromatogram of the extract shows major peaks at 28.03 and 35.13 min retention times with AU values of 0.010 and 0.014, respectively (Figure 8A). MS/MS analysis of these peaks showed that they are cyanidin-3-glucoside and cyanidin-3-(6″-malonyl)glucoside, respectively (Figure 8B,C,D). Another major anthocyanin found was at retention time 38.35 min, corresponding to peonidin-3-(6″-malonyl)glucoside. Identification of peaks from the MS/MS total ion chromatogram of the two extracts is summarized in Table 3. Condensed flavanol−anthocyanin derivatives were also identified in the extracts at an earlier retention time between 17 and 19 min corresponding to catechin-(4,8)-cyanidin-3-malonylglucoside and catechin-(4,8)-cyanidin-3,5-diglucoside. Supporting Information provides the HPLC chromatograms at 520 nm from water extracts of different DDGS.

DISCUSSION

In the United States alone, 316 million metric tons of corn valued at US $66 billion were produced in 2010.[13] To date, very few studies have been reported on the extraction of natural compounds from DDGS.[27] In this study, we optimized the extraction of anthocyanin from DDGS as coproduct of biofuel production from two colored corn varieties and two DDGS processing methods. The total polyphenol concentration ranged from 4489.6 to 19 603.7 μg gallic acid equivalent/g DDGS. Previous study on the total polyphenol concentrations of DDGS extracted with or without microwave irradiation showed that the highest concentration of polyphenols was 12.0 mg gallic acid/g DDGS achieved by 50% aqueous ethanol at 150 °C with microwave irradiation for 15 min.[28] Our results cover this previously

DOI: 10.1021/acs.jafc.5b00128
J. Agric. Food Chem. 2015, 63, 3205−3218

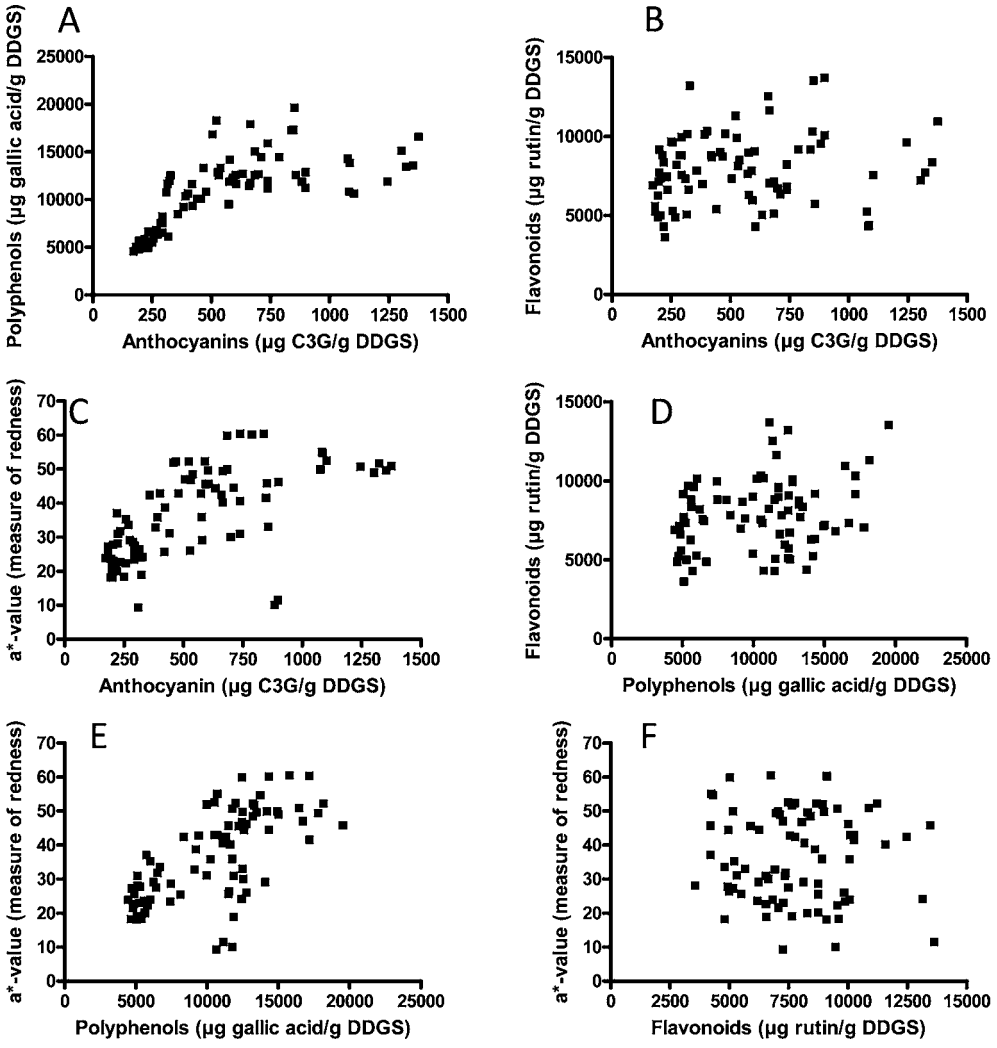

G

Correlations among parameters measured in DDGS extracts.

Comparison	P-value	Pearson r	95% confidence interval
Anthocyanins vs Polyphenols	**< 0.0001**	0.7191	0.5940 – 0.8103
Anthocyanins vs Flavonoids	0.1808	0.1502	-0.0705 – 0.3569
Anthocyanins vs a*-value	**< 0.0001**	0.6272	0.4736 – 0.7437
Polyphenols vs Flavonoids	**0.0138**	0.2725	0.0576 – 0.4634
Polyphenols vs a*-value	**< 0.0001**	0.6596	0.5115 – 0.7675
Flavonoids vs a*-value	0.7757	-0.0322	- 0.2488 – 0.1876

Figure 9. Correlations among parameters measured in DDGS extracts between total anthocyanins and total polyphenols (A), total anthocyanins and total flavonoids (B), total anthocyanins and *a**-value (C), total polyphenols and total flavonoids (D), total polyphenols and *a**-value (E), and total flavonoids and *a**-value (F). An insert table is presented to summarize the statistical parameters of correlation (G).

reported polyphenol concentration from DDGS extract; the slight difference can be explained by the use of different extraction conditions. To our knowledge, this is the first report that quantifies the amount of total monomeric anthocyanins and total flavonoid concentrations of different extracts from colored corn DDGS. Previous studies on the total anthocyanin concentrations of purple corn showed that the concentration of anthocyanin varied depending on which material was analyzed. Purple corncob gave the highest anthocyanin concentration of 1333 mg/100 g;[29] ground purple corn had a concentration of 6.02 mg/g[30] and 1277 μg/g,[31] while purple waxy corn kernel and cob had a concentration of 754 μg/g DW and 2534.1 μg/g DW, respectively.[32] Anthocyanin content of colored corn DDGS extracts ranged from 174.3 to 1573.4 μg C3G equivalent/g DDGS, which are comparable to what were previously reported on the anthocyanin level in purple corn kernel, indicating that the process of biofuel production did not affect the level of anthocyanin in DDGS. Dark corn cultivar had an anthocyanin concentration higher than that of purple corn cultivar, indicating the effect of cultivar in anthocyanin concentration, hence affecting the *a**-color parameters of the extracts, which was further supported by the generated color squares. In addition, DDGS obtained by the GC method yielded anthocyanin and polyphenol concentrations higher than those of the conventionally obtained DDGS, indicating the effect of DDGS processing methods on these compounds. The effect might be attributed to the temperature used during the liquefaction process.

DOI: 10.1021/acs.jafc.5b00128
J. Agric. Food Chem. 2015, 63, 3205−3218

Previous studies have shown that the major flavonoids found in purple corn were quercetin and hesperitin derivatives.[33] In addition, the concentration of flavonoids from purple corn was reported to be in the range of 1.18 to 2.66 g rutin equivalent/kg,[34] higher than what we found in this study. The difference could be attributed to the method of measuring flavonoid concentration as well as the solvent used in the extraction. We first reported here that extracts from colored corn DDGS are a potential source of different bioactive compounds. This result is economically important as it showed DDGS is a potential inexpensive source of these health-promoting compounds, and the left-over residue after bioactive extraction could still be used as an ingredient for animal diets.

Aside from the reported health benefits of anthocyanin, one of its major potential uses is as food colorant in the food industry. There is an increasing push in the food industry to replace the use of artificial food colorants with plant pigments. The maximum anthocyanin concentration was recorded after using 12.5% ethanol, 40:1 liquid-to-solid ratio, and 22 °C for C-PC; for GC-PC, 25% ethanol, 30:1 liquid-to-solid ratio, and 22 °C; and for GC-DC, 12.5% ethanol, 40:1 liquid-to-solid ratio, and 40 °C as extraction conditions. RSM analysis indicated that the optimum values for anthocyanin extraction were 12.5% ethanol, 40:1 liquid-to-solid ratio, and 22 °C. Analysis of variance of the regression equation for anthocyanin concentration as the dependent variable showed that a linear model ($P < 0.0001$) was significant for the C-PC sample; both linear and quadratic models were highly significant ($P < 0.0001$) for GC-PC and GC-DC samples. The R^2 for each model was 0.509 for C-PC, 0.640 for GC-PC, and 0.773 for GC-DC. Eigenvalues for the total experimental values were a mixture of positive and negative values for anthocyanin concentration, indicating that the stationary point is a saddle point.

Statistical analysis of the correlations among parameters measured in the DDGS extract showed that total anthocyanins and total polyphenols, total anthocyanins and *a**-value, total polyphenols and total flavonoids, and total polyphenols and *a**-value correlated (Figure 9) with each other with P-values of <0.0001, < 0.0001, 0.0138, and <0.0001, respectively. On the other hand, flavonoids did not correlate with anthocyanins and *a**-value of the extracts with P-values of >0.05. These results indicated that anthocyanins and polyphenols might have direct impact on the color of the extract while total flavonoids will have no impact on the color of the extract. These results further supported our observation of the effect of corn cultivars and DDGS processing methods on the total anthocyanins and total polyphenols of the extracts and the observation that total flavonoids were not affected.

A vast collection of color corn, as part of the maize germplasm bank collection at the University of Illinois, has shown that color corn stores well, maintains viability, and it is not more susceptible to degradation than white or yellow corn. However, more post-harvest studies are needed to measure and compare food grain quality— quantitative, qualitative, nutritive, and economic—of color corn versus white or yellow corn. Significant amounts of purple corn are processed for making cereals, tortillas, meal, chips, and other products.[13] Handling of purple corn (harvesting and drying) may be different from yellow dent corn because of its soft endosperm, but it is practiced commercially. Breeding efforts will be required to develop robust purple corn hybrids with good ethanol yields before they can be used by the biofuels industry; such efforts are underway at our institution.

In conclusion, the results suggested that anthocyanin extraction from colored corn DDGS can be optimized using 40:1 mL/g DDGS liquid-to-solid ratio, 22 °C extraction temperature, and 12.5% ethanol concentration. DDGS processing methods and corn cultivar affected total anthocyanins and polyphenols of the obtained extracts.

■ ASSOCIATED CONTENT

Supporting Information

HPLC chromatograms of water extracts from different DDGS (A) conventional-purple corn (C-PC), (B) granular starch hydrolysis-purple corn (GC-PC), and (C) granular starch hydrolysis-dark corn (GC-DC). This material is available free of charge via the Internet at http://pubs.acs.org.

■ AUTHOR INFORMATION

Corresponding Author

*228 ERML, MC-051, 1201 West Gregory Drive, Urbana, IL 61801. E-mail: edemejia@illinois.edu. Fax: +1-217-265-0925.

Funding

Kraft Foods provided funds to support this research.

Notes

The authors declare no competing financial interest.

■ ACKNOWLEDGMENTS

The authors thank Bo Kim and Melinda Holmes for technical assistance.

■ ABBREVIATIONS USED

C3G, cyanidin-3-glucoside; C-PC, conventional processing of purple corn; DDGS, distillers dried grains with solubles; GC-DC, granular starch hydrolysis processing of dark corn; GC-PC, granular starch hydrolysis processing of purple corn; RSM, response surface methodology

■ REFERENCES

(1) Hou, Z. H.; Qin, P. Y.; Zhang, Y.; Cui, S. H.; Ren, G. X. Identification of anthocyanins isolated from black rice (*Oryza sativa* L.) and their degradation kinetics. *Food Res. Int.* **2013**, *50*, 691−697.

(2) Wu, X. L.; Gu, L. W.; Prior, R. L.; McKay, S. Characterization of anthocyanins and proanthocyanidins in some cultivars of Ribes, Aronia, and Sambucus and their antioxidant capacity. *J. Agric. Food Chem.* **2004**, *52*, 7846−7856.

(3) Harakotr, B.; Suriharn, B.; Tangwongchai, R.; Scott, M. P.; Lertrat, K. Anthocyanin, phenolics and antioxidant activity changes in purple waxy corn as affected by traditional cooking. *Food Chem.* **2014**, *164*, 510−517.

(4) Bicudo, M. O. P.; Ribani, R. H.; Beta, T. Anthocyanins, phenolics acids and antioxidant properties of Juçara fruits (*Euterpe edulis* M.) along the on-tree ripening process. *Plant Foods Hum. Nutr. (N.Y., NY, U.S.)* **2014**, *69*, 142−147.

(5) Santos, V. D.; Bisen-Hersh, E.; Yu, Y. C.; Cabral, I. S. R.; Nardini, V.; Culbreth, M.; da Rocha, J. B. T.; Barbosa, F.; Aschner, M. Anthocyanin-rich açaí (*Eterpe oleracea* Mart.) extract attenuates Manganese-induced oxidative stress in rat primary astrocyte cultures. *J. Toxicol. Env. Health., Part A* **2014**, *77*, 390−404.

(6) Johnson, M. H.; de Mejia, E. G.; Fan, J. F.; Lila, M. A.; Yousef, G. G. Anthocyanins and proanthocyanidins from blueberry-blackberry fermented beverages inhibit markers of inflammation in macrophages and carbohydrate-utilizing enzymes in vitro. *Mol. Nutr. Food Res.* **2013**, *57*, 1182−1197.

(7) Fan, J. F.; Johnson, M. H.; Lila, M. A.; Yousef, G.; de Mejia, E. G. Berry and citrus phenolic compounds inhibit dipeptidyl peptidase IV: Implications in diabetes management. *J. Evidence-Based Complementary Altern. Med.* **2013**, *2013*, 479505.

DOI: 10.1021/acs.jafc.5b00128
J. Agric. Food Chem. 2015, 63, 3205−3218

(8) Kang, M. K.; Lim, S. S.; Lee, J. Y.; Yeo, K. M.; Kang, Y. H. Anthocyanin-rich purple corn extract inhibit diabetes-associated glomerular angiogenesis. *PLoS One.* **2013**, *8*, e79823.
(9) Gu, J.; Ahn-Jarvis, J. H.; Riedl, K. M.; Schwartz, S. J.; Clinton, S. K.; Vodovotz, Y. Characterization of black raspberry functional food products for cancer prevention human clinical trials. *J. Agric. Food Chem.* **2014**, *62*, 3997−4006.
(10) Fernandes, I.; Marques, F.; de Freitas, V.; Mateus, N. Antioxidant and antiproliferative properties of methylated metabolites of anthocyanins. *Food Chem.* **2013**, *141*, 2923−2933.
(11) Zeppa, G.; Bertolino, M.; Rolle, L. Quantitative descriptive analysis of Italian polenta produced with different corn cultivars. *J. Sci. Food Agric.* **2012**, *92*, 412−417.
(12) Lago, C.; Cassani, E.; Zanzi, C.; Landoni, M.; Trovato, R.; Pilu, R. Development and study of a maize cultivar rich in anthocyanins: Coloured polenta, a new functional food. *Plant Breed.* **2014**, *133*, 210−217.
(13) National Corn Growers Association. World of Corn Statistics Book, 2014. http://www.ncga.com/upload/files/documents/pdf/woc-2014.pdf (accessed, February 2015).
(14) Tres, A.; Heenan, S. P.; van Ruth, S. Authentication of dried distilled grain with solubles (DDGS) by fatty acid and volatile profiling. *LWT—Food Sci. Technol.* **2014**, *59*, 215−221.
(15) Liu, S. X.; Singh, M.; Inglett, G. Effect of incorporation of distillers' dried grain with solubles (DDGS) on quality of cornbread. *LWT—Food Sci. Technol.* **2011**, *44*, 713−718.
(16) Belyea, R. L.; Rausch, K. D.; Clevenger, T. E.; Singh, V.; Johnston, D. B.; Tumbleson, M. E. Sources of variation in composition of DDGS. *Anim. Feed Sci. Technol.* **2010**, *159*, 122−130.
(17) Aldai, N.; Klieve, A. V.; Dugan, M. E. R.; Kramer, J. K. G.; Ouwerkerk, D.; Aalhus, J. L.; et al. Evaluation of rumen fatty acid hydrogenation intermediates and differences in bacterial communities after feeding wheat- or corn-based dried distillers grains to feedlot cattle. *J. Anim. Sci. (Champaign, IL, U.S.)* **2012**, *90*, 2699−2709.
(18) Nuez-Ortin, W. G.; Yu, P. Nutrient variation and availability of wheat DDGS, corn DDGS and blend DDGS from bioethanol plants. *J. Sci. Food Agr.* **2009**, *89*, 1754−1761.
(19) Khuri, A. I.; Mukhopadhyay, S. Response Surface Methodology. *Wiley Interdiscip. Rev.: Comput. Stat.* **2010**, *2*, 128−149.
(20) Liu, K. Chemical composition of distillers grains, a review. *J. Agric. Food Chem.* **2011**, *59*, 1508−1526.
(21) Zou, T. B.; Xia, E. Q.; He, T. P.; Huang, M.y.; Jia, Q.; Li, H. W. Ultrasound-assisted extraction of mangiferin from Mango (*Mangifera indica* L.) leaves using response surface methodology. *Molecules* **2014**, *19*, 1411−1421.
(22) Shihadeh, J. K.; Huang, H.; Rausch, K. D.; Tumbleson, M. E.; Singh, V. Vacuum stripping of ethanol during high solids fermentation of corn. *Appl. Biochem. Biotechnol.* **2014**, *173*, 486−500.
(23) Lee, J.; Durst, R. W.; Wrolstad, R. E. Determination of total monomeric anthocyanin pigment content of fruit juices, beverages, natural colorants, and wines by the pH differential method: Collaborative study. *J. AOAC Int.* **2008**, *56*, 1896−1906.
(24) Heck, C. I.; Schmalko, M.; de Mejia, E. G. Effect of growing and drying conditions on the phenolic composition of mate tea (*Ilex paraguariensis*). *J. Agric. Food Chem.* **2008**, *56*, 8394−8403.
(25) Bower, A. M.; Hernandez, L. M. R.; Berhow, M. A.; de Mejia, E. G. Bioactive compounds from culinary herbs inhibit a molecular target for type 2 diabetes management, dipeptidyl peptidase IV. *J. Agric. Food Chem.* **2014**, *62*, 6147−6158.
(26) West, M. E.; Mauer, L. J. Color and chemical stability of a variety of anthocyanins and ascorbic acid in solution and powder forms. *J. Agri. Food Chem.* **2013**, *61*, 4169−4179.
(27) Liu, K. Chemical composition of distillers grains, a review. *J. Agric. Food Chem.* **2011**, *59*, 1508−1526.
(28) Inglett, G. E.; Rose, D. J.; Stevenson, D. G.; Chen, D.; Biswas, A. Total phenolics and antioxidant activity of water and ethanolic extracts from distilllers dried grains with solubles with or without microwave irradiation. *Cereal Chem.* **2009**, *86*, 661−664.
(29) Jing, P.; Noriega, V.; Schwartz, S. J.; Giusti, M. M. Effects of growing conditions on purple corncob (*Zea mays* L.) anthocyanins. *J. Agri. Food Chem.* **2007**, *55*, 8625−8629.
(30) Yang, Z. D.; Chen, Z. J.; Yuan, S. L.; Zhai, W. W.; Paio, X. S.; Piao, X. L. Extraction and identification of anthocyanin from purple corn (*Zea mays* L.). *Int. J. Food Sci. Technol.* **2009**, *44*, 2485−2492.
(31) Yang, Z. D.; Zhai, W. W. Optimization of microwave-assisted extraction of anthocyanins from purple corn (*Zea mays* L.) cob and identification with HPLC-MS. *Innovative Food Sci. Emerging Technol.* **2010**, *11*, 470−476.
(32) Harakotr, B.; Suriharn, B.; Tangwongchai, R.; Scott, M. P. Anthocyanin, phenolics and antioxidant activity changes in purple waxy corn as affected by traditional cooking. *Food Chem.* **2014**, *164*, 510−517.
(33) Pedreschi, R.; Cisneros-Zevallos, L. Phenolic profiles of Andean purple corn (*Zea mays* L.). *Food Chem.* **2005**, *100*, 956−963.
(34) Ramos-Escudero, F.; Munoz, A. M.; Alvarado-Ortiz, C.; Alvarado, A.; Yanez, J. A. Purple corn (*Zea mays* L.) phenolic profile and its assessment as an agent against oxidative stress in isolated mouse organs. *J. Med. Food* **2012**, *15*, 206−215.

DOI: 10.1021/acs.jafc.5b00128
J. Agric. Food Chem. 2015, 63, 3205−3218

MATERIALS AND METHODS

Materials. The alfalfa sample was harvested in the time period between the bud and initial flowering stage (10% bloom) from Gansu province of China and dried at environmental conditions. TRIzol reagent was purchased from Invitrogen (Carlsbad, CA, USA), whereas an IScript Advanced cDNA Synthesis kit was purchased from Bio-Rad (Hercules, CA, USA). RAW 264.7 mouse macrophage cells were obtained from the Chinese Academy of Sciences (Shanghai, China). Lipopolysaccharide (LPS) from *Escherichia coli* O111:B4 was obtained from Millipore (Bedford, MA, USA). Other reagents for isolation were of analytical grade without further purification.

Fractionation and Purification of Pectic Polysaccharide. After removal of the leaves, the dried alfalfa stem was milled into powders through a 200-mesh screen using an IKA mill (IKA, A11, Germany). Small molecules were removed from alfalfa stem powders by three 95% ethanol extractions at 75 °C for 2 h. Afterward, hot water (DD H_2O, 80 °C, 2 h; three times) and cold alkali (1 M NaOH, room temperature, 12 h; four times) were successively used to extract the water-soluble substances and hemicellulosic polysaccharides (Figure S1). The pectins were then extracted four times using a 20-fold volume of 1 M NaOH (w/v) at 80 °C with continuous stirring for 2 h. After neutralization with HCl solution, the extract was precipitated by using a 4-fold volume of 95% ethanol (v/v) and washed three times with 75% ethanol, followed by lyophilization to afford the crude pectic polysaccharides of alfalfa stem.

Further purification was carried out by membrane ultrafiltration (Minimate TFF system, Pall Corp., Port Washington, NY, USA) with defined exclusion limits of 10000 Da to obtain the pectic polysaccharide molecules of alfalfa stem (APPS) with MW >10000 Da. The cutoff polysaccharide was then purified by gel filtration chromatography on a Sephacryl S-400 Superfine column (80 × 1.6 cm i.d., Amersham Pharmacia Biotech, Uppsala, Sweden) eluted with DD H_2O at 1.0 mL/min. The collected eluates were combined and freeze-dried prior to further analysis (Figure S1).

Molecular Weight and Size Determination. The molecular weight and size of APPS were determined using a particle size analyzer (Zetasizer Nano-ZS90, Malvern Instruments Ltd., Malvern, Worcs, UK). In general, the well-dispersed APPS stock aqueous solution (2 mg/mL) was diluted to 1.00, 0.75, 0.50, 0.25, and 0.10 mg/mL. The Debye plot from static light scattering (SLS) was obtained to calculate the weight-averaged molecular weight (M_w) of APPS based on the Rayleigh equation (eq 1).[25]

$$\frac{KC}{R_\theta} = \left(\frac{1}{M_w} + 2A_2C\right) \times P(\theta) \tag{1}$$

In eq 1, K, M_w, A_2, C, and R_θ represent optical constant, sample molecular weight, second virial coefficient, concentration, and Rayleigh ratio, respectively. Representing the angular dependence of the sample scattering intensity, the value of $P(\theta)$ would reduce to 1 when the particles are much smaller than the wavelength of the incident light. The M_w (Da or g/mol) was determined from the intercept at zero concentration ($C \rightarrow 0$) according to $KC/R_\theta = 1/M_w$. The molecular size was simultaneously obtained along with the molecular weight determination at the concentration of 0.25 mg/mL.

Chemical Composition Analysis. APPS was analyzed for contents of total protein, carbohydrate, and uronic acid using bicinchoninic acid (BCA),[26] phenol–sulfuric acid,[27] and *m*-hydroxydiphenylsulfuric acid[28] methods, respectively.

The PMP derivation method was used to determine the monosaccharide and uronic acid compositions of APPS as described previously.[29] The obtained sugar derivatives were then determined by HPLC analysis at 250 nm with an Inertsil ODS-3 column (100 mm × 2.1 mm i.d., 2 μm, GL Sciences Inc., Tokyo, Japan) under the following chromatographic conditions: 30 °C, 0.1 M phosphate buffer (pH 6.7)/acetonitrile at a ratio of 80:20 (v/v), 0.3 mL/min.

Linkage Analysis by Methylation. APPS was first reacted with $NaBD_4$ to reduce the uronic acid residues according to a previously reported protocol.[30] The partially methylated alditol acetates (PMAAs) of APPS was prepared according to a modified Needs method[31] for the following determination using GC-MS (Agilent 7890A-5975C, Agilent Technology, Santa Clara, CA, USA), equipped with a HP-5 capillary column (30 m × 0.32 mm i.d., 0.25 μm film). The temperature of GC was increased from 50 to 150 °C at 30 °C/min, then to 220 °C at 3 °C/min, and finally to 300 °C at 30 °C/min and held for 10 min. The injector temperature was set at 250 °C, whereas the interface temperature was 280 °C. The MS parameters were set as ion source temperature at 300 °C, ionization energy at 70 eV, detector voltage at 1.5 kV, and mass range from 50 to 550. Glycosidic linkages of APPS were identified by comparing the mass spectrum patterns of PMAAs with the database of CCRC.[32] The molar ratios of individual linkage residues were calculated on the basis of peak areas and response factors for each sugar in the TIC as described previously.[33]

Spectroscopic Analysis. The infrared spectrum of APPS was measured on a FT-IR spectrometer (Nicolet 6700, Thermo Fisher, Waltham, MA, USA) using KBr pellets in the infrared region of 4000–400 cm^{-1} at a resolution of 4 cm^{-1}. One- and two-dimensional NMR analyses of APPS were carried out on an Avance Bruker III HD 600 MHz NMR spectrometer equipped with a 5 mm TCI CryoProbe at 25 °C using D_2O as the solvent to a final sample concentration of 40 mg/mL.

Transmission Electron Microscopy (TEM). In brief, a well-dispersed polysaccharide solution was first prepared using sodium dodecyl sulfate (SDS, 5 μg/mL) to a final concentration of 5 μg/mL. SDS aqueous solution was applied to dissolve APPS as the SDS solution could reduce the molecular aggregation.[34] A droplet of APPS solution (5 μL) was deposited on a carbon film specimen (200 mesh, Beijing Zhongjingkeyi Technology, Beijing, China) and dried at ambient temperature and humidity. The specimen was examined using TEM (Tecnai G2 Spirit BIOTWIN, FEI, Hillsboro, OR, USA) at an accelerating voltage of 120 kV to observe the morphology of APPS molecular assembly or the microstructures of APPS.

Isoconversional Thermal Characteristics. Pyrolysis characteristics of APPS were determined on a simultaneous thermal analyzer (SDT-Q600, TA Instruments, New Castle, DE, USA). In general, three different heating rates (including 5, 10, and 20 °C/min) were used to decompose the APPS sample from 50 to 600 °C under N_2 protection at a flow rate of 100 cm^3/min. The decomposition results were analyzed using the Flynn–Wall–Ozawa (FWO) method (eq 2) to obtain the experimental apparent activation energy (E_a)[35−37]

$$\log \beta = \log \frac{AE_a}{Rg(\alpha)} - 2.315 - 0.4567\frac{E_a}{RT} \tag{2}$$

where $g(\alpha) = \int_0^\alpha (d\alpha)/(f(\alpha))$, β is the heating rate, R is the general gas constant, A stands for the pre-exponential factor, E_a is the apparent activation energy, and T is the temperature at the conversion α. The experimental value of ln A was obtained by the compensation effect relationship (eq 3), the compensation parameters (a and b) of which could be deduced by a plot of ln A versus E_a from a model-fitting approach using the Coats–Redfern equation (eq 4) with T' being the average experimental temperature.

$$\ln A = aE_a + b \tag{3}$$

$$\ln \frac{g(\alpha)}{T^2} = \ln\left[\left(\frac{AR}{\beta E_a}\right)\left(1 - \frac{2RT'}{E_a}\right)\right] - \frac{E_a}{RT} \tag{4}$$

Both the FWO and Coats–Redfern methods were classified to model-free methods. By using these methods, the process is detectable in the form of a dependence of the activation energy E_a on the conversion rate α. The thermal analysis data were analyzed using the Universal Analysis 2000 software (version 4.5A, TA Instruments) and MS Excel 2013.

Anti-inflammatory Bioactivity Determination. The potential anti-inflammatory effect of APPS was evaluated by determining its potential inhibition of IL-1β, IL-6, and COX-2 gene expressions in the cultured RAW 264.7 mouse macrophage cells. Briefly, the aqueous solution of APPS was first prepared at two different treatment concentrations (10 and 50 μg/mL). RAW 264.7 cells were cultured in

DOI: 10.1021/acs.jafc.5b00494
J. Agric. Food Chem. 2015, 63, 3219−3228

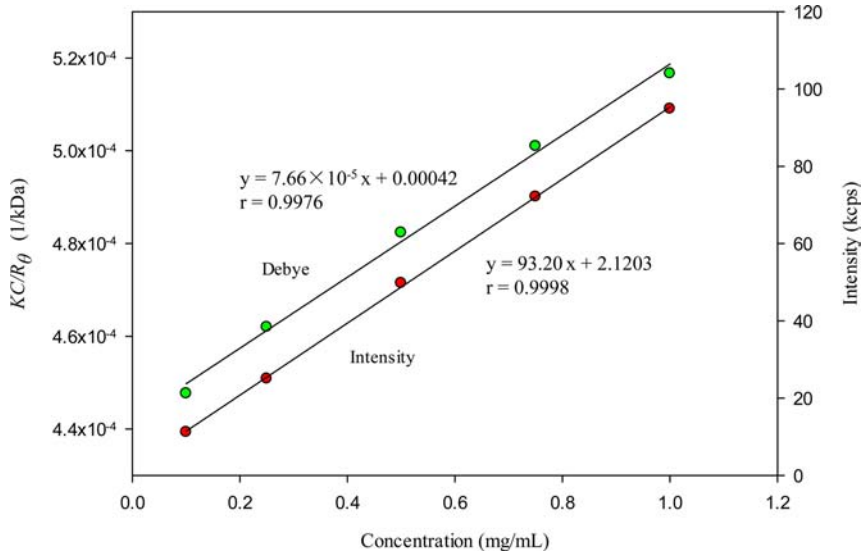

Figure 1. Debye plot of APPS for its molecular weight determination: angular dependences of KC/R_θ with K being the optical constant, C being the concentration, R_θ being the Rayleigh ratio, and θ being the scattering angle.

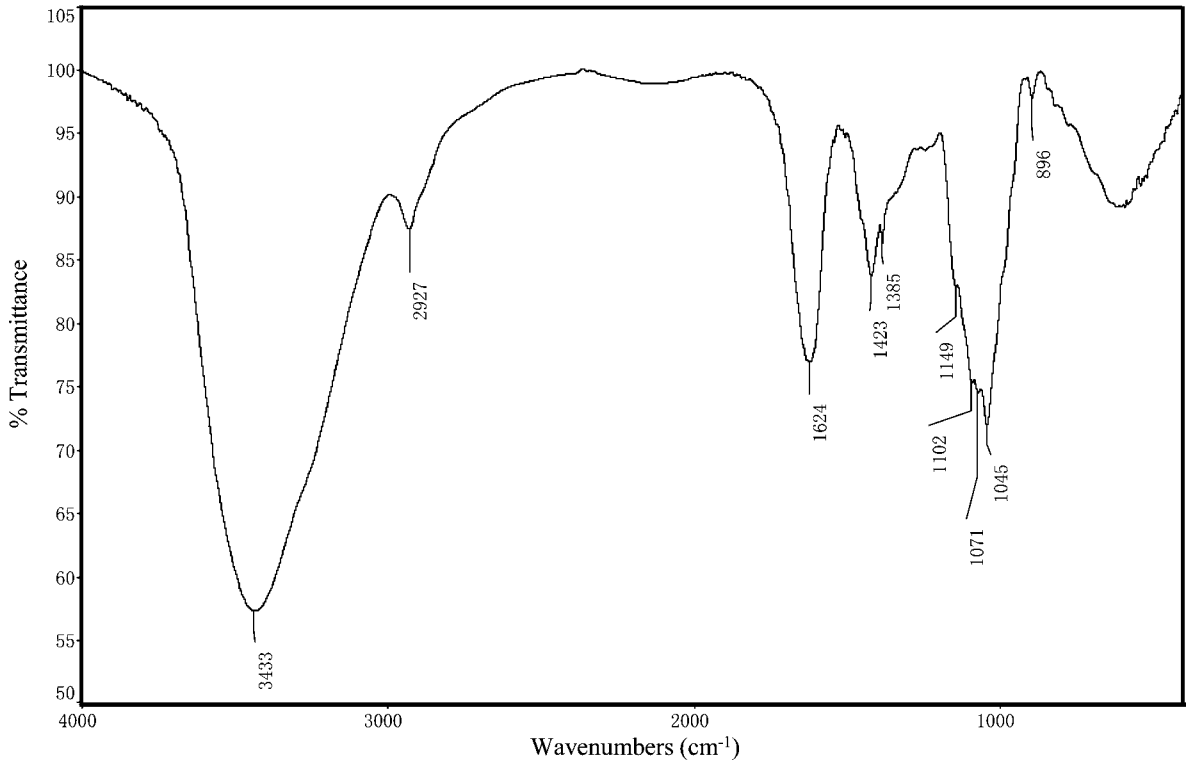

Figure 2. FT-IR spectrum of APPS.

6-well plates for 24 h to reach an 80% confluence before the treatment. After further incubation for 24 h, LPS was pipetted into the medium at a final concentration of 10 ng/mL and incubated for another 4 h at 37 °C under 5% CO_2.[38,39] Total RNA was isolated from the mouse peritoneal macrophages using a TRIzol reagent (Invitrogen) for further reverse transcription of cDNA and real-time PCR analysis using the IScript Advanced cDNA Synthesis kit on an ABI 7900HT Fast Real-Time PCR System (Applied Biosystems) with the following PCR conditions: 50 °C for 2 min, 95 °C for 10 min, and 46 cycles of amplification at 95 °C for 15 s and 60 °C for 1 min.

Statistical Analysis. Data were recorded as the mean ± SD for triplicate determination. The significance of differences between means were evaluated by one-way analysis of variance (ANOVA) and Tukey's test using SPSS for Windows (version rel. 18.0, SPSS Inc., Chicago, IL, USA) with statistical significance assigned at $P < 0.05$.

RESULTS AND DISCUSSION

Preparation of APPS. The crude hot alkali extractable fraction was about 3.31% dry weight of the alfalfa stem and contained 96.79% (w/w) of total carbohydrate including 10.03% uronic acid, whereas no protein was detected. A homogeneous polysaccharide fraction was purified from the crude extract by ultrafiltration and size exclusion chromatography (SEC) and designated APPS (Figure S2). APPS

DOI: 10.1021/acs.jafc.5b00494
J. Agric. Food Chem. 2015, 63, 3219−3228

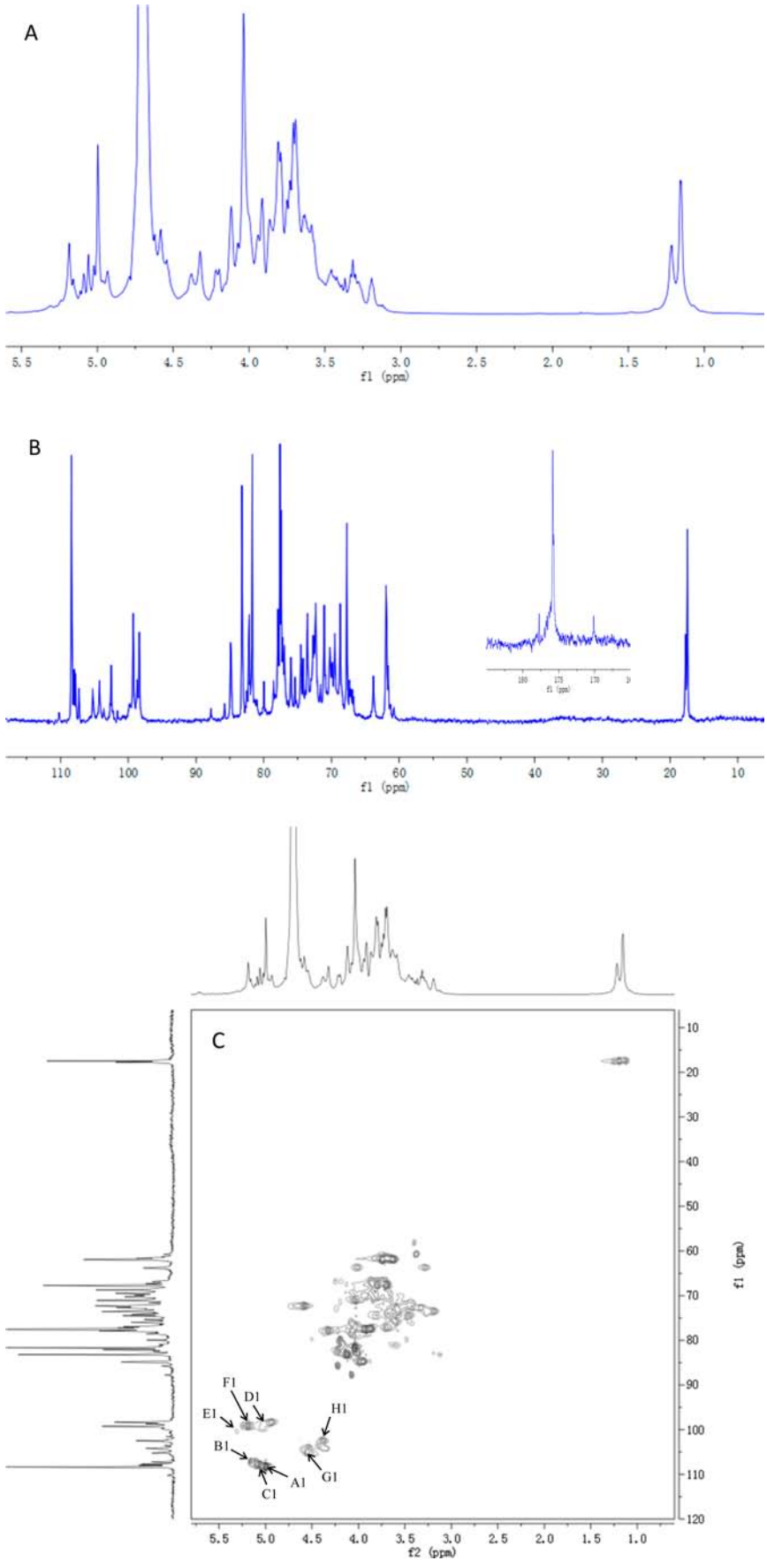

Figure 3. ^{1}H (A), ^{13}C (B), and HSQC (C) NMR spectra of APPS in D_2O solution at 25 °C. A1 means the correlation between C1 and H1 of residue A. The order of residues A, B, C...H is consistent with Table 1.

DOI: 10.1021/acs.jafc.5b00494
J. Agric. Food Chem. 2015, 63, 3219−3228

Table 1. ^{1}H and ^{13}C NMR Chemical Shifts of APPS Recorded in D_2O at 25 °C[a]

			chemical shift, δ						
no.	residue		1	2	3	4	5	6	COOH
A	1,5-α-L-Ara*f*	H	5.00	4.03	3.91	4.12	3.79, 3.69		
		C	106.81	81.75	79.01	83.11	67.62		
B	T-α-L-Ara*f*	H	5.16	4.17	3.86	4.22	4.01		
		C	107.09	80.87	78.39	85.71	63.64		
C	1,3,5-α-L-Ara*f*	H	5.06	4.04	3.86	3.96	3.74		
		C	107.83	79.93	84.68	84.84	67.55		
D	1,2-α-L-Rha*p*	H	5.03	3.92	3.67	3.33	3.82	1.21	
		C	98.56	77.53	70.67	72.71	69.08	17.45	
E	1,2,4-α-L-Rha*p*	H	5.31	4.20	4.03	3.99	3.71	1.25	
		C	100.42	79.95	70.97	79.30	67.55	17.55	
F	1,4-α-D-Gal*p*A	H	5.19	4.03	4.05	4.32	4.58		
		C	99.17	69.20	70.97	77.83	72.26		175.82
G	1,4-β-D-Gal*p*	H	4.53	3.42	3.58	3.99	3.62	3.73	
		C	102.31	72.47	73.04	79.30	75.43	61.81	
H	T-β-D-Gal*p*	H	4.38	3.18	3.47	3.70	3.62	3.64	
		C	102.60	73.49	74.43	69.93	75.43	61.83	

[a]Residues A, B, C...H are designated according to the decreasing order of proton peak intensity.

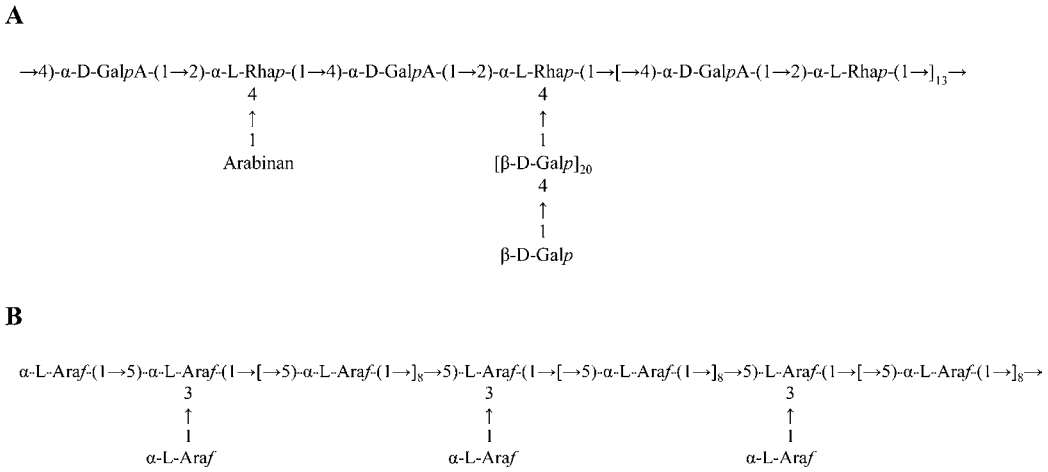

Figure 4. Proposed repeating units of APPS molecular structure: (A) schematic structure of APPS; (B) schematic structure of arabinan side chains in APPS.

consisted of rhamnose, galactose, galactouronic acid, and arabinose in a molar ratio of 2.4:1.4:1.0:3.4 (data not shown).

The M_w of APPS was calculated to be 2.38×10^3 kDa (or 2.38×10^6 g/mol) (Figure 1), whereas A_2 was calculated to be 7.66×10^{-5} from the gradient of the Debye plot, which indicated the aqueous solution of APPS was a stable system for the sake of A_2 over zero.[40] In addition, the average radius of APPS was simultaneously determined to be 123 nm.

Glycosidic Linkages of APPS. The result of PMAA analysis demonstrated that APPS was composed of eight different linkage residues including nonreducing terminals of arabinose (T-L-Ara*f*) and galactose (T-D-Gal*p*), the molar ratios of which are listed in Table S1 in the Supporting Information. The arabinose residues were primarily 1,5-L-Ara*f*, whereas the rhamnose residues were mainly 1,2-L-rhamnose (Rha*p*). Large percentages of 1,4-D-Gal*p* and 1,4-D-glactouronic acid (Gal*p*A) were also determined as the intrachain residues. The main branching points were at 1,3,5-L-Ara*f* and 1,2,4-L-Rha*p*. The ratio between terminal units and branching points was 0.97, indicating that the number of terminal units was approximately equal to the number of branching points in the polysaccharide. Additionally, the degree of branching (DB) value was 12% for APPS according to the equation DB = (NT + NB)/(NT + NB + NL),[41] where NT, NB, and NL are the numbers of the terminal residues, branch residues, and linear residues, respectively.

FT-IR Spectrum. Figure 2 shows the primary maxima of absorption bands in IR spectra of APPS. The strong absorption at 3433 cm^{-1} was dominated by the stretching vibrations of OH, whereas the band at 2927 cm^{-1} was attributed to stretching vibrations of CH_3. The signal at 1624 cm^{-1} was originated from the blending of water $\delta(H_2O)$, indicating H−O−H angle vibration. The bands at 1423 and 1385 cm^{-1} were assigned to be carboxylate groups of APPS.[42] Among them, the absorptions at 1624 and 1423 cm^{-1} were the characteristic peaks of pectin material, whereas no peak was detected at ~1750 cm^{-1}, indicating the absence of carboxyl ester groups.[43] In the region of 1200−950 cm^{-1}, several intense signals at 1149, 1102, 1071, and 1045 cm^{-1} contributed by the vibrations of glycosidic bonds and pyranoid rings.[43] Moreover, the band maximum at 1045 cm^{-1} was usually found in arabinogalacto-

DOI: 10.1021/acs.jafc.5b00494
J. Agric. Food Chem. 2015, 63, 3219−3228

rhamnoglycan, containing the dominant arabinose and rhamnose over the galactose units.[44]

Structural Characterization by NMR Analysis. Linkages between glycosyl residues in APPS were further investigated by NMR analyses, including ^{1}H NMR, ^{13}C NMR, and HSQC spectra (Figure 3), with the assistance of single-bond (COSY) and multiple-bond (TOCSY) proton−proton correlations (Figure S3). As shown in Figure 3C, eight cross peaks were presented in the anomeric region (^{1}H is from 4.3 to 5.5 ppm, whereas ^{13}C is in the range of 90−120 ppm) of the HSQC spectrum. The chemical shift assignments of ^{1}H and their corresponding ^{13}C were identified and are summarized in Table 1 from the above spectra according to the literature data for arabinofuranosides, arabinans, and pectins.[45−47] The backbone was indicated by the presence of the characteristic C-1 signals (Figure 3B) of α-(1→4)-Gal*p*A and α-(1→2)-Rha*p* at 99.17 and 98.56 ppm, respectively. According to the results of linkage analysis and the literature,[48,49] the intense peaks at 106.81, 81.75, 79.01, 83.11, and 67.62 ppm were assigned to C1, C2, C3, C4, and C5 of α-(1→5)-Ara*f*, respectively, which confirmed the prominence of an arabinan-like structure as a side chain. The pectic polysaccharides of the rhamnogalacturonan I class were reported to consist of repeating units →2)-α-L-Rha*p*-(1→4)-α-D-Gal*p*A-(1→ as backbone with side chains of either arabinan (average of 25−30 arabinose units) or galacto-oliosaccharides (average of 3−4 galactose units) attached to the *O*-4 position of →2)-α-L-Rha*p*-(1→ residues in the backbone.[50] On the basis of previous literature on the structure of pectic polysaccharides,[11,51,52] the results of methylation and NMR analysis indicated the proposed partial structure of APPS (Figure 4), which was mainly consistent with previous partial characterization of alfalfa pectic polysaccharide indicating large amounts of D-galacturonic acid and 2-*O*-(α-D-galactopyranosyluronic acid)-L-rhamnose based on partial acid hydrolysis and/or partial acetolysis analysis.[5] The primary difference between APPS and the previous arabinogalactorhamnoglycan type pectin was the degree of polymerization of the side chains.

Microscopic Morphology of APPS. TEM analysis was performed to observe the microstructure of APPS intuitively. As demonstrated in Figure 5, linear chains with minor branched structures were observed in APPS molecules under the experimental condition. The result was in agreement with that of methylation and NMR analyses that branching structure existed in APPS molecules.

Thermal Decomposition Analysis. Along with the structural properties, thermal decomposition characteristics also play an important role in the evaluation of polysaccharide applicability. In the present study, the thermal properties of APPS were assessed by thermogravimetry (TG), derivative thermogravimetry (DTG), and D^{2}TG (second-time derivatives). From the TG curves, two steps of weight loss were observed during three different heating rates (Figure 6A). In the first step, a small amount of weight loss (∼8%) occurred in the temperature range of 50−150 °C due to the loss of trapped water.[53] However, the structure of APPS was mainly pyrolyzed at the heating process of 200−400 °C, which resulted in ∼55% weight loss. Thereby, the weight at 150 °C was designated 100% dry weight of APPS for the degradation analysis.

The curves of TG, DTG, and D^{2}TG among three heating rates (β) were employed to calculate the thermal decomposition parameters of APPS in the 150−600 °C range (Figure 6B). Afterward, the pyrolysis properties of APPS were obtained from the β value of 0, which was deduced from each of the three temperatures (Figure 6C). Table 2 indicates the temperature of onset, maximum, and shift decomposition (T_o, T_p, and T_s) of APPS and their corresponding weight loss percentages (WL_o, WL_p, and WL_s). The decomposition of APPS was primarily started at 215.6 °C (T_o) and reached the maximum rate at 256.7 °C (T_p) with a loss of 12.80% dry weight (WL_p), whereas APPS experienced a rapid degradation in a narrow temperature range from the transition of 256.7 °C (T_p) to 328.0 °C (T_s). The major dry weight (51.12%) of APPS was lost in a 112.4 °C range of the heating process.

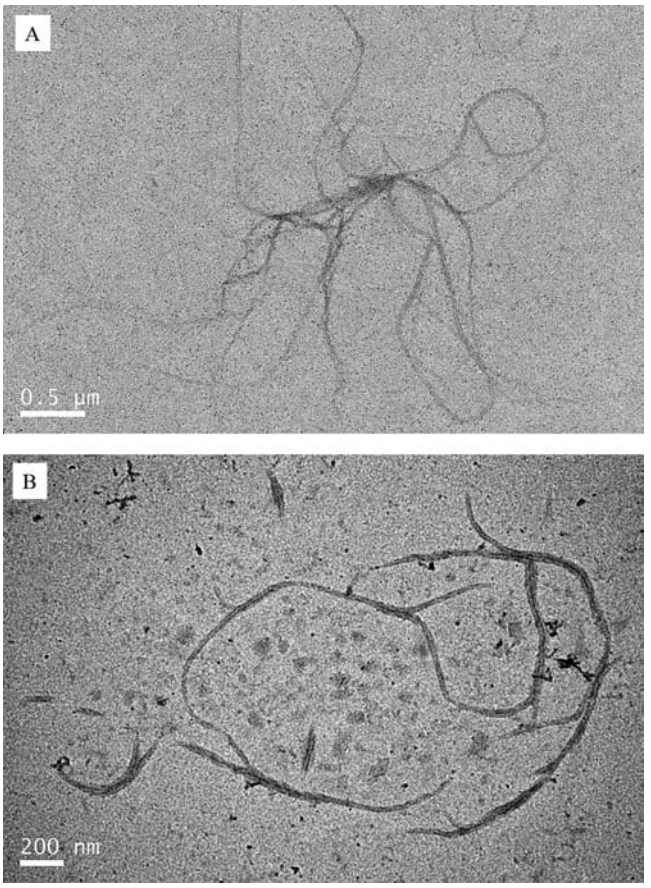

Figure 5. TEM images of APPS in sodium dodecyl sulfate (SDS) solution.

As shown in Figure 6D, the linear relationship and the fitted lines are nearly parallel in the conversion rate range of 0.3−0.7, which indicates approximate activation energies at different conversions and consequently implies the possibility of a single-reaction mechanism (or the unification of multiple-reaction mechanisms). However, the reaction mechanism could be different in the ranges of lower and higher conversion periods due to unsatisfied parallel lines at $\alpha < 0.3$ and $\alpha > 0.7$. The apparent activation energy (E_a) was thereby calculated to be 226.5 kJ/mol as listed in Table S2 in the Supporting Information, which was based on the FWO method at a conversion range from 0.3 to 0.7 with 0.1 increment (Figure 6D). The experimental pre-exponential factor (A) was obtained by the compensation effect relationship as eq 3 (Table S3). The compensation parameters of a and b were obtained from a plot of ln$A$ versus E_a using the Coats−Redfern equation (eq 4) (Figure S4).

The major decomposition occurred in temperature range of 215.6−328.0 °C (Figure 6A), which could be caused by the

DOI: 10.1021/acs.jafc.5b00494
J. Agric. Food Chem. 2015, 63, 3219−3228

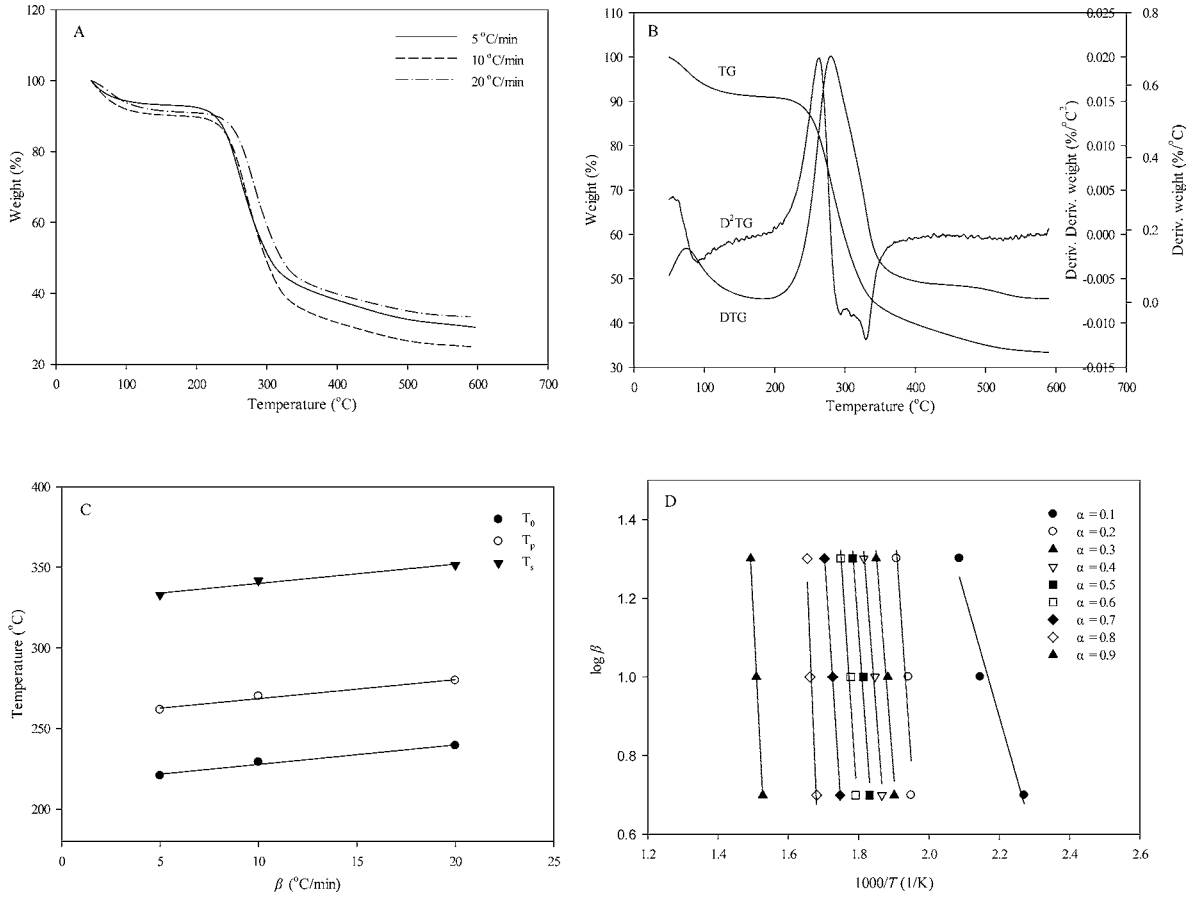

Figure 6. Thermal decomposition analysis of APPS: (A) TG curves of APPS at different heating rates; (B) determination of thermal decomposition parameters of APPS at a heating rate of 5 °C/min; (C) thermal degradation characteristics of APPS at different heating rates; (D) typical isoconversional plot of FWO method at different conversion rates.

Table 2. Thermal Degradation Characteristics of APPS[a]

sample	$T_{o\,\beta\to0}$ (°C)	WL_o (%)	$T_{p\,\beta\to0}$ (°C)	WL_p (%)	$T_{s\,\beta\to0}$ (°C)	WL_s (%)	$T_s - T_o$ (°C)	$WL_s - WL_o$ (%)
APPS	215.6	1.43	256.7	12.80	328.0	52.55	112.4	51.12

[a]Data are the mean temperatures from three different heating rates. T = temperature, WL = weight loss, subscript: o = onset, p = DTG peak, s = shift, $\beta\to0$ = extrapolated values to the heating rate of 0 °C/min.

degradation of polysaccharide structure.[20] Moreover, the E_a value of APPS was determined to be 226.5 kJ/mol, which revealed the good thermal stability of this pectic polysaccharide. The apparent activation energy (E_a) and pre-exponential factor (A) are the important parameters of the Arrhenius equation, where E_a might indicate a minimum energy requirement to initiate the decomposition reaction. These thermal decomposition characteristics are very important for the evaluation of the thermal stability of polysaccharides in their further application.

Anti-Inflammation Effects of APPS. The anti-inflammatory bioactivity of APPS was evaluated by determining its suppression effect of the IL-1β, IL-6, and COX-2 mRNA expressions in RAW 264.7 macrophage cells stimulated by LPS. As shown in Figure 7, the greater concentration of APPS was associated with a stronger suppression for IL-1β and IL-6 mRNA expressions, whereas increasing APPS concentration from 10 to 50 μg/mL increased the COX-2 mRNA expression. The results indicated the potential application of APPS in food and medicine fields to reduce the risk of chronic inflammatory diseases.

In summary, a pectic polysaccharide (APPS) was purified from the hot alkali extract of alfalfa stems and characterized for its chemical and molecular structures. APPS was composed of repeating units of →2)-α-L-Rha*p*-(1→4)-α-D-Gal*p*A-(1→ as the backbone and substituted at C-4 of Rha*p* with L-arabinosyl and D-galactosyl side chains, with a degree of branching value of 12%. The thermal stability and decomposition properties of APPS revealed the primary decomposition temperature range of 215.6−328.0 °C with an apparent activation energy (E_a) and a pre-exponential factor (A) of 226.5 kJ/mol and 2.10×10^{25}/s, respectively. APPS also showed a significant anti-inflammatory effect on LPS-stimulated RAW 264.7 mouse macrophage cells for suppression of IL-1β, IL-6, and COX-2 gene expressions. Compared with previous studies of alfalfa pectin,[5] the molecular structure of APPS was identified in combination with chemical characterization and morphological observation for the first time. The anti-inflammatory effect was also performed on a purified alfalfa pectic polysaccharide using an in vitro model. In addition, APPS showed a stronger potential anti-inflammatory effect compared with the pectic polysaccharide isolated from celery stalks.[54] Moreover, thermal degradation

DOI: 10.1021/acs.jafc.5b00494
J. Agric. Food Chem. 2015, 63, 3219−3228

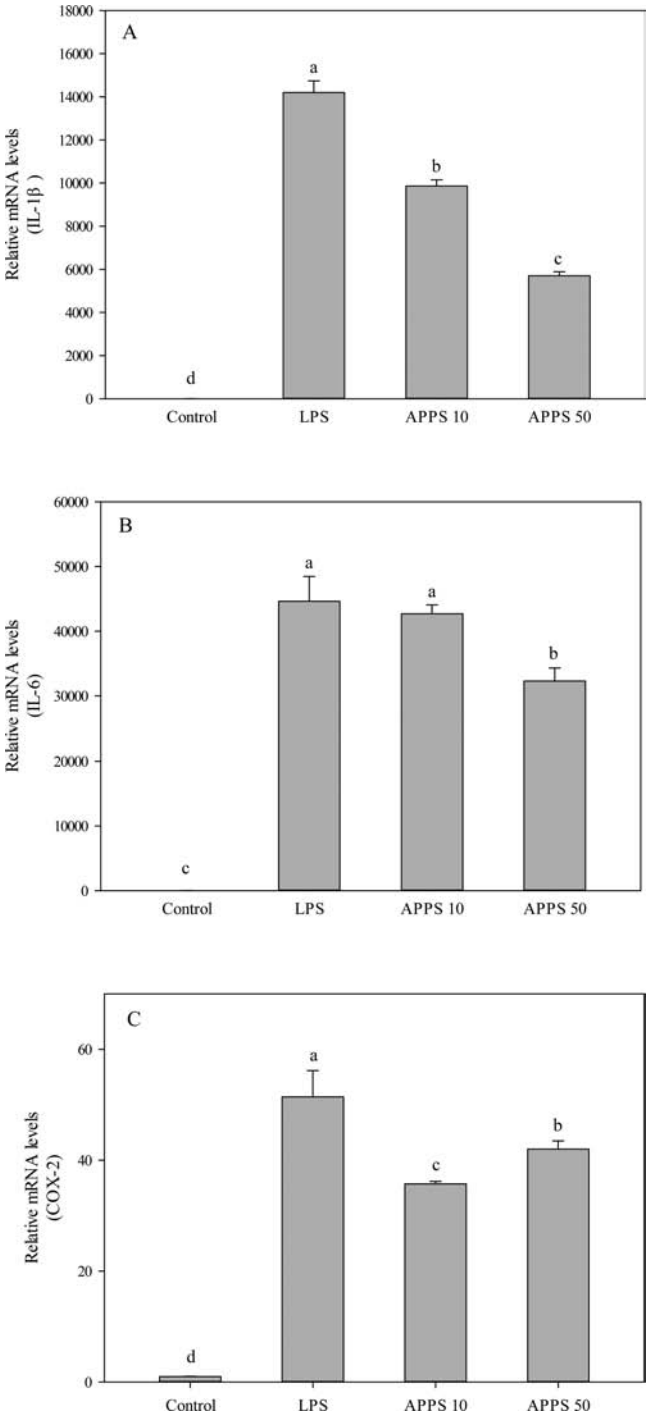

Figure 7. Effects of APPS on (A) IL-1β, (B) IL-6, and (C) COX-2 mRNA expressions in LPS -stimulated RAW 264.7 mouse macrophage cells. LPS represents cells treated with LPS at a final concentration of 10 ng/mL; APPS 10 and APPS 50 stand for the final treatment concentrations of APPS at 10 and 50 μg/mL followed by LPS inducement, respectively. The vertical bars represent the standard deviation (n = 3) of each data point. Different letters (a–d) represent significant differences (P < 0.05).

behavior was estimated to illustrate the stability for pectic polysaccharides from alfalfa for the first time. These results indicated the potential application of APPS in functional foods and dietary supplement products.

■ ASSOCIATED CONTENT

Supporting Information

Tables S1–S3 and Figures S1–S4. This material is available free of charge via the Internet at http://pubs.acs.org.

■ AUTHOR INFORMATION

Corresponding Author

*(L.Y.) Phone: (301) 405-0761. E-mail: lyu5@umd.edu.

Funding

This project was supported by a General Grant from the China Postdoctoral Science Foundation (Grant 2014M561476), a special fund for Agro-scientific Research in the Public Interest (Grant 201203069), a National High Technology Research and Development Program of China (Grants 2013AA102202 and 2013AA102207), SJTU 985-III disciplines platform and talent fund (Grants TS0414115001 and TS0320215001), and a grant from Wilmar (Shanghai) Biotechnology Research & Development Center Co., Ltd.

Notes

The authors declare no competing financial interest.

■ REFERENCES

(1) Hu, Y. G.; Cash, D. Global status and development trends of alfalfa. In *Alfalfa Management Guide for Ningxia*; Cash, D., Ed.; FAO: Rome, Italy, 2009; pp 1–3.

(2) Lamb, J. F. S.; Jung, H. J. G.; Sheaffer, C. C.; Samac, D. A. Alfalfa leaf protein and stem cell wall polysaccharide yields under hay and biomass management systems. *Crop Sci.* **2007**, *47*, 1407–1415.

(3) Aspinall, G. O.; McGrath, D. Hemicelluloses of lucerne. *J. Chem. Soc. C* **1966**, 2133–2139.

(4) Aspinall, G. O.; Fanshawe, R. S. Pectic substances from lucerne (*Medicago sativa*). Part I. Pectic acid. *J. Chem. Soc.* **1961**, 4215–4225.

(5) Aspinall, G. O.; Gestetner, B.; Molloy, J. A.; Uddin, M. Pectic substances from lucerne (*Medicago sativa*). Part II. Acidic oligosaccharides from partial hydrolysis of leaf and stem pectic acids. *J. Chem. Soc. C* **1968**, 2554–2559.

(6) Wang, S. P.; Dong, X. F.; Tong, J. M. Optimization of enzyme-assisted extraction of polysaccharides from alfalfa and its antioxidant activity. *Int. J. Biol. Macromol.* **2013**, *62*, 387–396.

(7) Dong, X. F.; Gao, W. W.; Su, J. L.; Tong, J. M.; Zhang, Q. Effects of dietary polysavone (alfalfa extract) and chlortetracycline supplementation on antioxidation and meat quality in broiler chickens. *Br. Poult. Sci.* **2011**, *52*, 302–309.

(8) Dong, X. F.; Gao, W. W.; Tong, J. M.; Jia, H. Q.; Sa, R. N.; Zhang, Q. Effect of polysavone (alfalfa extract) on abdominal fat deposition and immunity in broiler chickens. *Poult. Sci.* **2007**, *86*, 1955–1959.

(9) Voragen, A. J.; Coenen, G.; Verhoef, R.; Schols, H. Pectin, a versatile polysaccharide present in plant cell walls. *Struct. Chem.* **2009**, *20*, 263–275.

(10) Sila, D. N.; Van Buggenhout, S.; Duvetter, T.; Fraeye, I.; De Roeck, A.; Van Loey, A.; Hendrickx, M. Pectins in processed fruits and vegetables: Part II. Structure-function relationships. *Compr. Rev. Food Sci. Food Saf.* **2009**, *8*, 86–104.

(11) Dong, Q.; Liu, X.; Yao, J.; Dong, X.; Ma, C.; Xu, Y.; Fang, J.; Ding, K. Structural characterization of a pectic polysaccharide from *Nerium indicum* flowers. *Phytochemistry* **2010**, *71*, 1430–1437.

(12) Caffall, K. H.; Mohnen, D. The structure, function, and biosynthesis of plant cell wall pectic polysaccharides. *Carbohydr. Res.* **2009**, *344*, 1879–1900.

(13) Duan, J. Y.; Chen, V. L.; Dong, Q.; Ding, K.; Fang, J. L. Chemical structure and immunoinhibitory activity of a pectic polysaccharide containing glucuronic acid from the leaves of *Diospyros kaki*. *Int. J. Biol. Macromol.* **2010**, *46*, 465–470.

DOI: 10.1021/acs.jafc.5b00494
J. Agric. Food Chem. 2015, 63, 3219–3228

(14) Habibi, Y.; Heyraud, A.; Mahrouz, M.; Vignon, M. R. Structural features of pectic polysaccharides from the skin of *Opuntia ficus-indica* prickly pear fruits. *Carbohydr. Res.* **2004**, *339*, 1119−1127.
(15) Novosel'Skaya, I. L.; Voropaeva, N. L.; Semenova, L. N.; Rashidova, S. S. Trends in the science and applications of pectins. *Chem. Nat. Compd.* **2000**, *36*, 1−10.
(16) Vincken, J. P.; Schols, H. A.; Oomen, R. J. F. J.; McCann, M. C.; Ulvskov, P.; Voragen, A. G. J.; Visser, R. G. F. If homogalacturonan were a side chain of rhamnogalacturonan I. Implications for cell wall architecture. *Plant Physiol.* **2003**, *132*, 1781−1789.
(17) Fraeye, I.; Deroeck, A.; Duvetter, T.; Verlent, I.; Hendrickx, M.; Vanloey, A. Influence of pectin properties and processing conditions on thermal pectin degradation. *Food Chem.* **2007**, *105*, 555−563.
(18) Smout, C.; Sila, D. N.; Vu, T. S.; Van Loey, A. M. L.; Hendrickx, M. E. G. Effect of preheating and calcium pre-treatment on pectin structure and thermal texture degradation: a case study on carrots. *J. Food Eng.* **2005**, *67*, 419−425.
(19) Iqbal, M. S.; Massey, S.; Akbar, J.; Ashraf, C. M.; Masih, R. Thermal analysis of some natural polysaccharide materials by isoconversional method. *Food Chem.* **2013**, *140*, 178−182.
(20) Yao, F.; Wu, Q. L.; Lei, Y.; Guo, W. H.; Xu, Y. J. Thermal decomposition kinetics of natural fibers: activation energy with dynamic thermogravimetric analysis. *Polym. Degrad. Stab.* **2008**, *93*, 90−98.
(21) Liu, X. X.; Yu, L.; Liu, H. S.; Chen, L.; Li, L. Thermal decomposition of corn starch with different amylose/amylopectin ratios in open and sealed systems. *Cereal Chem.* **2009**, *86*, 383−385.
(22) Santos, J. C. O.; Santos, I. M. G.; Souza, A. G.; Prasad, S.; Santos, A. V. Thermal stability and kinetic study on thermal decomposition of commercial edible oils by thermogravimetry. *J. Food Sci.* **2002**, *67*, 1393−1398.
(23) De Wit, J. N. Thermal stability and functionality of whey proteins. *J. Dairy Sci.* **1990**, *73*, 3602−3612.
(24) Kapu Niak, J.; Ciesielski, W.; Kozio, J. J.; Tomasik, P. Thermogravimetry- and differential scanning calorimetry-based studies of the solid state reactions of starch polysaccharides with proteogenic amino acids. *Thermochim. Acta* **2001**, *372*, 119−128.
(25) Dollinger, G.; Cunico, B.; Kunitani, M.; Johnson, D.; Jones, R. Practical on-line determination of biopolymer molecular weights by high-performance liquid chromatography with classical light-scattering detection. *J. Chromatogr., A* **1992**, *592*, 215−228.
(26) Hill, H. D.; Straka, J. G. Protein determination using bicinchoninic acid in the presence of sulfhydryl reagents. *Anal. Biochem.* **1988**, *170*, 203−208.
(27) DuBois, M.; Gilles, K. A.; Hamilton, J. K.; Rebers, P. A.; Smith, F. Colorimetric method for determination of sugars and related substances. *Anal. Chem.* **1956**, *28*, 350−356.
(28) Blumenkrantz, N.; Asboe-Hansen, G. New method for quantitative determination of uronic acids. *Anal. Biochem.* **1973**, *54*, 484−489.
(29) Yan, W.; Niu, Y. G.; Lv, J. L.; Xie, Z. H.; Jin, L.; Yao, W. B.; Gao, X. D.; Yu, L. L. L. Characterization of a heteropolysaccharide isolated from diploid *Gynostemma pentaphyllum* Makino. *Carbohydr. Polym.* **2013**, *92*, 2111−2117.
(30) Pettolino, F. A.; Walsh, C.; Fincher, G. B.; Bacic, A. Determining the polysaccharide composition of plant cell walls. *Nat. Protoc.* **2012**, *7*, 1590−1607.
(31) Kim, J. S.; Reuhs, B. L.; Michon, F.; Kaiser, R. E.; Arumugham, R. G. Addition of glycerol for improved methylation linkage analysis of polysaccharides. *Carbohydr. Res.* **2006**, *341*, 1061−1064.
(32) CCRC. http://www.ccrc.uga.edu/specdb/ms/pmaa/pframe.html (accessed Oct 15, 2014).
(33) Rezanka, T.; Sigler, K. Structural analysis of a polysaccharide from *Chlorella kessleri* by means of gas chromatography-mass spectrometry of its saccharide alditols. *Folia Microbiol. (Praha)* **2007**, *52*, 246−252.
(34) Chen, L.; Cheung, P. C. K. Mushroom dietary fiber from the fruiting body of *Pleurotus tuber-regium*: fractionation and structural elucidation of nondigestible cell wall components. *J. Agric. Food Chem.* **2014**, *62*, 2891−2899.
(35) Liu, X. X.; Ma, H. X.; Yu, L.; Chen, L.; Tong, Z.; Chen, P. Thermal-oxidative degradation of high-amylose corn starch. *J. Therm. Anal. Calorim.* **2014**, *115*, 659−665.
(36) Flynn, J. H.; Wall, L. A. General treatment of the thermogravimetry of polymers. *J. Res. Natl. Bur. Stand.* **1966**, *70*, 487−523.
(37) Ozawa, T. A new method of analyzing thermogravimetric data. *Bull. Chem. Soc. Jpn.* **1965**, *38*, 1881−1886.
(38) Zhang, X. W.; Shang, P. P.; Qin, F.; Zhou, Q.; Gao, B. Y.; Huang, H. Q.; Yang, H. S.; Shi, H. M.; Yu, L. L. L. Chemical composition and antioxidative and anti-inflammatory properties of ten commercial mung bean samples. *LWT−Food Sci. Technol.* **2013**, *54*, 171−178.
(39) Huang, H. Q.; Cheng, Z. H.; Shi, H. M.; Xin, W. B.; Wang, T. T. Y.; Yu, L. L. L. Isolation and characterization of two flavonoids, engeletin and astilbin, from the leaves of *Engelhardia roxburghiana* and their potential anti-inflammatory properties. *J. Agric. Food Chem.* **2011**, *59*, 4562−4569.
(40) Casassa, E. F.; Markovitz, H. Statistical thermodynamics of polymer solutions. I. Theory of the second virial coefficient for a homogeneous solute. *J. Chem. Phys.* **1958**, *29*, 493−503.
(41) Hawker, C. J.; Lee, R.; Frechet, J. M. J. One-step synthesis of hyperbranched dendritic polyesters. *J. Am. Chem. Soc.* **1991**, *113*, 4583−4588.
(42) Ridley, B. L.; O'Neill, M. A.; Mohnen, D. Pectins: structure, biosynthesis, and oligogalacturonide-related signaling. *Phytochemistry* **2001**, *57*, 929−967.
(43) Èopíková, J.; Synytsya, A.; Èerná, M.; Kaasová, J.; Novotná, M. Application of FT-IR spectroscopy in detection of food hydrocolloids in confectionery jellies and food supplements. *Czech J. Food Sci.* **2000**, *19*, 51−56.
(44) Kac Uráková, M.; Capek, P.; Sasinková, V.; Wellner, N.; Ebringerová, A. FT-IR study of plant cell wall model compounds: pectic polysaccharides and hemicelluloses. *Carbohydr. Polym.* **2000**, *43*, 195−203.
(45) Ryden, P.; Colquhoun, I. J.; Selvendran, R. R. Investigation of structural features of the pectic polysaccharides of onion by ^{13}C-n.m.r. spectroscopy. *Carbohydr. Res.* **1989**, *185*, 233−237.
(46) Keenan, M. H. J.; Belton, P. S.; Matthew, J. A.; Howson, S. J. A ^{13}C-n.m.r. study of sugar-beet pectin. *Carbohydr. Res.* **1985**, *138*, 168−170.
(47) Joseleau, J.; Chambat, G.; Vignon, M.; Barnoud, F. Chemical and ^{13}C N.M.R. studies on two arabinans from the inner bark of young stems of *Rosa glauca*. *Carbohydr. Res.* **1977**, *58*, 165−175.
(48) Dourado, F.; Cardoso, S.; Silva, A.; Gama, F.; Coimbra, M. NMR structural elucidation of the arabinan from *Prunus dulcis* immunobiological active pectic polysaccharides. *Carbohydr. Polym.* **2006**, *66*, 27−33.
(49) Cardoso, S. M.; Silva, A. M.; Coimbra, M. A. Structural characterisation of the olive pomace pectic polysaccharide arabinan side chains. *Carbohydr. Res.* **2002**, *337*, 917−924.
(50) Willats, W. T.; McCartney, L.; Mackie, W.; Knox, J. P. Pectin: cell biology and prospects for functional analysis. In *Plant Cell Walls*; Carpita, N. C., Campbell, M., Tierney, M., Eds.; Springer: Dordrecht, The Netherlands, 2001; pp 9−27.
(51) Zheng, Y.; Mort, A. Isolation and structural characterization of a novel oligosaccharide from the rhamnogalacturonan of *Gossypium hirsutum* L. *Carbohydr. Res.* **2008**, *343*, 1041−1049.
(52) Habibi, Y.; Mahrouz, M.; Vignon, M. R. Arabinan-rich polysaccharides isolated and characterized from the endosperm of the seed of *Opuntia ficus-indica* prickly pear fruits. *Carbohydr. Polym.* **2005**, *60*, 319−329.
(53) Iqbal, M. S.; Akbar, J.; Saghir, S.; Karim, A.; Koschella, A.; Heinze, T.; Sher, M. Thermal studies of plant carbohydrate polymer hydrogels. *Carbohydr. Polym.* **2011**, *86*, 1775−1783.
(54) Ovodova, R. G.; Golovchenko, V. V.; Popov, S. V.; Popova, G. Y.; Paderin, N. M.; Shashkov, A. S.; Ovodov, Y. S. Chemical

DOI: 10.1021/acs.jafc.5b00494
J. Agric. Food Chem. 2015, 63, 3219−3228

composition and anti-inflammatory activity of pectic polysaccharide isolated from celery stalks. *Food Chem.* **2009**, *114*, 610−615.

DOI: 10.1021/acs.jafc.5b00494
J. Agric. Food Chem. 2015, 63, 3219−3228

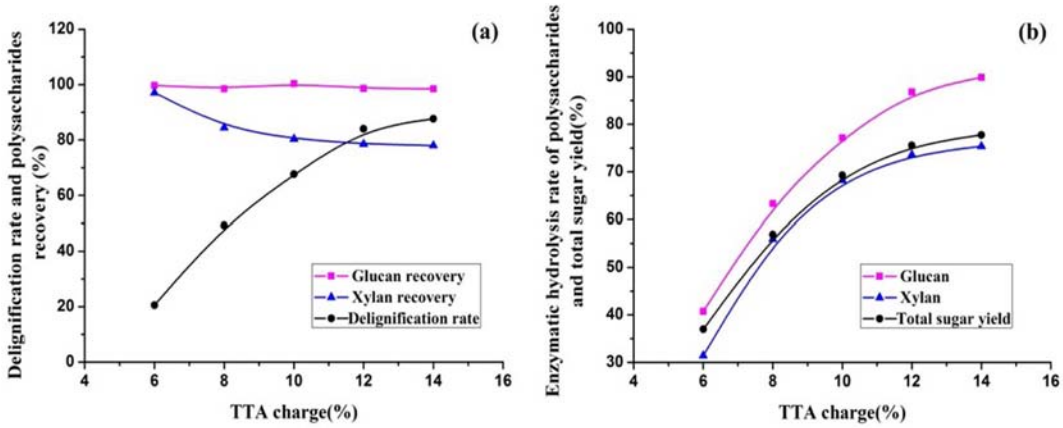

Figure 1. Effect of TTA charge on delignification rate, polysaccharide recovery, enzymatic hydrolysis rate of polysaccharides, and total sugar yield.

MATERIALS AND METHODS

Materials. The corn stover used in the present study was obtained from Qingdao, Shandong Province, China. Air-dried corn stover was milled using a plant grinder, and the particles between the sizes of 5 and 40 mesh were collected. The screened corn stover was stored in sealed plastic bags at room temperature.

Sodium hydroxide and sodium sulfite were purchased from Sinopharm Chemical Reagent Co. Ltd. The enzymes used for the enzymatic hydrolysis were Celluclast 1.5L (cellulase, enzyme activity 192 FPU/mL) and Novozyme 188 (β-glucosidase, enzyme activity 741 IU/mL) provided by Sigma-Aldrich China Inc. The enzymes activities were determined according to the method reported by Ghose.[22] All chemicals and enzymes were used as received.

Pretreatment of Corn Stover. The pretreatment of corn stover (50 g oven-dried) was carried out in a pot with a total volume of 1.5 L. Corn stover was subjected to pretreatment using sodium hydroxide (NaOH)−sodium sulfite (Na_2SO_3) with total titratable alkali charge of 6%, 8%, 10%, 12%, and 14%. The molar ratio of NaOH−Na_2SO_3 was 1:1. The ratio of pretreatment liquor to corn stover (oven-dried) charge was 4:1, 6:1, 8:1, 10:1, and 12:1, respectively. Both solution and corn stover were heated to the desired temperature in 20 min from 30 °C. The pretreatments were done at five levels in the range of 120−160 °C at holding time ranging from 10 to 50 min. After pretreatment, the bombs were cooled in water to room temperature. The solids were collected and washed with deionized water to remove residual chemicals and dissolved compounds and then used for determination of total solid, lignin, and polysaccharides prior to enzymatic hydrolysis.

PFI Refining. The pulp pretreated with alkali was beaten in a PFI mill. Beating conditions were as follows: pulp consistency 10%, beating gap 0.3 mm, revolutions in the range 1500−6000 rpm and increments of 1500 revolutions. The refined pulp was collected and stored in the refrigerator.

Enzymatic Hydrolysis. Enzymatic hydrolysis of the substrates was conducted on a 0.4 g (oven-dried) basis in a serum bottle with substrate consistency of 2% (W/V) at 50 °C using an incubator shaker at 95 rpm for 48 h. Sodium citrate buffer (pH = 4.8) was added to maintain the pH at 4.8, while 0.02% sodium azide was used in the mixture to inhibit the microbial infections. An enzyme cocktail of cellulase (20 PFU/g of dry biomass) and β-glucosidase (10 IU/g of dry biomass) was used for enzymatic hydrolysis.

Analysis Methods. *Chemical Component Analysis.* Cellulose, hemicellulose, and lignin contents of corn stover were determined according to the procedures described by National Renewable Energy Laboratory (NREL).[23] Acid and enzymatic hydrolysates were examined by high performance liquid chromatography (HPLC; model 1200, Agilent, USA). The HPLC system was equipped with a Bio-Rad Aminex HPX-87H column (300 mm × 7.8 mm) and refractive index detector. The column was run at 55 °C with sulfuric acid (0.005 M) as a mobile phase (0.5 mL/min), and the quantitative analysis was carried out using external standard calibration. Duplicate experiments were conducted, and the mean values were reported.

FTIR Analysis. The FTIR spectra of the untreated and pretreated corn stover were determined on a FTIR spectrometer (Nicolet 6700, Thermo Fisher Scientific Inc.). The samples were prepared by KBr pellet (the ratio of the samples to the KBr was 1:100). The resolution of the spectra was 4 cm^{-1} in the range of 400−4000 cm^{-1}, and 32 scans were taken for per sample.

SEM Analysis. The SEM analyses of the samples were conducted by scanning electron microscopy (S-4800, Hitachi, Japan) at different magnifications. The oven-dried dried samples were coated with platinum and treated with accelerating voltage of 3.0 kV.

RESULTS AND DISCUSSION

Optimization of the Alkali Dosage. The rates of delignification and polysaccharide retention after different pretreatments are presented in Figure 1a. Lignin is one of the major barriers for the enzymatic hydrolysis of lignocellulosic biomass. The efficiency of enzymatic hydrolysis was usually improved by the lignin removal.[24−26] The removal of lignin not only exposes more accessible cellulose but also reduces the strong surface interaction between lignin and enzyme. Figure 1a shows that the removal of lignin was improved by increasing the total titratable alkali (TTA) charge. When TTA charge was 14%, the removal of lignin was as high as 87.66%. Sodium hydrate has a certain effect on delignification. Sulfite also plays an important role in alkaline sulfite pretreatment process. The nucleophilic sulfite (SO_3^{2-}) in the pretreatment liquor lead to the sulfonation of lignin, as well as the break of α-benzyl ether linkages, α-alkyl ether linkages, and β-benzyl ether linkages on phenolic lignin units.[18] One can also observe that glucan and xylan decrease with the increase of TTA charge, and the degradation of glucan is less than that of xylan. One can infer that cellulose is more stable than hemicellulose under the alkaline sulfite pretreatment condition because of its high degree of polymerization and crystalline nature.[27] This is the main disadvantage of alkali-based pretreatment at present. So how to promote the deprivation of lignin and maximum preservation of hemicellulose will be an important research topic.

The enzymatic hydrolysis rates of polysaccharides and total sugar yield at different chemical charge are illustrated in Figure 1b. Undoubtedly, higher chemical charge will enhance the enzymatic hydrolysis rates of polysaccharides. When the TTA charge increased from 6% to 14%, the enzymatic hydrolysis rates of glucan and xylan increased more than one times. This

DOI: 10.1021/jf505433q
J. Agric. Food Chem. 2015, 63, 3229−3234

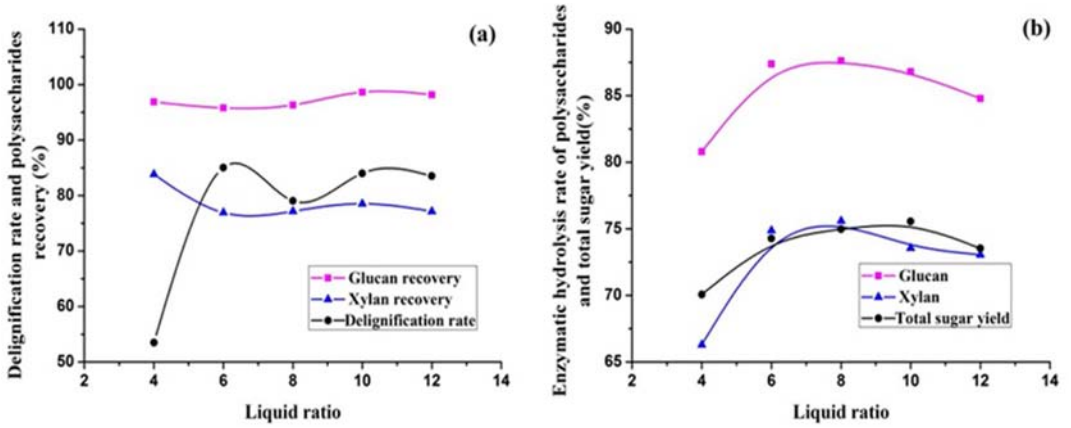

Figure 2. Effect of liquid/solid ratio on delignification rate, polysaccharide recovery, enzymatic hydrolysis rate of polysaccharides, and total sugar yield.

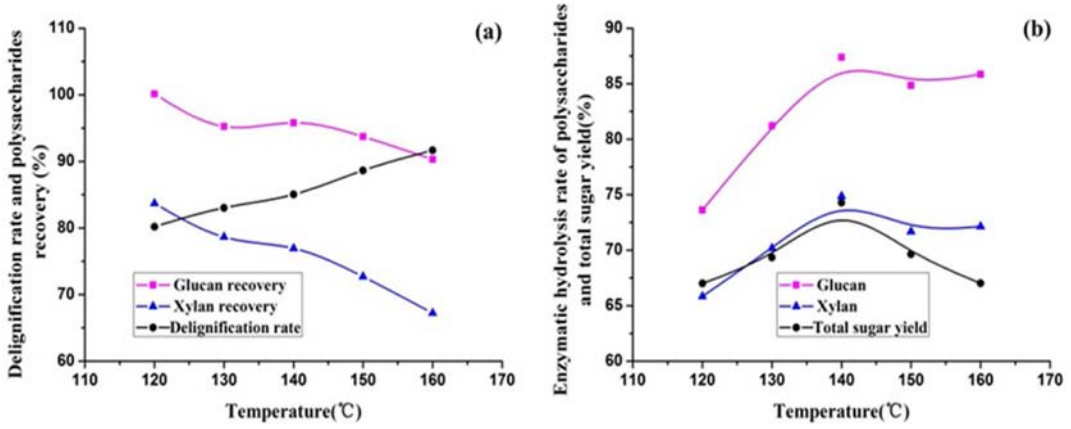

Figure 3. Effect of temperature on delignification rate, polysaccharide recovery, enzymatic hydrolysis rate of polysaccharides, and total sugar yield.

results from the destruction of cell walls and the dissolution of hemicellulose and lignin. It is obvious that the total sugar yield showed a rapid increase trend with the increase of alkali dosage and reached the maximum value when the TTA charge was 12%. However, the total sugar yield did not increase when we continued to increase the TTA charge to 14%. This was because the retention rate of glucan and xylan decreased in different degrees though the enzymatic hydrolysis rates of glucan and xylan increased 3.52% and 2.45%, respectively, when we continued to increase the TTA charge. Based on the data from Figure 1, one can conclude that 12% is the optimal dosage of chemicals for alkaline sulfite pretreatment.

Optimization of the Liquid/Solid Ratio. Figure 2a shows the impacts of liquid/solid ratio on the delignification rates and polysaccharide retention when TTA charge is 12%. About 85% of the lignin in the raw material was removed when the liquid/solid ratio was 6:1. However, when liquid/solid ratio was 4:1, the removal of lignin was only 53.48%. A high concentration of lignin in the pretreatment liquid can inhibit the dissolution of lignin in the raw material. But if the liquid/solid ratio is too high, the high liquid/solid ratio will reduce the concentration of chemicals and increase the difficulty of subsequent processing. In addition, the data showed that the role of liquid/solid ratio on polysaccharide retention is not significant.

According to the curves of enzymatic hydrolysis rates of polysaccharides and total sugar yield in Figure 2b, some details can be seen. With the increase of liquid/solid ratio, enzymatic hydrolysis rates of polysaccharides increased first and then decreased, and there was little difference when liquid/solid ratio ranged from 6 to 10. Total sugar yield showed the same trends. For example, the total sugar yields were 70.07% and 73.53%, respectively, when liquid/solid ratio was 4:1 and 6:1. In addition, the total sugar yield was only 74.28−75.56% when liquid/solid ratio ranged from 6 to 10. Therefore, the liquid/solid ratio of 6:1 was optimal.

Optimization of Temperature. Figure 3a shows the effect of temperature on the delignification rates and polysaccharide retention under the conditions of TTA charge at 12% and liquid/solid ratio of 6:1. The data show that lignin removal increased with the pretreatment temperature. For example, the removal of lignin increased from 80.19% to 91.66% when the temperature rose from 120 to 160 °C. This indicates that pretreatment temperature plays an important role in delignification. However, the retention of polysaccharides reduced with increasing pretreatment temperature. The degradation of xylan is higher than that of glucan in the same pretreatment conditions. This demonstrates that hemicellulose in corn stover is easier to degrade than cellulose in alkaline sulfite pretreatment.

The enzymatic hydrolysis rates of polysaccharides, increased first and then decreased, can be seen from Figure 3b. It is obvious that the enzymatic hydrolysis rate at 140 °C is much higher than that at 120 °C. This is mainly caused by the limited removal of hemicellulose and lignin at relatively low temper-

DOI: 10.1021/jf505433q
J. Agric. Food Chem. 2015, 63, 3229−3234

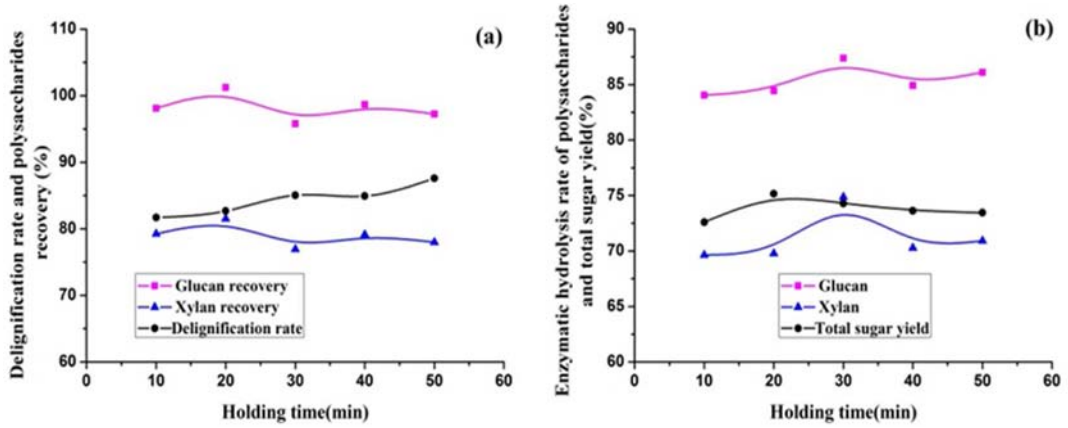

Figure 4. Effect of holding time on delignification rate, polysaccharide recovery, enzymatic hydrolysis rate of polysaccharides, and total sugar yield.

ature, which does not provide a loose enough structure of corn stover.[28] According to the curve of total sugar yield of pretreated corn stover in Figure 3, the highest sugar yield is obtained at 140 °C, which is 74.28%. Furthermore, temperature higher than 140 °C was not necessary nor recommended because higher temperature consumes more energy. Hence, 140 °C was recommended as the optimum pretreatment temperature.

Optimization of the Holding Time. In order to investigate the effect of holding time on delignification rates, polysaccharide retention, enzymatic hydrolysis rates, and total sugar yield, the pretreatments were done at holding time ranging from 10 to 50 min. Figure 4a shows the effect of holding time on and polysaccharide retention. One can observe that the delignification rates were increased with the increase of the holding time while the polysaccharides retention decreased. As seen in Figure 4b, increasing the holding time from 10 to 50 min only led to 2% increase in the enzymatic hydrolysis rates of glucan. When holding time was more than 20 min, the total sugar yield decreased because of the reduction in polysaccharide retention. The holding time of 20 min can obtain a better effect.

Comparison of Pretreatment between Alkaline Sulfite and Sodium Hydroxide. Optimum pretreatment conditions were obtained through the above optimization experiments: total titratable alkali of 12%, liquid/solid ratio of 6:1, temperature of 140 °C, and holding time of 20 min. Figure 5 shows the comparison between alkaline sulfite pretreatment and sodium hydroxide pretreatment under the optimum conditions. Delignification rates and polysaccharide retention rates of corn stover pretreated with alkaline sulfite are higher than those when we used sodium hydroxide alone. This is because the nucleophilic sulfite (SO_3^{2-}) and bisulfite (HSO_3^-) lead to the sulfonation of lignin. Sulfonation makes the lignin more hydrophilic. In addition, a lower sodium hydroxide charge reduces the degradation of cellulose and hemicellulose, which enhances the retention of carbohydrate. For example, compared with sodium hydroxide pretreatment, the retention of xylan is improved by more than 10%.

Figure 6 shows the enzymatic hydrolysis rates and total sugar yield of the corn stover pretreated by two different methods and then beaten with a PFI mill. One can observe that both the enzymatic hydrolysis rate of polysaccharides and total sugar yield are improved with the increase of revolutions. The shearing action in mechanical refining results in more internal delamination and surface fibrillation, which will disrupt the

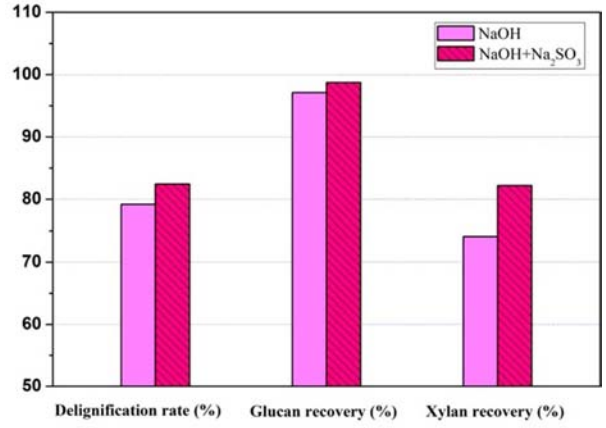

Figure 5. Comparison of alkaline sulfite pretreatment and sodium hydroxide pretreatment.

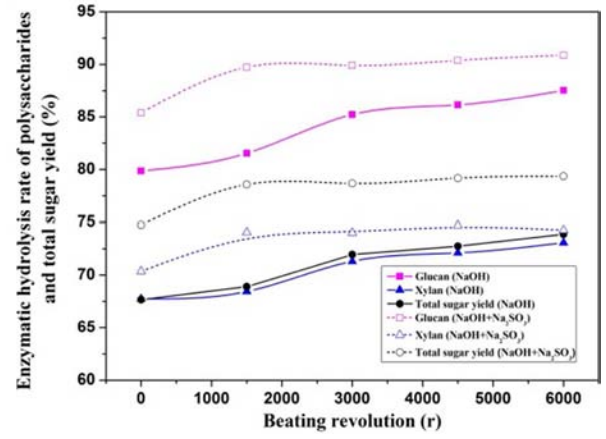

Figure 6. Effect of refining on enzymatic hydrolysis of polysaccharides and total sugar yield.

crystalline structure of the cellulose microfibrils, increase the accessible specific areas, and lead to a more efficient biomass digestibility.[29] Xu et al. found that beating degree of PFI refined substrates was strongly linear with final total sugar yields for the given pretreated corn stover.[30] Furthermore, it can achieve a relatively high enzymatic hydrolysis rate of polysaccharides with PFI refining at 1500 revolutions, and the total sugar yield was 78.58%. Compared with the sodium hydroxide pretreatment, the total sugar yield was increased by about 9.68%.

DOI: 10.1021/jf505433q
J. Agric. Food Chem. 2015, 63, 3229−3234

Mechanism Analysis for the Improvement of Corn Stover Enzymatic Hydrolysis Rate. *FTIR Analysis.* FTIR spectra of untreated and pretreated corn stover are shown in Figure 7. In particular, all the spectra are dominant by signals at

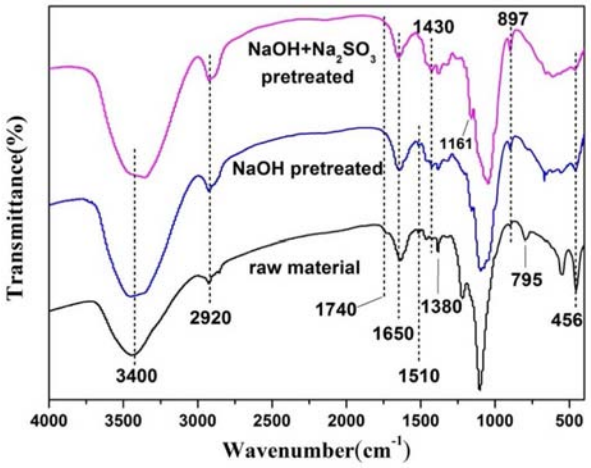

Figure 7. FTIR spectra of untreated and pretreated corn stover.

3400 and 2920 cm^{-1} due to the stretching vibrations of O−H and C−H corresponding to the aliphatic moieties in lignin and polysaccharides.[31] A shoulder at 1740 cm^{-1} is attributed to the acetyl and uronic ester groups on hemicellulose or linkages in lignin and ester hemicellulose feurilic and p-coumaric acid carboxylic groups.[32] The band at 1740 cm^{-1} being almost absent indicated that the pretreatment nearly cleaved this ester band from the hemicellulose and lignin. The lignin-associated peaks at 1510 and 795 cm^{-1} that were assigned to aromatic ring stretch vibrations in lignin were decreased, indicating the removal of the lignin after pretreatment. Furthermore, the band at 1510 cm^{-1} after alkaline sulfite pretreatment almost vanishes, which also indicates that the alkaline sulfite pretreatment is more efficient than sodium hydroxide on delignification. The carbohydrate-related peaks at 1380 and 1161 cm^{-1} were assigned to the C−H deformation in carbohydrate and C−O−C vibration in cellulose and hemicellulose.[33] After pretreatment, the intensity of these bands was decreased due to the degradation of cellulose and hemicellulose, and after sodium hydroxide pretreatment, the intensity decreased more severely than after alkaline sulfite pretreatment, which corresponded to the results obtained by sugar analysis. In addition, the peak at 897 cm^{-1} was associated with the β-glucosidic bonds of cellulose, and its increase after pretreatment was also because of the removal of lignin and hemicelluloses.[34] As can be seen from Figure 7, the band at 897 cm^{-1} after alkaline sulfite pretreatment is stronger than that after sodium hydroxide pretreatment, which indicated that the degradation of lignin and hemicellulose were relatively stronger in alkaline sulfite pretreatment. The decrease of the peak at 465 cm^{-1} (Si−O) was due to the removal of ash.

SEM Analysis. Pretreatment affects not only the chemical composition of the corn stover but also the physical appearance of the corn stover at the microscopic level. The scanning electron micrograph (SEM) images of untreated and pretreated corn stover are shown in Figure 8 at different magnifications. The surface of the corn stover that is untreated shown in Figure 8a,b is smooth and contiguous without pores. The tissue surface and cell wall were altered after pretreatment. Figure 8c,d

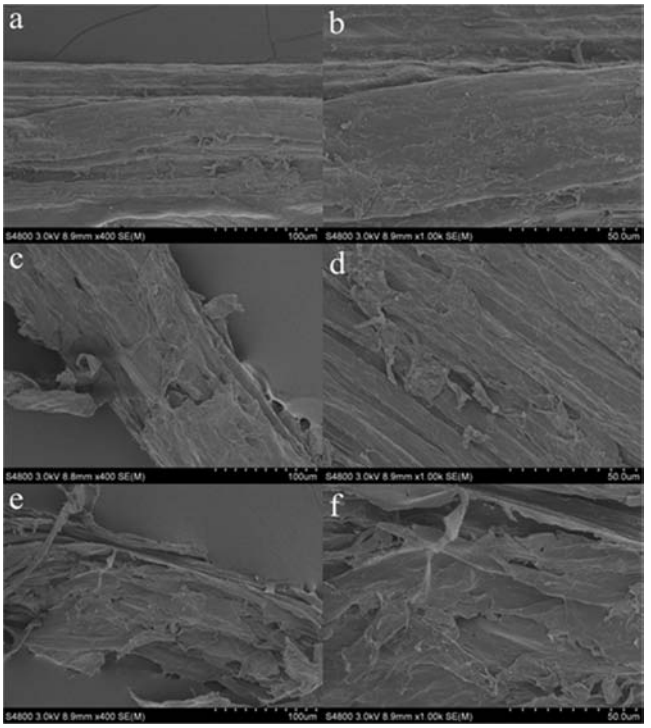

Figure 8. SEM of untreated and pretreated corn stover: (a, b) raw corn stover without pretreatment; (c, d) samples pretreated with NaOH pretreatment; (e, f) samples pretreated with alkali sulfite pretreatment. Pretreatment was performed at 140 °C with the liquid/solid ratio of 6 and 12% alkali.

shows images of corn stover after NaOH pretreatment. The smooth, contiguous surface of untreated stover has been perforated by the pretreatment processes. Alkaline pretreatments disrupt the lignocellulosic structure by dissolving lignin and hemicellulose. Treatment with Na_2SO_3 significantly alters the fibrillar structure. Coarse surfaces and porous areas are very evident. The microfibrils are separated from the initial connected structure and fully exposed. This would increase the external surface area and the porosity of the biomass.[35] These pores may increase the enzyme accessible surface area, which increases the enzyme digestibility of the corn stover.[36]

Conclusion. The optimum conditions of alkaline sulfite pretreatment for corn stover were as follows: total titratable alkali of 12%, liquid/solid ratio of 6:1, temperature of 140 °C, and holding time of 20 min. The delignification rate and the total sugar yield at the optimal condition were 82.45% and 74.73%, respectively, which was higher than those under only NaOH pretreatment, 79.20% and 67.67%. The corn stover pretreated under the optimum pretreatment conditions was beaten by PFI for 1500 rotations. After beating, the total sugar yield was 78.58%. Compared with 1500 rotations of PFI beating after sodium hydroxide pretreatment at the same amount of total titratable alkali, the total sugar yield improvement rate was 14.05%. Furthermore, lignin dissolved in the alkaline sulfite pretreatment exists in the form of lignosulfonate, which is a potential high-value coproduct. Thus, alkaline sulfite pretreatment is a suitable process for corn stover conversion to fermentable sugars.

DOI: 10.1021/jf505433q
J. Agric. Food Chem. 2015, 63, 3229−3234

AUTHOR INFORMATION

Corresponding Authors

*H. Wang. Phone: +86 532 80662725. Fax: +86 532 80662725. E-mail: wanghs@qibebt.ac.cn.

*M. Niu. E-mail: niumh@dlpu.edu.cn.

Funding

This research was funded by the Natural Science Foundation of China (Grant Nos. 21206184, 31370582, and 31370584) and the National High Technology Research and Development Program ("863" program) of China (Grant No. 2012AA022301).

Notes

The authors declare no competing financial interest.

REFERENCES

(1) Zhao, Y.; Wang, Y.; Zhu, J.; Ragauskas, A.; Deng, Y. Enhanced enzymatic hydrolysis of spruce by alkaline pretreatment at low temperature. *Biotechnol. Bioeng.* **2008**, *99* (6), 1320−1328.

(2) Sánchez, Ó. J.; Cardona, C. A. Trends in biotechnological production of fuel ethanol from different feedstocks. *Bioresour. Technol.* **2008**, *99* (13), 5270−5295.

(3) Bozell, J. J.; Petersen, G. R. Technology development for the production of biobased products from biorefinery carbohydrates-the US Department of Energy's "top 10" revisited. *Green Chem.* **2010**, *12* (4), 539−554.

(4) Wan, C.; Zhou, Y.; Li, Y. Liquid hot water and alkaline pretreatment of soybean straw for improving cellulose digestibility. *Bioresour. Technol.* **2011**, *102* (10), 6254−9.

(5) Gao, Z.; Mori, T.; Kondo, R. The pretreatment of corn stover with *Gloeophyllum trabeum* KU-41 for enzymatic hydrolysis. *Biotechnol. Biofuels* **2012**, *5* (1), 1−11.

(6) Chen, M.; Zhao, J.; Xia, L. Comparison of four different chemical pretreatments of corn stover for enhancing enzymatic digestibility. *Biomass Bioenergy* **2009**, *33* (10), 1381−1385.

(7) He, X.; Miao, Y.; Jiang, X.; Xu, Z.; Ouyang, P. Enhancing the enzymatic hydrolysis of corn stover by an integrated wet-milling and alkali pretreatment. *Appl. Biochem. Biotechnol.* **2010**, *160* (8), 2449−57.

(8) Mosier, N.; Wyman, C.; Dale, B.; Elander, R.; Lee, Y. Y.; Holtzapple, M.; Ladisch, M. Features of promising technologies for pretreatment of lignocellulosic biomass. *Bioresour. Technol.* **2005**, *96* (6), 673−86.

(9) Emmel, A.; Mathias, A. L.; Wypych, F.; Ramos, L. P. Fractionation of *Eucalyptus grandis* chips by dilute acid-catalysed steam explosion. *Bioresour. Technol.* **2003**, *86* (2), 105−115.

(10) Kim, T. H.; Lee, Y. Y. Fractionation of corn stover by hot-water and aqueous ammonia treatment. *Bioresour. Technol.* **2006**, *97* (2), 224−32.

(11) Millet, M. A.; Baker, A. J.; Scatter, L. D. Physical and chemical pretreatment for enhancing cellulose saccharification. *Biotechnol. Bioeng. Symp.* **1976**, *18* (6), 125−153.

(12) Camesasca, L.; Ramírez, M. B.; Guigou, M.; Ferrari, M. D.; Lareo, C. Evaluation of dilute acid and alkaline pretreatments, enzymatic hydrolysis and fermentation of napiergrass for fuel ethanol production. *Biomass Bioenergy* **2015**, *74* (0), 193−201.

(13) Park, N.; Kim, H.-Y.; Koo, B.-W.; Yeo, H.; Choi, I.-G. Organosolv pretreatment with various catalysts for enhancing enzymatic hydrolysis of pitch pine (*Pinus rigida*). *Bioresour. Technol.* **2010**, *101* (18), 7046−7053.

(14) Zhao, X.; Moates, G. K.; Wilson, D. R.; Ghogare, R. J.; Coleman, M. J.; Waldron, K. W. Steam explosion pretreatment and enzymatic saccharification of duckweed (*Lemna minor*) biomass. *Biomass Bioenergy* **2015**, *72* (0), 206−215.

(15) Lee, J. M.; Jameel, H.; Venditti, R. A. A comparison of the autohydrolysis and ammonia fiber explosion (AFEX) pretreatments on the subsequent enzymatic hydrolysis of coastal Bermuda grass. *Bioresour. Technol.* **2010**, *101* (14), 5449−5458.

(16) Wang, F.-Q.; Xie, H.; Chen, W.; Wang, E.-T.; Du, F.-G.; Song, A.-D. Biological pretreatment of corn stover with ligninolytic enzyme for high efficient enzymatic hydrolysis. *Bioresour. Technol.* **2013**, *144* (0), 572−578.

(17) Hansen, N. M.; Plackett, D. Sustainable films and coatings from hemicelluloses: A review. *Biomacromolecules* **2008**, *9* (6), 1493−1505.

(18) Yang, L.; Cao, J.; Mao, J.; Jin, Y. Sodium carbonate-sodium sulfite pretreatment for improving the enzymatic hydrolysis of rice straw. *Ind. Crops Prod.* **2013**, *43*, 711−717.

(19) Sixta, H. *Handbook of Pulp*; WILEY-VCH Verlag GmbH & Co. KGaA: Weinheim, Germany, 2006; Vol. *1*.

(20) von Schenck, A.; Berglin, N.; Uusitalo, J. Ethanol from Nordic wood raw material by simplified alkaline soda cooking pre-treatment. *Appl. Energy* **2013**, *102*, 229−240.

(21) Li, Q.; Gao, Y.; Wang, H.; Li, B.; Liu, C.; Yu, G.; Mu, X. Comparison of different alkali-based pretreatments of corn stover for improving enzymatic saccharification. *Bioresour. Technol.* **2012**, *125*, 193−199.

(22) Ghose, T. Measurement of cellulase activities. *Pure Appl. Chem.* **1987**, *59* (2), 257−268.

(23) Sluiter, A.; Hames, B.; Ruiz, R.; Scarlata, C.; Sluiter, J.; Templeton, D.; Crocker, D. *Determination of structural carbohydrates and lignin in biomass. Laboratory analytical procedure*; National Renewable Energy Laboratory: Golden, CO, 2008.

(24) Alvira, P.; Tomas-Pejo, E.; Ballesteros, M.; Negro, M. J. Pretreatment technologies for an efficient bioethanol production process based on enzymatic hydrolysis: A review. *Bioresour. Technol.* **2010**, *101* (13), 4851−61.

(25) Antoni, D.; Zverlov, V. V.; Schwarz, W. H. Biofuels from microbes. *Appl. Microbiol. Biotechnol.* **2007**, *77* (1), 23−35.

(26) Ban, W.; Wang, S.; Lucia, L. A. The relationship of pretreatment pulping parameters with respect to selectivity: optimization of green liquor pretreatment conditions for improved kraft pulping. *Pap. Puu* **2003**, *85*, 1−7.

(27) Gu, F.; Yang, L.; Jin, Y.; Han, Q.; Chang, H. M.; Jameel, H.; Phillips, R. Green liquor pretreatment for improving enzymatic hydrolysis of corn stover. *Bioresour. Technol.* **2012**, *124*, 299−305.

(28) Yang, L.; Cao, J.; Jin, Y.; Chang, H. M.; Jameel, H.; Phillips, R.; Li, Z. Effects of sodium carbonate pretreatment on the chemical compositions and enzymatic saccharification of rice straw. *Bioresour. Technol.* **2012**, *124*, 283−291.

(29) Jones, B. W.; Venditti, R.; Park, S.; Jameel, H.; Koo, B. Enhancement in enzymatic hydrolysis by mechanical refining for pretreated hardwood lignocellulosics. *Bioresour. Technol.* **2013**, *147*, 353−360.

(30) Xu, H.; Li, B.; Mu, X.; Yu, G.; Liu, C.; Zhang, Y.; Wang, H. Quantitative characterization of the impact of pulp refining on enzymatic saccharification of the alkaline pretreated corn stover. *Bioresour. Technol.* **2014**, *169*, 19−26.

(31) Sun, X.; Xu, F.; Sun, R.; Fowler, P.; Baird, M. Characteristics of degraded cellulose obtained from steam-exploded wheat straw. *Carbohydr. Res.* **2005**, *340* (1), 97−106.

(32) Kumar, R.; Mago, G.; Balan, V.; Wyman, C. E. Physical and chemical characterizations of corn stover and poplar solids resulting from leading pretreatment technologies. *Bioresour. Technol.* **2009**, *100* (17), 3948−3962.

(33) Xu, C.; Ma, F.; Zhang, X.; Chen, S. Biological pretreatment of corn stover by *Irpex lacteus* for enzymatic hydrolysis. *J. Agric. Food Chem.* **2010**, *58* (20), 10893−10898.

(34) Mou, H.; Li, B.; Fardim, P. Pretreatment of Corn Stover with the Modified Hydrotropic Method To Enhance Enzymatic Hydrolysis. *Energy Fuels* **2014**, *28* (7), 4288−4293.

(35) Kim, T. H.; Lee, Y. Y. Pretreatment and fractionation of corn stover by ammonia recycle percolation process. *Bioresour. Technol.* **2005**, *96* (18), 2007−2013.

(36) Mosier, N.; Hendrickson, R.; Ho, N.; Sedlak, M.; Ladisch, M. R. Optimization of pH controlled liquid hot water pretreatment of corn stover. *Bioresour. Technol.* **2005**, *96* (18), 1986−1993.

DOI: 10.1021/jf505433q
J. Agric. Food Chem. 2015, 63, 3229−3234

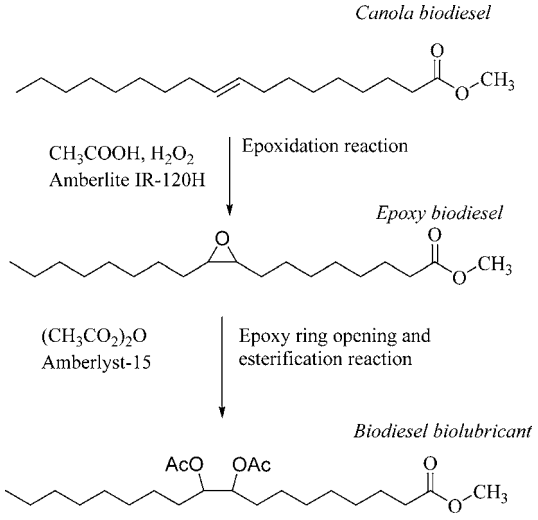

Figure 2. Reaction scheme for the synthesis of biodiesel derived biolubricant.

out using Amberlite IR-122 resin as catalyst.[18] Also, Amberlite IR-120H resin was found to be active catalyst for the epoxidation of polyunsaturated canola triglycerides.[12]

A few studies have been reported on the vicinal diacylation of epoxidized vegetable oils to obtain the product biolubricant. Hwang and Erhan[19] studied epoxy ring-opening by various linear and branched alcohols. Adhvaryu et al.[20] synthesized acylated soybean oil derivatives (biolubricants) using different carboxylic anhydrides and pyridine as catalysts. The synthesis method reported by Salimon et al.[21] for the acylation of ricinoleic acid includes sulfuric acid as a catalyst. Limited literature reports are available on the application of heterogeneous catalysts for the simultaneous oxirane ring-opening and diacylation of epoxidized triglycerides in vegetable oils to obtain biolubricant (i.e., esterified product). Application of solid metal oxide catalysts for the preparation of biolubricants from vegetable oils not only promote green technology but also minimize workup procedures to separate the product and the catalyst can be reused several times.[22,23]

The present investigation deals with the synthesis of biolubricants from canola oil and canola biodiesel by using heterogeneous catalysts (Figures 1 and 2). As per our knowledge, this report finds novelty with the preparation of

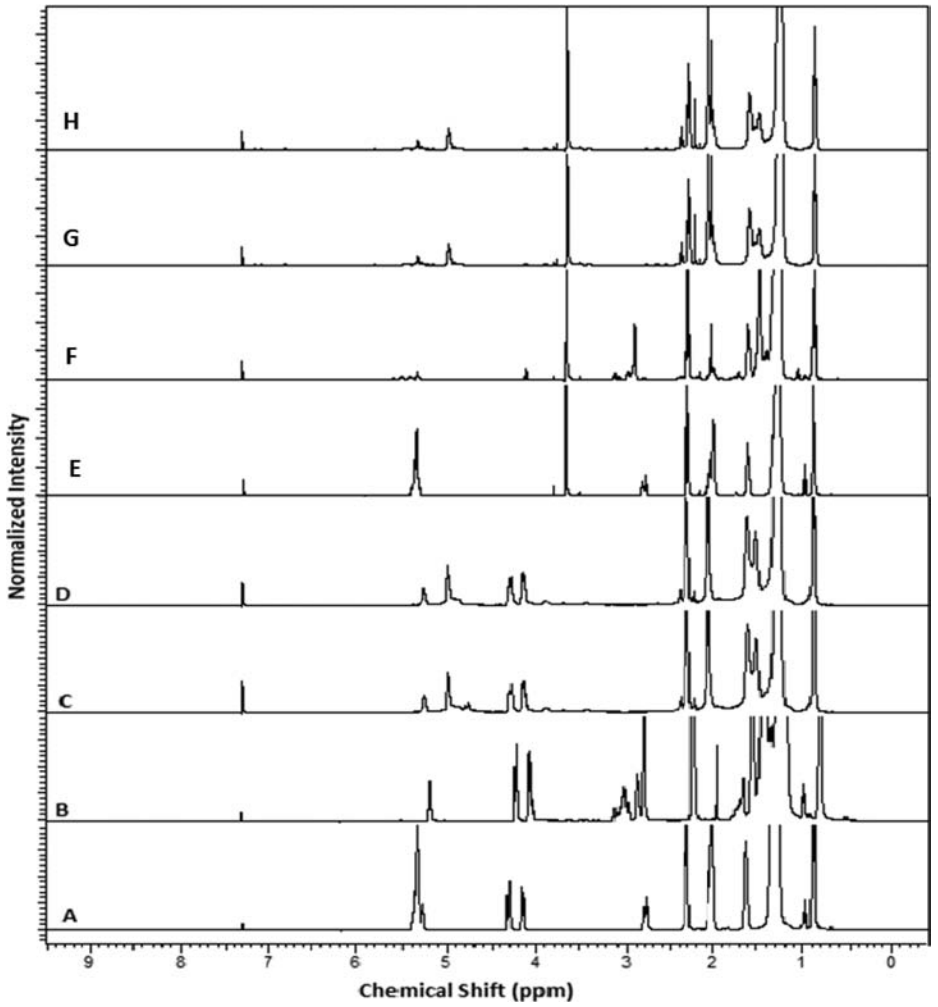

Figure 3. ^{1}H NMR spectra: (A) canola oil, (B) epoxidized canola oil, (C) biolubricant from canola oil, (D) D_2O exchanged biolubricant from canola oil, (E) canola biodiesel, (F) epoxidized canola biodiesel, (G) biolubricant from canola biodiesel, and (H) D_2O exchanged biolubricant from canola biodiesel.

DOI: 10.1021/jf505825k
J. Agric. Food Chem. 2015, 63, 3235−3242

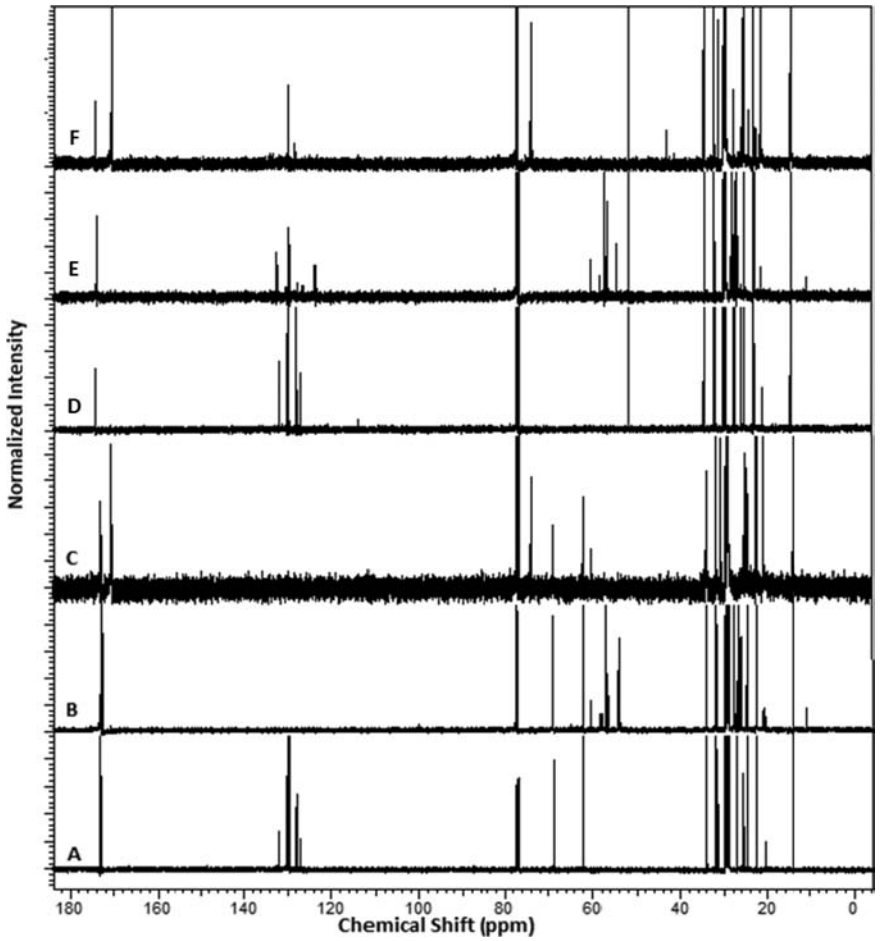

Figure 4. ^{13}C NMR spectra: (A) canola oil, (B) epoxidized canola oil, (C) biolubricant from canola oil, (D) canola biodiesel, (E) epoxidized canola biodiesel, and (F) biolubricant from canola biodiesel.

new value-added product biolubricant from canola biodiesel and the characteristic lubricity properties associated with it in comparison to canola oil biolubricant.

EXPERIMENTAL SECTION

Chemicals and Reagents. Edible grade canola oil (Loblaws Inc. Montreal, Canada), canola biodiesel (Milligan Biofuels Inc., Saskatoon, Canada), glacial acetic acid (reagent grade), 30 wt % hydrogen peroxide (GR grade) (EMD Chemicals Inc., Darmstadt, Germany), Amberlite IR-120H (Sigma-Aldrich, St. Louis, MO), Amberlyst-15 (Sigma-Aldrich, St. Louis, MO), Wijs' solution (VWR, San Diego, CA), ethyl acetate, and 33 wt % hydrobromic acid in acetic acid (EMD Chemicals Inc., Montreal, Canada) were purchased.

Analytical Methods. The iodine value (% unsaturation) analysis was carried out as per the AOCS Cd 1−25 standard method. The amount of epoxy content (oxirane oxygen) in the oil was calculated using AOCS Cd 9-57 volumetric titration method. Each experiment was repeated thrice and found to have ±3% error in the conversion. Equations 1 and 2 give the appropriate formulas employed for determining the change in the percentage unsaturation and the epoxy content in the oils during the course of the reaction.

$$\text{oxirane oxygen content} = \frac{\text{mL of HBr consumed} \times N \times 1.60}{\text{mass of sample, g}} \quad (1)$$

Where, N stands for HBr solution normality.

$$\text{epoxy conversion (\%)} = \frac{\text{oxirane value at O h} - \text{oxirane value at time } (t)}{\text{oxirane value at O h}} \times 100 \quad (2)$$

Kinematic viscosity, cloud point, and pour point were measured as per the ASTM methods. The oxidative stability measurements were carried out by AOCS methods. Lubricity of the products was performed according to ASTM methods. Thermogravimetric analysis was carried to determine the weight loss of materials. The details of the analysis procedure and equipment used for the determination of tribological properties of biolubricants are described in the literature.[6,23]

EXPERIMENTAL SETUP AND PROCEDURE

Epoxidation. The unsaturated fatty acids present in the feed stocks such as canola oil and canola biodiesel were epoxidized by using hydrogen peroxide and acetic acid.[6] A sample of 22.6 g of canola oil/biodiesel, acetic acid, and Amberlite IR −120H (22 wt % w.r.t to g of feed stock taken) were placed in a three neck round-bottom flask and maintained at 65 ± 2 °C. Then, aqueous hydrogen peroxide (30 wt %) was added with a molar ratio of 1.5:1 (unsaturation in canola oil/canola biodiesel: H_2O_2). The reaction was continued at 65 ± 2 °C for 8 h with rapid stirring. The oil phase was extracted using ethyl acetate as solvent and was separated by evaporation. The conversion was assessed by the iodine value (7.5 and 7.6 g of I_2/100 g for canola oil and biodiesel, respectively), oxirane content (5.6 and 5.8%), and glycol

DOI: 10.1021/jf505825k
J. Agric. Food Chem. 2015, 63, 3235−3242

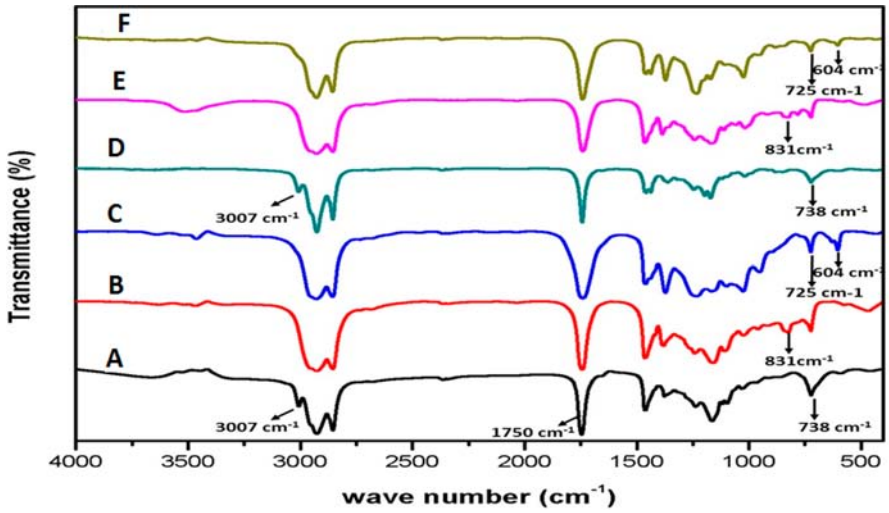

Figure 5. FTIR spectrum: (A) canola oil, (B) epoxidized canola oil, (C) biolubricant from canola oil, (D) canola biodiesel, (E) epoxidized canola biodiesel, and (F) biolubricant from canola biodiesel.

content (0.08 and 0.06 mol/100 g) of canola oil and canola biodiesel, respectively. Further, the product formation was also confirmed by spectroscopic techniques such as ^{1}H NMR, ^{13}C NMR, and FT-IR.

Epoxy Ring-Opening of Epoxidized Canola Oil/Epoxidized Biodiesel. The oxirane ring-opening and diacylation reactions were performed in a single pot. Typically, 30.0 g of epoxidized canola oil/epoxidized biodiesel, 45 g of acetic anhydride, and Amberlyst-15 (10 wt % of epoxidized product) were mixed in the three neck round-bottom flask and stirred for 15 h at 130 °C. The percentage epoxy conversion was measured periodically by the oxirane content method (eq 1), and the product formation was also identified with FTIR, ^{1}H NMR, and ^{13}C NMR analysis.

RESULTS AND DISCUSSION

Characterization of Products. *NMR Spectroscopy.* Figure 3 represents ^{1}H NMR spectra of starting materials and products. The olefinic hydrogens (H−C═C−H) of canola oil and canola biodiesel showed a chemical shift between 5.2 and 5.4 ppm. These proton shifts were found to be absent in the epoxidized canola oil and epoxidized canola biodiesel, indicating that all olefinic groups are converted to the epoxy group. ^{1}H NMR spectra of epoxidized canola oil and epoxidized canola biodiesel showed a chemical shift between 2.7 and 3.1 ppm due to the vicinity of epoxy oxygen.[12] The CH_2 proton α-to epoxy group showed a chemical shift at 1.9 ppm, while the β-CH_2 proton has a chemical shift at 1.6 ppm. The terminal $-CH_3$ proton indicates the chemical shift at 0.8−1.0 ppm. ^{1}H NMR spectra of canola oil biolubricant and biolubricant from canola biodiesel show a chemical shift at 5.0 ppm, which represents both CH− protons associated with the carbonyl group. The D_2O exchanged ^{1}H NMR spectrum of canola oil biolubricant, and biolubricant from canola biodiesel confirmed the absence of hydroxyl proton in the molecule which indicates the formation of diacylated product after the epoxy ring-opening step. Figure 3 confirmed the presence of methine proton of glycerol backbone by the signal appearing between 5.2 and 5.4 ppm and also the presence of $-COOCH_3$ proton that appeared at 3.7 ppm, which is characteristic of canola biodiesel.

Figure 4 represents ^{13}C NMR spectra of starting materials and products. Canola oil and canola biodiesel showed the signal appearing between 120 and 140 ppm due to the existence of olefinic carbon atoms. Epoxidized canola oil and epoxidized canola biodiesel exhibited no signal between 120 and 140 ppm, indicating the conversion of the olefinic carbon (−C═C−) to epoxy linkage, given by the signal appearing between 53 and 58 ppm. Biolubricant from canola oil and biolubricant from canola biodiesel showed no signal between 53 and 58 ppm, which indicates the conversion of epoxy linkage to ester linkage. This is indicated by a new signal at 170 ppm, which is attributed to carbonyl carbon. The presence of glycerol backbone in canola oil biolubricant is indicated by the shift at 62 and 68 ppm for α and β carbon atoms of the glycerol backbone, respectively. Figure 4 also confirmed the presence of $-CH_3$ carbon of $-COOCH_3$ that appeared at 51 ppm, which is characteristic of canola biodiesel. Therefore, the formation of canola oil biolubricant and canola biodiesel-derived biolubricant is confirmed by the NMR spectra.

FT-IR Spectroscopy. FT-IR transmittance spectra of the products and reactants were recorded to confirm the formation of biolubricant on the basis of functional groups present. FT-IR spectra are shown in Figure 5. Canola oil and canola biodiesel show the bands at 3007 and 738 cm^{-1}, which are due to the bending and stretching vibrations of H−C═C−H. No bands appeared at 3007 and 738 cm^{-1} indicating that −C═C− bonds in the oil are converted into epoxide. Epoxy band was found to appear at 831 cm^{-1}.[24] The FT-IR spectra of biolubricant from canola oil and biolubricant from canola biodiesel have no band at 831 cm^{-1}, indicating the absence of the epoxy group. However, two new bands appeared at 725 and 604 cm^{-1}, with also a corresponding increased intensity of the band at 1750 cm^{-1}. This confirmed the ester structure present in the products. Hence, FT-IR analysis indicated the formation of biolubricant from canola oil and canola biodiesel which was also confirmed by NMR results.

Low Temperature Properties. The cold flow temperature properties of the biolubricants from canola oil and canola biodiesel were represented by the cloud point and pour point. These properties of lubricants derived from vegetable oil are poor, hence, making it difficult to use in cold countries. It can be improved by reducing the aliphatic carbon chain length. Table 1 represents the low-temperature properties of epoxidized canola oil, epoxidized biodiesel, biolubricant from canola oil, and biolubricant from canola biodiesel. The epoxidized canola oil and epoxidized canola biodiesel have

DOI: 10.1021/jf505825k
J. Agric. Food Chem. 2015, 63, 3235−3242

Table 1. Tribological Properties of Products

entry	product	low temperature property: cloud point (°C)	low temperature property: pour point (°C)	kinematic viscosity (cSt): 40 °C	kinematic viscosity (cSt): 100 °C	oxidative stability (OIT) h
1	epoxidized canola oil	15	9	–	–	–
2	epoxidized canola biodiesel	6	0	–	–	–
3	biolubricant from canola oil	−3	−9	0	670	56.1
4	biolubricant from canola biodiesel	−12	−18	116	19	76.3

the cloud points of 15 and 6 °C and the pour points of 9 and 0 °C, respectively. It was found that cloud and pour point of epoxidized biodiesel are low as compared with epoxidized canola oil, which can be due to the presence of less number of aliphatic carbon atoms present in epoxidized biodiesel. Hence, an increase in the aliphatic carbon chain length reduced the low-temperature properties. Also, these low-temperature properties can be improved by adding the ester linkage in the epoxidized molecules, which promote steric hindrance. The cloud points of biolubricant from canola oil and biolubricant from canola biodiesel were found to be −3 and −12 °C, while pour points were −9 and −18 °C, respectively. Hence, it elucidates that biolubricant obtained from biodiesel has better low-temperature properties as compared to biolubricant obtained from canola oil, which can be due to the less steric hindrance. Hence, biolubricant from canola biodiesel is superior for low-temperature applications and has better future prospects for the automotive industry as compared to biolubricant from canola oil.

Viscosity. The viscosity of the fluid defines the effectiveness of the lubricant to lubricate the contact surface of the metals. The kinematic viscosity of canola biolubricant and biodiesel biolubricant were measured at 40 °C and found to be 0 and 116 cSt, whereas at 100 °C, it was found to be 670 and 19 cSt (Table 1). The viscosity index for biolubricant from canola biodiesel was found to be 185. High viscous nature of canola oil biolubricant is because of the addition of ester linkage in the oil at the unsaturation. The increase in the viscosity is also attributed to the intramolecular hydrogen bonding of the ester linkages.[25] Canola oil biolubricant is highly viscous and can be used as a lubricant for high temperature, high load, and high-speed operations like heavy machinery. However, biolubricant from canola biodiesel is less viscous as compared with biolubricant from canola oil. It might be because of less number of aliphatic carbon present in the biolubricant derived from canola biodiesel, which creates less steric hindrance and fewer hydrogen bondings as compared with the biolubricant derived from canola oil (Figure 2). Therefore, biolubricant derived from biodiesel can be used as lubricant for automobiles at low temperature. Hence, it can be anticipated that the biolubricant from biodiesel has a better future prospect for automobile sector.

Friction and Anti-Wear Properties. Lubricity testing was performed according to the report by Sripada et al.[26] All the samples were tested twice, and the average value is reported. The wear scar diameter of standard diesel sample was found to be 600 μm. With the addition of 1% of canola oil biolubricant to the standard diesel sample, the diameter of the wear scar was found to reduce to 130 μm, while 1% of biolubricant derived from canola biodiesel integrated in the standard diesel sample showed a wear scar diameter of 95 μm. It was noticed that canola oil biolubricant resulted in more wear scar on the steel test ball as compared with biolubricant from canola biodiesel (Figure 6). This can be due to the presence of more steric hindrance and intramolecular hydrogen bonding present in canola biolubricant, which increases the viscosity and hence decreases the solubility in the standard diesel sample and resulted in more wear scar diameter (130 μm). Furthermore, a lower number of aliphatic carbon atoms is present in biodiesel biolubricant as compared with canola biolubricant, which makes it less viscous and less nonpolar and, hence, increases the solubility in diesel fuel and results in less wear scar (95 μm). The better lubricity property of biodiesel biolubricant can also be explained by the presence of ester oxygen moieties in 1, 9, and 10 positions, which are free of hydrogen bonding and help to reduce the friction by developing the antifrictional film on metal surfaces.[27] Table 2 indicates that with the increase in lubricant content in pure diesel fuel, the wear scar on the steel test ball is decreased.

Table 2. Wear Scar Diameter of Bio-lubricants Diluted in Low Lubricity Diesel

biolubricant added in pure diesel (%)	wear scar diameter (μm): biolubricant from canola oil	wear scar diameter (μm): biolubricant from biodiesel
1	130	95
2	125	90
5	120	86
10	115	81

Thermogravimetric (TGA) Analysis. Thermal stability of canola oil, epoxdized canola oil, canola biolubricant, biodiesel,

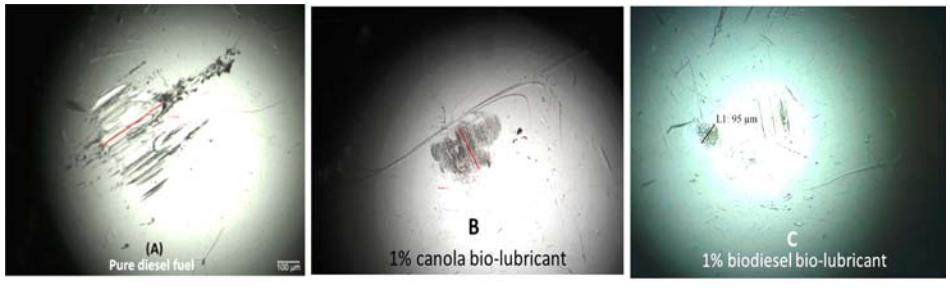

Figure 6. HFRR wear scar images of (A) standard diesel fuel, (B) 1% canola biolubricant, and (C) 1% biodiesel biolubricant.

DOI: 10.1021/jf505825k
J. Agric. Food Chem. 2015, 63, 3235−3242

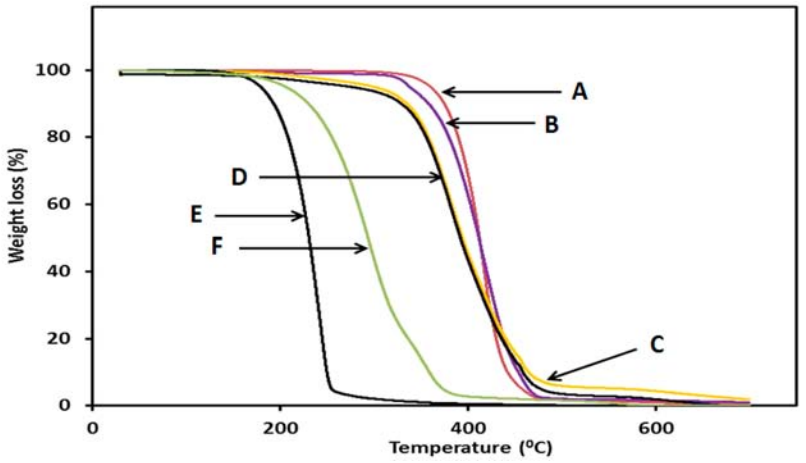

Figure 7. TGA thermogram of (A) canola oil, (B) epoxidized canola oil, (C) canola biolubricant, (D) biodiesel, (E) epoxidized biodiesel, and (F) biodiesel biolubricant.

epoxidized biodiesel, and biodiesel biolubricant was studied by thermo gravimetric differential thermal analyzer (TG/DTA). The detailed analysis procedure is described in the literature.[26] The graphs of weight loss against temperature are shown in Figure 7. It is clear from the graph that canola oil, epoxidized canola oil, and canola biolubricant are thermally stable below 305 °C. Maximum weight loss (90−95% wt) was observed in all these three materials at the temperatures 460, 461, and 530 °C, respectively. However, canola biodiesel, epoxidized canola biodiesel, and biodiesel biolubricant are found to be thermally stable below the temperatures 305, 160, and 194 °C, respectively, and about 90−95% weight loss was found for each sample at the temperatures 462, 251, 370 °C, respectively (Table 3). Hence, it is conclusive that canola biolubricant is thermally more stable as compared to biolubricant from canola biodiesel, which can be due to the presence of intra molecular hydrogen bonding. Thermogravimetric analysis (TGA) also confirms that canola biolubricant can be more useful for high-temperature applications, whereas biodiesel biolubricant is useful for low-temperature applications.

Table 3. Thermal Stability Data of Feed and the Products

	temperature (°C)		
product	stability	15−20 wt % loss	90−95 wt % loss
Canola oil	333	375	460
epoxidized canola oil	319	370	461
Canola biolubricant	309	364	530
biodiesel	309	360	462
epoxidized biodiesel	160	204	251
biodiesel biolubricant	194	247	370

Differential Scanning Calorimetry (DSC) Analysis. Figure 8 represents a DSC thermogram of epoxidized canola oil, epoxidized canola biodiesel, canola biolubricant, and biodiesel biolubricant. The exothermic crystallization peaks of epoxy canola oil and epoxy canola biodiesel appeared at −7 and −12 °C, respectively, because epoxy canola oil is well-stacked due to intramolecular forces.[25] Epoxy canola biodiesel crystallizes at lower temperature because of the presence of the *cis* epoxy linkage.[26] Biolubricant from canola oil shows the peak at −118 °C, and the biolubricant from biodiesel showed no peak for exothermic crystallization up to −140 °C, which can be due to the arrangement of the saturated molecules that influence the crystallization of the compound. Hence, biolubricant from biodiesel has better low-temperature properties.

Oxidation Stability Study. The oxidation stability of biolubricants depends on the degree of unsaturation present in the molecules which are very prone to oxidation. These oxidation processes of lubricants take place during the combustion process of the fuel inside the engine, hence it is a critical parameter.[28] Canola biolubricant showed a lower value of 56.1 h, whereas biodiesel biolubricant gave 76.3 h of oxidative induction time (Table 1). This increase in the oxidative stability is because of the existence of short chain ester linkage in canola biodiesel biolubricant as compared with canola biolubricant.[27] Hence, biodiesel biolubricant is close to 1.5 times more stable when compared with canola biolubricant, under similar oxidative conditions, which makes it more suitable for automotive applications.

Catalyst Reusability. In the present study, the two-step process was demonstrated for preparation of biolubricant, hence two different heterogeneous catalysts were used (i.e., Amberlite IR-120H and Amberlyst-15). The reusability of the catalysts was tested up to the third run. The reusability procedure was followed as in the literature.[6] The conversion decreased marginally in both the steps, and both the catalysts were used successfully up to three times.

In conclusion, in the present study two different biolubricants were prepared from canola oil and canola biodiesel using Amberlite IR-120H for the epoxidation step and Amberlyst-15 for the simultaneous ring opening and esterification step. NMR and FT-IR spectral analyses confirmed the formation of products. Biolubricant from canola biodiesel has good low temperatue properties (−12 °C and −18 °C), kinematic viscosity (19 cSt at 100 °C), low friction and antiwear scar (95 μm), and high oxidative stability (76.3 h). Therefore, biolubricant derived from biodiesel can be used for low temperature and general application like automotive lubricants. However, canola oil biolubricant has a cloud point of −3 °C and pour point of −9 °C, kinematic viscosity measured at 373 K is 670 cSt, friction and antiwear scar (130 μm), and oxidative stability (56.1 h). As biolubricant from canola oil has high thermal stability (305 °C), and is highly viscous, even at high temperature, it can be used at high temperature, heavy load, and high speed operations such as

DOI: 10.1021/jf505825k
J. Agric. Food Chem. 2015, 63, 3235−3242

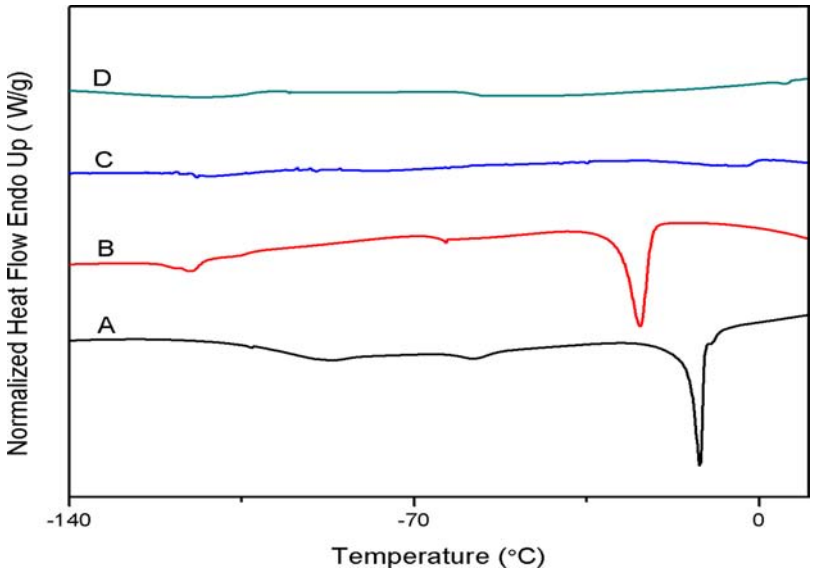

Figure 8. DSC thermogram of (A) epoxidized canola oil, (B) epoxidized canola biodiesel, (C) canola biolubricant, and (D) biodiesel biolubricant.

heavy machinery. This study shows that both the biolubricants are effective, attractive, renewable, and thus have good characteristics as industrial lubricants.

AUTHOR INFORMATION

Corresponding Author

*E-mail: ajay.dalai@usask.ca. Tel: +1 306 966 4771. Fax: +1 306 966 4777.

Funding

The authors acknowledge Saskatchewan Agricultural Development Fund (ADF) for providing funding for this research.

Notes

The authors declare no competing financial interest.

REFERENCES

(1) Vasiliadou, E.; Lemonidou, A. Parameters affecting the formation of 1,2-propanediol from glycerol over Ru/SiO_2 catalyst. *Org. Process Res. Dev.* **2011**, *15*, 925−931.

(2) Mang, T.; Dresel, W. *Lubricants and Lubrication*, 2nd completely revised and extended ed.; Wiley-VCH: Weinheim, Germany, 2007.

(3) Amani, M. A.; Davoudi, M. S.; Tahvildari, K.; Nabavi, S. M.; Davoudi, M. S. Biodiesel production from Phoenix dactylifera as a new feedstock. *Ind. Crops Prod.* **2013**, *43*, 40−43.

(4) Baroi, C.; Dalai, A. K. Simultaneous esterification, transesterification and chlorophyll removal from green seed canola oil using solid acid catalysts. *Catal. Today* **2013**, *207*, 74−85.

(5) Peterson, C. L. Vegetable oil as a diesel fuel: Status and research priorities. *Trans. ASAE* **1986**, *29*, 1413−1422.

(6) Sharma, R. V.; Dalai, A. K. Synthesis of bio-lubricant from epoxy canola oil using sulfated Ti-SBA-15 catalyst. *Appl. Catal., B* **2013**, *142*, 604−614.

(7) Kulkarni, M. G.; Dalai, A. K.; Bakhshi, N. N. Utilization of green seed canola oil for biodiesel production. *J. Chem. Technol. Biotechnol.* **2006**, *81*, 1886−1893.

(8) Lathi, P. S.; Mattiasson, B. Green approach for the preparation of biodegradable lubricant base stock from epoxidized oil. *Appl. Catal., B* **2007**, *69*, 207−212.

(9) Matthew, T. S.; Nader, S.; Bigyan, A.; Lambert, A. D. Influence of fatty acid composition on the tribological performance of two vegetable based lubricants. *J. Synth. Lubr.* **2007**, *24*, 101−110.

(10) Campanella, A.; Rustoy, E.; Baldessari, A.; Baltanas, M. A. Lubricants from chemically modified vegetable oils. *Bioresour. Technol.* **2010**, *101*, 245−254.

(11) Battersby, N. S.; Pack, S. E.; Watkinson, R. J. A correlation between the biodegradability of oil products in the CEC L-33-T-82 and modified sturm tests. *Chemosphere* **1992**, *24*, 1989−2000.

(12) Mungroo, R.; Pradhan, N. C.; Goud, V. V.; Dalai, A. K. Epoxidation of canola oil with hydrogen peroxide catalyzed by acidic ion exchange resin. *J. Am. Oil Chem. Soc.* **2008**, *85*, 887−896.

(13) Johansson, L. E.; Lundin, S. T. Copper catalysts in the selective hydrogenation of soybean and rapeseed oils: I. the activity of the copper chromite catalyst. *J. Am. Oil Chem. Soc.* **1979**, *56*, 974−980.

(14) Sinadinovic-Fiser, S.; Jankovic, M.; Petrovic, Z. S. Kinetics of *in situ* epoxidation of soybean oil in bulk catalyzed by ion exchange resin. *J. Am. Oil Chem. Soc.* **2001**, *78*, 725−731.

(15) Adhvaryu, A.; Erhan, S. Z. Epoxidized soybean oil as a potential source of high-temperature lubricants. *Ind. Crops Prod.* **2002**, *15*, 247−254.

(16) Goud, V. V.; Patwardhan, A. V.; Pradhan, N. C. Studies on the epoxidation of mahua oil (*Madhumicaindica*) by hydrogen peroxide. *Bioresour. Technol.* **2006**, *97*, 1365−1371.

(17) Dinda, S.; Patwardhan, A. V.; Goud, V. V.; Pradhan, N. C. Epoxidation of cottonseed oil by aqueous hydrogen peroxide catalysed by liquid inorganic acids. *Bioresour. Technol.* **2008**, *99*, 3737−3744.

(18) Meshram, P. D.; Puri, R. G.; Patil, H. V. Epoxidation of wild safflower (*Carthamusoxyacantha*) oil with peroxy acid in presence of strongly acidic cation exchange resin IR-122 as catalyst. *Int. J. ChemTech Res.* **2011**, *3*, 1152−1163.

(19) Hwang, H. S.; Erhan, S. Z. Modification of epoxidized soybean oil for lubricant formulations with improved oxidative stability and low pour point. *J. Am. Oil Chem. Soc.* **2001**, *78*, 1179−1184.

(20) Adhvaryu, A.; Liu, Z. S.; Erhan, S. Z. Synthesis of novel alkoxylated triacyl glycerols and their lubricant base oil properties. *Ind. Crops Prod.* **2005**, *21*, 113−119.

(21) Salimon, J.; Salih, N.; Yousif, E. Biolubricants: Raw materials, chemical modifications and environmental benefits. Eur. *J. Lipid Sci. Technol.* **2010**, *112*, 519−530.

(22) Fadhel, A. Z.; Pollet, P.; Liotta, C. L.; Eckert, C. A. Combining the benefits of homogeneous and heterogeneous catalysis with tunable solvents and near critical water. *Molecules* **2010**, *15*, 8400−8424.

(23) Sharma, R. V.; Soni, K. K.; Dalai, A. K. Preparation, characterization and application of sulfated Ti-SBA-15 catalyst for oxidation of benzyl alcohol to benzaldehyde. *Catal. Commun.* **2012**, *29*, 87−91.

(24) Vlcek, T.; Petrovic, Z. S. Optimization of the chemoenzymatic epoxidation of soybean oil. *J. Am. Oil Chem. Soc.* **2006**, *83*, 247−252.

DOI: 10.1021/jf505825k
J. Agric. Food Chem. 2015, 63, 3235−3242

(25) Zaher, F. A.; El-Kinawy, O. S.; Abdullah, R. The esterification of Jatropha oil using different short chain alcohols to produce esters to be used as biodiesel fuel. *Energy Source* **2012**, *34*, 2214−2219.
(26) Sripada, P. K.; Sharma, R. V.; Dalai, A. K. Comparative study of tribological properties of trimethylopropane-based biolubricants derived from methyl oleate and canola biodiesel. *Ind. Crop. Prod.* **2013**, *50*, 95−103.
(27) Dixit, S.; Kanakraj, S.; Rehman, A. Linseed oil as a potential resource for bio-diesel: A review. *Renew. Sust. Energy Rev.* **2012**, *16*, 4415−4421.
(28) Pedersen, J. R.; Ingemarsson, A.; Olsson, J. O. Oxidation of rapeseed oil, rapeseed methyl ester (RME) and diesel fuel studied with GS/MS. *Chemosphere* **1999**, *38*, 2467.

DOI: 10.1021/jf505825k
J. Agric. Food Chem. 2015, 63, 3235−3242

Table 1. List of Potato Species Used in This Study for Isolation of Patatins from Tubers

species	code of Gene Bank in Potato Research Institute Havlíčkův Brod	country of origin/geographic distribution
Solanum tuberosum L. cv. Desirée	EVIGEZ 07S0100243	Netherlands
Solanum andigenum Juz. & Bukasov	EVIGEZ 07S0300066	South America (Venezuela and Argentina)
Solanum goniocalyx Juz. & Bukasov	EVIGEZ 07S0300109	South America (Peru and Bolivia)
Solanum phureja Juz. & Bukasov	EVIGEZ 07S0300136	South America (Bolivia)
Solanum stenotomum Juz. & Bukasov	EVIGEZ 07S0300001	South America (Columbia and Argentina)

potato cultivars. Both groups showed similar values of the protein content, and three mass levels, 40.6, 41.8, and 42.9 kDa, of purified patatins were found by matrix-assisted laser desorption/ionization−mass spectrometry (MALDI−MS). The differences among these masses (~1.2 kDa) indicated a mass close to the molecular mass of patatin oligosaccharide, as mentioned above. However, the present study aiming at a detailed investigation of glycosylation profiles of patatins isolated from selected potato species showed the presence of more oligosaccharide structures. The data obtained by mass spectrometric analysis provided even evidence for differences in profiles of patatin *N*-glycans, and these results will be discussed.

MATERIALS AND METHODS

Plant Materials and Growth Conditions. For this work, tubers from selected potato species (for details see Table 1) were donated by the Gene Bank of Potato Research Institute Havlíčkův Brod, Czech Republic. In both experimental years (2011 and 2012), analyzed tubers were obtained by the following approach of cultivation: Plant *in vitro* reproduction was made on Murashige and Skoog (MS) agar medium containing 30 g L^{-1} sucrose without growth hormones.[21] Rooted *in vitro* plants were transferred to *in vivo* conditions of the greenhouse. Each potato plant (in total, five plants from each species) was cultivated in a pot with 10 L of potting soil to ensure harmonic nutritive conditions for a complete growing season. Potting soil in pots was kept in appropriate humidity by daily watering. Potato plants were cultivated during both seasons under chemical control against *Phytophthora infestans* and insect pests. All conditions of plant cultivation were the same in both experimental years. Obtained tubers were flushed in water and cut first longitudinally into identical halves and then into thin slices (~2 mm). The slices were frozen to −80 °C, freeze-dried (−50 °C, 0.040 mbar, 48 h, freeze-dryer Alpha 1-4 LSC, Martin Christ, Germany), and homogenized using a laboratory mill. Freeze-dried potato tuber meal (5 g) was extracted in 25 mM Tris−HCl buffer (50 mL, pH 7.4) for 30 min at 4 °C. The mixture was centrifuged (4 °C at 3600*g* for 15 min), and the supernatant was filtered.

Purification of Patatins. Chromatographic purification of patatins was achieved with the following three steps modified according to the procedure reported previously:[20] (1) Ion-exchange chromatography was completed on DEAE 52-Cellulose Servacel (15 mL, Serva, Germany) with 90 mL of starting buffer (25 mM Tris−HCl at pH 7.4). After application of the protein extract (10 mL), the column was washed with 60 mL of starting buffer to remove unbound proteins, and isocratic elution of bound proteins was performed with 30 mL of elution buffer (25 mM Tris−HCl at pH 7.4 + 0.5 M NaCl). (2) Affinity chromatography was performed on Concanavalin A Sepharose 4B (10 mL, GE Healthcare, Little Chalfont, U.K.). The column was equilibrated with 60 mL of starting buffer (25 mM Tris−HCl at pH 7.4 + 0.5 M NaCl). Elution of bound patatins was performed with 20 mL of buffer consisting of 25 mM Tris−HCl at pH 7.4 + 0.5 M NaCl + 100 mM α-methyl-D-glucoside. (3) Desalting of patatin proteins was achieved using molecular weight cut-off (MWCO) filters (3 kDa) according to the protocol of the manufacturer (Millipore). The purity of patatins (~99%) was verified by a means of sodium dodecyl sulfate−polyacrylamide gel electrophoresis (SDS−PAGE) and Experion automated electrophoretic system (see Supplementary Figure 1 of the Supporting Information).

Release of *N*-Glycans from Patatins. Lyophilyzed powder of patatin protein (500 μg) was dissolved in 25 mM ammonium bicarbonate (100 μL) and deglycosylated with *N*-glycosidase A (0.2 mU, Roche) at 37 °C for 20 h. Alternatively, the samples were digested first with trypsin (20 μg) at 37 °C for 4 h. Then, the digest was kept in a water bath at 85 °C for 5 min. After cooling, N-linked oligosaccharides were released from peptides again enzymatically by treatment with PNGase A (37 °C, 20 h). The reaction samples were mixed frequently during incubation.

Solid-Phase Extractions on Carbon Clean Cartridges. Prior to an extraction, the carbon cartridge columns (Supelclean-ENVI Carb SPE cartridges, Sigma-Aldrich) were first washed with 100% acetonitrile (ACN), following deionized water (5 mL of each). Then, digest (100 μL) was applied to a column with wet carrier and left to permeate, and after approximately 10 min, the carrier was rinsed with 5 × 1000 μL of deionized water. After that, glycans were eluted with 40% ACN (3 × 800 μL) and collected into separate tubes without using any pressure. All glycan fractions were evaporated and derivatized according to the procedure as described below.

Phenylhydrazine (PHN) Labeling. The derivatization with PHN (Sigma-Aldrich) was achieved according to the method previously reported,[22,23] with modified conditions as described next.

For MALDI−MS analysis, on-target labeling approach was applied: the fractions with glycans were dissolved in 20 μL of deionized water, and 1 μL of a sample solution was spotted onto the pre-deposited matrix ATT/PHN·HCl (2-aza-2-thiothymine/phenylhydrazine hydrochloride in a molar ratio of 2:1).[24] When the spot was partially dried, 0.4 μL of derivatization reagent (10 μL of PHN in 50 μL of deionized water and 5 μL of ACN) was added. During this time, the target was kept at a temperature of 50 °C until the spot had dried. These conditions prevent smearing of the spot after adding PHN reagent solution; when the reaction time is sped up and after 3−5 min, the sample is ready for measurement.

For electrospray ionization (ESI)−MS analysis, *N*-glycan pools were reconstituted in the mixture consisting of deionized water (50 μL), PHN (1 μL), and ACN (3 μL). The tube with the reaction mixture was kept at a temperature of 60 °C for 30 min under vigorous mixing.

Exoglycosidase Digestions. Selected glycan fractions were subjected to α-mannosidase or β-*N*-acetylglucosaminidase (*Canavalia ensiformis*, Jack beans; Sigma) treatment at 37 °C according to the protocol supplied by the manufacturer. After each time of incubation (from 20 min to 4 h), 1 μL of digested mixture was spotted on the MALDI target, derivatized, and analyzed under the same conditions as the glycan pool before exoglycosidase treatment.

MS. MALDI−MS analysis was performed on the MALDI-TOF/TOF instrument (Ultraflex III, Bruker) operated in the positive reflectron mode, and for each sample spot, 1200 shots were summed. The spectra were acquired using the FlexControl software. Parent ions of interest were selected for LIFT (MS/MS) experiments. MS^n data were recorded on an Orbitrap ELITE instrument (Thermo Fisher Scientific, Waltham, MA) equipped with a Nanospray Flex Ion Source using direct infusion in 50% acetonitrile at a flow rate of 300 nL/min. The resolution of all MS^n spectra was 240 000 (at m/z 400). Automatic gain control (AGC) target value of 1×10^6 or 50 000 ions and maximum injection time of 200 or 5000 ms were set for all MS or MS^n measurements, respectively. Higher energy collisional dissociation (HCD) was used to generate MS^2 ions of glycans. In the case of the MS^3 fragmentation scheme, collision-induced dissociation (CID) at a relative energy of 40% was used to generate glycan fragments, from which one was further selected for HCD fragmentation at different

DOI: 10.1021/acs.jafc.5b00426
J. Agric. Food Chem. 2015, 63, 3243−3250

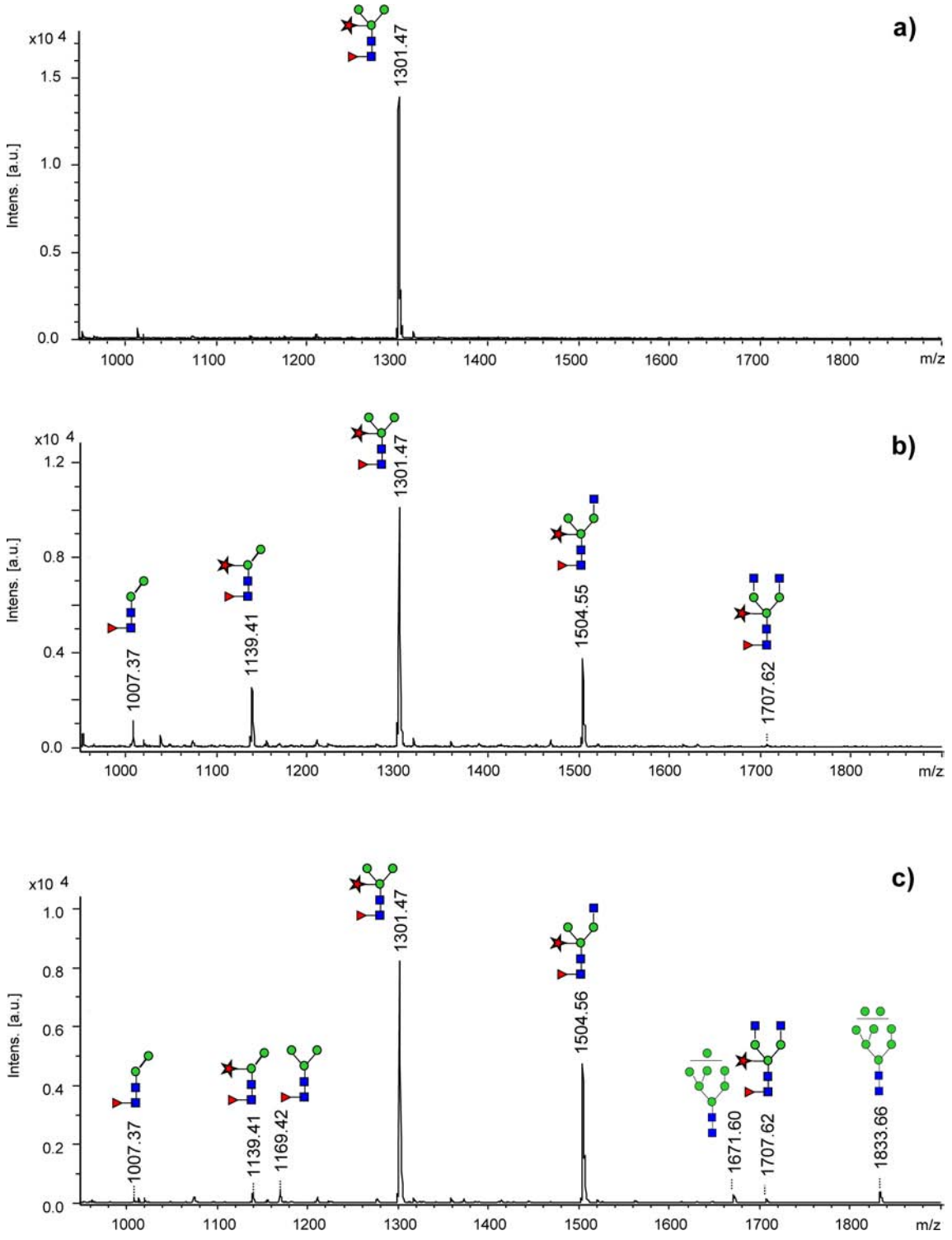

Figure 1. Representative MALDI-TOF/TOF-MS spectra of *N*-glycan profiles of patatin tubers from the following potato species: (a) *S. tuberosum* cv. Desirée, (b) *S. phureja* (collected in 2012), and (c) *S. stenotomum* (collected in 2012). All peaks are $[M + Na]^+$. *N*-Glycans were released with PNGase A from native patatins and labeled with PHN (+90.05 Da). Key symbols: (red triangles) Fuc, (blue squares) GlcNAc, (green circles) Man, and (orange stars) Xyl.

energies. The isolation window for all MS^n experiments was set to m/z 2. MS^n spectra were visualized and exported using Xcalibur Qual Browser (version 2.2, Thermo Fisher Scientific).

MS/MS spectra of *N*-glycans were interpreted manually. For the assignment of oligosaccharide fragment ions, the established nomenclature reported by Domon and Costello was followed.[25] The proposed oligosaccharide structures were derived from the single fragmentation patterns obtained for each precursor ions. For discrimination of single isomeric structures, previously reported rules were applied.[26]

Statistical Analysis. The MALDI measurements were repeated 3 times for each sample, and all experiments were repeated in triplicates for samples, with the exception of *S. tuberosum* L. (cv. Desirée). In the case of this cultivar, the experiments were repeated 5 times to confirm

DOI: 10.1021/acs.jafc.5b00426
J. Agric. Food Chem. 2015, 63, 3243−3250

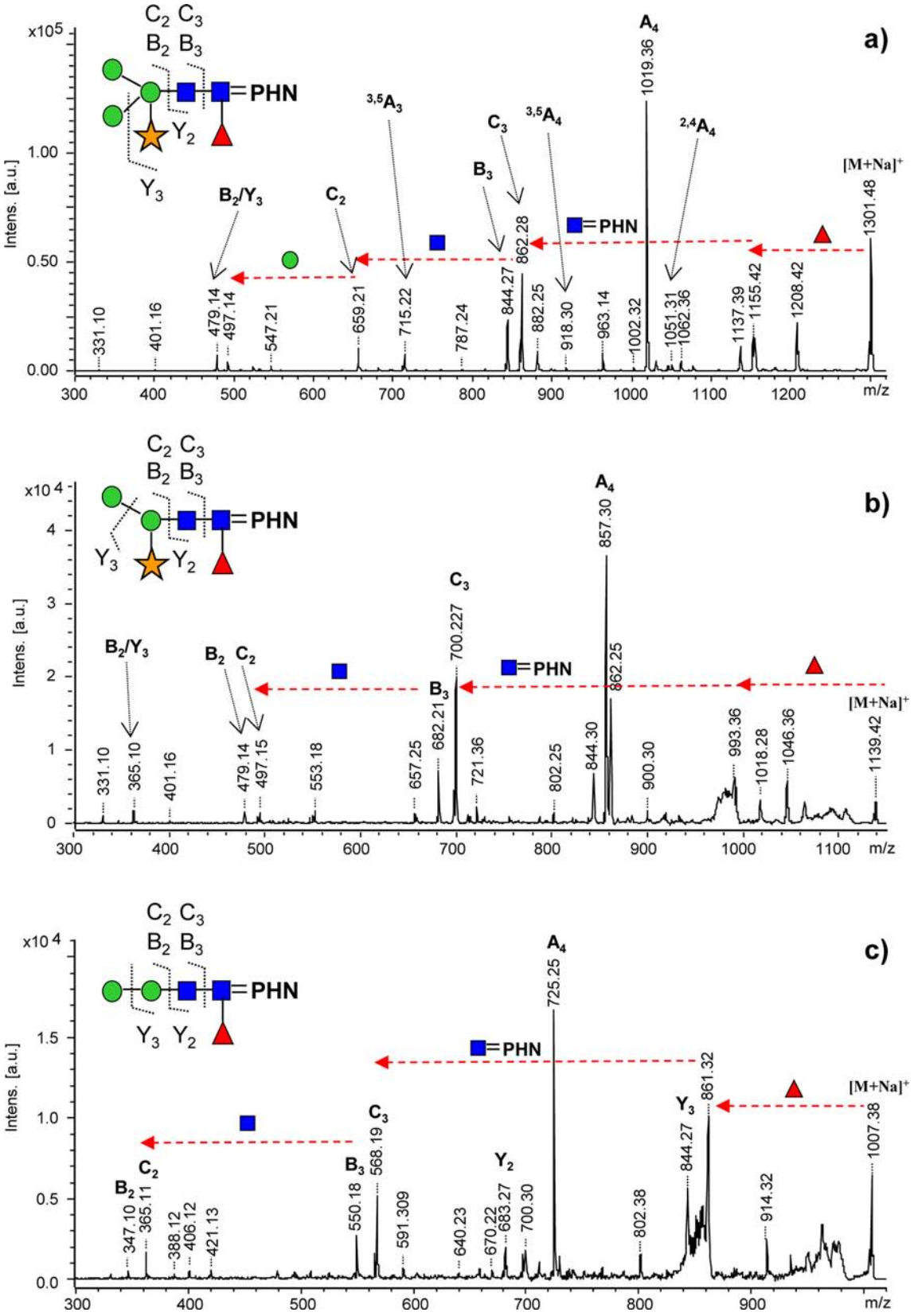

Figure 2. MALDI-TOF/TOF MS/MS spectra recorded for the glycans with precursor ions at (a) *m/z* 1301.4, (b) *m/z* 1139.4, and (c) *m/z* 1007.4. Fragment ions are sodiated.

the presence of only one oligosaccharide structure. The recorded MALDI−MS spectra were baseline-corrected and processed using the software tool of an instrument. The proportions of individual glycans that differentiated according to their *m/z* values were calculated from integrated MS peak intensities over the range of their isotopic envelopes and then normalized using Microsoft Excel software.

DOI: 10.1021/acs.jafc.5b00426
J. Agric. Food Chem. 2015, 63, 3243−3250

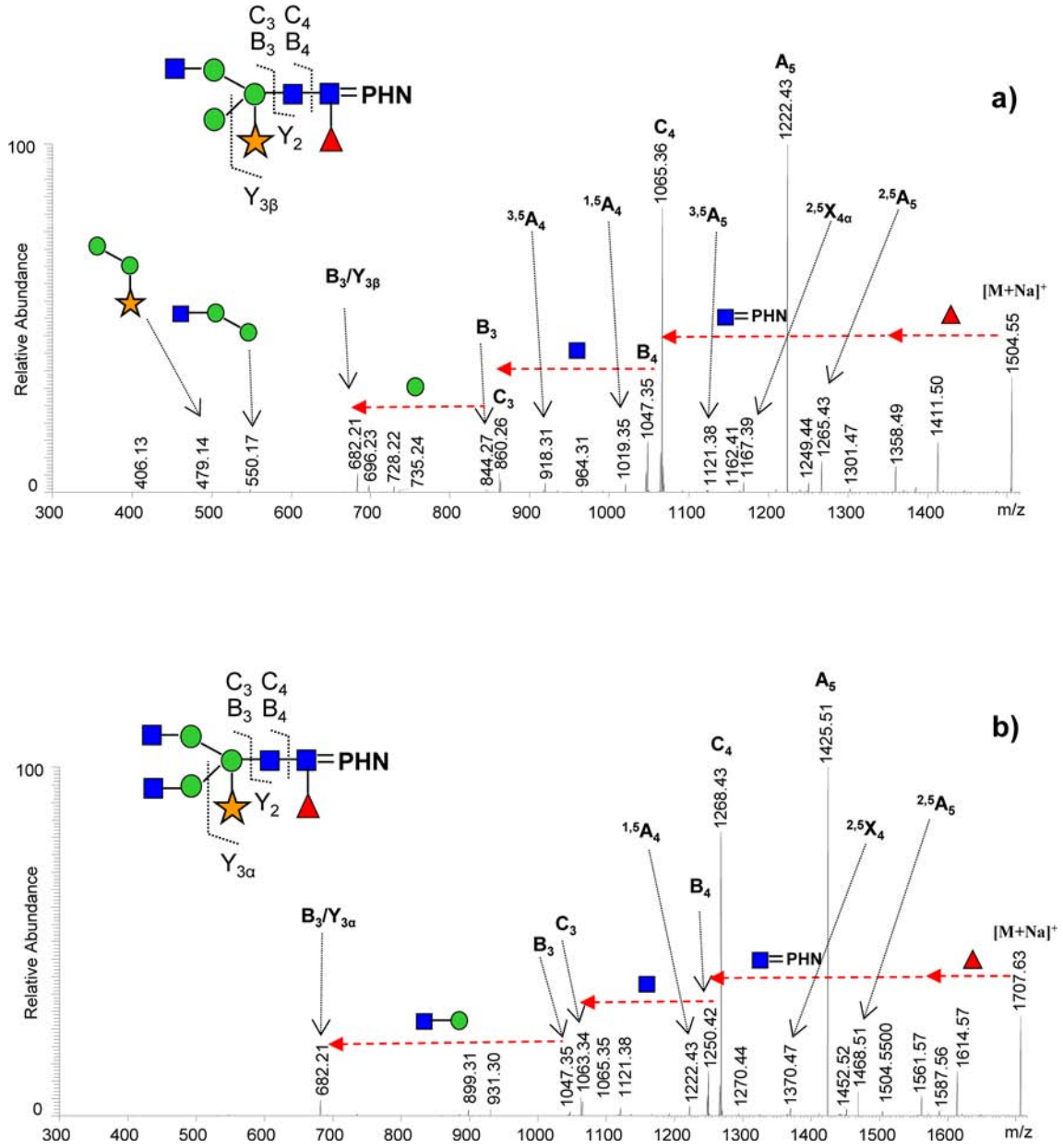

Figure 3. ESI−HCD spectra recorded for the glycans with precursor ions at (a) *m/z* 1504.5; and (b) *m/z* 1707.6. Fragment ions are sodiated.

RESULTS AND DISCUSSION

In this study, we examined *N*-glycans of patatins isolated from tubers of selected potato species from *Solanum* genus, as listed in Table 1. The selection of these potato groups was based on the knowledge reported recently that these types exhibit significant differences in the level of many tuber metabolites.[27] The oligosaccharides were released from purified patatins enzymatically with PNGase A, cleaned on carbon cartridges, and derivatized with PHN prior to mass spectrometric analysis. The principal method used for detection was highly sensitive MALDI−MS. This instrumental technique allows for the discrimination of different oligosaccharide classes. Besides, the abundance ratios of oligosaccharides can be calculated from a comparison of relative ion intensities corresponding to individual glycans. To confirm the type of cross-ring cleavages, additional MS/MS data were recorded on an Orbitrap ELITE instrument. The assignment of oligosaccharide types was based on monosaccharide composition, fragmentation patterns, exoglycosidase digestions, and knowledge of the glycan biosynthetic pathway in plants. Generally, only neutral oligosaccharides were detected and produced $[M + Na]^+$ ions when detected by MALDI−MS or Orbitrap when using a direct infusion. Most of the identified peaks showed 3-linked fucose at the GlcNAc of the reducing end (the resistance to PNGase F cleavage). The most abundant oligosaccharide in all samples was observed at *m/z* 1301.5 (Figure 1a), and its fragmentation pattern clearly corresponded to glycan with a composition of $Man_3(Xyl)GlcNAc_2(Fuc)$ (Figure 2a), the same structure as described previously in patatin isolated from potato tuber lipases.[19] This glycan was detected as only oligosaccharide in patatins isolated here from *S. tuberosum* cv. Desirée independently on the year of collection and from *Solanum goniocalyx* harvested in 2011 (Figure 1a). The glycoprotein obtained from *Solanum phureja* showed higher incidence of glycan at *m/z* 1139.4 (Figure 1b) and corresponded to the structure with composition $Man_2(Xyl)GlcNAc_2(Fuc)$ (Figure

DOI: 10.1021/acs.jafc.5b00426
J. Agric. Food Chem. 2015, 63, 3243−3250

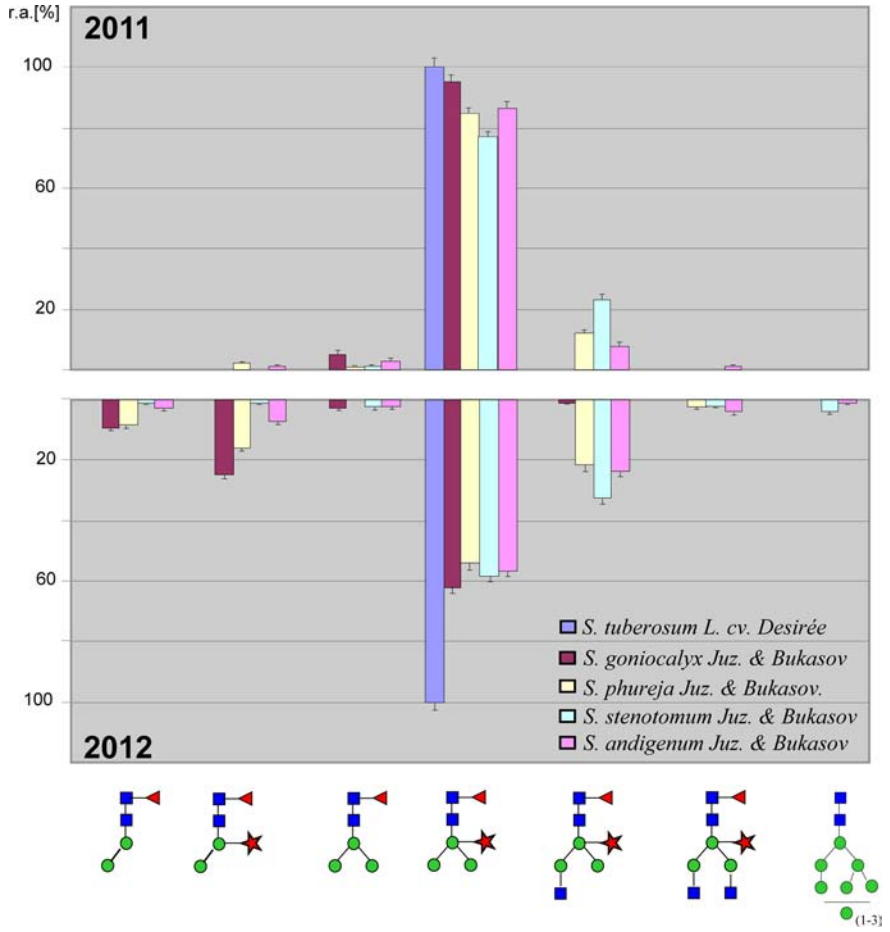

Figure 4. Schematic chart illustrating the occurrence of *N*-glycans detected by MALDI–MS in patatins isolated from five potato species (collected in years 2011 and 2012). The relative amounts of glycans calculated on the basis of their relative MS intensities as described in the Materials and Methods are presented as the mean ± standard deviation (SD) from at least three measurements.

2b). The peak with small intensity detected at m/z 1007.37 could be assigned to a glycan of similar structure as described above, however with no xylose linked on the core mannose (Figure 2c). The second highest peak in the spectra of most patatins was observed at m/z 1504.6 (e.g., panels b and c of Figure 1), and MS/MS data were supportive for the structure of the composition of $GlcNAcMan_3(Xyl)GlcNAc_2Fuc$ (Figure 3a). B and C fragment ions resulted from the loss of the chitobiose core, with m/z values detected at 1047.3 (B_4) or 1065 (C_4) or 844 (B_3) or 860 (C_3). Next the loss of 3-positioned hexose produced the fragment ions at m/z 682 (B_3/$Y_{3\beta}$) corresponding to the composition of the $GlcNAcMan_2Xyl$ residue (Figure 3a). Although two isomers could be possible for this glycan, according to the rules published previously,[23] only one isomer was detected: the preferential loss of 3-positioned hexose on the core mannose (m/z 682.21) was supportive for the prevalence of an isomer with GlcNAc moiety at the 6 position in mannose linked to the core mannose. Exoglycosidase treatment with β-*N*-acetylglucosaminidase confirmed the presence of the GlcNAc residue on the terminal end of oligosaccharides, and treatment with α-mannosidase produced glycans at m/z 1342.49, 1139.41, and 977.35 (e.g., see Supplementary Figure 2a of the Supporting Information). The parent ions of these products under MS/MS conditions produced the fragment ions supporting the attachment of the Xyl moiety on the core mannose (see panels a and b of Supplementary Figure 2 of the Supporting Information). Biantennary complex glycan detected at m/z 1707.6 was observed with lower abundance in some samples (e.g., panels b and c of Figure 1), and its precursor ions produced the fragment ions, indicating a structure with two GlcNAc residues at the non-reducing end (Figure 3b). The fragment ions recorded at m/z 682.2 (B_3/$Y_{3\alpha}$) were consistent with a loss of the GlcNAcMan residue from B_3 or C_3 ions and provided evidence for GlcNAc moieties on both mannoses linked at the core mannose.

In the MS/MS spectra of all detected glycans, the most dominant peak was associated with a loss of 282 mass units from each parent precursor ions (e.g., fragment ions detected at m/z 1019 in Figure 2a, fragment ions at m/z 1222 in Figure 3a, or ions at m/z 1425 in Figure 3b). The presence of these peaks in the MS/MS spectra of all detected glycans was not influenced by the type of monosaccharide residue(s) at the non-reducing end. Moreover, these fragment ions under MS^2 (Orbitrap) conditions produced the fragment ions as seen in the MS/MS spectra shown, e.g., in Figures 2 and 3 and provided again the support for cross-ring cleavages at the side from the reducing termini. On the basis of the above-mentioned facts, these dominant fragment ions could be explained by the loss of Fuc altogether with the cleavage $^{0,1}A$. The loss of the later mentioned residue from reducing termini ($^{0,1}A$-type cleavage) is commonly observed in the CID spectra of mammalian *N*-glycans when fucose on GlcNAc of the

DOI: 10.1021/acs.jafc.5b00426
J. Agric. Food Chem. 2015, 63, 3243–3250

reducing end is linked at the 6 position but never produced as major fragment ions.[23,28]

In the spectra of glycoproteins isolated from species *Solanum andigenum* and *Solanum stenotomum*, additional peaks appeared at m/z 1671.6 and 1833.7 (Figure 1c). Tandem mass spectra showed that these *N*-glycans had both antennae occupied with hexose residues only, and the fragmentation pattern was similar to that assigned to high-mannose structures as previously described.[28,29] Besides, sequential exoglycosidase treatment of the glycan pool with α-mannosidase caused the loss of hexose residue(s) and supported the structure with mannose residues on both antennae as depicted, e.g., in Figure 1c (m/z 1671 and 1833).

A lot of information regarding patatins as a glycoprotein with interesting properties was reported; however, most of this information is limited to only one type. The first report mentioning glycosylation pattern in patatin isolated from potato tubers was published more than 2 decades ago; two glycosylation sites at Asn60 and Asn90 were occupied with glycan of composition $Man_3(Xyl)GlcNAc_2(Fuc)$.[30] Although a few papers have studied the glycosylation of potato patatins, no evidence for the presence of other glycan structures has been reported up to now. Our present study provides evidence for the presence of other glycans in potato patatins, and the profile can differ with species level. The chart shown in Figure 4 illustrates identified *N*-glycans in the analyzed patatin samples. The major glycan structure found in all samples corresponded to the typical fucosylated plant glycan with xylose on the core mannose (m/z 1301). This glycan solely as one saccharide structure was found in *S. tuberosum* cv. Desirée (from both seasons) and *S. goniocalyx* (collected in 2011). It was reported previously that genotype (equally species and cultivar) is the predominant factor playing a role in the final expression of patatin proteins. However, the other factors, such as year, climate and soil conditions, fertilization, production system, and stress factors, represent also running factors with an ability to modify patatin proteins.[31] The patatin of *S. tuberosum* cv. Desirée did not show any significant change from one year to another. However, *N*-glycome profiles of other species altered with period. The most obvious change on this level was observed for *S. goniocalyx* (see Supplementary Figure 3a of the Supporting Information). This protein together with patatin of *S. phureja*, both collected in 2012, showed higher abundance of shorter glycans, $Man_2GlcNAc_2Fuc$ and $Man_2(Xyl)GlcNAc_2Fuc$. Whereas, in the samples from *S. stenotomum* and *S. andigenum* glycans with GlcNAc residue(s) on arm(s) were detected with higher intensity, $GlcNAc_{1-2}Man_3(Xyl)GlcNAc_2Fuc$. The above discussed species also showed the additional presence of high-mannose glycans with composition $Man_{7-9}GlcNAc_2$ glycans. These oligosaccharides have also never been described in patatins of potato tubers; on the other side, they are commonly found in mammals and not mentioned to be immunogenic.

Plants, among other properties, have great potentials as "biofactories" for the production of therapeutic proteins. Therefore, the number of plant recombinant proteins produced is increasing rapidly.[32] The immunogenicity of plant oligosaccharides in animals or humans is associated with the presence of an α(1,3)-fucose and a β(1,2)-xylose attached to the glycan core.[33] It was reported that the disappearance of sugar allergenic epitopes from plant oligosaccharides is offering a new possibility to produce safe proteins for therapeutic applications.[9] Although further studies are needed to follow carefully more conditions that may also influence the glycosylation profile and to provide better insight into biology of patatins, our data showed that the glycan profile of potato patatin among other factors alters with genotype/cultivar variability. The observed changes in profiles suggest that correct choice of species with careful monitoring of all conditions can enable the decrease of the presence of glycans with immunogenic sugar epitopes and potatoes as one of the most available and the low-cost crops can be used even more beneficially.

■ ASSOCIATED CONTENT

Supporting Information

Control of purity patatin samples using Experion automated electrophoretic system (Supplementary Figure 1), MALDI-TOF/TOF-MS and MS/MS spectra of patatin *N*-glycans obtained from *S. stenotomum* after exoglycosidase treatment (Supplementary Figure 2), and comparative MS spectra of *N*-glycans recorded from patatin of *S. goniocalyx* (Supplementary Figure 3). This material is available free of charge via the Internet at http://pubs.acs.org.

■ AUTHOR INFORMATION

Corresponding Author

*E-mail: zdrahal@sci.muni.cz.

Funding

This work was carried out with the support of Proteomics Core Facility of CEITEC − Central European Institute of Technology, ID number CZ.1.05/1.1.00/02.0068, financed from European Regional Development Fund.

Notes

The authors declare no competing financial interest.

■ REFERENCES

(1) Bertozzi, C. R.; Kiessling, L. L. *Science* **2001**, *291*, 2357−2364.
(2) Gomord, V.; Faye, L. *Curr. Opin. Plant Biol.* **2004**, *7*, 171−181.
(3) Wilson, I. B. H. *Curr. Opin. Struct. Biol.* **2002**, *12*, 569−577.
(4) Kornfeld, R.; Kornfeld, S. *Annu. Rev. Biochem.* **1985**, *54*, 631−664.
(5) Sears, P.; Wong, C. H. *Cell. Mol. Life Sci.* **1998**, *54*, 223−252.
(6) Wilson, I. B. H.; Zeleny, R.; Kolarich, D.; Staudacher, E.; Stroop, C. J. M.; Kamerling, J. P.; Altmann, F. *Glycobiology* **2001**, *11*, 261−274.
(7) Ree, R. van; Cabanes-Macheteau, M.; Akkerdaas, J.; Milazzo, J.-P.; Loutelier-Bourhis, C.; Rayon, C.; Villalba, M.; Koppelman, S.; Aalberse, R.; Rodriguez, R.; Faye, L.; Lerouge, P. *J. Biol. Chem.* **2000**, *275*, 11451−11458.
(8) Fötisch, K.; Vieths, S. *Glycoconjugate J.* **2001**, *18*, 373−390.
(9) Koprivova, A.; Stemmer, C.; Altmann, F.; Hoffmann, A.; Kopriva, S.; Gorr, G.; Reski, R.; Decker, E. L. *Plant Biotechnol. J.* **2004**, *2*, 517−523.
(10) Mullins, E.; Milbourne, D.; Petti, C.; Doyle-Prestwich, B. M.; Meade, C. *Trends Plant Sci.* **2006**, *11*, 254−260.
(11) Bach, S.; Yada, R. Y.; Bizimungu, B.; Fan, M.; Sullivan, J. A. *J. Agric. Food Chem.* **2013**, *61*, 3941−3948.
(12) Jørgensen, M.; Bauw, G.; Welinder, K. G. *J. Agric. Food Chem.* **2006**, *54*, 9389−9397.
(13) Rydel, T. J.; Williams, J. M.; Krieger, E.; Moshiri, F.; Stallings, W. C.; Brown, S. M.; Pershing, J. C.; Purcell, J. P.; Alibhai, M. F. *Biochemistry (Moscow)* **2003**, *42*, 6696−6708.
(14) Holk, A.; Rietz, S.; Zahn, M.; Quader, H.; Scherer, G. F. E. *Plant Physiol.* **2002**, *130*, 90−101.
(15) Senda, K.; Yoshioka, H.; Doke, N.; Kawakita, K. *Plant Cell Physiol.* **1996**, *37*, 347−353.
(16) Tonón, C.; Daleo, G.; Oliva, C. *Plant Physiol. Biochem.* **2001**, *39*, 849−854.

DOI: 10.1021/acs.jafc.5b00426
J. Agric. Food Chem. 2015, 63, 3243−3250

(17) Strickland, J. A.; Orr, G. L.; Walsh, T. A. *Plant Physiol.* **1995**, *109*, 667−674.
(18) Liu, Y.-W.; Han, C.-H.; Lee, M.-H.; Hsu, F.-L.; Hou, W.-C. *J. Agric. Food Chem.* **2003**, *51*, 4389−4393.
(19) Welinder, K. G.; Jørgensen, M. *J. Biol. Chem.* **2009**, *284*, 9764−9769.
(20) Bárta, J.; Bártová, V.; Zdráhal, Z.; Sedo, O. *J. Agric. Food Chem.* **2012**, *60*, 4369−4378.
(21) Murashige, T.; Skoog, F. *Physiol. Plant.* **1962**, *15*, 473−497.
(22) Lattova, E.; Perreault, H. *J. Chromatogr. A* **2003**, *1016*, 71−87.
(23) Lattová, E.; Perreault, H. *Mass Spectrom. Rev.* **2013**, *32*, 366−385.
(24) Lattová, E.; Chen, V. C.; Varma, S.; Bezabeh, T.; Perreault, H. *Rapid Commun. Mass Spectrom.* **2007**, *21*, 1644−1650.
(25) Domon, B.; Costello, C. *Glycoconjugate J.* **1988**, *5*, 397−409.
(26) Lattova, E.; Perreault, H.; Krokhin, O. *J. Am. Soc. Mass Spectrom.* **2004**, *15*, 725−735.
(27) Dobson, G.; Shepherd, T.; Verrall, S. R.; Griffiths, W. D.; Ramsay, G.; McNicol, J. W.; Davies, H. V.; Stewart, D. *J. Agric. Food Chem.* **2010**, *58*, 1214−1223.
(28) Lattová, E.; McKenzie, E. J.; Gruwel, M. L. H.; Spicer, V.; Goldman, R.; Perreault, H. *Rapid Commun. Mass Spectrom.* **2009**, *23*, 2983−2995.
(29) Lattová, E.; Tomanek, B.; Bartusik, D.; Perreault, H. *J. Proteome Res.* **2010**, *9*, 1533−1540.
(30) Sonnewald, U.; Sturm, A.; Chrispeels, M. J.; Willmitzer, L. *Planta* **1989**, *179*, 171−180.
(31) Bártová, V.; Diviš, J.; Bárta, J.; Brabcová, A.; Švajnerová, M. *Eur. J. Agron.* **2013**, *49*, 20−31.
(32) Fischer, R.; Stoger, E.; Schillberg, S.; Christou, P.; Twyman, R. M. *Curr. Opin. Plant Biol.* **2004**, *7*, 152−158.
(33) Bardor, M.; Faveeuw, C.; Fitchette, A.-C.; Gilbert, D.; Galas, L.; Trottein, F.; Faye, L.; Lerouge, P. *Glycobiology* **2003**, *13*, 427−434.

DOI: 10.1021/acs.jafc.5b00426
J. Agric. Food Chem. 2015, 63, 3243−3250

MATERIALS AND METHODS

Chemicals and Standards. All flavonoid standards used in the present study were purchased from Sigma-Aldrich Co. (St. Louis, MO). Methanol, formic acid, acetonitrile, and acetic acid (HPLC grade) were obtained from the Fisher Co. (Fairlawn, NJ). Deionized water (<18 MΩ resistance) was obtained from a Milli-Q Element water purification system (Millipore, Bedford, MA). Analytical-grade ethyl acetate was purchased from Beijing Chemical Reagent Plant (Beijing, China). All the other chemicals were purchased from Sigma-Aldrich Co. unless noted specially.

Plant Materials. *V. vinifera* L. cv. Cabernet Sauvignon grape berries from five commercial vineyards of the main wine-producing regions in China were obtained for the investigation of anthocyanin profile by HPLC–ESI-MS/MS (Table 1). All of the vineyards are located in a temperate continental arid climatic zone with the features of a cold–dry winter, abundant sunshine, and a big temperature difference between day and night. The Cabernet Sauvignon grapes collected at various developmental stages from Manasi of Xinjiang (XJM) in 2012 were used for quantitative polymerase chain reaction (PCR) analysis. The grape berries at commercial harvest from the same vineyard were used to separate *5GT* genes. The grape berry samples used for microsatellite analysis were collected in the years 2011 and 2012 from the five vineyards indicated in Table 2. Syrah and Chardonnay from Shang-Zhuang experimental station of China Agricultural University (Beijing, China) were taken as reference cultivars in the microsatellite analysis. The two cultivars were collected at harvest of the year 2013. To select representative grape samples, we performed the sampling according to the method described by Boulton et al.[16] Three 100-berry samples were selected at random from at least seven 10-cluster selections at similar positions on the 30 selected vines. The selected grape berries were washed, briefly dried, and then carried back to the laboratory under dry ice protection. The seeds were removed by hand. The skins were peeled and immediately put into liquid nitrogen and stored at −80 °C until further use.

Extraction and Analysis of Anthocyanins. The extraction of anthocyanins from grape skins was carried out according to the method of Liang et al.[17] Grape skin powder (0.5 g) was immersed in 10 mL of methanol containing 2% formic acid. This extraction was dispersed with the aid of ultrasonic vibration for 10 min and then shaken in the dark at 25 °C for 30 min at a rate of 150 rpm. The homogenate was centrifuged at 8000*g* for 20 min, and then the supernatant was collected. The residue was repeatedly extracted four times with the same solvent. The pooled extracts were evaporated to dryness by a rotary evaporator and finally redissolved in 10 mL of 10% ethanol solution (pH 3.7). The resulting suspensions were filtered through 0.22 μm filters (cellulose acetate and nitrocellulose, CAN) prior to HPLC–ESI-MS/MS analysis. For each sample, two independent extractions were performed.

HPLC–ESI-MS/MS experiments were carried out as reported in our previous work.[17] This analytical system used an Agilent 1200 series LC–MSD trap VL, equipped with a G1322A degasser, a G1312B bin pump, a G1367C HiP-ALS, a G1316B TCC, a G1314C VWD, and a Kromasil C18 column (250 × 4.6 mm, 5 μm). The compounds were eluted by using two solutions: (A) 6% (v/v) acetonitrile containing 2% (v/v) formic acid and (B) 54% acetonitrile containing 2% formic acid. The gradient was 10% B for 1 min, from 10 to 25% B for 17 min, isocratic 25% B for 2 min, from 25 to 40% for 10 min, from 40 to 70% for 5 min, and from 70 to 100% for 5 min, at a flow rate of 1.0 mL/min. The injection volumes were 30 μL, and the detection wavelength was 525 nm. The column temperature was 50 °C. MS conditions were as follows: ESI interface, positive ion model, 35 psi nebulizer pressure, 10 mL/min dry gas flow rate, 350 °C dry gas temperature, and scans at m/z 100–1000. All analyses were performed in duplicate. The identification and the peak assignment of anthocyanins were based on the comparison of their retention time (t_R), molecular ion, and products ions with those of the standards and the published data.[17−19] The concentration of each anthocyanin was expressed as the equivalent of malvidin 3-*O*-glucoside.

Microsatellite Analysis. The genomic DNA was separated using a DNeasy Plant Kit (Tiangen, Beijing, China) following the manufacturer's instructions. Samples were genotyped at six microsatellite loci proposed by the European project GENRES081 (http://www.eu-vitis.de/index.php): VVS2,[20] VVMD5 and VVMD7,[21] VVMD27,[22] and VrZAG62 and VrZAG79.[23] One primer of each pair was fluorescently labeled with the phosphoramidite dye. The 20 μL reaction system contained 50 ng of DNA, 1.0 U of Taq DNA polymerase (Takara), 1.5 mM Mg^{2+}, 200 μM of each dNTP, and 0.4 μM of each primer. The PCR reaction was performed at 94 °C for 5 min, 35 cycles at 94 °C for 30 s, 55 °C for 30 s, 72 °C for 90 s, and finally extension at 72 °C for 10 min and then cooling to 4 °C in a Techne TC-312 thermal cycler (UK). The separation and sizing of simple sequence repeat (SSR) alleles was completed on an ABI 3730XL DNA analyzer by Genewiz Biotechnology Co., Ltd. (Beijing, China). The data were analyzed with Gene-Marker software (Soft Genetics LLC, State College, PA). Allele sizes were adjusted to an exact number of bases using the algorithm as described by ref 24. SSR profiles were compared with a database (*Vitis* International Variety Catalogue (VIVC, http://www.vivc.de/index.php)) for cultivar identification.

Cloning of *5GT* Candidate Genes. Total RNA was separated from mature Cabernet Sauvignon grapes and the respective cDNA was synthesized using the method previously described.[25]

According to the nucleotide sequence (unpublished, communicated by Prof. Schwab) of the previously characterized functional *5GT-Cha*,[14] we used Cabernet Sauvignon genomic DNA as a template to amplify this gene (see primers for *Vv5GT1* in Table S1, Supporting Information). The PCR mixture (total volume 25 μL) contained 1 μL of DNA, 1 μL of each primer (20 μM), 12.5 μL of 2 × Taq PCR Master Mix (Tiangen, Beijing, China), and 9.5 μL of ddH_2O. Amplification was performed as described above. The PCR products were separated on 1.5% (w/v) agarose gel. The fragment was recovered and cloned into PMD19-T Easy vector (Takara, Japan) and subjected to sequence analysis. The resultant gene was designated as *Vv5GT1* (5-*O*-glucosyltransferase in *V. vinifera* L. Cabernet Sauvignon). Hausmann et al. found five candidate genes for 5GT in *Vitis* hybrid cv. Regent and suggested that one gene (gene 7) was the perfect candidate for anthocyanin 5GT through the investigation of their expression patterns.[26] The 5GT function of gene 7 was further confirmed by their subsequent study.[14] Here we used the 3′-RACE gene specific primers of the other four *Vitis 5GT* candidate genes (genes 5, 6, 8, and 9) to perform in-silico cloning in the database of Grape Genome Browse with the BLASTn program (http://www.genoscope.cns.fr/blat-server/cgi-bin/vitis/webBlat). The obtained sequences were blasted against the NCBI database (http://www.ncbi.nlm.nih.gov). The four in-silico sequences were taken as candidate *5GT* genes. Their specific primers were designed (Table S1, Supporting Information). The full-length cDNAs were obtained using the above Cabernet Sauvignon cDNA template by PCR amplification. The four PCR products all matched with their respective predicted sequences. They were named as *Vv5GT2* (grape genomic locus LOC100260432), *Vv5GT3* (LOC100265923), *Vv5GT4* (LOC100258380), and *Vv5GT5* (LOC100263517), respectively.

Sequence Analysis. Multiple sequence alignment was performed with ClustalX (http://www.clustal.org).[27] The phylogenetic tree was constructed using the neighbor–joining method in the MEGA4 package (http://www.megasoftware.net).[28] Bootstrap values (1000 replications) were performed to test the confidence of nodes.

Prokaryotic Expression and Purification of the Expressed Products. To determine whether these four candidate *Vv5GT*s are functional, we expressed these genes in *Escherichia coli* cells, respectively. Plasmids containing *Vv5GT* cDNAs were double-digested with *Xho*I and *BamH*I. The resulting DNA fragments were ligated with a pET-32a expression vector (Novagen, Madison, WI). The *E. coli* BL21 (DE3) with the recombinant plasmids was incubated into 500 mL of fresh Luria–Bertani medium containing 50 mg/L ampicillin and cultured at 37 °C until the optical density (OD_{600}) reached 0.6. Prokaryotic expression of the target genes was then induced by adding IPTG (isopropyl β-D-thiogalactoside) to a final concentration of 1 mM and further cultured overnight at 16 °C at a rate of 150 rpm. Cells were harvested by centrifugation, and the supernatant was discarded. The harvested cells were suspended in buffer A [50 mM NaH_2PO_4 (pH 8.0),

DOI: 10.1021/acs.jafc.5b00053
J. Agric. Food Chem. 2015, 63, 3251−3260

Table 1. Anthocyanins Identified from the Berry Skin of *Vitis vinifera* L. cv. Cabernet Sauvignon by HPLC−ESI-MS/MS (mg/kg of dry weight)[a]

peak	t_R (min)	anthocyanin compounds	$[M]^+$ (fragment MS^2) (m/z)	wine-growing regions in China (year harvested)							
				YNSR (2011)	YNMLS (2011)	SCMC (2010)	SCMC (2011)	XJM (2011)	XJM (2012)	GSQL-1 (2006)	GSQL-2 (2006)
1	2.89	delphinidin 3,5-*O*-diglucoside	627 (465, 303)	33.31 ± 2.27	59.09 ± 0.23	28.08 ± 2.76	55.59 ± 0.43	35.32 ± 1.93	37.5 ± 1.39	57.94 ± 4.28	65.19 ± 3.94
2	3.48	cyanidin 3,5-*O*-diglucoside	611 (449, 287)	trace	trace	trace	trace	–	–	–	–
3	3.83	delphinidin 3-*O*-glucoside	465 (303)	6540.37 ± 122.09	3910.18 ± 102.98	3195.97 ± 74.93	2376.58 ± 79.02	1840.21 ± 20.92	1357.61 ± 230.45	1901.89 ± 56.32	962.04 ± 31.24
4	5.31	peonidin 3,5-*O*-diglucoside	625 (463, 301)	27.32 ± 3.65	–	37.62 ± 4.63	21.05 ± 2.01	–	–	–	–
5	5.44	malvidin 3,5-*O*-diglucoside	655 (493, 331)	71.27 ± 3.12	66.61 ± 4.29	106.58 ± 9.28	120.49 ± 6.30	79.98 ± 2.93	–	–	–
6	5.67	cyanidin 3-*O*-glucoside	449 (287)	685.59 ± 13.98	631.03 ± 10.73	697.27 ± 22.09	294.29 ± 12.03	135.67 ± 9.36	183.4 ± 8.87	292.82 ± 8.32	150.42 ± 6.43
7	6.71	petunidin 3-*O*-glucoside	479 (317)	1621.76 ± 22.67	2008.97 ± 218.38	1842.42 ± 73.02	1474.75 ± 62.01	733.14 ± 7.92	1103.8 ± 12.37	1387.16 ± 8.37	658.49 ± 24.48
8	8.41	pelargonidin 3-*O*-glucoside	433 (271)	–	–	47.92 ± 2.90	–	–	–	–	–
9	9.02	peonidin 3-*O*-glucoside	463 (301)	1834.51 ± 41.65	1316.40 ± 75.35	2144.76 ± 65.09	1404.36 ± 62.10	657.21 ± 12.98	752.3 ± 9.32	787.70 ± 43.83	691.65 ± 65.31
10	10.03	malvidin 3-*O*-glucoside	493 (331)	9354.17 ± 314.30	8122.83 ± 276.28	8680.37 ± 45.92	9942.14 ± 321.02	6011.27 ± 232.98	7883.6 ± 293.47	5992.69 ± 265.98	5414.24 ± 178.33
11	11.23	delphinidin 3-*O*-acetylglucoside	507 (303, 465)	686.59 ± 21.09	1140.64 ± 83.29	922.12 ± 40.92	697.24 ± 32.09	478.12 ± 38.82	698.78 ± 32.45	422.65 ± 7.37	316.24 ± 9.42
12	14.74	cyanidin 3-*O*-acetylglucoside	491 (287, 449)	178.21 ± 45.87	225.32 ± 12.34	229.03 ± 10.84	105.49 ± 9.93	83.97 ± 8.39	135.32 ± 7.93	90.15 ± 8.32	107.52 ± 8.56
13	16.01	petunidin 3-*O*-acetylglucoside	521 (317, 479)	542.46 ± 3.98	813.11 ± 30.97	682.38 ± 32.91	532.68 ± 43.02	300.28 ± 12.04	457.3 ± 12.83	339.54 ± 19.21	278.24 ± 6.46
14	18.15	delphinidin 3-*O*-coumaroylglucoside	611 (303, 465)	177.64 ± 12.84	–	207.06 ± 20.10	–	170.85 ± 7.02	185.1 ± 12.38	428.10 ± 17.39	–
15	19.97	peonidin 3-*O*-acetylglucoside	505 (301, 463)	441.42 ± 19.76	501.38 ± 32.71	762.19 ± 20.80	583.12 ± 34.02	491.69 ± 34.75	476.2 ± 32.34	68.77 ± 3.21	326.40 ± 12.68
16	20.26	malvidin 3-*O*-acetylglucoside	535 (331, 493)	4531.46 ± 165.63	5150.13 ± 210.73	4820.22 ± 301.89	6132.99 ± 210.31	4849.27 ± 122.44	6105.28 ± 276.84	1650.99 ± 211.33	3424.19 ± 186.54
17	21.17	peonidin 3-*O*-caffeoylglucoside	625 (463, 301)	43.63 ± 1.57	22.82 ± 3.29	35.14 ± 3.81	–	–	–	29.52 ± 2.34	30.09 ± 1.86
18	21.98	malvidin 3-*O*-caffeoylglucoside	655 (493, 331)	–	35.17 ± 2.83	–	–	9.01 ± 0.96	15.67 ± 1.38	75.41 ± 6.38	23.37 ± 2.67
19	22.98	cyanidin 3-*O*-coumaroylglucoside	595 (449, 287)	52.89 ± 3.73	60.35 ± 2.97	166.49 ± 23.84	51.37 ± 4.02	51.64 ± 2.69	55.34 ± 3.49	74.82 ± 8.32	75.00 ± 4.45
20	24.36	petunidin 3-*O*-coumarylglucoside	625 (317, 479)	129.82 ± 20.09	141.01 ± 20.78	61.78 ± 4.82	141.06 ± 5.04	165.18 ± 7.92	160.24 ± 6.93	277.07 ± 9.42	45.16 ± 4.68
21	25.83	peonidin 3-*O*-(6-*O*-*cis*-*p*-coumaryl)glucoside	609 (463, 301)	25.81 ± 0.52	19.41 ± 1.83	142.58 ± 7.94	31.36 ± 3.01	16.90 ± 1.02	18.13 ± 0.93	27.81 ± 3.45	23.92 ± 2.78
22	26.84	malvidin 3-*O*-(6-*O*-*cis*-*p*-coumaryl)glucoside	639 (493, 331)	78.30 ± 3.81	68.04 ± 4.93	542.49 ± 23.89	130.74 ± 4.95	131.48 ± 8.04	122.38 ± 5.93	76.75 ± 2.93	51.17 ± 5.23
23	28.24	peonidin 3-*O*-(6-*O*-*trans*-*p*-coumaryl)glucoside	609 (463, 301)	261.02 ± 19.98	220.27 ± 20.78	42.63 ± 2.87	370.33 ± 12.03	353.15 ± 12.90	412.81 ± 9.45	243.10 ± 11.34	89.50 ± 4.78
24	28.77	malvidin 3-*O*-(6-*O*-*trans*-*p*-coumaryl)glucoside	639 (493, 331)	1346.13 ± 49.37	1321.77 ± 50.72	1683.12 ± 63.82	2099.68 ± 120.93	2360.64 ± 122.80	3301.94 ± 233.45	2080.21 ± 138.76	616.14 ± 13.76

[a]"–" indicates that the compound was not detected. YNSR, Shuori of Yunnan (28°34′ N and 98°47′ E); YNMLS, Meilishi of Yunnan (27°49′ N and 99°42′ E); SCMC, Mao County of Sichuan (32°0′ N and 103°42′ E). These three vineyards are all located in the high-altitude regions of southwestern China, where there is a particular dry−cool valley microclimate with a big temperature difference between daytime and nighttime. XJM, Manasi of Xinjiang (44°18′5 N and 86°13′ E). This vineyard is located in northwest China in a region with a semiarid climate, with high biologically effective day temperatures, a big temperature difference between daytime and nighttime, and low annual rainfall. GSQL, Qilian of Gansu (99°84′ E and 39°14′ N). This vineyard is located on the desert edge zones at an altitude of about 1214 m with a cool−arid climate and a big temperature difference between daytime and nighttime.

DOI: 10.1021/acs.jafc.5b00053
J. Agric. Food Chem. 2015, 63, 3251−3260

Table 2. Microsatellite DNA Profiles (allele sizes in bp) for Different Grape Samples Obtained for the Six Simple Sequence Repeat Loci

cultivar[a]	simple sequence repeat loci											
	VVS2		VVMD5		VVMD7		VVMD27		VrZAG62		VrZAG79	
Syrah	131	131	224	230	236	236	186	188	187	193	243	249
Chardonnay	135	141	232	236	236	240	178	186	187	195	241	243
Cabernet Sauvignon (YNSR)	137	149	230	238	236	236	172	186	187	193	245	245
Cabernet Sauvignon (YNMLS)	137	149	230	238	236	236	172	186	187	193	245	245
Cabernet Sauvignon (XJM)	137	149	230	238	236	236	172	186	187	193	245	245
Cabernet Sauvignon (GSQL)	137	149	230	238	236	236	172	186	187	193	245	245

[a]YNSR, Shuori of Yunnan (28°34′ N and 98°47′ E); YNMLS, Meilishi of Yunnan (27°49′ N and 99°42′ E); SCMC, Mao County of Sichuan (32°0′ N and 103°42′ E); XJM, Manasi of Xinjiang (44°18′5 N and 86°13′ E); GSQL, Qilian of Gansu (99°84′ E and 39°14′ N).

300 mM NaCl, 10 mM imidazole] and proteinase inhibitors including 1 mg/mL leupeptin, 0.5 mg/mL lysozyme, 0.5 mM phenylmethanesulfonyl fluoride (PMSF), and 0.4% (m/v) Triton X-100. The cell suspension was disrupted by sonication for 15 min, and the resulting cell debris were removed by centrifugation followed by filtration with a 0.45 μm filter (Millipore). The target proteins were purified by Ni-NTA His Bind Resin (Novagen, Madison, WI). The column was washed with 5 mL of washing buffer containing buffer A and 3 M imidazole in a proportion of 150:1 (pH 8.0) and then with elution buffer containing buffer A and 3 M imidazole in a proportion of 15:1 (pH 8.0). The high-concentration fractions were collected and purified using a stirred cell (Millipore) with a regenerated cellulose membrane [molecular weight cutoff (MWCO) 3000 Da; Millipore]. All steps were conducted at 4 °C. Sodium dodecyl sulfate−polyacrylamide gel electrophoresis (SDS−PAGE) was performed to estimate the relative purity of the recombinant proteins. The protein concentration was determined using the Bradford method.[29,30] Negative controls were carried out with *E. coli* BL21 (DE3) cells containing the empty expression vector pET-32a.

Enzyme Activity Assessment of Vv5GT Proteins. Six kinds of anthocyanidin 3-*O*-glucosides were respectively used as glycosyl acceptor. The reaction mixture (100 μL) was composed of 0.1 M potassium phosphate buffer (pH 8.0), purified recombinant protein (5 μL), 100 μM anthocyanidin 3-*O*-glucoside, and 2 mM UDP-glucose. The mixture was incubated in a 35 °C water bath for 30 min, and the reaction was terminated by adding an equal volume of methanol containing 1% (v/v) hydrochloric acid. Afterward, the reaction solution was filtered through 0.22 μm filters. The products were examined by means of HPLC−QQQ-MS/MS equipped with an Agilent series 1200 instrument and a Poroshell 120 EC-C18 column (150 × 2.1 mm, 2.7 μm, Agilent Technologies). The elution solution was composed of water (A) and acetonitrile/methanol (50:50, v/v, B), both with 0.1% formic acid. The elution gradient was from 10% to 46% B for 21 min, from 46% to 10% B 1 min later, with a flow rate at 0.4 mL/min; column cleanup and re-equilibration were at 90% A and 10% B for 5 min with a flow rate at 0.3 mL/min and a column temperature of 55 °C.

An Agilent 6410 QqQ instrument equipped with an electrospray ionization source was applied for identification and quantitation of the compounds. Spray voltage was set at 4 kV in positive mode, the source temperature was kept at 150 °C, gas temperature was 350 °C, gas flow was 12 L/h, and nebulizer pressure was 35 psi. The m/z^+ ions were selected as precursor ions of anthocyanins. SIM was used to find out the optimum fragmentor voltage. The target anthocyanins were detected under multiple reaction monitoring (MRM) mode. The catalytic activity of Vv5GT protein was assessed by the production of anthocyanidin diglucosides in the reaction system.

Biochemical Characterization of Vv5GT3. On the basis of the assessment of enzyme activity of various Vv5GT proteins, we found that only Vv5GT3 exhibited 5GT activity. To further understand the biochemical property of Vv5GT3, we altered some parameters of the above enzyme reaction protocols. In the reaction mixture using 60 μM peonidin 3-*O*-glucoside as glycosyl acceptor, the reaction was recorded from 0 to 23 h (Figure S3, Supporting Information); the amount of enzyme protein added was increased from 0 to 3.3 μg (Figure S4, Supporting Information); the reaction system was in the range of pH 6.5−10.0 (Figure S5a, Supporting Information), and the reaction temperature was set up from 25 to 45 °C (Figure S5b, Supporting Information). The K_m values were determined by varying the concentrations of cyanidin 3-*O*-glucoside (41.3−206.3 μM), delphinidin 3-*O*-glucoside (40.0−199.7 μM), malvidin 3-*O*-glucoside (37.8−189.1 μM), petunidin 3-*O*-glucoside (40.0−200.0 μM), pelargonidin 3-*O*-glucoside (38.8−194.2 μM), peonidin 3-*O*-glucoside (40.1−200.5 μM), quercetin 3-*O*-glucoside (861.4−4306.8 μM), delphinidin (118.1−590.5 μM), and quercetin (750.0−3750.0 μM), respectively, in the reaction mixture. The products were detected by HPLC−QQQ-MS/MS according to the above procedures, except that flavonols were identified in a negative ion mode. The K_m value was calculated from a double-reciprocal plot of initial velocity ($1/V$) against glycosyl acceptor concentration ($1/[S]$). The plot slope is K_m/V_{max}. All reactions were repeated in triplicate.

Subcellular Localization of Vv5GT3 Protein. The open reading frame of *Vv5GT3* was PCR-amplified, and the primers are listed in Table S1 (Supporting Information). Purified amplicon was digested with *BamH*I and *Hind*III and then fused to the upstream of the gene coding for green fluorescent protein (GFP) in the cauliflower mosaic virus 35S-EGFP-Ocs 3′ vector (*p*-EZS-NL vector, available online from https://deepgreen.dpb.carnegiescience.edu). Subcellular localization was conducted according to the protocol Zhu et al.[31]

Real-Time PCR. Quantitative real-time PCR was performed on a 7300 Real Time PCR System (Applied Biosystems) to investigate the expression pattern of *Vv5GT3* in developing Cabernet Sauvignon grape berries. *VvUbiquitin* (GenBank accession number AY684131) and *VvActin-7* (LOC100232866) were used as internal controls. The primers for real-time PCR are listed in Table S1 (Supporting Information). A total volume of 30 μL of reaction solution was composed of 15 μL of SYBR Premix Ex Taq and 0.5 μL of ROX reference dye (50×) (Takara), 13 μL of ddH_2O (TIANGEN), 0.5 μL of cDNA, and 1 μL of primer mixture (forward primer and reverse primer, 10 mM). For real-time PCR, the template cDNA was denatured at 95 °C for 30 s, followed by 40 cycles of amplification at 94 °C for 10 s and 60 °C for 31 s. The average cycle threshold (Ct) of *VvUbiquitin* and *VvActin-7* at each sampling point was determined, and their geomean value was used to calculate the transcript abundance of *Vv5GT3*, using the formula $2^{-\Delta Ct}$.[32] The mean and the standard derivation (SD) were estimated after $2^{-\Delta Ct}$ calculation.

RESULTS AND DISCUSSION

A total of 24 anthocyanins were detected in the skins of Cabernet Sauvignon grape berries. Among them, 20 anthocyandin 3-*O*-glucosides are commonly present in *V. vinifera* grapes. These anthocyanidin 3-*O*-glucosides include six individual anthocyanins, five acetylated anthocyanins, seven *p*-coumaroylated anthocyanins, and two caffeoylated anthocyanin (Table 1 and Figure 1a). Besides, four diglucosides of anthocyanidins were detected (Figure 1). The mass spectral data of peak 1 obtained with ESI-MS and ESI-MS/MS showed a molecular ion at m/z 627 ($[M]^+$) and two MS/MS fragment ions at m/z 465 ($[M - 162]^+$) and m/z 303 ($[M - 162 - 162]^+$), which were

DOI: 10.1021/acs.jafc.5b00053
J. Agric. Food Chem. 2015, 63, 3251−3260

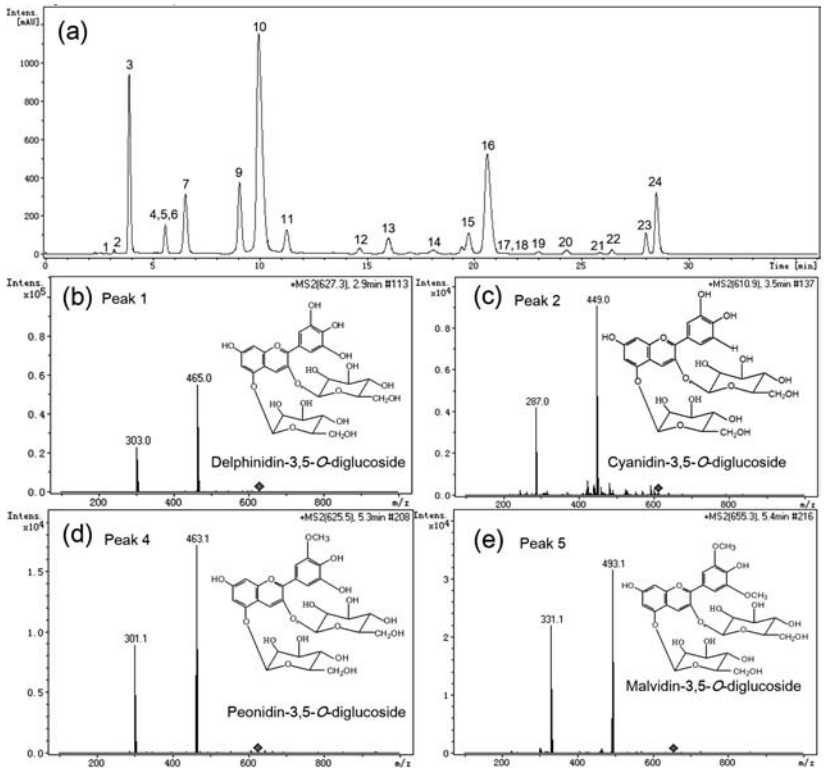

Figure 1. Detection of anthocyanidin 3,5-*O*-diglucosides in the skins of Cabernet Sauvignon grape berries from Deqin County of Yunnan Province in southwest China (28°34′ N and 98°47′ E). (a) Reverse-phase HPLC chromatogram of anthocyanins at 525 nm; the product ion mass spectra and chemical structures of (b) peak 1, (c) peak 2, (d) peak 4, and (e) peak 5. The compounds corresponding to the peak numbers are listed in Table 1.

compatible with a delphinidin-based structure linked to two hexose (m/z 162) units (Figure 1b). A similar fragmentation pattern was also reported previously.[19] So peak 1 was assigned as delphinidin 3,5-*O*-diglucoside. Similarly, peak 2 with a retention time of 3.50 min had a protonated ion of m/z 611 ($[M]^+$) and two fragment ions of m/z 449 ($[M - 162]^+$, cyanidin 3-*O*-glucoside) and m/z 287 ($[M - 162 - 162]^+$, cyanidin) by two successive losses of a hexose moiety. This compound was identified as cyanidin 3,5-*O*-diglucoside on the basis of fragmentation pattern and retention time (Figure 1c). Peak 4 had a molecular ion m/z 625, and two fragment ions of m/z 463 (peonidin 3-*O*-glucoside) and m/z 301 (peonidin), indicating that this compound is peonidin 3,5-*O*-diglucoside (Figure 1d); peak 5 with a retention time of 5.40 min had a protonated ion of m/z 655 ($[M]^+$) and two fragment ions of m/z 493 (malvidin 3-*O*-glucoside) and m/z 331 (malvidin), which correspond to malvidin 3,5-*O*-diglucoside (Figure 1e). Here, it needs to be noted that anthocyanidin 3,5-diglucoside has the identical molecular ion mass and fragmentation pattern with its 3,7-diglucoside, but they exhibit different retention times.[33−37] Previous study has found that malvidin 3,5-*O*-diglucoside elutes between delphinidin 3-*O*-glucoside and cyanidin 3-*O*-glucoside, whereas malvidin 3,7-*O*-diglucoside elutes between petunidin 3-*O*-glucoside and peonidin 3-*O*-glucoside,[34] which further demonstrates that peak 5 (Figure 1e) is malvidin 3,5-*O*-diglucoside. Moreover, in the present study, the identification of four anthocyanidin diglucosides was based on the analysis of *V. amurensis*, *Vitis davidii*, and *Vitis quinquangularis* grapes[17] with high levels of anthocyanidin 3,5-*O*-diglucosides, which also explains that these four compounds, corresponding to peaks 1, 2, 4, and 5, are 3,5-*O*-diglucosides of anthocyanidins, rather than 3,7-*O*-diglucosides. Additional investigation also revealed that the appearance of anthocyanidin 3,5-*O*-diglucoside in Cabernet Sauvignon grape berries is not an accident, and it has occurred in more than one wine-producing region in China (Table 1).

A few *V. vinifera* cultivars have been found to contain detectable anthocyandin 3,5-*O*-diglucosides.[3,15,38−41] However, so far no report has shown that anthocyanidin diglucosides are detected in Cabernet Sauvignon grapes, a *V. vinifera* cultivar widely planted in the wine-producing countries or regions of the world. Recent research also has demonstrated that *5GT* allele in this cultivar contains a three-base-pair deletion at nucleotide positions 901, 1182, and 1183, thus resulting in the loss of its function.[15] To test the real identity of the cultivar used in this study, we analyzed microsatellite DNA genotyping of the grapevines, using Syrah and Chardonnay cultivars as references. The obtained SSR loci were identical with microsatellite genotyping of Cabernet Sauvignon from grapevine SSR databases (http://www.vivc.de/index.php) (Table 2 and Figure S1, Supporting Information). Moreover, these grape samples from the five sampling vineyards all presented the same microsatellite profile. These facts demonstrate the authenticity of the Cabernet Sauvignon cultivar used in this study.

To explain why there are anthocyanidin 3,5-*O*-diglucosides in the Cabernet Sauvignon grapes grown in the wine-producing regions of China, we analyzed the DNA sequence of *Vv5GT1*, which was similar to the sequence of functional *5GT-Cha*.[14] The result showed that *Vv5GT1* had a nucleotide G deletion at position 902 when compared with the sequence of functional *5GT-Cha*. It is just this nucleotide deletion that caused a frameshift and a premature translation stop at codon 308 (TAA) at the C-terminus. That is, the deduced Vv5GT1 protein had a

DOI: 10.1021/acs.jafc.5b00053
J. Agric. Food Chem. 2015, 63, 3251−3260

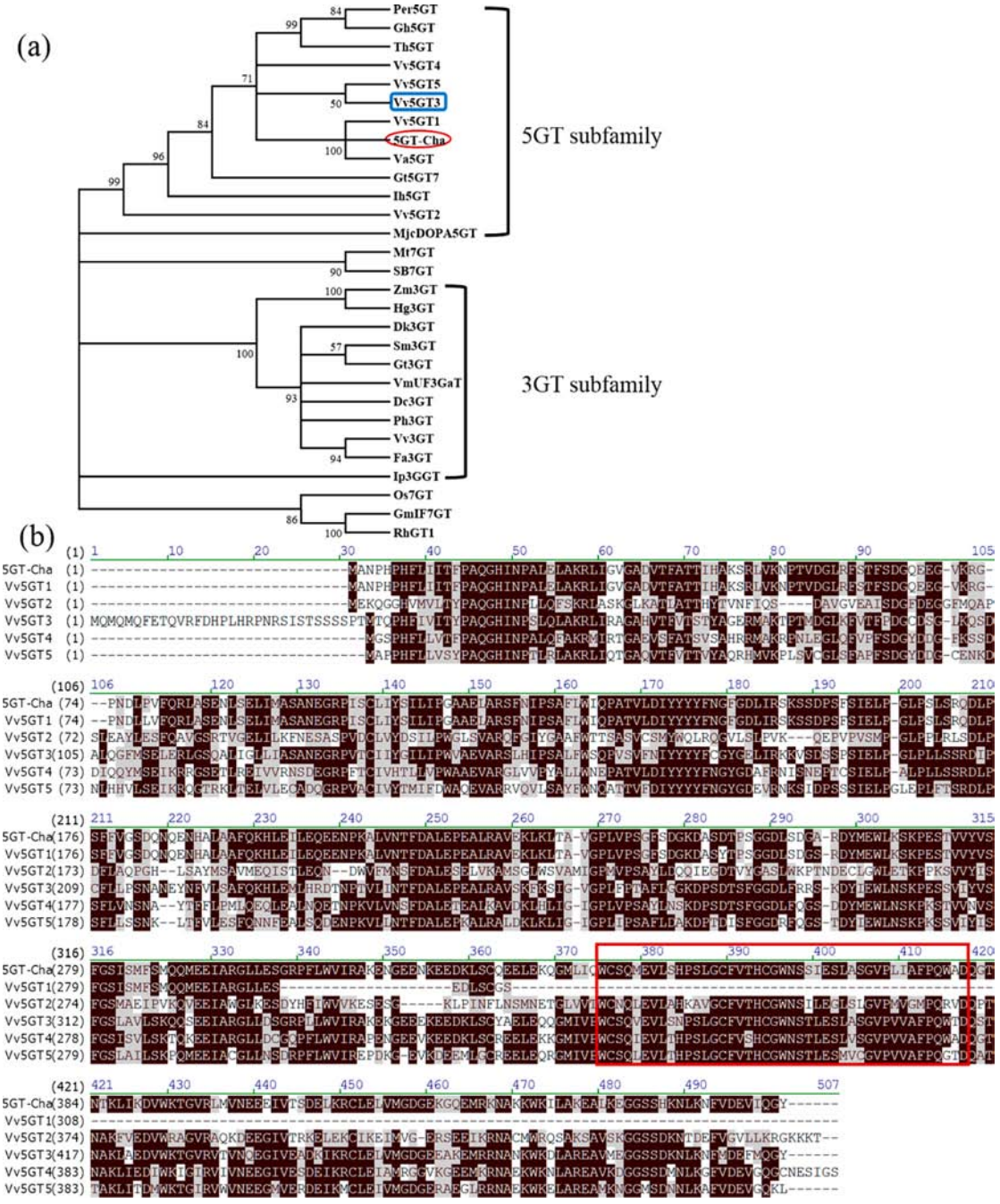

Figure 2. Phylogenetic analysis of glycosyltransferases and multiple alignment of deduced amino acid sequences of 5GTs. (a) Gene names refer to species and GenBank accession numbers are as follows. UDP-glucose:anthocyanin 5-*O*-glucoyltransferase (5GT): Vv5GT1, Vv5GT2, Vv5GT3, Vv5GT4, Vv5GT5 (present study); 5GT-Cha, the functional 5-*O*-glucosyltransferase from *Vitis vinifera* cv. Regent;[14] Per5GT, *Perilla frutescens* var. Crispa, BAA36421; Gh5GT, *Glandularia* × *hybrid*, BAA36423; Th5GT, *Torenia hybrid*, BAC54093; Va5GT, *V. amurensis*, AHL68667; Gt5GT7, *Gentiana*, AB363839; Ih5GT, *Iris* × *hollandica*, BAD06874; MjcDOPA5GT, *Mirabilis jalapa* cyclo-DOPA 5-*O*-glucosyltransferase, AB182643. UDP-glucose:flavonoid 3-*O*-glucoyltransferase (3GT): Zm3GT, *Zea mays*, P16167; Hg3GT, *Hordeum vulgare*, P14726; Dk3GT, *Diospyros kaki*, BAI40148; Sm3GT, *Solanum melongena*, Q43641; Gt3GT, *Gentiana triflora*, Q96493; Dc3GT1, *Dianthus caryophyllus*, BAD52003; Ph3GT, *Petunia* × *hybrid*, AAD55985; Vv3GT, *V. vinifera*, AAB81683; Fa3GT, *Fragaria* × *ananassa*, Q66PF5. Other GTs: GmIF7GT, *Glycine max* UDP-glucose:isoflavone 7-*O*-glucosyltransferase, BAF64416; Mt7GT, *Medicago truncatula* UDP-glycosyltransferase, AAW56091; Os7GT, *Oryza sativa* Japonica UDP-glycosyltransferase, BAD69345; SB7GT, *Scutellaria baicalensis* UDP-glucose:flavonoid 7-*O*-glucosyltransferase, AB031274; VmUF3GaT, *Vigna mungo* UDP-glucose:flavonoid 3-*O*-galactosyl transferase, AB009370; Ip3GGT, *Ipomoea purpurea* UDP-glucose:anthocyanidin 3-*O*-glucoside-2″-*O*-glucosyltransferase, AB192315; RhGT1, rose UDP-glucose:anthocyanidin 5,3-*O*-glucosyltransferase, AB201048. Bar = 0.1 amino acid substitutions/site. (b) Multiple alignment of deduced amino acid sequences of 5GTs. Dark and light shading indicate identical and similar amino acids, respectively. The box indicates the plant secondary product glycosyltransferase motif (PSPG box).

158-amino acid deletion at the C-terminus. This deletion region contained a characteristic motif for plant secondary product glucosyltransferase (PSPG box).[42] It is thus suggested that the 158-amino acid deletion led to the loss of gene function. In addition, *Vv5GT1* was also found to have 7-bp substitution in comparison with the functional *5GT-Cha*.

DOI: 10.1021/acs.jafc.5b00053
J. Agric. Food Chem. 2015, 63, 3251−3260

In an effort to find the genes that encode 5GT in the Cabernet Sauvignon grape berries, the other four candidate *Vv5GT*s (*Vv5GT2*−*Vv5GT5*) were separated. Phylogenetic analysis revealed that each of these genes is related to the 5GT subfamily of glycosyltransferase genes (Figure 2a). The molecular masses of their predicted proteins were approximately 50.4, 55.4, 52.1, and 51.9 kDa, respectively, consisting of 457,497, 469, and 463 amino acids. All of these four proteins contained a 44-amino acid consensus sequence at the C-terminus (Figure 2b), called the PSPG box, which was highly conserved among plant glycosyltransferases.[42] More importantly, these four candidate *Vv5GT*s could be transcribed since they were obtained using cDNA template.

To assess the catalytic activities of the four prokaryotically expressed proteins, we have used six individual anthocyanin 3-*O*-glucosides as glycosyl acceptors. No product was detected for the Vv5GT2, Vv5GT4, and Vv5GT5 proteins. Therefore, these three proteins were not further studied. Among the identified *Vv5GT* genes, only Vv5GT3 was an enzymatically active protein.

The substrate specificity and biochemical properties of the recombinant Vv5GT3 protein were analyzed using a wide variety of flavonoids as glycosyl acceptors and using UDP-glucose or UDP-galactose as glycosyl donors. Vv5GT3 exhibited an apparent 5GT activity with respect to malvidin 3-*O*-glucoside (K_m = 91.87 μM) (Figure S2a, Supporting Information), peonidin 3-*O*-glucoside (K_m = 373.88 μM), cyanidin 3-*O*-glucoside (K_m = 111.29 μM), delphinidin 3-*O*-glucoside (K_m = 53.54 μM), petunidin 3-*O*-glucoside (K_m = 114.57 μM), and pelargonidin 3-*O*-glucoside (K_m = 206.98 μM), respectively. As shown in Figure 3a,b, Vv5GT3 converted malvidin 3-*O*-glucoside (*m*/*z* 493) into malvidin 3,5-*O*-diglucoside (*m*/*z* 655) through adding a glycosyl group (*m*/*z* 162). Here, we also noticed that the retention time and fragmentation pattern of the product from the reaction of Vv5GT3 and malvidin 3-*O*-glucoside (Figure 3b) completely corresponded to those of the standard malvidin 3,5-*O*-diglucoside (Figure 3a), suggesting that Vv5GT3 acts at the 5-position of malvidin 3-*O*-glucoside, rather than at the 7-position. Judging from K_m value, Vv5GT3 had a higher affinity for anthocyanidin 3-*O*-glucosides. In general, the concentration of anthocyanidin 3-*O*-glucoside in the berry skins of Cabernet Sauvignon was in the range of 100−3500 mmol/kg, which exceeds the K_m values of Vv5GT3 for these compounds (53.54−373.88 μmol/L). Additionally, Vv5GT3 also could convert quercetin 3-*O*-glucoside (*m*/*z* 463) into quercetin 3,5-*O*-dglucoside (*m*/*z* 625) (Figure 3c,d). However, this enzyme showed a relatively low affinity for quercetin 3-*O*-glucoside (K_m = 4.51 mM) (Figure S2b, Supporting Information), indicating that anthocyandin 3-*O*-glucosides should be the preferred glycosyl acceptors in the catalytic reaction of Vv5GT3. Surprisingly, this enzyme transferred the glucosyl group of UDPG to the 3-position of either anthocyanidins (such as cyanidin, delphinidin, and malvidin) or flavonols (such as quercetin, kaempferol, and myricetin), but their K_m values were very high (1.61 mM for delphinidin and 3.12 mM for quercetin) (Figure S2c,d, Supporting Information). Figure 3e,f present the production of quercetin 3-*O*-glucoside (*m*/*z* 463) in the reaction system using quercetin (*m*/*z* 301) as the glycosyl acceptor. Meanwhile, we also detected quercetin 3,5-*O*-diglucoside (*m*/*z* 625) with a very low level in this reaction system (Figure 3f). However, the recombinant Vv5GT3 was found not to use UDP-galactose as a glycosyl donor (data not shown). These results indicate that Vv5GT3 has the activities of both 3GT and 5GT

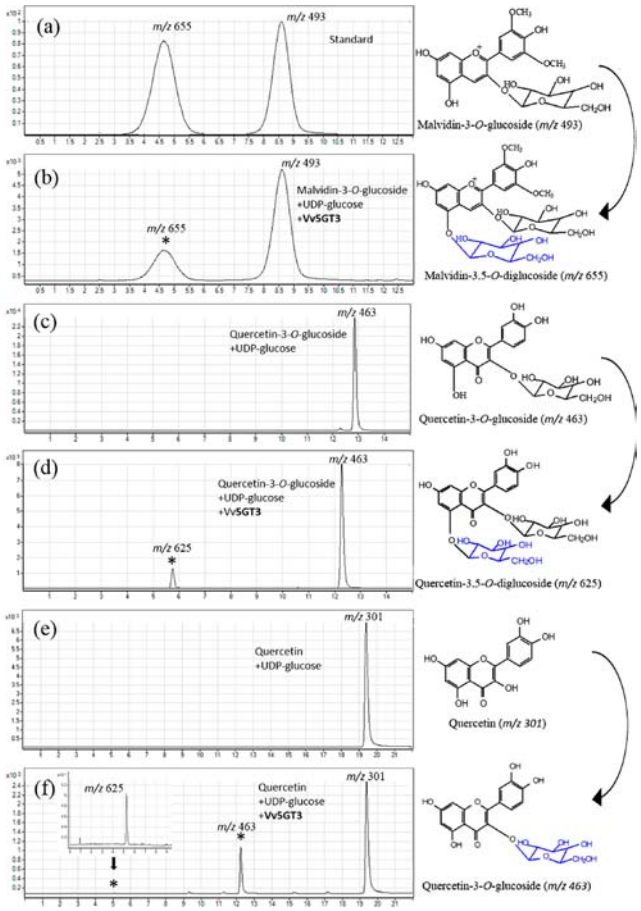

Figure 3. Enzymatic activity analyses of recombinant Vv5GT3 protein for glycosylation of malvidin 3-*O*-glucoside, quercetin 3-*O*-glucoside, and quercetin using HPLC−QQQ-MS/MS. (a) Authentic standards of malvidin 3-*O*-glucoside and malvidin 3,5-*O*-diglucoside. The product in the reaction systems containing (b) malvidin 3-*O*-glucoside, Vv5GT3, and UDP-glucose; (c) quercetin 3-*O*-glucoside + empty vector control + UDP-glucose; (d) quercetin 3-*O*-glucoside + Vv5GT3 + UDP-glucose; (e) quercetin + empty vector control + UDP-glucose; and (f) quercetin + Vv5GT3 + UDP-glucose. The asterisk indicates the product peak for each enzyme reaction.

and exhibits a broad substrate specificity. Such metabolic flexibility of Vv5GT3 might be one mechanism for producing the diversity of secondary plant metabolites.

To further understand the biochemical properties of Vv5GT3, we examined the effects of the reaction time course, enzyme amount, reaction temperature, and reaction system pH on the activity of Vv5GT3. TheVv5GT3 proteins continued to catalyze the glucosyltransfer reaction for about 11 h when incubated at 35 °C (Figure S3, Supporting Information), indicating that the enzyme is relatively stable and active. A linear relationship between the enzyme amount and the product concentration was also observed (Figure S4, Supporting Information). The highest catalytic activity of Vv5GT3 was around 35 °C and at pH 7.5−8.0 when we used peonidin 3-*O*-glucoside as the glycosyl acceptor (Figure S5a,b, Supporting Information).

Most of the anthocyanins accumulate in the vacuoles, and all structural genes involved in the anthocyanin biosynthesis are located on the endoplasmic reticulum membranes or in the cytoplasm, where the anthocyanins are directly produced.[43−45] To provide evidence regarding in vivo colocalization of the enzyme with its substrates, we examined the subcellular localization of

DOI: 10.1021/acs.jafc.5b00053
J. Agric. Food Chem. 2015, 63, 3251−3260

Vv5GT3 using transient expression of this gene fused with a *GFP* reporter gene in *Arabidopsis* protoplasts. The cytosol−nucleus double-localized PYR1 protein was taken as reference. GFP fluorescence was clearly observed in the cytoplasm (Figure 4), as we predicted.

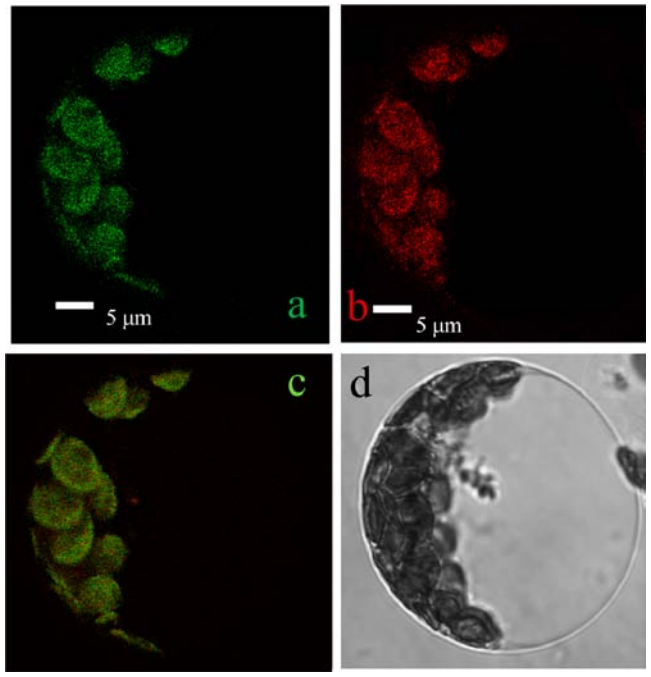

Figure 4. Confocal laser scanning microscopy of transiently expressed *Vv5GT3−GFP* fusions in *Arabidopsis* protoplasts. (a) Green fluorescent protein fluorescence of Vv5GT3−GFP. (b) Red fluorescent protein fluorescence of the nuclear−cytosol double-localized marker PYR1−RFP. (c) Merged image of parts a and b. (d) Light-microscopy image of intact protoplast. Bar: 5 μm.

Vv5GT3 was transcriptionally expressed during the development of Cabernet Sauvignon grape berries, and the relative expression amount was higher at preveraison than that at post-veraison (Figure 5). This may be related to the synthesis of flavonols, which occurs well before anthocyanin synthesis.

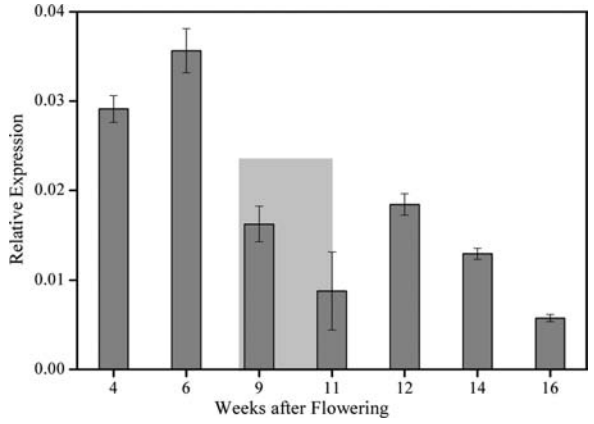

Figure 5. Relative expression levels of *Vv5GT3*. Expression analysis was performed on Cabernet Sauvignon grape berries at different development stages using quantitative real-time PCR (n = 3). The light gray background indicates the period of veraison from 10% to 100% of colored berries.

So far, most UGTs have been functionally characterized to be monofunctional. That is, 5GTs only can glycosylate flavonoid 3-*O*-glucosides but cannot take flavonoids like anthocyanidins, whereas 3GTs do not take anthocyanidin 5-*O*-glucoside as a glucosyl acceptor.[46] The present study showed a novel 5GT with catalytic activity at the 3-position of flavonoid. The following evidence could offer some explanations for this abnormal result. First, the primers cloning *Vv5GT3* are the same as gene 6 from the Regent cultivar,[26] and their nucleotide sequences have above 99% similarity. This gene 6 was found to be closely related to *5GT* genes in other plants based on the cluster analysis of sequences. Meanwhile, this gene can be transcribed in all the detected genotypes, independent of the existence of anthocyanidin 3,5-*O*-diglucoside.[26] Our study also revealed the occurrence of *Vv5GT3* transcription even in the early stage of Cabernet Sauvignon grape development, when grapes do not start to synthesize anthocyanins. It can be inferred that *Vv5GT3* might use the nonanthocyanins as glycosyl acceptors, such as flavonols. It may function to produce anthocyanidin diglucosides merely under a particular condition, such as under continental monsoon climate in the China's wine-producing regions. On the other hand, it should be completely possible to produce very low or trace levels of anthocyanidin diglucosides in *V. vinifera*, since there are *5GT*-like gene transcript and 3-*O*-anthocyanins existence in these cultivars. However, does the bifunctional property of *Vv5GT3* appear in other *V. vinifera* cultivars? Also, which catalytic activity of *Vv5GT3* is dominant in grape berries? Further study is under way.

In conclusion, we provided mass spectrometric and enzymatic evidence confirming the existence of anthocyanidin 3,5-*O*-diglucoside in *V. vinifera* L. Cabernet Sauvignon berries. This is the first report involving functional 5GT in Cabernet Sauvignon grapes. The identification of a new UGT with the activities of both 3GT and 5GT can be useful for better understanding anthocyanins' profile and their biosynthesis in *V. vinifera*. Our findings are also helpful for further investigations on the mechanism of the accumulation of anthocyanidin diglucosides in Cabernet Sauvignon berries in China's wine-producing regions.

■ ASSOCIATED CONTENT

Ⓢ Supporting Information

Primers used in this study, the SSR loci, and biochemical properties of Vv5GT3 protein. This material is available free of charge via the Internet at http://pubs.acs.org.

■ AUTHOR INFORMATION

Corresponding Author

*Tel: 86-10-62736191. Fax: 86-10-62738658. E-mail: panqh@cau.edu.cn.

Funding

This work is financially supported by the National Key Technology Support Program of China (Grant No. 2012BAD41B00) and the China Agricultural Research System for Grape Industry (CARS-30).

Notes

The authors declare no competing financial interest.

■ ABBREVIATIONS USED

HPLC−ESI-MS/MS, high-performance liquid chromatography−electrospray ionization tandem mass spectrometry; HPLC−QQQ-MS/MS, high-performance liquid chromatography coupled to triple quadrupole mass spectrometry; K_m,

DOI: 10.1021/acs.jafc.5b00053
J. Agric. Food Chem. 2015, 63, 3251−3260

Michaelis contant; PCR, polymerase chain reaction; SDS−PAGE, sodium dodecyl sulfate−polyacrylamide gel electrophoresis

REFERENCES

(1) Mattivi, F.; Guzzon, R.; Vrhovsek, U.; Stefanini, M.; Velasco, R. Metabolite profiling of grape: Flavonols and anthocyanins. *J. Agric. Food Chem.* **2006**, *54*, 7692−7702.

(2) Flamini, R.; Mattivi, F.; De Rosso, M.; Arapitsas, P.; Bavaresco, L. Advanced knowledge of three important classes of grape phenolics: Anthocyanins, stilbenes and flavonols. *Int. J. Mol. Sci.* **2013**, *14*, 19651−69.

(3) Picariello, G.; Ferranti, P.; Chianese, L.; Addeo, F. Differentiation of *Vitis vinifera* L. and hybrid red grapes by matrix-assisted laser desorption/ionization mass spectrometry analysis of berry skin anthocyanins. *J. Agric. Food Chem.* **2012**, *60*, 4559−4566.

(4) Li, Z.; Pan, Q.; Cui, X.; Duan, C. Optimization of anthocyanins extraction from wine grape skins using orthogonal test design. *Food. Sci. Biotechnol.* **2010**, *19*, 1047−1053.

(5) He, F.; Mu, L.; Yan, G. L.; Liang, N. N.; Pan, Q. H.; Wang, J.; Reeves, M. J.; Duan, C. Q. Biosynthesis of anthocyanins and their regulation in colored grapes. *Molecules* **2010**, *15*, 9057−9091.

(6) Sui, X.; Gao, X.; Ao, M.; Wang, Q. M.; Yang, D.; Wang, M.; Fu, Y.; Wang, L. cDNA cloning and characterization of UDP-glucose:anthocyanidin 3-*O*-glucosyltransferase in *Freesia hybrida*. *Plant Cell Rep.* **2011**, *30*, 1209−1218.

(7) Acevedo De la Cruz, A.; Hilbert, G.; Riviére, C.; Mengin, V.; Ollat, N.; Bordenave, L.; Decroocq, S.; Delaunay, J.-C.; Delrot, S.; Mérillon, J.-M.; Monti, J.-P.; Gomès, E.; Richard, T. Anthocyanin identification and composition of wild *Vitis* spp. accessions by using LC−MS and LC−NMR. *Anal. Chim. Acta* **2012**, *732*, 145−152.

(8) Giusti, M. M.; Rodríguez-Saona, L. E.; Griffin, D.; Wrolstad, R. E. Electrospray and tandem mass spectroscopy as tools for anthocyanin characterization. *J. Agric. Food. Chem.* **1999**, *47*, 4657−4664.

(9) Acevedo De la Cruz, A.; Hilbert, G.; Riviére, C.; Mengin, V.; Ollat, N.; Bordenave, L.; Decroocq, S.; Delaunay, J.-C.; Delrot, S.; Mérillon, J.-M.; Monti, J.-P.; Gomès, E.; Richard, T. Anthocyanin identification and composition of wild *Vitis* spp. accessions by using LC−MS and LC−NMR. *Anal. Chim. Acta* **2012**, *732*, 145−152.

(10) Zhu, L.; Zhang, Y.; Lu, J. Phenolic contents and compositions in skins of red wine grape cultivars among various genetic backgrounds and originations. *Int. J. Mol. Sci.* **2012**, *13*, 3492−3510.

(11) Zhao, Q.; Duan, C. Q.; Wang, J. Anthocyanins profile of grape berries of *Vitis amurensis*, its hybrids and their wines. *Int. J. Mol. Sci.* **2010**, *11*, 2212−2228.

(12) Stobiecki, M. Application of mass spectrometry for identification and structural studies of flavonoid glycosides. *Phytochemistry* **2000**, *54*, 237−256.

(13) Mazza, G. Anthocyanins in grapes and grape products. *Crit. Rev. Food Sci. Nutr.* **1995**, *35*, 341−371.

(14) Janvary, L.; Hoffmann, T.; Pfeiffer, J.; Hausmann, L.; Topfer, R.; Fischer, T. C.; Schwab, W. A double mutation in the anthocyanin 5-*O*-glucosyltransferase gene disrupts enzymatic activity in *Vitis vinifera* L. *J. Agric. Food Chem.* **2009**, *57*, 3512−3518.

(15) Yang, Y.; Labate, J. A.; Liang, Z.; Cousins, P.; Prins, B.; Preece, J. E.; Aradhya, M.; Zhong, G. Y. Multiple loss-of-function 5-*O*-glucosyltransferase alleles revealed in *Vitis vinifera*, but not in other *Vitis* species. *Theor. Appl. Genet.* **2014**, *127*, 2433−2451.

(16) Boulton, R. B.; Singleton, V. L.; Bisson, L. F.; Kunkee, R. E. Selection of state of ripeness for harvest and harvesting. In *Principles and Practices of Winemaking*; Boulton, R. B., Ed.; Chapman & Hall, International Thomson Publishing: New York, 1995; pp 52−60.

(17) Liang, N.-N.; Pan, Q.-H.; He, F.; Wang, J.; Reeves, M. J.; Duan, C. Phenolic profiles of *Vitis davidii* and *Vitis quinquangularis* species native to China. *J. Agric. Food Chem.* **2013**, *61*, 6016−6027.

(18) Han, F.-L.; Zhang, W.-N.; Pan, Q.-H.; Zheng, C.-R.; Chen, H.-Y.; Duan, C.-Q. Principal component regression analysis of the relation between CIELAB color and monomeric anthocyanins in young Cabernet Sauvignon wines. *Molecules* **2008**, *13*, 2859−2870.

(19) Wu, X.; Prior, R. L. Systematic identification and characterization of anthocyanins by HPLC−ESI-MS/MS in common foods in the United States: Fruits and berries. *J. Agric. Food Chem.* **2005**, *53*, 2589−2599.

(20) Thomas, M. R.; Scott, N. S. Microsatellite repeats in grapevine reveal DNA polymorphisms when analyzed as sequence-tagged sites (STSs). *Theor. Appl. Genet.* **1993**, *86*, 985−990.

(21) Bowers, J. E.; Dangl, G. S.; Vignani, R.; Meredith, C. P. Isolation and characterization of new polymorphic simple sequence repeat loci in grape (*Vitis vinifera* L). *Genome* **1996**, *39*, 628−633.

(22) Bowers, J. E.; Dangl, G. S.; Meredith, C. P. Development and characterization of additional microsatellite DNA markers for grape. *Am. J. Enol. Viticult.* **1999**, *50*, 243−246.

(23) Sefc, K. M.; Regner, F.; Turetschek, E.; Glossl, J.; Steinkellner, H. Identification of microsatellite sequences in *Vitis riparia* and their applicability for genotyping of different *Vitis* species. *Genome* **1999**, *42*, 367−373.

(24) Ghosh, S.; Karanjawala, Z. E.; Hauser, E. R.; Ally, D.; Knapp, J. I.; Rayman, J. B.; Musick, A.; Tannenbaum, J.; Te, C.; Shapiro, S. Methods for precise sizing, automated binning of alleles, and reduction of error rates in large-scale genotyping using fluorescently labeled dinucleotide markers. FUSION (Finland-US Investigation of NIDDM Genetics) Study Group. *Genome Res.* **1997**, *7*, 165−178.

(25) Zhang, Z.-Z.; Li, X.-X.; Zhu, B.-Q.; Wen, Y.-Q.; Duan, C.-Q.; Pan, Q.-H. Molecular characterization and expression analysis on two isogenes encoding 3-deoxy-D-arabino-heptulosonate 7-phosphate synthase in grapes. *Mol. Biol. Rep.* **2011**, *38*, 4739−4747.

(26) Hausmann, L.; Neumann, K.; Eibach, R.; Zyprian, E.; Topfer, R. Development of a molecular marker for an anthocyanin 5-*O*-glucosyltransferase homologous gene of *Vitis* ssp. correlated with anthocyanin 3,5-diglucoside formation in berry skin. *Acta Horticul.* **2009**, *827*, 457−460.

(27) Larkin, M. A.; Blackshields, G.; Brown, N. P.; Chenna, R.; McGettigan, P. A.; McWilliam, H.; Valentin, F.; Wallace, I. M.; Wilm, A.; Lopez, R.; Thompson, J. D.; Gibson, T. J.; Higgins, D. G. Clustal W and Clustal X version 2.0. *Bioinformatics* **2007**, *23*, 2947−2948.

(28) Tamura, K.; Dudley, J.; Nei, M.; Kumar, S. MEGA4: Molecular evolutionary genetics analysis (MEGA) software version 4.0. *Mol. Biol. Evol.* **2007**, *24*, 1596−1599.

(29) Bradford, M. M. A rapid and sensitive method for the quantitation of microgram quantities of protein utilizing the principle of protein−dye binding. *Anal. Biochem.* **1976**, *72*, 248−54.

(30) Fan, R. C.; Peng, C. C.; Xu, Y. H.; Wang, X. F.; Li, Y.; Shang, Y.; Du, S. Y.; Zhao, R.; Zhang, X. Y.; Zhang, L. Y. Apple sucrose transporter SUT1 and sorbitol transporter SOT6 interact with cytochrome b_5 to regulate their affinity for substrate sugars. *Plant Physiol.* **2009**, *150*, 1880−1901.

(31) Zhu, B. Q.; Cai, J.; Wang, Z. Q.; Xu, X. Q.; Duan, C. Q.; Pan, Q. H. Identification of a plastid-localized bifunctional nerolidol/linalool synthase in relation to linalool biosynthesis in young grape berries. *Int. J. Mol. Sci.* **2014**, *15*, 21992−22010.

(32) Reid, K. E.; Olsson, N.; Schlosser, J.; Peng, F.; Lund, S. T. An optimized grapevine RNA isolation procedure and statistical determination of reference genes for real-time RT-PCR during berry development. *BMC Plant Biol.* **2006**, *6*, 27.

(33) Giusti, M. M.; Rodríguez-Saona, L. E.; Griffin, D.; Wrolstad, R. E. Electrospray and tandem mass spectroscopy as tools for anthocyanin characterization. *J. Agric. Food Chem.* **1999**, *47*, 4657−4664.

(34) Alberts, P.; Stander, M. A.; de Villiers, A. Advanced ultra high pressure liquid chromatography−tandem mass spectrometric methods for the screening of red wine anthocyanins and derived pigments. *J. Chromatogr., Sect. A* **2012**, *1235*, 92−102.

(35) Alcalde-Eon, C.; Escribano-Bailón, M. T.; Santos-Buelga, C.; Rivas-Gonzalo, J. C. Changes in the detailed pigment composition of red wine during maturity and ageing: A comprehensive study. *Anal. Chim. Acta* **2006**, *563*, 238−254.

DOI: 10.1021/acs.jafc.5b00053
J. Agric. Food Chem. 2015, 63, 3251−3260

(36) Castillo-Muñoz, N.; Winterhalter, P.; Weber, F.; Gómez, M. V.; Gómez-Alonso, S.; García-Romero, E.; Hermosín-Gutiérrez, I. Structure elucidation of peonidin 3,7-*O*-*β*-diglucoside isolated from Garnacha Tintorera (*Vitis vinifera* L.) grapes. *J. Agric. Food. Chem.* **2010**, *58*, 11105−11111.
(37) Picariello, G.; Ferranti, P.; Garro, G.; Manganiello, G.; Chianese, L.; Coppola, R.; Addeo, F. Profiling of anthocyanins for the taxonomic assessment of ancient purebred *V. vinifera* red grape varieties. *Food Chem.* **2014**, *146*, 15−22.
(38) Liang, Z. C.; Owens, C. L.; Zhong, G. Y.; Cheng, L. L. Polyphenolic profiles detected in the ripe berries of *Vitis vinifera* germplasm. *Food Chem.* **2011**, *129*, 940−950.
(39) Vidal, S.; Hayasaka, Y.; Meudec, E.; Cheynier, V.; Skouroumounis, G. Fractionation of grape anthocyanin classes using multilayer coil countercurrent chromatography with step gradient elution. *J. Agric. Food Chem.* **2004**, *52*, 713−719.
(40) Heier, A.; Blaas, W.; Droß, A.; Wittkowski, R. Anthocyanin analysis by HPLC/ESI-MS. *Am. J. Enol. Viticult.* **2002**, *53*, 78−86.
(41) Li, Y.; Ma, R.; Xu, Z.; Wang, J.; Chen, T.; Chen, F.; Wang, Z. Identification and quantification of anthocyanins in Kyoho grape juicemaking pomace, Cabernet Sauvignon grape winemaking pomace and their fresh skin. *J. Sci. Food. Agric* **2013**, *93*, 1404−1411.
(42) Gachon, C. M. M.; Langlois-Meurinne, M.; Saindrenan, P. Plant secondary metabolism glycosyltransferases: The emerging functional analysis. *Trends. Plant. Sci.* **2005**, *10*, 542−549.
(43) Barceló, A. R.; Calderón, A.; Zapata, J.; Muñoz, R. The histochemical localization of anthocyanins in seeded and seedless grapes (*Vitis vinifera*). *Sci. Hortic.* **1994**, *57*, 265−268.
(44) Chen, J.-Y.; Wen, P.-F.; Kong, W.-F.; Pan, Q.-H.; Wan, S.-B.; Huang, W.-D. Changes and subcellular localizations of the enzymes involved in phenylpropanoid metabolism during grape berry development. *J. Plant Physiol.* **2006**, *163*, 115−127.
(45) Fan, R.-C.; Peng, C.-C.; Xu, Y.-H.; Wang, X.-F.; Li, Y.; Shang, Y.; Du, S.-Y.; Zhao, R.; Zhang, X.-Y.; Zhang, L.-Y. Apple sucrose transporter SUT1 and sorbitol transporter SOT6 interact with cytochrome b_5 to regulate their affinity for substrate sugars. *Plant Physiol.* **2009**, *150*, 1880−1901.
(46) Ogata, J.; Kanno, Y.; Itoh, Y.; Tsugawa, H.; Suzuki, M. Plant biochemistry: Anthocyanin biosynthesis in roses. *Nature* **2005**, *435*, 757−758.

DOI: 10.1021/acs.jafc.5b00053
J. Agric. Food Chem. 2015, 63, 3251−3260

of meat are well evaluated by LF-NMR measurements.[20,21] LF-NMR measurement is also a sensitive method for studying changes in water mobility and corresponding water populations in gel-like food matrixes such as cheese and tofu.[17,22] Different starch systems have been widely studied by LF-NMR. Tang et al. studied the molecular distribution of water in potato starch granules with LF-NMR, and they identified three proton fractions with different T_2 values, which were assigned to water molecules in different substructures of starch granules.[23,24] Bosmans et al. reported that there are three proton fractions in an unheated starch−gluten mixed system, and they used LF-NMR to study biopolymer dynamics, crumb firming, and several other physical properties of bread during its storage.[25−28] However, the soaking, steaming, and SSF processes of glutinous rice are currently not defined. In the present study, the soaking, steaming, and SSF processes of glutinous rice were studied by LF-NMR. On the basis of the intimate connection between proton dynamics and microstructure variations during SSF, we established a standardized SSF process of glutinous rice, which may aid in the real-time monitoring of other similar SSF processes of starch systems.

MATERIALS AND METHODS

Materials. Commercial glutinous rice from Jiangsu Province was obtained from a local market (approximately 77% amylopectin, 7.3% protein, and 13% water). The starter culture, sweet koji (Xiao Qu), was kindly provided by Suzhou Cereals, Oils and Foodstuffs Corporation (Suzhou, P. R. China). The starter culture contains *Rhizopus*, *Mucor*, and eight other strains of yeast. All other chemicals were of analytical grade and were obtained from Sigma-Aldrich Chemical Co. (St. Louis, MO, USA).

Preparation of Fermented Glutinous Rice. Glutinous rice was rinsed several times with water to remove powders and soluble matters, and then it was soaked in deionized water at a ratio of 1:3 (w/w) for 6 h at 20 °C. The water was then discarded, and the soaked glutinous rice was steamed in a Midea WSYH26A electric saucepan at 100 °C (Midea Co., Ltd., Guangdong, China) for 20 min. Glutinous rice was then cooled by rinsing with cold sterile water and mixed with sweet koji (preground into powder) at a ratio of 1:100 (w/w; 700 g of dry glutinous rice to 7 g of sweet koji powder). The inoculated glutinous rice was placed into a bowl, the central part of which was hollowed out to guarantee the oxygen supply for the bottom part. The inoculated glutinous rice was then incubated at 30 °C with humidity of 90% in an incubator. The fermentation normally lasts approximately 36−48 h. However, the fermentation duration was prolonged to 54 h to obtain a full understanding of the alternations that occur in glutinous rice during SSF.

Reducing Sugar (RS) Analysis. Estimation of the total reducing sugars was performed by the 3,5-dinitrosalicvlic acid (DNS) method.[29] Samples (1 g) taken out at different fermentation times were homogenized with 50 mL of distilled water. The mixture was then incubated in a water bath at 50 °C for 20 min for better extraction of reducing sugars. After incubation, the mixture was centrifuged in a CT15RT centrifugal filter system (Techcomp Co., Ltd., Shanghai, China) at 8000*g* for 5 min to obtain a supernatant. The supernatant was then diluted with water to 100 mL. Aliquots (1 mL) of the supernatant were placed into test tubes, and 2 mL of DNS reagent was added. The mixture was boiled for 5 min and then cooled to room temperature. Absorbance of the samples was recorded at 540 nm using a Multiskan GO spectrophotometer (Thermo Fisher Scientific Co., Ltd., Waltham, MA, USA). All of the experiments were conducted in triplicate.

Determinations of Titrable Acidity (TA). Fermented glutinous samples (25 g) from different fermentation times were homogenized with 225 mL of distilled water and incubated for 30 min for better extraction of acidoids. The TA (°T, expressed as Thorner degree; °T × 0.009 = lactic acid %) of the different samples was measured according to the method of Cen et al.[30] All of the experiments were conducted in triplicate.

Determinations of Moisture Content (MC). Samples (10 g) were taken from the central part of the rice and placed into a BAO-80A high temperature drying oven (STIK Co., Ltd., Shanghai, China). The drying process was conducted at 105 °C, and the samples were dried to a constant weight. MC was defined as the ratio of the weight loss during drying and the original weight of each sample. All of the experiments were conducted in triplicate.

Deuterium Oxide (D_2O) Experiments. To distinguish between exchanging protons and nonexchanging protons, deuterium oxide (D_2O) experiments were performed based on the method of Bosmans with slight modifications.[25] Raw glutinous rice (2 g) was soaked in excess D_2O for 12 h and subsequently decanted to a Labconco freezone 12 L console freeze-dry system (Labconco Co., Ltd., Kansas City, MO) for vacuum freeze-drying at a temperature of −50 °C for 24 h. The samples were then rehydrated by excess D_2O. For steamed rice, the samples were vacuum freeze-dried and then rehydrated by D_2O. Both cycles were repeated three times. Control experiments were performed with water instead of D_2O to correct for the impact of the exchange method on the proton distribution of the sample.

Low-Field Nuclear Magnetic Resonance Measurements. A 22.4 MHz NMR analyzer PQ001 (Niumag Co., Ltd., Shanghai, China) was used to perform low-field nuclear magnetic resonance (LF-NMR) measurements. Approximately 2.5 g of different fermented glutinous rice samples was taken from the central part of the rice curd and placed into 15 mm NMR glass tubes. The tubes were then heated to 32 °C in a water bath for 5 min and inserted into the NMR-probe. T_2 relaxation times were measured using the Carr−Purcell−Meiboom−Gill (CPMG) sequence. The T_2 measurements were performed with a τ-value of 100 μs (time between 90° and 180° pulses). Data from 5000 echoes were acquired as 16 scan repetitions, and the repetition time between two successive scans was 5 s. The relaxation measurements were performed at 32 °C.

MultiExp Inv Analysis software (Niumag Co., Ltd., Shanghai, China) was employed for data analysis. The MultiExp Inv Analysis software performs distributed exponential curve fitting. A continuous distribution of exponentials for a CPMG experiment is defined by the following equation:

$$R_{\mathrm{mag}}(t) = \sum_{j=1}^{n} P_{2j} \exp\left(\frac{-t}{T_{2j}}\right) + e(t) \quad (1)$$

where R_{mag} is the residual magnetization as a function of acquisition time t, P_{2j} and T_{2j} are the spin−spin relaxation amplitude and time, respectively, of the jth component, and e is the residual error. For a better fit, multiexponential fitting analysis was performed on the relaxation data according to a modified inversion method of Xiao et al.[31] The relaxation time T_{2i} and its corresponding water population (area ratio) M_{2i} were recorded. Each cycle (testing and inversion) required less than 2 min, and 10 parallel samples of each fermentation time were measured.

Statistical Analysis. Statistical analyses were carried using with SPSS version 18.0. To evaluate the difference between means, one-way ANOVA was used followed by Duncan's test. The significance levels were defined as * ($p < 0.05$) and ** ($p < 0.01$). A principal component analysis (PCA) model was performed using Simca-P+ software (Umetrics AB) to identify cluster patterns. Sigmoid fitting was performed with Origin 8.1. An adjusted determination coefficient (Adj R^2) was used to evaluate the fitting degree with Adj R^2 defined as follows:

$$\text{Adj } R^2 = 1 - \frac{(n-1)(1-R^2)}{n-m} \quad (2)$$

where R^2 is the original determination coefficient and n and m are the numbers of sample and variables, respectively.

DOI: 10.1021/acs.jafc.5b00769
J. Agric. Food Chem. 2015, 63, 3261−3270

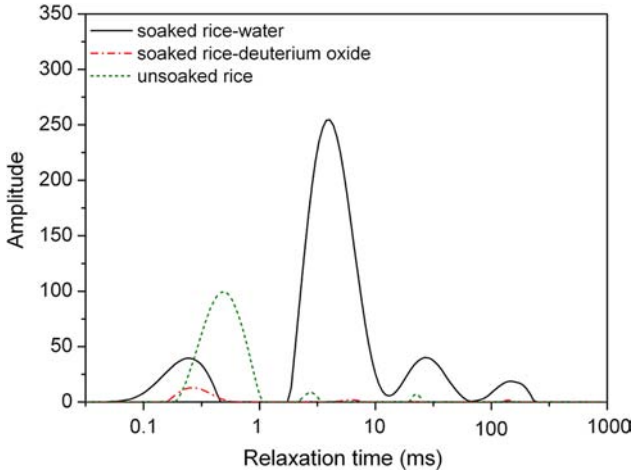

Figure 1. LF-NMR T_2 relaxation time distribution curves of unsoaked, soaked rice−water, and soaked rice−deuterium oxide samples.

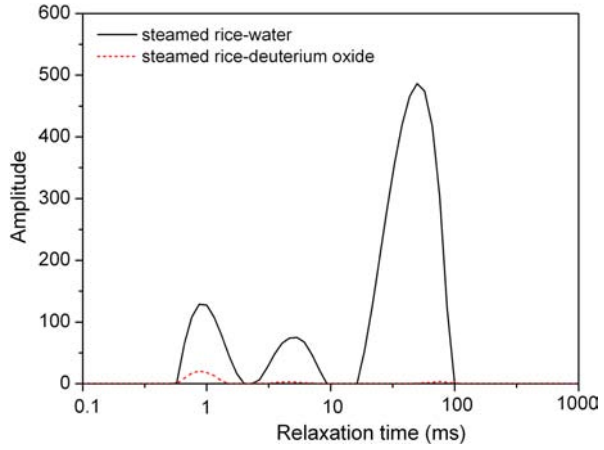

Figure 2. LF-NMR T_2 relaxation time distribution curves of steamed rice−water and steamed rice−deuterium oxide samples.

RESULTS AND DISCUSSION

LF-NMR Analysis of Raw, Soaked, and Steamed Glutinous Rice. The soaking and steaming pretreatments of glutinous rice are essential for further fermentation and sensory attributes of the final product. However, an in-depth understanding of the proton dynamics and interactions between water and macromolecules during soaking and steaming is still lacking. Figure 1 shows the relaxation time distribution curves of unsoaked glutinous rice (with 13% water content). Three proton fractions in raw glutinous rice were found in this study. As shown in Figure 1, T_{2b} was the fastest fraction, with a relaxation time of approximately 0.4 ms and accounted for more than 90% of the total signal. T_{21} was the intermediate fraction (approximately 5% of the total signal) with a relaxation time of approximately 5 ms, whereas T_{22} was the slowest and had the minimum fraction, with a relaxation time of approximately 25 ms (less than 1.5% of the total signal).

The interpretation and origin of the T_2 transverse relaxation of heterogeneous systems have been studied extensively. In general, multiexponential relaxation behavior of various food matrixes can be ascribed to different water fractions that exist in heterogeneous microstructures and protons of biopolymer.[13,15] Previous studies have shown that protons in starch systems can be differentiated into several distinct populations through their

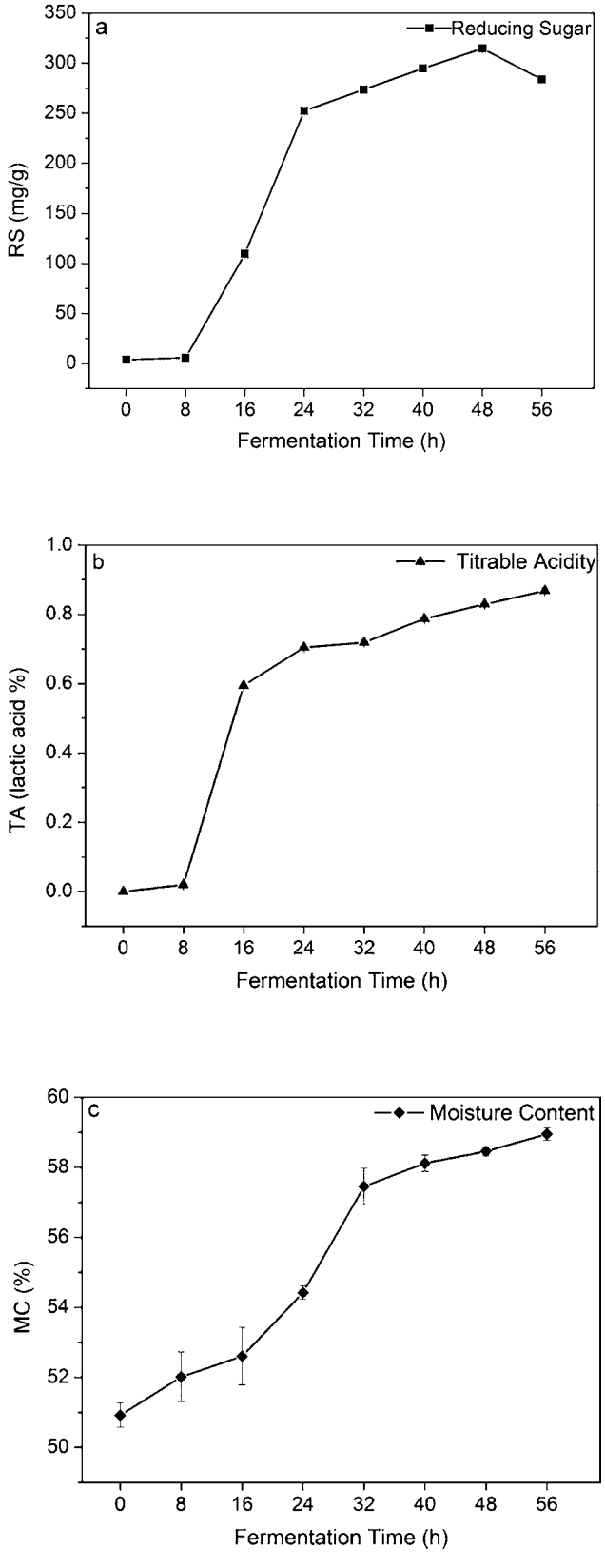

Figure 3. Variations of three traditional parameters during SSF: (a) total reducing sugar, (b) titrable acidity, (c) moisture content.

NMR relaxation behavior, which provides unique insight into the microstructure of the starch. Additionally, glutinous rice contains approximately 7.3% glutelin, which may also play a role in the formation of the microstructural network. The result

DOI: 10.1021/acs.jafc.5b00769
J. Agric. Food Chem. 2015, 63, 3261−3270

Table 1. Variations of Different T_2 Parameters During Solid-State Fermentation (n = 10)

fermentation time (h)	T'_{2b} (ms)	M'_{2b} (%)	T'_{21} (ms)	M'_{21} (%)	T'_{22} (ms)	M'_{22} (%)
0	0.79 ± 0.05 a	15.06 ± 0.07 f	5.20 ± 0.29 a	7.42 ± 0.34 d	51.26 ± 3.14 b	78.38 ± 1.04 a
8	0.81 ± 0.60 ab	12.79 ± 0.73 e	4.74 ± 0.57 ab	7.85 ± 0.53 e	35.69 ± 2.53 a	79.58 ± 0.42 a
16	1.01 ± 0.11 b	9.83 ± 1.15 d	5.82 ± 0.41 b	7.60 ± 0.18 de	37.16 ± 1.55 a	82.87 ± 1.76 b
24	2.11 ± 0.40 c	3.29 ± 0.89 c	10.65 ± 1.31 c	7.78 ± 0.25 e	67.76 ± 4.15 c	89.24 ± 2.99 c
32	2.55 ± 0.17 d	2.25 ± 0.15 b	11.25 ± 1.25 c	6.58 ± 0.20 c	79.04 ± 5.47 d	92.15 ± 0.98 d
40	2.86 ± 0.27 e	1.85 ± 0.05 ab	13.63 ± 0.89 d	6.10 ± 0.09 b	86.97 ± 0.01 e	92.35 ± 0.72 d
48	3.57 ± 0.28 f	1.56 ± 0.13 ab	13.44 ± 0.95 d	5.72 ± 0.28 a	98.70 ± 4.11 f	93.34 ± 0.52 d
56	3.56 ± 0.17 f	1.29 ± 0.05 a	13.25 ± 0.97 d	5.57 ± 0.22 a	113.48 ± 4.73 g	93.34 ± 0.47 d

[a]Results are presented as the mean ± standard deviation. Lowercase letters (a–g) in the same column indicate significant differences ($p < 0.05$).

of the D_2O experiment using raw samples is shown in Figure 1. The T_{21} and T_{22} fractions nearly disappeared in the soaked rice–D_2O sample, indicating that the protons of these two fractions were exchangeable. T_{2b}, the fastest fraction of the CPMG sequence, contained both nonexchangeable and exchangeable protons, which corresponded well with the report of Bosmans et al.[25] On the basis of the D_2O experiment and a previous study of waxy starch models, it is reasonable to propose the origin of three proton fractions in raw glutinous rice.[25] The slowest exchangeable fraction, T_{22}, was ascribed to mobile bulk water existing in the extragranular space between the granules. In view of its small proportion and fast relaxation time, this water fraction should exist as a thin layer between closely packed granules and is influenced by the interaction between biopolymer and water molecules. By diffusion from the bulk to the biopolymer interface acting as a relaxation sink, the T_2 values of the T_{22} water fraction are controlled by diffusive exchange. The intermediate component T_{21} can be ascribed to intragranular confined water that is in slow exchange with outside water on the NMR measurement time scale of a few hundred milliseconds such as water in amorphous growth rings of the granule.[24] This fraction should also include exchangeable protons of amylopectin and glutelin, including sulfydryl, hydroxyl, and carboxyl protons. According to the D_2O experiment, the T_{2b} fraction contained both nonexchangeable protons and exchangeable protons. Thus, the fastest fraction, T_{2b}, can be assigned to the nonexchangeable protons of amylopectin and glutelin, which do not have extensive contact with water such as CH protons in amorphous parts of the granule.[25] In addition, the T_{2b} fraction should also include water molecules trapped within starch or glutelin, which is regarded as an integral part of these macromolecules. The relaxation time of these water molecules is controlled by a rapid chemical exchange with the protons of biopolymers. Meanwhile, these water molecules are in slow exchange with outside water molecules,[13,17] which can be exchanged by D_2O and were mainly responsible for the signal loss of T_{2b} in the D_2O experiment.

Horigane et al. studied the soaking process of rice using gradient echo magnetic resonance imaging and found that despite the different penetration routes, water could diffuse to nearly all parts of the rice.[32] However, imaging cannot provide detailed information about changes in the proton distributions in the granular substructures. Figure 1 presents the relaxation time distribution curves of raw glutinous rice after soaking (with moisture content of approximately 40%). Because the soaking of rice does not involve irreversible chemical changes, we postulate that the assignments of different fractions were similar to that of unsoaked rice. Four fractions were detected in the soaked sample. The slowest fraction should be superficial water of the sample. This assignment was confirmed by the fact that this fraction vanished after using a hot-air blower to dry the soaked sample for 30 s (data not shown). The populations of the other three fractions showed a dramatic change in the soaked sample compared to the unsoaked sample. As shown in Figure 1, after soaking, the signal amplitude and relaxation time of the T_{22} fraction increased, which indicated that more water existed in the interstitial space of the granules. Moreover, the T_{21} fraction became the major fraction, and the T_{2b} fraction lost nearly half of its signal. Thus, the changes in the proton distribution were caused by water penetration because the moisture content of the rice increased to approximately 40%. Soaking allowed more water to penetrate into the granules and interact with protons of the T_{2b} fraction, and some T_{2b} protons became more mobile. The increase in the T_{21} population implied that the water absorbed by the starch mainly existed in the substructure of the granules.

The gelatinization of starch occurs when the starch granule is heated with water, and it is a process where the granule loses its crystallinity and its internal structure turns amorphous.[33] After gelatinization, the starch forms a three-dimensional network microstructure, which can be characterized by numerous holes and meshes with different diameters.[34] The multiexponential fitting relaxation curve of the steamed glutinous rice is shown in Figure 2 (with moisture content of 51%). The steamed sample still presented three fractions (T'_{2b}, T'_{21}, and T'_{22}), which were named after the order that they appeared in the time scale. The T'_{21} and T'_{22} fractions consisted of exchangeable protons because they had a low intensity in the D_2O experiment. The T'_{2b} fraction maintained part of its signal after exchanging with D_2O, indicating that it contained both exchangeable and nonexchangeable protons. Thus, the T'_{2b} fraction can be assigned to integrated water and protons of biopolymers, which were in the inner space of the starch–glutelin gel framework. The T'_{2b} population increased and accounted for approximately 15% of the total signal, which presumably reflected the swollen and broken granules. As the sample was heated in excess water, water was absorbed into the starch–glutelin gel framework and became an integral part of the biopolymer during gelatinization. In addition, protons of the biopolymers were embedded in the gel framework by gelatinization and contributed to the increase in the T'_{2b} population. The T'_{21} fraction, which accounted for approximately 7% of the total signal, can be ascribed to the water present in the small meshes of the rice microstructure and exchangeable protons of biopolymers. The T'_{22} fraction can be assigned to bulk water located in large meshes and can be considered to be controlled by diffusive exchange. For some starch systems that contain amylose, the heating process would lead to the merging of the T'_{21} and T'_{22} fractions and result in only two peaks. Unlike those starch systems, steamed glutinous

DOI: 10.1021/acs.jafc.5b00769
J. Agric. Food Chem. 2015, 63, 3261–3270

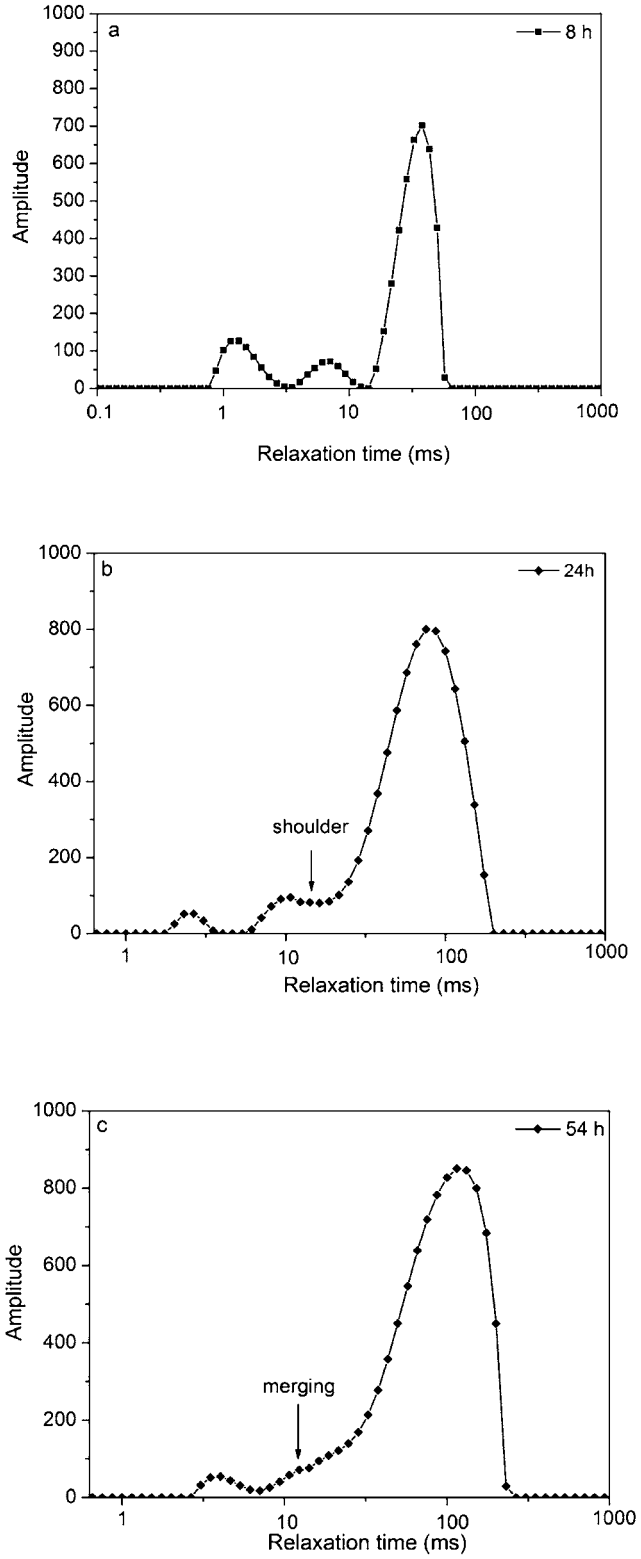

Figure 4. LF-NMR T_2 relaxation time distribution curves of samples at different fermentation times: (a) 8 h, (b) 24 h, (c) 54 h.

rice still presented three peaks, which was in accordance with the results derived from a waxy starch model.[25] Bosmans et al. suggested that the amylopectin has high swelling power and is disrupted more easily during heating. Heat-induced amylopectin gel forms a better developed three-dimensional network, microstructure with large meshes providing sufficient space for different proton fractions without averaging the diffusion.[25] The relaxation time of T'_{22} increased to approximately 51 ms, implying that the T'_{22} water was located in a more mobile microenvironment than in the raw and soaked samples due to the swelling and gelatinization effects of starch. Furthermore, more water was absorbed into the rice resulting in the T'_{22} fraction becoming the major fraction (accounted for approximately 78% of the total signal). Thus, the effects of soaking and steaming of glutinous rice is well reflected by the T_2 values, which provide detailed information about the proton dynamics during soaking and steaming.

Solid-State Fermentation of Glutinous Rice. The SSF of glutinous rice is a process by which starch is partially broken down and converted into reduced sugar (RS), alcohol, and other metabolites. During this process, filamentous fungi in koji are mainly responsible for generating hydrolases to convert starch to fermentable sugars for the subsequent ethanol fermentation performed by the yeast.[2] Figure 3a presents the changes of RS during fermentation. Because of the lag phase of fermentation, the RS remained at low levels (approximately 0.5 mg/g) in the first 8 h of fermentation before surging to more than 300 mg/g. After 48 h, the RS content decreased to 283 mg/g, indicating the start of the stationary phase. In addition to RS, microorganisms also produce organic acids such as lactic acid.[35] Figure 3b shows the variations of TA during SSF. In general, the TA presented similar tendency compared with RS, except that its surging point came earlier at approximately 8 h. Moisture content is another important parameter in SSF. Because of the metabolism of fungi and yeast, the MC of the glutinous rice increased from 50% to 57% during the fermentation period (Figure 3c). Compared to the LF-NMR measurements, the measurements of the three traditional parameters are time-consuming. In addition, the traditional parameters are unable to provide detailed information about biopolymer interactions, water dynamics, and microstructure changes during SSF.

The variation of the major fraction, T'_{22}, is shown in Table 1 and Figure 4. As mentioned previously, the T'_{22} fraction represents the water molecules that exist in large interstices or meshes of the microstructure of rice. During the first 8 h of fermentation, the T'_{22} relaxation time decreased significantly from 51 to 35 ms. We postulate that the decrease in T'_{22} relaxation was irrelevant to the changes of the microstructure because the effects of fermentation on rice should be insignificant considering the amount of water and metabolites (TA and RS) that they produced in the lag phase of fermentation. Starch retrogradation has been previously shown to result in a decrease of T_2 relaxation times in a starch system.[28] However, this assumption is not valid for the current conditions because the retrogradation of amylopectin belongs to the long-term retrogradation.[36] Thus, retrogradation did nearly not impact the T'_{22} relaxation time during the first 8 h of SSF. Considering the aforementioned facts, we propose that the decrease of T'_{22} relaxation time can be ascribed to the interactions between the water and macromolecules dissolved in the T'_{22} water. During the first 8 h, several macromolecules produced by microorganisms, such as maltodextrin, extracellular enzymes, and glutelin that were partially resolved by fungi, were dissolved and hydrated in the T'_{22} water fraction, which acted as a solution. The T'_{22} water molecules interacted with these macromolecules, leading to less mobility of the T'_{22} fraction and lower values of its relaxation time. After 8 h, the T'_{22} relaxation time presented an upward tendency, increasing

DOI: 10.1021/acs.jafc.5b00769
J. Agric. Food Chem. 2015, 63, 3261−3270

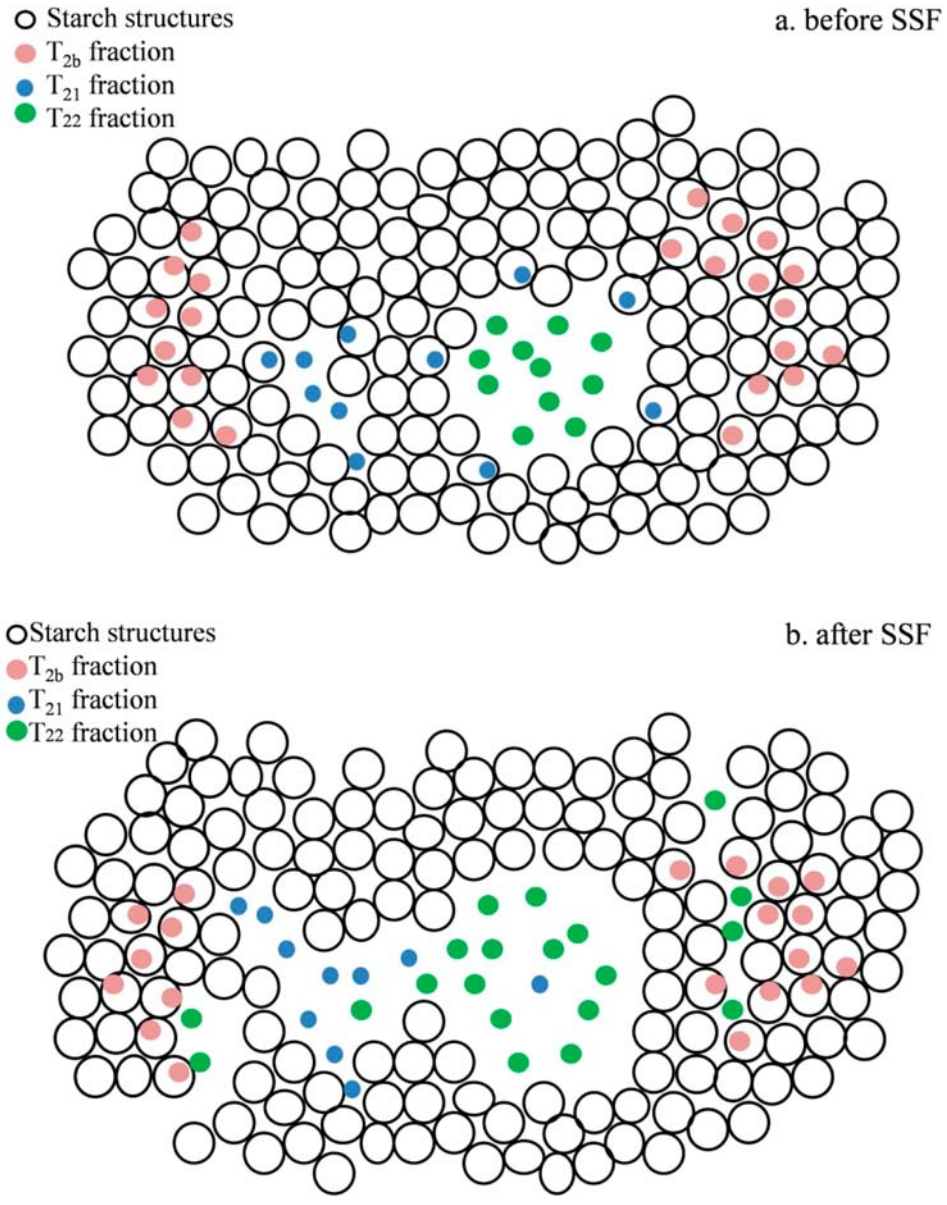

Figure 5. Simplified models to explain variations of the rice microstructure during SSF. Color-coded circles represent protons of different fractions: (a) before SSF, (b) after SSF.

from 35 to 113 ms, implying that the T'_{22} fraction was in a more mobile state. The significant influences of microorganisms on the microstructure of starch systems have been widely studied.[37,38] On the basis of variations in RS, TA, and MC, we speculate that the activities of fungi and yeast during fermentation lead to the change of microstructure and the increased T'_{22} relaxation time. To interpret the microstructure changes of glutinous rice, a simplified model was established. As shown in Figure 5, starch was consumed by microbial metabolism during fermentation, thus expanding the large interstices and meshes providing more space for the T'_{22} fraction. Moreover, the carbon dioxide produced by yeast may have also expanded the interstitial space of the microstructure.[38] Thus, we propose that these two factors increased the distance between the T'_{22} water molecules and the biopolymer interface, resulting in more mobile microenvironments in the T'_{22} fraction and higher values of its relaxation time. Although the MC of the sample increased by 7%, only the T'_{22} fraction population increased from 78% to 93% during SSF. This phenomenon indicated that the water produced by fermentation mainly diffused into the large meshes and became the T'_{22} water fraction, resulting in the increase of the T'_{22} population. As shown in Figure 4b, the rice microstructure became less homogeneous after fermentation because its peak broadened. This change also demonstrated the effects of fermentation on the microstructure of rice.

The intermediate fraction T'_{21} had a relaxation time that maintained an upward tendency. Although the lag phase of fermentation also influenced the T'_{21} fraction, which was reflected by the decrease in the relaxation time at 8 h, its impact was not as significant as that on the T'_{22} fraction because the relaxation time of the T'_{21} fraction at 16 h had exceeded its initial value. Similar to T'_{22} during fermentation, larger microenvironments were available for the T'_{21} fraction, leading to an increase of its relaxation time. Tang et al. found that the peak representing the intragranular water shifted to a longer

DOI: 10.1021/acs.jafc.5b00769
J. Agric. Food Chem. 2015, 63, 3261−3270

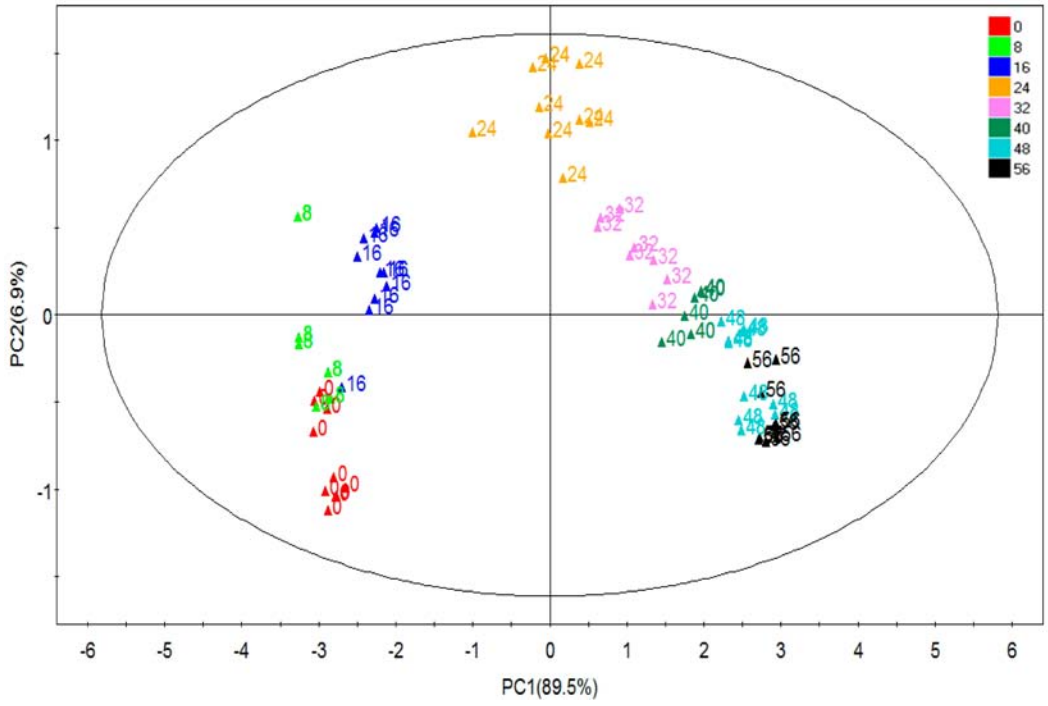

Figure 6. PCA plot obtained using distributed NMR T_2 relaxation data of all the samples (n = 80).

relaxation time during the acid hydrolysis of potato starch, and they ascribed the variation to an increased amount of water inside the granules.[24] However, the population of the T'_{21} fraction, which was different from that of the T'_{22} fraction, fluctuated during the first 24 h and then decreased slightly to approximately 5.6%. It was difficult to obtain detailed information on the variation of the T'_{21} population during fermentation because it was assigned to both water in the small meshes of the gel and exchangeable protons of biopolymers. Nevertheless, the T'_{21} population did not change considerably during fermentation. Moreover, the peaks of T'_{21} and T'_{22} were correlated with the fermentation time. After 24 h, there was a shoulder between the T'_{21} and T'_{22} fractions (Figure 4b). At 54 h, these two peaks completely merged into one (Figure 4c). Ideally, the distribution of proton relaxation times should be equivalent to the distribution of proton fractions in different microcompartments. However, the NMR signals of neighboring compartments can be averaged by the fast water diffusion between them. As a consequence, most water fractions in different microcompartments cannot be distinguished in time domain NMR, and the fractions can only be distinguished if their microstructural barriers exist because they can hinder the intercompartment water diffusion.[23] Thus, the independent signals of T'_{21} and T'_{22} fractions rely on the barriers that hinder the water exchange between them. The signals of the T'_{21} and T'_{22} water fractions were averaged by the fast diffusion between them, leading to the merging the T'_{21} and T'_{22} peaks. The diffusion averaging of the T'_{21} and T'_{22} fractions strongly indicated that the barriers between these two fractions were digested by fermentation, thereby reflecting the influence of SSF on the microstructure of rice (Figure 5b).

The T'_{2b} relaxation time increased from 0.8 to 3.6 ms, which may also be explained by the effects of SSF on the microstructure of rice. Before SSF, the strands of starch and protein network were well structured, thus preventing water molecules from penetrating in and interacting with the T'_{2b} fraction. Because of the activities of the microorganisms in fermentation, the structure of the starch and protein network may have been eroded by amylase and organic acid, allowing water to penetrate in and interact with the T'_{2b} fraction (Figure 5b). As more T'_{2b} protons associated with water penetrated into the fraction, the T'_{2b} population decreased from 15% to 1.3% along with increasing fermentation time.

LF-NMR provides unique insight into the soaking and SSF processes of glutinous rice. The variations of T_2 values during SSF can be ascribed to the microstructure changes of the rice. A PCA was performed using the T_2 parameters from different time intervals of the fermented samples to summarize the variation in the LF-NMR relaxation data. PC1 explained 89.5% of the variation in the data and clearly discriminated according to the different fermentation times (Figure 6). PC2 explained 6.9% of the variation in the data, which was considered to be largely due to the variation among replicates. There was a significant separation between the 16 and 24 h samples, indicating that the exponential phase of fermentation evaluated by LF-NMR began at approximately 16 h, which was 8 h later than suggested by the TA and RS measurements. It is reasonable that only metabolism proceeding to a certain extent may significantly change the microstructure. Thus, the microstructure changes were not significant until 24 h. The mixing of samples from 48 and 56 h implied that the sample microstructure did not change considerably during the stationary phase though fermentation. The mean values of the T_2 parameters were employed to establish mathematical models for SSF of glutinous rice. As shown in Figure 7, a cubic curve was the best fit for the relationship between the T'_{22} relaxation time and fermentation time. The relationships between the other parameters and fermentation time can be well explained by Boltzmann fitting, which is expressed by following equation:

DOI: 10.1021/acs.jafc.5b00769
J. Agric. Food Chem. 2015, 63, 3261−3270

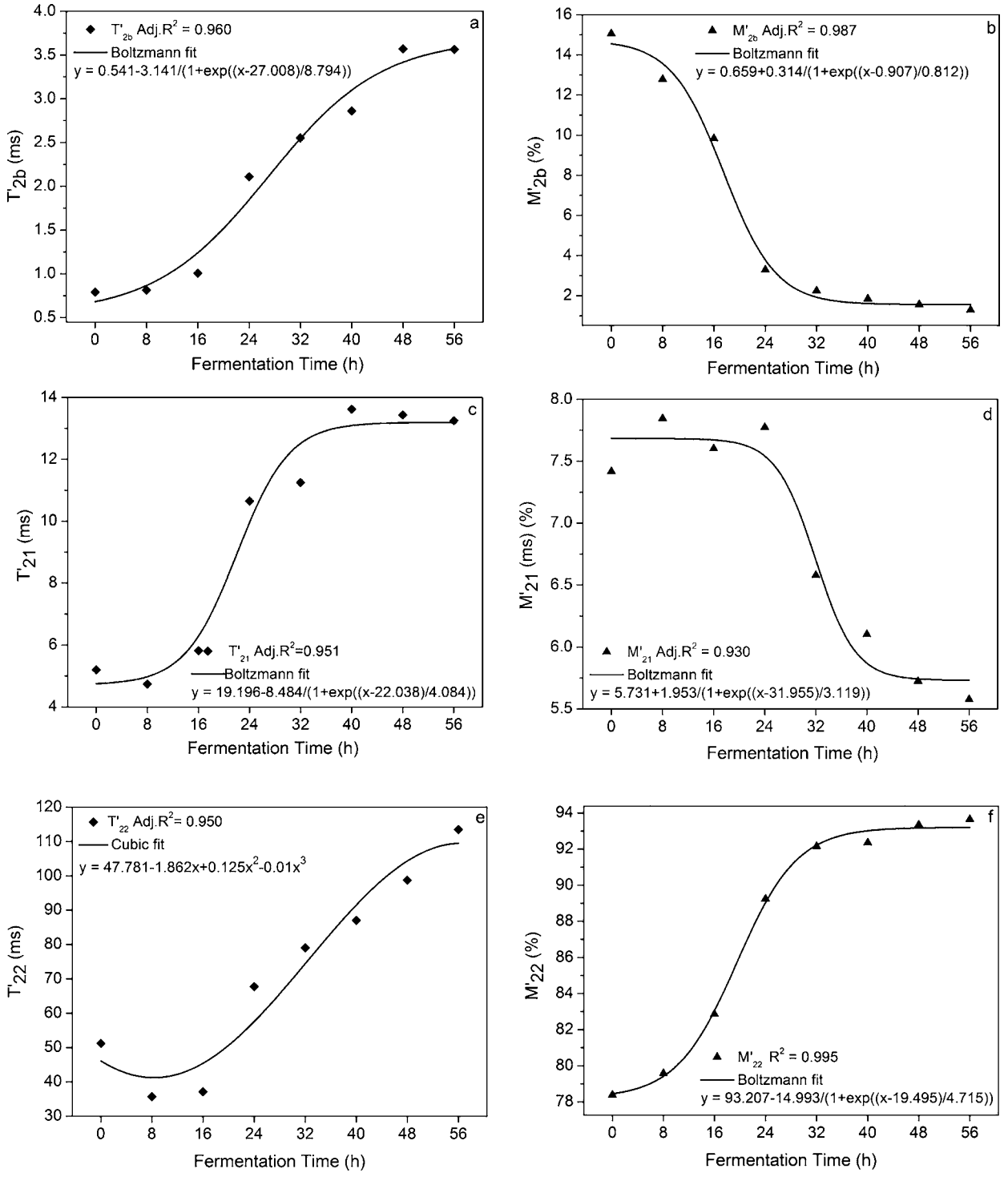

Figure 7. Fitting curves and equations of different T_2 parameters (n = 8) versus fermentation time: (a) T'_{2b}, (b) M'_{2b}, (c) T'_{21}, (d) M'_{21}, (e) T'_{22}, and (f) M'_{22}.

$$y = \frac{A_1 - A_2}{1 + e^{(X - X_0)/dx}} + A_2 \quad (3)$$

Interestingly, the fitting curves of the T_2 parameters were similar to the microbial growth curve. In conclusion, the present study demonstrated that the effects of SSF on glutinous rice can penetrate into the inner space and significantly change the microstructure rather than just affecting the surface. Thus, LF-NMR can be used to monitor the SSF of starch systems.

AUTHOR INFORMATION

Corresponding Author

*Phone: +86 25 84396989. Fax: +86 25 84399090. E-mail: dongms@njau.edu.cn.

Funding

This work was cofinanced by the High-Tech Research and Development Program of China (nos. 2011AA100903 and 2013BAD18B01-4) and the National Natural Science Foundation of China (nos. 31201422 and 31371807). This study was

DOI: 10.1021/acs.jafc.5b00769
J. Agric. Food Chem. 2015, 63, 3261−3270

also supported by the Project Funded by the Priority Academic Program Development of Jiangsu Higher Education Institutions (PAPD).

Notes

The authors declare no competing financial interest.

■ ACKNOWLEDGMENTS

We would like to thank the technical support from the Key Laboratory of Meat Processing and Quality Control, Ministry of Education (Nanjing, P. R. China).We also thank Huang Lu and Yang Peiqiang for their illuminating discussions on this study.

■ ABBREVIATIONS USED

SSF solid-state fermentation; LF-NMR low-field nuclear magnetic resonance; RS reducing sugar; DNS (3, -dinitrosalicvlic acid); TA titrable acidity; MC moisture content; D_2O deuterium oxide; CPMG Carr−Purcell−Meiboom−Gill; PCA principal component analysis; Adj R^2 adjusted determination coefficient

■ REFERENCES

(1) Bellon-Maurel, V.; Orliac, O.; Christen, P. Sensors and measurements in solid state fermentation: a review. *Process Biochem.* **2003**, *38*, 818−816.

(2) Zhu, Y.; Tramper, J. Koji—Where East Meets West in Fermentation. *Biotechnol. Adv.* **2013**, *31*, 1448−1457.

(3) Martins, S.; Mussatto, S.; Martínez-Avila, G.; Montañez-Saenz, J.; Aguilar, C.; Teixeira, J. Bioactive phenolic compounds: production and extraction by solid-state fermentation. A review. *Biotechnol. Adv.* **2011**, *29*, 365−373.

(4) Xiao, Y.; Xing, G.; Rui, X.; Li, W.; Chen, X.; Jiang, M.; Dong, M. Enhancement of the antioxidant capacity of chickpeas by solid state fermentation with *Cordyceps militaris* SN-18. *J. Funct. Foods* **2014**, *10*, 210−222.

(5) Chen, B.; Wu, Q.; Xu, Y. Filamentous fungal diversity and community structure associated with the solid state fermentation of Chinese Maotai-flavor liquor. *Int. J. Food Microbiol.* **2014**, *179*, 80−84.

(6) Lv, X.; Weng, X.; Zhang, W.; Rao, P.; Ni, L. Microbial diversity of traditional fermentation starters for Hong Qu glutinous rice wine as determined by PCR-mediated DGGE. *Food Control* **2012**, *28*, 426−434.

(7) Feng, Y.; Chen, Z.; Liu, N.; Zhao, H.; Cui, C.; Zhao, M. Changes in fatty acid composition and lipid profile during koji fermentation and their relationships with soy sauce flavour. *Food Chem.* **2014**, *158*, 438−444.

(8) Liu, G.; Sheng, Y.; Dai, C. Factors affecting γ-linolenic acid content in fermented glutinous rice brewed by *Rhizopus* sp. *Food Microbiol.* **2004**, *21*, 299−304.

(9) Chen, H. Principles of solid-state fermentation engineering and its scale-up. In *Modern Solid State Fermentation—Theory and Practice*; Chen, H., Eds.; Springer: New York, 2013; pp 97−105.

(10) Jiang, H.; Liu, G.; Xiao, X.; Mei, C.; Ding, Y.; Yu, S. Monitoring of solid-state fermentation of wheat straw in a pilot scale using FT-NIR spectroscopy and support vector data description. *Microchem. J.* **2012**, *102*, 68−74.

(11) Soons, Z. I. T. A.; Streefland, M.; Straten, G.; Boxtel, A. J. B. Assessment of near infrared and "software sensor" for biomass monitoring and control. *Chemom. Intell. Lab. Syst.* **2008**, *94*, 166−174.

(12) Cozzolino, D.; Parker, M.; Dambergs, R. G.; Herderich, M.; Gishen, M. Chemometrics and visible-near infrared spectroscopic monitoring of red wine fermentation in a pilot scale. *Biotechnol. Bioeng.* **2006**, *95*, 1101−1107.

(13) Hills, B. P.; Takacs, S. F.; Belton, P. S. A new interpretation of proton NMR relaxation time measurements of water in food. *Food Chem.* **1990**, *37*, 95−111.

(14) Mariette, F.; Lucas, U. NMR signal analysis to attribute the components to the solid/liquid phases present in mixes and ice creams. *J. Agric. Food Chem.* **2005**, *53*, 1317−1327.

(15) Belton, P. S.; Hills, B. P.; Raimbaud, E. R. The effects of microstructure and exchange on proton NMR relaxation in agarose gels. *Mol. Phys.* **1988**, *63*, 825−842.

(16) Han, M.; Wang, P.; Xu, X.; Zhou, G. Low-field NMR study of heat-induced gelation of pork myofibrillar proteins and its relationship with microstructural characteristics. *Food Res. Int.* **2014**, *62*, 1175−1182.

(17) Gianferri, R.; Maioli, M.; Delfini, M.; Brosio, E. A low-resolution and high-resolution NMR integrated approach to investigate the physical structure and metabolic profile of Mozzarella di Bufala Campana cheese. *Int. Dairy J.* **2007**, *17*, 167−176.

(18) Bertram, H. C.; Karlsson, A. H.; Rasmussen, M.; Pedersen, O. D.; Dønstrup, S.; Andersen, H. J. Origin of multiexponential T_2 relaxation in muscle myowater. *J. Agric. Food Chem.* **2001**, *49*, 3092−3100.

(19) Bertram, H. C.; Dønstrup, S.; Karlsson, A. H.; Aandersen, H. J. Continuous distribution analysis of T_2 relaxation in meat—an approach in the determination of water-holding capacity. *Meat Sci.* **2002**, *60*, 279−285.

(20) Bertram, H. C.; Aaslyng, M. D.; Andersen, H. J. Elucidation of the relationship between cooking temperature, water distribution and sensory attributes of pork—a combined NMR and sensory study. *Meat Sci.* **2005**, *70*, 75−81.

(21) Bertram, H. C.; Andersen, R. H.; Andersen, H. J. Development in myofibrillar water distribution of two pork qualities during 10-month freezer storage. *Meat Sci.* **2007**, *75*, 128−133.

(22) Li, T.; Rui, X.; Chen, X.; Jiang, M.; Dong, M. Water distribution in tofu and application of T_2 relaxation measurements in determination of tofu's water-holding capacity. *J. Agric. Food Chem.* **2014**, *62*, 8594−8601.

(23) Tang, H. R.; Godward, J.; Hill, B. P. The distribution of water in native starch granules—a multinuclear NMR study. *Carbohydr. Polym.* **2000**, *43*, 375−387.

(24) Tang, H. R.; Brun, A.; Hill, B. P. A proton NMR relaxation study of the gelatinisation and acid hydrolysis of native potato starch. *Carbohydr. Polym.* **2001**, *46*, 7−18.

(25) Bosmans, G. M.; Lagrain, B.; Delceu, J. L.; Fierens, E.; Hill, B. P.; Delcour, J. A. Assignments of proton populations in dough and bread using NMR relaxometry of starch, gluten, and flour model systems. *J. Agric. Food Chem.* **2012**, *60*, 5461−5470.

(26) Bosmans, G. M.; Lagrain, B.; Fierens, E.; Delcour, J. A. Impact of amylases on biopolymer dynamics during storage of straight-dough wheat bread. *J. Agric. Food Chem.* **2013**, *61*, 6525−6532.

(27) Bosmans, G. M.; Lagrain, B.; Ooms, N.; Fierens, E.; Delcour, J. A. Biopolymer interactions, water dynamics, and bread crumb firming. *J. Agric. Food Chem.* **2013**, *61*, 4646−4654.

(28) Hager, A. S.; Bosman, G. M.; Delcour, J. A. Physical and molecular changes during the storage of gluten-free rice and oat bread. *J. Agric. Food Chem.* **2014**, *62*, 5682−5689.

(29) Miller, G. Use of dinitrosalicylic acid reagent for determination of reducing sugar. *Anal. Chem.* **1959**, *31*, 426−428.

(30) Cen, C.; Rui, X.; Lu, Z.; Li, W.; Dong, M. Enhanced shelf-life of tofu by using bacteriocino genic *Weissella hellenica* D1501 as bioprotective cultures. *Food Control* **2014**, *46*, 203−209.

(31) Xiao, Z.; Wang, Z.; Liu, T. Application of multi-exponential inversion method to NMR measurements. *Pet. Sci.* **2004**, *1*, 19−22.

(32) Horigane, A. K.; Takahashi, H.; Maruyama, S.; Ohtsubo, K.; Yoshida, M. Water penetration into rice grains during soaking observed by gradient echo magnetic resonance imaging. *J. Cereal Sci.* **2006**, *44*, 307−316.

(33) Parada, J.; Aguilera, J. M. Effect of native crystalline structure of isolated potato starch on gelatinization behavior and consequently on glycemic response. *Food Res. Int.* **2012**, *45*, 238−243.

(34) Utrilla-Coello, R. G.; Bello-Péreza, L. A.; Vernon-Carterb, E. J.; Rodriguez, E.; Alvarez-Ramirezb, J. Microstructure of retrograded

DOI: 10.1021/acs.jafc.5b00769
J. Agric. Food Chem. 2015, 63, 3261−3270

starch: quantification from lacunarity analysis of SEM micrographs. *J. Food Eng.* **2013**, *116*, 775−781.
(35) Zhang, Z.; Jin, B.; Kelly, J. M. Production of lactic acid from renewable materials by *Rhizopus* fungi. *Biochem. Eng. J.* **2007**, *35*, 251−263.
(36) Chen, L.; Ren, F.; Zhang, Z.; Tong, Q.; Rashed, M. M. A. Effect of pullulan on the short-term and long-term retrogradation of rice starch. *Carbohydr. Polym.* **2015**, *115*, 415−421.
(37) Falade, A. T.; Emmambux, M. N.; Buys, E. M.; Taylor, J. R. N. Improvement of maize bread quality through modification of dough rheological properties by lactic acid bacteria fermentation. *J. Cereal Sci.* **2014**, *60*, 471−476.
(38) Lampignano, V.; Laverse, J.; Mastromatteo, M.; Del Nobile, M. A. Microstructure, textural and sensorial properties of durum wheat bread as affected by yeast content. *Food Res. Int.* **2013**, *50*, 369−376.

DOI: 10.1021/acs.jafc.5b00769
J. Agric. Food Chem. 2015, 63, 3261−3270

representing the deviation from ideality. These two coefficients are linked by the equation

$$K_i = \frac{y_i}{x_i} = \frac{\gamma_i \times P^0_{i(T)}}{P_T} \quad (3)$$

where x_i and y_i are molar fractions in the liquid and gas phases, respectively, $P^0_{i(T)}$ is the vapor pressure of pure component i at a given temperature T (Pa), and P_T is the total pressure (Pa).

Generally, K_i is measured at fixed temperature, pressure, and volume after the system reaches equilibrium. The most widely used methods for determining the partition coefficient can be divided into three groups: differential methods,[21−23] dynamic headspace methods,[24,25] and static methods.[26−33] No available methods are valid for complex matrices or for all aroma compounds regardless of their volatility. Moreover, some determination methods are technically difficult to implement or require external calibration.[34]

H_2S as a pure compound is very volatile, with a vapor pressure of 1698 kPa at 290 K.[35] Therefore, existing methods are not appropriate for the determination of its partition coefficient. Indeed, its very high volatility makes precise calibration and quantification by chromatographic methods very difficult, so the first step of this study was the development of a novel method that could be described as a "semistatic method" specifically to measure the partition coefficient of H_2S. The values of K_{H_2S} were first determined in water to validate the method and for comparison with published data. The method was then applied to synthetic media that simulated must, fermenting musts at different stages of fermentation, and wine. The effect of temperature on the partition coefficient of H_2S (K_{H_2S}) was also assessed. Finally, a model was established to calculate K_{H_2S} in enological conditions throughout alcoholic fermentation.

MATERIALS AND METHODS

Gas Standard. The H_2S standard gas was manufactured by Air Products SA (Paris, France): it consists of a gas cylinder of 3.074 Nm^3 at 162 bar with a precise H_2S concentration of 9.21% (i.e., 92 100 ppmV) in nitrogen.

H_2S standard gas was diluted with a binary gas dilutor LNI SONIMIX 6000C1 from LNI Schmidlin SA (Geneva, Switzerland), based on high-precision mass flow controllers and mechanical pressure regulators, with a glass dilution chamber and fluidics for perfect homogeneity. Air zero (99.9999% purity) for H_2S dilution was purchased from LINDE (Saint-Priest, France).

Dissolved H_2S Measurement. H_2S dissolved in liquid phases was assayed in situ using an amperometric microsensor purchased from AMT Analysenmesstechnik GmbH (Rostock, Germany). This H_2S probe allows precise and rapid measurement of the liquid concentrations of H_2S and total dissolved sulfides, without sampling and without reagents. The instrument consists of a box for reading and data treatment, linked to an amperometric microsensor covered with a membrane, and another separate probe for pH and temperature measurement. The probe is equipped with a type III microsensor for H_2S measurement in the range from 0.01 to 3 mg/L. The precision is better than 2% of the measured value, and the response time ($t_{90\%}$) is <200 ms.

Media Composition. A buffer solution was prepared containing 6 g/L of citric acid and 6 g/L of malic acid adjusted to pH 3.3 (with NaOH). For the model solution simulating a must, glucose was added to 220 g/L. For the model solution simulating a wine, the buffer solution was made up to 13.2% (v/v) ethanol. For the model solutions simulating musts at different stages of fermentation, the buffer solution was made up to (a) 175 g/L glucose and 2.7% (v/v) ethanol, (b) 132.5 g/L glucose and 5.3% (v/v) ethanol, or (c) 87.5 g/L glucose and 8% (v/v) ethanol. The resulting five media corresponded to 0, 20, 40, 60, and 100% progression of fermentation.

Determination of Gas−Liquid Partition Coefficients. The gas−liquid partition coefficient of H_2S was determined by a "semistatic" method: a gas phase for which the H_2S concentration was perfectly known and constant was continuously bubbled through the stirred liquid phase until the system was driven to equilibrium using the device shown in Figure 1. The concentration of H_2S in the liquid phase was continuously measured with the microsensor. A specially designed glass reactor with a total volume of 0.75 L (shown in Figure 1) was first filled with the liquid phase (500 mL) and regulated to the desired temperature (10, 15, 20, or 25 °C), within ±0.1 °C, by circulating water through the heating/cooling jacket fed by a cryostat Polystat cc1 (Huber, Offenburg, Germany). When the desired temperature was reached in the liquid phase, the gas supply to the reactor was opened with the lowest concentration of H_2S in the gas (H_2S_g; 112 ppmV at ambient temperature). All pipes connecting gas outside and inside the reactor were Sulfinert. Gas was sparged at 2000 NmL min^{-1} in the reactor through a stainless steel 316 L cylindrical porous distributor with a mean pore diameter of 0.5 μm. The liquid phase was stirred magnetically at 250 rpm. The concentration of H_2S in the liquid phase (H_2S_l) was recorded every minute for 20 min. Equilibrium was reached in the liquid phase after 15 min. The value of H_2S at equilibrium ($H_2S_l^*$) was calculated as the mean of five instantaneous values (one value per minute for 5 min after the first 15 min required to reach equilibrium). The procedure for measuring the equilibrium concentration of H_2S in the liquid phase was then repeated for four other values of H_2S_g: 135.4, 158.7, 205.4, and 263.7 ppmV of H_2S at ambient temperature. The H_2S concentrations in the gas studied were thus varied from 112 to 263.7 ppmV, which corresponds to a partial pressure from 1.13×10^{-2} to 2.67×10^{-2} kPa (respecting Henry's law, <200 kPa).[36] At the end of each measurement series (five values of H_2S_g), the reactor was drained. The reactor and the measuring probes (H_2S, pH, and temperature) were thoroughly rinsed with distilled water. The reactor was then refilled with fresh solution for a new set of measurements.

Each set of measurements was done in triplicate, except for media simulating 20, 40, and 60% progression of fermentation, which were measured in duplicate.

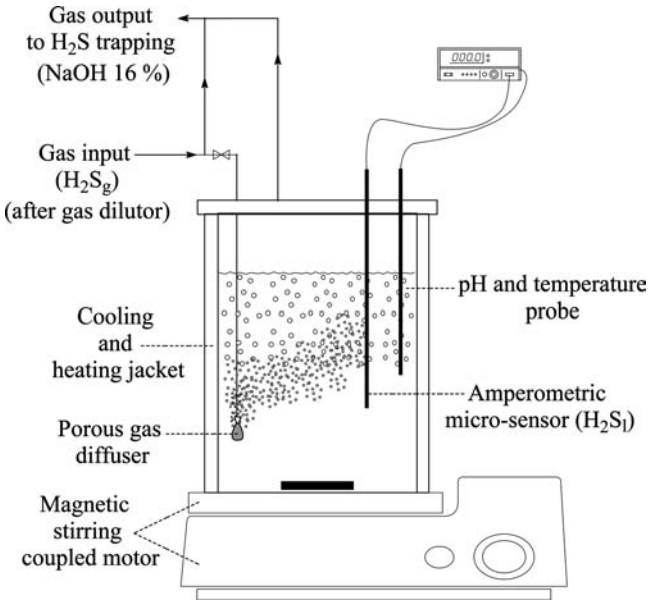

Figure 1. Schematic representation of the stirred reactor and associated sensors used for determination of the gas−liquid partition coefficient of H_2S.

DOI: 10.1021/jf505733a
J. Agric. Food Chem. 2015, 63, 3271−3278

At equilibrium, the concentration of H_2S in the gas phase at the reactor inlet ($H_2S_{g(in)}$) was equal to the concentration of H_2S in the gas phase at the reactor outlet ($H_2S_{g(out)}$); in the liquid phase, the H_2S concentration reached an equilibrium (H_2S_l*). The partition coefficient was calculated using eq 2 with H_2S_l* = H_2S_l, assuming that, at low partial pressure (<200 kPa), the solubility of H_2S is strictly given by Henry's law.[36] Losses, which correspond to the amount of compound not accounted for by the measured concentrations of each phase, were not considered; losses were the results of leakage from the sample container, adsorption onto container surfaces, loss during sampling, and/or faulty measurement. Losses from leaks were easy to detect and repair because H_2S is very odorant. Losses due to adsorption onto container surfaces also were minimal because inert materials (Sulfinert tubes, glass, stainless steel 316L) were used. Also, in situ measurement of H_2S using a microsensor is associated with much smaller errors than all methods that involve sample collection, such as chromatography.

RESULTS AND DISCUSSION

Gas–Liquid Partition Coefficient of H_2S in Water. The method for determining the coefficient of gas–liquid partition was applied to distilled water at pH 3.3. It was assumed that the gas was at the temperature of the liquid during bubbling. The concentration values given by the gas dilutor (in ppmV) were systematically transformed to mg/L and adjusted for the temperature using the general equation

$$H_2S_g\ (g/m^3) = \frac{H_2S_g\ (ppmV) \times (1.2187 \times 10^{-2}) \times MW}{273.15 + T\ (°C)} \quad (4)$$

where H_2S_g (g/m^3) is the concentration of H_2S in gram per cubic meter of ambient air, H_2S_g (ppmV) is the volume of H_2S per 10^6 volumes of ambient air, MW is the molecular weight of the H_2S (34.01 g mol^{-1} for H_2S), and T (°C) is the ambient air temperature in degrees Celsius.

The corrected values of H_2S_g for the four studied temperatures are given in Table 1. H_2S_l* increased proportionally with the H_2S concentration in the gas whatever the temperature between 10 and 25 °C (Figure 2). The probe gave stable values of H_2S concentration at equilibrium in the liquid (H_2S_l*) for each set of H_2S gas concentrations (H_2S_g). This indicates that there was no accumulation of H_2S, the species to be assayed, in the environment of the sensor. Also, H_2S_l* increased linearly with H_2S_g such that Henry's law was respected whatever the partial pressure of H_2S in the gas input. As the relationship between H_2S_l* and H_2S_g at each temperature was linear, K_{H_2S} corresponded directly to the slope of each regression line (Figure 2). The ratio H_2S_g/H_2S_l* and the value of the gas–liquid partition coefficient of H_2S in water at pH 3.3 were calculated from these results for the four temperatures tested (Table 2). The H_2S_g/H_2S_l* ratio was almost independent of H_2S_g, indicating that even when the concentration of H_2S in the gas increases, the system stayed in the infinite dilution state and that Henry's law was respected. The value of K_{H_2S} obtained at 25 °C was compared with published values for water at the same temperature.

Table 1. Values of H_2S_g Corrected for the Temperature and Corresponding to the Values of H_2S_g at the Output of the Gas Dilutor

H_2S_g from gas dilutor: temperature (°C)	H_2S_g (mg/L) 112.0 ppmV	135.4 ppmV	158.7 ppmV	205.4 ppmV	263.7 ppmV
10	0.164	0.199	0.233	0.302	0.387
15	0.162	0.195	0.229	0.296	0.380
20	0.159	0.192	0.225	0.291	0.374
25	0.156	0.189	0.221	0.286	0.368

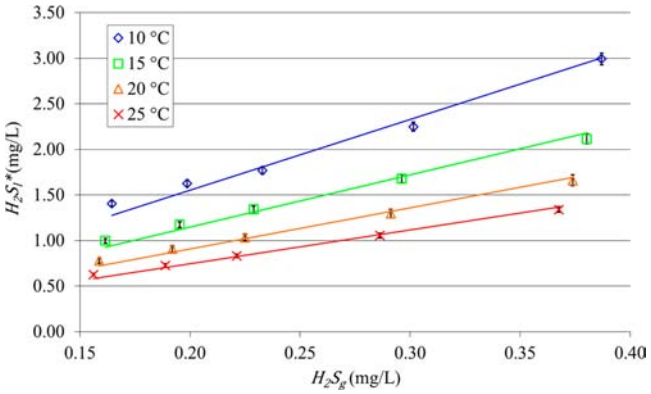

Figure 2. Changes in the H_2S concentration at equilibrium in water at pH 3.3 as a function of H_2S concentration in the gas phase, at 10, 15, 20, and 25 °C.

A compilation of published Henry's law data gives a value of k_H^{cp} = 0.1 mol kg^{-1} bar^{-1} for H_2S in water at 25 °C.[36−45] k_H^{cp} is defined as

$$k_H^{cp} = \frac{c_{l(i)}}{p_{g(i)}} \quad (5)$$

where c_l is the concentration of a species (i) in the liquid phase and $p_{g(i)}$ is the partial pressure of that species in the gas phase.

Henry's law constant can also be assimilated to the partition coefficient at infinite dilution of the species of interest expressed as the dimensionless ratio between its aqueous-phase concentration (c_l) and its gas-phase concentration (c_g)

$$k_H^{cc} = \frac{c_{l(i)}}{c_{g(i)}} = k_H^{cp} \times R \times T = \frac{1}{K_i} \quad (6)$$

where R is the gas constant and T is the temperature.

From eq 6, with R = 8.314 m^3·Pa mol^{-1} K^{-1} = 8.314 × 10^{-2} L·bar mol^{-1} K^{-1} and T = 25 °C = 298.15 K

$$K_{(H_2S)} = 1/(k_H^{cp} \times R \times T)$$
$$= 1/(0.1 \times (8.314 \times 10^{-2}) \times 298.15)$$
$$= 0.403$$

This value of 0.403 for K_{H_2S} obtained from the data in the literature differs substantially from the value of 0.265 that we obtained experimentally. This difference may be a consequence of these values of gas–liquid ratios not being determined at the same pH; indeed, the effect of the pH of the water is critical. Three ionic forms of H_2S coexist in the liquid phase (H_2S, HS^-, S^{2-}) with pK_1 = 6.97 and pK_2 = 12.90; their relative abundance depends of the pH (see Figure 3). At pH <5.0, H_2S is present in the form of an undissociated molecule, soluble in water. As the pH increases above pH 5.0, the concentration of the undissociated H_2S decreases, in a predictable manner, by dissociating to form the acid sulfide ion (HS^-); under alkaline conditions at pH >9.0, HS^- further dissociates, giving sulfide ions (S^{2-}). HS^- and S^{2-} are completely unable to partition

DOI: 10.1021/jf505733a
J. Agric. Food Chem. 2015, 63, 3271−3278

Table 2. $H_2S_g/H_2S_l^*$ Ratio for Each Condition (H_2S_g and Temperature) and Gas–Liquid Partition Coefficient of H_2S (K_{H_2S}) in Water at pH 3.3 for the Four Temperatures Considered

H_2S_g (ppmV)	10 °C	15 °C	20 °C	25 °C
112.0	0.117 ± 0.002	0.162 ± 0.004	0.204 ± 0.007	0.250 ± 0.006
135.4	0.122 ± 0.003	0.166 ± 0.004	0.211 ± 0.008	0.260 ± 0.006
158.7	0.132 ± 0.003	0.170 ± 0.004	0.218 ± 0.008	0.266 ± 0.006
205.4	0.134 ± 0.003	0.176 ± 0.005	0.225 ± 0.008	0.272 ± 0.007
263.7	0.129 ± 0.003	0.180 ± 0.005	0.225 ± 0.008	0.274 ± 0.007
K_{H_2S}	0.129 ± 0.003	0.174 ± 0.005	0.221 ± 0.008	0.269 ± 0.006
R^2	0.9821	0.9860	0.9887	0.9911

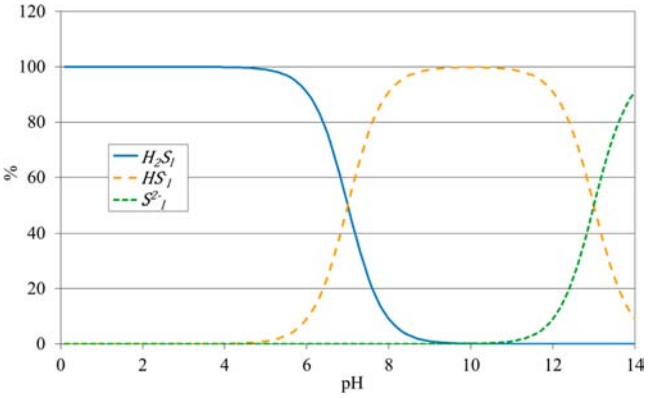

Figure 3. Changes in the equilibrium between the ionic species H_2S, HS^-, and S^{2-} as a function of pH.

from the water to the gas phase. Consequently, any H_2S in the gas phase coming into contact with an alkaline aqueous medium will, in addition to partitioning into the water, dissociate to the stable ionic species and continue to do so until the partitioning and dissociation reactions reach an equilibrium; this equilibrium state may or may not include the existence of H_2S in the gas phase. With knowledge about this phenomenon, $H_2S_l^*$ values observed experimentally at different pH values can be extrapolated. This approach is possible by using the concentration $H_2S_l^*$ at equilibrium in water at pH 3.3 and 25 °C and the proportion of the H_2S species in water according to the pH value:

$$H_2S^*_{l(pH_X)} = H_2S^*_{l(pH3.3)} \times H_2S_l\% \quad (7)$$

with

$$H_2S\% = \frac{10^{(-pH_X+pK_1)}}{[1 + 10^{(-pH_X+pK_1)}] + 10^{(pH_X-pK_2)}} \quad (8)$$

with $pK_1 = 6.97$ and $pK_2 = 12.90$.[39]

The K_{H_2S} for different pH values at 25 °C can then be calculated, on the assumption that H_2S_g is not affected by changes to the pH. Table 3 gives the results for calculated $H_2S_l^*$ and K_{H_2S} values in water for six values of pH in the range from 3.3 to 9.0 at 25 °C; Figure 4 shows the results of iterative

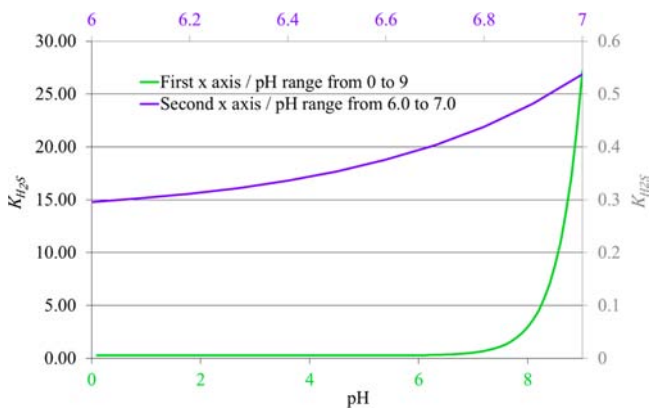

Figure 4. Changes in the K_{H_2S} value in water at 25 °C as a function of pH (first x axis for pH range from 0 to 9 and second x axis for pH range from 6 to 7. Results were obtained from iterative calculation step by step (0.1 pH unit).

calculation step by step (0.1 pH unit) of the changes in K_{H_2S} in water at 25 °C as a function of pH up to pH 9.0, the value at which <1% of H_2S is present in solution. By such calculations, K_{H_2S} was 0.403 (as reported in the literature) for the water at 25 °C when the pH was 6.7 (Figure 4), a pH consistent with that of distilled or deionized water. In all cases, published values fall within the range of K_{H_2S} values calculated from experimental results obtained at pH 3.3 and extrapolated.[36−45] These calculations and observations validate the experimental approach to measuring the partition coefficient of H_2S between liquid and gas. Therefore, this original semistatic method can be

Table 3. Values of K_{H_2S} in Water at Various pH Values and at 25 °C

pH	H_2S_g: H_2S_g:	112.0 ppmV 0.156 mg/L	135.4 ppmV 0.189 mg/L	158.7 ppmV 0.221 mg/L	205.4 ppmV 0.286 mg/L	263.7 ppmV 0.368 mg/L	K_{H_2S}
3.3	$H_2S_l^*$	0.625 ± 0.015	0.727 ± 0.017	0.831 ± 0.020	1.05 ± 0.025	1.34 ± 0.032	0.269 ± 0.006
5		0.619	0.720	0.823	1.040	1.327	0.271
6		0.568	0.661	0.755	0.955	1.218	0.296
7		0.312	0.363	0.415	0.525	0.670	0.538
8		0.057	0.066	0.076	0.095	0.122	2.957
9		6.188×10^{-3}	7.197×10^{-3}	8.227×10^{-3}	1.040×10^{-2}	1.327×10^{-2}	27.15

DOI: 10.1021/jf505733a
J. Agric. Food Chem. 2015, 63, 3271−3278

applied to study changes to the H_2S gas−liquid partition coefficient (K_i) during winemaking fermentations.

GasLliquid Partition Coefficient of H_2S in Enological Conditions. Hydrogen sulfide is weakly acidic, and no reactivity has been described between H_2S and any of the species present in media simulating enological solutions (water, citric and malic acids, glucose, and ethanol) at the pH values and temperatures studied in this work. The effects of glucose and ethanol on K_{H_2S} were measured in model solutions simulating fermenting must at the beginning (22% w/v glucose and no ethanol) and end (no glucose and 13% v/v ethanol) of fermentation. As in water at pH 3.3, the H_2S concentration at equilibrium in the synthetic must (A) as in the synthetic wine (B) increased proportionally with the H_2S concentration in the gas at all temperatures considered between 10 and 25 °C (Figure 5). Thus, Henry's law was respected whatever the partial pressure of H_2S in the gas input, and the probe gave stable values of H_2S concentration at equilibrium (H_2S_l*) for each H_2S concentration in the gas (H_2S_g), indicating that there was no accumulation of H_2S around the sensor.

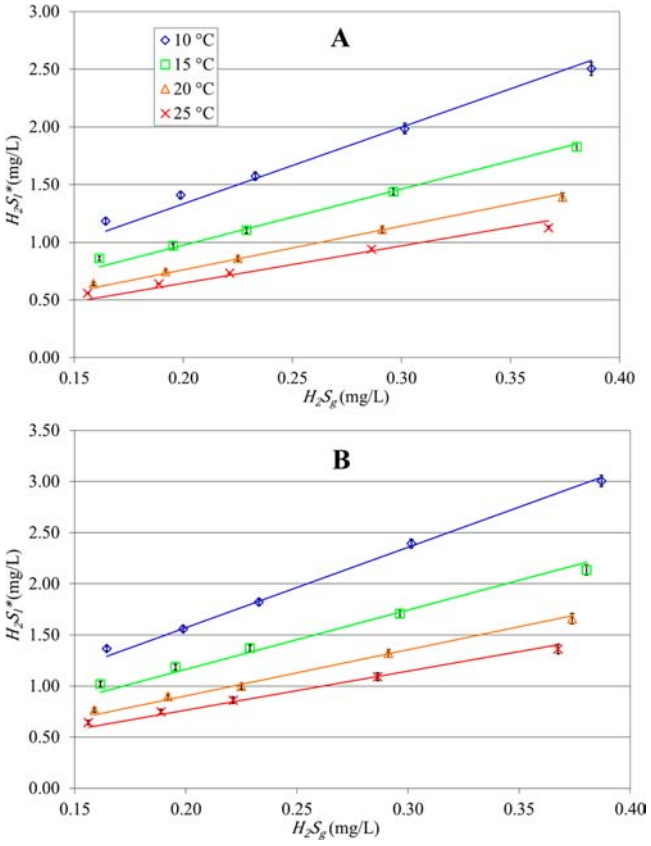

Figure 5. Changes in the H_2S concentration at equilibrium in synthetic must (A) and synthetic wine (B) as a function of the H_2S concentration in the gas phase, at 10, 15, 20, and 25 °C.

The partition coefficients of H_2S in both model solutions (Table 4) were different from those in aqueous solution (Table 2). The effects of the composition of the solution on the partitioning properties of volatile compounds were analyzed by calculating release ratios, expressed as

$$\%\, K_{H_2S_{m/w}} = \frac{K_{H_2S_m} - K_{H_2S_w}}{K_{H_2S_w}} \times 100 \quad (9)$$

where K_{H_2Sm} is the partition coefficient of H_2S in the model solution and K_{H_2Sw} is its partition coefficient in water at the same pH. A positive value indicates that the solute enhances release, whereas a negative value is associated with retention.

The presence of glucose in the model solution raised the partition coefficient of H_2S (Table 4), as observed for other volatile compounds with sucrose.[46,47] Indeed, in our conditions, simulating a grape must, the average (four studied temperatures) relative increase was 17%. However, the salting-out effect of glucose on H_2S was smaller than that observed on aromatic molecules (higher alcohols and esters) in the same enological simulating solutions.[48] The release of H_2S from glucose solution observed here resulted from a salting-out effect of glucose, which forms hydrogen bonds with water molecules, thereby decreasing the activity of the water, lowering the free water content and decreasing the solubility of aroma compounds.[49] Unlike glucose, the presence of 13% ethanol (a typical concentration in wines) did not substantially affect K_{H_2S} values (Table 4); the effect of ethanol on H_2S solubility was very much smaller than the salting-out effect caused by the presence of sugar.

Therefore, at constant temperature, changes in the value of K_{H_2S} during fermentation were mainly due to the decreasing sugar concentration (Figure 6). The gas−liquid partition not only depended on the composition of the liquid phase but was also strongly affected by the temperature (Figure 6). Indeed, the effect of temperature on K_{H_2S} was larger than that of the changes in matrix composition. However, the effect of temperature on the K_i of H_2S was as expected: the concentration ratio increased with the temperature.

Modeling of the Gas−Liquid Partitioning of H_2S during Winemaking Fermentations. The next objective of this work was to develop a model of the evolution of this partition coefficient (K_{H_2S}) between the gas and liquid phases during fermentation.

Table 4. Values of K_i for H_2S in Synthetic Must and Wine at Four Temperatures and Comparison to Values in Water (% $K_{im/w}$)

		10 °C	15 °C	20 °C	25 °C
synthetic must	K_{H_2S}	0.150 ± 0.003	0.205 ± 0.004	0.263 ± 0.007	0.309 ± 0.003
	R^2	0.9846	0.9911	0.9937	0.9726
	$\%K_{H_2S_{m/w}}$	16.7	17.7	19.0	14.9
synthetic wine	K_{H_2S}	0.127 ± 0.002	0.172 ± 0.004	0.221 ± 0.007	0.262 ± 0.009
	R^2	0.9962	0.9841	0.9925	0.9882
	$\%K_{H_2S_{m/w}}$	−1.2	−1.2	0.3	−2.6

DOI: 10.1021/jf505733a
J. Agric. Food Chem. 2015, 63, 3271−3278

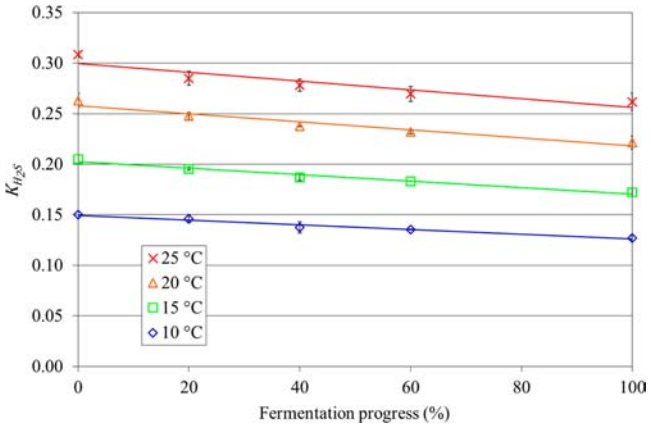

Figure 6. Changes in the K_{H_2S} as a function of the progress of fermentation at 10, 15, 20, and 25 °C.

A multiple linear regression method was chosen to describe the evolution of K_{H_2S} from characteristics of the liquid composition (glucose and ethanol concentrations) and the temperature. The general formula of the multiple linear model adopted was

$$K_{H_2S} = \beta_0 + \beta_1 \times [\text{glucose}] + \beta_2 \times [\text{ethanol}] + \beta_3 \times T + \varepsilon \quad (10)$$

where β_0 is the intercept (or constant), β_1, β_2, and β_3 are the coefficients corresponding to the effects of glucose concentration ([glucose] in g/L), ethanol concentration ([ethanol] in g/L), and temperature (T in °C), respectively, and ε is an independent $N(0,\sigma^2)$ error term.

Model parameters were determined simultaneously by multiple linear regression analysis (Excel software from Microsoft Pack Office Pro 2013) based on the values of K_{H_2S} obtained from all experiments including those in water: thus, all 60 values of measured K_{H_2S} were used to determine β_0–β_3 with the significance threshold set at 0.05. Estimated coefficients of the model parameters identified from eq 10 and test of significance are presented in Table 5. β_1 is of predictive value with a low P value (<0.05); the positive value of this parameter is consistent with the salting-out effect of sugar observed in the experiments. Conversely, the high P value (>0.05) of β_2 reflects the nonrepresentative effect of ethanol on H_2S solubilization. The strong effect of temperature on the K_{H_2S} was confirmed by the very low P value obtained for the β_3 parameter. The high value of β_3 itself reflects the predominant effect of temperature on the partition coefficient of H_2S. As ethanol had only a negligible effect, eq 10 can be written as

$$K_{H_2S} = 3.37 \times 10^{-2} + 1.35 \times 10^{-4} \times [\text{glucose}] + 9.43 \times 10^{-3} \times T \quad (11)$$

The adjusted R^2 (0.9644) indicates that the three variables combined predict >96% of the K_{H_2S} (Figure 7). The mean relative error between model prediction values and the experimentally measured values was calculated as follows:

$$\varepsilon = \frac{1}{n}\Sigma_{j=1}^{n}\frac{|K_{ij}^{\text{measured}} - K_{ij}^{\text{predicted}}|}{K_{ij}^{\text{measured}}} \times 100\% \quad (12)$$

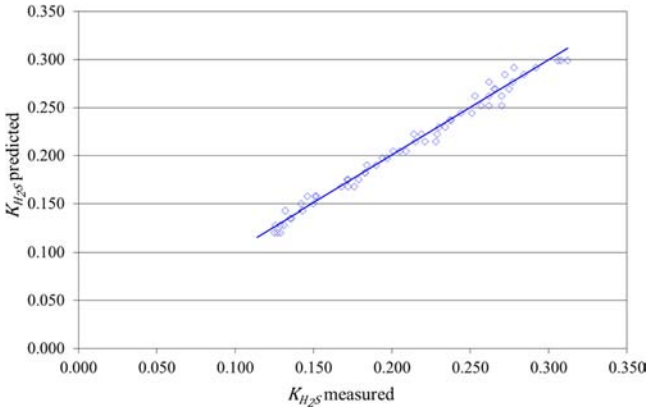

Figure 7. Comparison of measured K_{H_2S} (all media) and K_{H_2S} calculated from the model.

The average differences between experimental and predicted values of R^2 were <4%, demonstrating that H_2S gas–liquid partitioning was accurately predicted by the model based on the effects of modifications to the matrix and temperature.

Prediction of the partition coefficient of H_2S during fermentation will allow the calculation of the total production of this volatile compound from a single measurement (of its concentration in the gas or in the liquid phase). This will be particularly useful in cases of online monitoring of this extremely volatile compound in the fermentation gas, as described for carbonyl compounds but now possible for sulfur compounds with a flame photometric detector on the online monitoring system.[50] The ability to calculate total H_2S production and to differentiate between the amount remaining in the liquid and that lost in the CO_2 should help both improve our understanding of yeast metabolism and optimize fermentation control. Indeed, from a microbiological point of view, the total amount produced needs to be considered, whereas, from a technological point of view, the concentration remaining in the wine is more important. Minimizing the total amount of H_2S produced during fermentation and also the residual amounts after fermentation are important issues that may now soon be resolved.

Table 5. Estimated Coefficients of the Model Parameters Identified from Equation 10 by Multiple Linear Regression and Significance Testing

	coefficient	standard error	t stat	P value
β_0 (intercept)	3.37×10^{-2}	9.25×10^{-3}	3.6444	1.61×10^{-3}
β_1	1.35×10^{-4}	3.21×10^{-5}	4.2225	3.21×10^{-4}
β_2	-7.25×10^{-5}	7.27×10^{-5}	−0.9972	0.3305
β_3	9.43×10^{-3}	4.16×10^{-4}	22.6435	9.97×10^{-16}

DOI: 10.1021/jf505733a
J. Agric. Food Chem. 2015, 63, 3271−3278

AUTHOR INFORMATION

Corresponding Author

*(V.F.) Phone: +33 4 99 61 22 74. Fax: +33 4 99 61 28 57. E-mail: farines@supagro.inra.fr.

Notes

The authors declare no competing financial interest.

SYMBOLS AND ABBREVIATIONS USED

- c_l concentration of a species in the liquid phase (mol m^{-3} or g m^{-3})
- c_l^* concentration of a species at equilibrium in the liquid phase (mol m^{-3} or g m^{-3})
- c_g concentration of a species in the gas phase (mol m^{-3} or g m^{-3})
- n_i moles of the individual gas component (i) in the gas mixture (mol)
- H_2S_g H_2S concentration in the gas phase at equilibrium (g m^{-3})
- $H_2S_l^*$ H_2S concentration in the liquid phase at equilibrium (g m^{-3})
- H_i Henry's law coefficient: $H_i = \lim_{xi \to 0} K_i$ (dimensionless)
- i pure component
- k_H^{cc} Henry's constant: liquid concentration/gas concentration (dimensionless)
- k_H^{cp} Henry's constant: liquid concentration/partial pressure (mol m^{-3} Pa^{-1})
- K_i partition coefficient: gas concentration/liquid concentration (dimensionless)
- MW molecular weight (g mol^{-1})
- p_g partial pressure of a species in the gas phase (Pa)
- P_T total pressure (Pa)
- $P_{i(T)}^0$ vapor pressure of pure component (i) at a given temperature T (Pa)
- R gas constant (= 8.314 m^3·Pa mol^{-1} K^{-1})
- T temperature (°C or K)
- x_i molar fraction of individual gas component (i) in a liquid (dimensionless)
- y_i molar fraction of individual gas component (i) in a gas mixture (dimensionless)

REFERENCES

(1) Swiegers, J. H.; Pretorius, I. S. Modulation of volatile sulfur compounds by wine yeast. *Appl. Microbiol. Biotechnol.* **2007**, *74*, 954−960.

(2) Ribéreau-Gayon, P.; Glories, Y.; Maujean, A.; Dubourdieu, D. The chemistry of wine: stabilization and treatments. In *Handbook of Enology*, 2nd ed.; Wiley: Chichester, UK, 2006.

(3) Acree, T. E.; Sonoff, E. P.; Splittstoesser, D. F. Effect of yeast strain and type of sulfur compound on hydrogen sulfide production. *Am. J. Enol. Vitic.* **1972**, *23*, 6−9.

(4) Kumar, G. R.; Ramakrishnan, V.; Bisson, L. F. Survey of hydrogen sulfide production in wine strains of *Saccharomyces cerevisae*. *Am. J. Enol. Vitic.* **2010**, *61* (3), 365−371.

(5) Mendes-Ferreira, A.; Barbosa, C.; Falco, V.; Leao, C.; Mendes-Faia, A. The production of hydrogen sulphide and other aroma compounds by wine strains of *Saccharomyces cerevisiae* in synthetic media with different nitrogen concentrations. *J. Ind. Microbiol. Biotechnol.* **2009**, *36*, 571−583.

(6) Spiropoulos, A.; Tanaka, J.; Flerianos, I.; Bisson, L. F. Characterisation of hydrogen sulfide formation in commercial and natural wine isolates of *Saccharomyces*. *Am. J. Enol. Vitic.* **2000**, *51* (3), 233−248.

(7) Rauhut, D.; Kurbel, H. The production of H_2S from elemental sulfur, residues during fermentation and its influence on the formation of sulfur metabolites causing off-flavors in wines. *Wein−Wiss.* **1994**, *49*, 27−36.

(8) Acree, T. E.; Sonoff, E. P.; Splittstoesser, D. F. Determination of hydrogen sulfide in fermentation broths containing SO_2. *Appl. Microbiol.* **1971**, *22* (1), 110−112.

(9) Stratford, M.; Rose, A. H. Hydrogen sulfide production from sulfite by *Saccharomyces cerevisiae*. *J. Gen. Microbiol.* **1985**, *131*, 1417−1424.

(10) Giudici, P.; Kunkee, R. E. The effect of nitrogen deficiency and sulfur-containing amino acids on the reduction of sulfate to hydrogen sulfide by wine yeasts. *Am. J. Enol. Vitic.* **1994**, *45* (1), 107−112.

(11) Thomas, D.; Surdin-Kerjan, Y. Metabolism of sulfur amino acids in *Saccharomyces cerevisiae*. *Microbiol. Mol. Biol. Res.* **1997**, *61* (4), 503−532.

(12) Bell, S. J.; Henschke, P. A. Implications of nitrogen nutrition for grapes, fermentation and wine. *Aust. J. Grape Wine Res.* **2005**, *11*, 242−295.

(13) Jiranek, V.; Langridge, P.; Henschke, P. A. Regulation of hydrogen sulfide liberation in wine-producing *Saccharomyces cerevisiae* strains by assimillable nitrogen. *Appl. Environ. Microbiol.* **1995**, *61*, 461−467.

(14) Moreira, N.; Mendes, F.; Pereira, O.; Guedes de Pinho, P.; Hogg, T.; Vasconcelos, I. Volatile sulphur compounds in wines related to yeast metabolism and nitrogen composition of grape musts. *Anal. Chim. Acta* **2005**, *11*, 139−173.

(15) Wang, X. D.; Bohlscheid, J. C.; Edwards, C. G. Fermentative activity and production of volatile compounds by *Saccharomyces* grown in synthetic grape juice media deficient in assimilable nitrogen and/or pantothenic acid. *J. Appl. Microbiol.* **2003**, *94*, 349−359.

(16) Mendes-Ferreira, A.; Barbosa, C.; Ines, A.; Mendes-Faia, A. The timing of diammonium phosphate supplementation of wine must affects subsequent H_2S release during fermentation. *J. Appl. Microbiol.* **2010**, *108*, 540−549.

(17) Edwards, C. G.; Bohlscheid, J. C. Impact of pantothenic acid addition on H_2S production by *Saccharomyces* under fermentative conditions. *Enzyme Microb. Technol.* **2007**, *41*, 1−4.

(18) Hagen, K. M.; Keller, M.; Edwards, C. G. Survey of biotin, pantothenic acid, and assimilable nitrogen in winegrapes from the Pacific Northwest. *Am. J. Enol. Vitic.* **2008**, *59* (4), 432−436.

(19) Bohlscheid, J. C.; Edwards, C. G. Interactive effects of nitrogen and biotin on yeast growth, fermentation rate, and volatile production. *Am. J. Enol. Vitic.* **2004**, *55*, 310A.

(20) Butzke, C. E.; Park, S. K. Impact of fermentation rate changes on potential hydrogen sulfide concentrations in wine. *J. Microbiol. Biotechnol.* **2011**, *21* (5), 519−524.

(21) Raal, J. D. Characterization of differential ebulliometers for measuring activity coefficients. *AIChE J.* **2000**, *46* (1), 210−220.

(22) Eckert, C. A.; Sherman, S. R. Measurement and prediction of limiting activity coefficients. *Fluid Phase Equilib.* **1996**, *116* (1−2), 333−342.

(23) Alessi, P.; Fermeglia, M.; Kikic, I. Significance of dilute regions. *Fluid Phase Equilib.* **1991**, *70* (2−3), 239−250.

(24) Duhem, P.; Vidal, J. Extension of the dilution method to measurements of high activity coefficients at infinite dilution. *Fluid Phase Equilib.* **1978**, *2*, 231−235.

(25) Dufour, C.; Bayonove, C. L. Interactions between wine polyphenols andaroma substances. An insight at the molecular level. *J. AgricFood Chem.* **1999**, *47*, 678−684.

(26) Buttery, R. G.; Ling, L. C.; Guadagni, D. G. Volatilities of aldehydes, ketones, and esters in dilute water solution. *J. AgricFood Chem.* **1969**, *17*, 385−389.

(27) Nahon, D. F.; Harrison, M.; Roozen, J. P. Modeling flavor release from aqueous sucrose solutions, using mass transfer and partition coefficients. *J. AgricFood Chem.* **2000**, *48* (4), 1278−1284.

(28) Kolb, B.; Welter, C.; Bichler, C. Determination of partition coefficients by automatic equilibrium heaspace gas chromatography by vapor phase calibration. *Chromatographia* **1992**, *34* (5/8), 235−240.

DOI: 10.1021/jf505733a
J. Agric. Food Chem. 2015, 63, 3271−3278

(29) Whitehead, P. G.; Sandler, S. I. Headspace gas chromatography for measurement of infinite dilution activity coefficients of C-4 alcohols in water. *Fluid Phase Equilib.* **1999**, *157* (1), 111−120.
(30) Chaintreau, A.; Grade, A.; Munozbox, R. Determination of partition-coefficients and quantitation of headspace volatile compounds. *Anal. Chem.* **1995**, *67* (18), 3300−3304.
(31) Ettre, L. S.; Welter, C.; Kolb, B. Determination of gas-liquid partition-coefficients by automatic equilibrium headspace-gas-chromatography utilizing the phase ratio variation method. *Chromatographia* **1993**, *35* (1−2), 73−84.
(32) Jouquand, C.; Ducruet, V.; Giampaoli, P. Partition coefficients of aroma compounds in polysaccharide solutions by the phase ratio variation method. *Food Chem.* **2004**, *85* (3), 467−474.
(33) Gosset, J. M. Measurement of Henry' law constants for C1 and C2 chlorinated hydrocarbons. *Environ. Sci. Technol.* **1987**, *21*, 202−208.
(34) Athes, V.; Lillo, M. P. Y.; Bernard, C.; Perez-Correa, R.; Souchon, I. Comparison of experimental methods for measuring infinite dilution volatilities of aroma compounds in water/ethanol mixtures. *J. Agric. Food Chem.* **2004**, *52* (7), 2021−2027.
(35) Lide, D. R.; Frederikse, H. P. R. *CRC Handbook of Chemistry and Physics*, 76th ed.; Lide, D. R., Frederikse, H. P. R., Eds.; CRC Press: Boca Raton, FL USA, 1995.
(36) Carroll, J. J.; Mather, A. E. Phase equilibrium in the system water-hydrogen sulphide: hydrate-forming conditions. *Can. J. Chem. Eng.* **1991**, *69* (5), 1206−1212.
(37) Sander, R. Henry's law constants. In *NIST Chemistry WebBook Standard Reference Database 69*; Mallard, P. J., Linstrom, W. G., Eds.; National Institute of Standards and Technology: Gaithersburg, MD, USA, 2011.
(38) De Bruyn, W. J.; Swartz, E.; Hu, J. H.; Shorter, J. A.; Davidovits, P.; Worsnop, D. R.; Zahniser, M. S.; Kolb, C. E. Henry's law solubilities and Setchenow coefficients for biogenic reduced sulfur species obtained from gas-liquid uptake measurements. *J. Geophys. Res.* **1995**, *100D*, 7245−7251.
(39) Dean, J. A. *Lange's Handbook of Chemistry*; McGraw-Hill: New York, 1999.
(40) Carroll, J. J.; Mather, A. E. The solubility of hydrogen sulphide in water from 0 to 90 °C and pressures to 1 MPa. *Geochim. Cosmochim. Acta* **1989**, *53*, 1163−1170.
(41) Kavanaugh, M. C.; Trussell, R. R. Design of aeration towers to strip volatile contaminants from drinking water. *J. Am. Water Works Assoc.* **1980**, *72*, 684−692.
(42) Edwards, T. J.; Maurer, G.; Newman, J.; Prausnitz, J. M. Vapor-liquid equilibria in multicomponent aqueous solutions of volatile weak electrolytes. *AIChE J.* **1978**, *24*, 966−976.
(43) Wilhelm, E.; Battino, R.; Wilcock, R. J. Low-pressure solubility of gases in liquid water. *Chem. Rev.* **1977**, *77*, 219−262.
(44) Hine, J.; Weimar, R. D. Carbon basicity. *J. Am. Chem. Soc.* **1965**, *87*, 3387−3396.
(45) Loomis, A. G. Solubilities of gases in water. In *International Critical Tables of Numerical Data, Physics, Chemistry and Technology*; West, E. W., Dorsey, C. J., Bichowsky, N. E., Klemenc, F. R., Washburn, A., Eds.; McGraw-Hill: New York, 1928; Vol. III.
(46) Lubbers, S.; Guichard, E. The effects of sugars and pectin on flavour release from a fruit pastille model system. *Food Chem.* **2003**, *81*, 269−273.
(47) Nahon, D. F.; Harrison, M.; Roozen, J. P. Modeling flavor release from aqueous sucrose solutions, using mass transfer and partition coefficients. *J. Agric. Food Chem.* **2000**, *48*, 1278−1284.
(48) Morakul, S.; Athes, V.; Mouret, J. R.; Sablayrolles, J. M. Comprehensive study of the evolution of gas−liquid partitioning of aroma compounds during wine alcoholic fermentation. *J. Agric. Food Chem.* **2010**, *58* (18), 10219−10225.
(49) Nahon, D. F.; Koren, P. A. N. Y.; Roozen, J. P.; Posthumus, M. A. Flavor release from mixtures of sodium cyclamate, sucrose, and an orange aroma. *J. Agric. Food Chem.* **1998**, *46*, 4963−4968.
(50) Mouret, J. R.; Perez, M.; Angenieux, M.; Nicolle, P.; Farines, V.; Sablayrolles, J. M. On-line based kinetic analysis of higher alcohol and ester synthesis during winemaking fermentations. *Food Bioprocess Technol.* **2014**, *7*, 1235−1245.

DOI: 10.1021/jf505733a
J. Agric. Food Chem. 2015, 63, 3271−3278

increased bioavailability of (*Z*)-lycopenes caused by a better solubility in chylomicrons is often proposed to be the reason for this observation.[12] On the other hand, various processes during digestion are hypothesized to trigger the isomerization of lycopene and β-carotene.[13] Especially the gastric milieu is considered to be the main reason for the isomerization of carotenoids,[14] because a strong formation of (*Z*)-isomers at gastric pH as well as at elevated physiological temperatures was observed in several studies.[13,14] However, this cannot explain the dominant role of (*all-E*)-β-carotene in human plasma in the presence of only trace amounts of β-carotene isomers. Instead, enzymatic systems that could remove (*Z*)-isomers were discussed in the literature to form products such as (9*Z*)-retinoic acid.[7] Furthermore, the difference in the distribution of (*Z*)-lycopenes determined in various human tissues cannot be clarified by these hypotheses at all.[14]

Therefore, the physical and chemical quenching of carotenoids was investigated in detail, to identify possible mechanisms for the contradictory ratios of carotenoid (*Z*)-isomers in human plasma and tissues. The present work focused on the underlying isomerization processes and allowed insights to additional synergistic effects between lycopene and β-carotene.

MATERIALS AND METHODS

Chemicals. Chemicals with highest purities were obtained from Sigma-Aldrich (Taufkirchen, Germany) and Carl Roth GmbH (Karlsruhe, Germany) unless otherwise indicated. (15*Z*)-β-Carotene, (9*Z*)-β-carotene, (15*Z*)-lycopene, and (5*Z*)-lycopene were synthesized according to the literature.[15] Performed modifications were described in previous works.[16,17] (7*Z*,9*Z*)-Lycopene and (7*Z*)-lycopene were synthesized as well using the same Wittig strategy. In contrast to the literature, geraniol served as the educt for both these isomers.[15] Pure (*E*)-citral was generated after oxidation by activated manganese dioxide.[18] The following steps were more or less identical to the literature, with exception of the final Lindlar hydrogenation, where a ratio of Lindlar catalyst to Lindlar poison of 1:23000 (w:w) was used to accomplish an almost complete reaction. 11.0 mg of 7-*cis*-lycopene and 18.4 mg of (7*Z*,9*Z*)-lycopene were obtained with isomeric purities of 91% (7*Z*) and 83% (7*Z*,9*Z*). Standards were verified by 1D-, 2D-NMR spectra and HPLC−UV analyses. (*all-E*)-Lycopene was isolated from tomato paste according to the below described extraction method, followed by precipitation with methanol. Analytical parameters for identification and characterization as well as NMR data are summarized in Table S1 in the Supporting Information. 1,4-Dimethylnaphthalene-1,4-endoperoxide was synthesized according to Wasserman et al.[19] Peroxidase from horseradish (HRP) with an activity of about 150 U/mg was purchased as a lyophilized beige powder from Sigma-Aldrich (Taufkirchen, Germany). NMR solvents were purchased from ARMAR Chemicals (Döttingen, Switzerland) with a purity of 99.8 atom % D. Methanol and methyl *tert*-butyl ether as HPLC solvents were purchased from Sigma-Aldrich (HPLC grade ≥99.8%).

Fruit and Vegetable Samples. In this study, different fruits and vegetables were characterized for their content and isomeric composition of carotenoids. Samples of watermelon, papaya, persimmon, broccoli, eggplant, grapefruit, tomato, spinach, zucchini, and red pepper were purchased from local markets and food stores with different origins.

Preparation of Fruits and Vegetables. Fresh fruit and vegetable materials were homogenized at 0 °C with a mixer for 1 min under reduced light, if necessary with addition of water. Per sample between 15 and 30 g of the homogenate was frozen at −21 °C followed by lyophilization for 3 to 4 days. Dry plant materials were extracted overnight by addition of *n*-hexane/acetone/ethanol (50/25/25) containing 0.01% butylated hydroxytoluene performed on an orbital shaker (170 U/min). Saponification was performed for about 20 h at room temperature by addition of a methanolic potassium hydroxide solution (10%) to the filtrated extracts, thus allowing an effective separation of fatty compounds and chlorophylls. Alkaline extracts were washed 5 times with a 2% sodium chloride solution and were dried under an argon stream. Obtained precipitates were dissolved and diluted in mobile phase (methanol/methy *tert*-butyl ether, 50/50) followed by HPLC−UV analyses. This method was fully adopted from prior works.[16,17] Thermally induced or photoinduced isomerization processes were excluded during the whole preparation by working under reduced light and using aluminum foil or dark glassware. Temperature never exceeded 25 °C. Detailed investigations confirmed that the native isomeric composition was not influenced during storage and all steps of preparation.

Preparation of Human Plasma. A total of 15 human plasma samples of healthy donors between 22 and 35 years of age were obtained in cooperation with the university medical center Halle/Kröllwitz (Halle/Saale, Germany). All participants signed a written informed consent. Sample preparation was performed in compliance with the literature.[11] Plasma was obtained after centrifugation of blood samples for 10 min at 4 °C (2375 rpm, 454*g*). Separated plasma was stored on ice until preparation. 1 mL of plasma was diluted with 1 mL of doubly distilled water. Protein precipitation was performed by intensive shaking after addition of 2 mL of ethanol. Plasma carotenoids were extracted with 4 mL of *n*-hexane on a shaking device (Vortex) for 20 min. After centrifugation (15 min, 4500 rpm, 3400*g*) 3.8 mL of the organic layer was transferred to amber glassware vials and dried under an argon stream. For HPLC−UV analyses, the residues were dissolved in 200 μL of mobile phase (methanol/methyl *tert*-butyl ether, 50/50). All samples were prepared in duplicate.

Singlet Oxygen Assay. Transformation of (*all-E*)-lycopene and (*all-E*)-β-carotene was observed after treatment with various amounts of singlet oxygen, generated in situ, to gain a better understanding of chemical and physical isomerization processes. Concentration of singlet oxygen was referred to absolute amounts of carotenoids after incubation. First, separate incubations were performed with either lycopene or β-carotene as pure substances to investigate their individual isomerization processes. Then mixed incubations were used to determine possible synergistic effects between lycopene and β-carotene.

Singlet oxygen was generated in situ by thermal degradation of 1,4-dimethylnaphthalene-1,4-endoperoxide (DMNEP). This compound was synthesized according to Wasserman et al.,[19] followed by flash chromatography (silica gel 60; *n*-hexane/EtOAc, 7:3) to yield a mixture of educt and DMNEP (1:1). NMR experiments confirmed reproducible release ratios of molecular singlet oxygen during treatment at 40 °C for 20 min (about 37.7% of total applied amounts). For follow-up studies about 25 mg of DMNEP was diluted in 50 mL of *n*-hexane to yield an absolute concentration of 0.59 nmol/μL singlet oxygen or 0.059 nmol/μL for diluted solutions (1:10), respectively.

2.5 mg portions of lycopene and β-carotene were dissolved in 50 mL of hexane to final concentrations of 50 μg/mL. Aliquots (300 μL) were transferred to dark glass vials, and various volumes of DMNEP (0.059 nmol/mL, 0, 10, 25, 50, 100, 150, 200, 250 μL; 0.59 nmol/mL, 50, 100, 200, 500, 1000, 2200 μL) were added. For standardization, vials were filled up in each case to 2.5 mL with *n*-hexane. The resulting solutions were stirred for 20 min at 40 °C and were directly quenched on ice after treatment. After drying under an argon stream, residues were taken up in 400 μL of mobile phase (methanol/MTBE, 50/50) followed by HPLC−UV analyses.

H_2O_2/HRP and ABTS/H_2O_2/HRP Assay. Carotenoids were treated with H_2O_2 and horseradish peroxidase in model systems to simulate oxidative effects in vivo. Kinetics were analyzed by HPLC−UV and photometric measurements. Here, a protocol based on works of Özyürek et al. with some modifications was established.[20] First, 2.2 mg portions of carotenoid standards were dissolved in 4 mL of acetone to final concentrations of 0.55 mg/mL of lycopene and β-carotene, respectively. 5 mg of horseradish peroxidase (HRP, Sigma-Aldrich, ∼150 U/mg) was dissolved in 5 mL of H_2O/EtOH (1:1), resulting in HRP solution with 150 U/mL. 0.32 mM H_2O_2 solution was prepared

DOI: 10.1021/acs.jafc.5b00377
J. Agric. Food Chem. 2015, 63, 3279−3287

Table 1. Contents of β-Carotene and Lycopene and Their Isomeric Composition in Various Fruits and Vegetables and in Human Plasma, Expressed as Percentage of Total β-Carotene or Lycopene

	β-carotene				lycopene	
sample	content, μg/g FW	(*all-E*), %	(9Z), %	ratio (*all-E*)/(9Z)	content, μg/g FW	(*all-E*), %
broccoli	4.8	84.1	9.7	8.8	nd	
eggplant	0.4	85.4	7. 7	11.5	nd	
spinach	49.6	86.4	7.4	11.7	nd	
zucchini	1.6	84.0	8.4	10.1	nd	
pepper (red)	15.8	88.6	6.0	14.7	nd	
tomato	4.7	85.9	2.6	33.1	67.9	78.7
grapefruit (pink)	3.4	89.8	0.7	137.1	26.2	78.7
papaya	0.7	86.8	3.6	24.0	29.1	80.4
persimmon	0.2	76.0	3.8	20.0	3.2	79.9
watermelon	0.3	91.3	2.9	31.6	59.3	78.9
human plasma (n = 15)	1.0 nmol/mL	89.3	1.7	59.0	2.8 nmol/mL	37.3

from a 35% H_2O_2 solution (Sigma-Aldrich) by dilution in EtOH. Incubation solutions consisted of water (0.5 mL), ethanol (0.5, 0.4, 0.3, 0.2, 0.1, and 0 mL), and 0.1 mL of carotenoid solution. Various amounts of 0.32 mM H_2O_2 solution (0, 0.1, 0.2, 0.3, 0.4, and 0.5 mL) and constant levels of HRP solution (0.05 mL) in ethanol (150 U/mL) were also added to dark glass vials. The resulting solutions (final volume of always 1.15 mL) were shaken at room temperature for 30 min followed by photometric analyses with a Jasco UV/vis spectrophotometer V-530. Carotenoid concentrations were determined at 470 nm for lycopene and 450 nm for β-carotene. To analyze the isomeric composition the incubation solutions were extracted with dichloromethane (500 μL for two times) and dried under argon stream. Residues were taken up in 400 μL of mobile phase (methanol/MTBE, 50/50) followed by HPLC−UV analyses.

A similar model system was established to investigate quenching of radical species by carotenoids. 46.6 mg of 2,2′-azino-bis(3-ethylbenzthiazoline-6-sulfonic acid) (ABTS) was dissolved in 20 mL of H_2O to a final concentration of 2.33 mg/mL (4.25 mM). First, 0.1 mL of ABTS solution was incubated with HRP (0.05 mL) and H_2O_2 (volumes as described before) after addition of H_2O (0.4 mL) and EtOH (volumes as described before) with a total volume of 1.05 mL for 30 min at room temperature. After formation of the green to blue colored radical ($ABTS^{\bullet+}$), 0.1 mL of carotenoid solution was added and shaken for an additional 10 min. Isomeric composition and degradation rates were analyzed after extraction and preparation as described above.

All described experiments were performed with pure lycopene and β-carotene standard solutions first. Subsequently, mixtures of both carotenoids were incubated in the model systems to determinate possible synergistic effects, maintaining the same concentration of total carotenoids to give comparable results to the single carotenoid incubation.

Analytical HPLC−UV and HPLC−DAD. Carotenoid profiles were determined for all samples by the following HPLC system. The HPLC apparatus (Jasco, Groß-Umstadt, Germany) consisted of a quaternary gradient pump (PU-2089 Plus) with degasser, a column oven (Jetstream Plus), an autosampler (AS-2055 Plus), and a UV detector (UV-2075 Plus) operating at a wavelength of 450 nm. For DAD analyses, a Jasco MD-2015 Plus detector was used. Chromatographic separations were performed on a stainless steel column packed with RP-C30 material (YMC carotenoid, 5 μm, 250 × 4.6 mm, YMC Europe, Dinslaken, Germany) connected to a C30 guard column (5 μm, 250 × 4.0 mm, YMC Europe, Dinslaken, Germany) using a flow rate of 0.65 mL min^{-1}. Chosen column temperature was 20 °C. The mobile phase used was methanol (solvent A) and methyl *tert*-butyl ether (solvent B). Samples were injected at 40% B (held for 5 min), and gradient was then changed to 83% B in 50 min. Afterward gradient changed to 100% B in 5 min (held for 10 min) and to 40% B in 5 min (held for 10 min). Retention time of the carotenoid isomers was checked with the authentic references where possible. Further identification and characterization was performed by HPLC−DAD and HPLC−MS/MS analyses, as described in previous works.[16,17] In particular, the Q ratios were calculated by division of the absorption at the subsidiary "(Z)-peak" by the absorption at the absorption maxima. Based on these spectral characteristics, further isomers were assigned according to data from the literature.[11,15,21,22] A representative chromatogram is given in Figure S1 in the Supporting Information to verify the applicability of the established method. Additionally, all data required for the identification or characterization of altogether 16 carotenoid isomers are summarized in Table S1 in the Supporting Information.

For all samples (model incubations and biological samples), the isomeric composition was calculated by integration of all identified lycopene and β-carotene peaks first. Then, the areas of the separate peaks were divided by the sum of all lycopene and β-carotene values to express them as the percentage of total lycopene and β-carotene concentrations. Absolute concentrations and ratios of β-carotene and lycopene were determined by external calibration using (*all-E*) standard compounds analyzed at 450 nm.

High Performance Liquid Chromatography Mass Spectrometry (LC−MS/MS). The HPLC apparatus (Jasco, Groß-Umstadt, Germany) consisted of a pump (PU-2080 Plus) with degasser and quaternary gradient mixer, a column oven (Jasco Jetstream II), and an autosampler (AS-2057 Plus). Mass spectrometric detection was conducted on an API 4000 QTrap LC-MS/MS system (Applied Biosystems/MDS Sciex, Concord, ON, Canada) equipped with an API source using an atmospheric pressure chemical ionization (APCI) interface in negative mode. Nitrogen was used as sheath and auxiliary gas. The optimized parameters for mass spectrometry of lycopene were Q1 536.7 amu, Q3 467.6 amu, DP −75 V, CE −27 eV, CXP −12 V. β-Carotene showed no fragmentation in Q3 (Q1 536.7 amu, DP −60 V). The analytical parameters with respect to the used column and temperature were as described above for the analytical HPLC−UV and HPLC−DAD.

Nuclear Magnetic Resonance Spectroscopy (NMR). ^1H and ^{13}C NMR spectra were recorded on a Varian Unity Inova 500 instrument operating at 500 MHz for ^1H and 125 MHz for ^{13}C and on a Varian VXR 400 spectrometer at 400 MHz for ^1H and 100 MHz for ^{13}C, respectively. $SiMe_4$ was used as a reference for calibrating the chemical shift.

Statistical Analysis. Analyses of carotenoid concentrations and isomeric composition were performed in duplicate for each sample and resulted in coefficients of variation less than 5% in fruits and vegetables. Mean variation coefficients for carotenoid concentrations in human plasma samples were below 10% (maximal coefficients of variation <20%). Determination of the isomeric composition in human plasma resulted in coefficients of variation less than 10% for all measured isomers with concentrations of more than 1.5%. Confidence intervals were calculated with a probability value of 95%.

DOI: 10.1021/acs.jafc.5b00377
J. Agric. Food Chem. 2015, 63, 3279−3287

RESULTS AND DISCUSSION

Identification of Carotenoid Isomers. Identification of various lycopene and β-carotene isomers was performed according to Heymann et al. by comparison of retention times on HPLC−UV using commercially available and independently synthesized references.[16,17] Additional LC/APCI-MS analyses and HPLC−DAD with Q ratio characterization was also used. The present synthesized (7Z)- and (7Z,9Z)-lycopene were added to the established analytical method. All representative data are summarized in Tables S2 and S3 in the Supporting Information. A total of 8 authentic reference standards verified the established analytical method as a powerful instrument for the determination of the carotenoid profile in model solutions and in biological samples, thus allowing a detailed description of isomerization processes in further experiments.

Carotenoid Profile of Various Fruits and Vegetables. First, various fruits and vegetables were analyzed for their carotenoid content as well as their isomeric lycopene and β-carotene composition. The results are summarized in Table 1. Tomatoes contained, with about 68 μg/g fresh weight, the highest lycopene concentration compared to the other analyzed food samples. This level was slightly higher than expected from the literature, where usually concentrations between 20 and 50 μg/g were reported.[4] In the present study, an almost complete array of lycopene isomers was determined in comparison to other works, which might explain the increased total concentration with respect to the literature. Moreover, the natural deviation between different tomato varieties has an impact on carotenoid biosynthesis, too.[23] Furthermore, about the half of all analyzed tomatoes were cultivated under field-grown conditions, which also has a great impact on the rate of lycopene biosynthesis.[16] All other results, e.g., determined in watermelons or pink grapefruits, complied with published data very well.[4,24] Contents of β-carotene showed no significant differences compared to data from comparable studies, e.g., analyses of spinach, zucchini, and eggplant resulted in concentrations of 49.55 μg/g, 1.60 μg/g, and 0.41 μg/g fresh weight, while O'Neill et al. determined 44.89 μg/g, 1.80 μg/g, and 0.50 μg/g fresh weight,[24] respectively. In contrast to the literature, the analysis of pepper led to considerably higher amounts of β-carotene (15.76 μg/g vs 4.8 μg/g).[24] Here, the high levels of β-carotene in pepper fruits might result naturally from the specific cultivation variety, but can be influenced also by many other factors, e.g., light, temperature, or humidity.

The determination of the isomeric pattern of unprocessed food samples resulted in ratios between 70 and 91% of the (*all-E*)-isomers, as apparent from Table 1. This reflects their predominant occurrence in nature, and has been reported in the literature before.[13,25] Mean concentrations of (*all-E*)-β-carotene and of (*all-E*)-lycopene of all analyzed food samples deviated only in a small range, e.g., for (*all-E*)-β-carotene between 84.0 and 91.3%. Only in persimmons lower levels of about 76% were observed. Additionally, (*all-E*)-lycopene was determined with concentrations from 78.7 to 80.4%. On the other hand, (*Z*)-isomers of β-carotene and lycopene accounted only for about 15% and 20%, respectively, as has been described in the literature before.[26,27] However, the present detailed studies on carotenoid isomers projected a significant difference in the observed (9Z)-β-carotene concentration between lycopene free and lycopene containing fruits and vegetables. While mean levels between 6.0 and 9.7% were determined in samples such as broccoli (9.7%), spinach (7.4%), or red pepper (6.0%), the (9Z)-β-carotene concentration never exceeded 4.0% in lycopene rich samples like tomato (2.6%), grapefruit (0.7%), or watermelon (2.9%). Thus, the (9Z)-β-carotene concentration allowed for a clear differentiation between lycopene free and lycopene containing samples, as shown in Figure 1.

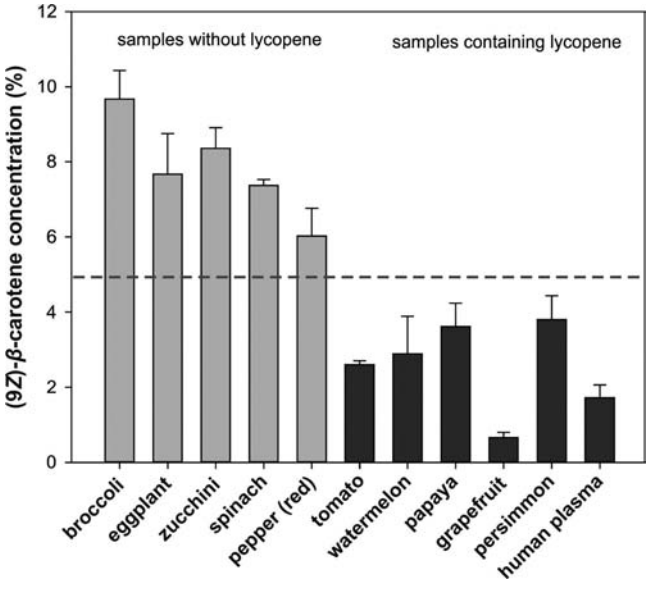

Figure 1. (9Z)-β-Carotene concentrations (expressed as percentage of total β-carotene) in lycopene free (gray bars) and lycopene containing (black bars) fruits and vegetables, and in human plasma samples.

Especially leafy green vegetables were reported for raised (*Z*)-isomer concentrations compared to others,[28] resulting in decreased (*all-E*)/(9Z) ratios (8.8 to 14.7, Table 1). Here, especially chlorophyll was proposed to act as a sensitizer that triggers the isomerization during photosynthesis.[29] Nevertheless, the isomerization process of β-carotene seems to be suppressed in the presence of lycopene. Our recent studies on the photoinduced isomerization process of carotenoids confirmed this observation. While energy-rich illumination resulted in significantly higher levels of (9Z)-β-carotene in field-grown spinach,[17] no difference in the isomeric β-carotene composition was observed between field- and greenhouse-grown tomato samples. As a consequence for the later, only the increased concentrations of (*Z*)-lycopenes led to a differentiation of light regimens during growing.[3,16] This means that, most likely, lycopene was able to minimize (i.e., quench) the photoinduced isomerization of (*all-E*)-β-carotene and thereby preserves its biological function as a vitamin-A precursor.[4]

Carotenoid Profile of Human Blood Plasma. The results of the analyses of plasma samples from 15 healthy subjects (age from 22 to 39) are also summarized in Table 1. Comparable to analyzed food samples, (*all-E*)-β-carotene dominated with a mean concentration of 89.3%, while (9Z)-β-carotene was determined at only 1.7%. (13Z)-β-Carotene represented the predominant (*Z*)-isomer with concentrations between 5.1 and 11.3%. These results completely complied with observations from the literature.[30,31] On the contrary, (*all-E*)-lycopene just occurred with a concentration of 37.3%, while (5Z)-lycopene was the dominant (*Z*)-isomer (29.8%) followed

DOI: 10.1021/acs.jafc.5b00377
J. Agric. Food Chem. 2015, 63, 3279−3287

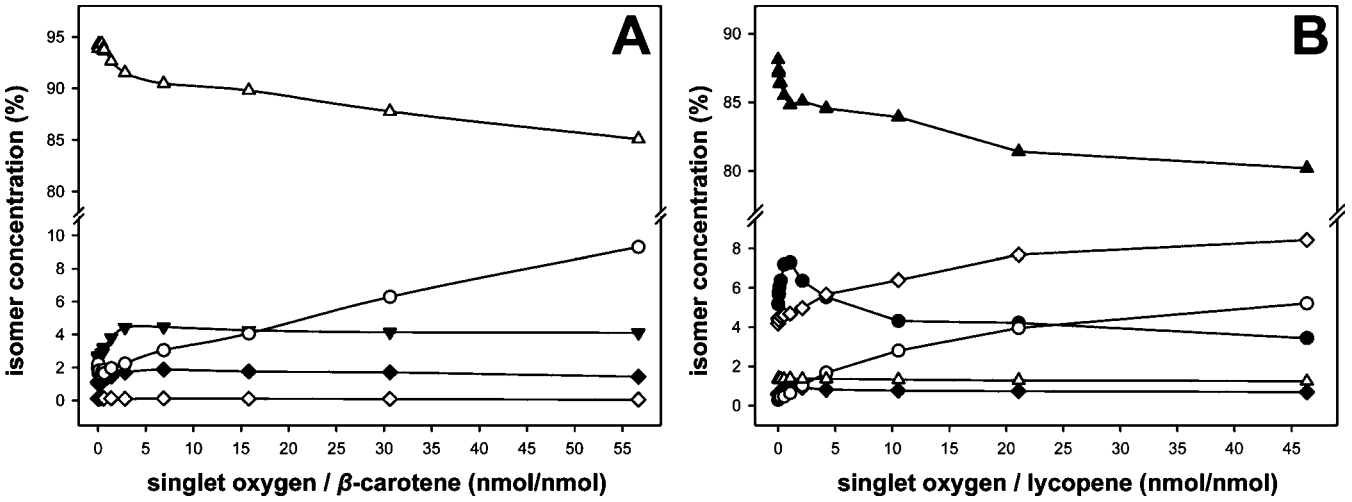

Figure 2. Concentrations of β-carotene (A) and lycopene (B) isomers during treatment with singlet oxygen of various concentrations, expressed as percentage of total β-carotene and lycopene (%). Kinetic products were formed especially at low levels, while thermodynamically controlled products dominated at high levels. A: (15*Z*)-β-carotene (◆), (13*Z*)-β-carotene (▼), (9*Z*,13*Z*)-β-carotene (◇), (*all-E*)-β-carotene (Δ), (9*Z*)-β-carotene (○). B: (15*Z*)-lycopene (◆), (13*Z*)-lycopene (●), (9*Z*)-lycopene (○), (7*Z*)-lycopene (Δ), (*all-E*)-lycopene (▲), (5*Z*)-lycopene (◇).

by (13*Z*) (14.1%), which was in line with the literature, too.[11,14,31]

Interestingly, the ratio of (*all-E*)- to (9*Z*)-β-carotene in human plasma was in the same range as for lycopene containing fruits (Figure 1). The chromatographic pattern of β-carotene was quite similar to lycopene containing fruits such as tomatoes or watermelon, characterized by very low levels of the (9*Z*)-isomer. This indicated that the suggested protective effect of lycopene on other carotenoids might be applicable for human plasma samples, too. Different from fruits, significantly higher amounts of (5*Z*)-lycopene were found in vivo.

Incubation of Lycopene and β-Carotene with Singlet Oxygen as Model System. The isomerization process during individual incubations of (*all-E*)-β-carotene (A) and (*all-E*)-lycopene (B) with singlet oxygen is illustrated in Figure 2. As expected from the literature, only physical quenching but no chemical quenching was observed during the reaction with singlet oxygen.[32]

The concentration of (*all-E*)-lycopene was degraded from initially 88.1% to 80.2%, while especially (9*Z*)-lycopene (from 0.3% to 5.2%) and (5*Z*)-lycopene (from 4.2% to 8.4%) were generated in high amounts. On the contrary, (7*Z*)- (1.4% to 1.2%) and (15*Z*)-lycopene (0.6% to 0.7%) just slightly changed at constant low levels during incubation. The isomerization process of (13*Z*)-lycopene was characterized by a strong increase (maximum of 7.3%) at singlet oxygen concentrations up to 1.05 nmol per nmol of lycopene, while it was degraded at higher singlet oxygen amounts to reach an equilibrium concentration of about 3.4%. In contrast, the formation of (5*Z*)- and (9*Z*)-lycopene showed almost linear increases with rising singlet oxygen concentrations. The remaining isomers showed no significant changes.

Comparable to lycopene the concentration of (*all-E*)-β-carotene was reduced from 94.2% to 85.1%. Only (9*Z*)-β-carotene (from 2.0% to 9.3%) significantly increased in an almost linear fashion. (13*Z*)-β-Carotene and (15*Z*)-β-carotene were formed only at low concentrations up to 2.8 nmol of singlet oxygen per nmol of β-carotene and reached subsequently equilibrium states at about 4.5% (13*Z*) and 1.9% (15*Z*). All other β-carotene isomers showed no significant changes.

These model systems illustrated defined processes during incubation of carotenoids with singlet oxygen. Obviously, the isomerization proceeded in two stages. In the first stage at low singlet oxygen concentrations, the isomerization progress was similar to thermally induced processes as described by Kuki et al., where mainly the kinetically controlled products such as (15*Z*)- and (13*Z*)-β-carotene as well as (15*Z*)- and (13*Z*)-lycopene were formed preferentially.[26,33] The second part of the reaction at high amounts of singlet oxygen (>10.5 nmol/nmol of β-carotene, >4.2 nmol/nmol of lycopene) was characterized by a dominant increase of the thermodynamic products like (9*Z*)-β-carotene and (5*Z*)-lycopene. These isomers are normally observed during high energy processing of foods, e.g., during high pressure sterilization or irradiation with UV light.[16,27,36] The results were in line with theoretical studies on the enthalpies of carotenoid isomers.[34,35] Accordingly, (9*Z*)-β-carotene has the highest rotational barrier to reisomerize to the (*all-E*) configuration compared to all other isomers ($\Delta E_r^{\ddagger}$ = 26.0 kcal/mol).[35] Thus, (9*Z*)-β-carotene is the most stable isomer that is only formed during high energetic stimulation. Rotational barriers for reisomerization of (13*Z*)-β-carotene ($\Delta E_r^{\ddagger}$ = 21.5 kcal/mol) and (15*Z*)-β-carotene ($\Delta E_r^{\ddagger}$ = 20.6 kcal/mol) are significantly lower, which explains equilibrium at high singlet oxygen concentrations, associated with their lower stabilities.[35] The same accounts for lycopene, where (13*Z*)- and (15*Z*)-lycopene were calculated to be the kinetically controlled products, whereas (9*Z*)- and especially (5*Z*)-lycopene represent the thermodynamically controlled products. Taken together, the present results illustrate that the energy input by singlet oxygen is located somewhere between thermal and photochemical excitation. Furthermore, the singlet oxygen induced isomerization of carotenoids is far more complex than illustrated in the literature so far, where only the complete transformation of (15*Z*)- and (13*Z*)-isomers to the (*all-E*)-configuration was reported for the interaction with singlet oxygen.[8,37]

The similar isomeric pattern in the single incubations changed abruptly in mixed β-carotene/lycopene reactions, where only lycopene displayed almost the same isomerization progress as shown before. Various ratios were chosen (38%, 56%, 64%, and 73% lycopene) with the total carotenoid

DOI: 10.1021/acs.jafc.5b00377
J. Agric. Food Chem. 2015, 63, 3279−3287

concentration maintained at the same level as used in the single carotenoid incubation. Specific formation rates of the 4 β-carotene isomers were calculated by linear fitting. In the case of (13*Z*) and (15*Z*) only the linear ranges at the start of the incubations were used for calculation to allow comparability. As depicted in Figure 3, the rates for (9*Z*) decreased with

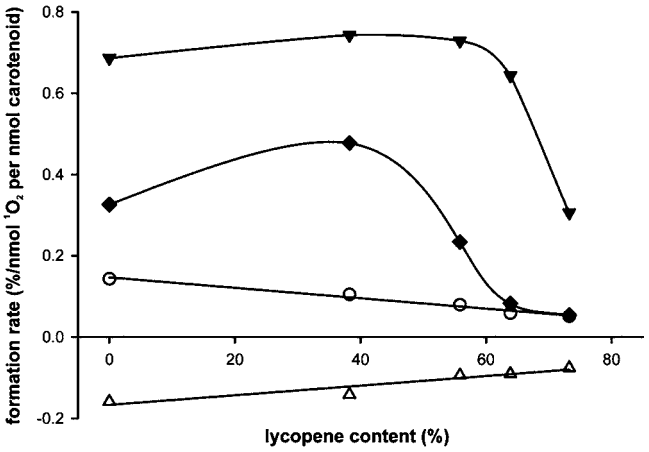

Figure 3. Formation rates of (*all-E*)- (Δ), (9*Z*)- (○), (13*Z*)- (▼), and (15*Z*)-β-carotene (◆) in β-carotene/lycopene reaction mixtures during quenching of singlet oxygen dependent on the lycopene content. Rates were calculated by linear regression during the linear formation progress of all isomers.

increasing lycopene concentrations from 0.143%/nmol of singlet oxygen per nmol of carotenoid (0% lycopene) to just 0.051%/nmol of singlet oxygen per nmol of carotenoid (73% lycopene), thus suppressing the formation to about one-third. The opposite effect was observed for the isomerization of (*all-E*)-β-carotene, where rates decreased from −0.1589 to −0.0757%/nmol of singlet oxygen per nmol of carotenoid. At lycopene contents of more than 50% the formation of (15*Z*)- and (13*Z*)-isomers was effectively suppressed, while smaller amounts of lycopene clearly led to increased formation compared to lycopene free systems. In line with the theoretical studies by Guo et al.,[35] lycopene reduces the potential energy levels during the physical quenching of singlet oxygen. Low-energy processes rather result in the formation of kinetically controlled products, i.e., (13*Z*) and (15*Z*)-β-carotene. Only very high amounts of lycopene significantly minimized the energy levels, leading to reduced formation of both isomers. In contrast, even small amounts of lycopene were able to suppress the formation of (9*Z*)-β-carotene with the highest activation energy within all mono-(*Z*)-isomers,[35] thus preventing the generation of this thermodynamic product at low energy levels.

These findings proved that lycopene was able to suppress the singlet oxygen induced isomerization of (*all-E*)-β-carotene probably as a result of its higher quenching activity.[2] Consequently, β-carotene is preserved in its (*all-E*) configuration and maintains its potential as a vitamin A precursor in vivo. Singlet oxygen naturally occurs in air, where it is generated during various reactions especially with oxygen and UV light.[38] The presence of sensitizers, such as chlorophyll during photosynthesis, or oxidation stress could also lead to singlet oxygen in vivo.[6] Unfortunately the determination of singlet oxygen concentrations is a technically challenging problem as reported by Kanofsky. Consequently, only quantum yields and lifetime experiments were described in the literature.[39] Thus, it is hard to assess if the used concentrations of singlet oxygen in our model systems might be applicable for biological systems.

Incubation with H_2O_2 and Horseradish Peroxidase (HRP). For simulation of reactions between carotenoids and reactive radical oxygen species first a model system of H_2O_2 and horseradish peroxidase (HRP) was used. In theory, carotenoid peroxides are formed from H_2O_2 that is enzymatically catalyzed by HRP. This reaction should result in a loss of total carotenoids as a measure for chemical quenching and decomposition. However, no relevant changes in extinction were found (data not shown). Amounts of carotenoids stayed at a constant level with the pattern of isomers nearly unchanged. Consequently neither chemical nor physical quenching was detected. It can only be speculated that the missing specificity of HRP to carotenoids was the reason for the lack in reactivity.

Incubation with H_2O_2 and Horseradish Peroxidase (HRP) and ABTS. Alternatively, the protective effect of lycopene on radical induced β-carotene isomerization was confirmed by experiments with ABTS radicals in the presence of hydrogen peroxide. In contrast to the reaction of carotenoids with singlet oxygen, the interaction with free radicals led to strong chemical quenching as reported in the literature.[40] This was evidenced by a strong degradation of both carotenoids. However, at high concentrations, lycopene was degraded completely, whereas loss of β-carotene was only partially. Figure 4 shows that, in β-carotene/lycopene mixed incubations

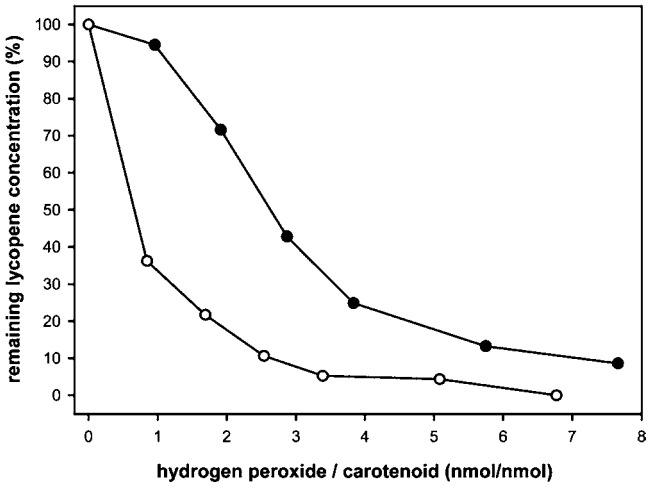

Figure 4. Degradation of lycopene in β-carotene/lycopene reaction mixtures during incubation with ATBS radicals and hydrogen peroxide. Values are expressed as remaining concentration of lycopene (%) compared to the initial concentration (β-carotene/lycopene ratio 4/1 (○) and 1/2 (●)).

(initial lycopene content 20%, see Figure 4 (○)), degradation of 54% of lycopene was already reached at 1.4 equiv of radical concentration, while at 2.8 equiv of lycopene was almost completely degraded. Parallel to degradation, lycopene showed also strong isomerization indicating physical quenching processes (data not shown). Higher lycopene proportions (initial lycopene content 67%, see Figure 4 (●)) shifted the degradation to higher radical concentrations. In contrast, even at 7.5 equiv of β-carotene degradation reached only 50%. This enabled us to study the effect of radicals on the physical quenching of lycopene in detail. The absolute degradation rates were calculated by comparison of the measured concentrations

DOI: 10.1021/acs.jafc.5b00377
J. Agric. Food Chem. 2015, 63, 3279−3287

to the initial starting carotenoid concentration during this study.

Figure 5A shows for single β-carotene reaction mixtures that increasing concentrations of ABTS radicals and hydrogen peroxide led to a strong degradation of (*all-E*)-β-carotene (from 95.4% to 70.8%) paralleled by considerable increases of (9*Z*)- (from 0.6% to 5.1%) and (13*Z*)-β-carotene (from 3.0% to 22.3%) by a factor of almost 10. (15*Z*)-β-Carotene concentration increased from 0.4% to 1.6%. The isomerization progress was immediately induced at low radical concentrations (★ at about 0.5 nmol of hydrogen peroxide per nmol of carotenoid). At high concentrations at about 6.0 nmol of hydrogen peroxide per nmol of carotenoid almost equilibrium states were reached for (*all-E*), (13*Z*), and (15*Z*), while (9*Z*) still increased in a linear fashion. A similar formation progress was described by Jeevarajan et al. and Gao et al., who both identified carotenoid radical cations and dications as precursors for the isomerization during radical quenching reactions.[41,42] In mixed lycopene/β-carotene incubations, the isomerization pattern of β-carotene changed significantly. Almost no degradation of (*all-E*)-β-carotene was observed as long as lycopene was still present at adequate concentrations, suppressing the isomerization of β-carotene at low hydrogen peroxide concentrations. Specifically, a mixed carotenoid solution with an initial lycopene content of 20% showed constant (*all-E*) levels up to concentrations of 1.7 nmol of hydrogen peroxide per nmol of carotenoid (Figure 5B). After that point (★) the strong isomerization coincided with the complete consumption of lycopene (see Figure 4 (○)), i.e., 79% of total lycopene was consumed at 2.5 nmol of hydrogen peroxide per nmol of carotenoid. From this point β-carotene (*Z*)-isomers quickly increased, comparable to the single incubations. A higher percentage of lycopene (67%, Figure 5C) moved the point of induction to even higher concentrations of hydrogen peroxide per carotenoid. In this system, 87% lycopene was degraded at concentrations of 5.8 nmol of hydrogen peroxide per nmol of carotenoid (Figure 4 (●)). This means that, only after complete oxidative breakdown of lycopene and thereby the loss of its high antioxidative quenching capacity, β-carotene (*Z*)-isomers are formed in significant amounts.

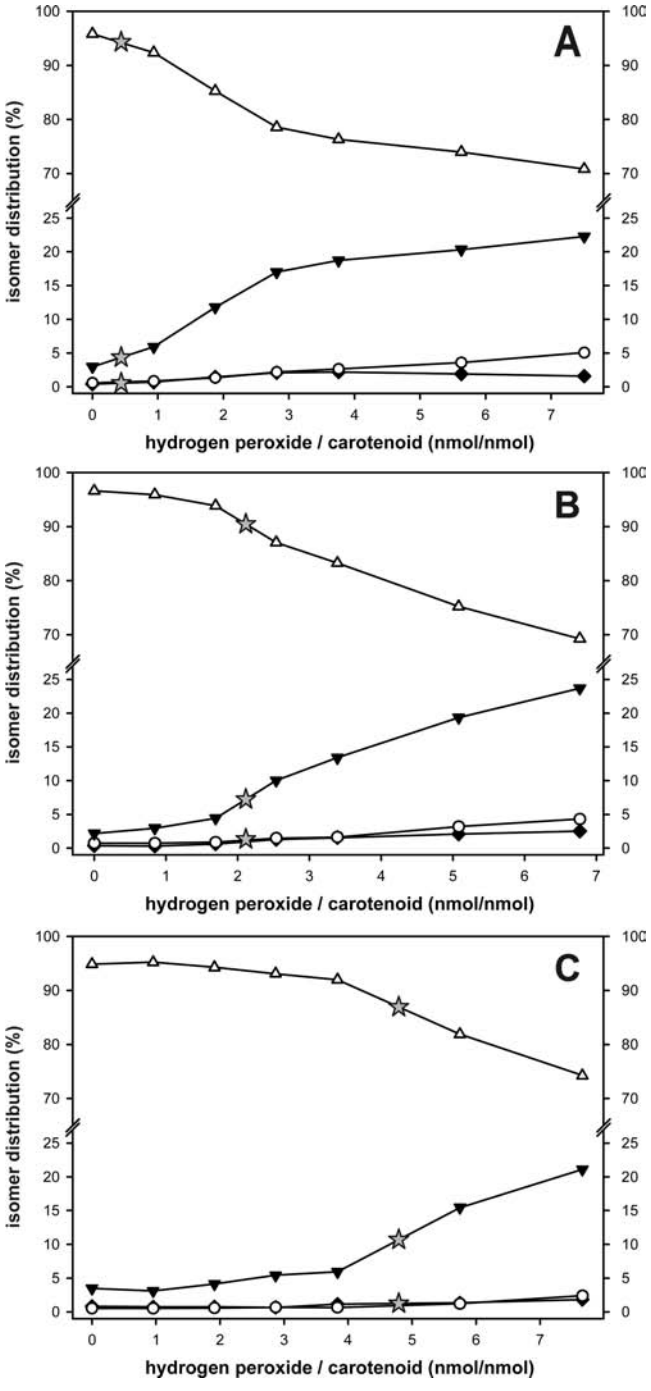

Figure 5. Isomerization progress during incubation of pure β-carotene (A) and in the presence of lycopene (B, 20%; C, 67%) with ATBS radicals and hydrogen peroxide. Gray stars indicate first observed significant changes in the isomeric pattern. (15*Z*)-β-Carotene (◆), (13*Z*)-β-carotene (▼), (*all-E*)-β-carotene (Δ), (9*Z*)-β-carotene (○).

The isomeric composition of β-carotene and lycopene in vivo is extensively discussed in the literature, because of the strong discrepancy in the (*Z*)-isomer concentrations. For a long time, the high content of (*Z*)-lycopene was related to a supposedly increased solubility and thus bioavailabilty of these compounds.[30,43] However, later studies disproved these results[44,45] and proposed isomerization processes during digestion to be the most plausible explanation for the differences in the isomeric pattern in vivo.[14] Indeed, under gastric pH the isomerization of lycopene was triggered to a much higher extent compared to the relatively stable β-carotene.[13] Furthermore, the supplementation of almost exclusively (*all-E*)-lycopene resulted in a strong increase of the (9*Z*)-lycopene plasma levels, which substantiated in vivo isomerization processes.[46] Moreover, thermal effects during digestion are suggested to explain the determined isomeric composition in vivo, too.[47] Various model systems showed that lycopene is more susceptible to thermal energy than β-carotene.[47] Additionally, the crystalline structure of the carotenoids in the food matrices was reported to have an enormous impact on the bioavailability and therefore on the isomerization in the gastric milieu, too. For example, lycopene is embedded in crystalline form in the chromoplasts of tomatoes, which effectively protects the configuration from external influences such as acids or thermal energy.[47,48] On the contrary, the liquid crystals in mango or papaya were shown to be transferred into the gastric micelles much more easily thus allowing an accelerated isomerization with respect to their thermodynamic characteristics.[34,49,50] On the other hand, (*all-E*)-lycopene was suggested to aggregate in the intestine to form crystals. This notion would lead to a reduced bioavailability and consequently

DOI: 10.1021/acs.jafc.5b00377
J. Agric. Food Chem. 2015, 63, 3279−3287

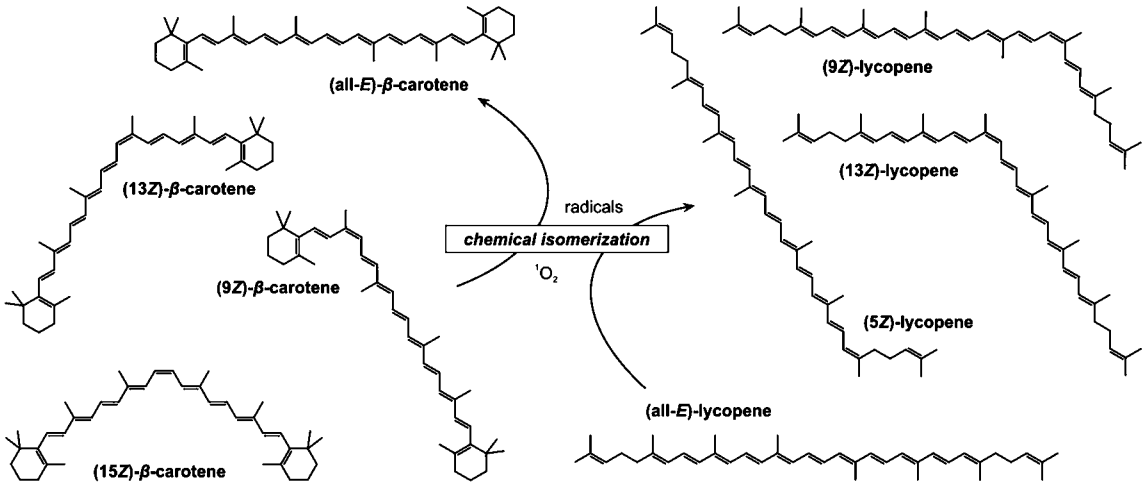

Figure 6. Lycopene effectively reduces or even inhibits the singlet oxygen or free radical induced isomerization of β-carotene.

to an accumulation of (Z)-isomers (with an assumed better solubility) in the human blood.[51]

Nevertheless, all known hypotheses are not able to explain the variable ratio of (Z)-lycopenes in various human organs and tissues, e.g., while about 80% of total lycopene was determined as (Z)-isomers in tissues of the lymph or prostata, only between 30 and 50% was isomerized in samples from the lung or serum.[31,43,52]

The present results strongly underpin the excellent quenching abilities of lycopene to explain these observations. All experiments clearly demonstrated that lycopene was able to reduce (singlet oxygen) or even to inhibit (radicals) the formation of (Z)-β-carotene isomers. It must be concluded that these findings are also true for in vivo systems. Here, oxidative stress in the form of singlet oxygen and radicals triggers the isomerization of carotenoids, as proposed earlier in the literature.[31,52] Lycopene acts as the effective quenching shield to protect other carotenoids against oxidative stress, i.e., β-carotene is preserved in its biologically active (all-E)-configuration, as illustrated in Figure 6.[4] During this process, lycopene gets highly isomerized and degraded. This rationale is also confirmed by studies of Stahl et al., who determined increased (9Z)-lycopene serum levels after consumption of processed tomato juice that contained only traces of this isomer.[31] Thus, the bioavailability theory to explain the different isomerization extent of specific carotenoids might be of minor relevance, if not of no relevance, to in vivo systems. In contrast, our lycopene protective theory is also capable of understanding the deviating (Z)-lycopene isomer concentrations found in specific human tissues, as different metabolic activities also entail different levels of oxidative stress.

In summary, our studies confirmed the outstanding quenching capabilities of lycopene in the reaction with radicals and activated oxygen species. This characteristic protects other carotenoids as β-carotene from degradation and isomerization, and explains the isomeric carotenoid patterns found in foods, but also in vivo.

■ ASSOCIATED CONTENT

Supporting Information

Analytical and spectroscopic data of carotenoid isomer references. This material is available free of charge via the Internet at http://pubs.acs.org.

■ AUTHOR INFORMATION

Corresponding Author

*E-mail marcus.glomb@chemie.uni-halle.de. Fax ++049-345-5527341.

Notes

The authors declare no competing financial interest.

■ ACKNOWLEDGMENTS

We thank the team of Prof. Dr. M. Girndt from the department of internal medicine II, Martin-Luther-University Halle-Wittenberg, Germany, for obtaining the human plasma samples.

■ REFERENCES

(1) Edge, R.; McGarvey, D. J.; Truscott, T. G. The carotenoids as anti-oxidants — a review. *J. Photochem. Photobiol., B* **1997**, *41*, 189−200.

(2) Di Mascio, P.; Kaiser, S.; Sies, H. Lycopene as the most efficient biological carotenoid singlet oxygen quencher. *Arch. Biochem. Biophys.* **1989**, *274*, 532−538.

(3) Conn, P. F.; Schalch, W.; Truscott, T. The singlet oxygen and carotenoid interaction. *J. Photochem. Photobiol., B* **1991**, *11*, 41−47.

(4) Namitha, K. K.; Negi, P. S. Chemistry and Biotechnology of Carotenoids. *Crit. Rev. Food Sci. Nutr.* **2010**, *50*, 728−760.

(5) Voutilainen, S.; Nurmi, T.; Mursu, J.; Rissanen, T. H. Carotenoids and cardiovascular health. *Am. J. Clin. Nutr.* **2006**, *83*, 1265−1271.

(6) Ramel, F.; Birtic, S.; Cuine, S.; Triantaphylides, C.; Ravanat, J.-L.; Havaux, M. Chemical Quenching of Singlet Oxygen by Carotenoids in Plants. *Plant Physiol.* **2012**, *158*, 1267−1278.

(7) Stahl, W.; Sies, H. Physical quenching of singlet oxygen and cis-trans isomerization of carotenoids. *Ann. N.Y. Acad. Sci.* **1993**, *691*, 10−19.

(8) Foote, C. S.; Chang, Y. C.; Denny, R. W. Chemistry of singlet oxygen. XI. Cis-trans isomerization of carotenoids by single oxygen and a probable quenching mechanism. *J. Am. Chem. Soc.* **1970**, *92*, 5218−5219.

(9) Fiedor, J.; Fiedor, L.; Haeßner, R.; Scheer, H. Cyclic endoperoxides of β-carotene, potential pro-oxidants, as products of chemical quenching of singlet oxygen. *Biochim. Biophys. Acta, Bioenerg.* **2005**, *1709*, 1−4.

(10) Palozza, P.; Krinsky, N. I. β-Carotene and α-tocopherol are synergistic antioxidants. *Arch. Biochem. Biophys.* **1992**, *297*, 184−187.

(11) Schierle, J.; Bretzel, W.; Buhler, I.; Faccin, N.; Hess, D.; Steiner, K.; Schuep, W. Content and isomeric ratio of lycopene in food and human blood plasma. *Food Chem.* **1997**, *59*, 459−465.

DOI: 10.1021/acs.jafc.5b00377
J. Agric. Food Chem. 2015, 63, 3279−3287

(12) Honest, K. N.; Zhang, H. W.; Zhang, L. F. Lycopene: Isomerization Effects on Bioavailability and Bioactivity Properties. *Food Rev. Int.* **2011**, *27*, 248−258.
(13) Re, R.; Fraser, P. D.; Long, M.; Bramley, P. M.; Rice-Evans, C. Isomerization of Lycopene in the Gastric Milieu. *Biochem. Biophys. Res. Commun.* **2001**, *281*, 576−581.
(14) Holloway, D. E.; Yang, M.; Paganga, G.; Rice-Evans, C. A.; Bramley, P. M. Isomerization of dietary lycopene during assimilation and transport in plasma. *Free Radical Res.* **2000**, *32*, 93−102.
(15) Hengartner, U.; Bernhard, K.; Meyer, K.; Englert, G.; Glinz, E. Synthesis, isolation, and NMR-spectroscopic characterization of fourteen (Z)-isomers of lycopene and of some acetylenic didehydro- and tetradehydrolycopenes. *Helv. Chim. Acta* **1992**, *75*, 1848−1865.
(16) Heymann, T.; Raeke, J.; Glomb, M. A. Photoinduced isomerization of lycopene and application to tomato cultivation. *J. Agric. Food Chem.* **2013**, *61*, 11133−11139.
(17) Heymann, T.; Westphal, L.; Wessjohann, L.; Glomb, M. A. Growing and Processing Conditions Lead to Changes in the Carotenoid Profile of Spinach. *J. Agric. Food Chem.* **2014**, *62*, 4960−4967.
(18) Frederico, D.; Donate, P. M.; Constantino, M. G.; Bronze, E. S.; Sairre, M. I. A Short and Efficient Synthesis of Crocetin-dimethyl ester and Crocetindial. *J. Org. Chem.* **2003**, *68*, 9126−9128.
(19) Wasserman, H. H.; Larsen, D. L. Formation of 1,4-Endoperoxides from Dye-Sensitized Photooxygenation of Alkyl-Naphthalenes. *J. Chem. Soc., Chem. Commun.* **1972**, 253−254.
(20) Ozyürek, M.; Bektaşoğlu, B.; Güçlü, K.; Güngör, N.; Apak, R. Simultaneous total antioxidant capacity assay of lipophilic and hydrophilic antioxidants in the same acetone-water solution containing 2% methyl-beta-cyclodextrin using the cupric reducing antioxidant capacity (CUPRAC) method. *Anal. Chim. Acta* **2008**, *630*, 28−39.
(21) Lee, M. T.; Chen, B. H. Separation of lycopene and its cis isomers by liquid chromatography. *Chromatographia* **2001**, *54*, 613−617.
(22) Vecchi, M.; Englert, G.; Maurer, R.; Meduna, V. Separation and Characterization of the Cis-Isomers of Beta, Beta-Carotene. *Helv. Chim. Acta* **1981**, *64*, 2746−2758.
(23) Kuti, J. O.; Konuru, H. B. Effects of genotype and cultivation environment on lycopene content in red-ripe tomatoes. *J. Sci. Food Agric.* **2005**, *85*, 2021−2026.
(24) O'Neill, M. E.; Carroll, Y.; Corridan, B.; Olmedilla, B.; Granado, F.; Blanco, I.; van den Berg, H.; Hininger, I.; Rousell, A. M.; Chopra, M.; Southon, S.; Thurnham, D. I. A European carotenoid database to assess carotenoid intakes and its use in a five-country comparative study. *Br. J. Nutr.* **2001**, *85*, 499−507.
(25) Singh, P.; Goyal, G. K. Dietary lycopene: its properties and anticarcinogenic effects. *Compr. Rev. Food Sci. Food Saf.* **2008**, *7*, 255−270.
(26) Colle, I.; Lemmens, L.; van Buggenhout, S.; van Loey, A.; Hendrickx, M. Effect of Thermal Processing on the Degradation, Isomerization, and Bioaccessibility of Lycopene in Tomato Pulp. *J. Food Sci.* **2010**, *75*, 753−759.
(27) Knockaert, G.; Pulissery, S. K.; Colle, I.; van Buggenhout, S.; Hendrickx, M.; van Loey, A. Lycopene degradation, isomerization and in vitro bioaccessibility in high pressure homogenized tomato puree containing oil: Effect of additional thermal and high pressure processing. *Food Chem.* **2012**, *135*, 1290−1297.
(28) Watanabe, K.; Kon, M.; Takahashi, B.; Hirota, S. Cis-trans isomers of β-carotene in fresh vegetables and fruits. *Food Sci. Technol. Res.* **1999**, *5*, 308−310.
(29) O'Neil, C. A.; Schwartz, S. J. Photoisomerization of.beta.-Carotene by Photosensitization with Chlorophyll Derivatives as Sensitizers. *J. Agric. Food Chem.* **1995**, *43*, 631−635.
(30) Boileau, T. W.; Boileau, A. C.; Erdman, J. W. Bioavailability of all-trans and cis-isomers of lycopene. *Exp. Biol. Med.* **2002**, *227*, 914−919.
(31) Stahl, W.; Schwarz, W.; Sundquist, A. R.; Sies, H. Cis Trans Isomers of Lycopene and Beta-Carotene in Human Serum and Tissues. *Arch. Biochem. Biophys.* **1992**, *294*, 173−177.
(32) Sies, H.; Stahl, W. Vitamins E and C, beta-carotene, and other carotenoids as antioxidants. *Am. J. Clin. Nutr.* **1995**, *62*, 1315−1321.
(33) Kuki, M.; Koyama, Y.; Nagae, H. Triplet-sensitized and thermal isomerization of all-trans, 7-cis, 9-cis, 13-cis and 15-cis isomers of beta -carotene: configurational dependence of the quantum yield of isomerization via the T1 state. *J. Phys. Chem.* **1991**, *95*, 7171−7180.
(34) Chasse, G. A.; Mak, M. L.; Deretey, E.; Farkas, I.; Torday, L. L.; Papp, J. G.; Sarma, D. S. R.; Agarwal, A.; Chakravarthi, S.; Agarwal, S.; Rao, A. V. An ab initio computational study on selected lycopene isomers. *J. Mol. Struct.: THEOCHEM* **2001**, *571*, 27−37.
(35) Guo, W. H.; Tu, C. Y.; Hu, C. H. Cis-Trans Isomerizations of beta -Carotene and Lycopene: A Theoretical Study. *J. Phys. Chem. B* **2008**, *112*, 12158−12167.
(36) Knockaert, G.; Pulissery, S. K.; Lemmens, L.; van Buggenhout, S.; Hendrickx, M.; van Loey, A. Carrot β-Carotene Degradation and Isomerization Kinetics during Thermal Processing in the Presence of Oil. *J. Agric. Food Chem.* **2012**, *60*, 10312−10319.
(37) Manitto, P.; Speranza, G.; Monti, D.; Gramatica, P. Singlet oxygen reactions in aqueous solution. Physical and chemical quenching rate constants of crocin and related carotenoids. *Tetrahedron Lett.* **1987**, *28*, 4221−4224.
(38) Schmidt, R. Photosensitized Generation of Singlet Oxygen. *Photochem. Photobiol.* **2006**, *82*, 1161.
(39) Kanofsky, J. R. Measurement of Singlet-Oxygen In Vivo: Progress and Pitfalls. *Photochem. Photobiol.* **2011**, *87*, 14−17.
(40) Böhm, F.; Edge, R.; Truscott, G. Interactions of dietary carotenoids with activated (singlet) oxygen and free radicals: potential effects for human health. *Mol. Nutr. Food Res.* **2012**, *56*, 205−216.
(41) Gao, G.; Wei, C. C.; Jeevarajan, A. S.; Kispert, L. D. Geometrical Isomerization of Carotenoids Mediated by Cation Radical/Dication Formation. *J. Phys. Chem.* **1996**, *100*, 5362−5366.
(42) Jeevarajan, A. S.; Wei, C.-C.; Kispert, L. D. Geometrical isomerization of carotenoids in dichloromethane. *J. Chem. Soc., Perkin Trans. 2* **1994**, 861−869.
(43) Boileau, A. C.; Merchen, N. R.; Wasson, K.; Atkinson, C. A.; Erdman, J. W., Jr. cis-Lycopene is more bioavailable than trans-lycopene in vitro and in vivo in lymph-cannulated ferrets. *J. Nutr.* **1999**, *129*, 1176−1181.
(44) Sicilia, T.; Bub, A.; Rechkemmer, G.; Kraemer, K.; Hoppe, P. P.; Kulling, S. E. Novel lycopene metabolites are detectable in Plasma of preruminant calves after lycopene supplementation. *J. Nutr.* **2005**, *135*, 2616−2621.
(45) Unlu, N. Z.; Bohn, T.; Francis, D. M.; Nagaraja, H. N.; Clinton, S. K.; Schwartz, S. J. Lycopene from heat-induced cis-isomer-rich tomato sauce is more bioavailable than from all-trans-rich tomato sauce in human subjects. *Br. J. Nutr.* **2007**, *98*, 140−146.
(46) Stahl, W.; Sies, H. Uptake of lycopene and its geometrical isomers is greater from heat-processed than from unprocessed tomato juice in humans. *J. Nutr.* **1992**, *122*, 2161−2166.
(47) Zechmeister, L. Cis-trans Isomerization and Stereochemistry of Carotenoids and Diphenyl-polyenes. *Chem. Rev.* **1944**, *34*, 267−344.
(48) Harris, W. M.; Spurr, A. R. Chromoplasts of Tomato Fruits. I. Ultrastructure of Low-Pigment and High- Beta Mutants. *Am. J. Bot.* **1969**, *56*, 369.
(49) Schweiggert, R. M.; Mezger, D.; Schimpf, F.; Steingass, C. B.; Carle, R. Influence of chromoplast morphology on carotenoid bioaccessibility of carrot, mango, papaya, and tomato. *Food Chem.* **2012**, *135*, 2736−2742.
(50) Takehara, M.; Nishimura, M.; Kuwa, T.; Inoue, Y.; Kitamura, C.; Kumagai, T.; Honda, M. Characterization and Thermal Isomerization of (all-E)-Lycopene. *J. Agric. Food Chem.* **2014**, *62*, 264−269.
(51) Britton, G. Structure and properties of carotenoids in relation to function. *FASEB J.* **1995**, *9*, 1551−1558.
(52) Clinton, S. K.; Emenhiser, C.; Schwartz, S. J.; Bostwick, D. G.; Williams, A. W.; Moore, B. J.; Erdman, J. W., Jr. cis-trans Lycopene isomers, carotenoids, and retinol in the human prostate. *Cancer Epidemiol., Biomarkers Prev.* **1996**, *5*, 823−833.

DOI: 10.1021/acs.jafc.5b00377
J. Agric. Food Chem. 2015, 63, 3279−3287

DOPC reverse micelles improved the activity of α-tocopherol or trolox, a water-soluble analogue of α-tocopherol, at low concentrations (10 μM) but decreased their activity at higher concentrations (100 μM). Because lecithin is a mixture of different types of individual phospholipids, the objective of this study was to examine the impact of DOPC and DOPE both individually and in combination on the antioxidant activity of α-tocopherol or trolox. The experiments were conducted at PC and PE concentrations above and below their critical micelle concentrations to determine the impact of reverse micelles on the antioxidant activity of α-tocopherol and trolox. In addition to the investigation of the influence of association colloids formed by phospholipid, α-tocopherol regeneration by different types of phospholipids was also examined.

MATERIALS AND METHODS

Materials. Soybean oil was purchased from a local store and stored at −20 °C. Medium-chain triacylglycerols (MCT) were purchased from Sasol North America Inc. (Houston, TX, USA). 1,2-Dioleoyl-*sn*-glycero-3-phosphocholine (DOPC), 1,2-dioleoyl-*sn*-glycero-3-phosphocholine (DOPE), and 1,2-dioleoyl-*sn*-glycero-3-phosphoethanolamine-*N*-(7-nitro-2-1,3-benzoxadiazol-4-yl) (ammonium salt) (NBD-PE) were purchased from Avanti Polar Lipids, Inc. (Alabaster, AL, USA). Silicic acid, activated charcoal, α-tocopherol, α-tocopherol quinone, and trolox were purchased from Sigma-Aldrich Co. (St. Louis, MO, USA). All other reagents were of HPLC grade or purer. Distilled and deionized water was used in all experiments.

Preparation of Stripped Soybean Oil. To avoid the influence of the minor compounds such as tocopherols, phospholipids, free fatty acids, and mono- and diacylglycerols, which are originally in the commercial oil, stripped soybean oil (SSO) was prepared as described by Cui et al.[18] Briefly, a chromatographic column (3.0 cm diameter, 35 cm long) was used to isolate soybean oil triacylglycerols. Three layers were packed into the column sequentially. The bottom layer was packed with 22.5 g of silicic acid (washed with distilled and deionized water and activated at 110 °C for 24 h). Activated charcoal (5.6 g) was then used for the middle layer and another 22.5 g of silicic acid for the top layer. Commercial soybean oil (30 g) was mixed with 30 mL of hexane and the mixture was passed through the column using 270 mL of hexane for elution. The solvent was then removed by a vacuum rotary evaporator (Rotavapor R 110, Buchi, Flawil, Switzerland) at 38 °C, and the remaining solvent was evaporated by nitrogen flushing. The removal of polar lipids was verified by a thin layer chromatography method according to the Association of Official Analytical Chemists (AOAC).[20] HPLC analysis also detected no tocopherols in SSO (method described below). The water content decreased from about 250 ppm to about 20 ppm as determined by Karl Fischer analysis using a 831 KF Coulometer (Metrohm, Riverview, FL, USA).[21] Unless noted, SSO mentioned in the following experiments was a mixture of 25% stripped soybean oil and 75% MCT.

Sample Preparation. The experiment was separated to five parts. Part 1 included the addition of 20 or 1000 μM DOPC or DOPE into SSO. Part 2 included the addition of 20 or 1000 μM DOPC or DOPE to SSO containing100 μM α-tocopherol or trolox. Part 3 included the addition of 1000 μM DOPC or DOPE to the commercial soybean oil. Part 4 included the addition of 1000 μM DOPC or DOPE to SSO containing 0.95 μM NBD-PE and 0−100 μM α-tocopherol or trolox. Part 5 included the addition of 800 μM DOPC, DOPE, or ethanolamine to MCT or SSO containing 800 μM α-tocopherol quinone. According to the different parts, appropriate amounts of antioxidants (α-tocopherol, α-tocopherol quinone, or trolox) were dissolved in ethanol and then pipetted into empty beakers followed by removal of solvent by nitrogen flushing. SSO was then added, and the sample was magnetically stirred overnight. According to different experimental parts, the appropriate amounts of NBD-PE, DOPC, and/or DOPE in chloroform, individually or at different ratios, were pipetted into empty beakers, and chloroform was removed by nitrogen flushing. SSO containing antioxidants was added and magnetically stirred at room temperature for 5 h for NBD-PE fluorescence study or overnight for lipid oxidation studies. For the lipid oxidation studies, 1 mL samples were aliquoted into 10 mL headspace vials, sealed with aluminum caps with PTFE/silicone septa, and stored in the dark at 55 °C.

Measurement of Lipid Oxidation. At various sampling times, lipid oxidation was determined by monitoring lipid hydroperoxides and headspace hexanal formation. Lipid hydroperoxides were measured as primary oxidation products according to the method of Shantha and Decker.[22] In short, 2.8 mL of a mixture of methanol/butanol (2:1, v/v) was added to oil samples of known weight. Then 15 μL of 3.94 M ammonium thiocyanate and 15 μL of 0.072 M Fe^{2+} (ferrous sulfate) were added, and the solution was vortexed. After a 20 min reaction time, the absorbance was measured at 510 nm using a Genesys 20 spectrophotometer (ThermoSpectronic, Waltham, MA, USA). The concentration of lipid hydroperoxides was calculated from a cumene hydroperoxide standard curve ranging from 0.7 to 17 mM. Samples with hydroperoxide concentrations >17 mM were diluted with methanol/butanol (2:1, v/v) before measurements.

Headspace hexanal was measured as a secondary lipid oxidation products using a GC-17A Shimadzu gas chromatograph equipped with an AOC-5000 autosampler (Shimadzu, Kyoto, Japan) as described by Chen et al.[17] In short, a 30 m × 0.32 mm Equity DB-1 column with a 1 μm film thickness was used for separations. Oil samples (1 mL) in 10 mL headspace vials were heated at 55 °C for 8 min in the autosampler heating block. A 50/30 μm DVB/Carboxen/PDMS solid-phase microextraction (SPME) fiber needle was injected into the sample vial for 2 min to adsorb volatiles, and then the fiber was placed into the 250 °C injector port for 3 min at a split ratio of 1:5. The GC separations were 10 min at 65 °C for each sample. Helium was used as a carrier gas, with a total flow rate of 15.0 mL/min. A flame ionization detector at 250 °C was used to detect hexanal, and concentrations were determined from peak areas using a standard curve made from SSO containing known hexanal concentrations from 2 to 800 μM.

Fluorescence Measurement of SSO Containing Reverse Micelles and Antioxidants. The concentration of NBD-PE in SSO was varied to get appropriate fluorescence intensity with minimal self-quenching, and the optimal concentration of the probe was found to be 0.95 μM. The measurements were carried out as described by Kittipongpittaya et al.[23] Basically, the sample was transferred to a triangular Suprasil quartz cuvette (Sigma-Aldrich Co., St. Louis, MO, USA). The steady-state emission intensity of spectra, determined as the emission signal intensity (counts per second) measured by a photomultiplier, was recorded with a PTI spectrofluorometer (PTI, Ontario, Canada). The spectral bandwidths for both excitation and emission slits were set to 2 nm for excitation at 468 nm. The integration time was set to 1 s.

Determination of α-Tocopherol Concentration by HPLC. Oil samples (20−30 mg) were dissolved in 1 mL of isoproponal and 1 mL of methanol and then passed through a 0.2 μm filter (Fisher Scientific, Pittsburgh, PA, USA). Sample (20 μL) was then injected to a Shimadzu HPLC system equipped with a Beckman Ultrasphere C18 reversed phase column (150 mm × 4.6 mm, 5 μm). The mobile phase was isocratic methanol at a flow rate of 1 mL/min. A Waters 474 scanning fluorescent detector (Waters, Milford, MA, USA) was used to detect α-tocopherol at an excitation wavelength of 290 nm and an emission wavelength of 330 nm. Peak integration was performed using Shimadzu EZstart software (version 7.2). α-Tocopherol in the samples was identified and quantified by comparing their relative retention times and peak areas with those of authentic compounds.

Cyclic Voltammetry Measurements. Cyclic voltammetry measurements were performed according to the method described by Wilson and co-workers.[24] Briefly, a BASi model C-3 cell stand with a planar 1 mm diameter glassy carbon working electrode, a Ag/AgCl reference electrode, and a Pt wire auxiliary electrode was used. Tetrabutylammonium hexafluorophosphate (Bu_4NPF_6; 0.5 M) in dichloromethane was used as a salt bridge. DOPC, DOPE, and α-tocopherol (1 mM) were freshly dissolved in dichloromethane before measurements.

DOI: 10.1021/acs.jafc.5b00243
J. Agric. Food Chem. 2015, 63, 3288−3294

Statistical Analysis. All experiments used triplicate samples (three samples taken at each time point), and each experiment was repeated at least two times. Data were presented as the mean value ± standard deviation. Data results were analyzed by analysis of variance (ANOVA) using SPSS 17.0 (SPSS Inc., Chicago, IL, USA). The differences between mean values were compared using Duncan's multiple-range test with a significance level of $p < 0.05$.

RESULTS AND DISCUSSION

Impact of DOPC and DOPE on SSO Oxidation. There are two reasons for choosing 20 and 1000 μM DOPE in the first experiment. First, 20 and 1000 μM represent concentrations below and above the critical micelle concentration (CMC) for DOPE because the CMC for DOPE is 200 μM.[18] Second, these concentrations are within the range of what is found in refined commercial oils. In this experiment, we found that at 55 °C, DOPE had the same lag phase (4 days) as the stripped soybean oil control when its concentration (20 μM) was below its CMC (200 μM). On the other hand, when DOPE concentration (1000 μM) was above its CMC (200 μM), it had pro-oxidant activity with a lag phase of 2 days.

When 20 μM DOPC was added to the SSO at the same concentration as DOPE, the lag phase was also similar to the control. DOPC above its CMC (1000 μM) was pro-oxidative, which agrees with previous results.[17] Samples containing 1000 μM DOPE showed slower rates of lipid hydroperoxides and hexanal formation than DOPC, but both had the same lag phase. Lag phase is the most important indicator of oil quality because after the lag phase, the oil is rancid. This indicates that both DOPE and DOPC are pro-oxidative at concentrations above their CMCs, at which they form association colloids. This pro-oxidative activity of phospholipids caused by the formation of reverse micelles during storage at 55 °C agrees with our previous results using SSO stored at 37 and 45 °C.[17,18]

Impact of DOPC and DOPE on the Oxidation of SSO Containing α-Tocopherol or Trolox. There has been a lot of research done on the impact of phospholipids on bulk oil oxidation. However, no agreement has been made on their roles as studies report both antioxidative and pro-oxidative activity.[6,8,9,25] Our previous results showed that when DOPE is above its CMC, it is pro-oxidative, whereas DOPE below its CMC does not affect oxidation rates. However, those results were based on a SSO system, which was almost pure triacylglycerols. Here, we used a system consisting of SSO and 100 μM α-tocopherol or trolox, which enabled us to investigate on how DOPC and DOPE reverse micelles affect the ability of antioxidants to alter lipid oxidation in bulk oil.

In the case of α-tocopherol (Figure 2), the lag phases of hydroperoxides and hexanal formation in the presence and absence of 20 μM DOPC were 17 and 21 days, respectively. It was somewhat unexpected that 20 μM DOPC decreased the activity of α-tocopherol because 20 μM DOPC had no impact on lipid oxidation rates by itself (Figure 1A, 1B). A potential reason that 20 μM DOPC could be pro-oxidative is that this concentration was very close to the CMC of DOPC and addition of α-tocopherol could cause the formation of some pro-oxidative reverse micelles. In the presence of 1000 μM DOPC, where large amounts of reverse micelles were present, the hydroperoxides and hexanal formation lag phase reduced from 21 days (α-tocopherol only) to 12 days. DOPC reverse micelles themselves had pro-oxidant activity (Figure 1), which would be expected to diminish the antioxidant activity of α-tocopherol. In addition, it is worth noting that compared to

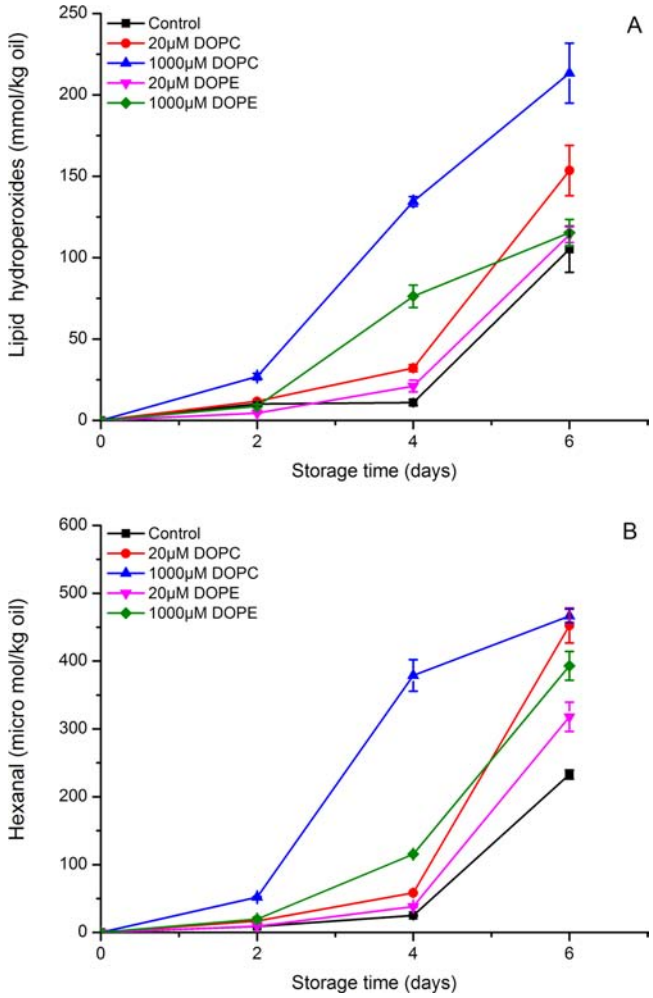

Figure 1. Formation of lipid hydroperoxides (A) and headspace hexanal (B) of SSO with 20 or 1000 μM DOPC or DOPE concentrations at 55 °C. Data points represent means (n = 3) ± standard deviations.

SSO alone, which had a lag phase of 4 days (Figure 1), the combination of 1000 μM DOPC and α-tocopherol still had a longer lag phase (12 days) and thus a net antioxidant effect.

As for DOPE, the activity of α-tocopherol was increased at DOPE concentrations both below (20 μM) and above (1000 μM) its CMC with antioxidant activity increasing with increasing DOPE concentrations as determined by both lipid hydroperoxides and headspace hexanal. This suggested that the ability of DOPE to increase the activity of α-tocopherol was independent from the presence of reverse micelles. The synergy seen between PE and α-tocopherol has been reported earlier,[8,9] but no clear mechanism was presented.

In the case of trolox (Figure 3), the lag phases of both hydroperoxides and hexanal formation in the presence and absence of 20 μM DOPC were the same, being 60 days. In the presence of reverse micelles formed by 1000 μM DOPC, the lag phase reduced from 60 days (trolox only) to 28 days for hydroperoxide formation and to 31 days for hexanal formation. This was as expected because of the pro-oxidative activity of DOPC reverse micelles. As for DOPE, the activity of trolox was increased at DOPE concentrations both below (20 μM) and above (1000 μM) the CMC with antioxidant activity increasing with increasing DOPE concentrations as determined by both lipid hydroperoxides and headspace hexanal. This again

DOI: 10.1021/acs.jafc.5b00243
J. Agric. Food Chem. 2015, 63, 3288−3294

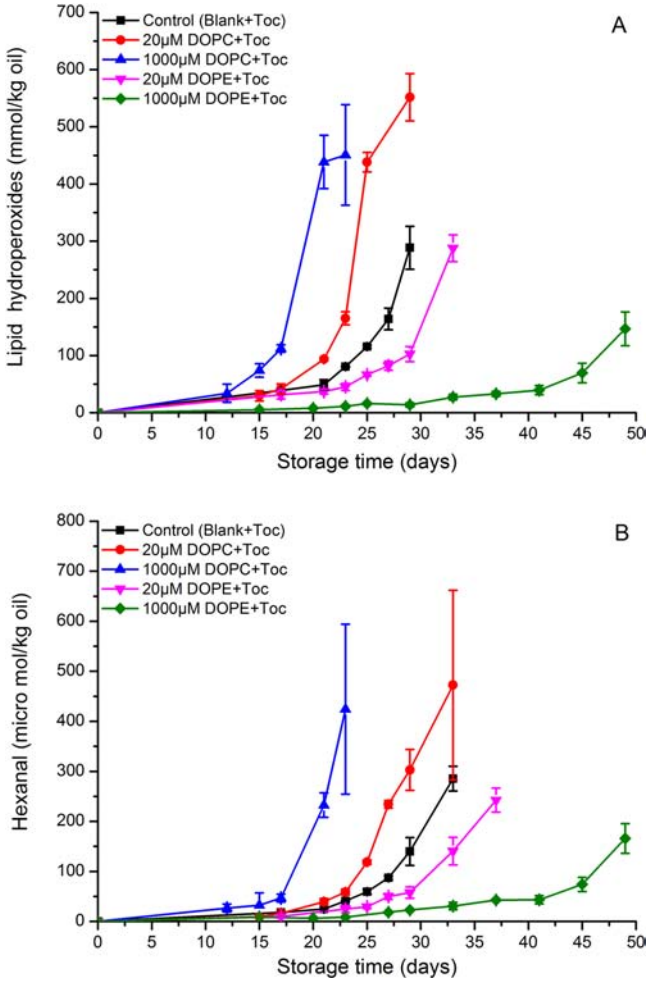

Figure 2. Formation of lipid hydroperoxides (A) and headspace hexanal (B) of SSO containing 100 μM α-tocopherol with addition of 20 or 1000 μM DOPC or DOPE at 55 °C. Data points represent means (n = 3) ± standard deviations.

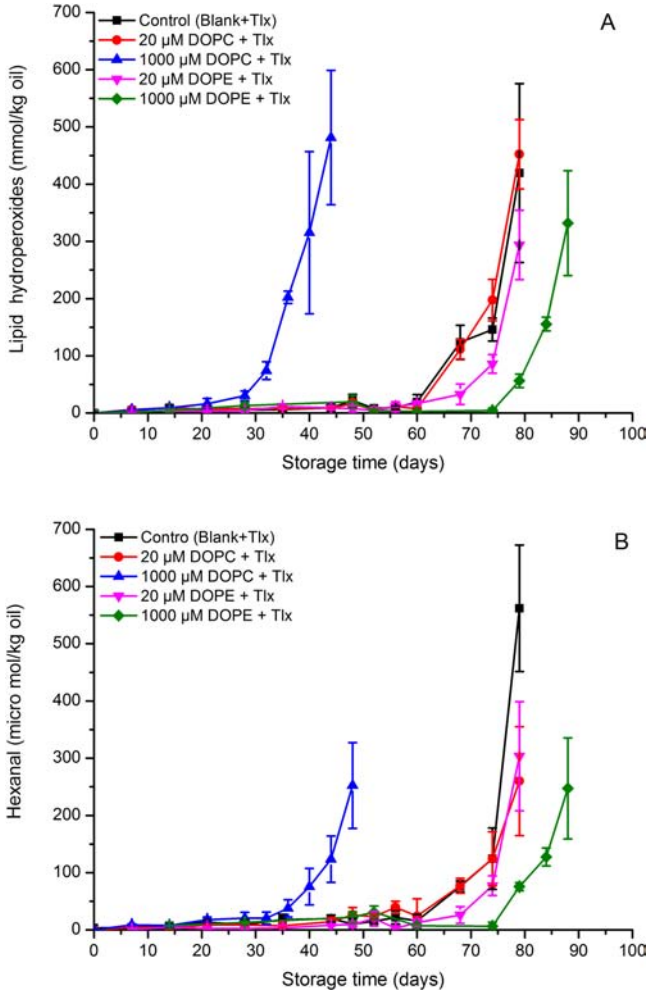

Figure 3. Formation of lipid hydroperoxides (A) and headspace hexanal (B) of SSO containing 100 μM trolox with addition of 20 or 1000 μM DOPC or DOPE at 55 °C. Data points represent means (n = 3) ± standard deviations.

suggested that DOPE was increasing the activity of trolox regardless of the presence of reverse micelles. In addition, the lag phases of all treatments with trolox were longer than those with α-tocopherol, which agreed with the antioxidant polar paradox theory.[26]

Impact of DOPC and DOPE Combinations on the Oxidation of SSO Containing α-Tocopherol. Previously, we reported that the combination of DOPC and DOPE at concentrations above their CMC could form mixed reverse micelles and was pro-oxidative in SSO.[18] Because PE was found to increase the activity of α-tocopherol, a further investigation on the combinations of these two phospholipids was carried out to see their overall impact on α-tocopherol. The lag phases of hexanal formation of different compositions of DOPC and DOPE above the CMC (1000 μM in total) with 100 μM α-tocopherol are shown in Figure 4. As the proportion of DOPE increased from 0 to 10, 30, 50, 60, and 100%, the corresponding lag phases increased from 17 to 21, 28, 28, 36, and 42 days, respectively. These different overall effects in hexanal lag phases with different DOPC/DOPE ratios were due to a combination of the pro-oxidative effect of the phospholipids reverse micelles and the ability of PE to increase the activity of α-tocopherol. This suggested that the addition of PE could improve the oxidative stability of refined soybean oil,

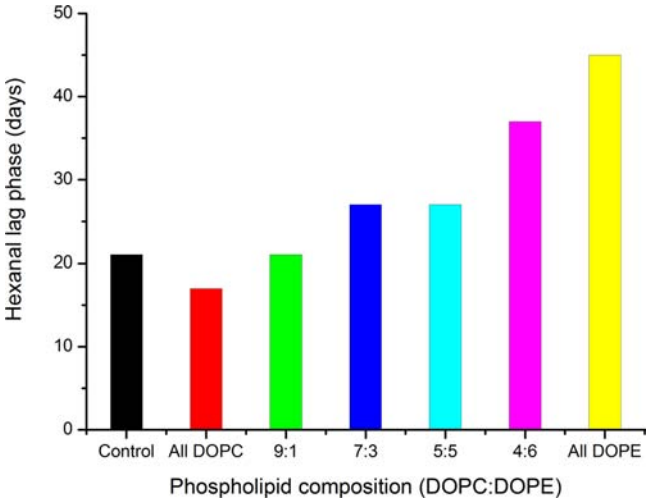

Figure 4. Headspace hexanal lag phases of SSO containing 100 μM α-tocopherol with addition of DOPC and DOPE at different ratios (1000 μM in total) at 55 °C.

which would naturally contain tocopherols. We tested this hypothesis with commercial soybean oil naturally containing

DOI: 10.1021/acs.jafc.5b00243
J. Agric. Food Chem. 2015, 63, 3288−3294

2000 μM (800 ppm) mixed tocopherols in which we added 1000 μM DOPC or DOPE (Figure 5). The control and the oil

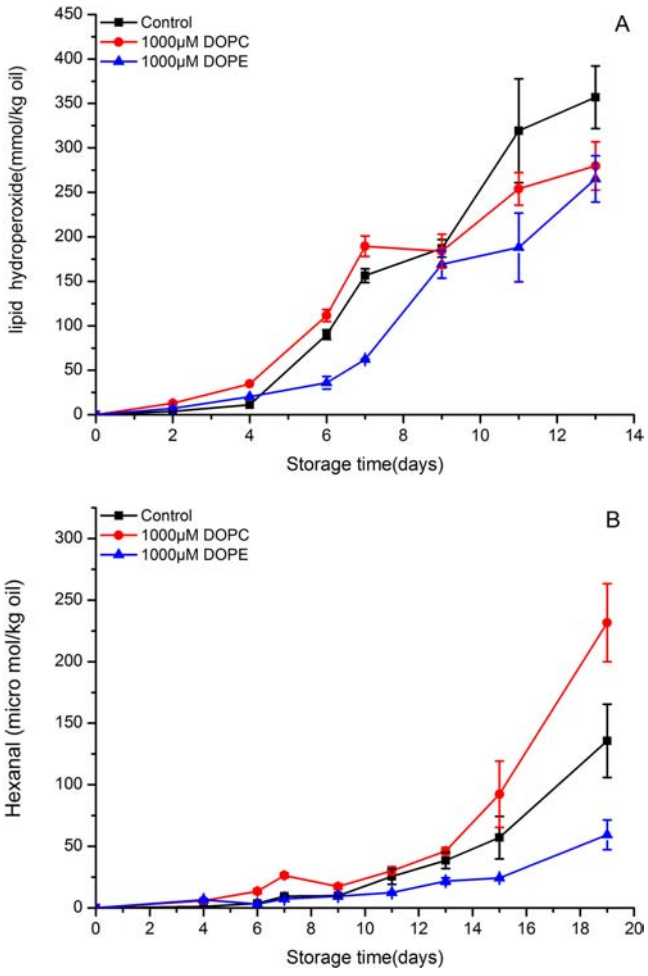

Figure 5. Formation of lipid hydroperoxides (A) and headspace hexanal (B) of commercial soybean oil with addition of 1000 μM DOPC or DOPE at 55 °C. Data points represent means (n = 3) ± standard deviations.

with the addition of DOPC had the same lipid hydroperoxides lag phase of 4 days and a hexanal lag phase of 9 days, whereas the oil with the addition of DOPE increased the lipid hydroperoxide lag phase to 6 days and the hexanal lag phase to 15 days.

Location of Antioxidants in the Presence of DOPE and DOPC Reverse Micelles. Physical locations of antioxidants in bulk oil can influence their antioxidant activities. NBD-PE was used to investigate whether or not DOPC and DOPE reverse micelles have an impact on antioxidant locations. NBD-PE is a surface-active phospholipid with a fluorophore group covalently attached to the headgroup of PE. This probe has been widely used in biological and model membranes as fluorescent analogues of native lipids, and the location of the probe in those models is believed to be at the interfacial region of the membrane.[27] In our experiments, 0.95 μM NBD-PE and 1000 μM DOPE or DOPC were added into bulk oil. With those concentrations, the ratio of fluorophore to surfactant was about 1:1000, which helped avoid probe aggregation and thus self-quenching effects.

When DOPC and DOPE reverse micelles were not present, the emission intensity of the probe decreased with increasing α-tocopherol concentration (data not shown), showing that α-tocopherol has the ability to quench the probe. On the other hand, when α-tocopherol is not present, the phospholipids alone (DOPC or DOPE) did not cause any changes of probe emission intensity (data not shown). In the presence of both DOPC and DOPE reverse micelles, increasing trolox concentration decreased the emission intensity of the NBD-PE probe (Figure 6), indicating that trolox was in close contact

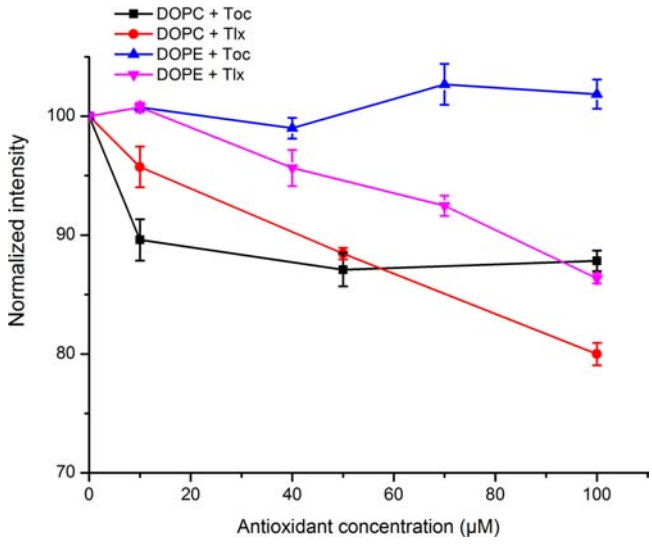

Figure 6. Normalized fluorescence intensity of NBD-PE in SSO with addition of 1000 μM DOPC or DOPE and different concentrations of α-tocopherol or trolox.

with the probe, thus quenching its fluorescence. However, the combination of DOPE reverse micelles and α-tocopherol did not cause a significant difference in NBD-PE emission intensity with increasing α-tocopherol concentrations. When the combination DOPC reverse micelles and α-tocopherol was present, the emission intensity of the probe decreased with the addition of α-tocopherol at first, but did not further decrease as α-tocopherol concentration increased from 10 to 100 μM. These results suggested that α-tocopherol did not accumulate in the DOPE reverse micelle but did accumulate in the DOPC reverse micelles. These data indicated that water-soluble trolox partitioned more readily into DOPE reverse micelles. Trolox also partitioned into DOPC reverse micelles, and at the concentration used in the antioxidant studies (100 μM), more trolox than α-tocopherol was in the reverse micelles. Because the micelle interface could be a major site of lipid oxidation reactions due to the presence of surface active hydroperoxides and water-soluble transition metals, the greater concentration of the antioxidant at the interface could explain why trolox was more effective than α-tocopherol. However, DOPE was found to increase the activity of α-tocopherol even though DOPE reverse micelles were not found to increase α-tocopherol concentrations at the micelle interface. This suggests that DOPE's ability to increase the activity of α-tocopherol was not due to changes in its physical location.

Effect of DOPE on α-Tocopherol Regeneration. Another potential mechanism by which DOPE could increase the activity of α-tocopherol would be through its ability to regenerate oxidized α-tocopherol back to its active, reduced

DOI: 10.1021/acs.jafc.5b00243
J. Agric. Food Chem. 2015, 63, 3288−3294

form. The hypothesis that phospholipids regenerate tocopherols was tested by monitoring the ability of DOPC, DOPE, and ethanolamine, the headgroup of PE, to react with α-tocopherol quinone, an oxidation product of α-tocopherol, in both MCT (Figure 7A) and SSO (Figure 7B) at 55 °C. In MCT (Figure 7A) where no lipid oxidation occurs, the treatments with DOPE and ethanolamine but not DOPC promoted the regeneration of α-tocopherol quinone to α-tocopherol, indicating that the ethanolamine headgroup of PE can reduce α-tocopherol quinone. In SSO (Figure 7B), only the treatment with DOPE and α-tocopherol quinone resulted in the formation of α-tocopherol. Also, the quantity of α-tocopherol regenerated by DOPE in SSO was smaller than that in MCT. This could be because in SSO, lipid oxidation was occurring, which could consume α-tocopherol once it was produced by DOPE and α-tocopherol quinone. This was confirmed by monitoring the hydroperoxide formation in SSO (Figure 7B, right *y* axis). DOPE with α-tocopherol quinone was still within the hydroperoxide lag phase after 8 days of storage, whereas all other treatments and the α-tocopherol quinone control had a lag phase of 2 or 4 days. This indicated that the newly produced α-tocopherol by DOPE and α-tocopherol quinone were being consumed to retard lipid oxidation in SSO, thus decreasing the accumulation of α-tocopherol compared to the nonoxidizing MCT.

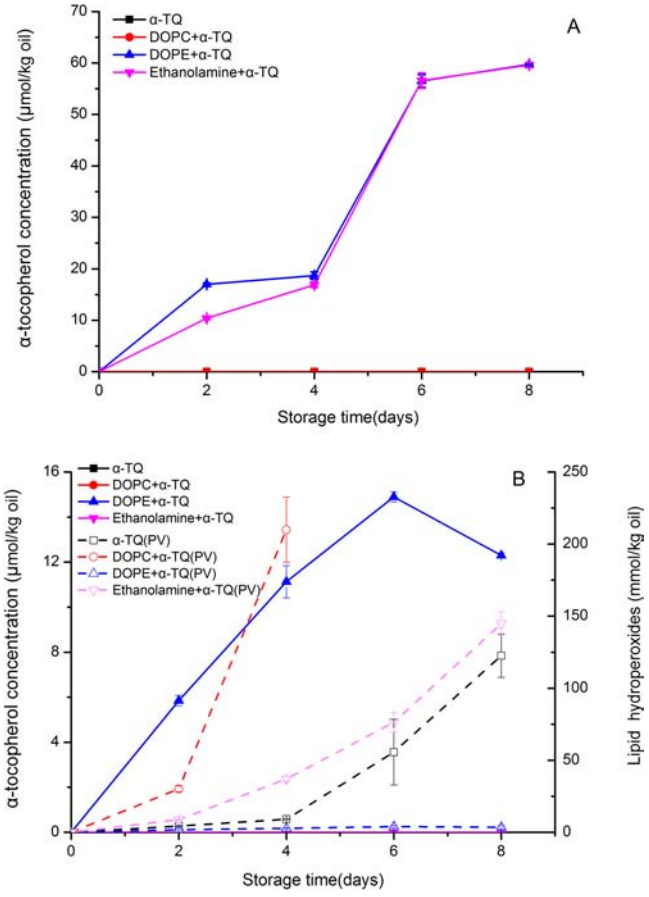

Figure 7. Formation of α-tocopherol (solid lines) by 800 μM DOPC, DOPE, or ethanolamine with 800 μM α-tocopherol quinone at 55 °C in MCT (A) and SSO (B); formation of lipid hydroperoxides (B, dashed lines) of SSO containing 800 μM DOPC, DOPE, or ethanolamine with 800 μM α-tocopherol quinone at 55 °C.

A potential mechanism by which DOPE could regenerate α-tocopherol quinone is by electron transfer. The potential for such an electron transfer reaction can be evaluated by measuring oxidation−reduction potentials via cyclic voltammetry.[28] Using this method, α-tocopherol exhibited an oxidation peak at about 600 mV, which was close to that reported in the literature.[29] However, there were no oxidation or reduction peaks detected for DOPC or DOPE (data not shown). This suggested that DOPE did not regenerate α-tocopherol through direct electron transfer. Recently, Doert et al.[10] also reported that α-tocopherol regeneration by primary amines can be explained by an ionic mechanism rather than by a radical mechanism. In their study, they found that a 1% addition of L-β,γ-dipalmitoyl-α-phosphatidylethanolamine (PE) and 1,2-dipalmitoylgycero-3-phosphoryl-L-serine (PS), but not L-β,γ-dipalmitoyl-α-phosphatidylcholine (PC) or L-β,γ-dipalmitoyl-α-inositol (PI), regenerated α-tocopherol quinone to α-tocopherol in toluene at 100 °C. In our case, this reaction was confirmed with about 10 times lower concentration of PE (0.07%) in both bulk oil and MCT at a much lower temperature (55 °C). The concentrations used in this study are much closer to concentrations expected in refined, commercial oils.

Conclusion. In this study, the impact of two types of phospholipids, DOPC and DOPE, both individually and in combinations on the antioxidant activity of α-tocopherol or trolox in bulk oil was investigated. It was found that DOPC reverse micelles decreased the antioxidant activity of α-tocopherol and trolox. DOPE reverse micelles did not cause changes in the physical location of α-tocopherol, but increased its antioxidant activity through regeneration of oxidized α-tocopherol by its primary amine headgroup. The addition of DOPE to commercial soybean oil inhibited lipid oxidation, whereas DOPC was ineffective. These results indicated that in bulk oils the primary amine headgroup of DOPE increased the antioxidant activity of α-tocopherol by regeneration of the α-tocopherol quinone. To get a better efficiency of natural antioxidants such as tocopherols in bulk oil, decreasing PC reverse micelles and increasing PE could help stabilize the food oils.

AUTHOR INFORMATION

Corresponding Author

*(E.A.D.) Phone: (413) 545-1062. Fax: (413) 545-1262. E-mail: edecker@foodsci.umass.edu.

Notes

The authors declare no competing financial interest.

REFERENCES

(1) Frankel, E. N. Lipid oxidation: mechanisms, products and biological significance. *J. Am. Oil Chem. Soc.* **1984**, *61*, 1908−1917.

(2) Ito, N.; Hirose, M.; Fukushima, S.; Tsuda, H.; Shirai, T.; Tatematsu, M. Studies on antioxidants: their carcinogenic and modifying effects on chemical carcinogenesis. *Food Chem. Toxicol.* **1986**, *24*, 1071−1082.

(3) Ford, S. M.; Hook, J. B.; Bond, J. T. The effects of butylated hydroxyanisole and butylated hydroxytoluene on renal function in the rat. II. Effects on organic acid and base transport. *Food Cosmetics Toxicol.* **1980**, *18*, 21−26.

(4) Branen, A. L. Toxicology and biochemistry of butylated hydroxyanisole and butylated hydroxytoluene. *J. Am. Oil Chem. Soc.* **1975**, *52*, 59−63.

(5) Frankel, E. N. Antioxidants in lipid foods and their impact on food quality. *Food Chem.* **1996**, *57*, 51−55.

DOI: 10.1021/acs.jafc.5b00243
J. Agric. Food Chem. 2015, 63, 3288−3294

(6) Judde, A.; Villeneuve, P.; Rossignol-Castera, A.; Guillou, A. Antioxidant effect of soy lecithins on vegetable oil stability and their synergism with tocopherols. *J. Am. Oil Chem. Soc.* **2003**, *80*, 1209−1215.
(7) Bandarra, N.; Campos, R.; Batista, I.; Nunes, M. L.; Empis, J. Antioxidant synergy of α-tocopherol and phospholipids. *J. Am. Oil Chem. Soc.* **1999**, *76*, 905−913.
(8) Takenaka, A.; Hosokawa, M.; Miyashita, K. Unsaturated phosphatidylethanolamine as effective synergist in combination with α-tocopherol. *J. Oleo Sci.* **2007**, *56*, 511−516.
(9) Kashima, M.; Cha, G.-S.; Isoda, Y.; Hirano, J.; Miyazawa, T. The antioxidant effects of phospholipids on perilla oil. *J. Am. Oil Chem. Soc.* **1991**, *68*, 119−122.
(10) Doert, M.; Jaworska, K.; Moersel, J.-T.; Kroh, L. Synergistic effect of lecithins for tocopherols: lecithin-based regeneration of α-tocopherol. *Eur. Food Res. Technol.* **2012**, *235*, 915−928.
(11) Hidalgo, F. J.; Nogales, F.; Zamora, R. Changes produced in the antioxidative activity of phospholipids as a consequence of their oxidation. *J. Agric. Food Chem.* **2005**, *53*, 659−662.
(12) Zamora, R.; Hidalgo, F. J. Coordinate contribution of lipid oxidation and maillard reaction to the nonenzymatic food browning. *Crit. Rev. Food Sci.* **2005**, *45*, 49−59.
(13) Hidalgo, F. J.; León, M. M.; Zamora, R. Antioxidative activity of amino phospholipids and phospholipid/amino acid mixtures in edible oils as determined by the Rancimat method. *J. Agric. Food Chem.* **2006**, *54*, 5461−5467.
(14) Zamora, R.; León, M. M.; Hidalgo, F. J. Free radical-scavenging activity of nonenzymatically-browned phospholipids produced in the reaction between phosphatidylethanolamine and ribose in hydrophobic media. *Food Chem.* **2011**, *124*, 1490−1495.
(15) Hidalgo, F. J.; León, M. M.; Zamora, R. Effect of tocopherols in the antioxidative activity of oxidized lipid−amine reaction products. *J. Agric. Food Chem.* **2007**, *55*, 4436−4442.
(16) Shimajiri, J.; Shiota, M.; Hosokawa, M.; Miyashita, K. Synergistic antioxidant activity of milk sphingomyeline and its sphingoid base with α-tocopherol on fish oil triacylglycerol. *J. Agric. Food Chem.* **2013**, *61*, 7969−7975.
(17) Chen, B.; Han, A.; McClements, D. J.; Decker, E. A. Physical structures in soybean oil and their impact on lipid oxidation. *J. Agric. Food Chem.* **2010**, *58*, 11993−11999.
(18) Cui, L.; Kittipongpittaya, K.; McClements, D. J.; Decker, E. Impact of phosphoethanolamine reverse micelles on lipid oxidation in bulk oils. *J. Am. Oil Chem. Soc.* **2014**, 1−7.
(19) Chen, B.; Han, A.; Laguerre, M.; McClements, D. J.; Decker, E. A. Role of reverse micelles on lipid oxidation in bulk oils: impact of phospholipids on antioxidant activity of α-tocopherol and Trolox. *Food Funct.* **2011**, *2*, 302−309.
(20) Association of Official Analytical Chemists (AOAC). Polar components in frying fats. Official Method 982.27, Chapter 41.1.34.
(21) Felgner, A.; Schlink, R.; Kirschenbühler, P.; Faas, B.; Isengard, H.-D. Automated Karl Fischer titration for liquid samples − water determination in edible oils. *Food Chem.* **2008**, *106*, 1379−1384.
(22) Shantha, N. C.; Decker, E. A. Rapid, sensitive, iron-based spectrophotometric methods for determination of peroxide values of food lipids. *J. AOAC Int.* **1994**, *77*, 421−424.
(23) Kittipongpittaya, K.; Panya, A.; Cui, L.; McClements, D.; Decker, E. Association colloids formed by multiple surface active minor components and their effect on lipid oxidation in bulk oil. *J. Am. Oil Chem. Soc.* **2014**, 1−11.
(24) Wilson, G. J.; Lin, C. Y.; Webster, R. D. Significant differences in the electrochemical behavior of the α-, β-, γ-, and δ-tocopherols (vitamin E). *J. Phys. Chem. B* **2006**, *110*, 11540−11548.
(25) Koprivnjak, O.; Škevin, D.; Valić, S.; Majetić, V.; Petričević, S.; Ljubenkov, I. The antioxidant capacity and oxidative stability of virgin olive oil enriched with phospholipids. *Food Chem.* **2008**, *111*, 121−126.
(26) Porter, W. L. Paradoxical behavior of antioxidants in food and biological systems. *Toxicol. Ind. Health* **1993**, *9*, 93−122.
(27) Chattopadhyay, A.; Mukherjee, S.; Raghuraman, H. Reverse micellar organization and dynamics: a wavelength-selective fluorescence approach. *J. Phys. Chem. B* **2002**, *106*, 13002−13009.
(28) Panya, A.; Kittipongpittaya, K.; Laguerre, M.; Bayrasy, C.; Lecomte, J.; Villeneuve, P.; McClements, D. J.; Decker, E. A. Interactions between α-tocopherol and rosmarinic acid and its alkyl esters in emulsions: synergistic, additive, or antagonistic effect? *J. Agric. Food Chem.* **2012**, *60*, 10320−10330.
(29) Akoh, C. C.; Min, D. B. *Food Lipids: Chemistry, Nutrition, And Biotechnology*; CRC Press: Boca Raton, FL, USA, 2008.

DOI: 10.1021/acs.jafc.5b00243
J. Agric. Food Chem. 2015, 63, 3288−3294

Table 1. Selected Enterobacteriaceae Strains Associated with Necrotizing Enterocolitis

bacterial strain	ATCC no.	abbreviation	origin[a]
Escherichia coli EC1000[b]	NA[c]	EC1000	NA
Citrobacter freundii	8090[T d]	CF8090	NA
Cronobacter sakazakii	BAA-894	CSBAA894	human
	29544[T]	CS29544	human throat
Cronobacter muytjensii	51329[T]	CM51329	NA
Enterobacter cloacae subsp. *cloacae*	13047[T]	EC13047	human spinal fluid
Escherichia coli O1:K1:H7	11775[T]	EC11775	human urine
Escherichia coli K12[b]	29425	EC29425	NA
Klebsiella pneumoniae subsp. *pneumoniae*	13883[T]	KP13883	NA
Klebsiella oxytoca	13182[T]	KO13182	human pharyngeal tonsil
Shigella dysenteriae	13313[T]	SD13313	human

[a]Origin as listed on ATCC Web site (http://www.atcc.org/). [b]Control strains classified as nonpathogenic Biosafety Level 1. [c]NA, information is not available. [d]Organism designated as the species ATCC type strain.

with the incidence of necrotizing enterocolitis in mice[24] and infants.[18−20] Bacterial strains were purchased from the American Type Culture Collection (ATCC, Manassas, VA, USA). Confirmation of bacterial identity was completed prior to the bacterial growth assays. Briefly, bacterial cultures were inoculated from frozen stock (12.5% glycerol, v/v) into brain−heart infusion (BHI; Difco, Franklin Lakes, NJ, USA) broth and incubated overnight aerobically with shaking at 200 rpm at 37 °C. Genomic DNA was isolated from stationary bacterial cultures. Briefly, a 1.8 mL aliquot was centrifuged at 10000*g* in a 2 mL centrifuge tube containing approximately 100 mg of 0.25 μm silicon beads (RPI Corp., Mount Prospect, IL, USA) for 1 min and the bacterial pellet was resuspended in nanopure water. The tubes were boiled for 5 min (additional kill step for pathogens) and were then centrifuged at 7000*g* for 5 min. The bacterial pellet was resuspended in nanopure water and vortexed at maximum speed for 10 min. The lysed bacterial cells were centrifuged at 12000*g* for 3 min, and the supernatant was frozen at −20 °C. An approximately 1400 bp amplicon of DNA was amplified from the crude DNA extract by 16S rRNA specific primers, 8F (5′-AGAGTTTGATCCTGGCTCAG-3′) and 1391R (5′-GACGGGCGGTGWGTRCA-3′).[25,26] The PCR reaction mixture contained 3 μL of target DNA, 5 μL of each primer (10 mM), and 25 μL of EconoTaq Plus 2X Master Mix (Lucigen Corp., Middleton, WI, USA). The PCR cycling parameters consisted of an initial step of 5 min at 95 °C, followed by 35 cycles (30 s at 95 °C, 60 s at 54 °C, and 2 min at 72 °C) and an extension step at 72 °C for 7 min. PCR products were purified using the Zymoclean DNA Clean & Concentrator Kit (Zymo Research Corp., Irvine, CA, USA) according to the manufacturer's instructions. Sanger sequencing was done with either primer (8F or 1391R) using an ABI 3730XL capillary sequencer (Life Technologies). The sequences were trimmed for quality and uploaded to the BLAST database (NCBI) to determine identity (>97% similarity). All strains were confirmed as the species indicated in Table 1.

Bacterial Growth Assays. Bacterial growth due to the addition of a carbohydrate was determined using a Bioscreen C (Growth Curves USA, Piscataway, NJ, USA). Bacterial cultures were inoculated from frozen stock (12.5% glycerol, v/v) into BHI broth and grown overnight aerobically with shaking at 200 rpm and 37 °C. A 1% (v/v) inoculum was passed into 5 mL of ZMB-1 broth,[27] a chemically defined medium allowing for carbohydrate utilization experiments, supplemented with 1% glucose and incubated overnight aerobically with shaking at 200 rpm at 37 °C. To prepare the bacterial inoculum for the Bioscreen C growth assay, bacterial cultures were centrifuged at 4000*g* for 10 min and washed twice with phosphate-buffered saline (PBS; MP Biomedicals, Santa Ana, CA, USA), pH 7.4. The washed bacterial pellets were resuspended in 5 mL of carbohydrate-free ZMB-1 broth. The final bacterial inoculum was prepared by transferring a 1% (v/v) volume of ZMB-1 suspended cells into a fresh aliquot of ZMB-1 broth. The honeycomb plate was prepared with each well containing a total of 300 μL: 225 μL of washed cells in ZMB-1 broth and 25 μL of 10% (w/v) sugar solution (Table 2), and 50 μL of mineral oil (to prevent evaporation). Plates were preincubated anaerobically (90% N_2, 5% CO_2, 5% H_2; Coy Laboratory Products, Grass Lake, MI, USA) for 1 h prior to the addition of mineral oil. Plates were incubated anaerobically for 24, 48, 72, or 96 h (varied by experiment). Optical density at 600 nm was measured at 30 min intervals, which were preceded by 30 s of shaking at maximum speed. Each carbohydrate was tested with a minimum of three independent replications.

Enrichment of Enterobacteriaceae Consortia. The following protocol was utilized to enrich and isolate Enterobacteriaceae from feces of weaned piglets (n = 10) aged 42 days. Fresh fecal samples (~1 g) were collected from piglets raised at the University of Illinois Swine

Table 2. Carbohydrate Substrates Supplemented as a Sole Carbon Source for Bacterial Growth Assays

carbohydrate source		abbreviation	purpose	supplier
monosaccharide	glucose	Glu	control	Fisher
	fructose	Fru	nonrepressor	Sigma-Aldrich
	galactose	Gal	component[a]	Acros Organics
	N-acetylneuramic acid (sialic acid)	SA	component	Carbosynth
	N-acetylglucosamine	GlcNAc	component	Sigma-Aldrich
	L-fucose	L-fuc	component	Sigma-Aldrich
disaccharide	lactose	Lac	component	Fisher
	sucrose	Suc	control	Fisher
trisaccharide	2′-fucosyllactose	2′-FL	HMO[b]	Inalco
	6′-sialyllactose	6′-SL	HMO	Inalco
tetrasaccharide	lacto-*N*-neotetraose	LNnT	HMO	Abbott Nutrition
polysaccharide	short-chain fructooligosaccharides	FOS	prebiotic	GTC Nutrition
	inulin	Inu	prebiotic	Sensus
	galactooligosaccharides-vivinal	GOS-V	prebiotic	Friesland Foods Domo
	galactooligosaccharides-purimune	GOS-P	prebiotic	GTC Nutrition
	ultrapurified galactooligosaccharides-purimune	UGOS-P	prebiotic	37
	maltodextrin	Mal	prebiotic	Ross Products
	polydextrose	PDX	prebiotic	Danisco

[a]Component sugars are mono- or disaccharides present in HMO sugars. [b]HMO, human milk oligosaccharides.

DOI: 10.1021/jf505721p
J. Agric. Food Chem. 2015, 63, 3295−3302

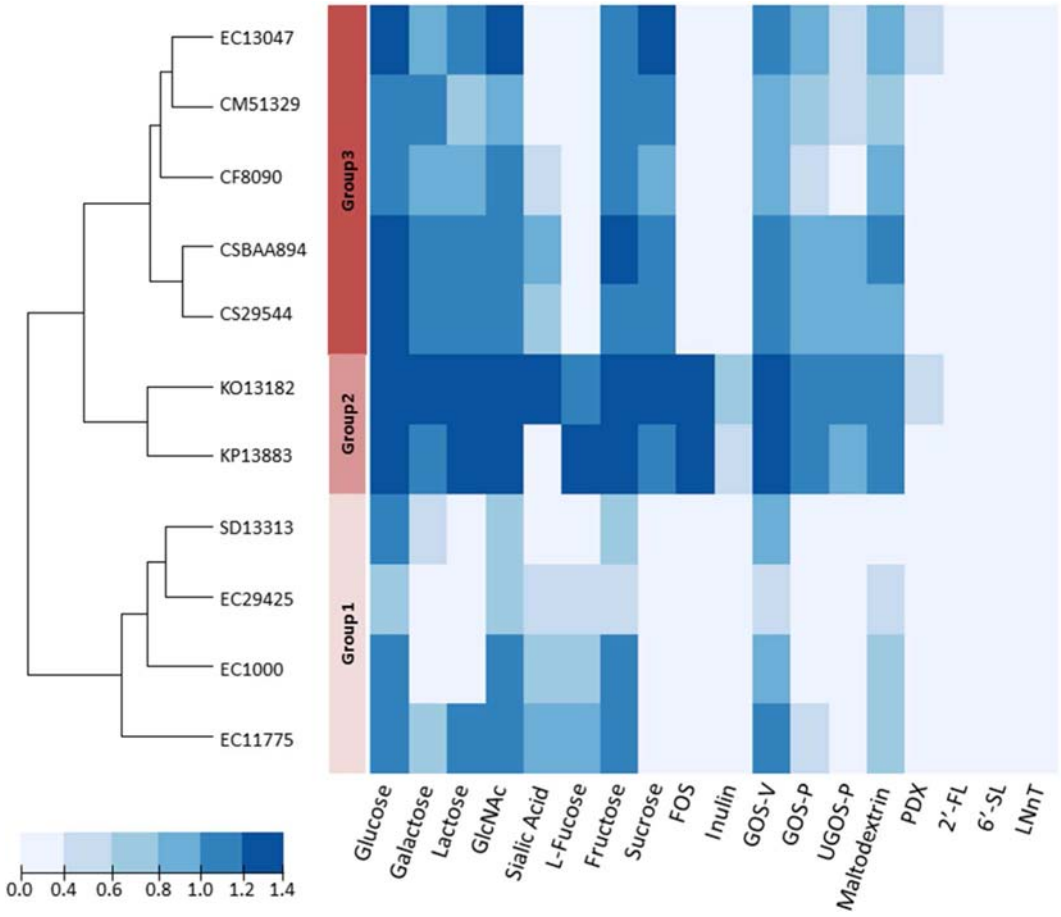

Figure 1. Maximal growth, OD 600 nm, achieved on 1% carbohydrate (glucose, galactose, lactose, *N*-acetylglucosamine (GlcNAc), *N*-acetylneuraminic acid (sialic acid), L-fucose, fructose, sucrose, sc-fructooligosacharides (FOS), inulin, galactooligosaccharides-vivinal (GOS-V), galactooligosaccharides-purimune (GOS-P), ultra-purified galactooligosaccharides-purimune (GOS-P), maltodextrin, polydextrose (PDX), 2′-fucosyllactose (2′-FL), 6′-siallyllactose (6′-SL), and lacto-*N*-neotetraose (LNnT)) in ZMB-1 media. No growth was observed in the absence of carbohydrates. Blank is corrected by subtraction of wells containing no cells and no carbohydrate. Dendrogram shows relatedness by pattern of growth. Average of three or more independent experiments.

Research Center. Samples were collected from their source (piglets) and stored on ice until use.

Enrichment of an Enterobacteriaceae consortium was performed as follows. Approximately 200 mg of feces was added to 2 mL (10-fold dilution) of prewarmed sterile buffered peptone water (BPW), pH 7.0. The fecal slurry was vortexed vigorously for complete homogenization. The BPW slurry was incubated overnight aerobically with shaking at 200 rpm and 37 °C. Following incubation the BPW fecal slurry was vortexed and set aside for 4 min to allow settling of the solid material. A 1 mL aliquot was combined with 9 mL (10-fold dilution) of Enterobacteriaceae Enrichment (EE) Broth (Oxoid, Basingstoke, UK) and incubated for 24 h aerobically with shaking at 200 rpm and 37 °C. A 5 mL aliquot of EE cultures was used for a Bioscreen C growth assay (procedure same as above). Upon completion of the Bioscreen C growth assay, 150 μL of cell suspension was centrifuged at 12000*g* for 3 min. A 100 μL aliquot was collected for HPLC analysis and stored at −20 °C. The remaining fermentate was pipetted off, and the cell pellets were frozen at −20 °C for archiving.

High-Performance Liquid Chromatography (HPLC). Selected fermentates from the in vitro growth assays were analyzed by HPLC using an Agilent Technologies 1260 Infinity HPLC (Agilent, Santa Clara, CA, USA) equipped with a refractive index detector using a Rezex ROA-Organic Acid H+ (8%) column (Phenomenex Inc., Torrance, CA, USA). The column was eluted with 0.005 N H_2SO_4 at a flow rate of 0.6 mL/min at 50 °C. Baseline samples were diluted 10-fold (20 μL of 10% sugar stock solution with 180 μL of ZMB-1), whereas fermentate samples were diluted 4-fold (50 μL of fermentate with 150 μL of water) prior to analysis.

Co-substrate Growth Assay. Bacterial growth resulting from the combination of a fermentable carbohydrate and an HMO was determined using a Bioscreen C as previously described. Washed cells were grown in ZMB-1 media supplemented with 1% (w/v) fermentable carbohydrate (Glu, Lac, or Mal) and 1% HMO (2′-FL, 6′-SL, or LNnT). Plates were incubated anaerobically for 48 or 72 h (varied by experiment). Each combination of carbohydrates was tested with three independent replications.

The impact to bacterial growth due to the presence or absence of HMOs was evaluated using a growth curve regression script written in MATLAB (version R2013a, The MathWorks, Natick, MA, USA) with the curve fitting toolbox. This script implements the modified logistic regression model, which provides a quantitative assessment of bacterial growth.[28] Additional heuristics were included in the modified logistic regression model to more accurately approximate the bacterial growth curves: (a) the death phase of the bacterial growth curve was not included in the regression, and (b) a threshold to detect cases where no growth occurred was set to an OD = 0.4 (600 nm). All regressions were judged by "goodness of fit" metrics, which were provided by the MATLAB curve fitting toolbox. Acceptable regression curves were selected on the basis of an $R^2 > 0.98$.

The growth curve was distilled into four calculable parameters: lag time (amount of time for bacteria to enter exponential growth phase), maximum specific growth rate (μ_{max}), doubling time (db time, also known as generation time), and delta OD (ΔOD, 600 nm). The lag

DOI: 10.1021/jf505721p
J. Agric. Food Chem. 2015, 63, 3295−3302

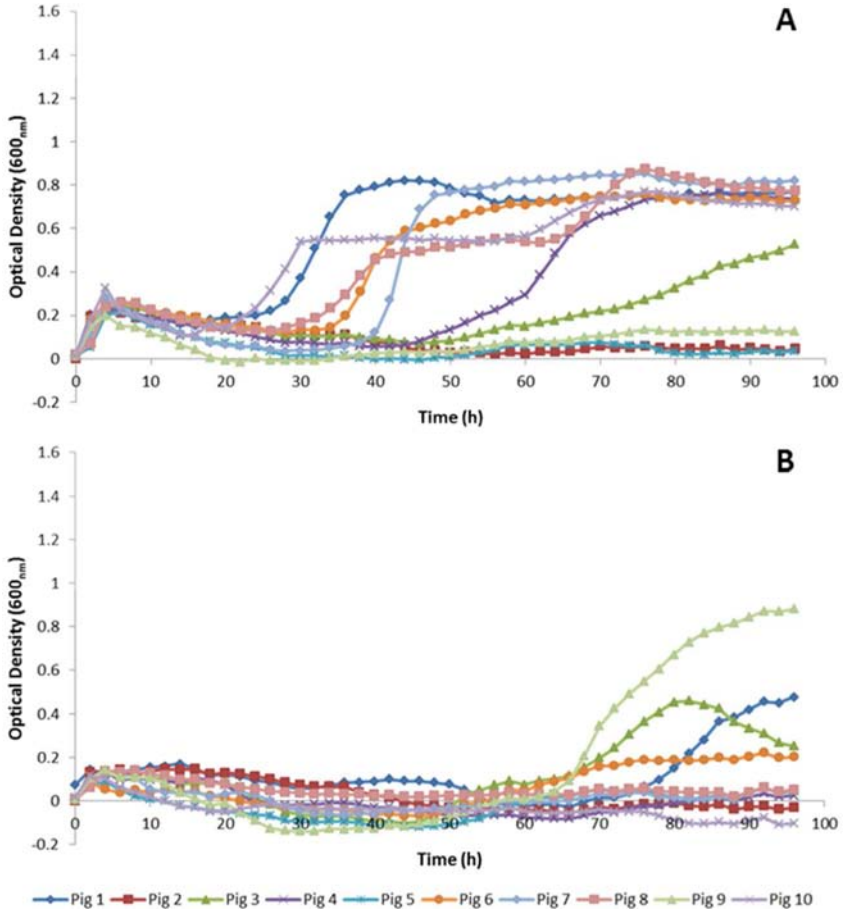

Figure 2. Growth curves of enriched piglet fecal Enterobacteriaceae consortia (n = 10), OD 600 nm, achieved at 96 h on 1% carbohydrate in ZMB-1 media: (A) ultra-purified purimune galactooligosaccharides (UGOS-P); (B) lacto-*N*-neotetraose (LNnT). Blank is corrected by subtraction of wells containing no cells and no carbohydrate. One independent Enterobacteriaceae consortia enriched per piglet.

time is defined as the x-intercept of the tangent line at the inflection point of the logistic regression curve (LRC) and is reported in hours. The maximum specific growth rate is defined as the slope of the tangent line at the inflection point of the LRC and is reported in hours^{-1}. The db time is mathematically related to the maximum specific growth rate and can be calculated using eq 1 (reported in hours):

$$\text{db time} = \frac{\ln(2)}{\mu_{\max}} \quad (1)$$

The ΔOD is calculated as the difference between the asymptote of the logistic curve (maximum OD) and the minimum OD and is reported as unit OD 600 nm.

Statistical Analysis. Statistical differences in bacterial growth parameters due to the presence/absence of HMO were determined using SAS (version 9.2, SAS Institute, Cary, NC, USA). Following satisfaction of the requirements of normality and homogeneity of variance, the bacterial parameters were evaluated using the generalized linear model (GLM). In cases when statistical significance was seen ($p < 0.05$), a post hoc mean separation was done using Dunnett's test. This test determines the statistical significance of the difference of each treatment (addition of HMO) to the control (fermentable sugar). Data visualized by heat map and dendrogram were conducted in R[29] using the gplots package.[30] The presented dendrogram (Figure 1) shows relatedness of organisms by their pattern of growth.

RESULTS

In Vitro Growth of Selected Carbohydrates. Nine pathogenic and two nonpathogenic Enterobacteriaceae strains (Table 1) were evaluated for their ability to grow in vitro using a selection of carbohydrates as a sole carbon source (Table 2). Preliminary experiments revealed that all tested Enterobacteriaceae were able to grow anaerobically in ZMB-1 supplemented with 1% glucose, whereas no growth was observed in the absence of a carbohydrate (data not shown). The resulting carbohydrate utilization data are displayed as a heat map (Figure 1). Interestingly, three distinct groups were identified on the basis of the observed patterns of growth and demonstrated significant overlap with phylogeny.[31] Group 1 is represented by the closely related *E. coli* strains and *Shigella dysenteriae*. Group 2 is represented by the two *Klebsiella* strains. Whereas the two *Cronobacter sakazakii* strains are grouped together, the other three strains, *Citrobacter freundii*, *Cronobacter muytjensii* and *Enterobacter cloacae*, in group 3 are not grouped according to phylogeny.

Bacterial strains that are represented by group 1 are EC1000, EC11775, EC29425, and SD13313. Their inability to utilize Suc and Lac (except EC11775) and weakened ability to grow in the presence of almost all carbohydrates tested are likely driving their clustering. Within the in vitro testing environment, these organisms were observed to grow on Glu, Fru, and GlcNAc; however, they did not grow in the presence of the tested prebiotics or HMOs.

The bacterial strains included in group 2 are KP13883 and KO13182. These two *Klebsiella* strains were strong utilizers of all carbohydrates tested except the HMOs. The unique ability

DOI: 10.1021/jf505721p
J. Agric. Food Chem. 2015, 63, 3295−3302

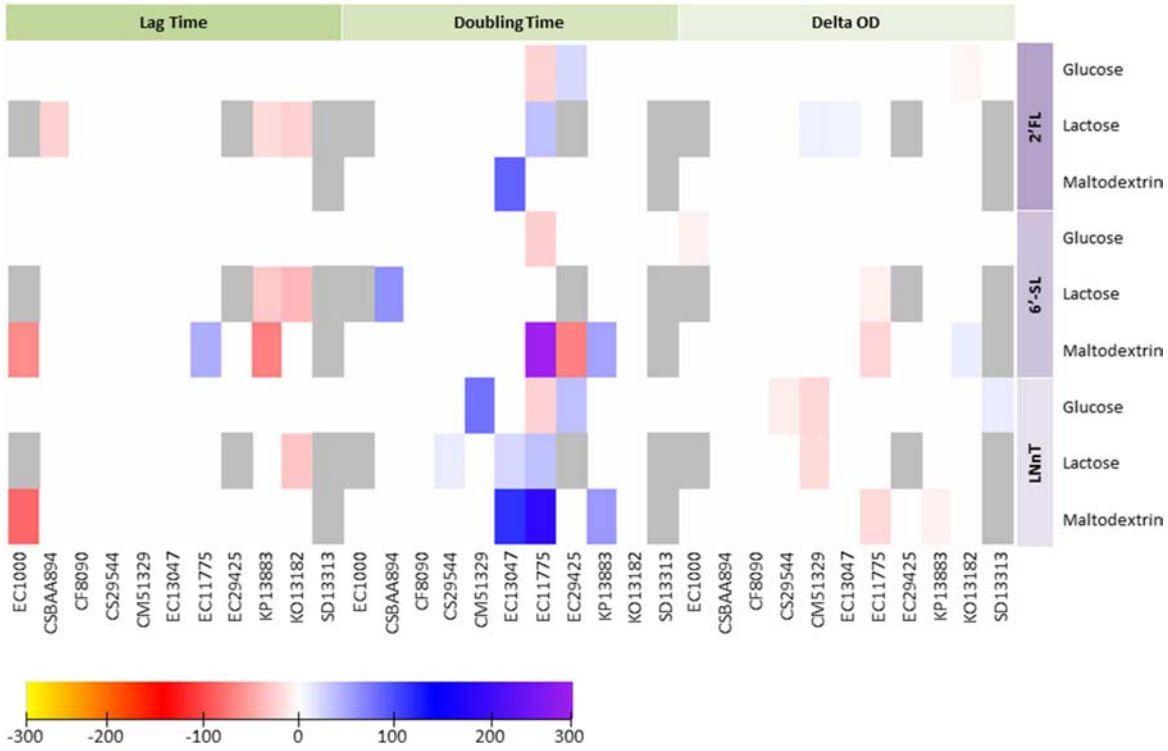

Figure 3. Statistically significant percent change in growth parameters determined from co-substrate bacterial growth. Bacterial cultures were grown in ZMB-1 with 1% fermentable carbohydrate (glucose, lactose, and maltodextrin) and 1% HMO (2′-fucosyllactose (2′-FL), 6′-sialyllactose (6′-SL), lacto-*N*-neotetraose (LNnT)). Heat map was generated on the basis of the percent change of either an increase or a decrease in the growth parameters of co-substrate wells compared to wells containing only the fermentable carbohydrate (ANOVA with Dunnett's mean separation). No growth was observed in the absence of carbohydrates. Blank is corrected by subtraction of wells containing no cells and no carbohydrate. Average of three independent experiments. Only organisms that were found to have a statistically significant percent change are shown. An organism's inability to grow in either lactose or maltodextrin is represented by gray boxes.

for KP13883 and KO13182 to utilize FOS and Inu for growth likely contributed to their clustering. Interestingly, only SA and PDX were differentially fermented between KP13883 and KO13182. Because KO13182 was observed to have a minimal increase in optical density in ZMB-1 supplemented with 1% LNnT (OD_{av} = 0.386), the bacterial growth curve was scrutinized. It was determined that an OD = 0.4 was an appropriate threshold because curves below this OD did not have a "characteristic" logistic curve with a distinct lag, exponential, or stationary phase. Additionally, the increase in OD occurred incrementally throughout the duration of the experiment (up to 96 h) until the maximum OD reading observed. We hypothesize that this small increase in growth was due to the presence of a small fraction of mono- or disaccharides in the LNnT we used. To test this hypothesis, the fermentate samples (n = 3) from KO13182 grown in ZMB-1 supplemented with 1% LNnT were analyzed by HPLC. The average percent decrease of LNnT detected in the fermentate as compared to the baseline (1% LNnT in ZMB-1) was 11.22 ± 0.29% (SEM) and was not considered significant.

Bacterial strains that are represented by group 3 are CSBAA894, CF8090, CS29544, CM51329, and EC13047. Interestingly, all five bacterial strains were unable to grow on L-fuc, fructooligosaccharides, and HMOs. Additionally, CF8090, CSBAA894, and CS29544 were observed to weakly grow on SA, whereas EC13047 and CM51329 were unable to utilize SA for growth. Conversely, these strains readily utilized Lac and Gal. Both CSBAA894 and CS29544 were observed to be GOS utilizers due to their ability to ferment the UGOS-P.

Enterobacteriaceae Consortia Growth. Enterobacteriaceae consortia were enriched from the feces of 42-day-old piglets (n = 10) who were weaned prior to fecal collection. These fecal consortia (PFEC) readily utilized Glu, Gal, Lac, GlcNAc, SA, and Mal for growth (data not shown). Interestingly, seven PFEC were capable of growing on UGOS-P with an extended lag time (Figure 2A), with three of the seven PFEC (4, 8, and 10) demonstrating multiphasic growth on UGOS-P. None of the PFEC grew when 2′-FL or 6′-SL (OD < 0.3) was supplemented as a sole carbon source. Conversely, three PFEC (1, 3, and 9) grew using 1% LNnT as a sole carbon source, albeit with a significant lag time (>60 h, Figure 2B). Subsequent HPLC analysis of the fermentate of all PFEC and two controls (EC29425 or no bacteria added) indicated that all of the PFEC, including the seven (piglets 2, 4, 5, 6, 7, 8, and 10) that did not show detectable growth (all OD < 0.25, Figure 2B), utilized at least some LNnT. More specifically, approximately 39 ± 8.8% of the LNnT disappeared from the fermentate of the seven PFEC that did not grow (OD < 0.25) on LNnT, and 62.8−97.7% of LNnT disappeared from the three PFEC that grew on LNnT (OD > 0.4). By contrast, the bacteria-free control (10.05 g/L) and EC29425 (9.4 g/L) showed no change in LNnT.

In Vitro Co-substrate Growth. Because HMOs are not the sole carbohydrates present in the diet of infants, we investigated the impact of providing various fermentable carbohydrates in combination with the HMOs on the growth of selected Enterobacteriaceae strains. Bacterial strains were grown in ZMB-1 supplemented with 1% of a fermentable

DOI: 10.1021/jf505721p
J. Agric. Food Chem. 2015, 63, 3295−3302

carbohydrate (Glu, Lac, or Mal) and compared to 1% fermentable carbohydrate + 1% HMO (2′-FL, 6′-SL, or LNnT). The impact on bacterial growth was evaluated by determination of the bacterial lag time, doubling time, and ΔOD and is presented in Figures S1−S3, respectively. To ease comparisons, the statistically significant percent of change between the experimental condition (addition of HMO) and control condition (fermentable carbohydrate) was illustrated using a heat map (Figure 3).

Combining individual HMOs with another fermentable carbohydrate affected lag time in only a few instances. The lag time for EC1000 was significantly decreased in the presence of Mal supplemented with 6′-SL and LNnT but not 2′-FL. Conversely, only Lac supplemented with 2′-FL caused a significant decrease in CSBAA894's lag time. Interestingly, both KP13883 and KO13182 had shorter ($p < 0.05$) lag times with all three HMOs in the presence of Lac, although it was more pronounced with 6′-SL ($p < 0.005$). Uniquely, EC11775 had a significantly increased lag time (6 h) when grown in the presence of Mal and 6′-SL.

The bacterial db time was differentially affected depending on the strain/carbohydrate combination. Several strains exhibited an increase in db time in the presence of an HMO. Specifically, the db time was significantly longer when an HMO was combined with Mal (EC13047:2′-FL and LNnT, EC11775 and KP13883:6′-SL and LNnT). Additionally, several strains (CS29544, EC13047, and EC11775) were significantly affected by the presence of LNnT in combination with Lac but to a lesser degree. Interestingly, only two strains (EC11775 and EC29425) had a significant decrease in db time. A significant decrease in db time for EC11775 was observed only when Glu was in combination with all three HMOs, whereas EC29425's db time decreased 69.7% when Mal was combined with 6′-SL. The largest percent change in db time was observed for EC11775 when Mal was combined with 6′-SL and LNnT (increases of 284 and 186%, respectively).

High-throughput experiments use the ΔOD to describe the magnitude of bacterial growth achieved over the course of a carbohydrate utilization experiment. It was observed that the ΔOD was differentially affected on the basis of the strain/carbohydrate combinations; however, the percent change was minimal (range from −25 to 10%). In general, the ΔOD was decreased in the presence of an HMO; however, no clear pattern was found. Interestingly, the ΔOD of CM51329 was significantly increased when Lac was in combination with 2′-FL. Conversely, when Glu and Lac were in combination with LNnT the ΔOD of CM51329 was significantly decreased.

DISCUSSION

Human milk oligosaccharides are believed to contribute to the health and development of the infant GI tract by multiple mechanisms. During the establishment of the intestinal microbiota,[2,11] HMOs function as prebiotics by selecting for certain *Bifidobacterium* and *Bacteroides* species. Although it has been assumed that HMOs do not support the growth of Enterobacteriaceae, which are thought to promote the inflammatory response that occurs during NEC, the ability of various members of this family to utilize individual HMOs has not been thoroughly examined. In this study, we assessed the ability of several Enterobacteriaceae strains and enriched piglet fecal Enterobacteriaceae consortia to utilize 2′-FL, 6′-SL, and LNnT as a sole carbohydrate for growth. Additionally, we examined the impact of adding glucose, lactose, and maltodextrin on HMO utilization by the various Enterobacteriaceae strains.

Several Enterobacteriaceae tested were able to readily utilize mono- or disaccharides (Glu, Gal, Lac, Fru, and Suc) for growth; however, growth on prebiotic carbohydrates (FOS, Inu, UGOS-P, Mal, and PDX) was lessened or absent (Figure 1). Utilization of prebiotics for growth may be limited due to an organisms' inability to transport larger carbohydrates (>3 monomers) intracellularly. Therefore, the presence of extracellular glycosidases may assist transportation by cleaving the prebiotics into mono- or disaccharides. The extracellular glycosidases from *Bifidobacterium bifidum* have been studied extensively. The extracellular lacto-*N*-biosidase allows for the intracellular transport of lacto-*N*-biose by removing the terminal galactose from type 1 HMOs.[13] We hypothesized that KP13883 and KO13182 likely possess several extracellular glycosidases due to their ability to use a wide range of prebiotics (FOS, Inu, UGOS-P, Mal, and PDX) tested regardless of chain length. On the basis of the inability of any of the selected Enterobacteriaceae to detectably grow when 2′-FL, 6′-SL, or LNnT was the sole carbon source, we also hypothesized that these organisms do not possess the appropriate HMO-specific transporter or extracellular enzymes necessary for catabolism. Our data do demonstrate the potential of cross-feeding, whereby commensal GI organisms could liberate monosaccharides from HMOs, thereby providing a substrate for pathogenic Enterobacteriaceae. Ng and collegues[32] demonstrated that *Salmonella enterica* subsp. *enterica* serovar Typhimurium and *Clostridium difficile* advantageously catabolize liberated muco-glycans in a *Bacteroides thetaiotaomicron* monoassociated mouse model. *Salmonella* Typhimurium and *C. difficile* were observed to have a growth advantage and induction of genes associated with the sialic acid (*nan*) operon when *B. thetaiotaomicron* was present.[32]

Analysis of the infant fecal microbiome in infants diagnosed with NEC detected a bloom in proteobacteria (>50% relative abundance) in the GI of infants diagnosed with NEC.[17−21] Interestingly, an analysis of an infants' GI metabolome pre-NEC and following diagnosis revealed a significant increase in carbohydrate utilization genes mapped to members of the Enterobacteriaceae family.[21] Although none of the selected Enterobacteriaceae were able to grow on the HMOs tested, it would be premature to assume that no Enterobacteriaceae strains are capable of utilizing HMOs for growth. Therefore, Enterobacteriaceae consortia were enriched with piglet feces, a rich source of Enterobacteriaceae, and evaluated for their ability to ferment selected carbohydrates including 2′-FL, 6′-SL, and LNnT. All PFEC tested were able to ferment HMO-associated mono- and disaccharides, whereas there was no detectable growth when 2′-FL or 6′-SL was supplied as a sole carbon source (data not shown). Conversely, all PFEC were observed to reduce LNnT detectably; however, not all PFEC had detectable growth (Figure 2B). Those PFEC that had detectable growth showed the largest reduction in LNnT (>63%); meanwhile, the other seven PFEC with no detectable growth converted only <40% of LNnT. Therefore, supplementation of preterm infant formula with LNnT may require further study. Additionally, seven PFEC were observed to utilize UGOS-P for growth (Figure 2B). Because galactooligosaccharides supplementation of infant formula did not cause a reduction in the incidence of NEC,[33] we conclude that supplementation poses no additional risk.

DOI: 10.1021/jf505721p
J. Agric. Food Chem. 2015, 63, 3295−3302

Considering that supplementation of HMOs in infant formula would likely be done in the presence of additional carbohydrates, we evaluated the impact of Enterobacteriaceae growth on Glu, Lac, and Mal in combination with HMOs. Although the inclusion of HMOs would likely not affect Glu utilization in vivo, Glu was included as a control. On the other hand, colonic lactose fermentation has been observed in premature infants.[34,35] Maltodextrin was also included because it is often added to infant formula. Because all included Enterobacteriaceae showed no detectable growth when 2′-FL, 6′-SL, or LNnT was provided as the sole carbon source, any change in growth was not attributed to direct fermentation of the tested HMOs. The resulting bacterial growth was analyzed using a logistic regression analysis to obtain the lag time, db time, and ΔOD. On the basis of these three parameters, two patterns can be used to determine the impact of growth in the presence of HMOs. A decrease in lag time and db time and an increase in ΔOD would indicate an environment that favors bacterial growth, whereas an increase in lag time and db time and a decrease in ΔOD would indicate an environment that disfavors growth. Interestingly, no strain/carbohydrate combination tested had a significant fold change in all three parameters that favored growth. Conversely, EC11775 was the only organism to have a significant fold change in all three parameters that did not favor growth. The combination of Mal and 6′-SL led to a significant increase in lag time (44%) and db time (284%) and a significant decrease in ΔOD (−23%). Hunt and colleagues[36] reported that pooled HMOs in combination with glucose and lactose resulted in an enhanced growth of *Staphylococcus epidermidis* and *Staphylococcus aureus* breast milk isolates. The two *Staphylococcus* species did not directly catabolize the pooled HMO fraction, but rather metabolized amino acids.[36] It appears that 6′-SL, an acidic HMO, may disturb EC11775's ability to grow on complex carbohydrates; however, the impact of 6′-SL on gene expression was not tested.

In conclusion, this study demonstrates that individual Enterobacteriaceae strains do not detectably grow in the presence of 2′-FL, 6′-SL, and LNnT, whereas three PFEC did have detectable growth when LNnT was added as a sole carbon source. Conversely, no PFEC had detectable growth on 2′-FL and 6′-SL. In addition, no Enterobacteriaceae strain had significantly enhanced growth in all three calculated bacterial growth parameters (lag time, db time, and ΔOD) when HMOs were combined with a fermentable carbohydrate. On the other hand, Mal in the presence of 6′-SL did not favor the growth of EC11775. Therefore, we conclude that supplementation of preterm infant formula with 2′-FL and 6′-SL should not lead to an increase in Enterobacteriaceae; however, supplementation with LNnT may require further exploration.

■ ASSOCIATED CONTENT

Supporting Information

Figures S1−S3. This material is available free of charge via the Internet at http://pubs.acs.org.

■ AUTHOR INFORMATION

Corresponding Author

*(M.J.M.) Phone: (217) 244-1973. Fax: (217) 265-0925. E-mail: mille216@illinois.edu.

Funding

This study was funded by Abbott Nutrition. J.L.H. also received financial support by the Agnes and Bill Brown Fellowship in Microbiology from the University of Illinois—Urbana-Champaign.

Notes

The authors declare the following competing financial interest(s): M.J.M. has received grant funding from Abbott Nutrition.

■ ACKNOWLEDGMENTS

We thank Taksawan Thongaram for the purification of galactooligosaccharides-purimune and Daniel E. Hoeflinger for development and implementation of the modified logistic regression script written in MATLAB.

■ REFERENCES

(1) Coppa, G. V.; Zampini, L.; Galeazzi, T.; Gabrielli, O. Prebiotics in human milk: a review. *Dig. Liver Dis.* **2006**, *38* (Suppl. 2), S291−S294.
(2) Walker, A. Breast milk as the gold standard for protective nutrients. *J. Pediatr.* **2010**, *156*, S3−S7.
(3) Coppa, G. V.; Gabrielli, O.; Pierani, P.; Catassi, C.; Carlucci, A.; Giorgi, P. L. Changes in carbohydrate composition in human milk over 4 months of lactation. *Pediatrics* **1993**, *91*, 637−641.
(4) Kunz, C.; Rudloff, S.; Baier, W.; Klein, N.; Strobel, S. Oligosaccharides in human milk: structural, functional, and metabolic aspects. *Annu. Rev. Nutr.* **2000**, *20*, 699−722.
(5) Ninonuevo, M. R.; Park, Y.; Yin, H.; Zhang, J.; Ward, R. E.; Clowers, B. H.; German, J. B.; Freeman, S. L.; Killeen, K.; Grimm, R.; Lebrilla, C. B. A strategy for annotating the human milk glycome. *J. Agric. Food Chem.* **2006**, *54*, 7471−7480.
(6) Albrecht, S.; Schols, H. A.; van Zoeren, D.; van Lingen, R. A.; Groot Jebbink, L. J.; van den Heuvel, E. G.; Voragen, A. G.; Gruppen, H. Oligosaccharides in feces of breast- and formula-fed babies. *Carbohydr. Res.* **2011**, *346*, 2173−2181.
(7) Eiwegger, T.; Stahl, B.; Schmitt, J.; Boehm, G.; Gerstmayr, M.; Pichler, J.; Dehlink, E.; Loibichler, C.; Urbanek, R.; Szepfalusi, Z. Human milk-derived oligosaccharides and plant-derived oligosaccharides stimulate cytokine production of cord blood T-cells in vitro. *Pediatr. Res.* **2004**, *56*, 536−540.
(8) He, Y.; Liu, S.; Leone, S.; Newburg, D. S. Human colostrum oligosaccharides modulate major immunologic pathways of immature human intestine. *Mucosal Immunol.* **2014**, *7*, 1326−1339.
(9) Newburg, D. S.; Ruiz-Palacios, G. M.; Morrow, A. L. Human milk glycans protect infants against enteric pathogens. *Annu. Rev. Nutr.* **2005**, *25*, 37−58.
(10) Angeloni, S.; Ridet, J. L.; Kusy, N.; Gao, H.; Crevoisier, F.; Guinchard, S.; Kochhar, S.; Sigrist, H.; Sprenger, N. Glycoprofiling with micro-arrays of glycoconjugates and lectins. *Glycobiology* **2005**, *15*, 31−41.
(11) Coppa, G. V.; Zampini, L.; Galeazzi, T.; Facinelli, B.; Ferrante, L.; Capretti, R.; Orazio, G. Human milk oligosaccharides inhibit the adhesion to Caco-2 cells of diarrheal pathogens: *Escherichia coli*, *Vibrio cholerae*, and *Salmonella fyris*. *Pediatr. Res.* **2006**, *59*, 377−382.
(12) Ruiz-Palacios, G. M.; Cervantes, L. E.; Ramos, P.; Chavez-Munguia, B.; Newburg, D. S. *Campylobacter jejuni* binds intestinal H(O) antigen (Fuc alpha 1, 2Gal beta 1, 4GlcNAc), and fucosyloligosaccharides of human milk inhibit its binding and infection. *J. Biol. Chem.* **2003**, *278*, 14112−14120.
(13) Wada, J.; Ando, T.; Kiyohara, M.; Ashida, H.; Kitaoka, M.; Yamaguchi, M.; Kumagai, H.; Katayama, T.; Yamamoto, K. Bifidobacterium bifidum lacto-*N*-biosidase, a critical enzyme for the degradation of human milk oligosaccharides with a type 1 structure. *Appl. Environ. Microbiol.* **2008**, *74*, 3996−4004.
(14) Asakuma, S.; Hatakeyama, E.; Urashima, T.; Yoshida, E.; Katayama, T.; Yamamoto, K.; Kumagai, H.; Ashida, H.; Hirose, J.; Kitaoka, M. Physiology of consumption of human milk oligosaccharides

DOI: 10.1021/jf505721p
J. Agric. Food Chem. 2015, 63, 3295−3302

ides by infant gut-associated bifidobacteria. *J. Biol. Chem.* **2011**, *286*, 34583−34592.
(15) Sela, D. A.; Garrido, D.; Lerno, L.; Wu, S.; Tan, K.; Eom, H. J.; Joachimiak, A.; Lebrilla, C. B.; Mills, D. A. *Bifidobacterium longum* subsp. *infantis* ATCC 15697 α-fucosidases are active on fucosylated human milk oligosaccharides. *Appl. Environ. Microbiol.* **2012**, *78*, 795−803.
(16) Marcobal, A.; Barboza, M.; Froehlich, J. W.; Block, D. E.; German, J. B.; Lebrilla, C. B.; Mills, D. A. Consumption of human milk oligosaccharides by gut-related microbes. *J. Agric. Food Chem.* **2010**, *58*, 5334−5340.
(17) Claud, E. C.; Walker, W. A. Hypothesis: inappropriate colonization of the premature intestine can cause neonatal necrotizing enterocolitis. *FASEB J.* **2001**, *15*, 1398−1403.
(18) Wang, Y.; Hoenig, J. D.; Malin, K. J.; Qamar, S.; Petrof, E. O.; Sun, J.; Antonopoulos, D. A.; Chang, E. B.; Claud, E. C. 16S rRNA gene-based analysis of fecal microbiota from preterm infants with and without necrotizing enterocolitis. *ISME J.* **2009**, *3*, 944−954.
(19) Mai, V.; Young, C. M.; Ukhanova, M.; Wang, X.; Sun, Y.; Casella, G.; Theriaque, D.; Li, N.; Sharma, R.; Hudak, M.; Neu, J. Fecal microbiota in premature infants prior to necrotizing enterocolitis. *PLoS One* **2011**, *6*, No. e20647.
(20) Smith, B.; Bode, S.; Petersen, B. L.; Jensen, T. K.; Pipper, C.; Kloppenborg, J.; Boye, M.; Krogfelt, K. A.; Molbak, L. Community analysis of bacteria colonizing intestinal tissue of neonates with necrotizing enterocolitis. *BMC Microbiol.* **2011**, *11*, 73.
(21) Claud, E. C.; Keegan, K. P.; Brulc, J. M.; Lu, L.; Bartels, D.; Glass, E.; Chang, E. B.; Meyer, F.; Antonopoulos, D. A. Bacterial community structure and functional contributions to emergence of health or necrotizing enterocolitis in preterm infants. *Microbiome* **2013**, *1*, 20-2618-1-20.
(22) Nanthakumar, N. N.; Fusunyan, R. D.; Sanderson, I.; Walker, W. A. Inflammation in the developing human intestine: a possible pathophysiologic contribution to necrotizing enterocolitis. *Proc. Natl. Acad. Sci. U.S.A.* **2000**, *97*, 6043−6048.
(23) Marcobal, A.; Sonnenburg, J. L. Human milk oligosaccharide consumption by intestinal microbiota. *Clin. Microbiol. Infect.* **2012**, *18* (Suppl. 4), 12−15.
(24) Carlisle, E. M.; Poroyko, V.; Caplan, M. S.; Alverdy, J. A.; Liu, D. Gram negative bacteria are associated with the early stages of necrotizing enterocolitis. *PLoS One* **2011**, *6*, No. e18084.
(25) Lane, D. J.; Pace, B.; Olsen, G. J.; Stahl, D. A.; Sogin, M. L.; Pace, N. R. Rapid determination of 16S ribosomal RNA sequences for phylogenetic analyses. *Proc. Natl. Acad. Sci. U.S.A.* **1985**, *82*, 6955−6959.
(26) Lane, D. J. 16S/23S rRNA sequencing. In *Nucleic Acid Techniques in Bacterial Systematics*; Wiley: New York, 1991; pp 115−175.
(27) Zhang, G.; Mills, D. A.; Block, D. E. Development of chemically defined media supporting high-cell-density growth of lactococci, enterococci, and streptococci. *Appl. Environ. Microbiol.* **2009**, *75*, 1080−1087.
(28) Zwietering, M. H.; Jongenburger, I.; Rombouts, F. M.; van't Riet, K. Modeling of the bacterial growth curve. *Appl. Environ. Microbiol.* **1990**, *56*, 1875−1881.
(29) R Development Core Team R. *A Language and Environment for Statistical Computing*; Vienna, Austria, 2011; ISBN 3-900051-07-0.
(30) Warnes, G. R.; Bolker, B.; Bonebakker, L.; Gentleman, R.; Liaw, W. H. A.; Lumley, T.; Maechler, M.; Magnusson, A.; Moeller, S.; Schwartz, M.; Venables, B. gplots: Various R Programming Tools for Plotting Data, 2015; http://cran.r-project.org/web/packages/gplots/index.html.
(31) Paradis, S.; Boissinot, M.; Paquette, N.; Belanger, S. D.; Martel, E. A.; Boudreau, D. K.; Picard, F. J.; Ouellette, M.; Roy, P. H.; Bergeron, M. G. Phylogeny of the Enterobacteriaceae based on genes encoding elongation factor Tu and F-ATPase β-subunit. *Int. J. Syst. Evol. Microbiol.* **2005**, *55*, 2013−2025.
(32) Ng, K. M.; Ferreyra, J. A.; Higginbottom, S. K.; Lynch, J. B.; Kashyap, P. C.; Gopinath, S.; Naidu, N.; Choudhury, B.; Weimer, B. C.; Monack, D. M.; Sonnenburg, J. L. Microbiota-liberated host sugars facilitate post-antibiotic expansion of enteric pathogens. *Nature* **2013**, *502*, 96−99.
(33) Srinivasjois, R.; Rao, S.; Patole, S. Prebiotic supplementation in preterm neonates: updated systematic review and meta-analysis of randomised controlled trials. *Clin. Nutr.* **2013**, *32*, 958−965.
(34) Kien, C. L.; Liechty, E. A.; Myerberg, D. Z.; Mullett, M. D. Dietary carbohydrate assimilation in the premature infant: evidence for a nutritionally significant bacterial ecosystem in the colon. *Am. J. Clin. Nutr.* **1987**, *46*, 456−460.
(35) Kien, C. L.; McClead, R. E.; Cordero, L., Jr. In vivo lactose digestion in preterm infants. *Am. J. Clin. Nutr.* **1996**, *64*, 700−705.
(36) Hunt, K. M.; Preuss, J.; Nissan, C.; Davlin, C. A.; Williams, J. E.; Shafii, B.; Richardson, A. D.; McGuire, M. K.; Bode, L.; McGuire, M. A. Human milk oligosaccharides promote the growth of staphylococci. *Appl. Environ. Microbiol.* **2012**, *78*, 4763−4770.
(37) Thongaram, T. *Probiotic Metabolism of Human Milk Oligosaccharides (HMOs) and Prebiotics*. Doctoral dissertation, University of Illinois at Urbana-Champaign, 2014.

DOI: 10.1021/jf505721p
J. Agric. Food Chem. 2015, 63, 3295−3302

with a low level exposure to BPA.[2] Recent studies of the National Toxicology Program (NTP) and the U.S. Food and Drug Administration (FDA) pointed out the potential BPA effects on brain, behavior, and prostate gland in fetuses, infants, and young children.[15] Indeed, BPA can affect the hormone-mediated neurologic and behavioral development in early life.[15−19] In addition, high BPA exposure has been associated with heart disease, diabetes, abnormally high levels of liver enzymes, and alterations of the thyroid function.[20−22] For these reasons, BPA containing baby bottles have been banned in Europe since March 2011.[23] Diet remains the predominant source of exposure for both phthalates and BPA especially for infants, since these compounds have been found in breast milk and in baby formulas.[24−27] The present paper analyzes the presence of DEHP, DnBP, and BPA in infant formulas to assess possible neonatal exposure and to reduce the gap of knowledge in this field.

MATERIALS AND METHODS

Sampling. Fifty infant formula samples were collected at different neonatal nurseries in Naples 53 hospital during three months (May−July 2013). Liquid ready to use (n = 22) and powder (n = 28) milk samples were collected. Among them, there were seven special milk samples, that is, milks for infant with gastrointestinal problems (n = 3), rice milk formulas (n = 3), and a premature formula. Liquid samples were packed in polyethylene terephthalate (PET) and Tetrapak, whereas milk powders were contained in aluminum (Al) containers. The infant formula samples were collected in glass vials and were rapidly transferred to the laboratory of the Department of Agriculture, where analytical samples were obtained for the different procedures. All samples were labeled. For DEHP and DnBP analysis, aliquots (15 mL) of liquid milk were lyophilized and stored a −18 °C until analyses, whereas powder sample aliquots (1 g) were just stored in the dark. For BPA determination, aliquots (5 mL) of liquid milk were stored at −18 °C until analyses, whereas powder sample aliquots (2 g) were reconstituted with high-performance liquid chromatography (HPLC) water (15 mL), were split into 5 mL aliquots, and were stored at −18 °C until analyses. For each reconstituted vial, an additional 5 mL vial with HPLC water was stored at −18 °C as a negative control to avoid possible bias because of a contamination of HPLC water.

DEHP and DnBP. *Chemical Reagents.* Acetonitrile, n-hexane, acetone for organic trace analysis, and anhydrous Na_2SO_4 were supplied by Merck (Darmstadt, Germany). Florisil (60/100 mesh) was furnished by Supelco (Bellefonte, PA, U.S.), and Bondesil (PSA 40UM) was furnished by Varian (Palo Alto, CA, U.S.). Standard solutions of DEHP and DnBP were purchased from Sigma-Aldrich (St. Louis, MO, U.S.).

Instrumental Parameters. The analyses of phthalates (PAEs, phthalic acid esters) were carried out by a Shimadzu GC-17 (Shimadzu, Kyoto, Japan) capillary gas chromatography with a flame ionization detector (GC-FID) and an HP-5 (cross-linked 5% PHME siloxane, 30 m length, 0.32 i.d., 0.25 μm film thickness) glass-capillary column. Helium was used as the carrier, and a hydrogen/air mixture was used to sustain the flame. The volume of injection was 1 μL in splitless mode, and the injector and detector temperatures were 260 and 310 °C, respectively. The temperature program was 100 °C for 1 min, increase of 15 °C/min up to 280 °C, and retention of this temperature for 10 min.

DEHP and DnBP Measurement. Because of PAE ubiquity, any contact with plastic was avoided. All the glassware was thoroughly washed, was rinsed twice with acetone and n-hexane, was heated at 250 °C for 2 h, and finally was stored away from any environmental contamination. In accordance with the method by Cirillo et al.,[25] the lyophilized samples were (1) extracted three times with 15 mL of acetonitrile in an ultrasound bath for 15 min; (2) centrifuged at 2000 rpm for 10 min, and the acetonitrile layer was transferred to a separatory funnel; and (3) added with 10 mL of n-hexane saturated with acetonitrile, and the funnel was vigorously shaken for 5 min. The acetonitrile phase was transferred into a flask and was dried under vacuum at 55 °C. The extracts were reconstituted by 5 mL of n-hexane and were purified through a column containing 2 g of Florisil activated for 2 h at 200 °C, 0.5 g of Bondesil, and 1 g of anhydrous Na_2SO_4. The column was eluted three times with 10 mL of n-hexane/acetone mixture (100:5 v/v). The eluates were collected in a flask, were evaporated under vacuum at 40 °C, and were reconstituted with 1 mL of n-hexane for GC analysis. The calibration curves were obtained using standard solutions at 0.625, 1.250 and 2.500, 5.00 and 10.00 μg/mL for DEHP and at 0.312, 0.625, 1.250, 2.500, and 5.00 μg/mL for DnBP. The regression coefficients (R) were >0.99 for both contaminants. The PAE concentrations in the samples were obtained by comparing the relevant peak areas with calibration curve. Limits of detection (LODs) and quantification (LOQs) were evaluated as the mean blank value plus three blank standard deviations and LOQ was evaluated as 3 times the LOD. LODs and LOQs were 5.0 ng/g and 15.0 ng/g for DEHP and 7.5 ng/g and 22.5 ng/g for DnBP, respectively. A run without sample was carried out every six determinations to reduce the instrumental background due to contamination. Moreover, solvents used to wash the syringe were frequently replaced. The intra- and interday repeatabilities of the method were evaluated by injecting standard solutions at three different concentration levels (2.50, 5.00, and 10.00 μg/mL for DEHP and 1.25, 2.50, and 5.00 μg/mL for DnBP) five times during a day (intraday) and during five consecutive days (interday). The intraday repeatability ranged from 7.0 to 9.5% for DEHP and from 5.5 to 8.5% for DnBP, whereas interday repeatability varied from 6.0 to 8.5% for DEHP and from 4.5 to 6.5% for DnBP. Samples with DEHP and DnBP concentrations lower than LOD were used for recovery tests. Three liquid and three powder milk samples (each in triplicate) were spiked with standard solutions at concentration 2.0, 4.0, and 8.0 μg/mL for DEHP and 1.0, 2.0, and 4.0 μg/mL for DnBP and then were processed as milk samples. Recoveries were 98 ± 10% for DEHP and 98 ± 9% for DnBP. Because of the ubiquity of these compounds, a blank sample (only solvents) for each batch was analyzed, and the average concentration value was subtracted from PAE detected values.

Bisphenol A. *Chemical Reagents.* Acetonitrile, methanol, and water (HPLC grade) were supplied by Merck (Darmstadt, Germany). Solid-phase extraction cartridges (Bond Elut C18 SPE, 1 g/6 mL) were purchased from Agilent Technologies (Palo Alto, CA, U.S.). A BPA standard (purity ≥99%) was purchased from Sigma-Aldrich (St. Louis, MO, U.S.).

Instrumental Parameters. BPA detection was performed through an HPLC (LC-10AT VP Shimadzu, Kyoto, Japan) equipped with a fluorescence detector (Shimadzu RF-10A XL) and a reversed-phase column (Ascentis C18 Length × i.d.: 15 cm × 4.6 mm; particle size: 5 μm, Supelco, Bellefonte, PA). The column was kept at a constant temperature of 40 °C. The

DOI: 10.1021/jf505563k
J. Agric. Food Chem. 2015, 63, 3303−3310

mobile phase consisted of 60% of acidified water (1% of acetic acid), 35% of acetonitrile, and 5% of methanol. The flow rate of mobile phase was set at 0.950 mL/min (isocratic run). The fluorimetric detection was carried out at an excitation wavelength of 275 nm and an emission wavelength of 305 nm.

BPA Measurement. BPA measurement was performed by adapting the procedure by Sun et al.[9] An aliquot of each sample (5 mL) was inserted into a 250 mL glass round-bottom flask and was added with acetonitrile (20 mL). Flasks were placed onto a Heidolph Promax 2020 shaker for 25 min. The content of each flask was then filtered through a filter paper and was transferred into a separatory funnel. The flask was rinsed with 5 mL of acetonitrile, which was added to the funnel. Afterward, 35 mL of *n*-hexane was also added to the separatory funnel, and the resulting mixture was shaken for 25 min. The acetonitrile layer was removed from the funnel and was stored in a round-bottom flask, whereas the hexane layer was washed twice with acetonitrile (first with 15 mL, then with 10 mL) which was collected and added in the same round-bottom flask. The solvent was removed from the extract through a rotavapor, and then the flask was washed with 3 mL of a methanol:water (5:95 v/v) solution to be processed by solid-phase extraction (SPE). SPE cartridges were first conditioned with 5 mL of methanol and then with 5 mL of water. Later, the sample was loaded, and the elution was carried out at a flow rate of 3−4 mL/min using a Supelco Visiprep SPE vacuum manifold. The cartridges were then washed with 2 mL of a methanol:water solution (30:70 v/v) and were dried under 152 vacuum pump for 1 min. Finally, the BPA retained in the cartridge was eluted with 3 mL of a methanol:water (80:20 v/v) solution. The eluate was dried by a rotavapor, was dissolved with 1 mL of methanol, and finally was collected in an amber vial before the HPLC analysis. A calibration curve with a correlation coefficient of 0.998 was obtained by injecting standard solutions of BPA at concentrations of 10.0, 20.0, 30.0, 40.0, and 50.0 μg/L. An instrumental LOD equal to 0.003 μg/g dry weight (dw) was calculated using the standard deviation of the response (σ) and the slope of the calibration curve (S) according to the formula 3.3 σ/S. Similarly, an LOQ equal to 0.009 μg/g dw was calculated as 10 σ/S. Recovery percentages at three concentration levels were assessed on six samples (three liquid and three powder milk samples with BPA level below the LOD) by spiking each sample with BPA solutions in methanol at concentrations of 50.0, 100.0, and 1000.0 μg/L. The recoveries were 87 ± 3%. BPA quantification was performed comparing the peak areas obtained in the samples with the BPA standard calibration curve.

For each batch of samples, a blank sample was processed according to the procedures mentioned previously. A total of 16 blanks were analyzed, and all of them showed BPA concentrations well below the LOD value.

BPA Confirmation by LC MS/MS. Because BPA measurements could be affected by matrix-related interferences, a confirmation by Liquid Chromatography Tandem Mass Spectrometry (LC MS/MS) was carried out according to the Shao et al. method.[28]

Instrumental Parameters. Identification was carried out using an alliance 2695 (Waters, U.S.) liquid chromatography equipped with a Quattro Ultima Pt (Micromass, U.K.) tandem mass spectrometer and a symmetry C-18 column (150 mm × 2.1 mm i.d., 3.5 m). The temperature of the column oven was set at 40 °C, the flow rate was 0.2 mL/min, and the injection volume was 10 μL. Mobile phases consisted of methanol and water with 0.1% ammonia. The methanol was linearly increased from 10 to 55% in 10 min, then was increased to 85% in 10 min, was held for 7.5 min, and finally was brought back to 10% and was held for 15 min before the following injection. The mass spectrometer was operated in negative mode electrospray ionization in multiple-reaction monitoring (MRM) mode. The capillary voltage was 3.5 kV, the cone voltage was 70 V, and the multiplier voltage was 650 V. Nitrogen was used as nebulizing, desolvation, and cone gas. In particular, the nebulizing gas was adjusted to the maximum, whereas the flow of the desolvation gas and cone gas was set to 550 L/h and 80 L/h, respectively. The source temperature and the desolvation gas temperature were held at 100 and 300 °C, respectively. The RF lenses 1 and 2 were set at 50 and 0.5, the ion energy 1 and the ion energy 2 were both 0.5, the entrance and exit were zero, and the collision gradient was 3.2 eV. Ultra High Purity (UHP) argon was used as the collision gas for the tandem mass spectrometric analysis, and the pressure in the collision chamber was kept at 2.8×10^{-3} mbar. A calibration curve in the concentration range 1−100 ng/g was obtained by linear regression of the normalized (to the internal standard area) standard solution areas against BPA concentrations. The correlation coefficient was ≥0.999. The intra- and interday repeatabilities of the method were evaluated by injecting standard solutions at three different concentration levels (10, 50, and 100 ng/g) five times during a day (intraday) and during five consecutive days (interday). The intraday reproducibility ranged from 4.0 to 6.5%, while interday reproducibility varied from 4.5 to 6.2%.

Statistical Analysis. A power calculation was undertaken to determine an appropriate sample size for this study. On the basis of literature data,[29] considering DEHP as the most abundant phthalate in infant formula, a two-sided test power calculation was performed. Double of the range value was used as the sigma (0.780 μg/g dry weight). This power calculation indicated that 11 samples in each group would be necessary to detect a 15% difference in the DEHP concentration with a power of 80% at a 5% level of significance. Data distribution was assessed with the Shapiro Wilk's test. A two-sample t test was performed with SPSS 20.0 software (IBM) to assess the differences between DEHP, DnBP, and BPA concentrations in liquid and powder milks. Significance was set at $p < 0.05$. The concentrations below LOD were assumed to be equal to LOD.

Dietary Intake Assessment for Italian Infants (Age 0−4 Months). Daily intake was estimated as

$$\text{Intake} = (C \times V)/\text{BW}$$

where C is concentration, V is volume of milk per day, and BW is body weight. This equation was used to evaluate DEHP, DnBP, and BPA exposure of young children through artificial milk. Dietary exposure was calculated using the blueprint to the budget method (BM) model[30] in accordance with Food and Agriculture Organization of the United Nations/World Health Organization (FAO/WHO) and with the help of weight growth charts by WHO[31] and pediatric nutrition suggestions for our range of age. We considered two possible scenarios: (1) median concentrations of contaminants, infants with average weight to development at the 50th percentile or at the 97th percentile (according to the growth curve by WHO[31]) who introduce daily a medium quantity of milk (medium case); (2) maximum concentrations of contaminants, children who have grown at the 50th percentile or at the 97th percentile and introduce daily a higher quantity of milk (worst case).

DOI: 10.1021/jf505563k
J. Agric. Food Chem. 2015, 63, 3303−3310

RESULTS

Most milk samples showed detectable levels of DEHP (80%, 86% of liquid and 96% of powder milks), DnBP (90%, 82% of liquid milks and 96% of powder milks), and BPA (60%, 43% of liquids milks and 67% of powder milks) (Table 1). The average concentration of DEHP in all milk samples was 1.327 ± 0.724 μg/g dw, and in particular, it was 1.112 ± 0.716 μg/g dw in liquid milks and 1.496 ± 0.729 μg/g dw in powder milks. For DnBP, the average concentration in all milk samples was 0.354 ± 0.305 μg/g dw, namely, 0.384 ± 0.385 μg/g dw in liquid milks and 0.330 ± 0.229 μg/g dw in powder milks. The average concentration of BPA in all milk samples was 0.021 ± 0.022 μg/g dw; it was 0.019 ± 0.037 μg/g dw in liquid milks and 0.023 ± 0.028 μg/g dw in powder milks (Table 1). DEHP concentrations varied from 0.092 to 3.552 μg/g (median 1.136 μg/g), DnBP concentrations varied from 0.008 to 1.624 μg/g (median 0.244 μg/g), and BPA concentrations varied from 0.003 to 0.169 μg/g (median = 0.008 μg/g) (Table 1). Similar concentrations of the three analytes were found in liquid and powder milks, even though containers were of different types. DEHP, DnBP, and BPA concentrations in the HLPC water samples stored as negative controls for reconstituted powder milk were below the LODs.

The concentrations of DEHP, DnBP, and BPA in liquid and powder milks together with the type of packaging are reported in Tables 2 and 3, respectively. Estimates of dietary exposure to DEHP, DnBP, and BPA in the medium and worst cases are shown in Tables 4 and 5. The daily intake of DEHP in the medium case ranged from 19.34 to 24.85 μg/kg body weight (bw) day at the 50th percentile and from 17.54 to 21.14 μg/kg bw day at the 97th percentile. In the worst case, DEHP intake varied between 42.57 at 54.68 μg/kg bw day at the 50th percentile and 38.61 at 46.52 μg/kg bw day at the 97th percentile (Tables 4 and 5). Estimates of dietary exposure to DnBP in the medium case ranged from 4.15 μg/kg bw day to 5.34 μg/kg bw day at the 50th percentile and from 3.77 μg/kg bw day to 4.54 μg/kg bw day at the 97th percentile. In the worst case, the DnBP intake varied between 13.62 and 17.50 μg/kg bw day at the 50th percentile and between 12.35 and 14.89 μg/kg bw day at the 97th percentile (Tables 4 and 5). BPA intakes in the medium and worst cases are shown in Tables 4 and 5. In the medium case, values ranged from 0.14 to 0.17 μg/kg bw day at the 50th percentile and from 0.12 to 0.15 μg/kg bw day at the 97th percentile. In the worst case, the BPA intake varied between 0.99 and 1.27 μg/kg bw day at the 50th percentile and between 0.90 and 1.08 μg/kg bw day at the 97th percentile. Both in the medium and worst cases, the highest intake occurred at the 30th day of life because the amount of consumed milk starts increasing while the baby's weight is still pretty low. As for BPA, for both DnBP and DEHP, the higher values of intake occurred in children at 30 days of age (Tables 4 and 5).

DISCUSSION

Our data indicate the presence of DEPH, DnBP, and BPA in infant formulas. Data relevant to all contaminants showed a wide variability, but no significant differences between liquid and powder milks were found, even though samples were packed in different types of containers. This finding would suggest that DEHP, DnBP, and BPA contamination could arise from raw materials or from manufacturing processes rather than from different packaging. Phthalates, in particular, may

Table 1. Di(2-ethylhexyl)phthalate (DEHP), Di-*n*-butylphthalate (DnBP) and Bisphenol A (BPA) Concentrations in μg/g Dry Weight[a]

	DEHP				DnBP				BPA			
sample	POS (%)	mean ± sd	median	min−max	POS (%)	mean ± sd	median	min−max	POS (%)	mean ± sd	median	min−max
liquid milk (n = 22)	86	1.112 ± 0.716	0.926	0.092−2.919	82	0.384 ± 0.385	0.280	0.008−1.624	43	0.019 ± 0.037	0.003	0.003−0.169
powder milk (n = 28)	96	1.496 ± 0.729	1.159	0.702−3.552	96	0.330 ± 0.229	0.212	0.101−0.812	67	0.023 ± 0.028	0.011	0.003−0.108
total (n = 50)	80	1.327 ± 0.724	1.136	0.092−3.552	90	0.354 ± 0.305	0.244	0.008−1.624	60	0.021 ± 0.022	0.008	0.003−0.169

[a]Mean ± sd, median, and range. There were no significant differences between liquid and powder milk (coupled t test, $p < 0.05$).

DOI: 10.1021/jf505563k
J. Agric. Food Chem. 2015, 63, 3303−3310

Table 2. Concentrations of Di(2-ethylhexyl)phthalate (DEHP), di-*n*-butylphthalate (DnBP) and Bisphenol A (BPA) in Liquid Milk Samples and Type of Packaging

type	packaging	DEHP (μg/g dry weight)	DnBP (μg/g dry weight)	BPA (μg/g dry weight)
infant formula	Tetrapak	0.696	0.075	0.003
		1.831	0.067	0.003
infant formula	PET	0.092	0.082	0.030
		0.219	0.084	0.020
		0.633	0.142	0.009
		2.067	0.0075	0.003
		1.456	0.287	0.003
		0.301	0.067	0.003
		2.099	0.624	0.003
		0.784	0.482	0.058
		0.606	0.216	0.014
		1.877	0.787	0.003
		1.202	0.351	0.003
		0.923	0.899	0.017
		0.256	0.14	0.018
		0.929	0.088	0.003
		2.919	1.624	0.169
		0.852	0.423	0.030
		1.428	0.384	0.003
		0.796	0.807	0.003
		1.137	0.272	0.003
		1.371	0.548	0.003

Table 3. Concentrations of Di(2-ethylhexyl)phthalate (DEHP), Di-*n*-butylphthalate (DnBP) and Bisphenol A (BPA) in Powder Milk Samples in Aluminium Packaging

type	DEHP (μg/g dry weight)	DnBP (μg/g dry weight)	BPA (μg/g dry weight)
infant formula	1.408	0.321	0.003
	1.134	0.199	0.003
	0.702	0.155	0.003
	0.871	0.212	0.028
	1.274	0.161	0.008
	0.883	0.137	0.003
	3.552	0.809	0.011
	2.909	0.765	0.100
	1.023	0.101	0.009
	1.142	0.356	0.022
	0.981	0.392	0.003
	1.024	0.161	0.003
	0.922	0.337	0.043
	1.052	0.709	0.054
	1.018	0.575	0.026
	2.341	0.187	0.012
	0.982	0.123	0.003
	1.723	0.118	0.016
	1.899	0.704	0.003
	1.175	0.148	0.035
	2.409	0.349	0.041
infant formula for gastrointestinal problems	1.213	0.301	0.003
	1.897	0.812	0.108
	1.821	0.201	0.018
rice milk formula	1.723	0.211	0.003
	2.871	0.321	0.003
	0.951	0.184	0.046
premature formula	0.997	0.201	0.003

contaminate milk during the production or preparation of formulas. A main source of contamination results from migration of phthalates from products in contact with food during processing. Several studies concerned the migration of DEHP from the PVC tubing of the milking machine used in dairy farms.[32−34] PVC tubing contains up to 40% DEHP by weight. A Norwegian study showed a clear difference in DEHP levels between raw milk collected by hand milking (about 5 μg/

DOI: 10.1021/jf505563k
J. Agric. Food Chem. 2015, 63, 3303−3310

Table 4. Medium Case, Estimated Daily Dietary Intake of Di(2-ethylhexyl)phthalate (DEHP), Di-*n*-butylphthalate (DnBP) and Bisphenol A (BPA) in Newborns Fed with Liquid or Powder Formulae According to the 50th and 97th of Infant Weight Growth Curve by WHO (2006)

	infant's average weight (kg)		milk assumption (g dry weight/day)		DEHP intake (μg/kg bw day)		DnBP intake (μg/kg bw day)		BPA intake (μg/kg bw[b] day)	
age (days)	50th pctl[a]	97th pctl	50th pctl	97th pctl	50th pctl	97th pctl	50th pctl	97th pctl	50th pctl	97th pctl
15	3.70	4.75	67.61	76.06	20.78	18.21	4.46	3.91	0.15	0.13
30	4.25	5.45	92.96	101.41	24.85	21.14	5.34	4.54	0.17	0.15
45	4.76	6.20	101.41	109.86	24.23	20.15	5.20	4.33	0.17	0.14
60	5.41	6.84	98.59	105.63	20.72	17.54	4.45	3.77	0.15	0.12
75	5.76	7.26	105.63	112.68	20.83	17.64	4.47	3.79	0.15	0.12
90	6.10	7.65	112.68	126.76	20.98	18.82	4.51	4.04	0.15	0.13
120	6.70	8.35	114.08	129.58	19.34	17.63	4.15	3.79	0.14	0.12

[a]pctl, percentile. [b]kg bw, kg body weight.

Table 5. Worst Case, Estimated Daily Dietary Intake of Di(2-ethylhexyl)phthalate (DEHP), di-*n*-butylphthalate (DnBP) and Bisphenol A (BPA) in Newborns Fed with Liquid or Powder Formulae, According to the 50th and 97th of Infant Weight Growth Curve by WHO (2006)

	infant's average weight (kg)		milk assumption (g dry weight/day)		DEHP intake (μg/kg bw day)		DnBP intake (μg/kg bw day)		BPA intake (μg/kg bw[b] day)	
age (days)	50th pctl[a]	97th pctl	50th pctl	97th pctl	50th pctl	97th pctl	50th pctl	97th pctl	50th pctl	97th pctl
15	3.70	4.75	67.61	76.06	45.74	40.07	14.64	12.82	1.06	0.93
30	4.25	5.45	92.96	101.41	54.68	46.52	17.50	14.89	1.27	1.08
45	4.76	6.20	101.41	109.86	53.32	44.33	17.06	14.19	1.24	1.03
60	5.41	6.84	98.59	105.63	45.60	38.61	14.59	12.35	1.06	0.90
75	5.76	7.26	105.63	112.68	45.85	38.83	14.67	12.42	1.06	0.90
90	6.10	7.65	112.68	126.76	46.18	41.43	14.78	13.26	1.07	0.96
120	6.70	8.35	114.08	129.58	42.57	38.80	13.62	12.41	0.99	0.90

[a]pctl, percentile. [b]kg bw, kg body weight.

kg) and machine milking involving PVC tubing (30 μg/kg in milking chamber and 50 μg/kg in collection tank).[33]

Dietary Intake Assessment for Italian Infants (Age 0−4 Months). To assess postnatal exposure to phthalates and BPA, the estimation of daily dietary intake of these contaminants was carried out in 0−4 month old children, as milk is the only food introduced in this age group. Four possible nutrition scenarios were possible, namely, nutrition with infant powder, liquid formula, breast milk, or a combination of these, but we only considered artificially fed babies assuming liquid or powder formulas (or both). The European Food Safety Authority (EFSA) established a tolerable daily intake (TDI) of 50 μg/kg bw for DEHP and 10 μg/kg bw for DnBP.[35,36] As expected, the highest intakes of DEHP and DnBP were estimated among infants with growth at the 50th percentile, who have a lower body weight than those at the 97th percentile.

Daily intake of DEHP in the medium case varied between 20 and 25% and between 18 and 21% of TDI at 50th and 97th percentile, respectively. In the worst case, intake was also lower than TDI, except for the 50th percentile infants aged 30 and 45 days (Table 5).

Daily intake of DnBP in the medium case varied between 42 and 53% and between 38 and 45% of TDI at 50th and 97th percentile, respectively. In the worst case, instead, intake always exceeded TDI, up to 175%. Muller et al.[37] estimated for 0−6 month old Danish infants a daily intake via infant formulas of 9.8 μg/kg bw/day for DEHP and 16.4 μg/kg bw/day for DnBP.[37] Our values for DEHP intake were higher than Muller's both in the medium and in the worst cases, whereas DnBP intake levels were lower in the medium case and similar in the worst case. Our estimates of DEHP and DnBP daily intake were higher than those reported by MAFF[29] for infants 0−3 months old, that is, 13 μg/kg bw/day for DEHP and 2.4 μg/kg bw/day for DnBP. Our estimated BPA daily intakes were well below the temporary tolerable daily intake (t-TDI) established by EFSA in 2015 (4.0 μg/kg bw). In the medium case, our intake ranges were 3.5−4.3% and 3.0−3.8% of t-TDI for the 50th and 97th percentile respectively, which increased in the worst case to 25−31% and 23−28% of t-TDI for the 50th and 97th percentile, respectively. The results reported in the worst case are consistent with oral exposure data shown in Draft Scientific Opinion on the risks to public health related to the presence of bisphenol A (BPA) in foodstuff by EFSA.[38] Diet is the main source of exposure to BPA in infants aged 0−4 months.[38] Minor pathways of introduction could be the inhalation or ingestion of dust, dermal contact, and the mouthing of toys. Until a few years ago, babies could introduce BPA from polycarbonate baby bottles, especially when bottles were heated and reused multiple times.[2,7] The EU Regulation No. 321/2011 imposed not to use BPA in the manufacture of baby bottles, thus reducing exposure. In 2008, a report of the U.S. National Toxicology Program (NTP) provided daily exposure estimates for infants, children, and adults on the basis of realistic scenarios.[39] The highest daily exposure to BPA was estimated to occur in infants and children. Formula-fed infants (0−6 months of age) had estimated daily intakes of 1−11 μg/kg bw. In 2010, the FAO and WHO jointly held an Expert Meeting on BPA, whose final report was published in 2011.[40] The report identified 0−6 month infants fed with liquid formulas in polycarbonate bottles as the subpopulation with the highest dietary exposure to BPA, namely, 2.4 μg/kg bw per day

DOI: 10.1021/jf505563k
J. Agric. Food Chem. 2015, 63, 3303−3310

(average) and 4.5 μg BPA/kg bw per day (95th percentile). In 2012, a probabilistic exposure assessment using data from recent Canadian surveys suggested that daily exposure to BPA in children ranged from 0.083 μg/kg bw (0−1 month old) to 0.164 μg/kg bw (children 4−7 months of age).[41] Our data resemble those of Health Canada but are lower than those of NTP and FAO/WHO, probably because the problem of BPA migration from baby bottles in Europe has been solved. The different packages (Tetrapak, PET, and aluminum) represent a possible bias of the present study. However, the studied contaminants can be found not only in Tetrapak and PET but also in aluminum packages, as these are often internally coated with plastic derivatives.

Our data show a widespread contamination of infant formulas from the three investigated contaminants, either of environmental or process origin. Our findings demonstrate that infant formulas may represent a main source for the simultaneous exposure to DEHP, DnBP, and BPA in babies. This risk is particularly relevant for DEHP and DnBP because intake from formulated milk could exceed in the worst case the TDI from EFSA. In conclusion, potential hazards exist for infants fed with baby formula, as these endocrine disruptors show the highest toxicity in infant population. TDIs for the three investigated contaminants set by EFSA refers to adult and infant populations, indiscriminately, but since children and infants are developing individuals, providing a specific TDI could be worthwhile as TDIs intended to children would help the protection of the most vulnerable part of the population from a severe public health hazard.

AUTHOR INFORMATION

Corresponding Author

*E-mail: tcirillo@unina.it. Phone: +39 081 2539450. Fax: +39 081 2539407.

Notes

The authors declare no competing financial interest.

REFERENCES

(1) Cobellis, L.; Latini, G.; De Felice, C.; Razzi, S.; Paris, I.; Ruggieri, F.; Mazzeo, P.; Petraglia, F. High plasma concentrations of di-(2-ethylhexyl)-phthalate in women with endometriosis. *Hum. Reprod.* **2003**, *18*, 1512−1515.

(2) Jenkins, S.; Raghuraman, N.; Eltoum, I.; Carpenter, M.; Russo, J.; Lamartiniere, C. A. Oral exposure to bisphenol A increases dimethylbenzanthracene induced mammary cancer in rats. *Environ. Health Perspect.* **2009**, *117*, 910−915.

(3) Habert, R.; Muczynski, V.; Lehraiki, A.; Lambrot, R.; Lécureuil, C.; Levacher, C.; Coffigny, H.; Pairault, C.; Moison, D.; Frydman, R.; Rouiller-Fabre, V. Adverse effects of endocrine disruptors on the foetal testis development: focus on the phthalates. *Histochem. Cytobiol.* **2009**, *47*, 67−74.

(4) Latini, G.; Del Vecchio, A.; Massaro, M.; Verrotti, A.; De Felice, C. Phthalate exposure and male infertility. *Toxicology* **2006**, *226*, 90−98.

(5) Latini, G.; Knipp, G.; Mantovani, A.; Marcovecchio, M. L.; Chiarelli, F.; Söder, O. Endocrine disruptors and human health. *Mini-Rev. Med. Chem.* **2010**, *10*, 846−55.

(6) Sathyanarayana, S.; Alcedo, G.; Saelens, B. E.; Zhou, C.; Dills, R. L.; Yu, J.; Lanphear, B. Unexpected results in a randomized dietary trial to reduce phthalate and bisphenol A exposures. *J. Exposure Sci. Environ. Epidemiol.* **2012**, *23*, 378−384.

(7) Wang, J.; Jenkins, S.; Lamartiniere, C. Cell proliferation and apoptosis in rat mammary glands following combinational exposure to bisphenol A and genistein. *BMC Cancer* **2014**, *14*, 379.

(8) Latini, G. Monitoring phthalate exposure in humans. *Clin. Chim. Acta* **2005**, *361*, 20−29.

(9) Sun, C.; Leong, L. P.; Barlow, P. J.; Chan, S. H.; Bloodworth, B. C. Single laboratory validation of a method for the determination of Bisphenol A; Bisphenol A diglycidyl ether and its derivatives in canned foods by reversed-phase liquid chromatography. *J. Chromatogr., A* **2006**, *1129*, 145−148.

(10) Latini, G.; Del Vecchio, A.; Massaro, M.; Verrotti, A.; De Felice, C. In utero exposure to phthalates and fetal development. *Curr. Med. Chem.* **2006**, *13*, 2527−2534.

(11) Yavasoğlu, N. U.; Köksal, C.; Dağdeviren, M.; Aktuğ, H.; Yavasoğlu, A. Induction of oxidative stress and histological changes in liver by subacute doses of butyl cyclohexyl-phthalate. *Environ. Toxicol.* **2012**, *29*, 345−53.

(12) Lovekamp-Swan, T.; Davis, B. J. Mechanisms of phthalate ester toxicity in the female reproductive system. *Environ. Health Perspect.* **2003**, *111*, 139−145.

(13) Singh, S.; Li, S. S. Epigenetic effects of environmental chemicals bisphenol a and phthalates. *Int. J. Mol. Sci.* **2012**, *13*, 10143−10153.

(14) Oldring, P. K.; Castle, L.; O'Mahony, C.; Dixon, J. Estimates of dietary exposure to bisphenol A (BPA) from light metal packaging using food consumption and packaging usage data: a refined deterministic approach and a fully probabilistic (FACET) approach. *Food Addit. Contam., Part A: Chem., Anal., Control, Exposure Risk Assess.* **2014**, *31*, 466−489.

(15) FDA (Food and Drug Administration). *Update on Bisphenol A for Use in Food Contact Applications*; Silver Spring, MD, 2010.

(16) Bashore, T. M.; Bates, E. R.; Berger, P. B.; Clark, D. A.; Cusma, J. T.; Dehmer, G. J.; Kern, M. J.; Laskey, W. K.; O'Laughlin, M. P.; Oesterle, S.; Popma, J. J.; O'Rourke, R. A.; Abrams, J.; Bates, E. R.; Brodie, B. R.; Douglas, P. S.; Gregoratos, G.; Hlatky, M. A.; Hochman, J. S.; Kaul, S.; Tracy, C. M.; Waters, D. D.; Winters, W. L., Jr. Task Force on Clinical Expert Consensus Documents. American College of Cardiology/Society for Cardiac Angiography and Interventions Clinical Expert Consensus Document on cardiac catheterization laboratory standards: A report of the American College of Cardiology Task Force on Clinical Expert Consensus Documents. *J. Am. Coll. Cardiol.* **2001**, *37*, 2170−2214.

(17) Chapin, R. E.; Adams, J.; Boekelheide, K.; Gray, L. E., Jr; Hayward, S. W.; Lees, P. S.; et al. NTP344 CERHR expert panel report on the reproductive and developmental toxicity of bisphenol A. *Birth Defects Res., Part B: Dev. Reprod. Toxicol.* **2008**, *83*, 157−395.

(18) Hengstler, J. G.; Foth, H.; Gebel, T.; Kramer, P. J.; Lilienblum, W.; Schweinfurth, H.; Völkel, W.; Wollin, K. M.; Gundert-Remy, U. Critical evaluation of key evidence on the human health hazards of exposure to bisphenol A. *Crit. Rev. Toxicol.* **2011**, *41*, 263−291.

(19) Vom Saal, F. S.; Hughes, C. An extensive new literature concerning low-dose effects of bisphenol A shows the need for a new risk assessment. *Environ. Health Perspect.* **2005**, *113*, 926−933.

(20) Belcher, S. M.; Chen, Y.; Yan, S.; Wang, H. S. Rapid estrogen receptor-mediated mechanisms determine the sexually dimorphic sensitivity of ventricular myocytes to 17β-estradiol and the environmental endocrine disruptor bisphenol A. *Endocrinology* **2012**, *153*, 712−720.

(21) Rubin, B. S. Bisphenol A: an endocrine disruptor with widespread exposure and multiple effects. *J. Steroid Biochem. Mol. Biol.* **2011**, *127*, 27−34.

(22) Sriphrapradang, C.; Chailurkit, L. O.; Aekplakorn, W.; Ongphiphadhanakul, B. Association between bisphenol A and abnormal free thyroxine level in men. *Endocrine* **2013**, *44*, 441−447.

(23) Commission Directive 2011/08/EU. Official Journal of the European Union. http://eurlex.europa.eu/LexUriServ/LexUriServ.do?uri=OJ:L:2011:026:0011:0014:EN:PDF (accessed Aug 02, 2014).

(24) Cirillo, T.; Fasano, E.; Castaldi, E.; Montuori, P.; Amodio Cocchieri, R. Children's exposure to Di(2 ethylhexyl)phthalate and dibutylphthalate plasticizers from school meals. *J. Agric. Food Chem.* **2011**, *59*, 10532−10538.

(25) Cirillo, T.; Fasano, E.; Esposito, F.; Montuori, P.; Amodio Cocchieri, R. Di(2-ethylhexyl)phthalate (DEHP) and di-n-butylph-

DOI: 10.1021/jf505563k
J. Agric. Food Chem. 2015, 63, 3303−3310

thalate (DBP) exposure through diet in hospital patients. *Food Chem. Toxicol.* **2013**, *51*, 434−438.
(26) Latini, G.; De Felice, C.; Verrotti, A. Plasticizers; infant nutrition and reproductive health. *Reprod. Toxicol.* **2004**, *19*, 27−33.
(27) Latini, G.; Wittassek, M.; Del Vecchio, A.; Presta, G.; De Felice, C.; Angerer, J. Lactational exposure to phthalates in Southern Italy. *Environ. Int.* **2009**, *35*, 236−239.
(28) Shao, B.; Han, H.; Hu, J. Y.; Zhao, J.; Wu, G. H.; Xue, Y.; Ma, Y. L.; Zhang, S. J. Determination of alkylphenol and bisphenol A in beverages using liquid chromatography/electrospray ionization tandem mass spectrometry. *Anal. Chim. Acta* **2005**, *530*, 245−252.
(29) MAFF (Ministry of Agriculture, Forestry and Fisheries). Phthalates in infant formulae − follow up survey. Food surveillance information fact sheet, MAFF: UK, 1998; No. 168.
(30) WHO (World Health Organization). Dietary exposure assessment of chemicals in food. In *Principles and Methods for the Risk Assessment of Chemicals in Food Environmental Health Criteria 240*; Sheffer, M, Ed.; Wissenchaftliche Verlagsgesellschaf: Stuttgart, Germany, 2009; Chapter 6;http://whqlibdoc.who.int/ehc/WHO_EHC_240_9_eng_Chapter6.pdf (accessed June 08, 2014).
(31) WHO (World Health Organization). Child Growth standards. http://www.who.int/childgrowth/standards/weight_for_age/en/ (accessed Aug 02, 2014).
(32) Castle, L.; Gibert, J.; Eklund, T. Migration of plasticizer from poly(vinylchloride) milk tubing. *Food Addit. Contam.* **1990**, *7*, 591.
(33) Feng, Y. L.; Zhu, J.; Sensenstein, R. Development of a headspace solid phase microextraction method combined with gas chromatography mass spectrometry for the determination of phthalate esters in cow milk. *Anal. Chim. Acta* **2005**, *538*, 41−48.
(34) Ruuska, R. M.; Korkeala, H.; Liukkonen-Lilja, H.; Suortti, T.; Salminen, K. Migration of contaminants from milk tubes and teat liners. *J. Food Protect.* **1987**, *50*, 316.
(35) EFSA (European Food Safety Authority).. *EFSA J.* **2005**, *242*, 1−17.
(36) EFSA (European Food Safety Authority).. *EFSA J.* **2005**, *243*, 1−20.
(37) Müller, A. K.; Nielsen, E.; Ladefoged, O. Human exposure to selected phthalates in Denmark. Institute of Food Safety and Nutrition: Denmark, 2003.
(38) EFSA (European Food Safety Authority). Scientific Opinion on the risks to public health related to the presence of bisphenol A (BPA) in foodstuffs. http://www.efsa.europa.eu/en/efsajournal/pub/3978.htm (accessed Feb 19, 2015).
(39) NTP-CERHR (National Toxicological Program - Center for the Evaluation of Risks to Human Reproduction). *Monograph on the potential human reproductive and developmental effects of bisphenol A*; USA, 2008; No. 08−5994.
(40) FAO-WHO (Food and Agricultural Organization of the United Nations and World Health Organization). Joint FAO/WHO Expert Meeting to Review Toxicological and Health Aspects of Bisphenol A, Ottawa, Canada, 2011.
(41) Health Canada. Assessment of Bisphenol A (BPA) Exposure from Food Sources, 2012.

DOI: 10.1021/jf505563k
J. Agric. Food Chem. 2015, 63, 3303−3310

Table 1. Abbreviations and Structural Formulas of Some Uncommon Chemicals

Abbreviation	Chemical name	Chemical structural formula
PEITC	Phenylethyl isothiocyenate	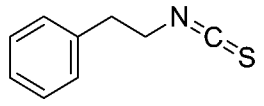
PEITC-GSH	S-(N-Phenylethylthiocarbamoyl)-glutathione	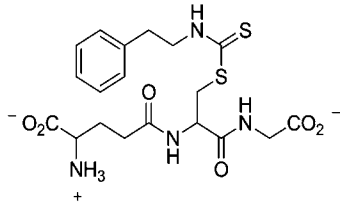
PEITC-CYS-CLY	S-(N-Phenylethylthiocarbamoyl)-cysteinylglycine	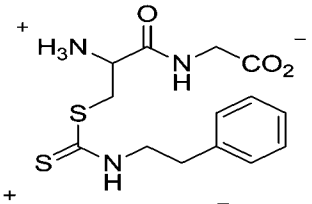
PEITC-CYS	S-(N-Phenylethylthiocarbamoyl)-cysteine	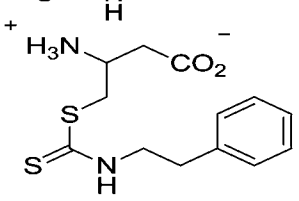
PEITC-NAC	N-Acetyl-S-(N-Phenylethylthiocarbamoyl)-cysteine	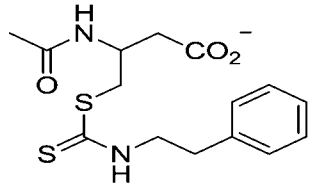

■ ACTIVATION OF APOPTOSIS PATHWAYS

Apoptosis, a form of programmed cell death, is a pivotal defense against the occurrence of cancer and is essential for metazoans in maintaining tissue homeostasis. In principle, there are two alternative pathways that initiate apoptosis: one is mediated by mitochondria, referred to as the "intrinsic pathway";[25] the other is mediated by death receptors on the cell surface, referred to as the "extrinsic pathway".[26] In addition, a third apoptotic pathway, the "endoplasmic reticulum (ER) stress" pathway, has been described recently.[27] All of these mechanisms of apoptosis are associated with caspase activation damage sensing and proapoptotic signaling.

■ THE INTRINSIC (MITOCHONDRIAL) PATHWAY

Mitochondria have been shown to have a vital role in apoptotic signal transduction.[28,29] Emerging evidence suggests that PEITC can cause oxidative mitochondrial damage by enhancing the intracellular ROS to a toxic level.[30−32] Possible explanations for these findings are that (1) PEITC conjugates with GSH, and the conjugate compounds export from cancer cells;[33] (2) time-dependent ROS accumulation induced by PEITC could induce ROS-mediated lipid peroxidation of mitochondrial membrane, such as oxidation of cardiolipin,[30] followed by the loss of membrane integrity ($\Delta\Psi$m), and release apoptosis-inducing factor (AIF) as well as apoptogenic cytochrome *c*; (3) cytokines influx into the cytosol, and then activate caspase family members that are executionary arm of apoptotic

DOI: 10.1021/jf504627e
J. Agric. Food Chem. 2015, 63, 3311−3322

Table 2. Other Abbreviations Used

abbreviation	name
GSH	c-glutamate-cysteine-glycine
NAC	*N*-acetylcysteine
ΔΨm	membrane integrity
AIF	apoptosis-inducing factor
PTP	permeability transition pore
Bcl-2	B-cell leukemia/lymphoma-2
TRAIL	tumor necrosis factor-related apoptosis-inducing ligand
DR4	death receptor 4/TNF-related apoptosis-inducing ligand
DR5	death receptor 5/TNF-related apoptosis-inducing ligand
Fas L	Fas ligand
FADD	Fas-associated death domain
NF-κB	nuclear factor kappa B
PI3K	phosphatidylinositol 3 kinase
TLR3	toll-like receptor 3
JNK	Jun N-terminal kinase
MKK7	mitogen-activated protein kinase 7
MAPK	p38 mitogen-activated protein kinase
CDK	cyclin-dependent kinase
ATM/ATR	ataxia telangiectasia mutated/ataxia telangiectasia and Rad3-related
DMEs	drug metabolizing enzymes
GSTs	*S*-transferases
QR	quinonereductase
γGCS	γ-glutamyl cysteine-synthetase
HO-1	heme oxygenase1
NQO1	NAD(P)H quinone oxidoreductase1
MDR	multidrug resistance
DNM	daunomycin
VBL	vinblastine
ABCG2	breast cancer resistance protein
MRP-1	multidrug resistance associated protein-1
Pgp-1	P-glycoprotein-1
NPEITC	novel alkyne-tagged ITC

machinery.[34,35] The permeability transition pore (PTP) is an unselective voltage-dependent mitochondrial channel and is central to mitochondrial vital functions. PTP opening can dissipate the transmembrane inner potential, trigger matrix swelling, release cytochrome *c*, and subsequently elicit cell apoptosis.[36] Studies from our own laboratory have shown that cell apoptosis of MCF-7 induced by PEITC is associated with ROS-mediated PTP opening. Ca^{2+} can also open PTP, leading to the rapid loss of transmembrane inner potential.[37] Further studies are needed to define whether calcium overload contributes to PEITC-induced PTP activity.

The Bcl-2 (B-cell leukemia/lymphoma-2) family proteins include both antiapoptotic members (such as Bcl-2 and Bcl-xL) and proapoptotic members (such as Bax and Bid). They are distributed not only in the mitochondrial outer membrane but also in the cell membrane, ER, and nuclear membrane. Studies have found that Bcl-2 proteins reside upstream of irreversible cellular damage and focus the greatest efforts at the level of mitochondria.[38] PEITC can regulate intracellular location of proapoptotic proteins or antiapoptotic proteins promoting the release of cytochrome *c* from the mitochondria.[39] For example, PEITC induced apoptosis via downregulation of Bcl-2/XIAP and triggering the mitochondrial pathway in MCF-7 cells.[40] Similar results have shown that PEITC triggered apoptosis through promotion of Bax and Bid expression, leading to the decreased levels of ΔΨm and release of cytochrome *c*, and then activating the caspase-dependent cell death.[41,42] Moreover, in ovarian cancer OVCAR-3 cells, PEITC decreased the level of prosurvival Bcl-2 protein while simultaneously increasing the level of proapoptotic Bax protein, which in turn caused activation of caspase-9 and -3 leading to cell apoptosis.[43]

THE EXTRINSIC (RECEPTOR-MEDIATED) PATHWAY

The death receptor pathways for caspase activation are referred to as the extrinsic apoptosis pathways.[35] Tumor necrosis factor-related apoptosis-inducing ligand (TRAIL) has the unique activity of activating cell death exclusively in tumor cells. TRAIL can bind with two death receptors (DRs), DR4 (TRAIL-R1) and DR5 (TRAIL-R2), both of which are type I transmembrane proteins.[44,45] Studies have shown that PEITC can enhance TRAIL-induced apoptosis through downregulation of cell survival proteins and upregulation of the death receptors (DR4 and DR5). For example, in human oral cancer HN22 cells, PEITC activates p38 MAPK through increasing phospho-p38 MAPK. As p38 MAPK are the upstream targets of DR5, the function of DR5 regulating apoptosis induced by PEITC is strongly associated with the p38 MAPK pathway.[46] However, another study found that PEITC increased the expression of DR4 and DR5 by downregulating the phosphorylation of ERK 1/2, neither phospho-JNK nor phospho-p38 MAPK. One possible explanation for these contrary findings is that the different kind of cell types might have different pathway responses when cells are exposed to PEITC.[47] Previous studies have demonstrated that PEITC can enhance the intracellular ROS and induce apoptosis. And, a recent study demonstrated that PEITC enhanced TRAIL-induced apoptosis through the upregulation of DR5 receptors on the ROS-induced-p53.[48] Fas is another cell surface death receptor involved in the transduction of apoptotic signals in both normal and cancer cells. Fas ligand (Fas L) binding followed by Fas-receptor (Fas) oligomerization leads to formation of a death-inducing signal complex and recruitment of the adapter molecule Fas-associated death domain (FADD). FADD recruits and aggregates the pro form of caspase-8, leading to the activation of caspase-8, and then cleaved procaspase-3 and procaspase-9.[49] PEITC can sensitize the human bladder carcinoma cells leading to Fas-mediated apoptosis. The intracellular GSH out of the cells provides a potential mechanism for PEITC-induced apoptosis.[15] But the concise pathogenesis is still not clear.

THE "ENDOPLASMIC RETICULUM (ER) STRESS" PATHWAY

Recently, the "ER stress" pathway has been recognized as the third apoptotic pathway.[50] ER stress, induced by the accumulation of unfolded or malfolded proteins, activates various apoptotic pathways.[27]

Very recent studies demonstrated that PEITC induced cell apoptosis in a concentration-dependent, ROS/Ca^{2+}-independent manner.[51,52] Similar results showed that PEITC promoted Ca^{2+} movement by inducing phospholipase C-dependent Ca^{2+} release from endoplasmic reticulum and Ca^{2+} entry via store-operated Ca^{2+} channels in PEITC-treated human prostate cancer cells (PC3).[14,51] Moreover, the rapid increase of cytosolic Ca^{2+} may cause elevation of mitochondrial Ca^{2+} and decrease of Ca^{2+} in endoplasmic reticulum, and such imbalance of Ca^{2+} may trigger a variety of cascades leading to cell death.[53]

DOI: 10.1021/jf504627e
J. Agric. Food Chem. 2015, 63, 3311−3322

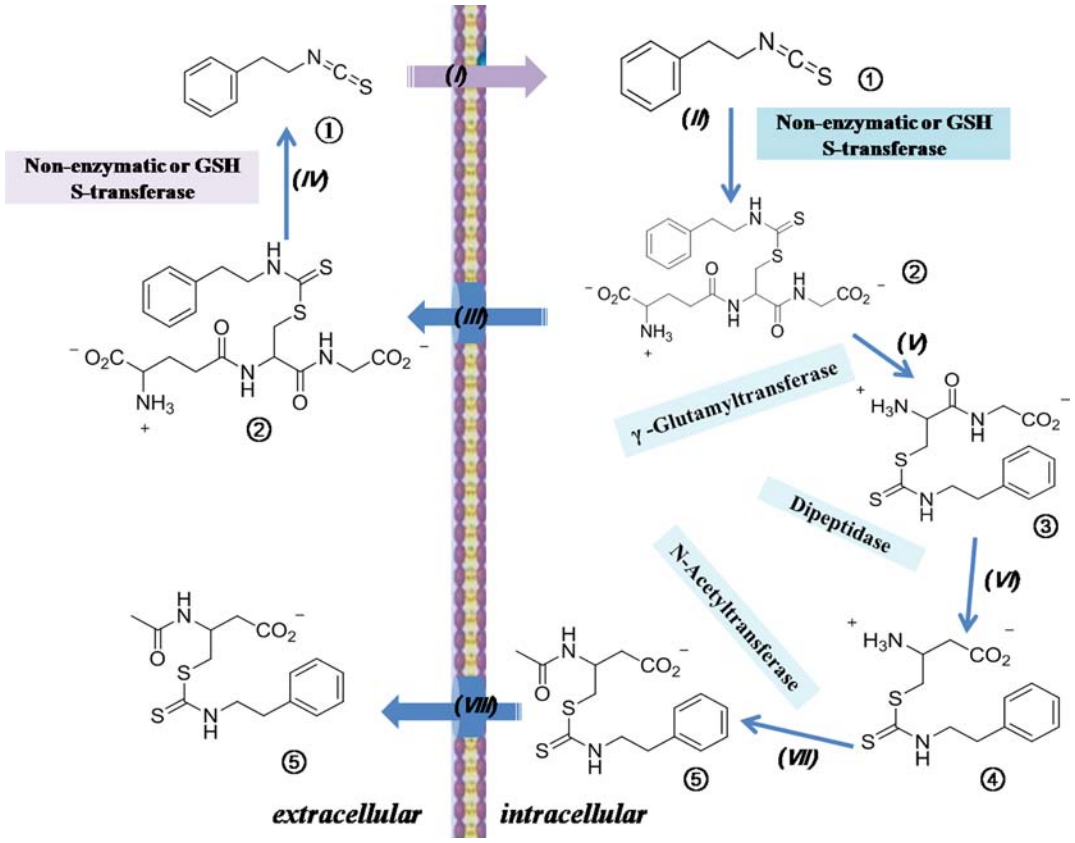

Figure 1. Metabolism of phenylethyl isothiocyanate by the mercapturic acid pathway. (I) PEITC (①) initially diffuses into cells and (II) and is rapidly conjugated to glutathione (GSH) via the action of glutathione *S*-transferases (GST). (III) The GSH conjugates (②) are exported from the cells via efflux pumps, and then (IV) the conjugates are hydrolyzed to the free PEITC, which is able to re-enter the cell. (V) But the intracellular PEITC−GSH is subsequently converted to the cysteinylglycine conjugate (③) by the action of γ-glutamyl transpeptidase and then (VI) converted to the cysteine conjugate (④) by the action of γ-glutamyl transpeptidase. (VII) Finally, the PEITC−cysteine conjugates are converted to NAC conjugates by the action of *N*-acetyltransferase and (VIII) excreted in the urine.

In addition to Ca^{2+} accumulation, inhibition of proteasomal activity and disruption of protein disulfide bond formation may trigger ER stress response. Various studies showed that PEITC significantly inhibited proteasome activities, including chymotrypsin-like, trypsin-like, and caspase-like, by inhibition of rapid accumulation of p53 and IκB nuclear factor-kappa B.[54,55] For example, PEITC can selectively induce degradation of α- or β-tubulin proteasome in different cancers, including non-small lung cancer A549 cells,[56] prostate cancer cells,[57] and breast cancer cells.[58] Interestingly, PEITC inhibits proteasome activity presumably through direct binding, suggesting that the proteasome, like tubulin, may serve as a molecular target of PEITC.

Taken together, the predominant apoptotic pathway targeted by PEITC may differ between cell types. The exact mechanism is difficult to determine because of the cross-talk between the different apoptotic pathways (Figure 2).

INHIBITION OF THE SURVIVAL PATHWAYS

The following section will summarize studies that investigated the effect of PEITC on survival pathways (Figure 3). Nuclear factor kappa B (NF-κB), phosphatidylinositol 3 kinase (PI3K), and p38 mitogen-activated protein kinase (MPKC) pathways are important for cell survival, proliferation, and differentiation.

THE NF-κB SURVIVAL PATHWAY

The NF-κB survival pathway plays a key role in cancer chemoprevention due to its involvement in tumor cell growth, proliferation, invasion, and survival.[59−61] NF-κB is sequestered in the cytoplasm in resting cells by combining with inhibitor proteins (IκB proteins). In response to stimulating factors, IκB was phosphorylated by the inhibitor of κB (IKK) kinase complex and further degraded, thus releasing active NF-κB dimers and allowing NF-κB to translocate to nucleus.[62] PEITC has been shown to have promising anti-inflammatory properties through the ubiquitous NF-κB signaling pathway.[16,63,64] For example, Xu et al. demonstrated the role of PEITC on NF-κB transcriptional activation and NF-κB-regulated gene expression in vitro.[59] A similar result showed that PEITC induced cell death by inhibition of NF-kB and EGFR activities in prostate cancer cells.[65] In these studies, PEITC exhibited its anti-inflammatory activity via the direct suppression of IκB kinase α/β (IKKα/β) phosphorylation, IκBα phosphorylation, and subsequent p65 NF-κB nuclear translocation.[66] Studies have demonstrated that Toll-like receptor 3 (TLR3) is one of the primary sensors of double stranded (ds) RNA and mediates NF-κB activation.[18] More recently, another study showed that PEITC could activate prosurvival NF-κB pathway by inhibiting TLR3 mediated IRF3 signaling.[67] However, the biochemical details of PEITC on IRF3 signaling are needed in further step.

Interestingly, PEITC and curcumin can exert their additive inhibitory effects on cell proliferation and ultimately lead to

DOI: 10.1021/jf504627e
J. Agric. Food Chem. 2015, 63, 3311−3322

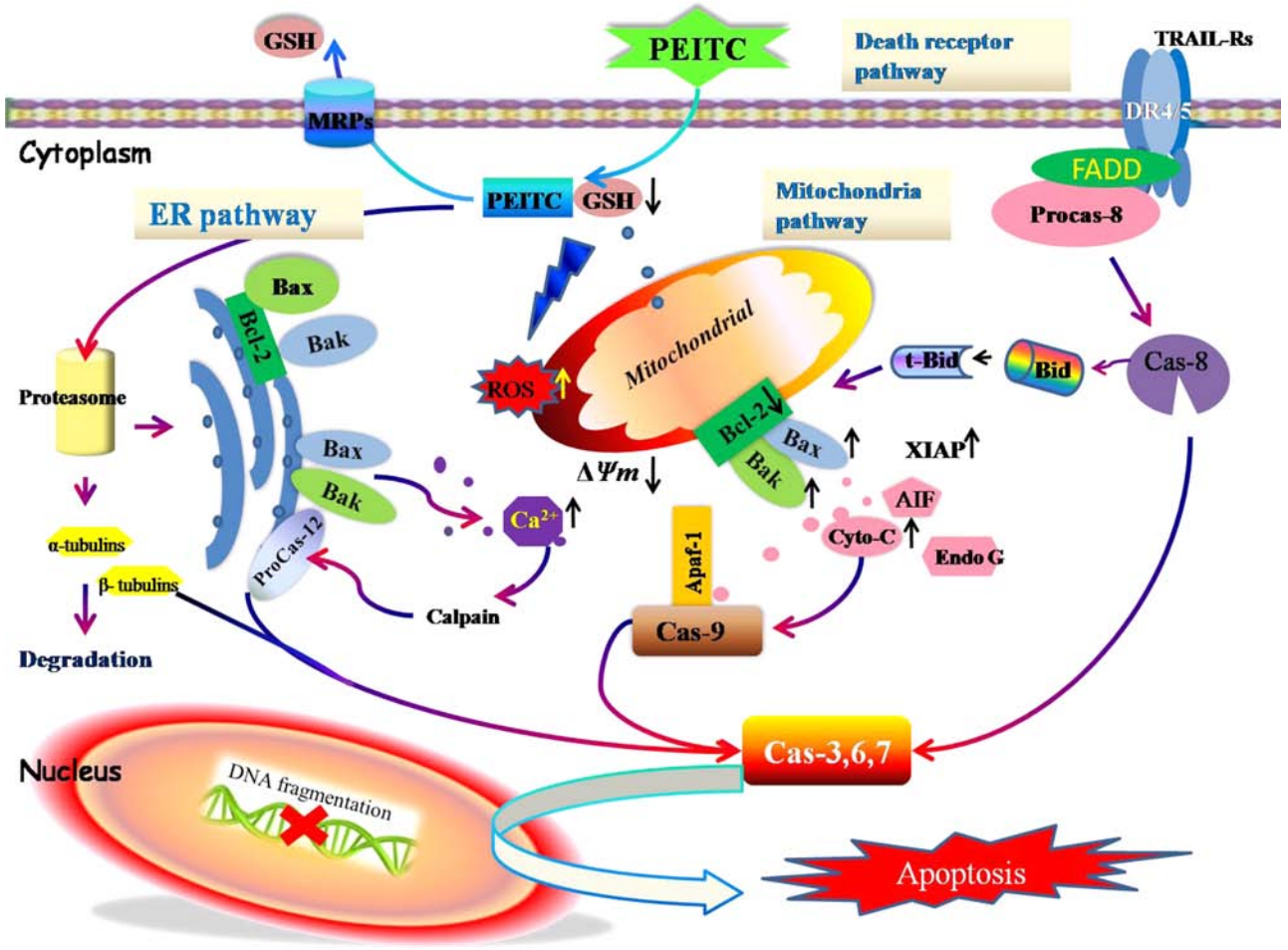

Figure 2. Signaling and molecular pathway of apoptosis in carcinoma cells. (1) In the mitochondrial pathway, PEITC-induced cell apoptosis interacts with the Bcl-2 family of proteins and then releases cytochrome *c*, AIF, and endo G, thereby forming the apoptosome which activates caspase-9 and is capable of proteolytically processing caspase-3 to induce apoptosis. (2) In the death receptor pathway, PEITC targets upregulation of death receptors which can interact with their ligands and recruit adaptor protein and initiator procaspases-8. Then, the active initiator caspase-8 activates the effector caspase-3 to induce apoptosis or to initiate degradation of Bid and to yield cytochrome *c* releasing from mitochondria. (3) In the ER pathway, PEITC induces cytoplasmic Ca^{2+} concentration, as a result of ER stress, resulting in the activation of caspase-12. Also, PEITC can induce degradation of proteasome, which may disrupt protein disulfide bond formation and trigger ER stress response.

programmed cell death of tumor cells by significant inhibition of NF-kB cell survival signal pathway and EGFR signaling pathway.[65] By contrast, others showed that MAPK/ERK signaling pathway, not NF-κB signaling pathway, was associated with apoptosis induced by PEITC plus cisplatin in HeLa cells.[68]

THE AKT SURVIVAL PATHWAY

Akt (also known as protein kinase B or PKB) comprises three closely related isoforms, Akt1, Akt2, and Akt3 (or PKB$\alpha/\beta/\gamma$ respectively).[69] It is a serine-threonine kinase intimately involved in the regulation of cell survival and is activated by recruitment to the cell membrane through PI3K.

Several research teams have demonstrated that PEITC can inhibit the PI3K/Akt signaling pathway and the downstream in recent years.[17,70] For example, PEITC inhibited ovarian tumor growth in vivo by suppressing the EGFR-AKT pathway.[71] Also, Xiao et al. demonstrated that PEITC treatment caused a decrease in survival of human umbilical vein endothelial cells by suppression of VEGF, downregulation of VEGF receptor 2 protein levels, and inactivation of prosurvival serine-threonine kinase Akt.[72] Very recent studies demonstrated that PEITC inhibited hypoxia-induced accumulation of HIF-1α and VEGF expression in human glioma cells, at least partly through the PI3K/AKT pathway.[73] Similar results showed that PEITC could target the Akt/JNK/Mcl-1 pathway. An in vivo study showed that the activity of the Akt is inhibited by PEITC, leading to Jun N-terminal kinase (JNK) activation, and culminating in Mcl-1 downregulation.[17] Moreover, PEITC can suppress the activating of Akt/mTOR, a downstream of Akt pathway.[74] Data from treatment of LNCaP and PC-3 cells with PEITC showed that levels of S2448-phosphorylated mTOR and phosphorylation of mTOR downstream target p70s6k (T389) decreased in both cell lines.[75]

THE MAPK SURVIVAL PATHWAY

Various studies have shown that PEITC can inhibit invasion and migration in cancer cells by MAPK (JNK, ERK1/2, and p38) pathways.[74,76] Indeed, in ovarian cancer cells, PEITC can inhibit Akt, ERK1/2 survival signaling, and c-Myc while simultaneously activating proapoptotic p38 and JNK1/2.[43] A similar result showed that PEITC exerted an inhibitory effect on the ERK1/2, mitogen-activated protein kinase 7 (MKK7), and MAP kinase3 (MEKK3) in human gastric cancer cells. Thus, suppressing MAPK pathways might be one of the

DOI: 10.1021/jf504627e
J. Agric. Food Chem. 2015, 63, 3311−3322

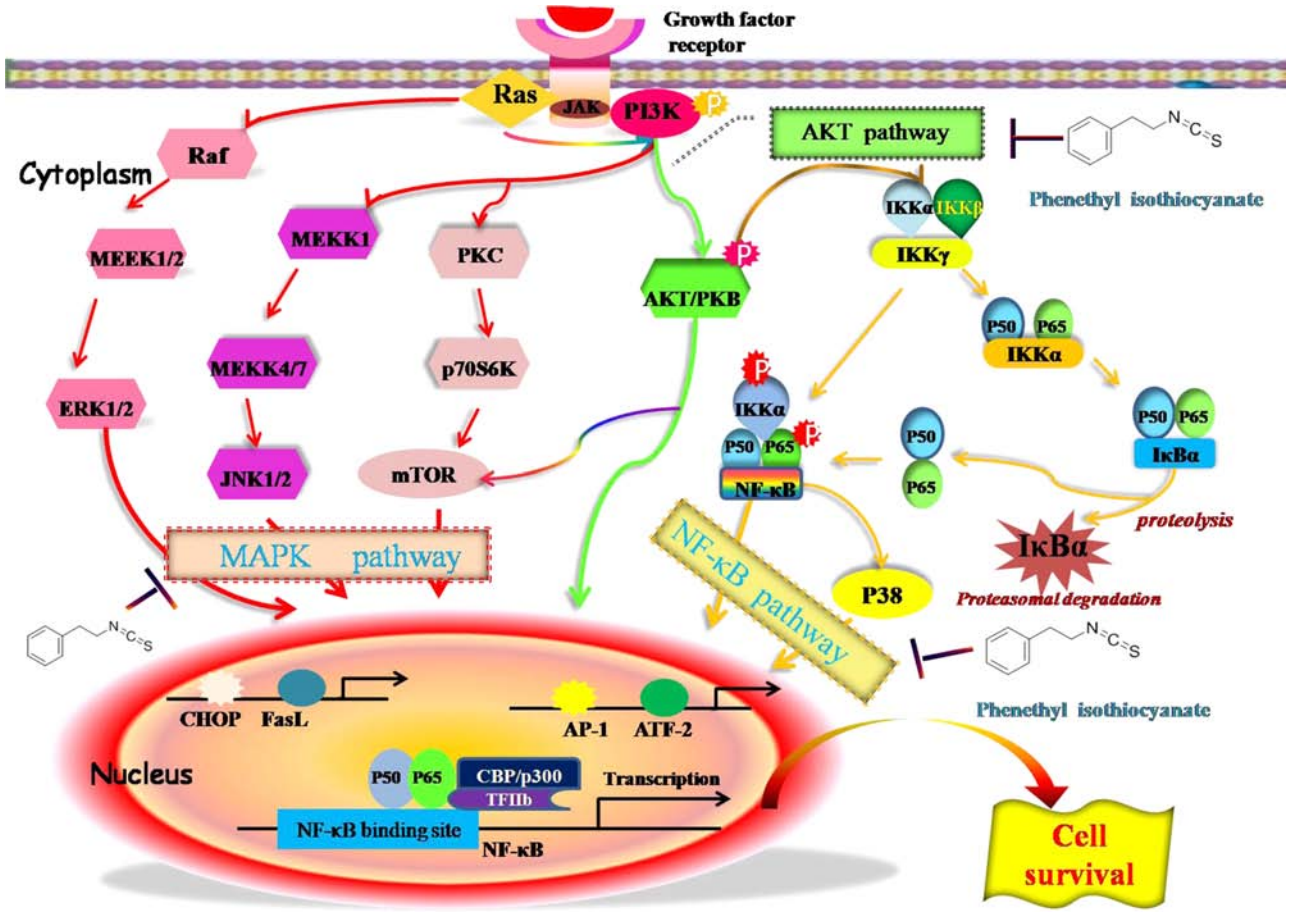

Figure 3. Regulation of survival signaling pathways by phenethyl isothiocyanate. Inactivation of survival pathways, including NF-κB, AKT, and MAPK pathways by PEITC, is considered as one important chemopreventive mechanism. (1) NF-κB is normally sequestrated by IκB which is subjected to phosphorylation by IκK. Phosphorylation of IκB by IκK increases degradation of IκB, and then the NF-κB translocates into the nucleus and activates the transcription of target genes involved in cell survival. PEITC has been shown to inhibit activation of NF-κB through inhibiting IκK. (2) PEITC can suppress the activating of AKT/PKB pathway and AKT/mTOR, a downstream of Akt pathway, by suppression of activating phosphorylations of Akt and mTOR. (3) MAPK signaling pathways such as ERK, JNK, and PKC can regulate the transcriptional activities of transcription factors that are induction of transcription of target genes. PEITC can downregulate the protein levels of MAPK pathways, such as ERK1/2, protein kinase C (PKC), and JNK1/2, and inhibit transcription survival genes.

mechanisms of migration and invasion of cancer cells inhibited by PEITC.[16]

Previous research has demonstrated that some agents inducing PKC activation can also stimulate MAPK, suggesting that there is a crosstalk between PKC and MAPK signaling pathway.[77,78] More recently, it has been shown that the functions of PEITC in migration and invasion of human gastric cancer AGS cells might be via inhibiting PKC/MAPK pathway by molecular targeting of PKC.[77] Similarly, in androgen-independent PC-3 cells, PEITC exhibited remarkable efficacy in sensitizing the cells to undergo cell death partly by modulating the activities of PKC.[79] Interestingly, some studies had demonstrated that upregulation of Nrf2/ARE-dependent gene expression by PEITC is likely mediated by the MAPK pathway.[78] Similar results have shown that PEITC inhibits the HIF-1α expression through inhibiting the MAPK signaling pathway.[73] As HIF-1 and Keap1/Nrf2 are involved in the expression of more than a hundred genes,[80,81] it is urgent to know whether cellular HIF-1α, Nrf2, and/or Keap1 proteins are direct targets of PEITCs. In conclusion, PEITC have the potential function to prevent invasion and metastasis in a wide range of tumor types by inhibition of the MAPK signaling pathway.

INDUCE OF CELL CYCLE ARREST

Cell cycle progression is a sequential process that directs dividing carcinoma cells through the G1, S, G2, and M phases.[82] The ability of PEITC to regulate the cell cycle and inhibit proliferation contributes to its chemopreventive capacity and is mediated through indirect targeting of cyclins, proteins responsible for the progression of the cell cycle, cyclin-dependent kinase (CDK) molecules, and their inhibitors (Figure 4).[83]

INDUCE OF G1/S PHASE CELL CYCLE ARREST

Recent studies have demonstrated the effect of PEITC on suppressing cell proliferation of cancer cells by causing G1/S phase cell cycle arrest in many cancers, such as human colorectal cancer,[84] oral squamous carcinoma,[42] and prostate cancer.[85] One possible explanation for these findings was that PEITC could lead to G0/G1 phase arrest by substantial reduction levels of cell cycle related proteins, such as CDC25A, CDK6, phospho-Rb, cyclin D, CDK2, and cyclin E proteins, but increase the expression of cyclin-dependent kinase inhibitors p15, p53, p27, and p21.[42] For example, in PC-3 cells, PEITC effectively blocked the G1-phase progression by

DOI: 10.1021/jf504627e
J. Agric. Food Chem. 2015, 63, 3311−3322

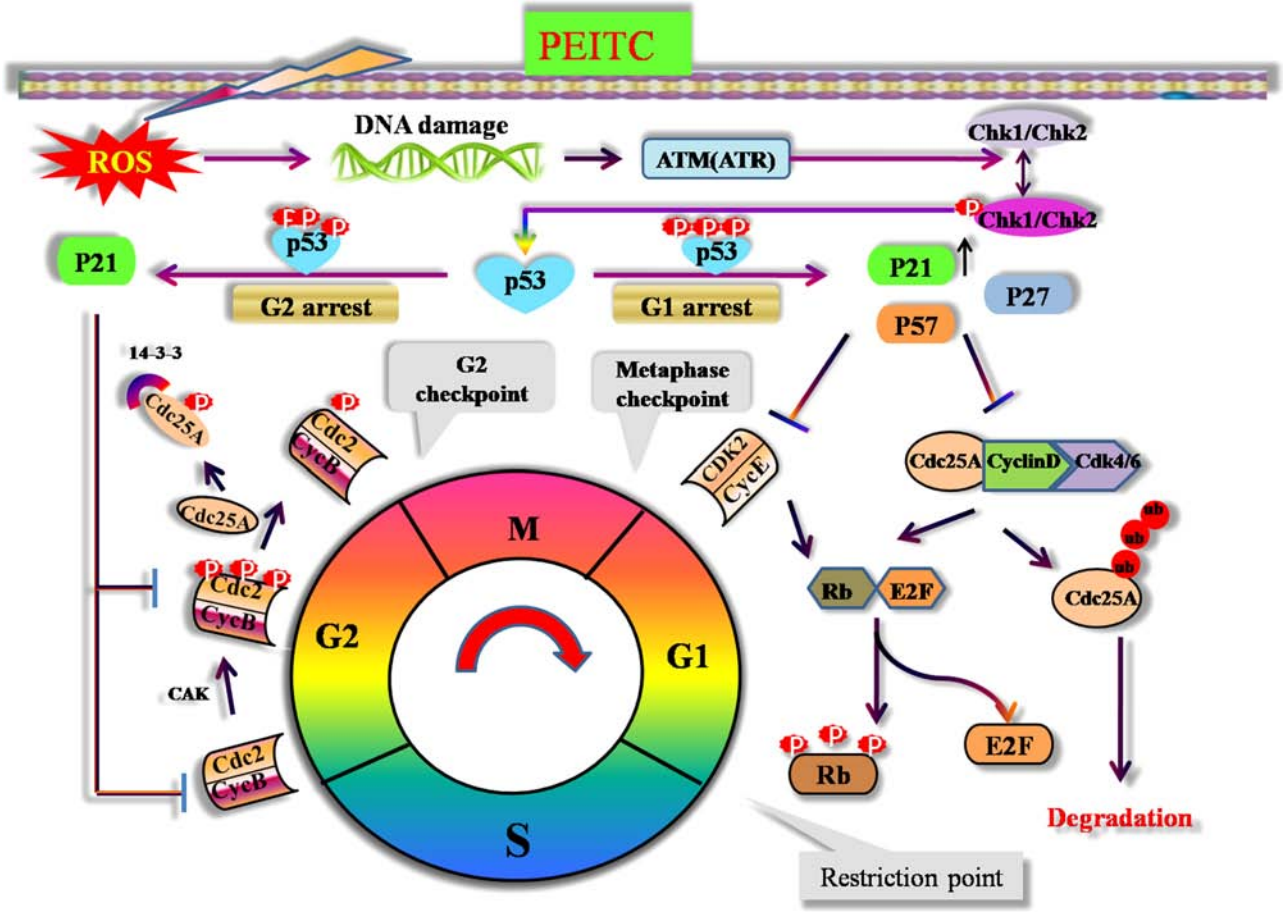

Figure 4. The proposed model of PEITC mechanisms of action for cell cycle arrest. The cell cycle is broadly divided into four phases (G1, S, G2, and M) culminating in cell duplication. Each phase of the cell cycle is regulated by a different complement of CDK−cyclin complexes. PEITC can lead to cell cycle arrest by direct reductions of the levels of cell cycle related proteins and indirect activation of the ATM/ATR pathway.

the combined activity of cyclin D1/CDK4, -6, and cyclin E/CDK2. In addition, decreasing phosphorylated Rb proteins activated the cell cycle progression.[85]

However, PEITC arrested the cells in the G1 phase by downregulation of cyclins through the activation of the p38 MAPK signaling pathway.[84] One possible explanation for these findings was that the p38MAPK stress kinase pathway was activated in response to DNA damage, and that the cell cycle checkpoint function was essential in cells with defective p53.[86] Moreover, several studies have demonstrated that the BAG family molecular chaperone regulator 3 (BAG3) belongs to a family of cochaperones and has been shown to play a relevant role in the survival, growth, and invasiveness of different tumor types.[87,88] Interestingly, a recent study found that PEITC promoted BAG3 silencing which sensitized EqS04b cells death and cell cycle arrest in G0/G1.[89]

■ INDUCTION OF G2/M PHASE CELL CYCLE ARREST

Furthermore, in a myeloma xenograft mouse model, PEITC caused G2/M cell cycle arrest by decreasing expression of key G2/M-regulating proteins including cyclin B1, p-cdc2, Cdc25C, p53, p27, and 14-3-3ε.[90] In vitro cell culture studies showed that PEITC induced time- and dose-dependent G2/M arrest by decline of cell cycle-related proteins, Cdk1 and Cdc25C.[91] Similarly, PEITC induced cell cycle arrest at the G2/M phase by inhibiting the levels of cell cycle regulatory proteins such as cyclin A and B1, while promoting the level of Chk1 and p53.[92] Another study found that the antiproliferative effects of PEITC in Caco-2 cells were attributed to the activation of the G2/M DNA damage checkpoint and sustained G2/M phase cell cycle arrest through upregulation of p21.[93] Several studies have demonstrated that the ataxia telangiectasia mutated/ataxia telangiectasia and Rad3-related (ATM/ATR) pathway plays important roles in maintaining genome integrity by triggering cell cycle arrest and DNA damage repair.[94,95] It indicated that the ATM/ATR pathway might be a therapeutic target in cancer therapy. Indeed, in oral cancer cells, PEITC induced G2/M phase arrest via a GSH redox stress and oxidative DNA damage-induced ATM-Chk2-p53-related pathway.[90]

A particularly interesting feature of PEITC was that PEITC-NAC, one of the metabolic products, had equal effectiveness with PEITC as an inhibitor of tumorgenesis by NNK while being less irritating and pungent than PEITC.[96−98] Therefore, PEITC-NAC, a prodrug of PEITC, has been introduced in a number of preclinical studies.[99] A recent study observed that PEITC-NAC had an effect on cell-cycle progression by downregulation of Cdk1 and cyclin B1 protein expression.[100] However, more detailed mechanism is needed to identify the chemopreventive activity and metabolic products of PEITC in humans.

■ INFLUENCE OF DMES

Drug metabolizing enzymes (DMEs) play central roles in xenobiotics (such as drugs) metabolism, elimination, and

DOI: 10.1021/jf504627e
J. Agric. Food Chem. 2015, 63, 3311−3322

detoxification in the human body. In general, DMEs protect or defend the body against the potential harmful insults from the environment.[101] PEITC has been attributed to its ability to disrupt multiple steps of the carcinogenic process: preventing genetic damage by the inhibition of carcinogen-activating phase I enzymes[102,103] and induction of carcinogen-detoxifying phase II enzymes.[10,15,104] Moreover, it could accumulate membrane drug transporters, such as MRP-1 and Pgp-1.[105]

INHIBITION OF PHASE I CYP DMES

PEITC could influence several CYP families by binding with their amino acid residues. Specifically, PEITC can activate or inhibit the expression of CYPs including CYP1A1, CYP1A2,[106] CYP2B1, CYP2E1,[107] CYP1A2, CYP2C9, CYP2D6, CYP2C19, CYP2B6, CYP2E1, CYP2A6, CYP3A4, and CYP3A5.[102,108] There can be many reasons behind the difference in their impacts. The main mechanism might be that PEITC could influence several CYP families by binding with their amino acid residues, and they had difference in binding affinity with the active group of PEITC. PEITC may react with α-amino groups in N-terminal residues and ξ-amino containing lysines through alkylation, thus forming thiourea.[109] Also, several recent studies have shown that PEITC reacts with the N-terminal of proline, and binds to hydroxyl group-containing residues of tyrosine.[110]

INDUCTION OF PHASE II DMES

The phase II metabolizing or conjugating enzymes consist of many superfamily of enzymes such as glutathione *S*-transferases (GSTs) and quinonereductase (QR).[101,111] PEITC was a substrate of GSTs, including Al-1, M1-1, M4-4, and P1-1. GSTs promote the thiol group of GSH to the electrophonic central carbon of the PEITC group to form dithiocarbamates (PEITC−GSH).[112] In animal models, treatment with PEITC resulted in an increase of NQO-1, GST, and UGT activities in the rat liver.[113] An earlier animal experiment had a similar result that PEITC could largely enhance UGT activities in liver.[114]

Nrf2, the key mediator of drug-induced changes in phase II metabolizing, can also be activated by ITCs.[115] When cells are exposed to oxidative stresses, chemicals, and UVR, Nrf2 dissociates from Keap1 and translocates into the nucleus, thereby activating ARE. PEITC can induce Nrf2-ARE-mediated phase II enzyme and its downstream gene expression, including γ-glutamyl cysteine-synthetase (γGCS), heme oxygenase1 (HO-1), and NAD(P)H quinone oxidoreductase1 (NQO1).[80,104] One of the mechanisms might be that PEITC induces the expression of ARE-mediated phase II enzymes via the c-Jun N-terminal kinase-1 (JNK1) and Nrf2-dependent pathways.[116]

REVERSE OF MULTIDRUG RESISTANCE

Multidrug resistance (MDR) is largely responsible for ineffective chemotherapy. P-glycoprotein/MDR1 (ABCB1) and MRP2 (ABCC2) are the uptake and efflux transporters of drugs. P-gp and MRP1 both transport a number of natural product chemotherapeutic agents, existing substrate preferences. Increased expression of P-gp, encoded by MDR1 gene, might account for MDR.[117,118] PEITC is effective in reducing and eliminating drug resistance including paclitaxel,[119] fludarabine,[31] metformin,[120] and cisplatin[68,121] in many types of tumor. The potential mechanism of PEITC reversing MDR might be inhibiting MRP1 by increasing the cellular accumulation of daunomycin (DNM) and vinblastine (VBL).[122,123] Moreover, breast cancer resistance protein (ABCG2) is an ATP-binding cassette transporter that plays an important role in drug absorption and disposition in the development of multidrug resistance in cancer cells. Studies have shown that PEITC is a substrate for BCRP and is a specific inhibitor of BCRP.[124]

On the other hand, the cellular accumulation or the drug-resistance effect of PEITC is regulated by multidrug resistance associated protein-1 (MRP-1) and P-glycoprotein-1 (Pgp-1). When the overexpression of MRP1 and P-gp cells is exposed to PEITC, the agent was rapidly exported, depending on accumulation in cells mainly in forms of GSH and cysteinylglycine conjugates.[105] In a word, PEITC can inhibit MDR proteins, but on the other hand, PEITC is regulated by these proteins.

Overall, this review summarized the work performed over the past 20+ years on PEITC absorption, metabolism, and cancer chemoprevention. Taken together, we have discussed the molecular signaling mechanisms of PEITC actions on some well-established mechanisms such as the following pathways: induction of apoptosis by intrinsic, extrinsic, and ER stress pathways; inhibition of the survival pathways, and cell cycle arrest; and reduction of the incidence of cancer by modulation of drug-metabolizing enzymes, including phase I and phase II. Recently, a novel alkyne-tagged ITC (NPEITC) was synthesized for the development of a "click" chemistry-based method to identify the protein targets for PEITC, which may pave the road for understanding the biological functions of PEITC as chemopreventive agents.[125] In addition to the well characterized effects on apoptosis, cell proliferation, and cell cycle, PEITCs can target angiogenesis, cell attachment,[126] and autophagic cell death.[9] Further investigation is required to answer whether normal dietary intake or pharmacological administration of PEITC is sufficient to modulate these pathways in vivo.

AUTHOR INFORMATION

Corresponding Author

*Department of Clinical Pharmacology, Xiangya Hospital; Institute of Clinical Pharmacology, Hunan Key Laboratory of Pharmacogenetics, Central South University, Changsha, Hunan 410078, P. R. China. Tel: +86 731 84805380. Fax: +86 731 82354476. E-mail: hhzhou2003@163.com.

Notes

The authors declare no competing financial interest.

ACKNOWLEDGMENTS

The authors thank Weijing Gong and Mouze Liu for their helpful advice during the development of this project.

REFERENCES

(1) Brown, K. K.; Hampton, M. B. Biological targets of isothiocyanates. *Biochim. Biophys. Acta* **2011**, *1810* (9), 888−94.

(2) Suzuki, R.; Iwasaki, M.; Hara, A.; Inoue, M.; Sasazuki, S.; Sawada, N.; Yamaji, T.; Shimazu, T.; Tsugane, S. Japan Public Health Center-based Prospective Study, G. Fruit and vegetable intake and breast cancer risk defined by estrogen and progesterone receptor status: the Japan Public Health Center-based Prospective Study. *Cancer Causes Control* **2013**, *24* (12), 2117−28.

(3) Han, B.; Li, X.; Yu, T. Cruciferous vegetables consumption and the risk of ovarian cancer: a meta-analysis of observational studies. *Diagn. Pathol.* **2014**, *9* (1), 7.

DOI: 10.1021/jf504627e
J. Agric. Food Chem. 2015, 63, 3311−3322

(4) Tse, G.; Eslick, G. D. Cruciferous vegetables and risk of colorectal neoplasms: a systematic review and meta-analysis. *Nutr. Cancer* **2014**, *66* (1), 128−39.
(5) Telang, U.; Morris, M. E. Effect of orally administered phenethyl isothiocyanate on hepatic gene expression in rats. *Mol. Nutr. Food Res.* **2010**, *54* (12), 1802−6.
(6) Brennan, P.; Hsu, C. C.; Moullan, N.; Szeszenia-Dabrowska, N.; Lissowska, J.; Zaridze, D.; Rudnai, P.; Fabianova, E.; Mates, D.; Bencko, V.; Foretova, L.; Janout, V.; Gemignani, F.; Chabrier, A.; Hall, J.; Hung, R. J.; Boffetta, P.; Canzian, F. Effect of cruciferous vegetables on lung cancer in patients stratified by genetic status: a mendelian randomisation approach. *Lancet* **2005**, *366* (9496), 1558−60.
(7) Izzotti, A.; Larghero, P.; Cartiglia, C.; Longobardi, M.; Pfeffer, U.; Steele, V. E.; De Flora, S. Modulation of microRNA expression by budesonide, phenethyl isothiocyanate and cigarette smoke in mouse liver and lung. *Carcinogenesis* **2010**, *31* (5), 894−901.
(8) Khor, T. O.; Keum, Y. S.; Lin, W.; Kim, J. H.; Hu, R.; Shen, G.; Xu, C.; Gopalakrishnan, A.; Reddy, B.; Zheng, X.; Conney, A. H.; Kong, A. N. Combined inhibitory effects of curcumin and phenethyl isothiocyanate on the growth of human PC-3 prostate xenografts in immunodeficient mice. *Cancer Res.* **2006**, *66* (2), 613−21.
(9) Powolny, A. A.; Bommareddy, A.; Hahm, E. R.; Normolle, D. P.; Beumer, J. H.; Nelson, J. B.; Singh, S. V. Chemopreventative potential of the cruciferous vegetable constituent phenethyl isothiocyanate in a mouse model of prostate cancer. *J. Natl. Cancer Inst.* **2011**, *103* (7), 571−84.
(10) Cheung, K. L.; Khor, T. O.; Huang, M. T.; Kong, A. N. Differential in vivo mechanism of chemoprevention of tumor formation in azoxymethane/dextran sodium sulfate mice by PEITC and DBM. *Carcinogenesis* **2010**, *31* (5), 880−5.
(11) Nakamura, T.; Kitamoto, N.; Osawa, T.; Kato, Y. Immunochemical detection of food-derived isothiocyanate as a lysine conjugate. *Biosci., Biotechnol., Biochem.* **2010**, *74* (3), 536−40.
(12) Kang, L.; Ding, L.; Wang, Z. Y. Isothiocyanates repress estrogen receptor alpha expression in breast cancer cells. *Oncol. Rep.* **2009**, *21* (1), 185−92.
(13) Gupta, P.; Srivastava, S. K. Antitumor activity of phenethyl isothiocyanate in HER2-positive breast cancer models. *BMC Med.* **2012**, *10*, 80.
(14) Jan, C.-R.; Chen, C.-Y.; Wang, S.-C.; Kuo, S.-Y. Phenethyl isothiocyanate induces Ca2+ movement and cytotoxicity in PC3 human prostate cancer cells. *J. Taiwan Inst. Chem. Eng.* **2011**, *42* (6), 895−901.
(15) Pullar, J. M.; Thomson, S. J.; King, M. J.; Turnbull, C. I.; Midwinter, R. G.; Hampton, M. B. The chemopreventive agent phenethyl isothiocyanate sensitizes cells to Fas-mediated apoptosis. *Carcinogenesis* **2004**, *25* (5), 765−72.
(16) Yang, M. D.; Lai, K. C.; Lai, T. Y.; Hsu, S. C.; Kuo, C. L.; Yu, C. S.; Lin, M. L.; Yang, J. S.; Kuo, H. M.; Wu, S. H.; Chung, J. G. Phenethyl isothiocyanate inhibits migration and invasion of human gastric cancer AGS cells through suppressing MAPK and NF-kappaB signal pathways. *Anticancer Res.* **2010**, *30* (6), 2135−43.
(17) Gao, N.; Budhraja, A.; Cheng, S.; Liu, E. H.; Chen, J.; Yang, Z.; Chen, D.; Zhang, Z.; Shi, X. Phenethyl isothiocyanate exhibits antileukemic activity in vitro and in vivo by inactivation of Akt and activation of JNK pathways. *Cell Death Dis.* **2011**, *2*, e140.
(18) Sahu, R. P.; Zhang, R.; Batra, S.; Shi, Y.; Srivastava, S. K. Benzyl isothiocyanate-mediated generation of reactive oxygen species causes cell cycle arrest and induces apoptosis via activation of MAPK in human pancreatic cancer cells. *Carcinogenesis* **2009**, *30* (10), 1744−53.
(19) Ji, Y.; Morris, M. E. Determination of phenethyl isothiocyanate in human plasma and urine by ammonia derivatization and liquid chromatography−tandem mass spectrometry. *Anal. Biochem.* **2003**, *323* (1), 39−47.
(20) Liebes, L.; Conaway, C. C.; Hochster, H.; Mendoza, S.; Hecht, S. S.; Crowell, J.; Chung, F. L. High-performance liquid chromatography-based determination of total isothiocyanate levels in human plasma: application to studies with 2-phenethyl isothiocyanate. *Anal. Biochem.* **2001**, *291* (2), 279−89.
(21) Ji, Y.; Kuo, Y.; Morris, M. E. Pharmacokinetics of dietary phenethyl isothiocyanate in rats. *Pharm. Res.* **2005**, *22* (10), 1658−66.
(22) Chung, F. L.; Morse, M. A.; Eklind, K. I.; Lewis, J. Quantitation of human uptake of the anticarcinogen phenethyl isothiocyanate after a watercress meal. *Cancer Epidemiol. Biomarkers Prev.* **1992**, *1* (5), 383−8.
(23) Conaway, C. C.; Wang, C. X.; Pittman, B.; Yang, Y. M.; Schwartz, J. E.; Tian, D.; McIntee, E. J.; Hecht, S. S.; Chung, F. L. Phenethyl isothiocyanate and sulforaphane and their N-acetylcysteine conjugates inhibit malignant progression of lung adenomas induced by tobacco carcinogens in A/J mice. *Cancer Res.* **2005**, *65* (18), 8548−57.
(24) Adesida, A.; Edwards, L. G.; Thornalley, P. J. Inhibition of human leukaemia 60 cell growth by mercapturic acid metabolites of phenylethyl isothiocyanate. *Food Chem. Toxicol.* **1996**, *34* (4), 385−92.
(25) Wu, C. C.; Bratton, S. B. Regulation of the intrinsic apoptosis pathway by reactive oxygen species. *Antioxid. Redox. Signaling* **2013**, *19* (6), 546−58.
(26) Francis, H.; McDaniel, K.; Han, Y.; Liu, X.; Kennedy, L.; Yang, F.; McCarra, J.; Zhou, T.; Glaser, S.; Venter, J.; Huang, L.; Levine, P.; Lai, J. M.; Liu, C. G.; Alpini, G.; Meng, F. Regulation of the extrinsic apoptotic pathway by microRNA-21 in alcoholic liver injury. *J. Biol. Chem.* **2014**, *289* (40), 27526−39.
(27) Reuter, S.; Eifes, S.; Dicato, M.; Aggarwal, B. B.; Diederich, M. Modulation of anti-apoptotic and survival pathways by curcumin as a strategy to induce apoptosis in cancer cells. *Biochem. Pharmacol.* **2008**, *76* (11), 1340−51.
(28) Schriewer, J. M.; Peek, C. B.; Bass, J.; Schumacker, P. T. ROS-mediated PARP activity undermines mitochondrial function after permeability transition pore opening during myocardial ischemia-reperfusion. *J. Am. Heart Assoc.* **2013**, *2* (2), e000159.
(29) Loor, G.; Kondapalli, J.; Iwase, H.; Chandel, N. S.; Waypa, G. B.; Guzy, R. D.; Vanden Hoek, T. L.; Schumacker, P. T. Mitochondrial oxidant stress triggers cell death in simulated ischemia-reperfusion. *Biochim. Biophys. Acta* **2011**, *1813* (7), 1382−94.
(30) Trachootham, D.; Zhou, Y.; Zhang, H.; Demizu, Y.; Chen, Z.; Pelicano, H.; Chiao, P. J.; Achanta, G.; Arlinghaus, R. B.; Liu, J.; Huang, P. Selective killing of oncogenically transformed cells through a ROS-mediated mechanism by beta-phenylethyl isothiocyanate. *Cancer Cell* **2006**, *10* (3), 241−52.
(31) Trachootham, D.; Zhang, H.; Zhang, W.; Feng, L.; Du, M.; Zhou, Y.; Chen, Z.; Pelicano, H.; Plunkett, W.; Wierda, W. G.; Keating, M. J.; Huang, P. Effective elimination of fludarabine-resistant CLL cells by PEITC through a redox-mediated mechanism. *Blood* **2008**, *112* (5), 1912−22.
(32) Xiao, D.; Powolny, A. A.; Moura, M. B.; Kelley, E. E.; Bommareddy, A.; Kim, S. H.; Hahm, E. R.; Normolle, D.; Van Houten, B.; Singh, S. V. Phenethyl isothiocyanate inhibits oxidative phosphorylation to trigger reactive oxygen species-mediated death of human prostate cancer cells. *J. Biol. Chem.* **2010**, *285* (34), 26558−69.
(33) Tusskorn, O.; Prawan, A.; Senggunprai, L.; Kukongviriyapan, U.; Kukongviriyapan, V. Phenethyl isothiocyanate induces apoptosis of cholangiocarcinoma cells through interruption of glutathione and mitochondrial pathway. *Naunyn Schmiedebergs Arch. Pharmacol.* **2013**, *386* (11), 1009−16.
(34) Nunez, G.; Benedict, M. A.; Hu, Y.; Inohara, N. Caspases: the proteases of the apoptotic pathway. *Oncogene* **1998**, *17* (25), 3237−45.
(35) Reed, J. C. Mechanisms of Apoptosis. *Am. J. Pathol.* **2000**, *157* (5), 1415−30.
(36) Cao, X. H.; Zhao, S. S.; Liu, D. Y.; Wang, Z.; Niu, L. L.; Hou, L. H.; Wang, C. L. ROS-Ca(2+) is associated with mitochondria permeability transition pore involved in surfactin-induced MCF-7 cells apoptosis. *Chem.-Biol. Interact.* **2011**, *190* (1), 16−27.
(37) Brenner, C.; Moulin, M. Physiological roles of the permeability transition pore. *Circ. Res.* **2012**, *111* (9), 1237−47.
(38) Arisan, E. D.; Kutuk, O.; Tezil, T.; Bodur, C.; Telci, D.; Basaga, H. Small inhibitor of Bcl-2, HA14−1, selectively enhanced the apoptotic effect of cisplatin by modulating Bcl-2 family members in MDA-MB-231 breast cancer cells. *Breast Cancer Res. Treat.* **2010**, *119* (2), 271−81.

DOI: 10.1021/jf504627e
J. Agric. Food Chem. 2015, 63, 3311−3322

(39) Martin, K. R. Targeting apoptosis with dietary bioactive agents. *Exp. Biol. Med. (Maywood)* **2006**, *231* (2), 117−29.
(40) Lee, J. W.; Cho, M. K. Phenethyl isothiocyanate induced apoptosis via down regulation of Bcl-2/XIAP and triggering of the mitochondrial pathway in MCF-7 cells. *Arch. Pharm. Res.* **2008**, *31* (12), 1604−12.
(41) Rose, P.; Armstrong, J. S.; Chua, Y. L.; Ong, C. N.; Whiteman, M. Beta-phenylethyl isothiocyanate mediated apoptosis; contribution of Bax and the mitochondrial death pathway. *Int. J. Biochem. Cell Biol.* **2005**, *37* (1), 100−19.
(42) Chen, P. Y.; Lin, K. C.; Lin, J. P.; Tang, N. Y.; Yang, J. S.; Lu, K. W.; Chung, J. G. Phenethyl Isothiocyanate (PEITC) Inhibits the Growth of Human Oral Squamous Carcinoma HSC-3 Cells through G(0)/G(1) Phase Arrest and Mitochondria-Mediated Apoptotic Cell Death. *Evidence-Based Complementary Altern. Med.* **2012**, *2012*, 718320.
(43) Satyan, K. S.; Swamy, N.; Dizon, D. S.; Singh, R.; Granai, C. O.; Brard, L. Phenethyl isothiocyanate (PEITC) inhibits growth of ovarian cancer cells by inducing apoptosis: role of caspase and MAPK activation. *Gynecol. Oncol.* **2006**, *103* (1), 261−70.
(44) Huong, L. D.; Shim, J.-H.; Choi, K.-H.; Shin, J.-A.; Choi, E.-S.; Kim, H.-S.; Lee, S.-J.; Kim, S.-J.; Cho, N.-P.; Cho, S.-D. Effect of *β*-Phenylethyl Isothiocyanate from Cruciferous Vegetables on Growth Inhibition and Apoptosis of Cervical Cancer Cells through the Induction of Death Receptors 4 and 5. *J. Agric. Food Chem.* **2011**, *59* (15), 8124−31.
(45) Gibson, S. B.; Oyer, R.; Spalding, A. C.; Anderson, S. M.; Johnson, G. L. Increased expression of death receptors 4 and 5 synergizes the apoptosis response to combined treatment with etoposide and TRAIL. *Mol. Cell. Biol.* **2000**, *20* (1), 205−12.
(46) Huong, L. D.; Shin, J. A.; Choi, E. S.; Cho, N. P.; Kim, H. M.; Leem, D. H.; Cho, S. D. beta-Phenethyl isothiocyanate induces death receptor 5 to induce apoptosis in human oral cancer cells via p38. *Oral Dis.* **2012**, *18* (5), 513−9.
(47) Huong le, D.; Shim, J. H.; Choi, K. H.; Shin, J. A.; Choi, E. S.; Kim, H. S.; Lee, S. J.; Kim, S. J.; Cho, N. P.; Cho, S. D. Effect of beta-phenylethyl isothiocyanate from cruciferous vegetables on growth inhibition and apoptosis of cervical cancer cells through the induction of death receptors 4 and 5. *J. Agric. Food Chem.* **2011**, *59* (15), 8124−31.
(48) Lee, D. H.; Kim, D. W.; Lee, H. C.; Lee, J. H.; Lee, T. H. Phenethyl isothiocyanate sensitizes glioma cells to TRAIL-induced apoptosis. *Biochem. Biophys. Res. Commun.* **2014**, *446* (4), 815−21.
(49) Liou, C. M.; Tsai, S. C.; Kuo, C. H.; Ting, H.; Lee, S. D. Cardiac Fas-dependent and mitochondria-dependent apoptosis after chronic cocaine abuse. *Int. J. Mol. Sci.* **2014**, *15* (4), 5988−6001.
(50) Momoi, T. Caspases involved in ER stress-mediated cell death. *J. Chem. Neuroanat.* **2004**, *28* (1−2), 101−5.
(51) Chen, I. S.; Mok, K. T.; Chou, C. T.; Liu, S. I.; Kuo, C. C.; Hsu, S. S.; Chang, H. T.; Tsai, J. Y.; Liao, W. C.; Jan, C. R. Effect of phenethyl isothiocyanate on Ca2+ movement and viability in MDCK canine renal tubular cells. *Hum. Exp. Toxicol.* **2012**, *31* (12), 1251−61.
(52) Huang, S. H.; Hsu, M. H.; Hsu, S. C.; Yang, J. S.; Huang, W. W.; Huang, A. C.; Hsiao, Y. P.; Yu, C. C.; Chung, J. G. Phenethyl isothiocyanate triggers apoptosis in human malignant melanoma A375.S2 cells through reactive oxygen species and the mitochondria-dependent pathways. *Hum. Exp. Toxicol.* **2014**, *33* (3), 270−83.
(53) Tusskorn, O.; Senggunprai, L.; Prawan, A.; Kukongviriyapan, U.; Kukongviriyapan, V. Phenethyl isothiocyanate induces calcium mobilization and mitochondrial cell death pathway in cholangiocarcinoma KKU-M214 cells. *BMC Cancer* **2013**, *13*, 571.
(54) Mi, L.; Gan, N.; Chung, F. L. Isothiocyanates inhibit proteasome activity and proliferation of multiple myeloma cells. *Carcinogenesis* **2011**, *32* (2), 216−23.
(55) Pawlik, A.; Szczepanski, M. A.; Klimaszewska, A.; Gackowska, L.; Zuryn, A.; Grzanka, A. Phenethyl isothiocyanate-induced cytoskeletal changes and cell death in lung cancer cells. *Food Chem. Toxicol.* **2012**, *50* (10), 3577−94.
(56) Xiao, Z.; Mi, L.; Chung, F. L.; Veenstra, T. D. Proteomic analysis of covalent modifications of tubulins by isothiocyanates. *J. Nutr.* **2012**, *142* (7), 1377S−81S.
(57) Yin, P.; Kawamura, T.; He, M.; Vanaja, D. K.; Young, C. Y. Phenethyl isothiocyanate induces cell cycle arrest and reduction of alpha- and beta-tubulin isotypes in human prostate cancer cells. *Cell Biol. Int.* **2009**, *33* (1), 57−64.
(58) Cang, S.; Ma, Y.; Chiao, J. W.; Liu, D. Phenethyl isothiocyanate and paclitaxel synergistically enhanced apoptosis and alpha-tubulin hyperacetylation in breast cancer cells. *Exp. Hematol. Oncol.* **2014**, *3* (1), 5.
(59) Xu, C.; Shen, G.; Chen, C.; Gelinas, C.; Kong, A. N. Suppression of NF-kappaB and NF-kappaB-regulated gene expression by sulforaphane and PEITC through IkappaBalpha, IKK pathway in human prostate cancer PC-3 cells. *Oncogene* **2005**, *24* (28), 4486−95.
(60) Chen, C. Y.; Su, C. M.; Huang, Y. L.; Tsai, C. H.; Fuh, L. J.; Tang, C. H. CCN1 Induces Oncostatin M Production in Osteoblasts via Integrin-Dependent Signal Pathways. *PLoS One* **2014**, *9* (9), e106632.
(61) Zhao, Y.; Xu, Y.; Zhang, J.; Ji, T. Cardioprotective effect of carvedilol: inhibition of apoptosis in H9c2 cardiomyocytes via the TLR4/NF-kappaB pathway following ischemia/reperfusion injury. *Exp. Ther. Med.* **2014**, *8* (4), 1092−6.
(62) Yu, Z.; Guo, W.; Ma, X.; Zhang, B.; Dong, P.; Huang, L.; Wang, X.; Wang, C.; Huo, X.; Yu, W.; Yi, C.; Xiao, Y.; Yang, W.; Qin, Y.; Yuan, Y.; Meng, S.; Liu, Q.; Deng, W. Gamabufotalin, a bufadienolide compound from toad venom, suppresses COX-2 expression through targeting IKKbeta/NF-kappaB signaling pathway in lung cancer cells. *Mol. Cancer* **2014**, *13* (1), 203.
(63) Huang, C. S.; Lin, A. H.; Liu, C. T.; Tsai, C. W.; Chang, I. S.; Chen, H. W.; Lii, C. K. Isothiocyanates protect against oxidized LDL-induced endothelial dysfunction by upregulating Nrf2-dependent antioxidation and suppressing NFkappaB activation. *Mol. Nutr. Food Res.* **2013**, *57* (11), 1918−30.
(64) Yang, Y.-T.; Shi, Y.; Jay, M.; Di Pasqua, A. J. Enhanced toxicity of cisplatin with chemosensitizer phenethyl isothiocyanate toward non-small cell lung cancer cells when delivered in liposomal nanoparticles. *Chem. Res. Toxicol.* **2014**, *27* (6), 946−8.
(65) Kim, J. H.; Xu, C.; Keum, Y. S.; Reddy, B.; Conney, A.; Kong, A. N. Inhibition of EGFR signaling in human prostate cancer PC-3 cells by combination treatment with beta-phenylethyl isothiocyanate and curcumin. *Carcinogenesis* **2006**, *27* (3), 475−82.
(66) Prawan, A.; Saw, C. L.; Khor, T. O.; Keum, Y. S.; Yu, S.; Hu, L.; Kong, A. N. Anti-NF-kappaB and anti-inflammatory activities of synthetic isothiocyanates: effect of chemical structures and cellular signaling. *Chem.-Biol. Interact.* **2009**, *179* (2−3), 202−11.
(67) Zhu, J.; Ghosh, A.; Coyle, E. M.; Lee, J.; Hahm, E. R.; Singh, S. V.; Sarkar, S. N. Differential effects of phenethyl isothiocyanate and D,L-sulforaphane on TLR3 signaling. *J. Immunol.* **2013**, *190* (8), 4400−7.
(68) Wang, X.; Govind, S.; Sajankila, S. P.; Mi, L.; Roy, R.; Chung, F. L. Phenethyl isothiocyanate sensitizes human cervical cancer cells to apoptosis induced by cisplatin. *Mol. Nutr. Food Res.* **2011**, *55* (10), 1572−81.
(69) Hers, I.; Vincent, E. E.; Tavare, J. M. Akt signalling in health and disease. *Cell. Signalling* **2011**, *23* (10), 1515−27.
(70) Kar, S.; Palit, S.; Ball, W. B.; Das, P. K. Carnosic acid modulates Akt/IKK/NF-kappaB signaling by PP2A and induces intrinsic and extrinsic pathway mediated apoptosis in human prostate carcinoma PC-3 cells. *Apoptosis* **2012**, *17* (7), 735−47.
(71) Loganathan, S.; Kandala, P. K.; Gupta, P.; Srivastava, S. K. Inhibition of EGFR-AKT axis results in the suppression of ovarian tumors in vitro and in preclinical mouse model. *PLoS One* **2012**, *7* (8), e43577.
(72) Xiao, D.; Singh, S. V. Phenethyl isothiocyanate inhibits angiogenesis in vitro and ex vivo. *Cancer Res.* **2007**, *67* (5), 2239−46.
(73) Gupta, B.; Chiang, L.; Chae, K.; Lee, D. H. Phenethyl isothiocyanate inhibits hypoxia-induced accumulation of HIF-1alpha

DOI: 10.1021/jf504627e
J. Agric. Food Chem. 2015, 63, 3311−3322

and VEGF expression in human glioma cells. *Food Chem.* **2013**, *141* (3), 1841−6.
(74) Cavell, B. E.; Syed Alwi, S. S.; Donlevy, A. M.; Proud, C. G.; Packham, G. Natural product-derived antitumor compound phenethyl isothiocyanate inhibits mTORC1 activity via TSC2. *J. Nat. Prod.* **2012**, *75* (6), 1051−7.
(75) Bommareddy, A.; Hahm, E. R.; Xiao, D.; Powolny, A. A.; Fisher, A. L.; Jiang, Y.; Singh, S. V. Atg5 regulates phenethyl isothiocyanate-induced autophagic and apoptotic cell death in human prostate cancer cells. *Cancer Res.* **2009**, *69* (8), 3704−12.
(76) Yan, H.; Zhu, Y.; Liu, B.; Wu, H.; Li, Y.; Wu, X.; Zhou, Q.; Xu, K. Mitogen-activated protein kinase mediates the apoptosis of highly metastatic human non-small cell lung cancer cells induced by isothiocyanates. *Br. J. Nutr.* **2011**, *106* (12), 1779−91.
(77) Soetikno, V.; Sari, F. R.; Sukumaran, V.; Lakshmanan, A. P.; Mito, S.; Harima, M.; Thandavarayan, R. A.; Suzuki, K.; Nagata, M.; Takagi, R.; Watanabe, K. Curcumin prevents diabetic cardiomyopathy in streptozotocin-induced diabetic rats: possible involvement of PKC-MAPK signaling pathway. *Eur. J. Pharm. Sci.* **2012**, *47* (3), 604−14.
(78) Das, B. N.; Kim, Y. W.; Keum, Y. S. Mechanisms of Nrf2/Keap1-dependent phase II cytoprotective and detoxifying gene expression and potential cellular targets of chemopreventive isothiocyanates. *Oxid. Med. Cell. Longevity* **2013**, *2013*, 839409.
(79) Mukherjee, S.; Bhattacharya, R. K.; Roy, M. Targeting protein kinase C (PKC) and telomerase by phenethyl isothiocyanate (PEITC) sensitizes PC-3 cells towards chemotherapeutic drug-induced apoptosis. *J. Environ. Pathol. Toxicol. Oncol.* **2009**, *28* (4), 269−82.
(80) Saw, C. L.; Cintron, M.; Wu, T. Y.; Guo, Y.; Huang, Y.; Jeong, W. S.; Kong, A. N. Pharmacodynamics of dietary phytochemical indoles I3C and DIM: Induction of Nrf2-mediated phase II drug metabolizing and antioxidant genes and synergism with isothiocyanates. *Biopharm. Drug Dispos.* **2011**, *32* (5), 289−300.
(81) Zhang, Z.; Qiu, L.; Lin, C.; Yang, H.; Fu, H.; Li, R.; Kang, Y. J. Copper-dependent and -independent hypoxia-inducible factor-1 regulation of gene expression. *Metallomics* **2014**, *6* (10), 1889−93.
(82) Aragon, C.; Lopez-Corcuera, B. Glycine transporters: crucial roles of pharmacological interest revealed by gene deletion. *Trends Pharmacol. Sci.* **2005**, *26* (6), 283−6.
(83) Traka, M.; Mithen, R. Glucosinolates, isothiocyanates and human health. *Phytochem. Rev.* **2008**, *8* (1), 269−82.
(84) Cheung, K. L.; Khor, T. O.; Yu, S.; Kong, A. N. PEITC induces G1 cell cycle arrest on HT-29 cells through the activation of p38 MAPK signaling pathway. *AAPS J.* **2008**, *10* (2), 277−81.
(85) Chiao, J. W.; Wu, H.; Ramaswamy, G.; Conaway, C. C.; Chung, F. L.; Wang, L.; Liu, D. Ingestion of an isothiocyanate metabolite from cruciferous vegetables inhibits growth of human prostate cancer cell xenografts by apoptosis and cell cycle arrest. *Carcinogenesis* **2004**, *25* (8), 1403−8.
(86) Reinhardt, H. C.; Aslanian, A. S.; Lees, J. A.; Yaffe, M. B. p53-deficient cells rely on ATM- and ATR-mediated checkpoint signaling through the p38MAPK/MK2 pathway for survival after DNA damage. *Cancer Cell* **2007**, *11* (2), 175−89.
(87) Chiappetta, G.; Basile, A.; Barbieri, A.; Falco, A.; Rosati, A.; Festa, M.; Pasquinelli, R.; Califano, D.; Palma, G.; Costanzo, R.; Barcaroli, D.; Capunzo, M.; Franco, R.; Rocco, G.; Pascale, M.; Turco, M. C.; De Laurenzi, V.; Arra, C. The anti-apoptotic BAG3 protein is expressed in lung carcinomas and regulates small cell lung carcinoma (SCLC) tumor growth. *Oncotarget* **2014**, *5* (16), 6846−53.
(88) Franaszczyk, M.; Bilinska, Z. T.; Sobieszczanska-Malek, M.; Michalak, E.; Sleszycka, J.; Sioma, A.; Malek, L. A.; Kaczmarska, D.; Walczak, E.; Wlodarski, P.; Hutnik, L.; Milanowska, B.; Dzielinska, Z.; Religa, G.; Grzybowski, J.; Zielinski, T.; Ploski, R. The BAG3 gene variants in Polish patients with dilated cardiomyopathy: four novel mutations and a genotype-phenotype correlation. *J. Transl. Med.* **2014**, *12*, 192.
(89) Cotugno, R.; Gallotta, D.; d'Avenia, M.; Corteggio, A.; Altamura, G.; Roperto, F.; Belisario, M. A.; Borzacchiello, G. BAG3 protects bovine papillomavirus type 1-transformed equine fibroblasts against pro-death signals. *Vet. Res.* **2013**, *44*, 61.
(90) Yeh, Y. T.; Yeh, H.; Su, S. H.; Lin, J. S.; Lee, K. J.; Shyu, H. W.; Chen, Z. F.; Huang, S. Y.; Su, S. J. Phenethyl isothiocyanate induces DNA damage-associated G2/M arrest and subsequent apoptosis in oral cancer cells with varying p53 mutations. *Free Radical Biol. Med.* **2014**, *74*, 1−13.
(91) Xiao, D.; Johnson, C. S.; Trump, D. L.; Singh, S. V. Proteasome-mediated degradation of cell division cycle 25C and cyclin-dependent kinase 1 in phenethyl isothiocyanate-induced G2-M-phase cell cycle arrest in PC-3 human prostate cancer cells. *Mol. Cancer Ther.* **2004**, *3* (5), 567−75.
(92) Wu, C. L.; Huang, A. C.; Yang, J. S.; Liao, C. L.; Lu, H. F.; Chou, S. T.; Ma, C. Y.; Hsia, T. C.; Ko, Y. C.; Chung, J. G. Benzyl isothiocyanate (BITC) and phenethyl isothiocyanate (PEITC)-mediated generation of reactive oxygen species causes cell cycle arrest and induces apoptosis via activation of caspase-3, mitochondria dysfunction and nitric oxide (NO) in human osteogenic sarcoma U-2 OS cells. *J. Orthop. Res.* **2011**, *29* (8), 1199−209.
(93) Visanji, J. M.; Duthie, S. J.; Pirie, L.; Thompson, D. G.; Padfield, P. J. Dietary isothiocyanates inhibit Caco-2 cell proliferation and induce G2/M phase cell cycle arrest, DNA damage, and G2/M checkpoint activation. *J. Nutr.* **2004**, *134* (11), 3121−6.
(94) Huang, S. M.; Lu, K. T.; Wang, Y. C. ATM/ATR and SMAD3 pathways contribute to 3-indole-induced G(1) arrest in cancer cells and xenograft models. *Anticancer Res.* **2011**, *31* (1), 203−8.
(95) Jang, S. H.; Lim, J. W.; Morio, T.; Kim, H. Lycopene inhibits Helicobacter pylori-induced ATM/ATR-dependent DNA damage response in gastric epithelial AGS cells. *Free Radical Biol. Med.* **2012**, *52* (3), 607−15.
(96) Kassie, F.; Melkamu, T.; Endalew, A.; Upadhyaya, P.; Luo, X.; Hecht, S. S. Inhibition of lung carcinogenesis and critical cancer-related signaling pathways by N-acetyl-S-(N-2-phenethylthiocarbamoyl)-l-cysteine, indole-3-carbinol and myo-inositol, alone and in combination. *Carcinogenesis* **2010**, *31* (9), 1634−41.
(97) Kassie, F.; Matise, I.; Negia, M.; Lahti, D.; Pan, Y.; Scherber, R.; Upadhyaya, P.; Hecht, S. S. Combinations of N-Acetyl-S-(N-2-Phenethylthiocarbamoyl)-L-Cysteine and myo-inositol inhibit tobacco carcinogen-induced lung adenocarcinoma in mice. *Cancer Prev. Res.* **2008**, *1* (4), 285−97.
(98) Hecht, S. S.; Upadhyaya, P.; Wang, M.; Bliss, R. L.; McIntee, E. J.; Kenney, P. M. Inhibition of lung tumorigenesis in A/J mice by N-acetyl-S-(N-2-phenethylthiocarbamoyl)-L-cysteine and myo-inositol, individually and in combination. *Carcinogenesis* **2002**, *23* (9), 1455−61.
(99) Yang, Y. M.; Jhanwar-Uniyal, M.; Schwartz, J.; Conaway, C. C.; Halicka, H. D.; Traganos, F.; Chung, F. L. N-acetylcysteine conjugate of phenethyl isothiocyanate enhances apoptosis in growth-stimulated human lung cells. *Cancer Res.* **2005**, *65* (18), 8538−47.
(100) Hwang, E. S.; Lee, H. J. Effects of phenylethyl isothiocyanate and its metabolite on cell-cycle arrest and apoptosis in LNCaP human prostate cancer cells. *Int. J. Food Sci. Nutr.* **2010**, *61* (3), 324−36.
(101) Rushmore, T. H.; Kong, A. N. Pharmacogenomics, regulation and signaling pathways of phase I and II drug metabolizing enzymes. *Curr. Drug Metab.* **2002**, *3* (5), 481−90.
(102) Gross-Steinmeyer, K.; Stapleton, P. L.; Tracy, J. H.; Bammler, T. K.; Strom, S. C.; Eaton, D. L. Sulforaphane- and phenethyl isothiocyanate-induced inhibition of aflatoxin B1-mediated genotoxicity in human hepatocytes: role of GSTM1 genotype and CYP3A4 gene expression. *Toxicol. Sci.* **2010**, *116* (2), 422−32.
(103) Ji, Y.; Morris, M. E. Effect of organic isothiocyanates on breast cancer resistance protein (ABCG2)-mediated transport. *Pharm. Res.* **2004**, *21* (12), 2261−9.
(104) Hu, Y.; Lu, W.; Chen, G.; Zhang, H.; Jia, Y.; Wei, Y.; Yang, H.; Zhang, W.; Fiskus, W.; Bhalla, K.; Keating, M.; Huang, P.; Garcia-Manero, G. Overcoming resistance to histone deacetylase inhibitors in human leukemia with the redox modulating compound beta-phenylethyl isothiocyanate. *Blood* **2010**, *116* (15), 2732−41.
(105) Callaway, E. C.; Zhang, Y.; Chew, W.; Chow, H. H. S. Cellular accumulation of dietary anticarcinogenic isothiocyanates is followed by

DOI: 10.1021/jf504627e
J. Agric. Food Chem. 2015, 63, 3311−3322

transporter-mediated export as dithiocarbamates. *Cancer Lett.* **2004**, *204* (1), 23−31.
(106) Konsue, N.; Ioannides, C. Modulation of carcinogen-metabolising cytochromes P450 in human liver by the chemo-preventive phytochemical phenethyl isothiocyanate, a constituent of cruciferous vegetables. *Toxicology* **2010**, *268* (3), 184−90.
(107) Hollenberg, P. F.; Kent, U. M.; Bumpus, N. N. Mechanism-based inactivation of human cytochromes p450s: experimental characterization, reactive intermediates, and clinical implications. *Chem. Res. Toxicol.* **2008**, *21* (1), 189−205.
(108) Nakajima, M.; Yoshida, R.; Shimada, N.; Yamazaki, H.; Yokoi, T. Inhibition and inactivation of human cytochrome P450 isoforms by phenethyl isothiocyanate. *Drug Metab. Dispos.* **2001**, *29* (8), 1110−3.
(109) Mi, L.; Di Pasqua, A. J.; Chung, F. L. Proteins as binding targets of isothiocyanates in cancer prevention. *Carcinogenesis* **2011**, *32* (10), 1405−13.
(110) Cross, J. V.; Rady, J. M.; Foss, F. W.; Lyons, C. E.; Macdonald, T. L.; Templeton, D. J. Nutrient isothiocyanates covalently modify and inhibit the inflammatory cytokine macrophage migration inhibitory factor (MIF). *Biochem. J.* **2009**, *423* (3), 315−21.
(111) Ku, K. M.; Choi, J. H.; Kim, H. S.; Kushad, M. M.; Jeffery, E. H.; Juvik, J. A. Methyl jasmonate and 1-methylcyclopropene treatment effects on quinone reductase inducing activity and post-harvest quality of broccoli. *PLoS One* **2013**, *8* (10), e77127.
(112) Kolm, R. H.; Danielson, U. H.; Zhang, Y.; Talalay, P.; Mannervik, B. Isothiocyanates as substrates for human glutathione transferases: structure-activity studies. *Biochem. J.* **1995**, *311* (Pt 2), 453−9.
(113) Abdull Razis, A. F.; Mohd Noor, N.; Konsue, N. Induction of epoxide hydrolase, glucuronosyl transferase, and sulfotransferase by phenethyl isothiocyanate in male Wistar albino rats. *Biomed. Res. Int.* **2014**, *2014*, 391528.
(114) Van der Logt, E. M.; Roelofs, H. M.; van Lieshout, E. M.; Nagengast, F. M.; Peters, W. H. Effects of dietary anticarcinogens and nonsteroidal anti-inflammatory drugs on rat gastrointestinal UDP-glucuronosyltransferases. *Anticancer Res.* **2004**, *24* (2B), 843−9.
(115) Xu, C.; Li, C. Y.; Kong, A. N. Induction of phase I, II and III drug metabolism/transport by xenobiotics. *Arch. Pharm. Res.* **2005**, *28* (3), 249−68.
(116) Keum, Y. S.; Owuor, E. D.; Kim, B. R.; Hu, R.; Kong, A. N. Involvement of Nrf2 and JNK1 in the activation of antioxidant responsive element (ARE) by chemopreventive agent phenethyl isothiocyanate (PEITC). *Pharm. Res.* **2003**, *20* (9), 1351−6.
(117) Suzuki, H.; Sugiyama, Y. Role of metabolic enzymes and efflux transporters in the absorption of drugs from the small intestine. *Eur. J. Pharm. Sci.* **2000**, *12* (1), 3−12.
(118) Tang, T.; Song, X.; Liu, Y. F.; Wang, W. Y. PEITC reverse multi-drug resistance of human gastric cancer SGC7901/DDP cell line. *Cell Biol. Int.* **2014**, *38* (4), 502−10.
(119) Flores, M. L.; Castilla, C.; Avila, R.; Ruiz-Borrego, M.; Saez, C.; Japon, M. A. Paclitaxel sensitivity of breast cancer cells requires efficient mitotic arrest and disruption of Bcl-xL/Bak interaction. *Breast Cancer Res. Treat.* **2012**, *133* (3), 917−28.
(120) Chan, D. K.; Miskimins, W. K. Metformin and phenethyl isothiocyanate combined treatment in vitro is cytotoxic to ovarian cancer cultures. *J. Ovarian Res.* **2012**, *5* (1), 19.
(121) Di Pasqua, A. J.; Hong, C.; Wu, M. Y.; McCracken, E.; Wang, X.; Mi, L.; Chung, F. L. Sensitization of non-small cell lung cancer cells to cisplatin by naturally occurring isothiocyanates. *Chem. Res. Toxicol.* **2010**, *23* (8), 1307−9.
(122) Tseng, E.; Kamath, A.; Morris, M. E. Effect of organic isothiocyanates on the P-glycoprotein- and MRP1-mediated transport of daunomycin and vinblastine. *Pharm. Res.* **2002**, *19* (10), 1509−15.
(123) Hu, K.; Morris, M. E. Effects of benzyl-, phenethyl-, and alpha-naphthyl isothiocyanates on P-glycoprotein- and MRP1-mediated transport. *J. Pharm. Sci.* **2004**, *93* (7), 1901−11.
(124) Ji, Y.; Morris, M. E. Membrane transport of dietary phenethyl isothiocyanate by ABCG2 (breast cancer resistance protein). *Mol. Pharmaceutics* **2005**, *2* (5), 414−419.
(125) Fu, Y.; Mi, L.; Sanda, M.; Silverstein, S.; Aggarwal, M.; Wang, D.; Gupta, P.; Goldman, R.; Appella, D. H.; Chung, F.-L. A click chemistry approach to identify protein targets of cancer chemo-preventive phenethyl isothiocyanate. *RSC Adv.* **2014**, *4* (8), 3920.
(126) Hudson, T. S.; Perkins, S. N.; Hursting, S. D.; Young, H. A.; Kim, Y. S.; Wang, T. C.; Wang, T. T. Inhibition of androgen-responsive LNCaP prostate cancer cell tumor xenograft growth by dietary phenethyl isothiocyanate correlates with decreased angiogenesis and inhibition of cell attachment. *Int. J. Oncol.* **2012**, *40* (4), 1113−21.

DOI: 10.1021/jf504627e
J. Agric. Food Chem. 2015, 63, 3311−3322

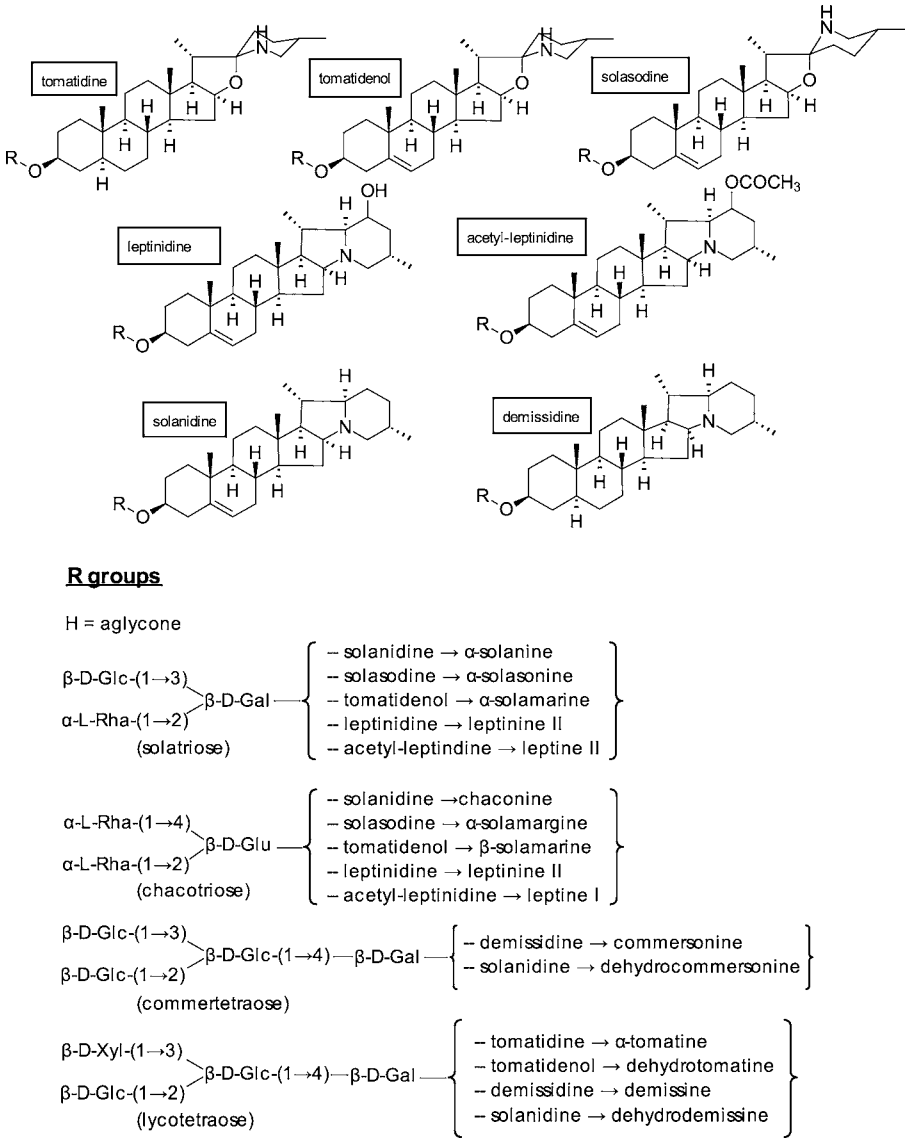

Figure 1. Structures of the aglycones and glycoalkaloids found in *Solanum*.[137,140,141]

combination, and as part of the diet against cancer cells and tumors. To help stimulate needed studies further, the main objective of this review is to unify the scattered information on the anticarcinogenic potential of the food-related glycoalkaloids. It should be noted that glycoalkaloids are reported to exhibit other beneficial as well as adverse effects in animals and humans. These aspects are beyond the scope of this review. They are comprehensively covered in our previous publications.[3−7]

CHEMISTRY AND PREVALENCE OF GLYCOALKALOIDS IN FOOD

Eggplants. *Solanum melongena* Linn. is an herbaceous plant with coarsely lobed leaves, white to purple flowers, and widely consumed fruit that can be eaten raw, cooked, or pickled.[8] The following selected studies show that eggplants contain several classes of bioactive compounds, including anthocyanidins, flavonoids, saponins, and glycoalkaloids. Individual or combinations of the bioactive compounds are probably responsible for the reported analgesic, antianaphylactic, anti-inflammatory, antioxidant, antipyretic, intraocular pressure reducing, central nervous system depressing, hypolipodemic, and hypotensive properties of eggplants, reviewed by Das and Barua and Sun et al.[8,9] We do not know whether eggplants also possess anticarcinogenic properties.

The fruits of the eggplant are one of the most widely consumed vegetables in the world, with the most popular species being Southeast Asia-domesticated *S. melongena* L.[10] These authors used liquid chromatography−mass spectrometry methods to compare the contents of the major eggplant glycoalkaloids (solamargine and solasonine) of *S. melongena* to the allied accession of the Africa-cultivated *S. aethiopicum* and *S. macrocarpon*. The results show that (a) fruits of *S. aethiopicum* and *S. melongena* contained (in mg/100 g fresh weight) 0.58−4.56 α-solamargine and 0.17−1.0 α-solasonine and (b) the corresponding much higher values for *S. macrocarpon* are 124−197 and 16−23, respectively, suggesting that this accession might not be safe for consumption. A related study of 10 eggplant lines and three allied species (*S. aethiopicum*, *S. integrifolium*, and *S. sodomaeum*) confirmed that the allied species had higher glycoalkaloid content than the widely consumed eggplants and that the glycoalkaloid content

DOI: 10.1021/acs.jafc.5b00818
J. Agric. Food Chem. 2015, 63, 3323−3337

generally increased during fruit development and ripening.[11] Bajaj et al.[12] used colorimetry to determine an average glycoalkaloid content of 21 eggplant varieties, whose concentrations (in mg/100 g fresh weightt) ranged from 6.25 to 20.5 or 3.3-fold variation from the lowest to the highest value. These authors also found that the crude protein content ranged from 0.77 to 3.63 (4.7-fold variation) and that high-glycoalkaloid eggplants tasted bitter. A British study used colorimetry to determine the average glycoalkaloid content of two eggplant samples of about 8 mg/100 g fresh weight.[13] Kintia and Shvets[14] isolated and characterized three steroidal saponins from seeds of Moldavian *S. melongena*. These compounds probably contribute to the observed bioactivities of eggplants. An Egyptian study[15] used colorimetry and thin-layer chromatography (TLC) to identify three glycoalkaloids (solamargine, solasonine, and solanine) in *S. melongena* fruit, whose concentrations varied with the harvesting season. These authors also found that fruit infected with *Botrytis cinerea* fungi contained the solanine hydrolysis product β-solanine. French scientists used colorimetry and TLC to determine the total glycoalkaloid and furastanol saponin content of six eggplant varieties, the concentrations of which (in mg/100 g fresh weight) ranged from 1.0 to 7.2 and 3.0 to 11.2, respectively.[16,17] Eanes et al.[18] developed an HPLC method for the separation and determination of the following eggplant glycoalkaloids: solamargine, solasonine, chaconine, and solanine and their aglycones, solasodine and solanidine. Extracts of *S. melongena* and *S. linnaeanum* were used to determine the method of recovery, limit of detection, and limit of quantification. In agreement with our studies with potato[19] and tomato[20] glycoalkaloids, grilling or boiling of eggplants did not result in significant changes in the total glycoalkaloid (solamargine plus solasonine) content.[21]

Potatoes. Nikolic et al.[22] describe a liquid−liquid system for the acid hydrolysis of potato glycoalkaloids from potato sprouts that yields 1.46 g of solanidine per 100 g of dried sprouts. Attoumbre et al.[23] describe a centrifugal partition chromatography procedure for the isolation of solanidine from glycoalkaloid hydrolysates of potato skins and sprout extracts. Kuo et al.[24] found that adding auxin phytohormones to cell culture tissues of the *Solanum lyratum* plant induced increases in the production of solanidine and solasodine levels, suggesting the availability of a new method for the production of steroidal alkaloids. Friedman and Levin[7] reviewed analytical methods for investigating potato glycoalkaloids and bioactive calystegine alkaloids. Figure 2 shows the glycoalkaloid content of fresh and processed potatoes.

Tomatoes. The glycoalkaloid known as tomatine consists of a mixture of two glycoalkaloids: α-tomatine and dehydrotomatine (Figure 1). In the present study, we will use the term tomatine for the 10:1 mixture. Both compounds are present in tomato fruit and leaves. Immature green tomatoes contain up to 500 mg of tomatine per kilogram of dry weight. The tomatine content of cherry tomatoes (grape tomatoes, minitomatoes) is several fold greater than that of larger size standard varieties. Because tomatine is largely degraded as the tomato ripens, the levels in red tomatoes are much lower, up to about 5 mg/kg. Consumers of high-tomatine green tomatoes and pickled green tomatoes consume high amounts of tomatine. A red tomato variant indigenous to the Andes mountains of Peru has a very high tomatine content, 500−5000 mg/kg dry wt.[25] These tomatoes are consumed without apparent acute toxic effects. Figure 3 lists the α-tomatine content of a small sampling of fresh and processed tomatoes.

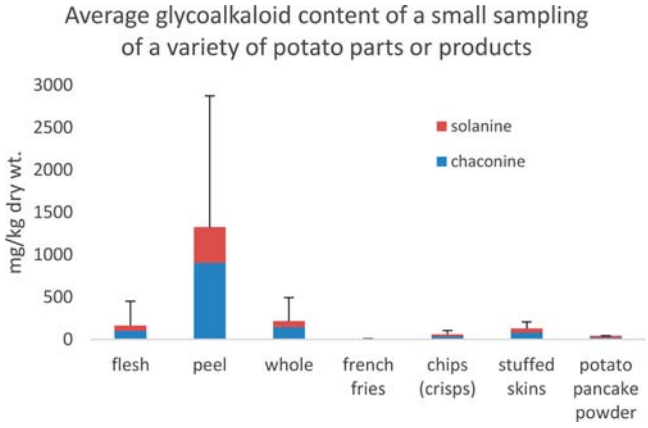

Figure 2. Makeup of total glycoalkaloids in a small sampling of a variety of potatoes and potato products. Due to the large standard deviations, ANOVA showed no statistical differences. Adapted from ref 6. Copyright 2006 American Chemical Society.

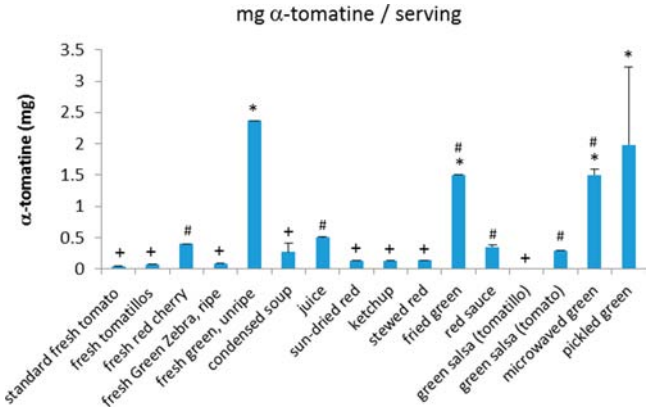

Figure 3. α-Tomatine content per serving of a variety of fresh and processed tomato (or tomatillo) products. Bars sharing the same symbol are not significantly different; $p < 0.05$. Adapted from ref 20. Copyright 1995 American Chemical Society.

The use of gene manipulation to introduce desirable traits into tomatoes, such as tolerance to stress and pesticides and resistance to phytopathogens, raises questions about the tomatine content of the transgenic tomatoes. Our results,[5] and those by other investigators,[26,27] indicate that tomatine levels of transgenic tomatoes were not significantly different from those observed in the standard varieties grown under the same field conditions. By contrast, a long-term (10 year) study revealed that organically grown tomatoes had higher average tomatine content than their standard counterparts, suggesting that soil composition and environmental conditions seem to affect the tomatine content in tomato.[28] The tomatine levels of tomatoes in both cropping systems ranged from 4.29 to 111.85 μg/g dry wt or a 26-fold variation from the highest to the lowest value. A related study found that the tomatidine content of 11 analyzed samples was higher in conventional tomatoes than that in organic tomatoes.[29] These results suggest the possibility of future anticancer and anticholesterol studies with selected high-tomatine and high-tomatidine red tomatoes.

We carried out studies designed to optimize the acid hydrolysis of the tetrasaccharide chain of tomatine to products

DOI: 10.1021/acs.jafc.5b00818
J. Agric. Food Chem. 2015, 63, 3323−3337

with three, two, one, and zero sugar groups.[30] A 20 min hydrolysis of tomatine in 1 N HCl at 100 °C was used for the formation of the trisaccharide β1-tomatine, the disaccharide γ-tomatine, and the monosaccharide δ-tomatine. Efforts to isolate the other theoretical possible trisaccharide, β2-tomatine, were unsuccessful, apparently because its xylose sugar is degraded during hydrolysis. A 70 min hydrolysis time achieved complete removal of the tetrasaccharide side chain to produce the aglycone tomatidine. Because tomatine was stable to acid hydrolysis at 37 °C, it may be stable in the acidic pH environment of the human gut. The hydrolysis products are formed by sequentially cleaving the sugars from lycotetraose (Figure 1).

With this background on the structures and composition of glycoalkaloids from eggplants, potatoes, and tomatoes and some of their hydrolysis products (metabolites), we will now briefly describe reported studies designed to determine the anticarcinogenic properties and mechanisms of action of the eggplant glycoalkaloids α-solamargine and α-solasonine, their common aglycone solasodine, the potato glycoalkaloids α-chaconine and α-solanine and hydrolysis products including the aglycone solanidine, and the tomato glycoalkaloids α-tomatine and hydrolysis products including aglycone tomatidine against cancer cells in culture (in vitro) and some animal and human tumors in vivo.

ANTICARCINOGENIC PROPERTIES OF EGGPLANT GLYCOALKALOIDS

Here, we briefly review mechanistic aspects associated with eggplant glycoalkaloids produced in some eggplant varieties. In addition to eggplants, numerous herbal and medicinal plants synthesize solamargine and solasonine. In fact, most of the anticancer studies mentioned below were done with glycoalkaloids isolated from these sources and not from eggplants. Because the glycoalkaloids from different plant sources are identical, we will also mention selected anticancer studies in cells, rodents, and human using glycoalkaloids from herbal and medicinal plants grown in different parts of the world. These include *S. incanum*,[31] *S. lycocarpum*,[32] and *S. nigrum*.[33]

Structural and Immune Effects in Apoptosis. Apoptosis is a genetically controlled (encoded), regulated, and conserved form of cell death, where the cell first undergoes nuclear and cytoplasm condensation with blebbing of the plasma membrane, DNA fragmentation, and breakdown of membrane-enclosed fragments known as apoptotic bodies, which are then engulfed rapidly by neighboring cells or macrophages.[34] The cell activity thus participates in its own destruction. In many cells, but apparently not with tomatine (see below), activation of caspases by eggplant glycoalkaloids may be the ultimate effector mechanism in apoptotic pathways. TNF exhibits antiproliferative effects against various cancer cell lines in vitro and in vivo.[34,35]

The trisaccharide solamargine and the corresponding mono- and diglycosides preferentially inhibited the uptake of tritiated thymidine by cancer cells relative to that by normal lymphocyte cells.[36] These results and the observed morphological changes in the cells indicate that the action against the cancer cells involves cell lysis. On the basis of a structure−activity and molecular modeling study, Chang et al.[37] concluded that the 2′-rhamnose moiety of solamargine [(22*S*,25*R*)-spiro-5-ene-3β-yl-α-L-rhamnopyranosyl-(1→2glu)-*O*-α-L-rhamnopyranosyl(1→4glu-β-D-glucopyranose)-solasodine] acts by penetrating the cell membrane by diffusion and then triggers death by apoptosis of human hepatoma Hep3B cells by changing the dihedral angle of the glycosidic bond, suggesting that the carbohydrate side chains of glycoalkaloids seem to govern the affinity to steroid human necrosis factor receptors and gene expression associated with carcinogenesis. A related study suggests that cells in the G(2)/M phases are highly susceptible to solamargine-mediated apoptosis and that parallel upregulation of tumor necrosis factor receptors TNFR-I or TNFR-II on the Hep3B cells may be an independent mechanism of solamargine-mediated apoptosis.[38]

Blankemeyer et al.[39] used a cell assay to measure the changes in membrane potentials of frog embryos induced by solamargine and solasonine. Experiments with solasonine at pH 6 and 8 suggest that the unprotonated form of solasonine is involved in the membrane potential effect and that the relative potencies of the two glycoalkaloids are similar for the observed frog embryo effects.

Solamargine and solasodine inhibit cell-mediated immune functions [(antibody-dependent cellular cytotoxicity (ADCC) and natural killer cell (NK)] activity of human peripheral mononuclear cells, possibly suggesting that enhancement of the immune system could contribute to apoptosis.[40] In vivo studies support this suggestion.[41] These authors found that groups of mice administered solasodine rhamnosyl glycosides one-half an hour after Sarcoma 180 inoculation caused total remission of the cancer, whereas mice treated with sarcoma but without the glycosides all died within 20 days. Moreover, 10 of 12 of cured mice were resistant to the reintroduction of terminal doses of cancer. Because, in addition to apoptosis, the glycosides stimulated lasting immunity against cancer similar to that observed with a vaccine containing *Corynbacterium parvum*, it seems that the stimulation of immunity contributed to the observed in vivo anticancer effects. It seems that solasodine glycosides could contribute to the management of diseases such as malignancy and also be used as a prevention therapy. Below, we mention the role of immunity in the bioactivity of glycoalkaloids.

Gastric Cancer Cells. Ding et al.[33] isolated six glycoalkaloids from *Solanum nigrum*. The following four induced cytotoxicity and apoptosis in the gastric cancer cell line MGC-803: solasonine, β1-solasonine, solamargine, and solanigroside P. The number and location of the α-L-rhamnose moiety and the type of sugar in the side chain as well as the presence of an OH group on the steroidal alkaloid backbone influenced relative potency. The suggested mechanism of apoptosis seems to be related to the recognized anticarcinogenic events: activation of caspase-3, cell cycle arrest, upregulation of the ratio of antiapoptotic Bax to Bcl-2 proteins, and downregulation of the mutant p53 gene.

Leukemia Cells. In an effort to define how solamargine mediates cytotoxicity via oncosis in human K562 leukemia and squamous cell carcinoma KB cells, Sun et al.[42] used the MTT assay to measure cytotoxicity and the release of lactate dehydrogenase (LDH) and the uptake of propidium iodide (PI) to determine leakage of cytoplasm content. Cytotoxicity and membrane disruption were triggered rapidly within minutes at the same rate by 10 μM solamargine, suggesting that apoptosis seems to be initiated by plasma membrane perturbation. These authors[34] also reported that exposure of the leukemia cells to 10 μM solamargine for 30 min induced a 7-fold increase in intracellular calcium concentration, down-expression of Bcl-2 and upregulation of Bax, caspase-3, and caspase-9 activities. These results and the observed decrease in

DOI: 10.1021/acs.jafc.5b00818
J. Agric. Food Chem. 2015, 63, 3323−3337

membrane potential and release of cytochrome c suggest that an induced lysosomal−mitochondrial death pathway is involved in the cytotoxicity. Because the cells do not show an early increase in reactive oxygen species (ROS) production before apoptosis, the lysosomal rupture does not seem to be associated with oxidative stress.

Liver Cancer Cells. Solamargine isolated from *Solanum nigrum* inhibited the growth and induced apoptosis of human hepatoma Hep G2 and SMMC-7721 cells lines via cell cycle arrest at G2/M phase and upregulation of caspase-3 expression, the so-called executioner caspase and mediator of DNA fragmentation and nuclear condensation, suggesting that the glycoalkaloid could be used to treat liver cancer.[43]

Lung Cancer Cells. Solamargine exhibited superior cytotoxicity in four human lung cancer cell lines, with IC_{50} values ranging from 3 to 7.2 μM, and increased binding of TNF-α and TNF-β to the lung cancer cells.[35] The glycoalkaloid induced release of cytochrome c, downregulation of anti-apoptotic Bcl-2 and Bcl-xL proteins, increase in caspase-3 activity, and DNA fragmentation.[35] These observations and the additional finding that TNF-resistant lung cancer cells became susceptible after exposure to solamargine suggest that the compound should be studied for its therapeutic value against human lung cancers.

Other investigators reported that the anticarcinogenic activity of solamargine is associated with the downregulation of HER-2 and upregulation of Fas and tumor necrosis factor receptor (TFNR) expression, which triggers the mitochondrial-mediated cell apoptosis pathway and sensitizes human lung cancer cell and A540 adenocarcinoma cells to chemotherapy, and that it potentiated the death of lung cancer H661 cells induced by the drugs herceptin and epirubicin[44,45] as well as the death of lung and breast cancer cells induced by the drug cisplatin.[46,47]

A detailed mechanistic study[48] revealed that solamargine inhibited growth and induced apoptosis of non-small-cell lung cancer cells in a time- and dose-dependent manner and increased phosphorylation of p38 mitogen-activated protein kinase (p38 MAPK) in a time-dependent manner. It also inhibited phosphorylation and protein expression of signal transducer and activator of transcription 3 (Stat3), which was abrogated by SB203580, a specific inhibitor of p38 MAPK, and induced protein expression of the p21 cyclin-dependent kinase inhibitors. Although silencing of Stat3 had no further effect, exogenous expression of Stat3 overcame the effect on cell proliferation. These results show that solamargine inhibits proliferation and induces apoptosis in lung cancer cells through p38 MAPK-mediated suppression of phosphorylation and protein expression of Stat3, followed by induction of Stat3's downstream effector, p21.

Osteosarcoma Cells. An investigation by Li et al.[49] on the role of the p53 gene in the proapoptotic action of solamargine in human U2OS cells using the microculture tetrazolium (MTT) and several other bioassays found that solamargine-induced apoptosis was associated with chromatin condensation, formation of apoptotic bodies, exposure of phosphatidylserine on the extracellular surface, increase in mRNA and protein levels of p53 and Bax (a proapoptotic protein), reduction in the expression of Bcl-2 (an antiapoptotic protein), loss of mitochondrial membrane potential, release of cytochrome c, and activation of caspase-3 and -9 enzymes. These results suggest that solamargine activates the mitochondria-mediated apoptotic pathway via both p53 transcription-dependent and -independent mechanisms. The authors conclude that the mechanism by which solamargine activates the p53 gene remains unclear.

Multiple Cancer Cell Lines. The Chinese medicinal herbs *Solanum incanum* and *Solanum nigrum* Linn. contain the steroidal glycoalkaloids solamargine, solanine, and solasonine. An ethanol extract of *S. nigrum* was found to inhibit the growth of MCF-7 breast cancer and to induce apoptosis of tumor cells.[50] Solanine isolated from this plant was found to inhibit tumors in the following cell lines (IC_{50} values in μg/mL): Hep G2 human carcinoma (14.5), SGC-7901 human gastric carcinoma (>50), and LS-174 human large intestine cancer cells (>50). The inhibitory action of solanine was accompanied by a decrease in the content of Bcl-2 protein in the Hep G2 cells. These data show that Hep G2 cells showed the greatest sensitivity to inhibition by solanine.

Munari et al.[32] evaluated the antiproliferative effects of solamargine and solasonine against the following tumor cell lines: murine melanoma (B16F10) and human colon carcinoma (HT29), breast adenocarcinoma (MCF-7), cervical adenocarcinoma (HeLa), hepatocellular liver carcinoma (Hep G2), and glioblastoma (MO59J, U343, and U251). Solamargine showed the most pronounced activity, with IC_{50} values ranging from 4.58 to 18.23 μg/mL. The lowest IC_{50} values (highest activities) were observed against Hep G2, with an IC_{50} value for solamargine of 4.58 and for solasonine of 6.01. These results show that the test substances behaved as broad-spectrum anticarcinogens.

Three solasodine glycoside derivatives prepared by trans-glycosylation exhibited strong cytotoxicity against four cancer cell lines, suggesting that they might serve as lead candidates for cancer chemotherapy.[51]

Multiple Drug Resistance. Multidrug resistance (MDR) is one of the major causes of the failure of conventional treatments of cancer. MDR is often associated with the expression of P-glycoprotein (P-gp), which acts as a drug efflux pump to transport intracellular drugs out of cells, thus imparting drug resistance to tumor cells.[52] These authors found that solamargine has broad-spectrum cytotoxic activity against multiple MDR cell lines (human myelogenous leukemia K562 cell line and its multidrug resistant counterpart K562/AO2) and that the P-gp−actin association pathway might be involved in the apoptosis, suggesting that the glycoalkaloid bypasses the MDR mechanism.

Enhancement of Cancer Drug Potencies. Solamargine synergistically enhanced the effects of cancer drugs including methotrexate, 5-florouracil, cisplatin,[46,47] and epirubicin[45,53] in several cancer cell lines, suggesting that it may have potential use in combination therapy for breast and lung cancers.

Mouse Cancers. A mixture of solasodine glycosides was effective in vivo against murine Sarcoma 180 (S180).[54] Mice in terminal stages of cancer became symptom free by a single dose. Because rhamnose inhibited the therapeutic effect, the authors suggest that the binding of glycosides to tumor cells may be mediated through the rhamnose carbohydrate of the trisaccharide side chain of solamargine.

Human Cancers. A 0.005% solasodine glycoside cream applied topically was effective in causing regression of human basal cell carcinomas (BCCs) and squamous cell carcinomas (SCCs) without adverse effect on the liver, kidneys, or blood system.[55] A solamargine-rich extract from *S. incanum* induced apoptosis in human SCC cells cells by upregulating the expression of TNFRs and Fas and downstream adaptors of TNF-α and Fas signaling pathways, triggering the mitochon-

DOI: 10.1021/acs.jafc.5b00818
J. Agric. Food Chem. 2015, 63, 3323−3337

drial apoptotic pathway, upregulating cytochrome c and Bax, and downregulating Bcl-X(L).[31] A once-daily application of a topical solamargine gel to the skin caused the disappearance of UVB-induced microinvasive SCCs in 27 of 30 hairless mice within 10 weeks. In addition, the gel cured 10 of 13 patients with actinic keratosis (AK) after 16 weeks. The authors suggest that the extract may be an ideal candidate for the treat of AK with minimal side effects on normal skin. Goldberg et al.[56] effectively treated cancer of the human penis, called Bowen's disease (in situ squamous cell carcinoma of the skin), with low concentrations of a mixture of solasodine glycosides and liquid nitrogen.

Punjabi et al.[57] evaluated, in a double-blind randomized study, the safety and efficacy of a cream containing a 0.005% mixture of solasodine glycosides (Zycure) for the treatment of basal cell carcinoma in humans (males, $n = 50$; females, $n = 44$) at 10 centers in the United Kingdom. The primary efficacy end point was histologically confirmed clearance of the basal cell carcinoma at the end of 8 week treatment. The results show that the treatment is a safe therapy for basal cell carcinoma, with a cure rate of 66% at 8 weeks and 78% at a 1 year follow-up.

In a related in vivo study, Tiossi et al.[58] used an extract of *Solanum lycocarpum* fruit containing 45% each of solamargine and solasonine to prepare a topical formulation and to optimize its penetration in vitro to porcine skin and in vivo to the skin of hairless mice. The results showed that pH 6.5 was optimal for delivery and penetration of skin in both animal models, suggesting that the formulation might be useful for topical therapy of skin disorders.

A review of the literature[59] concludes that there is insufficient evidence at present to make recommendations on the topical use of solasodine glycoalkaloids for skin cancers. Continued research on the efficacy of treatments is needed, including histologic confirmation of clearance, long-term follow-up, and comparison with surgical outcomes.

Solasodine. The aglycones solasodine and tomatidine isolated from the South African medicinal plant *Solanum aculeastrum* Dunal inhibited the growth of HeLa, MCF7, and HT29 cancer cell lines.[60] The IC_{50} value of the two compounds combined was lower (they were more active) than the value for solasodine but not for that of tomatidine.

ANTICARCINOGENIC PROPERTIES OF POTATO GLYCOALKALOIDS

Here, we will briefly describe reported anticarcinogenic properties and mechanisms of the bioactive potato compounds in cells (listed alphabetically) and laboratory animals.

***α*-Chaconine.** *Cervical, Liver, Hepatoma, and Stomach Cancer Cells.* Friedman et al.[2] describe methods for the isolation of large amounts of pure *α*-chaconine and *α*-solanine from Dejima potatoes and for the extraction and analysis of total glycoalkaloid content from five fresh potato varieties (Dejima, Jowon, Sumi, Toya, and Vora Valley). These compounds were then evaluated in experiments using a MTT assay to assess the anticarcinogenic effects of (a) the isolated pure glycoalkaloids separately, (b) artificial mixtures of the two glycoalkaloids, and (c) the total glycoalkaloids isolated from each of the five potato varieties. All samples tested reduced the number of the following human cell lines: cervical (HeLa), liver (Hep G2), lymphoma (U937), and stomach (AGS and KATO III) cancer cells and normal liver (Chang) cells. The results show that (a) the effects of the glycoalkaloids were concentration-dependent in the range of 0.1−10 μg/mL (0.117−11.7 nmol/mL), (b) *α*-chaconine was more active than *α*-solanine, (c) some mixtures exhibited synergistic effects, whereas others produced additive ones, (d) the different cancer cells varied in their susceptibilities to destruction, and (e) the destruction of normal liver cells was generally lower than that of liver cancer cells. The decreases in cell populations were also observed visually by phase contrast microscopy (Figure 4). This

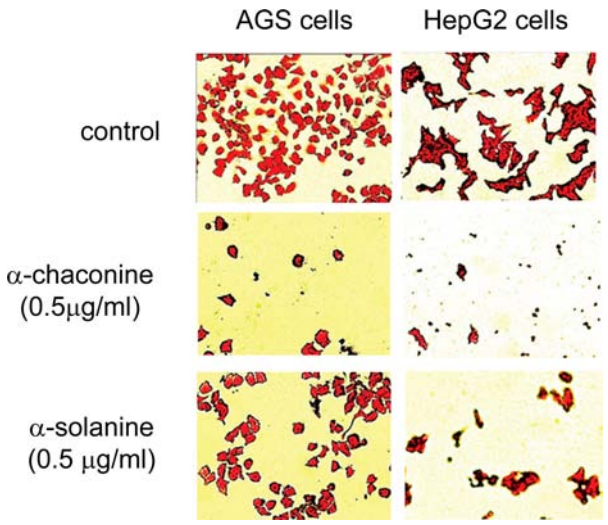

Figure 4. Morphological changes induced by glycoalkaloid treatments in Hep G2 and AGS cancer cells (×400 magnification). The cells were pretreated with either *α*-chaconine and *α*-solanine (0.5 μg/mL) for 48 h and stained with sulforhodanine B (0.4% w/v) for 30 min. Morphological alterations were recorded from phase-contrast microscopic observations. Adapted from ref 2. Copyright 2005 American Chemical Society.

study demonstrated for first the time the individual and synergistic anticancer properties of the two major glycoalkaloids present in all commercial potato varieties and processed potato products (chips, fries, skins).

Colon and Liver Cancer Cells. As part of an effort to improve plant-derived foods such as potatoes, eggplants, and tomatoes, the antiproliferative activities against human colon (HT29) and liver (Hep G2) cancer cells of a series of structurally related individual compounds were examined for the first time using a MTT assay.[1] The objective was to assess the roles of the carbohydrate side chain and aglycone part of *Solanum* glycosides in influencing inhibitory activities. Evaluations were carried out with four concentrations each (0.1, 1, 10, and 100 μg/mL) of the potato trisaccharide glycoalkaloids *α*-chaconine and *α*-solanine; the disaccharides *β*(1)-chaconine, *β*(2)-chaconine, and *β*(2)-solanine; the monosaccharide *γ*-chaconine and their common aglycone solanidine; the potato tetrasaccharide glycoalkaloid dehydrocommersonine; the potato aglycone demissidine; the tomato tetrasaccharide glycoalkaloid *α*-tomatine, the trisaccharide *β*1-tomatine, the disaccharide *γ*-tomatine, the monosaccharide *δ*-tomatine, and their common aglycone tomatidine; the eggplant glycoalkaloids *α*-solamargine and *α*-solasonine and their common aglycone solasodine; and the steroidal alkaloid jervine. All compounds were active in the assay, with the glycoalkaloids being the most active, and the hydrolysis products, less so. The effectiveness against the liver cells was greater than that against the colon cells. Potencies of *α*-tomatine and *α*-chaconine at a

DOI: 10.1021/acs.jafc.5b00818
J. Agric. Food Chem. 2015, 63, 3323−3337

concentration of 1 μg/mL against the liver carcinoma cells were higher than those observed with the anticancer drugs doxorubicin and camptothecin. This comprehensive report on anticarcinogenic potencies of a large number of glycoalkaloids and their hydrolysis products (metabolites) seems to have stimulated worldwide interest in the anticarcinogenic properties of potato and tomato glycoalkaloids and their mechanisms of action, as indicated by the numerous studies originating from different countries described below.

Colon Cancer Cells. α-Chaconine induced apoptosis of HT-29 human colon cancer cells in a time- and concentration-dependent manner.[61] The authors also showed that caspase-3 activity and the active form of caspase-3 were increased 12 h after α-chaconine treatment. In addition, caspase inhibitors prevented α-chaconine-induced apoptosis, whereas apoptosis was potentiated by an extracellular signal-regulated kinase (ERK) inhibitor. Results from the same study indicated that α-chaconine reduced the phosphorylation of ERK. It therefore seems that α-chaconine induces apoptosis of HT-29 cells through inhibition of ERK followed by activation of caspase-3.

Prostate Cancer Cells. Reddivari et al.[62] found that α-chaconine at 5 μg/mL and gallic acid at 15 μg/mL (a) exhibited potent antiproliferative properties and increased cyclin-dependent kinase inhibitor p27 levels in two prostate cancer cell lines, LNCaP and PC3, (b) induced poly[adenosine diphosphate (ADP)] ribose polymerase cleavage and caspase-dependent apoptosis in LNCaP cells and caspase-independent apoptosis through nuclear translocation of endonuclease G in both LNCaP and PC-3 cells, and (c) activated JNK, a response that played a major role in the induction of caspase-dependent apoptosis in LNCaP cells. These observations suggest that apoptosis induced by whole potato extracts in prostate cancer cell lines may be, in part, due to α-chaconine and gallic acid.

Inhibition of Angiogenesis of Bovine Aortic Endothelial Cells. In a study by Lu et al.,[63] α-chaconine inhibited the proliferation of bovine aortic endothelial cells (BAECs) in a dose-dependent manner, and nontoxic doses markedly suppressed cell migration, invasion, and tube formation. α-Chaconine also reduced the expression and activity of MMP-2, involved in angiogenesis (blood flow to cancer cells), and potently suppressed the phosphorylation of JNK, phosphatidylinositide-3 kinase (PI3K), and Akt, but it did not affect the phosphorylation of ERK and p38. Furthermore, the authors demonstrated that α-chaconine significantly increased the cytoplasmic level of inhibitors of IκBα and decreased nuclear factor κB (NF-κB), suggesting that it could inhibit NF-κB activity. It seems that α-chaconine inhibits migration, invasion, and tube formation of BAECs by reducing MMP-2 activity and JNK and PI3K/Akt signaling pathways and inhibiting NF-κB activity, suggesting its potential for use in antiangiogenic cancer therapy.

Reduction of Metastasis in Lung Carcinoma Cells. Metastasis is the spread of cancer cells from the initial or primary site of the disease to another part of the body. Shih et al.[64] found that α-chaconine (a) inhibited lung adenocarcinoma A549 cell invasion, migration, and phosphorylation of c-Jun N-terminal kinase (JNK) and Akt, (b) did not affect phosphorylation of extracellular signal regulating kinase (ERK) and p38, and (c) significantly decreased the nuclear level of NF-κB and the binding ability of NF-κB, suggesting that the inhibition of cell metastasis occurs by a reduction of matrix metalloproteinase-2 (MMP-2) and matrix metalloproteinase-9 (MMP-9) activities involving suppression of the phosphoinositide 3-kinase/Akt/NF-κB (PI3K/Akt/NF-κB) signaling pathway

α-Solanine. *Digestive System Cancer Cells.* Ji et al.[65] evaluated the effect of α-solanine isolated form the nightshade plant (*Solanum nigrum* Linn.) on the IC_{50} values of three digestive system tumor cell lines. The results show that (a) the IC_{50} values for the cell lines Hep G2, SGC-7901, and LS-174 were 14.47, >50, and >50 μg/mL, respectively, (b) the induced apoptosis rate in Hep G2 cells was 6.0, 14.4, 17.3, 18.9, and 32.2%, respectively, (c) cells in the G(2)/M phases of the cell cycle disappeared, whereas the number of cells in the S phase increased significantly for treated groups and the expression of Bcl-2 protein decreased. The target of solanine in inducing apoptosis in Hep G2 cells seems to be mediated by the inhibition of the expression of Bcl-2 protein.

Liver Cancer Cells. α-Solanine markedly increased in a dose-dependent manner the content of caspase-3 and concurrently decreased that of Bcl-2 in Hep G2 liver cancer cells. This observation suggests that α-solanine induces cell apoptosis by suppressing the activity of Bcl-2 and activating the caspase-3 protease.[66] Studies by Ji et al.[65] suggest that solanine-induced apoptosis in Hep G2 cells is turned on by reduction of the cell membrane potential, which opens ion channels that transport calcium ions down a concentration gradient, resulting in an increase in their concentration in the cell.

Pancreatic Cancer Cells In Vitro and In Vivo. Studies by Sun et al.[66] on the mechanism that may govern the anticarcinogenic activity of α-solanine in pancreatic cancer cells in vitro and in a nu/nu nude mouse model against human pancreatic cells show that the glycoalkaloid (a) inhibited the growth of the cancer cells through caspase-3-dependent mitochondrial apoptosis, (b) promoted the opening of the mitochondrial membrane permeability transition pore (MPTP) by downregulating the Bcl-2/Bax ratio, which resulted in the release of cytochrome c and Smac from the mitochondria into the cytosol to process the caspase-3 zymogen into its activated form, and (c) decreased the expression of tumor metastasis proteins, specifically MMP-2 and MMP-9, in the cells.

In a related study, Lv et al.[67] investigated the anticarcinogenic effect of α-solanine against human pancreatic cancer cells in vitro and in vivo. In vitro, α-solanine (a) inhibited the proliferation of PANC-1, sw1990, MIA PaCa-2 cells in a dose-dependent manner as well as cell migration and invasion at nontoxic doses; (b) suppressed the expression of MMP-2/9, extracellular inducer of matrix metalloproteinase CD44, eNOS, and E-cadherin in PANC-1 cells, (c) significantly decreased vascular endothelial growth factor (VEGF) expression and tube formation of endothelial cells, (d) suppressed phosphorylation of Akt, mTOR, and Stat3, and (e) enhanced phosphorylation of β-catenin and markedly decreased tran-nuclear translocation of NF-κB, β-catenin, and TCF-1. In vivo, administration of α-solanine (6 μg/g for 2 weeks) in a xenograft mouse model induced decreases in tumor volume and weight by 61 and 43%, respectively, as well as MMP-2/9, proliferating cell nuclear antigen (PCNA), and VEGF expression. These results indicate that the beneficial in vitro and in vivo effects seem to occur via the suppression of proliferation, angiogenesis, and metastasis. It seems that solanine might be an effective compound for the treatment of human pancreatic cancer.

Prostate Cancer Cells. An in vitro investigation of the effects of α-solanine on human androgen-independent prostate cancer cell line PC-3 showed that α-solanine suppressed the growth of the cells in a dose- and time-dependent manner and that the

DOI: 10.1021/acs.jafc.5b00818
J. Agric. Food Chem. 2015, 63, 3323−3337

cells were arrested in S phase.[68] The protein level of IκBα was increased and that of Bcl-2 was decreased at all tested concentrations (30, 40, and 50 μg/mL), suggesting that the antiprostate cancer effect occurred via inhibition of cell proliferation, arrest of the cells in S phase, induction of apoptosis, upregulation of the expression of IκBα, and downregulation of Bcl-2.

Shen et al.[69] investigated the mechanism involved in the suppression of human prostate cancer cell line (PC-3) metastasis by α-solanine. The results show that α-solanine reduces the viability of PC-3 cells. Treatment with a nontoxic dose markedly suppresses cell invasion and significantly elevates the expression of epithelial marker E-cadherin, and it concomitantly decreases the expression of mesenchymal marker vimentin, suggesting that the glycoalkaloid suppresses the epithelial−mesenchymal transition (EMT). The authors also showed that α-solanine reduces the mRNA level of MMP-2, MMP-9, and extracellular inducer of matrix metalloproteinase (EMMPRIN), but it increases the expression of reversion-inducing cysteine-rich protein with kazal motifs (RECK) and tissue inhibitor of metalloproteinase-1 (TIMP-1) and TIMP-2. In addition, it suppresses the phosphorylation of phosphatidylinositide-3 kinase (PI3K), Akt, and ERK. Furthermore, α-solanine downregulates oncogenic microRNA-21 (miR-21), upregulates tumor suppressor miR-138 expression and reduces ERK and PI3K/Akt signaling pathways, and regulates expression of miR-21 and miR-138. It seems that the inhibition of PC-3 cell invasion by α-solanine might, in part, result from blocking EMT and the expression of MMPs. These findings have therapeutic potential for suppressing invasion of prostate cancer cells.

Inhibition of Breast Cancer in Mice. Mohsenikia et al.[70] investigated α-solanine toxicity in vitro and in vivo and assessed its protective and therapeutic effects on a typical mouse model of breast cancer. The results show that α-solanine significantly suppressed the proliferation of mouse mammary carcinoma cells both in vitro and in vivo; at a concentration of 5 mg/kg, the tumor rate in the treated group was 0 compared with a 75% rate in the untreated controls. The average tumor size and weight were significantly lower in treated mice than that in corresponding controls. Moreover, α-solanine induced an increased in Bax protein expression in the breast tumor compared with that its respective control group and induced decreased expression of the antiapoptotic Bcl-2 protein and a decrease in proliferative and angiogenic parameters. These results demonstrate the chemoprotective and chemotherapeutic potential of α-solanine in a breast cancer model that operates through apoptosis induction and cell proliferation and angiogenesis inhibition.

Inhibition of Human Melanoma Cell Migration and Invasion. Lu et al.[71] examined the effect of α-solanine on the metastasis of melanoma cancer cells in vitro. The results show that α-solanine (a) inhibited proliferation of human melanoma cell line A2058 in a dose-dependent manner, (b) markedly suppressed cell migration and invasion and reduced the activity of MMP-2 and MMP-9, involved in the migration and invasion of cancer cells, at a nontoxic dose, (c) potently suppressed the phosphorylation of JNK, PI3K, and Akt but did not affect phosphorylation of extracellular signal regulating kinase (ERK), and (d) significantly decreased the nuclear level of NF-κB and inhibited NF-κB activity. Collectively, the results suggest that α-solanine inhibited migration and invasion of A2058 cells by reducing MMP-2/9 activities and inhibiting JNK and PI3K/Akt signaling pathways and NF-κB activity.

Disruption of Cell Membranes. Hep G2 cells treated with α-solanine showed typical signs of apoptosis associated with a lowered membrane potential of the mitochondria and an increased concentration of Ca^{2+}.[72] It seems that α-solanine opens up channels in the membrane by lowering the membrane potential that then leads to the transport of Ca^{2+} ions down their concentration gradient, resulting in an increase in the concentration of calcium ions in the cell and initiating the mechanism apoptosis.

Solanidine. *Solanidine and Solanidine Analogues.* Here, we will mention several aspects of solanidine biology and chemistry that may be relevant to the theme of the present review. A structure−function relationship study of the biological activities (cell cycle arrest, apoptosis) on human osteosarcoma 1547 cells revealed a correlation between the experimental and theoretical data that highlighted the importance of the heterosugar moiety and the 5,6 double bond in these activities.[73] Six synthetic solanidine analogues exhibited strong anticancer activities and multidrug resistance reversal effects in a hypodiploid population of HeLa murine lymphoma cells, suggesting that the modified solanidine skeleton is a suitable substrate for the design and synthesis of further innovative drug candidates with anticancer activities.[52]

Inhibition of Multidrug Resistance. Because intrinsic or acquired resistance of tumor cells to multiple cytotoxic drugs (multidrug resistance, MDR) is a major cause of failure of cancer chemotherapy, Lavie et al.[74] examined the ability of steroidal alkaloids of plant origin, namely, the *Veratrum* sp. alkaloid cyclopamine and the *Lycopersicon* sp. Aglycone (alkaloid) tomatidine, to act as chemosensitizers in multidrug-resistant NCI AdrR human adenocarcinoma. The results show that the alkaloids inhibited P-gp-mediated drug transport and multidrug resistance, suggesting that these plant-derived compounds may serve as chemosensitizers in combination chemotherapy with conventional cytotoxic drugs for treating multidrug-resistant cancer.

■ ANTICARCINOGENIC PROPERTIES OF THE TOMATO GLYCOALKALOID TOMATINE

Here, we will briefly mention results of reported studies on the anticarcinogenic potential of α-tomatine in vitro and in vivo.

Early Studies on the Inhibition of Multiple Cancer Cells. Lee et al.,[1] using the MTT in vitro assay, found that commercial tomatine is a strong inhibitor of growth for both human colon and liver cancer cell lines, as evidenced by the dose-dependent (0.1−100 μg/mL) inhibition of HT29 colon cancer cells at levels ranging from 38.0 to 81.5% and of human Hep G2 liver cancer cells from 46.3 to 89.2%. The anticarcinogenic activity against human liver cancer cells at a tomatine concentration of 1 μg/mL was higher than the activity observed with the commercial anticancer drug doxorubicin.

Friedman et al.[75] also investigated six green and three red tomatoes extracts for their ability to induce cell death in human cancer and normal cells using a microculture MTT assay. Compared to the untreated controls, the high-tomatine green tomato extracts strongly inhibited the following human cancer cell lines: breast (MCF-7), colon (HT-29), gastric (AGS), and hepatoma (liver) (Hep G2) as well as normal human liver cells (Chang). In another study, we discovered that the activity of α-tomatine generally decreases upon removal of one or more of the four carbohydrate groups of the lycotetraose side chain.[76]

DOI: 10.1021/acs.jafc.5b00818
J. Agric. Food Chem. 2015, 63, 3323−3337

For example, the activity of α-tomatine against the PC-3 prostate cancer cells was about 200 times greater than that of the aglycone tomatidine. Tomatidine is, however, active against the foodborne pathogen *Staphylococcus aureus*,[77] suggesting that the two bioactivities seem to be governed by different mechanisms.

Our systematic studies on the bioactivity of tomatine at microgram levels against multiple human cancer cells seems to have stimulated interest from a number of investigators mentioned below to explore the biomarkers and associated signaling pathways that may be associated with the anticarcinogenic effects of tomatine.

Leukemia Cells. α-Tomatine inhibited human leukemia MOLT-4 cells by activating cell cycle checkpoints without damaging single or double DNA strands in the cells.[78] The slowing of the cell cycle seems to involve caspase-independent cell death associated with an increase in the tumor suppressor protein p53 and the proapoptotic protein PUMA (p53 upregulated modulator of apoptosis) as well as other biomarkers associated with cell cycle regulation. A related study found that α-tomatine-mediated anticancer activity against human chronic myeloid leukemia cells in vitro and in a transplanted mouse tumor operated through cell cycle- and caspase-independent pathways.[79]

Prostate Cancer Cells. α-Tomatine inhibited PC-3 prostate cancer cells with an IC_{50} value of 1.67 μM.[80,81] Cytotoxicity occurred after an hour of treatment and was mainly due to induction of apoptosis, as evidenced by decreased mitochondrial membrane potential, increased nuclear condensation, polarization of F-actin potential, cell membrane permeability, cytochrome c expression, induction of activation of caspase-3, -8, and -9, inhibition of NF-κB nuclear translocation, and a decrease in NF-κB/p50 and NF-κBp65 in the nuclear fraction.

Suppression of NF-κB activation by α-tomatine in PC-3 prostate cancer cells seems to occur through the inhibition of IκBα kinase activity, leading to sequential suppression of IκBα phosphorylation, IκBα degradation, NF-κB/p65 phosphorylation, and NF-κB p50/p65 nuclear translocation.[82] As expected, α-tomatine also reduced TNF-α-induced activation of the prosurvival mediator Akt. Its inhibition of NF-κB activation was accompanied by significant reduction in the expression of NF-κB-dependent antiapoptotic (c-IAP1, c-IAP2, Bcl-2, Bcl-xL, XIAP, and survivin) proteins. It seems that NF-κB plays a role in prostate cancer and that agents that suppress its activation may inhibit development or progression of this malignancy.

Inhibition of Lung Cancer Cell Migration and Invasion. Shih et al.[83] found that α-tomatine (a) inhibited cell invasion, migration, and phosphorylation of Akt and extracellular signal-regulated kinase 1 and 2 (ERK1/2) in human lung adenocarcinoma A549 cells, (b) did not affect phosphorylation of JNK and p38, (c) decreased nuclear levels of NF-κB, c-Fos, and c-Jun, and (d) inhibited the binding abilities of NF-κB and activator protein-1 (AP-1). Metastasis inhibition occurs by reducing the effects of MMP-2, MMP-9, and uPA (urokinase-type-plasminogen activator) through the PI3K/Akt or ERK1/2 signaling pathway and inhibiting NF-κB or AP-1 binding activities.

A related study[84] confirmed that α-tomatine suppressed invasion and migration of human non-small-cell lung cancer NCI-H460 cells through inactivation of the FAK/PI3K/Akt signaling pathway and lowering the binding activity of NF-κB. Cytotoxicity occurred through inactivation of the signaling pathway and enhancement of IkBα protein expression to reduce NF-κB DNA binding activity, resulting in the downregulation of MMP-7 expression, inhibition of cell migration, and interference with the rearrangement of the actin cytoskeleton by decreasing the expression of the pFAK protein.

Inhibition of Fish and Mouse Tumors. Feeding 2000 ppm of tomatine and 224 ppm of the multiorgan carcinogen dibenzo[*a*,*l*]pyrene (DBP) to rainbow trout for 9 months resulted in a reduced incidence of liver and stomach tumors by 41.3 and 36.3%, respectively, as compared to the incidence of tumors observed with DBP alone.[85] This seems to be the first report on the inhibition of tumor growth by dietary α-tomatine.

Intraperitoneally (ip) administered α-tomatine (5−10 mg/kg) significantly attenuated the growth of androgen-independent PC-3 prostate cancer cells in mice.[82] Tumor suppression was associated with increased apoptosis and with reduced nuclear translocation of the p50 and p65 components of the NF-κB signaling pathway. It seems that α-tomatine can inhibit the growth of prostate cancer tumors in vivo without inducing overt toxicity.

An evaluation of the antitumor activity of α-tomatine against PC-3 cell tumors grown subcutaneously and orthotopically in mice showed that ip administration of α-tomatine significantly attenuates the growth of PC-3 cell tumors grown at both sites.[82] Analysis of tumor material indicates that the tumor-suppressing effects were accompanied by increased apoptosis and lower proliferation of tumor cells as well as reduced nuclear translocation of the p50 and p65 components of NF-κB.

Intraperitoneal-injected α-tomatine at 1 mg/kg slowed the growth of mammary carcinoma (Ehrlich tumors) in mice.[86] The combination of α-tomatine (1 mg/kg) and the cancer drug doxorubicin (2 mg/kg) acted synergistically and extended survival of the mice with the Ehrlich tumors. The activity against the tumors, which are derived from adenocarcinoma of the mammary gland, seems to involve the immune system in the inhibition of tumor progression. This suggestion seems plausible based on reports by other investigators that tomatine contributes to the protective immunity of rodents (see below).

Kim et al.[87] determined the effect of commercial α-tomatine on CT-26 colon cancer cells in vitro and in vivo in an intracutaneously transplanted mouse tumor. Cytotoxicity experiments showed that α-tomatine induces about 50% lysis of the cancer cells at 3.5 μM after 24 h treatment. Large proportions of cells were found to be in the Annexin V (+)/propidium iodide (+) phase of cell death, implying late-phase apoptotic/necrotic status. α-Tomatine induced cell death in CT-26 cancer cells through caspase-independent signaling pathways. This conclusion was supported by western blot analysis showing localization of apoptosis-inducing mitochondrial protein (AIF) in the nucleus, downregulation of the apoptosis inhibitor survivin, and failure to detect the active form of caspase-3, -8, and -9 produced by proteolytic cleavage in CT-26 cancer cells.

The ip-administered α-tomatine (5 mg/kg body weight) also markedly inhibited growth of the tumor without causing body and organ weight changes. It seems that the reduced tumor growth in the mice by 38% after 2 weeks was the result of increased caspase-independent apoptosis associated with increased nuclear translocation of AIF and decreased survivin expression in tumor tissues. It seems that α-tomatine in pure form and in tomatine-rich green tomatoes might prevent colon cancer.

DOI: 10.1021/acs.jafc.5b00818
J. Agric. Food Chem. 2015, 63, 3323−3337

In addition to the cited mechanistic aspects involving proapoptotic biomarkers and signaling pathways, it seems likely that tomatine–cholesterol interactions, tomatine-induced stimulation of the immune system, and disruption of cancer cell membranes might also contribute to the mechanisms that govern its anticarcinogenicity.

We will now briefly mention the possible scientific basis for these suggestions.

Stimulation of the Immune System. α-Tomatine can act as a powerful adjuvant to elicit an antigen-specific cell-mediated immune response to the circumsporozoite (CS) protein, a major pre-erythrocyte stage malaria vaccine candidate antigen, requiring both CD80 and CD86 costimulation to form antigen-specific cellular immunity.[88] Heal et al.[89] found that α-tomatine contributed to protective immunity elicited by a malaria vaccine candidate via $CD8^+$ T cell release of antigen-specific IFN-γ in a *Plasmodium berghei* (malaria) rodent model. It seems that stimulation of the immune system might also contribute the anticarcinogenic effects of α-tomatine.

α-Tomatine–Cholesterol Interactions in Breast and Leukemia Cancer Cells. Sucha et al.[90] observed that the inhibition of cell proliferation and viability of human breast adenocarcinoma MCF-7 cells in culture at concentrations of 6 and 9 μM was followed by a recovery of cells. The recovery was not caused by the biotransformation of α-tomatine in the cells but by a substantial decrease in the concentration of α-tomatine in the culture medium due to its binding with cholesterol. Additional experiments on the regulation of the mechanism of action of α-tomatine revealed a loss of ATP in α-tomatine-treated cells but no DNA damage, no changes in the levels of the proteins p53 and p21(WAF1/Cip1), and no apoptosis (neither activated caspase-8 and -9, sub-G1 peak, nor morphological signs). The authors suggest that these results support the conclusion that α-tomatine does not induce apoptosis in the MCF-7 cell line in culture.

Another study found that treatment of human myeloid leukemia HL-60 cells with α-tomatine resulted in growth inhibition and apoptosis in a concentration-dependent manner, that both events were partially abrogated by added cholesterol, and that α-tomatine inhibited the growth of HL-60 xenografts in vivo.[91] The authors suggest that interactions between α-tomatine and cell membrane-associated cholesterol might be involved in mediating the in vivo anticarcinogenic effect of α-tomatine. These results and the reported strong affinity of α-tomatine to cholesterol in an artificial cell membrane,[92] and to plasma cholesterol in vivo,[93−96] imply that the affinity of the glycoalkaloid to cancer cell membrane cholesterol might be a factor governing the mechanism of apoptosis.

Disruption of Cell Membranes. As part of an effort designed to establish the mechanism of action of glycoalkaloids in cells, frog embryos and frog skin were exposed to varying concentrations of α-tomatine and tomatidine.[97] α-Tomatine increased the fluorescence-measured membrane permeability of frog embryos by about 600% compared with control values; the corresponding value for tomatidine was about 150%. The glycoalkaloid also diminished sodium-active transport in frog skin by about 16% compared with control values, as estimated from the change in the interstitial short-circuit current. Tomatidine had no effect on frog skin. These observations suggest that the sugar side chain present in α-tomatine but not in tomatidine influences membrane permeability of cells. As these findings complement similar results with glycoalkaloids from potatoes[98,99] and eggplants,[39] it is likely that the disruption of cancer cell membranes associated with changes in ion flux and interstitial currents of the membranes may contribute to the anticarcinogenic mechanisms governing their action in animal and human cells in vitro and in vivo.

In a related study involving membrane potentials, Taveira et al.[100] found that tomatine-containing tomato leaf extracts and the isolated α-tomatine and tomatidine pure compounds at nontoxic concentrations preserved the mitochondria membrane potential, decreased reactive oxygen species of SY5Y glutamate-insulted neuronal cells, and interacted with nicotinic receptors. The authors suggest that this study provides novel insights into the neuroprotective effect of glutamate-induced neurotoxicity and demonstrates the low toxicity of both compounds.

■ DIETARY SIGNIFICANCE AND RESEARCH NEEDS

Overall, the cited studies seem to indicate that the molecular, signaling, biomarker, immunomodulating, cholesterol-chelating, and membrane-disruptive events at the cellular and molecular levels associated with apoptosis and cell migration and invasion might not be the same for the different cancer cell lines. They imply that both intrinsic and extrinsic proapoptosis pathways are involved and that α-tomatine may protect against the development and progression of several cancers (multiorgan protection). This is not surprising because, as mentioned earlier, carcinogenesis is a sequential multistage cellular process consisting of tumor initiation, promotion, and progression, characterized by dysregulation of multiple genes resulting in multiple adverse symptoms. Each stage involves signaling pathways and both the same and different associated biomarkers. The structurally different glycoalkaloids and their aglycones might impact the cancer cell components at different rates.

Antineoplastic glycoalkaloids complement and extend our knowledge of the mechanisms of alterations in the gene and/or protein levels of the Bcl-2 family members and other cell death mechanisms that are active in cancer cells following treatment with glycoalkaloids and numerous other natural compounds.[101,102] This overview is intended to stimulate interest in the use of both pure and food-containing glycoalkaloids at nontoxic levels to help protect against or ameliorate multiorgan carcinogenesis.

With respect to potatoes, unofficial worldwide guidelines recommend a guideline for total glycoalkaloid content of 20 mg/100 g fresh weight.[6,7] On the basis of the anticarcinogenic results discussed earlier, it seems that this level in commercial potatoes might help to protect against multiple cancers. Epidemiological studies are, however, needed to demonstrate this possibility. Guidelines for maximum glycoalkaloid content of eggplants and tomatoes have not been established.

Because, compared to the other glycoalkaloids, tomatine exhibits low toxicity in animals and humans, future experimental and epidemiological studies should concentrate on the tomato compounds.[4,25] Plant scientists are challenged to develop high-tomatine red tomatoes. High-tomatine red tomatoes will contain two anticarcinogenic compounds: the antioxidative red pigment lycopene and tomatine.[103] The potential payoff will be better human health.

Future studies need to address the following additional food and medical aspects:

- Determine whether in vitro anticarcinogenic effects of pure glycoalkaloids and glycoalkaloid-containing plant foods can be duplicated in humans.

DOI: 10.1021/acs.jafc.5b00818
J. Agric. Food Chem. 2015, 63, 3323−3337

- Determine how bioactivities vary depending on whether glycoalkaloids are tested or consumed in the free-state or as part of a mixture or a food.
- Determine, using epidemiology, the presumptive connection between glycoalkaloid consumption and lower risk of cancer in humans.
- Determine whether glycoalkaloid metabolites formed after absorption into the circulation possess anticarcinogenic properties.
- Validate, via dietary interventions, predicted anticarcinogenic properties based on mathematical modeling[104] or molecular interaction networks.[105]
- Define additive and synergistic effects of glycoalkaloids with other anticarcinogenic food-related plant foods and bioactive compounds, including pigmented rice brans and its anticarcinogenic constituent γ-oryzanol;[106−110] black and green teas and their anticarcinogenic epigallocatechin gallate (ECGC) and theaflavin constituents;[111−113] mushroom polysaccharides;[29,114] and multifunctional jujube fruit (Chinese dates) and jujube fruit and seed compounds jujuboside B and betulinic acid.[115−118] It seems that consumption of glycoalkaloid-containing food, pigmented rice, and teas with a high content of catechins and theaflavins might ameliorate carcinogensis[119−121] and that tea flavonoids might alleviate both cancer and infectious disease;[122] as noted above, lycopene- and tomatine-containing tomatoes might mitigate both carcinogenesis and cardiovascular disease. Combinations of food and bioactive food ingredients that act additively or synergistically will decrease the amounts needed for effective, safe, and tasty food formulations.
- Evaluate the efficacy of glycoalkaloids against multidrug-resistant cancers.
- Because inhibition of hedgehog signaling decreases tumor growth, determine whether inhibition of hedgehog signaling by tomatidine or tomatine can help to inhibit carcinogenesis.[123,124]
- Will α-tomatine, which is reported to inhibit the herpes simplex virus via insertion into the viral envelope, also inhibit the human papillomavirus that causes cervical cancer?[125,126]
- Encourage growers to produce tomatoes with a high content of tomatine using antisense RNA methods to suppress the genes that degrade tomatine. Create tomatine-containing potatoes.[127−130]
- Determine the anticarcinogenic potential of numerous glycoalkaloids present in tubers, leaves, and sprouts of uncultivated and wild-type potatoes.[131−137]
- Do glycoalkaloids contribute to the anticarcinogenic properties of anthocyanin-rich color-fleshed and high-antioxidant potatoes?[138,139]

AUTHOR INFORMATION

Corresponding Author

*E-mail: Mendel.Friedman@ars.usda.gov; Phone: 510-559-5615.

Notes

The author declares no competing financial interest.

ACKNOWLEDGMENTS

I take great pleasure in thanking my collaborators whose names appear in the cited references and Carol E. Levin for facilitating the preparation of the manuscript.

ABBREVIATIONS USED

AIF, apoptosis-inducing factor; AK, actinic keratosis; Akt, protein kinase B; Annexin V-FITC, annexin V conjugated with fluorescein isothiocyanate, for detection of cell apoptosis; AP-1, activator protein-1; Bax, a proapoptotic proteins; BCC, basal cell carcinoma; Bcl-2, Bcl-xL, antiapoptotic proteins; BAEC, bovine aortic endothelial cells; c-Fos, apoptosis signaling protein; c-IAP1, c-IAP2, antiapoptotic proteins; DBP, dibenzo-[*a*,*l*]pyrine-carcinogen; ERK, extracellular signal-regulated kinase; FAK, focal adhesion kinase; Fas, proapoptotic protein; EMT, epithelial mesenchymal transition; IC_{50}, concentration of the test substance that inhibited 50% of the cancer cells; IFN-γ, interferon-gamma; IgG, immunoglobulin; ip, intraperitoneal; JNK, c-Jun N-terminal kinase; LDH, lactate dehydrogenase; MAPK, mitogen-activated protein kinase; MDR, multidrug resistance; miR-21, microRNA-21; MMP, matrix metalloproteinase; MPTP, mitochondrial membrane permeability transition pore; MTT, a tetrazolium dye, 3-(4,5-dimethylthiazol-2-yl)-2,5-diphenyltetrazolium bromide; NF-κB, nuclear factor kappa-light-chain-enhancer of activated B cells; NP-40, Tergitol-type NP-40 detergent; NSCLC, non-small-cell lung cancer; PCNA, proliferating cell nuclear antigen; P-gp, p-glycoprotein; PI, propidium iodide; PS, phosphatidylserine; PI3K, phosphatidylinositol-4,5-bisphosphate 3-kinase; PI3K/AKT/mTOR, an intracellular signaling pathway; PUMA, proapoptotic protein; RECK, reversion-inducing cysteine-rich protein with kazal motifs; SCC, squamous cell carcinoma; TCF-1, transcription protein; TFNR-I, TFNR-II, tumor necrosis factor receptors; TIMP-1, tissue inhibitor of metalloproteinase-1; TNF-α, TNF-β, tumor necrosis factors; VEGF, vascular endothelial growth factor; uPA, urokinase type plasminogen activator; XIAP, X-chromosome-linked inhibitor of apoptosis

REFERENCES

(1) Lee, K.-R.; Kozukue, N.; Han, J.-S.; Park, J.-H.; Chang, E.-Y.; Baek, E.-J.; Chang, J.-S.; Friedman, M. Glycoalkaloids and metabolites inhibit the growth of human colon (HT29) and liver (HepG2) cancer cells. *J. Agric. Food Chem.* **2004**, *52*, 2832−2839.

(2) Friedman, M.; Lee, K. R.; Kim, H. J.; Lee, I. S.; Kozukue, N. Anticarcinogenic effects of glycoalkaloids from potatoes against human cervical, liver, lymphoma, and stomach cancer cells. *J. Agric. Food Chem.* **2005**, *53*, 6162−6169.

(3) Friedman, M.; McDonald, G. M. Potato glycoalkaloids: chemistry, analysis, safety, and plant physiology. *Crit. Rev. Plant Sci.* **1997**, *16*, 55−132.

(4) Friedman, M. Tomato glycoalkaloids: role in the plant and in the diet. *J. Agric. Food Chem.* **2002**, *50*, 5751−5780.

(5) Friedman, M. Analysis of biologically active compounds in potatoes (*Solanum tuberosum*), tomatoes (*Lycopersicon esculentum*), and jimson weed (*Datura stramonium*) seeds. *J. Chromatogr.* **2004**, *1054*, 143−155.

(6) Friedman, M. Potato glycoalkaloids and metabolites: roles in the plant and in the diet. *J. Agric. Food Chem.* **2006**, *54*, 8655−8681.

(7) Friedman, M.; Levin, C. E. Glycoalkaloids and calystegine alkaloids in potatoes. In *Advances in Potato Chemistry and Technology*, 2nd ed.; Singh, J., Kaur, L., Eds.; Academic Press: Boston, MA, 2015.

(8) Das, M.; Barua, N. Pharmacological activities of *Solanum melongena* Linn. (Brinjal plant). *Int. J. Green Pharm.* **2013**, *7*, 274−277.

DOI: 10.1021/acs.jafc.5b00818
J. Agric. Food Chem. 2015, 63, 3323−3337

(9) Sun, J.; Gu, Y. F.; Li, M. M.; Su, X. Q.; Li, H.; Li, J.; Tu, P. F. Research advances on chemical constituents of *Solanum melongena* and their pharmacological activities. *Chin. Tradit. Herb. Drugs* **2013**, *44*, 2615−2622.
(10) Sánchez-Mata, M. C.; Yokoyama, W. E.; Hong, Y.-J.; Prohens, J. α-Solasonine and α-solamargine contents of gboma (*Solanum macrocarpon* L.) and scarlet (*Solanum aethiopicum* L.) eggplants. *J. Agric. Food Chem.* **2010**, *58*, 5502−5508.
(11) Mennella, G.; Lo Scalzo, R.; Fibiani, M.; D'Alessandro, A.; Francese, G.; Toppino, L.; Acciarri, N.; de Almeida, A. E.; Rotino, G. L. Chemical and bioactive quality traits during fruit ripening in eggplant (*S. melongena* L.) and allied species. *J. Agric. Food Chem.* **2012**, *60*, 11821−11831.
(12) Bajaj, K. L.; Kaur, G.; Chadha, M. L. Glycoalkaloid content and other chemical constituents of the fruits of some eggplant (*Solanum melongena*. L.) varieties. *J. Plant Foods* **1979**, *3*, 163−168.
(13) Jones, P. G.; Fenwick, G. R. The glycoalkaloid content of some edible solanaceous fruits and potato products. *J. Sci. Food Agric.* **1981**, *32*, 419−421.
(14) Kintia, P. K.; Shvets, S. A. Melongosides n, o and p: steroidal saponins from seeds of *Solanum melongena*. *Phytochemistry* **1985**, *24*, 1567−1569.
(15) Hammouda, F. M.; Rizk, A. M.; Ahmed, S. S.; Mayergi, H. A.; Lashin, S. M.; Nofal, M. A. Alkaloidal constituents of eggplant *Solanum melongena* in response to seasonal variation and fungal infection. *Ann. Agric. Sci.* **1985**, *30*, 617−626.
(16) Aubert, S.; Daunay, M. C.; Pochard, E. Saponosides stéroïdiques de l'aubergine (*Solanum melongena* L.) I. Intérêt alimentaire, méthodologie d'analyse, localisation dans le fruit. *Agronomie* **1989**, *9*, 641−651.
(17) Aubert, S.; Daunay, M. C.; Pochard, E. Saponosides stéroïdiques de l'aubergine (*Solanum melongena* L.) II. Variations des teneurs liées aux conditions de récolte, aux génotypes et à la quantité de graines des fruits. *Agronomie* **1989**, *9*, 751−758.
(18) Eanes, R. C.; Tek, N.; Kirsoy, O.; Frary, A.; Doganlar, S.; Almeida, A. E. Development of practical HPLC methods for the separation and determination of eggplant steroidal glycoalkaloids and their aglycones. *J. Liq. Chromatogr. Relat. Technol.* **2008**, *31*, 984−1000.
(19) Friedman, M.; Dao, L. Distribution of glycoalkaloids in potato plants and commercial potato products. *J. Agric. Food Chem.* **1992**, *40*, 419−423.
(20) Friedman, M.; Levin, C. E. α-Tomatine content in tomato and tomato products determined by HPLC with pulsed amperometric detection. *J. Agric. Food Chem.* **1995**, *43*, 1507−1511.
(21) Scalzo, R. L. O.; Fibiani, M.; Mennella, G.; Rotino, G. L.; Dal Sasso, M.; Culici, M.; Spallino, A.; Braga, P. C. Thermal treatment of eggplant (*Solanum melongena* L.) increases the antioxidant content and the inhibitory effect on human neutrophil burst. *J. Agric. Food Chem.* **2010**, *58*, 3371−3379.
(22) Nikolic, N. C.; Stankovic, M. Z.; Markovic, D. Z. Liquid-liquid systems for acid hydrolysis of glycoalkaloids from *Solanum tuberosum* L. tuber sprouts and solanidine extraction. *Med. Sci. Monit.* **2005**, *11*, Br200−205.
(23) Attoumbre, J.; Giordanengo, P.; Baltora-Rosset, S. Solanidine isolation from *Solanum tuberosum* by centrifugal partition chromatography. *J. Sep. Sci.* **2013**, *36*, 2379−2385.
(24) Kuo, C. I.; Chao, C. H.; Lu, M. K. Effects of auxins on the production of steroidal alkaloids in rapidly proliferating tissue and cell cultures of *Solanum lyratum*. *Phytochem. Anal.* **2012**, *23*, 400−404.
(25) Friedman, M. Anticarcinogenic, cardioprotective, and other health benefits of tomato compounds lycopene, α-tomatine, and tomatidine in pure form and in fresh and processed tomatoes. *J. Agric. Food Chem.* **2013**, *61*, 9534−9550.
(26) Fletcher, S. P.; Geyer, B. C.; Smith, A.; Evron, T.; Joshi, L.; Soreq, H.; Mor, T. S. Tissue distribution of cholinesterases and anticholinesterases in native and transgenic tomato plants. *Plant Mol. Biol.* **2004**, *55*, 33−43.
(27) Rotino, G. L.; Acciarri, N.; Sabatini, E.; Mennella, G.; Lo Scalzo, R.; Maestrelli, A.; Molesini, B.; Pandolfini, T.; Scalzo, J.; Mezzetti, B.; Spena, A. Open field trial of genetically modified parthenocarpic tomato: seedlessness and fruit quality. *BMC Biotechnol.* **2005**, *5*, No. 32.
(28) Koh, E.; Kaffka, S.; Mitchell, A. E. A long-term comparison of the influence of organic and conventional crop management practices on the content of the glycoalkaloid α-tomatine in tomatoes. *J. Sci. Food Agric.* **2013**, *93*, 1537−1542.
(29) Caprioli, G.; Logrippo, S.; Cahill, M. G.; James, K. J. High-performance liquid chromatography LTQ-Orbitrap mass spectrometry method for tomatidine and non-target metabolites quantification in organic and normal tomatoes. *Int. J. Food Sci. Nutr.* **2014**, *65*, 942−947.
(30) Friedman, M.; Kozukue, N.; Harden, L. A. Preparation and characterization of acid hydrolysis products of the tomato glycoalkaloid α-tomatine. *J. Agric. Food Chem.* **1998**, *46*, 2096−2101.
(31) Wu, C.-H.; Liang, C.-H.; Shiu, L.-Y.; Chang, L.-C.; Lin, T.-S.; Lan, C.-C. E.; Tsai, J.-C.; Wong, T.-W.; Wei, K.-J.; Lin, T.-K.; Chang, N.-S.; Sheu, H.-M. *Solanum incanum* extract (SR-T100) induces human cutaneous squamous cell carcinoma apoptosis through modulating tumor necrosis factor receptor signaling pathway. *J. Dermatol. Sci.* **2011**, *63*, 83−92.
(32) Munari, C. C.; de Oliveira, P. F.; Campos, J. C.; Martins Sde, P.; Da Costa, J. C.; Bastos, J. K.; Tavares, D. C. Antiproliferative activity of *Solanum lycocarpum* alkaloidic extract and their constituents, solamargine and solasonine, in tumor cell lines. *J. Nat. Med.* **2014**, *68*, 236−241.
(33) Ding, X.; Zhu, F.; Yang, Y.; Li, M. Purification, antitumor activity in vitro of steroidal glycoalkaloids from black nightshade (*Solanum nigrum* L.). *Food Chem.* **2013**, *141*, 1181−1186.
(34) Sun, L.; Zhao, Y.; Li, X.; Yuan, H.; Cheng, A.; Lou, H. A lysosomal−mitochondrial death pathway is induced by solamargine in human K562 leukemia cells. *Toxicol. In Vitro* **2010**, *24*, 1504−1511.
(35) Liu, L.-F.; Liang, C.-H.; Shiu, L.-Y.; Lin, W.-L.; Lin, C.-C.; Kuo, K.-W. Action of solamargine on human lung cancer cells—enhancement of the susceptibility of cancer cells to TNFs. *FEBS Lett.* **2004**, *577*, 67−74.
(36) Daunter, B.; Cham, B. E. Solasodine glycosides. In vitro preferential cytotoxicity for human cancer cells. *Cancer Lett.* **1990**, *55*, 209−220.
(37) Chang, L.-C.; Tsai, T.-R.; Wang, J.-J.; Lin, C.-N.; Kuo, K.-W. The rhamnose moiety of solamargine plays a crucial role in triggering cell death by apoptosis. *Biochem. Biophys. Res. Commun.* **1998**, *242*, 21−25.
(38) Kuo, K.-W.; Hsu, S.-H.; Li, Y.-P.; Lin, W.-L.; Liu, L.-F.; Chang, L.-C.; Lin, C.-C.; Lin, C.-N.; Sheu, H.-M. Anticancer activity evaluation of the *Solanum* glycoalkaloid solamargine. Triggering apoptosis in human hepatoma cells. *Biochem. Pharmacol.* **2000**, *60*, 1865−1873.
(39) Blankemeyer, J. T.; McWilliams, M. L.; Rayburn, J. R.; Weissenberg, M.; Friedman, M. Developmental toxicology of solamargine and solasonine glycoalkaloids in frog embryos. *Food Chem. Toxicol.* **1998**, *36*, 383−389.
(40) Berek, L.; Szabó, D.; Petri, I. B.; Shoyama, Y.; Lin, Y. H.; Molnár, J. Effects of naturally occurring glucosides, solasodine glucosides, ginsenosides and parishin derivatives on multidrug resistance of lymphoma cells and leukocyte functions. *In Vivo* **2001**, *15*, 151−156.
(41) Cham, B. E.; Chase, T. R. Solasodine rhamnosyl glycosides cause apoptosis in cancer cells. Do they also prime the immune system resulting in long-term protection against cancer? *Planta Med.* **2012**, *78*, 349−353.
(42) Sun, L.; Zhao, Y.; Yuan, H.; Li, X.; Cheng, A.; Lou, H. Solamargine, a steroidal alkaloid glycoside, induces oncosis in human K562 leukemia and squamous cell carcinoma KB cells. *Cancer Chemother. Pharmacol.* **2011**, *67*, 813−821.
(43) Ding, X.; Zhu, F.-S.; Li, M.; Gao, S.-G. Induction of apoptosis in human hepatoma SMMC-7721 cells by solamargine from *Solanum nigrum* L. *J. Ethnopharmacol.* **2012**, *139*, 599−604.

DOI: 10.1021/acs.jafc.5b00818
J. Agric. Food Chem. 2015, 63, 3323−3337

(44) Liang, C. H.; Liu, L. F.; Shiu, L. Y.; Huang, Y. S.; Chang, L. C.; Kuo, K. W. Action of solamargine on TNFs and cisplatin-resistant human lung cancer cells. *Biochem. Biophys. Res. Commun.* **2004**, *322*, 751−758.
(45) Liang, C.-H.; Shiu, L.-Y.; Chang, L.-C.; Sheu, H.-M.; Tsai, E.-M.; Kuo, K.-W. Solamargine enhances HER2 expression and increases the susceptibility of human lung cancer H661 and H69 cells to trastuzumab and epirubicin. *Chem. Res. Toxicol.* **2008**, *21*, 393−399.
(46) Shiu, L. Y.; Chang, L. C.; Liang, C. H.; Huang, Y. S.; Sheu, H. M.; Kuo, K. W. Solamargine induces apoptosis and sensitizes breast cancer cells to cisplatin. *Food Chem. Toxicol.* **2007**, *45*, 2155−2164.
(47) Shiu, L. Y.; Liang, C. H.; Huang, Y. S.; Sheu, H. M.; Kuo, K. W. Downregulation of HER2/neu receptor by solamargine enhances anticancer drug-mediated cytotoxicity in breast cancer cells with high-expressing HER2/neu. *Cell Biol. Toxicol.* **2008**, *24*, 1−10.
(48) Zhou, Y.; Tang, Q.; Zhao, S.; Zhang, F.; Li, L.; Wu, W.; Wang, Z.; Hann, S. Targeting signal transducer and activator of transcription 3 contributes to the solamargine-inhibited growth and -induced apoptosis of human lung cancer cells. *Tumour Biol.* **2014**, *35*, 8169−8178.
(49) Li, X.; Zhao, Y.; Ji, M.; Liu, S. S.; Cui, M.; Lou, H. X. Induction of actin disruption and downregulation of P-glycoprotein expression by solamargine in multidrug-resistant K562/A02 cells. *Chin. Med. J.* **2011**, *124*, 2038−2044.
(50) Son, Y. O.; Kim, J.; Lim, J. C.; Chung, Y.; Chung, G. H.; Lee, J. C. Ripe fruits of *Solanum nigrum* L. inhibits cell growth and induces apoptosis in MCF-7 cells. *Food Chem. Toxicol.* **2003**, *41*, 1421−1428.
(51) Cui, C. Z.; Wen, X. S.; Cui, M.; Gao, J.; Sun, B.; Lou, H. X. Synthesis of solasodine glycoside derivatives and evaluation of their cytotoxic effects on human cancer cells. *Drug Discovery Ther.* **2012**, *6*, 9−17.
(52) Zupkó, I.; Molnár, J.; Réthy, B.; Minorics, R.; Frank, É.; Wölfling, J.; Molnár, J.; Ocsovszki, I.; Topcu, Z.; Bitó, T.; Puskás, L. G. Anticancer and multidrug resistance-reversal effects of solanidine analogs synthetized from pregnadienolone acetate. *Molecules* **2014**, *19*, 2061−2076.
(53) Shiu, L. Y.; Liang, C. H.; Chang, L. C.; Sheu, H. M.; Tsai, E. M.; Kuo, K. W. Solamargine induces apoptosis and enhances susceptibility to trastuzumab and epirubicin in breast cancer cells with low or high expression levels of HER2/neu. *Biosci. Rep.* **2009**, *29*, 35−45.
(54) Cham, B. E.; Daunter, B. Solasodine glycosides. Selective cytotoxicity for cancer cells and inhibition of cytotoxicity by rhamnose in mice with sarcoma 180. *Cancer Lett.* **1990**, *55*, 221−225.
(55) Cham, B. E.; Daunter, B.; Evans, R. A. Topical treatment of malignant and premalignant skin lesions by very low concentrations of a standard mixture (BEC) of solasodine glycosides. *Cancer Lett.* **1991**, *59*, 183−192.
(56) Goldberg, L. H.; Landau, J. M.; Moody, M. N.; Vergilis-Kalner, I. J. Treatment of Bowen's disease on the penis with low concentration of a standard mixture of solasodine glycosides and liquid nitrogen. *Dermatol. Surg.* **2011**, *37*, 858−861.
(57) Punjabi, S.; Cook, L. J.; Kersey, P.; Marks, R.; Cerio, R. Solasodine glycoalkaloids: a novel topical therapy for basal cell carcinoma. A double-blind, randomized, placebo-controlled, parallel group, multicenter study. *Int. J. Dermatol.* **2008**, *47*, 78−82.
(58) Tiossi, R. F. J.; Da Costa, J. C.; Miranda, M. A.; Praça, F. S. G.; McChesney, J. D.; Bentley, M. V. L. B.; Bastos, J. K. In vitro and in vivo evaluation of the delivery of topical formulations containing glycoalkaloids of *Solanum lycocarpum* fruits. *Eur. J. Pharm. Biopharm.* **2014**, *88*, 28−33.
(59) Clark, C. M.; Furniss, M.; Mackay-Wiggan, J. M. Basal cell carcinoma: an evidence-based treatment update. *Am. J. Clin. Dermatol.* **2014**, *15*, 197−216.
(60) Koduru, S.; Grierson, D. S.; Van De Venter, M.; Afolayan, A. J. Anticancer activity of steroid alkaloids isolated from *Solanum aculeastrum*. *Pharm. Biol.* **2007**, *45*, 613−618.
(61) Yang, S. A.; Paek, S. H.; Kozukue, N.; Lee, K. R.; Kim, J. A. α-Chaconine, a potato glycoalkaloid, induces apoptosis of HT-29 human colon cancer cells through caspase-3 activation and inhibition of ERK 1/2 phosphorylation. *Food Chem. Toxicol.* **2006**, *44*, 839−846.
(62) Reddivari, L.; Vanamala, J.; Safe, S. H.; Miller, J. C., Jr. The bioactive compounds α-chaconine and gallic acid in potato extracts decrease survival and induce apoptosis in LNCaP and PC3 prostate cancer cells. *Nutr. Cancer* **2010**, *62*, 601−610.
(63) Lu, M. K.; Chen, P. H.; Shih, Y. W.; Chang, Y. T.; Huang, E. T.; Liu, C. R.; Chen, P. S. α-Chaconine inhibits angiogenesis in vitro by reducing matrix metalloproteinase-2. *Biol. Pharm. Bull.* **2010**, *33*, 622−630.
(64) Shih, Y.-W.; Chen, P.-S.; Wu, C.-H.; Jeng, Y.-F.; Wang, C.-J. α-Chaconine-reduced metastasis involves a PI3K/Akt signaling pathway with downregulation of NF-κB in human lung adenocarcinoma A549 cells. *J. Agric. Food Chem.* **2007**, *55*, 11035−11043.
(65) Ji, Y. B.; Gao, S. Y.; Ji, C. F.; Zou, X. Induction of apoptosis in HepG2 cells by solanine and Bcl-2 protein. *J. Ethnopharmacol.* **2008**, *115*, 194−202.
(66) Sun, H.; Lv, C.; Yang, L.; Wang, Y.; Zhang, Q.; Yu, S.; Kong, H.; Wang, M.; Xie, J.; Zhang, C.; Zhou, M. Solanine induces mitochondria-mediated apoptosis in human pancreatic cancer cells. *BioMed. Res. Int.* **2014**, *2014*, No. 805926.
(67) Lv, C.; Kong, H.; Dong, G.; Liu, L.; Tong, K.; Sun, H.; Chen, B.; Zhang, C.; Zhou, M. Antitumor efficacy of α-solanine against pancreatic cancer in vitro and in vivo. *PLoS One* **2014**, *9*, No. e87868.
(68) Zhang, J.; Shi, G. W. [Inhibitory effect of solanine on prostate cancer cell line PC-3 in vitro]. *Zhonghua Nankexue* **2011**, *17*, 284−287.
(69) Shen, K. H.; Liao, A. C.; Hung, J. H.; Lee, W. J.; Hu, K. C.; Lin, P. T.; Liao, R. F.; Chen, P. S. α-Solanine inhibits invasion of human prostate cancer cell by suppressing epithelial−mesenchymal transition and MMPs expression. *Molecules* **2014**, *19*, 11896−11914.
(70) Mohsenikia, M.; Alizadeh, A. M.; Khodayari, S.; Khodayari, H.; Kouhpayeh, S. A.; Karimi, A.; Zamani, M.; Azizian, S.; Mohagheghi, M. A. The protective and therapeutic effects of α-solanine on mice breast cancer. *Eur. J. Pharmacol.* **2013**, *718*, 1−9.
(71) Lu, M. K.; Shih, Y. W.; Chang Chien, T. T.; Fang, L. H.; Huang, H. C.; Chen, P. S. α-Solanine inhibits human melanoma cell migration and invasion by reducing matrix metalloproteinase-2/9 activities. *Biol. Pharm. Bull.* **2010**, *33*, 1685−1691.
(72) Gao, S. Y.; Wang, Q. J.; Ji, Y. B. Effect of solanine on the membrane potential of mitochondria in HepG2 cells and $[Ca^{2+}]_i$ in the cells. *World J. Gastroenterol.* **2006**, *12*, 3359−3367.
(73) Trouillas, P.; Corbière, C.; Liagre, B.; Duroux, J. L.; Beneytout, J. L. Structure−function relationship for saponin effects on cell cycle arrest and apoptosis in the human 1547 osteosarcoma cells: a molecular modelling approach of natural molecules structurally close to diosgenin. *Bioorg. Med. Chem.* **2005**, *13*, 1141−1149.
(74) Lavie, Y.; Harel-Orbital, T.; Gaffield, W.; Liscovitch, M. Inhibitory effect of steroidal alkaloids on drug transport and multidrug resistance in human cancer cells. *Anticancer Res.* **2001**, *21*, 1189−1194.
(75) Friedman, M.; Levin, C. E.; Lee, S.-U.; Kim, H.-J.; Lee, I.-S.; Byun, J.-O.; Kozukue, N. Tomatine-containing green tomato extracts inhibit growth of human breast, colon, liver, and stomach cancer cells. *J. Agric. Food Chem.* **2009**, *57*, 5727−5733.
(76) Choi, S. H.; Ahn, J.-B.; Kozukue, N.; Kim, H.-J.; Nishitani, Y.; Zhang, L.; Mizuno, M.; Levin, C. E.; Friedman, M. Structure−activity relationships of α-, β1-, γ-, and δ-tomatine and tomatidine against human breast (MDA-MB-231), gastric (KATO-III), and prostate (PC3) cancer cells. *J. Agric. Food Chem.* **2012**, *60*, 3891−3899.
(77) Chagnon, F.; Guay, I.; Bonin, M. A.; Mitchell, G.; Bouarab, K.; Malouin, F.; Marsault, E. Unraveling the structure−activity relationship of tomatidine, a steroid alkaloid with unique antibiotic properties against persistent forms of *Staphylococcus aureus*. *Eur. J. Med. Chem.* **2014**, *80*, 605−620.
(78) Kúdelová, J.; Seifrtová, M.; Suchá, L.; Tomšík, P.; Havelek, R.; Rezácová, M. α-Tomatine activates cell cycle checkpoints in the absence of DNA damage in human leukemic MOLT-4 cells. *J. Appl. Biomed.* **2013**, *11*, 93−103.

DOI: 10.1021/acs.jafc.5b00818
J. Agric. Food Chem. 2015, 63, 3323−3337

(79) Chao, M. W.; Chen, C. H.; Chang, Y. L.; Teng, C. M.; Pan, S. L. α-Tomatine-mediated anti-cancer activity in vitro and in vivo through cell cycle- and caspase-independent pathways. *PLoS One* **2012**, *7*, No. e44093.
(80) Lee, S.-T.; Wong, P.-F.; Cheah, S.-C.; Mustafa, M. R. α-Tomatine induces apoptosis and inhibits nuclear factor-κB activation on human prostatic adenocarcinoma PC-3 cells. *PLoS One* **2011**, *6*, No. e18915.
(81) Lee, S. T.; Wong, P. F.; Hooper, J. D.; Mustafa, M. R. α-Tomatine synergises with paclitaxel to enhance apoptosis of androgen-independent human prostate cancer PC-3 cells in vitro and in vivo. *Phytomedicine* **2013**, *20*, 1297−1305.
(82) Lee, S. T.; Wong, P. F.; He, H.; Hooper, J. D.; Mustafa, M. R. α-Tomatine attenuation of in vivo growth of subcutaneous and orthotopic xenograft tumors of human prostate carcinoma PC-3 cells is accompanied by inactivation of nuclear factor-κB signaling. *PLoS One* **2013**, *8*, No. e57708.
(83) Shih, Y.-W.; Shieh, J.-M.; Wu, P.-F.; Lee, Y.-C.; Chen, Y.-Z.; Chiang, T.-A. α-Tomatine inactivates PI3K/Akt and ERK signaling pathways in human lung adenocarcinoma A549 cells: effect on metastasis. *Food Chem. Toxicol.* **2009**, *47*, 1985−1995.
(84) Shieh, J.-M.; Cheng, T.-H.; Shi, M.-D.; Wu, P.-F.; Chen, Y.; Ko, S.-C.; Shih, Y.-W. α-Tomatine suppresses invasion and migration of human non-small cell lung cancer NCI-H460 cells through inactivating FAK/PI3K/Akt signaling pathway and reducing binding activity of NF-κB. *Cell Biochem. Biophys.* **2011**, *60*, 297−310.
(85) Friedman, M.; McQuistan, T.; Hendricks, J. D.; Pereira, C.; Bailey, G. S. Protective effect of dietary tomatine against dibenzo-[*a*,*l*]pyrene (DBP)-induced liver and stomach tumors in rainbow trout. *Mol. Nutr. Food Res.* **2007**, *51*, 1485−1491.
(86) Tomsik, P.; Micuda, S.; Sucha, L.; Cermakova, E.; Suba, P.; Zivny, P.; Mazurova, Y.; Knizek, J.; Niang, M.; Rezacova, M. The anticancer activity of α-tomatine against mammary adenocarcinoma in mice. *Biomed. Pap.* **2013**, *157*, 153−161.
(87) Kim, S. P.; Nam, S. H.; Friedman, M. The tomato glycoalkaloid α-tomatine induces caspase-independent cell death in mouse colon cancer CT-26 cells and transplanted tumors in mice. *J. Agric. Food Chem.* **2015**, *63*, 1142−1150.
(88) Morrow, W. J. W.; Yang, Y.-W.; Sheikh, N. A. Immunobiology of the tomatine adjuvant. *Vaccine* **2004**, *22*, 2380−2384.
(89) Heal, K. G.; Taylor-Robinson, A. W. Tomatine adjuvantation of protective immunity to a major pre-erythrocytic vaccine candidate of malaria is mediated via $CD8^+$ T cell release of IFN-γ. *J. Biomed. Biotechnol.* **2010**, *2010*, No. 834326.
(90) Sucha, L.; Hroch, M.; Rezacova, M.; Rudolf, E.; Havelek, R.; Sispera, L.; Cmielova, J.; Kohlerova, R.; Bezrouk, A.; Tomsik, P. The cytotoxic effect of α-tomatine in MCF-7 human adenocarcinoma breast cancer cells depends on its interaction with cholesterol in incubation media and does not involve apoptosis induction. *Oncol. Rep.* **2013**, *30*, 2593−2602.
(91) Huang, H.; Chen, S.; Van Doren, J.; Li, D.; Farichon, C.; He, Y.; Zhang, Q.; Zhang, K.; Conney, A. H.; Goodin, S.; Du, Z.; Zheng, X. α-Tomatine inhibits growth and induces apoptosis in HL-60 human myeloid leukemia cells. *Mol. Med. Rep.* **2015**, *11*, 4573−4578.
(92) Walker, B. W.; Manhanke, N.; Stine, K. J. Comparison of the interaction of tomatine with mixed monolayers containing phospholipid, egg sphingomyelin, and sterols. *Biochim. Biophys. Acta, Biomembr.* **2008**, *1778*, 2244−2257.
(93) Friedman, M.; Fitch, T. E.; Levin, C. E.; Yokoyama, W. H. Feeding tomatoes to hamsters reduces their plasma low-density lipoprotein cholesterol and triglycerides. *J. Food Sci.* **2000**, *65*, 897−900.
(94) Friedman, M.; Fitch, T. E.; Yokoyama, W. E. Lowering of plasma LDL cholesterol in hamsters by the tomato glycoalkaloid tomatine. *Food Chem. Toxicol.* **2000**, *38*, 549−553.
(95) Raj, V.; Johnson, T.; Joseph, K. Cholesterol aided etching of tomatine gold nanoparticles: a non-enzymatic blood cholesterol monitor. *Biosens. Bioelectron.* **2014**, *60*, 191−194.
(96) Choi, K. M.; Lee, Y. S.; Shin, D. M.; Lee, S.; Yoo, K. S.; Lee, M. K.; Lee, J. H.; Kim, S. Y.; Lee, Y. M.; Hong, J. T.; Yun, Y. P.; Yoo, H. S. Green tomato extract attenuates high-fat-diet-induced obesity through activation of the AMPK pathway in C57BL/6 mice. *J. Nutr. Biochem.* **2013**, *24*, 335−342.
(97) Blankemeyer, J. T.; White, J. B.; Stringer, B. K.; Friedman, M. Effect of α-tomatine and tomatidine on membrane potential of frog embryos and active transport of ions in frog skin. *Food Chem. Toxicol.* **1997**, *35*, 639−646.
(98) Blankemeyer, J. T.; Atherton, R.; Friedman, M. Effect of potato glycoalkaloids α-chaconine and α-solanine on sodium active transport in frog skin. *J. Agric. Food Chem.* **1995**, *43*, 636−639.
(99) Blankemeyer, J. T.; Stringer, B. K.; Rayburn, J. R.; Bantle, J. A.; Friedman, M. Effect of potato glycoalkaloids, α-chaconine and α-solanine on membrane-potential of frog embryos. *J. Agric. Food Chem.* **1992**, *40*, 2022−2025.
(100) Taveira, M.; Sousa, C.; Valentao, P.; Ferreres, F.; Teixeira, J. P.; Andrade, P. B. Neuroprotective effect of steroidal alkaloids on glutamate-induced toxicity by preserving mitochondrial membrane potential and reducing oxidative stress. *J. Steroid Biochem. Mol. Biol.* **2014**, *140*, 106−115.
(101) Christodoulou, M. I.; Kontos, C. K.; Halabalaki, M.; Skaltsounis, A. L.; Scorilas, A. Nature promises new anticancer agents: interplay with the apoptosis-related BCL2 gene family. *Anticancer Agents Med. Chem.* **2014**, *14*, 375−399.
(102) Zhivotovsky, B.; Orrenius, S. Cell cycle and cell death in disease: past, present and future. *J. Int. Med.* **2010**, *268*, 395−409.
(103) Gajowik, A.; Dobrzyńska, M. M. Lycopene—antioxidant with radioprotective and anticancer properties. A review. *Rocz. Panstw. Zakl. Hig.* **2014**, *65*, 263−271.
(104) Finotti, E.; Bersani, E.; Friedman, M. Application of a functional mathematical index for antibacterial and anticarcinogenic effects of tea catechins. *J. Agric. Food Chem.* **2011**, *59*, 864−869.
(105) Westergaard, D.; Li, J.; Jensen, K.; Kouskoumvekaki, I.; Panagiotou, G. Exploring mechanisms of diet-colon cancer associations through candidate molecular interaction networks. *BMC Genomics* **2014**, *15*, No. 380.
(106) Kim, S. P.; Kang, M. Y.; Nam, S. H.; Friedman, M. Dietary rice bran component γ-oryzanol inhibits tumor growth in tumor-bearing mice. *Mol. Nutr. Food Res.* **2012**, *56*, 935−944.
(107) Choi, S. P.; Kim, S. P.; Nam, S. H.; Friedman, M. Antitumor effects of dietary black and brown rice brans in tumor-bearing mice: relationship to composition. *Mol. Nutr. Food Res.* **2013**, *57*, 390−400.
(108) Chen, M.-H.; Choi, S. H.; Kozukue, N.; Kim, H.-J.; Friedman, M. Growth-inhibitory effects of pigmented rice bran extracts and three red bran fractions against human cancer cells: relationships with composition and antioxidative activities. *J. Agric. Food Chem.* **2012**, *60*, 9151−9161.
(109) Nam, S. H.; Choi, S. P.; Kang, M. Y.; Koh, H. J.; Kozukue, N.; Friedman, M. Bran extracts from pigmented rice seeds inhibit tumor promotion in lymphoblastoid B cells by phorbol ester. *Food Chem. Toxicol.* **2005**, *43*, 741−745.
(110) Nam, S. H.; Choi, S. P.; Kang, M. Y.; Kozukue, N.; Friedman, M. Antioxidative, antimutagenic, and anticarcinogenic activities of rice bran extracts in chemical and cell assays. *J. Agric. Food Chem.* **2005**, *53*, 816−822.
(111) Friedman, M.; Mackey, B. E.; Kim, H.-J.; Lee, I.-S.; Lee, K.-R.; Lee, S.-U.; Kozukue, E.; Kozukue, N. Structure−activity relationships of tea compounds against human cancer cells. *J. Agric. Food Chem.* **2007**, *55*, 243−253.
(112) Fujiki, H.; Sueoka, E.; Watanabe, T.; Suganuma, M. Synergistic enhancement of anticancer effects on numerous human cancer cell lines treated with the combination of EGCG, other green tea catechins, and anticancer compounds. *J. Cancer Res. Clin. Oncol.* **2014**, DOI: 10.1007/s00432-014-1899-5.
(113) Fei, X.; Shen, Y.; Li, X.; Guo, H. The association of tea consumption and the risk and progression of prostate cancer: a meta-analysis. *Int. J. Clin. Exp. Med.* **2014**, *7*, 3881−3891.

DOI: 10.1021/acs.jafc.5b00818
J. Agric. Food Chem. 2015, 63, 3323−3337

(114) Kim, S. P.; Kang, M. Y.; Kim, J. H.; Nam, S. H.; Friedman, M. Composition and mechanism of antitumor effects of *Hericium erinaceus* mushroom extracts in tumor-bearing mice. *J. Agric. Food Chem.* **2011**, *59*, 9861−9869.
(115) Friedman, M. Bioactive compounds from *Ziziphus jujuba* and allied species. In *Chinese Dates (Jujubes): A Traditional Functional Food*; Shi, J., Ed.; CRC Press: Boca Raton, FL, 2015.
(116) Xu, M. Y.; Lee, S. Y.; Kang, S. S.; Kim, Y. S. Antitumor activity of jujuboside B and the underlying mechanism via induction of apoptosis and autophagy. *J. Nat. Prod.* **2014**, *77*, 370−376.
(117) Sun, Y. F.; Song, C. K.; Viernstein, H.; Unger, F.; Liang, Z. S. Apoptosis of human breast cancer cells induced by microencapsulated betulinic acid from sour jujube fruits through the mitochondria transduction pathway. *Food Chem.* **2013**, *138*, 1998−2007.
(118) Choi, S.-H.; Ahn, J.-B.; Kim, H.-J.; Im, N.-K.; Kozukue, N.; Levin, C. E.; Friedman, M. Changes in free amino acid, protein and flavonoid content in jujube (*Ziziphus jujube*) fruit during eight stages of growth and antioxidative and cancer cell inhibitory effects by extracts. *J. Agric. Food Chem.* **2012**, *60*, 10245−10255.
(119) Friedman, M.; Kim, S.-Y.; Lee, S.-J.; Han, G.-P.; Han, J.-S.; Lee, K.-R.; Kozukue, N. Distribution of catechins, theaflavins, caffeine, and theobromine in 77 teas consumed in the United States. *J. Food Sci.* **2005**, *70*, C550−C559.
(120) Friedman, M.; Levin, C. E.; Choi, S.-H.; Kozukue, E.; Kozukue, N. HPLC analysis of catechins, theaflavins, and alkaloids in commercial teas and green tea dietary supplements: comparison of water and 80% ethanol/water extracts. *J. Food Sci.* **2006**, *71*, C328−C337.
(121) Friedman, M.; Levin, C. E.; Lee, S.-U.; Kozukue, N. Stability of green tea catechins in commercial tea leaves during storage for 6 months. *J. Food Sci.* **2009**, *74*, H47−H51.
(122) Friedman, M. Overview of antibacterial, antitoxin, antiviral, and antifungal activities of tea flavonoids and teas. *Mol. Nutr. Food Res.* **2007**, *51*, 116−134.
(123) Zhao, C.; Chen, A.; Jamieson, C. H.; Fereshteh, M.; Abrahamsson, A.; Blum, J.; Kwon, H. Y.; Kim, J.; Chute, J. P.; Rizzieri, D.; Munchhof, M.; VanArsdale, T.; Beachy, P. A.; Reya, T. Hedgehog signalling is essential for maintenance of cancer stem cells in myeloid leukaemia. *Nature* **2009**, *458*, 776−779.
(124) Shi, Y.; Moura, U.; Opitz, I.; Soltermann, A.; Rehrauer, H.; Thies, S.; Weder, W.; Stahel, R. A.; Felley-Bosco, E. Role of hedgehog signaling in malignant pleural mesothelioma. *Clin. Cancer. Res.* **2012**, *18*, 4646−4656.
(125) Conesa-Zamora, P. Immune responses against virus and tumor in cervical carcinogenesis: treatment strategies for avoiding the HPV-induced immune escape. *Gynecol. Oncol.* **2013**, *131*, 480−488.
(126) Thorne, H. V.; Clarke, G. F.; Skuce, R. The inactivation of herpes simplex virus by some *Solanaceae* glycoalkaloids. *Antiviral Res.* **1985**, *5*, 335−343.
(127) Kozukue, N.; Misoo, S.; Yamada, T.; Kamijima, O.; Friedman, M. Inheritance of morphological characters and glycoalkaloids in potatoes of somatic hybrids between dihaploid *Solanum acaule* and tetraploid *Solanum tuberosum*. *J. Agric. Food Chem.* **1999**, *47*, 4478−4483.
(128) Iijima, Y.; Watanabe, B.; Sasaki, R.; Takenaka, M.; Ono, H.; Sakurai, N.; Umemoto, N.; Suzuki, H.; Shibata, D.; Aoki, K. Steroidal glycoalkaloid profiling and structures of glycoalkaloids in wild tomato fruit. *Phytochemistry* **2013**, *95*, 145−157.
(129) Itkin, M.; Rogachev, I.; Alkan, N.; Rosenberg, T.; Malitsky, S.; Masini, L.; Meir, S.; Iijima, Y.; Aoki, K.; de Vos, R.; Prusky, D.; Burdman, S.; Beekwilder, J.; Aharoni, A. GLYCOALKALOID METABOLISM1 is required for steroidal alkaloid glycosylation and prevention of phytotoxicity in tomato. *Plant Cell* **2011**, *23*, 4507−4525.
(130) Ohyama, K.; Okawa, A.; Fujimoto, Y. Biosynthesis of steroidal alkaloids in Solanaceae plants: incorporation of 3β-hydroxycholest-5-en-26-al into tomatine with tomato seedlings. *Bioorg. Med. Chem. Lett.* **2014**, *24*, 3556−3558.
(131) Kozukue, N.; Yoon, K.-S.; Byun, G.-I.; Misoo, S.; Levin, C. E.; Friedman, M. Distribution of glycoalkaloids in potato tubers of 59 accessions of two wild and five cultivated *Solanum* species. *J. Agric. Food Chem.* **2008**, *56*, 11920−11928.
(132) Kirui, G. K.; Misra, A. K.; Olanya, O. M.; Friedman, M.; El-Bedewy, R.; Ewell, P. T. Glycoalkaloid content of some superior potato (*Solanum tuberosum* L.) clones and commercial cultivars. *Arch. Phytopathol. Plant Prot.* **2009**, *42*, 453−463.
(133) Valcarcel, J.; Reilly, K.; Gaffney, M.; O'Brien, N. Effect of genotype and environment on the glycoalkaloid content of rare, heritage, and commercial potato varieties. *J. Food Sci.* **2014**, *79*, T1039−1048.
(134) Manrique-Carpintero, N. C.; Tokuhisa, J. G.; Ginzberg, I.; Veilleux, R. E. Allelic variation in genes contributing to glycoalkaloid biosynthesis in a diploid interspecific population of potato. *Theor. Appl. Genet.* **2014**, *127*, 391−405.
(135) Shakya, R.; Navarre, D. A. LC-MS analysis of solanidane glycoalkaloid diversity among tubers of four wild potato species and three cultivars (*Solanum tuberosum*). *J. Agric. Food Chem.* **2008**, *56*, 6949−6958.
(136) Sagredo, B.; Lorenzen, J.; Casper, H.; Lafta, A. Linkage analysis of a rare alkaloid present in a tetraploid potato with *Solanum chacoense* background. *Theor. Appl. Genet.* **2011**, *122*, 471−478.
(137) Mweetwa, A. M.; Hunter, D.; Poe, R.; Harich, K. C.; Ginzberg, I.; Veilleux, R. E.; Tokuhisa, J. G. Steroidal glycoalkaloids in *Solanum chacoense*. *Phytochemistry* **2012**, *75*, 32−40.
(138) Madiwale, G. P.; Reddivari, L.; Stone, M.; Holm, D. G.; Vanamala, J. Combined effects of storage and processing on the bioactive compounds and pro-apoptotic properties of color-fleshed potatoes in human colon cancer cells. *J. Agric. Food Chem.* **2012**, *60*, 11088−11096.
(139) Vinson, J. A.; Demkosky, C. A.; Navarre, D. A.; Smyda, M. A. High-antioxidant potatoes: acute in vivo antioxidant source and hypotensive agent in humans after supplementation to hypertensive subjects. *J. Agric. Food Chem.* **2012**, *60*, 6749−6754.
(140) Lawson, D. R.; Green, T. P.; Haynes, L. W.; Miller, A. R. Nuclear magnetic resonance spectroscopy and mass spectrometry of solanidine, leptinidine, and acetylleptinidine. Steroidal alkaloids from *Solanum chacoense* Bitter. *J. Agric. Food Chem.* **1997**, *45*, 4122−4126.
(141) Distl, M.; Wink, M. Identification and quantification of steroidal alkaloids from wild tuber-bearing solanum species by HPLC and LC-ESI-MS. *Potato Res.* **2009**, *52*, 79−104.

DOI: 10.1021/acs.jafc.5b00818
J. Agric. Food Chem. 2015, 63, 3323−3337

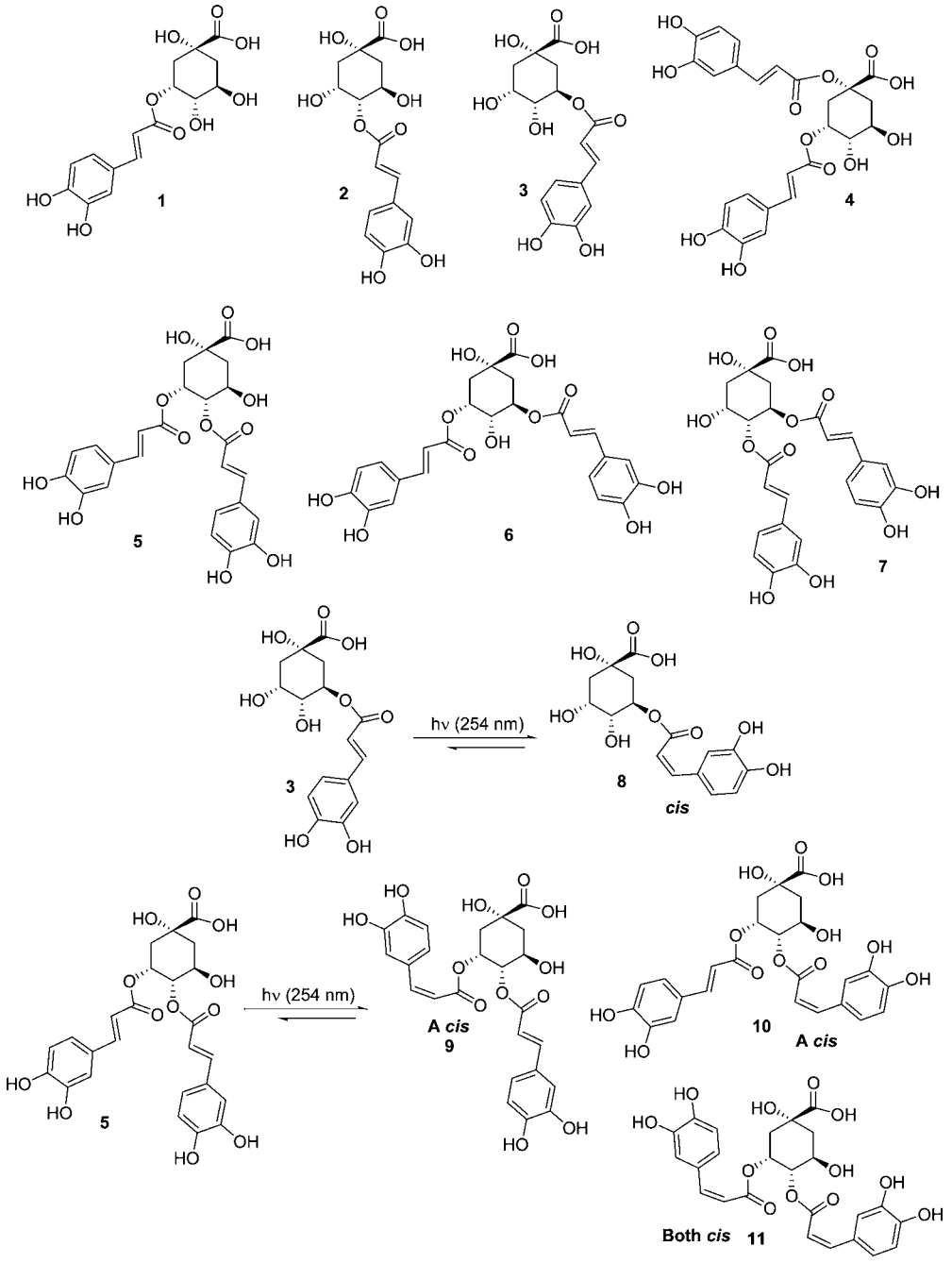

Figure 1. Representative structures of CGAs and *trans*−*cis* isomerization of 5-caffeoylquinic acid (**3**) and 3,4-dicaffeoylquinic acid (**5**).

optimized using 5-CQA (**3**) with a capillary temperature of 365 °C, a dry gas flow rate of 10 L/min, and a nebulizer pressure of 10 psi. High-resolution LC−MS was carried out using the same high-performance liquid chromatography (HPLC) equipped with a MicrOTOF focus mass spectrometer (Bruker Daltonics, Bremen, Germany) fitted with an electrospray ionization (ESI) source, and internal calibration was achieved with 10 mL of a 0.1 M sodium formate solution injected through a six-port valve prior to each chromatographic run. Calibration was carried out using the enhanced quadratic mode, and the mass error was below 5 ppm.

HPLC. Separation was achieved on a 150 × 3 mm inner diameter, 5 μm, diphenyl column, with a 5 × 3 mm inner diameter guard column of the same material (Varian, Darmstadt, Germany). Solvent A was water/formic acid (1000:0.005, v/v), and solvent B was methanol. Solvents were delivered at a total flow rate of 500 μL/min. The gradient profile was from 10 to 70% B linearly in 60 min, followed by 10 min isocratic, a return to 10% B at 90 min, and 10 min isocratic to re-equilibrate.[14]

Nuclear Magnetic Resonance (NMR). ^{1}H NMR spectra were acquired on a JEOL ECX-400 spectrometer operating at 400 MHz at room temperature in methanol-d_4 using a 5 mm probe.

UV Irradiation. The prepared samples of CGAs (0.5 mg/mL methanol) were placed in a photoreactor a LZC-4 V photoreactor (Luzchem, Ottawa, Canada) under a shortwave UV lamp and irradiated at 254 nm.

^{1}H NMR Data of Photoisomerized 1,3-Dicaffeoylquinic Acid Dervatives (Cycloaddition Products). CD_3OD, δ (ppm): 1.69 (1H, dd, J = 11.45 and 10.99 Hz), 2.08 (1H, dd, J = 15.45 and 1.85 Hz), 2.39 (1H, m), 2.93 (1H, m), 3.59 (1H, dd, J = 9.62 and 3.21 Hz), 3.88 (2H, d, J = 6.87 Hz), 4.0 (2H, d, J = 7.33 Hz), 4.15 (1H, dd, J = 8.24 and 3.2 Hz), 5.06 (1H, m), 6.30 (1H, dd, J = 8.24 and 1.83 Hz), 6.34 (1H, dd, J = 8.24 and 1.83 Hz), 6.39 (2H, dd, J = 8.70 and 1.83 Hz), and 6.51 (1H, dd, J = 8.24 and 4.1 Hz).

DOI: 10.1021/acs.jafc.5b00838
J. Agric. Food Chem. 2015, 63, 3338−3347

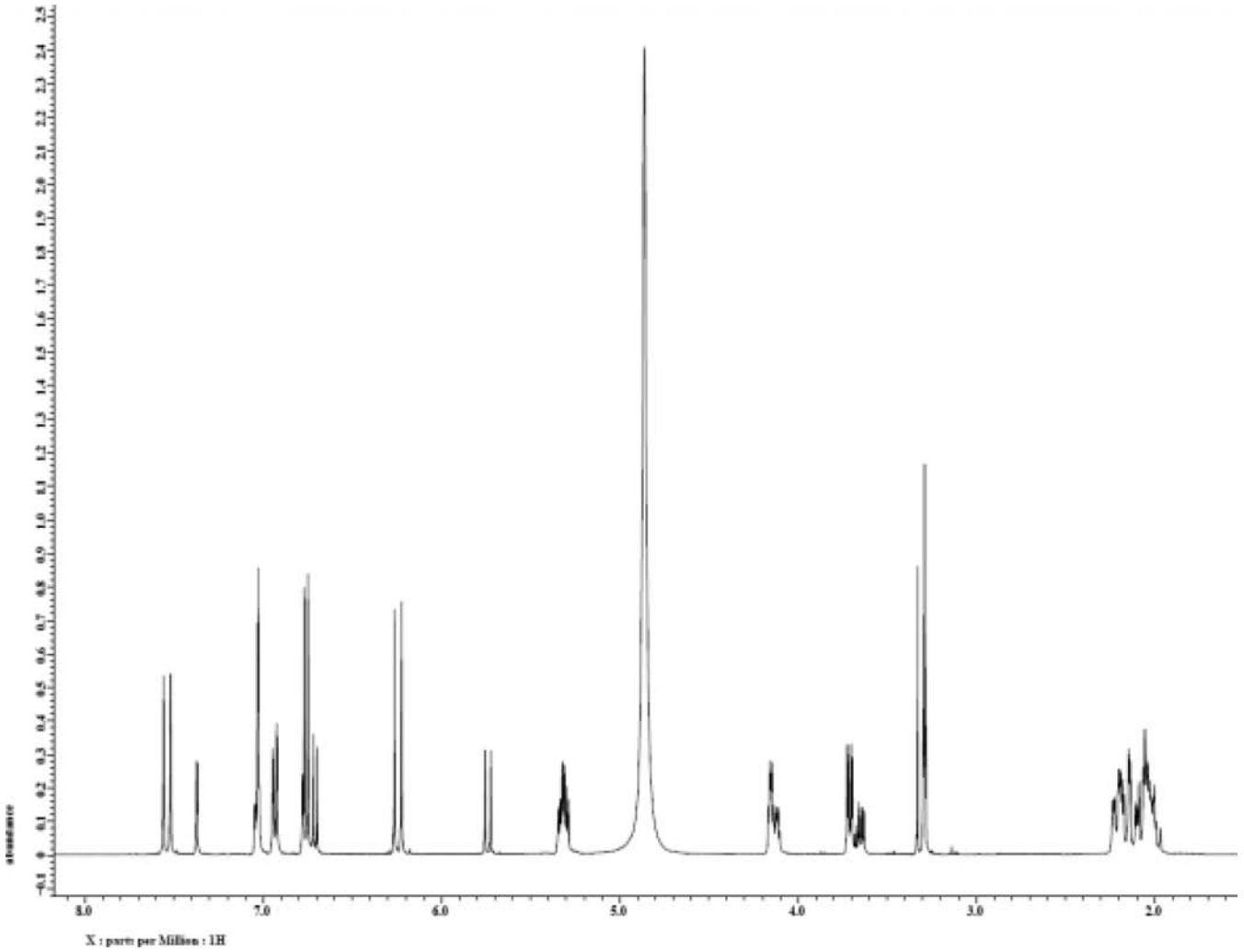

Figure 2. ^{1}H NMR spectrum (400 MHz) of UV-irradiated (2 h) 5-caffeoylquinic acid (**3**) in MeOH-d^4.

Table 1. Concentrations of the CGA Isomers at the Photostationary Equilibrium

number	CGA	*cis* isomer (%)	*trans* isomer (%)	*cis* isomer (%)	[2 + 2] cycloaddition product (%)
1	3-CQA	30	70	nd[a]	nd
2	4-CQA	30	70	nd	nd
3	5-CQA	28	72	nd	nd
4	1,3-diCQA	0	1	0	99
5	3,4-diCQA	10	48.5	41.5	nd
6	3,5-diCQA	11.8	40.2	48	nd
7	4,5-diCQA	8	51	41	nd

[a]nd = not detected.

Statistical Analysis. Statistical analyses of the data were performed with the software package of IBM SPSS Statistics 20.0. The distribution of the data set was analyzed by descriptive statistics and the Kolmogorov−Smirnov test. The correlation studies were performed by Pearson's correlation for the Gaussian (normal) distributed data set (5-CQA, **3**), and Spearman correlation coefficient test was performed for the non-Gaussian data set (e.g., *cis*-5-CQA, **8**) (see the Table S1 of the Supporting Information). A value of $p < 0.05$ was considered statistically significant.

RESULTS AND DISCUSSION

Photochemistry of hydroxycinnamates have been investigated previously.[15−19] We have reported on numerous occasions that plant material exposed to UV light, in particular, leaf material of coffee leaves,[7] *S. rebaudiana*,[9] *L. sativa*,[10] *R. hirta*,[12] *I. paraguariensis*,[13] etc., contains small amounts of *cis*-caffeoyl and *cis*-feruloylquinic acids. We suggested that these plant constituents were obtained through a photochemical *trans*−*cis* isomerization induced by UV light and could show that, in model systems, such an isomerization indeed takes place.

To investigate this process further, we decided to establish the photostationary equilibrium of this reaction using the most common mono- and dicaffeoylquinic acids encountered in our diet. The photostationary equilibrium is defined as an equilibrium composition at which forward and backward rate constants of the photochemical reaction are equal. Hence, at which point, no further changes in concentrations of starting

DOI: 10.1021/acs.jafc.5b00838
J. Agric. Food Chem. 2015, 63, 3338−3347

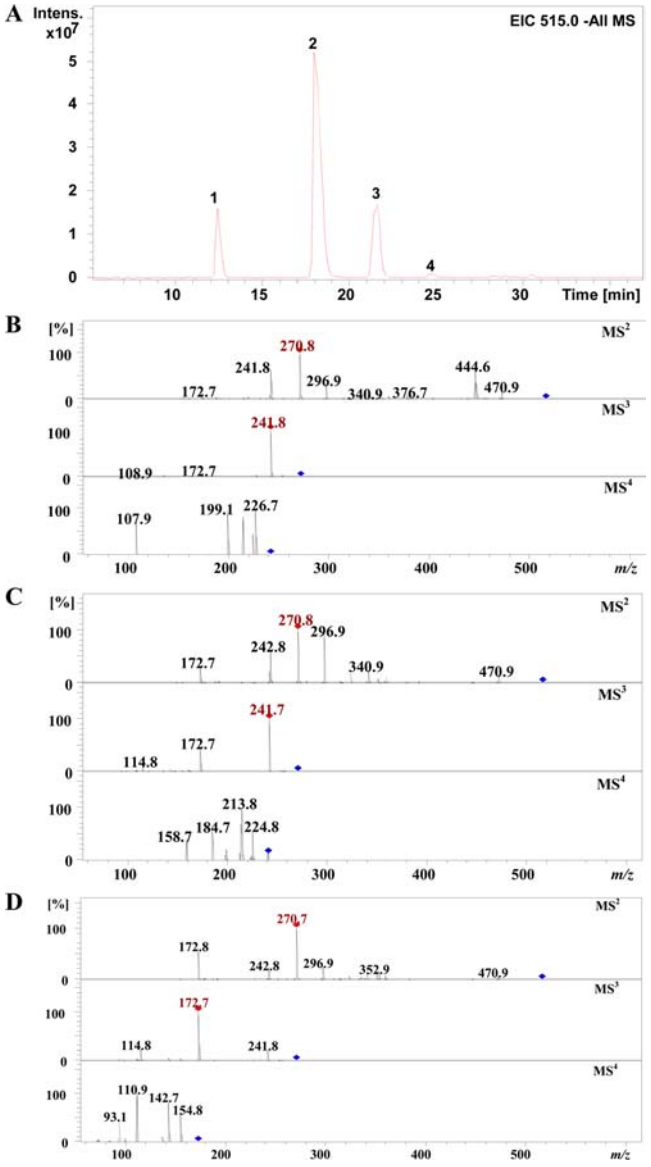

Figure 3. (A) Extracted ion chromatogram and (B–D) MS^4 spectra of [2 + 2] cycloaddition products of 1,3-dicaffeoylquinic acids at m/z 515 in negative-ion mode.

material and product are observed. For this purpose, we irradiated 3-CQA (**1**), 4-CQA (**2**), 5-CQA (**3**), 3,4-diCQA (**5**), 3,5-diCQA (**6**), 4,5 diCQA (**7**), and 1,3-diCQA (**4**) in a photochemical reactor with irradiation at 254 nm and analyzed samples by LC–tandem MS at time intervals of 15 min. Two examples of the photoisomerization are shown in Figure 1. As a further experiment, dried leaf samples were irradiated at 254 nm for 15 min, showing after sample workup an increase of *cis*-5-CQA of 20%. Using a combination of retention times, UV spectra (the *cis* derivatives show an additional shoulder) and tandem MS data compounds were assigned as described previously.[7] Quantitation of *trans* and *cis* derivatives was carried out using integration of the extracted ion chromatograms at m/z 353 or 515, respectively. To validate this quantitation procedure, we additionally obtained ^{1}H NMR spectra from irradiated samples and integrated the olefinic protons of both *cis* and *trans* isomers, both being readily identified by their $^3J_{HCCH}$ coupling constant of 16.5 Hz for the *trans* isomer and 11.2 Hz for the *cis* isomers (Figure 2). Quantitation results for the relative amounts

Table 2. Concentrations of CGAs in *Stevia* Leave Extracts

origin	variety	harvesting	year	5-CQA (**3**) (g/100 g of dry weight)	*cis*-5CQA (**8**) (g/100 g of dry weight)	4,5-diCQA (**7**) (g/100 g of dry weight)	*cis*-4,5-diCQA (g/100 g of dry weight)	*cis*-4,5-diCQA (g/100 g of dry weight)
Italy	3	II	Aug 11, 2011	2.692	0.147	1.155	0.008	0.015
Greece	4	I	2011	2.465	0.174	1.234	0.008	0.017
Spain	4	II	2011	2.063	0.136	1.275	0.029	0.058
Italy	4	I	July 07, 2011	1.843	0.12	1.232	0.022	0.028
Greece	2	II	Sept 20, 2010	2.634	0.138	1.681	0.045	0.045

DOI: 10.1021/acs.jafc.5b00838
J. Agric. Food Chem. 2015, 63, 3338–3347

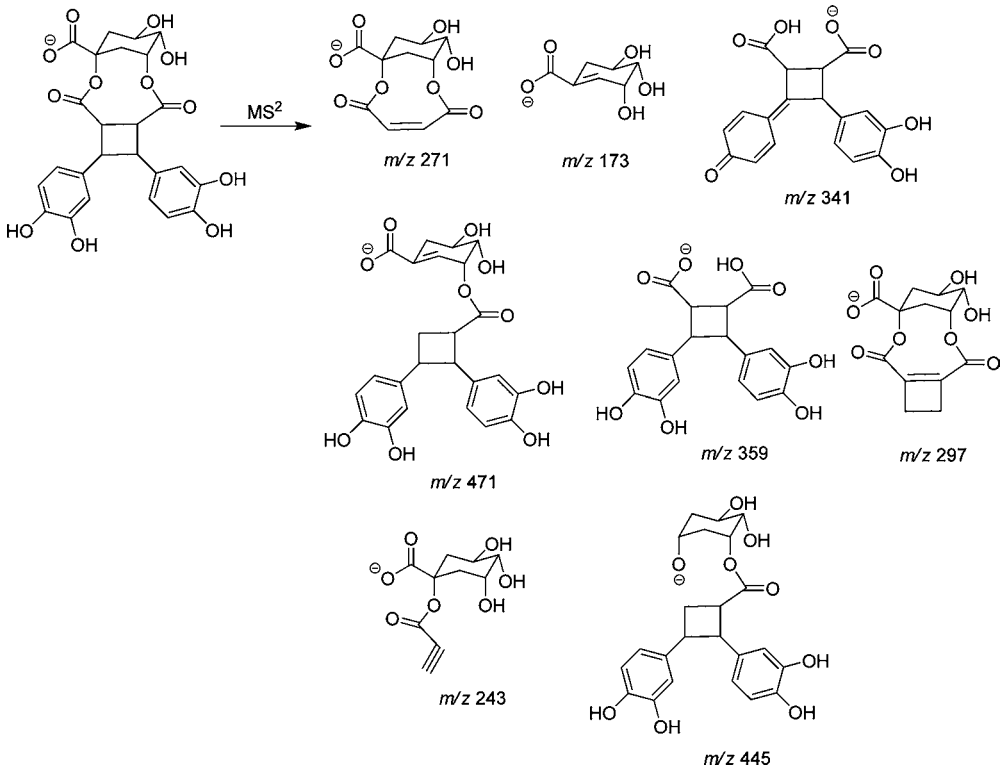

Figure 4. Fragmentation pattern of [2 + 2] cycloaddition products of 1,3-dicaffeoylquinic acids.

of *trans* versus *cis* isomers were found to be ±5% if NMR and LC−MS data were compared to one another. If, after three measurements, no further changes of the concentration of *trans* and *cis* isomers were observed, we assigned this equilibrium concentration to the photostationary equilibrium. It has to be noted that, for dicaffeoylquinic acids, three distinct isomeric *cis*-caffeoyl derivatives are produced as photoproducts, with the di-*cis* derivatives produced as a minor product. Interestingly, always one of two possible *cis* isomers is produced as a major product in the photoisomerization of dicaffeoylquinic acids, indicating preferential isomerization of one caffeoyl moiety over the other in a ratio of around 4:1. Currently, because tandem MS spectra of *cis* and *trans* derivatives are identical and NMR spectroscopic analysis suffers from extensive signal overlap, no clear assignment of regiochemistry was possible. Data are given in Table 1.

All compounds, except 1,3-diCQA (**4**, cynarin), showed exclusively *trans*−*cis* isomerization. 1,3-diCQA (**4**) in contrast showed, after irradiation, first the expected four geometric isomers and, after 30 min of irradiation at 254 nm, the appearance of four further reaction products, one of them a major product, at m/z 515. MS^2 spectra with 515 as a precursor ion revealed a base peak at 191, as expected for a quinic acid derivative.[6−10,12,13,20,21] No fragment ion at m/z 353 characteristic of a dicaffeoylquinic acid was observed.[20] Further fragments at m/z 271, 242, and 297 were observed (Figures 3−6).

These data indicate that a [2 + 2] photochemical cycloaddition reaction has taken place in cynarin, producing a cyclobutane diaryl diester of quinic acid. Such head-to-head photodimers of caffeic acid have been named truxinic acid. Of the theoretically possible eight isomeric cyclobutane derivatives, four isomeric structures were formed (Figures 3−6). The identity of the diaryl cyclobutane derivative was furthermore confirmed using, first, a hydrolysis experiment of the cynarin photoproduct. After base hydrolysis with aqueous NaOH, the LC−MS/MS analysis revealed two isomeric products at m/z 359 with fragment ions at m/z 341, 311, and 267.

For further structural anaylsis, the major photoproduct was isolated by preparative HPLC in an estimated purity of 85% and subjected to detailed NMR analysis. In the ^{1}H NMR spectra, the cyclobutane protons are observed as a higher order four-spin ABXY spectrum with chemical shifts at 2.56, 2.71, 3.21, and 3.35 ppm. Simulation of the higher order spectra revealed coupling constants of ^3J = 3.6, 5.1, 4.7, and 3.2 Hz, respectively. These data show that the major compound has a *cis* diaryl relationship and a *cis* diester relationship and must be assigned to either compound **3** or **8** (in Figure 5). The *cis* diaryl relationship appears to be a consequence of aromatic interactions in the lowest energy cynarin conformer.

The unique photochemical behavior of 1,3-diCQA (**4**) can be rationalized in terms of Schmidt's law.[22,23] Schmidt's law states that, in solid-state photochemical [2 + 2] cycloaddition, a critical distance between 32 and 40 pm of the two reacting olefinic chromophores must be reached to allow for formation of two new C−C σ bonds.[22−24]

Photochemical Mechanism and Fluorescence Spectra of CGAs. Zhu et al.[5] carried out a detailed investigation on the photochemistry of caffeic acid and 5-CQA (**3**). Their main conclusions were as follows. Hydroxycinnamic acids do not possess an accessible triplet state. Following irradiation, photoionization takes place, producing a hydroxycinnamic acid radical cation with a low quantum yield of around 0.02. Comments or experiments exploring the possibility of a singlet excited state were not carried out. Surprisingly, no fluorescence data of purified CGAs have been reported in the literature.

Because olefin *trans*−*cis* isomerization generally involves a triplet excited state as a key intermediate, the data by Zhu et al.[5] should actually not allow for an isomerization reaction. The possibility that photoisomerization proceeds via a long-lived radical cation intermediate should be ruled out because, in the

DOI: 10.1021/acs.jafc.5b00838
J. Agric. Food Chem. 2015, 63, 3338−3347

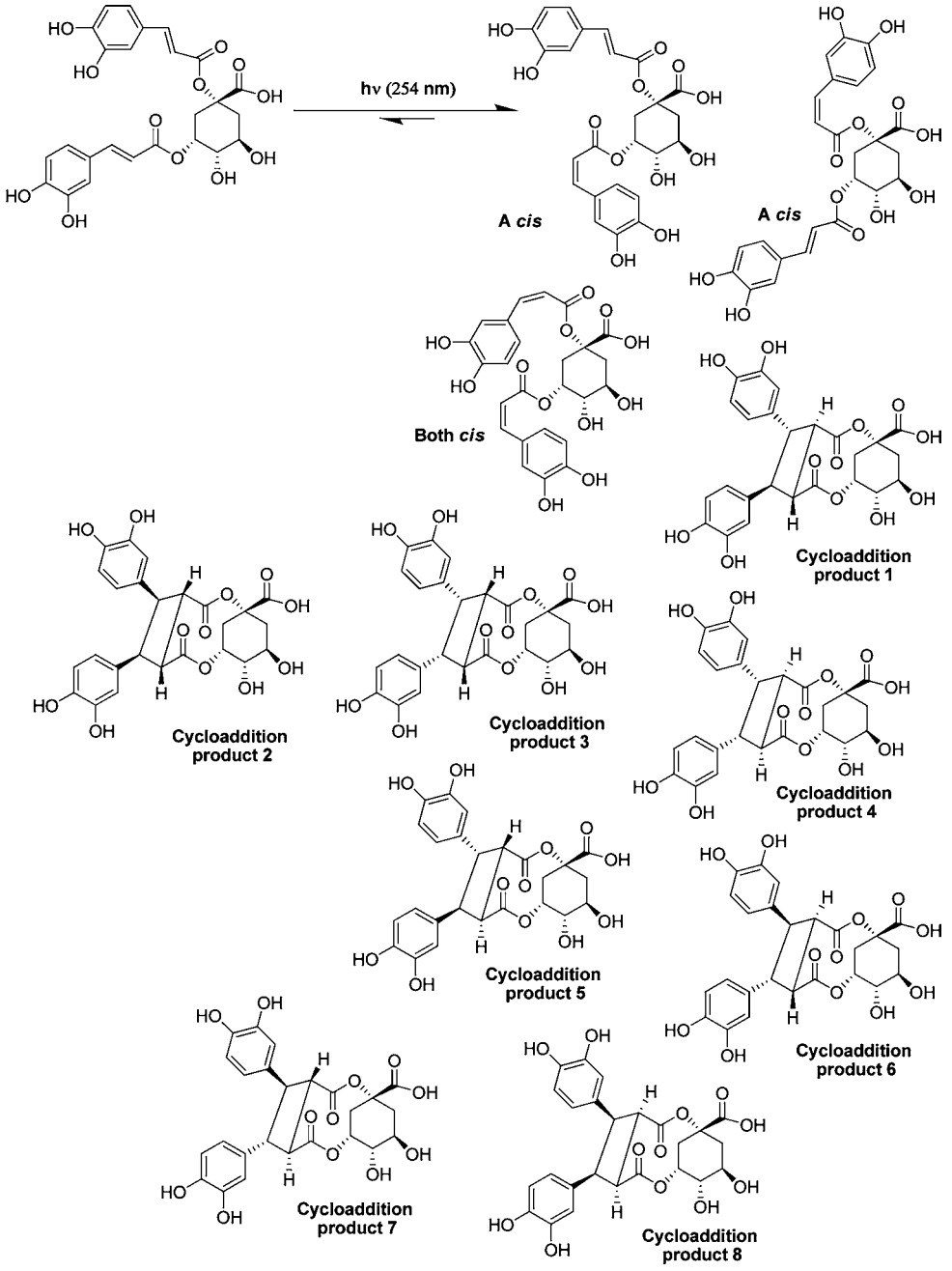

Figure 5. Formation of the photoisomerized [2 + 2] cycloaddition products of 1,3-dicaffeoylquinic acids.

model systems, it would be expected that side reactions with nucleophilic CGAs or with nucleophilic solvents form minor side products, which were never observed. To probe the presence of a radical cation, the photoisomerization was carried out in the presence of oxygen, and using LC−MS, CGAs quenched by O_2 were searched for in extracted ion chromatograms. However, no intermediates with m/z values of 385 and 537 could be detected. However, several other groups have demonstrated that *trans*−*cis* isomerization can occur as well from a singlet excited state.[25−27] To support this hypothesis, fluorescence spectra of all investigated CGAs were recorded. All mono- and dicaffeoylquinic acids displayed upon irradiation at 320 or 260 nm a weak fluorescence at 440 nm, supporting the presence of a singlet state (Figure 7).

***trans*−*cis* Isomerization in Agricultural Practice.** As a next step in our investigations, we decided to address the problem of whether the formation of *cis*-caffeoylquinic acids plays a role in agricultural practice. Furthermore, we wanted to investigate whether the formation of *cis*-caffeoylquinic acids would serve as a useful marker for UV exposure of plant tissues.

As an example, we used cultivation of *S. rebaudiana*, a plant cultivated mainly for its *ent*-kaurene-type terpenoids, better known as steviol glycosides, which are around 200 times sweeter than sucrose. We have recently reported on the presence of CGAs in *S. rebaudiana*. Within a European Union (EU) project (DIVAS), *S. rebaudiana* was cultivated in eight locations in the Mediterranean region of Europe over a period of 2 years using six different botanical varieties of *Stevia*. The leaves were harvested between 2 and 3 times annually from July to September, producing a total of 120 different samples of *S. rebaudiana* leaves. Agricultural parameters, including climatic conditions, are available through records of the nearest official weather station.

DOI: 10.1021/acs.jafc.5b00838
J. Agric. Food Chem. 2015, 63, 3338−3347

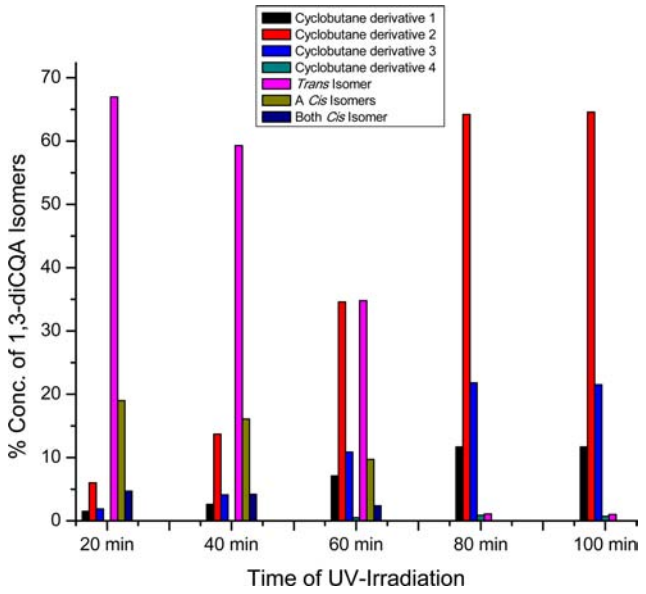

Figure 6. Concentrations of 1,3-dicaffeoylquinic acid isomers with time after UV irradiation.

For all 120 samples and an additional 30 samples of *Stevia* leaves obtained commercially, 5-CQA (**3**), *cis*-5-CQA, 3,4-diCQA (**5**), and two isomers of *cis*-3,4-diCQA were quantified in all samples. All further *cis*-CQA derivatives were present in the samples; however, for most data, their quantity was found to be below the limit of quantitation. A selection of data is shown in Table 2.

The first important question to be addressed involves the biosynthetic origin of the *cis*-CQA derivatives. For this purpose, initially, the statistical pattern and type of statistical distribution of the quantitative data were analyzed. Both 5-CQA (**3**) and 3,4-diCQA (**5**) concentrations show a Gaussian distribution profile over the 120 samples analyzed, as judged by the Kolmogorov–Smirnov test (Figure 8). In contrast, quantitative data for *cis*-5-CQA (**8**) and *cis*-3,4-diCQA were found to exhibit a non-Gaussian distribution.

For a large data set of quantitative data for three mono-CQA and four diCQA concentrations, we could recently show that concentrations of all CGA isomer concentrations in a plant correlate linearly with one another, pointing to a common stimulus of biosynthetic production in the plant. We applied this linearity test to this data set and observe that concentrations of 5-CQA (**3**) and *cis*-5-CQA (**8**) and concentrations of 3,4-diCQA (**5**) and their *cis* derivatives do not exhibit a linear concentration dependency. This points toward two distinct stimuli and pathways of their biosynthetic production.

In contrast, concentrations of the two *cis*-3,4-diCQA isomers and concentrations of *cis*-5-CQA and the *cis*-3,4-diCQA derivatives show a linear concentration dependency (see Figure S1 of the Supporting Information). This should be interpreted as all *cis*

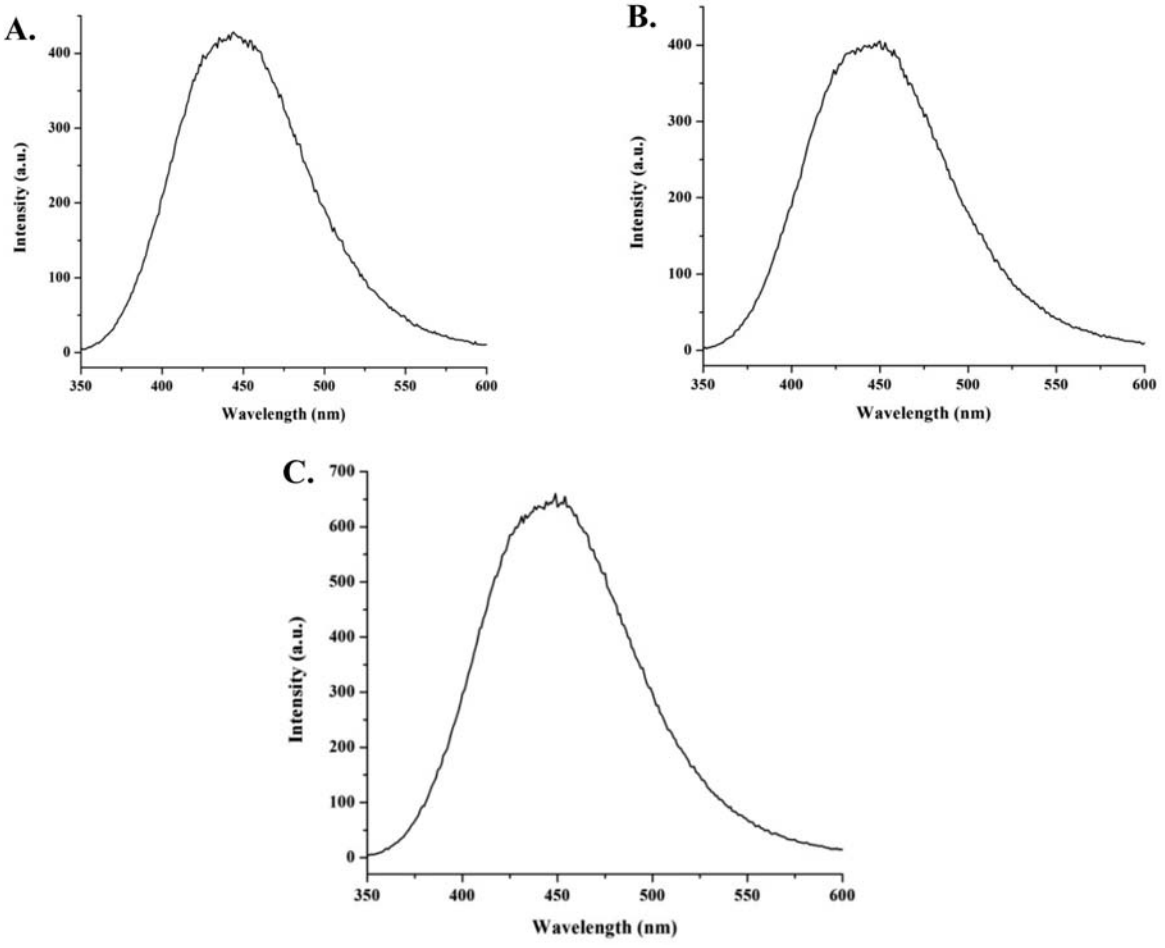

Figure 7. Fluorescence spectra of (A) 3-caffeoylquinic acid (**1**), (B) 4-caffeoylquinic acid (**2**), and (C) 5-caffeoylquinic acid (**3**) with excitation wavelength at 320 nm.

DOI: 10.1021/acs.jafc.5b00838
J. Agric. Food Chem. 2015, 63, 3338−3347

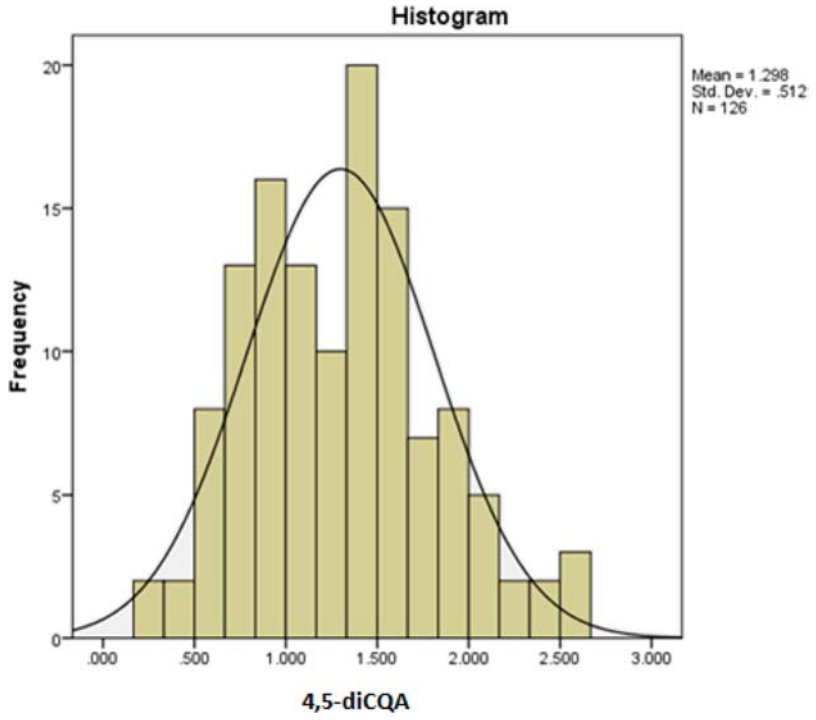

Figure 8. Histogram of 5-caffeoylquinic acid, showing the normal distribution of the data set.

derivatives sharing the same external stimulus for production. This stimulus is different from that of *trans*-CQA biosynthesis. We suggest that the stimulus of *cis*-CQA production is direct irradiation by UV light of exposed leaves.

To substantiate this hypothesis, we correlated available UV irradiation data with *cis*-CQA concentrations. As a first set of data, we looked at changes of *cis*-CQA concentrations in different harvests. For two set of samples, three harvests were carried out from June to September of crops grown at the same locations. For the last harvest in September, the number of sunshine hours affecting the plants was always considerably lower if compared to the two early harvests from June to August. Sunshine hours were available through the weather databases of the nearest airport weather station.[28,29] Representative data are shown in Figure 9, where, in two bar charts, the total *cis*-CQA concentration is given for three harvests in two different locations and, additionally, the ratio of *trans*-/*cis*-CQA concentrations at the three different harvests.

A more global picture including all available data was obtained by the log of *trans*-/*cis*-5-CQA concentrations against the number of sunshine hours in the month prior to sample collection for six locations, where, in 2010 and 2011, a total of 10 harvests were collected. The data plotted in this manner display a linear relationship with the quotient *trans*-/*cis*-5-CQA concentration clearly depending upon the number of sunshine hours 4 weeks prior to the harvest. The same observation can be made if correlating sunshine hours 2 weeks prior to the harvest with the quotient *trans*-/*cis*-5-CQA concentration. If longer periods prior to the harvest are taken into consideration, the difference in sunshine hours levels out and samples are more difficult to distinguish. The more sunshine hours the plant leaves were exposed to, the smaller the quotient and, therefore, the higher the relative amount of *cis*-5-CQA concentrations (Figure 10). It should as well be noted that the *trans*-/*cis*-5-CQA concentration does in no case exceed the theoretical maximum value, as determined in the measurement of the photostationary equilibrium values.

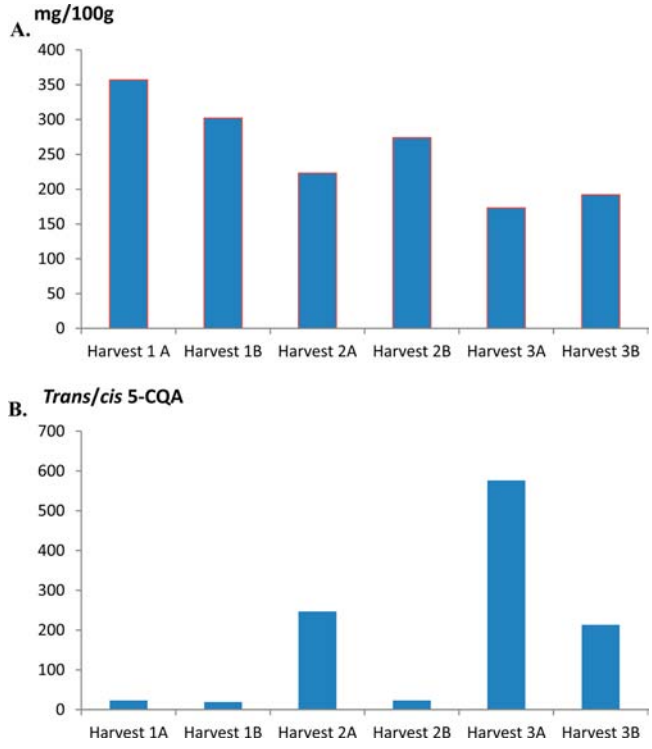

Figure 9. (A) Amount of 5-caffeoylquinic acid (**3**) (mg/100 g of dry leaves) and (B) *trans*/*cis* ratio from three harvests from location a (TCV) and location b (Amfilikeia) during 2011.

In conclusion, we have shown that all *trans*-CQAs investigated undergo photochemical *trans*−*cis* photoisomerization. The photostationary equilibrium for seven derivatives was determined for the first time. The only exception to this reaction

DOI: 10.1021/acs.jafc.5b00838
J. Agric. Food Chem. 2015, 63, 3338−3347

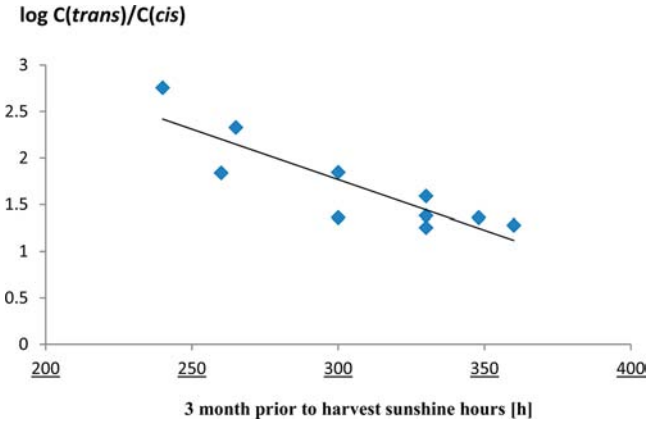

Figure 10. Plot of log $C(trans)/C(cis)$ against sunshine hours (prior to sample collection).

pathway was 1,3-diCQA (**4**, cynarin), which, following *trans*−*cis* photoisomerization, undergoes a [2 + 2] photocycloaddition to produce a diaryl cyclobutane derivative of quinic acid.

In a data set comprising 120 samples of *S. rebaudiana* grown in different locations, it could be convincingly demonstrated that the production of *cis*- and *trans*-CQA derivatives must follow two distinctly different pathways. The production of *cis* derivatives was shown to correlate with the number of sunshine hours, to which plant leaves were exposed in the month prior to harvest, suggesting that *cis*-CQA concentrations can serve as useful and promising markers of UV exposure of plant material in agricultural practice.

■ ASSOCIATED CONTENT

Supporting Information

Correlation coefficients of *cis* isomers according to Spearman's rule (Table S1) and linear dependency of (A) *cis*-5-caffeoylquinic acid (*cis*-5-CQA) with 5-caffeoylquinic acid (5-CQA) and (B) two isomers of *cis*-4,5-dicaffeoylquinic acid (*cis*-4,5-diCQAs) (Figure S1). This material is available free of charge via the Internet at http://pubs.acs.org.

■ AUTHOR INFORMATION

Corresponding Author

*Telephone: 49-421-200-3120. Fax: 49-421-200-3229. E-mail: n.kuhnert@jacobs-university.de.

Funding

The research leading to these results has received funding from the European Union's Seventh Framework Programme managed by Research Executive Agency (REA) http://ec.europa.eu/research/rea (FP7/2007−2013) under Grant Agreement 232250.

Notes

The authors declare no competing financial interest.

■ ACKNOWLEDGMENTS

The authors acknowledge the technical assistance of Anja Müller. All agricultural cooperatives active in the DIVAS project are thanked for the provision of *Stevia* leaf samples.

■ REFERENCES

(1) DeLuca, H. F. The vitamin D story: A collaborative effort of basic science and clinical medicine. *FASEB J.* **1988**, *2*, 224−236.

(2) Bintsis, T.; Litopoulou-Tzanetaki, E.; Robinson, R. K. Existing and potential applications of ultraviolet light in the food industry—A critical review. *J. Sci. Food Agric.* **2000**, *80*, 637−645.

(3) Morrison, I. M.; Robertson, G. W.; Stewart, D.; Wightman, F. Determination and characterization of cyclodimers of naturally occurring phenolic acids. *Phytochemistry* **1991**, *30*, 2007−2011.

(4) Sisa, M.; Bonnet, S. L.; Ferreira, D.; Van der Westhuizen, J. H. Photochemistry of flavonoids. *Molecules* **2010**, *15*, 5196−5245.

(5) Zhu, H.; Zhao, H.; Zhang, Z.; Wang, W.; Yao, S. Laser flash photolysis study on antioxidant properties of hydroxycinnamic acid derivatives. *Radiat. Environ. Biophys.* **2006**, *45*, 73−77.

(6) Clifford, M. N.; Marks, S.; Knight, S.; Kuhnert, N. Characterization by LC−MS^n of four new classes of *p*-coumaric acid-containing diacyl chlorogenic acids in green coffee beans. *J. Agric. Food Chem.* **2006**, *54*, 4095−4101.

(7) Clifford, M. N.; Kirkpatrick, J.; Kuhnert, N.; Roozendaal, H.; Salgado, P. R. LC−MS^n analysis of the *cis* isomers of chlorogenic acids. *Food Chem.* **2008**, *106*, 379−385.

(8) Jaiswal, R.; Patras, M. A.; Eravuchira, P. J.; Kuhnert, N. Profile and characterization of the chlorogenic acids in green Robusta coffee beans by LC−MS^n: Identification of seven new classes of compounds. *J. Agric. Food Chem.* **2010**, *58*, 8722−8737.

(9) Karakoese, H.; Jaiswal, R.; Kuhnert, N. Characterization and quantification of hydroxycinnamate derivatives in *Stevia rebaudiana* leaves by LC−MS^n. *J. Agric. Food Chem.* **2011**, *59*, 10143−10150.

(10) Jaiswal, R.; Kiprotich, J.; Kuhnert, N. Determination of the hydroxycinnamate profile of 12 members of the Asteraceae family. *Phytochemistry* **2011**, *72*, 781−790.

(11) Jaiswal, R.; Matei, M. F.; Deshpande, S.; Kuhnert, N. Identification and characterization of hydroxycinnamates of six *Galium* species from the Rubiaceae family. In *Handbook of Chemical and Biological Plant Analytical Methods*; Hostettmann, K., Stuppner, A., Marston, A., Chen, S., Eds.; John Wiley and Sons, Ltd.: Chichester, U.K., 2014; pp 505−524.

(12) Jaiswal, R.; Deshpande, S.; Kuhnert, N. Profiling the chlorogenic acids of *Rudbeckia hirta*, *Helianthus tuberosus*, *Carlina acaulis* and *Symphyotrichum novae-angliae* leaves by LC−MS^n. *Phytochem. Anal.* **2011**, *22*, 432−441.

(13) Jaiswal, R.; Sovdat, T.; Vivan, F.; Kuhnert, N. Profiling and characterization by LC−MS^n of the chlorogenic acids and hydroxycinnamoylshikimate esters in mate (*Ilex paraguariensis*). *J. Agric. Food Chem.* **2010**, *58*, 5471−5484.

(14) Jaiswal, R.; Kuhnert, N. Identification and characterization of the phenolic glycosides of *Lagenaria siceraria* Stand. (bottle gourd) fruit by liquid chromatography−tandem mass spectrometry. *J. Agric. Food Chem.* **2014**, *62*, 1261−1271.

(15) Dranik, L. I.; Shubert, T. A. The spectral investigation of *cis* and *trans* isomers of certain oxycinnamic acids. *Dokl. Akad. Nauk SSSR* **1969**, *185*, 705.

(16) Dranik, L. I.; Shubert, T. A. *Cis*−*trans* isomerization of esters of hydroxycinnamic acids. *Dokl. Akad. Nauk SSSR, Ser. Biochem. Sect.* **1970**, *193*, 202−205.

(17) Dranik, L. I.; Shubert, T. A. Photochemical transformation of cynarin 1,5-dicaffeoylquinic acid. *Dokl. Akad. Nauk SSSR, Ser. Biochem. Sect.* **1970**, *193*, 202−205.

(18) Haskins, F. A.; Williams, L. G.; Gorz, H. J. Light-induced *trans* to *cis* conversion of *β*-D-glucosyl *o*-hydroxycinnamic acid in *Melilotus alba* leaves. *Plant Physiol.* **1964**, *39*, 777−781.

(19) Kahnt, G. *Trans*−*cis*-equilibrium of hydroxycinnamic acids during irradiation of aqueous solutions at different pH. *Phytochemistry* **1967**, *6*, 755−758.

(20) Clifford, M. N.; Knight, S.; Kuhnert, N. Discriminating between the six isomers of dicaffeoylquinic acid by LC−MS^n. *J. Agric. Food Chem.* **2005**, *53*, 3821−3832.

(21) Clifford, M. N.; Johnston, K. L.; Knight, S.; Kuhnert, N. Hierarchical scheme for LC−MS^n identification of chlorogenic acids. *J. Agric. Food Chem.* **2003**, *51*, 2900−2911.

(22) Schmidt, G. M. J. Topochemistry. Part III. The crystal chemistry of some *trans*-cinnamic acids. *J. Chem. Soc.* **1964**, 2014−2021.

(23) Schmidt, G. M. J. Photodimerization in the solid state. *Pure Appl. Chem.* **1971**, *27*, 647−678.

DOI: 10.1021/acs.jafc.5b00838
J. Agric. Food Chem. 2015, 63, 3338−3347

(24) Cohen, M. D. The photochemistry of organic solids. *Angew. Chem., Int. Ed. Engl.* **1975**, *14*, 386−393.
(25) Kikuchi, A.; Saito, H.; Mori, M.; Yagi, M. Photoexcited triplet states of new UV absorbers, cinnamic acid 2-methylphenyl esters. *Photochem. Photobiol. Sci.* **2011**, *10*, 1902−1909.
(26) Marin, M. L.; Miguel, A.; Santos-Juanes, L.; Arques, A.; Amat, A. M.; Miranda, M. A. Involvement of triplet excited states in the electron transfer photodegradation of cinnamic acids using pyrylium and thiapyrylium salts as photocatalysts. *Photochem. Photobiol. Sci.* **2007**, *6*, 848−852.
(27) Wang, H.; Zhai, B.; Tang, W.; Yu, J.; Song, Q.; Photosensitized, Z−E isomerization of cinnamate by covalently linked 2-(3′,4′-dimethoxybenzoyl)benzyl moiety via triplet−triplet energy transfer. *Chem. Phys.* **2007**, 333, 229−235.
(28) http://weather.org/ (accessed Aug 2013).
(29) http://www.weatheronline.co.uk/ (accessed Aug 2013).

DOI: 10.1021/acs.jafc.5b00838
J. Agric. Food Chem. 2015, 63, 3338−3347

The measurement of the terpene patterns of a total of 40 cultivars in combination with sensory evaluations pointed out that sensory sensation such as sweet and nonbitter taste, sweetish, flowery, and nutty odor impressions correlate with a high popularity of the cultivars. As a marker for low popularity, the substances β-myrcene, β-caryophyllene, and humulene as well as a high content of total terpenoids were determined.[21]

In contrast to the roots, the terpene patterns of carrot leaves have hardly been studied. Habegger and Schnitzler[22,23] and Hampel et al.[24,25] studied the biosynthesis of VOCs in relation to the leaves and roots. No correlation of metabolite patterns between leaves and roots was found.

As monoterpenes are related to plant defense, Ibrahim[26] et al. studied the influence of temperature and exogenous limonene treatment on the headspace volatiles emitted from leaves. There are also only a few publications on the effects of VOCs of the leaves in the process of plant−herbivore interaction. For example Seljasen[27] determined an influence of *Psyllid* attack on the terpene pattern of the plant besides effects on the bitter compounds falcarindiol and 6-methoxymellein.

Regardless of the immense number of publications dealing with flavor compounds of carrots, no consensus about typical carrot volatile patterns exists. The lack of agreement in defining the essential chemical compounds of carrot aroma is depicted by analyzing 12 publications that give compilations of volatiles.[1,11,12,15,18,26,30−35] Altogether 124 different VOCs were reported. However, not a single compound out of the compilation of 124 is mentioned in all of the 12 papers coincidently. Consensus exists only in 11 out of 12 studies for five terpenoid compounds: sabinene, limonene, terpinolene, β-caryophyllene, and α-humulene. In addition frequently mentioned volatiles are the following: β-pinene (10×), α-pinene, γ-terpinene, and *p*-cymene (each 9×).

In summary it can be stated that the knowledge about VOC patterns of roots is present in particular in relation to the sensory quality, while leaves have been relatively unexamined. Especially the aspect of metabolic diversity in species is yet little-known. For carrot breeding approaches aiming to obtain good sensory properties in combination with high resistance to pests or diseases, knowledge of the usable biodiversity and the genotype−environment interactions (G × E) of VOCs is an important prerequisite.

In the present study for the first time 10 carrot cultivars, representing the main root colors white, yellow, red, orange, and purple and growing in a three-year field experiment, were analyzed with regard to the qualitative and quantitative composition of the VOCs of both roots and leaves. The influence of cultivar, harvest year, correlation between the VOCs, and the comparison between leaf and root metabolite patterns was examined using multivariate statistical methods.

MATERIALS AND METHODS

Chemicals. The reference substances hexanal, hexanol, limonene, γ-terpinene, humulene, and myristicine were purchased from Sigma-Aldrich Germany, Steinheim, Germany. The substances α-pinene, β-pinene, sabinene, β-myrcene, terpinolene, and β-caryophyllene were from Carl Roth Co KG, Karlsruhe, Germany. (*E*)-2-Hexenal was from Merck KGaA, Darmstadt, Germany, and bornyl acetate was delivered from CHEMOS GmbH, Regenstauf, Germany.

Plant Material. The leaves and roots of 10 carrot cultivars (*Daucus carota* L.) of different origin and color from a triennial field trial study at the experimental field station in Quedlinburg were included in the analysis. Cultivar specifications are given in Table 1. The seeds were sown (100 seeds/m) by a seed drill as plots in flat beds with two rows, each of them 3 m long and with a row distance of 45 cm by a seed drill. Plots were arranged in a randomized block design with four agronomical replications (biological replications). Chemical analyses were performed using 10 healthy and untouched marketable roots. Washed carrot leaves without the petioles as well as roots were sliced, immediately frozen with liquid nitrogen, and stored until analysis at −80 °C.

Table 1. Origin and Relevant Characters of Carrot Cultivars Used in the Study

abbr	cultivar	source[a]	status[b]	root color	root type
1	White Satin	Bejo	F_1	white	Flakkeer
2	Blanche[c]	INH 126	OP	white	Danvers/ Flakkeer
3	Yellowstone	Bejo	OP	yellow	Flakkeer
4	BL710015	Seminis	BL	yellow	Nantes
5	Nutrired	Seminis	OP	red	Nantes/Flakkeer
6	Pusa Kesar	WGRU 6755	LR	red	Flakkeer
7	Santa Cruz	Seminis	OP	orange	Chantenay
8	Nerac	Bejo	F_1	orange	Nantaise
9	Deep Purple	Bejo	F_1	purple	Flakkeer
10	Anthonina	Seminis	OP	purple	Flakkeer

[a]Bejo Zaden B.V. (NL), Seminis (USA), INH-Institute National Horticulture, Angers (F), WGRU-Wellesbourne Genetic Resources Unit, University of Warwick (UK). [b]OP, open pollinated cultivar; F_1, hybrid cultivar,; BL, breeding line; LR, land race. [c]Blanche 1/2 long des Voges.

Volatile Analysis by Headspace SPME−Gas Chromatography. After thawing the plant material, samples were homogenized for 1 min in a 20% NaCl solution (leaves/NaCl solution = 1:10, w/v, and roots/NaCl solution = 1:1.5) in a Waring blender. The homogenate was filtered using gauze. For each sample, four 20 mL headspace vials each containing 4 g of solid NaCl for saturation were filled with a 10 mL aliquot of the supernatant and sealed with a magnetic crimp cap including a septum. For automated headspace SPME−GC, a 100 μm polydimethylsiloxane fiber (Supelco, Bellefonte, PA, USA) and a MPS2 autosampler (Gerstel, Mühlheim, Germany) were used. After an equilibration time of 10 min at 35 °C using the shaker (300 rpm) the fiber was exposed to the headspace for 15 min at 35 °C. Desorption was performed within 2 min in splitless mode and 3 min with split at 250 °C. An Agilent Technologies 6890 GC equipped with an HP-5 ms column (0.25 mm i.d., 30 m length, and 0.5 μm film thickness) and FID were used for separation and detection. Carrier gas was hydrogen using a flow rate of 1.1 mL min^{-1}. The temperature program was the following: 45 °C (5 min), from 45 to 210 °C at 3 °C min^{-1} and held 25.5 min at 210 °C. The volatiles were identified by parallel runs of selected samples on an identically equipped GC-MS by library search (NIST and MassFinder), retention indices, and coelution of authentic samples (except for germacrene). All samples were run with four agronomical replications.

Data Processing and Statistics. The commercial software ChromStat2.6 (Analyt, Müllheim, Germany) was used for raw data processing.[28,29] Data inputs for ChromStat 2.6 were raw data from the percentage reports (retention time/peak area data pairs) performed with the software package Chemstation (version Rev.B.02.01.-SR1 [260]) by Agilent. Using ChromStat2.6, the chromatograms were divided in up to 200 time intervals, each of which represented a peak (substance) occurring in at least one chromatogram of the analysis set. The peak detection threshold was set on the 10-fold value of noise. The values are given as raw data (peak area in counts), which also can be described as relative concentration because of the normalized sample preparation. The semiquantitation by the software ChromStat 2.6 was focused on 15 VOCs summarized in Table 2.

A primary data analysis of normality gave a non-Gaussian distribution for most of the VOCs (data not shown). Therefore, a nonparametric Kruskal−Wallis procedure using the software SY-

DOI: 10.1021/acs.jafc.5b00704
J. Agric. Food Chem. 2015, 63, 3348−3356

Table 2. Carrot VOCs and Known Properties

no.	compound	abbreviation leaf/root	ref	properties[a]
1	hexanal	1H/2H	34	SC
2	(*E*)-2-hexenal	1E2H/2E2H	22, 23[b]	SC, fu
3	hexanol	1Hol/2Hol		SC
4	*α*-pinene	1aP/2aP	10, 16, 18, 22,[b] 23,[b] 26,[b]31, 32, 34, 42, 43, 45, 46	SC, CIC
5	sabinene	1Sa/2Sa	10, 16, 18, 22,[b] 23,[b] 26,[b] 30, 32, 34, 42, 43, 45, 46	SC, CIC
6	*β*-pinene	1bP/2bP	10, 16, 18, 26,[b] 30, 31, 32, 34, 42, 43, 45, 46	SC, CIC
7	*β*-myrcene	1bM/2bM	10, 16, 18, 22,[b] 23,[b] 26,[b] 30, 31, 32,34, 42, 43, 45, 46,	SC, CIC, av, ab
8	limonene	1L/1L	10, 16, 18, 22,[b] 23,[b] 26,[b] 30, 31, 32, 34, 42, 43, 45, 46	SC, CIC, av, ab
9	*γ*-terpinene	1gT/2gT	10, 16, 18, 26,[b] 30, 31, 32, 34, 42, 43, 45, 46	SC, CIC, av, ab
10	terpinolene	1Te/2Te	10, 16, 18, 26,[b] 30, 31, 32, 34, 42, 43, 45, 46	SC, CIC, av
11	bornyl acetate	1Ba/2Ba	10, 16, 26,[b] 30, 31, 32, 42, 43, 45, 46	SC
12	*β*-caryophyllene	1bC/2bC	10, 16, 18, 22,[b] 23,[b]26,[b] 30, 31, 32, 34, 42, 43, 45, 46	SC, CIC
13	humulene	1Hu/2Hu	18, 26,[b] 30, 31, 32, 34, 44, 46	SC, SIC, ab
14	germacrene	1Ge/2Ge	22,[b]23[b]	ab
15	myristicine	1My/2My	10, 16, 32, 42,43	

[a]SC, semiochemical after www.pherobase.com; CIC, aroma character impact compound in carrot roots; av, antiviral; ab, antibacterial; fu, fungicide. [b]Identified in leaves.

STAT13 (Systat Software, Inc., Chicago, IL, USA) was used to compare the VOC data of different cultivars for the single harvest years and additionally over the three years in summary. The Pearson correlation was performed with STATISTICA7.1. (StatSoft Europe GmbH, Hamburg, Germany). The heat map was constructed with the open source software Multi Experiment Viewer (MEV; http://www.tm4.org).

RESULTS AND DISCUSSION

Selection of Metabolite Targets. In this research the quantities of 15 compounds identified in both leaves and roots were used for further processing. The reasons to focus on the substances listed in Table 2 are the following. First, the selected VOCs are of high abundance in most of the samples, which is a result of the chosen volatile extraction method (HS-SPME). Second, these substances are identified by mass spectrometry (library search) and additional coelution of authentic reference substances. The only exception is germacrene, for which no reference was available. Third, the selection includes nine aroma compounds which are described in the literature as so-called "character impact compounds" (CIC) in carrot roots.[18] Additionally the compilation includes all of the mutual compounds published for carrots in the literature (from 11 studies) mentioned above. Finally, the substances listed in Table 2 are known to be involved in various biological activities that are of interest in plant genetics and breeding activities.

Cultivar and Harvest Year Affect the Contents of Volatile Metabolites. The data set of VOC patterns containing 10 cultivars, three harvest years, and four agronomical replications each is visualized by a heat map in Figure 1. Both qualitative and quantitative differences in VOC pattern were observed between cultivars as well as the harvest years. Qualitative differences are defined as values below the detection threshold of the SPME-GC-FID method used (7 counts) and are depicted as black spots in the heat map. For example, bornyl acetate (1BA) has never been detected in leaves over the three years in the cultivars 'White Satin', 'Yellowstone', 'Nutrired', 'Santa Cruz', 'Deep Purple', 'Pusa Kesar', and 'Anthonina', while in the remaining three cultivars low to medium levels were found. In roots hexanal (2H) is detected in only some samples of four cultivars at low concentrations ('Nutrired', 'Pusa Kesar', 'Santa Cruz', 'Nerac'). The compounds (*E*)-2-hexenal and 1-hexanol are exclusively present in the leaves only.

In general, the variability of metabolites seems to be determined by the cultivar especially in roots (Figure 1, Tables 3 and 4). Particularly the content of the monoterpenes *α*-pinene (2aP), sabinene (2Sa), *β*-pinene (2bP), *β*-myrcene (2bM), limonene (2L), and terpinene (2Te) decreases in the order white, yellow, red, orange, and purple. In contrast, the monoterpene terpinolene (2Te) shows high concentrations in roots of all cultivars. The most abundant VOC in leaves is *β*-myrcene (1bM), with a mean of 10 883 counts and a maximum of 30 884 counts (sample 9.1.3). In roots the highest concentration was found for the monoterpene terpinolene (2Te), with a mean of 15 331 counts and a maximum of 82 569 counts (sample 3.3.1). In general, the concentrations of VOCs were found in a similar concentration range in leaves and roots, although the sample preparation procedure for leaves works with a higher relation between tissue and NaCl solution by a factor of 6.67.

The statistical comparison of VOC patterns of the genotypes for the single harvest years and over the three years is summarized for both leaves and roots in Tables 3 and 4, respectively.

Leaves. The 10 cultivars show significant differences for 11 of the 15 leaf volatiles during the first year, differing from the compounds (*E*)-2-hexenal (1E2H), limonene (1L), *β*-caryophyllene (1bC), and humulene (1Hu) (Table 3). In the second harvest year the two VOCs *β*-caryophyllene (1bC) and humulene (1Hu) are not significantly different between the cultivars, whereas the third cultivation year was characterized by significant cultivar differences for all of the 15 VOCs. The statistical analysis for three years in summary shows nine significant metabolites.

The volatile bornyl acetate (1Ba) was detected in low to medium amounts in three out of the 10 cultivars (Figure 1). In all three years this compound was semiquantified only in the cultivar 'Nerac', while cv. 'Blanche', cv. 'BL 710015', and cv. 'Pusa Kesar' showed bornyl acetate only in the first year and not in all replicas. All other cultivars expressed no bornyl acetate. Thus, this compound seems to be a characteristic metabolite for discrimination of the mentioned cultivars. The partial expression in the cultivars 'Blanche', 'BL710015', and 'Pusa Kesar' suggests strong influences of the harvest year. Two of the compounds, hexanol (1Hol) and *β*-pinene (1bP), were not detectable in year 2, suggesting also an influence of the climatic conditions. The calculation over the whole period of three years gives no significances for six compounds (1aP, 1Sa, 1bM, 1L, 1gT, and 1Te), which suggests a stable expression independently from the environmental influences. In conclusion the VOC selection shows significant differences between the tested cultivars. A partially strong variation between the years suggests additional influences of the climatic conditions. On the other hand six VOCs (1aP, 1Sa, 1bM, 1L, 1gT, and 1Te) were expressed in equal relations between the cultivars over the three

DOI: 10.1021/acs.jafc.5b00704
J. Agric. Food Chem. 2015, 63, 3348−3356

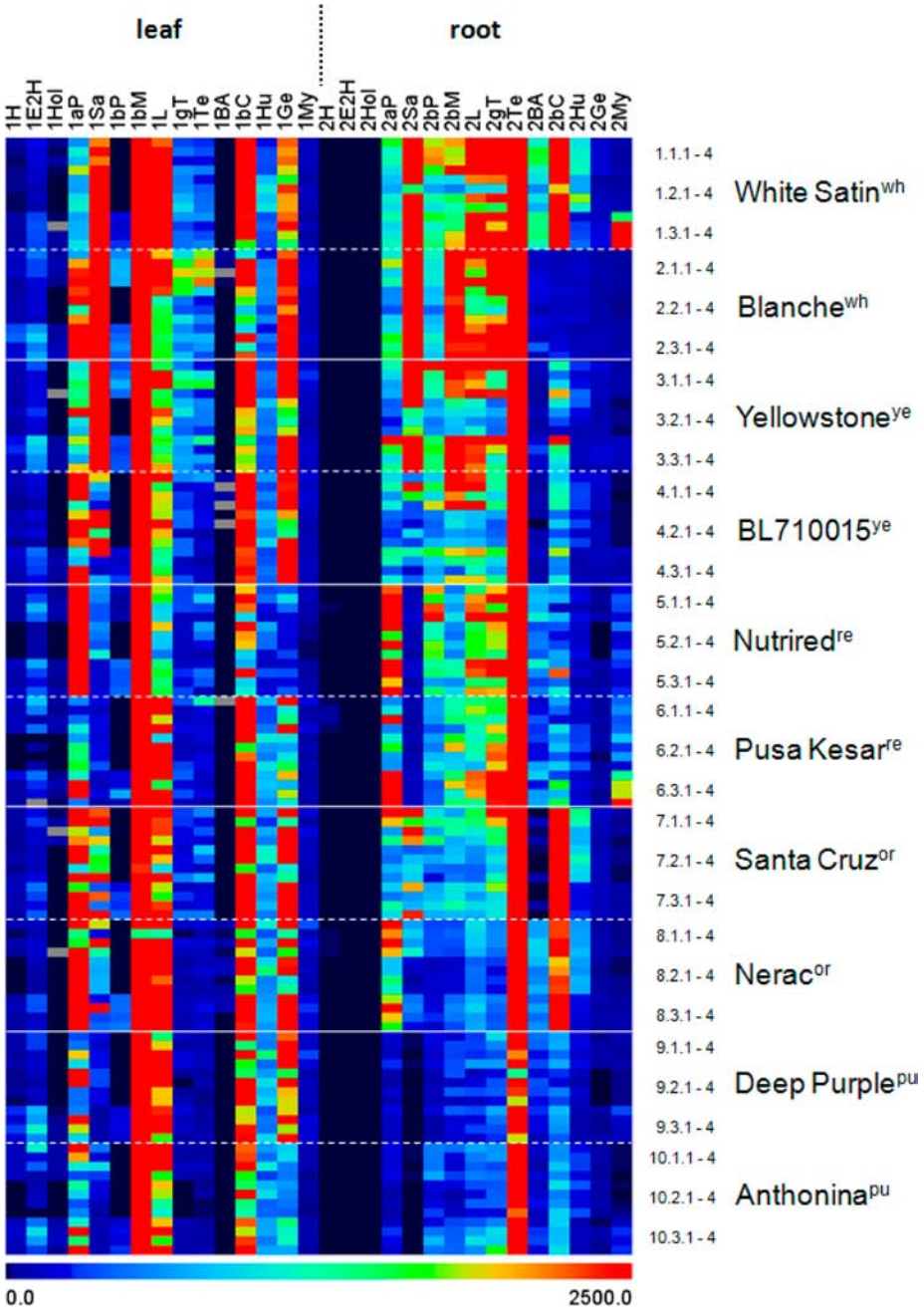

Figure 1. Heat map for 15 VOCs in leaves and roots separately, estimated for 10 cultivars, three harvest years, and four agronomical replications each. Color code for relative VOC concentrations in counts of peak area (color bar on bottom position): black = 0; red = 2500; gray = missing value. Sample code: "1.1.1−4" corresponds to "cultivar 1 (White Satin). harvest year 1. agronomical replications 1−4". Root color: ^{wh} is white; ^{ye} is yellow; ^{re} is red; ^{or} is orange; ^{pu} is purple.

years. It appears plausible that these six VOCs and bornyl acetate seem to be suitable for discrimination of carrot cultivars on the leaf metabolite level.

Roots. In contrast to leaves the VOCs (*E*)-2-hexenal and hexanol were not detected in root samples (Table 4). The root volatile hexanal (2H) showed a unique behavior because it was detected only in year 1 and exclusively for the cultivars 'Nutrired', 'Pusar Kesar', and 'Nerac'. The compound hexanal is discussed in the literature not only in association with plant defense[36] but also with stress responses.[36,37] The presence in the first year on one hand and the absence in the years 2 and 3 on the other hand suggests an association with the dryer and warmer climatic conditions in cultivation year 1.

Considering a year by year comparison, all of the 13 detected VOCs are significant between the tested cultivars. However, a statistical analysis of root volatiles based on the average of the three years showed differences between the cultivars for 10 of the 13 VOCs (Table 4). The high variation between the years with even qualitative differences for hexanal suggests influences of the environmental conditions similar to the discussion for leaf volatiles. The calculation for root VOCs over three cultivation years shows an equal relation in expression for 2Sa, 2BA, and 2bC, which can be interpreted as independence from the environmental conditions for these compounds. This seems to be suitable for discrimination of carrot cultivars on the basis

DOI: 10.1021/acs.jafc.5b00704
J. Agric. Food Chem. 2015, 63, 3348−3356

Table 3. Comparison of 15 VOCs in 10 Carrot Cultivars over Three Years Semiquantified in Leaves with the Kruskal–Wallis Test for Significance

					comparison of cultivars with the Kruskal–Wallis test[a]							
		relative concentration in counts			year 1		year 2		year 3		three years	
VOC	N	mean	min	max	KW	*p*	KW	*p*	KW	*p*	KW	*p*
1H	119	78.64	0.00	436.10	29.92	0.00	35.52	0.00	25.32	0.00	52.87	0.00
1E2H	119	293.02	0.00	1148.68	16.84	0.05 a	25.26	0.00	22.69	0.01	65.00	0.00
1Hol	117	19.72	0.00	122.74	29.76	0.00	n.d.		28.91	0.00	48.52	0.00
1aP	120	3091.50	170.28	16698.30	23.62	0.00	23.67	0.00	23.57	0.01	3.44	0.18 a
1Sa	120	2847.22	42.45	23520.00	33.05	0.00	35.32	0.00	34.76	0.00	4.22	0.18 a
1bP	120	146.91	0.00	779.97	38.68	0.00	n.d.		25.51	0.00	72.34	0.00
1bM	120	10882.67	1386.72	30883.60	32.13	0.00	29.23	0.00	28.29	0.00	5.05	0.08 a
1L	120	2544.55	505.88	7546.98	12.66	0.18 a	20.95	0.01	26.43	0.00	1.85	0.40 a
1gT	120	355.61	0.00	1946.50	29.93	0.00	35.35	0.00	32.45	0.00	1.82	0.40 a
1Te	120	347.24	12.13	2200.45	28.16	0.00	29.27	0.00	29.94	0.00	2.26	0.32 a
1BA	116	5.45	0.00	129.54	34.18	0.00	37.86	0.00	18.46	0.03	6.33	0.04
1bC	120	2748.58	731.49	7367.16	14.94	0.09 a	15.5	0.08 a	24.14	0.00	6.71	0.04
1Hu	120	583.55	127.72	1458.86	11.69	0.23 a	14.44	0.11 a	29.14	0.00	20.21	0.00
1Ge	120	2307.55	159.27	8162.69	24.14	0.00	26.69	0.00	29.25	0.00	13.57	0.00
1My	120	109.85	14.59	366.68	17.32	0.04	25.54	0.00	30.85	0.00	21.17	0.00

[a]KW, Kruskal–Wallis test statistics; n.d., not detected; significance differences at $p < 0.05$. "a" indicates nonsignificant differences between the cultivars.

Table 4. Comparison of 15 VOCs in 10 Carrot Cultivars over Three Years Expressed in the Roots with the Kruskal–Wallis Test for Significance

					comparison of cultivars with the Kruskal–Wallis test[a]							
		relative concentration in counts			year 1		year 2		year 3		three years	
VOC	N	mean	min	max	KW	*p*	KW	*p*	KW	*p*	KW	*p*
2H	119	1.22	0.00	32.49	32.71	0.00	n.d.		n.d.		17.42	0.00
2aP	120	1275.54	42.49	6863.78	30.74	0.00	35.24	0.00	34.19	0.00	14.52	0.00
2Sa	120	1954.64	0.00	11910.60	36.71	0.00	37.52	0.00	37.35	0.00	3.47	0.18 a
2bP	120	851.18	34.01	4420.85	35.08	0.00	33.98	0.00	32.78	0.00	11.04	0.00
2bM	120	1364.68	63.95	6751.40	36.01	0.00	33.56	0.00	34.11	0.00	6.74	0.03
2L	120	1442.71	133.96	5968.89	33.21	0.00	35.41	0.00	35.41	0.00	16.36	0.00
2gT	120	1507.68	207.77	4667.84	32.52	0.00	34.54	0.00	32.22	0.00	12.46	0.00
2Te	120	15331.34	1336.56	82568.70	34.76	0.00	34.57	0.00	35.55	0.00	14.75	0.00
2BA	115	389.59	0.00	1582.50	35.06	0.00	31.93	0.00	32.09	0.00	0.47	0.79 a
2bC	120	1624.62	82.46	8636.64	33.61	0.00	32.67	0.00	32.07	0.00	4.57	0.10 a
2Hu	120	339.50	41.70	1786.43	32.15	0.00	32.31	0.00	32.05	0.00	31.98	0.00
2Ge	120	72.41	0.00	236.68	34.78	0.00	34.32	0.00	32.06	0.00	6.71	0.04
2My	119	243.56	6.31	3117.78	33.21	0.00	31.96	0.00	34.01	0.00	36.57	0.00

[a]KW, Kruskal–Wallis test statistics; n.d., not detected; significance differences at $p < 0.05$. "a" indicates nonsignificant differences between the cultivars.

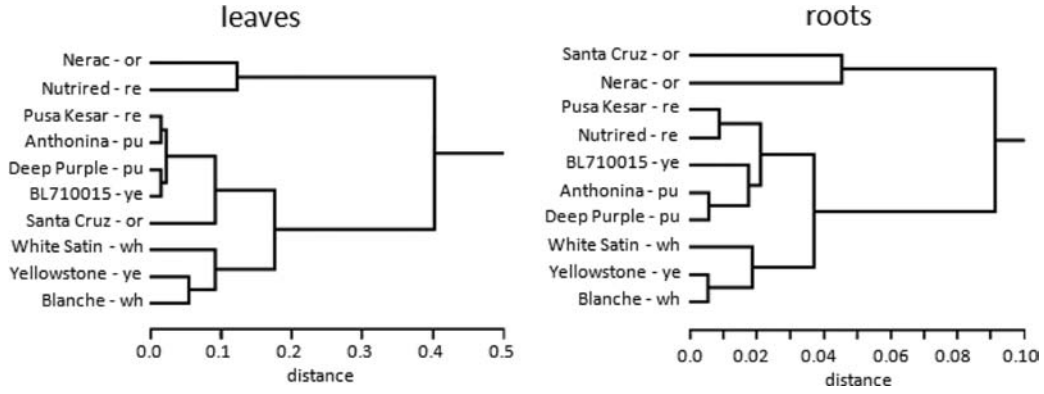

Figure 2. Hierarchical clustering (Pearson correlation coefficient, average linkage method) separately for leaves (left) and roots (right), on the basis of 15 VOCs as means of year and replicas ($N = 3$). Root color code: wh, white; ye, yellow; or, orange; re, red; pu, purple.

DOI: 10.1021/acs.jafc.5b00704
J. Agric. Food Chem. 2015, 63, 3348–3356

Table 5. Pearson Correlation among VOCs for Leaves and Roots[a]

Leaves															
VOC	1H	1E2H	1Hol	1aP	1Sa	1bP	1bM	1L	1gT	1Te	1BA	1bC	1Hu	1Ge	1My
1H	1														
1E2H	0.81	1													
1Hol	0.56	0.59	1												
1aP	0.01 a	0.08 a	0.13 a	1											
1Sa	0.18 a	0.05 a	0.10 a	−0.13 a	1										
1bP	0.42	0.37	0.39	0.35	0.54	1									
1bM	0.32	0.21	0.11 a	−0.31	0.29	0.21	1								
1L	−0.10 a	−0.05 a	−0.11 a	−0.01 a	0.01 a	0.02 a	0.19 a	1							
1gT	0.21	0.08 a	0.08 a	−0.13 a	0.95	0.49	0.35	0.01 a	1						
1Te	0.15 a	0.11 a	0.12 a	0.03 a	0.84	0.52	0.22	0.04 a	0.82	1					
1BA	−0.14 a	−0.14 a	−0.16 a	0.21	0.03 a	−0.02 a	−0.18 a	0.22	−0.06 a	0.06 a	1				
1bC	−0.08 a	−0.12 a	−0.14 a	−0.09 a	−0.03 a	−0.11 a	0.11 a	0.37	0.04 a	0.14 a	0.26	1			
1Hu	−0.24	−0.28	−0.35	0.01 a	−0.10 a	−0.25	0.07 a	0.37	−0.10 a	−0.07 a	0.31	0.53	1		
1Ge	0.24	0.10 a	−0.05 a	−0.09 a	0.36	0.30	0.40	0.16 a	0.37	0.32	0.17 a	0.36	0.24	1	
1My	−0.11 a	0.09 a	−0.11 a	0.11 a	0.29	0.29	0.24	0.22	0.28	0.31	0.27	0.38	0.26	0.85	1

Roots															
VOC	2H	2E2H	2Hol	2aP	2Sa	2bP	2bM	2L	2gT	2Te	2BA	2bC	2Hu	2Ge	2My
2H	1														
2E2H	n.d.	1													
2Hol	n.d.	n.d.	1												
2aP	0.11 a	n.d.	n.d.	1											
2Sa	−0.15 a	n.d.	n.d.	−0.01 a	1										
2bP	−0.03 a	n.d.	n.d.	0.51	0.41	1									
2bM	−0.08 a	n.d.	n.d.	0.11 a	0.77	0.43	1								
2L	0.11 a	n.d.	n.d.	0.43	0.72	0.71	0.74	1							
2gT	−0.05 a	n.d.	n.d.	0.49	0.60	0.62	0.56	0.79	1						
2Te	−0.11 a	n.d.	n.d.	0.36	0.69	0.62	0.66	0.94	0.72	1					
2BA	0.06 a	n.d.	n.d.	0.42	0.12 a	0.34	−0.12 a	0.38	0.33	0.33	1				
2bC	−0.10 a	n.d.	n.d.	0.07 a	0.28	0.22	−0.02 a	0.27	0.22	0.18 a	0.49	1			
2Hu	0.11 a	n.d.	n.d.	−0.02 a	0.13 a	0.11 a	−0.11 a	0.03 a	0.07 a	−0.11 a	0.32	0.69	1		
2Ge	−0.16 a	n.d.	n.d.	−0.04 a	0.63	0.42	0.53	0.58	0.35	0.50	0.19 a	0.60	0.35	1	
2My	0.05 a	n.d.	n.d.	0.23	0.07 a	0.08 a	0.03 a	0.33	0.36	0.34	0.45	0.26	−0.11 a	0.22	1

[a]Pearson correlation coefficients are significant for values >0.19, $N = 100$. "a" represents nonsignificant correlation coefficients for $p < 0.05$. n.d., not detected.

J. Agric. Food Chem. 2015, 63, 3348−3356
DOI: 10.1021/acs.jafc.5b00704

of the root metabolom. The occurrence of hexanal as a stress indicator should be tested in further experiments.

Correlation between Metbaolite Patterns and Root Color. The used cultivars are characterized by five different root colors: white, yellow, red, orange, and purple. Because especially the white and yellow cultivars 'White Satin', 'Blanche', 'Yellowstone', and 'BL71005' show a distinct increased level of the root compounds sabinene (2Sa), β-myrcene (2bM), limonene (2L), and γ-terpinene (2gT) (Figure 1), a correlation analysis was performed using the values for every cultivar as a mean of yearly and agronomical replications.

The cluster analysis of the leaf volatiles (Figure 2) results in two main clusters, with the cultivars 'Nerac' and 'Nutrired' in one and the remaining cultivars in a second cluster. The second cluster again is subdivided into two subclusters with the cultivars 'Blanche', 'Yellowstone', and 'White Satin' as one and the five others as a second group, respectively.

For the root volatiles (Figure 2) also two main clusters were specified but with different cultivars than in leaves. Cluster one contains the cultivars 'Santa Cruz' and 'Nerac', both with orange roots. The second cluster comprises the remaining eight cultivars. Similar to the leaf volatiles the second cluster is subdivided into two subclusters, one exactly the same as for leaves with the cultivars 'Blanche', 'Yellowstone', and 'White Satin'. The VOC patterns of roots partly correlate with the root color for orange, red, and purple carrots, whereas in leaves no clear correlation of VOC pattern and root color occurs. It is noteworthy that the two white cultivars 'White Satin' and 'Blanche' carry totally different patterns regarding the terpene acetate (2BA), the sesquiterpenes (2bC, 2Hu), and the phenylpropanoid myristicine in replica 3 (2My).

Correlations among the Volatile Compounds. A Pearson correlation analysis shows that 48 coefficients (out of 105 possible single correlations) with significant values exist between the individual compounds in leaves and 46 (out of 78) in roots, respectively (Table 5).

In leaves the three compounds hexanal (1H), (*E*)-2-hexenal (1E2H), and hexanol (1Hol) correlate among each other positively with high to medium values. High correlation coefficients occur for the pairs sabinene (1Sa) and γ-terpinene (1gT) (0.95), sabinene (1Sa) and terpinolene (1Te) (0.84), and terpinolene (1Te) and γ-terpinene (1gT) with a value of 0.82. The concentration of the phenylpropene myristicine (1My) correlates with 10 VOCs with significant positive values. The highest coefficient (0.85) occurs between myristicine (1My) and the sesquiterpene germacrene (1Ge) (Table5).

In roots the two lipoxygenase (LOX) products (*E*)-2-hexenal (2E2H) and hexanol (2Hol) were not detected, while hexanal (2H) was found sporadically in low concentrations only in three cultivars ('Nutrired', 'Pusa Kesar', and 'Nerac') (Figure 1). The highest correlation coefficient (0.94) occurs between the compounds limonene (2L) and terpinolene (2Te) (Table 5). Also in roots the compound myristicine (2My) is correlating positively with seven other volatiles.

Differences in Volatile Patterns between Leaf and Root. Earlier findings by Habegger and Schnitzler[22,24] and Hampel et al.[25] proved that the biosynthesis in leaves and roots may be independent from each other. To check the relation between the organs, a correlation was performed between the set of leaf and root VOCs, separately for every harvest year and also as the mean over three years. In contrast, the results in our study show that six out of the 13 VOCs correlate between leaves and roots over all years (Table 6).

Table 6. Pearson Correlation of Individual VOCs between Leaves and Roots[a]

	three years	year 1	year 2	year 3
VOC	n = 120	n = 40	n = 40	n = 40
H	0.03 a	0.23 a	n.d.	n.d.
aP	0.53	0.55	0.48	0.52
Sa	0.66	0.67	0.76	0.87
bP	0.13 a	0.11 a	n.d.	0.05 a
bM	0.23	0.19 a	0.27 a	0.15 a
L	−0.05 a	−0.07 a	−0.04 a	−0.14 a
gT	0.46	0.48	0.45	0.63
Te	0.42	0.46	0.41	0.77
BA	0.11 a	0.02 a	0.28 a	0.09 a
bC	0.15 a	0.04 a	0.38	0.12 a
Hu	0.19 a	−0.11 a	0.38	0.10 a
Ge	0.29	0.11 a	0.36	0.32
My	−0.22	−0.11 a	−0.34	−0.44

[a]Pearson correlation coefficients are significant for values > 0.19, N = 120. "a" represents nonsignificant correlation coefficients for $p < 0.05$. n.d., not detectable.

Also Figure 1 indicates differences between the two plant organs. The most distinct difference was found for the three C6 compounds (green leaf compounds, LOX) hexanal (H), (*E*)-2-hexenal (E2H), and hexanol (Hol). While these compounds are present in leaves with highly abundant peaks, hexanal (2H) occurs in roots only in three cultivars ('Nutrired', 'Pusa Kesar', 'Nerac') in the first cultivation year. Positive correlations were found for the compounds α-pinene (aP), sabinene (Sa), γ-terpinene (gT), and terpinolene (T) for both the individual years and three-year average (Table 6). Correlations for either individual years or the mean of three years were evidenced for β-myrcene (bM), β-caryophyllene (bC), humulene (Hu), germacrene (Ge), and myristicine (My). Myristicine (My) generally is negatively correlated between the plant organs for three years and the single years 2 and 3. The overall level as well the variability is much higher in roots than in leaves for this compound (Figure 1). The closest correlation between leaves and roots occurs for the volatile sabinene (Sa), with high correlation coefficients in all years and the mean of three years.

Consequences for Metabolic Studies and Cultivar Breeding. The diversity of volatile patterns shows more noticeable differences in roots than in leaves (Figure 1). Between the cultivars both qualitative and quantitative differences in VOC pattern exist. A genotype−environment (G × E) interaction was evidenced for the VOC patterns. On the one hand for a number of VOCs the analyses showed a similar expression over the years (e.g., 1gT, 1aP, 1My, 1L, 2Hu, 2bP, 2Ba) and seem to indicate a discrimination of the cultivars. On the other hand a group of analyzed VOCs (e.g., 1bP, 1Hol, 2My, 2Hu) are highly influenced by environmental factors such as soil temperature and water availability determined as "harvest year".

The 10 analyzed cultivars belong to five different root color types. The root color depends on the proportion of the nonvolatile metabolites such as lycopene, carotene, lutene, and anthocyanins. Due to noticeable differences in root color, also an influence on metabolic patterns may be expected. Even if there are some quantitative differences between monoterpenes especially in roots (Figure 1), a correlation analysis based on 30 VOCs in leaves and roots indicates only a partial clustering regarding root color (Figure 2). In particular, the two white

DOI: 10.1021/acs.jafc.5b00704
J. Agric. Food Chem. 2015, 63, 3348−3356

cultivars 'White Satin' and 'Blanche' present completely different patterns regarding terpene acetate (2Ba), the sesquiterpenes (2bC, 2Hu, 2Ge), and the phenylpropanoid myristicine (2My). But these differences may be influenced by other factors such as breeding status because the very old cultivar 'Blanche' belongs to the so-called open pollinated cultivars, whereas 'White Satin' represents a modern F1 hybrid.

The 15 quantified VOCs are derived from three different biosynthetic pathways. The compounds hexanal (H), (*E*)-2-hexenal (E2H), and hexanol (Hol) are generated by the LOX pathway, whereas myristicin (My) is synthesized according to the phenylpropanoid pathway. The remaining VOCs are terpenoids (mono- and sesquiterpenes as well as one terpene acetate). In leaves the three LOX-derived compounds (1H, 1E2H, 1Hol) are highly positively correlated with each other. In roots this type of metabolites is not present or only sporadically detected, which may be a hint on the different ecological requirements of the two different plant organs regarding plant defense. As an example, the three mentioned compounds are known for an inhibiting effect on fungi such as *Botrytis cinerea*.[38,39] Some high correlation coefficients between monoterpenes are caused by the synthesis in the same pathway. For example the cyclic monoterpenes sabinene (1Sa), γ-terpinene (1gT), and terpinolene (1Te), which correlate highly in leaves, are synthesized via the α-terpinyl cation.[40] The same relationship exists between limonene (2L) and terpinolene (2Te), which correlate with a coefficient of 0.94 in roots. Interestingly, numerous correlations of the phenylpropanoid myristicine in leaves and roots to mono- and sesquiterpenes exist. In recent literature no connection of these two biosynthetic pathways has been established yet.

Habegger and Schnitzler[22,23] analyzed the essential oils extracted from leaves and roots separately to study correlations between the two plant organs and make predictions from the patterns of the leaf VOCs for the composition of the roots for plant breeding. The authors draw the conclusion that the metabolic patterns in both plant organs develop independently. The present study gives a more detailed picture. At least seven of the VOCs correlate between leaves and roots (over three years), six positively and one negatively (myristicine). It is known that this compound (My) is involved in the formation of bitter taste in carrots.[41] Therefore, the development of a new method to predict the bitter taste in carrot roots based on the analytical data of the leaves may be an important approach for early selection in breeding programs. The results obtained in this study give basic information for research and breeding regarding quality including flavor, resistance against diseases, and availability of VOCs in nutrition. Currently, our research activities are directed to reveal the genetic background of the described VOCs including candidate gene approaches, marker development, and genetic mapping.

■ ASSOCIATED CONTENT

Supporting Information

The supporting material describes the common climatic and experimental conditions at the experimental field in Quedlinburg as well as the specific conditions over the three harvest years. This material is available free of charge via the Internet at http://pubs.acs.org.

■ AUTHOR INFORMATION

Corresponding Author

*(D. Ulrich) Phone: (49) 3946-47231. Fax: (49) 3946-47300. E-mail: detlef.ulrich@jki.bund.de.

Funding

The project was funded by DFG Schu 566/10-1.

Notes

The authors declare no competing financial interest.

■ ACKNOWLEDGMENTS

The authors wish to thank Kirsten Weiß, Ines Kasten, Martina Hoppe, and Barbara Sell for excellent technical assistance.

■ ABBREVIATIONS USED

CIC, character impact compound; FID, flame ionization detector; GC-MS, gas chromatography/mass spectrometry; MS, mass spectrometry; LOX, lipoxygenase; HS-SPME, headspace solid phase microextraction; VOCs, volatile organic compounds

■ REFERENCES

(1) Sulaeman, A.; Driskell, J. Carrot flavor. In *Handbook of Fruit and Vegetable Flavors*; Hui, Y. H.; et al., Eds.; John Wiley & Sons, Inc.: Hoboken, USA, 2010; pp 751−773.

(2) Behr, H. C. *AMI Markt Bilanz Gemüse 2012*; Agrarmarkt Informations-Gesellschaft mbH, 2012.

(3) Bino, R. J.; Hall, R. D.; Fiehn, O.; Kopka, J.; Saito, K.; Draper, J.; Nikolau, B. J.; Mendes, P.; Roessner-Tunali, U.; Beale, M. H.; Trethewey, R. N.; Lange, B. M.; Wurtele, E. S.; Sumner, L. W. Potential of metabolomics as a functional genomics tool. *Trends Plant Sci.* **2004**, *9*, 418−425.

(4) Ulrich, D.; Olbricht, K. Fruit Organoleptic Properties and Potential for Their Genetic Improvement. In *Breeding for Fruit Quality*; Jenks, M. A.; Bebeli, P. J., Eds.; John Wiley & Sons, Inc.: Hoboken, NJ, USA, 2011; pp 41−59.

(5) Hartmann, T. From waste products to ecochemicals: Fifty years research of plant secondary metabolism. *Phytochemistry* **2007**, *68*, 2831−2846.

(6) Goff, S. A.; Klee, H. J. Plant volatile compounds: Sensory cues for health and nutritional value? *Science* **2006**, *311*, 815−819.

(7) Arimura, G.; Kost, C.; Boland, W. Herbivore-induced, indirect plant defences. *BBA-Mol. Cell Biol. L* **2005**, *1734*, 91−111.

(8) Bruce, T. J.; Matthes, M. C.; Napier, J. A.; Pickett, J. A. Stressful "memories" of plants: Evidence and possible mechanisms. *Plant Sci.* **2007**, *173*, 603−608.

(9) Laothawornkitkul, J.; Taylor, J. E.; Paul, N. D.; Hewitt, C. Biogenic volatile organic compounds in the Earth system. *New Phytol.* **2009**, *183*, 27−51.

(10) Buttery, R. G.; Seifert, R. M.; Guadagni, D. G.; Black, D. R.; Ling, L. C. Characterization of some volatile constituents of carrots. *J. Agric. Food Chem.* **1968**, *16*, 1009−1015.

(11) Duan, H.; Barringer, S. A. Changes in furan and other volatile compounds in sliced carrot during air-drying. *J. Food Process. Pres.* **2012**, *36*, 46−54.

(12) Kreutzmann, S.; Thybo, A. K.; Edelenbos, M.; Christensen, L. P. The role of volatile compounds on aroma and flavour perception in coloured raw carrot genotypes. *Int. J. Food Sci. Technol.* **2008**, *43*, 1619−1627.

(13) Simon, P. W. Genetic variation for volatile terpenoids in roods of carrot, *Daucus carota*, backcrosses and F-generations. *Phytochemistry* **1982**, *21*, 875−879.

(14) Simon, P. W. Genetic variation for volatile terpenoids in roots of Carrot, *Daucus carota*, inbreds and Fl hybrids. *Phytochemistry* **1982**, *21*, 1299−1303.

DOI: 10.1021/acs.jafc.5b00704
J. Agric. Food Chem. 2015, 63, 3348−3356

(15) Simon, P. W.; Peterson, C. E.; Lindsay, R. C. Genotype, soil, and climate effects on sensory and objective components of carrot flavor. *J. Am. Soc. Hortic. Sci.* **1982**, *107*, 644−648.
(16) Simon, P. W. In *Carrot Flavor: Effects of Genotype, Growing Conditions, Storage, and Processing. In Evaluation of Quality of Fruits and Vegetables*; Pattee, H. E., Ed.; AVI Publishing Co Inc.: Kansas City, MO, USA, 1985; pp 315−328.
(17) Howard, L. R.; Braswell, D.; Heymann, H.; Lee, Y.; Pike, L. M.; Aselage, J. Sensory attributes and instrumental analysis relationships for strained processed carrot flavor. *J. Food Sci.* **1995**, *60*, 145−148.
(18) Edelenbos, M.; Christensen, L. P.; Kjeldsen, F. Characterisation of aroma volatiles in carrots using GC-Olfactometry and aroma extract dilution. In *Flavour Research at the Dawn of the Twenty-First Century*; Le Quere, J. L.; Etievant, P. X., Eds.; Lavoisier: Londres, 2003; pp 588−591.
(19) Ulrich, D.; Nothnagel, T. Effective screening of aroma pattern in carrots. *Acta Hortic.* **2006**, *712*, 907−910.
(20) Ulrich, D.; Nothnagel, T.; Hoberg, E.; Straka, P. Analysis of aroma types by rapid GC methods in carrot breeding research. In *Flavour Research at the Dawn of the Twenty-First Century*, Le Quere, J. L.; Etievant, P. X., Eds.; Lavoisier: Londres, 2003; pp 440−444.
(21) Ulrich, D.; Borschel, K.; Hoberg, E.; Quilitzsch, R.; Schütze, W.; Bauer, D.; Fleck, M. Vergleichende Qualitätsuntersuchungen von alten und neuen Gemüsesorten zur Entwicklung von Zuchtzielen für den ökologischen Gemüsebau. http://orgprints.org/7551, 2004.
(22) Habegger, R.; Schnitzler, W. H. Aroma compounds in the essential oil of carrots (Daucus carota L. ssp sativus). 1. Leaves in comparison with roots. *J. Appl. Bot.−Angew. Bot.* **2000**, *74*, 220−223.
(23) Habegger, R.; Schnitzler, W. H. Aroma compounds in the essential oil of carrots (Daucus carota L. ssp. *sativus*). 2. Intra-leaf distribution. *J. Appl. Bot.−Angew. Bot.* **2000**, *74*, 229−232.
(24) Hampel, D.; Mosandl, A.; Wust, M. Biosynthesis of mono- and sesquiterpenes in carrot roots and leaves (*Daucus carota* L.): metabolic cross talk of cytosolic mevalonate and plastidial methylerythritol phosphate pathways. *Phytochemistry* **2005**, *66*, 305−311.
(25) Hampel, D.; Mosandl, A.; Wüst, M. Biosynthesis of mono- and sesquiterpenes in strawberry fruits and foliage: ^{2}H labeling studies. *J. Agric. Food Chem.* **2006**, *54*, 1473−1478.
(26) Ibrahim, M. A.; Nissinen, A.; Prozherina, N.; Oksanen, E. J.; Holopainen, J. K. The influence of exogenous monoterpene treatment and elevated temperature on growth, physiology, chemical content and headspace volatiles of two carrot cultivars (*Daucus carota* L.). *Environ. Exp. Bot.* **2006**, *56*, 95−107.
(27) Seljasen, R.; Vogt, G.; Olsen, E.; Lea, P.; Hogetveit, L.; Tajet, T.; Meadow, R.; Bengtsson, G. Influence of field attack by carrot psyllid (*Trioza apicalis* Forster) on sensory quality, antioxidant capacity and content of terpenes, falcarindiol and 6-methoxymellein of carrots (*Daucus carota* L.). *J. Agric. Food Chem.* **2013**, *61*, 2831−2838.
(28) Ulrich, D. Fruit and vegetable flavour improvement by selection and breeding: possibilities and limitations. In *Fruit and Vegetable Flavour*; Brückner, B., Wyllie, S. G., Eds.; Woodhead Publishing Limited: Cambridge, England, 2008; pp 167−179.
(29) Ulrich, D.; Nothnagel, T.; Olbricht, K. Examination of volatile patterns of fruit and vegetables using a non-targeted analysis approach. *Acta Hortic.* **2008**, *804*, 659−662.
(30) Shamaila, M.; Durance, T.; Girard, B. Water blanching effects on headspace volatiles and sensory attributes of carrots. *J. Food Sci.* **1996**, *61*, 1191−1195.
(31) Seljasen, R. *Effects of handling on sensory quality of carrots (Daucus carota L.) in relation to chemical parameters;*Thesis Department of Horticulture and Crop Sciences: As, Norway, 2000; Vol. *20*, pp 1−33.
(32) Kjeldsen, F.; Christensen, L. P.; Edelenbos, M. Quantitative analysis of aroma compounds in carrot (*Daucus carota* L.) cultivars by capillary gas chromatography using large-volume injection technique. *J. Agric. Food Chem.* **2001**, *49*, 4342−4348.
(33) Alasalvar, C.; Grigor, J. M.; Zhang, D.; Quantick, P. C.; Shahidi, F. Comparison of volatiles, phenolics, sugars, antioxidant vitamins, and sensory quality of different colored carrot varieties. *J. Agric. Food Chem.* **2001**, *49*, 1410−1416.
(34) Jensen, S. M.; Christensen, L. P.; Edelenbos, M.; Kjeldsen, F. Quantitative analysis of volatile compounds in vegetables by gas chromatography using large-volume injection technique. In *Flavour Research at the Dawn of the Twenty-First Century*; Le Quere, J. L.; Etievant, P. X., Eds.; Lavoisier: Londres, 2003; pp 642−645.
(35) Hoberg, E.; Ulrich, D. Quality of old and new carrot cultivars from ecological cultivation. In *Flavour Science. Recent Advances and Trends*; Bredie, W.; Petersen, M. A., Eds.; Elsevier B. V.: Amsterdam, 2006; pp 545−548.
(36) Matsui, K. Green leaf volatiles: hydroperoxide lyase pathway of oxylipin metabolism. *Curr. Opin. Plant Biol.* **2006**, *9*, 274−280.
(37) Dominguez, T.; Luisa Hernandez, M.; Pennycooke, J. C.; Jimenez, P.; Manuel Martinez-Rivas, J.; Sanz, C.; Stockinger, E. J.; Sanchez-Serrano, J. J.; Sanmartin, M. Increasing omega-3 desaturase expression in tomato results in altered aroma profile and enhanced resistance to cold stress. *Plant Physiol.* **2010**, *153*, 655−665.
(38) Archbold, D. D.; Hamilton-Kemp, T. R.; Barth, M. M.; Langlois, B. E. Identifying natural volatile compounds that control gray mold (*Botrytis cinerea*) during postharvest storage of strawberry, blackberry, and grape. *J. Agric. Food Chem.* **1997**, *45*, 4032−4037.
(39) Hamilton-Kemp, T. R.; Archbold, D. D.; Langlois, B. E.; Collins, R. W. Antifungal activity of E-2-hexenal on strawberries and grapes. *Abstr. Pap. Am. Chem. S.* **1998**, *216*, U34.
(40) Degenhardt, J.; Kollner, T. G.; Gershenzon, J. Monoterpene and sesquiterpene synthases and the origin of terpene skeletal diversity in plants. *Phytochemistry* **2009**, *70*, 1621−1637.
(41) Kramer, M.; Bufler, G.; Ulrich, D.; Leitenberger, M.; Conrad, J.; Carle, R.; Kammerer, D. Effect of ethylene and 1-methylcyclopropene on bitter compounds in carrots (*Daucus carota* L.). *Postharvest Biol. Technol.* **2012**, *73*, 28−36.
(42) Heatherbell, D. A.; Wrolstad, R. E.; Libbey, L. M. Carrot volatiles. 1. Characterization and effects of canning and freeze drying. *J. Food Sci.* **1971**, *36*, 219−224.
(43) Heatherbell, D. A.; Wrolstad, R. E. Carrot volatiles. 2. Influence of variety, maturity and storage. *J. Food Sci.* **1971**, *36*, 225−227.
(44) Seifert, R. M.; Buttery, R. G. Characterization of some previously unidentified sesquiterpenes in carrot roots. *J. Agric. Food Chem.* **1978**, *26*, 181−183.
(45) Simon, P. W.; Peterson, C. E.; Lindsay, R. C. Genetic and environmental influences on carrot flavor. *J. Am. Soc. Hortic. Sci.* **1980**, *105*, 416−420.
(46) Habegger, R.; Muller, B.; Hanke, A.; Schnitzler, W. H. Aroma compounds in different varieties of carrot. *Gartenbauwissenschaft* **1996**, *61*, 225−229.

DOI: 10.1021/acs.jafc.5b00704
J. Agric. Food Chem. 2015, 63, 3348−3356

although as the pH exceeds 10.2, hydrolysis of the ester on the benzene ring takes place.[11]

The anionic form of MS-M (4-methoxy-6-methyl-1,3,5-triazin-2-ylcarbamoyl)[(2-(methoxycarbonyl)phenylsulfonyl]-amidate **2** (Figure 1), however, is much less prone to hydrolysis than its neutral form,[12] and there are several reports of alkali or alkali earth metal salts of sulfonylurea compounds prepared by reaction of the corresponding *N*-protonated sulfonylureas with a solution of a corresponding base, such as alkali metal carbonates, alkali metal hydroxides, and alkaline earth metal hydroxides.[13−18] Ammonium and quaternary ammonium salts of sulfonylureas have also been synthesized by treating the corresponding *N*-protonated sulfonylurea with ammonia, ethanolamine, or ammonium salt solution.[14,19,20] We have not found evidence that these salts have been commercialized.

Another challenging problem with sulfonylureas is obtaining a stable liquid formulation.[21] During storage, sulfonylurea herbicides (in the form of concentrated formulations of dissolved active ingredients) precipitate out of solution and crystal growth takes place. In these cases, solubility limits effective application or use of concentrates of the active herbicide.

In 2011 we presented a strategy of converting a herbicide into an ionic liquid (IL, currently defined as a salt which melts below 100 °C[22]) and applied the approach to a variety of herbicides (e.g., 2,4-D, MCPA, triclopyr, cyhalofop, glyphosate, and dicamba).[23−30] These herbicidal ionic liquids (HILs) were comprised of an active compound in ionic form, possessed low melting points (below 100 °C[22]), and were designed with dual functionality where both cation and anion added to the beneficial properties of the salt. Such combinations of two active chemicals in a single entity demonstrated improved (or in a few cases simply the same) herbicidal activity, while the physicochemical properties were modified. The second actives (cations) were chosen from food or cosmetic grade antibacterial cations, antifungal cations, surfactants, etc. These herbicides possessed greatly reduced volatility, showed improved efficacy, and demonstrated lower water solubility resulting in reduced environmental mobility.

We noted that the MS-M anion (Figure 1) fits the normal design rules for choosing ions that will form HILs (asymmetric, charge delocalized[27]) and, therefore, hypothesized that a similar strategy could be employed for the conversion of MS-M into the HILs, to improve its stability and precipitation problems. Here we report a series of new MS-M IL herbicides where we have paired the MS-M anion with several cations of a second biological activity, including: additional biological activity (e.g., 4,4-dialkyl morpholinium[31]), antimicrobial activity (e.g., quaternary ammonium,[32,33] pyridinium,[34,35] and imidazolium,[35] with longer alkyl chain lengths), penetration enhancers (e.g., linear saturated long chain alkyl substituents, soya[32]), or herbicidal activity (pyperidinium and morpholinium cations with longer *N*-alkyl group substituents[31]). Greenhouse testing and field studies of the synthesized compounds were evaluated to establish their herbicidal activity.

MATERIALS AND METHODS

Materials. All materials were used as supplied unless otherwise noted. Deionized (DI) water was obtained from a commercial deionizer (Culligan, Northbrook, IL, USA) with a specific resistivity of 16.82 MΩ·cm at 25 °C. KOH and all solvents (methanol, DMSO, acetonitrile, acetone, isopropanol, ethyl acetate, chloroform, toluene, hexane) were purchased from Aldrich (European market, Poznan, Poland) and used without further purification. Galmet 20 SG was obtained from P.U.H. Chemirol (Chemirol Sp. z o.o., Mogilno, Poland) and contained 20% metsulfuron methyl (CAS 74223-64-6) and 5% dimethylamine (CAS 124-40-3) as active components.

Bis(2-hydroxyethyl)oleylmethylammonium chloride (Ethoquad O/12, purity 75%) was obtained from Akzo Nobel (Akzo Nobel Head Office, Amsterdam, Netherlands). 2-Hydroxyethyltrimethylammonium chloride (purity > 98%), 1-dodecylpyridinium chloride, hydrate (purity 98%), 1-butyl-3-methylimidazolium chloride (purity 98%), 4-methylmorpholine (purity 98%), 1-bromodecane (purity 98%), tetrabutylphosphonium chloride (purity 96%), and dimidium bromide indicator (purity 95%) were obtained from Sigma-Aldrich (Sigma-Aldrich, St. Louis, MO, USA). Compounds 1-methyl-1-propylpiperidinium chloride (purity 99%), 1-allyl-3-methylimidazolium chloride (purity 98%), 1-butyl-1-methylpyrrolidinium chloride (purity 99%), and trihexyltetradecylphosphonium chloride (purity > 95%) were received from Ionic Liquids Technologies GmbH (IoLiTec, Heilbronn, Germany).

4-Decyl-4-methylmorpholinium bromide was synthesized via quaternization reaction of 4-methylmorpholine and 1-bromodecane as follows. 100 mL of acetonitrile was placed into a 250 mL round-bottom flask equipped with a Teflon-coated stirring bar and a condenser. 4-Methylmorpholine (0.10 mol) and 1-bromodecane (0.11 mol) were added to the acetonitrile, and the reactants were stirred for 48 h at 60 °C. After 48 h the solvent was removed using a vacuum evaporator. After solvent removal, 200 mL of ethyl acetate was added to the residue and the product precipitated as a white solid. The product was carefully separated by vacuum filtration through a glass filter funnel, thoroughly washed with small portions of ethyl acetate (6 × 10 mL) to remove unreacted 1-bromodecane, and dried under reduced pressure at 50 °C for 24 h.

Methods. *Thermal Gravimetric Analysis (TGA).* Thermal gravimetric analysis was performed using a Mettler Toledo Star^e TGA/DSC1 unit (Leicester, UK) under nitrogen. Samples between 2 and 10 mg were placed in aluminum pans and heated from 30 to 450 °C at a heating rate of 10 °C/min.

Differential Scanning Calorimetry (DSC). Thermal transition temperatures were determined by DSC with a Mettler Toledo Star^e DSC1 (Leicester, UK) unit, under nitrogen. Samples between 5 and 15 mg were placed in aluminum pans and heated from 25 to 120 °C at a heating rate of 10 °C/min, cooled with an intracooler at a cooling rate of 10 °C/min to −100 °C, and then heated again to 120 °C.

Melting Point. The melting point for the compound **10** was obtained using a BÜCHI melting point apparatus B-540 (BÜCHI Labortechnik AG, Postfach, Switzerland). A sample of the test substance was placed into a glass capillary tube and then heated at a constant heating rate (3 °C/min). Melting was determined visually with an accuracy ±1 °C.

Nuclear Magnetic Resonance Spectroscopy (NMR). ^{1}H NMR spectra were recorded on a Mercury Gemini 300 spectrometer operating at 300 MHz. ^{13}C NMR spectra were obtained with the same instrument at 75 MHz. TMS was used as the internal standard.

Elemental Analyses (CHN). Elemental analyses were performed at the Adam Mickiewicz University, Poznan (Poland).

Water Content. The water content was determined using an Aquastar volumetric Karl Fischer titrator EMD Millipore (Billerica, MA, USA) with Composite 5 solution as the titrant and anhydrous methanol as the solvent.

Purity Assay by EN ISO 2871-1:2010. As an alternative measure of purity, an assay was performed by direct two-phase volumetric titration according to EN ISO 2871-1:2010.[36] The salts were titrated with a standard solution of sodium dodecyl sulfate ($Na[CH_3(CH_2)_{11}SO_4]$) in a water−chloroform ($H_2O-CHCl_3$) biphasic system (or water−methanol−chloroform in the case of compounds with limited solubility in water). The titration was conducted with the indicator (dimidium bromide). In a 50 mL volumetric flask, 0.1 g of the MSM salt was dissolved in water (or in a mixture of water and methanol). Then, a 10 mL sample was taken from the prepared solution and blended with 15 mL of chloroform and 5 mL of pre-mixed indicator. The resulting biphasic system was titrated with a 0.004 M sodium

DOI: 10.1021/jf505782p
J. Agric. Food Chem. 2015, 63, 3357−3366

dodecyl sulfate. After addition of a titrant increment, the sample was stirred vigorously for 15 min to allow reaction of the titrant with the analyzed compound and its extraction into the organic phase (chloroform). After 15 min, the two phases were separated and the color analyzed. This was repeated until the pink color disappeared from the chloroform lower phase at the equivalence point, and a one-drop excess of titrant formed a violet complex. The purity was calculated using equation 1:

$$\%\ \text{purity} = \frac{(V_K C_d V_d \text{MW}) \times 100}{m V_p \times 1000} \quad (1)$$

where % purity is the cationic content (% of available), V_K is the total volume of the prepared solution of analyzed substance in mL; C_d is the concentration of the titrant solution of sodium dodecyl sulfate, $Na[CH_3(CH_2)_{11}SO_4]$ in mol/L; V_d is the volume of the titrant solution in mL; MW is the molecular weight of the analyzed compound in g/mol; m is the mass of the tested sample in g; and V_p is the volume of titrated analyte in mL.

Solubility Measurements. The solubilities were determined via *Vogel's Textbook of Practical Organic Chemistry* protocol.[37] A sample of each HIL (0.1 g) was added to a certain volume of each solvent, and the samples were thermostated (MEMMERT Water Bath, model WNB 7, Schwabach, Germany) at 25 °C. Based on the volume of solvent used, 3 types of behavior were recorded: "soluble" applies to compounds which dissolved in 1 mL of solvent, "limited solubility" applies to compounds that dissolved in 3 mL of solvent, and "not soluble" applies to compounds which did not dissolve in 3 mL of solvent.

Statistics. A total of 5 experiments were statistically analyzed, including 2 greenhouse experiments (on *Chemopodium album* and *Brassica napus*) and 3 field experiments (field trials conducted in 2012 and 2013 in fields near Szczecinek and Szamotuly) on *Matricaria inodora, Viola arvensis, Polygonum convolvulus, Galeopsis tetrahit, Capsella bursa pastoris, P. rhoeas, Veronica persica, S. media*, and *Myosotis arvensis*. In order to study the effect of the applied plant protection product on the value of weed destruction, a statistical analysis for each greenhouse and each field experiment was carried out. Each experiment was performed in a completely randomized design with $r = 3$ or 4 replications in greenhouse experiments and $r = 4$ replications in all field trials. For each experiment the following number of groups (v, also called conditions) was used: $v = 7$ groups for greenhouse trials (six HILs, **6**–**8** and **10**–**12** and the Galmet 20 SG control) and $v = 6$ for field trials (five HILs, **6**–**8**, **10**, and **11** and the Galmet 20 SG control) to determine if there was a significant difference between the efficacy data collected under each condition. For each experiment, the degree of freedom (df) that indicates the total number of data points collected (n) and the number of groups being compared (v) is reported in the American Psychological Association (APA) format, $df = v - 1; n - v$. This means that for the greenhouse trials with seven groups being compared with each other and three replicates collected for each of the groups, there were a total of $n = 7 \times 3 = 21$ data points and, therefore, df = 6; 14. Similarly, for the greenhouse trials with seven groups being compared with each other but four replicates collected for each, df = 6; 21. For the field study, only six groups were compared with each other, with four replicates collected for each of the groups resulting in $n = 24$ data points and df = 5; 18.

The program package R (3.0.2) was used for the statistical calculations (R Development Core Team, 2013[38]). Only normally distributed data can be analyzed by analysis of variance (ANOVA). Here, the Shapiro–Wilk test was used first to test the null hypothesis that "the samples come from a normal distribution" against the alternative hypothesis "the samples do not come from a normal distribution". In the case of normal distribution, the Fligner–Killeen test of homogeneity of variances was used to test the null hypothesis that the variances in each of the groups–for each treatment in one trial–ere the same. Before performing the test, a "significance level" (or test's threshold value, α) of 0.01 was chosen, followed by calculation of a function of the observed sample results (p-value), and the null hypothesis was tested at the chosen α-level of 0.01. When the p-value obtained was more than the significance level (α), the tests suggested that the observed data were consistent with the assumption that the null hypothesis was true. Subsequently, to study differences between studied treatments, a one-way analysis of variance (ANOVA) was applied. When the p-value was less than 0.01, the null hypothesis that the data were normally distributed was rejected and the non-parametric Kruskal–Wallis (K–W) rank sum test that does not assume a normal distribution of the samples (unlike the analogous one-way ANOVA) was applied.

Both ANOVA and the non-parametric Kruskal–Wallis (K–W) rank sum test are statistical procedures used for comparing sample means. The results allow for comparison of many sample distributions using significance level α- and p-values; however, the null hypothesis in the case of ANOVA was different: "there is no relationship between the groups" against the alternative hypothesis "there is relationship between the groups". For quantification, the F score (also called F-statistic), equal to the ratio between the variance of the group means/the mean of the variances within the group, indicates how significant the effect of the independent variable is. For both ANOVA and the non-parametric Kruskal–Wallis tests, we reported significance level α-level, p-value, and F-score.

ANOVA (or K–W) tests indicate whether we have an overall difference between the groups but not which specific groups, differed. In order to compare the HILs Galmet 20 SG and determine which groups have significant differences, we computed a post hoc test (Tukey's post hoc test or Wilcoxon rank sum test). Post hoc tests were only run when statistically significant differences between HILs and Galmet 20 SG-treatments were found (i.e., ANOVA resulted in an overall significant difference in group means). As a quantitative result of post hoc tests, we report the Honest Significant Difference (HSD) which represents the minimum difference between two group means that must exist before the difference is to be considered statistically significant. The results of the statistical tests are shown by marking the individual value of each treatment by an appropriate letter.

Syntheses. *General Synthesis (Method A) of **3**–**10** and **12**.* In a 50 mL round-bottom flask equipped with a Teflon-coated magnetic stirring bar, 0.01 mol of the corresponding halide of the desired cation was dissolved in 10 mL of anhydrous methanol followed by adding an equimolar amount of potassium hydroxide dissolved in 5 mL of anhydrous methanol. The mixture was then stirred for 1 h at room temperature. The inorganic potassium halide byproduct precipitated as a white solid and was carefully separated by vacuum filtration through a glass filter funnel. The filtrate (the free base of the desired cation) was carefully transferred to a 50 mL round-bottom flask equipped with a Teflon-coated magnetic stirring bar followed by addition of a stoichiometric amount of MS-M (2-[(4-methoxy-6-methyl-1,3,5-triazin-2-yl)amino]oxomethyl]sulfamoylbenzoic acid methyl ester), which was added all at once. The mixture was then stirred for another 1 h at room temperature, and the solvent was removed using a rotary evaporator followed by adding 20 mL of acetone to the residue. After filtration and evaporation of the solvent from the filtrate, the products were dried under reduced pressure at 50 °C for 48 h.

The synthesized salts were dried under vacuum (10 mbar) at 50 °C for 48 h and stored over P_4O_{10}. The water contents of the dried salts were measured by Karl Fischer titration and found to be less than 500 ppm. The obtained salts were stable in air and in contact with water and tested organic solvents. NMR spectra descriptions, purity assays, and elemental analyses for compounds **3**–**10** and **12** are provided in the Supporting Information.

*General Synthesis (Method B) of **4**, **7**, and **11**.* In a 50 mL round-bottom flask equipped with a Teflon-coated magnetic stirring bar, 0.01 mol of the corresponding chloride of the desired cation was dissolved in 10 mL of water followed by adding an equimolar amount of the potassium salt of MS-M (2-[(4-methoxy-6-methyl-1,3,5-triazin-2-yl)amino]oxomethyl]sulfamoylbenzoic acid methyl ester) dissolved in 10 mL of water. The mixture was then stirred for 24 h at room temperature, and the water was removed using a rotary evaporator. Then, 20 mL of anhydrous acetone was added to the residue. After filtration and evaporation of the solvent from the filtrate, the products

DOI: 10.1021/jf505782p
J. Agric. Food Chem. 2015, 63, 3357–3366

Scheme 1. Synthetic strategies to prepare MS-M-based salts: Method A (top)—acid base reaction with corresponding hydroxides (prepared from the appropriate halide salt if the hydroxide was not commercially available) and Method B (bottom)—metathesis.

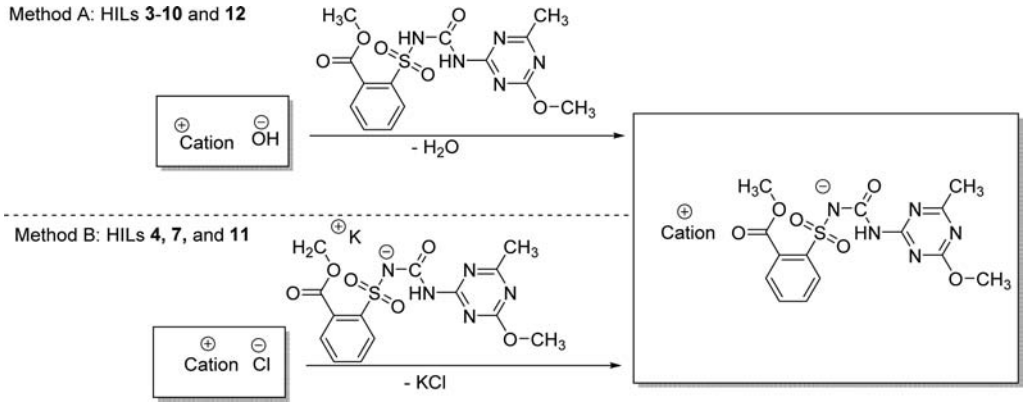

were dried under reduced pressure at 50 °C for 48 h. NMR spectra descriptions, purity assays, and elemental analyses for compounds **4**, **7**, and **11** are provided in the Supporting Information.

Greenhouse and Field Trials. Common lambsquarters (*C. album*) and oilseed rape (*B. napus*) plants were grown in 0.5 L plastic pots filled with peat-based potting material under controlled environmental conditions: a temperature of 20 ± 2 °C, relative humidity of 60%, and photoperiod of 16/8 h day/night. The plants were thinned to five per pot 10 days after emergence and watered as needed.

Plants were treated at the 6–8 leaf growth stage, and a complete randomized design was used with four replicates for each treatment. HIL herbicides were mixed with deionized water ca. 24 h before application, and the plants were treated with the aqueous solution only once, at a 4 g ae/ha (active equivalents applied per hectare) rate. The applications were conducted using a moving sprayer (APORO, Poznan, Poland) with a TeeJet VP 110/02 flat-fan nozzle (TeeJet Technologies, Wheaton, IL, USA) capable of delivering 200 L/ha of spray solution at 0.2 MPa operating pressure. The sprayer was moved above the plants at a 40 cm distance and at a constant speed of 3.1 m/s. A control group of plants was treated with standard Galmet 20 SG herbicide at the same application rate. Untreated plants were used for comparison and included in all experiments. Efficacy was evaluated using the fresh weight reduction method 2 weeks after treatment (2 WAT). Data were expressed as percent of fresh weight reduction compared with untreated plants.

Field trials were carried out in two consecutive years, 2012 and 2013, at winter wheat fields located near Szczecinek (northwestern part of Poland) and Szamotuly (western part of Poland). Herbicide treatments were applied to plants as aqueous solutions prepared *ca.* 24 h before application, and the plants were treated at an 8 g ae/ha rate. Treatments were applied using a knapsack sprayer (APORO, Poznan, Poland) equipped with TeeJet DG110/02 VS flat-fan nozzles (TeeJet Technologies, Wheaton, IL, USA) capable of delivering 200 L/ha of spray solution at 0.3 MPa operating pressure. Weed control was evaluated visually 4 weeks after herbicide applications (4 WAT) using a scale of 0 (no effect) to 100% (complete weed destruction).

RESULTS/DISCUSSION

Synthesis of MS-M-Based Ionic Liquids. Ten MS-M-based salts (Table 1) were prepared utilizing structurally variable quaternary ammonium cations (bis(2-hydroxyethyl)-methyloleylammonium, 2-hydroxyethyltrimethylammonium), pyridinium (1-dodecylpyridinium), pyrrolidinium and piperidinium cations (1-butyl-1-methylpyrrolidinium and 1-methyl-1-propylpiperidinium), imidazolium cations with saturated and unsaturated side chains (1-allyl-3-methylimidazolium and 1-butyl-3-methylimidazolium), a morpholinium cation (4-decyl-4-methylmorpholinium), and structurally different phosphonium cations (trihexyltetradecylphosphonium and tetrabutylphosphonium). All of the target MS-M HILs (except **11**) were synthesized by direct reaction between the cation hydroxide and MS-M free acid (Scheme 1, Method A); when the hydroxide form of the cation was not commercially available it was obtained by ion exchange of the cation halide with KOH. Two of the HILs prepared by method A (**4** and **7**) and **11** were additionally synthesized by a metathesis route, i.e., reaction of the cation chloride with the potassium salt of MS-M (Scheme 1, Method B), to verify the possibility of using this method.

The compounds were all obtained in high yields (>90%), and 9 of the 10 compounds (**3**–**12**) were liquids at room temperature, while 1 (**10**) was a low-melting crystalline solid with a melting point of 62–64 °C. (This compound had a tendency to supercool when melted.) The structures of all compounds were confirmed by ^{1}H and ^{13}C NMR spectroscopy. Elemental analysis helped to validate the identity and purity of the synthesized compounds and all compounds were obtained with high purities (>95%), see Table 1. The detailed synthesis of the compounds and their characterization data are provided in the Results/Discussion.

Thermal Properties. Glass transitions were observed below 16 °C for all of the prepared HILs with no observed crystallization or melting events (except for **10** as discussed below) as commonly seen for similar alkylammonium and phosphonium ILs. Analysis of structure vs glass transition relationships revealed a known trend where the longer the alkyl chain substituent on the nitrogen or phosphorus the lower the glass transition of the resulting salt. The lowest glass transition temperature (T_g = −45 °C) was observed for the HIL with the bis(2-hydroxyethyl)methyloleylammonium cation **3**, which has the long unsaturated *N*-oleyl alkyl chain (C_{18} alkyl). The second lowest glass transition was found for trihexyltetradecylphosphonium **11** (T_g = −32 °C), which contains a C_{14} alkyl group, while cation **5**, 1-dodecylpyridinium with a C_{12} alkyl group, was exhibited (T_g = −18 °C).

Glass transitions for all other compounds except **10**, which was a crystalline low-melting solid, were similar and varied between 1 and 7 °C. The 4-decyl-4-methylmorpholinium solid salt **10** had a melting point of 62–64 °C (determined using a melting point apparatus) and the highest glass transition (T_g = 16 °C) of all of the compounds prepared. This HIL also exhibited supercooling behavior, where a melting transition was observed on first heating but could not be reproduced within

DOI: 10.1021/jf505782p
J. Agric. Food Chem. 2015, 63, 3357–3366

Table 1. New MS-M-Based Herbicidal Ionic Liquids

Salt	Cation	Synthetic Method	T_g[a] (°C)	$T_{onset\ 5\%}$[b] (°C)	T_{onset}[c] (°C)	Yield %	Form at 25 °C
3	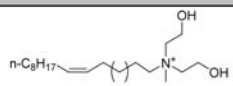 Bis(2-hydroxyethyl)methyloleylammonium	*A*	-45	180	300	90	Yellow liquid
4	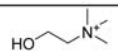 2-Hydroxyethyltrimethylammonium	*A and B*	4	150	135, 270[d], 400[e]	98	Colorless liquid
5	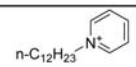 1-Dodecylpyridinium	*A*	-18	195	398	97	Colorless liquid
6	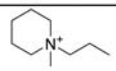 1-Methyl-1-propylpiperidinium	*A*	5	176	285	96	Colorless liquid
7	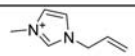 1-Allyl-3-methylimidazolium	*A and B*	1	190	304	91	Yellow liquid
8	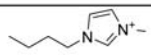 1-Butyl-3-methylimidazolium	*A*	7	182	313	99	Colorless liquid
9	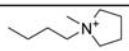 1-Butyl-1-methylpyrrolidinium	*A*	-1	167	283	90	Colorless liquid
10	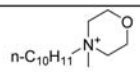 4-Decyl-4-methylmorpholinium	*A*	16, (T_m = 62-64)[f]	196	268	93	Crystalline solid
11	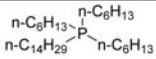 Trihexyltetradecylphosphonium	*B*	-32	194	393	98	Colorless liquid
12	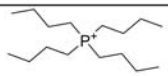 Tetrabutylphosphonium	*A*	-1	195	220, 410[d]	96	Yellow Liquid

[a]Glass transition temperature. [b]Onset to 5 wt % total mass loss decomposition. [c]Onset to 50 wt % mass loss first-stage decomposition. [d]Onset to 50 wt % mass loss of second-stage decomposition. [e]Onset to 50 wt % mass loss of third-stage decomposition. [f]Melting point determined using a melting point apparatus (see Materials and Methods); DSC analysis did not detect a melting point fot this compound due to glass formation.

the design of the DSC experiment over several heating/cooling cycles.

Most of the investigated salts exhibited simple thermal decomposition behavior with a single decomposition step. However, cholinium salt **4** exhibited a three-step decomposition, and the tetrabutylphosphonium salt (**12**) had a two-step decomposition.

Generally, the HILs decomposed between 150 and 200 °C, with cholinium MS-M (**4**) and other aliphatic alkyl ammonium MS-M HILs (**6** and **9**) being the least thermally stable. HILs with morpholinium (**10**) and phosphonium (**11**, **12**) cations exhibited the highest thermal stability. Moreover, it was noticed that all unsubstituted aromatic HILs exhibited higher stabilities of ca. 20 °C, compared to aliphatic salts, varying from 182 (for imidazoliums **7** and **8**) to 195 °C (for pyridinum **5**).

From these results it could be concluded that the phosphonium salts were more thermally stable than their ammonium equivalents and that the aromatic HILs tend to be more stable than those aliphatic, although the latter also have high thermal stability. In general, the thermal stability for each group of salts was more dependent on the structure of the cation core than on the presence of or chain length of the *N*-alkyl substituents.

Solubilities. The solubilities of the prepared HILs were tested in ten solvents, varying from low polarity to high polarity with both protic and aprotic solvents studied, Table 2. The solvents chosen for study were selected in order of decreasing polarity expressed as the Snyder polarity index: water, 9.0; methanol, 6.6; DMSO, 6.5; acetonitrile, 6.2; acetone, 5.1; isopropanol, 4.3; ethyl acetate, 4.3; chloroform, 4.1; toluene, 2.3; hexane, 0.0.

Ionic liquids are generally miscible with liquids with medium to high dielectric constants and immiscible with apolar compounds.[39] Thus, as expected, all tested compounds were

DOI: 10.1021/jf505782p
J. Agric. Food Chem. 2015, 63, 3357−3366

Table 2. Solubilities of the Prepared HILs in Ten Representative Solvents

salt	cation	water (9.0)[a]	methanol (6.6)	DMSO (6.5)	acetonitrile (6.2)	acetone (5.1)	isopropanol (4.3)	ethyl acetate (4.3)	chloroform (4.1)	toluene (2.3)	hexane (0.0)
3	bis(2-hydroxyethyl) methyloleylammonium	S[b]	S	S	S	S	S	S	S	S	N
4	2-hydroxyethyltrimethylammonium	S	S	S	S	L	N	N	S	N	N
5	1-dodecylpyridinium	L	S	S	S	S	S	S	S	L	N
6	1-methyl-1-propylpiperidinium	S	S	S	S	S	S	N	S	N	N
7	1-allyl-3-methylimidazolium	S	S	L	S	S	S	N	S	N	N
8	1-butyl-3-methylimidazolium	S	S	S	L	L	L	N	L	N	N
9	1-butyl-1-methylpyrrolidinium	S	S	S	S	S	S	N	S	N	N
10	4-decyl-4-methylmorpholinium	L	S	S	L	L	L	N	L	N	N
11	trihexyltetradecylphosphonium	N	S	S	S	S	S	S	S	S	N
12	tetrabutylphosphonium	S	S	S	S	S	S	S	S	N	N

[a]Snyder polarity index. [b]S: soluble. L: limited solubility. N: not soluble.

soluble in polar protic methanol and aprotic DMSO, though 1-allyl-3-methylimidazolium **7** had limited solubility in DMSO. Slightly less polar aprotic acetonitrile and acetone also dissolved all compounds albeit two, 1-butyl-3-methylimidazolium **8** and 4-decyl-4-methylmorpholinium **10**, demonstrated limited solubility in both acetonitrile and acetone, and HIL 2-hydroxyethyltrimethylammonium **4** was less soluble in acetone. Interestingly, only phosphonium HILs (**11**, **12**) and two of the ammonium HILs, bis(2-hydroxyethyl)methyloleylammonium **3** and 1-dodecylpyridinium **5**, were soluble in ethyl acetate. Isopropanol did not work as good as methanol, though it dissolved all HILs (some to the certain limits) except 2-hydroxyethyltrimethylammonium **4**. The chlorinated solvent, chloroform, even though of relatively low polarity, dissolved all HILs, although 1-butyl-3-methylimidazolium **8** and 4-decyl-4-methylmorpholinium **10** had limited solubilities. For nonpolar solvents, all tested compounds were insoluble in hexane and only bis(2-hydroxyethyl)methyloleylammonium **3** out of ammonium HILs and trihexyltetradecylphosphonium **11** were freely soluble in toluene. HILs with bis(2-hydroxyethyl)-methyloleylammonium **3** and the phosphonium cations, trihexyltetradecylphosphonium and tetrabutylphosphonium **11** and **12**, had solubility in almost all of the tested solvents.

Efficacy. Greenhouse tests were conducted using MS-M HILs **6**−**8** and **10**−**12**, and field trials were conducted with HILs **6**−**8** and **10** and **11**. Both types of trials were compared to the use of a commercial formulation of Galmet 20 SG and to control plants which were not treated.

Greenhouse Experiments. The HILs were studied for their herbicidal activity against dicotyledonous weeds (common lambsquarters and rapeseed) in a greenhouse. HILs **6**−**8** and **10**−**12** were selected for efficacy comparison against free MS-M as a commercial product Galmet 20 SG. The tests were conducted under controlled conditions of temperature 20 ± 2 °C, relative humidity 60%, and photoperiod 16/8 h day/night.

Common lambsquarters and rapeseed plants were separated into three groups: (1) those sprayed with the MS-M HILs (as aqueous solutions), (2) those sprayed with commercially available Galmet 20 SG (at the same application rate, 4 g ae/ha), and (3) those not sprayed (the control group). Two weeks after treatment (2 WAT), plants from four pots were selected from each group and their fresh weight was determined. The efficacy data is expressed as percent fresh weight reduction compared to untreated plants (see Methods and Materials for additional detail).

The HIL forms of MS-M applied to lambsquarters (*C. album*) showed a much higher activity that the Galmet 20 SG commercial herbicide, except for **6** whose activity was slightly lower than that of the reference herbicide. All HILs except **6** demonstrated at least twice the activity of commercial Galmet 20 SG, with **11** and **12** as much as 2.5 times more effective. On rapeseed, the herbicidal activities of HILs **6** and **7** were, respectively, 5% and 13% lower than that of Galmet 20 SG. HIL **11** demonstrated activity comparable to commercial analog, and HILs **8**, **10**, and **12** were substantially more effective (ca. 1.5 times greater activity).

Statistically, the HIL forms of MS-M applied to lambsquarters (*C. album*) showed significant differences in the mean effects of action for the tested substances in ANOVA. For HILs

Figure 2. Greenhouse efficacy of HILs **6**−**8** and **10**−**12** compared to Galmet 20 SG on lambsquarters.

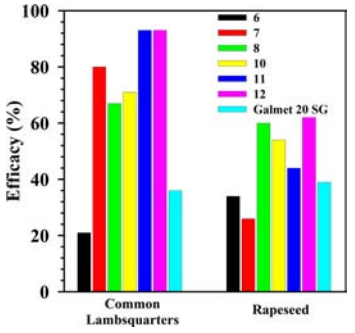

Figure 3. Greenhouse efficacy (measured as fresh weight reduction 2 weeks after treatment) of MS-M HILs **6** (black), **7** (red), **8** (green), **10** (yellow), **11** (blue), and **12** (fuschia) compared to Galmet 20 SG (aqua) on common lambsquarters and rapeseed at an application rate of 4 g ae/ha.

DOI: 10.1021/jf505782p
J. Agric. Food Chem. 2015, 63, 3357−3366

used on *C. album*, values of $F = 51.87$ and p-value = 0.000 were obtained, indicating a high significant difference between the treatment with HILs and commercial Galmet 20 SG, while for HILs used on *B. napus*, $F = 11.91$ and p-value = 0.000 (Table 3) the difference between the treatment with HILs and commercial Galmet 20 SG was significant but not that large. To determine which HILs among all the experiments had significant differences, post hoc comparisons using the Tukey HSD test ($\alpha = 0.05$) were conducted and indicated that the mean score for both *C. album* and *B. napus* treated with Galmet 20 SG was significantly lower than those plants treated with some of the HILs. The details are provided as follows.

On *C. album*, the mean value of Galmet 20 SG (36 ± 23) was significantly lower than the mean effects for all HILs except **6**. Specifically, the mean values of plants treated with HIL **11** (93 ± 23) and HIL **12** (94 ± 23) were the highest and significantly higher than the mean effects of action of HIL **8** (67 ± 23) and HIL **10** (71 ± 23).

On *B. napus*, Galmet 20 SG-treated plants gave a significantly lower mean effect (39 ± 9) than HIL **8** and HIL **12**. HIL **12** in this trial gave the highest mean effect on weed destruction (67 ± 9), which was significantly different than the mean effects of action of HILs **6**, 7, and **11**.

Table 3. Weed Control (%, 4 WAT) in *C. album* and *B. napus* Greenhouse Tests

	C. album[b]	*B. napus*
General analysis: degrees of freedom (df), F value, and significance value (p)		
analysis	ANOVA	ANOVA
df	6; 21	6; 14
F	51.87	11.91
p-value	0.000	0.000
Mean values for treatments results of post hoc tests ($\alpha = 0.05$)		
# of replications	4	3
general mean	65.9	46.3
6	21 c[d]	34 d
7	80 ab	26 d
8	67 b	60 ab
10	71 b	54 abc
11	93 a	44 bcd
12	94 a	67 a
standard[a]	36 c	39 cd
HSD for treatments with observed statistical differences		
±B[c]	23	9
HSD	231[b]	20

[a]Galmet 20 SG (% active metsulfuron-methyl − 20%) was used as the reference herbicide. [b]Analysis after Box-Cox transformation of data ($\lambda = 1.64$). [c]Treatment mean ± B gives lower and upper 95% confidence bounds (CI). [d]The same letter in the column means no statistical differences between treatments.

Field Trials. After greenhouse testing, HILs **6**−**8** and **10** and **11** were studied for their herbicidal activity in the field. The trials (a 2-year field investigation) were conducted in 2012 and 2013 in the winter wheat fields near Szczecinek (northwestern part of Poland) and Szamotuly (western part of Poland). The tests were conducted on a variety of weeds, particularly on mayweed (*M. inodora*), field pansy (*V. arvensis*), wild buckwheat (*P. convolvulus*), hemp nettle (*G. tetrahit*), shepherd's purse (*C. bursa pastoris*), field poppy (*P. rhoeas*), chickweed (*S. media*), field forget-me-not (*M. arvensis*), and persian speedwell (*V. persica*).

The herbicides were applied at a rate of 8 g ae/ha at the beginning of stem elongation, the end of tillering stage, or the BBCH (Biologische Bundesanstalt, Bundessortenamt and Chemische Industrie) 30 stage on the plant phenological development stage scale for cereals. All herbicidal treatments were conducted with an application rate of 8 g ae/ha. Weed control was evaluated visually 4 weeks after herbicide applications (4 WAT) using a scale of 0 (no effect) to 100% (complete weed destruction). The results are presented in Table 4.

Overall, the results were slightly different from the greenhouse data. In the field, the HILs tested and Galmet 20 SG were all 100% effective against *M. inodora*, *V. arvensis*, *P. convolvulus*, *G. tetrahit*, and *S. media*. The HILs were more effective that Galmet 20 SG for *C. bursa pastoris*, *P. rhoeas*, *V. persica*, and *M. arvensis*, demonstrating they can be used for weed control in winter wheat fields.

The efficacy of the HILs in greenhouse and field trials depended on species. On rapeseed the herbicidal activities of the HILs were only slightly higher than that of the commercial herbicide, while on lambsquarters (*C. album*) all but one of the HILs exhibited at least twice the activity of commercial Galmet 20 SG. In three field studies over 2 years (winter wheat fields), the herbicidal activity of the HILs again varied depending on the plant species but all tested HILs were at least as effective and in some cases more effective than the reference herbicide.

Statistically, for all field trials, the analyzed HILs **6**−**8**, **10**, and **11** demonstrated high efficiency (some as high as 100%) in plant reduction (Table 4). ANOVA test indicated significant differences in the mean effects of the action of the HILs used on *M. inodora*-2012[b] ($F = 4.364$; p-value = 0.0089), *V. arvensis*-2012[b] ($F = 4.687$; p-value = 0.0065), *P. rhoeas*-2013[c] ($F = 8.907$; p-value = 0.0002), and *V. persica*-2013[c] ($F = 13.15$; p-value = 0.0000), Table 4.

To determine which HILs in all of the experiments had significant differences, post hoc comparisons using the Tukey HSD test ($\alpha = 0.05$) were conducted similarly to those noted above for the greenhouse trials. The post hoc comparisons ($\alpha = 0.05$) indicated that the mean scores for *V. arvensis* treated with HIL **6** (90 ± 4) and HIL **11** (93 ± 4) were significantly different from the identical plants treated with Galmet 20 SG (81 ± 4, Table 4). The mean score for *P. rhoeas*-2013[c] treated with Galmet 20 SG (64 ± 5) was significantly lower than all HILs except HIL **11**; the identical situation occurred in the *V. persica*-2013[c] field trial. Although the mean values of the weed destruction for *M. inodora*-2012[b] treated with HILs **6**, **8**, and **11** were higher than in the case of Galmet 20 SG (90 ± 3), the differences were not statistically significant. For *M. inodora*-2012[b], the highest mean effect of action was observed for HIL **11** (95 ± 3), which was significantly different from the mean effects for HILs 7 and **10**.

P. rhoeas-2013[c] treated with HIL 7 (66 ± 5) and HIL **10** (68 ± 5) had mean scores significantly lower than the identical plant treated with HIL **6** (85 ± 5). The mean effect of action for HIL **10** (78 ± 5) used on *V. persica*-2013[c] was significantly higher than in the case of HILs 7 and **11**. While the Kruskal−Wallis tests used to analyze the other field experiments did not indicate significant differences between treatments, it is worth noting that in all cases HILs were 100% or almost 100% effective. Taken together, these results suggest that for some plants the efficacies of some of the HILs were significantly higher than Galmet 20 SG.

DOI: 10.1021/jf505782p
J. Agric. Food Chem. 2015, 63, 3357−3366

Table 4. Weed Control (%, 4 WAT) in Winter Wheat from 2012 to 2013 Szczecinek and 2013 Szamotuly Field Trials

	M. inodora			*V. arvensis*			*P. convolvulus*	*G. tetrahit*	*C. bursa pastoris*	*P. rhoeas*	*V. persica*	*S. media*		*M. arvensis*	
treatment	2012[b]	2013[c]	2013[b]	2012[b]	2013[c]	2013[b]	2012[b]	2012[b]	2012[b]	2013[c]	2013[c]	2013[c]	2013[b]	2013[c]	2013[b]
General analysis: degrees of freedom (df), *F* value, and significance value (*p*)															
analysis	AN[d]	K–W[e]	K–W	AN	*f*	K–W	K–W	*f*	K–W	AN	AN	K–W	*f*	K–W	K–W
df	5; 18	5	5	5; 18		5	5		5	5; 18	5; 18	5		5	5
F/χ^2	4.364	7.667	1.305	4.687		9.570	3.790		2.302	8.907	13.150	5.000		5.000	19.087
p-value	0.0089	0.1756	0.9344	0.0065		0.8838	0.5800		0.8060	0.0002	0.0000	0.4159		0.4159	0.0019
Mean values for treatments/results of post hoc tests (α = 0.05)															
general mean	90.8	99.5	97.0	87.4	100.0	96.8	96.8	100.0	94.7	72.0	68.1	99.8	100.0	99.7	93.3
6	92 ab[h]	100 a	98 a	90 a	100	90 a	95 a	100	94 a	85 a	71 abc	99 a	100	100 a	87 a
7	88 b	100 a	96 a	85 ab	100	98 a	97 a	100	95 a	66 bc	66 bc	100 a	100	98 a	100 a
8	91 ab	100 a	97 a	88 ab	100	98 a	97 a	100	96 a	76 ab	76 ab	100 a	100	100 a	92 a
10	89 b	99 a	98 a	89 ab	100	98 a	97 a	100	96 a	68 bc	78 a	100 a	100	100 a	96 a
11	95 a	100 a	97 a	93 a	100	98 a	97 a	100	96 a	74 abc	63 cd	100 a	100	100 a	100 a
standard[a]	90 ab	98 a	96 a	81 b	100	99 a	98 a	100	91 a	64 c	55 d	100 a	100	100 a	85a
HSD for treatments with observed statistical differences															
±B[g]	3			4						5	5				
HSD	6			9						12	11				

[a]Galmet 20 SG ($\%_{active}$ metsulfuron-methyl -20%). [b]Szczecinek. [c]Szamotuły. [d]One-way ANOVA was applied. [e]Non-parametric Kruskal–Wallis (K–W) rank sum test was applied. [f]The measured effectiveness of 100%; ANOVA or non-parametric Kruskal–Wallis tests not applicable. [g]Treatment mean ± B gives lower and upper 95% confidence bounds (CI). [h]The same letter in the column means no statistical differences between treatments.

J. Agric. Food Chem. 2015, 63, 3357−3366
DOI: 10.1021/jf505782p

■ ASSOCIATED CONTENT

Supporting Information

^{1}H, ^{13}C, and ^{31}P spectra, purity assays, and elemental analyses of all compounds. This material is available free of charge via the Internet at http://pubs.acs.org.

■ AUTHOR INFORMATION

Corresponding Authors

*Robin D. Rogers, Tel.: 1-514-3982851. E-mail: Robin.Rogers@mcgill.ca.

*Juliusz Pernak, Tel.: 00148-61-6653682. E-mail: juliusz.pernak@put.poznan.pl.

Funding

Studies were supported by Grant PBS2/A1/9/2013, The National Centre for Research and Development, Warszawa, Poland.

Notes

The authors declare the following competing financial interest(s). Robin D. Rogers has partial ownership of 525 Solutions. J. Pernak, J. Shamshina, T. Praczyk, G. Gurau, and R. D. Rogers are named inventors on related patent applications. Julia Shamshina and Gabriela Gurau are employees of 525 Solutions. The University of Alabama maintains approved Conflict Of Interest Management Plans.

■ ABBREVIATIONS

AHAS, enzyme acetohydroxyacid synthase; MS-M, herbicide "metsulfuron-methyl"; pK_a, acid dissociation constant; pH, acidity of solution; 2,4-D, 2,4-dichlorophenoxyacetic acid; MCPA, 2-methyl-4-chlorophenoxyacetic acid; IL, ionic liquids; HILs, herbicidal ionic liquids; TGA, thermal gravimetric analysis; DSC, differential scanning calorimetry; NMR, nuclear magnetic resonance spectroscopy; EN ISO, International Standard, in English; % purity, cationic content (% of available); MW, molecular weight; ae, active equivalents; WAT, weeks after treatment; BBCH, Biologische Bundesanstalt, Bundessortenamt and Chemische Industrie; T_g, glass transition temperature; $T_{5\%onset}$, onset to 5 wt % total mass loss decomposition; $T_{50\%onset}$, onset to 50 wt % total mass loss decomposition; T_m, melting point; S, compound is soluble; L, compound has limited solubility; N, compound is not soluble

■ REFERENCES

(1) Levitt, G. Agricultural Sulfonamides. U.S. Patent 4,383,113, Nov 30, 1979.

(2) Count on DuPont. http://www.dupont.com/products-and-services/crop-protection/cereals-protection/articles/count-on-dupont.html, last accessed Oct 1, 2014.

(3) For a review, see: Obrigawitch, T. T.; Cook, G.; Wetherington, J. Assessment of Effects on Non-target Plants from Sulfonylurea Herbicides Using Field Approaches. *Pestic. Sci.* **1998**, *52*, 199−217.

(4) McCourt, J. A.; Pang, S. S.; Guddat, L. W.; Duggleby, R. G. Elucidating the specificity of binding of sulfonylurea herbicides to acetohydroxyacid synthase. *Biochemistry* **2005**, *44*, 2330−2338.

(5) Blair, A. M.; Martin, T. D. A review of the activity, fate and mode of action of sulfonylurea herbicides. *Pestic. Sci.* **1988**, *22*, 195−219.

(6) Brown, H. M. Mode of action, crop selectivity and soil relations of the sulfonylurea herbicides. *Pestic. Sci.* **1990**, *29*, 263−281.

(7) Berger, B. M.; Wolfe, N. L. Hydrolysis and biodegradation of sulfonylurea herbicides in aqueous buffers and anaerobic water-sediment systems: assessing fate pathways using molecular descriptors. *Environ. Toxicol. Chem.* **1996**, *15*, 1500−1507.

(8) Wauchope, R. D.; Butler, T. M.; Hornsby, A. G.; Augustijn-Beckers, P. W. M.; Burt, J. P. The SCS/ARS/CES Pesticide Properties Database for Environmental Decision-Making. In *Reviews of Environmental Contamination and Toxicology*; Springer-Verlag Publishers: New York, 1992.

(9) Song, N.; Wang, D.; Shan, Z.; Shi, L. Influence of pH and Dissolved Organic Matter on Photolysis of Metsulfuron-Methyl. *Proc. Environ. Sci.* **2013**, *18*, 585−591.

(10) Sarmah, A. K.; Sabadie, J. Hydrolysis of Sulfonylurea Herbicides in Soils and Aqueous Solutions: a Review. *J. Agric. Food Chem.* **2002**, *50*, 6253−6265.

(11) Sarmah, A. K.; Kookana, R. S.; Duffy, M. J.; Alston, A. M.; Harch, B. D. Hydrolysis of triasulfuron, metsulfuron-methyl and chlorsulfuron in alkaline soil and aqueous solutions. *Pest. Manag. Sci.* **2000**, *56*, 463−471.

(12) Wang, H.; Xu, J.; Yates, S. R.; Zhang, J.; Gan, J.; Ma, J.; Wu, J.; Xuan, R. *Chemosphere* **2010**, *78*, 335−341.

(13) Chen, C. C.; Tocker, S. Process for preparing sulfonylurea salts. Patent WO1989001477, Aug 17, 1988.

(14) Sandell, L. S. Process for preparation of sulfonylurea solution formulations. U.S. Patent 4,599,412, Mar 21, 1985.

(15) Moore, E. P. Herbicidal complexes with ureas. U.S. Patent 4,659,823, Nov 12, 1985.

(16) Föry, W. Sulfonylurea salts as herbicides. Patent WO 1997041112, Apr 14, 1997.

(17) Ort, O.; Bauer, K.; Bieringer, H. Sulfonylureas and their use as herbicides and growth regulators. U.S. Patent 5,688,745, Jun 6, 1995.

(18) Process for preparing sulfonylurea salts. Patent EP 0304282, Aug 17, 1988.

(19) Schnabel, G.; Willms, L.; Bauer, K.; Bieringer, H. Nitrogen-substituted phenylsulfonylureas; processes for their preparation, and their use as herbicides and plant growth regulators. U.S. Patent 5,696,053, May 30, 1995.

(20) Wysong, R. D.; Chen, C. C.; Tseng, C. A.; Tirol, A. A. Quaternary ammonium salts of a sulfonylurea. U.S. Patent 6,225,260 B1, May 20, 1999.

(21) Reap, J. J. Liquid sulfonylurea herbicide formulations. Patent EP 2114143 A1, Aug 31, 2006.

(22) In *Ionic Liquids: Industrial Applications for Green Chemistry*; Rogers, R. D., Seddon, K. R., Eds.; ACS Symposium Series 818; American Chemical Society: Washington, DC, 2002.

(23) Pernak, J.; Syguda, A.; Materna, K.; Janus, E.; Kardasz, P.; Praczyk, T. 2,4-D based herbicidal ionic liquids. *Tetrahedron* **2012**, *68*, 4267−4273.

(24) Praczyk, T.; Kardasz, P.; Jakubiak, E.; Syguda, A.; Materna, K.; Pernak, J. Herbicidal Ionic Liquids with 2,4-D. *Weed Sci.* **2012**, *60*, 189−192.

(25) Pernak, J.; Syguda, A.; Janiszewska, D.; Materna, K.; Praczyk, T. Ionic liquids with herbicidal anions. *Tetrahedron* **2011**, *67*, 4838−4844.

(26) Pernak, J.; Shamshina, J.; Tadeusz, P.; Syguda, A.; Janiszewska, D.; Smiglak, M.; Gurau, G.; Daly, D. T.; Rogers, R. D. PCT Int. Appl. WO006313A2, 2012.

(27) Cojocaru, O. A.; Shamshina, J. L.; Gurau, G.; Syguda, A.; Praczyk, T.; Pernak, J.; Rogers, R. D. Ionic liquid forms of the herbicide dicamba with increased efficacy and reduced volatility. *Green Chem.* **2013**, *15*, 2110−2120.

(28) Pernak, J.; Niemczak, M.; Giszter, R.; Shamshina, J.; Gurau, G.; Cojocaru, O. A.; Praczyk, T.; Marcinkowska, K.; Rogers, R. D. Glyphosate-Based Herbicidal Ionic Liquids with Increased Efficacy. *ACS Sustainable Chem. Eng.* **2014**, *2*, 2845−2851.

(29) Kordala-Markiewicz, R.; Rodak, H.; Markiewicz, B.; Walkiewicz, F.; Sznajdrowska, A.; Materna, K.; Marcinkowska, K.; Praczyk, T.; Pernak, J. Phenoxy herbicidal ammonium ionic liquids. *Tetrahedron* **2014**, *32*, 4784−4789.

(30) Pernak, J.; Niemczak, M.; Zakrocka, K.; Praczyk, T. Herbicidal ionic liquid with dual-function. *Tetrahedron* **2013**, *69*, 8132−8136.

(31) Brycki, B.; Dega-Szafran, Z.; Mirska, I. Synthesis and antimicrobial activities of some quaternary morpholinium chlorides. *Pol. J. Microbiol.* **2010**, *59*, 49−53.

DOI: 10.1021/jf505782p
J. Agric. Food Chem. 2015, 63, 3357−3366

(32) Singer, E. J. Biological evaluation. In *Cationic Surfactants: Analytical and Biological Evaluation*; Cross, J., Singer, E. J., Eds.; Marcel Dekker: New York, 1994.
(33) Pernak, J.; Smiglak, M.; Griffin, S. T.; Hough, W. L.; Wilson, T. B.; Pernak, A.; Zabielska-Matejuk, J.; Rogers, R. D. Long alkyl chain quaternary ammonium-based ionic liquids and potential application. *Green Chem.* **2006**, *8*, 798−806.
(34) Docherty, K. M.; Kulpa, C. F., Jr. Toxicity and antimicrobial activity of imidazolium and pyridinium ionic liquids. *Green Chem.* **2005**, *7*, 185−189.
(35) Pernak, J.; Branicka, M. The Properties of 1-Alkoxymethyl-3-hydroxypyridinium and 1-Alkoxymethyl-3-dimethylaminopyridinium chlorides. *J. Surfactants Deterg.* **2003**, *6*, 119−123.
(36) International Standards Organization. *International Standard ISO 2871-1: Surface active agents−Detergents−Determination of cationic-active matter content−Part 1: High-molecular-mass cationic-active matter*, 2nd ed.; ISO: Geneva, Switzerland, 2010; Reference Number ISO 2871-1:2010(E).
(37) In *Vogel's Textbook of Practical Organic Chemistry*, 4th ed.; Vogel, A. I., Furniss, B. S., Eds.; Wiley, John & Sons, Inc.: New York, 1984.
(38) http://www.r-project.org/, last accessed Feb 23, 2015.
(39) Freemantle, M. *An Introduction to Ionic Liquids*, 1st ed.; RSC Publishing: Cambridge, UK, 2010.

DOI: 10.1021/jf505782p
J. Agric. Food Chem. 2015, 63, 3357−3366

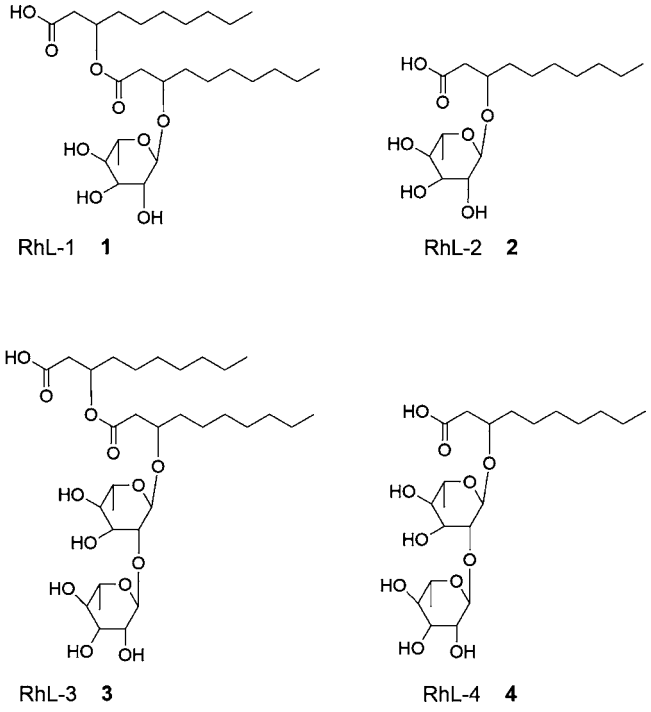

Figure 1. Representative molecular structures of four main groups of rhamnolipids, RhL-1−RhL-4.

the economic production of anti-zoospore chemicals and potentially valuable co-products from rhamnolipids.

MATERIALS AND METHODS

Materials. Ethanol, ethyl acetate, citric acid, sodium citrate, acetic acid, sodium bicarbonate, sodium hydroxide, sulfuric acid, sodium methoxide methanol solution (25%, w/w), cellulase (EC 3.2.1.4) from *Trichoderma reesei* [American Type Culture Collection (ATCC) 26921], and cellobiase from *Aspergillus niger* were purchased from Sigma-Aldrich (St. Louis, MO). Milli-Q water (Millipore, Billerica, MA) was used. V8 high-fiber 100% vegetable juice from Campbell Soup Company (Camden, NJ) was purchased from a local store. All other reagents were of analytical grade.

HPLC−MS Analysis. HPLC analysis was performed with the Hewlett-Packard LC1100 series equipment (Agilent Technologies, Santa Clara, CA). The column used was a 250 × 4.6 mm inner diameter, 5 μm, Supelcosil LC-18 (Supelco, Bellefonte, PA). The column temperature was controlled at 24 °C. Several mobile-phase solvents were used in this study for different sample groups. For clarity, they are described with the specific samples in later sections. The mobile phase flow rate used was always the same at 0.4 mL/min. All chromatographic peaks were confirmed to appear during the retention time period of 5−45 min. MS analysis was made with a Bruker Esquire-LC system. Compounds were ionized by electrospray ionization (ESI). The detection was made in the "smart mode" with the following conditions: gas flow pressure, 40 psi; gas flow rate, 8 mL/min; drying gas temperature, 365 °C; target m/z, 750; trap drive, 60%; compound stability, 75%; and under the wide-mode optimization.

Production and Purification of Rhamnolipids. Rhamnolipids were produced by *P. aeruginosa* fermentation. Inoculum was grown for 8 h in a 30 g/L tryptic soy broth (TSB) medium in a shaker operating at 34 °C and 250 rpm. A total of 10 mL inoculum was added to 90 mL of TSB solution and similarly grown for 18 h to prepare the preculture. The entire (100 mL) preculture was added to a 3 L fermentor (BIOFLO 110, New Brunswick Scientific, Edison, NJ) with 1 L of medium and agitated at 600 rpm with two six-blade turbines. The pH was maintained at 6.2 ± 0.1 by automatic addition of 1 N H_2SO_4 or NaOH. The dissolved oxygen concentration was kept at 10% (±3%) by controlled bubbling of pure oxygen; the temperature was controlled at 32.0 ± 0.1 °C. The fermentation medium contained 100 g/L glycerol, 6 g/L KH_2PO_4, 5.73 g/L NH_4Cl, 5 g/L yeast extract, 5 g/L peptone, 1.5 g/L NaCl, 0.9 g/L $MgSO_4{\cdot}7H_2O$, 0.1 g/L $FeSO_4{\cdot}7H_2O$, 0.03 g/L $CaCl_2{\cdot}2H_2O$, 0.03 g/L $MnCl_2{\cdot}4H_2O$, and 2 mL/L of a trace element solution. The trace element solution had 0.75 g/L $MnSO_4{\cdot}H_2O$, 0.75 g/L $ZnSO_4{\cdot}7H_2O$, 0.15 g/L H_3BO_3, 0.08 g/L $FeCl_3{\cdot}6H_2O$, 0.08 g/L $CoCl_2{\cdot}6H_2O$, 0.075 g/L $CuSO_4{\cdot}5H_2O$, and 0.05 g/L Na_2MoO_4.

The rhamnolipids produced in the fermentation broth were mainly RhL-1 and RhL-3. A glass chromatography column (600 × 50 mm inner diameter) was used for separation of RhL-1 and RhL-3. The height of silica gel in the column was about 500 mm. The mobile phase was a chloroform/methanol/water (100:23:3, v/v/v) mixture. The column was flushed with about 1.4 L mobile phase. The eluate was collected in 40 consecutive fractions of 25 mL. The 40 fractions were air-dried separately. RhL-1 was in the fractions 3−15, and RhL-3 was in the fractions 17−35, which was confirmed with HPLC−MS analysis.

Generation of Free Diacids from Rhamnolipids. Free diacids were generated in two steps: ethyl diacids were first formed and then hydrolyzed to free diacids, according to the route shown in Figure 2.

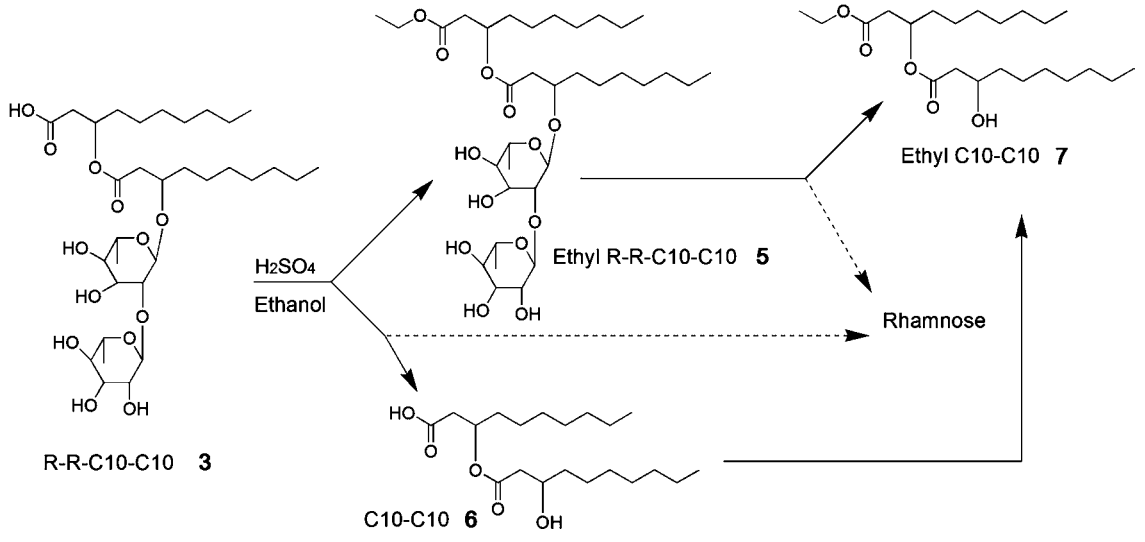

Figure 2. Reaction scheme for generating ethyl diacids from RhL-3, illustrated with R−R−C_{10}−C_{10} as the structural example.

DOI: 10.1021/acs.jafc.5b00033
J. Agric. Food Chem. 2015, 63, 3367−3376

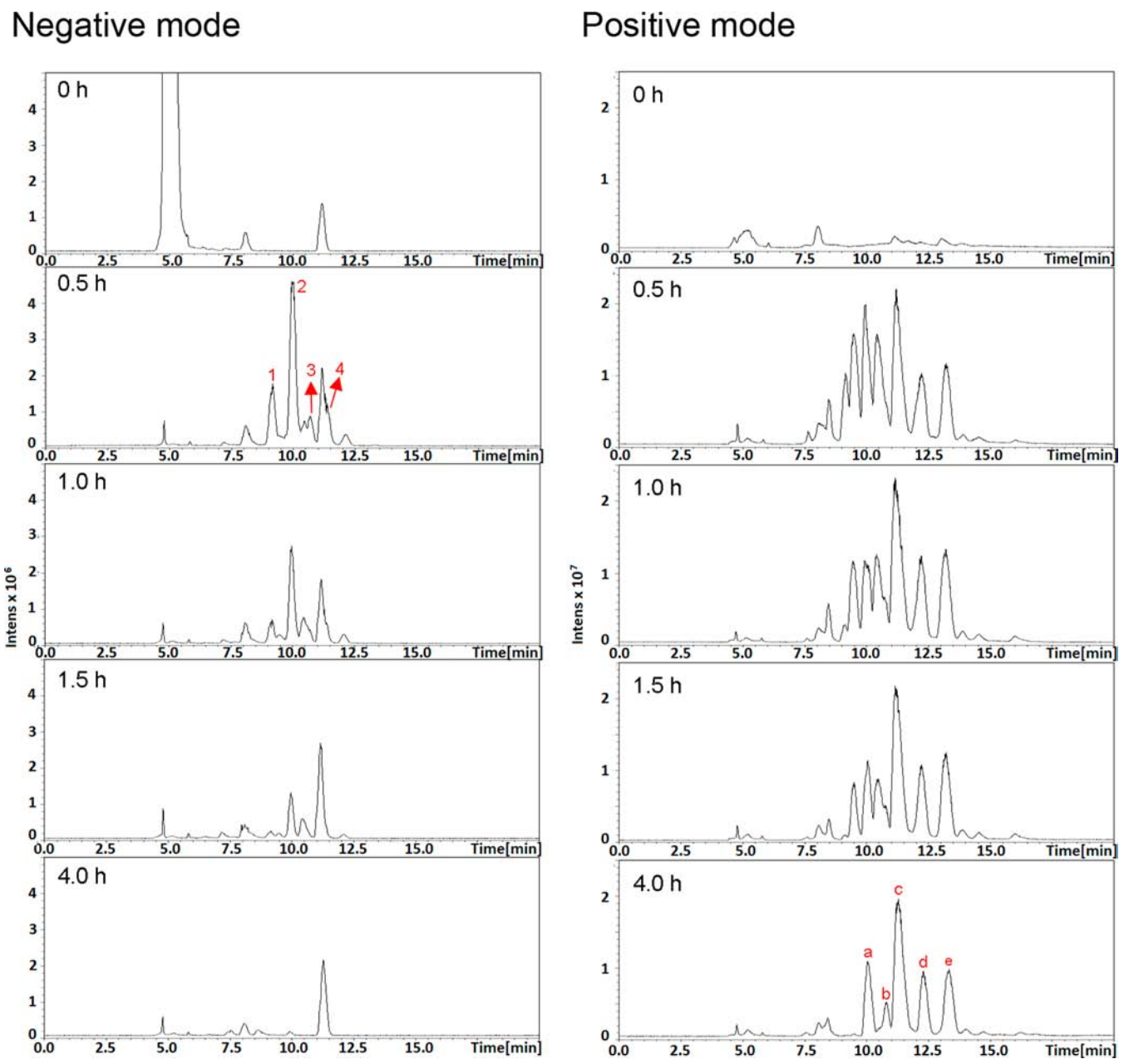

Figure 3. Total ion chromatograms from HPLC−MS analysis of samples during the generation of ethyl diacids from RhL-3.

For the production of ethyl diacids, 100 mg of RhL-3 and 5 mL of ethanol were charged into a 20 mL glass vial. Then, 0.2 mL of sulfuric acid was added dropwise. The mixture was reacted for 4 h in a 70 °C shaking water bath operating at 150 rpm. The reaction progress was followed by taking samples (typically 50 μL) at 0.5, 1.0, 1.5, 2.0, and 4.0 h. The sulfuric acid in these samples was neutralized by the addition of 100 μL of saturated aqueous solution of sodium bicarbonate. The neutralized samples were dried and extracted with ethyl acetate. The ethyl acetate phase was collected and dried, and the residue was redissolved in 95% methanol in water and then subjected to HPLC−MS analysis, which was performed with an isocratic flow (0.4 mL/min) of the following mobile phase: methanol/4 mM aqueous ammonium acetate (95:5).

Free diacids were then obtained in the second reaction step, by hydrolysis of the ethyl diacids with an aqueous sodium hydroxide solution. Typically, 2.5 mL of ethyl diacid solution (10 mg/mL in ethanol) was mixed with 1.5 mL of water. Then, 1 mL of sodium hydroxide stock solution (10 mg/mL in water) was added. The reaction mixture was shaken at 150 rpm and 25 °C for 2 h. The mixture was then neutralized with acetic acid, dried, and extracted with ethyl acetate to remove the remaining salt. The synthesized free diacids in the ethyl acetate extract were characterized by MS analysis with the following conditions: positive mode; gas flow pressure, 10 psi; gas flow rate, 8 mL/min; drying gas temperature, 310 °C; target m/z, 381; trap drive, 100%; compound stability, 100%; and under the normal-mode optimization.

Conversion of RhL-1 and RhL-3 to RhL-2 and RhL-4. A total of 100 mg of RhL-3 (or RhL-1) and 5 mL of aqueous NaOH solution (40 g/L) were reacted in a 20 mL glass vial for 4 h at 25 °C in a shaker operating at 150 rpm. Samples (50 μL each) were taken at 0.5, 1.0, 1.5, 2.0, and 4.0 h and neutralized with 50 μL of anhydrous acetic acid. The samples were dried and then dissolved with 40% methanol in water for HPLC−MS analysis. The mobile phase used for these samples was a gradient of (A) methanol and (B) 4 mM aqueous ammonium acetate according to the following: a 5 min isocratic hold at 40% A, a 20 min gradient to increase A from 40 to 95%, a 10 min isocratic hold at 95% A, a 15 min gradient to decrease A from 95 to 40%, and a 5 min isocratic hold at 40% A. The total run time was 55 min for each

DOI: 10.1021/acs.jafc.5b00033
J. Agric. Food Chem. 2015, 63, 3367−3376

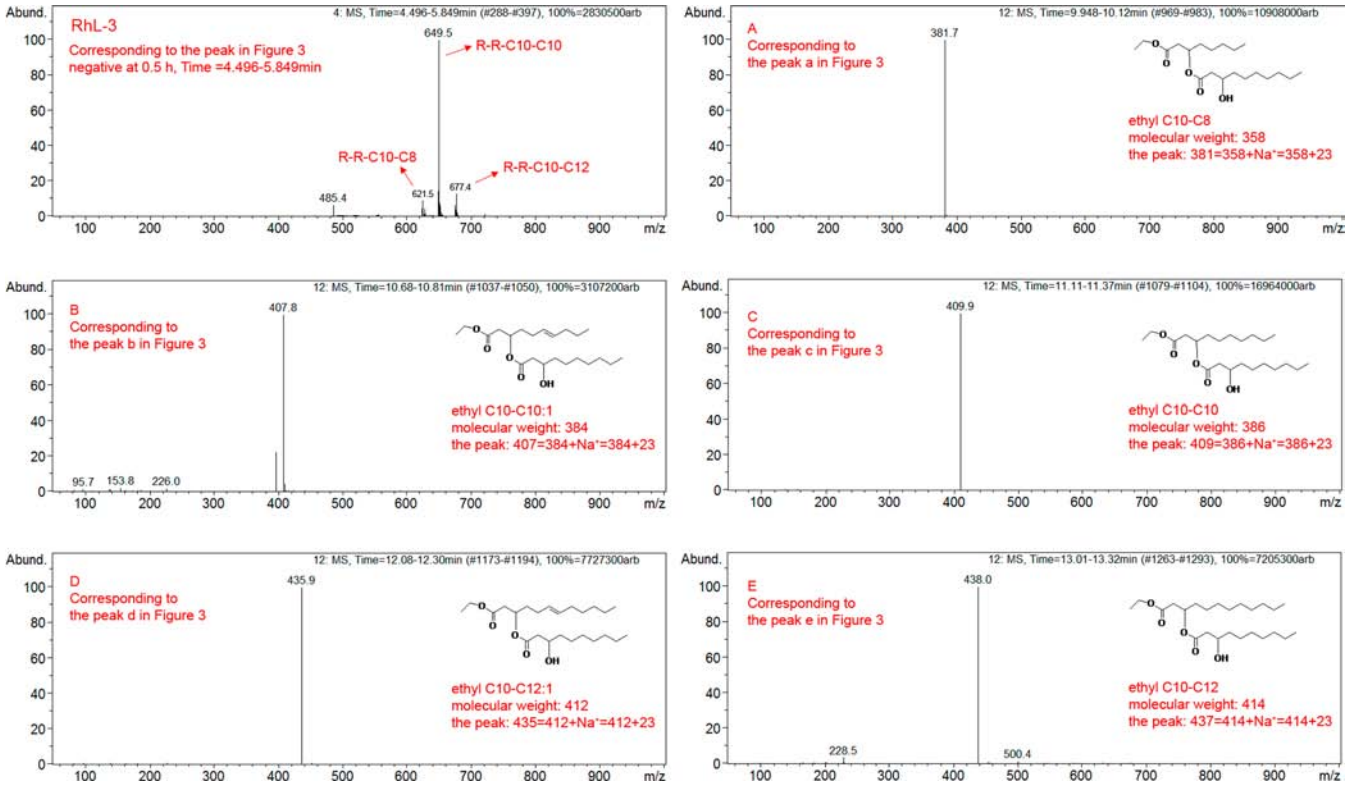

Figure 4. MS spectra for some isolated peaks shown in Figure 3, confirming the structures of the RhL-3 reactants and the five ethyl diacid products.

sample. MS analysis was in the negative mode, while other operating parameters were as described previously.

Enzymatic Conversion of RhL-3 to RhL-1. Into a 20 mL glass vial, 5 mL of RhL-3 solution (0.5 mg/mL in water) and 5 mL of enzyme solution (cellulase or cellobiase in 0.05 M citrate buffer at pH 4.8) were added. For cellulase, the concentration was 1 mg/mL (8.9 units/mL), assayed with cellulose as the substrate at pH 5.0 and 37 °C for 2 h of incubation time; 1.0 unit liberates 1.0 μmol/min glucose from cellulose. For cellobiase, the enzyme solution was prepared by adding 50 μL of cellobiase to 5 mL of citrate buffer. The reaction mixture was shaken at 150 rpm and 37 °C for 24 h. Samples (1 mL) were taken at 6 and 24 h. The samples were dried and redissolved in acetonitrile/water (40:60) for HPLC−MS analysis. The mobile phase used for these samples was a gradient of (A) acetonitrile and (B) 4 mM aqueous ammonium acetate according to the following: a 3 min isocratic hold at 40% A, a 17 min gradient to increase A from 40 to 95%, and a 10 min isocratic hold at 95% A. MS analysis was conducted in the negative mode as described previously.

Anti-zoospore Test. *P. sojae* was cultured on V8 juice agar. Zoospores were obtained by washing a 7-day-old plate culture with tap water, once every 30 min for a total of 6 h. Multiple 2 mL plastic tubes were used for the anti-zoospore test. Each tube was filled with 100 μL of rhamnolipid solution that had a concentration varying among 20, 40, 60, 80, 100, 120, 160, and 250 mg/L. A total of 50 μL of water and 50 μL of zoospore suspension were added to the tubes. The zoospore suspension had about 1×10^5 zoospores/mL as measured by counting with a hemocytometer under a light microscope coupled with a DP71 digital camera (Olympus America, Inc., Center Valley, PA). Immediately after the addition of zoospores, the tube was gently swirled for mixing for 5 s, followed by extraction of one drop of the mixture and placement on a glass slide for observation of zoospore motility under the microscope. The critical anti-zoospore concentration was defined in this study as the lowest rhamnolipid concentration at which the motility of all observed zoospores was stopped.

RESULTS AND DISCUSSION

Generation of Free Diacids from Rhamnolipids. There are several hypotheses as to why bacteria produce rhamnolipids.[19−21] None assumes that rhamnolipids are specifically produced to kill fungal zoospores.[19−21] The mechanism of the anti-zoospore effects of rhamnolipids is poorly understood. There have been no studies on the correlation of rhamnolipid molecular structures with their anti-zoospore effects. It was recognized at an early stage of this study that the structures of the diacid residue of RhL-1 and RhL-3 are somewhat similar to another class of biosurfactants, corynomycolic acids, which also have branched β-hydroxyl fatty acid structures.[22−24] On the other hand, other well-known biosurfactants, such as sophorolipids and surfactin, which have no strong anti-zoospore properties,[7] do not have the diacid structure. It was therefore hypothesized that, upon initial breakdown of rhamnolipids in natural environments, the free diacids generated may play a role in lysing zoospores (and/or other biological activities). If so, the anti-zoospore and/or other biological activities of the diacids may offer some longer term benefits to the rhamnolipid-producing bacteria, such as *P. aeruginosa*. Free diacids were therefore synthesized from rhamnolipids for the later anti-zoospore evaluation.

The reaction scheme for production of ethyl diacids from RhL3 precursors is shown in Figure 2. The total ion spectra from HPLC−MS analysis of the samples taken along the reaction of ethyl diacid production are shown in Figure 3. In the negative detection mode, RhL-3, with the free carboxyl group, is expected to give a strong signal. This is seen with the 0 h sample, as the large peak at the retention time of 4.5−5.5 min. The isolated mass spectrum for this large RhL-3 peak is given in Figure 4, showing three major structures: R−R−C_{10}−C_8, R−R−C_{10}−C_{10}, and R−R−C_{10}−C_{12}. In fact, five groups of

DOI: 10.1021/acs.jafc.5b00033
J. Agric. Food Chem. 2015, 63, 3367−3376

Table 1. Components of RhL-1−RhL-4 and the Free Diacids Detected in this Study

RhL-1 from fermentation	RhL-2 (produced from RhL-1)
$R-C_{10}-C_8$ or $R-C_8-C_{10}$	$R-C_8$
$R-C_{10}-C_{10:1}$ or $R-C_{10:1}-C_{10}$	$R-C_{10}$
$R-C_{10}-C_{10}$	$R-C_{12}$
$R-C_{10}-C_{12:1}$ or $R-C_{12:1}-C_{10}$ or $R-C_{10:1}-C_{12}$ or $R-C_{12}-C_{10:1}$	
$R-C_{10}-C_{12}$ or $R-C_{12}-C_{10}$	

RhL-3 from fermentation	RhL-4 (produced from RhL-3)	diacids (produced from RhL-3 and RhL-1/RhL-3 mixture)
$R-R-C_{10}-C_8$ or $R-R-C_8-C_{10}$	$R-R-C_8$	$C_{10}-C_8$ or C_8-C_{10}
$R-R-C_{10}-C_{10:1}$ or $R-R-C_{10:1}-C_{10}$	$R-R-C_{10}$	$C_{10}-C_{10:1}$ or $C_{10:1}-C_{10}$
$R-R-C_{10}-C_{10}$	$R-R-C_{12}$	$C_{10}-C_{10}$
$R-R-C_{10}-C_{12:1}$ or $R-R-C_{12:1}-C_{10}$ or $R-R-C_{10:1}-C_{12}$ or $R-R-C_{12}-C_{10:1}$		$C_{10}-C_{12:1}$ or $C_{12:1}-C_{10}$ or $C_{10:1}-C_{12}$ or $C_{12}-C_{10:1}$
$R-R-C_{10}-C_{12}$ or $R-R-C_{12}-C_{10}$		$C_{10}-C_{12}$ or $C_{12}-C_{10}$

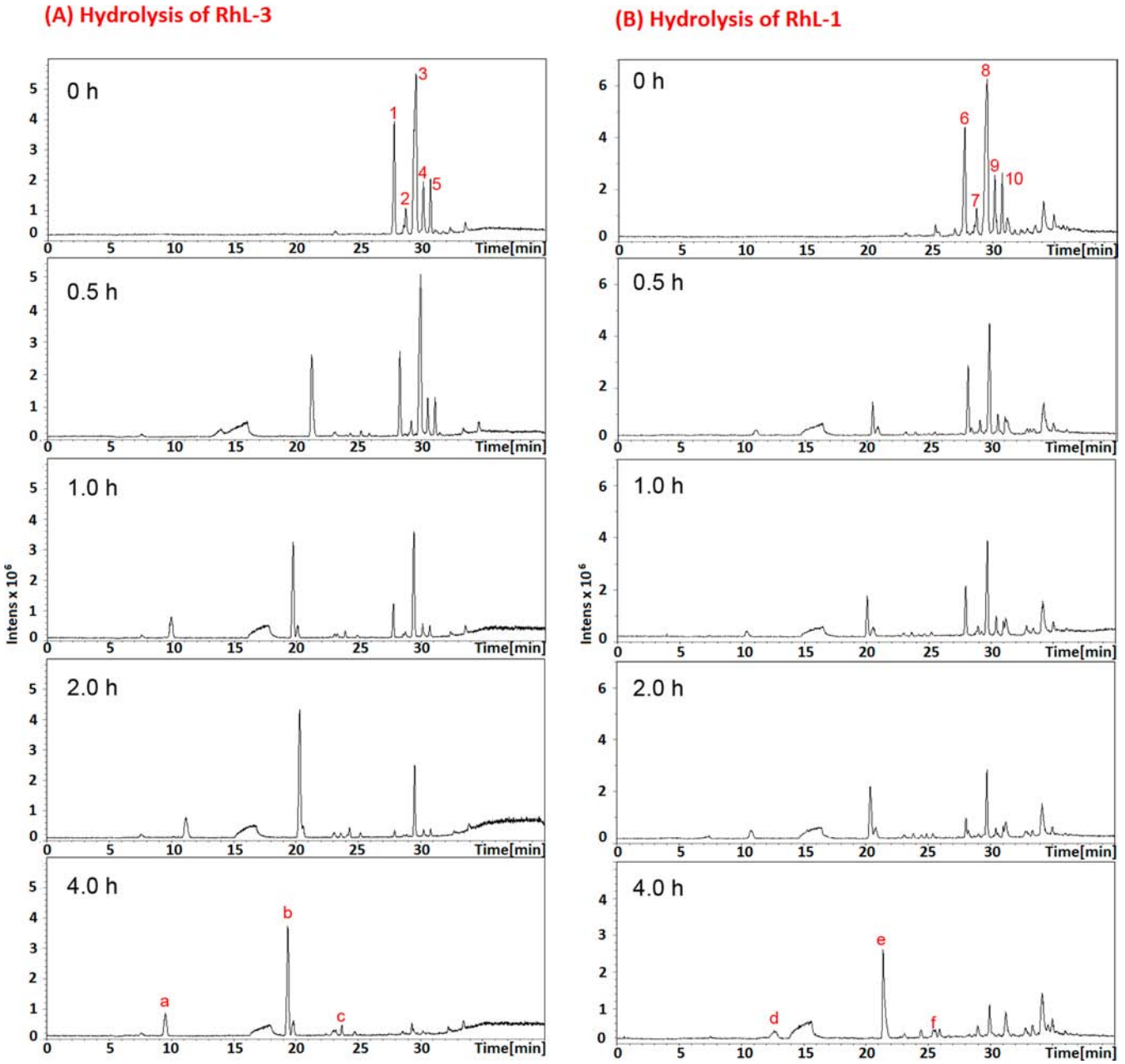

Figure 5. Total ion chromatograms from HPLC−MS analysis of samples from the hydrolysis reaction of (A) RhL-3 to RhL-4 and (B) RhL-1 to RhL-2.

DOI: 10.1021/acs.jafc.5b00033
J. Agric. Food Chem. 2015, 63, 3367−3376

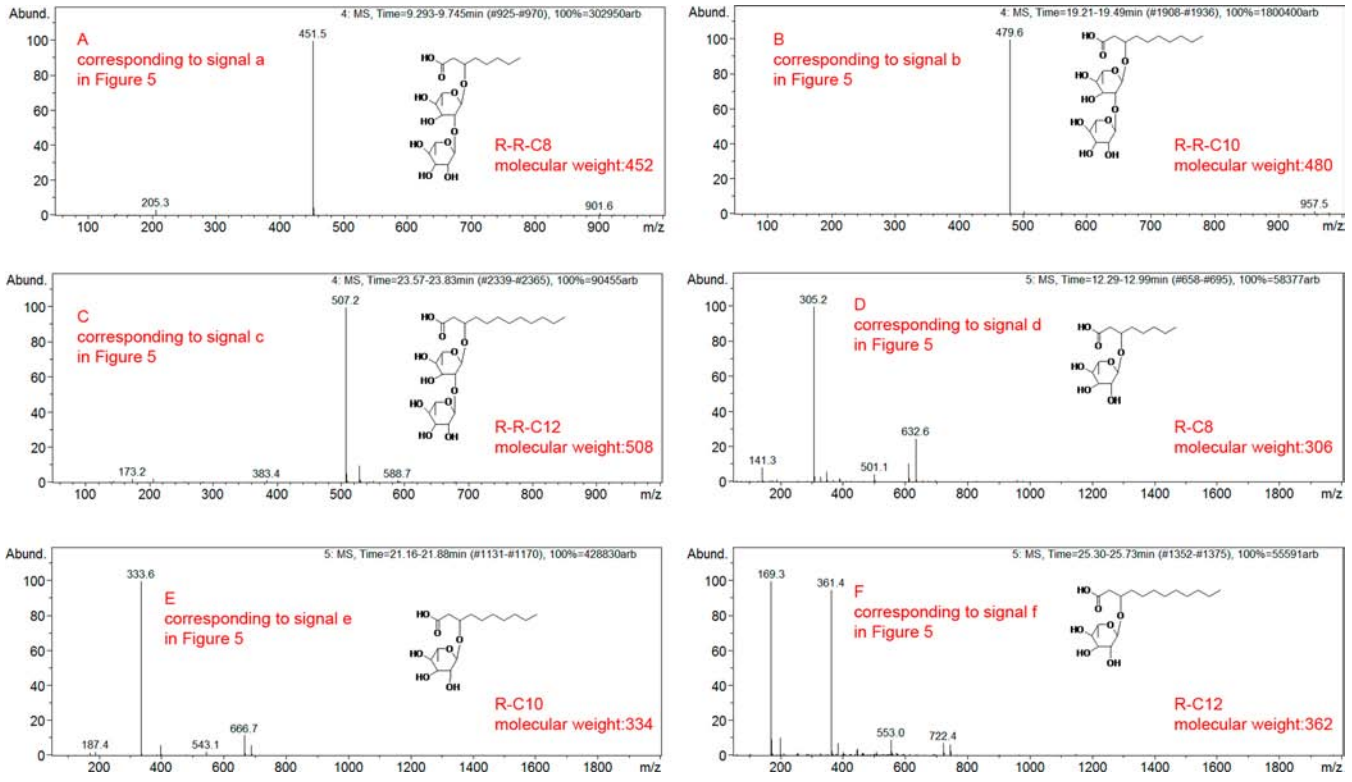

Figure 6. (A–F) MS spectra for the isolated product peaks, shown in Figure 5.

structures have been detected in RhL-3 produced in our laboratory, as given in Table 1. They are more clearly shown in Figures 5 and 7 in later sections. The two smaller groups of congeners are not apparent in this spectrum for the isolated peak.

In the negative-mode spectrum for the sample taken after 0.5 h of reaction, a group of new signals, labeled as 1–4 in Figure 3, appears in the retention time range of 8.5–11.5 min. According to their mass spectra, the new signals correspond to the ethylated rhamnolipids: (1) ethyl R–R–C_{10}–C_8, (2) ethyl R–R–C_{10}–C_{10}, (3) ethyl R–R–C_{10}–$C_{12:1}$, and (4) ethyl R–R–C_{10}–C_{12}. Among the five detectable structures in RhL-3, the group of R–R–C_{10}–$C_{10:1}$ and R–R–$C_{10:1}$–C_{10} is present in the smallest quantity; the ethylated rhamnolipid of this group is not seen in the negative-mode spectra in Figure 3.

The above four new peaks are seen to decrease in intensity with a longer reaction time and nearly disappear after 4.0 h. The results indicate that rhamnolipid ethylation is a fast reaction and the ethyl rhamnolipids formed are further converted to other products. These final products are more clearly seen in the positive-mode spectra in Figure 3. In the positive-mode spectrum for the 0 h sample, the signal of RhL-3 is much weaker than the signal in the negative-mode spectrum. However, more new peaks appear in the positive-mode spectrum for the 0.5 h sample. These peaks correspond to not only the ethyl rhamnolipids, which give strong signals at both negative and positive modes, but also the ethyl diacids formed by the reaction. For the 4.0 h sample, five peaks, labeled as a–e, remain in the positive-mode spectrum. These peaks are from the five synthesized ethyl diacids, as confirmed by the corresponding mass spectra shown in Figure 4 for the five isolated peaks.

Structures of the free diacids subsequently obtained by hydrolysis of the ethyl diacids with sodium hydroxide are summarized in Table 1. The synthesized free diacids were used in the later anti-zoospore study.

Besides ethyl diacids, rhamnose can be obtained as a byproduct. The production of rhamnose by sulfuric acid hydrolysis of rhamnolipids has been reported[25,26] and is not investigated in detail here. Currently, the commercial rhamnose is obtained through an extraction and hydrolysis process.[25,26] Rhamnose-containing materials are first extracted from plant materials, such as oak bark and citrus peels. Rhamnose is then produced by hydrolyzing these extracts. This labor-intensive process needs toxic, corrosive chemicals and produces undesirable waste products. The co-production of rhamnose from rhamnolipids represents an alternative route.

RhL-3 was used as the starting material to generate free diacid for easier tracking of the progress of reactions involving more manageable numbers of rhamnolipids and ethyl rhamnolipids. However, RhL-1 and RhL-3 have the same fatty acid residue (Table 1), and the diacids can be obtained from the mixture of RhL-1 and RhL-3. This process of generating diacids directly from the rhamnolipid mixture collected from fermentation, without the preceding chromatographic separation into RhL-1 and RhL-3, was also carried out in this study. The ethyl diacids obtained have the same final HPLC–MS positive-mode spectrum as that in Figure 3 (data not shown).

Generation of RhL-2 and RhL-4 from RhL-1 and RhL-3. RhL-2 and RhL-4, with one β-hydroxyalkanoic acid as the hydrophobic moiety, have been reported to be produced in the bacterial fermentation but typically make up very small fractions of the rhamnolipid mixtures.[17,18] In the rhamnolipids produced in our laboratory, the contents of RhL-2 and RhL-4 are very low, not observed in our MS analysis. RhL-1 and RhL-3, with two ester-linked β-hydroxyalkanoic acids as the hydrophobic moiety, are the most common groups of rhamnolipids. These

DOI: 10.1021/acs.jafc.5b00033
J. Agric. Food Chem. 2015, 63, 3367–3376

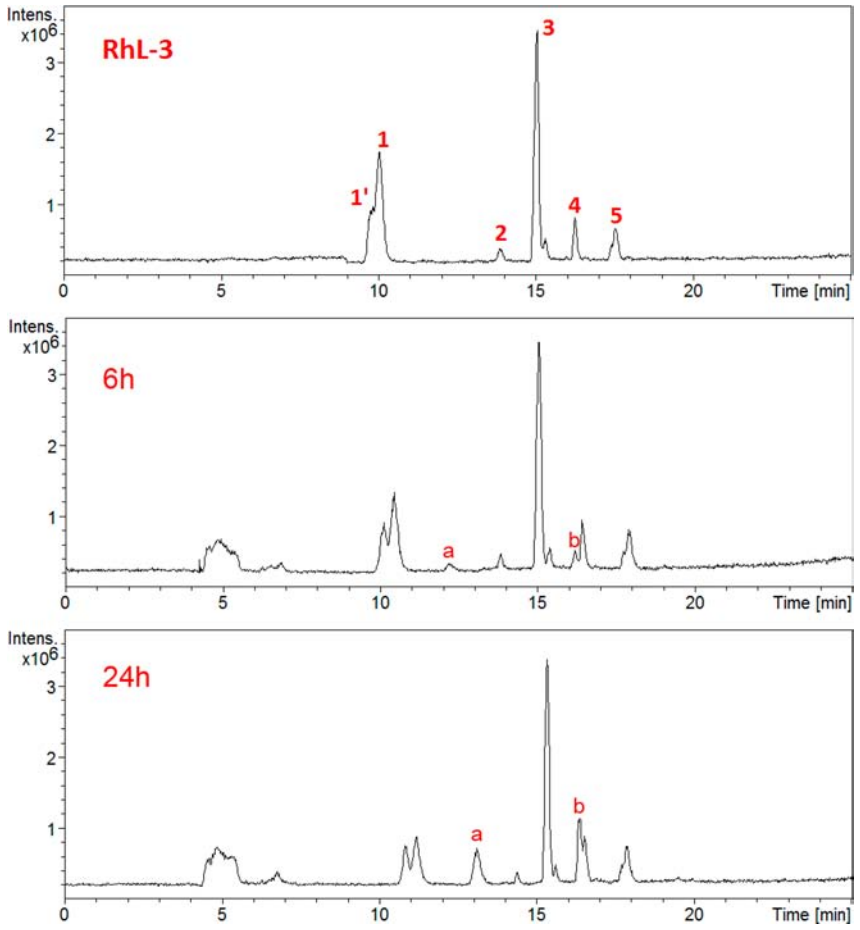

Figure 7. Total ion chromatograms from HPLC−MS analysis of samples from the cellobiase-catalyzed conversion of RhL-3 to RhL-1.

were the groups studied for rhamnose production and anti-zoospore effects in previous literature reports.[7,25] It was desirable to evaluate the anti-zoospore effect of RhL-2 and RhL-4, as compared to that of RhL-1 and RhL-3. The results might provide some insights into the potential importance of the unique diacid structure in rhamnolipids to the biological activities of the biosurfactants. In addition, if RhL-2 and RhL-4 would be found to have superior anti-zoospore property, there might be advantages to tailor the bacterial strain and fermentation conditions to produce RhL-2 and RhL-4, instead of RhL-1 and RhL-3. For example, RhL-2 and RhL-4 have smaller molecular weights than RhL-1 and RhL-3. The molar yield of RhL-2 and RhL-4 can be higher from the same amount of substrate.

RhL-1 and RhL-3 were hydrolyzed with sodium hydroxide to produce RhL-2 and RhL-4. The progress of the hydrolysis reaction is illustrated by the HPLC−MS results shown in Figure 5 for the samples taken at 0, 0.5, 1.0, 2.0, and 4.0 h. For the 0 h samples, the peaks numbered as 1−5 correspond to the five major structures in RhL-3 and those numbered as 6−10 correspond to the five structures in RhL-1. These structures are summarized in Table 1. As shown in Figure 5A, with increasing reaction time, peaks 1−5 of RhL-3 all decrease in intensity simultaneously and three new peaks, labeled as a−c, appear in the spectrum for the 4.0 h sample. The mass spectra corresponding to peaks a−c are shown in panels A−C of Figure 6, confirming that these new peaks formed are dirhamnolipids with the RhL-4 structure, i.e., R−R−C_8, R−R−C_{10}, and R−R−C_{12}. Similarly, three new peaks d−f are formed from hydrolysis of RhL-1, as shown in Figure 5B, and their corresponding mass spectra are shown in panels D−F of Figure 6, confirming that the new compounds produced are monorhamnolipids with the RhL-2 structure, i.e., R−C_8, R−C_{10}, and R−C_{12}. There are other possible RhL-2 and RhL-4 structures (i.e., R−$C_{10:1}$, R−$C_{12:1}$, R−R−$C_{10:1}$, and R−R−$C_{12:1}$) in addition to the three RhL-2 rhamnolipids formed from hydrolysis of RhL-1 and the three RhL-4 rhamnolipids from RhL-3. However, these structures are not seen in the product spectra. It should be noted that the broad signal appearing around 16−18 min of retention time in both panels A and B of Figure 5 (except for the 0 h starting reactants of RhL-3 and RhL-1) is from the sodium acetate present in the reaction mixture samples. The final reaction mixture required further purification techniques to collect only the RhL-2 and RhL-4 produced. Purification was performed by silica column chromatography, to remove the salt and hydroxyl fatty acids (see part 3 of the Supporting Information). The hydroxyl fatty acids collected were analyzed, and their structures were confirmed by MS (see part 3 of the Supporting Information). RhL-2 and RhL-4 thus produced were used in the later anti-zoospore tests. Industrial uses of the hydroxyl fatty acids obtainable from this simple base-catalyzed hydrolysis potentially improve the overall process economics of rhamnolipid production and applications.

Enzymatic Conversion of RhL-3 to RhL-1. Rhamnolipids mostly include RhL-1 and RhL-3, and the ratio of RhL-1/RhL-3 affects the rhamnolipid mixture physical properties. The monorhamnose RhL-1 is less hydrophilic than its dirhamnose

DOI: 10.1021/acs.jafc.5b00033
J. Agric. Food Chem. 2015, 63, 3367−3376

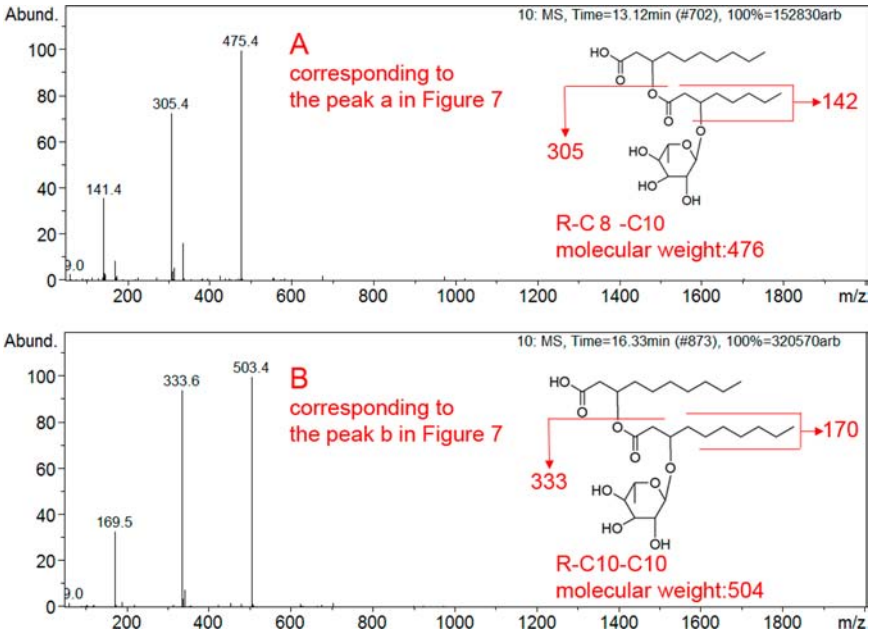

Figure 8. MS spectra for the isolated product peaks a and b in Figure 7.

RhL-3 counterpart with the same fatty acid residue. Accordingly, the critical micelle concentration (cmc) of RhL-1 is usually lower than that of RhL-3. For example, at pH 7, the cmc of RhL-1 is about 0.035 mM, while that of RhL-3 is about 0.110 mM.[23,27−29] These different properties might make different rhamnolipid mixtures more suitable for different applications. There are several ways to alter the ratio of RhL-1/RhL-3. This ratio varies with the fermentation conditions.[30,31] For example, mixtures of higher RhL-1 contents can be produced using vegetable oil as the carbon source in the fermentation.[31] The disadvantage is that the total yield of rhamnolipids also changes significantly with different fermentation substrates and/or conditions. A second approach is to first separate RhL-1 and RhL-3 and then blend them at different ratios, but the initial separation cost is high, usually relying on silica column chromatography. In current work, an enzymatic method was studied to convert RhL-3 to RhL-1. The enzymatic method not only suggests a way to tailor this ratio but also provides valuable information on the breakage of the glycosidic bond in RhL-3 *in vitro* with an enzyme as the catalyst. The latter is helpful to the understanding of the degradation of rhamnolipids in nature.

Both cellulase and cellobiase (β-glucosidase, EC 3.2.1.21) were tested for converting RhL-3 to RhL-1. No RhL-3 conversion could be detected with the cellulase alone. It is possible that the β-glucosidase activity was too low in the cellulase preparation used for this study. Note that β-glucosidase activity is mainly responsible for the intended hydrolysis of R−R disaccharide in RhL-3. On the other hand, RhL-3 hydrolysis was observed to take place with the cellobiase as the catalyst, as shown in Figure 7, in which RhL-3 rhamnolipids appear as a group of peaks 1 (and 1′)−5, similar to those in earlier figures. However, here, peak 1, which in earlier figures was described as the structure R−R−C_{10}−C_8 without differentiation of the order of the two fatty acid residues C_{10} and C_8, can clearly be seen to consist of two overlapping peaks. Peak 1′, which appears slightly earlier, has the structure of R−R−C_{10}−C_8, and the following peak 1 is R−R−C_8−C_{10}, as confirmed by MS analysis. With increasing reaction time, up to 24 h, the intensities of peaks 1 and 1′ are seen to clearly decrease but not the intensities of other peaks 2−5. Furthermore, two new peaks a and b appear and increase in intensity with the progress of reaction. The mass spectra for these new peaks a and b are shown in Figure 8, indicating that peak a is a combination of R−C_{10}−C_8 and R−C_8−C_{10} and peak b is R−C_{10}−C_{10}. According to the product peaks formed, R−R−C_{10}−C_8, R−R−C_8−C_{10}, and R−R−C_{10}−C_{10} were hydrolyzed by cellobiase to their corresponding monorhamnolipid counterparts, while no conversion was detected for R−R−C_{10}−$C_{12:1}$ and R−R−C_{10}−C_{12}. The conversions of R−R−C_8−C_{10} and R−R−C_{10}−C_8 appear to be the most significant, with the R−R−C_8−C_{10} conversion likely being faster. This is supported by two observations: the intensity of fragment R−C_8−C_{10} (m/z 305) is stronger than that of fragment R−C_{10}−C_8 (m/z 329) in Figure 8A, and peak 1 intensity decreases faster than peak 1′ intensity in Figure 7. It is possible that the enzymatic conversion is related to the fatty acid chain length. R−R−C_8−C_{10} and R−R−C_{10}−C_8 have the shortest chain length and are hydrolyzed the most. R−R−C_{10}−C_{10} is also hydrolyzed. The longest fatty acid chains in R−R−C_{10}−$C_{12:1}$ and R−R−C_{10}−C_{12} might have affected the affinity of these rhamnolipids for the active site of the enzyme. Cellobiase is supposed to act on the cellobiose released during enzymatic breakdown of cellulose. Rhamnose is not present in usual cellulose. The observed results of RhL-3 conversion with cellobiase suggest that the enzyme can also hydrolyze the dirhamnose residue of RhL-3 but not those with fatty acid residues longer than C_{10}−C_{10}.

Anti-zoospore Tests. RhL-1−RhL-4 and the synthesized diacids were investigated for their anti-zoospore effects. The results are shown in Table 2. RhL-1−RhL-4 have similar anti-zoospore effects, although RhL-1 appears to be most potent. This is inconsistent with the previous report that RhL-3 has better anti-zoospore property than RhL-1.[7,8] The discrepancies might arise from different choices for zoospores and different rhamnolipid compositions used in the various studies. More importantly, RhL-2 and RhL-4 are found to have anti-zoospore effects similar to RhL-1 and RhL-3. This finding sheds some

DOI: 10.1021/acs.jafc.5b00033
J. Agric. Food Chem. 2015, 63, 3367−3376

Table 2. Anti-zoospore Effects of RhL-1−RhL-4 and the Diacids Evaluated at Different Concentrations[a]

concentration (mg/L)	10	20	30	40	50	60	80	125
RhL-1	−	*	*	*	*	*	*	*
RhL-2	−	−	*	*	*	*	*	*
RhL-3	−	−	−	*	*	*	*	*
RhL-4	−	−	−	*	*	*	*	*
diacids (e.g., C_{10}−C_{10})	−	−	−	−	−	−	−	*

[a]"−", moving zoospores were observable; "*", all zoospores ceased moving; most were lysed.

light on the anti-zoospore mechanism of rhamnolipids. It does not support the hypothesis that the unique diacid structure of rhamnolipids plays a critical role in the anti-zoospore effect.

A wide range of cmc has been reported for rhamnolipid mixtures, because of the varying structures, e.g., 5−40 mg/L for RhL-1 and RhL-3 with two hydrophobic tails and around 200 mg/L for RhL-2 and RhL-4 with only one hydrophobic tail.[32] In this study, the critical anti-zoospore concentrations to stop movement of all zoospores for RhL-1−RhL-4 are found to be in the range of 20−40 mg/L (Table 2), which are much lower than the cmc of about 200 mg/L for RhL-2 and RhL-4. Therefore, while micelles might be present in the test solutions of RhL-1 and RhL-3 at their critical anti-zoospore concentrations, micelles were unlikely to be formed in the test solutions of RhL-2 and RhL-4 at those concentrations (30 and 40 mg/L). The finding implies that micelle formation and the associated solubilization of membrane lipids or other hydrophobic cell components are not an essential mechanism responsible for the anti-zoospore effect.

The diacids also exhibit the anti-zoospore effect (Table 2). The diacids are more effective against zoospores than most of the other biosurfactants tested in the literature;[7] more than 1000 mg/L of those biosurfactants (sophorolipids, trehalose lipid, and surfactin) are required to totally cease zoospore movement,[7] while approximately 125 mg/L diacids are required. Diacids are more hydrophobic and less soluble than RhL-1−RhL-4. The diacids make a clear solution in water at 100 mg/L but form a slightly white, turbid suspension at 1000 mg/L. The hydrophobicity of the diacids might affect their interactions with the surface of zoospores; the rhamnose residue in rhamnolipids lowers this hydrophobicity and significantly enhances the anti-zoospore effect of the biosurfactants. Overall, the results indicate that rhamnolipids are very effective against the zoospores of *P. sojae* and that, when applied to natural environments, the degradation intermediates, including RhL-2 and RhL-4 (which have lost one fatty acid residue) and the free diacids separated from the rhamnose residue, can continue to exert the anti-zoospore effect.

In summary, although RhL-1 and RhL-3 are produced in large quantities in *P. aeruginosa* fermentation, RhL-2 and RhL-4 and the free diacids can be synthesized from RhL-1 and RhL-3 using the methods developed in this study. Rhamnose, a valuable co-product, can be obtained from some of the conversion reactions developed. β-Hydroxy fatty acids can also be produced when generating RhL-2 and RhL-4 from RhL-1 and RhL-3. The possibility of adjusting the ratio of RhL-1/RhL-3 in the rhamnolipid mixture to better suit the specific application is further demonstrated using the cellobiase enzyme as a catalyst, and the enzyme is shown to have higher selectivity toward dirhamnolipids with shorter fatty acid chains. RhL-1−RhL-4 and the free diacids are all found to be very effective in damaging the zoospores of *P. sojae*, with RhL-1 being the most effective and the diacids the least effective among them. The results indicate that the combined structure of β-hydroxy fatty acid and sugar significantly enhances the anti-zoospore effect. This finding may be helpful to the further development of anti-zoospore chemicals. These results also indicate that, when applied to natural environments, the degradation intermediates, including the RhL-2 and RhL-4 that have lost one fatty acid residue (from RhL-1 and RhL-3) and the free diacids separated from the rhamnose residue, can all continue to exert the anti-zoospore effect.

■ ASSOCIATED CONTENT

Supporting Information

Mass spectra of ethyl rhamnolipids (part 1), proton nuclear magnetic resonance (^{1}H NMR) of ethyl diacids and free diacids (part 2), and mass spectra of hydroxyl fatty acids (part 3). This material is available free of charge via the Internet at http://pubs.acs.org.

■ AUTHOR INFORMATION

Corresponding Author

*Telephone: 330-972-7252. Fax: 330-972-5856. E-mail: lukeju@uakron.edu.

Funding

This work was supported by grants from the U.S. Department of Agriculture under the Biomass Research and Development Initiative (Award 2009-10001-05112), the U.S. Department of Transportation, Office of the Secretary (Grant DTOS59-07-G-00050), and the Ohio Soybean Council (Project 13-2-17).

Notes

The authors declare no competing financial interest.

■ ACKNOWLEDGMENTS

The authors are very grateful to Dr. Paul F. Morris of Bowling Green State University (Bowling Green, OH) for providing the *P. sojae* seed culture and the detailed instructions and demonstration on culturing and forming zoospores. The authors thank Krutika Invally and Jacob Kohl for helping to take zoospore photos.

■ REFERENCES

(1) *Ohio Soybean Industry Overview*; http://www.soyohio.org (accessed March 3, 2015).

(2) Canaday, C.; Schmitthenner, A. Effects of chloride and ammonium salts on the incidence of phytophthora root and stem rot of soybean. *Plant Dis.* **2010**, *94*, 758−765.

(3) Lee, S.; Mian, M. R.; Mchale, L. K.; Wang, H.; Wijeratne, A. J.; Sneller, C. H.; Dorrance, A. E. Novel quantitative trait loci for partial resistance to *Phytophthora sojae* in soybean PI 398841. *Theor. Appl. Genet.* **2013**, *126*, 1121−1132.

(4) Yousef, L. F.; Wojno, M.; Dick, W. A.; Dick, R. P. Lipid profiling of the soybean pathogen *Phytophthora sojae* using fatty acid methyl esters (FAMEs). *Fungal Biol.* **2012**, *116*, 613−619.

(5) Dorrance, A. E.; Mills, D.; Robertson, A. E.; Draper, M. A.; Giesler, L.; Tenuta, A. Phytophthora root and stem rot of soybean. *Plant Health Instr.* **2007**, DOI: 10.1094/PHI-I-2007-0830-07.

(6) Tyler, B. M. *Phytophthora sojae*: Root rot pathogen of soybean and model oomycete. *Mol. Plant Pathol.* **2007**, *8*, 1−8.

(7) Stanghellini, M. E.; Miller, R. M. Biosurfactants, their identity and potential efficacy in the biological control of zoosporic plant pathogens. *Plant Dis.* **1997**, *81*, 4−12.

DOI: 10.1021/acs.jafc.5b00033
J. Agric. Food Chem. 2015, 63, 3367−3376

(8) Sha, R.; Jiang, L.; Meng, Q.; Zhang, G.; Song, Z. Producing cell-free culture broth of rhamnolipids as a cost-effective fungicide against plant pathogens. *J. Basic Microb.* **2012**, *52*, 458−466.
(9) Foley, P.; Beach, E. S.; Zimmerman, J. B. Derivation and synthesis of renewable surfactants. *Chem. Soc. Rev.* **2012**, *41*, 1499−1518.
(10) Heyd, M.; Franzreb, M.; Berensmeier, S. Continuous rhamnolipid production with integrated product removal by foam fractionation and magnetic separation of immobilized *Pseudomonas aeruginosa*. *Biotechnol. Prog.* **2011**, *27*, 706−716.
(11) Banat, I. M.; Makkar, R. S.; Cameotra, S. Potential commercial applications of microbial surfactants. *Appl. Microbiol. Biotechnol.* **2000**, *53*, 495−508.
(12) Wu, J.-Y.; Yeh, K.-L.; Lu, W.-B.; Lin, C.-L.; Chang, J.-S. Rhamnolipid production with indigenous *Pseudomonas aeruginosa* EM1 isolated from oil-contaminated site. *Bioresour. Technol.* **2008**, *99*, 1157−1164.
(13) Wen, J.; Stacey, S. P.; Mclaughlin, M. J.; Kirby, J. K. Biodegradation of rhamnolipid, EDTA and citric acid in cadmium and zinc contaminated soils. *Soil Biol. Biochem.* **2009**, *41*, 2214−2221.
(14) Frank, N.; Lißner, A.; Winkelmann, M.; Hüttl, R.; Mertens, F. O.; Kaschabek, S. R.; Schlömann, M. Degradation of selected (bio-) surfactants by bacterial cultures monitored by calorimetric methods. *Biodegradation* **2010**, *21*, 179−191.
(15) Heyd, M.; Kohnert, A.; Tan, T.-H.; Nusser, M.; Kirschhöfer, F.; Brenner-Weiss, G.; Franzreb, M.; Berensmeier, S. Development and trends of biosurfactant analysis and purification using rhamnolipids as an example. *Anal. Bioanal. Chem.* **2008**, *391*, 1579−1590.
(16) Haba, E.; Pinazo, A.; Jauregui, O.; Espuny, M.; Infante, M. R.; Manresa, A. Physicochemical characterization and antimicrobial properties of rhamnolipids produced by *Pseudomonas aeruginosa* 47T2 NCBIM 40044. *Biotechnol. Bioeng.* **2003**, *81*, 316−322.
(17) Trummler, K.; Effenberger, F.; Syldatk, C. An integrated microbial/enzymatic process for production of rhamnolipids and L-(+)-rhamnose from rapeseed oil with *Pseudomonas* sp. DSM 2874. *Eur. J. Lipid Sci. Technol.* **2003**, *105*, 563−571.
(18) Lang, S.; Wullbrandt, D. Rhamnose lipids—Biosynthesis, microbial production and application potential. *Appl. Microbiol. Biotechnol.* **1999**, *51*, 22−32.
(19) Ron, E. Z.; Rosenberg, E. Natural roles of biosurfactants. *Environ. Microbiol.* **2001**, *3*, 229−236.
(20) Abdel-Mawgoud, A. M.; Lépine, F.; Déziel, E. Rhamnolipids: Diversity of structures, microbial origins and roles. *Appl. Microbiol. Biotechnol.* **2010**, *86*, 1323−1336.
(21) Maier, R. M. Biosurfactants: Evolution and diversity in bacteria. *Adv. Appl. Microbiol.* **2003**, *52*, 101−121.
(22) Gastambide-Odier, M.; Lederer, E. Biosynthesis of corynomycolic acid from two molecules of palmitic acid. *Nature* **1959**, *184*, 1563−1564.
(23) Wang, H. Solution and interfacial characterization of rhamnolipid biosurfactants and their synthetic analogues. Ph.D. Thesis, Department of Chemistry and Biochemistry, University of Arizona, Tucson, AZ, 2011.
(24) Rosenberg, E.; Ron, E. High-and low-molecular-mass microbial surfactants. *Appl. Microbiol. Biotechnol.* **1999**, *52*, 154−162.
(25) Linhardt, R. J.; Bakhit, R.; Daniels, L.; Mayerl, F.; Pickenhagen, W. Microbially produced rhamnolipid as a source of rhamnose. *Biotechnol. Bioeng.* **1989**, *33*, 365−368.
(26) Giani, C.; Wullbrandt, D.; Rothert, R.; Meiwes, J. *Pseudomonas aeruginosa* and its use in a process for the biotechnological preparation of L-rhamnose. U.S. Patent 5,658,793, 1997.
(27) Sánchez, M.; Aranda, F. J.; Espuny, M. J.; Marqués, A.; Teruel, J. A.; Manresa, Á.; Ortiz, A. Aggregation behaviour of a dirhamnolipid biosurfactant secreted by *Pseudomonas aeruginosa* in aqueous media. *J. Colloid Interface Sci.* **2007**, *307*, 246−253.
(28) Parra, J.; Guinea, J.; Manresa, M.; Robert, M.; Mercade, M.; Comelles, F.; Bosch, M. Chemical characterization and physicochemical behavior of biosurfactants. *J. Am. Oil Chem. Soc.* **1989**, *66*, 141−145.
(29) Lebrón-Paler, A. Solution and interfacial characterization of rhamnolipid biosurfactant from *P. aeruginosa* ATCC 9027. Ph.D. Thesis, Department of Chemistry, University of Arizona, Tucson, AZ, 2008.
(30) Lotfabad, T. B.; Abassi, H.; Ahmadkhaniha, R.; Roostaazad, R.; Masoomi, F.; Zahiri, H. S.; Ahmadian, G.; Vali, H.; Noghabi, K. A. Structural characterization of a rhamnolipid-type biosurfactant produced by *Pseudomonas aeruginosa* MR01: Enhancement of di-rhamnolipid proportion using gamma irradiation. *Colloids Surf., B* **2010**, *81*, 397−405.
(31) Abalos, A.; Pinazo, A.; Infante, M.; Casals, M.; Garcia, F.; Manresa, A. Physicochemical and antimicrobial properties of new rhamnolipids produced by *Pseudomonas aeruginosa* AT10 from soybean oil refinery wastes. *Langmuir* **2001**, *17*, 1367−1371.
(32) Nitschke, M.; Costa, S. G.; Contiero, J. Rhamnolipid surfactants: An update on the general aspects of these remarkable biomolecules. *Biotechnol. Prog.* **2005**, *21*, 1593−1600.

DOI: 10.1021/acs.jafc.5b00033
J. Agric. Food Chem. 2015, 63, 3367−3376

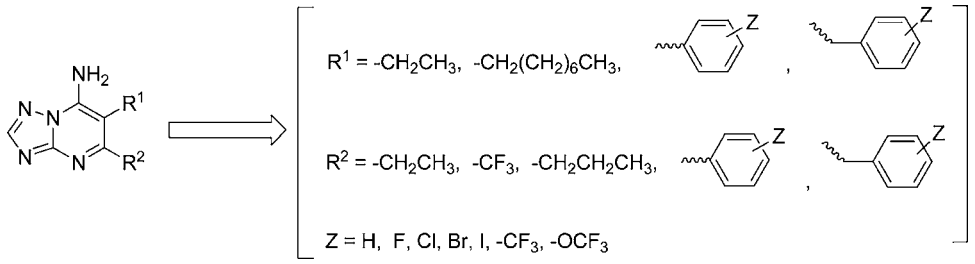

Figure 1. Design of the title compounds.

and discovery of novel ametoctradin analogues and fungicides targeting the bc_1 complex.

MATERIALS AND METHODS

General Methods. Unless otherwise noted, all chemical reagents were commercially available from Acros Organics and/or Sigma-Aldrich and treated with standard methods before used. ^{1}H NMR spectra were recorded in $CDCl_3$ or DMSO-d_6 solution on a varian Mercury 600 or 400 MHz spectrometer. Chemical shifts were recorded in parts per million (ppm), with TMS as the internal reference. The following abbreviations were used to designate chemical shift multiplicities: *s* = singlet, *d* = doublet, *t* = triplet, *m* = multiplet, *br* = broad; MS spectra were determined with a Tracems2000 organic mass spectrometer, and signals were given in *m*/*z*. Melting points were measured on a Buchi B-545 melting point apparatus. Element analyses (EA) were measured on a Vario ELIII CHNSO elemental analyzer. The silica gel (200−300 mesh) for flash column chromatography was purchased from QingDao Marine Chemical Factory in China.

General Procedure for the Preparation of Intermediate 2.[18−20] Under a nitrogen atmosphere, THF (tetrahydrofuran, 30 mL) and anhydrous acetonitrile (25 mmol) was mixed and stirred for 5 min at −78 °C. BuLi (2.M) was added into the mixture and stirred for 1 h at −78 °C. Then, different substituent benzyl bromide was added dropwise slowly and then the mixture was stirred for 20 min and monitored by TLC detection. After 20 min, the reaction was complete. The resulting suspension was then diluted with water (15 mL) and extracted with ethyl acetate (2 × 25 mL). The combined organic extracts were washed with brine (2 × 25 mL), dried with Na_2SO_4, and concentrated, and the residue was purified by flash chromatography on silica gel to provide the desired product.

General Procedure for the Preparation of Intermediate 3.[18−20] A mixture of solid potassium methoxide (1.75g) and *o*-xylene (2.7 mL) was stirred and heated with reflux. When the mixture changed to light yellow, as monitored by HPLC detection, only 10% of **2** (total 10 mmol) and ester (total 20 mmol) were added in 5 min and then stirred for 15 min. The complete addition required another 10 min. The reaction mixture was refluxed 2.5 h and was allowed to warm room temperature. Water (3.3 mL) was added to the reaction mixture with pH equal to 5−6 adjusted by adding 20% hydrochloric acid. Then it was extracted with ethyl acetate (3 × 15 mL). The combined organic extracts were washed with brine 15 mL and dried with Na_2SO_4 to yield 2-propionyldecanonitrile.

General Procedure for the Preparation of the Title Compounds 4a ∼ z. A mixture of **3** (3 mmol), 1,2,4-triazol-3-amine (3 mmol), and *o*-xylene (2.5 mL) was quickly stirred, and then $ClSO_3H$ (0.6 mmol) was slowly added dropwise. The reactive temperature was heated to 160 °C under reflux for 12−16 h as monitored by TLC detection. The mixture was cooled to room temperature, and the product was precipitated in the form of colorless crystals. Water (5 mL) was added to the reaction mixture with pH equal to 8−9 adjusted by adding 20% triethylamine. Finally, the precipitate was purified by flash chromatography on silica gel to provide the desired product. Due to the complexity of reaction, the yield of some compound is lower than 10%. Our purpose was to obtain a certain compound to assay its activity. So, we did not to optimize the reaction condition to increase the yield.

5-Ethyl-6-octyl-1,2,4-triazolo[1,5-*a*]pyrimidin-7-amine (ametoctradin). Yield: 76%; mp 197.7−198.7 °C; ^{1}H NMR (600 MHz, d_6-DMSO) δ 8.33 (s, 1H), 7.71 (s, 2H), 2.74 (q, *J* = 7.2 Hz, 2H), 2.63−2.56 (m, 2H), 1.41 (d, *J* = 13.8 Hz, 4H), 1.33−1.19 (m, 11H), 0.86 (t, *J* = 6.6 Hz, 3H); MS: *m*/*z* = 275.33 (M+).

6-Octyl-5-(*p*-tolyl)-1,2,4-triazolo[1,5-*a*]pyrimidin-7-amine (4a). Yield: 10%; mp 156−158 °C; ^{1}H NMR (600 MHz, d_6-DMSO): δ 8.44 (s, 1H), 8.01 (s, 2H), 7.34 (d, *J* = 7.2 Hz, 2H), 7.28 (d, *J* = 7.2 Hz, 2H), 2.56 (s, 2H), 2.38 (s, 3H), 1.33 (s, 2H), 1.25 (d, *J* = 12.0 Hz, 2H), 1.23−1.16 (m, 2H), 1.08 (dd, *J* = 42.6, 6.0 Hz, 6H), 0.83 (t, *J* = 7.2 Hz, 3H); MS: *m*/*z* = 337.27 (M+). Anal. Calcd for $C_{20}H_{27}N_5$: C, 71.18; H, 8.06; N, 20.75. Found: C, 71.22; H, 8.102; N, 20.50.

6-Octyl-5-(3-(trifluoromethyl)phenyl)-1,2,4-triazolo-[1,5-*a*]pyrimidin-7-amine (4b). Yield: 11%; mp 130−131 °C; ^{1}H NMR (600 MHz, $CDCl_3$): δ 8.42 (s, 1H), 7.78 (s, 1H), 7.73 (dd, *J* = 15.6, 7.2 Hz, 2H), 7.62 (t, *J* = 7.8 Hz, 1H), 6.00 (s, 2H), 2.60−2.55 (m, 2H), 1.58−1.46 (m, 2H), 1.23 (dd, *J* = 25.2, 19.8 Hz, 10H), 0.86 (t, *J* = 67.2 Hz, 3H). Anal. Calcd for $C_{20}H_{24}F_3N_5$: C, 61.37; H, 6.18; N, 17.89. Found: C,61.35; H, 6.070; N, 18.01.

5-(3-Chlorophenyl)-6-octyl-1,2,4-triazolo[1,5-*a*]-pyrimidin-7-amine (4c). Yield: 7%; mp 154−155 °C; ^{1}H NMR (600 MHz, d6-DMSO): δ 8.47 (s, 1H), 8.12 (s, 2H), 7.58−7.47 (m, 3H), 7.42 (d, *J* = 7.2 Hz, 1H), 2.53 (d, *J* = 7.8 Hz, 1H), 1.39- 1.28 (m, 2H), 1.21 (dd, *J* = 13.8, 7.2 Hz, 2H), 1.17- 0.99 (m, 8H), 0.83 (t, *J* = 7.2 Hz, 3H); MS: *m*/*z* = 357.26 (M+). Anal. Calcd for $C_{19}H_{24}ClN_5$: C, 63.77; H, 6.76; N, 19.57. Found: C, 63.61; H, 6.783; N, 19.31.

5-Ethyl-6-propyl-1,2,4-triazolo[1,5-*a*]pyrimidin-7-amine (4d). Yield: 64%; mp 179−181 °C; ^{1}H NMR (400 MHz, d_6-DMSO): δ 8.34 (s, 1H), 7.74 (s, 2H), 2.75 (d, *J* = 7.2 Hz, 2H), 2.58 (s, 2H), 1.45 (s, 2H), 1.23 (t, *J* = 7.2 Hz, 3H), 0.98 (t, *J* = 6.8 Hz, 3H); MS: *m*/*z* = 205.06 (M+). Anal. Calcd for $C_{10}H_{15}N_5$: C, 58.51; H, 7.37; N, 34.12. Found: C, 58.32; H, 7.379; N, 34.22.

6-Benzyl-5-phenyl-1,2,4-triazolo[1,5-*a*]pyrimidin-7-amine (4e). Yield: 33%; mp 249−251 °C; ^{1}H NMR (400 MHz, d_6-DMSO): δ 8.49 (s, 1H), 8.05 (s, 2H), 7.64−7.27 (m,

DOI: 10.1021/acs.jafc.5b00228
J. Agric. Food Chem. 2015, 63, 3377−3386

5H), 7.27−7.19 (m, 2H), 7.18−7.09 (m, 1H), 6.96 (d, J = 7.2 Hz, 2H), 4.01 (s, 2H); MS: m/z = 300.09 (M+). Anal. Calcd for $C_{18}H_{15}N_5$: C, 71.74; H, 5.02; N, 23.24. Found: C, 71.80; H, 5.169; N, 23.07.

6-Benzyl-5-(3,3,3-trifluoropropyl)-1,2,4-triazolo[1,5-*a*]pyrimidin-7-amine (4f). Yield: 39%; mp 212−214 °C; ^{1}H NMR (600 MHz, d_6-DMSO): δ 8.44 (s, 1H), 8.06 (s, 2H), 7.29 (t, J = 7.2 Hz, 2H), 7.20 (t, J = 7.2 Hz, 1H), 7.12 (d, J = 7.2 Hz, 2H), 4.11 (s, 2H), 2.93−2.80 (m, 2H), 2.61 (dd, J = 16.2, 10.8 Hz, 2H); MS: m/z = 321.08 (M+). Anal. Calcd for $C_{15}H_{14}F_3N_5$: C, 56.07; H, 4.39; N, 21.80. Found: C, 56.24; H, 4.514; N, 21.65.

6-(4-Bromobenzyl)-5-ethyl-1,2,4-triazolo[1,5-*a*]-pyrimidin-7-amine (4g). Yield: 53%; mp 239−241 °C; ^{1}H NMR (600 MHz, d_6-DMSO): δ 8.39 (s, 1H), 7.88 (s, 2H), 7.46 (d, J = 8.4 Hz, 2H), 7.08 (d, J = 8.4 Hz, 2H), 4.05 (s, 2H), 2.61 (q, J = 7.2 Hz, 2H), 1.09 (t, J = 7.2 Hz, 3H); MS: m/z = 332.96 (M+). Anal. Calcd for $C_{14}H_{14}BrN_5$: C, 50.62; H, 4.25; N, 21.08. Found: C, 50.73; H, 4.103; N, 21.99.

5-Ethyl-6-(4-fluorobenzyl)-1,2,4-triazolo[1,5-*a*]-pyrimidin-7-amine (4h). Yield: 85%; mp 216−218 °C; ^{1}H NMR (600 MHz, d_6-DMSO): δ 8.39 (s, 1H), 7.87 (s, 2H), 7.15 (t, J = 7.2 Hz, 2H), 7.09 (t, J = 9.0 Hz, 2H), 4.06 (s, 2H), 2.63 (q, J = 7.2 Hz, 2H), 1.09 (t, J = 7.2 Hz, 3H); MS: m/z = 271.06 (M+). Anal. Calcd for $C_{14}H_{14}FN_5$: C, 61.98; H, 5.20; N, 25.81. Found: C, 62.15; H, 5.269; N, 25.56.

6-(3-Bromobenzyl)-5-ethyl-1,2,4-triazolo[1,5-*a*]-pyrimidin-7-amine (4i). Yield: 52%; mp 211−212 °C; ^{1}H NMR (600 MHz, d_6-DMSO): δ 8.40 (s, 1H), 7.89 (s, 2H), 7.39 (d, J = 7.8 Hz, 1H), 7.34 (s, 1H), 7.24 (t, J = 7.8 Hz, 1H), 7.09 (d, J = 7.8 Hz, 1H), 4.09 (s, 2H), 2.63 (q, J = 7.2 Hz, 2H), 1.10 (t, J = 7.2 Hz, 3H); MS: m/z = 332.93 (M+). Anal. Calcd for $C_{14}H_{14}BrN_5$: C, 50.62; H, 4.25; N, 21.08. Found: C, 50.73; H, 4.103; N, 20.99.

5-Ethyl-6-(2-fluorobenzyl)-1,2,4-triazolo[1,5-*a*]-pyrimidin-7-amine (4j). Yield: 66%; mp 209−211 °C; ^{1}H NMR (600 MHz, d_6-DMSO): δ 8.40 (s, 1H), 7.89 (s, 2H), 7.26 (dd, J = 13.2, 6.6 Hz, 1H), 7.20 (t, J = 9.0 Hz, 1H), 7.05 (t, J = 7.2 Hz, 1H), 6.84 (t, J = 7.8 Hz, 1H), 4.06 (s, 2H), 4.47 (q, J = 7.2 Hz, 2H), 1.08 (t, J = 7.2 Hz, 3H); MS: m/z = 271.03 (M+). Anal. Calcd for $C_{14}H_{14}FN_5$: C, 61.98; H, 5.20; N, 25.81. Found: C, 61.82; H, 5.347; N, 25.80.

6-(2-Bromobenzyl)-5-ethyl-1,2,4-triazolo[1,5-*a*]-pyrimidin-7-amine (4k). Yield: 59%; mp 228−239 °C; ^{1}H NMR (600 MHz, d_6-DMSO): δ 8.40 (s, 1H), 7.90 (s, 2H), 7.67 (d, J = 7.8 Hz, 1H), 7.23 (t, J = 7.2 Hz, 1H), 7.17 (t, J = 7.8 Hz, 1H), 6.73 (d, J = 7.8 Hz, 1H), 4.06 (s, 2H), 2.48 (d, J = 7.5 Hz, 1H), 1.08 (t, J = 7.2 Hz, 3H); MS: m/z = 332.99 (M+). Anal. Calcd for $C_{14}H_{14}BrN_5$: C, 50.62; H, 4.25; N, 21.08. Found: C, 50.75; H, 4.234; N, 21.29.

5-Ethyl-6-(3-fluorobenzyl)-1,2,4-triazolo[1,5-*a*]-pyrimidin-7-amine (4l). Yield: 65%; mp 226−228 °C; ^{1}H NMR (600 MHz, d_6-DMSO): δ 8.39 (s, 1H), 7.88 (s, 2H), 7.31 (dd, J = 14.4, 7.8 Hz, 1H), 7.02 (t, J = 7.8 Hz, 1H), 6.95 (t, J = 10.2 Hz, 2H), 4.10 (s, 2H), 2.63 (q, J = 7.2 Hz, 2H), 1.10 (t, J = 7.2 Hz, 3H); MS: m/z = 271.08 (M+). Anal. Calcd for $C_{14}H_{14}FN_5$: C, 61.98; H, 5.20; N, 25.81. Found: C, 61.92; H, 5.467; N, 25.71.

5-Ethyl-6-(3-iodobenzyl)-1,2,4-triazolo[1,5-*a*]-pyrimidin-7-amine (4m). Yield: 87%; mp 214−215 °C; ^{1}H NMR (600 MHz, d_6-DMSO): δ 8.39 (s, 1H), 7.88 (s, 2H), 7.55 (d, J = 15.6 Hz, 2H), 7.08 (s, 2H), 4.06 (s, 2H), 2.62 (dd, J = 13.8, 6.5 Hz, 2H), 1.10 (t, J = 7.2 Hz, 3H); MS: m/z = 378.92 (M+). Anal. Calcd for $C_{14}H_{14}IN_5$: C, 44.34; H, 3.72; N, 18.47. Found: C, 44.59; H, 3.550; N, 18.50.

6-(2-Chlorobenzyl)-5-ethyl-1,2,4-triazolo[1,5-*a*]-pyrimidin-7-amine (4n). Yield: 59%; mp 225−227 °C; ^{1}H NMR (600 MHz, d_6-DMSO): δ 8.40 (s, 1H), 7.89 (s, 2H), 7.50 (d, J = 7.8 Hz, 1H), 7.25 (t, J = 7.8 Hz, 1H), 7.19 (t, J = 7.8 Hz, 1H), 6.75 (d, J = 7.8 Hz, 1H), 4.09 (s, 2H), 2.55−2.46 (m, 5H), 1.08 (t, J = 7.2 Hz, 3H); MS: m/z = 287.01 (M+). Anal. Calcd for $C_{14}H_{14}ClN_5$: C, 58.44; H, 4.90; N, 24.34. Found: C, 58.17; H, 4.710; N, 24.21.

5-Ethyl-6-(4-(trifluoromethoxy)benzyl)-1,2,4-triazolo-[1,5-*a*]pyrimidin-7-amine (4o). Yield: 69%; mp 212−213 °C; ^{1}H NMR (600 MHz, d_6-DMSO): δ 8.40 (s, 1H), 7.89 (s, 2H), 7.25 (dd, J = 23.4, 8.4 Hz, 4H), 4.11 (s, 2H), 2.63 (q, J = 7.2 Hz, 2H), 1.10 (t, J = 7.2 Hz, 3H); MS: m/z = 337.02 (M+). Anal. Calcd for $C_{15}H_{14}F_3N_5O$: C, 53.41; H, 4.18; N, 20.76. Found: C, 53.53; H, 4.336; N, 20.56.

6-(3-Chlorobenzyl)-5-ethyl-1,2,4-triazolo[1,5-*a*]-pyrimidin-7-amine (4p). Yield: 80%; mp 217−218 °C; ^{1}H NMR (600 MHz, d_6-DMSO): δ 8.40 (s, 1H), 7.89 (s, 2H), 7.30 (t, J = 7.8 Hz, 1H), 7.26 (d, J = 8.4 Hz, 1H), 7.20 (s, 1H), 7.05 (d, J = 7.8 Hz, 1H), 4.10 (s, 2H), 2.63 (q, J = 7.2 Hz, 2H), 1.10 (t, J = 7.2 Hz, 3H); MS: m/z = 287.02 (M+). Anal. Calcd for $C_{14}H_{14}ClN_5$: C, 58.44; H, 4.90; N, 24.34.

6-(3,4-Dichlorobenzyl)-5-ethyl-1,2,4-triazolo[1,5-*a*]-pyrimidin-7-amine (4q). Yield: 48%; mp 256−257 °C; ^{1}H NMR (600 MHz, d_6-DMSO): δ 8.40 (s, 1H), 7.89 (s, 2H), 7.52 (d, J = 8.4 Hz, 2H), 7.41 (s, 1H), 7.06 (d, J = 7.8 Hz, 1H),4.08 (s, 2H), 2.62 (d, J = 7.8 Hz, 2H), 1.11 (t, J = 7.2 Hz, 3H); MS: m/z = 321.19 (M+). Anal. Calcd for $C_{14}H_{13}Cl_2N_5$: C, 52.19; H, 4.07; N, 21.74. Found: C, 52.23; H, 4.251; N, 21.49.

5-Benzyl-6-phenyl-1,2,4-triazolo[1,5-*a*]pyrimidin-7-amine (4r). Yield: 17%; mp 251−252 °C; ^{1}H NMR (600 MHz, d_6-DMSO): δ 8.45 (s, 1H), 7.47 (ddd, J = 24.0, 15.6, 7.8 Hz, 4H), 7.33 (d, J = 4.2 Hz, 1H), 7.25 (d, J = 6.6 Hz, 2H), 7.17 (t, J = 7.2 Hz, 2H), 7.13 (d, J = 7.2 Hz, 1H), 6.94 (d, J = 7.2 Hz, 2H), 3.78 (s, 2H); MS: m/z = 300.07 (M+). Anal. Calcd for $C_{18}H_{15}N_5$: C, 71.74; H, 5.02; N, 23.24. Found: C, 71.64; H, 5.270; N, 23.13.

5-Benzyl-6-(4-fluorophenyl)-1,2,4-triazolo[1,5-*a*]-pyrimidin-7-amine (4s). Yield: 19%; mp 248−250 °C; ^{1}H NMR (600 MHz, d_6-DMSO): δ 8.44 (s, 1H), 7.48 (s, 2H), 7.31−7.24 (m, 4H), 7.18 (t, J = 7.2 Hz, 2H), 7.14 (d, J = 7.2 Hz, 1H), 6.94 (d, J = 7.2 Hz, 2H), 3.78 (s, 2H); MS: m/z = 318.07 (M+). Anal. Calcd for $C_{18}H_{14}FN_5$: C, 67.70; H, 4.42; N, 21.93. Found: C, 67.74; H, 4.250; N, 21.88.

5-Benzyl-6-(4-chlorophenyl)-1,2,4-triazolo[1,5-*a*]-pyrimidin-7-amine (4t). Yield: 5%; mp 262−263 °C; ^{1}H NMR (600 MHz, d_6-DMSO): δ 8.44 (s, 1H), 7.52 (d, J = 8.4 Hz, 4H), 7.25 (d, J = 8.4 Hz, 2H), 7.18 (t, J = 7.2 Hz, 2H), 7.14 (d, J = 7.2 Hz, 1H), 6.95 (d, J = 7.2 Hz, 2H), 3.78 (s, 2H); MS: m/z = 334.01 (M+). Anal. Calcd for $C_{18}H_{14}ClN_5$: C, 64.38; H, 4.20; N, 20.86. Found: C, 64.17; H, 4.308; N, 20.67.

6-Benzyl-5-ethyl-1,2,4-triazolo[1,5-*a*]pyrimidin-7-amine (4u). Yield: 80%; mp 229−230 °C; ^{1}H NMR (400 MHz, $CDCl_3$) δ 8.40 (s, 1H), 7.88 (s, 2H), 7.27 (d, J = 7.2 Hz, 2H), 7.19 (d, J = 6.4 Hz, 1H), 7.12 (d, J = 6.4 Hz, 2H), 4.08 (s, 2H), 2.80−2.57 (m, 2H), 1.09 (t, J = 7.2 Hz, 3H); MS: m/z = 253.09 (M+). Anal. Calcd for $C_{14}H_{15}N_5$: C, 66.38; H, 5.97; N, 27.65. Found: C, 66.41; H, 5.842; N, 27.60.

5-Ethyl-6-phenyl-1,2,4-triazolo[1,5-*a*]pyrimidin-7-amine (4v). Yield: 60%; mp 216−218 °C; ^{1}H NMR (400 MHz, $CDCl_3$) δ 8.43 (s, 1H), 7.66−7.50 (m, 2H), 7.47 (d, J =

DOI: 10.1021/acs.jafc.5b00228
J. Agric. Food Chem. 2015, 63, 3377−3386

7.2 Hz, 1H), 7.35 (s, 2H), 7.29 (s, 2H), 2.40 (dd, J = 14.8, 7.2 Hz, 2H), 1.06 (t, J = 7.6 Hz, 3H); MS: m/z = 238.09 (M+). Anal. Calcd for $C_{13}H_{13}N_5$: C, 65.25; H, 5.48; N, 29.27. Found: C, 65.25; H, 5.48; N, 29.27.

5-Ethyl-6-(4-fluorophenyl)-1,2,4-triazolo[1,5-*a*]-pyrimidin-7-amine (4w). Yield: 57%; mp 224−225 °C; ^{1}H NMR (400 MHz, d_6-DMSO): δ 8.43 (s, 1H), 7.35 (dd, J = 20.4, 8.0 Hz, 5H), 2.40 (dd, J = 14.8, 7.2 Hz, 2H), 1.07 (t, J = 7.6 Hz, 3H); MS: m/z = 256.07 (M+). Anal. Calcd for $C_{13}H_{12}FN_5$: C, 60.69; H, 4.70; N, 27.22. Found: C, 60.72; H, 4.822; N, 27.41.

6-(4-Chlorophenyl)-5-ethyl-1,2,4-triazolo[1,5-*a*]-pyrimidin-7-amine (4x). Yield: 47%; mp 235−236 °C; ^{1}H NMR (400 MHz, d_6-DMSO): δ 8.42 (s, 1H), 7.57 (d, J = 8.0 Hz, 2H), 7.43 (s, 2H), 7.36 (d, J = 8.0 Hz, 2H), 2.40 (dd, J = 15.2, 7.6 Hz, 2H), 1.06 (t, J = 7.6 Hz, 3H); MS: m/z = 272.05 (M+). Anal. Calcd for $C_{13}H_{12}ClN_5$: C, 57.04; H, 4.42; N, 25.59. Found: C, 57.01; H, 4.527; N, 25.31.

6-(4-Bromophenyl)-5-ethyl-1,2,4-triazolo[1,5-*a*]-pyrimidin-7-amine (4y). Yield: 39%; mp 242−244 °C; ^{1}H NMR (400 MHz, d_6-DMSO): δ 8.42 (s, 1H), 7.70 (d, J = 8.0 Hz, 2H), 7.44 (s, 2H), 7.30 (d, J = 8.0 Hz, 2H), 2.47−2.23 (m, 2H), 1.07 (t, J = 7.6 Hz, 3H); MS: m/z = 316.01 (M+). Anal. Calcd for $C_{13}H_{12}BrN_5$: C, 49.07; H, 3.80; N, 22.01. Found: C, 49.01; H, 3.926; N, 22.09.

6-Phenyl-5-(trifluoromethyl)-1,2,4-triazolo[1,5-*a*]-pyrimidin-7-amine (4z). Yield: 11%; mp 279−280 °C; ^{1}H NMR (400 MHz, d_6-DMSO): δ 8.67 (s, 1H), 8.05 (s, 2H), 7.50 (d, J = 5.2 Hz, 3H), 7.36 (d, J = 7.2 Hz, 2H); MS: m/z = 279.03 (M+). Anal. Calcd for $C_{12}H_8F_3N_5$: C, 51.62; H, 2.89; N, 25.08. Found: C, 51.48; H, 3.128; N, 25.35.

Enzyme Assays. The preparation of succinate−cytochrome c reductase (SCR, mixture of respiratory complex II and bc_1 complex) from porcine heart was essentially as reported.[21] The activity of SCR was measured by monitoring the increase in absorbance of cytochrome c_1 at 550 nm, by using the extinction coefficient of 18.5 mM^{-1} cm^{-1}. The succinate−ubiquinone reductase (complex II) activity was measured by monitoring the decrease in absorbance of 2,6-dichlorophenolindophenol (DCIP) at 600 nm, by using the extinction coefficient of 21 mM^{-1} cm^{-1}. The reaction mixture may be scaled down to 1.8 mL with final concentrations of PBS (pH 7.4), 100 mM; EDTA, 0.3 mM; succinate, 20 mM; oxidized cytochrome c_1, 60 uM (or DCIP, 53 uM); and appropriate amounts of enzyme to start the reaction. The ubiquinol−cytochrome c_1 reductase (bc_1 complex) activity in catalyzing the oxidation of DBH_2 by cytochrome c_1 was assayed in 100 mM PBS (pH 7.4), 0.3 mM EDTA, 750 uM lauryl maltoside (*n*-dodecyl-β-D-maltoside), 20−120 uM DBH_2, 100 uM oxidized cytochrome c_1, and an appropriate amount of SCR. The preparation of DBH_2 from DB was carried out according to the procedure described in previous publications, and the concentration of DBH_2 was determined by measuring the absorbance difference between 288 and 320 nm by using an extinction coefficient of 4.14 mM^{-1} cm^{-1} for the calculation. For the steady-state studies, the reaction was carried out in the absence or presence of various concentrations of the inhibitor.[21]

Data Analysis. The concentrations at 50% inhibition (absolute IC_{50} values) for experiments with SCR were obtained from a nonlinear regression of the activity data according to a four parameter logistic model. The absolute IC_{50} was calculated according to eq 1.

$$y = \min + \frac{\max - \min}{1 + 10^{x - \log IC_{50}}} \quad (1)$$

Sigma Plot software 9.0 was used to determine all kinetic constants.

Computational Methods and Binding-Free-Energy Calculations. *Molecular Docking.* The three-dimensional (3D) structure of bc_1 complex was obtained from PDB database (PDB ID: 1PPJ, from bovine). The AutoDock 4.2 program[22] was applied to dock ametoctradin and its derivates into the Q_o and or Q_i site of the bc_1 complex. The Gasteiger charges were used for these inhibitors. To select the best set of docking parameters and to test the reliability of the docking results, the antimycin and stigmatellin were first docked into the Q_i and Q_o site, respectively. In the docking process, a conformational search was performed for the antimycin/stigmatellin molecule using the Solis and Wets local search method, and the Lamarckian genetic algorithm (LGA)[23,24] was applied for the conformational search of the binding complex of antimycin/stigmatellin with bc_1 complex. Among a series of docking parameters, the grid size was set to be 40 × 40 × 40, and the used grid space was the default value of 0.375 Å. The interaction energy that resulted from probing the cyt *b* with the antimycin/stigmatellin molecule was assessed by the standard AutoDock scoring function. Among a set of 100 candidates of the docked complex structures, the best one was first selected according to the interaction energy and was then compared with the conformation of antimycin/stigmatellin extracted from the crystal structure. By tuning the docking parameters, the final antimycin/stigmatellin-bc_1 complex was obtained, based on the smallest root-mean-square deviation (rmsd) of the docked conformation of antimycin/stigmatellin from its conformation in the crystal structure. The RMSD between the selected conformation and previously noted in the X-ray crystal structure is 0.84 for stigmatellin and 0.89 for antimycin (data not shown), confirming the reliability of docking parameters. The same docking parameters were adopted to perform molecular docking of other compounds.

Molecular Dynamics Simulations. All the complex structures derived from molecular docking were used as starting structures for further energy minimizations using the Sander module of the Amber8 program before the final binding structures were achieved. The Amber ff99 force field was used for amino acid and General Amber force field was used for ligands. For temperature regulation, the Langevin thermostat was used to maintain a temperature of 300 K. The bcc charges were used as the atomic charges for ligands. There are two stages for energy minimization. First, the ligand was minimized with the protein fixed. Second, the backbone atoms of the protein were fixed, and other atoms were relaxed. The final minimization was performed with both the ligand and the protein relaxed. In each step, the energy minimization was executed by using the steepest descent method for the first 1000 cycles, and the conjugated gradient method for the subsequent 3000 cycles, with a convergence criterion of 0.1 kcal mol^{-1} $Å^{-1}$. The atomic coordinates were saved every picosecond. Then, an additional 10 ns MD simulation was performed for ametoctradin-Q_o and ametoctradin-Q_i complex. In order to reduce the computational cost, only 20 ps MD simulations were performed for 12 newly synthesized analogues.

MM/PBSA Calculation. For ametoctradin-Q_o and ametoctradin-Q_i, 100 snapshots of the simulated structure within the

DOI: 10.1021/acs.jafc.5b00228
J. Agric. Food Chem. 2015, 63, 3377−3386

Scheme 1. Synthetic Route of the Title Compounds: (a) Bu^{n}Li THF −78 °C Ice Bath; (b) CH_3OK *o*-Xylene Reflux Stirred; (c) $ClSO_3H$ *o*-Xylene Stirred Reflux

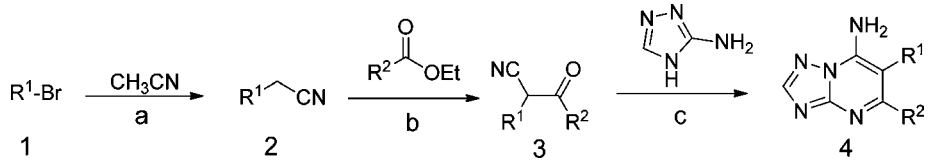

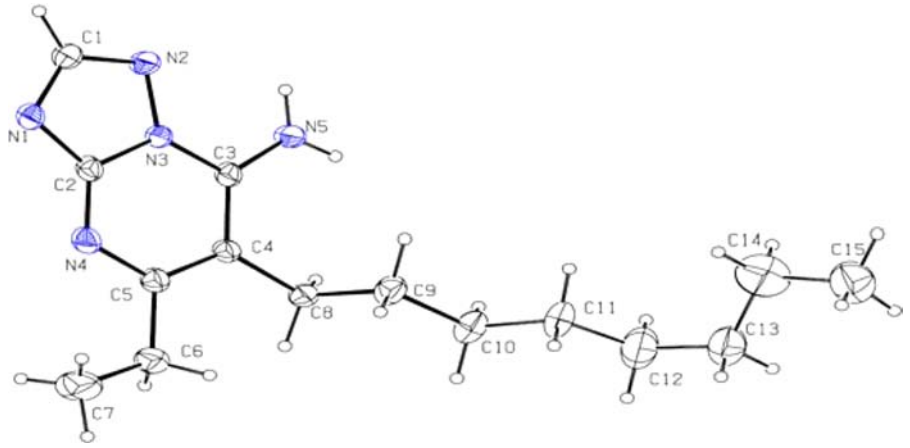

Figure 2. X-ray crystal structure of ametoctradin.

stable MD trajectory were selected and minimized to perform the MM/PBSA calculations (see below). For newly synthesized analogues, the last snapshot of the MD simulation was minimized to a convergence criterion of 0.1 kcal mol^{-1} Å^{-1}. Then, the ΔH calculation was performed on the minimized complex, as described elsewhere.[25,26]

In this method, the binding free energy of the protein−ligand complex (ΔG_{bind}) is obtained from the difference between the free energies of the protein−ligand complex (ΔG_{cpx}), the unbound receptor ($\triangle G_{rec}$), and the free ligand ($\triangle G_{lig}$) as follows:

$$\Delta G_{bind} = \triangle G_{cpx} - \triangle G_{rec} - \triangle G_{lig} \quad (2)$$

The binding free energy (ΔG_{bind}) can be evaluated as the sum of the changes in the molecular mechanical (MM) gas-phase binding energy (ΔE_{MM}), solvation free energy (ΔG_{sol}), and entropic contribution ($-T\Delta S$). The ΔE_{MM} was evaluated as a sum of electrostatic energy (ΔE_{ele}) and van der Waals interaction energy (ΔE_{vdw}).

$$\Delta G_{bind} = \Delta E_{MM} + \Delta G_{sol} - T\Delta S \quad (3)$$

$$\Delta E_{MM} = \Delta E_{ele} + \Delta E_{vdw} \quad (4)$$

The solvation free energy ΔG_{sol} was composed of two parts:

$$\Delta G_{sol} = \Delta G_{PB} + \Delta G_{np} \quad (5)$$

$$\Delta G_{np} = \gamma SASA + \beta \quad (6)$$

The electrostatic contribution to the solvation free energy (ΔG_{PB}) is evaluated by Poisson−Boltzmann (PB) methods. The nonpolar solvation energy, ΔG_{np}, can be estimated by an empirical relation of $\Delta G_{np} = \gamma SASA + \beta$, where SASA and is defined as the solvent-accessible surface area, and the solvation parameters γ and β were set to 0.00542 kcal·mol^{-1} Å^{-2} and 0.92 kcal·mol^{-1}, respectively. The dielectric constant for the molecule and surrounding solvent were set to 1 and 80, and the probe radius of the solvent was set to 1.4 Å.

The entropy contribution to the binding free energy can be divided into two parts: the solvation free entropy (ΔS_{solv}) and the conformational free entropy (ΔS_{conf}).

$$\Delta S_{sol} = \Delta S_{solv} + \Delta S_{conf} \quad (7)$$

The solvation free entropy is gained by the tendency of water molecules to minimize their contacts with hydrophobic groups in protein. The conformational free entropy is related to the change of the number of rotatable bonds during the binding process. The detailed computational procedure used to evaluate the entropy contribution ($-T\Delta S$) to the binding free energy was as previously described.[26]

RESULTS AND DISCUSSION

Synthetic Chemistry of the Title Compounds. As shown in Scheme 1, the target compounds **4a** ∼ **z** were smoothly prepared by a three-step synthetic route using bromide compound as starting materials. Compound **2**, resulting from the reaction of bromide compound with acetonitrile, underwent an elimination reaction with substituent ester to afford the key intermediates β-ketonitriles (**3**). By performing the cyclization reaction with 1,2,4-triazol-3-amine, compound **3** was successfully transformed into the corresponding substituted 1,2,4-triazolo[1,5-*a*]pyrimidine derivates **4a** ∼ **z**.

The structures of all synthesized compounds were characterized by element analyses, ^{1}H NMR, and GC-MS techniques. The crystal structure of ametoctradin was determined by X-ray diffraction analysis (CCDC 981965). As shown in Figure 2, the crystal structure showed that ametoctradin had an extended conformation.

Inhibition Effect against *bc*$_1$ Complex of Compounds 4a ∼ z. SCR is the mixture of respiratory complex II and the *bc*$_1$ complex (complex III), which was also deemed to form complex II−complex III supercomplexes.[27] Complex II (also

DOI: 10.1021/acs.jafc.5b00228
J. Agric. Food Chem. 2015, 63, 3377−3386

Table 1. Percent Inhibition and IC_{50} Value of the Title Compounds against Porcine SCR

no.	R^1	R^2	% inhibition (100 μM)	IC_{50} (μM)
4a	$CH_3(CH_2)_6CH_2$[a]	4-CH_3−Ph	82%	0.12 ± 0.01
4b	$CH_3(CH_2)_6CH_2$[a]	3-CF_3−Ph	75.5%	36.33 ± 1.23
4c	$CH_3(CH_2)_6CH_2$[a]	3-Cl-Ph	77.6%	0.15 ± 0.01
4d	$CH_3CH_2CH_2$[a]	CH_3CH_2	24.1%	/[b]
4e	$PhCH_2$	Ph	<10%	/
4f	$PhCH_2$	$CF_3CH_2CH_2$	12.6%	/
4g	4-Br-$PhCH_2$	CH_3CH_2	68.9%	24.89 ± 1.32
4h	4-F-$PhCH_2$	CH_3CH_2	23.0%	/
4i	3-Br-$PhCH_2$	CH_3CH_2	72.5%	26.82 ± 1.44
4j	2-F-$PhCH_2$	CH_3CH_2	29.3%	/
4k	2-Br-$PhCH_2$	CH_3CH_2	57.5%	82.62 ± 1.35
4l	3-F-$PhCH_2$	CH_3CH_2	16.7%	/
4m	3-I-$PhCH_2$	CH_3CH_2	84.1%	10.90 ± 1.27
4n	2-Cl-$PhCH_2$	CH_3CH_2	48.2%	/
4o	4-CF_3O-$PhCH_2$	CH_3CH_2	94.3%	5.56 ± 1.13
4p	3-Cl-$PhCH_2$	CH_3CH_2	65.0%	42.27 ± 1.24
4q	34-Cl_2−$PhCH_2$	CH_3CH_2	92.8%	4.00 ± 1.14
4r	Ph[a]	$PhCH_2$	<10%	/
4s	4-F-Ph[a]	$PhCH_2$	16.3%	/
4t	4-Cl-Ph[a]	$PhCH_2$	12.3%	/
4u	$PhCH_2$	CH_3CH_2	<10%	/
4v	Ph[a]	CH_3CH_2	36.7%	/
4w	4-F-Ph[a]	CH_3CH_2	14.2%	/
4x	4-Cl-Ph[a]	CH_3CH_2	70.0%	33.20 ± 1.30
4y	4-Br-Ph[a]	CH_3CH_2	76.4%	25.14 ± 1.26
4z	Ph[a]	CF_3	37.9%	/
ametoctradin	$CH_3(CH_2)_6CH_2$[a]	CH_3CH_2	100%	0.30 ± 0.02

[a]Meaning that the substituted 2 could be purchased. [b]Not tested.

known as succinate-ubiquinone oxidoreductase, SQR) first passes electrons from succinate to ubiquinone, and then the cytochrome bc_1 complex passes electrons from reduced ubiquinone to cytochrome c_1. The activity of complex II in SCR was selectively determined using succinate and dichlorophenolindophenol (DCIP) as substrates, and the activity of only the cytochrome bc_1 complex in SCR was determined using decylubiquinol (DBH_2) and cytochrome c_1 as substrates, whereas the overall activity of SCR (both complex II and bc_1 complex) was determined using succinate and cytochrome c_1 as substrates.[28,29]

The results indicated that all of the compounds exhibited no effect on the activity of complex II (data not shown) but markedly inhibited the activities of the bc_1 complex and SCR. As shown in Table 1, some compounds showed very high percent inhibition, such as **4a** (82%), **4q** (92.8%), **4o** (94.3%), **4m** (84.1%), against porcine SCR. To reduce the time and workload of the biological assay, the IC_{50} values of some compounds were not determined when its percent inhibition was less than 50%. Among the **26** newly synthesized compounds, **4a** was identified as the most potent inhibitor with a IC_{50} value of 0.12 μM against SCR from porcine heart mitochondria (Table 1), which indicated that the potency of **4a** against porcine SCR is nearly twice as much as ametoctradin (0.3 μM). In addition, when R^1 was $-CH_2(CH_2)_6CH_3$ and or substituent $-CH_2Ph$, the inhibitor always displayed much higher potency against porcine SCR, such as compound **4a**, **4c**, **4m**, **4o**, and **4q**. Remarkably, 2-substituent and or 3-substituent benzyl derivatives in R^1 displayed lower antifungal activity compared with the 4-substituent. These results indicated that the substituent on R^1 will affect the bioactive conformation of inhibitors, which would lead to different binding free energy of a ligand toward the protein and would be discussed in the following section.

Binding Mode of Ametoctradin. Although ametoctradin has been known as inhibitor of cytochrome bc_1 complex for many years, its detailed binding mode is still unknown so far. Many existing studies have shown that molecular docking is a very powerful technique to predict the binding mode of ligands;[30−34] therefore, the AutoDock4.2 program was integrated with the molecular dynamic simulations and MM/PBSA calculation to uncover the detailed binding mode of ametoctradin.

Before docking, sequence alignment of cytochrome bc_1 complex from different species was performed (the data were included in the Supporting Information). The bovine cytochrome b (1PPJ)[35] showed about 50.92% sequence identity with yeast (3CX5),[36] 74.67% with chicken (1BCC),[11] 49.08% with *Rhodobacter capsulates* (1ZRT),[37] and 48.02% with *Paracoccus denitrificans* (2YIU).[38] In addition, the residues around the Q_o-site region are highly conserved. Up to now, most crystal structures of inhibitor-bound bc_1 complex are from vertebrate heart, such as bovine and chicken. Previously, we used the bovine bc_1 complex (PDB ID: 1PPJ) as the receptor model to study the binding mode of some new Q_o-site inhibitors, which successfully guided the design of a series of new subnanomolar, even picomolar, Q_o site inhibitors of bc_1 complex.[39,40] Hence, the bovine PDB crystal structure (1PPJ) was selected herein as receptor model.

As mentioned before, there are two binding sites in the cytochromore bc_1 complex, a quinone reduction site near the negative side of the membrane (Q_i site) and a quinol oxidation

DOI: 10.1021/acs.jafc.5b00228
J. Agric. Food Chem. 2015, 63, 3377−3386

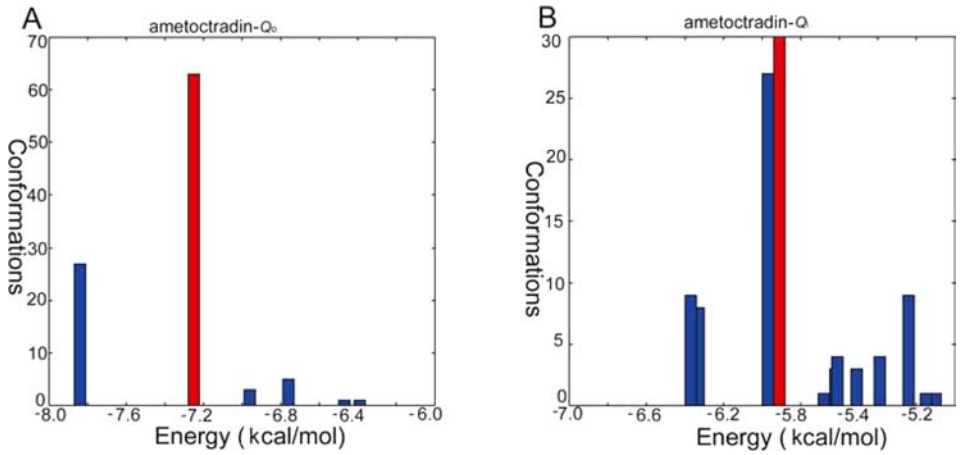

Figure 3. Binding energy of ametoctradin with bc_1 complex in Q_o (A) and Q_i (B) site. The red and blue histogram means the right and wrong binding mode, respectively. The figure was directly obtained from AutoDock cluster analysis with default parameters. Based on our knowledge, the 1,2,4-triazolo[1,5-*a*]pyrimidine ring in ametoctradin should locate into the $Q_{o/i}$-site, and then this binding mode cluster was defined as right. On the contrary, it was defined as wrong when 1,2,4-triazolo[1,5-*a*]pyrimidine ring pointed to other position in $Q_{o/i}$-site, such as the entrance of $Q_{o/i}$-site.

Table 2. Binding Free Energy of Ametoctradin in the Q_o and Q_i site (kcal/mol)

	AutoDock binding energy	ΔE_{ele}[a]	ΔE_{VDW}[a]	ΔE_{np}[a]	ΔE_{pol}[a]	ΔH_{PB}[a]
ametoctradin-Q_i	−6.0	−15.49	−38.97	−5.16	38.50	−21.11
ametoctradin-Q_o	−7.0	−18.27	−46.23	−5.10	45.15	−24.46

[a]Obtained from 10 ns MD simulation.

site close to the positive side of the membrane (Q_o site). Then, we, respectively, docked ametoctradin into the Q_o and Q_i sites, and obtained two ametoctradin-bound complexes, ametoctradin−Q_o and ametoctradin−Q_i complex (Figure 1S, Supporting Information). As shown in Figure 3, the Q_o site binding energy of ametoctradin (about −7.0 kcal/mol) was more favorable than the Q_i site binding energy (about −6.0 kcal/mol), showing that ametoctradin might be a Q_o site inhibitor. Then, we performed 10 ns molecular dynamics (MD) simulations for ametoctradin−Q_o and ametoctradin−Q_i complex (Figure 2S, Supporting Information), and the 100 snapshots obtained from the last 1 ns of each complex were used to calculate the binding free energy using MM/PBSA module. As shown in Table 2, the binding energies (ΔH) of ametoctradin−Q_o and ametoctradin−Q_i are −24.46 and −21.11 kcal/mol, respectively. It is necessary to point out that, if we prolonged the simulation time (e.g., 12 ns), ametoctradin would leave from the ametoctradin−Q_i complex, whereas the ametoctradin−Q_o complex remains very stable (data not shown). On the basis of these results, we proposed that ametoctradin should bind into the Q_o site of bc_1 complex.[41]

It is very interesting to compare the MD-simulated ametoctradin−Q_o complex with the existing crystal structures of Q_o site inhibitor-bound bc_1 complex. According to the reported crystal structures of Q_o site inhibitor-bound bc_1 complex,[4] the E271 and F274 would always form an H-bond and hydrophobic interaction with the inhibitor, indicating that both residues played an important role in the binding of Q_o site inhibitors.[39,40,42] For example, stigmatellin forms an H-bond with E271 and H161 and hydrophobic interaction with F274 (PDB code: 1PPJ)[35] (Figure 4A). As shown in Figure 4B, the amine group of ametoctradin also formed an H-bond with E271, and the aliphatic chain of ametoctradin formed a hydrophobic interaction with F274, F128, I146, L149, and L294 when binding into the Q_o site. As we knew, the long

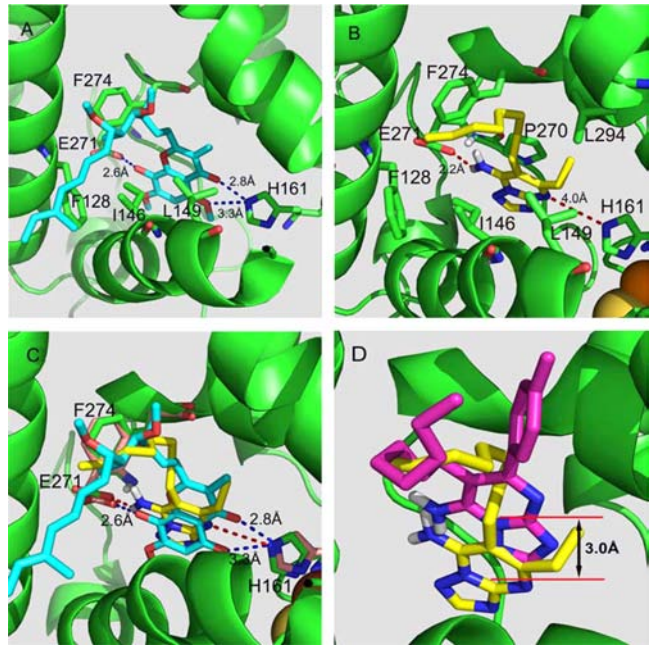

Figure 4. (A) Binding mode of stigmatellin in the Q_o site. The blue line represents the H-bond distance between stigmatellin and residue. (B) Binding mode of ametoctradin in the Q_o site. The red line represents the H-bond distance between ametoctradin and residue. (C) The overlay of ametoctradin and stigmatellin in the Q_o site. For clarity, only the key residues were shown. The blue line represents the H-bond distance between stigmatellin and the residue. (D) The overlay of ametoctradin and **4a** in the Q_o site.

aliphatic substituent in antimycin and stigmatellin adopted an extended conformation in the crystal complex structure (PDB code: 1PPJ). Therefore, it was reasonable that the octyl group in ametoctradin also took on an extended conformation, and

DOI: 10.1021/acs.jafc.5b00228
J. Agric. Food Chem. 2015, 63, 3377−3386

then 1,2,4-triazolo[1,5-*a*]pyrimidine ring in ametoctradin formed a hydrophobic interaction with P270. However, the distance between ametoctradin and H161 is 4.0 Å, which could account for the reason why ametoctradin (IC_{50} = 0.3 μM) has lower binding affinity than stigmatellin (IC_{50} = 2.4 nM for bc_1 complex from bovine heart) (Figure 4C,D).[43,44]

As we know,[45] the G143A mutation showed a nearly killing effect upon all of strobilurin inhibitors, whereas ametoctradin did not show cross-resistance to strobilurin fungicides.[16,17] The resistance mechanism for G143A mutation was that residue A143 would create steric hindrance between the methoxyacrylamide moiety of inhibitor and cytochrome *b*.[44,46] Schiffer et al.[47,48] had pointed out that the residue mutation would lead to less effect upon ligand activity with longer distance between ligand and residue. Therefore, we monitored the distance between ametoctradin with G143. As shown in Figure 5A, the closest distance between Gly143 and ametoctradin was about 4.2 Å, while it decreased to 3.6 Å with azoxystrobin (1SQB). The binding free energy of azoxystrobin upon G143A mutant and wild type bc_1 complex were, respectively, −23.59 kcal/mol and −26.74 kcal/mol (IC_{50} = 21 nM toward wild type bc_1 complex from yeast; IC_{50} = 1394 nM toward G143A mutant bc_1 form yeast[44]), which accounted for the resistance mechanism of G143A mutation to azoxystrobin. On the contrary, the closest distance between Gly143 in wide type bc_1 complex and ametoctradin was about 4.2 Å, while the closest distance between A143 in mutant bc_1 complex and ametoctradin decreased to 3.7 Å (Figure 5B). As a result, the binding free energy of ametoctradin upon G143A mutant and wild type bc_1 complex were −25.61 kcal/mol and −21.68 kcal/mol, respectively, which means G143A mutation increased the binding affinity of ametoctradin. These results showed that the established binding mode of ametoctradin should be reasonable.

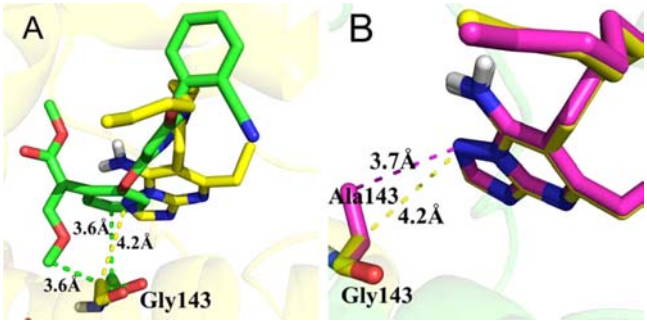

Figure 5. (A) Binding mode overlay between ametoctradin (yellow sticks) and azoxystrobin (PDB code 1SQB, green sticks). (B) The binding mode overlay of ametoctradin with wide type bc_1 complex (yellow stick) and G143A mutation (magenta stick). For clarity, only Gly143 or Ala143 was shown as a stick.

Binding-Free-Energy Calculation. In order to further confirm the binding mode of ametoctradin and understand the structure−activity relationships of ametoctradin analogues at the atomic level, we carried out molecular docking for 12 newly synthesized analogues with determined IC_{50} values and calculated their binding free energies using MM/PBSA method for the resulted analogue−Q_o and analogue−Q_i complex (Table 3), respectively.

For the analogue−Q_o complex, the correlation coefficients (R^2) between the experimental binding free energies (ΔG_{exp}, derived from the experimental binding affinities) and the calculated energy terms are 0.20 for enthalpy contribution (ΔH) and 0.64 for entropy compensation ($-T\Delta S$). Although these individual correlations are very low, the overall calculated binding free energies (ΔG_{cal}) correlated very well (R^2 = 0.96) with the experimental binding free energies (ΔG_{exp}) (Figure 6).

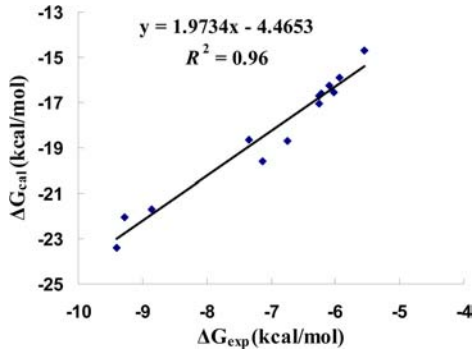

Figure 6. Correlation between the ΔG_{cal} and ΔG_{exp}.

Table 3. Individual Energy Terms of the Calculated Free Energy of Title Compounds (kcal/mol)

	Q_o			Q_i			
no.	ΔH	$-T\Delta S$	ΔG_{cal}	ΔH	$-T\Delta S$	ΔG_{cal}	ΔG_{exp}[a]
4a	−31.98	8.59	−23.39	−30.20	8.05	−22.15	−9.41
4b	−28.24	11.67	−16.57	−29.31	11.35	−17.96	−6.03
4c	−31.15	9.10	−22.05	−30.38	8.37	−22.01	−9.27
4g	−31.94	14.88	−17.06	−23.97	5.83	−18.14	−6.26
4i	−30.45	13.87	−16.58	−23.26	4.00	−19.26	−6.21
4k	−29.76	15.07	−14.69	−24.76	4.03	−20.73	−5.55
4m	−33.06	14.37	−18.69	−22.80	3.83	−18.97	−6.74
4o	−35.45	15.89	−19.58	−30.73	10.93	−19.80	−7.10
4p	−29.97	14.06	−15.91	−21.63	5.60	−16.03	−5.94
4q	−30.67	12.01	−18.66	−21.94	5.66	−16.28	−7.34
4x	−29.59	13.36	−16.23	−25.88	7.91	−17.97	−6.09
4y	−30.34	13.64	−16.70	−26.78	10.69	−18.14	−6.25
ametoctradin	−32.94	11.26	−21.68	−29.32	9.27	−20.05	−8.86
R^2[b]	0.20	0.64	0.96	0.06	0.21	0.0047	1.00

[a] $\Delta G_{exp} = -RT \times \ln IC_{50}$. [b] The correlation between ΔG_{exp} and the individual energy terms of the calculated free energy

DOI: 10.1021/acs.jafc.5b00228
J. Agric. Food Chem. 2015, 63, 3377−3386

However, for the analogue−Q_i complex, when the compounds were docked into the Q_i site, the corresponding R^2 values between ΔG_{exp} and the calculated energy terms were decreased to 0.06 for ΔH, 0.21 for $-T\Delta S$, and 0.0047 for ΔG_{cal}, respectively. Therefore, these molecular docking and binding free energy calculation results further confirmed that ametoctradin and its analogues should binding to the Q_o site of bc_1 complex.

It is very interesting to analyze the contribution of the individual energy terms. Although the enthalpy contribution (ΔH) always reflects the direct interaction between ligand and receptor, and plays an important role in the binding of ligand, the binding free energy arises from a more complex interplay between the enthalpy (ΔH) and entropy ($-T\Delta S$) terms. For the composition of enthalpy (ΔH) term, the ΔE_{VDW} (ranging from −43.83 to 49.27 kcal/mol) and the ΔE_{pol} (ranging from 31.25 to 45.10 kcal/mol) are two largest components of the binding free energy for each complex (Table 1S, Supporting Information). For the analogues bearing R^1 = $-CH_2(CH_2)_6CH_3$, their entropy term($-T\Delta S$, ranging from 8.59 to 11.67 kcal/mol) is lower than that of other compounds, but their binding affinity is higher than that of other compounds, such as **4a** (IC_{50} = 0.12 μM) and **4c** (IC_{50} = 0.15 μM). These result indicated that the R^1 group has an important role in the entropy compensation, which is a critical aspect for the binding of ametoctradin and its analogues.

The mode of ametoctradin−Q_o complex is shown in Figure 4B. As shown in Figure 4B, the octyl (R^1 group) of ametoctradin pointed to the outside of the Q_o pocket, whereas its ethyl (R^2) group inserted inside the Q_o pocket. As a result, when R^2 was a bulky group, such as substituted phenyl (4-CH_3−Ph, 3-CF_3−Ph, and 3-Cl-Ph), the compound (**4a**, **4b**, and **4c**) would move up about 3.0 Å compared to ametoctradin (Figure 4D) due to steric clash. It should be pointed out that this movement will lead to an entropy compensation, which is favorable to the binding of inhibitors.

In summary, a series of novel 1,2,4-triazolo[1,5-*a*]pyrimidine derivates **4a** ∼ **z** were designed and synthesized using ametoctradin as a lead compound. The in vitro assay indicated that compound **4a**, 6-octyl-5-*p*-tolyl-1,2,4-triazolo[1,5-*a*]-pyrimidine-7-amine, is a new inhibitor of bc_1 complex with higher binding affinity (IC_{50} = 0.12 μM) against porcine bc_1 complex than ametoctradin (IC_{50} = 0.30 μM). In addition, the results of molecular docking, molecular dynamics simulations, and MM/PBSA calculations strongly supported that ametoctradin and its analogues should bind to the Q_o site rather than the Q_i site of cytochrome bc_1 complex. Inside the Q_o pocket, ametoctradin and its analogues formed an H-bond with E721 and hydrophobic interactions with F274, F128, I146, L149, and L294.

On the basis of the results obtained from the present study, the following guidance for the future inhibitor design could be proposed: (1) 1,2,4-triazolo[1,5-*a*]pyrimidine should be substituted to form an H-bond with H161, a key residue for the binding of inhibitor; (2) Introduction of a bulky and hydrophobic group onto R^2 position is favorable to the binding due to their contribution to the entropy compensation.

■ ASSOCIATED CONTENT

Supporting Information

Supplemental cluster results showed the sequence alignment of bc_1 complex from different species. Figure 1S describes the binding mode of ametoctradin in the Q_i site, and Figure 2S describes the RMSD change during MD simulations for ametoctradin-Q_o/Q_i. Table 1S shows the individual energy terms of the calculated free energy of title compounds. This material is available free of charge via the Internet at http://pubs.acs.org.

■ AUTHOR INFORMATION

Corresponding Author

*E-mail: gfyang@mail.ccnu.edu.cn. Tel.: 86-27-67867800. Fax: 86-27-67867141.

Funding

The research was supported in part by the National Key Technologies R&D Program (2011BAE06B05) and the National Natural Science Foundation of China (No. 21472065).

Notes

The authors declare no competing financial interest.

■ REFERENCES

(1) Kim, H.; Xia, D.; Yu, C. A.; Xia, J. Z.; Kachurin, A. M.; Zhang, L.; Yu, L.; Deisenhofer, J. Inhibitor binding changes domain mobility in the iron-sulfur protein of the mitochondrial bc1 complex from bovine heart. *Proc. Natl. Acad. Sci. U.S.A.* **1998**, *95*, 8026−8033.

(2) Gao, X. G.; Wen, X. L.; Yu, G. A.; Esser, L.; Tsao, S.; Quinn, B.; Zhang, L.; Yu, L. D.; Xia, D. The crystal structure of mitochondrial cytochrome bc_1 in complex with famoxadone: the role of aromatic-aromatic interaction in inhibition. *Biochemistry.* **2002**, *41*, 11692−11702.

(3) Berry, E. A.; Huang, L. S. Observations concerning the quinol oxidation site of the cytochrome bc_1 complex. *FEBS Lett.* **2003**, *555*, 13−20.

(4) Esser, L.; Quinn, B.; Li, Y. F.; Zhang, M. Q.; Elberry, M.; Yu, L. D.; Yu, C. A.; Xia, D. Crystallographic studies of quinol oxidation site inhibitors: a modified classification of inhibitors for the cytochrome bc_1 complex. *J. Mol. Biol.* **2004**, *341*, 281−302.

(5) Wang, F.; Hui, L.; Wang, L.; Yang, W. C.; Wu, J. W.; Yang, G. F. Design, syntheses, and kinetic evaluation of 3-(phenylamino)-oxazolidine-2,4-diones as potent cytochrome bc_1 complex inhibitors. *Bioorg. Med. Chem.* **2011**, *19*, 4608−4615.

(6) Berry, E. A.; Huang, L. S. Conformationally linked interaction in the cytochrome bc_1 complex between inhibitors of the Q_o site and the Rieske iron-sulfur protein. *Biochim. Biophys. Acta* **2011**, *1807*, 1349−1363.

(7) Huang, L. S.; Shen, J. T.; Wang, A. C.; Berry, E. A. Crystallographic studies of the binding of ligands to the dicarboxylate site of Complex II, and the identity of the ligand in the "oxaloacetate-inhibited" state. *Biochim. Biophys. Acta* **2006**, *1757*, 1073−1083.

(8) Mitchell, P. Possible molecular mechanisms of the protonmotive function of cytochrome systems. *J. Theor. Biol.* **1976**, *62*, 267−327.

(9) Berry, E. A.; Huang, L. S.; Lee, D. W.; Daldal, F.; Nagai, K.; Minagawa, N. Ascochlorin is a novel, specific inhibitor of the mitochondrial cytochrome bc_1 complex. *Biochim. Biophys. Acta* **2010**, *1797*, 360−370.

(10) Gutierrez-Cirlos, E. B.; Merbitz-Zahradnik, T.; Trumpower, B. L. Inhibition of the yeast cytochrome bc_1 complex by ilicicolin H, a novel inhibitor that acts at the Q_N site of the bc_1 complex. *J. Biol. Chem.* **2004**, *279*, 8708−8714.

(11) Zhang, Z.; Huang, L.; Shulmeister, V. M.; Chi, Y. I.; Kim, K. K.; Hung, L. W.; Crofts, A. R.; Berry, E. A.; Kim, S. H. Electron transfer by domain movement in cytochrome bc_1. *Nature.* **1998**, *392*, 677−684.

(12) Iwata, S.; Lee, J. W.; Okada, K.; Lee, J. K.; Iwata, M.; Rasmussen, B.; Link, T. A.; Ramaswamy, S.; Jap, B. K. Complete structure of the 11-subunit bovine mitochondrial cytochrome bc_1 complex. *Science.* **1998**, *281*, 64−71.

(13) Esser, L.; Yu, C. A.; Xia, D. Structural Basis of Resistance to Anti-Cytochrome bc1 complex Inhibitors: Implication for Drug Improvement. *Curr. Pharm. Design.* **2014**, *20*, 704−724.

DOI: 10.1021/acs.jafc.5b00228
J. Agric. Food Chem. 2015, 63, 3377−3386

(14) Berry, E. A.; Guergova-Kuras, M.; Huang, L.; Crofts, A. R. Structure and function of cytochrome bc_1 complexes. *Annu. Rev. Biochem.* **2000**, *69*, 1005−1075.
(15) Gao, X.; Wen, X.; Esser, L.; Quinn, B.; Yu, L.; Yu, C. A.; Xia, D. Structural basis for the quinone reduction in the bc_1 complex: a comparative analysis of crystal structures of mitochondrial cytochrome bc_1 with bound substrate and inhibitors at the Q_i site. *Biochemistry.* **2003**, *42*, 9067−9080.
(16) Gold, R.; Scherer, M.; Rether, J.; Speakman, J.; Navé, B.; Levy, T.; Storer, R.; Marris. D. Initium® -An Innovative Fungicide of a New Chemical Class for the Control of Oomycetes, *Proceedings of BCPC Congress*, Glasgow, U.K., November 9−11, 2009.
(17) Chai, B. S.; Fu, C. X.; Sun, X. F.; Li, Q.; Li, Z. N.; Li, Z. N. Synthesis of Ametoctradin and Its Bioactivity. *Agrochemicals.* **2012**, *51*, 645−674.
(18) Grammenos, W.; Gewehr, M.; Mueller, B.; Blettner, C.; Blasco, J. T. I. 5, 6-Dialkyl-7-Aminotriazolopyrimidines, their Preparation and their Use for Controlling Harmful Fungi, and Compositions Comprising these Compounds. U.S. Patent No. US20080119493, 2005.
(19) Dietz, J.; Grotz, T.; Grammenos, W.; Muller, B.; Lohmann, J. K.; Renner, J.; Ulmschneider, S.; Tormo, I. B. J. Use of Substituted Triazolopyrimidines for Controlling Phytopathogenic Harmful Fungi. Patent No. WO 2007113136, 2007.
(20) Vogelbacher, U. J.; Otto, P.; Rack, M. Method for the production of beta-ketonitriles. U.S. Patent No. US20100105903, 2008.
(21) King, T. E. Preparations of succinate-cyto-chrome reductase and the cytochrome bc_1 particle, and reconstitution of succinate-cytochrome c reductase. *Methods Enzymol.* **1967**, *10*, 216−225.
(22) Morris, G. M.; Huey, R.; Lindstrom, W.; Sanner, M. F.; Belew, R. K.; Goodsell, D. S.; Olson, A. J. Autodock4 and AutoDockTools4: automated docking with selective receptor flexiblity. *J. Comput. Chem.* **2009**, *30*, 2785−2791.
(23) Morris, G. M.; Goodsell, D. S.; Halliday, R. S.; Huey, R.; Hart, W. E.; Belew, R. K.; Olson, A. J. Automated docking using a lamarckian genetic algorithm and an empirical binding free energy function. *J. Comput. Chem.* **1998**, *19*, 1639−1662.
(24) Sitkoff, D.; Sharp, K. A.; Honig, B. Accurate calculation of hydration free energies using macroscopic solvent models. *J. Phys. Chem.* **1994**, *98*, 1978−1988.
(25) Connolly, M. L. Analytical molecular surface calculation. *J. Appl. Crystallogr.* **1983**, *16*, 548−558.
(26) Pan, Y. M.; Gao, D. Q.; Zhan, C. G. Modeling the catalysis of anti-cocaine catalytic antibody: competing reaction pathways and free energy barrier. *J. Am. Chem. Soc.* **2008**, *130*, 5140−5149.
(27) Chen, J.; Chen, C. L.; Alevriadou, B. R.; Zweier, J. L.; Chen, Y. R. Excess NO predisposes mitochondrial succinate−cytochrome c reductase to produce hydroxyl radical. *Biochim. Biophys. Acta* **2011**, *1807*, 491−502.
(28) Zhu, X. L.; Xiong, L.; Li, H.; Song, X. Y.; Liu, J. J.; Yang, G. F. Computational and Experimental Insight into the Molecular Mechanism of Carboxamide Inhibitors of Succinate-Ubquinone Oxidoreductase. *ChemMedChem.* **2014**, *9*, 1512−1521.
(29) Li, H.; Zhu, X. L.; Yang, W. C.; Yang, G. F. Comparative Kinetics of Q_i Site Inhibitors of Cytochrome bc_1 Complex: Picomolar Antimycin and Micromolar Cyazofamid. *Chem. Biol. Drug Des.* **2013**, *83*, 71−80.
(30) Zhu, X. L.; Yang, W. C.; Yu, N. X.; Yang, S. G.; Yang, G. F. Computational Simulations of Structural Role of the Active-site W374C Mutation of Acetyl-Coenzyme-A Carboxylase: Multi-drug Resistance Mechanism. *J. Mol. Model.* **2011**, *17*, 495−503.
(31) Zhu, X. L.; Hao, G. F.; Zhan, C. G.; Yang, G. F. Computational Simulations of the Interactions between Acetyl-Coenzyme-A Carboxylase and Clodinafop: Resistance Mechanism Due to Active and Nonactive Site Mutations. *J. Chem. Inf. Model.* **2009**, *49*, 1936−1943.
(32) Hao, G. F.; Zhu, X. L.; Ji, F. Q.; Zhang, L.; Yang, G. F.; Zhan, C. G. Understanding Mechanism of Drug Resistance Due to a Codon Deletion in Protoporphrinogen Oxidase through Computational Modeling. *J. Phys. Chem. B* **2009**, *113*, 4865−4875.
(33) Hao, G. F.; Yang, G. F.; Zhan, C. G. Computational Mutation Scanning and Drug Resistance Mechanisms of HIV-1 Protease Inhibitors. *J. Phys. Chem. B* **2010**, *114*, 9663−9676.
(34) Chen, H.; Zhang, Y.; Ye, C.; Feng, T. T.; Han, J. G. Insight into the binding modes and inhibition mechanisms of adamantyl-based 1,3-disubstituted urea inhibitors in the active site of the human soluble epoxide hydrolase. *J. Biomol. Struct. Dyn.* **2014**, *32*, 1231−1247.
(35) Huang, L. S.; Cobessi, D.; Tung, E. Y.; Berry, E. A. Binding of the Respiratory Chain Inhibitor Antimycin to the Mitochondrial bc_1 Complex: A New Crystal Structure Reveals an Altered Intramolecular Hydrogen-bonding Pattern. *J. Mol. Biol.* **2005**, *351*, 573−597.
(36) Solmaz, S. R.; Hunte, C. Structure of complex III with bound cytochrome c in reduced state and definition of a minimal core interface for electron transfer. *J. Biol. Chem.* **2008**, *283*, 17542−17549.
(37) Berry, E. A.; Huang, L. S.; Saechao, L. K.; Pon, N. G.; Valkova-Valchanova, M.; Daldal, F. X-Ray Structure of Rhodobacter Capsulatus Cytochrome bc_1: Comparison with its Mitochondrial and Chloroplast Counterparts. *Photosynth. Res.* **2004**, *81*, 251−275.
(38) Kleinschroth, T.; Castellani, M.; Trinh, C. H.; Morgner, N.; Brutschy, B.; Ludwig, B.; Hunte, C. X-ray structure of the dimeric cytochrome bc_1 complex from the soil bacterium Paracoccus denitrificans at 2.7-Å resolution. *Biochim. Biophys. Acta* **2011**, *1807*, 1606−1615.
(39) Hao, G. F.; Wang, F.; Li, H.; Zhu, X. L.; Yang, W. C.; Huang, L. S.; Wu, J. W.; Berry, E. A.; Yang, G. F. Computational Discovery of Picomolar Q_o Site Inhibitors of Cytochrome bc_1 Complex. *J. Am. Chem. Soc.* **2012**, *134*, 11168−11176.
(40) Zhao, P. L.; Wang, L.; Zhu, X. L.; Huang, X.; Zhan, C. G.; Wu, J. W.; Yang, G. F. Subnanomolar Inhibitor of Cytochrome bc_1 Complex Designed by Optimizing Interaction with Conformationally Flexible Residues. *J. Am. Chem. Soc.* **2010**, *132*, 185−194.
(41) Zhu, X. L.; Zhang, M. M.; Yang, G. F. Synthesis and fungicidal activity of novel ametoctradin derivates, *248th American Chemical Society National Meeting & Exposition*, San Francisco, California, August 10−14, 2014 (http://abstracts.acs.org/chem/248nm/program/view.php?obj_id=261551&terms).
(42) Xiao, Y. M.; Esser, L.; Zhou, F.; Li, C.; Zhou, L. H.; Yu, C. A.; Qin, Z. H.; Xia, D. Studies on Inhibition of Respiratory Cytochrome bc_1 Complex by the Fungicide Pyrimorph Suggest a Novel Inhibitory Mechanism. *PLoS One* **2014**, *9*, e93765.
(43) Biagini, G. A.; Fisher, N.; Berry, N.; Stocks, P. A.; Meunier, B.; Williams, D. P.; Bonar-Law, R.; Bray, P. G.; Owen, A.; O'Neill, P. M.; Ward, S. A. Acridinediones: Selective and Potent Inhibitors of the Malaria Parasite Mitochondrial bc_1 Complex. *Mol. Pharmacol.* **2008**, *73*, 1347−55.
(44) Fisher, N.; Meunier, B. Re-examination of inhibitor resistance conferred by Q_o-site mutations in cytochrome *b* using yeast as a model system. *Pest Manag. Sci.* **2005**, *61*, 973−978.
(45) Mutations associated with Qo-I-resistance (2014). http://www.frac.info.
(46) Gisi, U.; Sierotzki, H.; Cook, A.; McCaffery, A. Mechanisms influencing the evolution of resistance to Q_o inhibitor fungicides. *Pest Manag. Sci.* **2002**, *58*, 859−867.
(47) Özen, A.; Haliloglu, T.; Schiffer, C. A. HIV-1 Protease and Substrate Coevolution Validates the Substrate Envelope as the Substrate Recognition Pattern. *J. Chem. Theory Comput.* **2012**, *8*, 703−714.
(48) Altman, M. D.; Ali, A.; Reddy, G. S.; Nalam, M. N.; Anjum, S. G.; Cao, H.; Chellappan, S.; Kairys, V.; Fernandes, M. X.; Gilson, M. K.; Schiffer, C. A.; Rana, T. M.; Tidor, B. HIV-1 protease inhibitors from inverse design in the substrate envelope exhibit subnanomolar binding to drug-resistant variants. *J. Am. Chem. Soc.* **2008**, *130*, 6099−6113.

DOI: 10.1021/acs.jafc.5b00228
J. Agric. Food Chem. 2015, 63, 3377−3386

Table 1. RSM Central Composite Design of Three Factors and Five Levels and the Experimental Responses (PC and AC) of β-CD-Assisted Extraction from Vine Shoots

run	β-CD concentration, β (mg/mL)		time, t (h)		temperature, T (°C)		PC (mg of GAE/g of DM)	AC (μMTE)
factorial design	20	(−1)	1.5	(−1)	40	(−1)	0.43	800.96
	40	(+1)	1.5	(−1)	40	(−1)	0.69	1190.57
	20	(−1)	5	(+1)	40	(−1)	0.93	1250.79
	40	(+1)	5	(+1)	40	(−1)	0.96	1130.34
	20	(−1)	1.5	(−1)	60	(+1)	1.43	1340.51
	40	(+1)	1.5	(−1)	60	(+1)	1.65	1710.88
	20	(−1)	5	(+1)	60	(+1)	1.75	1540.44
	40	(+1)	5	(+1)	60	(+1)	2.48	1740.37
center points	30	(0)	3.25	(0)	50	(0)	1.04	1220.06
	30	(0)	3.25	(0)	50	(0)	1.29	1390.49
	30	(0)	3.25	(0)	50	(0)	1.14	1370.00
	30	(0)	3.25	(0)	50	(0)	1.38	1270.04
	30	(0)	3.25	(0)	50	(0)	1.20	1240.55
	30	(0)	3.25	(0)	50	(0)	1.15	1410.99
star points	13.82	(−α)	3.25	(0)	50	(0)	0.85	1120.72
	46.82	(+α)	3.25	(0)	50	(0)	1.05	1390.49
	30	(0)	0.30	(−α)	50	(0)	0.36	1090.60
	30	(0)	6.19	(+α)	50	(0)	2.02	1460.97
	30	(0)	3.25	(0)	33.18	(−α)	0.56	940.66
	30	(0)	3.25	(0)	66.82	(+α)	1.76	1740.37

shoots were cut into cylinders of 1 cm height and a mean diameter of 5 mm.

Dry Matter (DM) Content. Vine shoots were dried in a convictive oven at 105 °C for 48 h for the measurement of the DM content. The DM of Syrah, Cabernet Sauvignon, Cabernet Franc, and Tempranillo vine shoots was found to be 60, 65, 57, and 69%, respectively.

Solid−Liquid Extraction. The solid−liquid extraction process of polyphenols from cylindrical vine shoots was performed with a solid/liquid ratio of 1:20 (w/v).[8] After β-CD aqueous extraction at different concentration, time, and temperature combinations, extracts were centrifuged at 5000 rpm for 15 min. β-CD aqueous concentrations were prepared by dissolving the required weight of β-CD in the specific water volume in a 50 °C water bath under stirring.

Total Polyphenol Content (PC). The total PC was determined by the Folin−Ciocalteu colorimetric assay.[11] A total of 1 mL of Folin−Ciocalteu reagent (10-fold diluted) was mixed to 200 μL of extract. Then, 800 μL of sodium carbonate (75 g/L) was added. The mixture was incubated for 10 min at 60 °C and then 10 min at room temperature. The absorbance was measured at 750 nm by the ultraviolet/visible (UV/vis) spectrophotometer (UV- 9200, BioTECH Engineering Management, U.K.). The calibration curve was drawn with GA. PC was expressed as milligrams of gallic acid equivalent (GAE) per gram of DM.

Antioxidant Capacity (AC). The AC of vine shoot extracts was measured by means of the DPPH assay.[12] A total of 50 μL of vine shoot extracts or standard (Trolox) was added to 1.45 mL of DPPH radical (0.06 mM). After an incubation of 30 min at room temperature, the absorbance was measured at 515 nm. The DPPH value of the extracts was expressed in micromolar Trolox equivalent per milliliter (μMTE).

HPLC. The HPLC analyses were conducted for the identification and quantification of polyphenols from vine shoot extracts.[13] The HPLC−diode array detection (DAD) analyses of polyphenols were carried out with a HPLC system (Waters Alliance, Milford, MA) equipped with a quaternary Waters e2695 pump. A UV−vis photodiode array spectrophotometer Waters 2998 was used, with the control system and data collection Empower 3 software. HPLC analyses of polyphenols were carried out on a Discovery C_{18}, 5 μm, 250 × 4.6 mm, column (Supleco, Bellefonte, PA) with a C_{18}, Supelguard Discovery 18, 20 × 4 mm, 5 μm, precolumn (Supelco, Bellefonte, PA) at 30 °C. Separation of 100 μL of cane extract was performed at a flow rate of 0.5 mL min^{-1}. Mobile phase A consisting of 0.1% (v/v) formic acid in water and mobile phase B consisting of 100% acetonitrile were used. The elution profile had the following proportions (v/v) of solvent B: 5 min, 15−20%; 45 min, 20−44.5%; 1 min, 100%; kept at 100% of B for 9 min; and followed by 5 min of stabilization at 15%. Spectrophotometric detection was performed at 280 nm.

Experimental Design. The optimization of the β-CD-assisted extraction process of polyphenol from vine shoots was conducted by RSM. The independent variables were β-CD concentration, time, and temperature. They were coded at five levels (−α, −1, 0, 1, and +α), in a central composite design (2^3 + star) of 20 experiments, including six center points. Table 1 (first four columns) shows the central composite design with the range of variables and their coded values. Two responses were studied: PC and AC. Data analyses were carried out using STATGRAPHICS Plus 4.0 for Windows and were fitted to a second-degree regression equation of the form

$$Y = a_0 + \sum_{n=1}^{3} a_n X_n + \sum_{n=1}^{3} a_{nn} X_n^2 + \sum_{n=1}^{2} \sum_{m=n+1}^{3} a_{nm} X_n X_m \quad (1)$$

where Y is the response, a_0, a_n, a_m, and a_{nm} are the constant, linear, quadratic, and two factor interaction coefficients, respectively.

Statistical Analysis. Each extraction process was repeated on three different vine shoot samples. Means and standard deviations (error bars in the figures) of data were calculated. Variance analyses (ANOVA) and least significant difference (LSD) test were performed by STATGRAPHICS Centurion XV (StatPoint Technologies, Inc.).

RESULTS AND DISCUSSION

Experimental Design and Statistics. The effect of time, temperature, and β-CD concentration (β) on polyphenol extraction from vine shoots was studied. The RSM design was conceived taking into consideration the solubility limitation of β-CD at concentrations above 50 mg/mL[10] and temperature limitation because of the possible heat degradation/oxidation of polyphenols. RSM is a statistical and mathematical method employed for the development, improvement, and optimization of extraction processes.[14] Table 1 shows the experimental design and combinations of the coded variables with their responses (PC and AC). Total PC ranged from 0.36 to 2.48 mg

DOI: 10.1021/acs.jafc.5b00672
J. Agric. Food Chem. 2015, 63, 3387−3393

of GAE/g of DM, while AC was between 800.96 and 1740.37 μMTE.

The relation between the responses and the experimental parameters (β, t, and T) was demonstrated by statistical analyses to fit second-order polynomial equations shown in Table 2. The analyses of the predicted values, calculated from the regression equations, showed a high correlation with experimental values and resulted in the calculation of the coefficients of determination (R^2), which were shown to have high levels of adequacy (Table 2).

Effect of the Time, Temperature, and β-CD Concentration on PC. According to the pareto chart (Figure 1a) and the response surface plot (Figure 1b), time, temperature and β-CD concentration have linear positive effects on polyphenol extraction from vine shoots. No quadratic effects were observed nor interaction between the parameters. Excluding insignificant parameters, the regression equation becomes

$$\mathrm{PC} = -2.0886 + 0.0116057\beta + 0.196472t + 0.0461738T \quad (2)$$

The positive effect of t, T, and β was expected. The temperature augments molecular diffusion; it decreases solvent viscosity, enhancing the solute solubilization and diminishing surface tension.[15] CDs are likely to form, within their lipophilic cavities and through non-covalent forces, inclusion complexes with hydrophobic polyphenols, increasing thus their water solubility.[16,17] Time comes immediately after the temperature factor in terms of its significance (Figure 1a). It plays an important role in the diffusion process, which is a relatively slow operation of three steps: (1) internal diffusion of the solvent, (2) solubilization of the target molecule, and (3) diffusion of the solubilized molecules to the surface of the particle.[18] The significant positive effect of time is therefore expected for polyphenol extraction from vine shoots.

Effect of the Time, Temperature, and β-CD Concentration on AC. Similar to PC, AC is positively affected by the time, temperature, and β-CD concentration (Figure 2a). As shown in Figure 2b, the increase in the β-CD concentration and time of the extraction process linearly augments AC up to 1740.37 μMTE. The temporary locking of polyphenols within CD cavities stabilizes host molecules from oxidation, light, and heat degradation,[16] which probably gave linear positive effects for t, T, and β. Excluding insignificant parameters, the regression equation becomes

$$\mathrm{AC} = -812.072 + 25.3102\beta + 198.619t + 24.1344T - 4.893\beta t \quad (3)$$

Comparing the significance of the studied parameters, it can be noticed that the effect of time was more significant for extracting higher PCs but had less effect on their AC. This might be due to the oxidation phenomena that is likely to occur when subjecting polyphenols to high temperatures (>50 °C) for long durations. In contrast, the β-CD concentration played a more important role for conserving the AC of polyphenols than enhancing their quantity (PC) (Figures 1a and 2a).

Multiple Response Optimization. Figure 3 shows the overlay plots for PC and AC at 66.6 °C (optimal temperature). As marked by the black dot, the optimal conditions for the maximization of PC are 46.8 mg/mL β-CD for 6.2 h, while those for AC are 46.8 mg/mL β-CD for 0.7 h. These are the quantitative and qualitative optimums, respectively. However, for industrial applications of vine-shoot-derived polyphenols, it

Table 2. Second-Order Polynomial Equations for PC and AC, Including Insignificant Parameters, with R^2 Also Shown for the Equations

	regression equation (including insignificant parameters)	regression coefficient, R^2 (%)
PC	$= 0.161426 - 0.0072592\beta - 0.0819191t - 0.0149214T - 0.000469537\beta^2 + 0.00206658\beta t + 0.000806414\beta T + 0.0122602t^2 + 0.00273404tT + 0.000280171T^2$	94.6
AC	$= -48.9255 + 12.2366\beta + 262.684t - 2.86155T - 0.106453\beta^2 - 4.893\beta t + 0.389216\beta T - 0.959765t^2 - 1.15653tT + 0.190782T^2$	88.7

DOI: 10.1021/acs.jafc.5b00672
J. Agric. Food Chem. 2015, 63, 3387−3393

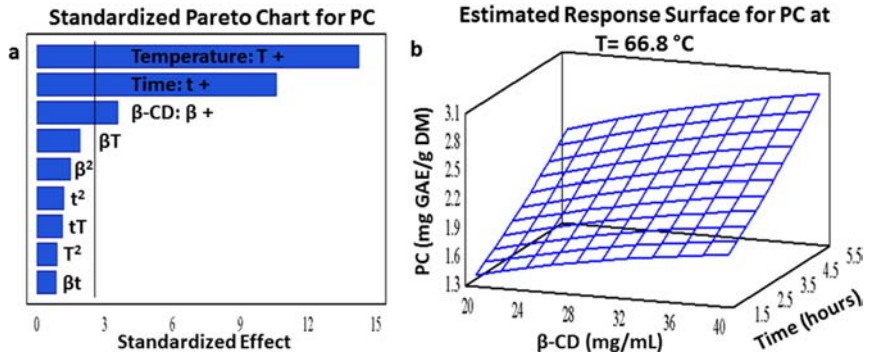

Figure 1. (a) Standardized pareto chart and (b) estimated response surface for PC.

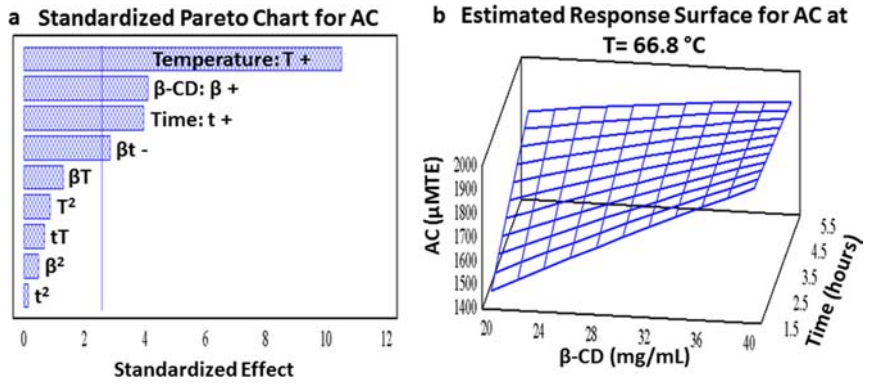

Figure 2. (a) Standardized pareto chart and (b) estimated response surface for AC.

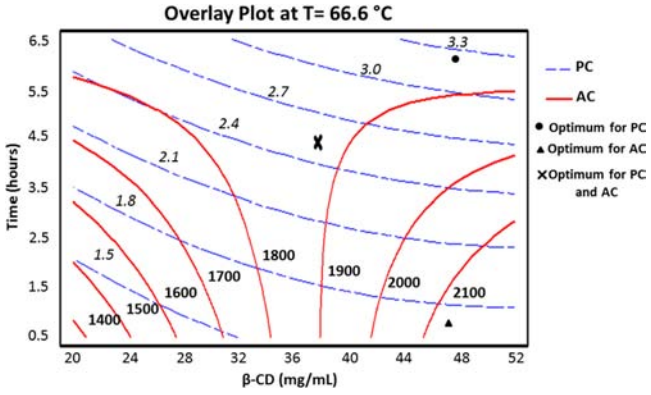

Figure 3. Superposition plots of PC and AC. The optimums for (●) PC, (▲) AC and (×) both responses are also shown.

is important to maintain the AC of the molecules through the extraction process. The simultaneous maximization of the polyphenol quantity (PC) and their quality (AC) is therefore primordial. Moreover, the optimization of the process is likely to diminish its cost. The simultaneous optimum for both responses was obtained with 37.7 mg/mL β-CD for 4.4 h at 66.6 °C. It permitted the decrease in β-CD consumption (from 46.8 to 37.7 mg/mL), thus reducing the overall cost of the process. The suggested multiple optimum is therefore an economic choice for industrial purposes that decreases the time and β-CD consumption, maintaining a high AC of concentrated polyphenol extracts. To verify the exactitude of the model, the optimal conditions for the optimization of both of the responses (PC and AC) were repeated. The extraction process of polyphenols from Syrah vine shoots was conducted at 66.6 °C for 4.4 h with a 37.7 mg/mL aqueous β-CD solvent. Experimental results were compared to those predicted by the model. As shown in Table 3, the difference of the values

Table 3. Predicted and Experimental Results of PC and AC at the Multiple Optimum Conditions (66.6 °C, 4.4 h, and 37.7 mg/mL β-CD)

multiple optimum	predicted	experimental	mean absolute error
PC (mg of GAE/g of DM)	2.5	2.45	0.14
AC (μMTE)	1881.3	1864	48.7

obtained by experimentation and model prediction are within the range of the mean absolute error, suggesting a good agreement of the model with experimental results.

Consequently, 66.6 °C and 37.7 mg/mL aqueous CD seem to be adequate optimal conditions for the maximization of both PC and AC. In the studied domain, all of the quadratatic effects (t^2, T^2, and β^2) of the parameters were insignificant. Time, temperature, and β-CD concentration had positive linear impacts on PC and AC (Figures 1a and 2a). The β-CD concentration in water is an experimental condition limited by its solubility and economic impact. Similarly, the temperature elevation is governed by the oxidation and/or degradation phenomena that it causes to polyphenols and also by its energy consumption that affects the overall cost of the process. Because of all of the aforementioned reasons, the linear extrapolation of the time parameter was possible because it was suspected to further increase PC and AC. Figure 4 shows PC and AC as a function of long periods of time (from 5 to 54 h) at 66.6 °C and 37.7 mg/mL β-CD. The highest PC and AC, 5.8 mg of GAE/g of DM and 3147 μMTE, respectively, were reached after 48 h of extraction. Beyond this time, PC

DOI: 10.1021/acs.jafc.5b00672
J. Agric. Food Chem. 2015, 63, 3387−3393

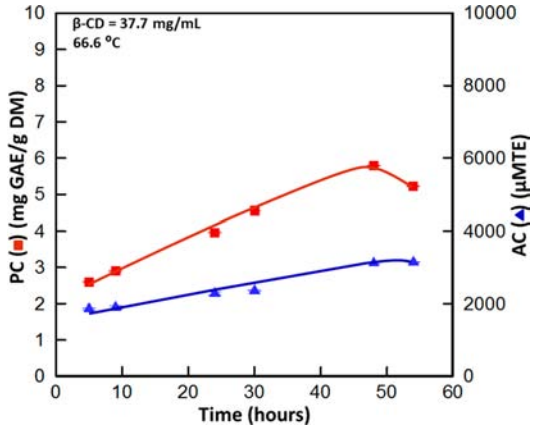

Figure 4. PC and AC as a function of time at 66.6 °C and 37.7 mg/mL β-CD.

diminishes, probably because of polyphenol degradation caused by exposure to a relatively high temperature for a long period of time.

The linear extrapolation of time permitted the amelioration of PC and AC by 2.3 and 1.7 times, respectively, enabling the obtainment of the highest concentration of bioactive polyphenols (5.8 mg of GAE/g of DM) with β-CD-assisted extraction (37.7 mg/mL) after 48 h at 66.6 °C.

β-CD and Organic Solvent Extraction. The efficiency of β-CD in the extraction of antioxidant polyphenols has been evaluated in comparison to organic solvent extraction with 50% ethanol/water, shown to be the optimal ethanolic mixture compared to 0, 25, and 75% ethanol/water in terms of polyphenol extraction from vine shoots.[8]

As shown in Figure 5, a PC of 2.6 mg of GAE/g of DM was reached after 0.5 h of extraction with 50% ethanol/water, while

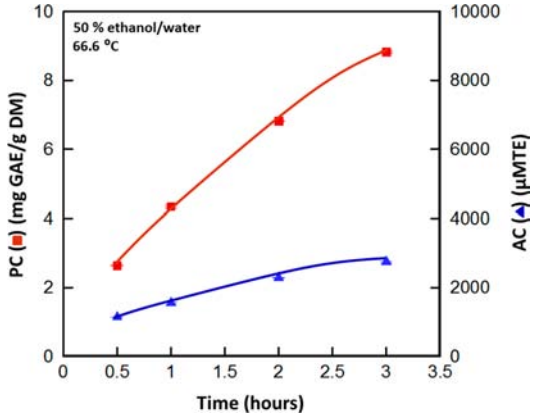

Figure 5. PC and AC as a function of time at 66.6 °C and 50% ethanol/water.

it took 5 h with β-CD (37.7 mg/mL) (Figure 4) and 10 h with pure water (data not shown) to attain the same phenolic yield. Ethanol is likely to enhance the polyphenol extraction process because it acts on both the solvent properties and the matrix. It influences the polarity of the solvent and its capacity to solubilize lipophilic polyphenols. Moreover, ethanol can chemically and biophysically alter biological membranes by affecting cell permeability.[19] The faster kinetics of polyphenol extraction with ethanol is therefore expected because it affects membrane permeability and, thus, facilitates molecular diffusion. With regard to the AC of the extracted molecules, a comparison was performed between polyphenols obtained by ethanol extraction and those by β-CD (37.7 mg/mL). For the same polyphenol yield (2.6 mg of GAE/g of DM), AC of 1000 μMTE was found with water, AC of 1100 μMTE was found with ethanol, and AC of 1864 μMTE was obtained with β-CD. The oxidation or degradation phenomena affecting polyphenol AC was more likely to occure in water and ethanol/water mixtures than with β-CD-containing solvent. This observation was maintained with higher polyphenol yields. For 5.8 mg of GAE/g of DM, AC of 2000 μMTE was found with ethanol compared to AC of 3146 μMTE obtained with β-CD. After 48 h of extraction at 66.6 °C with 50% ethanol/water mixture, PC of 24 mg of GAE/g of DM and AC of 6000 μMTE were obtained (data not shown). In comparison to β-CD, AC was only ameliorated 1.9 times, even when PC was 4.13 times higher. The negative effect of the ethanol and temperature combination on the polyphenol AC was highlighted within 48 h of extraction. Better antioxidant power and stability were reported for polyphenols encapsuled with CD compared to methanol extract.[20] The difference of AC among ethanol and β-CD extracts might result from (1) the difference in the composition and diversity of the extracted polyphenols and (2) the encapsulation role of β-CD in the protection of polyphenol from possible degradation by oxidation, heat, and UV light.[21] The identification and quantification of polyphenols from β-CD- and hydroethanolic-assisted extractions were conducted by HPLC. Both extracts had the same initial total PC of 5.8 mg of GAE/g of DM but different antioxidant activities (Table 4). As shown in Table 4, GA, HBA, FA, and TCA were identified in the β-CD extract obtained at the following conditions (37.7 mg/mL, 48 h, and 66.6 °C). Higher concentrations of polyphenols were identified in β-CD compared to the hydroethanolic extract. For instance, FA and HBA were by far better extracted with β-CD-containing solvent compared to 50% ethanol (Table 4). The higher yield of polyphenols and their improved diversity could be the reason for the enhanced AC activity observed with the β-CD extracts (3146 μMTE) compared to the hydroethanolic extracts (2000 μMTE).

With regard to the lower price of β-CD compared to ethanol and the higher quantity of ethanol used per experiment (7.8 g of ethanol equivalent to 50% ethanol/water mixture versus 0.754 g of β-CD equivalent to 37.7 mg/mL taken at the optimal conditions), it is more economic for industrial purposes to use β-CD. The importance of this latter is not limited to the extraction process because polyphenol encapsulation by β-CD

Table 4. PC of β-CD- and Ethanol-Assisted Extracts from Syrah Vine Shoots[a]

	GA (μg/g of DM)	HBA (μg/g of DM)	FA (μg/g of DM)	TCA (μg/g of DM)	AC (μMTE)	PC (mg of GAE/g of DM)
β-CD	2100 a	6.5 a	17.6	72.5 a	3146 a	5.8
50% ethanol	1958 b	1.7 b	nd	60.2 b	2000 b	5.8

[a]nd corresponds to non-detectable. GA, gallic acid; HBA, 4-hydroxybenzoic acid; FA, ferulic acid; TCA, *trans*-cinnamic acid; AC, antioxydant capacity; and PC, polyphenol content. Different letters (a, b, and c) indicate significant statistical difference between means.

DOI: 10.1021/acs.jafc.5b00672
J. Agric. Food Chem. 2015, 63, 3387−3393

Table 5. PC of Syrah, Cabernet Sauvignon, Cabernet Franc, and Tempranillo Vine Shoot Extracts[a]

	GA (μg/g of DM)	HBA (μg/g of DM)	FA (μg/g of DM)	TCA (μg/g of DM)	PA (μg/g of DM)	R (μg/g of DM)	AC (μMTE)	PC (mg of GAE/g of DM)
Syrah	2100 a	6.5	17.6 a	7.25	nd	nd	3146 a	5.8 a
Cabernet Sauvignon	1792 b		4.43 b		64.1 a	1929.7 a	4800 b	7.5 b
Cabernet Franc	2162 c		7 c		73.2 a	2230.8 b	3700 c	7.5 b
Tempranillo	1463 d				66 a	2300.2 c	7000 d	7.5 b

[a]nd corresponds to non-detectable. GA, gallic acid; HBA, 4-hydroxybenzoic acid; FA, ferulic acid; TCA, *trans*-cinnamic acid; PA, protocatechuic acid; R, resveratrol; AC, antioxydant capacity; and PC, polyphenol content. Different letters (a, b, and c) indicate significant statistical difference between means.

heightens their stability, masks their unpleasant taste, and improves their bioavailability and half-life.[21] Therefore, their removal is unnecessary, as is the case for organic solvents, after the extraction process, especially when they will be expected to be used in industrial applications. In comparison to organic solvent (50% ethanol), β-CD-assisted extraction was shown to be an efficient method in terms of antioxidant polyphenol extraction from vine shoots.

Comparison of Vine Shoot Cultivars. β-CD-assisted extraction of polyphenols was conducted on three other vine shoot cultivars proposed by a local viticulture for the valorization of their shoots: Cabernet Sauvignon, Cabernet Franc, and Tempranillo. The comparison was realized using the optimal conditions found with Syrah (β-CD, 37.7 mg/mL; *T*, 66.6 °C; and *t*, 48 h). Different diversities and quantities of polyphenols were identified among the extracts (Table 5). For example, in Tempranillo cultivar, three polyphenols were identified: GA, PA, and R. Among all of the studied vine shoots, Tempranillo had the highest concentration of R (2300.2 μg/g of DM), Cabernet Franc had the highest concentrations of GA (2162 μg/g of DM), and Syrah had the highest concentrations of FA (17.6 μg/g of DM) and HBA (6.5 μg/g of DM). All cultivars had the same PA content (73.2 μg/g of DM). No correlation was shown between the identified molecules and the antiradical capacities of the extract AC. However, all vine shoot cultivars were shown to be a rich source of highly antioxidant polyphenols. GA, PA, FA, TCA, HBA, and R were found by many authors in vine shoot extracts.[1,22,23] Our study focused on the differences between Syrah, Cabernet Sauvignon, Cabernet Franc, and Tempranillo cultivars in terms of their AC, PC, and diversity. All in all, we have clearly shown that β-CD-assisted extraction is an environmentally friendly process for the extraction of polyphenols with a high radical-scavenging capacity. At an industrial scale and compared to organic solvent, β-CDs are cheaper and safer for several applications and processes. This type of natural antioxidant molecule extraction is quite efficient in terms of quantity and quality of the polyphenols extracted from vine shoots. However, a potential co-extraction of phytochemicals is likely to occur when using β-CDs. Future studies on the identification and characterization of these phytochemicals is essential to consider this process as GRAS.

AUTHOR INFORMATION

Corresponding Author

*Telephone: +96178821568 or +330781419515. E-mail: hibarajha@net.usj.edu.lb.

Funding

The authors acknowledge the Research Council of Saint Joseph University of Beirut for financial support through Project FS54.

Notes

The authors declare no competing financial interest.

ACKNOWLEDGMENTS

The authors acknowledge Château Kefraya, Bekaa, Lebanon, for logistic support.

ABBREVIATIONS USED

β-CD, β-cyclodextrin; PC, polyphenol content; AC, antioxidant capacity; *t*, time; *T*, temperature; GA, gallic acid; HBA, 4-hydroxybenzoic acid; FA, ferulic acid; TCA, *trans*-cinnamic acid; PA, protocatechuic acid; R, resveratrol; GRAS, generally recognized as safe; RSM, response surface methodology; DPPH, 2,2-diphenyl-picrylhydrazyl; Trolox, (±)-6-hydroxy-2,5,7,8-tetramethylchromane-2-carboxylic acid; HPLC, high-performance liquid chromatography; DM, dry matter; μMTE, micromolar trolox equivalent per milliliter; GAE, gallic acid equivalent; DAD, diode array detection; UV, ultraviolet

REFERENCES

(1) Max, B.; Salgado, J. M.; Cortés, S.; Domínguez, J. M. Extraction of phenolic acids by alkaline hydrolysis from the solid residue obtained after prehydrolysis of trimming vine shoots. *J. Agric. Food Chem.* **2009**, *58*, 1909−1917.

(2) Çetin, E. S.; Altinöz, D.; Tarçan, E.; Göktürk Baydar, N. Chemical composition of grape canes. *Ind. Crops Prod.* **2011**, *34*, 994−998.

(3) Rajha, H. N.; El Darra, N.; Hobaika, Z.; Boussetta, N.; Vorobiev, E.; Maroun, R. G.; Louka, N. Extraction of total phenolic compounds, flavonoids, anthocyanins and tannins from grape byproducts by response surface methodology. Influence of solid−liquid ratio, particle size, time, temperature and solvent mixtures on the optimization process. *Food Nutr. Sci.* **2014**, *5*, 397−409.

(4) Cacace, J. E.; Mazza, G. Mass transfer process during extraction of phenolic compounds from milled berries. *J. Food Eng.* **2003**, *59*, 379−389.

(5) Bonilla, F.; Mayen, M.; Merida, J.; Medina, M. Extraction of phenolic compounds from red grape marc for use as food lipid antioxidants. *Food Chem.* **1999**, *66*, 209−215.

(6) Shi, J.; Nawaz, H.; Pohorly, J.; Mittal, G.; Kakuda, Y.; Jiang, Y. Extraction of polyphenolics from plant material for functional foods—Engineering and technology. *Food Rev. Int.* **2005**, *21*, 139−166.

(7) Wang, L.; Weller, C. L. Recent advances in extraction of nutraceuticals from plants. *Trends Food Sci. Technol.* **2006**, *17*, 300−312.

(8) Rajha, H. N.; Boussetta, N.; Louka, N.; Maroun, R. G.; Vorobiev, E. A comparative study of physical pretreatments for the extraction of polyphenols and proteins from vine shoots. *Food Res. Int.* **2014**, *65*, 462−468.

(9) Szente, L.; Szejtli, J. Cyclodextrins as food ingredients. *Trends Food Sci. Technol.* **2004**, *15*, 137−142.

(10) Ratnasooriya, C. C.; Rupasinghe, H. P. Extraction of phenolic compounds from grapes and their pomace using β-cyclodextrin. *Food Chem.* **2012**, *134*, 625−631.

DOI: 10.1021/acs.jafc.5b00672
J. Agric. Food Chem. 2015, 63, 3387−3393

(11) Singleton, V. L.; Orthofer, R.; Lamuela-Raventós, R. M.; Lester, P. Analysis of total phenols and other oxidation substrates and antioxidants by means of Folin−Ciocalteu reagent. *Methods Enzymol.* **1999**, *299*, 152−178.
(12) Brand-Williams, W.; Cuvelier, M. E.; Berset, C. Use of a free radical method to evaluate antioxidant activity. *LWT—Food Sci.Technol.* **1995**, *28*, 25−30.
(13) Vergara, C.; von Baer, D.; Mardones, C.; Wilkens, A.; Wernekinck, K.; Damm, A.; Macke, S.; Gorena, T.; Winterhalter, P. Stilbene levels in grape cane of different cultivars in southern Chile: Determination by HPLC−DAD−MS/MS method. *J. Agric. Food Chem.* **2012**, *60*, 929−933.
(14) Myers, R. H.; Montgomery, D. C.; Anderson-Cook, C. M. *Response Surface Methodology: Process and Product Optimization Using Designed Experiments*, 3rd ed.; John Wiley & Sons: Hoboken, NJ, 2009; Vol. *705*.
(15) Ibañez, E.; Herrero, M.; Mendiola, J. A.; Castro-Puyana, M. Extraction and characterization of bioactive compounds with health benefits from marine resources: Macro and micro algae, cyanobacteria, and invertebrates. In *Marine Bioactive Compounds*; Hayes, M., Ed.; Springer: New York, 2012; pp 55−98.
(16) Del Valle, E. M. Cyclodextrins and their uses: A review. *Process Biochem.* **2004**, *39*, 1033−1046.
(17) Loftsson, T.; Brewster, M. E. Pharmaceutical applications of cyclodextrins. 1. Drug solubilization and stabilization. *J. Pharm. Sci.* **1996**, *85*, 1017−1025.
(18) Mazza, G. *Functional Foods: Biochemical and Processing Aspects*; CRC Press: Boca Raton, FL, 1998; Vol. *1*.
(19) Goldstein, D.; Chin, J. Interaction of ethanol with biological membranes. *Fed. Proc.* **1981**, *40* (7), 2073−2076.
(20) Mantegna, S.; Binello, A.; Boffa, L.; Giorgis, M.; Cena, C.; Cravotto, G. A one-pot ultrasound-assisted water extraction/cyclodextrin encapsulation of resveratrol from *Polygonum cuspidatum*. *Food Chem.* **2012**, *130*, 746−750.
(21) Fang, Z.; Bhandari, B. Encapsulation of polyphenols—A review. *Trends Food Sci. Technol.* **2010**, *21*, 510−523.
(22) Delgado-Torre, M. P.; Ferreiro-Vera, C.; Priego-Capote, F.; Pérez-Juan, P. M.; Luque de Castro, M. D. Comparison of accelerated methods for the extraction of phenolic compounds from different vine-shoot cultivars. *J. Agric. Food Chem.* **2012**, *60*, 3051−3060.
(23) Karacabey, E.; Mazza, G. Optimisation of antioxidant activity of grape cane extracts using response surface methodology. *Food Chem.* **2010**, *119*, 343−348.

DOI: 10.1021/acs.jafc.5b00672
J. Agric. Food Chem. 2015, 63, 3387−3393

Table 1. Analyzed Compounds Associated with Oxidized Aroma, Their Odor Descriptors and Odor Thresholds

compound	odor descriptor	odor threshold (μg/L)
(*E*)-2-alkenals		
(*E*)-2-heptenal	soapy, fatty	4.6[a,9]
(*E*)-2-hexenal	green apple	4[a,9]
(*E*)-2-nonenal	green, fatty, sawdust	0.17[a,14]
(*E*)-2-octenal	fatty, nutty	3[a,9]
Strecker aldehydes		
methional	cooked potato-like	0.5[b,7]
2-methylpropanal	malty	6[b,9]
3-methylbutanal	malty	4.6[b,2]
2-phenylacetaldehyde	honey, floral	1[b,9]
furans		
furaneol	caramel	37[b,15]
homofuraneol	caramel	10[b,15]
sotolon	curry, seasoning	15[b,12]
aldehydes		
benzaldehyde	bitter almond-like	2000[a,16]
furfural	sweet, bread	14 100[b,17]
hexanal	grassy, green	20[a,16]
5-methylfurfural	sweet, bitter almond	2000[a,16]
alcohols		
maltol	caramel	5000[b,18]
methionol	cooked potato-like	1000[b,17]
eugenol	clove-like	6[b,17]

[a]Odor detection threshold determined in water. [b]Odor detection threshold determined in model wine (10% aqueous ethanol, 7 g/L glycerol, pH 3.2).

techniques were described: a HPLC and UPLC method[21,22] and a liquid−liquid extraction followed by GC-MS analysis.[23] In another paper, analysis of sotolon together with furaneol and maltol was performed via GC-MS after isolation of the volatiles via SPE.[24]

The aim of this work was to develop a highly sensitive GC-MS/MS method which allows simultaneous quantitation of 18 compounds involved in wine oxidation in a single run. This required quantifying a number of compounds which are present in trace quantities including (*E*)-2-alkenals, various Strecker aldehydes (methional, 2-phenylacetaldehyde, 3-methylbutanal, 2-methylpropanal), methionol, eugenol, maltol, as well as furans (sotolon, furaneol, homofuraneol). The comprehensive method was validated in an oxidized red, white, and model wine, and its application was demonstrated through the analysis of a 14 year old white wine which was stored under five different closures to study the effects of the formation of these flavor compounds.

MATERIALS AND METHODS

Chemicals. 3-Hydroxy-4,5-dimethyl-2(5*H*)-furanone (sotolon) (≥99%), 4-hydroxy-2,5-dimethyl-3(2*H*)-furanone (furaneol) (≥98%), 2-phenylacetaldehyde (≥95%), furfural (≥98%), 5-methylfurfural (≥98%), hexanal (≥97%), (*E*)-2-hexenal (≥95%), (*E*)-2-heptenal (≥97%), (*E*)-2-octenal (≥94%), (*E*)-2-nonenal (≥93%), 3-(methylthio)-propanal (methional) (98%), 3-(methylthio)-propanol (methionol) (≥98%), 3-methylbutanal (97%), 2-methylpropanal (98%), 4-allyl-2-methoxyphenol (eugenol) (≥98%), benzaldehyde (≥99%), and 3-hydroxy-2-methyl-4*H*-pyran-4-one (maltol) (≥99%) were supplied by Sigma-Aldrich (Castle Hill, NSW, Australia). *O*-(2,3,4,5,6-Pentafluorobenzyl)hydroxylamine hydrochloride (≥99%), used as a derivatization reagent, was also purchased from Sigma-Aldrich. d_4-Furfural was purchased from CDN Isotopes (SciVac PTY. Ltd., Hornsby, NSW, Australia). 2-Phenyl-d_5-acetaldehyde was prepared from 2-phenyl-d_5-ethanol using the method for *formyl*, α-[$^{13}C_2$]-2-phenylacetaldehyde.[25] d_5-Benzaldehyde was present as a byproduct (5%) in the 2-phenyl-d_5-acetaldehyde sample and formed as a result of C−C bond cleavage during the oxidation of 2-phenyl-d_5-ethanol as had been found previously.[26]

All chromatographic solvents were of HPLC grade; all chemicals were of analytical reagent grade unless otherwise stated; water was obtained from a Milli-Q purification system (Millipore, North Ryde, NSW, Australia). Sulfuric acid (95−97%, synthesis grade) was from Merck (Merck Pty. Ltd., Australia, Kilsyth, VIC, Australia). BondElut EN resins (styrene-divinylbenzene polymer), prepacked in 500 mg cartridges (6 mL total volume), were obtained from Agilent (Agilent Technologies Australia Pty Ltd., Mulgrave, VIC, Australia). All prepared solutions were % v/v with the balance made up with redistilled ethanol and prepared freshly prior to analysis.

Synthesis of 3-(Methyl-d_3-thio)-1-d_2-propanol (d_5-Methionol). Methyl 3-mercapto-propionate (3.94 g, 33 mmol), K_2CO_3 (7.2 g, 52 mmol), and CD_3I (5 g, 35 mmol) in THF (75 mL) were stirred for 7 days at room temperature in a sealed pressure vessel. The mixture was filtered, dried (Na_2SO_4), and filtered again into a fresh round-bottomed flask. The solution was cooled to 0 °C, $LiAlD_4$ (1.25 g, 30 mmol) was added, and the solution was stirred at room temperature overnight. The mixture was quenched with saturated NH_4Cl, and the organic layer was separated, dried (Na_2SO_4), and concentrated in vacuo. The residue was purified by vacuum distillation (85−95 °C; 12 mmHg) to give d_5-methionol (1.78 g, 54%). GC-MS, *m*/*z* (%): 94 (100), 110 (51), 64 (9), 33 (6), 78 (4).

Synthesis of 3-(Methyl-d_3-thio)-propanal (d_3-Methional). d_3-Methional was prepared using a modified version of the method of Sen et al.[27] d_3-Methionol was prepared as described for d_5-methionol above using $LiAlH_4$ in place of $LiAlD_4$. d_3-Methionol (2.6 g, 24 mmol), pyridinium chlorochromate (7.7 g, 36 mmol), and CH_2Cl_2 (125 mL) were stirred for 4 h. The mixture was loaded directly onto silica gel (150 g) and eluted using 30% Et_2O/pentane → 70% Et_2O/pentane to give d_3-methional (0.4 g, 15%). GC-MS, *m*/*z* (%): 51 (100), 46 (41), 79 (30), 64 (30), 50 (24), 107 (20).

Synthesis of 4-Hydroxy-2,5-dimethyl-d_6-3(2*H*)-furanone (d_6-Furaneol). Furaneol (2.0 g, 16 mmol), D_2O (12 mL), and 40 w/v% NaOD/D_2O (8 mL) were stirred for 4 days at 50 °C. The solution was salted (NaCl), acidified to pH 2 using DCl/D_2O, and extracted with anhydrous Et_2O. The combined organic layers were dried (Na_2SO_4) and concentrated in vacuo to give d_6-furaneol (870 mg, 41%). GC-MS, *m*/*z* (%): 134 (100), 46 (62), 60 (32), 88 (26), 78 (4).

Synthesis of d_5-5-Ethyl-4-hydroxy-2-methyl-3(2*H*)-furanone (d_5-Homofuraneol). Homofuraneol was synthesized using the method of Blank et al.[28] Homofuraneol (0.3 g, 2 mmol), D_2O (6 g, 0.3 mol), and 40 wt % NaOD/D_2O (1.0 g, 10 mmol) were stirred for 4 days in a sealed pressure vessel under nitrogen. The solution was acidified to pH 3 using DCl (2.7 M), salted (NaCl), and extracted with anhydrous Et_2O. The combined organic layers were dried (Na_2SO_4) and concentrated in vacuo to give d_5-homofuraneol (160 mg, 54%). GC-MS, *m*/*z* (%): 147 (100), 46 (62), 73 (53), 101 (30), 132 (26).

Synthesis of 3-Hydroxy-4-methyl-5-(methyl-d_3)-2(5*H*)-furanone-5-*d* (d_4-Sotolon). D_2O (5 mL) and 37% w/w DCl/D_2O (0.5 mL) was added to 2-ketobutyric acid (1.25 g, 12 mmol), and the solution was stirred for 1 h. The solution was salted (NaCl), extracted with anhydrous Et_2O, dried (Na_2SO_4), filtered, and then concentrated in vacuo. Additional D_2O (5 mL) and 37% w/w DCl/D_2O (5 mL) was added to the resultant 3,3-d_2-2-ketobutyric acid (0.9 g) in a 50 mL glass high-pressure vessel with a Teflon screw cap seal. The solution was chilled under N_2, and d_4-acetaldehyde (1.0 g, 21 mmol) was added. The vessel was sealed and stirred for 7 days, after which further D_2O (5 mL) was added and the solution was salted (NaCl). The product was extracted using Et_2O and washed with brine (6 × 2 mL), and the organic layer was dried (Na_2SO_4) and concentrated in vacuo to give the product (1.5 g, 92%). GC-MS, *m*/*z* (%): 87 (100), 59 (75), 132 (45), 46 (39), 76 (14), 114 (5).

DOI: 10.1021/jf505803u
J. Agric. Food Chem. 2015, 63, 3394−3401

Synthesis of (*E*)-2-Octenal-5,6,7,8-d_9 (d_9-(*E*)-2-Octenal). d_9-(*E*)-2-Octenal was prepared in five steps from d_9-bromobutane as per Heading.[29]

Synthesis of (*E*)-2-Hexenal-3,4,4,5,5,6,6,6-d_8 (d_8-(*E*)-2-Hexenal). d_8-(*E*)-2-Hexenal was prepared from the reduction of d_8-ethyl hexanoate to d_8-hexenol using lithium aluminum hydride and then converted to the aldehyde using the Swern oxidation as described in Grant-Preece et al.[30]

Wine. The wine studied was a Semillon from the Clare Valley region in South Australia, processed entirely in a stainless steel tank with no oak treatment. SO_2 was added postfermentation as well as dimethyl dicarbonate (Velcorin) at 10 μg/L, with the basic composition at bottling of pH 3.16, titratable acidity (as tartaric acid, pH 8.2) 6.1 g/L, volatile acidity 0.56 g/L as acetic acid, free sulfur dioxide 28 mg/L, and total sulfur dioxide 100 mg/L. The wine was bottled with the same closures used by an earlier closure trial[31] and had various flavor compound additions as described in Capone et al.[32] The bottled wines were kept in an inverted position in a near constant temperature storage facility (ca. 15 °C). The closures studied are shown in Table 2.

Table 2. Wine Samples Included in the Study, Bottled in 1999

code	closure	headspace	volume
Amp. N_2	glass ampule	N_2, 3 mL	50 mL
Amp. air	glass ampule	air, 3 mL	50 mL
SC	screw cap, ROTE	air, 3 mL	750 mL
NC 1	natural cork, 44 mm	air, 3 mL	750 mL
NC 2	natural cork, 38 mm	air, 3 mL	750 mL
Syn 1	synthetic extruded	air, 3 mL	750 mL
Syn 2	synthetic extruded	air, 3 mL	750 mL

Gas Chromatography–Mass Spectrometry. GC analysis was performed on an Agilent 7000 Triple Quadrupole GC-MS/MS system, equipped with an Agilent Multimode injector. The column used was a VF-200 ms from J&W Scientific, 30 m × 0.25 mm i.d., with 0.25 μm film thickness. The carrier gas was helium at a constant flow rate of 1.6 mL/min. The extract (2 μL) was injected in splitless mode, with a pressure of 16.95 psi, septum purge flow was 3 mL/min, and splitless time was 1 min. The injector temperature was 180 °C for 1 min and then heated to 260 °C at 250 °C min^{-1}. The oven temperature started at 40 °C, was held for 1 min, then raised to 220 °C at 10 °C/min, and finally heated to 270 °C at 100 °C/min. After each analytical run, backflushing was performed at 270 °C for 7.24 min at a pressure of 25 psi (back inlet pressure 1 psi). The temperature of the transfer line was 240 °C, and nitrogen (1.5 mL/min) was used as the collision gas. The mass spectrometer was operated in electron ionization mode at 70 eV with multiple reaction monitoring (MRM), with the monitored transitions listed in Table 3. Data acquisition and analyses were performed using the MassHunter Workstation software version B.05.01 supplied by the manufacturer (Agilent Technologies Australia Pty Ltd., Mulgrave, VIC, Australia).

Method Development. In order to determine the retention time and the characteristic mass fragments of the compounds, full scan analysis (m/z 50–350) was performed individually on each of the reference compounds as well as on the labeled standards. The aldehydes (10 mL of a 10 mg/L aqueous solution) were separately reacted with *O*-(2,3,4,5,6-pentafluorobenzyl)-hydroxyl-amine hydrochloride (1 mL of a 10 mg/mL aqueous solution) to obtain the oxime derivatives, these were then extracted with a Bond Elut ENV (200 mg) cartridge and eluted with 3 mL of dichloromethane (DCM), and after solvent evaporation to 200 μL the concentrated extract was subjected to GC-MS/MS analysis. The compounds that were quantified in their free forms were individually injected directly as solvent extracts, all in a concentration of 10 mg/L. The full scan experiments showed the precursor ions, and then MS/MS experiments were conducted on the precursor ions to determine their product ions. Once the selection of product ions was established, extracts of wine samples containing additions of the reference compounds and standards (100 μg/L) were injected using a ramp between 0 to 50 eV to determine the optimum collision energies for each of the different transitions (see Table 3).

Sample Preparation for GC-MS/MS Analysis. Isolation of the volatile analytes was performed according to Culleré et al. for quantitation of sotolon, furaneol, and maltol with the following modifications.[19] An ethanolic solution (30 μL) containing the labeled standards in concentrations from 1 to 60 μg/mL, depending on the expected concentration, was added to the wine sample (20 mL) and equilibrated for 15 min. To the spiked wine sample 1 mL of an aqueous solution containing the derivatization agent *O*-(2,3,4,5,6-pentafluorobenzyl)-hydroxylamine hydrochloride at 10 mg/mL was added, and the sample was stirred with a magnetic stir bar for 15 min. Ammonium sulfate (3 g) was then added to the samples prior to loading on the Bond Elut ENV SPE cartridge (500 mg, 6 mL volume) previously conditioned with 5 mL of dichloromethane, 5 mL of methanol, and finally 5 mL of model wine (13% v/v ethanol solution in water saturated with potassium hydrogen tartrate and adjusted to pH 3.3 with aqueous tartaric acid solution). Excess reagent was removed from the cartridge by loading 6 mL of a 0.05 M sulfuric acid solution. Analytes were finally eluted with dichloromethane (6 mL), and the organic layer was concentrated under a nitrogen stream to 200 μL at 40 °C using a turbovap (Turbo Vap LV Evaporator, Zymark). For wine analysis three individual bottles of each wine were analyzed.

RESULTS AND DISCUSSION

Method Development. *Sample Preparation.* For isolation of the different compounds various SPE materials (Bond Elut C18, SDBL, Licholut EN) and wine volumes (2, 5, 10, and 20 mL) were tested (data not shown), with the highest retention of the compounds achieved using a styrene-divinylbenzene polymer cartridge (Bond Elut ENV 500 mg) loaded with 20 mL of wine. The derivatization procedure with PFBHA had been previously investigated thoroughly by Culleré et al.,[19] who showed that the derivatization performed directly on the SPE cartridge was optimal, as derivatizing before the extraction caused interference in the MS spectra with other wine carbonyls that were also derivatized. However, since our method utilizes MS/MS analysis and measures only the specific mass transitions selected, the interference of other wine carbonyls did not constitute a problem. This fact, combined with the observation that derivatization conducted directly in the wine, showed a greater response for the underivatized compounds, allowing us to choose the latter procedure. The issue of a possible incomplete derivatization, and therefore inaccurate quantitation, was addressed by using isotopically labeled analogues of the analytes as internal standards, prior to the derivatization step. After loading the wine sample on the cartridge, the excess derivatizing agent along with other unwanted impurities were removed with 6 mL of a solution of dilute sulfuric acid (0.05 M). The elution of the target compounds was performed with dichloromethane (6 mL), followed by concentration under a stream of nitrogen to a final volume of 200 μL.

Isotopically Labeled Analogues. The synthesis of nine deuterium-labeled analogues including d_5-homofuraneol, d_4-sotolone, d_6-furaneol, d_5-methionol, d_3-methional, d_5-benzaldehyde, 2-phenyl-d_5-acetaldehyde, (*E*)-2-d_9-octenal, and d_8-(*E*)-2-hexenal was carried out in house for accurate quantitation of the compounds of interest.

Isotopically labeled standards were not available for some compounds; therefore, some standards were also used to determine other structurally similar compounds as follows. For the quantitation of 2-methylpropanal and 3-methylbutanal, d_5-benzaldehyde was used as an internal standard. The labeled

DOI: 10.1021/jf505803u
J. Agric. Food Chem. 2015, 63, 3394–3401

Table 3. Mass Spectral Transitions and Collision Energies Selected for Analysis of the Compounds for Aldehydes

	first transition parent ion (m/z) to product ion (m/z) (quantifier)	collision energy (V)	second transition parent ion (m/z) to product ion (m/z) (qualifier)	collision energy (V)
benzaldehyde[a]	301−181	22	301−271	6
d_5-benzaldehyde[a]	305−181	22	305−276	6
eugenol	163.8−149	10	164−131	14
furaneol	128−85	4	128−57	12
d_6-furaneol	134−88	5	134−60	7
furfural[a]	291−181	22	291−248	6
d_4-furfural[a]	295−181	22	295−251	6
(*E*)-2-heptenal[a]	307−181	22	307−250	2
hexanal[a]	295−181	18	295−252	2
(*E*)-2-hexenal[a]	293−181	20	293−250	2
d_8-(*E*)-2-hexenal[a]	301−181	20	301−251	2
homofuraneol	142−127	4	142−99	4
d_5-homofuraneol	147−132	4	147−101	4
maltol	126−97	14	126−97	14
methional[a]	299−181	20	299−102	6
d_3-methional[a]	302−181	12	302−105	4
methionol	106−59	2	106−88	2
d_5-methionol	111−64	4	111−45	4
5-methylfurfural[a]	305−181	22	304.7−262	8
2-methylpropanal[a]	267−181	24	267−250	2
3-methylbutanal[a]	281−181	24	281−239	2
(*E*)-2-nonenal[a]	335−181	22	335−250	8
(*E*)-2-octenal[a]	321−181	22	321−250	2
d_9-(*E*)-2-octenal[a]	330−181	16	330−250	2
2-phenylacetaldehyde[a]	315−181	22	315−117	16
2-phenyl-d_5-acetaldehyde[a]	320−181	22	320−122	16
sotolon	128−83	2	128−72	2
d_4-sotolon	132−87	4	132−76	4

[a]The parent ion is the derivative form.

Table 4. Method Validation and Calibration Data

	slope[a]	R^2	linearity range (μg/L)	LOQ (μg/L)	LOD (μg/L)
benzaldehyde	6.464 ± 0.182	0.992	0.1−500	0.01	0.005
eugenol	4.909 ± 0.142	0.993	0.5−1000	0.50	0.100
furaneol	0.774 ± 0.013	0.998	5−1000	5.00	2.000
furfural	0.180 ± 0.002	0.999	0.1−1000	0.10	0.005
(*E*)-2-heptenal	1.284 ± 0.046	0.996	0.01−100	0.01	0.005
hexanal	0.040 ± 0.001	0.998	0.01−500	0.01	0.005
(*E*)-2-hexenal	0.701 ± 0.019	0.997	0.01−100	0.01	0.005
homofuraneol	0.652 ± 0.009	0.997	10−1000	10.00	2.500
maltol	0.410 ± 0.047	0.993	20−1000	20.00	5.000
methional	0.298 ± 0.014	0.997	0.01−500	0.01	0.005
methionol	6.870 ± 0.115	0.998	10−2000	10.00	3.000
5-methylfurfural	0.119 ± 0.001	0.999	0.01−1000	0.01	0.005
2-methylpropanal	0.246 ± 0.004	0.997	0.01−100	0.01	0.005
3-methylbutanal	0.305 ± 0.004	0.997	0.01−100	0.01	0.005
(*E*)-2-nonenal	0.387 ± 0.006	0.997	0.01−500	0.01	0.005
(*E*)-2-octenal	1.187 ± 0.043	0.997	0.01−100	0.01	0.005
2-phenylacetaldehyde	0.754 ± 0.051	0.999	0.01−1000	0.01	0.005
sotolon	0.940 ± 0.005	0.999	5−1000	5.00	2.000

[a] Slope ± standard error.

standard of sotolon was also used for determination of eugenol and maltol. d_3-Methional was also used to quantitate hexanal. For the determination of 5-methylfurfural the internal standard d_4-furfural was used, and d_9-(*E*)-2-octenal was the standard for (*E*)-2-nonenal and (*E*)-2-heptenal.

GC Parameters. Six GC columns with different polarity (DB-35 ms, Solgel-Wax, DB-FFAP, DB-Wax, DB-5, DB-1701, VF-200 ms) were investigated (data not shown), and the majority of them gave unsatisfactory results for the compound sotolon in terms of peak shape and thus detection limits. The best chromatographic results, especially for sotolon, were

DOI: 10.1021/jf505803u
J. Agric. Food Chem. 2015, 63, 3394−3401

Table 5. Concentrations (μg/L) of Volatile Compounds in Semillon White Wine Stored under Different Closures for 14 Years

compound (μg/L)[a]	Amp. (N_2)	Amp. (air)	SC (screw cap)	NC 1 (natural cork 1)	NC 2 (natural cork 2)	Syn 1 (synthetic closure 1)	Syn 2 (synthetic closure 2)
(*E*)-2-alkenals							
(*E*)-2-heptenal	0.104 (0.010)	0.101 (0.010)	0.100 (0.002)	0.106 (0.001)	0.112 (0.010)	0.105 (0.002)	0.104 (0.004)
(*E*)-2-hexenal	0.024 (0.010)	0.017 (0.010)	0.026 (0.010)	0.035 (0.010)	0.038 (0.020)	0.072 (0.010)	0.087 (0.001)
(*E*)-2-nonenal	0.054 (0.030)	<0.01	0.017 (0.006)	<0.01	0.032 (0.009)	0.016 (0.007)	0.012 (0.002)
(*E*)-2-octenal	0.014 (0.004)	<0.01	0.012 (0.004)	0.011 (0.005)	0.018 (0.003)	0.017 (0.001)	0.014 (0.001)
Strecker aldehydes							
methional	0.69 (0.05)	4.32 (0.35)	1.09 (0.06)	3.77 (4.76)	4.87 (3.47)	18.30 (0.66)	22.80 (0.41)
2-methylpropanal	62.60 (1.97)	88.90 (6.68)	56.00 (1.48)	72.80 (16.60)	91.00 (21.00)	101.00 (9.65)	114.00 (0.01)
3-methylbutanal	4.22 (0.97)	12.20 (1.03)	3.81 (0.33)	12.80 (10.50)	27.50 (18.6)	64.00 (2.80)	99.50 (8.1)
2-phenylacetaldehyde	2.80 (0.10)	4.73 (0.43)	2.880 (0.003)	9.16 (7.06)	12.60 (6.93)	26.50 (0.55)	18.80 (0.47)
furans							
furaneol	25.20 (6.43)	16.70 (1.47)	27.20 (1.16)	23.40 (8.95)	15.60 (6.77)	6.01 (1.49)	3.45 (1.50)
homofuraneol	212.00 (72.68)	61.40 (6.03)	118.00 (4.97)	94.70 (32.2)	76.30 (30.59)	20.30 (1.27)	4.67 (0.58)
sotolon	<2	<2	<2	<2	<2	6.90 (0.14)	16.80 (1.70)
aldehydes							
benzaldehyde	24.6 (2.5)	7.2 (1.0)	18.8 (0.6)	25.6 (11.3)	24.5 (3.5)	7.8 (0.2)	23.0 (4.93)
furfural	1096.0 (121.0)	1149.0 (33.0)	1000.0 (56.3)	1284.0 (50.4)	1082.0 (401.0)	1311.0 (77.6)	1126.0 (76.7)
hexanal	1.0 (0.3)	0.9 (0.1)	0.7 (0.1)	1.0 (0.3)	1.5 (0.4)	1.46 (0.1)	2.1 (0.2)
5-methylfurfural	46.6 (0.9)	42.2 (0.6)	41.9 (0.3)	42.1 (1.9)	44.8 (0.8)	40.3 (1.3)	33.4 (2.5)
alcohols							
maltol	150.0 (14.7)	149.0 (7.4)	160.0 (1.8)	165.0 (12.9)	158.0 (14.3)	117.0 (10.9)	79.0 (7.0)
methionol	483.0 (14.3)	466.0 (16.4)	494.0 (9.6)	470.0 (17.6)	470.0 (5.7)	471.00 (0.01)	351 (45.3)
eugenol	1.8 (0.6)	1.5 (0.5)	2.0 (0.3)	1.4 (0.3)	1.9 (0.6)	1.3 (0.1)	1.4 (0.1)

[a]Mean values are shown, and standard deviation is in brackets ($n \geq 3$). For each closure three different bottles were measured.

achieved on a VF-200 ms column (30 m × 0. 25 mm i.d., with 0.25 μm film thickness). The injection type selected was liquid mode, and several inlet parameters were assessed, including splitless, split, pulsed splitless, as well as programmable temperature vaporization, with the splitless mode giving the greatest signal-to-noise. The injection in splitless mode was then tested at different temperatures ranging between 160 and 240 °C, and 180 °C was selected as the temperature giving the greatest sensitivity.

MS Parameters. The full scan MS analysis of the individual compounds showed a good signal for the molecular ion of each of the compounds analyzed. MS/MS experiments revealed the characteristic fragmentation of each of the compounds, and the most intense fragment was chosen as a quantifier. The second most intense fragment of each compound was chosen as a qualifier, and the fragmentation of the ions, together with the collision energies selected are shown in Table 3.

As the quantitation of 18 compounds and 10 internal standards requires the recording of 56 mass transitions, the sensitivity could potentially be compromised due to the number of data points that are needed to be collected. To minimize the number of recorded transitions and therefore maximize the sensitivity, the MS/MS experiments were grouped into three time segments over the GC-MS/MS run.

Method Validation. *Linearity.* Linearity was evaluated across a series (15 points) of duplicate standard additions of each of the compounds ranging over a concentration range from 0.01 to 2000 μg/L, depending on the expected concentration of the compound, and validated in red, white, and model wine (13% v/v ethanol solution in water saturated with potassium hydrogen tartrate and adjusted to pH 3.3 with aqueous tartaric acid solution). As shown in Table 4, good linearity was achieved for each of the compounds with coefficient of determination (R^2) values ranging between 0.992 and 0.999.

Repeatability. To assess the precision of the method, seven identical samples were spiked with all of the 18 compounds at two different concentrations (10 and 250 μg/L) in red, white, and model wine, and the relative standard deviation of the calculated concentrations was under 5% in all cases (data not shown).

Recovery. Control samples were spiked with all of the analytes at two different concentrations (10 and 100 μg/L) as well as a nonspiked sample, to determine the concentration in the blank, and the mean recoveries were between 92% and 105% (data not shown).

Limit of Detection. The LOD (S/N = 3) and LOQs (S/N = 10) were determined by calculating the signal-to-noise (S/N) ratio in a spiked nonoxidized wine and a model wine matrix. For some of the derivatized compounds the specific mass transition measured showed hardly any noise, which is a common occurrence for GC-MS/MS analysis. Therefore, the LOD could not be calculated in the conventional way. The limit of quantitation values were determined by measuring seven replicates of unspiked samples and the same number of replicates for samples containing increasing concentrations of the analytes and assessing whether they were significantly different ($P < 0.05$).

For all of the compounds included in the analysis the detection limits (Table 4) were lower than their odor detection threshold and ranged between 0.01 (for derivatized aldehydes) and 10 μg/L (for sotolon).

Analysis of Wines. After validation was complete, the GC-MS/MS method was applied to study a 14 year old white wine (bottled in 1999) under different closures (two natural corks, two synthetic corks, and a screw cap) to determine which of the selected compounds would most be affected by oxidation.

DOI: 10.1021/jf505803u
J. Agric. Food Chem. 2015, 63, 3394−3401

Wines stored under the same closures had been assessed by a trained sensory descriptive analysis panel at a much earlier stage of storage,[31,33,34] with the two wines bottled with synthetic closures being rated much higher in oxidized aroma than the screw cap-sealed wine and the cork-sealed wines being intermediate in scores. This set of samples also included wines stored in glass ampules sealed under nitrogen or air, and the color differences among the samples were clearly visible, indicating the degree of oxidation that occurred. The color of the wine ranged from light yellow in the case of the wines sealed in glass ampules to a dark brown for wines under synthetic corks. In order to account for possible bottle to bottle variations with the same closures, the analysis for each type of closure was carried out on three different bottles.

As expected from the immense differences in color highlighted by visual inspection of the wines, most of the compounds analyzed were found to be present in significantly different ($P < 0.05$) concentrations depending on the closures (Table 5). Among the Strecker aldehydes, the concentration of 2-phenylacetaldehyde, 3-methylbutanal, and methional was significantly higher in the wines sealed with natural corks than in those stored in glass ampules. Notably, the highest concentration of these three compounds was found in the wines stored under the synthetic closures, with 3-methylbutanal reaching concentrations of almost 100 μg/L in Syn 1 compared to around 4 μg/L found in the wines stored in glass ampules under nitrogen. Similarly, for methional and 2-phenylacetaldehyde the wine sealed in glass ampules showed concentrations below 5 μg/L, which increased by a factor of 4 in the wines sealed with synthetic closures (Syn 1 and Syn 2). For each of these flavor compounds (methional, phenylactaldehyde, and 3-methylbutanal) the wines sealed with natural corks had the second highest concentration. The wine sealed under screw cap contained a very low concentration of Strecker aldehydes, which were even lower than in the glass ampule sealed with air, and was very similar to that of the glass ampule sealed under nitrogen. This result is not surprising and is most likely attributed to the differences in volume among the wine vessels: the ratio of the head space to the wine volume was higher for the ampules since the volume of the ampules was 50 mL with 3 mL of headspace, in contrast to that of the wine bottles, where the ratio was much lower since the bottles had a 750 mL volume. Escudero et al. showed that methional is an impact odorant of oxidized wines, giving the wine a cooked vegetable off-flavor.[7] Their study showed that wines spiked with methionol or methionine resulted in an increase in the methional concentration and therefore explains that the possible formation pathway during wine oxidation is the direct peroxidation of methionol or a Strecker degradation of methionine. The same pathway was reported for the formation of 2-phenylacetaldehyde from phenylalanine, which also has a low odor threshold and an aroma described as "honey-like".[35,36]

Four (*E*)-2-alkenals with different chain length were measured, and only (*E*)-2-hexenal and (*E*)-2-nonenal were found in significantly different concentrations among closures, with no significant differences observed in both (*E*)-2-octenal and (*E*)-2-heptenal concentrations. The control ampule sealed under nitrogen contained the highest concentration of (*E*)-2-nonenal compared to all other closure samples, suggesting nonoxygen-induced changes may be contributing to the formation, whereas (*E*)-2-hexenal was about 3−4 times higher in wines sealed with synthetic closures and 1.5 times higher in wines sealed with natural corks compared with that of the control. The (*E*)-2-alkenals have been reported to be important contributors to oxidative off flavor.[5] A positive correlation between the (*E*)-2-octenal content and a "rotten apple" sensory note of oxidized wines was shown by Escudero et al., and (*E*)-2-decenal and (*E*)-2-nonenal were also found to be related to other oxidized wine notes,[4] whereas (*E*)-2-nonenal was associated with a "sawdust" aroma.[14] The concentration of the C_6 compound hexanal was higher only in the wine under synthetic cork Syn 2, whereas in all other samples this compound was not found in significantly different quantities.

The furanones, furaneol and homofuraneol, were found in higher concentration in the control wines (N_2) in comparison to all of the other closures. Homofuraneol was found in very high concentration in the control ampule sealed under nitrogen (212 μg/L) and much lower in all other samples, with the wines sealed with synthetic corks having the lowest concentrations of 20 and 4 μg/L (Syn 1 and Syn 2). The changes for furaneol were less drastic, but again the synthetic corks resulted in significantly lower concentrations than the ampouled controls, suggesting oxidative degradation of these compounds.

The "caramel"-like smelling compound maltol, which is commonly extracted from toasted oakwood used in the aging of wines,[37] was found to be present in approximately one-half the concentration in the wine sealed with the synthetic closure (Syn 2) compared to that of the glass ampules, and the wine sealed in Syn 1 also contained a lower concentration. There was no significant difference observed for all other closures, and the concentration of maltol found was well below its odor detection threshold of 5000 μg/L.[13] Methionol was found in a concentration of almost 500 μg/L in all samples (odor threshold 1000 μg/L[17]), with the only significant difference being with the wine sealed with the synthetic closure 2 (Syn 2), which contained 350 μg/L.

Sotolon has been shown to be a key odorant of aged Sherry wines, Ports, and botrytized wines and has also been reported as a contributor to the oxidative off-flavor of table wines.[5,10,22] In our study this compound was only found in increased concentrations and above its aroma detection threshold in the wines sealed with the synthetic closure 2 (Syn 2).

The compound furfural was present at a high concentration in each of the wines, whereas the structurally similar compound 5-methylfurfural was found at the highest concentration in the wine stored under nitrogen in the glass ampules (N_2) and at the lowest concentration in the wine under synthetic closure (Syn 2).

In previous studies using Maccabeo and Chardonnay wines it was shown that the levels of eugenol increased upon wine oxidation,[38] and gas chromatography-olfactometry (GC-O) investigations showed eugenol as an important odor linked to oxidation.[5] Our results with Semillon are in contrast to these findings, as there were no significant differences in concentration among the wines stored under different closures for this compound even though the wines were clearly and visibly affected by oxidation.

The role of different flavor compounds in contributing to wine aroma was clearly observed through the analysis of 14 year old white wines sealed under different closures and comparison to the reported aroma detection thresholds. The wines had naturally aged and oxidized via varied oxygen ingress over extended bottle storage. In agreement with the literature, 2-phenylacetaldehyde and methional were found in increased concentrations in the wines exposed to high oxygen levels,

DOI: 10.1021/jf505803u
J. Agric. Food Chem. 2015, 63, 3394−3401

which were significantly above their odor thresholds and could therefore add to the oxidative "off-flavor" in Semillon wine.

In conclusion, validation and application of a novel GC-MS/MS method is described that enables the simultaneous quantitation of 18 oxidation-related compounds in wines at mg/L, μg/L, and ng/L levels. The preparation of samples is simple and requires only a small volume of wine. An added advantage is the use of deuterated analogues as internal standards which ensures accuracy of the method. The reliability was established using validation criteria such as linearity, repeatability, and reproducibility. This method, to the best of our knowledge, is the first developed for assessing oxidation-related compounds using GC-MS/MS, and its effectiveness was proven through quantitation of 18 compounds in a white wine closure study. Hence, the GC-MS/MS method will provide new insights when used for future storage and shelf-life studies of wines and related beverages.

AUTHOR INFORMATION

Corresponding Author

*Phone: +61 88313 6689. Fax: +61 88313 6601. E-mail: dimitra.capone@awri.com.au.

Present Address

‡Christine M. Mayr: Cara Technology Limited, Leatherhead Enterprise Centre, Randalls Road, Leatherhead, Surrey, KT22 7RY, United Kingdom.

Funding

The Australian Wine Research Institute (AWRI), a member of the Wine Innovation Cluster in Adelaide, is supported by Australian grapegrowers and winemakers through their investment body, by the Australian Grape and Wine Authority (AGWA), with matching funds from the Australian Government.

Notes

The authors declare no competing financial interest.

ACKNOWLEDGMENTS

We thank our collaborators Agilent Technologies for their generous support, in particular, Jim Tsiotinas and Nick B. Harden for the loan of the GC-MS/MS system. We also thank Dr. Dan Johnson for his efforts in ensuring the success of the Agilent collaboration and Dr. Markus Herderich for manuscript evaluation. We would also like to thank Dr. Mark A. Sefton and Dr. Gordon Elsey for their contributions toward the deuterium-labeled standard synthesis used in this study and Dr. Sefton and Peter Godden for their contribution to the white wine closure study.

ABBREVIATIONS USED

PFBHA, *O*-(2,3,4,5,6-pentafluorobenzyl)hydroxylamine hydrochloride; GC, gas chromatography; MS, mass spectrometry; SPE, solid-phase extraction; THF, tetrahydrofuran; MRM, multiple reaction monitoring; LOD, limit of detection; LOQ, limit of quantitation; GC-O, gas chromatography-olfactometry

REFERENCES

(1) Waterhouse, A. L.; Laurie, V. F. Oxidation of wine phenolics: A critical evaluation and hypotheses. *Am. J. Enol. Vitic.* **2006**, *57*, 306−313.

(2) Ugliano, M. Oxygen contribution to wine aroma evolution during bottle aging. *J. Agric. Food Chem.* **2013**, *61*, 6125−6136.

(3) Ferreira, S.; Hogg, T.; de Pinho, P. G. Identification of key odorants related to the typical aroma of oxidation-spoiled white wines. *J. Agric. Food Chem.* **2003**, *51*, 1377−1381.

(4) Escudero, A.; Asensio, E.; Cacho, J.; Ferreira, V. Sensory and chemical changes of young white wines stored under oxygen. An assessment of the role played by aldehydes and some other important odorants. *Food Chem.* **2002**, *77*, 325−331.

(5) Escudero, A.; Cacho, J.; Ferreira, V. Isolation and identification of odorants generated in wine during its oxidation: a gas chromatography − olfactometric study. *Eur. Food Res. Technol.* **2000**, *211*, 105−110.

(6) Balboa-Lagunero, T.; Arroyo, T.; Cabellos, J. M.; Aznar, M. Sensory and olfactometric profiles of red wines after natural and forced oxidation processes. *Am. J. Enol. Vitic.* **2011**, *62*, 527−535.

(7) Escudero, A.; Hernández-Orte, P.; Cacho, J.; Ferreira, V. Clues about the role of methional as character impact odorant of some oxidized wines. *J. Agric. Food Chem.* **2000**, *48*, 4268−4272.

(8) Ferreira, V.; Escudero, A.; López, R.; Cacho, J. Analytical characterization of the flavor of oxygen-spoiled wines through the gas chromatography-ion-trap mass spectrometry of ultratrace odorants: Optimization of conditions. *J. Chromatogr. Sci.* **1998**, *36*, 331−339.

(9) Culleré, L.; Cacho, J.; Ferreira, V. An assessment of the role played by some oxidation-related aldehydes in wine aroma. *J. Agric. Food Chem.* **2007**, *55*, 876−881.

(10) Martin, B.; Etiévant, P. X.; Le Quéré, J. L.; Schlich, P. More clues about sensory impact of sotolon in some Flor Sherry wines. *J. Agric. Food Chem.* **1992**, *31*, 475−478.

(11) Silva Ferreira, A. C.; Barbe, J.-C.; Bertrand, A. 3-Hydroxy-4,5-dimethyl-2(5*H*)-furanone: a key odorant of the typical aroma of oxidative aged Port wine. *J. Agric. Food Chem.* **2003**, *51*, 4356−4363.

(12) Collin, S.; Nizet, S.; Bouuaert, T. C.; Despatures, P. M. Main odorants in jura flor-sherry wines. Relative contributions of sotolon, abhexon, and theaspirane-derived compounds. *J. Agric. Food Chem.* **2012**, *60*, 380−387.

(13) Ferreira, V.; Ortín, N.; Escudero, A.; López, R.; Cacho, J. Chemical characterization of the aroma of Grenache rosé wines: aroma extract dilution analysis, quantitative determination, and sensory reconstitution studies. *J. Agric. Food Chem.* **2002**, *50*, 4048−4054.

(14) Chatonnet, P.; Dubourdieu, D. Identification of substances responsible for the 'sawdust' aroma in oak wood. *J. Sci. Food Agric.* **1998**, *76*, 179−188.

(15) Kotseridis, Y.; Razungles, A.; Bertrand, A.; Baumes, R. Differentiation of the aromas of Merlot and Cabernet Sauvignon wines using sensory and instrumental analysis. *J. Agric. Food Chem.* **2000**, *48*, 5383−5388.

(16) Etiévant, P. X.. Wine. In *Volatile Compounds in Foods and Beverages*; Maarse, H., Ed.; Marcel Dekker: New York, 1991; Vol. *14*, pp 483−546.

(17) Ferreira, V.; López, R.; Cacho, J. F. Quantitative determination of the odorants of young red wines from different grape varieties. *J. Sci. Food Agric.* **2000**, *80*, 1659−1667.

(18) Cutzach, I.; Chatonnet, P.; Dubourdieu, D. Study of the formation mechanisms of some volatile compounds during the aging of sweet fortified wines. *J. Agric. Food Chem.* **1999**, *47*, 2837−2846.

(19) Culleré, L.; Cacho, J.; Ferreira, V. Analysis for wine C5−C8 aldehydes through the determination of their O-(2,3,4,5,6-pentafluorobenzyl)oximes formed directly in the solid phase extraction cartridge. *Anal. Chim. Acta* **2004**, *524*, 201−206.

(20) Ferreira, V.; Culleré, L.; Loscos, N.; Cacho, J. Critical aspects of the determination of pentafluorobenzyl derivatives of aldehydes by gas chromatography with electron-capture or mass spectrometric detection: Validation of an optimized strategy for the determination of oxygen-related odor-active aldehydes in wine. *J. Chromatogr. A* **2006**, *1122*, 255−265.

(21) Gabrielli, M.; Buica, A.; Fracassetti, D.; Stander, M.; Tirelli, A.; du Toit, W. J. Determination of sotolon content in South African white wines by two novel HPLC−UV and UPLC−MS methods. *Food Chem.* **2015**, *169*, 180−186.

DOI: 10.1021/jf505803u
J. Agric. Food Chem. 2015, 63, 3394−3401

(22) Guichard, E.; Pham, T. T.; Etievant, P. Quantitative determination of sotolon in wines by high-performance liquid chromatography. *Chromatographia.* **1993**, *37*, 539−542.
(23) Blank, I.; Sen, A.; Grosch, W. Potent odorants of the roasted powder and brew of Arabica coffee. *Z. Lebensm.-Unters. Forsch.* **1992**, *195*, 239−245.
(24) Ferreira, V.; Jarauta, I.; López, R.; Cacho, J. Quantitative determination of sotolon, maltol and free furaneol in wine by solid-phase extraction and gas chromatography-ion-trap mass spectrometry. *J. Chromatogr. A* **2003**, *1010*, 95−103.
(25) Schuh, C.; Schieberle, P. Characterization of the key aroma compounds in the beverage prepared from Darjeeling black tea: quantitative differences between tea leaves and infusion. *J. Agric. Food Chem.* **2006**, *54*, 916−924.
(26) Fernandes, R. A.; Kumar, P. PCC-mediated novel oxidation reactions of homobenzylic and homoallylic alcohols. *Tetrahedron Lett.* **2003**, *44*, 1275−1278.
(27) Sen, A.; Grosch, W. Synthesis of six deuterated sulfur containing odorants to be used as internal standards in quantification assays. *Z. Lebensm.-Unters. Forsch.* **1991**, *192*, 541−547.
(28) Blank, I.; Fay, L. B.; Lakner, F. J.; Schlosser, M. Determination of 4-Hydroxy-2,5-dimethyl-3(2*H*)-furanone and 2(or 5)-ethyl-4-hydroxy-5(or 2)-methyl-3(2*H*)-furanone in pentose sugar-based Maillard model systems by isotope dilution assays. *J. Agric. Food Chem.* **1997**, *45*, 2642−2648.
(29) Heading, H. J. Development of SIDA protocols for quantification of aldehydes in wine. Ph.D. Thesis, Flinders University of South Australia, 2007; pp 31−34.
(30) Grant-Preece, P. A.; Pardon, K. H.; Capone, D. L.; Cordente, A. G.; Sefton, M.; Jeffery, D. W.; Elsey, G. M. Synthesis of wine thiol conjugates and labelled analogues: fermentation of the glutathione conjugates of 3-mercaptohexan-1-ol yields the corresponding cysteine conjugate and free thiol. *J. Agric. Food Chem.* **2010**, *58*, 1383−1389.
(31) Godden, P.; Francis, I. L.; Field, J.; Gishen, M.; Coulter, A.; Valente, P.; Hoj, P.; Robinson, E. M. C. Wine bottle closures: physical characteristics and effect on composition and sensory properties of a Semillon wine 1. Performance up to 20 months post-bottling. *Aust. J. Grape Wine Res.* **2001**, *7*, 64−105.
(32) Capone, D.; Sefton, M.; Pretorius, I.; Høj, P. Flavour "scalping" by wine bottle closures-the "winemaking" continues post vineyard and winery. *Aust. N. Z. Wine Ind. J.* **2003**, *18*, 18−20.
(33) Godden, P. AWRI trial of the technical performance of various types of wine closure. *Aust. Grapegrower Winemaker* **1999**, *425*, 59−64.
(34) Godden, P.; Francis, L.; Field, J.; Gishen, M.; Coulter, A.; Valente, P.; Høj, P.; Robinson, E. Results of an AWRI trial investigating the technical performance of various types of wine closure: Part 2-Wine composition up to 20 month post-bottling. *Aust. Grapegrower Winemaker* **2001**, *7*, 89−98.
(35) Pripis-Nicolau, L.; de Revel, G.; Bertrand, A.; Maujean, A. Formation of flavor components by the reaction of amino acid and carbonyl compounds in mild conditions. *J. Agric. Food Chem.* **2000**, *48*, 3761−3766.
(36) Grant-Preece, P.; Fang, H.; Schmidtke, L. M.; Clark, A. Sensorially important aldehyde production from amino acids in model wine systems: Impact of ascorbic acid, erythorbic acid, glutathione and sulphur dioxide. *Food Chem.* **2013**, *141*, 304−312.
(37) Cutzach, I.; Chatonnet, P.; Henry, R.; Dubourdieu, D. Identification of volatile compounds with a " toasty " aroma in heated oak used in barrelmaking. *J. Agric. Food Chem.* **1997**, *45*, 2217−2224.
(38) Ferreira, V.; Escudero, A.; Fernández, P.; Cacho, J. F. Changes in the profile of volatile compounds in wines stored under oxygen and their relationship with the browning process. *Z. Lebensm.-Unters. Forsch. A* **1997**, *205*, 392−396.

DOI: 10.1021/jf505803u
J. Agric. Food Chem. 2015, 63, 3394−3401

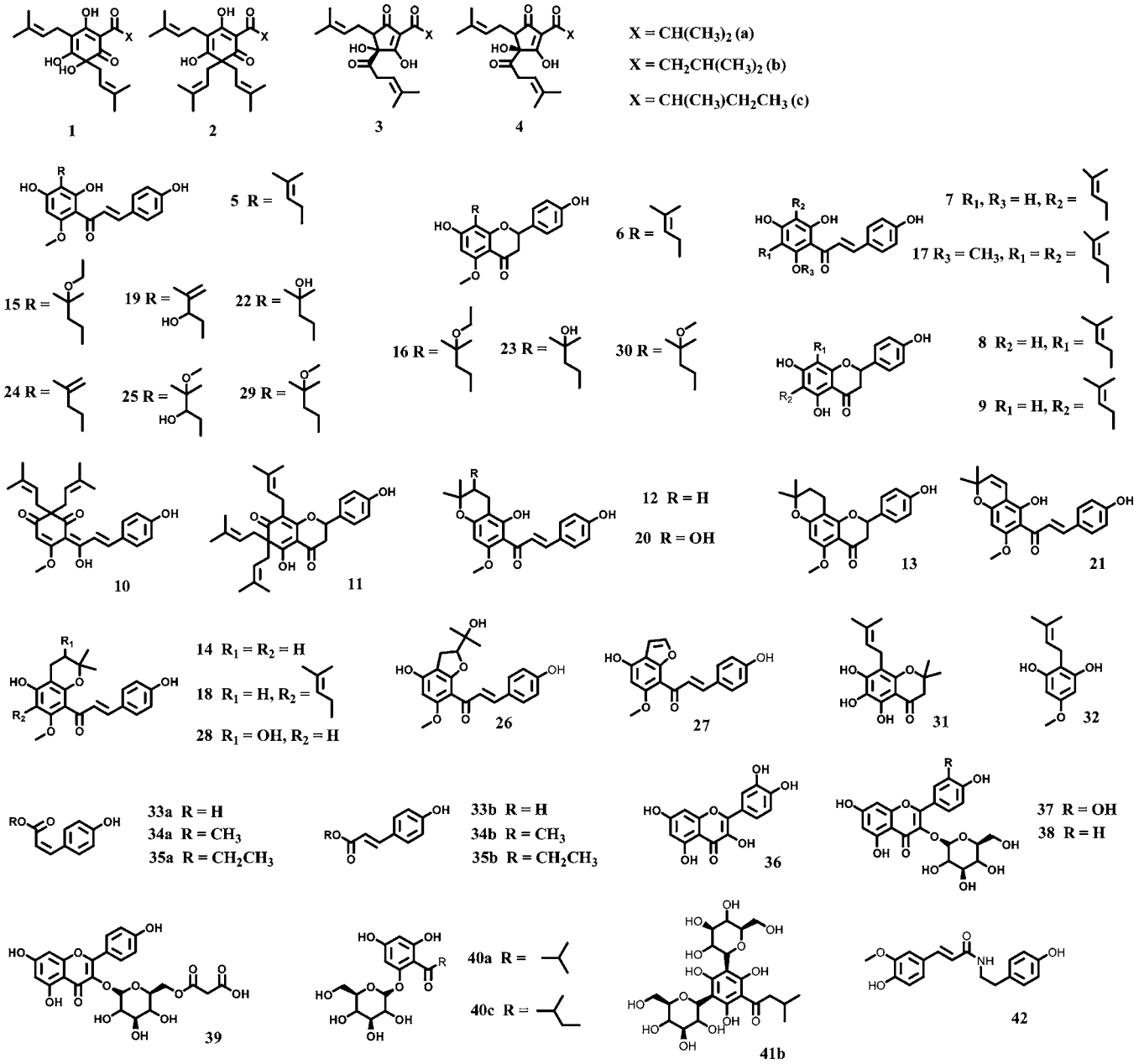

Figure 1. Chemical structures of key taste compounds identified in the hop hard resin fraction: cohumulon (**1a**), *n*-humulon (**1b**), adhumulon (**1c**), colupulon (**2a**), *n*-lupulon (**2b**), adlupulon (**2c**), *cis*-isocohumulon (**3a**), *cis*-isohumulon (**3b**), *cis*-isoadhumulon (**3c**), *trans*-isocohumulon (**4a**), *trans*-isohumulon (**4b**), *trans*-isoadhumulon (**4c**), xanthohumol (**5**), isoxanthohumol (**6**), desmethylxanthohumol (**7**), 8-prenylnaringenin (**8**), 6-prenylnaringenin (**9**), 4′-hydroxytunicatachalcone (**10**), isoxantholupon (**11**), 1″,2″-dihydroxanthohumol C (**12**), 1″,2″-dihydroisoxanthohumol C (**13**), 1″,2″-dihydroxanthohumol K (**14**), xanthohumol P (**15**), isoxanthohumol P (**16**), 5′-prenylxanthohumol (**17**), 1″,2″-dihydroxanthohumol F (**18**), xanthohumol D (**19**), xanthohumol B (**20**), xanthohumol C (**21**), xanthohumol H (**22**), isoxanthohumol H (**23**), xanthohumol N (**24**), 2″-hydroxy-xanthohumol M (**25**), xanthohumol I (**26**), xanthohumol O (**27**), xanthohumol L (**28**), xanthohumol M (**29**), isoxanthohumol M (**30**), 2″,3″-dehydrocyclohumulohydrochinon (**31**), 1-methoxy-4-prenylphloroglucinol (**32**), *cis*-/*trans*-*p*-coumaric acid (**33a**/**b**), *cis*-/*trans*-*p*-coumaric acid methyl ester (**34a**/**b**), *cis*-/*trans*-*p*-coumaric acid ethyl ester (**35a**/**b**), quercetin (**36**), quercetin-3-*O*-*β*-D-glucopyranoside (**37**), kaempferol-3-*O*-*β*-D-glucopyranoside (**38**), kaempferol-3-*O*-*β*-D-(6″-malonyl)glucopyranoside (**39**), 1-*O*-*β*-D-(2-methylpropanoyl)phloroglucinol glucopyranoside (co-multifidol glucopyranoside) (**40a**), 1-*O*-*β*-D-(2-methylbutyryl)phloroglucinol glucopyranoside (ad-multifidolglucopyranoside) (**40c**), phloroisovalerophenon-3,5-di-*C*-*β*-D-glucopyranoside (*n*-multifidol-di-*C*-glucopyranoside) (**41b**), and *trans*-*N*-feruloyltyramine (**42**).

Germany). Water for high-performance liquid chromatography (HPLC) and medium-pressure liquid chromatography (MPLC) separation was purified by means of a Milli-Q water advantage A 10 water system (Millipore, Molsheim, France), and bottled water was used for sensory studies (Evian, Danone, Wiesbaden, Germany). Solvents for HPLC were of HPLC grade and for LC-MS were of MS grade (J.T.Baker, purchased through Sigma-Aldrich).

Hop pellets type 90 and spent hop pellets, which were obtained after supercritical carbon dioxide extraction of hops, were delivered from Joh. Barth & Sohn GmbH & Co. KG (Nuremberg, Germany); XanthoFlav 15, XanthoFlav 75, hop tannin extracts (from both aroma and bitter hops), and resin extracts (from both aroma and bitter hops) were obtained from Hopsteiner (Simon H. Steiner GmbH, Mainburg, Germany). A novel *ε*-extract was produced in cooperation with Joh. Barth & Sohn GmbH & Co. KG and NateCO_2 GmbH & Co. KG

DOI: 10.1021/acs.jafc.5b00239
J. Agric. Food Chem. 2015, 63, 3402−3418

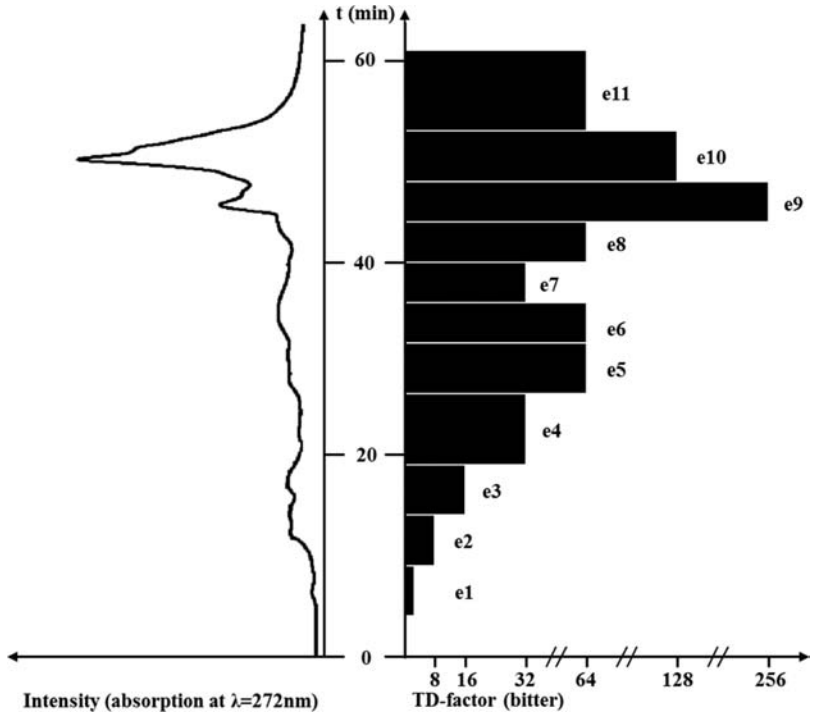

Figure 2. RP-MPLC chromatogram (left) and taste dilution chromatogram (right) of the ε-resin fraction isolated from spent hops.

(Wolnzach, Germany) by means of a supercritical CO_2 extraction using ethanol as a modifier.[27] Reference substances for individual iso-α-acids were purified from an iso-α-acid extract (30%; Hopsteiner), and purified α- and β-acids were isolated from an ethanolic hop extract (Hopsteiner, Simon H. Steiner GmbH, Mainburg, Germany) following the protocol reported recently.[28] Xanthohumol was purified from a commercial xanthohumol extract, and isoxanthohumol was prepared from xanthohumol by alkaline cyclization as reported recently.[28] 8-Prenylnaringenin was prepared from isoxanthohumol by demethylation using scandium trifluoromethanesulfonate.[29] Experimental brewing trails were conducted in the Research Brewery St. Johann St. Johann GmbH & CO. KG (Train-St. Johann, Germany). Unhopped "zero" beer was obtained from the Chair of Brewing and Beverage Technology, Technische Universität München (Freising, Germany).

Preparative Isolation of Soft Resin and δ- and ε-Hard Resin. According to the literature with some modifications,[30] spent hops (100 g) were exhaustively extracted with methanol/diethyl ether (1/5, v/v; 900 mL) for 1 h while stirring. After the addition of hydrochloric acid (300 mL; 0.1 mol/L), the mixture was stirred for additional 10 min and then filtered (320 mm, Macherey-Nagel, Düren, Germany), and the organic layer was extracted with hydrochloric acid (3 × 100 mL; 0.1 mol/L) before the solvent was separated in vacuum. To remove waxes, the residue was solubilized in methanol (400 mL), and, after incubation at −20 °C overnight and filtration (round filter paper, 320 mm, Roth, Karlsruhe, Germany), the solution was applied onto 55 μm, 70A, Strata C18-E Giga Tube cartridges (10 g, 60 mL; Phenomenex, Aschaffenburg, Germany), conditioned with methanol. Chlorophylls were separated by flushing the cartridges with methanol (150 mL), and the effluent was collected and separated from solvent in vacuum. The resin obtained was suspended in hexane and filtered (185 mm, Macherey-Nagel, Düren, Germany). The filtrate was collected and separated from solvent in vacuum to give the soft resin (91.9% yield), whereas the residue was extracted with hexane (50 mL) to give the nonsoluble hard resin (8.1% yield). Following a literature protocol for ε-resin isolation,[31,32] the hard resin was suspended in water at 40 °C during ultrasonification. After filtration (185 mm, Macherey-Nagel, Düren, Germany), the aqueous phase was collected, whereas the residue was again suspended in water (40 °C). After this process was repeated three times, the combined aqueous layer was freeze-dried to obtain the δ-resin (20.2% of total hard resin), whereas lyophilization of the residual material afforded the ε-resin (79.8% of total hard resin).

Fractionation of the ε-Resin by Medium-Pressure Liquid Chromatography (MPLC). Aliquots of the ε-resin (0.5 g) were dissolved in methanol/water (40/60, v/v; 20 mL) and separated on a 460 × 16 mm glass column (Büchi, Flawil, Switzerland) filled with 25−40 μm LiChroprep RP18 material (Merck KGaA, Darmstadt, Germany) using an MPLC system (Büchi Sepacore, Flawil, Switzerland) consisting of two C-605 pumps, a C-620 control unit, a C-660 fraction collector, a 6-way-injection valve, and a C-635 UV detector monitoring the effluent at 272 nm. Data acquisition was performed by means of Sepacore Control Chromatography Software, Version 1.0. Operating with a flow rate of 30.0 mL/min and using 0.1% aqueous formic acid as solvent A and methanol containing 0.1% formic acid as solvent B, chromatography was performed starting with 40% solvent B for 1 min and, then, increasing solvent B to 60% within 6 min, to 70% within 30 min and, finally, to 100% within an additional 20 min, followed by isocratic elution for 20 min. After 86.0 min, solvent B decreased again to 40% and was kept for 10 min prior to the next injection. A total of 11 fractions (e1−e11) were collected, separated from solvent in vacuum, and then used for a taste dilution analysis[33−35] to locate fractions e2 (yield: 3.4%), e3 (yield: 3.0%), e4 (yield: 3.2%), e5 (yield: 3.6), e6 (yield: 3.2%), e7 (yield: 2.6%), e8 (yield: 2.7%), e9 (yield: 18.4%), e10 (yield: 31.3%), and e11 (yield: 22.9%) with the highest bitter impact (Figure 2).

Isolation of Key Bitter Molecules from MPLC Fractions of ε-Resin. MPLC fractions were separated by means of preparative HPLC on a 250 × 21.2 mm, 5 μm, Luna Phenyl-Hexyl column (Phenomenex, Aschaffenburg, Germany) operated with a flow rate of 15 mL/min and using 0.1% aqueous formic acid and acetonitrile containing 0.1% formic acid as solvents. Separation of MPLC fractions e2 to e11 gave subfractions e2-1 to e2-14, e3-1 to e3-13, e4-1 to e4-5, e5-1 to e5-5, e6-1 to e6-11, e7-1 to e7-16, e8-1 to e8-8, e9-1 to e9-9, e10-13 to e10-13, and e11-1 to e11-15, all of which were collected, separated from solvent in vacuum, and subjected to a taste dilution analysis (Figure 3).

Structure Determination of Bitter Compounds in ε-Resin Subfractions. The individual ε-resin subfractions isolated above were directly analyzed by means of LC-TOF-MS and 1D/2D-NMR spectroscopy and, if needed, further purified by means of rechromatography using a semipreparative 250 × 10.0 mm Hypersil RP-18 column (Thermo Hypersil GmbH, Kleinostheim, Germany) using a solvent

DOI: 10.1021/acs.jafc.5b00239
J. Agric. Food Chem. 2015, 63, 3402−3418

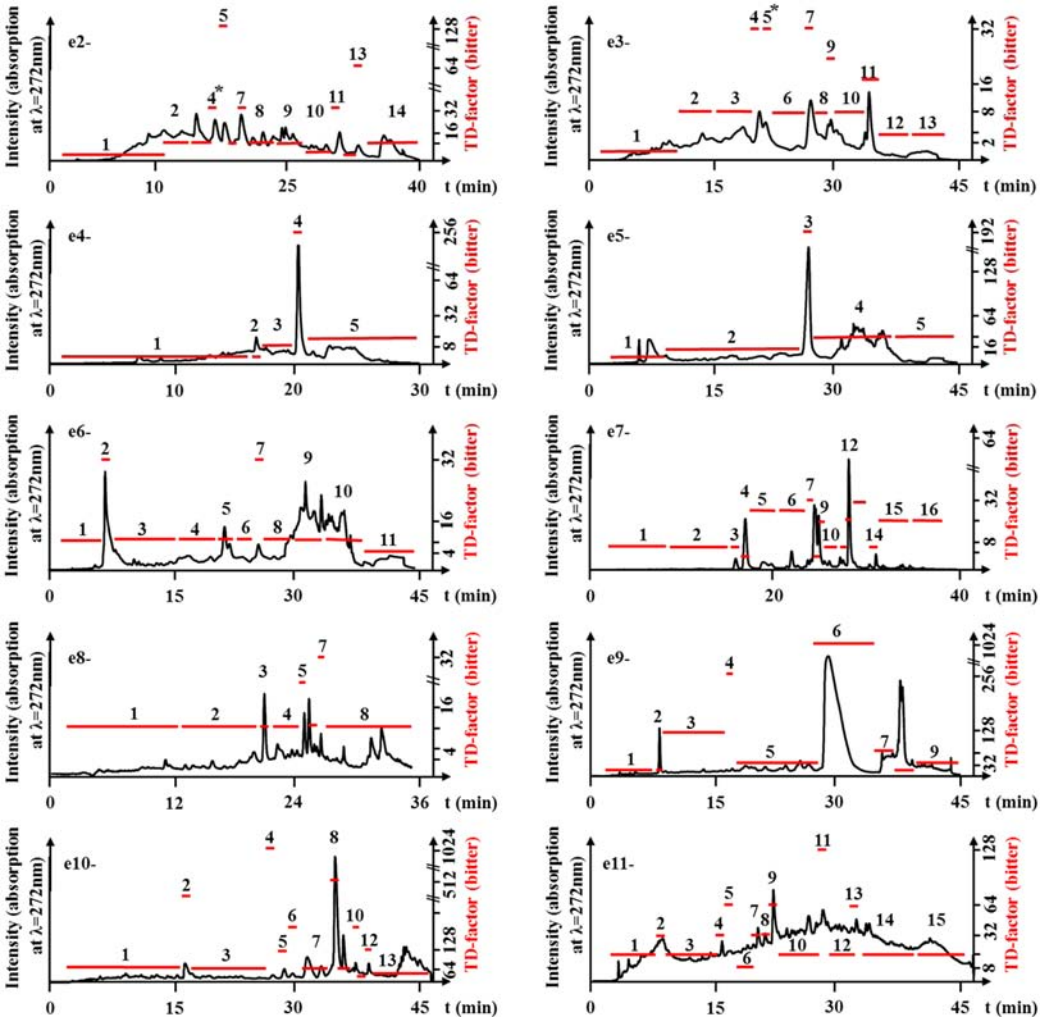

Figure 3. RP-HPLC-TDA chromatogram of the ε-resin subfractions e2−e11 isolated from spent hops. * Fraction with an astringent taste.

gradient of aqueous 0.1% formic acid and methanol containing 0.1% formic acid (flow rate: 4.7 mL/min). Compounds **5**−**7**, **9**−**12**, **14**, **17**−**22**, **25**−**29**, **31**−**34**, **36**, **37**, **40a**, and **42**−**44** were isolated from the subfractions as summarized in Table 1 in a purity of more than 98% and, after the solvent was separated in vacuum and freeze-dried twice, were used for structure determination by means of UV/vis, LC-MS/MS, UPLC-TOF-MS, and 1D/2D NMR, as well as for sensory experiments. Based on the comparison of spectroscopic (UV/vis, LC-TOF-MS, ^{1}H/^{13}C NMR) and chromatographic data with those recorded for references, previously reported compounds were confirmed as xanthohumol (**5**),[24] isoxanthohumol (**6**),[24] desmethylxanthohumol (**7**),[25] 6-prenylnaringenin (**9**),[24] 1″,2″-dihydroxanthohumol C (**12**),[23,36,37] 1″,2″-dihydroxanthohumol K (**14**),[36,37] 5′-prenylxanthohumol (**17**),[24,25] xanthohumol D (**19**),[25] xanthohumol B (**20**),[24,25] xanthohumol C (**21**),[24] xanthohumol H (**22**),[23,36,37] 2″-hydroxyxanthohumol M (**25**),[38] xanthohumol I (**26**),[23,36,37] xanthohumol O (**27**),[39] xanthohumol L (**28**),[39] *cis*-/*trans*-*p*-coumaric acid (**33a**/**b**),[29] *cis*-/*trans*-*p*-coumaric acid methyl ester (**34a**/**b**),[29] quercetin (**36**),[40] quercetin-3-*O*-β-D-glucopyranoside (**37**),[41] 1-*O*-β-D-(2-methylpropanoyl)-phloroglucinol glucopyranoside (co-multifidol glucopyranoside) (**40a**),[43] *trans*-*N*-feruloyltyramine (**42**),[23,36,37] cohumulon (**41a**),[13] *n*-humulon (**41b**),[13] adhumulon (**41c**),[13] colupulon (**44a**),[13] *n*-lupulon (**44b**),[13] and adlupulon (**44c**).[13] The chemical structures of compounds **10**, **11**, **18**, **29**, **31**, and **32** have been determined by means of UV/vis, LC-MS, and 1D/2D NMR experiments and, to the best of our knowledge, have not been earlier reported (Figure 4).

4′-Hydroxytunicatachalcone, 10 (Figure 4). UV/vis (ACN/water; 0.1% formic acid): λ_{max} = 406 nm. LC-MS (ESI$^-$): *m*/*z* (%) 421 (12, [M − H]$^-$), 119 (100), 93 (3), 217 (2), 245 (1). LC-TOF-MS (ESI$^-$): *m*/*z* 421.2014 ([M − H]$^-$, measured), *m*/*z* 421.2015 ([M − H]$^-$, calcd for $C_{26}H_{29}O_5^-$). ^{1}H NMR (500 MHz, MeOD; COSY): δ (ppm) 1.56 [s, 4 × 3H, H−C(4″, 4″a, 5″, 5″a)], 2.58 [m, 3H, H−C(1″, 1″a)], 3.99 [s, 3H, H−C(1‴)], 4.84 [m, 2H, H−C(2″, 2″a)], 5.56 [s, 1H, H−C(6)], 6.85 [m, 2H, *J* = 8.9 Hz, H−C(3′, 5′)], 7.54 [m, 2H, *J* = 8.9 Hz, H−C(2′, 6′)], 7.61 [d, 1H, *J* = 15.7 Hz, H−C(3)], 7.88 [d, 1H, *J* = 15.7 Hz, H−C(2)]. ^{13}C NMR (125 MHz, MeOH; HSQC, HMBC): δ (ppm) 17.9 [C(5″, 5″a)], 25.8 [C(4″, 4″a)], 39.5 [C(1″, 1″a)], 57.1 [C(1‴)], 62.6 [C(8)], 98.9 [C(6)], 106.1 [C(10)], 116.6 [C(3′, 5′)], 118.8 [C(2″, 2″a)], 119.1 [C(3)], 128.1 [C(1′)], 131.8 [C(2′, 6′)], 136.2 [C(3″, 3″a)], 145.9 [C(2)], 161.9 [C(4′)], 174.3 [C(5)], 180.3 [C(4)], 199.8 [C(7)], 205.9 [C(9)].

Isoxantholupon, 11 (Figure 4). UV/vis (ACN/water; 0.1% formic acid): λ_{max} = 308 nm. LC-MS (ESI$^-$): *m*/*z* (%) 475.2 (100, [M − H]$^-$), 243 (95), 119 (55), 363 (29), 286 (26), 257 (15). LC-TOF-MS (ESI$^-$): *m*/*z* 475.2492 ([M − H]$^-$, measured), *m*/*z* 475.2484 ([M − H]$^-$, calcd for $C_{30}H_{35}O_5^-$). ^{1}H NMR (500 MHz, MeOD; COSY): δ (ppm) 1.51/1.53/1.56/1.59 [s, 4 × 3H, H−C(4‴, 4‴a, 5‴, 5‴a)], 1.55 [s, 3H, H−C(4″)], 1.61 [s, 3H, H−C(5″)], 2.60/2.62 [d, 2 × 2H, *J* = 6.75 Hz, *J* = 7.35 Hz, H−C(1‴, 1‴a)], 2.96 [dd, 1H, *J* = 7.0 Hz, *J* = 18.2 Hz, H−C(3eq)], 3.00 [d, 2H, *J* = 7.0 Hz, H−C(1″)], 3.16 [dd, 1H, *J* = 9.8 Hz, *J* = 18.2 Hz, H−C(3ax)], 4.71/4.82 [t, 2 × 2H, *J* = 6.75 Hz, *J* = 7.35 Hz, H−C(2‴, 2‴a)]; 4.89 [t, 2H, *J* = 7.0 Hz, H−C(2″)]; 5.3 [dd, 1H, *J* = 4.0 Hz, *J* = 9.8 Hz, H−C(2)], 6.82 [m, 2H, *J* = 8.9, H−C(3′, 5′)], 7.28 [m, 2H, *J* = 8.9, H−C(2′, 6′)]. ^{13}C NMR (125 MHz, MeOD; HSQC, HMBC): δ (ppm) 17.9/18.1 [C(4″, 4‴, 4‴a)], 22.2 [C(1″)], 25.9/26.0 [C(5″, 5‴, 5‴a)], 38.5 [C(3)], 39.1/39.7 [C(1‴, 1‴a)], 61.9 [C(6)], 78.3 [C(2)],

DOI: 10.1021/acs.jafc.5b00239
J. Agric. Food Chem. 2015, 63, 3402−3418

Table 1. Orosensory Quality and Human Recognition Threshold Concentration of Taste Compounds Identified in Hops' Hard Resin and Hop Extracts

compound (no.)[a]	sensory quality[b]	fraction no.[c]	TC[d] [μmol/L]
cis-p-coumaric acid (**33a**)	as	e2-4	22
trans-p-coumaric acid (**33b**)	as	e2-4	22
quercetin-3-*O*-*β*-D-glc*p*[e] (**37**)	bi/as	e2-5; –[f]	28/2
kaempferol-3-*O*-*β*-D-glc*p* (**38**)	bi/as	–[f]	29/1
kaempferol-3-*O*-*β*-D-(6″-malonyl)-glc*p* (**39**)	bi/as	–[f]	35/5
co-multifidol glc*p* (**40a**)	bi	e2-7; –[f]	5
ad-multifidol glc*p* (**40c**)	bi	–[f]	10
n-multifidol di-*C*-glc*p* (**41b**)	bi	–[f]	37
trans-N-feruloyltyramine (**42**)	bi	e2-11	10
xanthohumol L (**28**)	bi	e2-13	8
xanthohumol I (**26**)	bi	e3-4	29
quercetin (**36**)	as	e3-5	15
1-methoxy-4-prenylphloroglucinol (**22**)	bi	e3-7	44
cis-p-coumaric acid methyl ester (**34a**)	bi	e3-7	184
trans-p-coumaric acid methyl ester (**34b**)	bi		189
cis-p-coumaric acid ethyl ester (**35a**)	bi	–[g]	195
trans-p-coumaric acid ethyl ester (**35b**)	bi	–[g]	198
xanthohumol O (**27**)	bi	e3-9	9
1″,2″-dihydroxanthohumol K (**14**)	bi	e3-11; e4-4; e7-3	16
isoxanthohumol (**6**)	bi	e4-2; e5-3; e6-5; e9-2	16
xanthohumol H (**22**)	bi	e6-7; e7-4	25
isoxanthohumol H (**23**)	bi	–[g]	25
xanthohumol B (**20**)	bi	e7-7	15
2″-hydroxyxanthohumol M (**25**)	bi	e7-8	9
xanthohumol D (**19**)	bi	e7-9	24
2″,3″-dehydrocylcohumulohydrochinon (**31**)	bi	e7-11	22
desmethylxanthohumol (**7**)	bi	e7-12	16
1″,2″-dihydroxanthohumol F (**18**)	bi	e7-14	12
xanthohumol M (**29**)	bi	e8-3; e9-4	14
isoxanthohumol M (**30**)	bi	–[g]	19
6-prenylnaringenin (**9**)	bi	e8-5	10
8-prenylnaringenin (**8**)	bi	–[g]	8
xanthohumol (**5**)	bi	e8-7; e9-6; e10-2	10
1″,2″-dihydroxanthohumol C (**12**)	bi	e10-4; e11-4	8
xanthohumol C (**21**)	bi	e10-5; e11-5	6
1″,2″-dihydroisoxanthohumol C (**13**)	bi	–[g]	6
4′-hydroxytunicatachalcone (**10**)	bi	e10-6	7
n-humulon (**1b**)	bi	e10-8; e11-8	21
adhumulon (**1c**)	bi	e10-9; e11-9	21
5′-prenylxanthohumol (**17**)	bi	e10-10; e11-8	7
isoxantholupon (**11**)	bi	e10-12	6
colupulon (**2a**)	bi	e11-7	17
n-lupulon (**2b**)	bi	e11-11	35
adlupulon (**2c**)	bi	e11-13	37
xanthohumol N (**24**)	bi	–[g]	13
xanthohumol P (**15**)	bi	–[g]	20
isoxanthohumol P (**16**)	bi	–[g]	24

[a]Chemical structures are given in Figure 1. [b]Sensory quality: astringent (as), bitter (bi). [c]Number of HPLC fraction referring to Figure 3. [d]Taste recognition threshold concentrations (TC) were determined in aqueous ethanolic solution (5%, v/v; pH 4.4). [e]glc*p*: glucopyranoside. [f]Compound isolated from hop tannin extract. [g]Compound synthesized.

105.3 [C(10)], 114.8 [C(8)], 116.5 [C(3′, 5′)], 118.9/119.0 [C(2‴, 2‴a)], 123.5 [C(2″)], 129.1 [C(2′, 6′)], 130.3 [C(1′)], 131.9 [C(3″)], 136.1/136.2 [C(3‴, 3‴a)], 159.2 [C(4′)], 165.7 [C(9)], 185.7 [C(4)], 198.6 [C(7)].

*1″,2″-Dihydroxanthohumol F, **18** (Figure 4).* UV/vis (ACN/water; 0.1% formic acid): λ_{max} = 326 nm. LC-MS (ESI$^-$): *m/z* (%) 421 (100, [M − H]$^-$), 119 (98), 365 (10). LC-TOF-MS (ESI$^-$): *m/z* 421.2008 ([M − H]$^-$, measured), *m/z* 421.2015 ([M − H]$^-$, calcd for $C_{26}H_{29}O_5^-$). ^{1}H NMR (500 MHz, MeOD; COSY): *δ* (ppm) 1.22 [s, 2 × 3H, H−C(4″, 5″)], 1.68 [s, 3H, H−C(4‴)], 1.76 [s, 3H, H−C(5‴)], 1.79 [t, 2H, *J* = 6.8 Hz, H−C(2″)], 2.65 [t, 2H, *J* = 6.8 Hz, H−C(1″)], 3.30 [2H, H−C(1‴)], 3.61 [s, 3H, H−C(1‴)], 5.20 [m, 1H, H−C(2‴)], 6.80 [m, 2H, H−C(3′, 5′)], 6.82 [d, 1H, *J* = 15.9 Hz, H−C(2)], 7.25 [d, 1H, *J* = 15.9 Hz, H−C(3)], 7.43 [m, 2H, H−C(2′, 6′)]. ^{13}C NMR (125 MHz, MeOH; HSQC, HMBC): *δ* (ppm) 17.98 [C(5‴)], 18.20 [C(1″)], 23.53 [C(1‴)], 25.91 [C(4‴)], 26.79 [C(4″, 5″)], 33.12 [C(2″)], 63.09 [C(1‴)], 75.38 [C(3″)], 106.57 [C(8)], 115.06 [C(6)], 116.43 [C(10)], 116.97 [C(3′, 5′)], 124.76 [C(2‴)], 127.03 [C(1′)], 127.48 [C(3)], 131.48 [C(2′, 6′)], 131.92 [C(3‴)], 147.57 [C(2)], 151.71 [C(9)], 156.33 [C(5)], 156.44 [C(7)], 161.50 [C(4′)], 198.33 [C(4)].

*Xanthohumol M, **29** (Figure 4).* UV/vis (ACN/water; 0.1% formic acid): λ_{max} = 368 nm. LC-MS (ESI$^-$): *m/z* (%) 385 (100, [M − H]$^-$), 119 (87), 265 (2), 163 (1). LC-TOF-MS (ESI$^-$): *m/z* 385.1664 ([M − H]$^-$, measured), *m/z* 353.1657 ([M − H]$^-$, calcd for $C_{22}H_{25}O_6^-$). ^{1}H NMR (500 MHz, MeOD; COSY): *δ* (ppm) 1.23 [s, 6H, H−C(4″, 5″)], 1.65 [m, 2H, H−C(2″)], 2.57 [m, 2H, H−C(1″)], 3.28 [s, 3H, H−C(6″)], 3.91 [s, 3H, H−C(1‴)], 6.04 [s, 1H, H−C(6)], 6.83 [m, 2H, *J* = 8.5 Hz, H−C(3′, 5′)], 7.50 [m, 2H, *J* = 8.5 Hz, H−C(2′, 6′)], 7.67 [d, 1H, *J* = 15.6 Hz, H−C(3)], 7.80 [d, 1H, *J* = 15.6 Hz, H−C(2)]. ^{13}C NMR (125 MHz, MeOD; HSQC, HMBC): *δ* (ppm) 18.6 [C(1″)], 26.4 [C(4″, 5″)], 39.4 [C(2″)], 50.6 [C(6″)], 57.1 [C(1‴)], 77.5 [C(3″)], 92.5 [C(6)], 110.8 [C(8)], 117.8 [C(3′, 5′)], 126.7 [C(3)], 129.3 [C(1′)], 132.1 [C(2′, 6′)], 144.3 [C(2)], 161.9 [C(4′)], 163.3 [C(5)], 164.7 [C(9)], 167.1 [C(7)], 195.0 [C(4)].

*2″,3″-Dehydrocyclohumulonhydrochinon, **31** (Figure 4).* UV/vis (ACN/water; 0.1% formic acid): λ_{max} = 280 nm. LC-MS (ESI$^-$): *m/z* (%) 291 (100, [M − H]$^-$), 289 (95, [M − 3H]$^-$), 207 (25, [M − H]$^-$), 235 (21), 136 (20). LC-TOF-MS (ESI$^-$): *m/z* 291.1222 ([M − H]$^-$, measured), *m/z* 291.1238 ([M − H]$^-$, calcd for $C_{16}H_{19}O_5^-$). ^{1}H NMR (500 MHz, MeOD; COSY): *δ* (ppm) 1.41 [s, 6H, H−C(1′, 2′)], 1.64 [s, 3H, H−C(4″)], 1.76 [s, 3H, H−C(5″)], 2.67 [s, 2H, H−C(3)], 3.20 [d, 2H, *J* = 7.3 Hz, H−C(1″)], 5.15 [m, 1H, *J* = 7.3 Hz, H−C(2″)]. ^{13}C NMR (125 MHz, MeOD; HSQC, HMBC): *δ* (ppm) 16.6 [C(5″)], 21.2 [C(1″)], 24.5 [C(4″)], 25.5 [C(1′, 2′)], 49.5 [C(3)], 78.0 [C(2)], 101.0 [C(10)], 107.8 [C(8)], 122.8 [C(2″)], 129.9 [C(3″)], 147.6 [C(5)], 151.7 [C(9)], 154.1 [C(7)], 197.3 [C(4)].

*1-Methoxy-4-prenylphloroglucinol, **32** (Figure 4).* UV/vis (ACN/water; 0.1% formic acid): λ_{max} = 292 nm. LC-MS (ESI$^-$): *m/z* (%) 207 (100, [M − H]$^-$), 137 (25), 121 (14), 109 (10), 149 (9). LC-TOF-MS (ESI$^-$): *m/z* 207.1035 ([M − H]$^-$, measured), *m/z* 207.1027 ([M − H]$^-$, calcd for $C_{12}H_{15}O_3^-$). ^{1}H NMR (500 MHz, MeOD; COSY): *δ* (ppm) 1.65 [s, 3H, H−C(4′)], 1.75 [s, 3H, H−C(5′)], 3.2 [d, 2H, *J* = 7.3 Hz, H−C(1′)], 3.83 [s, 3H, H−C(1″)], 5.21 [m, 1H, *J* = 7.3 Hz, H−C(2′)], 5.42 [s, 1H, H−C(2)], 6.04 [s, 1H, H−C(6)]. ^{13}C NMR (125 MHz, MeOD; HSQC, HMBC): *δ* (ppm) 17.8 [C(5′)], 22.0 [C(1′)], 25.9 [C(4′)], 56.2 [C(1″)], 93.4 [C(6)], 99.8 [C(2)], 105.9 [C(4)], 123.2 [C(2″)], 132.4 [C(3′)], 159.6 [C(1)], 167.9 [C(5)], 173.3 [C(3)].

DOI: 10.1021/acs.jafc.5b00239
J. Agric. Food Chem. 2015, 63, 3402−3418

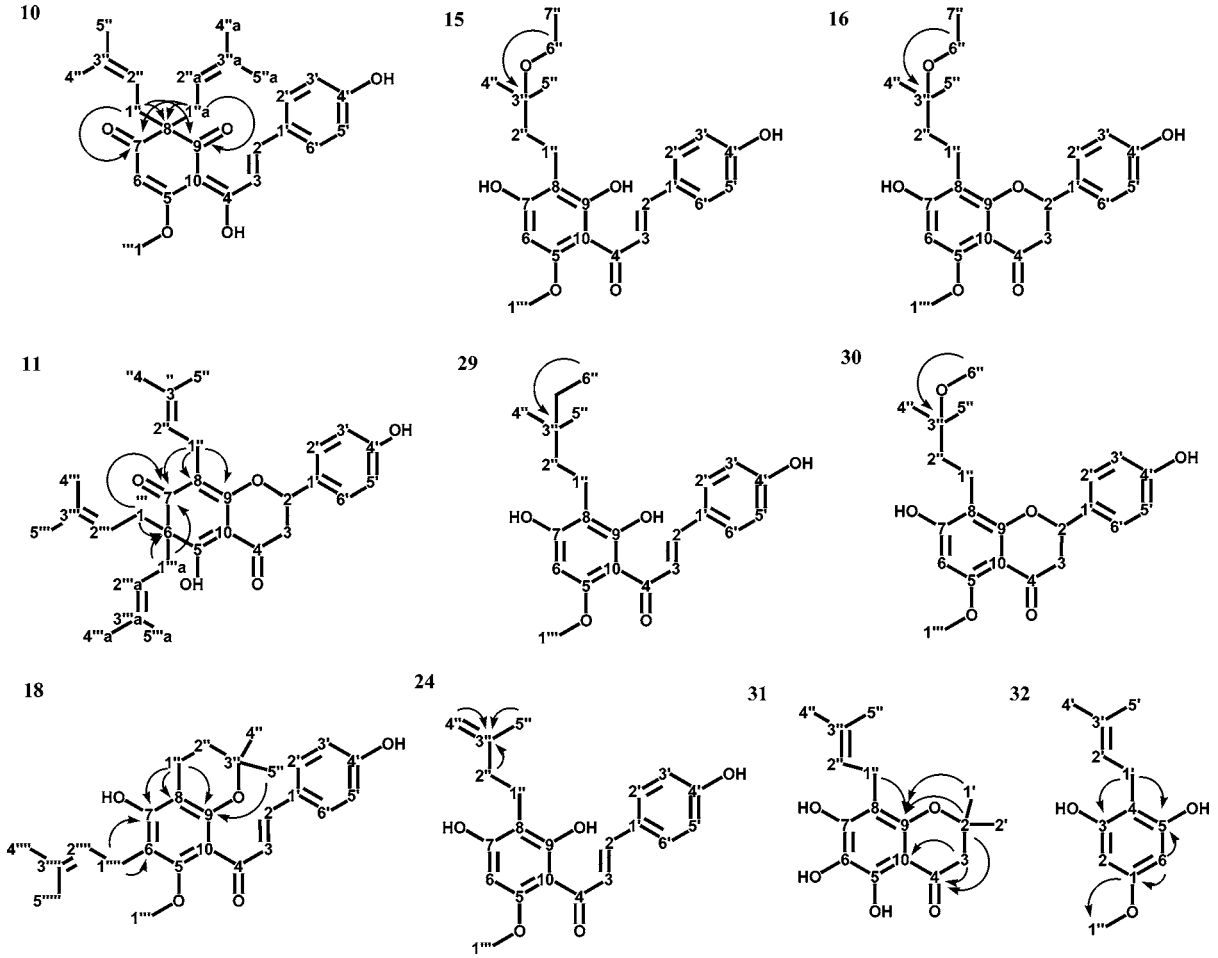

Figure 4. Chemical structures of compounds **10**, **11**, **15**, **17**, **18**, **24**, and **29**−**32** with heteronuclear key correlations (HMBC experiment) highlighted.

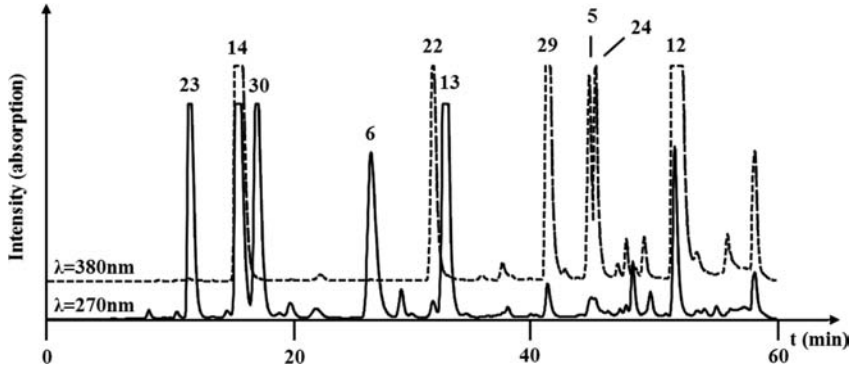

Figure 5. RP-HPLC/UV chromatogram of a methanolic solution of xanthohumol (**5**) after treatment (45 min, rt) with hydrobromic acid solution (33% in acetic acid). Numbering of compounds refer to structures given in Figure 1

Isolation of Compounds from Hop Tannin Extract. Aliquots of the hop tannin extract (200 μL), diluted with water (500 μL), were separated by means of HPLC on a 250 × 21.2 mm, 5 μm, Luna Phenyl-Hexyl column (Phenomenex, Aschaffenburg, Germany) operated with a flow rate of 15 mL/min and using 0.1% aqueous formic acid and acetonitrile containing 0.1% formic acid as solvents. Chromatography was performed by starting with 5% solvent B for 0.5 min, then increasing solvent B to 15% within 0.5 min, and, after keeping at 15% for 34.0 min, solvent B was increased to 25% within additional 7 min, then increased to 100% within 1 min, followed by isocratic elution for 3.0 min. After 46 min, solvent B decreased again to 5% within 1.0 min and was kept for 3.0 min prior to the next injection. The compounds eluting at 24.5 (**37**), 27.0 (**40a**), 30.0 (**38**), and 32.0 min (**39**) were collected and separated from solvent in vacuum and freeze-dried twice. For preparative isolation of additional compounds, the following gradient was used: 5% solvent B for 0.5 min and then increasing solvent B to 15% within 0.5 min. Solvent B was kept for 41.0 min at 15% and, finally, increased to 100% within an additional minute, followed by isocratic elution for 3.0 min. After 46 min, solvent B decreased again to 5% within 1.0 min and was kept for 3.0 min prior to the next injection. Compounds eluting after 31.5 (**40a**), 32.3 (**38**), 33.0 (**40c**), and 33.3 min (**41b**) were collected, separated from solvent under vacuum, and freeze-dried twice. Compounds **37**−**41b** (>98% purity) were analyzed by means of UV/vis, LC-MS/MS, UPLC-TOF-MS, and 1D/2D NMR. Based on the comparison of spectroscopic and chromatographic data with those recorded for references, previously reported compounds were confirmed as

DOI: 10.1021/acs.jafc.5b00239
J. Agric. Food Chem. 2015, 63, 3402−3418

quercetin-3-*O*-*β*-D-glucopyranoside (**37**),[41] kaempferol-3-O-*β*-D-glucopyranoside (**38**),[41] kaempferol-3-*O*-*β*-D-(6″-malonyl)glucopyranoside (**39**),[42] 1-*O*-*β*-D-(2-methylpropanoyl)phloroglucinol glucopyranoside (co-multifidol glucopyranoside, **40a**),[43] 1-*O*-*β*-D-(2-methylbutyryl)-phloroglucinol glucopyranoside (ad-multifidolglucopyranoside, **40c**),[43] and phloroisovalerophenon-3,5-di-*C*-*β*-D-glucopyranoside (*n*-multifidol-di-C-glucopyranoside) (**41b**).[43]

Synthetic Preparation of Xanthohumol Derivatives 12−14, 22−24, 29, and 30. An aliquot (50 mg) of xanthohumol (**5**) was solved in a mixture of hydrobromic acid solution (33% in acetic acid; 5 mL) and methanol (5 mL) and stirred for 45 min at room temperature. The reaction mixture was separated by semipreparative HPLC on a 250 × 10.0 mm Hypersil RP-18 column (Thermo Hypersil GmbH, Kleinostheim, Germany) using water (0.1% formic acid) as solvent A and methanol (0.1% formic acid) as solvent B at a flow rate of 4.7 mL/min. Chromatography was performed using the following gradient: 62% solvent B for 4.5 min, then increasing solvent B to 64% within 5.5 min. After 3.0 min solvent B was increased to 70% within 10 s, then to 72% within 5.3 min, to 80% within 0.5 min, kept for 6.0 min and, finally, to 100% within an additional 1.5 min, followed by isocratic elution for 2.5 min. After 29.0 min, solvent B decreased again to 62% within 1 min and was kept for 3.0 min prior to the next injection. Besides xanthohumol (**5**) and isoxanthohumol (**6**), the effluent of the peaks of compounds **12−14**, **22−24**, **29**, and **30** (Figure 5) was collected and, after the solvent was removed in vacuum and freeze-dried twice, the individual compounds (>98% purity) were used for sensory and identification experiments (UV/vis, LC-MS/MS, UPLC-TOF-MS, 1D/2D NMR). Based on the comparison of spectroscopic (UV/vis, LC-TOF-MS, $^{1}H/^{13}C$ NMR) and chromatographic data (retention time) with those recorded for reference substances, compounds reported earlier in the literature were identified as 1″,2″-dihydroxanthohumol C (**12**),[23,36,37] 1″,2″-dihydroisoxanthohumol C (**13**),[45] 1″,2″-dihydroxanthohumol K (**14**),[36,37] xanthohumol H (**22**),[23,36,37] and isoxanthohumol H (**23**).[39] Furthermore, compound **29** was identified as xanthohumol M based on the comparison with the compound isolated above form the *ε*-resin, whereas compounds **24** and **30** have not been previously reported (Figure 4).

*Xanthohumol N, **24** (Figure 4).* UV/vis (ACN/water; 0.1% formic acid): λ_{max} = 368 nm. LC-MS (ESI$^-$): *m/z* (%) 353 (100, [M − H]$^-$), 119 (35), 163 (15), 233 (12), 283 (8). LC-TOF-MS (ESI$^-$): *m/z* 353.1394 ([M − H]$^-$, measured), *m/z* 353.1394 ([M − H]$^-$, calcd for $C_{21}H_{21}O_5^-$). ^{1}H NMR (500 MHz, MeOD; COSY): *δ* (ppm) 1.79 [s, 3H, H−C(5″)], 2.18 [m, 2H, *J* = 8.1, H−C(2″)], 2.69 [m, 2H, *J* = 8.1, H−C(1″)], 3.28 [s, 3H, H−C(6″)], 3.90 [s, 3H, H−C(1‴)], 4.66 [s, 2H H−C(4″)], 6.03 [s, 1H, H−C(6)], 6.83 [m, 2H, *J* = 8.7 Hz, H−C(3′, 5′)], 7.50 [m, 2H, *J* = 8.7 Hz, H−C(2′, 6′)], 7.67 [d, 1H, *J* = 15.5 Hz, H−C(3)], 7.80 [d, 1H, *J* = 15.5 Hz, H−C(2)]. ^{13}C NMR (125 MHz, MeOD; HSQC, HMBC): *δ* (ppm) 22.1 [C(1″)], 22.6 [C(5″)], 37.9 [C(2″)], 56.2 [C(1‴)], 91.6 [C(6)], 106.5 [C(10)], 109.7 [C(8)], 110.1 [C(4″)], 116.9 [C(3′, 5′)], 125.9 [C(3)], 128.5 [C(1′)], 131.2 [C(2′, 6′)], 143.3 [C(2)], 161.0 [C(4′)], 162.5 [C(5)], 163.9 [C(7)], 166.2 [C(9)], 194.1 [C(4)].

*Isoxanthohumol M, **30** (Figure 4).* UV/vis (ACN/water; 0.1% formic acid): λ_{max} = 289 nm. LC-MS (ESI$^-$): *m/z* (%) 385 (8, [M − H]-), 119 (100), 265 (19), 165 (6), 163 (5), 197(4). LC-TOF-MS (ESI$^-$): *m/z* 385.1664 ([M − H]$^-$, measured), *m/z* 353.1657 ([M − H]$^-$, calcd for $C_{22}H_{25}O_6^-$). ^{1}H NMR (400 MHz, MeOD; COSY): *δ* (ppm) 1.13 [s, 6H, H−C(4″, 5″)], 1.60 [m, 2H, H−C(2″)], 2.53 [m, 2H, H−C(1″)], 2.66 [dd, 1H, *J* = 3.0, *J* = 16.9, H−C(3eq)], 3.00 [dd, 1H, *J* = 12.9, *J* = 16.9, H−C(3ax)], 3.06 [s, 3H, H−C(6″)], 3.80 [s, 3H, H−C(1‴)], 5.30 [dd, 1H, *J* = 3.0, *J* = 12.9, H−C(2)], 6.13 [s, 1H, H−C(6)], 6.81 [m, 2H, *J* = 8.7 Hz, H−C(3′, 5′)], 7.33 [m, 2H, *J* = 8.7 Hz, H−C(2′, 6′)]. ^{13}C NMR (100 MHz, MeOD; HSQC, HMBC): *δ* (ppm) 18.1 [C(1″)], 25.6/27.2 [C(4″, 5″)], 38.7 [C(2″)], 46.2 [C(3)], 49.3 [C(6″)], 56.0 [C(1‴)], 76.4 [C(3″)], 80.1 [C(2)], 93.5 [C(6)], 105.9 [C(10)], 110.5 [C(8)], 116.2 [C(3′, 5′)], 129.0 [C(2′, 6′)], 131.4 [C(1′)], 158.9 [C(4′)], 161.9 [C(5)], 163.9 [C(9)], 164.4 [C(7)], 192.9 [C(4)].

Synthetic Preparation of *cis*/*trans*-*p*-Coumaric Acid Ethyl Ester (35a/b). An aliquot (10 mL) of an ethanolic solution of *trans*-*p*-coumaric acid (**33b**; 100 mmol/L) was acidified with 0.1 mL of sulfuric acid. The solution was stirred under reflux for 24 h. Afterward the reaction mixture was subjected to a solid phase extraction using ethanol as an eluent. A HPLC separation with two injections of the crude extract after 0.0 and 3.0 min, using a gradient as follows, was applied to achieve fast separation of the *cis*- and *trans*-isomers: 41% solvent B for 20 min and, then, increasing solvent B to 100% within 0.5 min, followed by an isocratic elution for 1 min. After 21.5 min, solvent B decreased again to 41% within 0.1 min and was kept for 3.0 min prior to the next injection. After removing the solvent in vacuum and freeze-drying twice, compounds **35a** and **35b** were isolated (>98% purity) and were used for sensory experiments as well as UV/vis, TOF-MS, and 1D/2D NMR. Based on the comparison of spectroscopic and chromatographic data with those recorded for references, compounds reported earlier in the literature were identified as *cis*-/*trans*-*p*-coumaric acid ethyl ester (**35a**/**b**).[29]

Synthetic Preparation of Xanthohumol P (15). An aliquot (25 mg) of xanthohumol (**5**) and Amberlyst 15 (1 g) was stirred in ethanol (10 mL) for 4 h at 80 °C. HPLC purification of **15** was achieved using a gradient as follows: 30% solvent B for 2.0 min and, then, increasing solvent B to 80% within 12.5 min and, finally, increasing solvent B to 100% within 1.0 min, followed by isocratic elution for 2.5 min. After 16.0 min, solvent B decreased again to 30% within 1.0 min and was kept for 3.0 min prior to the next injection. The compound eluting after 15.3 min was isolated (>98% purity) and, after the solvent was removed in vacuum and freeze-dried twice, was used for sensory experiments. Structure verification by means of UV−vis, LC-MS/MS, UPLC-TOF-MS, and 1D/2D NMR undoubtedly identified the compound as xanthohumol P, **15** (Figure 4), which has to the best of our knowledge not been described yet in the literature. In addition, compounds **6** and **12−14** were isolated from the reaction mixture.

*Xanthohumol P, **15** (Figure 1).* UV/vis (ACN/water; 0.1% formic acid): λ_{max} = 367 nm. LC-MS (ESI$^-$): *m/z* (%) 399 (57, [M − H]$^-$), 119 (100), 353 (64), 232 (20), 174 (13). LC-TOF-MS (ESI$^-$): *m/z* 399.1802 ([M − H]$^-$, measured), *m/z* 399.1808 ([M − H]$^-$, calcd for $C_{23}H_{27}O_6^-$). ^{1}H NMR (400 MHz, MeOD; COSY): *δ* (ppm) 1.18 [t, 3H, H−C(7″)], 1.23 [s, 6H, H−C(4″, 5″)], 1.65 [m, 2H, *J* = 7.1, *J* = 8.5, H−C(2″)], 2.58 [m, 2H, *J* = 7.1, *J* = 8.5), H−C(1″)], 3.53 [dd, 2H, H−C(6″)], 3.90 [s, 3H, H−C(1‴)], 6.03 [s, 1H, H−C(6)], 6.87 [m, 2H, *J* = 8.7 Hz, H−C(3′, 5′)], 7.50 [m, 2H, *J* = 8.7 Hz, H−C(2′, 6′)], 7.67 [d, 1H, *J* = 15.5 Hz, H−C(3)], 7.80 [d, 1H, *J* = 15.5 Hz, H−C(2)]. ^{13}C NMR (100 MHz, MeOD; HSQC, HMBC): *δ* (ppm) 16.3 [C(7″)], 17.8 [C(1″)], 26.3 [C(4″, 5″)], 39.0 [C(2″)], 56.2 [C(1‴)], 57.5 [C(6″)], 76.4 [C(3″)], 91.7 [C(6)], 106.5 [C(10)], 110.0 [C(8)], 116.9 [C(3′, 5′)], 125.9 [C(3)], 128.5 [C(1′)], 131.3 [C(2′, 6′)], 143.4 [C(2)], 161.1 [C(4′)], 162.4 [C(5)], 163.8[C(9)], 166.2 [C(7)], 194.1 [C(4)].

Alkaline Isomerization of Compounds 9, 12, 15, and 29. An aliquot (10 mg) of the compound **9**, **12**, **15**, and **29**, respectively, was dissolved in 5 mL of methanol and, after adjusting the pH to a value of 14 with potassium hydroxide (0.1 mol/L), stirred for 30 min in a closed glass vial at 60 °C. The reaction mixture was diluted with water and subjected to a solid phase extraction using 55 *μ*m, 70A, Strata C18-E Giga Tube cartridges (200 mg, 3 mL; Phenomenex, Aschaffenburg, Germany) and methanol as an eluent, prior to HPLC separation on a 250 × 21.2 mm, 5 *μ*m, Luna Phenyl-Hexyl column (Phenomenex, Aschaffenburg, Germany). The HPLC system was operated with a flow rate of 15 mL/min, using 0.1% aqueous formic acid and acetonitrile containing 0.1% formic acid as solvents, and using a gradient as follows: 20% solvent B for 2.5 min and then increasing solvent B to 100% within 20.0 min followed by isocratic elution for 2.5 min. After 25.0 min, solvent B decreased again to 20% within 2.0 min and was kept for 3.0 min prior to the next injection. After the solvent was removed in vacuum and freeze-dried twice, compounds **7**, **8**, **13**, **16**, and **30** (>98% purity) were used for sensory experiments and structure determination. Based on the comparison of spectroscopic (UV/vis, LC-TOF-MS, $^{1}H/^{13}C$ NMR) and chromatographic data (retention time) with those recorded for reference substances, the following compounds were identified: desmethylxanthohumol (**7**),[25] 8-prenylnaringenin (**8**),[25] 1″,2″-dihydroisoxanthohumol C (**13**),[45] and isoxanthohumol M (**30**). To the best of our knowledge, isoxanthohumol P, **16** (Figure 4), has not been earlier reported in the literature.

DOI: 10.1021/acs.jafc.5b00239
J. Agric. Food Chem. 2015, 63, 3402−3418

Table 2. Concentrations of Taste-Active Soft and Hard Resin Components in Commercial Hop Products

	concn (μmol/100 g)											
	tannin extract		hard resin		pellets	Xantho Flav extract		resin extract		soft resin		
tastant[a]	aroma hops	bitter hops	Perle	Taurus	Herkules	15%	75%	aroma hops	bitter hops	Perle	Taurus	ε-extract
1a	799.5	559.0	681.4	694.9	15987	590.1	578.3	8727	8216	5820	5786	251.7
1b	798.2	818.3	857.3	833.2	15964	731.6	639.2	12139	11665	9533	12327	423.8
1c	378.8	363.9	362.0	450.9	7573	342.6	307.3	5403	4898	3904	4083	173.9
2a	730.4	650.7	679.7	785.6	14605	815.6	644.4	14808	14720	12603	19220	614.2
2b	644.6	441.1	453.7	724.8	12892	825.9	606.5	15763	9396	7971	11818	456.5
2c	279.1	233.9	212.6	428.8	5584	419.4	268.7	5101	3783	4259	6364	188.9
3a	8.91	4.54	2.89	2.64	178.1	1.47	3.04	14.09	7.13	14.56	5.28	0.70
3b	6.91	5.88	16.05	17.40	137.9	2.76	4.93	57.21	41.93	15.85	21.09	1.07
3c	10.83	13.54	19.14	14.03	216.6	6.33	5.00	129.45	96.96	28.90	16.85	1.60
4a	0.98	0.34	1.47	0.66	19.7	0.21	0.69	6.18	6.57	2.86	3.86	0.46
4b	<0.01	<0.01	<0.01	<0.01	<0.01	<0.01	<0.01	<0.01	<0.01	<0.01	<0.01	<0.01
4c	<0.01	<0.01	<0.01	<0.01	<0.01	<0.01	<0.01	<0.01	<0.01	<0.01	<0.01	<0.01
5	101.3	100.5	62811	33031	4993	35953	207646	1082	736.1	35.18	629.6	8601
6	30.83	45.44	7202	4817	265.7	13916	9754	112.8	98.08	1.57	126.5	7671
7	<0.01	17.14	93.68	15.61	57.25	<0.01	670.1	<0.01	5.50	<0.01	<0.01	21.06
8	11.41	18.05	3449	653.6	57.84	1319	3478	32.23	25.26	1.18	34.80	658.9
9	55.26	49.97	6532	1067	139.1	2524	13873	73.35	57.15	3.01	52.50	1154
10	<0.01	<0.01	16383	241.4	34.56	156.1	140.2	4.84	36.83	2.18	1193	<0.01
11	<0.01	<0.01	<0.01	<0.01	1575	8142	<0.01	<0.01	<0.01	<0.01	<0.01	6879
12	<0.01	<0.01	20347	4571	3.56	140.3	70.73	0.98	1.08	2.26	41.16	66.13
13	<0.01	<0.01	733.3	218.5	<0.01	317.5	<0.01	<0.01	<0.01	<0.01	<0.01	<0.01
14	<0.01	<0.01	7540	21723	6.55	112.9	717.5	2.01	<0.01	2.38	<0.01	37.74
15	<0.01	<0.01	919.8	363.4	180.3	601.9	397.4	11.26	11.43	0.55	<0.01	453.6
16	5.00	<0.01	341.2	271.4	32.09	896.0	752.1	5.95	2.82	<0.01	13.67	762.1
17	20.94	<0.01	4107	20445	464.0	1149	504.7	58.27	90.45	20.48	1320	7155
18	<0.01	<0.01	511.6	1967	<0.01	<0.01	<0.01	<0.01	<0.01	<0.01	<0.01	87.09
19	<0.01	33.88	1651	1139	758.4	2306	1797	14.41	12.02	<0.01	114.2	438.5
20	<0.01	<0.01	1017	745.7	133.2	1004	570.1	20.24	8.45	<0.01	<0.01	259.7
21	14.43	7.33	370.5	5165	303.7	983.8	815.1	42.05	31.31	11.90	74.18	1206
22	<0.01	<0.01	7331	1032	8.9	<0.01	1171	<0.01	<0.01	<0.01	<0.01	50.85
23	7.58	<0.01	1715	466.8	<0.01	<0.01	98.55	<0.01	<0.01	<0.01	<0.01	41.41
24	<0.01	3.02	1316	1238	166.2	1562	330.5	16.89	12.26	0.21	6.56	245.5
25	<0.01	<0.01	2797	2491	116.0	<0.01	<0.01	<0.01	<0.01	<0.01	<0.01	<0.01
26	<0.01	<0.01	289.2	601.9	34.27	2854	4548	17.57	7.08	<0.01	<0.01	681.3
27	<0.01	<0.01	1459	626.3	97.36	757.9	850.4	<0.01	21.19	<0. 01	<0.01	<0.01
28	27.97	41.93	983.5	2138	67.85	1676	11656	27.61	17.65	<0.01	<0.01	569.3
29	<0.01	<0.01	20354	1344	<0.01	23.96	22.40	1.02	<0.01	0.47	15.94	15.52
30	<0.01	<0.01	827.3	110.0	261.1	1429	95.80	0.56	3.73	<0.01	<0.01	38.88
31	<0.01	<0.01	<0.01	1924	<0.01	<0.01	<0.01	<0.01	<0.01	<0.01	<0.01	<0.01
32	<0.01	<0.01	<0.01	1022	68.38	1568	1418	<0.01	<0.01	<0.01	<0.01	2086
33a/b	<0.01	<0.01	1065	2357	227.2	<0.01	2997	156.4	<0.01	<0.01	<0.01	<0.01
34a/b	<0.01	<0.01	1777	3801	<0.01	276.8	<0.01	<0.01	<0.01	<0.01	<0.01	691.0
35a/b	<0.01	42.55	<0.01	<0.01	<0.01	<0.01	229.7	<0.01	<0.01	2.59	<0.01	183.5
36	<0.01	127.5	1041	507.8	26.12	<0.01	1239	27.16	<0.01	<0.01	<0.01	<0.01
37	9775	5927	831.4	4189	5622	2063	661.8	28.98	55.21	3.32	293.7	<0.01
38	14541	4623	3436	5447	31869	82522	45105	197.5	15.06	<0.01	401.5	<0.01
39	4280	813.2	254.88	1318	250.0	351.8	124.4	12.02	<0.01	<0.01	<0.01	<0.01
40a	1363	4802	297.88	2906	4639	1864	2968	20.42	79.87	3.85	129.9	3408
40c	585.1	1235	219.35	1820	1415	1178	800.6	19.94	21.80	1.31	146.6	124.08
41b	428.7	1038	<0.01	252.0	263.2	348.1	<0.01	8.95	<0.01	<0.01	<0.01	<0.01
42	<0.001	<0.01	2999	1637	100.6	380.7	1264	17.19	7.27	<0.01	<0.01	<0.01

[a]Numbering of molecules is referring to structures given in Figure 1.

*Isoxanthohumol P, **16** (Figure 1).* UV/vis (ACN/water; 0.1% formic acid): λ_{max} = 287 nm. LC-MS (ESI^-): *m/z* (%) 399 (10, $[M-H]^-$), 119 (100), 265 (21). LC-TOF-MS (ESI^-): *m/z* 399.1804 ($[M-H]^-$, measured), *m/z* 399.1808 ($[M-H]^-$, calcd for $C_{23}H_{27}O_6^-$). ^{1}H NMR (400 MHz, MeOD; COSY): δ (ppm) 1.12 [s, 6H, H−C(4″, 5″)], 1.12 [t, 3H, H−C(7″)], 1.60 [m, 2H, H−C(2″)], 2.54 [m, 2H, H−C(1″)], 2.67 [dd, 1H, *J* = 3.2, *J* = 16.9, H−C(3eq)], 3.02 [dd, 1H, *J* = 12.8, *J* = 16.9, H−C(3ax)], 3.34 [dd, 2H, H−C(6″)], 3.79 [s, 3H, H−C(1‴)], 5.32 [dd, 1H, *J* = 3.2, *J* = 12.8, H−C(2)], 6.12 [s, 1H, H−C(6)], 6.81 [m, 2H, *J* = 8.8 Hz, H−C(3′, 5′)], 7.33 [m, 2H, *J* = 8.8 Hz, H−C(2′, 6′)]. ^{13}C NMR (100 MHz, MeOD; HSQC, HMBC): δ (ppm) 15.8 [C(7″)], 17.5 [C(1″)], 25.3/27.1 [C(4″)/C(5″)], 38.0 [C(2″)], 45.9 [C(3)], 55.3

DOI: 10.1021/acs.jafc.5b00239
J. Agric. Food Chem. 2015, 63, 3402−3418

Table 3. Concentration of Hop-Derived Taste Components in a Commercial Pilsner-Type Beer and Beer Samples I–IV from a Brewing Trial Using ε-Extract and Spent Hops, Respectively

	concn (μmol/L)[c]				
tastant[a]	Pilsner beer[b]	beer I	beer II	beer III	beer IV
1a	1.30	3.34	23.56	11.63	7.50
1b	0.99	0.68	28.14	6.85	4.55
1c	0.17	0.16	4.53	1.10	0.83
2a	0.08	1.45	0.95	0.44	0.34
2b	0.05	0.04	0.37	0.08	0.10
2c	0.01	0.02	0.10	<0.01	0.02
3a	16.49	17.63	0.96	6.34	2.07
3b	24.32	26.17	1.65	9.09	3.31
3c	9.71	7.16	0.55	1.93	0.83
4a	5.10	5.23	0.83	3.86	1.10
4b	6.24	7.44	0.69	3.86	1.24
4c	<0.01	<0.01	<0.01	<0.01	<0.01
5	0.04	0.31	56.12	4.16	2.86
6	5.54	<0.01	4.02	0.46	0.92
7	0.01	0.08	0.10	0.21	0.07
8	0.05	<0.01	<0.01	0.02	0.01
9	0.06	0.09	3.25	0.50	0.80
10	<0.01	0.59	0.08	0.11	0.17
11	<0.01	0.39	<0.01	<0.01	<0.01
12	<0.01	0.05	0.06	0.04	0.02
13	0.03	0.18	10.44	3.35	2.55
14	0.01	<0.01	1.16	0.91	1.25
15	<0.01	0.01	1.61	0.30	0.12
16	0.04	0.03	0.87	9.84	9.68
17	<0.01	0.22	4.12	0.47	0.11
18	<0.01	<0.01	<0.01	0.07	<0.01
19	<0.01	<0.01	3.69	0.76	0.67
20	0.01	0.04	4.00	0.88	1.02
21	0.01	0.28	3.84	0.98	0.74
22	0.01	0.05	0.94	0.65	1.20
23	0.02	2.27	78.97	96.74	110.8
24	<0.01	0.02	0.12	0.03	0.08
25	<0.01	<0.01	<0.01	<0.01	11.43
26	0.03	0.02	<0.01	<0.01	<0.01
27	<0.01	<0.01	0.18	0.87	0.29
28	0.05	<0.01	8.62	32.37	9.33
29	<0.01	0.03	0.01	0.01	0.01
30	0.01	0.22	8.87	12.71	13.15
31	<0.01	0.20	4.02	<0.01	0.96
32	0.10	0.22	8.29	7.07	6.17
33a/b	0.01	34.83	48.32	69.36	46.24
34a/b	<0.01	0.03	0.104	0.12	0.09
35a/b	0.01	<0.01	1.83	0.51	2.06
36	0.01	0.49	0.947	15.14	0.79
37	3.54	1.42	4.64	566.4	46.82
38	12.03	4.50	9.42	663.3	43.74
39	0.38	0.12	0.364	24.08	2.03
40a	3.93	0.69	20.85	261.7	45.36
40c	0.90	0.12	8.52	142.0	17.93
41b	0.13	0.16	0.717	111.1	6.67
42	0.48	1.02	7.59	23.71	7.57

[a]Chemical structures are given in Figure 1. [b]Commercial Pilsner-type beer. [c]Beers I–IV were produced by the Research Brewery St. Johann (Germany) and their International Bitterness Units (IBU) adjusted as follows: beer I (reference) was produced using an Isohop extract (30%) added to the beer to adjust an IBU value of 23. Beers II–IV were produced using the same wort as for beer I just differing in the hop products. For beer II (27 IBU) and beer IV (27 IBU), an ε-extract was added to the wort postboiling and at the beginning of the kettle boiling, respectively. Beer III (51 IBU) was made by adding spent hops, obtained by exhaustive carbon dioxide extraction, to the wort prior to boiling.

[C(6″)], 56.4 [C(1‴)], 75.6 [C(3″)], 79.8 [C(2)], 93.8 [C(6)], 105.3 [C(10)], 109.9 [C(8)], 115.8 [C(3′, 5′)], 128.4 [C(2′, 6′)], 130.6 [C(1′)], 158.2 [C(4′)], 161.2[C(5)], 163.3 [C(9)], 163.2 [C(7)], 192.4 [C(4)].

Quantitation of Bitter Compounds in Hop Extracts and Beer by LC-MS/MS. For quantitation of bitter compounds, aliquots of hop pellets (1.5 g), hop extracts (100 mg), and samples (40 mg) of the advanced hop extracts XanthoFlav 15, XanthoFlav 75, and polyphenol extracts, respectively, were exhaustively extracted for 1 h with methanol (4 × 25 mL) during ultrasonification. After filtration, the extracts were diluted (1:100) with methanol and, after membrane filtration (0.45 μm, Sartorius, Göttingen, Germany), samples (5 μL) were directly injected into a Dionex UltiMate 3000 series UHPLC system consisting of two pumps, a degasser, a column compartment, and an autosampler (Dionex, Idstein, Germany) connected to an API 4000 Q-TRAP mass spectrometer (SCIEX, Darmstadt, Germany) which was equipped with an electrospray ionization (ESI) source and operated in negative ionization mode.

For the analysis of beer samples, the beverage was degassed by ultrasonification and membrane filtered (0.45 μm, Sartorius, Göttingen, Germany), and aliquots (5 μL) were directly injected into the SCIEX LC-MS system. The temperature of the autosampler was set to 5 °C and of the column compartment to 40 °C. The declustering potential (DP), the cell exit potential (CXP), and the collision energy (CE) of the mass spectrometer were optimized for each substance to induce fragmentation of the pseudo molecular ion $[M - H]^-$ to the corresponding target product ions after collision-induced dissociation. Quantitative analysis was performed by means of multiple reaction monitoring (MRM) mode using optimized fragmentation parameters and retention times of the corresponding reference compounds. The ion spray voltage was set to −4500 V, and dwell time for each mass transition was 2.5×10^{-3} s. Nitrogen was used as the collision gas (4×10^{-5} Torr). Using unhopped beer as a blank matrix, 8-point external matrix calibration curves were recorded for the individual analytes **1**–**42** in low (2.5 nmol/L to 200 μmol/L) and high concentrations (0.2 mmol/L to 20 mmol/L) by means of UPLC-MS/MS. Quantitation of the co- and ad-congeners of α-acids (**1**), β-acids (**2**), and *cis*-/*trans*-iso-α-acids (**3**, **4**) was performed by using the calibration curve of the *n*-congeners. Calibration functions were forced through zero, thus leading to correlation coefficients of >0.99 for all the reference compounds in unhopped beer. Concentrations of *cis*-/*trans*-*p*-coumaric acid (**33a**/**b**) were corrected for amounts detected in the nonhopped beer (control). The limit of detection was determined to be 0.3 nmol/L (S/N ratio: 3) for all compounds (**1**–**42**), and the limit of quantification was accordingly estimated to be 0.001 μmol/L (S/N ratio: 10).[46] Data processing and integration was performed by means of Analyst software version 1.5 (AB Sciex Instruments, Darmstadt, Germany). As stationary phase, a 150 × 2.0 mm, 4 μm, Synergi Hydro-RP column (Phenomenex, Aschaffenburg, Germany) was used. The mobile phase consisted of acetonitrile (0.1% formic acid) as solvent A and water (0.1% formic acid) as solvent B. Using a flow rate of 0.6 mL/min, chromatographic separation was achieved (Figure 5) by gradient elution increasing solvent A from 10 to 40% within 15 min and further increased to 60% in 13 min, to 70% in 20 min, and finally to 100% within 2 min. It was maintained at 100% for 1 min, following by readjustment to 10% within 5 min and re-equilibrated for 4 min prior to the next injection.

Sensory Analysis. *General Conditions and Panel Training.* Twelve subjects (7 women and 5 men, ages 23–29 years), who gave

DOI: 10.1021/acs.jafc.5b00239
J. Agric. Food Chem. 2015, 63, 3402–3418

consent to participate in the sensory tests of the present investigation and had no history of known taste disorders, participated for at least two years in weekly training sessions and were recruited from the Chair of Food Chemistry and Molecular Sensory Science (Freising, Germany). To familiarize the subjects with the bitter taste of hop-derived compounds and to get them trained in recognizing bitterness by using the sip-and-spit method,[33] xanthohumol (**5**) and *trans*-isocohumulone (**4a**) were used as references. The sensory experiments were performed at 20−22 °C. To prevent cross-modal interactions with olfactory or visual inputs, the panelists used nose clips and yellow light or whenever necessary red light, respectively, was used.

Pretreatment of Fractions and Pure Compounds. Prior to sensory analysis, the fractions or isolated compounds were suspended in water, and, after removal of the volatiles under high vacuum (<5 hPa), were freeze-dried twice. ^{1}H NMR spectroscopy, GC/MS, and high-performance ion chromatographic analysis of an aliquot revealed that fractions treated by that procedure are essentially free of solvents and buffer compounds used. Formic acid, which is GRAS listed as a flavoring agent for food and feed applications, was used to adjust the pH value of solutions to be sensorially evaluated, because trace amounts of this acid do not influence the sensory profile of the test solution.

Sensory Analysis of Isolated Hop Resins. The individual resin fractions isolated from hops as described above were evaluated in their bitter intensity. To achieve this, each resin sample was taken up in 5% aqueous ethanol adjusted to pH 4.4 with trace amounts of 10% aqueous formic acid. The bitter intensity of these solutions was judged on a scale from 0 (not detectable) to 5 (strongly detectable).

Taste Dilution Analysis (TDA)..[33−35] An aliquot of each fraction isolated from hops was freeze-dried twice and dissolved in water containing 5% ethanol (pH 4.4) in "natural" concentration ratios matching the amounts present in 2.0 g of hops hard resin. After each fraction had been sequentially diluted 1 + 1 with water (pH 4.4), the serial dilutions of each of these fractions were presented to the sensory panel in order of ascending concentration. Using a duo test, panelists were asked to determine the dilution step at which a difference between sample and blank could be detected. This so-called taste dilution (TD) factor[33] determined by the 12 sensory assessors was averaged and did not differ by more than plus/minus one dilution step between the trained individuals.

Bitter Recognition Threshold Concentrations. Bitter taste threshold concentrations of the purified compounds were determined by 12 panelists using a duo test. The geometric mean of the last and the second to last concentrations was calculated and taken as the individual recognition threshold. The threshold value of the sensory group was approximated by averaging the threshold values of the individuals in three independent sessions and did not differ by more than plus/minus one dilution step. Based on the three independent repetitions, the confidence interval (α = 0.05) was calculated for each compound.

Taste Re-Engineering Experiments. To investigate the impact of the hop constituents on the bitter perception of beer, four taste recombinants were produced by spiking unhopped "zero" beer with bitter taste molecules in concentrations as determined in a standard Pilsner-type beer (Table 3) by means of LC-MS/MS. Recombinant A: "zero" beer was spiked with iso-α-acids (**3a−c**, **4a−c**). Recombinant B: recombinant A was spiked with xanthohumol (**5**) and isoxanthohumol (**6**). Recombinant C: recombinant A was spiked with prenylated flavonoids **5−32**. Recombinant D: recombinant A was spiked with compounds **5−42**. Using a linear 5-point scale, the bitterness of these recombinants A−D was then compared with that of a standard Pilsner-type beer (reference).

Sensomics Heatmapping. Data analysis was performed within the programming and visualization environment R (version 2.13.2).[47] The sensomics heatmap was calculated using the heatmap.2 function of R based on the concentration data after scaling the sum of all sensometabolites to an equal value for each beer sample. The dendrograms were constructed by means of an agglomerative linkage algorithm specifying the distance between two clusters as the increase in the error sum of squares after fusing two clusters into a single cluster and seeking for a minimum distance at each clustering step.[48]

Liquid Chromatography/Mass Spectrometry (LC-MS/MS). For compound identification, mass and product ion spectra were acquired on an API 4000 Q-Trap triple quadrupole/linear ion trap mass spectrometer (SCIEX, Darmstadt, Germany). Isolated fractions were dissolved in methanol/water (50/50, v/v) and directly introduced into the mass spectrometer by flow infusion using a syringe pump. Data were acquired in full-scan mode with negative electrospray ionization (−4500 V). Both quadrupoles operated at unit mass resolution. Nitrogen served as curtain gas (30 psi) and as turbo gas (450 °C). Fragmentation of the pseudo molecular ions $[M-H]^-$ into specific product ions was induced by collision with nitrogen (4.5×10^{-5} Torr). Data acquisition and instrumental control were performed with Analyst 1.5 software (SCIEX).

UPLC/Time-of-Flight Mass Spectrometry (UPLC/TOF-MS). Mass spectra of the compounds were measured on a Synapt G2 HDMS mass spectrometer (Waters, Manchester, U.K.) coupled to an Acquity UPLC core system consisting of a binary solvent manager, sample manager, and column oven. The compounds were dissolved in acetonitrile (1 mL), and aliquots (1−5 μL) were injected into the UPLC-TOF-MS system equipped with a 2 × 150 mm, 1.7 μm, BEH C18 column (Waters). Operated with a flow rate of 0.3 mL/min at 40 °C, the following gradient was used for chromatography: starting with a mixture (5/95, v/v) of acetonitrile and aqueous formic acid (0.1%, pH 2.5), the acetonitrile content was increased to 100% within 5 min and held at 100% for 1 min. Measurements were performed using negative ESI and the resolution modus consisting of the following parameters: capillary voltage −3.0 kV, sampling cone 30, extraction cone 4.0, source temperature 150 °C, desolvation temperature 450 °C, cone gas 30 L/h, and desolvation gas 850 L/h. The instrument was calibrated over an m/z range of 100−1200 using a solution of sodium formate (0.5 mM) in a 2-propanol/water mixture (9/1, v/v). All data were lock mass corrected using leucine enkephalin as the reference (m/z 554.2615, $[M-H]^-$). Data processing was performed by using MassLynx 4.1 (Waters) and the tool "elemental composition".

Nuclear Magnetic Resonance Spectroscopy (NMR). 1D/2D-^{1}H and ^{13}C NMR spectra were acquired on a 400 MHz DRX and a 500 MHz Avance III spectrometer (Bruker, Rheinstetten, Germany), respectively. CD_3OD, D_2O, or DMSO-d_6 was used as solvent, and chemical shifts are reported in parts per million relative to the solvent signal. For signal assignment, 2D-NMR experiments (COSY, HMQC, HMBC) were carried out using the pulse sequences taken from the Bruker software library. Data processing was performed by using XWin-NMR software (version 3.5; Bruker, Rheinstetten, Germany) as well as MestReNova 5.1.0-2940 (Mestrelab Research S.L., Santiago de Compostela, Spain).

RESULTS AND DISCUSSION

As the use of the hop's hard resin fraction for beer manufacturing was reported to reveal beers with an intense and pleasant bitter profile,[26] the sensory impact of the hard resin fractions should be evaluated. To achieve this, the hard resin fraction was isolated from hops,[30] chlorophylls and hop waxes were separated by means of solid phase extraction, and the resin was separated to give the water-soluble δ-resin and the nonsoluble ε-resin fraction by extraction with water at 40 °C.[31,32] Aliquots of the δ-resin, ε-resin, hard resin, soft resin, and total hop resin, respectively, were solubilized in 5% ethanolic solution in their "natural" concentration ratio (0.2/0.8/1/9/10; w/w), and the pH was adjusted to 4.4 to match the pH value of a standard beer. The trained sensory panelists, who were asked to rate the bitter intensity on a linear scale from 0 (not detectable) to 5.0 (very intense), judged the bitterness of the soft resin solution with the highest score of 4.25 (±0.25), followed by the ε-resin and the hard resin with 0.51 (±0.08) and 0.5 (±0.25), whereas bitterness was almost not detectable (0.08 ± 0.04) in the solution containing the δ-resin (data not shown). These data confirm the previously reported major bitter contribution of the soft resin

DOI: 10.1021/acs.jafc.5b00239
J. Agric. Food Chem. 2015, 63, 3402−3418

components and indicated the ε-resin to account for the bitterness of the hop's hard resin fraction. The ε-resin was, therefore, further separated to locate and identify the key bitter molecules in that hydrophobic fraction.

Identification of Key Bitter Compounds in the ε-Resin. Fractionation of the ε-resin by means of MPLC on RP18 material revealed 11 fractions (e1−e11), which were dissolved in 5% ethanolic solution in their natural concentration ratio and, then, evaluated in their bitter impact by means of a taste dilution analysis (TDA).[33−35] Fractions e5, e6, and e8−e11 were judged with the highest TD factors of 64 and 256, respectively, followed by fractions e2−e4 judged with TD factors between 6 and 32 (Figure 2). Aimed at locating the key contributors to the bitter taste of fractions e2−e11, each MPLC fraction was separated by means of preparative RP-HPLC and the subfractions were again analyzed by means of TDA to locate most intense bitter tastants (Figure 3).

Comparison of spectroscopic data (UV/vis, LC-MS/MS, $^{1}H/^{13}C$ NMR) of xanthohumol (**5**) in subfractions e8-7, e9-6, and e10-2, isoxanthohumol (**6**) in subfractions e4-2, e5-3, e6-5, and e9-2, desmethylxanthohumol (**7**) in subfraction e7-12, 8-prenyl- (**8**) and 6-prenylnaringenin (**9**) in subfraction e8-5, 5′-prenylxanthohumol (**17**) in subfractions e10-10 and e11-8, xanthohumol D (**19**) in e7-9, xanthohumol B (**20**) in e7-7, and xanthohumol C (**21**) in e10-5 and e11-5 with the literature data[24,25] confirmed the identity of these compounds in the ε-resin (Table 1). In addition, 1″,2″-dihydroxanthohumol C (**12**) was identified in subfractions e10-4 and e11-4, 1″,2″-dihydroxanthohumol K (**14**) in e4-2, e5-3, and e7-3, xanthohumol H (**22**) in e6-7 and e7-4, xanthohumol I (**26**) in e3-4, and 2″-hydroxyxanthohumol M (**25**) in e7-8 (Table 1), the spectroscopic data of which confirmed previously published data.[23,36−38,45] Another polar bitter compound in fraction e2 was identified as co-multifidol glucopyranoside **40a**[43] in subfraction e2-7 (Table 1). Some trace amounts of α-acids (**1a**/**b**/**c**) were identified in e10-8/9 and e11-8/9, and β-acids (**2a**/**b**/**c**) in e11-7, e11-11, and e11-13, thus indicating some residual amounts of soft resin components in the hard resin fraction. Next to these bitter compounds, some astringent molecules were identified as *cis*/*trans*-*p*-coumaric acid (**33a**/**b**)[49] in subfraction e2-4, quercetin (**36**)[40] in e3-5, and quercetin-3-*O*-β-D-glucopyranoside (**37**)[41] in e2-5 (Table 1). The bitter molecules ad-multifidol glucopyranoside (**40c**)[43] and *n*-multifidol-di-*C*-glucopyranoside (**40b**)[44] as well as the astringent molecules *trans*-*N*-feruloyltyramine (**42**),[23,36,37] kaempferol-3-*O*-β-D-glucopyranoside (**38**),[41] and kaempferol-3-*O*-β-D-(6″-malonyl)glucopyranoside (**39**)[42] were isolated from a hop polyphenol extract and were also identified as hard resin constituents (Table 2). For unequivocal structure elucidation by means of NMR spectroscopy, glycosides **37**−**41** were isolated in larger quantities from the hop tannin extract.

In contrast to the above-mentioned taste molecules, compounds **10**, **11**, **18**, **23**, **27**−**29**, **31**, and **32** isolated from the ε-resin have not yet been identified as natural phytochemicals in hops and beer, respectively. Although not yet reported as hop components, xanthohumol O (**27**), xanthohumol L (**28**), and isoxanthohumol H (**23**) were found earlier as metabolites in feces of xanthohumol-fed rats.[39] The chemical structures of the previously not reported hop bitter constituents **10**, **11**, **18**, **29**, **31**, and **32** were determined by means of LC-MS and 1D/2D-NMR experiments.

NMR analysis of compound **29**, isolated from subfractions e8-3 and e9-4, showed similar ^{1}H and ^{13}C shifts as found for xanthohumol H (**22**), thus suggesting a similar chemical structure. However, an additional proton signal for H−C(6″) resonating at 3.28 ppm with an integral of three protons and an additional ^{13}C resonance signal for C(6″) at 50.6 ppm indicated compound **29** as the 3″-methoxy adduct of xanthohumol H (**22**). This was confirmed by the heteronuclear coupling observed between carbon atom C(3″) and the protons of the methyl group H−C(6″) in the HMBC spectrum (Figure 4). To confirm the natural occurrence of **29** and to exclude any artifact formation during workup, hop was extracted with ethanol instead of methanol. LC-MS/MS analysis of this ethanolic extract unequivocally identified xanthohumol M (**29**) in hops.

Compound **18** showed similar ^{1}H and ^{13}C NMR shifts for the naringenin moiety and the cyclic prenylic side chain as found for 1″,2″-dihydroxanthohumol K (**14**) and 1″,2″-dihydroxanthohumol C (**12**), respectively. But in comparison to **12** and **14**, any ^{1}H NMR signal for H−C(6) was lacking, whereas additional signals were observed for a second prenyl side chain as known for 5′-prenylxanthohumol (**17**). The HMBC spectrum indicated a heteronuclear coupling between carbon atom C(6) and the protons at C(1‴) and confirmed the attachment of a prenyl side chain to carbon C(6) (Figure 4). The hypsochromic shift of the UV maximum of xanthohumol (**5**) and 1″,2″-dihydroxanthohumol C (**12**), respectively, from ∼370 to 326 nm was well in line with the intramolecular cyclization of the prenyl side chain attached to carbon C(8) with the hydroxyl group bound to carbon C(9).[50] In consequence, the structure of this previously unknown compound was assigned as 1″,2″-dihydroxanthohumol F, **18** (Figure 4).

The spectroscopic data of compound **10**, showing major differences compared to those reported for other hop constituents in the past, indicated the presence of two prenyl side chains, a *p*-coumaroyl moiety, and a methoxy group in the HSQC spectrum. The HMBC spectrum revealed both prenyl side chains to be attached to carbon C(8) and to show connectivity to two keto functions, thus indicating a cyclohexenedione structure (Figure 4). In contrast to the keto function at C(4) as found in xanthohumol derivatives, carbon C(4) showed a ^{13}C chemical shift as expected for a hydroxylated carbon. However, the proton signal of H−C(2) showed an extraordinarily strong low-field shift as found for xanthohumol due to the *peri*-effect[51] caused by the keto function at C(9). Taking all spectroscopic data into consideration, the target bitter compound was identified as the previously not reported 4′-hydroxytunicatachalcone, **10** (Figure 4), which is the 4′-hydroxy derivative of tunicatachalcone identified earlier.[52]

The ^{1}H and ^{13}C NMR spectrum of compound **11** showed very similar chemical shifts as found for 5′-prenylxanthohumol (**17**) but additional resonance signals indicating the presence of another prenylic side chain and a keto function. Furthermore, an HSQC experiment revealed compound **11** to be a flavonoid showing the characteristic proton resonances at 2.96 and 3.16 ppm for the diastereotopic protons H−C(3). The HMBC spectrum showed a heteronuclear coupling between carbon C(9) and one prenylic side chain, and between carbonyl carbon C(7), resonating at 198.6 ppm, to three prenylic side chains (Figure 4). Taking all spectroscopic data into consideration, the structure of compound **11** was determined to be 5-hydroxy-2-(4-hydroxyphenyl)-6,6,8-triprenyl-6*H*-chroman-4,7-dione, coined isoxantholupon, **11** (Figure 4), which to the best of our knowledge has not previously been reported.

Compared to xanthohumol (**5**), compound **31** was missing the typical ^{1}H shifts of the *p*-coumaric acid moiety. Furthermore, the

DOI: 10.1021/acs.jafc.5b00239
J. Agric. Food Chem. 2015, 63, 3402−3418

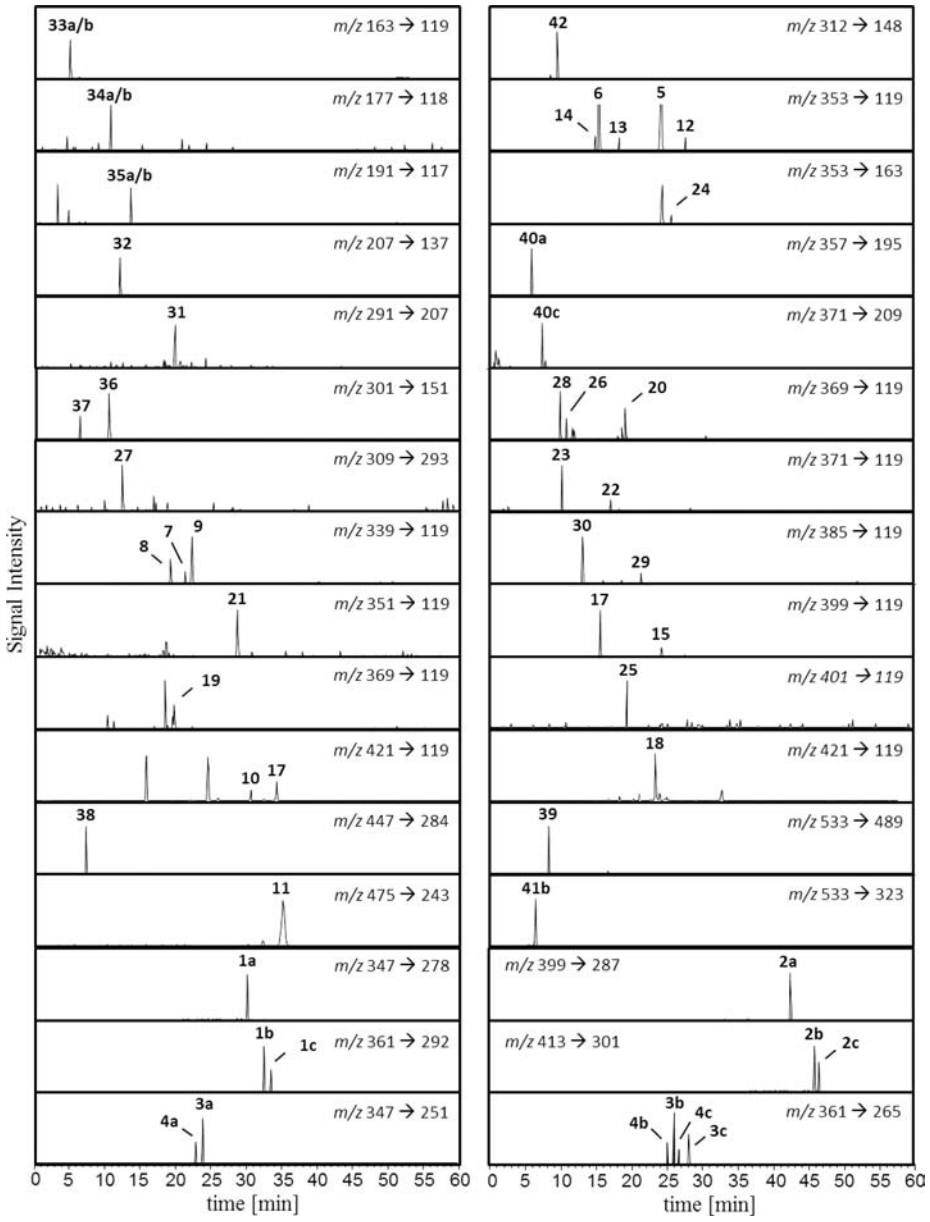

Figure 6. RP-HPLC-MS/MS mass chromatogram of taste compounds in hop extract. Numbering of compounds refers to chemical structures given in Figure 1.

spectra also showed that a substitution had occurred at carbon atom C(6) due to the lacking proton signal at this carbon atom. But interestingly, compound **31** exhibited typical ^{1}H shifts of an intact prenylic side chain as well as signals of two chemically identical methyl groups which showed no ^1J-coupling with any other proton. A long-range coupling of carbon C(9) and the methyl protons H−C (1′, 2′) in the HMBC spectrum revealed the structure of compound **31** to be 2,2-dimethyl-5,6,7-trihydroxy-8-(3-methylbut-2-enyl)chroman-4-one, which is coined 2″,3″-dehydrocyclohumulohydrochinone, **31** (Figure 4), due to its structural similarity with humulohydrochinon.[53] As LC-MS-MS analysis undoubtedly confirmed the presence of this compound in hops and excluded its formation as workup artifact (data not shown), compound **31** is considered a previously not reported hop constituent.

The ^{1}H NMR data of compound **32**, showing a molecular composition of $C_{12}H_{16}O_3$ (TOF-MS), revealed large similarities with those recorded for xanthohumol (**5**), but showed an additional singlet at 5.4 ppm and lacked the typical aromatic proton shifts of the *p*-coumaric acid moiety. Heteronuclear couplings in the HMBC spectrum indicated that a prenylic side chain is attached at carbon C(4) and that a methoxy group is connected to carbon C(1). Taking all spectroscopic data into account, the target compound was identified as the previously not reported 1-methoxy-4-prenylphloroglucinol, **32** (Figure 4). It is proposed in the literature that xanthohumol is biosynthesized from coumaroyl-CoA and three malonyl-CoA to form chalconaringenine, followed by a prenylation reaction to form first desmethylxanthohumol (**7**) and, thereafter, xanthohumol (**5**) by additional methylation.[54] Interestingly, the occurrence of compound **32** in hops provides evidence that the prenylation and methoxylation of the phloroglucin moiety during the biosynthesis of **5** can occur prior to its reaction with *p*-coumaroyl-CoA.

Synthetic Preparation of Xanthohumol Derivatives 12−16, 22−24, 29, and 30. In order to screen the hop fractions for additional xanthohumol derivatives, xanthohumol P

DOI: 10.1021/acs.jafc.5b00239
J. Agric. Food Chem. 2015, 63, 3402−3418

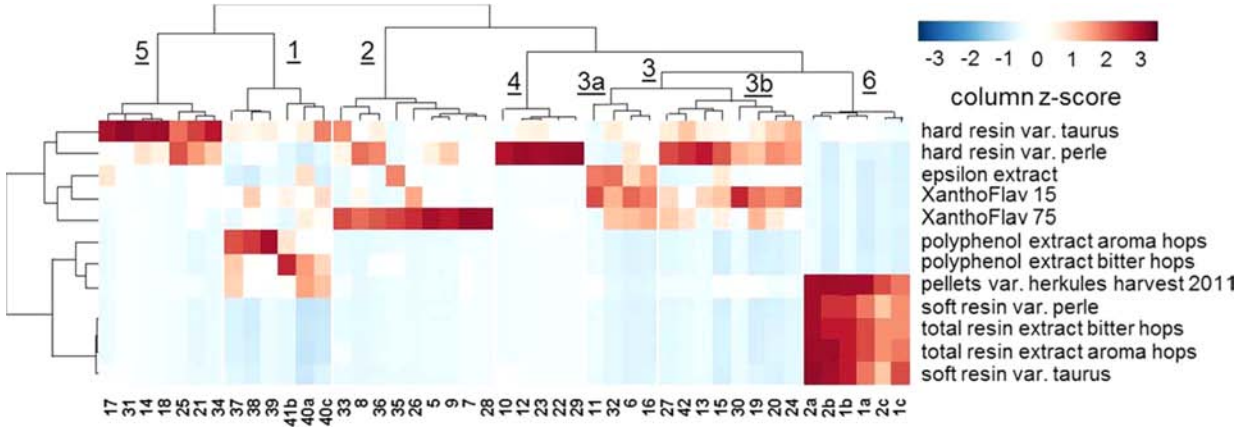

Figure 7. Sensomics heatmapping of concentrations of taste compounds in hop products/extracts taken from Table 3. The dendrogram is based on an agglomerative linkage algorithm.[48] Numbering of compounds refers to structures given in Figure 1

(**15**) was synthesized by heating an ethanolic solution of xanthohumol (**5**) for 4 h at 80 °C in the presence of the acidic cation exchanger Amberlyst 15, while isoxanthohumol P (**16**) and isoxanthohumol M (**30**) were obtained after alkaline isomerization of xanthohumol P (**15**) and xanthohumol M (**29**), respectively. Reaction of xanthohumol (**5**) with hydrobromic acid in methanol/acetic acid revealed, besides compounds **6**, **15**, **16**, **29**, and **30**, additional major transformation products, namely, **12**, **14**, and **22**−**24** (Figure 5). These compounds were identified as 1″,2″-dihydroxanthohumol C (**12**) and K (**14**), and xanthohumol H (**22**) by LC-MS and 1D/2D-NMR experiments as well as by cochromatography with the corresponding reference substance (Figure 4). Isoxanthohumol H (**23**) and 1″,2″-dihydroisoxanthohumol C (**13**) were isolated and identified by comparing the LC-MS and NMR data to those reported in literature.[39,45] Reaction product **24** exhibited similar ^{1}H and ^{13}C shifts as found for the naringenin substructure in xanthohumol (**5**) but with a different proton signal pattern recorded for the prenylic side chain. Instead of two nonaromatic signals integrating for three protons, only one signal at 1.79 ppm with an integral of three protons was observed. In addition, resonance signals integrating for two protons were observed at 2.18 and 4.66 ppm, respectively, suggesting that the double bond in **24** is located between C(3″) and C(4″). The heteronuclear coupling between C(3″) and H−C(4″) observed in the HMBC spectrum (Figure 4) confirmed the structure of **24** as xanthohumol N (Figure 1), which to the best of our knowledge has not yet been reported earlier.

Sensory Evaluation of Purified Hop Components. Prior to sensory analysis, the purity of each compound was confirmed by HPLC-MS as well as ^{1}H NMR spectroscopy to be more than 98%. To determine the human threshold concentrations for the bitter sensation induced by the hop derivatives identified, aqueous solutions of target compounds were evaluated in serial dilutions by means of a duo test (Table 1). The bitter threshold concentrations determined for the α-acids (**1**), β-acids (**2**), xanthohumol (**5**), and isoxanthohumol (**6**) by means of the duo test were comparable to those recorded recently by means of a triangular test,[15−17] thus confirming the suitability of the duo test setup.

Except for the *p*-coumaric acid esters (**34a**/**b**, **35a**/**b**), the human bitter threshold concentrations were relatively low and ranged from 5 to 44 μmol/L (Table 1). Comparably high threshold concentrations (>20 μmol/L) were found for compounds **15**, **16**, **19**, **22**, **23**, **26**, and **30** exhibiting a modified prenylic side chain, while an intramolecular cyclization (**12**, **14**, **20**, **28**) seemed not to influence the bitter threshold levels. More lipophilic molecules like compound **12** that elute later on RP-18 material seem to have a lower human threshold concentration than structurally related earlier eluting substances like compound **14**. Interestingly, the polar *O*-β-D-glycosides of the multifidol congeners **40a** and **40c** feature surprisingly low human threshold concentrations of 5 and 10 μmol/L, respectively (Table 1). As the α/β-acids, iso-α-acids, xanthohumol, and isoxanthohumol activate three bitter taste receptors, namely, hTAS2R1, hTAS2R14, and hTAS2R40 receptor,[21] these data suggest the involvement of another bitter taste receptor responding to the bitter β-glycosides **40a** and **40c**. One candidate receptor would be the hTAS2R16, which has been reported to be activated by β-glycosides like salicin.[55]

Quantitation and Sensomics Heatmapping of Hop-Derived Bitter Compounds in Hop Products and Beer. To gain insight into the occurrence and concentrations of the individual hop-derived bitter compounds in beer, compounds **1**−**42** (Figure 1) were quantitated in hop extracts as well as a Pilsner-type beer by means of HPLC-MS/MS in a single chromatographic run. Operating the mass spectrometer in the multiple reaction monitoring (MRM) mode, a highly selective and sensitive quantitation of the analytes could be accomplished (Figure 6).

As expected, xanthohumol (**5**) was the most predominant compound (>30 mmol/100 g) found in the hard resin (Table 2). With the exception of the very lipophilic isoxantholupon (**11**) and *cis*-/*trans*-*p*-coumaric acid ethyl ester (**35a**/**b**), all other compounds identified above were found in the hard resin as well. 1-Methoxy-4-prenyl-phloroglucinol (**32**) and 2″,3″-dehydrocyclohumulohydrochinon (**31**) were only detectable in the hard resin isolated from the bitter hop variety Taurus (Table 2). As expected, trace amounts of most of the prenylated flavonoid were found in the soft resins too. Only the nonpolar 4′-hydroxytunicatachalcone (**10**) and 5′-prenylxanthohumol (**17**), respectively, were observed in considerable amounts of 1193 and 1320 μmol/100 g in the soft resin of the bitter hop variety Taurus. Analysis of the commercially available pure resin extracts contained high amounts of >700 μmol/100 g of xanthohumol (**5**), whereas all other compounds (**6**−**42**) were present in comparatively low amounts (Table 2).

Quantitative analysis of the XanthoFlav 75% extract revealed, next to xanthohumol (**5**), high concentrations of isoxanthohumol (**6**, 9754 μmol/100 g), desmethylxanthohumol (**7**, 13873

DOI: 10.1021/acs.jafc.5b00239
J. Agric. Food Chem. 2015, 63, 3402−3418

μmol/100 g), xanthohumol L (**28**, 11656 μmol/100 g), and kaempferol-3-*O*-β-D-glycopyranoside (**38**, 45105 μmol/100 g). With the exception of xanthohumol (**1**), the XanthoFlav 15% extract did not differ much in its composition from the xanthohumol enriched extract XanthoFlav 75%. The only significant difference was the presence of much higher amounts (8142 vs 3.87 μmol/100 g) of isoxantholupon (**11**) in the extract XanthoFlav 15%. The ε-extract[27] contained quite the same compounds as the XanthoFlav extracts, however, xanthohumol (**5**) and isoxanthohumol (**6**) were present in comparably low amounts of 8601 and 7671 μmol/100 g, respectively, and the polar compounds **10**, **34**−**39**, **41b**, and **42** were not detectable at all (Table 2).

Commercially available tannin extracts revealed very high amounts of the flavonol glycosides **37**−**39** (813.2−14541 μmol/100 g) and the intensely bitter tasting multifidol glycosides **40a**, **40b**, and **41b** (428.7−4802 μmol/100 g). Interestingly, the extract prepared from an aroma hop variety has higher amounts of the flavononol glycosides **37**−**39** (18.60 vs 11.36 mmol/100 g), whereas the extract made from a bitter hop variety showed higher levels of the multifidol glycosides **40a**, **40b**, and **41b** (2.38 vs 7.08 mmol/100 g). Both extracts contained only minor amounts (<105 μmol/100 g) of xanthohumol (**5**) and its derivatives.

To examine the multivariate distances between the individual sensometabolites throughout the set of different hop products, the concentrations determined for hard resin-derived compounds (**5**−**42**) were scaled, followed by a hierarchical cluster analysis to arrange the taste compounds into six clusters labeled 1−6 as visualized in a sensomics heatmap (Figure 7). Cluster 1 consisted of the glycosides **37**−**41b** present in high concentrations in the tannin extracts and in hop pellets, thus demonstrating the quantitative dominance of glycosides over the xanthohumol derivatives. Cluster 2 comprised xanthohumol (**5**), desmethylxanthohumol (**7**), its isomerization products 8-(**8**) and 6-prenylnaringenin (**9**), xanthohumol I (**26**), *cis*-/*trans*-*p*-coumaric acid ethyl ester (**35a**/**b**), and quercetin (**36**) being the characteristic attribute of the XanthoFlav extract 75%. In comparison, the large cluster 3 consisted of isoxanthohumol (**6**), isoxantholupon (**11**), isoxanthohumol P (**16**), and 1-methoxy-4-prenylphloroglucinol (**32**) separating in subcluster 3a and 1″,2″-dihydroisoxanthohumol C (**13**), xanthohumol P (**15**), xanthohumol D (**19**), xanthohumol B (**20**), xanthohumol N (**24**), xanthohumol O (**27**), isoxanthohumol M (**30**), and *N*-*trans*-feruloyltyramine (**42**) in subcluster 3b. Whereas higher concentrations of compounds in subcluster 3a seem to be characteristic for the ε-extract and the XanthoFlav 75% extract, the extract XanthoFlav 15% and the hard resins showed high concentrations of compounds of subcluster 3b. Interestingly, the hard resin fraction prepared from the hop varieties Taurus and Perle showed significant differences in clusters 4 and 5. Compounds 4′-hydroxytunicatachalcone (**10**), 1″,2″-dihydroxanthohumol C (**14**), xanthohumol H (**22**), isoxanthohumol H (**23**), and xanthohumol M (**29**) are grouped in cluster 4 and are representative for the Perle hard resin, whereas 1″,2″-dihydroxanthohumol K (**14**), 5′-prenylxanthohumol (**17**), xanthohumol C (**21**), 2″-hydroxyxanthohumol M (**25**), 2″,3″-dehydrocyclohumulohydrochinon (**31**), and *cis*-/*trans*-*p*-coumaric acid methyl ester (**34a**/**b**), classified in cluster 5, seem to be typical for the Taurus hard resin. As expected, the α-acids (**1a**/**b**/**c**) and β-acids (**2a**/**b**/**c**) are characteristic for the total resin extract and the soft resin and are therefore grouping together in cluster 6. These data clearly show that the various hop products are distinctive for their content of specific hard resin derived compounds and are a useful resource to adjust levels of desired compounds in final hop-containing products like beer.

The quantitative analysis of a traditional Pilsner beer (Table 3) confirmed that the iso-α-acids (**3a**/**b**/**c**, **4a**/**b**/**c**) are the quantitatively predominant bitter tasting compounds[12−14] with concentrations between 5.0 and 24.5 μmol/L.[56] Due to the isomerization reaction during wort boiling, significant amounts (5.5 μmol/L) of isoxanthohumol (**6**) are present in the beer sample. Next to the iso-α-acids (**3a**/**b**/**c**, **4a**/**b**/**c**) and isoxanthohumol (**6**), the glycosides (**37**−**41b**) are the third largest group with concentrations between 0.9 and 4.0 μmol/L. All other xanthohumol and isoxanthohumol derivates (**5**, **8**−**30**) are present in concentrations below 0.6 μmol/L. With the exception of the iso-α-acids (**3a**/**b**/**c**, **4a**/**b**/**c**), none of the other compounds were detected in beer above their taste threshold concentration (Table 1). In order to investigate whether the subthreshold prenylated flavonoids and glycosides contribute additively to the beer's bitterness, taste re-engineering experiments were performed in the following.

Taste Re-Engineering Experiments. Samples of unhopped "zero" beer were spiked with natural concentrations (Table 3) of the individual purified iso-α-acids **3** and **4** to give recombinant A, the iso-α-acids (**3a**−**c**, **4a**−**c**), xanthohumol (**5**), and isoxanthohumol (**6**) to give recombinant B, the iso-α-acids (**3a**−**c**, **4a**−**c**) and the prenylated flavonoids **5**−**32** to give recombinant C, and the iso-α-acids (**3a**−**c**, **4a**−**c**) plus all the identified compounds **5**−**42** to give recombinant D. Using a linear 5-point scale, the bitterness of these recombinants A−D was then compared with that of a standard Pilsner-type beer as reference (Figure 8). Without any further addition, the bitterness

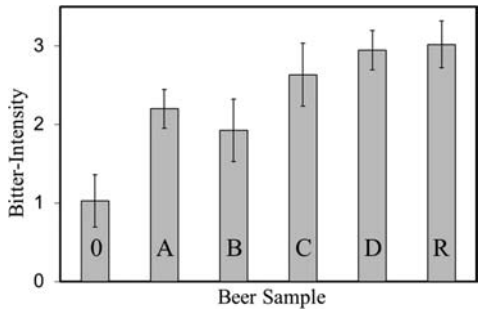

Figure 8. Bitter taste intensity of (R) standard Pilsner-type (reference), (0) unhopped "zero" beer and "zero" beer spiked with (A) iso-α-acids (**3a**/**b**/**c**, **4a**/**b**/**c**), (B) iso-α-acids (**3a**/**b**/**c**, **4a**/**b**/**c**), xanthohumol (**5**), and isoxanthohumol (**6**), (C) iso-α-acids (**3a**/**b**/**c**, **4a**/**b**/**c**) and compounds **5**−**35** and **42**, and (D) iso-α-acids (**3a**/**b**/**c**, **4a**/**b**/**c**) and all hard resin-derived compounds **5**−**42** (Table 1). Confidence interval (α = 5%).

of the "zero" beer was rated with a low score of 1.03 ± 0.33 compared to the reference Pilsner-type beer (3.02 ± 0.29), thus demonstrating that a majority of the beer's bitterness is due to hop-derived components while a marginal portion of remaining bitterness comes from other sources such as, e.g., yeast and malt. Recombinant A containing the iso-α-acids showed an increased intensity of 2.20 ± 0.25 for a scratchy bitterness which was perceived with an instantaneous onset but a short offset. Addition of xanthohumol (**5**) and isoxanthohumol (**6**) to recombinant A induced a marginally decreased bitter intensity of recombinant B (1.93 ± 0.40) which was reported by the panelists to exhibit a more long lasting and less sharp bitter profile when compared to

DOI: 10.1021/acs.jafc.5b00239
J. Agric. Food Chem. 2015, 63, 3402−3418

recombinant A. Recombinant C containing iso-α-acids plus compounds **5**−**32** showed a typical beer-like, well-rounded bitterness with a medicinal-herbal-like off-taste, and the bitter intensity increased and was determined to be 2.64 ± 0.25. Sensory evaluation of the total taste recombinant D revealed a bitterness of 2.95 ± 0.26, which did not differ significantly from the bitter intensity of the reference beer (3.02 ± 0.29) and was described as beer-like, long lasting, and well-rounded without any specific off-taste. Taking all these sensory data into account, iso-α-acids (**3a**−**c**, **4a**−**c**) and the identified compounds **5**−**42** were demonstrated for the first time to be truly sufficient for constructing the authentic bitter percept of beer. The knowledge on the structure and concentration of these bitter compounds paves the way for the targeted manufacturing of tailored taste profiles of beer and hop-containing foods and beverages.

Sensory and Quantitative Analysis of Hop-Derived Taste Compounds in Beer Manufactured with ε-Extract and Spent Hops, Respectively. It has been recently reported that the use of hop's hard resin instead of the soft resin fraction for beer production revealed a beer exhibiting an intense and pleasant bitter character.[26] As the above-mentioned ε-extract was found to be enriched in bitter tasting prenylated flavonoids, it was interesting to quantitate the bitter molecules and to sensorially evaluate the bitter taste of a beer manufactured by using this ε-extract as the only hop source. To achieve this, four different beers (beers I−IV) were produced and their International Bitterness Units (IBU) were determined by a trained sensory panel.[57] Beer I was produced as a bitter reference using an Isohop extract (30%) added to the final, fermented beer to adjust an IBU value of 23. Beers II−IV were produced using the same wort as for beer 1 just differing hop products. For manufacturing of beer II (27 IBU) and beer IV (27 IBU), the ε-extract was added to the wort postboiling and at the beginning of the kettle boiling, respectively. Beer III (51 IBU) was made by adding spent hops, which were obtained by exhaustive carbon dioxide extraction, to the wort prior to boiling. Descriptive sensory analysis revealed beer I (23 IBU) and beer IV (27 IBU) as well-rounded with a pleasant and typical Pilsner-type bitter profile. In comparison, beer III produced from spent hops (51 IBU) was described by the trained panelists as strongly bitter with a harsh bitter and irritating character perceived at the back of the tongue, while beer II (27 IBU) was reported to exhibit a medicinal or herbal bitter taste profile.

To gain some more insight into the concentrations of the individual hop-derived bitter compounds in beer, compounds **1**−**42** were quantitated in beers I−IV and a standard Pilsner-type beer by means of HPLC-MS/MS in a single chromatographic run (Table 3). Analysis of beer I revealed about 60 μmol/L iso-α-acids (**3**, **4**) as well as small amounts of 4′-hydroxytunicatachalcone (**10**) and isoxantholupon (**11**). Van Opstaele[58] already described that iso-α-acids extracts also contain some other hop-derived compounds which are accordingly introduced into a beer spiked with an iso-α-acids extract. All other compounds of the hard resin (**5**−**9**, **12**−**42**) were present just in trace amounts or were not detectable. In comparison, beer II contained significant amounts of the nonisomerized xanthohumol derivatives **5**, **12**, **14**, **15**, **17**, **19**−**22**, **24**, and **28**, besides α-acids (**1**) and β-acids (**2**), being well in line with manufacturing the beer by using a xanthohumol derivative enriched extract after wort boiling. Adding the ε-extract at the beginning of the wort boiling procedure (beer IV) resulted in rather low amounts of xanthohumols but significantly increased amounts of isoxanthohumol derivatives, namely, isoxanthohumol (**6**), 6-prenylnaringenin (**9**), 8-prenylnaringenin (**8**), isoxanthohumol H (**23**), and isoxanthohumol M (**30**). Interestingly, high concentrations of isoxanthohumol P (**16**) and *cis*-/*trans*-*p*-coumaric ethyl ester (**35a**/**b**) were found in beer IV, which might be explained by postfermentation reactions with ethanol produced by yeast.

The concentrations of most compounds (**5**−**35**) found in beer III, which was produced with spent hops only, did not significantly differ from those found in beer IV, thus confirming that all target compounds are already present in the spent material and are extracted and/or isomerized during kettle boiling. Interestingly, *trans*-*N*-feruloyltyramine (**42**), quercetin (**36**), and the bitter glycosides **37**−**41b** were also found in beer III in up to 10-fold higher concentrations than in beer IV. With the exception of the multifidol glycosides **40a** and **40c**, these very polar compounds were not present in the ε-extract and are extracted during wort boiling from spent hops. As beer III and beer IV showed quite similar concentrations of prenylated flavonoids (Table 3), but do differ drastically in the content of glycosides **37**−**41**, it is assumed that the overall harsh and unpleasant bitter taste sensation perceived for beer IV is due to the rather high levels of these glycosides.

With the exception of isoxanthohumol (**6**) and 8-prenylnaringenin (**8**), the concentrations of compounds **5**−**42** were much higher in beer IV than in the standard Pilsner-type beer, e.g., beer IV contained 68, 240, and 5500 times higher levels of xanthohumol, isoxanthohumol P, and isoxanthohumol H when compared to the standard Pilsner beer (Table 3). Since prenylated flavonoids have been shown to possess health beneficial effects in vitro[23,45,59,60] but a 60-fold enrichment of xanthumol derivatives is necessary to benefit from the proposed activities,[61] these results impressively demonstrate the possibility to produce beverages strongly enriched with prenylated hop flavonoids.

■ ASSOCIATED CONTENT

Ⓢ Supporting Information

Chromatographic parameters for HPLC separation of MPLC subfractions. Spectroscopic data of all hard resin derived compounds. Comprehensive spectroscopic data of isolated hop compounds. Table S1: Optimized mass spectrometric parameters for the quantitative analysis of taste-active hop-derived compounds by means of LC-MS/MS using negative electrospray ionization (ESI^-). This material is available free of charge via the Internet at http://pubs.acs.org.

■ AUTHOR INFORMATION

Corresponding Author

*Phone: +49-8161/71-2902. Fax: +49-8161/71-2949. E-mail: thomas.hofmann@tum.de.

Funding

We are grateful to the Barth-Haas-Group GmbH & Co. KG, Nuremberg, Germany, for their generous financial support.

Notes

The authors declare no competing financial interest.

■ ACKNOWLEDGMENTS

We are grateful to Christina Schönberger (Barth-Haas-Group) and Martin Biendl (Hopsteiner; Simon H. Steiner GmbH, Mainburg, Germany) for providing hop samples, to Andreas Gahr for providing the beer samples produced at the Research Brewery St. Johann (Train St. Johann, Germany), and to Cynthia Almaguer and Martina Gastl (Chair of Brewing and Beverage

DOI: 10.1021/acs.jafc.5b00239
J. Agric. Food Chem. 2015, 63, 3402−3418

Technology, Technische Universität München, Germany) for providing unhopped "zero" beer. The authors wish to thank SCIEX Darmstadt, Germany, for providing technical and application support.

REFERENCES

(1) Fritsch, H. T.; Schieberle, P. Identification based on quantitative measurements and aroma recombination of the character impact odorants in a Bavarian Pilsner-type beer. *J. Agric. Food Chem.* **2005**, *53*, 7544−7551.

(2) Kaltner, D.; Steinhaus, M.; Mitter, W.; Biendl, M.; Schieberle, P. (R)-Linalool as key flavor for hop aroma in beer and its behavior during beer staling. *Monatsschr. Brauwiss.* **2003**, *56*, 192−196.

(3) Palamand, S. R.; Aldenhoff, J. M. Bitter tasting compounds of beer. Chemistry and taste properties of some hop resin compounds. *J. Agric. Food Chem.* **1973**, *21*, 535−543.

(4) Schieberle, P. Primary odorants of pale lager beer. Differences to other beers and changes during storage. *Z. Lebensm.-Unters. Forsch.* **1991**, *193*, 558−565.

(5) Collin, S.; Nizet, S.; Gros, J. Le houblonnage à cru des bières spéciales belges est bien plus qu'une simple dissolution des composés aromatiques du houblon. *Cerevisia* **2012**, *36*, 119−124.

(6) Praet, T.; Van Opstaele, F.; Jaskula-Goiris, B.; Aerts, G.; De Cooman, L. Biotransformation of hop-derived aroma compounds by saccharomyces cerevisiae upon fermentation. *Cerevisia* **2012**, *36*, 125−132.

(7) Gros, J.; Nizet, S.; Collin, S. Occurrence of odorant polyfunctional thiols in the super alpha *Tomahawk* hop cultivar. Comparison with the thiol-rich *Nelson Sauvin* bitter variety. *J. Agric. Food Chem.* **2011**, *59*, 8853−8865.

(8) Dunkel, A.; Steinhaus, M.; Kotthoff, M.; Nowak, B.; Krautwurst, D.; Schieberle, P.; Hofmann, T. Nature's chemical signatures in human olfaction: A foodborne perspective for future biotechnology. *Angew. Chem., Int. Ed.* **2014**, *53*, 7124−7143.

(9) Jaskula, B.; Kafarski, P.; Aerts, G.; De Cooman, L. A kinetic study on the isomerization of hop α-acids. *J. Agric. Food Chem.* **2008**, *56*, 6408−6415.

(10) Verzele, M.; De Keukeleire, D. *Chemistry and analysis of hop and beer bitter acids*; Elsevier: Amsterdam, London, New York, Tokyo, 1991.

(11) De Keukeleire, D. Fundamentals of beer and hop chemistry. *Quim. Nova* **2000**, *23*, 108−112.

(12) Kowaka, M.; Kokubo, E. Composition of bitter substances of hops and characteristics of beer bitterness. *J. Am. Soc. Brew. Chem.* **1976**, *35*, 16−21.

(13) Verzele, M.; Jansen, H. E.; Ferdinandus, A. Organoleptic trials with hop bitter substances. *J. Inst. Brew.* **1970**, *76*, 25−28.

(14) Fritsch, A.; Shellhammer, T. H. Alpha-acids do not contribute bitterness to lager beer. *J. Am. Soc. Brew. Chem.* **2007**, *65*, 26−28.

(15) Haseleu, G.; Intelmann, D.; Hofmann, T. Identification and RP-HPLC-ESI-MS/MS quantitation of bitter-tasting β-acid transformation products in beer. *J. Agric. Food Chem.* **2009**, *57*, 7480−7489.

(16) Intelmann, D.; Kummerlowe, G.; Haseleu, G.; Desmer, N.; Schulze, K.; Frohlich, R.; Frank, O.; Luy, B.; Hofmann, T. Structures of storage-induced transformation products of the beer's bitter principles, revealed by sophisticated NMR spectroscopic and LC-MS techniques. *Chem.—Eur. J.* **2009**, *15*, 13047−13058.

(17) Haseleu, G.; Intelmann, D.; Hofmann, T. Structure determination and sensory evaluation of novel bitter compounds formed from β-acids of hop (*Humulus lupulus L.*) upon wort boiling. *Food Chem.* **2009**, *116*, 71−81.

(18) De Keukeleire, D.; Verzele, M. The absolute configuration of the isohumulones and the humulinic acids. *Tetrahedron.* **1971**, *27*, 4939−4945.

(19) Hänsel, R.; Schulz, J. Demethylxanthohumol: isolation from hops and cyclization to give flavanones (in German). *Arch. Pharm.* **1988**, *321*, 37−40.

(20) Heller, W. and Forkmann, G. Biosynthesis of flavonoids. In *The flavonoids: Advances in research since 1986*; Harborne, J. B., Ed.; Chapman and Hall: London, 1994; pp 499−536.

(21) Intelmann, D.; Batram, C.; Kuhn, C.; Haseleu, G.; Meyerhof, W.; Hofmann, T. Three TAS2R bitter taste receptors mediate the psychophysical responses to bitter compounds of hops (*Humulus lupulus* L.) and beer. *Chemosens. Percept.* **2009**, *2*, 1936−5802.

(22) Taniguchi, Y.; Taniguchi, H.; Yamada, M.; Matsukura, Y.; Koizumi, H.; Furihata, K.; Shindo, K. Analysis of the components of hard resin in hops (*Humulus lupulus L.*) and structural elucidation of their transformation products formed during the brewing process. *J. Agric. Food Chem.* **2014**, *62*, 11602−11612.

(23) Chadwick, L. R.; Nikolic, D.; Burdette, J. E.; Overk, C. R.; Bolton, J. L.; van Breemen, R. B.; Fröhlich, R.; Fong, H. H. S.; Farnsworth, N. R.; Pauli, G. F. Estrogens and congeners from spent hops. *J. Nat. Prod.* **2004**, *67*, 2024−2032.

(24) Stevens, J. F.; Ivancic, M.; Hsu, V. L.; Deinzer, M. L. Prenylflavonoids from *Humulus lupulus*. *Phytochemistry* **1997**, *44*, 1575−1585.

(25) Stevens, J. F.; Taylor, A. J.; Nickerson, G. B.; Ivancic, M.; Henning, J.; Haunold, A.; Deinzer, M. L. Prenylflavonoid variation in *Humulus lupulus*: Distribution and taxonomic significance of xanthogalenol and 4′-*O*-Methylxanthohumol. *Phytochemistry* **2000**, *53*, 759−775.

(26) Almaguer, C.; Gastl, M.; Dresel, M.; Hofmann, T.; Becker, T. Comparison of the quality parameters of hop hard resins. Poster EBC Congress, Glasgow, Scotland, 2011.

(27) Schulmeyr, J.; Dresel, M.; Hofmann, T. Hop resin-based substance. *PCT Int. Appl.* WO2012100953 (A1), 2012.

(28) Intelmann, D.; Haseleu, G.; Hofmann, T. LC-MS/MS quantitation of hop-derived bitter compounds in beer using the ECHO technique. *J. Agric. Food Chem.* **2009**, *57*, 1172−1182.

(29) Wilhelm, H.; Wessjohann, L. A. An efficient synthesis of the phytoestrogen 8-prenylnaringenin from xanthohumol by a novel demethylation process. *Tetrahedron* **2006**, *62*, 6961−6966.

(30) Drawert, F. Resin fractionation: modified Wöllmer method (in German). In *Brautechnische Analysenmethoden: Band I+II (MEBAK)*; Drawert, F., Ed.; MEBAK: Freising-Weihenstephan: 1979; pp 212−233.

(31) Stevens, R. The chemistry of hop constituents. *Chem. Rev.* **1967**, 19−71.

(32) Walker, T. K.; Zakomorny, M.; Blakebrough, N. Delta resin, a water-soluble, bitter, bacteriostatic portion of resin of hops. *J. Inst. Brew.* **1952**, *58*, 439−442.

(33) Frank, O.; Ottinger, H.; Hofmann, T. Characterization of an intense bitter-tasting 1H,4H-quinolizinium-7-olate by application of the taste dilution analysis, a novel bioassay for the screening and identification of taste-active compounds in foods. *J. Agric. Food Chem.* **2001**, *49*, 231−238.

(34) Brock, A.; Hofmann, T. Identification of the key astringent compounds in spinach (*Spinacia oleracea*) by means of the taste dilution analysis. *Chem. Percept.* **2008**, *1*, 268−281.

(35) Frank, O.; Blumberg, S.; Kunert, C.; Zehentbauer, G.; Hofmann, T. Structure determination and sensory analysis of bitter-tasting 4-vinylcatechol oligomers and their identification in roasted coffee by means of LC-MS/MS. *J. Agric. Food Chem.* **2007**, *55*, 1945−1954.

(36) Chadwick, L. R.; Pauli, G. F.; Farnsworth, N. R. The pharmacognosy of *Humulus lupulus L.* (Hops) with an emphasis on estrogenic properties. *Phytomed.* **2004**, *13*, 119−31.

(37) Chadwick, L. R.; Fong, H. H. S.; Farnsworth, N. R.; Pauli, G. CCC sample cutting for isolation of prenylated phenolics from hops. *J. Liq. Chromatogr. Relat. Technol.* **2005**, *28*, 1959−1969.

(38) Zhao, F.; Watanabe, Y.; Nozawa, H.; Deikonnya, A.; Kondo, K.; Kitanaka, S. Prenylflavonoids and phloroglucinol derivatives from hops (*Humulus lupulus*). *J. Nat. Prod.* **2005**, *68*, 43−49.

(39) Nookandeh, A.; Frank, N.; Steiner, F.; Ellinger, R.; Schneider, B.; Gerhauser, C.; Becker, H. Xanthohumol metabolites in faeces of rats. *Phytochemistry* **2004**, *65*, 561−570.

(40) Wackerbauer, K.; Kramer, P.; Siepert, J. Phenolic aromatic substances in beer. Phenolic carboxylic acid and phenols in the raw material and beer preparation. *Brauwelt* **1982**, *122*, 618−626.

DOI: 10.1021/acs.jafc.5b00239
J. Agric. Food Chem. 2015, 63, 3402−3418

(41) Vancraenenbroeck, R.; Vanclef, A.; Lontie, R. Characterization of flavonols and glucoside of phloroisobutyrophenone in hops. *Proc. Congr.—Eur. Brew. Conv.* **1965**, 360−371.
(42) Schwarz, B.; Hofmann, T. Sensory-guided decomposition of red currant juice (*Ribes rubrum*) and structure determination of key astringent compounds. *J. Agric. Food Chem.* **2007**, *55*, 1394−1404.
(43) Bohr, G.; Gerhäuser, C.; Knauft, J.; Zapp, J.; Becker, H. Anti-inflammatory acylphloroglucinol derivatives from hops (*Humulus lupulus*). *J. Nat. Prod.* **2005**, *68*, 1545−1548.
(44) Honma, D.; Tagashira, M.; Kanda, T. 2-Acylphloroglucinol-4,6-di-*C*-*β*-*D*-glucopyranoside having antioxidant action. *U.S. Pat. Appl. Publ.* JP 2008 174458, 2008.
(45) Gerhäuser, C.; Alt, A. P.; Klimo, K.; Knauft, J.; Frank, N.; Becker, H. Isolation and potential cancer chemopreventive activities of phenolic compounds of beer. *Phytochem. Rev.* **2003**, *1*, 369−377.
(46) Kane, M. A.; Folias, A. E.; Napoli, J. L. HPLC/UV quantitation of retinal, retinol, and retinyl esters in serum and tissues. *Anal. Biochem.* **2008**, *378*, 71−79.
(47) R Development Core Team. *R: A language and environment for statistical computing*; R Foundation for Statistical Computing: Vienna, Austria, 2008; http://www.R-project.org.
(48) Ward, J. H. Hierarchical Grouping to optimize an objective function. *J. Am. Stat. Assoc.* **1963**, *58*, 236−244.
(49) McMurrough, I.; Cleary, K.; Murray, F. Applications of high-performance liquid chromatography in the control of beer bitterness. *J. Am. Soc. Brew. Chem.* **1986**, *44*, 101−108.
(50) Chadwick, L. R. *Estrogens and congeners from hops*. Dissertation, University of Illinois, Chicago, IL, 2004.
(51) Kuznetsov, A. G.; Bush, A. A.; Rybakov, V. B.; Babaev, E. V. An improved synthesis of some 5-substituted indolizines using regiospecific lithiation. *Molecules* **2005**, *10*, 1074−1083.
(52) Andrei, C. C.; Ferreira, D. T.; Faccione, M.; De Moraes, L. A. B.; Carvalho, M. G.; Braz-Filho, R. C-Prenylflavonoids from roots of *Tephrosia tunicata*. *Phytochemistry* **2000**, *55*, 799−804.
(53) Riedl, W.; Nickl, J. C,C-Hydrogenolysis of hop bitter compounds (in German). *Chem. Ber.* **1956**, *89* (8), 1838−1849.
(54) Nagel, J.; Culley, L. K.; Lu, Y.; Liu, E.; Matthews, P. D.; Stevens, J. F.; Page, J. E. EST Analysis of hop glandular trichomes identifies an *O*-methyltransferase that catalyzes the biosynthesis of xanthohumol. *Plant Cell* **2008**, *20*, 186−200.
(55) Bufe, B.; Hofmann, T.; Krautwurst, D.; Raguse, J.-D.; Meyerhof, W. The human TAS2R16 receptor mediates bitter taste in response to *β*-glucopyranosides. *Nat. Genet.* **2002**, *32*, 397−401.
(56) De Clippeleer, J.; De Cooman, L.; Aerts, G. Beer's bitter compounds − A detailed review on iso-alpha-acids: Current knowledge of the mechanisms for their formation and degradation. *Brew. Sci.* **2014**, *67*, 167−182.
(57) Research Brewery St. Johann and Barth-Haas-Group, Internal report, 2012.
(58) Van Opstaele, F. *Hoppy aroma of beer: Characterisation of sensorially differentiated hop aromas and evaluation in brewing practice*. Dissertation, Katolieke Universiteit Leuven, Heverlee, Belgium, 2011.
(59) Fraga, C. G. *Plant phenolics and human health - Biochemistry, nutrition, and pharmacology*; John Wiley & Sons: Hoboken, NJ, 2010.
(60) Piendl, A.; Biendl, M. On the physiological impact of polyphenols and hop bitter compounds in beer (in German). *Brauwelt* **2000**, *140*, 526−537.
(61) Hieronymus, S. *For the love of hops. The practical guide to aroma, bitterness and the culture of hops*; Brewers Publications: Boulder, CO, 2012.

DOI: 10.1021/acs.jafc.5b00239
J. Agric. Food Chem. 2015, 63, 3402−3418

discourages barrel rejuvenation.[20,24,25] For these reasons, winemakers tend to favor replacement of old barrels.

Previous studies have demonstrated that a thermal gradient occurs within barrel staves during toasting, with temperatures ranging from approximately 175 to 105 °C, at 0−4 and 12−16 mm stave depths, respectively.[26] The middle and outer parts of staves may therefore retain considerable aroma potential since the thermal degradation of oak macromolecules (i.e., lignin, cellulose, and hemicellulose) that results in the formation of oak derived volatile compounds is temperature dependent[8,27] and may therefore occur to a lesser extent, if at all, at the comparatively lower toasting temperatures achieved across a stave. The aim of this study was therefore to investigate whether decommissioned barrels can be reclaimed and utilized as a previously untapped source of quality oak for wine maturation, i.e., to determine the aroma potential of oak battens prepared from the staves of old barrels. During the barrel reclaim process, the inner wine-affected portion of staves is discarded, to lessen the risk of "burnt" characters forming during toasting, as well as the microbial load. However, since spoilage bacteria have previously been found at stave depths of 8 mm,[25] the temperature profiles achieved during toasting were also measured, to evaluate the potential for viable spoilage yeast to remain in reclaimed oak.

MATERIALS AND METHODS

Chemicals. Chemicals were purchased from Sigma-Aldrich. Solvents were of HPLC grade from Merck (Darmstadt, Germany). Reference compounds included *cis*- and *trans*-oak lactone, guaiacol, 4-methylguaiacol, eugenol, vanillin, furfural, and 5-methylfurfural. [$^2H_4$]-(3*S*,4*S* and 3*R*,4*R*)-3-methyl-4-*O*-β-D-glucopyranosyloctanoic acid was synthesized in house as previously reported.[28]

Preparation of Reclaimed Oak Battens. Oak battens (48 in total, each approximately 900 × 70 × 6 mm^3) were prepared from randomly selected decommissioned oak barrels (12 French and 12 American) held in stock by Ausvat Pty. Ltd. (Willunga, Australia). Decommissioned barrels (which had been used for ≥5 years) were disassembled, and individual staves (1 from each barrel) were reclaimed to produce oak battens (Supporting Information, Figure 1), i.e., the wine-affected oak was removed and discarded, and the remaining oak split laterally to give two battens (i.e., "inner" and "outer" battens from the middle and outer portions of the stave, respectively), which were then trimmed to remove barrel grooves and planed to expose the fresh grain of the wood. Each batten was then divided lengthways and one-half subjected to far-infrared (FIR) toasting (on each side, sequentially), according to in-house operating procedures employed by Ausvat Pty. Ltd. Temperature profiles were characterized during toasting by positioning thermocouples (HOBO, Onset Computer Corporation, Bourne, MA, USA) on each face of one batten, approximately halfway along the batten (Supporting Information, Figure 1d). A thermocouple was also positioned within the batten itself (via a hole drilled laterally through the side of the batten). Temperature measurements were recorded at 10 s intervals. Two reclaimed American oak battens (both inner battens) were discarded following FIR toasting as they did not meet quality assurance requirements (i.e., due to inconsistent toasting); this reduced the number of samples for this treatment from 12 to 10.

Preparation of Oak Extracts. Oak shavings (approximately 20 g per sample) were prepared from untoasted and toasted battens using a hand-held plane. For the quantitation of oak lactone glycoconjugates, shavings (0.5 g) from untoasted battens were soaked in an aqueous 50% methanol solution (10 mL) with the addition of deuterated (3*S*,4*S* and 3*R*,4*R*)-3-methyl-4-*O*-β-D-glucopyranosyloctanoic acid (96 μg/mL in water, 10 μL) as an internal standard. Samples were then sonicated for 60 min, centrifuged (4,300*g* for 5 min), and a portion of the supernatant filtered through a 0.45 μm GHP membrane (Acrodisc, PALL Life Sciences, Cheltenham, Australia) prior to analysis. Preparation of the internal standard has been reported previously.[28] For quantitation of oak volatiles, spectroscopic analysis, and difference testing, shavings (2 g) from toasted battens were soaked in an aqueous 20% ethanol solution (100 mL, saturated with potassium bitartrate, pH adjusted to 3.5 with tartaric acid) for a week at room temperature and in darkness. Samples were then filtered prior to analysis.

Quantitation of Oak Lactone Glycoconjugates by Liquid Chromatography−Tandem Mass Spectrometry (HPLC-MS/MS). Three glycoconjugate precursors to oak lactone, namely, (3*S*,4*S*)-3-methyl-4-*O*-(6′-*O*-galloyl)-β-D-glucopyranosyloctanoic acid, (3*S*,4*S*)-*cis*- and (3*S*,4*R*)-*trans*-3-methyl-4-*O*-β-D-glucopyranosyloctanoic acid, and 3-methyl-4-*O*-(6′-*O*-α-L-rhamnosyl)-β-D-glucopyranosyloctanoic acid, hereafter referred to as galloylglucoside, glucoside, and rutinoside, respectively, were quantified in extracts of untoasted reclaimed oak according to the stable isotope dilution assay (SIDA) methods reported previously.[11,28] These publications describe the preparation of deuterated (3*S*,4*S* and 3*R*,4*R*)-3-methyl-4-*O*-β-D-glucopyranosyloctanoic acid, method validation, and instrumental operating conditions. Analyses were carried out using an Agilent 1200 HPLC system coupled to an AB Sciex 4000 Q TRAP hybrid tandem mass spectrometer (Agilent, Palo Alto, CA, USA).

Quantitation of Oak Volatiles by Gas Chromatography−Mass Spectrometry (GC-MS). The concentrations of *cis*- and *trans*-oak lactone, guaiacol, 4-methylguaiacol, eugenol, vanillin, furfural, 5-methylfurfural, 4-ethylguaiacol, and 4-ethylphenol in extracts of toasted reclaimed oak were quantified according to SIDA methods reported previously.[5,29−31] These publications describe the preparation of deuterated internal standards (d_4-*cis*- and d_4-*trans*-oak lactone, d_3-guaiacol, d_3-4-methylguaiacol, d_3-vanillin, d_4-furfural, and d_4-4-ethylphenol), method validation, and instrumental operating conditions. Analyses were performed by the Australian Wine Research Institute's (AWRI) Commercial Services Laboratory (Adelaide, Australia) using an Agilent 6890 gas chromatograph coupled to a 5973 mass selective detector (Agilent, Palo Alto, CA, USA) and electron impact ionization.

Sensory Analysis by Difference Testing. Difference tests were performed on a 2011 unwooded Chardonnay, with and without the addition of an oak extract (one French oak extract and one American oak extract, selected at random and spiked at 50 mL/L), using the triangle test method[32] and a panel of 30 judges aged between 18 and 55, with similar numbers of males and females. Wines were presented to the panel using a balanced, randomized presentation order, comprising all possible configurations (i.e., AAB, ABA, BAA, BBA, BAB, and ABB, where A denotes unspiked wine and B denotes spiked wine) an equal number of times. Wines (25 mL) were served at 22−24 °C, in covered ISO tasting glasses (215 mL) with randomly assigned three-digit codes. Panelists smelled the samples and were asked to identify the sample which was different.

Analysis of Toasted Oak by Attenuated Total Reflectance Mid-infrared (ATR-MIR) Spectroscopy. Oak extracts (ca. 0.5 mL) were scanned using a platinum diamond ATR single reflection sampling module cell mounted on a Bruker Alpha instrument (Bruker Optics GmbH, Ettlingen, Germany). Extracts of toasted reclaimed oak (n = 46, as above) and toasted French (n = 12) and American (n = 12) oak chips or powders (sourced from Oak Solutions Group, Tanunda, Australia and Oak Chips Incorporated, Piketon, OH, USA) prepared as for reclaimed oak extracts (as above) were analyzed. MIR spectra were recorded on OPUS software, version 6.5, provided by Bruker Optics. The spectrum of each sample was obtained by taking the average of 64 scans at a resolution of 8 cm^{-1} and acquired between 4000 and 375 cm^{-1}, with a scanner velocity of 7.5 kHz and a background of 64 scans. Background reference spectra were recorded using deionized water. The Unscrambler X software (v. 10.1, CAMO ASA, Norway) was used for principal component analysis (PCA) in order to determine any relevant and interpretable structure in the MIR data associated with the different treatments as well as to detect outlier samples. PCA models were developed using full cross-validation (leave one out).

Statistical Analysis. Chemical data were analyzed by one-way analysis of variance (ANOVA) using GenStat (10th edition, VSN International Limited, Herts, UK). Mean comparisons were performed

DOI: 10.1021/acs.jafc.5b00339
J. Agric. Food Chem. 2015, 63, 3419−3425

by least significant difference (LSD) multiple comparison test at $P < 0.05$.

RESULTS AND DISCUSSION

Inner and outer battens were prepared from randomly selected staves taken from decommissioned French and American oak barrels. The history of each barrel, e.g., cooperage conditions, barrel age, and prior usage, was not known, but compositional variation was expected due to differences in oak origin,[15] species,[14,15] and seasoning conditions,[16] so a range of samples (i.e., staves from 12 French and 12 American oak barrels) was deliberately chosen, to achieve a broad representation of used barrels. Aroma potential was determined by measuring (i) the concentrations of glycoconjugate precursors of oak lactone present in untoasted reclaimed oak; (ii) the concentrations of several oak volatiles present in toasted reclaimed oak; and (iii) the MIR spectra of extracts of new and reclaimed oak. Difference tests were also carried out to establish the sensory impact of reclaimed oak.

Oak Lactone Glycoconjugate Content of Untoasted Reclaimed Oak. Oak lactone is considered one of the most important oak derived volatile compounds and is known to occur in oak wood in both free and glycosidically bound precursor forms,[11,33−35] with three glycoconjugates of 3-methyl-4-hydroxyoctanoic acid (i.e., the ring-opened form of oak lactone) having previously been identified in oak wood: a galloylglucoside, a glucoside, and a rutinoside.[34] Pyrolysis of the galloylglucoside and glucoside at 235 °C for 30 min gave significant amounts of oak lactone;[35] thus, quantitation of glycoconjugates in untoasted oak wood provides a measure of aroma potential.

A recent study investigated the oak lactone glycoconjugate profiles of several French oak woods and found the galloylglucoside to be the predominant precursor.[11] Similar results were observed in the current study (Table 1). The galloylglucoside (quantified as glucoside equivalents) was the most abundant precursor present in reclaimed oak battens, irrespective of the geographical origin of oak. The galloylglucoside content of reclaimed French oak wood ranged from 0.11 to 317 μg/g, while higher levels were observed for reclaimed American oak: 0.18 to 403 μg/g. No significant differences were observed between the galloylglucoside levels of inner and outer battens. Mean glucoside concentrations were less than 25 μg/g for both French and American reclaimed oak, with significantly higher glucoside levels observed in inner vs outer reclaimed American oak battens ($P < 0.05$). Mean rutinoside concentrations (again quantified as glucoside equivalents) were approximately 10 μg/g for reclaimed French oak wood, but considerably higher levels, i.e. 55 to 60 μg/g, were measured in reclaimed American oak wood. That higher precursor levels were observed in reclaimed American oak was not surprising, given that American oak wood typically imparts higher concentrations of oak lactone than French oak wood.[7,14,15,18,26] Several samples of reclaimed oak (i.e., battens from two French oak staves and one American oak stave) gave extremely low levels (<2 μg/g) of each precursor (data not shown), but this could reflect natural variation in oak composition rather than exhaustion of oak flavor since relatively low levels have also been observed in new oak wood.[11] Importantly, the glycoconjugate levels observed in reclaimed oak were comparable to those reported in the literature for new oak wood (Table 1), suggesting reclaimed battens should be capable of releasing commercially significant quantities of oak lactone after toasting.

Table 1. Concentrations of Galloylglucoside, Glucoside, and Rutinoside Precursors of Oak Lactone Present in Extracts of Untoasted New and Reclaimed French and American Oak

oak samples		concentration (μg/g) galloylglucoside	glucoside	rutinoside
new French oak[11]		6.7−353.9	1.0−26.2	0.2−20.2
reclaimed French oak (inner)	mean[a]	137	13	9
	range	0.50−283.7	0.20−37.6	0.06−82.6
reclaimed French oak (outer)	mean[a]	151	13	10
	range	0.11−316.6	0.03−28.8	0.01−89.4
new American oak[28]			4.9−42.0	
reclaimed American oak (inner)	mean[a]	237	24	55
	range	0.18−402.5	0.03−51.4	0.02−169.9
reclaimed American oak (outer)	mean[a]	208	11	60
	range	0.23−334.3	0.01−23.4	0.04−147.5

[a]Values are the means from 12 samples.

FIR Toasting of Reclaimed Oak. Toasting plays an important role in the cooperage process and is largely responsible for the generation of oak volatiles. However, the volatile composition of oak wood is dependent on the temperature and duration of toasting. Chatonnet[27] monitored the evolution of oak volatiles from "light" through to "very heavy" levels of toasting and found thermal degradation of lignin and hemicellulose, and the formation of oak volatiles commenced from "medium" toasting. While the degree of toasting is hard to define and is usually judged empirically by individual coopers,[5] oak flavor research provides examples of "medium toast" conditions, which typically involve heating oak wood for at least 30 min at surface temperatures greater than 160 °C.[26,27,36] In this study, FIR heating was employed to simultaneously straighten and toast reclaimed battens. Battens were toasted on each side (sequentially), during which the temperature profiles on each face of, and within, a reclaimed batten were measured (Figure 1). A temperature differential was observed across the batten, such that the hottest temperatures measured were at the batten surface being toasted, being up to 225 °C by Probe 1 initially, then more than 250 °C by Probe 3. The lowest temperatures measured were at the opposite batten face, i.e., approximately 100 °C by Probe 3 initially, then more than 150 °C by Probe 1. The internal batten temperature (recorded by Probe 2) reached approximately 125 °C, then almost 200 °C, during toasting of each side of the batten. Traditional cooperage involves toasting partially assembled barrels over an open fire. Previous studies have shown that the temperature profile across the depth of a barrel stave, typically 30 mm, decreases rapidly, giving poor generation of volatiles much below the surface, i.e., deeper than 6 mm.[26] In contrast, temperatures capable of thermally degrading oak macromolecules (i.e., lignin and cellulose) and oak lactone glycoconjugates were observed across the batten, which can be explained by the relatively thin depth of the batten (i.e., < 7 mm). Importantly, the temperatures achieved during FIR toasting, i.e., between 150 and 250 °C (Figure 1), would also be sufficient to reduce any microbial load,[37,38] thereby preventing the carryover of yeast and/or bacteria during the barrel reclamation process. The concentrations of 4-ethylphenol and 4-ethylguaiacol were measured in toasted

DOI: 10.1021/acs.jafc.5b00339
J. Agric. Food Chem. 2015, 63, 3419−3425

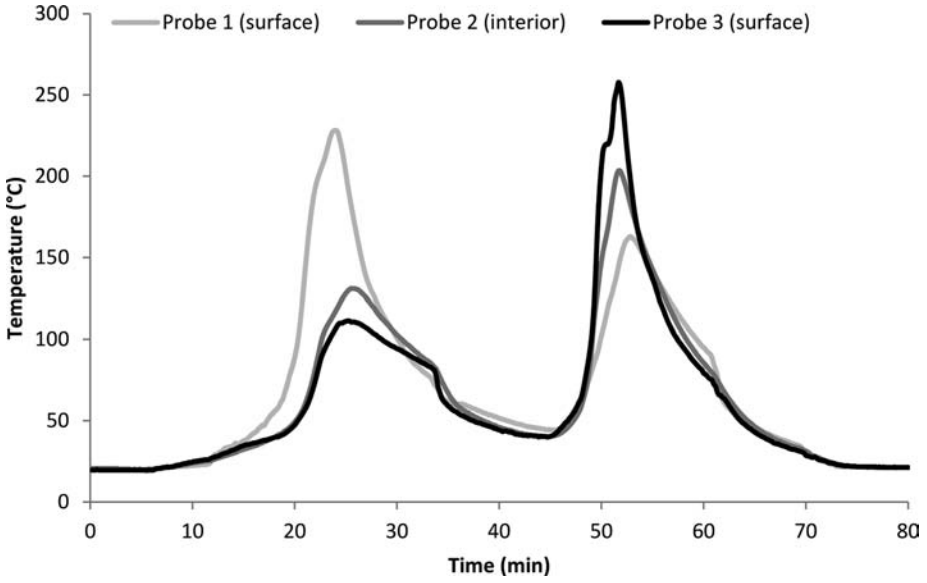

Figure 1. Temperature profiles (surface and interior) achieved during far-infrared toasting of reclaimed oak battens.

Table 2. Concentrations of Oak Derived Volatile Compounds Present in Extracts of Toasted New and Reclaimed French and American Oak

		concentration (μg/g)							
oak samples		*cis*-oak lactone	*trans*-oak lactone	guaiacol	4-methyl guaiacol	eugenol	vanillin	furfural	5-methyl furfural
new French oak[13,17,36]		nd[a], 0.05, 11.4	nd, 0.01, 6.8	18.5, 2.3, 12.9	1.3, 3.8, 10.2	0.7, 2.3	107, 53, 190	108, 963	14, 148
reclaimed French oak (inner)	mean[b]	10	13	5	2	4	87	1072	106
	range	nd–20.2	nd–43.2	2.2–11.6	0.8–4.9	3.0–7.7	58–105	786–1376	64–178
reclaimed French oak (outer)	mean[b]	15	27	4	2	4	91	946	105
	range	nd–33.4	nd–73.1	1.5–5.6	0.8–3.0	2.7–6.3	64–115	511–1134	54–213
new American oak[13,17,36]		12.3, 32.0, 47.9	5.3, 3.3, 4.9	13.5, 4.2, 9.2	0.9, 2.1, 7.9	6.1, 4.2	127, 42, 140	55, 1539	6, 237
reclaimed American oak (inner)	mean[c]	25	3	6	2	4	108	808	83
	range	nd–41.4	nd–9.1	0.8–12.3	0.6–5.6	2.3–5.5	70–137	412–1134	41–135
reclaimed American oak (outer)	mean[c]	26	2	7	3	4	117	824	77
	range	nd–65.5	nd–7.3	2.7–11.1	1.6–4.3	2.6–6.2	76–136	592–1122	43–136

[a]nd = not detected. [b]Values are the means from 12 samples. [c]Values are the means from 10 samples (two battens discarded after FIR toasting).

reclaimed oak, as markers of *Brettanomyces* spoilage.[39] 4-Ethylphenol was not detected in any samples, and only trace levels of 4-ethylguaiacol, i.e., $\leq$ 5.1 μg/g were observed (Supporting Information, Table 1). These results indicate that no carryover of *Brettanomyces*-derived volatile phenols occurred during the preparation of reclaimed oak battens, albeit this may simply reflect the absence of spoilage in the decommissioned barrels that were processed. The removal of wine affected oak (i.e., oak that was in contact with wine) should effectively remove any potential wine spoilage microorganisms since the maximum penetration of microbes into the oak surface appears to be limited by the depth of liquid infiltration to approximately 6 mm.[39] Therefore, the likelihood of battens being a source of contaminating microorganisms is very low.

Volatile Composition of Toasted Reclaimed Oak. To further assess the aroma potential of reclaimed oak, the concentrations of several important oak volatiles were measured in extracts (50% aqueous methanol) of toasted reclaimed oak battens and compared with concentrations reported in the literature for extracts of (new) toasted oak wood (Table 2).

For reclaimed French oak, *cis*- and *trans*-oak lactone levels of up to 33.4 and 73.1 μg/g were observed, respectively. No significant differences were observed between the mean oak lactone concentrations of inner vs outer battens, irrespective of geographical origin. Mean oak lactone levels were comparable or exceeded concentrations reported for new oak wood. Previous studies have shown that the ratio of *cis*- to *trans*-oak lactone isomers present in oak wood differs by region and species.[14,15] While *cis*-oak lactone is usually the predominant isomer, toasted sessile oak (*Quercus petraea*) from central France was found to have a significantly higher proportion of *trans*-oak lactone,[27] and similar results were observed for some reclaimed French oak samples in the current study. Reclaimed American oak contained several-fold higher concentrations of *cis*-oak lactone than *trans*-oak lactone, in agreement with previous findings.[7] Three samples of reclaimed French oak had no detectable oak lactone, including two samples that corresponded to the untoasted battens that gave very low glycoconjugate precursor concentrations (data not shown). Again, this might be indicative of flavor exhaustion, but low levels (i.e., $\leq$ 1 μg/g) of oak lactone have been reported in

DOI: 10.1021/acs.jafc.5b00339
J. Agric. Food Chem. 2015, 63, 3419–3425

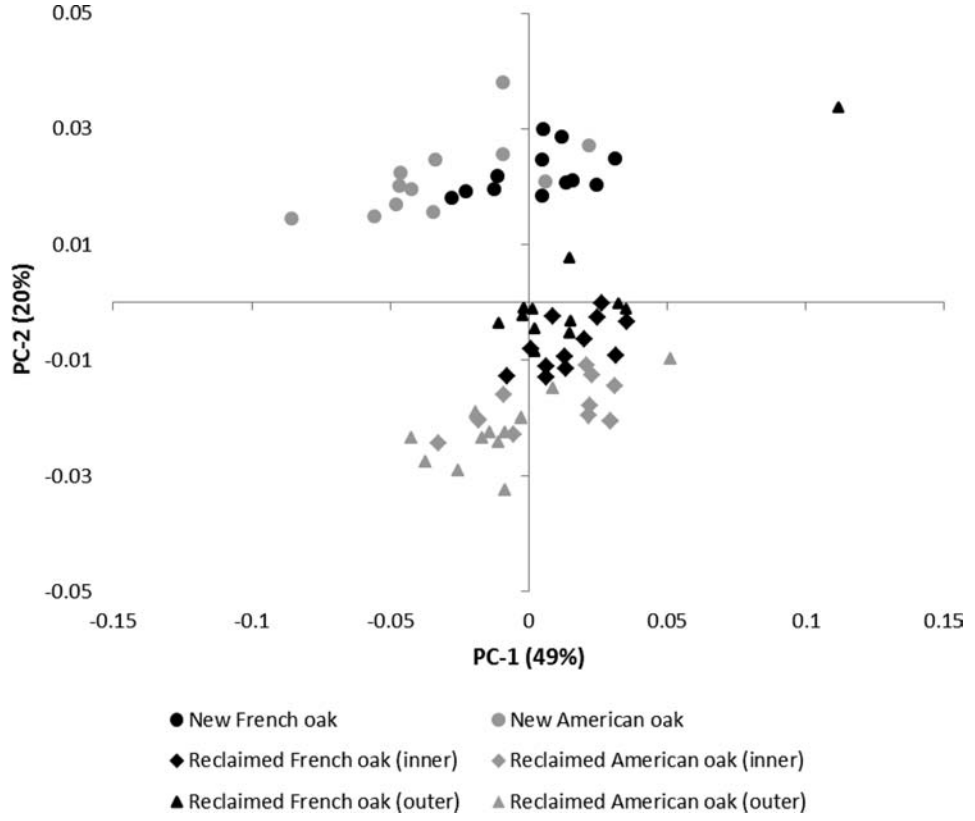

Figure 2. Score plot of the first two PCs derived from the MIR spectra of toasted samples of new and reclaimed French and American oak.

(new) French oak wood,[36] especially pedunculate oak (*Quercus robur*),[15] so this might simply reflect natural variation. Similarly, oak lactone could not be detected in some reclaimed American oak samples. Although American oak usually contains high levels of oak lactone,[17,29] Spillman and colleagues reported low levels of oak lactone in American oak wood samples sourced from Ohio.[16]

Similar guaiacol, 4-methylguaiacol, and eugenol concentrations, up to 12.3, 5.6, and 7.7 μg/g, respectively, were observed in French and American reclaimed oak samples. Vanillin levels ranged from 58 to 115 μg/g in reclaimed French oak, with slightly higher levels, i.e., 70 to 137 μg/g, observed in reclaimed American oak. In general, the concentrations of volatile phenols were comparable to the levels reported for new French and American oak wood[13,17,36] or in the case of eugenol, slightly higher. Again, there were no significant differences observed between the concentrations of these volatiles measured in inner vs outer battens. The influence of toasting temperature on the volatile phenol content of oak has been demonstrated previously, with higher toasting temperatures tending to favor volatile phenol formation.[17] Since oak wood has a low coefficient of thermal conductivity, the size of oak wood is also important, and increased surface area exposure to heat also encourages the formation of volatile phenols,[17] albeit volatiles are subject to volatilization if temperatures are too high.[13,16,17] The toasting temperatures achieved in the current study are comparable to those reported in previous studies involving toasting of oak staves at 200 °C and oak chips at 170 °C.[13,36]

Furfural and 5-methylfurfural were present in reclaimed oak samples at considerably higher concentrations than that for most other oak volatiles. Furfural concentrations ranged from 511 to 1376 μg/g in reclaimed French oak and from 412 to 1134 μg/g in reclaimed American oak. 5-Methylfurfural was less abundant; the levels ranged between 54 and 213 μg/g for reclaimed French oak and 41 and 136 μg/g for reclaimed American oak. These concentrations were again within or above the concentrations reported for new oak wood.

While the oak volatile profiles of reclaimed oak battens further demonstrated their suitability for oak maturation of wine, difference tests were performed to confirm their potential impact on wine aroma. Extracts of either reclaimed French oak or reclaimed American oak (selected at random) were added to a 2011 unwooded Chardonnay at 50 mL/L, i.e., the equivalent of a 1 g/L oak addition and presented as triangle tests to a panel of 30 judges. Seventeen and 20 panelists correctly differentiated wine samples with and without the addition of reclaimed French and American oak extracts, respectively, demonstrating the perceptible aroma impact of reclaimed oak, at the 99% confidence level.

ATR-MIR Analysis of Extracts of New and Reclaimed Toasted Oak. Quantitation of oak lactone precursors and oak volatiles enabled direct but limited comparisons to be made between the aroma potential of new and reclaimed oak wood. ATR-MIR analysis of extracts of new and reclaimed toasted oak was therefore performed as a more holistic approach to compositional analysis. No visual differences were observed in the MIR spectra obtained for extracts of new and reclaimed oak (data not shown), so PCA was performed on spectral data to investigate qualitative differences in oak composition. Figure 2 shows the score plot of the first two principal components (PC), which accounted for 69% of the variation between oak extracts. Two distinct sample clusters were observed: new oak samples were clustered in the upper quadrants, whereas

DOI: 10.1021/acs.jafc.5b00339
J. Agric. Food Chem. 2015, 63, 3419−3425

reclaimed oak samples were clustered in the lower quadrants. This suggests that, despite commercially significant levels of key oak volatiles being observed in reclaimed oak, other compositional differences existed that differentiated new and reclaimed oak wood, by spectral analysis. This could comprise volatile compounds other than those measured and/or nonvolatile oak constituents, such as oak tannins. Interestingly, some differentiation according to geographical origin (i.e., French vs American oak wood) was observed, in agreement with previous research.[40] However, no differentiation of extracts from inner vs outer reclaimed battens was apparent. Instead, extracts derived from inner and outer battens were overlaid, confirming their compositional uniformity.

Despite spectral analysis indicating that some compositional differences exist between new and reclaimed oak, HPLC-MS/MS and GC-MS analyses demonstrated comparable levels of the oak lactone glycoconjugates and oak volatiles that were measured. Difference tests then confirmed the addition of reclaimed oak extracts to wine had a perceptible impact on aroma. Collectively, these results establish the aroma potential of reclaimed oak, and therefore, its suitability as a raw material for oak maturation of wine, particularly given that winemakers can selectively reclaim barrels with a track record of favorable maturation performance. Furthermore, the temperatures achieved during toasting preclude any carryover of spoilage yeast, such as *Brettanomyces*. The reclamation process converts each 225 L barrel into approximately 8 m^2 of reclaimed oak battens, at a cost of AUD$ 150 or between 10 and 20% the price of a new barrique; thus, it is also economically viable.

■ ASSOCIATED CONTENT

Supporting Information

Concentrations of 4-ethylguaiacol and 4-ethylphenol in toasted samples of reclaimed French and American oak; images depicting the transformation of a barrel stave into oak battens during the barrel reclamation process; and the distribution of total oak lactone glycoconjugate precursor concentrations present in reclaimed French and American oak. This material is available free of charge via the Internet at http://pubs.acs.org.

■ AUTHOR INFORMATION

Corresponding Author

*Tel: + 61 8 8313 7360. Fax: + 61 8 8313 7716. E-mail: kerry.wilkinson@adelaide.edu.au.

Funding

S.L. and A.C. thank the Waite Research Institute and the Australian Grape and Wine Authority for research scholarships.

Notes

The authors declare the following competing financial interest(s): As the Chief Executive Officer of Ausvat Pty. Ltd., Peter Warren declares a financial conflict of interest.

■ ACKNOWLEDGMENTS

The authors gratefully acknowledge The Australian Wine Research Institute's Commercial Services Laboratory for GC-MS analysis.

■ REFERENCES

(1) Maga, J. A. The contribution of wood to the flavour of alcoholic beverages. *Food Rev. Int.* **1989**, *5*, 39−99.

(2) Sauvageot, F.; Feuillat, F. The influence of oak wood (*Quercus robur* L., *Q. petraea* Liebl.) on the flavour of Burgandy Pinot noir. An examination of variation amoung individual trees. *Am. J. Enol. Vitic.* **1999**, *50*, 447−455.

(3) Sefton, M. A.; Francis, I. F.; Williams, P. J. Volatile norisoprenoid compounds as constituents of oak woods used in wine and spirit maturation. *J. Agric. Food Chem.* **1990**, *38*, 2045−2049.

(4) Nishimura, K.; Ohnishi, M.; Masuda, M.; Koga, K.; Matsuyama, R. Reactions of Wood Components during Maturation. In *Flavour of Distilled Beverages: Origin and Development*; Piggott, J. R., Ed.; Ellis Horwood: Chichester, England, 1983.

(5) Spillman, P. J.; Pollnitz, A. P.; Liacopoulos, D.; Skouroumounis, G. K.; Sefton, M. A. Accumulation of vanillin during barrel aging of white, red, and model wines. *J. Agric. Food Chem.* **1997**, *45*, 2584−2589.

(6) Cutzach, I.; Chatonnet, P.; Henry, R.; Dubourdieu, D. Identifying new volatile compounds in toasted oak. *J. Agric. Food Chem.* **1999**, *47*, 1663−1667.

(7) Pérez-Coello, M. S.; Sanz, J.; Cabezudo, M. D. Determination of volatile compounds in hydroalcoholic extracts of French and American oak wood. *Am. J. Enol. Vitic.* **1999**, *50*, 162−165.

(8) Chatonnet, P.; Boidron, J. N.; Pons, M. Maturation of red wines in oak barrels: evolution of some volatile compounds and their aromatic impact. *Sci. Aliments* **1990**, *10*, 565−587.

(9) Boidron, J. N.; Chatonnet, P.; Pons, M. Influence du bois sur certaines substances odorantes des vins. *Conn. Vigne Vin* **1988**, *22*, 275−294.

(10) Spillman, P. J.; Sefton, M. A.; Gawel, R. The contribution of volatile compounds derived during oak barrel maturation to the aroma of a Chardonnay and Cabernet Sauvignon wine. *Aust. J. Grape Wine Res.* **2004**, *3*, 227−235.

(11) Wilkinson, K. L.; Prida, A.; Hayasaka, Y. Role of glycoconjugates of 3-methyl-4-hydroxyoctanoic acid in the evolution of oak lactone in wine during oak maturation. *J. Agric. Food Chem.* **2013**, *61*, 4411−4416.

(12) Prida, A.; Heymann, H.; Balanuta, A.; Puech, J.-L. Relation between chemical composition of oak wood used in cooperage and sensory perception of model extracts. *J. Sci. Food Agric.* **2009**, *89*, 765−773.

(13) Fernández de Simón, B.; Cadahía, E.; Muiño, I.; Del Álamo, M.; Nevares, I. Volatile composition of toasted oak chips and staves and of red wine aged with them. *Am. J. Enol. Vitic.* **2010**, *61*, 157−165.

(14) Mosedale, J. R.; Puech, J.-L.; Feuillat, F. The influence on wine flavor of the oak species and natural variation of heartwood components. *Am. J. Enol. Vitic.* **1999**, *50*, 503−512.

(15) Doussot, F.; De Jéso, B.; Quideau, S.; Pardon, P. Extractives content in cooperage oak wood during natural seasoning and toasting; influence of tree species, geographic location, and single tree effects. *J. Agric. Food Chem.* **2002**, *50*, 5955−5961.

(16) Spillman, P. J.; Sefton, M. A.; Gawel, R. The effect of oak wood source, location of seasoning and coopering on the composition of volatile compounds in oak-matured wines. *Aust. J. Grape Wine Res.* **2004**, *10*, 216−226.

(17) Campbell, J. I.; Sykes, M.; Sefton, M. A.; Pollnitz, A. P. The effects of size, temperature and air contact on the outcome of heating oak fragments. *Aust. J. Grape Wine Res.* **2005**, *11*, 348−354.

(18) Pérez-Prieto, L. J.; López-Roca, J. M.; Martínez-Cutillas, A.; Pardo-Minguez, F.; Gómez-Plaza, E. Maturing wine in oak barrels. Effects of origin, volume, and age of the barrel on the wine volatile composition. *J. Agric. Food Chem.* **2002**, *50*, 3272−3276.

(19) Pérez-Prieto, L. J.; López-Roca, J. M.; Martínez-Cutillas, A.; Pardo-Minguez, F.; Gómez-Plaza, E. Extraction and formation dynamic of oak-related volatile compounds from different volume barrels to wine and their behavior during bottle storage. *J. Agric. Food Chem.* **2003**, *51*, 5444−5449.

(20) Garde-Cerdán, T.; Ancín-Azpilicueta, C. Effect of oak barrel type on the volatile composition of wine: Storage time optimization. *LWT Food Sci. Technol.* **2006**, *39*, 199−205.

(21) Towey, J. P.; Waterhouse, A. L. The extraction of volatile compounds from French and American oak barrels in Chardonnay during three successive vintages. *Am. J. Enol. Vitic.* **1996**, *47*, 163−172.

DOI: 10.1021/acs.jafc.5b00339
J. Agric. Food Chem. 2015, 63, 3419−3425

(22) Garde Cerdan, T.; Lorenzo, C.; Carot, J. M.; Esteve, M. D.; Climent, M. D.; Salinas, M. R. Effects of composition, storage time, geographic origin and oak type on the accumulation of some volatile compounds and ethylphenols in wines. *Food Chem.* **2010**, *122*, 1076−1082.
(23) Spillman, P. J.; Pollnitz, A. P.; Liacopoulos, D.; Pardon, K. H.; Sefton, M. A. Formation and degradation of furfuryl alcohol, 5-methylfurfuryl alcohol, vanillyl alcohol and their ethyl ethers in barrel-aged wines. *J. Agric. Food Chem.* **1998**, *46*, 657−663.
(24) Malfeito-Ferreira, M.; Laureano, P.; Barata, A.; D'Antuono, I.; Slender, H.; Loureiro, V. Effect of different barrique sanitation procedures on yeasts isolated from the inner layers of wood. *Am. J. Enol. Vitic.* **2004**, *55*, 304A.
(25) Oelofse, A.; Pretorius, I. S.; du Toit, M. Significance of *Brettanomyces* and *Dekkera* during winemaking: A synoptic review. *S. Afr. J. Enol. Vitic.* **2008**, *29*, 128−144.
(26) Hale, M. D.; McCafferty, K.; Larmie, E.; Newton, J.; Swan, J. S. The influence of oak seasoning and toasting parameters on the composition and quality of wine. *Am. J. Enol. Vitic.* **1999**, *50*, 495−502.
(27) Chatonnet, P.; Boidron, J. N.; Pons, M. Incidence du traitement thermique du bois de chêne sur sa composition chemique: 2. Évolution de certains composés en function de l'intensite de brûlage. *Conn. Vigne Vin* **1989**, *23*, 223−250.
(28) Fudge, A. L.; Elsey, G. M.; Hayasaka, Y.; Wilkinson, K. L. Quantitative analysis of β-D-glucopyranoside of 3-methyl-4-hydroxyoctanoic acid, a potential precursor to *cis*-oak lactone, in oak extracts using liquid chromatography-tandem mass spectrometry based stable isotope dilution analysis. *J. Chromatogr., A* **2008**, *1215*, 51−56.
(29) Pollnitz, A. P.; Jones, G. P.; Sefton, M. A. Determination of oak lactones in barrel-aged wines and in oak extracts by stable isotope dilution analysis. *J. Chromatogr., A* **1999**, *857*, 239−246.
(30) Pollnitz, A. P. The Analysis of Volatile Wine Components Derived from Oak Products during Winemaking and Storage. Ph.D. Thesis, The University of Adelaide, 2000.
(31) Pollnitz, A. P.; Pardon, K. H.; Sykes, M.; Sefton, M. A. The effects of sample preparation and gas chromatograph injection techniques on the accuracy of measuring guaiacol, 4-methylguaiacol and other volatile oak compounds in oak extracts by stable isotope dilution analyses. *J. Agric. Food Chem.* **2004**, *52*, 3244−3252.
(32) Meilgaard, M. C.; Civille, G. V.; Carr, B. T. *Sensory Evaluation Techniques*, 3rd ed.; CRC Press: New York, 1999.
(33) Masson, E.; Baumes, R.; Le Guernevé, C.; Puech, J.-L. Identification of a precursor of β-methyl-γ-octalactone in the wood of sessile oak (*Quercus petraea* (Matt.) Liebl.). *J. Agric. Food Chem.* **2000**, *48*, 4306−4309.
(34) Hayasaka, Y.; Wilkinson, K. L.; Elsey, G. M.; Raunkjær, M.; Sefton, M. A. Identification of natural oak lactone precursors in extracts of American and French oak woods by liquid chromatography-tandem mass spectrometry. *J. Agric. Food Chem.* **2007**, *55*, 9195−9201.
(35) Wilkinson, K. L.; Elsey, G. M.; Prager, R. H.; Tanaka, T.; Sefton, M. A. Precursors to oak lactone II: Synthesis, separation and cleavage of four β-D-glucopyranosides of 3-methyl-4-hydroxyoctanoic acid. *Tetrahedron* **2004**, *60*, 6092−6100.
(36) Alañón, M. E.; Díaz-Maroto, M. C.; Pérez-Coello, M. S. Analysis of volatile composition of toasted and non-toasted commercial chips by GC-MS after an accelerated solvent extraction method. *Int. J. Food Sci. Technol.* **2012**, *47*, 816−826.
(37) Schmid, F.; Grbin, P.; Yap, A.; Jiranek, V. Relative efficacy of high-pressure hot water and high-power ultrasonics for wine oak barrel sanitization. *Am. J. Enol. Vitic.* **2011**, *62*, 519−526.
(38) Wilker, K. L.; Dharmadhikari, M. R. Treatment of barrel wood infected with acetic acid bacteria. *Am. J. Enol. Vitic.* **1997**, *48*, 516−520.
(39) Chatonnet, P.; Dubourdieu, D.; Boidron, J.-N.; Pons, M. The origin of ethylphenols in wines. *J. Sci. Food Agric.* **1992**, *60*, 165−178.
(40) Li, S.; Wilkinson, K. L.; Cozzolino, D. The use of near infrared reflectance spectroscopy to identify the origin of oak shavings used in wine aging. *Food Measure* **2014**, *8*, 356−361.

DOI: 10.1021/acs.jafc.5b00339
J. Agric. Food Chem. 2015, 63, 3419−3425

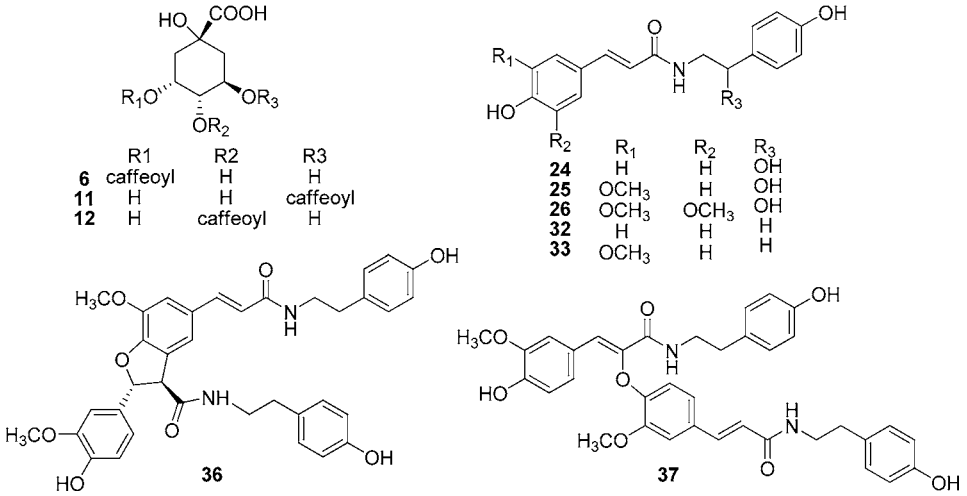

Figure 1. Structures of the 10 reference compounds. The notations for compounds are corresponding to the peak numbers in the HPLC chromatograms as listed in Figures 4 and 5.

A hybrid ion trap time-of-flight mass spectrometer (IT-TOF-MS) integrates the mass spectrometric functions of both ion trap and time-of-flight mass equipment, which could provide accurate structural information for both pseudomolecular ions and tandem fragment ion species. Hence, the analytical platform of the hyphenation of high performance liquid chromatography (HPLC) and IT-TOF-MS has been widely accepted as a powerful tool for targeted and nontargeted analysis of chemical constituents in complicated matrices, for instance, herbal medicine extract, vegetable extract, and food additive extract.[17−21]

In the current study, we aimed to characterize and compare the chemical compositions among the different parts of eggplant, using HPLC coupled with diode array detection (DAD) and IT-TOF-MS. Meanwhile, HPLC-DAD was exploited to simultaneously quantitate seven PAs along with three CAs in the roots of eggplant from different habitats. The results obtained are expected to provide a comprehensive understanding for the different parts of eggplant as well as a reliable tool for the quality control of medicinal materials derived from eggplant.

MATERIALS AND METHODS

Chemicals and Materials. Seven PAs, including *N-trans-p*-coumaroyloctopamine, *N-trans*-feruloyloctopamine, *N-trans*-sinapoyloctopamine, *N-trans-p*-coumaroyltyramine, *N-trans*-feruloyltyramine, grossamide, and cannabisin F, were previously purified and identified from the roots of eggplant in our laboratory, and their structures were established according to extensive spectroscopic and chemical methods.[5,22] Three CAs, namely 3-*O*-caffeoylquinic acid, 4-*O*-caffeoylquinic acid, and 5-*O*-caffeoylquinic acid (Figure 1), were purchased from the National Institutes for Food and Drug Control (Beijing, China). The purity of each compound was determined to be greater than 98% by normalization of the peak areas detected by HPLC-DAD analysis, and confirmed using NMR analysis.

LC-MS grade methanol, acetonitrile, and formic acid were supplied by Merck (Darmstadt, Germany). Ultrapure water was prepared in-house by a Milli-Q Integral water purification system (Millipore, Bedford, MA, USA). All the other reagents were of analytical grade and provided by Beijing Chemical Works (Beijing, China).

Seventeen batches (SM201201−SM201217) of the roots of eggplant were collected from Beijing, Heilongjiang, Guangdong, Henan, Shandong, Hebei, Jiangxi, and Inner Mongolia provinces in China. The stems, leaves, fruit pulps, and peels of SM201217 were also collected and subjected for qualitative analysis. All of the original plants were identified as *S. melongena* by one of the authors (P.-F.T.). The voucher specimens (Nos. SM201201−SM201217) are deposited in Modern Research Center for Traditional Chinese Medicine, Beijing University of Chinese Medicine (Beijing, China).

Sample Preparation. Stock solution was prepared by mixing the 10 reference compounds in methanol to make desired concentrations: 69.45 μg/mL for 3-*O*-caffeoylquinic acid, 1032.40 μg/mL for 5-*O*-caffeoylquinic acid, 125.70 μg/mL for 4-*O*-caffeoylquinic acid, 304.80 μg/mL for *N-trans-p*-coumaroyloctopamine, 812.30 μg/mL for *N-trans*-feruloyloctopamine, 95.80 μg/mL for *N-trans*-sinapoyloctopamine, 376.70 μg/mL for *N-trans-p*-coumaroyltyramine, 589.30 μg/mL for *N-trans*-feruloyltyramine, 52.80 μg/mL for grossamide, and 10.20 μg/mL for cannabisin F, respectively. After that, serial concentration levels of working solutions were obtained by 10-, 16.6-, 25-, 50-, 100-, 166-, 250-, and 500-fold diluting the stock solution with methanol, successively.

Immediately after harvesting, the fresh fruits were separated into pulps and peels (ca. 1−2 mm thick) using a kitchen peeler. The pulps were further cut into small cubes (ca. 1−3 cm). The peels and pulp samples were stored separately at −80 °C under an inert nitrogen atmosphere in ziplock bags. Both of the peels and the chopped pulps were freeze-dried for 48 h. The roots, stems, and leaves were dried in the shade for a couple of days. Afterward, all the dried materials were pulverized and griddled through 50 mesh sieves prior to extraction. The pulverized roots, stems, leaves, peels, and pulps were accurately weighed (approximately 1.0 g for each) and extracted with 25 volumes (w/v) of 50% aqueous methanol by maintaining them in an ultrasonic water bath at room temperature for 1 h, and an aliquot (0.05 mL) of acetic acid was added as an acidic modifier into the solvent to enhance the extraction of peels and pulps. Following extraction, 50% aqueous methanol was added to compensate for the lost weight during the extraction. Each supernatant was filtered through a nylon membrane (0.22 μm, Jinteng Experiment Equipment Co. Ltd., Tianjin, China) and subjected for LC-DAD-IT-TOF-MS analysis.

LC-DAD-IT-TOF-MS Analysis. The liquid chromatographic analysis was conducted on a Shimadzu LC system (Shimadzu, Kyoto, Japan) consisting of two LC-20AD$_{XR}$ solvent delivery units, a SIL-20AC$_{XR}$ autosampler, a CTO-20AC column oven, a SPD-M20A DAD module, a DGU-20A$_{3R}$ degasser, and a CBM-20A controller. A hybrid ion trap time-of-flight mass spectrometer (Shimadzu) equipped with an electrospray ionization (ESI) interface was connected to the LC system via a PEEK tube (0.13 mm i.d.) to perform high-resolution tandem mass spectrometry. Chromatographic separations were carried out on an SB-C$_{18}$ column (250 × 4.6 mm i.d., 5 μm, Agilent Technologies, Palo Alto, CA, USA), and the column oven was maintained at 30 °C. The mobile phase was composed of methanol (A) and 0.1% aqueous formic acid (B), and delivered at a total flow

DOI: 10.1021/acs.jafc.5b00023
J. Agric. Food Chem. 2015, 63, 3426−3436

rate of 1.0 mL/min following a gradient program: 0−10 min, 10−20% A; 10−18 min, 20−30% A; 18−30 min, 30−40% A; 30−40 min, 40−45% A; 40−44 min, 45−41% A; 44−60 min, 41−60% A; 60−65 min, 60−65% A; 65−66 min, 65−95% A; 66−76 min, 95% A. A roughly 20% portion of the effluent was introduced into the ESI interface by splitting the effluent via two PEEK tubes with a length ratio of 1:4. UV absorption over 190−400 nm was recorded by DAD unit, and fixed wavelengths of 280 and 325 nm were used for the simultaneous determination of seven PAs and three CAs, respectively. The injection volume was set at 10 μL. At the end of each run, the initial composition of the mobile phase (10% A) was permitted to re-equilibrate the whole system for 10 min.

In the mass spectrometer domain, an accurate ion axis was calibrated using the sodium trifluoroacetate clusters as a reference. Nitrogen was used as the nebulizing gas and drying gas, whereas ultrahigh purity argon (Ar) was used as the cooling gas and the collision gas for collision-induced dissociation (CID). The mass spectrometric parameters were set as below: ionization polarity, positive; nebulizing gas flow rate, 1.5 L/min; drying gas pressure, 100 MPa; detector voltage, 1.40 kV; curved desolvation line (CDL) voltage, constant level; CDL temperature, 200 °C; block heater temperature, 200 °C; interface voltage, 1.4 kV; and IT vacuum, 1.9×10^{-2} Pa. Positive mass spectra were recorded in the full scan and automatic multiple stage fragmentation scan modes over a range of m/z 100−1000 for all MS^1, MS^2, and MS^3 spectra acquisition. The ion accumulation time was set at 100 ms. The collision energy of CID was set at 50%. Data acquisition and processing were performed with the LCMS solution version 1.1 software package (Shimadzu). The accuracy of the assigned chemical formula was determined using a mass difference tolerance of ± 5 ppm, which was calculated by the deviation between the experimental mass and calculated mass.

Quantitative Method Validation. LC-DAD measurement was used to carry out simultaneous quantitation of 10 analytes, including 3-*O*-caffeoylquinic acid, 5-*O*-caffeoylquinic acid, 4-*O*-caffeoylquinic acid, *N*-*trans*-*p*-coumaroyloctopamine, *N*-*trans*-feruloyloctopamine, *N*-*trans*-sinapoyloctopamine, *N*-*trans*-*p*-coumaroyltyramine, *N*-*trans*-feruloyltyramine, grossamide, and cannabisin F, in SM201201−SM201217, and systematic validation assays were conducted for the developed quantitative method.

Linearity, LLOQ, and LOD. The linearity was assayed using external calibration curves with more than seven concentration levels for each analyte, and each level was conducted in triplicate. Calibration curve generation was performed by plotting the peak area (y) of an analyte against the theoretical concentration (x) over the respective calibration concentration range. The acceptance criterion for each regressive curve was a correlation coefficient (R^2) greater than 0.99. The lower limit of quantitation (LLOQ) and limit of detection (LOD) were termed as the concentration levels at a signal-to-noise ratio (S/N) of about 10 and 3, respectively.

Precision and Repeatability. Intra- and interday variations were chosen to achieve the precision assay for the proposed method. For intraday variability evaluation, 50-fold diluted stock solution (analyte concentrations, μg/mL: 1.39 for 3-*O*-caffeoylquinic acid, 20.65 for 5-*O*-caffeoylquinic acid, 2.51 for 4-*O*-caffeoylquinic acid, 6.10 for *N*-*trans*-*p*-coumaroyloctopamine, 16.25 for *N*-*trans*-feruloyloctopamine, 1.92 *N*-*trans*-sinapoyloctopamine, 7.53 for *N*-*trans*-*p*-coumaroyltyramine, 11.79 for *N*-*trans*-feruloyltyramine, 1.06 for grossamide, and 0.20 for cannabisin F, respectively) was selected and run for six replicates within a single day, while, for interday assay, the same solution was examined in triplicate per day for a consecutive 3 days. The precision was expressed using the relative standard deviation (RSD, %) of the replicate measurements.

For the repeatability assay, one batch of eggplant (SM201217) was selected to prepare extract sample in six replicates, which were subsequently measured using the aforementioned method. Stability assay was achieved by storing the selected sample (SM201217) at room temperature and analyzing at 0, 4, 8, 12, 16, 20, and 24 h, successively. The RSD value was taken as a measure of repeatability and stability.

Recovery Assay. The recovery was implemented to assess the accuracy of the method, and it was carried out by spiking a known amount of mixed standards into pulverized material (SM201217) prior to extraction. The follow-up extractions and HPLC-DAD analysis were then performed in the same manner as mentioned above. Three quantity levels (low, medium, and high) were set, and three replications at each level were conducted. The recoveries and RSDs were calculated using the following formulas: recovery (%) = (amount found − original amount)/amount spiked × 100% and RSD (%) = (SD/mean) × 100%, respectively.

RESULTS AND DISCUSSION

Optimization of Chromatographic Parameters and Extraction Procedure. Chromatographic conditions including analytical column, mobile phase, and elution program were systematically optimized to obtain optimal peak capacity and acceptable resolution for the investigated analytes between their adjacent peaks in the HPLC chromatogram. Several reverse phase (RP) columns were screened, such as Eclipse XDB-C_{18} (250 × 4.6 mm i.d., 5 μm, Agilent, Santa Clara, USA), Shim-pack XR-ODS II (75 × 2.0 mm i.d., 1.8 μm, Shimadzu, Kyoto, Japanese), and Agilent SB-C_{18} column. Finally, an Agilent SB-C_{18} column was chosen due to its superiorities at satisfactory separations for all investigated analytes, acceptable peak shape, and low system back-pressure over the other two columns. The mobile phase was selected between acetonitrile−water and methanol−water, and the latter combination exhibited greater separation potency for all analytes. Aiming to enhance the resolution and to improve the peak shape of the target compounds, formic acid was introduced into water as a mobile phase additive (final concentration, 0.1%, v/v). Fortunately, formic acid could also act as the ionic modifier to advance the overall mass response of the components in eggplant. Afterward, the gradient elution program was carefully optimized to achieve baseline separation for all analytes.

The extraction factors including solvent and extraction duration were optimized. Serial concentrations of aqueous methanol (20, 50, 70, and 100%) were compared with extraction efficiency, and the results suggested that 50% aqueous methanol resulted in the highest overall peak intensity. The extraction duration was compared among 30, 60, and 90 min, and the extraction yield of the investigated analytes did not increase after 60 min. Moreover, ultrasonic-assisted extraction was adopted by taking into account convenience. On the other side, the addition of 0.05 mL of acetic acid into 25 mL of 50% aqueous methanol could significantly enhance the overall response of those investigated compounds in the chromatograms of peels and pulps, which is possibly attributed to the fact that the abundant alkaline compounds like amides, in peels and pulps; thus, the acidified aqueous methanol extracts of the peels and pulps were subjected for LC-DAD-IT-TOF-MS analysis. Collectively, the extraction workflow was described in the Sample Preparation section.

Chemical Profiling of the Different Parts of Eggplant. *UV Absorption Characteristics and Mass Fragmentation Pathways.* Seven PA-type reference compounds, including *N*-*trans*-*p*-coumaroyloctopamine (**24**), *N*-*trans*-feruloyloctopamine (**25**), *N*-*trans*-sinapoyloctopamine (**26**), *N*-*trans*-*p*-coumaroyltyramine (**32**), and *N*-*trans*-feruloyltyramine (**33**), grossamide (**36**), and cannabisin F (**37**), were introduced to propose the mass fragmentation patterns along with UV absorption characteristics of this primary chemical type in eggplant. The UV spectra of the five *trans*-configurational PAs, including *N*-*trans*-*p*-coumaroyloctopamine (**24**), *N*-*trans*-feruloyloctopamine

DOI: 10.1021/acs.jafc.5b00023
J. Agric. Food Chem. 2015, 63, 3426−3436

Table 1. Retention Times, UV Data, Distribution, Mass Spectral Data, Molecular Formulae, and Plausible Identities of Detected Compounds in Different Parts of *S. melongena* Using LC-PDA-IT-TOF-MS

				$[M + H]^+$ (MS^1)							
compound[a]	t_R (min)	UV data, λ_{max} (nm)	distribution[b]	exptl	calcd	error (ppm)	MS^2	MS^3	molecular formula	plausible identity[c]	ref
1	4.863	280	ro, st, le, pu, pe	182.0814	182.0812	1.10	165.0583; 136.0757		$C_9H_{11}NO_3$	tyrosine	31
2	6.900	279	pe	251.1399	251.1390	2.79	234.1134	163.0409	$C_{13}H_{18}N_2O_3$	*N-cis*-caffeoylputrescine	
3	9.058	281	ro, st, le, pu, pe	166.0855	166.0863	−4.82	120.0764		$C_{19}H_{11}NO_2$	phenylalanine	31
4	9.867	279	pe	235.1438	235.1441	−1.28	218.1181	147.0436	$C_{13}H_{18}N_2O_2$	*N-cis-p*-coumaroylputrescine	
5	10.412	317, 292	ro, st, le, pu, pe	251.1400	251.1390	3.98	234.1150	163.0382	$C_{13}H_{18}N_2O_3$	*N-trans*-caffeoylputrescine	16
6	11.733	323	ro, st, le, pu, pe	355.1040	355.1024	4.51	163.0367		$C_{16}H_{18}O_9$	3-*O*-caffeoylquinic acid*	11
7	12.010	279	pu, pe	265.1547	265.1547	0.00	177.0553	145.0322	$C_{14}H_{20}N_2O_3$	*N-cis*-feruloylputrescine	
8	13.658	289	pu, pe	235.1438	235.1441	−1.28	218.1179	147.0448	$C_{13}H_{18}N_2O_2$	*N-trans-p*-coumaroylputrescine	16
9	14.462	279	ro, st, le, pu, pe	205.0968	205.0972	−1.95	188.0713	146.0653	$C_{11}H_{12}N_2O_2$	tryptophan	31
10	16.258	316	ro, st, le, pu, pe	265.1553	265.1547	2.26	177.0565	145.0322	$C_{14}H_{20}N_2O_3$	*N-trans*-feruloylputrescine	16
11	17.412	324	ro, st, le, pu, pe	355.1038	355.1024	3.94	163.0393	145.0322	$C_{16}H_{18}O_9$	5-*O*-caffeoylquinic acid*	11
12	18.678	324	ro, st, le, pu, pe	355.1033	355.1024	2.53	163.0394		$C_{16}H_{18}O_9$	4-*O*-caffeoylquinic acid*	11
13	19.628	279	le, pu, pe	474.2607	474.2599	4.85	222.1126	165.0557	$C_{25}H_{35}N_3O_6$	N^1,N^8-dihydrocaffeoylspermidine	16
14	20.713	520	pe	611.1616	611.1607	1.47	465.1010; 303.0495	257.0447	$C_{27}H_{31}O_{16}^+$	delphinidin-3-rutinoside (tulipanin)	25
15	21.165	277	le, pu, pe	472.2437	472.2442	−1.06	310.2124; 220.0961	163.0388	$C_{25}H_{33}N_3O_6$	N^1-caffeoyl-N^8-hydrocaffeoylspermidine	16
16	21.945	289	le, pu, pe	472.2435	472.2442	0.00	310.2124; 222.1125	165.0557	$C_{25}H_{33}N_3O_6$	N^1-hydrocaffeoyl-N^8-caffeoylspermidine	16
17	23.547	314	le, pu, pe	470.2283	470.2286	−0.64	308.1964; 220.0958	163.0413	$C_{25}H_{31}N_3O_6$	N^1,N^8-dicaffeoylspermidine	16
18	23.628	275	ro, st, le	300.1223	300.1230	−2.33	282.1081	147.0456	$C_{17}H_{17}NO_4$	*N-cis-p*-coumaroyloctopamine*	22
19	24.038	325	ro, st, le, pu, pe	369.1177	369.1180	−0.81	177.0556	145.0322	$C_{17}H_{20}O_9$	feruloylquinic acid	16
20	25.100	292	ro, le	316.1174	316.1179	−1.58	298.1077	163.0418	$C_{17}H_{17}NO_5$	*N-trans*-caffeoyloctopamine*	22
21	25.913	276	ro	330.1332	330.1336	−1.21	312.1219; 177.0552	145.0293	$C_{18}H_{19}NO_5$	*N-cis*-feruloyloctopamine*	22
22	27.033	345	ro, st, le	193.0500	193.0495	2.59	133.0299		$C_{10}H_8O_4$	isoscopoletin	24
23	27.218	317	ro	346.1270	346.1285	−4.33	328.179	177.0578	$C_{18}H_{19}NO_6$	*N-trans*-feruloylnoradrenline*	22
24	29.283	292, 310	ro, st, le	300.1236	300.1230	2.00	282.1150; 147.0453	119.0478	$C_{17}H_{17}NO_4$	*N-trans-p*-coumaroyloctopamine*	22
25	31.083	290, 318	ro, st, le	330.1346	330.1336	3.03	312.1216	177.0580	$C_{18}H_{19}NO_5$	*N-trans*-feruloyloctopamine*	22
26	32.285	290, 319	ro, st	358.1293	358.1296	−0.84	207.0659	175.0380	$C_{19}H_{21}NO_6$	*N-trans*-sinapoyloctopamine*	22
27	33.223	343	st, le	207.0644	207.0652	−3.86	151.0704		$C_{11}H_{10}O_4$	6,7-dimethoxycoumarin	6
28	33.327	276	ro, st, le	284.1276	284.1281	−1.76	147.0443		$C_{17}H_{17}NO_3$	*N-cis-p*-coumaroyltyramine*	6
29	34.147	292	ro, st, le	300.1216	300.1230	−4.66	163.0418		$C_{17}H_{17}NO_4$	*N-trans*-caffeoyltyramine	27
30	35.105	275	ro, st, le	314.1393	314.1387	1.91	177.0557	145.0276	$C_{18}H_{19}NO_4$	*N-cis*-feruloyltyramine*	22
31	35.570	292	ro, st, le	330.1323	330.1336	−3.94	177.0557	145.0322	$C_{18}H_{19}NO_5$	*N-trans*-feruloyldopamine	10
32	39.700	292, 310	ro, st, le	284.1288	284.1281	2.46	147.0449	119.0497	$C_{17}H_{17}NO_3$	*N-trans-p*-coumaroyltyramine*	22
33	41.740	290, 318	ro, st, le	314.1391	314.1387	1.27	177.0556	145.0285	$C_{18}H_{19}NO_4$	*N-trans*-feruloyltyramine*	22
34	42.390	292	ro, st	344.1477	344.1492	−4.36	207.0647	175.0375	$C_{19}H_{21}NO_5$	*N-trans*-sinapoyltyramine*	22
35	43.015	317	ro, st, le	344.1508	344.1492	4.65	177.0553	145.0304	$C_{19}H_{21}NO_5$	*N-trans*-feruloyl-3-methoxytyramine*	22
36	60.917	320	ro, st, le	625.2562	625.2544	2.88	462.1883	325.1039	$C_{36}H_{36}N_2O_8$	grossamide*	5
37	64.292	316	ro, st, le	625.2572		4.48	488.1618; 462.1889	351.0842	$C_{36}H_{36}N_2O_8$	cannabisin F*	5

[a]The notation for compounds refers to Figure 4. [b]ro, root; st, stem; le, leaves; pu, pulp; pe, peel. [c]Compounds marked with * were unambiguously identified with reference compounds; the others were identified on the basis of UV and mass spectra.

DOI: 10.1021/acs.jafc.5b00023
J. Agric. Food Chem. 2015, 63, 3426−3436

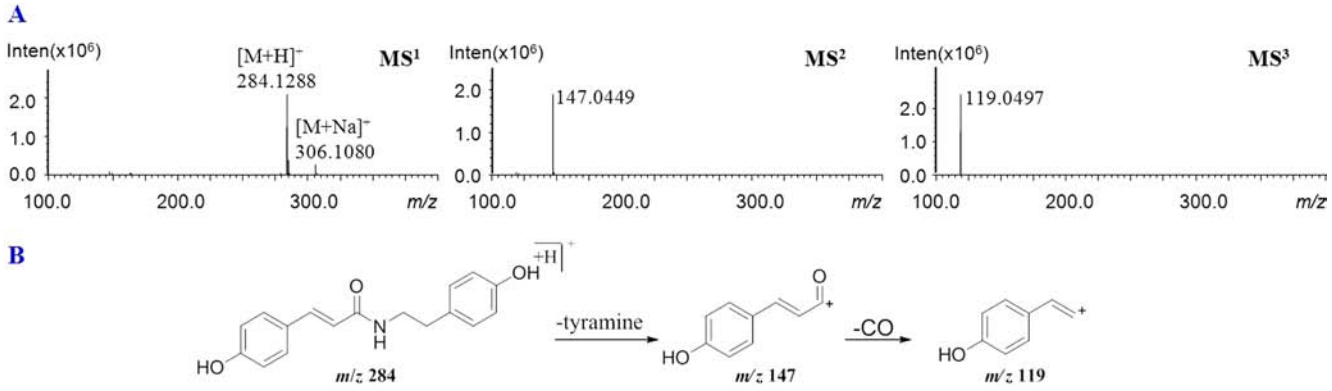

Figure 2. Tandem mass spectra (MS^1, MS^2, and MS^3) under positive ionization mode (A) and proposed schematic of mass fragmentation pathways (B) of *N-trans-p*-coumaroyltyramine (**32**).

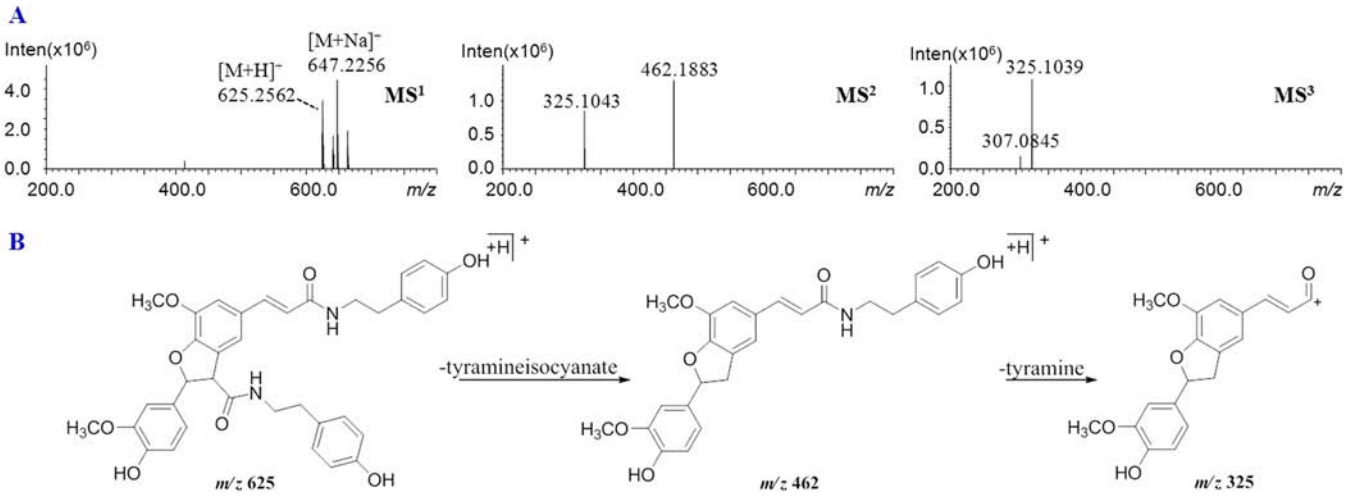

Figure 3. Tandem mass spectra (MS^1, MS^2, and MS^3) under positive ionization mode (A) and proposed schematic of mass fragmentation pathways (B) of grossamide (**36**).

(**25**), *N-trans*-sinapoyloctopamine (**26**), *N-trans-p*-coumaroyltyramine (**32**), and *N-trans*-feruloyltyramine (**33**), showed two common primary absorption peaks at around 290 and 315 nm (Table 1), whereas the typical UV absorption peak of two lignanamides (also known as *bis*-phenylpropanoid amides), grossamide (**36**) and cannabisin F (**37**), was observed at around 318 nm due to their big conjugated systems. These characteristics of the chromophores aided in further detection and identification of PAs in the extract.

The protonated ion and sodium adduct molecular ion of *N-trans-p*-coumaroyltyramine (**32**) were observed at *m/z* 284.1288 ($[M + H]^+$) and 306.1080 ($[M + Na]^+$) (Figure 2A), respectively, corresponding to the molecular formula of $C_{17}H_{17}NO_3$. When the protonated molecular ion was transmitted to a CID cell, the prominent product ions were yielded at *m/z* 147.0449 (element composition: $C_9H_7O_2$) and 119.0497 (element composition: C_8H_7O), indicating the dissociation at the amide group along with a subsequent neutral cleavage of the CO (28 amu) group (Figure 2B). Similarly, the successive neutral losses of the phenylethylamine (octopamine for *N-trans-p*-coumaroyloctopamine (**24**)/*N-trans*-feruloyloctopamine (**25**)/*N-trans*-sinapoyloctopamine (**26**) and tyramine for *N-trans*-feruloyltyramine (**33**), respectively) and CO moiety were detected for all of the compounds **24**−**26**, **32**, and **33** via the dissociation of the amide core (C−N bond) and α-cleavage of the carbonyl group (Table 1). In the case of lignanamides, the sodium adduct ion and protonated molecular ion of grossamide (**36**) were observed at *m/z* 647.2256 ($[M + Na]^+$) and 625.2562 ($[M + H]^+$), respectively, agreeing well with the molecular formula of $C_{36}H_{36}N_2O_8$. In the MS^2 spectrum of the protonated molecular ion, the dominant daughter ion species were detected at *m/z* 462.1883 and 325.1039 (Figure 3A), indicating the successive neutral cleavages of $C_9O_2NH_9$ and C_8ONH_{11} moieties (Figure 3B). Corresponding to the chemical structure of grossamide (**36**), we assumed that the α-cleavage of the carbonyl group at the C−C bond and the subsequent dissociation of the other amide group at the C−N bond gave rise to the generation of the prominent product ions at *m/z* 462.1883 and 325.1039 (Figure 3B). Cannabisin F (**37**) exhibited a similar mass spectral profile with grossamide (**36**) (Table 1). Therefore, the diagnostic fragmentation pathways of lignanamides were speculated as the α-cleavage of the carbonyl group at the C−C bond and the subsequent dissociation of the other amide group (Figure 3B).

On the other hand, the characteristic UV absorption of CAs was featured at approximately 324 nm. The protonated molecular ion of compounds 3-*O*-caffeoylquinic acid (**6**), 5-*O*-caffeoylquinic acid (**11**), and 4-*O*-caffeoylquinic acid (**12**) was observed at *m/z* 355.10, and the characteristic product ion was yielded at *m/z* 163.04 via dissociating the ester group at the C−O bond (Table 1), which could be adopted as a diagnosis for mining and identification of CAs in eggplant.

DOI: 10.1021/acs.jafc.5b00023
J. Agric. Food Chem. 2015, 63, 3426−3436

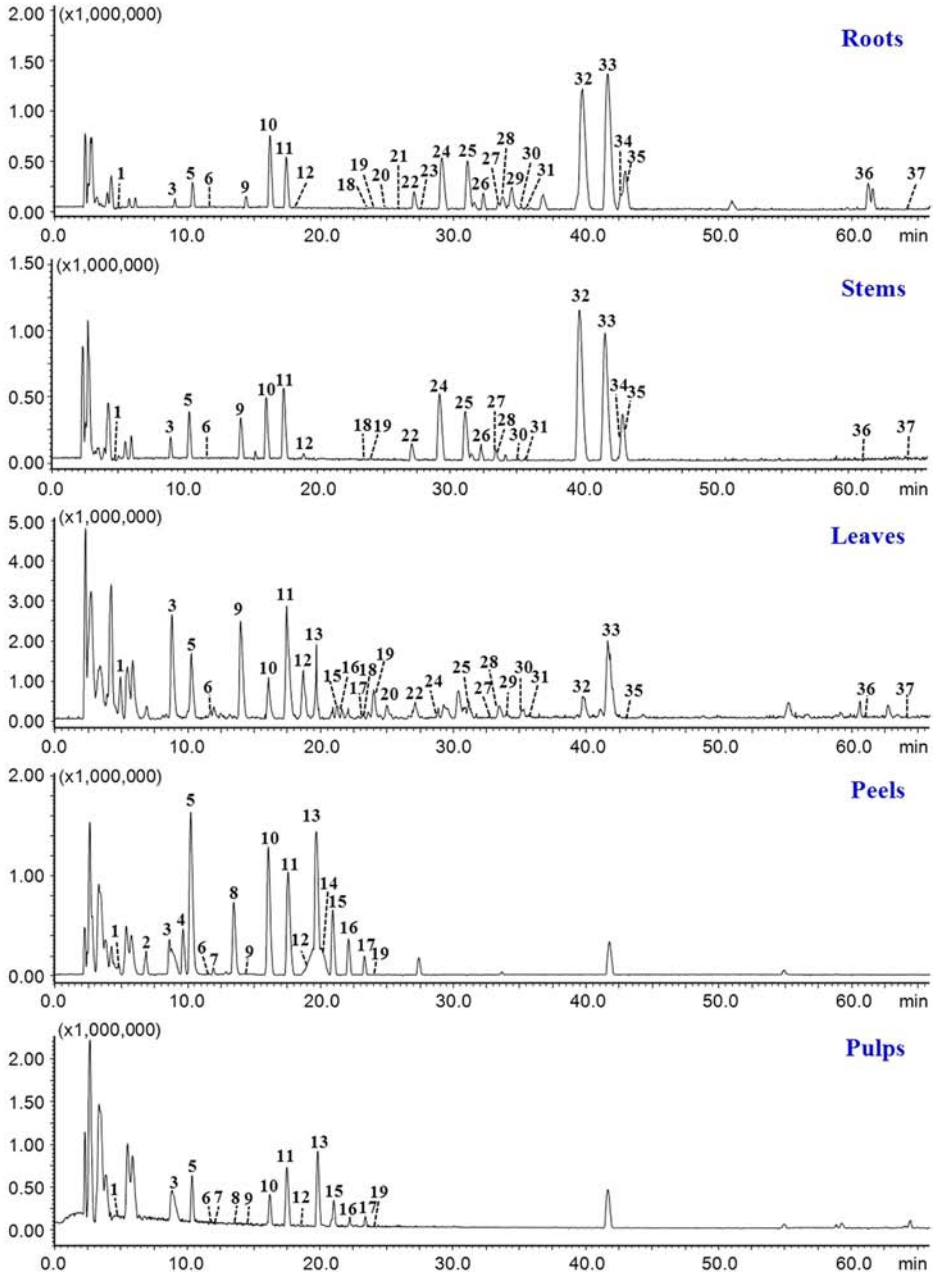

Figure 4. Representative total ion current (TIC) chromatograms of extracts of different parts of eggplant under positive ionization mode. The notation and identification of peaks are included in Table 1.

Characterization of Components in Eggplant. A total of 37 compounds were detected in the different parts of eggplant. The retention times, the wavelengths of maximum absorptions, precursor ions, molecular weights, molecular formulas, prominent fragment ions, plausible identities, and the distribution of each detected compound in different parts are illustrated in Table 1.

Phenylpropanoids and amines could be regarded as the biosynthetic precursors of PAs. PAs in eggplant can be tentatively divided into four types based on the different precursors,[4] including (1) type I, simple conjugates of hydroxycinnamic acid and arylamine, such as tyramine, octopamine, noradrenaline, anthranilate, and dopamine; (2) type II, dimers of type I compounds, also named lignanamides or *bis*-phenylpropanoid amides, which can be recognized as the conjugates of one lignan and two arylamines, such as grossamide (**36**) and cannabisin F (**37**); (3) type III, conjugates of hydroxycinnamic acid and putrescine; (4) type IV, phenylpropanoid polyamine conjugates, for instance, spermidine hydroxycinnamic acid amides.

First, in comparison with the UV spectral profiles, mass spectra, and retention times with the authentic compounds, the seven PAs, including *N-trans-p*-coumaroyloctopamine, *N-trans*-feruloyloctopamine, *N-trans*-sinapoyloctopamine, *N-trans-p*-coumaroyltyramine, *N-trans*-feruloyltyramine, grossamide, and cannabisin F, matched well with compounds **24**, **25**, **26**, **32**, **33**, **36**, and **37**, respectively (Figure 4 and Table 1).

The protonated molecular ions of type I PAs were usually observed as even numbers between m/z 280 and 350, and the predominant product ions were the cation of hydroxycinnamyl moieties. Following careful analysis of the spectral profiles, compounds **18**, **20**, **21**, **23**−**26**, and **28**−**35** were assigned into

DOI: 10.1021/acs.jafc.5b00023
J. Agric. Food Chem. 2015, 63, 3426−3436

this type. The fragment ion at m/z 147.04 (element composition: $C_9O_2H_7$) could be adopted as the diagnosis to search and identify the conjugates of coumaric acid and arylamine, e.g., compounds **24** and **32**. The positive quasi-molecular ion of compound **18** was yielded at m/z 300.1223, indicating a molecular formula of $C_{17}H_{17}NO_4$, and the primary product ion was detected at m/z 147.0456, identical with compound **32**; thus, this compound was assigned as *N-cis-p*-coumaroyloctopamine. Given that the steric hindrance could prevent the conjugation between the carbonyl group and the phenyl plane of the caffeoyl group, a hypsochromic shift might occur for the PAs with the *Z*-configuration of the C=C bond in comparison with *E*-configurational type I PAs; hence, the identity of compound **18** (absorption peak: 275 nm) was confirmed with the assistance of this rule. Interestingly, the precursor and product ions of compound **28** were the same as those of compound **32**, suggesting a pair of isomers for these compounds; consequently, it is reasonable to assume compound **28** as *N-cis-p*-coumaroyltyramine (Table 1). The product ion of m/z 163.0418, which was generated from the quasi-molecular ion (m/z 316.1174 $[M + H]^+$) of compound **20**, was calculated as $C_9O_3H_7$, corresponding to the cation of the caffeoyl group. In combination with the maximal absorption observed at 292 nm, compound **20** was thereby identified as *N-trans*-caffeoyloctopamine. Similarly, compound **29**, which shared an identical product ion (m/z 163.0418) with compound **20**, was correspondingly identified as *N-trans*-caffeoyltyramine. Compounds **21**, **23**, **30**, **31**, and **35** generated a common fragment of $C_{10}O_3H_9$ (calculated from m/z 177.06), indicating that ferulic acid was one of the two precursors for each compound. Integrating the UV chromatograms (maximum absorptions around 290 nm and/or 315 nm), the putative identities of compounds **23**, **31**, and **35** were elucidated in Table 1, whereas the absorption peaks at around 276 nm supported the identities of compounds **21** and **30** as *N-cis*-feruloyloctopamine and *N-cis*-feruloyltyramine (Table 1), respectively. Similar to compound **26**, signals at m/z 207.06 and 175.04 were observed as the prominent product ions for compound **34**, while its positive pseudomolecular ion ($[M + H]^+$) was detected at m/z 344.1477 (Table 1), 60 Da more than that of compound **32** (m/z 284.1228). The element composition of compound **34** was calculated as $C_{19}H_{21}NO_5$, and its maximum absorption peak was detected at 292 nm; therefore, the structure of compound **34** was plausibly assigned as *N-trans*-sinapoyltyramine.

Except for compounds **36** and **37**, no additional type II PAs were found from eggplant in the current study.

Type III PAs were defined as the conjugates of hydroxycinnamic acid and putrescine; hence, their pseudomolecular ions should be observed as odd numbers among m/z 230−270, and the cation of hydroxycinnamyl moieties might usually be yielded as the predominant fragments. Compounds **2**, **4**, **5**, **7**, **8**, and **10** were plausibly assorted to type III PAs. Taking compound **8**, for instance, the positive quasi-molecular ion was observed at m/z 235.1438, and the primary product ions were detected at m/z 218.1179 and 147.0448, corresponding to the neutral losses of a NH_3 molecule (17 u) and a putrescine molecule (88 u), respectively. Referring to the description above, m/z 147.0448 indicated the presence of a coumaryl group, and compound **8** was thereby tentatively identified as *N-trans-p*-coumaroylputrescine. As aforementioned, the product ion at m/z 163.04 could be utilized as the diagnostic product ion for the identification of caffic acid derivatives; therefore, compounds **2** and **5** were tentatively identified as *N-cis*-caffeoylputrescine and *N-trans*-caffeoylputrescine. Because the maximal absorption of compounds **2** and **5** was exhibited at 279 and 292 nm, respectively, the identity of compound **5** was tentatively assigned as *N-trans*-caffeoylputrescine, while *N-cis*-caffeoylputrescine was tentatively assigned to compound **2** (Table 1). Similarly, compounds **4**, **7**, and **10** were tentatively identified as *N-cis-p*-coumaroylputrescine, *N-cis*-feruloylputrescine, and *N-trans*-feruloylputrescine, respectively (Table 1).

The fragmentation patterns of type IV PAs have been previously proposed by Handrick et al.,[23] and the dissociation of the amide group at the C−N bond along with the α-cleavage of the middle amino group of spermidine were demonstrated as the primary features. With the assistance of the descriptions in ref 23, compounds **13** and **15**−**17** were picked out as the conjugates of spermidine and various hydroxycinnamic acids. Taking compound **17** as the representative one to describe the structural characterization process, the positive quasi-molecular ion ($[M + H]^+$) was generated at m/z 470.2283, suggesting a molecular formula as $C_{25}H_{31}N_3O_6$, and the fragment ions were observed at m/z 220.0958 and 163.0413. Identical with compound **5**, the fragment at m/z 163.0413 indicated the occurrence of cafferoyl substitution in compound **17**, and the other product ion of m/z 220.0958 was attributed to the α-cleavage of the middle amino group of spermidine (Table 1). Collectively, compound **17** was tentatively assigned as *N,N′*-dicaffeoylspermidine, which was previously identified from the fruits of eggplant.[11] Correspondingly, compound **15**, which yielded identical fragment ions (m/z 220.0961 and 163.0388) yet a different quasi-molecular ion (m/z 472.2437, 2 u more than that of compound **17**) with compound **17**, was tentatively identified as N^1-caffeoyl-N^8-hydrocaffeoylspermidine (Table 1). Moreover, the putative identities of compounds **13** and **16**, which shared identical product ions (m/z 222.11 and 165.06), were elucidated as N^1,N^8-dihydrocaffeoylspermidine and N^1-hydrocaffeoyl-N^8-caffeoylspermidine (Table 1), respectively.

CAs are widely distributed in the plant kingdom, and compounds **6**, **11**, and **12** were unambiguously identified as 3-*O*-caffeoylquinic acid, 5-*O*-caffeoylquinic acid, and 4-*O*-caffeoylquinic acid, respectively, by comparing with the retention times, mass spectral profiles, and UV spectra with the standards. In addition, compound **19** generated positive pseudomolecular and dominant product ions at m/z 369.1177 and 177.0556, respectively, both of which were 14 u more than those of compound **6**; thus, compound **19** was tentatively identified as feruloylquinic acid (Table 1).

The quasi-molecular ions of compounds **22** and **27** were detected at m/z 193.0500 and 207.0644, respectively, suggesting the molecular formulas as $C_{10}H_8O_4$ and $C_{11}H_{10}O_4$. In comparison with the information archived in refs 6 and 24, compounds **22** and **27** were proposed as isoscopoletin and 6,7-dimethoxycoumarin, respectively, both of which were previously isolated from the roots of eggplant.[6,24] The MS^1 spectrum of compound **14** showed the quasi-molecular ion at m/z 611.1616 ($[M]^+$), suggesting a molecular formula as $C_{27}H_{31}O_{16}$, and 520 nm was observed as the maximal absorption wavelength in the UV spectrum, indicating this compound as an anthocyanin analogue. The primary fragments were observed at m/z 465.1010 and 303.0495 in the MS^2 spectrum, by expelling the rhamose (146 amu) and glucose (162 amu) moieties, successively (Table 1). In comparison with the mass spectral profile documented in ref 25, compound **14**

DOI: 10.1021/acs.jafc.5b00023
J. Agric. Food Chem. 2015, 63, 3426−3436

was plausibly identified as tulipanin. In addition, compounds **1**, **3**, and **9** were characterized as tyrosine, phenylalanine, and tryptophan, respectively (Table 1), by referring to some available databases (HMDB, METLIN, and MassBank).

Compounds **1**−**4**, **7**, **9**, **29**, and **31** were reported in eggplant for the first time. PAs and CAs were observed as the primary components in different parts (Figure 4); thus, these two kinds of ingredients were hypothesized as the prominent efficacy material basis of eggplant. Moreover, a comparison was performed for the chemical profiles among the different parts of eggplant. First, high similarity was observed for the total ion current (TIC) chromatograms of the roots and stems (Figure 4A and B), which may provide chemical evidence for their combinatory use in traditional Chinese medical practices. Significant differences were detected for fruits versus the other parts, suggesting a unique usage. PAs were detected in all parts of eggplant. Type I and II PAs were only found in the roots, stems, and leaves; nonetheless, the fruits, including the peel and pulp parts, were wealthy of putrescine and spermidine derivatives (type III and IV PAs) (Figure 4). Collectively, it is not surprising that the various usages corresponding to the different parts were widely mentioned in the literature.[2]

In terms of fruits, compounds **2**, **4**, and **14** were only detected in the peel parts rather than the pulp parts, and a higher abundance of most PAs was observed in the peel parts rather than the pulp parts, for instance, compounds **5**, **7**, **8**, **10**, **13**, and **15**−**17** (Figure 4). In sight of the bioactivities of PAs and delphinidin-3-rutinoside (**14**) that revealed promising antioxidant potency,[14] we may conclude that the fruit peels of eggplant could exhibit a higher nutritional value than the pulp portion; however, it is a pity that the peels are usually deserted during cooking.

Simultaneous Determination of Seven PAs and Three CAs in the Roots of Eggplant. *Method Validation.* Given the abundant distribution of compounds **6**, **11**, **12**, **24**−**26**, **32**, **33**, **36**, and **37**, these 10 compounds were selected as the indicators to carry out quantitative analysis for the roots of eggplant.

In the linearity assays, calibration curves of all analytes showed good linear regression (R^2 > 0.999) within their respective test concentration ranges. The LODs and LLOQs of all investigated compounds ranged from 0.03 to 0.19 and 0.08 to 0.30 μg/mL, respectively. The overall intra- and interday variations were determined as less than 0.08 and 0.69%, respectively. Results of repeatability assay demonstrated the proposed method to be repeatable with RSDs less than 4.44% (n = 6). RSDs of the 10 analytes were less than 3.96% (n = 6) with 24 h in the stability assay, indicating that the sample solution could stay stable during measurement. Moreover, the recovery assay showed that the developed method showed satisfactory accuracy with recoveries ranging from 96.17 to 105.00%. Above all, the developed method was proved to be precise, accurate, and sensitive for the simultaneous quantitative investigation of the 10 analytes in the roots of eggplant.

Quantitative Analysis of the 10 Compounds in the Roots of Eggplant. The validated method was applied to simultaneously quantitate the 10 analytes in 17 batches of roots of eggplant (SM201201−SM201217). Figure 5 shows the typical HPLC-DAD chromatograms of the mixed standards as well as a representative extract of eggplant roots (SM201217) detected at 325 nm (0−20 min, red trace) and 280 nm (20−66 min, blue trace). The results of the quantitative analysis are summarized in Table 2. As shown in Table 2, the contents of

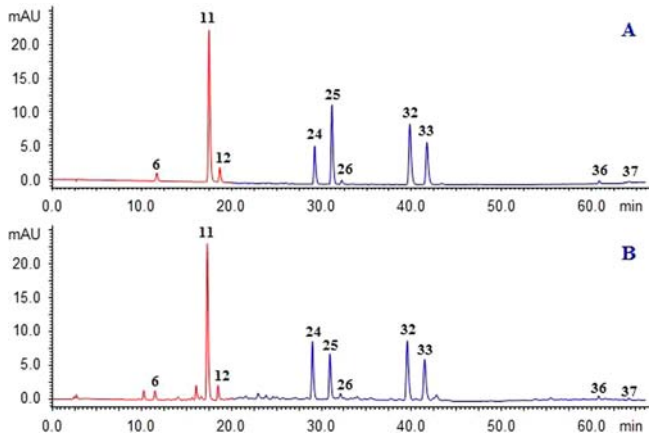

Figure 5. Representative combined HPLC-UV chromatograms (0−20 min: 325 nm, red trace; 20−66 min: 280 nm, blue trace) of mixed standards (A) and the extract of roots of *S. melongena* (B).

the 10 analytes exhibited big variations among different samples, suggesting that it is critical to carry out quality control of this herbal medicine. 5-*O*-Caffeoylquinic acid (**11**), *N*-*trans*-*p*-coumaroyloctopamine (**24**), *N*-*trans*-feruloyloctopamine (**25**), *N*-*trans*-*p*-coumaroyltyramine (**32**), and *N*-*trans*-feruloyltyramine (**33**) were found as the five most abundant compounds in the roots of eggplant, among which the content of 5-*O*-caffeoylquinic acid (**11**) (86.4−1434.8, μg/g) was detected to be higher than the other components in most samples, whereas the two lignanamides (grossamide (**36**), 12.8−161.9 μg/g, and cannabisin F (**37**), 3.0−26.5 μg/g) were determined as the minor components.

The inconsistency of the chemical compositions in different samples was identified by the quantitative analysis, and it might result from diverse factors, such as climate, temperature, soil,[26] cultural practices, and harvest maturity in different provinces.[11] PAs consist of cinnamic acid derivatives and amines, and the shikimate biosynthetic pathway is the key source for their phenylpropenyl groups,[28] which is mediated by several enzymes, such as phenylalanine ammonia lyase (PAL), hydroxycinnamoyl-CoA:shikimate hydroxycinnamoyl transferase (HST), hydroxycinnamoyl-CoA:quinate hydroxycinnamoyl transferase (HQT), shikimate dehydrogenase, and so on. The first committed step in the biosynthesis of most phenylpropanoids by converting phenylalanine derived from the shikimate pathway to *trans*-cinnamic acid and ammonia and HQT was responsible for the formation of chlorogenic acid.[29] As a consequence, the activities and contents of these enzymes, as well as some other enzymes that were involved in the biosynthesis of CAs and anthocyanins, might play key roles for the different chemical profiles of PAs among eggplant from different areas. Eggplant has been reported to be well adapted to high rainfall and high temperatures;[30] thus, humidity and temperature were expected as the determinant factors for the activities of the enzymes aforementioned were active under such conditions. Further research is needed to verify the assumption.

In summary, the mass fragmentation patterns of PAs were proposed with the combination of reference compounds and high resolution tandem mass spectrometry. A total of 37 compounds, including 27 PAs and 10 other compounds, were detected and identified from different parts of eggplant using LC-DAD-IT-TOF-MS, in which 22 compounds were identified from the roots, stems, and leaves and 21 compounds from the

DOI: 10.1021/acs.jafc.5b00023
J. Agric. Food Chem. 2015, 63, 3426−3436

Table 2. Contents (Mean ± SD, μg/g) of the 10 Analytes in the Roots of *S. melongena* from Different Habitats

no.	habitats	6[a]	11	12	24	25	26	32	33	36	37
SM201201	Xinyang, Henan	69.84 ± 0.61	864.10 ± 0.36	101.92 ± 0.43	201.84 ± 0.30	236.91 ± 0.62	55.94 ± 0.34	145.51 ± 0.46	201.72 ± 0.47	17.33 ± 0.92	4.14 ± 0.94
SM201202	Xinyang, Henan	61.46 ± 0.52	562.41 ± 0.11	71.73 ± 0.52	129.71 ± 0.63	227.34 ± 0.56	37.87 ± 0.45	242.10 ± 0.22	473.59 ± 0.40	17.48 ± 0.89	4.56 ± 0.99
SM201203	Xinyang, Henan	70.62 ± 0.49	347.25 ± 0.28	87.27 ± 0.67	232.92 ± 0.66	127.71 ± 0.77	40.83 ± 0.38	168.20 ± 0.42	169.40 ± 0.23	26.53 ± 0.69	6.01 ± 0.80
SM201204	Xinyang, Henan	16.15 ± 0.41	273.68 ± 0.31	25.51 ± 0.51	203.20 ± 0.53	410.19 ± 0.68	48.62 ± 0.51	174.71 ± 0.33	446.11 ± 0.56	21.22 ± 0.78	6.61 ± 0.33
SM201205	Leping, Jiangxi	68.87 ± 0.57	744.33 ± 0.05	112.62 ± 0.44	321.89 ± 0.52	206.34 ± 0.59	32.73 ± 0.55	233.37 ± 0.26	274.13 ± 0.55	36.60 ± 0.92	6.24 ± 0.56
SM201206	Heyuan, Guangdong	4.64 ± 0.60	42.23 ± 0.34	6.04 ± 0.43	115.02 ± 0.46	145.36 ± 0.70	24.61 ± 0.64	94.49 ± 0.63	99.01 ± 0.63	16.56 ± 0.74	3.02 ± 0.66
SM201207	Qingdao, Shandong	43.22 ± 0.45	514.22 ± 0.25	74.58 ± 0.11	256.28 ± 0.35	344.91 ± 0.53	64.09 ± 0.37	295.35 ± 0.44	477.46 ± 0.73	94.61 ± 0.46	21.58 ± 0.91
SM201208	Beijing	50.85 ± 0.67	526.30 ± 0.12	89.21 ± 0.53	452.19 ± 0.44	185.64 ± 0.33	26.00 ± 0.43	194.02 ± 0.33	132.52 ± 0.53	22.20 ± 0.77	3.07 ± 0.93
SM201209	Beijing	8.10 ± 0.84	135.90 ± 0.22	11.73 ± 0.83	174.21 ± 0.64	104.78 ± 0.67	12.71 ± 0.56	157.15 ± 0.56	155.58 ± 0.75	123.60 ± 0.55	22.21 ± 0.99
SM201210	Xuchang, Henan	56.46 ± 0.41	684.76 ± 0.31	86.64 ± 0.63	121.02 ± 0.45	140.01 ± 0.43	30.62 ± 0.27	139.57 ± 0.46	292.01 ± 0.46	12.82 ± 0.71	5.24 ± 0.86
SM201211	Shijiazhuang, Hebei	17.94 ± 0.71	530.29 ± 0.16	45.09 ± 0.55	366.32 ± 0.34	517.52 ± 0.55	55.38 ± 0.37	126.41 ± 0.67	320.60 ± 0.23	62.43 ± 0.67	18.78 ± 0.83
SM201212	Yichun, Heilongjiang	20.58 ± 0.42	962.21 ± 0.20	54.21 ± 0.11	271.64 ± 0.66	302.32 ± 0.37	56.82 ± 0.55	250.52 ± 0.53	390.93 ± 0.77	119.03 ± 0.60	25.49 ± 0.74
SM201213	Yichun, Heilongjiang	5.40 ± 0.51	335.93 ± 0.25	14.72 ± 0.64	56.27 ± 0.11	83.93 ± 0.67	11.70 ± 0.74	83.24 ± 0.47	219.28 ± 0.56	43.69 ± 0.87	7.50 ± 0.77
SM201214	Chifeng, Inner Mongolia	12.76 ± 0.45	380.77 ± 0.42	28.84 ± 0.58	468.72 ± 0.47	162.09 ± 0.27	15.43 ± 0.36	535.51 ± 0.38	283.11 ± 0.27	161.91 ± 0.63	31.13 ± 0.79
SM201215	Yichun, Heilongjiang	4.68 ± 0.11	86.41 ± 0.67	7.48 ± 0.81	104.19 ± 0.61	92.01 ± 0.66	15.28 ± 0.78	132.12 ± 0.36	203.31 ± 0.43	33.11 ± 0.68	9.22 ± 0.87
SM201216	Beijing	32.37 ± 0.23	1434.82 ± 0.01	110.10 ± 0.52	582.90 ± 0.16	277.60 ± 0.47	44.23 ± 0.41	338.77 ± 0.52	217.04 ± 0.74	77.12 ± 0.78	26.49 ± 0.65
SM201217	Xinyang, Henan	51.04 ± 0.42	677.34 ± 0.27	89.21 ± 0.74	260.24 ± 0.11	324.20 ± 0.58	57.61 ± 0.52	208.30 ± 0.41	346.82 ± 0.54	33.34 ± 0.90	10.31 ± 0.78

[a]The notation for compounds refers to Figures 4 and 5.

DOI: 10.1021/acs.jafc.5b00023
J. Agric. Food Chem. 2015, 63, 3426−3436

peels and pulps of the fruits. Compounds **1**−**4**, **7**, **9**, **29**, and **31** were reported in eggplant for the first time. PAs and CAs were observed as the primary components in each part of eggplant. Moreover, an LC-DAD-based method was developed and validated for the simultaneous determination of seven PAs along with three CAs in the roots of eggplant, and different wavelengths were applied for PAs and CAs to obtain a satisfactory response. Variations were observed for the contents of the 10 analytes in the roots of eggplant from different habitats. Taken together, the results of this study could provide a new insight for the efficacy material basis of eggplant and also offer a reliable tool for the quality control of the roots of eggplant.

■ ASSOCIATED CONTENT

Supporting Information

Calibration curves, linear ranges, LODs, and LLOQs (Table S1) and validation data of the HPLC-UV quantitative method (Table S2) for the 10 analytes. Mass spectra (MS^1, MS^2, and MS^3) and the proposed schematic of mass fragmentation pathways of *N-trans-p*-coumaroylputrescine (**8**), N^1,N^8-dicaffeoylspermidine (**17**), N^1-caffeoyl-N^8-hydrocaffeoylspermidine (**15**), N^1,N^8-dihydrocaffeoylspermidine (**13**), and N^1-hydrocaffeoyl-N^8-caffeoylspermidine (**16**) (Figures S1−S5). This material is available free of charge via the Internet at http://pubs.acs.org.

■ AUTHOR INFORMATION

Corresponding Authors

*Phone/Fax: +86 10 64286350. E-mail: drlj666@163.com.
*Phone/Fax: +86 10 82802750. E-mail: pengfeitu@163.com.

Author Contributions

§J.S. and Y.-L.S. contributed equally to this research.

Funding

This work was financially supported by the Program for New Century Excellent Talents in University (NCET-13-0693, to J.L.), the TCM support project from the Ministry of Industry and Information Technology of P.R. China (to J.L.), the National Key Technology R&D Program "New Drug Innovation" of China (2013ZX09402201001, to J.L.), and the National Natural Science Foundation of China (No. 81403073, to Y.-L.S.).

Notes

The authors declare no competing financial interest.

■ REFERENCES

(1) Sarker, R. H.; Yesmin, S.; Hoque, M. I. Multiple shoot formation in eggplant (*Solanum melongena* L.). *Plant Tissue Cult. Biotechnol.* **2006**, *16*, 53−61.

(2) Editorial Committee of the Administration Bureau of Traditional Chinese Medicine. *Chinese Materia Medica (Zhong Hua Ben Cao)*; Shanghai Science and Technology Press: Shanghai, 1999; Vol. *19*, pp 307−308.

(3) Sun, J.; Gu, Y. F.; Li, M. M.; Su, X. Q.; Li, H.; Li, J.; Tu, P. F. Research advances on chemical constituents of *Solanum melongena* and their pharmacological activities. *Chin. Tradit. Herb. Drugs* **2013**, *44*, 2615−2622.

(4) Bassard, J. E.; Ullmann, P.; Bernier, F.; Werck-Reichhart, D. Phenolamides: bridging polyamines to the phenolic metabolism. *Phytochemistry* **2010**, *71*, 1808−1824.

(5) Sun, J.; Gu, Y. F.; Su, X. Q.; Li, M. M.; Huo, H. X.; Zhang, J.; Zeng, K. W.; Zhang, Q.; Zhao, Y. F.; Li, J.; Tu, P. F. Anti-inflammatory lignanamides from the roots of *Solanum melongena* L. *Fitoterapia* **2014**, *98*, 110−116.

(6) Liu, X. C.; Luo, J. G.; Kong, L. Y. Phenylethyl cinnamides as potential α-glucosidase inhibitors from the roots of *Solanum melongena*. *Nat. Prod. Commun.* **2011**, *6*, 851−853.

(7) Lee, C.; Kim, J.; Lee, H.; Lee, S.; Kho, Y. Two new constituents of *Isodon excisus* and their evaluation in an apoptosis inhibition assay. *J. Nat. Prod.* **2001**, *64*, 659−660.

(8) Pan, P. C.; Cheng, M. J.; Peng, C. F.; Huang, H. Y.; Chen, J. J.; Chen, I. S. Secondary metabolites from the roots of *Litsea hypophaea* and their antitubercular activity. *J. Nat. Prod.* **2010**, *73*, 890−896.

(9) Takahashi, T.; Miyazawa, M. Synthesis and structure-activity relationships of phenylpropanoid amides of serotonin on tyrosinase inhibition. *Bioorg. Med. Chem. Lett.* **2011**, *21*, 1983−1986.

(10) Wu, Z.; Zheng, L.; Li, Y.; Su, F.; Yue, X.; Tang, W.; Ma, X.; Nie, J.; Li, H. Synthesis and structure−activity relationships and effects of phenylpropanoid amides of octopamine and dopamine on tyrosinase inhibition and antioxidation. *Food Chem.* **2012**, *134*, 1128−1131.

(11) Whitaker, B. D.; Stommel, J. R. Distribution of hydroxycinnamic acid conjugates in fruit of commercial eggplant (*Solanum melongena* L.) cultivars. *J. Agric. Food Chem.* **2003**, *51*, 3448−3454.

(12) Luthria, D. L. A simplified UV spectral scan method for the estimation of phenolic acids and antioxidant capacity in eggplant pulp extracts. *J. Funct. Foods* **2012**, *4*, 238−242.

(13) Honda, T.; Zushi, K.; Matsuzoe, N. Inheritance of anthocyanin pigment and photosensitivity in eggplant (*Solanum melongena* L.) fruit. *Environ. Control Biol.* **2012**, *50*, 75−80.

(14) Azuma, K.; Ohyama, A.; Ippoushi, K.; Ichiyanagi, T.; Takeuchi, A.; Saito, T.; Fukuoka, H. Structures and antioxidant activity of anthocyanins in many accessions of eggplant and its related species. *J. Agric. Food Chem.* **2008**, *56*, 10154−10159.

(15) Lattanzio, V. High-performance liquid chromatography of free and bound phenolic acids in the egg-plant (*Solanum melongena* L.). *J. Chromatogr.* **1982**, *250*, 143−148.

(16) Wu, S. B.; Meyer, R. S.; Withaker, B. D.; Litt, A.; Kennelly, E. J. A new liquid chromatography-mass spectrometry based strategy to integrate chemistry, morphology, and evolution of eggplant species. *J. Chromatogr. A* **2013**, *1314*, 154−172.

(17) Xu, J.; Duan, J.; Xue, C.; Feng, T.; Dong, P.; Sugawara, T.; Hirata, T. Analysis and comparison of glucocerebroside species from three edible sea cucumbers using liquid chromatography-ion trap-time-of-flight mass spectrometry. *J. Agric. Food Chem.* **2011**, *59*, 12246−12253.

(18) Grace, M. H.; Warlick, C. W.; Neff, S. A.; Lila, M. A. Efficient preparative isolation and identification of walnut bioactive components using high-speed counter-current chromatography and LC-ESI-IT-TOF-MS. *Food Chem.* **2014**, *158*, 229−238.

(19) Xie, T.; Liang, Y.; Hao, H.; A, J.; Xie, L.; Gong, P.; Dai, C.; Liu, L.; Kang, A.; Zheng, X.; Wang, G. Rapid identification of ophiopogonins and ophiopogonones in *Ophiopogon japonicus* extract with a practical technique of mass defect filtering based on high resolution mass spectrometry. *J. Chromatogr. A* **2012**, *1227*, 234−244.

(20) Wu, L.; Hao, H.; Wang, G. LC/MS based tools and strategies on qualitative and quantitative analysis of herbal components in complex matrixes. *Curr. Drug Metab.* **2012**, *13*, 1251−1265.

(21) Xu, J.; Duan, J.; Xue, C.; Feng, T.; Dong, P.; Sugawara, T.; Hirata, T. Analysis and comparison of glucocerebroside species from three edible sea cucumbers using liquid chromatography-ion trap-time-of-flight mass spectrometry. *J. Agric. Food Chem.* **2011**, *59*, 12246−12253.

(22) Sun, J.; Huo, H. X.; Zhang, J.; Huang, Z.; Zheng, J.; Zhang, Q.; Zhao, Y. F.; Li, J.; Tu, P. F. Phenylpropanoid amides from the roots of *Solanum melongena* L. (Solanaceae). *Biochem. Syst. Ecol.* **2015**, *58*, 265−269.

(23) Handrick, V.; Vogt, T.; Frolov, A. Profiling of hydroxycinnamic acid amides in Arabidopsis thaliana pollen by tandem mass spectrometry. *Anal. Bioanal. Chem.* **2010**, *398*, 2789−2801.

(24) Yoshihara, T.; Takamatsu, S.; Sakamura, S. Three new phenolic amides from the roots of eggplant (*Solanum melongena* L.). *Agric. Biol. Chem.* **1978**, *42*, 623−627.

DOI: 10.1021/acs.jafc.5b00023
J. Agric. Food Chem. 2015, 63, 3426−3436

(25) Sadilova, E.; Stintzing, F. C.; Carle, R. Anthocyanins, colour and antioxidant properties of eggplant (*Solanum melongena* L.) and violet pepper (*Capsicum annuum* L.) peel extracts. *Z. Naturforsch., C* **2006**, *61*, 527−535.
(26) Wang, M.; Wu, C.; Cheng, Z.; Meng, H.; Zhang, M.; Zhang, H. Soil chemical property changes in eggplant/garlic relay intercropping systems under continuous cropping. *PLoS One* **2014**, *9*, 1−13.
(27) Zhang, J.; Guan, S.; Sun, J.; Chen, P.; Feng, R.; Chen, X.; Wu, W.; Yang, M.; Guo, D. Characterization and profiling of phenolic amides from *Cortex Lycii* by ultra-high performance liquid chromatography coupled with LTQ-Orbitrap mass spectrometry. *Anal. Bioanal. Chem.* **2015**, *407*, 581−595.
(28) Georgiev, L.; Chochkova, M.; Totseva, I.; Seizova, K.; Marinova, E.; Ivanova, G.; Ninova, M.; Najdenski, H.; Milkova, T. Anti-tyrosinase, antioxidant and antimicrobial activities of hydroxycinnamoylamides. *Med. Chem. Res.* **2013**, *22*, 4173−4182.
(29) Navarre, D. A.; Payyavula, R. S.; Shakya, R.; Knowles, N. R.; Pillai, S. S. Changes in potato phenylpropanoid metabolism during tuber development. *Plant Physiol. Biochem.* **2013**, *65*, 89−101.
(30) Hanson, P. M.; Yang, R. Y.; Tsou, S. C. S.; Ledesma, D.; Engle, L.; Lee, T. Diversity in eggplant (*Solanum melongena*) for superoxide scavenging activity, total phenolic, and ascorbic acid. *J. Food Compos. Anal.* **2006**, *19*, 594−600.
(31) Chong, E. S.; McGhie, T. K.; Heyes, J. A.; Stowell, K. M. Metabolite profiling and quantification of phytochemicals in potato extracts using ultra-high-performance liquid chromatography-mass spectrometry. *J. Sci. Food Agric.* **2013**, *93*, 3801−3808.

DOI: 10.1021/acs.jafc.5b00023
J. Agric. Food Chem. 2015, 63, 3426−3436

MATERIALS AND METHODS

Materials. Duck (*Anas platyrhynchos*) breasts were purchased from Suguo supermarket in Nanjing, China, and stored at −20 °C until use. Protamex (1.5 AU of N/g) was purchased from Novo Co. (Novozyme Nordisk, Bagsvaerd, Denmark). 1,1-Diphenyl-2-picrylhydrazyl free radical (DPPH•) and L-glutathione reduced (GSH) were obtained from Sigma Chemical Co. (St. Louis, MO). Acetonitrile (ACN) and formic acid were of chromatographic grade, and other chemicals used were of analytical grade.

Preparation of Enzymatic Hydrolysate from Duck Meat. Frozen duck breasts were thawed at 4 °C overnight, and then the skin and connective tissue were removed. The meat was chopped into pieces and mixed with distilled water to give a final protein content of 4% (w/v). The mixture was then homogenized for 1 min at 8000 rpm using a homogenizer (IKA T25 digital ultraturrax, IKA, Germany) with cooling in ice. The pH of the mixture was adjusted to 6.0 with a pH meter (FiveEasy 20, Mettler Toledo, Swiss), and Protamex was added at an enzyme-to-substrate ratio of 0.75/100 (w/w) after a preincubation at 50 °C for 10 min. During the reaction, the pH of the mixture was adjusted to 6.0 every 20 min by addition of 4 mol/L HCl solution. Enzymatic hydrolysis of the meat proteins was performed for 4 h to achieve an optimum level of hydrolysis and was then immediately heated at 100 °C for 10 min to terminate the hydrolysis. The reaction mixture was cooled to room temperature and then centrifuged (Allegra 64R centrifuge, Bechman Coulter, United States) at 10000*g* for 10 min. The supernatant was collected, lyophilized, and stored at 4 °C for further use.

Measurement of DPPH• Scavenging Activity. The DPPH• scavenging activity was evaluated according to the procedure described by Ajila et al.[22] with a slight modification. The sample group was obtained by mixing 0.5 mL of sample (1.0 mg/mL) with 0.5 mL of 0.2 mmol/L DPPH• dissolved in ethanol, the blank group consisted of aliquots of samples mixed 1:1 (v/v) with ethanol, and the control group consisted of aliquots of ethanol mixed 1:1 (v/v) with 0.2 mmol/L DPPH•. The mixtures were shaken and kept in the dark for 30 min at room temperature. Then the absorbance was measured at 517 nm using a multifunctional microplate reader (model Spectral Max M2e, Molecular Devices, United States). The DPPH• scavenging activity was calculated as follows:

$$\text{DPPH radical scavenging activity (\%)} = \left(1 - \frac{A_s - A_b}{A_c - A_b}\right) \times 100$$

where A_s, A_c, and A_b represent the absorbances of the sample, control, and blank groups.

Measurement of Fe^{2+}-Chelating Ability. The Fe^{2+}-chelating ability was measured according to the procedure described by Zhu et al.[23] with a slight modification. Briefly, 0.5 mL of sample (1.0 mg/mL) was mixed with 0.05 mL of $FeCl_2$ (2 mmol/L) and 0.2 mL of ferrozine (5 mmol/L). The mixture was kept at room temperature for 10 min prior to measurement of the absorbance at 562 nm. The chelating activity was calculated as follows:

$$\text{Fe}^{2+}\text{-chelating ability (\%)} = \frac{A_c - A_s}{A_c} \times 100$$

where A_s represents the absorbance of the samples and A_c represents the absorbance of the control in which distilled water replaced the sample solution.

Hydroxyl Radical (•OH) Scavenging Activity. The •OH scavenging activity was assayed according to the procedure described by You et al.[24] Briefly, 1 mL of sample (1.0 mg/mL) was thoroughly mixed with 0.6 mL of 1,10-phenanthroline monohydrate (5 mmol/L), 0.4 mL of phosphate buffer (0.2 mol/L, pH 7.4), 0.6 mL of $FeSO_4$ (50 mmol/L), and 0.6 mL of EDTA (15 mmol/L). Then 0.4 mL of 0.1% H_2O_2 was added. The mixture was incubated at 37 °C for 1 h prior to measurement of the absorbance at 536 nm. The •OH scavenging activity was calculated as follows:

$$\text{hydroxyl radical scavenging activity (\%)} = \frac{A_s - A_d}{A_n - A_d} \times 100$$

where A_s is the absorbance of the samples, A_d is the absorbance of the damaged group without sample solution, and A_n is the absorbance of the nondamaged group without H_2O_2.

Peptide Fractionation by Ultrafiltration. A 2.0 g mass of the lyophilized DMH was dissolved in 350 mL of distilled water and then fractionated by centrifuge tubes fixed with ultrafiltration membranes having molecular weight cutoffs (MWCOs) of 30000 and 10000 (Amicon Ultra-15, Millipore Co., Billerica, MA), consecutively. MWCO-1, MWCO-2, and MWCO-3 represent the fractions with molecular weight distributions of >30000, 30000−10000, and <10000, respectively. Each fraction was collected, lyophilized, and used for determination of DPPH• scavenging activity.

Peptide Separation by Gel Filtration Chromatography. MWCO-3 (1.0 mg/mL) in a 0.5 mL aliquot was subjected to a size exclusion chromatograph (5 × 5 cm) packed with Sephadex G-25 (Amersham Biosciences, Uppsala, Sweden) to fractionate peptides according to their molecular sizes. The column was eluted with distilled water at a flow rate of 0.5 mL/min and monitored at 280 nm. All fractions were collected and lyophilized for the determination of their DPPH• scavenging activity after being redissolved in distilled water. The strongest antioxidant activity fraction was further separated by ion exchange chromatography.

Peptide Separation by Ion Exchange Chromatography. The fraction (1.0 mg/mL) exhibiting the highest antioxidant activity in a 0.5 mL aliquot was loaded onto an anion exchange column (Mono Q 5/50 GL, internal diameter 5 mm, length 50 mm) equilibrated with 20 mmol/L Tris−HCl buffer (pH 8.0) and eluted with a linear salt gradient (0−0.3 mol/L NaCl, over a 15 min period) in the same buffer at a flow rate of 1 mL/min and monitored at 280 nm. Each fraction was pooled and lyophilized for determination of antioxidant activity.

Identification of Antioxidant Peptides by LC−MS/MS. The most effective fraction derived from ion exchange chromatography was first desalted using an OASIS HLB cartridge (Waters Inc., United States). The peptides were then analyzed by nano-LC−MS/MS with a coupled Dionex Ultimate 3000 nano-LC system (Thermo Fisher Scientific Ltd., Fremont, CA) and a linear quadrupole ion trap Orbitrap (LTQ Orbitrap XL) mass spectrometer (Thermo Electron, Bremen, Germany) equipped with a nanoelectrospary ion source. Briefly, 2 μL of sample was injected, in triplicate, onto an Acclaim PepMap 100 column (75 μm × 2 cm, nanoViper C18, 3 μm, 100 Å) (Dionex, Sunnyvale, CA) for nano-LC separation at a flow rate of 300 nL/min. Mobile phases used for LC were (A) 0.1% formic acid in water and (B) 0.08% formic acid in 80% ACN. Gradient elution was carried out according to the following process: 0−8 min, isocratic elution 2% solvent B; 8−12 min, linear gradient 2%−15% solvent B; 12−93 min, linear gradient 15%−45% solvent B; 93−98 min, linear gradient 45%−98% solvent B; 98−121 min, isocratic elution 98% solvent B; 121−122 min, isocratic elution 2% solvent B. The mass spectrometer operated in positive ion mode, with a capillary temperature of 200 °C and a capillary voltage of 2.2 kV, in the mass range from m/z 350 to 1800 in the Orbitrap with a resolution of 60000 at m/z 400, allowing the sequential isolation of the five signal intensity ions for high-energy collisional dissociation (HCD) at a collision energy of 35 V. MS/MS was performed using the dynamic exclusion mode to exclude the previously selected ions during the repeated cycle of 60 s.

The acquired MS/MS data were analyzed using PEAKS de novo sequencing (PEAKS Studio 6.0, BSI, Canada). Basic parameter settings included a precursor mass tolerance of 10 ppm, a product mass tolerance of 0.02 Da, and a "no-enzyme" constraint. Oxidation of Met was used as a variable modification. Only those with a "de novo" peak studio score over 75% (average local confidence, ALC) were considered. The proteome of duck (*Anas*) was downloaded from the Uniprot protein database.

Synthetic Peptides. The peptide sequences derived from duck meat were synthesized by the solid-phase peptide procedure, using the

DOI: 10.1021/jf506120w
J. Agric. Food Chem. 2015, 63, 3437−3444

Table 1. Antioxidant Activities of DMH Prepared Using Protamex

	concn (mg/mL)	DPPH• scavenging activity[a] (%)	•OH scavenging activity[a] (%)	Fe^{2+}-chelating activity (%)
hydrolysate	1.0	82.09 ± 1.41 b	36.54 ± 2.38 b	78.57 ± 1.40
GSH	1.0	94.94 ± 0.82 a	75.35 ± 1.56 a	

[a]Different letters (a, b) in the same column indicate significant differences ($p < 0.05$).

Fmoc-protected amino acid synthesis method. These peptides were provided by Gen Script (Nanjing) Co., Ltd. Their purity was >95%.

Statistical Analysis. All the tests were repeated in triplicate. Data were evaluated using SAS 8.1 software. Values were expressed as the mean ± standard deviation (SD). The mean values were analyzed using the one-way analysis of variance (ANOVA) test. Duncan's multiple range tests were employed to determine any significant difference between treatments. The significant difference was determined with a 95% confidence interval ($p < 0.05$).

RESULTS AND DISCUSSION

Antioxidant Activity of DMH. The antioxidant properties of peptides result from their free radical scavenging, metal ion chelating, and single oxygen quenching activities.[25] In this study, the antioxidant activities of DMH were evaluated by DPPH• scavenging activity, •OH scavenging activity, and Fe^{2+}-chelating ability (Table 1).

DPPH• is a stable free radical that shows maximum absorbance at 517 nm. When DPPH radicals encounter proton-donating substrates such as antioxidants, the radicals are scavenged and the absorbance is reduced.[26] DMH showed high DPPH• scavenging activity at a concentration of 1.0 mg/mL (82.09%), whereas 1.0 mg/mL GSH exhibited nearly 95% scavenging activity on the DPPH radical (Table 1). This value is somewhat higher than that of many other protein hydrolysates. The chicken breast protein hydrolysate prepared by papain exhibited about 50% DPPH• scavenging activity at a concentration of 1.28 mg/mL.[10] The DPPH• scavenging activities in various hydrolysates (1.0 mg/mL) of round scad muscle were as follows: Alcalase (39.36%), Nnutral (32.33%), trypsin (39.37%), papain (40.21%), and pepsin (32.63%). These values are lower than that found for DMH.[27] Bougatef et al.[28] reported that smooth hound muscle hydrolysates prepared using low molecular weight (LMW) alkaline protease exhibited 76.7% DPPH• scavenging activity at a concentration of 3.0 mg/mL. Thus, we can infer that DMH contained antioxidant peptides that were capable of scavenging radicals.

•OH is the most reactive radical that can induce severe damage to adjacent biomolecules and thereby cause aging, cancer, and other diseases.[29] Therefore, removal of •OH could be one of the most effective defenses against these various diseases. The •OH scavenging activity for GSH (1.0 mg/mL) was about 75%. DMH exhibited a comparable higher •OH scavenging capacity, reaching a scavenging activity of 36.54% at a concentration of 1.0 mg/mL, comparable to that of bullfrog skin protein hydrolysate (34.5%) prepared using papain at a concentration of 1.5 mg/mL,[30] but lower than the pepsin hydrolysate from duck skin byproducts with about 50% •OH scavenging activity at a concentration of 0.55 mg/mL.[19] Thus, we can infer that DMH contained some antioxidant peptides which could convert free radicals to more stable products and terminate the radical chain reactions.

Transition-metal ions such as iron and copper ions are strong agents to catalyze the generation of free radicals via the Fenton reaction.[25] Thus, the chelation of metal ions contributes to antioxidation. As shown in Table 1, the hydrolysate exhibited an effective chelating effect on Fe^{2+} (78.57%).

Purification of Antioxidant Peptides from DMH. DMH was separated into three groups using ultrafiltration membranes (MWCO = 30000 and 10000): MWCO-1 (MW > 30000), MWCO-2 (MW = 10000−30000), and MWCO-3 (MW < 10000). The DPPH• scavenging activities were 29.01 ± 0.60%, 34.42 ± 1.61%, and 83.17 ± 0.73% at 1.0 mg/mL for MWCO-1, MWCO-2, and MWCO-3, respectively (Table 2). The lower molecular weight fraction had higher DPPH• scavenging activity than the higher molecular weight fractions. Therefore, the MWCO-3 fraction was selected for further study.

Table 2. Purification of Antioxidant Peptides from DMH (1.0 mg/mL)

step	DPPH• scavenging activity (%)	purification (fold)	recovery rate (%)
crude	82.09 ± 1.41	1.00	100
ultrafiltration			
>30 kDa	29.01 ± 0.60	0.35	8.21
10−30 kDa	34.42 ± 1.61	0.42	9.53
<10 kDa	83.17 ± 0.73	1.01	69.57
gel filtration chromatography (fraction B)	88.64 ± 1.98	1.08	40.90
ion exchange chromatography (fraction B5)	93.63 ± 0.13	1.14	6.71

The results of the separation of the MWCO-3 fraction by size exclusion chromatography is shown in Figure 1A, where peptides were separated into three fractions (A, B, and C) according to their molecular sizes. The DPPH• scavenging activities of these fractions, after lyophilization and solubilization, are presented in Figure 1B. We found that fractions A, B, and C had radical scavenging activities on DPPH of 40.86 ± 1.10%, 88.64 ± 1.98%, and 33.47 ± 1.18%, respectively, at 1.0 mg/mL, with fraction B showing the highest DPPH• scavenging activity compared to the other fractions.

Fraction B was further separated by anion exchange chromatography into six fractions (B1, B2, B3, B4, B5, and B6) (Figure 2A). Fraction B5 showed the highest DPPH• scavenging activity with a value of 93.63% (Figure 2B). Fraction B5 was further purified and identified by nano-LC−MS/MS for amino acid sequencing.

The DPPH• scavenging activity and stage of purification of the peptides are summarized in Table 2. DMH, MWCO-3, B, and B5 exhibited quite the same DPPH• scavenging activity at a concentration of 1.0 mg/mL; the purification of B5 was 1.14-fold (Table 2). Apart from the antioxidant peptides produced by Protamex, DMH and MWCO-3 may contain antioxidants that are naturally present in meat (e.g., amino acids, carnosine, anserine, conjugated linoleic acid, α-tocopherol, carotenoids, ubiquinone, uric acid, and polyamines)[31] or that are generated by endogenous enzymes during rigor mortis and resolution of rigor mortis.[32] Sacchetti et al.[33] reported that the hydrophilic and lipophilic fractions of poultry meat showed radical scavenging activity. The hydrophilic antioxidants present in

DOI: 10.1021/jf506120w
J. Agric. Food Chem. 2015, 63, 3437−3444

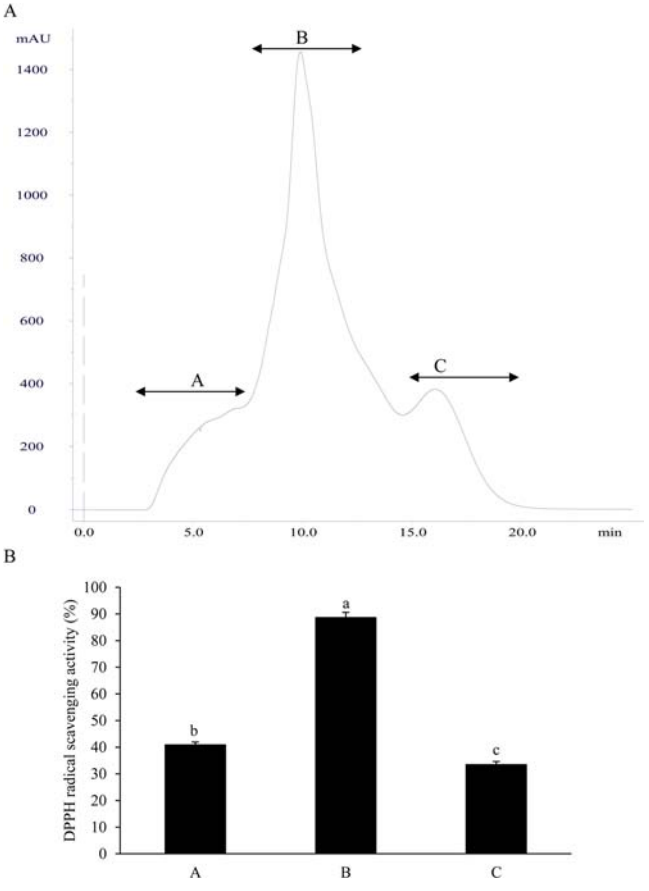

Figure 1. (A) Size exclusion chromatography of antioxidant peptide from duck meat hydrolysate by a Sephadex column packed with Sephadex G-25. Elution was done at 0.5 mL/min with distilled water using a UV detector at 280 nm. (B) DPPH radical scavenging activity of fractions obtained by size exclusion chromatography.

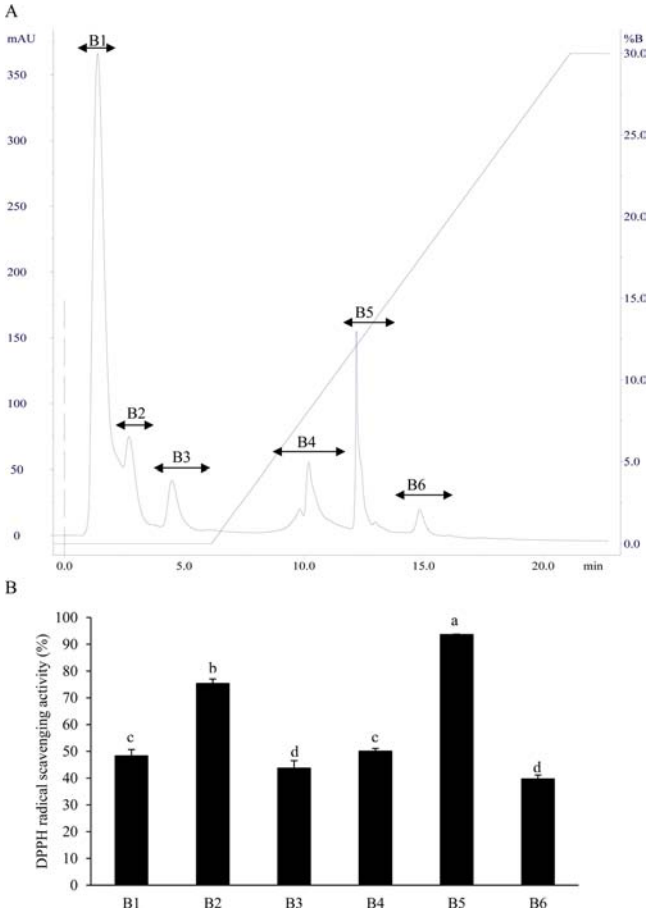

Figure 2. (A) Anion exchange chromatography of active fraction B obtained from a Sephadex G-25 column by Mono Q 5/50 GL. The elution was performed at a 1 mL/min flow rate with a linear NaCl gradient (0−0.3 M) in 20 mM Tris−HCl buffer (pH 8.0) using a UV detector at 280 nm. (B) DPPH radical scavenging activity of fractions obtained by ion exchange chromatography.

meat were thought to be endogenous and could be representative of peptides, uric acid, ascorbate, antioxidant enzymes, and polyamines or exogenous.[33] The lipophilic antioxidants in meat are represented by carotenoids, α-tocopherol, and ubiquinone.[33] These antioxidants may increase the antioxidant activity of DMH and MWCO-3, leading to their DPPH$^{\bullet}$ scavenging activity being close to those of fractions B and B5.

Identification of Antioxidant Peptides by Tandem Mass Spectrometry. For amino acid sequence identification, fraction B5 was further purified and identified by LC−MS/MS. Twenty-nine peptides were found in fraction B5 (data not shown). All the sequences of the peptides identified in this work were searched in BLAST (http://blast.ncbi.nlm.nih.gov/Blast.cgi), among which seven peptides showed 100% homology with the duck (*Anas*) proteome. The MS/MS spectra of these seven peptides are shown in Figure 3. The seven peptides were synthesized to evaluate their DPPH$^{\bullet}$ scavenging activities, $^{\bullet}$OH scavenging activities, and Fe^{2+}-chelating abilities. They had different potencies of antioxidant activities. The highest DPPH$^{\bullet}$ scavenging activity was found to be about 90% at a 1.0 mg/mL concentration of peptides LQAEVEELRAALE, GYDLGEAEFARIM, and IEDPFDQD-DWGAWKK, which was similar to that of GSH. In addition, the LQAEVEELRAALE peptide showed the highest Fe^{2+}-chelating ability, with a value of 87.13%. Peptides NWDDMEK and IEDPFDQDDWGAWKK exhibited the highest $^{\bullet}$OH scavenging activity, with values of 43.34% and 46.51%, at a concentration of 1.0 mg/mL, lower than that of the positive control GSH of about 74.68% (Table 3).

The antioxidant activity of peptides is closely related to their molecular weight, amino acid composition, sequences, and hydrophobicity.[34,35] The identified peptides were in a molecular weight range of 938.38−1851.86 that consisted of 7−15 amino acid residues (Table 3). The results confirmed that typical antioxidant peptides usually contain 2−20 amino acid residues with molecular weights of less of 6000.[4] Other research groups have purified and identified antioxidant peptides which had molecular weights similar to those found in this study, e.g., peptides from tuna backbone protein hydrolysates (1519),[36] venison protein hydrolysates (985, 1121),[7] hoki frame protein hydrolysates (1801),[8] duck skin byproduct hydrolysates (941.43),[19] and yellowfin sole frame protein hydrolysates (1300).[5]

It has been reported that hydrophobic amino acids have significant effects on radical scavenging.[34] For peptides, a high content of hydrophobic amino acids could increase their antioxidant activity.[37] Similar results have also been reported by Ren et al.,[38] who found that hydrophobic peptides contributed more to the antioxidant activities of peptides than the hydrophilic peptides. Zarei et al.[39] identified nine antioxidant peptides with high DPPH$^{\bullet}$ scavenging activities and found that

DOI: 10.1021/jf506120w
J. Agric. Food Chem. 2015, 63, 3437−3444

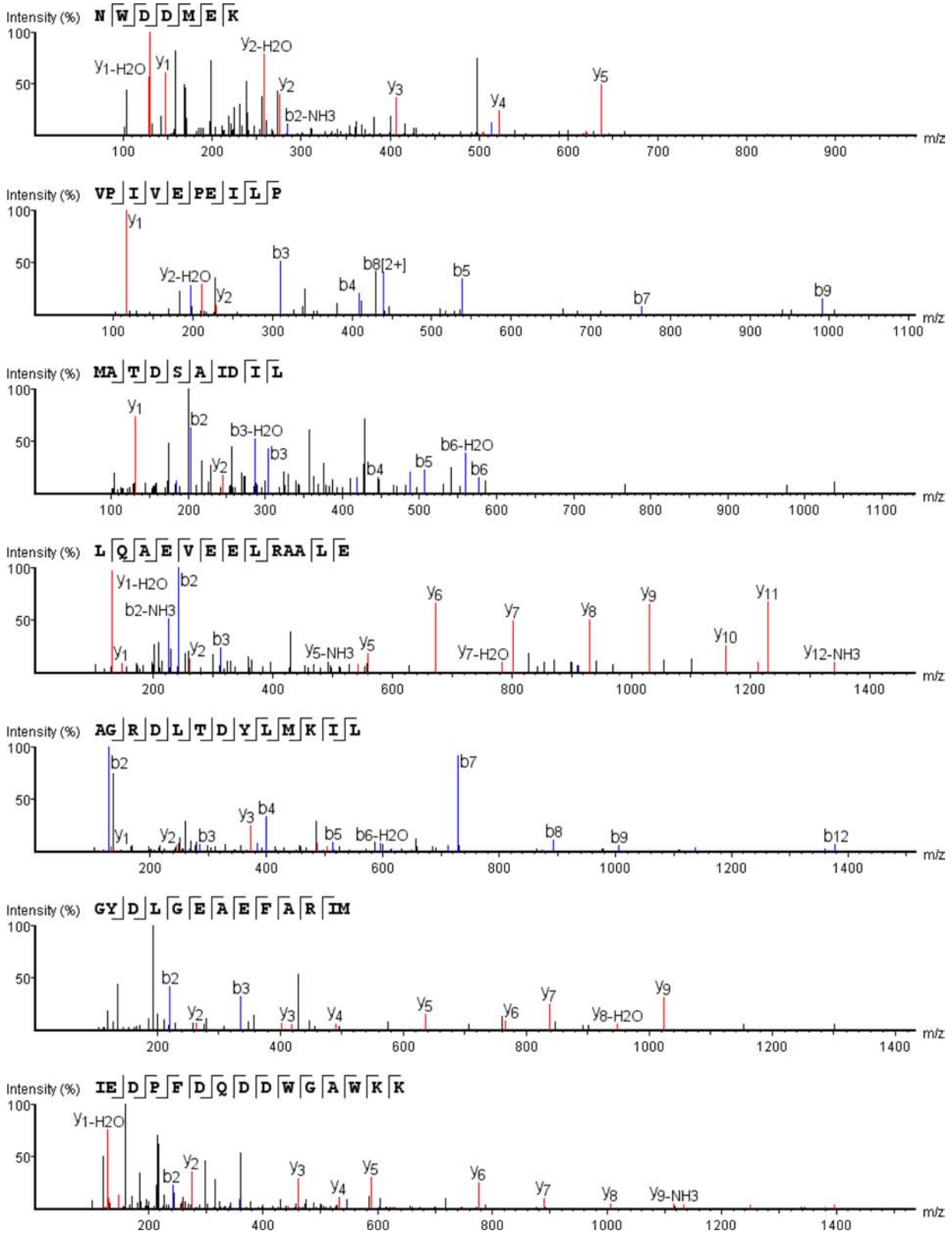

Figure 3. MS/MS spectra of seven peptides identified by a nano-LC system coupled to a linear quadrupole ion trap Orbitrap (LTQ Orbitrap XL) mass spectrometer.

the content of hydrophobic amino acids of each peptide was more than 50%. In the current study, the content of hydrophobic amino acids of NWDDMEK was less than 29%, whereas the percentage of hydrophobic amino acids of other peptides was about 50%. In addition, the existence of leucine (L) and isoleucine (I) at N-termini could increase the accessibility of peptides to the nonpolar phase, allowing full antioxidant capacity.[40] Glycine (G) has been suggested to play a vital role in the antioxidant activity of some peptides.[41−44] In the present study, LQAEVEELRAALE, GYDLGEAEFARIM,

DOI: 10.1021/jf506120w
J. Agric. Food Chem. 2015, 63, 3437−3444

Table 3. Antioxidant Activities and Characteristics of Peptides Isolated from Fraction B5 Using Anion Exchange Chromatography and Identified by LC−MS/MS

no.	peptide	av local confidence (%)	intensity	MW	accession	DPPH• scavenging activity[a] (%)	•OH scavenging activity[a] (%)	Fe^{2+}-chelating activity[a] (%)
1	NWDDMEK	96	3.21×10^6	938.4	gi 483524575	16.36 ± 1.03 g	43.34 ± 0.74 c	37.20 ± 3.28 d
2	VPIVEPEILP	83	1.17×10^6	1106.7	gi 483524470	54.54 ± 1.02 f	31.12 ± 0.34 d	6.28 ± 1.26 f
3	MATDSAIDIL	77	4.43×10^7	1050.5	gi 514730283	75.47 ± 0.79 e	20.00 ± 1.06 e	14.48 ± 1.00 e
4	LQAEVEELRAALE	92	8.89×10^7	1471.8	gi 514730283	93.36 ± 0.53 b	20.52 ± 0.61 e	87.13 ± 0.47 a
5	AGRDLTDYLMKIL	90	1.29×10^6	1007.2	gi 483524575	85.45 ± 0.23 d	30.75 ± 0.20 d	74.74 ± 0.24 b
6	GYDLGEAEFARIM	83	1.26×10^6	1472.7	gi 483507988	91.81 ± 1.84 bc	31.30 ± 0.31 d	58.94 ± 0.52 c
7	IEDPFDQDDWGAWKK	95	1.15×10^8	1851.9	gi 483507332	90.39 ± 0.65 c	46.51 ± 0.16 b	
8	GSH					95.24 ± 0.45 a	74.68 ± 0.63 a	

[a]Different letters (a−g) in the same column indicate significant differences ($p < 0.05$).

and IEDPFDQDDWGAWKK were found to have higher DPPH• scavenging activity, presumably due to the L, G, or I at the N-terminal. Furthermore, the amino acid sequence of the peptide might play an important role in the antioxidant activity. The peptide segment EEL contained in the peptide LQAEVEELRAALE with high Fe^{2+}-chelating ability was previously identified as part of the antioxidant peptides EELDNALN and VPSIDDQEELM generated from the hydrolysis of porcine myofibrillar proteins using papain for 24 h. The peptides EELDNALN and VPSIDDQEELM exhibited DPPH• scavenging activity and metal-chelating activity.[11] The segment EEL was also present in the peptidic sequence of the antioxidant peptide YVEEL generated from the hydrolysis of milk proteins.[44] Alanine (A) and leucine (L) might be responsible for the metal-chelating activity of peptides, evidenced by the fact that two peptides isolated from tuna dark muscle hydrolysates with DPPH• scavenging activity and Fe^{2+}-chelating ability contained A and L.[45]

However, the peptide NWDDMEK, with a low content of hydrophobic amino acid residues, had a high hydroxyl radical scavenging activity. Apart from its agreement with the reported antioxidant peptide size, this could be mainly explained by the existence of tryptophan (W) in the peptide sequence. The indolyl-containing amino acid W had the capacity to donate protons to electron-deficient radicals.[25] A study conducted by Tsopmo et al.[46] claimed that W released from human milk upon gastrointestinal digestion may have the potential to act as a powerful radical scavenger.

Antioxidant peptides prepared by enzymes have potential application as antioxidant agents in nutritional supplements and food systems. There are antioxidant applications of commercially available nutraceuticals in some countries, such as LIQUAMEN prepared from molva, which helps in reducing oxidative stress.[47] Khaled et al.[48,49] studied the antioxidant activities of the sardinelle protein hydrolysates (SPHs). In an in vitro test, the SPHs showed high DPPH• scavenging activity and metal-chelating activity. While in an in vivo test, the treatment of rats with SPHs reduced the malondialdehyde (MDA) concentration and increased the activities of antioxidant enzymes (superoxide dismutase, glutathione peroxidase, and catalase) and high-density lipoprotein cholesterol. Egg-yolk protein hydrolysates (0.5 mg/mL) with 83.5% DPPH• scavenging activity and 74.2% •OH scavenging activity effectively inhibited 2-thiobarbituric acid reactive substance (TBARS) formation from ground beef and tuna homogenates.[50] Potato protein hydrolysates with radical scavenging and metal ion chelating ability also inhibited lipid oxidation in muscle foods.[51] In our study, antioxidant peptides such as LQAEVEELRAALE, IEDPFDQDDWGAWKK, AGRALTAYLMKIL, and GYDLGEAEFARIM showed high free radical scavenging activity and metal ion chelating ability (Table 3), with potential use in food systems and nutraceuticals. However, the application of these peptides in foods and animal models should be further studied to confirm the speculation.

■ ASSOCIATED CONTENT

Supporting Information

DPPH• scavenging activity of each fraction from gel filtration chromatography and ion exchange chromatography. This material is available free of charge via the Internet at http://pubs.acs.org.

■ AUTHOR INFORMATION

Corresponding Author

*Phone: +86-25-84396808. Fax: +86-25-84396808. E-mail: mhuang@njau.edu.cn.

Funding

This research was funded by the Special Fund for Agro-scientific Research in the Public Interest (Grant 201303083-2) and National Natural Science Foundation of China (Grants 31171706 and 31371794).

Notes

The authors declare no competing financial interest.

■ ACKNOWLEDGMENTS

We thank Dr. Ron Tume (CSIRO Food and Nutrition Flagship, QLD, Australia) for his helpful discussion and manuscript revision.

■ ABBREVIATIONS USED

DPPH•, 1,1-diphenyl-2-picrylhydrazyl radical; •OH, hydroxyl radical; GSH, L-glutathione reduced; nano-LC−ESI LTQ-Orbitrap MS/MS, nano liquid chromatography equipped with electrospray ionization and connected to a linear quadrupole ion trap Orbitrap mass spectrometer

DOI: 10.1021/jf506120w
J. Agric. Food Chem. 2015, 63, 3437−3444

REFERENCES

(1) Ghouleh, I. A.; Khoo, N. K. H.; Knaus, U. G.; Griendling, K. K.; Touyz, R. M.; Thannickal, V. J.; Barchowsky, A.; Nauseef, W. M.; Kelley, E. E.; Bauer, P. M.; Darley-Usmar, V.; Shiva, S.; Cifuentes-Pagano, E.; Freeman, B. A.; Gladwin, M. T.; Pagano, P. J. Oxidases and peroxidases in cardiovascular and lung disease: New concepts in reactive oxygen species signaling. *Free Radical Biol. Med.* **2011**, *51*, 1271−1288.

(2) Qian, Z. J.; Jung, W. K.; Byun, H. G.; Kim, S. K. Protective effect of an antioxidative peptide purified from gastrointestinal digests of oyster, *Crassostrea gigas* against free radical induced DNA damage. *Bioresour. Technol.* **2008**, *99*, 3365−3371.

(3) Girgih, A. T.; He, R.; Malomo, S.; Offengenden, M.; Wu, J.; Aluko, R. E. Structural and functional characterization of hemp seed (*Cannabis sativa* L.) protein-derived antioxidant and antihypertensive peptides. *J. Funct. Foods* **2014**, *6*, 384−394.

(4) Sarmadi, B. H.; Ismail, A. Antioxidative peptides from food proteins: A review. *Peptides* **2010**, *31*, 1949−1956.

(5) Jun, S. Y.; Park, P. J.; Jung, W. K.; Kim, S. K. Purification and characterization of an antioxidant peptide from enzymatic hydrolysate of yellowfin sole (*Limanda aspera*) frame protein. *Eur. Food Res. Technol.* **2004**, *219*, 20−26.

(6) Je, J. Y.; Park, P. J.; Kim, S. K. Antioxidant activity of a peptide isolated from Alaska pollack (*Theragra chalcogramma*) frame protein hydrolysate. *Food Res. Int.* **2005**, *38*, 45−50.

(7) Kim, E. K.; Lee, S. J.; Jeon, B. T.; Moon, S. H.; Kim, B.; Park, T. K.; Han, J. S.; Park, P. J. Purification and characterisation of antioxidative peptides from enzymatic hydrolysates of venison protein. *Food Chem.* **2009**, *114*, 1365−1370.

(8) Kim, S. Y.; Je, J. Y.; Kim, S. K. Purification and characterization of antioxidnat peptide from hoki (*Johnius belengerii*) frame protein by gastrointestinal digestion. *J. Nutr. Biochem.* **2007**, *18*, 31−38.

(9) You, L. J.; Zhao, M. M.; Regenstein, J. M.; Ren, J. Y. Purification and indentification of antioxidative peptides from loach (*Misgurnus anguillicaudatus*) protein hydrolysate by consecutive chromatography and electrospray ionization-mass spectrometry. *Food Res. Int.* **2010**, *43*, 1167−1173.

(10) Sun, Y.; Pan, D.; Guo, Y.; Li, J. Purification of chicken breast protein hydrolysate and analysis of its antioxidant activity. *Food Chem. Toxicol.* **2012**, *50*, 3397−3404.

(11) Saiga, A.; Tanabe, S.; Nishimura, T. Antioxidant activity of peptides obtained from porcine myofibrillar proteins by protease treatment. *J. Agric. Food Chem.* **2003**, *51*, 3661−3667.

(12) Wang, Q.; Li, W.; He, Y.; Ren, D.; Kow, F.; Song, L.; Yu, X. Novel antioxidative peptides from the protein hydrolysate of oysters (*Crassostrea talienwhanensis*). *Food Chem.* **2014**, *145*, 991−996.

(13) Zhu, C. Z.; Zhang, W. G.; Zhou, G. H.; Xu, X. L.; Kang, Z. L.; Yin, Y. Isolation and identification of antioxidant peptides from jinhua ham. *J. Agric. Food Chem.* **2013**, *61*, 1265−1271.

(14) Samaranayaka, A. G. P.; Li-Chan, E. G. P. Food-derived peptidic antioxidants: A review of their production, assessment, and potential applications. *J. Funct. Foods* **2011**, *3*, 229−254.

(15) Schaafsma, G. Safety of protein hydrolysates, fractions thereof and bioactive peptides in human nutrition. *Eur. J. Clin. Nutr.* **2009**, *1*, 8.

(16) Himaya, S. W. A.; Ryu, B.; Ngo, D. H.; Kim, S. K. Peptide isolated from Japanese flounder skin gelatin protects against cellular oxidative damage. *J. Agric. Food Chem.* **2012**, *60*, 9112−9119.

(17) You, L.; Zhao, M.; Liu, R. H.; Regenstein, J. M. Antioxidant and antiproliferative activities of loach (*Misgurnus anguillicaudatus*) peptides prepared by papain digestion. *J. Agric. Food Chem.* **2011**, *59*, 7948−7953.

(18) Nazeer, R. A.; Kumar, N. S. S.; Ganesh, R. J. In vitro and in vivo studies on the antioxidant activity of fish peptides isolated from the croaker (*Otolithes ruber*) muscle protein hydrolysate. *Peptides* **2012**, *35*, 261−268.

(19) Lee, S. J.; Kim, Y. S.; Hwang, J. W.; Kim, E. K.; Moon, S. H.; Jeon, B. T.; Jeon, Y. J.; Kim, J. M.; Park, P. J. Purification and characterization of a novel antioxidative peptide from duck skin by-products that protects liver against oxidative damage. *Food Res. Int.* **2012**, *49*, 285−295.

(20) Lee, S. J.; Kim, E. K.; Hwang, J. W.; Oh, H. J.; Cheong, S. H.; Moon, S. H.; Jeon, B. T.; Lee, S. M.; Park, P. J. Purification and characterisation of an antioxidative peptide from enzymatic hydrolysates of duck processing by-products. *Food Chem.* **2010**, *123*, 216−220.

(21) Lee, S. J.; Kim, K. H.; Kim, Y. S.; Kim, E. K.; Hwang, J. W.; Lim, B. O.; Moon, S. H.; Jeon, B. T.; Jeon, Y. J.; Ahn, C. B.; Park, P. J. Biological activity from the gelatin hydrolysates of duck skin by-products. *Process Biochem.* **2012**, *47*, 1150−1154.

(22) Ajila, C. M.; Gassara, F.; Brar, S. K.; Verma, M.; Tyagi, R. D.; Valéro, J. R. Polyphenolic antioxidant mobilization in apple pomace by different methods of solid-state fermentation and evaluation of its antioxidant activity. *Food Bioprocess Technol.* **2010**, *5*, 2697−2707.

(23) Zhu, C. Z.; Zhang, W. G.; Kang, Z. L.; Zhou, G. H.; Xu, X. L. Stability of an antioxidant peptide extracted from Jinhua ham. *Meat Sci.* **2014**, *96*, 783−789.

(24) You, L.; Zhao, M.; Regenstein, J. M.; Ren, J. Changes in the antioxidant activity of loach (*Misgurnus anguillicaudatus*) protein hydrolysates during a simulated gastrointestinal digestion. *Food Chem.* **2010**, *120*, 810−816.

(25) Zhang, M.; Mu, T. H.; Sun, M. J. Purification and identification of antioxidant peptides from sweet potato protein hydrolysates by Alcalase. *J. Funct. Foods* **2014**, *7*, 191−200.

(26) Escudero, E.; Aristoy, M. C.; Nishimura, H.; Arihara, K.; Toldra, F. Antihypertensive effect and antioxidant activity of peptide fractions extracted from Spanish dry-cured ham. *Meat Sci.* **2012**, *91*, 306−311.

(27) Jiang, H.; Tong, T.; Sun, J.; Xu, Y.; Zhao, Z.; Liao, D. Purification and characterization of antioxidative peptides from round scad (*Decapterus maruadsi*) muscle protein hydrolysate. *Food Chem.* **2014**, *154*, 158−163.

(28) Bougatef, A.; Hajji, M.; Balti, R.; Lassoued, I.; Triki-Ellouz, Y.; Nasri, M. Antioxidant and free radical-scavenging activities of smooth hound (*Mustelus mustelus*) muscle protein hydrolysates obtained by gastrointestinal proteases. *Food Chem.* **2009**, *114*, 1198−1205.

(29) Jeong, H. J.; Park, J. H.; Lam, Y.; de Lumen, B. O. Characterization of lunasin isolated from soybean. *J. Agric. Food Chem.* **2003**, *51*, 7901−7906.

(30) Qian, Z. J.; Jung, W. K.; Kim, S. K. Free radical scavenging activity of a novel antioxidative peptide purified from hydrolysate of bullfrog skin, *Rana catesbeiana Shaw*. *Bioresour. Technol.* **2008**, *99*, 1690−1698.

(31) Bernardini, R. D.; Harnedy, P.; Bolton, D.; Kerry, J.; O'Neil, E.; Mullen, A. M.; Hayes, M. Antioxidant and antimicrobial peptidic hydrolysates from muscle protein source and by-products. *Food Chem.* **2011**, *124*, 1296−1307.

(32) Lafarga, T.; Hayes, M. Bioactive peptides from meat muscle and by-products: Generation, functionality and application as functional ingredients. *Meat Sci.* **2014**, *98*, 227−239.

(33) Sacchetti, G.; Mattia, C. D.; Pittia, P.; Martino, G. Application of a radical scavenging activity test to measure the total antioxidant activity of poultry meat. *Meat Sci.* **2008**, *80*, 1081−1085.

(34) Rajapakse, N.; Mendis, E.; Jung, W. K.; Je, J. Y.; Kim, S. K. Purification of a radical scavenging peptide from fermented mussel sauce and its antioxidant properties. *Food Res. Int.* **2005**, *38*, 175−182.

(35) Escudero, E.; Mora, L.; Fraser, P. D.; Aristoy, M. C.; Toldra, F. Identification of novel antioxidant peptides generated in Spanish dry-cured ham. *Food Chem.* **2013**, *138*, 1282−1288.

(36) Je, J. Y.; Qian, Z. J.; Byun, H. G.; Kim, S. K. Purification and characterization of an antioxidant peptide obtained from tuna backbone protein by enzymatic hydrolysis. *Process Biochem.* **2007**, *42*, 840−846.

(37) Zhang, Y.; Duan, X.; Zhuang, Y. Purification and characterization of novel antioxidant peptides from enzymatic hydrolysates of tilapia (*Oreochromis niloticus*) skin gelatin. *Peptides* **2012**, *38*, 13−21.

(38) Ren, J.; Zhao, M.; Shi, J.; Wang, J.; Jiang, Y.; Cui, C.; Kakuda, Y.; Xue, S. J. Purification and identification of antioxidant peptides from grass carp muscle hydrolysates by consecutive chromatography and

DOI: 10.1021/jf506120w
J. Agric. Food Chem. 2015, 63, 3437−3444

electrospray ionization-mass spectrometry. *Food Chem.* **2008**, *108*, 727−736.
(39) Zarei, M.; Ebrahimpour, A.; Abdul-Hamid, A.; Anwar, F.; Bakar, F. A.; Philip, R.; Saari, N. Identification and characterization of papain-generated antioxidant peptides from palm kernel cake proteins. *Food Res. Int.* **2014**, *62*, 726−734.
(40) Ranathunga, S.; Rajapakse, N.; Kim, S. K. Purification and characterization of antioxidative peptide derived from muscle of conger eel (*Conger myriaster*). *Eur. Food Res. Technol.* **2006**, *222*, 310−315.
(41) Chen, H. M.; Muramoto, K.; Yamauchi, F.; Nokihara, K. Antioxidant activity of designed peptides based on the antioxidative peptide isolated from digests of a soybean protein. *J. Agric. Food Chem.* **1996**, *44*, 2619−2623.
(42) Mendis, E.; Rajapakse, N.; Kim, S. K. Antioxidant properties of a radical-scavenging peptide purified from enzymatically prepared fish skin gelatin hydrolysate. *J. Agric. Food Chem.* **2005**, *53*, 581−587.
(43) Rajapakse, N.; Mendis, E.; Byun, H. G.; Kim, S. K. Purification and in vitro antioxidative effects of giant squid muscle peptides on free radical-mediated oxidative systems. *J. Nutr. Biochem.* **2005**, *16*, 562−569.
(44) Pihlanto, A. Antioxidative peptides derived from milk proteins. *Int. Dairy J.* **2006**, *16*, 1306−1314.
(45) Hus, K. C. Purification of antioxidant peptides prepared from enzymatic hydrolysates of tuna dark muscle by-product. *Food Chem.* **2010**, *122*, 42−48.
(46) Tsopmo, A.; Diehl-Jones, B. W.; Aluko, R. E.; Kitts, D. D.; Elisia, I.; Friel, J. K. Tryptophan released from mother's milk has antioxidant properties. *Pediatr. Res.* **2009**, *66*, 614−618.
(47) Chalamaiah, M.; Dinesh Kumar, B.; Hemalatha, R.; Jyothirmayi, T. Fish protein hydrolysates: Proximate composition, amino acid composition, antioxidant activities and applications: A review. *Food Chem.* **2012**, *135*, 3020−3038.
(48) Khaled, H. B.; Ktari, N.; Ghorbel-Bellaaj, O.; Jridi, M.; Lassoued, I.; Nasri, M. Composition, functional properties and in vitro antioxidant activity of protein hydrolysates prepared from sardinelle (*Sardinella aurita*) muscle. *J. Food Sci. Technol.* **2014**, *51*, 622−633.
(49) Khaled, H. B.; Ghlissi, Z.; Chtourou, Y.; Hakim, A.; Ktari, N.; Fatma, M. A.; Barkia, A.; Sahnoun, Z. Effect of protein hydrolysates from sardinelle (*Sardinella aurita*) on the oxidative status and blood lipid profile of cholesterol-fed rats. *Food Res. Int.* **2012**, *45*, 60−68.
(50) Sakanaka, S.; Tachibana, Y. Active oxygen scavenging activity of egg-yolk protein hydrolysates and their effects on lipid oxidation. *Food Chem.* **2006**, *95*, 243−249.
(51) Wang, L. L.; Xiong, Y. L. Inhibition of lipid oxidation in cooked beef patties by hydrolyzed potato protein in related to its reducing and radical scavenging ability. *J. Agric. Food Chem.* **2005**, *53*, 9186−9192.

DOI: 10.1021/jf506120w
J. Agric. Food Chem. 2015, 63, 3437−3444

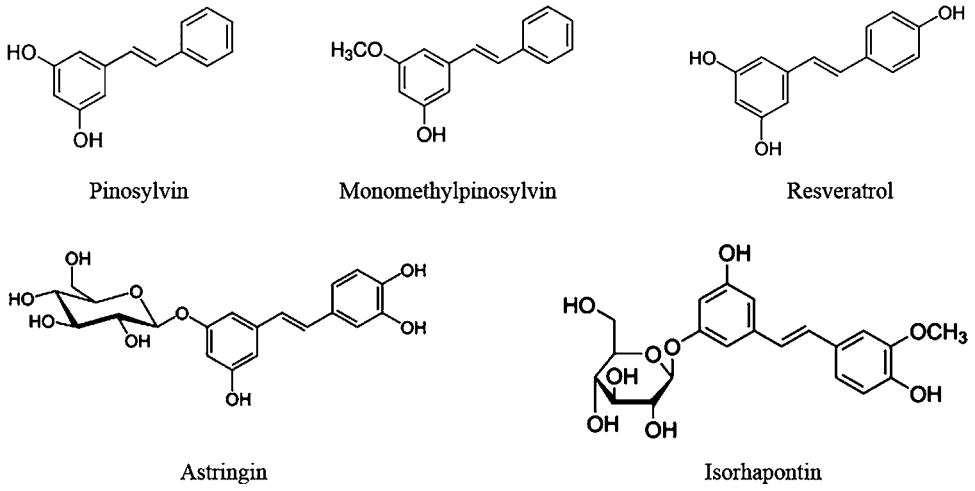

Figure 1. Chemical structures of pinosylvin, monomethylpinosylvin, resveratrol, astringin, and isorhapontin.

Table 1. Primer and Probe Sequences

gene	oligonucleotide	sequence 5′→3′
murine iNOS	forward primer	CCTGGTACGGGCATTGCT
	reverse primer	GCTCATGCGGCCTCCTT
	probe	CAGCAGCGGCTCCATGACTCCC
murine HO-1	forward primer	CCCTCACAGATGGCGTCACT
	reverse primer	GCGGTGTCTGGGATGAGCTA
	probe	CCTGCAGAGACACCCCGAGGGA
murine GAPDH	forward primer	GCATGGCCTTCCGTGTTC
	reverse primer	GATGTCATCATACTTGGCAGGTTT
	probe	TCGTGGATCTGACGTGCCGCC

The aim of the present study was to investigate the anti-inflammatory properties of the knot extract of *P. sylvestris* and to identify the active constituents and molecular mechanisms behind the immunomodulatory effects. The results reveal that two pine stilbenes, pinosylvin and monomethylpinosylvin, are powerful anti-inflammatory compounds both in vitro and in vivo.

MATERIALS AND METHODS

Chemicals. A knotwood extract of *P. sylvestris* and the purified stilbenes, pinosylvin and monomethylpinosylvin, were prepared at Åbo Akademi University. Knots removed from pine stems were freeze-dried and ground to pass through a 2 mm screen. The ground dry knot material was extracted in an accelerated solvent extractor (ASE) apparatus in two stages: (1) with hexane at 90 °C for 3 × 5 min to remove most of the lipophilic extractives and (2) with ethanol/water (95:5 by vol) at 100 °C for 3 × 5 min. The second extract containing primarily the hydrophilic extractives was evaporated to dryness in a vacuum. This extract was used in the biotests. The extract was analyzed by gas chromatography (GC) and gas chromatography−mass spectrometry (GC-MS) after silylation (1). The extract contained the following identified components, in wt % of dry knot material: monomethylpinosylvin, 12%; resin acids, 12%; oxidized resin acids, 11%; pinosylvin, 5%; nortrachelogenin (NTG), 7%; and matairesinol, 2%.

Pinosylvin and methylpinosylvin were isolated from the hydrophilic knot extract using flash chromatography (Biotage Flash 40i, Biotage AB, Uppsala, Sweden) with silica columns, using a step gradient with cyclohexane/acetone. Further purification was achieved by crystallization. The purity of the pinosylvin determined by GC was 89% and that of methylpinosylvin, 94%.

Resveratrol was bought from Tocris Bioscience (Ellisville, MO, USA), and astringin and isorhapontin were from Polyphenols Laboratoires AS (Sandnes, Norway). Rabbit polyclonal iNOS (sc-650), COX-2 (sc-1745), β-actin (sc-1616-R), and HO-1 (sc-1797) antibodies and HPR-conjugated goat polyclonal anti-rabbit antibody and donkey polyclonal anti-goat antibody were purchased from Santa Cruz Biotechnology Inc. (Santa Cruz, CA, USA). All other reagents were from Sigma Chemical Co. (St. Louis, MO, USA) unless otherwise stated.

Cell Culture. Murine J774 macrophages (American Type Culture Collection, Rockville, MD, USA) were cultured at 37 °C in 5% CO_2 atmosphere and grown in Dulbecco's modified Eagle's medium (DMEM) with glutamax-I containing 10% heat-inactivated fetal bovine serum, penicillin (100 units/ml), streptomycin (100 μg/mL), and amphotericin B (250 ng/mL) (Invitrogen, Paisley, UK). Cells were seeded on 96-well plates for the XTT-test and on 24-well plates for the measurements of NO, MCP-1, and IL-6 production and HO-1 and iNOS expression. Cell monolayers were grown for 72 h to confluence before the experiments were started, and the compounds of interest were added in fresh culture medium. Any potential cytotoxicity of the tested compounds was determined by measuring cell viability using the Cell Proliferation Kit II (Roche Diagnostics, Mannheim, Germany).

Preparation of the Stable HEK293pGL4.32NFκB Cell Line. To investigate drug effects on the activation of transcription factor NF-κB and on NF-κB-mediated transcription, the HEK-293 cells (ATCC, Manassas, VA, USA) were stably transfected with a luciferase reporter construct, pGL4.32[*luc2P*/NF-κB-RE/Hygro]. The plasmid was purchased from Promega Corp. (Madison, WI, USA) and contained five copies of an NF-κB response element that drives transcription of the luciferase reporter gene.

DOI: 10.1021/jf504606m
J. Agric. Food Chem. 2015, 63, 3445−3453

Nitrite Assays. NO production was determined by measuring the accumulation of nitrite, a stable metabolite of NO in aqueous milieu, by the Griess reaction.[13]

Western Blot Analysis. At the indicated time points, cells were rapidly washed with ice-cold phosphate-buffered saline (PBS) and solubilized in cold lysis buffer containing 10 mM Tris-HCl, pH 7.4, 5 mM EDTA, 50 mM NaCl, 1% Triton-X-100, 0.5 mM phenylmethanesulfonyl fluoride, 1 mM sodium orthovanadate, 20 μg/mL leupeptin, 50 μg/mL aprotinin, 5 mM sodium fluoride, 2 mM sodium pyrophosphate, and 10 μM *n*-octyl-β-D-glucopyranoside. After incubation for 15 min on ice, the lysates were centrifuged (12000*g*, 4 °C for 10 min), and the supernatants were collected and stored in SDS sample buffer at −20 °C. An aliquot of the supernatant was used to determine the protein concentration according to the Coomassie blue method.[14]

Protein samples (20 μg of lysates) were analyzed according to the standard Western blotting protocol as described previously.[15] The membrane was incubated with the primary antibody in the blocking solution overnight at 4 °C and with the secondary antibody in the blocking solution for 1 h at room temperature. Bound antibody was detected using SuperSignal West Pico or Dura chemiluminescent substrate (Pierce, Rockford, IL, USA) and Image Quant LAS 4000 mini imaging system (GE Healthcare Bio-Sciences AB, Uppsala Sweden). The quantitation of the chemiluminescent signal was carried out with Imaging Quant TL software (GE Healthcare).

RNA Extraction and Quantitative RT-PCR. Total RNA was extracted with the GenElute Mammalian Total RNA Miniprep Kit (Sigma-Aldrich). Reverse transcription of RNA to cDNA and PCR reactions were carried out as previously described.[16] Primers and probes (Table 1) for iNOS, heme oxygenase-1 (HO-1), and glyceraldehyde-3-phosphate dehydrogenase (GAPDH, used as a housekeeping gene) were designed with Primer Express Software (Applied Biosystems, Foster City, CA, USA) and supplied by Metabion (Martinsried, Germany).

Luciferase Activity. Firefly luciferase activity was measured using the luciferase assay reagent (Promega), and the results were normalized to the total cellular protein. The protein content was measured using the Coomassie blue method.

ELISA. IL-6 and MCP-1 concentrations in the culture medium were measured by enzyme-linked immunosorbent assay (ELISA) using reagents from R&D Systems Europe Ltd. (Abingdon, UK).

Carrageenan-Induced Paw Edema in the Mouse. The anti-inflammatory effects were studied by measuring carrageenan-induced paw edema in male C57BL/6 mice (Harlan Laboratories BV, Venray, The Netherlands). The study was carried out in accordance with the legislation for the protection of animals used for scientific purposes (Directive 2010/63/EU) and approved by the National Animal Experiment Board (license ESLH-2009-07700/Ym-23). Animals were housed under conditions of optimum light, temperature, and humidity (12:12 h light−dark cycle, 22 ± 1 °C, 50−60%) with food and water provided ad libitum. Male mice were divided into six groups: control group, L-NIL group (50 mg/kg), pinosylvin group (100 mg/kg), monomethylpinosylvin group (100 mg/kg), resveratrol group (100 mg/kg), and dexamethasone group (2 mg/kg). Doses were selected on the basis of our preliminary experiments and data found in the literature.[17,18] Mice were dosed by intraperitoneal injection with 150 μL of normal saline or the tested compound at 2 h before carrageenan was applied. The mice were anesthesized by intraperitoneal injection of 0.5 mg/kg of medetomidine (Domitor 1 mg/mL, Orion Oyj, Espoo, Finland) and 75 mg/kg of ketamine (Ketalar 10 mg/mL, Pfizer Oy Animal Health, Helsinki, Finland), and thereafter the mice received a 30 μL intradermal injection into one hind paw of normal saline containing λ-carrageenan 1.5% (w/v). The contralateral paw received 30 μL of saline, and it was used as a control. Edema was measured 6 h after carrageenan injection by using a plethysmometer (Ugo Basile, Comerio, Italy). Carrageenan-induced edema is expressed as the difference in the volume change between the carrageenan-treated paw and the control paw.

Statistics. Results are expressed as the mean ± standard error of mean (SEM). Statistical significance of the results was calculated by one-way ANOVA with Dunnett's post test (dose curves) or Bonferroni's post test (multiple comparisons) by using GraphPad InStat 3 for Windows XP (Graph-Pad Software, San Diego, CA, USA). Differences were considered significant at * = $p < 0.05$, ** = $p < 0.01$, and *** = $p < 0.001$. EC_{50} values were calculated with GraphPadPrism 6 for Windows (Graph-Pad Software).

RESULTS

Effects of *P. sylvestris* Knotwood Extract, Pinosylvin, and Monomethylpinosylvin on iNOS Protein Expression and NO Production. Neither NO production nor iNOS expression was detectable in resting J774 macrophages. When the cells were activated through the Toll-like receptor 4 (TLR4) pathway by exposure to bacterial lipopolysaccharide (LPS, 10 ng/mL), both iNOS expression and NO production were significantly enhanced. The *P. sylvestris* knotwood extract inhibited iNOS protein expression and NO production in a dose-dependent manner (Figure 2), and about 50% inhibition was achieved at a concentration of 3 μg/mL.

P. sylvestris knotwood extract is rich in stilbenes particularly pinosylvin [5% (w/w)] and monomethylpinosylvin [12% (w/w)], and we continued by investigating the effects of these compounds on iNOS expression and NO production. Both pinosylvin and monomethylpinosylvin inhibited iNOS ex-

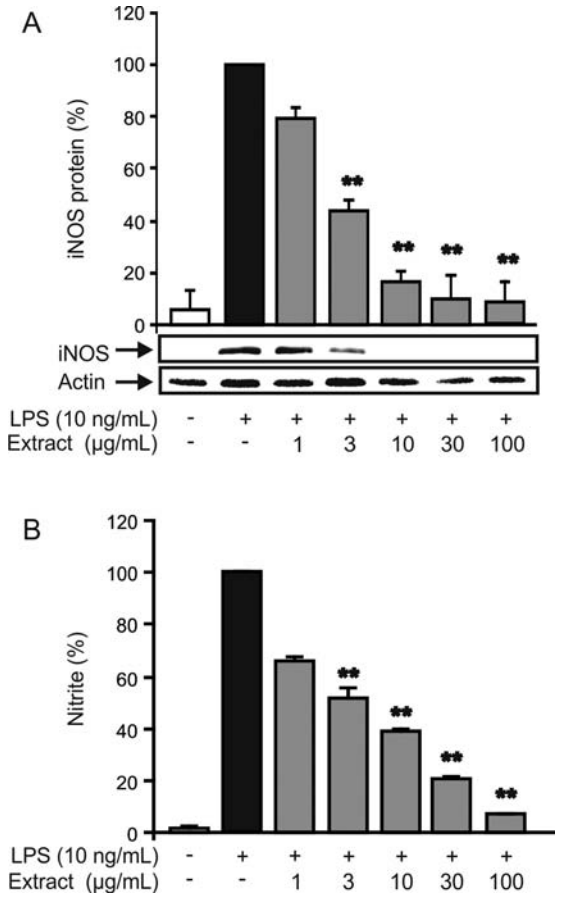

Figure 2. Effects of the *Pinus sylvestris* knot extract on LPS-induced (A) iNOS protein expression and (B) NO production in J774 macrophages as measured after a 24 h incubation. iNOS expression was measured by Western blot, and NO production was determined by measuring its metabolite nitrite in the culture medium by the Griess reaction. Values are expressed as the mean ± SEM, $n = 4$; (**) $p < 0.01$ as compared to cells incubated with LPS only.

DOI: 10.1021/jf504606m
J. Agric. Food Chem. 2015, 63, 3445−3453

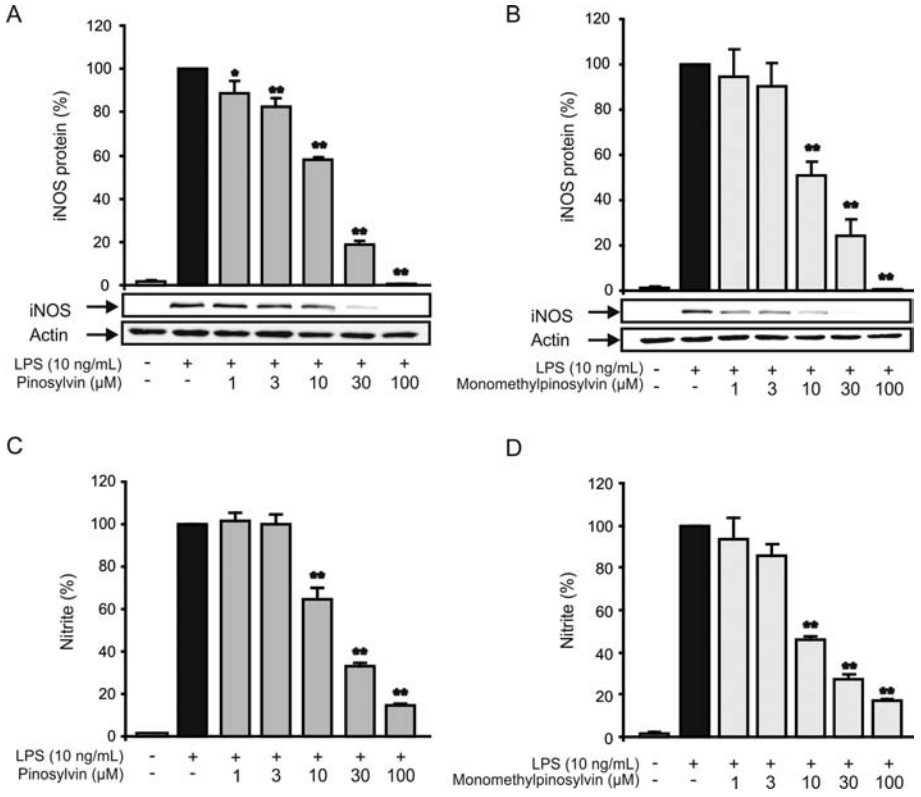

Figure 3. Effects of pinosylvin (A, C) and monomethylpinosylvin (B, D) on LPS-induced (A, B) iNOS protein expression and (C, D) NO production in J774 macrophages as measured after 24 h of incubation. iNOS expression was measured by Western blot, and NO production was determined by measuring its metabolite, nitrite, in the culture medium by the Griess reaction. Values are expressed as mean ± SEM, $n = 4$; (*) $p < 0.05$ and (**) $p < 0.01$ as compared to cells incubated with LPS only.

pression and NO production in a dose-dependent manner (Figure 3). Pinosylvin decreased iNOS expression with an EC_{50} value of 15 μM and monomethylpinosylvin with an EC_{50} value of 12 μM, whereas the EC_{50} values for inhibition of NO production were 13 μM for pinosylvin and 8 μM for monomethylpinosylvin. The effect was comparable to that of a well-known anti-inflammatory drug, dexamethasone, which decreased NO production by about 65% at a concentration of 10 μM.

After demonstrating that the stilbene components of the extract decreased iNOS expression and NO production, we also tested the effects of three other naturally occurring stilbene derivatives on iNOS protein expression and NO production: resveratrol as a positive control (this compound has been extensively evaluated in recent years) and astringin and isorhapontin, which have also been identified in extracts from Nordic conifers.[19] Resveratrol inhibited iNOS expression (EC_{50} = 18 μM) and NO production (EC_{50} = 6 μM) in activated macrophages in a dose-dependent manner (Figure 4), but the two other stilbenes (astringin and isorhapontin) were ineffective.

Effects of *P. sylvestris* Knotwood Extract, Pinosylvin, and Monomethylpinosylvin on iNOS mRNA Levels. In subsequent studies, we used quantitative RT-PCR to investigate the effects of *P. sylvestris* extract, pinosylvin, monomethylpinosylvin, and resveratrol (which was used as a control compound) on iNOS mRNA expression. J774 cells were incubated with the studied compounds for 2 h before LPS was added to activate the cells, and then mRNA levels were measured after a 6 h incubation with LPS. This time point was chosen according to the time curve of iNOS mRNA, where the maximal iNOS mRNA levels were detected at 6 h after the addition of LPS. *P. sylvestris* extract (100 μg/mL) and all tested stilbenes (100 μM) significantly lowered mRNA levels by 51−79% as seen in Figure 5.

Effects of *P. sylvestris* Knotwood Extract, Pinosylvin, and Monomethylpinosylvin on NF-κB-Mediated Transcription. To study in more detail their mechanisms of action, we investigated the effects of *P. sylvestris* extract, pinosylvin, and monomethylpinosylvin on NF-κB-mediated transcription because NF-κB is an important transcription factor for the iNOS gene. We used human embryonic kidney 293 cells that had been genetically modified to express luciferase (LUC) gene under the control of an NF-κB response element containing five NF-κB binding sites. *P. sylvestris* extract, pinosylvin, monomethylpinosylvin, and resveratrol (which was used as a control compound) significantly inhibited NF-κB-mediated transcription (measured as luciferase activity) (Figure 6). MG-132, a known NF-κB inhibitor, was also included in the experiments, and it reduced LUC-activity by >90%.

Effects of *P. sylvestris* Knotwood Extract, Pinosylvin, and Monomethylpinosylvin on Heme Oxygenase-1 Expression. HO-1 is a factor known to regulate NF-κB activation in macrophages.[20,21] Interestingly, the knotwood extract and the two purified stilbenes, pinosylvin and monomethylpinosylvin, as well as resveratrol all enhanced the HO-1 mRNA and protein levels in macrophages exposed to LPS (Figure 7). The HO-1 inducer hemin was used as a control compound.

Effects of *P. sylvestris* Knotwood Extract, Pinosylvin, and Monomethylpinosylvin on MCP-1 and IL-6 Production. We investigated whether *P. sylvestris* extract and the

DOI: 10.1021/jf504606m
J. Agric. Food Chem. 2015, 63, 3445−3453

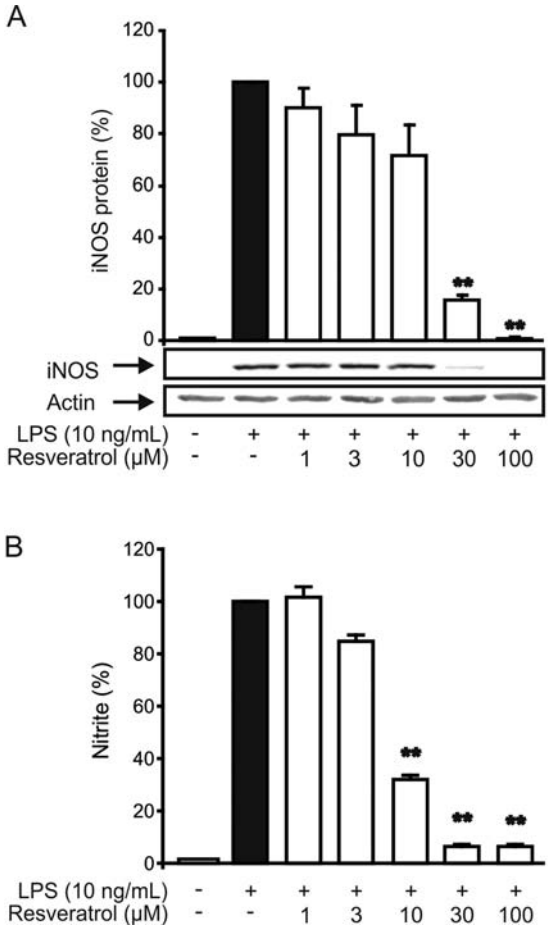

Figure 4. Effects of resveratrol on LPS-induced (A) iNOS protein expression and (B) NO production in J774 macrophages as measured after 24 h of incubation. iNOS expression was measured by Western blot, and NO production was assayed by measuring its metabolite, nitrite, in the culture medium by the Griess reaction. Values are expressed as mean ± SEM, $n = 4$; (**) $p < 0.01$ as compared to cells incubated with LPS only.

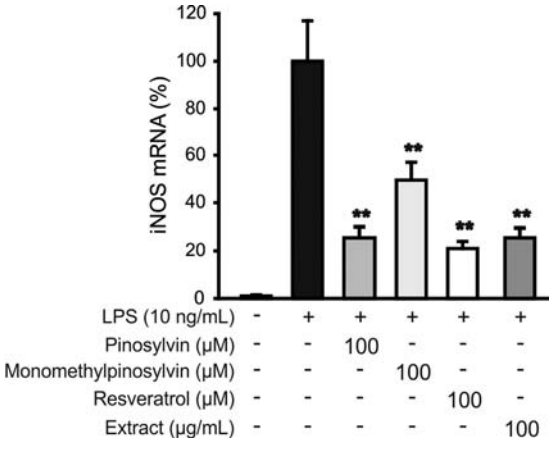

Figure 5. Effects of pinosylvin, monomethylpinosylvin, resveratrol, and the *P. sylvestris* knot extract on iNOS mRNA expression. J774 macrophages were stimulated with LPS in the presence or in the absence of the compounds and the extract for 6 h, and iNOS mRNA expression was measured by quantitative RT-PCR. The results were normalized against GAPDH mRNA and are expressed as mean ± SEM, $n = 4$; (**)$p < 0.01$ as compared to cells incubated with LPS only.

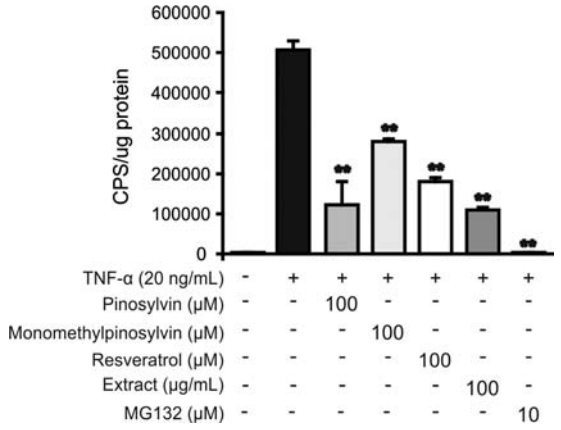

Figure 6. Effects of pinosylvin, monomethylpinosylvin, resveratrol, and the *P. sylvestris* knot extract on NF-κB-dependent transcription in HEK-293 cells transfected with luciferase reporter construct. HEK-pNF-κB(*luc2P*)hygro cells were stimulated with TNFα and treated with the extract or the compounds of interest or with the known NF-κB inhibitor MG132 for 5 h, and luciferase activity was measured. Results are expressed as mean ± SEM, $n = 4$; (**) $p < 0.01$ as compared to cells incubated with TNFα only.

stilbenes isolated from the extract would exert effects on other important inflammatory mediators by determining if they could modify the productions of the chemokine MCP-1 (Figure 8) and the pro-inflammatory cytokine IL-6 (Figure 9) in activated J774 macrophages. The extract of *P. sylvestris* reduced MCP-1 production in a dose-dependent manner with an EC_{50} value of 11 μg/mL. Furthermore, also pinosylvin (EC_{50} = 35 μM), monomethylpinosylvin (EC_{50} = 35 μM), and resveratrol (EC_{50} = 19 μM) reduced MCP-1 production. *P. sylvestris* extract (EC_{50} = 26 μg/mL) and monomethylpinosylvin (EC_{50} = 25 μM) had a moderate dose-dependent inhibitory effect also on IL-6 production. Similarly, resveratrol reduced IL-6 production with an EC_{50} value of 21 μM. Pinosylvin evoked about 30% inhibition on IL-6 production at a concentration of 30 μM. We also tested the effects of *P. sylvestris* extract, pinosylvin, and monomethylpinosylvin on COX-2 levels in activated macrophages, but none of the compounds had any inhibitory effect on the expression levels of COX-2 protein.

Effects of Pinosylvin and Monomethylpinosylvin on Carrageenan-Induced Paw Edema in the Mouse. Because both pinosylvin and monomethylpinosylvin displayed anti-inflammatory effects in the in vitro studies, we decided to test if they could also exhibit in vivo anti-inflammatory properties by using a carrageenan-induced paw inflammation model in the mouse. Intraperitoneal administration of known anti-inflammatory compounds, that is, the iNOS inhibitor L-NIL (50 mg/kg) and the glucocorticoid dexamethasone (2 mg/kg), reduced carrageenan-induced paw edema by >80%. Interestingly, also pinosylvin (100 mg/kg) and monomethylpinosylvin (100 mg/kg) decreased carrageenan-induced inflammation by almost 80%, whereas the inhibitory effect of resveratrol (100 mg/kg; used as a control compound) was only 50% (Figure 10).

DISCUSSION

The present study investigated the anti-inflammatory properties of knotwood extract of *P. sylvestris* and two of its stilbene constituents, pinosylvin and monomethylpinosylvin. We found that the knotwood extract of *P. sylvestris* inhibited LPS-induced NO production in activated macrophages in a dose-dependent

DOI: 10.1021/jf504606m
J. Agric. Food Chem. 2015, 63, 3445−3453

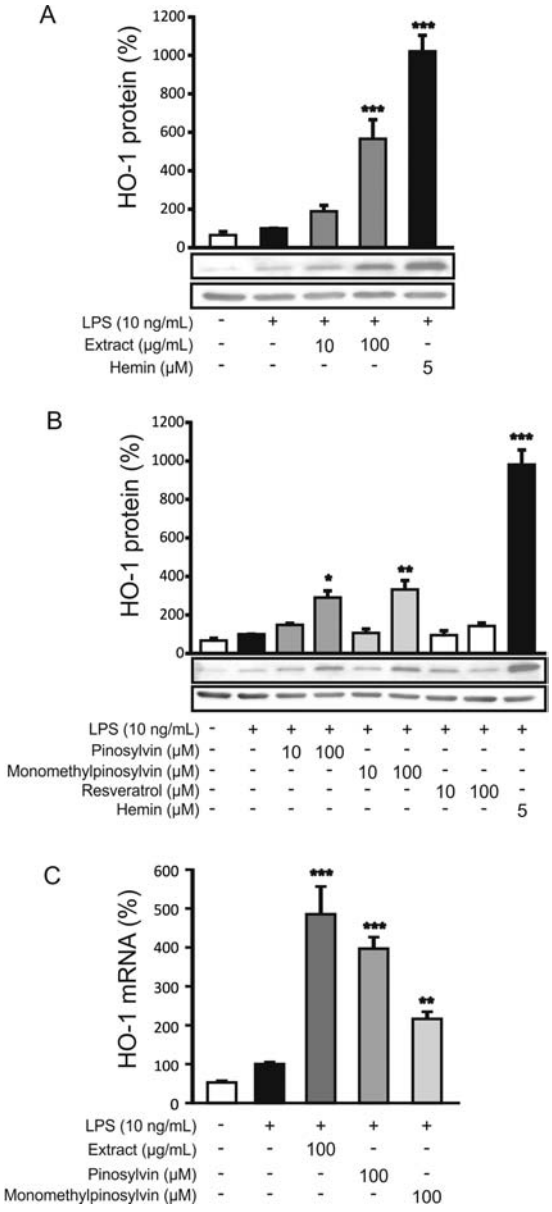

Figure 7. Effects of pinosylvin, monomethylpinosylvin, resveratrol, and the *P. sylvestris* knot extract on HO-1 protein expression (A, B) and mRNA expression (C). J774 macrophages were stimulated with LPS in the presence or in the absence of the compounds or the extract for 6 h, and HO-1 protein expression was measured by Western Blot or for 4 h and HO-1 mRNA expression was measured by quantitative RT-PCR. The results were normalized against GAPDH mRNA. The values are expressed as mean ± SEM, $n = 4$; (**) $p < 0.01$ as compared to cells incubated with LPS only.

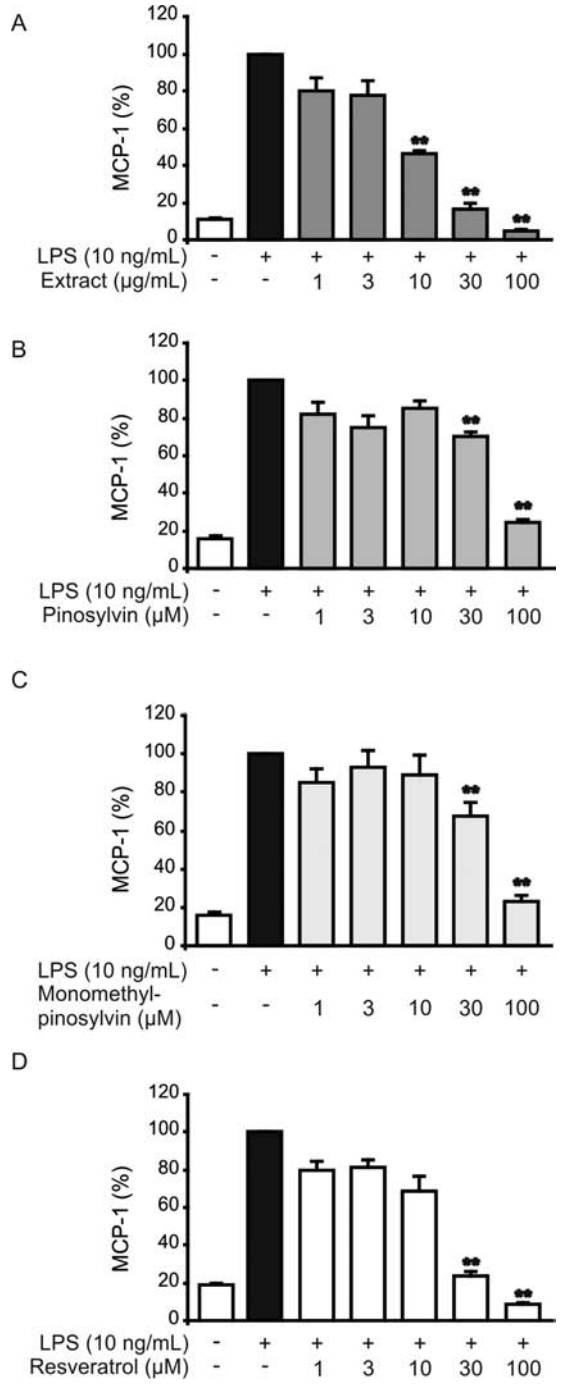

Figure 8. Effects of the *P. sylvestris* knot extract (A), pinosylvin (B), monomethylpinosylvin (C), and resveratrol (D) on MCP-1 production. J774 macrophages were stimulated with LPS for 24 h and thereafter the incubations were terminated and MCP-1 production was determined by ELISA. Results are expressed as mean ± SEM, $n = 4$; (**) $p < 0.01$ as compared to cells incubated with LPS only.

manner. This was attributable to the inhibitory effect on iNOS expression in response to inflammatory stimuli as both the iNOS protein and the mRNA levels were decreased. In addition, a clear reduction was observed in the expression of inflammatory genes IL-6 and MCP-1. Importantly, the anti-inflammatory effects of pinosylvin and monomethylpinosylvin were also found in vivo in a standard carrageenan-induced inflammatory paw edema model.

The immunomodulatory effects of *P. sylvestris* knot have not been reported earlier. It has been shown previously that the extract of *P. sylvestris* leaf buds could reduce NO production and iNOS mRNA expression in LPS and IFN-γ-stimulated murine macrophages but exerted no effects on COX-2 expression or PGE_2 production.[22] Karonen et al. have also reported that pine bark extracts possess anti-inflammatory properties,[23] but in these previous studies, the active constituents were not identified.

The knotwood extract was found to contain 5% (w/w) of pinosylvin and 12% of monomethylpinosylvin. The effects of these two stilbene derivatives on NO production and iNOS

DOI: 10.1021/jf504606m
J. Agric. Food Chem. 2015, 63, 3445−3453

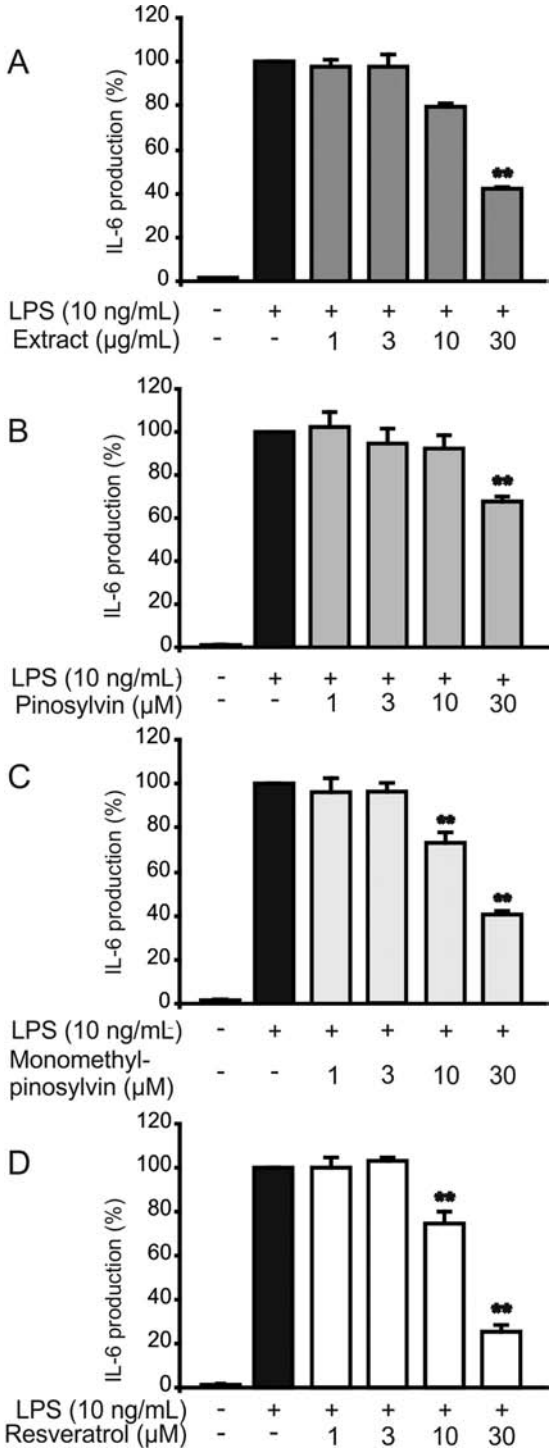

Figure 9. Effects of the *P. sylvestris* knot extract (A), pinosylvin (B), monomethylpinosylvin (C), and resveratrol (D) on IL-6 production. J774 macrophages were stimulated with LPS for 24 h, and thereafter the incubations were terminated and IL-6 production was determined by ELISA. Results are expressed as mean ± SEM, $n = 4$; (**) $p < 0.01$ as compared to cells incubated with LPS only.

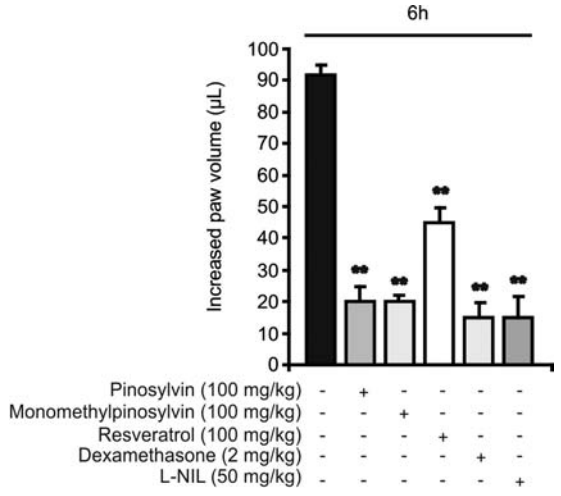

Figure 10. Effects of pinosylvin, monomethylpinosylvin, and resveratrol on carrageenan-induced paw inflammation in the mouse. Pinosylvin, monomethylpinosylvin, resveratrol, and control compounds L-NIL and dexamethasone were administered ip 2 h prior to carrageenan (1.5%) being injected into the paw. The contralateral paw was injected with the solvent and served as the control. Paw edema was measured before and 6 h after the carrageenan injection. Edema is expressed as the differences in the volume change between the carrageenan treated paw and the control paw. Results are expressed as mean ± SEM, $n = 6$; (**) $p < 0.01$.

expression were qualitatively similar to the effects of the extract, and thus it is likely that they account for the anti-inflammatory effects observed with the extract. Therefore, we continued the experiments with pinosylvin and monomethylpinosylvin, but we also included a well-known stilbene, resveratrol, as a control compound. In addition, two other stilbenes present in trees, astringin and isorhapontin, were also investigated.

Previously it has been shown that resveratrol could inhibit LPS-induced NO production in macrophages,[24−28] a result confirmed also in the present study. Furthermore, this effect was found to be shared by pinosylvin and monomethylpinosylvin. The present pinosylvin result is in line with the previous report from Park et al.[29] Some other natural substances from the stilbenoid group, namely, *cis*-mulberroside A, rhapontigenin, and piceatannol, have also been demonstrated to be able to decrease iNOS expression.[24,25,30] There are a few published studies on the structure−activity relationship of stilbenes on LPS-induced NO production which suggest that the structural balance between functional oxygen groups on the benzene rings is important for the biological activity.[24] In the previous study, the presence of a glucoside moiety was also found to reduce anti-inflammatory activity.[25] Here, the ineffectiveness of astringin and isorhapontin as compared to the other tested stilbenes may be explained by the fact that they are glycosylated forms and are perhaps poorly transported into the cell. It was decided to include astringin and isorhapontin in the present study because these compounds have also been reported to be present in Nordic conifers in addition to pinosylvin and monomethylpinosylvin.[19] There were no major differences between the potencies of pinosylvin, monomethylpinosylvin, and resveratrol on NO production or iNOS expression.

No previous data on the anti-inflammatory effects of monomethylpinosylvin have been reported, and there are only a few earlier reports on the corresponding properties of pinosylvin. Pinosylvin inhibited LPS-induced expression of pro-inflammatory cytokines IL-8 and TNF-α in THP-1 cells via the NF-κB signaling pathway.[31] Another study revealed that pinosylvin could reduce prostaglandin E_2 production in activated RAW 264.7 cells.[32]

DOI: 10.1021/jf504606m
J. Agric. Food Chem. 2015, 63, 3445−3453

The present study extends the previous data by showing that the extract of *P. sylvestris* and also pinosylvin and monomethylpinosylvin were able to inhibit the iNOS-NO pathway in activated macrophages. The compounds suppressed also iNOS mRNA levels, which proves that a transcriptional mechanism is behind the inhibitory effect on iNOS expression. NF-κB is one of the key transcription factors regulating iNOS transcription. In the present study, we found that NF-κB-mediated transcription was inhibited by the extract of *P. sylvestris* and its two stilbene constituents, pinosylvin and monomethylpinosylvin, which may, at least partly, explain their inhibitory effects on iNOS and other NF-κB-dependent genes.

HO-1 has been shown to play a role in cellular and tissue defense against oxidative stress, possessing potent anti-inflammatory and cytoprotective properties.[33] In the present study, we found that the knot extract and its active stilbenes increased HO-1 expression in activated macrophages. This may represent a putative mechanism for their anti-inflammatory action and explain how they were able to decrease the NF-κB activity and reduce inflammatory gene expression. Some other compounds of natural origin have been reported to affect HO-1.[33] There is also one study reporting that resveratrol could induce HO-1 in human aortic smooth muscle cells, which supports our original findings on the protective effects of pinosylvin and monomethylpinosylvin through HO-1 expression.[34]

Additionally, it was important to determine whether our findings in vitro could be translated into an anti-inflammatory effect in vivo. We chose to test the effects of pinosylvin and monomethylpinosylvin in carrageenan-induced paw inflammation, which is a widely used experimental model of acute inflammation in preclinical pharmacological studies. The carrageenan-induced inflammatory response in the paw has been reported to be mediated partly by increased NO production because it is sensitive to the anti-inflammatory properties of iNOS inhibitors.[35,36] In the current study, the iNOS inhibitor, L-NIL, also reduced significantly carrageenan-induced acute inflammation. The inhibitory responses of pinosylvin and monomethylpinosylvin were comparable to that of L-NIL and another control compound, dexamethasone, which is a very efficacious anti-inflammatory drug that also inhibits iNOS expression.[37] In the present study, resveratrol was observed to inhibit carrageenan-induced paw edema, although this effect was not detected in the previous study of Gentilli et al.[38] The difference in the dosing of resveratrol in these studies may explain the different results. Gentilli and co-workers injected resveratrol shortly before the carrageenan challenge, whereas we administered the drug 2 h before carrageenan. However, it is noteworthy that pinosylvin and monomethylpinosylvin were more potent than resveratrol in combatting carrageenan-induced paw inflammation. As far as we are aware, there is only one previous study in which pinosylvin has been tested in an inflammatory model in vivo, in adjuvant arthritis in the rat.[18] The results support our present findings that pinosylvin possesses a significant anti-inflammatory action also in vivo.

In conclusion, the most interesting novel finding in this study was that pinosylvin and monomethylpinosylvin were found to have anti-inflammatory properties in vivo, possibly via a mechanism involving the stimulation of HO-1 levels leading to inhibition of NF-κB activity and ultimately to the suppression of inflammatory gene expression. These findings extend our understanding of the potential beneficial properties of naturally occurring stilbenes and may provide new insights in the development of novel anti-inflammatory treatments. In addition, the immunomodulatory potential of pinosylvin and its derivatives as well as their detailed mechanisms of action should be evaluated in further studies.

AUTHOR INFORMATION

Corresponding Author

*(E.M.) Fax: +358 3 3640 558. E-mail: eeva.moilanen@uta.fi.

Funding

This work was financially supported by the FuBio program funded by Finnish Bioeconomy Cluster Ltd. and The Finnish Funding Agency for Technology and Innovation (TEKES). M.L. is a doctoral student in the National Doctoral Programme of Musculoskeletal Disorders and Biomaterials.

Notes

The authors declare no competing financial interest.

ACKNOWLEDGMENTS

The authors warmly thank Meiju Kukkonen, Petra Miikkulainen, Elina Jaakkola, and Salla Hietakangas for excellent technical assistance, Heli Määttä for skillful secretarial help, and Dr. Ewen MacDonald for professional language editing of the manuscript.

ABBREVIATIONS USED

COX-2, cyclooxygenase-2; GAPDH, glyceraldehyde-3-phosphate dehydrogenase; HO-1, heme oxygenase 1; IFNγ, interferon-γ; iNOS, inducible nitric oxide synthase; IL-6, interleukin-6; L-NIL, L-N^6-(1-iminoethyl)lysine hydrochloride; LPS, lipopolysaccharide; MCP-1, monocyte chemotactic protein-1; NF-κB, nuclear factor kappa B; NO, nitric oxide; NOS, nitric oxide synthase; PGE_2, prostaglandin E_2; XTT, sodium 3′-[1-(phenylaminocarbonyl)-3,4-tetrazolium]bis(4-methoxy-6-nitro)benzenesulfonic acid hydrate

REFERENCES

(1) Holmbom, B.; Willför, S.; Hemming, J.; Pietarinen, S.; Nisula, S.; Eklund, P.; Sjöholm, R. Knots in trees − a rich source of bioactive polyphenols In *ACS Symposium Series 954*; Argyropoulos, D., Ed.; American Chemical Society: Washington, DC, USA, 2007; pp 350−362.

(2) Willför, S.; Hemming, J. E.; Reunanen, M. H.; Holmbom, B. Phenolic and lipophilic extractives in scots pine knots and stemwood. *Holzforschung* **2003**, *57*, 359−372.

(3) Välimaa, A. L.; Honkalampi-Hämäläinen, U.; Pietarinen, S.; Willfor, S.; Holmbom, B.; von Wright, A. Antimicrobial and cytotoxic knotwood extracts and related pure compounds and their effects on food-associated microorganisms. *Int. J. Food Microbiol.* **2007**, *115*, 235−243.

(4) Kulkarni, S. S.; Canto, C. The molecular targets of resveratrol. *Biochim. Biophys. Acta* **2014**, DOI: 10.1016/j.bbadis.2014.10.005.

(5) Djoko, B.; Chiou, R. Y.; Shee, J. J.; Liu, Y. W. Characterization of immunological activities of peanut stilbenoids, arachidin-1, piceatannol, and resveratrol on lipopolysaccharide-induced inflammation of RAW 264.7 macrophages. *J. Agric. Food Chem.* **2007**, *55*, 2376−2383.

(6) Wang, K. T.; Chen, L. G.; Tseng, S. H.; Huang, J. S.; Hsieh, M. S.; Wang, C. C. Anti-inflammatory effects of resveratrol and oligostilbenes from *Vitis thunbergii* var. *taiwaniana* against lipopolysaccharide-induced arthritis. *J. Agric. Food Chem.* **2011**, *59*, 3649−3656.

(7) de la Lastra, C. A.; Villegas, I. Resveratrol as an anti-inflammatory and anti-aging agent: mechanisms and clinical implications. *Mol. Nutr. Food Res.* **2005**, *49*, 405−430.

DOI: 10.1021/jf504606m
J. Agric. Food Chem. 2015, 63, 3445−3453

(8) Scatena, R.; Bottoni, P.; Pontoglio, A.; Giardina, B. Pharmacological modulation of nitric oxide release: new pharmacological perspectives, potential benefits and risks. *Curr. Med. Chem.* **2010**, *17*, 61−73.
(9) Kanwar, J. R.; Kanwar, R. K.; Burrow, H.; Baratchi, S. Recent advances on the roles of NO in cancer and chronic inflammatory disorders. *Curr. Med. Chem.* **2009**, *16*, 2373−2394.
(10) Lyons, C. R.; Orloff, G. J.; Cunningham, J. M. Molecular cloning and functional expression of an inducible nitric oxide synthase from a murine macrophage cell line. *J. Biol. Chem.* **1992**, *267*, 6370−6374.
(11) Korhonen, R.; Lahti, A.; Kankaanranta, H.; Moilanen, E. Nitric oxide production and signaling in inflammation. *Curr. Drug Targets Inflamm. Allergy* **2005**, *4*, 471−479.
(12) Pautz, A.; Art, J.; Hahn, S.; Nowag, S.; Voss, C.; Kleinert, H. Regulation of the expression of inducible nitric oxide synthase. *Nitric Oxide* **2010**, *23*, 75−93.
(13) Green, L. C.; Wagner, D. A.; Glogowski, J.; Skipper, P. L.; Wishnok, J. S.; Tannenbaum, S. R. Analysis of nitrate, nitrite and [^{15}N]nitrate in biological fluids. *Anal. Biochem.* **1982**, *126*, 131−138.
(14) Bradford, M. M. A rapid and sensitive method for the quantitation of microgram quantities of protein utilizing the principle of protein-dye binding. *Anal. Biochem.* **1976**, *72*, 248−254.
(15) Leppänen, T.; Jalonen, U.; Korhonen, R.; Tuominen, R. K.; Moilanen, E. Inhibition of protein kinase Cdelta reduces tristetraprolin expression by destabilizing its mRNA in activated macrophages. *Eur. J. Pharmacol.* **2010**, *628*, 220−225.
(16) Lahti, A.; Jalonen, U.; Kankaanranta, H.; Moilanen, E. c-Jun NH_2-terminal kinase inhibitor anthra(1,9-*cd*)pyrazol-6(2*H*)-one reduces inducible nitric-oxide synthase expression by destabilizing mRNA in activated macrophages. *Mol. Pharmacol.* **2003**, *64*, 308−315.
(17) Yatkin, E.; Polari, L.; Laajala, T. D.; Smeds, A.; Eckerman, C.; Holmbom, B.; Saarinen, N. M.; Aittokallio, T.; Mäkelä, S. I. Novel lignan and stilbenoid mixture shows anticarcinogenic efficacy in preclinical PC-3M-luc2 prostate cancer model. *PLoS One* **2014**, *9*, No. e93764.
(18) Macickova, T.; Drabikova, K.; Nosal, R.; Bauerova, K.; Mihalova, D.; Harmatha, J.; Pecivova, J. In vivo effect of pinosylvin and pterostilbene in the animal model of adjuvant arthritis. *Neuro Endocrinol. Lett.* **2010**, *31* (Suppl. 2), 91−95.
(19) Pietarinen, S.; Willför, S.; Hemming, J.; Holmbom, B. Knotwood and bark extracts: strong antioxidants from waste materials. *J. Wood Sci.* **2006**, *52*, 436−444.
(20) Ryter, S. W.; Alam, J.; Choi, A. M. Heme oxygenase-1/carbon monoxide: from basic science to therapeutic applications. *Physiol. Rev.* **2006**, *86*, 583−650.
(21) Oh, G. S.; Pae, H. O.; Lee, B. S.; Kim, B. N.; Kim, J. M.; Kim, H. R.; Jeon, S. B.; Jeon, W. K.; Chae, H. J.; Chung, H. T. Hydrogen sulfide inhibits nitric oxide production and nuclear factor-kappaB via heme oxygenase-1 expression in RAW264.7 macrophages stimulated with lipopolysaccharide. *Free Radical Biol. Med.* **2006**, *41*, 106−119.
(22) Vigo, E.; Cepeda, A.; Gualillo, O.; Perez-Fernandez, R. In-vitro anti-inflammatory activity of *Pinus sylvestris* and *Plantago lanceolata* extracts: effect on inducible NOS, COX-1, COX-2 and their products in J774A.1 murine macrophages. *J. Pharm. Pharmacol.* **2005**, *57*, 383−391.
(23) Karonen, M.; Hämäläinen, M.; Nieminen, R.; Klika, K. D.; Loponen, J.; Ovcharenko, V. V.; Moilanen, E.; Pihlaja, K. Phenolic extractives from the bark of *Pinus sylvestris* L. and their effects on inflammatory mediators nitric oxide and prostaglandin E2. *J. Agric. Food Chem.* **2004**, *52*, 7532−7540.
(24) Cho, D. I.; Koo, N. Y.; Chung, W. J.; Kim, T. S.; Ryu, S. Y.; Im, S. Y.; Kim, K. M. Effects of resveratrol-related hydroxystilbenes on the nitric oxide production in macrophage cells: structural requirements and mechanism of action. *Life Sci.* **2002**, *71*, 2071−2082.
(25) Matsuda, H.; Kageura, T.; Morikawa, T.; Toguchida, I.; Harima, S.; Yoshikawa, M. Effects of stilbene constituents from rhubarb on nitric oxide production in lipopolysaccharide-activated macrophages. *Bioorg. Med. Chem. Lett.* **2000**, *10*, 323−327.
(26) Tsai, S. H.; Lin-Shiau, S. Y.; Lin, J. K. Suppression of nitric oxide synthase and the down-regulation of the activation of NFkappaB in macrophages by resveratrol. *Br. J. Pharmacol.* **1999**, *126*, 673−680.
(27) Liu, F. C.; Hung, L. F.; Wu, W. L.; Chang, D. M.; Huang, C. Y.; Lai, J. H.; Ho, L. J. Chondroprotective effects and mechanisms of resveratrol in advanced glycation end products-stimulated chondrocytes. *Arthritis Res. Ther.* **2010**, *12*, R167.
(28) Shakibaei, M.; Csaki, C.; Nebrich, S.; Mobasheri, A. Resveratrol suppresses interleukin-1beta-induced inflammatory signaling and apoptosis in human articular chondrocytes: potential for use as a novel nutraceutical for the treatment of osteoarthritis. *Biochem. Pharmacol.* **2008**, *76*, 1426−1439.
(29) Park, E. J.; Min, H. Y.; Chung, H. J.; Ahn, Y. H.; Pyee, J. H.; Lee, S. K. Pinosylvin suppresses LPS-stimulated inducible nitric oxide synthase expression via the MyD88-independent, but TRIF-dependent downregulation of IRF-3 signaling pathway in mouse macrophage cells. *Cell. Physiol. Biochem.* **2011**, *27*, 353−362.
(30) Zhang, Z.; Shi, L. Anti-inflammatory and analgesic properties of *cis*-mulberroside A from *Ramulus mori*. *Fitoterapia* **2010**, *81*, 214−218.
(31) Lee, J.; Jung, E.; Lim, J.; Lee, J.; Hur, S.; Kim, S. S.; Lim, S.; Hyun, C. G.; Kim, Y. S.; Park, D. Involvement of nuclear factor-kappaB in the inhibition of pro-inflammatory mediators by pinosylvin. *Planta Med.* **2006**, *72*, 801−806.
(32) Park, E. J.; Min, H. Y.; Ahn, Y. H.; Bae, C. M.; Pyee, J. H.; Lee, S. K. Synthesis and inhibitory effects of pinosylvin derivatives on prostaglandin E2 production in lipopolysaccharide-induced mouse macrophage cells. *Bioorg. Med. Chem. Lett.* **2004**, *14*, 5895−5898.
(33) Motterlini, R.; Foresti, R. Heme oxygenase-1 as a target for drug discovery. *Antioxid. Redox Signal.* **2013**, *20*, 1810−1826.
(34) Juan, S. H.; Cheng, T. H.; Lin, H. C.; Chu, Y. L.; Lee, W. S. Mechanism of concentration-dependent induction of heme oxygenase-1 by resveratrol in human aortic smooth muscle cells. *Biochem. Pharmacol.* **2005**, *69*, 41−48.
(35) Handy, R. L.; Moore, P. K. A comparison of the effects of L-NAME, 7-NI and L-NIL on carrageenan-induced hindpaw oedema and NOS activity. *Br. J. Pharmacol.* **1998**, *123*, 1119−1126.
(36) Salvemini, D.; Wang, Z. Q.; Wyatt, P. S.; Bourdon, D. M.; Marino, M. H.; Manning, P. T.; Currie, M. G. Nitric oxide: a key mediator in the early and late phase of carrageenan-induced rat paw inflammation. *Br. J. Pharmacol.* **1996**, *118*, 829−838.
(37) Hämäläinen, M.; Lilja, R.; Kankaanranta, H.; Moilanen, E. Inhibition of iNOS expression and NO production by anti-inflammatory steroids. Reversal by histone deacetylase inhibitors. *Pulm. Pharmacol. Ther.* **2008**, *21*, 331−339.
(38) Gentilli, M.; Mazoit, J. X.; Bouaziz, H.; Fletcher, D.; Casper, R. F.; Benhamou, D.; Savouret, J. F. Resveratrol decreases hyperalgesia induced by carrageenan in the rat hind paw. *Life Sci.* **2001**, *68*, 1317−1321.

DOI: 10.1021/jf504606m
J. Agric. Food Chem. 2015, 63, 3445−3453

c-EPS from their cell wall.[22] However, there have been few studies focusing on the anticancer activity and chemical characterization of c-EPS produced by LAB.[23] Recently, the *Lactobacillus helveticus* MB2-1 strain, which produces abundant EPS, was isolated in our laboratory from traditional Sayram ropy fermented milk (SRFM) in the southern Xinjiang region of China.[2] In vitro antioxidant activity assays demonstrated that the c-EPS and three r-EPS fractions (r-LHEPS-1, r-LHEPS-2, and r-LHEPS-3) had strong scavenging activities against four free radicals.[24,25] In addition, we found that all of the r-EPS fractions, especially r-LHEPS-2, exerted high inhibitory activity in vitro against BGC-823 human gastric cancer cells. Furthermore, we elucidated the fine structure of purified r-LHEPS-2, which showed a →4,6-D-Man*p*-(1 → 6)-D-Man*p*-(1 → 4)-D-Gal*p*-(1→ backbone with a single T-D-Glc*p*-(1 → 4)-D-Man*p*-(1 → 6)-D-Glc*p*-(1→ side-branch on the O-6 of the → 4,6-D-Man*p*-(1→ residue.[26]

In the present work, the c-EPS from *L. helveticus* MB2-1 was prepared and characterized by gas chromatography (GC), gas chromatography−mass spectrometry (GC−MS), nuclear magnetic resonance (NMR), atomic force microscopy (AFM), and scanning electron microscopy (SEM). Furthermore, the in vitro anticancer activity of c-EPS against human HepG-2 liver cancer, BGC-823 gastric cancer, and HT-29 colon cancer cells was evaluated.

MATERIALS AND METHODS

Microorganism and Reagents. The *L. helveticus* MB2-1 strain was isolated from SRFM. This strain was grown in liquid medium (1000 mL) containing 80 g of whey and 5 g of yeast extract and adjusted to pH 6.7 with 2.0 M NaOH. HepG-2, BGC-823, and HT-29 cancer cells and human colonic epithelial HCoEpiC cells were obtained from the Cell Bank of the Shanghai Institute of Cell Biology (Shanghai, China). Dulbecco's modified Eagle's medium (DMEM), fetal bovine serum (FBS), and 3-(4,5-dimethylthiazol-2-yl)-2,5-diphenyl-2*H*-tetrazolium bromide (MTT) were purchased from Gibco/Invitrogen (Gibco BRL, Grand Island, NY). Dimethyl sulfoxide (DMSO), methyl iodide (CH_3I), 5-fluorouracil (5-FU), penicillin, streptomycin, rhamnose, arabinose, mannose, fucose, glucose, galactose, xylose, and inositol were obtained from Sigma Chemical Co. (St. Louis, MO). DEAE-cellulose 52 and Sephadex G-100 were purchased from Whatman Co. (Maidstone, Kent, UK), and T-series dextrans were purchased Pharmacia Co. Ltd. (Uppsala, Sweden). All other reagents were of analytical grade.

Observation of *L. helveticus* MB2-1 Capsules. The presence of capsules on the cell surface of *L. helveticus* MB2-1 was confirmed by observation by transmission electron microscopy (TEM) using an H-7650 TEM (Hitachi High Technologies Corporation, Tokyo, Japan) operating at 80 kV. The sample was prepared by mounting the cells onto a copper grid, immersing the samples in 2% phosphotungstic acid (pH 7.0) and drying at room temperature.

Isolation and Purification of c-EPS. The c-EPS was isolated and purified according to our previous method, with minor modifications.[23] After growth at 40 °C for 24 h, the cultures were centrifuged at 12 000*g* and 4 °C for 15 min. The viscous cell precipitates were washed twice with 0.85% NaCl and then centrifuged as above. The centrifuged precipitates were resuspended in 1 M NaCl and treated with a JY92-IIN cell sonicator (Ningbo Scientz Biotechnology Co., Ltd., Ningbo, China) at 40 W and 4 °C for 3 min. After centrifugation to eliminate insoluble material, the supernatants were combined and then concentrated using a Laborota 4000 efficient rotary evaporator (Heidolph Instruments GmbH & Co, Schwabach, Germany). The final concentrated supernatant was mixed with three volumes of ice-cold ethanol and stirred vigorously. After standing overnight at 4 °C, the precipitate was collected by centrifugation and dialyzed using a dialysis bag (8000−14 000-Da molecular weight (MW) cutoff) in distilled water for 48 h at 4 °C before being lyophilized using a Heto Power Dry LL3000 freeze-dryer (Thermo Electron Co., Bath, UK). The freeze-dried crude c-EPS was fractionated with a DEAE-cellulose column (2.6 × 30 cm) and was eluted stepwise with distilled water and 0.1, 0.3, and 0.5 M NaCl solutions at a flow rate of 60 mL/h. The fractions were assayed for carbohydrate content by the phenol−sulfuric acid method.[27] The peak fractions containing c-EPS were pooled, dialyzed, and lyophilized. Further purification of c-EPS was performed using a Sephadex G-100 column (2.6 × 100 cm), which was eluted with distilled water at a flow rate of 12 mL/h. The fraction containing purified c-EPS was collected, dialyzed, and lyophilized.

Purity and Molecular Weight Estimation of c-EPS. The purity and MW of the c-EPS were determined by high-performance size-exclusion chromatography (HPSEC) with an Agilent 1200 series system (Palo Alto, CA) equipped with a TSK gel G4000 PW XL column (300 × 7.8 mm, Tosoh Corp., Tokyo, Japan) and an evaporative light-scattering detector (ELSD).[25] Twenty microliters of purified c-EPS (1 mg/mL) was injected and was eluted with distilled water at 50 °C at a flow rate of 0.7 mL/min. The linear regression was calibrated using the T-series dextran standards (T-500, T-200, T-100, T-50, and T-10).

Basic Component Analysis of c-EPS. The total sugar content was measured by the phenol−sulfuric acid method mentioned above.[27] Protein, uronic acid, and sulfate group quantities were determined according to our previous method.[25]

Analysis of Monosaccharide Composition. Five milligrams of purified c-EPS was hydrolyzed with 2 mL of 2 M trifluoroacetic acid (TFA) at 120 °C for 2 h.[5] The hydrolysates were then subjected to aldononitrile acetate precolumn derivatization for GC determination of the monosaccharide composition. GC was performed on an Agilent 6890N GC (Palo Alto, CA) equipped with a flame ionization detector (FID) and a HP-5 capillary column (30 m × 0.32 mm i.d., 0.25 mm, J&W Scientific Inc., Folsom, CA). N_2 was used as the carrier gas at a flow rate of 1 mL/min, and the temperatures of the injector and detector were set to 250 °C and 280 °C, respectively. The following chromatographic conditions were used: the initial column temperature was held at 100 °C for 5 min, increased at a rate of 5 °C/min to 150 °C, held at 150 °C for 5 min, and then subsequently increased at 5 °C/min to 240 °C, where it was held at 240 °C for 2 min. Arabinose, mannose, rhamnose, fucose, glucose, galactose, and xylose standards were prepared for comparison, and inositol was used as an internal standard.

Ultraviolet−Visible (UV−vis) and Fourier-Transform Infrared (FT-IR) Spectroscopy. UV−vis spectroscopy analyses were conducted with a U-4100 spectrophotometer (Hitachi Ltd., Japan). The c-EPS solution was prepared by suspending the sample in distilled water at a concentration of 1.0 mg/mL for UV−vis measurement over a wavelength range of 190−700 nm. FT-IR was recorded from a sample in a KBr pellet on a FT-IR spectrophotometer (Nicolet Nexus470, Thermo Nicolet Co., WI), and the spectrum from 400 to 4000 cm^{-1} was recorded.[25]

Methylation Analysis and Mass Spectrometry. Five milligrams of purified c-EPS was completely methylated using methyl iodide and solid sodium hydroxide in dimethyl sulfoxide, as described in our previous report.[23] Briefly, the permethylated c-EPS was hydrolyzed with 2 M TFA at 120 °C for 2 h. Next, the partially methylated monosaccharides were reduced with $NaBH_4$ for 2 h at room temperature and acetylated with pyridine−acetic anhydride (1:1, v/v) at 100 °C for 1 h. The resulting methylated alditol acetate derivatives were analyzed by GC−MS. GC−MS analysis was performed on an Agilent 5975MSD-6890 GC−MS (Agilent Technologies, Santa Clara, CA) equipped with a HP-5 capillary column and using He as the carrier gas. The initial oven temperature was 100 °C, which was then increased by 6 °C/min to 250 °C, where it was held for 5 min.

Nuclear Magnetic Resonance Spectroscopy Analysis. The NMR spectrum of the c-EPS solution was recorded with D_2O as the solvent using a Bruker AVANCE AV-500 spectrometer (Bruker Group, Fällanden, Switzerland) operating at 500 MHz.[28] The residual solvent signal was used as an internal standard. Both one-dimensional (1D) ^1H and ^{13}C NMR experiments were performed, and the

DOI: 10.1021/acs.jafc.5b01086
J. Agric. Food Chem. 2015, 63, 3454−3463

operating temperature was 323 K. The delay (D_1) and acquisition (AQ) times were 4.00 and 2.92 s for the ^{1}H NMR spectra and 1.08 and 2.00 s for ^{13}C NMR, respectively. The chemical shift (δ) values are given in parts per million (ppm), and coupling constants (J) are given in hertz. Two-dimensional (2D) ^{1}H−^{1}H correlated spectroscopy (COSY), ^{1}H−^{13}C heteronuclear single quantum coherence (HSQC), ^{1}H−^{13}C heteronuclear multiple quantum coherence (HMBC), and nuclear Overhauser effect spectroscopy (NOESY) measurements were used to assign signals and to determine the sequence of sugar residues.

Colorimetric Triple Helix Determination with Congo Red. The conformational structure of the purified c-EPS was established by helix−coil transition analysis according to Villares's procedure.[29] Briefly, the purified c-EPS was dissolved at 1 mg/mL in various NaOH solutions (0.05−0.4 M), and these samples were added to a Congo red solution (40 μM). Spectra were recorded at room temperature (25 °C) with a UV−vis spectrophotometer (U-4100, Hitachi Ltd., Japan).

Atomic Force Microscopy. A c-EPS solution (1 mg/mL) was prepared by adding purified c-EPS to distilled H_2O. The aqueous solution was stirred at 50 °C for approximately 1 h in a sealed bottle under N_2 until the c-EPS dissolved completely. After cooling to room temperature, the solution was diluted to a final concentration of 0.01 mg/mL. Approximately 5 μL of the diluted c-EPS solution was dropped onto the surface of a mica sample carrier and allowed to dry at room temperature. Later, the AFM image was collected using a Bruker Dimension Icon AFM (Bruker Biosciences, Billerica, MA) equipped with Bruker ScanAsyst-Air PeakForce tapping-mode AFM tips. The scan resolution and rate were 512 × 512 and 1 Hz, respectively.

Scanning Electron Microscopy. The morphology of the purified c-EPS was observed using an S-3000 scanning electron microscope (Hitachi Science Systems, Ltd., Hitachinaka, Japan) at an accelerating voltage of 30 kV. For SEM analysis, the sample was mounted on a metal stub and sputtered with gold. Micrographs were recorded at 2000× magnification to ensure clear images.

In Vitro Anticancer Activity. The inhibitory effects of purified c-EPS on the HepG-2, BGC-823, and HT-29 cancer cell lines and on human colonic epithelial HCoEpiC cells in vitro were evaluated using the MTT assay on a 96-well plate.[20] Briefly, 100 μL of cancer cells (2 × 10^5 cells/mL) was cultured at 37 °C for 24 h in DMEM supplemented with 10% FBS, penicillin (100 U/mL), and streptomycin (100 mg/L) under 5% CO_2. The cells were then treated with various concentrations of purified c-EPS (0, 50, 100, 200, 400, and 600 μg/mL) and 5-FU (50 μg/mL) for 24, 48, and 72 h. At the end of each treatment, 10 μL of MTT (5 mg/mL) was added, and the cells were incubated for another 4 h. The liquid was then removed, and 100 μL of DMSO was added to the well. After dissolving the formazan crystals that formed, the absorbance was measured in a Synergy-2 microplate reader (BioTek Instruments, Inc., Burlington, VT) at 570 nm. The inhibitory rate was expressed as follows:

$$\text{inhibitory rate (\%)} = [1 - (A_{\text{sample}} - A_{\text{blank}})/(A_{\text{control}} - A_{\text{blank}})] \times 100$$

where A_{control} and A_{blank} are the absorbance values of the system without the addition of c-EPS and without cells, respectively.

Statistical Analysis. The obtained results were analyzed using SPSS version 16.0 (SPSS Inc., Chicago, IL). All data were analyzed by one-way analysis of variance (ANOVA). Significant differences were determined by Tukey's honest significant difference (Turkey's HSD) post hoc test. Half-maximal (50%) inhibitory concentration (IC_{50}) values were calculated by probit regression analysis. Statistical significance was set to $p < 0.05$. In all cases, there were three replicates ($n = 3$).

RESULTS AND DISCUSSION

Visualization of Capsules. When cells of *L. helveticus* MB2-1 were stained using a negative dyeing method and examined with an optical microscope under an oil-immersion lens, the capsules appeared as unstained, colorless halos surrounding the *L. helveticus* MB2-1 cells against a light violet-gray background, while the bacterial cells stained distinctly violet (Figure 1a). Further visualization by TEM of the stained cells revealed a clearly visible cell wall with fibrillose materials on the bacterial surface, confirming the formation of capsules by *L. helveticus* MB2-1 (Figures 1b and 1c).

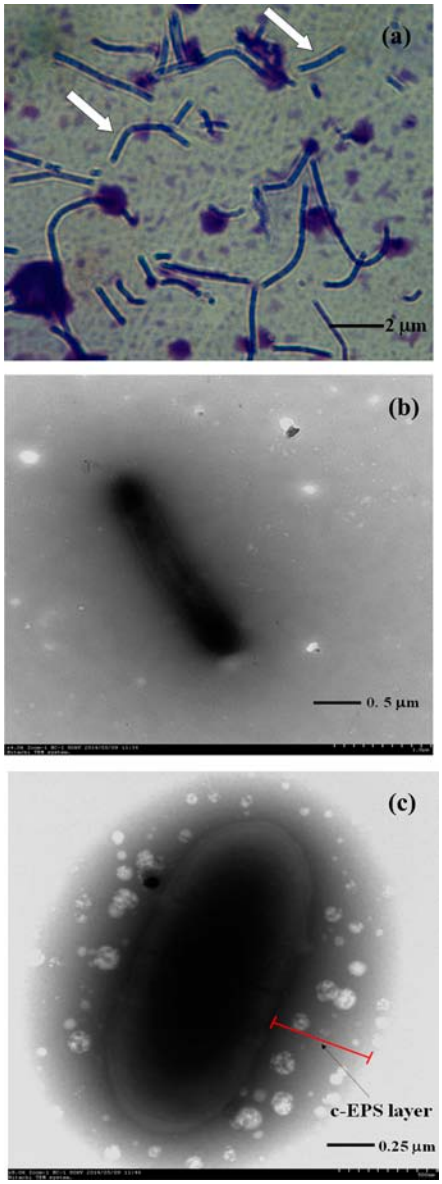

Figure 1. Micrographs showing the capsules of *L. helveticus* MB2-1 cells grown in whey medium. The capsules appear as unstained, colorless halos surrounding the bacterial cells when observed by optical microscopy (a) and as fibrillose materials attached to the bacterial surface when observed by TEM (b and c).

Isolation and Composition Analysis of c-EPS. The crude c-EPS of *L. helveticus* MB2-1 was obtained by ultrasonic extraction; the supernatant fraction was subsequently extracted with cold ethanol and fractionated first on a DEAE-cellulose 52 anion exchange chromatography column (Figure 2a) and then subjected to chromatography on a Sephadex G-100 gel filtration column (Figure 2b) for further purification. The corresponding chromatogram showed only one peak for c-EPS, indicating that the ultrasonically extracted c-EPS may be a

DOI: 10.1021/acs.jafc.5b01086
J. Agric. Food Chem. 2015, 63, 3454−3463

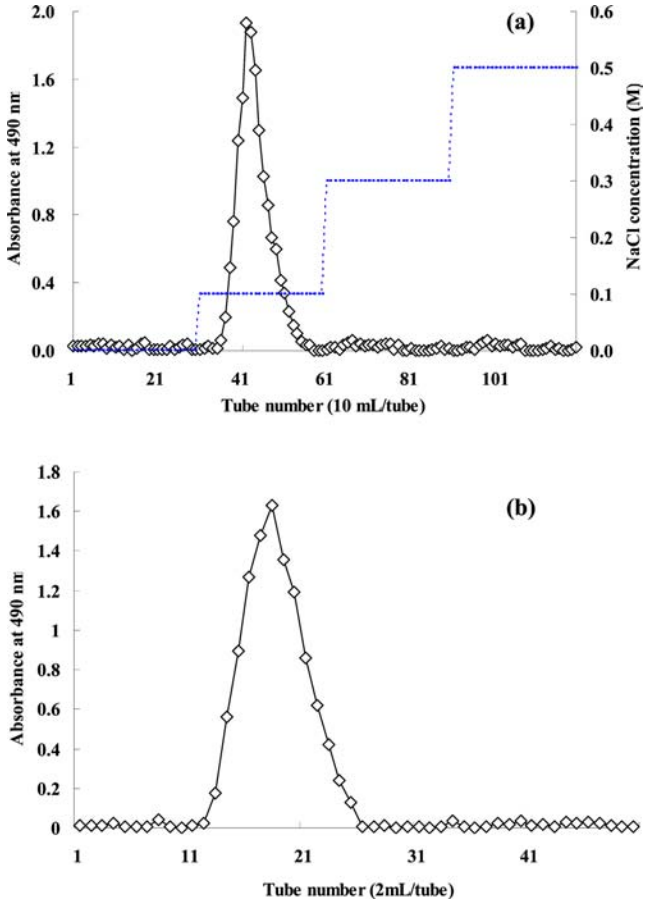

Figure 2. DEAE-cellulose 52 anion exchange chromatogram (a) and Sephadex G-100 gel filtration chromatogram (b) of crude c-EPS.

homogeneous polysaccharide. The recovery rate of c-EPS was 88.75%. Further HPSEC analysis of the purified c-EPS fraction showed a single sharp, symmetrical peak (Figure 3a), confirming that the purified c-EPS was homogeneous. According to the elution curve of the standards, the MW of the purified c-EPS was estimated to be 1.83×10^5 Da, which was less than those of the three r-EPS fractions isolated from *L. helveticus* MB2-1 (approximately 2.00×10^5 Da).[25] This MW was also lower than those of c-EPS from *L. pentosus* LPS26 (2.00×10^6 Da),[30] *L. plantarum* EP56 (8.50×10^5 Da),[31] and *L. rhamnosus* JAAS8 (5.50×10^5 Da).[13] The total carbohydrate content of the c-EPS was 95.45%. The uronic acid and sulfated group contents were 1.48% and 0.89%, respectively (Table 1). The lack of absorption by the purified c-EPS at 280 and 260 nm in the UV−vis spectrum demonstrated the absence of both proteins and nucleic acids in the polysaccharide (Figure 3b). Additionally, the c-EPS showed the same optical rotation, $[\alpha]_D^{20} = -56.8°$ (c 0.5, water), in different low concentrations of ethanol using an analytical AUTOPOL IV automatic polarimeter (RUDOLPH Research, Flanders, NJ) at room temperature.

Determination of the monomer composition was conducted after acid hydrolysis (Figure 3c). Quantitative monosaccharide analysis of the purified c-EPS revealed the presence of glucose, mannose, galactose, rhamnose, and arabinose at a molar ratio of 3.12:1.01:1.00:0.18:0.16 (Table 1). Glucose represented the greatest proportion compared to the other monosaccharides, corroborating previous reports for c-EPS or r-EPS from LAB of food origin, where glucose was often found in equal or greater

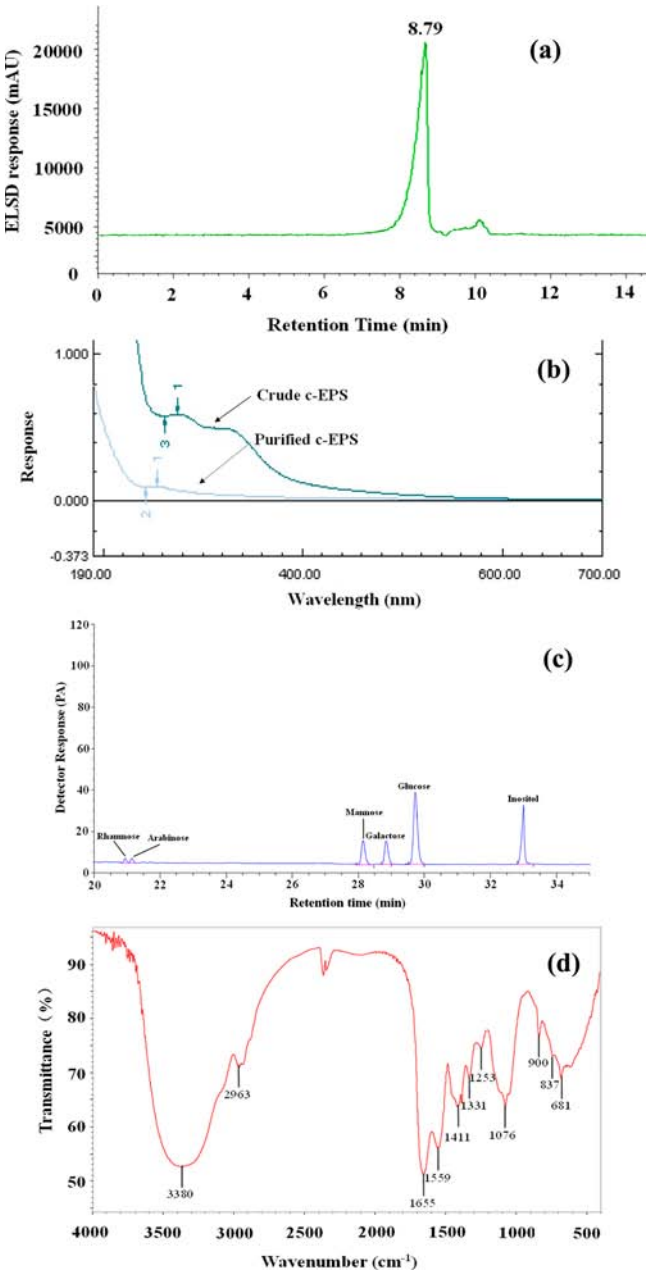

Figure 3. An HPSEC chromatogram of purified c-EPS (a), a UV−vis spectrum of purified c-EPS (b), a GC chromatogram of the monosaccharide composition (c), and a FT-IR spectrum (d) of purified c-EPS.

proportions than other monosaccharides.[14,15] The presence of different sugar moieties suggested that the polysaccharide was a HePS. A similar result was found by Rodríguez-Carvajala et al.,[30] who reported that glucose and rhamnose were the predominant components of c-EPS produced by *L. pentosus* LPS26. Tallon, Bressollier, and Urdaci[31] reported that the c-EPS from *L. plantarum* EP56 was composed mainly of glucose and galactose. Moreover, *N*-acetylglucosamine, *N*-acetylgalactosamine, and phosphoric acid have also commonly been reported as constituents of EPS produced by LAB.[13,14] However, this result was different from that obtained by Svensson, Zhang, Huttunen, and Widmalm,[32] who reported that the c-EPS from *Leuconostoc mesenteroides* ssp. *cremoris* PIA2 was a HoPS containing repeating units of linear galactose

DOI: 10.1021/acs.jafc.5b01086
J. Agric. Food Chem. 2015, 63, 3454−3463

Table 1. Monosaccharide Composition and the Carbohydrate, Protein, Uronic Acid, and Sulfate Group Contents of the Crude and Purified c-EPSs

					sugar component (molar ratio)[a]				
sample	carbohydrate (%)	protein (%)	uronic acid (%)	sulfate (%)	Gal	Glc	Man	Rha	Ara
crude c-EPS	84.09	6.49	3.46	1.79	1.00	3.36	1.22	0.12	0.15
purified c-EPS	96.23	–[b]	1.48	0.89	1.00	3.12	1.01	0.18	0.16

[a]Individual components were identified and quantified based on the elution of known standards, and the data are presented as the molar ratio for each sugar. [b]Not detected.

residues. Taken together, these results suggest that the monosaccharide constituents and molar ratios of c-EPS from LAB may be affected by the strain type.

Structural Analysis of Purified c-EPS. To investigate the functional groups of the purified c-EPS, an FT-IR spectrum was recorded over an absorbance range of 4000 to 500 cm^{-1}. As shown in Figure 3d, the spectrum of purified c-EPS displayed an intense, broad band at approximately 3380 cm^{-1}, which was assigned to the hydroxyl stretching vibration. The absorption band at 2963 cm^{-1} was due to the C−H stretching vibration.[33] The band at approximately 1655 cm^{-1} was due to bound water.[34] Peaks at 1559, 1411, and 1331 cm^{-1} were characteristic of carboxyl groups or carboxylates, indicating that c-EPS was an acidic polysaccharide. This result was consistent with its uronic acid content, which was quantified using the carbazole−sulfuric acid method using D-glucuronic acid as a standard.[23] The absorption peaks at 1253 and 1076 cm^{-1} were attributed to the stretching vibrations of the pyranose ring. Moreover, the band at 900 cm^{-1} indicated the β-pyranose form of the glucosyl residue, and the band at 837 cm^{-1} suggested the β-pyranose form of the mannose residue.[5] Finally, a characteristic absorption peak at 681 cm^{-1} indicated the existence of α-configurations in the purified c-EPS.[20]

The fully methylated c-EPS was hydrolyzed with TFA, converted into alditol acetates, and analyzed via GC−MS (Table 2). The analysis revealed the presence of five components. The c-EPS showed three major peaks of 2,4,6-Me_3Glc*p*, 2,3,4-Me_3Man*p*, and 2,3,6-Me_3Gal*p*, which originated from (1 → 3)-linked glucopyranose, (1 → 6)-linked mannopyranose, and (1 → 4)-linked galactopyranose residues, respectively. Trace amounts of 2,3,4,6-Me_4Rha*p* and 2,3,6-Me_3Ara*p* were also detected, indicating the presence of D-Rha*p*-(1 →)-linked rhamnopyranose and (1 → 4)-linked arabinopyranose residues, respectively. The molar ratio of the (1 → 3)-linked glucopyranose, (1 → 6)-linked mannopyranose, (1 → 4)-linked galactopyranose, (1 →)-linked rhamnopyranose and (1 → 4)-linked arabinopyranose residues was 3.29:1.21:1.00:0.12:0.09. No branched structures were found in c-EPS, suggesting that c-EPS may be a linear glucomannogalactan. The trace amounts of Rha*p*-(1 →) and (1 → 4)-Ara*p* linkages are also most likely randomly located within the c-EPS chains.

Table 2. Methylation Analysis of Purified c-EPS from *L. helveticus* MB2-1

retention time (min)	methylated sugar	primary mass fragments (*m*/*z*)	molar ratio	deduced linkage
14.024	2,3,6-Me_3Ara*p*	43.1, 45, 71, 87, 101.1, 117, 128.9, 161.1	0.09	(1→4)-D-Ara*p*
14.835	2,3,4,6-Me_4Rha*p*	43.1, 45, 72, 89, 101.1, 115, 131, 161.1	0.12	T-D-Rha*p*-(1→
15.457	2,4,6-Me_3Glc*p*	43.1, 71.1, 101.1, 128.9, 161.1, 205.1, 244.9, 280.9, 341	3.29	(1→3)-D-Glc*p*
15.813	2,3,4-Me_3Man*p*	43.1, 65, 85, 117, 139, 159.1,201.1, 231, 261.1, 281.9	1.21	(1→6)-D-Man*p*
18.052	2,3,6-Me_3Gal*p*	43.1, 71, 101.1, 125, 145.1, 173.1, 205.1, 245.2, 281.1	1.00	(1→4)-D-Gal*p*

The signals in the ^1H and ^{13}C NMR spectra of the purified c-EPS were assigned based on the component and methylation analyses and on values reported in the literature.[20,23,26,32] As shown in Figure 4a, three clear chemical shift signals from anomeric protons were found at δ 4.80, 4.50, and 4.37 ppm in the ^1H NMR spectrum. The signals at δ 3.40−4.20 represent the signal peak of the remaining proton, which is formed of multiple overlapping signal peaks. The signal at δ 4.71 was from the hydrogen of D_2O. This spectrum indicated that the purified c-EPS contained three residues (named **A**, **B**, and **C**). Based on their chemical shifts (δ) and the values of the coupling constant (J) for the anomeric signals in the ^1H NMR spectrum, residue **A** was determined to have an α-configuration (the $J_{1,2}$ values were 3−4 Hz), while residues **B** and **C** had β-configurations (the $J_{1,2}$ values were 7−8 Hz). The molar ratio of **A**, **B**, and **C** was approximately 1.03:1.00:3.15 when estimated using the ratio of the peak areas from the integration of the H-1 signals for residues **A**, **B**, and **C**. Based on the results of the aforementioned methylation analysis, the signal at δ 4.80 ppm corresponded to 2,3,6-Me_3Gal*p*, and the signals at 4.50 and 4.37 ppm corresponded to 2,3,4-Me_3Man*p* and 2,4,6-Me_3Glc*p*, respectively. The ^{13}C NMR spectrum (Figure 4b) showed that the C-1 signals of the three residues were detectable at δ 105.96, 105.83, and 102.28 ppm, respectively. The ^{13}C NMR chemical shifts in the anomeric carbon region also suggested three types of linkages for the galactose, glucose, and mannose residues.

Complete assignments for the ^1H and ^{13}C chemical shifts of c-EPS are shown in Supporting Information and were completed using 2D $^1H-^1H$ COSY, $^1H-^{13}C$ HSQC, $^1H-^{13}C$ HMBC, and NOESY experiments based on methylation analysis and data from the literature.[3,4,26,35] The single-bond correlations between the protons and the corresponding carbons obtained from the HSQC spectrum (Figure S1, Supporting Information) of c-EPS in D_2O enabled all of the ^{13}C NMR signals to be assigned. The signal at δ105.96 ppm (**C**) was attributed to the C-1 of →3)-β-D-Glc*p*-(1 → , δ105.83 ppm (**B**) to the C-1 of →6)-β-D-Man*p*-(1 → , and δ102.28 ppm (**A**) to the C-1 of →4)-α-D-Gal*p*-(1 →. These signals cross-correlate to the proton signals at δ4.37, 4.50, and 4.80, respectively. The results from the COSY spectrum (Figure S2, Supporting Information), based on stepwise magnetization transfers from the anomeric protons, aided in the assignment of the chemical shifts of other protons. The linkage of the residues was obtained from the HMBC spectrum (data not shown). The sequence of the glycosyl residues of c-EPS was also confirmed

DOI: 10.1021/acs.jafc.5b01086
J. Agric. Food Chem. 2015, 63, 3454−3463

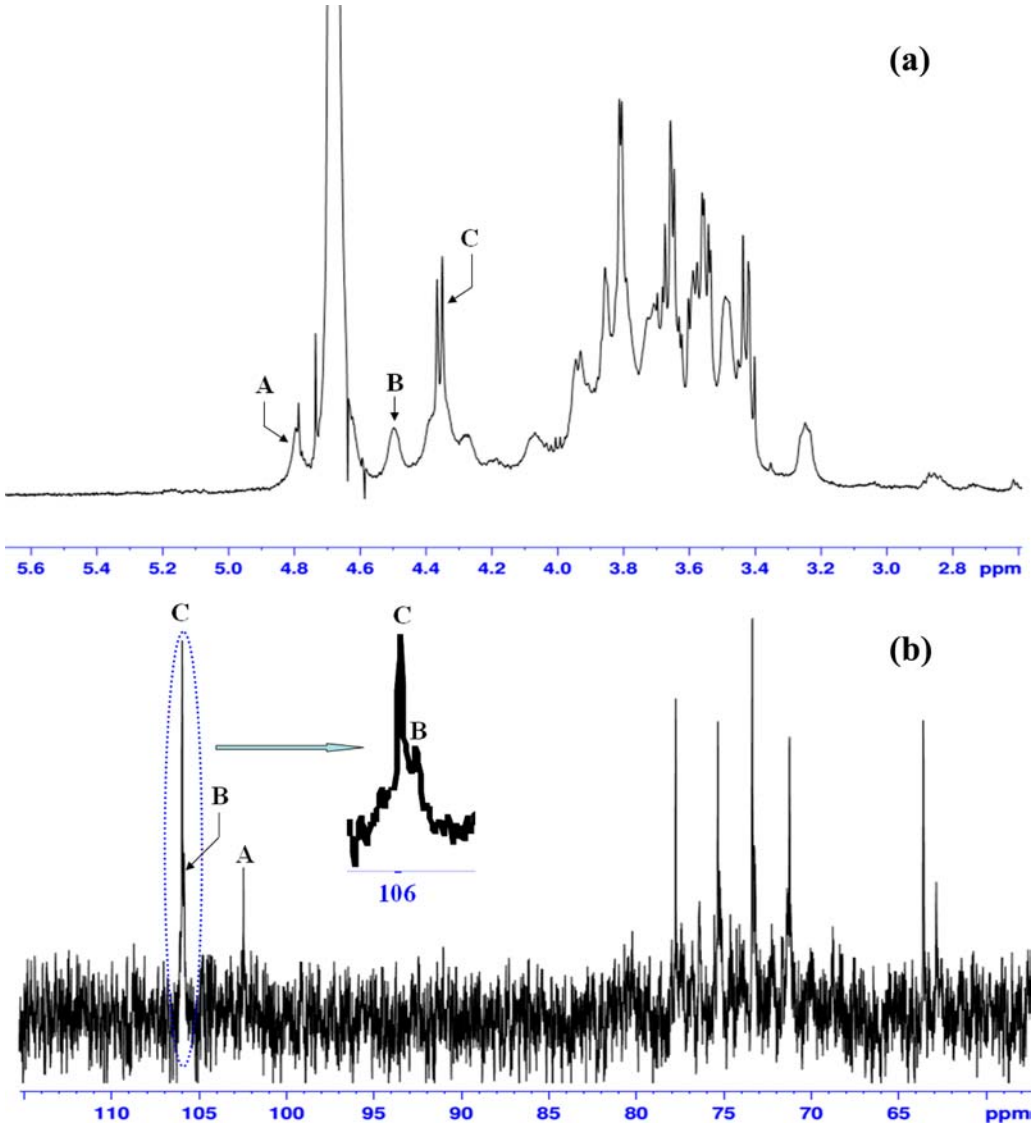

Figure 4. 500-MHz 1D ^{1}H (a) and ^{13}C (b) NMR spectra of purified c-EPS from *L. helveticus* MB2-1. Anomeric protons and carbon atoms are labeled with **A**, **B**, and **C** according to their decreased and increased chemical shifts, respectively.

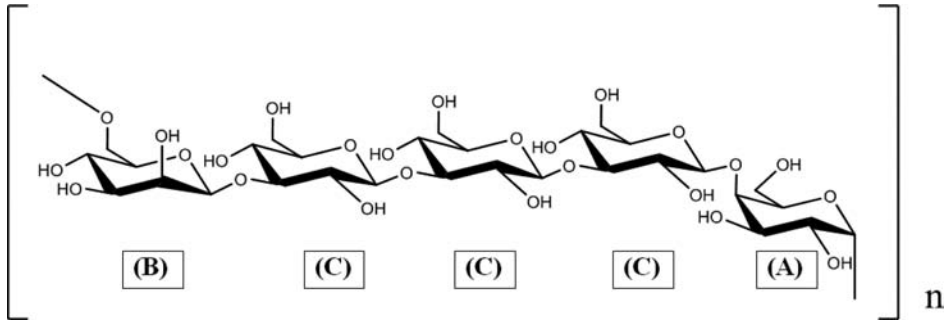

Figure 5. Proposed structure of purified c-EPS from *L. helveticus* MB2-1.

by the NOESY experiment. Inspection of the NOESY spectrum (Figure S3, Supporting Information) showed that the **A** H-1 to **B** H-6, **B** H-1 to **C** H-6, **C** H-1 to **C** H-3, and **C** H-1 to **A** H-4 were in agreement with the **A**-(1 → 6)-**B**, **B**-(1 → 3)-**C**, **C**-(1 → 3)-**C**, and **C**-(1 → 4)-**A** linkages, respectively. These results suggest that c-EPS is a linear glucomannogalactan containing repeating units of →6)-*β*-D-Man*p*-(1 → 3)-*β*-D-Glc*p*-(1 → 3)-*β*-D-Glc*p*-(1 → 3)-*β*-D-Glc*p*-(1 → 4)-*α*-D-Gal*p*-(1 →. In summary, the predicted repeating unit of c-EPS was determined (Figure 5), and the value of "*n*" for the number of repeating structural units in c-EPS was approximately 231.

Conformational and Morphological Characterization. Polysaccharides are considered to exist in an ordered three-dimensional structure, generally a triple-stranded helical

DOI: 10.1021/acs.jafc.5b01086
J. Agric. Food Chem. 2015, 63, 3454−3463

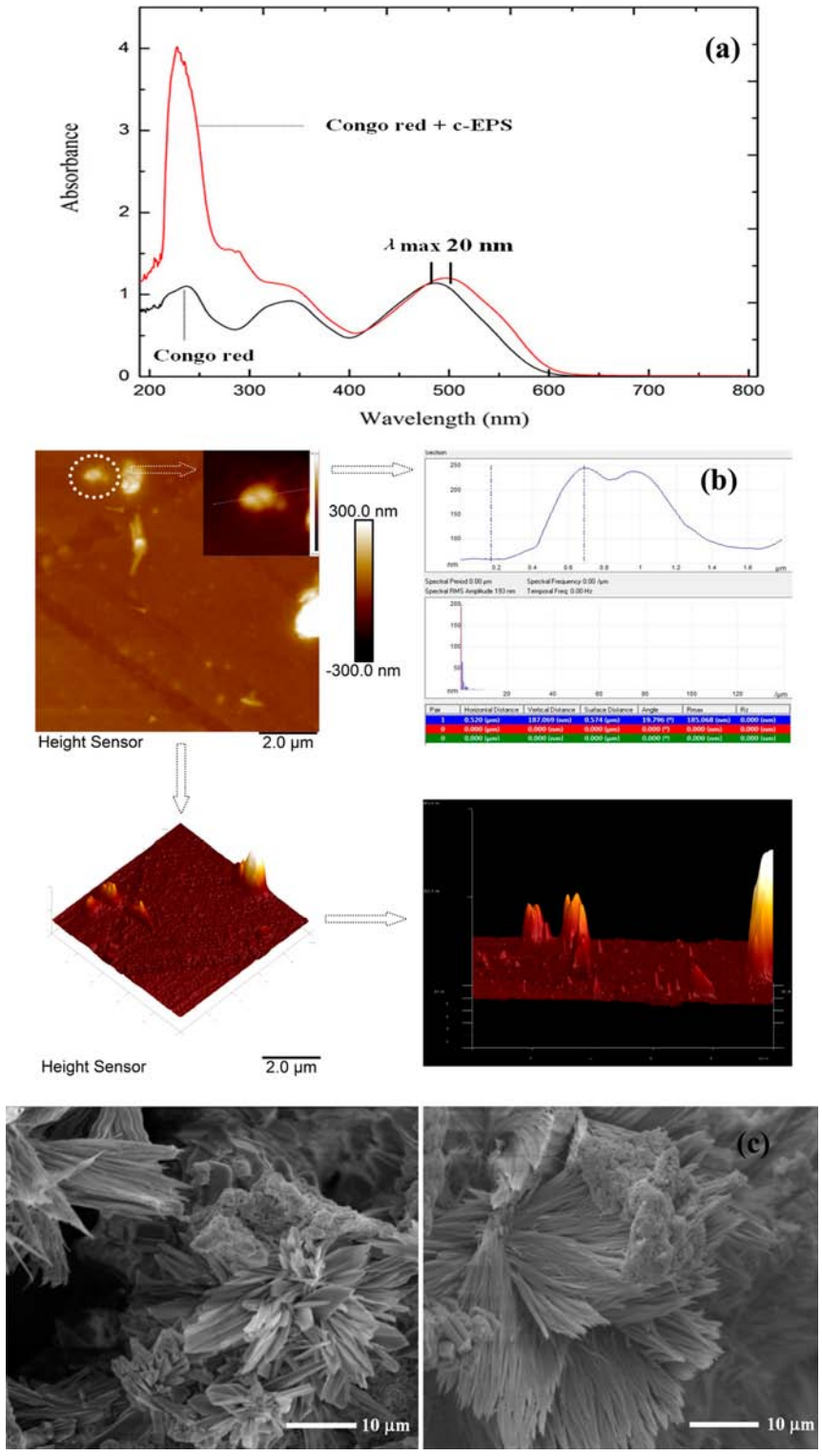

Figure 6. Absorption spectra of Congo red (control) and of Congo red with purified c-EPS (a), AFM (b), and SEM (c) images of purified c-EPS.

conformation, and they form a complex with Congo red in dilute NaOH solutions (less than 1 M). The complexation of polysaccharides with Congo red is denoted by a bathochromic shift in the visible absorption maxima (λ_{max}) of the Congo red spectrum. Hence, a polysaccharide displaying a triple-stranded helical conformation exhibits a shift in the UV absorption spectrum, whereas no shift should be observed for other conformations. Purified c-EPS from *L. helveticus* MB2-1 was complexed with Congo red at different NaOH concentrations. Laminarin and dextran were used as triple-stranded helical and random-coil controls (data not shown), respectively, and Congo red in NaOH was evaluated as the negative control. The absorption spectra of Congo red in NaOH and the c-EPS complexes with Congo red are shown in Figure 6a. The c-EPS solution exhibited a significant bathochromic shift of approximately 20 nm in the λ_{max} between 0.05 and 0.4 M

DOI: 10.1021/acs.jafc.5b01086
J. Agric. Food Chem. 2015, 63, 3454−3463

NaOH. These results suggested that purified c-EPS formed a complex with Congo red, which could be ascribed to its arrangement in a triple-stranded helical conformation.

Recently, EPS has been extensively studied by AFM, which is a powerful tool to observe the conformation of individual macromolecules and the molecular structure and dynamics of EPS.[36−38] Topographical AFM images of c-EPS are shown in Figure 6b. The c-EPS deposited from a 10 μg/mL aqueous solution exhibited rounded-to-spherical lumps with different sizes, and the formation of chains was also visible. However, the tight packing of the molecules suggested that they had a strong affinity for water molecules and had pseudoplastic behavior. Our findings for c-EPS showed rounded lumps with a maximum lump height of 250 nm. SEM is also a very powerful tool to study the three-dimensional and surface morphology of biomacromolecules, and it aids in understanding their common physical properties.[39] Micrographs of the microstructure and surface morphology of purified c-EPS are shown in Figure 6c. The c-EPS predominantly appeared as regular, feather-like structural units. This result differed from the work of Yadav, Prappulla, Jha, and Poonia,[40] who reported that EPS from *L. fermentum* CFR 2195 exhibited flake-like structural units and was highly compact. The different shape and structure, or surface topography, of the polysaccharides was most likely caused by differences in the physicochemical properties of the EPS and by differences in sample extraction, purification, or preparation.[41]

In Vitro Anticancer Activity of Purified c-EPS. The inhibitory effects of purified c-EPS from *L. helveticus* MB2-1 on three cancer cell lines and on human colonic epithelial HCoEpiC cells were measured using an MTT assay after the cells were treated with increasing concentrations (0, 50, 100, 200, 400, and 600 μg/mL) of c-EPS or with the positive control (5-FU, 50 μg/mL) for 24, 48, and 72 h. As shown in Figure 7a and 7b, the inhibitory effects of purified c-EPS on HepG-2 and BGC-823 cells significantly increased with increasing concentration and treatment time ($p < 0.05$). At the lowest concentration (50 μg/mL) and with an incubation period of 24 h, the inhibition rates of c-EPS against HepG-2 and BGC-823 cells were 9.03 ± 0.81% and 8.85 ± 0.78%, respectively. At the highest tested concentration (600 μg/mL), the inhibitory effects of c-EPS increased to 40.98 ± 0.62% and 38.75 ± 0.74% for HepG-2 and BGC-823, respectively. However, the inhibitory effects of c-EPS on HepG-2 and BGC-823 cells were all lower than that of the positive control (5-FU) at the same time points and concentrations. The inhibitory effect of c-EPS on HT-29 cells was also demonstrated to be dose- and time-dependent (Figure 7c). The inhibition rate against the HT-29 cells was significantly higher than against the other two cell lines at all c-EPS concentrations; for HT29 cells, the highest inhibition rates of c-EPS were comparable to those of 5-FU (80.05 ± 3.04%) after 72 h. Moreover, the strong inhibition of the HT-29 cells by c-EPS was evidenced by its IC_{50} value (250 μg/mL), which was much lower than those for the HepG-2 (1,520 μg/mL) and BGC-823 (2,878 μg/mL) cells. The anticancer activity of c-EPS against the HT-29 cells was also higher than that observed when the cells were treated with two r-EPSs that were isolated from the culture supernatant of *L. plantarum* 70810 at the same concentration and time.[20] These results indicated that c-EPS from *L. helveticus* MB2-1 has moderate anticancer activities against HepG-2 and BGC-823 cells and significant inhibitory effects on HT-29 cells. However, the level of c-EPS-mediated cytotoxicity in human colonic

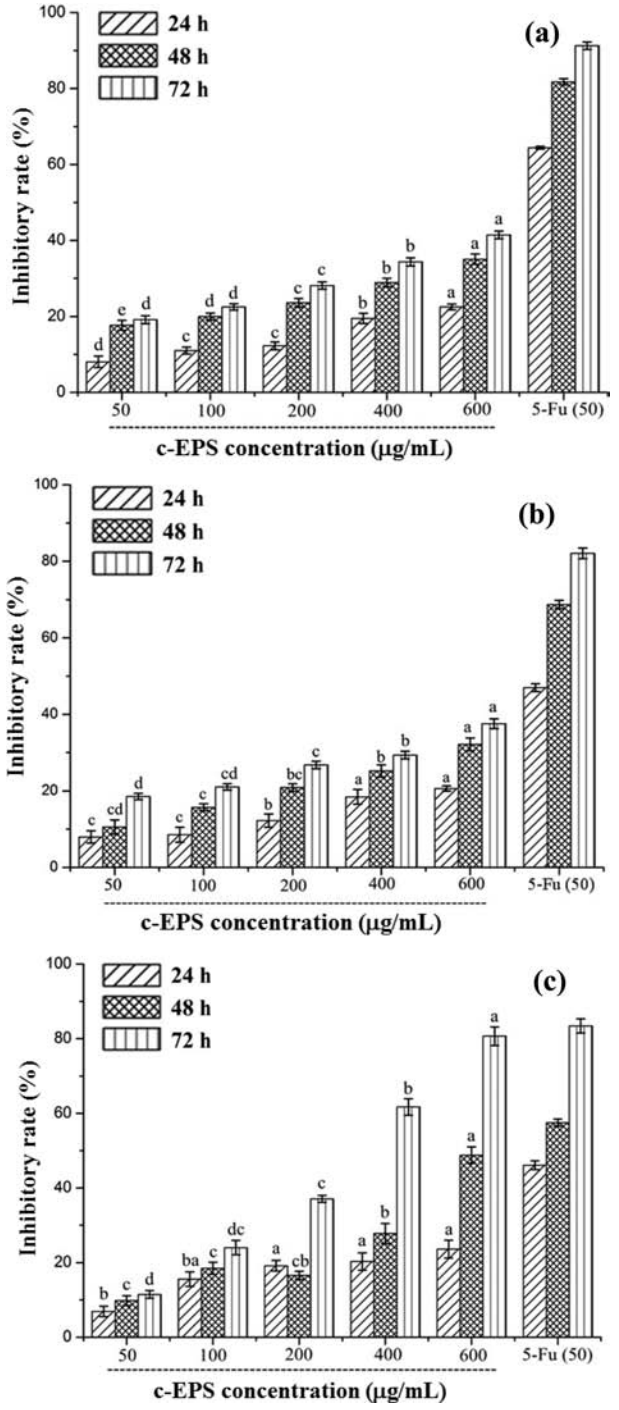

Figure 7. Anticancer effects of purified c-EPS on HepG-2 (a), BGC-823 (b), and HT-29 (c) cells. All values are expressed as the mean ± the standard deviation (SD) of three replicates. Different alphabets (a−d) in superscript donate significant difference ($p < 0.05$) and are determined by Turkey's HSD using SPSS (version 16.0).

epithelial HCoEpiC cells was not dramatic. Even at the highest dose (600 μg/mL), the level of cytotoxicity induced by a 72-h incubation of normal colonic cells with c-EPS was only 3.50 ± 0.89% (data not shown). Therefore, c-EPS possessed high anticolon cancer activity in vitro, but it was not cytotoxic to normal colon cells.

The anticancer activity of polysaccharides is related to their chemical composition, MW, chain conformation, and even charge characteristics.[16,25] Together with our previous study,

DOI: 10.1021/acs.jafc.5b01086
J. Agric. Food Chem. 2015, 63, 3454−3463

although the MW of c-EPS was similar to that of r-LHEPS-2 from *L. helveticus* MB2-1 and to those of r-EPS1 and r-EPS2 from *L. plantarum* 70810, the chemical composition and structure of c-EPS were significantly different from those of the other EPSs obtained. The c-EPS exhibited a triple-stranded helical conformation that is known to be beneficial for the anticancer activity of polysaccharides.[20,25,26] Other physicochemical properties of polysaccharides, such as the presence of uronic acid, sulfate groups, glucose, and β-type glycosidic linkages, are also conducive to increasing their anticancer activity.[14,42,43] NMR analysis revealed that r-LHEPS-2, r-EPS1, and r-EPS2 consisted predominantly of α-mannose residues and contained a minor portion of glucose and galactose residues in the β-configuration, whereas c-EPS contained mainly β-glucose residues with a minor portion of mannose and galactose residues in the α-configuration in its repeating units.[20,26] Such structural variability may profoundly affect the biological activities of EPS molecules. Therefore, certain structural properties of the purified c-EPS, such as a triple-stranded helical conformation, the presence of glucose as the major monosaccharide component, and β-type glycosidic linkages, may contribute to its multiple anticancer activities.

Currently, research on LAB c-EPS is garnering increased attention. Herein, purified c-EPS from *L. helveticus* MB2-1 was prepared and characterized. This novel c-EPS was a linear glucomannogalactan with an estimated MW of 1.83×10^5 Da. Further study revealed that the c-EPS contained repeating units of →6)-β-D-Man*p*-(1 → 3)-β-D-Glc*p*-(1 → 3)-β-D-Glc*p*-(1 → 3)-β-D-Glc*p*-(1 → 4)-α-D-Gal*p*-(1→ and trace amounts of (1 →)-Rha*p* and (1 → 4)-Ara*p* residues. Additionally, the c-EPS displayed a triple-stranded helical conformation. Morphological characterization by AFM and SEM showed that the c-EPS formed aggregates of regular feather-like units, where rounded lumps with a maximum height of 250 nm were observed. This morphology indicated good structural stability that may be utilized for film production and for the generation of edible nanostructures for the encapsulation of drug and food additives. In vitro anticancer analysis demonstrated that the c-EPS had significant anticancer activity against HepG-2, BGC-823, and especially HT-29 cancer cells. Therefore, these results suggest that the c-EPS produced by *L. helveticus* MB2-1 may be suitable for use in foods and in natural anticancer drugs.

■ ASSOCIATED CONTENT

Supporting Information

2D ^{1}H−^{13}C HSQC, ^{1}H−^{1}H COSY, and NOESY spectra of c-EPS from *L. helveticus* MB2-1. This material is available free of charge via the Internet at http://pubs.acs.org.

■ AUTHOR INFORMATION

Corresponding Author

*Tel: +86 25 84396989. Fax: +86 25 84399090. E-mail: dongms@njau.edu.cn.

Funding

This work was cofinanced by the National Natural Science Foundation of China (nos. 31201422 and 31371807), the Fundamental Research Funds for the Central Universities (no. KYZ201419), the Key Projects in the National Science & Technology Pillar Program of China (no. 2013BAD18B01-4), and the High-Tech Research and Development Program of China (no. 2011AA100903). It was also supported by a project funded by the Priority Academic Program Development of Jiangsu Higher Education Institutions (PAPD).

Notes

The authors declare no competing financial interest.

■ REFERENCES

(1) Axelsson, L. Lactic acid bacteria: Classification and physiology. In *Lactic acid bacteria microbiological and functional aspects*; Salminen, S., Wright, A. V., Ouwehand, A., Eds.; CRC Press: Boca Raton, FL, 2004; pp 1−66.

(2) Li, W.; Mutuvulla, M.; Chen, X.; Jiang, M.; Dong, M. Isolation and identification of high viscosity-producing lactic acid bacteria from a traditional fermented milk in Xinjiang and its role in fermentation process. *Eur. Food Res. Technol.* **2012**, *235*, 497−505.

(3) Landersjö, C.; Yang, Z.; Huttunen, E.; Widmalm, G. Structural studies of the exopolysaccharide produced by *Lactobacillus rhamnosus* strain GG (ATCC 53103). *Biomacromolecules.* **2002**, *3*, 880−884.

(4) Nordmark, E.; Yang, Z.; Huttunen, E.; Widmalm, G. Structural studies of an exopolysaccharide produced by *Streptococcus thermophilus* THS. *Biomacromolecules.* **2005**, *6*, 105−108.

(5) Li, W.; Ji, J.; Rui, X.; Yu, J.; Tang, W.; Chen, X.; Jiang, M.; Dong, M. Production of exopolysaccharides by *Lactobacillus helveticus* MB2-1 and its functional characteristics in vitro. *LWT–Food Sci. Technol.* **2014**, *59*, 732−739.

(6) Yang, L.; Lin, W.; Lu, T. Characterization and prebiotic activity of aqueous extract and indigestible polysaccharide from *Anoectochilus formosanus*. *J. Agric. Food Chem.* **2012**, *60*, 8590−8599.

(7) Liu, C.; Tseng, K.; Chiang, S.; Lee, B.; Hsu, W.; Pan, T. Immunomodulatory and antioxidant potential of *Lactobacillus* exopolysaccharides. *J. Sci. Food Agric.* **2011**, *91*, 2284−2291.

(8) Hu, J.; Nie, S.; Wu, Q.; Li, C.; Fu, Z.; Gong, J.; Cui, S.; Xie, M. Polysaccharide from seeds of *Plantago asiatica* L. affects lipid metabolism and colon microbiota of mouse. *J. Agric. Food Chem.* **2013**, *62*, 229−234.

(9) Hu, X. Q.; Huang, Y. Y.; Dong, Q. F.; Song, L. Y.; Yuan, F.; Yu, R. M. Structure characterization and antioxidant activity of a novel polysaccharide isolated from pulp tissues of *Litchi chinensis*. *J. Agric. Food Chem.* **2011**, *59*, 11548−11552.

(10) Pan, D.; Mei, X. Antioxidant activity of an exopolysaccharide purified from *Lactococcus lactis* subsp. *lactis* 12. *Carbohydr. Polym.* **2010**, *80*, 908−914.

(11) Adamsen, L.; Quist, M.; Midtgaard, J.; Andersen, C.; Moller, T.; Knutsen, L.; Tveteras, A.; Rorth, M. The effect of a multidimensional exercise intervention on physical capacity, well-being and quality of life in cancer patients undergoing chemotherapy. *Support. Care Cancer* **2006**, *14*, 116−127.

(12) Wagner, A. D.; Grothe, W.; Haerting, J.; Kleber, G.; Grothey, A.; Fleig, W. E. Chemotherapy in advanced gastric cancer: A systematic review and meta-analysis based on aggregate data. *J. Clin. Oncol.* **2006**, *24*, 2903−2909.

(13) Yang, Z.; Li, S.; Zhang, X.; Zeng, X.; Li, D.; Zhao, Y.; Zhang, J. Capsular and slime-polysaccharide production by *Lactobacillus rhamnosus* JAAS8 isolated from Chinese sauerkraut: Potential application in fermented milk products. *J. Biosci. Bioeng.* **2010**, *110*, 53−57.

(14) Badel, S.; Bernardi, T.; Michaud, P. New perspectives for *Lactobacilli* exopolysaccharides. *Biotechnol. Adv.* **2011**, *29*, 54−66.

(15) Jolly, L.; Vincent, S. J. F.; Duboc, P.; Neeser, J. Exploiting exopolysaccharides from lactic acid bacteria. *Antonie van Leeuwenhoek* **2002**, *82*, 367−374.

(16) Ruas-Madiedo, P.; Hugenholtz, J.; Zoon, P. An overview of the functionality of exopolysaccharides produced by lactic acid bacteria. *Int. Dairy J.* **2002**, *12*, 163−171.

(17) Kim, S. P.; Park, S. O.; Lee, S. J.; Nam, S. H.; Friedman, M. A polysaccharide isolated from the liquid culture of *Lentinus edodes* (Shiitake) mushroom mycelia containing black rice bran protects mice against a *Salmonella* lipopolysaccharide-induced endotoxemia. *J. Agric. Food Chem.* **2013**, *61*, 10987−10994.

DOI: 10.1021/acs.jafc.5b01086
J. Agric. Food Chem. 2015, 63, 3454−3463

(18) Li, C.; Li, W.; Chen, X.; Feng, M.; Rui, X.; Jiang, M.; Dong, M. Microbiological, physicochemical and rheological properties of fermented soymilk produced with exopolysaccharide (EPS) producing lactic acid bacteria strains. *LWT–Food Sci. Technol.* **2014**, *57*, 477−485.
(19) Zhang, S.; Nie, S.; Huang, D.; Huang, J.; Feng, Y.; Xie, M. A polysaccharide from *Ganoderma atrum* inhibits tumor growth by induction of apoptosis and activation of immune response in CT26-bearing mice. *J. Agric. Food Chem.* **2014**, *62*, 9296−9304.
(20) Wang, K.; Li, W.; Rui, X.; Chen, X.; Jiang, M.; Dong, M. Structural characterization and bioactivity of released exopolysaccharides from *Lactobacillus plantarum* 70810. *Int. J. Biol. Macromol.* **2014**, *67*, 71−78.
(21) Zhang, S.; Nie, S.; Huang, D.; Feng, Y.; Xie, M. A novel polysaccharide from *Ganoderma atrum* exerts antitumor activity by activating mitochondria-mediated apoptotic pathway and boosting the immune system. *J. Agric. Food Chem.* **2014**, *62*, 1581−1589.
(22) Vinogradov, E.; Valence, F.; Maes, E.; Jebava, I.; Chuat, V.; Lortal, S.; Grard, T.; Guerardel, Y.; Sadovskaya, I. Structural studies of the cell wall polysaccharides from three strains of *Lactobacillus helveticus* with different autolytic properties: DPC4571, BROI, and LH1. *Carbohyd. Res.* **2013**, *379*, 7−12.
(23) Wang, K.; Li, W.; Rui, X.; Chen, X.; Jiang, M.; Dong, M. Characterization of a novel exopolysaccharide with antitumor activity from *Lactobacillus plantarum* 70810. *Int. J. Biol. Macromol.* **2014**, *63*, 133−139.
(24) Li, W.; Ji, J.; Xu, X.; Hu, B.; Wang, K.; Xu, D.; Dong, M. Extraction and antioxidant activity in vitro of capsular polysaccharide from *Lactobacillus helveticus* MB2-1 in Sayram yogurt from Xinjiang. *Food Sci.* **2012**, *33*, 34−38.
(25) Li, W.; Ji, J.; Chen, X.; Jiang, M.; Rui, X.; Dong, M. Structural elucidation and antioxidant activities of exopolysaccharides from *Lactobacillus helveticus* MB2-1. *Carbohydr. Polym.* **2014**, *102*, 351−359.
(26) Li, W.; Ji, J.; Tang, W.; Rui, X.; Chen, X.; Jiang, M.; Dong, M. Characterization of an antiproliferative exopolysaccharide (LHEPS-2) from *Lactobacillus helveticus* MB2-1. *Carbohydr. Polym.* **2014**, *105*, 334−340.
(27) Dubois, M.; Gilles, K. A.; Hamilton, J. K.; Rebers, P. A.; Smith, F. Colorimetric method for determination of sugars and related substances. *Anal. Chem.* **1956**, *28*, 350−356.
(28) Li, W.; Xiang, X.; Tang, S.; Hu, B.; Tian, L.; Sun, Y.; Ye, H.; Zeng, X. Effective enzymatic synthesis of lactosucrose and its analogues by β-D-galactosidase from *Bacillus circulans*. *J. Agric. Food Chem.* **2009**, *57*, 3927−3933.
(29) Villares, A.; García-Lafuente, A.; Guillamón, E.; Mateo-Vivaracho, L. Separation and characterization of the structural features of macromolecular carbohydrates from wild edible mushrooms. *Bioact. Carbohydr. Diet. Fibre* **2013**, *2*, 15−21.
(30) Rodríguez-Carvajala, M. A.; Ignacio Sánchez, J.; Campelo, A. B.; Martínez, B.; Rodríguez, A.; Gil-Serrano, A. M. Structure of the high-molecular weight exopolysaccharide isolated from *Lactobacillus pentosus* LPS26. *Carbohyd. Res.* **2008**, *343*, 3066−3070.
(31) Tallon, R.; Bressollier, P.; Urdaci, M. C. Isolation and characterization of two exopolysaccharides produced by *Lactobacillus plantarum* EP56. *Res. Microbiol.* **2003**, *154*, 705−712.
(32) Svensson, M. V.; Zhang, X.; Huttunen, E.; Widmalm, G. Structural studies of the capsular polysaccharide produced by *Leuconostoc mesenteroides* ssp. *cremoris* PIA2. *Biomacromolecules* **2011**, *12*, 2496−250.
(33) Cui, J.; Qiu, J. Production of extracellular water-insoluble polysaccharide from *Pseudomonas* sp. *J. Agric. Food Chem.* **2012**, *60*, 4865−4871.
(34) Niu, Y.; Yan, W.; Lv, J.; Yao, W.; Yu, L. Characterization of a novel polysaccharide from tetraploid *Gynostemma pentaphyllum* makino. *J. Agric. Food Chem.* **2013**, *61*, 4882−4889.
(35) Bubb, W. A. NMR spectroscopy in the study of carbohydrates: Characterizing the structural complexity. *Concepts Magn. Reson. A* **2003**, *19*, 1−19.
(36) Francius, G.; Alsteens, D.; Dupres, V.; Lebeer, S.; Keersmaecker, S. D.; Vanderleyden, J.; Gruber, H. J.; Dufrene, Y. F. Stretching polysaccharides on live cells using single molecule force spectroscopy. *Nat. Protoc.* **2009**, *4*, 939−946.
(37) Marszalek, P. E.; Dufrêne, Y. F. Stretching single polysaccharides and proteins using atomic force microscopy. *Chem. Soc. Rev.* **2012**, *41*, 3523−3534.
(38) Wang, Y.; Li, C.; Liu, P.; Ahmed, Z.; Xiao, P.; Bai, X. Physical characterization of exopolysaccharide produced by *Lactobacillus plantarum* KF5 isolated from Tibet Kefir. *Carbohydr. Polym.* **2010**, *82*, 895−903.
(39) Costa, N. E.; Wang, L.; Auty, M. E.; Hannon, J. A.; McSweeney, P. L. H.; Beresford, T. P. Rheological, microscopic and primary chemical characterisation of the exopolysaccharide produced by *Lactococcus lactis* subsp. *cremoris* DPC6532. *Dairy Sci. Technol.* **2012**, *92*, 219−235.
(40) Yadav, V.; Prappulla, S. G.; Jha, A.; Poonia, A. A novel exopolysaccharide from probiotic *Lactobacillus fermentum* CFR2195: Production, purification and characterization. *Biotechnol. Bioinform. Bioeng.* **2011**, *1*, 415−421.
(41) Xu, S.; Xu, X.; Zhang, L. Effect of heating on chain conformation of branched β-glucan in water. *J. Phys. Chem. B* **2013**, *117*, 8370−8377.
(42) Ma, L.; Qin, C.; Wang, M.; Gan, D.; Cao, L.; Ye, H.; Sun, Y.; Zeng, X. Preparation, preliminary characterization and inhibitory effect on human colon cancer HT-29 cells of an acidic polysaccharide fraction from *Stachys floridana* Schuttl. ex Benth. *Food Chem. Toxicol.* **2013**, *60*, 269−276.
(43) Wang, Y.; Fang, J.; Ni, X.; Li, J.; Liu, Q.; Dong, Q.; Duan, J.; Ding, K. Inducement of cytokine release by GFPBW2, a novel polysaccharide from fruit bodies of *Grifola frondosa*, through dectin-1 in macrophages. *J. Agric. Food Chem.* **2013**, *61*, 11400−11409.

DOI: 10.1021/acs.jafc.5b01086
J. Agric. Food Chem. 2015, 63, 3454−3463

Corporation, Jiangmen, China. The material was identified by Professor R. M. Yu, College of Pharmacy, Jinan University, Guangzhou, Guangdong, China.

Experimental Reagents and Materials. Sephadex G-25 and DEAE cellulose-52 were obtained from Whatman, Ltd. Sephacryl S-300 HR was obtained from Amersham Biosciences. XAD-7 macroporous adsorption resin, dimethyl sulfoxide (DMSO), 3-(4,5-dimethylthiazol-2-yl)-2,5-diphenyltetrazolium bromide (MTT), penicillin G, and streptomycin were obtained from Sigma Chemical Co. (St. Louis, MO). Ascorbic acid (vitamin C, Vc), chlorosulfonic acid (CSA), pyridine (Pyr), hydrogen peroxide (H_2O_2), potassium ferricyanide [$K_3Fe(CN)_6$], and ferrous sulfate ($FeSO_4$) were obtained from Guangzhou Chemical Reagent Company, China. Human lung adenocarcinoma cell line A549 was obtained from Shanghai Institutes for Biological Sciences, Chinese Academy of Sciences. RPMI-1640 medium and fetal bovine serum (FBS) were purchased from Hyclone (Logan, UT). All reagents were of analytical grade.

Extraction, Isolation, and Purification of Compound 1. The dried powder of cultured *C. militaris* (500 g) was extracted in 0.5 L of distilled water using a domestic blender for 5 min. The mixture was added to a solution of simulated gastric juice (9.5 L, pH 1.5), which was used to mimic the conditions of the stomach according to the method by Golovchenko et al.,[11] with some modifications. Simulated gastric juice contained HCl (1.34 g/L), NaCl (2.16 g/L), KH_2PO_4 (0.63 g/L), $CaCl_2$ (0.12 g/L), KCl (0.39 g/L), and pepsin (0.53 g/L). Extraction was conducted for 4 h at 37 °C. After the filtered extract was centrifuged at 5000*g* for 15 min, the supernatant was concentrated with a rotary evaporator at 60 °C under vacuum. The mixture was obtained by ethanol precipitation at the final concentration of 80% (v/v) of ethanol at 4 °C overnight and then centrifuged at 5000*g* for 15 min to precipitate proteins and high-molecular-weight polysaccharides.[12] The supernatant (CMPA) was collected and lyophilized.

CMPA was fractionated on XAD-7 macroporous adsorption resin column (2.6 × 95 cm) and eluted with distilled water at a flow rate of 2 mL/min.[13] The elute (20 mL) was collected and then determined by the phenol−sulfuric acid method. Fractions 10−30 corresponding to the major peak were combined, concentrated, dialyzed (molecular weight cut-off of 500 Da), and lyophilized to obtain CMPA90.

CMPA90 was dissolved in distilled water, filtered through a filter (0.45 μm), purified on a DEAE cellulose-52 anion-exchange column (2.6 × 40 cm), and eluted with distilled water and a linear gradient from 0 to 1.0 M NaCl at a flow rate of 0.5 mL/min. The eluate (5 mL/tube) was collected automatically, and carbohydrates were assayed by the phenol−sulfuric acid method. A sharp peak was collected, dialyzed, and further purified by a Sephadex G-25 column (1.6 × 70 cm), eluting with distilled water. The flow rate was maintained at 0.3 mL/min. Consequently, a polysaccharide was obtained and coded CMPA90-1 (**1**), with $[\alpha]_D^{20} = -95.5°$ (*c* 1.0, H_2O).

Analytical Methods. The content of total sugar and uronic acid was determined by the phenol−sulfuric acid colorimetric method and the carbazole−sulfuric acid method, respectively.[14,15] Optical rotation was assayed by a Jasco P-1020 polarimeter. The sulfur content was determined by Wang's method.[9] The calibration curve was prepared with sodium sulfate as the standard. The degree of substitution (DS) was calculated on the basis of the following equation:

$$DS = \frac{1.62S\%}{32 - 1.02S\%}$$

Determination of Homogeneity and Molecular Weight. Gel permeation chromatography (GPC) was used to determine the homogeneity and molecular weights of samples. Standard dextrans (blue dextran, T-200, T-70, T-40, T-10, T-7, and T-4) and glucose were passed through a Sephacryl S-300 HR column (1.6 × 70 cm), and elution volumes were plotted against the logarithms of their respective molecular weights. Elution volumes of samples were then plotted in the same graph, and molecular weights of the polysaccharides were measured.[16]

Monosaccharide Composition Analysis. Compound **1** (5 mg) was dissolved in 2 mL of 2 M trifluoroacetic acid (TFA) in a sealed tube and hydrolyzed at 110 °C for 6 h. The excess acid was evaporated with a rotary evaporator after the hydrolysis was completed. The monosaccharide contents were measured by high-performance anion-exchange chromatography coupled with pulsed amperometric detection (HPAEC−PAD). The hydrolysate (1 mg/mL) was used for the ionic chromatography analysis by HPAEC−PAD on the Dionex ICS-2500 system, followed by the elution with a mixture of water and NaOH (200 mM) in the volume ratio of 92:8.[17]

Partial Hydrolysis. Compound **1** (30 mg) was partially hydrolyzed with 0.05 M TFA at 100 °C for 6 h. The hydrolysate was dialyzed in a dialysis bag (molecular weight cut-off of 500 Da) against distilled water for 48 h. The fraction out of the dialysis bag was collected. The excess TFA in the fraction was removed by co-distillation with MeOH, and the fraction was evaporated with a rotary evaporator, named fraction 1. The fraction in the dialysis bag was evaporated to dryness and then hydrolyzed with 0.5 M TFA. The hydrolysate was dialyzed, and the fraction out of the dialysis bag (namely, fraction 2) and the fraction in the dialysis bag (namely, fraction 3) were concentrated. Fractions 1, 2, and 3 were hydrolyzed with 2 M TFA and determined with HAPEC−PAD.[16]

Periodate Oxidation−Smith Degradation. Compound **1** (15 mg) was dissolved in 5 mL of distilled water, and 25 mL of $NaIO_4$ (15 mM) was added. The solution was kept in the dark at 4 °C. Aliquots (0.1 mL) were taken out at 6 h intervals, diluted to 5 mL with distilled water, and measured in a spectrophotometer at 223 nm, until the value became stable. The consumption of HIO_4 was analyzed by a spectrophotometric method, and the production of formic acid was determined by titration with NaOH (0.060 M). The residue was collected and reduced with $NaBH_4$ (30 mg) overnight.[16] After neutralization and dialysis, the retentate was lyophilized and hydrolyzed with TFA (2 M) at 100 °C for 6 h. The products were acetylated and then determined by gas chromatography (GC).[18]

Methylation Analysis. To analyze the glycosyl linkages, compound **1** (20 mg) was methylated 6 times according to the method described in the literature.[19] Disappearance of the OH band (3200−3700 cm^{-1}) in the infrared (IR) spectrum indicated the implementation of complete methylation. The methylated products were hydrolyzed, reduced, and acetylated to produce alditol acetates, which were analyzed by gas chromatography−mass spectrometry (GC−MS).[20] Peaks of methylated products were identified by their mass spectra. The relative molar ratios of products were estimated from the peak areas and corresponding response factors in GC.

Nuclear Magnetic Resonance (NMR) Spectroscopy. Compound **1** (60 mg) was dried in a vacuum over P_2O_5 for 6 h and then deuterium-exchanged by lyophilization with D_2O 3 times to completely replace H with D. After that, the sample was dissolved in D_2O at room temperature for 3 h before NMR analysis. One-dimensional (1D) and two-dimensional (2D) NMR spectra were obtained on an AMX 500 MHz FT NMR spectrometer (Bruker, Germany).

Sulfated Modification of Compound 1. CSA (6 mL) was added dropwise into anhydrous pyridine (12 mL) filled in a three-necked flask, under continuous stirring and cooling in an ice water bath.[9] All chemical reactions were completed in 40 min, and the sulfating reagent was obtained. Compound **1** (500 mg) was suspended in 20 mL of anhydrous formamide at room temperature, and then the mixture was stirred for 30 min. After the sulfating reagent was added, the mixture was kept stirred for 2 h at 70 °C. The product was neutralized with 2.0 M NaOH solution at room temperature, then concentrated, and precipitated with 95% ethanol (3 times volume). The sediment was then redissolved in water and intensively dialyzed against tap water (24 h) and then distilled water (48 h) to remove pyridine, salt, and potential degradation products.[6] Consequently, a sulfated polysaccharide, namely, CMPA90-M1 (**2**) was collected after lyophilization and saved in a dryness box.

FTIR Analysis. The IR spectra of compounds **1** and **2** were determined using a FTIR spectrometer (PerkinElmer, Waltham, MA). The dried powder of each sample was ground with KBr powder and then pressed into 1 mm pellets for FTIR measurement in a frequency range of 4000−500 cm^{-1}.

Ultrastructures of Compounds 1 and 2. SEM images of compounds **1** and **2** were obtained by environmental scanning electron

DOI: 10.1021/jf505915t
J. Agric. Food Chem. 2015, 63, 3464−3471

microscopy (ESEM, Philips XL-30, Netherlands). The dried powder of each sample was directly placed on separate specimen holders by double-sided adhesive tape and then sputtered with gold powder using a sputter coater.[21] Finally, the samples were observed with 2000- and 10 000-fold magnification at 5.0 kV under a high vacuum condition.

The ultrastructures of compounds **1** and **2** were also observed using AFM (BioScope Catylyst NanoScope V, Bruker, Billerica, MA). Each sample was dissolved in doubly distilled water (1 μg/mL) and stirred by a magnetic stirrer apparatus for 4 h. After that, the solution (5 μL) was dropped onto a freshly cleaved mica substrate and allowed to air-dry at room temperature. The AFM was determined in the contact mode.[22] A tube-type piezoelectric scanner (4 × 4 μm) and a Si_3N_4 probe (Olympus, Japan) were employed, and images were obtained simultaneously with 256 × 256 pixels at a scanning rate of 1.0 Hz per line.

Measurement of DPPH Radical-Scavenging Activity. The free-radical-scavenging capacity was measured using the DPPH test according to the method of Braca et al.[23] Briefly, each compound **1** and **2** solution (10 μL) at varying concentrations (0, 25, 50, 100, 200, 400, 800, and 1600 μg/mL) was added to DPPH ethanol solution (190 μL, 0.2 mM). For the positive control, the sample was substituted by Vc. The solution was kept at room temperature for 30 min, and the absorbance was measured at 517 nm. The percentage of DPPH radical-scavenging capability was calculated according to the following equation:

$$\text{scavenging ability } (\%) = [(A_0 - A_1)/A_0] \times 100\%$$

where A_0 was the absorbance in the absence of the sample and A_1 was the absorbance in the presence of the sample.

Measurement of Hydroxyl Radical-Scavenging Activity. The hydroxyl radical-scavenging activity was examined using the method described previously.[17] Vc was used as the positive control. All values were determined in the replicates. The percentage of hydroxyl radical-scavenging activity was calculated from the following equation:

$$\text{scavenging ability } (\%) = [(A_2 - A_1)/(A_0 - A_1)] \times 100\%$$

where A_0 was the absorbance of the blank control (without H_2O_2), A_1 was the absorbance in the absence of the sample, and A_2 was the absorbance in the presence of the sample.

Measurement of Reducing Power. The reducing power was tested referring to the ferric-reducing antioxidant power (FRAP) assay.[24] Samples (0−1600 μg/mL, 2.5 mL) were mixed with 2.5 mL of 0.2 M phosphate buffer (pH 6.6) and 5 mL of 1% (w/v) potassium ferricyanide $[K_3Fe(CN)_6]$. After incubation at 50 °C for 20 min, the reaction mixture was mixed with 2.5 mL of 10% (w/v) trichloroacetic acid. The mixture was then centrifuged at 5000*g* for 10 min. A total of 2.5 mL of the supernatant was mixed with the same volume of distilled water and 0.5 mL of 0.1% (w/v) ferric chloride. The absorbance of the resulting solution was measured at 700 nm after 10 min. Vc was used as the positive control.

Measurement of Ferrous-Ion-Chelating Activity. The ferrous-ion-chelating activity was estimated using the formation of the ferrous iron−ferrozine complex.[25] Samples at different concentrations (0−1600 μg/mL) were mixed with deionized water (3.7 mL), and then reacted with 0.1 mL of 2.0 mM $FeSO_4$ and 0.2 mL of 5.0 mM ferrozine. After the reaction for 10 min, the absorption was measured at 562 nm. For the positive control, the sample was substituted with ethylenediaminetetraacetic acid (EDTA). The chelating activity on ferrous ions was calculated as the following equation:

$$\text{chelating ability } (\%) = [(A_0 - A_1)/A_0] \times 100\%$$

where A_0 was the absorbance of the control (deionized water, instead of the sample) and A_1 was the absorbance of the sample mixed with reaction solution.

Cell Culture and Cytotoxicity Assay. A549 cells were cultured in RPMI-1640 medium containing 10% FBS, 100 units/mL penicillin G, and 100 μg/mL streptomycin in a cell incubator with 5% CO_2 at 37 °C. Experiments were performed when cell growth was approximately 80% confluent. Three independent experiments were performed. The cytotoxicity of compound **1** against the A549 cell line was determined using the MTT assay.[26] Briefly, A549 cells in logarithmic phase were seeded in 96-well culture dishes at a density of 3000 cells/well. After 24 h, the cells were treated with compounds **1** and **2** (final concentrations of 5.6, 16.7, 50, 150, and 450 μg/mL). Cisplatin was used as the positive control. After treatment of 48 h, 20 μL of MTT (5 mg/mL) was added to each well and the cells were incubated for another 4 h at 37 °C. After the media were removed, 200 μL of DMSO was added to each well to dissolve the cellular crystalline deposits and the absorbance was determined spectrophotometrically at 570 nm. The inhibition rate (I%) was calculated according to the formula below.

$$\text{inhibition rate } (I\%) = \frac{A_{570\text{ nm,control}} - A_{570\text{ nm,sample}}}{A_{570\text{ nm,control}} - A_{570\text{ nm,blank}}} \times 100\%$$

Statistical Analysis. Data were analyzed using statistical analysis software SPSS 11.5 and expressed as the mean value ± standard deviation (SD) for three independent experiments. Statistical significance was defined as $p < 0.05$ by analysis of variance (ANOVA), followed by Dunnett's tests.

RESULTS AND DISCUSSION

Isolation, Purification, and Chemical Composition of Compound 1. Crude polysaccharide (20.18 g) was obtained from the cultured fruiting bodies of *C. militaris*. The subsequent purification led to a single and symmetrical sharp peak of compound **1** by analysis of gel-filtration chromatography on a Sephacryl S-300 HR column with the phenol−sulfuric acid assay. The resulting compound **1** also showed the same optical rotation in varying low-content aqueous ethanol. The uronic acid content of compound **1** was below the detection limit. The average molecular weight of compound **1** was determined as 9.3 kDa by the GPC method on a Sephacryl S-300 HR column. The total sugar content of compound **1** was 98.4% (w/w), and the result of the *m*-hydroxybiphenyl colorimetric test was negative.

Structural Characterization of Compound 1. Compound **1** was acidically hydrolyzed, and three monosaccharides, arabinose, mannose, and galactose, were identified in the hydrolysate of compound **1** by HAPEC−PAD analysis, with relative ratios of 1.00:2.89:2.03, respectively. The partial acid hydrolysis of compound **1** afforded three fractions (1, 2, and 3), which were subsequently analyzed by HAPEC−PAD (Table 1).

Table 1. Results of HAPEC−PAD Analysis for the Degradation Products of Compound 1

	molar ratios		
	arabinose	mannose	galactose
CMPA90-1	1.00	2.89	2.03
fraction 1	nd[a]	1.00	nd
fraction 2	2.33	1.00	nd
fraction 3	nd	nd	1.00
Smith degradation	1.00	nd	3.15

[a]nd = not detected.

The component of fraction 3 (the precipitate in the sack) indicated that galactose might be the structural backbone of compound **1**. The results of fractions 1 and 2 suggested that compound **1** had the branched structure consisting of arabinose and mannose, with mannose as the terminal unit.

The results of periodate oxidized−Smith degradations were analyzed by GC and shown in Table 1. No mannose was found in the resulting oxidation products; thus, the linkage manner of mannose could be (1 →), (1 → 2), (1 → 6), (1 → 2,6),

DOI: 10.1021/jf505915t
J. Agric. Food Chem. 2015, 63, 3464−3471

(1 → 4), and (1 → 4,6), which might lead to oxidization of mannose into glycerol and erythritol. The presence of arabinose and galactose revealed that at least partial residues of arabinose and galactose were linked by the manners of (1 → 3), (1 → 2,3), (1 → 2,4), (1 → 3,4), or (1 → 2,3,4), which are stable under the condition of the oxidation.[27] The results of methylation analysis (Table 2) showed the presence of five

Table 2. GC−MS Results of Methylated Products of Compound 1

methylation product	retention time (min)	molar ratio	mass fragments (m/z)	linkage type
2,5-Me_2-Ara	15.22	1.00	87, 101, 117, 129, 189	1 → 3
2,3-Me_2-Ara	16.28	1.08	87, 113, 117, 129, 233	1 → 5
2,3,4,6-Me_4-Man	17.06	3.22	71, 87, 101, 117, 129, 161, 205	T →
3,4,6-Me_3-Man	17.84	0.89	71, 87, 101, 129, 161, 189	1 → 2
2,4-Me_2-Gal	18.94	6.19	43, 87, 117, 129, 189	1 → 3,6

components, namely, 2,5-Me_2-Ara, 2,3-Me_2-Ara, 2,3,4,6-Me_4-Man, 3,4,6-Me_3-Man, and 2,4-Me_2-Gal, with a molar ratio of 1.00:1.08:3.22:0.89:6.19, respectively. On the basis of the standard data in the Complex Carbohydrate Research Center (CCRC) spectral database for partially methylated alditol acetates (PMAAs), the linkage manners of arabinose were deduced as (1 → 3) and (1 → 5), while those of mannose were (1 →) and (1 → 2) and the those of galactose were (1 → 3,6). This finding was consistent with the linkage of terminal and branched residues. Moreover, the molar ratios also showed a good correlation with the monosaccharide composition analysis of compound **1** described above.

As shown in Figure 1, the characteristic absorption peaks of the polysaccharide are shown in the IR spectrum of compound

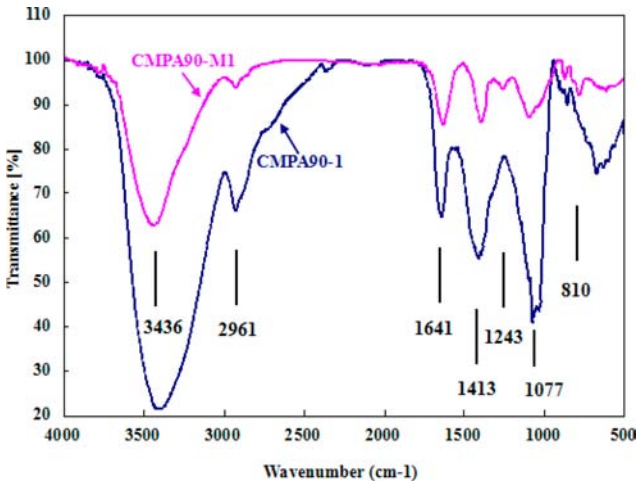

Figure 1. FTIR spectra of compounds **1** and **2**.

1 at 3436, 2961, 1641, 1413, and 1077 cm^{-1}. The absence of the absorbance band near 1243 and 810 cm^{-1} indicated the lack of sulfate ester in compound **1**. The absorption peaks at 866 and 896 cm^{-1} confirmed the co-existence of α- and β-glycosidic bonds. No band around 1740 cm^{-1} was observed, confirming that compound **1** did not contain uronic acid.[17,28]

NMR Spectroscopy Analysis. The planar structure of compound **1** was established by analysis of its 1D and 2D NMR spectra, together with comparison to the reported NMR data.[29−32] Five pairs of ^1H and ^{13}C signals of anomeric CH attributed to five different types of glycosidic bonds were assigned at δ 5.04/105.89, 5.12/104.15, 5.07/100.60, 5.10/99.33, and 4.98/98.08 ppm based on their chemical shifts and the corresponding heteronuclear single-quantum coherence (HSQC) correlations (Figure 2A). These five types of glycosidic bonds indicated the existence of five structural residues in compound **1**, i.e., residues A−E. According to ^1H and ^{13}C NMR spectra of standard arabinose (data not shown)[30] as well as the HSQC correlations, residue A was determined as an arabinose residue and the remaining signals of residue A were assigned as δ 81.53/δ 4.01(CH-2), 78.35/4.05 (CH-3), 86.86/4.12 (CH-4), and 68.40/3.85 (CH_2-5). Similarly, the NMR signals of the other residues were assigned (Table 3).

Five residues were connected together by the analysis of the heteronuclear multiple-bond correlation (HMBC) spectrum (Figure 2B) of compound **1**. In the HMBC spectrum, the following correlations were observed: E H-6 (δ 3.75) and B C-1 (δ 104.15), D H-2 (δ 4.10) and C C-1 (δ 100.60), B H-3 (δ 3.74) and C C-1 (δ 100.60), A H-1 (δ 5.04) and A C-4 (δ 86.86), A H-1 (δ 5.04) and A C-2 (δ 81.53), C H-1 (δ 5.07) and B C-3 (δ 81.11), C H-1 (δ 5.07) and D C-2 (δ 75.50), E H-1 (δ 4.98) and E C-2 (δ 70.62), B H-1 (δ 5.12) and E C-6 (δ 67.20), and A H-1 (δ 5.04) and E C-6 (δ 67.20). The cross-peaks at δ 3.75/104.15 and 5.12/67.20 were observed in HMBC. Because the signal at δ 3.75 corresponded to H-6 in residue E, the signal at δ 104.15 corresponded to C-1 in residue B, the signal at δ 5.12 corresponded to H-1 in residue B, and the signal at δ 67.20 corresponded to C-6 in residue E, it could be concluded that the residues E and B were connected to each other as E-(6 → 1)-B. Moreover, the cross-peaks at δ 5.07/75.50 and 4.10/100.60 were assigned to the inter-residue C H-1, D C-2 and the inter-residue D H-2, C C-1, respectively, indicating that the residues C and D were connected to each other as C-(1 → 2)-D. Similarly, the following sequences were established: E-(6 → 1)-A and C-(1 → 3)-B. Therefore, the structure of compound **1** was established, with a backbone composed of (1 → 3)-linked α-D-galactose and three branches, all of which substitute at O-6 of α-D-galactose, consisting of (1 → 2)-linked α-L-mannose, (1 → 5)-linked α-L-arabinose, and (1 → 3)-linked β-L-arabinose, with α-L-mannose as the terminal unit (Figure 3).

Structure Analysis of Compound 2. Compound **2** was prepared from compound **1** by the CSA−Pyr method.[6] The GPC analysis of compound **2** showed a single and symmetric sharp peak, and the average molecular weight of compound **2** was determined as 8.9 kDa. The specific rotation of compound **2** was determined as $[\alpha]_D^{20} = -35.7°$ (c 1.0, H_2O). The sulfur content was 3.9% (w/w), and the DS value was 0.23 in compound **2**. In comparison to compound **1**, two characteristic absorption bands attributed to sulfate groups occurred in the FTIR spectrum of compound **2**, one at 1243 cm^{-1}, corresponding to an asymmetrical S═O stretching vibration, and the other at 810 cm^{-1}, corresponding to a symmetrical C−O−S vibration associated with a C−O−SO_3 group, which indicated that the sulfate groups were successfully introduced into compound **2**.[33]

Ultrastructures of Compounds 1 and 2. Chemical modification could change the spatial structure of polysaccharides and, thus, affect the structure−activity relationship.[34] SEM of compounds **1** and **2** at magnifications of 2000 and 10 000 showed that compound **1** had a rough surface with a sheet-like

DOI: 10.1021/jf505915t
J. Agric. Food Chem. 2015, 63, 3464−3471

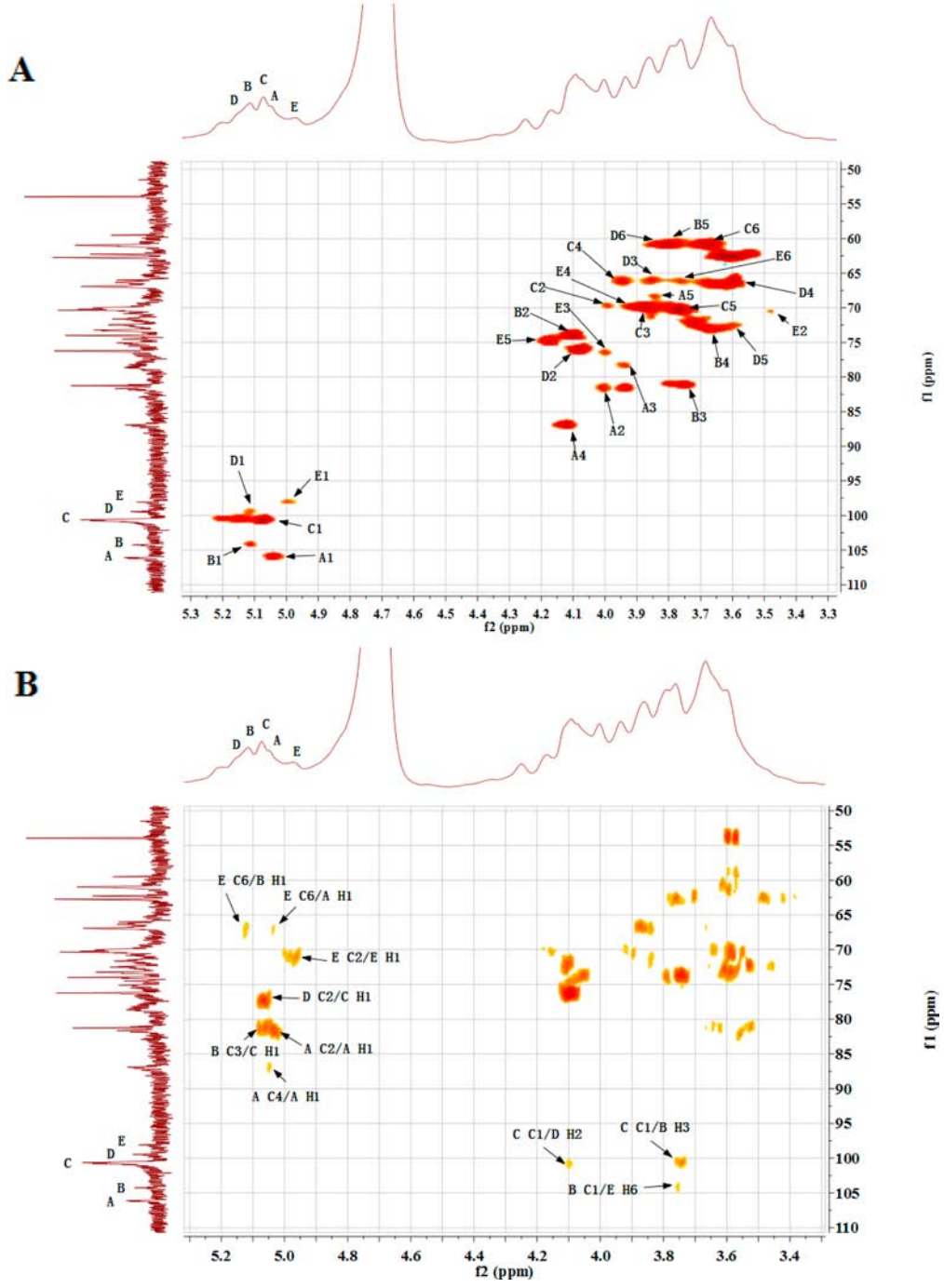

Figure 2. (A) $^{1}H-^{13}C$ HSQC spectrum of compound 1. (B) $^{1}H-^{13}C$ HMBC spectrum of compound **1**.

Table 3. Assignment of ^{13}C and ^{1}H NMR Chemical Shifts of Compound 1

	chemical shifts (ppm)					
sugar residue	C_1/H_1	C_2/H_2	C_3/H_3	C_4/H_4	C_5/H_5	C_6/H_6
A, → 5)-α-L-Ara(1 →	105.89/5.04	81.53/4.01	78.35/4.05	86.86/4.12	68.40/3.85	
B, → 3)-β-L-Ara(1 →	104.15/5.12	73.92/4.10	81.11/3.74	73.04/3.68	61.10/3.80	
C, α-L-Man(1 →	100.60/5.07	69.40/4.00	69.89/3.87	66.20/3.95	72.50/3.72	60.86/3.68
D, → 2)-α-L-Man(1 →	99.33/5.10	75.50/4.10	66.03/3.85	65.99/3.59	72.80/3.61	60.86/3.85
E, → 3,6)-α-D-Gal(1 →	98.08/4.98	70.62/3.48	76.00/4.05	70.01/3.95	74.78/4.17	67.20/3.75

appearance composed of many small lumpish particles and irregular pores, while compound **2** appeared to be a smooth surface with pore openings, which consisted mainly of randomly distributed individual spherical particles, with diameters of approximately 2 μm (panels A and B of Figure 4). The different surface topography of the polysaccharides was probably due to

DOI: 10.1021/jf505915t
J. Agric. Food Chem. 2015, 63, 3464−3471

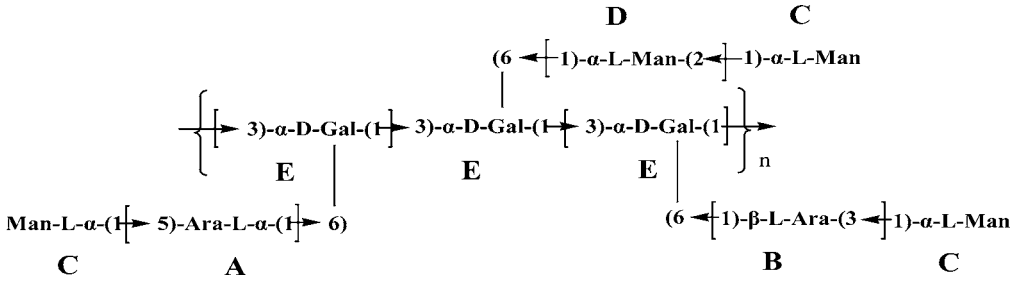

Figure 3. Predicted structure of compound **1**.

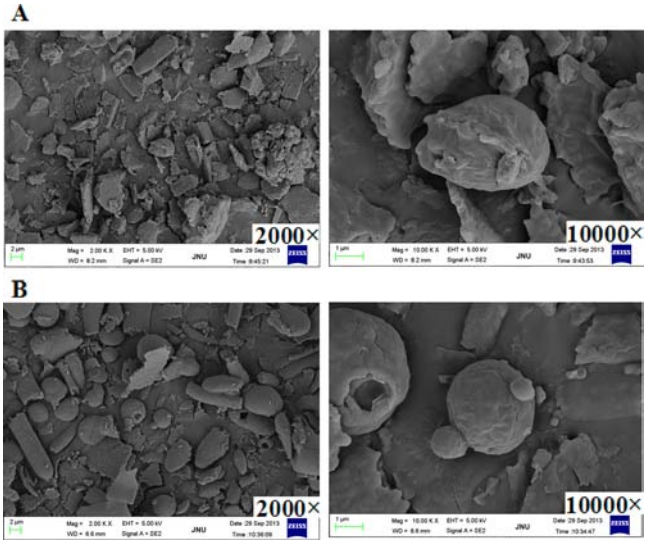

Figure 4. SEM images of compounds (A) **1** and (B) **2**.

the sulfated modification and changes of physicochemical properties; therefore, SEM could be set as a characteristic to qualitatively identify sulfated polysaccharides.

AFM has been applied as a valuable metrological tool to characterize surface topology on the nanometer scale of particles, macromolecules absorbed to surfaces, biopolymers, and the linear and circular triple helix structures of polysaccharides.[34]

Herein, AFM images showed that compound **1** aggregated to form homogeneous, smooth, and elastic dome-shaped particles (diameter ranged from 150 to 300 nm, and height was approximately 15 nm), while compound **2** particles aggregated to form a coral-like structure, with dimensions ranging from 500 to 1000 nm in length, from 100 to 300 nm in width, and from 2 to 3 nm in height (panels A and B of Figure 5). The size of polysaccharide chains of both compounds **1** and **2** was over 1.0 nm, which was larger than the usual size (approximately 0.1−1.0 nm).[34] Aggregation of polysaccharides occurs from their side branches entangling each other, and the substitution of the hydroxyl group of polysaccharides by the sulfate group can cause twisting and converting of the sugar ring conformation, which leads to a decrease of the size of the resulting sulfated polysaccharides.

Scavenging Activity of Compounds 1 and 2 against DPPH Radicals. As a stable free-radical compound with maximum absorbance at 517 nm, DPPH has been widely used to determine the free-radical-scavenging capacity of various antioxidative samples.[35] As shown in Figure 6A, compounds **1** and **2** and Vc scavenged DPPH radicals to different degrees in the given concentration range. IC_{50} values of compound **2** and Vc were 285.33 and 104.17 μg/mL, respectively.

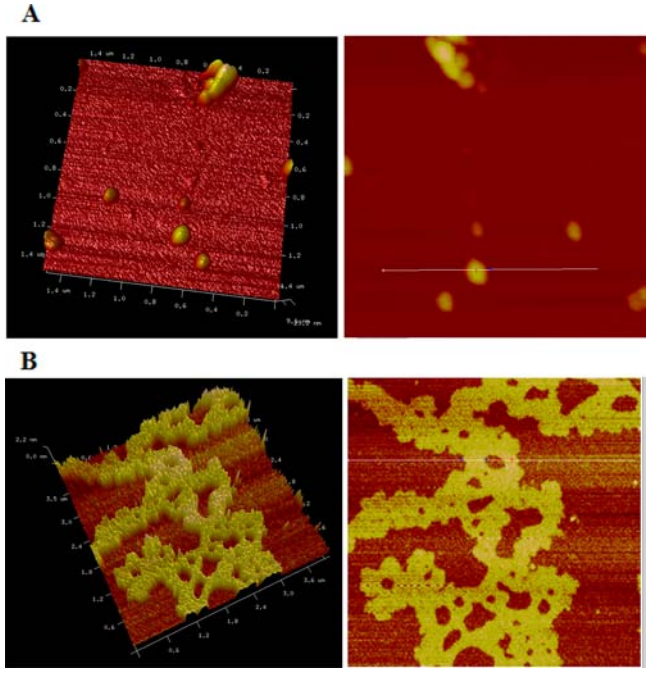

Figure 5. AFM images of compounds (A) **1** and (B) **2**.

Scavenging Activity of Compounds 1 and 2 against Hydroxyl Radicals. The hydroxyl radical generated by the Fenton reaction in this system was scavenged by samples with antioxidant activity. The scavenging activity of compounds **1** and **2** and Vc against hydroxyl radicals is shown in Figure 6B. IC_{50} values of compound 2 and Vc were 405.62 and 136.54 μg/mL, respectively.

Reducing Power of CMPA90-1 and CMPA90-M1. Figure 6C depicted the increase in the reducing power of compounds **1** and **2** and Vc at the gradient concentrations. Higher absorbance of the reaction mixture indicated a stronger reducing power of samples. The reducing abilities of compounds **1** and **2** and Vc at 400 μg/mL were 0.49, 0.82, and 1.21, respectively.

Ferrous-Ion-Chelating Effect of Compounds 1 and 2. The chelating abilities of compounds **1** and **2** and EDTA on Fe^{2+} are shown in Figure 6D. In the range of concentrations from 25 to 1600 μg/mL, they were found to possess a more potent chelating effect on Fe^{2+} in a concentration-dependent manner. EC_{50} values of compound 2 and EDTA were 385.68 and 107.14 μg/mL, respectively.

Cytotoxicity of Compounds 1 and 2 against A549 Cells. The cytotoxicity induced by compounds **1** and **2** was investigated in human cancer cell line A549 using the MTT assay. As shown in Figure 7, compounds **1** and **2** exhibited the capability of antiproliferation in A549 cells, with the IC_{50} values

DOI: 10.1021/jf505915t
J. Agric. Food Chem. 2015, 63, 3464−3471

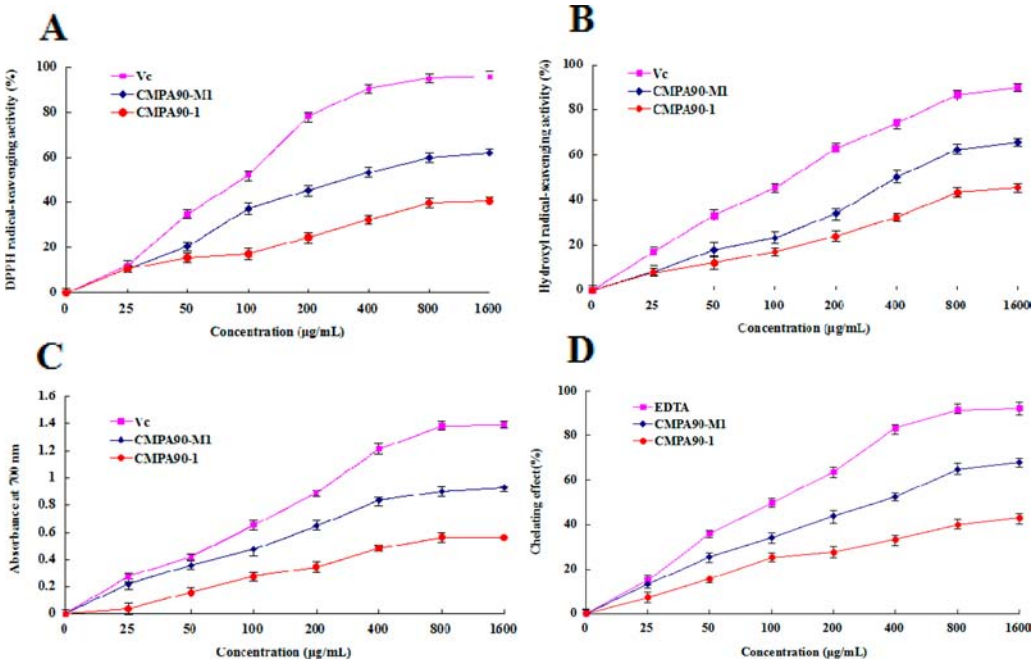

Figure 6. Antioxidant activities of compounds **1** and **2**: (A) DPPH radical-scavenging activity, (B) hydroxyl radical-scavenging activity, (C) reducing power, and (D) ferrous-ion-chelating effect. Values are the mean ± SD of three separate experiments.

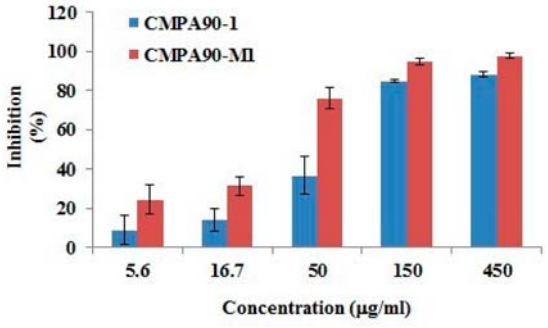

Figure 7. Inhibitory effects of compounds **1** and **2** on human tumor cell growth. A549 cells were treated by compounds **1** and **2** at different concentrations for 48 h in 96 well plates. The absorbance of the culture was measured at 570 nm. Data are presented as the mean ± SD of three separated experiments.

of 39.08 and 17.33 μg/mL, respectively. Cisplatin exhibited the capability of antiproliferation against A549 cells, with the IC_{50} value of 0.70 μg/mL.

In conclusion, a novel polysaccharide (**1**) was isolated from the cultured fruiting bodies of *C. militaris* containing predominantly D-galactose, L-mannose, and L-arabinose. The results showed that the structural characteristics of compound **1** are different from those of the polysaccharides previously found from *Cordyceps* sp. in monosaccharide ratios, molecular weights, etc.[1,2,4,36,37] Sulfation of compound **1** by the CSA−Pyr method led to its sulfate derivative (**2**). SEM and AFM exhibited that the ultrastructure of compound **2** differed greatly from that of compound **1**, which could result in an improvement of antioxidant and cytotoxic activities. Relative to compound **1**, compound **2** showed more noticeable free-radical-scavenging activity, ferrous-ion-chelating ability, and reducing power and stronger antiproliferative effect on A549 cells. The results of this study indicate that some specific substitutions occurring on original groups of polysaccharides might alter or improve their physicochemical and biological properties. This research may provide new insights into the development and application of polysaccharides from *C. militaris*.

AUTHOR INFORMATION

Corresponding Authors

*Telephone: +86-20-85222069. E-mail: tzhujh@jnu.edu.cn.
*Telephone: +86-20-85228205. E-mail: tsly@jnu.edu.cn.
*Telephone: +86-20-85220386. Fax: +86-20-85224766. E-mail: tyrm@jnu.edu.cn.

Funding

This research work was financially supported by the Major National Science and Technology Projects/Significant New Drugs Creation (2011ZX09102-001-33).

Notes

The authors declare no competing financial interest.

ACKNOWLEDGMENTS

The authors thank Dr. Dongbo Yu from The University of Chicago Medical Center, Chicago, IL, for proofreading the manuscript.

REFERENCES

(1) Won, S. Y.; Park, E. H. Anti-inflammatory and related pharmacological activities of cultured mycelia and fruiting bodies of *Cordyceps militaris*. *J. Ethnopharmacol.* **2005**, *96*, 555−561.

(2) Yu, R. M.; Song, L. Y.; Zhao, Y.; Bin, W.; Wang, L.; Zhang, H.; Wu, Y. H.; Ye, W. C.; Yao, X. S. Isolation and biological properties of polysaccharide CPS-1 from cultured *Cordyceps militaris*. *Fitoterapia* **2004**, *75*, 465−472.

(3) Yu, R. M.; Yin, Y.; Yang, W.; Ma, W. L.; Yang, L.; Chen, X. J.; Zhang, Z.; Ye, B.; Song, L. Y. Structural elucidation and biological activity of a novel polysaccharide by alkaline extraction from cultured *Cordyceps militaris*. *Carbohydr. Polym.* **2009**, *75*, 166−171.

(4) Wang, M.; Meng, X. Y.; Yang, R. L.; Qin, T.; Wang, X. Y.; Zhang, K. Y. *Cordyceps militaris* polysaccharides can enhance the immunity

DOI: 10.1021/jf505915t
J. Agric. Food Chem. 2015, 63, 3464−3471

and antioxidation activity in immunosuppressed mice. *Carbohydr. Polym.* **2012**, *89*, 461−466.
(5) You, L. J.; Gao, Q.; Feng, M. Y.; Yang, B.; Ren, J. Y.; Gu, L. J.; Cui, C.; Zhao, M. M. Structural characterization of polysaccharides from *Tricholoma matsutake* and their antioxidant and antitumor activities. *Food Chem.* **2013**, *138*, 2242−2249.
(6) Jin, M. L.; Lu, Z. Q.; Huang, M.; Wang, Y. M.; Wang, Y. Z. Sulfated modification and antioxidant activity of exopolysaccahrides produce by *Enterobacter cloacae* Z0206. *Int. J. Biol. Macromol.* **2011**, *48*, 607−612.
(7) Zhao, X. N.; Hu, Y. L.; Wang, D. Y.; Guo, L. W.; Yang, S. J.; Fan, Y. P.; Zhao, B. K.; Wang, Y. L.; Abula, S. Optimization of sulfated modification conditions of tremella polysaccharide and effects of modifiers on cellular infectivity of NDV. *Int. J. Biol. Macromol.* **2011**, *49*, 44−49.
(8) Guo, Z. H.; Hu, Y. L.; Wang, D. Y.; Ma, X.; Zhao, X. N.; Zhao, B. K.; Wang, J. M.; Liu, P. Sulfated modification can enhance the adjuvanticity of lentinan and improve the immune effect of ND vaccine. *Vaccine* **2009**, *27*, 660−665.
(9) Wang, L.; Li, X. X.; Chen, Z. X. Sulfated modification of the polysaccharides obtained from defatted rice bran and their antitumor activities. *Int. J. Biol. Macromol.* **2009**, *44*, 211−214.
(10) Niu, Y. G.; Xie, Z. H.; Zhang, H.; Sheng, Y.; Yu, L. L. Effects of structural modifications on physicochemical and bile acid-binding properties of *Psyllium*. *J. Agric. Food Chem.* **2013**, *61*, 596−601.
(11) Golovchenko, V. V.; Khramova, D. S.; Ovodova, R. G.; Shashkov, A. S.; Ovodov, Y. S. Structure of pectic polysaccharides isolated from onion *Allium cepa* L. Using a simulated gastric medium and their effect on intestinal absorption. *Food Chem.* **2012**, *134*, 1813−1822.
(12) Hua, Y. L.; Gao, Q.; Wen, L. R.; Yang, B.; Tang, J.; You, L. J.; Zhao, M. M. Structural characterisation of acid- and alkali-soluble polysaccharides in the fruiting body of *Dictyophora indusiata* and their immunomodulatory activities. *Food Chem.* **2012**, *132*, 739−743.
(13) Yang, B.; Prasad, K. N.; Xie, H. H.; Lin, S.; Jiang, Y. M. Structural characteristics of oligosaccharides from soy sauce lees and their potential prebiotic effect on lactic acid bacteria. *Food Chem.* **2011**, *126*, 590−594.
(14) Dubois, M.; Gilles, K. A.; Hamilton, J. K.; Rebers, P. A.; Smith, F. Colorimetric method for determination of sugars and related substances. *Anal. Chem.* **1956**, *28*, 350−356.
(15) Bitter, T.; Muir, H. M. A modified uronic acid carbazole reaction. *Anal. Biochem.* **1962**, *4*, 330−334.
(16) Hu, X. Q.; Huang, Y. Y.; Dong, Q. F.; Song, L. Y.; Yuan, F.; Yu, R. M. Structure characterization and antioxidant activity of a novel polysaccharide isolated from pulp tissues of *Litchi chinensis*. *J. Agric. Food Chem.* **2011**, *59*, 11548−11552.
(17) Yuan, F.; Yu, R. M.; Yin, Y.; Shen, J. R.; Dong, Q. F.; Zhong, L.; Song, L. Y. Structure characterization and antioxidant activity of a novel polysaccharide isolated from *Ginkgo biloba*. *Int. J. Biol. Macromol.* **2010**, *46*, 436−439.
(18) Yang, B.; Wang, J. S.; Zhao, M. M.; Liu, Y.; Wang, W.; Jiang, Y. M. Identification of polysaccharides from pericarp tissues of litchi (*Litchi chinensis* Sonn.) fruit in relation to their antioxidant activities. *Carbohydr. Res.* **2006**, *341*, 634−638.
(19) Hakomori, S. A rapid premethylation of glycolipid, and polysaccharide catalyzed by methylsulfinyl carbanion in dimethyl sulfoxide. *J. Biochem.* **1964**, *55*, 205−208.
(20) Sassaki, G. L.; Lacomini, M.; Gorin, P. A. Methylation−GC−MS analysis of arabinofuranose- and galactofuranose-containing structures: Rapid synthsis of partially O-methylated alditol acetate atandards. *An. Acad. Bras. Cienc.* **2005**, *77*, 223−234.
(21) Chen, S. H.; Chen, H. X.; Tian, J. G.; Wang, Y. W.; Xing, L. S.; Wang, X. Chemical modification, antioxidant and α-amylase inhibitory activities of corn silk polysaccharides. *Carbohydr. Polym.* **2013**, *98*, 428−437.
(22) Wang, X. M.; Sun, R. G.; Zhang, J.; Chen, Y. Y.; Liu, N. N. Structure and antioxidant activity of polysaccharide POJ-U1a extracted by ultrasound from *Ophiopogon japonicus*. *Fitoterapia* **2012**, *83*, 1576−1584.
(23) Braca, A.; Tommasi, N. D.; Bari, L. D.; Pizza, C.; Politi, M.; Morelli, I. Antioxidant principles from *Bauhinia terapotensis*. *J. Nat. Prod.* **2001**, *64*, 892−895.
(24) Yuan, Y. V.; Carrington, M. F.; Walsh, N. A. Extracts from dulse (*Palmaria palmata*) are effective antioxidants and inhibitors of cell proliferation in vitro. *Food Chem. Toxicol.* **2005**, *43*, 1073−1081.
(25) Dinis, T. C.; Madeira, V. M.; Almeida, L. M. Action of phenolic derivatives (acetaminophen, salicylate, and 5-aminosalicylate) as inhibitors of membrane lipid peroxidation and as peroxyl radical scavengers. *Arch. Biochem. Biophys.* **1994**, *315*, 161−169.
(26) Hu, X. J.; Song, L. Y.; Huang, L. J.; Zhen, Q.; Yu, R. M. Antitumor effect of a polypeptide fraction from *Arca subcrenata in vitro* and *in vivo*. *Mar. Drugs* **2012**, *10*, 2782−2794.
(27) Abdel-Akher, M.; Hamilton, J. K.; Montgomeny, R.; Smith, F. A new procedure for the determination of the fine structure of polysaccharides. *J. Am. Chem. Soc.* **1952**, *74*, 4970−4971.
(28) Sun, Y. X.; Liang, H. T.; Zhang, X. T.; Tong, H. B.; Liu, J. C. Structural elucidation and immunological activity of a polysaccharide from the fruiting body of *Armillaria mellea*. *Bioresour. Technol.* **2009**, *100*, 1860−1863.
(29) Bi, H. T.; Gao, T. T.; Li, Z. H.; Ji, L.; Yang, W.; Iteku, B. J.; Liu, E. X.; Zhou, Y. F. Structural elucidation and antioxidant activity of a water-soluble polysaccharide from the fruit bodies of *Bulgaria inquinans* (Fries). *Food Chem.* **2013**, *138*, 1470−1475.
(30) Kang, J.; Cui, S. W.; Phillips, G. O.; Chen, J.; Guo, Q. B.; Wang, Q. New studies on gum ghatti (*Anogeissus latifolia*) Part III: Structure characterization of a globular polysaccharide fraction by 1D, 2D NMR spectroscopy and methylation analysis. *Food Hydrocolloids* **2011**, *25*, 1999−2007.
(31) Patraa, P.; Dasa, D.; Beherab, B.; Maiti, T. K.; Islama, S. S. Structure elucidation of an immunoenhancing pectic polysaccharide isolated from aqueous extract of pods of green bean (*Phaseolus vulgaris* L.). *Carbohydr. Polym.* **2012**, *87*, 2169−2175.
(32) Mandal, E. K.; Maity, K.; Maity, S.; Gantait, S. K.; Behera, B.; Maiti, T. K.; Sikdar, S. R.; Islama, S. S. Chemical analysis of an immunostimulating (1 → 4)-, (1 → 6)-branched glucan from an edible mushroom, *Calocybe indica*. *Carbohydr. Res.* **2012**, *347*, 172−177.
(33) Maciel, J. S.; Chaves, L. S.; Souza, B. Structural characterization of cold extracted fraction of soluble sulfated polysaccharide from red seaweed *Cracilaria birdiae*. *Carbohydr. Polym.* **2008**, *77*, 559−565.
(34) Wang, Y. F.; Peng, Y. H.; Wei, X. L.; Yang, Z. W.; Xiao, J. B.; Jin, Z. Y. Sulfation of tea polysaccharides: Synthesis, characterization and hypoglycemic activity. *Int. J. Biol. Macromol.* **2010**, *46*, 270−274.
(35) Benvenuti, S.; Pellati, F.; Melegari, M.; Bertelli, D. Polyphenols, anthocyanins, ascorbic acid, and radical scavenging activity of Rubus, Ribes, and Aronia. *J. Food Sci.* **2004**, *69*, 164−169.
(36) Lee, J. S.; Kwon, J. S.; Yun, J. S.; Pahk, J. W.; Shin, W. C.; Lee, S. Y. Structural characterization of immunostimulating polysaccharide from cultured mycelia of *Cordyceps militaris*. *Carbohydr. Polym.* **2010**, *80*, 1011−1017.
(37) Jing, Y. S.; Cui, X. L.; Chen, Z. Y.; Huang, L. J.; Song, L. Y.; Yu, R. M. Elucidation and biological activities of a new polysaccharide from cultured *Cordyceps militaris*. *Carbohydr. Polym.* **2014**, *102*, 288−296.

DOI: 10.1021/jf505915t
J. Agric. Food Chem. 2015, 63, 3464−3471

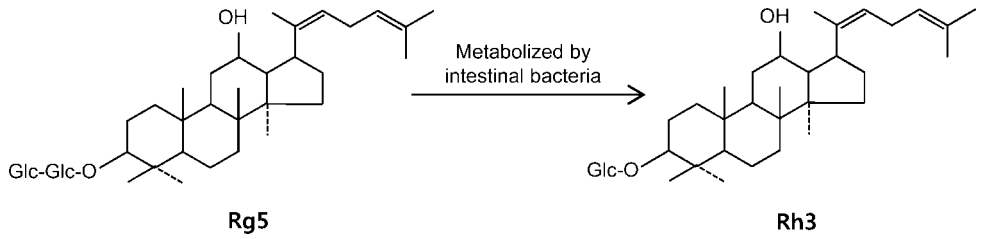

Figure 1. Chemical structure of ginsenoside Rg5 and Rh3.

Table 1. Primers Used in RT-PCR Reactions

gene	forward primer (5′ → 3′)	reverse primer (5′ → 3′)	size (bp)
TNF-α	CCTATGTCTCAGCCTCTTCT	CCTGGTATGAGATAGCAAAT	354
iNOS	CCCTTCCGAAGTTTCTGGCAGCAGC	GCCTGTCAGAGCCTCGTGGCTTTGG	450
IL-6	CCACTTCACAAGTCGGAGGCTT	CCAGCTTATCTGTTAGGAGA	395
HO-1	ATACCCGCTACCTGGGTGAC	TGTCACCCTGTGCTTGACCT	209
SIRT1	CACCGATCCTCGAACAATTC	CCCAGCTCCAGTCAGAACTA	640
GAPDH	ATGTACGTAGCCATCCAGGC	AGGAAGGAAGGCTGGAAGAG	420

radical-scavenging activities.[14−17] After intake, Rg5 is metabolized by intestinal bacteria and transformed to Rh3, which is taken up by the body.[16] Some evidence shows that Rh3 has anti-inflammatory effects in a chronic dermatitis model[16] and neuroprotective effects in a scopolamine-induced memory deficit model,[18] but its effect on neuroinflammation has not been well explored. Therefore, we examined the anti-inflammatory effect of Rh3 in LPS-induced microglia and investigated its underlying molecular mechanism.

MATERIALS AND METHODS

Isolation of Ginsenoside Rh3. Heated red ginseng extract was prepared as previously described,[18,19] and its main constituent ginsenoside Rg5 was isolated following a previously described procedure.[19,20] Briefly, ginsenoside Rg5 (0.2 g) was incubated with human fecal suspension (approximately 1 g) in anaerobic medium (0.5 L) according to a previously described method.[21] The reaction mixture was extracted with *n*-BuOH (1 L) twice and evaporated (dried extract, 0.15 g). The *n*-BuOH extract was subjected to silica gel column chromatography (2 × 15 cm), eluted with a stepwise gradient of $CHCl_3$ and methanol, and then underwent further chromatography on silica gel columns, employing the same eluent systems, to yield ginsenoside Rh3 (43 mg) (Figure 1). The extracted ginsenoside Rh3 was identified by comparison to an authentic standard by nuclear magnetic resonance spectrometry (Bruker AMX 400, 400 MHz) and fast atom bombardment mass spectrometry (FAB-MS). Ginsenoside Rh3 (purity, >95%), colorless powder (MeOH); melting point (mp), 161−162 °C; FAB-MS (*m*/*z*), 605 $(M + H)^+$.

Reagents. All reagents used for cell culture were obtained from Gibco BRL (Grand Island, NY). LPS (*Escherichia coli* serotype 055:B5), 5-aminoimidazole-4-carboxamide-1-β-D-ribofuranoside (AICAR), and nicotinamide were purchased from Sigma Chemical Co. (St Louis, MO). Antibodies against phospho-/total forms of mitogen-activated protein kinases (MAPKs) and Akt were purchased from Cell Signaling Technology (Beverley, MA). Antibodies against hemeoxygenase-1 (HO-1) and phospho-forms of janus kinase 1 (JAK1) and STAT1 were purchased from Santa Cruz Biotechnology (Santa Cruz, CA). Phosphatidylinositol 3-kinase (PI3K)/Akt- and JAK/STAT-specific inhibitors (LY294002, Ruxolitinib) were obtained from Calbiochem (La Jolla, CA) and MedChem Express (Princeton, NJ), respectively. Griess reagent for NO measurement, all of the reagents for reverse transcription polymerase chain reaction (RT-PCR), and oligonucleotides for electrophoretic mobility shift assay (EMSA) were purchased from Promega (Madison, WI).

Microglial Cell Cultures. Immortalized murine BV2 microglial cells[22] were grown and maintained in Dulbecco's modified Eagle's medium (DMEM) supplemented with 10% heat-inactivated fetal bovine serum, streptomycin (10 μg/mL), and penicillin (10 units/mL) at 37 °C. Primary microglial cells were cultured from the cerebral cortices of 1−2-day-old Sprague−Dawley rat pups as described previously.[23] The purity of microglial cultures was greater than 95%, which was confirmed by western blot and immunocytochemistry analyses using an antibody specific to ionized calcium-binding adapter protein-1 (data not shown). The use of rat for primary culture was approved by the Institutional Animal Care and Use Committee in the Medical School of Ewha Womans University (ESM13-0242).

Measurement of Cytokine and Nitrite Levels. BV2 cells (1×10^5 cells per well in a 24 well plate) or primary microglia (2.5×10^5 cells per well in a 48 well plate) were pretreated with Rh3 or AICAR for 1 h and stimulated with LPS (0.1 μg/mL for BV2 cells and 10 ng/mL for primary microglia). The supernatants of the cultured microglia were collected 24 h after LPS stimulation, and the concentrations of tumor necrosis factor (TNF)-α and interleukin (IL)-6 were measured by enzyme-linked immunosorbent assay (ELISA) as previously described.[24] Accumulated nitrite was measured in the cell supernatant by Griess reagent.

RT-PCR. BV2 cells (7.5×10^5 cells on a 6 cm dish) or rat primary microglia (7×10^6 cells on a 6 cm dish) were treated with LPS in the presence of Rh3, and total RNA was extracted with TRI reagent (Sigma). For RT-PCR, total RNA (1 μg) was reverse-transcribed in a reaction mixture containing 1 unit of RNase inhibitor, 500 ng of random primers, 3 mM $MgCl_2$, 0.5 mM dNTP, 1× RT buffer, and 10 units of reverse transcriptase (Promega). The synthesized cDNA was used as a template for PCR using GoTaq polymerase (Promega), and the primers are shown in Table 1. GAPDH was used as an internal control for normalizing target gene expression.

EMSA. Nuclear extracts from treated microglia were prepared as described previously.[24] Double-stranded DNA oligonucleotides containing the NF-κB or antioxidant response element consensus sequences (Promega) were end-labeled by [γ-^{32}P] ATP. Nuclear proteins (5 μg) were incubated with ^{32}P-labeled probe on ice for 30 min and resolved on a 5% acrylamide gel as previously described.[24]

Intracellular Reactive Oxygen Species (ROS) Measurement. Intracellular accumulation of ROS was measured with H_2DCF-DA (Sigma) by modifying previously reported methods.[25] In brief, BV2 microglial cells were stimulated with LPS for 16 h and stained with 20 μM H_2DCF-DA in Hank's balanced salt solution buffer for 1 h at 37 °C. 2′,7′-Dichlorofluorescein (DCF) fluorescence intensity was measured at 485 nm excitation and 535 nm emission on a fluorescence plate reader (Molecular Devices, Sunnyvale, CA). For image analysis of ROS production, BV2 cells were placed on coverslips and treated with Rh3 1 h prior to LPS treatment. Cells were stained with H_2DCF-

DOI: 10.1021/jf506110y
J. Agric. Food Chem. 2015, 63, 3472−3480

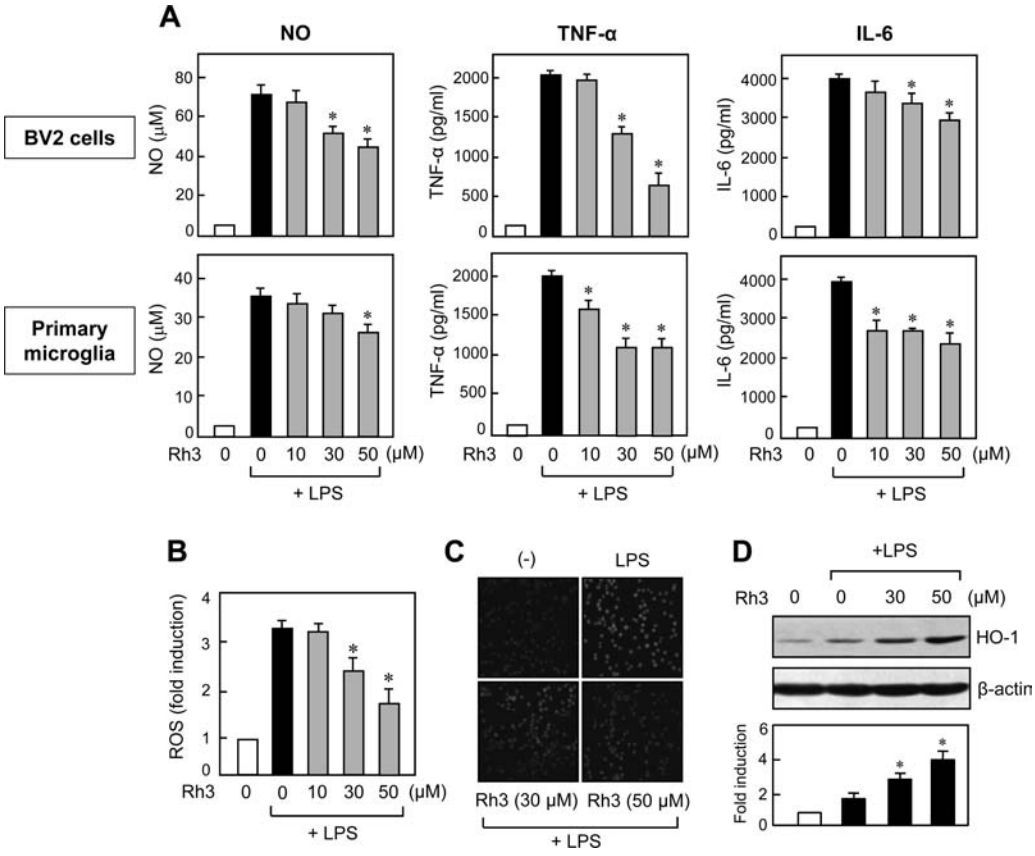

Figure 2. Rh3 inhibits NO, TNF-α, IL-6, and ROS production and enhances HO-1 expression in LPS-stimulated microglia. (A) BV2 cells or rat primary microglia were pretreated with Rh3 1 h prior to LPS (100 ng/mL) and incubated for 16 h. The supernatants were obtained, and the amounts of nitrite, TNF-α, and IL-6 were measured. (B) BV2 cells treated with the above conditions were stained with 20 μM H_2DCF-DA, and DCF fluorescence intensity was measured. (C) Confocal image analysis of intracellular ROS production. (D) Levels of HO-1 protein expression in BV2 cells were determined by western blot analysis. The data are expressed as the mean ± SEM for three independent experiments. (*) $p < 0.05$ versus cells treated with LPS alone.

DA for 1 h, mounted onto a microscope slide, and analyzed using confocal laser scanning microscopy.

Western Blot Analysis. Cell extracts were prepared as described previously.[24] Proteins were separated by 12% sodium dodecyl sulfate−polyacrylamide gel electrophoresis (SDS−PAGE) and transferred to nitrocellulose membrane (Amersharm, Piscataway, NJ). The membranes were blocked with 5% skim milk in 10 mM Tris−HCl containing 150 mM NaCl and 0.5% Tween 20 (TBST) and then incubated with primary antibodies (1:1000) recognizing the phospho- or total forms of extracellular signal-regulated kinase (ERK), p38 MAPK, c-Jun N-terminal kinase (JNK), or Akt. Primary antibodies recognizing JAK1, STAT1, or HO-1 were also used. β-Actin was used as the loading control for normalizing protein expression. After thoroughly washing with TBST, horseradish peroxidase-conjugated secondary antibodies (1:1000 dilution in TBST; New England Biolabs, Beverly, MA) were applied and blots were developed using an enhanced chemiluminescence detection kit (Thermo Fisher Scientific, Waltham, MA).

Knockdown of AMPK by Small Interfering RNA (siRNA). BV2 cells (0.5×10^5 cells per well in a 12 well plate) were transiently transfected with 100 pM AMPK siRNA using Ambion siPORT NeoFX transfection reagent following the protocols of the manufacturer (Ambion). A scrambled control siRNA was used as a negative control. The siRNA sequences were as follows: AMPK-α1 siRNA (5′-GCAGAAGUUUGUAGAGCAA-3′) and control siRNA (5′-AAUCGCAUAGCGUAUGCCGUU-3′). The cells were harvested 48 h after siRNA transfection, and the expression levels of AMPK protein were measured by western blotting.

Statistical Analysis. Unless otherwise stated, all experiments were performed with triplicate samples and repeated at least 3 times. Data are presented as the mean ± standard error of the mean (SEM), and statistical comparisons between groups were performed using one-way analysis of variance followed by Newman−Keuls multiple comparison test. p values less than 0.05 were deemed to indicate statistical significance.

RESULTS

Rh3 Inhibits LPS-Induced Production of NO, TNF-α, and IL-6 in BV2 Cells and Primary Cultured Microglia. BV2 cells were treated with Rh3 for 1 h before stimulation with LPS, and the effects of Rh3 on the LPS-induced production of NO and cytokines were examined. As shown in Figure 2A, Rh3 significantly inhibited NO, TNF-α, and IL-6 production in LPS-stimulated BV2 cells. The anti-inflammatory effects of Rh3 were also observed in rat primary microglia (Figure 2A). Rh3 did not have any cytotoxicity in the concentrations used in this study in both the BV2 and primary microglial cells at least for 48 h (data not shown).

Rh3 Suppresses LPS-Induced ROS Production and Upregulates HO-1 Expression. Previous studies indicate that ROS play a crucial role in oxidative and inflammatory responses.[1,4] To determine the effect of Rh3 on ROS production in LPS-stimulated BV2 cells, we measured intracellular ROS scavenging activities of Rh3 using the DCF-DA method. As shown in Figure 2B, Rh3 had an inhibitory effect on LPS-induced ROS production in BV2 cells. Confocal microscopic analysis also showed the inhibition of LPS-induced

DOI: 10.1021/jf506110y
J. Agric. Food Chem. 2015, 63, 3472−3480

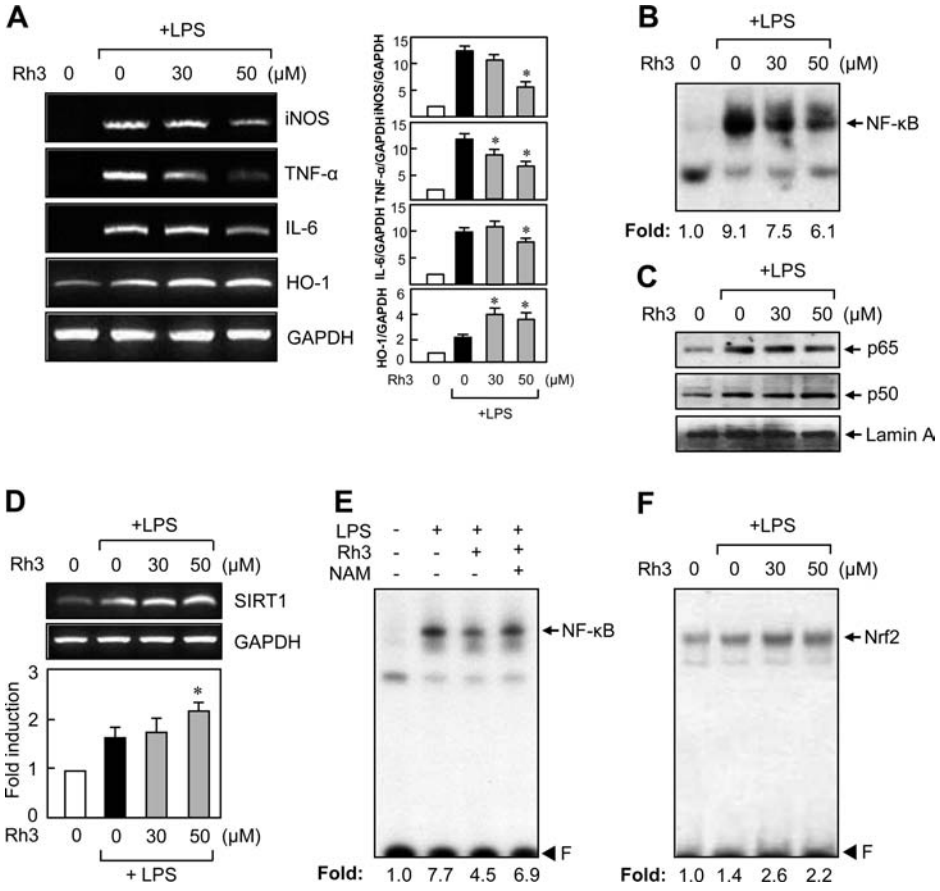

Figure 3. Rh3 suppresses LPS-induced mRNA expression of iNOS, TNF-α, and IL-6 and increases HO-1 expression by modulating NF-κB and Nrf2 activity. (A) To examine mRNA expression of iNOS, TNF-α, IL-6, and HO-1, BV2 cells were pretreated with Rh3 1 h before incubation with LPS (100 ng/mL) for 6 h. The mRNA levels of iNOS, TNF-α, IL-6, and HO-1 were determined by RT-PCR. The results are representative of three independent experiments (left panel). Quantitative analysis of mRNA expression was performed by densitometric analysis. GAPDH was used as an internal control. The data are expressed as the mean ± SEM for three independent experiments (right panel). (*) $p < 0.05$ versus cells treated with LPS alone. (B) EMSA for NF-κB DNA-binding activity. Nuclear extracts were prepared from BV2 cells after treatment with LPS (100 ng/mL) for 3 h in the presence or absence of Rh3, and gel shift assay was performed using NF-κB oligonucleotide probe. "F" indicates free probe. (C) Amount p65 or p50 protein was determined in the same nuclear extracts used in the EMSA, by western blot. Lamin A was used as the loading control for nuclear protein. (D) Effect of Rh3 on SIRT1 mRNA expression in BV2 cells stimulated with LPS for 3 h. The results are representative of three independent experiments. Quantitative analysis of mRNA levels of SIRT1 was performed by densitometric analysis. The data are expressed as the mean ± SEM for three independent experiments. (*) $p < 0.05$ versus cells treated with LPS alone. (E) Effect of nicotinamide (NAM) on NF-κB DNA-binding activity. Nuclear extracts were prepared from BV2 cells after treatment with LPS (100 ng/mL) for 3 h in the presence or absence of Rh3 (50 μM) or Rh3 (50 μM) + nicotinamide (50 μM), and EMSA was performed. (F) EMSA for Nrf2 DNA-binding activity.

ROS production by Rh3, which is consistent with DCF-DA data (Figure 2C). In addition, Rh3 significantly increased LPS-induced expression of HO-1 (Figure 2D), which is an important molecule involved in cellular defense against oxidative stress.[26,27]

Rh3 Inhibits LPS-Induced mRNA Expression of iNOS and Pro-inflammatory Cytokines and Increases HO-1 Expression by Modulating the NF-κB/Nrf2 Axis and Sirtuin 1 (SIRT1) Expression. Next, we examined the effect of Rh3 on the transcription of iNOS, TNF-α, IL-6, and HO-1 genes in LPS-stimulated BV2 cells. Rh3 significantly inhibited the mRNA expression of iNOS, TNF-α, and IL-6 and increased HO-1 mRNA expression (Figure 3A). A similar pattern of transcriptional regulation by Rh3 was observed in primary microglia (data not shown). These results suggest that Rh3 regulates the expression of iNOS, TNF-α, IL-6, and HO-1 at the mRNA level. To analyze the molecular mechanism underlying the anti-inflammatory effect of Rh3, we examined the effect of Rh3 on NF-κB, a key transcription factor modulating pro-inflammatory gene expression. Rh3 inhibited LPS-induced NF-κB DNA-binding activity (Figure 3B). However, it did not affect the nuclear translocation of p65 or p50 subunit protein (Figure 3C). Because SIRT1 is known to inhibit NF-κB signaling via deacetylation of the p65 subunit, we investigated whether Rh3 affects SIRT1 expression. RT-PCR analysis showed that Rh3 increased SIRT1 expression (Figure 3D). Next, to see whether the upregulation of SIRT1 led to NF-κB inhibition in Rh3-treated BV2 cells, we examined the effects of SIRT1 inhibitor, nicotinamide, on NF-κB activity. EMSA data showed that nicotinamide reversed the Rh3-mediated inhibition of NF-κB in LPS-stimulated BV2 cells (Figure 3E). The data suggest that SIRT1 is at least partly involved in Rh3-mediated inhibition of NF-κB signaling. Moreover, Rh3 increased Nrf2 binding to antioxidant response element, which is important for HO-1 gene expression (Figure 3F).

Rh3 Enhances AMPK Phosphorylation and Inhibits Phosphorylation of Akt and JAK1/STAT1 in LPS-

DOI: 10.1021/jf506110y
J. Agric. Food Chem. 2015, 63, 3472−3480

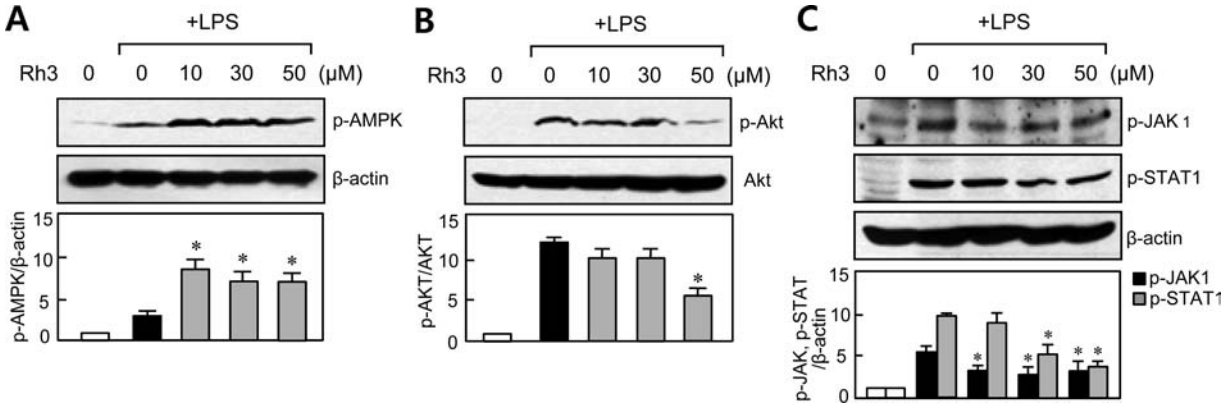

Figure 4. Rh3 enhances AMPK phosphorylation and inhibits the phosphorylation of Akt and JAK1/STAT1 in LPS-stimulated BV2 cells. Cell extracts were prepared from BV2 cells treated with LPS for 1 h in the absence or presence of Rh3 and were subjected to immunoblot analysis. The data show the effect of Rh3 on phosphorylation of (A) AMPK, (B) Akt, and (C) JAK1/STAT1. The results are representative of three independent experiments. p-Akt was normalized by total Akt, and p-AMPK, p-JAK1, and p-STAT1 were normalized by β-actin. Quantification data are shown in the bottom panel. The data are expressed as the mean ± SEM for three independent experiments. (*) $p < 0.05$ versus cells treated with LPS alone.

Stimulated BV2 Cells. To investigate the signaling pathways involved in the anti-inflammatory effect of Rh3, we examined the effect of Rh3 on the phosphorylation of AMPK, which is an important anti-inflammatory signaling molecule.[6−8] We found that Rh3 enhanced LPS-induced AMPK phosphorylation (Figure 4A). Next, we examined the effect of Rh3 on LPS-induced phosphorylation of three types of MAPKs, Akt (a downstream substrate of PI3K), JAK1, and STAT1, which are upstream signaling molecules that regulate gene expression of pro-inflammatory cytokines.[28−31] Rh3 had an inhibitory effect on Akt, JAK1, and STAT1 phosphorylation (panels B and C of Figure 4), but it did not affect the phosphorylation of MAPKs in LPS-induced BV2 cells (see Supplementary Figure 1 of the Supporting Information). To further investigate the role of PI3K/Akt and JAK1/STAT1 in Rh3-mediated anti-inflammation, we treated BV2 cells with PI3K/Akt or JAK/STAT pathway-specific inhibitors (LY294002, Ruxolitinib) before stimulation with LPS. We found that both inhibitors significantly inhibited the production of TNF-α, IL-6, NO, and ROS induced by LPS (see Supplementary Figure 2 of the Supporting Information). These results suggest that AMPK, PI3K/Akt, and JAK1/STAT1 signaling pathways are largely involved in the anti-inflammatory effect of Rh3 in LPS-stimulated BV2 cells.

AMPK Is an Upstream Signal of PI3K/Akt and JAK1/STAT1 and Mediates the Anti-inflammatory Effect of Rh3 in LPS-Stimulated BV2 Cells. To investigate a possible involvement of AMPK in Rh3-mediated anti-inflammation, BV2 cells were treated with AICAR, an AMPK activator. AICAR decreased LPS-induced phosphorylation of Akt and JAK1/STAT1 (Figure 5), suggesting that AMPK is an upstream signal of PI3K/Akt and JAK1/STAT1. In addition, AICAR, like Rh3, inhibited NO, TNF-α, IL-6, and ROS production, suppressed NF-κB DNA-binding activity, and upregulated SIRT1 (a negative regulator of NF-κB) expression (panels A−C of Figure 6). Furthermore, AICAR upregulated HO-1 expression by enhancing Nrf2 DNA-binding activity (panels D and E of Figure 6). These results suggest that Rh3 exerts anti-inflammatory/antioxidant effects in microglia by modulating AMPK. To confirm this possibility, we examined whether knockdown of AMPK by siRNA reversed the anti-inflammatory effect of Rh3. As shown in Figure 7, in comparison to the control siRNA group, AMPK siRNA

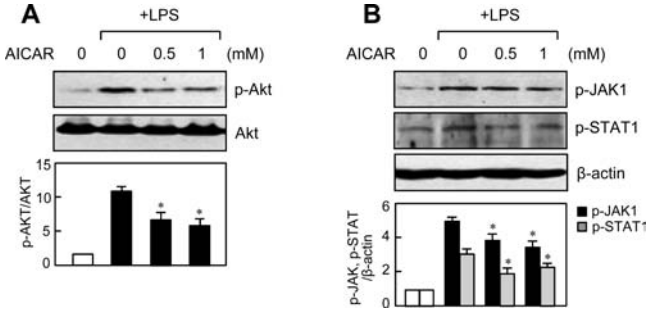

Figure 5. AICAR, an AMPK activator, has an inhibitory effect on LPS-induced phosphorylation of Akt, JAK1, and STAT1. (A) Cell extracts were prepared from BV2 cells treated with LPS for 1 h in the presence of AICAR and were subjected to immunoblot analysis using antibodies against phospho- or total forms of Akt. The total form of Akt was used as an internal control. (B) Effect of AICAR on the phosphorylation of JAK1 and STAT1. The results are representative of three independent experiments. Quantification data are shown in the bottom panel. The data are expressed as the mean ± SEM for three independent experiments. (*) $p < 0.05$ versus cells treated with LPS alone.

attenuated Rh3- and AICAR-mediated inhibition of TNF-α, IL-6, NO, and ROS production. We observed that AMPK siRNA also augmented LPS-induced inflammatory responses (Figure 7B). However, the percent increase of inflammatory responses induced by AMPK knockdown compared to control siRNA was much higher in the LPS + Rh3- or LPS + AICAR-treated group than the LPS-only group. These results collectively suggest that AMPK is at least partly involved in the anti-inflammatory effect of Rh3 in LPS-stimulated microglia.

■ DISCUSSION

In the present study, we demonstrated that Rh3 has an anti-inflammatory effect in activated microglia. Rh3 significantly inhibited the production of NO, TNF-α, and IL-6 in LPS-stimulated BV2 cells and rat primary microglia. In addition, Rh3 decreased levels of intracellular ROS, which is associated with upregulated antioxidant enzyme HO-1 expression. RT-PCR analysis showed that Rh3 regulated iNOS, TNF-α, IL-6, and HO-1 at a transcriptional level. Further mechanistic studies revealed that the inhibition of NF-κB and enhancement of Nrf2

DOI: 10.1021/jf506110y
J. Agric. Food Chem. 2015, 63, 3472−3480

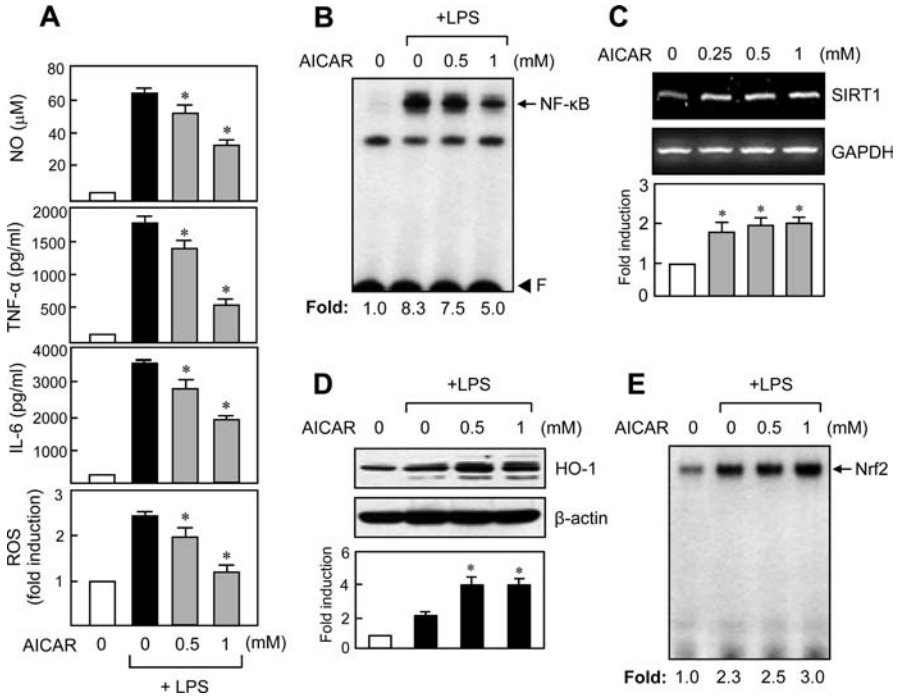

Figure 6. AICAR suppresses LPS-induced NO, TNF-α, IL-6, and ROS production and induces HO-1 expression by modulating NF-κB and Nrf2 DNA-binding activities. (A) BV2 cells were pretreated with AICAR 1 h prior to incubation with LPS (100 ng/mL) for 16 h, and the amounts of NO, TNF-α, and IL-6 released into the media and level of intracellular ROS were measured. The data are expressed as the mean ± SEM for three independent experiments. (*) $p < 0.05$ versus cells treated with LPS alone. (B) EMSA for NF-κB DNA-binding activity. Nuclear extracts were prepared from BV2 cells after treatment with LPS for 3 h in the presence of AICAR, after which EMSA was performed. The results are representative of three independent experiments. (C) Effect of AICAR on SIRT-1 mRNA expression was determined by RT-PCR analysis. (D) Levels of HO-1 protein were determined by western blot analysis. Quantification of three independent experiments is shown in the bottom panel. (E) EMSA for Nrf2 DNA-binding activity. The results are representative of three independent experiments.

pathways are involved in the anti-inflammatory effect of Rh3. We showed that upregulation of SIRT1 is responsible for NF-κB inhibition. Of interest, Rh3 inhibited the phosphorylation of PI3K/Akt and JAK1/STAT1 and upregulated AMPK. Finally, we found that AMPK modulated downstream signaling molecules, such as PI3K/Akt, JAK1/STAT1, and the NF-κB/Nrf2 axis, suggesting that AMPK plays a pivotal role in the anti-inflammatory mechanism of Rh3.

A number of studies indicate that the activity of AMPK can regulate the inflammatory responses induced by NF-κB.[6−8] AMPK does not directly target NF-κB but rather mediates the inhibition of NF-κB by modulating SIRT1, PGC-1α, p53, and FoxO.[6] For example, SIRT1 inhibits NF-κB signaling via deacetylation of the p65 subunit.[32,33] To confirm whether Rh3 acts through the AMPK-SIRT1-NF-κB signaling pathway, we compared the effects of Rh3 and AICAR, a chemical activator of AMPK. Indeed, we found that AICAR treatment increased SIRT1 expression and decreased NF-κB activity and expression of downstream pro-inflammatory genes, similar to Rh3 treatment. These findings suggest that the AMPK-SIRT1-NF-κB signaling pathways are at least partly involved in the anti-inflammatory mechanism of Rh3 in LPS-stimulated microglia.

In the present study, we also found the association of AMPK with other inflammatory signaling molecules, such as PI3K/Akt and JAK1/STAT1. AICAR inhibited the phosphorylation of Akt and JAK1/STAT1 in LPS-stimulated microglia, suggesting that AMPK is an upstream regulator of PI3K/Akt and JAK1/STAT1 signaling pathways. Consistent with this finding, several papers report that AMPK activation can inhibit JAK−STAT signaling. AMPK inhibits IL-6-stimulated STAT3 phosphorylation and pro-inflammatory gene expression in hepatocyte cell lines.[34] AMPK-mediated induction of an orphan nuclear receptor protein, small heterodimer partner, was suggested as one possible mechanism of STAT3 inhibition.[35] In addition, AMPK blocks IFN-γ-induced STAT1 expression in rat primary astrocytes and microglia.[11] As to the effect of AMPK on PI3K/Akt signaling, a recent study reports that AMPK activation blocks LPS/IFN-γ-induced phosphorylation of Akt and, thus, inhibits inflammation in mouse mesangial cells.[36] Therefore, our results suggest that AMPK activation by Rh3 may contribute to its anti-inflammatory effect via inhibition of PI3K/Akt and JAK1/STAT1 signaling pathways in LPS-stimulated microglia.

Besides its anti-inflammatory effect, Rh3 also showed an antioxidant effect in LPS-stimulated BV2 cells by decreasing ROS production and inducing HO-1 expression via the Nrf2/antioxidant response element (ARE) pathway. Previous studies demonstrate an AMPK-dependent inhibition of ROS synthesis in human umbilical vein endothelial cells (HUVECs), LPS-stimulated macrophages, and vascular smooth muscle cells.[37−39] Silencing of AMPK increases nicotinamide adenine dinucleotide phosphate (NADPH) oxidase expression and decreases antioxidant enzymes in HUVECs.[39,40] These studies suggest that AMPK activation limits excessive ROS synthesis by NADPH oxidase. Furthermore, some studies indicate that AMPK stimulates antioxidant Nrf2 signaling. Liu et al.[41] reports that AMPK induces HO-1 expression via the Nrf2 signaling pathway in endothelial cells. In addition, the crosstalk between Nrf2 and AMPK signaling pathways has been shown to be important for the anti-inflammatory effect of berberine in LPS-

DOI: 10.1021/jf506110y
J. Agric. Food Chem. 2015, 63, 3472−3480

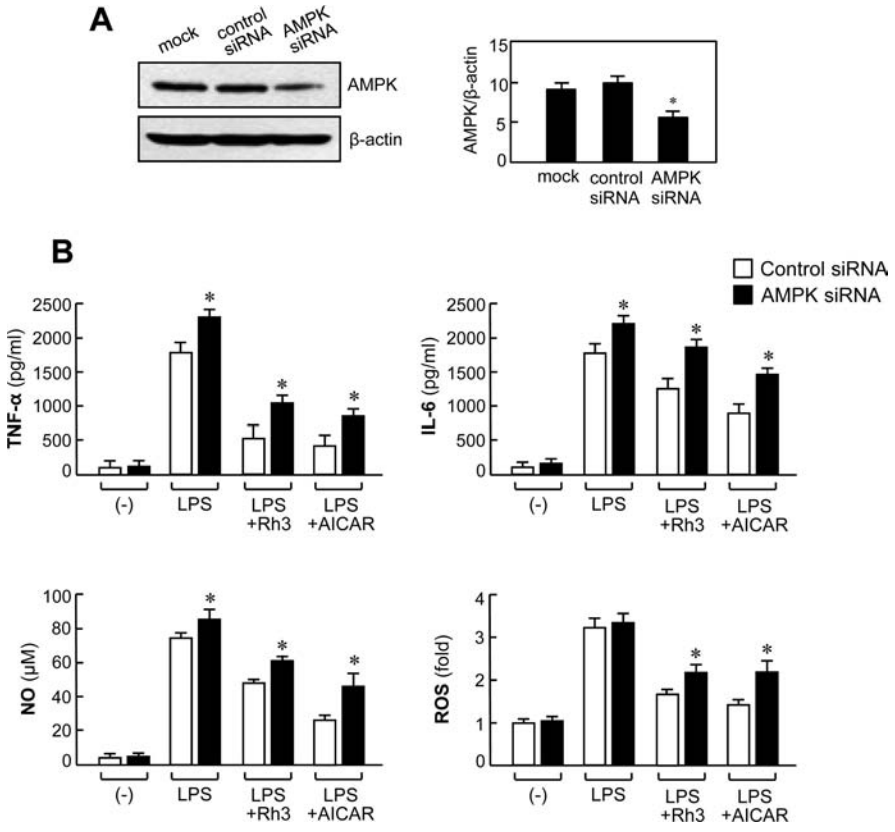

Figure 7. Knockdown of AMPK attenuates the anti-inflammatory effects of Rh3. (A) AMPK protein reduction by siRNAs was confirmed by western blotting. The data are representative of three independent experiments. Quantification data are shown in the right panel. (*) $p < 0.05$ versus the control siRNA-treated group. (B) Effects of AMPK siRNA on TNF-α, IL-6, NO, and ROS production in LPS-stimulated BV2 cells. Cells transfected with AMPK siRNA were treated with LPS (100 ng/mL) in the presence or absence of Rh3 (50 μM) or AICAR (1 mM) for 16 h, and the amounts of NO, TNF-α, and IL-6 released into the media and level of intracellular ROS were measured. Values are expressed as the mean ± SEM for three replicates using different cell cultures. (*) $p < 0.05$ versus the control siRNA-treated group.

stimulated macrophages and endotoxin-shocked mice.[42] Therefore, the results of the present study suggest that AMPK activation is largely involved in Rh3-mediated ROS inhibition and Nrf2/HO-1 upregulation, contributing to anti-inflammatory/antioxidant effects in LPS-stimulated microglia.

In summary, this study is the first to demonstrate the anti-inflammatory effect of Rh3 in LPS-stimulated microglia and its underlying molecular mechanisms. We showed that Rh3 inhibited microglial activation, at least partly, by modulating AMPK and its downstream signaling molecules, such as PI3K/Akt, JAK1/STAT1, and NF-κB/Nrf2. These findings suggest that Rh3 may offer therapeutic potential for the treatment of various neuroinflammatory disorders that are accompanied by microglial activation.

■ ASSOCIATED CONTENT

Supporting Information

Effect of Rh3 on the phosphorylation of three types of MAPKs in LPS-stimulated BV2 cells (Figure S1) and effect of PI3K/Akt- or JAK/STAT-specific inhibitor on TNF-α, IL-6, NO, and ROS production in LPS-stimulated BV2 cells (Figure S2). This material is available free of charge via the Internet at http://pubs.acs.org.

■ AUTHOR INFORMATION

Corresponding Author

*Telephone: 82-2-2650-5823. Fax: 82-2-2653-8891. E-mail: hskimp@ewha.ac.kr.

Author Contributions

†Yu Young Lee and Jin-Sun Park contributed equally to this work.

Funding

This research was supported by the Basic Science Research Program through the National Research Foundation of Korea (NRF) funded by the Ministry of Science, Information and Communications Technology (ICT) & Future Planning (Grants 2012R1A2A2A01045821 and 2012R1A5A2A32671866).

Notes

The authors declare no competing financial interest.

■ ABBREVIATIONS USED

AMPK, 5′-adenosine monophosphate-activated protein kinase; ARE, antioxidant response element; ERK, extracellular signal-regulated kinase; HO-1, heme oxygenase-1; iNOS, inducible nitric oxide synthase; JAK, janus kinase; JNK, c-Jun N-terminal kinase; MAPK, mitogen-activated protein kinase; NF-κB, nuclear factor-κB; PI3K, phosphatidylinositol 3-kinase; ROS, reactive oxygen species; siRNA, small interfering RNA; SIRT, sirtuin; STAT, signal transducer and activator of transcription; TNF, tumor necrosis factor

DOI: 10.1021/jf506110y
J. Agric. Food Chem. 2015, 63, 3472−3480

REFERENCES

(1) Glass, C. K.; Saijo, K.; Winner, B.; Marchetto, M. C.; Gage, F. H. Mechanisms underlying inflammation in neurodegeneration. *Cell* **2010**, *140*, 918−934.

(2) Graeber, M. B.; Streit, W. J. Microglia: Biology and pathology. *Acta. Neuropathol.* **2010**, *119*, 89−105.

(3) Cherry, J. D.; Olschowka, J. A.; O'Banion, M. K. Neuroinflammation and M2 microglia: The good, the bad, and the inflamed. *J. Neuroinflammation* **2014**, *11*, 98.

(4) Mosher, K. I.; Wyss-Coray, T. Microglial dysfunction in brain aging and Alzheimer's disease. *Biochem. Pharmacol.* **2014**, *88*, 594−604.

(5) Kannarkat, G. T.; Boss, J. M.; Tansey, M. G. The role of innate and adaptive immunity in Parkinson's disease. *J. Parkinson Dis.* **2013**, *3*, 493−514.

(6) Salminen, A.; Hyttinen, J. M. T.; Kaarniranta, K. AMP-activated protein kinase inhibits NF-κB signaling and inflammation: Impact on healthspan and lifespan. *J. Mol. Med.* **2011**, *89*, 667−676.

(7) Salminen, A.; Kaarniranta, K. AMP-activated protein kinase (AMPK) controls the aging process via an integrated signaling network. *Ageing Res. Rev.* **2012**, *11*, 230−241.

(8) Salt, I. P.; Palmer, T. M. Exploiting the anti-inflammatory effects of AMP-activated protein kinase activation. *Expert Opin. Invest. Drugs* **2012**, *21* (8), 1155−1167.

(9) Ramamurthy, S.; Ronnett, G. AMP-activated protein kinase (AMPK) and energy-sensing in the brain. *Exp. Neurobiol.* **2012**, *21* (2), 52−60.

(10) Giri, S.; Nath, N.; Smith, B.; Viollet, B.; Singh, A. K.; Singh, I. 5-aminoimidazole-4-carboxamide-1-β-4-ribofuranoside inhibits proinflammatory response in glial cells: A possible role of AMPK-activated protein kinase. *J. Neurosci.* **2004**, *24*, 479−487.

(11) Meares, G. P.; Qin, H.; Liu, Y.; Holdbrooks, A. T.; Benveniste, E. N. AMP-activated protein kinase (AMPK) restricts IFN-γ signaling. *J. Immunol.* **2012**, *190*, 372−380.

(12) Blumenthal, M. Asian ginseng: Potential therapeutic uses. *Adv. Nurse Pract.* **2001**, *2*, 26−28.

(13) Choi, I. H. Effects of *Panax ginseng* in neurodegenerative diseases. *J. Ginseng Res.* **2012**, *36*, 342−353.

(14) Lee, K. Y.; Lee, Y. H.; Kim, S. I.; Park, J. H.; Lee, S. K. Ginsenoside-Rg5 suppresses cyclin E-dependent protein kinase activity via up-regulating p21Cip/WAF1 and down-regulating cyclin E in SK-HEP-1 cells. *Anticancer Res.* **1997**, *17*, 1067−1072.

(15) Kang, K. S.; Kim, H. Y.; Baek, S. H.; Yoo, H. H.; Park, J. H.; Yokozawa, T. Study on the hydroxyl radical scavenging activity changes of ginseng and ginsenoside-Rb2 by heating processing. *Biol. Pharm. Bull.* **2007**, *30*, 724−728.

(16) Shin, Y. W.; Bae, E. A.; Kim, D. H. Inhibitory effect of ginsenoside Rg5 and its metabolite ginsenoside Rh3 in an oxazolone-induced mouse chronic dermatitis model. *Arch. Pharm. Res.* **2006**, *29*, 685−690.

(17) Kim, T. W.; Joh, E. H.; Kim, B.; Kim, D. H. Ginsenoside Rg5 ameliorates lung inflammation in mice by inhibiting the binding of LPS to toll-like receptor-4 on macrophages. *Int. Immunopharmacol.* **2012**, *12*, 110−116.

(18) Kim, E. J.; Jung, I. H.; Van Le, T. K.; Jeong, J. J.; Kim, N. J.; Kim, D. H. Ginsenosides Rg5 and Rh3 protect scopolamine-induced memory deficits in mice. *J. Ethnopharmacol.* **2013**, *146*, 294−299.

(19) Kim, W. Y.; Kim, J. M.; Han, S. B.; Lee, S. K.; Kim, N. D.; Park, M. K.; Kim, C. K.; Park, J. H. Steaming of ginseng at high temperature enhances biological activity. *J. Nat. Prod.* **2000**, *63*, 1702−1704.

(20) Kim, D. S.; Baek, N. I.; Park, J. D.; Lee, Y. H.; Jeong, S. Y.; Lee, C. B.; Kim, S. I. Preparation and structure determination of a new glycoside, (20*E*)-ginsenoside Rh3, and its isomer from diol-type ginseng saponins. *Yakhak Hoeji* **1995**, *39*, 85−93.

(21) Bae, E. A.; Han, M. J.; Choo, M. K.; Park, S. Y.; Kim, D. H. Metabolism of 20(*S*)- and 20(*R*)-ginsenoside Rg3 by human intestinal bacteria and its relation to in vitro biological activities. *Biol. Pharm. Bull.* **2002**, *25*, 58−63.

(22) Bocchni, V.; Mazzolla, R.; Barluzzi, R.; Blasi, E.; Sick, P.; Kettenmann, H. An immotalized cell line expresses properties of activated microglial cells. *J. Neurosci. Res.* **1992**, *31*, 616−621.

(23) Park, J. S.; Park, E. M.; Kim, D. H.; Jung, K.; Jung, J. S.; Lee, E. J.; Hyun, J. W.; Kang, J. L.; Kim, H. S. Anti-inflammatory mechanism of ginseng saponins in activated microglia. *J. Neuroimmunol.* **2009**, *209*, 40−49.

(24) Woo, M. S.; Jang, P. G.; Park, J. S.; Kim, W. K.; Joh, T. H.; Kim, H. S. Selective modulation of lipopolysaccharide-stimulated cytokine expression and mitogen-activated protein kinase pathways by dibutyryl-cAMP in BV2 microglial cells. *Brain Res. Mol. Brain Res.* **2003**, *113*, 86−96.

(25) Lee, K. M.; Kang, H. S.; Yun, C. H.; Kwak, H. S. Potential in vitro protective effect of quercetin, catechin, caffeic acid and phytic acid against ethanol-induced oxidative stress in SK-Hep-1 cells. *Biomol. Ther.* **2012**, *20*, 492−498.

(26) Syapin, P. J. Regulation of heme oxygenase-1 for treatment of neuroinflammation and brain disorders. *Br. J. Pharmacol.* **2008**, *115*, 623−640.

(27) Keum, Y. S. Regulation of Nrf2-mediated phase II detoxification and anti-oxidant genes. *Biomol. Ther.* **2012**, *20*, 144−151.

(28) Torres, M. Mitogen-activated protein kinase pathways in redox signaling. *Front. Biosci.* **2003**, *8*, d369−391.

(29) Jana, M.; Jana, A.; Liu, X.; Ghosh, S.; Pahan, K. Involvement of phosphatidylinositol 3-kinase-mediated up-regulation of IκBα in anti-inflammatory effect of gemfibrozil in microglia. *J. Immunol.* **2007**, *179*, 4142−4152.

(30) Darnell, J. E., Jr.; Kerr, I. M.; Stark, G. R. Jak-STAT pathways and transcriptional activation in response to IFNs and other extracellular signaling proteins. *Science* **1994**, *264*, 1415−1421.

(31) Shuai, K.; Liu, B. Regulation of JAK−STAT signaling in the immune system. *Nat. Immunol.* **2003**, *3*, 900−911.

(32) Yang, S. R.; Wright, J.; Bauter, M.; Seweryniak, K.; Kode, A.; Rahman, I. Sirtuin regulates cigarette smoke-induced proinflammatory mediator release via RelA/p65 NF-κB in macrophages in vitro and in rat lungs in vivo: Implications for chronic inflammation and aging. *Am. J. Physiol.: Lung Cell. Mol. Physiol.* **2007**, *292*, L567−576.

(33) Yang, Z.; Kahn, B. B.; Shi, H.; Xue, B. Macrophage α1 AMP-activated protein kinase (α1AMPK) antagonizes fatty acid-induced inflammation through SIRT1. *J. Biol. Chem.* **2010**, *285*, 19051−19059.

(34) Nerstedt, A.; Johansson, A.; Andersson, C. X. AMP-activated protein kinase inhibits IL-6-stimulated inflammatory response in human liver cells by suppressing phosphorylation of signal transducer and activator of transcription 3 (STAT3). *Diabetologia* **2010**, *53*, 2406−2416.

(35) Kim, Y. D.; Kim, Y. H.; Cho, Y. M. Metformin ameliorates IL-6-induced hepatic insulin resistance via induction of orphan nuclear receptor small heterodimer partner (SHP) in mouse models. *Diabetologia* **2012**, *55*, 1482−1494.

(36) Peairs, A.; Radjavi, A.; Davis, S.; Li, L.; Ahmed, A.; Giri, S.; Reilly, C. M. Activation of AMPK inhibits inflammation in MRL/lpr mouse mesangial cells. *Clin. Exp. Immunol.* **2009**, *156*, 542−551.

(37) Jeong, H. W.; Hsu, K. C.; Lee, J. W. Berberine suppresses pro-inflammatory responses through AMPK activation in macrophages. *Am. J. Physiol.: Endocrinol. Metab.* **2009**, *296*, E955−964.

(38) Sung, J. Y.; Choi, H. C. Aspirin-induced AMP-activated protein kinase activation regulates the proliferation of vascular smooth muscle cells from spontaneously hypertensive rats. *Biochem. Biophys. Res. Commun.* **2011**, *408*, 312−317.

(39) Colomb, S. L.; Moncada, S. AMPKα1 regulates the antioxidant status of vascular endothelial cells. *Biochem. J.* **2009**, *421*, 163−169.

(40) Wang, S.; Zhang, M.; Liang, B. AMPKα2 deletion causes aberrant expression and activation of NAD(P)H oxidase and consequent endothelial dysfunction *in vivo*: Role of 26S proteasomes. *Cir. Res.* **2010**, *106*, 1117−1128.

(41) Liu, X. M.; Peyton, K. J.; Shebib, A. R.; Wang, H.; Korthuis, R. J.; Durante, W. Activation of AMPK stimulates heme oxygenase-1 gene expression and human endothelial cell survival. *Am. J. Physiol.: Heart Circ. Physiol.* **2011**, *300*, H84−93.

DOI: 10.1021/jf506110y
J. Agric. Food Chem. 2015, 63, 3472−3480

(42) Mo, C.; Wang, L.; Zhang, J.; Numazawa, S.; Tang, H.; Tang, X.; Han, X.; Li, J.; Yang, M.; Wang, Z.; Wei, D.; Xiao, H. The crosstalk between Nrf2 and AMPK signal pathways is important for the anti-inflammatory effect of berberine in LPS-stimulated macrophages and endotoxin-shocked mice. *Antioxid. Redox Signaling* **2014**, *20* (4), 574−588.

DOI: 10.1021/jf506110y
J. Agric. Food Chem. 2015, 63, 3472−3480

Table 1. Viscosity, Electrical Conductivity of Solutions, and Average Fiber Diameters of Electrospun Nanofibers

solutions	% PVA[a] (w/v)	% β-CD[b] (w/w)	% RA (w/w)	viscosity[c] (Pa·s)	conductivity[c] (mS/cm)	AFD[c] (nm)
PVA	12			0.62 ± 0.04x	1.76 ± 0.02x	266 ± 59x
PVA/β-CD	10	30		0.78 ± 0.06y	1.76 ± 0.07x	282 ± 70y
PVA/RA	10		10	0.94 ± 0.16z	1.52 ± 0.09y	264 ± 61w
PVA/β-CD/RA	10	30	10	0.87 ± 0.08y	1.52 ± 0.04y	223 ± 49z

[a]With respect to solvent (water). [b]With respect to polymer (PVA). [c]Mean ± SD. The mean values with the same letter in a column are not significantly different ($P > 0.05$) at 95% confidence interval.

protection for active food components in the core from thermal, light, and other storage condition constraints.[16,18]

In this study, PVA and β-CD were chosen as the base material and RA as a core bioactive. The nanofiber encapsulation based on PVA has been extensively reported as a protecting coat for food materials.[16,18,24] The aim of this study was to use the electrospinning technique in order to develop a PVA/RA/β-CD nanofiber functional matrix that provides support of thermal stability and long shelf life of RA. The RA was incorporated separately into the PVA nanofibers for assessing the relation between the inclusion complex and the variation of the retained core. Furthermore, the RA in the nanofibers demonstrated the effect and influence on the morphology of the fibers and also determined release kinetics as a function of fiber material composition under room storage conditions.

MATERIALS AND METHODS

Materials. Poly(vinyl alcohol) (PVA) (Mw: 85 000−124 000, 99+ % hydrolyzed), retinyl acetate (RA), β-cyclodextrin (β-CD), and tetrabutyl ammonium hexafluorophosphate were purchased from Sigma-Aldrich (Castle-Hill, NSW 1765, Australia). Ethanol (100% proof) and acetonitrile (99.8%) were obtained from Chem-Supply (Gillman, SA 5013, Australia). All of the reagents used were of analytical grade and used as received. Milli-Q water was used throughout the experiments.

Preparation of the Solutions. The powdered PVA was dissolved in Milli-Q water at 75 °C using a magnetic stirrer (1 krpm) for 2 h to make up a 12% (w/v) solution.[12] In the same method, 10% (w/v) PVA solution was prepared containing a different concentration of retinyl acetate and β-CD inclusion complex. To this solution, 30% (w/w, with respect to polymer PVA) of β-CD was added at 75 °C with constant stirring for 10 min. Subsequently, the solution was cooled to 25 °C with stirring and 10% (w/w, respective to PVA) of retinyl acetate powder was added to make the PVA/retinyl acetate/β-CD solution. The solutions were stirred for a further 1 h at 25 °C prior to electrospinning.

Homogeneous and clear solutions were obtained for PVA and PVA/β-CD compositions. In contrast, these solutions turned turbid by addition of retinyl acetate. Finally, the prepared solution of PVA and composition with retinyl acetate and β-CD were electrospun separately at room temperature. The composition and rheological properties of the solutions are summarized in Table 1.

Electrospinning. The prepared solutions were placed in a 5 mL syringe connected with a stainless steel needle having an inner diameter of 0.5 mm. The solution in the syringe was pumped at 200 μL/h horizontally (model: KDS Legato 111, KD Scientific, Holliston, MA, USA), and the solutions were electrospun with an applied voltage of 18 kV using a homemade high voltage power supply. Then, the nanofibers were deposited on a grounded stationary metal collector covered with aluminum foil at 20 cm from the syringe nozzle to the tip. The electrospinning experiments were carried out at room temperature in an enclosed Plexiglas box.

Measurements and Characterization. Ionic conductivities of the polymer solutions were measured using a conductivity meter (METTLER TOLED: S230, Zurich, Switzerland) that was calibrated with 1413 μS/cm standard conductivity solution at room temperature. The viscosity of the solutions was measured with an AR2000 Advanced Rheometer (4 cm, 2° cone, TA Instruments, Delaware, USA) at 23 °C with a shear rate from 1 up to 1000 s^{-1}. The morphology and the fiber diameter of the electrospun nanofibers were analyzed by a field-emission scanning electron microscope (FE-SEM, Zeiss Supra 40 VP, Oberkochen, Germany). The nanofiber samples were coated with 15 nm of Au (EMITECH K975X) prior to SEM imaging. The average fiber diameter (AFD) for the samples was calculated by analysis of 100 fibers from the SEM images. The X-ray diffraction (XRD) patterns of powder PVA, β-CD, RA, and nanofiber membranes were obtained with a Bruker D8 Advance XRD with Cu Kα radiation at a scanning rate of 1°/min over a 2θ range of 5−40°. Thermal properties of the samples were investigated by using a differential scanning calorimeter (DSC) and a thermogravimetric analyzer (TGA) (DSC-TGA-2960 SDT V3.0F, TA Instruments Inc., Delaware, USA). For DSC analyses, the sealed 5 mg samples were initially equilibrated at 10 °C and then heated to 300 °C at a rate of 10 °C/min using nitrogen as a purge gas. TGA measurements were performed for electrospun nanofibers after 1 day of storage. The TGA data for 10 mg samples were recorded from room temperature to 600 °C at a heating rate of 10 °C/min, under a nitrogen atmosphere. X-ray photoelectron spectroscopy (XPS) (Kratos Axis Nova Analytical Ltd., Manchester, U.K.) was used to determine the surface chemistry of the nanofiber membranes. A monochromated Al Kα X-ray source was used at a power of 150 W. Elements were identified from survey spectra (0−1200 eV) with a detector pass energy of 160 eV. The atomic concentrations of the detected elements were calculated using integral peak intensities and the sensitivity factors supplied by the manufacturer.

Electrochemical Measurements. Electrochemical experiments were performed with a CH Instruments Model CH610 Electrochemical Analyzer. The electrochemical cell consisted of a three-electrode system: a glassy carbon (GC) working electrode (BASi MF-2012), a platinum wire (BASi MW-4130) auxiliary electrode, and a $Ag/AgNO_3$ reference electrode filled with 100 mM TBAP−acetonitrile (BASi MF-2062). The working electrode was cleaned with a polishing cloth (Buehler, Lake Bluff, IL, 60044, USA) impregnated with a 0.05 μm alumina slurry until a mirror-like surface was obtained. The polished electrodes were sonicated in acetonitrile to remove any alumina.

Sample Preparation. The nanofibers of PVA/RA and PVA/RA/β-CD-IC were measured frequently to determine the remaining retinyl acetate against the storage time. These nanofiber membranes were stored at room temperature in the laboratory for a certain period of time prior to analyses. Sample solutions of each type of nanofiber were prepared by soaking 40 mg of nanofibers in ethanol with sonication for 30 min at 25 °C to release the retinyl acetate into the solution.

The release rates of retinyl acetate from the nanofibers were monitored by square-wave voltammetry (SWV) using 0.1 M tetrabutyl ammonium hexafluorophosphate ($TBAPF_6$) in acetonitrile at 25 °C. The SWV conditions were as follows: step potential, 4 mV; amplitude, 25 mV; frequency, 15 Hz. The amount of retinyl acetate present in the nanofibers was monitored using a scanning potential range from 0 to 0.9 V. To perform the kinetic analysis, the signal obtained from each voltammogram was baseline subtracted and the value of the peak current (I_p) with the corresponding storage day was used for the subsequent analyses. The exact concentration of the released retinyl acetate was obtained using a calibration graph of retinyl acetate standard. The released amount was determined according to the

DOI: 10.1021/acs.jafc.5b00103
J. Agric. Food Chem. 2015, 63, 3481−3488

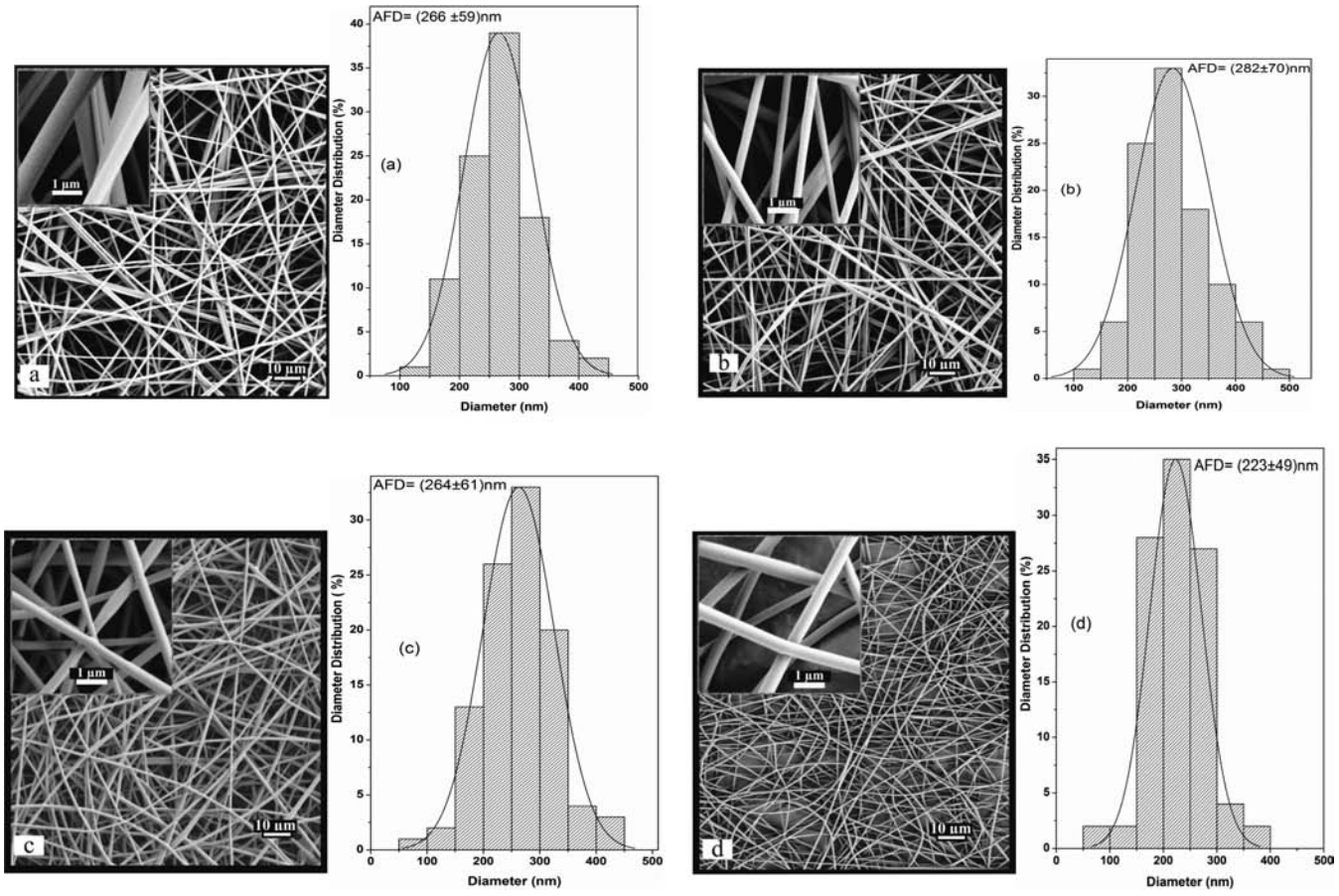

Figure 1. SEM images and fiber diameter distributions of the electrospun nanofibers obtained from (a) PVA, (b) PVA/β-CD, (c) PVA/RA, and (d) PVA/β-CD/RA. The insets show the high magnification images. The fiber diameter distributions of each are shown on the right.

decrease of peak current with respect to storage time. The release (%) is expressed by the equation

$$\text{Release (\%)} = 100 \times \frac{I_p(\text{Day } k) - I_p(\text{Day } k + t)}{I_p(\text{Day } k)}$$

where I_p(Day k) is the peak current for an earlier storage time compared to the peak current I_p(Day $k + t$) with longer storage time.

Statistical Analysis. All data were expressed as mean ± standard deviation. Statistical significance by analysis of variation (ANOVA) was used to determine the difference among samples' viscosity, conductivity, and AFD, $P < 0.05$.

RESULTS AND DISCUSSION

Measurements and Crystalline Structure. The PVA solutions containing retinyl acetate and retinyl acetate/β-CD-IC were electrospun from the aqueous solution mixture. The conductivity and shear viscosity of the PVA and PVA/β-CD with and without retinyl acetate solutions are shown in Table 1. The addition of 10% (w/w) RA to the PVA and PVA/β-CD solutions significantly affects the viscosity and the conductivity of the solutions, as shown in Table 1. The viscosity of PVA/β-CD has a higher value compared to the PVA. In the same manner, the viscosity of PVA/RA has the highest value compared to all the rest of the samples. In general, the conductivities of all the sample solutions are significantly different in the presence of RA ($P < 0.05$) and the mean fiber diameters also are significantly different as the compositions of the polymer solutions vary, as shown in Table 1. The results showed that the addition of RA did not change the morphology of the PVA and PVA/β-CD nanofibers; instead, the diameters of the nanofibers decreased slightly (Figure 1). Similar findings were observed in the range between 200 and 360 nm in other studies when PVA and PVA/β-CD were used for encapsulation of food flavors.[13,18] For comparison, both the PVA and PVA/β-CD nanofibers were produced in the same concentration solutions as fibers which have RA.

In the electrospinning, uniform nanofibers were obtained and no huge variation was encountered along the electrospun fibers in the whole sample. The representative SEM images and the fiber diameter distribution along with the average fiber diameter of PVA, PVA/β-CD-IC, PVA/RA, and PVA/RA/β-CD-IC nanofibers are depicted in Figure 1. The SEM images of electrospun nanofibers were obtained from homogeneous solutions of 12% (w/v) PVA in Milli-Q water and 30% (w/w) β-CD and 10% (w/w) RA with respect to PVA. Uniform nanofibers were obtained from all the solutions of the mixture. In the case of PVA/RA/β-CD-IC, nanofibers were mostly uniform and had smaller diameters. The fibers were also obtained without any aggregates of retinyl acetate on their surfaces, implying that RA was uniformly incorporated within the fibers. The result showed that incorporation of RA in the electrospun PVA and PVA/β-CD fibers had little effect upon the morphology. The average fiber diameter with the RA had smaller diameters compared to controls (Table 1 and Figure 1).

The X-ray diffraction pattern measurements were carried out in order to elucidate the form of crystalline aggregates in the nanofibers and the crystalline nature of the pure powder PVA samples. The nanofibers with samples of PVA, RA, and β-CD

DOI: 10.1021/acs.jafc.5b00103
J. Agric. Food Chem. 2015, 63, 3481−3488

were subjected to X-ray powder diffractometry at RT. The XRD patterns obtained are depicted in Figure 2. The β-CD has

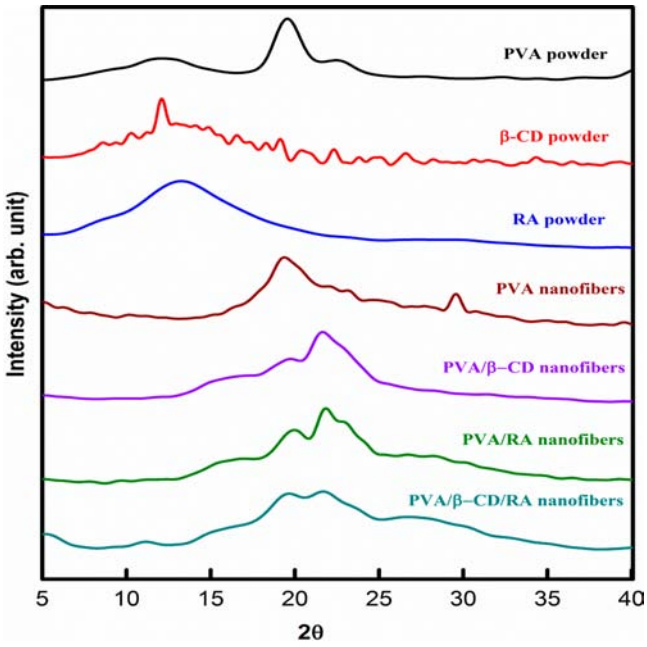

Figure 2. XRD spectra of received samples and electrospun nanofibers.

guest molecules which are localized separately from each other that affect the formation of crystals.[25] A wide spectral peak of the RA centered at 2θ = 13° suggests a semicrystalline structure. The diffractogram peak at 2θ = 19.5° for PVA powder and PVA nanofibers largely reveals their similarity. The PVA nanofibers preserve the semicrystalline nature of the powder after electrospinning except for a small additional peak at 2θ = 29.5°. These observed XRD diffraction peak results agree well with the literature. The reflection peak for electrospun PVA/β-CD and PVA/RA was detected at 2θ = 21.5° and shifted to the lower shoulder peak, which indicates the slight change in crystallinity. In addition, the PVA/RA/β-CD fibers had broad peaks at 2θ = 19.5° and 2θ = 21.5°, which is evidence of the existence of the introduced RA and β-CD in the PVA nanofiber matrix. In these spectra, the existence of RA is not apparent in the nanofibers of PVA/RA/β-CD and this implies that the RA incorporates in the form of RA/β-CD-ICs in the PVA nanofiber matrix. The existence of RA in the nanofibers of PVA/RA and PVA/RA/β-CD-IC affected the crystallization behavior of the nanofibers. This may need further study as to the reasons why RA has a greater tendency to alter the crystal structure of the final products. The absence of the peak for RA in the PVA/RA/β-CD nanofibers confirmed that the RA dispersed homogeneously in the PVA matrix and is deprived of the formation of crystal aggregates.

Thermal Analyses. The thermal stability was determined by thermogravimetric analysis in a temperature range of 25 °C up to 600 °C, as shown in Figure 3 for the TGA and DTGA curves. Thermogravimetric analysis revealed the thermal effects of PVA nanofibers with the presence of β-CD and RA at different concentrations. Figure 3a shows TGA curves of the PVA powder and the PVA nanofibers, with and without the composite β-CD and RA. All the samples exhibited three main weight loss steps. The first weight loss from 5 to 10%, which covers the temperature range of about 25−230 °C, corresponds to weakly physisorbed water (indicated in the inset of Figure 3a), while the loss in the range 230−400 °C is due to the decomposition of the PVA side chains with the decomposition of the main chain occurring at about 400−600 °C. A great deal of weight loss is observed in the range of the second stage of thermal decomposition, as shown in Figure 3, of the TGA and first order differential of the thermograms (DTGA). The powdered PVA shows a small weight loss in the first stage as compared with the nanofibers of PVA. For the electrospun nanofibers with β-CD, better thermal stability is observed than for the other samples (Figure 3b). This is evidence that β-CD improves the thermal stability of the encapsulate.[18,26]

The retinyl acetate weight loss was exhibited in four different stages. The first weight loss up to 100 °C corresponds to the evaporation of the adsorbed moisture. The second stage has 15% weight loss in the range 200−300 °C. The next 15% weight loss was observed in the range 300−430 °C. Moreover, the predominant and further weight loss was exhibited in the fourth stage in the range 430−600 °C. It is noticed that greater than 80% of the loss is observed after 300 °C. According to the

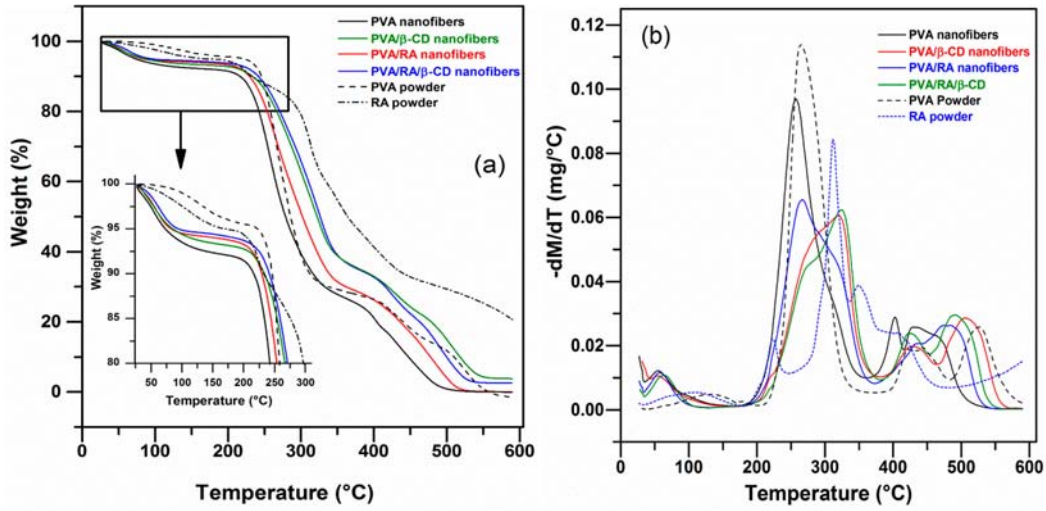

Figure 3. (a) TGA thermograms for the PVA and RA powders and the electrospun fibers and (b) first order derivatives of the TGA thermograms for powdered PVA and RA and the electrospun fibers.

DOI: 10.1021/acs.jafc.5b00103
J. Agric. Food Chem. 2015, 63, 3481−3488

TGA finding (Figure 3a), the RA in PVA/β-CD nanofibers has more thermal stability than the RA incorporated into PVA nanofibers. These results are consistent with results in other studies,[13,26] which include reports on how incorporating cyclodextrin inclusion improved the stability of the capsulate.

Differential scanning calorimetry (DSC) is used to identify if the guest molecules are incorporated inside the CD cavities.[25,27] The semicrystalline polymer of PVA has both the removal of its moisture and melting temperature (T_m), as depicted in Figure 4. Due to the introduction of RA, the

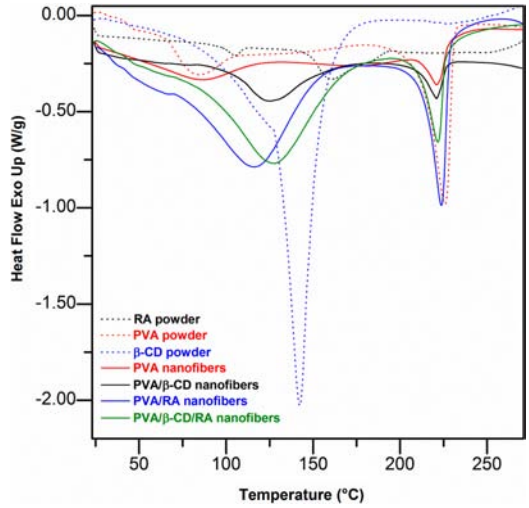

Figure 4. DSC thermograms of powders and electrospun nanofibers.

thermal behavior of PVA is expected to affect the composition interaction. Figure 4 shows the DSC curves of the powdered PVA and the electrospun nanofibers. The moisture content of the RA powder was removed at 105 °C, and the melting point at 160.6 °C was observed. The sharp melting point peak of β-CD appeared at 142.5 °C. The powder of PVA had moisture removed at 84 °C, whereas it occurred at 87 °C for the electrospun PVA nanofibers. The melting temperature of PVA powder and electrospun PVA nanofibers appeared at 221 and 225.5 °C, respectively. This result agrees with the literature value.[28] However, the melting point of PVA nanofibers increased by 4.5 °C, which may be due to the processing of the fibers. Generally, the melting point of the nanofibers is exhibited at the same temperature around 221 °C. The melting points of RA and β-CD powder were not observed in the nanofibers. This absence of the melting point suggested that RA incorporated inside the cavity and β-CD distributed through the nanofiber matrix for formation of inclusion complexation.

Several studies have elucidated the β-CD unique molecule delivery nature that can be used for vitamin A encapsulation to increase the thermal stability and control release.[29,30] For instance, the retinyl acetate without encapsulation starts to lose its stability earlier than 150 °C.[31] However, the stability of encapsulated retinyl acetate is improved in the range 230−300 °C without the presence of high chemical deterioration.[32,33]

XPS Characterization. X-ray photoelectron spectroscopy (XPS) was used to investigate chemical changes at the surface of the electrospun nanofibers and identify the atomic concentrations of the PVA, PVA/β-CD, PVA/RA, and PVA/RA/β-CD nanofibers. Accordingly, XPS survey spectra of the nanofibers were used to identify the surface elements present in ~10 nm of the outer surface of the samples. XPS wide energy surveys of PVA and PVA/β-CD nanofibers show different atomic concentrations of oxygen and carbon, namely, 65.6%/33.8% and 48.2%/49.0%, respectively (Table 2 and Figure 5).

Table 2. Surface Atomic Composition Measured by XPS

	total atomic composition (%)			
material	C	O	N	Na
PVA	65.6	33.9		0.5
PVA/β-CD	48.2	49.0	1.7	1.1
PVA/RA	42.7	54.6	0.8	2.0
PVA/RA/β-CD	41.7	56.2	2.0	0.2

The atomic composition identified of PVA nanofibers contains exclusively carbon, oxygen, and sodium. The electrospun PVA/β-CD nanofibers were analyzed to study the difference of compositions in detail (Figure 5b). In addition, the surface chemistry study by XPS investigated the variation of the surface composition with the presence of β-CD and retinyl acetate (Table 2). The XPS spectra of the PVA/RA and PVA/RA/β-CD nanofiber composites show four distinct peaks, corresponding to Na, N, C, and O, as shown in Figure 5c and d. Particularly, in the nanofibers of PVA/RA and PVA/RA/β-CD, increased concentrations of oxygen and slight variations of nitrogen were observed due to the introduction of retinyl acetate into the nanofibers (Figure 5c and d). The potential of using β-CD was assessed by observing its tendency to preserve oxygen against some common oxidation of the retinyl acetate. The electrospun nanofibers of PVA were used as a control for comparing the variation due to the introduction of functional groups from the RA and β-CD inclusion complex.

The result displayed a high oxygen atomic concentration, which is in agreement with the previous finding that the β-CD inclusion complex has a critical role to reduce loss of oxygen mainly in the form of oxidation that reduces the shelf life of the samples.[34,35] These results confirmed the formation of an inclusion complex and its preserving capacity to prolong the shelf life of the products.

Monitoring Release of Retinyl Acetate. The quantity and release kinetics of RA in electrospun nanofibers of PVA/RA and PVA/β-CD/RA were determined using the square-wave voltammogram peak current response against storage time under room storage conditions. The peak signal response of the retinyl acetate corresponds to the concentration of RA found in the nanofibers using the calibration graph of standard retinyl acetate (inset of Figure 7). The subsequent controlled release kinetics from the nanofibers.

A known amount of electrospun PVA/RA and PVA/β-CD/RA nanofibers was soaked in ethanol and sonicated to release the retinyl acetate. Subsequently, 600 μL of this solution was added into 0.1 M $TBAPF_6$ in acetonitrile solution in a 10 mL electrochemical cell. The SWV signal response revealed the amount of entrapped RA in the nanofibers according to the storage time, as shown in Figure 6. As can be seen from Figures 6 and 7, the concentration of RA in the nanofibers PVA/RA/β-CD and PVA/RA decreased with respect to increased storage time. Furthermore, the release rate was faster in both the PVA/RA/β-CD and PVA/RA nanofibers during the first 3 weeks as compared to the remaining times. Generally, the peak current signal suggested that the release rate of PVA/RA/β-CD-IC was slower than PVA/RA within the same storage conditions. This slower release rate for the PVA/RA/β-CD-IC nanofibers can be

DOI: 10.1021/acs.jafc.5b00103
J. Agric. Food Chem. 2015, 63, 3481−3488

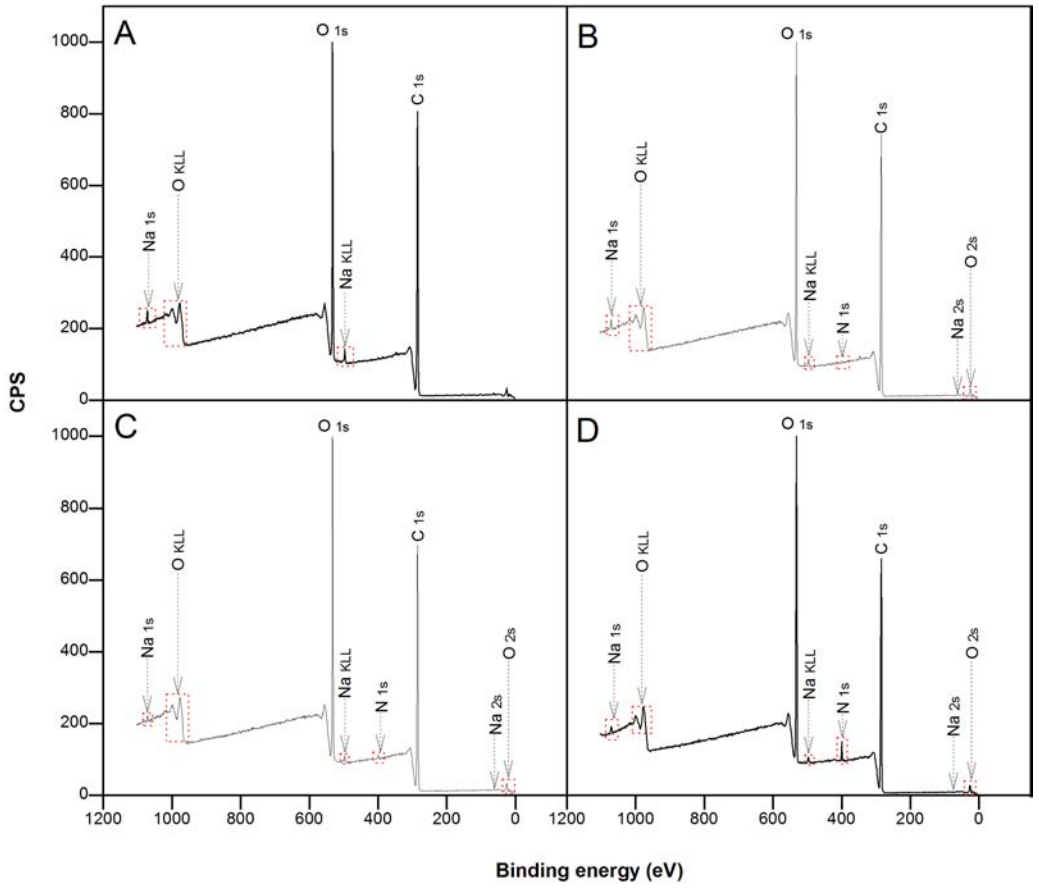

Figure 5. XPS spectrum of the (A) PVA, (B) PVA/β-CD, (C) nanofiber encapsulated retinyl acetate in PVA/RA, and (D) PVA/β-CD/RA.

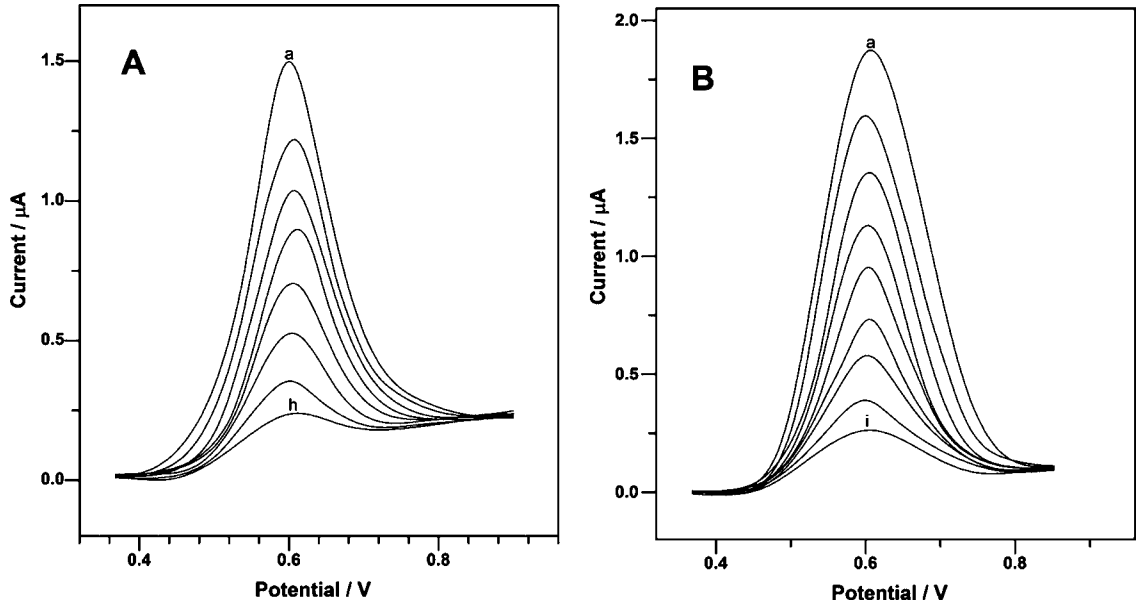

Figure 6. SWV of 40 mg of nanofiber membrane in 2 mL of ethanol. 600 μL aliquots were removed from each sample for analysis. (A) Fibers of PVA/RA and (B) fibers of PVA/RA/β-CD after storage time of a = day 1, b = day 8, c = day 23, d = day 35, e = day 46, f = day 54, g = day 61, h = day 80, and i = day 94. Experimental conditions: supporting electrolyte acetonitrile with 0.1 M $TBAPF_6$ with a glassy carbon electrode; scan from 0.0 to 0.9 V using an amplitude of 25 mV, step of 4 mV, and frequency of 15 Hz.

attributed to the effective host−guest complex formation between the retinyl acetate and the β-CD.

Since it is known that RA is highly unstable and sensitive to oxidation and light when it is stored without a coating matrix, studies carried out with RA shelf life tests aided in the formation of free-radicals, confirming that it has a short storage time due to subsequent loss of activity.[36,37] In contrast, RA encapsulated into 2-hydroxypropyl-β-CDs was stable for 3

DOI: 10.1021/acs.jafc.5b00103
J. Agric. Food Chem. 2015, 63, 3481−3488

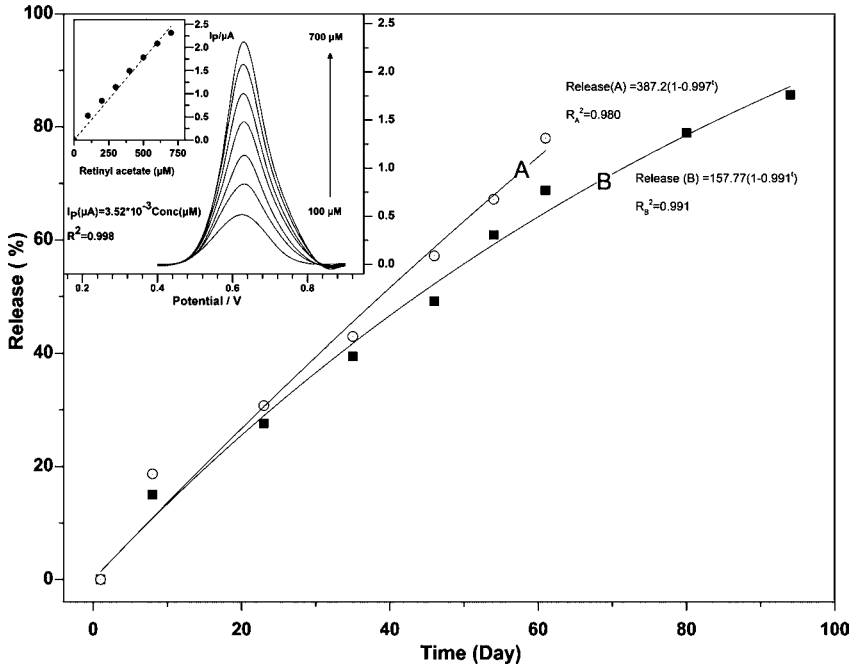

Figure 7. Releasing kinetics monitored by square-wave voltammograms of retinyl acetate in the nanofibers of (A) PVA/RA and (B) PVA/RA/β-CD. Inset: the calibration graph of retinyl acetate and graph equation used to calculate the corresponding concentration signal of retinyl acetate in the electrochemical cell released from nanofibers of PVA/RA and PVA/β-CD/RA. Experimental conditions same as those for Figure 6.

months of storage at room temperature.[38] In addition, RA encapsulated through nanoencapsulation into a polymer poly(ethylene glycol)−4-methoxycinnamoylphthaloylchitosan (PCPLC) increased its stability by 99% from free RA.[5] Similarly, the electrochemical detection results in Figure 7 showed these encapsulations protected RA to extend the shelf life.

These results demonstrate that electrospinning can be used as a method to fabricate nanofibrous structures for encapsulating bioactive retinyl acetate to prolong shelf life and thermal stability. This was achieved by encapsulating retinyl acetate inside the cavity of β-CD within the fibers to improve stabilities over longer time periods. Thus, electrospun nanofibers could be suitable for encapsulating food materials effectively and efficiently for prolonged shelf life and higher temperature stability and may be applicable in other areas such as the pharmaceutical and cosmetics industries, for edible food packaging, encapsulating antioxidants, food colors, flavors, and drugs.

AUTHOR INFORMATION

Corresponding Author

*E-mail: pkingshott@swin.edu.au. Phone: +61 (0)3 9214 5033.

Funding

The authors acknowledge financial support received from Free University of Bozen-Bolzano, Italy, and Swinburne University of Technology, Australia.

Notes

The authors declare no competing financial interest.

REFERENCES

(1) Gentili, A.; Caretti, F.; Bellante, S.; Ventura, S.; Canepari, S.; Curini, R. Comprehensive profiling of carotenoids and fat-soluble vitamins in milk from different animal species by LC-DAD-MS/MS hyphenation. *J. Agric. Food Chem.* **2013**, *61* (8), 1628−1639.

(2) Webster, R. D. Voltammetry of the liposoluble vitamins (A, D, E and K) in organic solvents. *Chem. Rec.* **2012**, *12* (1), 188−200.

(3) Loveday, S. M.; Singh, H. Recent advances in technologies for vitamin A protection in foods. *Trends Food Sci. Technol.* **2008**, *19* (12), 657−668.

(4) Taepaiboon, P.; Rungsardthong, U.; Supaphol, P. Vitamin-loaded electrospun cellulose acetate nanofiber mats as transdermal and dermal therapeutic agents of vitamin A acid and vitamin E. *Eur. J. Pharm. Biopharm.* **2007**, *67* (2), 387−397.

(5) Arayachukeat, S.; Wanichwecharungruang, S. P.; Tree-Udom, T. Retinyl acetate-loaded nanoparticles: dermal penetration and release of the retinyl acetate. *Int. J. Pharm.* **2011**, *404* (1−2), 281−288.

(6) Gonnet, M.; Lethuaut, L.; Boury, F. New trends in encapsulation of liposoluble vitamins. *J. Controlled Release* **2010**, *146* (3), 276−290.

(7) Champagne, C. P.; Patrick, F. Microencapsulation for the improved delivery of bioactive compounds into foods. *Curr. Opin. Biotechnol.* **2007**, *18* (2), 184−190.

(8) Swetank, Y. H.; Karthik, P.; Anandharamakrishnan, C. Effect of whey protein isolate and β-cyclodextrin wall systems on stability of microencapsulated vanillin by spray−freeze drying method. *J. Food Chem.* **2014**, *174*, 16−24.

(9) Gouin, S. Microencapsulation: industrial appraisal of existing technologies and trends. *Trends Food Sci. Technol.* **2004**, *15* (7), 330−347.

(10) Del Valle, E. M. M. Cyclodextrins and their uses: a review. *Process Biochem.* **2004**, *39* (9), 1033−1046.

(11) Bazhban, M.; Nouri, M.; Mokhtari, J. Electrospinning of cyclodextrin functionalized chitosan/PVA nanofibers as a drug delivery system. *Chin. J. Polym. Sci.* **2013**, *31* (10), 1343−1351.

(12) Uyar, T.; Hacaloglu, J.; Besenbacher, F. Electrospun polystyrene fibers containing high temperature stable volatile fragrance/flavor facilitated by cyclodextrin inclusion complexes. *React. Funct. Polym.* **2009**, *69* (3), 145−150.

(13) Kayaci, F.; Uyar, T. Electrospun zein nanofibers incorporating cyclodextrins. *Carbohydr. Polym.* **2012**, *90* (1), 558−568.

(14) Moreno, I.; González-González, V.; Romero-García, J. Control release of lactate dehydrogenase encapsulated in poly (vinyl alcohol) nanofibers via electrospinning. *Eur. Polym. J.* **2011**, *47* (6), 1264−1272.

DOI: 10.1021/acs.jafc.5b00103
J. Agric. Food Chem. 2015, 63, 3481−3488

(15) Kayaci, F.; Uyar, T. Encapsulation of vanillin/cyclodextrin inclusion complex in electrospun polyvinyl alcohol (PVA) nanowebs: Prolonged shelf-life and high temperature stability of vanillin. *Food Chem.* **2012**, *133* (3), 641−649.
(16) Marques, H. M. C. A review on cyclodextrin encapsulation of essential oils and volatiles. *Flavour Fragrance J.* **2010**, *25* (5), 313−326.
(17) Astray, G.; Gonzalez-Barreiro, C.; Mejuto, J. C.; Rial-Otero, R.; Simal-Gándara, J. A review on the use of cyclodextrins in foods. *Food Hydrocolloids* **2009**, *23* (7), 1631−1640.
(18) Kayaci, F.; Ertas, Y.; Uyar, T. Enhanced thermal stability of eugenol by cyclodextrin inclusion complex encapsulated in electrospun polymeric nanofibers. *J. Agric. Food Chem.* **2013**, *61* (34), 8156−8165.
(19) Kriegel, C.; Arecchi, A.; Arrechi, A.; Kit, K.; McClements, D. J.; Weiss, J. Fabrication, functionalization, and application of electrospun biopolymer nanofibers. *Crit. Rev. Food Sci. Nutr.* **2008**, *48* (8), 775−97.
(20) Fabra, M. J.; Lopez-Rubio, A.; Lagaron, J. M. High barrier polyhydroxyalcanoate food packaging film by means of nanostructured electrospun interlayers of zein. *Food Hydrocolloids* **2013**, *32* (1), 106−114.
(21) Mascheroni, E.; Fuenmayor, C. A.; Cosio, M. S.; Di Silvestro, G.; Piergiovanni, L.; Mannino, S.; Schiraldi, A. Encapsulation of volatiles in nanofibrous polysaccharide membranes for humidity-triggered release. *Carbohydr. Polym.* **2013**, *98* (1), 17−25.
(22) Li, F.; Scampicchio, M.; Mannino, S. Carbon nanotube-adsorbed electrospun nanofibrous membranes as coating for electrochemical sensors for sulfhydryl compounds. *Electroanalysis* **2011**, *23* (8), 1773−1775.
(23) Fuenmayor, C. A.; Lemma, S. M.; Mannino, S.; Mimmo, T.; Scampicchio, M. Filtration of apple juice by nylon nanofibrous membranes. *J. Food Eng.* **2014**, *122*, 110−116.
(24) Li, X.; Kanjwal, M. A.; Lin, L.; Chronakis, I. S. Electrospun polyvinyl-alcohol nanofibers as oral fast-dissolving delivery system of caffeine and riboflavin. *Colloids Surf., B* **2013**, *103*, 182−188.
(25) Celebioglu, A.; Uyar, T. Electrospinning of polymer-free nanofibers from cyclodextrin inclusion complexes. *Langmuir* **2011**, *27* (10), 6218−6226.
(26) Song, L. X.; Xu, P. A comparative study on the thermal decomposition behaviors between beta-cyclodextrin and its inclusion complexes of organic amines. *J. Phys. Chem. A* **2008**, *112* (45), 11341−11348.
(27) Nuchuchua, O.; Saesoo, S.; Sramala, I.; Puttipipatkhachorn, S.; Soottitantawat, A.; Ruktanonchai, U. Physicochemical investigation and molecular modeling of cyclodextrin complexation mechanism with eugenol. *Food Res. Int.* **2009**, *42* (8), 1178−1185.
(28) Ding, B.; Kim, H.-Y.; Lee, S.-C.; Shao, C.-L.; Lee, D.-R.; Park, S.-J.; Choi, K.-J. Preparation and characterization of a nanoscale poly(vinyl alcohol) fiber aggregate produced by an electrospinning method. *J. Polym. Sci., Part B: Polym. Phys.* **2002**, *40* (13), 1261−1268.
(29) Ghouchi-Eskandar, N.; Simovic, S.; Prestidge, C. A. Solid-state nanoparticle coated emulsions for encapsulation and improving the chemical stability of all-trans-retinol. *Int. J. Pharm.* **2012**, *423* (2), 384−391.
(30) Mathapa, B. G.; Paunov, V. N. Cyclodextrin stabilised emulsions and cyclodextrinosomes. *Phys. Chem. Chem. Phys.* **2013**, *15* (41), 17903−17914.
(31) Palmieri, G. F.; Wehrlé, P.; Duportail, G.; Stamm, A. Inclusion complexation of vitamin A palmitate with β-cyclodextrin in aqueous solution. *Drug Dev. Ind. Pharm.* **1992**, *18* (19), 2117−2121.
(32) Carlotti, M. E.; Rossatto, V.; Gallarate, M. Vitamin A and vitamin A palmitate stability over time and under UVA and UVB radiation. *Int. J. Pharm.* **2002**, *240* (1), 85−94.
(33) Kim, K.; Kim, D. High-performance liquid chromatography separation characteristics of molecular-imprinted poly (methacrylic acid) microparticles prepared by suspension polymerization. *J. Appl. Polym. Sci.* **2005**, *96* (1), 200−212.
(34) Krishnaswamy, K.; Orsat, V.; Thangavel, K. Synthesis and characterization of nano-encapsulated catechin by molecular inclusion with beta-cyclodextrin. *J. Food Eng.* **2012**, *111* (2), 255−264.
(35) Pinho, E.; Grootveld, M.; Soares, G.; Henriques, M. Cyclodextrins as encapsulation agents for plant bioactive compounds. *Carbohydr. Polym.* **2014**, *101*, 121−135.
(36) Afzal, M.; Walton, J. C. Oxidation of retinyl acetate and analogues by nitric oxide and nitrogen dioxide. *Bioorg. Med. Chem. Lett.* **1996**, *6* (19), 2329−2332.
(37) Lemma, S. M.; Scampicchio, M.; Bulbarello, A.; Mason, M.; Schweikert, L. Concerted determination of the hydrogen atom and electron transfer capacity of lipid soluble reducing agents. *Electroanalysis* **2014**, *26* (7), 1582−1587.
(38) Lin, H. S.; Chean, C. S.; Ng, Y. Y.; Chan, S. Y.; Ho, P. C. 2-hydroxypropyl-beta-cyclodextrin increases aqueous solubility and photostability of all-trans-retinoic acid. *J. Clin. Pharm. Ther.* **2000**, *25* (4), 265−269.

DOI: 10.1021/acs.jafc.5b00103
J. Agric. Food Chem. 2015, 63, 3481−3488

is able to produce by SSF of different agro-industrial byproducts more than 19 types of enzymes (cellulase, pectinase, protease, etc.) and several added-value bioactive products (citric acid, alcohols, etc.).[18] Most of the phenolic compounds occur primarily in conjugated form with one or more sugar residues linked to hydroxyl groups. Association with organic acids, amines, and lipids is also common.[19] These bounded forms of phenolics reduce their ability to function as good antioxidants because the resonance stabilization of free radicals is highly dependent on the availability of free hydroxyl groups on the phenolic rings.[1] The free phenolics can be released from the conjugated form via enzymatic hydrolysis with carbohydrate metabolizing enzymes (such as β-glucosidase) produced by fungi during SSF of lignocellulosic wastes, improving the health functionality of these phytochemicals in this way.[19] Enhancement of phenolic content and antioxidant potential using SSF was reported in cranberry[1] and apple pomaces,[19] pomegranate,[20] and pineapple[21] wastes and different cereals.[22] To our knowledge, there is no data available in the literature about the use of *Sambucus* berry pomaces as support in SSF processes for the production of value-added compounds. The hydrolytic enzyme complex excreted by *Aspergillus niger* in the SSF system, comprising mainly cellulase, pectinase, and protease, can also increase the lipid yields, hydrolyzing the polysaccharides from the seed cell walls and releasing the extra oil from its bounded forms, such as lipoproteins and lipopolysaccharides, which are otherwise nonextractable.[23] Therefore, the objective of the present work was to evaluate the influence of SSF by *A. niger* on phenolic contents and antioxidant activity in *Sambucus nigra* L. and *Sambucus ebulus* L. berry pomaces. Furthermore, the effect of fermentation time on the total fats and major lipid classes (neutral and polar) in bioprocessed substrates was also investigated. This solid-state bioprocessing approach can enhance the functional value of this berry byproduct.

MATERIALS AND METHODS

Chemicals. Folin−Ciocalteu's phenol reagent, gallic acid, sodium carbonate, acetic acid, acetonitrile, methanol, chlorogenic acid, rutin, cyanidin chloride, DPPH (1,1-diphenyl-2 picrylhydrazyl), the lipid standards, and other chemicals (used for the total fat extraction, fractionation, and preparation of fatty acid methyl esters (FAMEs)) were purchased from Sigma-Aldrich (Steinheim, Germany). The thin layer chromatography (TLC) plates (silica gel 60 F254, 20 × 20 cm) were purchased from Merck (Darmstadt, Germany). The FAMEs standard (37 component FAME Mix, SUPELCO) was obtained from Supelco (Bellefonte, PA, U.S.A.).

Raw Material. The freshly pressed berry pomaces were obtained in our laboratory from the fully ripened berries of wild *Sambucus nigra* L. (black or European elderberry) and *Sambucus ebulus* L. (dwarf elder, elderberry, or danewort) collected in September−October of 2013 in the northwest of Transylvania (Romania).

Culture Medium and Fermentation Conditions. The berry press residues of two *Sambucus* species were used as natural substrates for the SSF. The berry pomaces were homogenized with a high-power homogenizer (MICCRA D-9, Germany) and stored at −20 °C prior to use. The substrates were autoclaved for 30 min at 121 °C. The moisture content in the berry pomaces was 60% w/w. The fungal strain of *Aspergillus niger* (ATCC-6275; LGC Standards GmbH, Wesel Germany) was selected as a suitable fungus for solid-state fermentation due to its potential for higher enzyme production. *A. niger* was propagated according to the procedure developed by Oberoi et al.[23] The fungus was maintained on potato dextrose agar (PDA) plates at 4 °C. The culture of *A. niger* was grown on PDA Petri dish and incubated at 30 °C. The fungal spores were collected from the sporulation medium plates, inoculated into sterile distilled water, and stored in the freezer.

Solid-State Fermentation. Fifty grams of solid substrates (pH 5) in 500 mL Erlenmeyer flasks were thoroughly mixed and autoclaved at 121 °C for 30 min. The substrates were inoculated with spore suspension (2×10^7 spores/g of solid). After mixing, the flasks with inoculated substrates were incubated at 30 °C for 6 days. To carry out the chemical characterization, samples were withdrawn at the beginning and every 24 h and stored at −20 °C. The experiment was performed in triplicate. Because the lipid accumulation process in solid−state fermented medium is favored due to the low content of nitrogen or phosphorus sources and an excess of carbon source,[23] in this study, the solid substrates were not supplemented with any extra nutrient solution.

Extraction of Phenolic Compounds. Extraction was performed according to the method described by Veberic et al.[7] with some minor modifications. The samples of berry pomaces (1 g) were extracted with 20 mL of extraction mixture (hydrochloric acid/methanol/water in the ratio of 1:80:19) in an ultrasonic bath for 30 min at 40 °C. The mixtures were centrifuged at 4000*g* for 10 min, and the supernatants were filtered under vacuum through the glass frit. The filtrates were evaporated to dryness under vacuum. The resulting dried extracts were dissolved in methanol and then used for phenolic content and antioxidant activity measurements.

Determination of Total Phenolic Content. The content of total polyphenols (TP) was determined by the Folin−Ciocalteu method[24] using a Synergy HT Multi-Detection Microplate Reader with 96-well plates (BioTek Instruments, Inc., Winooski, VT, U.S.A.). A combination solution consisting of 25 μL sample extract, 125 μL of Folin−Ciocalteu reagent (0.2 N), and 100 μL of sodium carbonate (Na_2CO_3) solution (7.5% w/v) was homogenized and incubated at room temperature (25 °C) in the dark for 2 h. The absorbance was measured at 760 nm against a methanol blank. Gallic acid (0.01−1 mg/mL) was used as a standard, and the content of TP in the extract was expressed as gallic acid equivalents (GAE) in mg/g dry weight (DW) of pomace.

Phenolic Compound Analysis by High-Performance Liquid Chromatography-Diode Array Detection-Electrospray Ionization Mass Spectrometry (HPLC-DAD-ESI MS). An Agilent 1200 HPLC equipped with DAD detector, coupled with MS detector single quadrupole Agilent 6110 was used to confirm and quantify each individual phenolic compound. Separations were carried out using an Eclipse column, XDB C18 (4.6 × 150 mm, particle size 5 μm) (Agilent Technologies, U.S.A.) at 25 °C. All samples were analyzed in triplicate on the basis of the method described by Pop et al.[25] using as mobile phase 0.1% acetic acid/acetonitrile (99:1) in distilled water (v/v) (A) and 0.1% acetic acid in acetonitrile (v/v) (B) and the following gradient: 5% B (0−2 min), 5−40% B (2−18 min), 40−90% B (18−20 min), 90% B (20−24 min), 90−5% B (24−25 min), 5% B (25−30 min). The flow rate was 0.5 mL/min in all separations. For MS fragmentation, the ESI(+) module was applied, with a capillary voltage of 3000 V, at 350 °C and nitrogen flow of 8 L/min. Scan range was 100−1000 *m*/*z*. The eluent was monitored by DAD, and the

DOI: 10.1021/acs.jafc.5b00520
J. Agric. Food Chem. 2015, 63, 3489−3500

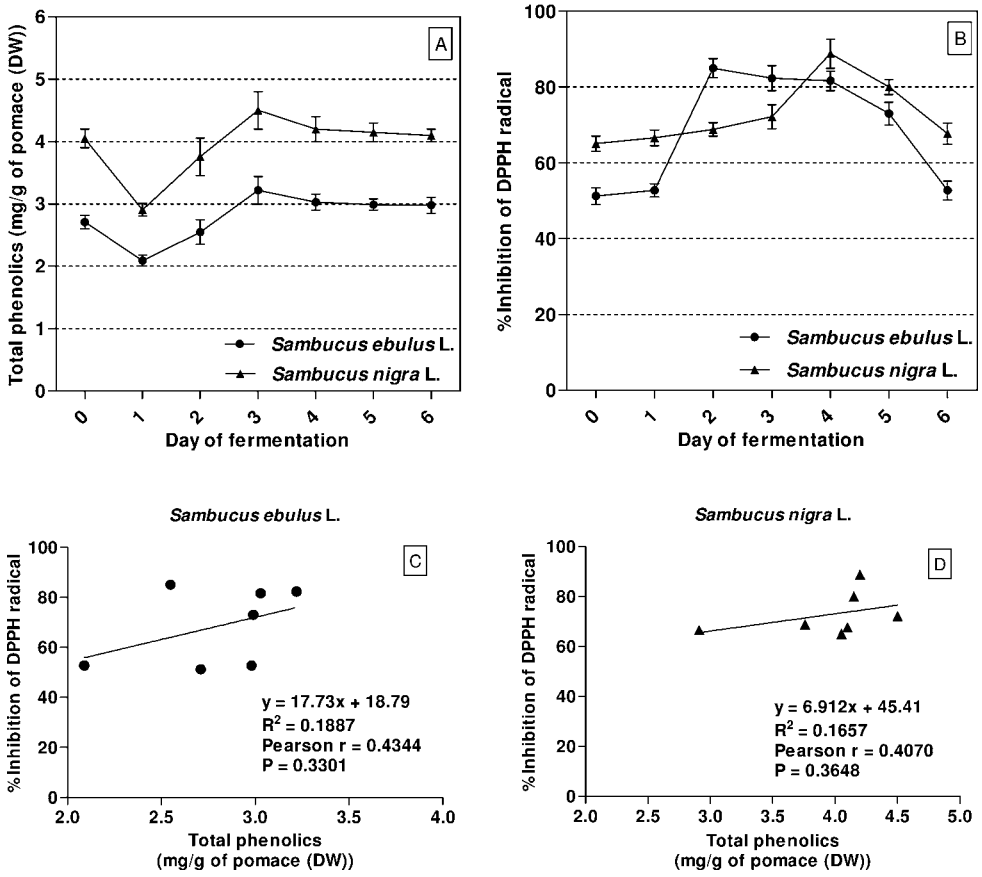

Figure 1. Total phenolic content (A), free radical scavenging activity of phenolics (B) and relationship between radical scavenging capacity (DPPH assay) and total phenolic content (C and D) of extracts from solid state fermented *S. ebulus* L. and *S. nigra* L. pomaces. Values are mean ± SD of three samples, analyzed individually in triplicate ($n = 3 \times 3$).

absorbance spectra (200−600 nm) were collected continuously during the course of each run. The flavonols were detected at 340 nm and the anthocyanins at 520 nm.[25] Data analysis was carried out by Agilent ChemStation Software (Rev B.04.02 SP1, Palo Alto, California, U.S.A.). The identification of the phenolics was made according to UV−visible spectra, retention time, cochromatography with authentic standards (when available), and mass spectra. The identified anthocyanins were quantified using cyanidin chloride as external standard and calculated as equivalents of cyanidin (mg cyanidin/100g dry weight (DW) of the substrate) (r^2 = 0.9935). Using the same quantification procedure, the chlorogenic acid was expressed in mg chlorogenic acid/100g DW of the substrate (r^2 = 0.9937) and quercetins were calculated as equivalents of rutin (mg rutin/100g DW of the substrate) (r^2 = 0.9981).[25]

Determination of the Antioxidant Activity with the DPPH Free Radical Scavenging Method. A method described by Mărghitaş et al.[26] with adaptation on the microplate reader was used to detect the 2,2-diphenyl-1-picrylhydrazyl (DPPH) radical scavenging activity of the examined extracts. Methanol extract (40 μL) was mixed with 200 μL of DPPH solution (0.02 mg/mL) and left to stand 15 min at room temperature and then the absorbance was measured at 517 nm. The percentage inhibition was calculated using the equation:

$$\text{Inhibition (\%)} = [1 - (\text{test sample absorbance/blank sample absorbance})] \times 100$$

Lipid Extraction. Total lipids (TLs) of berry pomaces were extracted from 5 g of samples, using a methanol/chloroform extraction method.[27]

Isolation of Neutral (TAGs, MAGs, 1, 2- and 1, 3-DAGs, FFAs, and SEs) and Polar lipid (PL) Fractions from TLs. Using a previously described method,[16,28,29] the TL extracts were fractionated by TLC into seven fractions. The separated bands (PLs, MAGs, 1, 2- and 1, 3-DAGs and FFAs) were scraped off, and extracted in a solvent mixture of chloroform/methanol (2:1, v/v). The TAG and SE bands were also scraped off and extracted with chloroform. After filtration and solvent evaporation, the dry residues were subjected to transesterification and gas chromatographic (GC) analysis. Trinonadecanoylglycerol (70 μg for TAGs) and nonadecanoic acid (10−50 μg for PLs, MAGs, DAGs, SEs and 200 μg for FFAs) were added as internal standards before the transesterification process.

Analysis of Fatty Acids and Calculation of Lipid Fractions Content in TLs. The isolated lipid fractions were transesterified into FAMEs using the acid-catalyzed method.[16] The FAMEs were analyzed with a gas chromatograph (GC) coupled to a mass spectrometer (MS): PerkinElmer Clarus 600 T GC-MS (PerkinElmer, Inc., Shelton, CT, U.S.A.)[27] on a Supelcowax 10 (60 m × 0.25 mm i.d., 0.25 μm film thickness; Supelco Inc., Bellefonte, PA, U.S.A.) capillary column. The temperature program was set as follows: initial temperature, 140 °C, then to 220 °C at 7 °C/min, and held at 220 °C for 23 min. The injector was set at 210 °C, with a 1:24 split ratio, and 0.5 μL was injected. The column flow rate (He) was 0.8 mL/

DOI: 10.1021/acs.jafc.5b00520
J. Agric. Food Chem. 2015, 63, 3489−3500

Table 1. Mean Polyphenolic Contents (mg/100g DW of the Substrate) of *S. nigra* L. and *S. ebulus* L. Pomaces During Solid-State Fermentation

	anthocyanins				cinnamic acid	quercetins	
identified compound ([M + H] + ion, fragments)	cyanidin 3-sambubioside-5-glucoside (743, 581, 449, 287)	cyanidin 3-sambubioside (581, 287)	cyanidin 3,5-diglucoside (611, 449, 287)	cyanidin 3-glucoside (449, 287)	5-caffeoylquinic acid (chlorogenic acid) (355, 181)	quercetin 3-rutinoside (rutin) (611, 303)	quercetin 3-glucoside (isoquercitrin) (465, 303)
peak	1	2	3	4	5	6	7
				Sambucus nigra L.			
day of fermentation							
0	44.94^{b} ± 2.50	4.46^{b} ± 0.15	18.70^{c} ± 1.10	7.90^{a} ± 0.35	4.16^{b} ± 0.20	40.25^{c} ± 2.10	25.45^{a} ± 1.30
1	34.99^{e} ± 1.65	2.76^{e} ± 0.10	11.04^{d} ± 0.48	3.48^{d} ± 0.18	0.82^{f} ± 0.06	30.92^{e} ± 1.28	14.13^{d} ± 0.65
2	38.58^{c} ± 2.10	3.34^{d} ± 0.16	21.44^{b} ± 1.10	5.09^{c} ± 0.30	3.17^{d} ± 0.18	42.77^{b} ± 1.85	18.83^{b} ± 0.80
3	46.88^{a} ± 2.20	4.62^{a} ± 0.18	23.04^{a} ± 1.18	5.93^{b} ± 0.26	4.49^{a} ± 0.22	45.50^{a} ± 1.90	19.03^{b} ± 0.85
4	46.45^{a} ± 2.25	4.40^{b} ± 0.20	18.80^{c} ± 1.10	2.41^{e} ± 0.15	3.52^{c} ± 0.20	34.00^{d} ± 1.65	16.18^{c} ± 0.80
6	37.02^{d} ± 1.72	4.16^{c} ± 0.20	11.68^{d} ± 0.60	1.80^{f} ± 0.10	2.98^{e} ± 0.21	31.07^{e} ± 1.55	13.10^{e} ± 0.65
				Sambucus ebulus L.			
day of fermentation							
0	28.90^{ab} ± 1.40	3.56^{a} ± 0.15	13.71^{a} ± 0.72	2.59^{a} ± 0.12	24.32^{ab} ± 1.20	12.80^{a} ± 0.65	9.85^{b} ± 0.45
1	23.78^{e} ± 1.20	2.43^{d} ± 0.13	13.38^{ab} ± 0.70	1.31^{e} ± 0.07	18.16^{d} ± 0.95	11.20^{b} ± 0.60	7.85^{d} ± 0.28
2	25.26^{d} ± 1.18	2.84^{c} ± 0.11	13.43^{ab} ± 0.65	1.75^{c} ± 0.09	23.85^{b} ± 1.10	12.39^{a} ± 0.70	9.92^{b} ± 0.40
3	29.61^{a} ± 1.62	2.94^{b} ± 0.14	13.75 ^{a} ± 0.75	2.06^{b} ± 0.10	25.04^{a} ± 1.15	13.01^{a} ± 0.65	10.69^{a} ± 0.45
4	28.64^{b} ± 1.45	2.46^{d} ± 0.11	13.50^{ab} ± 0.60	1.43^{d} ± 0.07	21.20^{c} ± 1.10	6.27^{cd} ± 0.35	8.54^{c} ± 0.40
6	27.52^{c} ± 1.40	2.19^{e} ± 0.11	13.19^{b} ± 0.65	1.28^{e} ± 0.08	20.50^{c} ± 1.15	5.82^{d} ± 0.30	7.34^{e} ± 0.35

The values represent the means of three samples, analyzed individually in triplicate ($n = 3 \times 3$). Totals with different superscript letters ($^{a\text{-}f}$) (within a column for the different *Sambucus* pomaces) were significantly different (repeated measures ANOVA "Tukey's Multiple Comparison Test", $p < 0.05$).

min. The EI (positive ion electron impact) mass spectra were recorded at 70 eV and a trap current of 100 μA with a source temperature of 150 °C. The mass scans were performed within the range of m/z: 22−395 (0.14 scans/s with an intermediate time of 0.02 s between the scans). The FAMEs were identified by comparing the retention times with those of known standards (37 components FAME Mix, Supelco no. 47885-U) and the resulting mass spectra to those in our database (NIST MS Search 2.0). Fatty acids were quantified by comparison to peak areas of the methyl nonadecanoate without application of any correction factor. The fatty acid compositions of lipid fractions were expressed as molar percentages of the fatty acids. The neutral (TAGs, MAGs, 1,2- and 1,3-DAGs, FFAs, and SEs) and polar lipid contents in TLs were calculated using an average molecular weight of fatty acids of the fraction in question and were expressed as weight percentages (wt %) in oils.

Statistical Analysis. All values were expressed as the mean ± standard deviation (SD) of three independent experiments with samples in triplicate. Correlations between the antioxidant activity and total phenolic content were examined using Pearson's correlation. Statistical differences among samples were estimated using Student's t test and ANOVA (repeated measures ANOVA; Tukey's Multiple Comparison Test; GraphPad Prism Version 5.0, Graph Pad Software Inc., San Diego, CA). A probability value of $p < 0.05$ was considered to be statistically significant.

RESULTS AND DISCUSSION

Total Phenolics. During the first 3 days of growth, both *Sambucus* species showed a similar trend, the total phenolics content decreased in the first 24 h and increased until the maximum yield (Day 3) (Figure 1A). Similar results were previously obtained by Correia et al.[21] in the production of phenolics by the solid-state bioconversion of pineapple waste using the *Rhizopus oligosporus*. The rapid fall of the observed measurable phenolics during the early stages of fermentation suggests that the most phenolics were present in bound form and only a small amount was in free soluble- form. However, it should be noted that under the given fermentation conditions the phenolics increased only with 18.82% for *S. ebulus* L. and 11.11% for *S. nigra* L. from initial values of 2.71 mg/g DW and 4.05 mg/g DW for unfermented pomaces to 3.22 mg/g DW and 4.50 mg/g DW for fermented pomaces. Vattem et al.[1] and Ajila et al.[19] reported that polyphenol content increases when the β-glucosidase activity increases, showing that this carbohydrate-cleaving enzyme plays an important role in the bioconversion or liberation of free phenolics from different pomaces during solid-state growth of *Phanerochaete chrysosporium*, *Lentinus edodes* , and *Rhizopus oligosporus*. According to previous studies,[1,21] the low nitrogen content of a media could act as a barrier for free phenolic compounds production. It can be concluded that to improve the TP production, the SSF should be carried out with the solid substrate supplemented with organic or inorganic nitrogen sources. Further investigation is needed. The measurable free phenolics for both berry wastes showed a slight decrease after 3 days of fermentation, probably due to the depletion of the nutrients and to the stress induced on the fungus. As response, it enabled the lignifying and tannin forming peroxidase enzymes in the fungus, causing the polymerization and lignification of the free phenolics and as an consequence, the intensity of the reaction of the molecules with Folin-Ciocalteu reagent decreased.[1] The ranges for obtained phenolic contents are in accordance with literature data,[4] indicating that significant amount of these biomolecules could be extracted from *Sambucus* berry pomaces, compared to whole berry or juice. Ozgen et al.[30] reported in their study on 14 purple- black American elderberry accessions (*Sambucus canadensis* L.) TP content values between 3.30 and 3.90 mg/g fresh weight, whereas Bermúdez-Soto and Tomás-

DOI: 10.1021/acs.jafc.5b00520
J. Agric. Food Chem. 2015, 63, 3489−3500

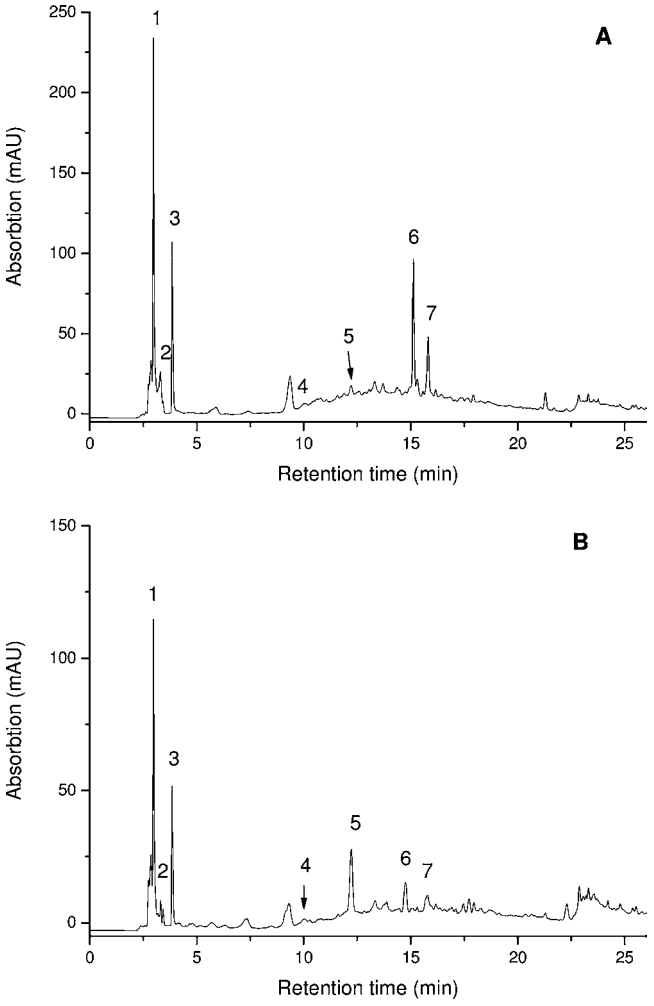

Figure 2. HPLC chromatograms (detected wavelength at 280 nm) of *A. niger* fermented (A) *S. nigra* L. (fourth day of SSF) and (B) *S. ebulus* L. (second day of SSF) berry pomaces: (1) cyanidin 3-sambubioside-5-glucoside; (2) cyanidin 3-sambubioside; (3) cyanidin 3,5-diglucoside; (4) cyanidin 3-glucoside; (5) 5-caffeoylquinic acid; (6) quercetin 3-rutinoside; (7) quercetin 3-glucoside.

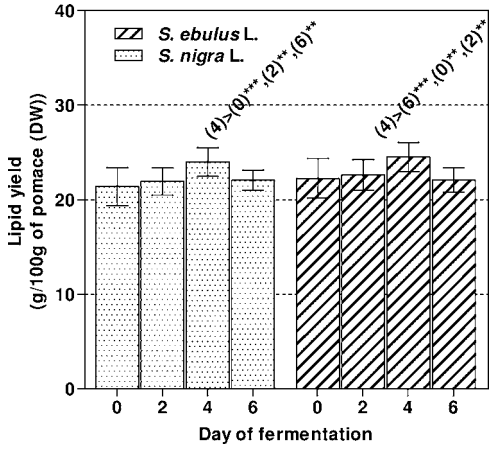

Figure 3. Time course of lipid production by strain *Aspergillus niger* from the *S. ebulus* L. and *S. nigra* L. berry press residues during solid-state fermentation. Results are given as mean ± SD (n = 3); ** p < 0.01, *** p < 0.001 (repeated measures ANOVA "Tukey's Multiple Comparison Test").

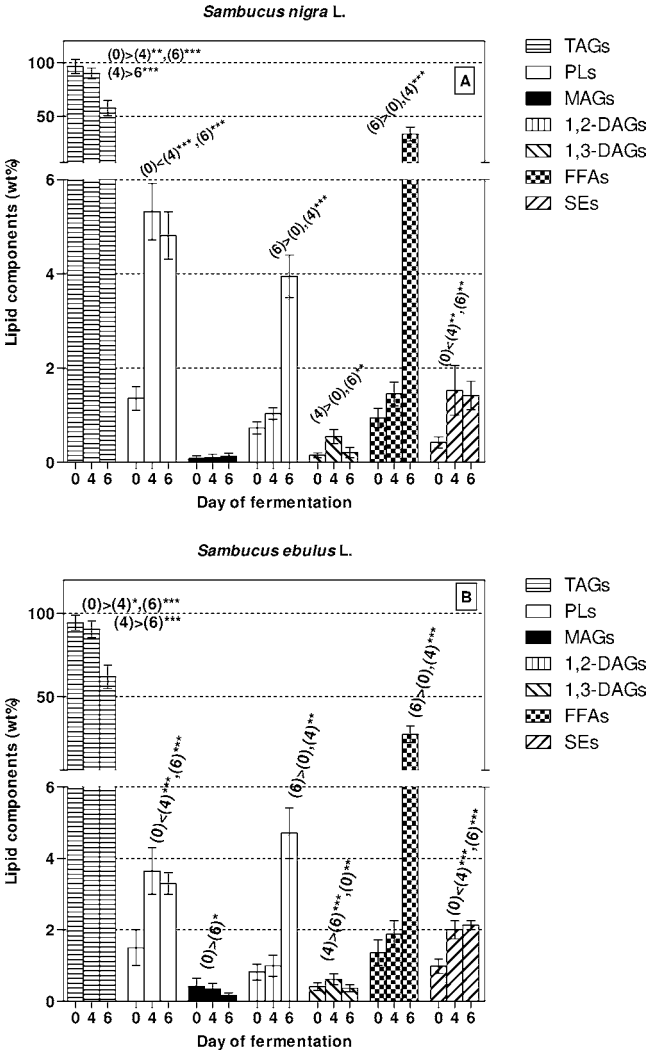

Figure 4. Lipid components in oils from the *S. nigra* L. (A) and *S. ebulus* L. (B) berry press residues during solid-state fermentation. Values are mean ± SD of three samples, analyzed individually in triplicate (n = 3 × 3); * p < 0.05, ** p < 0.01, *** p < 0.001 (repeated measures ANOVA "Tukey's Multiple Comparison Test"). TAGs − triacylglycerols, PL − polar lipids, MAG − monoacylglycerols, DAG − diacylglycerols, FFAs − free fatty acids, SEs − sterol esters.

Barberán[3] determined 30.50 mg/mL of elderberry juice concentrate. The TP amounts for aqueous and methanol extracts of *Sambucus ebulus* L. fruits reported by Ebrahimzadeh et al.[14] were 41.59 and 27.37 mg GAE/g of extract powder, respectively. In their study on anthocyanin and other polyphenolic profiles of different genotypes of *S. canadensis* and *S. nigra* L., Lee and Finn[31] reported TP contents between 277 and 582 mg GAE/100 g berries, depending on the growing seasons and cultivators. It should be mentioned that the phenolic compounds from the *Sambucus* berries coexist with different toxic and allergenic lectins. However, Jimenez et al.[9] showed that the negative effects of these lectins can be eliminated by a short-time heat treatment of berry-derived products, without any significant reduction in the content of the antioxidant compounds.

HPLC-DAD-MS Analysis of Phenolic Compounds. The contents of major phenolics in the berry press residues of two species of *Sambucus* were determined during fermentation (Table 1). The characteristic HPLC chromatograms are shown

DOI: 10.1021/acs.jafc.5b00520
J. Agric. Food Chem. 2015, 63, 3489−3500

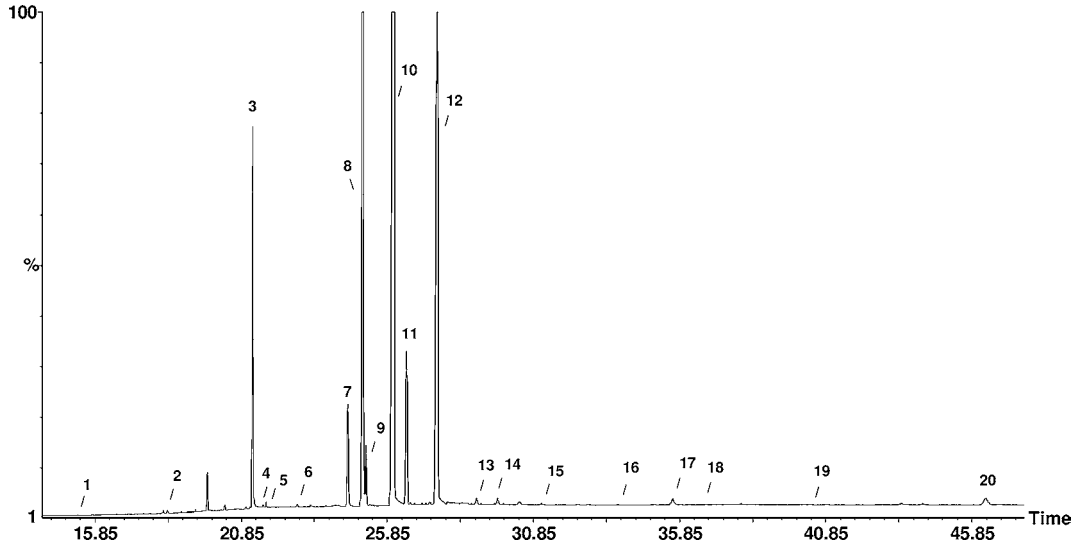

Figure 5. GC-MS chromatogram of FAMEs in the TLs of the *S. ebulus* L. berry pomaces after SSF with *A. niger* (the fourth day) analyzed with a Supelcowax 10 capillary column. Peak identification: (1) lauric (12:0); (2) myristic (14:0); (3) palmitic (16:0); (4) *cis*-7 hexadecenoic (16:1n-9); (5) palmitoleic (16:1n-7); (6) margaric (17:0); (7) stearic (18:0); (8) oleic (18:1n-9); (9) vaccenic (18:1n-7); (10) linoleic (18:2n-6); (11) nonadecanoic (19:0, internal standard); (12) α-linolenic (18:3n-3); (13) arachidic (20:0); (14) 11-eicosenoic (20:1n-9); (15) 11,14-eicosadienoic (20:2n-6); (16) eicosatrienoic (20:3n-3); (17) behenic (22:0); (18) erucic (22:1n-9); (19) tricosanoic (23:0); (20) lignoceric (24:0) acids.

in Figure 2. Both species contained seven dominant polyphenolics; four anthocyanins (cyanidin 3-sambubioside-5-glucoside, cyanidin 3-sambubioside, cyanidin 3,5-diglucoside and cyanidin 3-glucoside), cinnamic acid (chlorogenic acid) and two quercetins (rutin and isoquercitrin). The fruits of *Sambucus* contain an appreciable amount of cyanidin as a diglucoside (sambubioside), which is not common in most berries.[12] The proportion of the individual phenolics differed between species (Table 1). Cyanidin 3-sambubioside-5-glucoside was the major phenolic compound in both residues of the *Sambucus* species. The next predominant polyphenolics in *S. nigra* L. were rutin, isoquercitrin and cyanidin 3, 5-diglucoside, whereas in *S. ebulus* L. the second major phenolic compound was chlorogenic acid (Table 1 and Figure 2). The air-dried elderberries examined by Bridle and Garcia-Viguera[32] also had cyanidin 3-sambubioside-5-glucoside as the major anthocyanin. Our findings concerning the identity and number of quercetins in *S. nigra* L. press- residues match the literature data.[8] Quercetin-based glycosides were the major flavonol glycosides in both processed *Sambucus* residues. The identified flavonols were mostly rutinosides: from 61% (nonfermented) to 71% (the third day of fermentation) of total flavonol glycosides of *S. nigra* L. residues and from 56% (nonfermented) to 58% (the first day of fermentation) of total flavonol glycosides of *S. ebulus* L. residues, while the remainders were conjugated to glucose (Table 1). In most cases berry juice or air-dried, freeze-dried or frozen fruits were analyzed.[3,13,31] To our knowledge this is the first study investigating the variation of the amounts of phenolic compounds in wild-grown *S. nigra* L. and *S. ebulus* L. berry pomaces in correlation to fermentation days in solid-state system by *A. niger*. As shown in Table 1, at the beginning stage of fermentation (0—first day), the levels of all phenolic compounds decreased significantly ($p < 0.05$) (except cyanidin 3, 5-diglucoside from *S. ebulus* L. extract). After 24h, the contents of phenolics increased slightly during the course of SSF by day 3, after which the concentrations of individual polyphenols in both *Sambucus* berry residues decreased significantly ($p < 0.05$). In *S. ebulus* L. pomace extracts the level of cyanidin 3-sambubioside-5-glucoside increased significantly ($p < 0.05$) with 2.46% by day 3 from initial value before gradually decreasing for the remaining period of fermentation. The magnitude of this major anthocyanin change was higher for the *S. nigra* L. pomace, increased with 4.32% in the third before sharply decreasing in the sixth day (Table 1). The increase of the individual phenolic amounts during the first days of fermentation may be explained by the enzymatic release of bound phenolic compounds from the pomaces by means of lignin-degrading peroxidases and carbohydrate-cleaving enzymes expressed by the fungus during the initial stages of growth, to allow penetration of the tissues and the use of available nutrients from residues.[19] The decline of individual phenolic concentrations during the later course of growth could be due to polymerization of the released phenolic compounds. Qin et al.,[33] in their study on polyphenol and purine alkaloid contents during solid-state fermentation of pu-erh tea leaves, reported that most of the flavone glycosides were degraded after bioconversion with *Aspergillus* fungi.

Antioxidant Activity. The ability of phenolic compounds to inhibit DPPH (2,2′-diphenyl-1-picrylhydrazyl) free radical in methanol extracts of two *Sambucus* berry press residues during the course of solid-state bioprocessing was measured, and the results are shown in Figure 1B. In the methanolic extracts of *S. nigra* L. berry press residue the radical inhibition capacity increased by 36.50% by day 4 compared with the initial value (%I = 65) before sharply decreasing for the remaining period of the fungal growth. The increase in the radical inhibition activity was higher for the *S. ebulus* L. pomace, which increased with 66% in the second day versus initial value (%I = 51.20) before gradually decreasing by day 4 (Figure 1B). The literature shows that the antioxidant activity of *Sambucus* berries is mainly connected with the presence of flavonols and anthocyanins.[9,13,15] Moreover, Mandrone et al.[15] have determined a strong correlation between the antioxidant activity of *S. nigra* L. fruits and their cyanidin-3-sambubioside-5-glucoside composition. Phenolic compounds in fruits and their processing wastes have been ascribed important roles. Nontheless, there is

DOI: 10.1021/acs.jafc.5b00520
J. Agric. Food Chem. 2015, 63, 3489−3500

Table 2. Fatty Acid Compositions (Molar %) of Total Lipids and Individual Lipid Classes Produced by *Aspergillus niger* in Solid-State Fermentation of *S. ebulus* L. Berry Press Residues[a]

	Sambucus ebulus L.															
	fermentation time (day)															
	0	4	0	4	0	4	0	4	0	4	0	4	0	4	0	4
fatty acids	TLs		TAGs		PLs		MAGs		1,2-DAGs		1,3-DAGs		FFAs		SEs	
12:0	0.01	tr	0.03	0.01	0.06	0.37	0.77	0.75	0.05	0.02	0.05	0.09	0.29	0.05	0.46	0.28
14:0	0.07	0.03	0.06	0.02	0.34	1.01	1.75	2.18	0.13	0.06	0.37	0.43	0.35	0.16	1.52	0.95
16:0	7.70	6.02	6.79	5.10	25.30	18.99	20.66	18.64	9.71	5.45	8.71	10.66	12.53	13.38	51.55	35.79
16:1n-9	0.05	0.02	0.05	0.02	0.28	0.34	tr	1.39	0.15	0.07	0.13	0.22	0.30	0.20	1.76	1.01
16:1n-7	0.10	0.04	0.09	0.07	0.15	0.43	-	-	0.13	0.10	0.17	0.28	0.25	0.29	0.28	0.20
17:0	0.04	0.02	0.05	0.02	0.26	2.28	0.67	0.93	0.15	0.06	-	-	0.19	0.17	0.30	0.20
18:0	2.78	1.08	2.63	0.99	9.26	12.57	28.03	13.07	3.90	4.31	4.76	13.59	5.00	4.93	8.89	6.82
18:1n-9	20.22	23.30	15.71	18.10	18.77	15.92	10.09	17.06	21.37	22.73	23.04	22.34	17.40	18.15	13.82	22.39
18:1n-7	1.08	0.47	1.02	0.42	1.83	1.14	1.15	2.47	1.88	0.86	1.70	1.13	0.88	3.11	0.49	0.86
18:2n-6	43.11	45.19	43.99	46.32	33.94	31.40	19.26	25.52	51.46	43.02	40.34	34.67	30.51	31.39	11.19	21.88
18:3n-3	23.78	23.34	28.62	28.67	7.53	10.47	7.48	10.06	9.97	22.87	18.02	13.13	15.38	17.16	3.41	6.03
20:0	0.16	0.07	0.09	0.05	1.09	1.70	1.63	tr	0.17	0.09	0.50	0.84	0.97	0.40	2.00	1.14
20:1n-9	0.18	0.07	0.15	0.06	0.27	-	-	-	0.30	0.14	0.35	0.34	0.13	0.46	0.23	0.25
20:2n-6	tr	tr	-	-	tr	-	-	-	-	-	-	-	-	0.10	-	-
20:3n-3	tr	tr	-	-	tr	-	-	-	-	-	-	-	-	-	-	-
22:0	0.27	0.12	0.47	0.07	0.71	2.76	-	-	0.14	0.06	0.56	0.70	5.47	0.87	2.77	1.76
22:1n-9	0.02	0.01	-	-	0.23	0.61	8.51	7.92	0.50	0.17	1.31	1.57	0.10	-	1.35	0.46
23:0	0.02	0.01	-	-	-	-	-	-	-	-	-	-	-	0.07	tr	-
24:0	0.42	0.21	0.24	0.08	-	-	-	-	-	-	-	-	10.26	9.11	-	-
∑SFA	11.47^{a***}	7.56^{b}	10.36	6.34	37.01	39.68	53.50	35.58	14.24	10.04	14.95	26.32	35.05	29.14	67.48	46.93
∑ VLCSFAs(≥20C)	$0.87^{a}*$	0.41^{b}	0.80	0.21	1.80	4.46	1.63	-	0.31	0.15	1.06	1.54	16.70	10.45	4.77	2.90
∑MUFA	21.65^{b}	23.92^{a***}	17.02	18.66	21.52	18.45	19.75	28.84	24.33	24.07	26.69	25.88	19.06	22.21	17.92	25.16
∑PUFA	66.89^{b}	68.53^{a***}	72.61	75.00	41.47	41.88	26.75	35.58	61.43	65.89	58.36	47.80	45.89	48.65	14.60	27.91
∑n-3 PUFAs	$23.78^{a}*$	23.34^{b}	28.62	28.67	7.53	10.47	7.48	10.06	9.97	22.87	18.02	13.13	15.38	17.16	3.41	6.03
∑n-6 PUFAs	43.11^{b}	45.19^{a***}	43.99	46.32	33.94	31.40	19.26	25.52	51.46	43.02	40.34	34.67	30.51	31.49	11.19	21.88
n-6/n-3	1.81^{b}	1.94^{a**}	1.54	1.62	4.50	3.00	2.57	2.54	5.16	1.88	2.24	2.64	1.98	1.84	3.28	3.63
PUFAs/SFAs	5.83^{b}	9.07^{a***}	7.01	11.82	1.12	1.06	0.50	1.00	4.31	6.56	3.90	1.82	1.31	1.67	0.22	0.59

[a]The values represent the means of three samples, analyzed individually in triplicate ($n = 3 \times 3$). TLs − total lipids, TAGs − triacylglycerols, PLs − polar lipids, MAGs − monoacylglycerols, DAGs − diacylglycerols, FFAs − free fatty acids, SEs − sterol esters; SFAs − saturated fatty acids, MUFAs − monounsaturated fatty acids, PUFAs − polyunsaturated fatty acids, VLCSFAs − very long chain saturated fatty acids; tr. − trace.Different superscript letters (^{a,b}) in the same row mean significant differences between TLs of the two fermentation days. $^{*}p < 0.05$. $^{**}p < 0.01$. $^{***}p < 0.001$ (paired *t*-test). C12:0, lauric; C14:0, myristic; C16:0, palmitic; C16:1n-9, *cis*-7 hexadecenoic; C16:1n-7, palmitoleic; C17:0, margaric; C18:0, stearic; C18:1n-9, oleic; C18:1n-7,vaccenic; C18:2n-6, linoleic; C18:3n-3, α-linolenic; C20:0, arachidic; C20:1n-9, 11-eicosenoic; C20:2n-6, 11,14-eicosadienoic; C20:3n-3, eicosatrienoic; C22:0, behenic; C22:1n-9, erucic; C23:0, tricosanoic; C24:0, lignoceric acids.

DOI:10.1021/acs.jafc.5b00520
J. Agric. Food Chem. 2015, 63, 3489−3500

Table 3. Fatty Acid Compositions (Molar %) of Total Lipids and Individual Lipid Classes Produced by *Aspergillus niger* in Solid-State Fermentation of *S. nigra* L. Berry Press Residues[a]

	Sambucus nigra L.															
	fermentation time (day)															
	0	4	0	4	0	4	0	4	0	4	0	4	0	4	0	4
fatty acids	TLs		TAGs		PLs		MAGs		1,2-DAGs		1,3-DAGs		FFAs		SEs	
12:0	0.01	0.01	-	0.01	0.21	0.75	0.60	0.41	0.06	0.05	0.21	0.54	0.30	0.02	0.71	1.57
14:0	0.09	0.08	0.06	0.06	0.68	1.01	2.06	1.81	0.31	0.28	0.71	1.59	0.79	0.13	3.42	2.57
16:0	8.46	6.88	7.46	5.82	28.22	19.74	27.08	9.38	12.61	7.33	13.77	11.95	19.79	15.30	25.38	21.19
16:1n-9	0.04	0.05	0.06	0.05	0.40	0.91	-	-	0.31	0.41	tr	0.62	0.25	0.08	5.96	2.31
16:1n-7	0.06	0.06	0.06	0.06	0.29	0.69	tr	0.54	0.16	0.22	0.49	1.14	0.32	0.09	0.49	0.67
17:0	0.04	0.04	0.05	0.04	0.26	1.22	tr	0.86	0.07	-	-	-	0.34	0.09	0.91	0.44
18:0	2.40	1.02	1.99	1.10	8.85	13.81	20.12	6.93	4.51	5.23	6.31	10.85	6.90	4.29	18.99	6.80
18:1n-9	14.28	16.92	12.69	14.42	9.28	6.88	9.14	16.03	14.90	15.30	16.48	14.86	10.26	13.10	10.43	17.09
18:1n-7	0.85	0.64	0.77	0.79	1.24	1.14	4.09	0.52	1.37	0.90	1.64	0.92	0.74	1.07	0.32	0.77
18:2n-6	37.16	38.25	37.46	39.09	35.04	31.07	14.04	34.03	51.76	38.10	36.25	27.08	33.23	36.84	19.47	27.17
18:3n-3	36.05	35.59	39.10	38.26	10.20	16.57	7.43	25.21	12.48	31.83	20.07	26.95	25.28	28.23	9.23	13.68
20:0	0.17	0.10	0.15	0.10	1.17	1.47	-	-	0.33	-	0.57	1.61	0.71	0.25	2.63	4.09
20:1n-9	0.13	0.09	0.11	0.09	0.18	0.00	-	-	0.30	-	0.46	0.44	0.11	0.19	0.19	0.18
20:2n-6	tr	0.04	0.06	0.07	1.96	0.00	-	-	0.19	-	-	-	tr	0.09	-	-
20:3n-3	tr	0.02	-	0.04	0.28	0.00	-	-	-	-	-	-	0.06	0.05	-	-
22:0	0.15	0.14	-	0.02	1.73	4.73	1.86	4.27	0.22	0.36	1.69	1.46	0.44	0.14	0.98	1.47
22:1n-9	0.03	0.02	-	-	-	0.00	13.57	-	0.42	-	1.33	tr	0.10	-	0.74	-
23:0	tr	-	-	-	-	0.00	-	-	-	-	-	-	tr	-	0.17	-
24:0	0.08	0.06	-	-	-	0.00	-	-	-	-	-	-	0.37	0.05	-	-
∑SFA	11.40^{a***}	8.33^{b}	9.70	7.14	41.13	42.74	51.72	23.67	18.10	13.25	23.27	27.99	29.64	20.28	53.18	38.13
∑ VLCSFAs(≥20C)	$0.40^{a}*$	0.30^{b}	0.15	0.12	2.91	6.20	1.86	4.27	0.55	0.36	2.26	3.07	1.52	0.44	3.78	5.56
∑MUFA	15.39^{b}	17.77^{a***}	13.68	15.40	11.40	9.61	26.80	17.09	17.47	16.82	20.41	17.98	11.78	14.51	18.12	21.02
∑PUFA	73.21^{b}	73.90^{a**}	76.61	77.46	47.47	47.64	21.48	59.24	64.43	69.93	56.32	54.03	58.57	65.21	28.70	40.85
∑n-3 PUFAs	$36.05^{a}*$	35.61^{b}	39.10	38.30	10.48	16.57	7.43	25.21	12.48	31.83	20.07	26.95	25.35	28.29	9.23	13.68
∑n-6 PUFAs	37.16^{b}	38.29^{a***}	37.52	39.16	36.99	31.07	14.04	34.03	51.95	38.10	36.25	27.08	33.23	36.92	19.47	27.17
n-6/n-3	1.03^{b}	1.08^{a**}	0.96	1.02	3.53	1.88	1.89	1.35	4.16	1.20	1.81	1.00	1.31	1.31	2.11	1.99
PU*FAs/SFAs	6.42^{b}	8.87^{a***}	7.90	10.84	1.15	1.11	0.42	2.50	3.56	5.28	2.42	1.93	1.98	3.22	0.54	1.07

[a]The values represent the means of three samples, analyzed individually in triplicate ($n = 3 \times 3$). TLs − total lipids, TAGs − triacylglycerols, PLs − polar lipids, MAGs − monoacylglycerols, DAGs − diacylglycerols, FFAs − free fatty acids, SEs − sterol esters; SFAs − saturated fatty acids, MUFAs − monounsaturated fatty acids, PUFAs − polyunsaturated fatty acids, VLCSFAs − very long chain saturated fatty acids; tr. − trace. Different superscript letters (^{a,b}) in the same row mean significant differences between TLs of the two fermentation days. $^{*}p < 0.05$. $^{**}p < 0.01$. $^{***}p < 0.001$ (paired *t*-test). C12:0, lauric; C14:0, myristic; C16:0, palmitic; C16:1n-9, *cis*-7 hexadecenoic; C16:1n-7, palmitoleic; C17:0, margaric; C18:0, stearic; C18:1n-9, oleic; C18:1n-7,vaccenic; C18:2n-6, linoleic; C18:3n-3, α-linolenic; C20:0, arachidic; C20:1n-9, 11-eicosenoic; C20:2n-6, 11,14-eicosadienoic; C20:3n-3, eicosatrienoic; C22:0, behenic; C22:1n-9, erucic; C23:0, tricosanoic; C24:0, lignoceric acids.

J. Agric. Food Chem. 2015, 63, 3489−3500
DOI: 10.1021/acs.jafc.5b00520

confusing data about the correlation between antioxidant activity and TP contents. Several authors have reported that a high linear correlation exists between antioxidant potential and TP contents in berries and different pomaces.[12,19] However, on the other hand, some scientific reports also claim that there is a bad correlation between these two parameters,[12,34] which could be explained by the fact that different types of phenolic compounds may contribute differently to total antioxidant capacity of the analyzed plant matrix. The relationships between the free radical scavenging activity (DPPH assay) and total phenolic content of methanolic extracts from SSF *S. ebulus* L. and *S. nigra* L. berry press residues are shown in Figure 1C,D. In both bioprocessed pomaces the radical inhibition capacity of the extracts showed no significant correlations with the total phenolic content (R^2 = 0.1887, p = 0.3301 for *S. ebulus* L. and R^2 = 0.1657, p = 0.3648 for *S. nigra* L., respectively). Our results are in agreement with some earlier reports[1,21] which present weak correlations between these two parameters among different bioprocessed fruit byproducts. Due to the fact that these observations are common in studies that explore the ability of different fungi to produce enhanced levels of phenolic antioxidants, it can be concluded that the SSF process had an effect on the correlation between total phenolic content and the antioxidant potential of the fermented fruit byproducts. The possible explanation for this phenomenon could be that in certain stages of growth of fungi, the amount of the measurable phenolics decreases because of the polymerization of the free phenolics, caused by the stress induced on the fungus. Vattem et al.[1] and Di Majo et al.[34] claim that the inhibition of the free radicals tends to increase along with the order of polymerization.

Lipid Accumulation in SSF of the *S. ebulus* L. and *S. nigra* L. Berry Press Residues by *A. niger*. The lipid recovery for both the *Sambucus* berry press residues showed a similar trend (Figure 3). After a significant increase ($p < 0.05$) until day 4, there was a slight but statistically significant decrease ($p < 0.05$) in the TL content for the remaining days of fermentation. The extracted lipids increased with 12% for *S. nigra* L., and 10.50% for *S. ebulus* L. compared with initial values of 21.41g/100 g DW and 22.20 g/100 g DW of unfermented pomaces to the maximum amounts of 24 g/100 g DW and 24.53 g/100 g DW of fermented pomaces. The literature shows that the enzyme consortia (cellulase, pectinase, protease, etc.) secretion of the strains has a considerable impact on lipid yield, and a strong correlation between these two parameters was found. The enzyme productivity by *A. niger* is a function of culture conditions (temperature, pH, culture medium conditions), amount of available carbon source (glucose, cellulose, hemicellulose, pectin, etc.), and C/N ratio.[23,35] Previous research conducted on hydrolytic enzyme production by *A. niger* in SSF of different agro-residues have shown maximum cellulase and protease activities after 72 or 96 h,[23,36] when the enzyme secretion had almost stabilized or decreased. These observations are consistent with our results regarding the dynamics of the oil yields from Figure 3, with the maximum lipid amounts in day 4. At the early fermentation stage, fungi consume the readily available sugars (particularly glucose) and secrete hydrolytic enzymes; when the level of sugar monomer is too low, the strains start to use these enzymes to produce available sugars, resulting in a decrease of enzyme activity and lipid yield.[23] Oberoi et al.[23] used different crude enzyme extracts to improve the oil recovery from mustard seeds and reported that about 7% more oil was recovered when seeds were pretreated with enzyme consortium obtained from the individual culture of *A. niger*.

Neutral (TAGs, MAGs, 1,2- and 1,3-DAGs, FFAs, and SEs) and Polar Lipid (PL) Contents of Oils from the Solid-State Fermented Pomaces. Profiles of the different lipid classes in the oils of the SSF *S. ebulus* L. and *S. nigra* L. berry press residues are presented in Figure 4. The results showed that the major lipid fraction from SSF products (days 4 and 6) was TAG, constituting about 90−94% of the fermented berry-waste oils obtained in the early stages of fungal growth (within 4 days) and about 57−62% of the oils in the sixth day of fermentation. It should be noted that the proportions of FFAs increased significantly ($p < 0.05$) after the fourth day, from average values of 1.50% (*S. nigra* L.) and 1.90% (*S. ebulus* L.) to averages of 32% (*S. nigra* L.) and 27.50% (*S. ebulus* L.) of the total extracted lipids in the sixth day of SSF. The quality of the vegetable fat extracted from pomaces depends not only on the fatty acid composition but also on its lipid profile.[16] Due to the presence of lipase in the culture medium, TAGs are hydrolyzed to FFAs and DAGs or MAGs. A high amount of FFAs indicates a low quality of the oil. Accumulation of this lipid fraction in fats leads to an unacceptable flavor, which can be prevented by inactivation of the enzymes involved in the lipid degradation.[23] Among microorganisms, fungi are extensively recognized as the best lipase sources and are widely used in the food industry. It was reported that the lipase activity is induced by the presence of lipids in the medium.[37] The same authors had observed that in SSF system the lipase production by *Aspergillus niger* was partially associated with the fungal growth, the synthesis of this enzyme starting after the second day of fermentation. It is interesting to note that along fermentation processes, statistically significant ($p < 0.05$) increases (3-fold for *S. nigra* L. and around 2-fold for *S. ebulus* L.) in proportions of SEs were observed (Figure 5). These positive changes can be attributed to the ability of the *Aspergillus* strains to synthesize SEs. According to the study of Tőke et al.,[38] the filamentous fungi (especially *Aspergillus* spp.), in addition to their lipase production capacity, could produce significant amounts of sterol esterases under SSF conditions, enzymes able to efficiently catalyze the synthesis of sterol esters from phytosterols and free fatty acids. The free phytosterols and their esterified forms are known to reduce the cholesterol level in blood.[39] However, the sterol esters are generally preferred in the food and nutraceutical industry because of their better fat-solubility and compatibility.[38] Finally, analysis of the various lipid fractions demonstrated that the percentages of PLs also tends to increase (around 4-fold for *S. nigra* L. and more than 2-fold for *S. ebulus* L.) during fermentation processes (Figure 1 (A)). This observation is consistent with experimental data provided by Oliveira et al.[40] showing that in oleaginous microorganisms, during lipid turnover phase (which starts when the culture media is depleted of the carbon source), neutral lipid fraction (mainly composed of TAGs) are preferentially degraded, while significant amounts of membranar polar lipids are synthesized.

TLs Fatty Acid Compositions and Their Lipid Classes Obtained through Solid-State Fermented Products. The GC-MS analysis (results presented inTables 2 and 3) showed that the major fatty acid compositions of TLs from the solid-state fermented pomaces (day 4) were linoleic acid (C18:2n-6, 45.19% in *S. ebulus* L. and 38.25% in *S. nigra* L.), α-linolenic acid (C18:3n-3, 23.34% in *S. ebulus* L. and 35.59% in *S. nigra* L.), oleic acid (C18:1n-9, 23.30% in *S. ebulus* L. and 16.92% in

DOI: 10.1021/acs.jafc.5b00520
J. Agric. Food Chem. 2015, 63, 3489−3500

S. nigra L.) and palmitic acid (C16:0, 6.02% in *S. ebulus* L. and 6.88% in *S. nigra* L.) (Figure 5). The fermentation resulted in a slight increase of the linoleic (C18:2n-6) and oleic (C18:1n-9) acids levels (43.11% and 20.22% in *S. ebulus* L. and 37.16% and 14.28% in *S. nigra* L. unfermented pomaces, respectively). These results are in line with earlier findings showing that strains of *Aspergillus* produce lipids with significant amounts of oleic and linoleic acids.[41,42] As shown in Tables 2 and 3, statistically significant differences ($p < 0.05$) were found between the proportions of fatty acid classes of investigated TLs, extracted from *Sambucus* wastes before and after fermentation. Substantial decreases in the contents of saturated fatty acids (SFAs) were observed for both fermented residues (from 11.47% to 7.56% in *S. ebulus* L., and from 11.40% to 8.33% in *S. nigra* L., respectively). The differences were also statistically significant ($p < 0.05$) for the content of mono- (MUFAs) and polyunsaturated fatty acids (PUFAs), the average proportions in fermented substrates being slightly higher than those in the unfermented raw materials (Tables 2 and 3). The elevated levels of PUFAs from TLs of fermented berry press residues (68.53% in *S. ebulus* L. and 73.90% in *S. nigra* L.) determined in the present study are comparable to those of PUFA-rich vegetable oils, such as grape seed, sunflower, linseed, blackcurrant seed, safflower, and hemp seed oils.[43] The results also showed that the TLs of both bioprocessed wastes are characterized by high levels of PUFAs/SFAs (8.87−9.07) and low levels of n-6/n-3-PUFAs (1.08−1.94) ratios. Due to their high linoleic and α-linolenic acid contents, the unsaturated fats are more susceptible to the oxidation process.[16] The values of n-6/n-3 ratios reported in this study are close to the optimal range for human health (2/1−4/1), suggested by the nutritional scientists.[44] The profiles of fatty acids in TAGs were practically identical to the profiles of the TLs, with the same dominating fatty acids in both solid-state fermented pomaces (Tables 2 and 3). The fatty acid composition of all minor lipid classes was somehow affected by the fermentation period. The PL fractions of SSF berry wastes were poorer in palmitic (C16:0), oleic (C18:1n-9), and linoleic (C18:2n-6) acids and much richer in stearic (C18:0) and α-linolenic acids (C18:3n-3) compared with the unfermented pomaces (Tables 2 and 3). This enrichment process of PLs with n-3 PUFAs could be attributed to phospholipases produced by *Aspergillus* strains. In addition to the crucial role in the metabolism and biosynthesis of PLs, these enzymes are able to produce particular PLs or create novel molecular species of PLs with added-value characteristics (such as PLs esterified with n-3 fatty acids).[45] From the health point of view, the n-3 PUFAs have been shown to reduce the risk of coronary diseases and may be useful in the prevention and treatment of hypertension.[46] Moreover, in humans, α-linolenic acid can be converted to other biologically active PUFAs (eicosapentaenoic and docosahexaenoic acids) by a series of desaturation and elongation reactions.[47] All minor neutral lipid (NL) fractions (SEs, FFAs, MAGs, 1, 2- and 1, 3- DAGs) were highly unsaturated (Tables 1 and 2). In general, the fermentation process decreased SFAs, while unsaturated fatty acids (MUFAs + PUFAs) increased. Due to their nonionic molecular structures (with both hydrophilic and hydrophobic parts) MAGs and DAGs show excellent emulsifying properties, being successfully used in the food, cosmetic and pharmaceutical industries.[48] Moreover, DAGs play a significant role in the prevention of body fat accumulation and diseases associated with obesity. For this reason, they are considered as functional ingredients.[49] The SEs exhibited significantly higher SFA levels (38.13% in *S. nigra* L. and 46.93% in *S. ebulus* L.) than the other four NL fractions in fermented samples, because of the dominance of palmitic acid (C16:0) in their structures. Furthermore, it was observed that by the SSF process, the SE fractions were enriched in n-3 and n-6 essential fatty acids. The levels of n-3 PUFAs increased with 48% (in *S. nigra* L.) and 77% (in *S. ebulus* L.), while the amounts of n-6 PUFAs increased with 40% (in *S. nigra* L.) and 95% (in *S. ebulus* L.), respectively. A comprehensive study of 91 patients tested the benefit of omega-3 plant sterol esters (n-3-PSE) on lipid profile and other cardiovascular disease risk factors in subjects with mixed hyperlipidemia.[50] The study showed that n-3-PSE treatment decreased the serum triglyceride concentrations significantly (by 19%) without adversely affecting the plasma low-density lipoprotein cholesterol levels in mixed hyperlipidemic patients, after a 12 week intervention period.

This global characterization may potentially provide the basis for a sustainable integrated process of *Sambucus* berry pomaces exploitation as potential, inexpensive, and easily available sources of bioactive phytochemicals for the pharmaceutical and food industries.

AUTHOR INFORMATION

Corresponding Author

*E-mail: dan.vodnar@usamvcluj.ro. Tel.: +40-264-596 384 (ext. 213). Fax: +40-264-593-792.

Funding

This work was supported by a grant of the Romanian Ministry of Education, CNCS−UEFISCDI, project number PNII-RUPD-2012-3-0245 (contract no. 92/25.06.2013).

Notes

The authors declare no competing financial interest.

REFERENCES

(1) Vattem, D. A.; Lin, Y. T.; Labbe, R. G.; Shetty, K. Phenolic antioxidant mobilization in cranberry pomace by solid-state bioprocessing using food grade fungus *Lentinus edodes* and effect on antimicrobial activity against select food borne pathogens. *Innov. Food Sci. Emerg. Technol.* **2004**, *5*, 81−91.

(2) Dulf, F. V.; Andrei, S.; Bunea, A.; Socaciu, C. Fatty acid and phytosterol contents of some Romanian wild and cultivated berry pomaces. *Chem. Pap.* **2012**, *66*, 925−934.

(3) Bermúdez-Soto, M. J.; Tomás-Barberán, F. A. Evaluation of commercial red fruit juice concentrates as ingredients for antioxidant functional juices. *Eur. Food Res. Technol.* **2004**, *219*, 133−141.

(4) Radványi, D.; Juhász, R.; Kun, S.; Szabó-Nótin, B.; Barta, J. Preliminary study of extraction of biologically active compounds from elderberry (*Sambucus nigra* L.) pomace. *Acta Aliment.* **2013**, *42*, 63−72.

(5) Gray, A. M.; Abdel-Wahab, Y. H.; Flatt, P. R. The traditional plant treatment, *Sambucus nigra* (elder), exhibits insulin-like and insulin-releasing actions *in vitro*. *J. Nutr.* **2000**, *130*, 15−20.

(6) Roschek, B., Jr.; Fink, R. C.; McMichael, M. D.; Li, D.; Alberte, R. S. Elderberry flavonoids bind to and prevent H1N1 infection *in vitro*. *Phytochemistry* **2009**, *70*, 1255−1261.

(7) Veberic, R.; Jakopic, J.; Stampar, F.; Schmitzer, V. European Elderberry (*Sambucus nigra* L.) rich in sugars, organic acids, anthocyanins and selected polyphenols. *Food Chem.* **2009**, *114*, 511−515.

(8) Fazio, A.; Plastina, P.; Meijerink, J.; Witkamp, R. F.; Gabriele, B. Comparative analyses of seeds of wild fruits of *Rubus* and *Sambucus* species from Southern Italy: Fatty acid composition of the oil, total phenolic content, antioxidant and anti-inflammatory properties of the methanolic extracts. *Food Chem.* **2013**, *140*, 817−824.

DOI: 10.1021/acs.jafc.5b00520
J. Agric. Food Chem. 2015, 63, 3489−3500

(9) Jimenez, P.; Cabrero, P.; Basterrechea, J. E.; Tejero, J.; Cordoba-Diaz, D.; Cordoba-Diaz, M.; Girbes, T. Effects of short-term heating on total polyphenols, anthocyanins, antioxidant activity and lectins of different parts of dwarf elder (*Sambucus ebulus* L.). *Plant Foods Hum. Nutr.* **2014**, *69*, 168−174.
(10) Engels, G.; Brinckmann, J. European elder. *Herbal Gram.* **2013**, *97*, 1−7.
(11) European Herb Growers Association (Europam). Production of Medicinal and Aromatic Plants in Europe Status 2010. Vienna, Austria: *Europam*. 2010. Available: www.europam.net.
(12) Wu, X.; Gu, L.; Prior, R. L.; McKay, S. Characterization of anthocyanins and proanthocyanidins in some cultivars of *Ribes*, *Aronia*, and *Sambucus* and their antioxidant capacity. *J. Agric. Food Chem.* **2004**, *52*, 7846−7856.
(13) Dawidowicz, A. L.; Wianowska, D.; Baraniak, B. The antioxidant properties of alcoholic extracts from *Sambucus nigra* L. (antioxidant properties of extracts). *LWT-Food Sci. Technol.* **2006**, *39*, 308−315.
(14) Ebrahimzadeh, M. A.; Ehsanifar, S.; Eslami, B. *Sambucus ebulus elburensis* fruits: A good source for antioxidants. *Pharmacogn. Mag.* **2009**, *5*, 213−218.
(15) Mandrone, M.; Lorenzi, B.; Maggio, A.; La Mantia, T.; Scordino, M.; Bruno, M.; Poli, F. Polyphenols pattern and correlation with antioxidant activities of berries extracts from four different populations of Sicilian *Sambucus nigra* L. *Nat. Prod. Res.* **2014**, *28*, 1246−1253.
(16) Dulf, F. V.; Oroian, I.; Vodnar, D. C.; Socaciu, C.; Pintea, A. Lipid classes and fatty acid regiodistribution in triacylglycerols of seed oils of two *Sambucus* species (*S. nigra* L. and *S. ebulus* L.). *Molecules* **2013**, *18*, 11768−11782.
(17) Thomas, L.; Larroche, C.; Pandey, A. Current developments in solid-state fermentation. *Biochem. Eng. J.* **2013**, *81*, 146−161.
(18) Rodríguez-Couto, S. Exploitation of biological wastes for the production of value-added products under solid-state fermentation conditions. *Biotechnol. J.* **2008**, *3*, 859−870.
(19) Ajila, C. M.; Gassara, F.; Brar, S. K.; Verma, M.; Tyagi, R. D.; Valéro, J. R. Polyphenolic antioxidant mobilization in apple pomace by different methods of solid-state fermentation and evaluation of its antioxidant activity. *Food Bioprocess Technol.* **2012**, *5*, 2697−2707.
(20) Robledo, A.; Aguilera-Carbó, A.; Rodríguez, R.; Martinez, J. L.; Garza, Y.; Aguilar, C. N. Ellagic acid production by *Aspergillus niger* in solid state fermentation of pomegranate residues. *J. Ind. Microbiol. Biotechnol.* **2008**, *35*, 507−513.
(21) Correia, R. T.; McCue, P.; Magalhães, M.; Macêdo, G. R.; Shetty, K. Production of phenolic antioxidants by the solid-state bioconversion of pineapple waste mixed with soy flour using *Rhizopus oligosporus*. *Process Biochem.* **2004**, *39*, 2167−2172.
(22) Cai, S.; Wang, O.; Wu, W.; Zhu, S.; Zhou, F.; Ji, B.; Gao, F.; Zhang, D.; Liu, J.; Cheng, Q. Comparative study of the effects of solid-state fermentation with three filamentous fungi on the Total Phenolics Content (TPC), flavonoids, and antioxidant activities of subfractions from Oats (*Avena sativa* L.). *J. Agric. Food Chem.* **2011**, *60*, 507−513.
(23) Oberoi, H. S.; Babbar, N.; Dhaliwal, S. S.; Kaur, S.; Vadlani, P. V.; Bhargav, V. K.; Patil, R. T. Enhanced oil recovery by pre-treatment of mustard seeds using crude enzyme extract obtained from mixed-culture solid-state fermentation of Kinnow (*Citrus reticulate*) waste and wheat bran. *Food Bioprocess Technol.* **2012**, *5*, 759−767.
(24) Singleton, V. L.; Orthofer, R.; Lamuela-Raventos, R. M. Analysis of total phenols and other oxidation substrates and antioxidants by means of Folin−Ciocalteu reagent. *Methods Enzymol.* **1999**, *299*, 152−178.
(25) Pop, R. M.; Socaciu, C.; Pintea, A.; Buzoianu, A. D.; Sanders, M. G.; Gruppen, H.; Vincken, J. P. UHPLC/PDA−ESI/MS analysis of the main berry and leaf flavonol glycosides from different Carpathian *Hippophaë rhamnoides* L. varieties. *Phytochem. Anal.* **2013**, *24*, 484−492.
(26) Mărghitaş, L. A.; Stanciu, O. G.; Dezmirean, D. S.; Bobiş, O.; Popescu, O.; Bogdanov, S.; Campos, M. G. *In vitro* antioxidant capacity of honeybee-collected pollen of selected floral origin harvested from Romania. *Food Chem.* **2009**, *115*, 878−883.
(27) Mărgăoan, R.; Mărghitaş, L. A.; Dezmirean, D. S.; Dulf, F. V.; Bunea, A.; Socaci, S. A.; Bobis, O. Predominant and secondary pollen botanical origins influence the carotenoid and fatty acid profile in fresh honeybee-collected pollen. *J. Agric. Food Chem.* **2014**, *62*, 6306−6316.
(28) Dulf, F. V.; Pamfil, D.; Baciu, A. D.; Pintea, A. Fatty acid composition of lipids in pot marigold (*Calendula officinalis* L.) seed genotypes. *Chem. Cent. J.* **2013**, *7*, 8.
(29) Pintea, A.; Dulf, F. V.; Bunea, A.; Matea, C.; Andrei, S. Comparative analysis of lipophilic compounds in eggs of organically raised ISA Brown and Araucana hens. *Chem. Pap.* **2012**, *66*, 955−963.
(30) Ozgen, M.; Scheerens, J. C.; Reese, R. N.; Miller, R. A. Total phenolic, anthocyanin contents and antioxidant capacity of selected elderberry (*Sambucus canadensis* L.) accessions. *Pharmacogn. Mag.* **2010**, *6*, 198−203.
(31) Lee, J.; Finn, C. E. Anthocyanins and other polyphenolics in American elderberry (*Sambucus canadensis*) and European elderberry (*S. nigra*) cultivars. *J. Sci. Food Agric.* **2007**, *87*, 2665−2675.
(32) Bridle, P.; García-Viguera, C. Analysis of anthocyanins in strawberries and elderberries. A comparison of capillary zone electrophoresis and HPLC. *Food Chem.* **1997**, *59*, 299−304.
(33) Qin, J. H.; Li, N.; Tu, P. F.; Ma, Z. Z.; Zhang, L. Change in tea polyphenol and purine alkaloid composition during solid-state fungal fermentation of postfermented tea. *J. Agric. Food Chem.* **2012**, *60*, 1213−1217.
(34) Di Majo, D.; La Guardia, M.; Giammanco, S.; La Neve, L.; Giammanco, M. The antioxidant capacity of red wine in relationship with its polyphenolic constituents. *Food Chem.* **2008**, *111*, 45−49.
(35) Venkata Subhash, G.; Venkata Mohan, S. Lipid accumulation for biodiesel production by oleaginous fungus *Aspergillus awamori*: Influence of critical factors. *Fuel* **2014**, *116*, 509−515.
(36) Niu, X.; Qiu, S.; Wu, Y.; Yuan, J.; Xu, Y. Highly effective extraction of oil from soybean by pretreatment of solid-state fermentation with fungi. *Front. Chem. Sci. Eng.* **2011**, *5*, 122−125.
(37) Falony, G.; Armas, J. C.; Mendoza, J. C. D.; Hernández, J. L. M. Production of extracellular lipase from *Aspergillus niger* by solid-state fermentation. *Food Technol. Biotechnol.* **2006**, *44*, 235−240.
(38) Tőke, E. R.; Nagy, V.; Recseg, K.; Szakacs, G.; Poppe, L. Production and application of novel sterol esterases from *Aspergillus* strains by solid state fermentation. *J. Am. Oil Chem. Soc.* **2007**, *84*, 907−915.
(39) Dulf, F. V.; Unguresan, M. L.; Vodnar, D. C.; Socaciu, C. Free and esterified sterol distribution in four Romanian vegetable oil. *Not. Bot. Horti Agrobot. Cluj-Napoca* **2010**, *38*, 91−97.
(40) Oliveira, M. D. S.; Feddern, V.; Kupski, L.; Cipolatti, E. P.; Badiale-Furlong, E.; de Souza-Soares, L. A. Changes in lipid, fatty acids and phospholipids composition of whole rice bran after solid-state fungal fermentation. *Bioresour. Technol.* **2011**, *102*, 8335−8338.
(41) André, A.; Chatzifragkou, A.; Diamantopoulou, P.; Sarris, D.; Philippoussis, A.; Galiotou-Panayotou, M.; Komaitis, M.; Papanikolaou, S. Biotechnological conversions of bio-diesel-derived crude glycerol by *Yarrowia lipolytica* strains. *Eng. Life Sci.* **2009**, *9*, 468−478.
(42) Hui, L.; Wan, C.; Hai-tao, D.; Xue-jiao, C.; Qi-fa, Z.; Yu-hua, Z. Direct microbial conversion of wheat straw into lipid by a cellulolytic fungus of *Aspergillus oryzae* A-4 in solid-state fermentation. *Bioresour. Technol.* **2010**, *101*, 7556−7562.
(43) Dubois, V.; Breton, S.; Linder, M.; Fanni, J.; Parmentier, M. Fatty acid profiles of 80 vegetable oils with regard to their nutritional potential. *Eur. J. Lipid. Sci. Technol.* **2007**, *109*, 710−732.
(44) Abedi, E.; Sahari, M. A. Long-chain polyunsaturated fatty acid sources and evaluation of their nutritional and functional properties. *Food Sci. Nutr.* **2014**, *2*, 443−463.
(45) Casado, V.; Martín, D.; Torres, C.; Reglero, G. Phospholipases in food industry: a review. *Methods Mol. Biol.* **2012**, *861*, 495−523.
(46) Chojnacka, A.; Gładkowski, W.; Kiełbowicz, G.; Wawrzeńczyk, C. Enzymatic enrichment of egg-yolk phosphatidylcholine with α-linolenic acid. *Biotechnol. Lett.* **2009**, *31*, 705−709.
(47) Calder, P. C. Mechanisms of action of (n-3) fatty acids. *J. Nutr.* **2012**, *142*, 592−599.

DOI: 10.1021/acs.jafc.5b00520
J. Agric. Food Chem. 2015, 63, 3489−3500

(48) Feltes, M. M. C.; de Oliveira, D.; Block, J. M.; Ninow, J. L. The production, benefits, and applications of monoacylglycerols and diacylglycerols of nutritional interest. *Food Bioprocess Technol.* **2013**, *6*, 17−35.
(49) Lo, S.-K.; Tan, C.-P.; Long, K.; Yussof, M. S. A.; Lai, O.-M. Diacylglycerol oil-properties, processes and products: a review. *Food Bioprocess Technol.* **2008**, *1*, 223−233.
(50) Bitzur, R.; Cohen, H.; Cohen, T.; Dror, T. W.; Herzog, Y.; Lifshitz, Y.; Lubish, T.; Harats, D.; Rubinstein, A. The metabolic effects of omega-3 plant sterol esters in mixed hyperlipidemic subjects. *Cardiovasc. Drugs Ther.* **2010**, *24*, 429−437.

DOI: 10.1021/acs.jafc.5b00520
J. Agric. Food Chem. 2015, 63, 3489−3500

were expressed in δ (ppm) referring to the solvent residual peaks at δ_H 2.05, δ_C 29.8 for acetone-d_6, and coupling constants in Hertz. Silica gel (200−300 mesh) for column chromatography was purchased from the Qingdao Marine Chemical Company (Qingdao, China). Preparative high-speed counter-current chromatography (HSCCC) was performed on a TBE-300B instrument (Tauto Biotech, Shanghai, China) equipped with three preparative coils, a polytetrafluoroethylene tube (2.6 mm in diameter and total volume of 280 mL), and a 20 mL sample loop. The separation was carried out at 25 °C using a two-phase solvent system at flow rate of 3.0 mL/min, revolution speed of 900 rpm, and detection wavelength at 280 nm. Semipreparative high-performance liquid chromatography (HPLC) separation was carried out on a Lumtech instrument (Lumiere Tech. Ltd., Beijing, China) equipped with a K-501 pump (flow rate: 3 mL/min) and a K-2501 UV detector (detection was set at 280 nm) using a Luna-C18 column (250 mm × 10 mm i.d., 5 μm, Phenomenex Inc., Torrance, California). A BioTek PowerWave HT microplate spectrophotometer (BioTek Instruments Inc., Winooski, Vermont) was employed to measure the light absorption value.

Fungal Material. The pathogenic fungus *U. virens* UV-2 was kindly provided by Prof. Zhiyi Chen (Institute of Plant Protection, Jiangsu Academy of Agricultural Sciences, China). This fungus was isolated from the smut balls grown on the rice panicles collected in a paddy field of Jiangsu Province of China in the fall of 2008. A voucher specimen has been deposited in Prof. Chen's laboratory.

Fermentation, Extraction, and Isolation. The fungus *U. virens* UV-2 was grown on PDA (potato 200 g/L, dextrose 20 g/L, and agar 20 g/L) medium in Petri dishes at 28 °C for 8 days. Then, three agar plugs (0.5 cm × 0.5 cm) containing mycelia were added into a 1000 mL Erlenmeyer flask containing 300 mL of potato dextrose broth (potato 200 g/L, and dextrose 20 g/L) under aseptic condition and incubated at 28 °C in the dark for 7 days on a rotary shaker (150 rpm). This liquid culture was subsequently used to inoculate the solid rice medium, which was composed of rice and deionized water in a ratio of 1.0:1.1 (w/w) and autoclaved at 120 °C for 30 min before use. The fermentation was carried out in 50 1000 mL Erlenmeyer flasks each containing 100 g of rice and 110 mL of water, and incubated at 28 °C for about 2 months before harvest.

The moldy rice was collected and extracted with EtOAc at room temperature for 24 h (five times). The EtOAc extract was concentrated under vacuum at 38 °C on a rotatory evaporator to give a brownish residue (200 g). The crude extract was chromatographed over silica gel eluting with CH_2Cl_2:MeOH (9:1, v/v) to give four fractions (Fr. A−D). Fraction B (20 g) was repeatedly separated by preparative HSCCC using a two-phase solvent of petroleum ether−EtOAc−methanol−water (containing 0.01% oxalic acid) (5.0:5.0:6.5:4.5, v/v/v/v) to yield seven subfractions (Fr. B-1−B-7).

Fractions B-1−B-3, and B-5−B-7 were each purified by semi-preparative HPLC using MeOH-H_2O (0.01% oxalic acid) (80:20, v/v) as mobile phase to yield ustilaginoidin A, **8**, (1.3 mg, t_R 21.0 min) from Fr. B-1; ustilaginoidin G, **12**, (4.2 mg, t_R 10.0 min) from Fr. B-2; ustilaginoidin F, **11** (7.2 mg, t_R 13.0 min), ustilaginoidin P, **6** (0.8 mg, t_R 24.6 min), and ustilaginoidin L, **2** (5.5 mg, t_R 28.6 min) from Fr. B-3; ustilaginoidin E, **10**, (20.1 mg, t_R 23.0 min) from Fr. B-5; isochaetochromin B_2, **13** (3.5 mg, t_R 20.0 min), and ustilaginoidin M, **3** (27.9 mg, t_R 23.9 min), from Fr. B-6; and ustilaginoidin D, **9**, (46 mg, t_R 20.0 min) from Fr. B-7. Similarly, ustilaginoidin E_1, **7** (2.8 mg, t_R 18.0 min), ustilaginoidin O, **5** (7.2 mg, t_R 21.5 min), ustilaginoidin N, **4** (26.3 mg, t_R 23.0 min), and ustilaginoidin K, **1**, (1.6 mg, t_R 27.0 min) were isolated from Fr. B-4 by HPLC eluting with MeOH−H_2O (0.01% oxalic acid) (75:25, v/v).

Ustilaginoidin K, 1. Red amorphous powder; [α]20 D −46.7 (*c* 0.03, DMSO); UV (DMSO) λ_{max} (log ε) 281 (5.29), 295 (5.34), 329 (4.45), 424 (4.56) nm; CD (DMSO) 266 ($\Delta\varepsilon$ +62.13), 294.5 ($\Delta\varepsilon$ −72.43), 354 ($\Delta\varepsilon$ +8.26), 441 ($\Delta\varepsilon$ +1.16) nm; IR ν_{max} 3373, 2925, 2854, 1645, 1611, 1468, 1418, 1365, 1207, 1185, 1140, 1090, 839 cm^{-1}; ^1H NMR (CD_3COCD_3, 600 MHz) and ^{13}C NMR (CD_3COCD_3, 150 MHz) data, see Tables 1 and 2; HRESIMS *m/z* 541.11288 $[M-H]^-$ (calcd for $C_{30}H_{21}O_{10}$, 541.11402).

Table 1. ^1H NMR Data for Isolated Compounds 1−7 in Acetone-d_6

position	1 (600 MHz)	2 (600 MHz)	3 (600 MHz)	4 (400 MHz)	5 (600 MHz)	6 (600 MHz)	7 (600 MHz)
2					4.24 ddq (11.8, 3.1, 6.2)		4.51 ddq (11.8, 3.1, 6.2)
2′			3.95 dq (11.0, 6.1)	4.06 dq (11.0, 6.0)		4.53 dq (3.0, 6.2)	4.57 dq (3.2, 6.5)
3		6.12 s		6.10 s	2.78 dd (17.5, 11.8)	6.12 s	2.81 dd (17.4,11.8)
					2.70 dd (17.5, 3.1)		2.74 dd (17.4, 3.1)
3′			2.74 dq (11.0, 6.9)	2.74 dq (11.0, 6.8)		2.74 dq (3.0, 7.2)	2.75 dq (3.2, 7.4)
7	6.50 s	6.52 s	6.50 s	6.58 s	6.46 s	6.61 s	6.48 s
7′	6.50 s	6.50 s	6.40 s	6.47 s	6.56 s	6.50 s	6.48 s
10	6.34 s	6.38 s	6.30 s	6.36 s	5.92 s	6.37 s	5.910 s[a]
10′	6.34 s	6.33 s	5.92 s	5.89 s	6.30 s	5.89 s	5.914 s[a]
2-CH_3	2.23 s	2.26 s	2.29 s	2.28 s	1.30 d (6.2)	2.32 s	1.36 d (6.2)
2′-CH_3	2.23 s	2.28 s	1.33 d (6.1)	1.34 d (6.1)	2.28 s	1.25 d (6.5)	1.28 d (6.5)
3-CH_3	2.02 s		2.02 s				
3′-CH_3	2.02 s	2.03 s	1.24 d (6.9)	1.20 d (6.8)	1.99 s	1.15 d (7.3)	1.15 d (7.3)
5−OH			15.56 s				
5′−OH			15.56 s				
6-OH		9.95 s	9.97 s				
6′−OH		9.94 s	9.61 s				
8-OH		8.35 br.s	8.34 s				
8′−OH		8.35 br.s	8.34 s				

[a]Assignments within the same column may be interchanged.

DOI: 10.1021/acs.jafc.5b00694
J. Agric. Food Chem. 2015, 63, 3501−3508

Table 2. ^{13}C NMR Data for Isolated Compounds 1−7 in Acetone-d_6

position	1 (150 MHz)	2 (100 MHz)	3 (100 MHz)	4 (100 MHz)	5 (150 MHz)	6 (150 MHz)	7 (150 MHz)
2	166.2 C	170.9 C	166.6 C	170.9 C	74.1 CH	171.2 C	74.1 CH
2′	166.2 C	166.6 C	78.8 CH	78.9 CH	166.5 C	76.3 CH	76.2 CH
3	113.3 C	106.6 CH	113.2 C	106.6 CH	43.6 CH_2	106.5 CH	43.6 CH_2
3′	113.3 C	113.3 C	46.7 CH	46.7 CH	113.2 C	44.9 CH	44.9 CH
4	184.0 C	184.6 C	184.0 C	184.7 C	199.4 C	184.8 C	199.4 C
4′	184.0 C	184.0 C	201.7 C	201.6 C	184.0 C	203.5 C	203.3 C
4a	102.4 C	102.8 C	102.5 C	102.8 C	102.7 C	102.9 C	102.7 C
4a′	102.4 C	102.5 C	102.2 C	102.1 C	102.4 C	101.7 C	101.5 C
5	nd[a]	163.9 C	163.5 C	163.3 C	nd	164.0 C[b]	nd
5′	nd	163.5 C	165.2 C	163.3 C	nd	166.2 C[b]	nd
5a	105.9 C	105.8 C	105.52 C[c]	106.2 C[d]	105.2 C	105.9 C[e]	105.2 C[f]
5a′	105.9 C	105.3 C	105.45 C[g]	105.2 C[h]	106.1 C	105.7 C[i]	105.3 C[f]
6	159.5 C	160.3 C[j]	160.1 C[k]	159.6 C[l]	160.27 C	160.3 C[m]	160.3 C[n]
6′	159.5 C	160.3 C[o]	160.5 C[p]	160.4 C[q]	160.33 C	160.9 C[r]	160.4 C[n]
7	100.8 CH	101.4 CH	101.1 CH	101.4 CH	100.7 CH	101.6 CH	100.7 CH
7′	100.8 CH	101.1 CH	100.7 CH	100.7 CH	101.0 CH	100.9 CH	100.7 CH
8	160.1 C	160.8 C[j]	160.7 C[k]	160.6 C[l]	161.6 C	161.2 C[m]	161.6 C[s]
8′	160.1 C	160.6 C[o]	161.5 C[p]	161.4 C[q]	161.6 C	161.9 C[r]	161.7 C[s]
9	106.5 C	107.2 C	107.0 C[c]	107.1 C[d]	107.1 C	107.4 C[e]	107.1 C
9′	106.5 C	107.1 C	106.3 C[g]	106.8 C[h]	106.7 C	105.9 C[i]	107.1 C
9a	141.1 C	141.4 C	141.3 C	141.1 C	143.1 C	141.4 C	143.0 C
9a′	141.1 C	141.3 C	143.3 C	143.1 C	141.1 C	143.3 C	143.0 C
10	99.3 CH	99.5 CH	99.0 CH	99.7 CH	100.3 CH	99.4 CH	100.0 CH[t]
10′	99.3 CH	99.0 CH	100.0 CH	100.0 CH	99.1 CH	100.0 CH	100.1 CH[t]
10a	152.7 C	153.4 C	153.0 C	153.3 C	156.5 C	153.6 C	156.5 C
10a′	152.7 C	153.0 C	156.5 C	156.3 C	152.9 C	156.3 C	155.9 C
2-CH_3	18.6 CH_3	20.7 CH_3	18.7 CH_3	20.6 CH_3	20.8 CH_3	20.7 CH_3	20.9 CH_3
2′-CH_3	18.6 CH_3	18.7 CH_3	19.6 CH_3	19.7 CH_3	18.7 CH_3	16.5 CH_3	16.5 CH_3
3-CH_3	8.9 CH_3		8.9 CH_3				
3′-CH_3	8.9 CH_3	8.9 CH_3	9.7 CH_3	9.9 CH_3	8.9 CH_3	9.7 CH_3	9.7 CH_3

[a]nd: not detected. [b−t]Assignments within a same column may be interchanged.

Ustilaginoidin L, **2**. Orange amorphous powder; [α]20 D −106.0 (*c* 0.09, DMSO); UV (DMSO) λ_{max} (log ε): 276 (5.05), 295 (5.28), 341 (4.31), 420 (4.50); CD (DMSO) 266 (Δε +74.23), 294 (Δε −91.08), 352.5 (Δε +8.03), 440.5 (Δε +1.52) nm; IR ν_{max} 3734, 3381, 2924, 2854, 1645, 1621, 1461, 1366, 1254, 1203, 1141, 1022, 841 cm^{-1}; ^1H NMR (CD_3COCD_3, 600 MHz) and ^{13}C NMR (CD_3COCD_3, 100 MHz) data, see Tables 1 and 2; HRESIMS *m*/*z* 527.09573 $[M-H]^-$ (calcd for $C_{29}H_{19}O_{10}$, 527.09727).

Ustilaginoidin M, **3**. Orange amorphous powder; [α]20 D −54.5 (*c* 0.03,DMSO); UV (DMSO) λ_{max} (log ε): 274 (5.34), 296 (5.40), 329 (4.70), 420 (4.71); CD (DMSO) 266 (Δε +104.38), 294.5 (Δε −103.42), 347.5 (Δε +6.79), 435 (Δε +1.81) nm; IR ν_{max} 3392, 2927, 2854, 1709, 1637, 1590, 1507, 1457, 1364, 1262, 1204, 1142, 1089, 1024, 841 cm^{-1}; ^1H NMR (CD_3COCD_3, 600 MHz) and ^{13}C NMR (CD_3COCD_3, 100 MHz) data, see Tables 1 and 2; HRESIMS *m*/*z* 543.12852 $[M-H]^-$ (calcd for $C_{30}H_{23}O_{10}$, 543.12967).

Ustilaginoidin N, **4**. Orange amorphous powder; [α]20 D −78.4 (*c* 0.03, DMSO); UV (DMSO) λ_{max} (log ε): 274 (5.14), 295 (5.36), 343 (4.57), 417 (4.68); CD (DMSO) 266 (Δε +77.90), 294.5 (Δε −86.19), 347.5 (Δε +6.03), 429 (Δε +1.51) nm; IR ν_{max} 3375, 2927, 1706, 1635, 1589, 1456, 1364, 1262, 1204, 1183, 1148, 1089, 1025, 960, 843 cm^{-1}; ^1H NMR (CD_3COCD_3, 400 MHz) and ^{13}C NMR (CD_3COCD_3, 100 MHz) data, see Tables 1 and 2; HRESIMS *m*/*z* 529.11253 $[M-H]^-$ (calcd for $C_{29}H_{21}O_{10}$, 529.11402).

Ustilaginoidin O, **5**. Orange amorphous powder; [α]20 D −145.1 (*c* 0.03, DMSO); UV (DMSO) λ_{max} (log ε): 274 (5.22), 297 (5.32), 330 (4.53), 421 (4.62); CD (DMSO) 266 (Δε +91.09), 293.5 (Δε −96.23), 347.5 (Δε +6.13), 429.5 (Δε +1.64) nm; IR ν_{max} 3382, 1705, 1636, 1592, 1474, 1378, 1364, 1346, 1281, 1204, 1182, 1145, 1084, 840 cm^{-1}; ^1H NMR (CD_3COCD_3, 600 MHz) and ^{13}C NMR (CD_3COCD_3, 150 MHz) data, see Tables 1 and 2; HRESIMS *m*/*z* 529.11209 $[M-H]^-$ (calcd for $C_{29}H_{21}O_{10}$, 529.11402).

Ustilaginoidin P, **6**. Yellow amorphous powder; [α]20 D −269.1 (*c* 0.03, DMSO); UV (DMSO) λ_{max} (log ε): 270 (5.00), 297 (5.35), 329 (4.61), 420 (4.66); CD (DMSO) 266 (Δε +82.25), 294 (Δε −99.92), 346.5 (Δε +7.38), 423.5 (Δε +1.21) nm; IR ν_{max} 3392, 2970, 2927, 1685, 1637, 1590, 1421, 1365, 1206, 1139, 1091, 1028, 842 cm^{-1}; ^1H NMR (CD_3COCD_3, 600 MHz) and ^{13}C NMR (CD_3COCD_3, 150 MHz) data, see Tables 1 and 2; HRESIMS *m*/*z* 529.11130 $[M-H]^-$ (calcd for $C_{29}H_{21}O_{10}$, 529.11292).

Ustilaginoidin E$_1$, **7**. Yellow amorphous powder; [α]20 D −51.7 (*c* 0.03, DMSO); UV (DMSO) λ_{max} (log ε): 263 (4.73), 297 (5.06), 331 (4.58), 420 (4.53); CD (DMSO) 265.5 (Δε +52.42), 293.5 (Δε −52.65), 341 (Δε +3.82), 420.5 (Δε +0.78) nm; IR ν_{max} 3734, 3382, 2923, 1682, 1633, 1547, 1454, 1384, 1341, 1206, 1143, 1028, 996, 843, 802 cm^{-1}; ^1H NMR (CD_3COCD_3, 600 MHz) and ^{13}C NMR (CD_3COCD_3, 150 MHz) data, see Tables 1 and 2; HRESIMS *m*/*z* 531.12883 $[M-H]^-$ (calcd for $C_{29}H_{23}O_{10}$, 531.12967).

Antibacterial Assay. The antibacterial activities of the isolated compounds were evaluated against the plant/human pathogenic bacteria *Bacillus subtilis* ATCC 11562, *Staphylococcus hemolyticus* ATCC 29970, *Ralstonia solanacearum* ATCC11696, *Xanthomonas vesicatoria* ATCC 11633, *Agrobacterium tumefaciens* ATCC 11158, and *Pseudomonas lachrymans* ATCC 11921. Streptomycin sulfate was used as the positive control. The minimum inhibitory concentrations (MICs) and median inhibitory concentrations (IC_{50} values) of the tested substances were determined in sterile 96-well plates by the modified broth dilution-colorimetric assay.[30,31]

Cytotoxic Assay. Cytotoxicity was tested against five human carcinoma cell lines, including colon cancer cells (HCT-116), liver hepatocellular carcinoma cells (HepG2), gastric cancer cells (BGC-823),

DOI: 10.1021/acs.jafc.5b00694
J. Agric. Food Chem. 2015, 63, 3501−3508

nonsmall-cell lung carcinoma cells (NCI-H1650), and ovarian cancer cells (A2780), using the microculture tetrazolium (MTT) assay as described previously.[32] Taxol was used as the positive control, which showed inhibition on these cell lines with IC_{50} values of 3.0×10^{-2}, 1.2×10^{-2}, 4.1×10^{-3}, 3.6×10^{-2}, and 6.1×10^{-3} μM, respectively.

Inhibitory Activity Assay on the Radicle Elongation of Rice Seeds. The isolated compounds were evaluated for their inhibitory activities on the radicle elongation of rice (*Oryza sativa*) seeds. The seeds of two rice varieties (Lijiang, and Zhonghua 11), by courtesy of Prof. Zejian Guo (Department of Plant Pathology, China Agricultural University), were used.

The bioassay was performed using the method described by Aliferis and Jabaji[33] with some modifications. Five three-day-germinated rice seeds of each rice variety were sown directly onto the well containing 200 μL of working solution in a 24-well plate. The pure compounds were evaluated at 50, 100, 200, and 400 μg/mL dissolved in sterile distilled water containing a final concentration of 2.5% DMSO. The 2.5% DMSO in distilled water was used as the negative control and glyphosate (*N*-(phosphonomethyl)glycine) at 50, 100, 200, and 400 μg/mL as the positive control. Three replicates were used for each treatment. Plates were incubated in a moist chamber at 25 °C in the dark. The length of each root was measured after treatment for 48 h. The inhibition of radicle elongation was calculated as follows: Inhibition (%) = $[(Lc - Lt)/Lc] \times 100$, where Lc is the root length of the control group, and Lt is that of the treated.

All the experiments were repeated three times, and the results were expressed by their mean values and the standard deviations (SD). The data were submitted to analysis of variance to detect significant differences by PROC ANOVA of SAS (version 8.2). The term significant has been used to denote the differences for which $p \leq 0.05$.

RESULTS AND DISCUSSION

Column chromatography of the fungal extract, followed by HSCCC and HPLC purification, has led to the isolation of 13 ustilaginoidins, **1**–**13** (Figure 1).

Ustilaginoidin K, **1**, was isolated as a red amorphous powder. It showed a prominent pseudomolecular peak at m/z 541.11288 $[M\text{-}H]^-$ in the negative mode of HRESIMS, indicating its molecular formula as $C_{30}H_{22}O_{10}$. The UV spectrum showed maximal absorptions at 281, 295, 329, and 424 nm, which was similar to those of ustilaginoidin A, **8**,[4,6] suggesting the presence of a similar chromophore in **1**. The IR spectrum indicated the presence of hydroxyl group (3373 cm^{-1}), conjugated carbonyl group (1645 cm^{-1}), and aromatic double bond (1611 cm^{-1}). The ^{13}C NMR spectrum of **1** exhibited a total of 15 carbon signals including one carbonyl (δ_C 184.0), 12 sp^2-hybridized carbons, of which two methine carbons (δ_C 100.8, 99.3), five oxygenated quaternary carbons, and five nonoxygenated quaternary carbons were assigned, and two methyl groups (δ_C 18.6, 8.9). The ^1H NMR spectrum showed the presence of two aromatic protons (δ_H 6.50 and 6.34, each s) and two olefinic methyl groups (δ_H 2.23 and 2.02, each s). Taking into consideration of the molecular formula, **1** should have a symmetric structure. Comparison of the NMR data (Tables 1 and 2) with those of ustilaginoidin A, **8**,[6] which was also a symmetric dimer of naphtho-γ-pyrone, revealed their great similarities. However, the signal for the olefinic proton of the γ-pyrone ring in **8** was missing, whereas an additional olefinic methyl group (δ_H 2.02, s; δ_C 8.9) was present in **1**, which suggests that a methyl group was substituted at C-3/C-3′ of the γ-pyrone ring. This was corroborated by analysis of the HMBC spectrum (Figure 2), as correlations were seen from 2/2′-CH_3 (δ_H 2.23, s) to C-2/2′ (δ_C 166.2) and C-3/3′ (δ_C 113.3) and from 3/3′-CH_3 (δ_H 2.02) to C-2/2′, C-3/3′, and C-4/4′ (δ_C 184.0). Thus, compound **1** was established as 3,3′-dimethyl derivative of ustilaginoidin A.

Ustilaginoidin L, **2**, was isolated as an orange amorphous powder. It showed similar UV and IR absorptions to those of **1**,

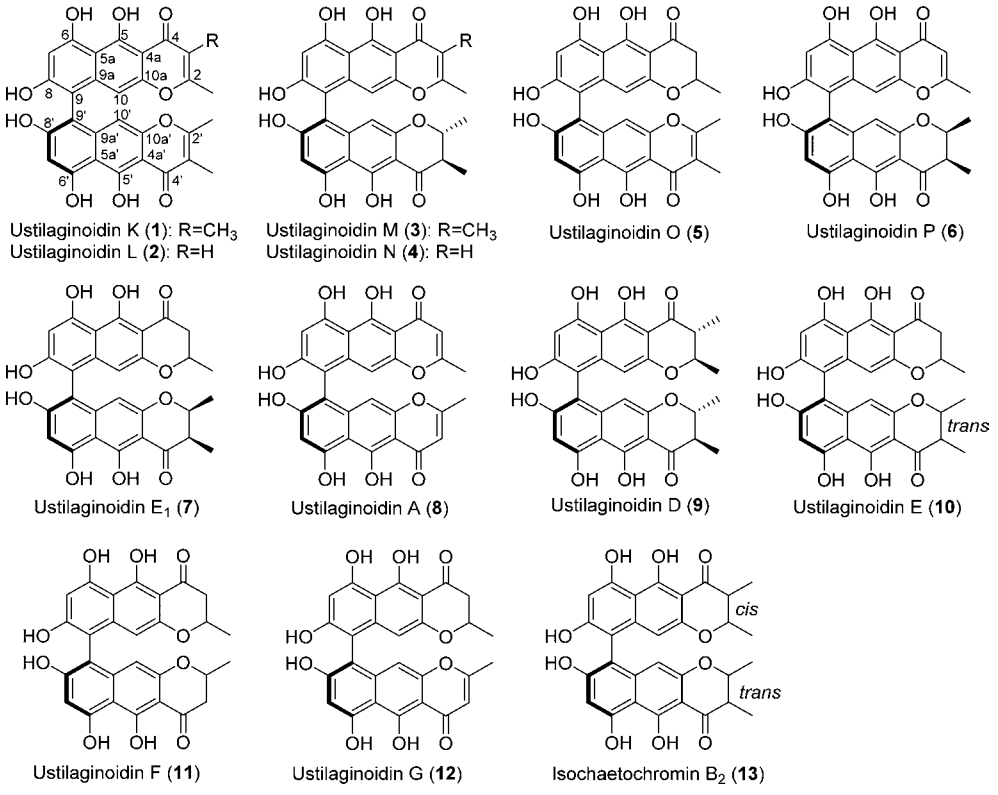

Figure 1. Structures of the isolated bis-naphtho-γ-pyrones (**1**–**13**).

DOI: 10.1021/acs.jafc.5b00694
J. Agric. Food Chem. 2015, 63, 3501−3508

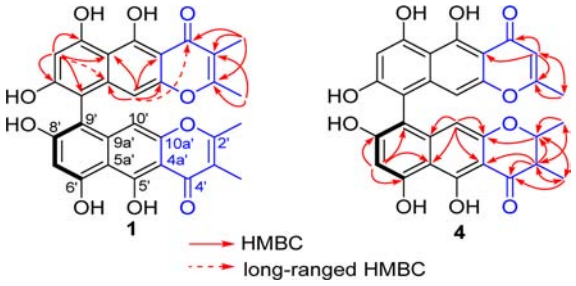

Figure 2. Selected HMBC (H → C) correlations of **1** and **4**.

indicating that **2** was a congener of **1**. The molecular formula of **2** was determined as $C_{29}H_{20}O_{10}$ by HRESIMS, containing one less CH_2 unit than that of **1**. In the ^{1}H NMR spectrum, four aromatic protons assignable to H-7 (δ_H 6.52, s), H-7′ (δ_H 6.50, s), H-10 (δ_H 6.38, s), and H-10′ (δ_H 6.33, s) were observed, suggesting the asymmetric nature of **2**. In addition, one olefinic proton resonated at δ_H 6.12 (s) and three olefinic methyl groups at δ_H 2.28, 2.26, and 2.03 (each s) were seen. Taking into consideration of the aforementioned data and the chemical shifts of the olefinic methine (δ_H 6.12, s; δ_C 106.6, CH) suggested that the methyl group at C-3 of **1** was replaced by that of a proton in **2**. This was confirmed by analysis of the HMBC spectrum, in which the correlations from 2-CH_3 (δ_H 2.26, s) to C-2 (δ_C 170.9, C) and the methine carbon (δ_C 106.6, C-3) were found. Thus, ustilaginoidin L, **2**, was a demethylated derivative of ustilaginoidin K, **1**.

The molecular formula of ustilaginoidin M, **3**, was established as $C_{30}H_{24}O_{10}$, bearing 2H more than that of **1**. The NMR data of **3** (Tables 1 and 2) comprised two sets of signals, each assignable to one naphtho-γ-pyrone moiety. Among them, one set of the signals was almost superimposable on that of ustilaginoidin K, **1**, while the other one was different from that of **1** in the γ-pyrone part, in which signals ascribed to a nonconjugated carbonyl group (δ_C 201.7, C), two methine groups (δ_H 3.95 (dq)/δ_C 78.8; δ_H 2.74 (dq)/δ_C 46.7), and two methyl groups (δ_H 1.33 (d)/δ_C 19.6; δ_H 1.24 (d)/δ_C 9.7) were discerned, indicating the presence of a 2,3-dimethyl-2,3-dihydro-γ-pyrone ring in **3**. The large coupling constant (11.0 Hz) between the two methine protons (H-2′ and H-3′) suggested the *trans* orientation of the 2′-CH_3 and 3′-CH_3 in the dihydro-γ-pyrone ring.[6] Thus, compound **3** was a dihydro derivative of ustilaginoidin K, **1**, as depicted in Figure 1. From a structural point of view, **3** was composed of one-half of ustilaginoidin K, **1**, and one-half of ustilaginoidin D, **9**.[6]

Ustilaginoidin N, **4**, was isolated as a congener of compound **3**. The molecular formula of **4** was $C_{29}H_{22}O_{10}$ as determined by HR-ESI−MS, which contained a CH_2 less than that of **3**. Inspection of the NMR data (Tables 1 and 2) suggested that both compounds were similar, except that the signal for one olefinic methyl group in **3** was replaced by that of an olefinic proton (δ_H 6.10, s) in **4**. The chemical shift of this proton together with its attached carbon (δ_C 106.6) as revealed by HSQC experiment, which indicated that the C-3 methyl group in **3** was replaced by a hydrogen atom in **4**. This conclusion was secured by the observed HMBC correlations from H-3 (δ_H 6.10, s) to C-2 (δ_C 170.9, C), 2- CH_3 (δ_C 20.6, CH_3), C-4 (δ_C 184.7, C), and C-4a (δ_C 102.8, C) (Figure 2). Therefore, ustilaginoidin N, **4**, was determined as the 3-desmethyl derivative of ustilaginoidin M, **3**.

Ustilaginoidin O, **5**, was isolated as an orange amorphous powder whose molecular formula was determined as $C_{29}H_{22}O_{10}$ by analysis of the pseudomolecular ion peak at m/z 529.11209 $[M-H]^-$ in the HRESIMS spectrum. The UV, IR, and NMR data of **5** were similar to those of ustilaginoidin G, **12**,[6] indicating it to be an ustilaginoidin-type compound. However, their NMR data differed in the γ-pyrone part. In the ^{1}H NMR spectrum of **5**, signals were observed for two olefinic methyl groups (δ_H 2.28, 1.99, each s), while those for the olefinic proton, as reported in ustilaginoidin G, **12**, were missing. This indicated that the olefinic proton (H-3′) of the γ-pyrone ring in ustilaginoidin G, **12**, was replaced by a 3′-methyl group in that of **5**. Therefore, compound **5** was elucidated as 3′-methylustilaginoidin G.

Ustilaginoidin P, **6**, was isolated as a minor compound, which had a same molecular formula as that of ustilaginoidin N, **4**. The NMR data of **6** resembled those of **4**, and both showed signals for a 2,3-dimethyl-2,3-dihydropyran-4-one and a 2-methyl-pyran-4-one moiety (Tables 1 and 2). However, the NMR data for the 2,3-dimethyl-2,3-dihydropyran-4-one ring in both compounds were notably different. H-2′ (δ_H 4.53, dq) of **6** significantly shifted to downfield compared to that of **4** (δ_H 4.06, dq), while large chemical shift differences between both compounds were observed at C-2′ (−2.6 ppm), C-3′ (−1.8 ppm), 2′-CH_3(−3.2 ppm), and C-4′ (+1.9 ppm). Thus, the stereochemistry of C-2′ in **6** should be different from that of **4**, that is to say, H-2′ and H-3′ were *cis*-configured in **6**, which was consistent with the observed small coupling constant (3.0 Hz)[6] between both protons. Therefore, ustilaginoidin P, **6**, was determined to be a 2′-epimer of ustilaginoidin N, **4**.

The new compound, ustilaginoidin E_1, **7**, was isolated as an isomer of ustilaginoidin E, **10**.[6] Both compounds showed nearly identical UV, IR, and MS spectra and similar NMR data. The differences were ascribed to the 2,3-dihydro-pyran-4-one ring, in which the vicinal methyl groups were *cis* oriented ($J_{H\text{-}2',\ H\text{-}3'}$= 3.2 Hz) in **7**, not like those of the *trans* isomer ($J_{H\text{-}2',\ H\text{-}3'}$ = 10.4 Hz) in ustilaginoidin E, **10**.[6] Furthermore, the NMR data of **7** were almost superimposable on those of **6** regarding the 2,3-dimethyl-2,3-dihydro-γ-pyrone ring located in the lower half of the molecule. Thus, ustilaginoidin E_1, **7**, was an epimer of ustilaginoidin E and also a dihydro derivative of ustilaginoidin P, **6**.

The absolute configuration of the 9/9′ axis of the new ustilaginoidins, **1**−**7**, was determined as *R* by comparing the CD spectra with the literature,[8] as these compounds all exhibited strong negative first (294 nm) and positive second (266 nm) Cotton effects. However, the absolute configuration of the chiral centers of the 2,3-dihydro-pyran-4-one ring in compounds **3**−**7** remains to be determined. This would require X-ray crystallographic analysis; however, no suitable crystals were obtained after several attempts to crystallize these metabolites in different solvent systems, which was not so surprising as until now, only the X-ray analysis of the 6-*O*-*p*-bromobenzoate of the 5,5′,6′,8,8′-pentamethyl ether of chaetochromin A has been reported.[8]

The known compounds were identified by comparison of the specific optical rotation, CD, NMR, and HRESIMS data with those reported in literature and included ustilaginoidin A, **8**,[4,6] ustilaginoidin D, **9**,[6] ustilaginoidin E, **10**,[6] ustilaginoidin F, **11**,[6] ustilaginoidin G, **12**,[6] and isochaetochromin B_2, **13**.[14]

Interestingly, all the isolated bis-naphtho-γ-prones from the cultured *U. virens* in the present study have a *R* configuration of the 9,9′-axis, and they only differed in the γ-pyrone ring, which was either a pyran-4-one or a 2,3-dihydropyran-4-one ring substituted with one or two methyl groups. In addition to

DOI: 10.1021/acs.jafc.5b00694
J. Agric. Food Chem. 2015, 63, 3501−3508

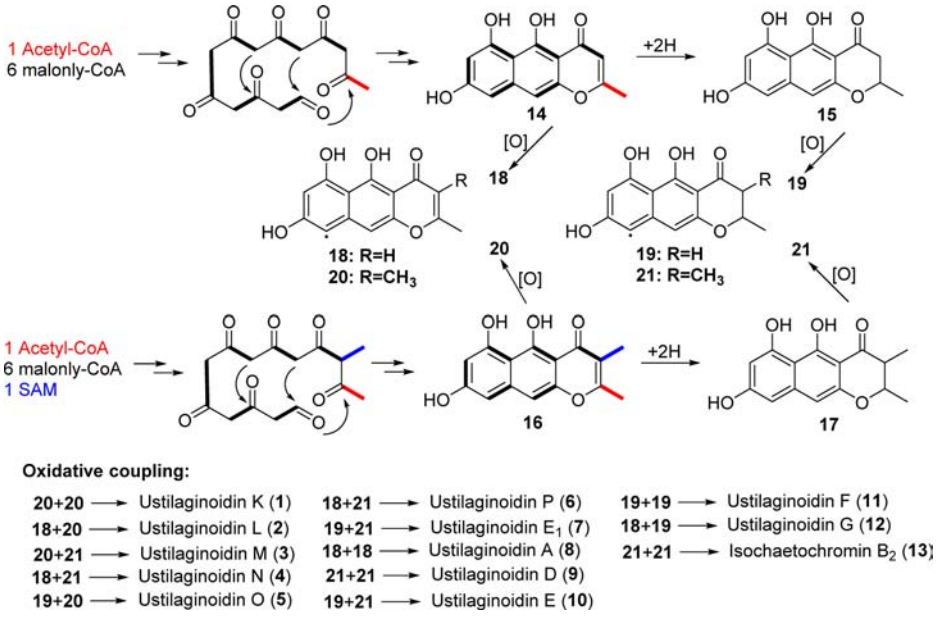

Figure 3. A plausible biosynthetic route for compounds **1**−**13**.

these structural types, some other analogues, such as ustilaginoidins B, C, H, I, and J, containing one or two hydroxymethyl groups at C-2 of the γ-pyrone rings, were reported from the extracts of rice false smut balls,[4−6] indicating a further oxidative reaction occurred in natural environment.

A hypothetical biosynthetic pathway for the isolated bis-naphtho-γ-pyrones was proposed (Figure 3). These metabolites should be dimers of heptaketides, by analogized with that of chaetochromin A,[34] a diastereomer of ustilaginoidin D. The condensation of one acetyl-CoA and six malonyl-CoA units, followed by cyclization, could form the heptaketide norrubrofusarin, **14**,[35] which could further undergo reduction to give its dihydro derivative, **15**. Similarly, the condensation of one acetyl-CoA, six malonyl-CoA, and one methyl unit donated by *S*-adenosylmethionine (SAM) would yield the other heptaketide, **16**, which could be further reduced to form its dihydro derivative, **17**. These heptaketide derivatives could be oxidized to give its corresponding radical intermediates, **18**, **19**, **20**, and **21**. The oxidative coupling of these monomeric naphtho-γ-pyrone radicals would yield the dimeric compounds (Figure 3), for instance, the coupling of **18** and **20** would yield ustilaginoidin L, **2**. In literature, the oxidative coupling between monomeric phenolic precursors was proposed to form the spirobisnaphthalenes.[36,37]

Some ustilaginoidins are mycotoxins. Ustilaginoidin A was reported to have teratogenic effects on mouse embryo limb bud and midbrain cells with IC_{50} values of 2.53 and 1.24 μM, respectively,[22] while ustilaginoidins A, D, E, and G were significantly cytotoxic to KB cells with IC_{50} values (μM) of 0.58, 0.42, 0.43, and 1.94, respectively.[23] Thus, in the current study, all the isolated ustilaginoidins were tested for their cytotoxicities against five human carcinoma cell lines including HCT-116, HepG2, BGC-823, NCI-H1650, and A2780. Only ustilaginoidins K, **1**, and L, **2**, showed inhibitory effects against the A2780 cells with IC_{50} values of 4.18 and 7.26 μM, respectively, whereas the other compounds were inactive with IC_{50} > 10 μM. It is worth mentioning that these compounds were 2−3-order less active than the positive control (taxol).

Meanwhile, the isolated compounds were screened for their inhibitory activities on seed radicle elongation of two rice varieties (Lijiang, and Zhonghua 11) (Table 3). Ustilaginoidins O, **5**, E, **10**, and F, **11**, and isochaetochromin B_2, **13**, showed inhibition at different test concentrations, though not as effective as that of positive control (glyphosate). Among them, ustilaginoidin F, **11**, showed the strongest activity against the tested rice seeds. In general, Lijiang variety was more susceptible to the compounds than Zhonghua 11.

The antibacterial effects of the isolated compounds were tested against six pathogenic bacteria including *A. tumefaciens*, *B. subtilis*, *P. lachrymans*, *R. solanacearum*, *S. hemolyticus*, and *X. vesicatorya* (Table 4). Among them, ustilaginoidins E, **10**, and G, **12**, showed inhibition against all the tested bacteria, while ustilaginoidins N, **4**, and D, **9**, displayed inhibitory activity against only four bacteria including *A. tumefaciens*, *B. subtilis*, *S. hemolyticus*, and *X. vesicatoria*. However, the other compounds were inactive at the highest test concentration of 64 μg/mL. Both ustilaginoidin D and isochaetochromin B_2 were previously reported to have inhibitory effects against *Mycobacterium phlei* with the same MIC value of 50.0 μg/mL.[16] Three related bis-naphtho-γ-pyrones, namely, isochaetomium A_2, chaetochromins A and B, possessing an a*S* axial chirality, showed antibacterial effects against *Escherichia coli*, *S. aureus*, and *B. subtilis*.[12]

In conclusion, 13 bis-naphtho-γ-pyrones, including the new ustilaginoidins K−P, **1**−**6**, and E_1, **7**, and the known ustilaginoidins A, **8**, D, **9**, E, **10**, F, **11**, and G, **12**, and isochaetochromin B_2, **13**, were isolated from the extract of rice false smut pathogen *U. virens*. Previous chemical investigation related to this pathogen was focused on chemical constituents of the smut balls grown on the infected rice panicles.[4−6] In the current study, chemical investigation of this fungus grown on solid rice medium was reported for the first time. This led to not only the identification of known ustilaginoidins that previously obtained from rice false smut balls, but also the discovery of new congeners. It is interesting that no hydroxymethyl derivatives were obtained in the current study; on the contrary, these metabolites were reported from the smut balls

DOI: 10.1021/acs.jafc.5b00694
J. Agric. Food Chem. 2015, 63, 3501−3508

Table 3. Inhibitory Activity of the Isolated Compounds on the Radicle Elongation of Rice Seeds

compound[a]	concentration (μg/mL)[b]	inhibitory rate of the radicle elongation of rice seeds (%)[c]	
		rice var. Lijiang	rice var. Zhonghua 11
ustilaginoidin O, **5**	50	32.97 ± 2.56 m	18.25 ± 3.37 lm
	100	40.07 ± 4.06 l	31.94 ± 1.96 i
	200	50.00 ± 3.50 k	41.80 ± 3.74 gh
	400	57.73 ± 3.42 i	44.44 ± 3.74 g
ustilaginoidin E, **10**	50	57.25 ± 1.02 i	24.87 ± 1.50 k
	100	57.73 ± 1.71 i	29.37 ± 3.37 ij
	200	60.14 ± 1.12 ghi	32.87 ± 2.34 i
	400	68.00 ± 1.27 e	39.81 ± 4.68 h
ustilaginoidin F, **11**	50	58.45 ± 0.68 hi	20.29 ± 0.00 l
	100	63.77 ± 1.83 f	38.04 ± 0.51 h
	200	72.22 ± 1.71 cd	67.39 ± 1.12 e
	400	78.26 ± 1.12 b	76.45 ± 1.69 c
isochaetochromin B_2, **13**	50	53.93 ± 0.66 j	5.75 ± 1.40 o
	100	59.54 ± 0.27 ghi	9.79 ± 0.37 n
	200	61.35 ± 0.42 fgh	14.68 ± 2.81 m
	400	62.32 ± 2.05 fg	26.46 ± 0.75 jk
CK^+ (glyphosate)[d]	50	69.89 ± 0.12 de	58.05 ± 1.60 f
	100	75.16 ± 1.46 bc	72.13 ± 3.87 d
	200	87.62 ± 0.43 a	81.29 ± 0.80 b
	400	90.49 ± 1.92 a	90.36 ± 0.80 a

[a]The other isolated compounds did not show inhibitory activity at the test concentrations. [b]The negative control (2.5% DMSO) showed no inhibition on radicle elongation of rice seeds. [c]The values were expressed as means ± SD (n = 3). Different letters indicated significant differences among treatments in each column including different compounds and their concentrations at $p \leq 0.05$. [d]Positive control.

Table 4. Antibacterial Activity of the Isolated Compounds

bacterium	MIC/IC_{50} (μg/mL)	compound[a]				
		ustilaginoidin N, **4**	ustilaginoidin D, **9**	ustilaginoidin E, **10**	ustilaginoidin G, **12**	CK^+ (*Streptomycin* sulfate)[b]
A. tumefaciens	MIC	16	32	64	64	5
	IC_{50}	2.41	5.37	6.62	5.37	1.41
B. subtilis	MIC	16	32	32	32	5.0
	IC_{50}	2.37	4.05	3.35	3.25	1.37
P. lachrymans	MIC	>64	>64	16	64	7.5
	IC_{50}	nd[c]	nd	5.57	8.22	2.34
R. solanacearum	MIC	>64	>64	16	64	5
	IC_{50}	nd	nd	4.19	10.64	1.21
S. hemolyticus	MIC	16	32	32	32	5
	IC_{50}	2.29	3.02	5.55	4.88	1.40
X. vesicatoria	MIC	16	32	32	64	10
	IC_{50}	4.09	3.53	6.11	9.61	2.59

[a]The other isolated compounds did not show inhibitory activity at 128 μg/mL. [b]Positive control. [c]nd: not detected.

collected in paddy field.[4−6] The cytotoxic and antibacterial activities of the isolated compounds were evaluated. Ustilaginoidins K, **1**, and L, **2**, were cytotoxic to A2780 cells, while ustilaginoidins N, **4**, D, **9**, E, **10**, and G, **12**, displayed inhibitory activities on the tested pathogenic bacteria. In addition, the in vitro phytotoxic activity of the bis-naphto-γ-pyrones on the inhibition of the rice radicle elongation was first reported. Ustilaginoidins O, **5**, E, **10**, and F, **11**, and isochaetochromin B_2, **13**, displayed moderate inhibition against the radicle elongation of rice seeds. Thus, *U. virens* was an intriguing producer of interesting bioactive ustilaginoidins. Further characterization of the physiological and ecological roles of the ustilaginoidins such as the role in the disease cycle of *U. virens* should be studied in detail.[38]

■ ASSOCIATED CONTENT

Supporting Information

IR, NMR, HRESIMS, and CD spectra for compounds **1**−**7**. This material is available free of charge via the Internet at http://pubs.acs.org.

■ AUTHOR INFORMATION

Corresponding Authors

*Phone: +86 10 62733609. Fax: +86 10 62733530. E-mail: dwlai@cau.edu.cn.

*Phone: +86 10 62731199. Fax: +86 10 62731062. E-mail: lgzhou@cau.edu.cn.

Funding

This work was supported by the Hi-Tech R&D Program of China (2011AA10A202), the National Basic Research Program of China (2013CB127805), the National Natural

DOI: 10.1021/acs.jafc.5b00694
J. Agric. Food Chem. 2015, 63, 3501−3508

Science Foundation of China (31471729 and 31271996), and the Chinese Universities Scientific Fund (2014RC020).

Notes

The authors declare no competing financial interest.

REFERENCES

(1) Tanaka, E.; Ashizawa, T.; Sonoda, R.; Tanaka, C. *Villosiclava virens* gen. nov., comb. nov., teleomorph of *Ustilaginoidea virens*, the causal agent of rice false smut. *Mycotaxon* **2008**, *106*, 491−501.

(2) Hu, M.; Luo, L.; Wang, S.; Liu, Y.; Li, J. Infection processes of *Ustilaginoidea virens* during artificial inoculation of rice panicles. *Eur. J. Plant Pathol.* **2014**, *139*, 67−77.

(3) Tang, Y. X.; Jin, J.; Hu, D. W.; Yong, M. L.; Xu, Y.; He, L. P. Elucidation of the infection process of *Ustilaginoidea virens* (teleomorph: *Villosiclava virens*) in rice spikelets. *Plant Pathol.* **2013**, *62*, 1−8.

(4) Shibata, S.; Ogihara, Y.; Ohta, A. Metabolic products of fungi. XXII. On ustilaginoidins. (2). The structure of ustilaginoidin A. *Chem. Pharm. Bull.* **1963**, *11*, 1179−1182.

(5) Shibata, S.; Ogihara, Y. Metabolic products of fungi. XXIII. Ustilaginoidins. 3. The structure of ustilaginoidins B and C. *Chem. Pharm. Bull.* **1963**, *11*, 1576−1578.

(6) Koyama, K.; Natori, S. Further characterization of seven bis(naphtho-γ-pyrone) congeners of ustilaginoidins, pigments of *Claviceps virens* (*Ustilaginoidea virens*). *Chem. Pharm. Bull.* **1988**, *36*, 146−152.

(7) Shibata, S.; Ogihara, Y. Absolute configurations of ustilaginoidins. *Tetrahedron Lett.* **1963**, *4*, 1777−1780.

(8) Koyama, K.; Natori, S.; Iitaka, Y. Absolute configurations of chaetochromin A and related bis(naphtho-γ-pyrone) mold metabolites. *Chem. Pharm. Bull.* **1987**, *35*, 4049−4055.

(9) Lu, S.; Tian, J.; Sun, W.; Meng, J.; Wang, X.; Fu, X.; Wang, A.; Lai, D.; Liu, Y.; Zhou, L. Bis-naphtho-γ-pyrones from fungi and their bioactivities. *Molecules* **2014**, *19*, 7169−7188.

(10) Sekita, S.; Yoshihira, K.; Natori, S. Chaetochromin, a bis-(naphthodihydropyran-4-one) mycotoxin from *Chaetomium thielavioideum*: Application of ^{13}C-^{1}H long-range coupling to the structure elucidation. *Chem. Pharm. Bull.* **1980**, *28*, 2428−2435.

(11) Koyama, K.; Natori, S. Chaetochromins B, C, and D; bis(naphtho-γ-pyrone) derivatives from *Chaetomium gracile*. *Chem. Pharm. Bull.* **1987**, *35*, 578−584.

(12) Xu, G.-B.; Yang, T.; Bao, J.-K.; Fang, D.-M.; Li, G.-Y. Isochaetomium A_2, a new bis(naphthodihydropyran-4-one) with antimicrobial and immunological activities from fungus *Chaetomium microcephalum*. *Arch. Pharmacal Res.* **2014**, *37*, 575−579.

(13) Zhang, Q.; Li, H. Q.; Zong, S. C.; Gao, J. M.; Zhang, A. L. Chemical and bioactive diversities of the genus *Chaetomium* secondary metabolites. *Mini Rev. Med. Chem.* **2012**, *12*, 127−148.

(14) Singh, S. B.; Zink, D. L.; Bills, G. F.; Teran, A.; Silverman, K. C.; Lingham, R. B.; Felock, P.; Hazuda, D. J. Four novel bis-(naphtho-γ-pyrones) isolated from *Fusarium* species as inhibitors of HIV-1 integrase. *Bioorg. Med. Chem. Lett.* **2003**, *13*, 713−717.

(15) Ugaki, N.; Matsuda, D.; Yamazaki, H.; Nonaka, K.; Masuma, R.; Omura, S.; Tomoda, H. New isochaetochromin, an inhibitor of triacylglycerol synthesis in mammalian cells, produced by *Penicillium* sp. FKI-4942: I. Taxonomy, fermentation, isolation, and biological properties. *J. Antibiot.* **2012**, *65*, 15−19.

(16) Kong, X.; Ma, X.; Xie, Y.; Cai, S.; Zhu, T.; Gu, Q.; Li, D. Aromatic polyketides from a sponge-derived fungus *Metarhizium anisopliae* mxh-99 and their antitubercular activities. *Arch. Pharmacal Res.* **2013**, *36*, 739−744.

(17) Ohtsubo, K. Oral toxicity of chaetochromin, a new mycotoxin produced by *Chaetomium virescens*, to mice. *Mycotoxins* **1980**, 28−29.

(18) Ito, Y.; Ohtsubo, K. Exencephaly in mice induced by feeding chaetochromin containing diet. *Mycotoxins* **1982**, 22−23.

(19) Ohtsubo, K. Hematopoietic injury and liver necrosis in the mice fed chaetochromin-containing moldy rice diet. *Mycotoxins* **1982**, 25−27.

(20) Ito, Y.; Ohtsubo, K. Teratogenicity of oral chaetochromin, a polyphenolic mycotoxin produced by *Chaetomium* spp., to mice embryo. *Bull. Environ. Contam. Toxicol.* **1987**, *39*, 299−303.

(21) Ohtsubo, K. Myocardial and hepatic necrosis and bone marrow suppression in mice induced by single administration of chaetochromin, a polyphenolic mycotoxin produced by *Chaetomium* spp. *J. Toxicol. Pathol.* **1989**, *2*, 163−174.

(22) Tsuchiya, T.; Sekita, S.; Koyama, K.; Natori, S.; Takahashi, A. Effect of chaetochromin A, chaetochromin D, and ustilaginoidin A, bis(naphtho-γ-pyrone) derivatives, on the mouse embryo limb bud and midbrain cells in culture. *Cong. Anom.* **1987**, *27*, 245−250.

(23) Koyama, K.; Ominato, K.; Natori, S.; Tashiro, T.; Tsuruo, T. Cytotoxicity and antitumor activities of fungal bis-(naphtho-γ-pyrone) derivatives. *J. Pharmacobiodyn.* **1988**, *11*, 630−635.

(24) Kawai, K.; Hisada, K.; Mori, S.; Nozawa, Y.; Koyama, K.; Natori, S. The impairing effect of chaetochromin A and related mycotoxins on mitochondrial respiration. *Mycotoxins* **1991**, 31−35.

(25) Mori, S.; Kawai, K.; Nozawa, Y.; Koyama, K.; Natori, S. The impairing effects of chaetochromin D on mitochondrial respiration and structure. *Mycotoxin Res.* **1993**, *9*, 85−93.

(26) Kawai, K.; Mori, S.; Hisada, K.; Nozawa, Y.; Koyama, K.; Natori, S. The induction of mitochondrial swelling by chaetochromin A, a bis-(naphtho-γ-pyrone) mycotoxin from *Chaetomium gracile*. *Mycotoxins* **1991**, 25−29.

(27) Mori, S.; Kawai, K.; Nozawa, Y.; Koyama, K.; Natori, S. Induction of mitochondrial swelling by chaetochromin A, a bis-(naphtho-γ-pyrone) mycotoxin from *Chaetomaum gracale* II. Relationship with uncoupling effect. *Mycotoxins* **1991**, 33−37.

(28) Ishii, R.; Horie, M.; Koyama, K.; Ishikawa, Y.; Kitanaka, S. Inhibitory effects of fungal bis-(naphtho-γ-pyrone) derivatives on nitric oxide production by a murine macrophage-like cell line, RAW 264.7, activated by lipopolysaccharide and interferon-γ. *Biol. Pharm. Bull.* **2005**, *28*, 786−790.

(29) Ugaki, N.; Yamazaki, H.; Uchida, R.; Tomoda, H. New isochaetochromin, an inhibitor of triacylglycerol synthesis in mammalian cells, produced by *Penicillium* sp. FKI-4942: II. Structure elucidation. *J. Antibiot.* **2012**, *65*, 21−24.

(30) Xu, L.; Zhou, L.; Zhao, J.; Li, J.; Li, X.; Wang, J. Fungal endophytes from *Dioscorea zingiberensis* rhizomes and their antibacterial activity. *Lett. Appl. Microbiol.* **2008**, *46*, 68−72.

(31) Xu, L.; Wang, X.-H.; Luo, R.-Y.; Lu, S.-Q.; Guo, Z.-J.; Wang, M.-A.; Liu, Y.; Zhou, L.-G. Secondary metabolites of rice sheath blight pathogen *Rhizoctonia solani* Kühn and their biological activities. *J. Integr. Agric.* **2015**, *14*, 80−87.

(32) Mosmann, T. Rapid colorimetric assay for cellular growth and survival: Application to proliferation and cytotoxicity assays. *J. Immunol. Methods* **1983**, *65*, 55−63.

(33) Aliferis, K. A.; Jabaji, S. Metabolite composition and bioactivity of *Rhizoctonia solani* sclerotial exudates. *J. Agric. Food. Chem.* **2010**, *58*, 7604−7615.

(34) Koyama, K.; Natori, S. Biosynthesis of chaetochromin A, a bis-(naphtho-γ-pyrone), in *Chaetomium* spp. *Chem. Pharm. Bull.* **1989**, *37*, 2022−2025.

(35) Frandsen, R. J. N.; Nielsen, N. J.; Maolanon, N.; Soerensen, J. C.; Olsson, S.; Nielsen, J.; Giese, H. The biosynthetic pathway for aurofusarin in *Fusarium graminearum* reveals a close link between the naphthoquinones and naphthopyrones. *Mol. Microbiol.* **2006**, *61*, 1069−1080.

(36) Shan, T.; Tian, J.; Wang, X.; Mou, Y.; Mao, Z.; Lai, D.; Dai, J.; Peng, Y.; Zhou, L.; Wang, M. Bioactive spirobisnaphthalenes from the endophytic fungus *Berkleasmium* sp. *J. Nat. Prod.* **2014**, *77*, 2151−2160.

(37) Krohn, K.; Michel, A.; Flörke, U.; Aust, H.-J.; Draeger, S.; Schulz, B. Biologically active metabolites from fungi, 5. Palmarumycins C_1−C_{16} from *Coniothyrium* sp.: Isolation, structure elucidation, and biological activity. *Liebigs Ann. Chem.* **1994**, *1994*, 1099−1108.

(38) Fan, J.; Guo, X. Y.; Huang, F.; Li, Y.; Liu, Y. F.; Li, L.; Xu, Y. J.; Zhao, J. Q.; Xiong, H.; Yu, J. J.; Wang, W. Epiphytic colonization of *Ustilaginoidea virens* on biotic and abiotic surfaces implies the widespread presence of primary inoculum for rice false smut disease. *Plant Pathol.* **2014**, *63*, 937−945.

DOI: 10.1021/acs.jafc.5b00694
J. Agric. Food Chem. 2015, 63, 3501−3508

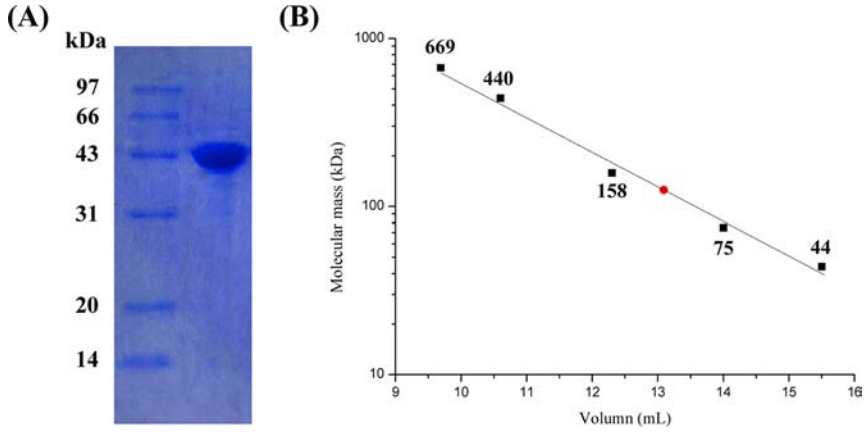

Figure 1. SDS−PAGE and gel filtration analysis of the purified recombinant enzyme. (A) SDS−PAGE of the protein stained with Coomassie Blue. Lane 1, molecular mass marker proteins; lane 2, the purified recombinant protein by metal-affinity chromatography. (B) Determination of the molecular mass of native protein. The column was calibrated with thyroglobulin (669 kDa), ferritin (440 kDa), aldolase (158 kDa), conalbumin (75 kDa), and ovalbumin (44 kDa) as reference proteins, and the native enzyme was eluted at a retention volume corresponding to 125 kDa (labeled by the red circle).

however, the values of most IFTases (DFA III forming) are less than 2000 units/mg.

In this work, a novel IFTase was characterized from *Arthrobacter* sp. 161MFSha2.1. The structure of depolymerized products from inulin was identified as DFA III by nuclear magnetic resonance (NMR) analysis. The enzymatic properties were studied in detail and were compared to those of other IFTases. The enzyme displays the highest thermostability and the second highest specific activity among the already characterized IFTases (DFA III forming), suggesting that it has great potential for industrial DFA III production.

MATERIALS AND METHODS

Chemicals and Reagents. The sugar standards, including DFA III, 1-ketose (GF_2), and nystose (GF_3), were from Wako Pure Chemical Industries (Osaka, Japan). Inulin was purchased from BENEO-Orafti NV (Tienen, Belgium). Chelating Sepharose Fast Flow, the resin for affinity chromatography, was obtained from Amersham Biosciences (Arlington Heights, IL). All other chemicals used in this study were at least of analytical grade, obtained from Sigma (St. Louis, MO) and Sinopharm Chemical Reagent (Shanghai, China).

Plasmids, Microorganisms, and Culture Conditions. The plasmid pET-22b(+) and *E. coli* BL21(DE3) were used as a vector and host to express the target gene, respectively. The *E. coli* strain was cultured in the Luria−Bertani (LB) medium. The LB medium used was composed of 5 g/L yeast extract, 10 g/L trypone, and 5 g/L NaCl (pH 7.5).

Gene Cloning and Expression. The nucleotide and protein sequence information were obtained from the National Center for Biotechnology Information (NCBI), with accession numbers NZ_KB895786 and WP_018778058, respectively. The full length of the encoding gene was designed to contain an in-frame 6× histidine-tag sequence before the stop codon and *Nde*I and *Xho*I restriction sites at the 5′ and 3′ termini. The designed DNA sequence was synthesized by Shanhai Generay Biotech Co., Ltd. (Shanghai, China) and was subcloned into the pET-22b(+) vector with the same restriction sites.

The recombinant plasmid was then transformed into *E. coli* BL21(DE3) for expression. A single colony of transformant was inoculated in LB medium plus ampicillin (100 μg/mL). When the cells were grown to an optimal density (600 nm) of 0.6 at 37 °C, protein expression was initiated by the addition of isopropyl-β-D-1-thiogalactopyranoside (IPTG) to a final concentration of 1 mM and the extracellular expression was performed at 28 °C for 72 h.

Purification of Recombinant IFTase. All purification steps were conducted at 4 °C. The culture broth was centrifuged at 10000*g* for 20 min to remove cell pellets. The supernatant containing 6× histidine-tagged recombinant proteins was directly loaded on Chelating Sepharose Fast Flow resin for metal-affinity chromatography using an ÄKTA purifier (GE Healthcare, Sweden). The purification was performed according to the protocol of the manufacturer (pET His Tag System, Novagen).

The protein concentration was calculated using the Bradford method, and the molecular mass was assessed by both sodium dodecyl sulfate−polyacrylamide gel electrophoresis (SDS−PAGE) and gel filtration. For SDS−PAGE, 12 and 5% (w/v) acrylamide were used for the separating and stacking gels, respectively, and Coomassie Brilliant Blue R250 was used for protein staining. For gel filtration, the native purified protein was loaded on a Superdex 200 10/300 GL gel filtration column (GE Healthcare, Sweden) and was eluted with 150 mM NaCl in 50 mM phosphate buffer (pH 6.5) at a flow rate of 0.5 mL min^{-1}.

Identification of the Reaction Product from Inulin. The reaction products from inulin by the recombinant enzyme were separated by high-performance liquid chromatography (HPLC, Agilent 1260 system, Santa Clara, CA) equipped with a refractive index detector and a preparative column, Carbomix H-NP5 (5 μm, 10 mm inner diameter × 300 mm, Sepax Technologies, Inc., Newark, DE). The column was eluted at 80 °C with a flow rate of 0.8 mL/min. The main product was collected and freeze-dried in the 4.5 L FreeZone freeze-dry system (Labconco Corp., Kansas City, MO).

The freeze-dried sample (30 mg) was dissolved in 0.45 mL of D_2O and analyzed by NMR using a Bruker Avance III 400 MHz Digital NMR spectrometer (Bruker, Karlsruhe, Germany). The NMR was operated at 400 MHz for ^{1}H NMR, ^{13}C NMR, and two-dimensional (2D) NMR spectra, including 2D ^{1}H shift correlated spectroscopy (^{1}H−^{1}H COSY), ^{1}H-detected heteronuclear single-quantum coherence (^{1}H−^{13}C HSQC), and ^{1}H-detected heteronuclear multiple-bond correlation (^{1}H−^{13}C HMBC). The sodium 4,4-dimethyl-4-silapentane-1-sulfonate (DSS) was used as a standard to reference the chemical shifts.

Enzyme Assay. The enzyme activity was determined by measuring the amount of produced DFA III from inulin. The reaction mixture was composed of 1 mL of solution containing phosphate buffer (pH 6.5), substrate inulin (10 g/L), and purified enzyme (6 nM). The reaction was conducted at 55 °C for 5 min and was stopped by boiling for 10 min. The generated DFA III was determined by HPLC [system, Agilent 1260; column, Asahipak NH2P-50-4E system, 4.6 mm inner diameter × 250 mm; column temperature, 25 °C; mobile phase, 65% (v/v) of acetonitrile; elution rate, 1 mL/min; and detector, refractive index detector]. One unit of enzyme activity was defined as the

DOI: 10.1021/jf506165n
J. Agric. Food Chem. 2015, 63, 3509−3515

Table 1. Chemical Shifts in ^{1}H and ^{13}C NMR Spectra

		δ_C (ppm)[a]			δ_H (ppm)[a]	
group	carbon atoms	main product	DFA III standard	DFA III standard reported previously[35]	main product	DFA III standard
α-Fru	1	66.36	66.36	66.2	3.68, 3.65	3.68, 3.65
	2	106.30	106.30	106.3		
	3	83.90	83.90	83.9	4.15	4.15
	4	78.09	78.09	78.1	3.87	3.87
	5	82.85	82.85	82.9	3.69	3.69
	6	63.33	63.33	63.3	3.89, 3.86	3.89, 3.86
β-Fru	1′	61.69	61.69	61.7	4.05, 4.02	4.05, 4.02
	2′	104.06	104.06	104.2		
	3′	84.59	84.95	84.5	4.09	4.09
	4′	74.98	74.98	75.0	4.65	4.65
	5′	81.73	81.73	81.8	4.31	4.31
	6′	63.81	63.81	63.8	3.85, 3.65	3.85, 3.65

[a]Chemical shifts were determined relative to the internal standard DSS ($\delta_C = \delta_H = 0.00$ ppm).

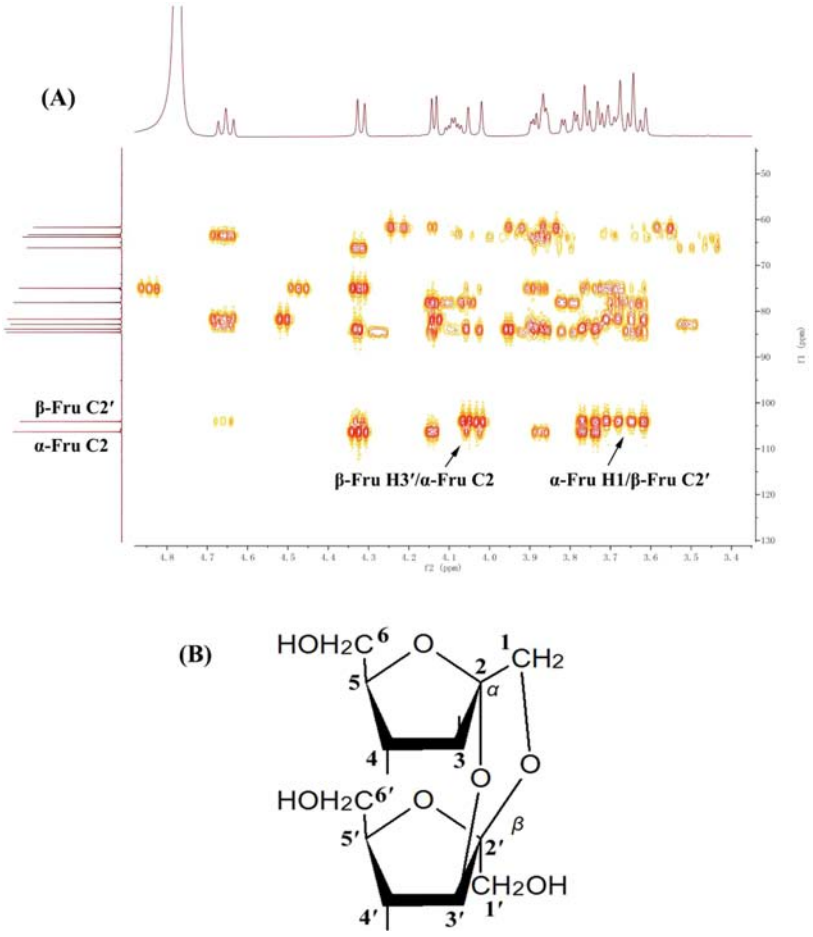

Figure 2. Identification of the structure of the main product produced from inulin by the recombinant enzyme. (A) $^{1}H-^{13}C$ HMBC spectrum of the purified main product. Connectivities of α-D-fructofuranose (2, 3′) β-D-fructofuranose and β-D-fructofuranose (2′, 1) α-D-fructofuranose were deduced by the correlation between α-D-Fru-C-2 and β-D-Fru-H-3′ and that between β-D-Fru-C-2′ and α-D-Fru-H-1, respectively. (B) Chemical structure of the main product.

amount of enzyme catalyzing the formation of 1 μmol of DFA III per minute at pH 6.5 and 55 °C.

Effect of the pH and Temperature. The optimum pH and temperature for recombinant IFTase (DFA III forming) were determined by assaying the enzyme activity in 50 mM different buffers (acetate buffer, pH 4.0−5.5; phosphate buffer, pH 6.0−7.0; and Tris−HCl buffer, pH 7.5−8.0) at 55 °C or at different temperatures (30−80 °C) in 50 mM phosphate buffer (pH 6.5). The thermostability was determined by calculating the residual activity of the enzyme, which was pre-incubated at 55, 60, 70, and 80 °C for 4 h. The initial activity without pre-incubation was taken as a control.

Conversion of Inulin to DFA III by Recombinant IFTase. Production of DFA III from inulin was studied in 100 mL of reaction volume using 80 nM recombinant enzyme at pH 6.5 and 55 °C. Different initial inulin concentrations were tested, including 50, 100, and 200 g/L.

DOI: 10.1021/jf506165n
J. Agric. Food Chem. 2015, 63, 3509−3515

RESULTS

Heterologous Expression and Protein Purification. The IFTase-encoding gene from *Arthrobacter* sp. 161MFSha2.1 is heterologously expressed in *E. coli* with a C-terminal 6× histidine tag. After expression by IPTG induction, extracellular inulin depolymerization activity is significantly detected, indicating that the recombinant enzyme is successfully secreted to the culture media. The culture supernatant is collected and loaded into a nickel-affinity column for enzyme purification. The recombinant enzyme is purified to homogeneity, showing a single band of 43 kDa in SDS−PAGE (Figure 1A). The molecular weight of the native enzyme determined by gel filtration is calculated to be 125 kDa (Figure 1B). These data indicate that the recombinant enzyme is a homotrimeric protein.

NMR Analysis of the Reaction Product. The ^{13}C and ^{1}H NMR spectra are shown in panels A and B of Figure S1 of the Supporting Information, respectively. The chemical shifts obtained from the spectra (shown in Table 1) are compared to the results of the DFA III standard. The ^{13}C NMR spectrum (see Figure S1A of the Supporting Information) shows 12 carbons containing two sugar carbons (106.3 and 104.1 ppm) with large downfield shifts and four methylene oxylated carbons (66.36, 63.81, 63.33, and 61.69 ppm) with upfield shifts, indicating the existence of two hexoses. The two hexose moieties are assigned as α-D-fructofuranose and β-D-fructofuranose by $^{1}H-^{1}H$ COSY (see Figure S3A of the Supporting Information) and $^{1}H-^{13}C$ HSQC (see Figure S3B of the Supporting Information). As shown in Figure 2, the C2 of α-D-fructofuranose (δ_C, 106.30 ppm) and the C2′ of β-D-fructofuranose (δ_C, 106.30 ppm) have HMBC correlation with the H3′ of β-D-fructofuranose (δ_H, 106.30 ppm) and the H1 of α-D-fructofuranose (δ_H, 106.30 ppm), respectively, indicating the α-D-fructofuranose (2, 3′) β-D-fructofuranose and α-D-fructofuranose (2′, 1) β-D-fructofuranose connectivities, respectively. Therefore, the produced compound is determined as α-D-fructofuranose-β-D-fructofuranose 2′,1:2,3′-dianhydride (DFA III).

Effect of the pH and Temperature on the Recombinant Enzyme. The purified recombinant IFTase (DFA III forming) from *Arthrobacter* sp. 161MFSha2.1 shows relatively high activity under acidic conditions and exhibits optimum activity at pH 6.5 in 50 mM phosphate buffer (Figure 3). Its relative activity is more than 80% of the maximal activity under the pH range of 5.0−6.5 and decreases sharply when pH is shifted to the alkaline side.

The optimal temperature of the recombinant enzyme is determined to be 55 °C (Figure 4A). The relative activity is kept at more than 95% of the maximal activity at the temperatures between 50 and 60 °C but decreases obviously at other temperatures. Although the relative activity is sensitive to the temperature (Figure 4A), the enzyme displays remarkably thermal stability (Figure 4B). When incubated at 55, 60, 70, and 80 °C for 4 h, the enzyme still retains 91, 86, 77, and 51% initial activity.

Reaction Product Analysis. The recombinant enzyme shows specific activity at 2391 units/mg at optimum reaction conditions (pH 6.5 and 55 °C). When the substrate inulin is depolymerized completely by using excess recombinant enzyme, the reaction mixtures analyzed by HPLC contain DFA III as the main product and some minor products composed of sucrose (GF), GF_2, and GF_3. In addition, the catalytic activities toward different types of fructosyl oligosaccharides, such as GF_2 and GF_3, are tested. The recombinant enzyme cannot act on GF_2 but hydrolyzed GF_3 to DFA III and GF, suggesting that the smallest substrate is GF_3.

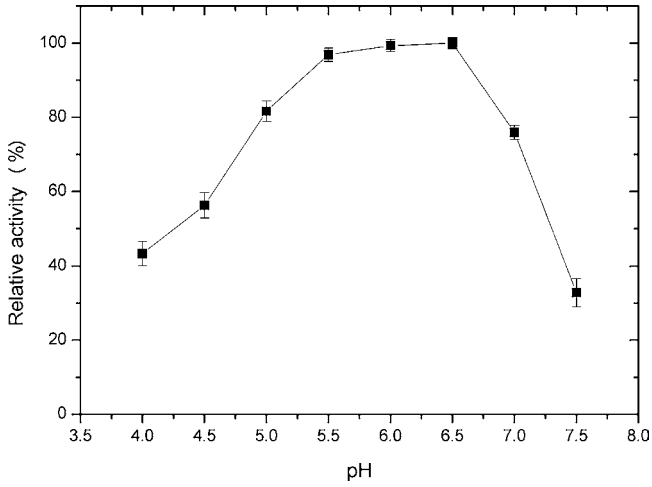

Figure 3. Effect of the pH on the recombinant enzyme activity. The enzyme was mixed with various buffers (50 mM): acetate buffer (pH 4.0−5.5), phosphate buffer (pH 6.0−7.0), and Tris−HCl buffer (pH 7.5−8.0). The maximal enzyme activity was set as a reference value of 100%, and relative activity was expressed as a percentage of the maximal activity. Each point represents the mean (n = 3) ± standard deviation.

Conversion of Inulin to DFA III by Recombinant IFTase. Under the optimum pH and temperature, biological production of DFA III is studied using 80 nM recombinant enzyme and various concentrations of substrate inulin. The conversion of inulin to DFA III reaches 88, 81, and 58% after reaction for 20 min, when the initial inulin concentration is set as 50, 100, and 200 g/L, respectively (Figure 5).

DISCUSSION

Thus far, there are two types of IFTases that have been identified, which depolymerize inulin to DFA III and DFA I (α-D-fructofuranose-β-D-fructofuranose 2′,1:2,1′-dianhydride), respectively.[16,34] Both types of IFTases have been mostly characterized from *Arthrobacter* species strains.[16] The genomic sequence of *Arthrobacter* sp. 161MFSha2.1 has recently been released in the GenBank database (accession number NZ_ARGU01000000). In the genome, there is an annotated gene encoding a hypothetical protein (accession number WP_018778058) proposed as fructotransferase. The protein displays relatively high homology with both IFTase (DFA III forming) and IFTase (DFA I forming). In this work, the protein was heterologously expressed in *E. coli*, and the recombinant protein was purified and characterized. The purified recombinant enzyme displayed depolymerization activity toward inulin. The reaction product from inulin was purified and determined as DFA III by NMR analysis. Thus, the enzyme was identified as IFTase (DFA III forming).

On the basis of the results of SDS−PAGE and gel filtration, the recombinant enzyme was suggested as a homotrimer. It was the same as the result of the crystal structure of *Bacillus* sp. IFTase (DFA III forming).[14] Also, the IFTase (DFA III forming) from *Arthrobacter* sp. A-6 was a trimeric enzyme.[21] However, other characterized IFTases were suggested as monomers or dimers. For examples, the IFTases from *A.*

DOI: 10.1021/jf506165n
J. Agric. Food Chem. 2015, 63, 3509−3515

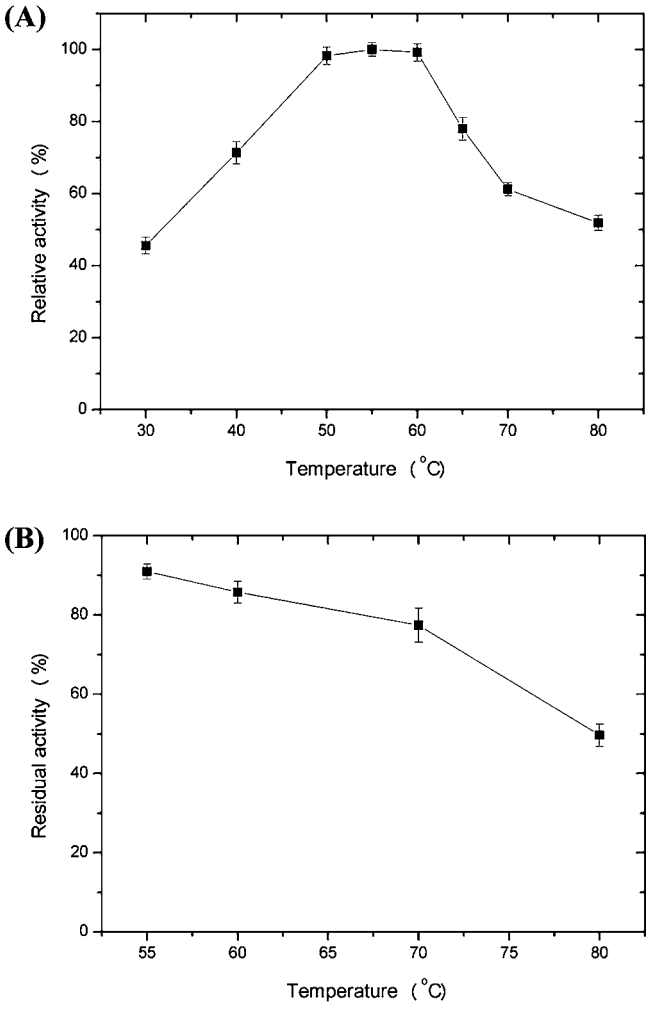

Figure 4. Effect of the temperature on the activity and stability of the recombinant enzyme. (A) Effect of the temperature on the enzyme activity. The maximal enzyme activity was set as a reference value of 100%, and relative activity was expressed as a percentage of the maximal activity. (B) Effect of the temperature on the enzyme stability. The effect on stability was studied by incubating the enzyme for 4 h at different temperatures, and the activity of the unincubated enzyme was taken as 100%. Each point represents the mean (n = 3) ± standard deviation.

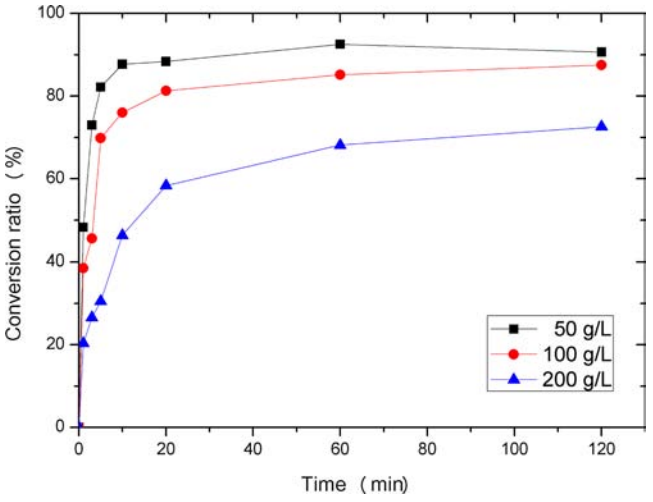

Figure 5. Production of DFA III from inulin by the recombinant enzyme. Three initial concentrations of inulin, 50, 100, and 200 g/L, were used for DFA III production.

aurescens SK 8.001,[27] *A. ureafaciens* D13-3,[25] *Flavobacterium* sp. LC-413,[28] and *A. globiformis* C11-1 were monomers,[17] and the IFTases from *Leifsonia* sp. T88-4,[31] *Arthrobacter* sp. L68-1,[24] *A. pascens* T13-2,[23] *Arthrobacter* sp. H65-7,[20] and *A. ilicis* OKU17B[19] were dimers.

The recombinant enzyme displayed maximal activity at pH 6.5 and 55 °C. The optimum pH and temperature were not much different from those of other reported IFTases (DFA III forming).[16] However, the IFTase (DFA III forming) from *Arthrobacter* sp. 161MFSha2.1 exhibited very high specific activity and significant thermostability when compared to others (Table 2). The specific activity reached 2391 units/mg, which was only less than that of IFTase (DFA III forming) from *Flavobacterium* sp. LC-413 (5728 units/mg).[28] Interestingly, the IFTases (DFA III forming) from non-*Arthrobacter* strains have relatively high specific activities (>1000 units/mg), except the IFTase from *Leifsonia* sp. T88-4 (644 units/mg).[16] By comparison, the IFTases from *Arthrobacter* strains show specific activities below 1000 units/mg, except the IFTases from *Arthrobacter* sp. A-6 (1,195 units/mg)[21] and the herein-reported *Arthrobacter* sp. 161MFSha2.1 (2391 units/mg).

On the contrary, the non-*Arthrobacter* IFTases (DFA III forming) with high specific activity usually display low thermostability (Table 2). For examples, the IFTases (DFA III forming) from *Nonomuraea* sp. ID06A0189[16] and *Leifsonia* sp. T88-4[31] were completely inactivated after incubation at 80 °C for 20 min and at 70 °C for 30 min, respectively; the IFTase from *Bacillus* sp. snu-7 was rapidly inactivated at 70 °C with half-life of only 6.6 min;[30] and the IFTase from *Flavobacterium* sp. LC-413 retained less than half of the initial activity when incubated above 75 °C for 30 min.[28] In comparison, some *Arthrobacter* IFTases exhibited higher thermostability. The IFTases (DFA III forming) from *A. aurescens* SK 8.001[27] and *Arthrobacter* sp. L68-1[24] were stable up to 70 and 80 °C, respectively, after 30 min of incubation, and the IFTase from *Arthrobacter* sp. A-6 retained more than half of the initial activity after 300 min of incubation at 70 °C.[21] Herein, a novel thermostable IFTase (DFA III forming) was reported having the highest thermostability, which was stable up to 80 °C for 4 h of incubation. Therefore, IFTase (DFA III forming) from *Arthrobacter* sp. 161MFSha2.1 has great potential for industrial application for DFA III production, because of both high specific activity and significant thermostability.

The smallest substrate was determined to be GF_3. IFTases (DFA III forming) from *A. aurescens* SK 8.001[26,27] and *Bacillus* sp. snu-7[29] displayed the smallest substrate as GF_3 and fructofuranosyl nystose (GF_4), respectively (Table 2). In this study, the recombinant enzyme degraded inulin to DFA III as a major product and small amounts of GF, GF_2, and GF_3. The result was the same as that of *A. ureafaciens* D13-3.[25] In comparison, the IFTases (DFA III forming) from *Arthrobacter* sp. L68-1,[24] *A. pascens* T13-2,[23] *Arthrobacter* sp. A-6,[21] and *Leifsonia* sp. T88-4[31] produced GF_3 and GF_4 as minor products. The IFTase from *A. aurescens* SK 8.001 produced small amounts of GF_2, GF_3, and GF_4.[26] The native crude IFTase from *Nonomuraea* sp. ID06A0189 could produce a very small amount of D-fructose,[33] while D-fructose was not produced from inulin by the purified recombinant enzyme.[32] The authors suggested that the *Nonomuraea* sp. ID06A0189 might also secrete other inulin-degrading enzymes to produce D-fructose.[32]

DOI: 10.1021/jf506165n
J. Agric. Food Chem. 2015, 63, 3509−3515

Table 2. Comparison of Biochemical Properties of Various Microbial IFTases (DFA III Forming)

microbial source	strain	native or recombinant	specific activity (units/mg)	thermostability[a]	minor reaction products from inulin	smallest substrate	reference
Arthrobacter strains	*Arthrobacter* sp. 161MFSha2.1	recombinant	2391	80 °C; 240 min	GF, GF_2, and GF_3	GF_3	this study
	A. aurescens SK 8.001	recombinant	NR[b]	70 °C; 60 min	GF_2, GF_3, and GF_4	GF_3	26
	A. aurescens SK 8.001	native	381	70 °C; 60 min	NR	GF_3	27
	A. ureafaciens D13-3	native	290	70 °C; 30 min	GF, GF_2, and GF_3	NR	25
	Arthrobacter sp. L68-1	native	NR	80 °C; 60 min	GF_3 and GF_4	NR	24
	A. pascens T13-2	native	NR	75 °C; 20 min	GF_3 and GF_4	NR	23
	Arthrobacter sp. A-6	native	1195	70 °C; >300 min 80 °C; <60 min	GF_3 and GF_4	NR	21
	Arthrobacter sp. H65-7	native	NR	70 °C; 20 min	NR	NR	20
	A. ilicis OKU17B	native	853	70 °C; 30 min	NR	NR	19
	A. globiformis C11-1	recombinant	227	NR	NR	NR	18
	A. globiformis C11-1	native	294	75 °C; 20 min	NR	NR	17
	A. ureafaciens	native	162.4	50 °C; 30 min	NR	NR	15
non-*Arthrobacter* strains	*Nonomuraea* sp. ID06A0189	recombinant	1991	70 °C; 20 min	NR	NR	32
	Nonomuraea sp. ID06A0189	native[c]	NR	70 °C; 20 min[c]	D-fructose, GF_2, GF_3, and GF_4[c]	NR	33
	Leifsonia sp. T88-4	native	644	60 °C; 30 min	GF_3 and GF_4	NR	31
	Bacillus sp. snu-7	recombinant	1276	60 °C; 103 min	NR	NR	30
	Bacillus sp. snu-7	native	48.5	60 °C; 10 min	GF_2 and GF_3	GF_4	29
	Flavobacterium sp. LC-413	native	5728	75 °C; 30 min	GF_2	NR	28

[a]The values showed that the enzyme could remain more than half of the initial activity after incubation at a specified temperature for a specified time. [b]NR = not reported. [c]The biochemical properties were characterized using crude enzyme.

■ ASSOCIATED CONTENT

Supporting Information

(A) ^{13}C and (B) ^{1}H NMR spectra of the main product produced from inulin by the recombinant enzyme (Figure S1) and (A) $^{1}H-^{1}H$ COSY and (B) $^{1}H-^{13}C$ HSQC spectra of of the main product produced from inulin by the recombinant enzyme (Figure S3). This material is available free of charge via the Internet at http://pubs.acs.org.

■ AUTHOR INFORMATION

Corresponding Author

*Telephone/Fax: 86-510-85919161. E-mail: wmmu@jiangnan.edu.cn.

Funding

This work was supported by the National Natural Science Foundation of China (NSFC) Project (31371788 and 21276001), the 863 Project (2013AA102102), the Fundamental Research Funds for the Central Universities (JUSRP51304A), and the Support Project of Jiangsu Province (BK20130001).

Notes

The authors declare no competing financial interest.

■ ABBREVIATIONS USED

DFA, difructose anhydride; IFTase, inulin fructotransferase; GF, sucrose; GF_2, 1-kestose; GF_3, nystose; GF_4, fructofuranosyl nystose; IPTG, isopropyl β-D-1-thiogalactopyranoside; LB, Luria−Bertani; SDS−PAGE, sodium dodecyl sulfate−polyacrylamide gel electrophoresis; HPLC, high-performance liquid chromatography; NCBI, National Center for Biotechnology Information; DSS, 4,4-dimethyl-4-silapentane-1-sulfonate

■ REFERENCES

(1) Nair, K. K.; Kharb, S.; Thompkinson, D. K. Inulin dietary fiber with functional and health attributes, a review. *Food Rev. Int.* **2010**, *26*, 189−203.

(2) Chi, Z. M.; Zhang, T.; Cao, T. S.; Liu, X. Y.; Cui, W.; Zhao, C. H. Biotechnological potential of inulin for bioprocesses. *Bioresour. Technol.* **2011**, *102*, 4295−4303.

(3) Chen, X. M.; Xu, X. M.; Jin, Z. Y.; Chen, H. Q. Expression of an endoinulinase from *Aspergillus ficuum* JNSP5-06 in *Escherichia coli* and its characterization. *Carbohydr. Polym.* **2012**, *88*, 748−753.

(4) Singh, R.S.; Dhaliwal, R.; Puri, M. Production of high fructose syrup from *Asparagus* inulin using immobilized exoinulinase from *Kluyveromyces marxianus* YS-1. *J. Ind. Microbiol. Biotechnol.* **2007**, *34*, 649−655.

(5) Hang, H.; Mu, W.; Jiang, B.; Zhao, M.; Zhou, L. L.; Zhang, T.; Miao, M. Recent advances on biological difructose anhydride III production using inulase II from inulin. *Appl. Microbiol. Biotechnol.* **2011**, *92*, 457−465.

(6) Kikuchi, H.; Nagura, T.; Inoue, M.; Kishida, T.; Sakurai, H.; Yokota, A.; Asano, K.; Tomita, F.; Sayama, K.; Senba, Y. Physical, chemical and physiological properties of difructose anhydride III produced from inulin by enzymatic reaction. *J. Appl. Glycosci.* **2004**, *51*, 291−296.

(7) Minamida, K.; Ohashi, M.; Hara, H.; Asano, K.; Tomita, F. Effects of ingestion of difructose anhydride III (DFA III) and the DFA III-assimilating bacterium *Ruminococcus* productus on rat intestine. *Biosci., Biotechnol., Biochem.* **2006**, *70*, 332−339.

(8) Minamida, K.; Shiga, K.; Sujaya, I. N.; Sone, T.; Yokota, A.; Hara, H.; Asano, K.; Tomita, F. Effects of difructose anhydride III (DFA III) administration on rat intestinal microbiota. *J. Biosci. Bioeng.* **2005**, *99*, 230−236.

(9) Hara, H.; Onoshima, S.; Nakagawa, C. Difructose anhydride III promotes iron absorption in the rat large intestine. *Nutrition* **2010**, *26*, 120−127.

(10) Mineo, H.; Amano, M.; Minaminida, K.; Chiji, H.; Shigematsu, N.; Tomita, F.; Hara, H. Two-week feeding of difructose anhydride III enhances calcium absorptive activity with epithelial cell proliferation in isolated rat cecal mucosa. *Nutrition* **2006**, *22*, 312−320.

DOI: 10.1021/jf506165n
J. Agric. Food Chem. 2015, 63, 3509−3515

(11) Nakamori, M.; Hien, V. T.; Khan, N. C.; Lam, N. T.; Dung, N. T.; Uotsu, N.; Shiomi, T.; Okuhara, Y.; Kise, M.; Shigematsu, N.; Yamamoto, S. Difructose anhydride III enhances bioavailability of water-insoluble iron in anemic Vietnamese women. *J. Nutr. Sci. Vitaminol.* **2010**, *56*, 191−197.
(12) Matsumoto, M.; Matsukawa, N.; Chiji, H.; Hara, H. Difructose anhydride III promotes absorption of the soluble flavonoid αG-rutin in rats. *J. Agric. Food Chem.* **2007**, *55*, 4202−4208.
(13) Sato, T.; Hanada, M.; Ohtani, M.; Nakai, T.; Teramura, M.; Sadoya, H.; Takahashi, T.; Hongo, A. Short communication: Effect of difructose anhydride III on serum immunoglobulin G concentration in newborn calves. *J. Dairy Sci.* **2012**, *95*, 5336−5339.
(14) Jung, W. S.; Hong, C. K.; Lee, S.; Kim, C. S.; Kim, S. J.; Kim, S. I.; Rhee, S. Structural and functional insights into intramolecular fructosyl transfer by inulin fructotransferase. *J. Biol. Chem.* **2007**, *282*, 8414−8423.
(15) Uchiyama, T.; Niwa, S.; Tanaka, K. Purification and properties of *Arthrobacter ureafaciens* inulase II. *Biochim. Biophys. Acta* **1973**, *315*, 412−420.
(16) Wang, X.; Yu, S.; Zhang, T.; Jiang, B.; Mu, W. From fructans to difructose dianhydrides. *Appl. Microbiol. Biotechnol.* **2015**, *99*, 175−188.
(17) Haraguchi, K.; Kishimoto, M.; Seki, K.; Hayashi, K.; Kobayashi, S.; Kainuma, K. Purification and properties of inulin fructotransferase (depolymerizing) from *Arthrobacter globiformis* C11-1. *Agric. Biol. Chem.* **1988**, *52*, 291−292.
(18) Haraguchi, K.; Mori, S.; Hayashi, K. Cloning of inulin fructotransferase (DFA III-producing) gene from *Arthrobacter globiformis* C11-1. *J. Biosci. Bioeng.* **2000**, *89*, 590−595.
(19) Kawamura, M.; Takahashi, S.; Uchiyama, T. Purification and some properties of inulin fructotransferase depolymerizing from *Arthrobacter ilicis*. *Agric. Biol. Chem.* **1988**, *52*, 3209−3210.
(20) Yokota, A.; Enomoto, K.; Tomita, F. Purification and properties of an inulin fructotransferase (depolymerizing) from *Arthrobacter* sp. H65-7. *J. Ferment. Bioeng.* **1991**, *72*, 262−265.
(21) Kim, H. Y.; Kim, C. W.; Choi, Y. J. Cloning and expression of inulin fructotransferase gene of *Arthrobacter* sp A-6 in *Escherichia coli* and *Bacillus subtilis*. *J. Microbiol. Biotechnol.* **2000**, *10*, 275−280.
(22) Jahnz, U.; Schubert, M.; Vorlop, K. D. Effective development of a biotechnical process: Screening, genetic engineering, and immobilization for the enzymatic conversion of inulin to DFA III on industrial scale. *Landbauforsch. Volkenrode* **2001**, *51*, 131−136.
(23) Haraguchi, K.; Yamanaka, T.; Ohtsubo, K. Purification and properties of a heat stable inulin fructotransferase (DFA III-producing) from *Arthrobacter pascens* T13-2. *Carbohydr. Polym.* **2002**, *50*, 117−121.
(24) Haraguchi, K.; Yoshida, M.; Ohtsubo, K. Thermostable inulin fructotransferase (DFA III-producing) from *Arthrobacter* sp. L68-1. *Carbohydr. Polym.* **2005**, *59*, 411−416.
(25) Haraguchi, K. Inulin fructotransferase (DFAIII-producing) from *Arthrobacter ureafaciens* D13-3. *Carbohydr. Polym.* **2010**, *82*, 742−746.
(26) Zhao, M.; Mu, W.; Jiang, B.; Hang, H.; Zhou, L.; Zhang, T. Cloning and extracellular expression of inulin fructotransferase from *Arthrobacter aurescens* SK 8.001 in *E. coli*. *J. Sci. Food Agric.* **2011**, *91*, 2715−2721.
(27) Zhao, M.; Mu, W.; Jiang, B.; Zhou, L.; Zhang, T.; Lu, Z.; Jin, Z.; Yang, R. Purification and characterization of inulin fructotransferase (DFA III-forming) from *Arthrobacter aurescens* SK 8.001. *Bioresour. Technol.* **2011**, *102*, 1757−1764.
(28) Cho, C. M.; Lee, S. O.; Hwang, J. S.; Jang, K. L.; Lee, T. H. Purification and characterization of an inulin fructotransferase from *Flavobacterium* sp LC-413. *J. Microbiol. Biotechnol.* **1997**, *7*, 121−126.
(29) Kang, S. I.; Kim, W. P.; Chang, Y. J.; Kim, S. I. Purification and properties of inulin fructotransferase (DFA III-producing) from *Bacillus* sp. snu-7. *Biosci., Biotechnol., Biochem.* **1998**, *62*, 628−631.
(30) Kim, C. S.; Hong, C. K.; Kim, K. Y.; Wang, X. L.; Kang, S. I.; Kim, S. I. Cloning, expression, and characterization of *Bacillus* sp. snu-7 inulin fructotransferase. *J. Microbiol. Biotechnol.* **2007**, *17*, 37−43.
(31) Haraguchi, K.; Yoshida, M.; Ohtsubo, K. Inulin fructotransferase (DFA III-producing) from *Leifsonia* sp. T88-4. *Carbohydr. Polym.* **2006**, *66*, 75−80.
(32) Pudjiraharti, S.; Ohtani, M.; Takano, N.; Abe, A.; Lisdiyanti, P.; Tanaka, M.; Sone, T.; Asano, K. *Nonomuraea* sp. ID06-A0189 inulin fructotransferase (DFA III-forming): Gene cloning, characterization and conservation among other *Nonomuraea* species. *J. Antibiot.* **2014**, *67*, 137−141.
(33) Pudjiraharti, S.; Takesue, N.; Katayama, T.; Lisdiyanti, P.; Hanafi, M.; Tanaka, M.; Sone, T.; Asano, K. Actinomycete *Nonomuraea* sp. isolated from Indonesian soil is a new producer of inulin fructotransferase. *J. Biosci. Bioeng.* **2011**, *111*, 671−674.
(34) Saito, K.; Tomita, F. Difructose anhydrides: Their mass-production and physiological functions. *Biosci., Biotechnol., Biochem.* **2000**, *64*, 1321−1327.
(35) Yokota, A.; Hirayama, S.; Enomoto, K.; Miura, Y.; Takao, S.; Tomita, F. Production of inulin fructotransferase (depolymerizing) by *Arthrobacter* sp. H65-7 and preparation of DFA III from inulin by the enzyme. *J. Ferment. Bioeng.* **1991**, *72*, 258−261.

DOI: 10.1021/jf506165n
J. Agric. Food Chem. 2015, 63, 3509−3515

Scheme 1. Synthesis and Structures of Coumarin-Fused Coumarins Employed in This Work

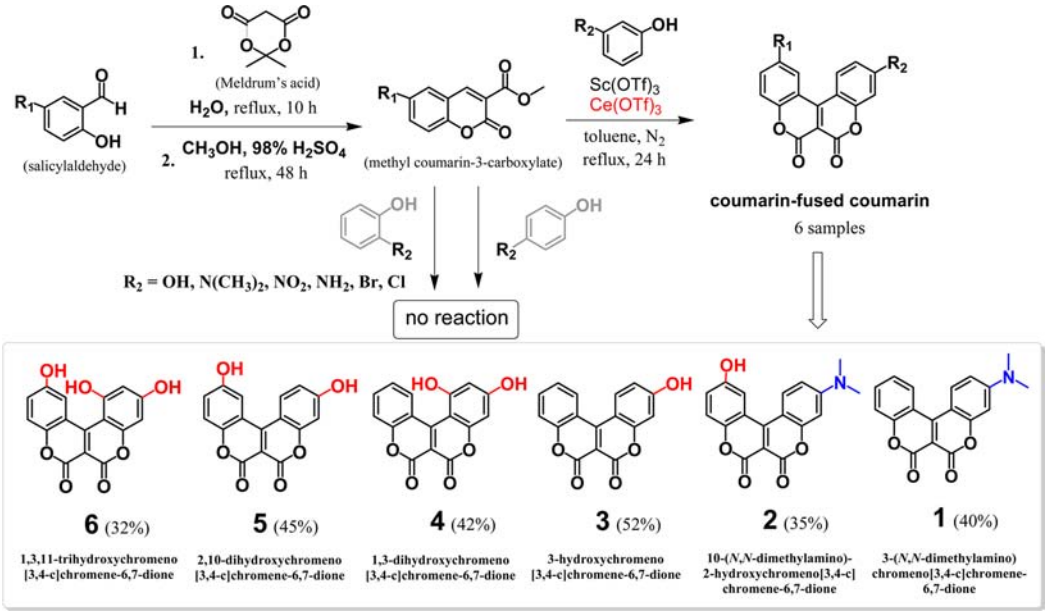

mmol) was refluxed in water (20 mL) under stirring for 10 h. Then, the mixture was cooled by ice water, and the precipitate was filtered and washed with ice water to obtain white or green product. The yields were higher than 93%.

Esterification of Coumarin-3-carboxylic Acids. To 20 mL of methanolic solution of coumarin-3-carboxylic acid (10 mmol), H_2SO_4 (98%, 0.6 mL) was added dropwisely under stirring. The above mixture was refluxed for 48 h and cooled to room temperature. After the solvent was evaporated under vacuum, the residue was purified by silica chromatography with ethyl acetate and petroleum ether (1:3, v/v) being eluent to afford a white product, yield >90%.

Oxidative Annulation for the Formation of Chromeno[3,4-*c*]chromene-6,7-diones. $Ce(OTf)_3$ (0.05 g), $Sc(OTf)_3$ (0.05 g), methyl coumarin-3-carboxylate (4 mmol), and phenol (2 mmol) were mixed in 10 mL of toluene and heated at 110 °C for 24 h under a protective atmosphere of N_2. Then, the mixture was cooled to room temperature by ice water, and the precipitate was purified by silica chromatography with methanol and dichloromethane being eluent to afford the product, yield 32%∼ 52%.

*3-(N,N-Dimethylamino)chromeno[3,4-c]chromene-6,7-dione (**1**).* R_f = 0.58 (CH_3OH:CH_2Cl_2 = 1:20, v/v), 0.25 g of red product, yield 40%. mp: 185−187 °C. ^{1}H NMR (400 MHz, $CDCl_3$) δ: 8.21 (d, J = 8.0 Hz, 1H), 8.07 (d, J = 9.6 Hz, 1H), 7.66 (t, J = 8.0 Hz, 1H), 7.37−7.40 (m, 2H), 6.72 (dd, J = 2.4 Hz, J = 9.2 Hz, 1H), 6.51 (d, J = 10.4 Hz, 1H), 3.15 (s, 6H). ^{13}C NMR (100 MHz, $CDCl_3$) δ: 157.8, 157.0, 156.7, 154.9, 152.8, 134.1, 130.0, 128.7, 124.2, 118.1, 109.9, 104.5, 100.6, 98.1, 40.1. MS: m/z 308.0925 [M+H$^+$].

*10-(N,N-Dimethylamino)-2-hydroxychromeno[3,4-c]-chromene-6,7-dione (**2**).* R_f = 0.21 (CH_3OH:CH_2Cl_2 = 1:20, v/v), 0.23 g of red product, yield 35%. mp: > 300 °C. ^{1}H NMR (400 MHz, DMSO-d_6) δ: 9.94 (s, 1H), 8.13 (d, J = 9.6 Hz, 1H), 7.67 (s, 1H), 7.20−7.34 (m, 2H), 6.90 (d, J = 9.6 Hz, 1H), 6.65 (s, 1H), 3.14 (s, 6H). ^{13}C NMR (100 MHz, DMSO-d_6) δ: 157.6, 156.4, 154.9, 152.1, 147.8, 130.3, 128.2, 122.9, 118.9, 116.3, 113.6, 110.5, 104.1, 100.2, 97.8, 42.0. MS: m/z 324.0877 [M + H$^+$].

*3-Hydroxychromeno[3,4-c]chromene-6,7-dione (**3**).* R_f = 0.63 (CH_3OH:CH_2Cl_2 = 1:10, v/v), 0.29 g of yellow product, yield 52%. mp: > 300 °C. ^{1}H NMR (400 MHz, DMSO-d_6) δ: 11.30 (s, 1H), 8.37 (d, J = 8.0 Hz, 1H), 8.29 (d, J = 9.2 Hz, 1H), 7.82 (t, J = 7.6 Hz, 1H), 7.47−7.51 (m, 2H), 6.96 (dd, J = 2.4 Hz, J = 9.2 Hz, 1H), 6.82 (d, J = 2.4 Hz, 1H). ^{13}C NMR (100 MHz, DMSO-d_6) δ: 164.5, 157.3, 155.7, 154.6, 152.7, 135.1, 131.5, 129.7, 125.1, 117.9, 115.6, 114.6, 107.6, 103.4. MS: m/z 281.0459 [M + H$^+$].

*1,3-Dihydroxychromeno[3,4-c]chromene-6,7-dione (**4**).* R_f = 0.52 (CH_3OH:CH_2Cl_2 = 1:10, v/v), 0.25 g of orange product, yield 42%. mp: > 300 °C. ^{1}H NMR (400 MHz, DMSO-d_6) δ: 11.23 (s, 1H), 11.02 (s, 1H), 7.98 (dd, J = 1.2 Hz, J = 8.4 Hz, 1H), 7.70 (td, J = 1.6 Hz, J = 8.4 Hz, 1H), 7.38 (dd, J = 1.2 Hz, J = 8.0 Hz, 1H), 7.32 (td, J = 1.2 Hz, J = 8.4 Hz, 1H), 6.42 (d, J = 1.2 Hz, 1H), 6.30 (d, J = 2.0 Hz, 1H). ^{13}C NMR (100 MHz, DMSO-d_6) δ: 164.8, 158.3, 157.2, 155.7, 154.3, 153.7, 134.3, 132.0, 122.7, 116.1, 115.8, 102.9, 100.2, 98.2, 94.8. MS: m/z 297.0405 [M + H$^+$].

*2,10-Dihydroxychromeno[3,4-c]chromene-6,7-dione (**5**).* R_f = 0.52 (CH_3OH:CH_2Cl_2 = 1:10, v/v), 0.25 g of orange product, yield 45%. mp: > 300 °C. ^{1}H NMR (400 MHz, DMSO-d_6) δ: 11.27 (s, 1H), 9.97 (s, 1H), 8.26 (d, J = 9.2 Hz, 1H), 7.70 (s, 1H), 7.24−7.38 (m, 2H), 6.98 (d, J = 8.4 Hz, 1H), 6.82 (s, 1H). ^{13}C NMR (100 MHz, DMSO-d_6) δ: 163.7, 157.3, 156.2, 154.3, 149.3, 147.9, 131.0, 123.3, 122.7, 119.5, 118.8, 114.2, 113.5, 107.4, 106.3, 103.4. MS: m/z 297.0403 [M + H$^+$].

*1,3,11-Trihydroxychromeno[3,4-c]chromene-6,7-dione (**6**).* R_f = 0.37 (CH_3OH:CH_2Cl_2 = 1:5, *v*:*v*), 0.20 g of red product, yield 32%. mp: > 300 °C. ^{1}H NMR (400 MHz, DMSO-d_6) δ: 9.63 (s, 1H), 9.37 (s, 1H), 9.33 (s, 1H), 7.31 (d, J = 8.8 Hz, 1H), 7.05 (dd, J = 2.8 Hz, J = 8.8 Hz, 1H), 6.62 (d, J = 2.8 Hz, 1H), 5.90 (s, 2H). ^{13}C NMR (100 MHz, DMSO-d_6) δ: 165.0, 160.0, 158.4, 156.3, 154.3, 151.3, 146.4, 125.9, 122.7, 121.2, 120.6, 119.5, 117.6, 112.6, 99.5. MS: m/z 313.0357 [M + H$^+$].

Cu^{2+}/GSH- and $^{\bullet}$OH-Induced Oxidations of DNA. Cu^{2+}/GSH-induced oxidation of DNA was carried out in a mixture of DNA (2.0 mg/mL), $CuSO_4$ (5.0 mM), and glutathione (GSH,

DOI: 10.1021/acs.jafc.5b00399
J. Agric. Food Chem. 2015, 63, 3516−3523

Scheme 2. TBARS Percentages (Data on the Column) in the Presence of 0.10 mM Coumarin-Fused Coumarins When the Oxidation of DNA (2.0 mg/mL) Is Caused by 5.0 mM Cu^{2+} and 3.0 mM GSH for 90 min (Right Column for Every Compound) or 4.0 mM H_2O_2 and 2.0 mM TCHQ for 30 min (Left Column for Every Compound)

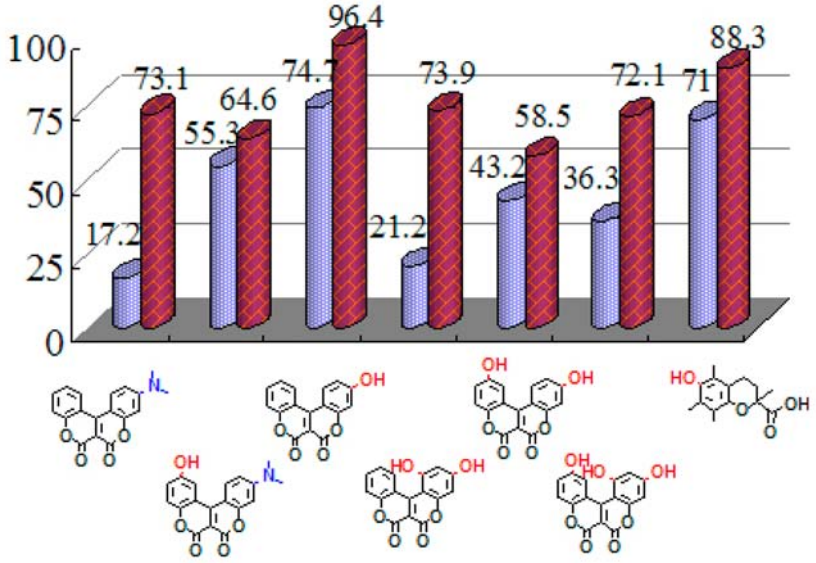

3.0 mM), which were dissolved in phosphate-buffered solution (PBS_1: 6.1 mM Na_2HPO_4, 3.9 mM NaH_2PO_4, pH = 7.0). The coumarin-fused coumarin was dissolved in dimethyl sulfoxide (DMSO) as the stock solution and added to the aforementioned solution. The final concentration of tested compound was 0.10 mM, and the volume of DMSO was less than 0.5% in the total volume of the solution. The mixture of DNA, Cu^{2+}, GSH, and coumarin-fused coumarin was delivered into test tubes in a total volume of 2.0 mL. The control experiment contained the same volume of DMSO without the tested compounds dissolved. The test tubes were incubated at 37 °C for initiating the DNA oxidation, and three of them were taken out at 90 min and cooled immediately. PBS_1 solution of EDTA (1.0 mL, 30.0 mM) was added to chelate Cu^{2+}, followed by adding 1.0 mL of thiobarbituric acid (TBA) solution (1.00 g of TBA and 0.40 g of NaOH dissolved in 100 mL of PBS_1) and 1.0 mL of 3.0% aqueous solution of trichloroacetic acid. The test tubes were heated in boiling water for 30 min and cooled to room temperature by ice water; subsequently, 1.5 mL of *n*-butanol was added and shaken vigorously to extract thiobarbituric acid reactive substance (TBARS) for measuring the absorbance at 535 nm.

$^{\bullet}OH$-induced oxidation of DNA was performed in a mixture of DNA (2.0 mg/mL), tetrachlorohydroquinone (TCHQ, 4.0 mM, dissolved in DMSO as the stock solution), and H_2O_2 (2.0 mM), which were dissolved in phosphate-buffered solution (PBS_2: 8.1 mM Na_2HPO_4, 1.9 mM NaH_2PO_4, 10.0 μM EDTA, pH = 7.4). The coumarin-fused coumarin was dissolved in DMSO as the stock solution and added to the aforementioned solution with a final concentration being 0.10 mM, while the volume of DMSO was less than 0.5% in the total volume of the solution. The solution of DNA, TCHQ, H_2O_2, and coumarin-fused coumarin was delivered into test tubes in a total volume of 2.0 mL. The control experimental system contained the same volume of DMSO without the tested compounds dissolved. The test tubes were incubated at 37 °C for initiating the oxidation of DNA, and three of them were taken out at 30 min and cooled immediately. Then, 1.0 mL of TBA solution (1.00 g of TBA and 0.40 g of NaOH dissolved in 100 mL of PBS_2) and 1.0 mL of 3.0% aqueous solution of trichloroacetic acid were added and heated in boiling water for 30 min. After the test tubes were cooled to room temperature by ice water, 1.5 mL of *n*-butanol was added and shaken vigorously to extract TBARS for measuring the absorbance at 535 nm. In the aforementioned two tests, the absorbances in the control experiment and in the presence of coumarin-fused coumarins were assigned as A_0 and A_{detect}, respectively. The effects of coumarin-fused coumarins on the oxidation of DNA were expressed by $A_{detect}/A_0 \times 100$, called TBARS percentage.

AAPH-Induced Oxidation of DNA Test. AAPH-induced oxidation of DNA was performed in a mixture of DNA (2.0 mg/mL, dissolved in PBS_2) and AAPH (40.0 mM, dissolved in PBS_2). The solution of DNA, AAPH, and a certain concentration of coumarin-fused coumarin (dissolved in DMSO as the stock solution) was delivered into test tubes in a total volume of 2.0 mL. The control experimental system contained the same volume of DMSO (0.5% of the total volume) without the tested compounds dissolved. The test tubes were incubated at 37 °C for initiating the oxidation of DNA, and three of them were taken out at every 2 h and cooled by ice water. Then, 1.0 mL of TBA solution (1.00 g of TBA and 0.40 g of NaOH dissolved in 100 mL of PBS_2) and 1.0 mL of 3.0% aqueous solution of trichloroacetic acid were added and heated in boiling water for 15 min. After the test tubes were cooled to room temperature, 1.5 mL of *n*-butanol was added and shaken vigorously to extract TBARS for measuring the absorbance at 535 nm. The absorbance of TBARS was plotted versus the reaction period.

Scavenging $ABTS^{+\bullet}$, DPPH, and Galvinoxyl Radicals. A 2.0 mL aqueous solution containing 4.0 mM ABTS salt and 1.41 mM $K_2S_2O_8$ was kept for 20 h to form $ABTS^{+\bullet}$ and then diluted by 100 mL of ethanol. The absorbance of $ABTS^{+\bullet}$ was around 1.00 at 734 nm ($\varepsilon_{ABTS^{+\bullet}} = 1.6 \times 10^4\ M^{-1}\ cm^{-1}$). DPPH and galvinoxyl radicals were dissolved in ethanol, respectively. The absorbances of DPPH and galvinoxyl radicals were around 1.00 at 517 nm ($\varepsilon_{DPPH} = 4.09 \times 10^3\ M^{-1}cm^{-1}$) and 428 nm ($\varepsilon_{galvinoxyl} = 1.4 \times 10^5\ M^{-1}cm^{-1}$), respectively. A certain concentration of DMSO solution of coumarin-fused coumarin

DOI: 10.1021/acs.jafc.5b00399
J. Agric. Food Chem. 2015, 63, 3516−3523

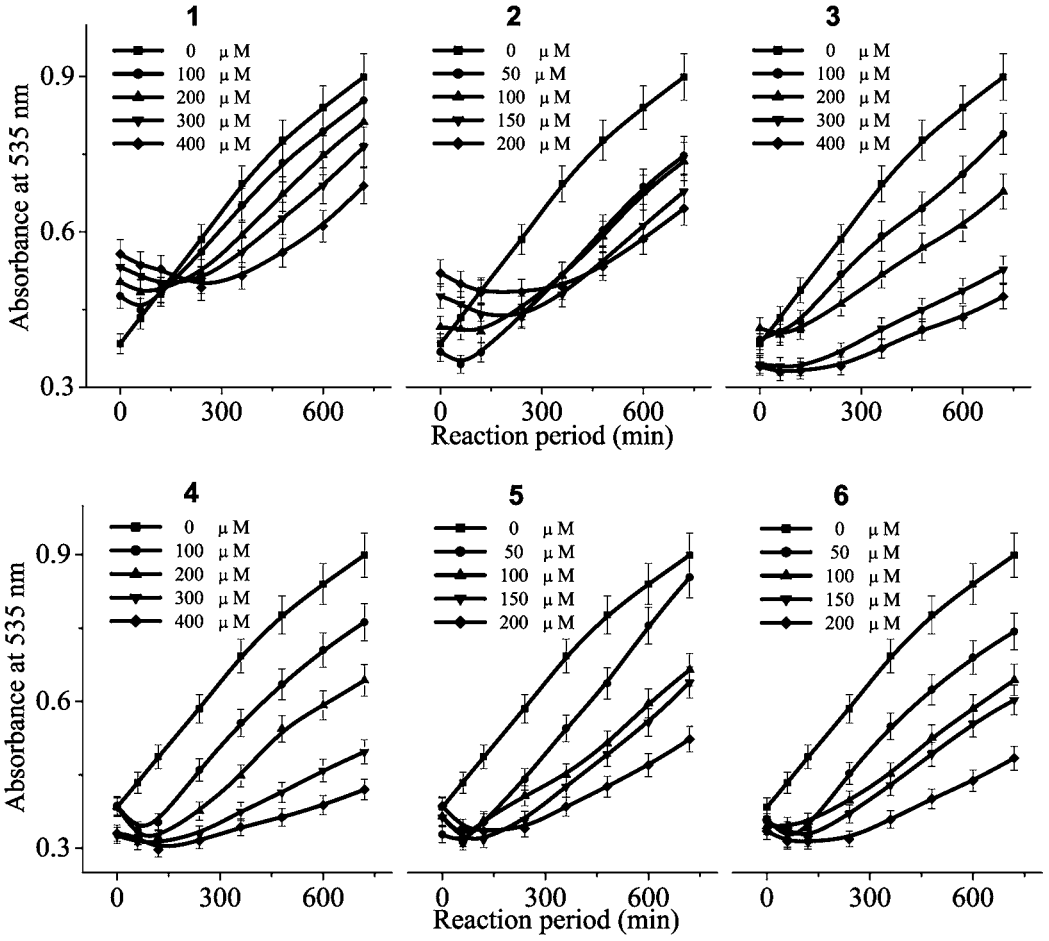

Figure 1. Variation of the absorbance of TBARS in the mixture of 2.0 mg/mL DNA, 40 mM AAPH, and various concentrations of coumarin-fused coumarins at 37 °C.

(0.1 mL) were added to 1.9 mL of $ABTS^{+\bullet}$, DPPH, and galvinoxyl radicals solution, respectively. The decreases of the absorbance of these radicals were recorded at 25 °C at a certain time interval.

Statistical Analysis. All the data were the average values from at least three independent measurements with the experimental error within 10%. The equations were analyzed by one-way ANOVA in Origin 6.0 professional software, and $p < 0.001$ indicated a significance difference.

RESULTS AND DISCUSSION

Synthesis of Coumarin-Fused Coumarins. Many efforts are contributed to develop synthetic protocols for constructing coumarin-fused heterocycles. The C═C in the lactone of coumarin possesses high reactivity for driving nucleophilic addition, leading to the formation of the fused heterocyclic[15] or spirocyclic coumarins.[16] For example, the C═C in the lactone can be shared with the C−C in cycloheptanone, forming a tricyclic fused coumarin as NO inhibitor.[17] In the synthetic operation, some novel techniques such as ultrasound vibration[18] and solvent-free heating[19] are widely used, but the formation of the lactone for coumarin-fused coumarin scaffold still depends upon appropriate catalysts. For example, the usage of cationic ruthenium complex catalyzes Diels−Alder reaction of enediynes can produce coumarin-fused polycycles.[20] The Cu(II) and Pb(II) are able to drive the cyclization of lactone,[21] and $Sc(OTf)_3$ can lead to the formation of chromeno[3,4-*c*]chromene- 6,7-dione, called coumarin-fused coumarin (see Scheme 1) in the yield of 33% with nitrobenzene being oxidant.[7] In this work, we follow our previously reported method[22] to apply $Ce(OTf)_3$ as the oxidant (instead of nitrobenzene) for catalyzing the annulation of methyl coumarin-3-carboxylate and *m*-substituted phenol. The mild oxidizability of $Ce(OTf)_3$ cannot oxidize the phenolic hydroxyl groups when resorcinol and phloroglucinol act as reactants in the synthesis of **3** ∼ **6**, and $Ce(OTf)_3$ can be conveniently removed in the purification of products via silica chromatography. The methyl 6-hydroxy-coumarin-3-carboxylate (a single coumarin scaffold) is prepared following a reported method,[23] and toluene is applied for the annulation between the single

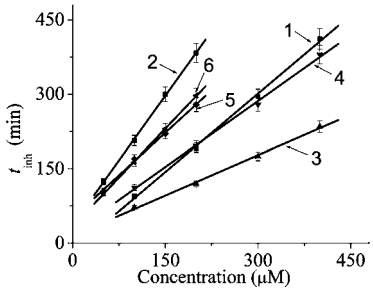

Figure 2. Linear relationships between concentrations of coumarin-fused coumarins and inhibition period (t_{inh}) in protecting DNA against AAPH-induced oxidation.

DOI: 10.1021/acs.jafc.5b00399
J. Agric. Food Chem. 2015, 63, 3516−3523

Table 1. Equations of t_{inh} ~ [Coumarin-Fused Coumarin] and *n* of Coumarin-Fused Coumarin in Protecting DNA against AAPH-Induced Oxidation[a]

compd	t_{inh} (min) = (n/R_i) [coumarin-fused coumarin (μM)] + constant[b]	n
1	t_{inh} = 1.05 (±0.05) [**1**] + 14.73 (±0.74)	3.53(±0.18)
2	t_{inh} = 1.74 (±0.09) [**2**] + 36.35 (±1.82)	5.85(±0.29)
3	t_{inh} = 0.54 (±0.03) [**3**] + 14.45 (±0.72)	1.81(±0.09)
4	t_{inh} = 0.89 (±0.04) [**4**] + 20.40(±1.02)	2.99(±0.15)
5	t_{inh} = 1.14 (±0.06) [**5**] + 50.73 (±2.54)	3.83(±0.19)
6	t_{inh} = 1.31 (±0.07) [**6**] + 33.52 (±1.68)	4.40(±0.22)

[a] $R_i = R_g = 1.4 \times 10^{-6}$ [AAPH] s^{-1} = 3.36 μM·min^{-1} when 40 mM AAPH was employed, thus, n = coefficient ×3.36 μM·min^{-1}. [b]The constant was generated from the linear regression analysis.

coumarin scaffold and *m*-substituted phenol because of the temperature controlled around 140 °C. We have attempted to enlarge the scale of suitable phenols for the annulation. As shown in Scheme 1, *ortho*- and *para*-substituted phenols are applied to carry out the reaction, and −OH, $-N(CH_3)_2$, and $-NH_2$ represent the electron-donating group (EDG), while $-NO_2$, −Br, and −Cl stand for the electron-withdrawing group (EWG). The annulation for forming coumarin-fused coumarin scaffold is not successful when the EDG or EWG (as R_2) locates at *ortho*- or *para*-position in the phenol because the first step in the formation of coumarin-fused coumarin is a transesterification between the methyl group in coumarin-3-carboxylate and the hydroxyl group in *meta*-substituted phenol, and then, the carbon atom at *para*-position in the phenol performs a C−C coupling reaction with the carbon atom in the lactone of coumarin. An EDG as $\mathbf{R_2}$ in the phenol is beneficial for the C−C coupling reaction, and other functional groups cannot take place in the same reaction. So, the limitation of the present synthetic protocol results in that only EDG at *meta*-position of phenol can successfully produce the coumarin-fused coumarin scaffold, and thus, we just explore the interaction of −OH (at the same or different benzene ring) and $-N(CH_3)_2$ (as a typical EDG) on the antioxidant effectiveness and do not mention coumarin-fused coumarins with other functional groups contained.

Inhibiting Cu^{2+}/GSH and •OH-Induced Oxidations of DNA. The glutathione radical (GS•) can be produced by the reaction of glutathione (GSH) and Cu^{2+},[24] while •OH can be produced by the reaction of H_2O_2 and tetrachlorohydroquinone (TCHQ).[25] DNA is susceptible to be oxidized by GS• and •OH, and the inhibitory effects on Cu^{2+}/GSH and •OH-induced oxidations of DNA are important index for an antioxidant. The oxidative products from the DNA oxidation can be readily detected after reacting with thiobarbituric acid (TBA).[26] Thus, a low percentage of thiobarbituric acid reactive substance (TBARS) (comparing with that in the control experiment as 100%) indicates that the antioxidant possesses high ability to inhibit the DNA oxidation. Scheme 2 outlines the TBARS percentage in the presence of 0.10 mM coumarin-fused coumarin added to the experimental systems of Cu^{2+}/GSH and •OH-induced oxidations of DNA with Trolox being the reference, which exhibits weak activities in inhibiting •OH- and Cu^{2+}/GSH-induced oxidation of DNA (TBARS% = 71.0 and 88.3, respectively).

The TBARS percentages of coumarin-fused coumarins in inhibiting •OH-induced oxidation of DNA are lower than those in inhibiting Cu^{2+}/GSH-induced oxidation of DNA. Hence, coumarin-fused coumarins possess higher abilities to inhibit •OH-induced oxidation of DNA than to inhibit Cu^{2+}/GSH-induced DNA oxidation. An antioxidant may inhibit Cu^{2+}/GSH-induced oxidation of DNA by chelating copper ions.[27] A single hydroxyl group such as Trolox (TBARS % = 88.3) and **3** (TBARS % = 96.4) cannot exhibit high activity for chelating Cu^{2+}, and antioxidant effectiveness is low in this case. With the amount of phenolic hydroxyl groups increasing, the TBARS % decreases from 73.9 of **4** to 58.5 of **5**. The comparison of TBARS % of **4** (73.9) with **6** (72.1) leads to an interesting conclusion that the hydroxyl group at benzene ring **A** seems not very active in inhibiting Cu^{2+}/GSH-induced DNA oxidation. But the lowest TBARS % of **5** (58.5) demonstrates that double hydroxyl groups locating at benzene rings **A** and **B**, respectively, exhibit the highest ability in this case. Taking **1** and **2** into consideration, it can be found that the TBARS % of **1** (73.1), similar to that of **4** (73.9), indicates that -$N(CH_3)_2$ (an EDG) at benzene ring **B** is equivalent to double hydroxyl groups for inhibiting Cu^{2+}/GSH-induced DNA oxidation. In addition, as in **2** (TBARS % = 64.6), -$N(CH_3)_2$ (at benzene ring **B**) and a hydroxyl group (at benzene ring **A**) are beneficial for chelating copper ion, and the decrease of the amount of copper ion cannot generate much more GS· for oxidizing DNA.

Scheme 2 also reveals that coumarin-fused coumarins are more active in inhibiting DNA oxidation caused by •OH than

Scheme 3. Rate Constant (*k*, Data on the Column) for Coumarin-Fused Coumarins and Trolox in Scavenging $ABTS^{+\bullet}$ (Left Column for Every Compound), DPPH (Middle Column for Every Compound) and Galvinoxyl Radical (Right Column for Every Compound)

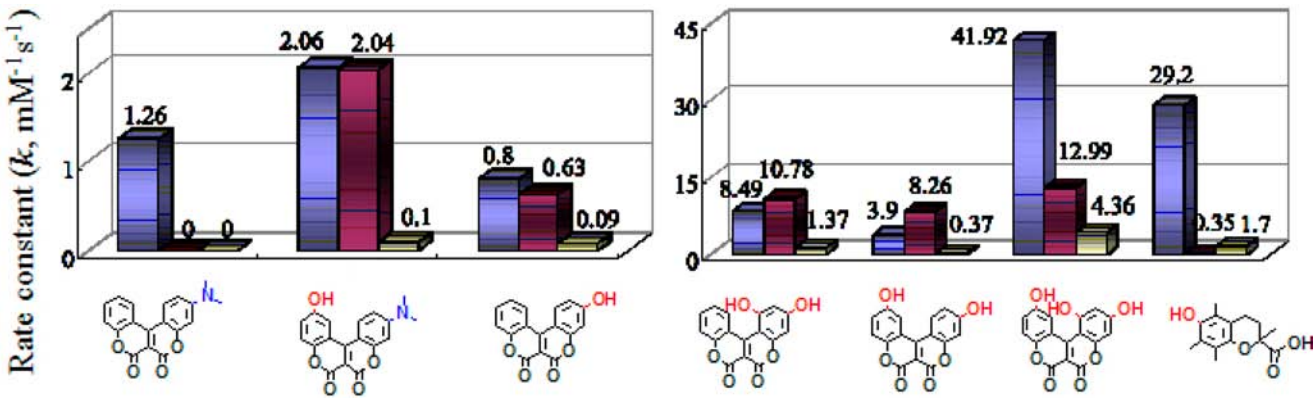

DOI: 10.1021/acs.jafc.5b00399
J. Agric. Food Chem. 2015, 63, 3516−3523

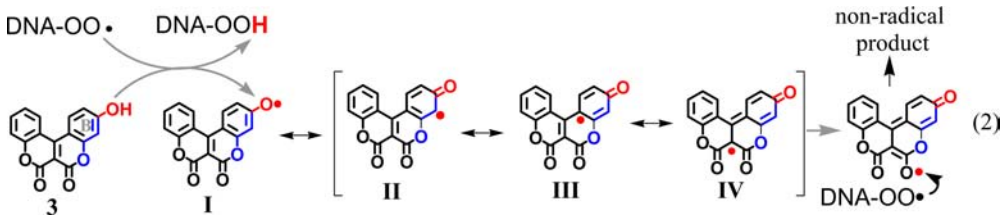

by Cu^{2+}/GSH. As we have pointed out in our previous work, the skeleton of a fused heterocycle is beneficial for the electrophilic addition by •OH.[9] Thus, the double latones in coumarin-fused coumarin may also be able to accommodate •OH, and thus, it may play antioxidative role in •OH-induced oxidation of DNA. Moreover, it can be found that more hydroxyl groups attaching to the benzene ring **B** increase the antioxidant effect of **4** (TBARS % = 21.2), and hydroxyl group at benzene ring **A** is not active because TBARS % of **6** (36.3, another hydroxyl group attaching to benzene ring **A** comparing with **4**) is higher than that of **4** (21.2). But all the efforts from phenolic hydroxyl groups on inhibiting •OH-induced oxidation of DNA cannot reach the level of the contribution from -$N(CH_3)_2$ at benzene ring **B** because **1** has the lowest TBARS % (17.2) among these compounds. On the other hand, TBARS % of **2** increases to 55.3, demonstrating again that the hydroxyl group attaching to benzene ring **A** may not be a positive factor in inhibiting •OH-induced oxidation of DNA.

Inhibiting AAPH-Induced Oxidation of DNA. The aforementioned experimental systems for evaluating antioxidant effectiveness are based on qualitative comparison. We have estimated a method for quantitatively expressing antioxidant effectiveness by using the experimental system of AAPH-induced oxidation of DNA.[9] As shown in Figure 1, an increase of the absorbance means that much more TBARS is generated for the longer reaction time than in the control experiment. But TBARS cannot be formed for a period when a coumarin-fused coumarin is added to the reaction system. Then, TBARS is produced as in the control experiment. The *inhibition period* (t_{inh}) is measured from the beginning of the reaction to the cross point of tangents for the inhibiting and the increasing period in TBARS absorbance line. Then, relationships between t_{inh} and concentrations of coumarin-fused coumarins are outlined in Figure 2 and expressed by the equation of $t_{inh} \sim$ [coumarin-fused coumarin] (see Table 1). Based on equations of $t_{inh} \sim$ [coumarin-fused coumarin], numbers of radical trapped by a coumarin-fused coumarins can be calculated by chemically kinetic method.

In view of chemical kinetics, the t_{inh} correlates proportionally with the concentration of an antioxidant as shown as eq 1.[28]

$$t_{inh} = (n/R_i)[\text{antioxidant}] \quad (1)$$

R_i refers to the initiation rate of the radical-induced reaction, and n is the *stoichiometric factor*. Both AAPH and the sodium salt of DNA are water-soluble compounds, and radicals generated from AAPH can attack DNA at water phase. R_i is thereby assumed to be equal to the radical generation rate (R_g, $R_g = (1.4 \pm 0.2) \times 10^{-6}$ [AAPH] s^{-1}[28]). The coefficient in the equation of $t_{inh} \sim$ [coumarin-fused coumarin] (see Table 1) is equivalent to (n/R_i) in eq 1. Hence, when R_i is equal to $R_g = 1.4 \times 10^{-6} \times 40$ mM·s^{-1} = 3.36 μM·min^{-1}, the n is the product of the coefficient in the equation (see Table 1) and R_i. The obtained n values of coumarin-fused coumarins are involved in Table 1 as well.

The usage of Trolox in AAPH-induced oxidation of DNA does not generate t_{inh}, and the n of Trolox cannot be obtained. As shown in Table 1, the n of **3** is 1.81, meaning that **3** can trap ~**2** radicals in protecting DNA against AAPH-induced oxidation. This can be understood by eq 2, in which DNA-OO• refers to the radical deriving from the DNA oxidation. DNA-OO· can abstract a hydrogen atom from hydroxyl group in **3**, producing a phenoxyl radical (**I**). The phenoxyl radical (**I**) accommodates the single electron via a series of resonance structures, **II**, **III**, and **IV**, and then to form another phenoxyl radical at C═O for quenching another DNA-OO•. So, two radicals trapped by **3** can be regarded as the contribution from the hydroxyl group and the adjacent lactone motif.

Moreover, the n values of **4**, **5**, and **6** are 2.99, 3.83, and 4.40, respectively, implying that **4**, **5**, and **6** (with 2, 2, and 3 hydroxyl groups, respectively) can trap ~3, ~4, and 4−5 radicals, respectively. The numbers of trapped radicals increase with the amount of hydroxyl group. But the n of **1** (3.53) is higher than that of **3** (1.81), indicating that -$N(CH_3)_2$ can improve the radical-scavenging property of the lactone motifs in the absence of hydroxyl group. So, the ring of lactone in the fused coumarin is an efficient radical-receptor in the presence of electron-donating group.[9] The n value of **2** is further increased to 5.85 by the hydroxyl group at benzene ring **A**, demonstrating that -$N(CH_3)_2$ in combination with hydroxyl group at different benzene rings can improve the ability to inhibit AAPH- induced oxidation of DNA.

Rate Constants in Scavenging Radicals. The radical-scavenging test reveals the direct interaction of an antioxidant with radicals, in which $ABTS^{+\bullet}$, DPPH, and galvinoxyl radicals are usually applied to evaluate the ability of the antioxidant to donate its hydrogen atom to *N*- and *O*-centered radicals, respectively. The expression on the radical-scavenging ability usually focuses on the amount of radicals trapped by the antioxidant.[29] We have developed a chemically kinetic method for measuring the rate constant (k) of the antioxidant quenching radicals.[30] Briefly, the concentrations of radicals decreases rapidly when coumarin-fused coumarins are mixed with radicals (see Supporting Information). The decay of the concentrations of radicals can be quantitatively expressed by eq 3, in which t represents the reaction time.

$$[\text{radical}] = Ae^{-(t/a)} + Be^{-(t/b)} + C \quad (3)$$

The differential operation is performed on eq 3 to obtain the reaction rate (r), −d[radical]/dt, as shown in eq 4.

$$-\text{d}[\text{radical}]/\text{d}t = r = (A/a)e^{-(t/a)} + (B/b)e^{-(t/b)} \quad (4)$$

If the reaction time is assigned to 0 (the beginning of the reaction), the reaction rate at $t = 0$ (r_0) can be calculated by eq 4. Meanwhile, [radical] and [antioxidant] at $t = 0$ are concentrations of radical and antioxidant at the beginning of the reaction. So, the rate constant (k) can be calculated by eq 5 (see Supporting Information).

DOI: 10.1021/acs.jafc.5b00399
J. Agric. Food Chem. 2015, 63, 3516−3523

$$r_0 = k[\text{radical}][\text{antioxidant}] \quad (5)$$

The rate constants (k) of coumarin-fused coumarins together with Trolox are outlined in Scheme 3. It can be found that k of **3** (only one hydroxyl group contained) in reducing $ABTS^{+\bullet}$ (0.80 $mM^{-1}\cdot s^{-1}$) is only 0.80 $mM^{-1}\cdot s^{-1}$, while those of **4** (two hydroxyl groups contained) and **6** (three hydroxyl groups contained) are 8.49 $mM^{-1}\cdot s^{-1}$ and 41.92 $mM^{-1}\cdot s^{-1}$, respectively. So, the ability of coumarin-fused coumarin to trap radical is related to the amount of hydroxyl group. The high k values of **3**, **4**, and **6** in trapping DPPH (0.63, 10.78, and 12.99 $mM^{-1}\cdot s^{-1}$, respectively) and galvinoxyl radical (0.09, 1.37, and 4.36 $mM^{-1}\cdot s^{-1}$, respectively) indicate that coumarin-fused coumarin prefers to donating the hydrogen atom in −OH to *N*- and *O*-centered radicals. In particular, three hydroxyl groups in **6** increase the radical-scavenging property even higher than that of Trolox. But k values of **4** (in trapping three radicals) are higher than those of **5**, implying that two hydroxyl groups locate at the different benzene rings are not beneficial for scavenging radicals. Moreover, **1** (without hydroxyl group contained) can reduce $ABTS^{+\bullet}$, indicating that $-N(CH_3)_2$ makes the scaffold of coumarin-fused coumarin a radical-scavenger.

In conclusion, $-N(CH_3)_2$ and the hydroxyl group play synergistically antioxidative role for coumarin-fused coumarin even though they do not locate at the same benzene ring. In particular, $-N(CH_3)_2$-involved coumarin-fused coumarin shows the highest activity in inhibiting $^{\bullet}OH$-induced oxidation of DNA even in the absence of a hydroxyl group. Therefore, $-N(CH_3)_2$ is an assisting group for the antioxidant effectiveness in the coumarin-fused heterocycles.

■ ASSOCIATED CONTENT

Ⓢ Supporting Information

NMR spectra of the synthetic compounds, the decay of the concentration of radicals together with the calculation of the rate constant (k) in quenching radicals. This material is available free of charge via the Internet at http://pubs.acs.org.

■ AUTHOR INFORMATION

Corresponding Author

*E-mail: zaiqun-liu@jlu.edu.cn.

Notes

The authors declare no competing financial interest.

■ REFERENCES

(1) Sandhu, S.; Bansal, Y.; Silakari, O.; Bansal, G. Coumarin hybrids as novel therapeutic agents. *Bioorg. Med. Chem.* **2014**, *22*, 3806−3814.

(2) Hamulakova, S.; Janovec, L.; Hrabinova, M.; Spilovska, K.; Korabecny, J.; Kristian, P.; Kuca, K.; Imrich, J. Synthesis and biological evaluation of novel tacrine derivatives and tacrine-coumarin hybrids as cholinesterase inhibitors. *J. Med. Chem.* **2014**, *57*, 7073−7084.

(3) Roussakia, M.; Zelianaios, K.; Kavetsou, E.; Hamilakis, S.; Hadjipavlou-Litina, D.; Kontogiorgis, C.; Liargkova, T.; Detsi, A. Structural modifications of coumarin derivatives: Determination of antioxidant and lipoxygenase (LOX) inhibitory activity. *Bioorg. Med. Chem.* **2014**, *22*, 6586−6594.

(4) Renuka, N.; Kumar, K. A. Synthesis and biological evaluation of novel formyl-pyrazoles bearing coumarin moiety as potent antimicrobial and antioxidant agents. *Bioorg. Med. Chem. Lett.* **2013**, *23*, 6406−6409.

(5) Pratap, R.; Ram, V. J. Natural and synthetic chromenes, fused chromenes, and versatility of dihydro benzo[*h*]chromenes in organic synthesis. *Chem. Rev.* **2014**, *114*, 10476−10526.

(6) Zheng, K.; Lin, W.; Tan, L.; Chen, H.; Cui, H. A unique carbazole−coumarin fused two-photon platform: Development of a robust two-photon fluorescent probe for imaging carbon monoxide in living tissues. *Chem. Sci.* **2014**, *5*, 3439−3448.

(7) Tasior, M.; Poronik, Y. M.; Vakuliuk, O.; Sadowski, B.; Karczewski, M.; Gryko, D. T. V-Shaped bis-coumarins: Synthesis and optical properties. *J. Org. Chem.* **2014**, *79*, 8723−8732.

(8) Pardo-Jiménez, V.; Barrientos, C.; Pérez-Cruz, K.; Navarrete-Encina, P. A.; Olea-Azar, C.; Nuñez-Vergara, L. J.; Squella, J. A. Synthesis and electrochemical oxidation of hybrid compounds: Dihydropyridine-fused coumarins. *Electrochim. Acta* **2014**, *125*, 457−464.

(9) Xi, G.-L.; Liu, Z.-Q. Coumestan inhibits radical-induced oxidation of DNA: Is hydroxyl a necessary functional group? *J. Agric. Food Chem.* **2014**, *62*, 5636−5642.

(10) Kim, Y.; Moon, Y.; Kang, D.; Hong, S. Synthesis of heterocyclic-fused benzopyrans *via* the Pd(II)-catalyzed C-H alkenylation/C-O cyclization of flavones and coumarins. *Org. Biomol. Chem.* **2014**, *12*, 3413−3422.

(11) Veselinović, J. B.; Veselinović, A. M.; Vitnik, Z. J.; Vitnik, V. D.; Nikolić, G. M. Antioxidant properties of selected 4-phenyl hydroxycoumarins: Integrated in vitro and computational studies. *Chem.-Biol. Interact.* **2014**, *214*, 49−56.

(12) Tanemossu, S. A. F.; Franke, K.; Arnold, N.; Schmidt, J.; Wabo, H. K.; Tane, P.; Wessjohann, L. A. Rare biscoumarin derivatives and flavonoids from *Hypericum riparium*. *Phytochemistry* **2014**, *105*, 171−177.

(13) Chen, J.; Liu, W.; Zhou, B.; Niu, G.; Zhang, H.; Wu, J.; Wang, Y.; Ju, W.; Wang, P. Coumarin- and rhodamine-fused deep red fluorescent dyes: Synthesis, photophysical properties, and bioimaging *in vitro*. *J. Org. Chem.* **2013**, *78*, 6121−6130.

(14) Su, H.; Gornitsky, M.; Velly, A. M.; Yu, H.; Benarroch, M.; Schipper, H. M. Salivary DNA, lipid, and protein oxidation in nonsmokers with periodontal disease. *Free Radical Biol. Med.* **2009**, *46*, 914−921.

(15) Miura, T.; Fujioka, S.; Iwasaki, H.; Ozeki, M.; Kojima, N.; Yamashita, M. Skeleton transformation of α-pyrone induced by 5-aryl substituent into ring-fused dihydrofuran. *Tetrahedron Lett.* **2014**, *55*, 1536−1539.

(16) Karthik, G.; Rajasekaran, T.; Sridhar, B.; Reddy, B. V. S. Highly regio- and diastereoselective three-component reaction of acyclic/cyclic donor-acceptor carbenoids for the synthesis of angularly fused furocoumarins and spirooxindolylfurocoumarins. *Tetrahedron* **2014**, *70*, 8148−8154.

(17) Jang, H.-L.; El-Gamal, M. I.; Choi, H.-E.; Choi, H.-Y.; Lee, K.-T.; Oh, C.-H. Synthesis of tricyclic fused coumarin sulfonates and their inhibitory effects on LPS-induced nitric oxide and PGE_2 productions in RAW264.7 macrophages. *Bioorg. Med. Chem. Lett.* **2014**, *24*, 571−575.

(18) Kanchithalaivan, S.; Sumesh, R. V.; Kumar, R. R. Ultrasound-assisted sequential multicomponent strategy for the combinatorial synthesis of novel coumarin hybrids. *ACS Comb. Sci.* **2014**, *16*, 566−572.

(19) Khoobi, M.; Ramazani, A.; Mahdavi, M.; Foroumadi, A.; Emami, S.; Joo, S. W.; Ślepokura, K.; Lis, T.; Shafiee, A. Efficient solvent-free synthesis of benzothiazine-fused pyrrolo[3,4-*c*]coumarins: Cycloaddition reactions between coumarin-based dihydrobenzothiazoles and isocyanides. *Helv. Chim. Acta* **2014**, *97*, 847−853.

(20) Yamamoto, Y.; Matsui, K.; Shibuya, M. Tandem Ruthenium-catalyzed transfer-hydrogenative cyclization/intramolecular Diels−Alder reaction of enediynes affording dihydrocoumarin-fused polycycles. *Org. Lett.* **2014**, *16*, 1806−1809.

(21) Moon, Y.; Kim, Y.; Hong, H.; Hong, S. Synthesis of heterocyclic-fused benzofurans *via* C-H functionalization of flavones and coumarins. *Chem. Commun.* **2013**, *49*, 8323−8325.

(22) Xi, G.-L.; Liu, Z.-Q. Solvent-free Povarov reaction for synthesizing ferrocenyl quinolines: Antioxidant abilities deriving from ferrocene moiety. *Eur. J. Med. Chem.* **2014**, *86*, 759−768.

DOI: 10.1021/acs.jafc.5b00399
J. Agric. Food Chem. 2015, 63, 3516−3523

(23) Mertens, M. D.; Hinz, S.; Müller, C. E.; Gütschow, M. Alkynylcoumarinyl ethers as MAO-B inhibitors. *Bioorg. Med. Chem.* **2014**, *22*, 1916−1928.
(24) Speisky, H.; Gómez, M.; Burgos-Bravo, F.; López-Alarcón, C.; Jullian, C.; Olea-Azar, C.; Aliaga, M. E. Generation of superoxide radicals by copper-glutathione complexes: Redox-consequences associated with their interaction with reduced glutathione. *Bioorg. Med. Chem.* **2009**, *17*, 1803−1810.
(25) Zhu, B. Z.; Kitrossky, N.; Chevion, M. Evidence for production of hydroxyl radicals by pentachlorophenol metabolites and hydrogen peroxide: A metal-independent organic Fenton reaction. *Biochem. Biophys. Res. Commun.* **2000**, *270*, 942−946.
(26) Sugden, K. D.; Wetterhahn, K. E. Direct and hydrogen peroxide-induced chromium(V) oxidation of deoxyribose in single-stranded and double-stranded calf thymus DNA. *Chem. Res. Toxicol.* **1997**, *10*, 1397−1406.
(27) Wang, Q.; Qian, Y.-P.; Dai, F.; Lu, D.-L.; Yan, W.-J.; Chen, Y.; Zhou, B. *ortho*-Dihydroxy chalcones as cupric ion-dependent prooxidants: Activity and mechanisms. *Food Chem.* **2013**, *141*, 1259−1266.
(28) Bowry, V. W.; Stocker, R. Tocopherol-mediated peroxidation: The prooxidation effect of vitamin E on the radical-initiated oxidation of human low-density lipoprotein. *J. Am. Chem. Soc.* **1993**, *115*, 6029−6044.
(29) Doulou, I.; Kontogiorgis, C.; Koumbis, A. E.; Evgenidou, E.; Hadjipavlou-Litina, D.; Fylaktakidou, K. C. Synthesis of stable aromatic and heteroaromatic sulfonyl-amidoximes and evaluation of their antioxidant and lipid peroxidation activity. *Eur. J. Med. Chem.* **2014**, *80*, 145−153.
(30) Wang, R.; Liu, Z.-Q. Solvent-free and catalyst-free Biginelli reaction to synthesize ferrocenoyl dihydropyrimidine and kinetic method to express radical-scavenging ability. *J. Org. Chem.* **2012**, *77*, 3952−3958.

DOI: 10.1021/acs.jafc.5b00399
J. Agric. Food Chem. 2015, 63, 3516−3523

been rarely used to study SS-mediated interactions of soy protein.

In this study, the protein forms rearranged by heating were identified by diagonal SDS-PAGE and MALDI-TOF/TOF MS. The SH contents of different subunits/polypeptides of soy protein were determined using thiol-specific fluorescent monobromobimane (mBBr) labeling combined with SDS-PAGE. The transformation of cysteine side chains between SH and SS was identified to discuss disulfide-mediated interaction of soy protein.

MATERIALS AND METHODS

Materials. Acrylamide, *N*,*N*′-methylenebis(acrylamide), sodium dodecyl sulfate (SDS), monobromobimane (mBBr), 4,4′-dithiodipyridine (DPS), *N*-ethylmaleimide (NEM), iodoacetamide (IAM), and dithiothreitol (DTT) were purchased from Sigma-Aldrich Trading Co., Ltd. (Shanghai, China). All other chemicals were of analytical reagent grade.

Soy Protein Preparation. Soybean Nannong 88-31 (moisture content, 9%) was used. Dehulled and milled soybean flour was treated with *n*-hexane five times to remove oil and was then dried at room temperature. The defatted soybean flour was treated with hexane/ethanol (1:2, v/v) at 4 °C for 1 h. The slurry was vacuum filtered, and the filter cake was treated with 95% (v/v) ethanol at 4 °C for 1 h to remove soluble sugars.[25] After drying at room temperature, the meal was dispersed in distilled water (1:10, w/v), and the pH was adjusted to pH 7.0 using 2 mol/L NaOH. After stirring for 1 h at 20 °C, the suspension was centrifuged at 15800*g* for 30 min at 4 °C. The supernatant was adjusted to pH 4.5 with 2 mol/L HCl and centrifuged at 4000*g* for 30 min at 4 °C. The precipitate was washed twice with distilled water and was resuspended in 5-fold (w/w) of the same and neutralized to pH 7.0 using 2 mol/L NaOH. After centrifuging at 15000*g* for 30 min at 4 °C to remove a small amount of insoluble substances, the supernatant was freeze-dried and then stored at 4 °C until use. Protein content in the prepared soy protein powder was 90% (w/w) as determined by using the micro-Kjeldahl method.

Heat Treatment of Soy Protein. Soy protein powder was suspended in 0.01 mol/L sodium phosphate buffer (pH 7.0). After centrifuging at 25000*g* for 30 min at 4 °C (Himac CR21GII, Hitachi, Tokyo, Japan) to remove a small amount of insoluble particles, the suspension (30 g/L) was obtained. The elongated screw-capped test tubes were filled with the soy protein solutions to prevent water evaporation. After heating in a water bath at 80 or 90 °C for different time lengths, the soy protein solutions were immediately cooled in an ice−water bath.

Sulfhydryl Content Determination by Colorimetric Method. The total free sulfhydryl content (SH_T) was determined according to the method of Ruan et al.[4] Soy protein solutions were diluted with the SDS buffer (pH 7.0) to make the final SDS concentration of 2% (w/v), and protein concentration was 3 g/L. The excess SH detecting reagent 4,4′-dithiodipyridine (DPS) (0.16 mmol/L) was added before the addition of SDS. The samples were vortexed and detected immediately at 324 nm against a buffer blank in a UV−vis spectrophotometer (UV-2450, Shimadzu, Kyoto, Japan) until the absorbance reached the maximum value (A_{324}). In the parallel reagent blank ($A_{324\,r}$), protein solution was replaced with 0.01 mol/L buffer (pH 7.0), mixed with DPS, and incubated for the same time. In the parallel protein blank ($A_{324\,p}$), DPS was replaced with water. SH_T was obtained as μmol SH/g soy protein. The calculation was

$$SH_T = (A_{324} - A_{324r} - A_{324p})/(\varepsilon \times L \times C) \times 10^6$$

where ε is the molar absorption coefficient ($M^{-1}\ cm^{-1}$), L is the light path (1 cm), and C is the protein concentration (g/L).

Sodium Dodecyl Sulfate−Polyacrylamide Gel Electrophoresis (SDS-PAGE). SDS-PAGE was performed on a vertical slab unit (Bio-Rad, purchased from Nanjing, China). A 12% resolving gel overlaid with a 3% stacking gel was used. Each sample was adjusted to the same concentration (Lowry method) and mixed with nonreducing 2× sample dissolving buffer (4% SDS, 20% glycerol, 0.125 mol/L Tris-HCl buffer (pH 6.8), 0.02% bromophenol blue). The samples were heated at 100 °C for 3 min and loaded onto SDS-PAGE gels. After running, the gel was fixed in methanol/water/acetic acid (5:5:1, v/v/v) overnight and stained for 2 h using 0.05% (w/v) Coomassie brilliant blue (CBB) R250. After staining, the gels were destained using a 10% (v/v) acetic acid solution until a clear background was obatined. The gels were scanned using a computing densitometer (Molecular Imager Chemi Doc XRS+, Bio-Rad, purchased from Nanjing, China). The CBB stained intensities of the protein bands were integrated using Image Lab software (Bio-Rad, purchased from Nanjing, China). The content of each band in soy proteins (*C*, g/g soy protein) was determined by comparing the individual band intensities with the total intensity of all bands in a lane. Molecular weights (MW) of the gel bands were estimated by molecular weight markers (Prestained Precision Plus, Bio-Rad, purchased from Nanjing, China), and the regression method is cubic spline.

mBBr Labeling Combined with SDS-PAGE. Soy protein was mixed with SDS buffer to make the final SDS concentration of 2%. The fluorescent labeling reagent monobromobimane (mBBr) was added immediately to label SH of soy protein in the dark.[26] After reaction finishing, the mixture was exposed to light to destroy unreacted mBBr because of susceptibility to photodegradation.[27] The mBBr-labeled protein was subjected to SDS-PAGE. After running, the gel was fixed in methanol/acetic acid/water (5:5:1, v/v/v) overnight with at least three solution changes. The fluorescence of bands was visualized with UV light excitation on a computing densitometer (Molecular Imager Chemi Doc XRS+, Bio-Rad, purchased from Nanjing, China). The same gel was stained with CBB R250 and scanned.

The fluorescence intensities were integrated by Image Lab software (Bio-Rad, USA). The allocation of free SH on the components of soy protein (SH^a, μmol SH/g soy protein) and the free SH content of the components (SH^c, μmol SH/g component) can be obtained as

$$SH^a = \frac{FI_i}{FI_T} \times SH_T \quad (1)$$

$$SH^c = \frac{SH^a}{C} \quad (2)$$

where FI_i is fluorescence intensities of individual band, FI_T is total fluorescence intensities of all bands in a lane, SH_T (μmol SH/g soy protein) is total free SH content of soy protein determined by colorimetric method, and *C* is content (by mass) of the component in soy proteins (g/g soy protein).

Diagonal SDS-PAGE. The mBBr-labeled protein dissolved in the nonreducing sample buffer was subjected to the first-dimensional electrophoresis. After running, the lane of interest was excised from the gel, immersed in distilled water (containing 50 mmol/L DTT) for 10 min at room temperature, and then boiled for 5 min to reduce SS. The reduced lane was placed on the top of another gel and overlaid with 0.5% low-melting agarose (Bio-Rad, purchased from Nanjing, China). Then the second-dimensional electrophoresis was conducted. The fluorescent spots were visualized with UV light excitation. Then the same gel was stained with CBB R250 and scanned. If the bands had SS in the first-dimensional electrophoresis lane, they would resolve into spots below the oblique diagonal line of the second-dimensional electrophoresis gel. If SS was not present in the bands of the first-dimensional electrophoresis lane, the spots in the second-dimensional electrophoresis gel would lie on an oblique diagonal line. The fluorescence intensities and CBB-stained intensities of the spots were integrated by Quantity One software (Bio-Rad, USA). The allocation of free SH on the spots (SH^a_{spot}, μmol SH/g soy protein) and the free SH content of the spots (SH^c_{spot}, μmol SH/g spot) can be obtained as

$$SH^a_{spot} = \frac{FI_{spot}}{FI_{T\,spot}} \times SH^a \quad (3)$$

$$SH^c_{spot} = \frac{SH^a_{spot}}{C_{spot}} \quad (4)$$

DOI: 10.1021/jf504519z
J. Agric. Food Chem. 2015, 63, 3524−3533

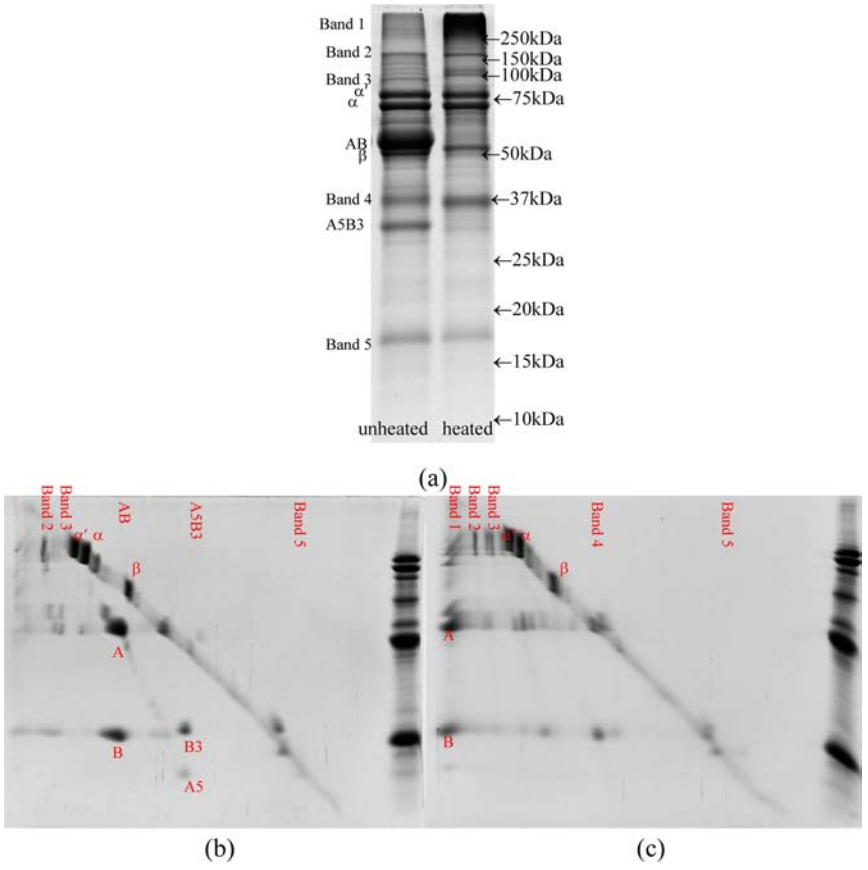

Figure 1. (a) Nonreducing SDS-PAGE pattern of unheated soy protein and heated soy protein (90 °C, 1800 s); diagonal SDS-PAGE pattern of unheated soy protein (b) and heated soy protein (90 °C, 1800 s) (c).

where FI_{spot} is the fluorescence intensity of the spot resolved from the original band, $FI_{T\ spot}$ is total fluorescence intensities of all spots resolved from the original band, SH^a (μmol SH/g soy protein) is the free SH allocation on the original band, and C_{spot} is the content (by mass) of the spot in soy protein (g/g soy protein).

In-Gel Tryptic Digests and Matrix-Assisted Laser Desorption/Ionization−Time-of-Flight/Time-of-Flight Mass Spectrometry (MALDI-TOF/TOF-MS). The SH of soy protein was blocked with NEM in the presence of 2% SDS. The NEM-modified soy protein was subjected to noreducing SDS-PAGE. After running, gel was stained with zinc negative staining. The zinc staining method was used to avoid protein fixation by organic solvent and interference of the dye.[28] Gels were first equilibrated in deionized water for 5 min, stained with 200 mmol/L imidazole, 0.1% SDS for 15 min, washed with deionized water for 1 min, and then developed with 0.1 mol/L $Zn(Ac)_2$ until sufficient contrast was obtained.

Gel pieces were excised from the gel and destained with 1% citric acid twice for 20 min by vortexing. The gel pieces were washed with three times for 10 min in deionized water and dehydrated in a vacuum centrifuge. The gel pieces were incubated with 10 mmol/L DTT at 56 °C for 45 min and subsequently with 60 mmo/L IAM at room temperature for 30 min to ensure complete reduction and carbamidomethylation of cysteine residues.[29] After deionized water washing and dehydration in a vacuum centrifuge, gel pieces were rehydrated on ice for 30 min with 20 μL of 10 μg/mL trypsin (Promega, V5111) in 25 mmol/L NH_4HCO_3 at pH 8.0. After the addition of 20 μL 25 mmol/L NH_4HCO_3, the samples were incubated for 20 h at 37 °C. The trypsin digests was collected, and the gel pieces were extracted with 50 μL of 0.1% trifluoroacetic acid in 60% acetonitrile by sonication for 15 min at room temperature. The extracts were combined with the trypsin digests and dried in a vacuum centrifuge. Peptides were redissolved in 3 μL of 0.1% trifluoroacetic acid.

The alternative SS reduction protocol without carbamidomethylation was also conducted:[20] The gel pieces were excised, destained, washed, and dehydrated. Protein digestion was carried out following the addition of trypsin. The resulting peptides were collected and dried. The SS were reduced by dissolving the dried peptides in 3 mmol/L DTT for 45 min at 56 °C. The peptides were dried again under vacuum and redissolved in 0.1% trifluoroacetic acid.

In the final step before MALDI-TOF/TOF analysis, 0.7 μL of peptide and 0.7 μL of 4-hydroxy-α-cyanocinnamic acid (used as a matrix) were loaded on a MALDI target and air-dried. The mass spectra were obtained with an ultrafleXtreme MALDI-TOF/TOF MS (Bruker Daltonics, Germany, purchased from Shanghai, China). All mass spectra were analyzed by flexAnalysis and Biotools software provided by Bruker Daltonics Corp (Germany).

Data Interpretation Using Database. The experimentally determined mass-to-charge ratio (m/z) values were used to search theoretically generated peptide masses from known protein sequences. Protein identification was performed by searching the National Center for Biotechnology Information (NCBI) nonredundant database using the Mascot search engine (www.matrixscience.com), which uses a probability-based scoring system. For database searches, the parameters were used as follows: average mass, 300 ppm peptide mass tolerance; 1.0 Da MS/MS mass tolerance; peptide charges of +1; trypsin as digesting enzyme with two missed cleavages allowed; carbamidomethylation of cysteine; oxidation of methionine; and NEM of cysteine as allowable variable modifications. Taxonomy was limited to green plants for both MALDI-TOF-MS and MS/MS ion searches.

Statistical Analysis. Three separate soy samples were used, and each sample was run in triplicate. Data were subjected to an analysis of variance (ANOVA) with SAS 9.1 package (SAS 2005). Significant differences among variables were determined by LSD all-pairwise multiple comparisons ($p < 0.05$). Data were expressed as the mean ± SD ($n = 3$).

RESULTS AND DISCUSSION

Newly Formed SS-Linked Products of Soy Protein by Heating. The unheated soy protein dissolved into several

DOI: 10.1021/jf504519z
J. Agric. Food Chem. 2015, 63, 3524−3533

bands in nonreducing SDS-PAGE (Figure 1a): subunits of β-conglycinin (α', α, β), AB (glycinin subunit), A5B3 (SS-linked portion of A4A5B3, one type of glycinin subunit), and some other bands.[30]

Diagonal SDS-PAGE was used to determine the SS-linked bands (Figure 1b). Table 1 shows the results of unheated soy protein. α', α, and β were positioned on the diagonal line, indicating that they had no SS; AB resolved into A and B, and A5B3 resolved into A5 and B3 below the diagonal line, indicating the presence of interchain SS between A and B; band 2 resolved into α' and α below the diagonal line and should be an SS-linked dimer of α' and/or α; band 3 resolved into A and B below the diagonal line and should be an SS-linked dimer of AB;[3,7] band 4 should be A4;[1] and band 5 was positioned on the diagonal line.

Table 1. Protein Composition of Bands of Unheated Soy Protein Examined by Diagonal SDS-PAGE and Identified by MALDI-TOF/TOF MS

	method		
	diagonal SDS-PAGE	MALDI-TOF/TOF-MS	
band		NBCI accession no.	protein species
1			
2	dimer of α' and/or α	gil9967361	α' subunit of β-conglycinin
		gil9967357	α subunit of β-conglycinin
3	dimer of glycinin subunit	gil33357661	glycinin G5/A3B4
		gil121276	glycinin G1
		gil255224	glycinin G4/A5A4B3
α'	α'	gil9967361	α' subunit of β-conglycinin
α	α	gil9967357	α subunit of β-conglycinin
AB	glycinin subunit	gil33357661	glycinin G5/A3B4
		gil15988117	glycinin G1/A1ab1b
		gil121276	
		gil351725363	glycinin G2/A2B1a
		gil255224	glycinin G4/A5A4B3
		gil121278	glycinin G3
β	β	gil21465631	β subunit of β-conglycinin
4	A4	gil255224	glycinin G4/A5A4B3
A5B3	A5B3	gil255224	glycinin G4/A5A4B3
5	Kunitz-type soybean trypsin inhibitor	gil157838208	Kunitz-type soybean trypsin inhibitor

The bands of unheated soy protein in nonreducing SDS-PAGE were subjected to in-gel digestion, and the tryptic peptides were analyzed by MALDI-TOF/TOF MS. The proteins identified from the bands are shown in Table 1. The bands of α', α, and β were matched to the corresponding subunits of β-conglycinin. All five species of glycinin subunit (G1−G5) were detected in the AB band. The A5B3 band was matched to G4. G4 was detected in the AB band, indicating the presence of another SS-linked form (A4B3) in G4, except for A5B3. A4B3 might be formed in the soy protein extraction process. α' and α were detected in band 2, in agreement with the result of diagonal SDS-PAGE. Band 2 could be a homodimer of α'/α or a heterodimer of α' and α. The dimer could be formed in the cotyledon cell of soybean or generated during the soy protein extraction process.[30,31] Three species of glycinin subunits (G1, G4, and G5) were detected in band 3, which could form homo/hetero dimers. Band 4 was matched to A4. Band 5 was matched to Kunitz trypsin inhibitor (KTI).

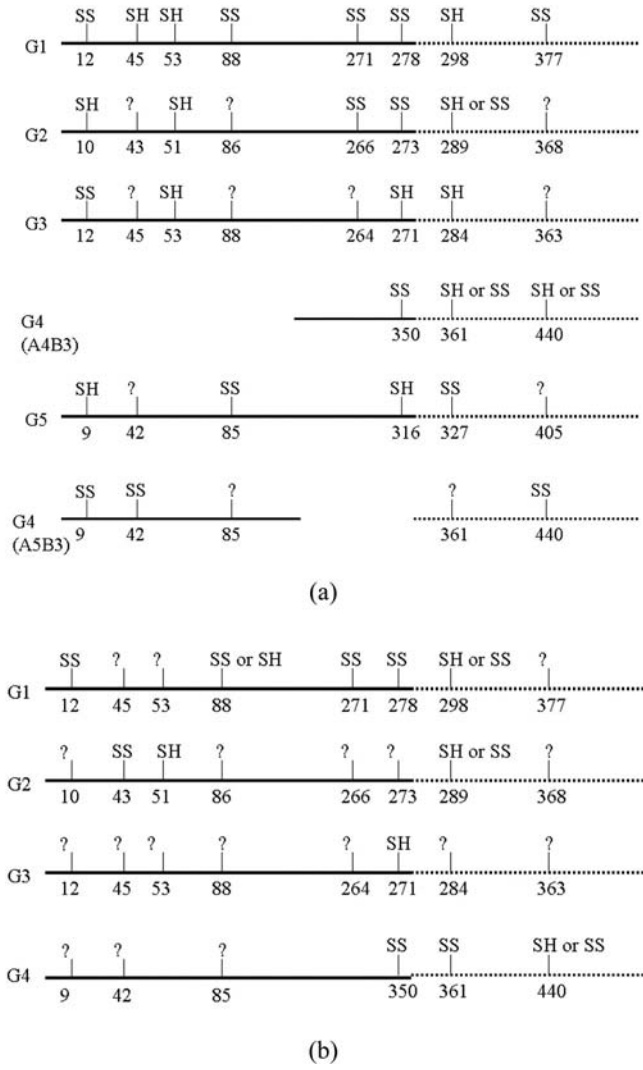

Figure 2. (a) Cysteine status (SH or SS) of glycinin subunit; (b) cysteine status (SH or SS) of polymer: solid line, acidic polypeptides (A); dotted line, basic polypeptides (B).

After heat treatment (90 °C, 1800 s), the glycinin subunits (AB and A5B3) disappeared completely, accompanied by the formation of band 1 on the top of the resolving gel and band 4 (Figure 1a). The newly formed SS-linked bands were also examined by diagonal SDS-PAGE (Figure 1c), and the result is shown in Table 2. Band 1 was a polymer composed of A, B, and small amounts of α' and α, which interacted with each other via intermolecular SS.[18] Band 4 resolved into two spots: the one on the diagonal line was A; the other below the diagonal line was B. This revealed that band 4 contained two components: monomer of A and SS-linked dimer of B (A&BB).

The proteins identified from the bands of heated soy protein (90 °C, 1800 s) in nonreducing SDS-PAGE are shown in Table 2. Five species of glycinin subunits (G1−G5) were detected in the polymer, indicating the complex heterogeneity of the polymer. Although G4/G5 has higher thermal stability than G2/G3/G1,[32,33] little effect has been seen for the formation of polymer. α' and α were not detected in the polymer, which might be because of their lower content in the polymer. Five species of glycinin subunits (G1−G5) were detected in the A&BB.

DOI: 10.1021/jf504519z
J. Agric. Food Chem. 2015, 63, 3524−3533

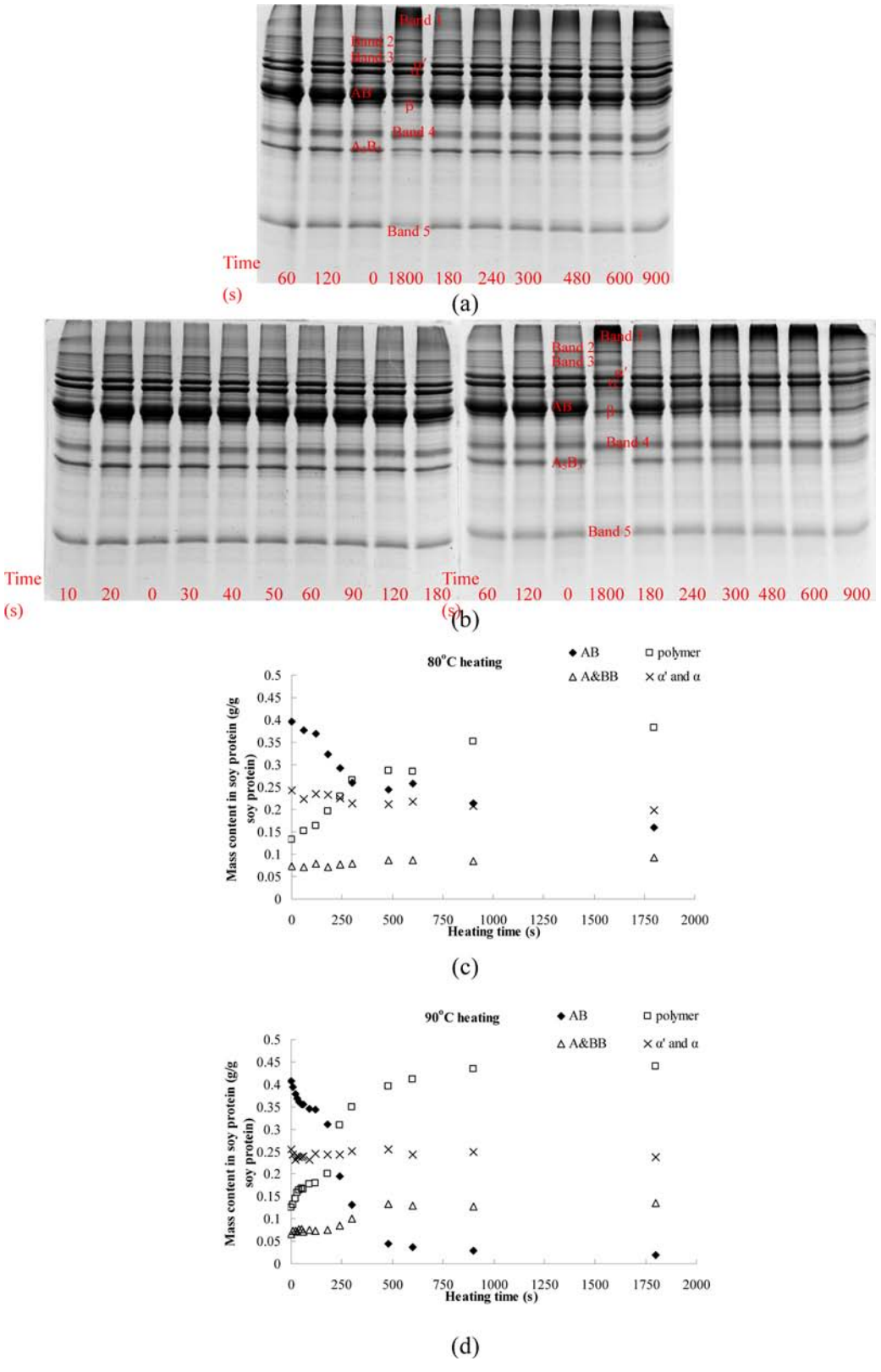

Figure 3. Nonreducing SDS-PAGE pattern of soy protein heated at 80 °C (a) and 90 °C (b) for different time lengths (0−1800 s); effect of heating temperature and time on relative mass content of AB, polymer, monomer of A and dimer of B (A&BB), and α' and α in soy protein (c, 80 °C; d, 90 °C).

The composition of band 2 (α' and α) was unchanged, indicating that the dimer of α' and/or α was stable by heating. The α', α, G1, and G2 were detected in band 3, and this oligomer might be a byproduct in the process of polymer formation.

In general, most of the glycinin was associated by intermolecular SS for forming polymer, and a small amount of glycinin was dissociated to form the A&BB by heating. Many researchers have found that heat-treated soy protein exhibited

DOI: 10.1021/jf504519z
J. Agric. Food Chem. 2015, 63, 3524−3533

Table 2. Protein Composition of the Bands of Heated Soy Protein (90 °C, 30 min) Examined by Diagonal SDS-PAGE and Identified by MALDI-TOF/TOF MS

	method		
	diagonal SDS-PAGE	MALDI-TOF/TOF-MS	
band		NBCI accession no.	protein species
1	polymer composed of A, B, and small amounts of α' and α	gil351725363	glycinin G2/A2B1a
		gil255224	glycinin G4/A5A4B3
		gil15988117	glycinin G1/A1ab1b
		gil121276	
		gil121278	glycinin G3
		gil33357661	glycinin G5/A3B4
2	dimer of α' and/or α	gil9967361	α' subunit of β-conglycinin
		gil9967357	α subunit of β-conglycinin
3	oligmer of A, B, α', and α	gil121276	glycinin G1
		gil351725363	glycinin G2/A2B1a
		gil9967361	α' of β-conglycinin
		gil9967357	α of β-conglycinin
α'	α'	gil9967361	α' subunit of β-conglycinin
α	α	gil9967357	α subunit of β-conglycinin
β	β	gil21465631	β subunit of β-conglycinin
4	SS-linked dimer of B and monomer of A (A&BB)	gil351725363	glycinin G2/A2B1a
		gil255224	glycinin G4/A5A4B3
		gil121278	glycinin G3
		gil121276	glycinin G1/A1ab1b
		gil33357661	glycinin G5/A3B4
5	Kunitz-type soybean trypsin inhibitor	gil157838208	Kunitz-type soybean trypsin inhibitor

bands with large molecular weight containing intermolecular SS, suggesting the presence of intermolecular SS due to the SH oxidation and/or SH−SS exchange reactions.[7,14−16]

Analysis of the Conversion of Cysteine Status between SH and SS. The glycinin subunit was associated so as to form polymer due to SH oxidation or SH−SS exchange reaction, leading to the conversion of cysteine side chain between SH and SS consequentially. The cysteine status (SH or SS) was examined by mass spectrometry analysis. The bands in nonreducing SDS-PAGE were subjected to in-gel tryptic digestion. The cysteine side chains in SH form were NEM-modified, causing a 125 Da mass increase of tryptic peptides. The SS were reduced and IAM-modified, causing a 57 Da mass increase of tryptic peptides. (Detailed information is shown in the Supporting Information).

The cysteine status of β-conglycinin of unheated soy protein was first examined. The α' and α subunits of β-conglycinin theoretically have only Cys7 (SH).[1] The peak at m/z 2798.5280 in the peptide map of the α' band represented the peptides containing NEM-modified Cys7, indicating the Cys7 (SH) of α'. The peak at m/z 2730.2954 in the peptide map of the dimer of α' or α represented the peptides containing IAM-modified Cys7 of α'. This indicated that the Cys7 (SH) of α' was oxidized to form an intersubunit SS of dimer of α' or α. Unluckily, the peptides containing Cys6 of α were not found in tryptic digests of α or dimer.

For the dimer of glycinin subunit of unheated soy protein, the cysteine status identified was (1) G5, A3, Cys9 (SH and SS), Cys85 (SS), Cys316 (SH); B4, Cys327 (SH and SS), Cys405 (SH); (2) G1, A1a, Cys12 (SS), Cys45 (SH), Cys88 (SH); B1b, Cys298 (SH); (3) G4, Cys440 (SH and SS). For G5, the presence of Cys9 (SH) and Cys327 (SH) indicated that the theoretical intrachain SS in A3 (Cys9−Cys42) or theoretical interchain SS between A3 and B4 (Cys85−Cys327) was likely to be broken by SH−SS exchange and then form an intersubunit SS. For G1, theoretical intrachain SS in A1a (Cys12−Cys45) and theoretical interchain SS between A1a and B1b (Cys88−Cys298) could be broken by SH−SS exchange to form intersubunit SS.

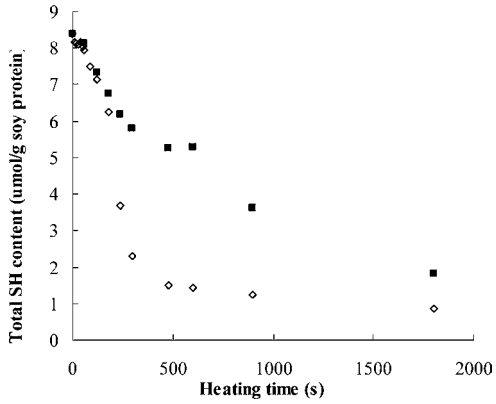

Figure 4. Effect of heating temperature and time on total free sulfhydryl content (SH_T) of soy proteins: (■) 80 °C; (◇) 90 °C.

The cysteine status identified from the AB band of unheated soy protein is shown in Figure 2a. For G1, the theoretical interchain SS between A1a and B1b should be Cys88−Cys298, but Cys298 (SH), Cys88 (SS), and Cys377 (SS) were identified. Because the glycinin subunit (AB) remained intact, Cys377 might have replaced Cys298 to form the Cys88−Cys377, resulting in Cys298 (SH). Cys271 (SS) and Cys278 (SS) suggested the presence of intrachain SS in A1a (Cys271−Cys278). Cys12 (SS) and Cys45 (SH) indicated that theoretical intrachain SS (Cys12−Cys45) in A1a might be broken. The theoretical SH in A1a (Cys53) was detected from tryptic peptides. For G2, the Cys289 (SH and SS) in B1a was identified, whereas Cys289 theoretically should be involved in interchain SS between A2 and B1a. Similarly, Cys284 of G3 theoretically involved in interchain SS between A1b and B2 was identified as SH. Interestingly, G4 was found in the AB band, indicating that A4 and B3 were linked by SS. The Cys350 (SS) in A4, Cys361 (SH and SS) in B3, and Cys440 (SH and SS) in B3 indicated that Cys350−Cys361 or Cys350−Cys440 could be the interchain SS between A4 and B3. For G5, Cys85 (SS) and Cys327 (SS) indicated the presence of interchain SS (Cys85−Cys327) between A3 and B4, and Cys316 (SH) in A3 was identified. Cys440 (SS) was identified from the peptide map of A5B3 band, indicating that Cys440 might be involved in the interchain SS between A5 and B3.

Figure 2b shows the cysteine status identified from polymer. Cys12 (SS), Cys271 (SS), Cys88 (SH and SS), and Cys298 (SH and SS) of G1 were identified in polymer. Cys298 of G1 was SH before heating. The presence of Cys298 (SS) in polymer, identified from the peptide containing IAM-modified Cys298 at $[M + H]^+$ 1724.90, indicated that the Cys298 (SH) was involved in SH−SS exchange or SH oxidation for forming intermolecular SS of polymer. The Cys88 of G1 was involved in Cys88−Cys377 between A1a and B1b before heating. The emergence of Cys88 (SH) in polymer, identified from the peptide containing NEM-modified Cys88 at $[M + H]^+$ 2751.2972, indicated that Cys88−Cys377 was most likely to be broken by SH−SS exchange for forming intermolecular SS. In addition, the possibility could not

DOI: 10.1021/jf504519z
J. Agric. Food Chem. 2015, 63, 3524−3533

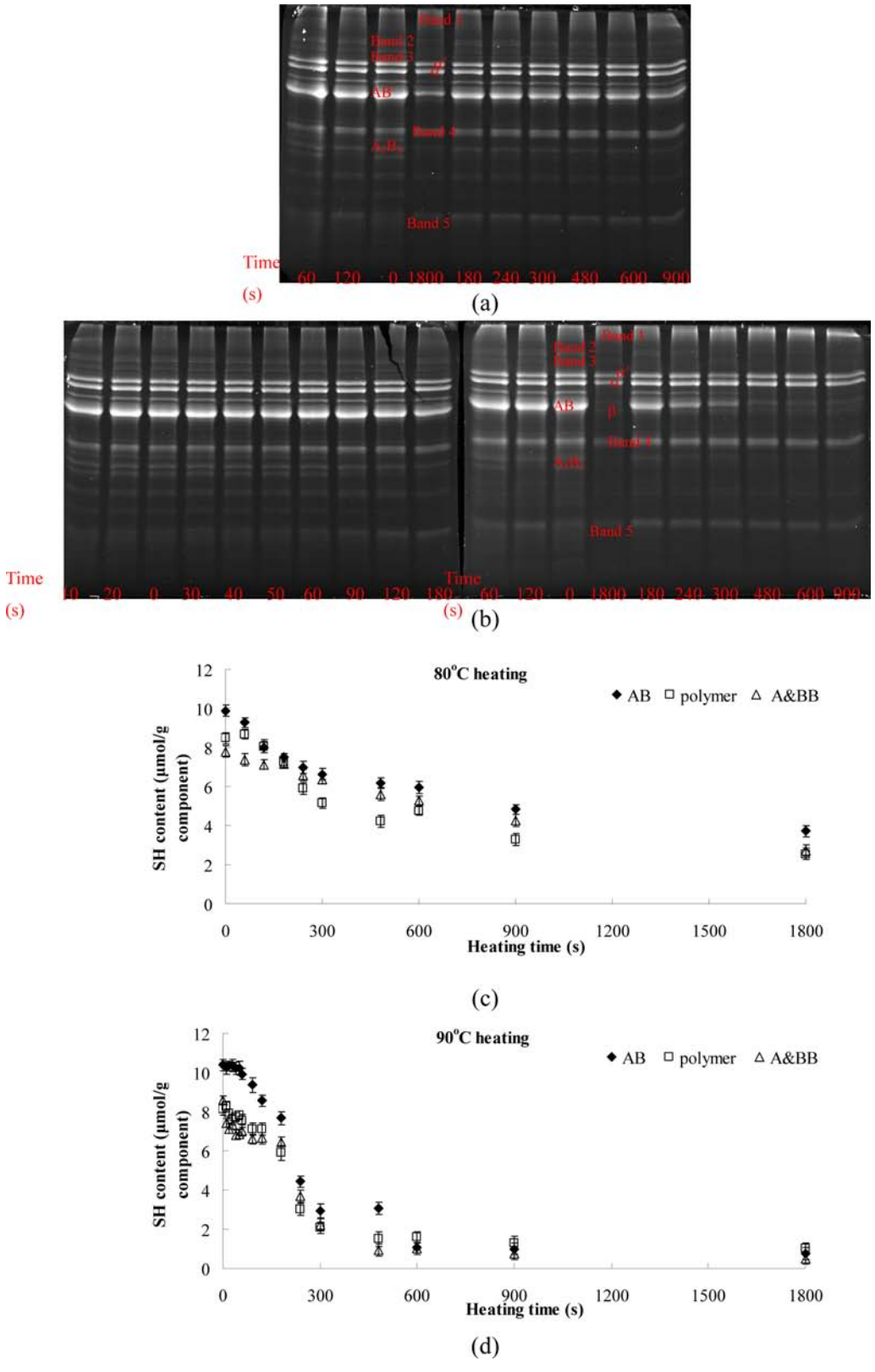

Figure 5. Fluorescence pattern of nonreducing SDS-PAGE of mBBr-labeled soy protein heated at 80 °C (a) and 90 °C (b) for different time lengths (0−1800 s); effect of heating time and temperature on SH contents of glycinin subunits (◆), polymer (□), and monomer of A and dimer of B (A&BB) (△) (c, 80 °C; d, 90 °C).

be eliminated that Cys12 and Cys271 in A1a were included in intermolecular SS of the polymer.

Cys289 (SH and SS) in B1a of G2 was identified in the polymer. The intensities of peptides containing NEM-modified Cys289 at $[M + H]^+$ 2062.0936 and 1662.9355 were higher than that of peptides containing IAM-modified Cys289 at $[M + H]^+$ 1764.9568 for G2 before heating. However, in the polymer the intensity of peptides containing NEM-modified Cys289 at

DOI: 10.1021/jf504519z
J. Agric. Food Chem. 2015, 63, 3524−3533

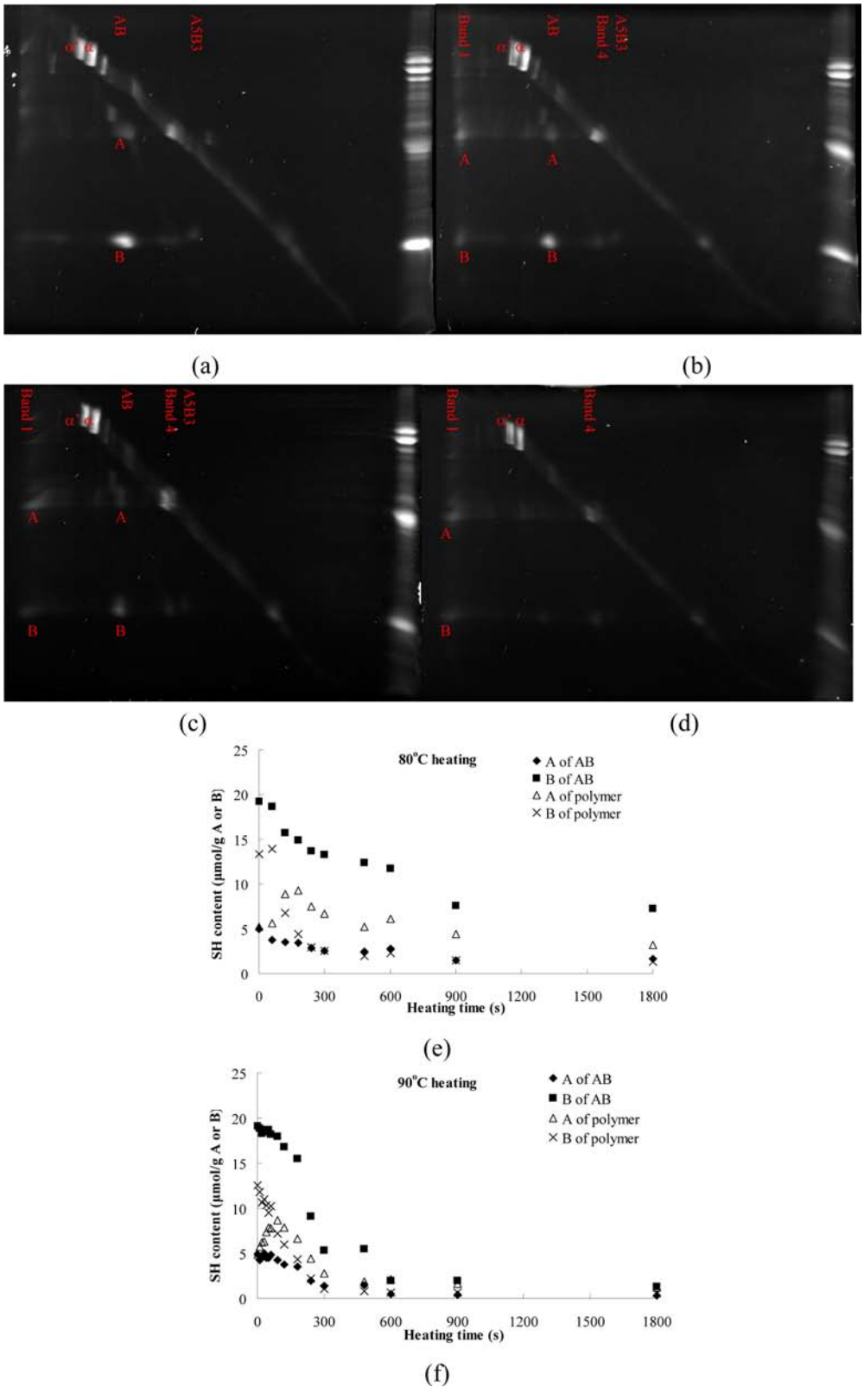

Figure 6. Fluorescence patterns of diagonal SDS-PAGE of soy protein (a, unheated; b, 80 °C, 1800 s; c, 90 °C, 300 s; d, 90 °C, 1800 s) (parts of the patterns are shown here); effect of heating time and temperature on the SH contents of acidic (A) polypeptide and basic (B) polypeptide in glycinin subunit (A, ◆; B, ■) and polymer (A, △; B, ×) (e, 80 °C; f, 90 °C).

$[M + H]^+$ 1792.9779 and 2062.0936 was adjacent to the intensity of peptides containing IAM-modified Cys289 at $[M + H]^+$ 1724.8674 and 1764.9508, suggesting that the Cys289 (SH) participated in SH−SS exchange or SH oxidation to form intermolecular SS of polymer. Cys440 of G4 was involved in Cys85−Cys440 and Cys350−Cys440 before heating. Cys440 (SH and SS) was identified in the polymer, suggesting that Cys440 (SH) was released by breaking the SS due to SH−SS exchange.

DOI: 10.1021/jf504519z
J. Agric. Food Chem. 2015, 63, 3524−3533

The cysteine status identified from the peptides map of A&BB contained (1) G1 (A1a, Cys12 (SS); B1b, Cys298 (SH)); (2) G2 (B1a, Cys289 (SH); A2, Cys273 (SH)); (3) G3 (A1b, Cys264 (SS)); (4) G4 (B3, Cys440 (SS)); and (5) G5 (B4, Cys405 (SH)). Cys440 (SS) in B3 of G4 suggested that Cys440 was one of the cysteine-forming SS between two monomers of B. Cys298 (SH) of G1, Cys289 (SH) of G2, and Cys405 (SH) of G5 might imply that the other cysteine of B, Cys377 of G1, Cys368 of G2, and Cys327 of G5, would be involved in SS between two monomers of B.

The cysteines identified from the peptides map of the oligomer (α', α, G1, and G2) of heated soy protein included (1) G1 (B1b, Cys298 (SH); A1a, Cys88 (SS)) and (2) G2 (B1a, Cys289 (SH and SS); A2, Cys266 (SH and SS), Cys273 (SS)). Cys88 (SS) of G1, Cys289 (SS) of G2, Cys266 (SS) of G2, and Cys273 (SS) of G2 were involved in the intermolecular SS of oligomer. (Cys86−Cys289) or (Cys266-Cys273) of G2 could be broken due to SH−SS exchange for forming intersubunit SS, resulting in Cys289 (SH) and Cys266 (SH).

In general, according to the cysteine status analysis, it was found that the interchain SS between A1a and B1b of G1 (Cys88−Cys298) was replaced by Cys88−Cys377, which might occur during the protein extraction process. Cys298 of G1, Cys289 of G2, and Cys440 of G4 were prone to participating in SH−SS exchange or SH oxidation for forming intermolecular SS of the polymer.

Evidence for SH Oxidation and SH−SS Exchange Reaction Supplied by SH Content Change of Subunit/Polypeptide. Soy protein heated at 80 and 90 °C for different times was subjected to nonreducing SDS-PAGE (Figure 3a,b). As shown, the glycinin subunits (AB and A5B3) progressively disappeared with heating time (0−1800 s).[7] The polymer and A&BB were gradually formed with heating time. The phenomena were further enhanced at higher temperature. The relative mass content of bands in soy proteins (C, g/g soy protein) was determined by comparing the individual band intensities with the total intensity of all bands in a lane (Figure 3c,d). The relative mass content of glycinin subunits decreased from 40 to 15% after heating at 80 °C for 1800 s, whereas at 90 °C glycinin subunits almost disappeared. More polymer was formed than A&BB. The relative contents of polymer and A&BB were approximately 45 and 13%, respectively, after heating at 90 °C for 30 min.

The total free SH content of soy protein (SH_T) was first determined and is shown in Figure 4. The SH_T of unheated soy protein was 8.4 μmol SH/g protein, which was in the wide range (0.2−14.8 μmol SH/g protein) reported in previous studies. The SH_T was decreased with heating time, which was promoted by increasing temperatures. This was in accordance with previous researches.[7,8,12] The decrease of SH_T indicated that the SH oxidation may be responsible for forming intermolecular SS of polymer. SH oxidation by molecular oxygen in aqueous solutions is suggested to be a common route for SS formation.[34] Sulfenic acids (RSOH) are formed by the oxidation of SH with dissolved molecular oxygen. Sulfenic acids exhibit potent electrophilic reactivity. Thiols can react with sulfenic acids to form SS.[35−38] SH−SS exchange is another way to break or form SS. The SH−SS exchange is a bimolecular nucleophilic substitution reaction (SN_2) in which the attacking nucleophile is the thiolate. The driving force of the reaction is the relatively low activation energy required for SH to break SS.[34,35]

Panels a and b of Figure 5 show the fluorescence pattern of nonreducing SDS-PAGE of mBBr-labeled soy protein. The SH contents of three major components (glycinin subunit, polymer, and A&BB) were calculated according to eqs 1 and 2, and the effects of heating time and temperature on the SH content are shown in Figure 5c,d. The SH content of all three major components was decreased obviously with heating time. An important feature was that the SH content of heat-generated products, polymer and A&BB, was lower than that of the principal-sourced proteins, glycinin subunit at heating phase. This confirmed that part of the intermolecular SS of polymer was formed by SH oxidation.

The fluorescence pattern of diagonal SDS-PAGE of mBBr-labeled soy protein (Figure 6a−d) and the corresponding CBB-stained patterns were also obtained (all heating samples were conducted but not all patterns are shown here). Panels e and f of Figure 6 show the SH content of A and B in glycinin subunit and polymer calculated according to eqs 3 and 4. The SH content of B (20 μmol/g B) was about 4 times higher than that of A (5 μmol/g A) in glycinin subunit before heating. The heat-induced decrease of SH content of B in glycinin subunit was more severe than that of A. The SH content of B in polymer was also decreased by heating, and much lower than the SH content of B in glycinin subunit, indicating the oxidation of SH of B. An important feature was that the SH content of A in polymer, which was lower than the SH content of B in polymer before heating, increased and exceeded the SH content of B after a short heating time and then remained higher than the SH content of B for prolonged heating. In addition, the SH content of A in polymer was always higher than the SH content of A in glycinin subunits. These results indicated that the SH was transferred from B to A when glycinin subunits were associated with form polymer, which was most likely due to the SH−SS exchange reaction between SH of B and SS of A.

As above, the SH of B in glycinin subunit was subjected to not only SH oxidation but also SH−SS exchange reaction for forming intermolecular SS of polymer. SH−SS exchange reaction was confirmed between SH of B and SS of A for the first time. The SH of B was suggested to be reactive for forming intermolecular SS of polymer, supporting the inference of Yamauchi et al.[39,40]

In this study, the disulfide-mediated interactions of soy protein during heat treatment were studied by nonreducing SDS-PAGE, diagonal SDS-PAGE, thiol-specific fluorescence labeling, and mass spectrometry analysis. The polymer was the major product composed of A, B, and small amounts of α' and α, which interacted with each other via intermolecular SS. The SH of B in the glycinin subunit was subjected to not only SH oxidation but also SH−SS exchange reaction for forming intermolecular SS of polymer. The SH of B (Cys298 of G1, Cys289 of G2, Cys440 of G4) identified by mass spectrometry was suggested to be reactive.

■ ASSOCIATED CONTENT

Supporting Information

Tabular information on unheated soy protein. This material is available free of charge via the Internet at http://pubs.acs.org.

■ AUTHOR INFORMATION

Corresponding Author

*(Y.H.) Fax: 86-0510-85329091. E-mail: yufeihuajiangnan@126.com or yfhua@jiangnan.edu.cn.

Funding

We gratefully acknowledge the financial support received from the Natural Science Foundation of China (31201380), the Natural Science Foundation of Jiangsu Province, People's Republic of China (BK2011151), the Open Project Program

DOI: 10.1021/jf504519z
J. Agric. Food Chem. 2015, 63, 3524−3533

of State Key Laboratory of Food Science and Technology, Jiangnan University (SKLF-ZZB-201202), and Doctor Candidate Foundation of Jiangnan University (JUDCF10025).

Notes

The authors declare no competing financial interest.

REFERENCES

(1) Utsumi, S.; Matsumura, Y.; Mori, T. Structure-function relationships of soy proteins. In *Food Proteins and Their Applications*; Damodaran, S., Paraf, A., Eds.; Dekker: New York, 1997; pp 257−291.

(2) Hou, H. J.; Chang, K. C. Structural characteristics of purified β-conglycinin from soybeans stored under four conditions. *J. Agric. Food Chem.* **2004**, *52*, 7931−7937.

(3) Wolf, W. J. Sulfhydryl content of glycinin: effect of reducing agents. *J. Agric. Food Chem.* **1993**, *41*, 168−176.

(4) Ruan, Q.; Chen, Y.; Kong, X.; Hua, Y. Comparative studies on sulfhydryl determination of soy protein using two aromatic disulfide reagents and two fluorescent reagents. *J. Agric. Food Chem.* **2013**, *61*, 2661−2668.

(5) Hou, D. H.; Chang, K. C. Structural characteristics of purified glycinin from soybeans stored under various conditions. *J. Agric. Food Chem.* **2004**, *52*, 3792−3800.

(6) Wu, S.; Murphy, P. A.; Johnson, L. A.; Fratzkea, A. R.; Reuber, M. A. Pilot-plant fractionation of soybean glycinin and β-conglycinin. *J. Am. Oil Chem. Soc.* **1999**, *76*, 285−293.

(7) Petruccelli, S.; Anon, M. C. Thermal aggregation of soy protein isolates. *J. Agric. Food Chem.* **1995**, *43*, 3035−3041.

(8) Shimada, K.; Cheftel, J. C. Determination of sulfhydryl groups and disulfide bonds in heat-induced gels of soy protein isolate. *J. Agric. Food Chem.* **1988**, *36*, 147−153.

(9) Wagner, J. R.; Gueguen, J. Surface functional properties of native, acid-treated, and reduced soy glycinin. 1. Foaming properties. *J. Agric. Food Chem.* **1999**, *47*, 2173−2180.

(10) Faris, R. J.; Wang, H.; Wang, T. Improving digestibility of soy flour by reducing disulfide bonds with thioredoxin. *J. Agric. Food Chem.* **2008**, *56*, 7146−7150.

(11) Wilson, S.; Blaschek, K.; de Mejia, E. G. Allergenic proteins in soybean: processing and reduction of P34 allergenicity. *Nutr. Rev.* **2005**, *63*, 47−58.

(12) Xu, Z.; Chen, Y.; Zhang, C.; Kong, X.; Hua, Y. The heat-induced protein aggregate correlated with trypsin inhibitor inactivation in soymilk processing. *J. Agric. Food Chem.* **2012**, *60*, 8012−8019.

(13) Utsumi, S.; Kinsella, J. E. Structure-function relationships in food proteins: subunit interactions in heat-induced gelation of 7S, 11S, and soy isolate proteins. *J. Agric. Food Chem.* **1985**, *33*, 297−303.

(14) Wang, J.; Xia, N.; Yang, X.; Yin, S.; Qi, J.; He, X.; Yuan, D.; Wang, L. Adsorption and dilatational rheology of heat-treated soy protein at the oil−water interface: relationship to structural properties. *J. Agric. Food Chem.* **2012**, *60*, 3302−3310.

(15) Cramp, G. L.; Kwanyuen, P.; Daubert, C. R. Molecular interactions and functionality of a cold-gelling soy protein isolate. *J. Food Sci.* **2008**, *73*, 16−24.

(16) Wang, C.; Damodaran, S. Thermal gelation of globular proteins: weight-average molecular weight dependence of gel strength. *J. Agric. Food Chem.* **1990**, *38*, 1157−1164.

(17) Yamagishi, T.; Miyakawa, A.; Noda, N.; Yamauchi, F. Isolation and electrophoretic analysis of heat-induced of mixed soybean 7S and 11S globulins. *Agric. Biol. Chem.* **1983**, *47*, 1229−1237.

(18) Ren, C.; Tang, L.; Zhang, M.; Guo, S. Structural characterization of heat-Induced protein particles in soy milk. *J. Agric. Food Chem.* **2009**, *57*, 1921−1926.

(19) Surroca, Y.; Haverkamp, J.; Heck, A. J. R. Towards the understanding of molecular mechanisms in the early stages of heat-induced aggregation of β-lactoglobulin AB. *J. Chromatogr., A* **2002**, *970*, 275−285.

(20) Holland, J. W.; Deeth, H. C.; Alewood, P. F. Analysis of disulphide linkages in bovine κ-casein oligomers using two-dimensional electrophoresis. *Electrophoresis* **2008**, *29*, 2402−2410.

(21) Chevalier, F.; Hirtz, C.; Sommerer, N.; Kelly, A. L. Use of reducing/nonreducing two-dimensional electrophoresis for the study of disulfide-mediated interactions between proteins in raw and heated bovine milk. *J. Agric. Food Chem.* **2009**, *57* (13), 5948−5955.

(22) Natarajan, S. S.; Xu, C.; Bae, H.; Caperna, T. J.; Garrett, W. M. Characterization of storage proteins in wild (*Glycine soja*) and cultivated (*Glycine max*) soybean seeds using proteomic analysis. *J. Agric. Food Chem.* **2006**, *54* (8), 3114−3120.

(23) Gomes, L. S.; Senna, R.; Sandim, V.; Silva-Neto, M. A. C.; Perales, J. E. A.; Zingali, R. B.; Soares, M. R.; Fialho, E. Four conventional soybean [*Glycine max* (L.) Merrill] seeds exhibit different protein profiles as revealed by proteomic analysis. *J. Agric. Food Chem.* **2014**, *62* (6), 1283−1293.

(24) Krishnan, H. B.; Nelson, R. L. Proteomic analysis of high protein soybean (*Glycine max*) accessions demonstrates the contribution of novel glycinin subunits. *J. Agric. Food Chem.* **2011**, *59*, 2432−2439.

(25) Wu, W.; Zhang, C.; Kong, X.; Hua, Y. Oxidative modification of soy protein by peroxyl radical. *Food Chem.* **2009**, *116*, 295−301.

(26) Rogers, L. K.; Leinweber, B. L.; Smith, C. V. Detection of reversible protein thiol modifications in tissues. *Anal. Biochem.* **2006**, *358*, 171−184.

(27) Kosower, E. M.; Kosower, N. S. Bromobimane probes for thiols. *Methods Enzymol.* **1995**, *251*, 133−148.

(28) Jin, X.; Chen, Y.; Lubman, D. M.; Misek, D.; Hanash, S. M. Capillary electrophoresis/tandem mass spectrometry for analysis of proteins from two-dimensional sodium dodecyl sulfate polyacrylamide gel electrophoresis. *Rapid Commun. Mass Spectrom.* **1999**, *13*, 2327−2334.

(29) Maeda, K.; Finnie, C.; Svensson, B. Identification of thioredoxin h-reducible disulphides in proteomes by differential labelling of cysteines: insight into recognition and regulation of proteins in barley seeds by thioredoxin h. *Proteomics* **2005**, *5*, 1634−1644.

(30) Petruccelli, S.; Anon, M. C. Soy protein isolate components and their interactions. *J. Agric. Food Chem.* **1995**, *43*, 1762−1767.

(31) Wadahama, H.; Iwasaki, K.; Matsusaki, M.; Nishizawa, K.; Ishimoto, M.; Arisaka, F.; Takagi, K.; Urade, R. Accumulation of β-conglycinin in soybean cotyledon through the formation of disulfide bonds between α′- and α-subunits. *Plant Physiol.* **2012**, *158*, 1395−1405.

(32) Lakemond, C. M. M.; de Jongh, H. H. J.; Gruppen, H.; Voragen, A. G. J. Differences in denaturation of genetic variants of soy glycinin. *J. Agric. Food Chem.* **2002**, *50*, 4275−4281.

(33) Tezuka, M.; Yagasaki, K.; Ono, T. Changes in characters of soybean glycinin groups I, IIa, and IIb caused by heating. *J. Agric. Food Chem.* **2004**, *52*, 1693−1699.

(34) Conte, M. L.; Carroll, K. S. The chemistry of thiol oxidation and detection. In *Oxidative Stress and Redox Regulation*; Jakob, U., Reichmann, D., Eds.; Springer: Dordrecht, The Netherlands, 2013.

(35) Nagy, P. Kinetics and mechanisms of thiol−disulfide exchange covering direct substitution and thiol oxidation-mediated pathways. *Antioxid. Redox Signal.* **2013**, *18* (13), 1623−1641.

(36) Owusu-Apenten, R. Colorimetric analysis of protein sulfhydyl groups in milk: applications and processing effects. *Crit. Rev. Food Sci. Nutr.* **2005**, *45*, 1−23.

(37) Rehder, D. S.; Borges, C. R. Cysteine sulfenic acid as an intermediate in disulfide bond formation and nonenzymatic protein folding. *Biochemistry* **2010**, *49*, 7748−7755.

(38) Bagiyan, G. A.; Koroleva, I. K.; Soroka, N. V.; Ufimtsev, A. V. Oxidation of thiol compounds by molecular oxygen in aqueous solutions. *Russ. Chem. Bull., Int. Ed.* **2003**, *52* (5), 1135−1141.

(39) Yamauchi, F.; Yamagishi, T.; Iwabuchi, S. Molecular understanding of heat-induced phenomena of soybean protein. *Food Rev. Int.* **1991**, *7*, 283−322.

(40) Yamagishi, T.; Yamauchi, F.; Shibasa, K. Isolation and partial characterization of heat-denatured products of soybean 11S globulin and their analysis by electrophoresis. *Agric. Biol. Chem.* **1980**, *44*, 1575−1582.

DOI: 10.1021/jf504519z
J. Agric. Food Chem. 2015, 63, 3524−3533

combined form polyelectrolyte complexes by molecular entanglements, ionic forces, hydrogen bonding, or hydrophobic forces.[17] The assembly of the protein-loaded CS/CRG magnetic nanoparticles was mediated by polyelectrolyte complexation under mild conditions, thus avoiding harmful organic solvents or high shear forces and retaining protein activity during immobilization.

Currently, because of high costs and complex methodology, enzyme immobilization has not yet been widely employed in industrial applications and is instead conducted either for the purpose of basic research or for use in technical processes.[9] Therefore, there is a need for the development of simple and green methods to facilitate the use of enzyme immobilization in industry. In the present work, we describe a simple, green, and novel method for the immobilization of pullulanase by adsorption. Chitosan was utilized as a flocculating agent to prepare pullulanase/chitosan complexes, which were then electrostatically coupled with Fe_3O_4/carrageenan nanoparticles. To prevent the adsorbed enzymes from leaking during repeated uses, which would restrict their application in enzyme immobilization, we further coated the immobilized enzymes with carrageenan by electrostatic interaction, expecting the interaction of chitosan, enzymes, and carrageenan to enhance the stability of the biocatalysts. Such structure was supposed to provide the advantage of high residual activity, besides the merit of enzyme recovery. To achieve these aims, the Fe_3O_4–κ-carrageenan nanoparticles were first prepared in situ under mild conditions without any surfactants. Pullulanase/chitosan mixtures were brought to complexing conditions by the slow addition of NaOH, and the effects of pH and protein/chitosan ratio on turbidity were investigated. The hybrid magnetic nanoparticles were then mixed with the pullulanase/chitosan complexes to obtain the immobilized enzymes and further coated with carrageenan. The effects of support/enzyme ratio on enzyme activity and protein loading were studied. Finally, the properties of the immobilized enzyme, such as kinetic behavior, pH and temperature profiles, thermal and operational stability, were also investigated.

MATERIALS AND METHODS

Materials. Pullulanase from *Klebsiella pneumoniae* and pullulan were purchased from Sigma-Aldrich. κ-Carrageenan (CRG, commercial grade) and chitosan (degree of deactylation = 90%) were obtained from Aladdin Industrial Co., Ltd. Ferric chloride hexahydrate ($FeCl_3 \cdot 6H_2O$), ferrous sulfate heptahydrate ($FeSO_4 \cdot 7H_2O$), and sodium hydroxide (NaOH) were obtained from Sinopharm Chemical Reagent Co., Ltd. (Shanghai, China). All other chemicals were analytic-grade and available from commercial sources.

Preparation of Hybrid Magnetic (Fe_3O_4–κ-Carrageenan) Nanoparticles. In situ synthesis of magnetic Fe_3O_4–κ-carrageenan nanoparticles was carried out as reported previously with minor modification.[12] In brief, 0.5 g of κ-carrageenan was dissolved in 100 mL of deoxygenated water, stirred until dissolved completely at 60 °C, and cooled to 40 °C. After cooling, 2 mL of $FeCl_3$ solution (0.2 M), freshly prepared in deoxygenated water, and 65 mg of $FeSO_4$ were immediately added to 20 mL of κ-carrageenan solution. To account for the possible oxidation of Fe^{2+}, ferrous ion was added in slight excess of the magnetite stoicheometric molar ratio (Fe^{3+}/Fe^{2+} = 2:1). After stirring the mixture for 15 min, 2.2 mL of 1 M sodium hydroxide was added, giving a final pH of over 10. The mixture immediately turned black, indicating that the Fe_3O_4–κ-carrageenan composite was successfully prepared.

Preparation of Pullulanase/Chitosan Complex Solutions. Chitosan powder was dispersed in 0.1% acetic acid solution (v/v) under magnetic stirring for 4 h at room temperature to prepare a 0.1% chitosan solution (w/v). Pullulanase was diluted with sodium acetate buffer (10 mM) to a final concentration of 1 mg/mL. Each solution was adjusted to a pH of 2.8. Turbidity titration of pullulanase/chitosan mixture was conducted by first mixing the two solutions at different ratios, ranging from 10:1 to 1:1, then slowly adjusting the pH to 8.0 with 0.1 M NaOH. Homogenous pullulanase (1 mg/mL) and chitosan solutions (0.1%, w/v) were used as blanks.[18]

Measurement of Turbidity. A UV–vis spectrophotometer (Shimadzu, Japan) with a 0.5 cm cuvette was used to measure turbidity at 600 nm. By the addition of gradated NaOH solutions (1, 0.5, 0.1 M), turbidimetric titration was carried out in increments of ∼0.1 pH unit up to a final pH of 8.0 under gentle stirring. Titrations were carried out at 25.0 ± 1.0 °C, and the pH (±0.01 pH unit) was monitored with a Mettler Toledo Delta 320 pH meter.[19]

Enzyme Immobilization. Fe_3O_4–κ-carrageenan nanoparticles were incubated with the pullulanase/chitosan complex solutions (pH 4.8) at 40 °C for 4 h under gentle stirring. After immobilization, successive washings with the buffer (pH 4.8) were conducted to remove the excess enzyme until no more activity was detected in the washing fractions. Then, the immobilized enzyme was further incubated with 0.1% (w/v) carrageenan solution (pH 4.8) at 40 °C for 1 h under gentle stirring and washed with the buffer several times.

The immobilized activity was calculated by taking the difference between the applied and the recovered activities. The amount of the immobilized protein was determined by subtracting the amount of protein remaining in the supernatant and washing solutions after 4 h of stirring from the amount of protein added to immobilization, according to the Bradford protein assay method reported previously.[20] The activity retention (AR) and enzyme loading efficiency were calculated according to the following equations:

$$\text{activity retention} = \frac{A_{\text{im}}}{A_0} \times 100 \quad (1)$$

where A_0 is the specific activity of free pullulanase and A_{im} is the specific activity of the immobilized enzyme.

$$\text{enzyme loading efficiency} = \frac{C_0V_0 - C_iV_i}{C_0V_0} \times 100\% \quad (2)$$

where C_0 and V_0 are the protein concentration and the volume of the free pullulanase solution added to immobilization, respectively, and C_i and V_i are the protein concentration and the volume of the supernatant solution after immobilization, respectively.

Characterization. A Zetasizer Nano ZS (Malvern Instruments, Malvern, UK) with a He/Ne laser of 633 nm wavelength was used to determine size distribution of freshly prepared nanoparticles; each sample was diluted to the appropriate concentration with ultrapure water, then placed in the electrophoretic cell at 20 °C. A high-performance digital imaging transmission electron microscopy (TEM) machine (JEM-2100 (HR), JEOL Ltd., Tokyo, Japan) was used to determine the particle size and morphology of the magnetic nanoparticles. Image-Pro Plus 6.0 (Media Cybernetics, Inc., Bethesda, Maryland, USA) was used to analyze the TEM micrographs to obtain the size distribution of nanoparticles. An average result of nanoparticle size was obtained by analyzing TEM images of 20 (total counts of particles: 200). Fourier transform-infrared (FT-IR) spectra were recorded using a Thermo Nicolet iS10 FT-IR Spectrometer (Thermo Electron Corp., Madison, WI, USA). X-ray diffraction (XRD) measurements were carried out with a BRUKER AXS GMBH D8 (Karlsruhe, Baden-Wuerttemberg, Germany) instrument; a continuous scan mode was used to collect 2θ data from 10 to 80°, at a constant rate of 4°/min. A vibrating-sample magnetometer (VSM, Lakeshore-7304, Westerville, Ohio, USA) was used to obtain magnetization curves at room temperature. Thermogravimetric analysis (TGA) was carried out with a Mettler Toledo SDTA 851e (Zürich, Canton of Zürich, Switzerland) instrument at a heating rate of 10 °C/min from 30 to 700 °C.

Activity Assay of Pullulanase. The activities of free and immobilized pullulanase were determined by the 3,5-dinitrosalicylic acid (DNS) method using pullulan as substrate.[2] In brief, 2 g of

DOI: 10.1021/jf505981t
J. Agric. Food Chem. 2015, 63, 3534–3542

pullulan was added into 100 mL of sodium acetate buffer (0.04 M, pH 4.4) to obtain a homogeneous pullulan solution (2%, w/v). Then 0.1 mL of free (50 μg/mL) or immobilized pullulanase (0.5 mg.d.s.mL^{-1}) solution was incubated with 1 mL of pullulan solution at a water bath of 50 °C for 30 min. The reaction was stopped by adding 1.5 mL of 3, 5-dinitrosalicylic acid (DNS). After incubation, the reaction mixtures were kept in boiling water for 10 min and then immediately cooled to room temperature. The reducing sugars were determined at an absorbance of 540 nm by the ultraviolet−visible (UV−vis) spectrophotometer. One unit of pullulanase activity was defined as the amount of enzyme that produced 1 μmol of reducing sugars (as maltotriose equivalents) in 1 min at 50 °C.

Kinetic Parameters of Free and Immobilized Enzyme. The kinetic properties of free and immobilized pullulanase were determined by using different substrate concentrations of 1−10 mg/mL. The kinetic constants K_m and V_m were calculated according to the Lineweaver−Burk plots.[21]

pH Stability. Stabilities of free and immobilized enzyme against pH were evaluated in light of the catalytic activity of enzyme by incubating enzyme at a pH range of 2.5−6.4 for 30 min at 50 °C, and their residual activities were determined.

Reusable Stability. The operational stability was assessed by incubating immobilized enzyme with pullulan (2%, w/v) in a water bath of 50 °C for 30 min, after which the activity was assayed immediately. After each reaction period, the immobilized pullulanase were removed from the reaction medium and washed with sodium acetate buffer (40 mM, pH 4.4). Then, the fresh pullulan solution was added again to start the reaction. The activity of the first run was defined as 100%.

Thermal Stability. The thermostabilities of free and immobilized pullulanases were tested in light of the optimum temperature and thermal inactivation courses. For the optimum temperature, enzymes were incubated in sodium acetate buffer (pH 4.4, 10 mM) in a water bath (20−65 °C) for 30 min, and their residually activities were determined. For the thermal inactivation courses, enzymes were incubated at 60 °C in 40 mM sodium acetate buffer (pH 4.4) for 6 h, and samples were withdrawn after incubation for 10, 20, 30, 60, 180, and 300 min, then immediately assayed for residual activity.

Statistical Analysis. The data expressed in various studies were plotted using Origin-8.5. Experiments were triplicated. Data represent the mean of three independent assays carried out in duplicate, and the results are presented as mean ± SD. Significant differences were determined statistically using one-way analysis of variance (ANOVA) posthoc Tukey test. Statistical significance was established at $p < 0.05$.

RESULTS AND DISCUSSION

Pullulanase/Chitosan Complexing Behavior as a Function of pH and Mixing Ratio. Chitosan is a well-known biopolymer commonly used in the formation of protein−polysaccharide complexes. Complex coacervates have many applications in the biotechnology, pharmaceutical, and food industries.[22] Amino groups in chitosan chains intensively interact with the carboxyl groups of enzymes largely by electrostatically driven forces, which in turn leads to the formation of a complex.[23] By controlling the conditions, this protein−polysaccharide complex could form nanoscale particles in soluble form in aqueous solution. For this reason, we first prepared pullulanase/chitosan complexes, then incubated them with magnetic nano−κ-carrageenan particles to prepare the nanoscale immobilized enzyme, and further coated them with carrageenan, expecting the interaction of biopolymers and enzymes to further prevent the adsorbed enzymes from leaking.

The complexing behavior of pullulanase/chitosan was affected by pH changes. The increase in absorbance at 600 nm upon addition of NaOH to the pullulanase/chitosan mixtures was indicative of the formation of colloidal dispersions via the self-assembly of the oppositely charged polyelectrolytes pullulanase and chitosan. Figure 1 shows the turbidity curves for the pullulanase/chitosan system. Below pH_c (the pH at

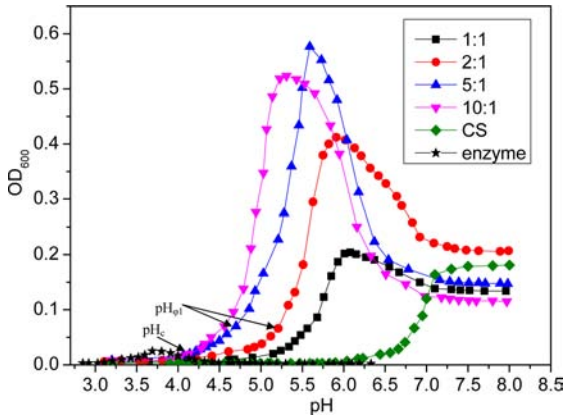

Figure 1. Turbidity curves for the pullulanase/chitosan system (C_p = 1 mg/mL) as a function of pullulanase/chitosan mixing ratio. Enzyme and chitosan (CS) solution at their corresponding concentrations were used as controls. The values of pH_c and $pH_{\varphi 1}$ were determined graphically as the intersection point of two tangents to the curve: pH_c corresponds to the pH value at which soluble complexes form, and $pH_{\varphi 1}$ corresponds to the pH value at which insoluble complexes form. Results are the mean of triplicates.

which soluble complexes form because of the local negative charges carried by proteins), the turbidity remained at the baseline because the electrostatic repulsive forces prohibited the formation of complexes. An abrupt increase in turbidity was observed with further addition of NaOH (at $pH_{\varphi 1}$), indicating the formation of insoluble complex particles. Before complexation with proteins, the chitosan solution was transparent until the pH increased to the pK_a of its amine (pH 6.3), where a protonated effect was observed. Therefore, the turbidity curve (Figure 1) for chitosan showed an abrupt increase at pK_a, followed by a maximum at around pH 7.0, and then reached the plateaus of turbidity, corresponding to the insolubility of chitosan.

Meanwhile, the pullulanase/chitosan interaction also can be affected by the mixing ratio. The decrease in pullulanase/chitosan ratio resulted in less negative charges being carried by proteins and more positive charges being carried by chitosan; as the consequence, $pH_{\varphi 1}$ shifted to higher pH values to achieve the charge neutralization.[24] At pullulanase/chitosan ratio = 2:1, the formation of soluble complex was distributed in a wide pH range from 4.0 (pH_c) to 5.27 ($pH_{\varphi 1}$). Ratios such as 5:1 and 10:1 had narrower pH ranges for soluble complex formation, whereas the 1:1 ratio yielded weak pullulanase−chitosan interactions that occurred near the deprotonation point of chitosan (pH 6.3). Therefore, the most flexible pH range for pullulanase−chitosan complex formation is seen using a mixing ratio of 2:1. From the view of charge neutralization (obtained at $pH_{\varphi 1}$), the negative charge of pullulanase (−12.5 mV, pH 4.8) was insufficient to neutralize the positive charge of chitosan solution (45.2 mV, pH 4.8) at the concentration of 0.1% (w/v), and the zeta potential of the complex was about 15.6 mV (pH 4.8), indicating the possibility that all the proteins were adsorbed in the chain of chitosan. Moreover, increased pH values led to the formation of insoluble complexes (pH 5.27), and there was almost no activity in the supernatant after centrifugation. These observations mean that the pullulanase was completely absorbed by chitosan at pH 5.27, indicating the

DOI: 10.1021/jf505981t
J. Agric. Food Chem. 2015, 63, 3534−3542

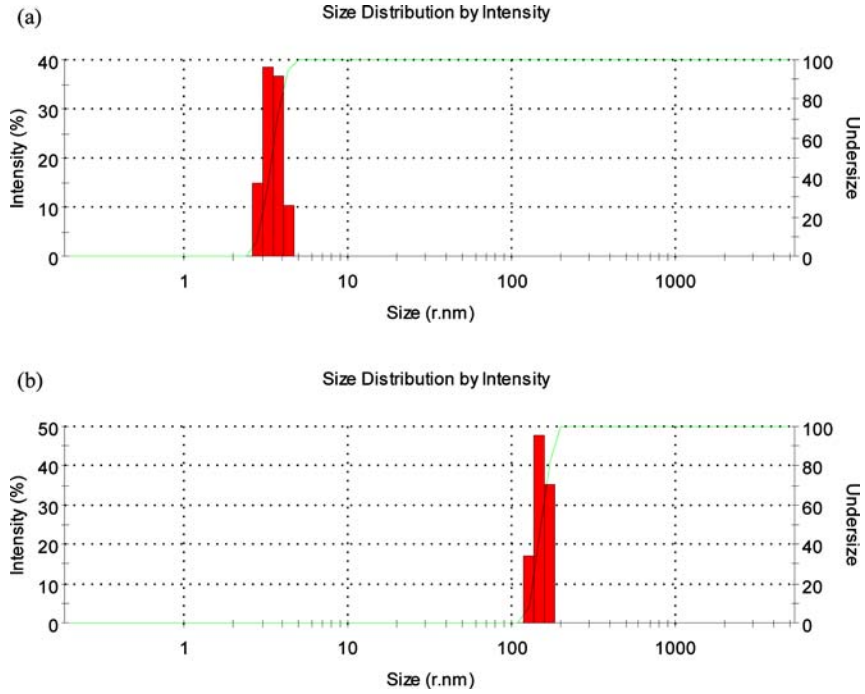

Figure 2. (a) Particle size distribution of the pullulanase/chitosan complex and (b) immobilized pullulanase.

high content of protein adsorbed by chitosan at pH 4.8 before phase separation.

In our research, the pullulanase/chitosan complexes formed at the ratio of 2:1 (pH 4.9) possessed an average diameter of 3.5 nm (Figure 2a), and after incubation of the complex with Fe_3O_4–κ-carrageenan nanoparticles, the immobilized enzyme showed an average diameter of 152 nm (Figure 2b). This indicated that the pullulanase/chitosan complexes take advantage of forming immobilized enzyme on the nanoscale because the diameter of immobilized enzyme was not in nanoscale when chitosan and pullulanase were added separately. Schematics for the fabrication process and the structure of the hybrid magnetic nanoparticles with immobilized pullulanase are shown in Figure 3.

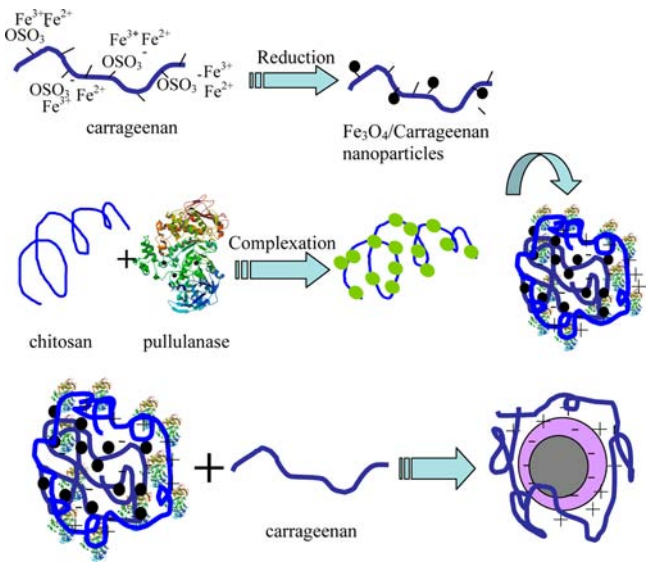

Figure 3. Schematic diagram of experimental design.

Characterization of Immobilized Enzymes. *Magnetic Properties.* At the first stage, the in situ synthesis of magnetic carrageenan nanoparticles involves the chelation of ferric (and ferrous) ions with the sulfate and hydroxyl groups of carrageenan at low pH, promoting the physical cross-linking of the carrageenan chains and formation of microgel; upon increasing pH, self-capped iron oxide nanoparticles are formed involving biopolymer molecules, with a number of the sulfate groups released. However, some sulfate groups still remain chelated to the nanoparticle surfaces, resulting in the high colloidal stability of this system.[12] This high colloidal stability results in a weak magnetic response of the nanoparticles to an external magnetic field. After the addition of the pullulanase/chitosan complex, the charge of the sulfate groups was neutralized, and the problem of weak magnetic response was solved. As shown in Figure 4, within the external magnetic field, immobilized enzymes aggregated completely in 15 s, whereas Fe_3O_4–κ-carrageenan nanoparticles moved slowly and finally aggregated completely in 8 min.

The hysteresis loops of Fe_3O_4–κ-carrageenan nanoparticles and immobilized enzymes were also calculated by a vibrating-sample magnetometer. As can be seen from Figure 4, both magnetic nanoparticles and immobilized enzymes exhibited superparamagnetic behavior. The saturation magnetization (M_s) of the immobilized enzymes was higher (42.6 emu/g) than that of the Fe_3O_4–κ-carrageenan nanoparticles (37.8 emu/g), whereas pure Fe_3O_4 was 98.1 emu/g. The excellent response to an applied magnetic field suggests that the immobilized enzymes meet the requirements for reuse in the food industries.

Morphology and Particle Size Distribution. Figure 5 shows a typical TEM image of immobilized enzymes. As can be seen from the picture, the average diameter of the immobilized enzymes was 156 nm, which is consistent with the result obtained on the zetasizer (Figure 2b). These results indicate that mixing of pullulanase/chitosan complex and magnetic carrageenan nanoparticles showed feasibility in the preparation

DOI: 10.1021/jf505981t
J. Agric. Food Chem. 2015, 63, 3534−3542

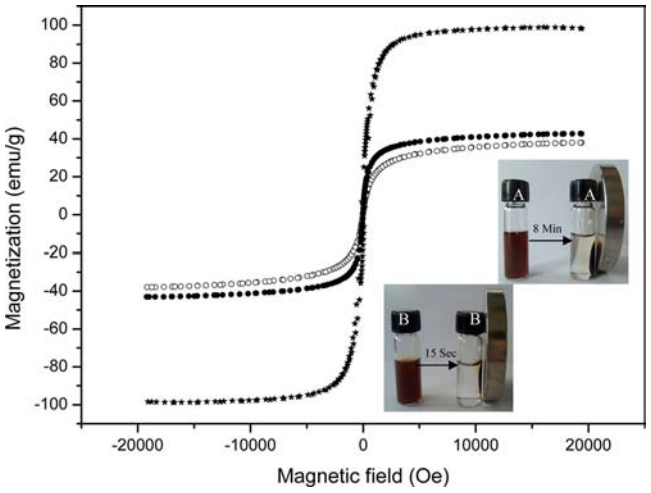

Figure 4. Magnetization curves for pure Fe_3O_4 (★), Fe_3O_4–carrageenan nanoparticles (○), and immobilized pulluanase (●). The inset shows the photograph of Fe_3O_4/carrageenan (A) and immobilized pullulanase (B) dispersion in water (left) and their magnetic response when placed in external magnetic field (right).

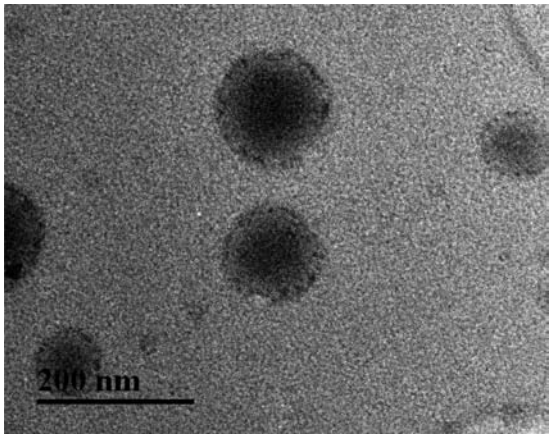

Figure 5. TEM micrographs of the immobilized pullulanase.

of nanoscale immobilized enzymes. The uniform and flexible environment of the pullulanase/chitosan complexes and magnetic carrageenan nanoparticles facilitated the homogeneous distribution of the enzymes.

FT-IR Analysis. FT-IR spectra of chitosan, carrageenan, immobilized enzymes, and Fe_3O_4 are shown in Figure 6. As can be seen from the figure, chitosan showed the typical peaks of amide I at 1651 cm^{-1}, amide II at 1597 cm^{-1}, and glycosidic bonds at 1080 cm^{-1}.[25] As for κ-carrageenan, the characteristic peaks at 1262, 847, 1068, and 928 cm^{-1} corresponded to the sulfate groups, galactose-4-sulfate, glycosidic linkage, and 3,6-anhydrogalactose, respectively.[26] The FT-IR spectrum of the immobilized enzymes exhibited the characteristic peaks of carrageenan at 1224, 1065, 929, and 845 cm^{-1} and the characteristic amide peak of chitosan, which converted into a single band at 1636 cm^{-1}. This verified the presence of carrageenan and chitosan in the biocatalyst. In the spectrum of the immobilized enzyme, the characteristic peak around 580 cm^{-1} was attributed to vibrations of the Fe–O bond of Fe_3O_4. Moreover, upon complexation of chitosan, carrageenan, and pullulanase, a new absorption band at 1530 cm^{-1}, assigned to NH_3^+ groups, was observed, which was absent in the spectra of

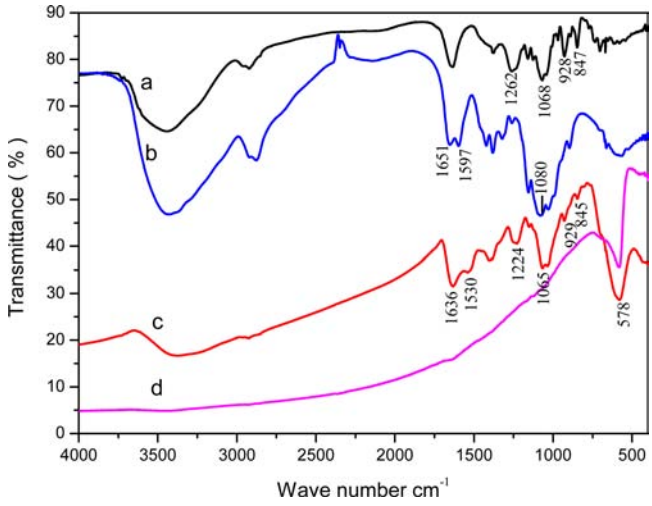

Figure 6. FT-IR spectra of chitosan (a, black trace), carrageenan (b, blue trace), immobilized pullulanase (c, red trace), and Fe_3O_4 (d, pink trace).

both chitosan and carrageenan. The spectra confirmed the successful formation of an immobilized enzyme.

XRD Patterns. XRD analysis of Fe_3O_4 and immobilized enzymes is shown in Figure 7. According to Joint Committee

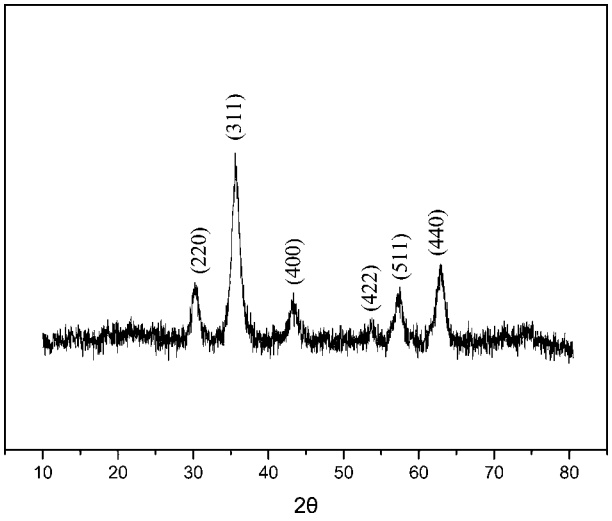

Figure 7. Wide-angle XRD patterns of immobilized pullulanase.

on Powder Diffraction Standards, JCPDS, entry 19-629, the powder XRD of immobilized enzymes matches the typical diffraction patterns observed for magnetite, which can be assigned to the six characteristic peaks at 2θ = 30.1, 35.4, 43.1, 53.2, 56.9, and 62.5°, corresponding to (220), (311), (400), (422), (511), and (440), respectively. Especially, the presence of the characteristic peak at 35.4° represents the formation of the spinel structure of Fe_3O_4, indicating that the immobilized enzyme still maintains its natural crystalline structure of Fe_3O_4 with no phase change.

Thermal Degradation. The thermal properties of pure Fe_3O_4, Fe_3O_4–κ-carrageenan nanoparticles, and immobilized enzymes studied by TGA are shown in Figure 8. Fe_3O_4 was thermally stable, and there was no weight loss in the interval of 200–800 °C (Figure 8a). For the Fe_3O_4–κ-carrageenan nanoparticles and immobilized enzymes, the derivative of

DOI: 10.1021/jf505981t
J. Agric. Food Chem. 2015, 63, 3534–3542

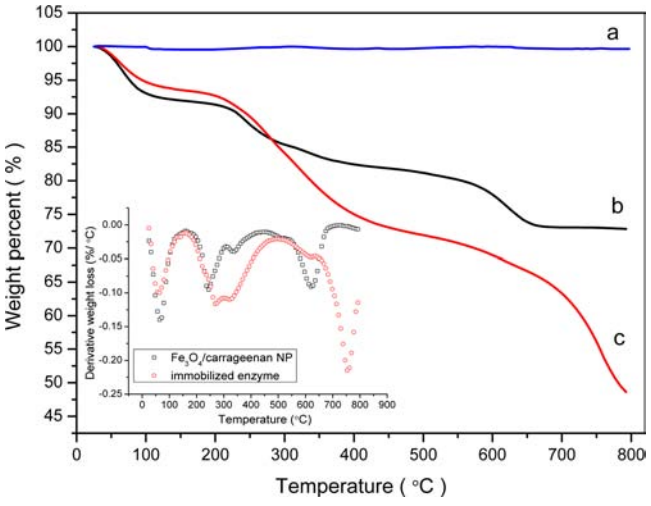

Figure 8. Thermogravimetric analysis of Fe_3O_4 (a, blue trace), Fe_3O_4–carrageenan nanoparticles (b, black trace), and immobilized pullulanase (c, red trace). The inset shows the derivative weight loss curves for Fe_3O_4–carrageenan nanoparticles and immobilized pullulanase.

weight-loss curves clearly indicated the inflection point of thermal decomposition, which was observed around 100, 240, 330, 620, and 750 °C (inset Figure 8). The weight loss below 200 °C was attributed to the loss of residual water.[27] The polysaccharide units of chitosan and carrageenan began to decompose at 200 °C.[28] In the interval of 200–800 °C, the degradation of carrageenan caused a weight loss of 18.41% estimated from the TGA curve of Fe_3O_4–κ-carrageenan nanoparticles (Figure 8b). At least three thermal events were observed: (i) From 200 to 300 °C, the degradation of carrageenan is associated with sulfur dioxide leaving and carbohydrate backbone fragmentation with weight loss of 5.80%. (ii) When the temperature increased to 450 °C, the degradation of carrageenan is related to polysaccharide decomposition with weight loss of 3.65%. (iii) The residual carrageenan or the intermediate compounds degradation caused a 8.96% weight loss that is continued until approximately 800 °C. Although in the interval of 200–800 °C, the degradation of chitosan, pullulanase and carrageenan (further coated) caused a 43.86% weight loss estimated from the TGA curves of Fe_3O_4–κ-carrageenan nanoparticles (Figure 8b) and immobilized enzymes (Figure 8c). At least three thermal degradations were also observed: an 8.28% weight loss from 200 to 300 °C, an 11.10% weight loss from 300 to 450 °C, and a 24.48% weight loss from 450 to 800 °C. Moreover, a new inflection point in the derivative weight-loss curve of immobilized enzymes was observed (inset Figure 8), which may be due to the complexation of chitosan, carrageenan, and pullulanase.

Reusability of Immobilized Pullulanase. Reusability of the immobilized enzyme is very important from the viewpoint of practical applications, and an improved stability makes the immobilized enzyme more advantageous than its free counterpart. However, as for absorption method, the leakage of enzymes from support in practice should be considered. To compare the stability of the immobilized pullulanase prepared as discussed in this paper with that of immobilized enzyme prepared by simply mixing magnetic carrageenan nanoparticles with pullulanase, we determined the reusability of the different immobilized enzymes. The activity of the immobilized pullulanase was assayed in 10 batches, and the same assay conditions were used for all batches. Activity of the first run was defined as 100%. In run 1, the immobilized enzyme was prepared as discussed in this paper. In run 2, the immobilized enzyme was prepared by simply mixing magnetic carrageenan nanoparticles with pullulanase. In run 3, the latter immobilized enzyme was further coated with carrageenan. As illustrated in Figure 9, the immobilized enzyme prepared in this paper (run

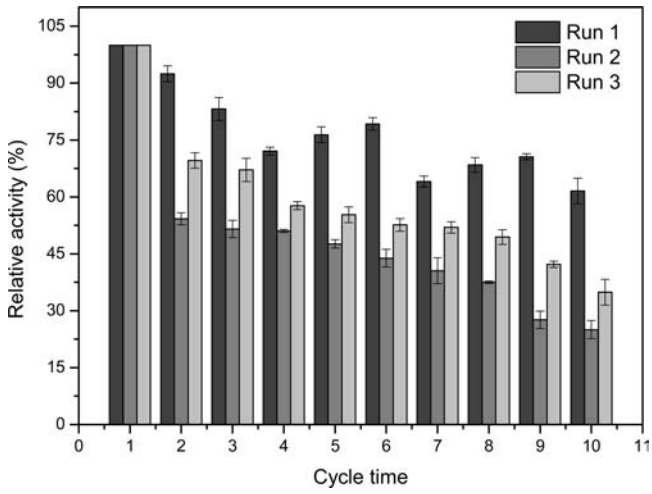

Figure 9. Reusability of the immobilized pullulanase. Experiments were triplicated, and the results are presented as mean ± SD.

1) showed the best reusability, retaining more than 76 and 61% of its original activity after 5 and 10 consecutive reuses, respectively. Pullulanase immobilized by simply mixing with magnetic carrageenan nanoparticles (run 2) exhibited a loss in activity of approximately 53 and 75% after 5 and 10 batch reactions, respectively. The immobilized enzyme prepared in run 3 also experienced a large loss in activity after 5 and 10 batch reactions (residual activity ≈ 52 and 34% of the initial value, respectively). Moreover, these enzymes undergo a fast decline in catalytic activity (residual activity ≈ 54 and 69% of the initial value) after the first use. In contrast, the immobilized enzyme prepared in this paper maintained its activity well (92% of the initial activity) after the first use. Obviously, the leakage of enzymes was remarkably abated.

Enzyme Immobilization and Loading Capacity. Activity retention, amount of protein immobilized, and loading efficiency after immobilization for different amounts of enzyme were summarized in Table 1. The amount of protein

Table 1. Activity Parameters of the Free and Immobilized Pullulanase[a]

applied activity (U.g.d.s.$^{-1}$)[b]	amount of protein immobilized (mg/g)	protein loading efficiency (%)	specific activity (u/mg)	activity retention (%)
37910	40.3 ± 2.4	70.7 ± 4.4	182.5 ± 3.9	51.2 ± 1.5
63183	51.2 ± 1.2	54.9 ± 3.8	222.1 ± 2.6	62.3 ± 2.5
126367	70.0 ± 1.5	40.8 ± 2.1	260.0 ± 6.0	72.9 ± 0.7
189550	76.4 ± 2.0	29.3 ± 2.3	290.2 ± 7.6	81.4 ± 1.5
379100	96.4 ± 2.1	23.9 ± 2.8	340.8 ± 6.4	95.6 ± 0.8
505467	102.6 ± 2.3	20.4 ± 2.6	320.6 ± 5.6	89.9 ± 0.9

[a]Experiments were triplicated, and the results are presented as mean ± SD. [b]d.s. corresponds to dry support.

DOI: 10.1021/jf505981t
J. Agric. Food Chem. 2015, 63, 3534–3542

immobilized increased when the loading efficiency decreased because saturation of the support was being achieved. The maximum quantity of pullulanase immobilized on 1 g of magnetic nanoparticles was 102 mg. Similarly, the activity retention increased from 51.19 to 95.58%, which implies that the activity of the enzyme was preserved well by this mild method; however, activity retention decreased with further increase of the bound protein. These results suggest that when a small amount of protein is immobilized on the support, its activity is totally expressed; however, when more proteins are attached, the enzyme molecules either become aggregated, forming a multilayer of enzyme molecules at the particle surface and blocking the active site, or the presence of neighboring enzyme molecules reduces the accessibility of substrate to the active sites,[29] resulting in decreased activity retention.

Effect of Immobilization on the pH Profile of Pullulanase. The effect of pH on the activity of free and immobilized pullulanase was estimated in the range of pH 2.5−6.4 (Figure 10a). The maximum pullulanase activity was

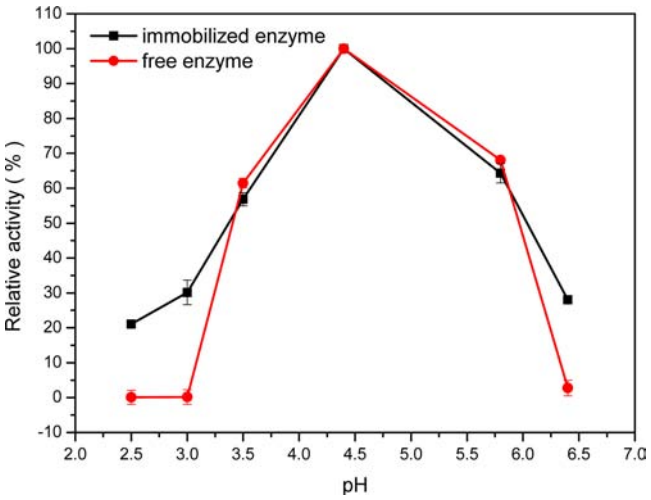

Figure 10. Effect of pH on pullulanase activity. Experiments were triplicated, and the results are presented as mean ± SD.

defined as 100%. It was observed that the activity of both free and immobilized pullulanase was greatly affected by pH, and the maximum activity was observed at pH 4.4 for both free and immobilized pullulanase. Compared with free pullulanase, the immobilized enzyme exhibited a better pH resistance at pH ≤ 3.0 and pH > 6. For example, at pH ≤ 3.0, there was a significant difference ($p < 0.01$) in enzyme activity: for the free enzyme, there almost no activity was detected, whereas for the immobilized enzyme, the relative activity was 21.05 and 30.14% at pH 2.5 and 3.0, respectively. Mechanisms of the decreased pullulanase activity might be attributed to the changed protein folding and binding modes (electrostatic or via hydrogen bonds).[7]

Catalytic Property (Activity and Kinetic Parameters) of Immobilized Pullulanase. Catalytic kinetics of the free and immobilized enzymes were further investigated. The Lineweaver−Burk plot for pullulan reduction (1−10 mg/mL) with free and immobilized pullulanase is shown in Figure 11. The apparent Michaelis constant, K_m, and the maximum reaction rates, V_m, of pullulanase calculated from the equations of these plots were summarized in Table 2. K_m relates to the affinity of substrate molecule and enzyme that depends upon

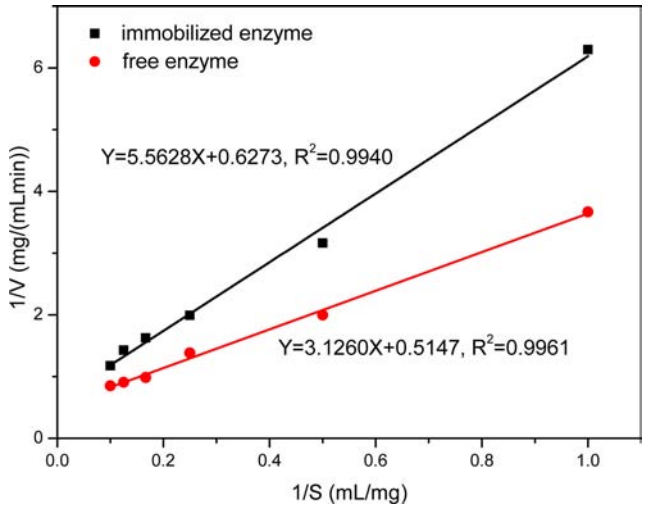

Figure 11. Lineweaver−Burk plots for the pullulan reduction with free and immobilized pullulanase (pH 4.4 at 50 °C). Results are the mean of triplicates.

Table 2. Kinetic Parameters of Free and Immobilized Pullulanase

enzyme type	K_m (mg/mL)	V_m (mg/(mL min))	enzymatic catalytic efficiency (V_m/ K_m)
free enzyme	6.073	1.942	0.319
immobilized enzyme	8.867	1.594	0.179

both partitioning and diffusional effects; V_m reflects the scale of mass transportation.[30] The K_m value of the immobilized enzyme (8.867 mg/mL) was higher than that of the free enzyme (6.073 mg/mL), and the V_m value of the immobilized enzyme (1.594 mg/(mL min)) was lower than that of the free enzyme (1.942 mg/(mL min)). The above results imply that the immobilized enzyme has an apparent lower affinity between enzyme and substrate, suggesting that it was more difficult for the substrate to diffuse and access the enzyme and that a higher concentration of substrate is needed when utilizing the immobilized enzyme. The lower affinity may be due to the negative effect of immobilization in terms of increased steric hindrance of the active site or substrate diffusion resistance.[31] Moreover, the lower affinity of the immobilized enzyme may be caused by the loss of enzyme flexibility necessary for substrate binding.[32] Therefore, a decrease in V_m of immobilized pullulanase was observed.

Thermal Stability of the Immobilized Pullulanase. The activity of free and immobilized pullulanase was assayed at temperatures in the range of 20−65 °C (pH 4.4). The maximum pullulanase activity was defined as 100%. As shown in Figure 12A, immobilization had no effect on the optimum temperature (50 °C) of pullulanase. A dramatic decrease in enzyme activity was observed in both systems when temperature went above 60 °C; however, the immobilized pullulanase showed higher activity than the free enzyme ($p < 0.01$). For example, at 65 °C, the relative activity of immobilized pullulanase was 66.7%, whereas that of free enzyme was only 25.5%. This result indicated that the immobilized enzyme possesses a better tolerance to heat.

The effect of temperature on the activity of free and immobilized enzyme at 60 °C versus the reaction time was also investigated. The initial activity was defined as 100%. As shown

DOI: 10.1021/jf505981t
J. Agric. Food Chem. 2015, 63, 3534−3542

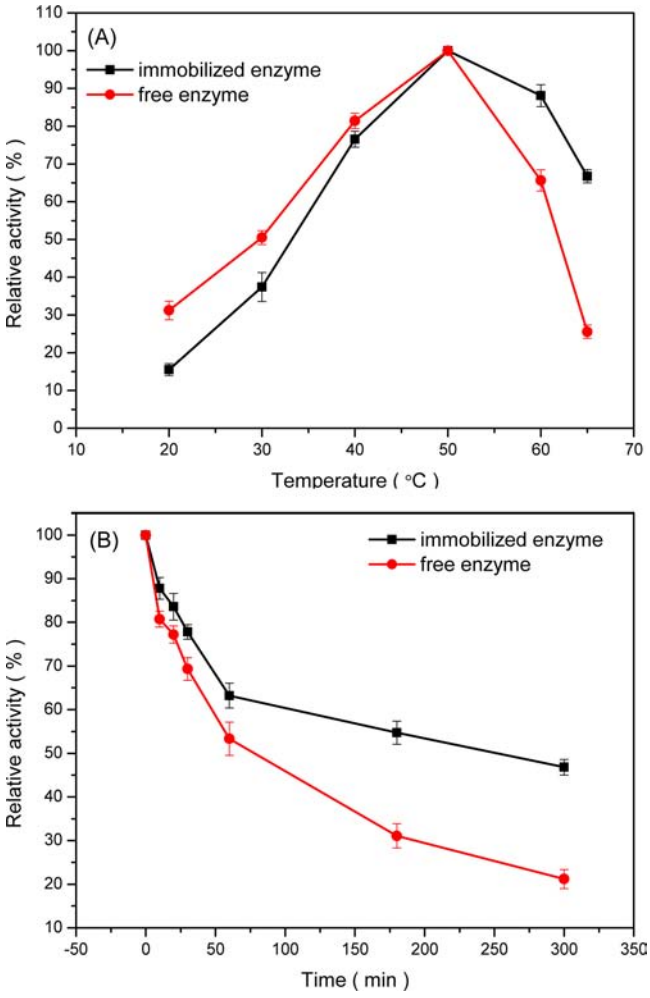

Figure 12. (A) Effect of temperature on activity of free and immobilized enzyme. (B) Thermal inactivation courses of free and immobilized enzyme (60 °C, pH 4.4). Experiments were triplicated, and the results are presented as mean ± SD.

in Figure 12B, the immobilized enzyme presented a higher thermal stability compared to the free enzyme. The rate of inactivation of the free enzyme was markedly higher than that of the immobilized enzyme. After 5 h, the immobilized enzyme retained more than 45% of its initial activity, whereas the free enzyme retained only 21% of its initial activity. This implies that immobilization had a positive effect on the thermal stability of pullulanase and was able to protect the active conformation of the enzyme from damage.[33] With this stabilizing effect, immobilized pullulanase exhibits an advantage in continuous applications in food industry.

AUTHOR INFORMATION

Corresponding Authors

*Phone:+86-510-85913299. Fax: +86-510-85913299. E-mail: jinlab2008@yahoo.com.

*Phone:+86-510-85320225. Fax: +86-510-85320225. E-mail: jiaoaq@jiangnan.edu.cn.

Notes

The authors declare no competing financial interest.

ACKNOWLEDGMENTS

We are grateful to Dr. Qingqing Liu for her technical assistance. This study was supported by the National Twelfth Five-Year Plan for Science & Technology Support of China (nos. 2012BAD37B02 and 2012BAD37B06).

REFERENCES

(1) Buchholz, K.; Seibel, J. Industrial carbohydrate biotransformations. *Carbohydr. Res.* **2008**, *343*, 1966−1979.

(2) Singh, R. S.; Saini, G. K.; Kennedy, J. F. Covalent immobilization and thermodynamic characterization of pullulanase for the hydrolysis of pullulan in batch system. *Carbohydr. Polym.* **2010**, *81*, 252−259.

(3) (a) Mateo, C.; Palomo, J. M.; Fernandez-Lorente, G.; Guisan, J. M.; Fernandez-Lafuente, R. Improvement of enzyme activity, stability and selectivity via immobilization techniques. *Enzyme Microb. Technol.* **2007**, *40*, 1451−1463. (b) Sheldon, R. A. Enzyme Immobilization: The Quest for Optimum Performance. *Adv. Synth. Catal.* **2007**, *349*, 1289−1307.

(4) Dessouki, A. M.; Issa, G. I.; Atia, K. S. Pullulanase immobilization on natural and synthetic polymers. *J. Chem. Technol. Biotechnol.* **2001**, *76*, 700−706.

(5) Kuroiwa, T.; Shoda, H.; Ichikawa, S.; Sato, S.; Mukataka, S. Immobilization and stabilization of pullulanase from Klebsiella pneumoniae by a multipoint attachment method using activated agar gel supports. *Process Biochem. (Oxford, U.K.)* **2005**, *40*, 2637−2642.

(6) Klein, M. P.; Nunes, M. R.; Rodrigues, R. C.; Benvenutti, E. V.; Costa, T. M.; Hertz, P. F.; Ninow, J. L. Effect of the support size on the properties of beta-galactosidase immobilized on chitosan: advantages and disadvantages of macro and nanoparticles. *Biomacromolecules* **2012**, *13*, 2456−2464.

(7) Wu, M.; He, Q.; Shao, Q.; Zuo, Y.; Wang, F.; Ni, H. Preparation and characterization of monodispersed microfloccules of TiO_2 nanoparticles with immobilized multienzymes. *ACS Appl. Mater. Interfaces* **2011**, *3*, 3300−3307.

(8) Garcia-Galan, C.; Berenguer-Murcia, Á.; Fernandez-Lafuente, R.; Rodrigues, R. C. Potential of Different Enzyme Immobilization Strategies to Improve Enzyme Performance. *Adv. Synth. Catal.* **2011**, *353*, 2885−2904.

(9) Zhao, G.; Wang, J.; Li, Y.; Chen, X.; Liu, Y. Enzymes Immobilized on Superparamagnetic Fe_3O_4@Clays Nanocomposites: Preparation, Characterization, and a New Strategy for the Regeneration of Supports. *J. Phys. Chem. C* **2011**, *115*, 6350−6359.

(10) Franzreb, M.; Siemann-Herzberg, M.; Hobley, T. J.; Thomas, O. R. T. Protein purification using magnetic adsorbent particles. *Appl. Microbiol. Biotechnol.* **2006**, *70*, 505−516.

(11) Wang, Y.; Li, B.; Zhou, Y.; Jia, D. In Situ Mineralization of Magnetite Nanoparticles in Chitosan Hydrogel. *Nanoscale Res. Lett.* **2009**, *4*, 1041−1046.

(12) Daniel-da-Silva, A. L.; Trindade, T.; Goodfellow, B. J.; Costa, B. F. O.; Correia, R. N.; Gil, A. M. In Situ Synthesis of Magnetite Nanoparticles in Carrageenan Gels. *Biomacromolecules* **2007**, *8*, 2350−2357.

(13) Li, J.; Wang, X. Binding of (−)-epigallocatechin-3-gallate with thermally-induced bovine serum albumin/iota-carrageenan particles. *Food Chem.* **2015**, *168*, 566−571.

(14) Rodrigues, S.; da Costa, A. M.; Grenha, A. Chitosan/carrageenan nanoparticles: effect of cross-linking with tripolyphosphate and charge ratios. *Carbohydr. Polym.* **2012**, *89*, 282−289.

(15) Yang, C.-Y.; Hsu, C.-H.; Tsai, M.-L. Effect of crosslinked condition on characteristics of chitosan/tripolyphosphate/genipin beads and their application in the selective adsorption of phytic acid from soybean whey. *Carbohydr. Polym.* **2011**, *86*, 659−665.

(16) (a) Feng, Z.; Shao, Z.; Yao, J.; Huang, Y.; Chen, X. Protein adsorption and separation with chitosan-based amphoteric membranes. *Polymer* **2009**, *50*, 1257−1263. (b) Dotto, G. L.; Pinto, L. A. A. Adsorption of food dyes onto chitosan: Optimization process and kinetic. *Carbohydr. Polym.* **2011**, *84*, 231−238. (c) Elmer, C.; Karaca, A. C.; Low, N. H.; Nickerson, M. T. Complex coacervation in pea

DOI: 10.1021/jf505981t
J. Agric. Food Chem. 2015, 63, 3534−3542

protein isolate−chitosan mixtures. *Food Res. Int.* **2011**, *44*, 1441−1446.
(d) Chang, Y. L.; Liu, T. C.; Tsai, M. L. Selective isolation of trypsin inhibitor and lectin from soybean whey by chitosan/tripolyphosphate/genipin co-crosslinked beads. *Inter. J. Mol. Sci.* **2014**, *15*, 9979−9990.
(17) Grenha, A.; Gomes, M. E.; Rodrigues, M.; Santo, V. E.; Mano, J. F.; Neves, N. M.; Reis, R. L. Development of new chitosan/carrageenan nanoparticles for drug delivery applications. *J. Biomed. Mater. Res., Part A* **2010**, *92A*, 1265−1272.
(18) Mattison, K. W.; Dubin, P. L.; Brittain, I. J. Complex Formation between Bovine Serum Albumin and Strong Polyelectrolytes: Effect of Polymer Charge Density. *J. Phys. Chem. B* **1998**, *102*, 3830−3836.
(19) Li, X.; Dong, D.; Hua, Y.; Chen, Y.; Kong, X.; Zhang, C. Soybean whey protein/chitosan complex behavior and selective recovery of kunitz trypsin inhibitor. *J. Agric. Food Chem.* **2014**, *62*, 7279−7286.
(20) Franzreb, M.; Siemann-Herzberg, M.; Hobley, T. J.; Thomas, O. R. Protein purification using magnetic adsorbent particles. *Appl. Microbiol. Biotechnol.* **2006**, *70*, 505−516.
(21) Liu, Q.; Hua, Y.; Kong, X.; Zhang, C.; Chen, Y. Covalent immobilization of hydroperoxide lyase on chitosan hybrid hydrogels and production of C6 aldehydes by immobilized enzyme. *J. Mol. Catal. B: Enzym.* **2013**, *95*, 89−98.
(22) Espinosa-Andrews, H.; Enriquez-Ramirez, K. E.; Garcia-Marquez, E.; Ramirez-Santiago, C.; Lobato-Calleros, C.; Vernon-Carter, J. Interrelationship between the zeta potential and viscoelastic properties in coacervates complexes. *Carbohydr. Polym.* **2013**, *95*, 161−166.
(23) de Vries, R.; Weinbreck, F.; de Kruif, C. G. Theory of polyelectrolyte adsorption on heterogeneously charged surfaces applied to soluble protein−polyelectrolyte complexes. *J. Chem. Phys.* **2003**, *118*, 4649.
(24) Yan, Y.; Seeman, D.; Zheng, B.; Kizilay, E.; Xu, Y.; Dubin, P. L. pH-Dependent aggregation and disaggregation of native beta-lactoglobulin in low salt. *Langmuir* **2013**, *29*, 4584−4593.
(25) Lawrie, G.; Keen, I.; Drew, B.; Chandler-Temple, A.; Rintoul, L.; Fredericks, P.; Grøndahl, L. Interactions between Alginate and Chitosan Biopolymers Characterized Using FTIR and XPS. *Biomacromolecules* **2007**, *8*, 2533−2541.
(26) Abad, L. V.; Relleve, L. S.; Aranilla, C. T.; Dela Rosa, A. M. Properties of radiation synthesized PVP-kappa carrageenan hydrogel blends. *Radiat. Phys. Chem.* **2003**, *68*, 901−908.
(27) Wang, J.; Zhao, G.; Li, Y.; Liu, X.; Hou, P. Reversible immobilization of glucoamylase onto magnetic chitosan nanocarriers. *Appl. Microbiol. Biotechnol.* **2013**, *97*, 681−692.
(28) Chen, J.-P.; Yang, P.-C.; Ma, Y.-H.; Wu, T. Characterization of chitosan magnetic nanoparticles for in situ delivery of tissue plasminogen activator. *Carbohydr. Polym.* **2011**, *84*, 364−372.
(29) de Fuentes, I. E.; Viseras, C. A.; Ubiali, D.; Terreni, M.; Alcántara, A. R. Different phyllosilicates as supports for lipase immobilisation. *J. Mol. Catal. B: Enzym.* **2001**, *11*, 657−663.
(30) Wilson, D. J.; Aldrich, C. C. A continuous kinetic assay for adenylation enzyme activity and inhibition. *Anal. Biochem.* **2010**, *404*, 56−63.
(31) Garcia−Galan, C.; Berenguer−Murcia, Á.; Fernandez−Lafuente, R.; Rodrigues, R. C. Potential of different enzyme immobilization strategies to improve enzyme performance. *Adv. Synth. Catal.* **2011**, *353*, 2885−2904.
(32) Chang, M.-Y.; Juang, R.-S. Activities, stabilities, and reaction kinetics of three free and chitosan−clay composite immobilized enzymes. *Enzyme Microb. Technol.* **2005**, *36*, 75−82.
(33) Zhang, S.; Gao, S.; Gao, G. Immobilization of beta-galactosidase onto magnetic beads. *Appl. Biochem. Biotechnol.* **2010**, *160*, 1386−1393.

DOI: 10.1021/jf505981t
J. Agric. Food Chem. 2015, 63, 3534−3542

the adsorption properties of anthocyanins; however, the purity of anthocyanins has not yet been significantly improved. This lack of improvement is most likely because the matrix of the most commercial adsorbent is hydrophobic (e.g., polystyrene), and the adsorption mechanism is mainly based on the hydrophobic interaction between adsorbents and anthocyanins. The hydrophobic affinity is non-specific, especially in aqueous solution.

There are multiple phenolic hydroxyl or hydrophilic sugar moieties in the structure of anthocyanins, which leads to the increasing hydrophilicity of anthocyanins. Therefore, hydrophilic adsorbents with amide, hydroxy, or other polar functional groups, such as polyamide or dextran, were selected for the preparation of anthocyanins with high purity, which were expected to have better adsorption selectivity toward anthocyanin.[25,26] However, in practical applications, these adsorbents did not exhibit good adsorption performance, because the extraction and separation of natural products based on the adsorption method usually occurs in aqueous solution, in which water molecules significantly destroy the polar affinity between adsorbents and adsorbates.[27−29] Hence, in aqueous solution, a rigid hydrophobic structure remains necessary, which is consistent with the results concerning the adsorption performance of peptide molecules in aqueous solution. In this consideration, the copolymerization of a monomer containing polar functional groups with styrene or divinylbenzene (DVB) becomes the most advantageous method. Commercial macroporous resins AB-8 and ADS-17 are examples of copolymerization of methacrylate and DVB. Nevertheless, to maintain skeleton stability, a sufficient cross-linking degree is indispensable for resin synthesis, which indicates that the content ratio of the polar monomer and hydrophobic monomer can only be modulated in a much smaller range, which definitely limits the application of these resins. In addition, the large difference in polarity between the two monomers means that the monomers do not readily copolymerize with each other to produce a uniform cross-linked network in free-radical polymerization. Therefore, some of the functional groups derived from the polar monomers were not uniformly distributed on the pore surface of the adsorbent, which indicates why the adsorption selectivity of the weak polar commercial adsorbent was improved at the expense of a decrease in adsorption capacity.[28]

To solve this problem, in the present study, we selected ethylene glycol dimethyl acrylate (EGDMA) as the monomer providing functional groups. EGDMA not only regulates the polarity of the adsorbent but also acts as cross-linking agent to copolymerize with DVB because it contains two polymerizable double bonds. Therefore, the necessary network structure of the adsorbent was maintained, whereas the concentration of the weak polar monomer can be adjusted across a larger scale. In this paper, a series of poly(EGDMA-*co*-DVB) with different EGDMA contents was synthesized. The resins with the best adsorption performance were screened out through static adsorption and desorption experiments. On this basis, the parameters of the dynamic adsorption and desorption experiments were optimized to achieve anthocyanins with high purity of 96%. The high-performance liquid chromatography (HPLC) fingerprint of the products is consistent with USP35-NF30. The established method of separation and purification of anthocyanins from bilberry will hopefully be applied in industrial production.

MATERIALS AND METHODS

Materials. EGDMA [analytical-reagent (AR) grade] and DVB (purity of 80%) were obtained from the Chemical Plant of Nankai University (Tianjin, China). 2,2′-Azobis(isobutyronitrile) (AIBN), toluene, 200 gasoline, poly(vinyl alcohol) (PVA), ethanol, hydrochloric acid, and sodium chloride were purchased from Tianjin Chemical Co. (Tianjin, China) and were all AR grade.

Bilberry fruits (frozen) was purchased from Sweden. Bilberry dry extract CRS was purchased from European Directorate for the Quality of Medicines & HealthCare (EDQM). The percentage content of cyanidin 3-*O*-glucoside chloride in bilberry dry extract CRS is 3.44 wt %.

HPLC-grade anhydrous formic acid, acetonitrile, and methanol were purchased from Concord Technology (Tianjin, China). All of the solutions prepared for HPLC were filtered through 0.45 μm nylon membranes before use.

Pretreatment of Commercial Adsorbents. The macroporous adsorbent Amberlite XAD-7 was purchased from Rohm and Hass (Philadelphia, PA). The macroporous adsorbents XAD-4, AB-8, and ADS-17 were purchased from Nankai Hecheng S&T (Tianjin, China). Before the adsorption experiments, the adsorbents were soaked in ethanol and then thoroughly washed with deionized water.

Synthesis of Adsorbents with Functional Groups. The beads were prepared using a suspension polymerization method. An organic solution composed of DVB, EGDMA, porogenic agent (toluene/200 gasoline = 70:30, w/w), and the initiator AIBN (0.5%, w/w) were mixed with the aqueous solution composed of poly(vinyl alcohol) (PVA, 1%, w/w) and sodium chloride (5%, w/w) in a 1000 mL three-necked round-bottomed flask equipped with a mechanical stirrer, reflux condenser, and thermometer. The round-bottomed flask was heated using a programmed heater. The mixture was stirred to yield a suspension of oil beads with a suitable size in the aqueous solution (100−120 rpm), heated at 65 °C for 4 h, and maintained at 85 °C for 6 h. The copolymer beads were filtered out, washed with a large amount of hot water followed by ethanol, then packed in a Soxhlet extractor, and eluted with petroleum ether.

The proportion between EGDMA and DVB was changed in the synthesis process to obtain polymeric adsorbents with different hydrophobic affinities. The adsorbents were named DE-5, DE-10, DE-20, DE-30, DE-40, corresponding to 5, 10, 20, 30, and 40% EGDMA contents in weight, respectively. The synthesis process is shown in Figure 1.

Determination of Pore Structure Parameters of Adsorbents. The pore structure parameters of the adsorbents were measured using an automatic surface area and pore size analyzer (Autosorb-1 MP,

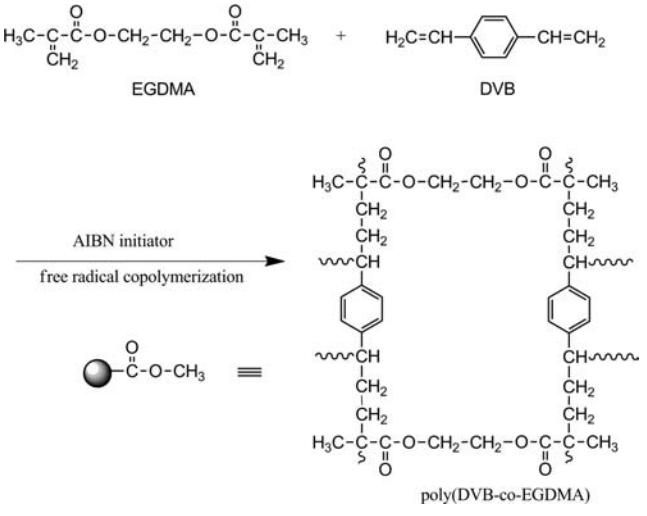

Figure 1. Synthesis process of poly(DVB-*co*-EGDMA) adsorbent, namely, DE resin.

DOI: 10.1021/jf506107m
J. Agric. Food Chem. 2015, 63, 3543−3550

Quantachrome Instruments, Boynton Beach, FL) based on the Brunauer–Emmett–Teller (BET) nitrogen adsorption method.

Determination of the Moisture Content Imbedded in the Adsorbents. The hydrated adsorbents disposed of deionized water were weighed accurately and then dried in an oven at 105 °C until a constant weight was attained. The following equation was used to calculate the moisture content (α, %) imbedded in the adsorbent:

$$\alpha = \frac{W_{wet} - W_{dry}}{W_{wet}} \times 100\% \quad (1)$$

where W_{wet} and W_{dry} are the weights (g) of the hydrated and dry adsorbents, respectively.

Characterization of Adsorbents. Infrared spectra of DE adsorbent were obtained from a Nicolet Magna 560 Fourier transform infrared (FTIR) spectrometer with a pellet of potassium bromide and adsorbent in the range of 500–4000 cm^{-1}. The inner surface morphology of the copolymer particles was investigated using a scanning electron microscope (SEM, Hitachi 3500N). The appearance of adsorbent beads was observed by an optical microscope (Olympus BX5).

HPLC Analysis of Anthocyanins. The HPLC analysis method of anthocyanins was based on USP35-NF30 with some adjustments. First, 0.1250 g of bilberry dry extract CRS was dissolved in the mixed solvent (hydrochloric acid/methanol = 2:98, v/v) and diluted to 25.0 mL. The reference solution was obtained by diluting 5.0 mL of the above solution to 20.0 mL with 10% phosphoric acid. The concentration of prepared reference solution is 1.25 mg/mL.

The analysis was performed on an Agilent 1200 series HPLC system with a 1200 diode array detector and 1200 quaternary pump with a degasser. A reversed-phase column (250 × 4.6 mm inner diameter) packed with Venusil ASB C_{18} (5 μm) was used for chromatographic analysis. The mobile phase was composed of mobile phase A (anhydrous formic acid/H_2O = 8.5:91.5, v/v) and mobile phase B (anhydrous formic acid/acetonitrile/methanol/H_2O = 8.5:22.5:22.5:41.5, v/v/v/v) and was used by the gradient program shown in Table 1. The flow rate was 1.0 mL/min. The detection wavelength was 535 nm. The entire column system was at a constant 30 °C using an Agilent 1200 thermostated column compartment.

Table 1. Gradient Program of HPLC Analysis of Anthocyanins

time (min)	mobile phase A (%)	mobile phase B (%)	elution
0–20	82 → 78	18 → 22	linear
20–35	78 → 72	22 → 28	linear
35–50	72 → 35	28 → 65	linear
50–51	35 → 0	65 → 100	linear
51–55	0	100	isocratic
55–56	0 → 82	100 → 18	linear
56–70	82	18	isocratic

The peaks corresponding to the anthocyanins and anthocyanidins were identified by the chromatogram supplied with bilberry extract CRS and USP35-NF30. The retention times and elution orders of the peaks are shown in Table 2. The chromatogram of bilberry extract CRS was used as a standard to calculate the concentration of anthocyanins in the tested solution, expressed as cyanidin 3-*O*-glucoside chloride, using the following expression:

$$c = \frac{Ac_r wV_r}{A_r V} \quad (2)$$

where c is the concentration (mg/mL) of anthocyanins (peaks 1–8, 10–15, and 17) in the chromatogram obtained with the test solution, c_r is the concentration (mg/mL) of reference solution, A is the sum of the areas of the peaks corresponding to the anthocyanins (peaks 1–8, 10–15, and 17) in the chromatogram obtained with the test solution, A_r is the area of the peak corresponding to cyanidin 3-*O*-glucoside chloride (peak 5) in the chromatogram obtained with reference solution, V and V_r are injection volumes (μL) of test solution and reference solution, respectively, and w is the percentage content of cyanidin 3-*O*-glucoside chloride in bilberry extract CRS.

Table 2. Anthocyanins/Anthocyanidins and Corresponding Retention Time in the HPLC Chromatogram

peak number	anthocyanins/anthocyanidins	retention time (min)
1	delphinidin 3-*O*-galactoside chloride	10.7
2	delphinidin 3-*O*-glucoside chloride	12.6
3	cyanidin 3-*O*-galactoside chloride	14.8
4	delphinidin 3-*O*-arabinoside chloride	15.9
5	cyanidin 3-*O*-glucoside chloride	18.0
6	petunidin 3-*O*-galactoside chloride	20.2
7	cyanidin 3-*O*-arabinoside chloride	21.6
8	petunidin 3-*O*-glucoside chloride	24.2
9	delphinidin chloride	27.0
10	peonidin 3-*O*-galactoside chloride	27.7
11	petunidin 3-*O*-arabinoside chloride	29.1
12	peonidin 3-*O*-glucoside chloride	32.1
13	malvidin 3-*O*-galactoside chloride	33.7
14	peonidin 3-*O*-arabinoside chloride	36.4
15	malvidin 3-*O*-glucoside chloride	38.3
16	cyanidin chloride	41.2
17	malvidin 3-*O*-arabinoside chloride	42.3
18	petunidin chloride	45.8
19	peonidin chloride	50.1
20	malvidin chloride	51.4

Preparation of Bilberry Crude Extraction Solution. According to the literature,[20,30,31] as the molecular forms of anthocyanins change with the pH value in aqueous solution, their stability also changes. The experimental results suggest that the stability of anthocyanins is optimal when the pH is 2.0; thus, the aqueous solution environment was maintained at pH 2.0 during the entire experimental process. The preparation of bilberry crude extraction was as follows: first, 500 g of bilberry frozen fruit was crushed into pulp in a cooking machine. Then, the pulp was transferred into a round-bottom flask with acidified 60% ethanol aqueous solution (adjust pH 2.0 with hydrochloric acid). The solid–liquid (fruit/extraction media, m/v) ratio was 1:3, and extraction was carried at 50 °C for 1 h twice. Collected supernatants were concentrated by rotary evaporation at 50 °C under vacuum for 1 h. The crude extraction solution was filtered using talcum powder to remove slime before use. The concentration of the solution obtained was 3.5 mg/mL, determined by the HPLC method.

Static Adsorption and Desorption Tests. The static adsorption tests were performed as follows: 1.0 g of hydrated test adsorbents was placed into a 100 mL flask with a lid, and 20 mL of the crude extract solution was added. The flask was then shaken (100 rpm) at a constant temperature of 25 °C until the adsorption equilibrium was reached. The concentrations of the anthocyanins in the solution before and after the adsorption were analyzed by HPLC. The following equation was used to quantify the equilibrium adsorption capacity (Q_e, mg/g of dry resin) of the adsorbent:

$$Q_e = \frac{(C_0 - C_e)V}{W_{wet}(1 - \alpha)} \quad (3)$$

where C_0 and C_e are the initial and equilibrium concentrations of anthocyanins in the solutions, respectively (mg/mL), V is the volume of the solution (mL), W_{wet} is the weight of the hydrated adsorbent (g), and α is the moisture content of the adsorbent (%).

After adsorption, the beads were washed with deionized water and then desorbed with 60% ethanol aqueous solution. The desorption ratio (D_d, %) was calculated using the following equation:

$$D_d = \frac{C_d V_d}{(C_0 - C_e)V} \times 100\% \quad (4)$$

DOI: 10.1021/jf506107m
J. Agric. Food Chem. 2015, 63, 3543–3550

Table 3. Structure Parameters of Adsorbents

adsorbent	DVB content (wt %)	structure	functional group	specific surface area(m^2/g)	moisture content (%)
XAD-4	100	poly(DVB)	none	780	61.8
AB-8	95	poly(MA-*co*-DVB)	ester group	750	67.5
ADS-17	60	poly(MA-*co*-DVB)	ester group	625	69.6
XAD-7	0	poly(EGDMA)	ester group	450	51.2
DE-5	95	poly(EGDMA-*co*-DVB)	ester group	854	67.0
DE-10	90		ester group	850	68.7
DE-20	80		ester group	842	70.1
DE-30	70		ester group	837	71.9
DE-40	60		ester group	828	73.4

where C_d is the concentration of anthocyanins in the desorption solution determined by HPLC (mg/L), V_d is the volume of the desorption solution (mL), and C_0, C_e, and V are the same as the parameters in eq 3.

To calculate the purity of the extract, the solid content was measured using the following method: the desorption solution measured accurately by HPLC was placed into a weighing bottle of constant weight, which was then placed in an oven to dry to constant weight at 105 °C to completely remove the solvent. The purity of the extract was calculated using the following equation:

$$\text{purity} = \frac{C_d V_d}{W - W_0} \times 100\% \quad (5)$$

where W is the total weight of the weighing bottle and residue solid after drying (g), W_0 is the weight of the weighing bottle (g), and C_d and V_d are the same as the parameters in eq 4.

Dynamic Adsorption and Elution Tests. Dynamic adsorption tests were performed as follows: the hydrated test adsorbent was packed into a glass column (Ø = 15 mm), and the bed volume (BV) was 30 mL. The solution prepared as described flowed through the adsorbent column.

The elution tests were performed as follows: after the adsorption equilibrium was reached, the adsorbate-laden column was first washed with deionized water and then eluted by desorption agents (pH 2.0).

The concentration of anthocyanins in the effluent solution was monitored by HPLC analysis, and the desorption ratio and purity of desorption solution were calculated using eqs 4 and 5.

Acquirement of Products and Repeated Tests. After the optimized process of dynamic adsorption and desorption tests was confirmed, experiments based on the selected adsorbent were performed 4 times under the optimized conditions.

RESULTS AND DISCUSSION

Characterization of Selected Commercial Adsorbents and Synthesized DE Adsorbents. The structural parameters of the commercial adsorbents and synthesized adsorbents were characterized, and the results are presented in Table 3. We know that a higher specific surface area of the adsorbent provides more sites for the adsorbate, thus improving the adsorption capacity. As demonstrated in Table 3, for the selected commercial adsorbents, with the increase of the polar moiety content, the DVB content decreased. The moisture content data reveals that the hydrophilicity of these adsorbents increased (except XAD-7), whereas the corresponding specific surface area declined remarkably, indicating the damage of the high cross-linking structure of the adsorbent. In contrast, the synthesized adsorbents with similar DVB content exhibited completely different trends; their specific surface area gradually decreased, but all remained at a relatively high level. From Table 3, it can be observed that, for the adsorbents AB-8 and DE-5 or ADS-17 and DE-40, whose DVB contents were almost equivalent, the specific surface area of the latter was greatly increased in comparison to that of the former. This finding suggested that EGDMA plays a supporting role for the adsorbent matrix instead of lowering the specific surface area because of the introduction of a weak polar monomer. In addition, we also noticed that the parameter of the adsorbent XAD-7 was unique. Although XAD-7 was composed entirely by the polymer of EGDMA and should have exhibited a high cross-linking degree, its specific surface area was reduced greatly because the chain of EGDMA is more flexible than that of DVB because of the existence of benzene. The weaker skeleton rigidity could cause a collapse of the pore structure of the adsorbents, thus reducing the specific surface area of the resin. It is inferred that the content of EGDMA should be controlled in a certain range. In addition, the moisture content of the DE adsorbent increased with increasing the EGDMA content, indicating the increasing hydrophilicity of this series of adsorbents.

The structure of adsorbents with different EGDMA contents was characterized by FTIR spectroscopy. The strong stretching vibration band at 1732 cm^{-1}observed in Figure 2 indicates that

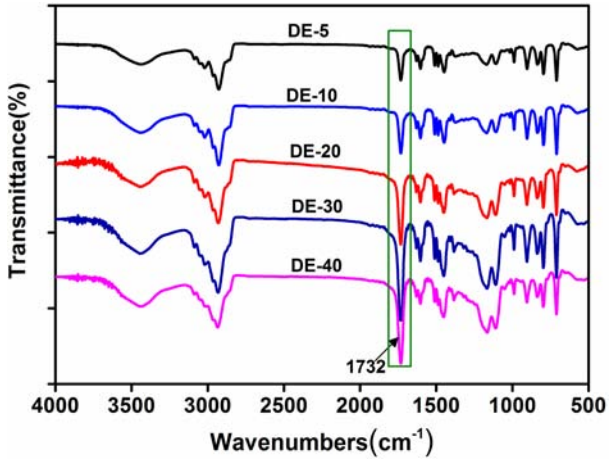

Figure 2. Infrared (IR) spectra of DE adsorbents with various EGDMA contents.

ester groups were successfully introduced into the DE adsorbents. The intensity of ester groups increased with increasing the EGDMA content, which indicates that adsorbents with different EGDMA contents were synthesized.

The optical microscope and SEM results of DE-20 are shown in Figure 3. The exterior of the beads had an intact spherical appearance, whereas the interior consisted of a distinct porous structure, which also indirectly demonstrated that the necessary high cross-linking structure of DE adsorbent was successfully sustained.

DOI: 10.1021/jf506107m
J. Agric. Food Chem. 2015, 63, 3543−3550

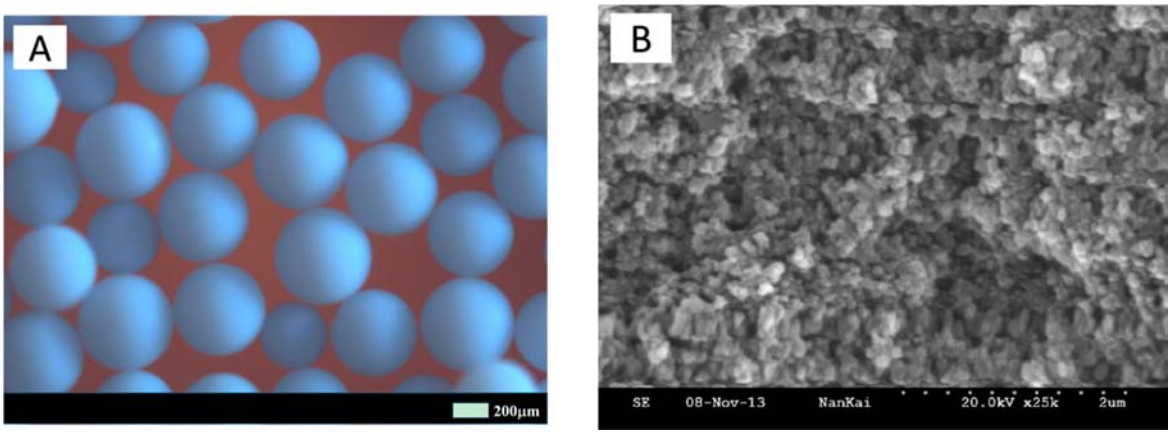

Figure 3. Images of adsorbent DE-20: (A) appearance of adsorbent beads observed under an optical microscope and (B) inner surface of the adsorbent under a SEM.

Results of Static Equilibrium Adsorption Experiments. Several representative commercial adsorbents were selected, and the static equilibrium adsorption and desorption experiment was conducted. The results are presented in Figure 4. The

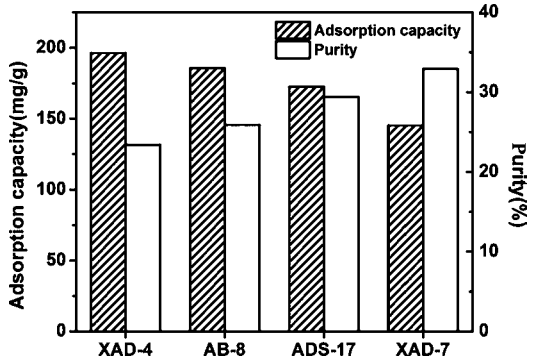

Figure 4. Adsorption capacity of four commercial resins (XAD-4, AB-8, ADS-17, and XAD-7) and purity of anthocyanins obtained through static adsorption experiments on these resins.

purity of the anthocyanins in the desorption solution increased significantly with increasing hydrophilicity of the selected adsorbents, indicating better adsorption selectivity. However, the adsorption capacity declined notably because of the decreasing specific surface area. Therefore, regulating the hydrophilicity of the resin on the premise of maintaining a high specific surface area is of great importance.

As demonstrated in Table 4, for DE resins, the adsorption capacity results agreed with those of the specific surface area, both showing slight declines with increasing polarity. Because of the introduction of EGDMA, the synthesized adsorbents exhibited better adsorption selectivity compared to commercial adsorbents, which was demonstrated by the purity of the anthocyanins in the eluent. The purity increased gradually and then decreased with increasing the EGDMA content because the interaction between the adsorbents and adsorbate also plays an important role in the adsorption selectivity in addition to the specific surface area. In addition, the synergistic dipolar and hydrophobic interactions can be used to explain this phenomenon very well. When the content of EGDMA exceeded 20%, the hydrophobic interaction decreased significantly caused by the decline of the percentage of DVB. There was not a sufficient driving force for the adsorbent to overcome the obstacles of the water molecules to bring the adsorbate molecule closer to the adsorbent matrix; the synergistic effect weakened, and thus, the adsorption ability decreased. Therefore, it is suggested that the synergistic dipolar and hydrophobic interaction between DE-20 and anthocyanins comes to an optimum point. All of these results confirmed that our strategy to regulate the adsorption selectivity of adsorbents by introducing EGDMA was successful. Consideration must be given to both the adsorption capacity and purity. The DE-20 adsorbent possessed the best selectivity, and its adsorption capacity and desorption ratio were acceptable. Hence, further experiments were performed using the DE-20 adsorbent.

Table 4. Results of Static Adsorption and Desorption of DE Resins

		eluent	
adsorbent	Q_e (mg/g)	purity (%)	desorption ratio (%)
DE-5	213.2	32.2	96.7
DE-10	210.9	34.5	95.4
DE-20	208.5	37.6	97.2
DE-30	194.6	35.3	97.4
DE-40	193.2	34.1	96.5

Effect of the Adsorption Rate on the Adsorption Property of DE-20 Adsorbent. To further investigate the adsorption property of the DE-20 adsorbent toward anthocyanins, adsorption curves were measured under different adsorption rates, and the results are presented in Figure 5.

If the solution flows through the column too fast, parts of the anthocyanins rapidly rush out of the column before interacting with the adsorbent, resulting in a decrease of the adsorption capacity. Reducing the rate of adsorption is beneficial for the adsorbate to thoroughly contact the adsorbents; however, when the flow rate is too low, the production period will be extended and the efficiency is reduced. In Figure 5, anthocyanins leaked early at 80 mL at a flow rate of 3 BV/h. When the flow rate was reduced to 2 BV/h, the leak point moved to 120 mL. In comparison to the leakage point corresponding to the adsorption rate of 1 BV/h, there was no obvious difference between the two adsorption curves. Considering both the experiment period and adsorption capacity, we select the flow rate of 2 BV/h, and the corresponding volume of the adsorption solution is 120 mL (4 BV).

DOI: 10.1021/jf506107m
J. Agric. Food Chem. 2015, 63, 3543−3550

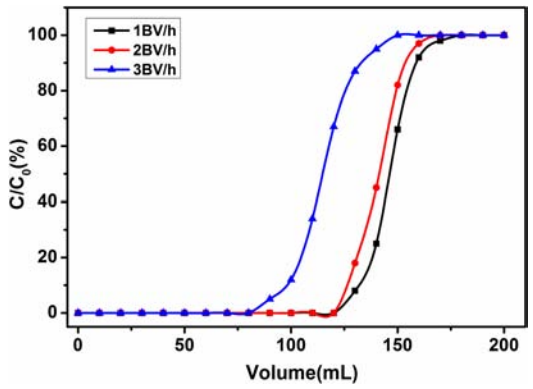

Figure 5. Dynamic leakage curves of anthocyanins on adsorbent DE-20 at different adsorption rates of 1, 2, and 3 BV/h.

Results of Gradient Dynamic Elution on DE-20 Adsorbent. The dynamic desorption experiments were conducted as described. After reaching the adsorption equilibrium, the adsorbent column was washed with deionized water and then desorbed by gradient elution with 10, 20, 30, and 60 vol % ethanol aqueous solutions in sequence; the results are presented in Figure 6.

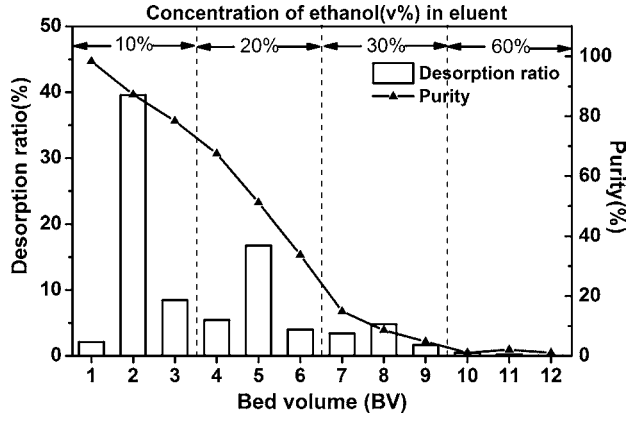

Figure 6. Purity and desorption ratio of anthocyanins obtained from gradient elution by ethanol aqueous solution at different concentrations of 10, 20, 30, and 60 vol % in sequence, as a function of the BV. The experiment was conducted on DE-20 resin, and consumption of ethanol aqueous solution of each concentration is 3 BV.

During the gradient elution process, the anthocyanins and other components laden on the adsorbent gradually migrated down according to their affinity to the adsorbents and elution. Figure 6 shows that approximately 40% of the anthocyanins can be desorbed when eluted by 10% ethanol solution in the second BV, which indicated that the affinity between anthocyanins and adsorbents was relatively weak, such that a low concentration of ethanol solution could break the bonding interaction. The purity of the anthocyanins in the desorption solution declined greatly with increasing the desorption volume, from 96% for the highest drops to less than 10%. Therefore, we concluded that a low concentration of ethanol solution was more suitable for obtaining anthocyanins at high purity. Considering the relatively low desorption ratio of 10% ethanol, we decided to perform the dynamic experiments in isocratic mode using ethanol aqueous solution of higher concentration as the desorption solvent.

Results of Isocratic Elution on DE-20 Adsorbent. Increasing the ethanol concentration in the eluent is one solution to effectively solve the trailing phenomenon observed in Figure 6. Therefore, we selected 20, 30, and 40% ethanol aqueous solution as the desorption solvent, and its suitable consumption is 3 BV. Figure 7 shows the results of isocratic elution with different desorption solvents on DE-20 adsorbent.

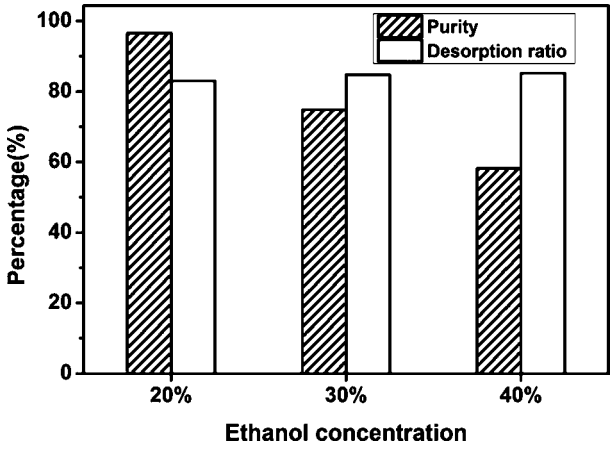

Figure 7. Purity and desorption ratio of anthocyanins eluted by ethanol aqueous solution of different concentrations (20, 30, and 40 vol %) in isocratic elution mode on DE-20 resin.

The desorption ratio and purity of the anthocyanins obtained are the most important factors in dynamic desorption experiments. According to Figure 7, we found that the desorption ratio was obviously improved to above 80% after increasing the concentration of ethanol in desorption solvent. A total of 83.2, 84.7, and 85.2% of the total anthocyanins can be obtained by eluting with 20, 30, and 40% ethanol solution, corresponding to purities of 96, 74, and 57%, respectively. It can be observed that the desorption ratio improved slightly under different elution conditions; however, the purity decreased remarkably with increasing the ethanol concentration in the desorption agents. These results can be explained by the different affinities of different components in bilberry toward adsorbents. The affinity between anthocyanin and the adsorbent was relatively weaker because anthocyanin is more hydrophilic, whereas the hydrophobic interaction between other impurities and adsorbents was much more intensive. In addition, the latter interaction was easier to break down using a higher ethanol concentration; thus, more impurities flowed out along with anthocyanins simultaneously, leading to the lower purity of anthocyanins.

In summary, the 20% ethanol aqueous solution (3 BV, pH 2.0) was selected as the most suitable desorption solvent, and the anthocyanin product was recycled at a high desorption ratio of 83% and high purity of 96%.

Results of Enrichment and Purification of Anthocyanins from Bilberry Based on DE-20 Resin. Briefly, the optimization of the purification process of anthocyanin on DE-20 adsorbent can be summarized as follows:

First, the hydrated adsorbent DE-20 is packed into a glass column (Ø = 15 mm), and the BV is 30 mL. Then, the crude extraction solution of anthocyanins (3.5 mg/mL) flows through the adsorbent DE-20 column at a flow rate of 2 BV/h. The adsorption capacity is 120 mL (4 BV). The adsorbate-laden column is then washed with 3 BV deionized water (pH 2.0),

DOI: 10.1021/jf506107m
J. Agric. Food Chem. 2015, 63, 3543−3550

followed by the elution of 20% ethanol aqueous solution (pH 2.0), at a flow rate of 2 BV/h. Finally, anthocyanins are successfully obtained at a high purity of 96% and high desorption rate of 83%.

Figure 8 shows a HPLC chromatogram of the highly pure anthocyanins and crude extraction solution of bilberry. The

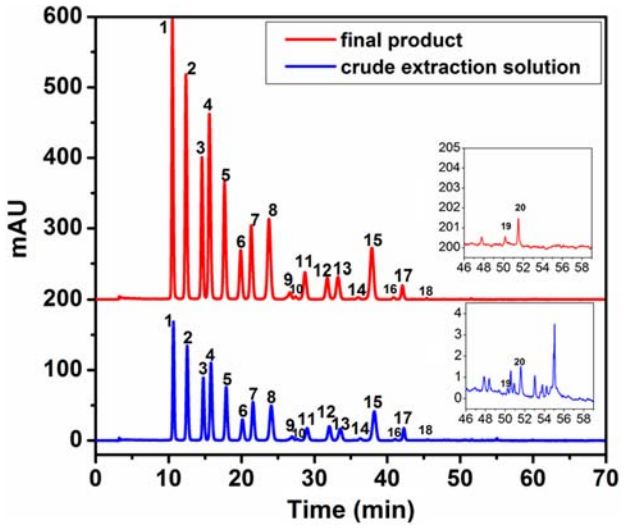

Figure 8. HPLC chromatograms for anthocyanins/anthocyanidins obtained from the final product (red line) and crude extraction solution (blue line), which are consistent with the HPLC chromatogram of USP35-NF30 (powdered bilberry extract). Peaks are numbered according to Table 2. Inset figures are magnified chromatograms for anthocyanidins numbered 19 and 20.

peaks of both of the chromatograms are consistent with USP35-NF30 (powdered bilberry extract), indicating that, in the entire process of extraction and purification, the composition of anthocyanins remains the same as in the fruit, except that the purity is improved remarkably and the amount of contained anthocyanidins is lower, which is also consistent with USP35-NF30.

Results of Repeatability of Anthocyanins on the Adsorbent DE-20. The results of repeatability of anthocyanins on the adsorbent DE-20 are listed in Table 5. Different

Table 5. Results of Purification and Repeatability of DE-20

test number	desorption ratio (%)	purity (%)
1	83.2	96.2
2	84.0	95.9
3	82.4	96.8
4	82.7	98.1
average	83.1	96.7
standard deviation (SD)	0.61	0.84

batches all exhibited good purification effects on the anthocyanins, which indicates that the method based on the synthesized macroporous adsorbent DE-20 was entirely practical for the purification of anthocyanins in bilberry.

Through a simple extraction and separation process, the content of anthocyanins increased from the original 0.5% in bilberry frozen fruits to high purity of 96% in the final product, which illustrates the effectiveness and practicality of the separation and purification method based on macroporous resin DE-20. For the first time, anthocyanins with high purity are achieved via separation technology based on macroporous polymeric adsorbents, which represents both a novel breakthrough and a method involving simple operation, low cost, and high efficiency, which is suitable for industrial-scale production. The product of anthocyanins with high purity is beneficial for further research concerning their medicinal and pharmacological applications.

AUTHOR INFORMATION

Corresponding Author

*Telephone/Fax: +86-2223503935. E-mail: wch2004@nankai.edu.cn.

Funding

The authors thank the financial support by the Tianjin Municipal Science and Technology Commission (Grant 13JCZDJC32900) and the Program for Changjiang Scholars and Innovative Research Team in University (PCSIRT) (IRT1257).

Notes

The authors declare no competing financial interest.

REFERENCES

(1) Hara, S.; Morita, R.; Ogawa, T.; Segawa, R.; Takimoto, N. Tumor suppression effects of bilberry extracts and enzymatically modified isoquercitrin in early preneoplastic liver cell lesions induced by piperonyl butoxide promotion in a two-stage rat hepatocarcinogenesis model. *Exp. Toxicol. Pathol.* **2014**, *66*, 225−234.

(2) Szakiel, A.; Paczkowski, C.; Huttunen, S. Triterpenoid content of berries and leaves of bilberry *Vaccinium myrtillus* from Finland and Poland. *J. Agric. Food Chem.* **2012**, *60*, 11839−11849.

(3) Latti, A. K.; Riihinen, K. R.; Kainulainen, P. S. Analysis of anthocyanin variation in wild populations of bilberry (*Vaccinium myrtillus* L.) in Finland. *J. Agric. Food Chem.* **2008**, *56*, 190−196.

(4) Wang, L. S.; Stoner, G. D. Anthocyanins and their role in cancer prevention. *Cancer Lett.* **2008**, *269*, 281−290.

(5) Hosseinian, F. S.; Beta, T. Saskatoon and wild blueberries have higher anthocyanin contents than other Manitoba berries. *J. Agric. Food Chem.* **2007**, *55*, 10832−10838.

(6) Jakobsdottir, G.; Nilsson, U.; Blanco, N.; Sterner, O.; Nyman, M. Effects of soluble and insoluble fractions from bilberries, black currants, and raspberries on short-chain fatty acid formation, anthocyanin excretion, and cholesterol in rats. *J. Agric. Food Chem.* **2014**, *62*, 4359−4368.

(7) Bornsek, S. M.; Ziberna, L.; Polak, T.; Vanzo, A.; Ulrih, N. P.; Abram, V.; Tramer, F.; Passamonti, S. Bilberry and blueberry anthocyanins act as powerful intracellular antioxidants in mammalian cells. *Food Chem.* **2012**, *134*, 1878−1884.

(8) Kalt, W.; Hanneken, A.; Milbury, P.; Tremblay, F. Recent research on polyphenolics in vision and eye health. *J. Agric. Food Chem.* **2010**, *58*, 4001−4007.

(9) Mauro, A. D.; Arena, E.; Fallico, B.; Passerini, A.; Maccarone, E. Recovery of anthocyanins from pulp wash of pigmented oranges by concentration on resins. *J. Agric. Food Chem.* **2002**, *50*, 5968−5974.

(10) Cretu, G. C.; Morlock, G. E. Analysis of anthocyanins in powdered berry extracts by planar chromatography linked with bioassay and mass spectrometry. *Food Chem.* **2014**, *146*, 104−112.

(11) Cassinese, C.; Combarieu, E. d.; Falzoni, M.; Fuzzati, N.; Pace, R.; Sardone, N. New liquid chromatography method with ultraviolet detection for analysis of anthocyanins and anthocyanidins in *Vaccinium myrtillus* fruit dry extracts and commercial preparations. *J. AOAC Int.* **2007**, *90*, 911−919.

(12) Baum, M.; Schantz, M.; Leick, S.; Berg, S.; Betz, M.; Frank, K.; Rehage, H.; Schwarz, K.; Kulozik, U.; Schuchmann, H.; Richling, E. Is the antioxidative effectiveness of a bilberry extract influenced by encapsulation? *J. Sci. Food Agric.* **2014**, *94*, 2301−2307.

DOI: 10.1021/jf506107m
J. Agric. Food Chem. 2015, 63, 3543−3550

(13) Kropat, C.; Betz, M.; Kulozik, U.; Leick, S.; Rehage, H.; Boettler, U.; Teller, N.; Marko, D. Effect of microformulation on the bioactivity of an anthocyanin-rich bilberry pomace extract (*Vaccinium myrtillus* L.) in vitro. *J. Agric. Food Chem.* **2013**, *61*, 4873−4881.
(14) Juadjur, A.; Winterhalter, P. Development of a novel adsorptive membrane chromatographic method for the fractionation of polyphenols from bilberry. *J. Agric. Food Chem.* **2012**, *60*, 2427−2433.
(15) Kahkonen, M. P.; Heinamaki, J.; Ollilainen, V.; Heinonen, M. Berry anthocyanins: Isolation, identification and antioxidant activities. *J. Sci. Food Agric.* **2003**, *83*, 1403−1411.
(16) McDougall, G. J.; Gordon, S.; Brennan, R.; Stewart, D. Anthocyanin-flavanol condensation products from black currant (*Ribes nigrum* L.). *J. Agric. Food Chem.* **2005**, *53*, 7878−7885.
(17) Du, Q.; Jerz, G.; Winterhalter, P. Isolation of two anthocyanin sambubiosides from bilberry (*Vaccinium myrtillus*) by high-speed counter-current chromatography. *J. Chromatogr. A* **2004**, *1045*, 59−63.
(18) He, J.; Giusti, M. M. High-purity isolation of anthocyanins mixtures from fruits and vegetables—A novel solid-phase extraction method using mixed mode cation-exchange chromatography. *J. Chromatogr. A* **2011**, *1218*, 7914−7922.
(19) Simmons, S. T. Commercial applicability of an innovative anthocyanin purification technique, utilizing mixed-mode solid-phase extraction. Master's Thesis, The Ohio State University, Columbus, OH, 2012.
(20) Scordino, M.; Mauro, A. D.; Passerini, A.; Maccarone, E. Adsorption of flavonoids on resins: cyanidin 3-glucoside. *J. Agric. Food Chem.* **2004**, *52*, 1965−1972.
(21) Buran, T. J.; Sandhu, A. K.; Li, Z.; Rock, C. R.; Yang, W. W.; Gu, L. Adsorption/desorption characteristics and separation of anthocyanins and polyphenols from blueberries using macroporous adsorbent resins. *J. Food Eng.* **2014**, *128*, 167−173.
(22) Wang, X.; Hansen, C.; Allen, K. Extraction of anthocyanins from black bean canning wastewater with macroporous resins. *J. Food Sci.* **2014**, *79*, E184−E188.
(23) Jampani, C.; Naik, A.; Raghavarao, K. S. Purification of anthocyanins from jamun (*Syzygium cumini* L.) employing adsorption. *Sep. Purif. Technol.* **2014**, *125*, 170−178.
(24) Chang, X. L.; Wang, D.; Chen, B. Y.; Feng, Y. M.; Wen, S. H.; Zhan, P. Y. Adsorption and desorption properties of macroporous resins for anthocyanins from the calyx extract of roselle (*Hibiscus sabdariffa* L.). *J. Agric. Food Chem.* **2012**, *60*, 2368−2376.
(25) Asenstorfer, R. E.; Hayasaka, Y.; Jones, G. P. Isolation and structures of oligomeric wine pigments by bisulfite-mediated ion-exchange chromatography. *J. Agric. Food Chem.* **2001**, *49*, 5957−5963.
(26) He, J.; Santos-Buelga, C.; Mateus, N.; de Freitas, V. Isolation and quantification of oligomeric pyranoanthocyanin-flavanol pigments from red wines by combination of column chromatographic techniques. *J. Chromatogr. A* **2006**, *1134*, 215−225.
(27) Zhao, R.; Yan, Y.; Li, M.; Yan, H. Selective adsorption of tea polyphenols from aqueous solution of the mixture with caffeine on macroporous crosslinked poly(*N*-vinyl-2-pyrrolidinone). *React. Funct. Polym.* **2008**, *68*, 768−774.
(28) Ma, N.; Wang, P.; Kong, X.; Shi, R.; Yuan, Z.; Wang, C. Selective removal of caffeine from tea extracts using macroporous crosslinked polyvinyl alcohol adsorbents. *J. Sep. Sci.* **2012**, *35*, 36−44.
(29) Ren, P.; Zhao, X.; Zhang, J.; Shi, R.; Yuan, Z.; Wang, C. Synthesis of high selectivity polymeric adsorbent and its application on the separation of ginkgo flavonol glycosides and terpene lactones. *React. Funct. Polym.* **2008**, *68*, 899−909.
(30) Ghidouche, S.; Rey, B.; Michel, M.; Galaffu, N. A rapid tool for the stability assessment of natural food colours. *Food Chem.* **2013**, *139*, 978−985.
(31) Welch, C. R.; Wu, Q.; Simon, J. E. Recent advances in anthocyanin analysis and characterization. *Curr. Anal. Chem.* **2008**, *4*, 75−101.

DOI: 10.1021/jf506107m
J. Agric. Food Chem. 2015, 63, 3543−3550

(TAG), increased.[19] Therefore, many mutants are impacted in the structure of subcellular organelles, e.g., ER, protein bodies, and amyloplasts, delimited by lipoprotein membranes. Surprisingly, no research was conducted on the relationships between endosperm lipids and maize vitreousness, especially by using normal maize inbred lines.

It is also important to consider endosperm programmed cell death (PCD). PCD starts at the center of the grain in the floury area to finally affect the entire endosperm.[20] Moreover, 10 days after pollination, endosperm faces hypoxia stress (DAP)[21] and desiccation at the end of development.[22] To delineate the biochemical basis of endosperm vitreousness, it is therefore more judicious to consider separately the floury and vitreous regions than the whole endosperm as was outlined for proteins.[23]

In this context, we report here the lipid composition of the vitreous and floury mature endosperms of dent and flint maize inbred lines. The results highlight a close relationship among starch lipids, amylose, and vitreousness. The differences observed in the composition and content of nonstarch lipids of vitreous and floury endosperm might be related to differences in their respective metabolic specificities and stress responses occurring along the PCD of developing endosperm.

MATERIALS AND METHODS

Plant Material, Vitreousness, and Milling Properties. Thirteen maize inbred lines were grown in the Limagrain station in Mons (France). Maize kernels from self-pollinated homozygote plants were collected in the middle third of the ear. For lipid analyses, grains were frozen in liquid nitrogen and stored at −80 °C. For vitreous area determination, 10 grains were cut vertically along the germ center. Sections were scanned, and pictures were analyzed with ImageJ software to determine total endosperm and vitreous areas. Vitreous endosperm mass percentage was measured after hand-dissection of 3 series of 4 grains. For semolina yield determination, a lab degerminator (Satake, Satake Europe LTD) was used in order to remove germ and bran, and to separate the vitreous from the other part of the grain. Vitreous areas and vitreous endosperm weight have a close ranking and are strongly correlated with the milling properties, i.e., semolina yield (Table S1, Supporting Information) $R = 0.79$ ($p < 0.01$) and $R = 0.82$ ($p < 0.001$), respectively. Principal component analysis of these texture parameters highlighted different groups of vitreousness that correspond to flint (L1 to L4) and dent (L05 to L13) phenotypes. In these inbred lines, L11 is a markedly different dent variety with a very low vitreousness (Figure S1 and Table S1, Supporting Information). The genetic diversity of the 13 inbred lines was characterized by the Nei-Li genetic distance matrix calculated with 3000 SNPs distributed on 10 chromosomes (Table S2, Supporting Information).

The floury and vitreous fractions were isolated using hand dissection after the removal of peripheral layers and the aleurone. The fractions were lyophilized and ground under liquid nitrogen. The protein content of isolated dried endosperm was determined by the Kjeldahl nitrogen determination method using a 5.7 factor for protein content.

Vitreous/floury statistical analyses were performed using Student's paired *t*-test. Error bars are standard deviations and represent differences between vitreous/floury fractions, as far as differences between maize inbred lines.

Starch and Amylose Content. Starch was quantified according to a modification of the Megazyme Total starch assay procedure. Briefly, 50 mg of flour was washed in 5 mL of 80% ethanol at 80 °C for 5 min. Starch was subsequently dispersed in 2 mL of DMSO for 10 min at 100 °C. Samples were hydrolyzed 6 min at 100 °C with 3 mL of a 50 mM, pH 7 thermostable α-amylase solution (100U/mL) in MOPS (3-(*N*-morpholino)propanesulfonic acid), before adding 4 mL of 200 mM ammonium acetate at pH 4.5 and 100 μL of amyloglucosidase (3300U/mL). The hydrolysis was conducted during 30 min at 50 °C. We added water up to 50 mL, and a diluted aliquot (10 X, 66 μL) was placed in the 96-well plate with 200 μL of GOPOD buffer and incubated for 20 min at 50 °C. Absorbance was read at 510 nm, and the subsequent glucose contents were determined using a standard curve. Glucose content was further converted to starch contents.

Amylose was quantified according to a modification of the Megazyme amylose/amylopectin assay procedure. Briefly, zeins were extracted from 25 mg of flour with 70% ethanol for 1 h. Starch was subsequently dispersed in 1 mL of DMSO for 15 min at 100 °C, and then we added 2 mL of 95% ethanol and 4 mL of absolute ethanol. After starch precipitation, the supernatant was removed. Starch was dispersed in 2 mL of DMSO for 15 min at 100 °C, then 0.6 M sodium acetate at pH 6.4 was added up to 25 mL. An aliquot was used for starch quantification, and another one was used for amylose quantification, after amylopectin and dextrin precipitation with concanavalin-A. Aliquots were hydrolyzed with α-amylase and amyloglucosidase in 100 mM sodium acetate at pH 4.5, then 40 μL was placed in 96-well plate with 200 μL of GOPOD buffer and incubated for 20 min at 50 °C. The amylose content was determined from the absorbance ratio at 510 nm.

Total Starch and Nonstarch Lipid Contents. Endosperm flour lipids were extracted by adding 1 mL of 2-propanol in 20 mg of flour. After 1 h at room temperature and centrifugation (3000*g*, 5 min), the pellet was extracted twice with 1 mL of chloroform/methanol 2:1 (v/v) for 1 h. The three supernatants containing nonstarch lipids were pooled and dried under nitrogen flux. Nonstarch lipids were methyl-esterified with 1 mL of 14% BF3 in methanol at 70 °C for 1 h in the presence of heptadecanoic acid (Sigma-Aldrich, France) as internal standard.

To quantify starch lipids, the residual defatted flour was dried and incubated in 5 mL of 2% sulfuric acid in methanol at 50 °C for 12 h in the presence of heptadecanoic acid as internal standard.[24] The resulting fatty acid methyl esters (starch and nonstarch) were analyzed by coupling gas chromatography with flame ionization detection (GC-FID Clarus680, PerkinElmer, France) using a DB225 (Agilent technologies, France) capillary column (30m × 0.32 mm, 0.25 μm) and a temperature gradient from 50 to 220 °C.

Starch and Nonstarch Lipid Composition. To determine the composition of nonstarch lipids, 1 g of endosperm flour (about 20 dissected grains) was extracted in 10 mL of 2-propanol for 1 h and centrifuged (3000*g*, 5 min). The pellet was extracted three times in chloroform−methanol (2/1) for 1 h. The supernatants were pooled and dried on a rotary evaporator. To remove nonlipid material, lipids were solubilized in 8 mL of chloroform−methanol (2/1), to which 2 mL of 0.9% NaCl in water were added.[25] The lower organic phase was collected and dried under nitrogen flux. Then, lipids were solubilized in 1 mL of chloroform containing 1% acetic acid and loaded on a silica (100 mg) cartridge (SupelClean LC-Si, Supelco, USA). Neutral lipids, galactolipids, and phospholipids were eluted with 1% chloroform-acetic acid, acetone, and methanol, respectively. Lipids were dried under nitrogen flux and solubilized in chloroform before UPLC analysis. An aliquot was taken for quantification by GC-FID as described above.

To analyze the starch lipid composition, 100 mg of thoroughly delipidated flour was dispersed in 1 mL of water during 5 min at 100 °C in water. Then, 4 mL of 1-propanol was added and mixed for 5 min at 100 °C. After centrifugation (3000*g*, 5 min), the pellet was washed with 80% 1-propanol in water. After centrifugation, the supernatants were pooled and dried under nitrogen flux, and the lipids were purified by phase partitioning in chloroform−methanol−0.9% NaCl as described above. Dried lipids were solubilized in 0.4 mL of chloroform before UPLC analysis. Lipids were analyzed on Dionex Ultimate 3000 UPLC equipped with an Uptisphere Strategy 2.2 μm 100 Å column (4.6 × 150 mm) and an evaporative light-scattering detector (Sedex80, Sedere, France). Lipids were eluted using a gradient from solvent A, chloroform, to solvent B, methanol−ammoniac 30%−chloroform 460:35:5 (v/v). The gradient started from 100% A to 20% B in 3 min, and then increased to 100% B in 9 min. After a plateau at 100% B for 3 min, the column was equilibrated in 100% A for 3 min. The analysis was carried out at 30 °C with a flow rate of 1.5 mL/min. Lipid content

DOI: 10.1021/acs.jafc.5b00293
J. Agric. Food Chem. 2015, 63, 3551−3558

was calculated in regard to a calibration curve obtained with lipid standards. Phosphatidylethanolamine (PE), phosphatidylcholine (PC), and phosphatidylinositol (PI) were from soybean (Avanti Polar Lipids Inc., USA). Bovine brain phosphatidylserine (PS), egg yolk phosphatidic acid (PA), 1-palmitoyl-lysophosphatidylcholine (C16 lysoPC), and linoleic acid were from Sigma-Aldrich Chimie (Lyon, France). 1-Heptanoyl-lysophosphatidylethanolamine (C17 lysoPE) was provided by Avanti Polar Lipids (Alabaster, Alabama, USA). Galactolipids, i.e., digalactosyldiacylglycerol (DGDG), and monogalactosyldiacylglycerol (MGDG) standards were purified from wheat flour as previously described.[26] Standard TAG were purified from the corresponding commercial sunflower oil on SiOH cartridges using stepwise elution with hexane−diethyl ether 99:1 and 95:5 (v/v).

RESULTS

Sequential Extraction Procedure Enabling Quantification and Characterization of Starch and Nonstarch Lipids of Maize Endosperm. The selected sample of 13 maize inbred lines displays a wide range of vitreousness and protein content (from 8.8 to 12.3% DW). The starch content varies from 71.2 to 74.5% DW (Table S1, Supporting Information). In maize endosperm, a part of the lipids are embedded in starch granules and are mainly composed by FFA and lysophospholipids.[27] They are not extractible using cold solvents, being only released after starch hydrolysis or by using hot water−alcohol solvents. Therefore, we developed a sequential extraction procedure where lipids are first thoroughly extracted with solvents at room temperature, i.e., nonstarch lipids, while the residual unextracted lipids, i.e., starch lipids, were extracted with hot water−1-propanol or released by acid methanolysis as fatty acid methyl esters (FAME). Compared to nonstarch lipids, starch lipids are characterized by a higher proportion of palmitic acid (about 40% vs about 18%). Conversely, nonstarch lipids contained a higher proportion of unsaturated fatty acids, namely, linoleic (18:2 n-6), linolenic (18:3 n-3) and oleic acids (18:1 n-9), than starch lipids (Figure 1a). These fatty acid compositions are in agreement with previous data obtained for purified maize starch and isolated maize endosperm.[28] Finally, when delipidated maize endosperms were extracted with hot aqueous 1-propanol, lipid analysis by normal-phase UPLC showed that these lipids are mainly composed of FFA and lysophospholipids, lysoPE, and especially lysoPC (Figure 1b and Figure S2a, Supporting Information) that specifies starch lipids.[27]

Starch lipid contents vary from 0.27 to 0.35% of endosperm DW (Table S3, Supporting Information). Therefore, about a third of endosperm lipids occur inside the starch granules. Related to starch contents, these values correspond to 0.37 and 0.49% of starch DW, respectively. These amounts are close to the value found for purified starch from a commercial maize hybrid, i.e., about 0.5%.[28] In contrast, nonstarch lipid contents vary from 0.47% to 0.83% of endosperm DW. In all inbred lines, nonstarch lipids are mainly composed of neutral lipids (79 to 95% of nonstarch lipids) (Table S3, Supporting Information) as previously observed in hybrids as well as in amylo- and waxy maize.[28] TAG and FFA compose the neutral lipids where only very small quantities of monoacyl (MAG)- and diacylglycerol (DAG) can be detected (Figure S2b, Supporting Information, and Figure 3b). This contrasts with the results obtained by Tan and Morrison[28] who found very low TAG levels, high amounts of FFA, and measurable levels of DAG and MAG. In regard to the results reported by Tan and Morisson,[28] the higher proportion of TAG vs FFA observed herein is probably due to our primary extraction with 2-propanol, which is known to inhibit lipases.[25] Finally, membrane lipids, i.e., galactolipids and phospholipids, were minor compounds and represented from 1 to 7.6% and from 2.5 to 13.6% of nonstarch lipids, respectively (Table S3, Supporting Information). Therefore, our sequential extraction procedure is a simple way to accurately determine the starch and nonstarch lipid contents and composition. It does not need extraction of starch, avoiding contamination by residual nonstarch lipids present inevitably on the surface of granules[28,29]

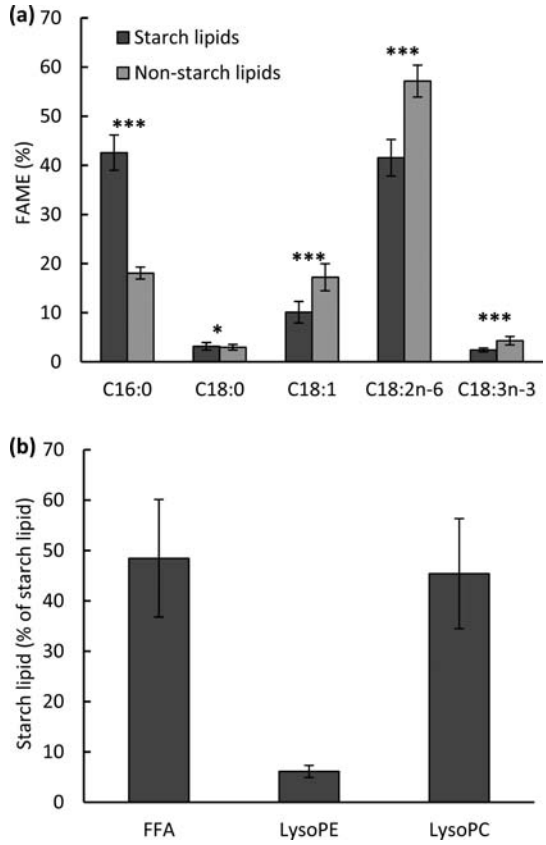

Figure 1. (a) Fatty acid composition of starch lipids and nonstarch lipids expressed as percentage of total FAME. Values are the average of two independent biological replicates for the 13 lines (error bar, SD; $n = 26$) (asterisks indicate significant difference; Student's t test; $^{*}P < 0.05$; $^{***}P < 0.001$). (b) Starch lipid composition of total endosperm expressed as percent of total starch lipids. FFA, free fatty acid; LysoPE, lysophosphatidylethanolamine; LysoPC, lysophosphatidylcholine. Mean values for the 13 lines (error bar, SD; $n = 13$).

FFA to Lysophospholipid Ratio of Starch Lipids Is a Marker of Vitreous and Floury Endosperm. In order to explore whether any relationship between biochemical composition and vitreousness can be assessed, the vitreous and floury regions were isolated by hand dissection. As previously shown in opaque and inbred maize lines,[23,30] protein contents were higher in the vitreous area, whereas higher starch contents were observed in the floury one (Table S4, Supporting Information). Similarly, slight but significant higher amylose levels were systematically evidenced in the starch of the vitreous endosperm when compared with the starch of the floury area (Table S4, Supporting Information). This result is in accordance with the higher amylose contents measured in maize hybrids and a QPM population with increased vitreousness.[31,32] Accordingly, starch lipids and

DOI: 10.1021/acs.jafc.5b00293
J. Agric. Food Chem. 2015, 63, 3551−3558

nonstarch lipids of vitreous and floury endosperm were quantified as FAME. When lipid contents are related to endosperm dry weight, the starch lipid content is not significantly different between the floury and vitreous regions. However, when lipid contents are related to starch dry weight content, a clear and significant trend for higher lipid content in the starch granules of the vitreous fraction than in the starch granules of the floury one is evidenced (Figure 2a).

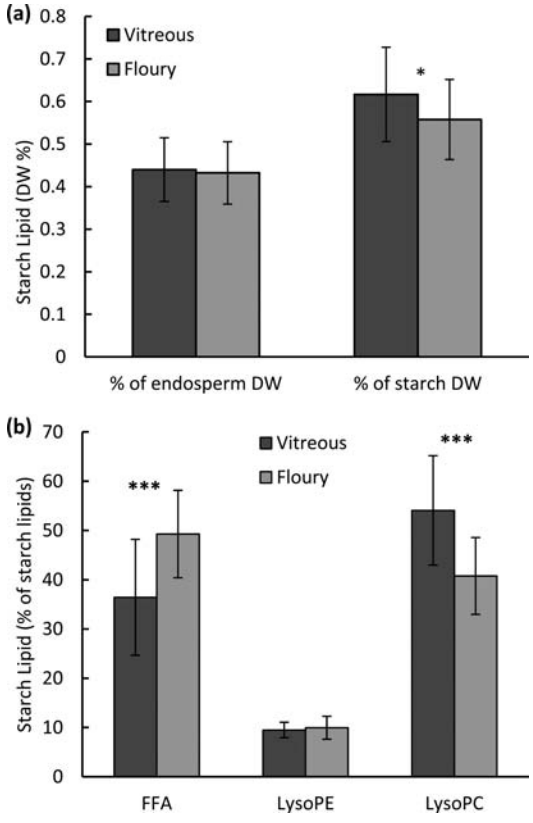

Figure 2. (a) Starch lipid content in vitreous and floury endosperm from the 13 lines expressed on endosperm and starch dry weight and expressed in dry weight percent. Values are averages of the 13 lines (error bar, SD; n = 13) (asterisks indicate significant difference; Student's t test; *P < 0.05). (b) Lipid content in vitreous and floury starch from the 13 lines expressed as percent of total starch lipid. FFA, free fatty acid; LysoPE, lysophosphatidylethanolamine; LysoPC, lysophosphatidylcholine. Values are averages of the 13 lines (error bar, SD; n = 13). (Asterisks indicate significant difference; Student's t test; **P < 0.01; ***P < 0.001.)

Interestingly, this increase of lipid contents comes with a major shift in the FFA to lysophosphopholipid ratio due to an increase of the lysoPC content, the major starch phospholipid (Figure 2b and Figure S2a, Supporting Information).

Partitioning of Storage and Membrane Lipids in Vitreous and Floury Endosperm. The highest nonstarch lipid contents are observed in the floury endosperm for each inbred line. Indeed, the mean nonstarch lipid amounts of the floury endosperms are almost twice those observed in the case of the vitreous endosperm, i.e., 1 and 0.6% endosperm DW, respectively (Figure 3a). This difference is mainly due to neutral lipids, the main lipid fraction of maize endosperm (Table S3 and Figure S2b, Supporting Information). Indeed, the amounts of membrane (polar) lipids are quite low in all inbred lines, and no significant differences are observed

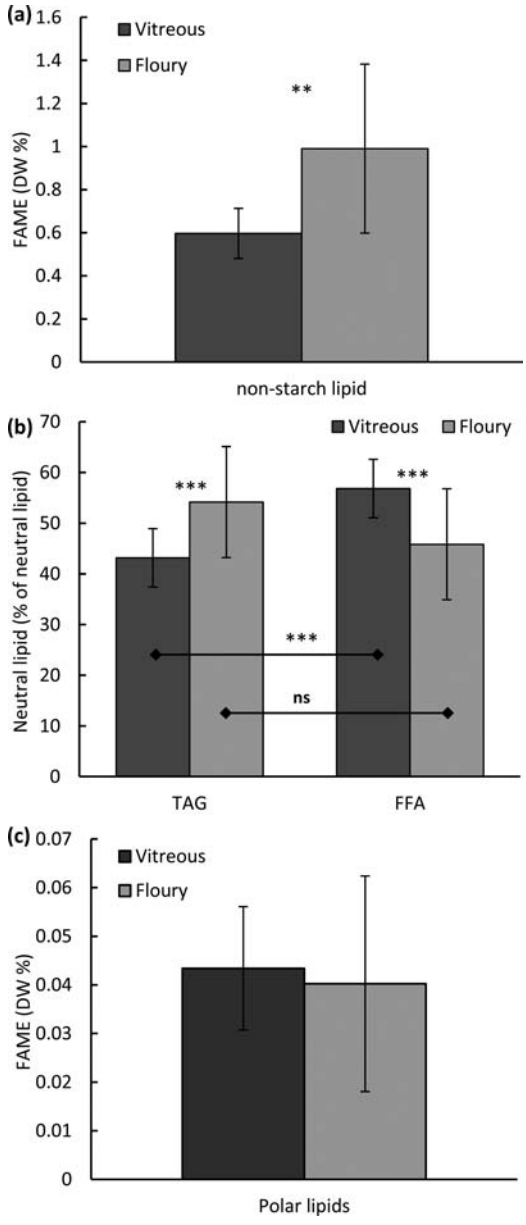

Figure 3. (a) Nonstarch lipid content in vitreous and floury endosperm from the 13 lines, expressed in dry weight percent of endosperm. Mean values for 13 lines (error bar, SD; n = 13) (asterisks indicate significant difference; Student's t test; **P < 0.01). (b) Vitreous and floury endosperm neutral lipid composition expressed as percent of total neutral lipids. TAG, triacylglycerol; FFA, free fatty acid. Values are averages of the 13 lines (error bar, SD; n = 13) (asterisks indicate significant difference; Student's t test; ***P < 0.001; ns, nonsignificant). (c) Polar lipid contents in vitreous and floury endosperm from the 13 lines expressed in dry weight percent of endosperm. Mean values for the 13 lines (error bar, SD; n = 13).

between the polar lipid contents of the vitreous and floury endosperms (Figure 3c). While the vitreous endosperm is significantly richer in FFA than in TAG, there is no significant difference between the FFA and TAG contents of floury endosperm (Figure 3b). Therefore, in regard to the vitreous endosperm, the higher amounts of neutral lipids in the floury endosperm are mainly due to TAG (Figure 3b).

Remarkably, the partition of nonstarch polar lipids between the vitreous and floury areas follows a different pattern. While the levels of total membrane lipids are not significantly different

DOI: 10.1021/acs.jafc.5b00293
J. Agric. Food Chem. 2015, 63, 3551−3558

between vitreous and floury endosperm (Figure 3c), their compositions, i.e., galactolipid to phospholipid ratio, differ significantly. Indeed, galactolipids represent 30% of membrane lipids in the floury region, whereas they represent 20% in the vitreous region (Figure 4a). Similarly, vitreous endosperm contains more phospholipids than the floury one, with 80% of phospholipids in vitreous endosperm and 70% in floury endosperm. These tendencies are observed in most lines except for L05 and L06 where the proportions of galactolipids and phospholipids in their floury and vitreous regions were similar (data not shown). We do not observe significant differences in the galactolipid composition of the vitreous and floury endosperm (Figure 4b). MGDG and DGDG are the major galactolipids, and in most maize lines, except for L02 and L13 (data not shown), we observe the same MGDG/DGDG ratio in the vitreous and floury endosperm (Figure 4b). Similarly, we do not observe significant differences in PE, PA, and lysoPC proportions between the floury and vitreous regions (Figure 4c). Conversely, a higher proportion of PC is observed in the vitreous endosperm, where it represents about 59% of phospholipids versus 54% in the floury part. This difference is partially balanced by a significant increase of PI level in floury areas, i.e., 12.6% of phospholipids vs 10.6% in vitreous endosperm.

Lipids of Vitreous Endosperm Display a Higher Level of PUFA than the Floury Endosperm. The fatty acid composition of vitreous and floury endosperm lipids display systematic differences. Acyl lipids of vitreous endosperm contained higher proportions of polyunsaturated fatty acid (PUFA) and lower levels of saturated and monounsaturated fatty acids (Figure 5). The proportions of linoleic acid and linolenic acid are significantly higher in the vitreous region. Nonstarch lipids consist of about 64% of PUFA in the vitreous region, whereas they represent at most 58% in the floury endosperm. In regard to the vitreous endosperm, the decrease of PUFA proportion in the floury endosperm is balanced by an increase of saturated and monounsaturated fatty acids, namely, palmitic, stearic, and oleic acids. We observed the same shift in fatty acid saturation level in both storage and membrane lipid classes. This shift was observed in starch lipid too, although it is less pronounced (data not shown). Therefore, a higher PUFA content in the lipid of the vitreous region than in the floury one is systematically observed in both starch and nonstarch lipids.

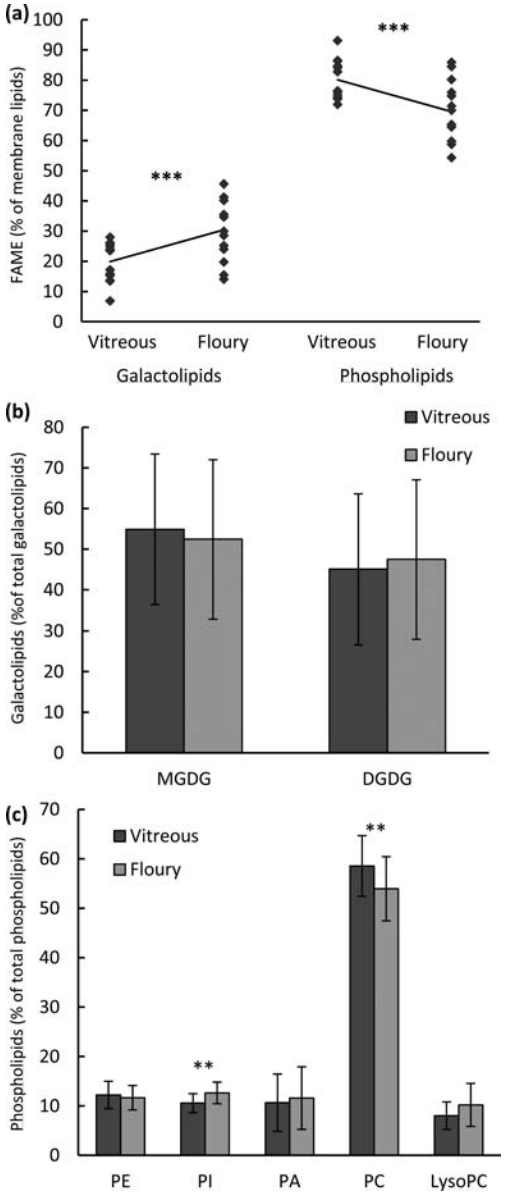

Figure 4. (a) Galactolipid and phospholipid levels in vitreous and floury endosperm of the 13 individual inbred lines (markers). The black line shows average lipid evolution. Lipids were quantified as FAME and expressed as percent of total polar lipids. Values are the average of two independent biological replicates (asterisks indicate significant difference; Student's *t* test; ***$P < 0.001$). (b) Vitreous and floury endosperm galactolipid composition expressed as a percent of total galactolipids. MGDG, monogalactosyldiacylglycerol; DGDG, digalactosydiacylglycerol. Values are the average of three independent biological replicates for the 13 lines (error bar, SD; $n = 39$). (c) Vitreous and floury endosperm phospholipid composition expressed as percent of total phospholipids. PE, phosphatidylethanolamine; PI, phosphatidylinositol; PA, phosphatidic acid; PC, phosphatidylcholine; LysoPC, lysophosphatidylcholine. Values are the average of three independent biological replicates for the 13 lines (error bar: SD; $n = 39$) (asterisks indicate significant difference; Student's *t* test; **$P < 0.01$).

DISCUSSION

Although lipids are minor compounds of the cereal endosperm, they play a major role in the assembly of the starch−protein matrix of mature kernels and therefore in grain texture (hardness). In this context, numerous research works were conducted on the lipids of wheat endosperms.[33] Surprisingly, only few research works were devoted to maize endosperm lipids and especially, no work had been realized on the relationships between endosperm lipids and vitreousness of maize seeds.

Endosperm lipids can be classified in starch and nonstarch lipids. Starch lipids are embedded in the starch granules and are extracted only with hot alcohol−water solvents or after starch hydrolysis.[27] They account for about 30% of total lipids and are characterized by a high palmitic acid content in regard to nonstarch lipids in agreement with previous results.[28] These starch lipids are almost exclusively composed of monoacyl-lipids, i.e., FFA and lysophospholipids, mainly lysoPC. In this inbred line population, no correlation could be found between these lipids and maize vitreousness or milling properties (semolina yield). Indeed, any significant correlation could be also observed between these physical properties and protein and starch contents as well. However, by considering separately the floury and vitreous regions obtained by hand dissection,

DOI: 10.1021/acs.jafc.5b00293
J. Agric. Food Chem. 2015, 63, 3551−3558

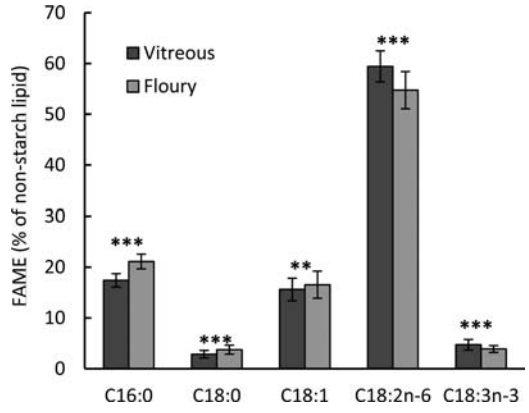

Figure 5. Fatty acid composition of nonstarch lipids quantified as FAME and expressed as percent of total fatty acid. Values are the average of two independent biological replicates for the 13 lines (error bar, SD; $n = 26$) (asterisks indicate significant difference; Student's t test; $^{**}P < 0.01$; $^{***}P < 0.001$).

significant differences were found. Starch lipid content was higher in the starch of vitreous endosperm than in the starch of floury endosperm. Similarly, the amylose content of starch is systemically higher in the vitreous than in the floury endosperm. This is in agreement with previous works reporting a relationship between the amylose and starch lipid contents when considering different groups, i.e., low-amylose (waxy), normal-amylose, and high-amylose maize starches. Indeed, higher amylose content is associated with higher starch lipid content.[34,35] Furthermore, our work shows that the higher lipid content of starches from vitreous endosperm than that of the starches of floury endosperm was mainly due to a shift in the FFA to lysoPC ratio. On the contrary, both FFA and lysophospholipid contents increased when comparing normal and high-amylose maize mutants emphasizing the difference between normal maize and mutants.[34,35] Starch lipids can form complexes with amylose in native starch granules[36,37] and impact amylose chain assemblies, starch crystallinity, and obviously play a role in the architecture of starch granules.[38] These changes of starch lipid content and composition may be compared with changes of the crystallinity and morphology of starch granules with an increase of endosperm vitreousness in QPM.[4,39] This also has to be compared with differences observed for the surface structure of starch granules isolated from the vitreous and floury endosperm regions of maize hybrids and the QPM population.[31] Therefore, the biosynthesis of starch lipids and its regulation can also be regarded as one of the significant molecular and cellular mechanisms determining maize endosperm vitreousness. Actually, the origin and the biological function of the monoacyl lipids entrapped in the starch granules are still unknown. Regarding lysoPC, it is the form used to import lipids from the ER into plastids for the synthesis of some plastid lipids.[40] Although it is not known if this way is operative in amyloplasts, it is interesting to note that the highest lysoPC level is observed in the vitreous endosperm where the synthesis of storage proteins, i.e., zeins, which occurs in the ER, is particularly more intense than in the floury region. Indeed, it is also in the vitreous endosperm where the highest level of PC, the precursor of lysoPC, is observed. Beside a role of these lipids in the synthesis of amyloplast membrane lipids as in plastids,[41−43] starch lipids could regulate the activity of enzymes involved in amylose and amylopectin synthesis. In this regard, it was shown that phospholipids could inhibit starch branching enzymes.[44]

Actually, differences in the biosynthesis of nonstarch lipids also exist between floury and vitreous endosperms. Indeed, nonstarch lipids are mainly composed by TAG and FFA for all inbred lines, and a higher accumulation of these lipids is observed in the floury than in the vitreous region of the maize endosperm. Concerning membrane lipids, galactolipids, and phospholipids, it was surprising to observe such low contents in all maize lines. Indeed, in wheat endosperm, with similar protein and starch content, the membrane lipid content[29,45]is more than 10 times the content found in maize endosperm (this work and ref 28). This low membrane lipid content in all inbred lines of our maize population seems to confirm and generalize the significant degradation of endosperm membrane lipids observed during endosperm development of a maize hybrid.[46] This specificity of endosperm maize development could be related to autophagy. Actually, autophagy and especially macroautophagy is a ubiquitous cellular mechanism that is involved in the degradation of damaged organelles and their membrane components.[47] Autophagy is operative in plants.[48,49] It is worthy to note that in maize endosperm the lipidation of an autophagy protein, i.e., Atg8, a marker of the formation of functional autophagosomes, starts almost at the same time[50] as membrane lipid degradation.[46] Furthermore, it is interesting to note that the decrease of TAG contents and the increase of FFA contents from mid to the end of endosperm development[46] occurs also at the onset of the expression of Atg8. Indeed, in animals as in plants, autophagy could be involved in TAG degradation.[51,52]

Whatever the origin and extent of the degradation of membrane lipids, it is worthwhile noting that there is a tendency toward higher galactolipid contents in the floury endosperm than in the vitreous one. This is in agreement with our observation that the floury endosperm has higher starch content than the vitreous one. Actually, galactolipids are specific compounds of the amyloplast membranes.[18] However, the higher phospholipid contents in the vitreous endosperm can be related to its higher protein content. Indeed, protein bodies, where protein accumulates, emerge from the ER, and their membrane lipids are composed by phospholipids. Finally, the lipid composition of the floury and vitreous endosperm could reflect some specificity in the regulation of their metabolism, which is essentially directed toward carbon and nitrogen storage.

In this regard, it is worthy to note that phospholipids of the floury endosperm display significantly higher PI level. Shank et al.[19] reported an increase of PI content in the Fl2 mutant that was also paralleled with an augmentation of TAG content. These relationships are not surprising since phospholipid and TAG biosynthetic pathways share common steps.[43] Shank et al.[19] showed that, in the Fl2 mutant, these lipid changes were related to UPR. UPR is a ubiquitous mechanism that controls the ER production of correctly folded protein and ER homeostasis.[53] Therefore, the PI and TAG increase observed in the floury endosperm in regard to the vitreous endosperm could suggest differences in the UPR responses between these endosperm regions. The lower proportion of PC in the floury endosperm also supports this. Indeed, studies on *C. elegans* report that PC decrease leads to UPR and is associated with an increase in saturated fatty acid.[54] Moreover, we observed that the lower proportion of PUFA, i.e., both linoleic and linolenic acids, in the floury endosperm than in the vitreous one is

DOI: 10.1021/acs.jafc.5b00293
J. Agric. Food Chem. 2015, 63, 3551−3558

systematically observed and is balanced by a significant increase of the proportion of both saturated and monounsaturated fatty acids. These differences could be related to differences of Δ12-desaturase activity. Actually, fatty acid saturation level and desaturase activity are good markers of cell stress in plants.[55,56] Therefore, the nonstarch lipid contents and compositions of the floury vs those of the vitreous endosperm can be linked to the stress occurring during endosperm development. Indeed, PCD starts early in the central region, which almost will correspond to the floury endosperm of the mature grain.[20,57] However, as outlined above for the membrane lipid and lysophospholipid partition, it could not be excluded that these differences in the fatty acid unsaturation level are also due to the metabolic specificities of the different endosperm regions. Indeed, the Δ12-desaturase activity seems centered in the endoplasmic reticulum of maize endosperm,[45] a compartment highly solicited for zein synthesis in the vitreous endosperm.

At this stage of the investigation, the role of nonstarch lipids of endosperm vitreousness cannot be clearly determined. It is, however, important to emphasize that lipids, especially membrane lipids, have to be considered in terms of surface potential in contrast with starch and proteins that have to be regarded in terms of volume occupancy. Actually, in dry mature wheat endosperm membrane lipids are mainly localized at the interface between the starch granule and the protein matrix,[58] and correlations have been found between the extractability of membrane lipids and wheat hardness.[59]

Although lipids are minor components of maize endosperm, this first analytical approach reveals that these compounds could be good markers of endosperm development. Indeed, the significant changes impacting the content and composition of lipids in relation to endosperm vitreousness are related to differences in the metabolism of cells that will lead to the vitreous and floury regions of the endosperm. The most important feature of this study is the probable important role of starch lipids, especially lysoPC, in determining with amylose the starch architecture and finally the starch−protein interactions.

■ ASSOCIATED CONTENT

Ⓢ Supporting Information

Vitreousness, semolina yield, and protein and starch content of maize endosperm; endosperm lipid composition; protein, starch, and amylose contents of vitreous and floury endosperm; principal component analysis (PCA) plots using semolina yield and vitreousness measurements (weight and surface, see Materials and Methods); and chromatogram of starch and nonstarch lipids from vitreous and floury endosperm. This material is available free of charge via the Internet at http://pubs.acs.org.

■ AUTHOR INFORMATION

Corresponding Author

*E-mail: Didier.Marion@nantes.inra.fr.

Funding

This work was supported by grants from the Fond Unique Interministériel (FUI GranoFlakes, F1204004C).

Notes

The authors declare no competing financial interest.

■ ABBREVIATIONS USED

DGDG, digalactosydiacylglycerol; ER, endoplasmic reticulum; FAME, fatty acid methyl ester; FFA, free fatty acids; QPM, quality protein maize; LysoPC, lysophosphatidylcholine; LysoPE, lysophosphatidylethanolamine; MGDG, monogalactosyldiacylglycerol; PA, phosphatidic acid; PC, phosphatidylcholine; PCD, programmed cell death; PI, phosphatidylinositol; PUFA, polyunsaturated fatty acid; quality protein maize; TAG, triacylglycerol; UPR, unfolded protein response

■ REFERENCES

(1) Azevedo, R. A.; Arruda, P. High-lysine maize: the key discoveries that have made it possible. *Amino Acids* **2010**, *39*, 979−989.

(2) Nuss, E. T.; Tanumihardjo, S. A. Maize: A paramount staple crop in the context of global nutrition. *Compr. Rev. Food Sci. Food Saf.* **2010**, *9*, 417−436.

(3) Sene, M.; Thevenot, C.; Hoffmann, D.; Benetrix, F.; Causse, M.; Prioul, J. L. QTLs for grain dry milling properties, composition and vitreousness in maize recombinant inbred lines. *Theor. Appl. Genet.* **2001**, *102*, 591−599.

(4) Salazar-Salas, N. Y.; Pineda-Hidalgo, K. V.; Chavez-Ontiveros, J.; Gutierrez-Dorado, R.; Reyes-Moreno, C.; Bello-Perez, L. A.; Larkins, B. A.; Lopez-Valenzuela, J. A. Biochemical characterization of QTLs associated with endosperm modification in quality protein maize. *J. Cereal Sci.* **2014**, *60*, 255−263.

(5) Schmidt, R. J.; Burr, F. A.; Aukerman, M. J.; Burr, B. Maize regulatory gene opaque-2 encodes a protein with a leucine-zipper motif that binds to zein DNA. *Proc. Natl. Acad. Sci. U.S.A.* **1990**, *87*, 46−50.

(6) Coleman, C. E.; Clore, A. M.; Ranch, J. P.; Higgins, R.; Lopes, M. A.; Larkins, B. A. Expression of a mutant alpha-zein creates the floury2 phenotype in transgenic maize. *Proc. Natl. Acad. Sci. U.S.A.* **1997**, *94*, 7094−7097.

(7) Kim, C. S.; Gibbon, B. C.; Gillikin, J. W.; Larkins, B. A.; Boston, R. S.; Jung, R. The maize Mucronate mutation is a deletion in the 16-kDa gamma-zein gene that induces the unfolded protein response. *Plant J.* **2006**, *48*, 440−451.

(8) Kim, C. S.; Hunter, B. G.; Kraft, J.; Boston, R. S.; Yans, S.; Jung, R.; Larkins, B. A. A defective signal peptide in a 19-kD alpha-zein protein causes the unfolded protein response and an opaque endosperm phenotype in the maize De*-B30 mutant. *Plant Physiol.* **2004**, *134*, 380−387.

(9) Holding, D. R.; Otegui, M. S.; Li, B. L.; Meeley, R. B.; Dam, T.; Hunter, B. G.; Jung, R.; Larkins, B. A. The maize floury1 gene encodes a novel endoplasmic reticulum protein involved in zein protein body formation. *Plant Cell* **2007**, *19*, 2569−2582.

(10) Wang, G. F.; Wang, F.; Wang, G.; Zhang, X. W.; Zhong, M. Y.; Zhang, J.; Lin, D. B.; Tang, Y. P.; Xu, Z. K.; Song, R. T. Opaque1 encodes a myosin XI motor protein that is required for endoplasmic reticulum motility and protein body formation in maize endosperm. *Plant Cell* **2012**, *24*, 3447−3462.

(11) Hunter, B. G.; Beatty, M. K.; Singletary, G. W.; Hamaker, B. R.; Dilkes, B. P.; Larkins, B. A.; Jung, R. Maize opaque endosperm mutations create extensive changes in patterns of gene. expression. *Plant Cell* **2002**, *14*, 2591−2612.

(12) Lee, J.; Ozcan, U. Unfolded protein response signaling and metabolic diseases. *J. Biol. Chem.* **2014**, *289*, 1203−1211.

(13) Wu, Y. R.; Holding, D. R.; Messing, J. Gamma-zeins are essential for endosperm modification in quality protein maize. *Proc. Natl. Acad. Sci. U.S.A.* **2010**, *107*, 12810−12815.

(14) Guo, X. M.; Ronhovde, K.; Yuan, L. L.; Yao, B.; Soundararajan, M. P.; Elthon, T.; Zhang, C.; Holding, D. R. Pyrophosphate-dependent fructose-6-phosphate 1-phosphotransferase induction and attenuation of Hsp gene expression during endosperm modification in quality protein maize. *Plant Physiol.* **2012**, *158*, 917−929.

(15) Mechin, V.; Thevenot, C.; Le Guilloux, M.; Prioul, J. L.; Damerval, C. Developmental analysis of maize endosperm proteome suggests a pivotal role for pyruvate orthophosphate dikinase. *Plant Physiol.* **2007**, *143*, 1203−1219.

(16) Prioul, J. L.; Mechin, V.; Damerval, C. Molecular and biochemical mechanisms in maize endosperm development: The

DOI: 10.1021/acs.jafc.5b00293
J. Agric. Food Chem. 2015, 63, 3551−3558

role of pyruvate-Pi-dikinase and Opaque-2 in the control of C/N ratio. *C. R. Biol.* **2008**, *331*, 772−779.
(17) Yu, Y.; Mu, H. H.; Wasserman, B. P.; Carman, G. M. Identification of the maize amyloplast stromal 112-kD protein as a plastidic starch phosphorylase. *Plant Physiol.* **2001**, *125*, 351−359.
(18) Myers, A. M.; James, M. G.; Lin, Q. H.; Yi, G.; Stinard, P. S.; Hennen-Bierwagen, T. A.; Becraft, P. W. Maize opaque5 encodes monogalactosyldiacylglycerol synthase and specifically affects galactolipids necessary for amyloplast and chloroplast function. *Plant Cell* **2011**, *23*, 2331−2347.
(19) Shank, K. J.; Su, P.; Brglez, I.; Boss, W. F.; Dewey, R. E.; Boston, R. S. Induction of lipid metabolic enzymes during the endoplasmic reticulum stress response in plants. *Plant Physiol.* **2001**, *126*, 267−277.
(20) Young, T. E.; Gallie, D. R. Programmed cell death during endosperm development. *Plant Mol. Biol.* **2000**, *44*, 283−301.
(21) Rolletschek, H.; Koch, K.; Wobus, U.; Borisjuk, L. Positional cues for the starch/lipid balance in maize kernels and resource partitioning to the embryo. *Plant J.* **2005**, *42*, 69−83.
(22) Sabelli, P. A.; Larkins, B. A. The development of endosperm in grasses. *Plant Physiol.* **2009**, *149*, 14−26.
(23) Landry, J.; Delhaye, S.; Damerval, C. Protein distribution pattern in floury and vitreous endosperm of maize grain. *Cereal Chem.* **2004**, *81*, 153−158.
(24) Welch, R. W. A micro-method for the estimation of oil content and composition in seed crops. *J. Sci. Food Agric.* **1977**, *28*, 635−638.
(25) Folch, J.; Lees, M.; Sloane Stanley, G. H. A simple method for the isolation and purification of total lipides from animal tissues. *J. Biol. Chem.* **1957**, *226*, 497−509.
(26) Bottier, C.; Gean, J.; Artzner, F.; Desbat, B.; Pezolet, M.; Renault, A.; Marion, D.; Vie, V. Galactosyl headgroup interactions control the molecular packing of wheat lipids in Lahgmuir films and in hydrated liquid-crystalline mesophases. *Biochim. Biophys. Acta* **2007**, *1768*, 1526−1540.
(27) Morrison, W. R. Lipids in cereal starches: a review. *J. Cereal Sci.* **1988**, *8*, 1−15.
(28) Tan, S. L.; Morrison, W. R. Distribution of lipids in the germ, endosperm, pericarp and tip cap of amylomaize, LG-11 hybrid maize and waxy maize. *J. Am. Oil Chem. Soc.* **1979**, *56*, 531−535.
(29) Hargin, K. D.; Morrison, W. R. The distribution of acyl lipids in the germ, aleurone, starch and non-starch endosperm of 4 wheat varieties. *J. Sci. Food Agric.* **1980**, *31*, 877−888.
(30) Dombrink-Kurtzman, M. A.; Bietz, J. A. Zein composition in hard and soft endosperm of maize. *Cereal Chem.* **1993**, *70*, 105−108.
(31) Dombrink-Kurtzman, M. A.; Knutson, C. A. A study of maize endosperm hardness in relation to amylose content and susceptibility to damage. *Cereal Chem.* **1997**, *74*, 776−780.
(32) Lee, K. M.; Bean, S. R.; Alavi, S.; Herrman, T. J.; Waniska, R. D. Physical and biochemical properties of maize hardness and extrudates of selected hybrids. *J. Agric. Food Chem.* **2006**, *54*, 4260−4269.
(33) Pauly, A.; Pareyt, B.; Fierens, E.; Delcour, J. A. Wheat (Triticum aestivum L. and T. turgidum L. ssp durum) kernel Hardness: I. current view on the role of puroindolines and polar lipids. *Compr. Rev. Food Sci. Food Saf.* **2013**, *12*, 413−426.
(34) Morrison, W. R.; Milligan, T. P.; Azudin, M. N. A relationship between the amylose and lipid contents of starches from diploid cereals. *J. Cereal Sci.* **1984**, *2*, 257−271.
(35) South, J. B.; Morrison, W. R.; Nelson, O. E. A relationship between the amylose and lipid contents of starches from various mutants for amylose content in maize. *J. Cereal Sci.* **1991**, *14*, 267−278.
(36) Morrison, W. R.; Law, R. V.; Snape, C. E. Evidence for inclusion complexes of lipids with V-amylose in maize, rice, and oat starches. *J. Cereal Sci.* **1993**, *18*, 107−109.
(37) Cheetham, N. W. H.; Tao, L. P. Solid state NMR studies on the structural and conformational properties of natural maize starches. *Carbohydr. Polym.* **1998**, *36*, 285−292.
(38) Perez, S.; Bertoft, E. The molecular structures of starch components and their contribution to the architecture of starch granules: A comprehensive review. *Starch/Stärke* **2010**, *62*, 389−420.
(39) Gibbon, B. C.; Wang, X. L.; Larkins, B. A. Altered starch structure is associated with endosperm modification in Quality Protein Maize. *Proc. Natl. Acad. Sci. U.S.A.* **2003**, *100*, 15329−15334.
(40) Mongrand, S.; Cassagne, C.; Bessoule, J. J. Import of lysophosphatidylcholine into chloroplasts likely at the origin of eukaryotic plastidial lipids. *Plant Physiol.* **2000**, *122*, 845−852.
(41) Jouhet, J.; Marechal, E.; Block, M. A. Glycerolipid transfer for the building of membranes in plant cells. *Prog. Lipid Res.* **2007**, *46*, 37−55.
(42) Moreau, P.; Bessoule, J. J.; Mongrand, S.; Testet, E.; Vincent, P.; Cassagne, C. Lipid trafficking in plant cells. *Prog. Lipid Res.* **1998**, *37*, 371−391.
(43) Li-Beisson, Y.; Shorrosh, B.; Beisson, F.; Andersson, M. X.; Arondel, V.; Bates, P. D.; Baud, S. b.; Bird, D.; DeBono, A.; Durrett, T. P.; Franke, R. B.; Graham, I. A.; Katayama, K.; Kelly, A. L. A.; Larson, T.; Markham, J. E.; Miquel, M.; Molina, I.; Nishida, I.; Rowland, O.; Samuels, L.; Schmid, K. M.; Wada, H.; Welti, R.; Xu, C.; Zallot, R. m.; Ohlrogge, J. Acyl-lipid metabolism. *Arabidopsis Book* **2013**, e0161.
(44) Vieweg, G. H.; Fekete, M. Effects of phospholipids on starch metabolism. *Planta* **1976**, *129*, 155−159.
(45) Finnie, S. M.; Jeannotte, R.; Morris, C. F.; Faubion, J. M. Variation in polar lipid composition among near-isogenic wheat lines possessing different puroindoline haplotypes. *J. Cereal Sci.* **2010**, *51*, 66−72.
(46) Tan, S. L.; Morrison, W. R. Lipids in the germ, endosperm and pericarp of the developing maize kernel. *J. Am. Oil Chem. Soc.* **1979**, *56*, 759−764.
(47) Feng, Y. C.; He, D.; Yao, Z. Y.; Klionsky, D. J. The machinery of macroautophagy. *Cell Res.* **2014**, *24*, 24−41.
(48) Bassham, D. C. Function and regulation of macroautophagy in plants. *BBA-Mol. Cell Res.* **2009**, *1793*, 1397−1403.
(49) Michaeli, S.; Galili, G. Degradation of organelles or specific organelle components via selective autophagy in plant cells. *Int. J. Mol. Sci.* **2014**, *15*, 7624−7638.
(50) Chung, T.; Suttangkakul, A.; Vierstra, R. D. The ATG autophagic conjugation system in maize: ATG transcripts and abundance of the ATG8-lipid adduct are regulated by development and nutrient availability. *Plant Physiol.* **2009**, *149*, 220−234.
(51) Settembre, C.; Ballabio, A. Lysosome: regulator of lipid degradation pathways. *Trends Cell Biol.* **2014**, *24*, 743−750.
(52) Hanamata, S.; Kurusu, T.; Kuchitsu, K. Roles of autophagy in male reproductive development in plants. *Front. Plant Sci.* **2014**, *5*, 457.
(53) Howell, S. H. Endoplasmic reticulum stress responses in plants. *Annu. Rev. Plant Biol.* **2013**, *64*, 477−499.
(54) Hou, N. S.; Gutschmidt, A.; Choi, D. Y.; Pather, K.; Shi, X.; Watts, J. L.; Hoppe, T.; Taubert, S. Activation of the endoplasmic reticulum unfolded protein response by lipid disequilibrium without disturbed proteostasis in vivo. *Proc. Natl. Acad. Sci. U.S.A.* **2014**, *111*, E2271−E2280.
(55) Upchurch, R. G. Fatty acid unsaturation, mobilization, and regulation in the response of plants to stress. *Biotechnol. Lett.* **2008**, *30*, 967−977.
(56) Los, D. A.; Mironov, K. S.; Allakhverdiev, S. I. Regulatory role of membrane fluidity in gene expression and physiological functions. *Photosynth. Res.* **2013**, *116*, 489−509.
(57) Sabelli, P. A. Replicate and die for your own good: Endoreduplication and cell death in the cereal endosperm. *J. Cereal Sci.* **2012**, *56*, 9−20.
(58) Al-Saleh, A.; Marion, D.; Gallant, D. J. Microstructure of mealy and vitreous wheat endosperms (Triticum durum L.) with special emphasis on location and polymorphic behavior of lipids. *Food Microstruct.* **1986**, *5*, 131−140.
(59) Morrison, W. R.; Law, C. N.; Wylie, L. J.; Coventry, A. M.; Seekings, J. The effect og group-5 chromosomes on the free polar lipids and breadmaking quality of wheat. *J. Cereal Sci.* **1989**, *9*, 41−51.

DOI: 10.1021/acs.jafc.5b00293
J. Agric. Food Chem. 2015, 63, 3551−3558

with some dietary polyphenols impaired the digestibility of many proteins, e.g., β-lactoglobulin. Using green tea catechins, Tantoush et al.[28] contrarily reported that the complexation could distinctly improve the pepsin digestibility of some food allergens. Venkatachalam and Sathe[29] reported that the presence of some phenolic compounds, including catechin and ellagic acid, did not adversely affect the in vitro pepsin hydrolysis of phaseolin (a 7S globulin from kidney bean). With in vivo experiments, Carbonaro et al.[31] also indicated that the binding of polyphenols produced an insignificant influence on the protein digestibility of proteins from several legumes. All these observations suggest that the influence of complexation with phenolic compounds on the protein digestibility is dependent on the type and nature of the tested proteins and even phenolic compounds. For legume storage proteins, the structural characteristics seem to play a vital role in their digestibility,[25,31] which might be highly affected by some pretreatments, including heating. From this viewpoint, it would be a very interesting subject to characterize the influence of complexation with curcumin on the in vitro digestibility of soy proteins.

The main objective of this study was systematically to investigate the complexation between nanoparticles of unheated and preheated (75−95 °C) SPI and curcumin. The correspondingly formed nanocomplexes were characterized in terms of surface characteristics, particle size, and microstructure, as well as the encapsulation efficiency of curcumin. Furthermore, the influence of the nanocomplexation on the storage stability and/or bioaccessibility of curcumin, as well as the in vitro digestibility of SPI, was also characterized using a gastrointestinal in vitro model. Our findings indicate that the nanocomplexation between SPI and curcumin not only provides a promising strategy to improve the stability and bioaccessibility of curcumin, but also can be applied to improve the nutritional value of soy proteins.

MATERIALS AND METHODS

Materials. Curcumin (~98% purity, from *Curcuma longa*) was purchased from Sigma-Aldrich Chemical Co. (St. Louis, MO). Defatted soy flour with low protein denaturation was obtained from Shandong Yuwang Industrial and Commercial Co. Ltd. (Yucheng, Shandong Province, China). All other chemicals were of analytical grade. SPI was prepared according to the conventional process as follows. In brief, the flour was dispersed in deionized water at a weight-to-volume ratio of 1:15, and the pH of the resultant slurry was adjusted to 8.0 using 2 M NaOH. The slurry was stirred for 2 h (if necessary, the pH was adjusted to 8.0 during the stirring) and then centrifuged at 8000*g* for 20 min to remove the insoluble material. The resulting supernatant was adjusted to pH 4.5 with 2 M HCl, and the isoelectric-precipitated curd was collected by centrifugation at 5000*g* for 20 min. The obtained precipitate was redispersed in deionized water at a weight-to-volume ratio of 1:5, and the pH of the dispersion was adjusted to 7.0 with 2 M NaOH. The final dispersion was lyophilized to produce the SPI. The protein content of this SPI was approximately 91.5% (wet basis), as determined using a Dumas combustion method (Elemental Analyzer rapid N cube, Germany), with a nitrogen conversion factor of 6.25.

Complexation of Curcumin with SPI. The SPI stock solution (5%, w/v) at pH 7.0 was prepared by dispersing the freeze-dried SPI sample in water under the stirring conditions for at least for 2 h. The heated SPI solutions were obtained by heating the same volume of the SPI stock solution in a water bath at 75, 85, and 95 °C for 15 min, and then immediately cooling to room temperature in an ice bath. Stock curcumin solution of 4.5 mg/mL concentration ([cur]) was prepared in ethyl alcohol absolute (if necessary, the preparation was centrifuged to remove the insoluble material). For the characterization of SPI−curcumin complexes, an amount of curcumin stock solution was added dropwise at a volume ratio of 1:50 to 5% (w/v) unheated or heated SPI solutions under magnetically stirred conditions. The final [cur] in the mixtures was about 88 μg/mL. The mixtures were further kept for 8 h on a magnetic stirrer at room temperature. Last, the insoluble curcumin was removed by centrifugation at 8000*g* for 20 min. The resultant supernatants were subject to the particle property characterization or freeze-dried to produce the SPI−curcumin complex powders.

To investigate the influence of variation in [cur] on the encapsulation efficiency (EE) and load amount (LA) of curcumin, increasing amount of the curcumin stock solution was added to a specific volume of 5% (w/v) unheated SPI solution. If necessary, a certain volume of ethanol was added to make sure that, in the final mixtures, the final ethanol and protein concentrations in the mixtures were constant at 30% (v/v) and 3.5% (w/v), respectively.

Determination of the Surface Hydrophobicity (H_0) and ζ-Potential of Proteins in Solutions. The H_0 of proteins in unheated and heated SPIs, before and after complexation with curcumin, was determined using a fluorescence probe, 1-anilinonaphthalene-8-sulfonate (ANS^-).[32] In brief, stock solutions of 8×10^{-3} M ANS^- and 1.5% (w/v) SPIs were prepared in 0.01 M phosphate buffer (pH 7.0). A 20 μL volume of ANS^- stock solution was added to 4 mL of the buffer containing increasing amounts (0−50 μL) of 1.5% (w/v) SPI solution. The relative fluorescence intensity (FI) was measured at 25 °C, with excitation and emission wavelengths of 390 and 470 nm, respectively. For each protein, the initial slope of the FI versus protein concentration plot was calculated by linear regression analysis and used as an index of H_0.

The ζ-potential of proteins in the unheated and heated SPI solutions at pH 7.0 was measured using a Zetasizer Nano ZS (Malvern Instruments Ltd., Malvern, Worcestershire, U.K.) in combination with a multipurpose autotitrator (model MPT-2, Malvern Instruments). Freshly prepared protein solutions were diluted to 0.1% (w/v) with the same applied buffer and filtered through a 0.45 μm HA Millipore membrane prior to analysis.

Differential Scanning Calorimetry (DSC). The thermal transition of unheated and heated SPIs was examined using a TA Q100-DSC thermal analyzer (TA Instruments, New Castle, DE) according to the process described in our previous work.[33] All the unheated and heated SPI samples with or without complexation with curcumin for the DSC examination were prepared by freeze-drying the corresponding solutions (5%, w/v). Approximately 2.0 mg of the freeze-dried samples was weighed into aluminum liquid pans (Dupont), and 10 μL of 0.05 M phosphate buffer (pH 7.0) was added. The pans were hermetically sealed and heated from 20 to 110 °C at a rate of 5 °C/min. A sealed empty pan was used as a reference. The denaturation temperature (T_d) and enthalpy change of the endotherm (ΔH) of the β-conglycinin and glycinin components in the samples were computed from the thermograms by Universal Analysis 2000, version 4.1D (TA Instruments-Waters LLC). All experiments were conducted in triplicate. The sealed pans containing protein samples and buffers were equilibrated at 25 °C for 12 h.

Particle Size Distribution and *z*-Average Diameter (D_z) Measurement. The particle size distribution of particles in unheated and heated SPI solutions, before and after the complexation with curcumin, was evaluated using the dynamic light scattering (DLS) technique. Each SPI solution was diluted to a protein concentration of about 0.1% (w/v) with 0.05 M phosphate buffer (pH 7.0) and filtered with a 0.22 μm filter. DLS analysis was performed at a fixed angle of 173° using a Zetasizer Nano-ZS instrument (Malvern Instruments) equipped with a 4 mW He−Ne laser (633 nm wavelength) at 25 °C. The D_z of the particles was calculated on the basis of the Stokes−Einstein equation, assuming protein particles to be spherical. Each determination was performed in duplicate, and the means were used for statistical analyses.

Atomic Force Microscopy (AFM). AFM images were acquired in tappng mode using a Dimension 3000 microscope (Digital Instruments-Veeco, Santa Barbara, CA) equipped with a "G" scanning head (maximum scan size 10 μm) and driven by a Nanoscope II Ia

DOI: 10.1021/acs.jafc.5b00448
J. Agric. Food Chem. 2015, 63, 3559−3569

controller. Various unheated and heated SPI solutions (5%, w/v), with and without complexation with curcumin, were diluted by 5000-fold with deionized water. A droplet (2 μL) of each diluted sample was immediately spread on a freshly cleaved mica disk in air for 30 min at ambient temperature. For imaging under ambient conditions, single-beam uncoated silicon cantilevers (type OMCL-AC, Olympus, and RTESP, Veeco) were used. The drive frequency was set at 300 kHz, and the scan rate was 1.2 Hz. Images were processed by Digital Nanoscope software (version 5.3 or 3, Digital Instruments). For each preparation condition, at least two samples were used for duplication. Approximately 10 images were obtained for each preparation.

Determination of the EE and LA of Curcumin. The EE (%) of curcumin in the SPI−curcumin complexes was estimated as the percentage of curcumin encapsulated in the proteins by the following equation:

$$\text{EE}\ (\%) = \left[1 - \frac{\text{amount of free curcumin (mg)}}{\text{total amount of added curcumin (mg)}}\right] \times 100 \quad (1,)$$

where the amount of free curcumin is determined from the precipitate obtained by centrifugation (see the section "Complexation of Curcumin with SPI"). The precipitate was extracted in 5 mL of ethanol with mild stirring for 5 min under magnetically stirred conditions and then centrifuged at 9000*g* for 15 min at 20 °C to remove the protein aggregates. The supernatant was subjected to spectrophotometric analysis at 426 nm with a UV754N UV−vis spectrophotometer, and the curcumin concentration was determined using an established standard curve of curcumin (with $R^2 > 0.999$).

The LA of curcumin was calculated by dividing the amount of encapsulated curcumin by the total protein amount in the system.

Stability Measurement. The storage stability of free curcumin in water and curcumin in the SPI−curcumin complexes in water (pH 7.0) was evaluated by monitoring the decrease in the kinetics of absorbance at 426 nm at 25 and 95 °C. The SPI−curcumin complex solutions (1%, w/v) were prepared by dispersing the freeze-dried samples in water under stirred conditions for more than 2 h. The free curcumin solution was prepared by dispersing 1.2 mL of the stock curcumin solution (4.5 mg/mL in ethanol) into 40 mL of water under the same conditions as for the SPI−curcumin complex solution. Then all the samples were centrifuged at 8000*g* for 20 min, and the supernatants were subjected to the storage stability experiment. The initial absorbance for all the cases was set as 100%. Each experiment was performed in duplicate, and the means were used for the statistical analyses.

Sequential in Vitro Gastric and Intestinal Digestion. An in vitro model that simulated sequential gastric and intestinal digestion was applied to evaluate the influence of digestion on the bioaccessibility of curcumin (free or encapsulated in the nanocomplexes with SPI) and/or in vitro protein digestibility of unheated and heated (at 95 °C) SPI according to the process described in our previous work[34] with a few modifications. In brief, 10 mL of SPI solutions, or solutions containing SPI−curcumin nanocomplexes at a protein concentration of 5.0% (w/v), was well mixed with 40 mL of 0.1 M HCl (pH 1.5) and preincubated in a shaker (at 37 °C) at a rate of 95 rpm for around 10 min. If necessary, the pH of the mixtures was adjusted to 1.5 with 1.0 M HCl. The curcumin content in the nanocomplexes was about 871.5−892 μg of curcumin/g of protein. Then 10 mg of pepsin powder was added and well mixed to start the simulated gastric digestion (0−60 min). After 60 min, the pH of the resultant pepsin digests was immediately adjusted to 7.0 with 4 M NaOH, and 250 mg of bile extract powder was added and well dispersed in the shaker for 10 min. Last, 20 mg of pancreatin powder was added to start the intestinal digestion (60−180 min). For free curcumin (control), the curcumin dispersion was prepared by mixing 500 μL of curcumin ethanol solution (4.5 g/L) with 25 mL of deionized water and then subjected to the same digestion process as above. At the end of the whole digestion, 1 mL of digest dispersions was collected and centrifuged at 10000*g* for 30 min at 10 °C. The amount of curcumin in the resultant supernatants and the whole digests was extracted and determined (see the next section).

Curcumin Extraction and Determination. Aliquots (200 μL) of the final digests (obtained after 180 min of digestion) or their supernatants (after centrifugation) were extracted two times with 2 mL of ethyl acetate for 5 min under vortexing conditions and then centrifuged at 5000*g* for 5 min. The absorbance of the pooled ethyl acetate extracts was determined at 420 nm with a UV−vis spectrophotometer, and the curcumin concentration in the extracts was calculated using an established standard curve of curcumin in ethyl acetate (with a coefficient factor of >0.999).

Characterization of the Digests of SPIs and Their Nanocomplexes with Curcumin. The hydrolysis of proteins in unheated and heated SPIs and or their nancomplexes with curcumin was characterized using sodium dodecyl sulfate−polyacrylamide gel electrophoresis (SDS−PAGE) and release of trichloroacetic acid (TCA)-soluble nitrogen. For SDS−PAGE experiments, aliquots (50 μL) of the digest samples at specific time periods of digestion (0−180 min) were taken and immediately mixed with 300 μL of sample buffer (2-fold), namely, 60 mM Tris−HCl buffer (pH 8.0) containing 2.0% (w/v) SDS, 25% (v/v) glycerol, 0.1% bromophenol blue, and 5% (v/v) β-mercaptoethanol. The electrophoresis was performed on a discontinuous buffered system using 12% separating gel and 4% stacking gel with some modification. The gel was stained with 0.1% Coomassie brilliant blue (R250) in a solution containing 45% methanol and 10% acetic acid for 40 min and further destained in a methanol/ehanol/water = 1/1/8 solution for 24 h.

To characterize the TCA-soluble nitrogen release, aliquots (1 mL) of the digests were taken after specific periods of digestion and immediately mixed with 2 mL of 20% TCA solution to precipitate the proteins with large molecular weights. The mixtures were placed for 10 min and then centrifuged at 5000*g* for 5 min. The nitrogen content of the resultant supernatants was determined by the micro-Kjeldahl method. The percentage of TCA-soluble nitrogen released during the digestion was estimated from the following equation:

$$\text{release of TCA-soluble nitrogen}\ (\%) = 100 - \frac{\text{amount of TCA-soluble nitrogen}}{\text{total amount of nitrogen}} \times 100 \quad (2)$$

The particle size distribution profiles of different digests were characterized using the DLS technique according to the same process as above. All the digests were diluted with the same background solvent to a concentration of about 0.05% (w/v) prior to the determination.

Statistical analysis. An analysis of variance (ANOVA) of the data was performed, and a least significant difference (LSD) with a confidence interval of 95% was used to compare the means.

RESULTS AND DISCUSSION

Formation and Characterization of SPI−Curcumin Nanocomplexes. Curcumin binds to hydrophobic clusters of proteins, mainly through hydrophobic interactions.[7,12,15,17,19,20,35] Heating can result in structural unfolding and denaturation of proteins, thus increasing their surface hydrophobicity (H_0). The improvement of the H_0 would be favorable for the binding of curcumin to the proteins. In the present work, the potential of both unheated and heated (at 75, 85, and 95 °C for 15 min) SPIs to form complexes with curcumin was investigated. As expected, increasing the temperature from 75 to 95 °C resulted in a progressive increase in protein denaturation of the β-conglycinin and/or glycinin components in the SPIs, as well as H_0; e.g., the H_0 considerably increased from 2248 to 5173 (Tables S1 and S2, Supporting Information). The observations about the influence of heating on the protein denaturation of SPI are in accordance with those of our previous findings.[33] In contrast, the ζ-

DOI: 10.1021/acs.jafc.5b00448
J. Agric. Food Chem. 2015, 63, 3559−3569

potential (−13.4 to −13.9 mV) of SPI at pH 7.0 was almost unchanged by the heating (Table S2). Figure 1 A shows the

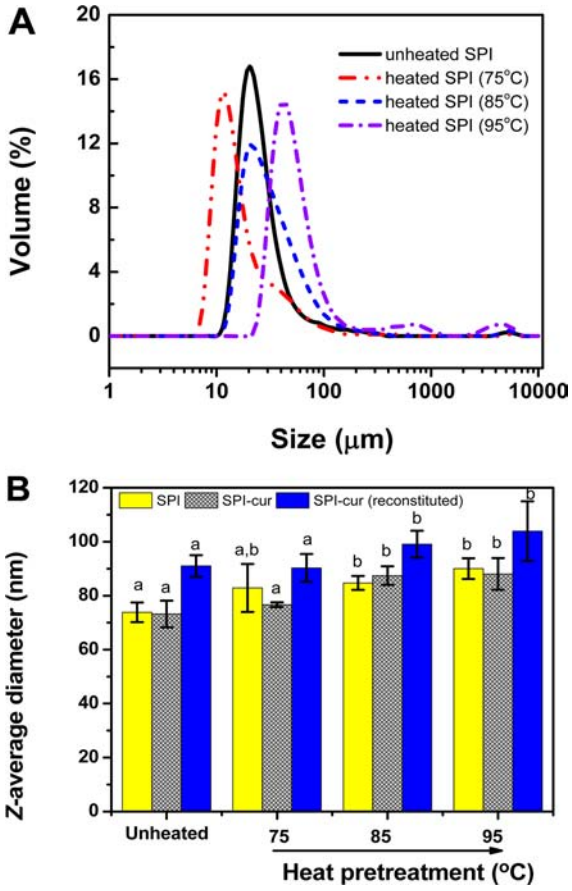

Figure 1. (A) Typical size distribution profiles of particles for unheated and heated SPI solutions. (B) *z*-average diameter of particles in unheated and heated (at 75, 85, and 95 °C for 15 min) SPI solutions or dispersions before and after nanocomplexation with curcumin. Different characters (a, b) on top of the columns represent a significant difference at $p < 0.05$ between the different treatments.

typical size distribution profiles of particles in unheated and heated SPI dispersions, and the *z*-average diameter (D_z) data are summarized in Figure 1B. Most of the particles in these unheated and heated SPI dispersions were present in the nanoparticle form, with D_z progressively but insignificantly increasing from 74 to 90 nm with the temperature of heating (Figure 1B). The progressive increase in D_z was closely associated with the heating-induced denaturation and subsequent aggregation. The D_z of the particles in unheated and heated SPIs is consistent with that of our previous findings.[24] This can be further confirmed by the AFM observations (Figure 2 A–D), where most of the particles in these SPIs were present in dissociated nanoparticles with heights of several nanometers.

After unheated or heated SPI (5%, w/v) was mixed with the curcumin stock solution (4.5 mg/mL, in 100% ethanol) at a volume ratio of 50:1, all the resultant dispersions were transparent and yellow in appearance (Figure 3 A), indicating formation of curcumin–SPI complexes at the nanoscale. Under the conditions, the EE of curcumin for all the preparations was within the range of 96.8–99.1%, and there was no significant difference in EE between the different preparations (Table S1, Supporting Information). The EE is comparable to that (>96%) of curcumin encapsulated in β-lactoglobulin nanoparticles produced by desolvation,[12] but considerably higher than that of curcumin encapsulated in casein nanocapsules by spray-drying (about 83.1%[19]) and in zein-based colloidal particles synthesized by an antisolvent precipitation (71–87%[14]). The differences in EE might be related to the differences in incorporated curcumin amount between these previous works and the present case. When all the SPI–curcumin nanocomplex preparations were freeze-dried and reconstituted, the transparency and yellow color of the resultant reconstituted dispersions were the same as those of the original counterparts (Figure 3), indicating good dispersion and curcumin stability of these formed nanocomplexes. As expected, the curcumin LAs of different dried samples were similar and within the range of 1.743–1.784 μg/mg of SPI (Table S1). The LA is much lower than that (19 μg/mg of casein) in the supernatant of curcumin encapsulated in casein nancapsules,[19] but close to 2 times greater than that (0.892 μg/mg of SPI) encapsulated in the same protein by spray-drying.[14] If the dried SPI–curcumin nanocomplex preparation in the present work is prepared at a protein concentration (*c*) of 1.0% (w/v), the solubility of curcumin in water will reach 17.43–17.84 mg/L, which is more than 1600-fold higher than that (approximately 11 μg/L) for free curcumin in water.[18]

To further unravel the potential of SPI to bind curcumin, we evaluated the complexation of unheated SPI with increasing amount of incorporated curcumin (in ethanol). When the fraction of curcumin-containing ethanol was above 0.3 (relative to the total volume of mixed dispersions), the dispersions exhibited a sol–gel state. Thus, the complexation of SPI with curcumin was performed at a final *c* value and ethanol volume fraction of 3.5% (w/v) and 0.3, respectively, with increasing [cur] from 0.0315 to 1.35 mg/mL of dispersion. From Figure 4, we can interestingly see that, as the [cur] increased, the EE progressively decreased from 98% to 78%, almost in an exponentially decaying way, while the LA of curcumin linearly increased from about 0.9 to 31 μg/mg of SPI. Similar changes in EE and LA with the increase in [cur] in the water–ethanol phase have been observed for the zein–curcumin composite colloidal particles.[14] At the highest [cur] (1.35 mg/mL) in the present work, the solubility of curcumin in water was enhanced by more than 98000-fold, as compared with the 11 μg/L free curcumin in water.[18] The solubility improvement was slightly lower than that (131000-fold) observed for a synthesized diblock copolymer micelle,[6] but considerably higher than those observed for hydrophobically modified starch and HP-γ-cyclodextrin (1670- and 4700-fold, respectively)[36,37] and camel β-casein (at least 2500-fold).[15] The [cur] of soluble curcumin in the supernatant of the 3.5% SPI dispersion at [cur] = 1.35 mg/mL was determined to be about 1.085 mg/mL, which was several-fold higher than the 136.7 μg/mL for the supernatant obtained by centrifuging the reconstituted spray-dried curcumin in casein nanocapsules (at 7.2 mg/mL casein[19]).

The influence of complexation with curcumin on DSC and surface characteristics, as well as the particle size of unheated and heated SPIs, was also investigated. The thermal denaturation of β-conglycinin and glycinin components in these SPIs was nearly unaffected by the complexation, but the complexation resulted in a considerable reduction in H_0, with the decreasing extent depending on the extent of heating (Tables S1 and S2, Supporting Information). The highest

DOI: 10.1021/acs.jafc.5b00448
J. Agric. Food Chem. 2015, 63, 3559–3569

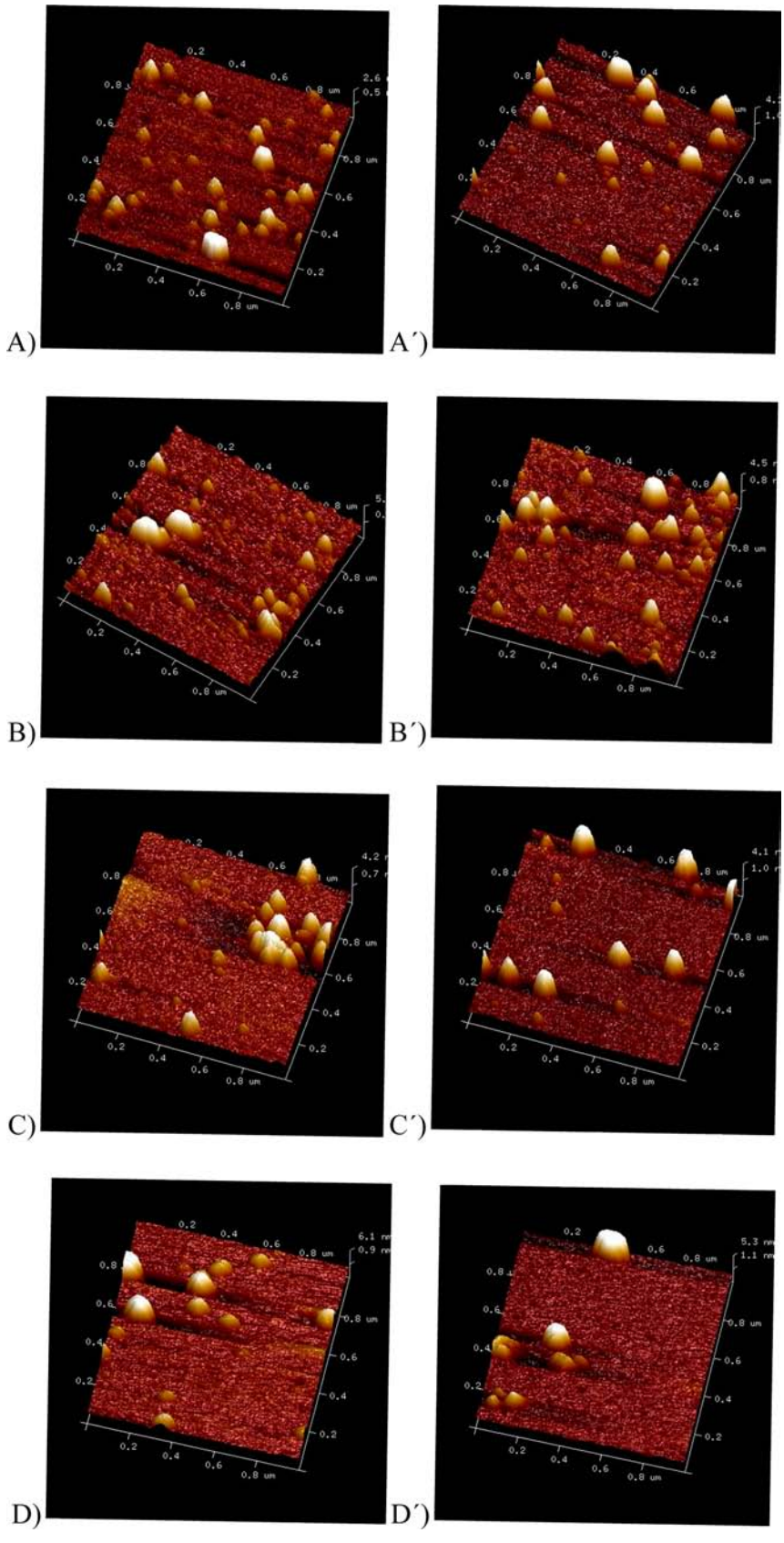

Figure 2. Typical AFM height images of particles in unheated and heated SPIs (A–D) and SPI–curcumin complexes (A′–D′). Panels A–D indicate the images of unheated SPI and SPIs heated at 75, 85, and 95 °C, respectively. Panels A′–D′ indicate the images of the SPI–curcumin complexes from unheated SPI or SPIs heated at 75, 85, and 95 °C, respectively.

DOI: 10.1021/acs.jafc.5b00448
J. Agric. Food Chem. 2015, 63, 3559–3569

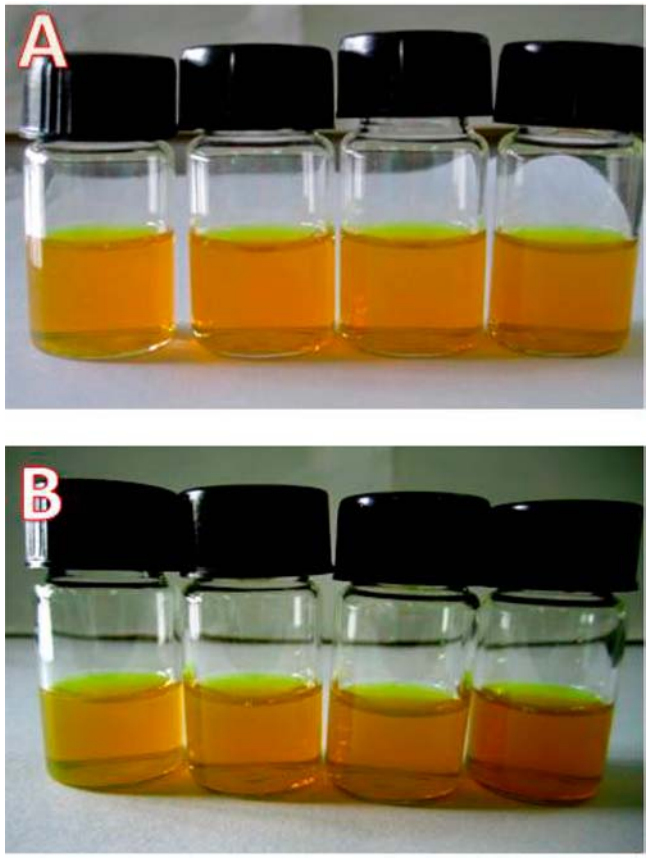

Figure 3. Visual observations of the original (A) and reconstituted (B) SPI–curcumin nanocomplexes in water. Unheated or heated SPI (5%, w/v) was mixed with the curcumin stock solution (4.5 mg/mL, in 100% ethanol) at a volume ratio of 50:1. The samples from left to right represent untreated SPI (control) and SPI preheated at 75, 85, and 95 °C, respectively.

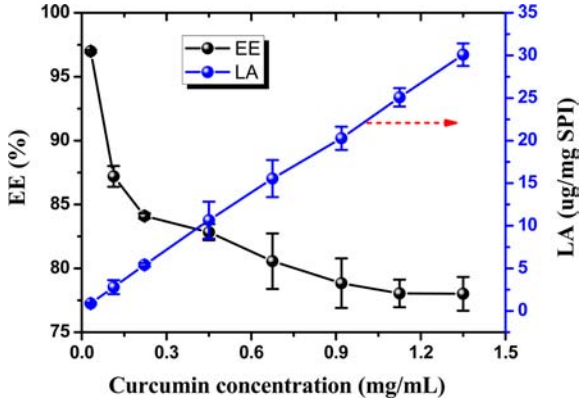

Figure 4. Influence of the curcumin concentration (in the mixed dispersions) on the encapsulation efficiency (EE) and load amount (LA) of curcumin in unheated SPI–curcumin nanocomplexes. The final c value and curcumin-containing ethanol volume fraction were kept constant at 3.5% (w/v) and 0.3, respectively. Each data point is the mean and standard deviation of triplicate measurements performed on separate samples.

reduction in H_0 was observed for the SPI heated at 85 °C among all the test preparations. Furthermore, the complexation also resulted in a slight but insignificant decline in the magnitude of ζ-potential in all the cases (Table S2). Curcumin molecules have two phenolic OH groups with pK_a values of 8.38 and 9.88 in aqueous solution, and are usually in the neutral form at around pH 7.0.[6] Thus, the decreased H_0 might be largely due to the masking of hydrophobic clusters of the proteins by binding with curcumin. Since the hydrophobic clusters are usually evenly distributed over the whole protein molecules, the complexation with curcumin will also mask some charged groups, thus causing the reduction in ζ-potential. The gradual decrease in the ζ-potential of the particles upon increasing the [cur] has also been observed for the complexation of zein colloidal particles with curcumin, though the complexation was performed at acidic pH values (3.5–4.1).[14] When these SPI–curcumin nanocomplexes were freeze-dried and reconstituted, the H_0 considerably increased (relative to that before the freeze-drying), but the magnitude of ζ-potential remarkably declined (Table S2), indicating that the additional freeze-drying markedly changed the surface properties of the SPI–curcumin nanocomplexes.

For any test SPI solution, the complexation with curcumin did not significantly change the size of particles in the aqueous solutions (Figure S1, Supporting Information), as could be further confirmed by the AFM observations of the particles (Figure 2). However, when the solutions containing SPI–curcumin complexes were freeze-dried and reconstituted, the particle size significantly increased relative to that before the freeze-drying (Figure S1), suggesting that the noticeable changes in surface characteristics of proteins after the freeze-drying led to protein aggregation or formation of larger particles. On the other hand, the complexation with curcumin did not affect the secondary structure of the proteins in unheated and heated SPIs, as evidenced by no discernible changes in the Fourier transform infrared (FTIR) spectra (Figure S2, Supporting Information). Previous works also indicated that no distinct conformational changes (at secondary and tertiary levels) occur for many proteins, e.g., β-lactoglobulin and BSA, upon complexation with curcumin or its derivatives.[12,17,20]

Storage Stability. Curcumin in aqueous solution is readily susceptible to hydrolysis or degradation, even at physiological pH.[8,9] Wang et al.[9] indicated that curcumin at neutral and basic pH values degraded by about 90%, within 30 min of storage at room temperature. This can be further confirmed in our experiment that free curcumin degraded by about 70% after storage of 30 min at 25 °C (Figure 5 A). If the storage was further elongated to 4 h, more than 80% of curcumin was degraded. In contrast, almost 90% of curcumin in the nanocomplexes with SPIs remained stable after storage for up to 4 h (Figure 5 A), indicating remarkable improvement of the degradation stability of curcumin. There was no noticeable difference in the degradation kinetics of curcumin between the nanocomplexes with unheated and heated (at 95 °C) SPIs (Figure 5 A). Tapal and Tiku[16] similarly reported that more than 80% of curcumin in the SPI–curcumin complexes was stable upon storage for up to 12 h in water or even in simulated gastric fluid and simulated intestinal fluid. A similar improvement of storage stability has also been observed for curcumin in complexes with serum albumins[8,9,38] and milk proteins including α_{s1}-casein and β-lactoglobulin.[11,12]

As expected, the degradation of curcumin, free or protein-bound, was greatly accelerated by increasing the temperature of storage to 95 °C (Figure 5 B). In this instance, the curcumin in all preparations (free or protein-bound) dramatically decreased within 30 min, and the rate of degradation gradually slowed upon further storage. However, at any specific time of storage,

DOI: 10.1021/acs.jafc.5b00448
J. Agric. Food Chem. 2015, 63, 3559–3569

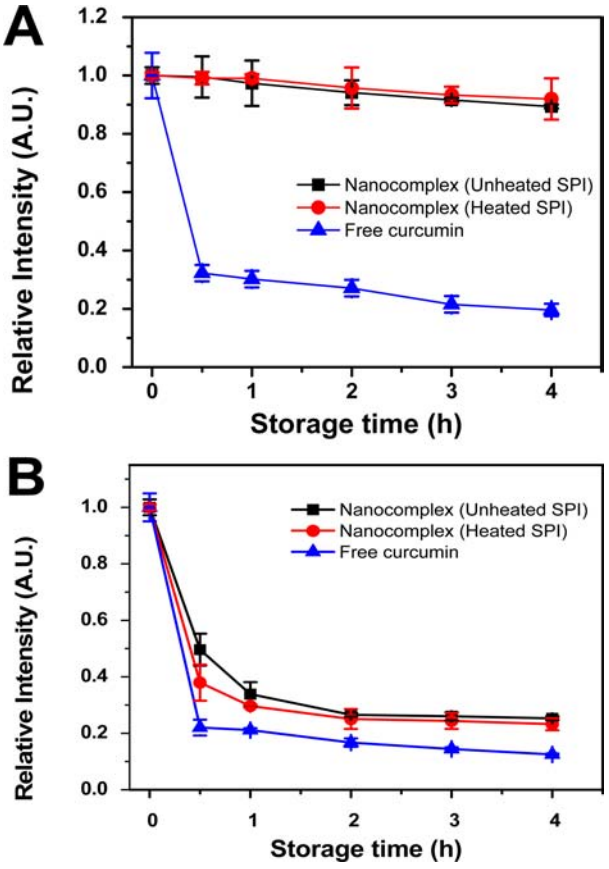

Figure 5. Degradation kinetics of free curcumin and curcumin in the nanocomplexes with unheated and heated (95 °C) SPIs in water at pH 7.0 upon storage for up to 4 h at 25 °C (A) and 95 °C (B). Data are presented as the means and standard deviations of triplicate measurements.

the amount of remaining curcumin was significantly higher for the SPI−curcumin nanocomplexes than for free curcumin (Figure 5 B). For example, approximately 25% of curcumin remained in the SPI−curcumin nanocomplexes after storage of 4 h at 95 °C, while it was about 12% for free curcumin. The observations indicated that the nanocomplexation of curcumin with SPI greatly improved the heat stability of curcumin.

Simulated Gastric and Intestinal Digestion. *Bioaccessibility and Stability of Curcumin.* During the digestion, the nanocomplexes of curcumin with SPI may undergo dramatic changes in environmental conditions (pH and ionic strength), action of proteases on the proteins, and even changes due to the presence of different active surfactants. After sequential processes of in vitro gastric (60 min) and intestinal (120 min) digestion, in the absence or presence of proteases, the bioaccessible amount of curcumin transferred to the aqueous phase of the digests for free curcumin and its nanocomplexes with SPI is shown in Figure 6 A. It should be noted that the bioaccessibility of curcumin might be dependent on its stability throughout the digestion process. If curcumin encapsulated in the nanocomplexes is susceptible to the digestion process, the stability of curcumin would be the prominent parameter affecting its bioaccessibility. Due to this consideration, we also evaluated the stability (against degradation) of curcumin upon digestion, as displayed in Figure 6 B.

Interestingly, it can be observed that the presence of proteases during digestion greatly improved the stability of curcumin, but the improvement was closely dependent on the present state of curcumin, free or bound (Figure 6 B). For free curcumin, about 88% of curcumin degraded after the digestion of 180 min without addition of proteases, whereas in the bound form case, it was only 30%. This observation is consistent with the observation of storage stability at ambient temperature (Figure 5 A), indicating strong stabilization of complexation with SPI toward degradation for curcumin. The presence of proteases considerably increased the amount of free curcumin that survived the whole digestion from 12% to 80%; for the curcumin in the nanocomplexes, there was no significant loss throughout the digestion in the presence of enzymes. The improvement of curcumin stability by the presence of enzymes during digestion might be largely attributed to the curcumin−

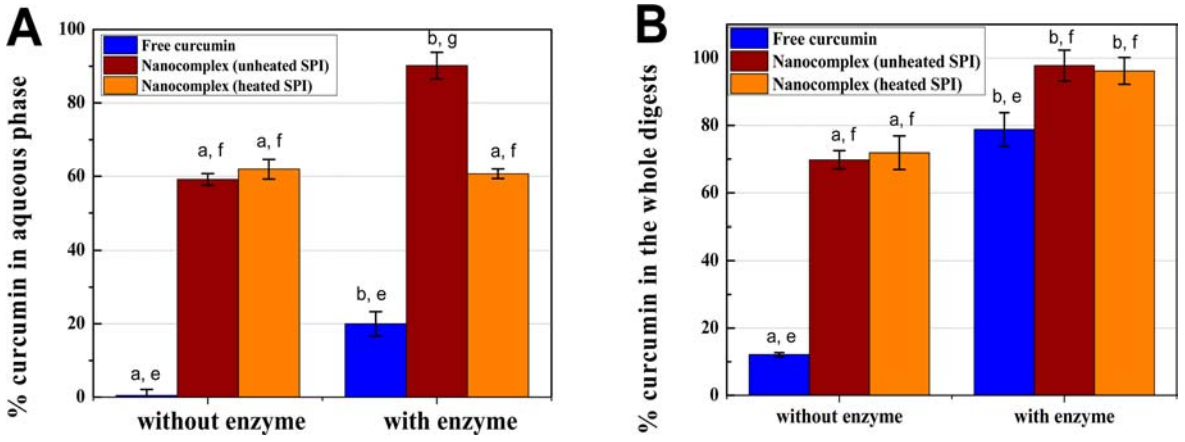

Figure 6. (A) Percentage of curcumin remaining in the aqueous phase for free curcumin and curcumin nanocomplexes with unheated and heated (at 95 °C) SPI after the whole simulated digestion of 180 min in the absence or presence of proteases. (B) Percentage of curcumin in the whole digests of free curcumin and curcumin nanocomplexes with unheated and heated SPI after the digestion of 180 min in the absence or presence of proteases. Data are presented as triplicate measurements on separate samples. Error bars represent standard deviations. Different letters (a, b) on top of the columns represent a significant difference at $p < 0.05$ among curcumin in free and complexed form due to the absence or presence of proteases. Different letters (e−g) on top of the columns represent a significant difference among the same set of samples without or with enzyme due to the different forms of curcumin (free or nanocomplexes with unheated or heated SPI).

DOI: 10.1021/acs.jafc.5b00448
J. Agric. Food Chem. 2015, 63, 3559−3569

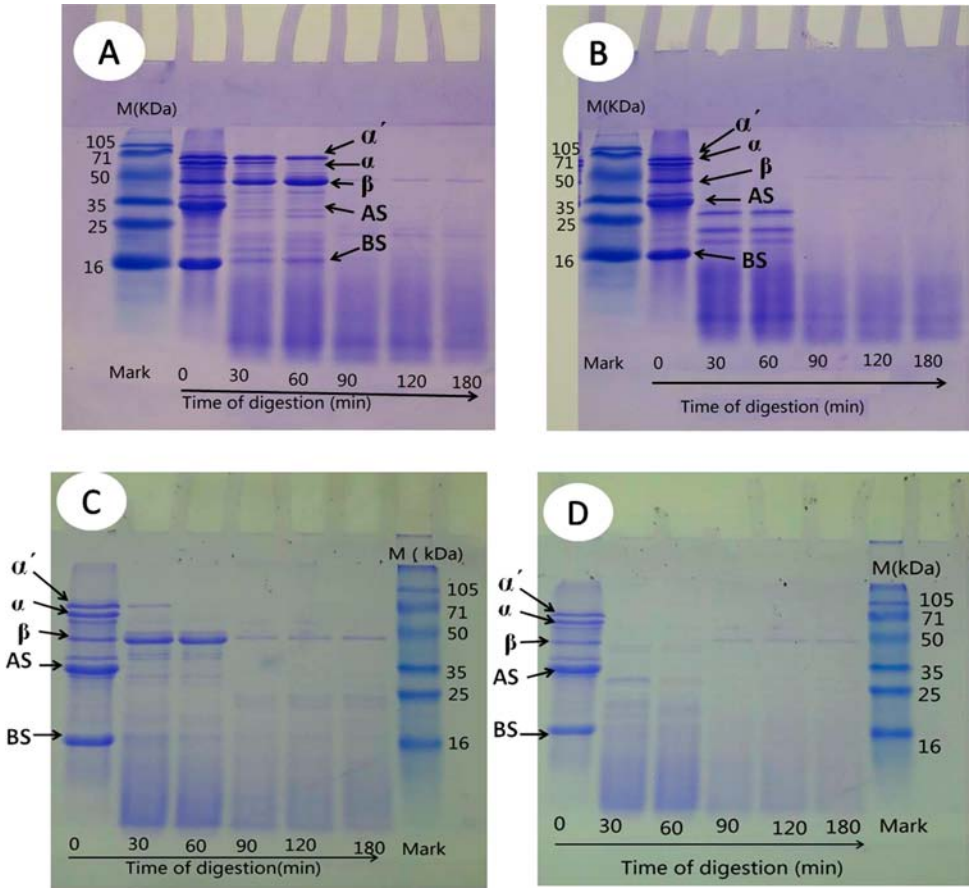

Figure 7. Changes in SDS−PAGE patterns of unheated (A, C) and heated (B, D) SP, during the digestion in SGF (0−60 min) and SIF (60−180 min) as a function of the digestion time. (A, B) Controls (without complexation with curcumin). (C, D) Nanocomplexes with curcumin. The symbols α', α, and β within the figure represent the major α'-, α-, and β-subunits of β-conglycinin, while AS and BS represent the acidic and basic subunits (or polypeptides) of glycinin, respectively.

protein interaction or complexation, since the enzymes are proteins themselves.

On the other hand, the bioaccessible amount of curcumin also highly depended on the present state of curcumin, as well as the presence or absence of enzymes (Figure 6 A). Without the enzymes during the digestion, only less than 1% of curcumin was transferred to the aqueous phase for free curcumin, indicating extremely low bioaccessibility. In contrast, the bioaccessibility of curcumin in the nanocomplexes with unheated and heated SPI reached approximately 60% (Figure 6 A). If the degradation of curcumin during the digestion is considered, the ideal bioaccessibility of curcumin in the nanocomplexes with SPI, in this case, may reach about 85%. In the presence of enzymes during the digestion, the bioaccessibility of free curcumin reached about 20% (Figure 6 A). Relative to the amount of undegraded curcumin, the ideal bioaccessibility for free curcumin would be around 25%. The presence of enzymes also significantly improved the bioaccessibility of curcumin in the nanocomplex with unheated SPI (from 60% to 90%), but did not significantly affect that with heated SPI (Figure 6 A). The difference in the improvement between the unheated and heated SPI might be due to the differences in their protein hydrolysis and protein aggregation.

Protein in Vitro Digestibility. The bioaccessibility of curcumin in the nanocomplexes with proteins may be associated with protease hydrolysis of the proteins during digestion. Furthermore, the complexation with curcumin also produces an influence on the digestibility of the proteins. During the simulated gastric fluid (SGF) and simulated intestinal fluid (SIF) digestion, the protease-induced hydrolysis of proteins in unheated or heated SPI, with or without complexation with curcumin, was characterized using SDS−PAGE and TCA-soluble nitrogen analyses, as displayed in Figures 7 and 8. As expected, the digestion resulted in a progressive hydrolysis of protein polypeptides in SPI, with dramatic changes observed in the SGF digestion, as evidenced by SDS−PAGE and the TCA method (Figures 7 and 8). By comparison between the unheated and heated SPI (without complexation with curcumin), it can be generally observed that (1) all the protein components in SPI were more susceptible to the gastric protease (pepsin) hydrolysis relative to the SIF hydrolysis and (2) the polypeptides of glycinin were much more easily digested by the protease hydrolysis than those from β-conglycinin (Figures 7 A,B and 8). The protease hydrolysis and TCA-soluble nitrogen release of unheated SPI during digestion are similar to those observed in our previous work.[34] Furthermore, the heat pretreatment could increase the susceptibility of β-conglycinin polypeptides to the pepsin hydrolysis, but it to a certain extent impaired the TCA-soluble nitrogen release during the SIF digestion (Figures 7 A,B and 8). The observations confirm the previous viewpoint that the protease susceptibility and/or in vitro digestibility of β-conglycinin or other vicilins is affected by the heat-induced protein denaturation (positive), as well as subsequent protein

DOI: 10.1021/acs.jafc.5b00448
J. Agric. Food Chem. 2015, 63, 3559−3569

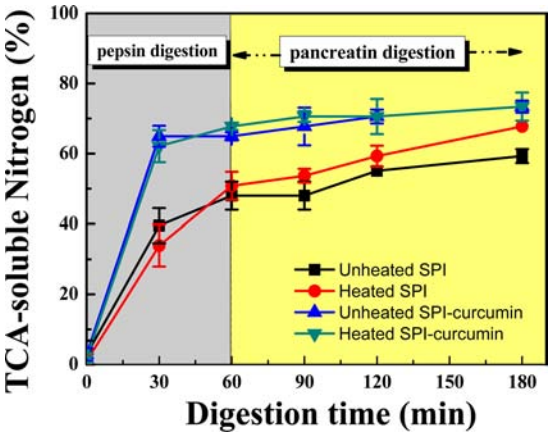

Figure 8. Release kinetics of TCA-soluble nitrogen during the sequential SGF and SIF digestion of unheated and heated SPI and its nanocomplexes with curcumin. Each data point is the mean and standard deviation of triplicate measurements on separate samples.

aggregation (negative).[25,26,29] The improvement of the susceptibility to pepsin hydrolysis by the heating could thus be largely attributed to the thermal denaturation of the protein, as similarly observed for phaseolin (a 7S globulin from kidney bean[25,29]). However, the influence of heating on the digestibility of these proteins is also dependent on the nature of their conformations and whether other components are present (e.g., in the protein isolate or flour form). For example, Deshphande and Damodaran[25] also pointed out that the vicilin from green peas with a flexible conformation underwent an undesirable change in conformation upon heating, and as a consequence, the heated vicilin exhibited more resistance to proteolysis than the native one. In fact, the undesirable change in conformation in this case can also be explained as the occurrence of a high extent of heat-induced protein aggregation. The importance of structural characteristics to the digestibility of legume proteins has also been confirmed using in vivo experiments with growing rats.[26]

On the other hand, in both unheated and heated SPI cases, the proteins in the nanocomplexes with curcumin were much more susceptible to the protease hydrolysis, especially during the gastric digestion (Figure 7). For example, the α'-subunit of β-conglycinin in the unheated SPI remained almost intact after 60 min of the SGF digestion, while that in its nanocomplex counterpart had been completely degraded even after 30 min of digestion. The improvement of protein hydrolysis by the nanocomplexation can be further confirmed by the TCA-soluble nitrogen release observations (Figure 8), wherein it can be observed that the release of TCA-soluble nitrogen during the SGF digestion was significantly higher in the nanocomplex case than in the controls. There was no significant difference in the TCA-soluble nitrogen release between the nanocomplexes with unheated and heated SPI (Figure 8). Since curcumin is a phenolic compound, the observations thus indicated that the nanocomplexation with curcumin greatly improved the protein digestibility of SPI, irrespective of heat pretreatment. A similar

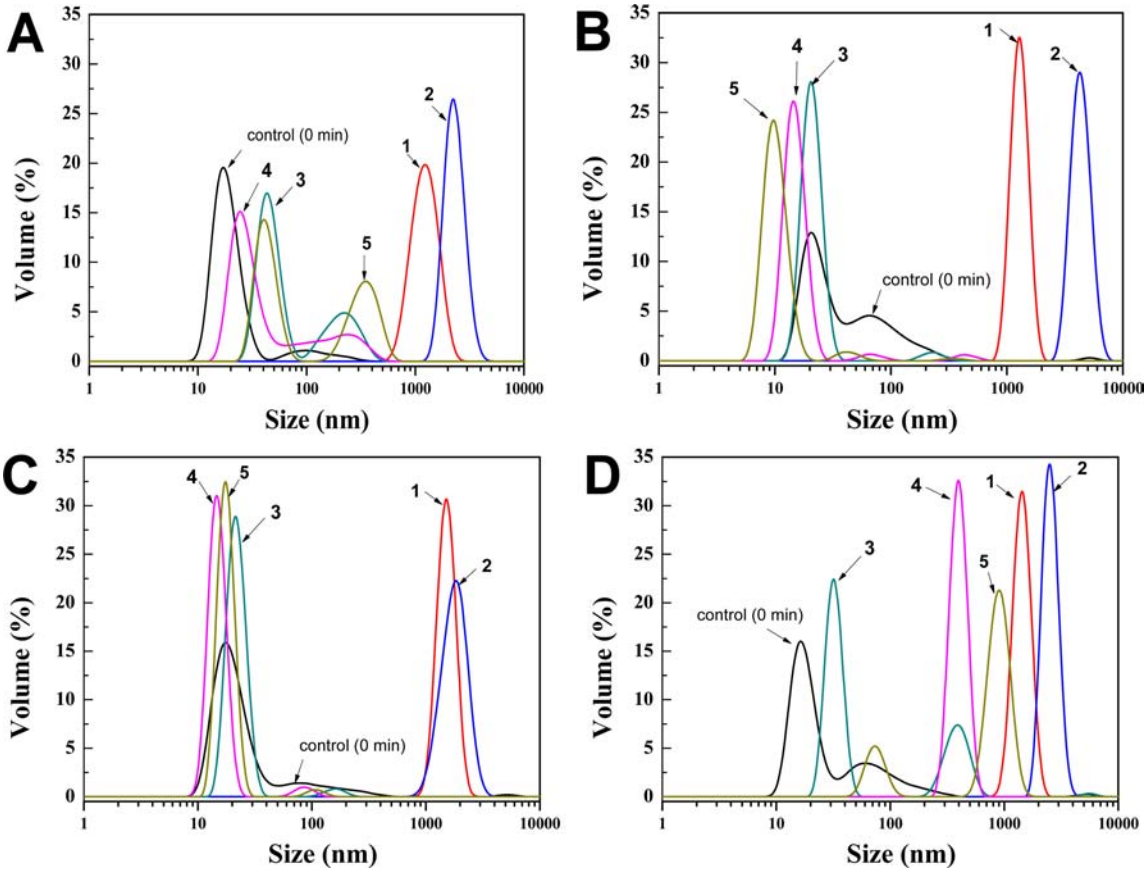

Figure 9. Typical particle size distribution profiles of unheated (A, C) and heated (B, D) SPI without (A, B) and with (C, D) complexation with curcumin as a function of the digestion time (0−180 min). The numbers 1−5 within the figures correspond to the digestion times of 30, 60, 90, 120, and 180 min, respectively. The digestion consisted of sequential SGF (0−60 min) and SIF (60−180 min) processes.

DOI: 10.1021/acs.jafc.5b00448
J. Agric. Food Chem. 2015, 63, 3559−3569

improvement of pepsin digestibility has been reported for some major food allergens when they interact with green tea catechins.[28] Tagliazucchi et al.[27] even observed that the complexation with some phenolic compounds distinctly improved the pepsin activity during simulated gastric digestion. However, some contrasting observations that the complexation with phenolic compounds may also produce an adverse or insignificant influence on the digestibility of many proteins, e.g., β-lactoglobulin[30] and legume proteins,[29,31] are available. Thus, the influence of complexation with phenolic compounds on the digestibility of proteins is a complex process related to the nature of both the phenolic compounds and proteins.

Hydrolysis-Induced Aggregation. The protease hydrolysis of proteins during digestion may lead to exposure of their hydrophobic clusters to the aqueous phase or release of hydrophobic peptides, thus resulting in protein aggregation.[39] Figure 9 shows changes in the particle size distribution profiles of unheated and heated SPI and its nancomplexes with curcumin upon increasing digestion time (0−180 min) in sequential in vitro SGF and SIF digestion. As expected, unheated SPI consisted of approximately two protein fractions with sizes centered at 17 (major) and 100 (minor) nm (Figure 9 A). The heat pretreatment led to a remarkable reduction of the 17 nm protein fraction and, concomitantly, a distinct increase of the fraction with a large size (∼100 nm) (Figure 9 A,B), indicating the occurrence of heat-induced aggregation of proteins. When both unheated and heated SPIs were subjected to the SGF digestion, it was observed that a new particle distribution peak occurred at a much larger size (>1000 nm) at the expense of all the initially present protein fractions (centered at 17 and 100 nm) (Figure 9 A,B). The observations clearly indicated that the pepsin hydrolysis resulted in aggregation of all the proteins. By comparison, we can approximately see that the extent of pepsin-induced aggregation was higher in the heated SPI case than in the unheated counterpart, and it also increased with increasing digestion time (0−60 min).

When the pepsin-treated digests of both unheated and heated SPI were further subjected to the SIF digestion for more than 30 min (and accordingly, the pH also changed from 1.2 to 6.8), the size of the formed aggregates (at 60 min) considerably decreased to much lower values (Figure 9 A,B), indicating disruption of the initially formed aggregates. However, the changing pattern of particle sizes was dependent on the type of proteins (unheated or heated) and the time of SIF digestion. In the unheated SPI case, minimal particle sizes (larger than that of the control) were observed at 120 min of digestion, while, in the heated case, the digestion with increasing time up to 180 min resulted in a progressive decrease in particle size (Figure 9 A,B). The observations suggest that although the heat pretreatment greatly increased the pepsin-induced aggregation of proteins, it facilitated the SIF digestion.

The particle size distribution of unheated and heated SPI was nearly unchanged by the nanocomplexation with curcumin, but the changing pattern of the particle size distributions upon protease hydrolysis, especially during the SIF digestion, was remarkably affected (Figure 9). In the unheated SPI case, the nanocomplexation with curcumin greatly favored the formation of smaller sizes of particles during the SIF digestion, as compared with the control (Figure 9 A,C). In this case, the particle sizes of the final digests seemed to be slightly dependent on the digestion time. In contrast, the situation is different in the heated SPI case, and in the latter case, it can be observed that increasing the digestion time during the SIF digestion resulted in a progressive increase in particle size (Figure 9 C,D). The observations indicated that, upon the sequential SGF and SIF digestion, the nanocomplexation of unheated SPI with curcumin greatly lessened the extent of protein aggregation occurring during the digestion, while the situation for the heated SPI was the reverse. Thus, the remarkably lower bioaccessibility of curcumin in the nanocomplex with heated SPI (relative to that with unheated SPI, Figure 6 A) could be largely attributed to the occurrence of protease-induced protein aggregation, especially in the SIF digestion.

In summary, we reported that SPI can easily form nanocomplexes with curcumin, thus remarkably improving its solubility (in the aqueous phase), stability, and even bioaccessibility. The complexation with curcumin did not distinctly change the size and morphology of the nanoparticles in SPI solutions, though the surface hydrophobicity of the proteins considerably decreased upon binding. Under the investigated conditions, the amount of loaded curcumin at a given c (e.g., 3.5%, w/v) was mainly dependent on the initial [cur] in the dispersion. Although the heated SPI exhibited a higher capacity to bind curcumin than unheated SPI, the bioaccessibility was significantly lower. The lower bioaccessibility of curcumin in the nanocomplexes with heated SPI relative to that with unheated SPI was largely attributed to the protein aggregation occurring during the SIF digestion. The present work reveals that SPI is an excellent nanovechicle for the delivery of water-insoluble bioactive ingredients, and the nanocomplexation exhibits a great potential to be applied in functional food formulations. However, the denatured or aggregated state of the proteins in SPI might produce a significant influence on the bioavailability of encapsulated bioactive ingredients. Further work is necessary to verify the effectiveness of curcumin in the nanocomplexes of SPI using in vivo digestion models.

■ ASSOCIATED CONTENT

Ⓢ Supporting Information

Tables listing the DSC characteristics of protein denaturation, EE, and content of curcumin in freeze-dried unheated and heated SPI and SPI−curcumin complex powders and surface hydrophobicity and ζ-potential of unheated and preheated SPI before and after complexation with curcumin and figures showing typical size distribution profiles of unheated and heated SPI and SPI−curcumin nanocomplexes and FTIR spectra for unheated SPI, unheated SPI−curcumin complexes, and free curcumin. This material is available free of charge via the Internet at http://pubs.acs.org.

■ AUTHOR INFORMATION

Corresponding Author

*Fax: (086)20-87114263. E-mail: chtang@scut.edu.cn.

Funding

This work was supported by the National Natural Science Foundation (NNSF) of China (Grants 31471695, 31171632, and 31130042).

Notes

The authors declare no competing financial interest.

DOI: 10.1021/acs.jafc.5b00448
J. Agric. Food Chem. 2015, 63, 3559−3569

REFERENCES

(1) Kaya-Celiker, H.; Mallikarjunan, K. Better nutrients and therapeutics delivery in food through nanotechnology. *Food Eng. Rev.* **2012**, *4*, 114−123.

(2) Yallapu, M. M.; Jaggi, M.; Charuhan, S. C. Curcumin nanoformulations: a future nanomedicine for cancer. *Drug Discovery Today* **2012**, *17*, 71−80.

(3) Sagalowicz, L.; Leser, M. E. Delivery systems for liquid food products. *Curr. Opin. Colloid Interface Sci.* **2010**, *15*, 61−72.

(4) Tang, C. H. Functional foods from spice turmeric. In *Plant Functional Foods*; Tang, C. H., Ed.; Chemical Industry Press: Beijing, China, 2004; pp 379−402.

(5) Anand, P.; Kunnumakkara, A. B.; Newman, R. A.; Aggarwal, B. B. Bioavailability of curcumin: problems and promises. *Mol. Pharmaceutics* **2007**, *4*, 807−818.

(6) Letchford, K.; Liggins, R.; Burt, H. Solubilization of hydrophobic drugs by methoxy poly (ethylene glycol)-block-polycaprolactone diblock copolymer micelles: theoretical and experimental data and correlations. *J. Pharm. Sci.* **2007**, *97*, 1179−1190.

(7) Sahu, A.; Kasoju, N.; Bora, U. Fluorescence study of the curcumin−casein micelle complexation and its application as a drug nanocarrier to cancer cells. *Biomacromolecules* **2008**, *9*, 2905−2912.

(8) Wang, Y. J.; Pan, M. H.; Cheng, A. L.; Lin, L. I.; Ho, Y. S.; Hsiech, C. Y.; Li, J. K. Stability of curcumin in buffer solutions and characterization of its degradation products. *J. Pharm. Biomed. Anal.* **1997**, *15*, 1867−1876.

(9) Leung, M. H. M.; Kee, T. W. Effective stabilization of curcumin by association to plasma proteins: human serum albumin and fibrinogen. *Langmuir* **2009**, *25*, 5773−5777.

(10) Yang, M.; Wu, Y.; Li, J.; Zhou, H.; Wang, X. Binding of curcumin with bovine serum albumin in the presence of *ι*-carrageenan and implications on the stability and antioxidant activity of curcumin. *J. Agric. Food Chem.* **2013**, *61*, 7150−7155.

(11) Sneharani, A. H.; Singh, S. A.; Rao, A. G. A. Interaction of α_{s1}-casein with curcumin and its biological implications. *J. Agric. Food Chem.* **2009**, *57*, 10386−10391.

(12) Sneharani, A. H.; Karakkat, J. V.; Singh, S. A.; Rao, A. G. A. Interaction of curcumin with *β*-lactoglobulin—stability, spectroscopic analysis, and molecular modeling of the complex. *J. Agric. Food Chem.* **2010**, *58*, 11130−11139.

(13) Tapal, A.; Tiku, P. K. Complexation of curcumin with soy protein isolate and its implications on solubility and stability of curcumin. *Food Chem.* **2012**, *130*, 960−965.

(14) Patel, A.; Hu, Y.; Tiwari, J. K.; Velikov, K. P. Synthesis and charcterisation of zein-curcumin colloidal particles. *Soft Matter* **2010**, *6*, 6192−6199.

(15) Esmaili, M.; Ghaffari, M.; Moosavi-Movahedi, Z.; Atri, M. S.; Sharifizadeh, A.; Farhadi, M.; Yousefi, R.; Chobert, J.-M.; Haertlé, T.; Moosavi-Movahedi, A. A. Beta casein-micelle as a nano vehicle for solubility enhancement of curcumin; food industry application. *LWT* **2011**, *44*, 2166−2172.

(16) Yazdi, S. R.; Corredig, M. Heating of milk alters the binding of curcumin to casein micelles. A fluorescence spectroscopy study. *Food Chem.* **2012**, *132*, 1143−1149.

(17) Bourassa, P.; Kanakis, C. D.; Pollissiou, M. G.; Tajmir-Riahi, H. A. Resveratrol, genistein, and curcumin bind bovine serum albumin. *J. Phys. Chem. B* **2010**, *114*, 3348−3354.

(18) Kiminaga, Y.; Nagatsu, A.; Akiyama, T.; Sugimoto, N.; Yamazaki, T.; Maitani, T.; Mizukami, H. Production of unnatural glucosides of curcumin with drastically enhanced water solubility by cell suspension cultures of *Catharanthus roseus*. *FEBS Lett.* **2003**, *555*, 311−316.

(19) Pan, K.; Zhong, Q.; Baek, S. J. Enhanced dispersibility and bioactivity of curcumin by encapsulation in casein nanocapsules. *J. Agric. Food Chem.* **2013**, *61*, 6036−6043.

(20) Sahoo, B. K.; Ghosh, K. S.; Dasgupta, S. Investigating the binding of curcumin derivatives to bovine serum albumin. *Biophys. Chem.* **2008**, *132*, 81−88.

(21) Zhang, L.; Qi, Z.; Huang, Q.; Zeng, K.; Sun, X.; Li, J.; Liu, Y.-N. Imprinted-like biopolymeric micelles as efficient nanovehicles for curcumin delivery. *Colloids Surf., B* **2004**, *123*, 15−22.

(22) Keerati-U-Rai, M.; Corredig, M. Effect of dynamic high pressure homogenization on the aggregation state of soy protein. *J. Agric. Food Chem.* **2009**, *57*, 3556−3562.

(23) Tang, C. H.; Ma, C. Y. Effect of high pressure treatment on aggregation and structural properties of soy protein isolate. *LWT* **2009**, *42*, 606−611.

(24) Liu, F.; Tang, C. H. Soy protein nanoparticle aggregates as Pickering stabilizers for oil-in-water emulsions. *J. Agric. Food Chem.* **2013**, *61*, 8888−8898.

(25) Deshpande, S. S.; Damodaran, S. Structure-digestibility relationship of legume 7S proteins. *J. Food Sci.* **1989**, *54*, 108−113.

(26) Carbonaro, M.; Cappelloni, M.; Nicoli, S.; Lucarini, M.; Carnovale, E. Solubility−digestibility relationship of legume proteins. *J. Agric. Food Chem.* **1997**, *45*, 3387−3394.

(27) Tagliazucchi, D.; Verzelloni, E.; Conte, A. Effect of some phenolic compounds and beverages on pepsin activity during simulated gastric digestion. *J. Agric. Food Chem.* **2005**, *53*, 8706−8713.

(28) Tantoush, Z.; Apostolovic, D.; Kravic, B.; Prodic, I.; Mihajlovic, L.; Stanic-Vucinic, D.; Cirkovic Velickovic, T. Green tea catechins of food supplements facilitate pepsin digestion of major food allergens, but hampers their digestion if oxidized by phenol oxidase. *J. Funct. Foods* **2012**, *4*, 650−660.

(29) Venkatachalam, M.; Sathe, S. Phaseolin *in vitro* pepsin digestibility: role of acids and phenolic compounds. *J. Agric. Food Chem.* **2003**, *51*, 3466−3472.

(30) Stojadinovic, M.; Radosavljevic, J.; Ognjenovic, J.; Vesic, J.; Prodic, I.; Stanic-Vucinic, D.; Cirkovic Velickovic, T. Binding affinity between dietary polyphenols and beta-lactoglobulin negatively correlates with the protein susceptibility to digestion and total antioxidant activity of complexes formed. *Food Chem.* **2013**, *136*, 1263−1271.

(31) Carbonaro, M.; Grant, G.; Cappelloni, M.; Pusztai, A. Perspectives into factors limiting in vivo digestion of legume proteins: antinutritional compounds or storage proteins? *J. Agric. Food Chem.* **2000**, *48*, 742−749.

(32) Haskard, C. A.; Li-Chan, E. C. Y. Hydophobicity of bovine serum albumin and ovalbumin determined using uncharged (PRODAN) and anionic (ANS^-) fluorescent probes. *J. Agric. Food Chem.* **1998**, *46*, 2671−2677.

(33) Tang, C. H.; Choi, S. M.; Ma, C. Y. Study of thermal properties and aggregation/denaturation. *Int. J. Biol. Macromol.* **2007**, *40*, 96−104.

(34) Tang, C. H.; Li, L.; Yang, X. Q. Influence of transglutaminase-induced cross-linking on *in vitro* digestibility of soy protein isolate. *J. Food Biochem.* **2006**, *30*, 718−731.

(35) Li, M.; Ma, Y.; Ngadi, M. O. Binding of curcumin to *β*-lactoglobulin and its effect on antioxidant characteristics of curcumin. *Food Chem.* **2013**, *141*, 1504−1511.

(36) Yu, H. L.; Huang, Q. R. Enhanced in vitro anti-cancer activity of curcumin encapsulated in hydrophbically modified starch. *Food Chem.* **2010**, *119*, 669−674.

(37) Baglole, K.; Boland, P.; Wagner, B. Fluorescence enhancement of curcumin upon inclusion into parent and modified cyclodextrins. *J. Photochem. Photobiol., A* **2005**, *173*, 230−237.

(38) Barik, A.; Priyadarsni, K. I.; Mohan, H. Photophysical studies on binding of curcumin to bovine serum albumin. *Photochem. Photobiol.* **2003**, *77*, 597−603.

(39) Inouye, K.; Nagai, K.; Takita, T. Coagulation of soy protein isolates induced by subtilisin Carlsberg. *J. Agric. Food Chem.* **2002**, *50*, 1237−1242.

DOI: 10.1021/acs.jafc.5b00448
J. Agric. Food Chem. 2015, 63, 3559−3569

assessment of uptake of silver particles. To avoid sample preparation artifacts, the silver coating is only treated with a drop of water and the particles in the eluted fraction are analyzed.

MATERIALS AND METHODS

Sample Preparation. Silver "pearls" meant for decoration of pastry were obtained from a local supermarket. The pearls were stored in a plastic vial. The ingredient list on the label clearly indicated that the product contains silver. Visual inspection suggested that the pearls have an interior that mainly consists of sugar and that they are covered with a smooth silver coating. TEM analysis was performed on the coating only and not on the entire pearl, while ICP-MS and SP-ICP-MS analyses were performed on the entire pearl.

As a positive control, the representative test material NM-300K (new number JRCNM03002a),[9] obtained from the nanomaterial repository of the European Commissions' Joint Research Centre, Institute for Health and Consumer Protection (JRC, Ispra, Italy), was analyzed by TEM, ICP-MS, and SP-ICP-MS using similar experimental conditions. NM-300K is distributed as a dispersion of silver nanoparticles in a glass vial, sealed under argon atmosphere with a nominal silver content of 10% w/w. Specific material characteristics are summarized in the JRC Scientific Report on NM-300K.[10]

For TEM analysis, silver pearls were treated with double-distilled water to separate the silver coating from the inner part. Each pearl was brought in contact with a 25 μL droplet of distilled water, placed on parafilm. The pearl was held with a pair of tweezers, which allowed moving the pearl in the water droplet. This resulted in a quick detachment of the silver coating that appeared to float onto the water droplet. Part of this coating was collected on an EM grid. A pointed piece of filter paper was used to dry the grid from beneath, which avoided removal of the silver particles of the grid. NM-300K samples were prepared by the grid-on-drop method.[11] For SP-ICP-MS analysis, each sugar pearl (±180 mg) was dissolved in 2 mL of Milli-Q water and 0.5 mL of the suspension was diluted in 50 mL of Milli-Q water. The latter suspension was 50 and 100 times further diluted for analysis (total dilution factors of 5000 and 10000, respectively). The NM-300K dispersion was diluted 2×10^{10} times for analysis. To determine the total silver concentration of the pearls by ICP-MS, one pearl (±180 mg) per sample was mineralized by microwave digestion (MarsXpress, CEM Corporation, NC, USA) in the presence of 8 mL of a mixture of HNO_3 (spA grade, ROMIL Ltd., Cambridge, UK) and bidistilled water (1:1, v/v). Digested samples were appropriately diluted with bidistilled water before ICP-MS analysis.

Each sample was prepared and analyzed on the same day because of the reported reactivity of silver nanoparticles which can compromise their stability.[12] All TEM experiments were done in duplicate to ensure repeatability of the results. The ICP-MS measurements to determine the total silver concentration were performed three times.

Because the X-rays generated in a TEM specimen can travel over a long distance and can cause fluorescence of other X-rays from for instance the EM-grid, two types of grids were used for the EDX analyses. Part of the silver pearls and NM-300K samples were collected on homemade 400 mesh pioloform- and carbon-coated copper EM-grids, which were pretreated (charged) with Alcian blue for 10 min to increase attachment of particles on the grid. To exclude that the copper signal in the EDX spectra originated from the particles, additional samples of the silver pearls and NM-300K were prepared on 400 Mesh holey polymer-coated nickel grids. Because Alcian blue contains copper as well, the nickel grids were not pretreated.

TEM Imaging and Analysis Conditions. Bright-field TEM images and diffraction patterns were recorded using a Tecnai Spirit microscope (FEI, Eindhoven, The Netherlands) operating at 120 kV. Digital micrographs were recorded using a bottom-mounted 4 × 4 K Eagle CCD-camera (FEI) at a magnification of 49000×, resulting in a pixel size of 0.2 nm, and were converted to .tif format using the TIA software (FEI, Eindhoven, The Netherlands). A systematic micrograph selection procedure was used and allowed unbiased random image collection as described by De Temmerman et al.[13]

Diffraction patterns of both the silver pearls and NM-300K were recorded and compared. The camera length was obtained by recording a diffraction pattern of 30 nm gold nanoparticles under the same experimental conditions.

Chemical analysis was performed using a Titan 80−300 "cubed" microscope (FEI, Eindhoven, The Netherlands) with a probe corrector operating at 200 kV. This microscope allowed obtaining analytical information with a high enough resolution to determine the elemental composition of each individual nanoparticle. The specimens were not plasma cleaned before analysis. The specimens were imaged in TEM and HAADF-STEM mode at magnifications ranging from 16000× to 320000×. In STEM mode, the probe current ranged between 100 and 500 pA. EDX elemental maps were acquired in STEM mode using a Super-X detector (FEI) which consisted of four windowless silicon drift detectors integrated into the objective lens. Each EDX map was acquired during 10−15 min. By selecting a specific region on an EDX map, an EDX spectrum was obtained in which the signal originated solely from this region.

Image Processing Conditions for Qualitative and Quantitative TEM Analysis. On the basis of visual inspection of the bright-field TEM images, the homogeneity and stability of the material under the applied conditions were examined. Furthermore, a qualitative description and a quantitative analysis of the material were performed on all samples. The quantitative analysis was performed on the basis of numerical parameters, which describe characteristic particle features (such as size, shape, surface properties, etc.).

Threshold-based detection of the nanomaterials was applied using iTEM software (Olympus, Münster, Germany) as described by De Temmerman et al.[13] and Verleysen et al.[14] This approach included optimizing the contrast and brightness of the image, applying a 10 × 10 smoothing filter, enclosing the particles in a region of interest (ROI), and setting the threshold to separate particles from the background based on their gray values. Particles consisting of less than 250 pixels, particles on the border of the ROI, and structures with an aberrant morphology, judged to be artifacts based on visual inspection, were omitted from analysis. There were 23 characteristic parameters measured for each particle.[13,14] The data collected for each characteristic parameter was represented as a number-based distribution using Sigmaplot software (Systat, Cosinus Computing, Drunen, The Netherlands).

Iterative curve fitting was applied on the distributions by maximum likelihood estimation using Fityk 0.9.8 software.[15,16] The parameters of the fitted function (height, center, width, etc.) can be used to describe the distribution, and the errors on these parameters were determined as described by Wojdyr[15] and Wolberg.[16]

TEM and HAADF-STEM micrographs, EDX spectra and elemental maps, and qualitative and quantitative analysis results were stored in a dedicated iTEM database, together with the specimen references and with the imaging conditions.

Validation of the Quantitative TEM Measurements. The measurement uncertainties associated with the quantitative TEM measurement of particle properties were estimated using a top-down approach based on measurements on NM-300K. The repeatability (within 1 day variability) and intermediate precision (day-to-day variability) for measurements on NM-300K were estimated as described by De Temmerman et al.[17] Three different vials were analyzed on 3 days within 1 week. On each day, three TEM specimens were prepared from one vial. From each TEM specimen, micrographs of seven regions on the grid were recorded and analyzed. The calibration of the microscope magnification using the cross-grating method was performed following ASTM-E766 guidelines.[18] The microscope was calibrated with the automatic HM magnification (Mi, SA) calibration procedure (FEI). The total intralaboratory uncertainty combined the repeatability, intermediate precision, and calibration uncertainties, and was calculated based on the mean of the measured medians of each of the 23 selected parameters.

ICP-MS Analysis Conditions. Total silver determination in the pearls was performed using a VG PQ-ExCell ICP-MS apparatus (Thermofisher Scientific, Winsford, UK). Silver was measured at the ^{107}Ag isotope. The sample batch was accompanied by three replicates of the certified reference material DOLT-4, in which the mass fraction of silver was certified (0.93 ± 0.07 mg/kg).

DOI: 10.1021/acs.jafc.5b00578
J. Agric. Food Chem. 2015, 63, 3570−3578

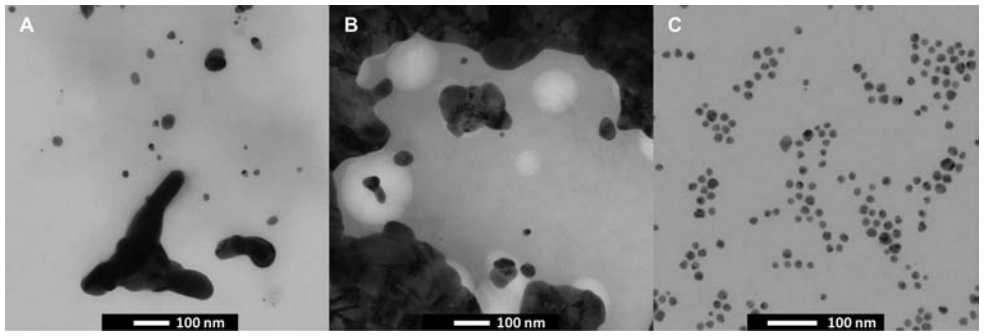

Figure 1. Representative TEM micrographs of nanoscale particles from (A,B) the coating of a pearl after treatment with distilled water, and from (C) the control sample NM-300K on a Cu grid. (A) and (B) are the result of independent experiments.

SP-ICP-MS Analysis Conditions. SP-ICP-MS analysis was performed using an Agilent 8800 ICP-MS apparatus (Agilent Technologies) equipped with a MicroMist nebulizer. The sample flow rate to the nebulizer was 0.5 mL/min. Data acquisition was performed using the MassHunter software in time-resolved analysis (TRA) mode. An acquisition time of 60 s per measurement and a dwell time of 3 ms were selected. Data were transferred to a CSV (comma-separated values) file, which was processed in Microsoft Excel for calculation of particle sizes and particle size distribution, particle number concentration, and particle mass concentration. Signals were treated as background if they were lower than 2500 counts per second. The corresponding size detection limit for silver was 13 nm, determined as the "mean +2.528 SD" of the Ag signal intensities (in cps) registered in 20 blank Milli-Q samples. This corresponded to a probability of 1% of false positive signals. The corresponding signal intensity was recalculated to particle size by taking into account the flow rate and nebulization efficiency during the analysis. NIST-8013 (gold nanoparticles) was used as particle calibration standard and diluted in Milli-Q water to a concentration of 50 ng/L. The calibration for silver was performed with a silver standard for ICP (Fluka Analytical) diluted to 1 and 2.5 μg/l.

RESULTS

Qualitative TEM Analysis. Visual inspection of TEM micrographs indicates that all TEM specimens prepared using Alcian blue treated Cu grids contain particles which are distributed over the complete grid surface, suggesting that the charge of the nanomaterial is compatible with the charge of the grid (Figure 1A–C). When using the Ni grids which were not treated with Alcian blue, only a small amount of particles remained attached to the grid surface and the particles tended to lie close to the border of the holes in the polymer film.

A simple treatment with water releases nanoscale particles from the coating of the pearls (Figure 1A,B). The micrographs show single as well as aggregated/agglomerated particles. In addition, large chunks of material were found abundantly on the EM-grids (Figure 1B). Most particles were round, suggesting a spherical 3D structure, although sometimes particles with a rectangular or triangular shape were detected as well. The aggregates and agglomerates tended to have a complex morphology. Diffraction contrast was observed in the particles. Even the single particles could consist of multiple crystallites. Sugar was found in all samples, on every part of the EM-grid, and caused intensity fluctuations in the background of the TEM images (Figure 1A,B). Identical results were obtained by duplicating the experiment.

The general appearance and the observed morphologies of the particles eluted from the silver pearls resembled the appearance and morphology of the representative test material NM-300K (Figure 1C). For NM-300K, a large amount of particles was found, evenly distributed over the complete grid surface (Figure 1C). Mainly single particles were found, although a few agglomerates were detected as well. The general morphology of the particles was round, suggesting a spherical 3D structure. Particles with a rectangular or triangular shape were sometimes detected as well. The agglomerates tended to be more or less equi-axed.

Electron Diffraction Analysis. All examined diffraction patterns of the particles eluted from the silver pearls show an excellent agreement with the diffraction pattern of silver (NM-300K) (Figure 2). However, the signal in the diffraction

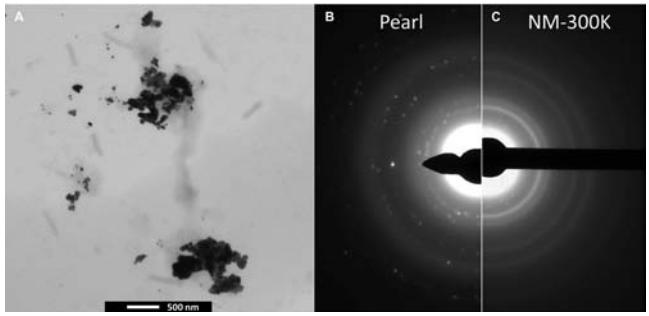

Figure 2. (A) TEM micrograph of nanoscale particles released from the coating of a pearl after treatment with distilled water, (B) corresponding diffraction pattern and agreement with (C) the electron diffraction pattern of NM-300K.

pattern cannot be attributed to nanoscale particles only. It cannot be excluded that a large part of the intensity in the diffraction pattern originated from larger (bulk) particles. If a small region which contained only nanoparticles was selected, the intensity in the corresponding diffraction pattern was too low to be observed.

Chemical Analyses by HAADF-STEM and EDX. The silver particles were easily detected on the HAADF-STEM images because their atomic number is relatively high compared to the background (Figure 3). The corresponding EDX elemental maps of silver clearly showed that the silver distribution coincided with the position of the particles on the HAADF-STEM images (Figure 3). To examine the presence of other chemical elements, EDX spectra of the particles were generated from the elemental maps and analyzed. Small amounts of oxygen and carbon, probably originating from the supporting film and from contamination, were always detected together with the particles. Comparison of copper and nickel grids excluded that the copper and nickel signals in the EDX spectra originated from the sample. In the specimens supported on a carbon and pioloform

DOI: 10.1021/acs.jafc.5b00578
J. Agric. Food Chem. 2015, 63, 3570–3578

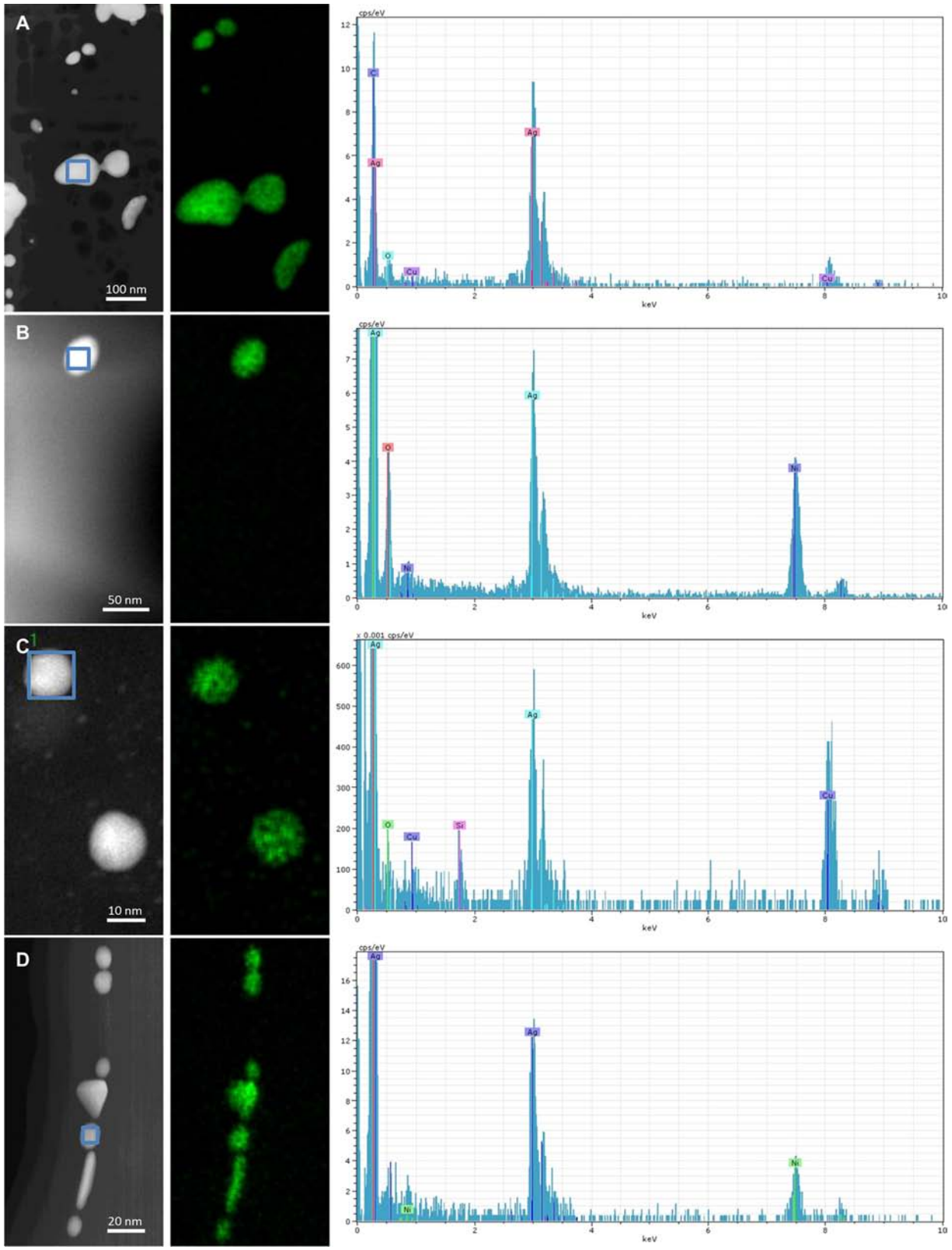

Figure 3. (left) HAADF-STEM images, (middle) corresponding EDX elemental maps of silver, and (right) EDX spectra recorded in the regions indicated on the HAADF-STEM images of (A) particles eluted from a pearl supported on a Cu grid, (B) particles eluted from a pearl supported on a Ni grid, (C) NM-300K supported on a Cu grid, and (D) NM-300K supported on a Ni grid.

coated Cu grid, Ni was not detected (Figure 3A,C), and in the specimens supported on a polymer coated Ni grid, Cu was not detected (Figure 3B,D).

In each specimen, EDX spectra of the background film typically contained oxygen, carbon, and silicon but no silver. These signals were measured over the complete grid area.

DOI: 10.1021/acs.jafc.5b00578
J. Agric. Food Chem. 2015, 63, 3570−3578

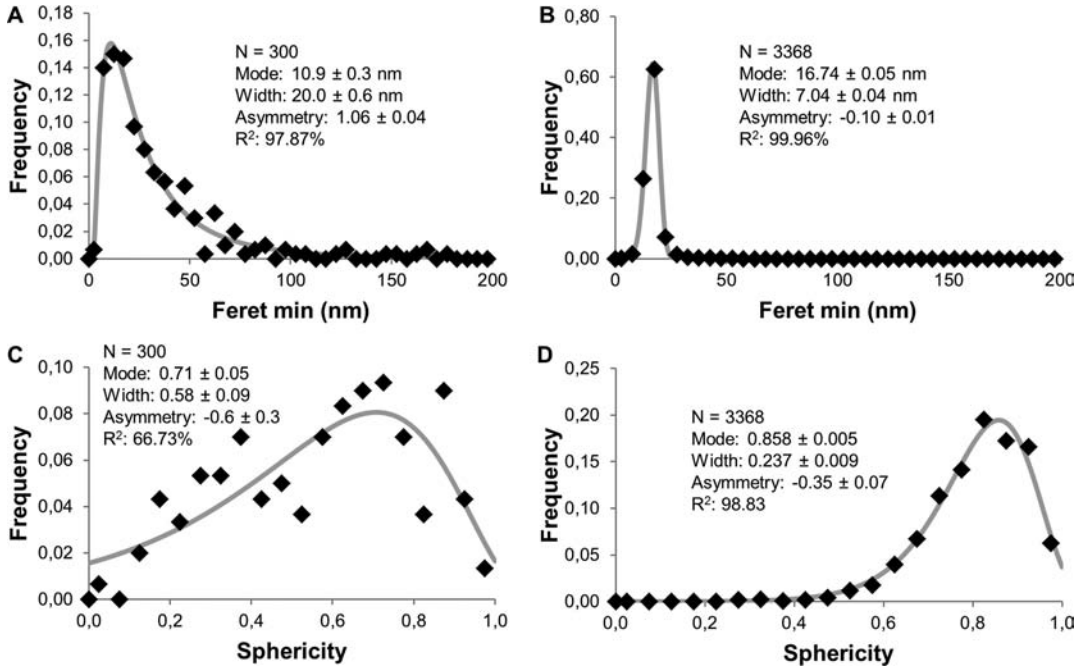

Figure 4. Combined results of two repetitions of the quantitative analysis of the particle size and shape. (A) Feret min distribution of the silver pearls, (B) Feret min distribution of NM-300K, (C) sphericity distribution of the silver pearls, and (D) sphericity distribution of NM-300K. N represents the number of measured particles.

Table 1. Standard and Expanded Measurement Uncertainties of 23 Quantitative Parameters Obtained by TEM in the Method Validation of NM-300K

			type A standard uncertainty			type B	
	mean median	stdev	u(r)	u(ip)	u(lab)	u(cal)	Ulab(x)
diameter mean (nm)	16.94	0.27	0.30	0.09	0.31	0.02	0.31
diameter max (nm)	17.88	0.28	0.31	0.09	0.33	0.02	0.33
diameter min (nm)	15.57	0.28	0.32	0.10	0.33	0.02	0.33
ECD (nm)	16.45	0.26	0.28	0.08	0.29	0.02	0.29
Feret mean (nm)	16.86	0.27	0.30	0.09	0.31	0.02	0.32
Feret max (nm)	17.90	0.29	0.32	0.10	0.33	0.02	0.33
Feret min (nm)	15.61	0.28	0.32	0.10	0.33	0.02	0.33
central distance mean (nm)	8.17	0.13	0.14	0.04	0.15	0.01	0.15
central distance max (nm)	9.05	0.16	0.17	0.05	0.18	0.01	0.18
central distance min (nm)	7.23	0.14	0.15	0.04	0.16	0.01	0.16
radius of inner circle (nm)	7.63	0.14	0.15	0.05	0.16	0.01	0.16
perimeter (nm)	53.21	1.22	1.33	0.40	1.39	0.06	1.40
area (nm^2)	212.70	6.71	7.25	2.18	7.57	0.51	7.58
convex area (nm^2)	216.70	6.89	7.52	2.26	7.85	0.52	7.87
convex perimeter (nm)	55.09	0.91	1.01	0.30	1.05	0.07	1.06
rectangle mean (nm^2)	284.05	9.29	10.31	3.10	10.76	0.68	10.78
rectangle max (nm^2)	293.91	9.66	10.71	3.22	11.18	0.71	11.20
rectangle min (nm^2)	271.92	9.06	9.84	2.97	10.28	0.65	10.30
aspect ratio	1.120	0.005	0.004	0.003	0.005	N/A[a]	0.005
convexity	0.983	0.001	0.001	0.000	0.001	N/A[a]	0.001
elongation	1.109	0.005	0.005	0.002	0.005	N/A[a]	0.005
shape Factor	0.956	0.003	0.003	0.001	0.003	N/A[a]	0.003
sphericity	0.813	0.008	0.008	0.003	0.008	N/A[a]	0.008

[a]Dimensionless measurand.

Quantitative TEM Analysis of the Physical Particle Properties. The particles were semiautomatically detected and measured on the BF-TEM images based on their mass thickness contrast. Because very similar size and shape distributions were obtained by duplicating the experiment, the distributions obtained from individual analyses (shown in Supporting Information, files 1 and 2 for the particles eluted from the pearls and NM-300K, respectively) were combined into single data sets (Figure 4).

The Feret min (i.e., the minimum distance of parallel tangents at opposing particle borders) distributions of the particles eluted from the pearls and of NM-300K lie almost entirely below

DOI: 10.1021/acs.jafc.5b00578
J. Agric. Food Chem. 2015, 63, 3570−3578

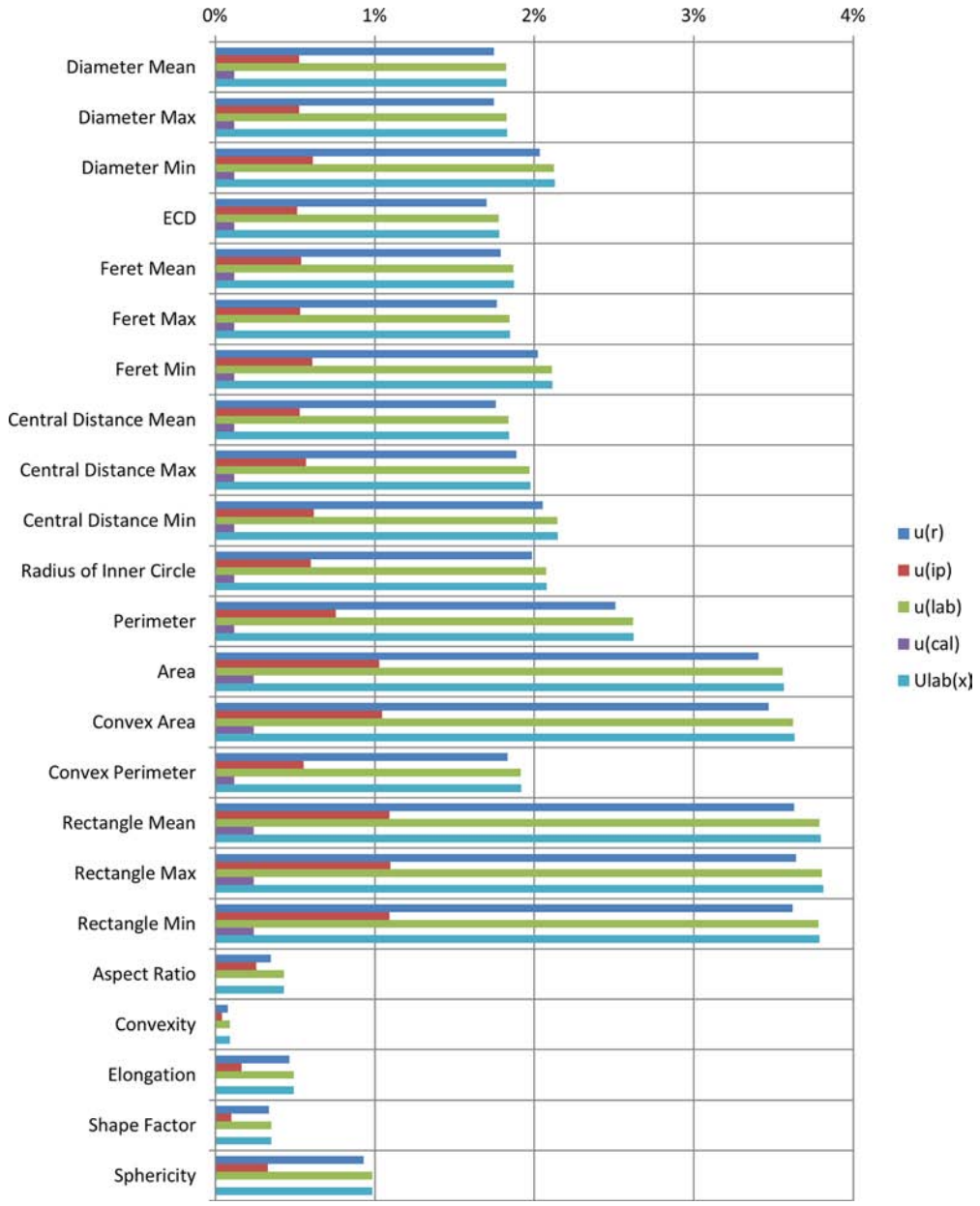

Figure 5. Relative standard and combined uncertainties (in %) for 23 parameters of NM-300K.

100 nm (Figure 4). A Feret min value smaller than 100 nm was measured for 94.70% and 99.94% of the particles eluted from the pearls and from NM-300K, respectively. The amount of particles with a Feret min value smaller than 10 nm was 14.57% and 1.60%, respectively.

As opposed to NM-300K, the particles eluted from the pearls have a log-normal Feret min distribution with tailing on the right-hand side. This tailing can be attributed to the occurrence of aggregates, agglomerates, and larger chunks of material. A log-normal function was fitted through the distributions. The center, width, and asymmetry of the fitted log-normal function are given together with the standard errors in Figure 4. The center represents the mode. The width is defined as two times the half-width at half-maximum (HWHM) at the left side of the mode. The log-normal function was selected because it is the most suitable physical model to describe the distribution which gives a high goodness-of-fit value. The agreement between the binned data and the fitted function is given by the R^2 value. The high amount of agreement between the log-normal functions fitted to the individual size distributions shown in Supporting Information files 1 and 2 justifies the combination of the data into single data sets.

The particles eluted from the pearls have a broader sphericity distribution than the particles of NM-300K, meaning that a larger fraction of the measured particles did not have spherical shape. The sphericity was larger than 0.67 for 40.73% and 89.47% and smaller than 0.33 for 18.87% and 0.42% of the particles eluted from the pearls and of NM-300K, respectively. In agreement with the classification of Krumbein and Sloss,[19] particles eluted from the pearls have a medium sphericity and particles of NM-300K have a high sphericity. Both log-normal sphericity distributions showed tailing on the left-hand side, which can be attributed to the occurrence of triangular and rectangular particles and aggregates and agglomerates. Tailing was significantly larger for the distribution of the particles eluted from the pearls due to the presence of larger chunks of material in this sample. A log-normal

DOI: 10.1021/acs.jafc.5b00578
J. Agric. Food Chem. 2015, 63, 3570−3578

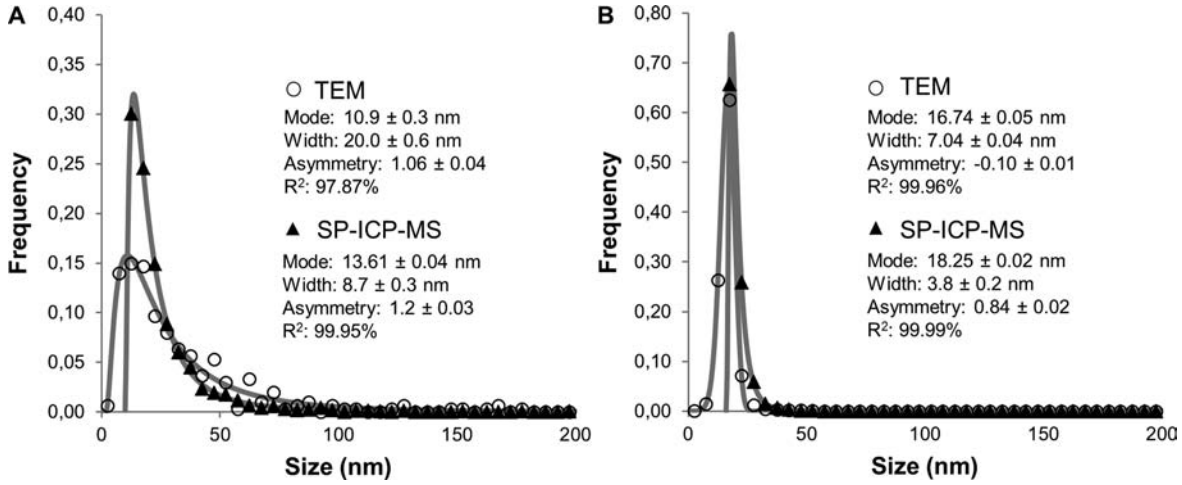

Figure 6. Comparison of TEM particle size measurement (Feret min) and SP-ICP-MS particle size measurement (volume equivalent spherical diameter) for (A) the particles eluted from the pearls and (B) NM-300K.

function was fitted through the data sets. The R^2 value, center, width, and asymmetry of the fitted log-normal function and associated standard errors are given in Figure 4. The R^2 value is relatively low for the sphericity distribution of the pearls due to the high amount of scatter of the data.

Combined Measurement Uncertainty. Table 1 and Figure 5 summarize the results of the determination of measurement uncertainties on NM-300K. Because no certified values are available for NM-300K, the trueness and trueness uncertainty could not be assessed. The mean median size, corresponding standard deviation, intralaboratory precision, calibration uncertainty, and combined laboratory uncertainties were determined.

The repeatability (u(r)) is the largest contribution to the combined uncertainty for all parameters. The intermediate precision (u(ip)) uncertainty and the calibration uncertainty contribute only for a small amount to the uncertainty budget. The total uncertainty budget is always smaller than 4%. For the 1D size parameters (e.g., diameter or Feret), the uncertainty budget is often lower than 2%.

ICP-MS Analysis. The mean silver concentration measured in the certified reference material DOLT-4, 1.02 ± 0.12 mg/kg (mean ± expanded uncertainty, k = 2), does not differ significantly from the certified value (0.93 ± 0.07 mg/kg). The mean total silver concentration in the pearls was 8.4 mg/kg, but the variation among pearls was elevated (RSD = 38%).

SP-ICP-MS Analysis. Figure 6 shows the number-based size distributions obtained by TEM (Feret min) and SP-ICP-MS (volume equivalent spherical diameter) for the particles eluted from the pearls and NM-300K. Because the detection limit of SP-ICP-MS for Ag is about 13 nm, only a part of the distributions was measured. Figure 6 shows that for both the particles eluted from the pearls and NM-300K, only one binned data point was obtained on the left side of the mode. Although the error on the estimation of the left side of the distribution is large, modes similar to those obtained by TEM were found by fitting a log-normal function through the distributions.

The calculated particle number concentration is 4.4 ± 0.5 × 10^9 particles/g of pearl. Note that particles smaller than 13 nm were not considered in this calculation. The mass concentration of the detected particles is 1.8 ± 0.6 μg/g of pearl. This corresponds to approximately 20% of the mean total silver concentration of the pearls.

DISCUSSION

Several TEM-based methods to analyze particle size, morphology, crystal structure, and chemical composition have been applied to formally prove that a fraction of silver nanoparticles is released from the coating of silver pearls, meant for decoration of pastry, after a simple treatment with distilled water. Generally, an extensive sample preparation method adapted for a specific nanomaterial−matrix combination is required to identify nanomaterials in a food matrix.[20] In this case, the simple treatment with distilled water is sufficient to identify the nanoparticles in the matrix by conventional TEM. Because the difference in atomic number of the particles and the matrix is large, the particles could be readily detected in the TEM and HAADF-STEM images, even without complete separation from the matrix.

TEM imaging allows visualizing the similarities in size and shape between the particles eluted from the silver pearls and the nanoparticles of the representative test materials NM-300K[10] (Figure 1). Because of the presence of both aggregated/agglomerated particles and larger chunks of (bulk) material extracted from the silver coating of the pearls, tailing of the number-based size distribution occurrs (Figure 4). Consequently, a modal Feret min diameter of 10.9 ± 0.3 nm, which is smaller than the median Feret min diameter of 23.3 nm, is obtained.

The abundant subpopulation of nanoparticles on a number-basis (Figure 4) highlights the importance of using counting techniques such as TEM, which can produce number-based distributions. The measurement of a mass-based distribution would make this fraction of nanoparticles seem insignificant compared to the fraction of larger particles. Scattering- and volume-based ensemble methods, such as dynamic light scattering (DLS) and centrifugal particle sizing, which are historically applied to estimate particle size distributions of food additives, tend to underestimate such subpopulation of small particles in polydisperse samples[21] and may even consider them as a background signal.

Although similar interplanar distances are found for the particles eluted from the pearls and NM-300K (Figure 2), the electron diffraction experiments do not irrefutably demonstrate that the fraction of nanoparticles consists of silver because the intensity in the diffraction patterns mainly originates from larger particles in the field of view. Instead of recording high resolution

DOI: 10.1021/acs.jafc.5b00578
J. Agric. Food Chem. 2015, 63, 3570−3578

TEM images and determining the interplanar distances from the corresponding fast Fourier transforms (FFTs), the composition of the particles is studied by analytical TEM. The coincidence between the positions of the nanoparticles detected on the HAADF-STEM images and on the EDX elemental silver maps, and the fact that no silver signal is found outside the detected particles, indicates that the spatial resolution of the EDX measurement is high enough to measure the composition of the individual nanoparticles. Comparison of samples deposited on copper and nickel grids excludes that the copper and nickel signals in the EDX spectra originates from the sample. It is assumed that the Si signal measured in all EDX spectra originates from the original samples or from storing the samples in glass vials.

Once identified, the number-based size and shape distributions of the particles could be determined by combining conventional BF-TEM imaging with image analysis. This method is validated for silver nanoparticles by estimating the measurement uncertainties of the quantitative TEM analysis of the representative test material NM-300K using a top-down approach. The obtained values of the different measurement uncertainties are in line with the results of earlier estimations of TEM measurement uncertainties.[17] By correlation analysis, the 23 measured parameters can be grouped into three classes representing size, shape, and surface properties (data not shown). The uncertainties of the measurements of the parameters within each class are similar (Figure 5), and the relative uncertainties of the 2D size parameters are twice as large as the 1D size parameters, as expected from propagation of error analysis. Consequently, each parameter within one class can be selected as a representative parameter to characterize the nanomaterial. The estimated expanded intralaboratory uncertainty of 1D size parameters is in the order of 2%, which allows precise determination of the Feret Min, relevant in the scope of EC regulations.[22,23]

Because 94.70% of the eluted particles have a Feret min diameter smaller than 100 nm, the eluted fraction classifies as a nanomaterial according to the EC regulations for novel food[22] and the EC Recommendation on the definition of a nanomaterial.[23] In future experiments, the nanofraction of particles in the original E174 food additive will be examined.

The guidance documents on the testing of manufactured nanomaterials[24] and on the risk assessment of the application of nanoscience and nanotechnologies in the food and feed chain[25] require that the size parameter of a nanomaterial is measured by at least two independent methods (one being electron microscopy) because the results obtained from different measurement techniques may differ because of the physical principles applied in the measurement method. Therefore, the TEM size measurements are independently confirmed using SP-ICP-MS. Because of its limit of quantification for Ag of about 13 nm, this method fails to detect a substantial fraction (about 26%) of the particles eluted from the pearls, which are detected by TEM. In this case, fitting a log-normal function to the incomplete distribution results in a mode (13.6 nm) similar to that obtained by TEM (10.9 nm). However, because the smallest particles are not detected by SP-ICP-MS, the uncertainty on the estimation of the left side of the distribution is large. Even so, SP-ICP-MS can be applied as a method to screen for the presence of a fraction of nanosized particles and allows determination of the particle number concentration ($4.4 \pm 0.5 \times 10^9$ particles/g of pearl) and the mass concentration of the detected particles (1.8 ± 0.6 μg/g of pearl). By combining these results with the ICP-MS results, the mass concentration of the detected particles is estimated to be about 20% of the mean total silver concentration of the pearls.

It is expected that the silver nanoparticles in the silver pearls do not increase or improve the function (metallic silver coloring) of the food additive and serve no technological function in the finished product. Dried NM-300K has a dark-blue color, and colloidal silver nanoparticles are typically yellow to gray depending on their size, concentration, and agglomeration state,[26,27] which would make intentional addition of a nanofraction to the coating of the silver particles ineffective. Therefore, the nanofraction can be considered as an unwanted contaminant fraction that counteracts the function of the food additive.

Even so, because of concerns about possible health effects of increased usage and exposure to silver nanoparticles,[4] this case study remains relevant. The oral uptake of silver nanoparticles in the food additive E174 is a factor that should be considered in future studies that examine possible health effects caused by exposure to nanosilver.

The presented approach to identify silver nanomaterials can be applied to analyze the size, shape, crystal structure, and chemical composition of the particles in the re-evaluation of food additives as foreseen in article 32 of Regulation (EC) no. 1333/2008.[7] This regulation requires that all food additives added to food for a technological purpose permitted in the EU before 20 January 2009 should be subjected to a new risk assessment by the European Food Safety Authority (EFSA) by 2020.

It remains debatable whether the silver food additive examined in this example should be labeled as nanomaterial. Because the food additive is intentionally produced and because it is composed of discrete functional parts, most of which have one or more dimensions of the order of 100 nm, it qualifies as an "engineered nanomaterial" according to EU Regulation 1169/2011 on the Provision of Food Information to Consumers.[28] This regulation specifies that besides information such as nutrition values, allergens, or country of origin, all ingredients present in the form of engineered nanomaterials shall be clearly indicated in the list of ingredients. The names of such ingredients shall be followed by the word "nano" in brackets. This mandatory labeling entered into force on 13 December 2014. However, because no significant change in production method, in starting materials used, or in particle size can be demonstrated for this already authorized food additive, one could consider that it is not a new additive, and thus at present it would not be subject to labeling requirements.

■ ASSOCIATED CONTENT

Supporting Information

Results of two repetitions of the quantitative analysis of the particle size and shape of a silver pearl. File 1: Feret min distribution of the first sample, Feret min distribution of the second sample, sphericity distribution of the first sample, and sphericity distribution of the second sample. File 2: Results of two repetitions of the quantitative analysis of the particle size and shape of NM-300K. Feret min distribution of the first sample, Feret min distribution of the second sample, sphericity distribution of the first sample, and sphericity distribution of the second sample. This material is available free of charge via the Internet at http://pubs.acs.org.

■ AUTHOR INFORMATION

Corresponding Author

*E-mail: eveline.verleysen@coda-cerva.be.

DOI: 10.1021/acs.jafc.5b00578
J. Agric. Food Chem. 2015, 63, 3570−3578

Author Contributions

E.V.: experimental design, sample preparation, TEM measurements, image analysis, writing, and editing the manuscript. E.V.D.: sample preparation, TEM measurements, validation NM-300K. N.W.: (SP)-ICP-MS analysis, writing the manuscript. P.J.D.T.: validation of NM-300K. M.A.D.F.: validation of NM-300K. J.M.: writing and editing the manuscript

Notes

The authors declare no competing financial interest.

■ ACKNOWLEDGMENTS

We thank Marina Ledecq (CODA-CERVA, Uccle, Belgium), Lotte Delfosse (CODA-CERVA, Tervuren, Belgium), and Dr. Maria Batuk (EMAT, UA, Antwerp, Belgium) for their technical assistance.

■ REFERENCES

(1) *Commission Regulation (EU) no. 1129/2011 of 11 November 2011 Amending Annex II to Regulation (EC) no. 1333/2008 of the Europen Parliament and of the Council by Establishing a Union List of Food Additives*; European Commission, 2011.

(2) *Commission Directive 95/45/EC of 26 July 1995 Laying down Specific Purity Criteria Concerning Colours for Use in Foodstuffs*; European Commission, 1995.

(3) Bouwmeester, H.; Dekkers, S.; Noordam, M. Y.; Hagens, W. I.; Bulder, A. S.; de Heer, C.; ten Voorde, S. E.; Wijnhoven, S. W. P.; Marvin, H. J.; Sips, A. J. Review of health safety aspects of nanotechnologies in food production. *Regul. Toxicol. Pharmacol.* **2009**, *53*, 52−62.

(4) SCENIHR. *Preliminary Opinion Nanosilver: Safety, Health and Environmental Effects and Role in Antimicrobial Resistance*; European Commission, 2013.

(5) *Scientific Opinion Inability to Assess the Safety of a Silver Hydrosol Added for Nutritional Purposes As a Source of Silver in Food Supplements and the Bioavailability of Silver from This Source Based on the Supporting Dossier Scientific Statement of the Panel on Food Additives and Nutrient Sources added to Food (ANS), Question no. EFSA-Q-2005−169, Adopted on 26 November 2008*; EFSA, 2008.

(6) *BfR Recommends That Nano-Silver Is Not Used in Foods and Everyday Products*; BfR Opinion no. 024/2010; Bundesinstitut für Risikobewertung, 28 December 2010; http://www.bfr.bund.de/cm/216/bfr_raet_von_nanosilber_in_lebensmitteln_und_produkten_des_taeglichen_bedarfs_ab.pdf.

(7) EC Regulation (EC) no. 1333/2008 of the European Parliament and of the Council of 16 December 2008 on food additives. *Official Journal of the European Union: Legislation* **2008**, *L354*, 16.

(8) EC Commission Regulation (EU) no. 257/2010 of 25 March 2010, Setting up a Programme for the Re-Evaluation of Approved Food Additives in Accordance with Regulation (EC) No 1333/2008 of the European Parliament and of the Council on Food Additives. *Official Journal of the European Union: Legislation* **2010**, *L80*, 19.

(9) Stefaniak, A. B.; Hackley, V. A.; Roebben, G.; Ehara, K.; Hankin, S.; Postek, M. T.; Lynch, I.; Fu, W. E.; Linsinger, T.; Thunemann, A. F. Nanoscale reference materials for environmental, health and safety measurements: needs, gaps and opportunities. *Nanotoxicology* **2013**, *7*, 1325.

(10) Klein, C. L.; Comero, S.; Stahlmecke, B.; Romazanov, J.; Kuhlbusch, T. A. J.; Van Doren, E.; De Temmerman, P. J.; Mast, J.; Wick, P.; Krug, H. F.; Locoro, G.; Hund-Rinke, K.; Kordel, W.; Friedrichs, S.; Maier, G.; Werner, J.; Linsinger, T.; Gawlik, B. M. *NM-Series of Representative Manufactured Nanomaterials: NM-300 Silver—Characterisation, Stability, Homogeneity*; European Commission Joint Research Centre, Institute for Health and Consumer Protection: Luxembourg, 2011; p 86.

(11) Mast, J.; Demeestere, L., Electron tomography of negatively stained complex viruses: application in their diagnosis. *Diagn. Pathol.* **2009**, *4* (5), DOI: 10.1186/1746-1596-4-5.

(12) McMahon, M.; Lopez, R.; Meyer, H., III; Feldman, L.; Haglund, R., Jr. Rapid tarnishing of silver nanoparticles in ambient laboratory air. *Appl. Phys. B: Laser Opt.* **2005**, *80* (7), 915−921.

(13) De Temmerman, P.-J.; Van Doren, E.; Verleysen, E.; Van der Stede, Y.; Francisco, M. A. D.; Mast, J. Quantitative characterization of agglomerates and aggregates of pyrogenic and precipitated amorphous silica nanomaterials by transmission electron microscopy. *J. Nanobiotechnol.* **2012**, *10* (1), 1−11.

(14) Verleysen, E.; De Temmerman, P.-J.; Van Doren, E.; Abi Daoud Francisco, M.; Mast, J. Quantitative characterization of aggregated and agglomerated titanium dioxide nanomaterials by transmission electron microscopy. *Powder Technol.* **2014**, *258*, 180−188.

(15) Wojdyr, M. Fityk: a general-purpose peak fitting program. *J. Appl. Crystallogr.* **2010**, *43*, 1126.

(16) Wolberg, J. *Data Analysis Using the Method of Least Squares: Extracting the Most Information from Experiments*. Springer: New York, 2006.

(17) De Temmerman, P.-J.; Lammertyn, J.; De Ketelaere, B.; Kestens, V.; Roebben, G.; Verleysen, E.; Mast, J. Measurement uncertainties of size, shape, and surface measurements using transmission electron microscopy of near-monodisperse, near-spherical nanoparticles. *J. Nanopart. Res.* **2014**, *16* (1), 1−22.

(18) *Standard Practice for Calibrating the Magnification of a Scanning Electron Microscope*; ASTM E766-14; ASTM International: West Conshohocken, PA, 2014.

(19) Krumbein, W. C.; Sloss, L. L. *Stratigraphy and Sedimentation*, 2nd ed.; Freeman: San Francisco, CA, 1963.

(20) Plathe, K. L.; von der Kammer, F.; Hassellöv, M.; Moore, J. N.; Murayama, M.; Hofmann, T.; Hochella, M. F., Jr. The role of nanominerals and mineral nanoparticles in the transport of toxic trace metals: field-flow fractionation and analytical TEM analyses after nanoparticle isolation and density separation. *Geochim. Cosmochim. Acta* **2013**, *102* (0), 213−225.

(21) Linsinger, T. P. J.; Roebben, G.; Gilliland, D.; Calzolai, L.; Rossi, F.; Gibson, N.; Klein, C. *Requirements on Measurements for the Implementation of the European Commission Definition of the Term "Nanomaterial"*; JRC Reference Reports, Publications Office of the European Union: Luxembourg, 2012.

(22) European Parliament and Council, Regulation (EC) no. 258/97 of the European Parliament and of the Council of 27 January 1997 Concerning Novel Foods and Novel Food Ingredients. *Official Journal of the European Union: Legislation*, **1997**, Vol. *L183*.

(23) EC, 2011a, Commission Recommendation of 18 October 2011 on the Definition of a Nanomaterial; 2011/696/EU; European Commission, 2011; pp 38−40.

(24) *OECD Guidance Manual for the Testing of Manufactured Nanomaterials: OECD Sponsorship Programme, First Revision*; OECD: Paris, 2010.

(25) EFSA Scientific Committee. Scientific Opinion: Guidance on the Risk Assessment of the Application of Nanoscience and Nanotechnologies in the Food and Feed Chain. *EFSA J.* **2011**, *9* (5), 2140.

(26) Mock, J.; Barbic, M.; Smith, D.; Schultz, D.; Schultz, S. Shape effects in plasmon resonance of individual colloidal silver nanoparticles. *J. Chem. Phys.* **2002**, *116* (15), 6755−6759.

(27) Mulfinger, L.; Solomon, S. D.; Bahadory, M.; Jeyarajasingam, A. V.; Rutkowsky, S. A.; Boritz, C. Synthesis and study of silver nanoparticles. *J. Chem. Educ.* **2007**, *84* (2), 322.

(28) European Parliament and Council (2011a), Regulation (EU) no. 1169/2011 of the European Parliament and of the Council of 25 October 2011 on the Provision of Food Information to Consumers, Amending Regulations (EC) no. 1924/2006 and (EC) no. 1925/2006 of the European Parliament and of the Council, and repealing Commission Directive 87/250/EEC, Council Directive 90/496/EEC, Commission Directive 1999/10/EC, Directive 2000/13/EC of the European Parliament and of the Council, Commission Directives 2002/67/EC and 2008/5/EC and Commission Regulation (EC) no. 608/2004. *Official Journal of the European Union: Legislation* **2011**, *L304*, 18−63.

DOI: 10.1021/acs.jafc.5b00578
J. Agric. Food Chem. 2015, 63, 3570−3578

peptide fraction and to the differences due to the countless brewing styles, preclude a reliable quantitative assessment of glutenlike harmful epitopes in beer and hence the possibility to establish beer (at least some types) as safe or hazardous for celiacs. The presence of immunoactive components, even in beer presumed to be gluten-free,[11] supports the precautionary exclusion of barley malt beers from the consumption by celiacs.

Wheat beer (also Weissbier or Weizen Beer) is a traditional beer produced with mixed barley malt and wheat adjunct (*Triticum aestivum*). According to the style, wheat can be malted (e.g., German Weissbier) or unmalted (e.g., Belgian Witbier). German regulations specify a share of at least 50% wheat malt for brewing Weissbier. Because of an average protein content higher than all-barley-malt beers (BMB) and to the sequence specificity of toxic epitopes from wheat prolamins, beer brewed with a large wheat grist bill is expected to be largely unsuitable for a strict gluten-free diet. However, ELISA determinations are heavily biased because of the commonly used gliadin standards, resulting in aberrant values (up to 47 000 ppm, i.e., ∼4.7 g/L) that are clearly inconsistent with the total protein content of wheat beer, which does not normally exceed the 2.5−2.8 g/L.[17] A gliadin-equivalent content of 250−400 ppm for wheat beer[13,18] appears to be a rather realistic range, as also determined by antibody-independent MS-based methods.[17]

Despite its relatively high commercial importance and an increasing trend of consumers' appreciation,[19] no attempt to elucidate the proteome of wheat beer has been reported so far. In this work, we explored the proteome of three commercial wheat beer samples (Weissbier style), hereafter referred to as WB#1, WB#2, and WB#3, by 2DE-MS. We primarily aimed to understand if homologous barley- and wheat-derived proteins survive the process of selection that determines the protein/peptide content of beer, or, on the contrary, that barley and wheat generate dissimilar protein patterns, with a focus on the set of potentially immunogenic proteins. The proteome and the peptidome of a representative Weissbier sample (WB#1) were investigated in detail using LC-MS/MS approaches. The gluten-equivalent content of WBs was determined using the G12 competitive ELISA method. Furthermore, we compared the IgA-immunoreactivity of WB proteins to that of a BMB sample by Western blot analysis, using sera from celiacs as the source of specific antigliadin antibodies.

MATERIALS AND METHODS

Samples and Chemicals. Three commercial trademarks of Weissbier (indicated as WB#1, WB#2, and WB#3; collectively as WBs) and an Italian BMB sample (double malt label) were purchased in a local supermarket. A commercial gluten-free beer, brewed with millet malt, was used as the control for the G12-based determinations. Relying on the producers' technical information, WBs were brewed according to the German style, using 50−60% of malted wheat as a grist adjunct. Chemicals were purchased from Sigma (St. Louis, MI, USA). HPLC-MS-grade solvents were from Carlo Erba (Milan, Italy). Total protein content of beers was measured in triplicate by the modified micro-Lowry protein assay (Sigma-Aldrich).

Extraction of the Protein/Peptide Fraction. The extraction protocol was optimized in order to limit the noncovalent interchain aggregation mediated by hydrophobic interactions. It consisted of the following steps: 20% TCA-insoluble proteins derived from 20 mL of degassed beer samples were redissolved in denaturing/reducing buffer (6 M guanidine, 50 mM Tris, 10 mM dithiothreitol, DTT, pH 8.0) and incubated for 30 min at 55 °C. Proteins were Cys-alkylated with iodoacetamide and then desalted with G-25 Econo-Pak 10 DG column (Biorad, Milan, Italy; exclusion limit = 6 kDa), eluting with 1% acetic acid. Proteins were quantified using the Bradford assay and lyophilized. For the shotgun proteomic analysis, the protein fractions (>6 kDa) were digested with proteomic-grade modified trypsin (Sigma) at a 1:100 (w/w) enzyme−substrate ratio in 50 mM ammonium bicarbonate, pH 8.0, overnight at 37 °C.

Peptides (<6 kDa) were isolated from an aliquot of beer using a G-25 Econo-Pak 10 DG column, eluting with 1% acetic acid, and then concentrated and purified from polar compounds using C18 Sep-pak cartridges (Waters, Mildord, MA, USA), eluting with 70% acetonitrile/0.1% TFA. Peptides were finally lyophilized.

1D and 2D Gel Electrophoresis. Beer proteins (15 μg) were separated by 1D SDS-PAGE using hand-cast 15% polyacrylamide gels mounted on a Mini-Protean Tetracell system (Biorad). For 2DE separations, freeze-dried protein extracts (400 μg) were dissolved in 340 μL of 8 M urea, 2% w/v CHAPS, 2% v/v IPG buffer, pH 3−10 (Amersham Biosciences/GE Healthcare, Uppsala, Sweden), containing traces of Bromophenol Blue and 20 mM DTT. Isoelectric focusing (IEF) was carried out on passively rehydrated IPG 18 cm 3−10 strips using a IPGphorII electrophoresis system (all from Amersham Biosciences). Proteins were focused up to a total of 32 000 V hrs, stepwise increasing the voltage up to 8000 V at 20 °C. Prior to the second dimension, the IPG strips were equilibrated for 15 min in equilibration buffer (50 mM Tris/HCl pH 8.8, 6 M urea, 30% v/v glycerol, 2% w/v SDS, traces of Bromophenol Blue, 10 mg/mL DTT), followed by 15 min in the same equilibration buffer containing 25 mg/mL iodoacetamide instead of DTT. The second dimension was run on 15% acrylamide gels using an Ettan DALTsix vertical system (Amersham Biosciences) using 15 mA/gel for 30 min and then 30 mA/gel. 1D- and 2DE-separated proteins were detected by Coomassie Brilliant Blue G-250 staining.

For peptide mass fingerprinting (PMF)-based identification, manually excised protein bands (1DE) or spots (2DE) were in-gel digested using 12.5 ng/mL proteomic-sequencing-grade trypsin (Sigma) as previously described.[5]

Size-Exclusion Chromatography. Size-exclusion liquid chromatography (SEC) separation of wheat beer proteins/peptides (100 μL of degassed beer) was carried out using a 152 A Gilson chromatograph (Gilson Inc., Middleton, WI, USA) equipped with a Superdex 75 HR 10/30 column (Amersham Biosciences), eluting with 50 mM sodium phosphate containing 150 mM NaCl, pH 7.2. The SEC separation was monitored by UV at 220 and 280 nm.

Reversed-Phase High-Performance Liquid Chromatography. HPLC separations of beer peptides were carried out using an Agilent 1100 HP Series (Agilent Technologies, Palo Alto, CA, USA) modular system equipped with a multiwave UV−vis detector. The stationary phase was a C18 reversed-phase (RP) column (250 cm × 2.1 mm i.d., Vydac, Hesperia, CA, USA). Separations were carried out at constant flow rate of 0.2 mL/min, applying a 5−60% solvent B (0.1% TFA in acetonitrile) linear gradient over 5−65 min. Solvent A was 0.1% TFA in Milli-Q water.

MALDI-TOF MS. MALDI-TOF MS analyses were carried out using a Voyager DE-Pro instrument (Perseptive Biosystem, Framingham, MA, USA) as previously described.[5] α-Cyano-4-hydroxycinnamic acid (10 mg/mL in 50% acetonitrile/0.1% TFA) was used as MALDI matrix. Spectra were elaborated with the Data Explorer software, version 4.0, supplied with the instrument. PMF was carried out using the MS-Fit tool of Protein Prospector (http://prospector.ucsf.edu).

HPLC-ESI-Q-TOF MS and MS/MS. Tryptic peptides (30 μg) arising from the entire pools of beer proteins and the peptide components (15 μg) were analyzed by HPLC-ESI-MS/MS analysis, using an Infinity 1290 UHPLC (Agilent Technologies, Santa Clara, CA, USA), equipped with a LUNA 5 μm C18(2) column (150 cm × 2 mm i.d., 100 Å, Phenomenex, Torrance, CA, USA) and coupled to a Q-Exactive Hybrid Quadrupole-Orbitrap mass spectrometer (Thermo Scientific, San Jose, CA, USA) that operated in the data-dependent acquisition mode (ddMS).[2] Source parameters: spray voltage, 3.2 kV; capillary temperature, 210 °C; S-lens RF level, 80; auxiliary gas temperature, 210 °C; sheath gas flow rate, 25; auxiliary gas flow rate, 12.

DOI: 10.1021/acs.jafc.5b00631
J. Agric. Food Chem. 2015, 63, 3579−3586

Full MS scans were acquired over the range m/z 350−1800, with a mass resolution of 70 000. The target value (AGC) was 3×10^6, and the maximum allowed accumulation time (IT) was 200 ms. For the ddMS^2 analyses, a top ten method was used: The ten most intense peaks (charge states 2, 3 and 4) were selected for sequencing and fragmented with a normalized energy of 20, 30, and 40%. AGC was 2×10^5. The ion-selection threshold was 20%, and the IT was 100 ms.

For the HPLC peptide separations, the elution gradient was 5% B isocratic for 5 min followed by 25 min to B 15%, 15 min to B 50% and 5 min to B 100%, maintained for 15 min. Eluents were (A) 0.1% FA in water and (B) 0.1% FA in ACN. The flow rate was 0.2 mL/min.

The raw spectra files were transformed into mgf files with the Mascot Distiller Software (version 2.5.1, Matrix Science Ltd., London, UK) and used to search the NCBI and Uniprot databases through Mascot, version 2.3 (Matrix Science, http://www.matrixscience.com) and the Batch-Tag Web (Protein Prospector) search engines. The searching parameters were the following: taxonomic restriction, none; for further confirmation searches were restricted to *Triticum*, *Hordeum* and *Saccharomyces* spp.; type of search, MS/MS ion search; enzyme, trypsin; max missed cleavages, 1; fixed modifications, carboamidomethylation (Cys); variable modifications, pyro-Glu formation (N-terminal Gln), Met-oxidation, deamidation (Gln); mass values, monoisotopic; precursor charge range, +2, +3, +4; parent ion tolerance, 10 ppm; fragment ion tolerance, 50 ppm. The peptide fraction was analyzed with the Batch-Tag Web engine using the same search parameters, except that no enzyme was selected during the search and "no fixed modification" was set for any of the amino acids. Output entries were separately validated by manual inspection of raw MS/MS spectra. Identifications were validated by manual inspection of the MS/MS spectra. Peptide identifications were considered successful when the measured molecular weight (MW) corresponded to the expected value, a sequence of at least three consecutive b- or y-fragment ions occurred in the spectrum, and the score corresponding to the identity was higher that 15 ($p < 0.05$). Outputs were homology filtered.

Western Immunoblotting with ECL Detection. Western blotting was carried out by transferring hordeum and wheat (positive controls), maize (negative control), and beer proteins separated by SDS-PAGE onto a 0.45 μm nitrocellulose membrane (Biorad). The membrane was blocked with 5% BSA. Pooled serum of four celiac subjects (age range = 5−36 years old, average = 24 years old), diluted 1:500 in T-TBS, was used as the source of primary IgA antigliadin antibodies. Secondary antibody was HPR-conjugated monoclonal antihuman IgA (Sigma) diluted 1:10,000 in T-TBS. Blots were developed with the ECL-plus kit (Amersham).

G12 Assay. Gluten content of beer samples was determined using the G12 assay kit, according to manufacturer's instructions (Biomedal SL, Sevilla, Spain). A standard curve was built with gliadin at various dilutions (0−120 ng/mL). To minimize possible protein−polyphenols interactions, beer samples were previously warmed for 40 min at 50 °C. Afterward, beer aliquots were diluted (1:50−1:200) in the dilution buffer (room temperature) and assayed in triplicate. Statistical analyses were carried out with the Excel 2010 software (Microsoft Co., WA, USA).

RESULTS AND DISCUSSION

Electrophoresis-Based Proteomic Analysis of Weissbier. The total protein content of Weissbier samples was 2.7−2.9 g/L (mean of three determinations), roughly 2-fold higher than BMB (1.4 g/L), as measured with the modified micro-Lowry assay. However, discrepancies can be found about the protein content of beer depending on the method of analysis.[1] After 20% TCA precipitation, polypeptides >6 kDa, here referred to as the protein fraction, were grossly separated from the low-molecular-weight (low-MW) peptides by SEC using G-25 Econo-Pak 10 DG columns.[9] Proteins from WB and BMB samples were analyzed with 1D SDS-PAGE, as shown in Figure 1. The main bands of WBs migrated with an apparent MW

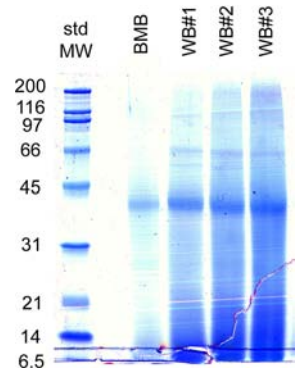

Figure 1. SDS-PAGE separation of proteins from Weissbier samples (WB#1, WB#2, and WB#3) compared to an all-barley-malt beer (BMB) sample. The band at ∼43 kDa and the quite broad band at low molecular weight are Z-type serpins and ns-LTP, respectively.

corresponding to that of BMB Z4 serpin and ns-LTPs. Indeed, the bands at ∼43 and ∼9.5 kDa were identified as barley Z4-serpin (UniProt Knowledge Base, UniProt: P06293) and ns-LTP1 (UniProt: P07597) by MALDI-TOF MS-based PMF after excision and in-gel trypsinolysis.

The cereal serpins (serine protease inhibitors) are Z-type cereal inhibitors that have been classified into five subfamilies, sharing 70−75% homology. Members within a subfamily share more than 89% sequence identity. Barley serpins are catalogued into three subfamilies, namely BSZ4, BSZ7, and BSZx, the latter having been never detected at the protein level.[20] Hexaploid *T. aestivum* wheat encodes a higher number of serpin proteoforms than the diploid barley. Actually, five different Z-type serpins, grouped into two subfamilies according to structural and functional homology with the barley serpins, have been cloned and sequenced in wheat.[21] Low-intensity peptides specific to wheat Z2A (UniProt: Q9ST57) and Z2B (UniProt: P93692) were detected among the tryptic digests of the band at ∼43 kDa, demonstrating that minor amounts of wheat serpins comigrated with the barley cognates (not shown). Similarly, minor signals of wheat ns-LTP1 co-occurred in the spectra with those of the barley homologue counterpart. These findings indicated that the brewing processes enrich specific homologous protein subsets of wheat and barley. PMF analysis demonstrated that a faint protein band of WBs at MW ≈ 65 kDa contained peptide ions specific to the Z-type serpins. In agreement with previous data, these bands have to be attributed to aggregates resulting from heat-induced covalent cross-linking of proteins.[22]

Although no appreciable difference was observed among the three WBs, a protein smear at MW = 28−40 kDa distinguished WBs from BMB. These diffuse bands were attributed to traces of gliadins and, at least in part, to enzymes of the yeast glycolytic pathway (e.g., triosophosphate isomerase). In fact, WBs supposedly contained significant amounts of haze-active yeast proteins because they are generally unfiltered and undergo an in-bottle refermentation following the addition of a viable yeast population (Hefeweizen beer style).

Z-serpins and ns-LTPs appeared as dominant diffuse zones in the 2DE gel of a representative Weissbier sample (WB#1, Figure 2). Substantially identical maps were observed for the other WB samples (not shown) and the BMB control, in-line with an early attempt to elucidate the protein profile of Weissbier.[23] The protein spots of Z-type serpins and ns-LTPs were identified by PMF, whereas minor protein spots were

DOI: 10.1021/acs.jafc.5b00631
J. Agric. Food Chem. 2015, 63, 3579−3586

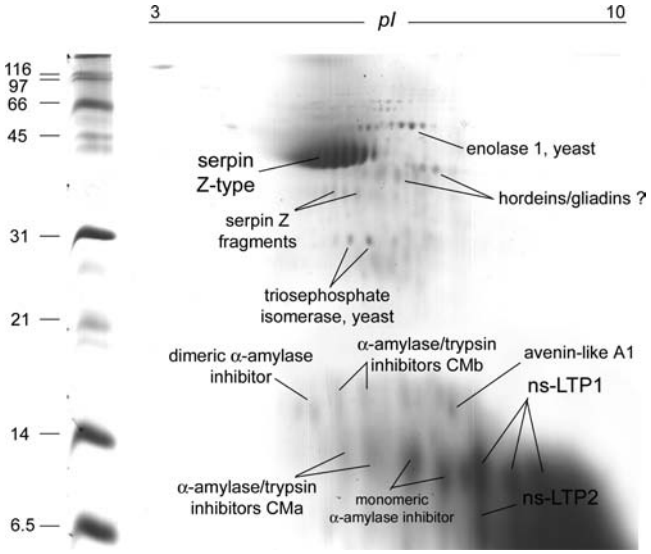

Figure 2. 2D electrophoresis (2DE) map of a representative Weissbier sample (WB#1). Major protein spots have been identified by PMF and on the basis of the MW/p*I* coordinates (also compare with ref 23).

tentatively assigned also relying on the MW/p*I* coordinates and by comparison with previous literature data.[24,25] Apparently, the respective broad spots only contained the barley Z-serpins and ns-LTPs. However, the probable comigrating wheat homologue proteins were not detected due to the lower relative abundance and to a certain degree of dispersion over numerous isoforms, which are additionally affected by variable nonenzymatic glycation.[26,27] Notably, a series of protein spots, previously described as α-amylase/trypsin inhibitors and aveninlike protein A1, was detected at MW = 13−17 kDa. Only protein traces possibly ascribable to hordeins/gliadins occurred at MW = 35−40 kDa and p*I* 7−7.5,[2] whereas fragments of barley Z4-serpin and proteoforms of yeast triosephosphate isomerase populated the MW range = 28−40 kDa.

Shotgun Proteomic Analysis of Weissbier. 2DE maps provided a general picture of the beer protein systems, evidencing the pattern of the main components and preserving the information about the protein integrity.[28] Nevertheless, beer is a complex biochemical system constituted by a heterogeneous protein fraction and polypeptides with peculiar properties (e.g., very high p*I*) that are in part severely glycated, hydrolyzed, or aggregated.[22]

The Weissbier proteome is expectedly even more complex than the BMB one because of the occurrence of hexaploid wheat as an additional source of gene-expression products. In cases like this, gel-free shotgun proteomics (bottom-up strategy) expands the analytical dynamic range, contributing to comprehensive protein inventories that include those less-abundant components hardly detectable by different strategies.[3,4,6,8,9] Thus, to deeply explore the proteome of Weissbier, the 2DE-based investigation was complemented with peptide-centric LC-ESI MS/MS-based shotgun proteomic analysis of a representative sample (WB#1). Overall, we identified 58 gene products with high confidence ($p < 0.05$), among which 41 (71%) were from *H. vulgare* and *T. aestivum*. The homology-filtered protein hits are listed in Table 1. The emPAI value, assigned by the Mascot search engine on the basis of the spectral count in a label-free fashion,[29] provided a rough estimate of the relative protein abundance.

Z-type serpins were by far the most represented proteins of WBs similar to those of the BMB.[9] Z4 and Z7 serpins were from barley, five serpin proteoforms from wheat. By summing the relevant emPAI values, Z-serpins were estimated to occur at an expression degree comparable to one between those of barley and wheat.

The search engine assigned three "unique" peptide matches to the barley ZX serpin, whose expression at the protein level has not been confirmed. These tryptic peptides actually were degenerate sequences that occur identical in both the Z4 and Z7 serpins. Therefore, ZX serpin was not computed within the list of the entries during the process of homology filtering. Similarly, several protein hits in Table 1 are indicative of a series of possible homologous gene products.

Barley and wheat ns-LTPs, especially the ns-LTP1 types, ranked as the second-most abundant protein family of Weissbier. Despite the important proportion of malted wheat used for brewing, the barley ns-LTPs appeared much more abundant than those of wheat, according to the electrophoretic and emPAI data, probably because of several differences of the primary structures (barley and wheat ns-LTP1 and ns-LTP2 share 74 and 65% identity, respectively) that might affect the stability of the ns-LTPs to proteases.[30] Anyhow, the proteins from both the sources are known to exhibit a relatively high resistance to proteases as well as to heat treatments.

As a general trend, similar to BMB, the process of protein selection during Weissbier production enriches a few classes of endosperm proteins generally categorized among the seed pathogenesis-related proteins, which are able to survive even the harshest brewing injuries.[31] Because of their functional role in the grain, pathogenesis-related proteins and protease inhibitors are also highly resistant to human physiological gastrointestinal digestion, and for this reason they could reach the gut in an immunologically active form and behave as type-I allergens in IgE-mediated food allergies.[32] To this purpose, α-amylases/trypsin inhibitors occurring as several isoforms in Weissbier are pest-resistance effectors besides being physiologically deputed to balance the accumulation and release of starch during the seed's transition from dormancy to germination. α-Amylases/trypsin inhibitors and thioredoxin are well established wheat IgE allergens, for instance in baker's asthma. Recently, it has been proposed that α-amylases/trypsin inhibitors are stronger elicitors of the innate immune response and could be involved in several inflammatory disorders of the gastrointestinal tract, including the recently emerged nonceliac gluten sensitivity.[33]

Probably because of an effect of suppression exerted by yeast proteins, hordeins appeared to be missing in Weissbier, whereas in BMB they have been detected, albeit at low amounts. Minor levels of gluten proteins, including wheat α/β- and γ-gliadins as well as high- and low-MW glutenin subunits, were clearly identified instead, demonstrating that Weissbier do contain prolamins that are potentially harmful for celiacs.

The relatively high number of gene products arising from *S. cerevisiae* (17 proteins, 29%) is consistent with the lack of the filtering step during brewing. Importantly, the great majority of the proteins identified are structurally and/or functionally related to components already described in BMB, thus actually validating the outcome of the analysis.

Peptidome Analysis of Weissbier. The analysis by SEC demonstrated that 75−80% of the protein fraction of WBs consisted of medium-/small-sized soluble polypeptides released from the barley and wheat malt, similar to results from BMB

DOI: 10.1021/acs.jafc.5b00631
J. Agric. Food Chem. 2015, 63, 3579−3586

Table 1. Identification of Wheat Beer Proteins by the Shotgun Proteomic Approach[a]

protein name[b]	UNIPROT ID	ACC #[c]	MW (Da)/p*I*	emPAI
serpin-Z4 (H)	SPZ4_HORVU	P06293	43277/5.7	9.13
serpin-Z1A (T)	SPZ1A_WHEAT	Q41593	43119/5.6	3.55
serpin-Z1B (T)	SPZ1B_WHEAT	P93693	43033/5.4	3.14
serpin-Z2A (T)	SPZ2A_WHEAT	Q9ST57	43311/5.5	3.11
serpin-Z2B (T)	SPZ2B_WHEAT	P93692	43011/5.2	2.75
serpin-Z1C (T)	SPZ1C_WHEAT	Q9ST58	42981/5.6	2.06
serpin-Z7 (H)	BSZ7_HORVU	Q43492	42821/5.4	1.04
serpin ZX (H)[d]	SPZX_HORVU	Q40066	42947/6.8	0.86
ns-lipid transfer protein 1 (H)	NLTP1_HORVU	P07597	12301/8.7	4.28
ns-lipid transfer protein 1 (T)	NLTP1_WHEAT	P24296	11898/8.5	1.81
ns-lipid transfer protein 2 (H)	NLT2_HORVU	P20145	10357/6.8	0.62
ns-lipid transfer protein 2 (T)	NLT2G_WHEAT	P82900	9831/8.9	0.50
glutenin high-MW subunit DY10 (T)	GLT0_WHEAT	P10387	69629/7.6	0.55
glutenin high-MW subunit PW212 (T)	GLT4_WHEAT	P08489	89174/5.8	0.16
glutenin low-MW subunit (T)	GLTA_WHEAT	P10385	41020/9.0	0.18
α/β-gliadin A-IV (T)	GDA4_WHEAT	P04274	34239/8.5	0.14
α/β-gliadin (T)	GDA7_WHEAT	P04727	36118/8.6	0.13
γ-gliadin (T)	GDB2_WHEAT	P08453	37122/7.6	0.12
γ-gliadin B (T)	GDBB_WHEAT	P06659	32967/8.1	0.15
B1-hordein	HOR1_HORVU	P06470	33423/8.9	0.38
B3-hordein (fragment)	HOR3_HORVU	P06471	30196/7.7	0.19
γ3-hordein	HOG3_HORVU	P80198	31189/6.7	0.15
late embryogenesis abundant protein-group 3 (T)	LEA3_WHEAT	Q03968	23238/8.8	0.45
barwin (T)	BARW_HORVU	P28814	13737/7.8	0.42
ABA-inducible protein PHV A1 (H)	LEA1_HORVU	P14928	21820/9.0	0.49
avenin like A2 (T)	AVLA2_WHEAT	P0CZ07	19702/8.4	0.23
avenin like B2 (T)	AVLB2_WHEAT	P0CZ05	32514/7.8	0.11
α-amylase inhibitor 0.19 (T)	IAA1_WHEAT	P01085	13337/6.7	0.85
α-amylase inhibitor 0.28 (T)	IAA2_WHEAT	P01083	16800/7.4	0.22
α-amylase/trypsin inhibitor CM2 (T)	IAAC2_WHEAT	P16851	15460/6.9	0.25
α-amylase/trypsin inhibitor CMb (H)	IAAB_HORVU	P32936	16526/5.8	0.38
α-amylase/trypsin inhibitor CM16 (T)	IAC16_WHEAT	P16159	15782/5.3	0.30
trypsin inhibitor Cme (H)	IAAE_HORVU	P01086	16135/7.5	0.67
α-amylase/trypsin inhibitor CM1 (T)	IAAC1_WHEAT	P16850	15517/7.5	0.29
α-amylase/trypsin BMAI-1	IAA1_HORVU	P16968	15816/5.4	0.21
α-amylase/trypsin inhibitor CMa (H)	IAAA_HORVU	P28041	15500/5.9	0.49
subtilisin-chymotrypsin inhibitor CI-1A (H)	ICIA_HORVU	P16062	8882/5.2	0.31
subtilisin-chymotrypsin inhibitor CI-1C (H)	ICIC_HORVU	P01054	8259/5.7	0.27
hordoindoline-B1	HINB1_HORVU	Q9FSI9	16122/8.7	0.11
puroindoline-B	PUIB_WHEAT	Q10464	16792/9.1	0.09
oleosin 18 kDa (H)[e]	OLEO1_HORVU	Q43769	19495/9.7	0.28
16.9 kDa class I heat shock protein 1 (S)	HS16A_WHEAT	P12810	16878/5.8	0.29
glyceraldehyde-3-phosphate dehydrogenase 1 (S)	G3P1_YEAST	P00360	35750/8.3	1.64
glyceraldehyde-3-phosphate dehydrogenase 2 (S)	G3P2_YEAST	P00358	35847/6.5	0.95
glyceraldehyde-3-phosphate dehydrogenase 3 (S)	G3P3_YEAST	P00359	35747/6.5	1.34
enolase 1 (S)	ENO1_YEAST	P00924	46816/6.2	0.75
enolase 2 (S)	ENO2_YEAST	P00925	46915/5.7	0.59
cell wall mannoprotein PST1 (S)	PST1_YEAS7	Q12355	45777/9.3	0.46
glucan 1,3-beta-glucosidase I/II (S)	EXG1_YEAST	P23776	51311/4.6	0.19
GPI-anchored protein YAR066W (S)	YA066_YEAST	P0CX18	20594/4.5	0.52
triosephosphate isomerase (S)	TPIS_YEAST	P00942	26796/5.7	0.18
fructose-bisphosphate aldolase (S)	ALF_YEAST	P14540	39621/5.5	0.10
putative protein YIL169C (S)	YIQ9_YEAST	P40442	99737/4.4	0.36
thioredoxin-1 (S)	TRX1_YEAST	P22217	11235/4.8	0.45
thioredoxin-2 (S)	TRX2_YEAST	P22803	11204/4.8	0.09
phosphoglycerate mutase 1 (S)	PMG1_YEAST	P00950	26709/8.8	0.12
alcohol dehydrogenase 4 (S)	ADH4_YEAS7	A6ZTT5	41084/5.9	0.11
pyruvate decarboxylase isozyme 1 (S)	PDC1_YEAST	P06169	61496/5.8	0.07

[a]emPAI values provide a gross quantitative estimation.[27] [b]H = *H. vulgare*; T = *T. aestivum*; S = *S. cerevisiae*. [c]UniProt accession number. [d]Not computed after homology filtering. [e]Peptide sequences (2) common to wheat oleosin.

DOI: 10.1021/acs.jafc.5b00631
J. Agric. Food Chem. 2015, 63, 3579−3586

(Figure 3). The peptide fraction (MW < 6 kDa) from the WB samples showed indistinct RP-HPLC patterns containing a

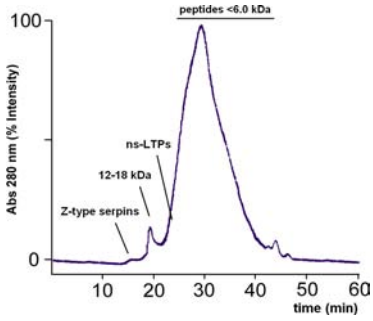

Figure 3. Size-exclusion chromatography of polypeptides from a representative Weissbier sample (WB#1). Fractions were collected and analyzed by SDS-PAGE or by MALDI-TOF MS.

multitude of unresolved, low-abundance peaks and a few dominant peaks, attributed to free aromatic amino acids (e.g., tryptophan), detected at λ = 280 nm, and possibly to polyphenols (not shown).[5] The low-MW peptide fraction of beer is extremely complex because of a series of concomitant factors, including the extreme heterogeneity of the parent proteins, which is further increased in Weissbier, the variable degree of heat-induced nonenzymatic glycation (Maillard reaction), and the unpredictable nature or lack of specificity of the proteolytic cleavage. The peptides from WB#1, representative of Weissbier samples, were analyzed by RP-HPLC-ESI-Q-Orbitrap MS/MS analysis coupled to the database search. Relying on the high resolution of the MS (and MS/MS) measurements and the power of the search engine, we identified 167 peptides deriving from 44 different proteins (Table S1). Many of the peptides were from metabolic proteins of *Saccharomyces* spp., confirming that yeast contributes to the proteome and peptidome of WBs much more than it does to the peptidome of BMB. A significant number of peptides (37) arose from α/β- and γ-gliadins and several other from low- and high-MW glutenin subunits. Therefore, the overall immunogenic potential of Weissbier is clearly incompatible with a gluten-free diet.

Some of the peptides could be encrypted in multiple protein entries because of the occurrence of repeated motifs within specific subfamilies of gluten proteins. In line with the parsimony principle, only protein entries representative of the subfamilies have been selected for cataloguing. The N-terminal region of α-gliadin that also is known to be resistant to proteolysis in sourdough[34] was particularly well-represented. Interestingly, no peptides from ω-gliadins were detected, mirroring the lack of fragments from the homologue C-hordeins in BMB.[6,9] In contrast, significant amounts of C-hordein-derived peptides have been recently described in a home-brewed beer.[35] Immunogenic-proteases-resistant toxic 33-mer 56−88 of α2-gliadin[36] was not detected, whereas N-terminal fragment 56−63 LQLQPFPQ of the same protein was clearly retrieved. (In Table S1 the sequence is indicated as 76−83, because the numbering includes the 1−20 signal peptide.) This result indicates that the 33-mer α2-gliadin peptide is at least partly hydrolyzed during brewing.

Pentapeptide QQPFP, common to other celiacogenic cereals and included in the 34−54 peptide of gliadins, is the main antigen of the R5 antibody used for assaying gluten in foods. QPFPQ, encrypted in the 56−63 α-gliadin fragment, is an additional epitope recognized by the R5,[37] whereas the extended sequence contains the QXQPFP consensus sequence for antigliadin IgA and IgG binding.[38−40] α-Gliadin fragment 33−54 (53−74 with the signal peptide) is part of toxic peptide 31−55, described as one of the main elicitors of the innate response in the immunopathogenesis of celiac disease.[41] Epitope DQ2.5-glut-L1[42] is partly contained in the low-MW glutenin-derived peptides.

Several other peptides of Weissbier harbored the restricted motifs associated with the induction of the celiac disease (e.g., PQQP).[43,44] However, many additional extended multivalent harmful epitopes,[36] distinctly sequenced in BMB,[9] were missing in Weissbier. We argue that this apparent incongruence is due in part to the intrinsic system complexity and to the pitfalls of the peptidomic pipeline. Specifically, the relatively high abundance of yeast-derived peptides in WBs overwhelmed the gluten-derived peptides, which additionally suffer from intrinsic low ionization efficiency. The effect of suppression exerted by yeast-derived peptides is confirmed by the relatively scarce presence of fragments of Z-type serpin and ns-LTPs, which in contrast are largely represented in BMB.[9] Also, it can not be ruled out that many gluten epitopes in Weissbier including the 33-mer are still encrypted within large-sized polypeptide fragments, so escaping MS/MS sequencing. To this purpose, it has to be underlined that several hundreds of peptide ions detected by MS remained unidentified. This demonstrates that the peptidomic picture emerging from the Weissbier system most likely is still the tip of an iceberg because the repertoire of peptide components is far from complete.

G12 Competitive ELISA and Western Blotting of Weissbier. G12 competitive ELISA determinations supported the relatively high abundance of gluten epitopes in WBs. The reliability of the ELISA methods based on the Mendez R5 and Skerritt antibodies for quantifying hordeins in beer has been questioned.[17] Moreover, it should be noted that the relationship between ELISA measurements of gluten and gluten toxicity is not clinically validated.[45] In an attempt to overcome these shortcomings, an assay has been introduced that is based on the G12 antibody raised against hexapeptide epitope QPQLPY of the α-gliadin 33-mer.[46] G12 antibody exhibits affinity to related toxic sequences from hydrolyzed prolamins of barley and rye and some cultivars of oats.[47] Because the standard curve is built using variable concentrations of gliadins, the assay of substrates containing mixed glutenlike epitopes also derived from different cereal species such as barley, as in the case of Weissbier, could result in an overestimation of the results. However, specifically targeting epitopes reactive against T-cell of celiac patients, the G12 ELISA determinations appear to correlate with the actual immune reactivity of gluten-containing foods.[11,48]

The gluten content of Weissbier samples assayed with the competitive G12 ELISA was 374, 372, and 382 ppm (mean of three determinations with different beer batches; standard deviations < 5%) for WB#1, WB#2, and WB#3, respectively, which is almost 10-fold higher than that of the BMB sample (41 ppm). Gluten-free beer, used as the control, contained 2.8 ppm gliadin equivalents.

Western blotting using a pool of sera from celiac patients as the source of antigliadin IgA antibodies confirmed the higher level of immunoreactive polypeptides in WB samples (Figure 4). Although the BMB sample only exhibited a responsive band because of a D-hordein,[9] WBs showed complex patterns of

DOI: 10.1021/acs.jafc.5b00631
J. Agric. Food Chem. 2015, 63, 3579−3586

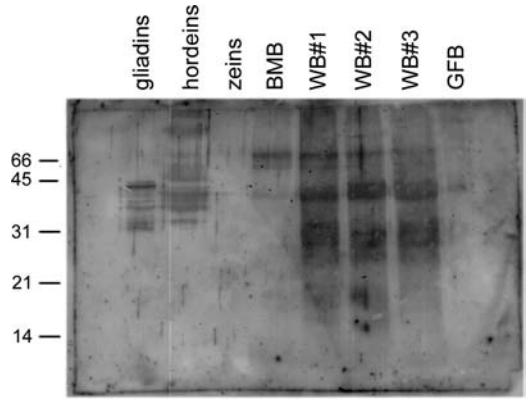

Figure 4. Western immunoblotting of Weissbier samples (WBs) compared to all-barley-malt (BMB) and gluten-free beers. SDS-PAGE-separated proteins were immunostained with pooled sera of celiac patients ($n = 4$) as the source of antigliadin IgA. Wheat (gliadins) and barley (hordeins) prolamins were used as the positive controls, whereas maize prolamins (zeins) were the negative control.

reactive components with the MW values expected for α/β-gliadins (34−38 kDa) in addition to responsive high-MW glutenin subunits, which are D-hordein homologues. WBs also showed a smear at MW < 30 kDa indicative of possible immunoreactive large-sized gluten fragments. Consistent with the G12 evaluation, the Western blotting analysis demonstrated a potential immunotoxicity of WBs significantly higher than that of BMB. The much higher gluten level of WBs compared to that of the lager/Pilsner BMB also supports previous ELISA and Western blotting assessments carried out with first-generation antigluten antibodies.[49]

CONCLUSIONS

The proteome of Weissbier, here explored for the first time, has shown a protein pattern in which the wheat-derived gene products mirror the homologue barley-derived proteins already catalogued in BMB. The correspondence between barley- and wheat-derived proteins was not trivially predictable, taking into account that biochemical events occurring during wheat malting are largely underinvestigated compared to the barley counterpart[50] and that wheat proteins significantly affect the properties of wheat beers.[51] Because of the contribution of hexaploid wheat, the brewing grist of Weissbier and, consequently, its proteome are substantially different from those of BMB. Proteolysis during malting and other brewing steps releases an even more heterogeneous peptide assortment that has been partly characterized in this study. Comprehensive profiling of the protein/peptide repertory is partly hampered by the abundance of interfering yeast-derived gene products that are present in relatively large amounts as a consequence of the brewing process (Hefeweizen beer). However, it emerged clearly that Weissbier contains a large number of protease-resistant and heat-stable proteins that are potential elicitors of IgE-mediated immunoreactions and sensitization events not related to celiac disease. The content of gluten epitopes in Weissbier, encrypted in either intact proteins or soluble hydrolyzed peptides, is much higher than that of lager/Pilsner BMB. The data presented herein demonstrate that although the compatibility of some lager BMB brands could be arguable[13] Weissbier is definitely incompatible with the celiacs' gluten-free diet.

ASSOCIATED CONTENT

Supporting Information

Table S1, LC-ESI MS/MS-based identification of low-molecular-weight peptides of wheat beer. This material is available free of charge via the Internet at http://pubs.acs.org.

AUTHOR INFORMATION

Corresponding Author

*Tel.: +39 0825 299218. Fax: +39 081 781585. E-mail: picariello@isa.cnr.it.

Notes

The authors declare no competing financial interest.

ACKNOWLEDGMENTS

The sera of celiac patients were kindly gifted by Dr. Carmen Gianfrani who is gratefully acknowledged.

REFERENCES

(1) Mills, E. N. C.; Kauffman, J. A.; Morgan, M. R. A.; Field, J. M.; Hejgaard, J.; Proudlove, M. O.; Onishi, A. Immunological Study of Hydrophobic Polypeptides in Beer. *J. Agric. Food Chem.* **1998**, *46*, 4475−4483.

(2) Perrocheau, L.; Rogniaux, H.; Boivin, P.; Marion, D. 2005. Probing heat-stable water-soluble proteins from barley to malt and beer. *Proteomics* **2005**, *5*, 2849−2858.

(3) Hao, J.; Li, Q.; Dong, J.; Yu, J.; Gu, G.; Fan, W. Identification of the major proteins in beer foam by mass spectrometry following sodium dodecyl sulfate-polyacrylamide gel electrophoresis. *J. Am. Soc. Brew. Chem.* **2006**, *64*, 166−174.

(4) Weber, D.; Cléroux, C.; Godefroy, S. B. Emerging analytical methods to determine gluten markers in processed foods-method development in support of standard setting. *Anal. Bioanal. Chem.* **2009**, *395*, 111−117.

(5) Picariello, G.; Bonomi, F.; Iametti, S.; Rasmussen, P.; Pepe, C.; Lilla, S.; Ferranti, P. Proteomic and peptidomic characterization of beer: Immunological and technological implications. *Food Chem.* **2011**, *124*, 1718−1726.

(6) Colgrave, M. L.; Goswami, H.; Howitt, C. A.; Tanner, G. J. What is in a beer? Proteomic characterization and relative quantification of hordein (gluten) in beer. *J. Proteome Res.* **2012**, *11*, 386−396.

(7) Konečná, H.; Müller, L.; Dosoudilová, H.; Potěšil, D.; Buršíková, J.; Sedo, O.; Márová, I.; Zdráhal, Z. Exploration of beer proteome using OFFGEL prefractionation in combination with two-dimensional gel electrophoresis with narrow pH range gradients. *J. Agric. Food Chem.* **2012**, *60*, 2428−2426.

(8) Fasoli, E.; Aldini, G.; Regazzoni, L.; Kravchuk, A. V.; Citterio, A.; Righetti, P. G. Les Maîtres de l'orge: the proteome content of your beer mug. *J. Proteome Res.* **2010**, *9*, 5262−5269.

(9) Picariello, G.; Mamone, G.; Nitride, C.; Addeo, F.; Camarca, A.; Vocca, I.; Gianfrani, C.; Ferranti, P. Shotgun proteome analysis of beer and the immunogenic potential of beer polypeptides. *J. Proteomics* **2012**, *75*, 5872−5882.

(10) Colgrave, M. L.; Goswami, H.; Blundell, M.; Howitt, C. A.; Tanner, G. J. Using mass spectrometry to detect hydrolysed gluten in beer that is responsible for false negatives by ELISA. *J. Chromatogr., A* **2014**, *1370*, 105−14.

(11) Real, A.; Comino, I.; Moreno, M. L.; López-Casado, M. Á.; Lorite, P.; Torres, M. I.; Cebolla, Á.; Sousa, C. Identification and in vitro reactivity of celiac immunoactive peptides in an apparent gluten-free beer. *PLoS One* **2014**, *9*, e100917.

(12) Van Landschoot, A. Gluten-free barley malt beers. *Cerevisia* **2011**, *36*, 93−97.

(13) Guerdrum, L. J.; Bamforth, C. W. Levels of gliadins in commercial beers. *Food Chem.* **2011**, *129*, 5−6.

(14) Appendix III: Draft revised codex standard for foods for special dietary use for persons intolerant to gluten. In *ALINORM 08/31/26,*

DOI: 10.1021/acs.jafc.5b00631
J. Agric. Food Chem. 2015, 63, 3579−3586

Report of the 29th Session of the Codex Committee on Nutrition and Foods for Special Dietary Uses, Bad Neuenahr-Ahrweiler, Germany, November 12−16, 2007; Codex Alimentarius Commission, Thirty first Session, Joint Fao/Who Food Standards Programme: Geneva, Switzerland, June 30−July 5, 2008.

(15) Food and Drug Administration, Health and Human Services.. Food labeling: gluten-free labeling of foods. Final rule. *Fed. Regist.* **2013**, *78*, 47154−47179.

(16) Tanner, G. J.; Blundell, M. J.; Colgrave, M. L.; Howitt, C. A. Quantification of Hordeins by ELISA: the correct standard makes a magnitude of difference. *PLoS One* **2013**, *8*, e56456.

(17) B. Tanner, G. J.; Colgrave, M. L.; Blundell, M. J.; Goswami, H. P.; Howitt, C. A. Measuring hordein (gluten) in beer−a comparison of ELISA and mass spectrometry. *PLoS One* **2013**, *8*, e56452.

(18) Hager, A. S.; Taylor, J. P.; Waters, D. M.; Arendt, E. K. Gluten free beer - a review. *Trends Food Sci. Technol.* **2014**, *36*, 44−54.

(19) Faltermaier, A.; Waters, D.; Becker, T.; Arendt, E.; Gastl, M. Common wheat (*Triticum aestivum* L.) and its use as a brewing cereal − a review. *J. Inst. Brew.* **2014**, *120*, 1−15.

(20) Roberts, T. H.; Marttila, S.; Rasmussen, S. K.; Hejgaard, J. Differential gene expression for suicide-substrate serine proteinase inhibitors (serpins) in vegetative and grain tissues of barley. *J. Exp. Bot.* **2003**, *54*, 2251−2263.

(21) Østergaard, H.; Rasmussen, S. K.; Roberts, T. H.; Hejgaard, J. Inhibitory serpins from wheat grain with reactive centers resembling glutamine-rich repeats of prolamin storage proteins. Cloning and characterization of five major molecular forms. *J. Biol. Chem.* **2000**, *275*, 33272−33279.

(22) Iimure, T.; Nankaku, N.; Kihara, M.; Yamada, S.; Sato, K. Proteome analysis of the wort boiling process. *Food Res. Int.* **2012**, *45*, 262−271.

(23) Dale, C. J.; Young, T. W. Fractionation of high molecular weight polypeptides from beer using two dimensional electrophoresis. *J. Inst. Brew.* **1988**, *94*, 28−32.

(24) Iimure, T.; Nankaku, N.; Hirota, N.; Tiansu, Z.; Hoki, T.; Kihara, M.; Hayashi, K.; Ito, K.; Sato, K. Construction of a novel beer proteome map and its use in beer quality control. *Food Chem.* **2010**, *118*, 566−574.

(25) Picariello, G.; Mamone, G.; Nitride, C.; Addeo, F.; Iimure, T.; Ferranti, P. Beer proteomics. In *Proteomics in Food: Principles and Applications*; Nollet, L., Toldrà, F., Eds.; Springer: New York, 2013; Vol. 2, pp 399−424.

(26) Petry-Podgórska, I.; Zídková, J.; Flodrová, D.; Bobálová, J. 2D-HPLC and MALDI-TOF/TOF analysis of barley proteins glycated during brewing. *J. Chromatogr., B: Anal. Technol. Biomed. Life Sci.* **2010**, *878*, 3143−3148.

(27) Mamone, G.; Picariello, G.; Addeo, F.; Ferranti, P. Proteomic analysis in allergy and intolerance to wheat products. *Expert Rev. Proteomics* **2011**, *8*, 95−115.

(28) Rogowska-Wrzesinska, A.; Le Bihan, M. C.; Thaysen-Andersen, M.; Roepstorff, P. 2D gels still have a niche in proteomics. *J. Proteomics* **2013**, *88*, 4−13.

(29) Ong, S. E.; Mann, M. Mass spectrometry-based proteomics turns quantitative. *Nat. Chem. Biol.* **2005**, *1*, 252−262.

(30) Zuidmeer, L.; van Ree, R. Lipid transfer protein allergy: primary food allergy or pollen/food syndrome in some cases. *Curr. Opin. Allergy Clin. Immunol.* **2007**, *7*, 269−273.

(31) Gorjanović, S. A review: biological and technological functions of barley seed pathogenesis-related proteins (PRS). *J. Inst. Brew.* **2009**, *115*, 334−360.

(32) García-Casado, G.; Crespo, J. F.; Rodríguez, J.; Salcedo, G. Isolation and characterization of barley lipid transfer protein and protein Z as beer allergens. *J. Allergy Clin. Immunol.* **2001**, *108*, 647−649.

(33) Junker, Y.; Zeissig, S.; Kim, S. J.; Barisani, D.; Wieser, H.; Leffler, D. A.; Zevallos, V.; Libermann, T. A.; Dillon, S.; Freitag, T. L.; Kelly, C. P.; Schuppan, D. Wheat amylase trypsin inhibitors drive intestinal inflammation via activation of toll-like receptor 4. *J. Exp. Med.* **2012**, *209*, 2395−2408.

(34) Garofalo, C.; Zannini, E.; Aquilanti, L.; Silvestri, G.; Fierro, O.; Picariello, G.; Clementi, F. Selection of sourdough lactobacilli with antifungal activity for use as biopreservatives in bakery products. *J. Agric. Food Chem.* **2012**, *60*, 7719−7728.

(35) Allred, L. K.; Voyksner, J. A.; Voyksner, R. D. Evaluation of Qualitative and Quantitative Immunoassays To Detect Barley Contamination in Gluten-Free Beer with Confirmation Using LC/MS/MS. *J. AOAC Int.* **2014**, *97*, 1615−1625.

(36) Shan, L.; Qiao, S. W.; Arentz-Hansen, H.; Molberg, Ø.; Gray, G. M.; Sollid, L. M.; Khosla, C. Identification and analysis of multivalent proteolytically resistant peptides from gluten: implications for celiac sprue. *J. Proteome Res.* **2005**, *4*, 1732−1741.

(37) Kahlenberg, F.; Sanchez, D.; Lachmann, I.; Tuckova, L.; Tlaskalova, H.; Mendez, E.; Mothes, T. Monoclonal antibody R5 for detection of putatively coeliac-toxic gliadin peptides. *Eur. Food Res. Technol.* **2006**, *222*, 78−82.

(38) Osman, A. A.; Günnel, T.; Dietl, A.; Uhlig, H. H.; Amin, M.; Fleckenstein, B.; Richter, T.; Mothes, T. B cell epitopes of gliadin. *Clin. Exp. Immunol.* **2000**, *121*, 248−254.

(39) Anderson, R. P.; Degano, P.; Godkin, A. J.; Jewell, D. P.; Hill, A. V. In vivo antigen challenge in celiac disease identifies a single transglutaminase-modified peptide as the dominant A-gliadin T-cell epitope. *Nat. Med.* **2000**, *6*, 337−342.

(40) Bateman, E. A.; Ferry, B. L.; Hall, A.; Misbah, S. A.; Anderson, R.; Kelleher, P. IgA antibodies of coeliac disease patients recognise a dominant T cell epitope of A-gliadin. *Gut* **2004**, *53*, 1274−1278.

(41) Shidrawi, R. G.; Day, P.; Przemioslo, R.; Ellis, H. J.; Nelufer, J. M.; Ciclitira, P. J. In vitro toxicity of gluten peptides in coeliac disease assessed by organ culture. *Scand. J. Gastroenterol.* **1995**, *30*, 758−763.

(42) Sollid, L. M.; Qiao, S. W.; Anderson, R. P.; Gianfrani, C.; Koning, F. Nomenclature and listing of celiac disease relevant gluten T-cell epitopes restricted by HLA-DQ molecules. *Immunogenetics* **2012**, *64*, 455−460.

(43) McLachlan, A.; Cullis, P. G.; Cornell, H. J. The use of extended amino acid motifs for focussing on toxic peptides in celiac disease. *J. Biochem., Mol. Biol. Biophys.* **2002**, *6*, 319−324.

(44) Tye-Din, J. A.; Stewart, J. A.; Dromey, J. A.; Beissbarth, T.; van Heel, D. A.; Tatham, A.; et al. Comprehensive, quantitative mapping of T cell epitopes in gluten in celiac disease. *Sci. Transl. Med.* **2010**, *2*, 41−51.

(45) Lester, D. R. Gluten measurement and its relationship to food toxicity for celiac disease patients. *Plant Methods* **2008**, *4*, 26.

(46) Shan, L.; Molberg, Ø.; Parrot, I.; Hausch, F.; Filiz, F.; Gray, G. M.; Sollid, L. M.; Khosla, C. Structural basis for gluten intolerance in celiac sprue. *Science* **2002**, *297*, 2275−2279.

(47) Morón, B.; Bethune, M. T.; Comino, I.; Manyani, H.; Ferragud, M.; López, M. C.; Cebolla, A.; Khosla, C.; Sousa, C. Toward the assessment of food toxicity for celiac patients: characterization of monoclonal antibodies to a main immunogenic gluten peptide. *PLoS One* **2008**, *3*, e2294.

(48) Comino, I.; Real, A.; Moreno, M. L.; Montes, R.; Cebolla, A.; Sousa, C. Immunological determination of gliadin 33-mer equivalent peptides in beers as a specific and practical analytical method to assess safety for celiac patients. *J. Sci. Food. Agric.* **2012**, *93*, 933−943.

(49) Kanerva, P.; Sontag-Strohm, T.; Lehtonen, P. Determination of Prolamins in Beers by ELISA and SDS-PAGE. *J. Inst. Brew.* **2005**, *111*, 61−64.

(50) Faltermaier, A.; Waters, D.; Becker, T.; Arendt, E. K.; Gastl, M. Protein modifications and metabolic changes taking place during the malting of common wheat (*Triticum aestivum* L.). *J. Am. Soc. Brew. Chem.* **2013**, *71*, 153−160.

(51) Depraetere, S. A.; Delvaux, F.; Coghe, S.; Delvaux, F. R. Wheat Variety and Barley Malt Properties: Influence on Haze Intensity and Foam Stability of Wheat Beer. *J. Inst. Brew.* **2004**, *110*, 200−206.

DOI: 10.1021/acs.jafc.5b00631
J. Agric. Food Chem. 2015, 63, 3579−3586

Table 1. ^{1}H and ^{13}C NMR Spectroscopic Data of 13 and 14[a]

13			14		
position	δ_H (int., mult., J in Hz)	δ_c	position	δ_H (int., mult., J in Hz)	δ_c
1	8.52 (1H, s)		1	ND[b]	
2		68.0	2		143.0
3	3.76 (1H, d, 13.5)	40.9	3		125.5
	3.59 (1H, d, 13.5)				
4		189.5	4		176.3
4a		117.7	4a		128.1
5	8.15 (1H, dd, 7.0, 1.5)	126.8	5	8.32 (1H, d, 8.0)	126.5
6	6.75 (1H, br. t, 7.0)	116.1	6	7.46 (1H, m)	125.7
7	7.30 (1H, td, 7.0, 1.5)	134.7	7	7.76 (1H, br. d, 3.5)[c]	134.1
8	7.06 (1H, br. d, 7.0)	114.7	8	7.76 (1H, br. d, 3.5)[c]	120.5
8a		149.6	8a		141.9
1′	12.26 (1H, s)		2′		162.6
2′		169.8	2″	4.46 (1H, dd, 11.8, 3.8)	58.9
4′		191.3	3″	2.78 (1H, m)	32.6
				1.09 (1H, m)	
4′a		117.9	4″	1.98 (1H, m)	24.2
				1.75 (1H, m)	
5′	8.02 (1H, dd, 7.0, 1.0)	125.4	5″	1.90 (1H, m)	27.0
				1.44 (1H, m)	
6′	7.01 (1H, br. t, 7.0)	121.5	6″	4.37 (1H, dd, 13.0, 5.0)	41.5
				3.14 (1H, dd, 13.0, 3.5)	
7′	7.40 (1H, td, 7.0, 1.5)	133.7			
8′	7.04 (1H, br. d, 7.0)	115.1			
8′a		141.0			

[a]Frequency was 500 MHz for ^{1}H NMR and 150 MHz for ^{13}C NMR in pyridine-d_5 for **13** and CD_3OD for **14**. [b]ND, not detected. [c]The chemical shifts of H-7 and H-8 overlapped.

fractions (G1−G9) were grouped according to the TLC profile. Fraction G3 (H_2O/MeOH, 6:4, v/v, 248.4 mg) was subjected to a semipreparative ODS-HPLC, using a linear gradient system of 5% MeCN (pH 2.65 by TFA, eluent A) and 60% MeCN (pH 2.65 by TFA, eluent B), from 100% A to 17% B for 30 min and increased to 100% B for 45 min, to yield fraction G3a (t_R 22.8 min, 5.2 mg), **2** (t_R 28.2 min, 9.1 mg), a mixture of **2** and **3** (t_R 28.8 min, 13.6 mg), a mixture of **4** and **5** (t_R 30.0 min, 10.1 mg), and **6** (t_R 33.5 min, 7.6 mg). Compound **1** (t_R 31.5 min, 2.4 mg) was isolated from fraction G3a (5.2 mg) by semipreparative ODS-HPLC, using a linear gradient system of 2% MeCN (pH 2.65 by TFA, eluent C) and 40% MeCN (pH 2.65 by TFA, eluent D), from 100% C to 17% D for 30 min.

Fraction G8 (H_2O/MeOH, 2:8, v/v, 1216.2 mg) was suspended in distilled water (100 mL) and partitioned with $CHCl_3$ (3 L, three times) to obtain G8-C ($CHCl_3$ layer, 779.4 mg). Fraction G8-C (779.4 mg) was subjected to semipreparative ODS-HPLC, using a linear gradient system of 30% MeOH (eluent E) and 70% MeOH (eluent F), from 100% E to 100% F for 30 min, to yield **7** (t_R 17.2 min, 4.0 mg), **8** (t_R 19.7 min, 7.6 mg), **9** (t_R 21.0 min, 75.0 mg), **10** (t_R 23.0 min, 67.5 mg), G8-C7 (t_R 24.7 min, 16.7 mg), G8-C8 (t_R 27.1 min, 20.2 mg), and G8-C9 (t_R 29.4 min, 32.1 mg). Through further purification by semipreparative ODS-HPLC, using a linear gradient system of 20% MeCN (pH 2.65 by TFA, eluent G) and 40% MeCN (eluent H), from 100% G to 100% H for 30 min and held at 100% H for 60 min, **11** (t_R 24.2 min, 1.1 mg), **12** (t_R 27.7 min, 3.0 mg), and **13** (t_R 29.5 min, 1.0 mg) from G8-C7 (16.7 mg), **14** (t_R 19.4 min, 1.1 mg) and **15** (t_R 26.8 min, 1.6 mg) from G8-C8 (20.2 mg), and **16** (t_R 31.4 min, 1.6 mg) from G8-C9 (32.1 mg) were isolated, respectively.

*Compound **9** (White Amorphous Powder).* $[\alpha]_D^{25}$ −0.03 (c 0.025, $CHCl_3$); UV $CHCl_3$ λ_{max} (nm) (log ε) 336 (3.82); ^{1}H NMR spectrum (500 MHz, pyridine-d_5, TMS) δ 8.48 (1H, d, J = 7.8 Hz, H-5), 7.42 (1H, t, J = 7.8 Hz, H-6), 7.71 (1H, t, J = 7.8 Hz, H-7), 7.83 (1H, d, J = 7.8 Hz, H-8), 4.02 (2H, t, J = 8.0 Hz, H-1′), 1.89 (2H, m, H-2′), 2.96 (2H, t, J = 7.0 Hz, H-3′); ^{13}C NMR (125 MHz, pyridine-d_5, TMS) δ 160.6 (C-2), 161.3 (C-4), 121.8 (C-4a), 127.0 (C-5), 126.6 (C-6), 134.6 (C-7), 127.9 (C-8), 150.8 (C-8a), 47.1 (C-1′), 19.8 (C-2′), 32.9 (C-3′); HRESI−MS (positive) m/z 187.0881 $[M + H]^+$ (calculated for $C_{11}H_{11}N_2O$, m/z 187.0871, +1.0 mDa).

*Compound **13** (White Amorphous Powder).* $[\alpha]_D^{25}$ −0.02 (c 0.013, $CHCl_3$); UV $CHCl_3$ λ_{max} (nm) (log ε) 348 (4.14); ^{1}H and ^{13}C NMR data shown in Table 1; HRESI−MS (positive) m/z 293.0916 $[M + H]^+$ (calculated for $C_{17}H_{13}N_2O_3$, m/z 293.0926, −1.0 mDa).

*Compound **14** (White Amorphous Powder).* $[\alpha]_D^{25}$ +0.08 (c 0.013, $CHCl_3$); UV $CHCl_3$ λ_{max} (nm) (log ε) 349 (4.04), 331 (4.01); ^{1}H and ^{13}C NMR data shown in Table 1; HRESI−MS (positive) m/z 277.0952 $[M + Na]^+$ (calculated for $C_{15}H_{14}N_2O_2Na$, m/z 277.0953, −0.1 mDa)

HPLC−ESI−MS/MS Analysis of 9, 13, and 14 in Chestnut Honey. The chestnut honey (20 g) was homogenized using a homogenizer (BM-2 Nissei biomixer) with MeOH (40 mL). After extraction for 24 h at room temperature, the mixture was filtered under vacuum through No. 2 filter paper (Whatman). The residue was extracted with EtOH (40 mL) for 24 h at 4 °C and then filtered under vacuum through No. 2 filter paper (Whatman). The MeOH and EtOH solutions were combined and concentrated under vacuum at 38 °C. The extracts were suspended in distilled water (60 mL) and partitioned with *n*-hexane (60 mL, three times) and EtOAc (60 mL, three times), successively. The EtOAc fraction was evaporated under vacuum at 38 °C. The EtOAc fraction (60 mg) was suspended in distilled water (50 mL) and partitioned with $CHCl_3$ (50 mL, three times). After evaporation under vacuum at 38 °C, the $CHCl_3$ fraction (11.5 mg) was dissolved in MeOH (4.6 mL). The fraction was analyzed using a high-performance liquid chromatography−electrospray ionization tandem mass spectrometer (HPLC−ESI−MS) (Shimadzu, Kyoto, Japan). Compounds **9**, **13**, and **14** were separated under the following HPLC conditions: column, MG III (C18, 3 μm, 3.0 × 100 mm^2) (Shiseido, Tokyo, Japan); flow rate, 0.2 mL/min (LC10AD, Shimadzu). The sample was eluted using a gradient system of 100% H_2O (containing 1% formic acid, eluent I) to 100% MeCN (containing 1% formic acid, eluent J), starting with 100% I, increasing

DOI: 10.1021/acs.jafc.5b01027
J. Agric. Food Chem. 2015, 63, 3587−3592

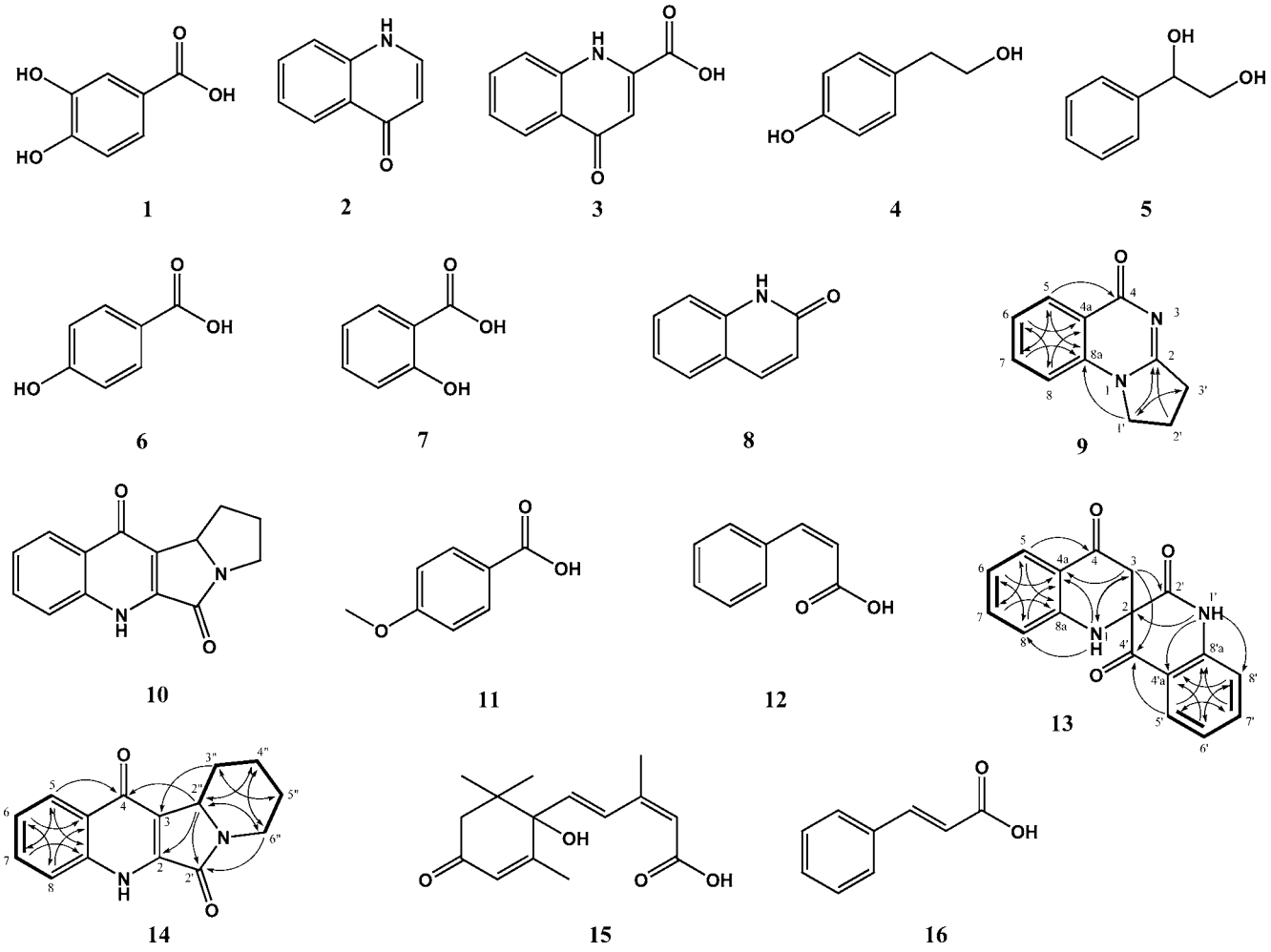

Figure 1. Structures of the isolated compounds from chestnut honey and the important $^{1}H-^{1}H$ correlation spectroscopy (COSY, bold lines) and heteronuclear multiple bond correlation (HMBC, arrows) correlations for **9**, **13**, and **14**.

to 20% J for 10 min, increasing to 50% J for 20 min, increasing to 100% J for 22 min, and holding at 100% J for 25 min. The mass spectrometer (positive ion mode) was set up for multiple reaction monitoring (MRM) to monitor m/z 187.0 → 92.1 for **9**, m/z 293.2 → 247.2 for **13**, and m/z 255.4 → 89.1 for **14** with the a dwell time of 0.1 s per transition. The optimal MS conditions for **9**, **13**, and **14** were employed; ESI source voltage 3.5 kV, detector voltage 45 V, heat block temperature 400 °C, and desolvation line temperature 250 °C. Nebulizing gas and drying gas flows were 3.0 L/min and 15.0 L/min, respectively. Argon was used as the collision gas at a pressure of 230 kPa. The optimized collision energies for **9**, **13**, and **14** were −36 eV, −26 eV, and −50 eV, respectively.

The content of **9**, **13**, and **14** in chestnut honey was analyzed quantitatively by HPLC−ESI−MS/MS analysis at the analytical scale. Sample and standard solutions were prepared just prior to analysis. The calibration curves (n = 6) were constructed using **9**, **13**, and **14** (0.1−50 ng) that were isolated from chestnut honey in this study. Accuracy and reproducibility were evaluated using the standard spike method. External standards of **9**, **13**, and **14** were added to aliquots of chestnut honey at three concentrations (n = 3) to determine their precision. The contents of **9**, **13**, and **14** in chestnut honey were determined in triplicate experiments.

RESULTS AND DISCUSSION

Thirteen known compounds isolated from chestnut honey were additionally identified as protocatechuic acid (**1**), 4(1*H*)-quinolinone (**2**), kynurenic acid (**3**), 4-(2-hydroxyethyl)phenol (**4**), 1-phenyl-1,2-ethanediol (**5**), *p*-hydroxybenzoic acid (**6**), salicylic acid (**7**), 2(1*H*)-quinolinone (**8**), 3-pyrrolidinyl kynurenic acid (**10**), 4-methoxybenzoic acid (**11**), *cis*-cinnamic acid (**12**), *trans*-abscisic acid (**15**), and *trans*-cinnamic acid (**16**) (Figure 2) based on NMR and MS spectroscopic data (Figure 1). All of these compounds have been found in chestnut honey or other honeys.[1,11−17]

The molecular formula of **9** was $C_{11}H_{10}N_2O$ (MW, 186), as established by a pseudomolecular ion peak in the HRESI−MS (positive). The ^{1}H NMR spectrum exhibited four sp^2 carbon proton signals of *ortho*-substituted benzene ring at δ 8.48 (1H, d, J = 7.8 Hz, H-5), 7.42 (1H, t, J = 7.8 Hz, H-6), 7.71 (1H, t, J = 7.8 Hz, H-7), and 7.83 (1H, d, J = 7.8 Hz, H-8). A propane moiety was also assigned by coupling patterns of three sp^3 methylene carbon protons at δ 4.02 (2H, t, J = 8.0 Hz, H-1′), 1.89 (2H, m, H-2′), and 2.96 (2H, t, J = 7.0 Hz, H-3′) in the ^{1}H NMR spectrum and their proton−proton correlations (bold lines) in the $^{1}H-^{1}H$ correlation spectroscopy (COSY) spectrum (Figure 1). This result was also supported by the ^{13}C NMR spectrum, which contained 11 carbon signals including eight sp^2 carbons with four quaternary carbons at δ 175.9−121.8 and three sp^3 carbons at δ 47.1 (C-1′), 32.9 (C-2′), and 19.8 (C-3′). Considering the molecular formula of **9**, the chemical shifts of four sp^2 quaternary carbons indicated that three of them were nitrogen-bearing carbons at δ 160.6 (C-2) and 150.8 (C-8a) with evidence of a carbonyl carbon at δ 161.3

DOI: 10.1021/acs.jafc.5b01027
J. Agric. Food Chem. 2015, 63, 3587−3592

(C-4). From the HRESI−MS and 1D NMR spectra, **9** was suggested to be quinazolinone connected with a propane moiety. The ^{1}H and ^{13}C NMR spectra of **9** were similar to those of 2,3-dihydropyrrolo[1,2-b]quinazolin-5(1*H*)-one, which has been synthesized as reported previously.[18] Complete NMR assignment and connectivity of **9** were further determined by ^{1}H−^{1}H COSY, heteronuclear single quantum correlation (HSQC), and heteronuclear multiple bond correlation (HMBC) experiments. Quinazolinone and propane moieties were also confirmed from the spectra. In particular, correlations (arrows) from H-1′ to C-8a and C-2 and from H-2′ to C-2 observed in the HMBC spectrum indicated that the propane moiety was connected with the 1 and 2 positions of the quinazolinone (Figure 1). Consequently, the structure of **9** was unambiguously determined to be 2,3-dihydropyrrolo[1,2-a]quinazolin-5(1*H*)-one (Figure 1). This compound has been synthesized, as reported previously.[19,20] However, this compound was identified for the first time in nature.

The molecular weight of **13** was determined to be 292 by the pseudomolecular ion peaks detected at *m*/*z* 293.1 $[M + H]^+$ and 315.1 $[M + Na]^+$ in the ESI−MS (positive) spectrum. The molecular formula ($C_{17}H_{12}N_2O_3$) was established by a pseudomolecular ion peak in the HRESI−MS (positive). The ^{1}H NMR spectrum of **13** showed the presence of eight proton signals occurring from two *ortho*-substituted benzene rings at δ 8.15−6.75. In addition, one methylene proton signal at δ 3.76 (1H, d, *J* = 13.5 Hz, H-3a) and 3.59 (1H, d, *J* = 13.5 Hz, H-3b) and two nitrogen-bearing proton signals at δ 8.52 (1H, s, H-1) and 12.26 (1H, s, H-1′) were observed. Considering the molecular formula and the chemical shifts of 17 carbon signals observed in the ^{13}C NMR spectrum of **13**, two *ortho*-substituted benzene ring moieties were assigned from 12 carbons at δ 149.6−114.7. Three carbonyl carbons at δ 189.5 (C-4), 169.8 (C-2′), and 191.3 (C-3′), one quaternary sp^3 carbon at δ 68.0 (C-2), and one sp^3 methylene carbon at δ 40.9 (C-3) were also observed, and four of them were nitrogen-bearing carbons at δ 169.8 (C-2′), 149.6 (C-8a), 141.0 (C-8′a), and δ 68.0 (C-2). From the MS and 1D-NMR data, the skeleton structures of **13** were suggested to be dihydroquinolinone and quinolinedione. In particular, the presence of one quaternary sp^3 carbon at δ 68.0 (C-2) indicated that **13** was a spiro compound consisting of dihydroquinolinone and quinolinedione. The complete NMR assignment and connectivity of **13** were further determined by the ^{1}H−^{1}H COSY, HSQC, and HMBC. The important correlations observed in ^{1}H−^{1}H COSY (bold lines) and the HMBC (arrows) spectra are shown in Figure 1, and the two partial structures of **13** were determined to be 2,3-dihydroquinolin-4(1*H*)-one and quinoline-2,4(1*H*,3*H*)-dione (Figure 1). In particular, correlations between H-1/C-8 and C-4a and H-3/C-4a were observed in the HMBC spectrum. Therefore, the planar structure of **13** was determined to be 3-dihydro-spiro[2(1*H*),3′(1′*H*)-diquinoline]-3′,4,4′-trione (spirodiquinolinone) (Figure 1), which is a new compound. However, structural determination for the absolute stereochemistry of **13** was impossible in the nuclear Overhauser effect spectroscopy experiment. Therefore, unambiguous determination of the absolute stereochemistry for **13** isolated in this study should be studied further with X-ray crystallography.

The molecular weight of **14** was determined to be 254 by the pseudomolecular ion peaks detected at *m*/*z* 255.1 $[M + H]^+$ and 277.1 $[M + Na]^+$ in the ESI−MS (positive) spectrum. The molecular formula ($C_{15}H_{14}N_2O_2$) was established by a pseudomolecular ion peak in the HRESI−MS (positive). The ^{1}H- and ^{13}C NMR spectra of **14** except for one methylene group were closely related to those of 3-(2′-pyrrolidinyl)-kynurenic acid isolated from chestnut reported previously[12] and in this study. That is, the ^{1}H NMR spectrum of **14** showed the presence of four *ortho*-substituted benzene ring proton signals at δ 8.32−7.46. In addition, one methine proton signal δ 4.46 (1H, dd, *J* = 11.8, 3.8 Hz, H-2″) and four methylene proton signals at δ 4.37−1.09 were observed. The ^{1}H NMR spectrum of **14** was supported by the ^{13}C NMR spectrum, which showed the presence of 15 carbon signals including 10 sp^2 carbons with six quaternary carbons at δ 176.3−120.5 and five sp^3 carbons at δ 58.9−24.2. Considering the molecular formula of **14**, the chemical shifts of six sp^2 quaternary carbons indicated that three of them were nitrogen-bearing carbons at δ 162.6 (C-2′), 143.0 (C-2), and 141.9 (C-8a) with two carbonyl carbons at δ 176.3 (C-4) and 162.6 (C-2′). The MS and 1D-NMR data suggested that the skeleton of **14** was kynurenic acid. In addition, a piperidine moiety was assigned as the partial structure from the split patterns of five sp^3 protons at δ 4.46−1.09 in the ^{1}H NMR spectrum and the correlations (bold lines) of H-2″/H-3″, H-3″/H-4″, H-4″/H-5″, and H-5″/H-6″ detected in the ^{1}H−^{1}H COSY spectrum (Figure 1). Therefore, the MS and 1D NMR data suggested that **14** was a pyrrolidinylkynurenic acid. The complete NMR assignment and connectivity of **14** were further determined by the HSQC and HMBC experiments. On the basis of the proton−carbon correlations (arrows) observed in the HMBC spectrum (Figure 1), **14** was determined to be 3-(2′-piperidine)-kynurenic acid (Figure 1), which is a new compound.

Qualitative and Quantitative Analyses of 9, 13, and 14 in Chestnut Honey. Several studies have already reported the presence of quinolinone alkaloids **2**, **3**, **8**, **10** in honey,[1,9−12] and these compounds were also confirmed in this study. We additionally isolated and identified three quinolinone derivatives **9**, **13**, and **14** from chestnut honey in this study. Compound **9** and its similar derivatives have been synthesized, as reported previously.[19] However, this is the first study where **9** was identified in nature. Furthermore, of the quinolone alkaloids isolated in the present study, **13** and **14** were determined to be new compounds. Thus, a further investigation on the occurrence and content of three compounds **9**, **13**, and **14** in chestnut honey was required. The three compounds **9**, **13**, and **14** were analyzed qualitatively and quantitatively by HPLC−ESI−MS. We used HPLC system and selective MRM detection of tandem MS using the isolated compounds as external standards to confirm the occurrence of three compounds in chestnut honey. The $CHCl_3$ fraction obtained after solvent fractionation of the chestnut honey MeOH and EtOH extracts was analyzed by MRM via HPLC−ESI systems. The three peaks of **9**, **14**, and **13** were detected at t_R 11.4, 17.0, and 14.3 min, respectively, on the MRM chromatogram of chestnut honey (Figure 2A−C). These data were in agreement with the retention times of authentic compounds (**9**, **14**, and **13**) purified from chestnut honey in the present study (Figure 2D). These results indicate that the occurrence of **9**, **13**, and **14** in chestnut honey was unambiguously revalidated.

The external calibration curve of each compound at a concentration range of 0.1−50 ng produced a good linear correlation (R^2 > 0.99). Therefore, the optical dilution of chestnut honey in MeOH was 1:920. The precision of **9** (3.5%), **14** (5.6%), and **13** (4.1%) ranged from 3.5−5.6%. The recovery percentage was calculated by comparing the slope of

DOI: 10.1021/acs.jafc.5b01027
J. Agric. Food Chem. 2015, 63, 3587−3592

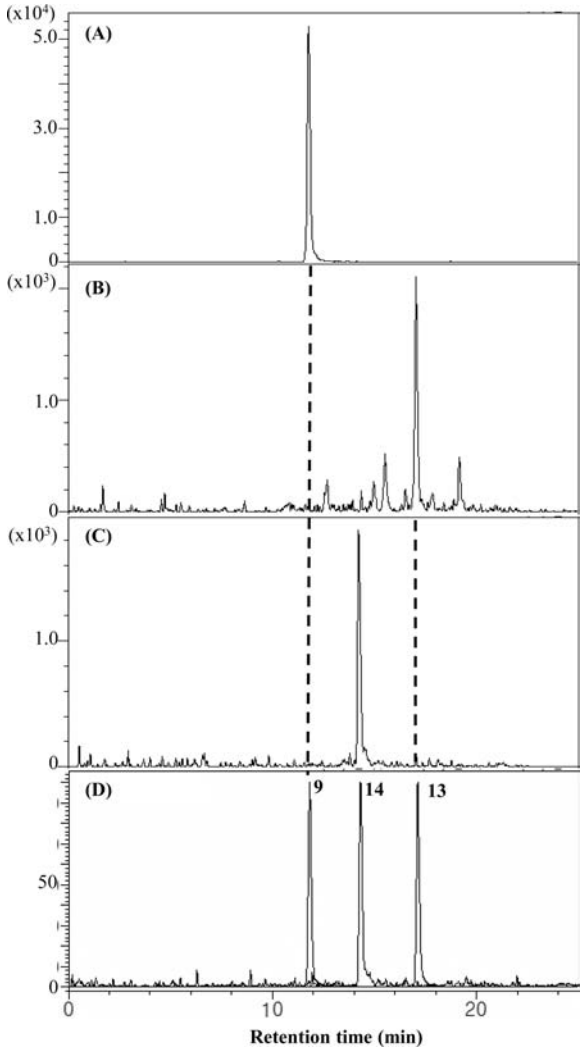

Figure 2. Multiple reaction monitoring (MRM) chromatograms of: (A) **9**, (B) **13**, and (C) **14** in chestnut honey and (D) standards.

the standard addition and the calibration curve for each compound. As a result of this analysis, the recovery of **9** (102.2 ± 3.9%), **13** (101.0 ± 3.44%), and **14** (98.8 ± 2.1%) ranged from 98.8−102.2%. Three compounds **9**, **13**, and **14** in chestnut honey were quantitatively analyzed by HPLC system and selective MRM detection of tandem MS. In the present study, the contents (μg/100 g) of **9**, **13**, and **14** in chestnut honey were 630.5 ± 62.5, 10.8 ± 0.7, and 734.8 ± 28.5, respectively. Compounds **9**, **13**, and **14** were present in very small amounts in chestnut honey when compared to quinolinone alkaloids **2** (2.3−211.5 mg/100 g) and **3** (8.1−64.4 mg/100 g), as reported previously.[11]

Quinoline alkaloids are widely distributed in nature and possess antimalarial, antimicrobial, anti-inflammatory, and analgesic activities.[21−23] In addition, kynurenic acid derivatives, which included **3**, **10**, and **14** identified in this study, are endogenous nonselective antagonists of α-7-nicotinic acetylcholine and *N*-methyl-D-aspartate receptors.[24] Furthermore, quinazolinone derivatives including **9** have anti-inflammatory and analgesic activities.[18] Therefore, quinolinone alkaloids including the two new compounds **13** and **14** identified in this study may be biologically active substances. These molecular-level investigations may offer very useful information for establishing the chemical profiles of honeys.

AUTHOR INFORMATION

Corresponding Author

*Phone: +82-62-530-2141. Fax: +82-62-530-2149. E-mail: nutrmoon@jnu.ac.kr.

Author Contributions

⊥J.Y.C. and S.H.B. contributed equally to this work.

Funding

This research was supported by the Rural Development Administration (PJ00826601).

Notes

The authors declare no competing financial interest.

REFERENCES

(1) Schievano, E.; Moelato, E.; Fachin, C.; Mammi, S. Characterization of markers of botanical origin and other compounds extracted from unifloral honeys. *J. Agric. Food Chem.* **2013**, *61*, 1747−1755.

(2) Gharzouli, K.; Amira, S.; Gharzouli, A.; Khennouf, S. Gastroprotective effects of honey and glucose−fructose−sucrose−maltose mixture against ethanol-, indomethacin-, and acidified aspirin-induced lesions in the rat. *Exp. Toxicol. Pathol.* **2002**, *54*, 217−221.

(3) Kassim, M.; Achoui, M.; Mustafa, M. R.; Mohd, M. A.; Yusoff, K. M. Ellagic acid, phenolic acids, and flavonoids in Malaysian honey extracts demonstrate in vitro anti-inflammatory activity. *Nutr. Res. (N.Y.)* **2010**, *30*, 650−659.

(4) Al-Wailli, N. S. Natural honey lowers plasma glucose, C-reactive protein, homocysteine, and blood lipids in healthy, diabetic, and hyperlipidemic subjects: Comparison with dextrose and sucrose. *J. Med. Food* **2004**, *7*, 100−107.

(5) Koc, A. N.; Silici, S.; Kasap, F.; Hormet-Oz, H. T.; Mavus-Buldu, H.; Ercal, B. D. Antifungal activity of the honey bee products against *Candida* spp. and *Trichosporon* spp. *J. Med. Food* **2011**, *14*, 128−134.

(6) Othman, N. H. Honey and cancer: Substainable inverse relationship particularly for developing nations—A review. *J. Evidence-Based Complementary Altern. Med.* **2012**, *2012*, No. 410406.

(7) Erejuwa, O. O.; Sulaiman, S. A.; Ab Wahab, M. S. Honey: A novel antioxidant. *Molecules* **2012**, *17*, 4400−4423.

(8) Ball, D. W. The chemical composition of honey. *J. Chem. Educ.* **2007**, *84*, 1643−1646.

(9) Beretta, G.; Caneva, E.; Facino, R. M. Kynurenic acid in honey from arboreal plants: MS and NMR evidence. *Planta Med.* **2007**, *73*, 1592−1595.

(10) Beretta, G.; Caneva, E.; Regazzoni, L.; Bakhtyari, N. G.; Facino, R. M. A solid-phase extraction procedure coupled to 1H NMR, with chemometric analysis, to seek reliable markers of the botanical origin of honey. *Anal. Chim. Acta* **2008**, *620*, 176−182.

(11) Beretta, G.; Artali, R.; Caneva, E.; Orlandini, S.; Centini, M.; Facino, R. M. Quinoline alkaloids in honey: Further analytical (HPLC−DAD−ESI−MS, multidimensional diffusion-ordered NMR spectroscopy), theoretical, and chemometric studies. *J. Pharm. Biomed. Anal.* **2009**, *50*, 432−439.

(12) Beretta, G.; Vistoli, G.; Caneva, E.; Anselmi, C.; Facino, R. M. Structure elucidation and NMR assignments of two new pyrrolidinyl quinolone alkaloids from chestnut. *Magn. Reson. Chem.* **2009**, *47*, 456−459.

(13) Gasic, U.; Keckes, S.; Dabic, D.; Trifkovic, J.; Milojkovic-Opsenica, D.; Natic, M.; Tesic, Z. Phenolic profile and antioxidant activity of Serbian polyfloral honeys. *Food Chem.* **2014**, *145*, 599−607.

(14) Alissandrakis, E.; Kibaris, A. C.; Tarantilis, P. A.; Harizanis, P. C.; Polissiou, M. Flavour compounds of Greek cotton honey. *J. Sci. Food Agric.* **2005**, *85*, 1444−1452.

(15) Jerković, I.; Marijanović, Z.; Kezić, J.; Gugić, M. Headspace, volatile, and semi-volatile organic compounds diversity and radical scavenging activity of ultrasonic solvent extracts from *Amorpha fruticosa* honey samples. *Molecules* **2009**, *14*, 2717−2728.

(16) Stephens, J. M.; Schlothauer, R. C.; Morris, B. D.; Yang, D.; Fearnley, L.; Greenwood, D. R.; Loomes, K. M. Phenolic compounds

DOI: 10.1021/acs.jafc.5b01027
J. Agric. Food Chem. 2015, 63, 3587−3592

and methylglyoxal in some New Zealand manuka and kanuka honeys. *Food Chem.* **2010**, *120*, 78−86.
(17) Tuberoso, C. I. G.; Bifulco, E.; Caboni, P.; Cottiglia, F.; Cabras, P.; Floris, I. Floral markers of strawberry tree (*Arbutus unedo* L.) honey. *J. Agric. Food Chem.* **2010**, *58*, 384−389.
(18) Azimvand, J. Synthesis of novel 1,2,3,5-tetrahydropyrrole[2,1-b]quinazoline-5-one analogs by using lithiation-intramolecular electrophilic reaction. *J. Chem. Pharm. Res.* **2012**, *4*, 3924−3928.
(19) Arya, V. P.; Dave, K. G.; Khadse, V. G.; Shenoy, S. J. Synthesis of new heterocycles: Part XXI. Synthesis of some quinazolones. *Indian J. Chem., Sect. B: Org. Chem. Incl. Med. Chem.* **1976**, *14B*, 879−882.
(20) Eun, S. M. Synthesis of quinazolin-4-one derivatives from 2-aminobenzamide. II. Reaction with γ-lactone and diketones. *Yakhak Hoechi* **1986**, *30*, 203−207.
(21) Michael, J. P. Quinoline, quinazoline, and acridone alkaloids. *Nat. Prod. Rep.* **2008**, *25*, 166−187.
(22) Marella, A.; Tanwar, O. P.; Saha, R.; Ali, M. R.; Srivastava, S.; Akhter, M.; Shaquiquzzaman, M.; Alam, M. M. Quinoline: A versatile heterocyclic. *Saudi Pharm. J.* **2013**, *21*, 1−12.
(23) Souto, A. L.; Tavares, J. F.; da Silva, M. S.; Diniz, M. F. F. M.; de Athayde-Filho, P. F.; Filho, J. M. B. Anti-inflammatory activity of alkaloids: An update from 2000 to 2010. *Molecules* **2011**, *16*, 8515−8534.
(24) Stone, T. W. Development and therapeutic potential of kyrurenic acid and kynurenine derivatives from neuroprotection. *Trends Pharmacol. Sci.* **2000**, *21*, 149−154.

DOI: 10.1021/acs.jafc.5b01027
J. Agric. Food Chem. 2015, 63, 3587−3592

hemagglutinating activity,[16] are both found in the seed meal after extraction of the valuable oil, constraining the development of castor as an alternative to petroleum for energy and as a raw material for a wide variety of industrial and consumer products.[17] The immunochemistry of ricin has been extensively studied, particularly to optimize therapeutic immunotoxins containing ricin A chain[18] and to define potentially protective and therapeutic antibodies.[19] Exploitation of ricin antibodies and the amplification afforded by the polymerase chain reaction (PCR) has contributed new tools for food defense.[20,21] In an earlier study, we used BLI to study the interaction of ricin and RCA-1 with antibodies.[22] In this report, we describe BLI and ELISA experiments to quantitate milk matrix effects and mitigate their impact on the analysis of a carbohydrate-binding protein, such as ricin.

MATERIALS AND METHODS

Chemicals, Biological Reagents, and Milk Samples. Analytical-reagent-grade chemicals and reverse-osmosis water filtered to 0.055 μS/cm were used in these studies. Ricin was obtained from Vector Laboratories (Burlingame, CA). Asialofetuin was obtained from Sigma (St. Louis, MO). The principal buffers and milk samples used in ELISAs and BLI were phosphate-buffered saline (PBS), PBS−0.05% (v/v) Tween-20 (PBST), and PBST with 10 mg/mL bovine serum albumin (BSA), and 0.01% (w/v) thimerosal (BPT).[4,22] For binding in the BLI system, both PBS and kinetics buffer (KB, PBST with 1 mg/mL BSA) were used at pH 7.4. Biotinylated mAbs were detected with horseradish peroxidase (HRP)−streptavidin (SA) conjugate (Invitrogen, Eugene, OR) at 0.3−1 μg/mL. Nonfat dry milk (NFDM), pasteurized and fortified with vitamins A and D (Safeway, Oakland, CA), was reconstituted (9.6 g/100 mL) and used immediately. Fresh milk labeled as fat-free (0% fat), reduced fat (2.1% fat), or whole (3.3% fat) milk was used before its sell-by date (Clover Stornetta Farms, Petaluma, CA). Milk samples and samples dialyzed against PBS were stored up to 1 week at 4 °C with the addition of 0.02% (w/v) NaN_3. Dialyses were conducted in SpectraPor 2 cellulose tubing, 10 mm flat width (Spectrum Laboratories, Rancho Dominguez, CA), and sealed with plastic clips or knots.

BLI. BLI studies were conducted using a model QK Octet biosensor and amine-reactive (AR) or SA sensor tips (ForteBio, Menlo Park, CA) to determine association and dissociation rate constants (k_a and k_d) and k_d/k_a, the equilibrium dissociation constant, K_D.[22] Binding rate constants were determined in three replicate experiments using five analyte concentrations in KB (2-fold dilutions from 10 μg/mL), unless otherwise noted. Regeneration of sensor tips following binding used a series of three 10 s immersions in 10 mM glycine−HCl at pH 1.7, alternating with PBS. The criterion for acceptable BLI data was fit of the sensorgrams to a 1:1 binding model, with $R^2 \geq 0.9$, and data are expressed as the mean ± standard deviation.

Analysis of Ricin Binding to ASF. ASF was immobilized on AR sensor tips at 20 μg/mL. Milk samples were diluted to 0.5% (v/v) and spiked with ricin at 1 μg/mL. Association steps were 600 or 1200 s, after which dissociation occurred in the same milk/buffer mixture. Replication was as follows: undialyzed (control) fresh milk, $n = 5$; dialyzed fresh milk, $n = 6$; and NFDM samples, $n = 3$.

BLI Sandwich Format. mAb 1797 was immobilized on AR sensor tips at 20 μg/mL. For the association step, sensor tips were dipped into wells containing ricin in buffer with or without reconstituted NFDM (2%, v/v). After ricin binding, sensors were moved immediately to wells containing b-mAb 1443, the same reagent used for detection in ELISA. Rate constants were normalized as a percent of values for the control buffer matrix ($n = 25$).

BLI Analysis Using Milk as a "Sink". Biotinylated mAb 1797 was immobilized on SA sensor tips at 10 μg/mL. After association under standard conditions (10 μg/mL ricin in KB), sensor tips were moved to wells containing buffer or reconstituted NFDM (10−100%, v/v) for the dissociation step.

MAbs and ELISA. The monoclonal antibodies that bind ricin were described previously.[3,23] MAbs were isolated from hybridoma culture supernatants by hydrophobic charge-induction chromatography on MEP-Hypercel (Pall Life Sciences, Port Washington, NY)[24] and affinity chromatography on Protein G-agarose (Pierce, Rockford, IL) in accordance with the protocols of the manufacturers. Purified mAbs were stored at 0.5−1 mg/mL in the presence of NaN_3 and a mixture of serine, cysteine, and acid protease inhibitors (Sigma). Biotinylated mAbs (b-mAbs) were prepared using *N*-hydroxysuccinimide (NHS)−biotin ester (Pierce) with an initial ester/antibody molar ratio of 10. ELISA was performed as described previously,[4] and data were fit to a logistic equation ($y = a_0 + a_1/(1 + (x/a_2)^{a_3})$) using SlideWrite, version 7.01 (Advanced Graphics, Rancho Santa Fe, CA). Coefficient a_2 is the analyte concentration at half-maximal binding (EC_{50}). Briefly summarized, analytical samples and immunoreagents (ricin, mAb dilutions, biotinylated mAbs, and diluted HRP−SA conjugate) were prepared and applied to ELISA wells with 30 min incubations. Spiked milk samples were incubated for 10 min before application to ELISA wells. Ricin-containing analyte and the first wash from ELISA are collected by a pipet and inactivated using sodium hypochlorite solution. After the analyte binding step and subsequent wash, biotinylated mAb (b-mAb 1443 at 100 ng/mL, unless noted otherwise) was added (100 μL/well) and incubated for 30 min. After an additional wash step, ELISAs were developed with HRP−SA and K-Blue tetramethylbenzidine substrate (Neogen, Lexington, KY). The reaction was stopped by the addition of 100 μL of 0.3 M HCl, and $A_{450\ nm} - A_{650\ nm}$ was determined using a M2 microplate reader (Molecular Devices, Sunnyvale, CA). Two or three well replicates were averaged for each ELISA data point, and experiments were conducted in triplicate, unless otherwise noted.

ELISA on Asialofetuin-Coated Microwells. Ricin (0, 1.25, 2.5, 5, 10, 20, 40, 80, and 100 ng/mL or a subset of these standards as shown on graphs) and b-mAb 1443 (100 ng/mL) were added sequentially, with intervening wash steps.

Effect of Milk in ELISA on ASF- and mAb 1797-Coated Microwells. Ricin (10 ng/mL) was prepared in neat and diluted 0% fat fresh milk in PBST + BSA. The ELISA was then conducted and developed under standard conditions with b-mAb 1443, HRP−SA, and substrate.

ELISA with Ricin-Spiked Milk or Milk Sequentially Applied. For the "spiked" condition, ricin (10 ng/mL) was added to buffer or to milk at various dilutions with a 10 min pre-incubation before application to wells and incubation for 30 min. In the "sequential" condition, ricin in buffer was applied to the wells. After incubation (30 min) and washing, the dilutions of milk were added to the wells for a further incubation of 30 min. For both conditions, plates were washed and b-mAb 1443 (100 ng/mL) was applied to detect bound ricin. Assays were developed with HRP−SA and substrate. To determine the time course for changes in ASF-bound ricin during the incubation with 1% milk in the "sequential" condition, 100 μL of milk was added to the ELISA wells containing ASF-bound ricin but removed at various times from 1 to 30 min and replaced with the standard ELISA buffer, BPT.

Sugar Effect on Ricin Binding to mAb 1797. Ricin was used as the analyte (20 ng/mL in control buffer or 0.133 M galactose or lactose). ELISA used mAb 1797-coated ELISA wells and b-mAb 1642 or b-mAb 1443 (100 ng/mL; $n = 2$, for each condition) as the detection antibody. Experiments were also conducted in kinetics buffer to mimic conditions used for BLI experiments. The dose−response effect of galactose was determined using 0, 14.7, 44.3, and 133 mM galactose.

Multiple Sample Comparisons. For multiple sample comparison of binding data under differing conditions, one-way analysis of variance (ANOVA) was used with Tukey's *post hoc* honestly significant difference (HSD) procedure to determine which means were significantly different (Statgraphics Centurion, version 15, Statpoint Technologies, Warranton, VA). A p value of <0.05 was considered significant.

Safety Information. Ricin is highly toxic and is regulated as a Select Agent (7 CFR Part 331 and 9 CFR Part 121). Special handling and inventory control are required.

DOI: 10.1021/acs.jafc.5b01136
J. Agric. Food Chem. 2015, 63, 3593−3598

RESULTS AND DISCUSSION

Immunosorbent Analysis of Ricin Binding to ASF. The binding of ricin to ASF was studied in sandwich ELISA, with ASF-coated wells and b-mAb 1443 as the detection antibody, as shown in Figure 1. In control experiments, ricin bound with

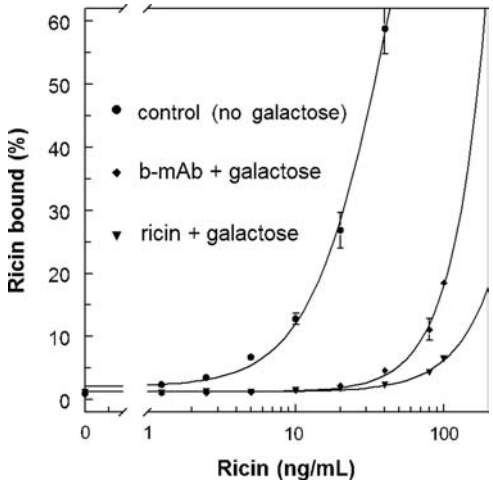

Figure 1. ELISA on ASF-coated microwells: (●) control, both ricin analyte and b-mAb 1443 applied in BPT; (◆) ricin applied as in the control and b-mAb 1443 applied in BPT containing 100 mM galactose; and (▼) ricin applied to wells in BPT containing 100 mM galactose and b-mAb applied as in the control.

EC_{50} = 30 ng/mL. When ricin was applied to the microwells as in the control but b-mAb 1443 was applied in buffer containing 100 mM galactose, binding was greatly reduced, with EC_{50} approximately 200 ng/mL. The presence of 100 mM galactose in the ricin sample solution reduced the binding more dramatically, to less than 5% of the control level (EC_{50} > 1000 ng/mL). This pattern of binding was expected from the known lectin activity of ricin,[25] and the reversibility of ricin binding reflects that ASF is only a moderate-affinity ricin receptor.[13]

Effect of Milk on Binding of Ricin to mAbs and ASF in ELISA. The effect of milk on the binding of ricin to mAbs and ASF was studied by ELISA using mAb- and ASF-coated microwells. The results of one set of assays are illustrated in Figure 2 and show that nonfat milk inhibits 50% of ricin binding at about 0.3% (v/v) for ASF. Comparable inhibition of binding to mAb 1797 occurred at a milk concentration of 55% (v/v). The effect of milk on ricin binding to ASF was further explored to determine whether the reduction of ricin binding to ASF by milk required that milk be present during initial ricin binding, the "spiked" milk condition. This condition was compared to a "sequential" ELISA in which milk was added to assay wells after the ricin-binding and wash steps were completed. The results are illustrated in Figure 3. The results show that milk does not have to be present during the binding step to have an inhibitory effect. The inset graph shows the time course for removal of previously ASF-bound ricin in the presence of milk. The process is nearly complete within 30 min, under the 1% milk condition. The effect of milk on ricin binding to ASF is consistent with the demonstration that milk could abrogate the effect of ricin on Vero cells.[6] Cellular and *in vivo* ribosome-inactivating activity begins with binding of ricin to cellular receptors.[26] We next conducted preliminary experiments that showed dialysis relieved the effect of milk

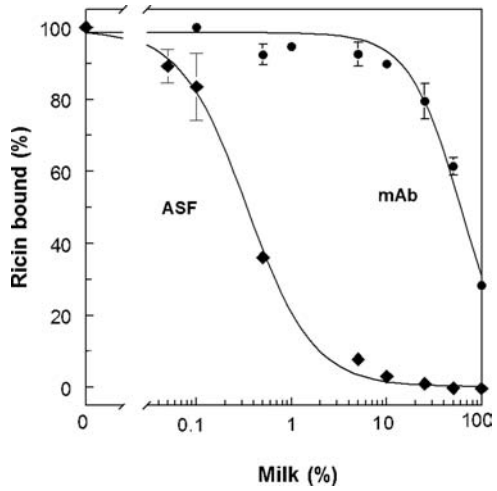

Figure 2. Effect of milk on ricin binding to ELISA wells coated with ASF or mAb 1797.

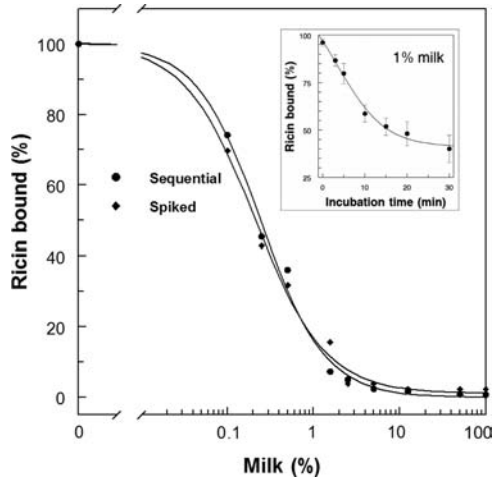

Figure 3. ELISAs using microplate wells coated with ASF conducted under two conditions: (◆) ricin (10 ng/mL) spiked into buffer or diluted milk applied to wells with 30 min of incubation and (●) ricin in buffer applied to the wells, incubated, and washed, followed sequentially by incubation with dilutions of milk. (Inset) Time course for removal of ASF-bound ricin during the incubation with 1% milk in the "sequential" condition.

on binding to ASF (data not shown). It seemed a reasonable hypothesis that sugars found in milk could account for this observation. Bovine milk contains approximately 48 g/L (0.14 M) lactose, β-D-galactopyranosyl-(1 → 4)-D-glucose,[27] the principal milk sugar, and we next tested the hypothesis.

Effect of Sugars on Ricin Capture by mAb 1797 in ELISA. Figure 4 shows the effect of sugars on the detection of ricin in ELISA using mAb 1797 for capture. When present in the analyte "capture" incubation step, galactose and lactose inhibited binding, producing about 20 and 40% inhibition, respectively, at 0.133 M. Means for galactose and lactose were significantly different from controls ($p < 0.05$, paired t test). Similar results were obtained when ELISAs used kinetics buffer (1 mg/mL), instead of PBST + BSA (10 mg/mL BSA), to mimic matrix conditions used in BLI studies described below. The inset graph shows a representative data set from three experiments determining the dose dependence of the galactose effect. Experiments were also performed with other capture/b-

DOI: 10.1021/acs.jafc.5b01136
J. Agric. Food Chem. 2015, 63, 3593−3598

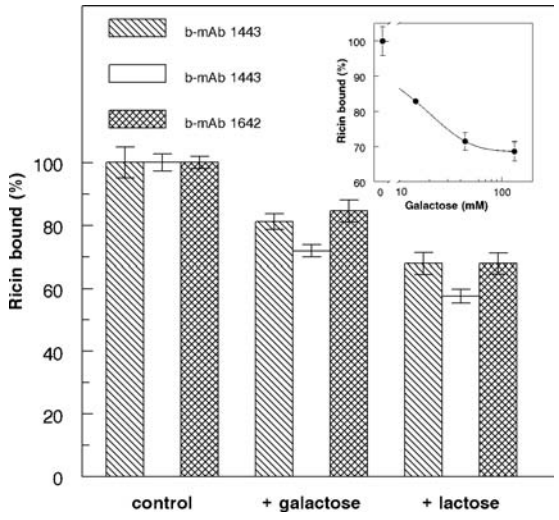

Figure 4. Effect of sugars on binding of 20 ng/mL ricin to mAb 1797, with b-mAb 1642 or b-mAb 1443. The cross-hatched bars illustrate results with ricin in KB, and the open bars illustrate results with ricin in BPT. (Inset) Galactose concentration dependence for ELISA in kinetics buffer with b-mAb 1443.

mAb detection sandwich ELISAs, but no significant sugar effects were observed (data not shown), suggesting that the inhibition observed with mAb 1797/b-mAb 1443 was epitope-dependent.

Studies Using BLI. To identify which steps in ricin binding to ASF and mAbs are affected by components of milk, we next determined rate constants for binding.

Ricin Binding to ASF. For these experiments, ASF was immobilized on AR sensor tips as ligand. The ricin analyte (1 μg/mL) was present in buffer or various types of milk (0.5%, v/v, in kinetics buffer), with or without prior dialysis versus PBS. The upper panel of Figure 5 shows the k_a values determined for ricin binding in four milk samples, undialyzed and dialyzed, and the lower panel of Figure 5 shows the dissociation constants. Multiple-sample comparison of the four control and four dialyzed milk samples indicated no significant differences among the means of either group of samples. For NFDM, the control sample k_a was significantly higher than the dialyzed ($p = 0.012$), but the difference was not significant for the other three samples. The values of k_d for all dialyzed fresh milk samples were lower than corresponding values for controls, but the difference was not significant for NFDM. Dialysis thus resulted in stronger binding of ricin in the fresh milk samples.

Ricin Binding to mAb 1797 in a BLI Sandwich Configuration. We wished to analyze ricin binding in BLI by mimicking ELISA conditions using the Octet biosensor. The first two layers of the "sandwich" were applied in turn as follows. Capture mAb 1797 was immobilized on AR sensors, and then sensors were moved to wells containing ricin in buffer with or without reconstituted NFDM (2%, v/v). After ricin binding, sensors were moved immediately to wells containing b-mAb 1443, for the upper layer of the sandwich, as for ELISA, although no secondary conjugate was used or needed in the BLI experiment that relied on the optical properties of the biolayer to provide a signal. The results are shown in Figure 6. Overall, the results indicate that ricin binds well to mAb 1797 in the presence or absence of milk, whether dialyzed against PBS or not. This is consistent with results that we reported[4] on the effectiveness of mAb 1797 as a capture antibody for ELISA

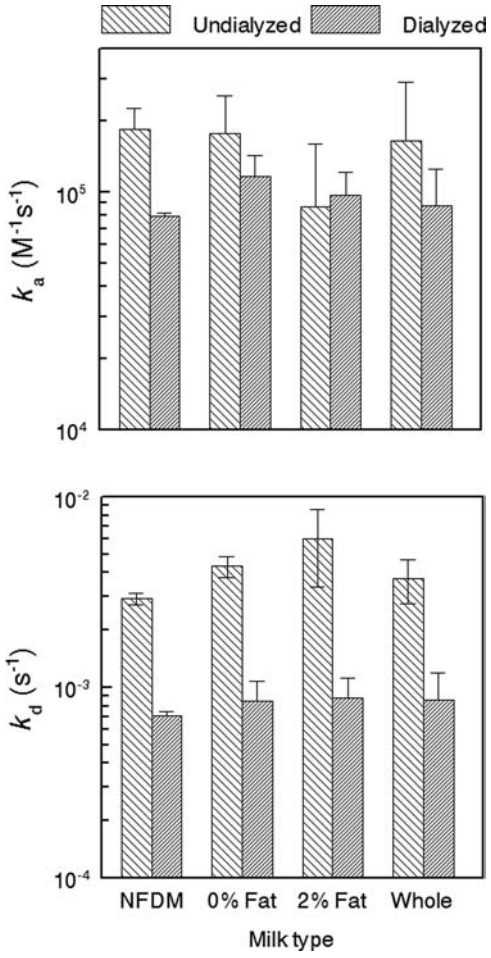

Figure 5. BLI analysis of ricin binding to ASF immobilized on AR sensor tips: (top panel) association constants, k_a, and (bottom panel) dissociation rate constants, k_d.

of ricin in food matrices. As in the ELISA, b-mAb 1443 is incubated in buffer, without milk, and is able to provide the upper layer of the sandwich on this platform. Once ricin is tightly bound to mAb 1797, it is available to bind b-mAb 1443. Ricin is thought to have three galactose-binding sites[28−30] and can therefore interact with ASF with much higher avidity than indicated by the relatively low association constants of individual sites. The higher affinity binding of mAb 1797 compared to ASF, even with lower probability of multiple site binding, overcomes the milk effect on dissociation of ricin from the antibody binding site.

Effect of Milk on Dissociation of Ricin from mAb 1797. The ELISA results above (Figure 3) indicated that milk inhibits the binding of ricin even in the "sequential" procedure. The effect of milk on dissociation of the ricin−mAb complex was studied using biotinylated mAb 1797 immobilized on SA sensors. To achieve greater accuracy near the limit of instrument sensitivity, this experiment included varying percentages of reconstituted NFDM in kinetics buffer during the dissociation step. These conditions were expected to minimize re-association of ricin with immobilized mAb, a procedure referred to as a sink method.[31]

Figure 7 shows the effect of analysis of ricin binding to mAb 1797 (b-mAb 1797 immobilized on SA sensor tips) in the absence or presence of milk. The association constant, k_a, was not affected significantly by the presence of milk, but the

DOI: 10.1021/acs.jafc.5b01136
J. Agric. Food Chem. 2015, 63, 3593−3598

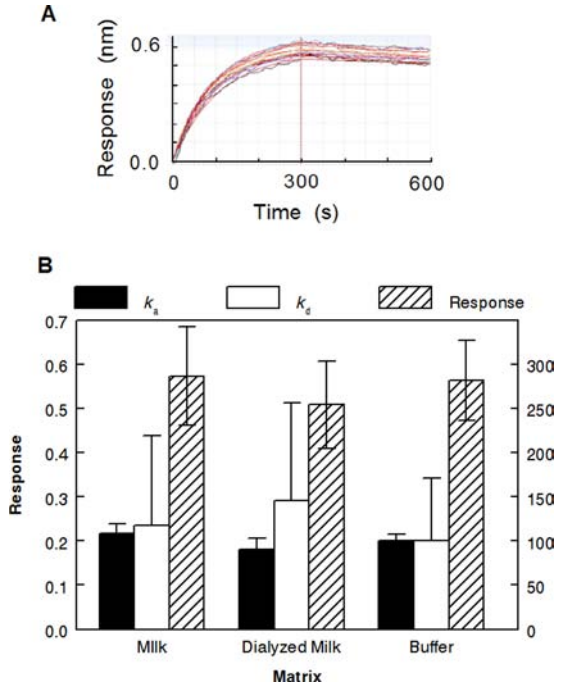

Figure 6. BLI analysis using a mAb sandwich: (A) typical sensorgrams from one set of experiments (ricin in dialyzed milk) and (B) response (biolayer thickness) and association and dissociation rates shown for three conditions.

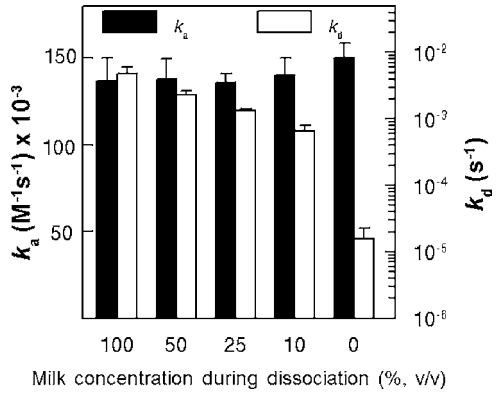

Figure 7. BLI analysis of ricin binding to b-mAb 1797 on SA sensor tips, with dissociation conducted under various conditions.

dissociation rate increased in the presence of milk. The multi-sample comparison test showed that the 50 and 100% milk samples were significantly different from the 0% control at the 95% confidence level, and the 25% sample was significantly different only at the 90% confidence level (Tukey's HSD test).

In this study, we demonstrated that the effect of milk on ricin binding to an antibody and a model receptor could be observed using BLI and ELISA, with complementary results. We also tested the use of a binding molecule as a "sink" to prevent the rebinding of analyte to a very high affinity ligand, mAb 1797. In this case, the sink was milk, a food. The "sink concept" in the context of well-based binding measurements refers to the use of a high-affinity ligand in solution that prevents rebinding of dissociated analyte to the sensing ligand.[31,32] The system can therefore emulate microfluidic-based systems that remove dissociating ligand from the sensor vicinity by flow. Because the antibody binding is fit well using a 1:1 binding model, this concept seemed relevant to the analysis of binding by mAb 1797. Even so, the contribution of divalent binding may also be significant, and increased dissociation in the presence of milk could result from abrogation of divalent binding. In either event, estimation of the dissociation rate constant was facilitated by the presence of a binder during dissociation. Although sensing techniques, such as BLI and surface plasmon resonance, use sophisticated, bulky instrumentation to measure optical properties of a surface that are influenced by the binding reactions in the "biolayer", miniaturized implementations of both sensor platforms have appeared in the marketplace. The practical use of these platforms in the field, in addition to the laboratory, will likely be realized in the near future, providing well-characterized, portable systems for detecting analytes that impact the safety and authenticity of the food supply. The results demonstrated that the effects of milk on the binding of ricin to carbohydrate receptors, as modeled by ASF, are mediated principally by dialyzable factors and that the use of high-affinity mAbs in ELISA mitigates the milk matrix effect on ricin analysis.

AUTHOR INFORMATION

Corresponding Author

*Telephone: +1-510-559-5783. Fax: +1-510-559-5880. E-mail: david.brandon@ars.usda.gov.

Funding

This study was undertaken under Project 2030-42000-048 of the National Research Program 108 (Food Safety) and was facilitated by the Western Regional Research Center student internship program (to Lisa M. Adams).

Notes

The authors declare no competing financial interest.

ACKNOWLEDGMENTS

The authors gratefully acknowledge Lily L. Yang for assistance with initial BLI studies, Anna M. Korn for antibody purification and biotinylation, and Matthew A. Taylor for assistance with ELISA (initially as a Bridge-to-Biosciences intern from City College of San Francisco).

ABBREVIATIONS USED

ANOVA, analysis of variance; AR, amine reactive; ASF, asialofetuin; b-mAb, biotinylated monoclonal antibody; BLI, biolayer interferometry; BPT, phosphate-buffered saline with Tween 20 with 10 mg/mL bovine serum albumin; BSA, bovine serum albumin; GFP, green fluorescent protein; HRP, horseradish peroxidase; HSD, honestly significant difference; NFDM, nonfat dry milk; RCA-1, *Ricinus communis* agglutinin-1; SA, streptavidin

REFERENCES

(1) Brandon, D. L.; Carter, J. M. Immunoassay. In *Handbook of Food Safety Engineering*; Sun, D.-W., Ed.; Blackwell: London, U.K., 2012; pp 279−312.

(2) Oste, R. E.; Brandon, D. L.; Bates, A. H.; Friedman, M. Effect of Maillard browning reactions of the Kunitz soybean trypsin inhibitor on its interaction with monoclonal antibodies. *J. Agric. Food Chem.* **1990**, *38*, 258−261.

(3) Brandon, D. L. Detection of ricin contamination in ground beef by electrochemiluminescence immunosorbent assay. *Toxins* **2011**, *3*, 398−408.

(4) Brandon, D. L.; Korn, A. M.; Yang, L. L. Immunosorbent analysis of ricin contamination in milk using colorimetric, chemiluminescent

DOI: 10.1021/acs.jafc.5b01136
J. Agric. Food Chem. 2015, 63, 3593−3598

and electrochemiluminescent detection. *Food Agric. Immunol.* **2014**, *25*, 160−172.
(5) He, X.; Lu, S.; Cheng, L. W.; Rasooly, R.; Carter, J. M. Effect of food matrices on the biological activity of ricin. *J. Food Prot.* **2008**, *71*, 2053−2058.
(6) Rasooly, R.; He, X.; Friedman, M. Milk inhibits the biological activity of ricin. *J. Biol. Chem.* **2012**, *287*, 27924−27929.
(7) Rasooly, R.; Hernlem, B.; Friedman, M. Low levels of aflatoxin B1, ricin, and milk enhance recombinant protein production in mammalian cells. *PLoS One* **2013**, *8*, No. e71682.
(8) Brandon, D. L.; Korn, A. M.; Yang, L. L. Detection of ricin contamination in liquid egg by electrochemiluminescence immunosorbent assay. *J. Food. Sci.* **2012**, *77*, T83−T88.
(9) Dawson, R. M.; Alderton, M. R.; Wells, D.; Hartley, P. G. Monovalent and polyvalent carbohydrate inhibitors of ricin binding to a model of the cell-surface receptor. *J. Appl. Toxicol.* **2006**, *26*, 247−252.
(10) Nagatsuka, T.; Uzawa, H.; Ohsawa, I.; Seto, Y.; Nishida, Y. Use of lactose against the deadly biological toxin ricin. *ACS Appl. Mater. Interfaces* **2010**, *2*, 1081−1085.
(11) Concepcion, J.; Witte, K.; Wartchow, C.; Choo, S.; Yao, D.; Persson, H.; Wei, J.; Li, P.; Heidecker, B.; Ma, W.; Varma, R.; Zhao, L. S.; Perillat, D.; Carricato, G.; Recknor, M.; Du, K.; Ho, H.; Ellis, T.; Gamez, J.; Howes, M.; Phi-Wilson, J.; Lockard, S.; Zuk, R.; Tan, H. Label-free detection of biomolecular interactions using biolayer interferometry for kinetic characterization. *Comb. Chem. High Throughput Screening* **2009**, *12*, 791−800.
(12) Lord, J. M.; Roberts, L. M. Ricin: Structure, synthesis, and mode of action. *Top. Curr. Genet.* **2005**, *11*, 215−233.
(13) Dill, K.; Olson, J. D. Picogram detection levels of asialofetuin via the carbohydrate moieties using the light addressable potentiometric sensor. *Glycoconjugate J.* **1995**, *12*, 660−663.
(14) Vitetta, E. S. Synergy between immunotoxins prepared with native ricin A chains and chemically-modified ricin B chains. *J. Immunol.* **1986**, *136*, 1880−1887.
(15) Dawson, R. M.; Paddle, B. M.; Alderton, M. R. Characterization of the asialofetuin microtitre plate-binding assay for evaluating inhibitors of ricin lectin activity. *J. Appl. Toxicol.* **1999**, *19*, 307−312.
(16) Roberts, L. M.; Lamb, F. I.; Pappin, D. J.; Lord, J. M. The primary sequence of *Ricinus communis* agglutinin. Comparison with ricin. *J. Biol. Chem.* **1985**, *260*, 15682−15686.
(17) McKeon, T. A.; Auld, D.; Brandon, D. L.; Leviatov, S.; He, X. Toxin content of commercial castor cultivars. *J. Am. Oil Chem. Soc.* **2014**, *91*, 1515−1519.
(18) Weidle, U. H.; Tiefenthaler, G.; Schiller, C.; Weiss, E. H.; Georges, G.; Brinkmann, U. Prospects of bacterial and plant protein-based immunotoxins for treatment of cancer. *Cancer Genomics Proteomics* **2014**, *11*, 25−38.
(19) O'Hara, J. M.; Kasten-Jolly, J. C.; Reynolds, C. E.; Mantis, N. J. Localization of non-linear neutralizing B cell epitopes on ricin toxin's enzymatic subunit (RTA). *Immunol. Lett.* **2013**, *158*, 7−13.
(20) He, X.; McMahon, S.; McKeon, T. A.; Brandon, D. L. Development of a novel immuno-PCR assay for detection of ricin in ground beef, liquid chicken egg and milk. *J. Food Prot.* **2010**, *73*, 695−700.
(21) He, X.; McMahon, S.; Henderson, T. D.; Griffey, S. M.; Cheng, L. W. Ricin toxicokinetics and its sensitive detection in mouse sera or feces using immuno-PCR. *PLoS One* **2010**, *5*, No. e12858.
(22) Brandon, D. L.; Adams, L. M.; Yang, L. L.; Korn, A. M. Antibody interactions with *Ricinus communis* agglutinins studied by biolayer interferometry. *Anal. Lett.* **2014**, *14*, 1747−1758.
(23) Brandon, D. L.; Hernlem, B. J. Development of monoclonal antibodies specific for *Ricinus* agglutinins. *Food Agric. Immunol.* **2009**, *20*, 11−22.
(24) Boschetti, E. Antibody separation by hydrophobic charge induction chromatography. *Trends Biotechnol.* **2002**, *20*, 333−337.
(25) Wu, J. H.; Singh, T.; Herp, A.; Wu, A. M. Carbohydrate recognition factors of the lectin domains present in the *Ricinus communis* toxic protein (ricin). *Biochimie* **2006**, *88*, 201−217.
(26) Spooner, R. A.; Lord, J. M. Ricin trafficking in cells. *Toxins* **2015**, *7*, 49−65.
(27) Scrimshaw, N. S.; Murray, E. B. The lactose content of milk and milk products. *Am. J. Clin. Nutr.* **1988**, *48*, 1099−1104.
(28) Frankel, A. E.; Burbage, C.; Fu, T.; Tagge, E.; Chandler, J.; Willingham, M. C. Ricin toxin contains at least three galactose-binding sites located in B chain subdomains 1α, 1β, and 2γ. *Biochemistry* **1996**, *35*, 14749−14756.
(29) Ganguly, D.; Mukhopadhyay, C. Extended binding site of ricin B lectin for oligosaccharide recognition. *Biopolymers* **2007**, *86*, 311−320.
(30) Steeves, R. M.; Denton, M. E.; Barnard, F. C.; Henry, A.; Lambert, J. M. Identification of three oligosaccharide binding sites in ricin. *Biochemistry* **1999**, *38*, 11677−11685.
(31) Abdiche, Y.; Malashock, D.; Pinkerton, A.; Pons, J. Determining kinetics and affinities of protein interactions using a parallel real-time label-free biosensor, the Octet. *Anal. Biochem.* **2008**, *377*, 209−217.
(32) Lowe, P. A.; Clark, T. J.; Davies, R. J.; Edwards, P. R.; Kinning, T.; Yeung, D. New approaches for the analysis of molecular recognition using the IAsys evanescent wave biosensor. *J. Mol. Recognit.* **1998**, *11*, 194−199.

DOI: 10.1021/acs.jafc.5b01136
J. Agric. Food Chem. 2015, 63, 3593−3598

stress in the target organs, is one of the mechanisms by which Cd induces its toxicity.[18] Several investigations have reported that Cd induces oxidative stress and causes oxidative damage by interrupting the antioxidant defense systems.[20,21] Moreover, the antioxidant defense system consists of enzymes such as superoxide dismutase (SOD), glutathione peroxidase (GPx), and catalase (CAT)[20] that have vital roles in maintaining cellular homeostasis by eliminating ROS.[22] Chronic exposure to Cd results in an imbalance between oxidants and antioxidants of the cell tissues, revealing oxidative damage in the liver and kidney.[23]

However, less attention has been paid to assessing the bioavailability and toxicity of Cd in human cells using a complete chain (soil−rice−human) transfer of Cd.

The bioaccessibility, bioavailability, and toxicity of Cd from rice can be determined by in vitro methods. The development of an in vitro Cd bioavailability model technique that revives gastric and small intestinal digestion in humans, coupled with intestinal epithelial cells (Caco-2), presents an advanced physiological measure for assessing Cd bioavailability issues.[24] Caco-2 cells under suitable and controlled conditions can differentiate into polarized enterocyte-like monolayers. After differentiation, they develop microvilli and in several ways work similarly to small intestinal epithelial cells.[25] Evaluations by different laboratories showed that the expressions of transporters by Caco-2 cells monolayers and the small intestine were similar.[26] This in vitro model is currently considered as the best approach, in terms of cost and time, to investigate the bioavailability of different food components as a prelude to in vivo study.[27] In the present study, this model was used in combination with a HL-7702 cell model to assess the bioaccessibility, bioavailability, and toxicity of Cd from contaminated polished rice grain.

Few studies have investigated the bioaccessibility and bioavailability of heavy metals in vegetables.[16,24,28] To the best of our knowledge, this is the first study reporting the transfer of Cd from two soils of different texture to rice and subsequent effects on bioaccessibility, bioavailability, and toxicity in humans.

The objectives of this study were to (i) assess the impact of different textured soils on Cd accumulation in polished rice; (ii) examine the relationship of Cd in polished rice with Cd bioavailability in soil using a Caco-2 cell model; and (iii) confirm the maximum limit of Cd that does not cause toxicity in human liver cells using in vitro digestion coupled with Caco-2/HL-7702 cell models.

MATERIALS AND METHODS

Chemicals and Reagents. $Cd(NO_3)_2$ was purchased from Sinopharm Chemical Reagent Co., Ltd. (Shanghai, China). Porcine pepsin, pancreatin, bile salts, and 3[4,5-dimethylthiazol-2-yl]-2,5-diphenyltetrazolium bromide (MTT) were purchased from Sigma-Aldrich (St. Louis, MO, USA). Dulbecco's modified Eagle medium (DMEM with glucose 4.5 g L^{-1}), trypsin−EDTA, phosphate-buffered saline (PBS), and fetal bovine serum (FBS) were purchased from Gibco Life Technologies (Grand Island, NY, USA). All enzyme testing kits were purchased from Nanjing KeyGen Biotech. Co., Ltd. (Nanjing, China). All reagents were prepared with deionized water (= 0.1 μS cm^{-1}) using a Milli-Q system (Millipore, Billerica, MA, USA).

Glass House Experiment, Sampling, and Analysis. *Soil Collection, Analysis, and Cd Spiking.* Two typical Chinese representative soils were used for investigation in this study. Samples of yellow (Periudic Argosols) soil and calcareous (Calcaric Regosols) soil were collected from the surface layer (0−20 cm) in Huzhou (119°14′−120° 29′ E; 30°22′−31°11′ N) and Ya'an counties (102°37′−103°12′ E, 29°23′−30°37′ N), respectively. The soils were air-dried and ground to pass through a 2 mm sieve. Both types of soil were analyzed for relevant physicochemical properties (Table 1).

Table 1. Selected Physical and Chemical Properties of the Soils

	yellow soil	calcareous soil
OM (g kg^{-1})	11.6 ± 0.72	21.8 ± 0.09
CEC (cmol kg^{-1})	12.05 ± 0.61	26.00 ± 1.34
pH	4.92 ± 0.06	8.11 ± 0.43
total N (g kg^{-1})	1.14 ± 0.07	1.46 ± 0.05
total P (g kg^{-1})	1.72 ± 0.08	1.00 ± 0.03
total K (g kg^{-1})	7.27 ± 0.19	9.53 ± 1.05
total Cd (mg kg^{-1})	0.47 ± 0.02	0.96 ± 0.03
total Zn (mg kg^{-1})	12.92 ± 0.85	33.9 ± 0.48
Fe(II) (mg kg^{-1})	25.4 ± 1.33	36.7 ± 2.18

Both soils were spiked with Cd as $Cd(NO_3)_2$ dissolved in an aqueous solution at loading rates of 2, 6, and 9 mg Cd kg^{-1} soil along with background value (CK). Distilled water was added to maintain soil moisture at 70% of its water-holding capacity. All of the Cd-spiked soil samples were aged for 1 year prior to usage for pot experiments and Cd analysis.

Glasshouse Experiment. A glasshouse experiment was conducted by growing rice (*Oryza sativa* L. var. Zhongzheyou 1) in pots during June−October 2012 at Zhejiang University, Hangzhou, China. Thirty-day-old seedlings were transplanted to plastic pots (20 cm diameter and 20 cm height). Each pot contained 5 kg of soil. All tests were conducted in triplicate under a completely randomized design. Fertilizers were applied (per pot) at rates of 180.5 mg of N (70% applied as the basal dose and 30% as the topdressing at the panicle initiation stage), 65.7 mg of P_2O_5, and 92 mg of K_2O.

Rice Sample Preparation. Plants were harvested at maturity and oven-dried at 65 °C for 45 h. Rice samples were manually threshed to separate rice grains. The biomass was determined by measuring the dry weight of grains. Brown rice was obtained by removing the husk using a laboratory dehusker (JLGJ4.5, Taizhou Cereal and Oil Instrument Co. Ltd., Zhejiang, China), which was then developed to polished rice using a laboratory polishing machine (JNMJ3, Taizhou Cereal and Oil Instrument Co. Ltd.). The polished rice sample was ground using a ball mill (Retsch, MM-301, Germany) and passed through a 60-mesh sieve and then kept at −20 °C prior to Cd analysis. Subsamples of the rice were cooked for 15−20 min with 1:2 rice/deionized water (w/v). The cooked rice sample was homogenized in a polytron homogenizer, and the homogenate was frozen and lyophilized before testing via the in vitro digestion/Caco-2/HL-7702 cell model.

Chemical Analysis. *Total Cd in Soil and Rice Grain.* A 0.20 g soil sample was digested with $HNO_3/HClO_4/HF$ (5:1:1). Similarly, 0.2 g of each rice sample was digested with HNO_3/H_2O_2 (4:1). The digested solution was transferred to a 25 mL volumetric flask, and the volume was made up with deionized water and filtered. Concentration of Cd in the filtrate was determined using inductively coupled plasma-mass spectrometry (ICP-MS, Agilent 7500a, Agilent Technologies, Santa Clara, CA, USA).

Cadmium Bioavailability and Toxicity Assays. *In Vitro Digestion of Rice Sample.* The method of Wei et al.[29] was used for in vitro digestion of rice samples. Briefly, 15 mL of mixed solution of 140 mM NaCl and 5 mM KCl was added to 5 g of cooked rice powder, and the pH was adjusted to 2.0 with 6 M HCl. For gastric digestion, 0.5 mL of pepsin (0.2 g of pepsin in 5 mL of 0.1 M HCl) was added, and the sample was incubated at 37 °C in a shaking water bath for 2 h. Before gastrointestinal digestion, the pH of the digester was raised to 5.0 with 1 M $NaHCO_3$ solution, 2.5 mL of pancreatin−bile solution (0.45 g of bile salts and 0.075 g of pancreatin in 37.5 mL

DOI: 10.1021/jf505557g
J. Agric. Food Chem. 2015, 63, 3599−3608

of 0.1 M $NaHCO_3$) was added, and the mixture was again incubated in a shaking water bath for 2 h at 37 °C. The sample was cooled in an ice bath for 10 min, and then the pH was adjusted to 7.2 with 0.5 M NaOH. The intestinal digester was heated for 4 min at 100 °C in a water bath to inhibit protease. The gastrointestinal digester was then cooled on ice and centrifuged at 3500*g* for 1 h at 4 °C. Then supernatant was transferred and pooled. Prior to the addition of rice soluble fraction to the cells, glucose (5 mM) and HEPES (50 mM) were added to the soluble fraction to make it similar to the culture media.

Cell Culture. The Caco-2 cells and HL-7702 cells were obtained from the Institute of Biochemistry and Cell Biology (SIBS, CAS, Shanghai, China) and used in assays at passage 20−41. Both cells were normally cultured in 25 cm^2 flasks (Corning Inc., Corning, NY, USA) and maintained in high glucose (4.5 g L^{-1}) DMEM, supplemented with 20% (v/v) heat-inactivated fetal bovine serum, 1% (v/v) nonessential amino acids, 4 mM L-glutamine, and 1% (v/v) and antibiotics (complete medium). The cells were incubated in a cell culture incubator (Heraeus, BB15, Germany) at 37 °C, 5% CO_2 in a humidified atmosphere, and the medium was changed every 48 h. Monolayers were subcultured with 7 and 4 day passage frequencies for Caco-2 cells and HL-7702 cells, respectively, by treatment with 0.25% trypsin−EDTA solution. For the Caco-2 cell model, 5×10^4 cells cm^{-2} in 1.5 mL of complete DMEM was seeded in permeable polycarbonate filters (24 mm diameter, 0.4 μm pore size, Costar Corp.), and 2.5 mL of complete DMEM was added in the basal compartment. For Cd toxicity assays HL-7702 cells were seeded in 6-well culture plates (Costar Corp.) at a density of approximately 5×10^3 cells/well. The medium was changed every 2 days, and the Caco-2 and HL-7702 cell cultures were maintained for 21 and 10 days to reach the stationary growth phase and to allow for maximal functional differentiation. Subsequently, the integrity of the Caco-2 cell monolayer was checked by measuring transepithelial electrical resistance (TEER) using a Millicell-ERS meter (Millipore Corp.) according to the manufacturer's protocols. Only those filters that had TEER values >250 Ωcm^2 at the beginning and the end of the experiment were included. The monolayer used in this study exhibited adequate TEER values of 520−610 Ωcm^2.

Cadmium Uptake Experiment in Caco-2 Cell. Before the Caco-2 uptake experiment, the growth medium was removed from each transwell and the Caco-2 cell layer was washed twice with phosphate-buffered saline (PBS) at a temperature of 37 °C and pH 7 to remove any unattached cells. Then 2.5 mL of standard transport solution (130 mM NaCl, 10 mM KCl, 1 mM MgSO4, 5 mM glucose, and 50 mM HEPES, pH 7.4) was added into the basolateral compartment, and the apical compartment was filled with 1.5 mL of rice soluble fraction. Cell cultures were incubated for 2 h at 37 °C, 5% CO_2, and 95% relative humidity.[29] After 2 h of incubation, basolateral compartments were collected to determine the Cd transport across the monolayer, and part of it was used to check the toxicity in the HL-7702 cells. In the apical chamber cell monolayer was washed with PBS to remove nonspecifically bound mineral and residual medium. The cells were lysed by the addition of 1 mL of deionized water in the well and then harvested.

The concentrations of Cd in cell retention (Cd fraction in the Caco-2 cell monolayer), the transport solution (Cd collected from basolateral compartment), and the gastrointestinal digestion solution (soluble added) from cooked rice sample were determined using the ICP-MS. Bioaccessibility of Cd was analyzed according to the method of Oomen et al.,[30] as follows:

$$\text{bioaccessibility \%} = \frac{\text{Cd mobilized from rice sample during digestion } (\mu g)}{\text{Cd present in rice sample before digestion } (\mu g)} \times 100\%$$

Cadmium Toxicity Assays in HL-7702 Cells. To assess the toxicity of Cd, HL-7702 cells cultured in 6-well plates were exposed to the transport solution from Cd uptake experiment for 3 h at 37 °C, 5% CO_2, and 95% relative humidity.[31] Hereafter, the cells were washed two times with PBS to remove extracellular bound Cd. The cell monolayer was lysed by the addition of 1 mL of 0.25% trypsin−EDTA in the well and then harvested. Cytological and biochemical assays were carried out on the cell lysate and culture medium for determination of markers of cell damage and TEM.

Cytotoxicity Assay. *MTT Assay.* Cytotoxicity induced by Cd was assessed by MTT assay. Exponentially growing HL-7702 cells were trypsinized and plated at 5×10^4 cells per well in 96-well plates overnight to allow attachment. Cell cultures were treated with different transport solutions from Cd uptake experiment for 3 h at 37 °C. Control groups consist of cells in media, which are processed identically and incubated simultaneously as treated groups. Following exposure, cells were incubated with MTT at 5 mg mL^{-1} for 4 h at 37 °C. Then the medium was replaced with 100 μL of DMSO agitated for 10 min at room temperature. Absorbance was measured at 570 nm using a microplate spectrophotometer system (Bio-Rad-680, Bio-Rad, Hercules, CA, USA). Cell viability was expressed as a percentage of the control group. Cell MTT response (percent of control) was calculated by using the following equation:

$$\%\ \text{of control} = \frac{\text{absorbance}_{\text{treatment}}}{\text{absorbance}_{\text{control}}} \times 100\%$$

LDH Release. Cadmium cytotoxicity in HL-7702 cells was also assessed by LDH release into the culture medium after 3 h of exposure to Cd containing transport solution. The LDH release into the culture medium was determined with a commercially available kit (Jiancheng Biochemical Co., Ltd., Nanjing, China). The change in absorbance was recorded at 440 nm using a microplate spectrophotometer system (Bio-Rad-680). LDH release (percent of control) was calculated from the equation

$$\%\ \text{of control} = \frac{(\text{U LDH/mg of cell protein})_{\text{treatment}}}{(\text{U LDH/mg cell protein})_{\text{control}}} \times 100\%$$

Enzyme Assays. The HL-7702 cell antioxidant (SOD, GPx) and oxidant (H_2O_2) enzyme and lipid peroxidation (MDA) activities were measured using respective cellular activity assay kits (Jiancheng Biochemical Co., Ltd.). SOD and GPx activities were expressed in terms of international units per mg cell protein. MDA and H_2O_2 enzyme activities were expressed as nanomoles per milligram of cell protein and millimoles per milligram of cell protein, respectively. The HL-7702 cell protein was determined using a semimicro adaptation of the Bio-Rad DC protein assay kit (Bio-Rad Laboratories) according to the manufacturer's instructions.

Transmission Electron Microscopy. To morphologically observe the alterations in Cd-contaminated HL-7702 cells, an ultrastructural analysis was performed following the procedure of Charqui et al.[32] Following Cd treatment, HL-7702 cells were harvested and fixed overnight in 4% (v/v) glutaraldehyde 0.1 M PBS and post fixed in 1% (v/v) osmium tetroxide for 1 h. Samples were then dehydrated by treating with a graded series of ethanol followed by acetone. Then samples were rinsed and impregnated with Spurr's resin overnight. The ultrathin sections were prepared and mounted on copper grids for viewing in a transmission electron microscope (JEOL TEM-1230EX) at an accelerating voltage of 60.0 kV.

Quality Control of Cadmium Analysis. Standard reference material (soil GSBZ 50013-88 and rice flour NCSZC 73008), approved by General Administration of Quality Supervision, Inspection and Quarantine of the People's Republic of China (AQSIQ), were used to check the accuracy of Cd analysis. The analytical results showed that the recoveries for SRMs were nearly 98 and 102.3%, respectively, and the precision and bias of the analysis were generally <5% for Cd.

Statistical Analysis. Data were analyzed using SPSS software version 18.0 (SPSS Inc., Chicago, IL, USA). Analysis of variance (ANOVA) was applied, with the least significant difference (LSD) test as a post hoc test, to compare the various means of different treatments in each series of experiments. Means were considered to be significantly different if the P value was smaller than 0.05 ($P < 0.05$).

DOI: 10.1021/jf505557g
J. Agric. Food Chem. 2015, 63, 3599−3608

RESULTS

Physicochemical Properties of Soils. Soils used in this study varied widely in their physicochemical characteristics (Table 1), which could influence the accumulation of Cd in rice grain. Total Cd and Zn concentrations (background value) in the YS were 0.47 and 12.92 mg kg^{-1}, whereas for CS, 0.96 and 33.9 mg kg^{-1}, respectively. Soil pH ranged from 4.92 for the yellow to 8.11 for the calcareous, namely, strongly acidic to mildly alkaline. The total organic matter was 11.6 g kg^{-1} in yellow and 22.6 g kg^{-1} in calcareous soil. The cation-exchange capacity (CEC) ranged from 12.05 cmol kg^{-1} for the yellow to 26.0 cmol kg^{-1} for the calcareous soil. Fe(II) in soil (background value) ranged from 25.4 to 36.7 mg kg^{-1} in yellow and calcareous soils, respectively.

Yield of Rice Grain. As compared to the control (nonspiked soils), rice grain yield appeared to increase at a low level of Cd (<2 mg kg^{-1}) in both soils, but the differences in grain yield were not statistically significant. The grain yield in YS decreased significantly at Cd loadings of 6 and 9 mg kg^{-1}, whereas in CS yield did not differ at all with Cd loading rates. Dry weights (DWs) of rice grain in relation to external Cd loading rates are summarized in Table 2.

Table 2. Effect of Cd Loading on Dry Weight (Grams per Pot) of Rice Grown in the Two Soils

Cd loading (mg kg^{-1})	YS[a]	CS[a]
CK	30.31 ± 0.76a	47.68 ± 1.97a
2	30.90 ± 0.58a	46.48 ± 2.32a
6	25.37 ± 0.73b	48.28 ± 1.22a
9	18.44 ± 1.68c	45.93 ± 2.70a

[a]YS refer to yellow soil and CS to calcareous soil. The results are expressed as the mean ± SD with three replications. Values within a column followed by a different letter are significantly different at $P < 0.05$.

Cd Concentration in Polished Rice Grain. The concentration of Cd in polished rice grain was significantly affected by soil type and increased with increasing external Cd loading (Figure 1). Cd concentration in rice was in the order straw > husk > polished rice and ranged from 0.98 to 86.11 mg kg^{-1}, from 0.26 to 22.48 mg kg^{-1}, and from 0.18 to 14.22 mg kg^{-1}, respectively. Cadmium accumulation in different rice parts was found to be significantly different due to the difference in Cd phytoavailability between the two soil types.

Bioaccessibility of Cd in Polished Rice Grain. The amount of Cd solubilized after in vitro digestion is an indicator of bioavailability. Increasing Cd loading rate had a significant effect on Cd bioaccessibility (Figure 2). Cadmium bioaccessibility in YS and CS rice ranged from 18.45 to 30.41% and from 6.89 to 11.43%, respectively. A significant increase was found in Cd bioaccessibility of polished rice from both soils at the higher loading rates (6 and 9 mg kg^{-1}) as compared to the control. These results suggest that most of the cadmium in CS rice at lower treatment levels remains nonbioaccessible and will not cause adverse health effects to local residents. However, in YS rice a considerable amount of cadmium was released during the in vitro digestion process.

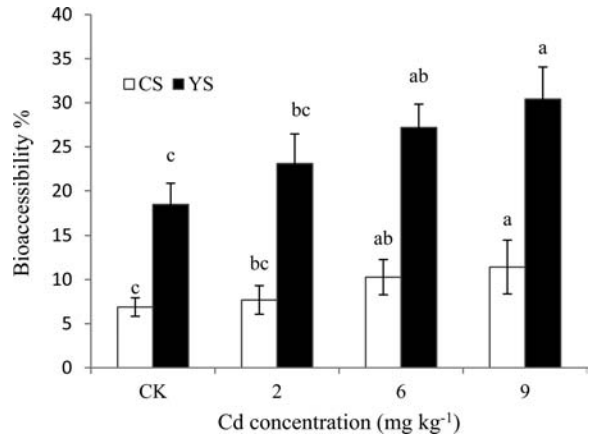

Figure 2. Effect of different Cd loading rates on bioaccessible fractions of Cd expressed as a percentage of the total concentrations in the polished rice grain. YS refers to yellow soil and CS to calcareous soil. The results are expressed as the mean ± SD with three replications. Different letters indicate significant differences at $P < 0.05$ as calculated by the least significant difference (LSD) test.

Cd Bioavailability of Polished Rice. Cd concentration in the bioaccessible fraction added to Caco-2 cells (soluble added), in cell monolayer (retention), basal medium (transport), and percentages of uptake are shown in Table 3. The

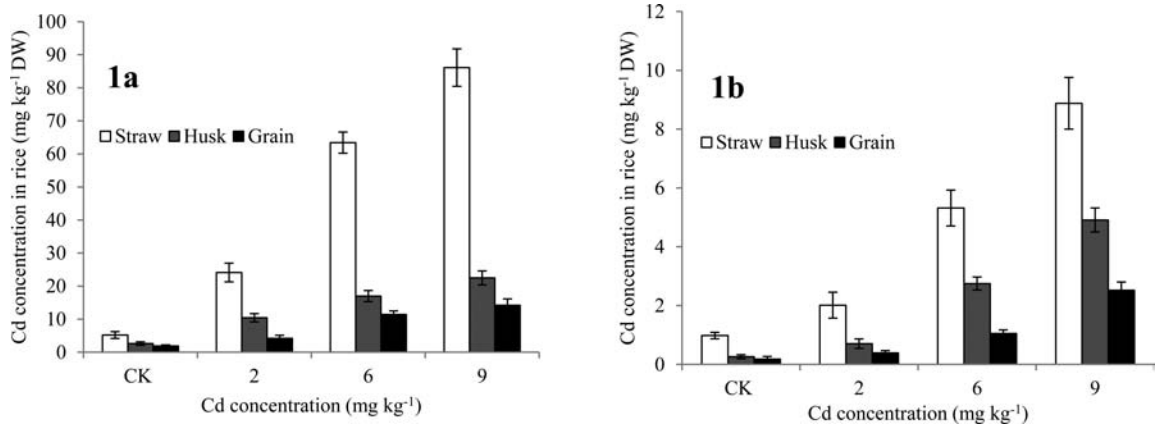

Figure 1. Cadmium concentration (mg kg^{-1} DW) in polished rice grain grown under different Cd loading rates in YS (a) and CS (b). The results are expressed as the mean ± SD. Different letters indicate significant differences at $P < 0.05$ as calculated by the least significant difference (LSD) test, $n = 3$. YS refers to yellow soil and CS to calcareous soil.

DOI: 10.1021/jf505557g
J. Agric. Food Chem. 2015, 63, 3599−3608

Table 3. Bioavailability: Total Cd Retention, Transport, and Uptake by Caco-2 Cells from Cooked Polished Rice[a]

Cd level	soluble added (μg)	retention (μg)	transport (μg)	retention %	transport %	cellular uptake %
			Yellow Soil			
CK	8.67 ± 1.57d	0.25 ± 0.12c	0.10 ± 0.05c	2.88 ± 0.37c	1.15 ± 0.22b	4.04 ± 0.46c
2	24.13 ± 3.36c	0.81 ± 0.14c	0.31 ± 0.05c	3.36 ± 0.33c	1.28 ± 0.34b	4.64 ± 0.68c
6	85.17 ± 6.08bc	4.14 ± 0.59bc	1.55 ± 0.22b	4.86 ± 0.74b	1.82 ± 0.57ab	6.68 ± 0.77b
9	108.12 ± 7.30a	6.61 ± 0.88a	2.71 ± 0.24a	6.11 ± 0.95a	2.51 ± 0.81a	8.62 ± 0.93a
			Calcareous Soil			
CK	0.31 ± 0.11c	0.01 ± 0.00c	0.00 ± 0.00c	1.61 ± 0.63a	0.16 ± 0.34a	1.77 ± 0.65a
2	0.75 ± 0.17c	0.01 ± 0.00c	0.00 ± 0.00bc	1.73 ± 0.81a	0.20 ± 0.37a	1.93 ± 0.37a
6	2.70 ± 0.77b	0.05 ± 0.02b	0.01 ± 0.00ab	1.85 ± 0.07a	0.26 ± 0.21a	2.11 ± 0.60a
9	7.20 ± 1.15a	0.14 ± 0.03a	0.02 ± 0.01a	1.94 ± 0.58a	0.31 ± 0.28a	2.25 ± 0.90a

[a]Results are expressed as the mean ± SD, $n = 3$. Values for each soil within a column followed by a different letter are significantly different at $P < 0.05$, as calculated by the least significant difference (LSD) test. Retention % or transport % is the percentage of Cd retention or transport in the total amount added (soluble added) Cellular uptake is calculated as [(retention + transport)/total Cd amount added to cell culture (soluble added)] × 100.

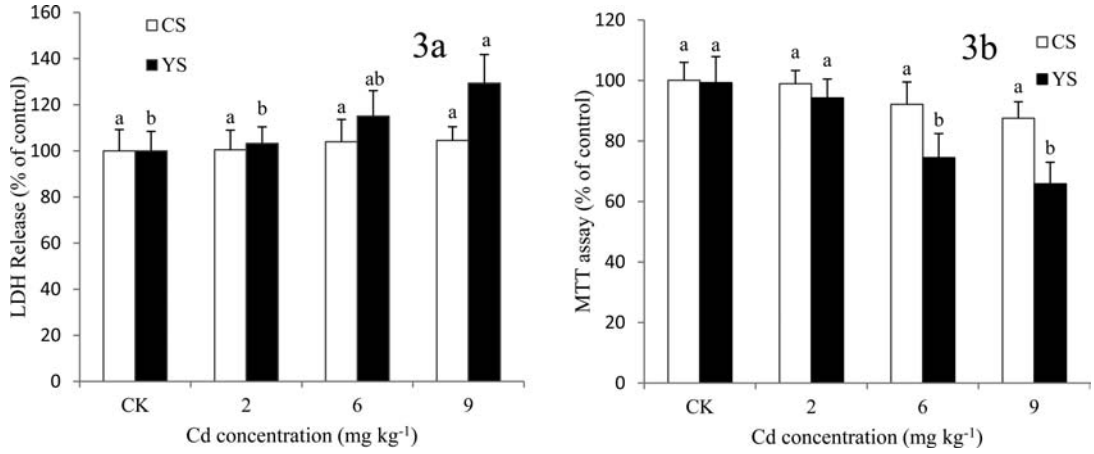

Figure 3. Effect of Cd loadings on LDH release (a) and MTT viability assay (b) in HL-7702 cells. Results are expressed as the mean ± SD. Different letters indicate significant differences at $P < 0.05$ as calculated by the least significant difference (LSD) test, $n = 3$.

Table 4. Toxicity Assays: Lipid Peroxidation (MDA), Oxidant Enzyme (H_2O_2), and Antioxidant Enzyme (SOD, GPx) Activities in HL-7702 Cells Treated with Different Concentrations of Cd Transported from Human Epithelial (Caco-2) Cells

		Cd concentration			
parameter	soil[a]	CK	2 mg kg^{-1}	6 mg kg^{-1}	9 mg kg^{-1}
MDA (nmol mg cell protein^{-1})	YS	2.92 ± 0.53b	2.93 ± 0.11b	3.00 ± 0.48ab	3.25 ± 0.39a
	CS	2.84 ± 0.17a	2.83 ± 0.28a	2.88 ± 0.30a	2.95 ± 0.28a
H_2O_2 (mmol mg cell protein^{-1})	YS	11.78 ± 0.83b	12.01 ± 0.19b	13.92 ± 0.92a	14.1 ± 0.35a
	CS	10.87 ± 1.00a	11.05 ± 0.84a	11.02 ± 0.96a	11.16 ± 1.13a
SOD (U mg cell protein^{-1})	YS	0.34 ± 0.08a	0.33 ± 0.01a	0.31 ± 0.1a	0.22 ± 0.08b
	CS	0.27 ± 0.03a	0.27 ± 0.07a	0.26 ± 0.04a	0.24 ± 0.08a
GPx (U mg cell protein^{-1})	YS	1.64 ± 0.24a	1.56 ± 0.38a	1.33 ± 0.40ab	1.15 ± 0.33b
	CS	1.01 ± 0.13a	0.97 ± 0.17a	0.91 ± 0.08a	0.87 ± 0.09a

[a]YS refers to yellow soil and CS to calcareous soil. Results are expressed as the mean ± SD, $n = 3$. Values within a row followed by a different letters are significantly different at $P < 0.05$, as calculated by the least significant difference (LSD) test.

results indicate that there were differences between the polished rice grains grown on two different soil types.

In the cell monolayer (retention), Cd concentration significantly varied from 0.25 to 6.61 μg and from 0.01 to 0.14 μg in YS and CS rice, respectively. Cadmium concentration in transport solution was increased, from 0.10 to 2.71 μg and from 0.00 to 0.02 μg, respectively, for YS and CS. Increasing Cd concentrations in the soluble fraction affected the percentages of Cd retention, transport, and uptake in YS rice, whereas for CS rice the percentages did not differ significantly from the control. Expressing retention, transport, and uptake of Cd calculated as percentage of the amount initially added revealed that in YS and CS rice, Cd retention (2.88−6.11 and 1.61−1.94%), transport (1.15−2.51 and 0.16−

DOI: 10.1021/jf505557g
J. Agric. Food Chem. 2015, 63, 3599−3608

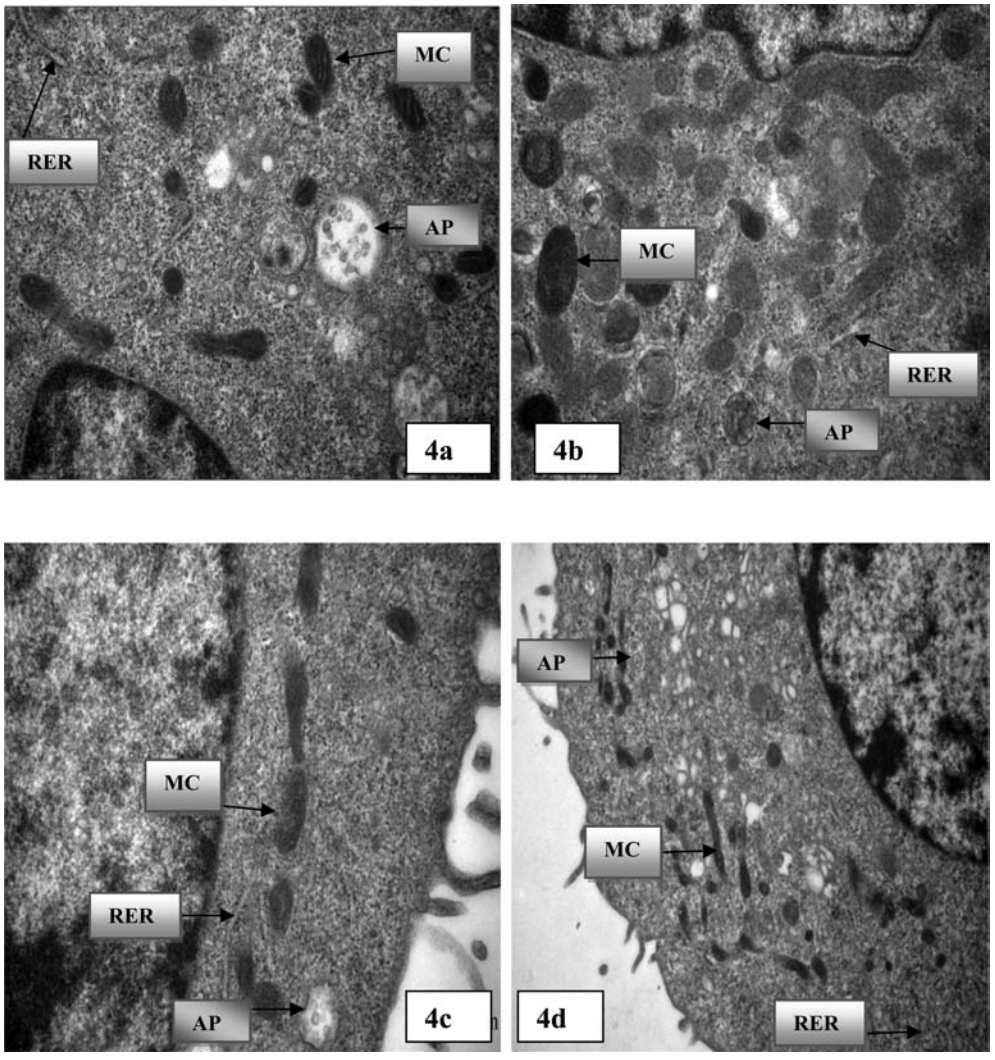

Figure 4. Electron microscopic graphs of HL-7702 cells: (a, b) TEM microscopic graphs of HL-7702 cells of YS at the control (CK) and Cd 9 mg kg^{-1} levels, respectively; (c, d) TEM microscopic graphs of HL-7702 cells of CS at the control (CK) and Cd 9 mg kg^{-1} levels, respectively. MC, mitochondria; RER, rough endoplasmic reticulum; AP, autophagy. YS refers to yellow soil and CS to calcareous soil.

0.31%), and uptake (4.04−8.62 and 1.77−2.25%) varied largely due to contrasting properties of the two soils.

Effect of Cadmium on Cytotoxicity Assays (LDH Release and MTT Viability Assay). To first establish the optimal experimental conditions for characterizing the effects of Cd on the human liver, HL-7702 cell membrane stability and viability were measured using LDH release and MTT assay as a function of increasing Cd concentrations in the transport solution. Statistical analysis of cytotoxic activities showed that Cd from CS rice did not have a significant effect on LDH release and MTT assay, but YS rice grown at Cd level >2 mg kg^{-1} significantly affected both LDH release and MTT assay. It was found that increasing Cd levels increased the LDH release in HL-7702 cells (Figure 3a) in CS and YS rice by 4 and 30%, respectively. The MTT assay to monitor the effects of different Cd concentrations transported from Caco-2 cells revealed that Cd from YS and CS rice suppressed cell stability by 12.47 and 34.14%, respectively (Figure 3b). A comparison of the two cytotoxicity assays showed that the LDH leakage assay was less sensitive than the MTT assay. However, both cytotoxicity assays showed initial cytotoxicity at the 6 mg kg^{-1} Cd level in YS rice (Figure 3).

Effect of Cadmium on Lipid Peroxidation and Enzymes (Oxidant + Antioxidant) Activities in HL-7702 Cells. The results for lipid peroxidation (MDA), oxidant (H_2O_2), and antioxidant (SOD, GPx) enzyme activities in normal human liver cells (HL-7702) due to Cd transported from Caco- 2 cells are shown in Table 4.

It was found that lipid peroxidation (MDA) in YS and CS rice was increased by 11.3 and 4%, respectively, from its respective control. As can be observed in the case of oxidant enzyme (H_2O_2), the YS and CS rice had a significant increase in H_2O_2 activity (by 19 and 2.66%, respectively, as compared to the control). The results showed that SOD activities in the YS and CS rice had decreases of 35 and 11%, whereas for GPx the decreases were about 30 and 13%, respectively, as compared to the control. In YS rice all toxicity assays showed a statistically significant effect at a Cd loading rate of 6 mg kg^{-1}. There was, however, no significant effect on lipid peroxidation and both enzyme activities on CS rice, indicating that a small amount of Cd transported from Caco-2 cells does not result in toxicity in HL-7702 cells.

Effect of Cd Stress on Ultrastructural Changes in HL-7702 Cells. Indeed, low doses (<1.55 μg) of Cd did not induce

DOI: 10.1021/jf505557g
J. Agric. Food Chem. 2015, 63, 3599−3608

apoptosis and toxicity in vitro in HL-7702 cells, as revealed by cytotoxicity assays and enzyme assays. A deeper understanding of Cd hepatotoxicity requires the identification of its intracellular localization and targets.

The TEM microscopic graphs of HL-7702 cells under CK and 9 mg kg^{-1} Cd stress from YS and CS rice are shown in Figure 4. As revealed by TEM microscopic graphs, the untreated (CK) HL-7702 cells exhibited large nuclei, surrounded by cytoplasm with healthy-looking mitochondria containing visible cristae, visible RER with attached granules, and autophagosome in their natural shape (Figure 4a,c). In YS rice treated cells (at the Cd rate of of 9 mg kg^{-1}) we found that Cd treatment promotes autophagy and swelling in mitochondria and rough endoplasmic reticulum. Cristae were not visible in mitochondria (Figure 4b). In CS rice TEM microscopic graphs of HL-7702 cells at the 9 mg kg^{-1} Cd level (Figure 4d) did not show any clear ultrastructural change in comparison to the control.

DISCUSSION

Significant amounts of Cd have been added and will continue to be added to the soils globally due to anthropogenic activities. Cadmium, a very toxic element, is of primary concern in soil and food contamination, particularly in rice cropping systems[33] as rice is the major crop that supplies food to a large portion of world population.[34] Therefore, rice grown on a Cd-contaminated soil has been an issue of human health concern. The present work is an attempt to improve our understanding about the health risk posed to humans from Cd accumulation in rice.

In the present study, it was observed that the yield of rice was not significantly decreased by Cd loading in CS, whereas in YS the rice yield was significantly decreased at the external Cd loading rates of 6 and 9 mg kg^{-1}. The observed effect of Cd on rice yield can be attributed to the adverse effects of Cd on physiological and biochemical functions in plants. Different mechanisms can explain this stimulatory effect of Cd on rice yield; for instance, metal ions may simulate the enzyme(s) activation in cytokinin metabolism, which enhances plant growth,[35] and a lower level of metal exposure may cause alterations in cytokinins and plant hormones that control the growth and development of plants.[36] Kaminek[36] found that cytokinins may delay senescence by maintaining photosynthetic activity and producing chlorophyll in plant leaves. However, previous studies also revealed that Cd could suppress plant growth by interfering with metabolic processes, inhibition of the proton pump, reduction of root elongation, and damage to photosynthetic machinery.[37,38] These results are in agreement with Rafiq et al.,[9] who observed that Cd at 8 mg kg^{-1} decreased polished rice grain yield by 11.7−168.5%, depending on soil type.

Cadmium loading at different rates significantly affected its accumulation in polished rice grains. Phytoavailability of Cd is related to soil properties, aging, and rate of Cd applied. Physicochemical characteristics of soil affected phytoavailability of Cd.[39] For example, changes in pH affect the sorption of Cd by soils and thereby its concentration in soil solution.[40] Rafiq et al.[9,39] stated that the Cd content of rice grain was highly dependent upon the soil pH, being highest at pH 4.85. An increase in soil pH decreases Cd concentration in soil solution or reduces it phytoavailability.[41] Other factors including exposure time, soil texture, and organic matter contents in soil also influence phytoavailability of Cd in soil.[9,39]

The bioaccessibility of Cd in polished rice grain was evaluated by simulated gastrointestinal digestion followed by a measurement of soluble Cd in the digester and thus covered only the first phase of the overall Cd absorption process. The soluble fraction obtained from the gastrointestinal digestion was used to carry out retention and transport experiments in Caco-2 cell models, and the transport solution was used to carry out the Cd toxicity experiment in the HL-7702 cell model. Both of these models offer a more physiological tool for determining Cd bioavailability and toxicity in food matrices, particularly when combined with a simulated digestion step. Cd bioaccessibility ranged from 6.89 to 30.41% for the rice investigated. These values are in the range reported by previous studies.[24,28,42,43] Our results are in agreement with Intawongse and Dean,[28] who observed a higher bioaccessibility for Cd and reported that it can be found in the gastric phase or the small intestinal phase depending on Cd concentration in a vegetable and the vegetable species. The metal bioaccessibility of food is controlled by many factors, such as microfibers of crystalline cellulase and phytates, phytochelatins, nutritional characteristics, and microbial processes.[44−46] The bioavailability of Cd (total uptake) from polished rice ranged from 1.77 to 8.62%, which is concordance with the previous reports.[24,42] The results indicated that soil type and Cd concentration in the soluble fraction had a significant effect on Cd bioavailability by Caco-2 cells. A possible explanation for the concentration-dependent Cd bioavailability in our study might be its chemical and physical properties related to essential metals such as iron (Fe) or zinc (Zn), which aid Cd transport and uptake in the cells by "ionic and molecular mimicry".[47] Whenever there is a deficiency of these essential elements, Cd absorption and toxicity are enhanced. Reeves and Chaney[48] reported that the association between subsistence rice population and food chain Cd disease may be linked to Fe and Zn deficiency commonly found in these rice-based diet consuming populations. The soils used in this study also supported this possibility as concentrations of Zn and Fe are lower in YS than in CS, which ultimately enhanced the bioavailability of Cd from rice grown in YS. Our findings suggest further investigations to assess the turnover pool of Cd in Caco-2 cells with marginal concentrations of iron and zinc. Regardless of soil type, our results indicated that rice from both soils had higher Cd retention percentages than transport. This finding is also in accordance with Zalups and Ahmed,[49] who reported that intestinal absorption of Cd is characterized by a rapid rate of metal accumulation within the intestinal mucosa and a low rate of diffusive transport into the circulatory system.

The main objective of the present study was to assess the toxicity of Cd in rice from YS and CS. The cytotoxicity assays revealed different profiles. In YS rice the MTT assay was more sensitive, which showed initial cytotoxicity at the Cd rate of 6 mg kg^{-1}, whereas the LDH leakage assay revealed Cd toxicity at a higher external loading rate (9 mg kg^{-1}). However, CS rice did not show any significant difference at all Cd levels for both cytotoxicity assays. The possible explanation can be that relatively low Cd concentrations (<1.55 μg) might enhance cell proliferation in a dose-dependent manner,[50] whereas at higher concentrations (>1.55 μg) Cd could induce apoptosis in many tissues, organs, and cells.[51,52] This finding is well in line with the result of Fotakis and Timbrell,[31] who compared the four in vitro cytotoxicity assays and found that only the MTT assay showed initial toxicity in HTC cells after 3 h of exposure to different Cd concentrations. This differential sensitivity can be

DOI: 10.1021/jf505557g
J. Agric. Food Chem. 2015, 63, 3599−3608

explained by the different nature of each assay. The LDH leakage assay is based on the release of the enzyme into the culture medium after cell membrane damage, whereas the MTT assay is mainly based on the enzymatic conversion of MTT in mitochondria.[31] It is thought that inhibition of the mitochondrial respiration induces active oxygen related cell death. Reactive oxygen species generated within the mitochondria can also damage mitochondrial components,[53] and therefore a cytotoxicity assay based on mitochondrial respiratory activity would give early signs of toxicity following exposure to a mitochondrial toxicant.

Cadmium-induced cytotoxicity is known to be intimately related to the generation of oxidative stress, so we have examined the lipid peroxidation (MDA), oxidant (H_2O_2), and antioxidant (SOD, GPx) effects of Cd in HL-7702 cells. The results clearly indicated that Cd at high concentrations (>1.55 μg) induced oxidative (MDA, H_2O_2) stress by inhibiting antioxidant (SOD, GPx) enzyme activities in human liver cells (HL-7702). These results are in agreement with Cuypers et al.,[54] who reported that Cd can induce oxidative stress via the inhibition of antioxidants. The production of oxidants as well as the protection against them is intrinsic to every living cell.

MDA, a well-known indicator of lipid peroxidation and oxidative stress, has been reported to increase in the liver and kidney upon exposure to Cd.[19] A statistically significant increase in MDA activity in YS rice due to Cd stress indicated oxidative stress in HL-7702 cells. These results are well in line with the previous findings.[51,55] The Cd-induced lipid peroxidation mechanism is multidirectional and may involve a decrease in the level of glutathione and the total pool of sulfhydryl groups and changes in the activities of antioxidant enzymes. Because Cd causes lipid peroxidation in numerous tissues both in vivo and in vitro,[56] it has been suggested that Cd may be able to initiate oxidative stress by producing hydroxyl radicals[57] and hydrogen peroxide.[53] Moreover, it has been shown that several oxidants and antioxidant defense systems protect cells from Cd-induced toxicity.[16]

To minimize oxidative damage, organisms have developed antioxidative mechanisms triggered by an increased ROS production. Oxidants such as ROS are balanced against this antioxidative defense system that consists of enzymes and metabolites in all subcellular compartments.[58] SOD and GPx are important antioxidant enzymes that protect against oxidative stress via elimination of ROS. Physiologically, SOD converts O_2 to H_2O_2 and thus protects against superoxide-induced damage.[59] GPx, in particular, is highly dependent on glutathione concentration. According to our findings, the major toxic effects of increasing doses of Cd involve decreased antioxidant enzyme levels. In our previous study we observed that Cd at 10 mg L^{-1} decreased the SOD and GPx activities in HL-7702 cells by 58 and 80.3%, respectively, which showed that Cd from salt solution had more toxic effects on HL-7702 cells than Cd transported from the rice soluble fraction.[51] These results agreed with previous studies.[55,60] According to Arroyo et al.,[61] Cd decreases the activity of antioxidant enzymes such as SOD, CAT, glutathione reductase (GR), and GPx. Moreover, Cd may increase the amount of free Cu and Fe ions that can promote oxidative stress via the Fenton reaction.[61] By these ways, Cd induces a pro-oxidative state in biological systems, resulting in the overproduction of ROS such as superoxide anion (O_2), hydroxyl radical (OH), and hydrogen peroxide (H_2O_2).

This study concludes that soil characteristics greatly influenced the bioavailability of Cd to rice and ultimately to Caco-2 cells. By selecting the proper soil type for rice cultivation, we may be able to avoid the dietary toxicity of Cd. This study also raises the possibility of a simple soil remediation method such as phytoextraction by using the coculture of Cd hyperaccumulator plants and rice, especially in acidic soils, to prevent further Cd disease. The results demonstrated that Cd is able to initiate oxidative stress and cell damage in human liver cell lines (HL-7702) when its transported concentration exceeds 1.55 μg. An effort was made to estimate the Cd bioavailability and toxicity in human (Caco-2, HL-7702 cells) from rice grown on Cd-contaminated soils, but further research to investigate the biochemistry and mechanism involved in the bioavailability and toxicity of Cd from rice would help resolve remaining questions and establish proper therapeutic approaches for acute and chronic intoxication of Cd.

AUTHOR INFORMATION

Corresponding Authors

*(X.Y.) E-mail: xeyang@zju.edu.cn. Phone/fax: +86-0571-88982907.

*(K.S.) E-mail: sunkewangwk@hotmail.com. Phone/fax: +86-0571-85131448.

Funding

This study was supported by the Ministry of Science and Technology of China (No. 2012AA100405), the Zhejiang Science and Technology Bureau (No. 2014C33240), Ministry of Environmental Protection of China (No. 2011467057), and the Fundamental Research Funds for the Central Universities of China.

Notes

The authors declare no competing financial interest.

ABBREVIATIONS USED

YS, yellow soil; CS, calcareous soil; SOD, superoxide dismutase; GPx, glutathione peroxidase; H_2O_2, hydrogen peroxide; MDA, malondialdehyde

REFERENCES

(1) He, Z. L.; Yang, X. E.; Stoffella, P. J. Trace elements in agro ecosystems and impacts on the environment. *J. Trace Elem. Med. Biol.* **2005**, *19*, 125−140.

(2) Xiao, W. D.; Yang, X. E.; He, Z. L.; Rafiq, M. T.; Hou, D. D.; Li, T. Q. Model for evaluation of the phytoavailability of chromium (Cr) to rice (*Oryza sativa* L.) in representative Chinese soils. *J. Agric. Food Chem.* **2013**, *61* (12), 2925−2932.

(3) Xiao, W. D.; Yang, X. E.; Zhang, Y. B.; Rafiq, M. T.; He, Z. L.; Aziz, R.; Li, T. Q. Accumulation of chromium in pak choi (*Brassica chinensis* L.) grown on representative Chinese soils. *J. Environ. Qual.* **2013**, *42* (3), 758−765.

(4) Li, K. Q.; Liu, J. G.; Lu, X. L. Uptake and distribution of cadmium in different rice cultivars. *J. Agro.-Environ. Sci.* **2003**, *22*, 529−532 (in Chinese, with English abstract)..

(5) Jin, T.; Nordberg, M.; Frech, W.; Dumont, X.; Bernard, A.; Ye, T.; Kong, Q.; Wang, Z.; Li, P.; Lundström, N.; Li, Y. Cadmium biomonitoring and renal dysfunction among a population environmentally exposed to cadmium from smelting in China (China Cad). *Biometals* **2002**, *15*, 397−410.

(6) Meharg, A. A.; Norton, G.; Deacon, C.; Williams, P.; Adomako, E. E.; Price, A.; Zhu, Y.; Li, G.; Zhao, F.; McGrath, S.; Villada, A.; Sommella, A.; De Silva, P. M. C. S.; Brammer, H.; Dasgupta, T.; Islam,

DOI: 10.1021/jf505557g
J. Agric. Food Chem. 2015, 63, 3599−3608

M. R. Variation in rice cadmium related to human exposure. *Environ. Sci. Technol.* **2013**, *47*, 5613−5618.
(7) Fang, Y.; Sun, X.; Yang, W.; Ma, N.; Xin, Z.; Fu, J.; Liu, X.; Liub, M.; Mariga, A. M.; Zhu, X.; Hu, Q. Concentrations and health risks of lead, cadmium, arsenic, and mercury in rice and edible mushrooms in China. *Food Chem.* **2014**, *147*, 147−151.
(8) Diao, W. P.; Ni, W. Z.; Ma, H. Y.; Yang, X. E. Cadmium pollution in paddy soil as affected by different rice (*Oryza sativa* L.) cultivars. *Bull. Environ. Contam. Toxicol.* **2005**, *75* (4), 731−738.
(9) Rafiq, M. T.; Aziz, R.; Yang, X.; Wendan, X.; Rafiq, M. K.; Ali, B.; Li, T. Q. Cadmium phytoavailability to rice (*Oryza sativa* L.) grown in representative Chinese soils. A model to improve soil environmental quality guidelines for food safety. *Ecotoxicol. Environ. Saf.* **2014**, *103*, 101−107.
(10) Peijnenburg, W. J. G. M.; Jager, T. Monitoring approaches to assess bioaccessibility and bioavailability of metals: matrix issues. *Ecotoxicol. Environ. Saf.* **2003**, *56*, 63−77.
(11) Shentu, J. L.; He, Z. L.; Yang, X. E.; Li, T. Q. Accumulation properties of cadmium in selected vegetable-rotation system of in southeastern China. *J. Agric. Food Chem.* **2008**, *56* (15), 6382−6388.
(12) Franz, E.; Römkens, P.; Van Raamsdonk, L.; Van Der Fels-Klerx, I. A chain modeling approach to estimate the impact of soil cadmium pollution on human dietary exposure. *J. Food Prot.* **2008**, *71*, 2504−2513.
(13) Kobayashi, E.; Suwazono, Y.; Dochi, M.; Honda, R.; Nishijo, M.; Kido, T. Estimation of benchmark doses as threshold levels of urinary cadmium, based on excretion of β2-microglobulin in cadmium polluted and non-polluted regions in Japan. *Toxicol. Lett.* **2008**, *179*, 108−112.
(14) Huang, S. S.; Liao, Q. L.; Hua, M.; Wu, X. M.; Bi, K. S.; Yan, C. Y.; Chen, B.; Zhang, X. Y. Survey of heavy metal pollution and assessment of agricultural soil in Yangzhong district, Jiangsu Province, China. *Chemosphere* **2007**, *67*, 2148−2155.
(15) He, M.; Ke, C. H.; Wang, W. X. Effects of cooking and subcellular distribution on the bioaccessibility of trace elements in two marine fish species. *J. Agric. Food Chem.* **2010**, *58*, 3517−3523.
(16) Intawongse, M.; Dean, J. R. Uptake of heavy metals by vegetable plants grown on contaminated soil and their bioavailability in the human gastrointestinal tract. *Food Addit. Contam.* **2006**, *23* (1), 36−48.
(17) Andersen, O.; Nielsen, J. B.; Sorensen, J. A.; Scherrebeck, L. Experimental localization of intestinal uptake sites for metals (Cd, Hg, Zn, Se) in vivo in mice. *Environ. Health Perspect.* **1994**, *102* (3), 199−206.
(18) Casalino, E.; Calzaretti, G.; Sblano, C.; Landriscina, C. Molecular inhibitory mechanisms of antioxidant enzymes in rat liver and kidney by cadmium. *Toxicology* **2002**, *30*, 37−50.
(19) Shaikh, Z. A.; Vutt Zaman, K. Oxidative stress as a mechanism of chronic cadmium-induced hepatotoxicity and renal toxicity and protection by antioxidants. *Toxicol. Appl. Pharmacol.* **1999**, *154*, 256−263.
(20) Saïdi, S. A.; Azaza, M. S.; Abdelmouleh, A.; Windmolders, P.; Pelt, J. V.; El-Feki, A. cytotoxicity evaluation and antioxidant enzyme expression related to heavy metals found in tuna by-products meal: an in vitro study in human and rat liver cell lines. *Exp. Toxicol. Pathol.* **2013**, *67*, 1025−1033.
(21) Nemmiche, S.; Chabane-Sari, D.; Kadri, M.; Guiraud, P. Cadmium chloride-induced oxidative stress and DNA damage in the human Jurkat T cell line is not linked to intracellular trace elements depletion. *Toxicol. in Vitro* **2011**, *51* (1), 191−198.
(22) Rudneva, I. I. Antioxidant system of Black Sea animals in early development. *Comp. Biochem. Physiol. Part C: Pharmacol., Toxicol. Endocrinol.* **1999**, *122*, 265−271.
(23) El-Missiry, M. A.; Shalaby, F. Role of β-carotene in ameliorating the cadmium-induced oxidative stress in rat brain and testis. *J. Biochem. Mol.* **2000**, *14*, 238−243.
(24) Fu, C.; Cui, Y. In vitro digestion/Caco-2 cell model to estimate cadmium and lead bioaccessibility/bioavailability in two vegetables: the influence of cooking and additives. *Food Chem. Toxicol.* **2013**, *59*, 215−421.
(25) Van Campen, D. R.; Glahn, R. P. Micronutrient bioavailability techniques: accuracy, problems and limitations. *Field Crops Res.* **1999**, *60*, 93−113.
(26) Maubon, N.; Le Vee, M.; Fossati, L.; Audry, M.; Le Ferrec, E.; Bolze, S.; Fardel, O. Analysis of drug transporter expression in human intestinal Caco-2 cells by real-time PCR. *Fundam. Clin. Pharmacol.* **2007**, *21* (6), 659−663.
(27) Hotz, C. Evidence for the usefulness of in vitro dialyzability, Caco-2 cell models, animal models, and algorithms to predict zinc bioavailability in humans. *Int. J. Vitam. Nutr. Res.* **2005**, *75*, 423−435.
(28) Intawongse, M.; Dean, J. R. Use of the physiologically-based extraction test to assess the oral bioaccessibility of metals in vegetable plants grown in contaminated soil. *Environ. Pollut.* **2008**, *152*, 60−72.
(29) Wei, Y. Y.; Shohag, M. J. I.; Wang, Y. Y.; Lu, L. L.; Wu, C. Y.; Yang, X. E. Effect of zinc sulfate fortification in germinated brown rice on seed zinc concentration, bioavailability, and seed germination. *J. Agric. Food Chem.* **2012**, *60*, 1871−1879.
(30) Oomen, A. G.; Hack, A.; Minekus, M.; Zeijdner, E.; Schoeters, G.; Verstraete, W.; Verstraete, W.; Van de Wiele, T.; Wragg, J.; Rompelberg, C. J.; Sips, A. J.; Van Wijnen, J. H. Comparison of five in vitro digestion models to study the bioaccessibility of soil contaminants. *Environ. Sci. Technol.* **2002**, *36*, 3326−3334.
(31) Fotakis, G.; Timbrell, J. A. Role of trace elements in cadmium chloride uptake in hepatoma cell lines. *Toxicol. Lett.* **2006**, *164* (2), 97−103.
(32) Charqui, A.; Zekri, S.; Jacquillet, G.; Rubera, K. I.; Ilie, K. M.; Belaid, A.; Duranton, C.; Tauc, M.; Hofman, P.; Poujeol, P.; El May, M. V.; Mograbi, B. Cadmium-induced autophagy in rat kidney: an early biomarker of subtoxic exposure. *Toxicol. Sci.* **2001**, *121* (1), 31−42.
(33) Reeves, P. G.; Chaney, R. L. Mineral nutrients status of female rats affects the absorption and organ distribution of cadmium from sunflower kernels (*Helianthus annuus* L.). *Environ. Res.* **2001**, *85*, 215−225.
(34) Chaney, R. L.; Reeves, P. G.; Angle, J. S. Rice plant nutritional and human nutritional characteristics role in human Cd toxicity. *Plant Nutr.* **2001**, *92*, 288−289.
(35) Peter, N.; Karoly, B.; Laszlo, G. Characterization of the stimulating effect of low-dose stressors in maize and bean seedlings. *J. Plant Physiol.* **2003**, *160*, 1175−1183.
(36) Kaminek, M. Progress in cytokinin research. *Trends Biotechnol.* **1992**, *10*, 159−162.
(37) Aidid, S. B.; Okamoto, H. Responses of elongation growth rate, turgor pressure and cell wall extensibility of stem cells of Impatiens balsamina to lead, cadmium and zinc. *Biometals* **1993**, *6*, 245−249.
(38) Ali, B.; Tao, Q. J.; Zhou, Y. F.; Gill, R. A.; Ali, S.; Rafiq, M. T.; Xu, L.; Zhou, W. 5-aminolevolinic acid mitigates the cadmium-induced changes in *Brassica napus* as revealed by the biochemical and ultra-structural evaluation of roots. *Ecotoxicol. Environ. Saf.* **2013**, *92*, 271−280.
(39) Rafiq, M. T.; Aziz, R.; Yang, X. E.; Xiao, W. D.; Stoffella, P. J.; Saghir, A.; Azam, M.; Li, T. Q. Phytoavailability of cadmium (Cd) to pak choi (*Brassica chinensis* L.) grown in Chinese soils: a model to evaluate the impact of soil Cd pollution on potential dietary toxicity. *PLoS One* **2014**, *7* (11), No. e111461.
(40) Naidu, R.; Kookana, R. S.; Sumner, M. E.; Harter, R. D.; Tiller, K. G. Cadmium sorption and transport in variable charge soils: a review. *J. Environ. Qual.* **1997**, *26*, 602−617.
(41) Vig, K.; Megharaj, M.; Sethunathan, N.; Naidu, R. Bioavailability and toxicity of cadmium to microorganisms and their activities in soil: a review. *Adv. Environ. Res.* **2003**, *8*, 121−135.
(42) Chan, D. Y.; Black, W. D.; Hale, B. A. Cadmium bioavailability and bioaccessibility as determined by in vitro digestion, dialysis and intestinal epithelial monolayers, and compared to in vivo data. *J. Environ. Sci. Health Part A* **2007**, *42*, 1283−1291.
(43) Yang, L.; Zhang, X. W.; Li, Y. H.; Li, H. R.; Wang, Y.; Wang, W. Y. Bioaccessibility and risk assessment of cadmium from uncooked rice

DOI: 10.1021/jf505557g
J. Agric. Food Chem. 2015, 63, 3599−3608

using an in vitro digestion model. *Biol. Trace Elem. Res.* **2012**, *145*, 81−86.
(44) Maulvault, A. L.; Machado, R.; Afonso, C.; Lourenco, H. M.; Nunes, M. L.; Coelho, I.; Langerholc, T.; Marques, A. Bioaccessibility of Hg, Cd and As in cooked black scabbard fish and edible crab. *Food Chem. Toxicol.* **2011**, *49*, 2808−2815.
(45) Zhang, Y.; Li, J. H.; Liu, X. R.; Jiang, F. L.; Tian, F. F.; Liu, Y. Spectroscopic and microscopic studies on the mechanisms of mitochondrial toxicity induced by different concentrations of cadmium. *J. Membr. Biol.* **2011**, *241*, 39−49.
(46) Sun, G. X.; Van de Wiele, T.; Alava, P.; Tack, F.; Laing, G. D. Arsenic in cooked rice: effect of chemical, enzymatic and microbial processes on bioaccessibility and speciation in the human gastrointestinal tract. *Environ. Pollut.* **2012**, *162*, 241−246.
(47) Vesey, D. A. Transport pathways for cadmium in the intestine and kidney proximal tubule: focus on the interaction with essential metals. *Toxicol. Lett.* **2010**, *198* (1), 13−19.
(48) Reeves, P. G.; Chaney, R. L. Marginal nutritional status of zinc, iron, and calcium increases cadmium retention in the duodenum and other organs of rats fed rice-based diets. *Environ. Res.* **2004**, *96*, 311−322.
(49) Zalups, R. K.; Ahmad, S. Molecular handling of cadmium in transporting epithelia. *Toxicol. Appl. Pharmacol.* **2003**, *186* (3), 163−188.
(50) Huang, D.; Zhang, Y.; Qi, Y.; Chen, C.; Ji, W. Global DNA hypomethylation, rather than reactive oxygen species (ROS), a potential facilitator of cadmium-stimulated K562 cell proliferation. *Toxicol. Lett.* **2008**, *179* (1), 43−47.
(51) Aziz, R.; Rafiq, M. T.; Yang, J.; Liu, D.; Lu, L.; He, Z.; Daud M. K.; Li, T. Q.; Yang, X. E. Impact assessment of cadmium toxicity and its bioavailability in human cell lines (Caco-2 and HL-7702). *BioMed. Res. Int.* **2014**, DOI: 10.1155/2014/839538.
(52) Yang, P.; Chen, H.; Tsai, J.; Lin, L. Cadmium induces Ca^{2+}-dependent necrotic cell death through calpain-triggered mitochondrial depolarization and reactive oxygen species mediated inhibition of nuclear factor-κB activity. *Chem. Res. Toxicol.* **2007**, *20* (3), 406−415.
(53) Koizumi, T.; Shirakura, G.; Kumagai, H.; Tatsumoto, H.; Suzuki, K. T. Mechanism of cadmium-induced cytotoxicity in rat hepatocytes: cadmium-induced active oxygen-related permeability changes of the plasma membrane. *Toxicology* **1996**, *114*, 124−134.
(54) Cuypers, A.; Plusquin, M.; Remans, T.; Jozefczak, M.; Keunen, E.; Gielen, H.; Opdenakker, K.; Nair, A. R.; Munters, E.; Artois, T. J.; Nawrot, T.; Vangronsveld, J.; Smeets, K. Cadmium stress: an oxidative challenge. *BioMetals* **2010**, *23* (5), 927−940.
(55) Jurczuk, M.1.; Brzóska, M. M.; Moniuszko-Jakoniuk, J.; Gałazyn-Sidorczuk, M.; Kulikowska-Karpińska, E. Antioxidant enzymes activity and lipid peroxidation in liver and kidney of rats exposed to cadmium and ethanol. *Food Chem. Toxicol.* **2004**, *42* (3), 429−438.
(56) El-Demerdash, F. M.; Yousef, M. I.; Kedwany, F. S.; Baghdadi, H. H. Cadmium-induced changes in lipid peroxidation, blood hematology, biochemical parameters and semen quality of male rats: protective role of vitamin E and β-carotene. *Food Chem. Toxicol.* **2004**, *42*, 1563−1571.
(57) O'Brien, P.; Salasinski, H. J. Evidence that the reactions of cadmium in the presence of metallothionein can produce hydroxyl radicals. *Arch. Toxicol.* **1998**, *72*, 690−700.
(58) Ognjanović, B. I.; Marković, S. D.; Pavlović, S. Z.; Žikić, R. V.; Štajn, A. S.; Saičić, Z. S. Combined effects of coenzyme Q10 and vitamin E in cadmium induced alterations of antioxidant defense system in the rat heart. *Environ. Toxicol. Pharmacol.* **2006**, *22*, 219−224.
(59) Matés, J. M. Effects of antioxidant enzymes in the molecular control of reactive oxygen species toxicology. *Toxicology* **2000**, *153*, 83−104.
(60) Yalin, S.; Comelekoglu, U.; Bagis, S.; Ozlen Sahin, N.; Ogenler, O.; Hatungil, R. Acute effect of single-dose cadmium treatment on lipid peroxidation and antioxidant enzymes in ovariectomized rats. *Ecotoxicol. Environ. Saf.* **2006**, *65* (1), 140−144.
(61) Arroyo, V. S.; Flores, K. M.; Ortiz, L. B.; Gómez-Quiroz, L. E.; Gutiérrez-Ruiz, M. C. Liver and cadmium toxicity. *J. Drug Metab.* **2012**, DOI: 10.4172/2157-7609.S5-001.

DOI: 10.1021/jf505557g
J. Agric. Food Chem. 2015, 63, 3599−3608

Table 1. Characteristics of Plant Food Supplements Tested Herein, Occurrence, and Estimated Intake of OTA

sample no.	dose form	daily consumption (g)	composition	*Vitis vinifera* (%)	OTA (μg/kg)	PDI[a] OTA (ng/kg bw)
1	capsule (powder)	1	dry extract of *Pinus pinaster* bark, dry extract of grape seed (*Vitis vinifera*)	29	nd[b]	<0.01
2	capsule (solution)	3	*Perilla frutescens*, gelatin, glycerin, extract of red grape, hydrogenated soybean oil, soy lecithin, E171, E172, E120, E306	10	5.23	0.26
3	ampoule	15	root fennel, yerba mate, grapes, pineapple	4.7	<LOQ[c]	<0.29
4	capsule (powder)	0.78	red grape seed, E400, L-glutathione, green tea, LDL Factors Plus, coenzyme Q10	8.5	<LOQ	<0.01
5	powder	2.4	ash, petiole cherry, olive leaves, pansy, meadowsweet, grape pomace, green tea, yerba mate, *Citrus aurantium*, kola nut	2	<LOQ	<0.05
6	powder	10	pineapple fruit powder, black currant fruit powder, fructose, calcium citrate, quinoa sprout powder, magnesium citrate, acerola juice powder, açai juice powder, goji berry extract, xanthan, mixed plant tocopherols, promegranate peel extract, red grape extract, green tea extract, tagetes extract, turmeric extract, black elderberry extract, coenzyme Q10, aloe vera leaf gel concentrate, zinc gluconate, manganese gluconate, copper gluconate, chromium chloride	0.8	<LOQ	<0.19
7	capsule (powder)	1	*Polygonum cuspidatum* extract, red grape seeds, vegetal magnesium stearate, silicon dioxide	10	<LOQ	<0.02
8	tablet	1.16	grape seed, rapeseed oil, gelatin, glycerin, sorbitol, glycerol monostearate, sunflower lecithin, tomato extract, lutein, extract flaxseed, bioretinol, vitamin E, rice flour, microcrystalline cellulose, dyes	7	nd	<0.01
9	tablet	1.6	dicalcium phosphate, microcrystalline cellulose, citrus bioflavonoids, vitamin C, potassium chloride, hydrolyzed marine collagen, blueberry, pineapple, vegetable fats, grape pomace (skins and seeds), red vine leaves, silicon dioxide, vitamin E, *Centella asiatica*, witch hazel, melioto, *Chrysanthemum American*, milk thistle, dandelion	5	20.23	0.54
10	tablet	1.94	cellulose, extract of grape skins and seeds, extract of Greek hay seed, extract of bean pod, extract of green tea leaves, extract of mate leaves, extract of kola nut, extract of green coffee bean, extract of dandelion root, extract of artichoke head, extract of cinnamon bark, carboxymethylcellulose sodium, iron oxide, magnesium stearate, silicon dioxide, hydroxypropylcellulose	11.5	nd	<0.02
11	capsule (powder)	0.46	dry extract of grape skins and seeds, dry extract of *Granata*, edible gelatin, maltodextrin, silicon dioxide and magnesium stearate, selenium yeast, iron oxide	29	5.19	0.04
12	tablet	1.24	dry extract of grape, leaves of *Lespedeza*, elderberry flowers, *Ortosifon* (leaves and flowers), microcrystalline cellulose, calcium phosphate, potassium phosphate, rutin, silicon dioxide, magnesium stearate, blueberry, vitamin B6, hydroxypropylmethylcellulose, microcrystalline cellulose, stearic acid, potassium silicate and aluminum, iron oxide	4	2.85	0.06
13	capsule (solution)	0.86	dry extract of grape seeds, L-tyrosine, edible gelatin, borage oil, wheat germ oil, glycerol, palm oil, DL-α-tocoferol acetate, flava wax, soybean oil, soy lecithin, beta-carotene, iron oxide, sodium selenite	8.3	nd	<0.01
14	syrup	4	mate leaves, fennel seed, grape pomace, pomegranate powder, maltodextrin, water, sucralose, chromium chloride, potassium sorbate, sodium benzoate	ni[d]	nd	<0.03
15	tablet	12	meadowsweet plant, extract of grape pomace, dandelion leaves, ash leaves, grapefruit, bitter orange pericarp, citric acid, sorbic acid, benzoic acid	52.3	<LOQ	<0.23
16	solution	0.69	microcrystalline cellulose, silicon dioxide, extract of vine leaves, E468, E1202, calcium hydrogen phosphate, hydroxypropyl methylcellulose, talc, magnesium stearate, titanium dioxide, iron oxide, hydrogenated vegetable fat	14	nd	<0.01
17	powder	2.5	grape pomace extract, grape juice concentrate, sorbitol, maltodextrin, fructooligosaccharides, natural aroma of black currants, citric acid, dry extracts of: stalk cherry, ash leaves, kola nut, maté leaves, olive leaves, orange peel, wild pansy flower, meadowsweet flowery, green tea leaves, saccharin	2	<LOQ	<0.05
18	tablet	9.75	grape pomace extract, sorbitol, dry extract of *Garcinia* fruit, maltodextrin, magnesium stearate, potassium iodide, chromium chloride	0.5	<LOQ	<0.19
19	ampoule	15	grape pomace, mate leaves, root of fennel, apple juice concentrate, pineapple juice concentrate	5	2.12	0.53
20	solution	10	grape pomace extract, purified water, glycerin, fluid extract of plants (cherry stem, nettle root, rhizome of Bermuda grass, leaves maté, marc), apple aroma, cocoa extract, acesulfame potassium, potassium sorbate, sodium benzoate	ni	<LOQ	<0.19
21	comfit	1.4	grape seeds extract, talc, calcium phosphate, microcrystalline cellulose, vitamin C, sodium carboxymethylcellulose, polyvinylpyrrolidone, E133, E104, E171, magnesium stearate vegetable, shellac, silicon dioxide, blueberry extract, camauba wax	7.2	<LOQ	<0.03
22	capsule (powder)	0.42	dry extract of grape must (*Vitis vinifera*), cellulose, magnesium stearate, silica dioxide, dry extract of *Polygonum cuspidatum* root, maltodextrin, hydroxypropyl methylcellulose, iron oxide, titanium dioxide	47.6	<LOQ	<0.01
23	tablet	1.10	microcrystalline cellulose, potassium phosphate, Java tea *Orthosiphon stamineus* (leaves), melioto (*Meliotus officinalis* leaves), bioflavonoids from lemon, corn starch, grape seeds (*Vitis vinifera*), rutin, hydroxypropyl methylcellulose, L-ascorbic acid, DL-α-tocopherol acetate, croscaramellose sodium, silicon dioxide, vegetable magnesium stearate, E171, E132	14.5	1.80	0.03
24	capsule (solution)	1.20	soybean oil (*Glycine max*), gelatin, grape seed (*Vitis vinifera*), glycerole, melioto flowers (*Melilotus officinalis*), rutin, hesperidin, soy lecithin, beeswax, colloidal silica, E172	25	1.94	0.04

[a]PDI, probable daily intake. [b]nd, not detected (LOD = 0.50 μg/kg). [c]LOQ, limit of quantitation (1.16 μg/kg). [d]ni, not indicated in the label.

J. Agric. Food Chem. 2015, 63, 3609−3614
DOI: 10.1021/acs.jafc.5b00326

MATERIALS AND METHODS

Reagents and Materials. Solid standard of OTA was purchased from Sigma-Aldrich (Milan, Italy). The stock solution (1 mg/mL) was prepared by weighing 1 mg of the toxin that was dissolved in 1 mL of toluene/acetic acid (99:1, v/v). To assess the exact concentration of the OTA stock solution, an aliquot was evaporated to dryness, redissolved in methanol at concentration of about 10 μg/mL, and spectrophotometrically tested (ε = 6330 cm^2/mmol, at λ = 332 nm). Standard solutions of OTA for HPLC calibration or spiking purposes were prepared by dissolving adequate amounts of the stock solution, previously evaporated to dryness under nitrogen stream, in the HPLC mobile phase. Acetonitrile, methanol, water (HPLC grade), and glacial acetic acid were purchased from Mallinckrodt Baker (Milan, Italy).

Sodium chloride (ACS grade), polyethylene glycol (PEG 8000), and sodium hydrogen carbonate ($NaHCO_3$, ACS grade) were purchased from Sigma-Aldrich. OchraTest immunoaffinity columns were purchased from Vicam (Watertown, MA). Filter paper and GF/A glass microfiber filters were obtained from Whatman (Maidstone, U.K.).

Commercial Samples. Commercially available PFS, food coloring agents, and leavening agents containing tartrates, all derived from *V. vinifera*, were purchase from retail stores in Bari province (Italy) or via the Internet for a total of 41 samples. The dose forms of PFS were tablet (seven samples), powder (three samples), solution (two samples), ampule (two samples), comfit (one sample), syrup (one sample), or capsule (eight samples). Food coloring agents were as powder (six samples) or liquid (seven samples), whereas the leavening agents containing tartrates (four) were as powder.

Samples from Distilleries. Eight additional samples were collected in two processing industries (distilleries) located in Puglia region (South Italy) that use wine lees (distillery 1), grape pomaces (distillery 2), and wine as starting materials for the production of ethyl alcohol, tartrates, dried grape seeds, and dried grape skins. In particular, grape pomaces or lees are mixed with wine or water and distilled to obtain ethyl alcohol. Dealcoholated pomaces or lees are washed with warm water to obtain a liquid borlanda. Washed pomaces are dried and separated into grape skins and grape seeds. Borlanda is used to precipitate and collect tartrates. Exhausted borlanda and exhausted lees are mixed and submitted to digestion in a purification plant constituted of an anaerobic fermenter to produce biogas followed by an aerobic fermenter containing activated sludge. Samples of 0.5−1 kg of starting materials (lees, grape pomaces) and final materials (dried grape seed, dried grape skins, tartrates, and mud) were collected and sent to our laboratory. These samples were collected in the same day, and they were considered sufficiently representative of the lot of pomaces or lees because they were homogenized during maceration or sedimentation processes in the winery.

All solid samples were ground before OTA extraction, powders were directly extracted, and liquid samples were used as such, whereas PFS available as capsules were opened to recover their content that was weighed and analyzed for OTA. Solid samples containing high humidity (grape pomaces and wine lees collected from distilleries) were dried before grinding. The list of the 49 samples analyzed for OTA is reported in Tables 1−3.

Determination of OTA. Each sample was analyzed as reported previously.[12] In particular, solid and liquid samples (5 g) were extracted with 30 mL of acetonitrile/water (60:40, v/v) by shaking for 60 min. Some liquid samples containing high levels of sugars showed two liquid layers after the addition of the extraction solvent. New aliquots of these samples were extracted with acetonitrile/methanol/water (90:90:80, v/v/v). The addition of methanol to the extraction solvent mixture prevents the formation of two liquid layers. After centrifugation (4000 rpm, 5 min) and filtration through a Whatman No. 4 filter paper, 6 mL of filtrate was diluted with 44 mL of water solution containing PEG (1%) and $NaHCO_3$ (5%), mixed, and filtered through Whatman GF/A glass microfiber. A 10 mL volume of diluted extract (equivalent to 0.2 g of solid sample or 0.17 g of liquid sample) was passed through an OchraTest immunoaffinity column at a flow rate of about 1 drop/s. The column was washed with 10 mL of water solution containing NaCl (2.5%) and $NaHCO_3$ (0.5%), followed by 10 mL of distilled water at a flow rate of 1−2 drops/s. The eluates were discarded, and OTA was recovered in a vial by passing 2 × 1 mL of methanol through the column. The purified extract was dried under nitrogen stream at about 50 °C and reconstituted with 500 μL of the HPLC mobile phase. One-hundred microliters, corresponding to 0.04 g of solid sample or 0.034 g of liquid sample, was injected into the HPLC apparatus by a full loop injection system. The HPLC determination and confirmation of OTA were performed according to the AOAC Official Method 2001.01.[16] The HPLC apparatus was an 1100 series equipped with a G1312A binary pump, a G1313A autosampler, a G1316A column thermostat set at 25 °C, a G1321A spectrofluorometric detector set at 333 nm (λ_{ex}) and 460 nm (λ_{em}), and a Chemstation G2170AA Windows 2000 operating system (Agilent, Waldbronn, Germany). The column used was a 150 mm × 3 mm i.d., 4 μm, Synergi Hydro-RP (Phenomenex, Torrance, CA, USA) with a 3 mm, 0.45 μm pore size guard filter (Rheodyne, Cotati, CA, USA). The mobile phase was an isocratic mixture of acetonitrile/water/acetic acid (99:99:2, v/v/v) eluted at a flow rate of 1.0 mL/min.

The identity and concentration of OTA in the purified extracts of two food supplements (#23 and #24) containing low levels of OTA were confirmed by LC−MS/MS by using the apparatus and analytical conditions reported elsewhere.[17]

Recovery Experiments. The performances of the analytical method were checked on blank samples of PFS based on red grape

Table 2. Occurrence of OTA in Food Coloring Agents and Leavening Agents Containing Tartrates Derived from *Vitis vinifera*

sample no.	physical state	product name	OTA (μg/kg)
25	solid	107 Anthocyan A55P	16.80
26	solid	Grape extract 25%	1.52
27	solid	Enocyanin 4% E163	32.00
28	liquid	Enocyanin 1% l-ws E163	<LOQ[a]
29	solid	Red anthocyan E163 95−96%	4.28
30	liquid	Exberry grape	nd[b]
31	liquid	Exberry grape	nd
32	solid	Exberry grape - powder	nd
33	liquid	Enocyanin	nd
34	liquid	Red anthocyan E163 0.5−1.5%	2.28
35	liquid	Enocyanin	<LOQ
36	liquid	Color prep-grade skin extact	<LOQ
37	liquid	Color prep-grade skin extact	1.93
38	solid	Cream of tartar E336	nd
39	solid	Leavening agent	nd
40	solid	Cream of tartar	nd
41	solid	Tartaric acid	nd

[a]LOQ, limit of quantitation (1.16 μg/kg). [b]nd, not detected (LOD = 0.50 μg/kg).

Table 3. Occurrence of OTA in Samples from Distilleries

sample no.	physical state	composition	OTA (μg/kg)
Distillery 1			
42	solid	lees	240.93
43	solid	mud	3.87
44	solid	tartrates	7.33
45	solid	tartrates	10.16
Distillery 2			
46	solid	grape pomace	46.50
47	solid	dried grape seeds	23.86
48	solid	dried grape skins	72.20
49	solid	tartrates	<LOQ[a]

[a]LOQ, limit of quantitation (1.16 μg/kg).

DOI: 10.1021/acs.jafc.5b00326
J. Agric. Food Chem. 2015, 63, 3609−3614

seeds (#1), food coloring agent based on grape powder (#32), and leavening agent containing tartrates obtained from grape (#39) spiked in triplicate with OTA at 5 and 20 μg/kg. Spiked samples were left overnight to allow for solvent evaporation.

RESULTS AND DISCUSSION

Method Performance. Analysis of spiked blank samples demonstrated that the method generated accurate and precise results. Recovery and repeatability results were in the range of 87−102% and 2−4%, respectively (Table 4), and the chromatograms of blank and spiked samples did not show matrix interfering peaks at retention time of OTA (Figure 2). Values of limit of detection (LOD) and limit of quantitation (LOQ), calculated as signal-to-noise ratios of 3:1 and 6:1, were 0.50 μg/kg and 1.16 μg/kg, respectively. Figure 2 shows the chromatograms of a PFS blank sample (#10) and two PFS samples naturally contaminated with OTA at 20.23 μg/kg (#9) and 5.19 μg/kg (#11). The identity and levels of OTA were confirmed in the purified extracts of two samples of PFS (#23 and #24) that were analyzed by LC−MS/MS.

Table 4. Recovery and Repeatability Results for OTA Determination in Spiked Samples. Results Are Mean of Three Replicates

sample	spiking level (μg/kg)	mean recovery (%)	SD[a]	RSD_r[b] (%)
PFS based on red grape seeds (#1)	5	88	2.9	3
	20	87	3.2	4
food coloring based on grape powder (#32)	5	102	1.7	2
	20	103	4.1	4
leavening agent containing tartrates derived from *V. vinifera* (#39)	5	99	3.8	4
	20	97	2.1	2

[a]SD, standard deviation. [b]RSD_r, within laboratory relative standard deviation.

Occurrence of OTA in Commercial Samples. Eighteen out of twenty-four PFS samples (75%) were found contaminated with OTA at levels ranging from <1.16−20.23 μg/kg (Table 1). For each sample of PFS, we have reported the dose form, daily consumption, composition, percentage of derivatives of *V. vinifera*, OTA level, and its calculated probable daily intake (PDI). Assuming that most of the OTA measured in positive PFS samples originated from *V. vinifera* used as ingredient, the calculated OTA level in this ingredient was in the range of <1.16−809.20 μg/kg. These levels of OTA are not surprising since levels up to 849.1 μg/kg of OTA were reported for samples of grape pomaces collected in South Italy.[12] The percentages of *V. vinifera*, mainly extracts of grape pomaces, in the PFS considered in this study were quite variable in the range of 0.5−52.3%, but no correlation was found between these percentages and OTA levels (R^2 = 0.01). This suggests that either OTA contamination of *V. vinifera* was variable or other ingredients used for PFS formulation could have contributed to OTA contamination. The calculated values of PDI of OTA for consumers of PFS analyzed in this study are reported in Table 1 and ranged from <0.007−0.54 ng/kg bw, which correspond to <0.04−3.2% of TDI (17.14 ng/kg bw) for this mycotoxin.

The occurrence of OTA in other kind of PFS was previously investigated by several authors.[18−20] In particular, six out of 62 PFS (10%) were found positive for OTA at levels <0.3−6 μg/kg with a calculated PDI of 0.15 ng/kg bw for the sample containing the highest OTA level (6 μg/kg).[18] OTA was also reported in 18 out of 50 samples (36%) of green coffee bean extracts-based PFS at levels in the range of <1−136.9 μg/kg.[19] Thirty-two samples (63%) of brewer's yeast food supplements were found contaminated with 0.03−1.53 μg/kg OTA.[20] OTA was also found, at different range levels, in dried fruits and botanicals such as medicinal plants (43% positive, up to 2340 μg/kg OTA), ginseng (40% positive, 0.4−1.8 μg/kg OTA), ginger (100% positive, 1.8−2.9 μg/kg OTA), red pepper (31%

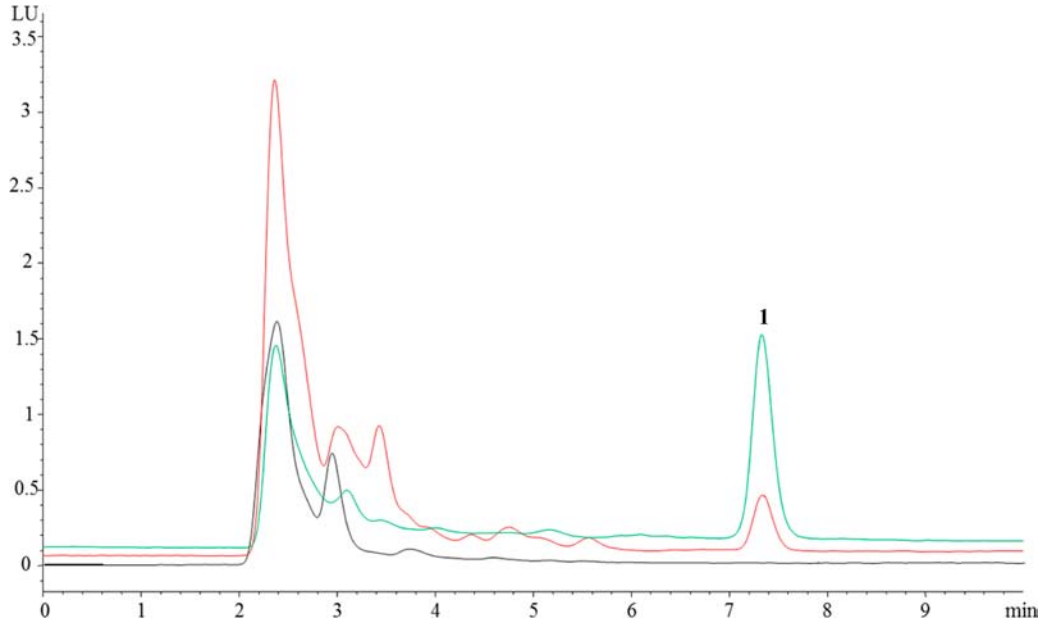

Figure 2. Chromatograms of a blank sample #10 (black) and samples #9 (green) and #11 (red) naturally contaminated with OTA (**1**) at 20.23 μg/kg and 5.19 μg/kg, respectively.

DOI: 10.1021/acs.jafc.5b00326
J. Agric. Food Chem. 2015, 63, 3609−3614

positive, 10.6−66.2 μg/kg OTA), and liquorice (45% positive, 0.3−217 μg/kg OTA).[21]

The consumption of PFS across different countries is not homogeneous, and their production, marketing, and control are regulated by every national legislation, although anyone can freely purchase products marketed on World Wide Web sites.[2] People living in the United States and northern Europe are the major consumers of PFS, mainly by people who are in good health and not by people who really need them.[22,23] Several research groups collected data on the habits of adult populations from different areas of the USA and EU to characterize the consumptions of PFS, but no clear information is yet available about average consumption in various age groups.[2,23−25] One of the problems that still prevents the creation of a reliable database is the extreme variability of the ingredients in the PFS available on the market. Some types of PFS may contain toxic compounds, which are constituents of plants used as ingredient of these types of PFS.[26] The results of our study indicate that OTA is widespread in PFS derived from *V. vinifera*; therefore, it should be considered as an additional safety issue for PFS.

Grape pomaces and wine lees are also used to manufacture either food coloring agents or tartrates. Anthocyanins (E 163), a food additive belonging to the functional class food coloring agents, can be produced from grape skin extracts.[27] Anthocyanins (E 163) refers to the food additives that are not sufficiently characterized and may contain both the glycosides (anthocyanins) and the aglycones (anthocyanidins).[27] Tartrates can be manufactured from grape pomaces or wine lees.[28] The results on the contamination of OTA in commercial samples of 13 food coloring agents and four leavening agents containing tartrates are reported in Table 2. Within the 13 food coloring agents, nine samples (69%) were contaminated with OTA at levels between <1.16−32.00 μg/kg, whereas none of the four samples of leavening agents containing tartrates were contaminated by OTA. As far as we know, this is the first report on the occurrence of OTA in food coloring agents manufactured from *V. vinifera*.

Occurrence of OTA in Samples from Distilleries. The results of the samples collected in the two distilleries that used grape pomaces or wine lees to produce tartrates, ethyl alcohol, grape skins, grape seeds, and biogas are reported in Table 3. All samples were contaminated, and the levels of OTA in tartrates were 2−4% of the level of OTA measured in the starting materials (wine lees or grape pomaces). The levels of OTA in samples of grape skins (72.20 μg/kg) and grape seeds (23.86 μg/kg) were comparable to that of the starting grape pomaces (46.50 μg/kg). These results confirm the stability of OTA during processing of grape pomaces to produce grape skins, ethyl alcohol, and grape seeds. Moreover, the levels of OTA measured in grape skins and grape seeds account for the total amount of OTA originally present in starting grape pomaces. This suggests that the toxin does not pass into ethyl alcohol during distillation of pomaces as previously reported on a laboratory scale.[12]

As shown in Table 3, a low level of OTA (3.87 μg/kg) was measured in the mud sample collected from the purification plant in spite of the high levels of OTA present in the starting wine lees (240.93 μg/kg). A possible explanation of this result could be a OTA degradation made by some of microorganisms used for anaerobic and aerobic digestion. In this case, the materials present in the purification plant could be a good source of OTA degrading microorganisms. Further investigations are necessary to support this hypothesis.

Maximum permitted levels of OTA are in force in Europe for some products derived from *V. vinifera* such as wine and grape juice (2 μg/kg) and raisins and sultanas (10 μg/kg).[28] The results reported herein demonstrate the high incidence and, for some samples, the high level of OTA in PFS and food coloring agents derived from *V. vinifera*, which require maximum permitted levels of OTA to be established also for these products.

AUTHOR INFORMATION

Corresponding Author

*E-mail: michele.solfrizzo@ispa.cnr.it. Phone: +39 080 5929367. Fax: +39 080 5929374.

Notes

The authors declare no competing financial interest.

ACKNOWLEDGMENTS

We thank Domenico Catalano for collecting samples from distilleries.

ABBREVIATIONS USED

OTA, ochratoxin A; PFS, plant food supplements; TWI, tolerable weekly intake; TDI, tolerable daily intake; PDI, probable daily intake

REFERENCES

(1) European Communities (2002) Directive 2002/46/EC of the European Parliament and of the Council of 10 June 2002 on the approximation of the laws of the Member States relating to food supplements. *Off. J. Eur. Comm.* **2002**, *L183*, 51−57.

(2) Garcia-Alvarez, A.; Egan, B.; de Klein, S.; Dima, L.; Maggi, F. M.; Isoniemi, M.; Ribas-Barba, L.; Raats, M. M.; Meissner, E. M.; Badea, M.; Bruno, F.; Salmenhaara, M.; Milà-Villarroel, R.; Knaze, V.; Hodgkins, C.; Marculescu, A.; Uusitalo, L.; Restani, P.; Serra-Majem, L. Usage of plant food supplements across six European countries: Findings from the PlantLIBRA consumer survey. *PLoS One* **2014**, *9*, 1−18.

(3) *Pomace*; Wikipedia: San Francisco, CA, 2014. http://en.wikipedia.org/wiki/Pomace (accessed January 16, 2015).

(4) Monagas, M.; Hernandez-Ledesma, B.; Gomez-Cordoves, C.; Bartolomé, B. Commercial dietary ingredients from *Vitis vinifera* L. leaves and grape skins: Antioxidant and chemical characterization. *J. Agric. Food Chem.* **2006**, *54*, 319−327.

(5) Shrikhande, A. J. Wine by-products with health benefits. *Food Res. Int.* **2000**, *33*, 469−474.

(6) Deng, Q.; Penner, M. H.; Zhao, Y. Chemical composition of dietary fiber and polyphenols of five different varieties of wine grape pomace skins. *Food Res. Int.* **2011**, *44*, 2712−2720.

(7) Jara-Palacios, M. J.; Gonzales-Manzano, S.; Escudero-Gilete, M. L.; Hernanz, D.; Dueñas, M.; Gonzales-Paramas, A. M.; Heredia, F. J.; Santos-Buelga, C. Study of zalema grape pomace: Phenolic composition and biological effects in *Caenorhabditis elegans*. *J. Agric. Food Chem.* **2013**, *61*, 5114−5121.

(8) Solfrizzo, M. Aspetti tossicologici e detossificazione dell'ocratossina A. *Inf. Fitopatol.* **2006**, *2*, 14−17.

(9) Visconti, A.; Perrone, G.; Cozzi, G.; Solfrizzo, M. Managing ochratoxin A risk in the grape-wine food chain. *Food Addit. Cont., Part A* **2008**, *25*, 193−202.

(10) Otteneder, H.; Majerus, P. Occurrence of ochratoxin A (OTA) in wines: Influence of the type of wine and its geographical origin. *Food Addit. Cont., Part A* **2000**, *17*, 793−798.

(11) Joergensen, K. Occurrence of ochratoxin A in commodities and processed food—A review of EU occurrence data. *Food Addit. Cont., Part A* **2005**, *S1*, 26−30.

DOI: 10.1021/acs.jafc.5b00326
J. Agric. Food Chem. 2015, 63, 3609−3614

(12) Solfrizzo, M.; Panzarini, G.; Visconti, A. Determination of ochratoxin A in grapes, dried vine fruits, and winery byproducts by high-performance liquid chromatography with fluorometric detection (HPLC−FLD) and immunoaffinity cleanup. *J. Agric. Food Chem.* **2008**, *56*, 11081−11086.
(13) Covarelli, L.; Beccari, G.; Marini, A.; Tosi, L. A review on the occurrence and control of ochratoxigenic fungal species and ochratoxin A in dehydrated grapes, non-fortified dessert wines, and dried vine fruit in the Mediterranean area. *Food Control* **2012**, *26*, 347−356.
(14) European Food Safety Authority (EFSA). Opinion of the scientific panel on contaminants in the food chain on a request from the commission related to ochratoxin A in food. *EFSA J.* **2006**, *365*, 1−56.
(15) European Food Safety Authority (EFSA). Scientific opinion. Statement on recent scientific information on the toxicity of ochratoxin A. *EFSA J.* **2010**, *8*, 1626−1633.
(16) Visconti, A.; Pascale, M.; Centonze, G. Determination of ochratoxin A in wine and beer by immunoaffinity column clenup and liquid chromatography analysis with fluorimetric detection: Collaborative study. *J. AOAC Int.* **2001**, *84*, 1818−1827.
(17) Lattanzio, V. M. T.; Solfrizzo, M.; Powers, S.; Visconti, A. Simultaneous determination of aflatoxins, ochratoxin A, and *Fusarium* toxins in maize by liquid chromatography/tandem mass spectrometry after multitoxin immunoaffinity cleanup. *Rapid Commun. Mass Spectrom.* **2007**, *21*, 3253−3261.
(18) Diana Di Mavungu, J.; Monbaliu, S.; Scippo, M. L.; Maghuin-Rogister, G.; Schneider, Y. J.; Larondelle, Y.; Callebaut, A.; Robbens, J.; Van Peteghem, C.; De Saeger, S. LC−MS/MS multi-analyte method for mycotoxin determination in food supplements. *Food Addit. Cont., Part A* **2009**, *26*, 885−895.
(19) Vaclavik, L.; Vaclavikova, M.; Begley, T. H.; Krynitsky, A. J.; Rader, J. I. Detemination of multiple mycotoxins in dietary supplements containing green coffee bean extracts using ultrahigh-performance liquid chromatography−tandem mass spectrometry (UHPLC−MS/MS). *J. Agric. Food Chem.* **2013**, *61*, 4822−4830.
(20) Gareis, M. Ochratoxin A in Brewer's yeast used as nutrient supplement. *Mycotoxin Res.* **2002**, *18*, 128−131.
(21) Trucksess, M. W.; Scott, P. M. Mycotoxins in botanicals and dried fruits: A review. *Food Addit. Cont., Part A* **2008**, *25*, 181−192.
(22) van den Berg, S. J. P. L.; Serra-Majem, L.; Coppens, P.; Rietjens, I. M. C. M. Safety assessment of plant food supplements (PFS). *Food Funct.* **2011**, *2*, 760−768.
(23) Rovira, M. A.; Grau, M.; Castañer, O.; Covas, M. I.; Schröder, H. Dietary supplement use and health-related behaviors in a Mediterranean population. *J. Nutr. Educ. Behav.* **2013**, *45*, 386−391.
(24) Dwyer, J.; Picciano, M. F.; Raiten, D. J. Collection of food and dietary supplement intake data: What we eat in America-NHANES. *J. Nutr.* **2003**, *133*, S590−600.
(25) Giammarioli, S.; Boniglia, C.; Carratù, B.; Ciarrocchi, M.; Chiarotti, F.; Mosca, M.; Sanzini, E. Use of food supplements and determinants of usage in a sample Italian adult population. *Public Health Nutr.* **2012**, *16*, 1768−1781.
(26) van den Berg, S. J. P. L.; Restani, P.; Boersma, M. G.; Delmulle, L.; Rietjens, I. M. C. M. Levels of genotoxic and carcinogenic compounds in plant food supplements and associated risk assessment. *Food Nutr. Sci.* **2011**, *2*, 989−1010.
(27) European Food Safety Authority (EFSA). Scientific opinion on the re-evaluation of anthocyanins (E 163) as a food additive. *EFSA J.* **2013**, *11*, 3145−3196.
(28) European Food Safety Authority (EFSA). Scientific opinion on the evaluation of the substances currently on the list in the annex to Commission Directive 96/3/EC as acceptable previous cargoes for edible fats and oils—Part II of III. *EFSA J.* **2012**, *10*, 2703−2854.
(29) European Commission. Commission Regulation (EC) No. 1881/2006 of 19 December 2006 setting maximum levels for certain contaminants in foodstuffs. *Off. J. Eur. Union* **2006**, *364*, 5−24.

DOI: 10.1021/acs.jafc.5b00326
J. Agric. Food Chem. 2015, 63, 3609−3614

Table 1. Antioxidative Enzymes and Their Functions (Modified from Lee et al., 2004)[99]

sr. no.	enzyme	function	typical reactions
1	superoxide dismutase (EC 1.15.1.1)	superoxide anion removal	$2O_2^- + 2H^+ \rightarrow H_2O_2 + O_2$
2	catalase (EC 1.11.1.6)	hydroperoxide removal	$2H_2O_2 \rightarrow 2H_2O + O_2$
3	glutathione peroxidase (EC 1.11.1.9)	hydroperoxide removal	$2\text{glutathione}_{red} + 2H_2O_2 \rightarrow 2\text{glutathione}_{ox} + 2H_2O$
4	glutathione *S*-transferase (EC 2.5.1.18)	lipid hydroperoxide removal	
5	glutathione disulfide reductase (EC 1.8.1.7)	oxidized glutathione reduction	$2\text{glutathione}_{ox} + NADPH \rightarrow 2\text{glutathione}_{red} + NADP^+$
6	peroxidase (EC 1.11.1.*x*)	decomposition of hydrogen peroxide and lipid hydroperoxide	

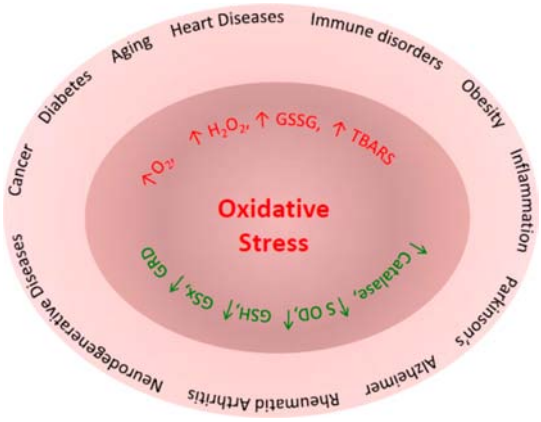

Figure 1. Oxidative stress and role in disease generation.

substances is plant material such as garlic, broccoli, green tea, soybeans, tomatoes, carrots, Brussels sprouts, kale, cabbages, onions, cauliflower, red beets, cranberries, cocoa, blackberries, blueberries, red grapes, prunes, and citrus fruits. With a huge market for functional foods comprising antioxidative attributes, there is renewed interest in the search for new diverse sources of antioxidants that can be safely used. Dairy products have also been reported to possess antioxidant properties (Table 2) and among various dairy supplements, probiotics have been recently known as potential sources of antioxidants.

PROBIOTICS

Probiotics are defined as "live microorganisms which when administered in adequate amounts, confer health benefits to the host".[8] Probiotics have established their efficacy as dietary factors that can regulate gastrointestinal functions, thereby imparting health benefits to consumers. Alleviation of lactose intolerance, prevention of different forms of diarrhea and urogenital infections, cholesterol reduction, reduction of atopic diseases, and modulation of the immune system are some of the functions attributed to probiotics.[9,10] Other benefits include prevention of cancer, particularly colon carcinoma and food allergy.[11,12] The competitive exclusion of pathogens and the reduction in number as well as metabolic activities of harmful organisms by probiotics have been demonstrated in vitro.[13] Lactobacilli are the major source of probiotics and are usually explained as Gram-positive bacteria, devoid of cytochromes and preferring anaerobic conditions, but are aero tolerant, fastidious, and strictly fermentative and produce lactic acid as the main product.[14] Various species and strains of lactobacilli, namely, *Lactobacillus acidophilus*, *Lactobacillus casei*, *Lactobacillus rhamnosus*, and *Lactobacillus helveticus* are considered as successful probiotics, and different variants have been available on the market for human consumption. *Bifidobacterium*, even though not grouped with lactic acid bacteria, is another genus with probiotic functions. *Bifidobacterium lactis* (*Bifidobacterium animalis* ssp. *lactis*) is a very commonly used probiotic, although it is not a normal inhabitant of the human gastrointestinal tract. *Bifidobacterium longum* ssp. *longum* (and ssp. *infantis*) and *Bifidobacterium breve* are mainly used in supplements.[15] Although various strains of lactobacilli and bifidobacteria have been known for various health beneficial effects, their role as antioxidants has been understudied.

Table 2. Antioxidant Values of Dairy and Dairy Products (Modified from Carlsen et al., 2010)[100]

sr. no.	product	antioxidant content[a] (mmol/100 mg)
1	buttermilk, special, 1.5% fat	0.04
2	buttermilk, skimmed	0.05
3	cheese, Gorgonzola dolce	0.54
4	cream, 22% fat	0.06
5	goat's milk	0.04
6	milk, 2%	0.04
7	ice cream, chocolate, regular fat	0.76
8	ice cream, regular fat, natural vanilla	0.05
9	ice cream with strawberry	0.21
10	milk, skimmed fermented with blueberries	0.42
11	sour cream	0.15
12	yogurt, original	0.06
13	yogurt, mixed wild berries	0.25
14	yogurt, strawberries	0.08
15	yogurt, frozen, fat-free, vanilla	0.06
16	yogurt, 99% fat-free, strawberry	0.11

[a]Values were estimated using the ferric reducing ability of plasma (FRAP) method.

APPLICATION OF PROBIOTICS IN FOOD

During the past 20 years, consumers' perception of functional foods including probiotics has changed. The presence of probiotics in commercial food products has been very well accepted and has been known for a number of health benefits. In this direction, industries worldwide are concentrating on applications of probiotics in food products as well as constructing a new era of "probiotic health" foods. Foods are considered better delivery vehicles for probiotic organisms than others due to the role played by the food matrix in maintaining the viability of organisms during the transition through the gastrointestinal tract. Dairy foods are considered natural carriers for lactobacilli and bifidobacteria due to their ability to utilize lactose and produce lactic acid.

DOI: 10.1021/jf506326t
J. Agric. Food Chem. 2015, 63, 3615−3626

Table 3. Description of Commonly Used Methods for Screening of in Vitro Antioxidant Potential of Natural Compounds

assay	principle	observation	refs
DPPH	antioxidants are able to reduce the free, stable, and purple-colored 2,2-diphenyl-1-picrylhydrazyl radical to the yellow-colored diphenylpicrylhydrazine	yellow color substance by spectrometry or visible	18, 19
ABTS	2,2′-azinobis(ethylbenzothiazoline 6-sulfonate) is oxidized by oxidants to its radical cation, $ABTS^{\bullet-}$, which is intensely colored, and antioxidant capacity is measured as the ability of test compounds to decolorize the ABTS radical directly	decoloration by spectrometry or visible observations	21, 22
hydroxyl radical scavenging activity	hydroxyl radical is indirectly confirmed by the hydroxylation of *p*-hydroxybenzoic acid in the presence of iron	spectrophotometric determination	23
FRAP	characterized by the ability of antioxidant to reduce ferric 2,4,6-tripyridyl-*s*-triazine complex $[Fe^{3+}-(TPTZ)_2]^{3+}$ to $[Fe^{2+}-(TPTZ)_2]^{2+}$ depending on the available reducing species followed by the alteration of color from yellow to blue in acidic condition (pH 3.6)	analyzed through spectrophotometer	24−26
ORAC	principle is based on decreasing intensity of fluorescent molecule such as *β*-phycoerythrin or fluorescein of the target along with time under reproducible and constant flux of peroxy radicals	analyzed by fluorometer	34−36

METHODS FOR ANTIOXIDANT ACTIVITY SCREENING OF PROBIOTICS

Various methodologies have been adopted to determine the antioxidative potential for natural compounds; however, it is important to use consistent and rapid methods. Each antioxidative activity assay has a specific target within the well-defined matrix. Each method has its own merits and demerits. In the absence of a universal method that can give unambiguous results, the best way is to use multiple methods instead of one. Some of the procedures involve the use of synthetic antioxidants or free radicals; few are specific for lipid peroxidation and require animal and plant cells, some have a broader scope, some require minimum preparation and information, and few methods produce speedy results.[16] The antioxidative activity of food products including probiotic products has been studied by using different in vitro and in vivo methods.

In Vitro Antioxidative Methods. The in vitro assays are based on determination of scavenging capacity against ROS such as superoxide anion scavenging assay, hydrogen peroxide scavenging assay, and scavenging activity against stable nonbiological radicals. Several assays have been used to assess the total antioxidant content in foods such as the 6-hydroxy-2,5,7,8-tetramethylchroman-2-carboxylic acid (Trolox) equivalent antioxidant capacity (TEAC) assay, the ferric-reducing antioxidant power assay (FRAP), and the oxygen radical absorbance capacity assay (ORAC) assay. However, it has been found that the most common and reliable methods are the 2,2-diphenyl-1-picrylhydrazyl (DPPH) and 2,2′-azinobis(3-ethylbenzothiazoline-6-sulfonic acid) (ABTS) methods; these methods are simple, rapid, sensitive, and reproducible and have been modified and improved as per research requirements.[17] A brief description of some antioxidant potential screening methods used for probiotics is presented here and summarized in Table 3.

DPPH Assay. This widely used discoloration method was first described by Blois (1958).[18] This assay is based on the premise that a hydrogen donor is an antioxidant. The antioxidants are able to reduce the free, stable, and purple-colored DPPH radical to the yellow-colored diphenylpicrylhydrazine, which is monitored by using a colorimeter. DPPH is usually used as a reagent to evaluate the free radical scavenging activity of antioxidants.[19]

ABTS Assay. The ABTS radical scavenging method was developed[20] and was then modified by others.[21] In this assay, ABTS is oxidized by oxidants to its radical cation, $ABTS^{\bullet+}$, which is intensely colored, and the antioxidant capacity is measured as the ability of test compounds to decolorize the ABTS radical directly. $ABTS^{\bullet+}$ radicals are more reactive than DPPH, whereas generation of its radical cation forms the basis of one of the spectrophotometric methods that have been applied for measuring the antioxidant property of pure substances, aqueous mixtures, and beverages.[22]

Hydroxyl Radical Scavenging Activity Assay. The hydroxyl radical ($^{\bullet}OH$) is the neutral form of the hydroxide ion (OH^-). This radical is known as the most reactive species and is known for lipid peroxidation and DNA damage.[23] In this assay, the hydroxyl radical is indirectly confirmed by the hydroxylation of *p*-hydroxybenzoic acid. However, iron plays a central role in the hydroxyl radical formation via the Fenton reaction.

FRAP Assay. The FRAP assay is characterized by the ability of an antioxidant to reduce ferric 2,4,6-tripyridyl-*s*-triazine complex $[Fe^{3+}-(TPTZ)_2]^{3+}$ to $[Fe^{2+}-(TPTZ)_2]^{2+}$ depending on the available reducing species followed by the alteration of color from yellow to blue in acidic condition (pH 3.6) and is analyzed through a spectrophotometer.[24−26] This method was employed to measure reducing power in plasma, but the assay subsequently has also been adapted and used for the assay of antioxidants in different foods or beverages,[27−32] teas, and fruits. A drawback of this method is that the antioxidant capacity of certain compounds which can react with ferrous ion (Fe^{2+}) and SH group-containing antioxidants cannot be measured.[33]

ORAC Assay. The ORAC assay uses the area-under-curve technique and combines the inhibition time and inhibition degree of free radical action by an antioxidant into a single quantity. On the other hand, similar methods use either inhibition time at a fixed inhibition degree or the inhibition degree at fixed time as the basis for quantifying the outputs.[34−36] ORAC evaluates antioxidant inhibition of peroxy radical-induced oxidations and thus reflects the classical radical chain-breaking antioxidant activity by hydrogen atom transfer (HAT).[37] The peroxy radicals are generated through thermal decomposition of 2,2′-azobis(2-amidinopropane) dihydrochloride (AAPH) in aqueous buffer. The principle of this method is based on decreasing the intensity of fluorescent molecules such as *β*-phycoerythrin or fluorescein of the target along with time under reproducible and constant flux of peroxy radicals.

ANTIOXIDATIVE POTENTIAL OF PROBIOTIC MICROORGANISMS AND FOODS

Each characteristic of probiotic organisms is first established using in vitro methods and subsequently in vivo experiments

DOI: 10.1021/jf506326t
J. Agric. Food Chem. 2015, 63, 3615−3626

Table 4. Summary of Antioxidative Potential of Intact Cells, Cell-free Extract, and Culture Supernatant of *Lactobacillus* sp. and *Bifidobacterium* sp.

species	intact cell[a]	ICFE[a,b]	culture supernatant[a]	antioxidative method used	ref
6 *Lactobacillus*, 2 *Streptococcus*, and 1 *Lactococcus*	−	+	−	microsome thibarbituric acid (MS-TBA) method	42
Lactobacillus acidophilus B, E, N1, 4356, LA-1, and Farr; *Lactobacillus bulgaricus*12 278, 448, 449, Lb, 1006, and 11 842; *Streptococcus thermophilus* 821, MC, 573, 3641, and 19 987; and *Bifidobacterium longum* B6 and 15 708	−	+	−	inhibition of ascorbate autoxidation, ferrous and copper ion chelating assay, hydroxyl and hydrogen peroxide radical scavenging activity, reducing power assay, superoxide dismutase activity, and SOD induction	43
L. acidophilus ATCC 4356 and *B. longum* ATCC 15708	+	+	−	thiobarbituric acid method (TBA), DPPH, plasma lipid peroxidation	52
Lactobacillus delbrueckii ssp. *lactis* RM2-5, RM6-5, and RM5-4, *Lactobacillus delbrueckii* ssp. *bulgaricus* 18, 10442, and Y-23, *Lactobacillus acidophilus* O16, L-1, and NCFM and *Lactobacillus casei* E10, 9018, and E5	+	+	−	oxygen radical absorbance capacity	44
*Lactobacillus*sp. L13, *L. acidophilus* 14 and 15, *L. casei* ssp. *casei* 19 and 63, *L. delbrueckii* ssp. *bulgaricus* 4 and 9, *L. helveticus* 6, *L. plantarum* 20, *L. fermentum* 141, 155, 156	+	+	−	DPPH assay by TLC, MS-TBA, and linoleic acid peroxidation assay	41
Lactobacillus fermentum	+	−	−	hydroxyl, DPPH, and superoxide anion radical scavenging activity assay	51
Bifidobacterium longum and *Lactobacillus delbrueckii* ssp. *bulgaricus*	+	+	−	DPPH radical scavenging activity, inhibition of lipid peroxidation in liposomes, measurement of malondialdehyde	45
Lactobacillus casei subsp.*casei* SY13 and *Lactobacillus delbrueckii* subsp. *bulgaricus* LJJ	+	+	−	measurement of linoleic acid peroxidation, chelating capacity of ferrous ion and reducing activity, DPPH and hydroxyl radical scavenging activity, superoxide anion scavenging activity	101
Bifidobacterium animalis 01	+	+	+	lipid peroxidation, DPPH, hydroxyl radical assay, superoxide anion assay	63
L. plantarum AS1	+	−	−	linoleic acid peroxidation and DPPH	78
39 *Lactobacillus* isolates	+	−	−	resistance to reactive oxygen species, hydrogen peroxide, hydroxyl radicals, superoxide anions, SOD activity, total antioxidative against linolenic acid (TAA_{LA})	39
Lactobacillus helveticus CD6	+	+	−	inhibition of ascorbate autoxidation, reducing activity assay, metal ion chelating assay, hydroxyl radical assay, DPPH, SOD activity and its induction	60
Lactobacillus paracasei Fn032 and *Lactobacillus rhamnosus* GG (LGG)	+	+	−	resistance to hydrogen peroxide and hydroxyl radicals, scavenging capacity against hydroxyl radical and superoxide anion	79
7 *Bifidobacterium*, 11 *Lactobacillus*, 6 *Lactococcus*, and 10 *Streptococcus thermophilus*	+	+	−	total antioxidative activity against ascorbic (TAA_{AA}) and TAA_{LA}, Trolox equivalent antioxidant capacity (TEAC), intracellular glutathione (TGSH), SOD	64

[a] +, use of each preparation (intact cells and ICFE of probiotic bacteria) for antioxidative activity; −, no use of each preparation (intact cells, ICFE, and culture supernatant of probiotic bacteria) for antioxidative activity. [b] ICFE, intracellular cell-free extract.

J. Agric. Food Chem. 2015, 63, 3615−3626
DOI: 10.1021/jf506326t

conducted in suitable animal models. On confirmation of the suitability of the organism, it is incorporated in suitable food products, and further studies are conducted using probiotic foods to establish its efficacy, survival under storage conditions, etc.[8] In vitro antioxidative studies have been conducted on different probiotic organisms (mainly lactobacilli and bifidobacteria), and food products containing probiotic organisms have also been studied. The following section reviews these studies, and a summary is presented in Table 4.

■ *LACTOBACILLUS* SP.

Lactobacillus rhamnosus. Different antioxidative capacities of *Lactobacillus* species to modify the bacterial profile and prevent the oxidative stress in the Fe-overloaded mice colon were studied.[38] The generation of hydrogen peroxide and hydroxyl radical as well as growth of Fe-dependent bacteria is encouraged by iron (Fe). Findings of this study showed that survival time of *L. rhamnosus* GG strain was significantly longer in the presence of H_2O_2 and hydroxyl radical as compared to non-antioxidative strains, *L. paracasei* Fn032 and *L. plantarum* Fn001, respectively. In addition, *L. paracasei* Fn032 and *L. plantarum* Fn001 were specific for free radical scavenging activities of their intracellular free extracts (ICFE). Scavenging activities increased to various extents when bacterial strains were exposed to gastric and pancreatic juice. However, Achuthan et al.[39] also reported the resistance of a total of 39 *Lactobacillus* cultures to ROS. Most of the isolates showed moderate to strong resistance toward 0.4 mM H_2O_2. The majority of cultures demonstrated high resistance to hydroxyl radicals, and isolate *L. plantarum* 21 (Lp21) was most resistant with log count reduction of 0.20-fold only. Of 39 isolates, *Lactobacillus* spp. S3 showed highest total antioxidative activity of 77.85 followed by 56.1 of isolate *L. plantarum* 55 (Lp55) in terms of percent inhibition of linolenic acid oxidation. Moreover, isolate *L. plantarum* 9 (Lp9) up-regulated the expression of superoxide dismutase (SOD) gene 2 in HT-29 cell at concentrations of 0.1 mM (1.997-fold) and 1.0 mM H_2O_2 (2.058-fold). In addition to this, cultures Lp9, *L. plantarum* 91 (Lp91), and Lp55 showed significant up-regulation in the expression of GPX-I gene to levels of 5.451-, 8.706-, and 10.083-fold, respectively, when HT-29 cells were challenged with 0.1 mM H_2O_2. On the other hand, CAT gene expression was also significantly regulated by all of the isolates used in this study in the presence of 0.1 mM H_2O_2.

Grompone et al.[40] developed a new, fast, predictive, and convenient in vitro method for the screening of antioxidative potential of new probiotic strains using the nematode *Caenorhabditis elegans* as host (model organism). In this study, a total of 78 strains of lactic acid bacteria (LAB) (*Lactobacillus* and *Bifidobacterium*) were examined. This collection is composed by 62 *Lactobacillus* strains belonging to *L. acidophilus*, *L. bulgaricus*, *L. casei*, *L. paracasei*, *L. plantarum*, and *L. rhamnosus* species, 9 *Streptococcus thermophilus* isolates, and 6 *Bifidobacterium* strains belonging to the *B. animalis*, *B. breve*, and *B. longum* species. The LAB stains used in this study were fed to *C. elegans*, and the survival rate of *C. elegans* was examined upon exposure to H_2O_2-induced stress by comparison with the protective effect exerted by *Escherichia coli* OP50. As a result of this screening, a *Lb. rhamnosus* strain (CNCM I-3690) demonstrated a high antioxidant capacity.

Kapila et al.[41] examined the antioxidative activity of ICFE of 13 strains of *Lactobacillus* sp. by using microsome–thiobarbituric acid (MS-TBA) and linoleic acid peroxidation methods. Maximum antioxidant capacity in terms of percent inhibition of oxidation was expressed in *L. casei* ssp. *casei* 19 (76.82%) followed by *L. acidophilus* 14 (62.21%), *Lactobacillus* sp. L13 (59.25%), *L. casei* ssp. *casei* 63 (53.30%), *L. helveticus* 6 (52.70%), and *L. delbrueckii* ssp. *bulgaricus* 4 (52.64%), whereas the remaining strains showed <50% activity. In addition to this, strain *L. casei* ssp. *casei* 19 showed 72.04% linoleic acid peroxidation followed by *L. acidophilus* 14 (51.74%), *Lactobacillus* sp. L13 (51.38%), and the remaining strains exhibited <50% activity.

Similarly, other authors[42] reported the antioxidative potential of ICFE of 19 strains of lactic acid bacteria (16 lactobacilli, 2 streptococci, 2 lactococci) of 570 strains using MS-TBA. However, the highest inhibitory activity of oxidation was observed in *Lactobacillus* sp. SBT-2028 (91%) followed by *L. casei* ssp. *pseudoplantarum* SBT-0624 (77%). The antioxidative potential of ICFE of 19 strains of LAB including *L. acidophilus* B, E, N1, 4356, LA-1, and Farr; *L. bulgaricus* 12, 278, 448, 449, Lb, 1006, and 11 842; *S, thermophilus* 821, MC, 573, 3641, and 19 987; and *B. longum* B6 and 15 708 was studied by using inhibition of ascorbate autoxidation, ferrous and copper ion chelating assays, hydroxyl and hydrogen peroxide radical scavenging activity, reducing power assay, SOD activity, and SOD induction assay.[43] All strains exhibited the inhibition of ascorbate autoxidation in the range of 7–12%. The strain *L. acidophilus* E showed the highest (33.1 mM) and *S. thermophilus* 3641 the lowest (0.5 mM) hydroxyl radical scavenging capacities, equivalent to that of uric acid. Furthermore, the reducing activity of *B. longum* B6 was found to be higher, equivalent to 225.3 μM cysteine and 50-fold higher than that of *S. thermophilus* 19 987, which had the reducing activity equivalent to 4.3 μM cysteine, whereas strains of *L. acidophilus* B, E, N1, and 4356 also showed the lowest reducing activity. Among the 19 strains of lactic acid bacteria tested, *L. bulgaricus* strains demonstrated higher metal ion Fe^{2+} chelating ability (ranging from 5.6 to 52.9 ppm) than *L. acidophilus*. On the other hand, *S. thermophilus* strains showed a very wide range of Fe^{2+} chelating ability ranging from 0.5 to 72.7 ppm. *S. thermophilus* 821 and 19 987 demonstrated the highest and lowest Fe^{2+} chelating abilities, respectively, whereas *B. longum* B6 and 15708 had high chelating activities for Fe^{2+} at 40.7 and 26.6 ppm, respectively.

Moreover, for copper ion chelation, *L. acidophilus* and *S. thermophilus* strains showed a wide range of chelation abilities ranging from 0 to 34.8 ppm and from 2.4 to 51.0 ppm, respectively. Six *L. bulgaricus* strains tested had high Cu^{2+} chelating abilities ranging from 13.2 to 48.3 ppm. Both *B. longum* B6 and 15 708 had not only high Fe^{2+} chelating ability but also high Cu^{2+} chelating ability (18.5 and 63 ppm, respectively). All of the strains were unable to inhibit the SOD activity, whereas SOD activity also was not induced when growth medium was supplemented with metal ions Mn^{2+}, Fe^{2+}, Cu^{2+}, or Zn^{2+}.

Saide and Gilliland[44] demonstrated antioxidative activity by evaluating the oxygen radical absorbance capacity of whole cells and ICFE of selected strains of lactobacilli species, which was expressed as Trolox equivalents per 10^9 cells. Cell-free extract of *L. delbrueckii* ssp. *lactis* RM5-4, *L. acidophilus* NCFM, *L. delbrueckii* ssp. *bulgaricus* 18, 10442, and Y-23 and *L. casei* 9018 exhibited higher oxygen radical absorbance capacity (total antioxidative capacity) than that of the intact cells.

Ou et al.[45] reported the comparative antioxidative potential of intact cells and ICFE of *B. longum* and *L. delbrueckii* ssp.

DOI: 10.1021/jf506326t
J. Agric. Food Chem. 2015, 63, 3615–3626

bulgaricus. In this direction, intact cells of both strains showed 71.3% and 70.4% and ICFE of both strains showed 72.6% and 75.1% DPPH radical scavenging activity respectively. On the other hand, both strains were capable to protect liposome lipid from oxidation and the inhibition rate ranged from 25−31% while no significant difference in lipid peroxidation by intact cells and ICFE of both strains was reported. There was significant reduction in malondialdehyde production in intestine 407 cells.

***Lactobacillus fermentum* ME-3.** The *L. fermentum* ME-3 strain has been comprehensively studied at University of Turku, Finland. It is a unique strain of *Lactobacillus* species, having at the same time antimicrobial and physiologically effective antioxidative properties and expressing health-promoting characteristics.[45] Research on *L. fermentum* ME-3 has established that the particular strain has double functional properties: antimicrobial activity against intestinal pathogens and high total antioxidative activity (TAA) and total antioxidative status (TAS) of intact cells and lysates. *L. fermentum* ME-3 is characterized by a complete glutathione system: synthesis, uptake, and redox turnover. The functional efficacy of the antimicrobial and antioxidative property has been proved by the eradication of *Salmonella* and the reduction of liver and spleen granulomas in *S. typhimurium*-infected mice treated with the combination of ofloxacin and *L. fermentum* ME-3.[46,47] It also revealed the antioxidative potential of probiotic *L. fermentum* ME-3 in soft cheese spreads containing different fatty acids. Moreover, *L. fermentum* E-3 and E-18 contained remarkable levels of glutathione and expressed Mn-SOD, which is of vital importance for the prevention of lipid peroxidation and secretion of hydrogen peroxide.[48] Few researchers[49] have worked on *L. fermentum* FTL2311 and *L. fermentum* FTL10BR strains isolated from miang, traditional fermented tea leaves, which liberate certain substances that possess antioxidative activity expressed in terms of TEAC and equivalent concentration (EC) values for free radical scavenging and reducing mechanisms, respectively. The culture supernatant of *L. fermentum* FTL2311 revealed TEAC and EC values of 22.54 ± 0.12 and 20.63 ± 0.17 μM/mg respectively, whereas that of *L. fermentum* FTL10BR yielded TEAC and EC values of 24.09 ± 0.12 and 21.26 ± 0.17 μM/mg, respectively. These two strains isolated from miang present high potential as promising health-promoting probiotics.[50] On the other hand, *L. fermentum* demonstrated higher free radical scavenging activities of against hydroxyl, superoxide, and DPPH radicals. Scavenging activities at populations of 10^6 and 10^9 CFU/mL for hydroxyl radical, superoxide radical, and DPPH were 7.35, 12.86, and 64.26% and 91.84, 80.56, and 87.89%, respectively.[51]

***Lactobacillus acidophilus*.** The antioxidative potential of intestinal lactic acid bacteria *L. acidophilus* ATCC 4356 was reported.[52] In this study, both intact cells and ICFE showed 28.1 and 45.3% inhibition of linoleic acid peroxidation, whereas 43.2 and 20.8% inhibition of DPPH radical scavenging activity, respectively. The cytotoxicity of 4-nitroquinoline-*N*-oxide (4NQO) to intestine 407 cells was reduced by intact cells up to 49%, whereas no inhibition was observed for ICFE. Findings of this study suggest that ICFE showed better antioxidative activity than intact cells.

***Lactobacillus plantarum*.** Studies by others[53] exhibited the antioxidative attributes of the intact cells of *L. plantarum* AS1 isolated from the South Indian fermented food *kallappam*. Strain AS1 showed 50.96% inhibition of linoleic acid peroxidation, whereas DPPH radical scavenging activity was found to be 29.15%. This study concluded that a significant antioxidant effect might be a reason for the reduction of cancerous tumors and related symptoms in rats (also discussed for in vivo studies).

The antioxidative property of *L. rhamnosus* in combination with *B. longum* containing fruit juice permeates such as lemon juice and mango and guava pulps was studied.[54] The superoxide anion radical scavenging capacity of *L. rhamnosus* GG was higher than those of several other bacteria such as *L. rhamnosus* Lc 705, *L. acidophilus* LA, *L. paracasei* YEC, *Bifidobacterium* sp. BB12, and *E. coli*.[55]

***Lactobacillus casei*.** Both intact cells and ICFE of *L. casei* KCTC 3260 demonstrated high antioxidative activity and inhibited lipid peroxidation by 46.2 and 72.9%, respectively. The culture had higher levels of chelating activity for both Fe^{2+} and Cu^{2+} ions at 10.6 and 21.8 ppm, respectively, which suggested that the antioxidative capacity of *L. casei* KCTC 3260 may be caused by chelating metal ions instead of SOD activation.[56] Moreover, Yoon and Byun[57] found that *L. casei* HY 2782 contained the highest level of glutathione sulfhydryl (GSH) among different probiotic strains tested. GSH levels in *L. casei* HY 2782 reached maximum values after 24 h of cultivation but decreased for 72 h. The effect of culture media on GSH activity was also studied, and it was found that GSH levels were significantly higher during cultivation in de Man Rogosa and Sharpe (MRS) broth than in tryptone phytone yeast extract broth or bromcresol purple dextrose broth. Significant positive correlation between antioxidative activity and cellular GSH contents was observed.

***Lactobacillus gasseri*.** Kim et al.[58] investigated the protective effect of the selected *L. gasseri* NLRI 312 against oxidative damage to cellular membrane lipid and DNA in the Jurkat cell line. *L. gasseri* NLRI 312 had a protective effect on the Jurkat cell lines in terms of oxidative damage, although supplementation had no effect on malondialdehyde (MDA) production. There was a 50% reduction in DNA damage after probiotic treatment of cell lines. Many peptides are identified in fermented milk, which contributes to the antioxidant potential of products. A κ-casein-derived peptide with DPPH radical scavenging activity has been found in milk fermented with *L. delbrueckii* ssp. *bulgaricus*.[59]

***Lactobacillus helveticus*.** *L. helveticus* CD6 producing a folic acid derivative 5-methyltetrahydrofolate (5-MeTHF) was studied for antioxidative activity. The ICFE of *L. helveticus* CD6 demonstrated antioxidative activity with the inhibition rate of ascorbate autoxidation in the array of 27.5%, which showed highest metal ion chelation ability for Fe^{2+} (0.26 ± 0.06 ppm) as compared to Cu^{2+}. The DPPH and hydroxyl radical scavenging activities of intact cells found to be 24.7 and 20.8%, respectively, proved its antioxidative potential. Moreover, it demonstrated 14.89% inhibition of epinephrine autoxidation, 20.9 ± 1.8 μg of cysteine equivalent reducing activity, and 20.8% hydroxyl radical scavenging effect. This study also reported the detection of SOD by using 10% nondenaturing polyacrylamide gel electrophoresis. It was observed that SOD activity was absent in the ICFE of *L. helveticus* CD6.[60]

Two strains each of lactobacilli (*L. rhamnosus* GD 11 and *L. plantarum* LA3) and bifidobacteria (*B. breve* A28 and *B. breve* A10) were studied for exopolysaccharide (EPS) production, antioxidative characteristics, and their role in gingival fibroblast. Among four cultures, *B. breve* A28 showed high EPS production at 122 mg/L. It also showed 72% DPPH free radical scavenging

DOI: 10.1021/jf506326t
J. Agric. Food Chem. 2015, 63, 3615−3626

activity and 88% iron ion chelation activity. The strain also showed 71% inhibition of lipid peroxidation.[61]

***Bifidobacterium* sp.** Several studies have been conducted on the antioxidative activity of *Bifidobacerium* sp. Lin and Chang[52] investigated the antioxidative potential of the intestinal lactic acid bacteria *B. longum* ATCC 15708. Both intact cells and ICFE, respectively, showed 32 and 48% inhibition of linoleic acid peroxidation and 52 and 42% DPPH radical scavenging activity. The cytotoxicity of 4NQO to intestine 407 cells was reduced by intact cells up to 89%, whereas no inhibition was observed for intracellular extract. Furthermore, intact cells and ICFE showed 16.2 and 34.3% inhibition rates of plasma lipid peroxidation for 10^9 cells of *B. longum* ATCC 15708. Another study[62] reported that *Bifidobacterium* was involved in the transformation of lignan glucosides. In this view, only 10 *Bifidobacterium* cultures partially hydrolyzed secoisolariciresinol diglucoside (SDG), giving both secoisolariciresinol (SECO) and the monoglucoside with yields <25% of 28 strains. *B. pseudocatenulatum* WC 01 gave highest SDG conversion to SECO, which exhibited 75% yield in cellobiose-based medium after 48 h. The antioxidative activity of *B. animalis* 01 culture supernatant, intact cells, and ICFE exhibited an inhibitory effect on linoleic acid peroxidation. The inhibitory effect was 30.48, 41.12, and 71.02% for culture supernatant, intact cells, and ICFE, respectively. Culture supernatant of *B. animalis* 01 demonstrated the highest DPPH scavenging effect (73.11%), which was significantly ($P < 0.05$) higher than that of MRS broth, whereas the relatively lowest DPPH free radical scavenging effect was found in intact cells among the tested groups. In addition, culture supernatant showed 78.32% hydroxyl radical and 86.39% superoxide anion radical scavenging activities, which were also significantly higher than that of MRS broth, whereas intact cells exhibit a weak scavenging effect.[63] Work by others[64] reported the in vitro antioxidative properties of 34 strains of *Bifidobacterium*, *Lactobacillus*, and *Lactococcus* against ascorbic and linolenic acid oxidation (TAA_{AA} and TAA_{LA}), TEAC, intracellular glutathione (TGSH), and SOD. Of these cultures *B. animalis* subsp. *lactis* DSMZ 23032, *L. acidophilus* DSMZ 23033, and *L. brevis* DSMZ23034 exhibited among the highest TAA_{AA}, TAA_{LA}, TEAC, and TGSH values.

Probiotic Products with Antioxidant Activity. Fermented milk was prepared from cow's, goat's, and camel's milk supplemented with probiotic bacteria *Pediococcus pentosus* and studied for antioxidative property and fatty acid profile.[65] The finding showed that probiotic fermented milk obtained from goat's milk has the highest DPPH radical scavenging activity (98%) followed by product from camel's milk (86%) and cow's milk (79%). Moreover, it has also been reported that different protein peptides present in fermented milk are responsible for increased radical scavenging activity.[66]

Recently the antioxidative potential of two synbiotic dairy products, namely, synbiotic lassi with honey and whey-based synbiotic drink with inulin and orange juice containing *L. helveticus* MTCC 5463 as probiotic strain, was evaluated.[67] Both products showed antioxidative activity in terms of hydroxyl radical scavenging activity, radical scavenging activity, and antiradical scavenging activity. The storage of products at 4 ± 1 °C had an adverse effect on these activities as for whey-based drink, the activity reduced for all parameters. The synbiotic yogurt samples containing *L. plantarum* and *L. fermentum* expressed radical scavenging in the form of DPPH radical inhibition of 85 and 82%, respectively, at day 1, and the values increased as the storage time increased.[68] In this study, fructooligosaccharide was used as prebiotic for preparation of synbiotic yogurt. To measure the antioxidant activity of probiotic strain *L. plantarum* NBIMCC 2415, which was used as starter culture for production of dried fermented products,[69] four methods for cell disintegration of strain *L. plantarum* NBIMCC 2415 were investigated such as temperature, alkaline, enzymatic, and ultrasound. An alkaline cell lysis method was found to be appropriate, and with this method *L. plantarum* NBIMCC 2415 showed high antioxidant activity (5.57 μmol TE/log N). The study concluded that meat starter culture *L. plantarum* NBIMCC 2415 was not only involved in fermentation process but also preserved the color, formed the flavor, and increased the meat products' shelf life as well. Antioxidative activity in soy milk fermented with LAB and bifidobacteria simultaneously was reported to be significantly higher than that fermented with either of the cultures individually. Unfermented soy milk showed hydrogen peroxide-scavenging effect. Freeze-dried product had significantly lesser reduction in the antioxidative activity of soy milk than spray-dried. The antioxidative activity of fermented soy milk reduced after drying.[70]

Some researchers worked on the effect of prebiotics (inulin, lactulose, and raffinose) on multiplication of some probiotic strains of *Lactobacillus* and *Bifidobacterium*, used in a pollen and honey medium for obtaining a bee bread-like product. The prebiotics were tested and compared to pollen and honey medium for the viability and total antioxidative activity. In this view, medium B2 supplemented with ground pollen and honey (inoculated with studied probiotic strain) showed ∼45% DPPH radical scavenging activity after 7 days of incubation.[71]

IN VIVO STUDIES IN ANIMAL MODEL

The effect of oral administration of live *B. breve* strain Yakult (BBY) on skin barrier perturbation caused by UV and ROS was studied in hairless mice.[72] Strain BBY prevented the UV-induced increase in transepidermal water loss (TEWL). It also significantly suppressed the hydrogen peroxide level, oxidation of proteins and lipids, and xanthine oxidase activity, induced by UV in the skin.

Wang et al.[51] reported that *L. fermentum* could keep pigs growing healthily by increasing SOD and GPX activities and decreasing MDA levels in serum. Similarly, increased activity of hepatic CAT was also observed with decreased MDA levels. The effect of supplemented diets on the generation of intestinal nitric oxide (NO_x) and antioxidant activities with two strains of *L. delbrueckii* subsp. *bulgaricus* B3 and A13, which produced highest (211 mg/L) and lowest (27 g/L) amounts of exopolysaccharide, was studied.[73] The result showed that the small intestinal glutathione (GSH) and thiobarbituric acid-reactive substances (TBARS) were increased by administration of the probiotic organisms, but amino acid levels did not change in either control or experimental groups. NO_x also increased in both samples. An excessive amount of NO_x may contribute to lipid peroxidation because of increased ROS and reactive nitrogen species. The antioxidative capacity of the small intestine was ameliorated by administration of two strains of *L. delbrueckii* subsp. *bulgaricus* B3 and A13. Probiotic Dahi was prepared by coculturing selected strains of *L. acidophilus* and *B. bifidum* and Dahi culture in standardized buffalo milk and evaluated for its antioxidative effects on rats.[74] The activities of SOD and CAT were determined in red blood cells (RBC) at monthly intervals and in liver and colorectal tissue at

DOI: 10.1021/jf506326t
J. Agric. Food Chem. 2015, 63, 3615−3626

the conclusion of the experiment. The SOD activity in RBC increased with probiotic Dahi but not with Indian Dahi. In addition, the CAT activity in RBC increased with probiotic Dahi as well as normal Dahi and the former was more efficacious. In the liver, the SOD activity was stimulated by probiotic Dahi, whereas in colorectal tissue, both normal and probiotic Dahi effectively stimulated SOD activity. Milk fermented with *L. acidophilus* and *B. bifidum* when fed to rats enhanced the activity of SOD and decreased TBARS accumulation in liver and colorectal tissues.

Probiotic Dahi containing *L. acidophilus* LaVK2 (La-Dahi) and *B. bifidum* BbVK3 (LaBb-Dahi) alleviated age-inflicted accumulation of oxidation products, antioxidant enzymes, and improved expression of biomarkers of aging in mice.[75] In this direction, La-Dahi or LaBb-Dahi increased CAT and GPX activities in RBCs and hepatic tissue and led to a significant decline in TBARS in plasma, kidney, and hepatic tissues and protein carbonyls in the plasma of mice. Probiotic Dahi also reversed the age-related decline in expression of biomarkers of aging, peroxisome proliferators activated receptor-α, senescence marker protein-30 (SMP-30), and Klotho in hepatic and kidney tissue. The findings of this study suggested that probiotic Dahi containing selected strains of LAB can be used as potential nutraceutical intervention to combat oxidative stress and molecular alterations associated with aging. On the other hand, in vivo antioxidant activities of selenium/zinc-enriched probiotics preparation were studied using indigenous dogs (30 day trial).[76] In this study, two probiotic strains, particularly *L. acidophilus* and *Candida utilis*, highly tolerant to high concentrations of inorganic selenium (Se), zinc (Zn), and bile salts and low pH conditions were used. The results of this study indicated that the SOD ($P < 0.01$) and TAOC ($P < 0.05$) activity in the group supplemented with Se/Zn-enriched probiotics were higher as compared to the control group. In addition, there were no significant variations in the increased activity of GPX in both control and experimental groups. The MDA activity of the experimental group was lower than that of the control after 15 days of trial. However, at 30 days of trial, the activities of GPX, SOD, and TAOC in the experimental group were superior to those in the control group, with all of them showing very significant differences ($P < 0.01$). The MDA level of the experimental group was significantly decreased in comparison with the control group ($P < 0.01$).

Furthermore, Dahi containing probiotic *L. acidophilus* NCDC14 and *L. casei* NCDC19 significantly suppressed STZ-induced oxidative damage in pancreatic tissues by inhibiting the lipid peroxidation and formation of nitric oxide and preserving the antioxidant pool such as glutathione content and activities of SOD, CAT, and GPX.[77] The same authors also reported that *L. acidophilus* and *L. casei* with Dahi increased the ability of Dahi to suppress STZ-induced diabetes in rats by inhibiting depletion of insulin as well as preserving diabetic dyslipidemia and inhibiting lipid peroxidation and nitrite formation.

The cholesterol-lowering and antioxidative potential of *L. casei* ssp. *casei* was studied,[41] and it was reported that the cholesterol levels were lower in the plasma of groups fed fermented milk by 2−11 and by 15−25% in groups fed lyophilized culture as compared to the group fed skim milk. The levels of TBARS were lower in the LDL fraction of plasma in rats fed fermented milk or culture than the control group fed skim milk.

The comparative effects of probiotic curd (*Acidophilus casei* Dahi) prepared using *L. acidophilus* and *L. casei* and normal curd (DRC-1, prepared using *Lactococcus lactis* spp. biovar. *diacetylactis*) on lipid peroxidation level (TBARS level) of 1,2-dimethylhydrazine-treated rats were studied.[78] The TBARS levels were estimated in tissues obtained from the liver and colon. The *A. casei* Dahi inhibited the lipid peroxidation in comparison to normal curd by reducing the TBARS level in both the liver and colon.

The in vivo antioxidative properties of *L. plantarum* AS1 isolated from South Indian fermented food *kallappam* were reported.[79] In this study, male albino rats were used and an increased level of lipid peroxide (LPO) products and increased activities of antioxidant enzymes (SOD, CAT, and glutathione *S*-transferase) and marker enzymes (alkaline phosphatase and acid phosphatase) in the colon and plasma of cancer-bearing animals have been observed. Strain AS1 showed its anticancer effect through its potent antioxidative attributes.

The antioxidative activities of three lactobacilli, *L. rhamnosus* GG, *L. paracasei* Fn032, and *L. plantarum* Fn001, in the colon of Fe-overloaded mice were evaluated.[80] In this study, decreased mucosal total antioxidative capacity and oxidative enzyme activity were observed in Fe-overloaded mice. *L. rhamnosus* GG significantly inhibited the increase of colonic mucosal free radicals and MDA content. Moreover, strain *L. paracasei* Fn032 inhibited only MDA, whereas *L. plantarum* Fn001 showed no significant antioxidative potential in vivo.

Sengul et al.[81] demonstrated the antioxidative activity of two exopolysaccharide producing probiotic strains, *L. delbrueckii* subsp. *bulgaricus* (first group: high-EPS producing) B3 and A13 (second group: low-EPS producing) on gut oxidative damage in a rat model of experimental colitis. It was reported that the activities of antioxidative enzymes such as SOD, CAT, and GPX were higher in both probiotic-treated groups compared to that of the colitis model group. Furthermore, lipid peroxidation was also significantly enhanced in both probiotics groups. In this direction, oxidative damage was associated with a high level of MDA activity and reduced activity of antioxidative enzymes in the colitis model group significantly. Activities of antioxidative enzymes and MDA contents in serum and liver of aging mice were evaluated[63] using culture supernatant, intact cells, and cell-free extract of *B. animalis* 01. Monoamine oxidase (MAO) activity and lipofuscin level in brains of aging mice were also characterized. Results showed that *B. animalis* 01 culture supernatant, intact cells, ICFE, and ascorbic acid significantly ($P < 0.05$) enhanced the activities of antioxidant enzymes (SOD, CAT, and GPX) and the TAOC level in mice sera. In addition, findings suggest that the culture supernatant was more effective than MRS broth in enhancing activities of antioxidant enzymes and reducing MDA content in mice sera while lipofuscin level and MAO activity in mouse brains also reduced. This study indicated that *B. animalis* 01 has the potential to be developed into a dietary antioxidant supplements.

Amaretti et al.[64] studied the in vivo antioxidative potential of strains *B. animalis* subsp. *lactis* DSMZ 23032, *L. acidophilus* DSMZ 23033, and *L. brevis* DSMZ 23034 within lactobacilli and bifidobacteria groups (total of 34 strains). Potential antioxidative probiotic formulations of the same stains were prepared and administered to rats at doses of 10^7, 10^8, and 10^9 CFU/day for 18 days. The probiotic strains colonized the colon of the rats during the trial and promoted intestinal saccharolytic metabolism. In this direction, selected probiotic strains

DOI: 10.1021/jf506326t
J. Agric. Food Chem. 2015, 63, 3615−3626

neutralized the oxidative stress induced in animal model. Although in basal condition, probiotic treatment did not modify the tested markers of oxidative stress. On the other hand, the increase of reactive oxygen metabolites (ROM) concentration and decrease in TAA and GSH levels were found in non-probiotic-supplemented doxorubicin (DOXO) administered rats, whereas no alteration was detected in animals supplemented with two higher probiotic concentrations as compared to that of not supplemented, not stressed rats.

Administration of *Lactobacillius* GG helped in increasing the efficacy of treatment of cholesterol-induced peroxidation damage in plasma lipoproteins as well as in liver.[82] *Lactobacillus* GG ameliorated alcohol-induced liver protein carbonyl deposition in rats.[83] The same study reported that alcohol and *L. rhamnosus* GG (LGG) fed rats had significantly less severe alcoholic steatohepatitis (ASH).

A rat intestinal isolate, *E. coli* CFR 16, having probiotic potential, was used to study the role of probiotics in 1,2-dimethylhydrazine (DMH)-induced oxidative damage in the colon of a rodent model. The results revealed that there was a reduction in the activity of antioxidant enzymes (SOD, CAT, and GPX), and there was increased lipid peroxidation in liver and intestinal tissues in animals treated with DMH only. Not only did the DMH-treated animals show reduced lipid peroxidation activity but also the activity of antioxidant enzymes was maintained at normal level. The colonic histological sections also showed significant protection.[84]

Selenium-enriched probiotics were used to study the effect on various health parameters such as growth, immune function, and selenoprotein gene expression along with antioxidant status in crossbred weanling piglets kept under high natural summer temperatures. The results indicated a high growth in the probiotic-treated group along with an increase in activity of blood GPX and expression of tissue thioredoxin reductase 1 mRNA.[85]

The effect of diet supplemented with *L. plantarum* along with bursin (a peptide isolated from bursa of Fabriciuos) immunization was studied for immune characteristics, antioxidant status, and intestinal microflora in broilers. The probiotic supplementation increased the antioxidant capacity by increasing activity of enzymes such as CAT in liver and GPX in serum and liver and decreased MDA content in serum.[86]

As mentioned earlier, in vivo antioxidative potential of *L. rhamnosus* strain CNCM I-3690 was also evaluated through transcriptomics study, which was correlated with an increase in signaling of the insulin-like pathway mediated by the DAF-16 transcriptional factor.[40]

IN VIVO STUDIES ON HUMAN VOLUNTEERS/CLINICAL STUDIES WITH HUMAN

To verify the antioxidative properties of probiotic organism *L. fermentum* ME-3, different clinical study designs (including double-blind, placebo-controlled, crossover studies) and different subjects (healthy volunteers, allergic patients, and those recovering from a stroke) have been conducted using capsules or foodstuffs.[46] Clinical studies have been carried out on volunteers with clinical symptoms because it was difficult to assess the impact of probiotics without clinical symptoms and thus related to its effect on host health. In this context, the functional efficiency of *L. fermentum* ME-3 was examined in the human gastrointestinal tract (GIT) of healthy volunteers by measuring the influence of two different formulations, that is, *L. fermentum* ME-3 fermented goat's milk and *L. fermentum* ME-3 capsules, on intestinal flora and oxidative stress markers of blood and urine after 3 weeks of consumption.[87] In this study, human body oxidative stress status was evaluated by measuring the total antioxidative activity (TAA), total antioxidative status (TAS), and ratio of glutathione oxidized (ox) and glutathione reduced (red) in blood serum. In the goat's milk-treated group, TAA and TAS were found to be 6 and 9%, respectively, as compared to control, but 4 and 2.5%, respectively, in probiotic capsule group as compared to placebo. Furthermore, the glutathione red-ox ratio was found to significantly decrease in both the study group and the control in the goat's milk trial. However, no significant decrease was demonstrated in the probiotic capsule treated group. On the other hand, fermented milk containing the *L. fermentum* ME-3 strain also exhibited the antioxidative (enhanced TAA) and antiatherogenic effects in healthy human volunteers.[50]

MECHANISMS OF PROBIOTICS AS ANTIOXIDANTS

Antioxidant supplements or foods containing antioxidants would greatly help in reducing oxidative damage, free radical scavenging rate, and reducing activity of SOD and GPX in the human body. Probiotics from the LAB family can be potential candidates for the production of functional foods or natural antioxidant supplements.[58,88] It has been reported that some probiotics result in increased activity of antioxidative enzymes or modulation of circulatory oxidative stress, which protects cells against carcinogen-induced damage. These enzymes include glutathione *S*-transferase, glutathione, glutathione reductase, GPX, SOD, and CAT.[53] Some authors hypothesize that probiotics exert their defensive effects against oxidative stress by re-establishment of the gut flora.[83,89] Most LAB have scavenging systems for oxygen free radicals. Some lactobacilli possess antioxidant activity and are able to decrease the risk of accumulation of ROS during ingestion of food.[42] Metabolic activities of probiotic bacteria may have shown the antioxidative effect through the scavenging of oxidant compounds or the prevention of their generation into the intestine.[90] Production of bioactive peptides has been considered an effective mode of antioxidative activity in foods containing probiotic bacteria. Peptides obtained from hydrolyzed food proteins have been shown to possess antioxidative activities, which can impart protection against the peroxidation of lipids or fatty acids.[91] It has been observed that the peptic digest of casein liberates small peptides with radical scavenging activity.[92] The antioxidant ability was considered due to the presence of histidine and some hydrophobic amino acids in high concentrations. Increased antioxidant activity of milk during fermentation with commonly used dairy starter cultures, including *Leuconostoc mesenteroides* ssp. *cremoris* strain, *L. jensenii*, and *L. acidophilus* has been observed.[93]

The intestinal *Lactobacillus* species are particularly foci for development of novel foods by food industry due to the increasing interest of consumer in healthy diet.[94] During the past decade, oxidative stress and antioxidative potency have been revealed as the key points in molecular regulation of cellular stress responses.[95] In the case of *Lactobacillus* spp., it has been concluded that their antimicrobial effect is also expressed via ROS such as hydrogen peroxide, superoxide anions (O_2^-), and hydroxyl radicals ($^-{}^\bullet OH$), which may have a selective influence on the intestinal microbiota, whereas a similar mechanism has been described for oral streptococci.[96] Some lactobacilli possess antioxidative activity and are able to decrease the risk of accumulation of ROS during the ingestion

DOI: 10.1021/jf506326t
J. Agric. Food Chem. 2015, 63, 3615−3626

of food.[41,97] *L. rhamnosus* strain GG was reported to have potent antioxidative activity by down-modulating the ROS production and phagocytic capacity of neutrophils.[98]

In conclusion, the antioxidative property of probiotics has been the subject of many studies in recent times, and a few patents have been granted recently in this area[102] on the use of *Bifidobacterium lactis* BS 05, *Lactobacillus acidophilus* LA 06, and *Lactobacillus brevis* LBR01. Strong evidence for the antioxidative activity of *Lactobacillus plantarum*, *L. helveticus*, *L. acidophilus*, *L. fermentum*, *L. casei*, *Lactobacillus* GG, and a few bifidobacteria and foods containing these organisms is put forward by the studies conducted. However, it should be noted that the antioxidative property is strain specific. Methods used in the study of such activity are modifications of those used for the determination of the antioxidative property of plant-based foods. It is necessary to harmonize methods for dairy-based foods as these foods are considered as the most suitable carriers of probiotics. The mechanisms of antioxidative action that have not been properly understood and elucidated could be the focus of probiotic research in years to come.

AUTHOR INFORMATION

Corresponding Author

*(V.M.) E-mail: vijendramishra.niftem@gmail.com. Phone: +91-0130-2281167.

Notes

The authors declare no competing financial interest.

REFERENCES

(1) Cheeseman, K. H.; Slater, T. F. An introduction to free radical biochemistry. In *Free Radical in Medicine*; Cheeseman, K. H., Slater, T. F., Eds.; Churchill Livingstone: New York, 1993; pp 481−93.

(2) Seifried, H. E.; Anderson, D. E.; Fisher, E. I.; Milner, J. A. A review of the interaction among dietary antioxidants and reactive oxygen species. *J. Nutr. Biochem.* **2007**, *18*, 567−579.

(3) Valko, M.; Leibfritz, D.; Moncol, J.; Cronin, M. T.; Mazur, M.; Telser, J. Free radicals and antioxidants in normal physiological functions and human disease. *Int. J. Biochem. Cell Biol.* **2007**, *39*, 44−84.

(4) Halliwell, B.; Gutteridge, J. M. The antioxidants of human extracellular fluids. *Arch. Biochem. Biophys.* **1990**, *280*, 1−8.

(5) Feed antioxidants, Market and markets.com, http://www.marketsandmarkets.com/Market-Reports/animal-feed-antioxidants-market-138013648.html, 2014.

(6) Mayne, S. T. Antioxidant nutrients and chronic disease: use of biomarkers of exposure and oxidative stress status in epidemiologic research. *J. Nutr.* **2003**, *133* (Suppl 3), S933−S940.

(7) Grajek, W.; Olejnik, A.; Sip, A. Probiotics, prebiotics and antioxidants as functional foods. *Acta Biochim. Polym.* **2005**, *52*, 665−671.

(8) FAO, WHO. *Guidelines for the Evaluation of Probiotics in Food*, report of a joint FAO/WHO working group on drafting guidelines for the evaluation of probiotics in food; London, ON, Canada, April 30 and May 1, 2002; pp 1−11.

(9) Andersson, H.; Asp, N.-G.; Bruce, A.; Roos, S.; Wadstrom, T.; Wold, A. E. Health effects of probiotics and prebiotics: a literature review on human studies. *Scand. J. Nutr.* **2001**, *45*, 58−75.

(10) Chapman, C. M.; Gibson, G. R.; Rowland, I. Health benefits of probiotics: are mixtures more effective than single strains? *Eur. J. Nutr.* **2011**, *50*, 1−17.

(11) Majamaa, H.; Isolauri, E. Probiotics: a novel approach in the management of food allergy. *J. Allergy Clin. Immunol.* **1997**, *99*, 179−185.

(12) Chong, E. S. A potential role of probiotics in colorectal cancer prevention: review of possible mechanisms of action. *World J. Microbiol. Biotechnol.* **2014**, DOI: 10.1007/s11274-013-1499-6.

(13) Mishra, V.; Prasad, D. N. Application of *in vitro* methods for selection of *Lactobacillus casei* strains as potential probiotics. *Int. J. Food Microbiol.* **2005**, *103*, 109−115.

(14) Stiles, M. E.; Holzapfel, W. H. Lactic acid bacteria of foods and their current taxonomy. *Int. J. Food Microbiol.* **1997**, *36*, 1−29.

(15) Vasiljevic, T.; Shah, N. P. Probiotics − from Metchnikoff to bioactives. *Int. Dairy J.* **2008**, *18*, 714−728.

(16) Carocho, M.; Ferreira, I. C. A review on antioxidants, prooxidants and related controversy: natural and synthetic compounds, screening and analysis methodologies and future perspectives. *Food Chem. Toxicol.* **2013**, *51*, 15−25.

(17) Gulcin, I.; Berashvili, D.; Gepdiremen, A. Antiradical and antioxidant activity of total anthocyanins from *Perillapankinen is* decne. *J. Ethnopharmacol.* **2005**, *101*, 287−293.

(18) Blois, M. S. Antioxidant determinations by the use of a stable free radical. *Nature* **1958**, *26*, 1199−1200.

(19) Elmastas, M.; Turkekul, I.; Ozturk, L.; Gulcin, I.; Isıldak, O.; Aboul-Enein, H. Y. The antioxidant activity of two wild edible mushrooms (*Morchella vulgaris* and *Morchella esculanta*). *Comb. Chem. High Throughput Screening* **2006**, *9*, 443−448.

(20) Rice-Evans, C. A.; Miller, N. J. Total antioxidant status in plasma and body fluids. *Methods Enzymol.* **1994**, *234*, 279−293.

(21) Re, R.; Pellegrini, N.; Proteggente, A.; Pannala, A.; Yang, M.; Rice-Evans, C. Antioxidant activity applying an improved ABTS radical cation decolorization assay. *Free Radical Biol. Med.* **1999**, *26* (9−10), 1231−1237.

(22) Gulcin, I. Antioxidant activity of L-adrenaline: an activity structure insight. *Chem.-Biol. Interact.* **2009**, *179*, 71−80.

(23) Halliwell, B.; Chirico, S. Lipid peroxidation: its mechanism, measurement and significance. *Am. J. Clin. Nutr.* **1993**, *57*, 715−725.

(24) Benzie, I. F.; Strain, J. J. The ferric reducing ability of plasma (FRAP) as a measure of "antioxidant power": the FRAP assay. *Anal. Biochem.* **1996**, *239*, 70−76.

(25) Benzie, I. F.; Strain, J. J. Ferric reducing/antioxidant power assay: direct measure of total antioxidant activity of biological fluids and modified version for simultaneous measurement of total antioxidant power and ascorbic acid concentration. *Methods Enzymol.* **1999**, *299*, 15−27.

(26) Antolovich, M.; Prenzler, P. D.; Patsalides, E.; McDonald, S.; Robards, K. Methods for testing antioxidant activity. *Analyst* **2002**, *127*, 183−198.

(27) Pellegrini, N.; Serafini, M.; Colombi, B.; Del Rio, D.; Salvatore, S.; Bianchi, M.; Brighenti, F. Total antioxidant capacity of plant foods, beverages, and oils consumed in Italy assessed by three different *in vitro* assays. *J. Nutr.* **2003**, *133*, 2812−2819.

(28) Benzie, I. F.; Szeto, Y. T. Total antioxidant capacity of teas by the ferric reducing/antioxidant power assay. *J. Agric. Food Chem.* **1999**, *47*, 633−636.

(29) Proteggente, A. R.; Pannala, A. S.; Paganga, G.; Van Buren, L.; Wagner, E.; Wiseman, S.; Van De Put, F.; Dacombe, C.; Rice-Evans, C. A. The antioxidant activity of regularly consumed fruit and vegetables reflects their phenolic and vitamin C composition. *Free Radical Res.* **2002**, *36*, 217−233.

(30) Bursal, E.; Gulcin, I. Polyphenol contents and *in vitro* antioxidant activities of lyophilised aqueous extract of kiwifruit (*Actinidia deliciosa*). *Food Res. Int.* **2011**, *44*, 1482−1489.

(31) Gulcin, I.; Topal, F.; Cakmakc, I. R.; Goren, A. C.; Bilsel, M.; Erdogan, U. Pomological features, nutritional quality, polyphenol content analysis and antioxidant properties of domesticated and three wild ecotype forms of raspberries (*Rubus idaeus* L.). *J. Food Sci.* **2011**, *76*, C585−C593.

(32) Gulcin, I.; Topal, F.; OzturkSarıkaya, S. B.; Bursal, E.; Goren, A. C.; Bilsel, M. Polyphenol contents and antioxidant properties of medlar (*Mespilus germanica* L.). *Records Nat. Prod.* **2011**, *5*, 158−175.

(33) Somogyi, A.; Rosta, K.; Pusztai, P.; Tulassay, Z.; Nagy, G. Antioxidant measurements. *Physiol. Meas.* **2007**, *28*, R41−R55.

(34) Miller, N. J.; Rice-Evans, C. A.; Davies, M. J.; Gopinathan, V.; Milner, A. A novel method for measuring antioxidant capacity and its

DOI: 10.1021/jf506326t
J. Agric. Food Chem. 2015, 63, 3615−3626

application to monitoring the antioxidant status in premature neonates. *Clin. Sci.* **1993**, *84*, 407−412.
(35) Glazer, A. N. Phycoerythrin fluorescence-based assay for reactive oxygen species. *Methods Enzymol.* **1990**, *186*, 161−168.
(36) Whitehead, T. P.; Thorpe, G. H. G.; Maxwell, S. R. J. Enhanced chemiluminescent assay for antioxidant capacity in biological fluids. *Anal. Chim. Acta* **1992**, *266*, 265−277.
(37) Ou, B.; Hampsch-Woodill, M.; Prior, R. L. Development and validation of an improved oxygen radical absorbance capacity assay using fluorescein as the fluorescent probe. *J. Agric. Food Chem.* **2001**, *49*, 4619−4626.
(38) Sun, J.; Hu, X. L.; Le, G. W.; Shi, Y. H. Inhibition of Fe-induced colon oxidative stress by lactobacilli in mice. *World J. Microbiol. Biotechnol.* **2013**, *29*, 209−216.
(39) Achuthan, A. A.; Duary, R. K.; Madathil, A.; Panwar, H.; Kumar, H.; Batish, V. K.; Grover, S. Antioxidative potential of lactobacilli isolated from the gut of Indian people. *Mol. Biol. Rep.* **2012**, *39*, 7887−97.
(40) Grompone, G.; Martorell, P.; Llopis, S.; González, N.; Genovés, S.; Mulet, A. P.; Fernández-Calero, T.; Tiscornia, I.; Bollati-Fogolín, M.; Chambaud, I.; Foligné, B.; Montserrat, A.; Ramón, D. Anti-inflammatory *Lactobacillus rhamnosus* CNCM I-3690 strain protects against oxidative stress and increases lifespan in *Caenorhabditis elegans*. *PLoS One* **2012**, *7* (12), No. 52493, DOI: 10.1371/journal.-pone.0052493.
(41) Kapila, S.; Vibha; Sinha, P. R. Antioxidative and hypocholesterolemic effect of *Lactobacillus casei* ssp. *Casei* (biodefensive properties of lactobacilli). *Indian J. Med. Sci.* **2006**, *60*, 361−370.
(42) Kaizu, H.; Sasaki, M.; Nakajama, H.; Suzuki, Y. Effect of antioxidative lactic acid bacteria on rats fed a diet deficient in vitamin. *J. Dairy Sci.* **1993**, *76*, 2493−2499.
(43) Lin, M. Y.; Yen, C. L. Antioxidative ability of lactic acid bacteria. *J. Agric. Food Chem.* **1999**, *47*, 1460−1466.
(44) Saide, J. A.; Gilliland, S. E. Antioxidative activity of lactobacilli measured by oxygen radical absorbance capacity. *J. Dairy Sci.* **2005**, *88*, 1352−1357.
(45) Ou, C. C.; Lu, T. M.; Tsai, J. J.; Yen, J. H.; Chen, H. W.; Lin, M. Y. Antioxidative effect of lactic acid bacteria: intact cells vs. intracellular extracts. *J. Food Drug Anal.* **2009**, *17* (3), 209−216.
(46) Mikelsaar, M.; Zilmer, M. *Lactobacillus fermentum* ME-3 − an antimicrobial and antioxidative probiotic. *Microb. Ecol. Health Dis.* **2009**, *21*, 1−27.
(47) Jarvenpaa, S.; Tahvonen, R. L.; Ouwehand, A. C.; Sandell, M.; Jarvenpaa, E.; Salminen, S. A probiotic, *Lactobacillus fermentum* ME-3, has antioxidative capacity in soft cheese spreads with different fats. *J. Dairy Sci.* **2007**, *90*, 3171−3177.
(48) Kullisaar, T.; Zilmer, M.; Mikelsaar, M.; Vihalemm, T.; Annuk, H.; Kairane, C.; Kilk, A. Two antioxidative lactobacilli strains as promising probiotics. *Milchwissenschaft* **1997**, *52*, 503−505.
(49) Kullisaar, T.; Songisepp, E.; Mikelsaar, M.; Zilmer, K.; Vihalemm, T.; Zilmer, M. Antioxidative probiotic fermented goats' milk decreases oxidative stress-mediated atherogenicity in human. *Br. J. Nutr.* **2003**, *90*, 449−456.
(50) Klayraung, S.; Okonogi, S. Antibacterial and antioxidant activities of acid and bile resistant strains of *Lactobacillus fermentum* isolated from miang. *Braz. J. Microbiol.* **2009**, *40*, 757−766.
(51) Wang, A. N.; Yi, X. W.; Yu, H. F.; Dong, B.; Qiao, S. Y. Free radical scavenging activity of *Lactobacillus fermentum in vitro* and its antioxidative effect on growing-finishing pigs. *J. Appl. Microbiol.* **2009**, *107*, 1140−1148.
(52) Lin, M. Y.; Chang, F. J. Antioxidative effect of intestinal bacteria *Bifidobacterium longum* ATCC 15708 and *Lactobacillus acidophilus* ATCC 4356. *Dig. Dis. Sci.* **2000**, *45*, 1617−1622.
(53) Kumar, M.; Kumar, A.; Nagpal, R.; Mohania, D.; Behare, P.; Verma, V.; Kumar, P.; Poddar, D.; Aggarwal, P. K.; Henry, C. J.; Jain, S.; Yadav, H. Cancer-preventing attributes of probiotics: an update. *Int. J. Food Sci. Nutr.* **2010**, *61*, 473−496.
(54) El-Nawawy, M. A.; El-Malkey, W.; Aumara, I. E. Production and properties of antioxidative fermented probiotic beverages with natural fruit juices. *Ann. Agric. Sci. (Cairo)* **2009**, *54*, 121−135.
(55) Ahotupa, M.; Saxelin, M.; Korpela, R. Antioxidative properties of *Lactobacillus* GG. *Nutr. Today* **1996**, No. Suppl. 1, S51−S52.
(56) Lee, J.; Hwang, K.; Chung, M. Y.; Chao, D. H.; Park, C. S. Resistance of *Lactobacillus casei* KCTC 3260 to reactive oxygen species (ROS): role for a metal ion chelating effect. *J. Food Sci.* **2005**, *70*, 388−391.
(57) Yoon, Y. H.; Byun, J. R. Occurrence of glutathione sulfhydryl (GHS) and antioxidant activities in probiotic *Lactobacillus* spp. *Asian-Australas. J. Anim. Sci.* **2004**, *17*, 1582−1585.
(58) Kim, H. S.; Jeong, S. G.; Ham, J. S.; Chae, H. S.; Lee, J. M.; Ahn, C. N. Antioxidative and probiotic properties of *Lactobacillus gasseri* NLRI-312 isolated from Korean infant feces. *Asian-Australas. J. Anim. Sci.* **2006**, *19*, 1335−1341.
(59) Kudo, Y.; Matsuda, S.; Igoshi, K.; Oki, T. Antioxidative peptide from milk fermented with *Lactobacillus delbrueckii* subsp. *bulgaricus* IFO13953. *J. Jpn. Soc. Nutr. Food Sci.* **2001**, *48*, 44−50.
(60) Ahire, J. J.; Mokashe, N. U.; Patil, H. J.; Chaudhari, B. L. Antioxidative potential of folate producing probiotic *Lactobacillus helveticus* CD6. *J. Food Sci. Technol.* **2013**, *50*, 26−34.
(61) Mendi, A.; Aslım, B. Antioxidant lactobacilli could protect gingival fibroblasts against hydrogen peroxide: a preliminary *in vitro* study. *Probiotics Antimicrob. Proteins* **2014**, *6* (3−4), 157−164.
(62) Roncaglia, L.; Amaretti, A.; Raimondi, S.; Leonardi, A.; Rossi, M. Role of bifidobacteria in the activation of the ligansecoisolariciresinol diglucoside. *Appl. Microbiol. Biotechnol.* **2011**, *92*, 159−168.
(63) Shen, Q.; Shang, N.; Li, P. *In vitro* and *in vivo* antioxidant activity of *Bifidobacterium animalis* 01 isolated from centenarians. *Curr. Microbiol.* **2011**, *62*, 1097−1103.
(64) Amaretti, A.; di Nunzio, M.; Pompei, A.; Raimondi, S.; Rossi, M.; Bordoni, A. Antioxidant properties of potentially probiotic bacteria: *in vitro* and *in vivo* activities. *Appl. Microbiol. Biotechnol.* **2013**, *97*, 809−817.
(65) Balakrishnan, G.; Agrawal, R. Antioxidant activity and fatty acid profile of fermented milk prepared by *Pediococcus pentosaceus*. *J. Food Sci. Technol.* **2012**, DOI: 10.1007/s13197-012-0891-9.
(66) Nishino, T.; Shibahara-Sone, H.; Kikuchi-Hayakawa, H.; Ishikawa, F. Transit of radical scavenging activity of milk products prepared by maillard reaction and *Lactobacillus casei* strain Shirota fermentation through the hamster intestine. *J. Dairy Sci.* **2000**, *83*, 915−922.
(67) Shah, C.; Mokashe, N.; Mishra, V. Preparation, characterization and *in vitro* antioxidative potential of synbiotic fermented dairy products. *J. Food Sci. Technol.* **2014**, DOI: 10.1007/s13197-014-1491-7.
(68) Madhu, A. N.; Amrutha, N.; Prapulla, S. G. Characterization and antioxidant property of probiotic and synbiotic yogurts. *Probiotics Antimicrob. Proteins* **2012**, *4*, 90−97.
(69) Nedelcheva, P.; Denkova, Z.; Denev, P.; Slavchev, A.; Krastanov, A. Probiotic strain *Lactobacillus plantarum* NBIMCC 2415 with antioxidant activity as a starter culture in the production of dried fermented meat products. *Biotechnol. Biotechnol. Equip.* **2010**, DOI: 10.2478/v10133-010-0016-4.
(70) Wang, Y. C.; Yu, R. C.; Chou, C. C. Antioxidative activities of soymilk fermented with lactic acid bacteria and bifidobacteria. *Food Microbiol.* **1998**, *23*, 128−135.
(71) Vamanu, E.; Vamanu, A.; Popa, O.; Babeanu, N. The antioxidant effect of a functional product based on probiotic biomass, pollen and honey. *Anim. Sci. Biotechnol.* **2010**, *43*, 331−336.
(72) Ishii, Y.; Sugimoto, S.; Izawa, N.; Sone, T.; Chiba, K.; Miyazaki, K. Oral administration of *Bifidobacterium breve* attenuates UV-induced barrier perturbation and oxidative stress in hairless mice skin. *Arch. Dermatol. Res.* **2014**, *306* (5), 467−473.
(73) Coskun, S.; Aslim, B.; Yuksedag, Z. N. Effect of two strains of *Lactobacillus delbrueckii* subsp. *bulgaricus* on nitric oxide generation and antioxidant status of rat small intestine. *Med. Chem. Res.* **2010**, *19*, 1082−1091.

DOI: 10.1021/jf506326t
J. Agric. Food Chem. 2015, 63, 3615−3626

(74) Rajpal, S.; Kansal, V. K. Probiotic Dahi containing *Lactobacillus acidophilus* and *Bifidobacterium bifidum* stimulates antioxidant enzyme pathways in rats. *Milchwissenschaft* **2009**, *64*, 287−290.
(75) Kaushal, D.; Kansal, V. K. Probiotic Dahi containing *Lactobacillus acidophilus* and *Bifidobacteriumbifidum* alleviates age-inflicted stress and improves expression of biomarkers of ageing mice. *Mol. Biol. Rep.* **2012**, *39*, 1791−1799.
(76) Ren, Z.; Zhao, Z.; Wang, Y.; Huang, K. Preparation of selenium/zinc-enriched probiotics and their effect on blood selenium and zinc concentrations, antioxidant capacities and intestinal microflora in canine. *Biol. Trace Elem. Res.* **2011**, *141*, 170−183.
(77) Yadav, H.; Jain, S.; Sinha, P. R. Oral administration of Dahi containing probiotic *Lactobacillus acidophilus* and *Lactobacillus casei* delayed the progression of streptozoocin-induced diabetes in rats. *J. Dairy Res.* **2008**, *75*, 189−195.
(78) Arvind; Sinha, P. R.; Singh, N. K.; Kumar, R. Effects of acidophilus casei Dahi (probiotic curd) on lipids in 1,2-dimethylhydrazine induced intenstinal cancer in rats. *Int. J. Probiotics Prebioitcs* **2009**, *4*, 195−200.
(79) Kumar, R. S.; Kanmani, P.; Yuvaraj, N.; Paari, K. A.; Pattukumar, V.; Thirunavukkarasu, C.; Arul, V. *Lactobacillus plantarum* AS1 isolated from south Indian fermented food *kallappam* suppress 1,2-dimethylhydrazine (DMH)-induced colorectal cancer in male wistar rats. *Appl. Biochem. Biotechnol.* **2012**, *166*, 620−631.
(80) Sun, J.; Hu, X. L; Le, G. W.; Shi, Y. H. Inhibition of Fe-induced colon oxidative stress by lactobacilli in mice. *World J. Microbiol. Biotechnol.* **2013**, *29*, 209−216.
(81) Sengul, N.; Isik, S.; Aslim, B.; Ucar, G.; Demirbag, A. The effect of exopolysaccharide-producing probiotic strains on gut oxidative damage in experimental colitis. *Dig. Dis. Sci.* **2011**, *56*, 707−714.
(82) Broccali, G.; Berti, M.; Pistolesi, E.; Cestaro, B. Study of the effect of *Lactobacillus* GG supplementation in combination with and without arginine aspartate on lipoproteins and liver peroxidation in cholesterol-fed rats. *Int. J. Food Sci. Nutr.* **2000**, *6*, 475−482.
(83) Forsyth, C. B.; Farhadi, A.; Jakate, S. M.; Tang, Y.; Shaikh, M.; Keshavarzian, A. *Lactobacillus* GG treatment ameliorates alcohol-induced intestinal oxidative stress, gut leakiness, and liver injury in a rat model of alcoholic steatohepatitis. *Alcohol* **2009**, *43*, 163−172.
(84) Pandey, S.; Singh, A.; Kumar, P.; Chaudhari, A.; Nareshkumar, G. Probiotic *Escherichia coli* CFR 16 producing pyrroloquinolinequinone (PQQ) ameliorates 1,2-dimethylhydrazine-induced oxidative damage in colon and liver of rats. *Appl. Biochem. Biotechnol.* **2014**, *173*, 775−786.
(85) Gan, F.; Chen, X.; Liao, S. F.; Lv, C.; Ren, F.; Ye, G.; Pan, C.; Huang, D.; Shi, J.; Shi, X.; Zhou, H.; Huang, K. Selenium-enriched probiotics improve antioxidant status, immune function, and selenoprotein gene expression of piglets raised under high ambient temperature. *J. Agric. Food Chem.* **2014**, *62* (20), 4502−4508.
(86) Shen, X.; Yi, D.; Ni, X.; Zeng, D.; Jing, B.; Lei, M.; Bian, Z.; Zeng, Y.; Li, T.; Xin, J. Effects of *Lactobacillus plantarum* on production performance, immune characteristics, antioxidant status and intestinal microflora of bursin-immunized broilers. *Can. J. Microbiol.* **2014**, *60* (4), 193−202.
(87) Songisepp, E.; Kals, J.; Kullisaar, T.; Mandar, R.; Hutt, P.; Zilmer, M.; Mikelsaar, M. Evaluation of the functional efficacy of an antioxidative probiotic in healthy volunteers. *Nutr. J.* **2005**, *4*, 22.
(88) Liu, J.; Huang, S. S.; Zhao, Z. Research on antioxidative capacity of lactic acid bacteria. *China Dairy Ind.* **2010**, *38* (5), 38−41.
(89) Nardone, G.; Compare, D.; Liguori, E.; Di Mauro, V.; Rocco, A.; Barone, M.; Napoli, A.; Lapi, D.; Iovene, M. R.; Colantuoni, A. Protective effects of *Lactobacillus paracasei* F19 in a rat model of oxidative and metabolic hepatic injury. *Am. J. Physiol. Gastrointest. Liver Physiol.* **2010**, *299*, G669−G676.
(90) Azcárate-Peril, M. A.; Sikes, M.; Bruno-Bárcena, J. M. The intestinal microbiota, gastrointestinal environment and colorectal cancer: a putative role for probiotics in prevention of colorectal cancer? *Am. J. Physiol.−Gastr. L.* **2011**, *301*, G401−G424.
(91) Saiga, A.; Tanabe, S.; Nishimura, T. Antioxidant activity of peptidesobtained from porcine myofibrillar proteins by protease treatment. *J. Agric. Food Chem.* **2003**, *12*, 3661−3667.
(92) Suetsuna, K.; Ukeda, H.; Ochi, H. Isolation and characterization of free radical scavenging activities peptides derived from casein. *J. Nutr. Biochem.* **2000**, *11*, 128−131.
(93) Virtanen, T.; Pihlanto, A.; Akkanen, S.; Korhonen, H. Development of antioxidant activity in milk whey during fermentation with lactic acid bacteria. *J. Appl. Microbiol.* **2007**, *102*, 106−115.
(94) Vaughan, E. E.; Mollet, B.; deVos, M. W. Functionality of probiotics and intestinal lactobacilli: light in the intestinal tract tunnel. *Curr. Opin. Biotechnol.* **1999**, *10*, 505−510.
(95) Demple, B.; Hidalgo, E.; Ding, H. Transcriptional regulation via redox-sensitive iron− sulphurcentres in an oxidative stress response. *Biochem. Soc. Symp.* **1999**, *64*, 119−128.
(96) Garcia-Mendoza, A.; Liebana, J.; Castillo, A.; de la Higuera, A.; Gutierrez, J. Post-hydrogen peroxide effect in peroxidogenic oral streptococci. *Microb. Ecol. Health Dis.* **1993**, *6*, 17−22.
(97) Peuhkuri, K.; Lahteenmaki, T.; Sievi, E.; Saxelin, M.; Vapaatalo, H.; Korpela, R. Antioxidative properties of *Lactobacillus* GG measured as prostacyclin and nitric oxide production in endothelial cell culture. *Nutr. Today* **1996**, *31* (Suppl.), S53−S54.
(98) Vong, L.; Loretz, R. J.; Assa, A.; Glogauer, M.; Sherman, P. M. Probiotic *Lactobacillusrhamnosus* inhibits the formation of neutrophill extracellular traps. *J. Immunol.* **2014**, *192* (4), 1870−1877.
(99) Lee, J.; Koo, N.; Min, D. B. Reactive oxygen species, aging and antioxidative nutraceuticals. *Compr. Rev. Food Sci. Food Saf.* **2004**, *3*, 21−33.
(100) Carlsen, M. H.; Halvorsen, B. L.; Holte, K.; Bohn, S. K.; Dragland, S.; Sampson, L.; Willey, C.; Senoo, H.; Umezono, Y.; Sanada, C.; Barikmo, I.; Berhe, N.; Willett, W. C.; Phillips, K. M.; Jacobs, D. R.; Blomhoff, R. The total antioxidant content of more than 3100 foods, beverages, spices, herbs and supplements used worldwide. *Nutr. J.* **2010**, *9*, 3.
(101) Zhang, S.; Liu, L.; Su, Y.; Li, H.; Sun, Q.; Liang, X.; Lv, J. Antioxidative activity of lactic acid bacteria in yogurt. *Afr. J. Microbiol. Res.* **2011**, *5* (29), 5194−5201.
(102) Mogna, G.; Strozzi,G. P.;Mogna, L.Probiotic bacteria having antioxidant activity and use thereof, U.S. 20140065116 A1, 2014.

DOI: 10.1021/jf506326t
J. Agric. Food Chem. 2015, 63, 3615−3626

and environmental safety of *Bt* rice. Results from this study will provide important information concerning the environmental safety of genetically modified (GM) strains of rice.

MATERIALS AND METHODS

Chemicals. Human chorionic gonadotropin (hCG) and methanesulfonate (MS-222) were purchased from Sigma Chemical Company (St. Louis, MO, USA). Commercial frog feed was obtained from Cargill Feed Co., LTD (Nanjing, People's Republic of China). Liver and kidney function detection kits and *Bt*-Cry1Ab/1Ac protein detection kits were purchased from JianCheng Bioengineering Institute (Nanjing, People's Republic of China) and EnviroLogix Inc., (Portland, OR, USA), respectively.

Test Materials. The HH1 transgenic rice line expressing the fusion gene Cry1Ab/1Ac exhibits resistance to stem borers, such as *Chilo suppressalis*, *Scirpophaga incertulas*, and *Cnaphalocrocis medinalis*.[4] The insecticidal activity of HH1 seeds were previously confirmed at the seedling stage.[26] The parental nontransformed control line (MH63) is an elite *Indica* restorer line for cytoplasmic male sterility commonly grown in China. These lines were simultaneously planted in two adjacent plots at a scientific research base at Jiangxi Academy of Agricultural Sciences (Nanchang, Jiangxi Province, People's Republic of China). Transgenic rice had not been previously planted in these plots. Crops were managed in accordance with regulations of the Agricultural Genetically Modified Organism (GMO) Safety Management of China. Rice was harvested at the end of October 2013, and grains were collected and stored at −20 °C until use. The conventional nutrient components of each rice line were analyzed by the Beijing Research Institute for Nutritional Resources, People's Republic of China.

Animals. Mature female and male *X. laevis* were maintained separately in glass tanks containing dechlorinated water at 21 ± 2 °C on a 12 h light/12 h dark cycle and were fed chopped pork liver once per week. One pair of parent frogs was chosen and injected with 100 IU hCG to induce breeding. After eggs were laid, the mating pair was removed from the breeding tank. Fertilized eggs were incubated at 22 ± 2 °C on a 12 h light/12 h dark cycle. Tadpoles were started on a daily diet of green algae and *D. magna* on day 5 after fertilization and switched to commercial frog feed when they completed metamorphosis. Approximately 2 months after metamorphosis, froglets with uniform body weight (∼4.30 g) and body length (∼32.0 mm) were used for experimentation. Frogs were treated in accordance with the NIH Guide for the Care and Use of Laboratory Animals.

Diet Formulation. Synthetic frog diets were produced based on the nutrient composition of a commercial frog feed. Two test diets contained 30% rice flour, whereas the control diet was formulated using cornstarch and soybean meal without rice. The detailed diet compositions are shown in Table 1.

Experimental Design. A total of 96 froglets were equally divided into three experimental groups of 32 according to body weight, and their sexes were not considered. Each group was randomly divided into four glass jars (20 × 34 × 24 cm) to give four replicates. Froglets were fed daily (∼3% weight/body weight). Fresh dechlorinated water was replenished every 2 days and monitored daily to stay at 20−22 °C. A 12 h light/12 h dark cycle was maintained throughout the course of the experiment. Animals were observed twice daily, and body weight and length (from the tip of the snout to the tip of cloaca) were measured every 15 days for 90 days. Animals were fasted overnight before being sacrificed.

Gross Necropsy and Histopathology. At the end of the experiment, the frogs were anesthetized by immersion in 1% MS-222. Before dissection, body weight and length were measured, and the gender was determined on the basis of gross gonadal morphology. A complete necropsy was then performed, and the following organs were excised and weighed: heart, liver, spleen, lung, kidneys, body fat, ovaries or testes, and intestines. Paired organs (lungs, kidneys, ovaries and testes) were weighed as a total of left and right. Additionally, the tissues (stomach, intestines (divided into duodenum, ileum, and rectum), liver, spleen, and gonad) of one male and one female from each glass jar were fixed for a minimum of 24 h in 4% phosphate-buffered formaldehyde before histological processing. Tissue samples were embedded in paraffin, and ∼4 to 6 μm thick sections were cut and stained with hematoxylin and eosin for light microscopy.

Table 1. Composition of Nutritionally Balanced Test and Control Diets for *X. laevis* Froglets

	amt of ingredient (%)		
ingredient	HH1	MH63	control
transgenic rice	30.0	0.00	0.00
nontransgenic rice	0.00	30.0	0.00
pregelatinized starch	8.00	8.00	8.00
corn	0.00	0.00	17.0
soybean meal	6.00	6.00	21.0
soybean oil	3.00	3.00	3.50
fish meal	52.0	52.0	38.0
wheat bran	0.00	0.00	5.00
meat and bone meal	0.00	0.00	6.00
rock flour	0.00	0.00	0.50
additive[a]	1.00	1.00	1.00
total	100	100	100

[a]Contents in mg/kg of diet: iron, 70; copper, 11; manganese, 70; zinc, 65; iodine, 0.49; selenium, 0.3; vitamin A, 8000 (IU); vitamin D, 2400 (IU); vitamin E, 20 (IU); vitamin K, 0.5 (IU); vitamin B1, 2; vitamin B2, 8; vitamin B6, 3.5; vitamin B12, 0.01; calcium pantothenate, 20; niacin, 35; folic acid, 0.75; biotin, 0.26.

Determination of Liver and Kidney Function. The liver and spleen from the remaining six froglets in each glass jar (a total of 24 samples per treatment) were used to determine the following parameters: alkaline phosphatase (AKP) activity, albumin (ALB), alanine aminotransferase (ALT) activity, aspartate aminotransferase (AST) activity, urea (BUN), cholinesterase (CHE) activity, total protein (TP), creatinine (CR), glutamic acid (GLU), total cholesterol (TC), and triglycerides (TG). All parameters were detected using kits provided by the JianCheng Bioengineering Institute. All of the detection kits used in this study use a corresponding standard substance to show assay validity prior to analysis. Moreover, these kits are used strictly according to the recommendations and protocols set by the manufacture.

Determination of Cry1Ab/1Ac Content. The Cry1Ab/1Ac protein content in rice grains, frog diets, frog tissues (stomach and intestine), and frog feces (∼0.20 g each) were determined using a *Bt*-Cry1Ab/1Ac protein kit with a detection limit of 0.1 ng/g total protein. Solid feces were collected immediately after the renewal of rearing water at the later stage of the present study. Before analysis, animal tissues were washed in phosphate-buffered saline/Tween-20 to remove *Bt* toxins from the outer surface, lyophilized, and then homogenized in 1 mL phosphate-buffered saline/Tween-20 using a micropestle and mortar on ice. After centrifugation and appropriate dilution of the supernatants, an ELISA was performed following the manufacturer's protocol. Optical density values were read using a microplate spectrophotometer (PowerWave XS2, BioTek, Winooski, VT, USA). A standard curve derived from purified Cry1Ab/1Ac samples was used to calculate Cry1Ab/1Ac levels.

Statistical Analyses. All data are presented as mean ± standard deviation (SD) unless indicated otherwise. Statistically significant differences in conventional nutrient compositions between HH1 and MH63 rice grains were analyzed by Student's *t* test. Body weights and lengths were analyzed using repeated measures analysis of variance (ANOVA), whereas a one-way ANOVA, followed by least significant difference (LSD) multiple comparison tests, was used to analyze differences in organ weight, as well as liver and kidney function among the three treatment groups. Differences were considered significant at $p < 0.05$.

DOI: 10.1021/jf5055547
J. Agric. Food Chem. 2015, 63, 3627−3633

Table 2. Nutrient Composition of Rice Grains and Diets for *X. laevis* Froglets

component	rice grain (n = 3)			diet (n = 1)		
	amt of component[a] in HH1[b]	amt of component[a] in MH63[b]	p value[c]	amt of component[a] in HH1	amt of component[a] in MH63	amt of component[a] in control
crude protein (%)	6.63 ± 0.24	6.85 ± 0.12	0.22	38.1	38.2	42.2
crude fat (%)	2.83 ± 0.58	2.90 ± 0.00	0.18	8.40	8.80	8.10
crude fiber (%)	6.97 ± 0.06	6.65 ± 0.50	0.17	3.30	3.20	3.00
crude ash (%)	11.8 ± 0.26	11.9 ± 0.06	0.89	11.2	11.4	10.7
calcium (g/kg)	0.66 ± 0.16	0.61 ± 0.13	0.71	3.50	3.50	2.40
phosphorus (%)	0.36 ± 0.01	0.37 ± 0.01	0.25	1.81	1.84	1.73

[a]Units for the amount of component are given in column 1. [b]Data are presented as mean ± SD. [c]Student's t test, $p < 0.05$.

RESULTS

Nutrient Composition of Rice Grains and Froglet Diets. Levels of conventional nutrients (crude protein, crude fat, crude fiber, crude ash, calcium, and phosphorus) were very similar in HH1 and MH63 rice grains (Table 2), and no statistical differences were observed between the two ($p > 0.05$). Moreover, the measured values of these same nutrients in the HH1 diet were comparable to those in the MH63 and control diets (Table 2).

General Health. Animal wellbeing was observed twice daily, and body weight and length were measured every 15 days for 90 days. No adverse effects on animal behavior were observed during the experiment. The mean body weights and body lengths of animals from each treatment are shown in Tables 3 and 4, respectively. Statistically significant differences were observed among the seven repeated measures within each treatment group from day 0 to day 90 ($p < 0.01$ for body weight and body length), but not among the three treatments ($p = 0.81$ for body weight, $p = 0.98$ for body length). Additionally, the only significant difference in organ weight among the three dietary groups was the relative weight of fat body, which was significantly higher in the HH1 group in comparison to control ($p < 0.05$, Table 5).

Table 3. Mean Body Weight over Time in *X. laevis* Froglets Fed Test versus Control Diets (n = 32)

time (days)	body weight (g)[a]		
	HH1	MH63	control
0	4.35 ± 0.01	4.36 ± 0.06	4.32 ± 0.04
15	6.02 ± 0.23	6.13 ± 0.30	5.85 ± 0.21
30	8.85 ± 0.25	9.33 ± 0.57	8.97 ± 0.27
45	12.0 ± 0.40	12.3 ± 1.01	12.2 ± 0.38
60	16.7 ± 0.39	17.2 ± 1.46	16.8 ± 0.56
75	21.2 ± 0.34	22.2 ± 2.11	22.5 ± 1.12
90	27.7 ± 2.17	27.4 ± 2.40	27.9 ± 1.67

[a]Data are presented as group mean values ± SD. Repeated measures ANOVA, $p < 0.05$.

Table 4. Mean Body Length over Time in *X. laevis* Froglets Fed Test versus Control Diets (n = 32)

time (days)	body length (mm)[a]		
	HH1	MH63	control
0	31.6 ± 0.44	31.7 ± 0.42	31.8 ± 0.19
15	34.8 ± 0.60	34.7 ± 0.48	33.9 ± 0.39
30	39.2 ± 0.27	39.5 ± 0.68	39.5 ± 0.51
45	43.2 ± 0.39	43.3 ± 0.98	43.7 ± 0.54
60	47.8 ± 0.42	48.3 ± 0.50	48.5 ± 0.53
75	52.5 ± 0.78	52.0 ± 1.74	52.2 ± 1.38
90	60.2 ± 1.55	59.3 ± 2.33	59.7 ± 1.64

[a]Data are presented as group mean values ± SD. Repeated measures ANOVA, $p < 0.05$.

Liver Function, Kidney Function, and Fat Metabolism. Parameters for liver and kidney function, as well as fat metabolism, are given in Table 6. There were no statistically significant differences among the three groups ($p > 0.05$).

Cry1Ab/1Ac Protein Content in Diets and Frogs' Digestive Tracts. Cry1Ab/1Ac was present in HH1 rice grain at an average concentration of 752 ± 78.0 ng/g and was not detectable (ND) in the nontransformed control strain MH63 (Table 7). The measured Cry1Ab/1Ac contents in the HH1, MH63, and control diets (221 ± 21.2 ng/g, ND, and ND, respectively; Table 7) were close to the predicted values (226, 0, and 0 ng/g, respectively). To investigate the degradation of Cry1Ab/1Ac protein in the frog digestive tract, intestinal contents and feces were collected, and the Cry1Ab/1Ac protein content was determined by ELISA. Cry1Ab/1Ac protein was detected in the intestinal contents (249 ± 16.9 ng/g) and in feces (160 ± 34.7 ng/g) of froglets fed on the HH1 diet but not in those fed on the MH63 or control diet (Table 7).

Gross Necropsy and Histopathology. Histological examinations of stomach, intestine (ileum), liver, kidneys, spleen, testes, and ovaries are shown in Figure 1. None of the three sections of intestines showed apparent pathological abnormalities; only representative images of ileum are shown in Figure 1. Overall, there were no gross pathological findings during the necropsies, and no group-related histopathological abnormalities were observed.

DISCUSSION

An integral part of the safety evaluation of GM plants is testing for substantial equivalence to the unmodified parent strain, which provides a starting point for the overall assessment.[27] In the present study, we analyzed the differences in nutrient composition between HH1 and MH63 before evaluating the effects of the GM rice strain on development of froglets. No significant differences in composition, including crude protein, crude fat, and crude ash levels, were found between the two rice lines or between diets containing them (Table 2). Schrøder et al. found significant differences in some nutritional composition indices between brown rice material from transgenic Cry1Ab and its corresponding parental line, but all differences were within the normal reference intervals.[7] Indeed, most studies have shown that transgenic *Bt* rice lines have nutrient compositions similar to those of their parental lines,[6,8,28] which is consistent with our results.

DOI: 10.1021/jf5055547
J. Agric. Food Chem. 2015, 63, 3627−3633

Table 5. Absolute and Relative Organ Weights and Intestinal Lengths in *X. laevis* Froglets Fed Test versus Control Diets[a]

	HH1	MH63	control	statistics[c]
		Absolute Measurements		
body (g)	27.7 ± 2.17	27.4 ± 2.40	27.9 ± 1.67	$t = 0.07$; $p = 0.93$
heart (g)	0.14 ± 0.01	0.14 ± 0.02	0.15 ± 0.02	$t = 0.41$; $p = 0.66$
liver (g)	1.70 ± 0.16	1.60 ± 0.16	1.64 ± 0.07	$t = 0.17$; $p = 0.84$
spleen (g)	0.03 ± 0.00	0.03 ± 0.00	0.03 ± 0.00	$t = 0.02$; $p = 0.98$
lung (g)	0.16 ± 0.01	0.16 ± 0.01	0.16 ± 0.02	$t = 0.07$; $p = 0.94$
kidney (g)	0.21 ± 0.03	0.21 ± 0.03	0.22 ± 0.01	$t = 0.16$; $p = 0.85$
fat body (g)	1.84 ± 0.14	1.82 ± 0.21	1.73 ± 0.06	$t = 0.20$; $p = 0.82$
ovary (g)	0.12 ± 0.02 (16)	0.11 ± 0.01 (13)	0.12 ± 0.02 (19)	$t = 0.11$; $p = 0.90$
testis (g)	0.05 ± 0.01 (16)	0.04 ± 0.01 (19)	0.05 ± 0.01 (13)	$t = 0.95$; $p = 0.39$
intestinal length (cm)	15.1 ± 1.11	15.0 ± 1.30	16.2 ± 1.76	$t = 1.94$; $p = 0.15$
		Relative Values[b]		
heart	0.51 ± 0.05	0.49 ± 0.04	0.52 ± 0.06	$t = 0.60$; $p = 0.55$
liver	6.06 ± 0.14	5.75 ± 0.20	5.70 ± 0.15	$t = 2.00$; $p = 0.14$
spleen	0.10 ± 0.01	0.11 ± 0.01	0.10 ± 0.01	$t = 0.75$; $p = 0.48$
lung	0.56 ± 0.04	0.58 ± 0.05	0.56 ± 0.04	$t = 0.27$; $p = 0.76$
kidney	0.74 ± 0.05	0.76 ± 0.07	0.77 ± 0.04	$t = 0.63$; $p = 0.54$
fat body	6.56 ± 0.22[b]	6.49 ± 0.39[ab]	6.00 ± 0.26[a]	$t = 3.99$; $p = 0.02$
ovary	0.44 ± 0.06 (16)	0.42 ± 0.06 (13)	0.48 ± 0.09 (19)	$t = 0.73$; $p = 0.49$
testis	0.18 ± 0.03 (16)	0.16 ± 0.02 (19)	0.17 ± 0.01 (13)	$t = 0.60$; $p = 0.55$
intestinal length	0.56 ± 0.02	0.58 ± 0.08	0.63 ± 0.02	$t = 2.47$; $p = 0.09$

[a]Data presented as group mean values ± SD ($n = 32$, except for ovaries and testes, where n is given in parentheses). Different Roman lowercase letters in the same row indicate a statistical difference of $p < 0.05$. [b]Relative values expressed as g or cm per 100 g of body weight. [c]One-way ANOVA, $p < 0.05$.

Table 6. Liver Function, Kidney Function, and Fat Metabolism in *X. laevis* Froglets Fed Test versus Control Diets ($n = 24$)

indices	HH1	MH63	control	statistics[a]
		Liver Function		
AKP (U/g protein)	195 ± 12.6	193 ± 31.1	167 ± 12.1	$t = 0.81$; $p = 0.45$
ALB (g/L)	7.31 ± 0.55	7.22 ± 0.58	7.04 ± 0.72	$t = 0.73$; $p = 0.49$
ALT (U/g protein)	860 ± 181	902 ± 224	813 ± 36.7	$t = 0.55$; $p = 0.58$
AST (U/g protein)	443 ± 66.5	432 ± 65.1	405 ± 22.0	$t = 0.75$; $p = 0.48$
BUN (mg/L)	1.82 ± 0.08	1.79 ± 0.08	1.72 ± 0.08	$t = 2.71$; $p = 0.08$
CHE (U/mg protein)	1.41 ± 0.15	1.40 ± 0.10	1.34 ± 0.12	$t = 0.06$; $p = 0.94$
TP (g/L)	9.27 ± 0.48	8.90 ± 0.21	9.10 ± 0.25	$t = 1.28$; $p = 0.28$
		Kidney Function		
BUN (mg/L)	3.49 ± 0.11	3.32 ± 0.18	3.36 ± 0.48	$t = 0.47$; $p = 0.63$
CR (μmol/L)	23.9 ± 4.07	25.1 ± 3.30	20.3 ± 5.56	$t = 2.82$; $p = 0.07$
GLU (μmol/g protein)	30.6 ± 4.34	28.25 ± 3.74	29.75 ± 0.82	$t = 0.74$; $p = 0.48$
		Fat Metabolism		
TC (mmol/L)	0.66 ± 0.05	0.69 ± 0.10	0.67 ± 0.16	$t = 0.19$; $p = 0.83$
TG (mmol/L)	2.32 ± 0.34	2.11 ± 0.10	2.06 ± 0.68	$t = 0.79$; $p = 0.46$

[a]One-way ANOVA, $p < 0.05$.

Table 7. Cry1Ab/1Ac Protein Content in Rice Grain, Diet, and Digestive Tract of *X. laevis* Froglets Fed Test versus Control Diets (ng/g)[a]

	HH1	MH63	control
rice grain ($n = 6$)	752 ± 78.0	ND	NA
diet ($n = 6$)	221 ± 21.2	ND	ND
intestinal tract ($n = 24$)	249 ± 16.9	ND	ND
feces ($n = 6$)	160 ± 34.7	ND	ND

[a]ND, not detectable; NA, not applicable.

The consequences and potential risks associated with expressed insecticidal proteins are of particular concern in any safety assessment.[29] Numerous experimental studies have consistently indicated that the health and performance of animals fed GM crop lines and isogenic non-GM crop lines are comparable.[30] The food and feed safety of *Bt* rice has been tested in many animals, including rats,[6−9] broilers,[10] pigs,[11] and carp,[12] and all of the above studies showed that the safety of the GM line and that of the parental line were comparable. For example, TT51 rice, the same *Bt* rice line as in the present study, showed no significant differences on reproduction performance of rats in comparison with MH63 and control.[9] Moreover, Xu et al. found that Cry1Ab/Ac fusion protein produced in *Escherichia coli* has no adverse effects in mice by gavage at a high dose level of 5 g/kg body weight.[31] Our results using *X. laevis* froglets were consistent, as there were no significant differences among the three dietary groups with respect to general health, including animal behavior, body weight (Table 3), and body length (Table 4). In addition, we assessed organ weight and relative organ weight, which are important indicators reflecting organ development. A change in organ weight can signal adverse effects from the external environment, including food.[32] Our findings show that the diet containing HH1 rice resulted in no significant differences in absolute or relative organ weights in comparison with the MH63 and control diets, except for an increase in the relative weight of fat bodies in the HH1 group in comparison to the control group (Table 5). Furthermore, pathology exams revealed no obvious lesions in any group (Figure 1), and

DOI: 10.1021/jf5055547
J. Agric. Food Chem. 2015, 63, 3627−3633

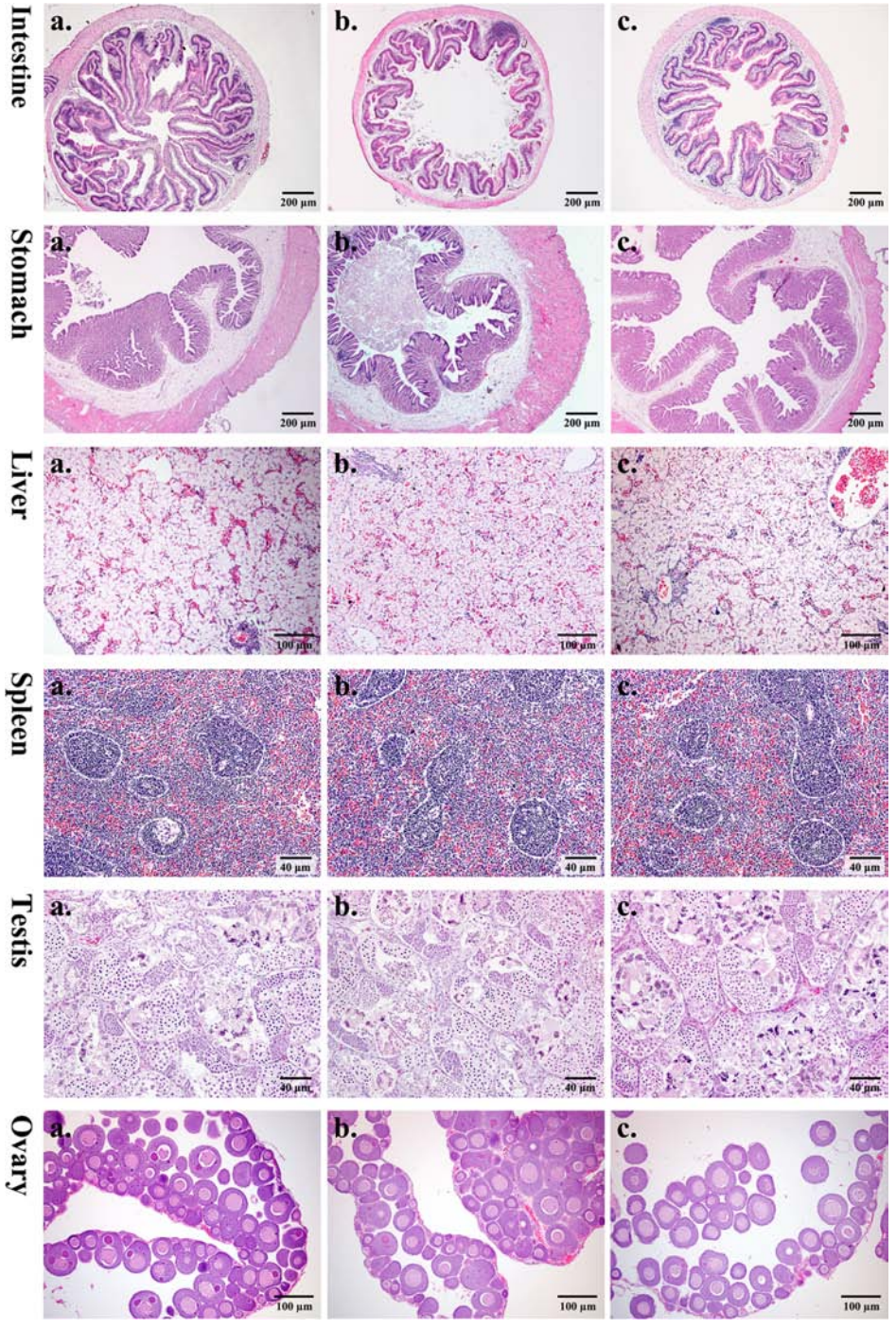

Figure 1. Histopathological staining of tissues from *X. laevis* froglets after consuming the HH1 test diet (a), MH63 test diet (b), or control diet (c) for 90 days. For intestine, only representative images of the ileum are shown.

liver function, kidney function, and fat metabolism (Table 6) were not significantly different among the groups. Taken together, these results indicate that Cry1Ab/Ac protein had no significant adverse effect on organ development.

The planting of GM crops brings huge economic and environmental benefits to humans; however, it also raises questions and concerns regarding their safety. Some people fear that foreign proteins will enter the food chain and eventually enter the human body, where they may cause potential harm to humans. They also fear that foreign proteins may be present in the feces of animals fed GM crops, where they may affect the environment. Whereas some researchers found that transgenic DNAs and proteins could not be detected in the gastrointestinal contents or feces of animals fed diets containing GM crops,[11,33,34] others were able to detect foreign transgenic proteins in the gastrointestinal contents and/or feces of pigs,[35] bovines,[36,37] deer,[38] and insects[39] that were fed transgenic crops or diets containing transgenic crops. The amount of transgenic protein ingested by livestock depends on the concentration of the protein in the feed, the amount of feed intake, and the species.[29] From previous studies we can conclude that *Bt* proteins can survive passage through an animal's gastrointestinal tract but are not transferred to the visceral organs or their products.[33,36] In the current study, Cry1Ab/1Ac

DOI: 10.1021/jf5055547
J. Agric. Food Chem. 2015, 63, 3627−3633

protein was detected in the intestinal contents and feces of froglets in the HH1 group (Table 7), indicating that they were exposed to Bt proteins by consuming a diet containing the Cry1Ab/1Ac protein. However, the microstructure of the digestive tract (Figure 1) and the froglets' overall development were not adversely affected. Our results, combined with those of others, demonstrate that expressed foreign *Bt* proteins do not produce harmful effects in the digestive tract or elsewhere after ingestion by animals.[29]

Consumption of *Bt* rice fed arthropods is the main route through which frogs are exposed to the rice-produced Cry proteins. Zhang et al. found that the Cry2Aa protein content in most of the arthropods collected from the Cry2Aa rice field were much lower than 200 ng/g dry weight.[22] Studies of *Bt* soybean and *Bt* maize showed that the plant-produced Cry proteins are diluted when moving through the foodweb.[39,40] Additionally, Wang et al. did not detect Cry1Ab/1Ac protein in the stomach and intestine of frogs collected from HH1 rice field.[26] In the present study, the Cry1Ab/1Ac protein concentration in the HH1 diet was 221 ± 21.2 ng/g (Table 7), which was much higher than the likely exposure under field conditions.

In this 90 day study, *X. laevis* froglets were exposed to *Bt* proteins by consuming a diet containing HH1 rice that carries the gene encoding Cry1Ab/1Ac. Froglet development was not adversely affected in comparison with froglets fed a diet containing the parental rice (MH63) or no rice. Combining this laboratory study with our previous field experiment,[26] we conclude that the planting of transgenic Cry1Ab/1Ac rice will not adversely affect the development of frogs.

AUTHOR INFORMATION

Corresponding Authors

*X.-P.C.: tel, +86-10-62815947; fax, +86-10-62896114; e-mail, cxpyuan@gmail.com.

*Y.-F.P.: tel, +86-10-62815947; fax, +86-10-62896114; e-mail, yfpeng@vip.qq.com.

Funding

This work was supported by the National GMO New Variety Breeding Program of the PRC (2012ZX08011-002 and 2014ZX08011-001) and a Priority Academic Program Development of Jiangsu Higher Education Institutions (PAPD).

Notes

The authors declare no competing financial interest.

ACKNOWLEDGMENTS

We thank Professor Yongjun Lin (Huazhong Agricultural University, Wuhan, People's Republic of China) for kindly providing transgenic rice seeds.

ABBREVIATIONS USED

AKP, alkaline phosphatase activity; ALB, albumin; ALT, alanine aminotransferase activity; AST, aspartate aminotransferase activity; BUN, urea; CHE, cholinesterase activity; TP, total protein; CR, creatinine; GLU, glutamic acid; TC, total cholesterol; TG, triglycerides

REFERENCES

(1) High, S. M.; Cohen, M. B.; Shu, Q. Y.; Altosaar, I. Achieving successful deployment of *Bt* rice. *Trends Plant Sci.* **2004**, *9* (6), 1360−1385.

(2) Hofmann, C.; Vanderbruggen, H.; Hofte, H.; Van Rie, J.; Jansens, S.; Van Mellaert, H. Specificity of *Bacillus thuringiensis* delta-endotoxins is correlated with the presence of high-affinity binding sites in the brush border membrane of target insect midgets. *Proc. Natl. Acad. Sci. U. S. A.* **1988**, *85* (21), 7844−7848.

(3) Chen, M.; Shelton, A.; Ye, G. Y. Insect-resistant genetically modified rice in China: from research to commercialization. *Annu. Rev. Entomol.* **2011**, *56*, 81−101.

(4) Wang, Y.; Zhang, G.; Du, J.; Liu, B.; Wang, M. Influence of transgenic hybrid rice expressing a fused gene derived from *cry1Ab* and *cry1Ac* on primary insect pests and rice yield. *Crop Prot.* **2010**, *29* (2), 28−33.

(5) Lu, C. The first approved transgenic rice in China. *GM crops* **2010**, *1* (3), 113−115.

(6) Wang, Z. H.; Wang, Y.; Cui, H. R.; Xia, Y. W.; Altosaar, I.; Shu, Q. Y. Toxicological evaluation of transgenic rice flour with a synthetic *cry1Ab* gene from *Bacillus thuringiensis*. *J. Sci. Food Agric.* **2002**, *82* (7), 738−744.

(7) Schrøder, M.; Poulsen, M.; Wilcks, A.; Kroghsbo, S.; Miller, A.; Frenzel, T.; Danier, J.; Rychlik, M.; Emami, K.; Gatehouse, A.; Shu, Q.; Engel, K. Z.; Altosaar, I.; Knudsen, I. A 90-day safety study of genetically modified rice expressing Cry1Ab protein (*Bacillus thuringiensis* toxin) in Wistar rats. *Food Chem. Toxicol.* **2007**, *45* (3), 339−349.

(8) Cao, S.; He, X.; Xu, W.; Luo, Y.; Yuan, Y.; Liu, P.; Cao, B.; Shi, H.; Huang, K. Safety assessment of transgenic *Bacillus thuringiensis* rice T1c-19 in Sprague-Dawley rats from metabonomics and bacterial profile perspectives. *IUBMB Life* **2012**, *64* (3), 242−250.

(9) Wang, E. H.; Yu, Z.; Hu, J.; Jia, X. D.; Xu, H. B. A two-generation reproduction study with transgenic Bt rice TT51 in Wistar rats. *Food Chem. Toxicol.* **2014**, *65*, 312−320.

(10) Qin, H. F. Safety assessment of rice genetically modified with *Cry1Ac* and *sck* by feeding studies on broilers. Dissertation, Chinese Academy of Agriculture Science, 2012 (in Chinese with English abstract).

(11) Cao, Z. H.; Wang, Z. B.; Gu, X. H. Residues and organ damage of exogenous gene and protein from transgenic *Bt* brown rice in growing pigs. *Chin. J. Anim. Nutr.* **2014**, *26* (7), 1908−1915 (in Chinese with English abstract) .

(12) Xu, Z. Y. Safety assessment of rice genetically modified with *Cry1Ac* and *sck* by feeding studies on carp (*Cyprinus carpio*). Dissertation, Chinese Academy of Agriculture Science, 2011 (in Chinese with English abstract).

(13) Bernal, C. C.; Aguda, R. M.; Cohen, M. B. Effect of rice lines transformed with *Bacillus thuringiensis* toxin genes on the brown planthopper and its predator *Cyrtorhinus lividipennis*. *Entomol. Exp. Appl.* **2002**, *102* (1), 21−28.

(14) Liu, W.; Lu, H. H.; Wu, W. X.; Wei, Q. K.; Chen, Y. X.; Thies, J. C. Transgenic Bt rice does not affect enzyme activities and microbial composition in the rhizosphere during crop development. *Soil Biol. Biochem.* **2008**, *40* (2), 475−486.

(15) Akhtar, Z. R.; Tian, J. C.; Chen, Y.; Fang, Q.; Hu, C.; Chen, M.; Peng, Y. F.; Ye, G. Y. Impacts of six *bt* rice lines on nontarget rice feeding thrips under laboratory and field conditions. *Environ. Entomol.* **2010**, *39* (2), 715−726.

(16) Li, Y.; Zhang, X.; Chen, X.; Romeis, J.; Yin, X.; Peng, Y. Consumption of Bt rice pollen containing Cry1C or Cry2A does not pose a risk to *Propylea japonica* (Thunberg) (Coleoptera: Coccinellidae). *Sci. Rep.* **2015**, *5*, 7679.

(17) Li, Y.; Chen, X.; Hu, L.; Romeis, J.; Peng, Y. Bt rice producing Cry1C protein does not have direct detrimental effects on the green lacewing *Chrysoperla sinica* (Tjeder). *Environ. Toxicol. Chem.* **2014**, *33* (6), 1391−1397.

(18) Viktorov, A. G. Transfer of Bt corn byproducts from terrestrial to stream ecosystems. *Russ. J. Plant Physiol.* **2011**, *58* (4), 543−548.

(19) Li, G.; Wang, Y.; Liu, B.; Zhang, G. Transgenic *Bacillus thuringiensis* (Bt) rice is safer to aquatic ecosystems than its non-transgenic counterpart. *PLoS One* **2014**, *9* (8), e104270.

DOI: 10.1021/jf5055547
J. Agric. Food Chem. 2015, 63, 3627−3633

(20) Wang, J.; Chen, X.; Li, Y.; Zhu, H.; Ding, J.; Peng, Y. Effect of straw leachates from Cry1Ca-expressing transgenic rice on the growth of *Chorella Pyrenoidosa*. *Environ. Toxicol. Chem.* **2014**, *33* (5), 1156−1162.
(21) Blaustein, A. R.; Han, B. A.; Relyea, R. A.; Johnson, P. T. J.; Buck, J. C.; Gervasi, S. S.; Kats, L. B. The complexity of amphibian population declines: understanding the role of cofactors in driving amphibian losses. *Ann. N. Y. Acad. Sci.* **2011**, *1223*, 108−119.
(22) Zhang, Q. L.; Li, Y. H.; Hua, H. X.; Yang, C. J.; Wu, H. J.; Peng, Y. F. Exposure degree of important non-target arthropods to Cry2Aa in *Bt* rice fields. *Chin. J. Appl. Ecol.* **2013**, *24* (6), 1647−1651 (In Chinese with English abstract) .
(23) Wang, Y.; Hu, H.; Huang, J.; Li, J.; Liu, B.; Zhang, G. Determination of the movement and persistence of Cry1Ab/1Ac protein released from *Bt* transgenic rice under field and hydroponic conditions. *Soil Biol. Biochem.* **2013**, *58*, 107−114.
(24) Wang, H.; Ye, Q.; Gan, J.; Wu, L. Biodegradation of Cry1Ab protein from Bt transgenic rice in aerobic and flooded paddy soils. *J. Agric. Food Chem.* **2007**, *55* (5), 1900−1904.
(25) Cong, L.; Qin, Z. F.; Jing, X. N.; Yang, L.; Zhou, J. M.; Xu, X. B. *Xenopus laevis* is a potential alternative model animal species to study reproductive toxicity of phytoestrogens. *Aquat. Toxicol.* **2006**, *77* (3), 250−256.
(26) Wang, J. M.; Chen, X. P.; Liang, Y. Y.; Zhu, H. J.; Ding, J. T.; Peng, Y. F. Influence of transgenic rice expressing a fused Cry1Ab/1Ac protein on frogs in paddy fields. *Ecotoxicology* **2014**, *23* (9), 1619−1628.
(27) Alexander, T. W.; Reuter, T.; Aulrich, K.; Sharma, R.; Okine, E. K.; Dixon, W. T.; McAllister, T. A. A review of the detection and fate of novel plant molecules derived from biotechnology in livestock production. *Anim. Feed Sci. Technol.* **2007**, *133*, 31−62.
(28) Li, X.; Huang, K.; He, X.; Zhu, B.; Liang, Z.; Li, H.; Luo, Y. Comparison of nutritional quality between Chinese indica rice with *sck* and *cry1Ac* genes and its nontransgenic counterpart. *J. Food Sci.* **2007**, *72* (6), S420−424.
(29) Aumaitre, A.; Aulrich, K.; Chesson, A.; Flachowsky, G.; Piva, G. New feeds from genetically modified plants: substantial equivalence, nutritional equivalence, digestibility, and safety for animals and the food chain. *Livest. Prod. Sci.* **2002**, *74* (3), 223−238.
(30) Van Eenennaam, A. L.; Young, A. E. Prevalence and impacts of genetically engineered feedstuffs on livestock populations. *J. Anim. Sci.* **2014**, *2* (10), 255−278.
(31) Xu, W.; Cao, S.; He, X.; Luo, Y.; Guo, X.; Yuan, Y.; Huang, K. Safety assessment of Cry1Ab/Ac fusion protein. *Food Chem. Toxicol.* **2009**, *47* (7), 1459−1465.
(32) Konarzewski, M.; Diamond, J. M. Evolution of basal metabolic rates and organ masses in laboratory mice. *Evolution* **1995**, *49* (6), 1239−1248.
(33) Ash, J.; Novak, C.; Scheideler, S. E. The fate of genetically modified protein from Roundup Ready soybeans in laying hens. *J. Appl. Poult. Res.* **2003**, *12* (2), 242−245.
(34) Alexander, T. W.; Reuter, T.; Okine, E.; Sharma, R.; McAllister, T. A. Conventional and real-time polymerase chain reaction assessment of the fate of transgenic DNA in sheep fed Roundup Ready rapeseed meal. *Br. J. Nutr.* **2006**, *96* (6), 997−1005.
(35) Chowdhury, E. H.; Kuribara, H.; Hino, A.; Sultana, P.; Mikami, O.; Shimada, N.; Guruge, K. S.; Saito, M.; Nakajima, Y. Detection of corn intrinsic and recombinant DNA fragments and Cry1Ab protein in the gastrointestinal contents of pigs fed genetically modified corn Bt11. *J. Anim. Sci.* **2003**, *81* (10), 2546−2551.
(36) Chowdhury, E. H.; Shimada, N.; Murata, H.; Mikami, O.; Sultana, P.; Miyazaki, S.; Yoshioka, M.; Yamanaka, N.; Hirai, N.; Nakajima, Y. Detection of Cry1Ab protein in gastrointestinal contents but not visceral organs of genetically modified Bt11-fed calves. *Vet. Human Toxicol.* **2003**, *45* (2), 72−75.
(37) Lutz, B.; Wiedemann, S.; Einspanier, R.; Mayer, J.; Albrecht, C. Degradation of Cry1Ab protein from genetically modified maize in the bovine gastrointestinal tract. *J. Agric. Food Chem.* **2005**, *53* (5), 1453−1456.
(38) Guertler, P.; Lutz, B.; Kuehn, R.; Meyer, H. H. D.; Einspanier, R.; Killermann, B.; Albrecht, C. Fate of recombinant DNA and Cry1Ab protein after ingestion and dispersal of genetically modified maize in comparison to rapeseed by fallow deer (*Dama dama*). *Eur. J. Wildlife Res.* **2008**, *54* (1), 36−43.
(39) Li, Y.; Romeis, J. Bt maize expressing Cry3Bb1 does not harm the spider mite, *Tetranychus urticae*, or its ladybird beetle predator, *Stethorus punctillum*. *Biol. Control* **2010**, *53* (3), 337−344.
(40) Yu, H.; Romeis, J.; Li, Y.; Li, X.; Wu, K. Acquisition of Cry1Ac protein by non-target arthropods in Bt soybean fields. *PLoS One* **2014**, *9* (8), e103973.

DOI: 10.1021/jf5055547
J. Agric. Food Chem. 2015, 63, 3627−3633

field.[32] Recently, a magnetic molecularly imprinted polymer using bare Fe_3O_4 as supporting matrix was applied to extraction of sulfonylurea herbicides.[33] However, the bare Fe_3O_4 magnetic nanoparticles is easy to agglomerate. If a protective layer is coated on the surface of bare Fe_3O_4 magnetic nanoparticles, the stability of Fe_3O_4 magnetic nanoparticles would have been largely improved. To address the question, we developed a new type of core−shell magnetic MIPs with SiO_2-coated Fe_3O_4 magnetic particles as supporting matrix and bensulfuron-methyl as the template molecule. The core−shell magnetic molecularly imprinted polymers have been synthesized as the sorbent materials of SPE and successfully applied to assessing sulfonylurea herbicide residues in food and environmental media. The objective of the study was to provide an efficient, selective, and accurate method for analyzing sulfonylurea herbicide at trace abundance in multiple media.

MATERIALS AND METHODS

Materials and Chemicals. The pesticides BSM (methy α-(4,6-dimethoxypryrimidin-2-yl-carbamoyl sulfamoyl)-*O*-toluate, 96.1%), triasulfuron (TS, *N*-(6-methoxy-4-methyl-1,3,5-triazin-2-yl-aminocarbonyl)-2-(2-chloroethoxy)-benzenesulfonamide, 95%), prosulfuron (PS, *N*-((3-(4-methoxy-6-methyl-1,3,5-triazin-2-yl) amino)carbonyl)-2-(3,3,3-trifluoropropyl)benzone sulfonamide, 95%), pyrazosulfuron-ethyl (PSE, ethyl-5-(4,6-dimethoxypyrimidin-2-yl-carbamoylsulfamoyl)-1-methylpyrazole-4-ca, 98%), and propazine (PPZ, 6-chloro-*n*,*n*′-bis-(1-methylethyl)-1,3,5-triazine-2,4-diamine, 97%) were obtained from Syngenta Nantong Crop Protection Co., Ltd. Fe_3O_4 (200 nm), trimethylolpropane trimethacrylate (TRIM) were purchased from Aladdin Co., Ltd. 3-Methacryloyloxypropyltrimethoxysilane (MPS) was purchased from Shanghai Jiachen Chemical Co., Ltd. HPLC grade acetonitrile was from ROE scientific INC. All other chemicals were of analytical grade provided by Nanjing Chemical Reagent Co., Ltd. Azodiisobutyronitrile (AIBN) was recrystallized by methanol. *N*,*N*-Dimethylformamide (DMF) was dried over 3 Å molecular sieves.

Instruments and Analytical Methods. The interaction between BSM and functional monomer MAA was studied by UV-2600 spectrophotometer (Shimadzu, Japan) at 190−280 nm. A series of solutions were prepared in acetonitrile in which the molar ratio of BSM and MAA was set at 0:1, 1:0, 1:1, 1:2, 1:4, 1:8, 1:10, 1:20, 1:30, 1:40, 1:50, and 1:60. The background UV absorbance of only BSM or MAA was taken out by the absorbance of solvent acetonitrile, and the background UV absorbance of other solutions was taken out by the absorbance of corresponding MAA. A TENSOR-27 FT-IR spectrometer (Bruker, Germany) with a 2 cm^{-1} resolution and a spectral range of 400−4000 cm^{-1} was employed to examine the FT-IR spectra of nanopaticle samples by a pressed tablet (sample: KBr = 1:100, w/w). The size and morphology of nanoparticle samples were analyzed using an S-4800 field emission scanning electron microscope (SEM, Hitachi High-Technologies Corporation, Japan) and a Tecnai 12 transmission electron microscope (TEM, Philips, Holland). Phase identification was done using X-ray polycrystal diffraction (XRD, Bruker-AXS Corporation, Germany) patterns, using a D8 Advance X-ray diffractometer with Cu $K_{\alpha 1}$ irradiation at $\gamma = 0.15418$ nm. The magnetic properties were studied using an EV7 vibrating sample magnetometer (VSM, ADE, US) operating at room temperature. All chromatographic measurements were performed using a HPLC system (Waters 2489, Waters Technologies Co. Ltd.), equipped with a 515 pump and a UV−vis detector. A C_{18} column (250 mm × 4.6 mm i.d., 5 μm) was used, with the mobile phase of acetonitrile−water (acidified with glacial acetic acid to pH 3.0) (60:40, v/v), detection at 235 nm, and a flow rate of 0.3 mL min^{-1}. The injection volume was 20 μL.

Preparation of Magnetic and Microsphere MIPs. Prior to use, the bare Fe_3O_4 magnetic nanoparticles were modified with negatively charged citrate groups.[34] Fe_3O_4 magnetic nanoparticles (2 g) were mixed in 150 mL (20 mM) of trisodium citrate and sonicated for 0.5 h, followed by magnetic stirring at 30 °C for 24 h. The obtained citric acid-modified Fe_3O_4 magnetic nanoparticles were washed several times with double-distilled water and acetone, isolated with a magnet, and dried under vacuum overnight.

The citric acid-modified Fe_3O_4 magnetic core was well protected by a silica film by Stöber method with a slight modification.[35] Fe_3O_4 magnetic nanoparticles (1 g) were mixed with 100 mL of 2-propanol and 20 mL of double-distilled water and sonicated for 30 min. Four milliliters of tetraethylorthosilicate (TEOS) and 2.5 mL of ammonium hydroxide were added to the mixture drop by drop. The mixture was stirred under a nitrogen atmosphere at room temperature for 20 h. The resultant product (Fe_3O_4@SiO_2) was separated with a magnet and rinsed with ethanol and double-distilled water several times, and dried under vacuum.

The Fe_3O_4@SiO_2 particles were allowed to react with MPS to introduce double bonds for polymerization. Briefly, 300 mg of Fe_3O_4@SiO_2 was added in 90 mL of toluene, sonicated for 10 min, and stirred vigorously. The mixing solution of 5 mL of MPS and 10 mL of toluene was then dropped into the resulting solution for 30 min. The stirring continued under a nitrogen atmosphere at 110 °C for 24 h. The product (vinyl-modified Fe_3O_4@SiO_2) was collected by a magnet, rinsed with methanol several times thoroughly, and dried under vacuum.

The synthesis procedure for bensulfuron-methyl (BSM)-imprinted microspheres with a molar ratio of BSM/methacrylic acid (MAA)/TRIM = 1:4:10 is described as follows. Prior to polymerization, the prearranged solution of bensulfuron-methyl (0.625 mM) and functional monomer (MAA, 2.5 mM) in 30 mL of anhydrous DMF was placed in a refrigerator and kept for 12 h to form the template−monomer complex. Vinyl-modified Fe_3O_4@SiO_2 (0.1 g), TRIM (6.25 mM), AIBN (50 mg), and 30 mL of DMF were mixed by ultrasonication for 15 min. The mixture and template−monomer complex were added into the flask and purged with high purity nitrogen for 10 min. To obtain a high cross-linking density, prepolymerization was undertaken at 50 °C for 6 h and then stirred at 60 °C for 24 h. After polymerization, the polymers (MIP1) were separated and washed with methanol/acetic acid (9:1, v/v) several times in a Soxhlet extraction apparatus until no template molecule (BSM) was detected by HPLC. The polymers were washed with double-distilled water several times until neutral and dried under vacuum. In parallel, nonimprinted microspheres (NIP1) were prepared in a similar way with no addition of template BSM. Meanwhile, in MIP2 (or NIP2) and MIP3 (or NIP3) preparation, vinyl-modified Fe_3O_4@SiO_2 was substituted by citric acid-modified Fe_3O_4 and Fe_3O_4@SiO_2, successively (Supporting Information, Table S1).

Molecular Simulation. Interactions between template BSM and functional monomer MAA were simulated using the Hyperchem 7.5 software package (Hypercube, Inc., USA). The structures of BSM, MAA, and their complexes were drawn using Chembiodraw Ultra 12.0 software. The three-dimensional structure of BSM and MAA were optimized. The minimum energies of the structures were analyzed iteratively until the convergence value was less than 0.01 kcal mol^{-1} and calculated through semiempirical quantum methods (PM3). The dimers of BSM and MAA were optimized, and the binding energies of BSM and MAA were calculated at the same level. The binding energy (ΔE) was defined as

$$\Delta E = E_{complex} - (E_{template} + E_{monomer})$$

Measurement of Adsorption Isotherm and Kinetic Adsorption Curve. Static equilibrium adsorption experiments were conducted: 10 mg of MIP1 or NIP1 was added into the centrifuge tubes containing 5 mL of methanol/water (3/7, v/v) solution with BSM concentration varying from 0.02 to 0.40 mM and shaken for 24 h at room temperature. The supernatant and polymer were separated by a permanent magnet. The BSM concentration in the supernatant was measured by HPLC.

MIP1 or NIP1 (10 mg) was mixed with 5 mL of methanol/water (3/7, v/v) solution with BSM at 0.2 mM and shaken at regular time intervals. The supernatant and polymer were separated by a permanent magnet. Concentrations of BSM in the supernatant were determined by HPLC. According to the BSM concentration before and after adsorption, the equilibrium amount of substrate bound to the polymer (Q, mg g^{-1}) was calculated by following eq 1:

DOI: 10.1021/jf506239b
J. Agric. Food Chem. 2015, 63, 3634−3645

$$Q = \frac{MV(C_0 - C_1)}{m} \quad (1)$$

where C_0 and C_1 represent the initial solution and final solution concentration (mM) of BSM, respectively; V is the solution volume (mL); m (mg) is the weight of the polymer particles; and M (g mol^{-1}) is the molar mass of the template. All average results from three independent tests were used for the following discussion.

In order to further study the binding properties of magnetic MIP1, experimental data were fitted to the Langmuir isotherms (eq 2), Freundlich isotherms (eq 3), and Langmuir−Freundlich isotherms (eq 4).

$$\frac{C_e}{Q_e} = \frac{C_e}{Q_m} + \frac{1}{Q_m K_L} \quad (2)$$

$$\log Q_e = (1/n)\log C_e + \log K_F \quad (3)$$

$$B = \frac{N_t a F^m}{1 + aF^m} \quad (4)$$

where Q_e (mg g^{-1}) and C_e (mg L^{-1}) are the amount adsorbed on magnetic MIP1 and concentration of BSM in the solution at equilibrium, respectively; Q_m (mg g^{-1}) is the theoretical maximum adsorption capacity; K_L (L mg^{-1}) is the Langmuir constant related to the affinity of adsorption sites; K_F (L mg^{-1}) and n are determined from a linear plot of log Q_e versus log C_e, demonstrating adsorption capacity and intensity, respectively; N_t is the total number of binding sites; a is related to the binding affinity (K_0) via $K_0 = a^{1/m}$, and m is the heterogeneity index that varies from 0 to 1 (m = 1 means the media is homogeneous).

Selectivity Experiment. To evaluate the specific recognition ability of MIP1 for BSM, 10 mg of MIP1 (or NIP1) was added into 10 mL centrifuge tubes containing 5 mL of methanol and water (3/7, v/v) solution with 0.2 mM of BSM, TS, PS, PSE, or PPZ. Meanwhile, 10 mg of MIP1 (or NIP1) was added into the mixed solution of these five pesticides with initial concentrations of 0.2 mM. Each mixture with MIP1 (or NIP1) was shaken at room temperature for 24 h. The supernatant was separated with a permanent magnet. Concentrations of BSM, TS, PS, PSE, and PPZ were determined by HPLC. The interrelated absorbed coefficient was evaluated by the following equation:

$$\text{Static distribution coefficient } K_d = \frac{C_p}{C_s} \quad (5)$$

where C_p is the concentration on the absorbed medium, and C_s is the final free concentration of the solution. The selectivity coefficient of MIP1 to BSM with respect to the competitor species can be obtained according to eq 6.

$$\text{Selectivity coefficient } k = \frac{K_d(SU_s)}{K_d(PPZ)} \quad (6)$$

where K_d (SU_s) stands for static distribution coefficient of the template or the structural analogues; and K_d (PPZ) is the static distribution coefficient of pesticide PPZ.

The value of the relative selectivity coefficient k' defined in eq 7 indicates the enhanced extent of adsorption affinity and selectivity of MIP1 to the template BSM.

$$k' = \frac{k_{MIP}}{k_{NIP}} \quad (7)$$

where k_{MIP} and k_{NIP} are the selectivity coefficients of MIP1 and NIP1, respectively.

Separation Enrichment of Sulfonylurea Herbicides. MIP1 was used directly as sorbents for sulfonylurea herbicides. Water samples (20 mL) and 100 mg of magnetic MIP1 particles were mixed in a centrifuge tube. After being shaken at room temperature for 3 h, MIP1 was removed by a permanent magnet, first washed with water, and then washed with 4 mL of methanol. The eluent solution was collected and filtered through a 0.45 μm filter before HPLC analysis.

MIP1 was used as sorbents to prepare the SPE cartridge. MIP1 particles (100 mg) were packed in an empty 3 mL solid phase extraction (SPE) cartridge. The SPE cartridge was capped with PTFE frits at the top and bottom, respectively. The MIP-SPE cartridge was washed with 10 mL of methanol−acetic acid (9:1, v/v) to remove residue and preconditioned with 5 mL of methanol and 5 mL of ultrapure water. Standard solution or sample solution was loaded onto the preconditioned MIP-SPE cartridge at a rate of 0.5 mL min^{-1}. After sample loading, the MIP-SPE cartridge was washed with 2 mL of methanol/water (3/7, v/v). The elution step was performed using 2 mL of methanol. The eluate was collected and filtered through a 0.45 μm filter before HPLC analysis. For comparison, C_{18} SPE (Supelco, 3 mL, 500 mg) was used with a similar protocol to that of the MIP-SPE columns.

Determination of Environmental Samples. Rice water (paddy soil water), soil, and rice grain were collected for analysis. Water sample was directly added into the centrifuge tube containing magnetic MIP or loaded onto the preconditioned MIP-SPE column. The soil was collected from a rice field, and the plant debris was removed from the soil. The soil was dried under natural conditions and passed through a 2 mm sieve. The soil sample was extracted ultrasonically with 20 mL of acetone−water (3:1, v/v) for 30 min and centrifuged. The extraction procedure was performed in triplicate. The supernatant was concentrated to remove acetone at 40 °C by a rotary evaporator. The residual water was loaded onto the preconditioned MIP-SPE column. The rice was ground. The rice grains were rinded in a grinder (FW177, Taisite Instrument Co. Ltd., China) and passed through a 0.38 mm sieve. The rice grain was soaked and ultrasonicated with dichloromethane three times, each time with 20 mL for 30 min. The extracting solution was centrifuged, and the supernatant was combined and concentrated by a rotary evaporator at 40 °C. The residue was redissolved in 1 mL of methanol and then diluted with 20 mL of water. The diluting solution was loaded onto the preconditioned MIP-SPE column. The MIP-SPE column was washed. The eluent was collected and analyzed using the methods indicated above. Each sample was repeated in triplicate.

To evaluate accuracy of the method, the spiked recoveries of samples were investigated. Test samples of soils (10.0 g) and ground rice grains (10.0 g) were prepared using an appropriate volume of standard mixture solution (each pesticide 1.0 mg·L^{-1}) to obtain the final concentrations of 0.1, 0.25, and 0.5 mg kg^{-1}, respectively. The spiked samples were incubated and left to stand for about an hour. The water samples were spiked with each herbicide at the concentrations of 0.05, 0.25, and 0.5 mg L^{-1}. Extraction, purification, and concentration were performed in the same way indicated above.

Statistic Analysis. All of the experiments were performed at least three repetitive independent treatments. The values were expressed as the means ± standard deviation. ANOVA was conducted using the mixed model procedure in SPSS statistics 20. The significance of the differences among the means was calculated by Turkey's test. Statistical significance was set at $p < 0.05$.

RESULTS AND DISCUSSION

Preparation of Imprinted Magnetic Microspheres. The schematic representation of MIP preparation is illustrated in Figure 1. The synthetic approach included the following procedures: (1) obtaining the shell−core structure of vinyl-modified Fe_3O_4@SiO_2; (2) self-assembly of the template and functional monomers; (3) polymerization in the presence of cross-linker, initiator and porogen; and (4) achieving recognition cavities in the polymer matrix by eluting template BSM.

To obtain highly stable and well-dispersed magnetic nanoparticles, silica was selected to encapsulate Fe_3O_4. Silica has a small dimension with extremely high surface-to-volume ratio.[25] It can screen the magnetic dipolar attraction between the magnetic Fe_3O_4 molecules in liquid media. Also, most of the template molecules are situated at the surface or are in the proximity of surface. Furthermore, since the silanol group stands on the Fe_3O_4 surface coated by silica, the modified Fe_3O_4 could increase

DOI: 10.1021/jf506239b
J. Agric. Food Chem. 2015, 63, 3634−3645

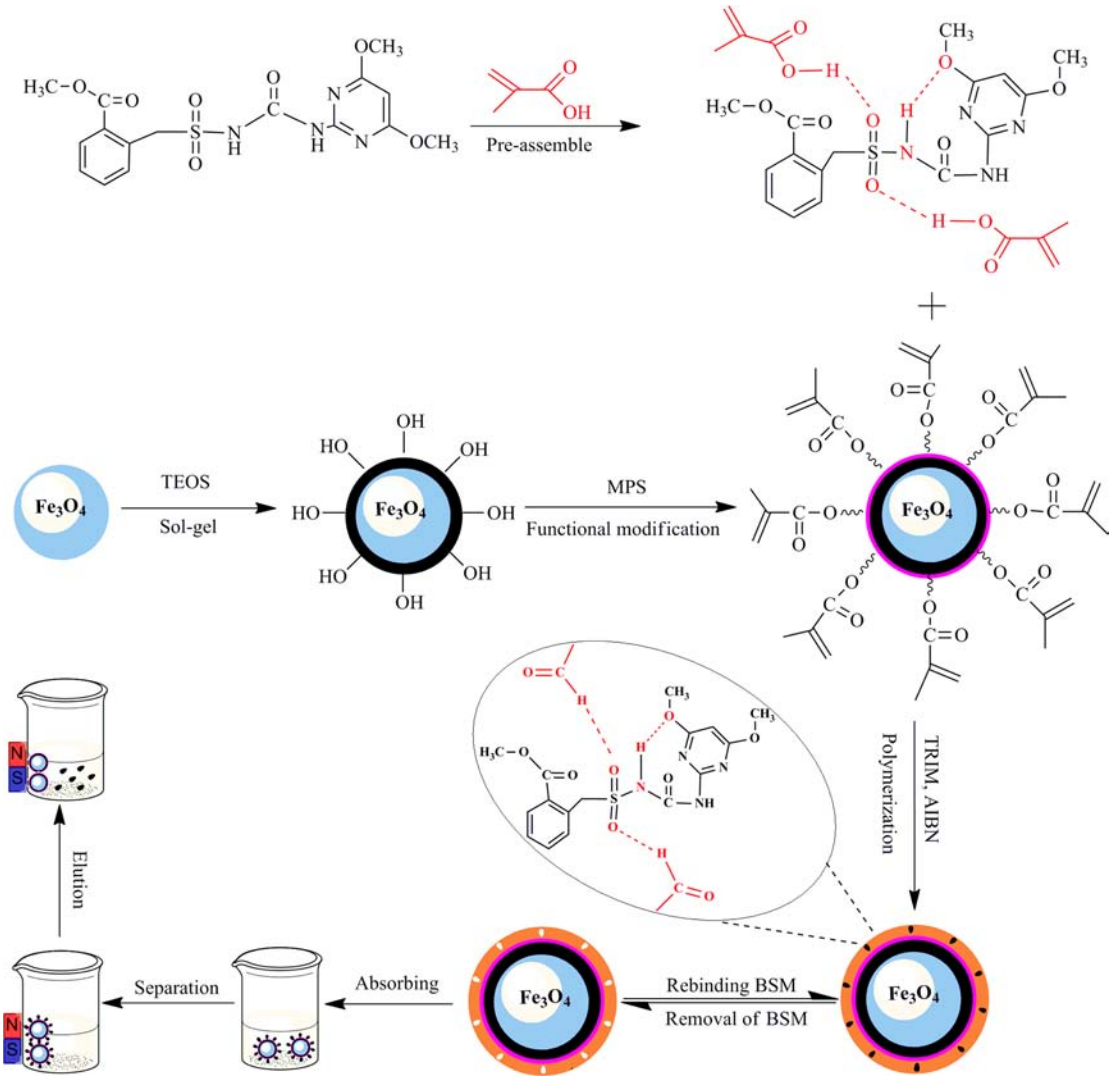

Figure 1. Schematic representation of the possible process of BSM imprinted polymers.

biocompatibility and bioconjugation with various groups. The silanol group on the Fe_3O_4@SiO_2 surface further reacted with MPS to introduce vinyl groups, which subsequently reacted with the functional monomer MAA. The copolymerization of terminal C═C double bonds of MPS with MAA can directly produce the network structures and form MIP nanospheres.

To investigate the modification of Fe_3O_4, a series of molecularly imprinted and nonimprinted polymers were prepared (Supporting Information, Table S1). All BSM-imprinted polymers (MIP) had much greater adsorption capacity for the template than the corresponding referenced polymers (NIP) (Supporting Information, Table S1). Among the three MIPs, MIP1 showed the greatest binding capacity for BSM, about twice as much as MIP2 and MIP3, suggesting that more recognition sites existed in MIP1 than in MIP2 and MIP3. MIP3 showed the lowest binding capacity for BSM among three MIPs. MIP1 was therefore selected for further investigation.

Interaction between BSM and MAA in Solution. In order to acquire the high adsorption capacity of MIP, interactions between the functional monomer and template were investigated. Since hydrogen-bonding can provide precise molecular recognition depending on both distance and direction between the monomer and template, it is commonly used for assembling the noncovalent MIP.[36] When BSM concentration is kept constant and the ratio of BSM/MAA increased from 1:0 to 1:60 (BSM/MAA), the maximum absorption wavelengths of BSM presented obviously red shifts, and the maximum absorbance intensity of BSM also largely decreased with the increasing molar ratio of MAA (Figure 2). The result indicated that hydrogen bonding existed between BSM and MAA, and affected the $\pi-\pi^*$ absorption band of BSM.

To confirm the hydrogen bonding between BSM and MAA, we employed a molecular simulation technique that is widely adopted to study molecular interactions between the template and functional monomer at the molecular level.[15,37−39] Simulated results showed that the binding energies (ΔE) of BSM with MAA were −11.14 and −17.03 kcal mol^{-1}, respectively, when BSM interacted with MAA at mole ratios of 1:1 and 1:2, indicating that the binding energy was lowest with −17.03 kcal mol^{-1} and that the complex with a mole ratio of 1:2 was most stable. Stable hydrogen bonding interactions between BSM and MAA were observed involving two intermolecular hydrogen bonds (at each O in the $-SO_2$-group) and an intramolecular hydrogen bond at O27 and H38 (Supporting Information, Figure S1). Although molecular simulation showed the theoretic binding sites and ratio between BSM and MAA, the

DOI: 10.1021/jf506239b
J. Agric. Food Chem. 2015, 63, 3634−3645

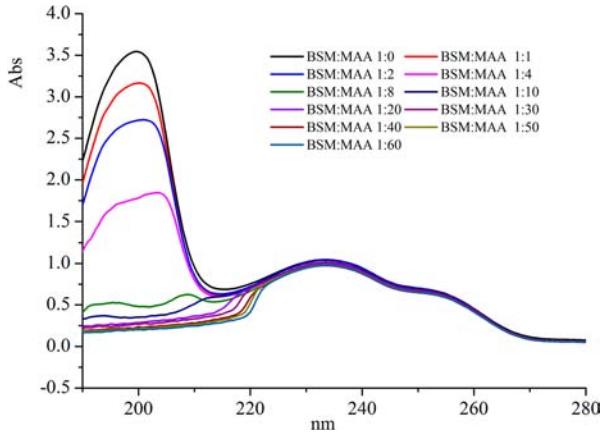

Figure 2. UV spectra of BSM with different molar ratios of MAA in acetonitrile. Concentration of BSM, 0.05 mmol L^{-1}; concentration of MAA for lines 1−11, 0, 0.05, 0.1, 0.2, 0.4, 0.5, 1, 1.5, 2, 2.5, and 3 mmol L^{-1} respectively. Corresponding pure MAA solutions as blank.

experimental approach affected the choice of the most appropriate ratio between them. Since the association between the monomer and template is governed by an equilibrium in the noncovalent approach, the functional monomers normally have to be added in excess relative to the number of moles of the template to favor the formation of the template−monomer complex. Therefore, the working molar ratio of the template to functional monomer was typically set with 1:4.[40]

Characterization of Core−Shell Magnetic Molecularly Imprinted Polymers. The TEM images showed that the size of Fe_3O_4 magnetic particles was around 200 nm with an irregular shape (Figure 3A). The diameter of the uniform spherical Fe_3O_4@SiO_2 with silica coating was extended to about 620 nm, corresponding to a 420 nm thickness of SiO_2 layers coated on the Fe_3O_4 particles (Figure 3B). The silica shell of Fe_3O_4@SiO_2 enhanced the biocompatibility and stability of Fe_3O_4 magnetic particles and prevented oxidation and aggregation of Fe_3O_4 magnetic particles. However, Fe_3O_4@SiO_2 provided the sites to react with MPS, which could offer vinyl end groups favorable for further grafting.[41] Furthermore, the uniform core−shell MIP was successfully constructed, and the MIP1 had a polymer layer with about 20 nm thickness (Figure 3C), revealing that the binding sites almost existed at the surface of Fe_3O_4@SiO_2-MIP. The MIP1 spheres appear more irregular, presumably due to the presence of the imprint. In contrast, NIP1 spheres appear smoother, showing more uniform appearance (Figure 3E). However, the MIP1 had a three-dimensional structure and appeared more porous and looser in comparison with that of NIP1. The result demonstrated the fixing of template BSM and functional monomer MAA on the Fe_3O_4@SiO_2 surface in the presence of the cross-linker, porogen, and initiator in the polymerization system (Figure 3D). This core−shell structure of MIP1 should be effective in mass transport for rebinding and releasing the template.

In FT-IR spectra, the peak at 580.54 cm^{-1} was attributed to the stretching vibrations of Fe−O (Figure 4A). In comparison with the infrared data of Fe_3O_4, the peaks at 804.41, 948.85, and 1089.67 cm^{-1} correspond to the stretching vibrations of Si−O, Si−O−H, and Si−O−Si, respectively (Figure 4B−D), pointing to the formation of silica coating on the surface of Fe_3O_4. The vibration at 1696.29 cm^{-1} in vinyl-modified Fe_3O_4@SiO_2 was the peak of carbonylic groups, indicating the successful modification using MPS on the Fe_3O_4@SiO_2 surface (Figure 4B). Meanwhile, the strong peaks of the C═O group at 1736.01 cm^{-1} and C−H

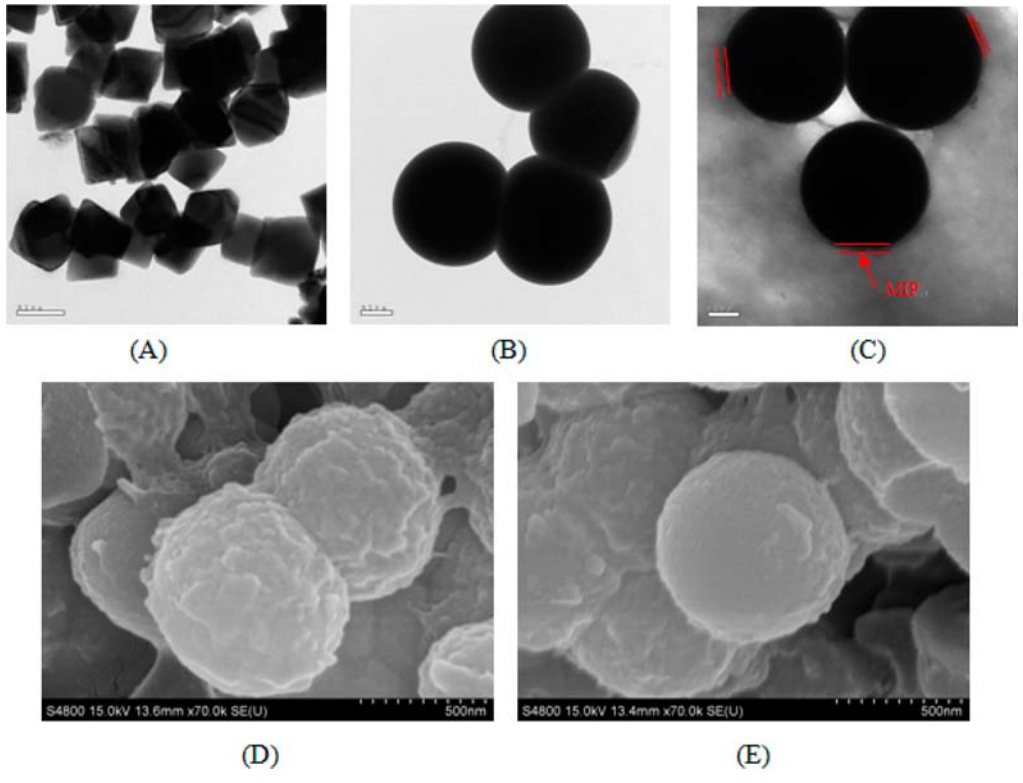

Figure 3. TEM images Fe_3O_4 (A), Fe_3O_4@SiO_2 (B), and MIP1 (C) with scale bars of 0.2 μm. SEM images of MIP1 (D) and NIP1 (E) with scale bars of 500 nm.

DOI: 10.1021/jf506239b
J. Agric. Food Chem. 2015, 63, 3634−3645

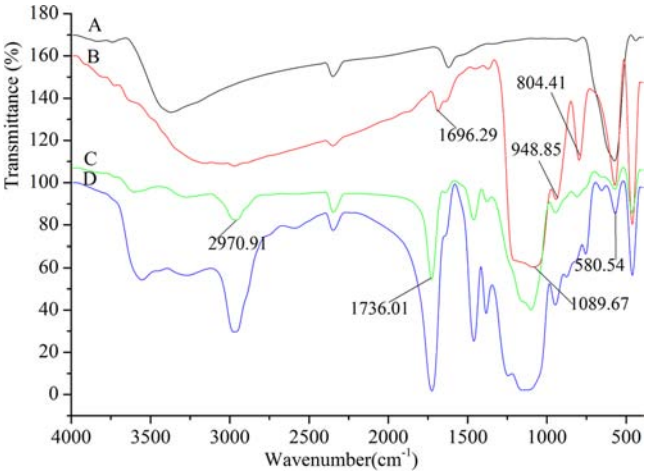

Figure 4. FT-IR spectra of Fe_3O_4 (A), vinyl-modified Fe_3O_4@SiO_2 (B), MIP1 (C), and NIP1 (D).

group of methyl at 2970.91 cm^{-1} (Figure 4C and D) indicated the successful grafting of a polymer layer on the vinyl-modified Fe_3O_4@SiO_2. In addition, MIP1 had the same characteristic peaks with NIP1, showing the complete removal of the template from MIP1.

XRD is a powerful tool for crystal structure characterization. The XRD patterns for the magnetic particles with and without coating were displayed in Supporting Information, Figure S2. These samples with specific diffraction peaks were highly crystalline materials, and the four particles contain Fe_3O_4 with a spinel structure.[42] The peak positions of the four samples remained unchanged, indicating that the step-by-step procedure of coating and polymerization made no crystalline structure change of Fe_3O_4. The intensities of the characteristic peaks in MIP1 slightly decreased owing to the encapsulation by the polymer layer.

VSM was applied to the characterization of the magnetic properties of the synthesized particles. The remnant magnetization (M_r) and coercivity (H_c) can be determined from the VSM data (Figure 5). The values of M_r and H_c were 5.44 emu g^{-1}

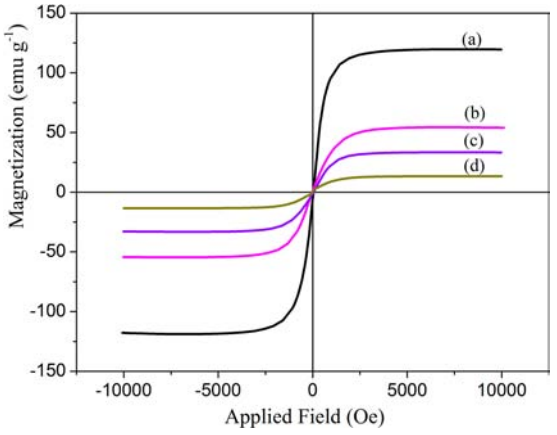

Figure 5. Magnetization curves at 298 K of Fe_3O_4 (a), Fe_3O_4@SiO_2 (b), vinyl-modified Fe_3O_4@SiO_2 (c), and MIP1 (d).

and 34.25 Oe for Fe_3O_4, 1.17 emu g^{-1} and 27.68 Oe for Fe_3O_4@SiO_2, 1.10 emu g^{-1} and 41.77 Oe for vinyl-modified Fe_3O_4@SiO_2 and 0.57 emu g^{-1} and 12.92 Oe for MIP1, respectively. The very weak hysteresis indicated that four samples had good superparamagnetism at room temperature. We were sure that all of the nanoparticle samples with good superparamagnetism can be redispersed rapidly as soon as the external magnetic field was removed. Furthermore, the saturation magnetization of Fe_3O_4@SiO_2 (54.3 emu g^{-1}) and vinyl-modified Fe_3O_4@SiO_2 (33.4 emu g^{-1}) were lower than that of Fe_3O_4 (119.5 emu g^{-1}) (Figure 5) because the small particle surface was inactive and the magnetic layer was not collinear with the magnetic field.[43] The saturation magnetization of MIP1 with an additional polymer layer was significantly decreased to 13.4 emu g^{-1}. However, the MIP1 remained strongly magnetic and could be isolated using an external magnet in a few seconds.

Adsorption Isotherms. The adsorption isotherm experiments were conducted with different initial concentrations of BSM ranging from 0.02 to 0.4 mM. The adsorbability of MIP1 continuously increased with the increment of BSM ranging from 0.02 to 0.35 mM and reached equilibrium at 0.35 mM (Figure 6A). The adsorption capacity of MIP1 (37.32 mg g^{-1}) was about 2.02-fold over that of NIP1 (18.45 mg g^{-1}) at 0.4 mM of BSM. The result confirmed that the arrangement of MAA in MIP1 was inherently different from that of NIP1.

The corresponding parameters fitting Langmuir, Freundlich, and Langmuir−Freundlich isotherm models to the experimental data were obtained (Figure 6B−D). The values of Q_m and K_L were 43.48 mg g^{-1} and 0.0083 L mg^{-1}, respectively; the values of n and K_F were 1.247 and 1.0007 L mg^{-1}, respectively; and the values of N_t and m were 98.67 mg g^{-1} and 1, respectively. K_0 is equal to a (3.517M^{-1}). Although the Freundlich model has been shown to be generally applicable to most noncovalently imprinted polymers,[28,44] it did not fit the experimental data well. The Langmuir isothermal equation with an R^2 value of 0.9267 seemed more desirable to describe the adsorption of BSM on magnetic MIP1 than the Freundlich isothermal equation (R^2 = 0.7532) and the Langmuir−Freundlich equation (R^2 = 0.7527). However, the isotherms (MIP1) showed 3 distinct regions: region 1, a low slope linear relationship at low concentration demonstrating weak adsorption; region 2, a higher slope linear relationship at intermediate concentrations; and region 3, a low slope linear relationship at high concentration, suggesting that sites were nearly saturated (Figure 6A).

Adsorption Kinetics. The adsorption kinetics of magnetic MIP1 was investigated at 0.2 mM BSM. An overall 5-fold increase was observed in adsorption capacity with magnetic MIP1 versus NIP1 (Figure 7). For MIP1 there was a fast rising adsorption during the first 60 min before the adsorption equilibrium was reached. In the first 60 min, the magnetic MIP1 attained up to 86% of equilibrium absorption amounts of BSM. These results indicated that most of the template was sorbed to the imprinted sites at a fast rate, suggesting that the binding sites of the magnetic MIP1 were on or near the surface. In contrast, the magnetic NIP1 showed a low affinity but similar equilibration time to that of MIP1 as there was a clear increase in amount sorbed from time 0 to 60 min.

Magnetic MIP Binding Specificity. In order to investigate the selectivity of magnetic MIP1 microspheres for sulfonylurea herbicides, binding experiments were conducted by choosing triasulfuron (TS), prosulfuron (PS), and pyrazosulfuron-ethyl (PSE) as the structural analogues of BSM template and propazine (PPZ) as a representative of different classes of compounds of dissimilar structure. NIP1 was used for comparison. The binding amounts of BSM for magnetic MIP1 were higher than those of the other three sulfonylurea herbicides and PPZ,

DOI: 10.1021/jf506239b
J. Agric. Food Chem. 2015, 63, 3634−3645

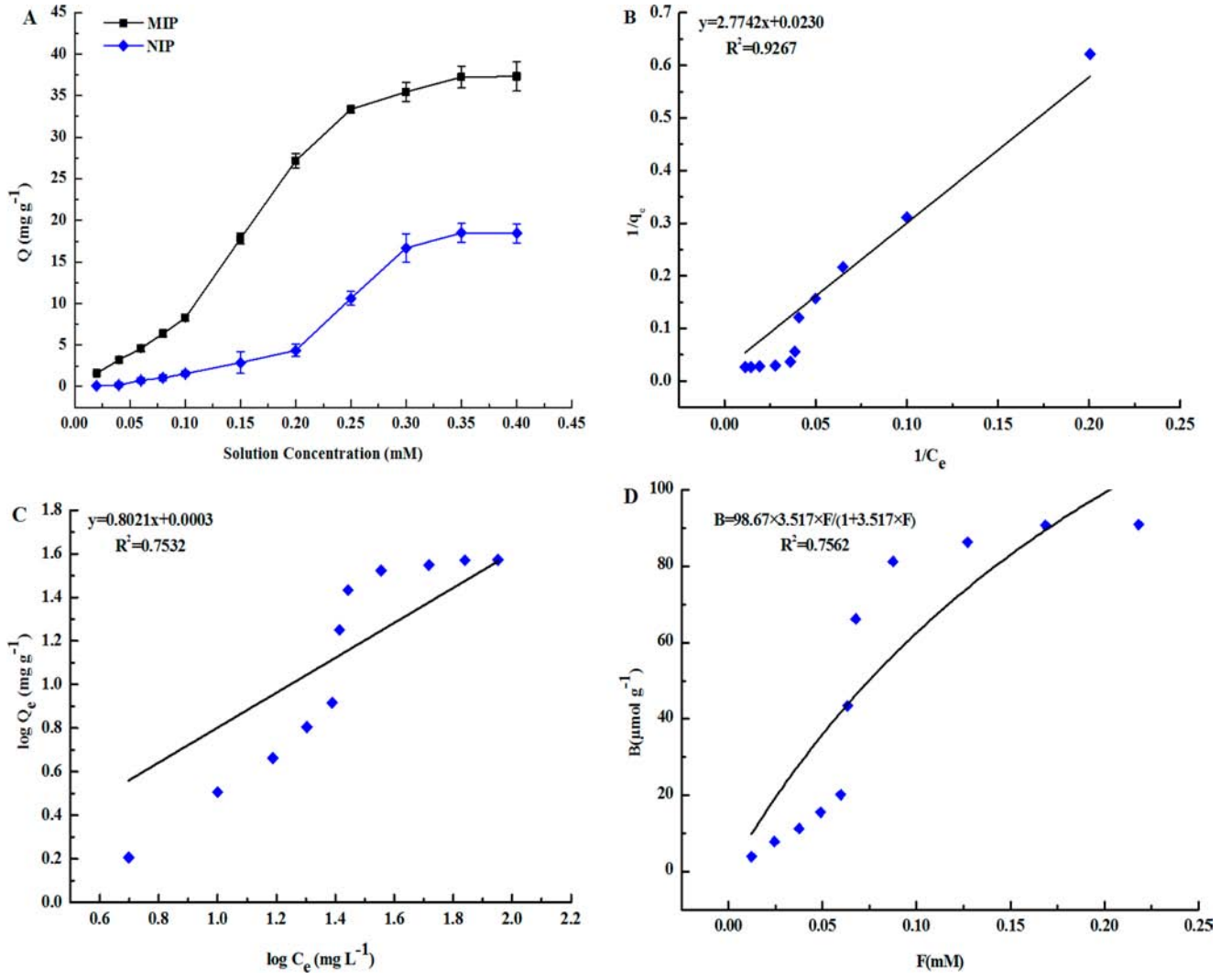

Figure 6. Adsorption isotherms (A) of BSM on MIP1 and NIP1, Langmuir plot (B), Freundlich plot (C), and Langmuir–Freundlich plot (D) to estimate the binding nature of MIP1. Experimental conditions: 0.02–0.4 mmol L^{-1} BSM with 10.0 mg of the polymers for 24 h, and the binding medium was 5 mL of methanol–water (30:70, v/v). The measurements were repeated three times.

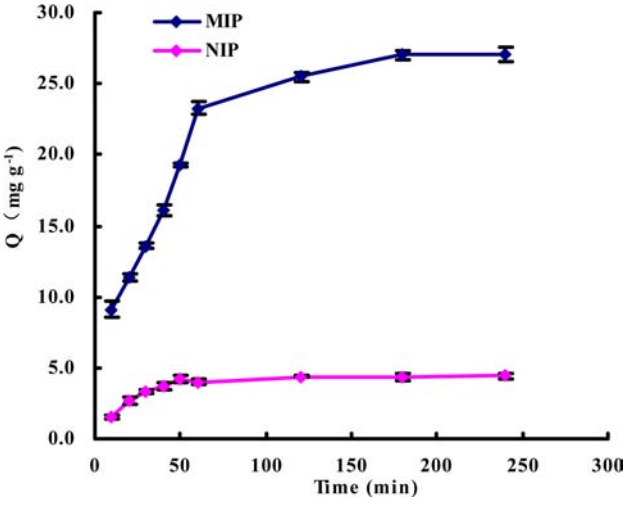

Figure 7. Adsorption kinetic curves of BSM on MIP1 and NIP1. Experimental conditions: 0.2 mmol L^{-1} BSM in the binding medium of 5 mL of methanol–water (3:7, v/v) with 10 mg of MIP1 or NIP1 for a certain time period. The measurements were repeated three times.

suggesting that the template molecule BSM had a relatively higher affinity for the imprinted polymer than others (Figure 8). It was possible that the specific sites existing in magnetic MIP1 were complementary in shape, size, and spatial distribution to template BSM. The template fitted the cavities well in the imprinted polymer.[45] Moreover, the absorption amounts of magnetic MIP1 toward the five pesticides were lower in the mixture (Figure 8B) than in individual solutions (Figure 8A). The phenomenon demonstrated that the binding sites were fixed in magnetic MIP1 and that the five compounds competed with each other in the mixed solution, leading to the reduced adsorption on magnetic MIP1. There were interactions of hydrogen bonding between the hydroxyl group in MAA and sulfonyl group in BSM (Supporting Information, Figure S1). Three analogous pesticides (TS, PS, and PSE) also have the group ($-SO_2-$) that is the same in BSM (Supporting Information, Figure S3). Therefore, the binding capacities of the analogues were much higher than that of PPZ, indicating that magnetic MIP1 also possessed high selectivity to the structural analogues of BSM. This was supported by the fact that the relative binding affinity was a function of compound structure (Supporting Information, Figure S1). PSE is most similar to BSM in molecular dimensions and

DOI: 10.1021/jf506239b
J. Agric. Food Chem. 2015, 63, 3634–3645

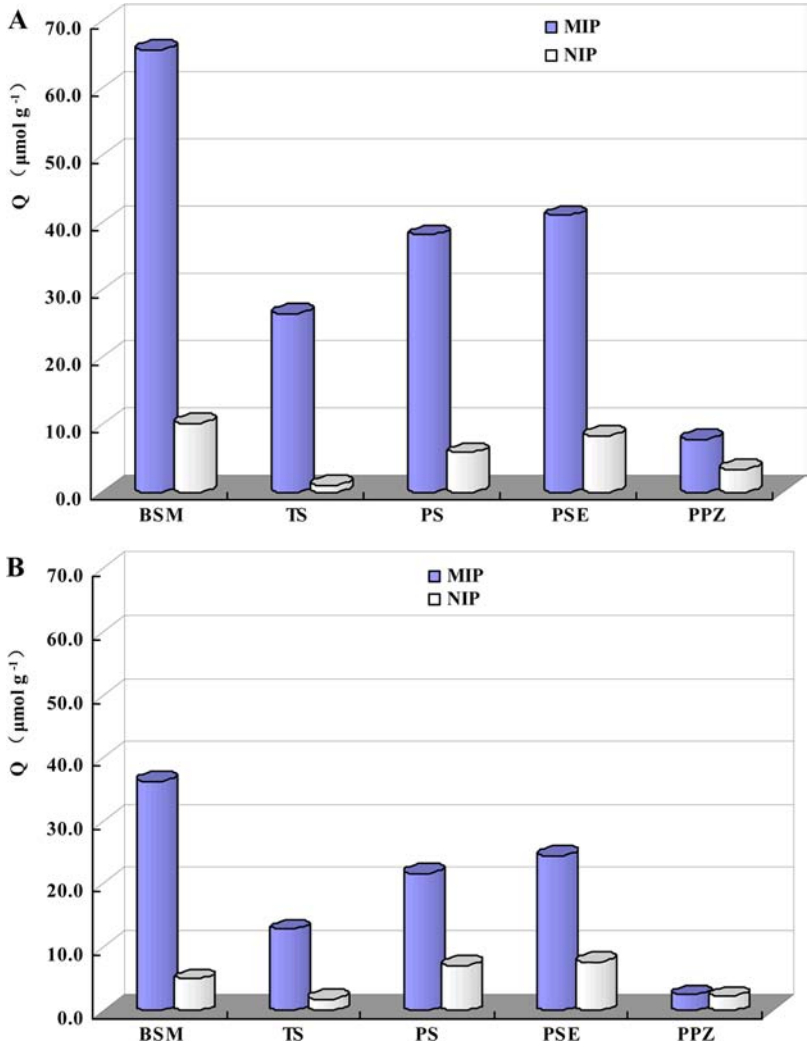

Figure 8. Adsorption selectivity of BSM onto MIP1 and NIP1 in single solution (A) and mixed solution (B). Ten milligrams of the polymers was suspended in 5 mL of methanol−water (3:7, v/v), in which the concentration of BSM, TS, PS, PSE, and PPZ was 0.2 mmol L^{-1} (A). Ten milligram polymers were suspended into 5 mL of mixed solution containing a mixture of BSM, TS, PS, PSE, and PPZ with a concentration of 0.2 mmol L^{-1} for each compound (B). The measurements were repeated three times. BSM, bensulfuron-methyl; TS, triasulfuron; PS, prosulfuron; PSE, pyrazosulfuron-ethyl; PPZ, propazine.

Table 1. Specific Recognition Properties of Magnetic MIP1 and NIP1

	MIP1			NIP1			
analytes	C_s (mM)	K_d	k	C_s (mM)	K_d	k	k'
BSM	0.127	0.573	22.038	0.190	0.053	2.208	9.981
TS	0.174	0.148	5.692	0.196	0.019	0.792	7.187
PS	0.157	0.278	10.692	0.186	0.077	3.208	3.333
PSE	0.151	0.327	12.577	0.185	0.083	3.458	3.637
PPZ	0.195	0.026	1	0.195	0.024	1	1

functional groups, and it had the highest binding affinity among the competing herbicides tested. The binding of PSE on magnetic MIP1 was greater than those of TS and PS. Compared with BSM, the mismatch of the structure and size with specific cavities might hinder TS entering the imprinted cavities and lead to the lowest binding capacity of TS among the four analogues. Since the three F atoms in PS bind to hydroxyl hydrogen in MAA, the binding affinity of magnetic MIP1 to PS was larger than that of TS. In addition, PPZ, with the least structural similarity to BSM, showed the lowest binding capacity (3 μmol g^{-1}) (Figure 8B). In contrast, there was no obvious difference of the NIP1 binding capacity for five herbicides, which likely depended on the same mechanism of nonspecific absorption.

To further assess the molecular recognition property for MIP1, the static distribution coefficient (K_d), selectivity coefficient (k), and relative selectivity coefficient (k') were calculated based on the data in Figure 8B by eqs 5−7. The k values of magnetic MIP1 showed a significant increase compared to the values of NIP1 due to the imprinting effect (Table 1). The k' for PPZ was much lower than that for TS, PS, and PSE, indicating that the magnetic MIP1 had a high binding affinity for these

DOI: 10.1021/jf506239b
J. Agric. Food Chem. 2015, 63, 3634−3645

Table 2. Results of the Determination and Recoveries of Water Spiked with Four Sulfonylurea Herbicides (n = 3)

		MIP as sorbents			MIP-SPE cartridge			C_{18} cartridge		
compound	spiked (μmol L^{-1})	observed (μmol L^{-1})	recovery (%)	RSD (%)	observed (μmol L^{-1})	recovery (%)	RSD (%)	observed (μmol L^{-1})	recovery (%)	RSD (%)
bensulfuron-methyl	0	nd[a]			nd[a]			nd[a]		
	0.05	0.044	87.81	3.20	0.051	102.00	0.83	0.038	76.20	8.18
	0.25	0.215	85.95	4.14	0.229	91.38	3.40	0.165	65.92	7.06
	0.5	0.456	91.15	1.13	0.438	87.62	2.50	0.326	65.22	7.04
triasulfuron	0	nd[a]			nd[a]			nd[a]		
	0.05	0.038	76.83	2.81	0.050	100.80	2.70	0.034	67.15	7.48
	0.25	0.169	67.46	2.48	0.209	83.42	2.09	0.159	63.08	5.35
	0.5	0.413	82.53	1.49	0.404	80.75	1.69	0.380	75.93	2.79
prosulfuron	0	nd[a]			nd[a]			nd[a]		
	0.05	0.036	72.47	1.76	0.042	83.73	1.40	0.030	59.90	3.86
	0.25	0.178	71.34	1.59	0.224	89.45	4.53	0.150	59.88	8.09
	0.5	0.417	83.39	2.01	0.417	83.34	7.60	0.301	60.13	7.68
pyrazosulfuron-ethyl	0	nd[a]			nd[a]			nd[a]		
	0.05	0.040	80.55	2.47	0.046	92.06	0.22	0.039	77.49	6.51
	0.25	0.195	77.96	7.22	0.206	82.18	8.74	0.197	78.94	4.14
	0.5	0.423	84.66	1.18	0.391	78.14	3.52	0.368	73.52	6.70

[a]nd: not detected.

Table 3. Results of the Determination and Recoveries of Rice Soil and Grain Spiked with Four Sulfonylurea Herbicides (n = 3)

			MIP-SPE cartridge			C18 cartridge		
sample	compound	spiked (μmol kg^{-1})	observed (μmol kg^{-1})	recovery (%)	RSD (%)	observed (μmol kg^{-1})	recovery (%)	RSD[c](%)
soil	bensulfuron-methyl	0	nd[a]			nd[a]		
		0.1	0.090	89.63	3.41	0.073	73.31	4.77
		0.25	0.240	95.78	2.24	0.182	72.95	1.37
		0.5	0.473	94.67	3.71	0.355	70.93	2.09
	triasulfuron	0	nd[a]			nd[a]		
		0.1	0.052	52.26	2.44	0.047	46.76	3.22
		0.25	0.128	51.18	2.91	0.106	42.31	3.25
		0.5	0.330	65.99	7.54	0.169	33.88	6.00
	prosulfuron	0	nd[a]			nd[a]		
		0.1	0.084	84.17	2.57	0.048	47.74	3.23
		0.25	0.222	88.65	2.34	0.165	65.95	8.71
		0.5	0.409	81.77	0.81	0.164	32.79	6.55
	pyrazosulfuron-ethyl	0	nd[a]			nd[a]		
		0.1	0.084	83.63	2.95	0.077	76.54	0.74
		0.25	0.202	80.77	4.55	0.185	73.99	3.17
		0.5	0.429	85.72	2.52	0.255	51.06	7.92
grain	bensulfuron-methyl	0	nd[a]			nd[a]		
		0.1	0.086	85.67	5.15	0.063	62.72	6.41
		0.25	0.229	91.50	5.12	0.164	65.70	4.01
		0.5	0.434	86.72	3.53	0.359	71.86	4.70
	triasulfuron	0	nd[a]			nd[a]		
		0.1	NDQ[b]			NDQ[b]		
		0.25	0.127	50.81	5.77	NDQ[b]		
		0.5	0.266	53.16	0.93	NDQ[b]		
	prosulfuron	0	nd[a]			nd[a]		
		0.1	0.073	73.21	7.08	0.062	61.64	8.56
		0.25	0.204	81.51	6.61	0.151	60.28	5.48
		0.5	0.407	81.42	1.61	0.358	71.67	7.37
	pyrazosulfuron-ethyl	0	nd[a]			nd[a]		
		0.1	0.075	75.24	4.28	0.052	51.83	4.89
		0.25	0.206	82.20	1.79	0.080	32.12	7.45
		0.5	0.428	85.50	6.19	0.247	49.38	5.35

[a]nd: not detected. [b]NDQ could be detected but could not be determined quantitatively. [c]RSD relative standard deviation.

analogues but not for the different class compound of dissimilar structure (PPZ). Therefore, the magnetic MIP1 can be used as group-recognition materials because of the similar adsorption properties for these structural analogues.

DOI: 10.1021/jf506239b
J. Agric. Food Chem. 2015, 63, 3634−3645

Methodological Validation and Application to Real Samples. The magnetic MIP-SPE cartridges were applied for purifying and concentrating the selected sulfonylurea herbicides in real samples. The washing step for the MIP-SPE is the key parameter for the method of sample pretreatment.[46] To obtain maximum selectivity and recovery of sulfonylurea herbicides in the washing step, water containing different percentages of methanol was tested. Two milliliters of methanol/water (45/55 or 35/65, v/v) led to lower recoveries among all ratios of methanol and water (Supporting Information, Figure S4). The recovery of BSM showed no significant difference at 30:70, 25:75, and 15:85 ($MeOH/H_2O$). For the recovery of PS, the use of 30:70 ($MeOH/H_2O$) showed no significant difference compared to 25:75, as well as 25:75 compared to 15:85. The recoveries of TS and PSE using 30:70 ($MeOH/H_2O$) were lower than 25:75 and 15:85 but were also reached or greater than 80%. As more interference in paddy soil and grain occurred, an appropriately high ratio of methanol in washing solution could provide high elution strength. Thus, 2 mL of methanol/water (30/70) was chosen as the washing solution in the experiment in order to eliminate the impurities and keep the recoveries of the four sulfonylurea herbicides. Under the optimized conditions of magnetic MIP-SPE coupled with HPLC, a good linearity was achieved for standards in the range of 0.04−0.8 μM for BSM, TS, PS, and PSE with correlation coefficients of 0.9996, 0.9954, 0.9936, and 0.9941, respectively (Supporting Information, Table S2). Their LODs were in the range of 6.4−9.5 nM.

The created methodology was applied to the rice water, paddy soil, and grain samples. Initial analyses confirmed that the three samples were free of sulfonylurea herbicides. The detecting signals of four sulfonylurea herbicides with MIP-SPE procedure (Supporting Information, Figure S5-Ac, Bc, and Cc) were stronger than that without the MIP-SPE procedure (Supporting Information, Figure S5-Ab, Bb, and Cb) in the water, soil, and grain samples. The analysis of blank samples showed that most of the interference substances were washed during the methanol/water (3/7, v/v) cleaning up process (Supporting Information, Figure S5-Aa, Ba, and Ca). Although there were some impurities after the soil sample was treated by magnetic MIP-SPE, they had the least impact on the quantitative determination of sulfonylurea herbicides (Supporting Information, Figure S5B).

The accuracy of the method was evaluated by the recovery test conducted with spiked samples. The relative recoveries of BSM, PS, and PSE with magnetic MIP-SPE as columns for the spiked rice water, soil, and grain were 78.14−102.00%, 80.77−95.78%, and 73.21−91.50%, respectively, and the relative standard deviations (RSDs) were 0.22−8.74%, 0.81−4.55%, and 1.61−7.08%, respectively (Tables 2 and 3). The recoveries of four herbicides for rice water using magnetic MIP as sorbents were slightly lower than those with the MIP-SPE column. The recoveries of TS in the three spiked samples were 50.81−100.80%, with RSDs ranging from 0.93% to 7.54% (Tables 2 and 3). The C_{18} column only had the nonspecific adsorption, resulting in much lower recoveries of sulfonylurea herbicides in the spiked samples. The results demonstrated that the magnetic MIP-SPE coupled with HPLC was an efficient and effective methodology for selective extraction and sensitive assessment of multiple sulfonylurea herbicides at a very low concentration.

Reusing MIPs. To verify the recyclability of MIP-SPE, regeneration (adsorption/desorption) cycles were conducted with four sulfonylurea herbicides. After MIP-SPE columns were used to analyzed samples in food or environmental media, the columns could be regenerated by washing with 5 mL of acetic acid, 5 mL of methanol, and 5 mL of water. The result showed that MIP-SPE columns could be used for six cycles at least, and the average recovery had only a loss of less than 5.5%, indicating that the selectivity of the MIP-SPE was specific and stable for four sulfonylurea herbicides in food and environmental media.

■ ASSOCIATED CONTENT

Ⓢ Supporting Information

Preparation composition of different polymers; linear range, method limit of detection (LOD) of MIP-SPE coupled with HPLC for four sulfonylurea herbicides; molecular simulation of interactions between BSM and MAA; XRD patterns at 298K of Fe3O4 (a), Fe3O4@SiO2 (b), vinyl-modified Fe3O4@SiO2 (c), and MIP1 (d); structures of four sulfonylurea herbicides (BSM, PSE, PS, and TS) and PPZ; recoveries of BSM, TS, PS, and PSE from the washing step using different ratios of methanol/water (v/v); and chromatograms of spiked sulfonylurea herbicides. This material is available free of charge via the Internet at http://pubs.acs.org.

■ AUTHOR INFORMATION

Corresponding Author

*Weigang No.1, Chemistry Building, College of Sciences, Nanjing Agricultural University, Nanjing 210095, China. Tel: +86-25-84395207. E-mail: hongyang@njau.edu.cn.

Funding

We acknowledge the Special Fund for Agro-scientific Research in the Public Interest (No. 201203022) from the Ministry of Agriculture of China. This work was supported by funding from Jiangsu Innovation Program for Graduate Education (KYLX_0580).

Notes

The authors declare no competing financial interest.

■ REFERENCES

(1) Weber, J. B.; Warren, R. L.; Swain, L. R.; Yelverton, F. H. Physicochemical property effects of three herbicides and three soils on herbicide mobility in field lysimeters. *Crop Prot.* **2007**, *26*, 299−311.

(2) Penmetsa, K. V.; Leidy, R. B.; Shea, D. Analysis of primisulfuron and triasulfuron in water and soil samples by micellar electrokinetic capillary chromatography. *J. Chromatogr., A* **1997**, *766*, 225−231.

(3) Cessna, A. J.; Donald, D. B.; Bailey, J.; Waiser, M.; Headley, J. V. Persistence of the sulfonylurea herbicides thifensulfuron-methyl, ethametsulfuron-methyl, and metsulfuron-methyl in farm dugouts (ponds). *J. Environ. Qual.* **2006**, *35*, 2395−2401.

(4) Yang, L.; Zhao, X.; Zhou, J. Selective enrichment and determination of nicosulfuron in water and soil by a stir bar based on molecularly imprinted polymer coatings. *Anal. Chim. Acta* **2010**, *670*, 72−77.

(5) Barros, J. F. C.; Basch, G.; Carvalho, M. D. Effect of reduced doses of a post-emergence herbicide to control grass and broad-leaved weeds in no-till wheat under Mediterranean conditions. *Crop Prot.* **2007**, *26*, 1538−1545.

(6) Font, N.; Hernández, F.; Hogendoorn, E. A.; Baumann, R. A.; Zoonen, P. V. Microwave-assisted solvent extraction and reversed-phase liquid chromatography−UV detection for screening soils for sulfonylurea herbicides. *J. Chromatogr., A* **1998**, *798*, 179−186.

(7) Chen, Z. L.; Kookana, R. S.; Naidu, R. Determination of sulfonylurea herbicides in soil extracts by solid-phase extraction and capillary zone electrophoresis. *Chromatographia* **2000**, *52*, 142−146.

(8) Mohajeri, S. A.; Hosseinzadeh, H.; Keyhanfar, F.; Aghamohammadian, J. Extraction of crocin from saffron (*Crocus sativus*) using molecularly imprinted polymer solid-phase extraction. *J. Sep. Sci.* **2010**, *33*, 2302−2309.

DOI: 10.1021/jf506239b
J. Agric. Food Chem. 2015, 63, 3634−3645

(9) Sahebnasagh, A.; Karimi, G.; Mohajeri, S. A. Preparation and evaluation of histamine imprinted polymer as a selective sorbent in molecularly imprinted solid-phase extraction coupled with high performance liquid chromatography analysis in canned fish. *Food Anal. Method* **2014**, *7*, 1−8.
(10) Mahony, J. O.; Nolan, K.; Smyth, M. R.; Mizailoff, B. Molecularly imprinted polymers—potential and challenges in analytical chemistry. *Anal. Chim. Acta* **2005**, *534*, 31−39.
(11) Rezaei, B.; Jafari, M. T.; Khademi, R. Selective separation and determination of primidone in pharmaceutical and human serum samples using molecular imprinted polymer-electrospray ionization ion mobility spectrometry (MIP-ESI-IMS). *Talanta* **2009**, *79*, 669−675.
(12) Alizadeh, T.; Akhoundian, M. Promethazine determination in plasma samples by using carbon paste electrode modified with molecularly imprinted polymer (MIP): Coupling of extraction, preconcentration and electrochemical determination. *Electrochim. Acta* **2010**, *55*, 5867−5873.
(13) Núñez, L.; Turiel, E.; Martin−Esteban, A.; Tadeo, J. L. Molecularly imprinted polymer for the extraction of parabens from environmental solid samples prior to their determination by high performance liquid chromatography−ultraviolet detection. *Talanta* **2010**, *80*, 1782−1788.
(14) Chianella, I.; Piletsky, S. A.; Tothill, I. E.; Chen, B.; Tuener, A. P. F. MIP−based solid phase extraction cartridges combined with MIP−based sensors for the detection of microcystin−LR. *Biosens. Bioelectron.* **2003**, *18*, 119−127.
(15) Rostamizadeh, K.; Vahedpour, M.; Bozorgi, S. Synthesis, characterization and evaluation of computationally designed nanoparticles of molecular imprinted polymers as drug delivery systems. *Int. J. Pharm.* **2012**, *424*, 67−75.
(16) Nilsson, J.; Spégel, P.; Nilsson, S. Molecularly imprinted polymer formats for capillary electrochromatography. *J. Chromatogr., B* **2004**, *804*, 3−12.
(17) Alizadeh, T.; Memarbashi, N. Evaluation of the facilitated transport capabilities of nano− and micro−sized molecularly imprinted polymers (MIPs) in a bulk liquid membrane system. *Sep. Purif. Technol.* **2012**, *90*, 83−91.
(18) Blanco-López, M. C.; Lobo-Castanon, M. J.; Miranda-Ordieres, A. J.; Tunon-Blanco, P. Electrochemical sensors based on molecularly imprinted polymers. *Trends Anal. Chem.* **2004**, *23* (1), 36−48.
(19) Alizadeh, T.; Zare, M.; Ganjali, M. R.; Norouzi, P.; Tavana, B. A new molecularly imprinted polymer (MIP)-based electrochemical sensor for monitoring 2, 4, 6-trinitrotoluene (TNT) in natural waters and soil samples. *Biosens. Bioelectron.* **2010**, *25*, 1166−1172.
(20) Zhu, Q. Z.; Haupt, K.; Knopp, D.; Niessner, R. Molecularly imprinted polymer for metsulfuron-methyl and its binding characteristics for sulfonylurea herbicides. *Anal. Chim. Acta* **2002**, *468*, 217−227.
(21) Bastide, J.; Cambon, J. P.; Breton, F.; Piletsky, S. A.; Rouillon, R. The use of molecularly imprinted polymers for extraction of sulfonylurea herbicides. *Anal. Chim. Acta* **2005**, *542*, 97−103.
(22) Fu, X. W.; Wu, Y. J.; Qu, J. R.; Hong, Y. Preparation and utilization of molecularly imprinted polymer for chlorsulfuron extraction from water, soil, and wheat plant. *Environ. Monit. Assess.* **2012**, *184* (7), 4161−4170.
(23) She, Y. X.; Cao, W. Q.; Shi, X. M.; Lv, X.L.; Liu, J. J.; Wang, R. Y.; Jin, F.; Wang, J.; Xiao, H. Class-specific molecularly imprinted polymers for the selective extraction and determination of sulfonylurea herbicides in maize samples by high-performance liquid chromatography−tandem mass spectrometry. *J. Chromatogr., B* **2010**, *878*, 2047−2053.
(24) Yilmaz, E.; Haupt, K.; Mosbach, K. The use of immobilized templates—a new approach in molecular imprinting. *Angew. Chem., Int. Ed.* **2000**, *39* (12), 2115−2118.
(25) Peng, Y.; Xie, Y.; Luo, J.; Nie, L.; Chen, Y.; Chen, L. N.; Du, S. H.; Zhang, Z. P. Molecularly imprinted polymer layer-coated silica nanoparticles toward dispersive solid-phase extraction of trace sulfonylurea herbicides from soil and crop samples. *Anal. Chim. Acta* **2010**, *674*, 190−200.
(26) Qu, J. R.; Zhang, J. J.; Gao, Y. F.; Yang, H. Synthesis and utilisation of molecular imprinting polymer for clean−up of propachlor in food and environmental media. *Food Chem.* **2012**, *135*, 1148−1156.
(27) Miao, S. S.; Wang, H. Z.; Lu, Y. C.; Geng, H. R.; Yang, H. Preparation of Dufulin imprinted polymer on surface of silica gel and its application as solid-phase extraction sorbent. *Environ. Sci.: Processes Impacts* **2014**, *16*, 932−941.
(28) Mehdinia, A.; Dadkhah, S.; Kayyal, T. B.; Jabbari, A. Design of a surface-immobilized 4-nitrophenol molecularly imprinted polymer via pre-grafting amino functional materials on magnetic nanoparticles. *J. Chromatogr., A* **2014**, *1364*, 12−19.
(29) Yadavalli, T.; Ramasamy, S.; Chandrasekaran, G.; Michael, I.; Therese, H. A.; Chennakesavulu, R. Dual responsive PNIPAM−chitosan targeted magnetic nanopolymers for targeted drug delivery. *J. Magn. Magn. Mater.* **2015**, *380*, 315−320.
(30) Jacinto, M. J.; Kiyohara, P. K.; Masunaga, S. H.; Jardim, R. F.; Rossi, L. M. Recoverable rhodium nanoparticles: synthesis, characterization and catalytic performance in hydrogenation reactions. *Appl. Catal., A: general* **2008**, *338*, 52−57.
(31) Zhao, X.; Shi, Y.; Wang, T.; Cai, Y. Q.; Jiang, G. B. Preparation of silica-magnetite nanoparticle mixed hemimicelle sorbents for extraction of several typical phenolic compounds from environmental water samples. *J. Chromatogr., A* **2008**, *1188*, 140−147.
(32) Li, X.; Zhang, B.; Li, W.; Lei, X. F.; Fan, X. L.; Tian, L. Preparation and characterization of bovine serum albumin surface-imprinted thermosensitive magnetic polymer microsphere and its application for protein recognition. *Biosens. Bioelectron.* **2014**, *51*, 261−267.
(33) Lerma-García, M. J.; Zougagh, M.; Ríos, A. Magnetic molecular imprint-based extraction of sulfonylurea herbicides and their determination by capillary liquid chromatography. *Microchim. Acta* **2013**, *180*, 363−370.
(34) Nigam, S.; Barick, K. C.; Bahadur, D. Development of citrate-stabilized Fe_3O_4 nanoparticles: Conjugation and release of doxorubicin for therapeutic applications. *J. Magn. Magn. Mater.* **2011**, *323*, 237−243.
(35) Tan, C. J.; Tong, Y. W. Preparation of superparamagnetic ribonuclease a surface imprinted submicrometer particles for protein recognition in aqueous media. *Anal. Chem.* **2007**, *79* (1), 299−306.
(36) Yao, Q.; Zhou, Y. Synthesis of TiO_2 hybrid molecular imprinted nanospheres linked by silane coupling agent. *J. Inorg. Organomet. Polym.* **2009**, *19*, 466−472.
(37) Dong, W.; Yan, M.; Liu, Z.; Wu, G. S.; Li, Y. M. Effects of solvents on the adsorption selectivity of molecularly imprinted polymers: Molecular simulation and experimental validation. *Sep. Purif. Technol.* **2007**, *53*, 183−188.
(38) Chen, L. N.; Jia, X. J.; Lu, Q.; Peng, Y.; Du, S. H.; Chen, Q. Highly efficient and selective enrichment of puerarin from Radix Puerariae by molecularly imprinted solid-phase extraction. *Sep. Purif. Technol.* **2010**, *71*, 324−330.
(39) Tang, K.; Gu, X.; Luo, Q.; Chen, S. W.; Wu, L. Y.; Xiong, J. H. Preparation of molecularly imprinted polymer for use as SPE adsorbent for the simultaneous determination of five sulphonylurea herbicides by HPLC. *Food Chem.* **2014**, *150*, 106−112.
(40) Vasapollo, G.; Sole, R. D.; Mergola, L.; Lazzoi, M. R.; Scardino, A.; Scorrano, S.; Mele, G. Molecularly imprinted polymers: present and future prospective. *Int. J. Mol. Sci.* **2011**, *12* (9), 5908−5945.
(41) Chang, L.; Chen, S.; Li, X. Synthesis and properties of core-shell magnetic molecular imprinted polymers. *Appl. Surf. Sci.* **2012**, *258*, 6660−6664.
(42) Heidari, H.; Razmi, H. Multi-response optimization of magnetic solid phase extraction based on carbon coated Fe_3O_4 nanoparticles using desirability function approach for the determination of the organophosphorus pesticides in aquatic samples by HPLC−UV. *Talanta* **2012**, *99*, 13−21.
(43) Xiao, D. L.; Dramou, P.; Xiong, N. Q.; He, H.; Yuan, D. H.; Dai, H.; Li, H.; He, X. M.; Peng, J.; Li, N. Preparation of molecularly imprinted polymers on the surface of magnetic carbon nanotubes with a pseudo template for rapid simultaneous extraction of four fluoroquinolones in egg samples. *Analyst* **2013**, *138*, 3287−3296.

DOI: 10.1021/jf506239b
J. Agric. Food Chem. 2015, 63, 3634−3645

(44) Umpleby, R. J., II; Baxter, S. C.; Bode, M.; Berch, J. K., Jr.; Shah, R. N.; Shimizu, K. D. Application of the Freundlich adsorption isotherm in the characterization of molecularly imprinted polymers. *Anal. Chim. Acta* **2001**, *435*, 35−42.
(45) Kong, X.; Gao, R. X.; He, X. W.; Chen, L. X.; Zhang, Y. K. Synthesis and characterization of the core−shell magnetic molecularly imprinted polymers (Fe_3O_4@MIPs) adsorbents for effective extraction and determination of sulfonamides in the poultry feed. *J. Chromatogr., A* **2012**, *1245*, 8−16.
(46) Mohajeri, S. A.; Ebrahimi, S. A. Preparation and characterization of a lamotrigine imprinted polymer and its application for drug assay in human serum. *J. Sep. Sci.* **2008**, *31*, 3595−3602.

DOI: 10.1021/jf506239b
J. Agric. Food Chem. 2015, 63, 3634−3645

may vary dependent upon soil properties, affecting the free concentration of plant-available PFAAs in soil solution.[21,27] Since sorption to soil particles cannot occur in nutrient solution experiments and consequently the well-established leaching of PFAAs in soil must necessarily remain unconsidered, it is possible that the exposure time-dependent uptake of PFAAs by the root surface may be overestimated. In addition, differing sorption characteristics of PFAAs on soil particles depending upon varying chain lengths and functional groups may have an impact on the uptake of PFAAs and consequently on the PFAA distribution pattern.[27] This may, in turn, have an effect upon the resulting accumulation potential of PFAAs in above-ground plant parts. In addition, the time period of exposition to PFAAs, particularly in regard to reproductive parts of plants, is shortened in nutrient solution experiments. To the best of our knowledge, there have not been any systematic studies of the accumulation of different PFAAs in fully mature maize plants. A pot experiment, in which the soil was spiked with PFAAs, was therefore designed to determine whether the soil plays an important role in the uptake of PFAAs by maize. The uptake of a mixture of 10 PFAAs from soil by maize plants was determined for two different concentration levels (0.25 mg/kg and 1.00 mg/kg soil) under controlled conditions in a pot experiment. The mixture of seven perfluoroalkyl carboxylic acids (C4 to C10) and three perfluoroalkyl sulfonic acids (C4, C6, and C8) was selected in order to study the effect of various chemical properties of PFAAs on the uptake and distribution of these molecules in maize. Those properties included different functional groups and chain lengths. A mixture of PFAAs was chosen to mimic real conditions since PFAAs occur in the environment, especially in hot-spot regions, in heterogeneous mixtures, not in the form of isolated single substances. Based on the PFAA concentrations applied in the soil and those measured in maize, the soil-to-plant transfer factors were calculated for each substance in the straw and kernels of maize. The PFAA concentration levels chosen for this study reflect those levels found in the soil of "hot-spot regions" in Germany, including regions in Hesse, North Rhine Westphalia, and Baden-Württemberg.[28−31]

MATERIALS AND METHODS

Chemicals. All standards—perfluoro-*n*-butanoic acid (PFBA), perfluoro-*n*-pentanoic acid (PFPeA), perfluoro-*n*-hexanoic acid (PFHxA), perfluoro-*n*-heptanoic acid (PFHpA), perfluoro-*n*-octanoic acid (PFOA), perfluoro-*n*-nonanoic acid (PFNA), perfluoro-*n*-decanoic acid (PFDA), potassium perfluoro-1-butanesulfonate (PFBS), sodium-perfluoro-1-hexanesulfonate (PFHxS), and sodium-perfluoro-1-octanesulfonate (PFOS) (chemical purity each ≥98%)—as well as mass-labeled internal standards—perfluoro-*n*-[1,2,3,4-$^{13}C_4$]-butanoic acid, perfluoro-*n*-[1,2-$^{13}C_2$]hexanoic acid, perfluoro-*n*-[1,2,3,4-$^{13}C_4$]octanoic acid, perfluoro-*n*-[1,2,3,4,5-$^{13}C_5$]nonanoic acid, perfluoro-*n*-[1,2-$^{13}C_2$]decanoic acid, and sodium perfluoro-1-[1,2,3,4-$^{13}C_4$]octanesulfonate (chemical purity each ≥98%, isotopic purity ≥99%) by Wellington Laboratories (Guelph, Canada)—were obtained from Campro Scientific (Berlin, Germany). Acetonitrile, methanol, and water with a purity of ≥99.97% as well as ammonium acetate were obtained from Biosolve BV (Valkenswaard, Netherlands). QuEChERS-Mix[32] used for cleanup during sample preparation containing $C_6H_5Na_3O_7 \cdot 2H_2O$ (15%) with a purity of ≥9.5%, $MgSO_4$ (62%) with a purity of ≥97.0%, and $C_6H_6Na_2O_7 \cdot 1.5\ H_2O$ (8%) with a purity of ≥99.0% were from Sigma-Aldrich Chemie GmbH (Steinheim, Germany), and NaCl (15%) with a purity of ≥99.5% was obtained from Merck (Darmstadt, Germany). Formic acid with a purity of ≥96.0% from Sigma-Aldrich (Steinheim, Germany) was used in water for conditioning and washing solid phase extraction (SPE) cartridges. Ammonium hydroxide, A.C.S. reagent for eluting PFAAs from cartridges, was obtained from Sigma-Aldrich. Unless otherwise noted, all chemicals and solvents were from Merck, Darmstadt, Germany and from Sigma-Aldrich, Taufkirchen, Germany of the quality, "purum" or "suprapur".[25]

Spiking Solution. The soil for cultivation of maize was spiked by first creating a 1 L stock solution with 10 different PFAAs at a concentration of 200 mg/L of each individual substance. The stock solution was made up of seven perfluoroalkyl carboxylic acids (PFBA, PFPeA, PFHxA, PFHpA, PFOA, PFNA, PFDA) as well as three perfluoroalkyl sulfonic acids (PFBS, PFHxS, PFOS). To improve the solubility of the substances, 220 mL of PFAA-free absolute ethanol (purity 100%) was added to the stock solution, and the PFASs were then dissolved individually beginning with the longer-chain followed by the shorter-chain molecules. PFAA-free ethanol was also added to all of the treatments in order to ensure the same physiological conditions for cultivation of all plants.[25]

Study Design. Maize (*Zea mays* L. cv. Amadeo, Kleinwanzlebener Saatzucht, German plant breeding company) was chosen for the pot experiment. This maize hybrid is suitable for use as grain maize and silage as well as a substrate for biogas plants and has been established as an experimental plant for plant physiology studies by the Institute of Plant Nutrition (Justus Liebig University Giessen, Germany). Each maize plant was cultivated in 12 kg of nutrient-poor subsoil in 12 L Ahr pots. The soil used in the experiment did not contain any PFAAs above the limit of quantification (LOQ) of 1 μg/kg soil and had the following properties: pH 7.2 (in 0.01 M $CaCl_2$), 18% clay, 34% silt, 48% sand (Supporting Information, Table S1). The soil was air-dried at room temperature for 5 days before use, sieved to a particle size <10 mm, and then weighed into the cultivation pots. To ensure an adequate supply of nutrients for the maize plants, 24 g of ground PFAA-free mineral fertilizer (<LOQ of 1 μg/kg) were mixed by hand into the soil (12 kg) in each pot; providing 2.88 g of nitrogen, 1.26 g of phosphorus, 3.36 g of potassium, 0.28 g of magnesium, and 1.44 g of sulfur per pot. After 8 weeks, 5 g of mineral fertilizer was again added to each pot (0.60 g of nitrogen, 0.26 g of phosphorus, 0.70 g of potassium, 0.06 g of magnesium, 0.30 g of sulfur). Additionally, micronutrients were supplied in optimum. The plants were divided into three different treatments. Allocation into the three groups was made 24 days after sowing of maize kernels. In two of the treatments, the soil was spiked with an aqueous solution of PFAA mixture at target concentrations of 0.25 mg and 1.00 mg of the individual substance per kg of soil. The spiking solution consisted of seven PFCAs and three PFSAs (see also Spiking Solution above). A third treatment served as the control. This treatment was not spiked in order to document cross-contamination of PFAAs throughout the entire experiment and sample preparation (blank-value determination). Throughout the experimental period, the moisture level of the soil in all three treatments was maintained at 60% of its maximal water-holding capacity in order to provide the plants with an adequate water supply and to maintain identical levels of moisture in all of the pots. Only deionized, PFAA-free water was used. Four replications per treatment were cultivated to maturity, and after 128 days straw and kernels were harvested. The samples were dried to a steady state in a drying cabinet at 39 °C and ground to a particle size <1.0 mm in a cross beater (hammer) mill (Retsch, Haan, Germany). To avoid cross-contamination during grinding, the mill was rinsed with 20 mL of ethanol (100%) after each use. Homogenized samples of 0.2 g of straw dry weight (DW) and 0.5 g of kernels DW were used in sample preparation for PFAA analysis.

Analytical Method for Plant Material. Samples of 0.2 g (straw) or 0.5 g (kernels) of dried and homogenized plant material (see also Study Design) were spiked with 50 μL of internal standard solution consisting of $^{13}C_4$-perfluorobutanoic acid, $^{13}C_2$-perfluorohexanoic acid, $^{13}C_4$-perfluorooctanoic acid, $^{13}C_5$-perfluorononanoic acid, $^{13}C_2$-perfluorodecanoic acid, and $^{13}C_4$-perfluorooctanesulfonate with a concentration of 100 μg/L and suspended in 2 mL of acetonitrile and 2 mL of water in a centrifuge tube (VWR, Darmstadt, Germany) and were vigorously shaken for 30 s by hand. The tube was then tightly closed and shaken on a mechanical shaker (Heidolph,

DOI: 10.1021/acs.jafc.5b00012
J. Agric. Food Chem. 2015, 63, 3646−3653

Schwabach, Germany) for 30 min. After the addition of 1.5 g of QuEChERS-Mix (see also Chemicals) developed by Anastassiades et al.[32] for the determination of pesticide residues in agricultural products, the sample was again shaken for 30 s by hand and centrifuged for 5 min at 1800*g*. Addition of the salt mixture to the sample resulted in a well-defined phase separation. The organic supernatant was mixed with 2 mL of water before enrichment of PFAAs by solid-phase extraction. Oasis WAX cartridges (60 mg of sorbent, 3 mL cartridge—Waters, Eschborn, Germany) that had been conditioned first with 2 mL of 0.1% formic acid in water (v/v) and then with 2 mL of methanol served as the solid phase. Finally, the organic supernatant mixed with water was applied. The cartridge was then washed first with 2 mL of 2% formic acid in water and then with 2 mL of methanol. Elution of the target components was performed with 2 mL of 0.1% ammonia in methanol (v/v). The extracts were evaporated to dryness at 39 °C under nitrogen gas (biostep, sample concentrator, Jahnsdorf, Germany) and reconstituted with 0.25 mL of methanol/water-mixture (50:50 v/v) by means of a vortex mixer (VWR, Darmstadt, Germany). The sample was then strained through a polyester filter (pore size 0.45 μm, Macherey and Nagel, Düren, Germany) attached to a 2 mL disposable syringe and then transferred to a sample vial. A matrix-free sample (blank value) was prepared and analyzed exactly as were the samples in order to determine any potential background contamination. Analysis was performed using HPLC-tandem mass spectrometry with negative ionization. Data were collected on an Alliance 2695 separation module coupled to a Quattro-Micro tandem-mass spectrometer (Waters, Eschborn, Germany). Separation was performed on a binary gradient of methanol and ammonium acetate solution (2 mM) using a Luna C18 HPLC column, 150 mm × 3 mm, 3 μm particle size (Phenomenex, Aschaffenburg, Germany). Chromatographic separation was performed on a gradient (0.3 mL/min) beginning with 55% solution A (10 mM ammonium acetate in methanol) and 45% solution B (10 mM ammonium acetate in water). The proportion of A increased to 95% in the first 4 min and then further increased from 95% to 98% from 6.5 to 6.6 min and was maintained at 98% from 6.6 min until 10 min. Initial conditions were repeated beginning at the 11th minute. The injected volume was 20 μL.

Statistical Analysis. Data were processed using the IBM SPSS Statistics package (version 20). Significant differences between concentrations of PFAAs in straw and kernels with homogeneous variance were evaluated by single-factor variance analysis (ANOVA) and the Tukey-HSD test. In cases of inhomogeneous variances, the data were first subjected to logarithmic transformation ($\log_{10}(x)$) in order to obtain homogeneous variances. The transformed data were then evaluated by single factor variance analysis and the Tukey-HSD test. The results of the comparison of means were then applied to the original data.

When comparing just two random samples with homogeneous variances, the *t* test was used, and in cases of inhomogeneous variances the Welch test was applied. Variance homogeneity was assessed with the Levene test and was shown to be $p > 0.05$. Soil-to-plant transfer factors (TF) of PFAAs were calculated for straw (eq 1) and kernels (eq 2) as follows:

$$\mathrm{TF}_{\mathrm{straw}} = \frac{\text{PFAA concentration in straw (mg/kg dry weight)}}{\text{PFAA concentration in soil (mg/kg dry weight)}} \quad (1)$$

$$\mathrm{TF}_{\mathrm{kernels}} = \frac{\text{PFAA concentration in kernels (mg/kg dry weight)}}{\text{PFAA concentration in soil (mg/kg dry weight)}} \quad (2)$$

Validation of Methods for Testing Plant Samples. Calibration solutions were prepared with substance concentrations between 0 and 100 μg/L (0, 20, 50, 100 μg/L). Samples that were found to contain higher concentrations than the highest calibration standard were diluted until the concentrations were within the calibration range. Quality assurance was carried out on two samples of our standard quality control plant materials (carrots, wheat) using 10 replicates of each material. As part of the validation of the PFAAs in-house method, quality assurance was carried out on two samples of our standard quality control plant materials (carrots, wheat) using 10 replicates of each sample (Hessian State Laboratory 2011). The concentrations of each of the compounds analyzed in each plant species were below the LOQ of 1 μg/kg. The samples were spiked with 10 μg/kg of each compound to be measured. The absolute recovery rate (mean) ranged between 85% for PFBS (carrots) and 112% for PFHxA (wheat). Coefficient of variation values between 1% (PFOA) and 9% (PFPeA, carrots) were determined (Stahl et al.).[20]

RESULTS AND DISCUSSION

PFAA Concentration of Maize Straw after Soil Spiking with Two Different PFAA Concentrations. *Spiking Concentration 0.25 mg/kg Soil per Individual Substance.* At this spiking level, PFBA exhibited the highest concentration (15 911 μg/kg DW) in maize straw. Concentrations of all PFCAs in the straw decreased significantly with increasing chain length (Figure 1A). Of all the PFSAs tested, PFBS was found at the highest concentration in the straw (962 μg/kg DW). With increasing chain length, PFSA concentrations significantly decreased in maize straw (Figure 1B).

Spiking Concentration 1.00 mg/kg Soil per Individual Substance. Similar to the lower spiking level, at a spiking level of 1.00 mg/kg soil, PFBA was found at the significantly highest level with a mean of 35 233 μg/kg DW in straw (Figure 1C). PFBS was found at a concentration of 1843 μg/kg DW (Figure 1D). Decreasing concentrations of both PFCAs and PFSAs in straw were detected as chain lengths of the PFAAs increased.

Comparison of Both Spiking Levels (0.25 mg and 1.00 mg/kg Soil). All 10 of the PFAAs tested were detected in the maize straw, both in the 0.25 mg and in the 1.00 mg spiked treatment. The PFAA concentrations of straw of the 1.00 mg treatment were always significantly higher than in the 0.25 mg-treated plants (Supporting Information, Figure S1). The concentration ratios of PFAAs (= PFAA $\text{concentration}_{1.00\ \mathrm{mg}}$/PFAA $\text{concentration}_{0.25\ \mathrm{mg}}$) increased with increasing chain length for both PFCAs and PFSAs in straw (Table 1).

PFAA Concentrations of Maize Straw Compared to Results from Other Carryover Experiments. Yoo et al.[33] applied PFAA-contaminated sewage sludge to agricultural soils and obtained results in grass that are comparable to ours. They found higher accumulation potentials for PFHxA, the shortest-chain substance they tested, than for longer-chain PFCAs (C7 to C14). In a nutrient solution experiment, Krippner et al.[25] showed a significantly higher uptake of shorter-chain PFAAs by the roots and a significantly higher translocation in young maize plants than of longer-chain PFAAs.[25] Felizeter et al.[17] also observed increased mobility and translocation of shorter-chain PFAAs within lettuce. The shorter-chain PFAAs accumulated in larger amounts in the above-ground parts of the plants. This finding was confirmed in a study on the basis of foliage-root-concentration factors (FRCF = $[\mathrm{PFAA}]_{\mathrm{foliage}}/[\mathrm{PFAA}]_{\mathrm{root}}$) > 1 for PFBA and PFPeA.[17] In a latter nutrient solution experiment, Felizeter et al.[26] reconfirmed their previous results from lettuce in tomato, cabbage, and zucchini plants. Those distinctly higher concentrations of shorter-chain PFAAs than longer chain molecules in the above-ground parts of plants can consequently be explained in terms of a lower sorption of shorter-chain PFAAs by soil particles[21,27] and thus a greater availability to the plants as well as to a higher mobility and translocation rate within the plants.[17,25,26]

PFAA Concentrations of Maize Kernels after Spiking the Soil with Two Different PFAA Concentrations.

DOI: 10.1021/acs.jafc.5b00012
J. Agric. Food Chem. 2015, 63, 3646−3653

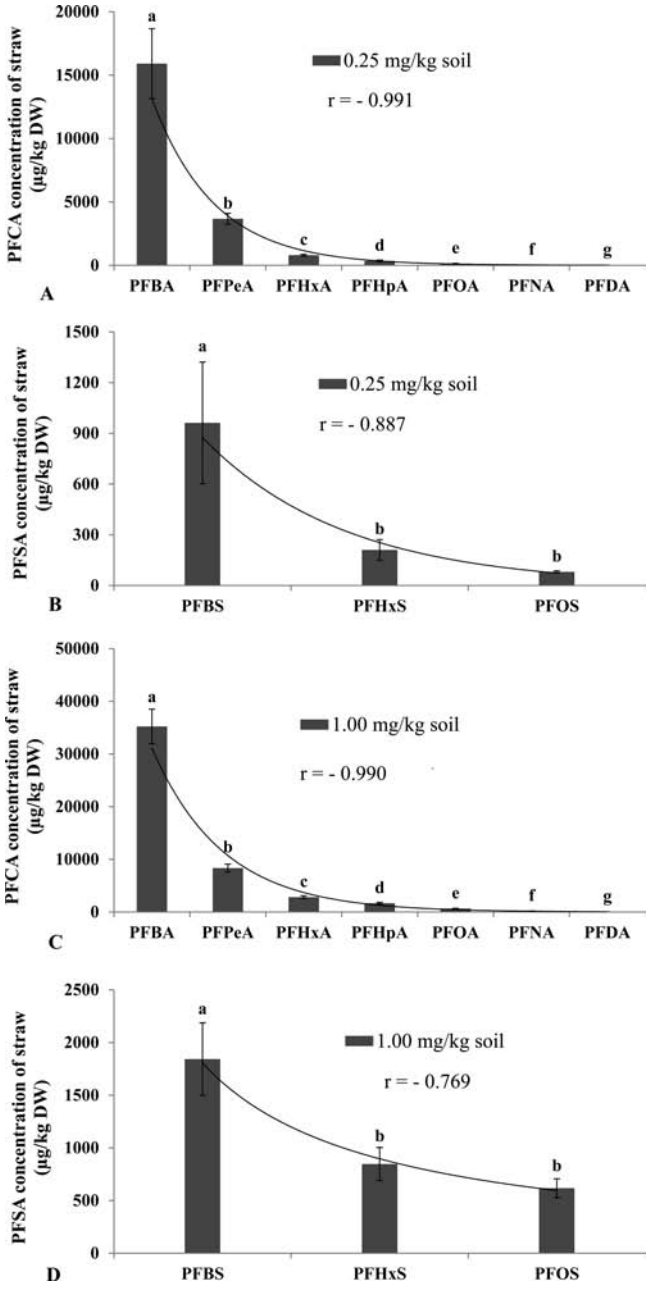

Figure 1. PFCA and PFSA concentrations of maize straw. PFCA (A) and PFSA (B) concentrations of maize straw after spiking the soil with 0.25 mg of the individual substances/kg soil; PFCA (C) and PFSA. (D) Concentrations of maize straw after spiking the soil with 1.00 mg of the individual substance/kg of soil. Paired comparison (Tukey-HSD), $p \leq 0.05$; mean value ($n = 4$) with standard error bars. Letters (a–g) indicate significant differences depending upon chain length; trend line (exponential), r = Spearman rank correlation coefficient; DW = dry weight.

Spiking Concentration 0.25 mg/kg Soil per Individual Substance. Of all PFAAs tested, the shorter-chain PFCAs PFBA, PFPeA, and PFHxA were found at the highest concentrations in maize kernels. The significantly highest concentrations in kernels were measured for PFPeA at 91.4 µg/kg, PFBA at 33.1 µg/kg, and PFHxA at 30.7 µg/kg DW. The concentrations of longer-chain PFCSs (≥C8) in the kernels were below the LOQ of 1 µg/kg DW (Figure 2A). Of all the

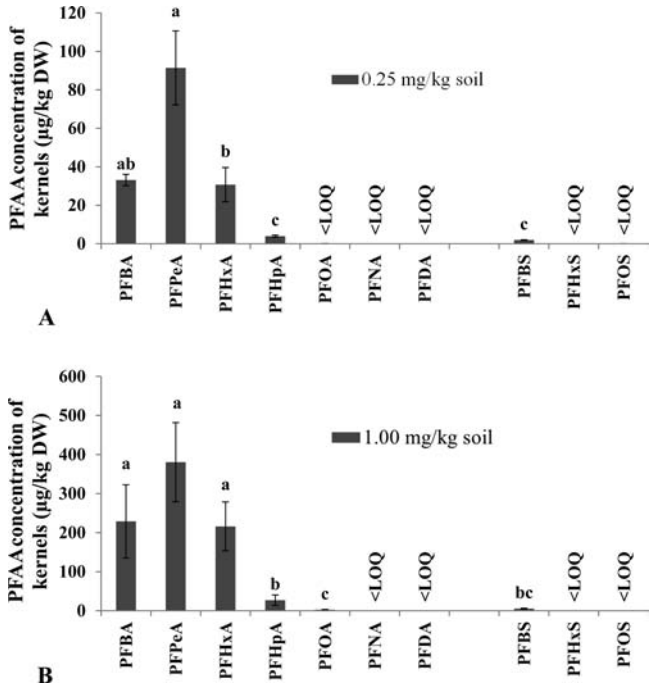

Figure 2. PFCA and PFSA concentrations of maize kernels. PFCA and PFSA concentrations of maize kernels after spiking the soil with (A) 0.25 mg and (B) 1.00 mg of the individual substances per kg of soil. Paired comparison (Tukey-HSD), $p \leq 0.05$; mean ($n = 4$) with standard error bars. Letters (a–c) indicate significant differences among PFAAs; DW = dry weight; LOQ = limit of quantification (1 µg/kg DW).

PFSAs, only PFBS was detected above the LOQ of 1 µg/kg DW in maize kernels, at a concentration of 1.93 µg/kg. At the soil-spiking level of 0.25 mg/kg, the concentrations of PFAAs detected in maize kernels were always lower than those found in the straw (Supporting Information, Table S2).

Spiking Concentration 1.00 mg/kg Soil per Individual Substance. A 4-fold higher spiking concentration resulted in significantly higher concentrations of maize kernels of 228 µg/kg, 380 µg/kg, and 216 µg/kg DW for PFCAs PFBA, PFPeA, and PFHxA compared to 27.1 µg/kg, 2.45 µg/kg and 5.44 µg/kg DW for PFHpA, PFOA, and PFBS.

PFNA and PFDA concentrations were below the LOQ of 1 µg/kg DW. As in the 0.25 mg/kg soil spiked treatment, the only PFSA that was detected in maize kernels above the LOQ

Table 1. PFAA Concentration Ratios of Both Spiking Concentrations (0.25 mg and 1.00 mg/kg soil)[a]

concentration ratio	PFBA	PFPeA	PFHxA	PFHpA	PFOA	PFNA	PFDA	PFBS	PFHxS	PFOS
straw	2.21	2.27	3.53	4.75	4.62	5.48	4.56	1.92	4.03	7.64
kernels	6.91*	4.16	7.03	6.85*				2.82		

[a]Concentration ratio = PFAA concentration$_{1.00mg}$/PFAA concentration$_{0.25mg}$; comparison of means (t test or Welch test). *No significant differences between spiking levels (0.25 mg and 1.00 mg/kg).

DOI: 10.1021/acs.jafc.5b00012
J. Agric. Food Chem. 2015, 63, 3646–3653

(1 μg/kg DW) was PFBS at a concentration of 5.44 μg/kg (Figure 2B). The concentrations of PFAAs in kernels at a spiking concentration of 1.00 mg/kg soil were always significantly lower than the PFAAs concentrations measured in the straw of maize (Supporting Information, Table S2).

Comparison of the Two Spiking Levels (0.25 and 1.00 mg/kg Soil). The spiking of 1.00 mg/kg soil resulted in 4-fold higher PFAA concentrations of maize kernels than concentrations of kernels of maize plants treated with 0.25 mg/kg soil. The concentration of PFHxA was 7-fold higher after spiking with 1.00 mg/kg soil than after spiking with 0.25 mg/kg soil (Table 1). A spiking concentration of 1.00 mg/kg did not result in significantly higher concentrations of PFBA or PFHpA of maize kernels than in 0.25 mg treated maize plants (Supporting Information, Figure S2). With a spiking concentration of 1.00 mg/kg soil, just as with 0.25 mg/kg soil, PFBS was the only PFSA detected above the LOQ of 1 μg/kg DW (Figure 2B). The concentration of PFBS of the kernels after spiking with 1.00 mg/kg soil was 5.44 μg/kg DW and therefore 2.5-fold higher than after spiking with 0.25 mg/kg soil (1.93 μg/kg DW; Table 1). The graphical depiction of individually measured values from every single experimental replication (n = 4 maize plants—evaluation of every individual plant) per spiking concentration shows that in individual maize plants comparable fingerprints of PFCAs existed in their kernels. PFPeA was found at the highest concentrations in maize kernels both after spiking with a concentration of 0.25 mg of the individual substances/kg soil (Figure 3A) and 1.00 mg/kg soil (Figure 3B). At a spiking concentration of 0.25 mg, a significantly lower concentration of PFHxA was found than that of PFPeA and PFBA in the kernels (Figure 3A). At a spiking level of 1.00 mg, no significant differences were found between PFBA, PFPeA, and PFHxA. However, at the lower spiking level, PFPeA tended to result in higher concentrations than PFBA and PFHxA in the kernels (Figure 3B). These data suggest that PFPeA was more translocated into the kernels than the other PFCAs tested (Figure 3B). Due to the small sample size (n = 4), it is presently not possible to confirm the greater mobility of PFPeA over other PFCAs in maize kernels statistically.

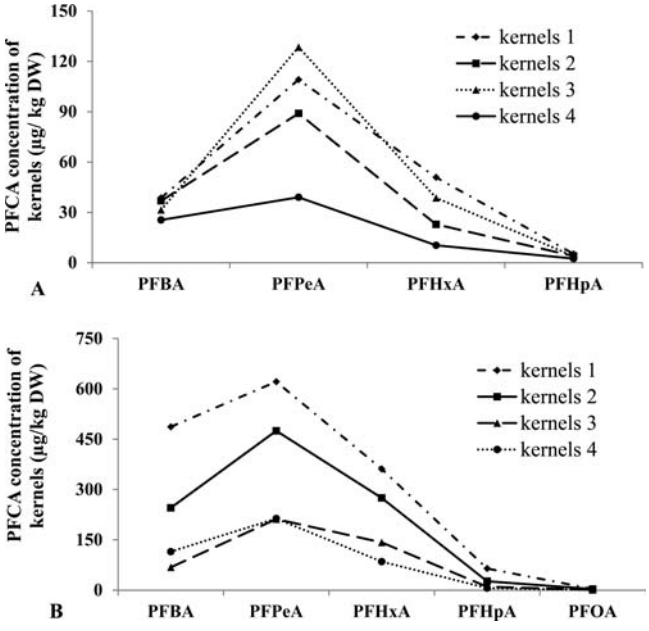

Figure 3. PFCA concentrations of maize kernels for each experimental repetition. PFCA concentrations of maize kernels after spiking the soil with (A) 0.25 mg and (B) 1.00 mg of the individual substances/kg soil in kernels from every maize plant (individual values). DW = dry weight.

PFAA Concentrations of Maize Kernels Compared to Results from Other Carryover Experiments. Only few systematic studies have been carried out on the translocation of PFAAs from soil to generative organs of plants.[18−20] These studies were all limited to the two key compounds, PFOA and PFOS. Stahl et al.[19,20] presented results comparable to those of the present report in a study of the uptake of PFOA and PFOS by the generative organs of various cultivated plants. Those studies showed that PFOA and PFOS concentrations were significantly lower in the kernels than in the vegetative organs of wheat, rye, barley, canola, and maize. Stahl et al.[19] also demonstrated a concentration-dependent carryover of PFOA and PFOS from soil to plants: The higher the soil concentrations of PFOA and PFOS, the higher the plant concentrations. In addition, PFOS concentrations were found to be always lower than PFOA concentrations in plants. Lechner and Knapp[18] also determined in zucchini plants that the concentrations of PFOA and PFOS were substantially lower for generative than for vegetative organs. Studying 14 different PFAAs (C4 to C14), Felizeter et al.[26] performed a study in which nutrient solution was spiked with PFAA concentrations between 0.001 and 1.00 μg/L. The authors showed that the edible-part-concentration factors (ECF = $\log([\mathrm{PFAA}]_{\text{edible part}}/[\mathrm{PFAA}]_{\text{nutrient solution}})$) were highest for short-chain PFAAs in generative plant parts of zucchini and tomato plants and as the chain length of PFCAs and PFSAs increased the ECF decreased. This present study, which represents the first systematic analysis of short-chain PFAAs under natural conditions in soil, demonstrates that shorter-chain PFAAs are also taken up by plants from the soil and are transferred to both vegetative and generative organs. This has, until now, only been shown for PFOA and PFOS.[18−20]

Accumulation potential of PFAAs in Maize Straw and Kernels after Spiking with Two Different PFAA Concentrations. *Soil-to-Plant Transfer Factors for PFAAs in Maize Straw.* Spiking with a concentration of 0.25 mg of the individual substances/kg of soil resulted in a transfer factor (TF_{straw}) of 63.6 for PFBA in the straw, 14.7 for PFPeA, 3.19 for PFHxA, 1.41 for PFHpA, and 3.85 for PFBS. In contrast, the transfer factors for PFOA, PFNA, PFDA, PFHxS, and PFOS were all <1.00. The PFAA transfer from soil to straw decreased with increasing chain length. Spiking with a concentration of 1.00 mg of the individual substances/kg of soil also showed that transfer factors of PFAAs to the straw were lower for molecules with longer chain lengths than for shorter-chained PFAAs (Table 2).

Comparison of the Two Spiking Levels (0.25 and 1.00 mg/kg Soil). Comparison of the two different spiking concentrations of 0.25 mg of the individual substances/kg soil and 1.00 mg of the individual substances/kg soil showed that a 4-fold increase in PFAA concentration in the soil significantly reduced the transfer factor of PFBA in the straw to 35.2 and of PFPeA to 8.33. For PFOS, the 4-fold increase in soil concentration resulted in a significant doubling of the transfer factor from 0.32 to 0.62. For PFHxA, PFHpA, PFOA, PFNA, PFDA, PFBS, and PFHxS, increasing soil concentration to 1.00 mg did not result in a significant change of the soil-to-plant transfer factors. However, increasing the chain length of the PFAAs did show a

DOI: 10.1021/acs.jafc.5b00012
J. Agric. Food Chem. 2015, 63, 3646−3653

Table 2. Transfer Factors of PFCAs and PFSAs in Maize Straw[a]

treatment	PFBA	PFPeA	PFHxA	PFHpA	PFOA	PFNA	PFDA	PFBS	PFHxS	PFOS
0.25 mg/kg	63.64 a	14.68 a	3.19 a	1.41 a	0.56 a	0.12 a	0.03 a	3.85 a	0.84 a	0.32 a
1.00 mg/kg	35.23 b	8.33 b	2.82 a	1.67 a	0.65 a	0.16 a	0.04 a	1.84 a	0.85 a	0.62 b
transfer ratio*	0.55	0.57	0.88	1.18	1.16	1.33	1.33	0.48	1.01	1.94

[a]Transfer factors for PFAAs in maize straw after spiking the soil with 0.25 mg and 1.00 mg of the individual substances/kg soil. Comparison of means (*t* test), $p \leq 0.05$; mean value ($n = 4$). Letters (a, b) indicate significant differences between transfer factors after spiking with two different concentrations. *The relationship of the transfer factors of PFAAs after spiking with 1.00 mg and transfer factors after spiking with 0.25 mg are represented (transfer ratio = PFAA concentration$_{1.00mg}$/PFAA concentration$_{0.25mg}$); LOQ = limit of quantification (1 μg/kg).

Table 3. Transfer Factors of PFCAs and PFSAs in Maize Kernels[a]

treatment	PFBA	PFPeA	PFHxA	PFHpA	PFOA	PFNA	PFOA	PFBS	PFHxS	PFOS
0.25 mg/kg	0.133 a	0.366 a	0.123 a	0.016 a	<LOQ	<LOQ	<LOQ	0.008 a	<LOQ	<LOQ
1.00 mg/kg	0.229 a	0.380 a	0.216 a	0.027 a	0.002	<LOQ	<LOQ	0.005 a	<LOQ	<LOQ
transfer ratio*	1.72	1.04	1.76	1.69				0.63		

[a]Transfer factors for PFAAs in maize kernels after spiking the soil with 0.25 mg and 1.00 mg of the individual substances/kg soil. Comparison of means (*t* test), $p \leq 0.05$; mean value ($n = 4$). Letters (a, b) indicate significant differences between transfer factors after spiking with two different concentrations. *The relationship of the transfer factors of PFAAs after spiking with 1.00 mg and transfer factors after spiking with 0.25 mg are represented (transfer ratio); LOQ = limit of quantification (1 μg/kg).

trend toward increasing transfer ratios (TR = PFAA $TF_{1.00mg}$/PFAA $TF_{0.25mg}$) (Table 2).

Soil-to-Plant Transfer Factors for PFAAs in Maize Kernels. With a spiking concentration of 0.25 mg/kg soil, the transfer factors for kernels ($TF_{kernels}$) were between 0.366 (PFPeA) and 0.008 (PFBS; Table 3). With a spiking concentration of 1.00 mg/kg soil, the transfer factors were between 0.380 (PFPeA) and 0.005 (PFBS). There were no significant differences between transfer factors of PFAAs in maize kernels after spiking at different concentration levels. It was not possible to calculate transfer factors for longer-chain PFCAs and PFSAs since the concentrations in the kernels were below the LOQ of 1 μg/kg DW (Table 3).

Soil-to-Plant Transfer Factors in Maize Straw Compared to Other Carryover Experiments. With calculation from the concentrations of PFOA and PFOS in soil and plants published by Stahl et al.,[19] a spiking level of 0.25 mg of the individual substances/kg soil results in transfer factors for PFOA and PFOS maize straw of $TF_{straw} > 0.27$ (PFOA) and > 0.13 (PFOS) and in maize kernels, $TF_{kernels} = 0.008$ (PFOA). PFOS was not detected in the kernels after spiking the soil with 0.25 mg/kg. At 1.00 mg/kg spiking level, the transfer factors in maize straw (TF_{straw}) for PFOA and PFOS were >0.12 (PFOA) and >0.10 (PFOS) and in kernels, $TF_{kernels}$ was 0.004 (PFOA) and 0.003 (PFOS). TF_{straw} calculated in the present study for PFOA (>0.56) and for PFOS (>0.32) were considerably higher than those reported by Stahl et al.[19] (Table 2). Possible explanations for the differences in PFOA and PFOS in maize straw are differences in maize cultivars and varying cultivation conditions as well as differences in the soil composition.[21] In the present study, just as described by Stahl et al.,[19] only a minimal transfer of PFOA and PFOS into the kernels was observed. PFOS concentrations of the generative organs of the plants were never above the LOQ at either spiking concentration. For PFOA, it was only possible to calculate a transfer factor in the kernels ($TF_{kernels}$) of 0.002 at the 1.00 mg spiking concentration (Table 3) because the amounts of PFOA in the 0.25 mg samples were below the LOQ of 1 μg/kg DW (Figure 2A). From pot experiment results, Lechner and Knapp[18] calculated transfer factors (TF = $[PFAA]_{plant\ (wet\ substance)}$/$[PFAA]_{soil\ (dry\ weight)}$) of PFOA and PFOS in carrots, potatoes, and cucumber grown in soil mixed with PFAAs-contaminated sewage sludge. Levels of contamination in the soil from the sewage sludge reached between 0.28 mg/kg and 0.81 mg/kg soil for PFOA and between 0.01 mg/kg and 0.56 mg/kg soil for PFOS. The highest transfer factors for vegetative plant parts were >0.17 (PFOS) and >0.40 (PFOA). The transfer factors in vegetative plant parts of zucchini plants were TF > 0.76 (PFOA) and > 0.12 (PFOS). Lechner and Knapp[18] calculated transfer factors of TF > 0.03 (PFOA) and TF < 0.01 (PFOS) in generative organs of zucchini plants. When comparing the transfer factors with this study, it must be noted that Lechner and Knapp[18] calculated the transfer factors of PFAA on a fresh weight basis. In a nutrient solution experiment with 14 different PFAAs (C4 to C14), Felizeter et al.[26] showed that the edible-part concentration factors (ECF = log ($[PFAA]_{edible\ part}$/$[PFAA]_{nutrient\ solution}$)) of the shorter-chain PFCAs PFBA, PFPeA, and PFHxA were on average close to 1 in the fruit of zucchini plants and >1 in the fruit of tomato plants after spiking the nutrient solution with PFAA concentrations between 0.01 and 1.00 μg/L. It must be noted, however, that nutrient solution experiments do not reflect field conditions, and the influence of the soil on uptake of PFAAs and its effect on the distribution of PFAAs within the plant are not considered. The subsoil used in the present study was a sandy loam with a low potential cation exchange capacity (CEC_{pot}) of <10 cmol/kg soil and a low organic carbon concentration of C_t < 0.275% (Table S1, Supporting Information). Zhao et al.[21] studied the phytotoxic effect of PFOA and PFOS on Chinese cabbage (*Brassica chinensis*) in different soils and found that the organic matter, followed by the CEC of the soil, has the greatest influence on sorption of PFOA and PFOS. The pH value and the proportion of clay have only minor influence.[21] In addition, climatic influences such as rainfall can alter the distribution of PFAAs in the soil profile. Different chain lengths and functional groups of the PFAAs can result in differences in the degree of leaching along the soil profile so that PFAAs may escape uptake by plant roots.[20] It must also be taken into consideration that, in addition to the soil properties, interactions of PFAAs among one another may occur, in particular when PFAA mixtures are present, and these may influence the sorption in the soil and

DOI: 10.1021/acs.jafc.5b00012
J. Agric. Food Chem. 2015, 63, 3646−3653

finally the uptake via roots and the distribution of PFAAs in maize plants.

Altogether, the results from the present study and the other studies cited here show that PFAAs accumulate to a greater degree in vegetative plant parts and only to a small degree in generative organs. Genotypic and culture-specific differences occur in regard to accumulation in vegetative and generative plant parts. However, the transfer factors for PFOA and PFOS in the generative organs of zucchini are higher than the transfer factors in maize kernels.

Analysis of the results of the present study with different spiking concentrations can be summarized as follows:

- The fingerprints of both spiking levels show that shorter-chain PFAAs predominate both in maize straw as well as in the kernels and are found at the significantly higher concentrations compared to longer-chain molecules.
- A comparison of the spiking concentration levels shows that a 4-fold increase in spiking (1.00 mg of the individual substances/kg soil versus 0.25 mg/kg soil) leads to a 4-fold higher concentration of PFCAs with chain lengths ≥ C6 (PFHxA, PFHpA, PFOA, PFNA, PFDA) and PFSAs with a chain length ≥ C6 (PFHxS, PFOS) in the straw of maize plants.
- In contrast, a 4-fold increase in spiking concentration does not lead to a 4-fold increase of PFBA, PFPeA, or PFBS in the straw, but only to a 2-fold increase.
- For PFOS, however, a 4-fold increase in spiking concentration leads to an 8-fold increase in concentration of the straw.
- Significant differences in concentrations of maize kernels dependent upon spiking concentration could only be shown for PFPeA, PFHxA, and PFBS.
- Regardless of spiking concentration, PFAA concentrations were always significantly lower in the kernels than in the straw.
- Shorter-chain PFAAs (≤C7) have the highest accumulation potentials in above-ground plant parts with transfer factors of >1.00 in straw and >0.01 in kernels.
- Of all the PFAAs tested, PFPeA showed the highest accumulation potential in maize kernels.

The results presented here confirm the results of previous nutrient solution experiments inasmuch as they also show that short-chain PFAAs are particularly mobile under the influence of soil. Shorter-chain PFAAs are preferentially taken up by maize plants from the soil and are stored in above-ground vegetative as well as in generative plant parts. Those molecules consequently exhibit the highest accumulation potentials in maize. Uptake and storage of these substances in above-ground plant parts of maize depend not only on chain length (C4 to C10) but also on the functional group: carboxylate or sulfonate. Significantly lower concentrations of PFCAs and PFSAs are observed with increasing chain length, and as a consequence, short-chain molecules have the highest transfer factors in maize straw and kernels. In addition, PFCAs are always found in higher concentrations than PFSAs in maize. In addition to different rates of uptake, this may be the result of different transport mechanisms for PFCAs and PFSAs from root to kernels, which will be the subject of future studies.

■ ASSOCIATED CONTENT

Supporting Information

Detailed description of the properties of the subsoil used in this study as well as the results of the statistical comparison between concentrations of PFAAs of maize after spiking the soil with different PFAA concentrations. This material is available free of charge via the Internet at http://pubs.acs.org.

■ AUTHOR INFORMATION

Corresponding Author

*Tel.: +49 611 7608532. Fax: +49 611 7608539. E-mail: thorsten.stahl@lhl.hessen.de.

Notes

The authors declare no competing financial interest.

■ ACKNOWLEDGMENTS

Special thanks to our technical staff, Rosa Maria Sobel and Maria Elisabeth Ebel, for their efforts in sample preparation and analysis. We are indebted to Anna Stein for preparation of the graphical abstract. We also wish to thank Barbara Gamb for her assistance in the literature search. We would also like to express our gratitude to Corinna Alles, Helga Tripp, and Lutz Wilming of the Institute of Plant Nutrition at Justus Liebig University Giessen, Germany, for assistance in culturing and harvesting the plants.

■ REFERENCES

(1) The European Parliament and the Council of the European Union. Directive 2006/122/EC of the European Parliament and of the Council of 12 December 2006 on restrictions on the marketing and use of certain dangerous substances and preparations (perfluorooctanesulfonates). *Off. J. Eur. Union* **2006**, *372*, 32−34.

(2) Zhao, Y. G.; Wonga, C. K. C.; Wonga, M. H. Environmental contamination, human exposure and body loadings of perfluorooctane sulfonate (PFOS), focusing on Asian countries. *Chemosphere* **2012**, *89*, 355−368.

(3) Valsecchi, S.; Rusconi, M.; Polesello, S. Determination of perfluorinated compounds in aquatic organisms: A review. *Anal. Bioanal. Chem.* **2013**, *405*, 143−157.

(4) Stahl, T.; Mattern, D.; Brunn, H. Toxicology of perfluorinated compounds. *Environ. Sci. Eur.* **2011**, *23*, 38.

(5) European Food Safety Authority (EFSA). Perfluorooctane sulfonate (PFOS), perfluorooctanoic acid (PFOA) and their salts. *EFSA J.* **2008**, *653*, 1−131.

(6) Gellrich, V.; Brunn, H.; Stahl, T. Perfluoroalkyl and polyfluoroalkyl substances (PFASs) in mineral water and tap water. *J. Environ. Sci. Health, Part A: Toxic/Hazard. Subst. Environ. Eng.* **2013**, *48*, 129−135.

(7) van Asselt, E. D.; Kowalczyk, J.; van Eijkeren, J. C.; Zeilmaker, M. J.; Ehlers, S.; Forst, P.; Lahrssen-Wiederholt, M.; van der Fels-Klerx, H. J. Transfer of perfluorooctane sulfonic acid (PFOS) from contaminated feed to dairy milk. *Food Chem.* **2013**, *141*, 1489−1495.

(8) Hong, S.; Khim, J. S.; Park, J.; Kim, M.; Kim, W.-K.; Jung, J.; Hyun, S.; Kim, J.-G.; Lee, H.; Choi, H. J.; Codling, G.; Giesy, J. P. In situ fate and partitioning of waterborne perfluoroalkyl acids (PFAAs) in the Youngsan and Nakdong River Estuaries of South Korea. *Sci. Total Environ.* **2013**, *445−446*, 136−145.

(9) Cai, M.; Zhao, Z.; Yang, H.; Yin, Z.; Hong, Q.; Sturm, R.; Ebinghaus, R.; Ahrens, L.; Cai, M.; He, J.; Xie, Z. Spatial distribution of per- and polyfluoroalkyl compounds in coastal waters from the East to South China Sea. *Environ. Pollut.* **2012**, *161*, 162−169.

(10) Kwok, K. Y.; Yamazaki, E.; Yamashita, N.; Taniyasu, S.; Murphy, M. B.; Horii, Y.; Petrick, G.; Kallerborn, R.; Kannan, K.; Murano, K.; Lam, P. K. S. Transport of Perfluoroalkyl substances (PFAA) from an arctic glacier to downstream locations: Implications for sources. *Sci. Total Environ.* **2013**, *447*, 46−55.

(11) Del Vento, S.; Halsall, C.; Gioia, R.; Jones, K.; Dachs, J. Volatile per− and polyfluoroalkyl compounds in the remote atmosphere of the western Antarctic Peninsula: An indirect source of perfluoroalkyl acids to Antarctic waters? *Atmos. Pollut. Res.* **2013**, *3*, 450−455.

DOI: 10.1021/acs.jafc.5b00012
J. Agric. Food Chem. 2015, 63, 3646−3653

(12) Zhang, W.; Zhang, Y.; Taniyasu, S.; Yeung, L. W. Y.; Lam, P. K. S.; Wang, J.; Li, X.; Yamashita, N.; Dai, J. Distribution and fate of perfluoroalkyl substances in municipal wastewater treatment plants in economically developed areas of China. *Environ. Pollut.* **2013**, *176*, 10−17.
(13) Stahl, T.; Gellrich, V.; Brunn, H. PFC contamination of groundwater and drinking water. *Water Waste*, Special Edition, **2012**, 18−20.
(14) Gomez-Canela, C.; Barth, J. A. C.; Lacorte, S. Occurrence and fate of perfluorinated compounds in sewage sludge from Spain and Germany. *Environ. Sci. Pollut. Res.* **2012**, *19*, 4109−4119.
(15) Kim, S. K.; Im, J. K.; Kang, Y. M.; Jung, S. Y.; Kho, Y. L.; Zoh, K. D. Wastewater treatment plants (WWTPs)-derived national discharge loads of perfluorinated compounds (PFCs). *J. Hazard. Mater.* **2012**, *201*−*202*, 82−91.
(16) Lin, A. Y.; Panchangam, S. C.; Ciou, P. S. High levels of perfluorochemicals in Taiwan's wastewater treatment plants and downstream rivers pose great risk to local aquatic ecosystems. *Chemosphere* **2010**, *80*, 1167−1174.
(17) Felizeter, S.; McLachlan, M. S.; de Voogt, P. Uptake of perfluorinated alkyl acids by hydroponically grown lettuce (*Lactuca sativa*). *Environ. Sci. Technol.* **2012**, *46*, 11735−11743.
(18) Lechner, M.; Knapp, H. Carryover of perfluorooctanoic acid (PFOA) and perfluorooctanesulfonate (PFOS) from soil to plant and distribution to the different plant compartments studied in cultures of carrots (*Daucus carota* ssp. sativus), potatoes (*Solanum tuberosum*), and cucumbers (*Cucumis sativus*). *J. Agric. Food Chem.* **2011**, *59*, 11011−11018.
(19) Stahl, T.; Heyn, J.; Thiele, H.; Hüther, J.; Failing, K.; Georgii, S.; Brunn, H. Carryover of perfluorooctanoic acid (PFOA) and perfluorooctane sulfonate (PFOS) from soil to plants. *Arch. Environ. Contam. Toxicol.* **2009**, *57*, 289−298.
(20) Stahl, T.; Riebe, R. A.; Falk, S.; Failing, K.; Brunn, H. A long-term lysimeter experiment to investigate the leaching of perfluoroalkyl substances (PFAAs) and the carryover from soil to plants − Results of a pilot study. *J. Agric. Food Chem.* **2013**, *61*, 1784−1793.
(21) Zhao, H.; Chen, C.; Zhang, X.; Chen, J.; Quan, X. Phytotoxicity of PFOS and PFOA to *Brassica chinensis* in different Chinese soils. *Ecotoxicol. Environ. Saf.* **2011**, *74*, 1343−1347.
(22) Kowalczyk, J.; Ehlers, S.; Forst, P.; Schafft, H.; Lahrssen-Wiederholt, M. Transfer of perfluorooctanoic acid (PFOA) and perfluorooctane sulfonate (PFOS) from contaminated feed into milk and meat of sheep: Pilot study. *Arch. Environ. Contam. Toxicol.* **2012**, *63*, 288−298.
(23) Kowalczyk, J.; Ehlers, S.; Oberhausen, A.; Tischer, M.; Forst, P.; Schafft, H.; Lahrssen-Wiederholt, M. Absorption, distribution, and milk secretion of the perfluoroalkyl acids PFBS, PFHxS, PFOS, and PFOA by dairy cows fed naturally contaminated feed. *J. Agric. Food Chem.* **2013**, *61*, 2903−2912.
(24) Van Asselt, E. D.; Kowalczyk, J.; van Eijkeren, J. C.; Zeilmaker, M. J.; Ehlers, S.; Forst, P.; Lahrssen-Wiederholt, M.; van der Fels-Klerx, H. J. Transfer of perfluorooctane sulfonic acid (PFOS) from contaminated feed to dairy milk. *Food Chem.* **2013**, *141*, 1489−1495.
(25) Krippner, J.; Brunn, H.; Falk, S.; Georgii, S.; Schubert, S.; Stahl, T. Effects of chain length and pH on the uptake and distribution of PFAAs in maize (*Zea mays*). *Chemosphere* **2014**, *94*, 85−90.
(26) Felizeter, S.; McLachlan, M. S.; de Voogt, P. Root uptake and translocation of perfluorinated alkyl acids by three hydroponically grown crops. *J. Agric. Food Chem.* **2014**, *62*, 3334−3342.
(27) Higgins, C. P.; Luthy, R. G. Sorption of perfluorinated surfactants on sediments. *Environ. Sci. Technol.* **2006**, *40*, 7251−7256.
(28) Weinfurtner, K.; Kördel, W.; Bücking, M. Untersuchungen zum Übergang aus PFT-belasteten Böden in Pflanzen. *Bodenschutz* **2008**, *3/08*, 88−92.
(29) State Agency for Nature, Environment and Consumer Protection in North Rhine-Westphalia. *Perfluorinated tenside soil testing of crop land exposed to the "GW Umwelt" waste mixture in North Rhine-Westphalia*. (http://www.lanuv.nrw.de/boden/pft_boden.htm) (accessed 2/28/2015).
(30) Hessian State Office of the Environment and Geology (HLUG). *Perfluorinated Chemicals (PFC) in Hesse. Research program of the HLUG*; HLUG: Wiesbaden, Germany, 2010; ISBN 978-3-89026-363-9.
(31) Press information: Department of the Environment Baden-Württemberg. Perfluorinated tensides (PFT) in effluent sludge in Baden-Württemberg − Background − Results − Perspectives. Press conference from August 3, 2007, Stuttgart.
(32) Anastassiades, M.; Lehotay, S. J.; Stajnbaher, D.; Schenck, F. J. Fast and easy multiresidue method employing acetonitrile extraction/partitioning and "dispersive solid-phase extraction" for the determination of pesticide residues in produce. *J. AOAC Int.* **2003**, *86*, 412−431.
(33) Yoo, H.; Washington, J. W.; Jenkins, T. M.; Ellington, J. J. Quantitative determination of perfluorochemicals and fluorotelomer alcohols in plants from biosolid-amended fields using LC/MS/MS and GC/MS. *Environ. Sci. Technol.* **2011**, *45*, 7985−7990.

DOI: 10.1021/acs.jafc.5b00012
J. Agric. Food Chem. 2015, 63, 3646−3653

Ion leakage was measured with a conductivity meter (DDS-11A, Shanghai, China) according to our previous method.[14] Ion leakage was expressed as relative conductivity. MDA content was measured according to the method of Hodges et al.,[19] and the result was expressed as nanomoles per gram of fresh weight (FW).

GB Content and BADH Activity Measurement. For GB content measure, 10 g of tissue sample was homogenized with 20 mL of methanol−chloroform extraction buffer (60% methanol, 25% chloroform) and then centrifuged at 10000*g* for 20 min at 4 °C. The aqueous phase was purified by an anionic resin (Dowex AG1 OH^-, 200−400 mesh, Dow Chemical Co., Midland, MI, USA). The GB fraction was eluted with 6 mol L^{-1} NH_4OH and then dried under nitrogen at 45 °C. The residue was dissolved with 2 mL of methanol. The GB content was assayed using high-performance liquid chromatography (Agilent 1100, Agilent Corp., Santa Clara, CA, USA) according to the method of Bessieres et al.[20] GB content was expressed as micrograms per gram of FW.

BADH activity was assayed according to the method of Arakawa et al.[21] with some modification. Ten grams of tissue sample was homogenized with 20 mL of 0.2 mmol L^{-1} potassium phosphate buffer (pH 7.4) and centrifuged at 13000*g* for 20 min at 4 °C. The assay mixture consisted of 0.5 mL of crude enzyme extract, 2.9 mL of 0.2 mmol L^{-1} potassium phosphate buffer (pH 7.4), and 0.5 mL of 10 mmol L^{-1} betaine aldehydede. One unit of BADH activity was defined as an increase of 0.01 in absorbance per minute at 340 nm.

Energy Metabolism Enzyme Assays. Crude mitochondria of loquat fruit samples were extracted for enzyme assay. H^+-ATPase and Ca^{2+}-ATPase activities were measured using our previous method.[16] One unit of H^+-ATPase and Ca^{2+}-ATPase activities was defined as the release of 1 μmol of phosphorus per minute under the assay conditions. Succinic dehydrogenase (SDH) activity was measured according to the method of Ackrell et al.[22] One unit of SDH activity was defined as an increase of 0.01 of absorbance at 600 nm per minute. CCO activity was measured according to our previous method.[16] One unit of CCO activity was defined as an increase of 0.1 of absorbance at 510 nm per minute.

ATP, ADP, and AMP Contents and Energy Charge (EC) Measurements. To analyze energy status, 2 g of loquat flesh tissue was ground with 5 mL of 0.6 mol L^{-1} perchloric acid. ATP, ADP, and AMP assays used high-performance liquid chromatography (Agilent 1100) according to the Jin et al.[16] method. ATP, ADP, and AMP contents were expressed as micrograms per gram of FW. EC was calculated using the formula EC = [ATP + 0.5 × ADP]/[ATP + ADP + AMP].

Protein Assay. Protein content of enzyme was measured using the Bradford[23] method. Specific activity of enzymes was expressed as units per milligram of protein.

Statistical Analysis. These experiments were carried out using a completely randomized design. Each treatment in the study was replicated three times. The experiment was carried out for twice and got the similar results. The data were from one experiment and expressed as the mean ± SE (standard error) of three replications. All statistical analyses were performed using SPSS software (version 14.0, SPSS Inc., Chicago, IL, USA). Data were analyzed by one-way analysis of variance. Mean separations were compared by Duncan's multiple-range tests. Differences at $p < 0.05$ were considered as significant.

RESULTS

Effect of LTC Treatment on CI, Ion Leakage, and MDA Content in Loquat Fruit. CI usually develops in loquat fruit during cold storage for a long time. Flesh internal browning was the most obvious symptom of CI in loquat (shown in the Tabove of Contents graphic). The CI index increased gradually after the first week in cold-stored loquat fruit. LTC treatment significantly ($p < 0.05$) inhibited CI increase during storage. As shown in Figure 1, CI index values were 57.3 and 36.2% lower in LTC-treated loquat than in control fruit in the third and fifth weeks, respectively. Ion leakage and MDA content in loquat fruit increased with storage time, which was associated with CI development during cold storage. The increasing tendencies of ion leakage and MDA were significantly ($p < 0.05$) prevented by LTC (Figure 2).

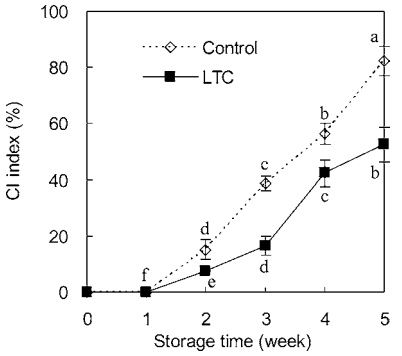

Figure 1. Effect of LTC treatment on CI index of loquat fruit during cold storage. Data are expressed as the mean of triplicate samples ± standard errors. Vertical bars represent the standard errors of the means. Significant differences are shown by different letters.

Effect of LTC Treatment on GB Content and BADH Activity in Loquat Fruit. The content of GB in control fruit decreased steadily during the whole storage time (Figure 3B). LTC treatment increased GB content after the first week in loquat fruit. GB contents were 30.1 and 27.5% higher in LTC-treated fruit than in control fruit in the third and fifth weeks, respectively. BADH activity increased until the third week and decreased slowly afterward in control fruits. LTC treatment significantly ($p < 0.05$) increased the activity of BADH during the whole storage time, which was 69.2% higher than in control loquat fruit at the end of storage.

Effect of LTC Treatment on Energy Metabolism Enzyme Activities in Loquat Fruit. H^+-ATPase and Ca^{2+}-ATPase activities decreased gradually during the whole storage time. LTC treatment significantly ($p < 0.05$) increased the activities of H^+-ATPase and Ca^{2+}-ATPase activities after the first week (Figure 4A,B). SDH activity increased until the second week and then decreased rapidly in control fruit. LTC treatment maintained higher activity of SDH, which was 32.7% higher than that in control loquat fruit at the end of the storage (Figure 4C). CCO activity declined slowly with storage time. LTC treatment could prevent the decrease of CCO activity in loquat fruit (Figure 4D).

Effect of LTC Treatment on Energy Status in Loquat Fruit. ATP content declined gradually with storage time, whereas ADP content increased mildly until the first week and decreased rapidly after the second week (Figure 5). In general, LTC treatment maintained higher contents of ATP and ADP in comparison with the control fruit. AMP content increased gradually in control loquat during the whole storage time. The increasing tendency was significantly ($p < 0.05$) prevented by LTC treatment during the whole storage time except the fourth week. According to the difference in ATP and ADP contents, energy charge in loquat fruit decreased during storage. LTC treatment maintained the high level of energy charge in loquat fruit.

DISCUSSION

LTC is a useful technique to maintain quality and reduce CI in postharvest industry of fruit and vegetables. Increasing evidence has shown that CI symptoms were alleviated in avocado,

DOI: 10.1021/acs.jafc.5b00605
J. Agric. Food Chem. 2015, 63, 3654−3659

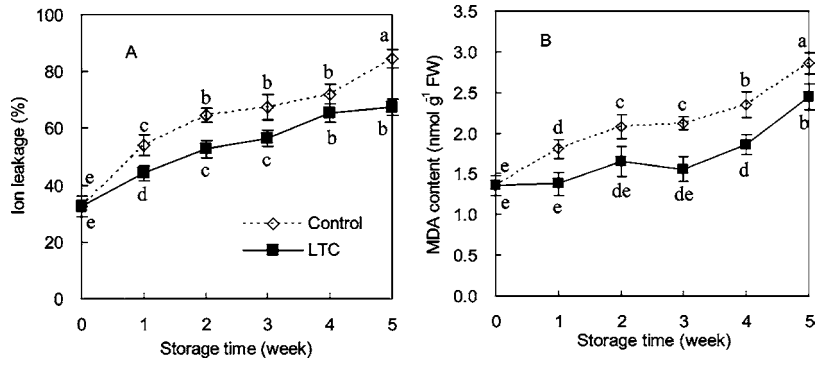

Figure 2. Effect of LTC treatment on ion leakage (A) and MDA content (B) of loquat fruit during cold storage. Data are expressed as the mean of triplicate samples ± standard errors. Vertical bars represent the standard errors of the means. Significant differences are shown by different letters.

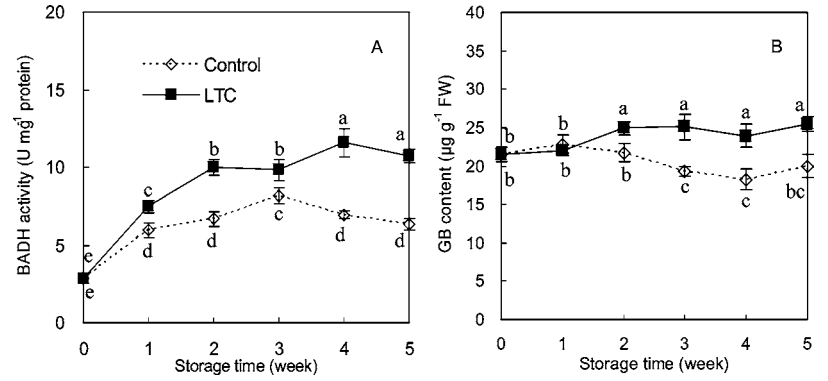

Figure 3. Effect of LTC treatment on BADH activity (A) and GB content (B) of loquat fruit during cold storage. Data are expressed as the mean of triplicate samples ± standard errors. Vertical bars represent the standard errors of the means. Significant differences are shown by different letters.

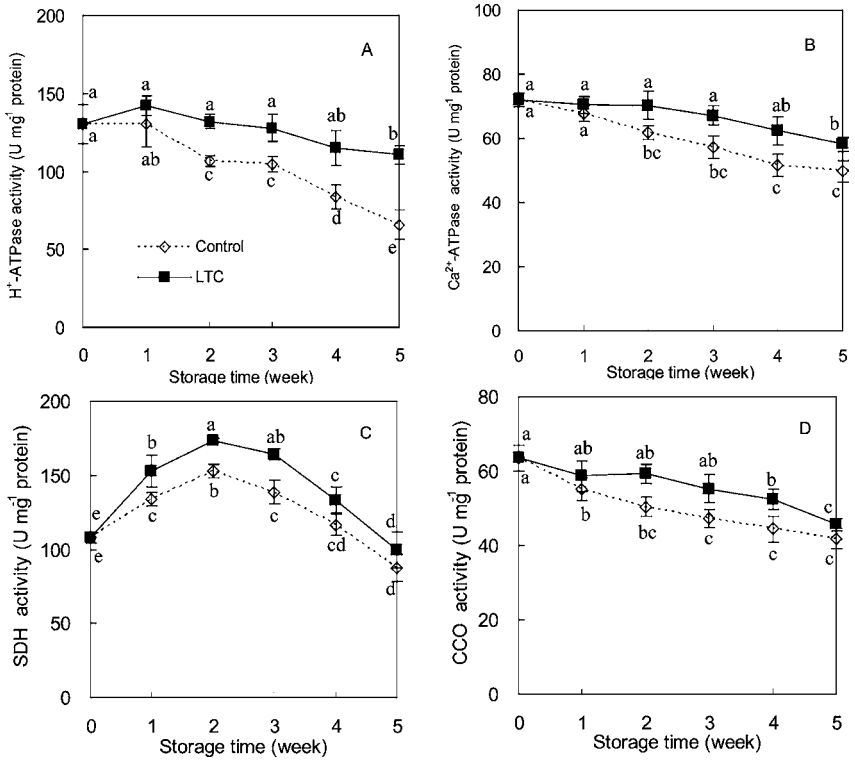

Figure 4. Effect of LTC treatment on activities of H^+-ATPase (A), Ca^{2+}-ATPase (B), SDH (C), and CCO (D) of loquat fruit during cold storage. Data are expressed as the mean of triplicate samples ± standard errors. Vertical bars represent the standard errors of the means. Significant differences are shown by different letters.

DOI: 10.1021/acs.jafc.5b00605
J. Agric. Food Chem. 2015, 63, 3654−3659

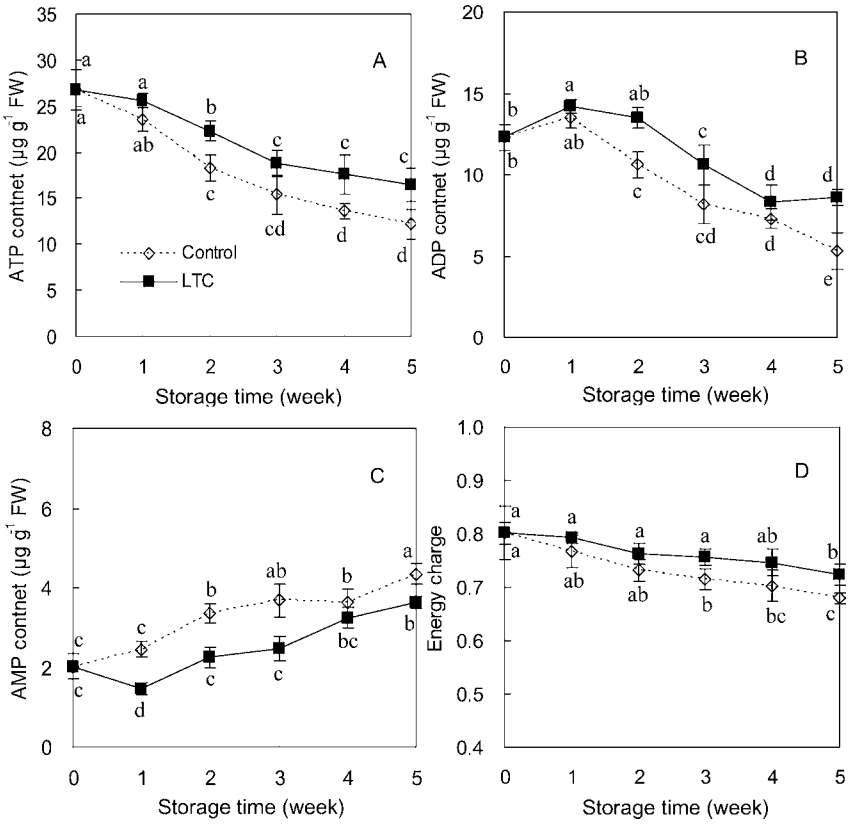

Figure 5. Effect of LTC treatment on contents of ATP (A), ADP (B), AMP (C), and energy charge (D) of loquat fruit during cold storage. Data are expressed as the mean of triplicate samples ± standard errors. Vertical bars represent the standard errors of the means. Significant differences are shown by different letters.

zucchini squash, and sweet potatoes by LTC treatment.[24] As to loquat fruit, Cai et al.[5] reported that 'Luoyangqing' loquats conditioned at 5 °C for 6 days had better quality and lower CI symptoms than control fruits. Our previous study found that conditioning at 10 °C for 6 days could be the optimum condition for 'Jiefangzhong' loquat. This different temperature condition for pretreatment is probably due to the different loquat cultivar response to low-temperature stress. The beneficial effects of LTC have been attributed to enhancing antioxidant system, reducing electrolyte leakage, and inducing lipid membrane unsaturation.

Moreover, LTC induced chilling tolerance by regulating the expression of transcripts related to secondary metabolism, hormone biosynthesis, and transcription factors.[25] Our study provided new evidence that LTC alleviated CI in cold-stored loquat fruit associated with accumulation of GB and energy status.

It has been indicated that GB accumulates in some plants responding to environmental stresses, including low temperature, water stress, or drought.[6] Some plants accumulate small molecular substances with cryoprotectant activity against cold stress. Glycine betaine is one of several such osmotic adjustment substances that has a protective function to proteins and enzyme activities and even stabilizes membranes under environmental stresses.[8] Previous evidence has suggested that there is a correlation between GB content and cold tolerance in higher plants. For example, endogenous GB was accumulated by cold acclimation treatment, which induced freezing tolerance in *Arabidopsis*.[7] Similarly, tolerance to low temperatures was also improved in tomato plant GB treatment.[26] In addition, Rajashekar et al.[9] found that exogenous abscisic acid treatment induced cold tolerance and improved freezing survival and regrowth in whole strawberry plants, which triggered endogenous GB accumulation. In our study, GB accumulation was associated with CI development in loquat fruit during cold storage. LTC treatment significantly reduced CI and a maintained higher level of GB content than those in control fruits. These results suggest that the accumulation of GB might contribute to the reduced CI in loquat fruits treated with LTC.

BADH is the key enzyme that plays the important role during GB metabolism. It had been reported that heat treatment resulted in a high expression of BADH gene in transgenic tomato, which was correlated with up-regulated GB accumulation.[27] Yang et al.[28] found that GB accumulation as a result of the introduction of the BADH gene into tobacco enhances the tolerance against high-temperature stress. Chen et al.[29] obtained similar results in maize, which indicated that GB accumulation caused by cold stress was associated with an increase in BADH activity. Our study showed that treatment with LTC maintained higher activity of BADH in loquat fruit. The decline of BADH activity in control fruit after the third week was possibly due to the senescence of loquat fruit, which may account for the low level of GB content. This suggested that the accumulation of GB in LTC-treated loquat fruit could be due to increased activity of BADH, the key enzyme involved in GB biosynthesis. It is worth mentioning that GB plays an important physiological role in stress tolerance involved in osmotic regulation, detoxication of reactive oxygen radicals, and protection of membrane integrity. These results indicated that

DOI: 10.1021/acs.jafc.5b00605
J. Agric. Food Chem. 2015, 63, 3654−3659

LTC induced cold tolerance of loquat due in part to regulating endogenous GB metabolism.

Energy supply in cells plays an important role in controlling fruit ripening, senescence, and physiological disorder after harvest.[11] Many studies have suggested that postharvest CI symptoms of various kinds of fruits, such as pears,[12] litchis,[13] longans,[30] and peaches,[14] mainly resulted from membrane damage related to the energy deficit under cold stress. In the present study, LTC treatment effectively maintained high levels of ATP and energy charge and reduced CI in cold-stored loquat fruit. Moreover, activities of energy metabolism enzymes were significantly higher in loquat fruits treated with LTC than in control fruits. This suggests that these enzymes played positive roles in the process of energy production. Similar results were also found in peach fruit in our previous study.[31] ATP and energy might play important roles in cell membrane protection and fatty acid biosynthesis. Under stress conditions, stress-resistant cultivars could maintain higher energy levels, resulting in a decrease in membrane leakage. Thus, our results indicated that LTC could enhance chilling tolerance in cold-stored loquat fruit by means of enhancing energy accumulation, preventing ion leakage increase, and protecting membrane function.

In conclusion, the results of this work suggest that treatment with LTC decreased CI in loquat fruit contributed to enhancing endogenous GB content and energy status. The GB accumulation plays an important role in enhancing cold tolerance in loquat fruit by LTC treatment, which was attributed to increasing BADH activity. Furthermore, the reduction of CI by LTC treatment may be due to induced enzyme activity related to energy metabolism. However, further studies are needed to evaluate other related enzyme activities and gene expression involved in metabolism of GB or energy.

AUTHOR INFORMATION

Corresponding Author

*(Y.Z.) Phone: +86-25-84399080. Fax: +86-25-84395618. E-mail: zhengyh@njau.edu.cn.

Funding

This study was supported by the National Natural Science Foundation of China (No. 31000824 and 31371862), the Jiangsu Provincial Scientific and Technical Supporting Program (SBE201330109), and the Qinglan Project of Jiangsu Province.

Notes

The authors declare no competing financial interest.

REFERENCES

(1) Zheng, Y. H.; Li, S. Y.; Xi, Y. F. Changes of cell wall substances in relation to flesh woodiness in cold-stored loquat fruits. *Acta Phytophysiol. Sin.* **2000**, *26*, 306−310.

(2) Hofman, P. J.; Stubbings, B. A.; Adkins, M. F.; Corcoran, R. J.; White, A.; Woolf, A. B. Low temperature conditioning before cold disinfestation improves 'Hass' avocado fruit quality. *Postharvest Biol. Technol.* **2003**, *28*, 123−133.

(3) Maul, P.; McCollum, G.; Guy, C. L.; Porat, R. Temperature conditioning alters transcript abundance of genes related to chilling stress in 'Marsh' grapefruit flavedo. *Postharvest Biol. Technol.* **2011**, *60*, 177−185.

(4) Jin, P.; Wang, K.; Shang, H.; Tong, J.; Zheng, Y. H. Low-temperature conditioning combined with methyl jasmonate treatment reduces chilling injury of peach fruit. *J. Sci. Food Agric.* **2009**, *89*, 1690−1696.

(5) Cai, C.; Xu, C. J.; Shan, L. L.; Li, X.; Zhou, C. H.; Zhang, W. S.; Ferguson, I.; Chen, K. S. Low temperature conditioning reduces postharvest chilling injury in loquat fruit. *Postharvest Biol. Technol.* **2006**, *41*, 252−259.

(6) Ashraf, M.; Foolad, M. R. Roles of glycine betaine and proline in improving plant abiotic stress resistance. *Environ. Exp. Bot.* **2007**, *59*, 206−216.

(7) Xing, W.; Rajashekar, C. B. Glycine betaine involvement in freezing tolerance and water stress in *Arabidopsis thaliana*. *Environ. Exp. Bot.* **2001**, *46*, 21−28.

(8) Sakamoto, A.; Murata, N. The role of glycine betaine in the protection of plants from stress: clues from transgenic plants. *Plant, Cell Environ.* **2002**, *25*, 163−171.

(9) Rajashekar, C. B.; Zhou, H.; Marcum, K. B.; Prakash, O. Glycine betaine accumulation and induction of cold tolerance in strawberry plants. *Plant Sci.* **1999**, *148*, 175−183.

(10) Sun, Y. J.; Jin, P.; Shan, T. M.; Xu, J.; Zheng, Y. H. Effect of glycine betaine treatment on postharvest chilling injury and active oxygen metabolism in loquat fruits. *Food Sci.* **2014**, *35*, 210−215 (in Chinese with English abstract).

(11) Jiang, Y. M.; Jiang, Y. L.; Qu, H. X.; Duan, X. W.; Luo, Y. B.; Jiang, W. B. Energy aspects in ripening and senescence of harvested horticultural crops. *Stewart Postharvest Rev.* **2007**, *4*, 1−5.

(12) Saquet, A. A.; Streif, J.; Bangerth, F. Energy metabolism and membrane lipid alterations in relation to brown heart development in 'Conference' pears during delayed controlled atmosphere storage. *Postharvest Biol. Technol.* **2003**, *30*, 123−132.

(13) Song, L. L.; Jiang, Y. M.; Gao, H. Y.; Li, C. T.; Liu, H.; You, Y. L. Effects of adenosine triphosphate on browning and quality of harvested litchi fruit. *Am. J. Food Technol.* **2006**, *1*, 173−178.

(14) Jin, P.; Zhu, H.; Wang, L.; Shan, T. M.; Zheng, Y. H. Oxalic acid alleviates chilling injury in peach fruit by regulating energy metabolism and fatty acid contents. *Food Chem.* **2014**, *161*, 87−93.

(15) Zhou, Q.; Zhang, C. L.; Cheng, S. C.; Wei, B. D.; Liu, X. Y.; Ji, S. J. Changes in energy metabolism accompanying pitting in blueberries stored at low temperature. *Food Chem.* **2014**, *164*, 493−501.

(16) Jin, P.; Zhu, H.; Wang, J.; Chen, J. J.; Wang, X. L.; Zheng, Y. H. Effect of methyl jasmonate on energy metabolism in peach fruit during chilling stress. *J. Sci. Food Agric.* **2013**, *93*, 1827−1832.

(17) Azevedo, I. G.; Oliveira, J. G.; da Silva, M. G.; Pereira, T.; Correa, S. F.; Vargas, H. P-type H^+-ATPases activity, membrane integrity, and apoplastic pH during papaya fruit ripening. *Postharvest Biol. Technol.* **2008**, *48*, 242−247.

(18) Cao, S.; Zheng, Y.; Wang, K.; Jin, P.; Rui, H. Methyl jasmonate reduces chilling injury and enhances antioxidant enzyme activity in postharvest loquat fruit. *Food Chem.* **2009**, *115*, 1458−1463.

(19) Hodges, D. M.; Delong, J. M.; Forney, C.; Prange, R. K. Improving the thiobarbituric acid reactive-substances assay for estimating lipid peroxidation in plant tissue containing anthocyanin and other interfering compounds. *Planta* **1999**, *207*, 604−611.

(20) Bessieres, M. A.; Gibon, Y.; Lefeuvre, J. C.; Larher, F. A single-step purification for glycinebetaine determination in plant extracts by isocratic HPLC. *J. Agric. Food Chem.* **1999**, *47*, 3718−3722.

(21) Arakawa, K.; Katkyama, M.; Takabe, T. Levels of betain and betaine aldehyde dehydrogenase activity in green leaves and etiolated leaves and roots of barley. *Plant Cell Physiol.* **1990**, *31*, 797.

(22) Ackrell, B. A.; Keamery, E. B.; Singer, T. P. Mammalian succinate dehydrogenase. *Methods Enzymol.* **1978**, *53*, 466−483.

(23) Bradford, M. M. A rapid and sensitive method for the quantitation of microgram quantities of protein utilizing the principle of protein dye binding. *Anal. Biochem.* **1976**, *72*, 248−254.

(24) Jin, P.; Cao, S. F.; Zheng, Y. H. Managing chilling injury in fruits. *Acta Hortic.* **2013**, *1012*, 1087−1095.

(25) Maul, P.; McCollum, G. T.; Popp, Mick; Guy, C. L.; Porat, R. Transcriptome profiling of grapefruit flavedo following exposure to low temperature and conditioning treatments uncovers principal molecular components involved in chilling tolerance and susceptibility. *Plant, Cell Environ.* **2008**, *31*, 752−768.

DOI: 10.1021/acs.jafc.5b00605
J. Agric. Food Chem. 2015, 63, 3654−3659

(26) Park, E.; Jeknic, Z.; Chen, T. H. H. Exogenous application of glycinebetaine increases chilling tolerance in tomato plants. *Plant Cell Physiol.* **2006**, *47*, 706−714.
(27) Li, M.; Li, Z.; Li, S.; Guo, S.; Meng, Q.; Li, G.; Yang, X. Genetic engineering of the biosynthesis of glycine betaine reduced the heat-enhanced photoinhibition by enhancing antioxidative defense to alleviate lipid peroxidation in tomato plants. *Plant Mol. Biol. Rep.* **2014**, *32*, 42−51.
(28) Yang, X. H.; Liang, Z.; Lu, C. M. Genetic engineering of the biosynthesis of glycinebetaine enhances photosynthesis against high temperature stress in transgenic tobacco plants. *Plant Physiol.* **2005**, *138*, 2299−2309.
(29) Chen, W. P.; Li, P. H.; Chen, T. H. H. Glycinebetaine increase chilling tolerance and reduces chilling-induced lipid peroxidation in *Zea mays* L. *Plant, Cell Environ.* **2000**, *23*, 609−618.
(30) Su, X. G.; Jiang, Y. M.; Duan, X. W.; Liu, H.; Li, Y. B.; Lin, W. B. Effects of pure oxygen on the rate of skin browning and energy status in longan fruit. *Food Technol. Biotechnol.* **2005**, *43*, 359−365.
(31) Jin, P.; Zhu, H.; Wang, J.; Chen, J. J.; Wang, X. L.; Zheng, Y. H. Effect of methyl jasmonate on energy metabolism in peach fruit during chilling stress. *J. Sci. Food Agric.* **2013**, *93*, 1827−1832.

DOI: 10.1021/acs.jafc.5b00605
J. Agric. Food Chem. 2015, 63, 3654−3659

Table 1. Detailed Information on Liquors

aroma type	full name	abbreviation	alcohol content (% vol)	geographic origin (province of China)
soy sauce	soy sauce finished liquor	SSFL	53	Guizhou
strong	strong finished liquor	SFL	52	Sichuan
light	light finished liquor	LFL	53	Shanxi
complex	complex finished liquor	CFL	50	Anhui
laobaiganxiang	laobaiganxiang finished liquor	LBGXFL	43	Hebei
roasted-sesame-like	roasted-sesame-like finished liquor	RSLFL	46	Shandong
herblike	herblike finished liquor	HLFL	54	Guizhou
fenxiang	fenxiang finished liquor	FXFL	52	Shaanxi
texiang	texiang finished liquor	TXFL	45	Jiangxi
chixiang	chixiang base distillate	CXBD	38	Guangdong
chixiang	chixiang finished liquor	CXFL	38	Guangdong

Gas chromatography−olfactometry (GC−O), often using aroma extract dilution analysis (AEDA) and Osme, coupled with careful quantitative analysis of the odor-active compounds and calculation of odor activity values (OAVs), has enabled significant advances in understanding of important odorants in alcoholic beverages. Aroma recombination and omission experiments are being extensively and successfully used to confirm the key aroma compounds of alcoholic beverages, such as beer,[8] brandy,[2] Chinese rice wine,[9] Chinese liquor,[10] whisky,[11] and wine.[12]

To our knowledge, no studies have reported on the contribution of aroma compounds to the characteristic aroma of chixiang aroma-type liquor. The aims of the present study were (i) to identify important odorants in chixiang aroma-type liquor by GC−O, (ii) to quantify these compounds by different pretreatment methods and various advanced analytic approaches, and (iii) to perform aroma recombination and omission/addition experiments to confirm the key aroma compounds of chixiang aroma-type liquor.

MATERIALS AND METHODS

Liquors. Detailed sample information is listed in Table 1. Only chixiang aroma-type finished liquor (CXFL) and its base distillate (CXBD) were used for GC−O analysis. All liquors (500 mL for each bottle) were stored at 4 °C until analysis.

Chemicals. All chemicals were of analytical reagent grade, with at least 97% purity. Ethyl acetate, ethyl 2-methylpropanoate, ethyl butanoate, ethyl 2-methylbutanoate, ethyl 3-methylbutanoate, 3-methylbutyl acetate, ethyl pentanoate, ethyl hexanoate, ethyl heptanoate, ethyl 2-hydroxypropanoate (ethyl lactate), ethyl octanoate, 3-methylbutyl hexanoate, ethyl nonanoate, ethyl decanoate, diethylbutanedioate, 1-propanol, 2-methylpropanol, 1-butanol, 3-methylbutanol, 1-pentanol, 1-hexanol, 1-heptanol, 1-octanol, propanoic acid, 3-methylbutanoic acid, pentanoic acid, hexanoic acid, heptanoic acid, octanoic acid, hexanal, heptanal, octanal, 1,1,3-triethoxypropane, 3-hydroxy-2-butanone, nonanal, 2-nonanone, (*E*)-2-octenal, 2-furancarboxaldehyde (furfural), 2-decanone, (*E*)-2-nonenal, (*E*)-2-decenal, (*E*)-2-undecenal, (*E*,*E*)-2,4-decadienal, styrene, benzeneacetaldehyde, ethyl benzoate, ethyl 2-phenylacetate, 2-phenylethyl acetate, benzyl alcohol, ethyl 3-phenylpropanoate, (*E*)-cinnamaldehyde, 3-(methylthio)-1-propanal (methional), 3-(methylthio)-1-propanol (methionol), 2-phenylethanol, γ-octalactone, γ-nonalactone, 4-methylguaiacol, phenol, 4-ethylguaiacol, 4-ethylphenol, and *O*-(2,3,4,5,6-pentafluorobenzyl)hydroxylamine hydrochloride (PFBHA) were purchased from Sigma−Aldrich Co., Ltd. (Shanghai, China). Acetic acid, 2-methylpropanoic acid, butanoic acid, and naphthalene were supplied by Alfa Aesar (Tianjin, China). Diethyl pimelate, diethyl suberate, and diethyl azelate were provided by ANPEL Scientific Instrument Co., Ltd. (Shanghai, China). Pentyl acetate (internal standard, IS1), 2,2-dimethylpropanoic acid (IS2), ethyl octanoate-d_{15} (IS3), *n*-hexyl-d_{13} alcohol (IS4), ethyl 2-phenylacetate-d_3 (IS5), and *p*-fluorobenzaldehyde (IS6) were purchased from ANPEL Scientific Instrument Co., Ltd. (Shanghai, China). IS1 was used as internal standard for compounds with high concentrations (ethyl acetate, ethyl lactate, 1-propanol, 2-methylpropanol, 3-methylbutanol, and 2-phenylethanol). IS2−IS6 were used as internal standards for fatty acids, esters, alcohols, benzoic compounds, and carbonyl compounds, respectively. The remaining compounds (1,1,3-triethoxypropane, γ-octalactone, and γ-nonalactone) were quantified with IS3. A C_5−C_{30} *n*-alkane mixture (Sigma−Aldrich, Shanghai, China) was used for determination of linear retention indices (RIs). Sodium chloride, sodium bicarbonate, sulfuric acid, anhydrous sodium sulfate, and absolute ethanol were from China National Pharmaceutical Group Corp. (Shanghai, China). Diethyl ether and pentane obtained from ANPEL Scientific Instrument Co., Ltd. (Shanghai, China) were freshly distilled before use.

Sample Preparation. According to literature,[10] a total of 50 mL of liquor sample was diluted to 10% ethanol by volume with Milli-Q water (Millipore, Bedford, MA), boiled for 5 min, and then cooled to room temperature in a 1 L flask, saturated with NaCl. The diluted liquor sample was extracted 3 times with 20 mL of a mixture of pentane/diethyl ether (1:1 by volume). The combined extracts were further separated into acidic/water-soluble fraction (AF) and neutral/basic fraction (NBF). Both fractions were dried with 5 g of anhydrous Na_2SO_4 overnight, concentrated to a final volume of 200 μL under a gentle stream of nitrogen, and then stored at −20 °C until analysis.

Gas Chromatographic−Olfactometric and −Mass Spectrometric Analysis. GC−O and GC−MS analysis were performed on an Agilent 6890 gas chromatograph equipped with an Agilent 5975 mass-selective detector (MSD) and an olfactometer (ODP 2, Gerstel, Germany). Samples were analyzed on both a DB-FFAP column (60 m × 0.25 mm i.d., 0.25 μm film thickness, J&W Scientific) and a DB-5 column (30 m × 0.25 mm i.d., 0.25 μm film thickness, J&W Scientific). The column carrier gas was helium at a constant flow rate of 2 mL/min. Each concentrated fraction (1 μL) was injected into the GC and the sniffing port with a split ratio of 1:1. The injector temperature was set at 250 °C. The oven temperature was held at 50 °C for 2 min, then programmed to 230 °C at a rate of 6 °C/min, and finally

DOI: 10.1021/jf506238f
J. Agric. Food Chem. 2015, 63, 3660−3668

held at 230 °C for 10 min. The temperature of the olfactory port was kept at 280 °C. Mass spectra in the electron ionization mode (EI) were recorded at 70 eV ionization energy. The temperature of the ion source was 230 °C, and the mass range was from 30 to 350 amu. Four trained panelists (two females and two males), three graduate students and one teacher from the Laboratory of Brewing Microbiology and Applied Enzymology at Jiangnan University, were selected for the GC−O study. During a GC run, a panelist placed his/her nose close to and above the top of the sniffing port, recorded the odor of the chromatographic effluent as well as retention time. Analyses were repeated in duplicate by each panelist.

Aroma Extract Dilution Analysis. For AEDA, each concentrated fraction, containing NBF and AF, was diluted stepwise with diethyl ether as the solvent in a series of 1:3, 1:9, 1:27, ..., 1:729 dilution. Each dilution was submitted to GC−O analysis under the same GC conditions described above until no odorant could be detected. The flavor dilution (FD) factor of each compound represented the maximum dilution in which the odorant could be perceived. Identification of each aroma compound was carried out by comparing with their odors, retention index (RI), and mass spectra with those of pure standards.

Quantitative Analysis of Aroma Compounds. *Gas Chromatography with Flame Ionization Detector.* Ethyl acetate, ethyl lactate, 1-propanol, 2-methylpropanol, 3-methylbutanol, and 2-phenylethanol (Table 3) were quantified by gas chromatography with flame ionization detector (GC-FID) according to ref 13. Liquor sample was spiked with IS1 to final concentration 176 mg/L. One microliter of disposed sample was injected into the GC in split mode 37:1. The correction factors calculated in 38% ethanol by volume are showed in Table 3. Nitrogen was used as carrier gas at a constant flow rate of 1 mL/min. The separations were performed on a DB-Wax column (30 m × 0.25 mm i.d. × 0.25 μm film thickness; J&W Scientific). The oven temperature was initially set at 60 °C for 3 min, ramped at 5 °C/min to 150 °C for 5 min, and then increased to 230 °C at 10 °C/min for 5 min. The injector and detector temperatures were set at 250 °C. All analyses were repeated in triplicate.

Liquid−Liquid Microextraction. Fatty acids were quantified by liquid−liquid microextraction (LLME) according to the method of Wang et al.[14] Diluted liquor sample (18 mL) with 6 μL of IS2 solution (3.41 mg/L final concentration) was saturated with NaCl and then extracted for 3 min with 1 mL of redistilled diethyl ether. The GC−MS conditions were set as for GC−O analysis on a DB-FFAP column (60 m × 0.25 mm i.d., 0.25 μm film thickness, J&W Scientific) described above. Selective ion monitoring (SIM) mass spectrometry was used to quantify the odorants. The ion monitored for IS2 was m/z 57. The standard curve for fatty acids was carried out by plotting the response ratio of standard compounds and IS2 against the concentration ratio (Table 3). The limits of detection (LOD) was calculated as the analyte concentration of a standard that produced a signal-to-noise ratio of 3. The recovery of target compounds was estimated according to ref 14.

Headspace Solid-Phase Microextraction−Gas Chromatography−Mass Spectrometry. As the methods reported,[10] each liquor sample was diluted with Milli-Q water (Millipore, Bedford, MA) to a final concentration of 10% ethanol by volume. A total of 8 mL of diluted solution with 10 μL of IS solution (IS3, IS4, and IS5 with concentrations of 87.8, 163, and 207 mg/L in ethanol, respectively) was put into a 20 mL screw-capped vial and then saturated with NaCl. An automatic headspace sampling system (MultiPurposeSample MPS 2 with a SPME adapter, from Gerstel Inc., Mülheim, Ruhr, Germany) with a 50/30 μm divinylbenzene/carboxen/poly(dimethylsiloxane) (DVB/CAR/PDMS) fiber (2 cm, Supelco Inc., Bellefonte, PA) was used to extract volatile odorants. The conditions of HS-SPME remained the same as in ref [10]. The GC−MS conditions were set as for GC−O analysis on a DB-FFAP column (60 m × 0.25 mm i.d., 0.25 μm film thickness, J&W Scientific) described above. The ions monitored for IS3, IS4, and IS5 were m/z 91 and 142, 64 and 78, and 104 and 46, respectively. The LOD and recovery of target compounds were detected by the method described above.

Quantitation of Carbonyl Compounds by Headspace Solid-Phase Microextraction−Gas Chromatography−Mass Spectrometry after Derivatization with O-(2,3,4,5,6-Pentafluorobenzyl)hydroxylamine Hydrochloride. Quantitation of carbonyl compounds after derivatization with PFBHA was performed by GC−MS on a DB-FFAP column (60 m × 0.25 mm i.d., 0.25 μm film thickness, J&W Scientific) modified from literature.[15] The liquor sample was diluted to 10% ethanol by volume. Eight milliliters of dilution was saturated with NaCl and added to a 20 mL standard headspace vial, and then 10 μL of a solution of IS6 (1.0724 mg/L in ethanol) and 120 μL of PFBHA (50 g/L in water) were added. The fiber used was three-phase fiber as described above. The sample was incubated at 65 °C for 10 min and extracted for 45 min at the identical temperature under stirring at a rotation speed of 250*g*, then transferred the fiber to the injector for desorption at 250 °C for 300 s. During the GC run (in splitless mode), a constant flow rate (1 mL/min) of the carrier gas (helium) was maintained. The injector temperature was held at 280 °C. The oven temperature was programed to 50 °C for 2 min and raised to 100 °C at a rate of 6 °C/min for 0.1 min, then to 160 °C at a rate of 2 °C/min for 0.1 min, and finally at 5 °C/min to 230 °C for 10 min. The mass spectrometer was operated in electron ionizationI mode at 70 eV with SIM. The ion monitored for IS6 after derivatization was m/z 319. Monitored ions of carbonyl compounds after derivatization are listed in Table 3. The standard curve and LOD, as well as recovery of carbonyl compounds, were measured by the method mentioned above.

Determination of Odor Thresholds. For the calculation of OAVs, odor thresholds of some aromas were determined in 46% ethanol/water solution by triangle tests based on ref 16.

Aroma Recombination of Chixiang Finished Liquor. Ethanol/water solution (38% ethanol by volume) was used as the matrix for recombination. The aroma compounds with OAVs ≥ 1 (Table 4) of CXFL were spiked into the matrix according to their occurring concentrations (Table 3). The overall aroma profiles of the CXFL liquor and reconstituted models were evaluated by 10 well-trained assessors (five males and five females, 30 years old on average), eight graduate students and two teachers from the Laboratory of Brewing Microbiology and Applied Enzymology at Jiangnan University. All of the assessors were trained for 2 months (45 min/day) to describe and recognize the odor qualities of approximately 30 odorants. Testing samples (20 mL) were presented to assessors in four-digit-coded, covered glasses in a sensory panel room at 20 ± 1 °C. The assessors rated eight aroma attributes to describe the overall aroma: fatty, grassy, sweet, alcoholic, floral, fruity, cheesy, and acidic. The intensity of each aroma attribute was rated on a 6-point scale, where 0 is none, 1 is very weak, 2 is weak, 3 is moderate, 4 is strong, and 5 is very strong. The

DOI: 10.1021/jf506238f
J. Agric. Food Chem. 2015, 63, 3660−3668

Table 2. Aroma Compounds Identified by Gas Chromatography−Olfactometry in Chixiang Aroma-type Finished Liquor and Its Base Distillate

	RI						FD factor	
no.	FFAP column	DB-5 column	aroma compd	descriptor	basis of ID[a]	fraction[b]	CXFL[c]	CXBD[c]
1	892	589	ethyl acetate	pineapple	MS, aroma, RI	NBF	81	81
2	961	750	ethyl 2-methylpropanoate	apple	MS, aroma, RI	NBF	243	27
3	1035	530	1-propanol	alcoholic	MS, aroma, RI	NBF + AF	3	3
4	1038	817	ethyl butanoate	pineapple	MS, aroma, RI	NBF	3	9
5	1045	860	ethyl 2-methylbutanoate	berry	MS, aroma, RI	NBF	9	9
6	1060	856	ethyl 3-methylbutanoate	apple	MS, aroma, RI	NBF	81	27
7	1071	803	hexanal	grassy	MS, aroma, RI	NBF	243	9
8	1087	620	2-methylpropanol	wine	MS, aroma, RI	NBF + AF	3	3
9	1102	878	3-methylbutyl acetate	banana	MS, aroma, RI	NBF	81	243
10	1128	913	ethyl pentanoate	apple	MS, aroma, RI	NBF	1	3
11	1137	669	1-butanol	alcoholic	MS, aroma, RI	NBF+AF		1
12	1199	902	heptanal	grassy	MS, aroma, RI	NBF	81	9
13	1232	789	3-methylbutanol	nail polish	MS, aroma, RI	NBF+AF	9	27
14	1235	1028	ethyl hexanoate	fruity	MS, aroma, RI	NBF	1	3
15	1255	892	styrene	plastic	MS, aroma, RI	NBF	3	
16	1256	763	1-pentanol	fruity	MS, aroma, RI	NBF+AF		1
17	1280	1003	octanal	fatty	MS, aroma, RI	NBF	729	27
18	1271	1128	1,1,3-triethoxypropane	vegetal	MS, aroma, RI	NBF	3	3
19	1304	717	3-hydroxy-2-butanone	buttery	MS, aroma, RI	NBF	9	3
20	1310	1115	ethyl heptanoate	fruity	MS, aroma, RI	NBF	9	3
21	1334	823	ethyl lactate	fruity	MS, aroma, RI	NBF+AF	3	3
22	1354	892	1-hexanol	floral	MS, aroma, RI	AF	1	1
23	1369	1121	nonanal	soapy	MS, aroma, RI	NBF	729	
24	1376	1089	2-nonanone	floral	MS, aroma, RI	NBF	9	3
25	1427	1203	ethyl octanoate	fruity	MS, aroma, RI	NBF	9	81
26	1437	1070	(*E*)-2-octenal	fatty	MS, aroma, RI	NBF	81	3
27	1459	601	acetic acid	vinegar	MS, aroma, RI	AF	81	243
28	1453	903	methional	cooked potato	MS, aroma, RI	NBF+AF	243	9
29	1442	978	1-heptanol	alcoholic	MS, aroma, RI	AF	1	3
30	1454	1238	3-methylbutyl hexanoate	fruity	MS, aroma, RI	NBF	1	9
31	1466	840	furfural	sweet, almond	MS, aroma, RI	NBF+AF		27
32	1479	1190	2-decanone	fruity	MS, aroma, RI	NBF	1	
33	1499	1289	ethyl nonanoate	fruity	MS, aroma, RI	NBF	3	27
34	1516	1160	(*E*)-2-nonenal	fatty	MS, aroma, RI	NBF	81	3
35	1530	675	propanoic acid	vinegar	MS, aroma, RI	AF	243	81
36	1539	1090	1-octanol	fruity	MS, aroma, RI	AF	1	3
37	1555	792	2-methylpropanoic acid	cheesy	MS, aroma, RI	AF	9	27
38	1602	802	butanoic acid	cheesy	MS, aroma, RI	AF	243	81
39	1610	1398	ethyl decanoate	fruity	MS, aroma, RI	NBF	1	3
40	1603	1273	(*E*)-2-decenal	fatty	MS, aroma, RI	NBF	9	1
41	1620	1052	phenylacetaldehyde	floral	MS, aroma, RI	NBF		9
42	1634	837	3-methylbutanoic acid	cheesy	MS, aroma, RI	AF	9	27
43	1640	1165	ethyl benzoate	floral	MS, aroma, RI	NBF	3	9
44	1655	1170	diethyl butanedioate	fruity	MS, aroma, RI	NBF	1	1
45	1695	977	methionol	cooked potato	MS, aroma, RI	NBF	1	1
46	1727	879	pentanoic acid	cheesy	MS, aroma, RI	AF	81	3
47	1742	1218	naphthalene	mothball	MS, aroma, RI	NBF	3	81
48	1744	1365	(*E*)-2-undecenal	fatty	MS, aroma, RI	NBF	3	1
49	1786	1254	ethyl 2-phenylacetate	rosy, honey	MS, aroma, RI	NBF	3	3
50	1801	1271	2-phenylethyl acetate	floral	MS, aroma, RI	NBF	3	9
51	1822	1327	(*E*,*E*)-2,4-decadienal	fatty	MS, aroma, RI	NBF	81	1
52	1825	971	hexanoic acid	sweaty, cheesy	MS, aroma, RI	AF	9	9
53	1858	1037	benzyl alcohol	floral	MS, aroma, RI	NBF+AF	3	3
54	1872	1348	ethyl 3-phenylpropanoate	floral	MS, aroma, RI	NBF	3	3
55	1906	1132	2-phenylethanol	rosy, honey	MS, aroma, RI	NBF+AF	27	243
56	1886	1215	γ-octalactone	coconut	MS, aroma, RI	NBF	9	9
57	1955	1103	heptanoic acid	rancid, unpleasant	MS, aroma, RI	AF	3	9
58	1959	1199	4-methylguaiacol	smoky	MS, aroma, RI	AF		3

DOI: 10.1021/jf506238f
J. Agric. Food Chem. 2015, 63, 3660−3668

Table 2. continued

no.	RI FFAP column	RI DB-5 column	aroma compd	descriptor	basis of ID[a]	fraction[b]	FD factor CXFL[c]	FD factor CXBD[c]
59	2007	991	phenol	phenol, medicinal	MS, aroma, RI	AF		3
60	2010	1297	4-ethylguaiacol	clove	MS, aroma, RI	AF		81
61	2018	1359	γ-nonalactone	coconut	MS, aroma, RI	NBF	243	81
62	2033	1281	(*E*)-cinnamaldehyde	cinnamon	MS, aroma, RI	NBF	1	3
63	2060	1168	octanoic acid	cheesy	MS, aroma, RI	AF	9	27
64	2185	1181	4-ethylphenol	smoky	MS, aroma, RI	AF		3

[a]MS, compounds were identified by MS spectra; aroma, compounds were identified by comparison to reference standards by GC−O; RI, compounds were identified on FFAP and DB-5 by comparison to reference standards. [b]Fraction(s) in which odorant was detected by GC−O after fractionation. AF, acidic/water-soluble fraction; NBF, neutral and basic fraction. [c]CXFL, chixiang aroma-type finished liquor; CXBD, chixiang aroma-type base distillate.

sensory data were analyzed by one-way analysis of variance (ANOVA) by use of SPSS15.0 (SPSS Inc., Chicago, IL).

Omission/Addition Tests. In triangular tests with forced choice, a recombinant model, in which one odorant or a class of odorants (Table 6) was omitted/added, was evaluated against two complete recombinants. The testing samples were arranged in a random four-digit code, and each test was repeated in triplicate. The assessors were asked to sniff the samples and estimate the differing one. The significance of the differences was evaluated by the method as reported.[17]

RESULTS AND DISCUSSION

Aroma Compounds by Gas Chromatography−Olfactometry in Chixiang Aroma-type Liquor. A total of 64 odorants were perceived by GC−O in chixiang finished liquor and its base distillate. In finished liquor (CXFL), 56 odorants could be detected by AEDA. Among them, octanal and nonanal obtained the highest FD factor (FD ≥729), which gave intense fatty and soapy aromas, respectively. A total of 61 aroma compounds were identified in base distillate (CXBD). 3-Methylbutyl acetate, acetic acid, and 2-phenylethanol (FD ≥ 243) had the highest FD factor, which elicited intense banana, vinegar, and rose- or honey-like aromas, respectively. As shown in Table 2, (*E*)-2-octenal, (*E*)-2-nonenal, (*E*)-2-decenal, (*E*)-2-undecenal, and (*E*,*E*)-2,4-decadienal were first detected in CXFL and CXBD liquors, which exhibited intense fatty aromas. Unsaturated aldehydes usually gave off-flavor in beer,[18,19] and they have been proposed as main note of the roasted mini-pig pork meat aroma.[20] Methionol was detected in both liquors (FD ≥ 1 in CXFL and CXBD), which was previously regarded as one of the characteristic aromas of chixiang aroma-type liquor.[5,7] Diethyl pimelate, diethyl suberate, and diethyl azelate were not detected by GC−O in either liquor.

Concentration of Aroma Compounds in Chixiang Aroma-type Liquor. To gain a deeper insight into the aroma of chixiang aroma-type liquor, a total of 59 compounds, 56 odorants detected by AEDA and three dibasic acid diethyl esters (diethyl pimelate, diethyl suberate, and diethyl azelate), were quantified in CXFL liquor (Table 3). As exhibited in Table 3, ethyl lactate had the highest concentration (585 mg/L), followed by ethyl acetate (385 mg/L) and 3-methylbutanol (354 mg/L). In addition, the data in Table 4 demonstrate that the highest concentrations of (*E*)-2-octenal, (*E*)-2-nonenal, (*E*)-2-decenal, (*E*)-2-undecenal, and (*E*,*E*)-2,4-decadienal were found in CXFL liquor among 10 aroma-type Chinese liquors. (*E*)-2-Octenal was the most abundant unsaturated aldehyde in CXFL liquor with concentration exceeding 400 μg/L, followed by (*E*)-2-decenal (375 μg/L) and (*E*)-2-nonenal (156 μg/L). The total concentration of five unsaturated aldehydes in CXFL liquor was the highest, up to 1040 μg/L, notably higher than any other aroma-type liquors. Besides, CXBD and DJ liquor had higher concentrations of 100−200 μg/L whereas total concentrations of these five unsaturated aldehydes in SSFL, SFL, LFL, CFL, LBGXFL, RSLFL, FXFL, and TXFL liquors were less than 100 μg/L, far lower than that in CXFL liquor (Table 4). Diethyl pimelate, diethyl suberate, and diethyl azelate were included in the quantification experiments because they were frequently described as important aroma compounds in the literature.[7] The concentrations of diethyl pimelate, diethyl suberate, and diethyl azelate were 687, 228, and 2310 μg/L, respectively.

Odor Activity Values. The thresholds were determined in 46% hydroalcoholic solution (by volume). As indicated in Table 5, odor thresholds of 24 aroma compounds were determined, and the odor thresholds in liquor ranged from 7.12 (methional) to 1 280 000 μg/L (diethyl azelate). So contribution to the liquor would depend not only on the concentration of an odorant but also its odor threshold.

To evaluate the contribution of quantified odorants to the overall aroma of the liquor, odor activity values (ratio of concentration to its odor threshold) were calculated for each aroma compound listed in Table 5. A total of 34 odorants were calculated with OAVs ≥1. These odorants should be important contributors to the characteristic aroma of CXFL liquor. The highest OAV in finished liquor was ethyl 2-methylpropanoate (OAV = 336), followed by ethyl octanoate (OAV = 157) and hexanal (OAV = 69). (*E*)-2-Decenal, (*E*)-2-octenal, (*E*,*E*)-2,4-decadienal, and (*E*)-2-nonenal, which give "fatty" flavor,[2,21] were detected with OAVs 31, 28, 5, and 3, respectively. The CXFL liquor was much higher than any other liquors in the OAVs of (*E*)-2-decenal, (*E*)-2-octenal, (*E*,*E*)-2,4-decadienal, and (*E*)-2-nonenal (Table 4). Noticeably, (*E*)-2-nonenal was detected with OAV > 1 only in the CXFL liquor. Two odorants, 2-phenylethanol (rose- or honey-like-aroma) and methionol (cooked potato), might contribute to the overall aroma according to their OAVs (>1). However, diethyl pimelate, diethyl suberate, and diethyl azelate were calculated with OAVs ≤ 1; therefore, they could not contribute to the overall aroma.

Aroma Recombination and Omission/Addition Experiments. To confirm that the aroma compounds were indeed the important odorants of chixiang aroma-type liquor, aroma recombination and omission/addition experiments were undertaken, based on the quantitative results of finished liquor. For this purpose, an aroma recombinate was prepared in a 38% hydroalcoholic solution (by volume), by addition of 34

DOI: 10.1021/jf506238f
J. Agric. Food Chem. 2015, 63, 3660−3668

Table 3. Standard Curve and Concentrations of 59 Aroma Compounds in Chixiang Aroma-type Finished Liquor

										CXFL[a]	
no.	aroma compd	quantified ion	IS	slope	intercept	n	R^2	LOD (μg/L)	recovery (%)	avg[b] (μg/L)	RSD[c] (%)
21	ethyl lactate[d]	1.04[e]	IS1							585000	7
1	ethyl acetate[d]	1.47[e]	IS1							385000	6
13	3-methylbutanol[d]	0.770[e]	IS1							354000	8
27	acetic acid[f]	43	IS2	52.2	2.39	6	0.993	2800	90	260000	8
8	2-methylpropanol[d]	0.720[e]	IS1							233000	6
55	2-phenylethanol[d]	0.830[e]	IS1							127000	7
3	1-propanol[d]	0.830[e]	IS1							88200	7
57	heptanoic acid[f]	60	IS2	6.12	1.38	6	0.993	2930	86	25600	7
2	ethyl 2-methylpropanoate	43	IS3	21.6	−1.41	7	0.998	3.65	95	19300	3
38	butanoic acid[f]	60	IS2	4.02	0.980	8	0.999	2580	88	19200	6
52	hexanoic acid[f]	60	IS2	2.71	0.740	7	0.996	938	95	17400	6
63	octanoic acid[f]	60	IS2	9.81	0.490	7	0.984	887	80	11300	8
37	2-methylpropanoic acid[f]	43	IS2	3.18	0.410	8	0.999	1960	84	9300	7
35	propanoic acid[f]	74	IS2	9.06	0.460	6	0.997	214	92	8560	9
53	benzyl alcohol	79	IS5	43.0	2.90	9	0.993	56.9	108	7130	8
44	diethyl butanedioate	101	IS3	7.95	−3.97	11	0.994	27.4	109	5100	3
22	1-hexanol	56	IS4	18.9	8.33	12	0.996	2.64	99	3820	5
4	ethyl butanoate	71	IS3	8.97	6.89	11	0.996	14.0	99	3690	3
46	pentanoic acid[f]	60	IS2	2.72	0.150	6	0.984	194	92	3470	8
20	ethyl heptanoate	88	IS3	0.390	5.51	12	0.990	16.2	85	3260	4
45	methionol	106	IS4	4.53	0.160	9	0.993	316	102	3090	6
9	3-methylbutyl acetate	43	IS3	1.71	4.91	11	0.999	50.6	110	2510	2
67	diethyl azelate	199	IS3	2.04	2.66	8	0.996	86.6	98	2310	2
25	ethyl octanoate	88	IS3	0.130	1.63	11	0.992	11.4	111	2030	3
43	ethyl benzoate	105	IS5	0.210	0.0300	11	0.999	2.33	99	1880	2
7	hexanal[g]	44	IS6	9.37	−1.51	12	0.999	32.7	87	1760	3
14	ethyl hexanoate	88	IS3	0.440	0.0800	7	0.997	2.92	91	1600	4
19	3-hydroxy-2-butanone[g]	240	IS6	28.7	−0.180	10	0.999	11.4	95	1390	6
12	heptanal[g]	70	IS6	4.60	0.210	7	0.998	70.8	99	1180	4
42	3-methylbutanoic acid[f]	60	IS2	1.21	0.0400	8	0.999	362	90	1090	7
33	ethyl nonanoate	88	IS3	0.120	1.11	10	0.998	13.4	110	950	5
61	γ-nonalactone	85	IS3	29.9	0.150	10	0.995	20.3	105	866	4
23	nonanal[g]	57	IS6	1.17	0.140	10	0.999	1.25	104	854	3
17	octanal[g]	43	IS6	0.750	0.790	7	0.997	10.7	98	759	2
65	diethyl pimelate	125	IS3	5.68	0.540	8	0.993	25.7	106	687	2
36	1-octanol	56	IS4	1.07	0.290	8	0.992	12.6	100	612	4
29	1-heptanol	70	IS4	4.19	−0.320	11	0.996	8.12	89	574	2
62	(*E*)-cinnamaldehyde	131	IS5	3.55	0.680	8	0.994	14.5	97	471	3
26	(*E*)-2-octenal[g]	250	IS6	2.46	1.25	10	0.999	1.61	102	422	9
40	(*E*)-2-decenal[g]	250	IS6	4.04	7.18	10	0.999	1.06	101	375	5
18	1,1,3-triethoxypropane	103	IS3	3.39	0.310	11	0.998	38.5	96	350	3
6	ethyl 3-methylbutanoate	88	IS3	2.96	0.640	8	0.996	4.04	101	344	3
54	ethyl 3-phenylpropanoate	104	IS5	0.290	0.660	11	0.999	14.2	109	314	5
24	2-nonanone[g]	58	IS6	1.39	0.100	11	0.996	8.50	104	252	4
66	diethyl suberate	185	IS3	0.160	0.410	7	0.994	10.8	101	228	2
32	2-decanone[g]	58	IS6	1.78	0.0800	12	0.997	3.33	94	183	6
39	ethyl decanoate	88	IS3	0.0400	0.0700	8	0.995	0.710	99	161	4
34	(*E*)-2-nonenal[g]	250	IS6	3.05	2.29	10	0.999	0.660	106	156	4
50	2-phenylethyl acetate	104	IS5	0.380	0.0300	11	0.998	0.800	96	147	5
56	γ-octalactone	85	IS3	19.2	0.120	8	0.991	2.89	90	132	2
49	ethyl phenylacetate	91	IS5	0.260	0.0300	11	0.997	0.570	94	125	2
10	ethyl pentanoate	88	IS3	0.440	0.0800	9	0.998	28.9	85	108	3
15	styrene	104	IS5	0.250	0.130	8	0.997	2.16	107	102	3
48	(*E*)-2-undecenal[g]	250	IS6	9.78	4.56	11	0.999	0.650	98	47.3	4
51	(*E*,*E*)-2,4-decadienal[g]	276	IS6	3.73	2.12	11	0.999	0.440	89	35.6	5
30	3-methylbutyl hexanoate	70	IS3	0.210	0.0200	11	0.999	3.39	115	24.5	4
5	ethyl 2-methylbutanoate	57	IS3	4.25	−0.280	7	0.992	0.790	93	10.3	2
28	methional[g]	299	IS6	14.3	0.0400	9	0.999	3.47	106	6.97	4
47	naphthalene	128	IS3	0.0200	0.0100	9	0.995	0.130	91	3.41	2

DOI: 10.1021/jf506238f
J. Agric. Food Chem. 2015, 63, 3660−3668

Table 3. continued

[a]CXFL, chixiang aroma-type finished liquor. [b]Average concentration of triplicates. [c]Relative standard deviation. [d]Quantified by GC-FID. [e]Calibration factors of aroma compounds detected by GC-FID. [f]Quantified by LLME combined with GC−MS. [g]Detected by GC−MS after derivatization with PFBHA.

Table 4. Concentrations and OAVs of Unsaturated Aldehydes in Different Aroma-type Chinese Liquors[a]

	(*E*)-2-octenal			(*E*)-2-nonenal			(*E*)-2-decenal			(*E*)-2-undecenal			(*E*,*E*)-2,4-decadienal			
liquor	avg[b] (μg/L)	OAV	RSD (%)	avg (μg/L)	OAV	RSD (%)	avg (μg/L)	OAV	RSD (%)	avg (μg/L)	OAV	RSD (%)	avg (μg/L)	OAV	RSD (%)	total (μg/L)
SSFL	22.2	1	9	13.2	<1	10	8.25	<1	9	6.88	<1	7	9.80	1	10	60.4
SFL	33.4	2	7	17.0	<1	9	9.45	<1	5	8.55	<1	7	7.59	<1	10	76.0
LFL	28.4	2	8	20.5	<1	6	10.2	<1	7	8.24	<1	8	9.79	1	9	77.2
CFL	18.9	1	10	10.1	<1	7	7.66	<1	8	7.10	<1	6	7.76	1	8	51.5
LBGXFL	27.1	2	6	14.4	<1	8	8.38	<1	7	12.2	<1	5	11.3	1	5	73.4
RSLFL	20.8	1	7	14.4	<1	5	15.4	1	6	10.6	<1	6	10.4	1	6	71.8
HLFL	33.7	2	9	25.7	<1	7	53.0	4	5	18.9	<1	9	28.5	4	5	160
FXFL	28.5	2	10	14.0	<1	8	10.8	<1	9	8.60	<1	5	8.93	1	7	70.9
TXFL	22.4	1	9	14.0	<1	7	12.1	<1	9	9.82	<1	10	6.93	<1	9	65.3
CXBD	96.4	6	6	16.2	<1	8	38.8	3	5	29.1	<1	8	13.0	1	9	194
CXFL	422	28	8	156	3	6	375	31	10	47.3	<1	12	35.6	5	8	1040

[a]Thresholds of (*E*)-2-octenal, (*E*)-2-nonenal, (*E*)-2-decenal, (*E*)-2-undecenal, and (*E*,*E*)-2,4-decadienal, determined on the basis of ref 16, were 15.1, 50.5, 12.1, 240, and 7.71 μg/L, respectively. [b]Average concentration of triplicates.

Table 5. Odor Activity Values of 59 Odorants in Chixiang Aroma-type Finished Liquor

no.	aroma compd	odor threshold (μg/L)	OAV
2	ethyl 2-methylpropanoate	57.5[a]	336
25	ethyl octanoate	12.9[a]	157
7	hexanal	25.5[a]	69
6	ethyl 3-methylbutanoate	6.89[a]	50
4	ethyl butanoate	81.5[a]	45
40	(*E*)-2-decenal	12.1	31
14	ethyl hexanoate	55.3[a]	29
26	(*E*)-2-octenal	15.1	28
9	3-methylbutyl acetate	93.9	27
38	butanoic acid	964[a]	20
17	octanal	39.6[a]	19
1	ethyl acetate	32600[a]	12
61	γ-nonalactone	90.7[a]	10
46	pentanoic acid	389[a]	9
8	2-methylpropanol	28300[a]	8
23	nonanal	122[a]	7
52	hexanoic acid	2520[a]	7
37	2-methylpropanoic acid	1580[a]	6
19	3-hydroxy-2-butanone	259	5
21	ethyl lactate	128000[a]	5
51	(*E*,*E*)-2,4-decadienal	7.71	5
55	2-phenylethanol	28900[a]	4
63	octanoic acid	2700[b]	4
10	ethyl pentanoate	26.8[a]	4
12	heptanal	410[a]	3
34	(*E*)-2-nonenal	50.5	3
54	ethyl 3-phenylpropanoate	125[a]	3
13	3-methylbutanol	179000[a]	2
57	heptanoic acid	13800[b]	2
3	1-propanol	54000[b]	2
27	acetic acid	160000[a]	2
45	methionol	2110	1
43	ethyl benzoate	1430[a]	1
42	3-methylbutanoic acid	1050[a]	1
28	methional	7.12	<1
35	propanoic acid	18100	<1
32	2-decanone	186	<1
24	2-nonanone	483[b]	<1
22	1-hexanol	5370[a]	<1
36	1-octanol	1100	<1
5	ethyl 2-methylbutanoate	18.0	<1
49	ethyl phenylacetate	407[a]	<1
33	ethyl nonanoate	3150[a]	<1
20	ethyl heptanoate	13200[a]	<1
48	(*E*)-2-undecenal	240	<1
53	benzyl alcohol	40900	<1
50	2-phenylethyl acetate	909[a]	<1
39	ethyl decanoate	1120[a]	<1
62	(*E*)-cinnamaldehyde	4800	<1
18	1,1,3-triethoxypropane	3700	<1
15	styrene	1400	<1
56	γ-octalactone	2820	<1
30	3-methylbutyl hexanoate	1400	<1
29	1-heptanol	26600	<1
47	naphthalene	159	<1
44	diethyl butanedioate	353000[a]	<1
65	diethyl pimelate	396000	<1
66	diethyl suberate	641000	<1
67	diethyl azelate	1280000	<1

[a]From ref 10. [b]From ref 30.

odorants with OAVs ≥ 1 listed in Table 5. Odor attributes of the recombinate and original liquor were evaluated by a sensory panel consisting of 10 trained assessors. As shown in Figure 1, the aroma of the recombinate showed good similarity for fatty, grassy, alcoholic, floral, fruity, cheesy, and acidic aromas, whereas sweet aroma was slightly lower in the reconstituted

DOI: 10.1021/jf506238f
J. Agric. Food Chem. 2015, 63, 3660−3668

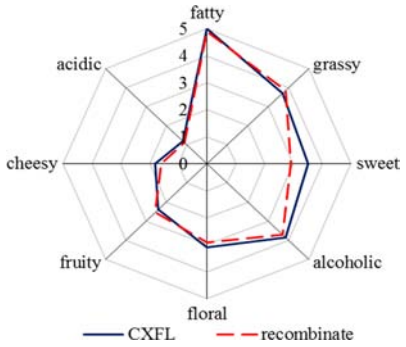

Figure 1. Aroma profile of chixiang aroma-type finished liquor (CXFL) and the complete aroma recombinate.

model. The overall aroma similarities of the reconstitution model with the original liquor were judged to be 4.3 out of 5.0 points. Consequently, this result indicated the success in mimicking the typical aroma of the investigated liquor.

To take deeper consideration of the aroma contribution of certain compounds, a total of 20 aroma omission models (Table 6) missing either a single component or a group of components were investigated by omission experiments. Each of the omission models was evaluated compared with the complete recombinate by a triangle test. The results of the descriptive study for 20 reconstitution samples are shown in Table 6.

Table 6. Omission Experiments from Complete Recombinate

no.	odorants omitted from the complete recombinate	n^a	significance[b]
1	(*E*)-2-octenal, (*E*)-2-nonenal, (*E*)-2-decenal, (*E,E*)-2,4-decadienal, octanal, and nonanal	10	***
1-1	(*E*)-2-nonenal	9	***
1-2	(*E*)-2-octenal	8	**
1-3	(*E*)-2-decenal	4	
1-4	(*E,E*)-2,4-decadienal	4	
1-5	octanal	5	
1-6	nonanal	3	
2	2-phenylethanol, ethyl 3-phenylpropanoate, and ethyl benzoate	8	**
2-1	2-phenylethanol	8	**
2-2	ethyl 3-phenylpropanoate	6	
2-3	ethyl benzoate	4	
3	hexanal, heptanal	7	*
3-1	hexanal	7	*
3-2	heptanal	4	
4	all esters	5	
5	2-methylpropanol, 3-methylbutanol, and 1-propanol	6	
6	fatty acids	5	
7	γ-nonalactone	3	
8	3-hydroxy-2-butanone	5	
9	methionol	3	

[a]Number of correct judgments from 10 assessors evaluating the aroma difference by triangle test. [b]Significance: *, significant ($\alpha \leq 0.05$); **, highly significant ($\alpha \leq 0.01$); ***, very highly significant ($\alpha \leq 0.001$).

The data (Table 6) suggested that all assessors were able to detect the omission of (*E*)-2-octenal, (*E*)-2-nonenal, (*E*)-2-decenal, (*E,E*)-2,4-decadienal, octanal, and nonanal with a very high significance ($\alpha \leq 0.001$). This result indicated the fairly important role of these fatty-smelling compounds for the overall chixiang aroma. Among them, model 1-1 (Table 6) without (*E*)-2-nonenal (fatty) was also evaluated with very high significance ($\alpha \leq 0.001$) in aroma compared to the complete recombinate, thereby pinpointing the crucial role of (*E*)-2-nonenal for the typical aroma of chixiang aroma-type liquor. (*E*)-2-Nonenal has already been detected in alcoholic beverages, such as beer,[22] whisky,[21] brandy,[2] and wine.[23] Researchers have indicated that (*E*)-2-nonenal was formed by lipid oxidation.[18,24] Pork meat contains abundant lipids,[20] which could lead to generation of (*E*)-2-nonenal during storage. When (*E*)-2-octenal was omitted from the complete recombinate, a high significance ($\alpha \leq 0.01$) was obtained. However, no significant difference was observed when (*E*)-2-decenal, (*E,E*)-2,4-decadienal, octanal, and nonanal were respectively omitted from the complete recombinate. Consequently, the fatty note present in the profile of overall aroma could be strongly linked to (*E*)-2-nonenal.

A model mixture without compounds 2-phenylethanol (rose- or honey-like), ethyl 3-phenylpropanoate (floral), and ethyl benzoate (floral) resulted in highly significant difference ($\alpha \leq 0.01$) in aromas. Furthermore, when only 2-phenylethanol (Table 6, model 2-1) was missing, the assessors could detect a highly significant difference ($\alpha \leq 0.01$), whereas the omission of only ethyl 3-phenylpropanoate (Table 6 model 2-2) or only ethyl benzoate (Table 6 model 2-3) could not be detected significantly. These results indicated that 2-phenylethanol could be responsible for the typical floral note of chixiang aroma-type liquor. 2-Phenylethanol has already been detected in Chinese liquor,[25,26] Chinese rice wine,[27] whisky,[21] and brandy.[2] Researchers have demonstrated that L-phenylalanine was the key precursor for formation of 2-phenylethanol through the Ehrlich pathway in alcoholic fermentation by yeast.[28,29]

A model mixture lacking both hexanal and heptanal (Table 6, model 3) was evaluated as significantly different ($\alpha \leq 0.05$) compared to the entire model mixture. A mixture lacking only heptanal (Table 6, model 3-2) was not detected as different from the complete recombinate, while a mixture lacking only hexanal (Table 6, model 3-1) was judged with significance ($\alpha \leq 0.05$). However, in model 4 lacking in all esters, the sensory panel was not able to detect a significant difference between the samples; thereby the fruity note present in the aroma profile of the entire model mixture (Figure 1) could not be correlated to certain aroma components. Fatty acids mostly demonstrated a vinegar or cheesy note; omission of this group of compounds was also determined with no significant difference by the assessors (Table 6, model 6). The same results also occurred with alcohols, γ-nonalactone, and 3-hydroxy-2-butanone, as exhibited in Table 6, models 5, 7, and 8, respectively. Additionally, methionol had been suggested as a characteristic aroma compound in chixiang aroma-type liquor.[5] Our study (Table 6, model 9) showed that this compound did not contribute significantly to the flavor of chixiang aroma-type liquor.

In addition, the complete recombinate was spiked with diethyl pimelate, diethyl suberate, and diethyl azelate and then compared with the complete recombinate. The addition of these compounds was correctly detected by only 4 of 20 assessors in triangle tests. As a consequence, no significant difference was determined for the addition of three dibasic acid diethyl esters, which agrees with the fact that the dibasic acid diethyl esters had not been detected by GC−O.

DOI: 10.1021/jf506238f
J. Agric. Food Chem. 2015, 63, 3660−3668

In conclusion, the aroma-active compounds in chixiang aroma-type liquors were successfully identified by GC−O analysis, and 34 odorants were further detected as important odorants according to quantitative study and OAVs. The aroma profile of chixiang aroma-type finished liquor could be successfully reconstituted by mixing 34 aroma compounds in concentrations measured in this study. Omission experiments further confirmed (*E*)-2-nonenal as the key odorant and revealed the significance of (*E*)-2-octenal and 2-phenylethanol for the overall aroma of chixiang aroma-type finished liquor. Methionol, diethyl pimelate, diethyl suberate, and diethyl azelate had no effects on aroma based on omission/addition experiments. Further research is needed to investigate whether nonvolatile compositions had effects on aroma, which may be of great importance in understanding "sweet" flavors in finished liquor.

AUTHOR INFORMATION

Corresponding Author

*Phone 86-510-85197082; fax 86-510-85918201; e-mail Wenlai.Fan@gmail.com or Wenlai.fan@163.com.

Funding

We appreciate financial support from the National High Technology Research and Development Programe of China (Program 863) under Grant 2013AA102108.

Notes

The authors declare no competing financial interest.

REFERENCES

(1) Fan, W.; Xu, Y.; Qian, M. C. Identification of aroma compounds in Chinese "Moutai" and "Langjiu" liquors by normal phase liquid chromatography fractionation followed by gas chromatography/olfactometry. In *Flavor Chemistry of Wine and Other Alcoholic Beverages*; Qian, M. C., Shellhammer, T. H., Eds.; American Chemical Society: Washington, DC, 2012; pp 303−338.

(2) Willner, B.; Granvogl, M.; Schieberle, P. Characterization of the key aroma compounds in Bartlett pear brandies by means of the sensomics concept. *J. Agric. Food Chem.* **2013**, *61*, 9583−9593.

(3) Li, D. Discussion on the formation of the specific style of soybean-flavor liquor. *Liquor Making Sci. Technol.* **2004**, *1*, 24−27.

(4) Shen, Y. *Manual of Chinese Liquor Manufacturers Technology*; Light Industry Publishing House of China: Beijing, China, 1996.

(5) Feng, Z.; Qiu, X. Analysis of the aroma compounds of Chinese *chixiang* aroma type liquor. *Niangjiu* **1995**, *4*, 75−82.

(6) Grosch, W. Evaluation of the key odorants of foods by dilution experiments, aroma models and omission. *Chem. Senses* **2001**, *26*, 533−545.

(7) Zhang, W.; He, S. Analysis of flavor components of soybean-flavor liquor. *Liquor Making Sci. Technol.* **2010**, *12*, 58−64.

(8) Langos, D.; Granvogl, M.; Schieberle, P. Characterization of the key aroma compounds in two Bavarian wheat beers by means of the sensomics approach. *J. Agric. Food Chem.* **2013**, *61*, 11303−11311.

(9) Chen, S.; Xu, Y.; Qian, M. C. Aroma characterization of Chinese rice wine by gas chromatography−olfactometry, chemical quantitative analysis, and aroma reconstitution. *J. Agric. Food Chem.* **2013**, *61*, 11295−11302.

(10) Gao, W.; Fan, W.; Xu, Y. Characterization of the key odorants in light aroma type Chinese liquor by gas chromatography−olfactometry, quantitative measurements, aroma recombination, and omission studies. *J. Agric. Food Chem.* **2014**, *62*, 5796−5804.

(11) Poisson, L.; Schieberle, P. Characterization of the key aroma compounds in an American bourbon whisky by quantitative measurements, aroma recombination, and omission studies. *J. Agric. Food Chem.* **2008**, *56*, 5820−5826.

(12) Mayr, C.; Geue, J.; Holt, H.; Pearson, W.; Francis, I. L. Characterization of the key aroma compounds in Shiraz wine by quantitation, aroma reconstitution, and omission studies. *J. Agric. Food Chem.* **2014**, 4528−4536.

(13) AQSIQ; SAC. Method of analysis for Chinese spirits. In *National Standard of the People's Republic of China*; Standardization Publishing House of China: Beijing, 2007; Vol. GB/T 10345−2007, pp 1−17.

(14) Wang, L.; Fan, W.; Xu, Y. Analysis of capillary chromatographic skeleton compounds in Chinese soy sauce aroma type liquor by liquid-liquid microextraction and aroma recombination. *Sci. Technol. Food Ind.* **2012**, 304−309.

(15) Saison, D.; De Schutter, D. P.; Delvaux, F.; Delvaux, F. R. Determination of carbonyl compounds in beer by derivatisation and headspace solid-phase microextraction in combination with gas chromatography and mass spectrometry. *J. Chromatogr., A* **2009**, *1216*, 5061−5068.

(16) Czerny, M.; Christlbauer, M.; Christlbauer, M.; Fischer, A.; Granvogl, M.; Hammer, M.; Hartl, C.; Hernandez, N. M.; Schieberle, P. Re-investigation on odour thresholds of key food aroma compounds and development of an aroma language based on odour qualities of defined aqueous odorant solutions. *Eur. Food Res. Technol.* **2008**, *228*, 265−273.

(17) Jellinek, G. *Sensory Evaluation of Food: Theory and practice*; Horwood: Chichester, U.K., 1985.

(18) Vanderhaegen, B.; Neven, H.; Verachtert, H.; Derdelinckx, G. The chemistry of beer aging: A critical review. *Food Chem.* **2006**, *95*, 357−381.

(19) Tan, Y.; Siebert, K. J. Quantitative structure−activity relationship modeling of alcohol, ester, aldehyde, and ketone flavor thresholds in beer from molecular features. *J. Agric. Food Chem.* **2004**, *52*, 3057−3064.

(20) Xie, J.; Sun, B.; Zheng, F.; Wang, S. Volatile flavor constituents in roasted pork of mini-pig. *Food Chem.* **2008**, *109*, 506−514.

(21) Poisson, L.; Schieberle, P. Characterization of the most odor-active compounds in an American bourbon whisky by application of the aroma extract dilution analysis. *J. Agric. Food Chem.* **2008**, *56*, 5813−5819.

(22) Carrillo, G.; Bravo, A.; Zufall, C. Application of factorial designs to study factors involved in the determination of aldehydes present in beer by on-fiber derivatization in combination with gas chromatography and mass spectrometry. *J. Agric. Food Chem.* **2011**, *59*, 4403−4411.

(23) Culleré, L.; Escudero, A.; Cacho, J.; Ferreira, V. Gas chromatography−olfactometry and chemical quantitative study of the aroma of six premium quality Spanish aged red wines. *J. Agric. Food Chem.* **2004**, *52*, 1653−1660.

(24) Belitz, H.-D.; Grosch, W.; Schieberle, P. *Food Chemistry*; Springer: Berlin, Heidelberg, and New Delhi, 2009.

(25) Fan, W.; Qian, M. C. Characterization of aroma compounds of Chinese "Wuliangye" and "Jiannanchun" liquors by aroma extract dilution analysis. *J. Agric. Food Chem.* **2006**, *54*, 2695−2704.

(26) Fan, W.; Qian, M. C. Headspace solid phase microextraction and gas chromatography−olfactometry dilution analysis of young and aged Chinese 'Yanghe Daqu' liquors. *J. Agric. Food Chem.* **2005**, *53*, 7931−7938.

(27) Chen, S.; Wang, D.; Xu, Y. Characterization of odor-active compounds in sweet-type Chinese rice wine by aroma extract dilution analysis with special emphasis on sotolon. *J. Agric. Food Chem.* **2013**, *61*, 9712−9718.

(28) Albertazzi, E.; Cardillo, R.; Servi, S.; Zucchi, G. Biogeneration of 2-phenylethanol and 2-phenylethylacetate important aroma components. *Biotechnol. Lett.* **1994**, *16*, 491−496.

(29) Etschmann, M.; Bluemke, W.; Sell, D.; Schrader, J. Biotechnological production of 2-phenylethanol. *Appl. Microbiol. Biotechnol.* **2002**, *59*, 1−8.

(30) Wang, X.; Fan, W.; Xu, Y. Comparison on aroma compounds in Chinese soy sauce and strong aroma type liquors by gas chromatography−olfactometry, chemical quantitative and odor activity values analysis. *Eur. Food Res. Technol.* **2014**, *239*, 813−825.

DOI: 10.1021/jf506238f
J. Agric. Food Chem. 2015, 63, 3660−3668

SPAD-502 readings in estimating leaf N. The latter might be the consequence of surface-based Chl often compared to mass-based N,[11,15] although the effect of leaf mass per area (LMA) on this relationship has been clearly demonstrated for ligneous species in general[16] or specifically for grapevine.[17] It should be mentioned here that grapevine was also used as a model plant to analyze the potential of optical leaf clips to nondestructively assess leaf Chl content,[18,19] independently of its relation to nitrogen.

Two major problems with the use of the SPAD-502 (N-tester) or equivalent leaf clips are their nonlinearity,[19] especially at optimal and supraoptimal N contents, and the influence of the variable LMA.[20] This sensor nonlinearity is independent of the additional nonlinearity due to the physiological saturation of leaf response to N.[21,22] Recently, in addition to single-parameter Chl leaf clips, both multiparameter leaf clips and multiparameter proximal sensors have become available.[21−23] Therefore, a bi- or multiparametric approach to estimating N can be attempted. Cartelat et al.[24] proposed the use of the nitrogen balance index (NBI), which is the ratio of Chl to epidermal flavonol (Flav) leaf content, for nitrogen nutrition of wheat in the context of precision agriculture. Ten years later, the advent of the new Dualex leaf clip and the proximal sensor Multiplex from FORCE-A has allowed for an easier assessment of this new nitrogen index and has permitted its extension to other crops, including both monocots[21,22,25,26] and dicots.[27,28] Nevertheless, there is a need for a proper quantitative calibration of this index to implement its use in crop diagnostics. Leaf Chl and flavonol contents on a surface basis are both dependent on leaf age and light experienced during growth.[29,30] They both increase with age and light during the first part of the season. During the second part, Chl tends to decrease while Flav remains constantly high.[29] The NBI index (Chl/Flav) is much less sensitive to phenology, and it reflects the N availability better than either of the two indicators used individually.[16,21,22,24,25,31,32]

Most important experiments on N fertilization were performed under controlled conditions in potted plants.[33−35] We wanted to test the NBI approach in vineyards under real viticultural practices for which this optical diagnostic approach was originally designed. There are no published calibrations for N measurements by these new devices, namely, the Dualex and the Multiplex. As the Dualex responds linearly to both Chl and Flav leaf contents,[19] the NBI index can potentially be quantitatively related to leaf N content. Therefore, the objectives of this paper are (1) to provide a calibration of the Dualex response to leaf N content, (2) to verify the robustness of the N estimation by NBI in grapevine as a diagnostic method, and (3) to propose a protocol for leaf sampling for optical diagnostics of N content in grapevine.

MATERIALS AND METHODS

Experimental Design and Sensors. Experiments were performed over a period of 5 years, parallel to the development of the new Dualex leaf clips. Therefore, both the SPAD-502 (Konica-Minolta, Tokyo, Japan) and the Dualex 4 Scientific (FORCE-A, Orsay, France) were used for the Chl measurements. SPAD-502 units were transformed into leaf Chl content on a surface basis (μg cm^{-2}) using the consensus formula from Cerovic et al.[19] The Dualex 4 Scientific Chl was used as given by the device because it was calibrated in μg cm^{-2} units.[19] Epidermal Flav values were measured by the Dualex leaf-clip version Dualex 3.3 (FORCE-A) and the version Dualex 4 Scientific. Absorbance in the UV at 375 nm due to flavonol presence in the epidermis was used as given by the device without transformation.

For the data set Leaves 2007, leaves were sampled at the Fort Chabrol vineyard in Epernay, Champagne, France (03°57′ E, 49°02′ N) in May 2007 just before flowering (BBCH 57).[36] No. 5 leaves counted from the tip of the shoots were chosen from Pinot noir vines. The first leaf having a central vein longer than 3 cm was considered as leaf no. 1. Six light-exposed and six shaded leaves were measured with the SPAD-502 from the abaxial leaf side once on the left-hand side (position 1) and once on the right-hand side (position 2) from the main vein (cf. Figure S2, Supporting Information). Total Chl for each spot was calculated from the SPAD-502 measurements using the consensus equation from Cerovic et al.[19] Flavonols were measured by the Dualex 3.3 on the same leaf spots as for Chl, but from both the adaxial and abaxial leaf sides. The mean Chl value from the two spots was calculated for each leaf. The mean Flav value was calculated for the two spots from the sum of the abaxial and adaxial sides. The NBI[24,37] was calculated from these mean Chl and Flav data for each leaf. A 1 cm^2 disk sampled from the spot in position 1 was used for Chl extraction and a 1 cm^2 disk sampled from the spot in position 2 for nitrogen content analysis.

For the Leaves 2009 data set, leaves were sampled on May 28 and 29, 2009, just before flowering (BBCH 57) at the Plumecoq experimental vineyard near Epernay, France (03°58′ E, 49°01′ N) belonging to the Champagne committee. A total of 59 no. 5 leaves counted from the shoot tip were sampled from Pinot noir (29 leaves) and Chardonnay (30 leaves) planted in 1996 and trained to a "Chablis" system, with three canes. Leaf Chl was measured with both the SPAD-502 and the Dualex 4 Scientific on the adaxial leaf side on the two spots, as for the Leaves 2007 data set (cf. Figure S1, Supporting Information). Flavonols were measured by both the Dualex 3.3 and the first version of the Dualex 4 Scientific on the same leaf spots on both leaf sides. The mean Chl value for the two spots was calculated for each leaf, both for Dualex 4 Scientific and for SPAD-502 measurements. The mean Flav value was calculated for the two spots from the sum of the abaxial and adaxial side measurements with the Dualex 3.3. The SPAD-502 measurements were transformed using the consensus equation from Cerovic et al.[19] The NBI index was calculated from the Chl and Flav data for each leaf. A 0.58 cm^2 disk sampled from the spot in position 1 was used for Chl extraction and a 0.58 cm^2 disk sampled from the spot in position 2 for nitrogen content analysis.

For the Plot 2009 data set, 60 leaves were sampled from each of the 27 commercial plots scattered around Epernay in Champagne. In total, 1620 leaves were measured. Plots from 0.3 to 1 ha, having different soils and cultural practices, planted with Pinot noir, Meunier, and Chardonnay of different ages were chosen. No. 5 leaves were sampled from three rows per plot from May 18 to May 27, 2009, just before flowering (BBCH 55−57). Two spots per leaf, as in the Leaves 2007 data set, were measured by the SPAD-502 for Chl and the Dualex 3.3 for Flav. The total Chl for each spot was calculated from the SPAD-502 measurements using the consensus equation from Cerovic et al.[19] The Chl, Flav, and NBI indices were calculated for each leaf as described in the Leaves 2009 data set. Two 0.58 cm^2 disks were sampled per leaf (both spots) for nitrogen content analysis (see below). The averages of the three optical indices, Chl, Flav, and NBI, and the N content were calculated for each plot from the 60-leaf data.

The Subplots 2012 data set was obtained at Chateau Gazin near Bordeaux, France (0°11′ E, 44°55′ N) on July 27, 2012, at the bunch closure stage (BBCH 79). The plot was planted with Merlot noir on SO4 in 1977 and trained as a double Guyot, with 1.25 m intrarow and 1.4 m interrow spacing. A total of 10 subplots were selected on the basis of a map of the NBI produced by a Multiplex-mounted system (FORCE-A) a few days before (cf. Figure S2, Supporting Information). Three leaves from three consecutive vines were measured by the most recent version of the Dualex 4 Scientific for both Chl and Flav. These nine-leaf batches were repeated three times on each of the 10 subplots. Thanks to the relative heterogeneity inside each of the chosen subplots (cf. Figure S1, Supporting Information), the nine-leaf batches could be used individually, producing a final data

DOI: 10.1021/acs.jafc.5b00304
J. Agric. Food Chem. 2015, 63, 3669−3680

set of 31 samples (3 × 10) + 1, because in the last subplot an extra batch of nine leaves was measured. Although only mature leaves on primary shoots were sampled, as in the three other data sets, there were two major differences: the exact node position on the shoot was not assessed, and only one spot on the leaf was measured; care was taken to only sample leaves from the same height of the canopy at which the Multiplex measurements were made, above the second wire. The details of the mounted Multiplex mapping of a vineyard are described in detail elsewhere (Diago et al., manuscript in preparation). They were not relevant for this study, where NBI maps were only used to choose the sampling sites that will allow a sufficiently large span of variable situations.

Chlorophyll Extraction. Leaf disks were collected immediately after the optical measurements. They were frozen in liquid nitrogen and stored at −80 °C until further processing. Disks were powdered in liquid nitrogen and extracted three times at room temperature with methanol (3 × 1.5 mL) containing calcium carbonate.[19] The three supernatants obtained by centrifugation (10000*g*, 5 min) were grouped, topped to 5 mL, and centrifuged again at 4100*g* for 5 min. The extinction coefficients for Chl in pure methanol of Porra et al.[38] were used to calculate the Chl concentration in the extracts.

Leaf Nitrogen Content. In the Leaf 2007 and Leaf 2009 data sets, individual leaf disks were freeze-dried, and after fine grinding, a 2−3 mg aliquot of the powder was analyzed by the Dumas method using isotope ratio mass spectrometry coupled with elemental analysis (EA−IRMS) using the analytical platform Metabolism-Metabolome of Labex Saclay Plant Science (France). This method measures the total N content, including nitrate. For the Plots 2009 data set, 120 disks were pooled together per plot and the aliquots were analyzed as described above. In the Subplots 2012 data set, nine whole leaves were pooled together per subplot sample after the optical measurements. Leaves were dried at 65 °C until a constant weight was obtained and then ground. Total leaf nitrogen content was determined in 50 mg aliquots for each subplot by the Kjeldahl method in a commercial laboratory (Laboratoire LCA, Bordeaux, France).

Statistical Analysis and Plotting. Data were treated, transformed, statistically analyzed, fitted, and plotted using a combination of software: Excel 2003 (Microsoft, Redmond, WA), Statistica 6 (StatSoft, Tulsa, OK), and Igor Pro 6.02 (WaveMetrics, Portland, OR). The accuracies of the fitted models and of the prediction of leaf N content from Chl and Flav contents and the NBI index were assessed by the coefficient of determination (R^2) and the root mean square error (RMSE):

$$\mathrm{RMSE} = [1/n \sum_{i=1}^{n} (\hat{y}_i - y_i)^2]^{1/2} \quad (1)$$

where $\hat{y}_i$ is the model-predicted value and y_i the measured value. "Major axis" regressions were used in all of the presented graphs, considering that the error is present in both plotted variables.[39]

Other descriptors listed in Tables 1 and 2 for the classification test are defined as usual,[40] using the true positive (TP), false positive (FP), false negative (FN), and true negative (TN) values present in the contingency table (Table 1) that compares the diagnostic test to the gold standard (here the wet chemistry N analysis):

$$\text{sensitivity} = \mathrm{TP}/(\mathrm{TP} + \mathrm{FN}) \quad (2)$$

$$\text{specificity} = \mathrm{TN}/(\mathrm{TN} + \mathrm{FP}) \quad (3)$$

$$\text{Youden index} = \text{sensitivity} + \text{specificity} - 1 \quad (4)$$

$$\text{accuracy index} = (\mathrm{TP} + \mathrm{TN})/(\mathrm{TP} + \mathrm{TN} + \mathrm{FP} + \mathrm{FN}) \quad (5)$$

The number of leaves needed to establish reliable sampling guidelines was calculated according to Dagnelie:[41]

$$\text{sample size} = k(\mathrm{CV})^2/\partial^2 \quad (6)$$

where CV is the coefficient of variation of the sample and ∂ the relative difference among plots that we want to detect. The parameter k is approximately 21 and 40 for acceptable errors of 10% and 5%, respectively.

Table 1. Example of a Contingency Table for the Calculation of the Youden Index[a]

	leaf nitrogen content		
	nitrogen + (N+)	nitrogen − (N−)	
optical index + (I+)	TP	FP	sum of I+
optical index − (I−)	FN	TN	sum of I−
	sum of N+	sum of N−	sample size (n)
	sensitivity	specificity	Youden index

	leaf nitrogen content		
	N+	N−	
I+	15	1	16
I−	1	10	11
	16	11	27
	0.94	0.91	0.85

[a]Data are for the chlorophyll index of the Plots 2009 data set (Figure 3): true positive (TP), false positive (FP), false negative (FN), and true negative (TN). For index definitions and calculation formulas, see the Materials and Methods.

Table 2. Statistics for the Calibration Models and Classification Test Indices for the Optical Indices[a]

optical index		Leaves 2007	Leaves 2009	Plots 2009	Subplots 2012
	N threshold (mg/g)	35	40	35	30
	sample size (n)	12	59	27	31
NBI	RMSE	2.5	3.7	1.7	1.8
	R^2	0.740	0.488	0.907	0.844
	sensitivity	0.71	0.79	0.94	0.77
	specificity	1	0.88	1	0.94
	Youden index	0.71	0.67*	0.94	0.71
	accuracy index	0.83	0.83	0.96	0.87
Chl	RMSE	2.2	4.5	2.0	2.6
	R^2	0.790	0.387	0.877	0.722
	sensitivity	0.71	0.74	0,94	0.85
	specificity	0.80	0.72	0.91	0.89
	Youden index	0.51	0.46***	0.85	0.74
	accuracy index	0.75	0.73	0.93	0.87
Flav	RMSE	4.1	7.6	2.3	3
	R^2	0.498	0.184	0.840	0.659
	sensitivity	0.71	0.44	0.94	0.77
	specificity	1	0.52	1	0.94
	Youden index	0.71	−0.04***	0.94	0.71
	accuracy index	0.83	0.48	0.96	0.87

[a]Samples were made of individual leaves for Leaves 2007 and Leaves 2009. Samples were averages of 60 leaves for Plots 2009 and averages of 9 leaves for Subplots 2012. RMSE is expressed in N units. All R^2 values were highly significant ($p < 0.001$). The t test was applied to verify the significance of the differences among the Youden indices of optical indices, both among data sets and among optical indices. The p values for the differences are indicated using asterisks: *, $p < 0.05$; ***, $p < 0.001$.

RESULTS AND DISCUSSION

Calibration of Optical Indices against Leaf N. Although the Dualex can be used on any crop or plant species, we decided to present here the specific case of grapevine, which is a crop and a ligneous species. We calibrated the Dualex against leaf nitrogen content as the "gold standard" by using natural variability of the nitrogen supply to grapevine due to soil heterogeneity, as opposed to controlled fertilization experi-

DOI: 10.1021/acs.jafc.5b00304
J. Agric. Food Chem. 2015, 63, 3669−3680

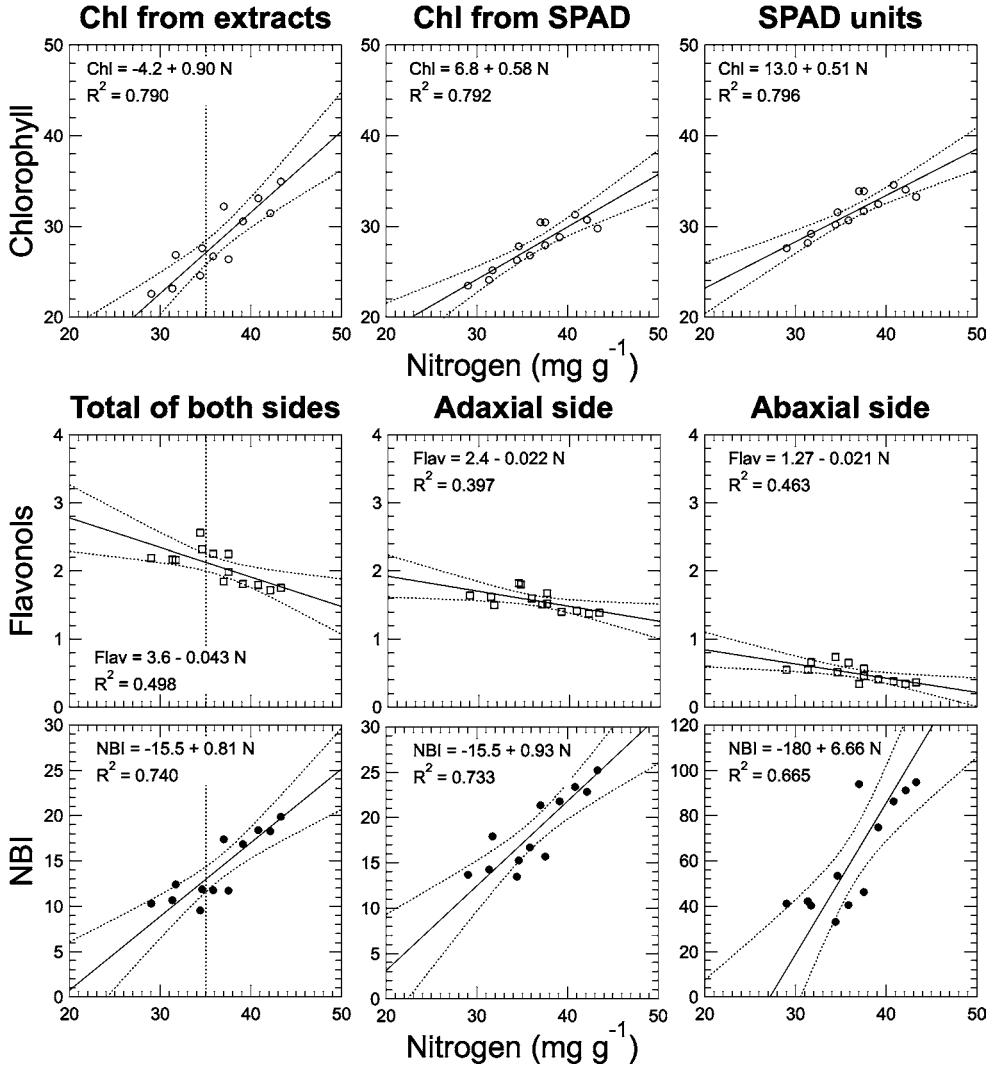

Figure 1. Dependence of optical indices on individual leaf nitrogen content for the Leaves 2007 data set. Each datum represents an individual leaf. The three top graphs are for Chl: total Chl content measured from extracts (left), Chl measured with the SPAD-502 (right), and Chl calculated from the SPAD-502 measurements using the consensus equation from Cerovic et al.[19] (center). Three Flav indices are presented in the middle row of the figure: Flav measured from the abaxial side of the leaf (right), Flav measured from the adaxial side of the leaf (center), and the sum of Flav of the two sides (left). All three NBI indices, total (left), adaxial (center), and abaxial (right), were calculated using the same transformed SPAD-502 measurements (center Chl graph). Regression models are indicated on the graphs by a full line, with dotted lines representing the 95% confidence interval bands. The vertical dotted line indicates the threshold limit used for the classification test presented in Table 2.

ments that usually yield a smaller number of data points and ambiguous results on ligneous perennials.[15] The responses of Chl, Flav, and NBI to N content in individual leaves are presented in Figures 1 and 2, and responses at the level of leaf populations, whole plots or subplots, are presented in Figures 3 and 4, respectively. All figures were plotted with the same N range for an easy visual comparison, although the different data sets did not have the same N average, span, or range. This is especially the case for Subplots 2012 (Figure 4) that was sampled two months later (end of July) than the other three data sets (end of May) (Figures 1−3). Linear regression models were sufficient and were the best in all cases. Determination coefficients (R^2) are indicated in the graphs and in Table 2. Table 2 also includes the corresponding RMSE. Using both criteria and for all three optical indices, Plots 2009 gave the best results with the smallest RMSE for the estimation of N content of 2.3, 2.0, and 1.7 mg g^{-1} for Flav, Chl, and NBI, respectively (Table 2). This is a consequence of the larger number of leaves averaged in the Plots 2009 data set. Data for the three cultivars were analyzed together. This showed the universality of the calibration, at least for these three cultivars. In all four data sets, Chl was better related to N than was Flav, with RMSE for Chl almost 2 times smaller for individual leaves. They were 2.2 vs 4.1 mg of N g^{-1} DW and 4.5 vs 7.6 mg of N g^{-1} DW, for Chl vs Flav, respectively (Table 2). The difference was much smaller in the case of plots and subplots where populations of leaves are sampled and averaged together, 2.0 vs 2.3 mg of N g^{-1} DW and 2.6 vs 3.0 mg of N g^{-1} DW, for Chl vs Flav (Table 2). Moreover, NBI was the best estimator of N content in all situations except for Leaves 2007, in which light-exposed and shaded leaves were mixed. There was a substantial decrease of NBI RMSE to 1.7 and 1.8 for plots and subplots and an increase in R^2 to 0.907 and 0.844 for Plots 2009 and Subplots 2012. Therefore, NBI, which is the ratio of Chl to Flav, improves the estimation of N even though it combines two estimators of inferior quality.

DOI: 10.1021/acs.jafc.5b00304
J. Agric. Food Chem. 2015, 63, 3669−3680

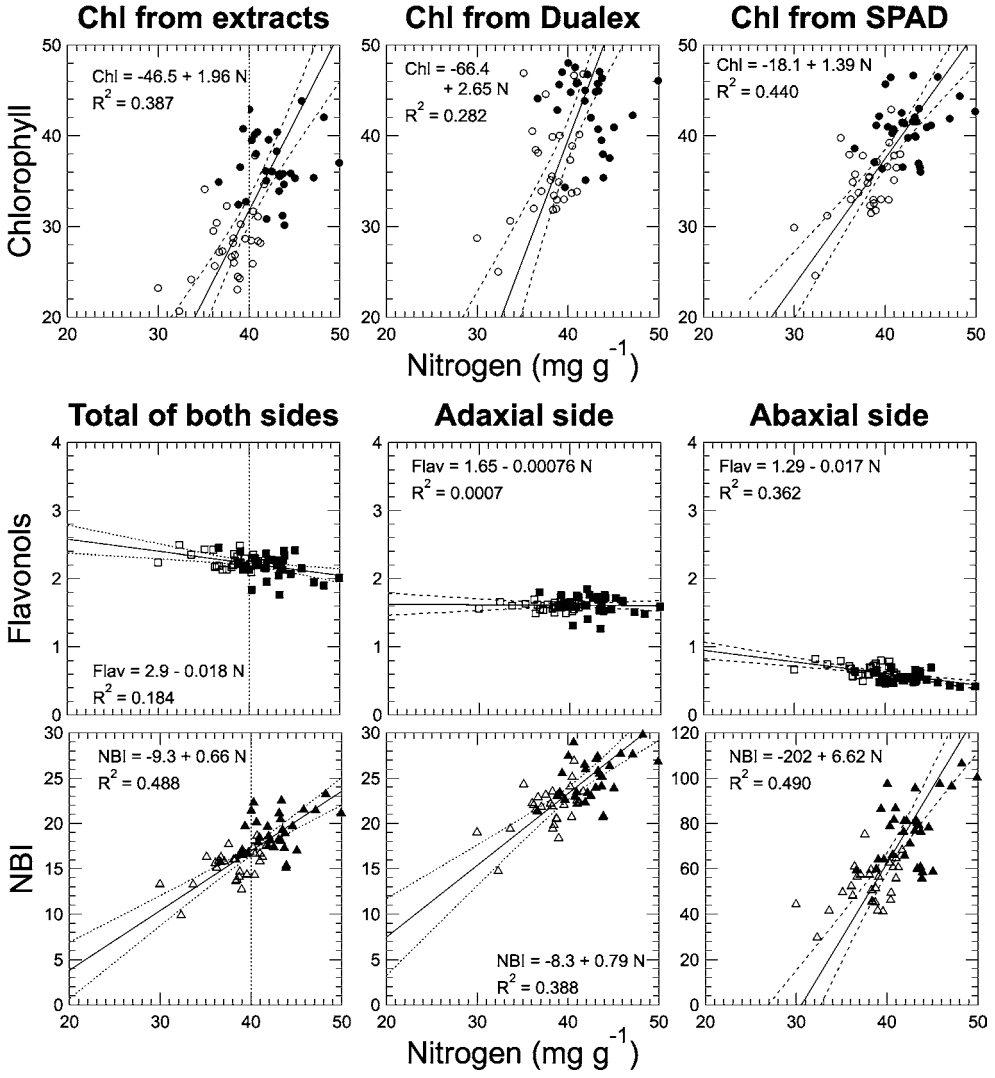

Figure 2. Dependence of optical indices on individual leaf nitrogen content for the Leaves 2009 data set. Each datum represents an individual leaf. Open symbols were used for Chardonnay and closed symbols for Pinot noir. The three top graphs are for Chl: total Chl content measured from extracts (left), Chl measured with the Dualex (center), and Chl calculated from the SPAD-502 measurements using the consensus equation from Cerovic et al.[19] (right). Three Flav indices are presented in the middle row of the figure: Flav measured from the abaxial side of the leaf (right), Flav measured from the adaxial side of the leaf (center), and the sum of Flav of the two sides (left). All three NBI indices, total (left), adaxial (center), and abaxial (right), were calculated using the same transformed SPAD-502 measurements (right Chl graph). Regression models are indicated on the graphs by a full line, with dotted lines representing the 95% confidence interval bands. The vertical dotted line indicates the threshold limit used for the classification test presented in Table 2.

The calibration at the population level, 60 leaves at the plot level (Figure 3) and 9 leaves at the subplot level (Figure 4), which is the agronomical pertinent situation, decreased the variability compared to individual leaf calibration (Figures 1 and 2). Plots 2009 and Subplots 2012 were two very different data sets. The former was obtained for Champagne on Pinot noir at flowering and the latter for Bordeaux on Merlot noir at bunch closure. The two month difference was the major factor governing the differences seen between the two.[16] Flavonol content in Subplots 2012 was greater because flavonols were accumulated with time and light exposure. Leaf N content was smaller because it was diluted with time and LMA increase.[6,42] This had a cumulated consequence on the NBI that also decreased. The data obtained here for Pinot noir (Figure 3) and Merlot noir (Figure 4) correspond to those obtained by Romero et al.[6] on Tempranillo. In both cases, the average N content decreased from 36 mg g^{-1} at the end of May to 28 mg g^{-1} at the end of July. Contrary to our expectations, a precisely controlled situation in which local Dualex sampling on leaf disks was compared to a chemically tested leaf N on the very same disk (Figures 1 and 2) did not produce better calibrations than the mixed-leaf N analysis (Figures 3 and 4). Pooled leaves from a single height without even counting the nodes (Figure 4) produced better results than single leaves (Figures 1 and 2).

Nitrogen Balance Index. The NBI correlates better with N content on a mass basis because it takes into account not only the surface-based variability in N investment in the photosynthetic machinery but also the variation in LMA. This advantageous relationship could be obtained by comparing surface-based Chl with surface-based N after its transformation with the LMA (surface-based N = mass-based N × LMA), but unfortunately, the estimation of LMA is destructive. In ligneous species light controls N investment in leaves to adjust photosynthesis to its light environment (photosynthetically

DOI: 10.1021/acs.jafc.5b00304
J. Agric. Food Chem. 2015, 63, 3669−3680

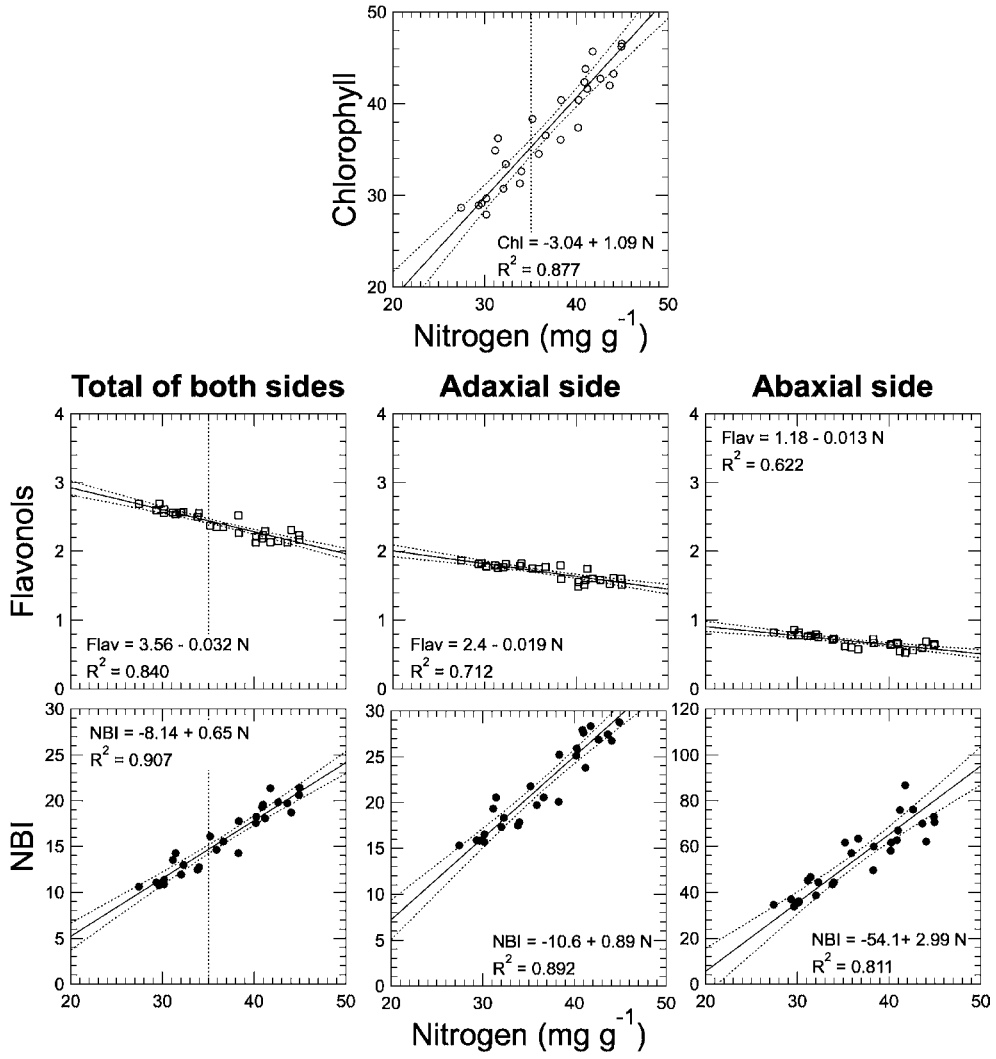

Figure 3. Dependence of optical indices on the mean nitrogen content for the Plots 2009 data set. Each datum represents a single plot characterized by the average of 60 leaves. The top graph is for Chl calculated from the SPAD-502 measurements using the consensus equation from Cerovic et al.[19] Three Flav indices are presented in the middle row of the figure: Flav measured from the abaxial side of the leaf (right), Flav measured from the adaxial side of the leaf (center), and the sum of Flav of the two sides (left). All three NBI indices, total (left), adaxial (center), and abaxial (right), were calculated using the same transformed SPAD-502 measurements (top Chl graph). Regression models are indicated on the graphs by a full line, with dotted lines representing the 95% confidence interval bands. The vertical dotted line indicates the threshold limit used for the classification test presented in Table 2.

active radiation (PAR) irradiance) by increasing LMA (mostly leaf thickness) without changing mass-based N.[43] This has been shown for grapevine,[34] for beech,[44] and for tropical trees.[45] This is why surface-based leaf Chl content obtained with leaf clips might not always correlate to leaf N. Surface-based Chl will reflect leaf N only when comparisons are made among leaves that developed under different N supplies but under the same light regime. Using Flav as a proxy for LMA[16,30] can compensate for different leaf light exposures. Therefore, the introduction of the NBI index will alleviate the frequent problem of surface-based Chl measurements compared to mass-based N (see, for example, the paper by Porro et al.[11]).

The abaxial Flav level was always lower than the adaxial level (Figures 1−4). Later in the season (Figure 4), both leaf sides had larger Flav contents, but the increase was more marked on the abaxial side. The single-sided Flav defines the single-sided NBI because Chl remains the same independent of the side from which it is measured (illustrated in Figure 4). Indeed, Chl in Figure 4 shows that there were no significant differences when it was measured from the adaxial or abaxial side, confirming that a single measurement is sufficient for leaf clips based on transmittance. In all four cases (Figures 1−4), the total NBI calculated using the sum of Flav of both leaf sides was better correlated to N (higher R^2) than single-sided NBI. In addition, it can be seen that sometimes single-sided NBI (adaxial NBI in Figures 1 and 3, abaxial NBI in Figure 2) gives estimations as good as the total NBI. Still, the absolute values of the total NBI are more stable. Single-sided measurements are important for the future use of noncontact fluorescence sensors such as the Multiplex that have a different response depending on the side or measurement[10] (Diago et al., manuscript in preparation), but this is outside the scope of the present paper.

Classification Test. For arable crops that have a quadratic response of yield to N supply, with saturation often above a threshold, the Cate−Nelson classification[46] can be used to separate the responding from the nonresponding regions in the yield-to-N supply curves. Here we have a linear relationship between optical indices and leaf N, so the Cate−Nelson

DOI: 10.1021/acs.jafc.5b00304
J. Agric. Food Chem. 2015, 63, 3669−3680

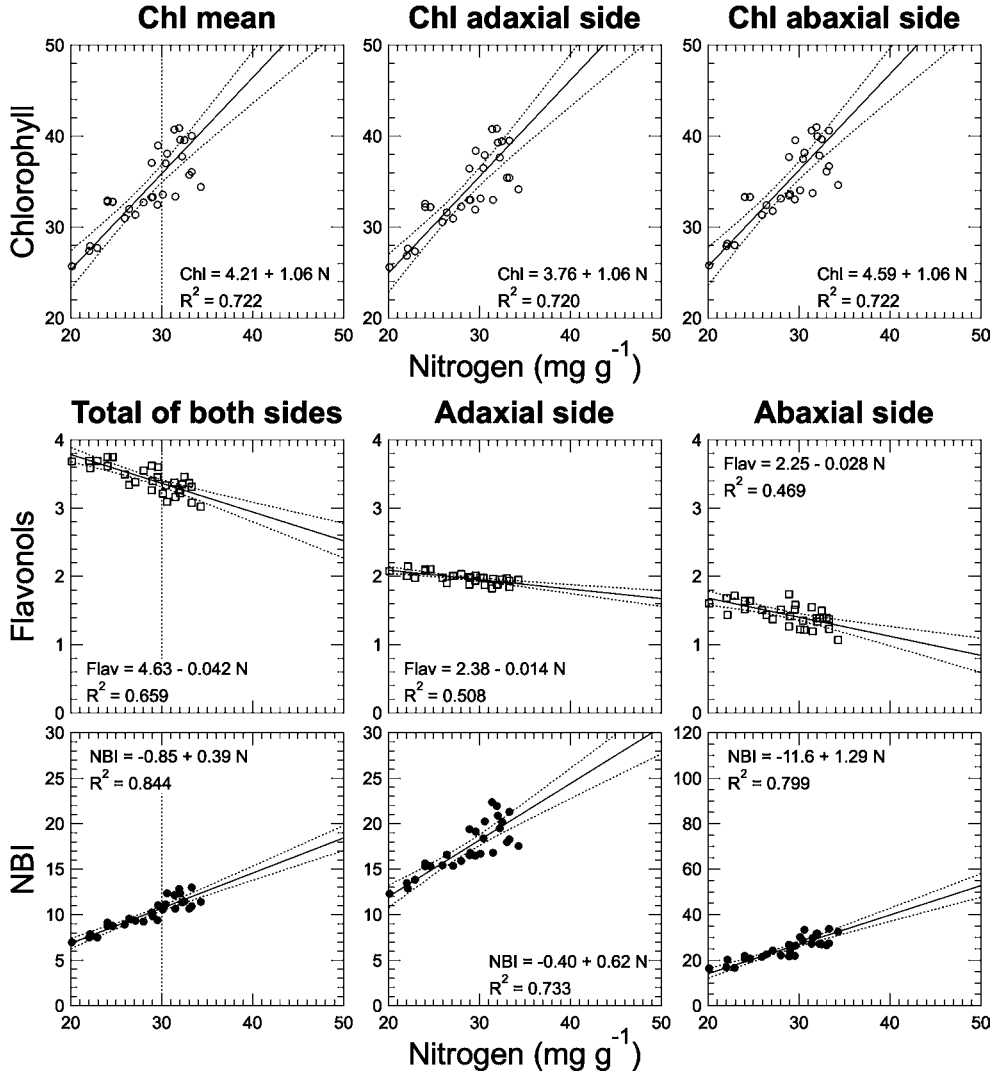

Figure 4. Dependence of optical indices on the mean nitrogen content of leaves for the Subplots 2012 data set. Each datum represents a subplot characterized by the average of nine leaves present on three adjacent vines. The three top graphs are for Chl measured with the Dualex 4 from the abaxial side of the leaf (right) and from the adaxial side of the leaf (center) and the mean Dualex Chl of the two leaf sides. Three Flav indices are presented in the middle row of the figure: Flav measured from the abaxial side of the leaf (right), Flav measured from the adaxial side of the leaf (center), and the sum of Flav of the two sides (left). The three NBI indices, total (left), adaxial (center), and abaxial (right), were calculated using the mean Dualex Chl and the adaxial and the abaxial Chl, respectively. Regression models are indicated on the graphs by a full line, with dotted lines representing the 95% confidence interval bands. The vertical dotted line indicates the threshold limit used for the classification test presented in Table 2.

statistical procedure was not well adapted. However, for practical purposes optical indices are usually used to diagnose deficiency and classify plots to those needing fertilization or not, thanks to their relationship to leaf N. This is why the presented continuous values (Figures 1−4) can also be analyzed on the basis of a cutoff value for sufficient leaf N. An evaluation of the test for this binary classification can be done by calculating the Youden index (Youden's J statistics, informedness)[40] (Table 1). This index is a commonly used measure for overall diagnostic effectiveness of a method. It is especially useful because it combines sensitivity and specificity, which are both prevalence-independent statistics. Leaf N content is considered here as the gold standard for N sufficiency. Generally, levels of N in leaf blades below 20 mg g^{-1} between flowering and véraison indicate deficiency[47] (see Table S1, Supporting Information). For the four different data sets, we had to apply different threshold values to have an acceptable prevalence (proportion of positive values) for the contingency table analysis. The threshold values (cutoffs) were chosen to have a prevalence of around 50%. In addition, they corresponded to the real situation generally recorded in the field (cf. Table S1). The individual leaf data sets (Figures 1 and 2) and the plot data set (Figure 3) for Champagne cultivars were obviously on the high N side; therefore, 35 and 40 mg g^{-1} thresholds were tested (Table 2). For the Leaves 2009 data set, we used a higher threshold (40 mg g^{-1}) because for the 35 mg g^{-1} threshold the prevalence was too large to be acceptable (0.89).[40] According to Youden,[40] the sample size was sufficient for comparisons except for the Leaves 2007 data set, which only had 12 leaves. No significant differences among indices (NBI vs Chl vs Flav) or among data sets (type of data sets) were found, apart from the Leaves 2009 data set, for which the Youden index for Flav was much lower than that for Chl and NBI (Table 2). In plant disease research, as in medicine, one would

DOI: 10.1021/acs.jafc.5b00304
J. Agric. Food Chem. 2015, 63, 3669−3680

favor tests that minimize false negatives, that is, tests that maximize sensitivity. On the contrary, farmers' adversity toward loss of yield would prefer an indicator that minimizes false positives, that is, which maximizes specificity. They prefer to fertilize even if it is not needed, rather than to lose some yield. In viticulture at the lower threshold (N-deficient vines), a viticulturist would behave like any other farmer, but at the higher threshold (N overfertilization), he should behave like a physician: he would favor an indicator that avoids false negatives because overly vigorous vines are more prone to diseases and produce grapes of lower technological quality.[4]

The Leaf 2009 data set, which had the largest dispersion of experimental points, is characteristic of the advantage of NBI over the use of Chl and Flav indices alone. Using a poor Flav index that has low sensitivity and specificity (Youden's $J = 0$) to divide a modest Chl index that has a modest sensitivity and specificity (Youden's $J = 0.46$) produced an NBI index that has a fair sensitivity (0.79) and a high specificity (0.88). The Youden index for NBI increased to 0.67, and accuracy reached 0.83. This is an outstanding achievement for an index that has an RMSE of 3.7 mg g^{-1}, which is 2 times larger than the plot (1.7) and subplot (1.8) RMSEs (Table 2). We can conclude that both the Youden index and the accuracy of the leaf-clip method are very good for N nutrition estimation in grapevine. There were two major reasons for this success. First, Dualex had a more linear response than SPAD-502 thanks to the choice of a less absorbed sensing wavelength.[19,48] However, the use of the consensus equation[19,48] for the transformation of SPAD-502 units also helped to obtain quantitative relationships. Second, grapevine is a crop usually fertilized with parsimony; therefore, leaves rarely attain the very high levels of N and Chl found in overfertilized grain crops.[49] Even then, it is expected that epidermal leaf Flav will continue to respond to increased N when Chl stops responding.[10,21,22]

Choice of the Representative Leaf and Growth Stage. Reliable estimation of N content will be dependent on several factors: the most representative leaf, the number of leaves to represent the management unit, the best plant, and the leaf phenological stage.[3,8] In a preliminary experiment, we measured all leaves of all primary shoots of a Merlot noir vine on three dates in July 2014. The within-plant coefficients of variation for Chl, Flav, and NBI were 25%, 12%, and 31%, respectively. Therefore, to discriminate a 10% difference in Chl content with an acceptable error of 10%, a minimum of 131 leaves would be needed to reliably sample a plot (250 leaves for an error of 5%)[41] (see the Materials and Methods). Fortunately, the variation among the leaves at the same node number is much smaller than that, ranging from 6.6% to 14%. By fixing the node position, the needed number of sampled leaves decreases to a minimum of 9 and a maximum of 45 for an acceptable error of 10% (41−78 leaves for an error of 5%). The intraleaf variability can be even smaller. Its coefficient of variation was often 4%, 6%, and 8.5% for Chl, Flav, and NBI, respectively. Therefore, with a measurement on a single well-defined position on a leaf, one could concentrate the sampling effort to different vines because it is advantageous to sample leaves from different plants in a sufficient number to obtain a smaller variance in N estimation.[8]

The leaf opposite the first cluster on node no. 4 counted from the base of the shoot is often used for N analysis.[11] At flowering this leaf corresponds to a just-matured leaf, but at later phenological stages it is not the best choice because it becomes very old. Therefore, attempts were made to replace it by the next leaf just above it, i.e., the leaf opposite the second cluster, or even the leaf four nodes above it.[5,50] It is obvious that a metabolically active younger leaf would be a better choice.[51] If 4−5 nodes are counted above the clusters, as preconized in Italy[50] for later growth stages, it would have forced us to select a leaf on node nos. 8−9 from the base. For a 13−14-leaf shoot, it will actually correspond to leaf no. 5 from the tip. Often used in phytopathology research,[52] leaf no. 5 from the tip is representative of the leaf that has just attained maturity. From an expanding carbon sink leaf, it becomes a carbon source leaf; therefore, it is more sensitive to deficiencies. The universally accepted node and the leaf position for N sampling that we recommend here is around the ninth node from the shoot base for a 14-node fully developed shoot. This leaf will be in the upper half of the vertical shoot positioning (VSP) trained vines, above the second wire in a three-wire trellis system, or just below the second wire in a two-wire trellis system. This would also be the best position for the noncontact on-the-go sensing with optical sensors such as the Multiplex[32] or the Crop Circle.[12]

In addition to postharvest autumnal fertilization, flowering is the best phenological stage for in-season fertilization[34] because at this stage it is still possible to correct for N deficiency by in-season amendments if needed. Véraison, the stage at which most diagnoses are often performed (Table S1, Supporting Information), is too late for efficient in-season amendment.[51] It can only be useful as information for viticultural practice decisions concerning next year's crop, such as the severity of pruning and potential interrow cropping. Therefore, performing leaf N diagnosis somewhere between flowering and bunch closure (BBCH 65−75) would be recommended.

Leaf Nitrogen Norms. For various plant species and independently of the growth stage, N contents in mature leaf tissue of less than 25, between 25 and 45, and above 60 (mg of N g^{-1} DW) are usually considered as deficient, sufficient, and excessive, respectively.[3] In grapevine, excess N can be even more damaging than deficiency because vines would be more subject to diseases and insect infestations.[53] Overfertilization usually produces grapes of lower quality.[4] Overfertilized plants are also prone to flowering abortion and a lack of fruit set.[3,54] Therefore, for grapevine these N thresholds were defined for individual countries or even wine-growing regions[55,56] (cf. Table S1, Supporting Information). For example, for Washington, the critical range proposed is 25−35 mg of N g^{-1} DW at bloom and 22.5−32.5 mg of N g^{-1} DW at véraison.[57] For Bordeaux, leaf N contents at véraison of 22.0, 26.2, and 34.1 mg of N g^{-1} DW were considered limited, mean, and excessive by Hilbert et al.[35] (cf. Table S1).

Calibrations performed in the present work allow us to propose the corresponding values of Chl and NBI for the consensus thresholds drawn from the literature at flowering and bunch closure (Table 3). On the basis of the literature survey, we have chosen 30 and 40 mg of N g^{-1} DW for the lower and upper thresholds at flowering and 22 and 32 mg of N g^{-1} DW at bunch closure. The corresponding Chl values are 30 and 40 μg cm^{-2} for flowering and 29 and 37 μg cm^{-2} for bunch closure. The corresponding NBI values are 11 and 18 for flowering and 8 and 11 for bunch closure.

When proposing the use of absolute thresholds, it is important to estimate the associated uncertainty. Several factors should be taken into account: leaf position (10% error), phenological phase at time of diagnosis (5%), inherent precision (or lack of precision) of the optical diagnostic

DOI: 10.1021/acs.jafc.5b00304
J. Agric. Food Chem. 2015, 63, 3669−3680

Table 3. Tentative Grapevine Leaf Content Norm Thresholds for Nitrogen (mg g^{-1}), Dualex Chlorophyll (μg cm^{-2}), and Dualex NBI Index at the Flowering and Bunch Closure Growth Stages

	deficient	sufficient (optimal)	excessive (overfertilized)
		Flowering	
nitrogen	<30	30−40	>40
chlorophyll	<30	30−40	>40
NBI index	<11	11−18	>18
		Bunch Closure	
nitrogen	<22	22−32	>32
chlorophyll	<29	29−37	>37
NBI index	<8	8−11	>11

method (10%), and the precision of the gold standard (5%). The differences in estimation of N content by the reference methods can be substantial because they do not analyze the same type of N. The Dumas combustion method includes all types of N (NH_4, NO_3, and protein and heterocyclic N). The N_2 produced is determined by mass spectroscopy or by thermal conductivity detection with reproducibility not better than 5%. The Kjeldahl digestion method, until now the industry standard, yields lower results than the Dumas method because it neglects heterocyclic N. It can be performed with or without NO_3 and NO_2 recovery, which changes the results among laboratories.[8] Therefore, if we want to use an absolute threshold calibrated against the gold standard, the overall uncertainty of optical estimation including all factors will not be smaller than 16%. The latter value was calculated as the square root of the sum of squares of individual errors assuming that individual errors were independent and uncorrelated. This is larger than the year-to-year variability of ±10% found by Failla et al.,[56] corresponding to an average of 20 mg of N g^{-1} DW ± 2 mg g^{-1}. The regional variability due to soil and climate and the year-to-year variability are what we are looking for, so they were not included in this calculation. In summary, with the best protocol, a plot can be declared N-deficient with certainty if it has an average Chl content lower than 25 μg cm^{-2} at flowering. It can be considered overfertilized if it has a Chl above 47 μg cm^{-2}.

Proposed Protocol. All of the above work incites us to propose a stringent sampling protocol comprising double-sided Dualex measurements on 40 light-exposed primary leaves positioned at the same canopy height, just above the first trellis wire in a two-wire trellis system, which corresponds to the middle of the canopy (i.e., node no. 9). The optimal procedure would be to divide the plot to be diagnosed into three equal parts and to walk through the two interrows that separate these parts. One should then sample (measure with the Dualex) one leaf from the three shoots of a vine, repeating this on five vines from each side of the interrow, left and right, and for the two interrows. This would yield measurements from 60 leaves all together (1 leaf × 3 shoots × 5 vines × 2 row sides × 2 interrows). A single measurement per leaf at the intervein position (Figure S1, Supporting Information) is sufficient. The representative average for the plot for Chl and for NBI (Chl divided by the sum of Flav of the two leaf sides) can be compared to the threshold criteria presented in Table 3. Alternatively, for smaller plots or for visually homogeneous plots, the sampling can be decreased to 36 leaves (1 leaf × 3 shoots × 3 vines × 2 row sides × 2 interrows). Thanks to the knowledge of leaf N dilution during the season,[5,6] a lookup table could also be constructed to correct for seasonal effects when diagnostics cannot be made at the optimal postflowering growth stage (the BBCH 65−75 window). To sum up, we propose to sample 36−60 leaves at flowering at a fixed node position, preferably node no. 9, or at the same height for VSP.

Limitations of Optical Nitrogen Estimation. Water availability influences nitrogen uptake[58] and therefore would influence leaf N content. One should make a distinction between the effect of water availability on nutrient analysis[59] and genuine leaf N content physiological dependence on rainfall.[58] In the first case, a water deficit simply precludes the use of petiole nitrate tests, and leaf N is also affected. In the second case, water availability, rainfall, or irrigation during canopy development interacts with nitrogen availability to optimize simultaneously both nitrogen and water use efficiency by adjusting the total leaf area, N per leaf area, and LMA. This represents the potential limit for the use of absolute values of NBI because Flav is also influenced by light and water stress.[60] As an alternative approach to NBI, Flav can be used to verify that sampled leaves belong to the same sun-exposed category that has the same LMA. In that case, Chl alone could be used as a proxy for N content even when expressed in surface-based units. Then the Chl index would perform sufficiently well and can be used as an absolute value. Knowing that only thoroughly trained and experienced technicians should be responsible for collecting plant tissue samples[8] and that very often this is not the case, this type of objective postacquisition filtering of optically acquired data could be very useful.

Other leaf-clip chlorophyll meters such as the SPAD-502 can also be used for N estimation.[11−15] They would best be used after an adequate transformation into leaf Chl content (cf. the Material and Methods). Still, the SPAD-502 leaf clip has an effective access length of only 1.3 cm because it was originally designed for rice leaves. This is why in the present study we performed the measurement with the SPAD-502 on the disks once they had been cut from the leaf. This can be a real problem for rapid in-field measurements if one wants to avoid leaf edges. To scarify one leaf among the two thousand leaves present on a vine by cutting it might not seem prohibitive, but it will greatly slow the diagnostic speed. The Dualex that was designed for grapevine leaves has an access length of 8 cm to attain the middle of even a 16 cm wide leaf.

The "nitrogen sufficiency index" approach[1] is another potential way to alleviate most of the problems of the use of absolute threshold values for the indices because it is related to a standard condition for the same index. It could mitigate the above-mentioned concerns about both the absolute NBI values and the environmental and phenological influences on N estimation, such as the variable growth rate and leaf age at the time of measurement. Unfortunately, the nitrogen sufficiency index cannot be applied to a ligneous species such as grapevine on a year-to-year basis due to a lack of overfertilized reference and to the latency in N deficiency expression. However, a new approach to explore within the framework of site-specific crop management could be to use a virtual-reference concept,[61] i.e., just the comparison of subplots or homogeneous zones to the one having the largest NBI value. Indeed, for spatial heterogeneity analysis and zoning, both Chl and NBI measurements are valuable, especially with tractor-mounted sensors such as the Multiplex.

Conclusion and Prospects. Technology-based optical sensing is the equivalent of visual estimation. Still, it is more objective and can be automated and georeferenced. It is well

DOI: 10.1021/acs.jafc.5b00304
J. Agric. Food Chem. 2015, 63, 3669−3680

adapted for site-specific crop management in replacement of plant tissue testing. In this paper we presented quantitative optically measured norms for grapevine N nutrition based on extensive studies of Chl and Flav using a new optical leaf clip. The knowledge of the growth stage and the sampling of leaves at a defined node are crucial for a reliable estimation of grapevine N status. The presented grapevine optically measured leaf N sufficiency level thresholds should be refined for different phenological stages, from flowering to véraison, by accumulation of data on different sites. The universality of Chl and NBI indices should be verified for different cultivars. Their robustness against year-to-year variability should also be verified by multiyear surveys on the same sites. Finally, for practical applications of these optical approaches in precision viticulture, indices obtained by mounted optical proximal sensors such as the Multiplex need to be calibrated and validated against the Dualex indices presented in this paper. Grapevine is just an example of the use of optical sensors for the applications of leaf Chl and NBI for crop N management. In viticulture, it is important to estimate vine nitrogen availability for three reasons. First, N affects yield, as in other crops. Second, it influences the grape fermentation potential.[35] Third, it defines the must quality via phenolic and technological grape maturity. The type of analysis presented in this paper can and should be repeated on other crops. Indeed, some data are already available for muskmelon.[28]

■ ASSOCIATED CONTENT

Supporting Information

Table S1 listing literature data for the total nitrogen content (% DW) in leaf blades at four phenological stages, Figure S1 showing the preferred positions for optical measurements on the leaf, and Figure S2 showing the NBI map of the plot at Chateau Gazin with sampling points indicated by green circles for data set Subplots 2012. This material is available free of charge via the Internet at http://pubs.acs.org.

■ AUTHOR INFORMATION

Corresponding Author

*Phone: +33169157224. Fax: +33169157353. E-mail: zoran.cerovic@u-psud.fr.

Funding

This work was supported by FORCE-A (Orsay) in a joint project with the Centre National de la Recherche Scientifique and Université Paris-Sud (Grant UPS N8780). In addition, the research leading to these results has recently received funding from the European Community's Seventh Framework Program (FP7/2007-2013) under Grant Agreement FP7-311775, Project Innovine.

Notes

The authors declare the following competing financial interest(s): Z.G.C. declares a double link to the FORCE-A company: as one of the co-authors of the Dualex patent that the company exploits and as a part-time consultant to the company. Other authors declare no competing financial interests.

■ ACKNOWLEDGMENTS

We thank the following institutions for giving us access to their vineyards: Moët & Chandon Champagne, the trade association Comité Champagne, and Chateau Gazin. We thank Dr. Gwendal Latouche for his useful advice on the manuscript and Dr. Zorana Ratkovic for proofreading the manuscript. Finally, we thank the anonymous reviewers for comments that helped improve the clarity of the paper.

■ ABBREVIATIONS USED

N, nitrogen; NBI, nitrogen balance index; Chl, chlorophyll; LMA, leaf mass per area; Flav, flavonol; RMSE, root mean squared error; UV, ultraviolet; DW, dry weight

■ REFERENCES

(1) Samborski, S. M.; Tremblay, N.; Fallon, E. Strategies to make use of plant sensors-based diagnostic information for nitrogen recommendations. *Agron. J.* **2009**, *101*, 800−816.

(2) Bramley, R. G. V. Precision Viticulture: managing vineyard variability for improved quality outcomes. In *Managing Wine Quality*; Reynolds, A. G., Ed.; CRC Press—Woodhead Publishing: Oxford, Cambridge, New Delhi, 2010; Vol. *1*, pp 445−480.

(3) Munson, R. D. Principles of plant analysis. In *Handbook of Methods for Plant Analysis*; Kalra, Y. P., Ed.; CRC Press: Boca Raton, FL, 1998; pp 1−24.

(4) Keller, M. Managing grapevines to optimize fruit development in a challenging environment: a climate change primer for viticulturists. *Aust. J. Grape Wine Res.* **2010**, *16*, 56−69.

(5) Romero, I.; Garcia-Escudero, E.; Martin, I. Leaf blade versus petiole analysis for nutritional diagnosis of *Vitis vinifera* L. cv. Tempranillo. *Am. J. Enol. Vitic.* **2013**, *64*, 50−64.

(6) Romero, I.; García-Escudero, E.; Martín, I. Effects of leaf position on blade and petiole mineral nutrient concentration of Tempranillo grapevine (*Vitis vinifera* L.). *Am. J. Enol. Vitic.* **2010**, *61*, 544−550.

(7) Christensen, P. Nutrient level comparisons of leaf petioles and blades in twenty-six grape cultivars over three years (1979 through 1981). *Am. J. Enol. Vitic.* **1984**, *35*, 124−133.

(8) Jones, J. B., Jr. *Laboratory Guide for Conducting Soil Tests and Plant Analysis*; CRC Press: Boca Raton, FL, 2001.

(9) Ohmart, C. P.; Matthiasson, S. K. Soil Management. In *California Code of Sustainable Winegrowing Workbook*; Sustainable Winegrowing Joint Committee, California Sustainable Winegrowing Alliance: San Francisco, CA, 2012; pp 1−23.

(10) Tremblay, N.; Wang, Z.; Cerovic, Z. G. Sensing crop nitrogen status with fluorescence indicators. A review. *Agron. Sustainable Dev.* **2012**, *32*, 451−464.

(11) Porro, D.; Dorigatti, C.; Stefanini, M.; Ceschini, A. Use of SPAD meter in diagnosis of nutritional status in apple and grapevine. *Acta Hortic.* **2001**, *564*, 243−252.

(12) Taskos, D. G.; Koundouras, S.; Stamatiadis, S.; Zioziou, E.; Nikolaou, N.; Karakioulakis, K.; Theodorou, N. Using active canopy sensors and chlorophyll meters to estimate grapevine nitrogen status and productivity. *Precis. Agric.* **2015**, *16*, 77−98.

(13) Tregoat, O.; Van Leeuwen, C.; Choné, X.; Gaudillière, J.-P. Etude du regime hydrique et de la nutrition azotée de la vigne par des indicateurs physiologiques. Influence sur le comportement de la vigne et la maturation du raisin (*Vitis vinifera* L. cv Merlot, 2000, Bordeaux). *J. Int. Sci. Vigne Vin* **2002**, *36*, 133−142.

(14) Lacroux, F.; Tregoat, O.; Van Leeuwen, C.; Pons, A.; Tominaga, T.; Lavigne-Cruège, V. r.; Dubourdieu, D. Effect of foliar nitrogen and sulphur application on aromatic expression of *Vitis vinifera* L. cv. Sauvignon blanc. *J. Int. Sci. Vigne Vin* **2008**, *42*, 125−132.

(15) Brunetto, G. Use of the SPAD-502 in estimating nitrogen content in leaves and grape yield in grapevines in soils with different texture. *Am. J. Plant Sci.* **2012**, *03*, 1546−1561.

(16) Meyer, S.; Cerovic, Z. G.; Goulas, Y.; Montpied, P.; Desmotes-Mainard, S.; Bidel, L.; Moya, I.; Dreyer, E. Relationships between optically assessed polyphenols and chlorophyll content and the dry mass per leaf area ratio of woody plants: a signature of the carbon and nitrogen balance within leaf? *Plant Cell Environ.* **2006**, *29*, 1338−1348.

(17) Poni, S.; Intrieri, C.; Silvestroni, O. Interaction of leaf age, fruiting, and exogenous citokinins in Sangiovese grapevines under non-irrigate conditions. II. Chlroprophyll and nitrogen content. *Am. J. Enol. Vitic.* **1994**, *45*, 278−284.

DOI: 10.1021/acs.jafc.5b00304
J. Agric. Food Chem. 2015, 63, 3669−3680

(18) Steele, M. R.; Gitelson, A. A.; Rundquist, D. A comparison of two techniques for nondestructive measurement of chlorophyll content in grapevine leaves. *Agron. J.* **2008**, *100*, 779−782.
(19) Cerovic, Z. G.; Masdoumier, G.; Ben Ghozlen, N.; Latouche, G. A new optical leaf-clip meter for simultaneous non-destructive assessment of leaf chlorophyll and epidermal flavonoids. *Physiol. Plant.* **2012**, *146*, 251−260.
(20) Peng, S.; Garcia, F. V.; Laza, R. C.; Cassman, K. G. Adjustment of specific leaf weight improves chlorophyll meter's estimation of rice leaf nitrogen concentration. *Agron. J.* **1993**, *85*, 987−990.
(21) Agati, G.; Foschi, L.; Grossi, N.; Volterrani, M. In field non-invasive sensing of the nitrogen status in hybrid bermudagrass (*Cynodon dactylon* × *C. transvaalensis* Burtt Davy) by a fluorescence-based method. *Eur. J. Agron.* **2015**, *63*, 89−96.
(22) Agati, G.; Foschi, L.; Grossi, N.; Guglielminetti, L.; Cerovic, Z. G.; Volterrani, M. Fluorescence-based versus reflectance proximal sensing of nitrogen content in *Paspalum vaginatum* and *Zoysia matrella* turfgrasses. *Eur. J. Agron.* **2013**, *45*, 39−51.
(23) Tremblay, N. Sensing technologies in horticulture: options and challenges. *Chron. Hortic.* **2013**, *53*, 10−14.
(24) Cartelat, A.; Cerovic, Z. G.; Goulas, Y.; Meyer, S.; Lelarge, C.; Prioul, J.-L.; Barbottin, A.; Jeuffroy, M.-H.; Gate, P.; Agati, G.; Moya, I. Optically assessed contents of leaf polyphenolics and chlorophyll as indicators of nitrogen deficiency in wheat (*Triticum aestivum* L.). *Field Crops Res.* **2005**, *91*, 35−49.
(25) Tremblay, N.; Wang, Z.; Bélec, C. Performance of Dualex in spring wheat for crop nitrogen status assessment, yield prediction and estimation of soil nitrate content. *J. Plant Nutr.* **2010**, *33*, 57−70.
(26) Zhang, Y.; Tremblay, N.; Zhu, J. A first comparison of Multiplex® for the assessment of corn nitrogen status. *J. Food Agric. Environ.* **2012**, *10*, 1008−1016.
(27) Goffart, J.-P.; Abras, M.; Abdallah, F. B. Gestion de la fertilisation azotée des cultures de plein champ. Perspectives d'amélioration de l'efficience d'utilisation de l'azote sur base du suivi du statut azoté de la biomasse aérienne. *Biotechnol. Agron. Soc. Environ.* **2013**, *17*, 221−230.
(28) Padilla, F. M.; Teresa Peña-Fleitas, M.; Gallardo, M.; Thompson, R. B. Evaluation of optical sensor measurements of canopy reflectance and of leaf flavonols and chlorophyll contents to assess crop nitrogen status of muskmelon. *Eur. J. Agron.* **2014**, *58*, 39−52.
(29) Louis, J.; Meyer, S.; Maunoury-Danger, F.; Fresneau, C.; Meudec, E.; Cerovic, Z. G. Seasonal changes in optically assessed epidermal phenolic compounds and chlorophyll contents in leaves of sessile oak (*Quercus petraea* Matt.(Liebl.)): towards signatures of phenological stage. *Funct. Plant Biol.* **2009**, *36*, 732−741.
(30) Louis, J.; Genet, H.; Meyer, S.; Soudani, K.; Montpied, P.; Legout, A.; Dreyer, E.; Cerovic, Z. G.; Dufrêne, E. Tree age-related effects on sun acclimated leaves in a chonosequence of beech (*Fagus sylvatica*) stands. *Funct. Plant Biol.* **2012**, *39*, 323−331.
(31) Debuisson, S.; Germain, C.; Garcia, O.; Panigai, L.; Moncomble, D.; Le Moigne, M.; Fadaili, E. M.; Evain, S.; Cerovic, Z. G. Using Multiplex® and Greenseeker™ to manage spatial variation of vine vigor in champagne. *10th International Conference on Precision Agriculture (ICPA)*, Denver, CO, July 18−21, 2010; International Society of Precision Agriculture: Monticello, IL, 2010; pp 1−21.
(32) Garcia, O.; Debuisson, S.; Morlet, M.; Germain, C.; Panigai, L.; Le Moigne, M.; Fadaili, E. M.; Ben Ghozlen, N.; Cerovic, Z. G. Using Multiplex® to manage nitrogen variability in champagne vineyards. *11th International Conference on Precision Agriculture (ICPA)*, Indianapolis, IN, July 15−18, 2012; International Society of Precision Agriculture: Monticello, IL, 2012; pp 1−10.
(33) Conradie, W. J. Distribution and translocation of nitrogen absorbed during early summer by two-year-old grapevines grown in sand culture. *Am. J. Enol. Vitic.* **1991**, *42*, 180−190.
(34) Keller, M.; Koblet, W. Dry matter and leaf area partitioning, bud fertility and second season growth of *Vitiis vinifera* L.: responses to nitrogen supply and limiting irradiance. *Vitis* **1995**, *34*, 77−83.
(35) Hilbert, G.; Soyer, J. P.; Molot, C.; Giraudon, J.; Milin, S.; Gaudillere, J. P. Effects of nitrogen supply on must quality and anthocyanin accumulation in berries of cv. Merlot. *Vitis* **2003**, *42*, 69−76.
(36) Meier, U. *Growth Stages of Mono- and Dicotyledonous Plants*; Federal Biological Research Centre for Agriculture and Forestry: Berlin, Germany, 2001; 158 pp.
(37) Cerovic, Z. G.; Moise, N.; Goulas, Y.; Latouche, G. Procédé et dispositif de détermination du rapport des teneurs en chlorophylle et en un composé chromophore d'un tissu végétal sans mesurer indépendamment ces teneurs. FR0757056, 2007; delivered Oct 20, 2009.
(38) Porra, R. J.; Thompson, W. A.; Kreidemann, P. E. Determination of accurate extinction coefficients and simultaneous equations for assaying chlorophyll *a* and *b* extracted with four different solvents: verification of the concentration of chlorophyll standards by atomic absorption spectroscopy. *Biochim. Biophys. Acta, Bioenerg.* **1989**, *975*, 384−394.
(39) Legendre, P.; Legendre, L. *Numerical Ecology*; Elsevier: Amsterdam, 1998; 853 pp.
(40) Youden, W. J. Index for rating diagnostic tests. *Cancer* **1950**, *3*, 32−35.
(41) Dagnelie, P. *Principes d'Expérimentation. Planification des Expériences et Analyse de leur Résultats*; Les Presses Agronomiques de Gembloux: Gembloux, Belgium, 2003; 398 pp.
(42) Wermelinger, B.; Koblet, W. Seasonal growth and nitrogen distribution in grapevine leaves, shoots and grapes. *Vitis* **1990**, *29*, 15−26.
(43) Poorter, H.; Niinemets, Ü.; Poorter, L.; Wright, I. J.; Villar, R. Causes and consequences of variation in leaf mass per area (LMA): a meta-analysis. *New Phytol.* **2009**, *182*, 565−588.
(44) Montpied, P.; Granier, A.; Dreyer, E. Seasonal time-course of gradients of photosynthetic capacity and mesophyll conductance to CO2 across a beech (*Fagus sylvatica* L.) canopy. *J. Exp. Bot.* **2009**, *60*, 2407−2418.
(45) Posada, J. M.; Lechowicz, M. J.; Kitajima, K. Optimal photosynthetic use of light by tropical tree crowns achieved by adjustment of individual leaf angles and nitrogen content. *Ann. Bot.* **2009**, *103*, 795−805.
(46) Cate, R. B.; Neslon, L. A. A simple statistical procedure for partitioning soil test correlation data into two classes. *Soil Sci. Soc. Am. Proc.* **1971**, *35*, 658−660.
(47) Roubelakis-Angelakis, K. A.; Kliewer, W. M. Nitrogen metabolism in grapevine. *Hortic. Rev.* **1992**, *10*, 407−452.
(48) Casa, R.; Castaldi, F.; Pascucci, S.; Pignatti, S. Chlorophyll estimation in field crops: an assessment of handheld leaf meters and spectral reflectance measurements. *J. Agric. Sci.* **2014**, 1−15.
(49) Dwyer, L. M.; Andersont, A. M.; Ma, B. L.; Stewart, D. W.; Tollenaar, M.; Gregorich, E. Quantifying the nonlinearity in chlorophyll meter response to corn leaf nitrogen concentration. *Can. J. Plant Sci.* **1995**, *75*, 179−182.
(50) Stringari, G.; Porro, D.; Failla, O.; Möller, F. A method to assess and manage leaf analysis standards according to genetic and environmental variability. *Acta Hortic.* **1997**, *448*, 145−153.
(51) Champagnol, F. *Eléments de Physiologie de la Vigne et Viticulture Générale*; Saint-Gely-du-Fesc, France, 1984; 352 pp.
(52) Bellow, S.; Latouche, G.; Brown, S. C.; Poutaraud, A.; Cerovic, Z. G. *In vivo* localization at the cellular level of stilbene fluorescence induced by *Plasmopara viticola* in grapevine leaves. *J. Exp. Bot.* **2012**, *63*, 3697−3707.
(53) Dordas, C. Role of nutrients in controlling plant diseases in sustainable agriculture. A review. *Agron. Sustainable Dev.* **2008**, *28*, 33−46.
(54) Vasconcelos, M. C.; Greven, M.; Winefield, C. S.; Trought, M. C. T.; Raw, V. The flowering process of *Vitis vinifera*: a review. *Am. J. Enol. Vitic.* **2009**, *60*, 411−434.
(55) Failla, O.; Scienza, A.; Stringari, G.; Porro, D.; Tarducci, S.; Di Dionisio, A. Indagine sullo stato nutrizionale dei vigneti in alcune zone toscane a denominazione d'origine per una proposta d'interpretazione

DOI: 10.1021/acs.jafc.5b00304
J. Agric. Food Chem. 2015, 63, 3669−3680

delle analisi fogliari e del terreno. *VigneVini Riv. Ital. Vitic. Enol.* **1995**, *12*, 15−25.
(56) Failla, O.; Stringari, G.; Porro, D.; Scienza, A. Stato nutrizionale di alcune zone viticole dell'Italia centro-settentrionale. *VigneVini Riv. Ital. Vitic. Enol.* **1993**, *3*, 77−82.
(57) Davenport, J. R.; Horneck, D. A. *Sampling Guide for Nutrient Assessment of Irrigated Vineyards in the Inland Pacific Northwest*; PNW622; Washington State University: Pullman, WA, 2011; pp 1−6.
(58) Farquhar, G. D.; Buckley, T. N.; Miller, J. M. Optimal stomatal control in relation to leaf area and nitrogen content. *Silva Fennica* **2002**, *36*, 625−637.
(59) Shellie, K. Influence of deficit irrigation on nutrient indices in wine grape (*Vitis vinifera* L.). *Agric. Sci.* **2012**, *03*, 268−273.
(60) Agati, G.; Brunetti, C.; Di Ferdinando, M.; Ferrini, F.; Pollastri, S.; Tattini, M. Functional roles of flavonoids in photoprotection: new evidence, lessons from the past. *Plant Physiol. Biochem.* **2013**, *72*, 35−45.
(61) Holland, K. H.; Schepers, J. S. Use of a virtual-reference concept to interpret active crop canopy sensor data. *Precis. Agric.* **2013**, *14*, 71−85.

DOI: 10.1021/acs.jafc.5b00304
J. Agric. Food Chem. 2015, 63, 3669−3680

Figure 1. Examples of fungicides structure.

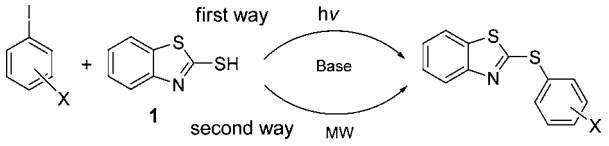

Figure 2. Methodologies employed for the arylation of 2-mercaptobenzotiazole.

DMSO (Carlo Erba) was also distilled under nitrogen and stored in molecular sieve 4 Å (Aldrich). Potato glucose agar (PGA) and Triadimefon were commercially available and used as received. Distilled water was sterilized before their use.

Photostimulated Reactions of Dihalobenzenes with Benzothiazole-2-thiolate Ions in DMSO. The following procedure is representative of these reactions. 2-Mercaptobenzothiazole (1.1 mmol) and *t*-BuOK (1.1 mmol) were added to 8 mL of degassed DMSO. Then, after 10 min when no more solid was present, benzothiazole-2-thiolate ions were ready for use (characterized by a yellow solution). Substrate (1.0 mmol) was added to the solution and the reaction mixture irradiated for 180 min. The reaction was then quenched by adding an excess of water. The solution was then extracted with dichloromethane and water (25 mL). The organic extract was analyzed by GC-MS, and the products were isolated by column chromatography.

A similar procedure was carried out for reactions with substrate excess, adding 1.0 mmol of 2-mercaptobenzothiazole and *t*-BuOK and 5.0 mmol of substrate. These reaction mixtures were irradiated for 30 min.

Microwave Assisted Reactions of Dihalobenzenes with Benzothiazole-2-thiolate Ions in Microwave Oven. 2-Mercaptobenzothiazole (0.5 mmol) and KOH (0.5 mmol) was added to 2 mL of water. Then, after 2 min when no more solid was present, the benzothiazole-2-thiolate ions were ready for use (characterized by a yellow solution). Substrate (0.6 mmol) was added to the solution and the reaction mixture irradiated for 2−7 min. The solid was extracted with dichloromethane. The organic extract was analyzed by GC-MS.

Data for 2-(Phenylthio)benzothiazole (2). The product was isolated as yellow oil after column chromatography using dichloromethane:petroleum ether (70:30). ^{1}H NMR (400 MHz, $CDCl_3$) δ: 7.27−7.57 (m, 5H), 7.62−7.82 (m, 3H), 7.90 (dd, J = 12.55 Hz, J = 8.17 Hz, 1H). ^{13}C NMR (100 MHz, $CDCl_3$) ppm: 121.1, 121.5, 122.2, 124.7, 124.9, 126.5, 130.3, 130.8, 135.7, 135.9, 153.3. HRMS $[MH]^+$ exact mass calculated for $C_{13}H_{10}S_2N$, 244.0249; found, 244.0317.

Data for 1,4-Bis(2-Mercaptobenzothiazol)benzene (3). The nucleophile excess was extracted from the reaction mixture by washing with water. The product was isolated as a white solid after filtrating and washing the precipitate with ethyl acetate; mp: 197.5−199.3 °C. ^{1}H NMR (400 MHz, DMSO-d_6) δ: 7.39 (td, J = 8.14 Hz, J = 1.15 Hz, 2H), 7.49 (td, J = 8.22 Hz, J = 1.27 Hz, 2H), 7.89 (ddd, J = 8.17 Hz; J = 1.00 Hz, J = 0.54 Hz, 2H), 7.92 (s, 4H), 8.00 (ddd, J = 8.05 Hz, J = 1.17 Hz, J = 0.55 Hz, 2H). ^{13}C NMR (100 MHz, DMSO-d_6) ppm: 121.7, 121.9, 125.0, 126.6, 132.1, 135.1, 135.5, 153.2. HRMS $[MH]^+$ exact mass calculated for $C_{20}H_{13}S_4N_2$, 408.9962; found, 408.9986.

Data for 2-(4-Bromophenylthio)benzothiazole[23] (4). The product was isolated as white solid after column chromatography using dichloromethane:petroleum ether (70:30); mp 55.6−56.8 °C. ^{1}H NMR (400 MHz, $CDCl_3$) δ: 7.29 (ddd, J = 7.97 Hz, J = 7.37 Hz, J = 1.21 Hz, 1H), 7.42 (ddd, J = 8.13 Hz, J = 7.28 Hz, J = 1.25 Hz, 1H), 7.56−7.64 (m, J = 3.00 Hz; J = 1.14 Hz, J = 0.52 Hz, 4H), 7.69 (ddd, J = 8.28 Hz, J = 0.53 Hz, 1H), 7.89 (dd, J = 8.28 Hz, J = 0.53 Hz, 1H). ^{13}C NMR (100 MHz, $CDCl_3$) ppm: 120.9, 122.1, 124.6, 125.2, 126.3, 129.1, 133.1, 135.6, 136.5, 139.1, 153.81, 168.0. HRMS $[MH]^+$ exact mass calculated for $C_{13}H_9S_2NBr$, 321.9354; found, 321.9356.

Data for 2-(4-Iodophenylthio)benzothiazole (5). The product was isolated as yellow oil after column chromatography using dichloromethane:petroleum ether (70:30). ^{1}H NMR (400 MHz, $CDCl_3$) δ: 7.28−7.32 (m, 1H), 7.40−7.45 (m. 3H), 7.56−7.78 (m, 2H), 7.80 (d, J = 8.12 Hz, 1H) 7.89 (dd, J = 8.12 Hz, J = 3.03 Hz, 1H). ^{13}C NMR (100 MHz, $CDCl_3$) ppm: 121.2, 122.5, 124.9, 126,7, 130.2, 130.3, 130.6, 135.7, 136.0, 136.9, 139.4, 154.1. HRMS $[MH]^+$ exact mass calculated for $C_{13}H_9S_2NI$, 369.9221; found, 369.9239.

Data for 2-(2-Chlorophenylthio)benzothiazole (6). The product was isolated as brown solid after column chromatography using dichloromethane:petroleum ether (70:30). ^{1}H NMR (400 MHz, $CDCl_3$) δ (ppm): 7.28−7.34 (td, 1H, J = 1.17 Hz, J = 8.69 Hz), 7.34−7.39 (dd, 1 H, overlapping, J = 1.23 Hz, J = 8.38 Hz), 7.39−7.46 (tt, 2H, overlapping, J = 1.23 Hz, J = 8.01 Hz), 7.66−7.72 (dt, 1H, J = 1.48 Hz, J = 7.54 Hz), 7.73−7.78 (dt, 1H, J = 8.26 Hz), 7.78−7.82 (dt, 1H, J = 1.97 Hz), 7.89−7.95 (dt, 1H, J=8.14 Hz). ^{13}C NMR (100 MHz, $CDCl_3$) (ppm): 120.93, 122.27, 124.63, 126.26, 128.65, 129.73, 131.71, 131.87, 134.19, 135.87, 136.92, 153.87, 166.97. HRMS $[MH]^+$ exact mass calculated for $C_{13}H_8S_2NCl$, 277.9865; found, 277.9860.

Data for 2-(3-Chlorophenylthio)benzothiazole[24] (7). The product was isolated as colorless oil after column chromatography using dichloromethane:petroleum ether (70:30). ^{1}H NMR (400 MHz, $CDCl_3$) δ: 7.28−7.34 (J = 1.17 Hz, J = 8.69 Hz, td, 1H), 7.37−7.44 (t, 1H, overlapping, J = 7.77 Hz), 7.37−7.44 (dd, 1H, overlapping, J = 1.23 Hz, J = 8.38 Hz), 7.44−7.50 (tt, 1H, overlapping, J = 1.23 Hz, J = 8.01 Hz), 7.58−7.64 (dt, 1H, J = 1.48 Hz, J = 7.54 Hz), 7.68−7.72 (d, 1H, J = 8.26 Hz), 7.72−7.74 (t, 1H, J = 1.97 Hz), 7.83−8.03 (d, 1H, J = 8.14 Hz). ^{13}C NMR (100 MHz, $CDCl_3$) ppm: 120.9, 122.3, 124.7, 126.3, 130.4, 130.9, 131.9, 132.9, 134.5, 135.4, 135.7, 153.7. HRMS $[MH]^+$ exact mass calculated for $C_{13}H_9S_2NCl$, 277.9865; found, 277.9860.

Data for 2-(4-Fluorophenilthio)benzothiazole (8). The product was isolated as brownish solid after column chromatography using dichloromethane:petroleum ether (70:30); mp 54.3−55.5 °C. ^{1}H NMR (400 MHz, $CDCl_3$) δ: 7.11−7.21 (m, 2H), 7.22−7.31 (m, 1H), 7.40 (ddd, J = 8.65 Hz, J = 7.30 Hz, J = 1.20 Hz, 1H), 7.65 (d, J = 8.17 Hz, 1H), 7.68−7.73 (m, 2H), 7.86 (d, J = 8.17 Hz, 1H). ^{13}C NMR (100 MHz, $CDCl_3$) ppm: 117.5, 117.7, 121.1, 122.3, 124.7, 126.8, 135.9, 138.1, 138.2, 154.2, 163.3, 165.8, 169.8. HRMS $[MH]^+$ exact mass calculated for $C_{13}H_9S_2NF$, 262.0155; found, 262.0169.

Bioassays of Fungicidal Activities. Five bunches of botrytized grape clusters (*Vitis vinifera* cv. Chardonnay) were randomly hand-harvested in a vineyard in the district Barrancas, Maipú, province Mendoza (Argentina) in 2010. Solutions of compounds **2**−**8** were prepared with ethanol and were sterilized by filtration with 0.2 μm GHP HPLC filter membrane. Those solutions were each incorporated into polystyrene Petri dishes which contained potato glucose agar (PGA) and the required amount of water to reach the desired concentration of each compound. Fungal growth in the presence of each compound was evaluated at four concentrations (12.5, 25, 50, and 100 μg mL^{-1}) in PGA. Then the culture media were allowed to solidify. The final concentration of ethanol was 1.2% of the final volume of media for all treatments and control. For this instance, ethanol, water, PGA, and HPLC filters, membranes, and syringes were previously sterilized by autoclave for 15 min at 120 °C. For each analysis, three replicates were performed. Radial growth was measured after incubation at 28 °C for 8 days in the dark. For all assays, the fungi were cultured on PGA/water (positive control) and PGA/water/

DOI: 10.1021/acs.jafc.5b00150
J. Agric. Food Chem. 2015, 63, 3681−3686

ethanol (ethanol control). More details are included in the Supporting Information.

RESULTS AND DISCUSSION

Synthesis under Light Irradiation. The photostimulated reaction of benzothiazole-2-thiolate anion with iodobenzene afforded 60% yields of monosubstitution product (**2**) within 180 min (Table 1, entry 1, photostimulated reactions). Photostimulated reaction between 2 mmol of 2-mercaptobenzothiazole and 1 mmol of *p*-diiodobenzene afforded mainly 65% yields of disubstitution product (**3**) within 180 min (Table 1, entry 2).

To decrease the formation of disubstitution product and to produce monosubstitution product with retention of halide, reactions were performed with different benzenedihalides using a relation substrate:nucleophile (1:1). However, the best yields were obtained using a relation substrate:nucleophile (5:1). Thus, benzothiazole-2-thiolate ions reacted with *p*-bromoiodobenzene at a relation substrate:nucleophile (1:1) and (5:1), affording 37% and 98% yields of monosubstitution product with retention of bromine (**4**), respectively (Table 1, entry 3). This reaction did not occur in the dark and was inhibited by *p*-dinitrobenzene (*p*-DNB), a well-known inhibitor of $S_{RN}1$ reactions.[17] These reactions and more details about the optimization for *p*-bromoiodobenzene with **1** are included in the Supporting Information.

Reaction of benzothiazole-2-thiolate anion with *p*-diiodobenzene in a relation (1:1) afforded disubstitution product within 60 min, but by reducing the concentration of benzothiazole-2-thiolate anion and reaction time (30 min), 25% yields of monosubstitution product with retention of iodine (**5**) was obtained. The reaction performed in a relation substrate:nucleophile (5:1) afforded 93% yields of **5** within 30 min (Table 1, entry 4).

Photostimulated reaction of *o*-chloroiodobenzene afforded 44% and 98% yields of monosubstitution product with retention of chloride (**6**) within 30 min (Table 1, entry 5) at a relation substrate:nucleophile (1:1) and (5:1), respectively.

Furthermore, benzothiazole-2-thiolate ions reacted with *m*-chloroiodobenzene and *p*-fluoroiodobenzene, rendering 58% (**7**) and 63% (**8**) yields, respectively, under irradiation during 180 min with a relation substrate:nucleophile (1:1) (Table 1, entries 6 and 7). It has been observed that *o*-chloroiodobenzene was less reactive than *m*-chloroiodobenzene, probably due to hindering.

By contrast, *p*-dibromobenzene, *p*-chlorobromobenzene, or *m*-clorobromobenzene did not react with benzothiazole-2-thiolate ions under these reaction conditions (Table 1, entries 8−10). It is clear that those substrates with reduction potential greater than −1.60 V[25] are able to initiate the reaction while those with lower potential such as *p*-dibromobenzene, *m*-chlorobromobenzene, and *p*-chlorobromobenzene remain unreacted (see reduction potential in the Supporting Information).

Synthesis under Microwave Radiation. As an alternative to reaction initiation and in search of an environmentally benign process, microwave irradiation was employed.[26] Microwave irradiation in polar solvents allows rapid heating to high temperatures enabling short reaction times and often improved yields.[27] The solvent polarity affects the rate of a reaction carried out in a microwave oven because polar molecules absorb microwave causes heating of the substance through frictional effects. It would follow that the rates at which a solvent absorbs microwave radiation depends on its loss factor. The larger the loss factor the greater the coupling with microwaves. Thus, solvents such as water, methanol, DMF,

Table 1. Reactions of Arylhalides with 1: Comparison between Light and Microwave Irradiation

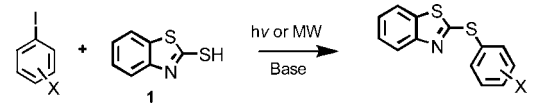

Entry	X	Product	Isolated Product (%) (Substrate recovered) hν/DMSO[a]	MW/H_2O[i]	IC_{50} μg mL^{-1}
1	H	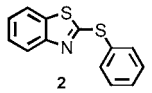 2	60 (34)	78 (20)	0.75
2	*p*-I[b]	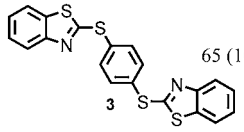 3	65 (10)	-	1.03
3	*p*-Br	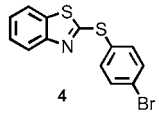 4	37 (50)[c] 98 (nq)[d]	88 (nq)	1.93
4	*p*-I	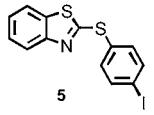 5	25 (68)[e] 93 (nq)[d]	72 (nq)[j]	0.97
5	*o*-Cl	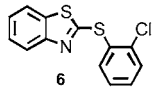 6	44 (50) 98 (nq)[d]	70 (nq)	0.69
6	*m*-Cl	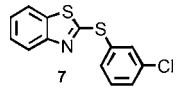 7	58 (30)	81 (nq)	0.65
7	*p*-F	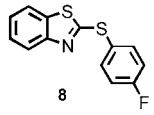 8	63 (34)	18 (nq)	1.17
8	*f*	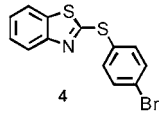 4	- (95)	- (96)	-
9	*g*	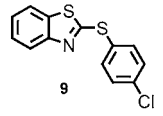 9	- (98)	- (97)	-
10	*h*	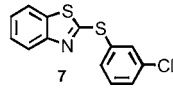 7	- (98)	- (95)	-

[a] *tert*-BuOK and **1** concentrations were 13.7 × 10^{-2} M, substrate concentration was 12.5 × 10^{-2} M. [b] Base and **1** concentrations were 27.5 × 10^{-2} M, 18% of **5**. [c] 4% of **2** and 2% of **3**. [d] Substrate concentration was 62.5 × 10^{-2} M, reaction time was 30 min. nq: not quantified. [e] Base and **1** concentrations were 7.5 × 10^{-2} M, reaction time was 45 min, 4% of **2**. [f] *p*-Dibromobenzene. [g] *p*-Chlorobromobenzene. [h] *m*-Chlorobromobenzene. [i] KOH and **1** concentrations were 25 × 10^{-2} M, substrate concentration was 30 × 10^{-2} M, TBABr, reaction time was 7 min. [j] Reaction time was 2 min.

DOI: 10.1021/acs.jafc.5b00150
J. Agric. Food Chem. 2015, 63, 3681−3686

DMSO, etc., are all heated rapidly when irradiated with microwaves.[28]

Arylation of commercial fungicides were also studied in a previous report, allowing the formation of new compounds with potential fungicide activity under microwave irradiation.[29] The synthesis of polyfluorinated 2-benzylthiobenzothiazole derivatives under microwave radiation has been also reported.[30] Recently, Peñéñory et al. reported that microwave irradiation promotes a quick aromatic nucleophilic substitution by a thermally induced electron transfer process to form new C−C bonds by the coupling of aryl radicals and enolate nucleophiles.[31]

The reaction of 0.5 mmol of the benzothiazole-2-thiolate anion with 0.6 mmol of iodobenzene in DMSO was made at low and high temperatures (60, 90, 120 °C), short times (5−60 min), and different microwave radiation modes, but the outcome was nucleophile decomposition in all conditions assessed, which did not allow achievement of the desired product (Table 2, entries 1 and 2).

Table 2. Optimization of 2[a] under Microwave Irradiation

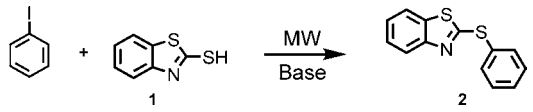

entry	conditions (time, min)[c]	product yields[b] (substrate recovered)
1	DMSO, 60 °C (5−60)[d]	decomposition
2	DMSO, 60−120 °C (5−60)	decomposition
3	DMF, 120 °C (20)[e,f]	**2**, − (97)
4	DMF, 120 °C (20)[g]	**2**, 5 (94)
5	DMF, 120 °C (20)[h]	**2**, 30 (65)
6	DMF, 120 °C (20)[i,j]	**2**, 70 (24)
7	H_2O/polyethylenglycol, 150 °C	**2**, − (95)
8	H_2O, 90 °C (20)[d,e,g,h,i,k]	**2**, − (96)
9	H_2O, 120 °C (20)[a,k]	**2**, 78 (20)
10	H_2O, 120 °C (10)[a,k]	**2**, 78 (20)
11	H_2O, 120 °C (7)[a,k]	**2**, 75 (16)

[a]Base and **1** concentrations were 25 × 10^{-2} M. [b]Yields of isolated products. [c]Dynamic mode and 150 W power was applied. [d]Pulsed mode. [e]With K_2CO_3 as base. [f]With *t*-BuOK as base. [g]With 1 equiv of KOH as base. [h]With 2 equiv of KOH. [i]With 3 equiv of KOH. [j]200 W power was applied. [k]With tetra-*n*-butylammonium bromide (TBABr).

Reaction of 2-mercaptobenzothiazole with iodobenzene in DMF at 120 °C using both K_2CO_3 and *t*-BuOK as base did not occur (Table 2, entry 3). Nevertheless, using KOH as base, the coupling reaction was observed (Table 2, entry 4). Moreover, reaction yields were increased using excess of KOH, proving 30 and 70% yields of (**2**) (Table 2, entries 5 and 6). Thus, this reaction was also carried out using a power of 200 W, and similar results were observed. Under N_2, no changes were observed.

To find an environmental friendly procedure, the reaction was performed in *t*-butanol, isopropyl alcohol, polyethylene glycol, or acetonitrile, which did not allow achieving the desired product. The reaction was also carried out using a solvent mixture which did not allow achievement of the desired product (Table 2, entry 7).

When the reaction was made using water as solvent at 90 °C with different bases and other conditions, no product was detected (Table 2, entry 8), while at 120 °C, the coupling reaction product was observed (Table 2, entries 9−11). Reactions were efficient using solvents with loss factor between 0.1 and 0.2. The best product yields were obtained using water as solvent at 120 °C under microwave irradiation for 7 min. So, subsequent reactions were performed using this last condition.

Thus, the reaction of **1** with *p*-bromoiodobenzene, *p*-diiodobenzene, *o*-chloroiodobenzene, *m*-chloroiodobenzene, and *p*-fluoriodobenzene, rendered 88% (**4**), 72% (**5**), 70% (**6**), 81% (**7**), and 18% (**8**) yields, respectively (Table 1, entries 3−7). Similar to photoestimulation, *p*-dibromobenzene, *p*-chlorobromobenzene, and *m*-clorobromobenzene did not react with **1** under these reaction conditions (Table 1, entries 8−10).

No disubstitution product was obtained from 2 mmol of benzothiazole-2-thiolate anion and 1 mmol of *p*-diiodobenzene using microwave irradiation because the nucleophile got decomposed (Table 1, entry 2). It is very important to notice that this reaction was efficient under photostimulation.

The use of microwave decreased reaction times considerably in comparison to photostimulation. The synthetic procedure reported here is simple and reproducible, and the products are obtained in high yields using water as solvent. It is worthy of mention that this novel process shows environmental and economic advantages over previously reported protocols.

Bioassays of Fungicidal Activity against *Botrytis cinerea*. *B. cinerea* is responsible for the gray mold disease on more than 200 host plants. This necrotrophic ascomycete displays the capacity to kill host cells through the production of toxins, reactive oxygen species, and the induction of a plant-produced oxidative burst.[32] It is well-known that Triadimefon inhibits *B. cinerea*'s growth as well. Triadimefon is widely used to control other fungal diseases. For this reason, it was used as assay control.[33]

Toxicity Test of Solvents on B. cinerea. Solvents used to dissolve tested compounds needed to be nontoxic against *B. cinerea*. Results showed that a solution of ethanol 1.2% final in potato glucose agar (PGA) culture media did not exhibit significant suppression on fungus growth (Figure 3, control with ethanol).

B. cinerea Growth Inhibition Assay. In vitro fungal growth inhibition assay modified from Huang et al. was performed.[33] Fungal growth in the presence of compounds **2**−**8** was evaluated at four concentrations (12.5, 25, 50, and 100 μg mL^{-1}) in PGA.[33] Results in Figure 3 show that all compounds assayed exhibited strong antifungal activity against *B. cinerea* at four concentrations.

Each treatment was performed in triplicate, and the effective concentration 50 (IC_{50}), defined as the concentration required to inhibit 50% of the fungal growth, was used to describe the inhibitory activity of the compounds. IC_{50} of the target compounds along with the standard drug for comparison are summarized in Table 1.

By analyzing the graphs at 12.5 μg mL^{-1}, it can be seen that compounds **2**, **3**, **4**, **6**, and **7** inhibit fungal growth better than Triadimefon. Apparently, the presence of a halogen, either Br, I, or F, in the aromatic ring does not cause large effects in terms of activity against *B. cinerea*. This can be seen if compounds **4**, **5**, and **8** are compared at 25 μg mL^{-1}.

Compounds **2**, **6**, and **7** are those that caused greater inhibition in fungus growth at different concentrations than Triadimefon (IC_{50} values: 0.75, 0.69, 0.65 vs 1.05 μg mL^{-1}). Furthermore, it is easy to see that compounds **6** and **7** showed three times more inhibition than Triadimefon at 25 μg mL^{-1}, presenting the highest antifungal activity.

DOI: 10.1021/acs.jafc.5b00150
J. Agric. Food Chem. 2015, 63, 3681−3686

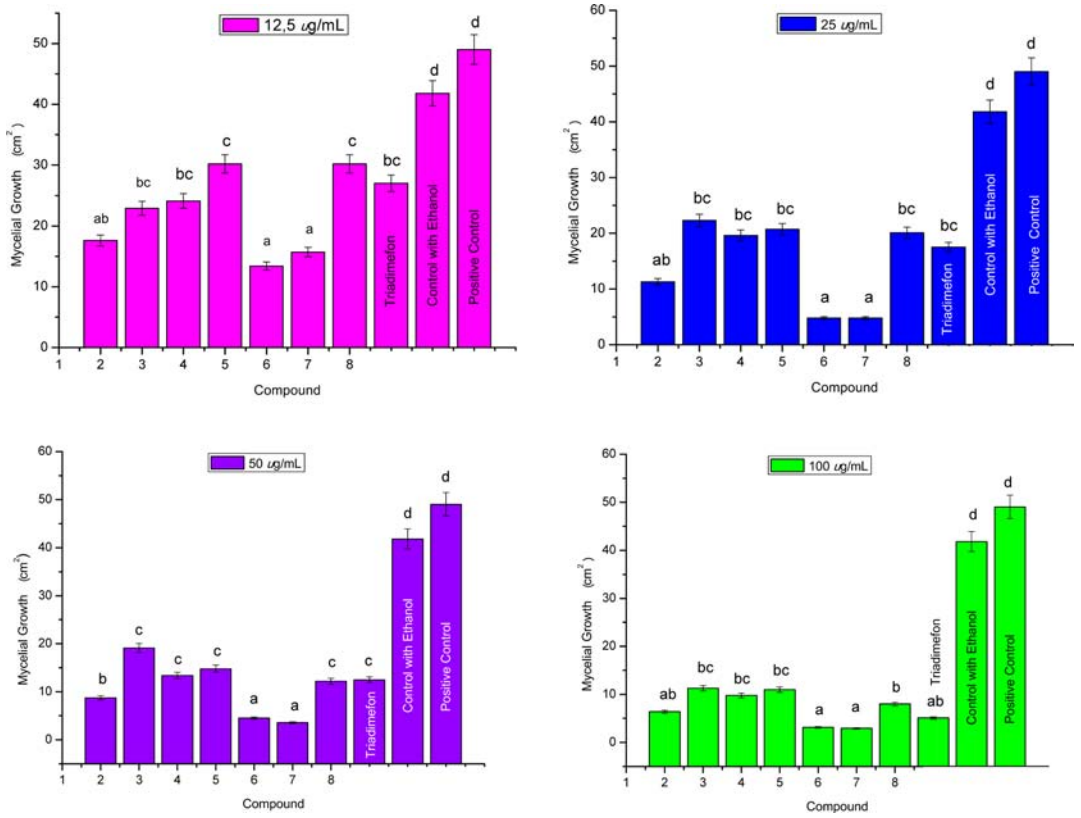

Figure 3. *Botrytis cinerea* growth inhibition assay of aryl-2-thiobenzothiazoles family at different concentrations. Radial growth areas were calculated using the formula for the area of a circle ($A = \pi r^2$) (cm^2). Different letters indicate significant differences ($p \leq 0.05$).

In conclusion, two alternative routes for the arylation of 2-mercaptobenzothiazole have been evaluated. The first pathway involved a photostimulated nucleophilic substitution, while the second consisted in a microwave assisted reaction. Both methodologies were shown to be complementary. Reactivity of the family of dihalobenzene explained by their reduction potentials was reported.

The synthetic procedures reported here are one-pot, reliable, simple, and highly reproducible processes. These are also energy efficient as they involves very short reaction times and in high reaction yields. The methodology using water and microwave irradiation is economical and eco-friendly. Moreover, thermal initiated $S_{RN}1$ reactions of dihalobenzene using controlled microwave heating to promote the reaction were reported.

All compounds assayed have an excellent growth inhibition for *B. cinerea* in the conditions employed. Furthermore, compounds **2**, **6**, and **7** inhibit fungal growth better than Triadimefon. Thus, these compounds could be used as alternative to Triadimefon for fungi control in plants. Further toxicity, persistence, and structure−activity relationship studies for those compounds are underway.

■ ASSOCIATED CONTENT

Supporting Information

General information, optimization of *p*-bromoiodobenzene with **1**, reduction potential, more details about bioassays of fungicidal activities, isolation and spectroscopy data for all compounds. This material is available free of charge via the Internet at http://pubs.acs.org.

■ AUTHOR INFORMATION

Corresponding Author

*Phone: +54 351 5353867. Fax: +54 351 4344971. E-mail: santiago@fcq.unc.edu.ar.

Funding

This work was supported in part by CONICET, SECYT, and ANPCyT.

Notes

The authors declare no competing financial interest.

■ ACKNOWLEDGMENTS

N.H.C. and M.S.B. gratefully acknowledges receipt of a fellowship from CONICET.

■ ABBREVIATIONS USED

GC-MS, Gas chromatography−mass spectroscopy detector; IC_{50}, half-maximal inhibitory concentration; DMSO, dimethyl sulfoxide; PGA, potato glucose agar; DMF, dimethylformamide; TBABr, tetra-*n*-butylammonium bromide

■ REFERENCES

(1) Azam, M. A. B.; Suresh, B. Biological Activities of 2-Mercaptobenzothiazole Derivatives: A Review. *Sci. Pharm.* **2012**, *80*, 789−823.

(2) (a) Roberts, T. R.; Hutson, D. H. *Metabolic Pathways of Agrochemicals, Part 2: Insecticides and Fungicides*; RSC, Cambridge, 1999. (b) Ten Have, A.; Dekkers, E.; Kay, J.; Phylip, L. H.; Van Kan, J. A. L. An aspartic proteinase gene family in the filamentous fungus *Botrytis cinerea* contains members with novel features. *Microbiology* **2004**, *150*, 2475−2489. (c) Hong, Y. S.; Martinez, A.; Liger-Belair, G.; Jeandet, P.; Nuzillard, J.-M.; Cilindre, C. *J. Exp. Bot.* **2012**, *63*, 5773−

DOI: 10.1021/acs.jafc.5b00150
J. Agric. Food Chem. 2015, 63, 3681−3686

5785. (d) Cilindre, C.; Jégou, S.; Hovasse, A.; Schaeffer, C.; Castro, A. J.; Clément, C.; Van Dorsselae, A.; Jeandet, P.; Marchal, R. Proteomic Approach To Identify Champagne Wine Proteins as Modified by *Botrytis cinerea* Infection. *J. Proteome Res.* **2008**, *7*, 1199−1208.

(3) Steel, C. C.; Blackman, J. W.; Schmidtke, L. M. Grapevine bunch rots: Impacts on wine composition, quality, and potential procedures for the removal of wine faults. *J. Agric. Food Chem.* **2013**, *61*, 5189−5206.

(4) Keri, R. S.; Patil, M. R.; Patil, S. A.; Budagumpi, S. A comprehensive review in current developments of benzothiazole-based molecules in medicinal chemistry. *Eur. J. Med. Chem.* **2015**, *89*, 207−251.

(5) Huang, S. T.; Hsei, I. J.; Chen, C. Synthesis and anticancer evaluation of bis(-benzimidazoles), bis(benzoxazoles), and benzothiazoles. *Bioorg. Med. Chem.* **2006**, *14*, 6106−6119.

(6) Singh, M.; Singh, S. K.; Gangwar, M.; Nath, G.; Singh, S. K. Design, synthesis and mode of action of some benzothiazole derivatives bearing an amide moiety as antibacterial agents. *RSC Adv.* **2014**, *4*, 19013−19023.

(7) Siddiqui, N.; Pandeya, S. N.; Khau, S. A.; Stables, J.; Rana, A.; Alam, M.; MdArshad, F.; Bhat, M. A. Synthesis and anticonvulsant activity of sulfonamide derivatives hydrophobic domain. *Bioorg. Med. Chem.* **2007**, *17*, 255−259.

(8) Akhtar, T.; Hameed, S.; Al-Masoudi, N.; Loddo, R.; Colla, P. In vitro antitumor and antiviral activities of new benzothiazole and 1,3,4-oxadiazole-2-thione derivatives. *Acta Pharm.* **2008**, *58*, 135−149.

(9) Palmer, F. J.; Trigg, R. B.; Warrington, J. V. Benzothiazolines as antituberculous agent. *J. Med. Chem.* **1971**, *14*, 248−251.

(10) Burger, A.; Sawhey, S. N. Antimalarials. III. Benzothiazole amino alcohols. *J. Med. Chem.* **1968**, *11*, 270−273.

(11) Suresh, C. H.; Rao, J. V.; Jayaveera, K. N.; Subudhi, S. K. Synthesis and anthelmintic activity of 3-(2-hydrozinobenzothiazole)-substituted indole-2-one. *Int. J. Pharm.* **2013**, *2*, 257−261.

(12) Siddiqui, N.; Alam, M.; Siddiqui, A. A. Synthesis and analgesic activity of some 2-[{4-(alkylthioureido)phenyl}sulphonamido]-6-substituted benzothiazoles. *Asian J. Chem.* **2004**, *16*, 1005−1008.

(13) Gurupadayya, B. M.; Gopal, M.; Padmashali, B.; Vaidya, V. P. Synthesis and bological activities of fuorobenzothiazoles. *Ind. J. Heterocy Chem.* **2005**, *15*, 169−172.

(14) Pattan, S. R.; Suresh, Ch.; Pujar, V. D.; Reddy, V. V. K.; Rasal, V. P.; Koti, B. C. Synthesis and antidiabetic activity of 2-amino[5″(4-sulphonylbenzylidene-2,4-thiazolidenedinone]-7-chloro-6-flourobenzothiazole. *Indian J. Chem.* **2005**, *44B*, 2404−2408.

(15) Singh, S. P.; Segal, S. Study of fungicidal activities of some benzothiazoles. *Indian J. Chem.* **1988**, *27B*, 941−943.

(16) Rao, A. J.; Rao, P. V.; Rao, V. K.; Mohan, C.; Raju, C. N.; Suresh Reddy, C. Microwave assisted one-pot synthesis of novel a-aminophosphonates and their biological activity. *Bull. Korean Chem. Soc.* **2010**, *31*, 1863−1868.

(17) (a) Bardagí, J. I., Vaillard, V. A., Rossi, R. A. In *Encyclopedia of Radicals in Chemistry, Biology & Materials*; Chatgilialoglu, C., Studer, A., Eds.; John Wiley & Sons Ltd.: Chichester, UK, 2012; pp 333−364. (b) Rossi, R. A.; Pierini, A. B.; Peñéñory, A. B. Nucleophilic Substitution Reactions by Electron Transfer. *Chem. Rev.* **2003**, *103*, 71−167. (c) Rossi, R. A.; Pierini, A. B.; Santiago, A. N. Aromatic Substitution by $S_{RN}1$ Reaction. In *Organic Reactions*; Paquette, L. A., Bittman, R., Eds.; Wiley & Sons: New York, 1999, *54*, pp 1−271.

(18) Uranga, J. G.; Montañez, J. P.; Santiago, A. N. Theoretical and experimental study on the reactivity of methyl dichlorobenzoates with sulfur-centered nucleophiles by electron transfer reactions. *Tetrahedron* **2012**, *68*, 584−589.

(19) Ramnathan, V. K.; Kotha, V. S. R. S. K.; Kotarkonda, R. G. Facile synthesis of 2-(substitutedbenzylsulfanyl)-benzothiazoles and their antimicrobial activity screening. *J. Heterocycl. Chem.* **2005**, *42*, 153−156.

(20) Aiello, S.; Wells, G.; Stone, E. L.; Kadri, H.; Bazzi, R.; Bell, D. R.; Stevens, M. F. G.; Matthews, C. S.; Bradshaw, T. D.; Westwell, A. D. Synthesis and Biological Properties of Benzothiazole, Benzoxazole, and Chromen-4-one Analogues of the Potent Antitumor Agent 2-(3,4-Dimethoxyphenyl)-5-fluorobenzothiazole. *J. Med. Chem.* **2008**, *51*, 5135−5139 and references therein..

(21) Inomata, H.; Toh, A.; Mitsui, T.; Fukuzawa, S. *N*-Heterocyclic carbene copper(I) complex-catalyzed direct C−H thiolation of benzothiazoles. *Tetrahedron Lett.* **2013**, *54*, 4729−4731.

(22) (a) Wang, X.; Li, Y.; Yuan, Y. The Direct Thiolation of Benzothiazole Catalyzed by Copper Complex in Superbase System. *Synthesis* **2013**, *45*, 1247−1255. (b) Correa, A.; Carril, M.; Bolm, C. Iron-Catalyzed S-Arylation of Thiols with Aryl Iodides. *Angew. Chem., Int. Ed.* **2008**, *47*, 2880−2883.

(23) Ranjit, S.; Lee, R.; Heryadi, D.; Shen, C.; Wu, J.; Zhang, P.-F.; Huang, K.-W.; Liu, X.-G. Copper-Mediated C−H Activation/C−S Cross-Coupling of Heterocycles with Thiols. *J. Org. Chem.* **2011**, *76*, 8999−9007.

(24) Murru, S.; Ghosh, H. K.; Sahoo, S. K.; Patel, B. Intra- and Intermolecular C−S Bond Formation Using a Single Catalytic System: First Direct Access to Arylthiobenzothiazoles. *Org. Lett.* **2009**, *11*, 4254−4257.

(25) Meites, L.; Zuman. P. *Handbook Series in Organic Electrochemistry*; CRC Press. New York, 1976; Vol. *1*.

(26) Tierney, J. P.; Lidstrom, P. *Microwave Assisted Organic Synthesis*; Blackwell Publishing: Oxford, UK, 2005.

(27) (a) Loupy, A. *Microwaves in Organic Synthesis*; Wiley-VCH, Verlag GmbH & Co. KGaA, Weinheim, Germany, 2006. (b) Kappe, C. O. Controlled Microwave Heating in Modern Organic Synthesis. *Angew. Chem., Int. Ed.* **2004**, *43*, 6250−6284.

(28) Ravichandran, S.; Karthikeyan, E. Microwave Synthesis —A Potential Tool for Green Chemistry. *Int. J. Chem. Technol. Res.* **2011**, *3*, 466−470.

(29) Herrera Cano, N.; Santiago, A. N. Different methodologies by arylations of arylchlorides. A convenient preparation of new triazolic fungicides. *Tetrahedron* **2014**, *70*, 280−285.

(30) Huang, W.; Yang, G. F. Microwave-assisted, one-pot syntheses and fungicidal activity of polyfluorinated 2-benzylthiobenzothiazoles. *Bioorg. Med. Chem.* **2006**, *14*, 8280−8285.

(31) Soria-Castro, S. M.; Caminos, D. A.; Peñéñory, A. B. An expedient route to heterocycles through α-arylation of ketones and arylamides by microwave induced thermal $S_{RN}1$ reactions. *RSC Adv.* **2014**, *4*, 17490−17497.

(32) Choquer, M.; Fournier, E.; Kunz, C.; Levis, C.; Pradier, J. M.; Simon, A.; Viaud, M. *Botrytis cinerea* virulence factors: new insights into a necrotrophic and polyphageous pathogen. *FEMS Microbiol. Lett.* **2007**, *277*, 1−10.

(33) Soylu, E. M.; Kurt, S.; Soylu, S. In vitro and in vivo antifungal activities of the essential oils of various plants against tomato grey mould disease agent *Botrytis cinerea*. *Int. J. Food Microbiol.* **2010**, *143*, 183−189.

DOI: 10.1021/acs.jafc.5b00150
J. Agric. Food Chem. 2015, 63, 3681−3686

In our pilot study, we first find that AIO can exert neuroprotection by blocking oligomer Aβ42- or NMDA-induced neurotoxicity and OA-induced tau protein hyperphosphorylation through inhibiting the expression of kinase p-ERK1/2. Meanwhile, it may reflect the potential activation of the Aβ-decomposing system, and this is also beneficial to synaptic plasticity. Consequently, AIO, which is abundant in mulberry and other fruits, is a suitable and promising candidate for the development of general food type neuroprotection on AD.

MATERIALS AND METHODS

Plant Material and Reagents. Dried mulberries (*Morus alba* L.) were purchased from Wuhan Qiangkang Pharmaceutical Co. Ltd. (Wuhan, China).

We also used the following in our procedures: poly-D-Lysine (Sigma), *N*-methyl-D- aspartate (Sigma), Neurobasal (Gibco), B27 (Invitrogen), Aβ42 peptide (American peptide), rabbit polyclonal anti-p-tau(Ser396) (1:500; Invitrogen), p-CDK5(1:500; Santa Cruz), P-GSK3α/β(1:500; Santa Cruz) rabbit polyclonal anti-p-tau(Ser235) (1:500; Santa Cruz), mouse monoclonal anti-AT270 (1:500; Santa Cruz), mouse monoclonal anti-tau5 (1:500; Millipore Biotechnology), rabbit polyclonal anti-ERK, JNK, p-ERK1/2, p-JNK1/2 (1:500; Cell Signaling), 6E10(1:1000; Signet), MTT(Sigma-Aldrich Chemical Co). Amaxa Rat Neuron Nucleofector Kit (Lonza), CellTiter-Glo Luminescent Cell Viability Assay (Promega), Microplate reader (IMark, Bio-Rad), AmaxaNucleofector (Lonza), GloMax Luminometer (Promega), ChemiDoc XRS ECL system (Bio-Rad).

Extraction and Purification of AIO from Mulberry. Dried mulberries (15.0 kg) were extracted three times using 5× volumes of 70% ethanol for 2 h at reflux. The filtrate was concentrated to dryness under vacuum at 50 °C to afford 70% ethanol extract. The 70% ethanol extract was suspended in 10 L of distilled water and successively partitioned three times with the same volume of hexane, $CHCl_3$, EtOAc, and *n*-butanol, which yielded hexane (123.0 g), $CHCl_3$ (148.0 g), EtOAc (78.0 g), *n*-BuOH (246.0 g) and water-soluble extracts, respectively, after organic solvent was removed under vacuum at 50 °C.

The chloroform-soluble fraction (148.0 g) was further purified by silica gel chromatography and eluted with a $CHCl_3$/MeOH gradient elution (the ratios of $CHCl_3$/MeOH were from 100:0 to 0:100). The $CHCl_3$/MeOH (20:1) elution (4.1 g) was subjected to a silica gel column, followed by a Sephadex LH-20 column and a semipreparative HPLC column (Cosmosil 5C18-MS- II, 10 ID × 250 mm), resulting in a yield of 27.0 mg for AIO.

Primary Culture of Rat Hippocampus Neurons. Primary hippocampus neurons were prepared from Sprague-Dawley rats at 18 embryonic days according to a previously established method with few modifications.[17] Briefly, hippocampus from fetal rat brains (free of meninges, olfactory bulbs, and striata) were pooled, chopped in Ca^{2+}- and Mg^{2+}-free HBSS, and incubated with 0.025% trypsin for 10 min at 37 °C. The enzymatic digestion was terminated by mixing the suspension with an equal volume of DMEM supplemented with 10% FBS. The cells were passed through 70 μm cell strainers (BD Falcon, Bedford, MA) and collected by brief centrifugation. The hippocampus neuron cells are resuspended in neurobasal medium with 2% B27, 0.5 mM glutamine, 25 μM glutamate, 50 units/mL penicillin, and 50 μg/mL streptomycin or transfected by GFP plasmid DNA using electroperation method. The dissociated cells were plated on 96 well plates or 6 well plates (precoated with 10 μg/mL poly-D-lysine) in seeding medium consisting of neurobasal medium supplemented with 2% B27. The cultures were maintained at 37 °C in a humidified incubator with 5% CO_2. One day following plating, the seeding medium was removed and replaced with maintenance medium (seeding medium without glutamate) and refreshed twice a week. Neurons are the principal surviving cell type under these serum-free culture conditions.

Oligomer Aβ_{42} Preparation. Briefly, Aβ_{42} peptide was dissolved in cold hexafluoro-2-propanol (HFIP) to a final concentration of 1 mM. The peptide was aliquoted and dried under vacuum. The aliquoted peptides were stored at −80 °C until use. For use in cell experiments, the peptide was dissolved in DMSO to a final concentration of 5 mM and then diluted to 100 μM in Ham's/F12 media.

Cell Viability Assay. Neuron cells(DIV14) in culture medium were pretreated by 10 μM AIO for 1 h before incubated by 10 μM oligomer Aβ_{42} for another 24 h or pretreated by 100 μM NMDA for 24 h then the AIO was used. After 24 h of treatment, 0.5 mg/mL MTT was subsequently added to each well. After 4 h of additional incubation, 100 μL of DMSO was added to dissolve the crystals. The absorption values at 570 nm were determined with a microplate reader. Experiments were performed in triplicate for each sample.

ATP Assay. ATP luminescence were detected followed the manufactured information with modification to evaluate the cells viability after Aβ_{42} or NMDA treatment. Neuron cells in culture medium were pretreated by 10 μM AIO for 1 h before treatment with 10 μM oligomer Aβ_{42} for another 24 h, or cells were pretreated by 100 μM NMDA for 24 h, and then the AIO was used. The plates and its contents were equilibrated at room temperature for approximately 30 min after 24 h of treatment. Cell titer reagent (100 μL) was added to each well in a 96-well plate, and the plate was shaken gently for 2 min to induce cell lysis. The plate was allowed to incubate at room temperature for 10 min to stabilize the luminescent signal, and then the luminescence was recorded.

OA and AIO Treatment. To investigate the effects of OA-induced neurotoxicity, the cultured neurons (DIV14) were preincubated with different concentrations of AIO (0, 0.1, 0.3, 1, 3, 10 μM) for 1 h, and then the neurons were treated with10 nM of OA for 24 h at 37 °C.

Western Blot Analysis. Neuron cells treated by AIO and OA or treated by AIO and oligomer Aβ42 were washed in cold PBS and then were lysed in a RIPA buffer that contained a mixture of protease inhibitors. Fifteen micrograms of total protein from each sample were run on a 12% SDS-PAGE gel and transferred to a nitrocellulose membrane. The membranes were incubated with appropriately diluted primary antibodies, followed by horseradish peroxidase-conjugated secondary antibodies against the corresponding species. Labeling was detected using the ECL system (Amersham Biosciences). Reported values are representative of three independent experiments.

Electroperation Transfection. The hippocampus neuron cells were counted, and the required number of cells was centrifuged (4×10^6 cells per sample) at 800 rpm for 5 min at room temperature. The supernatant was removed completely, and the cell pellet was resuspended carefully in 100 μL of room-temperature nucleofector solution per sample with 4 μg GFP plasmid DNA. The cell/DNA suspension was transferred into a certified cuvette (sample must cover the bottom of the cuvette without air bubbles). The cuvette with cell/DNA suspension was inserted into the Nucleofector Cuvette Holder, and the appropriate Nucleofector program was selected to finish the transfection.

Immunofluorescence and Confocal Microscopy. The transfected cells pretreated by 10 μM AIO 1 h before 10 μM oligomer Aβ42 treatment were washed with Dulbecco's phosphate buffered saline (DPBS, pH 7.4), fixed with 4% paraformaldehyde in 0.1 M phosphate buffer (pH 7.4) for 10 min, and then imaged with a confocal laser-scanning microscope (LSM510, Zeiss) using the 63× oil-immersion objective. The selected areas are zoomed according to requirement. Spine density was expressed as the number of spines per 10 μm of dendritic length.

Statistical Analysis. Data are expressed as the mean ± SD. Analyses were performed using Prism 5 software with a two-way ANOVA to identify significant effects. Differences were considered significant at $p < 0.05$, $n = 3$.

RESULTS

Structure Identification of AIO. AIO was obtained as a white powder. The ESI-MS showed the $[M - H]^-$ ion at m/z

DOI: 10.1021/acs.jafc.5b00396
J. Agric. Food Chem. 2015, 63, 3687−3693

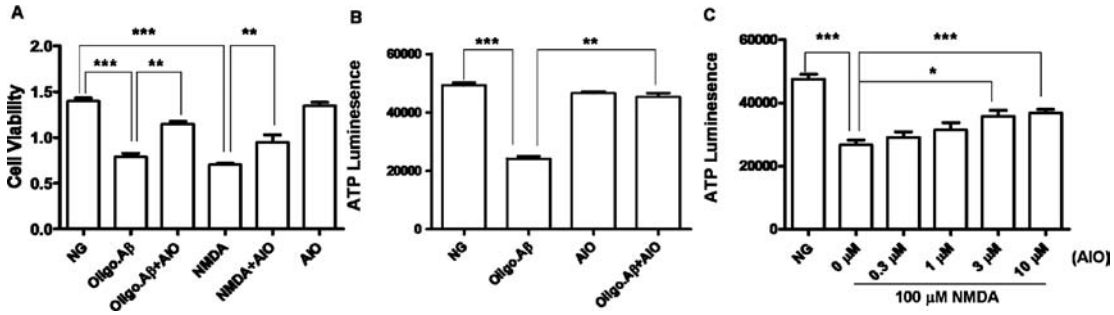

Figure 2. Neuroprotection of AIO on cultured neuron cells treated by oligomer Aβ42 or NMDA. (A) Neuron cells (DIV14) were pretreated with or without 10 μM AIO for 1 h before 10 μM oligomer Aβ42 treatment; or neurons were pretreated by 100 μM NMDA before treatment with or without 10 μM AIO; or neurons were treated by only AIO, then the cells were cultured for another 24 h to detect cell viability using MTT method. (B) Neuron cells (DIV14) were pretreated by 10 μM AIO for 1 h before 10 μM oligomer Aβ42 treatment, then the cells were cultured for another 24 h to detect the ATP level. (C) Neuron cells (DIV14) were pretreated by 100 μM NMDA for 1 h before different does of AIO treatment, and then the cells were cultured for another 24 h to detect the ATP level. * $P < 0.05$, **$P < 0.01$, ***$p < 0.001$, $n = 3$.

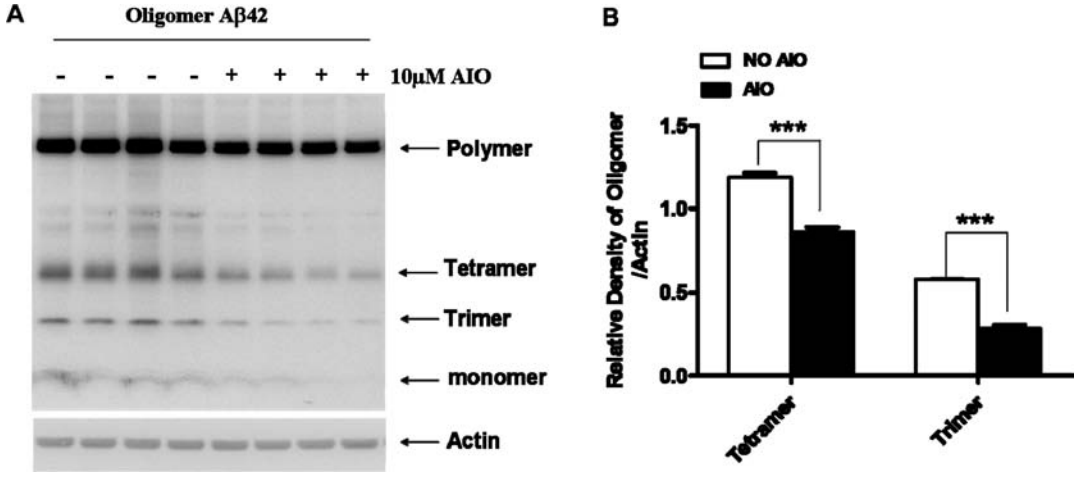

Figure 3. Effect of AIO on Aβ-decomposition system in cultured neurons. After pretreatment without or with 10 μM AIO for 1 h, rat hippocampus neurons (DIV 14) were treated by 10 μM oligomer Aβ42 for 24 h. After being washed with cold PBS, Aβ oligomers in the whole cell lysates were detected by Western blot analysis (12% sodium dodecyl sulfate polyacrylamine gel; a mouse anti-Aβ monoclonal antibody 6E10) and actin was used as a loading control in the same membrane. ***$p < 0.001$, $n = 4$.

323, and its molecular formula was drawn as $C_{20}H_{20}O_4$ from its ^{1}H and ^{13}C NMR. In the ^{1}H NMR (400 MHz, acetone-d_6), an ABX spin-coupling system was ascribed to the three protons of the benzene ring, with signals at 7.43 (H, d, J = 8.4 Hz), 6.99 (H, d, J = 2.4 Hz), and 6.81 ppm (H, dd, J = 8.4, 2.4 Hz), respectively. The proton signals at 5.13 (H, tq, J = 6.5, 1.4 Hz), 3.47 (2H, d, J = 6.4 Hz), 1.67 (3H, s), and 1.64 ppm (3H, d, J = 1.2 Hz) were ascribed to a prenyl group in the molecule. The signal at 3.83 ppm (3H, s) was ascribed to a methoxy group. In the ^{13}C NMR, there were 20 carbons, including a benzofuran, a prenyl, and a benzene ring. Compared to the reported data,[18] it was identified as artoindonesianin O (AIO), the chemical structure of which was given in Figure 1.

AIO Can Exert Neuroprotection after Oligomer Aβ42 or before NMDA Treatment on Hippocampus Neuron Cells. Previous study has demonstrated that oligomer Aβ42 is toxic to a neuron and that NMDA can induce excitotoxicity. In this study, we first investigated the cell viability using the MTT method. The result clearly showed that AIO can significantly enhance the cell viability after oligomer Aβ42 or before NMDA treatment; however, AIO alone has no impact on cell viability even at the concentration of 10 μM (Figure 2A). At the same time, we also detected the ATP level of neurons. We found that the ATP level of neuron was remarkably reduced after 10 μM oligomer Aβ42 treatment compared with negative control. To our surprise, the ATP level of neuron in AIO pretreatment group was enhanced compared with the 10 μM oligomer Aβ42 treatment group (Figure 2B). Excitotoxicity is a key mechanism of cell death following acute neuronal injury that involves deregulation of intracellular calcium. To model excitotoxicity, we used the agonist NMDA to activate NMDA receptors in primary neuron cells.[19] The cells at DIV 14 were pretreated with 100 μM NMDA for 1 h, except for the control group, followed by returning to conditioned media without or with different concentrations of AIO. The ATP level was detected after 24 h treatment. The result clearly showed that NMDA can reduce the cell ATP level, but in the 3 μM and 10 μM AIO groups, there is a remarkable reverse in the reduction (Figure 2C).

AIO May Reflect the Potential Activation of Aβ-Decomposing System. Because AIO could protect the neurons treated by oligomer Aβ42, we wanted to know whether AIO could partly activate the intracellular Aβ-decomposing system to exert its neouroprotection. Interestingly, AIO could significantly decrease cellular Aβ42 tetramer and trimer compared with no AIO treatment group (Figure 3A,B).

DOI: 10.1021/acs.jafc.5b00396
J. Agric. Food Chem. 2015, 63, 3687−3693

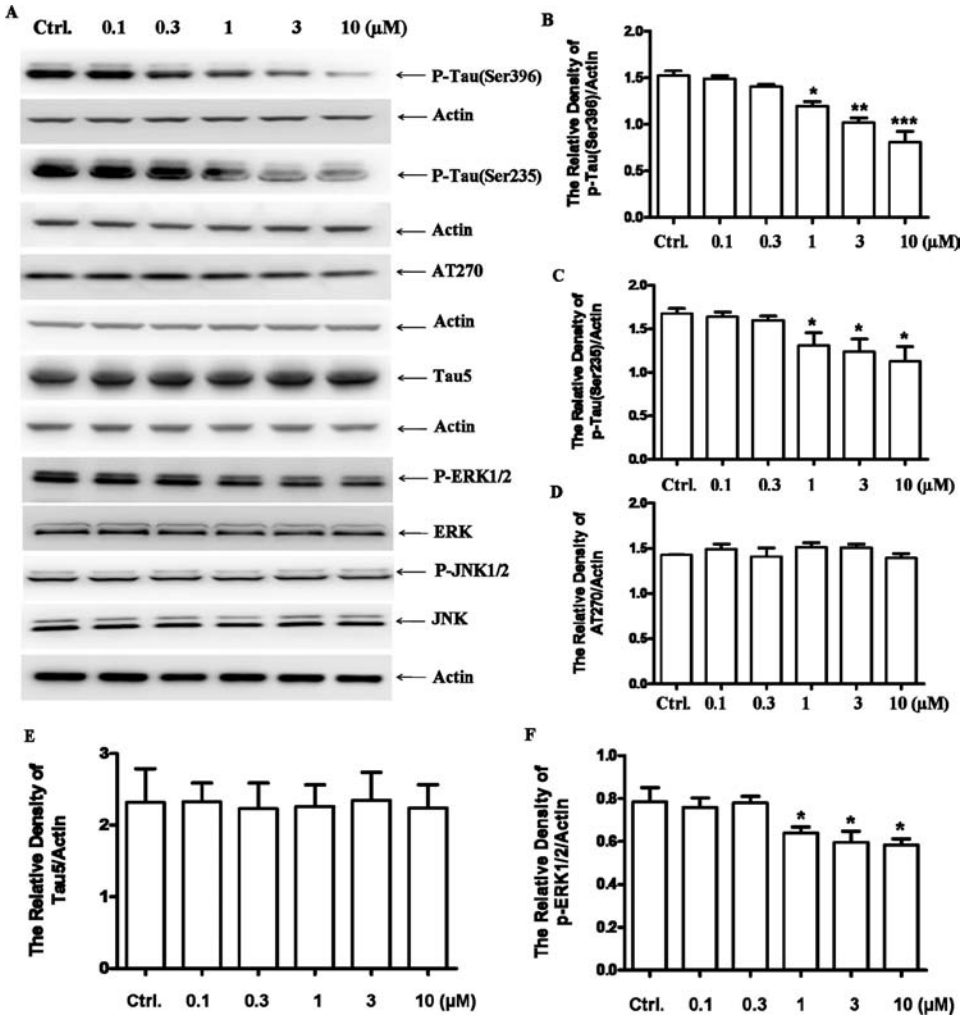

Figure 4. Expressions of okadamic acid (OA)-induced hyperphosphorylated tau-related proteins on neuron cells treated by AIO. Rat hippocampus neurons (DIV 14) were pretreated by various concentrations of AIO (0−10 μM) for 1 h, and then the cells were continuously treated by 25 nM OA for 24 h. Western blot analysis was used to detect the expressions of hyperphosphorylated tau, total tau, and its kinase (panel A). The optical density of the each band was as 1 arbitrary densitometry unit, normalized to actin for the same membrane (panels B−F). * $P < 0.05$, ** $P < 0.01$, *** $p < 0.001$ vs Control.

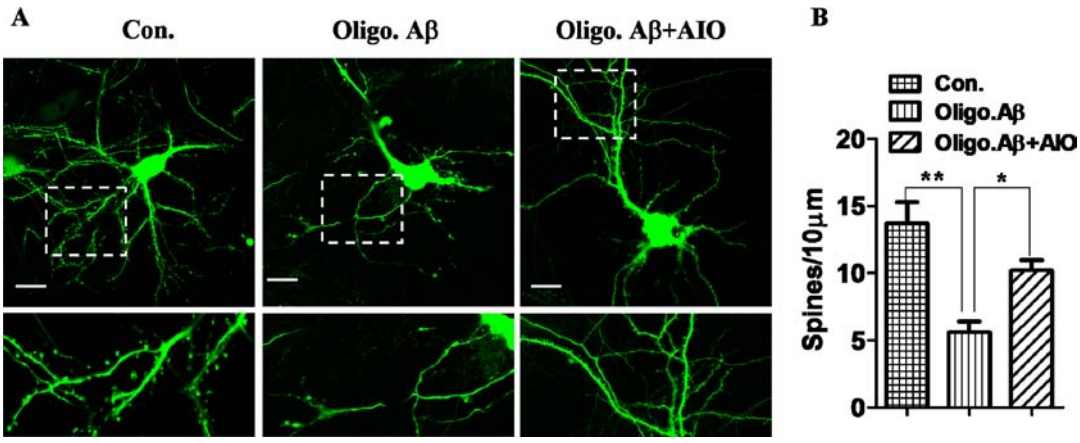

Figure 5. Morphological change on cultured neuron cells transfected by GFP after oligomer Aβ42 and AIO treatment. Neuron cells were transfected by GFP plasmid DNA on the cultured day, and then images of the cells were taken using a confocal microscope (63×) after 21 days of culture (panel A), in which cells were pretreated by 10 μM AIO for 1 h before 10 μM oligomer Aβ42 treatment. Graphical result of dendritic spines on cultured neuron cells (panel B). * $P < 0.05$, ** $P < 0.01$ vs control. Scale bar represents 10 μM.

AIO Attenuates OA-Induced Tau Hyperphosphorylation and Protects the Neuron from Neurotoxicity. On the basis of the above result, we wondered whether or not AIO could impact the tau hyperphosphorylation on cultured neuron

DOI: 10.1021/acs.jafc.5b00396
J. Agric. Food Chem. 2015, 63, 3687−3693

cells. OA was used to induce tau hyperphosphorylation.[20,21] Interestingly, we found that AIO could significantly reduce the expressions of tau hyperphosphorylation at Ser396 and Ser235 from dosage 1 to 10 μM. But it was almost no action about AT270 at Thr181 site (Figure 4A–D).

AIO Has No Obvious Effect on Total Tau (Tau5) Level. Because of the reduction of tau hyperphosphorylation at Ser396 and Ser235, we further investigated the expression of total tau using the same samples. As we expected, total tau did not change (Figure 4A). The quantity result of total tau was shown in Figure 4E.

AIO Inhibits the Expression of Hyper-Phosphorylated Tau Kinase on Neuron Cells. Tau hyperphosphorylation is mediated by several kinases, many of which show large overlap in their ability to phosphorylate tau at the same epitopes in AD.[22] It has been reported that the inhibition of PP2A by OA induced a dramatic increase in the phosphorylation/activation of ERK1/2, and thus, OA could promote the activity of ERK1/2 to phosphorylate the tau in vitro at many abnormal hyperphosphorylatation sites and cause neurotoxicity.[23] Our result showed that the expression of p-ERK1/2 was reduced after AIO treatment in a dose over 1 μM. At the same time, the total ERK did not change. Another kinase, p-JNK1/2, did not change (Figure 4A, 4F). Other related kinases, including p-CDK5 and p-GSK3α/β, remained unchanged (data not shown).

AIO Elevates the Number of Dendritic Spines on Neurons Treated with Oligomer Aβ42. Dendritic spines are related with synaptic plasticity and memory loss in AD. On the basis of the above result, we were curious to know that whether AIO can exert its neuroprotection to improve the synaptic plasticity. Our methods helped to find a compelling result. The numbers of dendritic spines were significantly reduced in the oligomer Aβ42-treated group compared with the control group. Moreover, in the combined AIO oligomer and Aβ42 treatment, the dendritic spines numbers were remarkably increased as expected (Figure 5A,B).

DISCUSSION

The past decade has witnessed an intense interest in herbal medicines, in which phytochemical constituents can have long-term health-promoting or medicinal qualities. Phytochemicals present in vegetables and fruits are believed to reduce the risk of several major diseases, including cardiovascular diseases, cancers, as well as Alzheimer's disease. Identification and characterization of new medicinal plants to cure neurodegenerative diseases has been a major and increasing scientific interest in recent years. In this pilot study, we first evaluated the neuroprotective activity of AIO extracted from mulberry in rat primary hippocampus neurons.

As we know, the formation of amyloid plaques is one of the major pathologies of AD. Aβ is produced by endoproteolysis of the parental amyloid precursor protein (APP), which is achieved by the sequential cleavage of APP by groups of enzymes or enzyme complexes termed β- and γ-secretases. Recent studies suggest that the buildup of oligomer Aβ may be an early event in the pathogenesis of AD.[24] Also it is the trigger to kill the cells in the AD brain. In this study, the ATP level and MTT method were used to evaluate the cells viability after oligomer Aβ42 treatment. Interestingly, we found that AIO could exert neuroprotection against oligomer Aβ42-induced neurotoxicity partly through the activation of the Aβ decomposition system, resulting in the reduction of cellular oligomerization. Excitotoxicity is a distinct mode of neuronal death that is attributed to increased presynaptic glutamate release. Disturbance of extracellular glutamate levels acting on NMDA receptors (NMDAR) results in enhanced calcium influx and death of the cells. Overactivation of NMDAR is a major cause of cell death following acute neuronal injury and is also implicated in neurodegenerative diseases, such as Parkinson, Huntington, and Alzheimer's disease.[17] As we expected, AIO can reverse the neuronal cell death induced by NMDA. All of those data clearly show for the first time that AIO has neuroprotection on hippocampus neuron cells.

Tau-based strategies have received little attention until recently despite that the presence of extensive tau pathology is central to Alzheimer's disease. The discovery of mutations within the tau gene that causes front-temporal dementia demonstrated that tau dysfunction, in the absence of amyloid pathology, was sufficient to cause neuronal loss and clinical dementia. Abnormal levels and hyperphosphorylation of tau protein have been reported to be the underlying cause of a group of neurodegenerative disorders collectively known as "tauopathies". The detrimental consequence is the loss of affinity between this protein and the microtubules, increased production of fibrillary aggregates, and the accumulation of insoluble intracellular neurofibrillary tangles in AD.[25] OA can induce microtubule-associated protein tau hyperphosphorylation leading to the pathological process of analogical AD.[23,26] OA selectively inhibits the serine/threonine phosphatases 2A thereby induces hyperphosphorylation of tau. Hyperphosphoryltion of tau is triggered by multiple mechanisms involving MAP kinases via ERK1/2, Jun N-terminal kinase and other cellular stress and so on. The consequence of tau hyperphosphorylation is neurotoxicity. Thus, the inhibitory effect on tau hyperphosphorylation may reduce the damage of axonal transport and thereby benefit cognitive function. In this study, we wonder whether AIO can impact the tau hyperphosphorylation induced by OA on neurons. Interestingly, we find that AIO significantly reduces the expression of hyperphosphorylation of tau at Ser396 and Ser235, which had been reported to have higher disease incidences in AD brain, but it remains unchanged at about AT270 at the Thr 181 site. Is the reduction of tau hyperphosphorylation at Ser396 and Ser235 followed by the reduction of total tau (tau5)? With this question, the level of total tau is evaluated using the same sample. As we expected, the total tau was not remarkably changed in this process. These studies provide evidence that targeting p-tau may represent an effective treatment strategy.

It is well-known that phosphorylation of tau at certain sites was involved in AD pathogenesis. Some kinases, including cyclin-dependent kinase 5, GSK3α/β, casein kinase 1, protein kinase A, and MAPKs, have been implicated in tau phosphorylation.[27] In this study, we want to know whether the decrease in hyperphosphorylated tau was due in part to an inhibition of tau kinases. The results showed that p-ERK1/2 was involved in the reduction of hyperphosphorylated tau after AIO treatment despite no change in the level of total ERK, but p-JNK1/2, p-CDK5, and p-GSK3α/β keep the basal level. AIO may possibly compete with OA to recover the activity of PP2A and reduce the ERK phosphorylation, but a detailed mechanism still needs to be clarified.

It is known that both Aβ and phosphorylation tau are correlated with synaptic and cognitive deficits.[28] Aβ toxicity is mediated not only by the fibrillar form of the protein but also by the soluble oligomers. The dendritic spines have been

DOI: 10.1021/acs.jafc.5b00396
J. Agric. Food Chem. 2015, 63, 3687–3693

assigned critical roles in the form of synaptic plasticity and memory. Dendritic spine defects are found in a number of cognitive disorders, including AD. Therefore, we hypothesized that the AIO is critical to synaptic function. In this study, we examined the relationship between AIO and synaptic defects induced by oligomer Aβ42. The result surprised us. In comparison, AIO treatment enhances the density of dendritic spines on neurons induced by oligomer Aβ42. Therefore, AIO may be possibly involved in the synaptic plasticity and may prevent memory loss.

Taken together, our results strongly suggest that AIO, a dietary phenolic compound from mulberry, is a potential nutritional candidate for protection against neurodegeneration through the reduction of tau hyperphosphorylation and improvements in the synaptic plasticity. More studies are still needed to elucidate the initial mechanisms that trigger the neuroprotection in order to design appropriate therapeutic interventions to block the progression of AD.

AUTHOR INFORMATION

Corresponding Author

*E-mail: hexiangjiu@163.com. Tel/Fax: 86-20-3935-2132.

Funding

The present work was supported by the National Natural Science Foundation of China under Grant (U1203103) and the grant from Colleges and Universities in Guangdong province 1000 cultivation of talents in China.

Notes

The authors declare no competing financial interest.

ACKNOWLEDGMENTS

The authors would like to thank for Dr. Yanfeng Zhao for her assistant in modification the manuscript.

ABBREVIATIONS USED

Aβ, β-amyloid; AIO, artoindonesianin O; AD, Alzheimer's disease; JNK, c-Jun N-terminal kinase; ERK, extracellular signal-regulated kinase; MAPKs, mitogen-activated protein kinases; CDK5, cyclin dependent kinase 5; OA, okadaic acid; NMDA, *N*-methyl-D- aspartate; GSK3, glycogen synthase kinase 3; DIV, days in vitro

REFERENCES

(1) Adanna, A. G.; Vanessa, M.; Li, C. Use of *Caenorhabditis elegans* as a model to study Alzheimer's disease and other neurodegenerative disease. *Front. Genet.* **2014**, *5*, 279.

(2) Kim, M. J.; Seong, A. R.; Yoo, J. Y.; Jin, C. H.; Lee, Y. H.; Kim, Y. J.; Lee, J.; Jun, W. J.; Yoon, H. G. Gallic acid, a histone acetyltransferase inhibitor, suppresses β-amyloid neurotoxicity by inhibiting microglial-mediated neuroinflammation. *Mol. Nutr. Food Res.* **2011**, *55*, 1798−1808.

(3) Markesbery, W. R. Oxidative stress hypothesis in Alzheimer's disease. *Free Radical Biol. Med.* **1997**, *23*, 134−147.

(4) Riemer, J.; Kins, S. Axonal transport and mitochondrial dysfunction in Alzheimer's disease. *Neurodegener. Dis.* **2013**, *12*, 111−124.

(5) Reitz, C. Dyslipidemia and the risk of Alzheimer's disease. *Curr. Atheroscler. Rep.* **2013**, *15*, 307.

(6) Lovestone, S.; Reynolds, C. H. The phosphorylation of tau: a critical stage in neurodevelopment and neurodegenerative processes. *Neuroscience* **1997**, *78*, 309−324.

(7) Ballatore, C.; Lee, V. M.; Trojanowski, J. Q. Tau-mediated neurodegeneration in Alzheimer's disease and related disorders. *Nat. Rev. Neurosci.* **2007**, *8*, 663−672.

(8) Avila, J.; Lucas, J. J.; Perez, M.; Hernandez, F. Role of tau protein in both physiological and pathological conditions. *Physiol. Rev.* **2004**, *84*, 361−384.

(9) Yang, X.; Yang, L.; Zheng, H. Hypolipidemic and antioxidant effects of mulberry (*Morus alba* L.) fruit in hyperlipidaemia rats. *Food Chem. Toxicol.* **2010**, *48*, 2374−2379.

(10) Jeong, J. C.; Jang, S. W.; Kim, T. H.; Kwon, C. H.; Kim, Y. K. Mulberry fruit (*Moris fructus*) extracts induce human glioma cell death in vitro through ROS-dependent mitochondrial pathway and inhibits glioma tumor growth *in vivo*. *Nutr. Cancer* **2010**, *62*, 402−412.

(11) Liu, L. K.; Chou, F. P.; Chen, Y. C.; Chyau, C. C.; Ho, H. H.; Wang, C. J. Effects of mulberry (*Morus alba* L.) extracts on lipid homeostasis *in vitro* and *in vivo*. *J. Agric. Food Chem.* **2009**, *57*, 7605−7611.

(12) Kang, T. H.; Hur, J. Y.; Kim, H. B.; Ryu, J. H.; Kim, Y. K. Neuroprotective effects of the cyanidin-3-O-beta-D-glucopyranoside isolated from mulberry fruit against cerebral ischemia. *Neurosci. Lett.* **2006**, *391*, 122−126.

(13) Kim, H. G.; Ju, M. S.; Shim, J. S.; Kim, M. C.; Lee, S. H.; Huh, Y.; Kim, S. Y.; Oh, M. S. Mulberry fruit protects dopaminergic neurons in toxin-induced Parkinson's disease models. *Br. J. Nutr.* **2010**, *104*, 8−16.

(14) Yang, Z. G.; Matsuzaki, K.; Takamatsu, S.; Kitanaka, S. Inhibitory effects of constituents from *Morus alba* var. *multicaulis* on differentiation of 3T3-L1 cells and nitric oxide production in RAW264.7 cells. *Molecules* **2011**, *16*, 6010−6022.

(15) Hwang, S. L.; Shih, P. H.; Yen, G. C. Neuroprotective effects of citrus flavonoids. *J. Agric. Food Chem.* **2012**, *60*, 877−885.

(16) Ngoungoure, V. L.; Schluesener, J.; Moundipa, P. F.; Schluesener, H. Natural polyphenols binding to amyloid: A broad class of compounds to treat different human amyloid diseases. *Mol. Nutr. Food Res.* **2015**, *59*, 8−20.

(17) Bhuiyan, M. I.; Islam, M. N.; Jung, S. Y.; Yoo, H. H.; Lee, Y. S.; Jin, C. Involvement of ceramide in ischemic tolerance induced by preconditioning with sublethal oxygen-glucose deprivation in primary cultured cortical neurons of rats. *Biol. Pharm. Bull.* **2010**, *33*, 11−17.

(18) Hakim, H.; NULinnuha, U. Z.; Syah, Y. M.; Ghisalberti, E. L. Artoindonesianins N and O, new prenylated stilbene and prenylated arylbenzofuran derivatives from *Artocarpus gomezianus*. *Fitoterapia* **2002**, *73*, 597−603.

(19) Jahani-AsI, A.; Pilon-Larose, K.; Xu, W.; MacLaurin, J. G.; Park, D. S.; McBride, H. M.; Slack, R. S. The mitochondrial inner membrane GTPase, optic atrophy 1(Opa1), restores mitochondrial morphology and promotes neuronal survival following excitotoxicity. *J. Biol. Chem.* **2011**, *286*, 4772−4782.

(20) Feng, L. J.; Shen, Y. X.; Sun, A. M.; Shen, Y. J.; Fang, S. Y.; Li, J. Endoplasmic reticulum stress in involved in okadaic acid-induced tau hyperphosphorylation and neurotoxic effects of okadaic acid. *Neural Regener. Res.* **2010**, *5*, 1534−1540.

(21) Sun, A. M.; Wang, H. P.; Shen, Y. J.; Shen, Y. X.; Fang, S. Y. Differential induction of tau hyperphoephorylation by OA treatment in primary cultured neurons and SH-SY5Y cell. *Chin. Pharmacol. Bull.* **2010**, *27*, 41−45.

(22) Duka, V.; Lee, J. H.; Credle, J.; Wills, J.; Oaks, A.; Smolinsky, C.; Shah, K.; Mash, D. C.; Masliah, E.; Sidhu, A. Identification of the sites of Tau hyperphosphorylation and activation of tau kinases in synucleinopathies and Alzheimer's diseases. *PLoS One* **2013**, *8*, 1−11.

(23) Kamat, P. K.; Shivika, R.; Suprida, S.; Rakesh, S.; Chandishwar, N. Molecular and cellular mechanism of okadaic acid(OKA)-induced neurotoxicity: A novel tool for Alzheimer's disease therapeutic application. *Mol. Neurobiol.* **2014**, *50*, 852−865.

(24) LaFerla, F. M.; Green, K. N.; Oddo, S. Intracellular amyloid-beta in Alzheimer's disease. *Nat. Rev. Neurosci.* **2007**, *8*, 499−509.

(25) Medina, M.; Avila, J. New perspectives on the role of Tau in Alzheimer's disease. Implication for therapy. *Biochem. Pharmacol.* **2014**, *88*, 540−547.

(26) Zhao, J. F.; Wang, D.; Li, L. M.; Zhao, W. H.; Zhao, C. Protective effects of humamin on okadaic acid-induced neurotoxicity in cultured cortical neurons. *Neurochem. Res.* **2014**, *39*, 2150−2159.

DOI: 10.1021/acs.jafc.5b00396
J. Agric. Food Chem. 2015, 63, 3687−3693

(27) Dolan, P. J.; Johnson, G. V. The role of tau kinases in Alzheimer's disease. *Curr. Opin. Drug Discovery Devel.* **2010**, *13*, 595−603.
(28) Chen, X.; Hu, J.; Jiang, L.; Xu, S.; Zheng, B.; Wang, C.; Zhang, J.; Wei, X.; Chang, L.; Wang, Q. Brilliant Blue G improves cognition in an animal model of Alzheimer's disease and inhibits amyloid-β-induced loss of filopodia and dendrite spines in hippocampal neurons. *Neuroscience* **2014**, *279*, 94−101.

DOI: 10.1021/acs.jafc.5b00396
J. Agric. Food Chem. 2015, 63, 3687−3693

suppression, and inhibition of α-glucosidase and tyrosinase.[18,21−29] Furthermore, it has been reported that regular consumption of coffee is associated with a lower risk of type 2 diabetes mellitus,[30] and 5-CQA in coffee may contribute to the beneficial effects of coffee on type 2 diabetes mellitus.[31] However, the inhibitory effects of CQA derivatives from kudingcha on α-glucosidase have never been reported before. As tea polyphenolic compounds strongly interact with proteins,[32] CQA derivatives from kudingcha may exhibit potential interactions with α-glucosidase. This should inevitably result in the change of enzyme molecular configuration and lead to the loss of catalytic activity, thereby reducing carbohydrate digestibility and protection against diabetes and obesity. Recently, we have reported the potent antioxidant activity of kudingcha polyphenols and isolated CQA derivatives from the leaves of *I. kudingcha* C.J. Tseng.[22,33−35] In this study, therefore, the inhibitory effects against α-glucosidase of six kinds of CQA derivatives (3-CQA, 4-CQA, 5-CQA, 3,4-diCQA, 3,5-diCQA, and 4,5-diCQA) present in kudingcha made from the leaves of *I. kudingcha* C.J. Tseng were investigated. Furthermore, the potential mechanisms of interactions between α-glucosidase and CQA derivatives were characterized by fluorescence spectroscopy and circular dichroism (CD) spectroscopy.

MATERIALS AND METHODS

Materials and Reagents. Kudingcha made from the leaves of *I. kudingcha* C.J. Tseng was obtained from Hainan Yexian Bio-Science Technology Co., Ltd. (Hainan, China), and the sample was ground by using a domestic blender, stored in sealed polyethylene bags, and kept in a refrigerator at −20 °C until use. α-Glucosidase from *Saccharomyces cerevisiae* (dialysis 48 h before use), 5-CQA, and 4-nitrophenyl α-D-glucopyranoside (≥99%) were purchased from Sigma-Aldrich Chemical Co. (St. Louis, MO, USA). Standards of 3-CQA, 4-CQA, 3,4-diCQA, 3,5-diCQA, and 4,5-diCQA (>95%) were prepared from kudingcha according to our reported methods.[22,34,35] The solvents used for chromatographic purpose were of high-performance liquid chromatography (HPLC) grade, and all other reagents were of analytical reagent grade.

Determination of Total Polyphenols Content and CQA Derivatives. The total polyphenols content was determined by using the Folin−Ciocalteu method according to the reported procedure.[22] The contents of CQA derivatives were measured by HPLC with an Agilent HPLC series 1100 (Agilent, Santa Clara, CA, USA) equipped with a model G1379A degasser, a model G1311A quatpump, a model G1316A column oven, a model G1315B diode array detector (DAD), and Chemstation software. The separation was completed on a TSK gel ODS-80TsQA column (4.6 × 250 mm, 5 μm, Tosoh Corp., Tokyo, Japan) with a gradient mobile phase consisting of ultrapure water (A), methanol (B), and 1.0% formic acid (C, v/v) at a flow rate of 0.5 mL/min. Elution was performed with a linear gradient as follows: 0−45 min, A from 60 to 35%, B from 20 to 45%, C 20%. The temperature of column oven was set at 40 °C, the injection volume was 20 μL, and CQA derivatives were detected at 326 nm with a DAD. The chromatographic peaks were identified by comparing the retention times and UV spectra of standards of CQA derivatives.

Preparation of CQA Derivatives. The preparation of CQA derivatives was performed according to the reported methods[22,33−35] with some modifications. Briefly, the kudingcha powder was extracted with water (10 for the ratio of extraction solvent to material, v/w) for 30 min at 95 °C. After extraction, the extract was centrifuged at 5000*g* for 10 min, and the resulting insoluble residue was treated twice as described above. The combined supernatants were concentrated by a rotary evaporator (Tokyo Rikakikai Co., Ltd., Tokyo, Japan) and lyophilized (Labconco, Kansas, MO, USA) to afford the crude extract. The crude extract was dissolved in deionized water and applied to a column (5 × 30 cm) of HP-20 macroporous resin. Then, the column was washed with 3 times bed volume of distilled water and eluted with 70% ethanol solution, respectively. The collected fractions (10 mL/tube) were analyzed by HPLC as described above, and the fractions containing CQA derivatives were combined, concentrated, and freeze-dried, affording kudingcha polyphenols. The CQA derivatives (3-CQA, 4-CQA, 5-CQA; 3,4-diCQA, 3,5-diCQA, and 4,5-diCQA) were further isolated from the kudingcha polyphenols by HPLC with a semipreparative HPLC column of YMC-Pack ODS-A (20 × 250 mm, 5 μm, YMC Co., Ltd., Kyoto, Japan) according to our reported methods.[22,34,35] The desired fractions containing 3-CQA, 4-CQA, 5-CQA; 3,4-diCQA, 3,5-diCQA, and 4,5-diCQA were combined, concentrated, and lyophilized, respectively. The structures of CQA derivatives were confirmed by electrospray ionization−mass spectrometry (ESI-MS), HPLC, and nuclear magnetic resonance (NMR) spectrometry.

Enzyme Inhibitory Activities Assay. The inhibitory activity against α-glucosidase was measured according to the reported method[26] with some modifications. Briefly, the reaction mixture contained 8 μL of test sample with different concentrations, 30 μL of 2.5 mM 4-nitrophenyl α-D-glucopyranoside as substrate, 20 μL of enzyme solution (0.2 U/mL), and 102 μL of 0.1 M phosphate buffer saline (pH 6.9). The reaction mixture was incubated at 37 °C for 15 min. The reaction was then terminated by the addition of 80 μL of 0.2 M Na_2CO_3 solution. The increase in absorbance at 405 nm due to enzymatic hydrolysis of 4-nitrophenyl α-D-glucopyranoside was monitored with a microplate reader (BioTek Instruments, Inc., Winooski, VT, USA). All samples were analyzed in triplicate. The inhibition percentage was calculated using the formula

$$\text{inhibition rate } (\%) = [((A_{c+} - A_{c-}) - (A_s - A_b)) / (A_{c+} - A_{c-})] \times 100$$

where A_{c+}, A_{c-}, A_s, and A_b are defined as the absorbances of 100% enzyme activity (only the solvent with the enzyme), 0% enzyme activity (only the solvent without enzyme), the test sample (with the enzyme), and a blank (only the sample), respectively. The effective concentration that could inhibit 50% of α-glucosidase activity is defined as IC_{50}.

Assay of Inhibitory Pattern of CQA Derivatives on α-Glucosidase Activity. The effects of CQA derivatives on α-glucosidase activity were investigated with increasing concentrations of enzyme substrate (4-nitrophenyl α-D-glucopyranoside, from 3.0 × 10^{-4} to 1.5 × 10^{-3} M) in the presence or absence of CQA derivatives. Then, the inhibition type was determined by Lineweaver−Burk plot analysis according to Michaelis−Menten kinetics.

Fluorescence Measurement. *General Procedure.* A quantitative analysis of the potential interaction between CQA derivative and α-glucosidase was performed by fluorometric titration as follows: 3.0 mL of solution containing appropriate concentration of α-glucosidase was titrated by the addition of different concentration of 5-CQA, 3,4-diCQA, 3,5-diCQA, or 4,5-diCQA solution. All samples were incubated at fixed temperature (293 or 310 K) for 0.5 h. Then, the fluorescence spectra were recorded with an F-7000 fluorescence spectrophotometer (Hitachi High-Technologies Corp., Tokyo, Japan) by using a 1.0 cm quartz cell and at an excitation wavelength of 280 nm, and the emission spectra were recorded from 300 to 450 nm. Spectral resolution for both excitation and emission was 5 nm. The three-dimensional (3D) fluorescence spectra of enzyme in the absence and presence of CQA derivatives were obtained by recording the excitation and the emission spectra in the range of 200−600 nm with an interval of 5 nm, respectively.

Analysis of Fluorescence Quenching Constant and Thermodynamic Parameters. The fluorescence quenching data were analyzed via the modified Stern−Volmer equation:[36]

$$\lg[(F_0 - F)/F] = \lg K_a + n \lg[Q]$$

Here, F_0 and F are the fluorescence intensities of the enzyme in the absence and presence of quencher, [Q] is the quencher concentration, K_a is the binding constant, and n is the number of the binding sites per

DOI: 10.1021/acs.jafc.5b00420
J. Agric. Food Chem. 2015, 63, 3694−3703

enzyme. The values of n and K_a can be calculated by the slope and intercept with the plots of $\lg(F_0 - F)/F$ against $\lg[Q]$.[37]

Considering that the enthalpy change (ΔH) does not vary significantly over the temperature range, it can be considered as a constant. ΔH and entropy change (ΔS) can be calculated using the van't Hoff equation

$$\ln K = -\frac{\Delta H}{RT} + \frac{\Delta S}{R}$$

$$\ln(K_2/K_1) = (1/T_1 - 1/T_2)\Delta H/R$$

$$\Delta G = \Delta H - T\Delta S$$

where R is the gas constant, T is the experimental temperature, K is the binding constant at the corresponding T, and ΔG is the free energy. Then ΔH, ΔS, and ΔG of interaction can be calculated from the equations above.

CD Measurement. The CD spectra of α-glucosidase and its complexes with CQA derivatives were recorded with the use of a Jasco-810 spectrophotometer (JASCO Corp., Tokyo, Japan) at room temperature. The spectra were measured in the far-UV region (190–250 nm) with a path length of 1.0 mm, a scan speed of 50 nm/min, and a response time of 4 s. In addition, three scans were accumulated for each spectrum. All working solutions were prepared with 20 mM phosphate buffer (pH 6.9). The enzyme concentration was set at 0.2 mg/mL (3×10^{-6} M), and the complexes were prepared by mixing the enzyme with CQA derivative (5-CQA or 3,5-diCQA) at molar ratios of 1:0.5, 1:1, and 1:2 (enzyme to CQA derivative). The resulting CD data were analyzed by curve-fitting program software CDPro using CONTIN, SELCON, and CDSSTR methods, as described by Sreerama and Woody,[38] to obtain the secondary structural contents of α-glucosidase.

Statistical Analysis. Data were expressed as the mean ± standard deviation (SD) of triplicates. The IC_{50} value was calculated from linear regression analysis. Any significant difference was determined by one-way analysis of variance (ANOVA) followed by t test for multiple comparisons at $P < 0.05$ level (SPSS Statistics 20.0, IBM, Armonk, NY, USA).

RESULTS

Inhibitory Activity of Kudingcha Polyphenols against α-Glucosidase. The effect of kudingcha polyphenols, partially purified polyphenols from the crude extract of *I. kudingcha* C.J. Tseng by chromatography of HP-20 macroporous resin, on α-glucosidase from *S. cerevisiae* was investigated. As shown in Figure 2A, the kudingcha polyphenols exhibited strong inhibitory activity against α-glucosidase. The IC_{50} value was determined to be 0.42 mg/mL. To further explore the inhibition type of kudingcha polyphenols against α-glucosidase, the kinetic reaction of α-glucosidase was investigated with different concentrations of enzyme. As shown in Figure 2B, it was found that the line obtained from the kinetic reaction plot passed through the origin point (0, 0) of the coordinate, indicating that the inhibition type of kudingcha polyphenols on α-glucosidase was reversible inhibition. As for irreversible inhibition, the inhibitor binds with enzyme covalently and forms a stable complex, making the enzyme inactivated. The enzyme will exhibit its activity only when a certain amount of enzyme is added to the reaction system. Therefore, the plot of enzyme concentration versus reaction velocity does not pass through the origin of the coordinate, whereas for reversible inhibition, which is characterized by the existence of equilibrium between enzyme and inhibitor, the plot may pass through the origin.[39,40] It is obvious that kudingcha polyphenols are reversible inhibitors of α-glucosidase.

As shown in Figure 3A, the kudingcha polyphenols contained 3-CQA (3.2 ± 0.15%), 4-CQA (2.1 ± 0.09%), 5-CQA (8.4 ± 0.13%), 3,4-diCQA (11.8 ± 0.25%), 3,5-diCQA (23.2 ± 1.61%), and 4,5-diCQA (25.6 ± 1.52%). Because the kudingcha polyphenols showed potent α-glucosidase inhibitory activity as mentioned above, CQA derivatives, the main polyphenols in *I. kudingcha* C.J. Tseng, were isolated by semipreparative HPLC from kudingcha polyphenols (78.4% for total polyphenol content determined by the Folin–Ciocalteu method). The purified CQA derivatives, with purity >95% (Figure 3B), were confirmed to be 3-CQA, 4-CQA, 5-CQA, 3,4-diCQA, 3,5-diCQA, and 4,5-diCQA by HPLC, ESI-MS, and ^{1}H NMR through comparison with the reported data.[22,34,35,41−43]

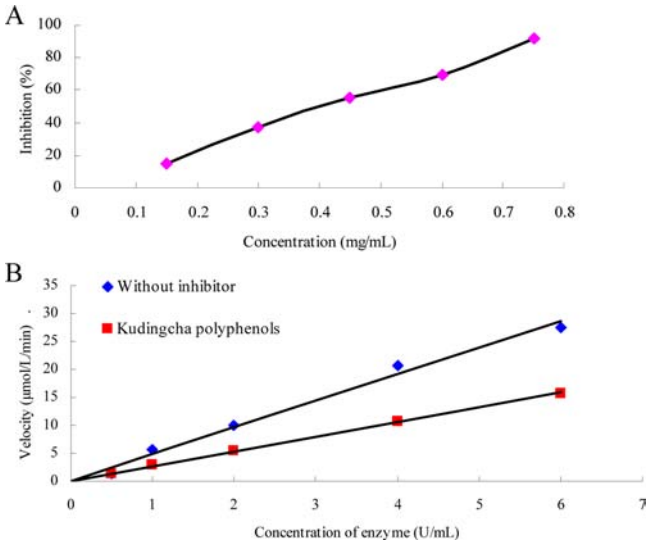

Figure 2. Inhibitory effect (A) and inhibition type (B) of kudingcha polyphenols on α-glucosidase.

Inhibitory Activities of CQA Derivatives against α-Glucosidase. The resulting CQA derivatives from *I. kudingcha* C.J. Tseng were further examined for their inhibition on α-glucosidase by evaluating their IC_{50} values. The results revealed that all of the CQA derivatives had inhibitory activity against α-glucosidase in a dose-dependent manner (Figure 4A). At a concentration of 1.0 mg/mL, α-glucosidase was almost inhibited (98%) by CQA derivatives. The IC_{50} values for 3-CQA, 4-CQA, 5-CQA, 3,4-diCQA, 3,5-diCQA, and 4,5-diCQA were determined to be 0.39, 0.34, 0.30, 0.27, 0.27, and 0.16 mg/mL, respectively. Notably, diCQA derivatives with double caffeoyl moieties exhibited higher inhibition activities than CQA derivatives with a single caffeoyl moiety, indicating that the addition of caffeoyl moiety significantly increased the inhibitory ability.

To characterize the inhibition pattern of α-glucosidase by CQA derivatives, the enzyme reactions were examined with increasing concentrations of substrate without or with a fixed concentration of inhibitor. As an example, Figure 4B shows the Lineweaver–Burk double-reciprocal plots of α-glucosidase kinetics with 4,5-diCQA as the inhibitor. It is obvious that the V_{max} for α-glucosidase decreased while the K_m (0.68 mM) remained unchanged in the presence of 4,5-diCQA, and the other CQA derivatives showed similar trends. Thus, the inhibition of α-glucosidase by CQA derivatives was non-competitive, in which the inhibitor and the substrate should bind simultaneously with the enzyme.

Fluorescence Spectra. Fluorescence spectroscopy and CD spectroscopy were used to explore the interactions between α-glucosidase and CQA derivatives. As the inhibitory activity of

DOI: 10.1021/acs.jafc.5b00420
J. Agric. Food Chem. 2015, 63, 3694−3703

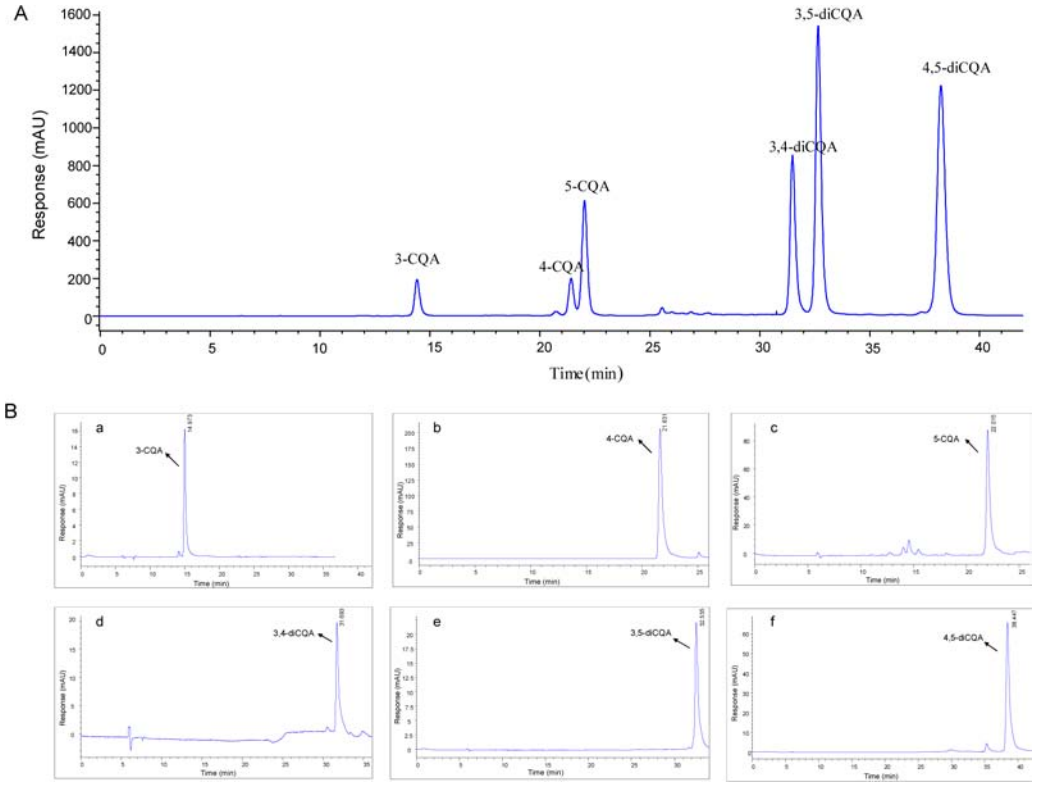

Figure 3. HPLC chromatograms of the extract (A) and six purified caffeoylquinic acids (B) from *Ilex kudingcha* C.J. Tseng.

diCQA derivatives was higher than that of CQA derivatives with a single caffeoyl moiety, 5-CQA, 3,4-diCQA, 3,5-diCQA, and 4,5-diCQA were used for further studies of interaction mechanisms.

Fluorescence spectroscopy is used to measure the interaction between a biomacromolecule and a small molecule ligand.[44] In a protein molecule, Trp has the most powerful activity to emit fluorescence and the intrinsic fluorescent intensity may change depending on the impact of the interaction between the protein and another molecule.[36] It contains 18 Trp residues in α-glucosidase (obtained from the Brookhaven Protein Data Bank, PDB ID: 1 VAD). Therefore, it is possible to use quenching of the intrinsic Trp fluorescence in enzyme to study the interactions between CQA derivatives and α-glucosidase.

Under our measurement condition (i.e., from 300 to 450 nm), all fluorescence emissions from CQA derivatives, buffer, and other reagents were so weak that their impact could be ignored. As shown in Figure 5, the fluorescence intensities of α-glucosidase decreased gradually with the addition of CQA derivatives at 37 °C, and the maximal absorption peak (near 332 nm) was red-shifted; thus, the CQA derivatives interacted with the enzyme (data at 20 °C not shown). As a result, the maximum emission wavelength was shifted from 332 to 360 nm for the addition of 5-CQA, from 332 to 352 nm for 3,4-diCQA, from 331 to 356 nm for 3,5-diCQA, and from 332 to 356 nm for 4,5-diCQA, respectively. These changes suggested that the interactions between the CQA derivatives and α-glucosidase led to a polarity variation for Trp residues in the enzyme and made the microenvironment change from hydrophilic to hydrophobic, thus resulting in greater exposure of Trp residues and unfolding of protein structure.[45,46]

The 3D fluorescence spectra have been used to investigate the characteristic conformational change of protein in recent years.[47] The 3D fluorescence contour maps of α-glucosidase and the mixtures with four CQA derivatives in different concentrations (0.01 and 0.025 mg/mL) are shown in Figure 6. The 3D spectra showed two distinct peaks in enzyme marked 1 ($\lambda_{ex}/\lambda_{em}$: 280 nm/330 nm) and 2 ($\lambda_{ex}/\lambda_{em}$: 230 nm/330 nm). Peak 1 corresponded to the characteristics of Trp and Tyr residues, and peak 2 provided spectral properties of the polypeptide backbone, which occur mainly due to the presence of the $\pi-\pi^*$ and $n-\pi^*$ transitions, respectively.[48,49] The two peaks were quenched by the addition of CQA derivative in a dose-dependent manner. The corresponding parameters (Table 1) indicated that the fluorescence intensity decreased with the addition of CQA derivatives, following a red shift of 10 nm in each of peaks 1 and 2. It was also found that the quenching effect showed a sequence as diCQA > 5-CQA, which was in accordance with the results of fluorescence experiments. These effects might be due to hydrophobic interactions between the aromatic ring and the hydrophobic moieties present, therefore inducing conformational changes in the α-glucosidase molecule.[14]

Fluorescence Binding Constant and Binding Site. To obtain the binding constant (K_a) and the number of binding site per enzyme (n) between CQA derivative and α-glucosidase, the fluorescence quenching data were analyzed according to the modified Stern–Volmer equation by using the Scatchard plots (Figure 5). The results are summarized as shown in Table 2. The results demonstrated that K_a was in the order diCQA > 5-CQA, indicating that introduction of the second caffeoyl moiety into CQA to form diCQA enhanced the binding affinity to the enzyme. As compared with tea polyphenol–protein interactions with K_a from 1.0×10^4 to 1.0×10^5 M^{-1},[50−52] the K_a values (10^6–10^8 M^{-1}) for interactions of CQA derivatives and α-glucosidase were quite high, indicating comparatively strong ligand–protein interactions.

DOI: 10.1021/acs.jafc.5b00420
J. Agric. Food Chem. 2015, 63, 3694−3703

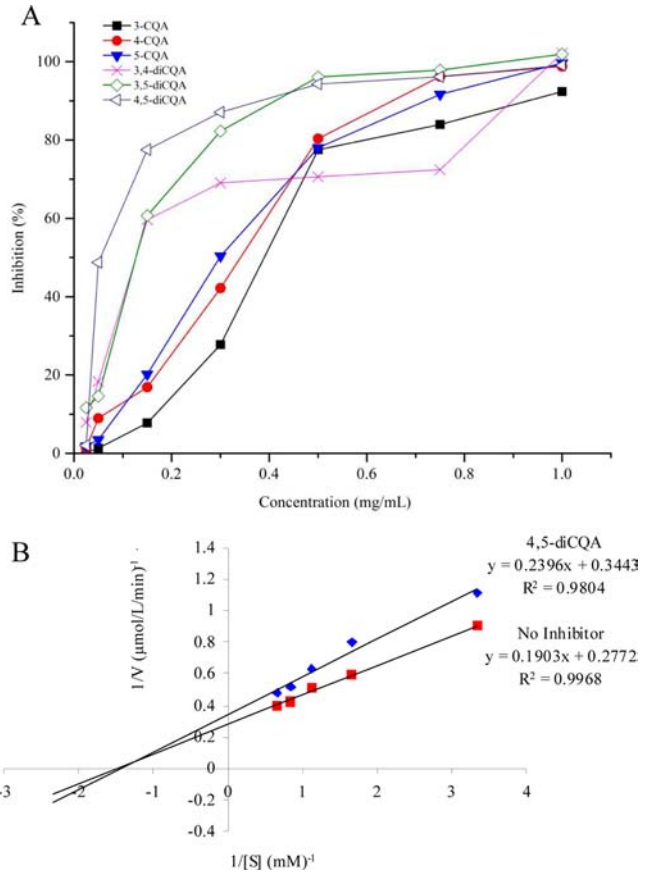

Figure 4. (A) Inhibitory effects of caffeoylquinic acids against the α-glucosidase-catalyzed hydrolysis of 4-nitrophenyl α-D-glucopyranoside at 37 °C and pH 6.9. Each point represents the means of triplicate experiments. (B) Lineweaver–Burk plots of the reaction of α-glucosidase in the presence and absence of 4,5-diCQA at the concentration of 5×10^{-4} M.

Thermodynamic Parameters and Binding Mode. The interactions between phenolic compounds and biomolecules may involve electrostatic interactions, van der Waals interactions, hydrophobic forces, hydrogen bonds, and so on. According to ΔH and ΔS data, the model of interaction between quencher and a protein molecule can be concluded.[53] More specifically, if $\Delta H > 0$ and $\Delta S > 0$, the main force would be hydrophobic force; if $\Delta H < 0$ and $\Delta S > 0$, it would be electrostatic force; if $\Delta H < 0$ and $\Delta S < 0$, it would be hydrogen bonding. According to the van't Hoff equation, the thermodynamic parameters were calculated and the results are presented in Table 2. Notably, the ΔH and ΔS values were both positive, indicating that hydrophobic forces played a major role in the bindings between CQA derivative and α-glucosidase. Furthermore, the negative value of ΔG suggested that the binding reaction was spontaneous.

CD Spectra. CD spectroscopy was conducted to evaluate the influence of 5-CQA and 3,5-diCQA on the secondary structure of α-glucosidase in the far-UV CD range (from 250 to 190 nm). As shown in Figure 7, the CD spectra of α-glucosidase were characterized mainly by two negative bands at 208 and 222 nm, which are caused by a negative Cotton effect characteristic of helical structure.[54,55] The CD spectra were analyzed by using the CDPro software package to afford the contents of four secondary structures: α-helix, β-sheet, turns, and unordered in the absence and presence of 5-CQA or 3,5-diCQA. As shown in Table 3, the secondary structure proportions for free α-glucosidase were α-helical, 21.8%; β-

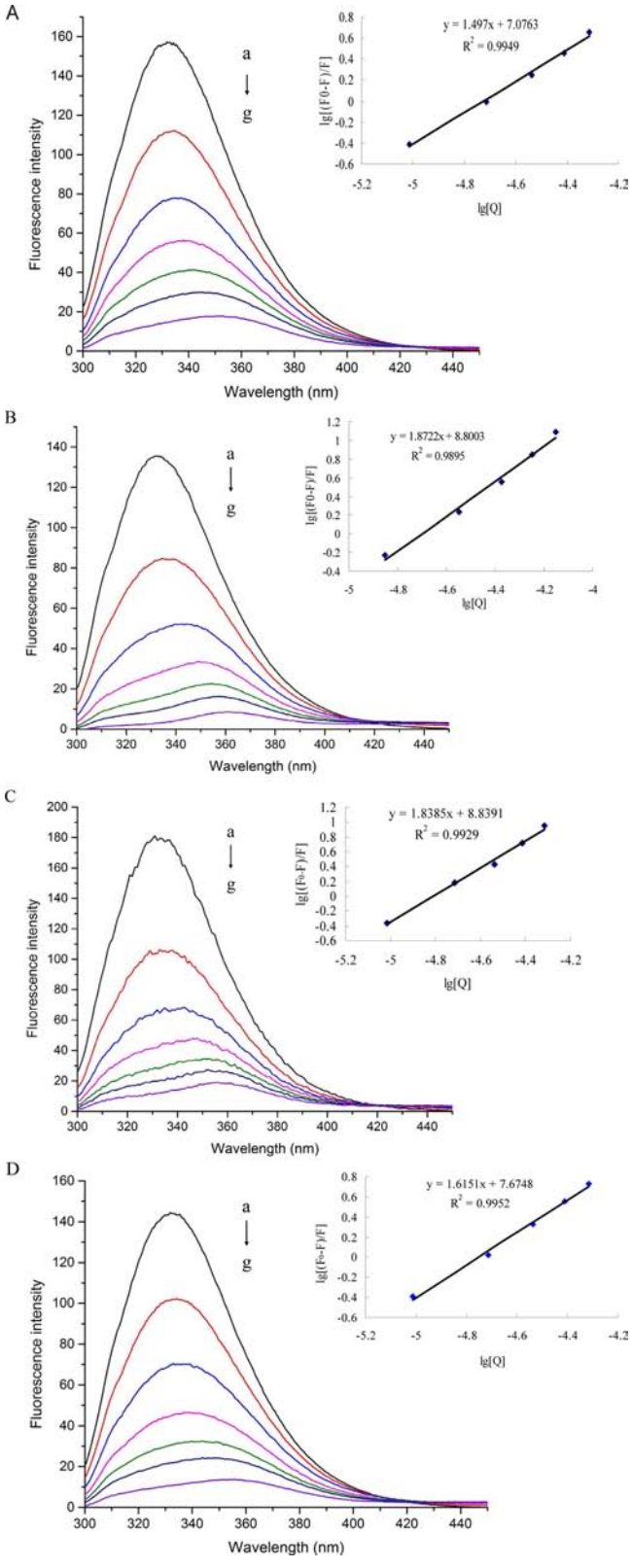

Figure 5. Fluorescence emission spectra of α-glucosidase in the presence of various concentrations of 5-CQA (A), 3,4-diCQA (B), 3,5-diCQA (C), and 4,5-diCQA (D). Conditions: T = 37 °C, λ_{ex} = 280 nm; α-glucosidase = 0.05 mg/mL; caffeoylquinic acid concentrations of 0, 0.005, 0.01, 0.015, 0.02, 0.025, and 0.03 mg/mL (a–g).

DOI: 10.1021/acs.jafc.5b00420
J. Agric. Food Chem. 2015, 63, 3694–3703

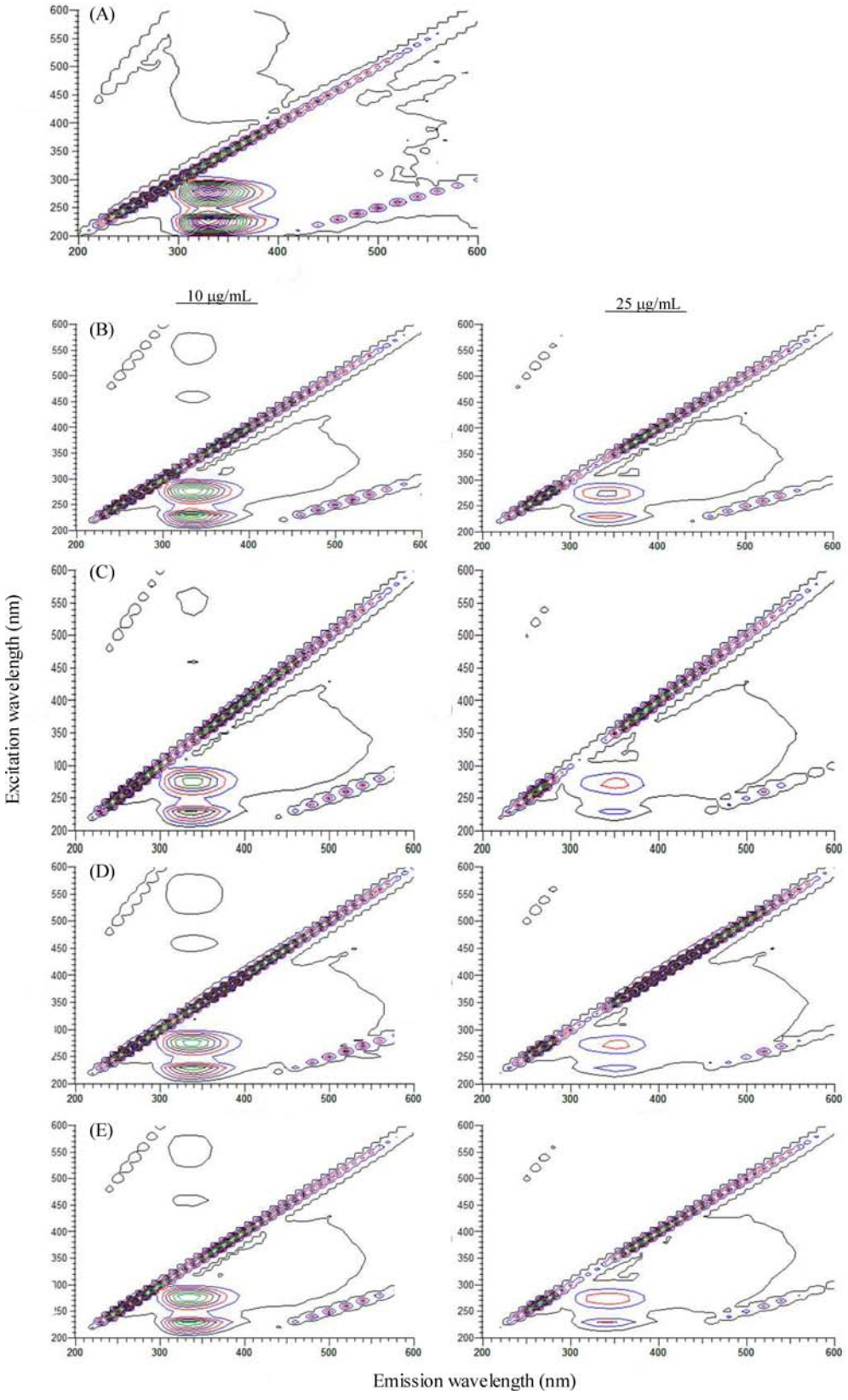

Figure 6. Three-dimensional fluorescence spectra of α-glucosidase (A) and the enzyme−CQA systems (5-CQA (B), 3,4-diCQA (C), 3,5-diCQA (D), and 4,5-diCQA (E)).

sheet, 18%; turn, 17.2%; and unordered, 25.7%. With the addition of 5-CQA or 3,5-diCQA to enzyme, the α-helix contents decreased to 15.9 and 16.4%, whereas the β-sheet contents increased to 27.5 and 31% and the unordered structure contents increased to 30.7 and 32.1%, respectively. In addition, it was found that the difference was not significant for the effects of 5-CQA and 3,5-diCQA on secondary structure contents of α-glucosidase. The decrease in α-helical contents

DOI: 10.1021/acs.jafc.5b00420
J. Agric. Food Chem. 2015, 63, 3694−3703

Table 1. Three-Dimensional Fluorescence Spectral Characteristic Parameters of α-Glucosidase and Enzyme−Caffeoylquinic Acid Systems

	peak 1 (nm)			peak 2 (nm)		
system	λ_{ex}	λ_{em}	intensity	λ_{ex}	λ_{em}	intensity
α-glucosidase (enzyme)	230	330	149.40	280	330	150.20
enzyme−5-CQA	230	330	51.68	280	330	55.83
enzyme−3,4-diCQA	230	340	73.46	280	340	79.01
enzyme−3,5-diCQA	230	340	60.21	280	340	65.05
enzyme−4,5-diCQA	230	330	65.14	280	330	68.98

Table 2. Binding Parameters and Relative Thermodynamic Variables for Caffeoylquinic Acid Derivatives (5-CQA, 3,4-diCQA, 3,5-diCQA, and 4,5-diCQA) Binding to α-Glucosidase at Different Temperatures

sample	temp (K)	K_a (L mol^{-1})	n	ΔG (kJ mol^{-1})	ΔH (kJ mol^{-1})	ΔS (J mol^{-1}K^{-1})
5-CQA	293	5.53×10^6	1.42	−37.82	34.04	245.26
	310	1.19×10^7	1.50	−41.99		
3,4-diCQA	293	7.93×10^7	1.70	−44.31	92.13	465.56
	310	6.31×10^8	1.87	−52.22		
3,5-diCQA	293	6.32×10^7	1.63	−43.76	106.18	511.74
	310	6.90×10^8	1.83	−52.45		
4,5-diCQA	293	2.18×10^7	1.53	−41.16	34.41	257.92
	310	4.73×10^7	1.62	−45.55		

and increase in contents of unordered structure suggested that the binding of CQA derivatives to α-glucosidase induced the unfolding of protein structure, which is consistent with the results obtained from fluorescence assay.

DISCUSSION

Natural α-glucosidase inhibitors from plant sources offer an attractive strategy to control postprandial hyperglycemia. To our knowledge, this is the first report on α-glucosidase inhibitory effects and mechanisms of CQA derivatives from *I. kudingcha* C.J. Tseng, although it has been used in China for the treatment of diabetes and coronary heart diseases in traditional natural medicine for a long time.[18]

In our previous works, we investigated the potent antioxidant activity of kudingcha polyphenols and purified and characterized the CQA derivatives present in *I. kudingcha* C.J. Tseng.[22,34,35] As many plant polyphenols with relatively high antioxidant activity exhibit inhibitory effects on digestive enzymes,[26,56] we examined the inhibitory activities of CQA derivatives from *I. kudingcha* C.J. Tseng against α-glucosidase from *S. cerevisiae* and further determined the potential interaction mechanisms in the present study. As a result, the inhibitory activities of CQA derivatives were in the order 4,5-diCQA > 3,5-diCQA ≈ 3,4-diCQA > 5-CQA > 4-CQA > 3-CQA by comparison of their IC_{50} values. The inhibitory activity of diCQA was higher than that of CQA derivative with a single caffeoyl moiety, indicating that the inhibitory activity of CQA derivative increases with increasing number of caffeoyl moieties. In addition, the inhibitory activity was affected by the substitution position of the caffeoyl moiety on quinic acid. The substitution at the 5-position exhibited relatively higher inhibitory activity than that at the 4-position, but it was relatively higher than that at the 3-position ($p < 0.05$). As for the three diCQA derivatives, 3,4-diCQA showed equal inhibitory activity to 3,5-diCQA ($p > 0.05$), but it was weaker than 4,5-diCQA ($p < 0.05$). The differences in the α-glucosidase inhibitory activities of CQA derivatives may be due to their differences in structures, particularly the distribution of caffeoyl group and its position in the quinic acid aromatic ring.[26] Such results are in agreement with the conclusions of previous structure−activity relationship investigations by other researchers.[16,23,57−59] For example, the α-glucosidase inhibitory activities of 3,4-diCQA, 3,5-diCQA, and 4,5-diCQA, separated from flower buds of *Tussilago farfara* L., were higher than that of 5-CQA.[57] For porcine pancreas α-amylase isozyme I, diCQA derivative exhibited higher inhibitory activity than mono-CQA derivatives and feruloylquinic acids.[58] Five CQA derivatives (5-CQA, 3,4-diCQA, 3,5-diCQA, methyl 3,4-di-*O*-caffeoylquinate (3,4-diCQM), and 3,5-diCQM) were isolated from *Lonicera fulvotomentosa* Hsu et S. C. Cheng, and their interactions with bovine serum albumin (BSA) were determined; their binding constants with BSA ranked in the following order: 3,4-diCQM > 3,5-diCQM ≈ 3,4-diCQA > 3,5-diCQA > 5-CQA (IUPAC numbering system: 4,5-diCQM > 3,5-diCQM ≈ 4,5-diCQA > 3,5-diCQA > 5-CQA).[59] It has also been reported that diCQA derivatives with double caffeoyl moieties had higher antioxidant capacity as compared to CQA derivative with a single caffeoyl moiety, indicating the addition of caffeoyl moiety significantly increased the antioxidative ability.[23] Furthermore, the inhibitory types of 3-CQA, 4-CQA, 5-CQA, 3,4-diCQA, 3,5-diCQA, and 4,5-diCQA from *I. kudingcha* C.J. Tseng for α-glucosidase were found to be noncompetitive in the present study. This is the first report on the inhibitory kinetics of the enzyme of six CQA derivatives from kudingcha, although the α-glucosidase inhibitory activities of several CQA derivatives from other herbs were investigated before.

Some polyphenols have a strong ability to interact with digestive enzymes on the basis of interactions between polyphenols and the protein, which reduce food digestibility.[60,61] Thus, we explored the interactions between the CQA derivative and α-glucosidase by fluorescence spectroscopy and

DOI: 10.1021/acs.jafc.5b00420
J. Agric. Food Chem. 2015, 63, 3694−3703

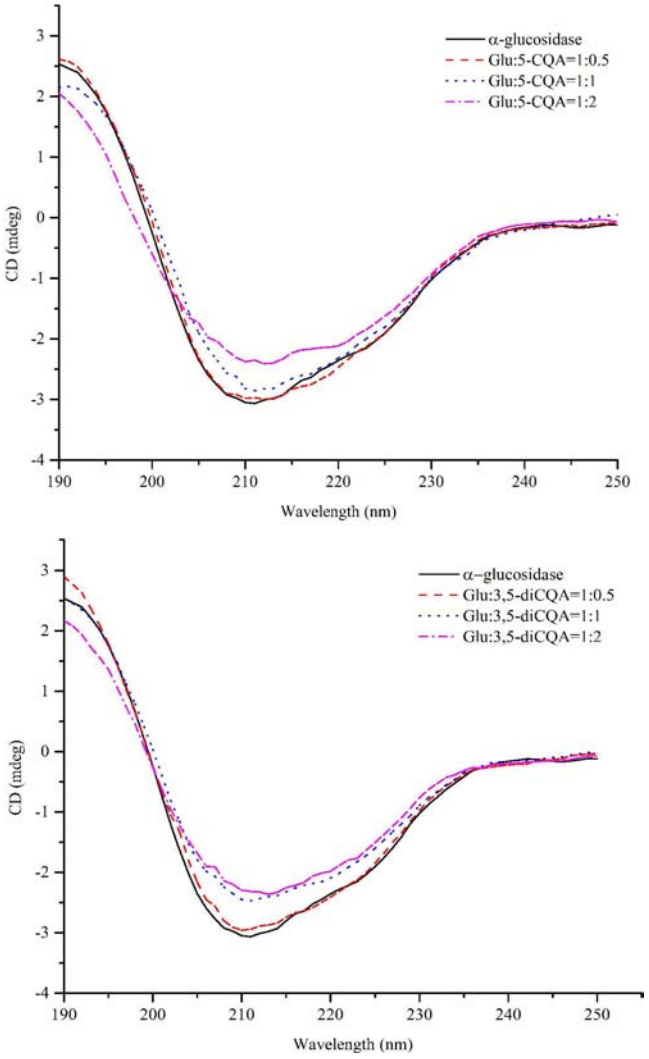

Figure 7. Circular dichroism spectra of free α-glucosidase and enzyme−caffeoylquinic acid complexes: free enzyme and enzyme−caffeoylquinic acid complexes in phosphate buffer solution with a protein concentration of 3×10^{-6} M and caffeoylquinic acid concentrations of 0, 1.5×10^{-6}, 3.0×10^{-6}, and 6×10^{-6} M.

Table 3. Secondary Structure Contents of α-Glucosidase and Its Complexes with 5-CQA and 3,5-diCQA by Circular Dichroism Spectroscopy at Room Temperature

secondary structural content	α-helix (%)	β-sheet (%)	turn (%)	unordered (%)
native α-glucosidase	21.8	18.0	17.2	25.7
glucosidase/5-CQA = 1:0.5	20.7	25.0	20.4	29.6
glucosidase/5-CQA = 1:1	18.5	31.4	22.6	33.1
glucosidase/5-CQA = 1:2	15.9	27.5	20.5	30.7
glucosidase/3,5-diCQA = 1:0.5	21.1	21.6	18.8	27.6
glucosidase/3,5-diCQA = 1:1	18.5	25.4	18.8	28.0
glucosidase/3,5-diCQA = 1:2	16.4	31.0	21.6	32.1

CD spectroscopy for the first time. As for fluorescence spectra, the decrease of fluorescence intensities and a red shift of maximal absorption peak were observed, indicating a conformational change in α-glucosidase. From the fluorescence analysis, the CQA derivative−α-glucosidase binding was achieved by hydrophobic interactions of the interior hydrophobic groups of enzyme and then might be stabilized by hydrogen bonding between polar groups (−OH, −SH, and −NH groups) of the enzyme with the −OH groups of CQA derivative. It has been reported that the integy moment of hydrophobicity descriptors (vsurf_ID4 and vsurf_ID7) in 5-CQA derivatives contributed to the inhibitory activity of α-glucosidase from *Bacillus stearothermophilus* or *S. cerevisiae*. The requirement of the hydrophilic properties on the van der Waals surface of the molecules by properly aligned polar and aromatic/hydrophobic regions for all highly active and less active compounds was confirmed by pharmacophore analysis.[28,62] The binding abilities of CQA derivatives were found to be quite high with a binding constant from 10^6 to 10^8 M^{-1}, and the order was diCQA derivative > CQA derivative with a single caffeoyl moiety, which is in accordance with the results of enzyme inhibition. Interactions between small molecules and enzymes may alter the conformation of the enzyme.[63,64] In our present study, the changes in secondary structures of α-glucosidase with the addition of 5-CQA or 3,5-diCQA were demonstrated by using CD spectroscopy. Thus, CQA derivatives may have a binding effect on α-glucosidase, changing the polarity and molecule conformation of enzyme, resulting in partial loss of the enzyme activity. These structural changes of α-glucosidase finally caused the inhibition of enzyme activity.

In conclusion, six kinds of CQA derivatives, 3-CQA, 4-CQA, 5-CQA, 3,4-diCQA, 3,5-diCQA, and 4,5-diCQA, separated from *I. kudingcha* C.J. Tseng were demonstrated to be effective noncompetitive α-glucosidase inhibitors. The diCQA derivatives exhibited relatively higher inhibition activity than CQA derivatives with a single caffeoyl moiety. Furthermore, the fluorescence spectra suggested that the interaction was spontaneous, and hydrophobic force might be primarily responsible for the interaction. The CD spectra revealed that the change in protein conformation occurred due to the binding of the α-glucosidase molecule to 5-CQA or 3,5-diCQA. All of the present results suggested that the CQA derivatives from *I. kudingcha* C.J. Tseng could be physiologically useful for suppressing postprandial hyperglycemia and therefore may be developed as functional foods for the prevention or treatment of diabetes and obesity.

AUTHOR INFORMATION

Corresponding Authors

*(X.Z.) Fax: +86 25 84396791. E-mail: zengxx@njau.edu.cn.
*(Y.S.) Fax: +86 25 84396791. E-mail: sunyi01@njau.edu.cn.

Funding

This work was supported by Grants-in-Aid for scientific research from the National Natural Science Foundation of China (31171666) and a project funded by the Priority Academic Program Development of Jiangsu Higher Education Institutions (PAPD).

Notes

The authors declare no competing financial interest.

REFERENCES

(1) Holman, R. R.; Sourij, H.; Califf, R. M. Cardiovascular outcome trials of glucose-lowering drugs or strategies in type 2 diabetes. *Lancet* **2014**, *383*, 2008−2017.

(2) Shi, Y. K.; Hu, F. B. The global implications of diabetes and cancer. *Lancet* **2014**, *383*, 1947−1948.

DOI: 10.1021/acs.jafc.5b00420
J. Agric. Food Chem. 2015, 63, 3694−3703

(3) Scheen, A. J.; Charbonnel, B. Effects of glucose-lowering agents on vascular outcomes in type 2 diabetes: a critical reappraisal. *Diabetes Metab.* **2014**, *40*, 176−185.
(4) Ceriello, A. Postprandial hyperglycemia and diabetes complications. *Diabetes* **2005**, *54*, 1−7.
(5) Ludwig, D. S. The glycemic index: physiological mechanisms relating to obesity, diabetes and cardiovascular disease. *JAMA, J. Am. Med. Assoc.* **2002**, *287*, 2414−2423.
(6) Goto, T.; Horita, M.; Nagai, H.; Nagatomo, A.; Nishida, N.; Matsuura, Y.; Nagaoka, S. Tiliroside, a glycosidic flavonoid, inhibits carbohydrate digestion and glucose absorption in the gastrointestinal tract. *Mol. Nutr. Food Res.* **2012**, *56*, 435−445.
(7) Ye, F.; Shen, Z.; Xie, M. α-Glucosidase inhibition from a Chinese medical herb (*Ramulus mori*) in normal and diabetic rats and mice. *Phytomedicine* **2002**, *9*, 161−166.
(8) Chiasson, J. L.; Josse, R. G.; Gomis, R.; Hanefeld, M.; Karasik, A.; Laakso, M. Acarbose for prevention of type 2 diabetes mellitus: the STOP-NIDDM randomised trial. *Lancet* **2002**, *359*, 2072−2077.
(9) Scheen, A. J. Voglibose for prevention of type 2 diabetes mellitus. *Lancet* **2009**, *373*, 1579−1580.
(10) Cheng, A. Y.; Fantus, I. G. Oral antihyperglycemic therapy for type 2 diabetes mellitus. *Can. Med. Assoc. J.* **2005**, *172*, 213−226.
(11) Fujusawa, T.; Ikegami, H.; Inoue, K.; Kawabata, Y.; Ogihara, T. Effect of two a-glucosidase inhibitors, voglibose and acarbose, on postprandial hyperglycemia correlates with subjective abdominal symptoms. *Metab., Clin. Exp.* **2005**, *54*, 387−390.
(12) Lacroix, I. M. E.; Li-Chan, E. C. Y. Overview of food products and dietary constituents with antidiabetic properties and their putative mechanisms of action: a natural approach to complement pharmacotherapy in the management of diabetes. *Mol. Nutr. Food Res.* **2014**, *58*, 61−78.
(13) Shin, E. J.; Hur, H. J.; Sung, M. J.; Park, J. H.; Yang, H. J.; Kim, M. S.; Kwon, D. Y.; Hwang, J. T. Ethanol extract of the *Prunus mume* fruits stimulates glucose uptake by regulating PPAR-γ in C2C12 myotubes and ameliorates glucose intolerance and fat accumulation in mice fed a high-fat diet. *Food Chem.* **2013**, *141*, 4115−4121.
(14) Li, Y. Q.; Zhou, F. C.; Gao, F.; Bian, J. S.; Shan, F. Comparative evaluation of quercetin, isoquercetin and rutin as inhibitors of α-glucosidase. *J. Agric. Food Chem.* **2009**, *57*, 11463−11468.
(15) Deutschlander, M. S.; van de Venter, M.; Roux, S.; Louw, J.; Lall, N. Hypoglycaemic activity of four plant extracts traditionally used in South Africa for diabetes. *J. Ethnopharmacol.* **2009**, *124*, 619−624.
(16) Gao, H.; Huang, Y. N.; Xu, P. Y.; Kawabata, J. Inhibitory effect on α-glucosidase by the fruits of *Terminalia chebula* Retz. *Food Chem.* **2007**, *105*, 628−634.
(17) Yan, D. H. Health functions, plant species and name evolution of Kuding tea. *Guizhou Agric. Sci.* **2007**, *35* (1), 114−116.
(18) Li, L.; Xu, L. J.; Ma, G. Z.; Dong, Y. M.; Peng, Y.; Xiao, P. G. The large-leaved kudingcha (*Ilex latifolia* Thunb and *Ilex kudingcha* C.J. Tseng): a traditional Chinese tea with plentiful secondary metabolites and potential biological activities. *J. Nat. Med.* **2013**, *67*, 425−437.
(19) De Mejia, E. G.; Song, Y. S.; Heck, C. I.; Ramirez-Mares, M. Yerba mate tea (*Ilex paraguariensis*): phenolics, antioxidant capacity and *in vitro* inhibition of colon cancer cell proliferation. *J. Funct. Foods* **2010**, *2*, 23−34.
(20) IUPAC Nomenclature of cyclitols. *Biochem. J.* **1976**, *153*, 23−31.
(21) Zhu, F.; Cai, Y. Z.; Sun, M.; Ke, J.; Lu, D.; Corke, H. Comparison of major phenolic constituents and in vitro antioxidant activity of diverse Kudingcha genotypes from *Ilex kudingcha*, *Ilex cornuta*, and *Ligustrum robustum*. *J. Agric. Food Chem.* **2009**, *57*, 6082−6089.
(22) Liu, L.; Sun, Y.; Laura, T.; Liang, X.; Ye, H.; Zeng, X. X. Determination of polyphenolic content and antioxidant activity of kudingcha made from *Ilex kudingcha* C.J. Tseng. *Food Chem.* **2009**, *112*, 35−41.
(23) Thuong, P. T.; Su, N. D.; Ngoc, T. M.; Hung, T. M.; Dang, N. H.; Thuan, N. D.; Bae, K.; Oha, W. K. Antioxidant activity and principles of Vietnam bitter tea *Ilex kudingcha*. *Food Chem.* **2009**, *113*, 139−145.
(24) Song, C.; Xie, C.; Zhou, Z.; Yu, S.; Fang, N. Antidiabetic effect of an active components group from *Ilex kudingcha* and its chemical composition. *Evidence-Based Complement. Altern. Med.* **2012**, *2012*, article ID 423690 (DOI: 10.1155/2012/423690).
(25) Murase, T.; Misawa, K.; Minegishi, Y.; Aoki, M.; Ominami, H.; Suzuki, Y.; Shibuya, Y.; Tadashi, H. Coffee polyphenols suppress diet-induced body fat accumulation by downregulating SREBP-1c and related molecules in C57BL/6J mice. *Am. J. Physiol.: Endocrinol. Metab.* **2011**, *300*, E122−E133.
(26) Ooi, K. L.; Muhammad, T. S. T.; Tan, M. L.; Sulaiman, S. F. Cytotoxic, apoptotic and anti-α-glucosidase activities of 3,4-di-*O*-caffeoyl quinic acid, an antioxidant isolated from the polyphenolic-rich extract of *Elephantopus mollis* Kunth. *J. Ethnopharmacol.* **2011**, *135*, 685−695.
(27) Iwai, K.; Kishimoto, N.; Kakino, Y.; Mochida, K.; Fujita, T. In vitro antioxidative effects and tyrosinase inhibitory activities of seven hydroxycinnamoyl derivatives in green coffee beans. *J. Agric. Food Chem.* **2004**, *52*, 4893−4898.
(28) Moorthy, N. S. H. N.; Ramos, M. J.; Fernandes, P. A. Studies on α-glucosidase inhibitors development: magic molecules for the treatment of carbohydrate mediated diseases. *Mini-Rev. Med. Chem.* **2012**, *12*, 1−8.
(29) Zhang, Z.; Luo, A. M.; Zhong, K.; Huang, Y. N.; Gao, Y.; Zhang, J.; Gao, H.; Xua, Z. J.; Gao, X. L. α-Glucosidase inhibitory activity by the flower buds of *Lonicera japonica* Thunb. *J. Funct. Foods* **2013**, *5*, 1253−1259.
(30) Van Dam, R. M. Coffee consumption and risk of type 2 diabetes, cardiovascular diseases, and cancer. *Appl. Physiol., Nutr., Metab.* **2008**, *33*, 1269−1283.
(31) Ong, K. W.; Hsu, A.; Tan, B. K. H. Chlorogenic acid stimulates glucose transport in skeletal muscle via AMPK activation: a contributor to the beneficial effects of coffee on diabetes. *PLoS One* **2012**, *7* (3), No. e32718, DOI: 10.1371/journal.pone.0032718.
(32) He, Q.; Lv, Y.; Yao, K. Effects of tea polyphenols on the activities of α-amylase, pepsin, trypsin and lipase. *Food Chem.* **2007**, *101*, 1178−1182.
(33) Sun, Y.; Xu, W. Q.; Zhang, W. Q.; Hu, Q. H.; Zeng, X. X. Optimizing the extraction of phenolic antioxidants from kudingcha made frrom *Ilex kudingcha* C.J. Tseng by using response surface methodology. *Sep. Purif. Technol.* **2011**, *78*, 311−320.
(34) Sun, Y.; Zhang, X.; Zhang, W. Q.; Zeng, X. X.; Hu, Q. H. Purification and structural identification of polyphenols in kudingcha. *Food Sci.* **2011**, *32* (11), 60−63.
(35) Wang, Q. C.; Zhang, X.; Zhang, W. Q.; Sun, X. Q.; Hu, B.; Sun, Y.; Zeng, X. X. Purification of caffeoylquinic acids from kudingcha made from *Ilex kudingcha* C.J. Tseng and their analysis by high performance liquid chromatography. *Food Sci.* **2013**, *34* (22), 119−122.
(36) Lakowicz, J. R. *Principles of Fluorescence Spectroscopy*; Springer: Berlin, Germany, 2007.
(37) Liang, L.; Tajmir-Riahi, H. A.; Subirade, M. Interaction of β-lactoglobulin with resveratrol and its biological implications. *Biomacromolecules* **2008**, *9*, 50−56.
(38) Sreerama, N.; Woody, R. W. Estimation of protein secondary structure from circular dichroism spectra: comparison of CONTIN, SELCON, and CDSSTR methods with an expanded reference set. *Anal. Biochem.* **2000**, *287*, 252−260.
(39) Chen, Q. X.; Song, K. K.; Qiu, L.; Liu, X. D.; Huang, H.; Guo, H. Y. Inhibitory effects on mushroom tyrosinase by *p*-alkoxybenzoic acids. *Food Chem.* **2005**, *91*, 269−274.
(40) Fei, Q. Q.; Gao, Y.; Zhang, X.; Sun, Y.; Hu, B.; Zhou, L.; Jabbar, S.; Zeng, X. X. Effects of oolong tea polyphenols, EGCG, and EGCG3″Me on pancreatic α-amylase activity in vitro. *J. Agric. Food Chem.* **2014**, *62*, 9507−9514.
(41) Clifford, M. N.; Johnston, K. L.; Knight, S.; Kuhnert, N. Hierarchical scheme for LC-MS^n identification of chlorogenic acids. *J. Agric. Food Chem.* **2003**, *51*, 2900−2911.

DOI: 10.1021/acs.jafc.5b00420
J. Agric. Food Chem. 2015, 63, 3694−3703

(42) Bravo, L.; Goya, L.; Lecumberri, E. LC/MS characterization of phenolic constituents of mate (*Ilex paraguariensis*, St. Hil.) and its antioxidant activity compared to commonly consumed beverages. *Food Res. Int.* **2007**, *40*, 393−405.
(43) Islam, M. S.; Yoshimoto, M.; Yahara, S.; Okuno, S.; Ishiguro, K.; Yamakawa, O. Identification and characterization of foliar polyphenolic composition in sweetpotato (*Ipomoea batatas* L.) genotypes. *J. Agric. Food Chem.* **2002**, *50*, 3718−3722.
(44) Rawel, H. A.; Meidtner, K.; Kroll, J. Binding of selected phenolic compounds to proteins. *J. Agric. Food Chem.* **2005**, *53*, 4228−4235.
(45) Kanakis, C. D.; Hasni, I.; Bourassa, P.; Tarantilis, P. A.; Polissiou, M. G.; Tajmir-Riahi, H. A. Milk β-lactoglobulin complexes with tea polyphenols. *Food Chem.* **2011**, *127*, 1046−1055.
(46) Ge, Y. S.; Jin, C.; Song, Z.; Zhang, J. Q.; Jiang, F. L.; Liu, Y. Multi-spectroscopic analysis and molecular modeling on the interaction of curcumin and its derivatives with human serum albumin: a comparative study. *Spectrochim. Acta, Part A* **2014**, *124*, 265−276.
(47) Yue, Y.; Liu, J.; Yao, M.; Yao, X.; Fan, J.; Ji, H. The investigation of the binding behavior between ethyl maltol and human serum albumin by multi-spectroscopic methods and molecular docking. *Spectrochim. Acta, Part A* **2012**, *96*, 316−323.
(48) Li, D.; Wang, Y.; Chen, J.; Ji, B. Characterization of the interaction between farrerol and bovine serum albumin by fluorescence and circular dichroism. *Spectrochim. Acta, Part A* **2011**, *79*, 680−686.
(49) Singha Roy, A.; Pandey, N. K.; Dasgupta, S. Preferential binding of fisetin to the native state of bovine serum albumin: spectroscopic and docking studies. *Mol. Biol. Rep.* **2013**, *40*, 3239−3253.
(50) Wu, X. L.; Dey, R.; Wu, H.; Liu, Z. G.; He, Q. Q.; Zeng, X. J. Studies on the interaction of -epigallocatechin-3-gallate from green tea with bovine β-lactoglobulin by spectroscopic methods and docking. *Int. J. Dairy Technol.* **2013**, *66*, 7−13.
(51) Ghosh, K. S.; Sahoo, B. K.; Dasgupta, S. Spectrophotometric studies on the interaction between (−)-epigallocatechin gallate and lysozyme. *Chem. Phys. Lett.* **2008**, *452*, 193−197.
(52) Yuksel, Z.; Avci, E.; Erdem, Y. K. Characterization of binding interactions between green tea flavanoids and milk proteins. *Food Chem.* **2010**, *121*, 450−456.
(53) Ross, P. D.; Subramanian, S. Thermodynamics of protein association reactions: forces contributing to stability. *Biochemistry* **1981**, *20*, 3096−3102.
(54) Teng, Y.; Ji, F.; Li, C.; Yu, Z.; Liu, R. Interaction mechanism between 4-aminoantipyrine and the enzyme lysozyme. *J. Lumin.* **2011**, *131*, 2661−2667.
(55) Besley, N. A.; Hirst, J. D. Theoretical studies toward quantitative protein circular dichroism calculations. *J. Am. Chem. Soc.* **1999**, *121*, 9636−9644.
(56) Dalar, A.; Konczak, I. Phenolic contents, antioxidant capacities and inhibitory activities against key metabolic syndrome relevant enzymes of herbal teas from Eastern Anatolia. *Ind. Crops Prod.* **2013**, *44*, 383−390.
(57) Gao, H.; Huang, Y. N.; Gao, B.; Xu, P. Y.; Inagaki, C.; Kawabata, J. α-Glucosidase inhibitory effect by the flower buds of *Tussilago farfara* L. *Food Chem.* **2008**, *106*, 1195−1201.
(58) Narita, Y.; Inouye, K. Inhibitory effects of chlorogenic acids from green coffee beans and cinnamate derivatives on the activity of porcine pancreas α-amylase isozyme I. *Food Chem.* **2011**, *127*, 1532−1539.
(59) Tang, D.; Li, H. J.; Li, P.; Wen, X. D.; Qian, Z. W. Interaction of bioactive components caffeoylquinic acid derivatives in Chinese medicines with bovine serum albumin. *Chem. Pharm. Bull.* **2008**, *56*, 360−365.
(60) Thielecke, F.; Boschmann, M. The potential role of green tea catechins in the prevention of the metabolic syndrome − a review. *Phytochemistry* **2009**, *70*, 11−24.
(61) Wu, X. L.; Wang, W. P.; Zhu, T.; Liang, T.; Lu, F. Q.; He, W. Y.; Zhang, H. P.; Liu, Z. G.; He, S. H.; Gao, K. P.; He, Z. D. Phenylpropanoid glycoside inhibition of pepsin, trypsin and α-chymotrypsin enzyme activity in Kudingcha leaves from *Ligustrum purpurascens*. *Food Res. Int.* **2013**, *54*, 1376−1382.
(62) Moorthy, N. S. H. N.; Ramos, M. J.; Fernandes, P. A. Comparative structural analysis of α-glucosidase inhibitors against difference species: a computational study. *Arch. Pharm.* **2012**, *345*, 265−274.
(63) Wu, X. L.; He, W. Y.; Zhang, H. P.; Li, Y.; Liu, Z. G.; He, Z. D. Acteoside: a lipase inhibitor from the Chinese tea *Ligustrum purpurascens* kudingcha. *Food Chem.* **2014**, *142*, 306−310.
(64) Wu, X. L.; He, W. Y.; Li, Y.; Zhang, H. P.; Liu, Z. G.; Wang, W. P.; Ye, Y.; Cao, J. J. Characterization of binding interactions of (−)-epigallocatechin-3-gallate from green tea and lipase. *J. Agric. Food Chem.* **2013**, *61*, 8829−8835.

DOI: 10.1021/acs.jafc.5b00420
J. Agric. Food Chem. 2015, 63, 3694−3703

Table 1. NMR Spectroscopic Data of Trichoharzianol (1)[a]

position	δ_C	DEPT	δ_H (J^b in Hz)	COSY	HMBC (correlated C)
1	52.7	C			
2	52.3	CH	1.94 (1H, m)	1′, 3	2′, 1, 9, 1-CH_3, 1′-CH_3
3	123.3	CH	5.65 (1H, ddd, J = 10.0, 4.0, 2.0)	2, 4	1, 4a
4	126.9	CH	5.90 (1H, dd, J = 10.0, 1.5)	3, 4a	3, 5, 2, 8a
4a	41.5	CH	1.93 (1H, m)	4, 5	3, 5
5	79.7	CH	3.72 (1H, dd, J = 10.0, 4.0)	4a,6	4′, 6, 4
6	73.6	CH	4.26 (1H, ddd, J = 6.5, 4.0. 3.0)	5, 7a, 7b	4a, 8
7	37.0	CH_2	2.06 (1Ha, m)	6, 7b, 8	5, 6, 8a, 8
			1.64 (1Hb, m)	6, 7a, 8	8a, 8
8	32.3	CH	1.60 (1H, m)	7a, 7b, 8-CH_3, 8a	8-CH_3
8a	40.6	CH	1.82 (1H, dd, J = 10.5, 9.0)	4a, 8	1, 4a, 7, 8, 1-CH_3
9	215.7	C			
10	41.1	CH_2	2.81 (1Ha, ddd, J = 19.0, 7.0, 4.0)	10b, 11	9, 11
			2.65 (1Hb, ddd, J = 19.0, 6.0, 4.0)	10a, 11	9, 11
11	58.1	CH_2	3.86 (2H, m)	10a, 10b	9, 10
1′	37.1	CH	1.10 (1H, m)	2, 1′-CH_3	1′-CH_3, 3′
2′	24.4	CH_2	1.43 (1Ha, m)	1′, 2′b, 3′	1′, 1′-CH_3, 3′
			0.74 (1Hb, m)	1′, 2′a, 3′	1′, 1′-CH_3, 3′
3′	12.4	CH_3	0.73 (3H, d, J = 4.5)	2′a, 2′b	1′, 2′
4′	107.9	C			
5′	26.2	CH_3	1.35 (3H, s)		4′, 6′
6′	28.6	CH_3	1.48 (3H, s)		4′, 5′
1-CH_3	19.2	CH_3	1.21 (3H, s)		9, 1, 2, 8a
8-CH_3	22.3	CH_3	0.64 (3H, d, J = 6.5)	8	8a, 8, 7
1′-CH_3	19.3	CH_3	0.90 (3H, d, J = 7.0)	1′	2, 7, 2′, 3′

[a]Data were recorded in $CDCl_3$ (500 MHz). [b]J values of coupling were determined by a homodecoupling experiment.

min, 55 °C annealing for 1 min, 72 °C extension for 2 min, and a final extension at 72 °C for 10 min. The amplified products were purified with a Gel/PCR DNA Fragment Extraction Kit (Geneaid, Taiwan) according to the guidance of the manufacturer and cloned into pGMEMT-Easy vectors (Promega Corporation, Madison, WI) for DNA sequencing. A BLASTN search was used to search for sequences of the closest match in the GenBank database.

C. gloeosporioides was purchased from the Plant Health Clinic, Department of Plant Pathology, Faculty of Agriculture, Kasetsart University, Kamphaeng Saen Campus, Nakhon Pathom, Thailand.

Fermentation. *T. harzianum* F031 from a slant culture was subcultured on PDA for 7 days. The 5 mm discs of growing colonies were cut from the margin of each plate and inoculated into an Erlenmeyer flask containing 250 mL of potato dextrose broth (PDB). After a 27-day incubation at room temperature, the stationary cultures were filtered through filter paper (Whatman No. 1) to obtain the culture filtrate.

Extraction and Purification. The combined culture filtrate (20 L) was exhaustively extracted with EtOAc (3× 1 L). The organic layers were combined, dried over Na_2SO_4, and evaporated under reduced pressure to yield the EtOAc extract (6.10 g). This material was fractionated by the solid-phase extraction (SPE), eluted with EtOAc–hexane and MeOH–EtOAc gradients (5% increasing polarity with 20 mL each). From the basic TLC profiles, four fractions (F1–F4) were obtained.

Fraction F1 (2.32 g, eluted with 5–30% EtOAc–hexane) was separated by CC (SiO_2), eluted with 20% EtOAc–hexane to provide 14 subfractions (S1–S14). Subfraction S3 (24.3 mg) was further purified by CC (SiO_2), eluted with 15% EtOAc–hexane to give compound **1** (12.7 mg) as a colorless amorphous solid. Subfraction S7 (38.4 mg) was separated by CC (SiO_2), eluted with 10% EtOAc–CH_2Cl_2. The product was further purified by CC (SiO_2), eluted with 10% EtOAc–hexane to afford compound **3** (4.2 mg) as a white solid. Subfraction S8 (119.2 mg) was separated by CC (SiO_2), eluted with 5% acetone–CH_2Cl_2 to obtain eight portions (C1–C8). Portion C4 (12.7 mg) was further purified by CC (SiO_2), eluted with 20% acetone–hexane to yield compound **4** (3.0 mg) as a white solid. Subfraction S10 (541.4 mg) was separated by CC (Sephadex LH 20), eluted with 50% MeOH–CH_2Cl_2 to afford four subfractions (D1–D4). Purification of subfraction D2 (326.1 mg) by two consecutive CC (SiO_2; first CC, 10% EtOAc–hexane; second CC, 40% EtOAc–hexane) resulted in compound **2** (8.3 mg), a colorless amorphous solid.

Trichoharzianol (**1**): colorless amorphous solid; $[\alpha]_D^{25}$ +121.5 (*c* 0.13, MeOH); IR ν_{max}, 3489, 1700, 1242, 1218 cm^{-1}; ^1H NMR (500 MHz, $CDCl_3$) and ^{13}C NMR (125 MHz, $CDCl_3$), see Table 1 and the Supporting Information; HRESIMS (*m*/*z*), 365.2686 $[M + H]^+$ (calcd for $C_{22}H_{38}O_4$, 365.2692).

Antifungal Activity Evaluation. The agar dilution method[20] was used to evaluate antifungal activity of the crude extract. The sample was prepared as a stock solution at 10 mg/mL in dimethyl sulfoxide (DMSO). PDA (9.8 mL) was sterilized, and the sample (200 μL) was added at 48 °C to obtain a final concentration of 200 μg/mL and then poured into a 9 cm diameter Petri dish. The dish was left at room temperature overnight. The disc (5 mm diameter), which was removed from the margin of a 3-day-old colony of *C. gloeosporioides*, was placed at the center of the PDA plate and inoculated at room temperature for 3 days. The diameter (in millimeters) of the mycelium growth was recorded and calculated as a percentage of growth inhibition = $(Y - X)/Y \times 100$, where Y is the growth diameter in the untreated control and X is the growth diameter in the treatment. The results of this quadruplicate experiment were reported as the antifungal activity.

The microdilution method, with 96 well microliter plates, was used to evaluate antifungal activity of the fractions and pure compounds.[31] The samples were prepared as 2-fold dilutions and added (50 μL) to each well, which contained the spore suspension (50 μL) and RPMI-1640 medium (100 μL), to give a final concentration of 1024–8 μg/mL for the fractions and 256–0.125 μg/mL for the pure compounds, again performed in quadruplicate. After the mixtures were incubated for 48 h at room temperature, 0.18% resazurin (10 μL) was added to each well and incubated continuously for 3–4 h. Amphotericin B (10 μg/mL, 50 μL) and 1% DMSO (50 μL) were used as a positive control and control, respectively. A positive result was indicated by a

DOI: 10.1021/acs.jafc.5b01258
J. Agric. Food Chem. 2015, 63, 3704–3708

color change from blue to pink. The lowest concentration at which the color did not change was taken to be the minimum inhibitory concentration (MIC).

RESULTS AND DISCUSSION

Extraction and Purification. The crude EtOAc extract (6.10 g) of broth culture was fractionated by SEP to provide four combined fractions (F1−F4) based on their TLC characteristics. Subfractions (S1−S14) were obtained from fraction F1 by CC (SiO_2). Subfractions S3, S10, S7, and S8 were further purified to afford compounds **1**, **2**, **3**, and **4**, respectively.

Structural Elucidations. Trichoharzianol (**1**) was shown to possess a molecular formula $C_{22}H_{37}O_4$ as determined by HR-TOF-MS, exhibiting a $[M + H]^+$ peak at m/z 365.2686 (calcd for $C_{22}H_{38}O_4$, 365.2692). Its IR spectrum displayed the absorption bands for hydroxyl (3489 cm^{-1}) and carbonyl (1700 cm^{-1}) groups. The ^1H NMR spectroscopic data (Table 1) displayed characteristics resembling those of eujavanical A.[32,33] However, the two methine protons (H-5 and H-6) were shifted downfield to δ_H 3.71 and 4.26, because they are connected to oxygen atoms of the acetonide group at C_5−C_6. The *gem*-dimethyl groups of acetonide appeared at δ 1.48 and 1.35. The significant downfield shifts of C-5 and C-6 (δ_C 79.7 and 73.6) supported the presence of an acetonide group at C_5−C_6.

The substituents were designated to be a 3-hydroxypropionyl group at C-1, a 1-methylpropyl group at C-2, two methyl groups at C-1 and C-8, and an acetonide group at C-5 and C-6. The assignments of the ^1H and ^{13}C NMR spectra were based on the correlation spectroscopy (COSY), heteronuclear single-quantum coherence (HSQC), and heteronuclear multiple-bond correlation (HMBC) data (see Table 1). The attachments of side chains on the decalin moiety were established by the analysis of the HMBC data. The location of the 3-hydroxylpropyl group at C-1 was suggested by the correlations of 1-CH_3 (δ_H 1.21) to C-9. H-2 (δ 1.94) showed correlations to C-2′ and 1′-CH_3, confirming the attachment of a 1-methylpropyl group at C-2. The correlations of a methyl (δ_H 1.21) to C-8a and C-2, together with another methyl (δ_H 0.64) to C-8a, C-8, and C-7, indicated the connections of two methyls at C-1 and C-8, respectively. Furthermore, the correlations between H-5 (δ_H 3.72) and H-6 (δ_H 4.26) to C4′ indicated the presence of an acetonide group at C-5−C-6.

The relative configuration of compound **1** was determined by the nuclear Overhauser effect spectrometry (NOESY) correlations as shown in Figure 2. The above data confirmed that compound **1** was an acetonide derivative eujavanicol A,[33] and the structure of trichoharzianol (**1**) was established as shown in Figure 1.

Eujavanicol A (**2**) was reported previously from *Eupenicillium javanicum*,[33] whereas 5-hydroxy-3-hydroxymethyl-2-methyl-7-methoxychromone (**3**) and 4,6-dihydroxy-5-methylphthalide (**4**) were found in the lichen *Graphis scripta*[34] and *Talaromyces flavus*,[35] respectively. Their structures were identified with spectroscopic data (UV, IR, NMR, and MS) and compared to those reported in the literature.

Antifungal Activity. The crude extract of *T. harzianum* F031 showed the antifungal activity against *C. gloeosporioides* with 76.6% inhibition by an agar dilution assay at a concentration of 0.2 mg/mL. After further fractionation and purification, the fractions and all the pure compounds were evaluated for their antifungal activity and their MIC values were determined by microdilution. Fraction A showed the highest antifungal activity against *C. gloeosporioides* with a MIC of 512 μg/mL, while fractions B−D exhibited MIC values of >1024 μg/mL. Trichoharzianol (**1**) showed the highest antifungal activity against *C. gloeosporioides* with MIC of 128 μg/mL (Table 2), followed by 5-hydroxy-3-hydroxymethyl-2-methyl-7-methoxychromone (**3**) (MIC of 256 μg/mL). It should be noted here that eujavanicol A (**2**) and 4,6-dihydroxy-5-methylphthalide (**4**) showed antifungal activity of >256 μg/mL.

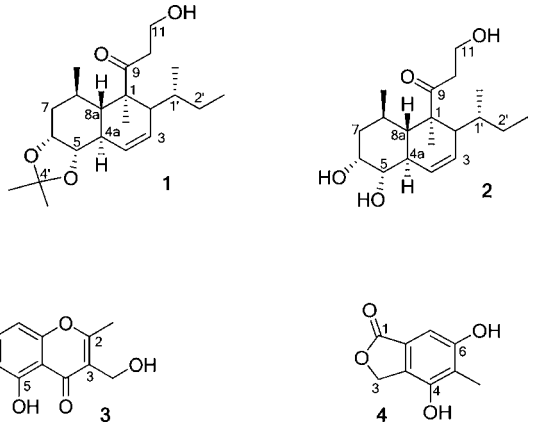

Figure 1. Structure of trichoharzianol (**1**), eujavanicol A (**2**), 5-hydroxy-3-hydroxymethyl-2-methyl-7-methoxychromone (**3**), and 4,6-dihydroxy-5-methylphthalide (**4**).

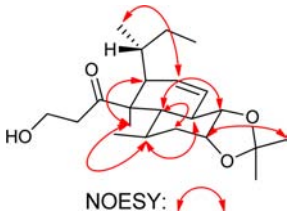

Figure 2. Selective NOESY correlation of trichoharzianol (**1**).

Table 2. Antifungal Activity against *C. gloeosporioides* of Compounds 1−4

compound	MIC (μg/mL)
trichoharzianol (**1**)	128
eujavanical A (**2**)	>256
5-hydroxy-3-hydroxymethyl-2-methyl-7-methoxychromone (**3**)	256
4,6-dihydroxy-5-methylphthalide (**4**)	>256

Trichoharzianol (**1**) is found to be a new and major component from *T. harzianum* F031 strain and shows the highest antifungal activity against *C. gloeosporioides*. In addition, eujavanicol A (**2**), 5-hydroxy-3-hydroxymethyl-2-methyl-7-methoxychromone (**3**), and 4,6-dihydroxy-5-methylphthalide (**4**) are reported from this strain for the first time.

ASSOCIATED CONTENT

Supporting Information

^1H and ^{13}C NMR spectra of trichoharzianol (**1**). This material is available free of charge via the Internet at http://pubs.acs.org.

DOI: 10.1021/acs.jafc.5b01258
J. Agric. Food Chem. 2015, 63, 3704−3708

AUTHOR INFORMATION

Corresponding Author

*Telephone: +66-7567-2989 and/or +66-7567-2090. Fax: +66-7567-2004. E-mail: worrapong@gmail.com.

Funding

This work was supported by Walailak University Fund and IFS-NRCT Scientific Collaboration on Establishment of the International Research Network in Thailand's Competent Fields.

Notes

The authors declare no competing financial interest.

ACKNOWLEDGMENTS

The authors thank the Utilization of Natural Products Research Unit and the Tropical Fruit Research Unit at Walailak University and the Center of Excellence for Innovation in Chemistry (PERCH-CIC) at Mahidol University for access to laboratory facilities.

REFERENCES

(1) Than, P. P.; Prihastuti, H.; Phoulivong, S.; Taylor, P. W. J.; Hyde, K. D. Chilli anthracnose disease caused by *Colletotrichum* species. *J. Zhejiang Univ., Sci., B* **2008**, *9*, 764−778.

(2) De los Santos-Villalobos, S.; Guzmán-Ortiz, D. A.; Gómez-Lim, M. A.; Délano-Frier, J. P.; De-Folter, S.; Sánchez-García, P.; Peña-Cabriales, J. J. Potential use of *Trichoderma asperellum* (Samuels, Liechfeldt et Nirenberg) T8a as a biological control agent against anthracnose in mango (*Mangifera indica* L.). *Biol. Control* **2013**, *64*, 37−44.

(3) Than, P. P.; Jeewon, R.; Hyde, K. D.; Pongsupasamit, S.; Mongkolporn, O.; Taylor, P. W. J. Characterization and pathogenicity of *Colletotrichum* species associated with anthracnose on chilli (*Capsicum* spp.) in Thailand. *Plant Pathol.* **2008**, *57*, 562−572.

(4) Bosquez-Molina, E.; Jesús, E. R.; Bautista-Baños, S.; Verde-Calvo, J. R.; Morales-López, J. Inhibitory effect of essential oils against *Colletotrichum gloeosporioides* and *Rhizopus stolonifer* in stored papaya fruit and their possible application in coatings. *Postharvest Biol. Technol.* **2010**, *57*, 132−137.

(5) Vinale, F.; Ghisalberti, E. L.; Sivasithamparam, K.; Marra, R.; Ritieni, A.; Ferracane, R.; Woo, S.; Lorito, M. Factors affecting the production of *Trichoderma harzianum* secondary metabolites during the interaction with different plant pathogens. *Lett. Appl. Microbiol.* **2009**, *48*, 705−711.

(6) Vinale, F.; Flematti, G.; Sivasithamparam, K.; Lorito, M.; Marra, R.; Skelton, B. W.; Ghisalberti, E. L. Harzianic acid, an antifungal and plant growth promoting metabolite from *Trichoderma harzianum*. *J. Nat. Prod.* **2009**, *72*, 2032−2035.

(7) Evidente, A.; Cabras, A.; Maddau, L.; Marras, F.; Andolfi, A.; Melck, D.; Motta, A. Viridenepoxydiol, a new pentasubstituted oxiranyldecene produced by *Trichoderma viride*. *J. Agric. Food Chem.* **2006**, *54*, 6588−6592.

(8) Verma, M.; Brar, S. K.; Tyagi, R. D.; Surampalli, R. Y.; Valéro, J. R. Antagonistic fungi, *Trichoderma* spp.: panoply of biological control. *Biochem. Eng. J.* **2007**, *37*, 1−20.

(9) Vinale, F.; Sivasithamparam, K.; Ghisalberti, E. L.; Marra, R.; Barbetti, M. J.; Li, H.; Woo, S. L.; Lorito, M. A novel role for *Trichoderma* secondary metabolites in the interactions with plants. *Physiol. Mol. Plant Pathol.* **2008**, *72*, 80−86.

(10) Claydon, N.; Hanson, J. R.; Truneh, A.; Avent, A. G. Harzianolide, a butenolide metabolite from cultures of *Trichoderma harzianum*. *Phytochemistry* **1991**, *30*, 3802−3803.

(11) Amagata, T.; Usami, Y.; Minoura, K.; Ito, T.; Numata, A. Cytotoxic substances produced by a fungal strain from a sponge: physico-chemical and structures. *J. Antibiot.* **1997**, *51*, 33−39.

(12) Vinale, F.; Marra, R.; Scala, F.; Ghisalberti, E. L.; Lorito, M.; Sivasithamparam, K. Major secondary metabolites produced by two commercial *Trichoderma* strains active against different phytopathogens. *Lett. Appl. Microbiol.* **2006**, *43*, 143−148.

(13) Song, F.; Dai, H.; Tong, Y.; Ren, B.; Chen, C.; Sun, N.; Liu, X.; Bian, J.; Liu, M.; Gao, H.; Liu, H.; Chen, X.; Zhang, L. Trichodermaketones A-D and 7-O-methylkoninginin D from the marine fungus *Trichoderma koningii*. *J. Nat. Prod.* **2010**, *73*, 806−810.

(14) Ishii, T.; Nonaka, K.; Suga, T.; Masuma, R.; Ōmura, S.; Shiomi, K. Cytosporone S with antimicrobial activity, isolated from the fungus *Trichoderma* sp. FKI-6626. *Bioorg. Med. Chem. Lett.* **2013**, *23*, 679−681.

(15) Evidente, A.; Ricciardiello, G.; Andolfi, A.; Sabatini, M. A.; Ganassi, S.; Altomare, C.; Favilla, M.; Melck, D. Citrantifidiene and citrantifidiol: bioactive metabolites produced by *Trichoderma citrinoviride* with potential antifeedant activity toward aphids. *J. Agric. Food Chem.* **2008**, *56*, 3569−3573.

(16) Aneja, M.; Gianfagna, T. J.; Hebbar, P. K. *Trichoderma harzianum* produces nonanoic acid, an inhibitor of spore germination and mycelial growth of two cacao pathogens. *Physiol. Physiol. Mol. Plant Pathol.* **2005**, *67*, 304−307.

(17) Macías, F. A.; Varela, R. M.; Simonet, A. M.; Cutler, H. G.; Cutler, S. J.; Eden, M. A.; Hill, R. A. Bioactive carotanes from *Trichoderma virens*. *J. Nat. Prod.* **2000**, *63*, 1197−1200.

(18) Ding, G.; Chen, L.; Chen, A.; Tian, X.; Chen, X.; Zhang, H.; Chen, H.; Liu, X. Z.; Zhang, Y.; Zou, Z. M. Trichalasins C and D from the plant endophytic fungus *Trichoderma gamsii*. *Fitoterapia* **2012**, *83*, 541−544.

(19) Luo, S. L.; Lo, C. T.; Shibu, M. A.; Leu, Y. L.; Jen, B. Y.; Peng, K. C. Study on the anthraquinones separated from the cultivation of *Trichoderma harzianum* strain Th-R16 and their biological activity. *J. Agric. Food Chem.* **2009**, *57*, 7288−7292.

(20) Evidente, A.; Cabras, A.; Maddau, L.; Serra, S.; Andolfi, A.; Motta, A. Viridepyronone, a new antifungal 6-substituted 2H-pyran-2-one produced by *Trichoderma viride*. *J. Agric. Food Chem.* **2003**, *51*, 6957−6960.

(21) Li, G. H.; Yang, Z. S.; Zhao, P. J.; Zheng, X.; Luo, S. L.; Sun, R.; Niu, X. M.; Zhang, K. Q. Three new acorane sesquiterpenes from *Trichoderma* sp. YMF1. 02647. *Phytochem. Lett.* **2011**, *4*, 86−88.

(22) Yamamoto, T.; Izumi, N.; Ui, H.; Sueki, A.; Masuma, R.; Nonaka, K.; Hirose, T.; Sunazuka, T.; Nagai, T.; Yamada, H.; Omura, S.; Shiomi, K. Wickerols A and B: novel anti-influenza virus diterpenes produced by *Trichoderma atroviride* FKI-3849. *Tetrahedron* **2012**, *68*, 9267−9271.

(23) Fukuda, T.; Uchida, R.; Ohte, S.; Inoue, H.; Yamazaki, H.; Matsuda, D.; Nonaka, K.; Masuma, R.; Katagiri, T.; Tomoda, H. Trichocyalides A and B, new inhibitors of alkaline phosphatase activity in bone morphogenetic protein-stimulated myoblasts, produced by *Trichoderma* sp. FKI-5513. *J. Antibiot.* **2012**, *65*, 565−569.

(24) Garo, E.; Starks, C. M.; Jensen, P. R.; Fenical, W.; Lobkovsky, E.; Clardy, J. Trichodermamides A and B, cytotoxic modified dipeptides from the marine-derived fungus *Trichoderma virens*. *J. Nat. Prod.* **2003**, *66*, 423−426.

(25) Mannina, L.; Segre, A. L.; Ritieni, A.; Fogliano, V.; Vinale, F.; Randazzo, G.; Maddau, L.; Bottalico, A. A new fungal growth inhibitor from *Trichoderma viride*. *Tetrahedron* **1997**, *53*, 3135−3144.

(26) Warin, I.; Chaiyawat, S.; Chiradej, C.; Montree, I.; Sorwaporn, K.; Kan, C. Bioactive compound of antifungal metabolite from *Trichoderma harzianum* mutant strain for the control of anthracnose of chili (*Capsicum annuum* L.). *Philipp. Agric. Sci.* **2009**, *92*, 392−397.

(27) Vinale, F.; Sivasithamparam, K.; Ghisalberti, E. L.; Marra, R.; Woo, S. L.; Lorito, M. *Trichoderma*-plant-pathogen interactions. *Soil Biol. Biochem.* **2008**, *40*, 1−10.

(28) Tarus, P. K.; Lang'at-Thoruwa, C. C.; Wanyonyi, A. W.; Chhabra, S. C. Bioactive metabolites from *Trichoderma harzianum* and *Trichoderma longibrachiatum*. *Bull. Chem. Soc. Ethiop.* **2003**, *17*, 185−190.

(29) Chakraborty, B. N.; Chakraborty, U.; Saha, A.; Dey, P. L.; Sunar, K. Molecular characterization of *Trichoderma viride* and *Trichoderma harzianum* isolated from soils of north bengal based on rDNA markers

DOI: 10.1021/acs.jafc.5b01258
J. Agric. Food Chem. 2015, 63, 3704−3708

and analysis of their PCR-RAPD profiles. *Global. J. Biotechnol. Biochem.* **2010**, *5*, 55−61.
(30) Lian, B.; Zang, J.; Hou, W.; Yuan, S.; Smith, D. L. PCR-based sensitive detection of the edible fungus *Boletus edulis* from rDNA ITS sequences. *Electron. J. Biotechnol.* **2008**, *11*, 1−8.
(31) Anaruma, N. D.; Schmidt, F. L.; Duarte, M. C. T.; Figueira, G. M.; Delarmelina, C.; Benato, E. A. Control of *Colletotrichum gloepsporioides* (penz.) Sacc. in yellow passion fruit using *Cymbopogon citratus* essential oil. *Braz. J. Microbiol.* **2010**, *41*, 66−73.
(32) Kobayashi, M.; Uehara, H.; Matsunami, K.; Aoki, S.; Kitagawa, I. Trichoharzin, a new polyketide produced by the imperfect fungus *Trichoderma harzianum* separated from the marine sponge *Micale cecilia*. *Tetrahedron Lett.* **1993**, *34*, 7925−7928.
(33) Nakadate, S.; Nozawa, K.; Horie, H.; Fujii, Y.; Nagai, M.; Hosoe, T.; Kawai, K. I.; Yaguchi, T.; Fukushima, K. Eujavanicols A-C, decalin derivatives from *Eupenicillium javanicum*. *J. Nat. Prod.* **2007**, *70*, 1510−1512.
(34) Tanahashi, T.; Takenaka, Y.; Nagakura, N.; Hamada, N. 2,3-Dialkylchromones from mycobiont cultures of the lichen *Graphis scripta*. *Heterocycles* **2000**, *53*, 1589−1593.
(35) Ayer, W. A.; Racok, J. The metabolites of *Talaromtces flavus*: part 1. metabolites of the organic extracts. *Can. J. Chem.* **1990**, *68*, 2085−2094.

DOI: 10.1021/acs.jafc.5b01258
J. Agric. Food Chem. 2015, 63, 3704−3708

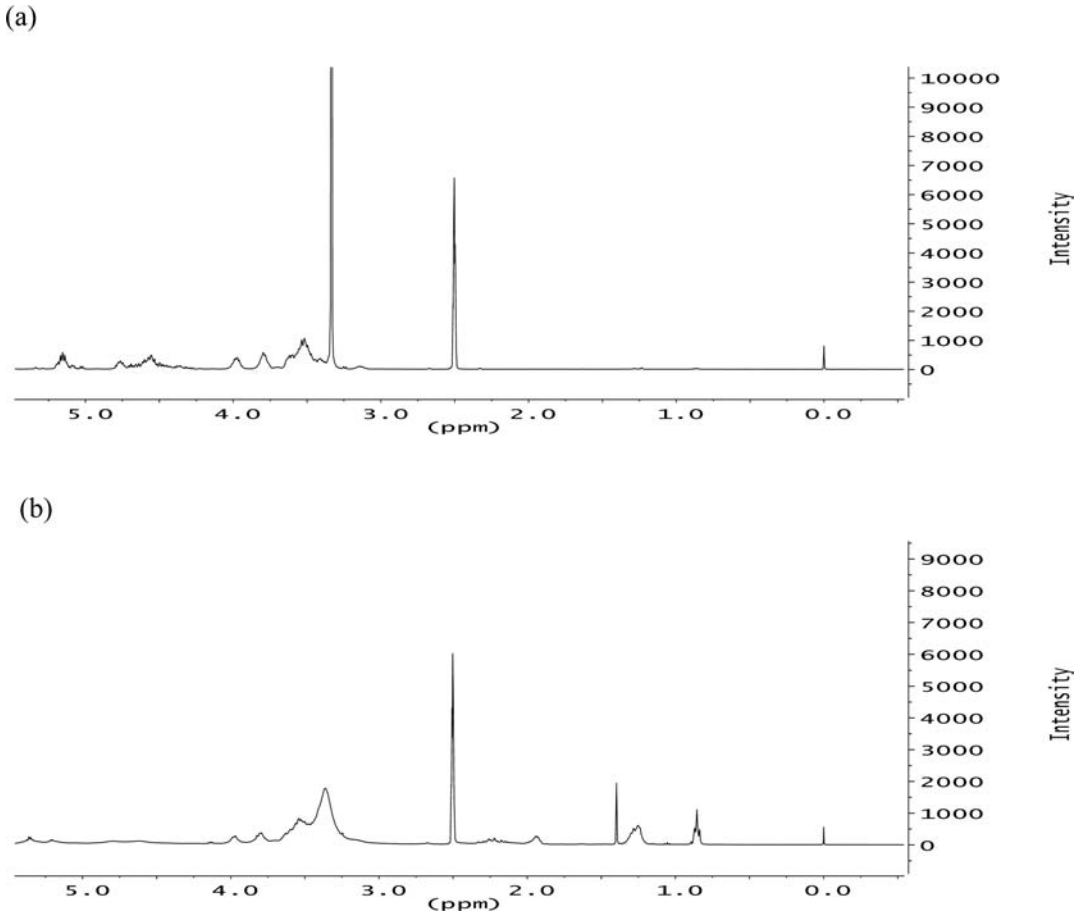

Figure 1. Proton NMR spectra of (a) unmodified inulin (Inutec H25P) and (b) OSA−inulin.

solutions to prevent solidification in the dropping funnel. Throughout the reaction, the pH was maintained at pH 8.3−8.5 through addition of aqueous sodium hydroxide (1, 3, or 10%, w/w). The reaction was continued until no further pH change was observed; typically, this was about 6 h. The reaction mixture was then brought to pH 6.0 by addition of 5% aqueous hydrochloric acid. The solid product was recovered by freeze-drying and washed by Soxhlet extraction with cyclohexane for 6 h prior to drying in a vacuum oven.

Characterization. *NMR Spectroscopy.* H^1 NMR spectra of ASA−inulins were recorded using a 500 MHz NMR Spectrometer at 25 °C. Each sample (5 mg) was added to 0.7 g of DMSO-d_6 then added into a 5 mm thin wall NMR tube and dissolved at 25 °C. The spectra were recorded using the Pulse Program ZG30 together with Mnova 7.0 software, with a 30° pulse and a delay of 1 s.

Fourier-Transform Infrared Spectroscopy. ASA−inulin samples were dried in an oven at 70 °C overnight. Sample (1 mg) was milled with 100 mg of dried KBr using an agate mortar and pestle for several minutes to obtain a fine powder. A thin pellet was produced using a 15 ton manual press and a P/N 03000 13 mm pellet die (maximum load 10.0 tons) from Specac Limited. The FTIR spectra were recorded in the range 4000−400 cm^{-1} using a PerkinElmer FTIR spectrometer RX 1, taking 16 scans at a resolution of 4 cm^{-1}. Spectral analysis and display were performed using the interactive PerkinElmer Read-IR3 software, version 3.0.

Critical Aggregation Concentration. *Dye Solubilization.* The CAC was determined using the dye solubilization technique as described previously.[7] Stock solutions of 1% ASA−inulins were prepared and diluted to give solutions of various concentrations. A 10 mg aliquot of the dye was added to 10 mL of inulin solution, and the samples were left agitating at 40 °C overnight. The solution was then filtered to remove insoluble dye particles using a Millex-GP 0.22 μm filter (Millipore Ireland Ltd.) into disposable UV grade 10 mm path length cuvettes (CXA-110-0053 from Fisher Scientific Ltd.). The absorbance of the solution was determined at a wavelength of 510 nm using a Lambda 25 UV/vis Spectrometer (PerkinElmer). The CAC was obtained from the point at which the absorbance first increased.

Dynamic Light Scattering. Dynamic light scattering measurements were recorded using the Zetasizer Nano ZS (Malvern Instruments Ltd., Malvern, UK) equipped with a 5 mW He−Ne laser (λ_0 = 632.8 nm) and a digital correlator at a 175° angle relative to the incident beam. The temperature was controlled at 25 ± 1 °C. Samples were prepared by serial dilution with filtered distilled water from a stock of 2.0 g/dL to create five sample concentrations in the range of 0.004−1 g/dL. Samples were filtered using a Millex-GP 0.22 μm filter (Millipore Ireland Ltd.). Solutions were placed in disposable plastic cells with a cross-sectional area of 1 cm^2. Fifteen runs were performed for each sample, and the collection time was 180 s. Zetasizer Software (version 6.20, ©2002−2010 Malvern Instruments Ltd.) was used for data analysis. The CAC was determined from the change in the slope of the plot of the intensity of scattered light as a function of concentration. The hydrodynamic diameter of the aggregates formed above the CAC was obtained from the Stokes−Einstein relationship using the instrument software.

Surface Tension. The surface tension of ASA−inulin solutions at varying concentrations was determined using a Tensiometer K8 with a 4 cm circumference Du Nouy ring (RI 01 from Krüss GmbH). All measurements were repeated three times, and the average taken. The temperature was kept constant at 25 ± 1 °C during all the measurements. The CAC was determined from the change in slope of the plot of equilibrium surface tension as a function of ASA−inulin concentration.

Emulsification Properties. Oil-in-water emulsions (15 %, w/w) were prepared by mixing 1.5 g of oil and 8 g of a 2.5% aqueous solution of alkenyl succinylated inulin and 0.5 g of water to make

DOI: 10.1021/acs.jafc.5b00333
J. Agric. Food Chem. 2015, 63, 3709−3715

2.35%. ASA−inulin emulsion samples contained in a 20 mL glass tube were homogenized using an IKA T25 Digital ultra-Turrax homogenizer at 24 000 rpm for 3 min. Emulsions were also prepared using Tween 20 for comparison. The droplet size of the emulsions was measured by laser diffraction immediately after preparation and after storing at room temperature for a period of up to 21 days using the Mastersizer-2000 (Malvern Instruments, UK). Two or three drops of the sample were introduced into the dispersion unit containing distilled water. The dispersion unit pump speed was 2000 rpm, and the obscuration was between 10 and 30%. The refractive index of the dispersing medium and the dispersed particles were 1.33 and 1.45, respectively. Measurements were carried out in duplicate and the average value reported.

RESULTS AND DISCUSSION

Characterization. Figure 1a,b shows the ^{1}H NMR spectra of the native and OSA−inulin samples, respectively. The prominent peaks at 2.5 and 3.35 ppm are from the solvent, i.e., DMSO and HDO, respectively, and the peaks from 3.4 to 5.3 ppm are from the inulin itself (Figure 1a).[7] ^{1}H NMR signals at 0.85, 1.26, and 1.94 ppm[10−12] correspond to the methyl and methylene groups of the octenylsuccinic anhydride (Figure 1b). The amount of alkenyl chains incorporated into the modified samples was calculated from the ratio of the area of the peak at 0.85 ppm to the area of the peaks from 3.4−5.3 ppm, and the results are shown in Table 1.

Table 1. Degree of Substitution of the Modified Inulins

sample	% substitution/mol
OSA	29.6
DSA	28.7
DDSA	22.7
TDSA	26.2
HDSA	39.8
ODSA	12.9

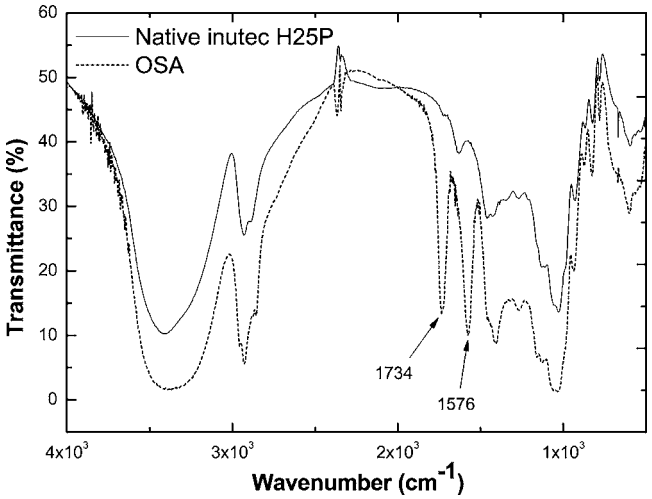

Figure 2. FTIR spectra of unmodified inulin (Inutec H25P) and OSA−inulin.

FTIR spectra of the native and OSA−inulin samples are presented in Figure 2. The peaks for the native inulin at 3398, 2930, and 1028 cm^{-1} indicate O−H stretching, CH_2 stretching, and C−O−C bending, respectively.[7,13] The spectrum of OSA−inulin shows two new peaks at 1576 and 1734 cm^{-1} caused by the formation of the ester linkage. Similar findings were found for the other modified samples (data not shown). The peaks

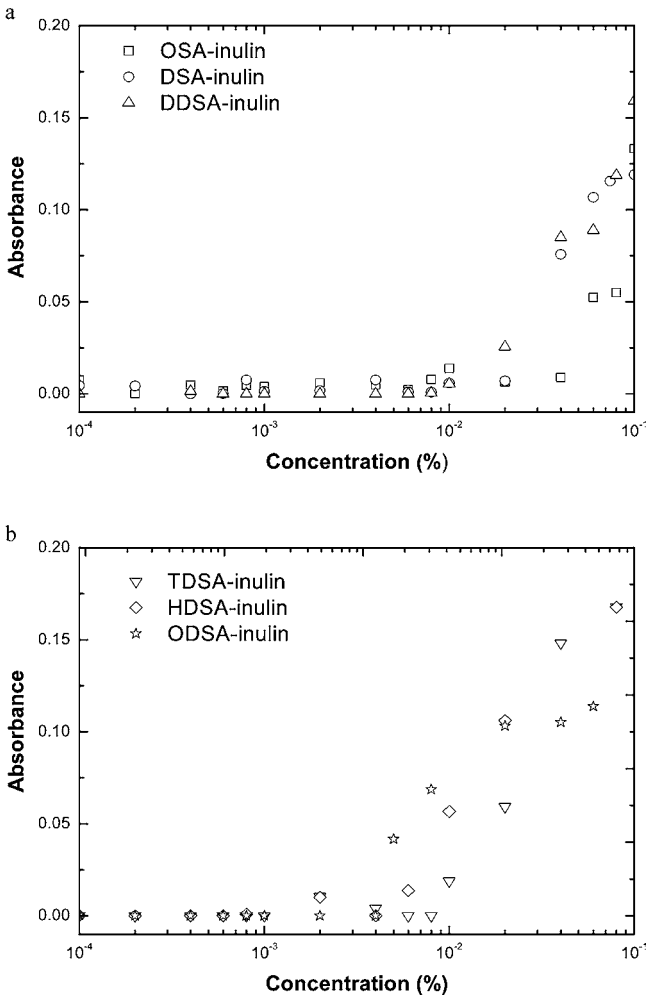

Figure 3. (a)Absorbance at 510 nm of OSA−, DSA−, and DDSA−inulin samples at varying concentrations in the presence of Sudan IV dye. (b) Absorbance at 510 nm of TDSA−, HDSA−, and ODSA−inulin samples at varying concentrations in the presence of Sudan IV dye.

Table 2. Critical Aggregation Concentrations of the Modified Inulin Samples Using Various Techniques

	CAC %		
sample	dynamic light scattering (intensity)	dye solubilisation	surface tension
OSA	0.08 ± 0.005	0.07 ± 0.01	0.07 ± 0.01
DSA	0.06 ± 0.005	0.04 ± 0.01	0.05 ± 0.01
DDSA	0.04 ± 0.01	0.02 ± 0.005	0.04 ± 0.01
TDSA	0.02 ± 0.005	0.009 ± 0.001	0.015 ± 0.005
HDSA	0.015 ± 0.005	0.007 ± 0.001	0.015 ± 0.005
ODSA	0.012 ± 0.005	0.0045 ± 0.0005	0.005 ± 0.001

are assigned to asymmetric COO− and ester carbonyl stretching, respectively.[13] In studies on starch modification, it has previously been reported that the CH_2 stretching band at 2930 cm^{-1} increased after modification because of the contribution from the carbon chain associated with the alkenyl succinic group.[14] However, the CH_2 stretching band at 2930 cm^{-1} for our modified inulins was not comparably enhanced, in agreement with the findings of Kokubun et al.[7]

Critical Aggregation Concentration. The absorbance values obtained for ASA−inulins in the presence of Sudan IV

DOI: 10.1021/acs.jafc.5b00333
J. Agric. Food Chem. 2015, 63, 3709−3715

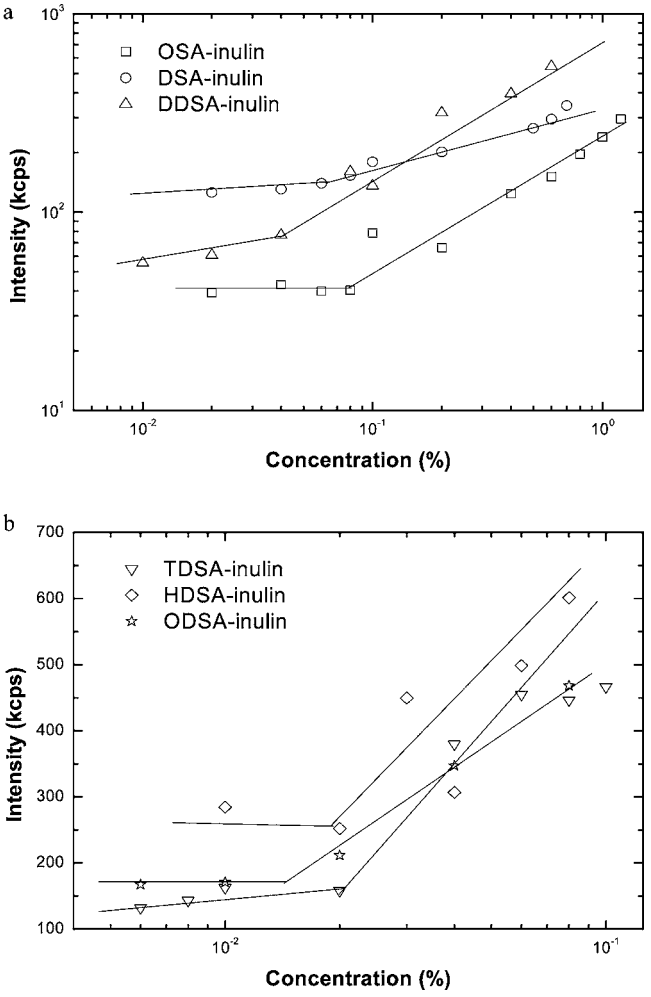

Figure 4. (a) Scattering intensity as a function of concentration for OSA-, DSA-, and DDSA-modified inulins. (b) Scattering intensity as a function of concentrations for TDSA-, HDSA-, ODSA-modified inulins.

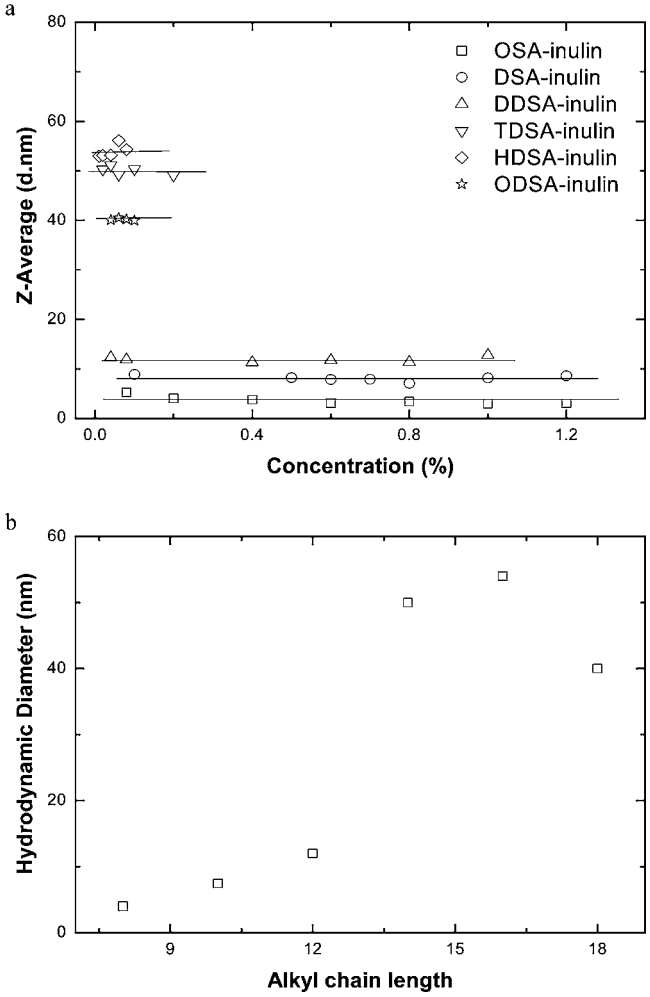

Figure 5. (a) Z-average hydrodynamic diameter as a function of concentration for modified inulins with different alkenyl chain lengths. (b) Z-average hydrodynamic diameter as a function of alkenyl chain length for ASA−inulins.

are given in Figure 3a,b. It is noted that the values increase significantly above a critical concentration which is attributed to the formation of micellar−like aggregates and the dissolution of the dye in their hydrophobic core.[7] The CAC values for all ASA−inulins are summarized in Table 2. It is generally seen that the CAC decreases as the alkenyl chain length increases as expected and also as noted by Kokubun et al.[7] and van Kempen et al.[5] for hydrophobically modified inulins. The actual CAC values for the OSA−inulins are lower than those reported by Kokubun et al.,[7] and this is attributed mainly to the fact that the present samples have a significantly higher degree of alkenylation. The values, however, are higher than those reported by van Kempen et al.[5] This is probably due to the fact that in our study modification was carried out using alkenyl succinic anhydride which leads to the incorporation of a free carboxylate group present in the surfactant headgroup giving an anionic charge. This was not the case for the samples produced by van Kempen et al., which were nonionic.[5] It is well-known that ionic surfactants have a higher critical micelle concentration (CMC) compared to nonionic surfactants because of the fact that for ionic surfactants electrostatic repulsions between the surfactant head groups in the micelle oppose the micellization process.

The scattering intensity of solutions of ASA−inulin samples are plotted as a function of concentration in Figure 4a,b. The sharp increase in the scattering intensity above a certain concentration is attributed to the CAC and the formation of aggregates. The CAC values are given in Table 2 and are of the same order of magnitude as the values obtained by dye solubilization.

The Z-average hydrodynamic diameters of ASA−inulin samples are given as a function of concentration in Figure 5a and are plotted as a function of alkenyl chain length in Figure 5b. It is noted that in general the size of the aggregates increases with the alkenyl chain length as might be expected. The value for ODSA−inulin is a little lower than might be expected from the trend shown, and this is probably due to the fact that it has a significantly lower degree of modification than the other samples. Kokubun et al.[7] reported higher values of 13 and 30 nm compared to values of 4 and 12 nm in this study for OSA- and DDSA-modified inulin samples, respectively. The main reason for the difference is the fact that the DP of the inulin used in the present study was 2−8, whereas in the study of Kokubun et al.,[7] the inulin had a DP of >10. van Kempen et al.[5] also used inulin with a DP of 2−8 and reported values of between 4.3 to 13.4 nm for C8−C18 modified inulins,

DOI: 10.1021/acs.jafc.5b00333
J. Agric. Food Chem. 2015, 63, 3709−3715

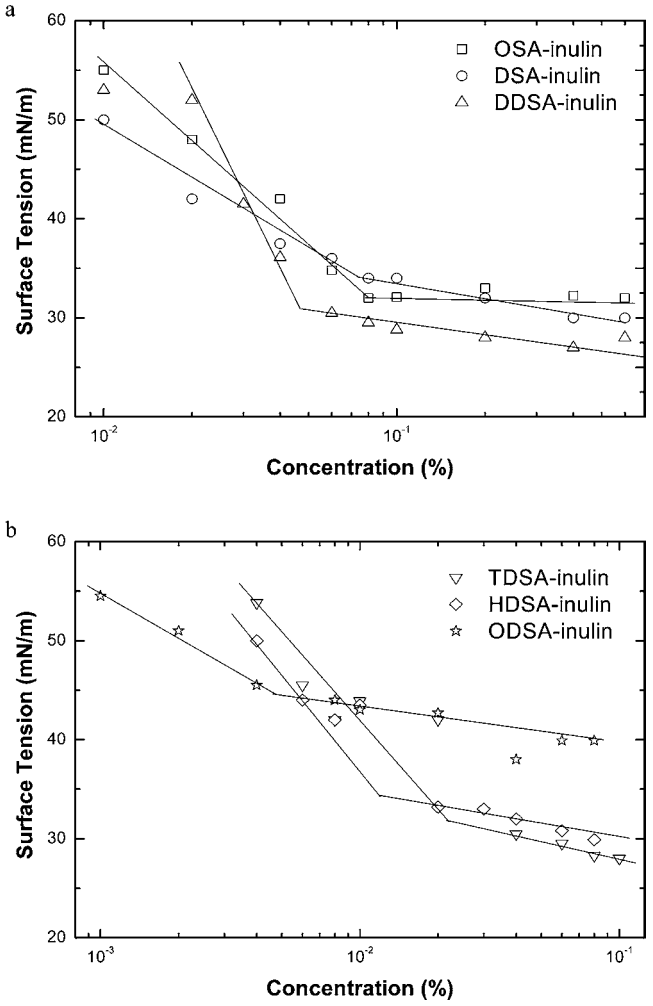

Figure 6. (a) Surface tension of OSA−, DSA−, and DDSA−inulin samples as a function of concentration. (b) Surface tension of TDSA−, HDSA−, and ODSA−inulin samples as a function of concentration.

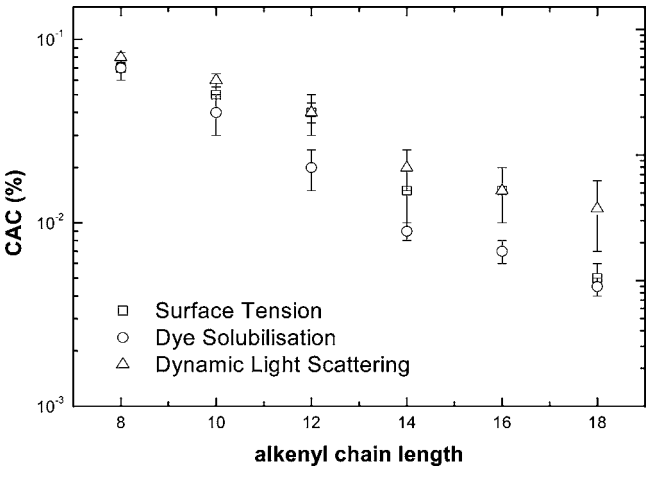

Figure 7. Critical aggregation concentrations of ASA−inulins as a function of alkenyl chain length.

consistent with the values reported here using inulin of a similar DP.

The surface tensions of ASA−inulins at the air−water interface are shown as a function of concentration in Figure 6a,b. The CAC value for each of the samples was obtained from the inflection in the curve, and the results are reported in Table 2. The values are in reasonable agreement with the values obtained using dye solubilization and dynamic light scattering methods. The surface tension was found to be between 31 and 34 mNm at the CAC for all of the samples, apart from ODSA−inulin which had a much higher value (43 mNm). This discrepancy may be due to its lower degree of modification. Kokubun et al.[7] reported values of ∼35−40 mNm for OSA−inulin and DDSA−inulin, and van Kempen et al.[5] reported

Table 3. Surface Excess (Γ) and Molecular Cross-Sectional Area (*A*) Determined at 25°C

surfactant	maximum surface excess (Γ) × 10^{-6} (mol/m^2)	molecular area (nm^2)
OSA	2.24	0.74
DSA	1.58	1.06
DDSA	2.52	0.66
TDSA	1.66	1.00
HDSA	1.94	0.86
ODSA	0.93	1.78

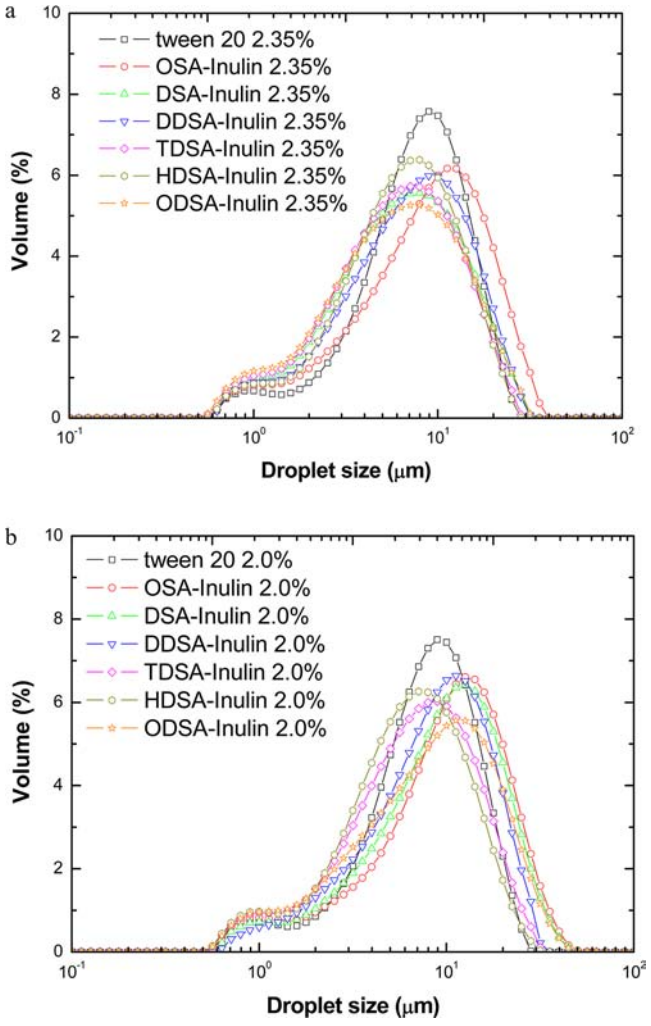

Figure 8. (a) Droplet size distributions of emulsions prepared with 2.35% Tween 20 and modified inulins with various lengths of alkenyl chain at room temperature on day 1. (b) Droplet size distributions of emulsions prepared with 2.35% Tween 20 and modified inulins with various lengths of alkenyl chain at 25 °C after storage at room temperature for 21days.

DOI: 10.1021/acs.jafc.5b00333
J. Agric. Food Chem. 2015, 63, 3709−3715

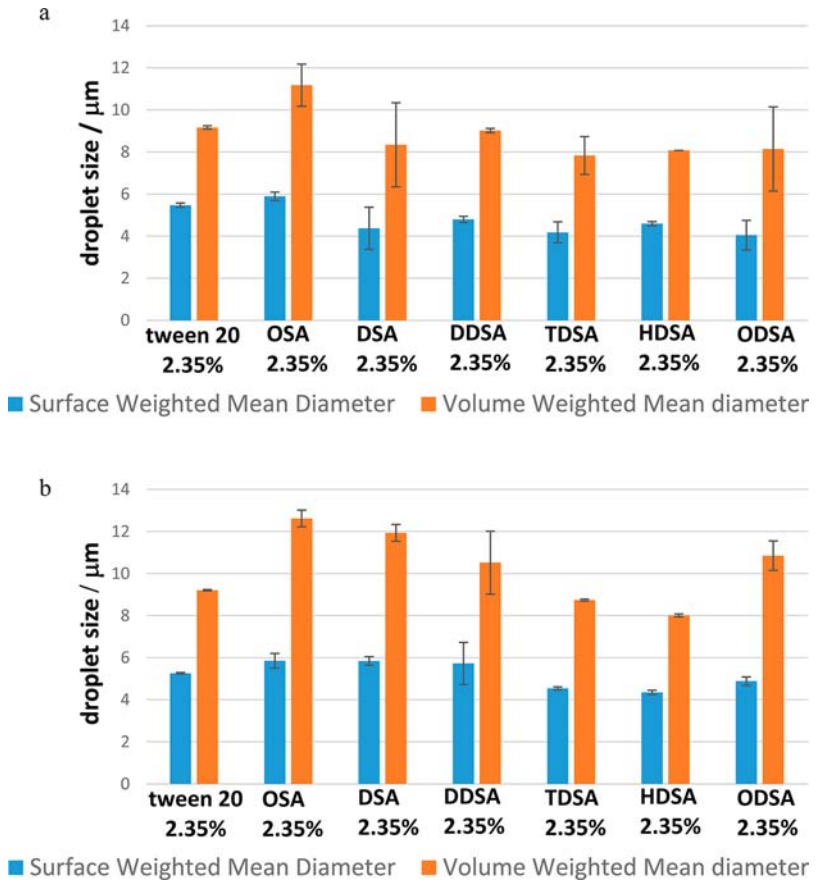

Figure 9. (a) Droplet size for 15% oil-in-water emulsions prepared using 2.35% modified inulins at room temperature on day 1. (b) Droplet size for 15% oil-in-water emulsions prepared using 2.35% modified inulins after storing at room temperature for 21 days.

values of ∼34−40 mNm for inulin samples modified with C8−C16 alkyl chains.

The CAC values for ASA−inulins obtained using the different techniques are plotted as a function of the alkyl chain length in Figure 7, which clearly shows the decrease in CAC with increasing alkyl chain length. The free energy decrease for the transfer of a $-CH_2-$ unit from the bulk phase to the micelle (ΔG_{mic}) can be calculated by eq 1, derived by Rosen[15,16] and represented as

$$\log \mathrm{CMC} = (\Delta G_{mic}/2.303RT)m + K_{mic} \quad (1)$$

where m is the number of carbons in the alkyl chain and K_{mic} is a constant for the same hydrophilic group. The calculated ΔG_{mic} per CH_2 is −0.79 kJ/mol at 25 °C. Zhang and Marchant[16] reported a ΔG_{mic} value for the *N*-alkylmaltoamide series of −1.86 kJ/mol at 25 °C. Using the same procedure, van Kempen et al.[5] obtained a value of −3.1 kJ/mol.

The surface excess, Γ, is related to surface tension by the Gibbs equation, which for a 1:1 ionic surfactant is given by eq 2,[5] represented as

$$\Gamma = -\left(\frac{1}{2RT}\right)\left(\frac{d\gamma}{d(\ln C)}\right) \quad (2)$$

Surface excess values were determined from the slope of the lines for the plot of γ−ln C just below the CAC,[5,17] and the results are shown in Table 3. The values obtained for the surface excess were used to calculate the surface area occupied by each molecule, A, using the equation

$$A = \frac{1}{\Gamma N_A} \quad (3)$$

where N_A is Avogadro's number.

The area occupied per molecule was found to vary between 0.66 and 1.06 nm^2 for the inulins modified using C8−C16 alkenyl chains and is of an order similar to the values reported by van Kempen et al.[5] of 0.46 to 0.91 nm^2 and by Stevens et al.,[4] who reported an area per molecule of 0.9 nm^2 for a hydrophobically modified inulin sample. The high value obtained for ODSA−inulin (1.78 nm^2) may be a consequence of is low solubility, which is likely to result in molecular aggregation. The values for A are larger than those reported for simple sugar-based surfactants with only one or two sugar residues. For example, Soultani et al.[18] reported values of 0.05−0.2 nm^2 for hydrophobically modified fructose and sucrose surfactants, whereas Garofalakis et al.[19] reported values of 0.29−0.68 nm^2 for surfactants based on xylose, galactose, sucrose, and lactose. For the modified inulins, the area occupied will ultimately depend on the number and position of the hydrophobic groups attached to the backbone. If there are several hydrophobic groups randomly distributed along the backbone, then the carbohydrate moieties would be expected to lie flat at the interface and occupy a much larger surface area than inulin molecules with the hydrophobic groups attached at one end.

Emulsion Stability. The droplet size distributions for the emulsions prepared using the various modified inulin samples and Tween 20 were determined shortly after preparation and after 21 days and are presented in Figure 8a,b, respectively. The

DOI: 10.1021/acs.jafc.5b00333
J. Agric. Food Chem. 2015, 63, 3709−3715

corresponding $d_{3,2}$ and $d_{4,3}$ values are given in Figure 9a,b. It was found that the modified inulin samples with alkylene chain lengths C10−C18 produced emulsions with slightly smaller droplet sizes than did C8 inulin and Tween 20. There was little change observed in the droplet size on storing for 21 days. This is consistent with the study by Kokubun et al.,[8] which showed that DDSA−inulin yielded emulsions with a droplet size smaller than OSA−inulins (both with DS 12 mol %).

The work described in this paper has demonstrated that inulin can be successfully modified in aqueous solution by alkylene succinic anhydrides with alkenyl chain lengths varying from C8−C18, and the derivatives have been shown to form micellarlike aggregates in solution. The CAC values have been found to decrease with increasing alkenyl chain length, whereas the hydrodynamic size of the aggregates has been shown to increase with increasing alkenyl chain length. It has also been shown that inulins are able to produce stable oil-in-water emulsions with a droplet size similar to those formed with Tween 20. The dye solubilization experiments have demonstrated that ASA−inulins are able to form micellarlike aggregates and dissolve hydrophobic compounds within their hydrophobic core. This coupled to the fact that they can stabilize oil-in-water emulsions makes them suitable candidates for the encapsulation and delivery of water-insoluble active compounds, with potential application in food, cosmetic, personal care, and pharmaceutical formulations.

AUTHOR INFORMATION

Corresponding Author

*Tel.: +44 1978 293083. E-mail: williamspa@glyndwr.ac.uk.

Notes

The authors declare no competing financial interest.

ACKNOWLEDGMENTS

The authors gratefully acknowledge colleagues at Bangor University for undertaking NMR measurements. I.R. and P.A.W. are grateful to the BBSRC Integrated Biorefining Research and Technology (IBTI) Club (Grant Reference No. BB/1005315/1) for financial support.

REFERENCES

(1) Meyer, D.; Blaauwhoed, J.-P. Inulin. In *Handbook of Hydrocolloids*; Philips, G. O., Williams, P. A., Eds.; Woodhead Publishing: Cambridge, U.K., 2009; pp 829−848.

(2) Rogge, T. M.; Stevens, C. V. Facilated synthesis of inulin esters by trans-esterification. *Biomacromolecules* **2004**, *5*, 1799−1803.

(3) Rogge, T. M.; Stevens, C. V.; Booten, C. V.; Levecke, B.; Vandamme, A.; Vercauteren, C.; Haelterman, B.; Corthouts, J.; D'hooge, C. Improved synthesis and physicochemical properties of alkoxylated inulin. *Top. Catal.* **2004**, *27*, 39−47.

(4) Stevens, C. V.; Meriggi, S.; Peristeropoulou, M.; Christoy, P. P.; Booten, K.; Levecke, B.; Vandamma, A.; Pittevils, N.; Tadros, T. F. Polymeric surfactants based on inulin, a polysaccharide extracted from chicory. 1. Synthesis and interfacial properties. *Biomacromolecules* **2001**, *2*, 1256−1259.

(5) van Kempen, S. E. H. J.; Schols, H. A.; van der Linden, E.; Sagis, L. M. C. Effect of variations in the fatty chain on functional properties of oligofructose fatty acid esters. *Food Hydrocolloids* **2014**, *40*, 22−29.

(6) Morros, J.; Levecke, B.; Rosa, I. M. Chemical hydrophobic modification of inulin in aqueous media: Synthesis of beta-hydroxyalkyl ethers of inulin. *Carbohydr. Polym.* **2010**, *81*, 681−686.

(7) Kokubun, S.; Ratcliffe, I.; Williams, P. A. Synthesis, characterization and self-assembly of biosurfactants based on hydrophobically modified inulins. *Biomacromolecules* **2013**, *14*, 2830−3836.

(8) Kokubun, S.; Ratcliffe, I.; Williams, P. A. Functional properties of hydrophobically modified inulin. In *Gums and Stabilisers for the Food Industry 17*, Proceedings of the Gums and Stabilisers for the Food Industry Conference, June 25−28, 2013, Glyndwr University, Wales, U.K. ; Williams, P.A., Philips, G.O., Eds.; Royal Society of Chemistry Special Publication No. 346; CPI Group: Croydon, U.K., 2014; pp 245−251.

(9) Evans, M.; Gallagher, J. A.; Ratcliffe, I.; Williams, P. A. Functional properties of hydrophobically modified inulin. In *Gums and Stabilisers for the Food Industry 17*, Proceedings of the Gums and Stabilisers for the Food Industry Conference, June 25−28, 2013, Glyndwr University, Wales, U.K. ; Williams, P.A., Philips, G.O., Eds.; Royal Society of Chemistry Special Publication No. 346; CPI Group: Croydon, U.K., 2014; pp 73−78.

(10) Verraest, D. L.; Peters, J. A.; Batelaan, J. G.; Vanbekkum, H. Carboxymethylation of inulin. *Carbohydr. Res.* **1995**, *271*, 101−112.

(11) Chi, H.; Xu, K.; Xue, D.; Song, C.; Zhang, W.; Wang, P. Synthesis of dodecenyl succinic anhydride (DDSA) corn starch. *Food Res. Int.* **2007**, *40*, 232−238.

(12) Tizzotti, M. J.; Sweedman, M. C.; Tang, D.; Schaefer, C.; Gilbert, R. G. New H-1 NMR Procedure for the Characterization of Native and Modified Food-Grade Starches. *J. Agric. Food Chem.* **2011**, *59*, 6913−6919.

(13) Fares, M. M.; Salem, M. S.; Khanfar, M. Inulin and poly (acrylic acid) grafted inulin for dissolution enhancement and preliminary controlled release of poorly water-soluble Irbesartan drug. *Int. J. Pharm. (Amsterdam, Neth.)* **2011**, *410*, 206−211.

(14) Bai, Y.; Shi, Y. C.; Wetzel, D. L. Fourier transform infrared (FT-IR) microspectroscopic census of single starch granules for octenyl succinate ester modification. *J. Agric. Food Chem.* **2009**, *57*, 6443−6448.

(15) Rosen, M. J. The relationship of structure to properties in surfactants IV. Effectiveness in surface or Interfacial Tension Reduction. *J. Colloid Interface Sci.* **1976**, *56*, 320−327.

(16) Zhang, T.; Marchant, R. E. Novel Polysaccharide Surfactants: The effect of Hydrophobic and Hydrophilic Chain Length on Surface Active Properties. *J. Colloid Interface Sci.* **1996**, *177*, 419−426.

(17) Becerra, N.; Toro, C.; Zanocco, A. L.; Lemp, E.; Gunther, G. Characterization of micelles formed by sucrose 6-O-monoesters. *Colloids Surf., A* **2008**, *327*, 134−139.

(18) Soultani, S.; Ognier, S.; Engasser, J. M.; Ghoul, M. Comparative study of some surface active properties of fructose esters and commercial sucrose esters. *Colloids Surf., A* **2003**, *227*, 35−44.

(19) Garofalakis, G.; Murray, B. S.; Sarney, D. B. Surface activity and critical aggregation concentration of pure sugar esters with different sugar headgroups. *J. Colloid Interface Sci.* **2000**, *229*, 391−398.

DOI: 10.1021/acs.jafc.5b00333
J. Agric. Food Chem. 2015, 63, 3709−3715

and 7.5−9.5% Na_2O), sodium periodate, and sulfuric acid (98%). Sodium borohydride, cetyltrimethylammonium bromide (CTAB), trimethoxy(octyl)silane (OTMS; 96%), glycerin, glycidyloxypropyltrimethoxysilane (GPTMS 99.7%), *p*-nitrophenol (pNP), *p*-nitrophenyl butyrate (pNPB), acetone, propylene carbonate, methyltetrahydrofuran (Me-THF), *tert*-butanol (*t*-BuOH), palmitic acid, ascorbyl palmitate, and TritonX-100 (laboratory grade) were purchased from Sigma−Aldrich (St. Louis, MO, USA). Lactulose was purchased from Carbosynth (Berkshire, United Kingdom). Lipases from *Pseudomonas stutzeri* (PsL) and *Alcaligenes* sp. (AsL), under the trade names Lipase TL and Lipase QL respectively, were kindly donated by Meito-Sangyio Ltd. (Fuchu, Japan). All other reagents and solvents were of the highest available purity and used as purchased.

Synthesis and Characterization of Supports. *Silica Synthesis.* Synthesis and functionalization of silica was carried out according to a previous work.[18] A typical reaction of synthesis is described below: a mixture with the following molar proportion of reagents: SiO_2:Na_2O:CTAB:EtAc:H_2O = 1:0.3:0.24:7.2:193 was heated at 80 °C for 48 h under quiescent conditions. Then the solid was calcined at 540 °C (heating rate: 1.5 °C min^{-1}) for 3 h and derivatized according to the requirements of the chemical surface.

Octyl Silica Derivatization (OS). One g of silica was activated under vacuum then was mixed with 30 mL of 10% OTMS in toluene solution and gently stirred under reflux for 6 h. After filtration, the solid was washed with acetone and abundant water (conditioning the silica surface for the enzyme) and finally dried at room temperature.[13]

Octyl-glyoxyl Silica Derivatization (OGS). The octyl and glyoxyl cobonded silica (OGS) particles were prepared in a similar way than OS, using a 10% GPTMS-OTMS mixture in a 1:1 proportion. After washing and filtration, the derivatized silica was oxidized by contacting the support with 0.1 M $NaIO_4$ solution for 2 h at 25 °C. Details of the grafting reaction can be found in Bernal et al.[13,19]

Biocatalyst Preparation. *As*L and *Ps*L were immobilized in the supports according to their chemical surface. For OS, the support was prepared at pH 7 to favor its hydrophobic interaction with the lipase, while for OGS preparation, the enzyme was first contacted with the support at pH 7 to favor hydrophobic interaction but, after that, the pH of the suspension was increased to 10 with the aim of favoring covalent bond formation between the glyoxyl groups of the activated silica and the lysine residues of the enzymes. Immobilization was carried out offering 160 and 200 IU of *Ps*L and *As*L per gram of support, respectively. More details about the immobilization process can be found in previous works.[13,18]

Assay of lipase activity was performed by measuring the increase in absorbance at 348 nm produced by the released *p*-nitrophenol in the hydrolysis of 0.4 mM *p*-nitrophenyl butyrate (*p*NPB) in 25 mM sodium phosphate buffer at pH 7.0 and 25 °C. One international unit of lipase activity (IU) was defined as the amount of enzyme that hydrolyzes 1 μmol of *p*NPB per minute under the conditions described above. Expressed activity was determined in IU per gram of biocatalyst.

Stability of Biocatalysts. Stability of the biocatalysts and the soluble lipases was evaluated under two nonreactive conditions: in 25 mM sodium phosphate buffer at pH 7.0 and 60 °C, and in 100% acetone, *t*-BuOH, Me−THF, and propylene carbonate at 40 °C without the addition of surfactant or activity stabilizers in both cases. Aliquots were withdrawn periodically under stirring in order to have a homogeneous biocatalyst suspension. The residual activity of the enzymes was measured as described previously, and half-life (period of time at which the enzyme have lost one-half of its initial activity) was determined.

Lactulose Palmitate Synthesis. Lactulose palmitate was synthesized at a 10 mL scale by esterification of lactulose (5 mM) with palmitic acid (2.5 mM) using different organic solvents: acetone, *t*-BuOH, propylene carbonate, and Me−THF at 40 °C. The reaction mixture contained 15 mg/mL of biocatalyst. Substrates and products of reactions were determined by HPLC using a C-18 column (Waters Symmetry C18, 5 μm 4.6 mm × 150 mm) and a UV−vis spectrophotometer detector (JASCO model AS-2089). Separation was achieved by eluting with acetonitrile:water mixtures as mobile phase at a flow rate of 1 mL/min with the following gradient program: 60:40 (v/v) for 6 min and then 95:5 (v/v) for 18 min. Detection was performed in a UV detector at 270 nm and the monoester of lactulose palmitate was analyzed by HPLC-MS (model 2020, Shimadzu, Kyoto, Japan) with photodiode detector (SPD M 20A) and mass analyzer (MS 2020) with electrospray ionization (ESI) system.

The monoester yield was calculated according to eq 1:

$$Y(\%) = \frac{[\text{monoester}] \times V_{\text{reactor}} \times MW_{\text{lactulose}}}{Wi_{\text{lactulose}}} \times 100 \quad (1)$$

where [monoester] is the lactulose palmitate monoester molar concentration, V_{reactor} is the reactor volume, $MW_{\text{lactulose}}$ is the molecular weight of lactulose, and $Wi_{\text{lactulose}}$ is the initial mass of lactulose in the reaction mixture.

Specific productivity (SP) was calculated according to eq 2:

$$SP = \frac{[\text{monoester}] \times MW_{\text{monoester}} \times V}{t \times W_{\text{biocatalyst}}} \quad (2)$$

where [monoester] is the lactulose palmitate monoester molar concentration, $MW_{\text{monoester}}$ is the molecular weight of the monoester, V is the reactor volume, t is the time of reaction, and $W_{\text{biocatalyst}}$ is the mass of biocatalyst in the reaction mixture.

Purification of lactulose monoester was carried out by scaling-up the HPLC procedure in a preparative column of Silica C-18 (particle size, 40−75 μm; and pore size, 70 Å). Reaction mixture was dissolved in acetone and injected into the column. Mobile phase consisted of acetonitrile and water mixtures at different ratios (60:40 for monoester and 95:5 for other products and residual palmitic acid). The flow rate was kept at 2.0 mL/min, and the injection volume was 0.5 mL. Fractions were analyzed by HPLC according to the methodology described above. Collected peak fractions were evaporated to dryness under reduced pressure at 55 °C.

Experimental Design. With the aim of evaluating the effect of reaction conditions in the lactulose palmitate monoester yield and specific productivity, an experimental design was carried out. For the 2^3 factorial design, temperature and substrates molar ratio were selected as variables: each of them were tested at 5 levels (high, centered, low, and two axials) coded −1.41, −1, 0, +1, and +1.41. The uncoded and coded values for each level of these variables are given in Table 1. The experimental setting (11 duplicate runs) was generated by Design-Expert 6.0.8 software. The reaction media were analyzed after 48 h by HPLC, as described above, analyzing the monoester yield (eq 1).

Table 1. Factors and Their Levels Selected for the 2^3 Full Factorial Design

variable	levels				
	−1.41	−1.00	0.00	1.00	1.41
	Acetone				
temperature (°C)	26.5	30.0	38.5	47.0	50.5
lactulose:palmitic acid molar ratio	0.60	1.00	2.00	3.00	3.41
	Propylene Carbonate				
temperature (°C)	54.1	50.0	40.0	30.0	26.0
lactulose:palmitic acid molar ratio	0.60	1.00	2.00	3.00	3.41

Response surface analysis was carried out from these experiments, and ANOVA analysis, the model adjustment for the final equations, and their graphic representation were done with the Design-Expert 6.0.8 software.

Error obtained between experimental and modeled data (E_y) was calculated according to eq 3:

$$E_y = \frac{\text{experimental yield}}{\text{predicted yield}} \times 100 \quad (3)$$

DOI: 10.1021/jf505222x
J. Agric. Food Chem. 2015, 63, 3716−3724

Table 2. Stability and Expressed Activity in Organic Solvents of *Pseudomonas stutzeri* (*Ps*L) and *Alcaligens* sp. (*As*L) Lipases Immobilized in Porous Octyl-silica (OS) and Octyl-glyoxyl-silica (OGS)[a]

	aqueous media	propylene carbonate		acetone		*t*-BuOH		Me−THF	
biocatalyst	EA IU g^{-1}	EA UI g^{-1}	$t_{1/2}$ (h)	EA IU g^{-1}	$t_{1/2}$ (h)	EA IU g^{-1}	$t_{1/2}$ (h)	EA IU g^{-1}	$t_{1/2}$ (h)
soluble-*Ps*L	2486*[b]		2.40		2.60		3.20		3.60
OGS-*Ps*L	87.0	96.0	4.00	150	30.3	163	91.3	21.0	47.0
OS-*Ps*L	100	300	2.80	365	2.60	410	33.6	75.0	21.0
soluble-*As*L	1355*[b]		3.20		1.90		3.20		8.00
OGS-*As*L	58.0	31.0	18.2	58.0	5.00	50.0	11.7	14.0	36.2
OS-*As*L	60.0	264	9.20	108	3.80	214	46.0	18.0	5.00

[a]EA: specific activity per unit mass of biocatalyst. $t_{1/2}$: half-life for every solvent at 40 °C. [b]*Enzyme activity of soluble enzyme expressed in IU per gram of commercial powder.

All experiments were done in triplicate and the standard deviation (σ_x) was calculated according to

$$\sigma_x = \pm\sqrt{0.5 \sum (x_i - x^2)} \quad (4)$$

where x_i is the individual value for every measure and x is the average value in the experiment.

Biocatalyst Reuse. Effect of time and biocatalyst:palmitic acid mass ratio was evaluated with the aim of optimizing the batch reaction of synthesis. At the selected conditions after the experimental design, reaction was carried out during 48 h with 100 IU/g palmitic acid or during 24 h with 200 IU/g palmitic acid. In both cases, the yield of monoester and specific productivity were evaluated (eqs 3 and 4).

Operating performance in successive batches was evaluated with the obtained biocatalysts under the optimum reaction conditions established by the experimental design. At the end of each batch, one aliquot was taken and analyzed by HPLC as previously described in order to determine the monoester yield and specific productivity. Between cycles, the reacted medium was filtered out and the retained biocatalyst washed with acetone and dried at 25 °C to remove residual substrate, products, and solvent prior to using it in the subsequent batch.

RESULTS AND DISCUSSION

Biocatalysts Characteristics. Synthesis of lactulose palmitate was performed with lipases from *Pseudomonas stutzeri* and *Alcaligenes* sp. because they exhibited good esterase activity when immobilized in octyl silica and glyoxyl-octyl silica.[13] Their expressed activities in aqueous media are shown in Table 2, indicating that the orientation into the support influenced the expressed activity and immobilization yield, which was reported in a previous work.[13] Considering that esterification reactions are conveniently conducted in organic solvents, expressed activity and stability at 40 °C was evaluated in acetone, *t*-BuOH, Me−THF, and propylene carbonate. Despite the fact that the activity of lipases in soluble form cannot be measured in organic solvent (the proteins precipitate), it can be seen that immobilization in octyl and octyl-glyoxyl silica favored the expressed activity of both enzymes (in comparison with expressed activity of the biocatalyst in aqueous medium) except when the activity was measured in Me−THF (Table 2). This behavior can be explained by the physicochemical characteristics of acetone, propylene carbonate, and *t*-BuOH, which could favor the opening of the lipase lid and preclude the essential water layer around the active site of the enzyme from being stripped off.[20] Thermal stability of biocatalysts in pure organic solvent (with water content corresponding to the equilibrium moisture) at 40 °C was increased by immobilization in most of cases, it being higher for the heterofunctional support OGS (Table 2). This trend is due to the extra stiffening caused by the covalent attachment of the lysine residues of the enzyme surface to the glyoxyl groups of the support.[13] The highest thermal stability was obtained in the presence of *t*-BuOH. This is due to its high viscosity that can decrease the conformational mobility of the protein, stabilizing its tridimensional structure.[17]

Palmitate Lactulose Synthesis. Sugar ester synthesis was carried out in the presence of pure solvent with the aim of favoring esterification over hydrolysis. Propylene carbonate, acetone, *t*-BuOH, and Me−THF were selected because polar solvents favor the solubility of lactulose, one of the main problems of synthesis of sugar fatty acid esters.[21] After 48 h of reaction, all biocatalysts catalyze the conversion of palmitic acid to palmitate ester (Figure 1); however, only the conversion to monoester was quantified because this molecule has better hydrophilic−lipophilic balance than di- and triester (synthesis yield of di- and triester under evaluated conditions was less than 2%). Monoester identification was reported in a previous work.[13] Immobilized lipases in OS exhibited a higher yield toward monoester synthesis in comparison with OGS-biocatalysts, probably because the lid of lipase in OS support is more open than in OGS silica, which promotes the catalysis.

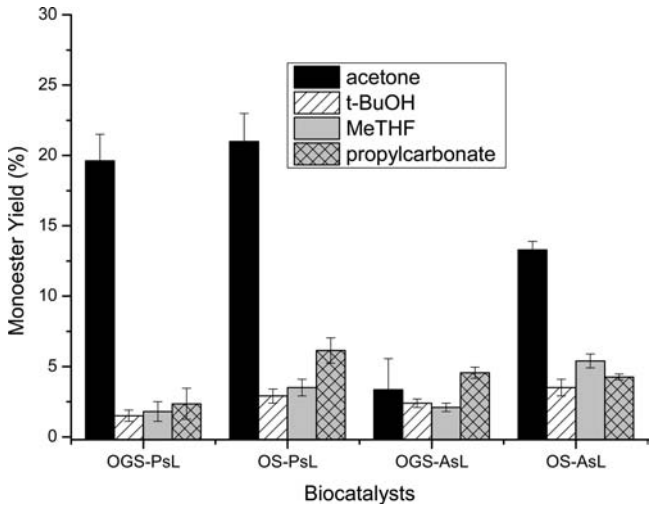

Figure 1. Monoester yield on lactulose palmitate synthesis with *Pseudomonas stutzeri* (*Ps*L) and *Alcaligens* sp. (*As*L) lipases immobilized in porous octyl-silica (OS) and octyl-glyoxyl-silica (OGS) at 40 °C after 48 h with lactulose:palmitic acid molar ratio of 1:2 in the presence of acetone (black), *t*-BuOH (hatched white), Me−THF (gray), and propylene carbonate (cross-hatched gray). Experiments were carried out by triplicate.

Yield of lactulose palmitate monoester synthesis depended on the solvent used as reaction medium (Figure 1), acetone

DOI: 10.1021/jf505222x
J. Agric. Food Chem. 2015, 63, 3716−3724

Table 3. Experimental Design and Results (Experimental and Predicted) Obtained Using a 2^3 Factorial Design for the Optimization of Yield Lactulose Palmitate Monoester Synthesis Catalyzed by Lipase from *Pseudomonas stutzeri* (*Ps*L) and *Alcaligenes* sp. (*As*L) Immobilized in Porous Octyl-silica (OS) and Octyl-glyoxyl-silica (OGS), Using Acetone As Solvent[a]

		OGS-*Ps*L		OS-*Ps*L		OGS-*As*L		OS-*As*L	
T	*r*	*E* (%)	*M* (%)	*E* (%)	*M* (%)	*E* (%)	*M* (%)	*E* (%)	*M* (%)
47.0	3.00	39.6	39.7	50.1	49.4	14.4	11.0	16.5	18.5
47.0	1.00	36.1	36.2	41.7	41.0	20.6	20.5	14.5	13.1
50.5	2.00	36.2	36.0	41.8	42.5	14.4	16.6	16.5	18.5
38.5	2.00	16.4	17.5	18.6	20.1	6.40	6.40	12.5	13.6
30.0	1.00	14.5	14.6	4.10	3.50	6.22	8.35	4.10	6.80
38.5	2.00	16.4	17.5	19.1	20.1	6.20	6.40	13.6	13.6
38.5	3.40	37.4	37.2	44.4	45.1	4.60	7.60	13.6	13.6
30.0	3.00	10.0	10.2	4.80	4.20	6.00	4.80	4.10	7.30
38.5	0.60	14.8	14.6	6.60	7.30	18.6	16.7	27.1	25.8
38.5	2.00	19.6	17.5	21.0	20.1	6.40	6.40	14.0	13.6
26.5	2.00	13.1	12.9	2.50	3.20	4.60	3.60	2.20	1.60

[a] *T*, temperature (°C); *r*, lactulose:palmitic acid molar ratio; *E*, experimental data; *M*, value predicted by model.

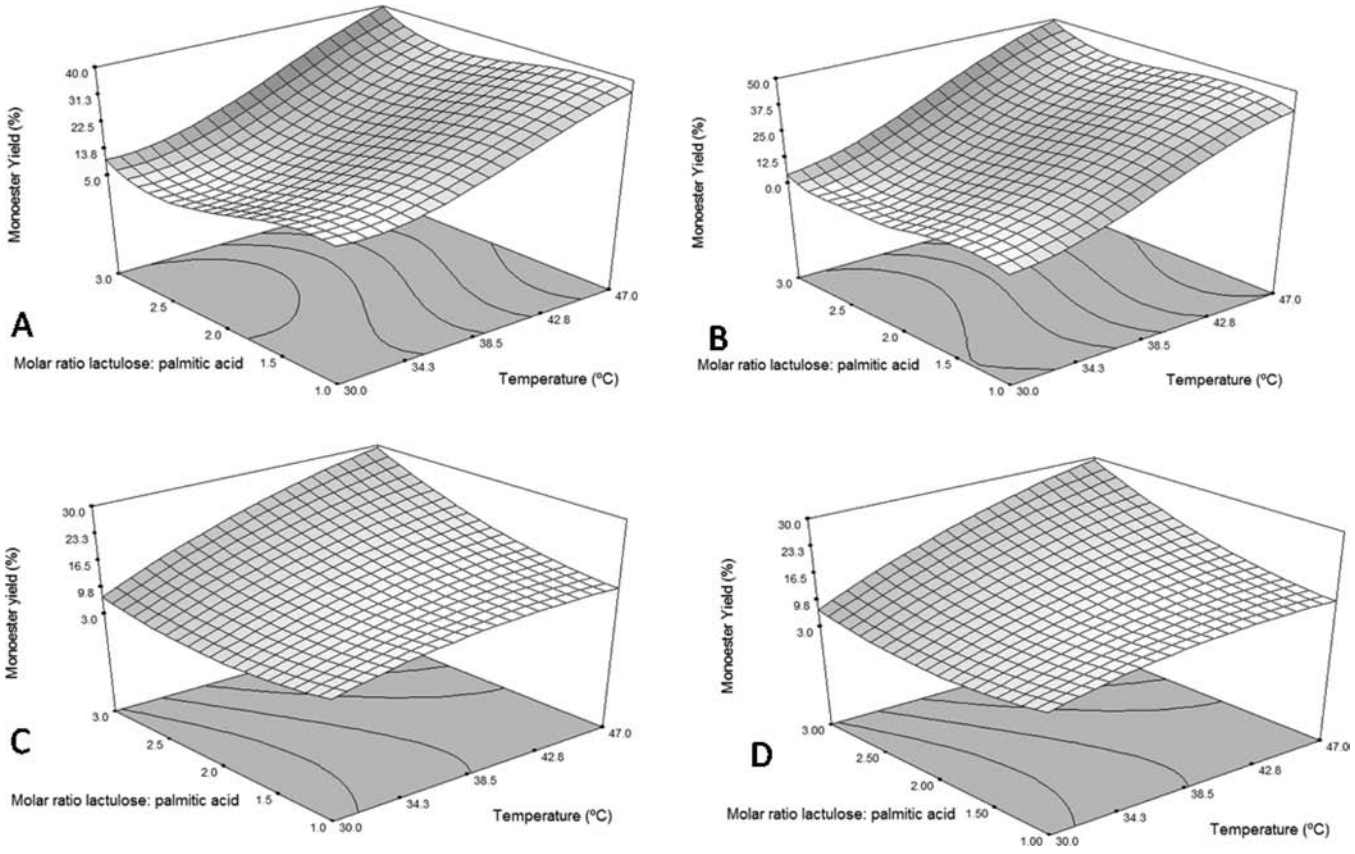

Figure 2. Response surface and contour graphics for the effect of temperature and lactulose:palmitic acid molar ratio on lactulose palmitate monoester yield with lipase from *Pseudomonas stutzeri* (*Ps*L) and from *Alcaligenes* sp. (*As*L) immobilized in porous octyl-silica (OS) and octyl-glyoxyl-silica (OGS), using acetone as solvent. (A) OGS-*Ps*L, (B) OS-*Ps*L, (C) OGS-*As*L, (D) OS-*As*L.

being the best solvent in all cases, probably because the balance between high polarity and low viscosity (Table 1) favors the persistence of the essential water layer around the active site of the lipase, the solubility of lactulose and the diffusion of substrates and products into and out of the biocatalyst. In propylene carbonate, the monoester yield was the second highest obtained, possibly because its viscosity is seven times higher than acetone, which reduces the diffusion rates of substrates and products. On the other hand, the reaction of palmitic acid to lactulose palmitate monoester is so slow when *t*-BuOH and Me−THF are used, probably because these solvents have high dielectric constants, similar to water (Table S1, Supporting Information), which favors hydrolysis[22,23] while slowing down esterification (Figure 1).

Effect of Reactions Conditions on Lactulose Palmitate Monoester Yield. Considering the results of monoester yield (Figure 1), the experimental design was done only with acetone and propylene carbonate according to the variables specified in Table 1.

DOI: 10.1021/jf505222x
J. Agric. Food Chem. 2015, 63, 3716−3724

Table 4. Experimental Design and Results (Experimental and Predicted) Obtained Using a 2^3 Factorial Design for the Synthesis Optimization of Lactulose Palmitate Monoester Synthesis Catalyzed by Lipase from *Pseudomonas stutzeri* and *Alcaligenes* sp. Immobilized in Porous Octyl-silica (OS) and Octyl-glyoxyl-silica (OGS), Using Propylene Carbonate As Solvent[a]

		OGS-*Ps*L		OS-*Ps*L		OGS-*As*L		OS-*As*L	
T	r	E (%)	M (%)	E (%)	M (%)	E (%)	M (%)	E (%)	M (%)
30.0	1.00	0.39	0.34	3.83	3.43	2.20	1.86	3.14	2.61
50.0	1.00	2.00	2.18	5.07	4.95	3.23	3.29	5.75	5.36
30.0	3.00	2.25	1.94	4.86	4.26	2.70	2.69	3.63	3.06
50.0	3.00	1.50	1.41	6.12	5.80	5.33	5.72	5.90	5.47
26.5	2.00	0.60	0.82	2.84	3.40	1.00	1.26	2.84	3.42
54.0	2.00	1.83	1.74	5.40	5.56	4.73	4.42	6.68	7.07
40.0	0.60	1.48	1.36	3.92	4.15	2.57	2.78	2.35	2.81
40.0	3.40	1.70	1.95	4.83	5.33	5.33	5.08	2.70	3.21
40.0	2.00	2.32	2.25	5.54	5.76	4.06	4.15	4.25	4.03
40.0	2.00	2.13	2.25	5.80	5.76	4.33	4.15	3.60	4.03
40.0	2.00	2.25	2.25	5.83	5.76	4.28	4.15	4.11	4.03

[a] T, temperature (°C); r, lactulose:palmitic acid molar ratio; E, experimental data; M, value predicted by model.

The evaluation of interactions between temperature and substrates molar ratio indicates that lipase from *P. stuzeri* exhibited a similar dependence on these variables, independently from the support used for its immobilization, when the esterification reaction is carried out in acetone. Values of monoester yield obtained are presented in Table 3. The adjustment of data with ANOVA analysis, using the Design-Expert 6.0.8 software, shows that they can be properly modeled by a third-order polynomial in the case of monoester yield (R^2: 0.9945 and 0.9968 for OGS-*Ps*L and OS-*Ps*L, respectively) Some terms were eliminated from the model because its statistical interaction could be irrelevant according to the p-value (T^2r and r^2T), allowing obtaining of the polynomial equations that model the reaction behavior (eqs 5−6):

OGS-*Ps*L in acetone

$$Y(\%) = 425.9T + 64.7r + 0.9T^2 - 45.3r^2 + 0.2Tr - 7.5 \times 10^{-3}T^3 + 8.2r^3 \quad (5)$$

OS-*Ps*L in acetone

$$Y(\%) = 515.6T + 103.7r + 1.3T^2 - 63.6r^2 + 0.2Tr - 0.01T^3 + 11.1r^3 \quad (6)$$

where Y is the monoester yield, r is the lactulose:palmitic acid molar ratio, and T is the temperature.

Data optimization using response surface methodology allowed obtaining of the conditions that maximized monoester yield, as presented in Figure 2 for all biocatalysts.[24,25] The graphical analysis indicates that yield is positively affected by temperature and molar ratio. These models predict that the highest values of monoester yield are obtained for both *Ps*L biocatalysts when the reaction is carried out at 47 °C and lactulose:palmitic acid molar ratio of 1:3, with predicted values of 39.7% and 49.4% for OGS-*Ps*L and OS-*Ps*L, respectively.

Biocatalysts obtained with lipases from *Alcaligenes* sp. exhibited a similar trend for yield, independently of the immobilization support, but those from *P. stutzeri* showed a different behavior when the reaction was carried out in acetone (Figure 2). In the latter case, the monoester yield was adjusted to a second-order polynomial (R^2: 0.9044 and 0.9447 for OGS-*As*L and OS-*Ps*L, respectively). Experimental and predicted data are shown in Table 3. The model equations obtained by ANOVA analysis for the behavior of biocatalyst of lipase from *Alcaligenes* sp. are presented below (eqs 7−8).

OGS-*As*L in acetone

$$Y(\%) = 28.5 - 1.1T - 8.3r + 0.04T^2 + 2.9r^2 - 0.18Tr \quad (7)$$

OS-*Ps*L in acetone

$$Y(\%) = -30.8 + 2.6T - 26.4r - 0.04T^2 + 3.2r^2 + 0.5Tr \quad (8)$$

where Y is the monoester yield, r is the lactulose:palmitic acid molar ratio, and T is the temperature.

In the case of OS-*As*L, the best reaction conditions were similar to those found with OGS-*Ps*L and OS-*Ps*L: 47 °C and molar ratio of substrate 1:3, although a lower value of yield was obtained (Y = 29.5%). In the case of OGS-*As*L, best reaction conditions were 47 °C and a molar ratio of substrate 1:1, at which 20.4% yield was obtained. Differences obtained among biocatalyst can be attributed to the fact that the lipase from *Alcaligenes* sp. is less sensitive to changes in its 3D structure caused by the immobilization by adsorption into hydrophobic surface because this lipase, different from the one from *P. stutzeri*, has only one lid.[26,27] The values are consistent with the response surface for every biocatalyst (Figure 2), showing that the maximum values are unique in both cases.

When propylene carbonate was used as solvent, the monoester yield trend obtained with both biocatalysts could be properly modeled by a second-order polynomial (eqs 10−12) that according to ANOVA analysis represent a good statistical adjustment between predicted and experimental values, as shown in Table 4.

OGS-*Ps*L in propylene carbonate

$$Y(\%) = -13.20 + 0.54T + 3.77r - 4.88 \times 10^{-3}T^2 - 0.38r^2 - 0.06Tr \quad R^2 = 0.938 \quad (9)$$

OS-*Ps*L in propylene carbonate

$$Y(\%) = -10.37 + 0.59T + 2.44r - 6.39 \times 10^{-3}T^2 - 0.51r^2 - 4.11 \times 10^{-4}Tr \quad R^2 = 0.867 \quad (10)$$

OGS-AsL in propylene carbonate

DOI: 10.1021/jf505222x
J. Agric. Food Chem. 2015, 63, 3716−3724

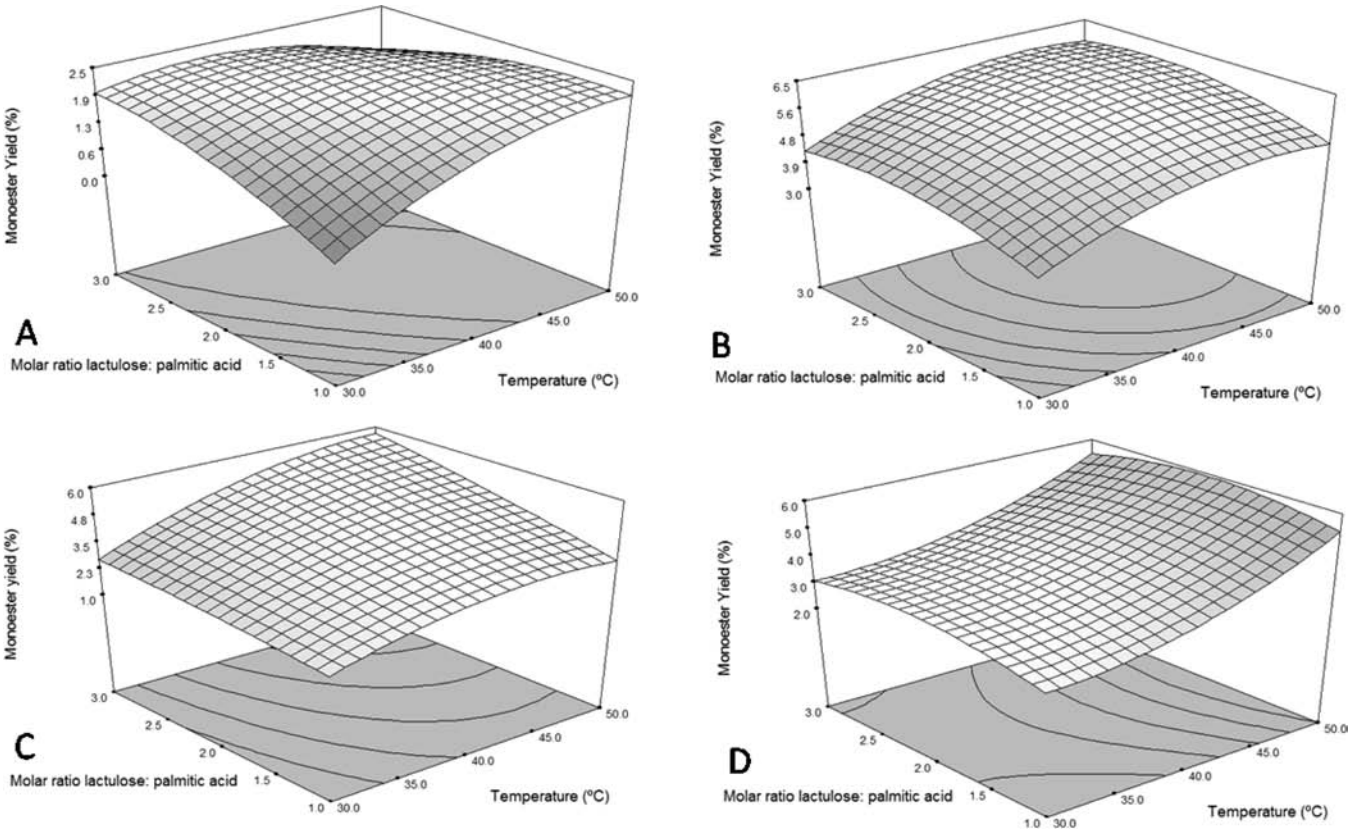

Figure 3. Response surface and contour graphics for the effect of temperature and lactulose:palmitic acid molar ratio on lactulose palmitate monoester yield with lipase from *Pseudomonas stutzeri* (*Ps*L) and from *Alcaligenes* sp. (*As*L) immobilized in porous octyl-silica (OS) and octyl-glyoxyl-silica (OGS), using propylene carbonate as solvent. (A) OGS-*Ps*L, (B) OS-*Ps*L, (C) OGS-*As*L, (D) OS-*As*L.

Table 5. Monoester Yield (Y) and Specific Productivity (P) Obtained in the Synthesis under Optimum Conditions of Lactulose Palmitate Monoester, With Lipases from *Pseudomonas stutzeri* (*Ps*L) and *Alcaligenes* sp. (*As*L) Immobilized in Porous Octyl-silica (OS) and Octyl-glyoxyl-silica (OGS)[a]

	acetone					propylene carbonate				
biocatalyst	T (°C)	r	Y (%)	P	E_y (%)	T °C	A:B	Y (%)	P	E_y (%)
OGS-*Ps*L	47.0	1:3	38.3	0.06	3.50	44.0	1:2.0	2.20	0.004	4.40
OS-*Ps*L	47.0	1:3	48.3	0.08	2.30	46.0	1:2.4	5.80	0.01	4.90
OGS-*As*L	47.0	1:1	20.7	0.04	1.50	37.8	1:3.0	4.40	0.007	6.40
OS-*As*L	47.0	1:3	30.9	0.05	3.30	50.0	1:2.0	5.60	0.01	5.10

[a] r, lactulose:palmitic acid molar ratio; P, specific productivity (g day^{-1} g catalyst^{-1}); E_y, yield error.

$$Y(\%) = -9.64 + 0.55T - 0.34r - 6.53 \times 10^{-3}T^2 - 0.11r^2 + 0.04Tr \quad R^2 = 0.967 \tag{11}$$

OGS-AsL in propylene carbonate

$$Y(\%) = 5.60 - 0.34T + 2.52r + 6.09 \times 10^{-3}T^2 - 0.51r - 8.57 \times 10^{-3}Tr \quad R^2 = 0.884 \tag{12}$$

where Y is the monoester yield, r is the lactulose:palmitic acid molar ratio, and T is the temperature.

Figure 3 shows the response surfaces for the yield of all biocatalysts during palmitate lactulose synthesis using propylene carbonate. In this case, a different response surface was obtained for each biocatalyst, indicating that the high viscosity of propylene carbonate (Table S1, Supporting Information) produced a more significant effect on the catalytic behavior of the immobilized lipases due to the extra stiffness in the 3D structure when they were immobilized into OGS support. This is reflected by the fact that the type of solvent and the reaction conditions (temperature and substrates molar ratio) at which the highest yield was obtained are different for each biocatalyst (Table 5); however, they were similar when lipases were immobilized in OS, which does not occur when acetone is used as reaction medium, showing the strong effect of the high viscosity of propylene carbonate in *P. stutzeri* lipase activity reducing the yield obtained with this enzyme more strongly than with the enzyme from *Alcaligenes* sp. In the same way, the yield was the lowest when the reaction was catalyzed by OGS-PsL and lower in propylene carbonate than in acetone, also showing the marked effect of viscosity on the performance of this lipase (Table 5).

Considering the results obtained at optimum conditions (Table 5), the effect of reaction time and biocatalyst to substrate mass ratio were evaluated. When the reaction time was decreased to one-half (down to 24 h), and the biocatalyst dose was doubled (up to 200 IU per gram of palmitic acid),

DOI: 10.1021/jf505222x
J. Agric. Food Chem. 2015, 63, 3716−3724

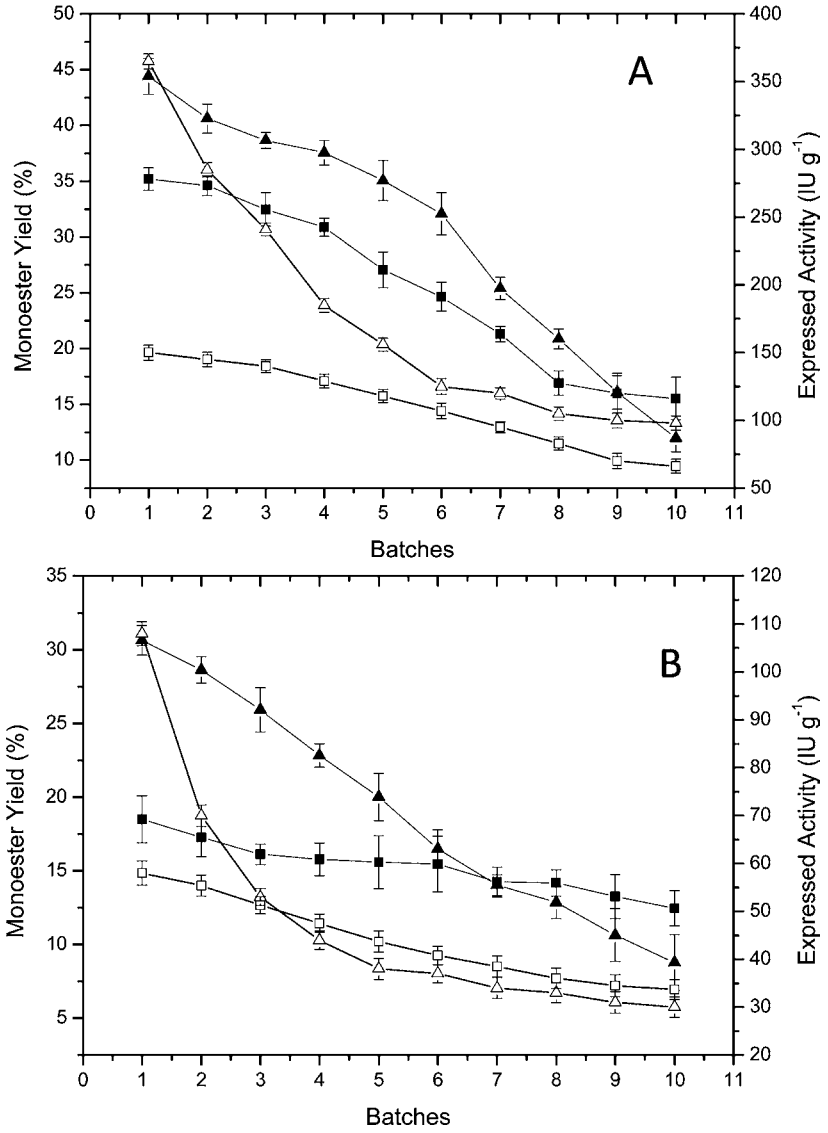

Figure 4. Monoester yield (filled symbols) and hydrolytic expressed activity (empty symbols) during reaction with lipase from *Pseudomonas stutzeri* (A) and from *Alcaligenes* sp. (B) immobilized in octyl-silica (OS) (triangles) and in octyl-glyoxyl-silica (OGS) (squares) in successive batch operation (24 h of operation in each batch) in the synthesis of lactulose palmitate monoester under optimal conditions. Experiments were carried out in triplicate.

similar monoester yields and specific productivities were obtained than those achieved in the experimental design, showing that the performance of the biocatalyst is determined by the enzyme dose and the reaction time, as expected. Differences in the values of yield and productivity between both conditions were lower than 5% (data not shown).

Operating Performance in Successive Batches. Considering the lactulose palmitate monoester yields obtained with all biocatalyst in acetone and propylene carbonate, the biocatalyst reuse was tested in successive 24 h batch operation, using acetone as reaction medium at the optimum reactions conditions (Table 5) with 200 IU per gram of palmitic acid. Yield and cumulative productivity of palmitate monoester synthesis obtained are presented in Figures 4 and 5. After 10 successive batches, monoester yields obtained with all lipase biocatalysts from *P. stutzeri* progressively decreased with each batch. (Figure 4A); however, in the last evaluated batch, the relative hydrolytic activity of OGS-*Ps*L biocatalyst remained higher than the one of OS-*Ps*L in the same batch (44.1% and 26.9% with respect to the initial batch, Figure 4A). On the other hand, lipase from *Alcaligenes* sp. exhibited a different behavior, showing similar values for monoester yield after each batch when immobilized in OGS support (Figure 4B), probably because in this case the additional stiffness provided by covalent bonding to the support precluded its inactivation; the opposite happened when this lipase was immobilized only by adsorption in OS support (67.4% and 28.6% respect to initial, OGS-*As*L and OS-*As*L, respectively, Figure 4B). This behavior was the expected for the lipases immobilized in two steps: adsorption by the hydrophobic pocket and then covalent bond formation with the lysine residues near to the active pocket.[13]

Evaluation of specific productivity in successive batches showed a similar trend regardless of the lipase (Figures 5). In this case, the biocatalysts obtained with octyl silica had a better behavior batch after batch, generating a higher increase in the cumulative productivity in comparison with the biocatalyst obtained with glyoxyl-octyl silica. This behavior can be explained considering the initial hydrolytic activity because

DOI: 10.1021/jf505222x
J. Agric. Food Chem. 2015, 63, 3716−3724

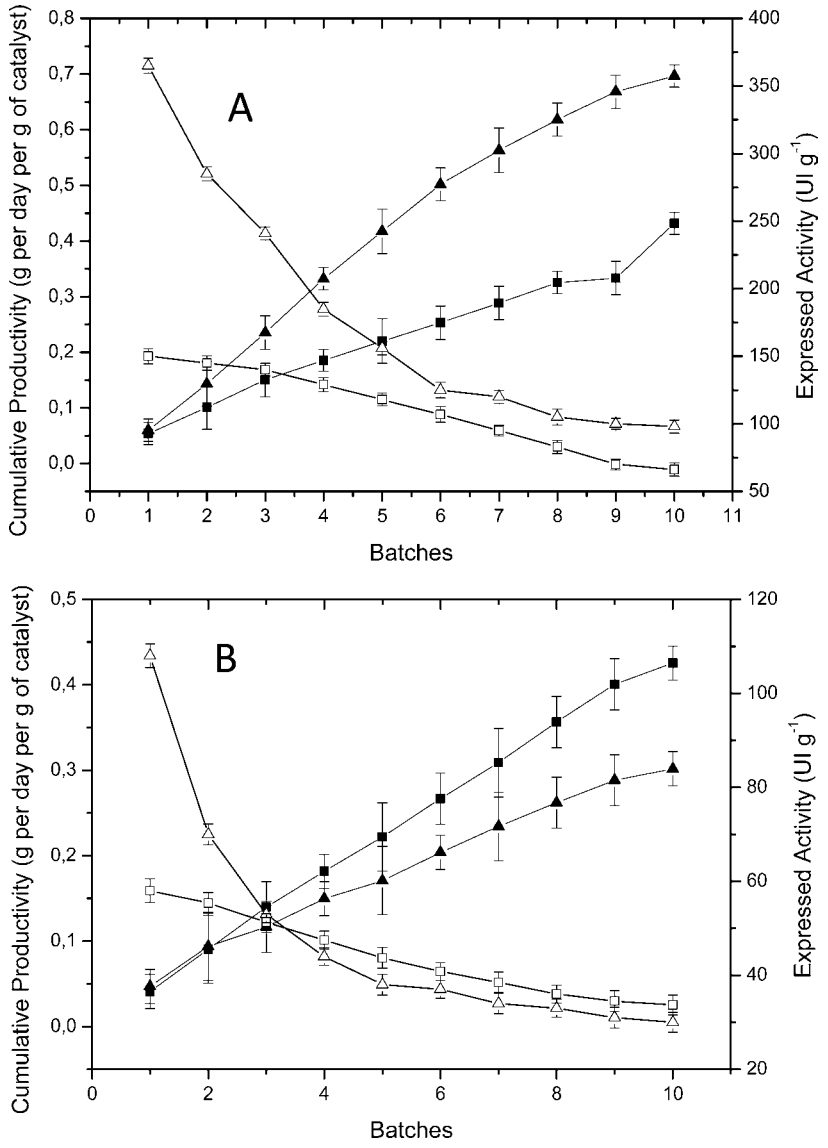

Figure 5. Cumulative productivity (filled symbols) and hydrolytic expressed activity (empty symbols) during reaction with lipase from *Pseudomonas stutzeri* (A) and from *Alcaligenes* sp. (B) immobilized in octyl-silica (OS) (triangles) and in octyl-glyoxyl-silica (OGS) (squares) in successive batch operation (24 h of operation in each batch) in the synthesis of lactulose palmitate monoester under optimal conditions. Experiments were carried out in triplicate.

biocatalysts immobilized by adsorption expressed a higher activity (OS-*Ps*L and OS-*As*L), making the increase in productivity faster than in the case of OGS-*As*L and OGS-*Ps*L (Figures 5). However, it was expected that the cumulative productivity of OGS-*As*L biocatalyst will be higher than OS-*As*L after many batches because in this case the operational stability was significantly higher that the OS-*As*L (Figure 5B).

Lipases from *Alcaligenes* sp. and *P. stutzeri* immobilized in silica with different functional groups were used for the synthesis of lactulose palmitate monoester with very good yields and specific productivities. Solvents, temperature, and substrates molar ratio influenced the biocatalyst performance, best results being obtained with both lipases when acetone was used as solvent.

Enzymatic immobilization influenced also the monoester yields and productivities obtained with each biocatalyst, showing that covalent immobilization into glyoxyl-octyl silica could produce a fairly active and robust biocatalyst able to be reused several times.

■ ASSOCIATED CONTENT

Ⓢ Supporting Information

Physicochemical properties of organic solvents. This material is available free of charge via the Internet at http://pubs.acs.org.

■ AUTHOR INFORMATION

Corresponding Author

*Phone: +56 322372025. Fax: +56 322273803. E-mail: claberz@gmail.com, /claudia.berna@ucv.cl.

Funding

Work financed and postdoctoral fellowship by Chilean Fondecyt grant 3130321.

Notes

The authors declare no competing financial interest.

■ ACKNOWLEDGMENTS

Generous donation of lipases from *Pseudomonas stutzeri* and *Alcaligenes* sp. from MEITO-SANGYO. Ltd. is acknowledged.

DOI: 10.1021/jf505222x
J. Agric. Food Chem. 2015, 63, 3716−3724

REFERENCES

(1) Nitschke, M.; Costa, S.G.V.A.O. Biosurfactants in food industry. *Trends Food Sci. Technol.* **2007**, *18*, 252−259.

(2) Garti, N.; Clement, V.; Fanun, M.; Leser, M. E. Some characteristics of sugar ester nonionic microemulsions in view of possible food applications. *J. Agric. Food Chem.* **2000**, *48*, 3945−3956.

(3) Chortyk, O. T.; Kays, S. J.; Teng, Q. Characterization of insecticidal sugar esters of Petunia. *J. Agric. Food Chem.* **1997**, *45*, 270−275.

(4) Queneau, Y.; Chambert, S.; Besset, C.; Cheaib, R. Recent progress in the synthesis of carbohydrate-based amphiphilic materials: the examples of sucrose and isomaltulose. *Carbohydr. Res.* **2008**, *343*, 1999−2009.

(5) Plou, F. J.; Cruces, M. A.; Ferrer, M.; Fuentes, G.; Pastor, E.; Bernabé, M.; Christensen, M.; Comelles, F.; Parra, J. L.; Ballesteros, A. Enzymatic acylation of di- and trisaccharides with fatty acids: choosing the appropriate enzyme, support and solvent. *J. Biotechnol.* **2002**, *96*, 55−66.

(6) Ferrer, M.; Soliveri, J.; Plou, J. M.; López-Cortés, N.; Reyes-Duarte, D.; Christensen, M.; Copa-Patiño, J. L.; Ballesteros, A. Synthesis of sugar esters in solvent mixtures by lipases from *Thermomyces lanuginosus* and *Candida antarctica* B and their antimicrobial properties. *Enzyme Microb. Technol.* **2005**, *36*, 391−398.

(7) Adlercreutz, P. Immobilisation and application of lipases in organic media. *Chem. Soc. Rev.* **2013**, *42*, 6406−6436.

(8) Blanco, R. M.; Terreros, P.; Fernandez-Perez, M.; Otero, C.; Diaz-Gonzalez, G. Functionalization of mesoporous silica for lipase immobilization: characterization of the support and the catalysts. *J. Mol. Catal. B: Enzym.* **2004**, *30*, 83−93.

(9) Karmee, S. K. Lipase catalyzed synthesis of ester-based surfactants from biomass derivatives. *Biofuels, Bioprod. Biorefin.* **2008**, *2*, 144−154.

(10) Adachi, S.; Kobayashi, T. Synthesis of esters by immobilized-lipase-catalyzed condensation reaction of sugars and fatty acids in water-miscible organic solvent. *J. Biosci Bioeng.* **2005**, *99*, 87−94.

(11) Walsh, M. K.; Bombyk, R. A.; Wagh, A.; Bingham, A.; Berreau, L. M. Synthesis of lactose monolaurate as influenced by various lipases and solvents. *J. Mol. Catal. B: Enzym.* **2009**, *60*, 171−177.

(12) Zaidan, U. H.; Rahman, M. B. A.; Othman, S. S.; Basri, M.; Abdulmalek, E.; Zaliha, R. N.; Rahman, R. A.; Salleh, A. B. Biocatalytic production of lactose ester catalysed by mica-based immobilised lipase. *Food Chem.* **2012**, *131*, 199−205.

(13) Bernal, C.; Illanes, A.; Wilson, L. Heterofunctional hydrophilic−hydrophobic porous silica as support for multipoint covalent immobilization of lipases: application to lactulose palmitate synthesis. *Langmuir* **2014**, *30*, 3557−3566.

(14) Wang, X.; Miao, S.; Wang, P.; Zhang, S. Highly efficient synthesis of sucrose monolaurate by alkaline protease Protex 6. *Bioresour. Technol.* **2012**, *109*, 7−12.

(15) Ye, R.; Hayes, D. G. Lipase-catalyzed synthesis of saccharide−fatty acid esters utilizing solvent-free suspensions: effect of acyl donors and acceptors, and enzyme activity retention. *J. Am. Oil Chem. Soc.* **2012**, *89*, 455−463.

(16) Chansanroj, K.; Betz, G. Sucrose esters with various hydrophilic−lipophilic properties: novel controlled release agents for oral drug delivery matrix tablets prepared by direct compaction. *Acta Biomater.* **2010**, *6*, 3101−3109.

(17) Aït-Aissa, A.; Aïder, M. Lactulose: production and use in functional food, medical and pharmaceutical applications. Practical and critical review. *Int. J. Food Sci. Technol.* **2014**, *49*, 1245−1253.

(18) Bernal, C.; Sierra, L.; Mesa, M. Improvement of thermal stability of β-galactosidase from *Bacillus circulans* by multipoint covalent immobilization in hierarchical macro-mesoporous silica. *J. Mol. Catal. B: Enzym.* **2012**, *84*, 166−172.

(19) Bernal, C.; Urrutia, P.; Illanes, A.; Wilson, L. Hierarchical meso-macroporous silica grafted with glyoxyl groups: opportunities for covalent immobilization of enzymes. *New Biotechnol.* **2013**, *30*, 500−506.

(20) Kamal, Z.; Yedavalli, P.; Deshmukh, M. V.; Rao, N. M. Lipase in aqueous-polar organic solvents: activity, structure, and stability. *Protein Sci.* **2013**, *22*, 904−915.

(21) Chang, S. W.; Shaw, J. F. Biocatalysis for the production of carbohydrate esters. *New Biotechnol.* **2009**, *26*, 109−116.

(22) Ou, G.; He, B.; Yuan, Y. Lipases are soluble and active in glycerol carbonate as a novel biosolvent. *Enzyme Microb Technol.* **2011**, *49*, 167−170.

(23) Izutsu, K.. *Electrochemistry in Nonaqueous Solutions*. Wiley-VCH: Weinheim, Germany, 2009; pp 1−83.

(24) Zhong, X.; Qian, J.; Liu, M.; Ma, L. *Candida rugosa* lipase-catalyzed synthesis of sucrose-6-acetate in a 2-butanol/buffer two-phase system. *Eng. Life Sci.* **2013**, *13*, 563−571.

(25) Galonde, N.; Brostaux, Y.; Richard, G.; Nott, K.; Jerôme, C.; Fauconnier, M.-L. Use of response surface methodology for the optimization of the lipase-catalyzed synthesis of mannosyl myristate in pure ionic liquid. *Process Biochem.* **2013**, *48*, 1914−1920.

(26) Chen, H.; Wu, J.; Yang, L.; Xu, G. Characterization and structure basis of *Pseudomonas alcaligenes* lipase's enantiopreference towards d,l-menthyl propionate. *J. Mol. Catal. B: Enzym.* **2014**, *102*, 81−87.

(27) Maraite, A.; Hoyos, P.; Carballeira, J. D.; Cabrera, A. C.; Ansorge-Schumacher, M. B.; Alcántara, A. R. Lipase from *Pseudomonas stutzeri*: Purification, homology modelling and rational explanation of the substrate binding mode. *J. Mol. Catal. B: Enzym.* **2013**, *87*, 88−98.

DOI: 10.1021/jf505222x
J. Agric. Food Chem. 2015, 63, 3716−3724

AF from *Streptomyces chartreusis* GS901 demonstrated slight reacting with this substrate.[2,18] In contrast, AbfD3 from *Thermobacillus xylanilyticus*, also a member of GH 51, was found to be extremely active on arabinoxylan.[19] Accordingly, it is difficult to find regularity in the substrate specificity of AFs. Consequently, the definition of substrate specificity of certain AFs needs amount of experimental attempts; however, this is cost- and labor-intensive.

Structure understanding and theoretical computation are popular assisting means in the research of various enzymes, including analysis of substrate specificity, rational design of stable protein, and mutation prediction on proteins.[20,21] For example, the programs like PREDIKIN and CaSPredictor were especially written for the prediction of substrate specificity in protein serine/threonine kinases, cytochrome P450, and caspases, achieving medium to good performances.[22−24] In the absence of computational tools, substantial and reliable crystal structures of substrate−enzyme complex were utilized with no hesitation for substrate-specificity analysis with the assist of the automated protocols like SOLVE, ARP/wARP, and REFMAC.[25] In the situation no experimental resulted structure is feasible; the closely related structure can be relied on for molecular modeling of the enzyme under study. And substrate specificity can also be analyzed according to the information obtained from ligand docking through software like Autodock.

We found some AF genes from different strains including *Celf_3321*, "AF domain-containing protein" from *Cellulomonas fimi* ATCC 484, by gene mining on the NCBI Web site (http://www.ncbi.nlm.nih.gov/). In this paper, we described the cloning and expression of this gene in *Escherichia coli* (*E. coli*), termed as *abfCelf*. The expressed enzyme AbfCelf displayed a relatively higher AF activity among the mined AFs. Then, AbfCelf was characterized, and the catalytic activities toward different substrates were determined after purification due to that the substrate specificity of GH 51 AFs was different. In case of no ready-made professional computational tools and crystal structure are available for AbfCelf, structure and mechanism based methods were applied to analyze substrate specificity to the greatest extent. The structure of AbfCelf was built by automated protein structure homology modeling from the Swiss Model server (http://swissmodel.expasy.org/). Substrates bind with the structure of AbfCelf by using Autodock 4.2, and supplementary analysis was conducted by using the discovery studio 4.0. The experimental results were compared with docking values, which helped to analyze substrate specificity of AbfCelf.

MATERIALS AND METHODS

Chemicals and Reagents. Substrates 4-nitrophenyl-α-L-arabinofuranoside (PNP-Abf), PNP-α-D-xylopyranoside, PNP-β-D-xylopyranoside, L-(+)-arabinose, and xylan (from beechwood) were purchased from Sigma-Aldrich Co., Ltd. (St. Louis, MO, U.S.A.). Sugar beet linear 1,5-α-arabinan, sugar beet red debranched arabinan, wheat flour arabinoxylan (medium viscosity), larch arabinogalactan, arabinan (sugar beet), arabinobiose, arabinotriose, and arabinotetraose were obtained from Megazyme International Ireland Co., Ltd. (Wicklow, Ireland). Gum arabic power and soluble starch were from Shanghai Hushi Co., Ltd. (Shanghai, China). Genomic DNA extraction kits, plasmid extraction kits, gel extraction kits, and Ni−Sepharose resin were purchased from Tiangen Biotech Co., Ltd. (Beijing, China). All other molecular cloning reagents were from Takara Biotechnology Co., Ltd. (Dalian, China). Other chemicals used in this study were of analytical grade or higher.

Strain, Media, and Plasmids. The strain used in this study, *C. fimi* ATCC 484, was obtained from own preservation, which was subcultured from a stock culture (50% glycerol) made from the original isolate. *E. coli* DH5α, *E. coli* BL21 (DE3), and the plasmid pET28a (+) were used for cloning and expression. Transformants were grown in Luria−Bertani (LB) medium (1% peptone, 1% NaCl, and 0.5% yeast extract) with 100 μg/mL kanamycin.

Sequence Analysis. Multiple nucleotide sequence alignment of gene *abfCelf* was performed with the DNAMAN program. The molecular weight and pI were predicted by using the Compute pI/Mw tool on the ExPASy Bioformatics Resources Portal (http://web.expasy.org/compute_pi/).

Cloning, Expression, and AbfCelf Purification. The coding sequence of *abfCelf* was amplified by polymerase chain reaction (PCR) with the following forward and reverse primers: forward primer for *abfCelf*, 5′-TTTGGATCCCCTCAGCGCGCCACCGT-3′; reverse primer for *abfCelf*, 5′-TTTGAATTCGCGGGTCAGGGTCGCCG-3′. The products of PCR reaction were cloned in the plasmid pET28a (+) containing both C- and N-terminal His_6-tags for purification of AbfCelf.

The recombinant plasmid was transformed into *E. coli* BL21 (DE3) and grown on solid LB medium. The transformation of *E. coli* strains was performed as described previously.[26]

The target protein was purified by using Ni−Sepharose through eluting with imidazole in a linear gradient from 10 to 500 mM. The active fractions were identified by 12.5% sodium dodecyl sulfate polyacrylamide gel electrophoresis (SDS−PAGE). Then, imidazole was ultrafiltered by using a 15 mL 10 kDa Millipore's Amicon Ultra-15 centrifugal filter device (Millipore, MA, U.S.A.). The concentrated active fractions were stored in 100 mM phosphate buffer (pH 7.0) containing 10% glycerol in several aliquots at −20 °C. One aliquot was used for enzyme activity verification as described in the following section.

AF Assay and Protein Measurement. The reaction system for AF activity determination consisted of 30 μL of PNP-Abf (7 mM) in 205 μL of sodium acetate buffer. An amount of 15 μL of diluted enzyme sample (10−50 dilution volume by 100 mM phosphate buffer according to the enzyme protein concentration) was incubated at 40 °C for 15 min, then the reaction was stopped by adding 850 μL of 1 M Na_2CO_3. Finally, absorbance at 405 nm was read by using a UV-1200 spectrophotometer (MAPADA, Shanghai, China). One unit of AF activity was defined as the amount of enzyme that liberates 1 μmol of 4-nitrophenol (PNP) per min in the reaction mixture under these assay conditions. The protein content was determined using Bradford reagent with bovine serum albumin (BSA) as standard. Standard curves of PNP and BSA are shown in Figure S1 in the Supporting Information. The molecular mass of the enzyme AbfCelf was determined by SDS−PAGE on a 12.5% polyacrylamide gel. Proteins were visualized by staining with the Coomassie brilliant blue R 250. All assays were performed in triplicate batches, and the results are presented as means ± standard deviation (SD).

Enzymatic Properties. The optimum pH was determined by detecting the enzyme activities in sodium acetate buffer (pH 4.0−6.0), sodium phosphate buffer (pH 6.0−8.0), and Tris−HCl buffer (pH 8.0−9.0) at 40 °C for 15 min. The optimum temperature was determined by measuring the enzyme activities of reactions incubated at temperatures ranging from 5 to 70 °C in 100 mM sodium acetate buffers (pH 6.0) for 15 min. To estimate pH stability, the enzyme was incubated in buffers ranging from pH 4.0 to 8.0 at 40 °C for various periods. And for temperature stability, the enzyme was incubated in 100 mM sodium acetate buffers (pH 6.0) at temperatures ranging from 40 to 60 °C for various phases. Then, the residual enzyme activity was measured under optimum condition.

The kinetic parameters, apparent K_m, and V_{max} values were determined through the Lineweaver−Burk plot method under optimum condition by using PNP-Abf at concentrations ranging from 0.02 to 2 mM for 5 min of reaction.[27]

Substrate Specificity. Substrate specificity was estimated with different synthetic PNP-glycosides, oligosaccharides, and polysacchar-

DOI: 10.1021/jf5059683
J. Agric. Food Chem. 2015, 63, 3725−3733

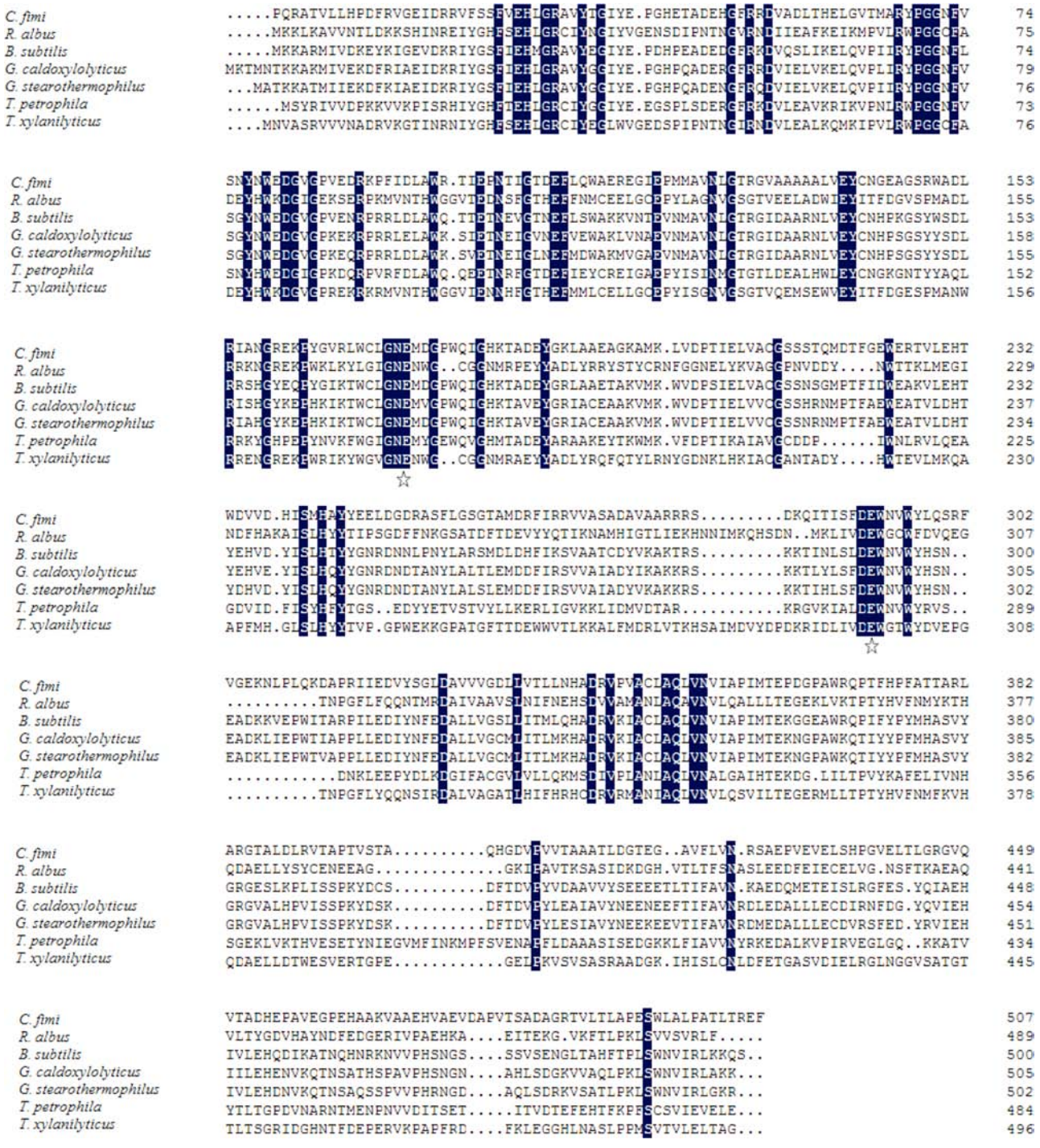

Figure 1. Multiple sequence alignment of AbfCelf with some GH 51 AFs. AbfCelf was compared with AFs from *R. albus* 8 (AEE64774), *B. subtilis* 168T$^+$ (CAA99595), *G. caldoxylolyticus* TK4 (ABI34800), *G. stearothermophilus* T-6 (AAD45520.2), *T. petrophila* RKU-1(ABQ46651), and *T. xylanilyticus* T3 (CAA76421). The catalytic residues are marked with asterisks. Residues that are identical in all sequences are shaded in blue.

ides. PNP-α-D-xylopyranoside and PNP-β-D-xylopyranoside were used as substrates with the method similar to AF assay.

For nonchromogenic substrates, the hydrolysis products were determined by high-performance anion-exchange chromatography (HPAEC) under the following conditions: system, Agilent 1100 series system (Agilent, CA, U.S.A.); column, Waters Sugar-pak1 column (300 mm × 6.5 mm; Waters, MA, U.S.A.); mobile phase, double-distilled deionized and degassed water; flow rate, 0.5 mL/min; column temperature, 80 °C. The eluted compounds were detected by refractive index. One unit of enzyme activity was defined as 1 μmol of L-arabinose produced per min. The nonchromogenic substrates included α-1,5-linked oligosaccharides, xylan from beechwood, linear 1,5-α-arabinan, wheat flour arabinoxylan, larch arabinogalactan, arabinan (sugar beet), gum arabic power, and starch soluble solutions. The substrate level was always 2% w/v.

Homology Modeling. The structure of AbfCelf was built by homology modeling from Swiss Model server with the crystal structure of AbfA from *Geobacillus stearothermophilus* T-6 (1QW9, http://www.rcsb.org/pdb/explore/explore.do?structureId=1QW9) as template. The structure, especially loops, was optimized for energy minimization by Modeler 9.12. Ramachandran plot (RC plot) analysis was used to validate the structure of AbfCelf by using PROCHECK.[28]

DOI: 10.1021/jf5059683
J. Agric. Food Chem. 2015, 63, 3725−3733

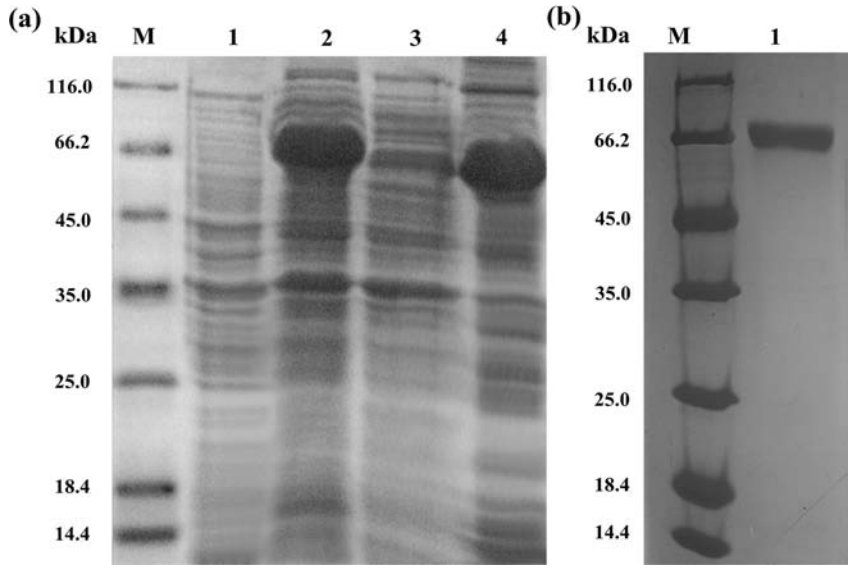

Figure 2. Expression and purification of AbfCelf. (a) Analysis of the protein expression (lanes: M, molecular marker; 1, crude cell lysate after cold osmotic shock of wild BL21; 2, crude cell lysate after cold osmotic shock; 3, soluble fraction of the crude cell lysate after cold osmotic shock; 4, insoluble fraction of the crude cell lysate after cold osmotic shock); (b) recombinant AbfCelf purified by Ni−Sepharose column.

Docking. Autodock 4.2 was selected as the docking tool to predict protein binding partners based on initial-stage flexible-body docking algorithm, according to the User's Guide.[29] The structure of AbfCelf was used as macromolecular receptor in the docking simulation. The structure of ligands was generated with Chemdraw software and the energy-minimized with ChemBio3D Ultra 11. The ligands were sugar molecules, including arabinobiose, arabinotriose, arabinotetraose, α-L-arabinofuranose, α-D-xylopyranose, β-D-xylopyranose, PNP-α-L-arabinofuranose, PNP-α-D-xylopyranose, and PNP-β-D-xylopyranose.

The amino acids of AbfCelf molecule which may form hydrogen bonds with ligands were selected as the flexible amino acid, and the grid box was selected as a certain radius, 40 Å, with the center coordinates of x, 68.676; y, 43.846; z, 75.444. The ligands were docked into AbfCelf with these parameters by using Autodock 4.2 with MGLTools. Binding energy (ΔG, kcal/mol) of Autodock, about ligand−receptor combination, was used as the final criterion to identify the best docking mode.

RESULTS

Sequence Analysis of *abfCelf*. The gene *abfCelf* (NC_015514) had an open reading frame of 1521 bp encoding a protein of 507 amino acids. The protein has a calculated molecular mass of 55.6 kDa and a calculated isoelectric point of 4.87.

AbfCelf was classified as a member of the GH 51 based on its protein sequence, which was also included in CAZy database (Carbohydrate Active enZYmes database, http://www.cazy.org). Moreover, the amino acid sequence of AbfCelf displayed 20.3%, 45.2%, 44.6%, 45.2%, 29.7%, and 22.7% identity with the sequences of AFs from *Ruminococcus albus* 8, *Bacillus subtilis* 168T$^+$, *G. caldoxylolyticus* TK4, *G. stearothermophilus* T-6, *Thermotoga petrophila* RKU-1, and *T. xylanilyticus* T3, respectively (Figure1). The sequence variation may be associated with loop regions and give rise to the diverse substrate-specificity characteristic.

The catalytic domain of AbfCelf comprised two key active sites, both Glu, which were conserved in all members of GH 51 family. On the basis of the results of sequence and structure alignment between AbfCelf and 1QW9, Glu^{173} is the acid/base, and Glu^{292} is the nucleophile.

Cloning, Expression, and AbfCelf Purification. The gene *abfCelf* was cloned and expressed in pET28a (+). Parts of the recombinant AbfCelf overexpressed in *E. coli* BL21 (DE3) were soluble and active (Figure 2a). The enzyme purified by Ni−Sepharose column is shown in Figure 2b, which indicated that the molecular weight of native protein after purification was about 66 kDa. The final preparation of purified AbfCelf was 0.19 mg/mL, and the specific activity measured under optimum condition was 19.4 U/mg.

Enzymatic Properties. The optimum reaction temperature of purified AbfCelf was at 40 °C (Figure 3a). AbfCelf could maintain most of the initial activity after incubation at 40 °C for 20 h while losing most activity mostly when incubated at 60 °C for 30 min (Figure 3b). AbfCelf reached the highest activity at pH 6.0, 40 °C in 100 mM sodium acetate buffer and achieved about 57.9% and 72.1% of the maximal activity at pH 5.0 and pH 7.0, respectively (Figure 3c). AbfCelf was stable at pH 6.0 compared with no activity remaining after 4 h of incubation at pH 4.0 (Figure 3d).

Kinetic parameters were measured at 40 °C, pH 6.0 for 5 min by the Lineweaver−Burk plot, which is shown in Figure S2 in the Supporting Information. The K_m, V_{max}, and k_{cat} toward PNP-Abf are 1.5 mM, 112.4 U/mg, and 123.6 s^{-1}, respectively. The K_m's of AbfD3 from *T. xylanilyticus*, ABF2 from *P. purpurogenum*, and AbfATK4 from *G. caldoxylolyticus* are 0.7 mM, 98.6 μM, and 0.17 mM, respectively.[16,18,19] The V_{max}'s of AF from *B. pumilus* PS213 and AbfD3 are 52.9 and 456 U/mg, respectively.[19,30] Compared with these reported GH 51 AFs, AbfCelf had an average kinetic value, indicating the affinity of AbfCelf toward PNP-Abf was in a medium level.

Substrate Specificity. The substrate specificity of the enzyme was tested by using several oligosaccharides, polysaccharides, heteropolysaccharide, and PNP-glycosides. Sugar beet arabinan, linear 1,5-α-arabinan, and wheat flour arabinoxylan were degraded by AbfCelf when the reaction time was prolonged to 2 h. In contrast, beechwood xylan, soluble starch, gum arabic, and larch arabinogalactan were resistant to the action of AbfCelf even though the enzyme was added in excess. Table 1 displays the specific activity of AbfCelf on different

DOI: 10.1021/jf5059683
J. Agric. Food Chem. 2015, 63, 3725−3733

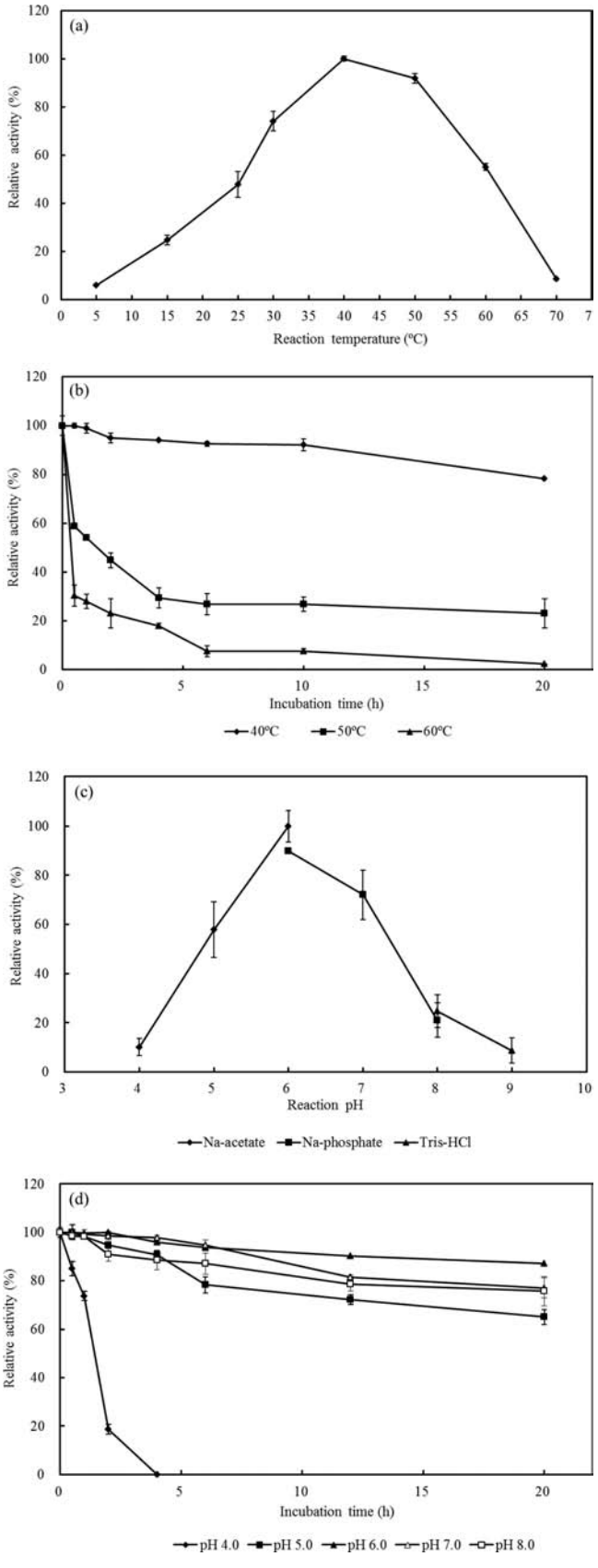

Figure 3. Biochemical properties of AbfCelf on pH and temperature. (a) Effect of temperature on enzyme activity. Reactions were conducted for 15 min in 100 mM, pH 6.0, sodium acetate buffer. (b) Effect of temperature on enzyme stability. The enzyme was incubated at temperatures ranging from 40 to 60 °C in 100 mM, pH 6.0, sodium acetate buffer for a period of time. (c) Effect of pH on enzyme activity. Activity was measured at 40 °C for 15 min at the indicated pH values in 100 mM of each buffer. (d) Effect of pH on enzyme stability. The enzyme was incubated at 40 °C in pH 4.0−8.0 100 mM buffers for a period of time. After that, residual activity was assayed at optimum temperature and pH. In all panels, the highest activity was taken as 100%. Reaction substrate was 0.84 mM PNP-Abf.

oligosaccharides and PNP-glycosides. AbfCelf was able to hydrolyze PNP-Abf and arabino-oligosaccharides, whereas no activity was detected toward PNP-α-D-xylopyranoside and PNP-β-D-xylopyranoside.

Homology Modeling. The structure of AbfCelf was built using the Swiss Model server with the chain B of 1QW9 as template. The sequence identity between template and target was 48.6%, and the QMEAN *Z*-score of the structure was −1.893, which was an evaluation parameter in homology modeling.[31,32] RC plot analysis showed that out of 502 residues, 84.4% were in most favored region, 14.4% in additionally allowed region, and 0.9% in generously allowed region. Only 0.3% of residues were in disallowed regions, indicating that the conformation was reliable.

As shown in Figure 4a, AbfCelf was organized into two domains: a characteristic $(\beta/\alpha)_8$ barrel (residues 19−382) and a 12-stranded β-sandwich with a jelly roll topology (residues 1−18 and 383−502). In Figure 4b, the coloring approximates the actual electrostatic potential. The catalytic area was hydrophobic, where binding clefts and protein surfaces conferred the extensive range of specificities.

Docking. After building the reliable structure of AbfCelf, substrate analysis can be carried out with the aid of the docking method. For the reason for lacking reliable tools (software), docking an enzyme with its macrosubstrate precisely is almost impossible today. Thus, this study examined only small oligosaccharides and PNP-glycosides in silico.

ΔG obtained from Autodock was used as a rapid evaluation of binding free energy.[29] Namely, the binding affinity between ligand and receptor can be expressed in terms of ΔG, which is given in Table 1. The negative number of ΔG means the positive binding affinity between the ligand and receptor. The more negative ΔG is, the larger is the binding constant.[33] In contrast, when ΔG was a positive number (e.g., arabinotetraose), the ligand could not combine into the receptor, and thus the docking cannot be finished. As Table 1 shows, the ΔG of arabinotetraose was the only one positive number in the total tested substrates. The ΔG's of other substrates and all products were negative numbers, among which arabinotriose, arabinobiose, and β-D-xylopyranose achieved the most negative numbers.

DISCUSSION

The strain *C. fimi* was sequenced in 2013, and the gene *Celf_3321* was marked as "AF domain-containing protein".[34] This work confirmed the gene segment encoding a GH 51 AF. Moreover, the AF from *C. fimi* was not reported before. Therefore, it is possible that this enzyme would be a novel AF with prospect activity that was worthy to be studied.

GH 51 AFs including AbfCelf can remove both α-1,2- and α-1,3-arabinofuranosyl moieties from arabinan and arabinoxylans. AbfCelf was also active on α-1,5-linked oligosaccharides, which is a characteristic of GH 43 AFs.[13] The substrate specificity of

DOI: 10.1021/jf5059683
J. Agric. Food Chem. 2015, 63, 3725−3733

Table 1. Activities of AbfCelf and Molecular ΔG Obtained by Using AutoDock 4.2

Substrate	Structure	ΔG (kcal/mol)	Product	Structure	ΔG (kcal/mol)	Specific activity (μmol min^{-1} mg^{-1})
Arabinobiose	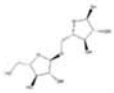	-8.87	α-L-arabinofuranose	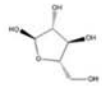	-6.3	4.07 ± 0.17
Arabinotriose	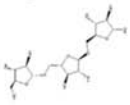	-8.95	Arabinobiose	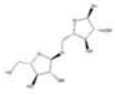	-8.87	0.09 ± 0.01
Arabinotetraose	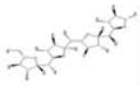	1.39	Arabinotriose	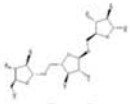	-8.95	0.05 ± 0.02
PNP-β-D-xylopyranose	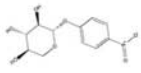	-6.76	β-D-xylopyranose	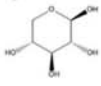	-7.21	< 0.01
PNP-α-D-xylopyranose	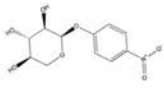	-6.17	α-D-xylopyranose		-7.13	< 0.01
PNP-α-L-arabinofuranose	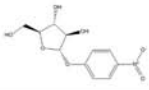	-6.79	α-L-arabinofuranose		-6.3	19.4

AbfCelf is partly different from some previously well-characterized GH 51 AFs such as AbfATK4 from *G. caldoxylolyticus* TK4.[16]

The substrates of AFs include natural polymeric polysaccharides and chromogenic PNP-glycosides. The formers are sugar beet arabinan, debranched arabinan, linear 1,5-α-arabinan, arabinogalactan, gum arabic, arabinoxylan (wheat/rye), xylan (larchwood/beechwood/oat spelt), CMC, mannan, glucomannan, and Avicel, etc. Many relative enzymes are necessary for the complete degradation of these natural substrates. On the other hand, different synthetic substrates were diffusely used also, such as PNP-α/β-L-arabinofuranoside, PNP-α/β-L-arabinopyranoside, PNP-α/β-D-xylopyranoside, PNP-α-D-galactopyranoside, PNP-α/β-D-glucopyranoside, PNP-β-D-fucopyranoside, PNP-α-L-rhamnopyranoside, PNP-β-D-glucosaminide, PNP-α-D-mannoside/mannopyranoside, PNP-α/β-D-galactoside, and so on. These PNP-glycosides can be degraded by a single enzyme, and therefore, they are used to detect the activity of such enzyme. Consequently, the substrates cover 30 kinds of various PNP-glycosides and polysaccharides for AFs, and the large number of substrates leads to large amount of experimental determination in the analysis of substrate specificity. Thus, structure understanding and theoretical computation were utilized to analyze the substrate specificity of GH 51 AFs in this paper.

Among many enzymatic reactions, product release or substrate binding is the rate-limiting step.[35] The more negative ΔG of substrate implied stronger substrate binding affinity in the active center, while the more negative ΔG of product signified the product released more difficultly. PNP-β-D-xylopyranose and PNP-α-D-xylopyranose bound into AbfCelf with ΔG below −6 kcal/mol, while that value of the product was below −7 kcal/mol (Table 1). Apparently, AbfCelf had a higher binding affinity with the product than these substrates, which meant product would occupy the active site and hinder the next binding of a new substrate molecule. In reality, the enzyme activity of AbfCelf on these pyranosidic synthetic substrates also cannot be detected. In these reactions, product release is the rate-limiting step.

AbfCelf displayed specific activity as only 0.05 U/mg toward arabinotetraose, the biggest substrate among the six tested ones, while obtained a positive ΔG of this substrate. In this case, substrate binding is the rate-limiting step, due to the difficulty for the substrate to enter the binding crevice of AbfCelf during docking.

Moreover, PNP-α-L-arabinofuranoside bound with AbfCelf easily and product α-L-arabinofuranoside released rapidly according to the ΔG in Table 1. The real AbfCelf activity on PNP-α-L-arabinofuranoside was coincident with this prediction. Additionally, AbfCelf exhibited a higher activity with arabinobiose than arabinotriose, which was in accord with the difference of ΔG between the substrate and product of docking experiment. Thus, ΔG, and the difference of ΔG between the substrate and product, could describe enzymatic reactions and suggest the reaction possibility.

The structure of AbfCelf is shown in Figure 4. Its $(\beta/\alpha)_8$ barrel, which exists commonly in various GH families, participated in substrate binding and catalysis. The circularly permuted form of the catalytic $(\beta/\alpha)_8$ barrel varied in location, size, and shape. There is correlation of specificity differences with sequence variation in the $\beta \rightarrow \alpha$ segments of the characteristic $(\beta/\alpha)_8$ barrel.[36] The β-sandwich of AbfCelf was previously functioned as a domain for binding the carbohydrate molecules, but lost such function during evolution.[25] The two catalytic residues (Glu173 and Glu292) were situated at C-terminal extensions of β-strands 4 and 7 in the $(\beta/\alpha)_8$ fold, which did superimpose perfectly with different GH 51 AFs. Other residues at $\beta \rightarrow \alpha$ 4, such as Gln171, Asn172, Trp178, Glu181, and Tyr189, that might contain specificity-denoting characteristics, participated in the interaction with sugar ligands.[37]

DOI: 10.1021/jf5059683
J. Agric. Food Chem. 2015, 63, 3725−3733

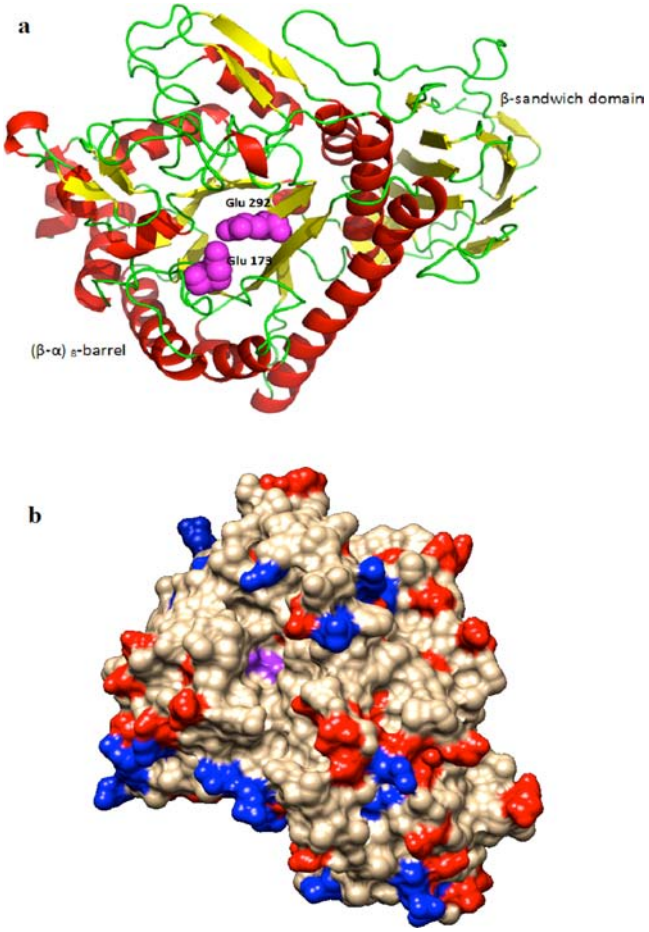

Figure 4. Structure of AbfCelf. (a) The structure of AbfCelf created by Swiss Model. The α-helices and β-sheets are shown in red and yellow, respectively. Loops and other secondary structures are shown in green. The catalytic residues, Glu[173] and Glu[292], are shown in purple balls. (b) The solvent-accessible surface of AbfCelf. Positive and negative residues are shown in blue and red, respectively. The catalytic area is shown in purple.

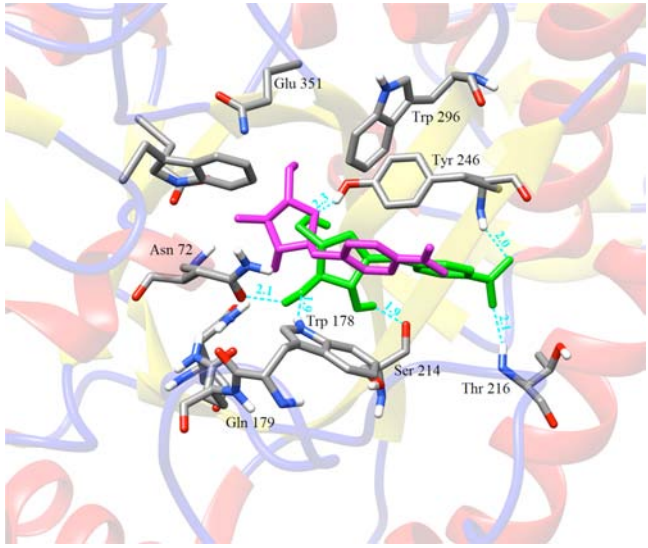

Figure 5. Interaction between ligands and key residues in the active site of AbfCelf. Overlapping of AbfCelf and the homologous structure (1QW9-B chain) in (wall-eyed) stereo. Residues are shown in stick model. PNP-Abf of AbfCelf by docking is in green, while that of template is magenta. Potential hydrogen bonds are shown as dotted blue lines; their length in angstroms is indicated. The α-helices and β-sheets are shown in red and yellow, respectively. Loops and other secondary structures are shown in blue.

The interaction between substrate and binding pocket of AbfCelf is shown in Figure 5. Some key residues were responsible for catalysis and substrate binding interactions like Glu27, Arg67, Asn172, Glu173, His242, Tyr244, Glu292, and Gln351, whose location and function are conserved in GH 51 AFs.[37] The result was in good agreement with sequence alignment in Figure 1.

AbfA crystal 1QW9 was used to test the rationality of docking method in simulating the interaction between enzyme and substrate. The conformation of the ligand with the lowest ΔG was overlapped with that of the 1QW9, which showed the main part of the substrate PNP-Abf in crystal and docking conjugate were partly coincided (Figure 5). Figure 5 also showed the hydrogen-bond network at the active site of AbfCelf. In the structure of covalent glycosyl-enzyme intermediate of AbfA, the arabinofuranose moiety was bound by a large number of hydrogen bonds, at least seven possible hydrogen bonds, which was also shown by Hövel et al.[25] In the AbfCelf complex, the whole PNP-Abf can form six hydrogen bonds and therefore was less tightly bonded than AbfA complex. Interestingly, AbfA hydrolyzed substrate with higher catalytic affinity according to its k_{cat}/K_m of 134 s^{-1} mM^{-1}, compared with that of AbfCelf, 82.4 s^{-1} mM^{-1}. The sequence identity between template and AbfCelf made difficulty in completely overlapping of the crystal and docking conjugate. In addition, the differences in side chains might also lead to the environmental diversity between crystallization and docking. AbfCelf shared less hydrogen bonds based on the docking experiment, and such results matched the lower catalytic efficiency and affinity determined experimentally, indicating the conformation of ligand docking into the binding site of AFs can be simulated in a general credibility.

Finally, the protein−ligand ΔG could manage to find putative ligands in silico and analyze the substrate specificity to some extent. Because L-arabinose residues are linked to form α-1,5-L-arabinan to which L-arabinofuranose units are attached, the lower protein−ligand ΔG of α-1,5-linked oligosaccharides exhibits potential hydrolytic activity against sugar beet arabinan, debranched arabinan, and linear arabinan.[38] Additionally, L-arabinosyl residues constitute side chains on the β-(1→4)-linked xylose backbones in xylans and arabinoxylans.[39] Accordingly, the ΔG of xylopyranoside gave a clue that PNP-xylopyranoside, xylan, and substituted xylan could be the putative ligands for AbfCelf so that some bifunctional AFs are discovered. This mainly depends on the credibility of the method.

In this study, AbfCelf was characterized and showed potent activity, 19.4 U/mg. Substrates were docked into the binding site to obtain the ΔG, indicating the reaction possibility. Then these prediction results were compared with experimental detected enzyme activity, which gave a clue of feasibility for substrate-specificity analysis in silico. After the present work, there is every possibility for us to screen virtually to select diverse bifunctional AFs with high active catalytic performance, thereby expanding the utilization and application in food industries. Also, before the characterization of an enzyme, the present approach to find putative substrates can save huge amounts of experimental labor, time, and cost. We hope to

DOI: 10.1021/jf5059683
J. Agric. Food Chem. 2015, 63, 3725−3733

develop better catalysts in this way for efficient production of L-arabinose and pectin in the future, and AFs will have greater prospects to provide desirable food production properties.

■ ASSOCIATED CONTENT

Supporting Information

Standard curves of PNP and BSA and Lineweaver−Burk plot of AbfCelf. This material is available free of charge via the Internet at http://pubs.acs.org.

■ AUTHOR INFORMATION

Corresponding Author

*Fax: +86-21-64252563. E-mail: jlxie@ecust.edu.cn.

Funding

This work was supported by the National Special Fund for State Key Laboratory of Bioreactor Engineering (2060204), partially supported by the National Natural Science Foundation of China (no. 31201296) and the Fundamental Research Funds for the Central Universities, People 's Republic of China.

Notes

The authors declare no competing financial interest.

■ REFERENCES

(1) Saha, B. C. Alpha-L-Arabinofuranosidases: biochemistry, molecular biology and application in biotechnology. *Biotechnol. Adv.* **2000**, *18* (5), 403−423.

(2) Matsuo, N.; Kaneko, S.; Kuno, A.; Kobayashi, H.; Kusakabe, I. Purification, characterization and gene cloning of two α-L-arabinofuranosidases from *Streptomyces chartreusis* GS901. *Biochem. J.* **2000**, *346*, 9−15.

(3) Bonnin, E.; Dolo, E.; Le Goff, A.; Thibault, J. F. Characterisation of pectin subunits released by an optimized combination of enzymes. *Carbohydr. Res.* **2002**, *337* (18), 1687−1696.

(4) Chen, J.; Yang, R. J.; Chen, M.; Wang, S. H.; Li, P.; Xia, Y.; Zhou, L.; Xie, J. L.; Wei, D. Z. Production optimization and expression of pectin releasing enzyme from *Aspergillus oryzae* PO. *Carbohydr. Polym.* **2014**, *101*, 89−95.

(5) Wang, S. H.; Yang, Y.; Yang, R. J.; Zhang, J.; Chen, M.; Matsukawa, S. G.; Xie, J. L.; Wei, D. Z. Cloning, characterization of a cold-adapted endo-1,5-α-L-arabinanase from *Paenibacillus polymyxa* and rational design for acidic applicability. *J. Agric. Food Chem.* **2014**, *62* (33), 8460−8469.

(6) Numan, M. T.; Bhosle, N. B. α-L-Arabinofuranosidases: the potential applications in biotechnology. *J. Ind. Microbiol. Biotechnol.* **2006**, *33* (4), 247−260.

(7) Gobbetti, M.; De Angelis, M.; Arnaut, P.; Tossut, P.; Corsetti, A.; Lavermicocca, P. Added pentosans in breadmaking: fermentations of derived pentoses by sourdough lactic acid bacteria. *Food Microbiol.* **1999**, *16* (4), 409−418.

(8) Voragen, A. G. J.; Rombouts, F. M.; Searle-van Leeuwen, M. F.; Schols, H. A.; Pilnik, W. The degradation of arabinans by endo-arabinanase and arabinofuranosidases purified from *Aspergillus niger*. *Food Hydrocolloids* **1987**, *1* (5), 423−437.

(9) Henrissat, B.; Davies, G. J. Glycoside hydrolases and glycosyltransferases. Families, modules, and implications for genomics. *Plant Physiol.* **2000**, *124* (4), 1515−1519.

(10) Lombard, V.; Ramulu, H. G.; Drula, E.; Coutinho, P. M.; Henrissat, B. The carbohydrate-active enzymes database (CAZy) in 2013. *Nucleic Acids Res.* **2014**, *42* (D1), D490−D495.

(11) Suzuki, H.; Murakami, A.; Yoshida, K. I. Motif-guided identification of a glycoside hydrolase family 1 α-L-arabinofuranosidase in *Bifidobacterium adolescentis*. *Biosci., Biotechnol., Biochem.* **2013**, *77* (8), 1709−1714.

(12) Davies, G.; Henrissat, B. Structures and mechanisms of glycosyl hydrolases. *Structure* **1995**, *3* (9), 853−859.

(13) Remond, C.; Boukari, I.; Chambat, G.; O'Donohue, M. Action of a GH 51 α-L-arabinofuranosidase on wheat-derived arabinoxylans and arabino-xylooligosaccharides. *Carbohyd. Polym.* **2008**, *72* (3), 424−430.

(14) Zhang, G.; Mao, L.; Zhao, Y.; Xue, Y.; Ma, Y. Characterization of a thermostable xylanase from an alkaliphilic *Bacillus* sp. *Biotechnol. Lett.* **2010**, *32* (12), 1915−1920.

(15) Apiraksakorn, J.; Nitisinprasert, S.; Levin, R. E. Grass degrading β-1, 3−1, 4-D-glucanases from *Bacillus subtilis* GN156: Purification and characterization of glucanase J1 and pJ2 possessing extremely acidic pI. *Appl. Biochem. Biotechnol.* **2008**, *149* (1), 53−66.

(16) Canakci, S.; Belduz, A. O.; Saha, B. C.; Yasar, A.; Ayaz, F. A.; Yayli, N. Purification and characterization of a highly thermostable α-L-arabinofuranosidase from *Geobacillus caldoxylolyticus* TK4. *Appl. Microbiol. Biotechnol.* **2007**, *75* (4), 813−820.

(17) Lee, S. F.; Forsberg, C. W. Purification and characterization of an α-L-arabinofuranosidase from *Clostridium acetobutylicum* ATCC 824. *Can. J. Microbiol.* **1987**, *33* (11), 1011−1016.

(18) Fritz, M.; Ravanal, M. C.; Braet, C. A family 51 α-L-arabinofuranosidase from *Penicillium purpurogenum*: purification, properties and amino acid sequence. *Mycol. Res.* **2008**, *112* (8), 933−942.

(19) Debeche, T.; Cummings, N.; Connerton, I.; Debeire, P.; O'Donohue, M. J. Genetic and biochemical characterization of a highly thermostable α-L-arabinofuranosidase from *Thermobacillus xylanilyticus*. *Appl. Environ. Microbiol.* **2000**, *66* (4), 1734−1736.

(20) Zhang, L. J.; Tang, X.; Cui, D. B.; Yao, Z.; Gao, B.; Jiang, S.; Wei, D. Z. A method to rationally increase protein stability based on the charge−charge interaction, with application to lipase LipK107. *Protein Sci.* **2014**, *23* (1), 110−116.

(21) Gonnelli, G.; Rooman, M.; Dehouck, Y. Structure-based mutant stability predictions on proteins of unknown structure. *J. Biotechnol.* **2012**, *161* (3), 287−293.

(22) Brinkworth, R. I.; Breinl, R. A.; Kobe, B. Structural basis and prediction of substrate specificity in protein serine/threonine kinases. *Proc. Natl. Acad. Sci. U.S.A.* **2003**, *100* (1), 74−79.

(23) De Voss, J. J.; Sibbesen, O.; Zhang, Z.; Ortiz de Montellano, P. R. Substrate docking algorithms and prediction of the substrate specificity of cytochrome P450cam and its L244A mutant. *J. Am. Chem. Soc.* **1997**, *119* (24), 5489−5498.

(24) Garay-Malpartida, H. M.; Occhiucci, J. M.; Alves, J.; Belizário, J. E. CaSPredictor: a new computer-based tool for caspase substrate prediction. *Bioinformatics* **2005**, *21* (suppl 1), 169−176.

(25) Hövel, K.; Shallom, D.; Niefind, K.; Belakhov, V.; Shoham, G.; Baasov, T.; Schomburg, D. Crystal structure and snapshots along the reaction pathway of a family 51 α-L-arabinofuranosidase. *EMBO J.* **2003**, *22* (19), 4922−4932.

(26) Wang, S. H.; Yang, Y.; Zhang, J.; Sun, J.; Matsukawa, S.; Xie, J. L.; Wei, D. Z. Characterization of abnZ2 (yxiA1) and abnZ3 (yxiA3) in *Paenibacillus polymyxa*, encoding two novel endo-1, 5-α-L-arabinanases. *Bioresour. Bioprocess.* **2014**, *1* (1), 1−11.

(27) Lineweaver, H.; Burk, D. The determination of enzyme dissociation constants. *J. Am. Chem. Soc.* **1934**, *56* (3), 658−666.

(28) Laskowski, R. A.; MacArthur, M. W.; Moss, D. S.; Thornton, J. M. PROCHECK: a program to check the stereochemical quality of protein structures. *J. Appl. Crystallogr.* **1993**, *26* (2), 283−291.

(29) Morris, G. M.; Huey, R.; Lindstrom, W.; Sanner, M. F.; Belew, R. K.; Goodsell, D. S.; Olson, A. J. AutoDock4 and AutoDockTools4: Automated docking with selective receptor flexibility. *J. Comput. Chem.* **2009**, *30*, 2785−2791.

(30) Degrassi, G.; Vindigni, A.; Venturi, V. A thermostable α-arabinofuranosidase from xylanolytic *Bacillus pumilus*: purification and characterisation. *J. Biotechnol.* **2003**, *101* (1), 69−79.

(31) Arnold, K.; Bordoli, L.; Kopp, J.; Schwede, T. The SWISS-MODEL workspace: a web-based environment for protein structure homology modelling. *Bioinformatics* **2006**, *22* (2), 195−201.

(32) Schwede, T.; Kopp, J.; Guex, N.; Peitsch, M. C. SWISS-MODEL: an automated protein homology-modeling server. *Nucleic Acids Res.* **2003**, *31* (13), 3381−3385.

DOI: 10.1021/jf5059683
J. Agric. Food Chem. 2015, 63, 3725−3733

(33) Williams, D.; Stephens, E.; O'Brien, D.; Zhou, M. Understanding noncovalent interactions: ligand binding energy and catalytic efficiency from ligand-induced reductions in motion within receptors and enzymes. *Angew. Chem.* **2004**, *43*, 6596−6616.
(34) Abt, B.; Foster, B.; Lapidus, A.; Clum, A.; Sun, H.; Pukall, R.; Klenk, H. Complete genome sequence of *Cellulomonas flavigena* type strain (134T). *Stand. Genomic Sci.* **2010**, *3* (1), 15.
(35) Garcia-Viloca, M.; Gao, J.; Karplus, M.; Truhlar, D. G. How enzymes work: analysis by modern rate theory and computer simulations. *Science* **2004**, *303* (5655), 186−195.
(36) Gottschalk, T. E.; Tull, D.; Aghajari, N.; Haser, R.; Svensson, B. Specificity modulation of barley α-amylase through biased random mutagenesis involving a conserved tripeptide in $\beta \rightarrow \alpha$ loop 7 of the catalytic (β/α) 8-barrel domain. *Biochemistry* **2001**, *40* (43), 12844−12854.
(37) Sakon, J.; Adney, W. S.; Himmel, M. E.; Thomas, S. R.; Karplus, P. A. Crystal structure of thermostable family 5 endocellulase E1 from *Acidothermus cellulolyticus* in complex with cellotetraose. *Biochemistry* **1996**, *35* (33), 10648−10660.
(38) Beldman, G.; Schols, H. A.; Pitson, S. M.; Searle-van Leeuwen, M. J. F.; Voragen, A. G. J. Arabinans and arabinan degrading enzymes. *Adv. Macromol. Carbohydr. Res.* **1997**, *1* (1), 64.
(39) Kormelink, F. J.; Gruppen, H.; Viëtor, R. J.; Voragen, A. G. Mode of action of the xylan-degrading enzymes from *Aspergillus awamori* on alkali-extractable cereal arabinoxylans. *Carbohydr. Res.* **1993**, *249* (2), 355−367.

DOI: 10.1021/jf5059683
J. Agric. Food Chem. 2015, 63, 3725−3733

Table 1. Structural Formula of the Title Compounds

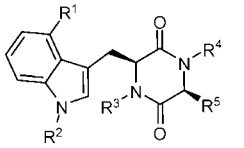

$R^1 = NO_2$, H;
$R^2 = CH_3$, H;
$R^3 = CH_3$, H;
$R^4 = CH_3$, H;

Compd.	R^1	R^2	R^3	R^4	R^5
1a	NO_2	H	H	H	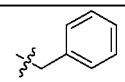
1b	NO_2	H	H	H	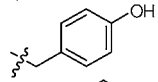
1c	NO_2	H	H	H	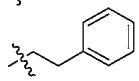
1d	NO_2	H	H	H	H
1e	NO_2	H	H	H	
2a (TC)	NO_2	H	CH_3	H	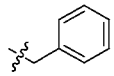
2b	NO_2	H	CH_3	H	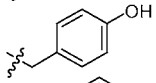
2c	NO_2	H	CH_3	H	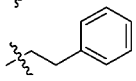
2d	NO_2	H	CH_3	H	H
2e	NO_2	H	CH_3	H	
2f	NO_2	H	CH_3	H	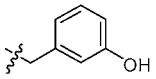
3a	H	H	H	H	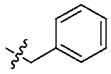
3b	H	H	H	H	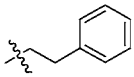
4a	NO_2	CH_3	CH_3	CH_3	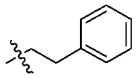
4b	NO_2	CH_3	CH_3	CH_3	H
4c	NO_2	CH_3	CH_3	CH_3	
4d	H	CH_3	CH_3	CH_3	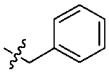

dried by distillation over CaH_2. Thin-layer chromatography (TLC) was performed on silica gel GF254 plates. Column chromatography was performed on silica gel (200−300 mesh). ^1H and ^{13}C nuclear magnetic resonance (NMR) spectra were recorded on a Bruker AVANCE AV400 (400 and 100 MHz). All NMR chemical shifts were referenced to residual solvent peaks or to tetramethylsilane (TMS) as an internal standard. All coupling constants J were quoted in hertz. High-resolution mass spectra (HRMS) were obtained on an IonSpec QFT mass spectrometer with electrospray ionization (ESI). Optical rotations were recorded on a PerkinElmer 341 polarimeter. Melting points were measured on an X4 apparatus.

Herbicidal Activities. The initial herbicidal activities of compounds **1**−**4** and TA against dicotyledon weeds, including *Brassica campestris* and *Amaranthus retroflexus*, and monocotyledon weeds, including *Echinochloa crus-galli* and *Digitaria sanguinalis*, were evaluated according to a previously reported procedure.[21−23]

All title compounds were screened at a adosage of 1500 g ha^{-1}. Then, compounds TA, **1a**, **2a**, and **2f** with higher herbicidal activities were further assayed at lower dosages of 750, 375, and 187.5 g ha^{-1}. Dichlobenil was selected as a positive control. All treatments were carried out in triplicate (Tables 4 and 5).

Treatment. The emulsions of tested compounds were prepared by dissolving them in 100 μL of *N*,*N*-dimethylformamide (DMF) with the addition of a little Tween 20 and diluting with proper water to the desired concentrations. Then, these emulsions were sprayed using a microsprayer. As negative control experiments, the mixture of the same amount of water, DMF, and Tween 20 with no compounds was also tested. Herbicidal activities of dichlobenil at the same concentrations as tested compounds were carried out as positive control experiments.

Pre-emergence. Sandy clay (100 g) in a plastic box (11 × 7.5 × 6 cm) was wetted with water. A total of 15 sprouting seeds of the weed under test were planted in fine earth (0.6 cm depth) in the glasshouse and sprayed with the test compound solution.

Post-emergence. Seedlings (one leaf and one stem) of the weed were sprayed with the tested compounds at the same rate as used for the pre-emergence test.

Data Collection. For both methods, the fresh weights of three parallel plants were determined 20 days later, and the percentage inhibition relative to the controls was calculated by eq 1

$$\text{inhibition}\ (\%) = (w_c - w_t)/w_c \times 100\% \quad (1)$$

where w_c is the wet weight of the negative control and w_t is the wet weight of the tested group.

Crop Selectivity. Compounds TA, **1a**, **2a**, and **2f** were selected for crop selectivity evaluation. Conventional wheat, corn, cotton, and peanut were respectively planted in plots (diameter = 12 cm) containing test soil and grown in a greenhouse at 20−25 °C. After the plants had reached the four-leaf stage, the spraying treatment was conducted at different dosages by diluting the formulations of tested compounds with water. The visual injury and growth state of the individual plant were observed at regular intervals. The fresh weights were determined 30 days later, and the percentage inhibition relative to the controls was calculated. Dichlobenil was selected as a positive control (Table 6).

Protoporphyrinogen Oxidase (PPO) and Acetohydroxyacid Synthase (AHAS) Inhibition Activity. The recombinant tobacco PPO enzyme (mtPPO) was expressed according to the established protocol.[24−27] Oxadiazon, fluazolate, and sulfentrazone were selected as positive controls. The product of the enzymatic reaction has a maximum excitation wavelength at 410 nm and a maximum emission wavelength at 630 nm. PPO activity was assayed by measuring the formation of protoporphyrin IX at room temperature using a fluorescence detector with the excitation and emission wavelengths set at 410 and 631 nm, respectively. The concentration of protoporphyrinogen IX was determined according to the absorption of protoporphyrin IX, and the concentration of protoporphyrin IX was calculated from the calibration graph. In each assay, the stock dimethyl sulfoxide (DMSO) solution (1% total volume) of inhibitor was added to the reaction system. The final inhibitor concentration ranged from 0.005 to 500 μM. The enzymatic reaction rate was measured in a reagent buffer of 100 mM potassium phosphate (pH 7.5), 5 mM dithiothreitol (DTT), 1 mM ethylenediaminetetraacetic acid (EDTA), Tween 80 (0.03%, v/v), 200 mM imidazole, 5 μM flavin adenine dinucleotide (FAD), and approximately 0−40 μg of protein. The IC_{50} value was determined by measuring PPO activity over a range of inhibitor concentrations at a fixed substrate concentration. IC_{50} values were calculated by fitting v versus $[I]$ data to a single binding site model described by eq 2

$$y = \min + \frac{\max - \min}{1 + 10^{x - \log IC_{50}}} \quad (2)$$

where y is the percentage of maximal rate, with max and min being the y values at which the curve levels off, x is the logarithm of the inhibitor

DOI: 10.1021/jf506153t
J. Agric. Food Chem. 2015, 63, 3734−3741

Table 2. ^{1}H NMR Data of Title Compounds 1−4

compound	^{1}H NMR
1a	1.98−2.11 (m, 1H, C$\underline{H}_2$), 2.70 (dd, J_1 = 13.6 Hz, J_2 = 5.3 Hz, 1H, C$\underline{H}_2$), 2.79 (dd, J_1 = 13.5 Hz, J_2 = 4.9 Hz, 1H, C$\underline{H}_2$), 3.02 (dd, J_1 = 14.5 Hz, J_2 = 4.2 Hz, 1H, C$\underline{H}_2$), 3.78 [m, 1H, diketopiperazine (DKP) C$\underline{H}$], 4.06 (d, J = 5.3 Hz, 1H, DKP C$\underline{H}$), 7.09 (d, J = 8.2 Hz, 3H, Ph-$\underline{H}$), 7.23 (q, J = 8.0 Hz, 2H, Ph-$\underline{H}$), 7.31 (t, J = 7.4 Hz, 2H, indole C$\underline{H}$), 7.65 (d, J = 2.8 Hz, 1H, indole C$\underline{H}$), 7.76 (t, J = 9.0 Hz, 2H, indole C$\underline{H}$, DKP N$\underline{H}$), 7.96 (s, 1H, DKP N$\underline{H}$), 11.72 (s, 1H, indole N$\underline{H}$)
1b	2.03 (dd, J_1 = 14.2 Hz, J_2 = 8.9 Hz, 1H, C$\underline{H}_2$), 2.55−2.62 (m, 1H, C$\underline{H}_2$), 2.69 (dd, J_1 = 13.7 Hz, J_2 = 4.7 Hz, 1H, C$\underline{H}_2$), 3.05 (dd, J_1 = 14.3 Hz, J_2 = 4.2 Hz, 1H, C$\underline{H}_2$), 3.69 (m, 1H, DKP C$\underline{H}$), 3.95 (m, 1H, DKP C$\underline{H}$), 6.64−6.77 (m, 2H, Ph-$\underline{H}$), 6.82−6.94 (m, 2H, Ph-$\underline{H}$), 7.14 (d, J = 1.8 Hz, 1H, indole C$\underline{H}$), 7.22 (t, J = 7.9 Hz, 1H, indole C$\underline{H}$), 7.56 (d, J = 2.8 Hz, 1H, indole C$\underline{H}$), 7.77 (t, J = 8.0 Hz, 2H, DKP N$\underline{H}$, indole C$\underline{H}$), 7.86 (d, J = 2.5 Hz, 1H, DKP N$\underline{H}$), 9.23 (s, 1H, O$\underline{H}$), 11.61−11.99 (m, 1H, indole N$\underline{H}$)
1c	1.37−1.50 (m, 2H, C$\underline{H}_2$), 1.61 (m, 1H, C$\underline{H}_2$), 1.95−2.05 (m, 1H, C$\underline{H}_2$), 2.12−2.30 (m, 2H, C$\underline{H}_2$), 3.70 (m, 1H, DKP C$\underline{H}$), 4.07 (m, 1H, DKP C$\underline{H}$), 7.03 (d, J = 7.5 Hz, 2H, Ph-$\underline{H}$), 7.17 (m, 2H, Ph-$\underline{H}$, indole C$\underline{H}$), 7.26 (t, J = 7.5 Hz, 2H, Ph-$\underline{H}$), 7.50 (d, J = 2.3 Hz, 1H, indole C$\underline{H}$), 7.71 (m, 2H, DKP N$\underline{H}$, indole C$\underline{H}$), 7.86 (s, 1H, DKP N$\underline{H}$), 8.07−8.17 (m, 1H, indole C$\underline{H}$), 11.86 (s, 1H, indole N$\underline{H}$)
1d	3.23−3.30 (m, 2H, C$\underline{H}_2$), 3.43−3.49 (m, 2H, DKP C$\underline{H}_2$), 3.84−3.95 (m, 1H, DKP C$\underline{H}$), 7.24 (t, J = 7.9 Hz, 1H, indole C$\underline{H}$), 7.51 (d, J = 2.6 Hz, 1H, indole C$\underline{H}$), 7.74−7.86 (m, 3H, DKP N$\underline{H}$, indole C$\underline{H}$), 7.91 (d, J = 3.1 Hz, 1H, DKP N$\underline{H}$), 11.86 (s, 1H, indole N$\underline{H}$)
1e	0.61−0.91 (m, 8H, *i*-butyl C$\underline{H}_2$, C$\underline{H}_3$), 1.01 (m, 1H, *i*-butyl C$\underline{H}$), 1.54 (m, 1H, DKP C$\underline{H}$), 3.27 (d, J = 8.2 Hz, 1H, indole-C$\underline{H}_2$), 3.57 (m, 1H, indole-C$\underline{H}_2$), 4.05 (m, 1H, DKP C$\underline{H}$), 7.21 (t, J = 7.9 Hz, 1H, indole C$\underline{H}$), 7.48 (s, 1H, indole C$\underline{H}$), 7.63−8.15 (m, 4H, DKP N$\underline{H}$, indole C$\underline{H}$), 11.81 (s, 1H, indole N$\underline{H}$)
2a	2.12 (m, 1H, C$\underline{H}_2$), 2.59−2.69 (m, 2H, C$\underline{H}_2$), 2.73 (s, 3H, DKP-C$\underline{H}_3$), 3.02 (m, 1H, C$\underline{H}_2$), 3.84 (m, 1H, DKP C$\underline{H}$), 3.94 (m, 1H, DKP C$\underline{H}$), 6.87−6.93 (m, 2H, Ph-$\underline{H}$), 7.18−7.32 (m, 5H, indole C$\underline{H}$, Ph-$\underline{H}$), 7.72−7.92 (m, 3H, DKP N$\underline{H}$, indole C$\underline{H}$), 11.75−11.94 (m, 1H, indole N$\underline{H}$)
2b	2.05 (m, 1H, C$\underline{H}_2$), 2.57 (m, 1H, C$\underline{H}_2$), 2.65−2.68(m, 1H, C$\underline{H}_2$) 2.70 (s, 3H, DKP-C$\underline{H}_3$), 3.00 (m, 1H, C$\underline{H}_2$), 3.78 (t, J = 6.2 Hz, 1H, DKP C$\underline{H}$), 3.84−3.88 (m, 1H, DKP C$\underline{H}$), 6.63−6.74 (m, 4H, Ph-$\underline{H}$), 7.17−7.28 (m, 2H, indole C$\underline{H}$), 7.72−7.77 (m, 1H, indole C$\underline{H}$), 7.77−7.83 (m, 2H, DKP N$\underline{H}$, indole C$\underline{H}$), 9.22 (s, 1H, O$\underline{H}$), 11.87 (s, 1H, indole N$\underline{H}$)
2c	0.84 (m, 1H, C$\underline{H}_2$), 1.44 (m, 1H, C$\underline{H}_2$), 2.24 (m, 1H, C$\underline{H}_2$), 2.34 (m, 1H, C$\underline{H}_2$), 2.83 (s, 3H, DKP-C$\underline{H}_3$), 3.36 (d, J = 5.7 Hz, 1H, C$\underline{H}_2$), 3.49−3.57 (m, 2H, DKP C$\underline{H}$, C$\underline{H}_2$), 4.04 (t, J = 5.2 Hz, 1H, DKP C$\underline{H}$), 6.97−7.04 (m, 2H, Ph-$\underline{H}$), 7.14−7.22 (m, 2H, Ph-$\underline{H}$, indole C$\underline{H}$), 7.26 (t, J = 7.5 Hz, 2H, Ph-$\underline{H}$), 7.43 (d, J = 2.5 Hz, 1H, indole C$\underline{H}$), 7.66 (d, J = 8.0 Hz, 1H, indole C$\underline{H}$), 7.74 (d, J = 7.8 Hz, 1H, indole C$\underline{H}$), 8.22 (d, J = 3.1 Hz, 1H, DKP N$\underline{H}$), 11.90 (m, 1H, indole N$\underline{H}$)
2d	2.72 (s, 3H, DKP-C$\underline{H}_3$), 2.93 (m, 1H, C$\underline{H}_2$), 3.31 (m, 1H, C$\underline{H}_2$), 3.43 (m, 2H, DKP C$\underline{H}_2$), 3.93 (t, J = 5.8 Hz, 1H, DKP C$\underline{H}$), 7.25 (t, J = 7.9 Hz, 1H, indole C$\underline{H}$), 7.46 (d, J = 2.5 Hz, 1H, indole C$\underline{H}$), 7.82 (d, J = 7.8 Hz, 3H, DKP N$\underline{H}$, indole C$\underline{H}$), 11.93 (s, 1H, indole N$\underline{H}$)
2e	0.65 (t, J = 6.7 Hz, 6H, *i*-butyl C$\underline{H}_3$), 0.99−1.13 (m, 2H, *i*-butyl C$\underline{H}_2$), 1.16−1.19 (m, 1H, *i*-butyl C$\underline{H}$), 2.76 (s, 3H, DKP-C$\underline{H}_3$), 3.35−3.36 (m, 2H, indole-C$\underline{H}_2$), 3.44−3.49 (m, 1H, DKP C$\underline{H}$), 3.97−4.06 (m, 1H, DKP C$\underline{H}$), 7.22 (t, J = 7.9 Hz, 1H, indole C$\underline{H}$), 7.44 (d, J = 2.5 Hz, 1H, indole C$\underline{H}$), 7.76 (dd, J_1 = 10.2 Hz, J_2 = 7.9 Hz, 2H, indole C$\underline{H}$), 8.09 (d, J = 3.3 Hz, 1H, DKP N$\underline{H}$), 11.70−12.04 (m, 1H, indole N$\underline{H}$)
2f	2.33 (dd, J_1 = 13.4 Hz, J_2 = 6.3 Hz, 1H, C$\underline{H}_2$), 2.44−2.49 (m, 1H, C$\underline{H}_2$), 2.58−2.71 (m, 4H, DKP-C$\underline{H}_3$, C$\underline{H}_2$), 2.85 (m, 1H, C$\underline{H}_2$), 3.74 (t, J = 6.5 Hz, 1H, DKP C$\underline{H}$), 3.97 (m, 1H, DKP C$\underline{H}$), 6.38 (d, J_1 = 7.6 Hz, 1H, Ph-$\underline{H}$), 6.47−6.55 (m, 1H, Ph-$\underline{H}$), 6.63 (dd, J_1 = 8.0 Hz, J_2 = 1.6, 1H, Ph-$\underline{H}$), 7.09 (t, J = 7.8 Hz, 1H, Ph-$\underline{H}$), 7.17 (d, J = 2.5 Hz, 1H, indole C$\underline{H}$), 7.24 (t, J = 7.9 Hz, 1H, indole C$\underline{H}$), 7.79 (t, J = 7.6 Hz, 2H, indole C$\underline{H}$), 7.88 (d, J = 3.2 Hz, 1H, DKP N$\underline{H}$), 9.39 (s, 1H, O$\underline{H}$), 11.88 (d, J = 2.5 Hz, 1H, indole N$\underline{H}$)
3a	1.86 (m, 1H, C$\underline{H}_2$), 2.45 (d, J = 3.0 Hz, 1H, C$\underline{H}_2$), 2.55 (d, J = 5.7 Hz, 1H, C$\underline{H}_2$), 2.77−2.88 (m, 1H, C$\underline{H}_2$), 3.86 (s, 1H, DKP C$\underline{H}$), 3.98 (s, 1H, DKP C$\underline{H}$), 6.71 (d, J = 7.2 Hz, 2H, Ph-$\underline{H}$), 6.94−7.02 (m, 2H, Ph-$\underline{H}$), 7.07 (t, J = 7.5 Hz, 1H, Ph-$\underline{H}$), 7.16 (m, 3H, indole C$\underline{H}$), 7.31 (t, J = 10.4 Hz, 1H, indole C$\underline{H}$), 7.49 (d, J = 7.8 Hz, 1H, indole C$\underline{H}$), 7.70 (s, 1H, DKP N$\underline{H}$), 7.90 (s, 1H, DKP N$\underline{H}$), 10.88 (s, 1H, indole N$\underline{H}$)
3b	0.88−0.99 (m, 1H, C$\underline{H}_2$), 1.22−1.28 (m, 1H, C$\underline{H}_2$), 1.80−1.88 (m, 2H, C$\underline{H}_2$), 3.02 (dd, J_1 = 14.4 Hz, J_2 = 4.7 Hz, 1H, C$\underline{H}_2$), 3.29 (d, J = 4.0 Hz, 1H, C$\underline{H}_2$), 3.58−3.63 (m, 1H, DKP C$\underline{H}$), 4.16 (m, 1H, DKP C$\underline{H}$), 6.75−6.81 (m, 2H, Ph-$\underline{H}$), 6.92−6.97 (m, 1H, Ph-$\underline{H}$), 6.99−7.04 (m, 1H, Ph-$\underline{H}$), 7.06 (d, J = 2.3 Hz, 1H, indole C$\underline{H}$), 7.08−7.13 (m, 1H, Ph-$\underline{H}$), 7.15−7.24 (m, 3H, indole C$\underline{H}$), 7.62 (d, J = 7.8 Hz, 1H, indole C$\underline{H}$), 8.06 (d, J = 2.3 Hz, 1H, DKP N$\underline{H}$), 8.14 (d, J = 2.2 Hz, 1H, DKP N$\underline{H}$), 10.89 (s, 1H, indole N$\underline{H}$)
4a	1.12−1.31 (m, 1H, C$\underline{H}_2$), 1.47−1.65 (m, 1H, C$\underline{H}_2$), 2.45 (m, 2H, C$\underline{H}_2$), 2.67 (s, 3H, DKP-C$\underline{H}_3$), 2.82 (s, 3H, DKP-C$\underline{H}_3$), 3.43 (m, 2H, C$\underline{H}_2$), 3.71 (s, 3H, indole-C$\underline{H}_3$), 3.71 (s, 1H, DKP C$\underline{H}$), 4.03 (t, J = 4.8, 1H, DKP C$\underline{H}$), 7.07 (d, J = 8.0 Hz, 2H, Ph-$\underline{H}$), 7.20−7.32 (m, 4H, indole C$\underline{H}$, Ph-$\underline{H}$), 7.48−7.55 (m, 1H, indole C$\underline{H}$), 7.67−7.73 (m, 1H, indole C$\underline{H}$), 7.77−7.86 (m, 1H, indole C$\underline{H}$)
4b	2.42 (d, J = 1.3 Hz, 3H, DKP-C$\underline{H}_3$), 2.54 (d, J = 2.0 Hz, 1H, DKP C$\underline{H}_2$), 2.81 (s, 3H, DKP-C$\underline{H}_3$), 3.27−3.31 (m, 1H, DKP C$\underline{H}_2$), 3.39 (d, J = 5.4 Hz, 1H, indole-C$\underline{H}_2$), 3.43 (d, J = 8.0 Hz, 1H, indole-C$\underline{H}_2$), 3.86 (m, 3H, indole-C$\underline{H}_3$), 4.04 (t, J = 5.0 Hz, 1H, DKP C$\underline{H}$), 7.32 (t, J = 8.0 Hz, 1H, indole C$\underline{H}$), 7.41 (s, 1H, indole C$\underline{H}$), 7.84 (d, J = 7.8 Hz, 1H, indole C$\underline{H}$), 7.92 (d, J = 8.2 Hz, 1H, indole C$\underline{H}$)
4c	0.81−0.91 (m, 6H, *i*-butyl C$\underline{H}_3$), 1.29 (m, 1H, *i*-butyl C$\underline{H}$), 1.53−1.68 (m, 2H, *i*-butyl C$\underline{H}_2$), 2.71 (s, 3H, DKP-C$\underline{H}_3$), 2.79 (s, 3H, DKP-C$\underline{H}_3$), 3.34−3.41 (m, 2H, indole-C$\underline{H}_2$), 3.74 (d, J = 5.7 Hz, 1H, DKP C$\underline{H}$), 3.86 (s, 3H, indole-C$\underline{H}_3$), 3.95 (t, J = 6.0 Hz, 1H, DKP C$\underline{H}$), 7.31 (t, J = 8.0 Hz, 1H, indole C$\underline{H}$), 7.56 (s, 1H, indole C$\underline{H}$), 7.81 (dd, J_1 = 8.0 Hz, J_2 = 1.0 Hz, 1H, indole C$\underline{H}$), 7.89 (dd, J_1 = 8.1 Hz, J_2 = 1.0 Hz, 1H, indole C$\underline{H}$)
4d	1.48 (m, 1H, C$\underline{H}_2$), 2.15−2.29 (m, 1H, C$\underline{H}_2$), 2.44 (d, J = 3.8 Hz, 3H, DKP-C$\underline{H}_3$), 2.77 (dd, J_1 = 14.9 Hz, J_2 = 3.9 Hz, 1H, C$\underline{H}_2$), 2.85 (d, J = 3.7 Hz, 3H, DKP-C$\underline{H}_3$), 2.94 (dd, J_1 = 14.8 Hz, J_2 = 4.1 Hz, 1H, C$\underline{H}_2$), 3.73 (d, J = 3.7 Hz, 3H, indole-C$\underline{H}_3$), 3.97 (m, 1H, DKP C$\underline{H}$), 4.17 (m, 1H, DKP C$\underline{H}$), 6.54−6.64 (m, 2H, Ph-$\underline{H}$), 7.03−7.24 (m, 6H, indole C$\underline{H}$, Ph-$\underline{H}$), 7.39 (d, J = 8.0 Hz, 1H, indole C$\underline{H}$), 7.48 (d, J = 7.6 Hz, 1H, indole C$\underline{H}$)

concentration, and IC_{50} is the concentration of the inhibitor that caused 50% of the total inhibition. Because the inhibitors belong to the class of competitive inhibitors, the calculated K_i value can be obtained by applying the following relationship among K_i, K_m, and IC_{50} at any saturating substrate concentration (S) by the following eq 3.

$$K_i = \frac{IC_{50}}{S/K_m + 1} \quad (3)$$

The expression vector pQE-GMwt, containing the wild-type *Escherichia coli* AHAS II gene, was provided by professor D. M. Chipman (Ben-Gurion University). The wild-type *E. coli* AHAS II was expressed from the plasmid pQE-GMwt. A single colony of the *E. coli* strain XL1-Blue, transformed with the plasmid pQE-GMwt, was inoculated in 20 mL of Luria−Bertani (LB) medium containing 100 μg mL^{-1} ampicillin. The culture was incubated overnight at 37 °C. The overnight medium was transferred into 500 mL of LB medium in a 2 L round-bottomed flask. Then, the culture was induced with 0.5 mM isopropyl-β-D-thiogalactoside (IPTG) when A_{600} reached 0.7−0.8. Cells were grown for an additional 3 h at 37 °C and harvested by centrifugation at 6000 rpm for 10 min. The cell pellet was suspended in 10 mL of solution (10 mM imidazole, 0.5 M KCl, 50 mM Tris−HCl at pH 8.0, and 20 μM FAD) for every gram. The solution was cooled in an ice bath and subjected to disruption in a SONICS VCX500 model ultrasonic processor with a 1.3 cm flat-tip probe for 60 cycles (1 s each with 9 s pauses). The disrupted cells were centrifuged at 27000*g* for 1 h at 4 °C to remove cellular debris. The purification of 6× His tag AHAS II was carried out to near homogeneity in a single step by nickel−nitrilotriacetic acid (Ni−NTA) affinity chromatography as described in QIAexpressionist (Qiagen).[28] The enzyme was stored in aliquots at −80 °C. One aliquot was analyzed by sodium dodecyl sulfate−polyacrylamide gel electrophoresis (SDS−PAGE), with protein concentrations determined by the method of Bradford.[29−32] The inhibitory activity of the title compounds against AHAS enzyme

DOI: 10.1021/jf506153t
J. Agric. Food Chem. 2015, 63, 3734−3741

Table 3. Melting Point and HRMS Data of Title Compounds 1−4

compound	mp (°C)	HRMS
1a	255.0−256.0	$(M + H)^+$ 379.1396
1b	256.5−258.0	$(M + H)^+$ 395.1356
1c	276.5−278.2	$(M + H)^+$ 393.1563
1d	294.0−296.2	$(M + H)^+$ 289.0937
1e	277.4−279.4	$(M + H)^+$ 345.1564
2a	252.0−254.0	$(M + H)^+$ 393.1551
2b	165.0−167.0	$(M + H)^+$ 409.1500
2c	236.5−238.0	$(M + H)^+$ 407.1715
2d	225.0−226.5	$(M + H)^+$ 303.1087
2e	267.5−269.5	$(M + H)^+$ 359.1719
2f	163.0−165.0	$(M + H)^+$ 409.1504
3a	254.5−256.5	$(M + H)^+$ 334.1551
3b	270.5−272.5	$(M + H)^+$ 348.1709
4a	255.0−257.0	$(M + H)^+$ 435.2020
4b	215.0−217.0	$(M + H)^+$ 331.1405
4c	250.0−252.5	$(M + H)^+$ 387.2023
4d	266.4−268.2	$(M + H)^+$ 376.2021

in vitro was measured according to Westerfeld[33−35] and Singh[36,37] methods. Chlorimuron ethyl and bispyribac sodium were selected as a positive control. The reaction mixture contained a 50 mM potassium phosphate buffer (pH 7.5), 10 mM $MgCl_2$, 1 mM thiamine diphosphate (ThDP), 10 μM FAD, 100 mM pyruvate, and the enzyme in the absence or presence of various concentrations of inhibitors. The mixture was preincubated at room temperature for 5 min before initiation of the reaction. Then, the reaction was started by the addition of AHAS enzyme and allowed to incubate at 37 °C for 1 h, before being stopped by the addition of 3 M H_2SO_4 ($^1/_{10}$ final volume). Acetolactate was converted to acetoin by incubation at 60 °C for 15 min. Acetoin was then quantified by measuring the absorbance at 525 nm after incubation at 60 °C for 15 min with 0.5% creatine and 5% (w/v) α-naphthol. The apparent inhibition constant (K_i) values were determined by fitting the data to eq 4. The K_i values represented the concentration of the inhibitor at 50% inhibition.

$$\nu_i = \nu_\infty + (\nu_0 - \nu_\infty)/(1 + [I]/K_i) \quad (4)$$

In eq 4, ν_i and ν_0 represented the rates in the presence or absence of inhibitor, respectively, and $[I]$ was the concentration of the inhibitor. If the initial analysis indicated that the residual activity (ν_∞) at a saturating inhibitor concentration was not significantly greater

Scheme 1. Synthesis of Title Compounds

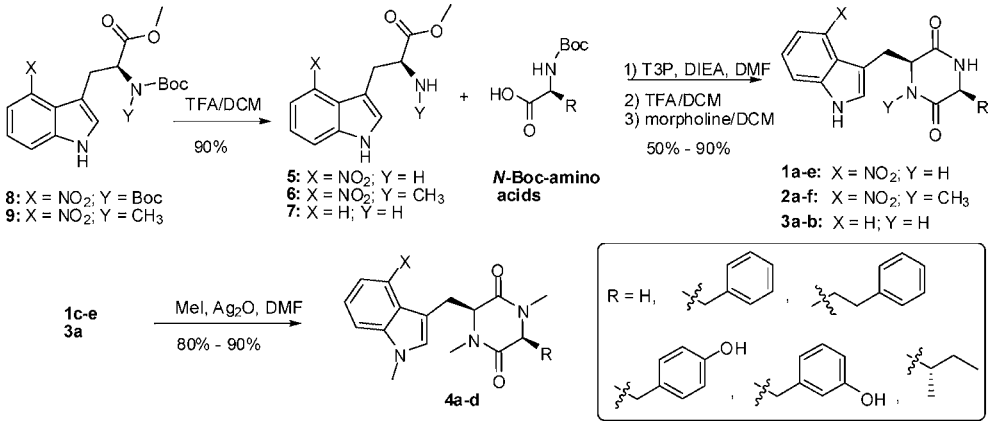

Table 4. Herbicidal Activity of Compounds (Percent Inhibition) (Rate = 1500 g ha^{-1})[a]

	BC		AR		EC		DS	
compound	pre	post	pre	post	pre	post	pre	post
1a	85.0 ± 1.2	30.0 ± 0.4	95.0 ± 1.3	5.0 ± 1.4	0.0	0.0	15.0 ± 0.8	20.0 ± 1.2
1b	0.0	15.0 ± 2.1	0.0	0.0	0.0	0.0	0.0	0.0
1c	10.0 ± 0.5	10.0 ± 1.1	0.0	0.0	0.0	0.0	0.0	0.0
1d	0.0	0.0	0.0	0.0	0.0	0.0	0.0	0.0
1e	0.0	10.0 ± 1.7	0.0	0.0	0.0	0.0	0.0	0.0
2a	100.0	100.0	100.0	61.3 ± 1.6	100.0	55.6 ± 2.1	100.0	50.0 ± 1.3
2b	5.0 ± 1.3	0.0	0.0	0.0	0.0	0.0	5.0 ± 0.6	0.0
2c	5.0 ± 0.9	0.0	10.0 ± 2.2	0.0	0.0	0.0	0.0	0.0
2d	0.0	0.0	10.0 ± 0.6	0.0	0.0	0.0	0.0	0.0
2e	0.0	5.0 ± 0.1	0.0	0.0	0.0	0.0	0.0	0.0
2f	100.0	100.0	95.0 ± 0.7	80.0 ± 2.4	100.0	20.0 ± 1.1	50.0 ± 0.8	65.0 ± 0.7
3a	10.0 ± 0.4	10.0 ± 1.1	0.0	0.0	0.0	0.0	0.0	0.0
3b	0.0	15.0 ± 0.7	0.0	10.0 ± 0.7	0.0	0.0	0.0	0.0
4a	10.0 ± 1.2	5.0 ± 0.5	0.0	0.0	0.0	0.0	0.0	0.0
4b	5.0 ± 1.0	0.0	0.0	0.0	0.0	0.0	0.0	0.0
4c	10.0 ± 0.8	15.0 ± 1.6	0.0	0.0	0.0	0.0	0.0	0.0
4d	10.0 ± 1.1	5.0 ± 0.8	0.0	0.0	0.0	0.0	0.0	0.0
TA	100.0	80.0 ± 1.5	100.0	70.0 ± 1.1	40.0 ± 0.9	30.0 ± 0.6	45.0 ± 1.4	10.0 ± 1.3
Dicb	100.0	20.0 ± 1.2	100.0	5.0 ± 1.5	95.4 ± 1.7	0.0	64.9 ± 2.1	0.0

[a]BC, *B. campestris*; AR, *A. retroflexus*; EC, *E. crus-galli*; DS, *D. sanguinalis*; post, post-emergence; pre, pre-emergence; and Dicb, dichlobenil.

DOI: 10.1021/jf506153t
J. Agric. Food Chem. 2015, 63, 3734−3741

Table 5. Further Herbicidal Activity of Compounds TA, 1a, 2a, and 2f (Percent Inhibition)[a,b]

compound	dosage (g ha^{-1})	BC		AR		AT		EC		DS		SG		SV		CV	
		pre	post	pre	post	pre	post	pre	post	pre	post	pre	post	pre	post	pre	post
1a	750	49.5 ± 1.1	15.6 ± 0.3	67.6 ± 0.7	17.9 ± 1.4	60.6 ± 1.1	15.0 ± 1.8	0.0	0.0	3.5 ± 0.5	14.6 ± 2.2	30.4 ± 1.7	29.1 ± 1.6	34.9 ± 0.9	0.0	0.0	0.0
	375	0.6 ± 0.2	10.5 ± 0.8	57.4 ± 1.2	14.4 ± 0.5	50.3 ± 1.7	10.0 ± 1.2	0.0	0.0	0.0	5.6 ± 1.3	18.3 ± 0.6	12.1 ± 1.2	7.3 ± 1.4	0.0	0.0	0.0
	187.5	0.0	9.2 ± 0.5	52.2 ± 0.8	6.8 ± 1.2	29.1 ± 1.3	2.1 ± 1.0	/	/	/	/	/	/	/	/	/	/
2a	750	88.1 ± 1.3	76.1 ± 1.5	91.9 ± 0.8	14.1 ± 0.4	56.0 ± 1.3	15.7 ± 1.2	100.0	0.0	3.5 ± 0.6	40.4 ± 0.7	90.2 ± 0.1	93.1 ± 0.3	89.7 ± 0.9	36.3 ± 0.5	71.1 ± 0.2	0.0
	375	86.0 ± 1.5	26.1 ± 2.4	91.2 ± 0.7	6.5 ± 0.1	41.8 ± 1.2	10.8 ± 0.6	100.0	2.2 ± 0.4	0.9 ± 1.2	14.6 ± 1.3	54.4 ± 1.1	88.5 ± 1.5	46.7 ± 0.3	21.4 ± 1.2	28.9 ± 0. 5	0.0
	187.5	68.9 ± 0.6	18.1 ± 1.1	83.1 ± 0.2	3.8 ± 1.3	36.5 ± 0.9	2.8 ± 1.5	/	/	/	/	/	/	/	/	/	/
2f	750	100.0	20.9 ± 1.8	100.0	3.5 ± 1.1	46.5 ± 0.7	59.2 ± 1.5	65.1 ± 1.3	0.0	20.9 ± 2.4	38.2 ± 1.3	38.2 ± 0.7	67.8 ± 1.8	51.3 ± 0.4	41.0 ± 0.8	0.0	0.0
	375	98.1 ± 1.5	13.0 ± 1.3	100.0	2.6 ± 0.7	39.4 ± 0.6	36.2 ± 0.7	30.7 ± 1.5	0.0	10.4 ± 1.9	12.2 ± 1.2	31.0 ± 1.5	42.6 ± 1.1	10.7 ± 0.9	11.5 ± 1.5	0.0	0.0
	187.5	86.2 ± 0.4	9.7 ± 1.0	100.0	1.2 ± 0.5	30.1 ± 1.3	16.6 ± 0.7	/	/	/	/	/	/	/	/	/	/
TA	750	100.0	52.1 ± 0.5	99.3 ± 0.1	3.8 ± 0.6	33.0 ± 1.3	15.2 ± 0.9	3.2 ± 0.7	22.2 ± 0.6	6.1 ± 1.4	0.0	51.5 ± 0.8	70.5 ± 0.7	41.8 ± 1.0	38.2 ± 0.6	0.0	0.0
	375	100.0	44.1 ± 0.4	96.3 ± 1.1	2.4 ± 0.3	29.4 ± 1.7	0.0	0.0	7.7 ± 0.4	0.0	0.0	48.5 ± 0.9	33.6 ± 1.8	33.0 ± 1.2	0.0	0.0	0.0
	187.5	98.1 ± 0.6	25.1 ± 1.5	94.9 ± 0.8	1.8 ± 0.6	17.0 ± 1.1	0.0	/	/	/	/	/	/	/	/	/	/
Dicb	750	100.0	8.8 ± 1.5	100.0	11.8 ± 0.7	73.4 ± 0.8	2.1 ± 1.4	55.6 ± 1.2	4.6 ± 1.1	0.0	0.0	61.6 ± 0.8	19.9 ± 0.4	22.4 ± 1.2	36.3 ± 0.6	55.6 ± 0.7	0.0
	375	100.0	5.9 ± 0.7	100.0	8.5 ± 0.9	57.1 ± 1.2	1.7 ± 0.6	24.6 ± 1.1	0.0	0.0	0.0	50.8 ± 0.9	15.8 ± 1.4	10.7 ± 2.1	0.0	2.2 ± 1.4	0.0
	187.5	87.6 ± 0.5	1.0 ± 0.1	96.3 ± 1.5	5.3 ± 0.6	42.9 ± 0.8	0.0	/	/	/	/	/	/	/	/	/	/

[a]BC, *B. campestris*; AR, *A. retroflexus*; AT, *A. theophrasti*; EC, *E. crus-galli*; DS, *D. sanguinalis*; SG, *S. glauca*; SV, *S. viridis*; CV, *Cernuella virigata*; post, post-emergence; pre, pre-emergence; and Dicb, dichlobenil. [b]"/" = not tested.

than zero, the data were reanalyzed with $\nu_\infty = 0$. K_i^{app} was calculated by nonlinear least squares and the simplex method for error minimization.[38−41] The K_i values were summarized in Table 7.

Antifungal Activity. Compounds **1**−**4** and TA were evaluated for their antifungal activities against *Candida albicans* [American Type Culture Collection (ATCC) 76615], *Candida utiliz*, *Saccharomyces cerevisia*, and *Aspergillus flavus* according to the National Committee for Clinical Laboratory Standards (NCCLS).[42] Fluconazole was selected as the control. A spore suspension in sterile distilled water was prepared from a 1-day-old culture of the fungi growing on Sabouraud agar (SA) media. The final spore concentration was 1−5 × 10^3 spore mL^{-1}. From the stock solutions of the tested compounds and reference antifungal fluconazole, dilutions in sterile RPMI 1640 medium (Neuronbc Laboraton Technology Co., Ltd., Beijing, China) were made resulting in 11 wanted concentrations (0.25−256 μg mL^{-1}) of each tested compound. These dilutions were inoculated and incubated at 35 °C for 24 h. The growth was monitored visually and spectrophotometrically. The lowest concentration (highest dilution) required to arrest the growth of fungi was regarded as the minimum inhibitory concentration (MIC). All of the antifungal activities were tested 3 times. The MICs were summarized in Table 8.

Data Collection. The tested compounds and reference drugs were prepared in Mueller−Hinton broth by 2-fold serial dilution to obtain the required concentrations of 512, 256, 128, 64, 32, 16, 8, 4, 2, 1, and 0.5 μg/mL. The data were collected only if three of the MIC values were consistent or three of the MICs were ranged in two neighboring concentrations (two MICs were consistent, and this concentration was collected).

RESULTS AND DISCUSSION

Chemistry. The total chemical synthesis of a series of thaxtomin analogues differs in R^1 and R^2 on indole, and R^3, R^4, and R^5 on the diketopiperazine ring are also synthesized. The detailed ^{1}H NMR (Table 2), ^{13}C NMR, optical rotation, and high-resolution mass spectra as well as melting point data (Table 3) of all title compounds are reported, and NMR and high-resolution mass spectrometry (HRMS) spectra are presented (see the Supporting Information).

The synthetic route of title compounds are given in Scheme 1. Compounds **8**[43] and **9**[20] were prepared according to the reported synthetic routes. Compounds **5** and **6** could be obtained in 90% yields by the deprotection of precursors **8** and **9** in solution of dichloromethane/trifluoroacetic acid (4:1, v/v) at room temperature for 30 min. The tryptophan methyl ester **7** was commercially available. The condensation of compounds **5**, **6**, and **7** with *N*-Boc-amino acid respectively in the presence of propylphosphonic acid anhydride (T3P), following by the deprotection of Boc moiety in dichloromethane/trifluoroacetic acid (4:1, v/v), afforded the key intermediates. The cyclization step[44] of the key intermediates with morpholine as a base in dichloromethane at room temperature for 48 h produced the target compounds **1a**−**1e**, **2a**−**2f**, **3a**, and **3b** in yields of 50−90%. The further methylation of compounds **1c**−**1e** and **3a** with MeI and Ag_2O afforded compounds **4a**−**4d** in yields of 80−90%.

Herbicidal Activities. The pre-emergence and post-emergence herbicidal activities in Table 4 manifest that substituents at R^1 and R^5 significantly affect the activities of title thaxtomin analogues, while the methylations of R^2, R^3, and R^4 show a weak influence on the herbicidal efficiency. It is observed that this series of compounds generally exhibits more effective pre-emergence herbicidal activities than post-emergence herbicidal activities. Compounds TA, **1a**, **2a**, and **2f** with the benzyl group and *m*-hydroxybenzyl groups at R^5 show significant pre-emergence herbicidal activity against dicotyledon

DOI: 10.1021/jf506153t
J. Agric. Food Chem. 2015, 63, 3734−3741

Table 6. Crop Selectivity of Compounds TA, 1a, 2a, and 2f (Post-emergence; Percent Inhibition)

compound	dosage (g ha^{-1})	wheat	corn	cotton	peanut
1a	750	4.1 ± 0.2	43.6 ± 0.5	0.0	7.7 ± 1.0
	375	0.0	13.4 ± 1.5	0.0	5.0 ± 0.7
2a	750	0.0	31.8 ± 0.8	0.0	26.2 ± 2.2
	375	0.0	24.1 ± 0.4	0.0	14.6 ± 0.8
2f	750	15.9 ± 1.6	27.1 ± 0.7	8.6 ± 0.4	36.0 ± 0.9
	375	13.3 ± 0.3	9.9 ± 0.4	0.0	22.4 ± 0.1
TA	750	17.5 ± 1.2	0.0	10.7 ± 0.8	36.8 ± 1.7
	375	0.0	0.0	0.0	24.5 ± 0.5
Dicb	750	7.6 ± 0.7	36.2 ± 1.2	0.0	25.0 ± 2.1
	375	4.7 ± 0.5	24.9 ± 0.4	0.0	7.9 ± 0.6

Table 7. PPO and AHAS Inhibition Activity of Compounds TA, 1a, 2a, and 2f (K_i, μM)[a]

compound	PPO	AHAS
1a	75.04 ± 7.43	–
2a	41.51 ± 2.38	–
2f	39.94 ± 1.83	–
TA	45.75 ± 0.42	–
chlorimuron ethyl	/	0.0221 ± 0.0064
bispyribac sodium	/	24.0 ± 15.8
oxadiazon	0.024 ± 0.0007	/
fluazolate	0.0062 ± 0.0009	/
sulfentrazone	0.030 ± 0.0006	/

[a]"–" = no activity, and "/" = not tested.

Table 8. Antifungal Data as MIC (μg mL^{-1}) for Compounds[a,b]

	fungi			
compound	*C. albicans*	*C. utiliz*	*S. cerevisiae*	*A. flavus*
1a	128	256	256	64
1b	32	256	512	128
1c	64	256	256	128
1d	64	128	128	128
1e	256	256	128	256
2a	64	64	64	64
2b	256	256	256	256
2c	128	128	128	64
2d	256	128	256	64
2e	128	128	128	128
2f	256	256	256	128
3a	256	256	256	128
3b	256	256	256	128
4a	128	64	128	128
4b	128	128	128	128
4c	256	256	128	256
4d	64	128	128	64
TA	256	128	64	128
fluconazole	4	16	16	256

[a]MICs were determined by the microbroth dilution method for microdilution plates. [b]*C. albicans*, *Candida albicans* (ATCC 76615); *C. utiliz*, *Candida utiliz*; *S. cerevisia*, *Saccharomyces cerevisia*; and *A. flavus*, *Aspergillus flavus*.

weeds *B. campestris* (≥85.0%) and *A. retroflexus* (≥95.0%). However, when the group at R^5 is exchanged by other substituents, such as *p*-hydroxybenzyl, phenylethyl, or alkyl groups or hydrogen (compounds **1b**–**1e** and **2b**–**2e**), the herbicidal properties disappear (percent inhibitions ≤15.0% to all weeds). Then, to investigate the influence of the nitro moiety at R^1, compounds **3a** and **3b** as controls were tested. The results manifest that the herbicidal activities disappear with the removal of the nitro group. Noticeably, compound **3a** exhibits rather decreased activities (≤10.0%) in comparison to its precursor **1a** with nitro on indole. Then, further methylations of ineffective compounds **1c**–**1e** and **3a** at R^2, R^3, and R^4 to afford compounds **4a**–**4d** lead no significant enhancements of their weed control competence. Besides, benzyl and *m*-hydroxybenzyl at R^5 of these thaxtomin analogues are more favorable for herbicidal activities than other substituents. Nitro at R^1 is essential for herbicidal efficacy, and the N-methylation of R^2, R^3, and R^4 is not helpful for herbicidal activity.

Compounds TA, **1a**, **2a**, and **2f** with effective activities were selected for further herbicidal testing at lower dosages (Table 5). The results indicate that compound **1a** shows moderate activity at 750 g ha^{-1} dosage to weeds but low activity at a lower dosage in most instances. Compounds TA, **2a**, and **2f** exhibit generally better weed control ability against dicotyledons (*B. campestris*, *A. retroflexus*, and *Abutilon theophrasti*) than monocotyledons, which are comparable or even better than positive control dichlobenil even at low dosage of 187.5 g ha^{-1}. Especially, TA and compound **2f** show excellent pre-emergence herbicidal activity against *B. campestris* and *A. retroflexus* with an inhibitory percent up to 86.2% at a dosage of 187.5 g ha^{-1}, which are superior to dichlobenil. Meanwhile, compound **2a** also exerts effective inhibition to monocotyledons *E. crus-galli*, *Setaria glauca*, and *Setaria viridis*. These results enable these compounds to be of much potential for further investigations as new herbicides.

Crop Selectivity. On the basis of the herbicidal activities mentioned above, compounds TA, **1a**, **2a**, and **2f** were selected for crop selectivity evaluation. As depicted in Table 6, four compounds display different crop selectivity to tested crops. Wheat and cotton exhibit absolute tolerance to compounds **1a** and **2a** with benzyl at R^5 by post-emergence application even at the dosage of 750 g ha^{-1}. Meanwhile, compound **2f** with *m*-hydroxybenzyl is safe for cotton at a dosage of 375 g ha^{-1}. Then, TA with *C*-hydroxyl diketopiperazine ring exerts no injury to corn at a high dosage of 750 g ha^{-1}, while wheat and cotton are also absolutely tolerant to TA at the dosage of 375 g ha^{-1}. However, peanut is susceptible to all four tested compounds. These results indicate that the substituents, especially the benzyl moiety at R^5 and the hydroxyl group on diketopiperazine, affect crop selectivity properties of thaxtomin analogues. The tested compounds may have the potential as herbicides in wheat, corn, and cotton fields.

PPO and AHAS Inhibition Activity. It was observed that the injury symptoms of thaxtomins in most instances were similar to known CBI dichlobenil. Meanwhile, the tested compounds also caused substantial wilting on all species following

DOI: 10.1021/jf506153t
J. Agric. Food Chem. 2015, 63, 3734–3741

post-emergence applications, which was similar to PPO or AHAS inhibitors. Thus, the PPO and AHAS inhibition experiments of compounds TA, **1a**, **2a**, and **2f** were carried out. Results shown in Table 7 indicate that TA, **1a**, **2a**, and **2f** all exhibit moderate PPO inhibitory activity but no AHAS inhibition. These results might be a reasonable explanation for why thaxtomins cause substantial wilting on weeds beside CBI mode of action and indicate that thaxtomins might act as multi-target herbicides.

Antifungal Activities. It is revealed that thaxtomins could inhibit the synthesis of cellulose, which is a major component of the fungal cell wall. This situation inspired us to evaluate the antifungal activity of title thaxtomin analogues. The MIC values in Table 8 manifested that the nitro group at R^1 is favorable for antifungal activities, and the introduction of the methyl moiety on indole and diketopiperazine at R^2, R^3, and R^4 has no significant influence on their bioactivities. Compounds **1**, **2**, and TA with nitro group R^1 give relatively better activities in contrast to compounds **3a** and **3b**. Especially the natural compound TC (**2a**) exhibits the most broad and effective antifungal efficacy among the tested compounds, with MICs of 64 μg mL^{-1} to all strains. Additionally, compounds **1b−1d** show moderate inhibition to *C. albicans* (MIC = 32−64 μg mL^{-1}); meanwhile, compounds **1a** and **2c−2d** could inhibit the growth of *A. flavus* at a concentration of 64 μg mL^{-1}. Subsequently, the N-methylations of R^2, R^3, and R^4 in compounds **1c−1e** and **3a** to synthesize compounds **4a−4d** do not result in improved antifungal activities. In summary, compound **2a** displays the broadest and most effective activities among the tested thaxtomin analogues and might be a potential lead compound for further development of novel antifungal agents.

In conclusion, a series of thaxtomin analogues were synthesized and evaluated for herbicidal property, PPO and AHAS inhibition, crop selectivity and antifungal activity. The greenhouse experiments indicate that nitro at R^1 and benzyl or *m*-hydroxybenzyl fragments at R^5 significantly affect herbicidal activities of thaxtomin analogues; meanwhile, N-methylations at R^2, R^3, and R^4 lead to a slight influence on the efficacy. Especially compounds TA, TC (**2a**), **1a**, and **2f** exhibit effective activities, which are comparable or even superior to positive control dichlobenil at a dosage of 187.5 g ha^{-1}. Moreover, the selected compounds show moderate PPO inhibition and satisfactory crop selectivity results. The above results indicate that the selected compounds TA, TC, **1a**, and **2f** might be potential lead compounds for future development of novel herbicides. Additionally, antifungal bioassays show that some compounds, especially TC, display effective inhibition to the tested fungi. Eventually, an attractive biological performance of thaxtomins mentioned above could prove to be of prime importance in future endeavors at understanding the mode of action of thaxtomins and developing new herbicides based on this natural resource backbone.

■ ASSOCIATED CONTENT

Supporting Information

General, synthetic procedures for the preparation of 4-nitro tryptophan methyl ester **5**, preparation of 4-nitro *N*-methyltryptophan methyl ester **6**, preparation of the title compounds **1a−1e**, preparation of the title compounds **2a−2f**, preparation of the title compounds **3a** and **3b**, preparation of the title compounds **4a−4d**, and preparation of TA, and NMR and HRMS spectra. This material is available free of charge via the Internet at http://pubs.acs.org.

■ AUTHOR INFORMATION

Corresponding Authors

*Telephone: +086-022-23501642. Fax: +86-022-23505369. E-mail: wangxinnk@nankai.edu.cn.

*E-mail: pwang@nankai.edu.cn.

Author Contributions

†Hongbo Zhang and Qingpeng Wang contributed equally to this work.

Author Contributions

⊥Xiande Yang, Xiaolin Lu, and Jiabao Zhang contributed equally to this work.

Funding

This research was supported by the National Natural Science Foundation of China (Grants 21102076, 91013013, and 31100587) and the Natural Science Foundation of Tianjin (Grant 10JCYBJC04100).

Notes

The authors declare no competing financial interest.

■ REFERENCES

(1) Duke, S. O.; Cantrell, C. L.; Meepagala, K. M.; Wedge, D. E.; Tabanca, N.; Schrader, K. K. *Toxins* **2010**, *2*, 1943−1962.

(2) Cantrell, C. L.; Dayan, F. E.; Duke, S. O. *J. Nat. Prod.* **2012**, *75*, 1231−1242.

(3) Hüter, O. F. *Phytochem. Rev.* **2011**, *10*, 185−194.

(4) Copping, L. G.; Duke, S. O. *Pest Manage. Sci.* **2007**, *63*, 524−554.

(5) Dayan, F. E.; Owens, D. K.; Duke, S. O. *Pest Manage. Sci.* **2012**, *68*, 519−528.

(6) King, R. R.; Calhoun, L. A. *Phytochemistry* **2009**, *70*, 833−841.

(7) Molesworth, P. P.; Gardiner, M. G.; Jones, R. C.; Smith, J. A.; Tegg, R. S.; Wilson, C. *Aust. J. Chem.* **2010**, *63*, 813−820.

(8) Krasnoff, S. B.; Lobkovsky, E. B.; Wach, M. J.; Loria, R.; Gibson, D. M. *J. Agric. Food Chem.* **2005**, *53*, 9446−9451.

(9) King, R. R.; Calhoun, L. A. *Magn. Reson. Chem.* **2009**, *47*, 273−276.

(10) King, R. R.; Calhoun, L. A. *Phytochemistry* **2009**, *70*, 833−841.

(11) Koivunen, M.; Marrone, P. U.S. Patent 20100167930 A1, 2010.

(12) King, R. R.; Lawrence, C. H.; Clark, M. C.; Calhoun, L. A. *J. Chem. Soc., Chem. Commun.* **1989**, 849−850.

(13) King, R. R.; Lawrence, C. H.; Gray, J. A. *J. Agric. Food Chem.* **2001**, *49*, 2298−2301.

(14) Lawrence, C. H.; Clark, M. C.; King, R. R. *Phytopathology* **1990**, *80*, 606−608.

(15) Goyer, C.; Charest, P. M.; Toussaint, V.; Beaulieu, C. *Can. J. Bot.* **2000**, *78*, 374−380.

(16) Fry, B. A.; Loria, R. *Physiol. Mol. Plant Pathol.* **2002**, *60*, 1−8.

(17) Leiner, R. H.; Fry, B. A. *Phytopathology* **1996**, *86*, 709−713.

(18) Bischoff, V.; Cookson, S. J.; Wu, S. *J. Exp. Bot.* **2009**, *60*, 955−965.

(19) Scheible, W. R.; Fry, B.; Kochevenko, A. *Plant Cell* **2003**, *15*, 1781−1794.

(20) Zhang, H.; Ning, X.; Hang, H.; Ru, X.; Li, H.; Li, Y.; Wang, L.; Zhang, Xiao.; Yu, S.; Qiao, Y.; Wang, Xin.; Wang, P. G. *Org. Lett.* **2013**, *15*, 5670−5673.

(21) Zhu, Y. Q.; Zou, X. M.; Hu, F. Z.; Yao, C. S.; Liu, B.; Li, Y. H.; Yang, H. Z. *J. Agric. Food Chem.* **2005**, *53*, 9566−9570.

(22) Li, H.; Zhu, Y.; Song, X.; Hu, F.; Liu, B.; Li, Y.; Niu, Z.; Liu, P.; Wang, Z.; Song, H.; Zou, X.; Yang, H. *J. Agric. Food Chem.* **2008**, *56*, 9535−9542.

(23) Xu, H.; Zhu, Y. Q.; Zou, X. M.; Liu, B.; Wang, Y.; Hua, F. Z.; Yang, H. Z. *Pest Manage. Sci.* **2012**, *68*, 276−284.

(24) Manelia, M. H.; Corrigalla, A. V.; Klumpb, H. H.; Davidsa, L. M.; Kirscha, R. E.; Meissnera, P. N. *Biochim. Biophys. Acta, Proteins Proteomics* **2003**, *1650*, 10−21.

(25) Dailey, T. A.; Dailey, H. A. *Protein Sci.* **1996**, *5*, 98−105.

DOI: 10.1021/jf506153t
J. Agric. Food Chem. 2015, 63, 3734−3741

(26) Corrigall, A. V.; Siziba, K. B.; Maneli, M. H.; Shephard, E. G.; Ziman, M.; Dailey, T. A.; Dailey, H. A.; Kirsch, R. E.; Meissner, P. N. *Arch. Biochem. Biophys.* **1998**, *358*, 251−256.
(27) Tan, Y.; Sun, L.; Xi, Z.; Yang, G. F.; Jiang, D. Q.; Yan, X. P.; Yang, X.; Li, H. Y. *Anal. Biochem.* **2008**, *383*, 200−204.
(28) Chen, Y. Z.; Gu, X. L.; Cao, Z. W. *J. Mol. Graphics Modell.* **2001**, *19*, 560−570.
(29) Balius, T. E.; Rizzo, R. C. *Biochemistry* **2009**, *48*, 8435−8448.
(30) Hao, G. F.; Yang, G. F.; Zhan, C. G. *J. Phys. Chem. B* **2010**, *114*, 9663−9676.
(31) Hou, T. J.; Yu, R. *J. Med. Chem.* **2007**, *50*, 1177−1188.
(32) Ishikita, H.; Warshel, A. *Angew. Chem., Int. Ed.* **2008**, *47*, 697−700.
(33) Kastenholz, M. A.; Pastor, M. G.; Cruciani, E. E.; Haaksma, J.; Fox, T. *J. Med. Chem.* **2000**, *43*, 3033−3044.
(34) Rocha, J. R.; Freitas, R. F.; Montanari, C. A. *Expert Opin. Drug Discovery* **2010**, *5*, 333−346.
(35) Naumann, T.; Matter, H. *J. Med. Chem.* **2002**, *45*, 2366−2378.
(36) Chuaqui, C.; Deng, Z.; Singh, J. *J. Med. Chem.* **2005**, *48*, 121−133.
(37) Deng, Z.; Chuaqui, C.; Singh, J. *J. Med. Chem.* **2004**, *47*, 337−344.
(38) Goodford, P. J. *J. Med. Chem.* **1985**, *28*, 849−857.
(39) Murcia, M.; Morreale, A.; Ortiz, A. R. *J. Med. Chem.* **2006**, *49*, 6241−6253.
(40) Murcia, M.; Ortiz, A. R. *J. Med. Chem.* **2004**, *47*, 805−820.
(41) Wang, T.; Wade, R. C. *J. Med. Chem.* **2001**, *44*, 961−971.
(42) Wang, Q.; Zhang, J.; Damu, G. L.; Wan, K.; Zhang, H.; Zhou, C. *Sci. China: Chem.* **2012**, *55*, 2134−2153.
(43) Xu, Z.; Hu, W.; Liu, Q. *J. Org. Chem.* **2010**, *75*, 7626−7635.
(44) Movassaghi, M.; Schmidt, M. A.; Ashenhurst, J. A. *Angew. Chem., Int. Ed.* **2008**, *47*, 1485−1487.

DOI: 10.1021/jf506153t
J. Agric. Food Chem. 2015, 63, 3734−3741

Therefore, the relationship between metabolites and quality remains to be explored. On the other hand, liquid chromatography−mass spectrometry (LC−MS) coupled with a multivariate statistical analysis of the metabolome (LC−MS-based metabolic profiling technique) has been used in the medical and microorganism/plant physiology fields as a comprehensive, sensitive, and nontargeted (nonbiased) approach.[19] This LC−MS-based metabolic profiling technique can elucidate the relationship between the previously undescribed metabolites in the green beans and the coffee quality.

Recently, we reported on the relationship between the metabolites and maturity levels[20] determined using the LC−MS-based metabolic profiling technique. In the present study, we have investigated the direct relationship between the metabolite properties and the resultant beverage quality (flavor score) and identified the metabolite markers (key compounds) responsible for the resultant beverage quality. The key compounds identified in this study can be utilized as objective criteria for selecting green beans and as indicators for improving beverage quality during technical processes such as roasting, brewing, and storing.

2. MATERIALS AND METHODS

2.1. Chemicals. LC−MS-grade acetonitrile, water, and formic acid were purchased from Wako Pure Chemical Industries, Ltd. (Osaka, Japan). High-performance-liquid-chromatography- (HPLC-) grade methanol, ethanol, and hexane and 6N HCl were purchased from Nacalai Tesque (Kyoto, Japan). 3-Methylbutanoic acid for food additives was purchased from Sigma-Aldrich (St. Louis, MO). Deuterated dimethyl sulfoxide (DMSO-d_6) was purchased from Eurisotop (Saint-Aubin, France).

2.2. Green and Roasted Coffee Beans. Forty varieties of green arabica coffee beans were obtained commercially, of which 36 were from Guatemala and 4 were uncharacterized. Each variety of green coffee beans (100 g) was roasted using a laboratory-scale roaster (Suntory laboratory and Suncafe laboratory, Kanagawa, Japan). The roasting degree was adjusted to a luminosity (L) value of 22−23 for all samples.

2.3. Sensory Evaluation. The sensory evaluation experiments were performed for metabolic profiling to identify the markers, for validating the applicability of the markers, and for determining the influence of the thermal degradation product of the markers on the resultant beverage quality (cup quality). All evaluations were conducted by an experienced Licensed Q grader, certified by the Coffee Quality Institute (CQI).

2.3.1. Metabolic Profiling. The sensory evaluation was performed basically in accordance with the Specialty Coffee Association of America (SCAA) cupping protocol.[21] For this study, 36 varieties of coffee beans from Guatemala were utilized. To avoid fatigue of the tongue, a maximum of six samples were compared at a time. A standard session consisted of six sets, with six samples per set (6 sets × 6 samples/set = 36 samples) and two cups from each sample. In addition, one control was used that was assigned 83 points (the mean score for all of the samples), which helped the grader in fixing the scale and scoring more accurately. The standard session was performed twice in a randomized order as blind analyses. The final cupping scores of each sample were given by summing the individual scores in the fragrance/aroma, flavor, aftertaste, acidity, body, balance, sweetness, uniformity, cleanliness, overall, and defects categories. The final scores were analyzed by multivariate statistical analysis.

2.3.2. Validation of the Applicability. The four uncharacterized coffee samples were evaluated (two cups from each sample) in accordance with the SCAA cupping protocol.

2.3.3. Influence of the Thermal Degradation Product of the Markers on the Cup Quality. Two varieties of coffee beans from Guatemala, one of good quality and the other of excellent quality, were studied. The ground powder (30 g) of each variety of roasted beans was extracted with hot water (300 mL, 97 °C). The coffee brew resulting from the coffee beans that were of good quality was used as the basic brew for studying the influence of 0.1 μ/L of flavor compound additives, whereas the brew prepared from the coffee beans of excellent quality was used for calibration reference. The panel assessed and scaled these brews with an SCAA cupping score. Only the aftertaste grades are provided in this article. The intensity values are assigned as line-scale values from 6 to 10 points in quarter point increments.

2.4. Metabolite Extraction and LC−MS Analysis for Metabolic Profiling. The green beans (10 g) frozen in liquid nitrogen were crushed with a small metal device by shaking using a Multibeads Shocker (Biomedical Science, Nagasaki, Japan) at 1100 rpm for 7 min, twice. The crushed powder (50 mg) was extracted with 1.5 mL of 70% methanol/H_2O for 1 h at 80 °C. After centrifugation at 10000 rpm for 10 min at 10 °C, the supernatants were diluted four times with 20% acetonitrile and filtered using a Ultrafree-MC filter units (0.22 μm, Polyvinylidene Fluoride (PVDF), Millipore, Billerica, MA) for use in the LC−MS analysis.

The LC−MS measurement of coffee metabolites was performed as described in our previous study,[20] on a Luna-C18 column (250 × 1.0 mm, 5-μm particle size, Phenomenex, Torrance, CA) using a LC−MS−ion trap (IT)−time-of-flight (TOF) instrument (Shimadzu, Kyoto, Japan).

2.5. Data Processing, Multivariate Statistical Analysis, and Correlation Plots. The data processing (peak picking and alignment) and normalization by the sum of total ion counts of each sample for the ion signals in positive mode were performed as described in our previous report.[20] The ion signals were subsequently filtered according to two criteria: (1) at least one group of a total of 36 categorical groups (36 varieties, n = 3) should exhibit <25% missing values and (2) relative standard deviation (RSD) values are <75%. As a result, 2649 valid peaks were obtained.

Multivariate statistical analysis was performed using the SIMCA P$^+$ version 13.0 software program (Umetrics, Umeå, Sweden). An orthogonal projection to latent structure (OPLS) regression model[22] was created to develop the sensory predictive model for the SCAA cupping score. Correlation plots between the cupping score and the extracted normalized signal intensity of the two markers were drawn.

2.6. LC−High-Resolution MS (LC−HR-MS) Analysis for the Isolation and the Structural Determination of the Markers. LC−HR-MS analyses of the coffee extracts and purified fractions were performed using a Q-Exactive hybrid quadrupole-orbitrap mass spectrometer (Thermo Fisher, San Jose, CA) with an electrospray ionization (ESI) source connected to a 10AV HPLC system (Shimadzu, Kyoto, Japan) on a KINETEX C18 column (250 mm × 2.1 mm, 1.7 μm, Phenomenex, Torrance, CA). For the LC analysis, the mobile phases A and B consisted of 0.1% formic acid/H_2O and 0.1% formic acid/acetonitrile, respectively. A flow rate of 0.2 mL/min; a gradient elution program of 5% B (0−2 min), 5−55% B (2−7.5 min), 55−100% B (7.5−17 min), 100% B (17−23 min), 100−5% B (23−24 min), and 5% B (24−32 min); and a column oven temperature of 40 °C were used. For the MS analysis, spray voltages of 3.5 kV (positive) and −3.5 kV (negative), a capillary temperature of 250 °C, a resolution power of 70000 for the full-scan MS event and MS/MS event, an m/z scan range of 80−1200, and a collision energy for MS/MS analysis of 15−45% (normalized) were used

2.7. Acid Hydrolysis of the Markers. To determine the configurations of the sugar moieties, the purified compounds (200 μg) were hydrolyzed by 6 N HCl (200 μL) at 100 °C for 60 min and analyzed using an HPLC−refractive index (RI) system on a Shodex SUGAR SP0810 column (8.0 mm × 300 mm, 7 μm, Showa Denko, Tokyo, Japan). For the LC analysis, isocratic elution of H_2O with a flow rate of 0.6 mL/min for 30 min was used. The column oven temperature was 80 °C. Identifications were carried out by comparing the chromatographic retention times of authentic sugars (D-glucose, D-fructose, D-galactose, and D-mannose), which were hydrolyzed and analyzed under the same conditions.

DOI: 10.1021/jf5054047
J. Agric. Food Chem. 2015, 63, 3742−3751

2.8. NMR Spectroscopy. For the structural determination of the markers, ^{1}H nuclear magnetic resonance (NMR) spectroscopy, ^{13}C NMR spectroscopy, total correlation spectroscopy (TOCSY), double quantum filter correlation spectroscopy (DQF-COSY), ^{1}H{^{13}C} heteronuclear single-quantum coherence (HSQC) spectroscopy, ^{1}H-{^{13}C} heteronuclear multiple bond correlation (HMBC) spectroscopy, nuclear Overhauser enhancement spectroscopy (NOESY), and rotational nuclear Overhauser effect spectroscopy (ROESY) spectra were obtained using a DMX-750 spectrometer (Bruker BioSpin, Rheinstetten, Germany) at 750 MHz. DMSO-d_6 was used as the solvent, and the chemical shifts were referenced to the solvent signal (δ 2.50 for ^{1}H and δ 39.43 for ^{13}C).

2.9. Quantitative Analysis of the Markers. The quantitative analyses of the markers in four green bean varieties were performed using LC−HR-MS. The purified compounds (markers) with concentrations of 0, 0.1, and 1 mg/L were used for standard calibration. Three replicates of the standards and of each sample were analyzed. The signal intensities at m/z 471.1714 (±10 ppm) were monitored in the negative mode.

2.10. Pyrolysis and Gas Chromatography (GC)−MS Analysis. Pyrolysis of the purified compounds was carried out using the Double-Shot PY-2020D pyrolyzer (Frontier Laboratories Ltd., Fukushima, Japan) at a temperature of 230 °C for 10 min. The thermally decomposed compounds were then separated directly using a 7890A GC system (Agilent Technologies, Santa Clara, CA) on a J&W DB-WAX etr fused silica capillary column (60 m × 0.32 mm i.d., df = 0.25 μm, Agilent Technologies) coupled with electron ionization (EI; 70 eV)−quadrupole (Q)-MS system using a 5075C inert XL MSD mass spectrometer (Agilent Technologies). The GC−MS analysis was conducted with a carrier gas (He) flow rate of 4.1 mL/min (at 40 °C), a transfer-line temperature of 250 °C, an ion-source temperature of 230 °C, a split ratio of 10:1, and an MS scan range of 33−450. The temperature program used was 40 °C for 2 min, raised to 250 °C by a 4 °C/min ramp, and finally kept at 250 °C for 5 min. The identifications were carried out by comparing the chromatographic retention times and mass spectral data of the target compounds with those of reference samples analyzed under the same conditions and by comparing the spectra with those obtained from the National Institute of Standards and Technology (NIST) library.

2.11. Extraction and Purification of the Markers for Structural Determination. Green coffee beans (*Coffea arabica*) (1.6 kg; Guatemala, Pacamara) frozen in liquid nitrogen were crushed using a Multibeads Shocker and defatted with 5 L of hexane. After being dried, the defatted powder was extracted with 8 L of 70% methanol/water for 2 h at 80 °C and filtered. The remaining powder was further extracted with 4 L of 70% methanol/water for 20 h at 4 °C and filtered. The combined filtrate was concentrated and loaded onto six types of columns, which are described below and in Figure S1 (Supporting Information), and the column eluents were analyzed by LC−HR-MS to detect the target compounds. **(1) HP-20 column** (1 L, Mitsubishi Chemical Co., Tokyo, Japan): The target compounds were eluted with water and 10% ethanol/water, and the eluents were separately concentrated to yield 250.8 and 11.4 g of powder, respectively. **(2) COSMOSIL C_{18}-OPN column** (1.2 L, 140 μm, Nacalai Tesque, Kyoto, Japan): The powder (250.8 g) from the water eluent of HP-20 was purified, and the target compounds were eluted with 0.1% formic acid/water and 0.1% formic acid/10% ethanol/water to yield 94.1 g of powder. **(3) COSMOSIL 75C18PREP column** (500 mL, 75 μm, Nacalai Tesque, Kyoto, Japan): The powder (11.4 g) obtained from the 10% ethanol/water eluent on HP-20 and the powder (94.1 g) obtained from the eluent on COSMOSIL C_{18}-OPN were combined and loaded. Fractions 2−9 (containing the target compounds) were concentrated to yield 20.2 g of powder. **(4) Develosil C30-UG-5 column** (20 × 250 mm, 5 μm, Nomura Chemical Co. Ltd., Aichi, Japan): The powder (20.2 g) was further purified. The fractionation was performed 17 times. Fractions 7−10 (containing compound **1**) and fractions 11−15 (containing compound **2**) were separately concentrated to yield 2.28 g (fraction 1A) and 2.00 g (fraction 1B), respectively, of powder. **(5) Shodex Asahipak NH2-P90 20F column** (20 × 300 mm, 5 μm, Showa Denko, Tokyo, Japan): Fraction 1A and fraction 2B were separately purified. Fraction 1A was purified by fractionating twice, and fractions 26−29 (containing compound **1**) were concentrated to yield 42.4 mg of powder (fraction 2A). Fraction 1B was purified by fractionating four times, and fractions 22−25 (containing compound **2**) were concentrated to yield 42.4 mg of powder (fraction 2B). **(6) Develosil C30-UG-5 column** (4.6 mm × 150 mm, 5 μm): Fractions 2A and 2B were separately purified. Fractions 8 and 9 (containing compound **1**) from fraction 2A and fraction 9 (containing compound **2**) from fraction 2B were separately concentrated to yield 2.3 and 6.0 mg, respectively, of a white powder.

3. RESULTS AND DISCUSSION

3.1. Metabolic Profiling. *3.1.1. Prediction of the Coffee Flavor Quality and Study of the Coffee-Flavor-Predicting Metabolite Markers.* The aim of this study is to identify the chemical compounds present in green coffee beans, which are the key compounds for the resultant beverage quality (cup quality). For this purpose, we purchased 36 varieties of green coffee beans from Guatemala that had different coffee qualities and roasted part of them under uniform conditions. Subsequently, an experienced Licensed Q grader evaluated their cup qualities and assigned SCAA cupping scores (Table 1) using the standardized SCAA protocol,[21] to ensure an accurate evaluation of the cup quality.

Table 1. Thirty-Six Coffee Green Beans from Guatemala Evaluated by the SCAA Cupping Score

SCAA cupping score (points)	
89	89.0
88	
87	
86	
85	
84	84.0, 84.0, 84.25
83	83.0, 83.0, 83.25, 83.25
82	82.0, 82.0, 82.0, 82.0, 82.0, 82.25, 82.25, 82.5, 82.75
81	81.0, 81.25, 81.25, 81.5, 81.5, 81.75, 81.75
80	80.0, 80.0, 80.75, 80.75, 80.75
79	79.0, 79.5, 79.5
78	78.25, 78.5
77	77.5
76	76.5

The rest of the green beans were subjected to LC−MS measurements using LC−MS−IT−TOF. The LC−MS spectra obtained were processed for peak picking and alignment, which resulted in a total of 2649 valid peaks.

We then applied a supervised multivariate statistical technique commonly used in metabolomics studies to isolate the most characteristic metabolite markers in our experiments. Using the SIMCA-P^{+} software program, a flavor (SCAA cupping score) prediction model was created, based on the OPLS regression analysis.[22] Although only 5.6% of the variation correlated with the first latent variable, the regression model appeared to be a good predictor of the scores, as indicated by the values of the correlation coefficient (R^2 = 0.957), the cross-

DOI: 10.1021/jf5054047
J. Agric. Food Chem. 2015, 63, 3742−3751

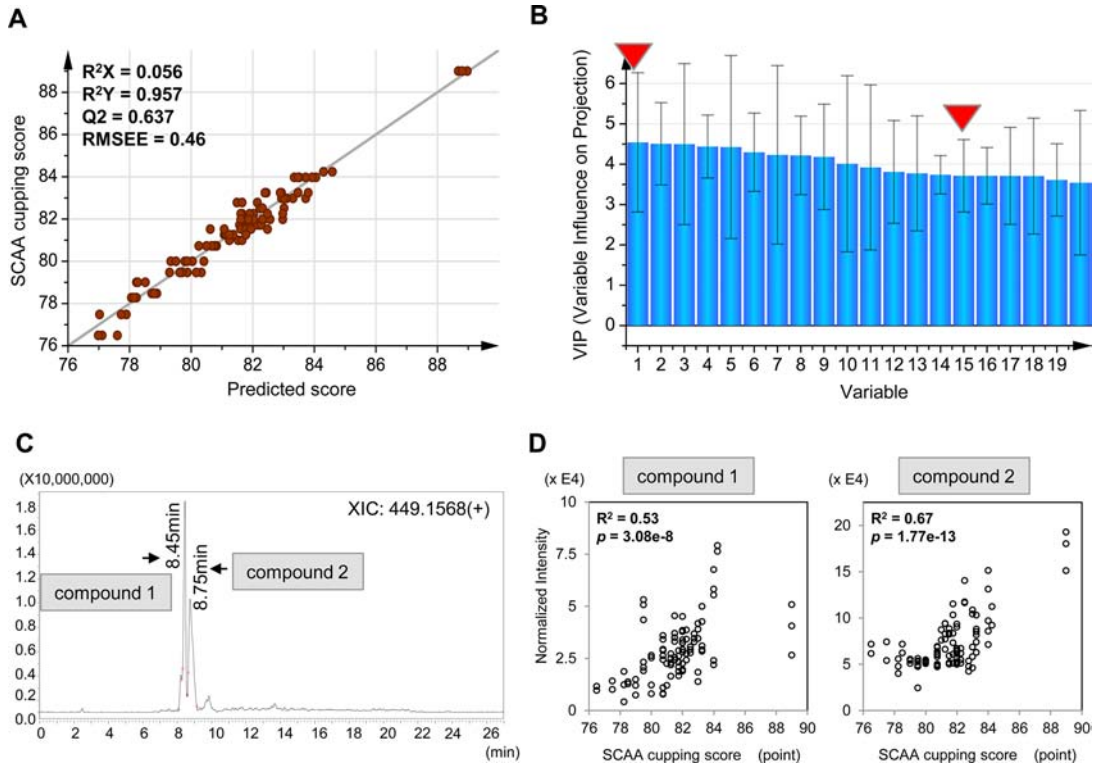

Figure 1. Two markers that strongly correlated with the SCAA cupping score studied by nontargeted metabolic analysis. (A) The OPLS model. The SCAA cupping score was predicted by the metabolomic information. (B) The VIP plot. The top 20 variables are shown. The red arrowhead indicated the two ion signals (markers) with m/z 449.1568(+). (C) The XIC for m/z 449.1568(+) derived from LC−MS−IT−TOF analysis of the coffee green extract (the green beans with SCAA score of 84 points). Two markers with the same m/z value (449.1568) were separately observed at RT 8.45 min (compound **1**) and RT 8.75 min (compound **2**). (D) The correlation plots between the SCAA score and the ion intensities of compound **1** (left) and compound **2** (right).

validated correlation coefficient (Q^2 = 0.637), and the root-mean-square error of estimation (RMSEE = 0.46) (Figure 1A).[23] This finding indicated that the metabolite data in the green beans could predict the SCAA cupping score (or cup quality) after the roasting and brewing processes.

The interpreted OPLS regression model was given by the variable influence on projection (VIP) parameter. We obtained a list of the metabolite ion signals ranked according to their VIP values (Figure 1B). As the higher-ranked metabolite signals are thought to substantially contribute to the regression, the top ranked m/z value of 449.1568 [retention time (RT) of 8.75 min] was considered to be most strongly correlated with the SCAA cupping score. Interestingly, in the VIP list, the signal for the 15th (m/z value of 449.1568) candidate was found to have the same m/z value as the top candidate, but a slightly different LC retention time (8.45 min). Indeed, the extracted chromatograms (XICs) displayed distinct peaks on top of each other (Figure 1C, RT 8.45 min, compound **1**; RT 8.75 min, compound **2**), suggesting that the two signals (markers) had different origins. Furthermore, the correlations between the SCAA scores and the ion intensities of these two markers were shown to be rather strong (for compound **1**, R^2 = 0.53, whereas for compound **2**, R^2 = 0.67) (Figure 1D). Overall, the data obtained indicated that an increasing amount of these two markers could either additively or independently contribute to the enhancement of the SCAA cupping score, raising the possibility that these were the potent precursors of coffee beverage flavor compounds.

3.2. Structural Determination and Quantification of the Markers. *3.2.1. Extraction and Purification.* Next, we purified and determined the chemical structures of the markers, to study their effectiveness in enhancing coffee flavor. The coffee green beans (1.6 kg) were extracted and subjected to several types of chromatography (Figure S1, Supporting Information). As an index of the ion at m/z 449.157 (±10 ppm) using LC−HR-MS, compounds **1** and **2** were successfully purified, resulting in 2.3 and 6.0 mg, respectively, of product.

3.2.2. Structural Determination. By LC−HR-MS, the molecular formulas of both compounds **1** and **2** were determined to be $C_{17}H_{30}O_{12}$ (compound **1**, m/z 449.1630 $[M + Na]^+$, error of −1.1 ppm; compound **2**, m/z 449.1631 $[M + Na]^+$, error of −0.9 ppm).

The LC−HR-MS/MS analyses revealed that both compounds **1** and **2** consisted of aglycone ($C_5H_{10}O_2$) and two hexose moieties with molecular masses of 426 (compounds **1** and **2**, precursor ion at m/z 471.171 $[M + HCO_2H - H]^-$ ($C_{18}H_{31}O_{14}$), fragment ions at m/z 425.167 $[M - H]^-$ ($C_{17}H_{29}O_{12}$), m/z 323.098 $[M -$ aglycone ($C_5H_{10}O_2$) $- H]^-$ ($C_{12}H_{19}O_{10}$), and m/z 161.044 $[M -$ aglycone $-$ (hexose $- H_2O) - H]^- = [$hexose $- H_2O - H]^-$ ($C_6H_9O_5$)).

Moreover, acid hydrolysis of compounds **1** and **2** indicated the presence of glucose in compound **1** and glucose and fructose in compound **2**, which were determined by comparison with pure sugars. The full assignments of the ^1H and ^{13}C NMR data of compounds **1** and **2**, established by one- and two-dimensional NMR spectra are reported in Tables 2 and 3, respectively.

3.2.2.1. Compound 1. The ^1H and ^{13}C NMR signals of compound **1** indicated a partial structure of 3-methylbutanoyl. In the ^1H NMR spectrum, two anomeric proton signals at δ

DOI: 10.1021/jf5054047
J. Agric. Food Chem. 2015, 63, 3742−3751

Table 2. ^{1}H and ^{13}C NMR Spectral Data of Compound 1 (DMSO-d_6), Compared with Literature Data

	compound 1		reference[a]	
	δ_H, (multi; J [Hz])	δ_C	δ_H, (multi; J [Hz])	δ_C
acyl moiety	3-methylbutanoyl		octanoyl	
1	–	171.16	–	174.1
2	2.24 (d; 7.0)	42.29	2.38 (m)	34.9
3	2.01 (m)	24.83	1.62 (tt; $J_{2',3'}$ 7.3)	25.6
4	0.92 (d; 6.7)	22.02	1.30-1.35 (m)	30.1
5	0.92 (d; 6.7)	22.02		30.1
6				32.8
7				23.7
8			0.90 (t; $J_{7',8'}$ 7.1)	14.4
sugar moiety	glucose moiety		glucose moiety	
1'	5.36 (d; $J_{1',2'}$ 8.2)	93.86	5.45 (d; $J_{1',2'}$ 7.8)	95.5
2'	3.11 (ov[b])	72.2	3.32 (dd; $J_{2',3'}$ 9.3)	73.3
3'	3.23 (dt; $J_{2',3'}$ 8.9, $J_{3',4'}$ 8.9)	76.33	3.41 (m)	77.7
4'	3.18 (dt; $J_{4',5'}$ 9.1)	69.15	3.42 (m)	70.8
5'	3.41 (ddd; $J_{5',6a'}$ 5.4, $J_{5',6b'}$ 1.2)	76.15	3.53 (m)	77.7
6'a	3.58 (dd; $J_{6a',6'b}$ 11.3)	67.77	3.76 (dd; $J_{5',6'a}$ 5.1, $J_{6'a,6'b}$ 11.4)	69.4
6'b	3.96 (dd)	–	4.14 (dd; $J_{5',6b'}$ 3.0)	–
	glucose moiety		glucose moiety	
1''	4.17 (d; $J_{1'',2''}$ 7.8)	102.94	4.31 (d; $J_{1'',2''}$ 7.8)	104.5
2''	2.95 (ddd; $J_{2'',3''}$ 8.7)	73.34	3.20 (dd; $J_{1'',2''}$ 9.1)	75.0
3''	3.11 (ov[b])	76.6	3.34 (dd; $J_{3'',4''}$ 8.8)	77.9
4''	3.04 (ov[b])	69.85	3.28 (dd; $J_{4'',5''}$ 8.8)	71.4
5''	3.04 (ov[b])	76.74	3.25 (m)	77.9
6''a	3.44 (ddd; $J_{5'',6'a}$ 5.9, $J_{6'a,6'b}$ 11.2)	60.89	3.65 (dd; $J_{5',6'a}$ 5.4, $J_{6'a,6'b}$ 12.1)	62.6
6''b	3.65 (ddd; $J_{5',6'b}$ 1.0)	–	3.85 (dd; $J_{5',6'b}$ 2.2)	–
	sugar OH-group			
2'(OH)	5.24 (d; $J_{2',2'(OH)}$ 5.5)			
3'(OH)	5.14 (d; $J_{3',3'(OH)}$ 4.9)			
4'(OH)	5.07 (d; $J_{4',4'(OH)}$ 5.7)			
2''(OH)	4.82 (d; $J_{2'',2''(OH)}$ 4.8)			
3''(OH)	4.90 (d; $J_{3'',3''(OH)}$ 4.9)			
4''(OH)	4.87 (d; $J_{4'',4''(OH)}$ 4.5)			
6''(OH)	4.44 (t; $J_{6''a,6''(OH)}$ 5.9, $J_{6''b,6''(OH)}$ 5.9)			

[a] 6-*O*-(*β*-D-Glucopyranosyl)-1-*O*-octanoyl-*β*-D-glucopyranose measured in CD_3OD.[24] [b] OV, overlapping signals.

5.36 and δ 4.17 were observed. Further, the ^{1}H and ^{13}C NMR data considered along with the results of acid hydrolysis suggested that the two hexose moieties could be assigned to glucose exhibiting a *β*-configuration, based on the values of coupling constants for inner glucose ($J_{1',2'}$ = 8.2 Hz) and terminal glucose ($J_{1'',2''}$ = 7.8 Hz). The ^{1}H and ^{13}C NMR data of the complete sugar moiety of compound **1** were consistent with those of 6′-*O*-(*β*-D-glucopyranosyl)-1′-*O*-acyl-*β*-D-glucopyranose.[24]

Comparison with literature values indicated 1 → 6 linkages of two glucose moieties,[25] and the anomeric proton H-1′ showed a downfield shift indicating an ester linkage of 3MA to the hydroxyl group at the C-1′ position in the inner glucose. Furthermore, the $^{1}H\{^{13}C\}$-HMBC analysis also showed a cross-peak between H-1′ of the inner glucose (δ 5.36) and the carbonyl carbon of the 3-methylbutanoyl moiety (δ 171.16) and between H-1″ of the terminal glucose (δ 4.17) and C-6′ of the inner glucose (δ 67.77). Therefore, compound **1** was deduced to be 6′-*O*-(*β*-D-glucopyranosyl)-1′-*O*-[3-methylbutanoyl]-*β*-D-glucopyranose (Figure 2).

3.2.2.2. Compound 2. Comparison of the ^{1}H and ^{13}C NMR results with the reported data in the literature suggested that

DOI: 10.1021/jf5054047
J. Agric. Food Chem. 2015, 63, 3742−3751

Table 3. ^{1}H and ^{13}C NMR Spectral Data of Compound 2 (DMSO-d_6), Compared with Literature Data

	compound 2		reference[a]	
	δ_H, (multi; J [Hz])	δ_C	δ_H, (multi; J [Hz])	δ_C
acyl moiety	3-methylbutanoyl		3-methylbutanoyl	
1	–	172.19	–	172.3
2	2.20 (m)	42.33	2.19 (m)	42.4
3	1.99 (m)	25.02	1.99 (m)	25.1
4	0.91 (d; 6.7)	22.03	0.90 (d; 6.7)	22.1
5	0.91 (d; 6.7)	22.03	0.90 (d; 6.7)	22.1
sugar moiety	glucose moiety		glucose moiety	
1'	5.17 (d; $J_{1',2'}$ 3.6)	91.38	5.17 (d; $J_{1',2'}$ 3.7)	91.5
2'	3.20 (ddd; $J_{2',3'}$ 9.6)	71.4	3.20 (dd; $J_{2',3'}$ 9.7)	71.5
3'	3.48 (dt; $J_{3',4'}$ 9.2)	72.55	3.48 (t; $J_{3',4'}$ 9.7)	72.7
4'	3.06 (dt; $J_{4',5'}$ 9.4)	70.03	3.06 (t; $J_{4',5'}$ 9.7)	70.1
5'	3.90 (m)	69.87	3.90 (m)	70.0
6'a	4.24 (dd; $J_{5',6a'}$ 1.3, $J_{6'a,6'b}$ 11.7)	63.36	4.24 (dd; $J_{5',6'a}$ 1.0, $J_{6'a,6'b}$ 10.0)	63.4
6'b	4.01 (dd; $J_{5',6'b}$ 6.0)	–	4.01 (dd; $J_{5',6'b}$ 6.0)	–
	fructose moiety		fructose moiety	
1''ab	3.38 (m)	62.03	3.38 (m)	62.2
2''	–	103.79	–	103.79
3''	3.87 (t; $J_{3'',4''}$ 8.1)	76.79	3.88 (d; $J_{3'',4''}$ 8.0)	76.9
4''	3.73 (m)	74.39	3.73 (m)	74.5
5''	3.59 (m)	82.65	3.58 (m)	82.7
6''a	3.54 (m)	62.5	3.55 (m)	62.6
6''b	3.57 (m)	–	3.55 (m)	–
	sugar OH-group			
2'(OH)	5.13 (d; $J_{2',2'(OH)}$ 6.0)			
3'(OH)	4.89 (d; $J_{3',3'(OH)}$ 4.8)			
4'(OH)	5.01 (d; $J_{4',4'(OH)}$ 5.7)			
1''(OH)	4.81 (t; $J_{1'',1''(OH)}$ 6.2)			
3''(OH)	4.56 (d; $J_{3'',3''(OH)}$ 8.1)			
4''(OH)	5.16 (d; $J_{4'',4''(OH)}$ 6.0)			
6''(OH)	4.40 (bt; $J_{6''a,6''(OH)}$, $J_{6''b,6''(OH)}$ 5)			

[a] 3-methylbutanoyl-6-O-α-D-glucopyranosyl-β-D-fructofuranoside measured in DMSO-d_6.[26]

compound **2** was a known compound.[26] Briefly, the ^{1}H and ^{13}C NMR data of compound **2** and compound **1** were consistent in terms of the acyl moiety, suggesting the presence of 3-methylbutanoyl. Further, the NMR signals from compound **2** suggested the presence of acyl-6-O-sucrose and glucose moieties,[27,28] in addition to providing indications of an ester linkage at position of 6′ of the glucose moiety. Compound **2** was concluded to be 3-methylbutanoyl-6-O-α-D-glucopyranosyl-β-D-fructofuranoside (Figure 2), and the data obtained were in good agreement with the data reported in the literature (see Tables 2).[26]

The two markers that strongly correlated with the SCAA cupping score were isolated from the green beans and determined to be 3-methylbutanoyl disaccharides (3MDs), 6′-O-(β-D-glucopyranosyl)-1′-O-[3-methylbutanoyl]-β-D-glucopyranose (compound **1**) and 3-methylbutanoyl-6-O-α-D-

DOI: 10.1021/jf5054047
J. Agric. Food Chem. 2015, 63, 3742−3751

glucopyranosyl-β-D-fructofuranoside (compound **2**). Although compound **2** is a known compound in coffee green beans,[26] to the best of our knowledge, the presence of compound **1** has not been reported so far. These markers were considered to be the isomers of the sugar-bound flavor precursors.

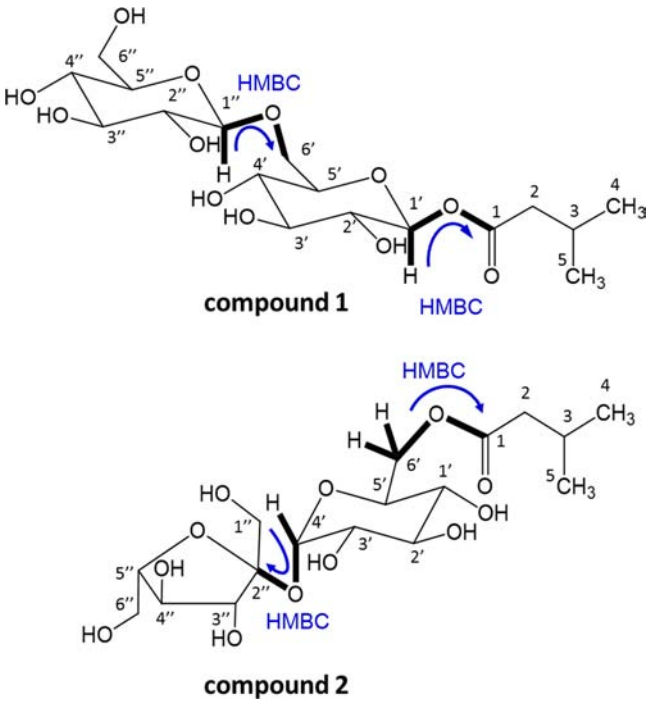

Figure 2. Structures of two markers, compound **1** (upper) and compound **2** (lower). $^{1}H\{^{13}C\}$-HMBCs are shown with thick lines.

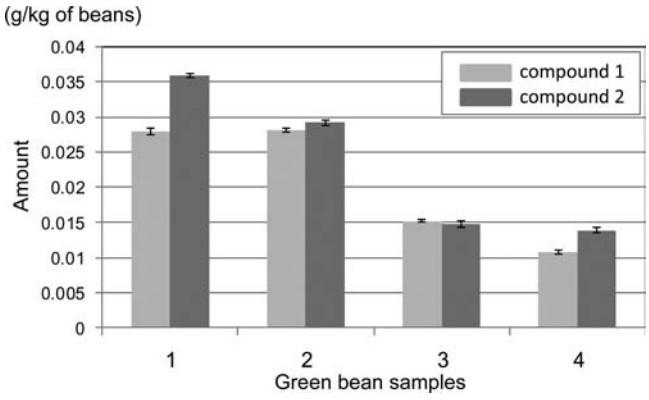

Figure 3. Quantitative analyses of compounds **1** and **2** in four green bean samples by LC–HR-MS.

3.2.3. Quantification. Quantitative analyses revealed that the amounts of 3MDs in four green beans were only 0.01–0.035 g/kg of beans (for both compounds **1** and **2**) (Figure 3). These amounts were only about 1/1000–1/5000 that of chlorogenic acid,[29] which is the major constituent in the coffee green beans. Despite the very small quantity, these were significant flavor-discrimination markers and could be the potent precursors for coffee beverage's flavor compounds that enhance the cup quality. The SCAA cupping score (cup quality) of four samples will be discussed in section 3.4.

3.3. Influence of 3MDs on the Cup Quality. Coffee flavors and aromas are developed during the roasting process.[30] However, the chemical changes in the metabolites during roasting are highly complicated and remain uncharacterized. On the other hand, in food chemistry, pyrolysis coupled with GC–MS has been utilized to study thermal degradation products to mimic processes such as roasting and heating.[31,32] We employed this technique to identify the thermal products of 3MDs and then studied the effects of the thermal products on the cup quality (SCAA cupping score) by model experiments.

3.3.1. Identification of Flavor/Aroma Compounds by Thermal Reaction of 3MDs. First, the thermal degradation products of 3MDs were studied. The two 3MDs were subjected to pyrolysis under the model conditions of roasting (230 °C, 10 min), and the products were detected by GC–MS. Thermal reaction of compound **1** produced compounds mainly consisting of 3-methylbutanoic acid (3MA) (RT 28.9 min), in addition to minor amounts of furfural (RT 22.0 min) and 5-hydroxymethylfurfural (5-HMF, RT 50.2 min), which were identified based on a NIST library search (Figure 4A). Furthermore, the structure of 3MA, which was the main product, was confirmed by comparing the chromatographic retention time and the mass spectral data obtained in the experiments with those corresponding to the standard compound. Interestingly, the pyrolysis of compound **2** produced mostly the same compounds as pyrolysis of compound **1** (Figure 4A). Thermal reactions of both markers mainly resulted in 3MA by hydrolysis (Figure 4B), along with the minor caramelized products furfural and 5-HMF. The caramelized products have been previously reported to be formed from sugars,[33,34] which are one of the main ingredients of green beans.[35] On the other hand, 3MA is a characteristic moiety of 3MDs. Therefore, in this article, we focus on 3MA and discuss its effect on coffee flavor.

3.3.2. Study of the Influence of 3MA on Cup Quality. The effect of the addition of 3MA to the basic coffee brew on the cup quality was investigated next. An experienced Licensed Q grader evaluated the base coffee brew with and without the 3MA additive, and the calibration reference brew (excellent quality), and then assigned aftertaste score, which is one of the axes described in the SCAA protocol. Aftertaste is a significant factor for coffee flavors and represents the impression (length and quality) of coffee flavors that remains after swallowing. Figure 5 shows that the aftertaste intensities increased with the addition of 3MA (0.1 μ/L). Therefore, it was concluded that the addition of 3MA improved the cup quality. The scorings for other attributes, such as acidity, body, and sweetness, need to be interpreted further.

These findings indicate that the two 3MDs are the precursors of 3MA, which significantly enhances the quality of coffee flavors. The two precursors could additively enhance the cup quality. In the literature, some other 3-methylbutanoyl sugar conjugates, such as 3-methylbutanoyl-1-*O*-β-D-glucopyranosyl-β-D-apiofuranoside[26] and 3′-*O*-β-D-glucopyranosyl-2′-*O*-3-methylbutanoyl-2β-(2-desoxy-atracty-ligenin)-β-D-glucopyranoside,[36,37] have been isolated from coffee green beans. These compounds would additively enhance the cup quality. The contribution ratio of these compounds toward the cup quality will be examined further.

3.4. Validation of the Applicability of 3MDs for Predicting the Cupping Score. To verify the applicability of the 3MDs as potent markers, we analyzed another sample set (validation sample set). As described in section 3.2.3, four varieties of uncharacterized coffee green beans, which were procured from different coffee-producing countries, contained

DOI: 10.1021/jf5054047
J. Agric. Food Chem. 2015, 63, 3742–3751

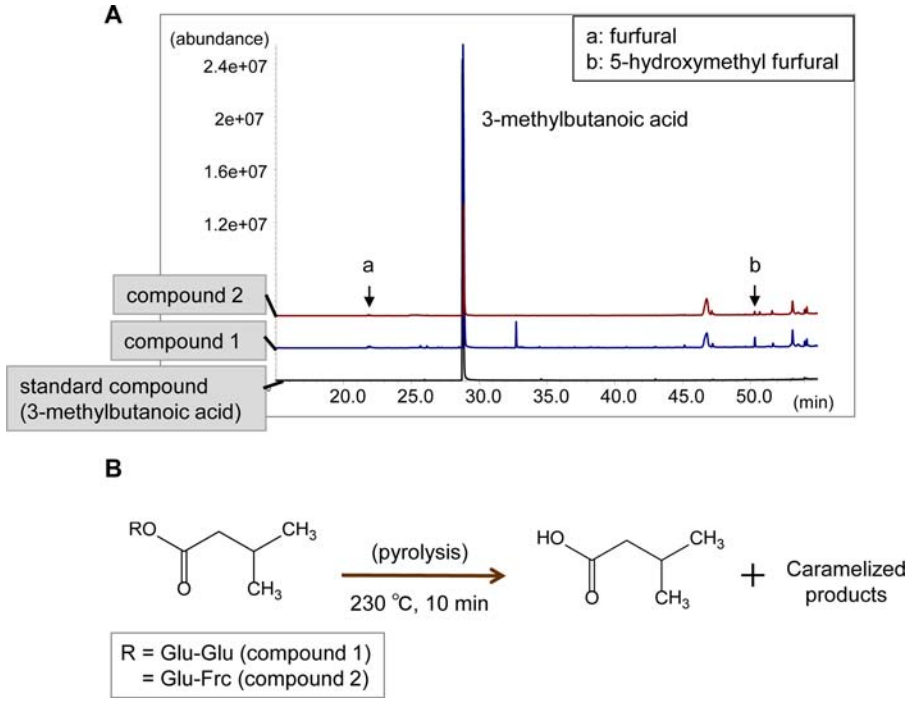

Figure 4. Pyrolysis-GC−MS analyses. (A) Total ion chromatograms of compounds **1** and **2** and the standard compound (3MA). (B) Thermal degradation of compounds **1** and **2** to produce 3MA and caramelized compounds.

Figure 5. Sensory evaluation (aftertaste score) of three coffee brew: the calibration reference brew, the base brew, and the base brew with 3MA additive (0.1 μL/L).

compounds **1** and **2** with different amounts (Figure 3). After we roasted these green beans under uniform conditions, an experienced Licensed Q grader evaluated the cup quality and assigned SCAA scores (Table 4). The results combined Figure 3 with Table 4 indicated that increasing amounts of 3MDs were associated with increasing SCAA cupping scores. Therefore, it was verified that the 3MDs were flavor-discrimination markers in the validation sample set. To highlight the applicability and importance of these markers for practical use, a number of sample sets, including a wide variety of coffee samples obtained from different production areas and countries (different cultivation condition), from different cultivars, and with different processing methods (washed or natural process method to produce green beans from cherries) will need to be examine further.

Table 4. SCAA Cupping Scores for the Validation Coffee Samples

coffee sample	SCAA cupping score
1	85.5
2	85
3	81
4	80

In summary, we focused on the metabolites in green beans to predict and contribute to the resultant beverage quality. We prepared samples from 36 varieties of coffee green beans that had distinct differences in quality (different SCAA cupping scores) and conducted nontargeted LC−MS-based metabolic profiling. It was validated that the LC−MS data of metabolites could predict the beverage quality through the roasting and brewing processes. Further, we successfully explored and identified two isomers of 3MDs, one of which is a novel structure that has not been reported in the literature so far, to the best of our knowledge. Although the 3MDs are present in very small quantities in the green coffee beans, they were found to be significant flavor-discrimination markers and were potent precursors for the flavor/aroma compounds in coffee beverages that enhance the cup quality. Other 3-methylbutanoyl sugar conjugates from coffee green beans have also been reported in the literature and could additively enhance the cup quality along with the 3MDs. The 3MDs could be used as universal criteria to evaluate and predict beverage quality from green beans in the presence or absence of other compounds.

■ ASSOCIATED CONTENT

Supporting Information

Detailed description of the purification of two markers. This material is available free of charge via the Internet at http://pubs.acs.org.

DOI: 10.1021/jf5054047
J. Agric. Food Chem. 2015, 63, 3742−3751

AUTHOR INFORMATION

Corresponding Authors

*Tel.: +81-75-962-9189. Fax: +81-75-961-2908. E-mail: Keiko_Iwasa@suntory.co.jp (K.I.).

*Tel.: +81-75-962-9189. Fax: +81-75-961-2908. E-mail: Koichi_Nakahara@suntory.co.jp (K.N.).

Notes

The authors declare no competing financial interest.

ACKNOWLEDGMENTS

We thank Dr. Takashi Iwashita and Shoko Mori (Suntory Foundation for Life Sciences) for the NMR measurements. We also thank Suncafé Ltd. (Kanagawa, Japan) for roasting the beans. We thank Nami Tomonaga (Kyushu University), and Noriko Ishibashi and Yuki Kaneko (Suntory SIC) for their technical support.

REFERENCES

(1) World Coffee Trade. International Coffee Organization, London, http://www.ico.org/trade_e.asp?section=About_Coffee (accessed Sep 25, 2014).

(2) *Coffee Meister Training Course Text Book*; Specialty Coffee Association of Japan: Tokyo, Japan, 2011; pp 36−39 (in Japanese).

(3) Rodrigues, C. L.; Maia, R.; Miranda, M.; Ribeirinho, M.; Nogueira, J. M. F.; Maguas, C. Stable isotope analysis for green coffee bean: A possible method for geographic origin discrimination. *J. Food Compos. Anal.* **2009**, *22*, 463−471.

(4) Alonso-Salces, R. M.; Serra, F.; Reniero, F.; Heberger, K. Botanical and geographical characterization of green coffee (*Coffea arabica* and *Coffea canephora*): Chemometric evaluation of phenolic and methylxanthine contents. *J. Agric. Food Chem.* **2009**, *57*, 4224−4235.

(5) Wei, F.; Furihata, K.; Koda, M.; Hu, F.; Kato, R.; Miyakawa, T.; Tanokura, M. ^{13}C NMR-based metabolomics for the classification of green coffee beans according to variety and origin. *J. Agric. Food Chem.* **2012**, *60*, 10118−10125.

(6) Choi, M. Y.; Choi, W.; Park, J. H.; Lim, J.; Kwon, S. W. Determination of coffee origins by integrated metabolomics approach of combining multiple analytical data. *Food Chem.* **2010**, *121*, 1260−1268.

(7) El-Abassy, R. M.; Donfack, P.; Materny, A. Discrimination between Arabica and Robusta green coffee using visible micro Raman spectroscopy and chemometric analysis. *Food Chem.* **2011**, *126*, 1443−1448.

(8) Alves, R. C.; Casal, S.; Alves, M. R.; Oliveira, M. B. Discrimination between arabica and robusta coffee species on the basis of their tocopherol profiles. *Food Chem.* **2009**, *114*, 295−299.

(9) Casal, S.; Alves, A. R.; Mendes, E.; Oliveira, M. B. P. P.; Ferreira, M. A. Discrimination between arabica and robusta coffee species on the basis of their amino acid enantiomers. *J. Agric. Food Chem.* **2003**, *51*, 6495−6501.

(10) Mendonca, J. C. F.; Franca, A. S.; Oliveira, L. S.; Nuncs, M. Chemical characterization of non-defective and defective green arabica and robusta coffees by electrospray ionization-mass spectrometry (ESI-MS). *Food Chem.* **2008**, *111*, 490−497.

(11) Santos, J. R.; Sarraguca, M. C.; Rangel, A. O. S. S.; Lopes, J. A. Evaluation of green coffee beans quality using near infrared spectroscopy: A quantitative approach. *Food Chem.* **2012**, *135*, 1828−1835.

(12) Farah, A.; Monterio, M. C.; Calado, V.; Franca, A. S.; Trugo, L. C. Correlation between cup quality and chemical attributes of Brazilian coffee. *Food Chem.* **2006**, *98*, 373−380.

(13) Koshiro, Y.; Zheng, X.; Wang, M.; Nagai, C.; Ashihara, H. Changes in content and biosynthetic activity of caffeine and trigonelline during growth and ripening of *Coffea arabica* and *Coffea canephora* fruits. *Plant Sci.* **2006**, *171*, 242−250.

(14) Clifford, M. N.; Kazi, T. The influence of coffee bean maturity on the content of chlorogenic acids, caffeine and trigonelline. *Food Chem.* **1987**, *26*, 59−69.

(15) Koshiro, Y.; Jackson, M. C.; Katahira, R.; Wang, M. L.; Nagai, C.; Ashihara, H. Biosynthesis of chlorogenic acids in growing and ripening fruits of *Coffea arabica* and *Coffea canephora* plants. *Z. Naturforsch. C* **2007**, *62*, 731−742.

(16) De Menezes, H. C. The relationship between the state of maturity of raw coffee beans and the isomers of caffeoylquinic acid. *Food Chem.* **1994**, *50*, 293−296.

(17) Craig, A. P.; Franca, A. S.; Oliveira, L. S. Discrimination between immature and mature green coffees by attenuated total reflectance and diffuse reflectance Fourier transform infrared spectroscopy. *J. Food Sci.* **2011**, *76*, C1162−C1168.

(18) De Abreu, H. M. C.; Nobile, P. M.; Shimidzu, M. M.; Yamamoto, P. Y.; Silva, E. A.; Colombo, C. A.; Mazzafera, P. Influence of air temperature on proteinase activity and beverage quality in *Coffea arabica*. *Braz. J. Bot.* **2012**, *35*, 357−376.

(19) Dettmer, K.; Aronov, P. A.; Hammock, B. D. Mass spectrometry based metabolomics. *Mass Spectrom. Rev.* **2007**, *26*, 51−78.

(20) Setoyama, D.; Iwasa, K.; Seta, H.; Shimidzu, H.; Fujimura, Y.; Miura, D.; Wariishi, H.; Nagai, C.; Nakahara, K. High-throughput metabolic profiling of diverse green *Coffea arabica* beans identified tryptophan as a universal discrimination factor for immature beans. *PLoS One* **2013**, *8*, e70098.

(21) Cupping Protocols. Specialty Coffee Association of America, Santa Ana, CA, http://www.scaa.org/?page=resources&d=cupping-protocols (accessed Sep 25, 2014).

(22) Wiklund, S.; Johansson, E.; Sjostrom, L.; Mellerowicz, E.; Edlund, U.; Shockcor, J. P.; Gottfries, J.; Moritz, T.; Trygg, J. Visualization of GC/TOF-MS-based metabolomics data for identification of biochemically interesting compounds using OPLS class models. *Anal. Chem.* **2008**, *80*, 115−122.

(23) Eriksson, L.; Johansson, E.; Kettaneh-Wold, N.; Trygg, J.; Wikström, C.; Wold, S. *Multi- and Megavariate Data Analysis. Part I: Basic Principles and Applications*; Umetrics: Umeå, Sweden. 2006.

(24) Wang, M.; Kikuzaki, H.; Jin, Y.; Zhu, N.; Csiszar, K.; Boyd, C.; Rosen, T. R.; Ghai, G.; Ho, C. Novel glycosides from Noni (*Morinda citrifolia*). *J. Nat. Prod.* **2000**, *63* (8), 1182−1183.

(25) Kaneko, T.; Ohtani, K.; Kasai, R.; Yamasaki, K.; Duc, N. M. *n*-Alkyl glycosides and *p*-hydroxybenzoyloxy glucose from fruits of *Crescentia cujete*. *Phytochemistry* **1998**, *47*, 259−263.

(26) Weckerle, B.; Gati, T.; Toth, G.; Schreier, P. 3-Methylbutanoyl and 3-methylbut-2-enoyl disaccharides from green coffee beans (*Coffea arabica*). *Phytochemistry* **2002**, *60*, 409−414.

(27) Thévenet, S.; Wernicke, A.; Belniak, S.; Descotes, G.; Bouchu, A.; Queneau, Y. Esterification of unprotected sucrose with acid chlorides in aqueous medium: Kinetic reactivity versus acyl- or alkoxycarbonyl-group migrations. *Carbohydr. Res.* **1999**, *318*, 52−66.

(28) Tchinda, A.; Tane, P.; Ayafor, J. F.; Connolly, J. D. Stigmastane derivatives and isovaleryl sucrose esters from *Vernonia guineensis* (Asteraceae). *Phytochemistry* **2003**, *63*, 841−846.

(29) Moon, J. K.; Yoo, H. S.; Shibamoto, T. Role of roasting conditions in the level of chlorogenic acid content in coffee beans: Correlation with coffee acidity. *J. Agric. Food Chem.* **2009**, *57*, 5365−5369.

(30) Illy, E. The complexity of coffee. One of life's simple pleasures is really quite complicated. *Sci. Am.*, **2002**, June, 86−91.

(31) Wnorowski, A.; Yaylayan, V. A. Influence of pyrolytic and aqueous-phase reactions on the mechanism of formation of maillard products. *J. Agric. Food Chem.* **2000**, *48*, 3549−3554.

(32) Xie, W.; Gu, X.; Luo, C.; Wang, G.; Tang, J. Study on the pyrolysis behavior of geranyl-β-D-glucopyranoside by gas chromatography-mass spectrometry. *Chin. J. Chromatogr.* **2006**, *24* (4), 339−342.

(33) Locas, C. P.; Yaylayan, V. A. Isotope labeling studies on the formation of 5-(hydroxymethyl)-2-furaldehyde (HMF) from sucrose by pyrolysis-GC/MS. *J. Agric. Food Chem.* **2008**, *56*, 6717−6723.

(34) Maga, J. A. Furans in foods. *CRC Crit. Rev. Food Sci. Nutr.* **1979**, *11*, 355−400.

DOI: 10.1021/jf5054047
J. Agric. Food Chem. 2015, 63, 3742−3751

(35) Balzer, H. H. Acids in coffee. In *Coffee: Recent Developments*, 1st ed.; Clarke, R. J., Vitztbum, O. G., Eds.; Blackwell Science: Cambridge, MA, 2001; Chapter 1B, p 23.
(36) Maier, H. G.; Wewetzer, H. Bestimmung von Diterpen-Glykosiden im Bohnenkaffee. *Z. Lebensm.-Unters. Forsch.* **1978**, *167*, 105−107.
(37) Bradbury, A. G. W.; Balzer, H. H. Carboxyatractyligenin and atractyligenin glycosides in coffee. *18th International Scientific Colloquium on Coffee*; ASIC: Bussigny, Switzerland, 1999; pp 71−77.

DOI: 10.1021/jf5054047
J. Agric. Food Chem. 2015, 63, 3742−3751

They were allowed access to water and standard rat chow ad libitum for 7 days to acclimatize and fasted overnight prior to the experiments.

Evaluation of Bioavailability of Collagen. The bioavailability of collagen was indirectly evaluated by the bioavailability of Hyp in collagen, which was determined using a pharmacokinetic method after oral administration to rats. Briefly, 30 rats were randomly divided into five groups of 6 each: group I (collagen, 4000 mg/kg bw, i.g.), group II (Hyp, 400 mg/kg bw, i.g.), group III (Hyp, 400 mg/kg bw, i.v.), group IV (NS, i.g.), and group V (NS, i.v.). Group I had the same Hyp dose as groups II and III because the Hyp content of the collagen was 10% (w/w).[13] Groups IV and V were given isometric NS as a control. Before and after treating with sample, ~0.5 mL of blood sample was drawn from orbit into heparinized tubes at different times for each rat. The plasma was obtained by centrifugation at 3000 g for 15 min.

The pharmacokinetic parameters of the area under the concentration−time curve (AUC), half-life ($t_{1/2}$), mean residence time (MRT), peak plasma concentration (C_{max}), and time to peak concentration (T_{max}) were calculated by the software BAPP 2.0 (Center for Drug Metabolism and Pharmacokinetics, China Pharmaceutical University, Nanjing, China). The relative (F_r) and absolute (F_s) bioavailability were calculated by the following equations,[15]

$$F_r = [AUC]_{col} D_{col} / [AUC]_{i.g.} D_{i.g.} \times 100\%$$

$$F_s = [AUC]_{col} D_{col} / [AUC]_{i.v.} D_{i.v.} \times 100\%$$

where $[AUC]_{col}$, $[AUC]_{i.g.}$, and $[AUC]_{i.v.}$ were the area under the concentration−time curve for Hyp in collagen, Hyp (i.g.), and Hyp (i.v.) from zero to infinity; D_{col}, $D_{i.g.}$, and $D_{i.v.}$ were the dose of Hyp in collagen, Hyp (i.g.) and Hyp (i.v.).

Separation of Collagen Peptides from Plasma. Another 20 rats were randomly divided into two groups of 10 each. One group was orally administered collagen at a dose of 4000 mg/kg bw. After 2 h, blood was drawn from the abdominal aorta under anesthesia and centrifuged to separate the plasma. The other group was given isometric NS as a control.

The plasma was filtered with Millipore's Amicon Ultra-15 centrifugal filter devices with the nominal molecular weight cut-offs of 3000 Da. The filtrate was loaded on a Sephadex G10 column (1.5 × 75 cm) and eluted with distilled water at 0.5 mL/min. The resulting fractions were then subjected to an Agilent ZORBAX Eclipse XDB-C18 column (9.4 × 250 mm, 5 μm) and eluted by acetonitrile (2% in 0−5 min, 2−10% in 5−10 min, 10−70% in 10−20 min) with 0.1% TFA at 2.5 mL/min. The absorbance at 220 nm was monitored.

Identification of Collagen Peptides. The collagen peptide was identified using Waters ACQUITY UPLC coupled to SYNAPT Q-TOF-MS with electrospray ionization. The sample was dissolved in distilled water, and 5 μL was then injected into a BEH130 C18 column (2.1 × 150 mm, 1.7 μm) and eluted with a linear gradient of acetonitrile (0−20% in 20 min) at 0.2 mL/min. The mass spectrometer was operated in the positive ion mode with a capillary voltage of 3.5 kV, ion source temperature of 100 °C, desolvation temperature of 300 °C, desolvation gas flow of 10 L/min, cone voltage of 45 V, cone gas flow of 1 L/min, and scanning range of 50−1000 *m*/*z*. The amino acid sequence was analyzed using BioLynx software.

Other Analytical Methods. The Hyp concentration in plasma was determined by the colorimetric method recommended by ISO.[16] Briefly, the plasma was hydrolyzed at 105 °C for 16 h with isometric 6 M H_2SO_4. After filtering and diluting, 2 mL of the plasma hydrolysates was mixed with 1 mL of Chloramine T, and the oxidation was allowed to proceed for 20 min at room temperature. Chromophore was then developed by the addition of 1 mL of Ehrlich's reagent and incubation for 20 min at 60 °C. The absorbance of the complex was measured at 558 nm.

The total amino acid profile of the plasma filtrate was analyzed using an amino acid analyzer after hydrolyzing under vacuum with 6 M HCl at 110 °C for 24 h in the presence of 1% phenol (v/v). The free amino acid profile was measured by the analyzer after deproteinizing by sulfosalicylic acid. The peptide-bound amino acid was calculated by subtracting the free amino acid from the total amino acid.[17]

Statistical Analysis. The data were presented as mean value ± standard deviation. Statistical analyses were performed using one-way analysis of variance. Multiple comparisons of means were done by the LSD test. A P value of <0.05 was considered significant. All computations were made with SPSS 15.0.

RESULTS AND DISCUSSION

Oral Bioavailability of Collagen. The plasma concentration−time curve for Hyp after oral administration of collagen is shown in Figure 1, and the derived pharmacokinetic parameters are presented in Table 1. A negligible amount of Hyp in plasma was observed before the ingestion of collagen. After ingestion, the Hyp increased significantly and reached a maximum (40.4 ± 5.46 μg/mL) at 2 h, which indicated that the collagen was digestible and absorbable in vivo. The peak was followed by a slow decrease, and only 14.7% of Hyp in plasma was retained at 24 h, which was calculated as the ratio of the Hyp concentration at 24 h to the peak concentration at 2 h. This was in agreement with Oesser's report that more than 85% radioactivity in plasma disappeared after oral administration of ^{14}C labeled collagen hydrolysate for 24 h.[9] Moreover, the $t_{1/2}$ (6.91 ± 1.09 h) and MRT (10.8 ± 1.73 h) of Hyp in collagen were significantly higher than the oral administration of Hyp (1.18 ± 0.22 h and 3.45 ± 0.13 h, respectively) because Hyp

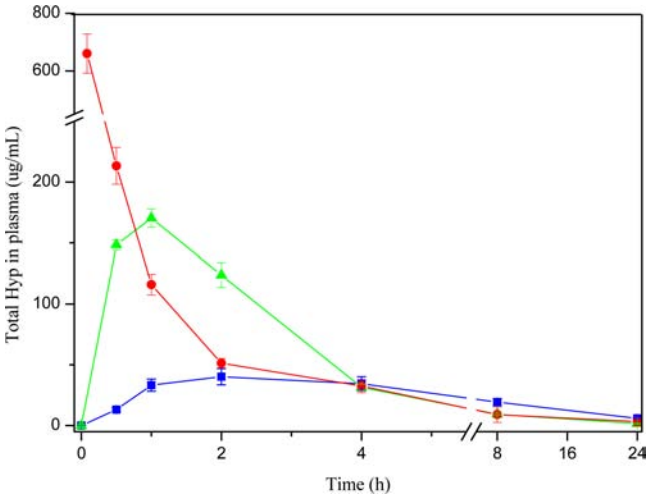

Figure 1. Plasma concentration−time curves for total Hyp in plasma after ingestion of collagen (blue, 4000 mg/kg bw, i.g.), Hyp (green, 400 mg/kg bw, i.g.), and Hyp (red, 400 mg/kg bw, i.v.).

Table 1. Pharmacokinetic Parameters of Hyp in Rat Plasma (n = 6) after Ingestion of Collagen (i.g.), Hyp (i.g.), and Hyp (i.v.)

	Hyp in collagen (i.g.)[a]	Hyp (i.g.)	Hyp (i.v.)
AUC (h·μg/mL)	436 ± 54.2 c	753 ± 16.1 b	877 ± 42.8 a
$t_{1/2}$ (h)	6.91 ± 1.09 a	1.18 ± 0.22 b	0.35 ± 0.04 c
MRT (h)	10.8 ± 1.73 a	3.45 ± 0.13 b	3.74 ± 0.61 b
C_{max} (μg/mL)	40.4 ± 5.46 c	173 ± 25.2 b	660 ± 68.0 a
T_{max} (h)	2.00 ± 0.00 a	0.83 ± 0.29 b	0.08 ± 0.00 c

[a]Mean value ± standard deviation from separate determination of six rats. Values with different superscripts in a row are significantly different at P < 0.05.

DOI: 10.1021/jf5057502
J. Agric. Food Chem. 2015, 63, 3752−3756

could be absorbed directly from the intestine, whereas there was the need for collagen to be digested into small peptides or free amino acids first.

The F_r and F_s of collagen were 57.8% and 49.6%, respectively, which were lower than 73−92% of animal protein (beef, casein, egg, milk, whey protein) and similar to 45−78% of cereal protein (wheat, corn, rice, oats).[18,19] These indicated the considerable digestibility and absorbability of collagen, although it was a high-molecular-weight scleroprotein with special structure and amino acid profile.[10,11]

Effect of Ingesting Collagen on the Amino Acid Profile of Plasma. The amino acid profiles of plasma filtrate before and after oral administration of collagen for 2 h are given in Table 2. All the free and peptide-bound amino acids in plasma significantly increased after ingestion of collagen, which indicated that the digested collagen could be absorbed in the forms of both free amino acid and peptide. When we compared the increased amount of peptide-bound amino acid with that of total amino acid, it was found that more than 63.4% of the amino acid residues in collagen were absorbed in the form of a peptide. The Glu absorbed in peptide form had the highest proportion (more than 97.5%), and there was a relatively high proportion of Asp, Phe, His, and Arg, whereas Hyp, Pro, Tyr and Hyl were very low.

Table 2. Amino Acid Profile of Plasma before and after Administration of Collagen for 2 h

	free amino acid (μg/mL)[a]		peptide-bound amino acid (μg/mL)	
	before	after	before	after
Hyp	1.24 ± 0.05	21.4 ± 1.50	0.39 ± 0.06	22.8 ± 0.26
Asp	0.86 ± 0.05	1.46 ± 0.03	6.84 ± 0.13	9.54 ± 0.04
Thr	14.6 ± 0.46	22.0 ± 0.38	8.70 ± 0.38	20.1 ± 0.18
Ser	12.3 ± 0.32	24.0 ± 0.30	4.44 ± 0.21	21.23 ± 0.35
Glu	6.42 ± 0.20	7.28 ± 0.05	69.8 ± 0.99	104 ± 0.84
Pro	7.67 ± 0.24	36.3 ± 0.58	4.58 ± 0.39	37.8 ± 2.67
Gly	9.68 ± 0.24	57.8 ± 0.62	9.16 ± 0.64	69.5 ± 1.30
Ala	22.2 ± 0.51	41.9 ± 0.33	12.5 ± 0.83	41.4 ± 1.54
Val	5.94 ± 0.08	9.82 ± 0.47	3.81 ± 0.11	11.1 ± 0.22
Met	1.15 ± 0.22	4.37 ± 0.09	0.38 ± 0.12	5.98 ± 0.82
Ile	3.01 ± 0.18	3.85 ± 0.25	2.21 ± 0.10	5.32 ± 2.10
Leu	5.31 ± 0.06	9.05 ± 0.27	3.52 ± 0.01	9.80 ± 0.63
Tyr	4.70 ± 0.19	5.08 ± 0.08	2.74 ± 0.02	3.08 ± 0.36
Phe	2.63 ± 0.58	3.30 ± 0.52	2.55 ± 0.29	5.22 ± 0.82
Hyl	0.00 ± 0.00	1.64 ± 0.20	0.00 ± 0.00	1.79 ± 0.12
His	4.02 ± 0.04	4.58 ± 0.28	4.63 ± 0.03	9.80 ± 0.04
Lys	27.8 ± 1.48	33.3 ± 0.11	13.03 ± 0.51	33.0 ± 0.69
Arg	11.0 ± 0.18	14.9 ± 0.73	3.39 ± 2.93	20.6 ± 1.88
total	141	302	152	431

[a]Mean value ± standard deviation from three separate determinations.

Referring to the amino acid profile of collagen,[13] it was observed that there was a good linear correlation between the increased amount of an amino acid in plasma and its content in collagen (R^2 = 0.9225) (Figure 2), which showed that the absorbed amount of an amino acid from the intestine depended on its content in collagen. Furthermore, Hyp was the closest to the regression curve among all the amino acids, which indicated that it was reasonable to indirectly evaluate the bioavailability of collagen by determining the bioavailability of Hyp in collagen.

Separation of Collagen Peptides. The plasma filtrate was first fractionated into three fractions (F_1, F_2, F_3) by a Sephadex G10 column (Figure 3a), in which molecules are separated by their size. All the fractions significantly increased after ingestion, which indicated the digested collagen could be absorbed within a wide range of molecular weights. These fractions were then separated by the Eclipse XDB C18 column, which was based on their hydrophobic or hydrophilic property (Figure 3b). Compared with the control, a number of new peaks emerged that were deemed the peptides or free amino acids derived from oral collagen. They were eluted in a lower range of acetonitrile concentrations, suggesting their low hydrophobicity.

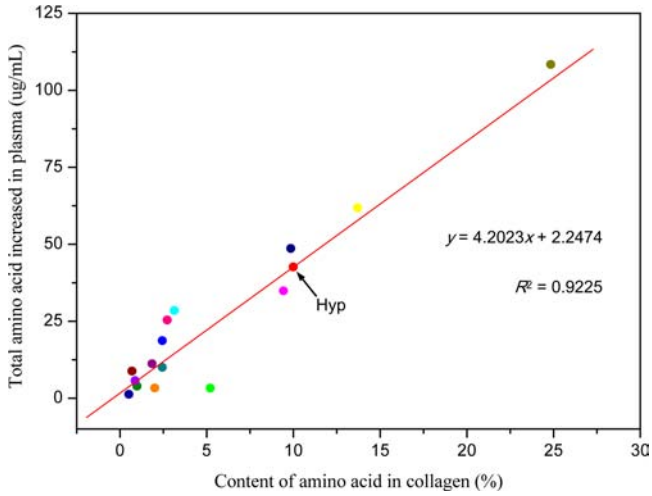

Figure 2. Correlation curve of the increased amount of amino acid in plasma (μg/mL) after ingestion of collagen against its content in collagen (%).

Identification of collagen peptides. The digested collagen in plasma was further identified by UPLC−ESI-MS with a BEH130 C18 column. The F_1 was high-molecular-weight peptides (>500 Da), and the F_3 was free amino acids. The observation was not in agreement with Iwai's report that no collagen peptide larger than Pro-Hyp-Gly could be found in plasma.[7]

From the F_2, 16 kinds of small peptides were identified: Ala-Asn, Ala-Hyp-Gly, Asp-Glu, Glu-Asn, Glu-Asp, Glu-Met, Gly-Pro-Hyp, Leu-Hyp, Leu-Met, Phe-Gly-Asn, Pro-Gly-Leu, Pro-Leu, Ser-Gly-Met, Ser-Hyp, Ser-Pro-Gly, Tyr-Met (Figure 4). These were quite different from previous reports,[1,7,8] which could be due to the differences of the collagen source, experimental animal, and detection method. It is known that oligopeptides are frequently degraded in a short time by peptidase in blood. For example, the half-lives of Ala-Tyr, Gly-Tyr, Ala-Gln, Gly-Gln, *N*-acetyl-Ser-Asp-Lys-Pro, and Pyr-His-Pro-NH_2 in blood were less than 10 min.[20,21] However, combined with the high percentage of collagen peptides in plasma (63.4%) 2 h after oral ingestion, it indicated that these collagen peptides might have a high resistance to digestion by the enzymes in plasma and the gastrointestinal tract.

It has been demonstrated that Pro-Hyp and Pro-Hyp-Gly had chemotactic activity to the human fibroblast, peripheral blood neutrophils, and monocytes.[22] This showed that collagen peptides acted as a biological messenger and triggered the synthesis of new collagen fibers and reorganization of the extracellular matrix by stimulating fibroblast cells. Pro-Hyp and Hyp-Gly had a stimulatory activity on the proliferation, migration, and hyaluronic acid synthesis of the skin fibroblast,[8,23,24] which indicated that collagen peptides modulated the cells and extracellular matrix in the skin. Asp-

DOI: 10.1021/jf5057502
J. Agric. Food Chem. 2015, 63, 3752−3756

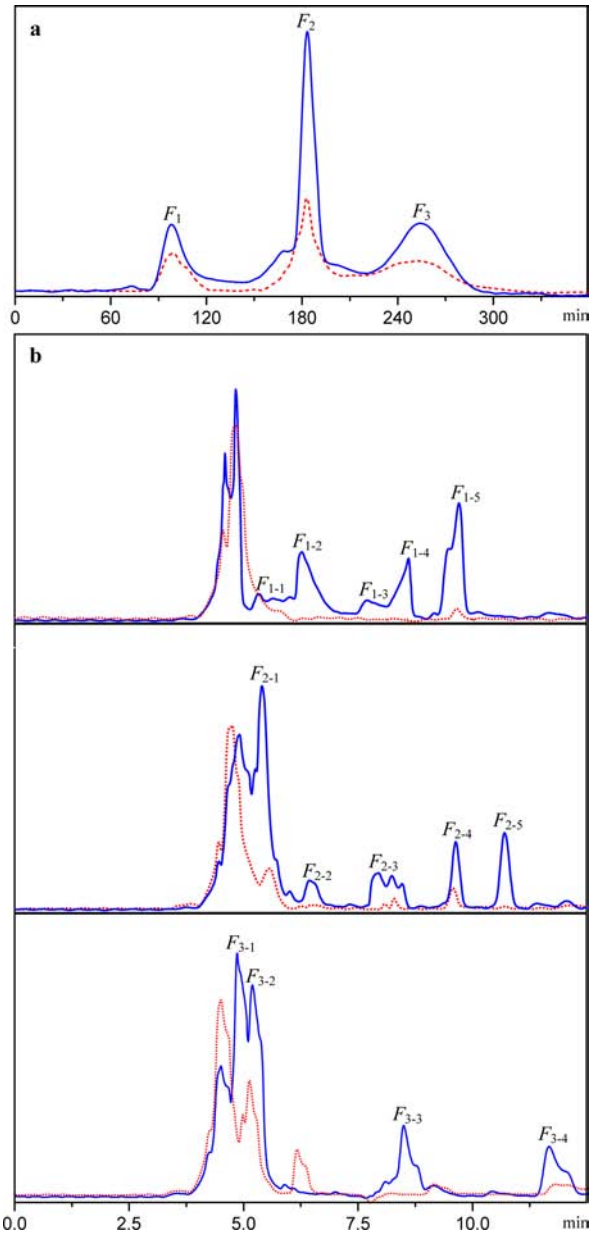

Figure 3. Chromatographic profiles of plasma filtrate before and after ingestion of collagen, using Sephadex G10 (a) and Eclipse XDB-C18 columns (b). Red, before; blue, after.

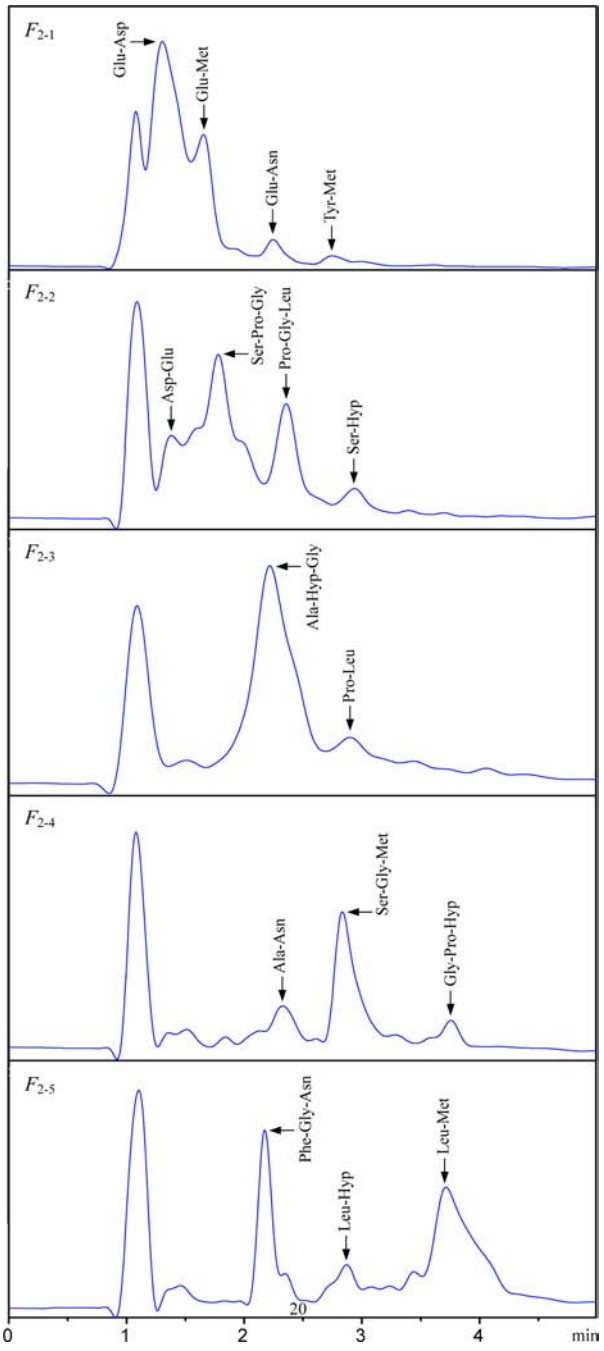

Figure 4. Chromatographic profiles of plasma filtrate fraction (F_2) with a BEH130 C18 column.

Gly-Glu-Ala could stimulate osteoblast-related gene expression of bone marrow cells.[25] Furthermore, Ala-Hyp and Gly-Pro-Val were potential inhibitors of angiotensin-converting enzyme, and Gly-Pro-Hyp was suggested to be involved in platelet aggregation,[26,27] suggesting their beneficial effects on hypertension and thrombosis. However, only a small part of the collagen peptides and their physiological effects are currently known about. It is necessary to obtain more detailed information on the physiological effects and molecular mechanisms of the collagen peptides in further investigation.

In conclusion, the bioavailability and bioavailable forms of collagen after oral administration to rat were investigated in this study. The bioavailability of collagen was lower than animal protein, but was comparable to cereal protein. Most of the digested collagen was absorbed in the form of a peptide rather than a free amino acid, and the absorbed amount of an amino acid depended on its content in collagen. Moreover, some collagen peptides in the plasma were purified and identified, but further studies are needed to investigate their physiological effects and molecular mechanisms.

AUTHOR INFORMATION

Corresponding Author

*Phone/fax: +86 511 88780201. E-mail: linwang@ujs.edu.cn.

Funding

This research was supported by the Natural Science Foundation of Jiangsu Province (BK20140545), Science and Technology Support Program of Jiangsu Province

DOI: 10.1021/jf5057502
J. Agric. Food Chem. 2015, 63, 3752−3756

(BE2014339), and Science and Technology Support Program of Zhenjiang City (NY2014023).

Notes

The authors declare no competing financial interest.

REFERENCES

(1) Ohara, H.; Matsumoto, H.; Ito, K.; Iwai, K.; Sato, K. Comparison of quantity and structures of hydroxyproline-containing peptides in human blood after oral ingestion of gelatin hydrolysates from different sources. *J. Agric. Food Chem.* **2007**, *55*, 1532−1535.

(2) Tanaka, M.; Koyama, Y.; Nomura, Y. Effects of collagen peptide ingestion on UV-B-induced skin damage. *Biosci., Biotechnol., Biochem.* **2009**, *73*, 930−932.

(3) Moskowitz, R. W. Role of collagen hydrolysate in bone and joint disease. *Semin. Arthritis Rheum.* **2000**, *30*, 87−99.

(4) Trentham, D. E.; Dynesius-Trentham, R. A.; Orav, E. J.; Combitchi, D.; Lorenzo, C.; Sewell, K. L.; Hafler, D. A.; Weiner, H. L. Effects of oral administration of type II collagen on rheumatoid arthritis. *Science* **1993**, *261*, 1727−1730.

(5) Matsuda, N.; Koyama, Y.; Hosaka, Y.; Ueda, H.; Watanabe, T.; Araya, T.; Irie, S.; Takehana, K. Effects of ingestion of collagen peptide on collagen fibrils and glycosaminoglycans in the dermis. *J. Nutr. Sci. Vitaminol.* **2006**, *52*, 211−215.

(6) Minaguchi, J.; Koyama, Y.; Meguri, N.; Hosaka, Y.; Ueda, H.; Kusubata, M.; Hirota, A.; Irie, S.; Mafune, N.; Takehana, K. Effects of ingestion of collagen peptide on collagen fibrils and glycosaminoglycans in Achilles tendon. *J. Nutr. Sci. Vitaminol.* **2005**, *51*, 169−174.

(7) Iwai, K.; Hasegawa, T.; Taguchi, Y.; Morimatsu, F.; Sato, K.; Nakamura, Y.; Higashi, A.; Kido, Y.; Nakabo, Y.; Ohtsuki, K. Identification of food-derived collagen peptides in human blood after oral ingestion of gelatin hydrolysates. *J. Agric. Food Chem.* **2005**, *53*, 6531−6536.

(8) Shigemura, Y.; Akaba, S.; Kawashima, E.; Park, E. Y.; Nakamura, Y.; Sato, K. Identification of a novel food-derived collagen peptide, hydroxyprolyl-glycine, in human peripheral blood by pre-column derivatisation with phenyl isothiocyanate. *Food Chem.* **2011**, *129*, 1019−1024.

(9) Oesser, S.; Adam, M.; Babel, W.; Seifert, J. Oral administration of ^{14}C labeled gelatin hydrolysate leads to an accumulation of radioactivity in cartilage of mice (C57/BL). *J. Nutr.* **1999**, *129*, 1891−1895.

(10) Asghar, A.; Henrickson, R. L.; Chichester, C. O.; Mrak, E. M.; Stewart, G. F. Chemical, biochemical, functional, and nutritional characteristics of collagen in food systems. In *Advances in Food Research*; Academic Press: New York, 1982; pp 231−372.

(11) Raghavan, R. N.; Muthukumar, T.; Somanathan, N.; Sastry, T. P. Biomimetic mineralization of novel silane crosslinked collagen. *Mater. Sci. Eng., C* **2013**, *33*, 1983−1988.

(12) Liang, Q.; Wang, L.; He, Y.; Wang, Z.; Xu, J.; Ma, H. Hydrolysis kinetics and antioxidant activity of collagen under simulated gastrointestinal digestion. *J. Funct. Foods* **2014**, *11*, 493−499.

(13) Zeng, S. K.; Zhang, C. H.; Lin, H.; Yang, P.; Hong, P. Z.; Jiang, Z. H. Isolation and characterisation of acid-solubilised collagen from the skin of Nile tilapia (*Oreochromis niloticus*). *Food Chem.* **2009**, *116*, 879−883.

(14) Wang, L.; An, X.; Xin, Z.; Zhao, L.; Hu, Q. Isolation and characterization of collagen from the skin of deep-sea redfish (*Sebastes mentella*). *J. Food Sci.* **2007**, *72*, 451−455.

(15) Tang, L.; Gong, Y.; Lv, C.; Ye, L.; Liu, L.; Liu, Z. Pharmacokinetics of aconitine as the targeted marker of Fuzi (*Aconitum carmichaeli*) following single and multiple oral administrations of Fuzi extracts in rat by UPLC/MS/MS. *J. Ethnopharmacol.* **2012**, *141*, 736−741.

(16) Anonymous. Meat and meat products - Determination of hydroxyproline content. *Int. Stand.* 1994, ISO 3496.

(17) Rhyu, M. R.; Kim, E. Y. Umami taste characteristics of water extract of *Doenjang*, a Korean soybean paste: Low-molecular acidic peptides may be a possible clue to the taste. *Food Chem.* **2011**, *127*, 1210−1215.

(18) Hoffman, J. R.; Falvo, M. J. Protein - which is best? *J. Sport. Sci. Med.* **2004**, *3*, 118−130.

(19) Kies, C. Bioavailability: a factor in protein quality. *J. Agric. Food Chem.* **1981**, *29*, 435−440.

(20) Ezan, E.; Carde, P.; Le Kerneau, J.; Ardouin, T.; Thomas, F.; Isnard, F.; de Paillette, E. D.; Grognet, J. M. Pharmcokinetics in healthy volunteers and patients of NAc-SDKP (seraspenide), a negative regulator of hematopoiesis. *Drug Metab. Dispos.* **1994**, *22*, 843−848.

(21) Matsui, T.; Tamaya, K.; Seki, E.; Osajima, K.; Matsumo, K.; Kawasaki, T. Absorption of Val-Tyr with *in vitro* angiotensin I-converting enzyme inhibitory activity into the circulating blood system of mild hypertensive subjects. *Biol. Pharm. Bull.* **2002**, *25*, 1228−1230.

(22) Zague, V. A new view concerning the effects of collagen hydrolysate intake on skin properties. *Arch. Dermatol. Res.* **2008**, *300*, 479−483.

(23) Shigemura, Y.; Iwai, K.; Morimatsu, F.; Iwamoto, T.; Oda, T. M. C.; Taira, T.; Park, E. Y.; Nakamura, Y.; Sato, K. Effect of Prolyl-hydroxyproline (Pro-Hyp), a food-derived collagen peptide in human blood, on growth of fibroblasts from mouse skin. *J. Agric. Food Chem.* **2009**, *57*, 444−449.

(24) Ohara, H.; Ichikawa, S.; Matsumoto, H.; Akiyama, M.; Fujimoto, N.; Kobayashi, T.; Tajima, S. Collagen-derived dipeptide, proline-hydroxyproline, stimulates cell proliferation and hyaluronic acid synthesis in cultured human dermal fibroblasts. *J. Dermatol.* **2010**, *37*, 330−338.

(25) Mizuno, M.; Kuboki, Y. Osteoblast-related gene expression of bone marrow cells during the osteoblastic differentiation induced by type I collagen. *J. Biochem.* **2001**, *129*, 133−138.

(26) Kim, S. K.; Byun, H. G.; Park, P. J.; Shahidi, F. Angiotensin I converting enzyme inhibitory peptides purified from bovine skin gelatin hydrolysate. *J. Agric. Food Chem.* **2001**, *49*, 2992−2997.

(27) Knight, C. G.; Morton, L. F.; Onley, D. J.; Peachey, A. R.; Ichinohe, T.; Okuma, M.; Farndale, R. W.; Barnes, M. J. Collagen-platelet interaction: Gly-Pro-Hyp is uniquely specific for platelet Gp VI and mediates platelet activation by collagen. *Cardiovasc. Res.* **1999**, *41*, 450−457.

DOI: 10.1021/jf5057502
J. Agric. Food Chem. 2015, 63, 3752−3756

a variety of techniques. The morphologies of the native forms of gums were compared with their DDSA derivatives using SEM analysis. DGK and its DDSA derivatives were characterized using attenuated total reflectance−Fourier transform infrared spectroscopy (ATR-FTIR), ^{1}H NMR, thermogravimetric analysis (TGA), differential scanning calorimetry (DSC) analysis, and rheological studies. The critical aggregation concentration (CAC) was determined by means of dye solubilization and surface tension. We tested the antibacterial properties of DDSA-DGK using Gram-positive and -negative bacteria and believe this to be the first instance of such experimentation.

MATERIALS AND METHODS

Materials. The GK sample was procured from Girijan Co-operative Corp. (GCC), Hyderabad, India. (2-Dodecen-1-yl)succinic anhydride (DDSA), sodium nitrate, sodium iodide, hydrochloric acid, cyclohexane, and absolute ethanol were obtained from Sigma-Aldrich Co. Ltd. (St. Louis, MO, USA). Sudan IV (dye content 80%) was obtained from Eastman Kodak Co. (Rochester, NY, USA). Deionized water was used for all analyses.

Preparation of DGK. The GK was powdered in a high-speed mechanical blender and later sieved using a bin (mesh size = 250 μm), so as to obtain fine and uniform samples. One gram portions of GK powder were accurately weighed and dispensed into clean glass beakers containing 1 L of deionized water. The gum solutions were placed on magnetic stirrers at room temperature and gently stirred overnight, after which they were allowed to stand at room temperature for 12 h to separate out any undissolved matter. The resulting gum solutions were subsequently centrifuged to obtain clear solutions. Three volumes of each of the gum solutions was deacetylated by mixing with 1 volume of 1 M NaOH. After incubation for 6 h at room temperature (with gentle agitation on a magnetic stirrer), 1 volume of 1 M HCl was added to neutralize the solution to a final pH of 7.0. The resulting DGK solution was dialyzed (dialysis tubing DTV 12000.09.000; M_w range = 12−14 kDa, Medicell International Ltd., London, UK) extensively against deionized water to remove residual salts. The centrifuged DGK solution was dialyzed against deionized water. After dialysis, the gum solution was centrifuged to remove any residual precipitates, and the clear solutions so obtained were freeze-dried and stored until further use. Deacetylation was monitored by FTIR analysis.[4]

Determination of Molecular Mass Distributions of DGK. The molecular mass distributions of DGK were determined using the technique of gel permeation chromatography (GPC) linked to multiangle laser light scattering (MALLS). Sodium nitrate (0.1 M) containing 0.005% sodium azide (biocide) was utilized as the eluent, and the solution was filtered using a GSWP 0.45 μm nylon filter (Millipore) and degassed by means of a vacuum degasser (CS 615; Cambridge Scientific Instruments, UK) before use. The samples of DGK (0.2 wt %) were prepared in 0.1 M $NaNO_3$ solution and left overnight on a roller to achieve complete dissolution. The GPC system consisted of a Suprema 3000 column with these specifications: dimensions, 300 mm × 8 mm; bead size, 10 μm; and pore size, 100 Å. The column was protected by a guard column (Polymer Standards Service GmbH, Mainz, Germany). The flow rate was set to 0.5 mL/min using a Waters Corp. HPLC pump in conjunction with a Rheodyne 7125 model injection system (loop volume = 200 μL). A Dawn DSP Laser Photometer and OPTILAB DSP Interferometric Refractometer (Wyatt Technology Corp., Santa Barbara, CA, USA) were used as detectors. The DGK samples were filtered through 0.45 μm nylon syringe filters before being injected into the HPLC column. All measurements were performed in triplicate. Molecular mass distributions and rms radius moments of the DGK were determined using the designated Astra software for Windows (4.90.08, QELSS 2. XX). Data were fitted using a first-order polynomial and the Zimm model. The refractive index increment (dn/dc) value for DGK was determined to be 0.140 mL/g.[20]

Synthesis of DDSA Derivative of DGK. DGK (15 g, lyophilized dry powder) was suspended in deionized water (100 mL) with gentle agitation and placed on a roller overnight (12 h). The pH of the solution was adjusted to 8.5 by adding 5% NaOH. A weighed quantity of DDSA (5 g) dissolved in absolute ethanol (30 mL) was slowly added to the gum solution. All reactions were performed in 500 mL, three-necked round-bottom flasks placed in a water bath to maintain a temperature of 25 °C. A propeller mixer (Heidolph type: STI) with a PTFE centrifugal stirrer shaft (6 mm diameter, 400 mm length) was used for continuous mixing of the solutions. The pH of the reaction mixtures was adjusted using 5% NaOH and a peristaltic pump. The reaction was continued for 7−8 h until the pH became stable at 8.5. The resultant product was neutralized with 5% HCl to pH 6.0 before being freeze-dried, yielding a white powder. The final product was purified by Soxhlet extraction for 6 h using cyclohexane as solvent. Finally, the DDSA-DGK was dried in an oven overnight at 70 °C.

SEM Analysis. The composition and morphology of the native GK, DGK, and DDSA-DGK were studied using a scanning electron microscope with a beam current of 12−40 nA and an acceleration voltage of 0.02−30 kV. The complete detection system is composed of an In-lens energy and angle selective backscatter detector (EsB), four-quadrant solid-state backscattered detector (AsB), and conventional secondary electron detector (Everhardt-Thornley) (Carl Zeiss, Ultra/Plus, Munich, Germany). Specimens were permanently mounted onto stubs using slow-drying Araldite or silver dag. The stubs with the specimens were then sputter-coated with a thin layer of gold to make the specimens conductive under high-vacuum conditions. The processed specimens were then subjected to SEM analysis.

ATR-FTIR Spectrometry. ATR-FTIR (Nicolet IZ10, Thermo Scientific, USA) was used to characterize the functional groups of GK, DGK, and DDSA-DGK. The spectrometer was equipped with a multireflection, variable angle, and horizontal ATR accessory.

Determination of the Degree of Substitution (DS). The DS of DDSA-DGK was determined by titration and ^{1}H NMR methods. The titration procedure adopted for the determination of the DS for DDSA-DGK was as reported for gum arabic and starch.[13,19] In brief, 1 g of DDSA-DGK was accurately weighed into a 50 mL beaker, after which 20 mL of deionized water was added. The resulting solution was magnetically stirred until complete dissolution was achieved. Subsequently, 0.05 M NaOH was added slowly until the solution pH reached 9.0. The resulting solution was then titrated against 0.05 M HCl. A control reaction was also performed with unmodified DGK. All of the experiments were carried out in triplicate, and average values were noted. The DS was determined using the equation

$$\mathrm{DS} = \frac{M_{\mathrm{DDSA}} MV}{(W - M_{\mathrm{DDSA}})MV} \times 100\% \quad (1)$$

where V is the volume of the titer, M is the molarity of the HCl solution, M_{DDSA} is the molecular weight of the DDSA (266 g/mol), and W is the weight of the DDSA-DGK sample.

^{1}H NMR Spectroscopy. The samples (DGK and DDSA-DGK, 5 mg each) were dissolved in D_2O or DMSO-d_6 and placed in NMR tubes. The ^{1}H NMR spectra were measured using a 500 MHz spectrometer (Bruker DRX-500, Rheinstetten, Germany) at 70 °C. The DS was determined by comparing the intensity (I) of the peak at δ 0.89 due to the $-CH_3$ group from the terminal end of the alkenyl chains with that of anomeric protons of the (1→4)-α-D-GalA-(1→2)-α-L-Rhap units of DGK from the ^{1}H NMR spectra by using the following equation:

$$\mathrm{DS} = \frac{[1/3 \times I_{(\mathrm{DDSA,methyl\ group})}]}{[I_{(1\rightarrow4)\text{-}\alpha\text{-D-GalA}-(1\rightarrow2)\text{-}\alpha\text{-L-Rhap,anomeric protons plus reducing end})}]} \times 100\% \quad (2)$$

The present study was compared to the determination of DS using ^{1}H NMR of DDSA and OSA derivatives of various polysaccharides such as inulin,[15] konjac glucomannan,[16] hyaluronic acid,[21,22] and starch.[13,23,24]

DSC. DSC experiments on DGK and DDSA-DGK were carried out using a Pyris Diamond S6 DSC (PerkinElmer, Boston, MA, USA).

DOI: 10.1021/jf505783e
J. Agric. Food Chem. 2015, 63, 3757−3765

The sample was heated from 30 to 400 °C with temperature increments of 10 °C in a nitrogen atmosphere, at a flow rate of 20 mL/min. Each sample (5 mg) was crimped in an aluminum DSC pan.

TG Analysis. The thermal stability and composition of the DGK and its DDSA derivative were determined using a Mettler Toledo apparatus (TGA/SDTA851, Columbus, OH, USA). The experimental atmosphere was nitrogen at a flow rate of 20 mL/min. The sample was heated from 30 to 800 °C.

Critical Aggregation Concentration (CAC). The CAC was determined using dye solubilization and surface tension techniques.

Dye Solubilization. CAC was determined by the dye solubilization technique using Sudan IV. A total of 10 mg of dye was added to 10 mL of the DGK and DDSA-DGK, at various concentrations in deionized water. The samples were mixed overnight at room temperature and filtered through Mille-GP 0.22 μm filters (Millipore Ireland Ltd.) into disposable, UV-grade, 10 mm path length cuvettes (CXA-110-0053, Fisher Scientific Ltd., Loughborough, UK). The absorbances of the solutions were measured at 510 nm using a Lambda 25 UV−vis spectrometer (PerkinElmer). All of the measurements were carried out in triplicate. The CAC was determined from the increase in absorbance. A blank solution of DGK was used as the control.

Surface Tension Measurements. The Du Noüy ring method was used to determine the surface tension of solutions of DGK and the DDSA-DGK derivative at different concentrations using a Kruss K8 surface tensiometer (Krüss GmbH, Hamburg, Germany). Measurements were carried out in triplicate, and the values were reported as means ± SD. The CAC was determined from the inflection in the plot of the surface tension versus concentration.

Rheological Study. Rheological measurements of both aqueous DGK and DDSA-DGK were performed using a rheometer (Physica MCR 51, Anton Paar GmbH, Graz, Austria). The solutions were characterized for their steady shear viscosity function, $\eta(r)$, using a unidirectional steady-shear flow, with shear rate ranging from 1 to 700 s^{-1} at 25 °C.

Antibacterial Activity Tests. *Bacterial Strains and Culture Media.* The bacterial strains of Gram-negative *Escherichia coli* (CCM 3954) and *Pseudomonas aeruginosa* (CCM 3955) and Gram-positive *Staphylococcus aureus* (CCM 3953) used in this study were obtained from the Czech Collection of Microorganisms, Masaryk University Brno, Czech Republic. Bacterial suspensions were always prepared fresh by growing a single colony overnight at 37 °C in a nutrient broth. All agar plates were freshly prepared before antibacterial testing. A sterilized cotton swab was dipped into the culture suspension, and the cells were spread homogeneously over the agar plates. These plates were immediately used for antibacterial activity tests.

Determining the Zone of Inhibition (ZOI). We determined the antibacterial activity of the DDSA derivative of DGK. The DDSA-DGK solutions (1, 2, 3, 4, and 10% each of DDSA-DGK) were pipetted onto sterilized membrane filters and placed on inoculated agar plates. In addition, 6 mm diameter circles of filter paper were also placed directly onto the inoculated agar plates. Similarly, samples of DGK solution (10%) without DDSA were used as controls. The samples and inoculated agar plates were then incubated for 24 h at 37 °C. The ZOI was determined as being the total diameter (mm) of DDSA-DGK filter paper sample plus the halo-zone where bacterial growth was inhibited. All measurements were performed in triplicate for the DDSA-DGK solutions, and average values were reported.

Statistical Analysis. All of the tests were performed in triplicate. Analysis of variance (ANOVA) was performed, and all experimental values were reported as means ± SD (n = 3). A Duncan test was conducted to examine significant differences among experimental mean values ($P < 0.05$).

RESULTS AND DISCUSSION

Molecular Mass Distribution of DGK. The estimated molar mass distributions (weight-average, M_w; number-average, M_n and z-average, M_z) and average mean square radius moments (R_n, R_w, and R_z, all in nm) of DGK are presented in Table 1. The data were obtained using GPC/MALLS and fitted with first-order polynomials using the Zimm method. The elution profiles of DGK juxtaposed against their corresponding molecular weight distributions (derived using GPC in conjunction with light scattering and refractive index detectors) are also shown in Figure 1. For DGK, the weight-average molecular weight was ascertained to be 1.827×10^6. The weight-average molecular mass of DGK was found to be higher compared to other tree gums reported in the literature.[20,25]

Table 1. Estimated Molar Mass Distributions and Average Mean Square Radius Moments of DGK Using GPC/MALLS and Data Fitting by First-Order Polynomials: Zimm Method[a]

M_n (g/mol)[b]	M_w (g/mol)[c]	M_z (g/mol)[d]	R_n (nm)[e]	R_w (nm)[f]	R_z (nm)[g]
1.537×10^6	1.827×10^6	2.062×10^6	87.0	91.8	95.3

[a]Eluent, 0.1 M $NaNO_3$; flow rate, 0.5 mL/min.; dn/dc, DGK, 0.140 mL/g. [b]M_n, number-average molecular mass. [c]M_w, weight-average molecular mass. [d]M_z, z-average molecular mass. [e]R_n, number−average mean square radius. [f]R_w, weight-average mean square radius. [g]R_z, z-average mean square radius.

Preparation and Characterization of DDSA Derivative of DGK. *Esterification of DGK.* The scheme for esterification of DGK with DDSA is presented in Figure 2. The major parameters that affected the formation of DDSA derivatives of the DGK were the concentration ratio of DDSA and DGK, pH, concentration of NaOH solution, reaction time, and temperature.[13−15] In the present study, the DDSA-DGK ratio was maintained at 3:1; the pH of the reaction mixture was kept between 8 and 9 using 3% NaOH; and the temperature was held between 25 and 30 °C for 8 h.

Confirmation of Esterification by ATR-FTIR. ATR-FTIR spectra of GK, DGK, and the DDSA-DGK are presented in Figure 3. Spectra of GK and DGK displayed peaks at 3300 cm^{-1} (relating to the OH group) and also peaks in the fingerprint region (corresponding to −C−O−C− stretching vibrations of various sugar moieties present in the gums) at 1159, 1082, and 1014 cm^{-1}, respectively. The band at 2923 cm^{-1} represents the characteristic vibration due to C−H stretching. The DDSA-DGK spectrum indicates that the peaks at 1726 cm^{-1} represent the −COOR group. The latter group is absent in the spectra of DGK and is the result of ester bond formation between the −COOH groups of DDSA and the −OH groups of the DGK in the derivatization process (Figure 3c). Compared with DGK spectra, the new absorption bands at 1726 and 1572 cm^{-1} appear after DDSA esterification of DGK corresponding to the C═O stretching vibration of an ester group and the asymmetric stretching vibration of a carbonyl group, respectively (Figure 3c). Furthermore, the predominant band at 2923 cm^{-1} representing aliphatic C−H stretching vibrations suggested the formation of DDSA-DGK (Figure 3c). The prominent peak observed in the DDSA derivative of DGK was a reflection of the high degree of substitution. Similar types of results were reported in the literature when corn starch,[13] inulin,[15] and gum arabic[19] were derivatized with DDSA to form DDSA derivatives of these polysaccharides.

SEM Analysis of GK, DGK, and DDSA-DGK. SEM images relating to the surface morphology of GK, DGK, and the DDSA-DGK derivative are shown in Figure 4. Irregular particles were observed on the surface of GK (Figure 4A),

DOI: 10.1021/jf505783e
J. Agric. Food Chem. 2015, 63, 3757−3765

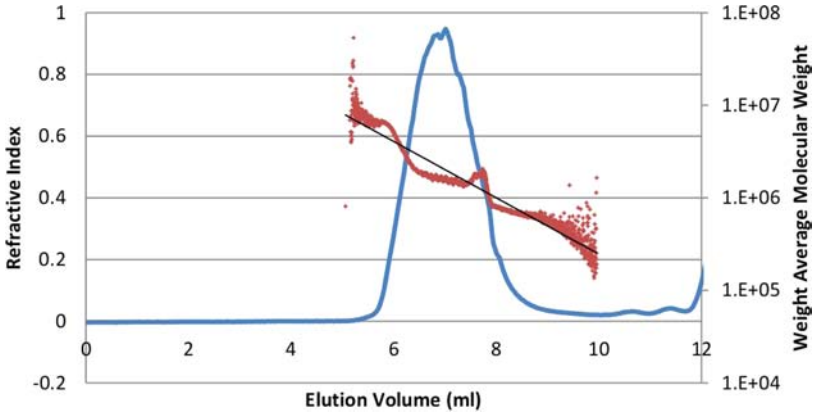

Figure 1. Refractive index and weight-average molecular mass GPC elution profiles of DGK.

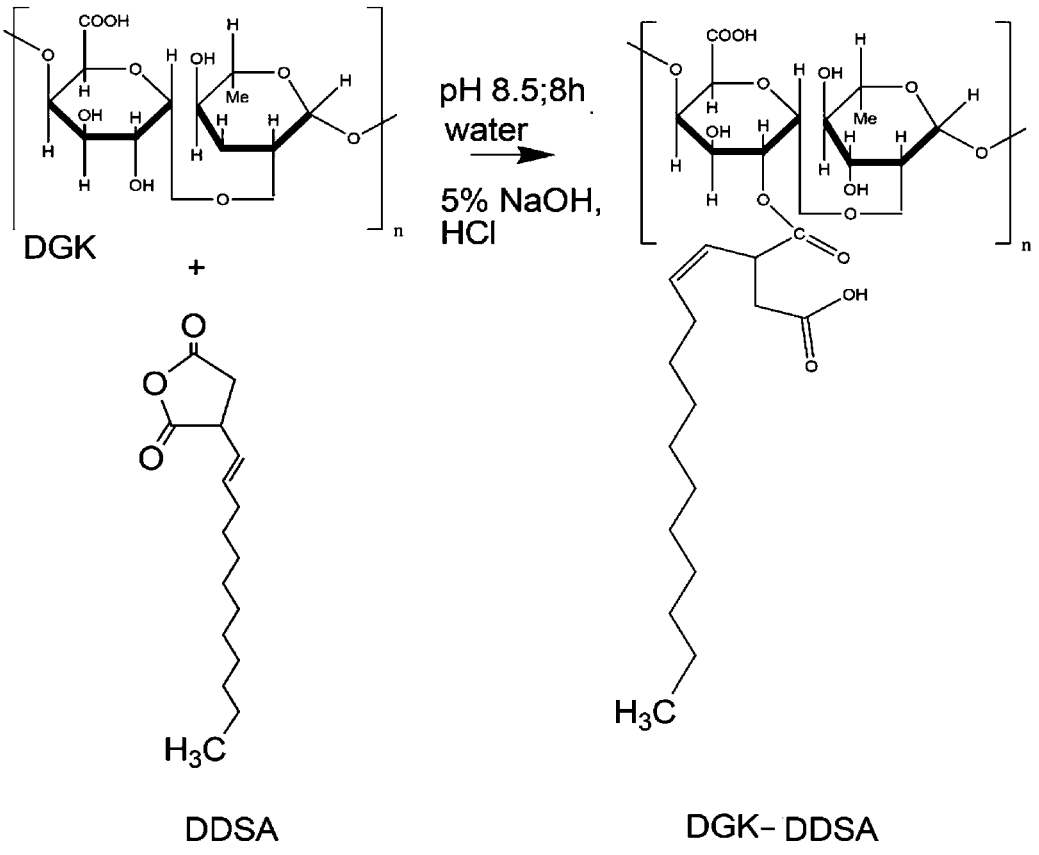

Figure 2. Schematic representation of reaction between DDSA and DGK and formation of the DDSA-DGK derivative.

and flake-like structures were displayed for DGK due to deacetylation of GK (Figure 4B). Significant changes, namely, highly porous structures and cavities, were observed after DDSA derivatization of DGK (Figure 4C). SEM analysis showed that the DDSA treatment caused some changes in the structure of the DGK. The SEM images of DDSA-DGK (Figure 4C) exhibited slightly rough surfaces with greater porosity, and many holes were observed, probably due to the DDSA treatment occurring on the surface of the DGK. This indicated that the esterification reaction had taken place. Similar types of morphological analysis have been reported for octenylsuccinic anhydride modified early "Indica" rice starch.[26]

Determination of the DS Using Titration and ^{1}H NMR Spectroscopy Methods. The DS of DDSA-DGK was determined to be 10.29% by means of titration using eq 1. ^{1}H NMR spectra of DGK and DDSA-DGK are presented in Figure 5. The DS can be calculated from the intensity of DDSA groups' signals as a ratio of the DGK anomeric protons, which are used as an internal reference. The proton signals at δ 3.2–3.7 were very broad and complex. They were attributed to protons of various sugar moieties present in the DGK.[4,27] Compared to the DGK, the DDSA-DGK derivative had several additional signals (Figure 5). It was seen that the peak at δ 0.89 in the ^{1}H NMR spectrum corresponded to the methyl protons of the DDSA group.[13,15] The peaks from δ 1.28 to 2.62 were due to the methylene and methenyl groups of the DDSA.[13,15] There was a multiplex at δ 5.54 and a shoulder with multiple peaks around at δ 5.4. These peaks were ascribed to protons of the double bond in the DDSA group. Signals from δ 4.5 to 5.2 observed in DGK were assigned to the anomeric proton.[27]

DOI: 10.1021/jf505783e
J. Agric. Food Chem. 2015, 63, 3757–3765

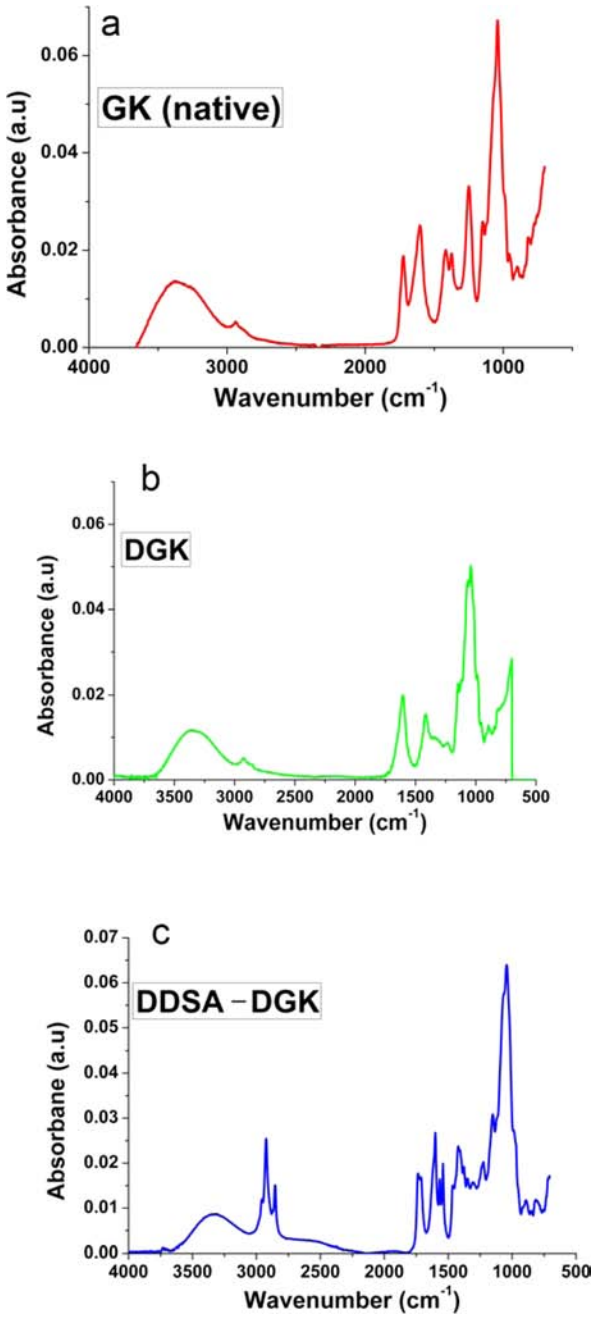

Figure 3. ATR-FTIR spectra of (a) GK, (b) DGK, and (c) DDSA-DGK.

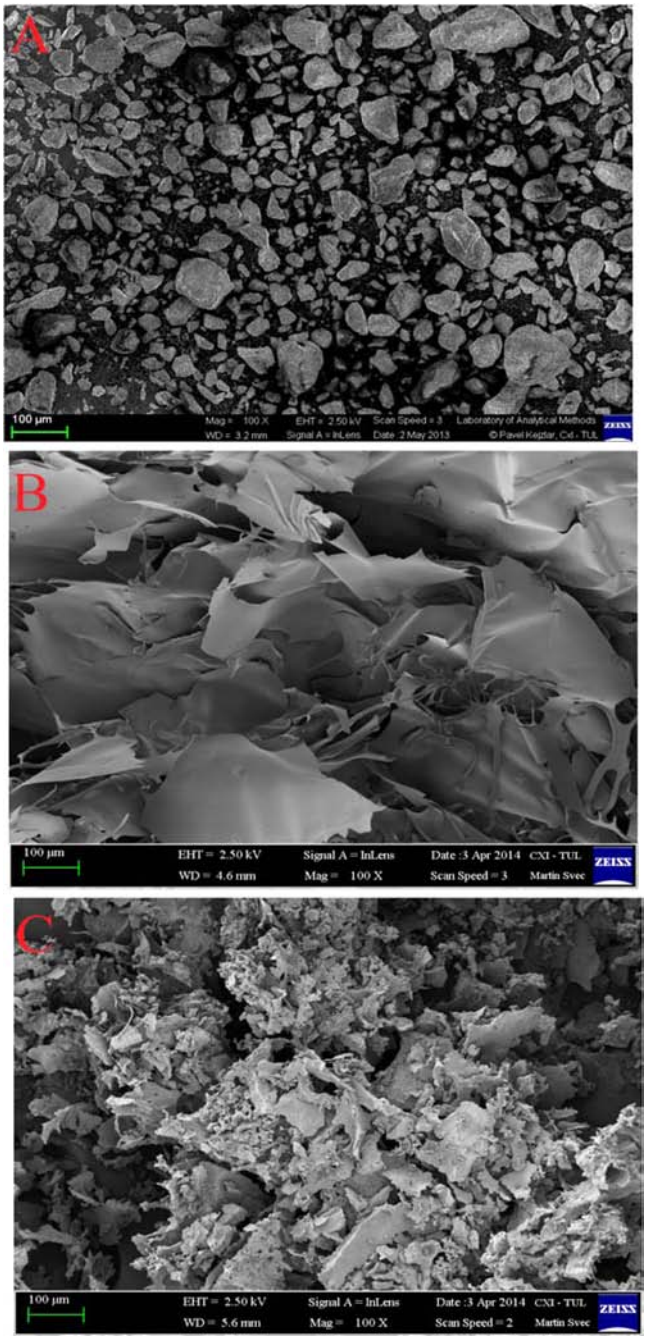

Figure 4. SEM micrographs of the surfaces of (A) GK, (B) DGK, and (C) DDSA-DGK, indicating the morphological changes during esterification.

After DDSA modification, the additional signals appeared in the δ 0.89−3.00 region of the DDSA-DGK spectrum. ^{1}H NMR spectroscopy was utilized for the determination of the DS of the OSA/DDSA anhydrides to many polysaccharides such as inulin,[15] konjac glucomannan,[16] hyaluronic acid,[21,22] and starch,[13,23,24] and the present study is in agreement with these reported methods in the literature.

It was not possible to determine which hydroxyl moieties the DDSA had reacted with or how evenly distributed the modification had been along the polymer chain. According to earlier studies on starches, both primary and secondary hydroxyl groups of the glucose repeating unit had been observed to react with the OSA/DDSA. This was also the case for other starches, hyaluronic acid, and most other polysaccharides, as reported in the literature.[21−24] In the DGK molecule, there are three hydroxyl groups available for chemical modification. They are located at the C-2, C-3, and C-6 positions. Hydroxyl groups at C-2 and C-6 are more active than those at C-3 because of their steric attributes. The extent of alkenyl chain incorporation (DS) was calculated from the ratio of the peak areas at δ 0.89 to the corresponding area from δ 3 to 5.5, due to the contribution of DGK, which we established had a DS of 10.25%. In the present investigation, the values of the DS for DDSA-DGK obtained by titration and ^{1}H NMR methods were 10.29 and 10.25%, respectively. Therefore, the figures obtained from the DS calculation by using both methods complement each other very well. These results are

DOI: 10.1021/jf505783e
J. Agric. Food Chem. 2015, 63, 3757−3765

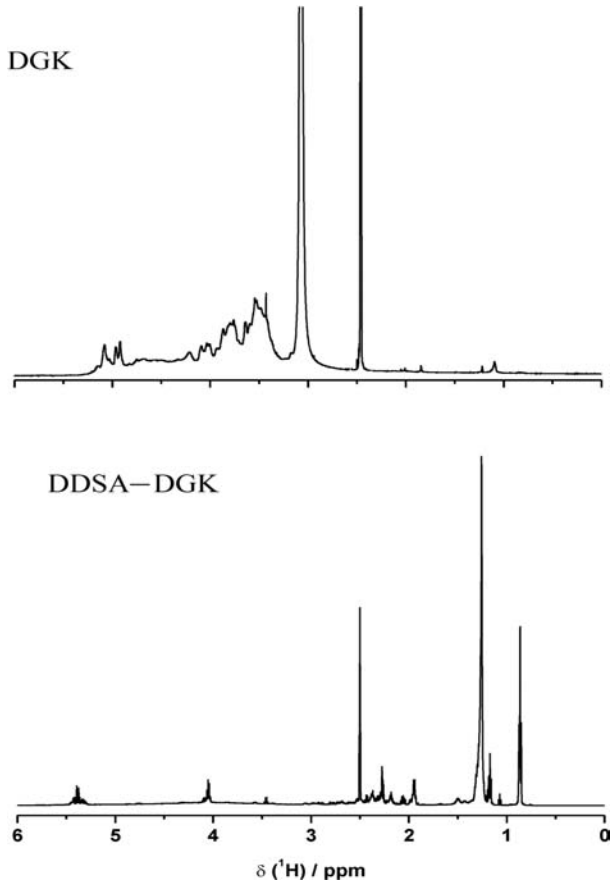

Figure 5. ^{1}H NMR spectra recorded for DGK and DDSA-DGK.

in agreement with those obtained for DDSA derivatives of starch,[13] inulin,[15] and gum arabic[19] previously reported in the literature.

TGA. The TGA and derivative thermogravimetric analysis (DTG) plots of DGK and the DDSA-DGK derivative are presented in Figure 6. TGA was performed in an inert nitrogen atmosphere. From the TGA curves, it is evident that the DDSA-DGK derivative decomposed in two major weight-loss steps as compared to DGK, which decomposed in a single step. The first stage of decomposition occurred in DDSA-DGK at 219 °C. This is attributed to breakage of ester bonds between DDSA and the gum at the aforementioned temperature and the

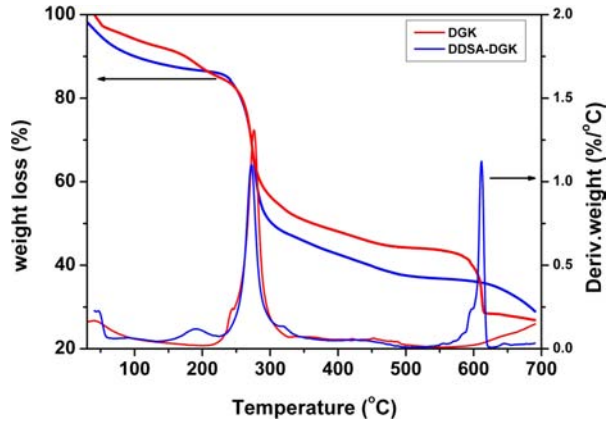

Figure 6. TGA and DGT curves as a function of temperature for DGK and DDSA-DGK.

release of alkyl chains from the DDSA. The second major degradation step shown by the DDSA derivative of DGK occurred at a peak decomposition temperature of 275 °C, this representing the bulk of the weight loss. This substantial weight reduction was due to breakages of main-chain linkages of DGK at this temperature. A similar behavior was reported for TGA of carboxymethyl starch/quaternary ammonium salt complexes, where two-step weight losses caused by the release of alkyl moieties associated with surfactant and the starch matrix were observed.[28] Thus, TGA indicates clearly that pristine DGK is more stable than its corresponding DDSA derivative. However, the DDSA derivatized samples exhibited lower weight loss until approximately 200 °C, owing possibly to the reduced water absorption of the modified samples. DGK in contrast showed a higher weight loss until 200 °C. However, the overall rate of decomposition of DDSA-DGK was faster compared to DGK and gave a low char yield of 20%. The comparative yield for pristine DGK was twice this value.

DSC. Figure 7 shows DSC thermal curves for both DGK and its derivative, DDSA-DGK. The DSC profiles reflect the

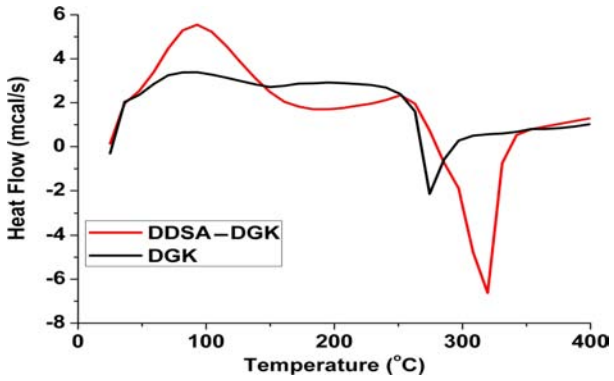

Figure 7. DSC thermograms of DGK and DDSA-DGK.

occurrence of exothermic and endothermic changes with increasing temperature. Thermograms for the DDSA-DGK indicate a broad endothermic transition over the range of 60–140 °C with a melting peak at around 93 °C. This can be attributed to the increased thermoplastic nature of DDSA modified DGK brought about by plasticizing alkenyl groups, probably through internal plasticization. The results suggest that the DDSA-DGK derivative has better thermoplasticity compared to pristine DGK. The decreased enthalpy value of the first transition (Figure 7) also suggests greater interaction between DGK and DDSA. DGK does show a very mild transition in this range, if viewed individually. The improved thermoplastic nature effected by alkyl group modified surfactants and the adoption of simple methodologies have been reported earlier.[28] Both samples exhibited exothermic peaks at higher temperatures, at 276 °C for DGK and at 319 °C for DDSA-DGK. These results suggest that modification by DDSA had improved the thermal stability. The enthalpy changes associated with the first and second transitions were 63 and −116 J/g for DDSA-DGK. In comparison, the DGK gave corresponding figures of 415 and −203 J/g. Furthermore, the results obtained indicate that hydrophobic groups of the DDSA reagent had weakened hydrogen bond formation in the DDSA-DGK derivative. This in turn enhanced structural flexibility, altered the gelatinization temperature, and brought about a

DOI: 10.1021/jf505783e
J. Agric. Food Chem. 2015, 63, 3757–3765

reduction in enthalpy, as had also been reported for OSA derivatives of starch.[29]

CAC. *Dye Solubilization.* Absorbance versus concentration plots for DGK and DDSA-DGK along with Sudan IV dye are presented in Figure 8. The absorbance of DGK does not

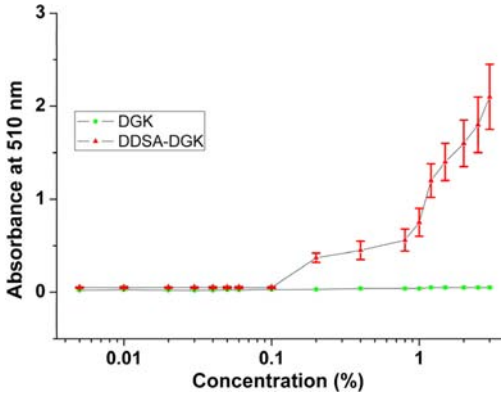

Figure 8. Concentration dependence of the UV−vis absorbances of DGK and DDSA-DGK in the presence of Sudan IV dye.

change over the concentration range studied, confirming that there is no interaction between DGK and the dye. For the DDSA-DGK sample, the absorbance values increase significantly above a certain concentration, indicating the formation of aggregates (Figure 8). The CAC was determined to be 0.1% for DDSA-DGK, the results obtained being in agreement with CAC values reported for DDSA derivatives of inulin[15] and gum arabic.[19]

Surface Tension Measurements. The surface tensions of DDSA-DGK solutions are plotted as a function of concentration in Figure 9. The surface tension of the DGK derivative

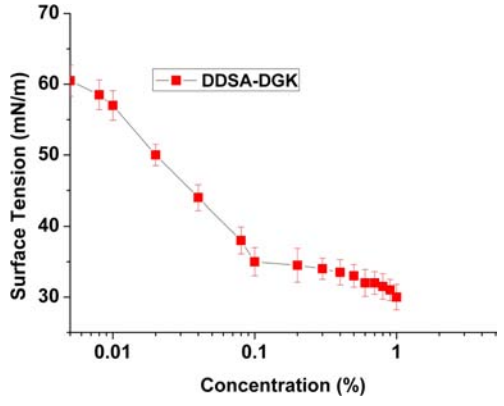

Figure 9. Surface tension of DDSA-DGK as a function of concentration.

was found to decrease with increasing concentration, but there was a distinct inflection in the curve, corresponding to the CAC. This was attributable to the formation of micelle-type aggregates brought about by hydrophobic association of the molecules through the alkyl chains, occurring at a concentration of 0.1%. This value is in good agreement with the result obtained from the dye solubilization experiment (Figure 8). The surface tension was found to be ∼30−35 mN/m at the CAC. The experimental values obtained concur with the CAC values reported in the literature for DDSA derivatives of inulin[15] and gum arabic.[19]

Rheological Properties. The flow behavior of DGK and DDSA-DGK at different concentrations (1, 2, and 3% w/w) was monitored, and the apparent viscosities were plotted as a function of shear rate. It was observed that for both DGK and DDSA-DGK in deionized water, the apparent viscosity increased with rising concentrations of both formulations (Figure 10). The apparent viscosity of the DDSA-DGK

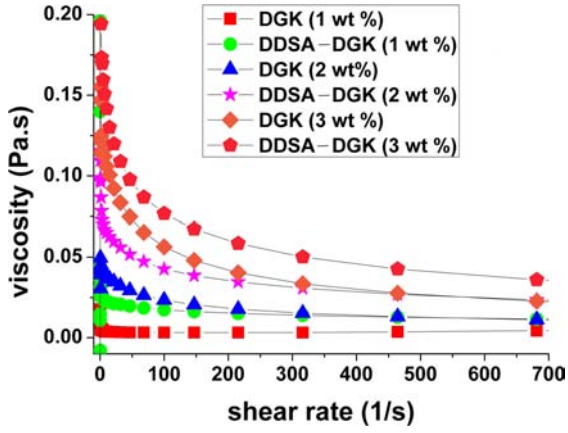

Figure 10. Plots of viscosity as a function of shear rate for DGK and DDSA-DGK of different concentrations (1, 2, and 3%).

derivative was significantly higher than that of DGK alone at the same concentration. This indicated that DDSA derivatization had indeed occurred and had resulted in a higher molecular weight. The higher viscosity values reported for OSA derivatives of starch[30,31] are in agreement with the results of our present study. It was also noted that the viscosities of both DGK and DDSA-DGK decreased sharply with increasing shear rate for all concentrations, eventually reaching a constant value at higher shear rates. The behavior was ascribed to the formation of aggregates through hydrogen bonding and polymer entanglement, producing a highly ordered arrangement of stiff molecules. This ultimately resulted in high viscosity at low shear rates, as reported in the literature for gum kondagogu.[32]

Antibacterial Properties. We tested the antibacterial activity of the DDSA-DGK against Gram-negative *E. coli* and *P. aeruginosa* and Gram-positive *S. aureus* bacteria. The results show that the control sample without DDSA does not display any antibacterial activity. Figure 11 and Table 2 summarize the results ZOI were determined.

The ZOI for Gram-negative *E. coli* and *P. aeruginosa* and Gram-positive *S. aureus* were 8.2 ± 0.8, 8.0 ± 0.8, and 8.2 ± 0.7 mm, respectively, for 1 wt % concentration of DDSA-DGK. The ZOI for DDSA-DGK against *E. coli*, *P. aeruginosa*, and *S. aureus* were seen to increase when the concentration of DDSA-DGK rose from 1 to 10 wt % in all three cases. Furthermore, the antibacterial ZOI for DDSA-DGK against Gram-negative *E. coli* and *P. aeruginosa* and Gram-positive *S. aureus* were observed to be almost equal for all three tested microorganisms of different bacterial strains (Table 2).

These results were in good agreement with earlier reported investigations about antibacterial properties of gum tragacanth/PVA nanofibers, Ag/montmorillonite/chitosan bionanocomposites, and PVA/carboxymethyl-chitosan/Ag-nanowires.[33−35] The present study suggests that antibacterial properties of DDSA-DGK are enhanced with increasing concentration. The improved antimicrobial action of DDSA-DGK may be related

DOI: 10.1021/jf505783e
J. Agric. Food Chem. 2015, 63, 3757−3765

Figure 11. Bacterial activity with zones of inhibition for various concentrations of DDSA-DGK (1, 2, 3, 4, and 10%): (A) *E. coli*; (B) *P. aeruginosa*; (C) *S. aureus*.

to the balance of hydrophilicity/hydrophobicity and the increased surface roughness of DGK after derivatization with DDSA, the latter helping to increase contact between the surfaces of the material and the bacteria. The current work is in agreement with the antibacterial action of poly(propylene)-modified Cu and Ag nanocomposites and polyethylene/triclosan/chlorohexidene composites[36,37] However, the antibacterial properties of DDSA are less well-known compared to those of Ag nanoparticles.[38] The biocidal attributes and toxicity of Ag nanoparicles have also been studied in detail recently.[39,40] With regard to nontoxicity, the present undertaking emphasizes that natural gum derivatized DDSA materials can be developed as the leading antibacterial agent, which could replace the toxic Ag and Cu of CuO-based polymeric materials in their role as antimicrobial agents. Given that gums are widely used in food and pharmaceutical applications as stabilizing and emulsifying agents,[2] the development of DDSA derivatized gums has potentially two major benefits, namely, as stabilizers and antibacterial agents in food and nonfood applications.

AUTHOR INFORMATION

Corresponding Author

*(Vinod V.T.P.) E-mail: vinod.padil@tul.cz or vinodvellorathekkaepadil@gmail.com. Phone: +420 607 393 502. Fax: +420 485 353 445.

Funding

The research reported in this paper was financially supported by the Ministry of Education, Youth and Sports within the framework of the targeted support of the "National Programme for Sustainability I"; the OPR & DI project (LO 1201), and the Centre for Nanomaterials, Advanced Technologies and Innovation CZ.1.05/2.1.00/01.0005.

Notes

The authors declare no competing financial interest.

ABBREVIATIONS USED

GK, gum karaya; DGK, deacetylated gum karaya; DDSA, (2-dodecen-1-yl)succinic anhydride; OSA, octenylsuccinic anhydride; DS, degree of substitution; GPC/MALLS, gel permeation chromatography/multiangle laser light scattering; ATR-FTIR, attenuated total reflectance−Fourier transform infrared spectroscopy; SEM, scanning electron microscopy; ^{1}H NMR, proton nuclear magnetic resonance spectroscopy; TGA, thermogravimetric analysis; DSC, differential scanning calorimetry; CAC, critical aggregation concentration; ZOI, zones of inhibition

REFERENCES

(1) Phillips, G. O.; Williams, P. A. Tree exudates gums: natural and versatile food additives and ingredients. *Food Ingred. Anal. Int.* **2001**, *23*, 26−28.

(2) Verbeken, D.; Dierchx, S.; Dewettinck, K. Exudate gums: occurrence, production and applications. *Appl. Microbiol. Biotechnol.* **2003**, *63*, 10−21.

(3) Pollard, M. A.; Kelley, R.; Fischer, P. A.; Windhab, E. J.; Eder, B.; Amado, R. Investigation of molecular weight distribution of LBG galactomannan for flours prepared from individual seeds, mixtures, and commercial samples. *Food Hydrocolloids* **2008**, *22*, 1596−1606.

(4) Vinod, V. T. P.; Sashidhar, R. B.; Suresh, K. I.; Rama Rao, B.; Vijaya Saradhi, U. V. R.; Prabhakar Rao, T. Morphological, physiochemical and structural characterization of gum kondagogu (*Cochlospermum gossypium*): a tree gum from India. *Food Hydrocolloids* **2008**, *22*, 899−915.

(5) Anderson, D. M. W.; McNab, C. G. A.; Anderson, C. G.; Braown, P. M.; Pringuer, M. A. Gum exudates from the genus *Sterculia* (gum karaya). *Int. Tree Crops J.* **1982**, *2*, 147−154.

(6) Le Cerf, D.; Irinei, F.; Muller, G. Solution properties of gum exudates from *Sterculia urens* (karaya gum). *Carbohydr. Polym.* **1990**, *13*, 375−386.

Table 2. Zone of Inhibition of Different Bacterial Strains Observed for DDSA-DGK

	zone of inhibition[a] (mm) at DDSA-DGK concentration of				
bacterial strain	1 wt %	2 wt %	3 wt %	4 wt %	10 wt %
E. coli	8.1 ± 0.8	9.2 ± 0.6	10.2 ± 0.5	11.1 ± 0.8	14.2 ± 0.8
P. aeruginosa	8.0 ± 0.8	10.5 ± 0.8	11.8 ± 0.7	12.8 ± 0.7	15.0 ± 0.6
S. aureus	8.2 ± 0.7	10.6 ± 0.8	12.0 ± 0.8	12.9 ± 0.6	15.0 ± 0.8

[a]Values are means ± SD, n = 3.

DOI: 10.1021/jf505783e
J. Agric. Food Chem. 2015, 63, 3757−3765

(7) Whistler, R. L. Exudate gums. In *Industrial Gums: Polysaccharides and Their Derivatives*; Whistler, R. L., Bemiller, J. N., Eds.; Academic Press: San Diego, CA, USA, 1993; pp 318−337.
(8) Weiping, W. Tragacanth and karaya. In *Handbook of Gydrocolloids*; Philips, G. O., Williams, P. A., Eds.; Woodhead: Cambridge, UK, 2000; pp 155−168.
(9) Brito, A. C. F.; Silva, D. A.; de Paula, R. C. M.; Feitosa, J. P. A. *Sterculia striata* exudate polysaccharide: characterisation, rheological properties and comparison with *Sterculia urens* (karaya) polysaccharide. *Polym. Int.* **2004**, *53*, 1025−1032.
(10) Brito, A. C. F.; Sierakowski, M. R.; Reicher, F.; Feitosa, J. P. A.; de Paula, R. C. M. Dynamic rheological study of *Sterculia striata* and karaya polysaccharides in aqueous solution. *Food Hydrocolloids* **2005**, *19*, 861−867.
(11) Stephen, A. M.; Churms, S. C. Polysaccharides and mucilages. In *Food Polysaccharides and Their Applications*; Stephen, A. M., Ed.; Dekker: New York, 1995; pp 377−440.
(12) Meer, W. In *Handbook of Water-Soluble Polysaccharides and Resins*; Davidson, R., Ed.; McGraw-Hill: New York, 1980; pp 3−4.
(13) Chi, H.; Xu, K.; Xue, D.; Song, C.; Zhang, W.; Wang, P. Synthesis of dodecenyl succinic anhydride (DDSA) corn starch. *Food Res. Int.* **2007**, *40*, 232−238.
(14) Zhou, J.; Ren, L.; Tong, J.; Xie, L.; Liu, Z. Surface esterification of corn starch films: Reaction with dodecenyl succinic anhydride. *Carbohydr. Polym.* **2009**, *78*, 888−893.
(15) Kokubun, S.; Ratcliffe, I.; Williams, P. A. Synthesis, characterization and self-assembly of biosurfactants based on hydrophobically modified inulins. *Biomacromolecules* **2013**, *14*, 2830−2836.
(16) Meng, F.; Zheng, L.; Wang, Y.; Liang, Y.; Zhong, G. Preparation and properties of konjac glucomannan octenyl succinate modified by microwave method. *Food Hydrocolloids* **2014**, *38*, 205−210.
(17) Sweedman, M. C.; Tizzotti, M. J.; Schäfer, C.; Gilbert, R. G. Structure and physicochemical properties of octenyl succinic anhydride modified starches: a review. *Carbohydr. Polym.* **2013**, *92*, 905−920.
(18) Segura-Campos, M.; Chel-Guerrero, L.; Betancur-Ancona, D. Synthesis and partial characterization of octenyl succinic starch from *Phaseolus lunatus*. *Food Hydrocolloids* **2008**, *22*, 1467−1474.
(19) Wang, H.; Williams, P. A.; Senan, C. Synthesis, characterization and emulsification properties of dodecenyl succinic anhydride derivatives of gum Arabic. *Food Hydrocolloids* **2014**, *37*, 143−148.
(20) Vinod, V. T. P.; Sashidhar, R. B. Solution and conformational properties of gum kondagogu (*Cochlospermum gossypium*) − a natural product with immense potential as a food additive. *Food Chem.* **2009**, *116*, 686−692.
(21) Tommeraas, K.; Mellergaard, M.; Malle, B. M.; Skagerlind, P. New amphiphilic hyaluronan derivatives based on modification with alkenyl and aryl succinic anhydrides. *Carbohydr. Polym.* **2011**, *85*, 173−179.
(22) Eenschooten, C.; Guillaumie, F.; Kontogeorgis, M.; Stenby, E. H.; Abdellaoui, K. S. Preparation and structural characterisation of novel and versatile amphiphilic octenyl succinic anhydride-modified hyaluronic acid derivatives. *Carbohydr. Polym.* **2010**, *79*, 597−605.
(23) Bai, Y.; Shi, Y.-C. Structure and preparation of octenyl succinic esters of granular starch, microporous starch and soluble maltodextrin. *Carbohydr. Polym.* **2011**, *83*, 520−527.
(24) Tizzotti, M. J.; Sweedman, M. C.; Tang, D.; Schaefer, C.; Gilbert, R. G. New ^{1}H NMR procedure for the characterization of native and modified food-grade starches. *J. Agric. Food Chem.* **2011**, *59*, 6913−6919.
(25) Mahendran, T.; Williams, P. A.; Phillips, G. O.; Al-Assaf, S.; Baldwin, T. C. New insights into the structural characteristics of the arabinogalactan-protein (AGP) fraction of gum Arabic. *J. Agric. Food Chem.* **2008**, *56*, 9269−9276.
(26) Song, X.; He, G.; Ruan, H.; Chen, Q. Preparation and properties of octenyl succinic anhydride modified early indica rice starch. *Starch/Staerke* **2006**, *58*, 109−117.
(27) Cheng, H. N.; Neiss, T. G. Solution NMR spectroscopy of food polysaccharides. *Polym. Rev.* **2012**, *52*, 81−114.
(28) Balsamo, V.; Lopez-Carrasquero, F.; Laredo, E.; Conto, K.; Contreras, J.; Feijoo, J. L. Preparation and thermal stability of carboxymethyl starch/quaternary ammonium salts complexes. *Carbohydr. Polym.* **2011**, *83*, 1680−1689.
(29) Bao, J. S.; Xing, J.; Philips, D. L.; Corke, H. Physical properties of octenyl succinic anhydride modified rice, wheat, and potatoes starches. *J. Agric. Food Chem.* **2003**, *51*, 2283−2287.
(30) Bhosale, R.; Singhal, R. Effect of octenylsuccinylation on physicochemical and functional properties of waxy maize and amaranth starches. *Carbohydr. Polym.* **2007**, *68*, 447−456.
(31) Song, X.-Y.; Zhu, Z.; Li, Z.; Zhu, Z. Characteristic and application of octenyl succinic anhydride modified waxy corn starch in sausage. *Starch /Staerke* **2010**, *62*, 629−636.
(32) Vinod, V. T. P.; Sashidhar, R. B.; Sarma, V. U. M.; Vijaya Saradhi, U. V. R. Compositional analysis and rheological properties of gum kondagogu (*Cochlospermum gossypium*): a tree gum from India. *J. Agric. Food Chem.* **2008**, *56*, 2199−2207.
(33) Ranjbar-Mohammadi, M.; Bahrami, S. H.; Joghataei, M. T. Fabrication of novel nanofiber scaffolds from gum tragacanth/poly (vinyl alcohol) for wound dressing application: In vitro evaluation and antibacterial properties. *Mater. Sci. Eng., C* **2013**, *33*, 4935−4943.
(34) Zhao, Y.; Zhou, Y.; Wu, X.; Wang, L.; Xu, L.; Wei, S. A facile method for electrospinning of Ag nanoparticles/poly (vinyl alcohol)/carboxymethyl-chitosan nanofibers. *Appl. Surf. Sci.* **2012**, *258*, 8867−8873.
(35) Shameli, K.; Ahmad, M. B.; Zargar, M.; Yunus, W. M. Z.; Ibrahim, N. A.; Moghaddam, M. G. Synthesis and characterization of silver/montmorillonite/chitosan bionanocomposites by chemical reduction method and their antibacterial activity. *Int. J. Nanomed.* **2011**, *6*, 271−284.
(36) Espana-Sanchez, B. L.; Avila-Orta, C. A.; Padilla-Vaca, F.; Neira-Velazquez, M. G.; Gonzalez-Moroues, P.; Rodriguez-Gonzalex, J. A.; Hernandez-Hernandez, E.; Rangel-Serrano, A.; Barriga-, E. D.; Yate, C. L.; Ziolo, R. F. Enhanced antibacterial activity of melt processed poly(propylene) Ag and Cu nanocomposites by argon plasma treatment. *Plasma Processes Polym.* **2014**, *11*, 353−365.
(37) Popelka, A.; Novak, I.; Lehocky, M.; Chodak, I.; Sedliacik, J.; Gajtanska, M.; Sedliacikova, M.; Vesel, A.; Junkar, I.; Kleinova, A.; Spirkova, M.; Bilek, F. Anti-bacterial treatment of polyethylene by cold plasma for medical purposes. *Molecules* **2012**, *17*, 762−785.
(38) Marambio-jones, C.; Hoek, E. M. V. A review of the antibacterial effects of silver nanomaterials and potential implications for human health and the environment. *J. Nanopart. Res.* **2010**, *12*, 1531−1551.
(39) Liu, J.; Hurt, R. H. Ion release kinetics and particle persistence in aqueous nano-silver colloids. *Environ. Sci. Technol.* **2010**, *44*, 2169−2175.
(40) Kittler, S.; Greulich, C.; Diendorf, J.; Koller, M.; Epple, M. Toxicity of silver nanoparticles increases during storage because of slow dissolution under release of silver ions. *Chem. Mater.* **2010**, *22*, 4548−4554.

DOI: 10.1021/jf505783e
J. Agric. Food Chem. 2015, 63, 3757−3765

processing conditions and could oxidatively modify side chains and polypeptide backbone of protein, resulting in its conformational changes.[26] Meanwhile, MDA can react with amino groups of proteins, producing strong intermolecular cross-links of the Schiff base type.[27] In our previous study,[25] the novel cold-set MP gel could be formed on the premise of the swelling of MP under 0.6 M NaCl and the non-disulfide covalent bond induced by MDA. The gelation mechanism of salted MP mainly involving simultaneous protein oxidation and internal cross-linking via MDA was also proposed.[25] On the basis of our previous findings, we thus postulated that incubation with MDA in MP-based emulsion systems may result in the formation of a new type of cold-set emulsion gel stabilized by MP. This speculation would provide foundational information for further exploring the potential impact of MDA in real meat emulsions during manufacturing and storage.

The objective of this study was to test the hypothesis that MDA affects the gelation of MP-stabilized emulsion under different ionic strength conditions. The consequential changes in emulsion gel in terms of the amount/fraction of protein entrapped/non-entrapped as well as mechanical properties (gel elasticity, strength, water-holding capacity), microstructure, and oxidative stability were all investigated to elucidate the structure-modifying effect of MDA.

MATERIALS AND METHODS

Materials. Longissimus muscle from three pork carcasses (48 h post-mortem) was purchased from a local commercial abattoir (Zhongshan, China); the pigs were slaughtered at about 6 months of age following standard industrial procedures. Fat was trimmed away, and muscle was cut into cubes, minced, vacuum packaged (ca. 100 g), and frozen at −80 °C until use (within 3 days). Commercially available Jinlongyu soybean oil (pure) produced by Yihai Kerry Food Co. (Shanghai, China) was purchased from a local supermarket. MDA solution was prepared by acid treatment of 1,1,3,3-tetramethoxypropane obtained from Sigma-Aldrich Chemical Co. (St. Louis, MO, USA). Nile Blue A and Nile Red were obtained from Sigma-Aldrich Chemical Co. All other chemicals were of analytical reagent grade.

Extraction of MP. Three batches of MP were prepared from different bags of raw muscle thawed at 4 °C according to the method of Park et al.[24] with slight modifications. The pH of MP suspension at 0.1 M NaCl in the last wash was adjusted to 6.25 before centrifugation. The pellet was finally suspended in 20 mM sodium phosphate buffer (pH 6.0) containing NaCl at different levels (0, 0.2, 0.4, and 0.6 M), and the protein concentration was determined according to the Biuret method using BSA as standard.

Emulsion Preparation. Oil-in-water (O/W) emulsions were prepared by dispersing 20 wt % soybean oil in 20 mM phosphate buffer (pH 6.0) containing 3% (w/v) MP at different NaCl levels (0, 0.2, 0.4, and 0.6 M). Coarse emulsions were prepared using a high-speed blender operating at 11000 rpm for 3 min (Ultra-Turrax, IKA-Labortechnik, Staufen, Germany). The coarse emulsions were further homogenized using a two-stage single-piston homogenizer (APV-1000, Albertslund, Denmark) at 30 MPa. Sodium azide (0.02 wt %) was then added to the emulsions to prevent microbial growth. Emulsions were placed in lightly sealed screw-cap vials or 2 mL centrifuge tubes and stored in a dark oven at 25 °C for 30 days.

Evaluation of Emulsions. *Particle Size Distribution.* The mean particle size and size distribution of emulsions were measured by a Mastersizer 2000 (Malvern Instruments Co. Ltd., Worcestershire, UK) at 25 °C. The refractive indices of soybean oil and phosphate buffer were taken as 1.456 and 1.330, respectively. The absorption index was 0.001. The particle sizes measured are reported as the volume-weighted mean diameter $d_{4,3}$ ($d_{4,3} = \sum n_i d_i^4 / \sum n_i d_i^3$), where n_i is the number of particles with diameter d_i.

Rheological Characterization. The rheological properties of the emulsions stabilized by MP at different ionic levels were characterized using a HAAKE MARS III Rheometer (Thermo Electron GmbH, Karlsruhe, Germany) with a parallel plate (diameter = 35 mm), at 25 °C. The gap between two plates was set to 1.0 mm. For determination of steady shear viscosities, shear rate was ramped from 1 to 200 s^{-1}. Shear stress, shear rate, and steady shear (apparent) viscosity (η) were recorded by a RheoWin 4 Data Manager. Dynamic viscoelastic properties were characterized using small-amplitude oscillatory frequency sweep mode. The frequency was oscillated from 0.1 to 100 rad/s, and all measurements were performed within the identified linear viscoelastic region and made at 0.5% strain. The elastic modulus (G'), loss modulus (G''), and loss tangent (tan δ) were recorded.

Preparation of MDA-Modified MP Emulsion Gels. MDA stock solution was freshly prepared by hydrolyzing 1,1,3,3-tetramethoxypropane according to the method described by Wu et al.[28] with minor modifications.[25] The concentration of MDA was determined by spectrophotometric measurements of the dilution 10^{-5} at 267 nm (ε = 31500).

MP emulsion in the presence of 0.6 M NaCl was mixed with MDA at different concentrations (0, 0.5, 2.5, 5, 10, 25, and 50 mM, final). The resulting mixtures were immediately transferred into tightly sealed glass vials (2.5 cm i.d., 5 cm height) and 2 mL centrifuge tubes and incubated at 25 °C in the dark for 24 h. After incubation, a series of treated samples with different states were obtained. To further investigate the influence of ionic strength, MP emulsions at different NaCl levels (0, 0.2, 0.4, and 0.6 M) were mixed with 10 mM MDA. The incubation condition used was the same as mentioned above. MP emulsion in the presence of 0.6 M NaCl treated without MDA was selected as control.

Evaluation of Gel Characteristics. *Low-Amplitude Dynamic Oscillatory Measurements.* Small-deformation rheological measurements using parallel plates (diameter = 35 mm, 1 mm gap) were investigated in a HAAKE MARS III Rheometer (Thermo Electron GmbH). Frequency sweep analysis between 0.1 and 100 rad/s (at 25 °C and 0.5% strain) was applied to investigate the viscoelastic properties.

Gel Strength. The gel strength of emulsion gels was measured using a cylinder measuring probe (P 0.5SS) attached to a TA.TX2 texture analyzer (Stable Micro System, Surrey, UK) at a constant probe speed of 1.0 mm/min at room temperature (25 ± 1 °C). Gel strength is defined as the initial force required to disrupt the gels. All samples were prepared in triplicate.

Water-Holding Capacity (WHC). WHC values of the emulsion gels were determined according to the method of Wu et al.,[12] with slight modifications. Briefly, gels (3 g) were centrifuged at 8000*g* for 30 min at 4 °C. WHC (%) was expressed as the final weight as a percentage of the weight before centrifugation.

Amount of Protein Entrapped. The amount of proteins entrapped was evaluated according to the method of Chanyongvorakul et al.[29] with modifications. After incubation, the emulsion gels in 2 mL centrifuge tubes were centrifuged (10000*g*, 30 min, 25 °C) and used to determine the amount of proteins entrapped. The protein concentration of separated aqueous layer, filtered through a 0.45 μm filter (Millipore Corp.), was determined according to the Bradford assay, using BSA as standard. The percent of entrapped proteins was calculated as (1 − protein concentration in separated aqueous layer/initial protein concentration in the aqueous phase) × 100.

Sodium Dodecyl Sulfate−Polyacrylamide Gel Electrophoresis (SDS-PAGE) Analysis. SDS-PAGE was performed on entrapped and non-entrapped proteins of the emulsion gels according to the method described Flores et al.,[30] under either nonreducing or reducing conditions. Both aqueous and creamed layers after centrifuging (10000*g*, 30 min, 4 °C) were collected and mixed with certain volumes of sample buffer (with and without 5% β-mercaptoethanol (β-ME)) to obtain a theoretical concentration of 1 mg mL^{-1} protein. Samples were vortexed and incubated at room temperature overnight. The ones with β-ME were boiled for 5 min before centrifugation (10000*g*, 10 min). Then, 24 μL of samples was loaded onto the polyacrylamide gel made of 12% running gel and 5% stacking gel and subjected to electrophoresis at a constant current of

DOI: 10.1021/jf505916f
J. Agric. Food Chem. 2015, 63, 3766−3777

25 mA per gel using a Mini-PROTEAN 3 Cell apparatus (Bio-Rad Laboratories, Hercules, CA, USA).

Confocal Laser Scanning Microscopy (CLSM). The microstructure of the MDA-modified emulsion gels was determined in a confocal laser scanning microscope (Zeiss, LSM 710, Germany), using Nile Red and Nile Blue A as fluorescence dyes for the protein and oil phases, respectively.[8] Each freshly prepared MDA-treated emulsion sample (1 mL) was stained with about 40 μL of fluorescence dye mixtures of Nile Blue A (0.1%, w/v) and Nile Red (0.1%, w/v) in 1,2-propanediol. The emulsion gels containing the dyes were directly formed in concave confocal microscope slides (Sail; Sailing Medical-Lab Industries Co. Ltd., Suzhou, China), covered with glycerol-coated coverslips (further sealed with tin foil), according to the same conditions mentioned above. Finally, the CLSM images were examined with a 100 magnification lens and an argon/krypton laser having an excitation line of 514 nm and a helium−neon laser (HeNe) with excitation at 633 nm for Nile Blue A and at 488 nm for Nile Red, respectively. Factually, most of the protein-coated oil droplets would be predominantly yellow in appearance of the overlay image (green + red = yellow).

Lipid Hydroperoxide Measurement. Lipid hydroperoxide was measured according to the method described by Tong et al.[31] with some modifications. Emulsions/emulsion gels were diluted in 4 volumes (w/v) of distilled water before homogenization (11000 rpm, 1 min). Aliquots (0.2 mL) of the dilution ere mixed with 1.5 mL of isooctane/2-propanol (3:1, v/v) and vortexed (10 s, three times). After centrifugation at 3400*g* for 2 min, the organic solvent phase (200 μL) was added to 2.8 mL of methanol/1-butanol (2:1, v/v), followed by 15 μL of 3.94 M ammonium thiocyanate and 15 μ L of ferrous iron solution (prepared by mixing 0.132 M $BaCl_2$ and 0.144 M $FeSO_4$). Twenty minutes later, the absorbance was measured at 510 nm using a UV−vis spectrophotometer (Genesys 10, Thermo Scientific, USA). Distilled water was used instead of diluted emulsion as a reagent blank. Hydroperoxide concentrations were determined using a standard curve made from hydrogen peroxide.

Statistical Analysis. Three batches of MP were prepared on different days, each used for independent trials (i.e., replicate preparation of MP, emulsion, and emulsion gel), and all of the experiments were repeated with three different batches of MP. Statistical calculation was investigated using the statistical package SPSS 11.5 (SPSS Inc., Chicago, IL, USA) for one-way ANOVA. The Student−Newman−Keuls test was used for comparison of mean values among determinations using a level of significance of 5%. Data were expressed as means ± standard deviations (SD) of triplicate determinations unless specifically mentioned.

RESULTS AND DISCUSSION

Emulsion Characteristics. *Particle Size Distribution and Physical Stability.* The particle size distributions and changes in the mean droplet diameter ($d_{4,3}$) for MP-stabilized emulsions at different NaCl levels were used to assess emulsifying ability and physical stability, as shown in Figure 1. The fresh emulsion stabilized by MP without addition of NaCl had an almost bimodal distribution with relatively small $d_{4,3}$ (Figure 1). The increase of NaCl concentration increased $d_{4,3}$ and caused a gradual shift of the size distribution peak to the right, indicating a decreased emulsifying capacity.[20] It has been reported that MP began to expand transversely when exposed to about 0.4−0.5 M NaCl and swell profusely at about 0.6 M NaCl due to enhanced electrostatic repulsion by Cl-binding to actomyosin.[25,32] Thus, the swollen MP in the presence of NaCl, on the one hand, decreased the protein adsorption rate on the droplets' surface due to increased steric hindrance; on the other hand, it increased protein−protein interactions,[18,25] resulting in the formation of a thicker layer surrounding the droplet (Figure 1A, inset) and, thus, the larger $d_{4,3}$ (Figure 1).

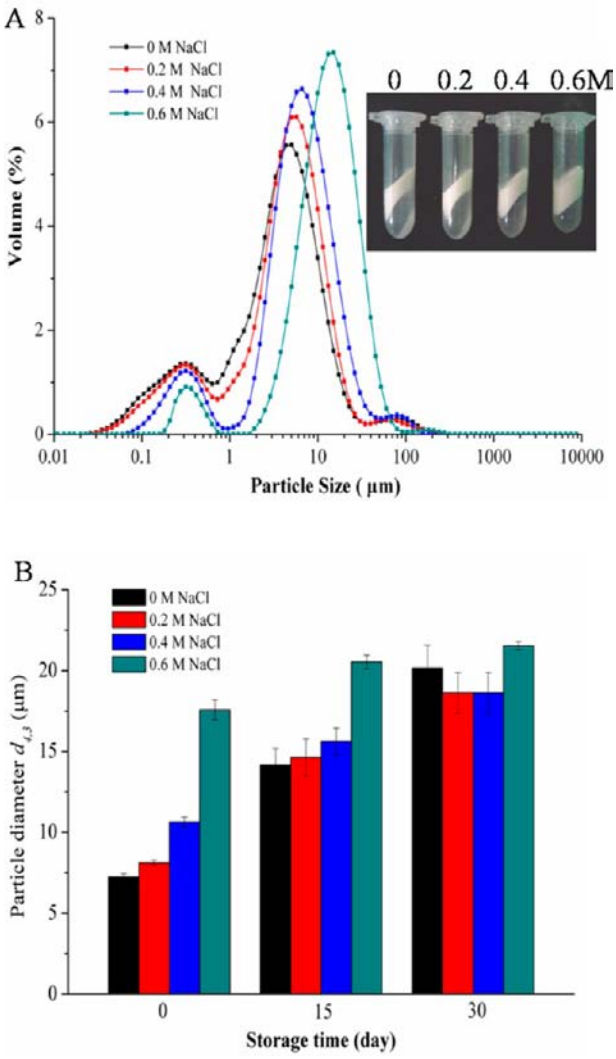

Figure 1. (A) Particle size distributions of fresh emulsions stabilized by MP at different NaCl levels (0−0.6 M). (Inset) Visual observation of fresh emulsions after centrifugation (10000*g*, 30 min). (B) Changes in mean particle diameter $d_{4,3}$ of emulsions during storage for 30 days.

To evaluate the physical stability of emulsions, the changes in the $d_{4,3}$ of emulsions were followed during storage (Figure 1B). As shown in Figure 1B, for the emulsion without NaCl, a marked increase in $d_{4,3}$ was observed with increasing storage time, reaching 20.16 μm at day 30, almost twice larger than that at day 0. Meanwhile, the emulsion exhibited an obvious phase separation (data not shown) after 30 days. These results indicated that MP-stabilized emulsion without NaCl was less stable after 30 days due to the coalescence of oil droplets, which were consistent with our previous study.[20] Compared to the emulsion without NaCl, the stability of emulsions in the presence of NaCl was obviously improved (Figure 1B). Specifically, when 0.6 M NaCl was added, the $d_{4,3}$ showed only a slight increase during the storage (Figure 1B) and no visible phase separation was found (data not shown), suggesting the enhanced stability of emulsions. As has been previously reported, more soluble MP with swollen appearance was available at high NaCl concentrations.[18,32] Therefore, the more hydrated absorbed protein layer with higher thickness around the droplets could be formed (Figure 1A, inset) due to enhanced protein−protein interactions, thus slowing the

DOI: 10.1021/jf505916f
J. Agric. Food Chem. 2015, 63, 3766−3777

coalescence of oil droplets and improving the emulsion stability (Figure 1B).[1,10]

Rheological Characterization. The rheological properties, including flow and dynamic viscoelastic properties of emulsions stabilized by MP at different NaCl levels, were characterized, as shown in Figure 2, panels A and B, respectively. All of the

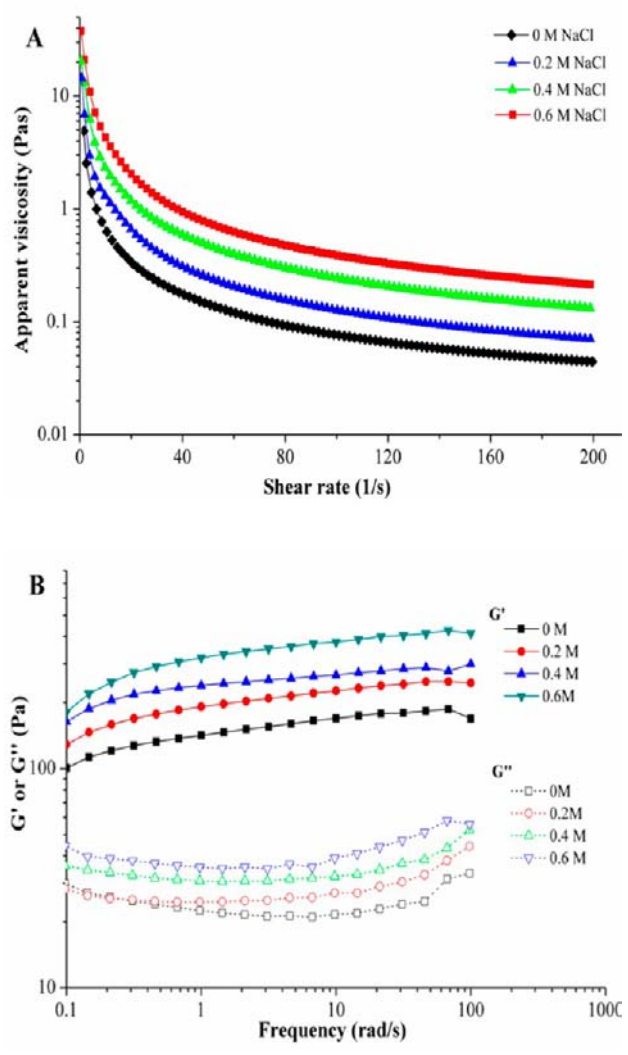

Figure 2. Variation of apparent viscosity (η) with shear rate (A) and of storage modulus (G')/loss modulus (G'') with frequency (B) for MP-stabilized emulsions at different NaCl levels (0−0.6 M).

emulsions exhibited shear-thinning behaviors at the tested shear rates in the range of 0.1−100 s^{-1}, with apparent viscosity (η) progressively decreasing upon increasing shear rate (Figure 2A). This phenomenon is supposed to be associated with the flocculation of fat droplets, as has been well addressed in previous studies.[10,33] Noticeably, at any test shear rate, η progressively increased with increasing NaCl from 0 to 0.6 M (Figure 2A). As has been aforementioned, the swelling of MP with increasing NaCl concentrations could enhance protein−protein interactions,[32] opposing the free flow of the emulsion in a shear field, thus increasing its apparent viscosity (Figure 2A). The increased system viscosity in turn retarded the migration of oil droplets and thus enhanced the emulsion stability (Figure 1B).

As to emulsion viscoelastic properties, in all cases, the storage modulus (G') was higher than the loss modulus (G'') in the test linear viscoelastic range (Figure 2B), suggesting the potential to form elastic gel or gel-like structure. The G' progressively increased with increasing oscillatory frequency (Figure 2B), as has also been observed in some other gel-like emulsions.[10,33] Furthermore, as expected, at any oscillatory frequency, the G' of emulsions stabilized by MP continuously and significantly increased with increasing NaCl concentration from 0 to 0.6 M (Figure 2B), indicating a gradual increase in the stiffness of emulsions. These results completely reproduced the general trends observed in the data from emulsion stability and steady viscosity (Figures 1B and 2A), further suggesting enhanced interdroplet interactions in the presence of 0.6 M NaCl, which contributed to an improvement in the emulsion stability.

Evaluation of MDA-Modified MP Emulsion Gels. *Visual Observation.* Figure 3 shows the images of MDA-modified MP emulsion either at various MDA concentrations (Figure 3A) or at different NaCl levels (Figure 3B). After incubation, vials containing samples were kept upside down for 10 min and photographed. As shown in Figure 3A, in the presence of 0.6 M NaCl, with the increasing addition of MDA, a transition from sol to gel was observed, and emulsion gel samples were obtained when the MDA concentration was >2.5 mM. Nevertheless, an "oil leak" phenomenon was also observed when samples were treated with MDA >25 mM (Figure 3A, bottom). These results indicated that MDA played a critical role in emulsion gel formation. Additionally, the necessity of NaCl in emulsion gel formation was further confirmed, as shown in Figure 3B. After being upside down for 10 min, the emulsion gel sample with 0.2 M NaCl collapsed (Figure 3B), indicating a weak gel structure. Thus, these results indicated that both MDA and NaCl played an important role in controlling gel formation and quality.

Low-Amplitude Dynamic Oscillatory Measurements. For better understanding of the influence of MDA and NaCl on the viscoelastic properties of emulsion gels, variations of G' and tan δ with frequency were recorded, using small strain measurement, as shown in Figure 4. For MDA-modified MP emulsion with 0.6 M NaCl, as can be seen from Figure 4A, G' in magnitude in the test linear viscoelastic range first continuously increased with increasing MDA concentration from 0 to 10 mM. At certain frequency (1 rad/s), G' of the sample treated with 10 mM MDA reached 1986 Pa, representing an evident increase in G' approximately 6.0 times compared to that of control, which indicated the elastic property of the sample was markedly enhanced and corresponded well to the formation of gel structure as shown in Figure 3A. This might be due to the development of protein−protein cross-links under MDA-induced oxidative stress,[25,27] resulting in an entanglement network between adsorbed and nonadsorbed proteins.[10] Nevertheless, further addition of MDA (25−50 mM) sharply decreased the G', suggesting a weakened gel structure, which might be related to the oil leakage (Figure 3A).[13] As has been extensively stated in the literature,[6,34] incorporated oil could functionalize as active filler, leading to a gel network with an enhanced rigidity, and thus the reduced oil incorporated would decrease the gel elasticity (25−50 mM MDA). In addition, the loss factor, tan δ, indicative of whether elastic or viscous properties were predominant, was further measured, as shown in Figure 4C. In all cases, it can be clearly seen that tan δ was almost independent of the frequency throughout the tested

DOI: 10.1021/jf505916f
J. Agric. Food Chem. 2015, 63, 3766−3777

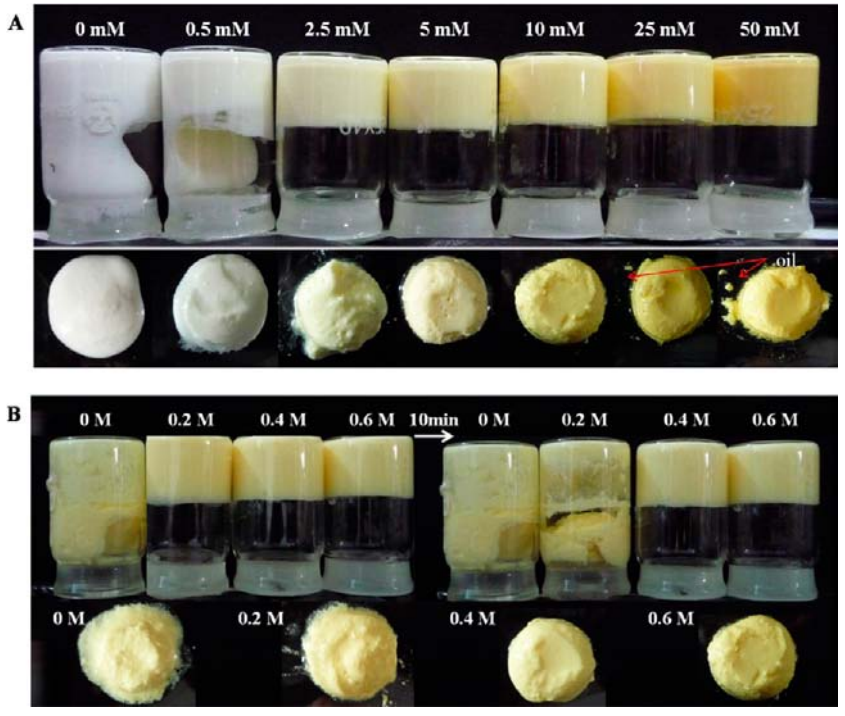

Figure 3. Visual observations of MDA-modified MP emulsions with various MDA concentrations (0−50 mM MDA, 0.6 M NaCl) (A) or at different NaCl levels (0−0.6 M NaCl, 10 mM MDA) (B).

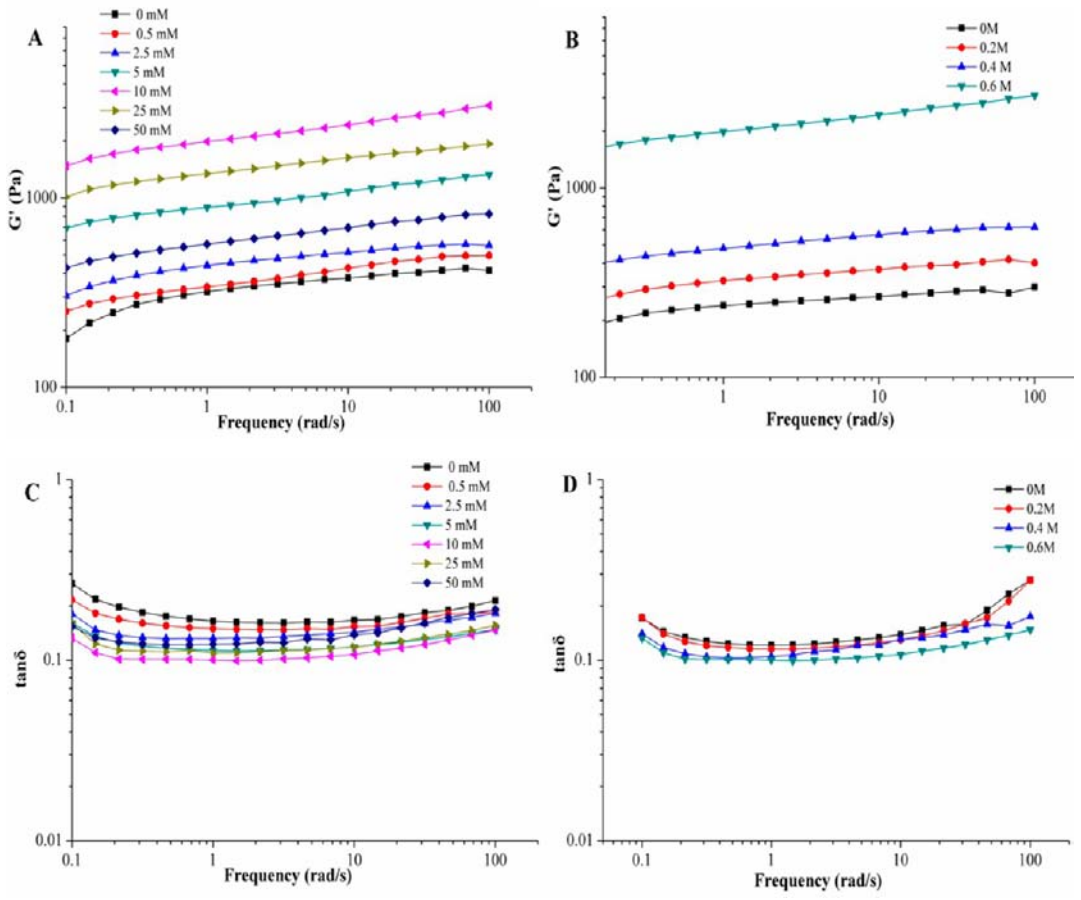

Figure 4. Typical dependence profiles of storage modulus (G') (A, B) and tan δ (C, D) on frequency for MDA-modified MP-stabilized emulsions at various MDA concentrations (A, C) or at different NaCl levels (B, D).

DOI: 10.1021/jf505916f
J. Agric. Food Chem. 2015, 63, 3766−3777

range and the tan δ values were <1 (Figure 4C), indicating all of the samples exhibited a predominant elastic behavior with frequency independency.[10] Furthermore, with increasing MDA concentrations from 0 to 10 mM, an evident decrease in the tan δ values was observed, suggesting enhanced elastic properties. However, when MDA concentration was >10 mM, the tan δ values increased. These results were in good agreement with previous analysis (Figures 3A and 4A).

As to the influence of NaCl, changes in G' and tan δ with frequency were also recorded, as presented in Figure 4, panels B and D, respectively. With increasing NaCl concentrations from 0 to 0.6 M, a dramatic increase in G' (Figure 4B) and an overall decrease in tan δ values (Figure 4D) were observed, respectively, indicating improved elastic properties of the emulsion gel. These results were again in line with visual observation (Figure 3B). As mentioned above, emulsions with thicker interfacial layer were obtained in the presence of 0.6 M NaCl (Figure 1A, inset) due to the profuse swelling of MP.[25,32] The thicker protein layer surrounding the oil droplets would increase the interdroplet interactions via several bridges, including ionic interaction and the stronger covalent bonds upon the presence of MDA,[27,35] which thus could promote the formation of emulsion gels with high elasticity (Figures 3B and 4). Nevertheless, in the absence of NaCl, protein fails to swell and disperses unevenly due to its low solubility.[25,32] Thus, the lack of effective molecular interaction between absorbed/nonabsorbed MP and MDA caused protein-coated oil droplet clusters, rather than a network,[25] thus resulting in the failure of gel formation and the low elasticity (Figures 3B and 4).

Gel Strength and WHC. To further evaluate the properties of formed emulsion gels, the gel strength and WHC were further measured and compared, as shown in panels A and B of Figure 5. In the presence of 0.6 M NaCl, the formed emulsion gel could be obtained when MDA concentration reached 2.5 mM (see Figure 3A). As can be seen from Figure 5A, with increasing MDA concentrations, emulsion gel strength remarkably increased, reaching a maximum of 1.09 N at 10 mM. This should be mainly attributed to the enhanced protein−protein interactions due to the swelling of MP and thus the increased inter- and intramolecular interaction within protein absorbed or unabsorbed under MDA-induced oxidative stress.[10,25,27,32] These analyses were in good agreement with the G' and tan δ data of emulsion gels (Figure 4A,C), which was related to the gel strength.[19] Nevertheless, with further addition of MDA (25−50 mM), a drastic decrease in gel strength was observed (Figure 5A), implying a collapse of gel structure. This might be mainly due to the occurrence of separated oil phase (Figure 3A, bottom) and was again in good agreement with gel elasticity (Figure 4A,C). In addition, the influence NaCl concentration on gel the strength in the presence of 10 mM MDA was also investigated as shown in Figure 5A. As expected, gel strength increased along with increasing NaCl levels (Figure 5A), which was largely due to the swollen appearance of MP promoting gel formation, and is in well consistent with results from G' (Figure 4B).

Furthermore, the gel WHC, which could reflect the spatial structure of the emulsion gel, showed a very similar trend as compared to gel strength, as shown in Figure 5B. This was also in good agreement with G' and tan δ data (Figure 4). As has been reported, the gel strength or stiffness played a prominent role in the water-holding property of gels;[8,12] thus, the progressive increase/decrease in WHC can be attributed to

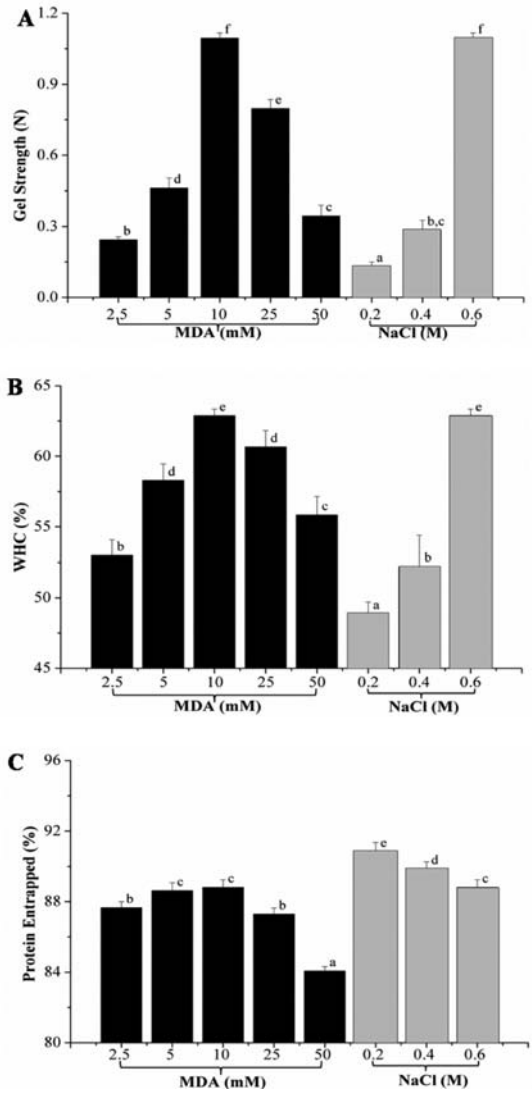

Figure 5. Gel strength (A) and WHC (B) of MDA-modified emulsion gels and protein entrapped (C) in MDA-modified emulsion gels at various MDA concentrations (black columns) or at different NaCl levels (gray columns). Columns with different letters are significantly different ($p < 0.05$).

compact/loose structure and strengthened/weakened gel structure with MDA/NaCl at different levels.

Amount of Protein Entrapped. The MDA-induced gelation of MP emulsions is closely associated with the ionic and covalent interactions between adsorbed and/or unadsorbed proteins, as mentioned above. Once the emulsion gel network is formed, the content of the proteins entrapped, including those adsorbed to the surface of oil droplets and some of the unabsorbed, can be approximately determined using centrifugation of the emulsions or emulsion gels.[9,29] Figure 5C shows the influence of MDA and NaCl on the amount of protein entrapped within the emulsion gel matrix. We could clearly see that in the presence of 0.6 M NaCl, the amount of entrapped proteins slightly but progressively increased as the MDA concentration increased from 2.5 to 10 mM, indicating more proteins participating in the gel network formation. This should be mainly due to the enhanced protein−protein interactions under MDA-induced oxidative stress, which reinforced the gel structure (Figures 4A,C and 5A,B), thus increasing the amount

DOI: 10.1021/jf505916f
J. Agric. Food Chem. 2015, 63, 3766−3777

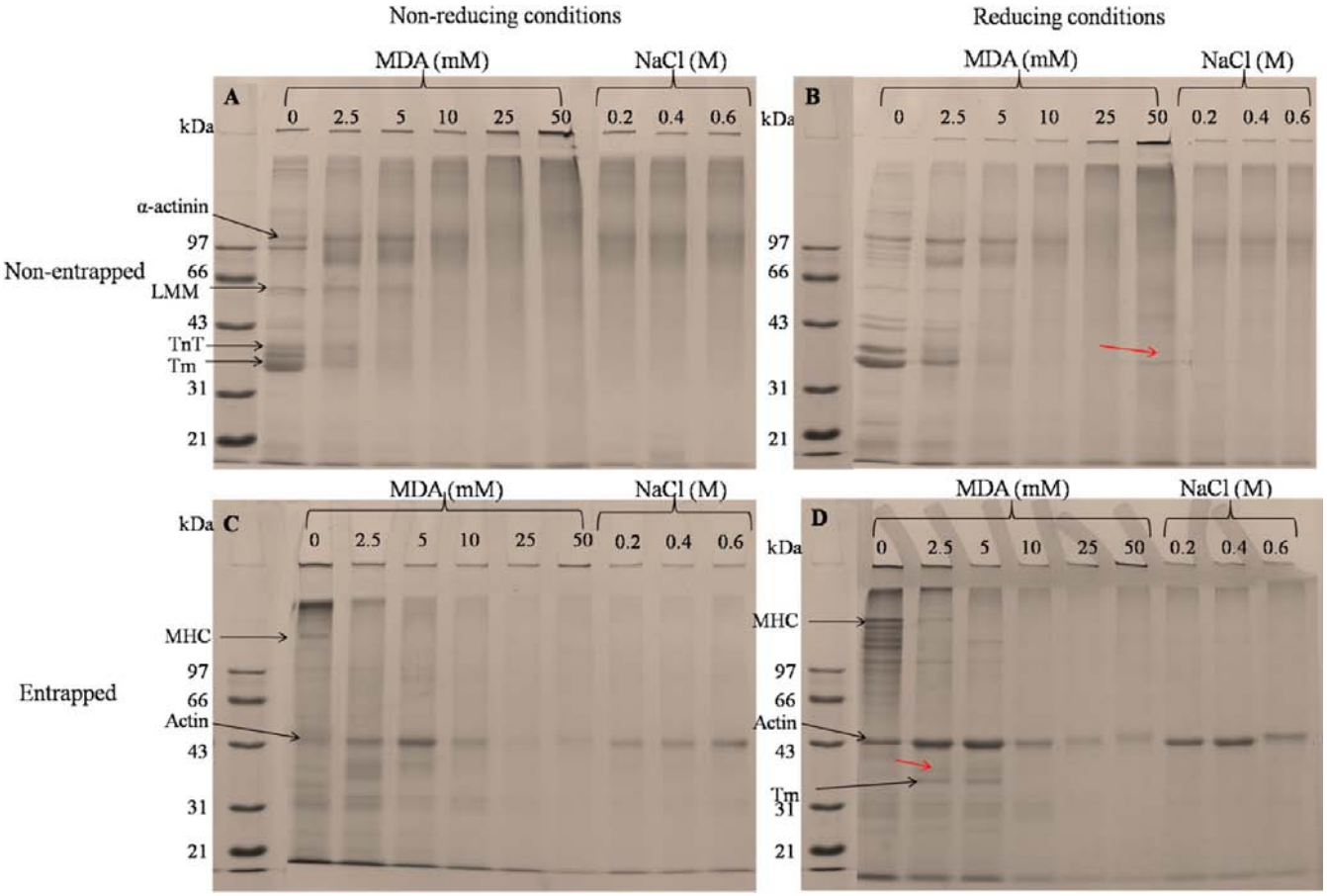

Figure 6. Representative SDS-PAGE patterns of the non-entrapped (A, B) and entrapped (C, D) protein in MDA-induced MP emulsion gels in the absence (nonreducing, A andC) or presence (reducing, B and D) of 5% β-ME. LMM, light meromyosin; MHC, myosin heavy chain; TnT, troponin T; Tm, tropomyosin.

of protein entrapped. Nevertheless, further addition in MDA (25−50 mM) caused a significant ($p < 0.05$) decrease in the amount of protein entrapped. As aforementioned, emulsion gel with separated oil phase and decreased gel elasticity and strength were observed when the MDA concentration added was >25 mM (Figures 3A, 4A, and 5A). Therefore, we could speculate that excessive covalent bonds might be formed when the addition of MDA exceeded 25 mM,[25] which could break protein−protein bonds or drag protein away from interface. Accordingly, the separated oil drops would lead to the protein separated from the gel matrix, no longer staying in the upper layer after centrifugation due to enhanced density and, thus, resulting in the decreased amount of protein entrapped (Figure 5C).

As to the influence of NaCl levels, the amount of protein entrapped decreased with increasing NaCl levels (Figure 5C), which seems to be inconsistent with the visual observation of emulsions after centrifugation (Figure 1A, inset). However, in fact, the amount of interfacial protein of emulsions (Figure 1A, inset) also decreased with increasing NaCl concentrations (data not shown). This could be explained by the fact that MP swells profusely at around 0.6 M NaCl, which decreased the protein adsorption rate on the droplet surface, thus decreasing the amount of interfacial protein of emulsions (data not shown). Furthermore, it is worth noting that, in the presence of 0.6 M NaCl, the amount of protein entrapped within the gel matrix (Figure 5C) was higher than that of interfacial protein of the corresponding emulsion (data not shown), suggesting that the unadsorbed proteins in the aqueous phase of the emulsion was involved in gel matrix formation.[34,36]

SDS-PAGE. Protein patterns of non-entrapped and entrapped proteins in the MDA-induced emulsion gels were examined by performing SDS-PAGE in either nonreducing or reducing conditions, as shown in Figure 6. Additionally, the control emulsion stabilized by MP in the presence of 0.6 M NaCl without MDA was also recorded for better comparison. As can be seen from Figure 6A, for non-entrapped proteins, in the absence of β-ME, basically four MP components—α-actinin, light meromyosin (LMM), troponin T (TnT), and tropomyosin (Tm)—were observed in the control sample (0 mM), within which TnT and Tm were predominant. Previous studies have already indicated that TnT and Tm were uncoagulable and did not contribute to muscle protein gel network formation.[12,37] With increasing concentration of MDA, the band intensities of four MP components progressively decreased or vanished (Figure 6A). Concomitantly, the band intensity of high molecular weight polymers (HMWP), which accumulated on the top part of the stacking gel or barely entered, increased accordingly (Figure 6A). However, in the presence of β-ME, most of these HMWP, but not reduced/lost bands, could be recovered, especially within the MDA range from 0 to 10 mM (Figure 6B). These results implied that HMWP formed were partially through disulfide bonds, rather than mainly non-disulfide covalent bonds as observed in other cases,[25,27] indicating that non-entrapped proteins were less influenced by MDA-induced oxidative modification, similar to

DOI: 10.1021/jf505916f
J. Agric. Food Chem. 2015, 63, 3766−3777

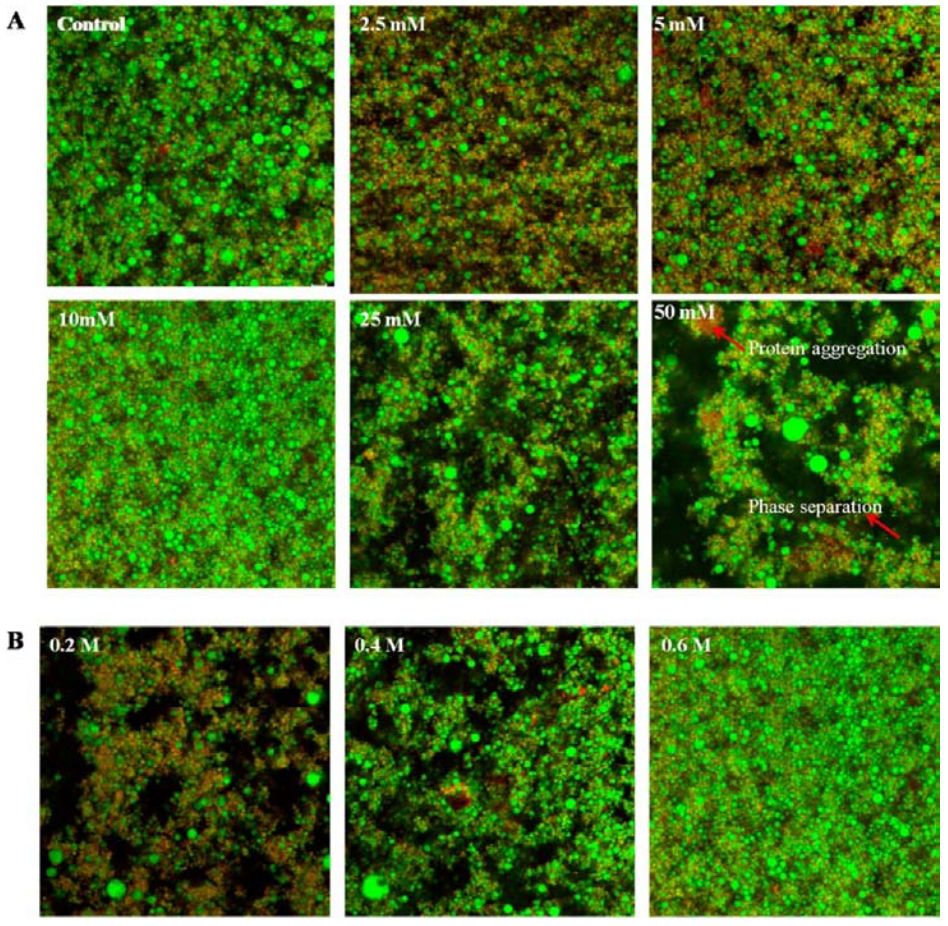

Figure 7. Typical CLSM images of MDA-induced MP emulsion gels at various MDA concentrations (A) or at different NaCl levels (B). All of the images were obtained with the dyes Nile Red (protein) and Nile Blue (oil phase), excited at 488 and 633 nm, respectively.

the previous study.[38] Moreover, when the concentration of MDA reached 50 mM, diffuse bands with molecular weight similar to that of Tm occurred again (Figure 6B), which might be related to the collapse of gel structure (Figure 4A,C).

For entrapped proteins, in the absence of β-ME, essentially myosin heavy chain (MHC) and actin were observed in the control sample (0 mM), and no clear bands corresponding to TnT or Tm, which have been discovered in the non-entrapped (Figure 6A), were obtained (Figure 6C). Nevertheless, MHC in all of the gel samples vanished, and all bands were lost with excessive addition of MDA (>25 mM), besides actin remaining faint (Figure 6C). However, no HMWP were detected with increasing MDA concentration (25−50 mM). This should be due to the over-cross-linking of proteins, leading to the formation of very high molecular weight polymers, which could not penetrate into the gel.[25,39] In the presence of β-ME, MHC in all gel samples could not be recovered (Figure 6D), suggesting that most cross-linking originated from myosin was not through disulfide bonds and the covalent bond in gel was too strong to break, which are similar to the previous reports that MDA can react with amino groups of proteins, producing strong intermolecular cross-links of the Schiff base type.[25−27] In addition, these results also indicated that oxidative modifications concerned more specifically the proteins adsorbed or entrapped, in agreement with a previous paper.[38] Interestingly, TnT and Tm, which have just been observed in the non-entrapped, although progressively reduced or lost with increasing addition of MDA, actually were obtained in the entrapped protein upon incubation with MDA (Figure 6C). These results, together with that obtained from changes in the non-entrapped, implied that within the MDA range of 2.5−10 mM, the reduced/lost protein composition (TnT and Tm) in non-entrapped might participate in the gel network formation under MDA-induced oxidative stress, thus turning into the entrapped proteins. Herein, the progressive entrapment of proteins with strong covalent bonds would provide structure reinforcement, which resulted in a gel matrix capable of sustaining higher stresses and therefore the higher gel strength (Figure 4). These analyses are also in good agreement with the increased amount of protein entrapped as previously stated (Figure 5).

As for the influence of NaCl level, increase in NaCl level did not change the protein pattern of either the non-entrapped or the entrapped (Figure 6), but slightly decreased the stability of actin (Figure 6D), as has been previously reported.[25,40]

Microstructure. The gel strength and WHC of the formed emulsion gels are, to a large degree, related to their gel microstructure. Therefore, the microstructure of the MDA-induced MP emulsion gels, formed at various MDA concentrations (2.5−50 mM) or at different NaCl levels (0.2, 0.4, and 0.6 M), was further characterized using CLSM, as displayed in Figure 7, panels A and B, respectively. In addition, the control emulsion in the presence of 0.6 M NaCl without MDA was also recorded and compared. As shown in Figure 7A, for the control emulsion, most of the oil droplets with similar sizes were evenly dispersed in the emulsion, indicating a

DOI: 10.1021/jf505916f
J. Agric. Food Chem. 2015, 63, 3766−3777

relatively stable state, which was in agreement with the $d_{4,3}$ data of emulsion (Figure 1B). In the presence of 0.6 M NaCl, when the concentration of MDA increased from 2.5 to 10 mM, the dispersed oil droplets coated with protein gradually got close, and the adjacent droplets even became tightly packed when the addition of MDA reached 10 mM. This might be attributed to enhanced protein−protein covalent binding among absorbed or nonabsorbed (Figure 6), forming a compact and homogeneous gel network with oil droplets perfectly adherent to the gel matrix (Figure 7A). These analyses were well consistent with the gel strength and WHC (Figure 5) and were also in good agreement with the data from low-amplitude dynamic oscillatory measurements (Figure 4), for it has been well accepted that the samples that have more compact and homogeneous microstructure possess the higher elastic modulus and lower tan δ.[10,19] Nevertheless, further increase in MDA concentration (25−50 mM) greatly changed the gel morphology, and a gel microstructure with obvious phase separation, accumulated protein aggregation, and oil droplets with larger size were observed. These results indicated the collapse of the gel microstructure, which was well consistent with the "oil leak" phenomenon observed (Figure 3A) as well as the sharp decrease in gel elasticity/strength and WHC (Figures 4 and 5).

As for the influence of NaCl, a more homogeneous gel microstructure was observed with increasing NaCl concentration (Figure 7B). It has been confirmed that the network of emulsion gels was closely related to the state of oil droplets in the original emulsions.[9] Thus, at low NaCl level (i.e., 0.2 M), the relative low emulsion apparent viscosity and small steric hindrance (Figures 1 and 2) easily led to the flocculation of oil droplets. Meanwhile, the protein absorbed or unabsorbed failed to swell profusely,[32,41] which resulted in the insufficient interaction between MP and MDA,[25] thus leading to the resultant discontinuously poor gel microstructure (Figure 7B). However, when the addition of NaCl increased, more stable oil droplets coated with MP were obtained, in a more swollen state, forming a more interactive gel network (Figure 7B).

Oxidative Stability of Emulsion Gels. With the fact of improved emulsion gel structure within a certain MDA range (2.5−10 mM) taken into consideration, the oxidative stability of MDA-modified MP emulsions was further studied, as shown in Figure 8. Lipid hydroperoxides, generally accepted as the first oxidation products, is the most used analysis for determining the initial oxidation rate.[42,43] Compared to the control emulsion, it is interesting to note that hydroperoxides of MDA-modified MP emulsion first decreased along with MDA from 0 to 10 mM, reaching a minimum at the 10 mM MDA level, before increasing sharply to a maximum at 50 mM (Figure 8A). These results indicated that MDA-induced gelation of MP emulsion obtained higher oxidative stability, depending on the MDA concentration. As aforementioned, the emulsion gels with enhanced gel quality (elasticity, strength, WHC) and better microstructure were obtained within MDA ranging from 2.5 to 10 mM (Figures 4, 5, and 7). Thus, the reinforced gel network between absorbed and unabsorbed protein might work as a physical barrier, separating the lipid substrates from the pro-oxidants present in the aqueous phase or retarding the oxygen diffusion within the systems, which thus could well protect the oil droplets (Figure 8A). A similar protective effect of gelation on emulsion oxidative stability has also been reported.[34] Nevertheless, the collapsed gel microstructure due to the formation of excessive covalent bonds led

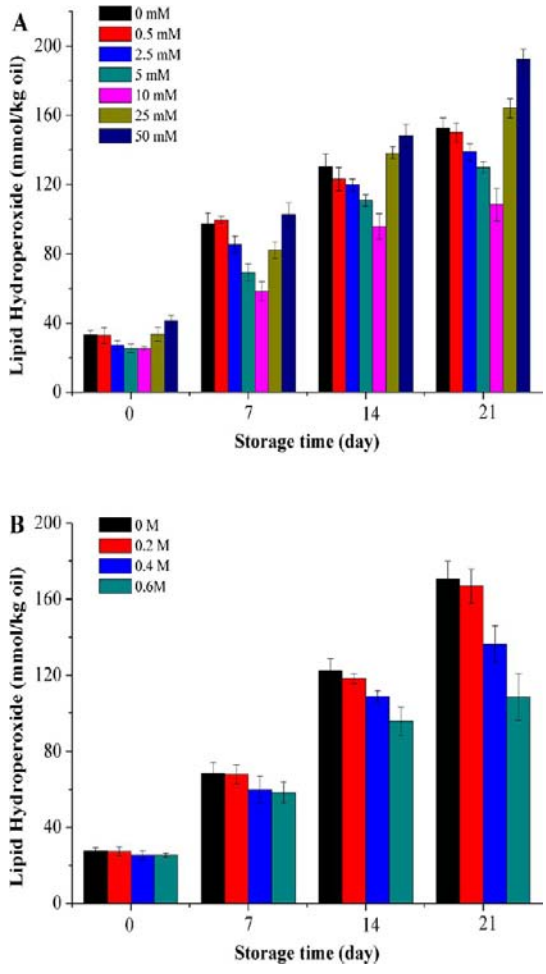

Figure 8. Changes in lipid hydroperoxides of emulsions gels stabilized by MP either at various MDA concentrations (A) or at different NaCl levels (B) during storage at 25 °C for 21 days.

to the "oil leak" (Figures 3 and 6), favoring the direct contact of oil with oxidizer, which thus decreased the oxidative stability of the system (25−50 mM MDA) (Figure 8A). As for the influence of NaCl, similarly, a lower amount of hydroperoxides at higher levels of NaCl was obtained (Figure 8B), which could also be largely attributed to the protective effect of improved gel properties (Figures 3−5). Additionally, the higher interfacial area of emulsions/emulsion gels at lower NaCl level (Figure1) might also promote interactions between lipids and pro-oxidants in the aqueous phase and thus the lower oxidative stability (Figure 8B).[34,44]

General Discussion. On the basis of the analyses above, we can conclude that addition of MDA could lead to the formation of emulsion gel stabilized by MP in the presence of NaCl. Meanwhile, the gel properties as well as the gel oxidative stability were enhanced at certain concentration ranges of MDA (Figures 4, 5, and 8). To clarify a reasonable understanding of either improved or deteriorated gel quality, a schematic illustration of the formation process of the MDA-induced MP emulsion gels is proposed and shown in Figure 9. In the absence of NaCl, MP fails to swell,[32] and thus emulsions with smaller size were obtained due to relatively quick absorption of protein to the oil droplet surface (Figure 1A). Nevertheless, the small steric hindrance of the protein at interface as well as the unevenly dispersed protein in aqueous phase due to its low

DOI: 10.1021/jf505916f
J. Agric. Food Chem. 2015, 63, 3766−3777

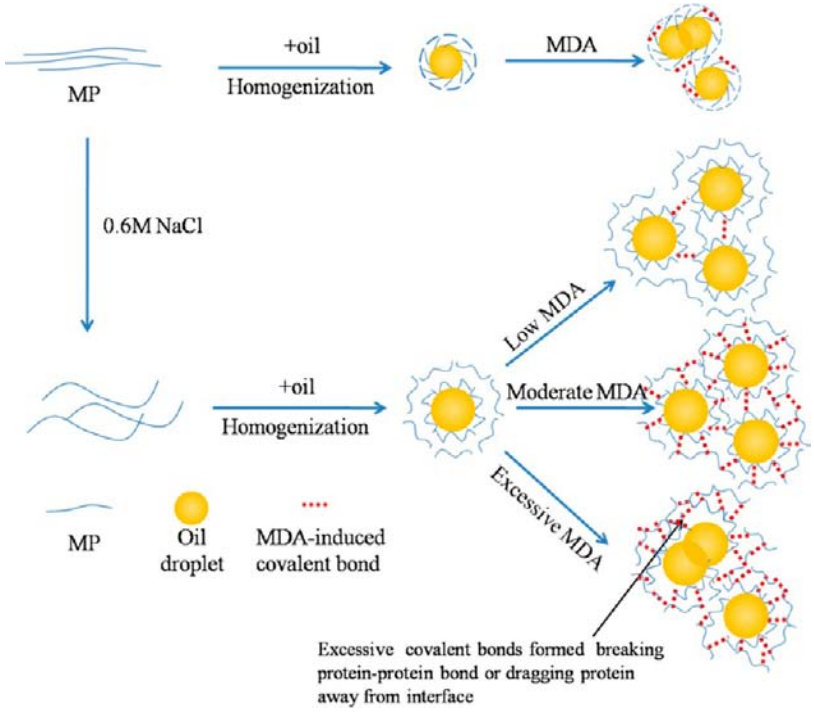

Figure 9. Schematic illustration of formation process of the MDA-induced emulsion gels stabilized by salted MP.

solubility made the droplet free to flow and easier to flocculate (Figures 1B and 2),[32] which further limited the interaction between MP (absorbed or unabsorbed) and MDA, leading to coagulation, rather than gelation of emulsion (Figure 3B). However, in the presence of 0.6 M NaCl, MP swells profusely,[18,32,45] and the swollen MP-stabilized emulsions with larger size possessed a thicker absorbed protein layer due to enhanced protein−protein interaction (Figure 1A),[18,25] which thus increased the physical stability of emulsions (Figure 1B). Upon incubation with MDA, the stretching structure of MP at 0.6 M NaCl first facilitates the interactions among absorbed and/or unabsorbed proteins,[38] forming strong covalent bonds (Figure 6), which thus promoted the gel formation (Figure 3A). Specifically, within MDA concentrations ranging from 2.5 to 10 mM, enhanced protein−protein cross-links were observed with more amounts of protein, even the unabsorbed protein fractions (i.e., Tm), being progressively entrapped (Figures 5C and 6), contributing to a more homogeneous and compact gel structure with higher gel elasticity, strength, and WHC (Figures 4, 5, and 7). Interestingly, with oil droplets perfectly adherent to the homogeneous gel matrix (Figure 7), the enhanced oxidative stability of gelled emulsion was also obtained (Figure 8). Nevertheless, further increase in MDA concentration (above 25 mM) led to the formation of excessive covalent bonds (Figure 6), breaking the protein−protein bonds or triggering the separation of the protein−oil interface, which thus resulted in the resultant "oil leak" as well as the collapse of gel structure (Figures 3−5 and 7). Accordingly, the gel oxidative stability was also remarkably decreased (Figure 8).

In conclusion, this work demonstrated an interesting discovery of the formation of cold-set, MDA-induced emulsion gels stabilized by salted MP, and the possible mechanism involved was also proposed. The gel was formed on the premise of the swelling of MP under certain ionic strengths and the non-disulfide covalent bonds formed via MDA. Within certain MDA ranges (2.5−10 mM), the oil droplets were perfectly adherent to the gel matrix due to the moderate amount of covalent bonds formed between absorbed and unabsorbed proteins, endowing the emulsion gel with a better quality. Meanwhile, the reinforced gel network was also responsible for enhanced oxidative stability of emulsion gels. Considering the real meat manufacturing or storage process, the link between MDA-induced protein oxidation and MP-stabilized emulsion gel is far from straightforward. However, the results presented in this paper could provide a new aspect for better understanding the effect of oxidation in meat protein/oil composite systems.

AUTHOR INFORMATION

Corresponding Author

*(M.Z.) Phone/fax: +86 20 87113914. E-mail: femmzhao@scut.edu.cn.

Funding

This work was supported by the National Natural Science Foundation of China (No. 31201387), the Natural Science Foundation of Guangdong Province (No. S2012040007533), and the Doctoral Fund of Ministry of Education of China (No. 20120172120017).

Notes

The authors declare no competing financial interest.

ACKNOWLEDGMENTS

We gratefully acknowledge and appreciate the assistance provided by Dr. Zhi-Li Wan.

REFERENCES

(1) Dickinson, E. Emulsion gels: the structuring of soft solids with protein-stabilized oil droplets. *Food Hydrocolloids* **2012**, *28*, 224−241.
(2) Gordon, A.; Barbut, S. Mechanisms of meat batter stabilization: a review. *Crit. Rev. Food Sci. Nutr.* **1992**, *32*, 299−332.

DOI: 10.1021/jf505916f
J. Agric. Food Chem. 2015, 63, 3766−3777

(3) Xiong, Y. L. Meat binding: emulsions and batters. In *Meat Processing Technology Series*; Osburn, W. N., Sebranek, J. G.,Schultz Kaster, C. M., Eds.; American Meat Science Association: Savoy, IL, USA, 2007; pp 1−28.
(4) Ziegler, G. R.; Foegeding, E. A. The gelation of proteins. *Adv. Food Nutr. Res.* **1990**, *34*, 203−298.
(5) Line, V. L. S.; Remondetto, G. E.; Subirade, M. Cold gelation of β-lactoglobulin oil-in-water emulsions. *Food Hydrocolloids* **2005**, *19*, 269−278.
(6) Chen, J.; Dickinson, E. Effect of surface character of filler particles on rheology of heat-set whey protein emulsion gels. *Colloid Surf. B* **1999**, *12*, 373−381.
(7) Sala, G.; Van Aken, G. A.; Stuart, M. A. C.; Van De Velde, F. Effect of droplet-matrix interactions on large deformation properties of emulsion-filled gels. *J. Texture Stud.* **2007**, *38*, 511−535.
(8) Tang, C.-H.; Chen, L.; Foegeding, E. A. Mechanical and water-holding properties and microstructures of soy protein isolate emulsion gels induced by $CaCl_2$, glucono-δ-lactone (GDL), and transglutaminase: Influence of thermal treatments before and/or after emulsification. *J. Agric. Food Chem.* **2011**, *59*, 4071−4077.
(9) Tang, C.-H.; Luo, L.-J.; Liu, F.; Chen, Z. Transglutaminase-set soy globulin-stabilized emulsion gels: influence of soyβ-conglycinin/glycinin ratio on properties, microstructure and gelling mechanism. *Food Res. Int.* **2013**, *51*, 804−812.
(10) Manoi, K.; Rizvi, S. S. Emulsification mechanisms and characterizations of cold, gel-like emulsions produced from texturized whey protein concentrate. *Food Hydrocolloids* **2009**, *23*, 1837−1847.
(11) Lee, S.-H.; Lefevre, T.; Subirade, M.; Paquin, P. Changes and roles of secondary structures of whey protein for the formation of protein membrane at soy oil/water interface under high-pressure homogenization. *J. Agric. Food Chem.* **2007**, *55*, 10924−10931.
(12) Wu, M.; Xiong, Y. L.; Chen, J.; Tang, X.; Zhou, G. Rheological and microstructural properties of porcine myofibrillar protein-lipid emulsion composite gels. *J. Food Sci.* **2009**, *74*, E207−E217.
(13) Wu, M.; Xiong, Y. L.; Chen, J. Role of disulphide linkages between protein-coated lipid droplets and the protein matrix in the rheological properties of porcine myofibrillar protein−peanut oil emulsion composite gels. *Meat Sci.* **2011**, *88*, 384−390.
(14) Acton, J. C.; Ziegler, G. R.; Burge, D. L., Jr.; Froning, G. W. Functionality of muscle constituents in the processing of comminuted meat products. *Crit. Rev. Food Sci. Nutr.* **1982**, *18*, 99−121.
(15) Asghar, A.; Samejima, K.; Yasui, T. Functionality of muscle proteins in gelation mechanisms of structured meat products. *Crit. Rev. Food Sci. Nutr.* **1985**, *22*, 27−106.
(16) Lund, M. N.; Heinonen, M.; Baron, C. P.; Estevez, M. Protein oxidation in muscle foods: a review. *Mol. Nutr. Food Res.* **2011**, *55*, 83−95.
(17) Zhang, W.; Xiao, S.; Ahn, D. U. Protein oxidation: basic principles and implications for meat quality. *Crit. Rev. Food Sci. Nutr.* **2013**, *53*, 1191−1201.
(18) Li, C.; Xiong, Y. L.; Chen, J. Protein oxidation at different salt concentrations affects the cross-linking and gelation of pork myofibrillar protein catalyzed by microbial transglutaminase. *J. Food Sci.* **2013**, *78*, 823−831.
(19) Xiong, Y. L.; Blanchard, S. P.; Ooizumi, T.; Ma, Y. Hydroxyl radical and ferryl-generating systems promote gel network formation of myofibrillar protein. *J. Food Sci.* **2010**, *75*, C215−C221.
(20) Sun, W.; Zhou, F.; Sun, D.-W.; Zhao, M. Effect of oxidation on the emulsifying properties of myofibrillar proteins. *Food Bioprocess Technol.* **2012**, *6*, 1703−1712.
(21) Zhou, F.; Zhao, M.; Zhao, H.; Sun, W.; Cui, C. Effects of oxidative modification on gel properties of isolated porcine myofibrillar protein by peroxyl radicals. *Meat Sci.* **2013**, *96*, 1432−1439.
(22) Estévez, M.; Kylli, P.; Puolanne, E.; Kivikari, R.; Heinonen, M. Oxidation of skeletal muscle myofibrillar proteins in oil-in-water emulsions: interaction with lipids and effect of selected phenolic compounds. *J. Agric. Food Chem.* **2008**, *56*, 10933−10940.
(23) Koutina, G.; Jongberg, S.; Skibsted, L. H. Protein and lipid oxidation in parma ham during production. *J. Agric. Food Chem.* **2012**, *60*, 9737−9745.
(24) Park, D.; Xiong, Y. L.; Alderton, A. L.; Ooizumi, T. Biochemical changes in myofibrillar protein isolates exposed to three oxidizing systems. *J. Agric. Food Chem.* **2006**, *54*, 4445−4451.
(25) Zhou, F.; Zhao, M.; Su, G.; Cui, C.; Sun, W. Gelation of salted myofibrillar protein under malonaldehyde-induced oxidative stress. *Food Hydrocolloids* **2014**, *40*, 153−162.
(26) Xiong, Y. L.; Park, D.; Ooizumi, T. Variation in the cross-linking pattern of porcine myofibrillar protein exposed to three oxidative environments. *J. Agric. Food Chem.* **2008**, *57*, 153−159.
(27) Buttkus, H. The reaction of myosin with malonaldehyde. *J. Food Sci.* **1967**, *32*, 432−434.
(28) Wu, W.; Zhang, C.; Hua, Y. Structural modification of soy protein by the lipid peroxidation product malondialdehyde. *J. Sci. Food Agric.* **2009**, *89*, 1416−1423.
(29) Chanyongvorakul, Y.; Matsumura, Y.; Sawa, A.; Nio, N.; Mori, T. Polymerization of β-lactoglobulin and bovine serum albumin at oil-water interfaces in emulsions by transglutaminase. *Food Hydrocolloids* **1997**, *11*, 449−455.
(30) Flores, M.; Barat, J. M.; Aristoy, M.; Peris, M. M.; Grau, R.; Toldrá, F. Accelerated processing of dry-cured ham. Part 2. Influence of brine thawing/salting operation on proteolysis and sensory acceptability. *Meat Sci.* **2006**, *72*, 766−772.
(31) Tong, L. M.; Sasaki, S.; McClements, D. J.; Decker, E. A. Antioxidant activity of whey in a salmon oil emulsion. *J. Food Sci.* **2000**, *65*, 1325−1329.
(32) Offer, G.; Trinick, J. On the mechanism of water holding in meat: the swelling and shrinking of myofibrils. *Meat Sci.* **1983**, *8*, 245−281.
(33) Tang, C.-H.; Liu, F. Cold, gel-like soy protein emulsions by microfluidization: emulsion characteristics, rheological and microstructural properties, and gelling mechanism. *Food Hydrocolloids* **2013**, *30*, 61−72.
(34) Sato, A.; Moraes, K.; Cunha, R. Development of gelled emulsions with improved oxidative and pH stability. *Food Hydrocolloids* **2014**, *34*, 184−192.
(35) Intarasirisawat, R.; Benjakul, S.; Visessanguan, W. Stability of emulsion containing skipjack roe protein hydrolysate modified by oxidised tannic acid. *Food Hydrocolloids* **2014**, *41*, 146−155.
(36) Kim, K.-H.; Renkema, J.; Van Vliet, T. Rheological properties of soybean protein isolate gels containing emulsion droplets. *Food Hydrocolloids* **2001**, *15*, 295−302.
(37) Samejima, K.; Ishioroshi, M.; Yasui, T. Heat induced gelling properties of actomyosin: effect of tropomyosin and troponin. *Agric. Biol. Chem.* **1982**, *46*, 535−540.
(38) Berton, C.; Ropers, M.-H.; Guibert, D.; Sole, V.; Genot, C. Modifications of interfacial proteins in oil-in-water emulsions prior to and during lipid oxidation. *J. Agric. Food Chem.* **2012**, *60*, 8659−8671.
(39) Coupland, J. N.; McClements, D. J. Lipid oxidation in food emulsions. *Trends Food Sci. Technol.* **1996**, *7*, 83−91.
(40) Thorarinsdottir, K. A.; Arason, S.; Geirsdottir, M.; Bogason, S. G.; Kristbergsson, K. Changes in myofibrillar proteins during processing of salted cod (*Gadus morhua*) as determined by electrophoresis and differential scanning calorimetry. *Food Chem.* **2002**, *77*, 377−385.
(41) Liu, Z.; Xiong, Y. L.; Chen, J. Identification of restricting factors that inhibit swelling of oxidized myofibrils during brine irrigation. *J. Agric. Food Chem.* **2009**, *57*, 10999−11007.
(42) Wan, Z.-L.; Wang, J.-M.; Wang, L.-Y.; Yang, X.-Q.; Yuan, Y. Enhanced physical and oxidative stabilities of soy protein-based emulsions by incorporation of a water-soluble stevioside−resveratrol complex. *J. Agric. Food Chem.* **2013**, *61*, 4433−4440.
(43) Sun-Waterhouse, D.; Zhou, J.; Miskelly, G. M.; Wibisono, R.; Wadhwa, S. S. Stability of encapsulated olive oil in the presence of caffeic acid. *Food Chem.* **2011**, *126*, 1049−1056.

DOI: 10.1021/jf505916f
J. Agric. Food Chem. 2015, 63, 3766−3777

(44) Waraho, T.; McClements, D. J.; Decker, E. A. Mechanisms of lipid oxidation in food dispersions. *Trends Food Sci. Technol.* **2011**, *22*, 3−13.
(45) Xiong, Y. L. Role of myofibrillar proteins in water-binding in brine-enhanced meats. *Food Res. Int.* **2005**, *38*, 281−287.

DOI: 10.1021/jf505916f
J. Agric. Food Chem. 2015, 63, 3766−3777

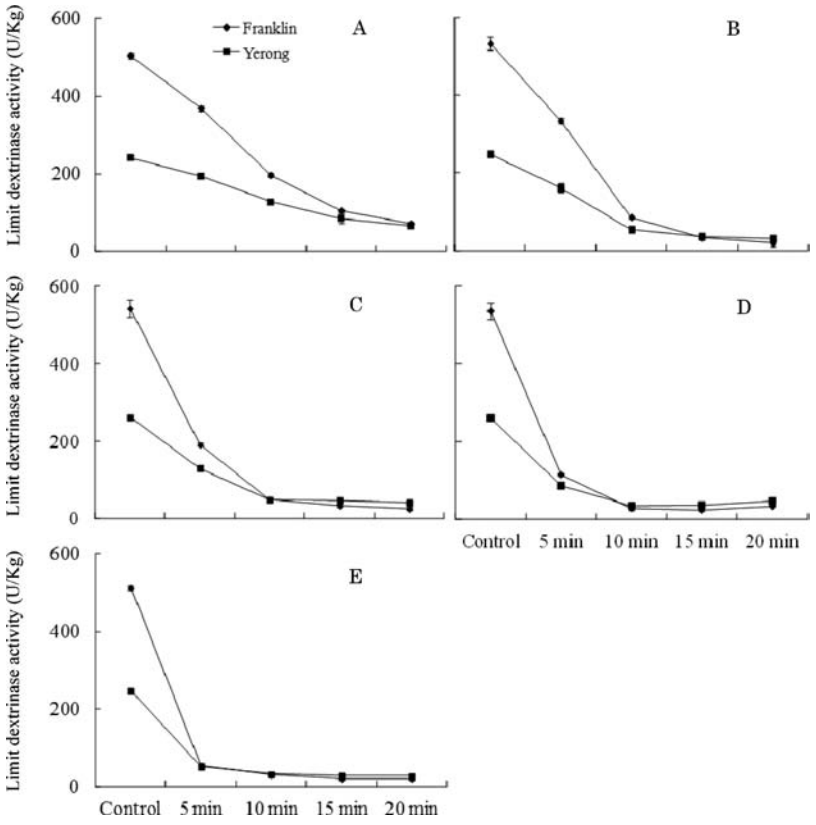

Figure 1. Limit dextrinase activity variation after thermo treatment at different temperatures for 0−20 min. A, B, C, D, and E: Limit dextrinase activity variation after thermo treatment at 54.5, 55.5, 56.5, 57.5, and 58.5 °C, respectively. Control: without thermo treatment.

the current study, a genetic diversity analysis was conducted for the identification of genotypes with high LD thermostability. Moreover, QTLs analysis of LD thermostability was carried out to identify relevant novel genes or genetic factors.

MATERIALS AND METHODS

Plant Materials and Sample Preparation. Fifty-one cultivated barley, 40 Tibetan wild barley genotypes, and a DH population consisted of 177 lines from a cross between Yerong and Franklin was used in this study.[32] Franklin is an Australian two-rowed malting barley cultivar, and Yerong is an Australian six-rowed feed barley variety. Seeds of Tibetan wild barley, collected from the Qinghai-Tibet Plateau of China, were kindly provided by Professor Dongfa Sun of Huazhong Agricultural University, China.

All materials were grown in the field of the experimental farm, Zhejiang University, Huajiachi campus, Hangzhou, China, in 2008−2009 and 2009−2010 winter barley growing seasons, except that the DH population was only cultivated in 2009−2010 growing season. Each genotype or DH line was sown in a 2 m row with 0.25 m between rows, with three replications. Field management, including fertilization, weed, and disease control, was the same as applied locally. At maturity, the plants were harvested and stored in a cool room at 4 °C. Grains were mixed and used for micromalting and LD activity assay after milled to pass through a 0.5 mm screen.

Grain samples (200 g) were micromalted in a Phoenix System Micromalting Apparatus (Adelaide, Australia) in the order of steeping, germination and kilning according to the method described by Dai et al. (2007),[33] with some modification in the steeping stage. Briefly, there were the following stages: 5 h steep and 8 h air-rest at 17 °C, 8 h steep and 12 h air-rest at 16 °C, 4 h steep, 5 h air-rest and 2 h steep at 15 °C followed by 96 h germination at 16 °C. Malting of all the genotypes and DH lines were milled to pass through a 0.5 mm screen for analysis.

Thermo Treatment and LD Activity Assay. LD activity was determined using the Limit-Dextrinase assay kit (Megazyme, Ireland). According to McCleary (1992)[34] and the Megazyme manual, LD was extracted from 0.25 g sample with 4.0 mL extracting solution, 0.1 mM sodium malate buffer (pH 5.5) containing 25 mM dithiothreitol, for 5 h at 40 °C. Thermo treatment in the current study referred to the method described by Evans et al. (2003)[14] and was conducted using a Memmert WNE450 water bath (Memmert, Germany). Specifically, 0.5 mL of supernatant was added to a plastic tube after centrifuging at 1000*g* and incubated in a water bath for thermo treatment. Thermo treatment was terminated with an ice−water bath for 10 min. LD activity of thermo-treated and nonthermo-treated (control) supernatants was determined using Limit-Dextrizyme tablets at 40 °C. One unit of LD activity is the amount of enzyme required to release one μmol of glucose reducing-sugar equivalents per min from pullulan under the defined assay conditions.

QTL Analysis. A genetic linkage map of the Yerong/Franklin DH population was composed of 496 DArT and 28 microsatellite markers.[32] QTLs were analyzed using MapQTL5.0 software package,[35] as described by Dai et al. (2011).[36] Briefly, QTLs were analyzed by interval mapping (IM) and approximate multiple QTLs model (MQM) of MapQTL5.0. Logarithm of the odds (LOD) threshold values (set as 3.0) applied to declare the presence of QTLs were

DOI: 10.1021/acs.jafc.5b00190
J. Agric. Food Chem. 2015, 63, 3778−3783

estimated by performing the genome wide permutation tests with at least 1000 permutations of the original data set for the trait. The percentage of variance explained by each QTL (R^2) was obtained using restricted MQM mapping implemented with MapQTL5.0.

Statistical Analysis. Each measurement was carried out with at least three replications. Statistical analysis was carried out using SPSS v16.0 for windows (SPSS Inc., Chicago, U.S.A.).

RESULTS

Effect of Thermo Treatment on LD Activity. In order to determine the optimal time and temperature for LD activities of the parental lines Franklin and Yerong, time- and temperature-dependent experiments were conducted. The LD activities of Franklin and Yerong after thermo treatments for 0−20 min at a set of temperature gradients are shown in Figure 1A−E, respectively. Under the control condition (without thermo treatment), LD activity of Franklin (521.9 U kg^{-1}) was significantly higher than that of Yerong (250.9 U kg^{-1}). LD activity of Franklin and Yerong declined by 26.9% and 19.8%, 37.3% and 34.9%, 64.8% and 50.1%, 78.6% and 66.8%, 89.2% and 79.0%, after 5 min thermo treatments at 54.5, 55.5, 56.5, 57.5, and 58.5 °C, respectively (Figure 1). The LD activity decreased sharply during the first 5 min of the thermo treatment, and thereafter, the rate of decline became much slower. Hence, the optimum treatment time at 5 min was chosen for comparing the difference in LD thermostability (expressed as a ratio of the remaining LD activities after 5 min thermo treatment to those in the control) between Franklin and Yerong.

LD thermostability of Franklin and Yerong responded differently to increasing temperatures (Figure 2). The LD thermostability of Franklin and Yerong were 68.5% and 71.8%, 73.1% and 80.2%, 59.2% and 64.3%, 62.7% and 65.1%, 47.9% and 58.5%, 35.2% and 49.9%, 33.4% and 43.0%, 21.4% and 33.2%, 19.4% and 30.5%, 10.8% and 21.0%, 7.9% and 17.2% after 5 min thermo treatments at 54, 54.5, 55, 55.5, 56, 56.5, 57, 57.5, 58, 58.5, 59 °C, respectively. According to the method of Arora et al. (1992),[37] we estimated the LT_{50} (lethal temperature of 50%), which is defined as the temperature at which 50% of LD activity lost after thermo treatment. In the current study, LT_{50} of Franklin and Yerong were 54.4 and 56.4 °C, respectively (Figure 2). In order to obtain a relative higher dose of thermo treatment, we chose 56.5 °C as the optimum temperature for thermo treatment in the current study rather than 55.5 °C, which was close to LT_{50} and similar to the results of Evans et al. (2003)[14] and Yang et al. (2009).[2]

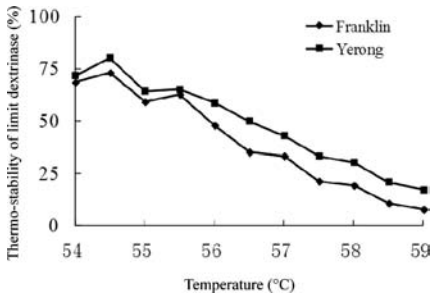

Figure 2. Thermostability variation of limit dextrinase after 5 min thermo treatment at different temperatures from 54 to 59 °C.

Difference in LD Thermostability in Cultivated and Wild Barley. In 2009, LD activity for the 40 wild barley (WB) genotypes ranged from 352.3 U kg^{-1} to 562.8 U kg^{-1}, with a mean of 448.0 U kg^{-1}, whereas LD activity for the 51 cultivated barley (CB) genotypes ranged from 366.2 U kg^{-1} to 787.6 U kg^{-1}, with a mean of 539.6 U kg^{-1} (Table 1). Thermostable LD activity of WB ranged from 229.7 U kg^{-1} to 457.4 U kg^{-1}, with a mean of 327.5 U kg^{-1}, and CB ranged from 177.4 U kg^{-1} to 488.8 U kg^{-1}, with a mean of 318.3 U kg^{-1}. Obviously, WB had lower average value of LD activity than CB. As for the mean of thermostable LD activity, both cultivated and wild barley were basically the same. The LD thermostability of WB ranged from 59.9% to 91.3%, with a mean of 73.3%, and CB ranged from 27.1% to 85.4%, with a mean of 59.8%. It is clear that WB had much larger LD thermostability value than CB. In addition, the coefficient of variation (CV) for LD, thermostable LD, and LD thermostability were slightly smaller in WB than those in CB (Table 1).

In 2010, the LD activity of WB and CB ranged from 285.6 U kg^{-1} to 604.8 U kg^{-1} and from 315.6 U kg^{-1} to 741.6 U kg^{-1}, with means of 405.4 U kg^{-1} and 514.8 U kg^{-1}, respectively. (Table 1). Thermostable LD activity of WB and CB ranged from 181.1 U kg^{-1} to 486.0 U kg^{-1} and from 172.8 U kg^{-1} to 555.6 U kg^{-1}, with means of 275.9 U kg^{-1} and 319.8 U kg^{-1}, respectively. However, for LD thermostability, WB and CB ranged from 50.5% to 80.4% and from 41.5% to 75.3%, with means of 67.8% and 61.3%, respectively. All the parameters in 2010 are very consistent to those in 2009, for instance, the maximum and mean LD thermostability of WB were higher than those of CB. Meanwhile, the CV values of WB were smaller uniformly.

Identification of QTL Associated with Thermostable LD. In view of the significant differences in LD activity and

Table 1. Genetic Diversity of Limit Dextrinase and Its Thermostability in Wild and Cultivated Barley Grown in 2008−2009 and 2009−2010

	2009						2010					
	LD[a] (U kg^{-1})		thermostable LD (U kg^{-1})		LD thermostability (%)		LD[a] (U kg^{-1})		thermostable LD (U kg^{-1})		LD thermostability (%)	
	WB[b]	CB[c]	WB	CB	WB	CB	WB	CB	WB	CB	WB	CB
min	352.3	366.2	229.7	177.4	59.9	27.1	285.6	315.6	181.1	172.8	50.5	41.5
max	562.8	787.6	457.4	488.8	91.3	85.4	604.8	741.6	486.0	555.6	80.4	75.3
mean	448.0	539.6	327.5	318.3	73.3	59.8	405.4	514.8	275.9	319.8	67.8	61.3
CV[d](%)	14.1	21.1	17.7	21.9	12.2	17.4	16.6	18.6	22.6	29.7	11.1	15.1

[a]LD, limit dextrinase. [b]WB, wild barley (n = 40). [c]CB, cultivated barley (n = 51). [d]CV, coefficient of variation. Thermo treatment: 0.5 mL supernatant of each genotype was treated in a water bath at 56.5 °C for 5 min.

DOI: 10.1021/acs.jafc.5b00190
J. Agric. Food Chem. 2015, 63, 3778−3783

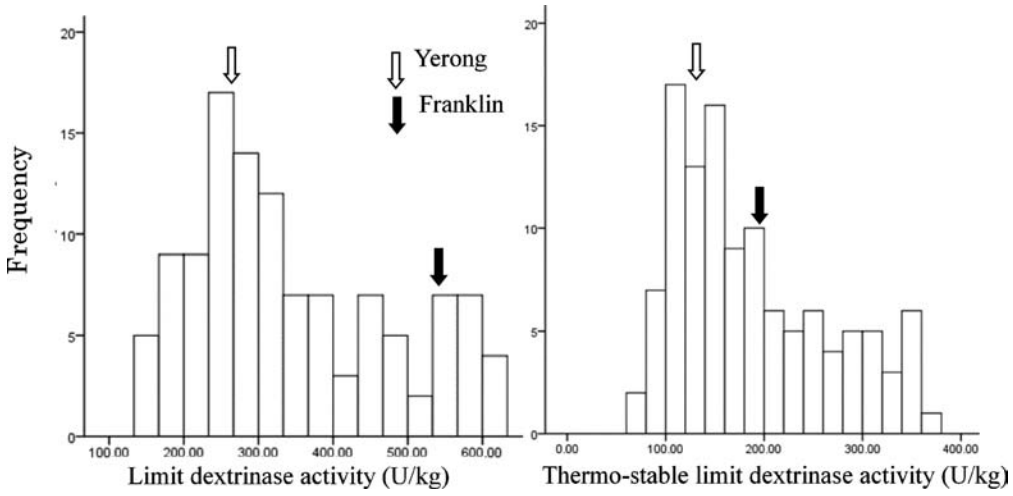

Figure 3. Frequency distribution for limit dextrinase and thermostable limit dextrinase activity in a DH population of Yerong/Franklin.

thermostability between Franklin and Yerong found in our preliminary study, we further conducted the QTL analysis using a DH population consisted of 177 lines from a cross between Yerong and Franklin (Li et al., 2008) in order to identify novel QTLs associated with LD activity and thermostability. Normal distributions of LD and thermostable LD activity exhibited no significant skewness and kurtosis (Figure 3). Transgression beyond the parental values was also observed. Moreover, some favorable combinations, such as high LD activity under both control conditions and thermo treatments, were found in this DH population.

A major QTL controlling LD activity in malt was identified on chromosome 7H under both control (*qLD2*) and thermo treatment (*qTS-LD3*) at the position of 58.7 cM on the genetic map with the nearest marker being bPb-2866 (Table 2). This QTL was able to explain 19.6% of the phenotypic variation of LD activity under thermo treatments, in comparison to 31.0% of the phenotypic variation of LD activity under control condition. Both of these QTLs are contributed by Franklin. In addition, a minor QTL (*qLD1*) controlling LD activity was identified at the position of 58.2 cM on chromosome 4H, with the nearest marker being bPb-0365. This QTL was not detected for LD activity under thermo treatment. Instead, two other minor QTLs were found, one on chromosome 1H (*qTS-LD1*) contributed by Franklin at 102.0 cM and the closest marker of HVHVA1, and another on chromosome 2H (*qTS-LD2*) contributed by Yerong at 83.7 cM and the nearest marker of bPb-5440 (Table 2). No significant QTL was identified for LD thermostability.

Table 2. Quantitative Trait Locus (QTLs) for Limit Dextrinase in the DH Population of Yerong/Franklin Grown in 2009−2010

treatment	QTL	chr.	nearest marker	position (cM)	LOD	R^2 (%)
control	*qLD1*	4H	bPb-0365	58.2	3.71	9.2
	qLD2	7H	bPb-2866	58.7	10.73	31.0
thermo treatment	*qTS-LD1*	1H	HVHVA1	102.0	4.03	9.9
	qTS-LD2	2H	bPb-5440	83.7	3.66	8.9
	qTS-LD3	7H	bPb-2866	58.7	7.49	19.6

DISCUSSION

In this study, we first investigated LD activity and thermostability of parental lines Franklin and Yerong under different temperature and time treatments in order to determine the optimal time and temperature for further research. It was found that both cultivars showed a rapid reduction of LD activity during the first 5 min of thermo treatment, and then leveled off over the course of another 15 min (Figure 1). Hence, we chose 5 min as the optimal time for thermo treatment. However, the time duration is shorter than those used in previous studies.[2,38,39] On the other hand, the optimal temperature was determined according to LT_{50}. Based on the influence of different temperature on LD activity, we chose 56.5 °C as the optimal temperature for thermo treatment. The results are basically consistent with some previous reports.[2,14] Under these thermo treatment conditions, we found Tibetan wild barley demonstrated much greater genotypic variation in LD thermostability than cultivated barley (Table 1), indicating that the wild barley is indeed an elite germplasm for barley breeders in developing cultivars with high LD thermostability.

The wide genetic diversity of LD and thermostable LD activity in the DH population (Figure 3) has enabled us to identify novel QTLs. The Yerong/Franklin DH population has already been used successfully for QTL analysis of waterlogging tolerance[32] and phytase activity.[36] A major QTL associated with LD and thermostable LD activity in malt was identified on chromosome 7H with the nearest marker bPb-2866 and a position of 58.2 cM on genetic map. The QTL is close to the LD gene with a position of 46 cM on chromosome 7H reported by Li et al. (1999).[13] Although there is no available sequence for bPb-2866, the sequence of a marker named bPb-8049 with available sequence has been found (http://www.diversityarrays.com/), which is close to bPb-2866 (2.36 cM) on the genetic map of Yerong/Franklin DH population.[18] We further mapped the sequences of LD gene (AF022725) and bPb-8049 to a synthetic assembly of the barley genome based on the WGS contigs assembly of cv. Morex, Barke and Bowman,[27] in an attempt to identify their physical locations. Interestingly, LD gene and bPb-8049 were mapped to contigs of barke_contig_281373 and barke_contig_275219, respectively. Their physical distance was 1.0 Mega base in the synthetic assembly of the barley genome. Thus, it may be suggested that the major QTL we identified on 7H is the LD gene in barley.

DOI: 10.1021/acs.jafc.5b00190
J. Agric. Food Chem. 2015, 63, 3778−3783

Two minor QTLs associated with thermostable LD activity were found to be located on the position of 83.7 cM on chromosome 2H (*qTS-LD2*) contributed by Yerong and 102.0 cM on chromosome 1H (*qTS-LD1*) contributed by Franklin, indicating that it should be exist a gene related to thermostable LD activity in Franklin other than the major QTL of LD activity in 7H. Recently, Huang et al. (2014)[17] identified two DArT markers related to LDI content, bPb-8347 on the 73.4 cM of chromosome 6H and bPb-8399 on the 25.7 cM of chromosome 2H. We compared the position of *qTS-LD1*, *qTS-LD2* and that of bPb-8347, bPb-8399. Although *qTS-LD2* and bPb-8399 are located on the same chromosome, their chromosome positions differ largely according to the consensus maps.[40] It was reported that the synergistic function of LD and *beta*-amylase caused increase of maltose in the mash liquor, and adding LD to mashes resulted in a substantial increase in levels of fermentable sugars.[41] *qTS-LD1* identified in this study coincides with a QTL determining malt-extract, which is located at the position of 91.9−106.5 cM on chromosome 1H.[42] Diastatic power is another important malt quality trait and is also a measure of combined activity of four starch-degrading enzymes, including α-amylase, *beta*-amylase, LD and α-glucosidase.[43] *qTS-LD2* identified in this study is close to a QTL determining diastatic power.[42]

Recent study has shown that only increases in LD activity may increase the production of fermentable sugar.[43] It might be because of the different amino acid substitution, considering the case of *beta*-amylase.[44] One of a possible mechanism is a single amino acid substitution, which improves the persistence of beta-amylase during mashing to result in slightly higher fermentable sugar production during mashing. The other type of mechanism is protein refold after a period of heating. Hence, there is a long way to go and much to be done to figure out the mechanism of LD thermostability. In short, the current study identified the novel QTLs associated with LD thermostability and again proved the wide diversity of Tibetan wild barley in LD thermostability. Moreover, the detected QTLs should be useful for a better understanding of the genetic control of LD activity and thermostability in malt.

AUTHOR INFORMATION

Corresponding Author

*E-mail: fdai@zju.edu.cn. Phone: +86 571 86971115. Fax: +86 571 86971117.

Funding

This study was supported by the Natural Science Foundation of China (31201166 and 31471480) and the Fundamental Research Funds for the Central Universities.

Notes

The authors declare no competing financial interest.

ACKNOWLEDGMENTS

We thank Professor D. Sun (Huazhong Agricultural University, China) for providing the Tibetan wild barley.

REFERENCES

(1) Manners, D. J.; Marshall, J. J.; Yellowlees, D. The specificity of cereal limit dextrinase. *Biochem. J.* **1970**, *116*, 539−541.

(2) Yang, X. Q.; Westcott, S.; Gong, X.; Evans, E.; Zhang, X. Q.; Lance, R. C. M.; Li, C. D. Amino acid substitutions of the limit dextrinase gene in barley are associated with enzyme thermostability. *Mol. Breed.* **2009**, *23*, 61−74.

(3) Sissons, M. J.; Lance, R. C. M.; Wallace, W. Bound and free forms of barley limit dextrinase. *Cereal Chem.* **1994**, *71*, 520−521.

(4) Stenholm, K.; Home, S. A new approach to limit dextrinase and its role in mashing. *J. Inst. Brew.* **1999**, *105*, 205−210.

(5) Sissons, M. J.; Taylor, M.; Proudlove, M. Barley malt limit dextrinase: Its extraction, heat stability, and activity during malting and mashing. *J. Am. Soc. Brew. Chem.* **1995**, *53*, 104−10.

(6) Manners, D. J.; Yellowlees, D. Studies on debranching enzymes. The limit dextrinase activity of extracts of certain higher plants and commercial malts. *J. Inst. Brew.* **1973**, *79*, 377−385.

(7) Lee, W. J.; Pyler, R. E. Barley malt limit dextrinase: varietal, environmental and malting effects. *J. Am. Soc. Brew. Chem.* **1984**, *42*, 11−17.

(8) Kristensen, M.; Svensson, B.; Larsen, J. Purification and characterization of barley limit dextrinase during malting. *Proc. Congr. Eur. Brew. Conv.* **1993**, *24*, 37−43.

(9) Longstaff, M. A.; Bryce, J. H. Development of limit dextrinase in germinated barley (*Hordeum vulgare* L.). *Plant Physiol* **1993**, *101*, 881−889.

(10) Gomes, I.; Gomes, J.; Steiner, W. Highly thermostable amylase and pullulanase of the extreme thermophilic eubacterium *Rhodothermus marinus*: production and partial characterization. *Bioresour. Technol.* **2003**, *90*, 207−214.

(11) Burton, R. A.; Zhang, X. Q.; Hrmova, M.; Fincher, G. B. A single limit dextrinase gene is expressed both in the developing endosperm and in germinated grains of barley. *Plant Physiol* **1999**, *119*, 859−887.

(12) Kristensen, M.; Lok, F.; Planchot, V.; Svendsen, I.; Leah, R.; Svensson, B. Isolation and characterization of the gene encoding the starch debranching enzyme limit dextrinase from germinating barley. *Biochim. Biophys. Acta, Protein Struct. Mol. Enzymol.* **1999**, *1431*, 538−546.

(13) Li, C. D.; Zhang, X. Q.; Eckstein, P.; Rossnagel, B. G.; Scoles, G. J. A polymorphic microsatellite in the limit dextrinase gene of barley (*Hordeum vulgare* L.). *Mol. Breed.* **1999**, *5*, 569−577.

(14) Evans, D. E.; van Wegen, B.; Ma, Y.; Eglinton, J. K. The impact of the thermostability of α-amylase, β-amylase and limit dextrinase on potential wort fermentability. *J. Am. Soc. Brew. Chem.* **2003**, *61*, 210−218.

(15) Wang, X. D.; Yang, J.; Zhang, G. P. Genotypic and environmental variation in barley limit dextrinase activity and its relation to malt quality. *J. Zhejiang Univ., Sci., B* **2006**, *7*, 386−392.

(16) Jin, X. L.; Cai, S. G.; Ye, L. Z.; Chen, Z. H.; Zhou, M. X.; Zhang, G. P. Association of *HvLDI* with limit dextrinase activity and malt quality in barley. *Biotechnol. Lett.* **2013**, *35*, 639−645.

(17) Huang, Y. Q.; Cai, S. G.; Ye, L. Z.; Han, Y.; Wu, D. Z.; Dai, F.; Li, C. D.; Zhang, G. P. Genetic architecture of limit dextrinase inhibitor (LDI) activity in Tibetan wild barley. *BMC Plant Biol.* **2014**, *14*, 117.

(18) Li, F.; Zhang, J. E.; Liu, H. M.; Tian, S. J.; Yang, X. G.; Ma, J. X.; Sun, M. X. Comparative study of activity and heat stability of limit dextrinase in 16 barley cultivars. *Cereal Chem.* **2008**, *85*, 271−275.

(19) Walker, J. W.; Bringhurst, T. A.; Broadhead, A. L.; Brosnan, J. M.; Pearson, S. Y. The survival of limit dextrinase during fermentation in the production of Scotch whisky. *J. Inst. Brew.* **2001**, *107*, 99−106.

(20) MacGregor, E. A. The proteinaceous inhibitor of limit dextrinase in barley and malt. *Biochim. Biophys. Acta, Proteins Proteomics* **2004**, *1696*, 165−170.

(21) Heisner, C. B.; Bamforth, C. W. Thioredoxin in barley: could it have a role in releasing limit dextrinase in brewery mashes? *J. Inst. Brew.* **2008**, *114*, 122−126.

(22) von Bothmer, R.; Seberg, O.; Jacobsen, N. Genetic resources in the Triticeae. *Hereditas* **1992**, *116*, 141−150.

(23) Nevo, E.; Chen, G. Drought and salt tolerances in wild relatives for wheat and barley improvement. *Plant, Cell Environ.* **2010**, *33*, 670−685.

(24) March, T. J.; Richter, D.; Colby, T.; Harzen, A.; Schmidt, J.; Pillen, K. Identification of proteins associated with malting quality in a subset of wild barley introgression lines. *Proteomics* **2012**, *12*, 2843−2851.

DOI: 10.1021/acs.jafc.5b00190
J. Agric. Food Chem. 2015, 63, 3778−3783

(25) Dai, F.; Qiu, L.; Xu, Y.; Cai, S. G.; Qiu, B. Y.; Zhang, G. P. Differences in phytase activity and phytic acid content between cultivated and Tibetan annual wild barley. *J. Agric. Food Chem.* **2010**, *58*, 11821−11824.
(26) Dai, F.; Nevo, E.; Wu, D. Z.; Comadran, J.; Zhou, M. X.; Qiu, L.; Chen, Z. H.; Beiles, A.; Chen, G. X.; Zhang, G. P. Tibet is one of the centers of domestication of cultivated barley. *Proc. Natl. Acad. Sci. U. S. A.* **2012**, *109*, 16969−16973.
(27) Dai, F.; Chen, Z. H.; Wang, X. L.; Li, Z. F.; Jin, G. L.; Wu, D. Z.; Cai, S. G.; Wang, N.; Wu, F. B.; Nevo, E.; Zhang, G. P. Transcriptome profiling reveals mosaic genomic origins of modern cultivated barley. *Proc. Natl. Acad. Sci. U. S. A.* **2014**, *111*, 13403−13408.
(28) Qiu, L.; Wu, D. Z.; Ali, S.; Cai, S. G.; Dai, F.; Jin, X. L.; Wu, F. B.; Zhang, G. P. Evaluation of salinity tolerance and analysis of allelic function of *HvHKT1* and *HvHKT2* in Tibetan wild barley. *Theor. Appl. Genet.* **2011**, *122*, 695−703.
(29) Wu, D. Z.; Qiu, L.; Xu, L. L.; Ye, L. Z.; Chen, M. X.; Sun, D. F.; Chen, Z. H.; Zhang, H. T.; Jin, X. L.; Dai, F.; Zhang, G. P. Genetic variation of *HvCBF* genes and their association with salinity tolerance in Tibetan annual wild barley. *PLoS One* **2011**, *6*, e22938.
(30) Ye, L. Z.; Dai, F.; Qiu, L.; Sun, D. F.; Zhang, G. P. Allelic diversity of a beer haze active protein gene in cultivated and Tibetan wild barley and development of allelic specific markers. *J. Agric. Food Chem.* **2011**, *59*, 7218−7223.
(31) Cai, S. G.; Wu, D. Z.; Jabeen, Z.; Huang, Y. Q.; Huang, Y. C.; Zhang, G. P. Genome-wide association analysis of aluminum tolerance in cultivated and Tibetan wild barley. *PLoS One* **2013**, *8*, e69776.
(32) Li, H. B.; Vaillancourt, R.; Mendham, N.; Zhou, M. X. Comparative mapping of quantitative trait loci associated with waterlogging tolerance in barley (*Hordeum vulgare* L.). *BMC Genomics*, **2008**, 9.10.1186/1471-2164-9-401
(33) Dai, F.; Wang, J. M.; Zhang, S. H.; Xu, Z. Z.; Zhang, G. P. Genotypic and environmental variation in phytic acid content and its relation to protein content and malt quality in barley. *Food Chem.* **2007**, *105*, 606−611.
(34) McCleary, B. V. Measurement of the content of limit dextrinase in cereal flours. *Carbohydr. Res.* **1992**, *227*, 257−268.
(35) Van-Ooijen, J. W. *MapQT® 5 Software for the mapping of quantitative trait loci in experimental populations*; Kyazma, B. V.: Wageningen, The Netherlands, 2004.
(36) Dai, F.; Qiu, L.; Ye, L. Z.; Wu, D. Z.; Zhou, M. X.; Zhang, G. P. Identification of a phytase gene in barley (*Hordeum vulgare* L.). *PLoS One* **2011**, *6*, e18829.
(37) Arora, R.; Wisniewski, M. E.; Scorza, R. Cold acclimation in genetically related (sibling) deciduous and evergreen peach (*Prunus persica* L. Batsch). I Seasonal changes in cold hardiness and polypeptides of bark and xylem tissues. *Plant Physiol.* **1992**, *99*, 1562−1568.
(38) Hu, S.; Yu, J.; Dong, J.; Evans, D. E.; Liu, J.; Huang, S.; Huang, S.; Fan, W.; Yin, H.; Li, M. Relationship between levels of diastatic power enzymes and wort sugar production from different barley cultivars during the commercial mashing process of brewing. *Starke* **2014**, *66*, 615−623.
(39) Henson, C. A.; Duke, S. H.; Vinje, M. A. A comparison of barley malt amylolytic enzyme thermostabilities and wort sugars produced during mashing. *J. Am. Soc. Brew. Chem.* **2014**, *72*, 51−65.
(40) Wenzl, P.; Li, H.; Carling, J.; Zhou, M.; Raman, H.; Paul, E.; Hearnden, P.; Maier, C.; Xia, L.; Caig, V.; Ovesna, J.; Cakir, M.; Poulsen, D.; Wang, J.; Raman, R.; Smith, K. P.; Muehlbauer, G. J.; Chalmers, K. J.; Kleinhofs, A.; Huttner, E.; Kilian, A. A high-density consensus map of barley linking DArT markers to SSR, RFLP and STS loci and agricultural traits. *BMC Genomics* **2006**, *7*, 206.
(41) MacGregor, A. W.; Bazin, S. L.; Macri, L. J.; Babb, J. V. Modelling the contribution of alpha-amylase, beta-amylase and limit dextrinase to starch degradation during mashing. *J. Cereal Sci.* **1999**, *29*, 161−169.
(42) Marquez-Cedillo, L. A.; Hayes, P. M.; Jones, B. L.; Kleinhofs, A.; Legge, W. G.; Rossnagel, B. G.; Sato, K.; Ullrich, E.; Wesenberg, D. M. QTL analysis of malting quality in barley based on the doubled-haploid progeny of two elite North American varieties representing different germplasm groups. *Theor. Appl. Genet.* **2000**, *101*, 173−184.
(43) Evans, D. E.; Redd, K.; Harysamow, S.; Elvig, N.; Koutoulis, A. Small scale comparison of the influence of malt quality on malt brewing with barley quality on barley brewing using Ondea Pro. *J. Am. Soc. Brew. Chem.* **2014**, *72*, 192−207.
(44) Ma, Y. F.; Langridge, P.; Logue, S. J.; Evans, D. E. Mutations of barley beta-amylase that improve substrate-binding affinity and thermostability. *Mol. Genet. Genomics* **2001**, *266*, 345−352.

DOI: 10.1021/acs.jafc.5b00190
J. Agric. Food Chem. 2015, 63, 3778−3783

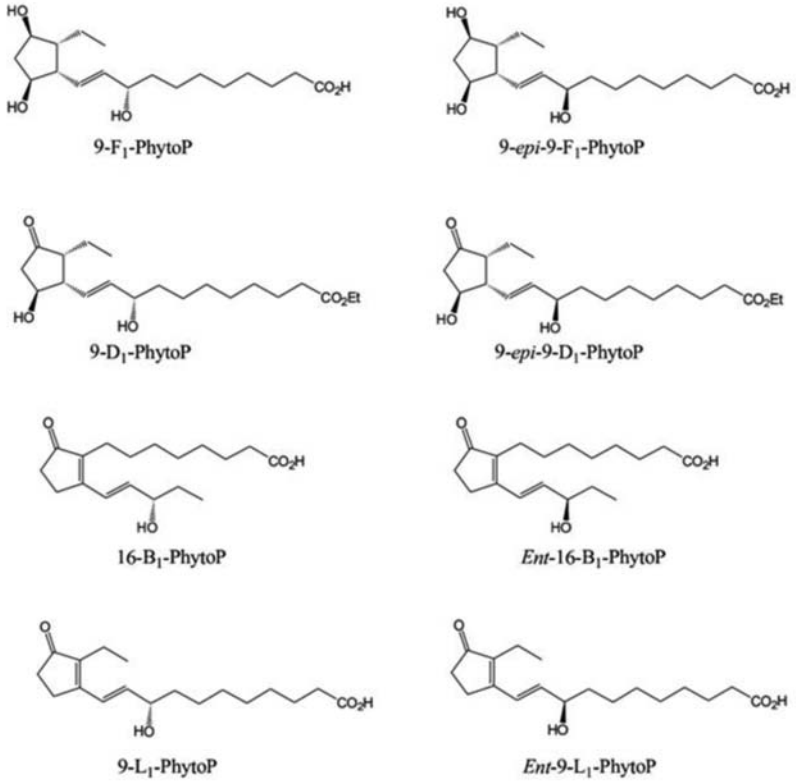

Figure 1. Chemical structures of 9-F_{1t}-PhytoP, 9-*epi*-9-F_{1t}-PhytoP, 9-*epi*-9-D_{1t}-PhytoP, 9-D_{1t}-PhytoP, 16-B_1-PhytoP, *ent*-16-B_1-PhytoP, 9-L_1-PhytoP, and *ent*-9-L_1-PhytoP.

Parchmann and Mueller[19] showed that α-linolenic acid (ALA, C18:3, ω-3), which is the main polyunsaturated fatty acid (PUFA) present in higher plants, is used for the synthesis of the C18-isoprostanes (IsoPs) in plants termed phytoprostanes (PhytoPs).[20−22] PhytoPs are classified according to a nomenclature system that conforms with the prostaglandins (PG) convention.[22−24] In this paper we will use the Taber/Roberts nomenclature (IUPAC), which is different from the one described by Mueller, so care must be taken by the reader to acknowledge the structure associated with the name.[23]

PhytoPs are not only excellent biomarkers of oxidative degradation of plant-derived foodstuffs but also biologically active molecules because they are components of an oxidant-injury-sensing, archaic signaling system that induces several plant defense mechanisms.[24,25] The levels of PhytoPs in plants increase under a variety of conditions, especially when free radical generation is enhanced.[26] Despite little being known of the biological effects of PhytoPs, they have been identified in urine and are found esterified to lipids in plasma in healthy men consuming vegetable oil.[27] Nevertheless, there is some evidence that they play a role in regulation of the immune function,[28] and according to Durand et al.[29] PhytoPs may contribute to the benefical effects of the Mediterranean diet, because they display potent anti-inflammatory and apoptosis-inducing activities similar to those of other prostanoids.

For these reasons, the aim of the experiment described was to increase our understanding of the PhytoPs profile present in Cornicabra extra virgin olive oil, as plant biomarker of oxidative stress in the olive tree. Moreover, special attention was paid to analyzing for the first time if the pit hardening phenological period is really a noncritical period to water deficit for olive fruit, because some individual PhytoP content in the extra virgin olive oil extracted could be affected and, subsequently, the oxidative stress of the tree.

MATERIALS AND METHODS

Plant Material, Experimental Conditions, and Treatments. The experiment was carried out in 2012 at the El Chaparrillo experimental farm, located in Ciudad Real (Spain) (39°00′ N, 3°56′ W; altitude 640 m). The plant material consisted of olive trees (*O. europaea* L. cv Cornicabra) planted in 1998 and spaced 7 m × 4.76 m (300 trees ha^{-1}). The first crop yield (>5 kg per tree) was obtained in 2003.

The soil is an alkaline (pH 8.1) and shallow Petrocalcic Palexeralfs with a clay loam texture, low electrical conductivity (0.2 dS m^{-1}), organic matter (1.05%), nitrogen (0.12%), and potassium (17×10^{-4} mol kg^{-1}) levels, and high cationic exchange capacity (0.186 mol kg^{-1}) level. A discontinuous petrocalcic horizon is located between 0.75 and 0.85 m. The soil volumetric water content for the first 0.3 m depth is 22.8% at field capacity (soil matric potential −0.03 MPa) and 12.1% at permanent wilting point (soil matric potential −1.5 MPa), and from 0.3 to 0.75 m it was 43.0 and 21.1%, respectively.

Irrigation was carried out daily and during the night using a drip irrigation system with four emitters (each delivering 8 L h^{-1}) per tree and irrigation water with an electrical conductivity of 2.9 dS cm^{-1}. Crop irrigation requirements (ETc) were estimated according to daily crop reference evapotranspiration (ETo), calculated using the Penman−Monteith equation,[30] and a crop factor based on the time of the year[31] and taking into consideration canopy size.[32]

Plants were irrigated from mid-May (day of the year, DOY, 134) to the end of September (DOY 273). Control plants (T0 treatment) were irrigated at 100% ETc of the previous week. When midday stem water potential (Ψ_{stem}) values of that week were below −1.2 MPa before pit hardening (phase I of fruit growth) or −1.4 MPa during and after pit hardening (phases II and III of fruit growth, respectively), irrigation amounts were increased 10% in order to ensure no irrigation-related stress.[33]

DOI: 10.1021/acs.jafc.5b00805
J. Agric. Food Chem. 2015, 63, 3784−3792

In addition to T0, two regulated deficit irrigation treatments (T1 and T2) were applied, which were calculated to avoid water deficit during phase I and III of fruit growth, maintaining Ψ_{stem} values around the threshold values indicated for T0 plants, and save irrigation water during the noncritical phenological period of pit hardening (phase II) developing different situations of water deficit (threshold Ψ_{stem} values of −2.00 and −3.00 MPa in T1 and T2 plants, respectively). The irrigation protocol in T1 and T2 plants was based on that proposed by Moriana et al.[33] Irrigation requirements were determined weekly on the basis of the Ψ_{stem} measurements, and irrigation was begun when measured Ψ_{stem} values were lower than the threshold values suggested. The first irrigation event was always 1 mm in both treatments. After each requirement determination the increase or decrease in the irrigation rate was related to the differences between the Ψ_{stem} measured and the threshold suggested as follows:

- When deviations were <10%, the variation in the irrigation was 0.25 mm day^{-1}.
- When deviations were between 10 and 20%, the variation in the irrigation was 0.5 mm day^{-1}.
- When deviations were between 20 and 30%, the variation in the irrigation was 1 mm day^{-1}.
- When deviations were >30%, the variation in the irrigation was 2 mm day^{-1}.

Irrigation was stopped if this approach indicated a negative application.

During the irrigation season (DOY 134−273), ETc was 202 mm and cumulative amounts of applied water in T0, T1, and T2 treatments, measured by means of flow meters integrated in the irrigation system, were 407, 196, and 141 mm, respectively. The orchard was managed under no-tillage conditions; weeds were controlled with postemergence herbicides. Pest control practices were those usually used by local growers.

Climate and Plant Water Status. Meteorological data, namely, air temperature, solar radiation, air relative humidity, rainfall, and wind speed 2 m above the soil surface, were collected in a nearby automatic weather station. Mean daily air vapor pressure deficit (VPD_m) was calculated according to the method of Allen et al.[30] Daily ETo was estimated using the Penman−Monteith equation.[30]

From DOY 173 to 276, midday (12 h solar time) stem water potential (Ψ_{stem}) was measured on the middle third of the trees, in fully developed leaves near the main trunk from two trees of each replicate, enclosing leaves in small black plastic bags covered with aluminum foil for at least 1 h before measurements in the pressure chamber (model 3005, Soil Moisture Equipment Co., Santa Barbara, CA, USA).

Oil Extraction. Olive fruits were harvested at mid-December (DOY 345). Extra virgin olive oil was extracted using an Abencor system, and the obtained oil was separated by decanting. Samples for analysis were filtered and stored at −18 °C in darkness using amber glass bottles without headspace until analysis.

Chemicals and Reagents. PhytoPs (Figure 1), including 9-F_{1t}-PhytoP, 9-*epi*-9-F_{1t}-PhytoP, *ent*-16-F_{1t}-PhytoP, *ent*-16-*epi*-16-F_{1t}-PhytoP, 9-D_{1t}-PhytoP, 9-*epi*-9-D_{1t}-PhytoP, *ent*-16-B_1-PhytoP, 16-B_1-PhytoP, *ent*-9-L_1-PhytoP, and 9-L_1-PhytoP, were synthesized according to our published procedures.[34−36] As internal standard, 8-iso-$PGF_{2\alpha}$d4 was used (Cayman Chemicals, Ann Arbor, MI, USA). Hexane was purchased from Panreac (Castellar del Vallés, Barcelona, Spain), bis(2-hydroxyethyl)amino-tris(hydroxymethyl)methane (Bis-Tris) was from Sigma-Aldrich (St. Louis, MO, USA) and LC-MS grade solvents, methanol and acetonitrile, were purchased from J. T. Baker (Phillipsburg, NJ, USA). The SPE cartridges used was Strata cartridge (Strata X-AW, 100 mg/3 mL), which was acquired from Phenomenex (Torrance, CA, USA).

Phytoprostanes Extraction. PhytoPs were extracted by using a dilution followed by a solid-phase extraction (SPE), as described previously.[21,37] Briefly, 1 mL of extra virgin olive oil samples was diluted in 10 mL of *n*-hexane, and this solution was rediluted in 2 mL of methanol, stirred, and then rediluted in 2 mL of Bis-Tris buffer (0.02 M, HCl, pH 7). Immediately after, the emulsion of each sample (oil + hexane + Bis-Tris buffer) was subjected to SPE using a Strata X-AW cartridge (100 mg/3 mL), which was, prior to the oil sample loading, conditioned and equilibrated with 2 mL of hexane, 2 mL of methanol, and 2 mL of Milli-Q water. Later, to remove undesired compounds, the cartridge was washed with a series of solvents in the following sequence: 2 mL of hexane, 2 mL of Milli-Q water, 2 mL of a solution of methanol/Milli-Q water (1:3), and 2 mL of acetonitrile. Retained compounds were eluted with 1 mL of methanol, which was evaporated by using a SpeedVac concentrator (Savant SPD121P, Thermo Scientific, Waltham, MA, USA). The residue of each sample was redissolved in 200 μL of a mixture of A/B solvents (90:10, v/v), employing a mixture of Milli-Q water/0.01% acetic acid as solvent A and a solution of methanol/0.01% acetic acid as solvent B. Reconstituted samples were sonicated for 10 min and passed through a 0.45 μm filter (Millipore, Beford, MA, USA) before 20 μL of each was analyzed by UHPLC-QqQ-MS/MS (Agilent Technologies, Waldbronn, Germany).

UHPLC-QqQ-MS/MS Analyses. Ten PhytoPs were analyzed by reversed phase using UHPLC coupled with a 6460 triple-quadrupole MS/MS (Agilent Technologies), as reported by Collado-González et al.[37] Briefly, chromatographic separation was carried out on a BEH C18 column (2.1 × 50 mm, 1.7 μm) (Waters, Milford, MA, USA), the temperature of which was 6 °C (both left and right sides of the column). The solvents used as mobile phase were water/acetic acid (99.99:0.01, v/v) (A) and methanol/acetic acid (99.99:0.01, v/v) (B). The MS analysis was applied in the multiple reaction monitoring (MRM negative) ESI mode. The injection volume was 20 μL, and elution was performed at a flow rate of 0.2 mL/min. The linear gradient started with 60% B at 0 min, rose to 62% B at 2 min and 62.5% B at 4 min to reach 65% B at 8 min and at 8.01 min returned to the initial conditions. In this way, the acquisition time was 8.01 min for each sample, with a postrun of 2 min for the column equilibration. ESI conditions and ion optics were as previously described.[37] Data acquisition and processing were performed using the MassHunter software version B.04.00 from Agilent Technologies. The eight detected PhytoPs were quantified using authentic standards: 9-F_{1t}-PhytoP, 9-*epi*-9-F_{1t}-PhytoP, 9-D_{1t}-PhytoP, 9-*epi*-9-D_{1t}-PhytoP, *ent*-16-B_1-PhytoP, 16-B_1-PhytoP, and *ent*-9-L_1-PhytoP, 9-L_1-PhytoP.

Statistical Design and Analysis. The design of the experiments was completely randomized with four replications, each replication consisting of five adjacent tree rows, each with nine trees. Measurements were taken on the inner trees of the central row of each replicate, which were very similar in appearance (leaf area, trunk cross-sectional area, height, ground shaded area, etc.), whereas the other trees served as border trees. Data were analyzed using SPSS software.[38] Analysis of variance was performed, and mean values were compared by a $Tukey_{0.05}$ test. Values for each replicate were averaged before the mean and standard error of each treatment were calculated. To check the regression model hypothesis (linearity, homoscedasticity, normality, and independency) Kolmogorov−Smirnov was used with the Liliefors correction and the Shapiro−Wilk tests for normality and the Levene test for homoscedasticity on the typified residuals. To do the Levene test, data were divided into two groups according to the median of the abscissa data.

RESULTS

Plant Water Status. During the irrigation season (DOY 134−273), average daily maximum and minimum air temperatures were 31.4 and 13.2 °C, respectively, with a mean relative humidity of 37%. VPD_m ranged from 0.09 to 3.50 kPa, and accumulated ETo was 849 mm (Figure 2). Rainfall achieved 96 mm, taking place in 10 daily episodes mainly during September (Figure 2).

Ψ_{stem} values for T0 plants were high and nearly constant, reaching mean values of −1.48 MPa during the measurement periods (−1.40 MPa during phase I and −1.50 during phases II and III) (Figure 3). During phases I and III of fruit growth Ψ_{stem} values for the three treatment plants were very similar and

DOI: 10.1021/acs.jafc.5b00805
J. Agric. Food Chem. 2015, 63, 3784−3792

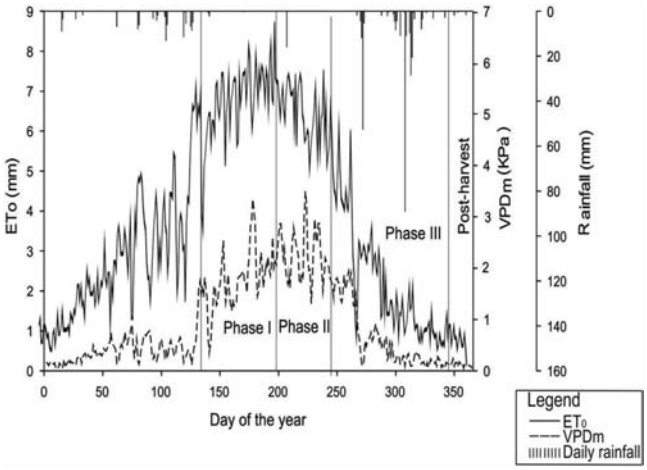

Figure 2. Daily crop reference evapotranspiration (ETo, solid line), mean daily air vapor pressure deficit (VPD_m, short-dash line), and daily rainfall (vertical bars) during year 2012.

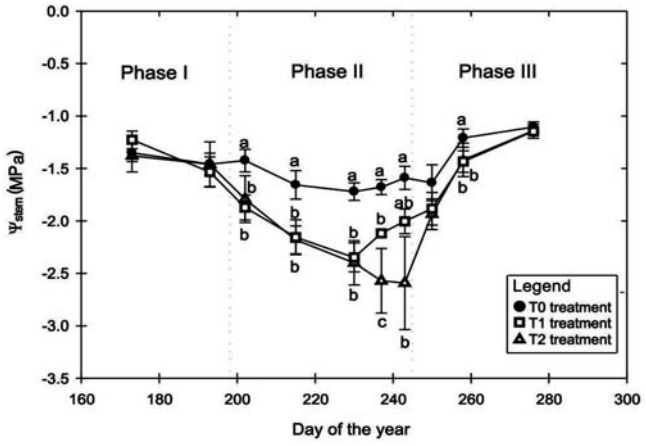

Figure 3. Midday stem water potential (Ψ_{stem}) in T0 (soild symbols), T1 (open squares), and T2 (open triangles) plants during the measurement period. Bars on data points are ±SE of the mean (not shown when smaller than symbols). Different letters on data points at each time indicate significant differences according to the Tukey test ($P \leq 0.05$). Each point is the mean of six values.

slightly increased during phase III of fruit growth (Figure 3). Ψ_{stem} values for T1 and T2 treatments significantly decreased during phase II at a similar rate of around 0.023 MPa day^{-1}, reaching minimum values of −2.35 and −2.59 MPa on DOY 230 and 243, respectively. However, differences between T1 and T2 plants in Ψ_{stem} values during this phenological period were significant only on DOY 237 (Figure 3).

Effect of Water Deficit on PhytoP Content. The PhytoPs profile of the extra virgin olive oil is shown in Figure 4 and Table 1, which indicates the presence of 9-F_{1t}-PhytoP, 9-*epi*-9-F_{1t}-PhytoP, 9-*epi*-9-D_{1t}-PhytoP, 9-D_{1t}-PhytoP, 16-B_1-PhytoP, *ent*-16-B_1-PhytoP, 9-L_1-PhytoP, and *ent*-9-L_1-PhytoP. It is important to emphasize that two series of PhytoPs, the 16-B_1-PhytoP and the 9-L_1-PhytoP, were not separated, using achiral chromatographic conditions. Each pair of enantiomers was quantified together (sum of both for each pair of enantiomers). PhytoPs were identified on the basis of their mass spectra considering their pseudomolecular ion (*m*/*z* 327.2, 325.2, and 307.2), their most characteristic fragmentations, and their

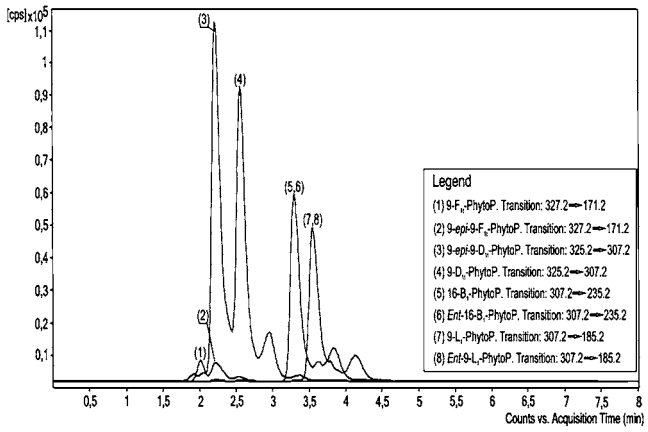

Figure 4. UHPLC-QqQ-MS/MS chromatograms of PhytoPs detected in olive oil. 9-F_{1t}-PhytoP (1), transition 327.2 → 171.2; 9-*epi*-9-F_{1t}-PhytoP (2), transition 327.2 → 171.2; 9-*epi*-9-D_{1t}-PhytoP (3), transition 325.2 → 307.2; 9-D_{1t}-PhytoP (4), transition 325.2 → 307.2; 16-B_1-PhytoP (5), transition 307.2 → 235.2; *ent*-16-B_1-PhytoP (6), transition 307.2 → 235.2; 9-L_1-PhytoP (7), transition 307.2 → 185.2; *ent*-9-L_1-PhytoP (8), transition 307.2 → 185.2.

Table 1. Multiple Reaction Monitoring (MRM) Transitions and Retention Time for Quantification of PhytoPs Using UHPLC-QqQ-MS/MS

phytoprostane	retention time (min)	precursor ion (*m*/*z*)	product ion (*m*/*z*)
9-F_{1t}-PhytoP	1.879	327.2	171.2
9-*epi*-9-F_{1t}-PhytoP	2.086	327.2	171.2
9-*epi*-9-D_{1t}-PhytoP	2.087	325.2	307.2
9-D_{1t}-PhytoP	2.380	325.2	307.2
16-B_1-PhytoP + *ent*-16-B_1-PhytoP	3.070	307.2	235.2
9-L_1-PhytoP + *ent*-9-L_1-PhytoP	3.294	307.2	185.2

elution order according to their retention times as described in Table 1.

The quantification of total PhytoPs in extra virgin olive oil oscillated from 9.18 to 19.31 ng/mL, the dominant PhytoP class being the F_{1t}-PhytoP and the D_1-PhytoPs class the minor components (Table 2). The total PhytoPs content in the extra virgin olive oil increased as a result of water deficit effect, although the differences between T1 and T2 contents were not significant (Table 2). However, the behavior observed in each PhytoP was not similar. In this sense, 9-F_{1t}-PhytoP, 9-*epi*-9-F_{1t}-PhytoP, and a racemic mixture of 16-B_1-PhytoP + *ent*-16-B_1-PhytoP showed a response to water deficit similar to that observed considering the total PhytoPs content, whereas the other PhytoPs (9-*epi*-9-D_{1t}-PhytoP, 9-D_{1t}-PhytoP, and a racemic mixture of 9-L_1-PhytoP + *ent*-9-L_1-PhytoP) showed similar levels in T0 and T1 olive oil, which were significantly lower than those observed in T2 oil (Table 2).

The observations of total PhytoPs and all individual PhytoPs in extra virgin olive oil from the three irrigation treatments showed significant first-order and second-order polynomic correlations with minimum Ψ_{stem} values in phase II of fruit growth, except when 9-F_{1t}-PhytoP was considered in the first-order correlation and a racemic mixture of 9-L_1-PhytoP + *ent*-9-L_1-PhytoP in the second-order polynomic correlation (Tables 3 and 4). Moreover, most equations in Tables 3 and 4 predict a negative PhytoP value under high Ψ_{stem} values.

DOI: 10.1021/acs.jafc.5b00805
J. Agric. Food Chem. 2015, 63, 3784−3792

Table 2. Effect of Irrigation Treatment (T0, T1, and T2) on the PhytoP Content (ng/mL) in Cornicabra Extra Virgin Olive Oil[a]

phytoprostane	T0	T1	T2	ANOVA
9-F_{1t}-PhytoP	5.24 ± 0.21 b	10.00 ± 2.02 a	9.73 ± 2.06 a	0.022
9-*epi*-9-F_{1t}-PhytoP	2.83 ± 0.21 b	4.86 ± 0.49 a	5.26 ± 0.93 a	0.006
9-*epi*-9-D_{1t}-PhytoP	0.13 ± 7.6 × 10^{-4} b	0.13 ± 0.21 b	0.26 ± 0.08 a	0.032
9-D_{1t}-PhytoP	nd	0.19 ± 0.05 b	0.45 ± 0.11 a	0.022
16-B_1-PhytoP + *ent*-16-B_1-PhytoP	0.32 ± 0.02 b	0.72 ± 0.19 a	0.75 ± 0.09 a	0.008
9-L_1-PhytoP + *ent*-9-L_1-PhytoP	0.66 ± 0.12 b	1.28 ± 0.06 b	2.88 ± 0.88 a	0.005
total	9.18 ± 0.31 b	17.18 ± 2.70 a	19.31 ± 3.38 a	0.006

[a]Means within a row followed by different letters are significantly different by Tukey's test ($P \leq 0.05$). nd, not detected.

Table 3. Intercept (a), Slope (b), Coefficient of Determination (r^2), Number of Data Points (n), and Mean Square Error (MSE) of First-Order Linear Equations ($y = a + bx$) between PhytoP Content (ng/mL) and Minimum Mid-day Stem Water Potential (Ψ_{stem}, MPa) in Phase II of Fruit Growth, Using All Data Pooled[a]

phytoprostane	a	b	r^2	n	MSE
9-F_{1t}-PhytoP	0.393^{ns}	−3.482^{ns}	0.3476^{ns}	9	5.555
	(4.180)	(1.803)			
9-*epi*-9-F_{1t}-PhytoP	0.087^{ns}	−1.857*	0.4719*	9	0.942
	(1.721)	(0.742)			
9-*epi*-9-D_{1t}-PhytoP	−0.119^{ns}	−0.128**	0.6917**	9	0.002
	(0.075)	(0.032)			
9-D_{1t}-PhytoP	−0.748***	−0.421***	0.9132***	9	0.004
	(0.114)	(0.049)			
16-B_1-PhytoP + *ent*-16-B_1-PhytoP	−0.252^{ns}	−0.373*	0.5520*	9	0.028
	(0.294)	(0.127)			
9-L_1-PhytoP + *ent*-9-L_1-PhytoP	−2.144^{ns}	−1.647*	0.4875*	9	0.696
	(1.480)	(0.638)			
total	−2.783^{ns}	−7.907*	0.5118*	9	14.560
	(6.767)	(2.919)			

[a]*, significant at $P < 0.05$; **, significant at $P < 0.01$; ***, significant at $P < 0.001$; and ^{ns}, nonsignificant. Standard error shown in parentheses.

Table 4. Equations, Coefficients of Determination (r^2), Number of Data Points (n), and Mean Square Error (MSE) of Second-Order Polynomic Equations ($y = a + bx + cx^2$) between PhytoP Content (ng/mL) and Stem Water Potential (Ψ_{stem}, MPa) in Phase II of Fruit Growth, Using All Data Pooled[a]

phytoprostane	a	b	c	r^2	n	MSE
9-F_{1t}-PhytoP	−44.840*	−43.250**	−8.432*	0.7838*	9	2.148
	(13.260)	(11.487)	(2.424)			
9-*epi*-9-F_{1t}-PhytoP	−21.063**	−20.452**	−3.943**	0.9270***	9	0.152
	(3.526)	(3.055)	(0.645)			
9-*epi*-9-D_{1t}-PhytoP	0.688*	0.582*	0.150*	0.8974**	9	6.9 × 10^{-4}
	(0.237)	(0.206)	(0.043)			
9-D_{1t}-PhytoP	−0.777^{ns}	−0.446^{ns}	−0.005^{ns}	0.9132***	9	0.005
	(0.627)	(0.543)	(0.115)			
16-B_1-PhytoP + *ent*-16-B_1-PhytoP	−2.836^{ns}	−2.644*	−0.482^{ns}	0.7494*	9	0.018
	(1.212)	(1.050)	(0.222)			
9-L_1-PhytoP + *ent*-9-L_1-PhytoP	−11.311^{ns}	−9.706^{ns}	−1.709^{ns}	0.5998^{ns}	9	0.634
	(7.205)	(6.241)	(1.317)			
total	−80.138**	−75.917**	− 14.420**	0.8760**	9	4.314
	(18.789)	(16.276)	(3.435)			

[a]*, significant at $P < 0.05$; **, significant at $P < 0.01$; ***, significant at $P < 0.001$; ^{ns}, nonsignificant. Standard error shown in parentheses.

In general, correlations for the second-order polynomic equations of minimum Ψ_{stem} versus PhytoPs were tighter than those of first-order equations, except when 9-D_{1t}-PhytoP or a racemic mixture of 9-L_1-PhytoP + *ent*-9-L_1-PhytoP was considered (Tables 3 and 4). In this respect, in the case of a racemic mixture of 9-L_1-PhytoP + *ent*-9-L_1-PhytoP versus Ψ_{stem} because the coefficient of determination of the second-order polynomic equation was not significant, and in the case of 9-D_{1t}-PhytoP because both equations showed similar coefficients of determination (Tables 3 and 4).

It is important to indicate that the PhytoPs that increased their contents in T1 and T2 extra virgin olive oil (9-F_{1t}-PhytoP, 9-*epi*-9-F_{1t}-PhytoP, and a racemic mixture of 16-B_1-PhytoP + *ent*-16-B_1-PhytoP) (Table 2) showed a second-order polynomic relationsship with respect to minimum Ψ_{stem} values characterized by two different phases (Figure 5). Above minimum Ψ_{stem} values of around −2.5 MPa, PhytoP values increased

DOI: 10.1021/acs.jafc.5b00805
J. Agric. Food Chem. 2015, 63, 3784−3792

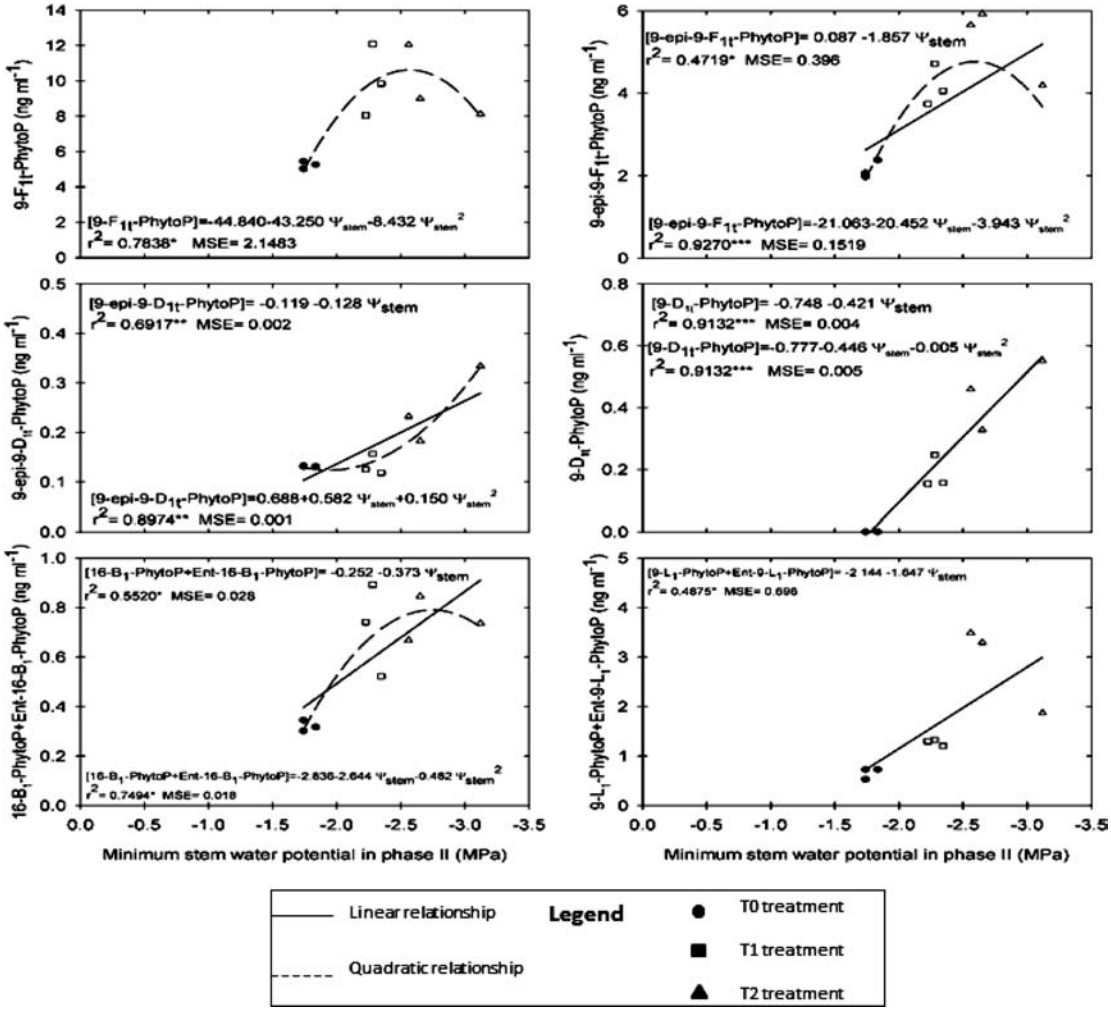

Figure 5. Relationship between PhytoPs content and minimum Ψ_{stem} values in T0 (solid circles), T1 (open squares), and T2 (open triangles) plants during phase II of fruit growth. Each value is the mean of three measurements.

sharply as minimum Ψ_{stem} decreased, and when minimum Ψ_{stem} values were below this threshold value, the relationship changed and any further reduction in minimum Ψ_{stem} was associated with a decrease in PhytoP contents. In contrast, the PhytoPs showed contents in T1 olive oil lower than in T2 (9-*epi*-9-D_{1t}-PhytoP, 9-D_{1t}-PhytoP, and a racemic mixture of 9-L_1-PhytoP + *ent*-9-L_1-PhytoP) and linear regression may be sufficient for modeling the relationship between Ψ_{stem} and PhytoP in the water stress range studied (minimum Ψ_{stem} values in phase II from −3.12 to −1.73 MPa) (Figure 5).

DISCUSSION

The fact that Ψ_{stem} values for T0 plants during phases I, II, and III of fruit growth were slightly below the threshold Ψ_{stem} values (Figure 3) could be because irrigation amounts were not properly managed when Ψ_{stem} values were below the threshold values. Nevertheless, Ψ_{stem} mean values in each fruit growth phase were quite high and nearly constant,[39−41] suggesting that T0 plants were not under irrigation-related stress during the experimental period.[33]

Despite Ψ_{stem} values for T1 and T2 plants during phase II decreased at a similar and slow rate,[42] minimum Ψ_{stem} values indicated that both treatment plants achieved substantial water deficit levels, but were more important in T2 plants at the end of this phenological period (Figure 3).[43,44]

In a previous paper, Collado-González et al.[37] showed in a branded extra virgin olive oil a different PhytoP profile from that shown in Table 2, because they identified 9-*epi*-9-D_{1t}-PhytoP, 9-D_{1t}-PhytoP, 16-B_1-PhytoP + *ent*-16-B_1-PhytoP, and *ent*-16-*epi*-16-F_{1t}-PhytoP + *ent*-16-F_{1t}-PhytoP. In other words, they additionally detected *ent*-16-*epi*-16-F_{1t}-PhytoP + *ent*-16-F_{1t}-PhytoP, even though did not detect 9-F_{1t}-PhytoP, 9-*epi*-9-F_{1t}-PhytoP, and 9-L_1-PhytoP + *ent*-9-L_1-PhytoP (Table 2). However, the level of total PhytoPs (14.64 ng/mL) in that branded extra virgin olive was within the range found under our experimental conditions in Cornicabra extra virgin olive oil (9.18−19.31 ng/mL). Taking into consideration that both olive oils were extra virgin and that analyses were performed with the same method, using synthetic standards, it is clear that these differences in composition can be ascribed to the decisive effect of cultivar, oil extraction technology, and/or storage conditions prone to autoxidation.[27]

To the best of our knowledge, no previous information exists on the effect of the water deficit on the PhytoPs content. In this sense, the increase in PhytoPs by water deficit effect during pit hardening (phase II of fruit growth) (Table 2) showed that this phenological period can be noncritical considering fruit yield,[18] but is clearly critical for PhytoPs content in olive oil. In this sense, Gómez del Campo and García[45] showed that virgin olive oils from deficit irrigated stress from the end of fruit drop to the

DOI: 10.1021/acs.jafc.5b00805
J. Agric. Food Chem. 2015, 63, 3784−3792

end of July exhibited significantly higher oxidative stability, which coincided with significantly higher contents in phenol derivatives, although deficit irrigation strategies in summer did not determine significant changes in the parameters legally established for evaluating the level of commercial quality of the virgin oils. Moreover, this increase in PhytoPs content could be related to the fact that under drought stress the frail balance between reactive oxygen species (ROS) and scavenging that defines the normal steady-state level of intracellular ROS suffers an upward shift enhancing ROS production due to stomatal closure and the concomitant limitation on CO_2 fixation.[46] A consequence of this enhanced ROS formation in plants is the formation of an array of lipid peroxidation products, including structural congeners of jasmonates, the PhytoPs.[24]

Because all PhytoPs are induced by oxidative stress (OS) from common precursors, the G_1-PhytoPs,[24,47] the fact that the behavior observed in each PhytoP in response to water deficit was not similar (Table 2) indicated that those which increased their contents in the T1 extra virgin olive oil might require a lower OS level to be induced from the precursor and could be used as early markers of water deficit in extra virgin olive oil.

From an nutritional point of view, the increase in total PhytoPs in T1 and T2 olive oil, nearly 2-fold with respect to control (T0) olive oil (Table 2), could be considered a potential beneficial aspect of the extra virgin olive oils from trees cultivated under water deficit conditions during pit hardening, because even though there is no detailed knowledge of the biological effects of PhytoPs, there is some evidence of their beneficial effects on human health, such as regulation of immune function[28,48] and anti-inflammatory and apoptosis-inducing activities.[29]

The fact that the relationships between 9-F_{1t}-PhytoP, 9-*epi*-9-F_{1t}-PhytoP or a racemic mixture of 16-B_1-PhytoP + *ent*-16-B_1-PhytoP and minimum Ψ_{stem} values in phase II were tighter using second-order polynomic equations, whereas the relations for 9-*epi*-9-D_{1t}-PhytoP or 9-D_{1t}-PhytoP using linear or quadratic equations showed similar levels of significance for their coefficients of determination and the relationship for a racemic mixture of 9-L_1-PhytyoP + *ent*-9-L_1-PhytyoP was defined only by a linear equation (Figure 5), could indicate different development levels of the same behavior. In this sense, Horner[49] indicated that the relationship between plant water status and secondary metabolite contents is defined by a quadratic relationship. Also, some authors showed that the relationship between plant water status and some metabolite contents is not defined by a linear correlation when a wide range of plant water status is considered.[50,51] Then, the first-order relationship between plant water deficit and PhytoPs content (Figure 5) could correspond to the first phase of the quadratic relationship proposed by Horner,[49] indicating that a more severe water deficit could be necessary to induce a decrease in the 9-*epi*-9-D_{1t}-PhytoP, 9-D_{1t}-PhytoP, or a racemic mixture of 9-L_1-PhytoP + *ent*-9-L_1-PhytoP content.

The fact that most equations in Tables 3 and 4 showed a negative intercept could contraindicate the use these equations under high Ψ_{stem} values because negative PhytoPs values could be predicted, which does not make sense from a metabolic or physiological point of view. Nevertheless, PhytoPs values could be predicted using these equations when Ψ_{stem} values were within the range of values used to determine these equations (minimum Ψ_{stem} values in phase II from −3.12 to −1.73 MPa). Therefore, using these Ψ_{stem} boundary values negative PhytoPs values are not predicted.

Overall, the results showed for the first time that pit hardening (phase II of olive fruit growth), a phenological period noncritical for fruit yield, is clearly critical for extra virgin olive oil composition because water deficit enhances the PhytoPs content, with the concomitant potential beneficial aspects on human health because they are bioavailable in humans according to previous results.[48] Also, qualitative and quantitative differences in PhytoPs content with respect to those reported by other authors indicate a decisive effect of cultivar, oil extraction technology, and/or storage conditions prone to autoxidation. The content of each individual PhytoP in the olive oil from T0, T1, and T2 treatments could define different phases of the same behavior. In this sense, when minimun Ψ_{stem} values in phase II were above −2.5 MPa, 9-F_{1t}-PhytoP, 9-*epi*-9-F_{1t}-PhytoP, and a racemic mixture of 16-B_1-PhytoP + *ent*-16-B_1-PhytoP values increased sharply as Ψ_{stem} decreased, and when Ψ_{stem} values were below this threshold value, the relationship changed and any further reduction in Ψ_{stem} was associated with a decrease in PhytoPs contents. In contrast, when minimun Ψ_{stem} values in phase II decreased from −1.73 to −3.12 MPa, the 9-*epi*-9-D_{1t}-PhytoP, 9-D_{1t}-PhytoP, and a racemic mixture of 9-L_1-PhytoP + *ent*-9-L_1-PhytoP increased, indicating that a more severe water deficit could be necessary to induce a decrease in their contents. Therefore, from a physiological and agronomical point of view, 9-F_{1t}-PhytoP, 9-*epi*-9-F_{1t}-PhytoP, and a racemic mixture of 16-B_1-PhytoP + *ent*-16-B_1-PhytoP could be considered as early candidate biomarkers of water stress in olive tree.

AUTHOR INFORMATION

Corresponding Author

*(A.G.-I.) Phone: +34 968396363. Fax: +34 968396213. E-mail: angelgil@cebas.csic.es.

Funding

This research was supported by MICINN (CICYT/FEDER AGL2013-45922-C2-1-R and AGL2013-45922-C2-2-R), CSIC 201170E041, Fundación Séneca (04486/GERM/06), and CYTED, Action 112RT0460 CORNUCOPIA grants to the authors. J.C.-G. was funded by a FPI grant.

Notes

The authors declare no competing financial interest.

ABBREVIATIONS USED

ALA, α-linolenic acid; DOY, day of the year; ETo, estimated according to daily crop reference evapotranspiration; ETc, crop irrigation requirements; IsoPs, isoprostanes; MRM, multiple reaction monitoring; OS, oxidative stress; PG, prostaglandin; PhytoPs, phytoprostanes; PUFAs, polyunsaturated fatty acids; RDI, regulated deficit irrigation; ROS, reactive oxygen species; SPE, solid phase extraction; Ψ_{stem}, stem water potential; UHPLC-QqQ-MS/MS, ultrahigh-performance liquid chromatography coupled to triple-quadrupole mass spectrometry

REFERENCES

(1) FAOSTAT. 2014, available at http://faostat.fao.org.

(2) International Olive Oil Council (IOOC). *Trade Standard Applying to Olives Oils and Pomace Oils*; Document COI/T.15/NC No 3/Rev. 8; IOOC: Madrid, Spain, 2015.

(3) De la Lastra, C. A.; Barranco, M. D.; Motilva, V.; Herrerias, J. M. Mediterranean diet and health: biological importance of olive oil. *Curr. Pharm. Des.* **2001**, *7*, 933−950.

(4) Abuznait, A. H.; Qosa, H.; Busnena, B. A.; El Sayed, K. A.; Kaddoumi, A. Olive-oil-derived oleocanthal enhances β-amyloid

DOI: 10.1021/acs.jafc.5b00805
J. Agric. Food Chem. 2015, 63, 3784−3792

clearance as a potential neuroprotective mechanism against Alzheimer's disease: in vitro and in vivo studies. *ACS Chem. Neurosci.* **2013**, *4*, 973−982.
(5) Galli, C.; Visioli, F. Antioxidant and other activities of phenolics in olives/olive oil, typical components of the Mediterranean diet. *Lipids* **1999**, *34* (Suppl.), S23−S26.
(6) Beauchamp, G. K.; Keast, R. S.; Morel, D.; Lin, J.; Pika, J.; Han, Q.; Lee, C.-H.; Smith, A. B.; Breslin, P. A. Phytochemistry: ibuprofen-like activity in extra-virgin olive oil. *Nature* **2005**, *437*, 45−46.
(7) Harwood, J. L.; Yaqoob, P. Nutritional and health aspects of olive oil. *Eur. J. Lipid Sci. Technol.* **2002**, *104*, 685−697.
(8) Stark, A. H.; Madar, P. Z. Olive oil as a functional food: epidemiology and nutritional approaches. *Nutr. Rev.* **2002**, *60*, 170−176.
(9) Waterman, E.; Lockwood, B. Active components and clinical applications of olive oil. *Altern. Med. Rev.* **2007**, *12*, 331−342.
(10) MAAMA. 2014, available at http://www.magrama.gob.es.
(11) Martin Vertedor, A.; Perez-Rodriguez, J.; Losada, H. P.; Fereres Castiel, E. Interactive responses to water deficits and crop load in olive (*Olea europaea* L., cv. Morisca). II: Water use, fruit and oil yield. *Agric. Water Manage.* **2011**, *98*, 950−958.
(12) Moriana, A.; Orgaz, F.; Pastor, M.; Fereres, E. Yield responses of a mature olive orchard to water deficits. *J. Am. Soc. Hortic. Sci.* **2003**, *128*, 425−431.
(13) Orgaz, F.; Fereres, E. El riego. In *El Cultivo del Olivo*, Barranco, D., Fernández-Escobar, R., Eds.; Mundi-Prensa: Barcelona, Spain, 2007; pp −-346.
(14) Katerji, N.; Mastrorilli, M.; Rana, G. Water use efficiency of crops cultivated in the Mediterranean region: review and analysis. *Eur. J. Agron.* **2008**, *28*, 493−507.
(15) Janick, J.; Naor, A. Irrigation scheduling and evaluation of tree water status in deciduous orchards. *Hortic. Rev.* **2006**, *32*, 111.
(16) Chalmers, D. J. A physiological examination of regulated deficit irrigation. *N. Z. Agric. Sci.* **1989**, *23*, 44−48.
(17) Inglese, P.; Barone, E.; Gullo, G. The effect of complementary irrigation on fruit growth, ripening pattern and oil characteristics of olive (*Olea europaea* L) cv. Carolea. *J. Hortic. Sci.* **1996**, *71*, 257−263.
(18) Goldhamer, D. A. Regulated deficit irrigation for California canning olives. *Acta Hortic.* **1999**, 369−372.
(19) Parchmann, S.; Mueller, M. J. Evidence for the formation of dinor isoprostanes E1 from α-linolenic acid in plants. *J. Biol. Chem.* **1998**, *273*, 32650−32655.
(20) Durand, T.; Bultel-Poncé, V.; Guy, A.; Berger, S.; Mueller, M. J.; Galano, J.-M. New bioactive oxylipins formed by non-enzymatic free-radical-catalyzed pathways: the phytoprostanes. *Lipids* **2009**, *44*, 875−888.
(21) Medina, S.; Dominguez-Perles, R.; Gil, J. I.; Ferreres, F.; Garcia Viguera, C.; Gil Izquierdo, A. A ultra-pressure liquid chromatography/triple quadrupole tandem mass spectrometry method for the analysis of 13 eicosanoids in human urine and quantitative 24 h values in healthy volunteers in a controlled constant diet. *Rapid Commun. Mass Spectrom.* **2012**, *26*, 1249−1257.
(22) Imbusch, R.; Mueller, M. J. Analysis of oxidative stress and wound-inducible dinor isoprostanes F(1) (phytoprostanes F(1)) in plants. *Plant Physiol.* **2000**, *124*, 1293−1303.
(23) Jahn, U.; Galano, J.-M.; Durand, T. A cautionary note on the correct structure assignment of phytoprostanes and the emergence of a new prostane ring system. *Prostaglandins, Leukotrienes Essent. Fatty Acids* **2010**, *82*, 83−86.
(24) Thoma, I.; Krischke, M.; Loeffler, C.; Mueller, M. The isoprostanoid pathway in plants. *Chem. Phys. Lipids* **2004**, *128*, 135−148.
(25) Vazquez Romero, A.; Verdaguer, X.; Riera, A. General approach to prostanes B1 by intermolecular Pauson-Khand reaction: syntheses of methyl esters of prostaglandin B1and phytoprostanes 16-B1-PhytoP and 9-L1-PhytoP. *Eur. J. Org. Chem.* **2013**, *2013*, 1716−1725.
(26) Loeffler, C.; Berger, S.; Guy, A.; Durand, T.; Bringmann, G.; Dreyer, M.; von Rad, U.; Durner, J.; Mueller, M. B1-phytoprostanes trigger plant defense and detoxification responses. *Plant Physiol.* **2005**, *137*, 328−340.
(27) Karg, K.; Dirsch, V.; Vollmar, A. M.; Cracowski, J.-L.; Laporte, F.; Mueller, M. J. Biologically active oxidized lipids (phytoprostanes) in the plant diet and parenteral lipid nutrition. *Free Radical Res.* **2007**, *41*, 25−37.
(28) Gutermuth, J.; Bewersdorff, M.; Traidl-Hoffmann, C.; Ring, J.; Mueller, M. J.; Behrendt, H.; Jakob, T. Immunomodulatory effects of aqueous birch pollen extracts and phytoprostanes on primary immune responses in vivo. *J. Allergy Clin. Immunol.* **2007**, *120*, 293−299.
(29) Durand, T.; Bultel Ponce, V.; Guy, A.; El Fangour, S.; Rossi, J.-C.; Galano, J.-M. Isoprostanes and phytoprostanes: bioactive lipids. *Biochimie* **2011**, *93*, 52−60.
(30) Allen, R. G.; Pereira, R. S.; Raes, D.; Smith, M. Crop evapotranspiration − guidelines for computing crop water requirements. *Irrigation and Drainage 56*; FAO: Rome, Italy, 1998.
(31) Orgaz, F.; Fereres, E. Riego. In *El cultivo del Olivo*; Barranco, D., Fernández-Escobar, R., Rallo, L., Eds.; Mundi-Prensa y Consejería de Agricultura y Pesca de la Junta de Andalucía: Madrid, Spain, 2004; pp 320−346.
(32) Fereres, E.; Castel, J. R. *Drip Irrigation Management*; Leaflet, Division of Agricultural Sciences, University of California, 1981; p 21259.
(33) Moriana, A.; Pérez-López, D.; Prieto, M. H.; Ramírez-Santa-Pau, M.; Pérez-Rodriguez, J. M. Midday stem water potential as a useful tool for estimating irrigation requirements in olive trees. *Agr. Water Manage.* **2012**, *112*, 43−54.
(34) El Fangour, S.; Guy, A.; Vidal, J.-P.; Rossi, J.-C.; Durand, T. A flexible synthesis of the phytoprostanes B1 type I and II. *J. Org. Chem.* **2005**, *70*, 989−997.
(35) Pinot, E.; Guy, A.; Fournial, A.; Balas, L.; Rossi, J.-C.; Durand, T. Total synthesis of the four enantiomerically pure diasteroisomers of the phytoprostanes E1 type II and of the 15-E2t-isoprostanes. *J. Org. Chem.* **2008**, *73*, 3063−3069.
(36) El Fangour, S.; Guy, A.; Despres, V.; Vidal, J.-P.; Rossi, J.-C.; Durand, T. Total syntheses of the eight diastereoisomers of the syn-anti-syn phytoprostanes F1 types I and II. *J. Org. Chem.* **2004**, *69*, 2498−2503.
(37) Collado-González, J.; Medina, S.; Durand, T.; Guy, A.; Galano, J.-M.; Torrecillas, A.; Ferreres, F.; Gil-Izquierdo, A. New UHPLC-QqQ-MS/MS method for quantitative and qualitative determination of free phytoprostanes in foodstuffs of commercial olive and sunflower oils. *Food Chem.* **2014**, *178*, 212−220.
(38) SPSS Inc. 2002. SPSS Professional Statistics. Business Intelligence Division, v.12. SPSS. Inc., Chicago.
(39) Dell'Amico, J.; Moriana, A.; Corell, M.; Girón, I. F.; Morales, D.; Torrecillas, A.; Moreno, F. Low water stress conditions in table olive trees (*Olea europaea* L) during pit hardening produced a different response of fruit and leaf water relations. *Agric. Water Manage.* **2012**, *114*, 11−17.
(40) Tognetti, R.; d'Andria, R.; Sacchi, R.; Lavini, A.; Morelli, G.; Albino, A. Deficitirrigation affects seasonal changes in leaf physiology and oil quality of *Olea europaea* (cultivars Frantoio and Leccino). *Ann. Appl. Biol.* **2007**, *150*, 169−186.
(41) Fernández, J. E.; Díaz-Espejo, A.; Infante, J. M.; Duran, P.; Palomo, M. J.; Chamorro, V.; Girón, I. F.; Villagarcía, L. Water relations and gas exchange in olive treesunder regulated deficit irrigation and partial root zone drying. *Plant Soil* **2006**, *284*, 273−291.
(42) Hale, M. G.; Orcutt, D. M. *The Physiology of Plants under Stress*; Wiley: New York, 1987.
(43) Alegre, S.; Marsal, J.; Mata, M.; Arbones, A.; Girona, J. Regulated deficit irrigation in olive trees (*Olea europaea* L. cv. Arbequina) for oil production. *Acta Hortic.* **2002**, 259−262.
(44) Iniesta, F.; Testi, L.; Orgaz, F.; Villalobos, F. J. The effects of regulated and continuous deficit irrigation on the water use, growth and yield of olive trees. *Eur. J. Agron.* **2009**, *30*, 258−265.
(45) Gómez del Campo, M.; García, J. M. Summer deficit-irrigation strategies in a hedgerow olive cv. Arbequina orchard: effect on oil quality. *J. Agric. Food Chem.* **2013**, *61*, 8899−8905.

DOI: 10.1021/acs.jafc.5b00805
J. Agric. Food Chem. 2015, 63, 3784−3792

(46) Cruz de Carvalho, M. H. Drought stress and reactive oxygen species: production, scavenging and signaling. *Plant Signal. Behav.* **2008**, *3*, 156−165.
(47) Sattler, S. E.; Mène Saffrané, L.; Farmer, E. E.; Krischke, M.; Mueller, M. J.; DellaPenna, D. Nonenzymatic lipid peroxidation reprograms gene expression and activates defense markers in *Arabidopsis* tocopherol-deficient mutants. *Plant Cell* **2006**, *18*, 3706−3720.
(48) Barden, A. E.; Croft, K. D.; Durand, T.; Guy, A.; Mueller, M. J. Flaxseed oil supplementation increases plasma F1-phytoprostanes in healthy men. *J. Nutr.* **2009**, *139*, 1890−1895.
(49) Horner, J. D. Nonlinear effects of water deficits on foliar tannin concentration. *Biochem. Syst. Ecol.* **1990**, *18*, 211−213.
(50) Gobbo Neto, L.; Gobbo-Neto, L.; Lopes, N. P. Medicinal plants: factors of influence on the content of secondary metabolites. *Quim. Nova* **2007**, *30*, 374.
(51) Mena, P.; Galindo, A.; Collado Gonzalez, J.; Ondoño, S.; Garcia Viguera, C.; Ferreres, F.; Torrecillas, A.; Gil Izquierdo, A. Sustained deficit irrigation affects the colour and phytochemical characteristics of pomegranate juice. *J. Sci. Food Agric.* **2013**, *93*, 1922−1927.

DOI: 10.1021/acs.jafc.5b00805
J. Agric. Food Chem. 2015, 63, 3784−3792

Table 1. Summary of Wheat–*Hordeum chilense* Addition and Substitution Lines and Their Chromosomal Composition

code	genotype	chromosomal composition
CS	*Triticum aestivum* L. cv. Chinese Spring	$2n = 6x = 42$
CS A7$\mathbf{H}^{ch}$	*T. aestivum* cv. Chinese Spring–*H. chilense* (H1) disomic addition line of chromosome 7$\mathbf{H}^{ch}$	$2n = 6x + 2 = 44$
CS A7$\mathbf{H}^{ch}\alpha$	*T. aestivum* cv. Chinese Spring–*H. chilense* (H1) ditelosomic addition line of 7$\mathbf{H}^{ch}\alpha$ chromosome arm	$2n = 6x + 2t = 42 + 2$ telos
CS A7$\mathbf{H}^{ch}\beta$	*T. aestivum* cv. Chinese Spring–*H. chilense* (H1) ditelosomic addition line of 7$\mathbf{H}^{ch}\beta$ chromosome arm	$2n = 6x + 2t = 42 + 2$ telos
CS(7**A**)7$\mathbf{H}^{ch}$	*T. aestivum* cv. Chinese Spring–*H. chilense* (H1) disomic substitution line of chromosome 7**A** by 7$\mathbf{H}^{ch}$	$2n = 6x = 42$
CS(7**B**)7$\mathbf{H}^{ch}$	*T. aestivum* cv. Chinese Spring–*H. chilense* (H1) disomic substitution line of chromosome 7**B** by 7$\mathbf{H}^{ch}$	$2n = 6x$
CS(7**D**)7$\mathbf{H}^{ch}$	*T. aestivum* cv. Chinese Spring–*H. chilense* (H1) disomic substitution line of chromosome 7**D** by 7$\mathbf{H}^{ch}$	$2n = 6x = 42$

improve nutritional and agronomic properties (e.g., resistance to abiotic or biotic stresses in the seed) while maintaining breadmaking characteristics and low allergen levels.

MATERIALS AND METHODS

Plant Materials. Introgression lines (chromosome additions or substitutions) for chromosome 7$\mathbf{H}^{ch}$ from *H. chilense* in bread wheat (*Triticum aestivum* cv. Chinese Spring (CS), $2n = 6x = 42$) used in this work were kindly provided by Steve Reader (John Innes Centre, Norwich, UK) and are summarized in Table 1. Seeds were germinated in Petri dishes on wet filter papers in darkness for 5 days at 4 °C followed by 24 h of incubation at 25 °C. All plants were grown in a greenhouse at 26 °C during the day and 22 °C at night with a photoperiod of long days (16 h of daylight–8 h of darkness).

Protein Extraction. Embryos were removed from mature grains using clean scalpels. Seven mature wheat grains from each line, which were pooled and harvested from five plants, were used for protein extraction. Endosperms were manually milled into a fine powder using a mortar and pestle. Total endosperm proteins were extracted from an equivalent pool of flour per line in a proportion of 600 μL of lysis buffer (7 M urea, 2 M thiourea, 4% 3-[(3-cholamidopropyl)-dimethylammonio]-1-propanesulfonate (CHAPS; Sigma-Aldrich, Madrid, Spain), 1% dithiothreitol (DTT; Sigma-Aldrich), and 1% protease inhibitor cocktail set VI (Calbiochem, Madrid, Spain) per each 20 mg of flour. About 20–30 mg of pooled flour per wheat line was used for independent protein extraction.

To this end, samples were homogenized in lysis buffer and sonicated using an ultrasonic homogenizer (Sonopuls HD2070, Bandelin Electronic, Berlin, Germany) three times during 20 s, leaving the samples for 1 min on ice between sonication intervals and then incubated for 30 min in an orbital rotator at 4 °C. Subsequently, the samples were clarified to remove insolubilized debris by centrifugation at 13000 rpm for 20 min, and the supernatant was recovered and used for analysis. Protein concentrations were determined with the Bradford assay (Sigma-Aldrich) using BSA as standard and according to the manufacturer's instructions for microplate procedure.

Two-Dimensional Gel Electrophoresis (2-DE) and Image Analysis. Three replicates per line were used for 2-DE analysis. For the first dimension, proteins were isoelectrofocused in IPG strips of 7 cm, 3–10 nonlinear pH gradient (Bio-Rad, Madrid, Spain). Immobilized pH gradient (IPG) strips were rehydrated in a total volume of 125 μL containing 100 μg of protein and rehydratation buffer (7 M urea, 2 M thiourea, 4% CHAPS, 20 mM DTT, 0.5% Triton X-100, 0.5 Bio-Lyte ampholytes pH 3–10 (Bio-Rad, Madrid, Spain)). Three strips per line sample were isoelectrofocused simultaneously in a Protean IEF Cell (Bio-Rad), using the following parameters: (1) linear voltage increment; (2) active rehydration at 50 V for 12 h; (3) 250 V for 15 min; (4) rapid ramp to 4000 V h; (5) slow ramp of voltage to 10000 V h; and (6) a final hold step at 500 V. After isoelectrofocusing, the IPG strips were equilibrated for 10 min in 2.5 mL of equilibration buffer I (50 mM Tris-HCl, pH 8.8, 6 M urea, 2% sodium dodecyl sulfate (SDS), 30% glycerol, and 2% (w/v) DTT), followed by 10 min in 2.5 mL of equilibration buffer II (50 mM Tris-HCl, pH 8.8, 6 M urea, 2% SDS, 30% glycerol, and 2.5% (w/v) iodoacetamide (Sigma-Aldrich)). The second dimension separation was performed on 12% SDS–polyacrylamide gels using Mini-PROTEAN 3 Dodeca Cell (Bio-Rad) that allowed running 12 gels under identical conditions. After electrophoresis, gels were rinsed briefly in mQ water and stained with Coomassie Brilliant Blue G-250 (Merck-Millipore, Madrid, Spain).[22] Gels were incubated for 20 h in Coomassie Blue G-250 working solution (8% ammonium sulfate, 2% phosphoric acid, 1% Coomassie Blue G-250, 20% methanol). Then, gels were washed for 1–3 min with 0.1 M Tris–phosphate, pH 6.5, briefly rinsed (<1 min) with 25% methanol, and finally washed overnight with 20% ammonium sulfate. Stained gels were rinsed in water and scanned in a GS800 calibrated densitometer (Bio-Rad). Gel images were analyzed with PDQuest version 7.2 software (Bio-Rad Discovery Series). All gels were analyzed all at once for analysis interlines. Spots were matched simultaneously among all gels from all analyzed lines, which allowed us to compare the same spot/protein among different lines.

Intensity levels of the spots were normalized by expressing the intensity of each protein spot in a 2-DE gel as a proportion of the total protein intensity detected for the entire gel. Spots detected by the software were matched among all gels. All data were manually reviewed for any discrepancies, and only reproducible spots were maintained in the final analysis. The normalized volume of each spot was calculated for each gel and used to calculate the differences in protein expression between lines. Both qualitative and quantitative changes were determined. For quantitative changes a minimum fold-change of 2 was set. For each of the comparisons analyzed, spot intensities were statistically analyzed among three replicate gels using a Student t test, and only significant data ($p < 0.05$) were considered as quantitative changes. Spots identified as qualitative (presence/absence) or quantitative (changes in intensity) changes were selected for identification by MALDI-TOF/TOF mass spectrometry. A heatmap was generated to compile and display the differential expression of the peptides using MeV-multiexperiment viewer software (http://www.tm4.org/mev.html).

Protein Identification by MALDI-TOF/TOF Mass Spectrometry. Spots were automatically excised in a ProPic station (Genomic Solutions, Bath, UK) and digested with modified porcine trypsin (sequencing grade; Promega, Madrid, Spain), by using a ProGest digestion station (Genomic Solutions). Gel pieces were distained twice for 30 min at 37 °C with 200 mM ammonium bicarbonate in 40% acetonitrile (ACN) and subsequently subjected to three consecutive dehydration/rehydration cycles with pure ACN and 25 mM ammonium bicarbonate in 50% ACN, respectively. Finally, gel pieces were dehydrated for 5 min with pure ACN and dried over 4 h at room temperature. Then, 20 μL of trypsin (12.5 ng/μL in 25 mM ammonium bicarbonate) was added to dried gel pieces and digestion proceeded at 37 °C for 12 h. Peptides were extracted from gel plugs by adding 1 μL of 10% (v/v) trichloroacetic acid (TCA) and incubating for 15 min. Then, they were desalted and concentrated by using μC-18 ZipTip columns (Millipore, Madrid, Spain) in a ProMS station (Genomic Solutions) and directly loaded onto the MALDI plate using α-cyanohydroxycinnamic acid as the matrix. Mass analysis of peptides of each sample was performed with a 4800 MALDI-TOF/TOF Analyzer (Applied Biosystems, Madrid, Spain) in automatic mode with the following settings: for the MS data, m/z range from 800 to 4000 with an accelerating voltage of 20 kV and delayed extraction, peak density of maximum 50 peaks per 200 Da, minimal S/N ratio of 10, and maximum peak at 65. Spectra were internally calibrated with peptides from trypsin autolysis ($M + H^+ = 842.509$, $M + H^+ = 2211.104$). For the MS/MS data, fragment selection criteria were a

DOI: 10.1021/jf5055672
J. Agric. Food Chem. 2015, 63, 3793–3802

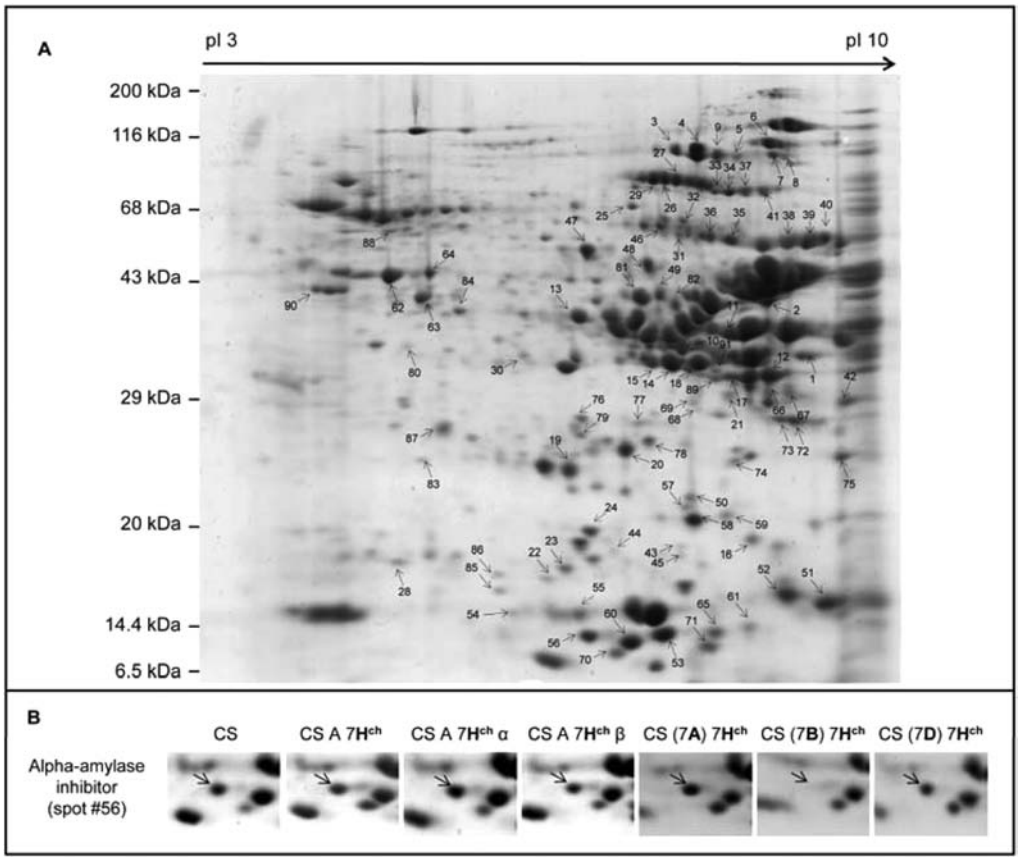

Figure 1. (A) Proteome map of wheat grains displaying all of the proteins that were found to be differentially expressed among wheat lines. (B) Example of a qualitative change among lines.

minimum S/N ratio of 5, a maximum number of peaks set at 65, and peak density of maximum 50 peaks per 200 Da. For each precursor selected for MS/MS analysis, fragment mass values in the range from 60 to 10 Da below precursor mass were used for peptide identification. Protein identification was assigned by peptide mass fingerprinting and confirmed by MS/MS analysis of at least three peptides in each sample. The Mascot 1.9 search engine (Matrixscience, London, UK) was used for protein identification running on GPS software (Applied Biosystems) against the Uniprot Viridiplantae database updated January 2013 (1,351,179 sequences; 457,681,928 residues). The search setting allowed one missed cleavage with the selected trypsin enzyme, a MS/MS fragment tolerance of 0.2 Da, and a precursor mass tolerance of 100 ppm. The 2D-PAGE analysis was carried out in the Servicio de Proteómica (SCAI, member of ProteoRed network, Universidad de Córdoba, Spain).

RESULTS

Identification of Differentially Expressed Proteins in *H. chilense* Chromosome 7 Addition and Substitution Lines in Bread Wheat. A 2-DE-PAGE comparative proteomics analysis was carried out to assess the effect of the addition of *H. chilense* chromosome pair 7$\mathbf{H}^{ch}$ or its 7$\mathbf{H}^{ch}\alpha$ or 7$\mathbf{H}^{ch}\beta$ chromosome arms and the selective substitutions of wheat chromosomes 7**A**, 7**B**, or 7**D** by chromosome 7$\mathbf{H}^{ch}$ from *H. chilense* on the proteome of wheat endosperm. Protein extracts of three biological replicates for each introgression line were run in separate gels and stained with Coomassie Brilliant Blue G-250. The gels were scanned and then analyzed to compare the proteomic profile of the seed endosperm of the different chromosome 7$\mathbf{H}^{ch}$ introgression lines. An example of the 2-DE gels is shown in Figure 1A.

A total of 319 spots were matched across all 2-DE gels and used for comparative analysis among wheat lines (data not shown). The differential protein expression levels were obtained by the comparisons between (1) each chromosome 7$\mathbf{H}^{ch}$ addition or substitution lines versus CS; (2) the addition of the whole chromosome 7$\mathbf{H}^{ch}$ versus the addition of only the 7$\mathbf{H}^{ch}\alpha$ or the 7$\mathbf{H}^{ch}\beta$ addition lines; and (3) among the different (7**A**)7$\mathbf{H}^{ch}$, (7**B**)7$\mathbf{H}^{ch}$, and (7**D**)7$\mathbf{H}^{ch}$ substitution lines ($p < 0.05$ and a minimum fold change of 2). Thus, a total of 91 spots were differentially expressed; 89 of them showed quantitative differences in expression between lines (Figure 1A; Table 2), and spots 90 and 91 uniquely presented qualitative differences, meaning that these peptides were present only in some of the lines but not in others (Figure 1B; Table 3; Supporting Information Supplementary Table 2). Only three spots showed both quantitative and qualitative differences (spots 56, 65, and 75; Table 3). The analysis of the differentially expressed spots was carried out by MALDI-TOF/TOF mass spectrometry and led to the identification of 91 proteins (Supplementary Tables 1 and 2). These proteins have been classified in 13 groups on the basis of their annotation: low molecular weight (LMW) glutenins, high molecular weight (HMW) glutenins, (α-, β-, γ-, and ω-) gliadins, avenin-like proteins, globulins, triticins, puroindolines, α-amylase/protease inhibitors, serpins, xylanase inhibitors, pathogenesis-related proteins (PRs), allergens and putative allergens, and other proteins (Figure 2).

Fifty-six percent of the differentially expressed spots belonged to the storage proteins category, which included the glutenins, gliadins, avenin-like proteins, globulins, and triticins. The most numerous changes were recorded in the globulin

DOI: 10.1021/jf5055672
J. Agric. Food Chem. 2015, 63, 3793−3802

Table 2. Summary of the Number of Qualitative and Quantitative Differences in the Abundance of the Peptides Identified in the 2DE Analysis[a]

	differences between addition lines and CS			differences between substitution lines and CS			differences among addition lines			differences among substitution lines		
	CSA7H^{ch} vs CS	CSA7H$^{ch}\alpha$ vs CS	CSA7H$^{ch}\beta$ vs CS	CS(7A)7H^{ch} vs CS	CS(7B)7H^{ch} vs CS	CS(7D)7H^{ch} vs CS	CSA7H$^{ch}\alpha$ vs CSA7H^{ch}	CSA7H$^{ch}\beta$ vs CSA7H^{ch}	CSA7H$^{ch}\beta$ vs CSA7H$^{ch}\alpha$	CS(7B)7H^{ch} vs CS(7A)7H^{ch}	CS(7D)7H^{ch} vs CS(7A)7H^{ch}	CS(7D)7H^{ch} vs CS(7B)7H^{ch}
quantitative changes	42↑ 0↓	26↑ 0↓	19↑ 4↓	28↑ 3↓	9↑ 7↓	7↑ 11↓	6↑ 16↓	5↑ 24↓	2↑ 8↓	1↑ 16↓	3↑ 31↓	5↑ 19↓
qualitative changes	0–0	0–0	0–0	0–0	0–2	0–3	0–0	0–0	0- 0	0–2	0–3	2–3
total changes	42	26	23	31	18	21	22	29	10	19	37	29

[a]The arrows indicate increase or decrease in expression levels. For the qualitative changes the first figure indicates the number of proteins found in A but not in B, and the second figure after the hyphen indicates the number of proteins found in B but not in A.

family, followed by the α-amylase/protease inhibitors, the (putative) allergens, and the HMW glutenins. The puroindolines and the LMW glutenins were the least affected proteins because only two spots corresponded to each of these categories (Figure 2).

Qualitative Changes in Protein Expression in *H. chilense* Chromosome 7 Addition and Substitution Lines in Bread Wheat. Only five spots appeared or disappeared when the 2-DE gels of the different chromosome 7**H**^{ch} substitution and addition lines were compared (Table 3). Chymotrypsin inhibitor WCI (spot 65), serpins 2 and 4 (spot 90), and avenin-like b6 (spot 91) were expressed only when chromosomes 7**D** was present, and the presence of chromosome 7**H**^{ch} does not compensate for its absence. In the case of spots 56 and 75, which corresponded to an α-amylase/trypsin inhibitor and Barperm1, respectively, their expression seemed to be related to the presence of chromosome 7**B**.

Quantitative Changes in the Wheat Endosperm Protein Expression Due to the Presence of the *H. chilense* Chromosome 7H^{ch}. The identification of the peptides by mass spectrometry allowed the classification of the 89 spots in 13 groups (Figures 2 and 3). A heatmap was generated with the aim of visualizing the differences in the peptide expression between all of the wheat lines analyzed. Rows and columns represented the spots from the gels and the comparisons between lines, respectively (Figure 3). The addition of chromosome 7 of *H. chilense* increased the quantity of most of the proteins, especially globulins, xylanase inhibitors, and several allergens, whereas the addition of only the 7**H**$^{ch}\alpha$ or 7**H**$^{ch}\beta$ arm introduced fewer changes in the proteome as expected (Figure 3; Table 2). As well as for the addition of the complete chromosome, the repression of protein abundance was rare or absent in the ditelosomic addition lines (Figure 3; Table 2). Hence, the disomic and ditelosomic additions and the (7**A**)7**H**^{ch} substitution led to an increase in protein abundance compared to CS, whereas, in contrast, (7**B**)7**H**^{ch} or (7**D**)7**H**^{ch} chromosome substitutions led to a similar number of proteins with increased or reduced expression (Figure 3; Table 2).

Among the 89 spots, 50 belong to the storage protein category including prolamins (glutenins, gliadins), avenin-like proteins, globulins, and triticins. The prolamin fraction scarcely changed between addition or substitution lines compared to CS; indeed, the ditelosomic addition of the 7**H**$^{ch}\alpha$ chromosome arm did not show any significant differences with CS in any of the prolamins. The most important changes in avenin-like proteins were detected when chromosome 7**A** was substituted by 7**H**^{ch}, whereas the (7**B**)7**H**^{ch} chromosome substitution did not alter their expression (Figure 3). In addition, it is worth remarking that the proteins with the highest number of differentially expressed spots were the globulins (28 spots; Figure 3; Supplementary Table 1). The 7**H**^{ch} addition or substitution lines displayed increased globulin content, especially remarkable in the addition lines. Only four spots identified as triticins were differentially expressed among lines. The (7**A**)7**H**^{ch} substitution presented the highest expression of triticins compared to CS, the addition lines and the other (7**B**)7**H**^{ch} or (7**D**)7**H**^{ch} chromosome substitutions (Figure 3; Supplementary Table 1).

Puroindolines, which are biochemical markers of grain softness,[23] were repressed only when chromosome 7**D** was substituted by 7**H**^{ch}, which suggests that the addition of neither chromosome 7**H**^{ch} itself nor the (7**A**)7**H**^{ch} or the (7**B**)7**H**^{ch}

DOI: 10.1021/jf5055672
J. Agric. Food Chem. 2015, 63, 3793−3802

Table 3. Summary of Peptides That Show Qualitative Changes in the Proteomics 2DE Analysis between Wheat Lines[a]

protein identification		comparison between lines					
spot	protein name	CS vs CS(7B) 7H^{ch}	CS vs CS(7D) 7H^{ch}	CS(7A)7H^{ch} vs CS(7D)7H^{ch}	CS(7B)7H^{ch} vs CS(7D)7H^{ch}	CS(7A)7H^{ch} vs CS(7B)7H^{ch}	CS(7D)7H^{ch} vs CS(7B)7H^{ch}
90	serpins 2 and 4		×	×	×		
65	chymotrypsin inhibitor WCI		×	×	×		
91	avenin-like b6		×	×	×		
56	α-amylase/trypsin inhibitor	×				×	×
75	Barperm1	×				×	×

[a]× indicates that the spot is present in the first wheat line of the comparison but not in the second. The identification of the peptides was carried out by MALDI-TOF/TOF mass spectrometry.

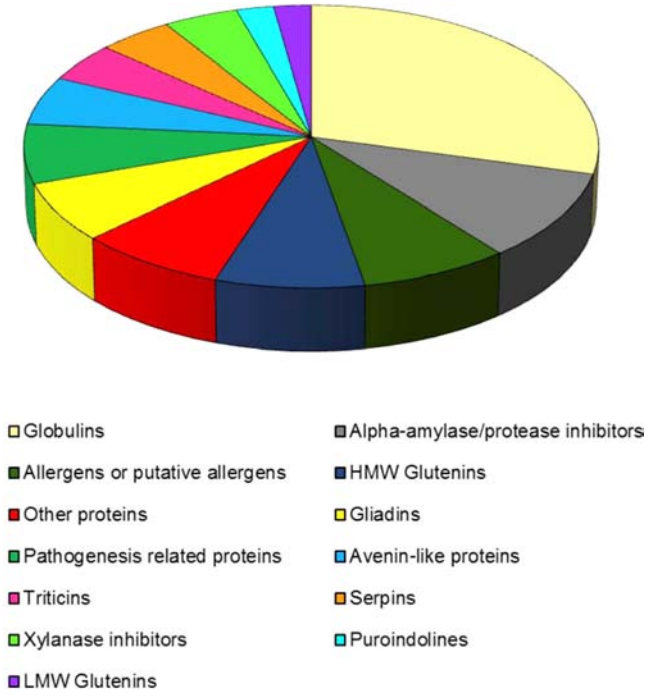

Figure 2. Classification of the proteins that displayed quantitative expression differences between wheat lines by 2-DE-PAGE analysis.

chromosome substitutions affected the abundance of these proteins (Figure 3).

Seventeen spots were classified as protease inhibitors, including α-amylase inhibitors, serpins, and xylanase inhibitors. The addition of chromosome 7H^{ch} induced the accumulation of six α-amylase/protease inhibitors, whereas only three of these types of proteins were enhanced in the ditelosomic addition of 7H^{ch}β and two of them in the 7H^{ch}α ditelosomic addition and the (7A)7H^{ch} chromosome substitution lines. Xylanase inhibitor expression increased in both chromosome 7H^{ch} addition and substitution lines. The (7D)7H^{ch} substitution line did not show any differences in serpin expression (Figure 3; Supplementary Table 1).

Pathogenesis-related proteins (PRs) showed higher expression in chromosome 7H^{ch} addition and in the (7A)7H^{ch} substitution lines. On the contrary, the addition of chromosome arm 7H^{ch}β and the 7B(7H^{ch}) or 7D(7H^{ch}) chromosome substitutions did not affect the quantity of these proteins (Figure 3; Supplementary Table 1).

Related to wheat allergens, the (7D)7H^{ch} substitution line expressed the lowest amount of allergens compared to the other substitution and addition lines for chromosome 7H^{ch} (Figure 3; Supplementary Table 1).

DISCUSSION

Breeding for improving nutrient content in crops is considered a sustainable and cost-effective strategy to address malnutrition in developing countries because it targets staple foods that are daily consumed.[24] Varieties of crops with naturally high content in nutrients can be used in crossbreeding with high-yielding commercial varieties and provide seeds with both desirable features: high yield and increased nutritional value. An example of this strategy could be the introgression of chromosome 7 from the wild barley *H. chilense* into wheat, which leads to an increment in the seed carotenoid concentration.[19]

Apart from the improvement of the nutritional composition, other aspects of flour quality must be considered to obtain wheat lines with commercial potential. Introgression lines from related wild species could produce in wheat unintended proteomic alterations associated with changes in the genome; therefore, the analysis of the proteome of these lines constitutes a helpful tool to decipher the protein composition and the viability of these lines for flour production and, specifically, breadmaking properties.

Although the addition of chromosome 7 from *H. chilense* into wheat is known to increase the seed carotenoid content,[19] none of the proteins identified in this study were related to carotenoid metabolism. This was most likely due to the fact that carotenoid-related proteins are low-abundance or membrane proteins. Consequently, they are rarely detected in 2D gels because large quantities of abundant soluble proteins obscure their detection.[25] Instead, changes in the expression of storage proteins were observed, including prolamins, avenin-like proteins, globulins and triticins, puroindolines, α-amylase/protease inhibitors, serpins, xylanase inhibitors, PRs, allergens, and other proteins (Figure 2).

In wheat, prolamins constitute the major components of the gluten protein fraction, which forms a viscoelastic network and is largely responsible for the ability to process wheat grains.[26] Prolamins comprise 80% of the endosperm protein and consist of the monomeric gliadins (α-, γ-, and ω-) and the polymeric glutenins, including HMW and LMW glutenins.[27] In bread wheat, glutenins and γ- and ω-gliadin genes are located on chromosomes of the homeologous group 1, whereas α- and β-gliadins are located on the short arm of the homeologous group 6.[28] Hence, the low number of changes identified in the prolamin fraction may be explained by the fact that the wheat chromosomes substituted in this study were 7A, 7B, and 7D (Figure 3; Supplementary Table 1) and suggests that the

DOI: 10.1021/jf5055672
J. Agric. Food Chem. 2015, 63, 3793−3802

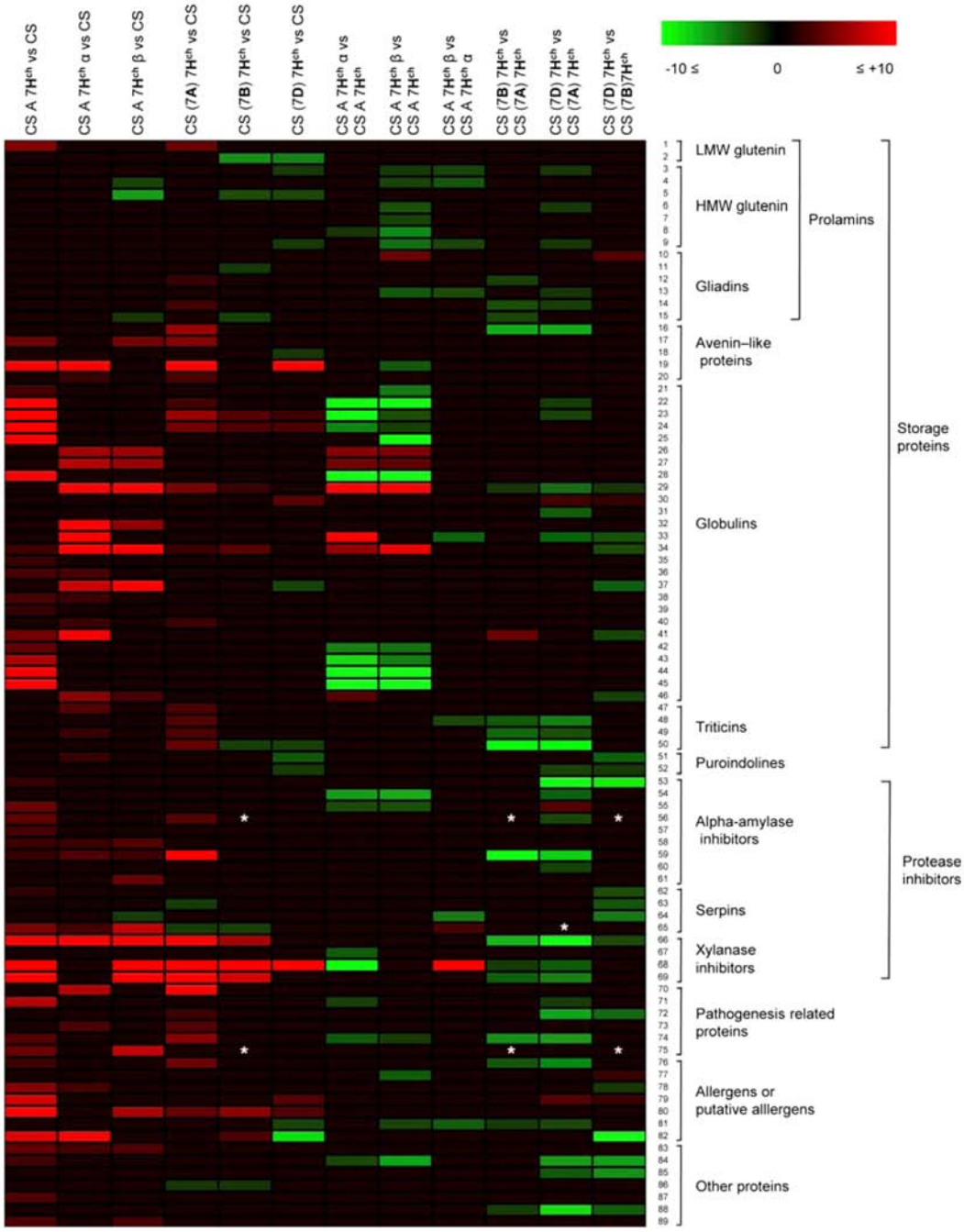

Figure 3. Heatmap depicting the quantitative comparison of the expression of the proteins across several wheat lines. Rows represent the spots from the gels, and the columns are the comparisons between wheat lines. Red, black, and green colors indicate up-regulated, unchanged, and down-regulated peptides, respectively. The asterisks indicate qualitative changes that are described in detail in Table 3 and Supplementary Table 2.

regulation of the synthesis of these proteins is scarcely controlled by genes/proteins located on chromosome 7 (Figure 3; Supplementary Table 1).

Avenin-like proteins are minor storage proteins that are rich in cysteine residues.[29,30] Overexpression of avenin-like b proteins improves dough mixing properties by their incorporation into glutenin polymers.[31] The most important changes in these proteins occurred in the (7**A**)7**H**^{ch} substitution line, which presented higher amounts of four avenin-like proteins. The substitution of 7**B** chromosome did not alter their expression at all, which could indicate that the avenin-like proteins were not located on this chromosome or that they are not regulated by chromosome 7**B** either (Figure 3).

Although globulins represent a small proportion of flour proteins (around 3%), most changes identified in this study were detected in the globulin fraction (Figure 3; Supplementary Table 1), which could be due to the presence of post-translational modifications of the same protein or the identification of monomers,[32,33] which could be the case of the charge trains composed by the spots 26−27 and 38−40 (Figure 1; Supplementary Table 1). As expected the addition of the whole chromosome 7**H**^{ch} was the line in which most of the globulins detected showed higher expression compared to CS

DOI: 10.1021/jf5055672
J. Agric. Food Chem. 2015, 63, 3793−3802

(Figure 3; Supplementary Table 1). Globulins have been demonstrated to be potential food allergens; for this reason the use of wheat lines with an increased content of these proteins (e.g addition lines) is not advisible when wheat is intended for human consumption.[14,34]

Triticin, a minor storage protein of wheat endosperm, is considered to be nutritionally rich due to the presence of lysine-rich decapeptide repeats.[13] Because lysine is the first nutritionally limiting essential amino acid in most cereals, several attempts have been carried out to obtain high-lysine mutants in cereals such as maize; however, in wheat these mutants could not be isolated yet, possibly because of its polyploidy.[13] In the present study, four spots identified as triticins were differentially expressed among lines. Triticins are heterotetramers;[13] therefore, the spots with different mobilities in the 2D gels might be s consequence of the identification of the different monomers. The (7**A**)7**H**^{ch} substitution line presented the highest quantity of triticins compared to CS and to the addition and to the other substitution lines, suggesting that chromosome 7**A** could have a role in the regulation of triticin expression (Figure 3; Supplementary Table 1).

Wheat cultivars with harder grains are best suited for breads, and those that have soft grain are best for cookies, cakes, and pastries.[11] The first biochemical marker of grain softness is fribialin, a mixture of two polypeptides, puroindolines a and b.[23] The hard texture of durum wheat grains is due to s lack of puroindolines and has been associated with the absence of genome **D**. Puroindoline genes are located on the short arm of chromosome 5**D** (*Hardness* locus, *Ha*),[35] but other genetic regions have been associated with kernel hardness, for example, in the long arm of 7**A** chromosome.[11,36] However, in our study, we identified a reduced expression of puroindolines only when chromosome 7**D** was substituted, but the substitution of neither chromosome 7**A** nor 7**B** by chromosome 7**H**^{ch} affected the abundance of these proteins (Figure 2; Supplementary Table 1). Therefore, chromosome 7**D** might be also implicated in puroindoline presence in grain. From the data we have obtained in the current work the concrete causes of the importance of chromosome 7**D** cannot be inferred, but the simplest plausible explanation could be that a transcription factor that regulates the puroindoline expression is encoded in this chromosome and its absence could be the cause for the differences detected. Other likely causes could be that chromosome 7**D** encodes a protein that stabilizes puroindolines. In any case, the reduced expression of puroindolines in substitution 7**H**^{ch} (7**D**) could be potentially used to get varieties with increased grain hardness.

Wheat grain accumulates a wide variety of α-amylase and other protease inhibitors, which have protective roles against insect proteases and abiotic stresses and also act as storage proteins. Interestingly, these proteins have a higher percentage of glutamine and proline and a more balanced amino acid composition than major gluten proteins,[12] which might be exploited for human nutrition. The drawback of these proteins is the fact that they cause IgE-mediated occupational and food allergies.[37−39] Therefore, the increment of these proteins might have a negative impact in bakers' safety and flour processing. The addition of chromosome 7**H**^{ch} induced the accumulation of six α-amylase/protease inhibitors, and two of them were also enhanced in the (7**A**)7**H**^{ch} substitution line (Figure 3; Supplementary Table 1). Although genes encoding for α-amylase inhibitors have been located in 7**B** or 7**D**,[12] the substitution of these chromosomes does not change the expression of most of these proteins, probably due to the complementation with the *H. chilense* chromosome. Interestingly, the absence of spot 56 (α-amylase/trypsin inhibitor CM2) in (7**B**)7**H**^{ch} chromosome substitution line (Figure 1; Supplementary Table 2) would confirm a role of chromosome 7**B** in the expression of this particular protein.

The wheat serine protease inhibitors (serpins) are suicide substrate inhibitors of chymotrypsin and cathepsin A that may function to protect the prolamins from the digestive proteinases of insects.[40,41] The serpins are synthesized by the Srp-A1, Srp-B1, and Srp-D1 genes located in the chromosomes 5**AL**, 5**BL**, and 5**DL** (McIntosh et al., 2013).[42] Spot 90 corresponding to a serpin protein was absent in (7**D**) 7**H**^{ch} lines, which could indicate that it might be encoded or regulated by molecular elements located on the 7**D** chromosome (Table 3).

Xylanases can improve loaf volume and crumb texture by solubilizing wheat cell wall polysaccharides and improving gluten performance. Hence, they are one of the most established baking enzymes, and commercial xylanase preparations are available for the breadmaking industry.[43] However, wheat flour naturally contains xylanase inhibitors that might limit the usefulness of those preparations. Therefore, lines with lower content in xylanase inhibitors could be interesting for breeding. Both addition and substitution lines for chromosome 7**H**^{ch} displayed an increase in xylanase inhibitors, whereas the 7**H**$^{ch}\alpha$ addition and the (7**D**)7**H**^{ch} substitution lines were less affected (Figure 3; Supplementary Table 1). Nevertheless, xylanase inhibitors also play a role in the plant's defense mechanism against pathogens.[44] Therefore, and in contrast to that for the breadmaking industry, lines with higher contents in xylanase inhibitors may be interesting for wheat breeding because they could be used to increase plant resistance to biotic stresses.

The PRs are induced specifically in response to infections by pathogens or by adverse environmental factors.[45] Although increased accumulation of PRs might be considered an advantage for plant defense, their accumulation in food products might have negative consequences in human health, because they may also be plant food allergens.[46,47] PRs showed higher expression in additions and in the (7**A**)7**H**^{ch} substitution lines, whereas, on the contrary, 7**H**^{ch} β arm addition and (7**B**)7**H**^{ch} or (7**D**)7**H**^{ch} substitutions did not affect their expression (Figure 3; Supplementary Table 1). Barperm1 (spot 75) belongs to the PRs family of thaumatin-like proteins, which is known to be differentially expressed in *T. aestivum* developing grains at different stages[48] and involved in seed development in barley.[49]

The abundance of allergens in wheat seeds is involved in hypersensivity reactions that cause food allergies.[14] In the present proteomic analysis of the introgression lines the allegens 1-Cys peroxiredoxin PER1 (spot 79) and glyceraldehyde-3-phosphate dehydrogenase (spot 82),[14,39] were 8-fold more abundant in the 7**H**^{ch} addition than in CS. The (7**D**)7**H**^{ch} substitution line presented minor amounts of glyceraldehyde-3-phosphate dehydrogenase compared to the other lines, which may indicate that this line is a good candidate to reduce the allergenic properties of wheat flour (Figure 3; Supplementary Table 1). Because the number of allergens with known sequences continuously increases, new families of storage and structural proteins and metabolic enzymes are added to the already firmly established protein families that contain allergens (Breiteneder and Radauer, 2004).[50] Therefore, the assessment

DOI: 10.1021/jf5055672
J. Agric. Food Chem. 2015, 63, 3793−3802

of the allergenic properties of the lines is a complex study that would require further analyses.

In summary, the current work showed how the addition or substitution of one particular exogenous chromosome such as chromosome 7$\mathbf{H}^{ch}$ from *H. chilense* can affect the seed endosperm proteomic profile in wheat. The addition of the 7$\mathbf{H}^{ch}\alpha$ arm in wheat was the most promising line for breeding purposes because it did not alter the content of most glutenins and gliadins, and it might therefore maintain, or even improve, dough properties for breadmaking. We also showed that the triticin content was increased in this line compared to CS, and consequently a higher content in lysine (the first nutritionally limiting essential amino acid in most cereals) may be present in seeds. Moreover, the 7$\mathbf{H}^{ch}\alpha$ addition line presented higher quantities of puroindolines, which might improve the plants' resistance to pathogens, and the lower xylanase inhibitor expression may provide more suitable flour for the bakery industry. Finally, it did not present a major increase in the abundance of allergens. Thus, the 7$\mathbf{H}^{ch}\alpha$ addition line seems to be the best option among all other chromosome 7$\mathbf{H}^{ch}$ introgressions to be used in breeding programs to increase the carotenoid content in wheat and not cause negative effects, but positive ones, in the wheat endosperm proteomic profile. On the other hand, the (7**A**)7$\mathbf{H}^{ch}$ substitution displayed enhanced avenin-like b and triticin expression, which may improve dough properties and the nutritional value of flour. Interestingly, (7**D**)7$\mathbf{H}^{ch}$, which showed a reduction in puroindoline proteins, could increase kernel hardness, which may be interesting for the bakery industry. As expected, the addition of the whole chromosome 7$\mathbf{H}^{ch}$ did not display a desirable proteomic profile, at least for human consumption, because there were no important changes that may improve flour quality for breadmaking, but the variation in globulins, α-amylase inhibitors, and other putative allergens could confer negative allergenic features to the wheat flour. The data obtained in this work could provide some indications on how changes in the wheat genome composition by breeding strategies, such as the introgression of related chromosome or chromosome segments, can affect the proteomic profile. This work illustrates the importance of the proteomic characterization of new breeding lines because it provides additional functional information and reveals changes that genomic analysis may not reflect, for example, changes in the expression of proteins that are not codified on the introgressed chromosomes.

■ ASSOCIATED CONTENT

Supporting Information

Supplementary Tables 1, 2, and 3 (proteins identified from the spots with differential expression levels among genotypes; protein score, protein score confidence interval (C. I. %), species, protein molecular weight (M. W), protein isoelectric point (P. I), accession number, peptide count, total ion score, and total ion confidence interval; information for the peptides includes calculated mass, observed mass, peptide start and end, sequences of peptides, ion score, confidence interval, modifications, and rank result type). This material is available free of charge via the Internet at http://pubs.acs.org.

■ AUTHOR INFORMATION

Corresponding Author

*(P.P.) Mail: Instituto de Agricultura Sostenible−CSIC, Av. Menéndez Pidal s/n, Campus Alameda del Obispo, Apdo. 4084, 14080 Córdoba, Spain. E-mail: pilar.prieto@ias.csic.es.

Author Contributions

†Co-first authors.

Funding

This research was supported by Grant ERC-StG-243118 from the FP7 and The European Regional Development Fund (FEDER) from the European Union.

Notes

The authors declare no competing financial interest.

■ ACKNOWLEDGMENTS

We are grateful for the technical assistance of Raquel González and Consuelo Gómez from the Unidad de Proteómica de la Universidad de Córdoba (Spain), a member of the ProteoRed network.

■ ABBREVIATIONS USED

2DE, two-dimensional electrophoresis; 2D-PAGE, two-dimensional polyacrylamide gel electrophoresis; ACN, acetonitrile; BSA, bovine serum albumin; CHAPS, 3-[(3-cholamidopropyl) dimethylammonio]-1-propanesulfonate; CS, *Triticum aestivum* cv. Chinese Spring; DTT, dithiothreitol; HMW, high molecular weight; IPG, immobilized pH gradient; LMW, low molecular weight; MS, mass spectrometry; PRs, pathogenesis related proteins; SDS, sodium dodecyl sulfate; TCA, trichloroacetic acid

■ REFERENCES

(1) Shiferaw, B.; Smale, M.; Braun, H.-J.; Duveiller, E.; Reynolds, M.; Muricho, G. Crops that feed the world 10. Past successes and future challenges to the role played by wheat in global food security. *Food Security* **2013**, *5*, 291−317.

(2) Reynolds, M.; Bonnett, D.; Chapman, S. C.; Furbank, R. T.; Manès, Y.; Mather, D. E.; Parry, M. A. Raising yield potential of wheat. I. Overview of a consortium approach and breeding strategies. *J. Exp. Bot.* **2010**, *62*, 439−452.

(3) Martín, A.; Martín, L. M; Cabrera, A. M; Ramirez, C.; Gimenez, M. J; Rubiales, D; Hernández, P; Ballesteros, J. The potential of *Hordeum chilense* in breeding *Triticeae* species. In *Triticeae III*; Jaradat, A. A., Ed.; Science: Enfield, NH, USA, 1998; pp 377−386.

(4) Zamir, D. Plant breeders go back to nature. *Nat. Genet.* **2008**, *40*, 269−270.

(5) Islam, N.; Woo, S. H.; Tsujimoto, H.; Kawasaki, H.; Hirano, H. Proteome approaches to characterize seed storage proteins related to ditelocentric chromosomes in common wheat (*Triticum aestivum* L.). *Proteomics* **2002**, *2*, 1146−1155.

(6) Islam, N.; Tsujimoto, H.; Hirano, H. Proteome analysis of diploid, tetraploid and hexaploid wheat: towards understanding genome interaction in protein expression. *Proteomics* **2003**, *3*, 549−557.

(7) Dumur, J.; Jahier, J.; Bancel, E.; Laurière, M.; Bernard, M.; Branlard, G. Proteomic analysis of aneuploid lines in the homeologous group 1 of the hexaploid wheat cultivar Courtot. *Proteomics* **2004**, *4*, 2685−2695.

(8) Collado-Romero, M.; Alós, E.; Prieto, P. Unravelling the proteomic profile of rice meiocytes during early meiosis. *Front. Plant Sci.* **2014**, *5*, 356.

(9) Tasleem-Tahir, A.; Nadaud, I.; Girousse, C.; Martre, P.; Marion, D.; Branlard, G. Proteomic analysis of peripheral layers during wheat (*Triticum aestivum* L.) grain development. *Proteomics* **2011**, *11* (3), 371−379.

DOI: 10.1021/jf5055672
J. Agric. Food Chem. 2015, 63, 3793−3802

(10) De Angelis, M.; Minervini, F.; Caputo, L.; Cassone, A.; Coda, R.; Calasso, M. P.; Divella, F.; Gobbetti, M. Proteomic analysis by two-dimensional gel electrophoresis and starch characterization of *Triticum turgidum* L. var. durum cultivars for pasta making. *J. Agric. Food Chem.* **2008**, *56* (18), 8619−8628.
(11) Nadolska-Orczyk, A.; Gasparis, S.; Orczyk, W. The determinants of grain texture in cereals. *J. Appl. Genet.* **2009**, *50* (3), 185−197.
(12) Altenbach, S. B.; Vensel, W. H.; Dupont, F. M. The spectrum of low molecular weight α-amylase/protease inhibitor genes expressed in the US bread wheat cultivar Butte 86. *BMC Res. Notes* **2011**, *4*, 242.
(13) Yadav, D.; Singh, N. K. Wheat triticin: a potential target for nutritional quality improvement. *Asian J. Biotechnol.* **2011**, *3* (1), 1−21.
(14) Larré, C.; Lupi, R.; Gombaud, G.; Brossard, C.; Branlard, G.; Moneret-Vautrin, D. A.; Rogniaux, H.; Denery-Papini, S. Assessment of allergenicity of diploid and hexaploid wheat genotypes: identification of allergens in the albumin/globulin fraction. *J. Proteomics* **2011**, *74*, 1279−1289.
(15) Oliver, R. E.; Cai, X.; Xu, S. S.; Chen, X.; Stack, R. W. Wheat-alien species derivatives: a novel source of resistance to *Fusarium* head blight in wheat. *Crop Sci.* **2005**, *45*, 1353−1360.
(16) Lukaszewski, A. J. Manipulation of the 1RS.1BL Translocation in wheat by induced homoeologous recombination. *Crop Sci.* **2010**, *40*, 216−225.
(17) Calderon, M. D. C.; Ramirez, M. D.; Martin, A.; Prieto, P. Development of *Hordeum chilense* 4Hch introgression lines in durum wheat: a tool for breeders and complex trait analysis. *Plant Breed.* **2012**, *131*, 733−738.
(18) Fedak, G. Intergeneric hybrids with *Hordeum*. In *Barley: Genetics, Biochemistry, Molecular Biology and Biotechnology*; Shewry, P. R., Ed.; CAB. International, Alden Press Ltd.: Oxford, UK, 1992; pp 45−68.
(19) Álvarez, J. B.; Martín, L. M.; Martín, A. Chromosomal localization of genes for carotenoid pigments using addition lines of *Hordeum chilense* in wheat. *Plant Breed.* **1998**, *117*, 287−289.
(20) Rubiales, D.; Reader, S. M.; Martín, A. Chromosomal location of resistance to *Septoria tritici* in *Hordeum chilense* determined by the study of chromosomal addition and substitution lines in Chinese Spring wheat. *Euphytica* **2000**, *115*, 221−224.
(21) Miller, T. E.; Reader, S. M.; Chapman, V. The addition of *Hordeum chilense* chromosomes to wheat. In *Proc. Int. Symp. Eucarpia on Induced Variability in Plant Breeding*; Broertjes, C., Ed.; Pudoc: The Netherlands, 1982; pp 79−81.
(22) Neuhoff, V.; Arold, N.; Taube, D.; Ehrhardt, W. Improved staining of proteins in polyacrylamide gels including isoelectric focusing gels with clear background at nanogram sensitivity using Coomassie Brilliant Blue G-250 and R-250. *Electrophoresis* **1988**, *9*, 255−262.
(23) Morris, C. F. Puroindolines: the molecular genetic basis of wheat grain hardness. *Plant Mol. Biol.* **2002**, *48*, 633−647.
(24) Dwivedi, S. L.; Sahrawat, K. L.; Rai, K. N.; Blair, M. W.; Andersson, M.; Pfieffer, W. Nutritionally enhanced staple food crops. *Plant Breed. Rev.* **2012**, *34*, 169−262.
(25) Chevalier, F. Highlights on the capacities of "gel-based" proteomics. *Proteome Sci.* **2010**, *8*, 23.
(26) Shewry, P. R.; Halford, N. G. Cereal seed storage proteins: structures, properties and role in grain utilization. *J. Exp. Bot.* **2002**, *53* (370), 947−958.
(27) Hurkman, W. J.; Tanaka, C. K. Extraction of wheat endosperm proteins for proteome analysis. *J. Chromatogr., B: Anal. Technol. Biomed. Life Sci.* **2007**, *849*, 344−350.
(28) Payne, P. I. Genetics of wheat storage proteins and the effect of allelic variation on breadmaking quality. *Annu. Rev. Plant Physiol.* **1987**, *38*, 141−153.
(29) Kan, Y.; Wan, Y.; Beaudoin, F.; Leader, D. J.; Edwards, K.; Poole, R.; Wang, D.; Mitchell, R. A. C.; Shewry, P. Transcriptome analysis reveals differentially expressed storage protein transcripts in seeds of *Aegilops* and wheat. *J. Cereal Sci.* **2006**, *44*, 75.
(30) De Caro, S.; Ferranti, P.; Addeo, F.; Mamone, G. Isolation and characterization of avenin-like protein type-B from durum wheat. *J. Cereal Sci.* **2010**, *52*, 426−431.
(31) Ma, F.; Li, M.; Li, T.; Liu, W.; Liu, Y.; Li, Y.; Hu, W.; Zheng, Q.; Wang, Y.; Li, K.; Chang, J.; Chen, M.; Yang, G.; Wang, Y.; He, G. Overexpression of avenin-like b proteins in bread wheat (*Triticum aestivum* L.) improves dough mixing properties by their incorporation into glutenin polymers. *PLoS One* **2013**, *8*, No. 7.
(32) Dupont, F. M.; Vensel, W. H.; Tanaka, C. K.; Hurkman, W. J.; Altenbach, S. B. Deciphering the complexities of the wheat flour proteome using quantitative two-dimensional electrophoresis, three proteases and tandem mass spectrometry. *Proteome Sci.* **2011**, *11*, 10.
(33) Koziol, A. G.; Loit, E.; McNulty, M.; MacFarlane, A. J.; Scott, F. W.; Altosaar, I. Seed storage proteins of the globulin family are cleaved post-translationally in wheat embryos. *BMC Res. Notes* **2012**, *5*, 385.
(34) MacFarlane, A. J.; Burghardt, K. M.; Kelly, J.; Simell, T.; Simell, O.; Altosaar, I.; Scott, F. W. A type 1 diabetes-related protein from wheat (*Triticum aestivum*). cDNA clone of *a wheat storage globulin, Glb1, linked to islet damage*. *J. Biol. Chem.* **2003**, *278* (1), 54−63.
(35) Jolly, C. J.; Rahman, S.; Kortt, A. A.; Higgins, T. J. V. Characterization of the wheat Mr 15000 "grain-softness protein" and analysis of the relationship between its accumulation in the whole seed and grain softness. *Theor. Appl. Genet.* **1993**, *86*, 589−597.
(36) Wilkinson, M.; Wang, Y.; Tosi, P.; Leverington, M.; Snape, J.; Mitchell, R. A. C.; Shewry, P. R. Identification and genetic mapping of variant forms of puroindoline b expressed in developing wheat grain. *J. Cereal Sci.* **2008**, *48*, 722−728.
(37) Kimoto, M.; Suzuki, M.; Komiyama, N.; Kunimoto, A.; Yamashita, H. Isolation and molecular cloning of a major wheat allergen, Tri a Bd 27K. *Biosci., Biotechnol., Biochem.* **2009**, *73*, 85−92.
(38) Hiemori, M.; Yosida, Y.; Kimoto, M.; Yamashita, H.; Takahashi, K.; Komiyama, N.; Tsuji, H. Investigation of multiple forms of Tri a Bd 27K, a major wheat allergen, by immunoblotting analysis. *Biosci., Biotechnol., Biochem.* **2010**, *74*, 199−202.
(39) Sander, I.; Rozynek, P.; Rihs, H. P.; van Kampen, V.; Chew, F. T.; Lee, W. S.; Kotschy-Lang, N.; Merget, R.; Bruning, T.; Raulf-Heimsoth, M. Multiple wheat flour allergens and cross-reactive carbohydrate determinants bind IgE in baker's asthma. *Allergy* **2011**, *66*, 1208−1215.
(40) Østergaard, H.; Rasmussen, S. K.; Roberts, T. H.; Hejgaard, J. Inhibitory serpins from wheat grain with reactive centers resembling glutamine-rich repeats of prolamin storage proteins. Cloning and characterization of five major molecular forms. *J. Biol. Chem.* **2000**, *275*, 33272−33279.
(41) Roberts, T. H.; Marttila, S.; Rasmussen, S. K.; Hejgaard, J. Differential gene expression for suicide-substrate serine proteinase inhibitors (serpins) in vegetative and grain tissues of barley. *J. Exp. Bot.* **2003**, *54*, 2251−2263.
(42) Breiteneder, H. A classification of plant food allergens. *J. Allergy Clin. Immunol.* **2004**, *113*, 821−830.
(43) Butt, M. S.; Tahir-Nadeem, M.; Ahmad, Z.; Sultan, M. T. Xylanases and their applications in baking industry. *Food Technol. Biotechnol.* **2008**, *6* (1), 22−31.
(44) Bellincampi, D.; Camardella, L.; Delcour, J. A.; Desseaux, V.; D'Ovidio, R.; Durand, A.; Elliot, G.; Gebruers, K.; Giovane, A.; Juge, N.; Sørensen, J. F.; Svensson, B.; Vairo, D. Potential physiological role of plant glycosidase inhibitors. *Biochim. Biophys. Acta, Proteins Proteomics* **2004**, *1696*, 265−274.
(45) Breiteneder, H. Thaumatin-like proteins a new family of pollen and fruit allergens. *Allergy* **2004**, *59* (5), 479−481.
(46) Asensio, T.; Crespo, J. F.; Sanchez-Monge, R.; Lopez-Torrejon, G.; Somoza, M. L.; Rodriguez, J.; Salcedo, G. Novel plant pathogenesis-related protein family involved in food allergy. *J. Allergy Clin. Immunol.* **2004**, 114896−114899.
(47) Niskanen, R.; Dris, R. Pathogenesis-related proteins − an important group of plant-derived allergens. *Food, Agric. Environ.* **2004**, *2* (2), 14−24.

DOI: 10.1021/jf5055672
J. Agric. Food Chem. 2015, 63, 3793−3802

(48) Guo, G.; Lv, D.; Yan, X.; Subburaj, S.; Ge, P.; Li, X.; Hu, Y.; Yan, Y. Proteome characterization of developing grains in bread wheat cultivars (*Triticum aestivum* L.). *BMC Plant Biol.* **2012**, *12*, 147.
(49) Muthukrishnan, S.; Liang, G. H.; Trick, H. N.; Gill, B. S. Pathogenesis-related proteins and their genes in cereals. *Plant Cell, Tissue Organ Cult.* **2001**, *64*, 93−114.
(50) McIntosh, R. A.; Yamazaki, Y.; Dubcovsky, J.; Rogers, W. J.; Morris, C.; Appels, R.; Xia, X. C. Catalogue of gene symbols for wheat. **2013** http://www.shigen.nig.ac.jp/wheat/komugi/genes/macgene/2013/GeneSymbol.pdf.10.1071/EC13072.

DOI: 10.1021/jf5055672
J. Agric. Food Chem. 2015, 63, 3793−3802

JOURNAL OF AGRICULTURAL AND FOOD CHEMISTRY

Addition/Correction

pubs.acs.org/JAFC

Correction to Nematicidal Activities of 4-Quinolone Alkaloids Isolated from the Aerial Part of *Triumfetta grandidens* against *Meloidogyne incognita*

Ja Yeong Jang, Quang Le Dang, Yong Ho Choi, Gyung Ja Choi, Kyoung Soo Jang, Byeongjin Cha, Ngoc Hoang Luu, and Jin-Cheol Kim*

J. Agric. Food Chem. **2015**, *63* (1), 68−74. DOI: 10.1021/jf504572h

During the review process of our paper, waltheriones E−L were reported from the roots of *Waltheria indica* in *Journal of Natural Products* **2014**, *77*, 2304−2311.

The use of the same name to describe two different compounds will bring some confusion to the scientific community. Therefore, we want to change the name of our new compound to 5′-methoxywaltherione A as follows: All instances of "waltherione E" in text, figures, and tables, should be changed to 5′-methoxywaltherione A. In addition, p 71, right-hand column, lines 3 and 4, should read "Thus, compound **1** was identified as 5′-methoxywaltherione A (Figure 2)." On p 72, paragraph 4, line 7, "waltherione A and E" should be "waltherione A and 5′-methoxywaltherione A".

Published: April 1, 2015

ACS Publications © 2015 American Chemical Society

DOI: 10.1021/acs.jafc.5b01535
J. Agric. Food Chem. 2015, 63, 3803−3803

JOURNAL OF AGRICULTURAL AND FOOD CHEMISTRY

Addition/Correction

pubs.acs.org/JAFC

Correction to Survey of Polyphenol Constituents in Grapes and Grape-Derived Products

Yanping Xu, James E. Simon, Cara Welch, JoLynne D. Wightman, Mario G. Ferruzzi, Lap Ho, Giulio M. Pasinetti, and Qingli Wu*

J. Agric. Food Chem. **2011**, *59* (19), 10586–10593. DOI: 10.1021/jf202438d

Dr. Giulio M. Pasinetti's name was misspelled in the original publication and is corrected here. In addition, a second affiliation for Dr. Pasinetti should have been included: Geriatric Research and Clinical Center, James J. Peters Veterans Affairs Medical Center, Bronx, New York 10468, United States.

Finally, the following disclosure is made:

This material is the result of work supported in part with resources and the use of facilities at the James J. Peters Veterans Affairs Medical Center, Bronx, NY, USA. In addition, G.M.P. holds a Career Scientist Award in the Research and Development unit and is the Director of the Basic and Biomedical Research and Training Program, GRECC, James J. Peters Veterans Affairs Medical Center. We also acknowledge that the contents of this paper do not represent the views of the U.S. Department of Veterans Affairs or the U.S. government.

Published: April 6, 2015

ACS Publications © 2015 American Chemical Society

DOI: 10.1021/acs.jafc.5b01552
J. Agric. Food Chem. 2015, 63, 3804–3804

livestock and poultry and reducing the exposure of humans to resistant bacteria. A challenging objective is to develop candidates that could be incorporated into natural, safe formulations to reduce both susceptible and resistant pathogens in animal feeds, food-animal environments, and human foods.

With this aim in mind, a critical assessment by Wright,[14] and additional publications mentioned below, describe the potential impact natural products could have on antibiotic drug discovery. There is general agreement that antibiotic discovery is in crisis and that the discovery of new natural-product-based antibiotics that can also combat the problems of resistance is needed urgently. To help stimulate the research needed to achieve these objectives, this review strives to integrate the widely scattered information on the origin, distribution in the food chain, and proposed approaches to inactivate resistant pathogens and the mechanisms of antimicrobial and resistant effects. Work so far, described here, provides a scientific basis, resource, and rationale for future progress designed to mitigate the adverse potential of resistant pathogens in animal feed, human food, and infectious diseases. Although the present review is largely limited to resistant pathogens, related aspects about susceptible organisms will be mentioned for comparison. The availability of novel and safe antibiotics provides more options for the treatment of livestock, poultry, animal feed, and human food and reduces the exposure of humans to resistant bacteria.

OCCURRENCE OF ANTIBIOTIC-RESISTANT BACTERIA IN THE FOOD CHAIN

Antibiotic-resistant bacteria are prevalent in different environments and can therefore be introduced into the food chain at different points. Here we will briefly describe the prevalence of antibiotic-resistant bacteria in the food chain.

Humans and Livestock. When the impact of resistant bacteria on the food chain is considered, an important area for investigation is people coming into contact with livestock and farms who are at risk of infection by antibiotic-resistant bacteria that are present in that environment. For example, a study in Thailand[15] found that, among 544 healthy adult food factory workers, 75% were positive for a particular resistant bacterium of interest, extended-spectrum β-lactamase (ESBL)-producing *E. coli*. The value for 30 healthy animal farm workers was 77.3%. Among the farm animals, the value was 76.7% in pigs and 40% in poultry broilers. The ESBL-producing *E. coli* was more prevalent in fresh meat samples than in fresh vegetables, in fresh than in cooked foods, and in water samples collected from animal farms than in those from canals and fish and shrimp ponds.

A study has also been conducted on the short-term exposure to resistant bacteria of 30 veterinary students on 40 pork farms, in which nasal swabs of the students and pigs were taken before and after the farm visits.[16] The findings of the study include that (a) methicillin-resistant *Staphylococcus aureus* (MRSA) was present in 30% of the pork farms and 22% of the students; (b) all students found to be MRSA-positive were initially negative; and (c) because the duration of MRSA exposure was brief, it most likely represents contamination of the nasal passages rather than biological colonization.[16]

A Japanese study on the prevalence of resistant pathogens from retail meats and food-animal feces found that (a) resistance to *Campylobacter coli* was higher than to *Campylobacter jejuni*; (b) MRSA was isolated from 3% of the meat samples (9 of 300); (c) vancomycin-resistant Enterococci (VRE) were not detected in any of the samples; (d) *S. aureus* isolates showed the highest resistance to ampicillin and tetracycline; and (e) three *C. jejuni* isolates from a hospital patient with diarrhea and two chicken samples that exhibited resistance to ciprofloxacin had identical pulsed-field gel electrophoresis patterns, suggesting that the resistant pathogen could have originated from the chicken meat.[17] This study shows that the prevalence of MRSA and VRE was low in food-producing animals and domestic meats in Japan. It also provides a good example of how and why antimicrobial-resistant pathogens should be monitored regularly to improve the management of the antimicrobial drug resistance associated with their transfer from food-producing animals to humans.

Related studies indicate that (a) resistant *E. coli* can contaminate meat products during slaughter and enter the food chain regardless of whether or not cattle are administered the antimicrobial growth promoter (AGP) chlortetracycline plus sulfmethazine, with most isolates from meat and environmental samples having similar genetic profiles to hides or digesta;[18,19] (b) a probable relationship exists between swine and human salmonellosis across the food chain;[20] and (c) banning the use of growth-promoting antibiotics seemed to result in decreases in the prevalence of some resistant bacteria in food animals.[21]

The method by which antibiotics are administered to humans or animals could potentially affect the levels of resistant bacteria. For example, a study by Zhang et al.[22] found that oral administration of the medicinal antibiotics ampicillin and tetracycline to mice resulted in increased levels (amplification and development) of antibiotic resistance (AR) in the gut microbiota. The effect may be minimized by intraperitoneal (ip) injection of the antibiotics.

Other Animals. A survey by Gorski et al.[23] of cold-blooded vertebrates (frogs, lizards, newts, salamanders, snakes, and toads) and associated surface waters in a produce-growing region of California to determine the diversity of *Salmonella* found that 66 isolates of 460 samples from amphibians and 119 water samples showed resistance, with 27 isolates resistant to more than one antibiotic and 6 isolates to three classes. The authors suggest that these species may serve as reservoirs of antibiotic resistance, determinants in the environment, and sources of contamination of leafy greens associated with produce recalls. Related studies found that fecal samples of birds and mammals may function as host reservoirs and potential vectors for the spread of resistant *E. coli* bacteria[24] and that the feces of stray dogs and coyotes are also a potential reservoir of resistant *E. coli* and *Salmonella* strains.[25] There is, therefore, a need for good agricultural practices to mitigate microbial risks from animal fecal deposits, especially in produce production areas.

Fresh Fruits and Vegetables. A review of the literature suggests that reducing microbial contamination of irrigation water and soil may help prevent and control produce contamination to produce (such as leafy greens and tomatoes).[26] A study by Oliveira et al.[27] on the transfer of *E. coli* O157:H7 from soil fertilized with contaminated compost or irrigated with contaminated water to the edible part (leaves) of lettuce indicates that microbial contamination takes place from both sources and persists for several months.[28] Holvoet et al.[29] reported a moderate prevalence of antimicrobial resistance in *E. coli* isolates from lettuce, irrigation water, and soil.

A survey of 29 commercial herbal supplements showed that tetracycline-resistant bacteria in onion powders and ground

DOI: 10.1021/acs.jafc.5b00778
J. Agric. Food Chem. 2015, 63, 3805−3822

garlic samples and that ginger, goldenseal, mustard, and rosemary contained low levels of resistant bacteria.[30] Related studies report that (a) raw tomatoes are a potential exposure risk for resistant *Enterococcus* spp.;[31] (b) Brazilian ready-to-eat (RTE) salad vegetables contained resistant *Salmonella enterica* isolates;[32] (c) factors other than streptomycin exposure seem to be responsible for resistant bacteria in apple orchards;[33] and (d) the use of fungicides such as fludioxonil for gray mold control in blackberries and strawberries may be a risk for the development of resistant strains in European and North American fields.[34]

Meat and Meat Products. Once livestock has been slaughtered to process into meat and meat products, the problem of antibiotic resistance remains. An Austrian study on the prevalence and genetic characteristics ESBL-producing bacteria, MRSA, and VRE reported the presence of 24 ESBL isolates in 20 of the 100 minced meat samples from a butcher's shop.[35] A Chinese study found that 210 samples collected from a large-scale swine farm contain MDR bacteria that could be transmitted to humans.[36] The large diversity of ESBL-producing *E. coli* may indicate a growing dissemination of ESBL genes in this microorganism from bovine and porcine origins.

A comprehensive review of the literature on the worldwide presence of livestock-associated MRSA indicates that (a) the slaughter process plays a decisive role in MRSA transmission from farm to fork; (b) heat treatment such as flaming and scalding during the slaughter process can significantly reduce the MRSA burden on carcasses; and (c) recontamination with MRSA might occur as a result of fecal contamination at evisceration or by human handling during meat processing.[37] These steps can be improved to minimize the transmission of MRSA from pig to pork.

Poultry Products. Poultry can also be a reservoir for resistant bacteria that can be transmitted to humans. There have therefore been studies conducted on the prevalence and characterization of resistant bacteria in poultry. For example, to assess whether the food chain might contribute to the epidemiology and the transmission of cephalosporin-resistant *E. coli*, Abgottspon et al.[38] used antibiotic susceptibility testing to characterize resistant bacteria isolated from domestic and imported poultry meat. They found that 21 of the 24 isolates were multidrug resistant and that multilocus sequence and phylogenetic group typing indicated a high heterogeneity among different isolates of the same sample.

A German study[39] found that *E. coli* from human stool samples was more resistant than chicken isolates, suggesting that a comparison of ESBL and the multilocus sequence type of the human and poultry isolates are not correlated and that chicken meat is not a major contributor to the colonization of ESBL-carrying Enterobacteriaceae in humans.

The results of a Canadian study[40] on the resistance of 193 *Salmonella* Enteritidis, Hadar, and Typhimurium serovars isolated from broiler production facilities indicated that >43% of the isolates were resistant to multiple antibiotics and that the resistant serovars were genetically diverse, suggesting that the presence of these strains is highly relevant to food safety and public health. A Romanian study found that 23% of 144 chicken carcasses contained MDR *E. coli* and *Salmonella* strains.[41] A Greek study on *E. coli* found in meat from retail stores showed that isolates from chicken had higher levels of resistance to ciprofloxacin (62.5%) than those in lamb/goat isolates,[42] which in turn were higher than those in beef isolates (27.9%).[43] Related studies on the prevalence of resistant pathogens in retail raw poultry in China are described by Yang et al.,[44] in Italy by Giacomelli et al.,[45] in Nigeria by Raufu et al.,[46] in the United Kingdom by McNeece et al.,[47] and in Vietnam by Ta et al.[48]

It is noteworthy that Sapkota et al.[49,50] observed lower levels of resistant bacteria in poultry farms in the United States that transitioned to organic practices without the use of antibiotics. A review of the literature by Smith-Spangler et al.[51] indicates that the risk of isolating bacteria resistant to three or more antibiotics was higher in conventional than in organic chicken or pork (risk difference 33%). By contrast, the study by Mollenkopf et al.[52] on resistant *E. coli* pathogens in organic (antibiotic-free) fresh retail chicken breast does not seem to support this conclusion, suggesting further studies are needed.

Because the consumption of poultry meat is reported to be a major source for foodborne diseases, Adzitey et al.[53] examined the prevalence of resistant *Campylobacter*, *Salmonella*, and *Listeria* isolated from ducks. The mean prevalence for *Campylobacter* is 53% in ducks, 31.6% in duck meat, and 94.4% in the duck-rearing and -processing environment; the lower values recorded for *Salmonella* suggest that ducks were more frequently contaminated with *Campylobacter* than with the other bacteria.

Collectively, the cited studies show that raw and processed poultry products are a major source of resistant pathogens.

Other Food Products. Other studies have been carried out on specific food groups or a range of food groups for comparison. For example, to help define the problem of antibiotic resistance in *E. coli*, the most common Gram-negative pathogen in humans, across a range of food types, Rasheed et al.[54] used the Kirby−Bauer method to determine the antibiotic sensitivity patterns of different foods collected randomly in India. The highest level of resistant bacteria (in %) was found in raw chicken (23.3), followed by vegetable salad (20), raw meat (13.3), raw egg surface (10), and unpasteurized milk (6.7), with an overall incidence of drug-resistant *E. coli* of 14.7. The authors suggest that, because pathogen cycling through food is common, it might pose a potential health risk to the consumer.

The results of a related study from Bangladesh suggested that RTE frozen food contaminated with susceptible and resistant bacteria could be a potential vehicle for transmitting foodborne disease.[55] An evaluation in Poland of the resistant profile of *Staphylococcus* spp. isolated from 858 RTE foods (cheeses, cured meats, sausages, smoked fish, salads) found that 54.9% of the isolates were resistant to at least one class of antibiotics, and, of these, 35.4% of the strains were multidrug resistant, suggesting that RTE food is an important route for the transmission of resistant bacteria.[56]

Fish and shellfish are reported to contain resistant pathogens.[57−60] Duran and Marshall[61] found that 13 commercial brands of RTE shrimp contained high levels of multiple resistant bacteria. The authors suggest that thawing of shrimp products before serving may result in consumer exposure to resistant bacteria and that the worldwide trade of shrimp products may help disseminate resistant pathogens.

Although the incidence of resistant bacteria has been found to be higher in retail meat (69.8%) than in dairy (62.5%) products,[62] many studies that have included dairy products have reported the presence of resistant organisms in retail cheeses, salads, ham, and raw meat,[63] in cow's milk and dairy products,[64] in goat's and sheep's milk,[65] and in Gouda cheese manufactured from raw milk.[66] The cited authors emphasize

DOI: 10.1021/acs.jafc.5b00778
J. Agric. Food Chem. 2015, 63, 3805−3822

the need to use improved hygienic conditions to reduce the prevalence of resistant bacteria in dairy products.

The resistance of egg shell *Salmonella* isolates, especially *Salmonella* Typhimurium, to antimicrobial drugs was shown to be serotype dependent and was greater than observed with *E. coli* isolates, suggesting the need to reduce resistant pathogens in shell eggs and shell egg processing water.[67]

In another study that involved a range of food types, Duffy et al.[68] compared the survival of susceptible and resistant strains of *E. coli* in various food matrices. Orange juice and yogurt were inoculated with antibiotic-sensitive (AS) and laboratory-created antibiotic-resistant mutants (MAR) of *E. coli* O157:H7 or *E. coli* O26, and their growth/survival was monitored at 37 °C or in storage at 4 °C. The strains were also inoculated into minced beef and their *D* values (time in minutes for a 1 log reduction of the bacteria) examined at 55 °C, with and without a prior heat shock at 48 °C. The results show that (a) the growth kinetics in the laboratory were similar for both susceptible and resistant bacteria and (b) *E. coli* O157 MAR died out significantly more quickly in orange juice and yogurt and was more heat-sensitive than the other verocytotoxigenic (VTEC) strains. The authors discuss the possible reasons for the observed difference in survival between resistant and VTEC organisms.

METHODS FOR TESTING BACTERIAL RESISTANCE

Many of the studies cited above required methods for the rapid identification of resistant bacteria. Although not discussed in detail here, the development of assays used to detect atypical and multidrug resistance, especially in ESBL and carbapenemase-expressing Enterobacteriaceae, is of worldwide importance. Reviews by Frickmann et al.[69] and Zboromyrska et al.[70] discuss the advantages of rapid assays based on MALDI-TOF mass spectrometry in combination with PCR/electrospray ionization mass spectrometry or minisequencing. A simple, inexpensive, and easy-to-perform assay to screen antimicrobial compounds from natural products or synthetic chemical libraries for their potential to work in tandem with antibiotics against multiple drug-resistant bacteria is based on measuring zones of inhibition in Petri plates.[71]

COMBATTING ANTIBIOTIC RESISTANCE WITH ALTERNATIVES TO TRADITIONAL MEDICAL ANTIBIOTICS

Because the occurrence of resistant pathogens is still a problem, and yet the rate of development of new antibiotics has declined, Allen et al.[72] suggest the need to discover alternatives to antibiotics used in both animal agriculture and human medicine. Suggested alternatives include modulating the gut microbial community, either through feed additives or fecal transplantation, phage therapy, phage lysins, bacteriocins, endolysins isolated from bacteria, and predatory bacteria as well as the alteration of the rumen population and fermentation with the aid of saponin plant glycosides and new natural antimicrobial compounds.[73,74]

Intervention (mitigation) strategies to reduce the prevalence of pathogens in sanitation facilities and in food animals have been described by Callaway et al.,[75] White et al.,[76] Clardy et al.,[77] Wang et al.,[78] Walsh and Fanning,[79] Fischbach and Walsh,[80] Doyle and Erickson,[81] Doyle et al.,[82] Hur et al.,[83] Oliveira et al.,[84] Capita and Alonso-Calleja,[85] Rutkowski and Brzezinski,[86] Allen et al.,[72] Brown et al.,[74] Gyawali and Ibrahim,[87] Jassim and Limoges,[88] and Linden et al.[89] Because bacteria can, in principle, evolve resistance to any antimicrobial, it is important to use antibiotics and alternatives judiciously[72] and to determine whether proposed new antimicrobials develop resistance in bacteria.

Many types of food and other natural products have been used for medicinal purposes for centuries; indeed, most drug-based antibiotics have been based on or derived from natural products. With the increase in antibiotic resistance, the interest in using the natural products themselves as antibiotics has increased. As an example of such a study, in 2004, we reported on the ability of five selected natural products to inhibit three resistant pathogens.[12] After demonstrating the lack of effectiveness of standard antibiotics against the acquired antibiotic resistance of *B. cereus* (NCTC10989), *E. coli* (NCTC1186), and *S aureus*, we showed that the following natural substances inhibited these three resistant pathogens: cinnamon oil, oregano oil, thyme oil, carvacrol (a major component of oregano and thyme oils), (*S*)-perillaldehyde, 3,4-dihydroxybenzoic (*β*-resorcylic acid), and dopamine (3,4-dihydroxyphenylethylamine).[12]

Exposure of the three pathogens to a dilution series of the test compounds showed that oregano oil was the most active substance. The oils and pure compounds exhibited exceptional activity against *B. cereus* vegetative cells, with oregano oil being active at nanogram per milliliter levels. In contrast, activities against *B. cereus* spores were low. Activities of the test compounds were in the following approximate order: oregano oil > thyme oil > > carvacrol (the main constituent of oregano oil) > cinnamon oil > perillaldehyde > dopamine > *β*-resorcylic acid. The order of susceptibilities of the three pathogens to inactivation was *B. cereus* > *S. aureus* > *E. coli*. The cited results show that all test substances were active, and some were highly active, against the resistant organisms.

In a related study, we found that the above-mentioned substances had bactericidal activity against a resistant non-pathogenic *Micrococcus luteus* strain.[90] Unlike the many standard antibiotics evaluated, all of the compounds were active against this organism. This organism can be used as a model to test the efficacy of potential antimicrobials against resistant bacteria. Other investigators reported that the combination of five molecules (*trans*-cinnamaldehyde, *β*-resorcylic acid, carvacrol, thymol, and eugenol) was more effective than individual compounds in overcoming resistant *Salmonella enterica* to one or more antibiotics, suggesting that the natural compounds could potentially be used as feed supplements to reduce antibiotic resistance in food animals.[91] The papers by Gibbons et al.[92] and Oluwatuyi et al.[93] and the above-cited study seem to have been some of the first reports on the inhibition of resistant pathogens by natural compounds and plant extracts. A discussion of the use of such essential oils is continued in the section below on essential oils and their constituents.

PURE NATURAL COMPOUNDS ISOLATED FOR USE AS ANTIBIOTICS

I will now briefly describe in alphabetical order the resistant effects of pure compounds isolated from natural sources and plant extracts. In some cases, the studies on the plant extracts and their pure compounds are linked, so they are dealt with together.

Baicalein. Baicalein is an active constituent isolated from the root of *Scutellaria baicalensis*. It is a flavonoid that has been used as a Japanese herbal supplement and has been shown to

DOI: 10.1021/acs.jafc.5b00778
J. Agric. Food Chem. 2015, 63, 3805−3822

significantly reverse ciprofloxacin resistance of MRSA.[94] It may also be an SOS response inhibitor of *S. aureus* (see section below on the SOS response as an antibiotic target).[95]

Chlorogenic Acid. The phenolic compound chlorogenic acid is commonly found in many plant materials, including coffee beans, grapes, and tea. The isolated compound was shown to have antibacterial and antibiofilm activities against clinical isolates of *Stenotrophomonas maltophilia*, including a resistant strain.[96] It could therefore be developed as a safe antibiotic alternative or for use in combination.

Other Phenolic Compounds. An evaluation of the structure−activity relationship (SAR) of pure phenolic compounds isolated from several mushroom species using molecular docking studies showed that (a) 2,4-dihydroxybenzoic and protocatechuic acids inhibited MRSA more than methicillin-susceptible *S. aureus*; (b) MRSA was inhibited by 2,4-dihydroxybenzoic, vanillic, and syringic acids at MICs of 0.5 mg/mL and by *p*-coumaric acid at an MIC of 1 mg/mL; and (c) these compounds at the same concentrations did not inhibit methicillin-susceptible *S. aureus*, suggesting that the presence of COOH, two OH groups in the para and ortho positions, and an OCH_3 group in the meta position of the benzene ring seems to govern anti-MRSA activity.[97,98] We previously reported on a similar SAR study of these and related phenolic compounds against four susceptible pathogens.[99]

An evaluation of anti-*Campylobacter* activities by an MIC assay using microdilution coupled with ATP measurement showed that (a) the natural phenolic compounds of plant origin produced significant, but variable, activities against both resistant and susceptible *Campylobacter*; (b) carnosic and rosmarinic acids showed the highest activity in pure forms and in enriched plant extracts; and (c) inactivation of the efflux pump genes in *Campylobacter* mutants significantly increased antimicrobial activity, suggesting that the drug efflux systems contribute to the resistance to the phenolic compounds.[100]

Phenolic compounds have also been tested for their efficacy in treating fungal infections. A quantitative structure−activity relationship (QSAR) of 11 natural phenolic compounds against four fluoconazole-resistant *Candida albicans* species may make it possible to predict the anti-*Candida* activity of new phenolic compounds in the search for antifungal candidates.[101]

***cis*-Cinnamic Acid.** Although both *cis* and *trans* isomers of cinnamic acid can be found in plants, the *trans* form is the more common. The transformation of *trans*-cinnamic acid to the *cis* isomer and isolation of *cis*-cinnamic acid allowed its antibacterial activity to be measured alone and in combination against resistant *Mycobacterium tuberculosis*.[102] Although both isomers were active against the resistant strain, the *cis* isomer showed greater activity, suggesting its potential value to treat tuberculosis.

Ellagitannins and Gallotannin. Ellagitannins, esters of hydrolyzable tannins, hexahydrodiphenoic acids, and monosaccharides, occur in fruits (blackberry, raspberry, strawberry, and pomegranate), nuts (almonds, walnuts), and seeds. A review by Lipińska et al.[103] on bioactive ellagitannins includes a section on reported inhibition of MRSA by ellagitannins from black raspberry.[104] A gallotannin (1,2,3-tri-*O*-galloyl-β-D-glucopyranose) isolated from the *Terminalia chebula* fruit exhibited efflux-pump inhibitory activity against multidrug-resistant uropathogenic *E. coli*.[105] Tannins from fruits and nuts merit further study for their potential to inhibit resistant bacteria.

Enterocin. The enterocins are bacteriocins that can be isolated from *Enterococcus faecium*. A test of the efficacy of the antimicrobial enterocin AS-48 alone and in combination with biocides such as benzalkonium chloride against three susceptible and three resistant *S. aureus* strains showed that (a) inactivation was greater in combination than with individual antimicrobials; (b) inactivation continued during storage; and (c) higher concentrations of antimicrobials were needed to inhibit the formation of biofilms.[106] Because bacteriocins and related peptide antibiotics are active against susceptible pathogens,[74,107] it would be interesting to determine whether or not they also inhibit resistant organisms.

Human Milk Protein−Lipid Complex (HAMLET). Human α-lactalbumin made lethal to tumor cells (HAMLET) is a protein−lipid complex isolated from human milk that has both tumoricidal and bactericidal activities. Sublethal concentrations of HAMLET potentiated the antimicrobial effect of common antibiotics (penicillins, macrolides, and aminoglycosides) against pneumococci.[108] A combination of HAMLET and antibiotics completely eliminated biofilms and colonization in mice of both susceptible and resistant strains of *Acinetobacter baumanii* and *Moraxella catarrhal*, suggesting the presence of a conserved HAMLET-activated pathway that circumvents antibiotic resistance in bacteria.

Pentacyclic Triterpenoids. Three triterpenoids isolated from the bark of the tree *Callicarpa farinosa* inactivated MRSA and methicillin-sensitive *S. aureus* with MIC values ranging from 2 to 512 μg/mL.[109] A genome-wide transcription analysis revealed that the antibiotic effects involved multiple novel cellular targets governing cell division resulting in destabilization of the bacterial cell membrane, suppression of protein synthesis, and inhibition of cell growth that led to cell death. This novel approach to inactivation of resistant bacteria merits further exploration.

Tomatidine. Hydrolytic removal of the tetrasaccharide side chain from the tomato glycoalkaloid α-tomatine results in the formation of the aglycone tomatidine.[110] Although inactive alone, tomatidine specifically enhances the inhibition of MRSA by aminoglycoside antibiotics by blocking the expression of several genes in the resistant bacteria,[111] suggesting that tomatidine is an aminoglycoside potentiator that acts as an antivirulence agent targeting both susceptible and resistant *S. aureus*. It would be of interest to find out whether the aglycones tomatidenol and solanidine derived from the tomato glycoalkaloid dehydrotomatine and potato glycoalkaloids α-chaconine and α-solanine, respectively,[112] would also enhance inhibition of MRSA.

PLANT EXTRACTS AS ANTIMICROBIALS

Essential Oils and Oil Compounds. We published a series of studies on the inactivation in vitro and in food of individual and multiple foodborne pathogens by plant essential oils and some of their bioactive compounds.[9,10,113−121] The following observations indicate that plant essential oils and some of their bioactive compounds are also strong inhibitors of resistant bacteria, reviewed by Yap et al.[7]

An evaluation of the bioactivity of oregano oil, carvacrol, and thymol against methicillin-susceptible and -resistant *Staphylococci* by Nostro et al.[122] showed that all three substances inhibited both types of pathogens to the same extent, with MIC values for carvacrol of 0.015−0.03%. The essential oil from the Korean *Thymus* plant and its components carvacrol and thymol inhibited both susceptible and resistant strains of *Streptococcus*

DOI: 10.1021/acs.jafc.5b00778
J. Agric. Food Chem. 2015, 63, 3805−3822

pneumoniae, *S. aureus*, *Salmonella* Enteritidis, and *Salmonella* Typhimurium with MIC values ranging from 0.125 to 8 mg/mL.[123] Carvacrol and thymol were highly effective in reducing the resistance of microbes, including *Salmonella* and *E. coli*, to several antibiotics; some combinations of the plant and medical antibiotics acted synergistically, suggesting that natural antibiotics can decrease the MIC of a diverse group of drug-resistant bacteria.[124] Subinhibitory concentrations of five natural antimicrobials including carvacrol individually and synergistically increased the susceptibility of resistant *Salmonella* Typhimurium to five medical antibiotics, suggesting the potential value of the natural compounds as feed supplements to reduce the resistance of *Salmonella* in food animals.[91] Carvacrol and cinnamaldehyde rapidly inactivated susceptible and resistant *Campylobacter jejuni* strains, suggesting that the same mechanism probably governs the inactivation of both types of pathogens.[125] These two compounds also inhibited resistant *Campylobacter* on chicken breast[126] and resistant *S. enterica* on celery and oysters,[127] suggesting that these plant antimicrobials have the potential to be used to decontaminate resistant pathogens on seafood, salads, and oysters. Carvacrol, cinnamaldehyde, and eugenol decreased a five-strain mixture of nalidixic acid-resistant *Salmonella* on shell eggs from log 8.0 log CFU/mL to undetectable levels, suggesting that the natural antimicrobials could be used as a wash treatment to reduce *Salmonella* Enteritidis on shell eggs.[128] Our studies also indicate that the antimicrobial efficacy of carvacrol is similar to that of oregano oil with a ~80% carvacrol content, suggesting that the minor components do not seem to contribute to the bioactivity.[9,129]

Tea tree oil (*Melaleuca alternifolia*) was shown to be effective as an adjunctive therapy in treating osteomyelitis and infected chronic wounds in human case studies and small clinical trials.[130] Other studies showed that tea tree oil did not induce bacterial resistance to antimicrobial agents, including carvacrol,[131] and that *Thymus maroccanus* essential oil and its major components carvacrol and thymol modified the susceptibility of resistant bacteria to antibiotics by a membrane-associated mechanism, thereby conferring antibiotic resistance to bacteria.[132] A follow-up study found that the oil can restore antibiotic activities of resistant Gram-negative bacteria by blocking the antibiotic efflux through inhibition of the functional assembly of the efflux pump component.[133]

Extracts of the Brazilian medicinal plant *Lippia origanoides*, containing about 20 compounds including carvacrol and thymol, potentiated the action of neomycin and amikacin against MRSA in vitro, suggesting that the plant could be a source of secondary metabolites for use in antibiotic chemotherapy of MRSA-caused infections.[134] In addition, a Korean study found that essential oils from two *Thymus magnus* plants and their bioactive constituents, carvacrol and thymol, restored the activity of several *Salmonella* and *S. aureus* bacteria to the quinolone antibiotic norfloxacin.[123]

As already mentioned, combinations of extracts or natural products, whether with other natural products or conventional antibiotics, can have a synergistic effect. For example, carvacrol in combination with methyl gallate isolated from *Galla rhois* exhibited enhanced activity against eight nalidixic acid-resistant pathogenic bacteria compared with the activities observed with the individual compounds.[135] These results indicate that carvacrol and methyl gallate alone or in combination have potential use against nalidixic acid-resistant bacteria. It was also reported that carvacrol, cinnamaldehyde, cinnamic acid, and eugenol in combination with antibiotics acted synergistically against 39 pathogenic microorganisms,[136] and cinnamon bark, lavender, and peppermint essential oils evaluated against *E. coli* reduced the resistance to several antibiotics, suggesting the possibility of their use to reverse β-lactam antibiotic resistance and potentially resulting in a reduced use of antibiotics.[137]

Carvacrol and thymol have also been tested against fungal pathogens and were shown to synergistically enhance the efficacy of the antifungal drug fluoconazole against resistant pathogenic *C. albicans* isolates by chemosensitizing the fungal cells to the drug and decreasing its efflux, suggesting their value in therapy for candidiasis.[138]

Essential oil components have also been tested for their use in animal feeds. For example, an in vitro study demonstrated the efficacy of essential oil compounds (carvacrol, thymol, linalool, nerolidol, cinnamaldehyde, eugenol, piperine, and capsaicin) to inhibit susceptible and resistant *Brachyspira intermedia*, the cause of intestinal spirochetosis in hens. Consumption of feed supplemented with coated *trans*-cinnamaldehyde cured the hens of the disease.[139]

Garlic Extracts. An evaluation of an ethanol garlic extract against 15 MDR and 5 non-MDR clinical isolates of *Mycobacterium tuberculosis* showed that the extract inhibited both types of isolates, with MIC values ranging from 1 to 3 mg/mL.[140] The authors suggest that garlic extracts have the potential to prevent/treat MDR tuberculosis.

In another study, an evaluation of the inhibitory activity of a garlic (*Allium sativum*) extract against MDR strains of *Streptococcus mutans* isolated from human carious teeth using disc sensitivity and broth dilution methods showed that (a) of 105 carious teeth tested, 92 (87.6%) isolates of *S. mutans* were recovered; (b) 28 (30.4%) were resistant to four or more antibiotics; and (c) all MDR and non-MDR isolates were susceptible to the garlic extract with MICs ranging from 4 to 32 μg/mL. These results suggest that mouthwashes or toothpaste containing the garlic extract have the potential to prevent human dental caries and possibly also infectious diseases originating from tooth decay.[141]

Organic Herbal Products. An evaluation of resistance in six pathogens from herbal products grown organically and conventionally (garlic, ginger, goldenseal, mustard, onions) revealed the prevalence of low resistance, suggesting that organic farming could contribute to reduced resistance in foodborne bacteria.[30]

It is not immediately apparent why organic food might contain low levels of resistant bacteria. One possible explanation is that, to protect themselves against phytopathogens in the absence of pesticides, organic plants produce greater amounts of bioactive secondary metabolites than do conventionally grown plants.

Honey and Propolis. The commercial honey preparation MEDIHONEY has been approved by the FDA as an antimicrobial to help heal traumatic wounds. MEDIHONEY was shown to inhibit the resistant Gram-negative bacterium *A. baumanii* and also MRSA in vitro with MIC values of 8.5 and 3.5%, respectively,[142] whereas "supermarket honey" induced bacterial and fungal growth. Related studies found that MEDIHONEY in combination with the antibiotic rifamycin acted synergistically against MRSA and clinical isolates of *S. aureus*, suggesting that the combination may be an effective therapy for chronic wound infections.[142,143] The bee product propolis, a resinous mixture, has also been reported to have antimicrobial properties. Indeed, ethanol extracts of the bee

DOI: 10.1021/acs.jafc.5b00778
J. Agric. Food Chem. 2015, 63, 3805−3822

products propolis and honey acted synergistically against resistant *S. aureus* and *E. coli*, as well as against the fungus *C. albicans*, suggesting the need to isolate the active antimicrobial ingredients from propolis and honey.[144] Three possible antimicrobial ingredients have been identified in honey, hydrogen peroxide, methylglyoxal, and the peptide defensin-1, and the low pH of honey may contribute to its activity.[145]

Mushroom Extracts. Purified phenolic compounds derived from mushrooms have been tested for their antibacterial activity against resistant strains. In addition, whole extracts have been used against clinical bacterial strains. For example, an ethyl acetate extract of the culture filtrate and fruiting bodies of the mushroom *Xylaria* showed significant antimicrobial activity against clinical MDR *S. aureus* and *Pseudomonas aeruginosa* strains, with MIC values (in μg/mL) of 225−625 and 120−625, respectively, suggesting that *Xylaria* mushrooms are a potential source of new antimicrobial compounds.[146]

Pepper Extracts. An investigation into edible pepper (*Piper nigrum*) and, in addition, the tropical vine *Telfairia occidentalis* plant extracts showed they were active against 29 pathogenic microorganisms in the absence and presence of the efflux pump inhibitor (EPI) phenylalanine-arginine-β-naphthylamide (PAβN), suggesting that these extracts may help control bacterial infection including MDR phenotypes.[147] Nanoliposomes containing the pepper compound piperine and the antibiotic gentamycin were effective against MRSA, with MIC values of 100 and 32 μg/mL, respectively.[148]

Pomegranate Extracts. Methanolic extracts of the pomegranate (*Punica granatum*) fruit pericarp acted synergistically with the antibiotic ciprofloxacin against resistant strains of *E. coli*, *Klebsiella pneumoniae*, and *P. aeruginosa*, suggesting that the observed synergy against ESBL- and MBL-producing Gram-negative bacteria may help provide an inexpensive alternative therapy against resistant pathogens.[149]

Red Cabbage Extracts. Methanol extracts of red cabbage exhibited antimicrobial activity against MDR bacteria that were resistant to 15 antibiotics as well as against human fungal pathogens.[150] The antimicrobial effects are probably due to the high anthocyanin content. Safe cabbage extracts merit evaluation for efficacy against in vivo infections.

Teas Extracts, Tea Catechins, and Theaflavins. We previously reported that commercial teas and their bioactive constituents, catechin and theaflavin, strongly inhibited susceptible *Bacillus cereus* bacteria and that the antimicrobial activity of a large number of teas correlated with their composition as determined by HPLC.[151] The antimicrobial efficacies of the teas correlated with their flavonoid contents determined by HPLC.[152] Table 2 illustrates the exceptional activity of freshly prepared teas and tea compounds against this pathogen at nanogram levels, suggesting that the mentioned pure black and green tea flavonoids might merit further study for their potential to inhibit resistant pathogens.

Other investigators reported that tea compounds also inhibited resistant bacteria. For example, aqueous extracts of Japanese green tea (*Camellia sinensis*) and the epigallocatechin gallate (ECGC) component inhibited oxacillin β-lactam resistance in MRSA. The tea polyphenolic compounds reduced the MIC values several hundred-fold.[153] These results indicate that teas and their bioactive compounds can inhibit both susceptible and resistant pathogens. Long-term storage of teas seems to degrade some of their bioactive compounds.[154] Yerba mate tea, an infusion made from the leaves of the tree *Ilex paraguariensis*, is a widely consumed nonalcoholic beverage in South America.[155] Burris et al.[156] found that low concentrations of the tea inhibited MSRA in culture and in beef.

Table 2. Bactericidal Activity of Tea Flavonoids Compared to Medicinal Antibiotics against *Bacillus cereus*, Where BA_{50} Equals Percent Concentration That Killed 50% of the Bacteria (Lower Number = Greater Activity[151])

compound	BA_{50} (nmol/well)	relative activities to least active compound, (−)-GC
(−)-gallocatechin-3-gallate	0.43	2307
theaflavin-3,3′-digallate	0.54	1837
(−)-epigallocatechin-3-gallate	0.68	1459
theaflavin-3′-gallate	1.8	551
rifampicin	2.1	472
vancomycin HCl	2.3	431
theaflavin-3-gallate	2.8	354
(−)-catechin-3-gallate	5.5	180
tetracycline HCl	12	83
clindamycin	19	52
(−)-epicatechin-3-gallate	22	45
gentamycin sulfate	75	13
chloramphenicol	180	5.5
theaflavin	283	3.5
(−)-epigallocatechin	800	1.2
(−)-gallocatechin (GC)	992	1.0

OTHER METHODS OF TREATING RESISTANT BACTERIA

It is worth mentioning here some of the other more biological and physical methods for combatting bacterial resistance, techniques that could perhaps be used in combination with some of the strategies described above.

Bacteriophages. Immersion of live oysters contaminated with the virulent multiple-antibiotic-resistant *Vibrio parahemolyticus* bacteria in a bacteriophage-containing bath induced a significant reduction in the growth of the pathogens, suggesting the potential use of the phage to avoid infection from aquaculture to consumption.[157] As noted above, carvacrol and thymol inactivated resistant *S. enterica* on contaminated oysters.[127] Will adding these antimicrobials to oyster-containing water tanks reduce microbial contamination?

Chlorine Disinfection. A chlorine dose of 100 mg/L effectively achieved complete removal of susceptible and resistant pathogens in various sites of two anaerobic swine wastewater systems, one anaerobic and the other aerobic.[158] The authors also report that ammonia present in the system can compete with chlorine to form monochloramine and that aeration helps remove ammonia, thus improving the efficacy of chlorine in overcoming antibiotic pollution. A related study[159] found that inactivation of both susceptible and resistant *Salmonella* Typhimurium in chlorinated water displayed nonlinear kinetics with a concave downward curve (R^2 = 0.964) that fit the power law model, with a shape parameter of 1.37. In addition, the *D* value for a single log reduction from an initial concentration of 5.36 log CFU/mL did not differ among the four resistant groups evaluated and ranged from 3.8 to 4.3 min,[159] suggesting that the resistance phenotype does not impart cross-protection to chlorine inactivation in chilled water.

Thermal Inactivation. An evaluation of the effect of temperature (55−70 °C) on 10 MDR and 10 non-multidrug-

DOI: 10.1021/acs.jafc.5b00778
J. Agric. Food Chem. 2015, 63, 3805−3822

Table 3. Summary of Antiresistant Formulations Described in the Text

pure compound	resistant pathogens inhibited
baicalein	*S. aureus, L. monocytogenes*
aminocoumarins	*S. aureus*
anchovy peptide	*B. cereus, E. coli, Salmonella* Typhi, *S. aureus*
capsaicin	*B. intermedia*
carnosic acid	*Campylobacter* strains, *E. faecalis, S. aureus*
catechins and theaflavins, tea	*L. monocytogenes, S. aureus*
carvacrol	*B. cereus, E. coli, S. aureus, C. albicans*
chlorogenic acid	*Campylobacter* strains, *S. aureus*
cinnamaldehyde	*B. cereus, B. intermedia, E. coli, S. aureus*
citral	*E. coli*
cinnamic acid	*M. tuberculosis*
curcumin	enhanced resistance response in *Salmonella*
dopamine	*B. cereus, E. coli, S. aureus*
ferulic acid	*Campylobacter* strains
gallic acid	*Campylobacter* strains
iberin	*P. aeruginosa*
ellagitannins	*S. aureus*
enterocin	*S. aureus*
gallotannin	*E. coli*
eugenol	*B. cereus, E. coli, S. aureus*
indolecarbinol	Gram-negative bacteria
linalool	*B. intermedia*
methyl gallate	multiple resistant bacteria
milk protein, human	*A. baumanii, Moraxella catarrhalis*
nerolidol	*B. cereus, B. intermedia, E. coli, S. aureus*
piperine	*B. intermedia, S. aureus*
perillaldehyde	*B. cereus, E. coli, S. aureus*
plumbagin	*E. coli*
rosmarinic acid	*Campylobacter* strains
β-resorcylic acid	*B. cereus, E. coli, S. aureus*
sinapinic acid	*Campylobacter* strains
shiknin	*E. coli*
syringic acid	*Campylobacter* strains
tannic acid	*E. coli*
thymol	*B. cereus, B. intermedia, E. coli, S. aureus, C. albicans*
tomatidine	*S. aureus*
triterpenoids	*S. aureus*
vanillic acid	*Campylobacter* strains
plant extracts	
cabbage	multiple MDR bacteria
garlic	*M. tuberculosis*
horseradish	*P. aeruginosa*
mushrooms	*Campylobacter, S. aureus, P. aeruginosa*
Lippia origanoides medicinal plant	*E. coli*
pepper	multiple resistant phenotypes
pomegranate	*E. coli, K. pneumoniae, P. aeruginosa*
Yerba mate tea	*S. aureus*
others	
bacterial quorum sensing	*Salmonella* strains
bacterial SOS response	*E. coli*
bacteriophage	*V. parahemolyticus*
chlorine	multiple pathogens
essential oils	*Campylobacter, E. coli, S. aureus, S. pneumoniae*
heat	*E. coli, Salmonella*
honey, propolis	*A. baumanii, E. coli, S. aureus*
hydrostatic pressure	*E. coli, Salmonella*
pulsed electric fields	*Salmonella*
UV light	*E. coli, Listeria*

resistant (NMDR) *Salmonella* strains isolated from cattle or cattle environments found that NMDR serotypes had a slightly higher heat resistance than MDR serotypes.[160] *Salmonella* Agona and *Salmonella* Anatum serotypes had the highest resistance. The *Salmonella* Agona serotype survived in ground beef patties cooked to an internal temperature of 71 °C. The authors conclude that drug resistance does not seem to affect the heat resistance of *Salmonella* and that serotype or strain is an important consideration in risk assessment of the pathogen's survival at cooking temperatures.

A related study evaluated the inactivation of rifampicin-resistant *E. coli* O157:H7 in pan-broiled or roasted beef at different temperatures.[161] The highest reduction of 5.5 log CFU/g was obtained in samples cooked in the kitchen oven set at 260 °C. The authors suggest that the observed results could facilitate the use of cooking methods to enhance the safety of beef products.

Pulsed Electric Fields (PEF). Repeated rounds of PEF treatment and outgrowth of survivors of *Salmonella enterica* serovar Typhimurium SL1344 resulted in a culture that showed higher resistance to PEF.[162] Additional studies showed that (a) the membranes of the resistant organisms were less susceptible to permeabilization (disruption) than those of the parental strain and (b) resistance to PEF was accompanied by higher tolerance to acidic pH, hydrogen peroxide, and ethanol, but not to heat. The authors suggest the need to study the mechanism of PEF resistance.

UV Disinfection. A Chinese study found that the exposure of resistant bacteria in reclaimed wastewater to UV light resulted in a 4 log CFU reduction of total heterotrophic bacteria. After a standing incubation for 22 h, however, the resistant bacteria mostly reactivated.[163] Related observations indicate that (a) exposure of *E. coli* in wastewater to solar and UV light in the presence of the photocatalyst TiO_2 for 30−60 min inactivated the organisms and that an antibiotic resistant test (Kirby−Bauer) on surviving colonies showed that the photocatalytic process affected the resistance of the strains to the target antibiotics differently;[164] and (b) acid-stressed resistant strains of *Listeria monocytogenes* were more resistant to disinfection in distilled water and a 9% sodium chloride solution by UV light than were unstressed and heat-resistant and heat-shocked strains.[165]

Hydrostatic Pressure. High-pressure processing of green onions inoculated with resistant *Salmonella* and *E. coli* O157:H7 to an average of 5−6 log CFU/g reduced the bacteria by 0.6−5 log CFU/g, depending on the pressure level and sample wetness state.[166] Because the pressure treatment had a minimal adverse effect on most sensory properties and color, it seems that hydrostatic pressure offers an approach to reduce the risk of consumption of contaminated onions. The application of pressure to inactivate resistant pathogens merits further study.[167]

Table 3 summarizes this section, showing the antimicrobial formulations and the respective resistant pathogens inhibited.

Bacterial Resistance Mechanisms. In their review on bacterial multidrug efflux pumps that govern the resistance of bacterial pathogens, Sun et al.[168] note that MDR refers to the capability of bacterial pathogens to withstand lethal doses of

DOI: 10.1021/acs.jafc.5b00778
J. Agric. Food Chem. 2015, 63, 3805−3822

drugs that are capable of eradicating nonresistant strains and that among the four general mechanisms that cause resistance (target alteration, drug inactivation, decreased permeability, and increased efflux), drug extrusion serves as an important mechanism of MDR. An understanding of the mechanism of extrusion is therefore of importance for the development of antiresistant interventions.[169,170] We will now briefly summarize some of the reported mechanisms that may govern resistant activities of several natural antimicrobials.

A study of the resistance mechanisms of phenolic compounds [(−)-epigallocatechin gallate and carnosic, chlorogenic, ferulic, gallic, rosmarinic, sinapinic, syringic, and vanillic acids] in resistant *Campylobacter* strains in the absence and presence of EPIs showed that (a) inactivation of the *cmeB* efflux gene rendered the bacteria more susceptible to the phenolic compounds; (b) mutations of the *cmeF* efflux and *cmeR* transcriptional repressor genes produced a moderate effect on the MICs; and (c) efflux pump inhibitors significantly reduced the MICs of the antimicrobials, suggesting that the antiresistant compounds can be developed for use in live poultry or processed meat to reduce transmission of the pathogens to humans.[171]

Three pure plant compounds (plumbagin from *Plumbago indica*, nordihydroguaretic acid from creosote bush, and shikonin from *Lithspermum erythrorhizon*) were able to inhibit substrate efflux from resistant pathogenic *E. coli* cells that is mediated by the multidrug efflux pump AcrB, suggesting that the gene docking used to predict the bioactivity could be used to preselect compounds with potential EPI activity.[172,173]

A study with indole-3-carbinol, a natural compound found in the edible plant family Cruciferae, found that the antimicrobial activity against Gram-negative bacteria was influenced more by the barrier action of the outer cell membrane lipopolysaccharide than by the action of efflux pumps. It was also found that the compound acted synergistically with ampicillin against drug-resistant isolates, possibly by the facilitated entry of the carbinol after the partial disruption of the cell wall by the antibiotic.[174]

The activity of the natural compound carnosic acid on the uptake/efflux of ethidium bromide is correlated with its ability to change the membrane potential gradient in *S. aureus* and *E. faecalis*, suggesting that the acid can function as an efflux pump modulator that can be used in combination therapies against resistant Enterococci and *S. aureus*.[175]

A study of the ability of the essential oil of *Thymus riartarum* to block efflux pump systems of six resistant Gram-negative bacteria showed that (a) the antimicrobial activity of the oil was significantly enhanced by the efflux pump inhibitor PAβN and (b) the oils also enhanced the susceptibility of resistant isolates to the antibiotic chloramphenicol, suggesting that it could be a candidate for a new drug that can restore the antimicrobial activity of antibiotics by chemosensitive and membranotropic effects.[176]

Collectively, the cited studies indicate that natural, food-compatible compounds have the potential to help overcome the resistance of antibiotics, an approach that merits further investigation.

STRATEGIES FOR COMBATTING BACTERIAL RESISTANCE

Conventional antibacterial actions can generally be divided into four mechanisms, three of which involve the inhibition or regulation of enzymes involved in cell wall biosynthesis, nucleic acid metabolism and repair, or protein synthesis, and the fourth involves the disruption of membrane structure. To combat resistance there are, however, some more unusual modes of action that could hinder the evolution of resistance, involving the disruption of bacterial quorum sensing or the bacterial SOS response.

Bacterial Quorum Sensing (QS) Inhibition. Instead of killing the bacteria, interruption of bacterial communication by QS, where individual cells release small signal molecules such *N*-acylhomoserine lactone (AHL), might also benefit microbial food safety.[177] To demonstrate this possibility, the cited authors determined the inhibition of QS in the opportunistic pathogen *Pseudomonas aeruginosa* by the horseradish (*Armoracia rusticana*) compound iberin. Real-time PCR (RT-PCR) and DNA microarray studies showed that iberin blocked the expression of the QS-regulated genes LasIR and RhIIR and downgraded QS-controlled rhamnolipid production in wild-type cultures of the bacterium, suggesting the need for an epidemiological study of the relationship between the ingestion of food known to contain QS inhibitors (such as cabbage, garlic, and horseradish) and the incidence/severity of bacterial infections.

In a related study, *trans*-cinnamaldehyde and tannic and salicylic acids strongly inhibited AHL synthase in *E. coli*,[178] suggesting that the inhibition of the enzyme by natural products may facilitate the discovery of novel anti-infectives based on anti-QS mechanisms. The results of another study demonstrated that cinnamon bark or lavender essential oils, acting as apparent QS inhibitors, individually and in combination with the antibiotic piperacillin, reduced bioluminescence expression in resistant *E. coli*, suggesting that the oils have the potential to reverse resistance to piperacillin in the bacteria via two mechanisms, alteration of the outer membrane permeability and inhibition of bacterial QS as a novel approach to reverse resistance.[179,180] A review by Koh et al.[181] discusses the use of autoinducers such as AHL to regulate the formation and release of virulence factors, biofilm formation, antibiotic production, the potential of numerous plant-derived products to inhibit QS, and the need to explore the synergistic effects of anti-QS antagonists and antibiotics and concludes that anti-QS is as important as antibacterial activity as it is not likely to cause resistance because it does not pose selection pressure.

Bacterial SOS Response Inhibition. Exposure of bacteria to stress (heat, pH, UV light, disinfectants, antimicrobials) may induce a so-called SOS response that facilitates their survival and that may result in the induction of genetic diversity, formation of reactive oxygen species (ROS), formation of biofilms, and stress-resistant subpopulations.[182,183]

The biphasic kinetics of heat and antimicrobial destruction of bacteria in a ground beef matrix described by Juneja et al.[184,185] support the possible significance of the SOS response in microbial foods safety. Other studies have also provided support for the importance of the SOS response. For example, aminocoumarins strongly inhibited fluoroquinolone-induced RecA genes and the SOS response (resistance development) in *S. aureus*, suggesting that the combination could be useful in anti-infective therapy.[186−188] In addition, baicalein, a flavone present in *Scutellariae baicalensis radix* (described above),[189] was found to be a potent inhibitor of the expression rifamycin-resistant genes and ROS and ATP levels in *S. aureus*, suggesting that it may be used to prevent mutations induced by antibiotics.[95] By contrast, the food ingredient curcumin

DOI: 10.1021/acs.jafc.5b00778
J. Agric. Food Chem. 2015, 63, 3805−3822

enhanced the ciprofloxacin-induced SOS response in *Salmonella* Typhimurium and *Salmonella* Typhi, thus significantly enhancing *Salmonella* pathogenesis.[190] Whether the SOS response can induce/prevent resistance in different antimicrobials merits further study.

More Conventional Mechanisms of Action. The section on mechanisms of resistance discussed some of the methods by which the compounds overcome the main mechanism of drug extrusion. Here, some of the experimental approaches designed to define the mechanisms that might govern the antimicrobial effects of some of the compounds and extracts described above are briefly mentioned. Most of the methods and mechanisms focused on here involve effects on the bacterial membrane.

Bacterial Membrane Disruption. Exposure of *B. cereus* to carvacrol results in the depletion of the intracellular ATP pool, a change in membrane potential, and an increase in the permeability of the cytoplasmic membrane for protons and potassium ions.[191] The loss of the ion gradient impairs essential metabolic processes in the cell and consequently leads to cell death. We have used the technique of autofluorescence spectra to determine the effect of carvacrol on another pathogen, *E. coli*.[129] The autofluorescence spectra and data showed significant changes at much lower concentrations of carvacrol (0.01 mM) than changes in membrane potential or release of ATP (ATP flux) after disruption of the bacterial cell membrane (1−2 mM), suggesting that autofluorescence detects physiological responses to carvacrol more efficiently than do changes in membrane potential or release of ATP.

We have also used molecular dynamics simulations to study the interactions of green tea catechins and black tea theaflavins with the lipid bilayer of artificial biological membranes.[192−194] The results showed that both catechins and theaflavins have a strong affinity for the lipid bilayer of the cell membranes via hydrogen bonding to the surface, with some able to penetrate underneath the surface. In addition, the molecular structure of the tea compounds influenced their configuration when binding to the bilayer surface, as well as their ability to form hydrogen bonds with the lipid headgroups. These studies help to define structure−function relationships and provide a better understanding of the antimicrobial mechanisms of the tea compounds at the molecular−cellular levels. Computer simulation methods can also be used to predict the antimicrobial and anticarcinogenic properties of natural bioactive compounds.[195−197]

Another study used a Langmuir trough equipped with a computer-controlled microbalance to measure the effect of carvacrol and four other natural antimicrobials on monolayers of model membranes composed of bacterial phospholipids.[198] Surface pressure−area (π−A) and surface potential−area ($\Delta\psi$−A) isotherms were measured to monitor changes in the thermodynamic and physical properties of the lipid monolayers. Carvacrol modified the three lipid monolayer structures by integrating into the monolayer, forming aggregates of antimicrobial−lipid complexes, reducing the packing effectiveness of the lipids, increasing the membrane fluidity, and altering the total dipole moment in the monolayer membrane model.

It has been reported that exposure of *B. cereus* to subinhibitory, nonlethal concentrations of carvacrol resulted in increased resistance of the bacteria to inhibition that was accompanied by a lowering of membrane fluidity associated with changes in their fatty acid and headgroup composition.[199] Similar changes in membrane fatty acid profiles observed by Di Pasqua et al.[200] and by Luz Ida et al.[201] suggest that the mechanism of the antimicrobial effect is associated with an alteration in membrane lipid profiles and damage to the cell envelope.

Some constituents of essential oils including carvacrol were analyzed for their mechanism of action against a range of pathogens using a novel whole-cell biosensor assay. The results suggest that the antimicrobial mechanism of action of carvacrol and related compounds involves damage to cell membranes and disruption to cellular metabolism and energy production.[202] Another set of studies examined the combination of carvacrol and low doses of γ-radiation against *B. cereus*. Various techniques were used to monitor the effects, and it was demonstrated that the combination synergistically inhibited *B. cereus* via disruption of cell membranes, with the combination being more effective than either treatment alone, suggesting that the treatment could be effective in contaminated food.[203,204]

Many other studies have indicated the involvement of membrane disruption in the mechanism of action of some natural products. For example, cinnamaldehyde at MIC induces cell death of *E. coli* and *S. aureus* that results from the lysis of the cell membrane;[205] the antimicrobial activity of a peptide from anchovy (*Engraulis japonicus*) seems to be associated with the disruption of membranes of *B. cereus*, *E. coli*, *Salmonella* Typhi, and *S. aureus*;[206] and an increase in resistance in *E. coli* strains stimulated by *Thymus maroccanus* essential oil was associated with changes in the composition of the microbial membrane, suggesting an adaptation or stimulation of the native resistance to the components of the natural oil.[132] The tea polyphenol (−)-epicatechin gallate (ECG) disrupts the secretion of virulent coagulase and α-toxin by *Staphylococcus aureus*,[207] suggesting action via disruption of the cytoplasmic membrane. Components of pomegranate rind were analyzed to investigate their antibacterial mode of action. The results indicate that the phenolic pomegranate compounds act by impairing the membrane structure of *L. monocytogenes*, suggesting their potential as food preservatives and in the reduction of listeriosis.[208] Bacterial membrane disruptive proteins have been widely reported as promising targets for potential antibacterial therapy, and a greater understanding of the composition and function of the complexes they form could aid antibiotic development.[132,209,210]

DNA Interactions and Other Mechanisms. Many modes of action are not at all well-defined or compounds may have multiple modes of action. For example, in a study on the effects of carvacrol and thymol on bacteria and fungi, it was reported that they induced their antimicrobial activity via a mechanism that involves the production of formaldehyde and its reaction products.[211]

Carvacrol and thymol have also been shown to bind to DNA via H-bonding of the OH group to the guanine N7, cytosine N3, and backbone phosphate group, with binding constants of $K = 1.55 \times 10^3$/M and 2.43×10^3/M, respectively, suggesting that the mechanism of formation of the DNA complexes can serve as a model for drug−DNA interactions.[212] The antibacterial activity of the wine compound resveratrol seems to result from the induction of cellular stress and not from direct membrane perturbation.[213]

The mechanism of action of essential oil components has been shown to be complex, possibly involving different mechanisms depending on the conditions. Indeed, cell death in *E. coli* caused by citral and carvacrol has been reported to be

DOI: 10.1021/acs.jafc.5b00778
J. Agric. Food Chem. 2015, 63, 3805−3822

associated with oxidative DNA damage, suggesting their possible value as alternative antimicrobials.[214]

Free fatty acids have antibacterial properties, and although their main target of action is the cell membrane, their mode of action is diverse, and they are less likely to induce resistance than conventional antibiotics, suggesting their potential for commercial use.[215]

The cited results provide insights into the mechanisms of the molecular interactions between naturally occurring antimicrobial compounds and, in most cases, the phospholipids of the bacterial cell membrane that govern activities. As described, the mechanisms can be complex, however, and are still not yet fully elucidated. Moroever, similar mechanisms might govern membrane disruption of susceptible and resistant pathogens by natural antimicrobials. A better understanding of the mechanisms that govern the antimicrobial activities of natural compounds will help in the design of approaches to inhibit resistant bacteria in different environments. It is largely not known whether the use of many of the natural antimicrobials will result in the development of resistance associated with standard antibiotics.

OUTLOOK AND AREAS FOR FUTURE RESEARCH

Antibiotic resistance often arises from the administration of subtherapeutic levels of antibiotics in animal feeds. Resistant microorganisms may be present in the animal waste, contaminating ground, surface, and irrigation waters and often contaminating fruits, vegetables, and other edible plant tissues. They suffuse throughout the food chain and can enter the human intestinal tract after the produce or the undercooked meat, poultry, and other food products are consumed. There is, therefore, a need to develop new alternatives to standard antibiotics, preferably based on safe, food-compatible plant compounds and extracts that can be effective against both susceptible and resistant bacteria. It is hoped that the present overview of multidisciplinary aspects of antibiotic resistance and its prevention will help meet this need. Largely unanswered questions are whether or not different classes of natural antimicrobials that have been found to be effective against susceptible pathogens will exhibit similar efficacy against resistant bacteria and fungi and whether antimicrobial activities in vitro will be duplicated in vivo after consumption by food-producing animals and by humans.

There are many areas in which further studies could help to address some specific aspects of antiresistance. For example, from a mechanistic point of view, it would be useful to devise strategies to bypass the bacterial membrane barrier comprising influx and efflux mechanisms to restore the activity of antibiotics against resistant bacteria,[216] and determine the relative potencies of structurally different efflux pump inhibitors in resistant pathogens.[175,217]

With regard to the whole food chain, it would be useful to investigate the efficacy of natural antimicrobials as a replacement for antibiotics in animal feed, where antibiotic resistance can arise. As indicated above, there may be differences in the prevalence of resistance between organic and conventional produce. It would be interesting to compare the prevalence of resistant bacteria in various conventional and organic foodstuffs.

The efficacy of many of these compounds is not known in vivo, and safety is paramount. Thus, the bioavailability, metabolism, and safety of antimicrobial compounds in animals and humans remains to be investigated further, and as does whether or not the resistant activities observed in vitro can be duplicated in vivo, especially in humans.

Another area concerning efficacy and safety that would be of interest for investigation is whether resistant formulations can also inhibit endotoxemias associated with human pathogens[218,219] and determining whether or not resistant pathogens release toxins to the same extent as susceptible pathogens.[220]

As discussed in this paper, many of the natural antimicrobials have additive and synergistic effects in combination with medicinal antibiotics, and these synergisitic effects merit further study in vivo. The same applies for their use as food additives. For example, it would be interesting to determine whether or not combinations of resistant food ingredients that act synergistically will be safer and will affect less the color, flavor, and taste of food than the individual compounds.[221] When considering their application as food additives, previous studies have investigated the use of certain natural products to reduce concurrently both resistant pathogens and carcinogenic heterocyclic amines in cooked meat.[119,222,223] Such investigations merit further study. It would be interesting to know if the consumption of compounds elicits a lower risk of infection and cancer in humans.

Some natural products that are inhibitors of bacterial resistance also have other beneficial properties. For example, carvacrol has analgesic, antiarthritic, antiallergic, anticarcinogenic, antidiabetic, cardioprotective, gastroprotective, hepatoprotective, and neuroprotective properties as well.[11] It would therefore be of interest to investigate any additional medicinal properties of the other food-compatible compounds and extracts described here. We are challenged to help solve these problems associated with microbial food safety and human health.

AUTHOR INFORMATION

Corresponding Author

*Phone: (510) 559-5615. E-mail: mendel.friedman@ars.usda.gov.

Notes

The authors declare no competing financial interest.

ACKNOWLEDGMENTS

I thank my colleagues whose names are shown in the cited references for excellent collaboration and Carol E. Levin for facilitating the preparation of the manuscript.

ABBREVIATIONS USED

AGP, antimicrobial growth promoters; AHL, *N*-acylhomoserine lactone; AR, antibiotic resistance; AS, antibiotic-sensitive; CFU, colony-forming units; *D* value, time in minutes to kill 90% of the bacteria or 1 log reduction; EPI, efflux pump inhibitor; ESBL, extended spectrum beta-lactamase; MAR, antibiotic-resistant mutants; MDR, multidrug resistant; MIC, minimum inhibitory concentration; MRSA, methicillin-resistant *Staphylococcus aureus*; NMDR, non-multidrug-resistant; PAβN, phenylalanine-arginine-β-naphthylamide resistant inhibitor; PEF, pulsed electric field; QS, quorum sensing; QSAR, quantitative structure−activity relationship; ROS, reactive oxygen species; RTE, ready-to-eat; VRE, vancomycin-resistant Enterococci; VTE, verocytotoxigenic bacteria

DOI: 10.1021/acs.jafc.5b00778
J. Agric. Food Chem. 2015, 63, 3805−3822

REFERENCES

(1) Chattopadhyay, M. K. Use of antibiotics as feed additives: a burning question. *Front. Microbiol.* **2014**, *5*, article 334 10.3389/fmicb.2014.00334

(2) He, L. Y.; Liu, Y. S.; Su, H. C.; Zhao, J. L.; Liu, S. S.; Chen, J.; Liu, W. R.; Ying, G. G. Dissemination of antibiotic resistance genes in representative broiler feedlots environments: identification of indicator ARGs and correlations with environmental variables. *Environ. Sci. Technol.* **2014**, *48*, 13120−13129.

(3) Udikovic-Kolic, N.; Wichmann, F.; Broderick, N. A.; Handelsman, J. Bloom of resident antibiotic-resistant bacteria in soil following manure fertilization. *Proc. Natl. Acad. Sci. U.S.A.* **2014**, *111*, 15202−15207.

(4) Xue, K. Superbug, an epidemic begins. *Harvard Mag.* **2014** (May−June), 40−49.

(5) Park, A. Man vs. microbe: we're losing the battle against bacteria. Can we win the war? *Time* **2014** (May 19).

(6) Blaser, M. J. *Missing Microbes: How the Overuse of Antibiotics Is Fueling Our Modern Plagues*; Henry Holt: New York, 2014; p 288.

(7) Yap, P. S.; Yiap, B. C.; Ping, H. C.; Lim, S. H. Essential oils, a new horizon in combating bacterial antibiotic resistance. *Open Microbiol. J.* **2014**, *8*, 6−14.

(8) CDC. Antibiotics resistance threats in the United States. http://www.cdc.gov/drugresistance/threat-report-2013/ (Jan 30, 2015).

(9) Friedman, M.; Henika, P. R.; Mandrell, R. E. Bactericidal activities of plant essential oils and some of their isolated constituents against *Campylobacter jejuni*, *Escherichia coli*, *Listeria monocytogenes*, and *Salmonella enterica*. *J. Food Prot.* **2002**, *65*, 1545−1560 http://www.ingentaconnect.com/content/iafp/jfp/2002/00000065/00000010/art00004.

(10) Friedman, M.; Henika, P. R.; Levin, C. E.; Mandrell, R. E. Antibacterial activities of plant essential oils and their components against *Escherichia coli* O157:H7 and *Salmonella enterica* in apple juice. *J. Agric. Food Chem.* **2004**, *52*, 6042−6048.

(11) Friedman, M. Chemistry and multi-beneficial bioactivities of carvacrol (4-isopropyl-2-methylphenol), a component of essential oils produced by aromatic plants and spices. *J. Agric. Food Chem.* **2014**, *62*, 7652−7670.

(12) Friedman, M.; Buick, R.; Elliott, C. T. Antibacterial activities of naturally occurring compounds against antibiotic-resistant *Bacillus cereus* vegetative cells and spores, *Escherichia coli*, and *Staphylococcus aureus*. *J. Food Prot.* **2004**, *67*, 1774−1778 http://www.ingentaconnect.com/content/iafp/jfp/2004/00000067/00000008/art00034.

(13) Friedman, M.; Henika, P. R.; Levin, C. E. Antimicrobial activities of red wine-based formulations containing plant extracts against *Escherichia coli* O157:H7 and *Salmonella enterica* serovar Hadar. *Food Control* **2015**, *50*, 652−658.

(14) Wright, G. D. Something old, something new: revisiting natural products in antibiotic drug discovery. *Can. J. Microbiol.* **2014**, *60*, 147−154.

(15) Boonyasiri, A.; Tangkoskul, T.; Seenama, C.; Saiyarin, J.; Tiengrim, S.; Thamlikitkul, V. Prevalence of antibiotic resistant bacteria in healthy adults, foods, food animals, and the environment in selected areas in Thailand. *Pathog. Global Health* **2014**, *108*, 235−245.

(16) Frana, T. S.; Beahm, A. R.; Hanson, B. M.; Kinyon, J. M.; Layman, L. L.; Karriker, L. A.; Ramirez, A.; Smith, T. C. Isolation and characterization of methicillin-resistant *Staphylococcus aureus* from pork farms and visiting veterinary students. *PLoS One* **2013**, *8*, article e53738 10.1371/journal.pone.0053738

(17) Hiroi, M.; Kawamori, F.; Harada, T.; Sano, Y.; Miwa, N.; Sugiyama, K.; Hara-Kudo, Y.; Masuda, T. Antibiotic resistance in bacterial pathogens from retail raw meats and food-producing animals in Japan. *J. Food Prot.* **2012**, *75*, 1774−1782.

(18) Alexander, T. W.; Inglis, G. D.; Yanke, L. J.; Topp, E.; Read, R. R.; Reuter, T.; McAllister, T. A. Farm-to-fork characterization of *Escherichia coli* associated with feedlot cattle with a known history of antimicrobial use. *Int. J. Food Microbiol.* **2010**, *137*, 40−48.

(19) Fluckey, W. M.; Loneragan, G. H.; Warner, R.; Brashears, M. M. Antimicrobial drug resistance of *Salmonella* and *Escherichia coli* isolates from cattle feces, hides, and carcasses. *J. Food Prot.* **2007**, *70*, 551−556 http://www.ingentaconnect.com/content/iafp/jfp/2007/00000070/00000003/art00003.

(20) Gomes-Neves, E.; Antunes, P.; Manageiro, V.; Gärtner, F.; Caniça, M.; da Costa, J. M. C.; Peixe, L. Clinically relevant multidrug resistant *Salmonella enterica* in swine and meat handlers at the abattoir. *Vet. Microbiol.* **2014**, *168*, 229−233.

(21) Mathew, A. G.; Cissell, R.; Liamthong, S. Antibiotic resistance in bacteria associated with food animals: a United States perspective of livestock production. *Foodborne Pathog. Dis.* **2007**, *4*, 115−133.

(22) Zhang, L.; Huang, Y.; Zhou, Y.; Buckley, T.; Wang, H. H. Antibiotic administration routes significantly influence the levels of antibiotic resistance in gut microbiota. *Antimicrob. Agents Chemother.* **2013**, *57*, 3659−3666.

(23) Gorski, L.; Jay-Russell, M. T.; Liang, A. S.; Walker, S.; Bengson, Y.; Govoni, J.; Mandrell, R. E. Diversity of pulsed-field gel electrophoresis pulsotypes, serovars, and antibiotic resistance among *Salmonella* isolates from wild amphibians and reptiles in the California Central Coast. *Foodborne Pathog. Dis.* **2013**, *10*, 540−548.

(24) Carroll, D.; Wang, J.; Fanning, S.; McMahon, B. J. Antimicrobial resistance in wildlife: implications for public health. *Zoonoses Public Health* **2015**, DOI: 10.1111/zph.12182.

(25) Jay-Russell, M. T.; Hake, A. F.; Bengson, Y.; Thiptara, A.; Nguyen, T. Prevalence and characterization of *Escherichia coli* and *Salmonella* strains isolated from stray dog and coyote feces in a major leafy greens production region at the United States-Mexico border. *PLoS One* **2014**, *9*, article e113433 10.1371/journal.pone.0113433

(26) Park, S.; Szonyi, B.; Gautam, R.; Nightingale, K.; Anciso, J.; Ivanek, R. Risk factors for microbial contamination in fruits and vegetables at the preharvest level: a systematic review. *J. Food Prot.* **2012**, *75*, 2055−2081.

(27) Oliveira, M.; Viñas, I.; Usall, J.; Anguera, M.; Abadias, M. Presence and survival of *Escherichia coli* O157:H7 on lettuce leaves and in soil treated with contaminated compost and irrigation water. *Int. J. Food Microbiol.* **2012**, *156*, 133−140.

(28) Mootian, G.; Wu, W. H.; Matthews, K. R. Transfer of *Escherichia coli* O157:H7 from soil, water, and manure contaminated with low numbers of the pathogen to lettuce plants. *J. Food Prot.* **2009**, *72*, 2308−2312 http://www.ingentaconnect.com/content/iafp/jfp/2009/00000072/00000011/art00010.

(29) Holvoet, K.; Sampers, I.; Callens, B.; Dewulf, J.; Uyttendaele, M. Moderate prevalence of antimicrobial resistance in *Escherichia coli* isolates from lettuce, irrigation water, and soil. *Appl. Environ. Microbiol.* **2013**, *79*, 6677−6683.

(30) Brown, J. C.; Jiang, X. Prevalence of antibiotic-resistant bacteria in herbal products. *J. Food Prot.* **2008**, *71*, 1486−1490 http://www.ingentaconnect.com/content/iafp/jfp/2008/00000071/00000007/art00025.

(31) Micallef, S. A.; Goldstein, R. E.; George, A.; Ewing, L.; Tall, B. D.; Boyer, M. S.; Joseph, S. W.; Sapkota, A. R. Diversity, distribution and antibiotic resistance of *Enterococcus* spp. recovered from tomatoes, leaves, water and soil on U.S. Mid-Atlantic farms. *Food Microbiol.* **2013**, *36*, 465−474.

(32) Taban, B. M.; Aytac, S. A.; Akkoc, N.; Akcelik, M. Characterization of antibiotic resistance in *Salmonella enterica* isolates determined from ready-to-eat (RTE) salad vegetables. *Braz. J. Microbiol.* **2013**, *44*, 385−391.

(33) Yashiro, E.; McManus, P. S., Effect of streptomycin treatment on bacterial community structure in the apple phyllosphere. *PLoS One* **2012**, *7*, article e37131 10.1371/journal.pone.0037131

(34) Li, X.; Fernandez-Ortuno, D.; Grabke, A.; Schnabel, G. Resistance to fludioxonil in *Botrytis cinerea* isolates from blackberry and strawberry. *Phytopathology* **2014**, *104*, 724−732.

(35) Petternel, C.; Galler, H.; Zarfel, G.; Luxner, J.; Haas, D.; Grisold, A. J.; Reinthaler, F. F.; Feierl, G. Isolation and characterization of multidrug-resistant bacteria from minced meat in Austria. *Food Microbiol.* **2014**, *44*, 41−46.

DOI: 10.1021/acs.jafc.5b00778
J. Agric. Food Chem. 2015, 63, 3805−3822

(36) Liu, Z.; Zhang, Z.; Yan, H.; Li, J.; Shi, L. Isolation and molecular characterization of multidrug-resistant *Enterobacteriaceae* strains from pork and environmental samples in Xiamen, China. *J. Food Prot.* **2015**, *78*, 78−88.
(37) Lassok, B.; Tenhagen, B. A. From pig to pork: methicillin-resistant *Staphylococcus aureus* in the pork production chain. *J. Food Prot.* **2013**, *76*, 1095−1108.
(38) Abgottspon, H.; Stephan, R.; Bagutti, C.; Brodmann, P.; Hachler, H.; Zurfluh, K. Characteristics of extended-spectrum cephalosporin-resistant *Escherichia coli* isolated from Swiss and imported poultry meat. *J. Food Prot.* **2014**, *77*, 112−115.
(39) Belmar Campos, C.; Fenner, I.; Wiese, N.; Lensing, C.; Christner, M.; Rohde, H.; Aepfelbacher, M.; Fenner, T.; Hentschke, M. Prevalence and genotypes of extended spectrum beta-lactamases in Enterobacteriaceae isolated from human stool and chicken meat in Hamburg, Germany. *Int. J. Med. Microbiol.* **2014**, *304*, 678−684.
(40) Diarra, M. S.; Delaquis, P.; Rempel, H.; Bach, S.; Harlton, C.; Aslam, M.; Pritchard, J.; Topp, E. Antibiotic resistance and diversity of *Salmonella enterica* serovars associated with broiler chickens. *J. Food Prot.* **2014**, *77*, 40−49.
(41) Dan, S. D.; Tabaran, A.; Mihaiu, L.; Mihaiu, M. Antibiotic susceptibility and prevalence of foodborne pathogens in poultry meat in Romania. *J. Infect. Dev. Countries* **2015**, *9*, 35−41.
(42) Lavilla Lerma, L.; Benomar, N.; Casado Munoz Mdel, C.; Galvez, A.; Abriouel, H. Antibiotic multiresistance analysis of mesophilic and psychrotrophic *Pseudomonas* spp. isolated from goat and lamb slaughterhouse surfaces throughout the meat production process. *Appl. Environ. Microbiol.* **2014**, *80*, 6792−6806.
(43) Gousia, P.; Economou, V.; Sakkas, H.; Leveidiotou, S.; Papadopoulou, C. Antimicrobial resistance of major foodborne pathogens from major meat products. *Foodborne Pathog. Dis.* **2011**, *8*, 27−38.
(44) Yang, B.; Cui, Y.; Shi, C.; Wang, J.; Xia, X.; Xi, M.; Wang, X.; Meng, J.; Alali, W. Q.; Walls, I.; Doyle, M. P. Counts, serotypes, and antimicrobial resistance of *Salmonella* isolates on retail raw poultry in the People's Republic of China. *J. Food Prot.* **2014**, *77*, 894−902.
(45) Giacomelli, M.; Salata, C.; Martini, M.; Montesissa, C.; Piccirillo, A. Antimicrobial resistance of *Campylobacter jejuni* and *Campylobacter coli* from poultry in Italy. *Microb. Drug Resist.* **2014**, *20*, 181−188.
(46) Raufu, I. A.; Fashae, K.; Ameh, J. A.; Ambali, A.; Ogunsola, F. T.; Coker, A. O.; Hendriksen, R. S. Persistence of fluoroquinolone-resistant *Salmonella enterica* serovar Kentucky from poultry and poultry sources in Nigeria. *J. Infect. Dev. Countries* **2014**, *8*, 384−388.
(47) McNeece, G.; Naughton, V.; Woodward, M. J.; Dooley, J. S. G.; Naughton, P. J. Array based detection of antibiotic resistance genes in Gram negative bacteria isolated from retail poultry meat in the UK and Ireland. *Int. J. Food Microbiol.* **2014**, *179*, 24−32.
(48) Ta, Y. T.; Nguyen, T. T.; To, P. B.; Pham da, X.; Le, H. T.; Thi, G. N.; Alali, W. Q.; Walls, I.; Doyle, M. P. Quantification, serovars, and antibiotic resistance of *Salmonella* isolated from retail raw chicken meat in Vietnam. *J. Food Prot.* **2014**, *77*, 57−66.
(49) Sapkota, A. R.; Hulet, R. M.; Zhang, G.; McDermott, P.; Kinney, E. L.; Schwab, K. J.; Joseph, S. W. Lower prevalence of antibiotic-resistant enterococci on U.S. conventional poultry farms that transitioned to organic practices. *Environ. Health Perspect.* **2011**, *119*, 1622−1628.
(50) Sapkota, A. R.; Kinney, E. L.; George, A.; Hulet, R. M.; Cruz-Cano, R.; Schwab, K. J.; Zhang, G.; Joseph, S. W. Lower prevalence of antibiotic-resistant *Salmonella* on large-scale U.S. conventional poultry farms that transitioned to organic practices. *Sci. Total Environ.* **2014**, *476*−*477*, 387−392.
(51) Smith-Spangler, C.; Brandeau, M. L.; Hunter, G. E.; Clay Bavinger, J.; Pearson, M.; Eschbach, P. J.; Sundaram, V.; Liu, H.; Schirmer, P.; Stave, C.; Olkin, I.; Bravata, D. M. Are organic foods safer or healthier than conventional alternatives? A systematic review. *Ann. Intern. Med.* **2012**, *157*, 348−366.
(52) Mollenkopf, D. F.; Cenera, J. K.; Bryant, E. M.; King, C. A.; Kashoma, I.; Kumar, A.; Funk, J. A.; Rajashekara, G.; Wittum, T. E. Organic or antibiotic-free labeling does not impact the recovery of enteric pathogens and antimicrobial-resistant *Escherichia coli* from fresh retail chicken. *Foodborne Pathog. Dis.* **2014**, *11*, 920−929.
(53) Adzitey, F.; Huda, N.; Rahmat Ali, G. R. Prevalence and antibiotic resistance of *Campylobacter*, *Salmonella*, and *L. monocytogenes* in ducks: a review. *Foodborne Pathog. Dis.* **2012**, *9*, 498−505.
(54) Rasheed, M. U.; Thajuddin, N.; Ahamed, P.; Teklemariam, Z.; Jamil, K. Antimicrobial drug resistance in strains of *Escherichia coli* isolated from food sources. *Rev. Inst. Med. Trop. Sao Paulo* **2014**, *56*, 341−346.
(55) Sultana, F.; Kamrunnahar; Afroz, H.; Jahan, A.; Fakruddin, M.; Datta, S. Multi-antibiotic resistant bacteria in frozen food (ready to cook food) of animal origin sold in Dhaka, Bangladesh. *Asian Pac. J. Trop. Biomed.* **2014**, *4*, S268−S271.
(56) Chajęcka-Wierzchowska, W.; Zadernowska, A.; Nalepa, B.; Sierpińska, M.; Łaniewska-Trokenheim, Ł. Retail ready-to-eat food as a potential vehicle for *Staphylococcus* spp. harboring antibiotic resistance genes. *J. Food Prot.* **2014**, *77*, 993−998.
(57) Elhadi, N. Prevalence and antimicrobial resistance of *Salmonella* spp. In raw retail frozen imported freshwater fish to Eastern Province of Saudi Arabia. *Asian Pac. J. Trop. Biomed.* **2014**, *4*, 234−238.
(58) Moore, J. E.; Huang, J.; Yu, P.; Ma, C.; Moore, P. J. A.; Millar, B. C.; Goldsmith, C. E.; Xu, J. High diversity of bacterial pathogens and antibiotic resistance in salmonid fish farm pond water as determined by molecular identification employing 16S rDNA PCR, gene sequencing and total antibiotic susceptibility techniques. *Ecotoxicol. Environ. Saf.* **2014**, *108*, 281−286.
(59) Kang, C. H.; Shin, Y.; Jeon, H.; Choi, J. H.; Jeong, S.; So, J. S. Antibiotic resistance of *Shewanella putrefaciens* isolated from shellfish collected from the West Sea in Korea. *Mar. Pollut. Bull.* **2013**, *76*, 85−88.
(60) Yu, L.; Zhou, Y.; Wang, R.; Lou, J.; Zhang, L.; Li, J.; Bi, Z.; Kan, B. Multiple antibiotic resistance of *Vibrio cholerae* serogroup O139 in China from 1993 to 2009. *PLoS One* **2012**, *7*, article e38633 10.1371/journal.pone.0038633.
(61) Duran, G. M.; Marshall, D. L. Ready-to-eat shrimp as an international vehicle of antibiotic-resistant bacteria. *J. Food Prot.* **2005**, *68*, 2395−2401 http://www.ingentaconnect.com/content/iafp/jfp/2005/00000068/00000011/art00020.
(62) Ahmed, A. M.; Shimamoto, T.; Shimamoto, T. Characterization of integrons and resistance genes in multidrug-resistant *Salmonella enterica* isolated from meat and dairy products in Egypt. *Int. J. Food Microbiol.* **2014**, *189*, 39−44.
(63) Pesavento, G.; Calonico, C.; Ducci, B.; Magnanini, A.; Lo Nostro, A. Prevalence and antibiotic resistance of *Enterococcus* spp. isolated from retail cheese, ready-to-eat salads, ham, and raw meat. *Food Microbiol.* **2014**, *41*, 1−7.
(64) Silveira-Filho, V. M.; Luz, I. S.; Campos, A. P.; Silva, W. M.; Barros, M. P.; Medeiros, E. S.; Freitas, M. F.; Mota, R. A.; Sena, M. J.; Leal-Balbino, T. C. Antibiotic resistance and molecular analysis of *Staphylococcus aureus* isolated from cow's milk and dairy products in northeast Brazil. *J. Food Prot.* **2014**, *77*, 583−591.
(65) Osman, K. M.; Zolnikov, T. R.; Samir, A.; Orabi, A. Prevalence, pathogenic capability, virulence genes, biofilm formation, and antibiotic resistance of *Listeria* in goat and sheep milk confirms need of hygienic milking conditions. *Pathog. Global Health* **2014**, *108*, 21−29.
(66) D'Amico, D. J.; Druart, M. J.; Donnelly, C. W. Comparing the behavior of multidrug-resistant and pansusceptible *Salmonella* during the production and aging of a Gouda cheese manufactured from raw milk. *J. Food Prot.* **2014**, *77*, 903−913.
(67) Musgrove, M. T.; Jones, D. R.; Northcutt, J. K.; Cox, N. A.; Harrison, M. A.; Fedorka-Cray, P. J.; Ladely, S. R. Antimicrobial resistance in *Salmonella* and *Escherichia coli* isolated from commercial shell eggs. *Poult. Sci.* **2006**, *85*, 1665−1669.
(68) Duffy, G.; Walsh, C.; Blair, I. S.; McDowell, D. A. Survival of antibiotic resistant and antibiotic sensitive strains of *E. coli* O157 and *E. coli* O26 in food matrices. *Int. J. Food Microbiol.* **2006**, *109*, 179−186.

DOI: 10.1021/acs.jafc.5b00778
J. Agric. Food Chem. 2015, 63, 3805−3822

(69) Frickmann, H.; Masanta, W. O.; Zautner, A. E. Emerging rapid resistance testing methods for clinical microbiology laboratories and their potential impact on patient management. *BioMed Res. Int.* **2014**, *2014*, article 375681 10.1155/2014/375681
(70) Zboromyrska, Y.; Ferrer-Navarro, M.; Marco, F.; Vila, J. [Detection of antibacterial resistance by MALDI-TOF mass spectrometry]. *Rev. Esp. Quimioter.* **2014**, *27*, 87−92 http://seq.es/seq/0214-3429/27/2/yuliya.pdf.
(71) Iqbal, J.; Siddiqui, R.; Kazmi, S. U.; Khan, N. A. A simple assay to screen antimicrobial compounds potentiating the activity of current antibiotics. *BioMed. Res. Int.* **2013**, *2013*, article 927323 10.1155/2013/927323
(72) Allen, H. K.; Trachsel, J.; Looft, T.; Casey, T. A. Finding alternatives to antibiotics. *Ann. N. Y. Acad. Sci.* **2014**, *1323*, 91−100.
(73) Patra, A. K.; Saxena, J. The effect and mode of action of saponins on the microbial populations and fermentation in the rumen and ruminant production. *Nutr. Res. Rev.* **2009**, *22*, 204−219.
(74) Brown, D. G.; Lister, T.; May-Dracka, T. L. New natural products as new leads for antibacterial drug discovery. *Bioorg. Med. Chem. Lett.* **2014**, *24*, 413−418.
(75) Callaway, T. R.; Anderson, R. C.; Edrington, T. S.; Genovese, K. J.; Harvey, R. B.; Poole, T. L.; Nisbet, D. J. Recent pre-harvest supplementation strategies to reduce carriage and shedding of zoonotic enteric bacterial pathogens in food animals. *Anim. Health Res. Rev.* **2004**, *5*, 35−47.
(76) White, D. G.; Zhao, S.; Singh, R.; McDermott, P. F. Antimicrobial resistance among Gram-negative foodborne bacterial pathogens associated with foods of animal origin. *Foodborne Pathog. Dis.* **2004**, *1*, 137−152.
(77) Clardy, J.; Fischbach, M. A.; Walsh, C. T. New antibiotics from bacterial natural products. *Nat. Biotechnol.* **2006**, *24*, 1541−1550.
(78) Wang, J.; Kodali, S.; Lee, S. H.; Galgoci, A.; Painter, R.; Dorso, K.; Racine, F.; Motyl, M.; Hernandez, L.; Tinney, E.; Colletti, S. L.; Herath, K.; Cummings, R.; Salazar, O.; Gonzalez, I.; Basilio, A.; Vicente, F.; Genilloud, O.; Pelaez, F.; Jayasuriya, H.; Young, K.; Cully, D. F.; Singh, S. B. Discovery of platencin, a dual FabF and FabH inhibitor with in vivo antibiotic properties. *Proc. Natl. Acad. Sci. U.S.A.* **2007**, *104*, 7612−7616.
(79) Walsh, C.; Fanning, S. Antimicrobial resistance in foodborne pathogens–a cause for concern? *Curr. Drug Targets* **2008**, *9*, 808−815.
(80) Fischbach, M. A.; Walsh, C. T. Antibiotics for emerging pathogens. *Science* **2009**, *325*, 1089−1093.
(81) Doyle, M. P.; Erickson, M. C. Opportunities for mitigating pathogen contamination during on-farm food production. *Int. J. Food Microbiol.* **2012**, *152*, 54−74.
(82) Doyle, M. E.; Hartmann, F. A.; Lee Wong, A. C. Methicillin-resistant staphylococci: implications for our food supply? *Anim. Health Res. Rev.* **2012**, *13*, 157−180.
(83) Hur, J.; Jawale, C.; Lee, J. H. Antimicrobial resistance of *Salmonella* isolated from food animals: a review. *Food Res. Int.* **2012**, *45*, 819−830.
(84) Oliveira, H.; Azeredo, J.; Lavigne, R.; Kluskens, L. D. Bacteriophage endolysins as a response to emerging foodborne pathogens. *Trends Food Sci. Technol.* **2012**, *28*, 103−115.
(85) Capita, R.; Alonso-Calleja, C. Antibiotic-resistant bacteria: a challenge for the food industry. *Crit. Rev. Food Sci. Nutr.* **2013**, *53*, 11−48.
(86) Rutkowski, J.; Brzezinski, B. Structures and properties of naturally occurring polyether antibiotics. *BioMed. Res. Int.* **2013**, *2013*, article 16251310.1155/2014/162513.
(87) Gyawali, R.; Ibrahim, S. A. Natural products as antimicrobial agents. *Food Control* **2014**, *46*, 412−429.
(88) Jassim, S. A. A.; Limoges, R. G. Natural solution to antibiotic resistance: bacteriophages 'The Living Drugs'. *World J. Microbiol. Biotechnol.* **2014**, *30*, 2153−2170.
(89) Linden, S. B.; Zhang, H.; Heselpoth, R. D.; Shen, Y.; Schmelcher, M.; Eichenseher, F.; Nelson, D. C. Biochemical and biophysical characterization of PlyGRCS, a bacteriophage endolysin active against methicillin-resistant *Staphylococcus aureus*. *Appl. Microbiol. Biotechnol.* **2015**, *99*, 741−752.
(90) Friedman, M.; Buick, R.; Elliott, C. T. Antimicrobial activities of plant compounds against antibiotic-resistant *Micrococcus luteus*. *Int. J. Antimicrob. Agents* **2006**, *28*, 156−158.
(91) Johny, A. K.; Hoagland, T.; Venkitanarayanan, K. Effect of subinhibitory concentrations of plant-derived molecules in increasing the sensitivity of multidrug-resistant *Salmonella enterica* serovar Typhimurium DT104 to antibiotics. *Foodborne Pathog. Dis.* **2010**, *7*, 1165−1170.
(92) Gibbons, S.; Oluwatuyi, M.; Veitch, N. C.; Gray, A. I. Bacterial resistance modifying agents from *Lycopus europaeus*. *Phytochemistry* **2003**, *62*, 83−87.
(93) Oluwatuyi, M.; Kaatz, G. W.; Gibbons, S. Antibacterial and resistance modifying activity of *Rosmarinus officinalis*. *Phytochemistry* **2004**, *65*, 3249−3254.
(94) Chan, B. C.; Ip, M.; Lau, C. B.; Lui, S. L.; Jolivalt, C.; Ganem-Elbaz, C.; Litaudon, M.; Reiner, N. E.; Gong, H.; See, R. H.; Fung, K. P.; Leung, P. C. Synergistic effects of baicalein with ciprofloxacin against NorA over-expressed methicillin-resistant *Staphylococcus aureus* (MRSA) and inhibition of MRSA pyruvate kinase. *J. Ethnopharmacol.* **2011**, *137*, 767−773.
(95) Peng, Q.; Zhou, S.; Yao, F.; Hou, B.; Huang, Y.; Hua, D.; Zheng, Y.; Qian, Y. Baicalein suppresses the SOS response system of *Staphylococcus aureus* induced by ciprofloxacin. *Cell. Physiol. Biochem.* **2011**, *28*, 1045−1050.
(96) Karunanidhi, A.; Thomas, R.; van Belkum, A.; Neela, V. In vitro antibacterial and antibiofilm activities of chlorogenic acid against clinical isolates of *Stenotrophomonas maltophilia* including the trimethoprim/sulfamethoxazole resistant strain. *BioMed Res. Int.* **2013**, *2013*, article 392058 10.1155/2013/584549
(97) Alves, M. J.; Ferreira, I. C.; Froufe, H. J.; Abreu, R. M.; Martins, A.; Pintado, M. Antimicrobial activity of phenolic compounds identified in wild mushrooms, SAR analysis and docking studies. *J. Appl. Microbiol.* **2013**, *115*, 346−357.
(98) Alves, M. J.; Ferreira, I. C.; Dias, J.; Teixeira, V.; Martins, A.; Pintado, M. A review on antimicrobial activity of mushroom (Basidiomycetes) extracts and isolated compounds. *Planta Med.* **2012**, *78*, 1707−1718.
(99) Friedman, M.; Henika, P. R.; Mandrell, R. E. Antibacterial activities of phenolic benzaldehydes and benzoic acids against *Campylobacter jejuni*, *Escherichia coli*, *Listeria monocytogenes*, and *Salmonella enterica*. *J. Food Prot.* **2003**, *66*, 1811−1821 http://www.ingentaconnect.com/content/iafp/jfp/2003/00000066/00000010/art00011.
(100) Klančnik, A.; Možina, S. S.; Zhang, Q. Anti-*Campylobacter* activities and resistance mechanisms of natural phenolic compounds in *Campylobacter*. *PLoS One* **2012**, *7*, article e51800 10.1371/journal.-pone.0051800
(101) Gallucci, M. N.; Carezzano, M. E.; Oliva, M. M.; Demo, M. S.; Pizzolitto, R. P.; Zunino, M. P.; Zygadlo, J. A.; Dambolena, J. S. In vitro activity of natural phenolic compounds against fluconazole-resistant *Candida* species: a quantitative structure-activity relationship analysis. *J. Appl. Microbiol.* **2014**, *116*, 795−804.
(102) Chen, Y. L.; Huang, S. T.; Sun, F. M.; Chiang, Y. L.; Chiang, C. J.; Tsai, C. M.; Weng, C. J. Transformation of cinnamic acid from trans- to cis-form raises a notable bactericidal and synergistic activity against multiple-drug resistant *Mycobacterium tuberculosis*. *Eur. J. Pharm. Sci.* **2011**, *43*, 188−194.
(103) Lipińska L, K. E. S. M. The structure, occurrence and biological activity of ellagitannins: a general review. *Acta Sci. Pol., Technol. Aliment.* **2014**, *13*, 289−299.
(104) Kim, S. K.; Kim, H.; Kim, S. A.; Park, H. K.; Kim, W. Anti-inflammatory and anti-superbacterial activity of polyphenols isolated from black raspberry. *Korean J. Physiol. Pharmacol.* **2013**, *17*, 73−79.
(105) Bag, A.; Chattopadhyay, R. R. Efflux-pump inhibitory activity of a gallotannin from *Terminalia chebula* fruit against multidrug-resistant uropathogenic *Escherichia coli*. *Nat. Prod. Res.* **2014**, *28*, 1280−1283.

DOI: 10.1021/acs.jafc.5b00778
J. Agric. Food Chem. 2015, 63, 3805−3822

(106) Caballero Gomez, N.; Abriouel, H.; Grande, M. J.; Perez Pulido, R.; Galvez, A. Combined treatments of enterocin AS-48 with biocides to improve the inactivation of methicillin-sensitive and methicillin-resistant *Staphylococcus aureus* planktonic and sessile cells. *Int. J. Food Microbiol.* **2013**, *163*, 96−100.
(107) Balciunas, E. M.; Castillo Martinez, F. A.; Todorov, S. D.; Franco, B. D. G. D. M.; Converti, A.; Oliveira, R. P. D. S. Novel biotechnological applications of bacteriocins: a review. *Food Control* **2013**, *32*, 134−142.
(108) Marks, L. R.; Clementi, E. A.; Hakansson, A. P. The human milk protein-lipid complex HAMLET sensitizes bacterial pathogens to traditional antimicrobial agents. *PLoS One* **2012**, *7*, article e43514.10.1371/journal.pone.0043514
(109) Chung, P. Y.; Chung, L. Y.; Navaratnam, P. Potential targets by pentacyclic triterpenoids from *Callicarpa farinosa* against methicillin-resistant and sensitive *Staphylococcus aureus*. *Fitoterapia* **2014**, *94*, 48−54.
(110) Friedman, M. Anticarcinogenic, cardioprotective, and other health benefits of tomato compounds lycopene, α-tomatine, and tomatidine in pure form and in fresh and processed tomatoes. *J. Agric. Food Chem.* **2013**, *61*, 9534−9550.
(111) Mitchell, G.; Lafrance, M.; Boulanger, S.; Séguin, D. L.; Guay, I.; Gattuso, M.; Marsault, E.; Bouarab, K.; Malouin, F. Tomatidine acts in synergy with aminoglycoside antibiotics against multiresistant *Staphylococcus aureus* and prevents virulence gene expression. *J. Antimicrob. Chemother.* **2012**, *67*, 559−568.
(112) Friedman, M. Potato glycoalkaloids and metabolites: roles in the plant and in the diet. *J. Agric. Food Chem.* **2006**, *54*, 8655−8681.
(113) Friedman, M.; Henika, P. R.; Levin, C. E.; Mandrell, R. E. Antimicrobial wine formulations active against the foodborne pathogens *Escherichia coli* O157:H7 and *Salmonella enterica*. *J. Food Sci.* **2006**, *71*, M245−M251.
(114) Rojas-Graü, M. A.; Avena-Bustillos, R. J.; Friedman, M.; Henika, P. R.; Martin-Belloso, O.; McHugh, T. H. Mechanical, barrier, and antimicrobial properties of apple puree edible films containing plant essential oils. *J. Agric. Food Chem.* **2006**, *54*, 9262−9267.
(115) Wong, S. Y. Y.; Grant, I. R.; Friedman, M.; Elliott, C. T.; Situ, C. Antibacterial activities of naturally occurring compounds against *Mycobacterium avium* subsp. *paratuberculosis*. *Appl. Environ. Microbiol.* **2008**, *74*, 5986−5990.
(116) Du, W. X.; Olsen, C. W.; Avena-Bustillos, R. J.; McHugh, T. H.; Levin, C. E.; Friedman, M. Effects of allspice, cinnamon, and clove bud essential oils in edible apple films on physical properties and antimicrobial activities. *J. Food Sci.* **2009**, *74*, M372−M378.
(117) Du, W.-X.; Olsen, C. W.; Avena-Bustillos, R. J.; McHugh, T. H.; Levin, C. E.; Mandrell, R.; Friedman, M. Antibacterial effects of allspice, garlic, and oregano essential oils in tomato films determined by overlay and vapor-phase methods. *J. Food Sci.* **2009**, *74*, M390−M397.
(118) Moore-Neibel, K.; Gerber, C.; Patel, J.; Friedman, M.; Ravishankar, S. Antimicrobial activity of lemongrass oil against *Salmonella enterica* on organic leafy greens. *J. Appl. Microbiol.* **2012**, *112*, 485−492.
(119) Rounds, L.; Havens, C. M.; Feinstein, Y.; Friedman, M.; Ravishankar, S. Plant extracts, spices, and essential oils inactivate *Escherichia coli* O157:H7 and reduce formation of potentially carcinogenic heterocyclic amines in cooked beef patties. *J. Agric. Food Chem.* **2012**, *60*, 3792−3799.
(120) Chen, C. H.; Ravishankar, S.; Marchello, J.; Friedman, M. Antimicrobial activity of plant compounds against *Salmonella* Typhimurium DT104 in ground pork and the influence of heat and storage on the antimicrobial activity. *J. Food Prot.* **2013**, *76*, 1264−1269.
(121) Todd, J.; Friedman, M.; Patel, J.; Jaroni, D.; Ravishankar, S. The antimicrobial effects of cinnamon leaf oil against multi-drug resistant *Salmonella* Newport on organic leafy greens. *Int. J. Food Microbiol.* **2013**, *166*, 193−199.
(122) Nostro, A.; Blanco, A. R.; Cannatelli, M. A.; Enea, V.; Flamini, G.; Morelli, I.; Roccaro, A. S.; Alonzo, V. Susceptibility of methicillin-resistant *staphylococci* to oregano essential oil, carvacrol and thymol. *FEMS Microbiol. Lett.* **2004**, *230*, 191−195.
(123) Shin, S.; Kim, J. H. In vitro inhibitory activities of essential oils from two Korean *Thymus* species against antibiotic-resistant pathogens. *Arch. Arch. Pharmacal Res.* **2005**, *28*, 897−901.
(124) Palaniappan, K.; Holley, R. A. Use of natural antimicrobials to increase antibiotic susceptibility of drug resistant bacteria. *Int. J. Food Microbiol.* **2010**, *140*, 164−168.
(125) Ravishankar, S.; Zhu, L.; Law, B.; Joens, L.; Friedman, M. Plant-derived compounds inactivate antibiotic-resistant *Campylobacter jejuni* strains. *J. Food Prot.* **2008**, *71*, 1145−1149 http://www.ingentaconnect.com/content/iafp/jfp/2008/00000071/00000006/art00006.
(126) Mild, R. M.; Joens, L. A.; Friedman, M.; Olsen, C. W.; McHugh, T. H.; Law, B.; Ravishankar, S. Antimicrobial edible apple films inactivate antibiotic resistant and susceptible *Campylobacter jejuni* strains on chicken breast. *J. Food Sci.* **2011**, *76*, M163−M168.
(127) Ravishankar, S.; Zhu, L.; Reyna-Granados, J.; Law, B.; Joens, L.; Friedman, M. Carvacrol and cinnamaldehyde inactivate antibiotic-resistant *Salmonella enterica* in buffer and on celery and oysters. *J. Food Prot.* **2010**, *73*, 234−240 http://www.ingentaconnect.com/content/iafp/jfp/2003/00000066/00000010/art00011.
(128) Upadhyaya, I.; Upadhyay, A.; Kollanoor-Johny, A.; Baskaran, S. A.; Mooyottu, S.; Darre, M. J.; Venkitanarayanan, K. Rapid inactivation of *Salmonella* Enteritidis on shell eggs by plant-derived antimicrobials. *Poult. Sci.* **2013**, *92*, 3228−3235.
(129) Friedman, M. Antibiotic activities of plant compounds against non-resistant and antibiotic-resistant foodborne human pathogens. *ACS Symp. Ser.* **2006**, *No. 931*, 167−183.
(130) Halcón, L.; Milkus, K. *Staphylococcus aureus* and wounds: a review of tea tree oil as a promising antimicrobial. *Am. J. Infect. Control* **2004**, *32*, 402−408.
(131) Thomsen, N. A.; Hammer, K. A.; Riley, T. V.; Van Belkum, A.; Carson, C. F. Effect of habituation to tea tree (*Melaleuca alternifolia*) oil on the subsequent susceptibility of *Staphylococcus* spp. to antimicrobials, triclosan, tea tree oil, terpinen-4-ol and carvacrol. *Int. J. Antimicrob. Agents* **2013**, *41*, 343−351.
(132) Fadli, M.; Chevalier, J.; Hassani, L.; Mezrioui, N. E.; Pages, J. M. Natural extracts stimulate membrane-associated mechanisms of resistance in Gram-negative bacteria. *Lett. Appl. Microbiol.* **2014**, *58*, 472−477.
(133) Fadli, M.; Chevalier, J.; Bolla, J. M.; Mezrioui, N. E.; Hassani, L.; Pages, J. M. *Thymus maroccanus* essential oil, a membranotropic compound active on Gram-negative bacteria and resistant isolates. *J. Appl. Microbiol.* **2012**, *113*, 1120−1129.
(134) Medeiros Barreto, H.; Cerqueira Fontinele, F.; Pereira de Oliveira, A.; Arcanjo, D. D.; Cavalcanti Dos Santos, B. H.; de Abreu, A. P.; Douglas Melo Coutinho, H.; Alves Carvalho da Silva, R.; Oliveira de Sousa, T.; Freire de Medeiros, M.; Lopes Cito, A. M.; Dantas Lopes, J. A. Phytochemical prospection and modulation of antibiotic activity in vitro by *Lippia origanoides* H.B.K. in methicillin resistant *Staphylococcus aureus*. *BioMed Res. Int.* **2014**, *2014*, article 305610.10.1155/2014/305610
(135) Choi, J. G.; Kang, O. H.; Lee, Y. S.; Oh, Y. C.; Chae, H. S.; Jang, H. J.; Shin, D. W.; Kwon, D. Y. Antibacterial activity of methyl gallate isolated from *Galla Rhois* or carvacrol combined with nalidixic acid against nalidixic acid resistant bacteria. *Molecules* **2009**, *14*, 1773−1780.
(136) Langeveld, W. T.; Veldhuizen, E. J.; Burt, S. A. Synergy between essential oil components and antibiotics: a review. *Crit. Rev. Microbiol.* **2014**, *40*, 76−94.
(137) Yap, P. S.; Lim, S. H.; Hu, C. P.; Yiap, B. C. Combination of essential oils and antibiotics reduce antibiotic resistance in plasmid-conferred multidrug resistant bacteria. *Phytomedicine* **2013**, *20*, 710−713.
(138) Ahmad, A.; Khan, A.; Manzoor, N. Reversal of efflux mediated antifungal resistance underlies synergistic activity of two monoterpenes with fluconazole. *Eur. J. Pharm. Sci.* **2013**, *48*, 80−86.

DOI: 10.1021/acs.jafc.5b00778
J. Agric. Food Chem. 2015, 63, 3805−3822

(139) Verlinden, M.; Pasmans, F.; Mahu, M.; Vande Maele, L.; De Pauw, N.; Yang, Z.; Haesebrouck, F.; Martel, A. In vitro sensitivity of poultry *Brachyspira intermedia* isolates to essential oil components and in vivo reduction of *Brachyspira intermedia* in rearing pullets with cinnamaldehyde feed supplementation. *Poult. Sci.* **2013**, *92*, 1202−1207.
(140) Hannan, A.; Ikram Ullah, M.; Usman, M.; Hussain, S.; Absar, M.; Javed, K. Anti-mycobacterial activity of garlic (*Allium sativum*) against multi-drug resistant and non-multi-drug resistant mycobacterium tuberculosis. *Pak. J. Pharm. Sci.* **2011**, *24*, 81−85 http://www.pjps.pk/wp-content/uploads/pdfs/CD-PJPS-24-1-11/Paper-15.pdf.
(141) Fani, M. M.; Kohanteb, J.; Dayaghi, M. Inhibitory activity of garlic (*Allium sativum*) extract on multidrug-resistant *Streptococcus mutans*. *J. Indian Soc. Pedod. Prev. Dent.* **2007**, *25*, 164−168.
(142) Tirado, D. J.; Hudson, N. R.; Maldonado, C. J. Efficacy of medical grade honey against multidrug-resistant organisms of operational significance: part I. *J. Trauma Acute Care Surg.* **2014**, *77*, S204−S207.
(143) Müller, P.; Alber, D. G.; Turnbull, L.; Schlothauer, R. C.; Carter, D. A.; Whitchurch, C. B.; Harry, E. J. Synergism between Medihoney and rifampicin against methicillin-resistant *Staphylococcus aureus* (MRSA). *PLoS One* **2013**, *8*, article e57679, 10.1371/journal.pone.0057679.
(144) Al-Waili, N.; Al-Ghamdi, A.; Ansari, M. J.; Al-Attal, Y.; Salom, K. Synergistic effects of honey and propolis toward drug multi-resistant *Staphylococcus aureus*, *Escherichia coli* and *Candida albicans* isolates in single and polymicrobial cultures. *Int. J. Med. Sci.* **2012**, *9*, 793−800.
(145) Kwakman, P. H.; Zaat, S. A. Antibacterial components of honey. *IUBMB Life* **2012**, *64*, 48−55.
(146) Ramesh, V.; Arivudainambi, U.; Thalavaipandian, A.; Karunakaran, C.; Rajendran, A. Antibacterial activity of wild *Xylaria* sp. strain R005 (Ascomycetes) against multidrug-resistant *Staphylococcus aureus* and *Pseudomonas aeruginosa*. *Int. J. Med. Mushrooms* **2012**, *14*, 47−53.
(147) Noumedem, J. A.; Mihasan, M.; Kuiate, J. R.; Stefan, M.; Cojocaru, D.; Dzoyem, J. P.; Kuete, V. In vitro antibacterial and antibiotic-potentiation activities of four edible plants against multidrug-resistant gram-negative species. *BMC Complement. Altern. Med.* **2013**, *13*, 190.
(148) Khameneh, B.; Iranshahy, M.; Ghandadi, M.; Ghoochi Atashbeyk, D.; Fazly Bazzaz, B. S.; Iranshahi, M. Investigation of the antibacterial activity and efflux pump inhibitory effect of co-loaded piperine and gentamicin nanoliposomes in methicillin-resistant *Staphylococcus aureus*. *Drug Dev. Ind. Pharm.* **2014**, DOI: 10.3109/03639045.2014.920025.
(149) Dey, D.; Debnath, S.; Hazra, S.; Ghosh, S.; Ray, R.; Hazra, B. Pomegranate pericarp extract enhances the antibacterial activity of ciprofloxacin against extended-spectrum beta-lactamase (ESBL) and metallo-beta-lactamase (MBL) producing Gram-negative bacilli. *Food Chem. Toxicol.* **2012**, *50*, 4302−4309.
(150) Hafidh, R. R.; Abdulamir, A. S.; Vern, L. S.; Abu Bakar, F.; Abas, F.; Jahanshiri, F.; Sekawi, Z. Inhibition of growth of highly resistant bacterial and fungal pathogens by a natural product. *Open Microbiol. J.* **2011**, *5*, 96−106.
(151) Friedman, M.; Henika, P. R.; Levin, C. E.; Mandrell, R. E.; Kozukue, N. Antimicrobial activities of tea catechins and theaflavins and tea extracts against *Bacillus cereus*. *J. Food Prot.* **2006**, *69*, 354−361 http://www.ingentaconnect.com/content/iafp/jfp/2006/00000069/00000002/art00015.
(152) Friedman, M. Overview of antibacterial, antitoxin, antiviral, and antifungal activities of tea flavonoids and teas. *Mol. Nutr. Food Res.* **2007**, *51*, 116−134.
(153) Stapleton, P. D.; Shah, S.; Anderson, J. C.; Hara, Y.; Hamilton-Miller, J. M.; Taylor, P. W. Modulation of β-lactam resistance in *Staphylococcus aureus* by catechins and gallates. *Int. J. Antimicrob. Agents* **2004**, *23*, 462−467.
(154) Friedman, M.; Levin, C. E.; Lee, S.-U.; Kozukue, N. Stability of green tea catechins in commercial tea leaves during storage for 6 months. *J. Food Sci.* **2009**, *74*, H47−H51.
(155) Heck, C. I.; de Mejia, E. G. Yerba mate tea (*Ilex paraguariensis*): a comprehensive review on chemistry, health implications, and technological considerations. *J. Food Sci.* **2007**, *72*, R138−R151.
(156) Burris, K. P.; Higginbotham, K. L.; Stewart, C. Aqueous extracts of yerba mate as bactericidal agents against methicillin-resistant *Staphylococcus aureus* in a microbiological medium and ground beef mixtures. *Food Control* **2015**, *50*, 748−753.
(157) Jun, J. W.; Kim, H. J.; Yun, S. K.; Chai, J. Y.; Park, S. C. Eating oysters without risk of vibriosis: application of a bacteriophage against *Vibrio parahaemolyticus* in oysters. *Int. J. Food Microbiol.* **2014**, *188*, 31−35.
(158) Qiang, Z.; Macauley, J. J.; Mormile, M. R.; Surampalli, R.; Adams, C. D. Treatment of antibiotics and antibiotic resistant bacteria in swine wastewater with free chlorine. *J. Agric. Food Chem.* **2006**, *54*, 8144−8154.
(159) Oscar, T. P.; Tasmin, R.; Parveen, S. Chlorine inactivation of nonresistant and antibiotic-resistant strains of *Salmonella* Typhimurium isolated from chicken carcasses. *J. Food Prot.* **2013**, *76*, 1031−1034.
(160) Stopforth, J. D.; Suhalim, R.; Kottapalli, B.; Hill, W. E.; Samadpour, M. Thermal inactivation *D*- and *z*-values of multidrug-resistant and non-multidrug-resistant *Salmonella* serotypes and survival in ground beef exposed to consumer-style cooking. *J. Food Prot.* **2008**, *71*, 509−515 http://www.ingentaconnect.com/content/iafp/jfp/2008/00000071/00000003/art00007.
(161) Shen, C.; Geornaras, I.; Belk, K. E.; Smith, G. C.; Sofos, J. N. Inactivation of *Escherichia coli* O157:H7 in moisture-enhanced nonintact beef by pan-broiling or roasting with various cooking appliances set at different temperatures. *J. Food Sci.* **2011**, *76*, M64−M71.
(162) Sagarzazu, N.; Cebrian, G.; Pagan, R.; Condon, S.; Manas, P. Emergence of pulsed electric fields resistance in *Salmonella enterica* serovar Typhimurium SL1344. *Int. J. Food Microbiol.* **2013**, *166*, 219−225.
(163) Huang, J. J.; Tang, F.; Xi, J. Y.; Pang, Y. C.; Hu, H. Y. [Inactivation and reactivation of antibiotic-resistant bacteria during and after UV disinfection in reclaimed water]. *Huanjing Kexue* **2014**, *35*, 1326−1331.
(164) Rizzo, L.; Della Sala, A.; Fiorentino, A.; Li Puma, G. Disinfection of urban wastewater by solar driven and UV lamp - TiO_2 photocatalysis: effect on a multi drug resistant *Escherichia coli* strain. *Water Res.* **2014**, *53*, 145−152.
(165) McKinney, J. M.; Williams, R. C.; Boardman, G. D.; Eifert, J. D.; Sumner, S. S. Effect of acid stress, antibiotic resistance, and heat shock on the resistance of *Listeria monocytogenes* to UV light when suspended in distilled water and fresh brine. *J. Food Prot.* **2009**, *72*, 1634−1640 http://www.ingentaconnect.com/content/iafp/jfp/2009/00000072/00000008/art00006.
(166) Neetoo, H.; Nekoozadeh, S.; Jiang, Z.; Chen, H. Application of high hydrostatic pressure to decontaminate green onions from *Salmonella* and *Escherichia coli* O157:H7. *Food Microbiol.* **2011**, *28*, 1275−1283.
(167) Reddy, N. R.; Marshall, K. M.; Morrissey, T. R.; Loeza, V.; Patazca, E.; Skinner, G. E.; Krishnamurthy, K.; Larkin, J. W. Combined high pressure and thermal processing on inactivation of type A and proteolytic type B spores of *Clostridium botulinum*. *J. Food Prot.* **2013**, *76*, 1384−1392.
(168) Sun, J.; Deng, Z.; Yan, A. Bacterial multidrug efflux pumps: mechanisms, physiology and pharmacological exploitations. *Biochem. Biophys. Res. Commun.* **2014**, *453*, 254−267.
(169) Blair, J. M.; Richmond, G. E.; Piddock, L. J. Multidrug efflux pumps in Gram-negative bacteria and their role in antibiotic resistance. *Future Microbiol.* **2014**, *9*, 1165−1177.

DOI: 10.1021/acs.jafc.5b00778
J. Agric. Food Chem. 2015, 63, 3805−3822

(170) Blair, J. M.; Webber, M. A.; Baylay, A. J.; Ogbolu, D. O.; Piddock, L. J. Molecular mechanisms of antibiotic resistance. *Nat. Rev. Microbiol.* **2015**, *13*, 42−51.
(171) Klančnik, A.; Gröblacher, B.; Kovač, J.; Bucar, F.; Možina, S. S. Anti-*Campylobacter* and resistance-modifying activity of *Alpinia katsumadai* seed extracts. *J. Appl. Microbiol.* **2012**, *113*, 1249−1262.
(172) Ohene-Agyei, T.; Mowla, R.; Rahman, T.; Venter, H. Phytochemicals increase the antibacterial activity of antibiotics by acting on a drug efflux pump. *Microbiol. Open* **2014**, *3*, 885−896.
(173) Du, D.; Wang, Z.; James, N. R.; Voss, J. E.; Klimont, E.; Ohene-Agyei, T.; Venter, H.; Chiu, W.; Luisi, B. F. Structure of the AcrAB-TolC multidrug efflux pump. *Nature* **2014**, *509*, 512−515.
(174) Sung, W. S.; Lee, D. G. Mechanism of decreased susceptibility for Gram-negative bacteria and synergistic effect with ampicillin of indole-3-carbinol. *Biol. Pharm. Bull.* **2008**, *31*, 1798−1801.
(175) Ojeda-Sana, A. M.; Repetto, V.; Moreno, S. Carnosic acid is an efflux pumps modulator by dissipation of the membrane potential in *Enterococcus faecalis* and *Staphylococcus aureus*. *World J. Microbiol. Biotechnol.* **2013**, *29*, 137−144.
(176) Fadli, M.; Bolla, J. M.; Mezrioui, N. E.; Pagès, J. M.; Hassani, L. First evidence of antibacterial and synergistic effects of *Thymus riatarum* essential oil with conventional antibiotics. *Ind. Crops Prod.* **2014**, *61*, 370−376.
(177) Jakobsen, T. H.; Bragason, S. K.; Phipps, R. K.; Christensen, L. D.; van Gennip, M.; Alhede, M.; Skindersoe, M.; Larsen, T. O.; Høiby, N.; Bjarnsholt, T.; Givskov, M. Food as a source for quorum sensing inhibitors: iberin from horseradish revealed as a quorum sensing inhibitor of *Pseudomonas aeruginosa*. *Appl. Environ. Microbiol.* **2012**, *78*, 2410−2421.
(178) Chang, C. Y.; Krishnan, T.; Wang, H.; Chen, Y.; Yin, W. F.; Chong, Y. M.; Tan, L. Y.; Chong, T. M.; Chan, K. G. Non-antibiotic quorum sensing inhibitors acting against *N*-acylhomoserine lactone synthase as druggable target. *Sci. Rep.* **2014**, *4*, 7245.
(179) Yap, P. S. X.; Krishnan, T.; Yiap, B. C.; Hu, C. P.; Chan, K. G.; Lim, S. H. E. Membrane disruption and anti-quorum sensing effects of synergistic interaction between *Lavandula angustifolia* (lavender oil) in combination with antibiotic against plasmid-conferred multi-drug-resistant *Escherichia coli*. *J. Appl. Microbiol.* **2014**, *116*, 1119−1128.
(180) Yap, P. S.; Krishnan, T.; Chan, K. G.; Lim, S. H. Some evidences on the mode of action of *Cinnamomum verum* bark essential oil, alone and in combination with piperacillin against a multi-drug resistant *Escherichia coli* strain. *J. Microbiol. Biotechnol.* **2014**, *2*410.4014/jmb.1407.07054.
(181) Koh, C. L.; Sam, C. K.; Yin, W. F.; Tan, L. Y.; Krishnan, T.; Chong, Y. M.; Chan, K. G. Plant-derived natural products as sources of anti-quorum sensing compounds. *Sensors* **2013**, *13*, 6217−6228.
(182) van der Veen, S.; Abee, T. Bacterial SOS response: a food safety perspective. *Curr. Opin. Biotechnol.* **2011**, *22*, 136−142.
(183) Gottschalk, S.; Ifrah, D.; Lerche, S.; Gottlieb, C. T.; Cohn, M. T.; Hiasa, H.; Hansen, P. R.; Gram, L.; Ingmer, H.; Thomsen, L. E. The antimicrobial lysine-peptoid hybrid LP5 inhibits DNA replication and induces the SOS response in *Staphylococcus aureus*. *BMC Microbiol.* **2013**, *13*, 192.
(184) Juneja, V. K.; Gonzales-Barron, U.; Butler, F.; Yadav, A. S.; Friedman, M. Predictive thermal inactivation model for the combined effect of temperature, cinnamaldehyde and carvacrol on starvation-stressed multiple *Salmonella* serotypes in ground chicken. *Int. J. Food Microbiol.* **2013**, *165*, 184−199.
(185) Juneja, V. K.; Yadav, A. S.; Hwang, C.-A.; Sheen, S.; Mukhopadhyay, S.; Friedman, M. Kinetics of thermal destruction of *Salmonella* in ground chicken containing *trans*-cinnamaldehyde and carvacrol. *J. Food Prot.* **2012**, *75*, 289−296.
(186) Heide, L. New aminocoumarin antibiotics as gyrase inhibitors. *Int. J. Med. Microbiol.* **2014**, *304*, 31−36.
(187) Schroder, W.; Goerke, C.; Wolz, C. Opposing effects of aminocoumarins and fluoroquinolones on the SOS response and adaptability in *Staphylococcus aureus*. *J. Antimicrob. Chemother.* **2013**, *68*, 529−538.
(188) Cirz, R. T.; Jones, M. B.; Gingles, N. A.; Minogue, T. D.; Jarrahi, B.; Peterson, S. N.; Romesberg, F. E. Complete and SOS-mediated response of *Staphylococcus aureus* to the antibiotic ciprofloxacin. *J. Bacteriol.* **2007**, *189*, 531−539.
(189) Woźniak, D.; Dryś, A.; Matkowski, A. Antiradical and antioxidant activity of flavones from *Scutellariae baicalensis radix*. *Nat. Prod. Res.* **2014**, DOI: 10.1080/14786419.2014.983920.
(190) Marathe, S. A.; Kumar, R.; Ajitkumar, P.; Nagaraja, V.; Chakravortty, D. Curcumin reduces the antimicrobial activity of ciprofloxacin against *Salmonella* Typhimurium and *Salmonella* Typhi. *J. Antimicrob. Chemother.* **2013**, *68*, 139−152.
(191) Ultee, A.; Kets, E. P.; Smid, E. J. Mechanisms of action of carvacrol on the food-borne pathogen *Bacillus cereus*. *Appl. Environ. Microbiol.* **1999**, *65*, 4606−4610 http://aem.asm.org/content/65/10/4606.long.
(192) Sirk, T. W.; Brown, E. F.; Friedman, M.; Sum, A. K. Molecular binding of catechins to biomembranes: relationship to biological activity. *J. Agric. Food Chem.* **2009**, *57*, 6720−6728.
(193) Sirk, T. W.; Brown, E. F.; Sum, A. K.; Friedman, M. Molecular dynamics study on the biophysical interactions of seven green tea catechins with lipid bilayers of cell membranes. *J. Agric. Food Chem.* **2008**, *56*, 7750−7758.
(194) Sirk, T. W.; Friedman, M.; Brown, E. F. Molecular binding of black tea theaflavins to biological membranes: relationship to bioactivities. *J. Agric. Food Chem.* **2011**, *59*, 3780−3787.
(195) Friedman, M. Antibacterial, antiviral, and antifungal properties of wines and winery byproducts in relation to their flavonoid content. *J. Agric. Food Chem.* **2014**, *62*, 6025−6042.
(196) Finotti, E.; Bersani, E.; Friedman, M. Application of a functional mathematical index for antibacterial and anticarcinogenic effects of tea catechins. *J. Agric. Food Chem.* **2011**, *59*, 864−869.
(197) Friedman, M.; Juneja, V. K. Review of antimicrobial and antioxidative activities of chitosans in food. *J. Food Prot.* **2010**, *73*, 1737−1761 http://www.ingentaconnect.com/content/iafp/jfp/2010/00000073/00000009/art00021.
(198) Nowotarska, S. W.; Nowotarski, K. I.; Friedman, M.; Situ, C. Effect of structure on the interactions between five natural antimicrobial compounds and phospholipids of bacterial cell membrane on model monolayers. *Molecules* **2014**, *19*, 7497−7515.
(199) Ultee, A.; Kets, E. P.; Alberda, M.; Hoekstra, F. A.; Smid, E. J. Adaptation of the food-borne pathogen *Bacillus cereus* to carvacrol. *Arch. Microbiol.* **2000**, *174*, 233−238.
(200) Di Pasqua, R.; Betts, G.; Hoskins, N.; Edwards, M.; Ercolini, D.; Mauriello, G. Membrane toxicity of antimicrobial compounds from essential oils. *J. Agric. Food Chem.* **2007**, *55*, 4863−4870.
(201) Luz Ida, S.; de Melo, A. N.; Bezerra, T. K.; Madruga, M. S.; Magnani, M.; de Souza, E. L. Sublethal amounts of *Origanum vulgare* L. essential oil and carvacrol cause injury and changes in membrane fatty acid of *Salmonella* Typhimurium cultivated in a meat broth. *Foodborne Pathog. Dis.* **2014**, *11*, 357−361.
(202) Chan, A. C.; Ager, D.; Thompson, I. P. Resolving the mechanism of bacterial inhibition by plant secondary metabolites employing a combination of whole-cell biosensors. *J. Microbiol. Methods* **2013**, *93*, 209−217.
(203) Ayari, S.; Dussault, D.; Millette, M.; Hamdi, M.; Lacroix, M. Response of *Bacillus cereus* to gamma-irradiation in combination with carvacrol or mild heat treatment. *J. Agric. Food Chem.* **2010**, *58*, 8217−8224.
(204) Ayari, S.; Dussault, D.; Hayouni, E.; Hamdi, M.; Lacroix, M. Radiation tolerance of *Bacillus cereus* pre-treated with carvacrol alone or in combination with nisin after exposure to single and multiple sub-lethal radiation treatment. *Food Control* **2013**, *32*, 693−701.
(205) Shen, S.; Zhang, T.; Yuan, Y.; Lin, S.; Xu, J.; Ye, H. Effects of cinnamaldehyde on *Escherichia coli* and *Staphylococcus aureus* membrane. *Food Control* **2015**, *47*, 196−202.
(206) Tang, W.; Zhang, H.; Wang, L.; Qian, H. Membrane-disruptive property of a novel antimicrobial peptide from anchovy (*Engraulis japonicus*) hydrolysate. *Int. J. Food Sci. Technol.* **2014**, *49*, 969−975.

DOI: 10.1021/acs.jafc.5b00778
J. Agric. Food Chem. 2015, 63, 3805−3822

(207) Shah, S.; Stapleton, P. D.; Taylor, P. W. The polyphenol (−)-epicatechin gallate disrupts the secretion of virulence-related proteins by *Staphylococcus aureus*. *Lett. Appl. Microbiol.* **2008**, *46*, 181−185.
(208) Li, G.; Xu, Y.; Wang, X.; Zhang, B.; Shi, C.; Zhang, W.; Xia, X. Tannin-rich fraction from pomegranate rind damages membrane of *Listeria monocytogenes*. *Foodborne Pathog. Dis.* **2014**, *11*, 313−319.
(209) Patil, S. D.; Sharma, R.; Srivastava, S.; Navani, N. K.; Pathania, R. Downregulation of yidC in *Escherichia coli* by antisense RNA expression results in sensitization to antibacterial essential oils eugenol and carvacrol. *PLoS One* **2013**, *8*, article e57370,10.1371/journal.-pone.0057370
(210) Ait-Ouazzou, A.; Espina, L.; Gelaw, T. K.; De Lamo-Castellví, S.; Pagán, R.; García-Gonzalo, D. New insights in mechanisms of bacterial inactivation by carvacrol. *J. Appl. Microbiol.* **2013**, *114*, 173−185.
(211) Altintas, A.; Tabanca, N.; Tyihak, E.; Ott, P. G.; Moricz, A. M.; Mincsovics, E.; Wedge, D. E. Characterization of volatile constituents from *Origanum onite*s and their antifungal and antibacterial activity. *J. AOAC Int.* **2013**, *96*, 1200−1208.
(212) Nafisi, S.; Hajiakhoondi, A.; Yektadoost, A. Thymol and carvacrol binding to DNA: model for drug-DNA interaction. *Biopolymers* **2004**, *74*, 345−351.
(213) Ferreira, S.; Silva, F.; Queiroz, J. A.; Oleastro, M.; Domingues, F. C. Resveratrol against *Arcobacter butzleri* and *Arcobacter cryaerophilus*: activity and effect on cellular functions. *Int. J. Food Microbiol.* **2014**, *180*, 62−68.
(214) Chueca, B.; Pagán, R.; García-Gonzalo, D. Oxygenated monoterpenes citral and carvacrol cause oxidative damage in *Escherichia coli* without the involvement of tricarboxylic acid cycle and Fenton reaction. *Int. J. Food Microbiol.* **2014**, *189*, 126−131.
(215) Desbois, A. P.; Smith, V. J. Antibacterial free fatty acids: activities, mechanisms of action and biotechnological potential. *Appl. Microbiol. Biotechnol.* **2010**, *85*, 1629−1642.
(216) Bolla, J. M.; Alibert-Franco, S.; Handzlik, J.; Chevalier, J.; Mahamoud, A.; Boyer, G.; Kiec-Kononowicz, K.; Pages, J. M. Strategies for bypassing the membrane barrier in multidrug resistant Gram-negative bacteria. *FEBS Lett.* **2011**, *585*, 1682−1690.
(217) Schweizer, H. P. Understanding efflux in Gram-negative bacteria: opportunities for drug discovery. *Expert Opin. Drug Discovery* **2012**, *7*, 633−642.
(218) Kim, S. P.; Nam, S. H.; Friedman, M. Rice hull smoke extract protects mice against a *Salmonella* lipopolysaccharide-induced endotoxemia. *J. Agric. Food Chem.* **2014**, *62*, 7753−7759.
(219) Kim, S. P.; Park, S. O.; Lee, S. J.; Nam, S. H.; Friedman, M. A polysaccharide isolated from the liquid culture of *Lentinus edodes* (shiitake) mushroom mycelia containing black rice bran protects mice against a *Salmonella* lipopolysaccharide-induced endotoxemia. *J. Agric. Food Chem.* **2013**, *61*, 10987−10994.
(220) Friedman, M.; Rasooly, R. Review of the inhibition of biological activities of food-related selected toxins by natural compounds. *Toxins* **2013**, *5*, 743−775.
(221) Rada, X.; Todd, J.; Friedman, M.; Patel, J.; Jaroni, D.; Ravishankar, S. Combining essential oils and olive extract for control of multi-drug resistant *Salmonella enterica* on organic leafy greens. *Food Control* **2015**, submitted for publication.
(222) Friedman, M.; Zhu, L.; Feinstein, Y.; Ravishankar, S. Carvacrol facilitates heat-induced inactivation of *Escherichia coli* O157:H7 and inhibits formation of heterocyclic amines in grilled ground beef patties. *J. Agric. Food Chem.* **2009**, *57*, 1848−1853.
(223) Rounds, L.; Havens, C. M.; Feinstein, Y.; Friedman, M.; Ravishankar, S. Concentration-dependent inhibition of *Escherichia coli* O157:H7 and heterocyclic amines in heated ground beef patties by apple and olive extracts, onion powder and clove bud oil. *Meat Sci.* **2013**, *94*, 461−467.

DOI: 10.1021/acs.jafc.5b00778
J. Agric. Food Chem. 2015, 63, 3805−3822

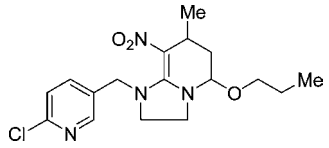

Figure 1. Molecular structure of IPP (1-((6-chloropydidin-3-yl)-methyl)-7-methyl-8-nitro-5-propoxy-1,2,3,5,6,7-hexahydroimidazo-[1,2-α-]-pyridine).

(BMM) in flasks, and 150 μL of an IPP stock solution (20 g L^{-1}) was added as the sole carbon source to give a final concentration of 30 mg L^{-1}. The method of enrichment, isolation, and identification of IPP-degrading bacteria and the composition of BMM media were followed in previous reports.[14−17]

The obtained enrichment suspension was streaked on the nutrient agar plates. All of the plates were incubated at 30 °C for 72 h. The morphologically distinct isolates were selected and preserved on a nutrient agar slant at 4 °C.The larger colonies were selected and streaked on the plate for further purification and study. A comparative 16S rRNA gene sequence analysis of IPP-degrading bacteria was performed according to the previous report,[14] and the amplified PCR product was sequenced by Sangon Biotechnology (Shanghai, China).

Biodegradation Assays. To illustrate the biodegradation pathway of IPP in an aquatic system, 250 mL glass flasks were used in all of the degradation studies and 150 μL of the IPP stock solution (20 g L^{-1}) was added to 100 mL of BMM solution to give a final concentration of 30 mg L^{-1}. Three replicates were conducted for all tests. After being cultured for 72 h, cells of *Sphingobacterium* sp. P1-3 were harvested by centrifugation (21 000*g*, 4 °C, 10 min) and washed twice with a 0.85% (w/w) sodium chloride solution.

The biodegradation experiments by IPP-degrading bacteria were carried out in a 250 mL flask on an environmental orbital shaker at 150 rpm. The factors of the pH value (from 6.0, 7.0, and 8.0) and IPP concentration (10, 30, and 50 mg L^{-1}) were studied upon IPP biodegradation. The cultivation and biodegradation experiments were carried out at 30 °C in the dark. At different time intervals (5, 10, 15, 20, 25, and 30 days), the incubation medium was harvested to determine its concentration and monitor its metabolites. The controlled IPP experiment was followed using the same procedures as mentioned above, except that the cells of *Sphingobacterium* sp. P1-3 were not added to BMM solution.

Extraction and Pretreatment. The cultivation was collected by centrifugation (21 000*g*, 4 °C, 10 min). The supernatant was extracted with dichloromethane three times.[14,18] The recovery of IPP ranged from 91.22 to 107.29%, and the relative standard deviation (RSD) was less than 7.58%. The results showed that the extraction method is feasible and satisfactory for the analysis of IPP residues. The dichloromethane extracts were combined and concentrated through a vacuum rotary evaporator at 40 °C until they were almost dry, and then the extracts were dissolved in 1 mL of methanol.

Analytical Procedures. Bacterial growth was analyzed by recording the increase in OD_{600} with a UV−vis spectrophotometer (Gold Spectrumlab 53, Lingguang, China).

IPP was determined with high-performance liquid chromatography (HPLC, Agilent 1260, Agilent Company, USA). The operation

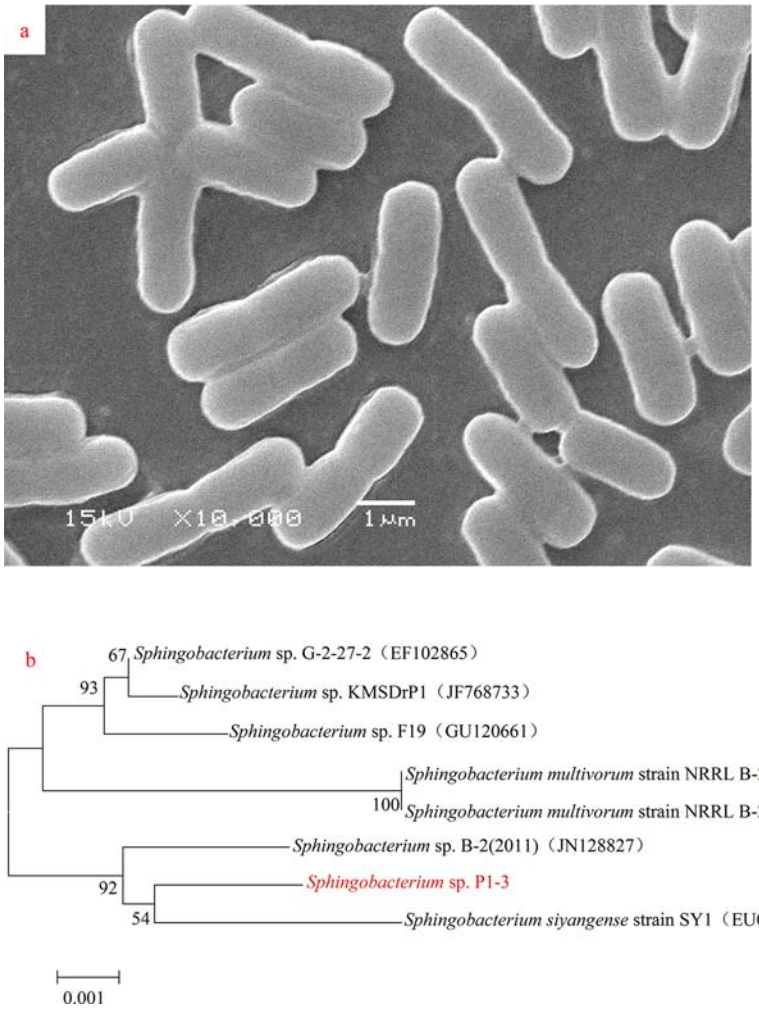

Figure 2. (a) Electron micrograph and (b) phylogenetic tree of strain P1-3 based on the 16S rRNA gene homology.

DOI: 10.1021/acs.jafc.5b00706
J. Agric. Food Chem. 2015, 63, 3823−3829

conditions were as follows: 354 nm, Agilent C_{18} column (3.5 μm, 4.6 × 250 mm^2), and 30 °C. The mobile phase was acetonitrile and pure water (50:50 v/v), and the flow rate was 1.0 mL min^{-1}.

IPP biodegradation intermediates were monitored and analyzed with HPLC (Agilent 1260, 268 nm, C_{18} column (3.5 μm, 4.6 × 250 mm^2)) at 30 °C. Acetonitrile with 0.1% (v/v) acetic acid (HPLC grade) and a mixture of 0.1% (v/v) acetic acid in water (HPLC grade) was used in a linear gradient program (minutes/% acetonitrile: 0/15, 7/15, 20/35, 40/100, 45/100, 50/15, 60/15). The flow rate was 1.0 mL min^{-1}.

LC-MS/MS analysis was conducted using a Dionex U3000 HPLC system coupled with a Bruker maXis 4G ion trap mass spectrometer with an electrospray ionization source (ESI). The separate conditions were in accordance with those used for HPLC analysis. The ion source temperature was controlled at 250 °C, and the capillary voltage was −4.5 kV. The analysis mode of ionization was electrospray ionization (ESI, positive). The operation conditions were as follows: collision energy, 10.0 eV; ISCID energy and ion energy, 5.0 eV; dry gas, 6 L min^{-1}; dry temperature, 180 °C; gas pressure, 1.5 bar. The continuous full scanning from m/z 50 to 500 Da was performed in positive ion mode.

IPP Degradation Kinetics and Calculation. IPP degradation by strain P1-3 followed a first-order exponential decay model. The rate constant from the first-order model was used to determine the DT50 (half-life value). DT50 was calculated by

$$-\ln \frac{c}{c_0} = kt \text{ or } \ln c = -kt + \ln c_0 \quad (1)$$

where C_0 is the initial concentration of IPP (mg L^{-1}), C is the real-time concentration of herbicide at a certain time, t is the incubation time (days), and k is the degradation rate constant of the herbicide (day^{-1}). DT50 and DT90 were calculated as $\ln 2/k$ and $\ln 10/k$, respectively.

RESULTS AND DISCUSSION

Isolation and Identification of IPP-Degrading Bacterium. There were 18 morphologically distinct isolates on the nutrient agar plate, and they could use IPP as the sole carbon and energy source. Isolate P1-3 had higher IPP-degrading activity among these isolates and was chosen for further study.

The physiological and biochemical characteristics are as follows: G$^-$, short rod (0.5−0.6 μm × 0.9−1.9 μm, Figure 2a), aerobic. Oxidase and catalase are positive, and strain P1-3 can utilize fructose, glucose, lactose, malt sugar, mannose, melibiose, starch, raffinose, and cellulose as the energy and carbon source. The colony of strain P1-3 was smooth, wet, and orange after 24 h of incubation.

The 16S rRNA gene sequences were compared by using BLAST similarity searches, and the closely related sequences were obtained from GenBank (Figure 2b). On the basis of the sequence identification of the 16S rRNA gene with GenBank, the highest similarity values of strain P1-3 were closely related to strain *Sphingobacterium* sp. G-2-27-2 (99% identity), *Sphingobacterium* sp. KMSDrP1 (99% identity), *Sphingobacterium multivorum* strain NRRL B-23206 (99% identity), *Sphingobacterium* sp. B-12 (99% identity), and *Sphingobacterium* sp. F19 (99% identity). Morphological and biochemical analysis in combination with phylogenetic analysis based on a partial 16S rRNA gene sequence indicated that strain P1-3 was a member of the genus *Sphingobacterium*. On the basis of these results, strain P1-3 was designated as *Sphingobacterium* sp. P1-3 (GenBank accession numbers KP657689).

Genus *Sphingobacterium* was originally proposed by Yabuuchi et al.;[19] it usually includes *Sphingobacterium multivorum, S. spiritivorum*, and *S. mizutae*. There are limited data showing that *Sphingobacterium* sp. was employed for biodegradation and bioremediation. Janbandhu and Fulekar reported that *Sphingobacterium* sp. had an effective phenanthrene-degrading ability.[20] *Sphingobacterium* sp. JCR5 was isolated from activated sludge; it could degrade 17α-ethynylestradiol, and the degradation rate reached 87%.[21] The results reported by Fang et al. showed that *Sphingobacterium* sp. strain D6 could utilize dichlorodiphenyltrichloroethane (DDT), dichlorodiphenyldichloroethane (DDD), and dichlorodiphenyldichloroethylene (DDE) (DDTs) as its sole carbon and energy source.[22] Strain D6 was also used for the remediation of DDT congeners and cadmium in soil. The degradation half-lives of DDTs in soils treated by strain D6 decreased by 8.1% to 68.0%, and strain D6 and *S. alfredii* could successfully control DDTs and Cd in contaminated soil.[23] In this study, the isolated bacterium capable of IPP degradation was unexpectedly affiliated with the family *Sphingobacterium*. This is the first report using *Sphingobacterium* sp. to biodegrade novel insecticide Paichongding, and there are limited data for IPP degradation by microorganisms.

Effect of Initial pH on IPP Biodegradation. The effect of initial pH on IPP degradation by *Sphingobacterium* sp. P1-3 was investigated in this study. The results of kinetic degradation data of IPP at a concentration of 30 mg L^{-1} in BBM at pH 6.0, 7.0, and 8.0 are shown in Figure 3a and Table 1. Throughout the whole experiment, the hydrolysis percentages of IPP were

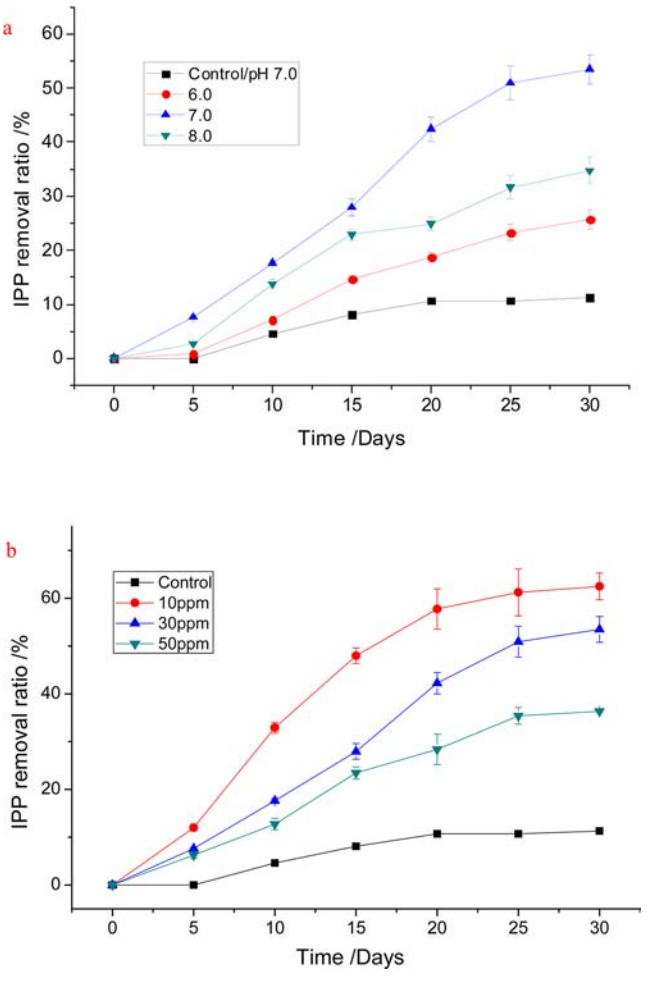

Figure 3. Effects of (a) pH and (b) the initial substrate concentration on IPP biodegradation by *Sphingobacterium* sp. P1-3.

DOI: 10.1021/acs.jafc.5b00706
J. Agric. Food Chem. 2015, 63, 3823−3829

Table 1. Kinetic Data of IPP Degradation by Strain P1-3 at Different pH Values and Concentrations

IPP (mg L^{-1})	pH	kinetic equations	k (day^{-1})	DT50	DT90	R^2
		Effect of pH				
30	6.0	$\ln c = 0.0110t + 3.40$	0.0110	63	209	0.9781
30	7.0	$\ln c = 0.0259t + 3.40$	0.0259	27	89	0.9892
30	8.0	$\ln c = 0.0147t + 3.40$	0.0147	47	157	0.9762
		Effect of Concentration				
10	7.0	$\ln c = 0.0372t + 2.30$	0.0372	19	62	0.9520
30	7.0	$\ln c = 0.0259t + 3.40$	0.0259	27	89	0.9892
50	7.0	$\ln c = 0.0162t + 3.91$	0.0162	43	142	0.9804
		Control				
30	7.0	$\ln c = 0.0046t + 3.40$	0.0046	151	501	0.9348

less than 6%. After incubation for 20 days, the degradation ratio of IPP reached 18.65% at pH 6.0, 42.41% at pH 7.0, and 24.88% at of pH 8.0. The biodegradation rate increases with increasing pH and reaches its maximum at pH 7.0. With further increases in pH, the biodegradation rate decreased and DT50 increased. The results showed that the neutral condition is favorable for IPP biodegradation by strain P1-3, whereas higher or lower pH inhibits degradation. The values of k and DT50 were found to be 0.0259 d^{-1} and 27 d, respectively, whereas DT50 of IPP in the control test was 151 d, which showed that strain P1-3 had a higher IPP degrading activity at pH 7.0 and the IPP degradation rate was highest when the pH value was 7.0. From Figure 3a, it also indicated that IPP could be hydrolyzed in the control test, which was in accordance with the previous report.[5] Compared to the biodegradation process, the hydrolysis ratio was relatively low.

Effect of IPP Concentration on Biodegradation. Figure 3b shows the result of the IPP removal ratio at pH 7.0 and 30 °C at different initial concentrations of 10, 30, and 50 mg L^{-1}. The biodegradation kinetic equations are shown in Table 1. The results show that both the biodegradation rate and the value of k decrease with increasing IPP concentration. The values of k and DT50 were 0.0372 d^{-1}, 19 d and 0.0162 d^{-1}, 43 d when the IPP concentration was 10 and 50 mg L^{-1}, respectively. When the IPP concentration increased, the first-order rate coefficient (k) decreased gradually, indicating that higher initial concentrations of IPP constrain the biodegradation rate, and the degradation rate and DT50 also declined, suggesting substrate inhibition (toxicity to microorganisms or enzymes). Compared to the results of the control experiments, it showed that the removal of IPP was due to bacterial activity and not abiotic degradation. The values of k and DT50 were 0.0046 d^{-1} and 151 d, respectively, in the control experiments.

Identification of Metabolites. The major degradation intermediates of IPP by strain P1-3 in aqueous solution were analyzed and identified by high-performance chromatography time-of-flight mass spectrometry, LC-MS and LC-MS/MS. In this study, five degradation metabolites were observed and analyzed. For each intermediate, its structure and formula were assumed on the basis of information derived from the retention time, elemental formula, its fragmentation pattern from MS^2 spectra, and a comparison with mass spectral data of the metabolite standard.

Novel insecticide IPP had a retention time of 16.87 min, and its mass spectrum showed that ion fragments of IPP were at m/z 367.1551 ($C_{17}H_{23}ClN_4O_3$) $[M + H]^+$, m/z 369.1543, and the ion fragment of m/z 367.1551, including daughter ions of 306.4454 (100), 308.4442 (21), and 137.1082 (50), which were accordance with the structure of standard IPP (Figure 4a).[1,2,5]

During the IPP degradation process by strain P1-3, five metabolites (M1−M5) were monitored and detected by HPLC with retention times of 1.1 min (M1), 32.8 min (M2), 21.2 min (M3), 35.0 min (M4), and 48.6 min (M5), which was accompanied by a decrease in IPP concentration. Among these five metabolites, M1 and M2 appeared first and their concentration increased, followed by the appearance of M3−M5. The content of M3−M5 also decreased gently after 20 days. These results showed that strain P1-3 could not only biodegrade novel insecticide IPP but also could degrade its metabolites (M1, M2, M3, M4, and M5).

According to the LC-MS/MS and MS^2 spectra of the metabolites, the metabolites of M1 and M4 were identified as 1-((6-chloropydidin-3-yl)methyl)-7-methyl-8-nitro- 5-hydroxy-1,2,3,5,6,7-hexahydroimidazo[1,2-α-]-pyridine (Figure 4b) and 1-((6-chloropydidin-3-yl)methyl)-7-methyl-8-amino-1,2,3,5,6,7-hexahydroimidazo [1,2-α-]-pyridine (Figure 4e). The protonated molecular ion clearly showed that there was an even number of nitrogen atoms of M4 and a mass unit loss of 46. This indicated that the oxygen atoms were lost from M1 to form amino product M4. M1 and M4 were also found via IPP degradation in soils as reported by Fu et al.[1,2]

Metabolite M2 was not the daughter of ion of IPP, and the loss of the 26 mass unit was likely a result of the hydroxylation of the nitro on IPP (Figure 4c). M2 had main two daughter ions (281.2967 and 326.3623). Hence, M2 was identified as 1-((6-chloropydidin-3-yl)methyl)-7-methyl-8- hydroxy-5-propoxy-1,2,3,5,6,7-hexahydroimidazo-[1,2-α-]-pyridine.

M3 was determined to be the denitration derivative of M1 based on the elemental formula fit, with the loss of a mass unit of 47 corresponding to $-NO_2$ and H. The M3 ions with m/z was 276.0900 and 278.0796 and matched elemental formula $C_{14}H_{14}ClN_3O$ (Figure 4d); thus M3 was identified as 1-((6-chloropydidin-3-yl) methyl)-7-methyl-5-carbonyl-1,2,3,5,6,7-hexahydroimidazo-[1,2-α-]-pyridine.

Intermediate M5, with m/z 142.1591 (Figure 4f), matched formula $C_7H_{15}N_3$ and was tentatively determined to be generated from M4. An analysis of the daughter ions generated from M5 showed that M5 was 8-amino-1,2,3,5,6,7-hexahydroimidazo-[1,2-α-]-pyridine.

IPP Biodegradation Pathway. On the basis of the five identified metabolites, a biodegradation pathway of IPP by *Sphingobacterium* sp. P1-3 in an aqueous system was proposed (Figure 5). The microbial transformation of IPP revealed four biodegradation patterns of the chloropydidine ring and tetrahydropyridine ring on the IPP parent compound: (i) elimination of propyl, methyl, or nitro; (ii) conversion of nitro to amino; (iii) conversion of nitro group to a hydroxyl; and (iv) cleavage of methyl.

Initially, the propyl group of IPP was de-esterified and hydrolyzed to form M1. Meanwhile, another biocatalyzed reaction was that IPP was hydrolated to generate M2 through the reduction of the nitro group on IPP. The nitro group of M1 was eliminated through the cleavage of the C−N bond, and the hydroxyl was oxidized at the tetrahydropyridine to produce

DOI: 10.1021/acs.jafc.5b00706
J. Agric. Food Chem. 2015, 63, 3823−3829

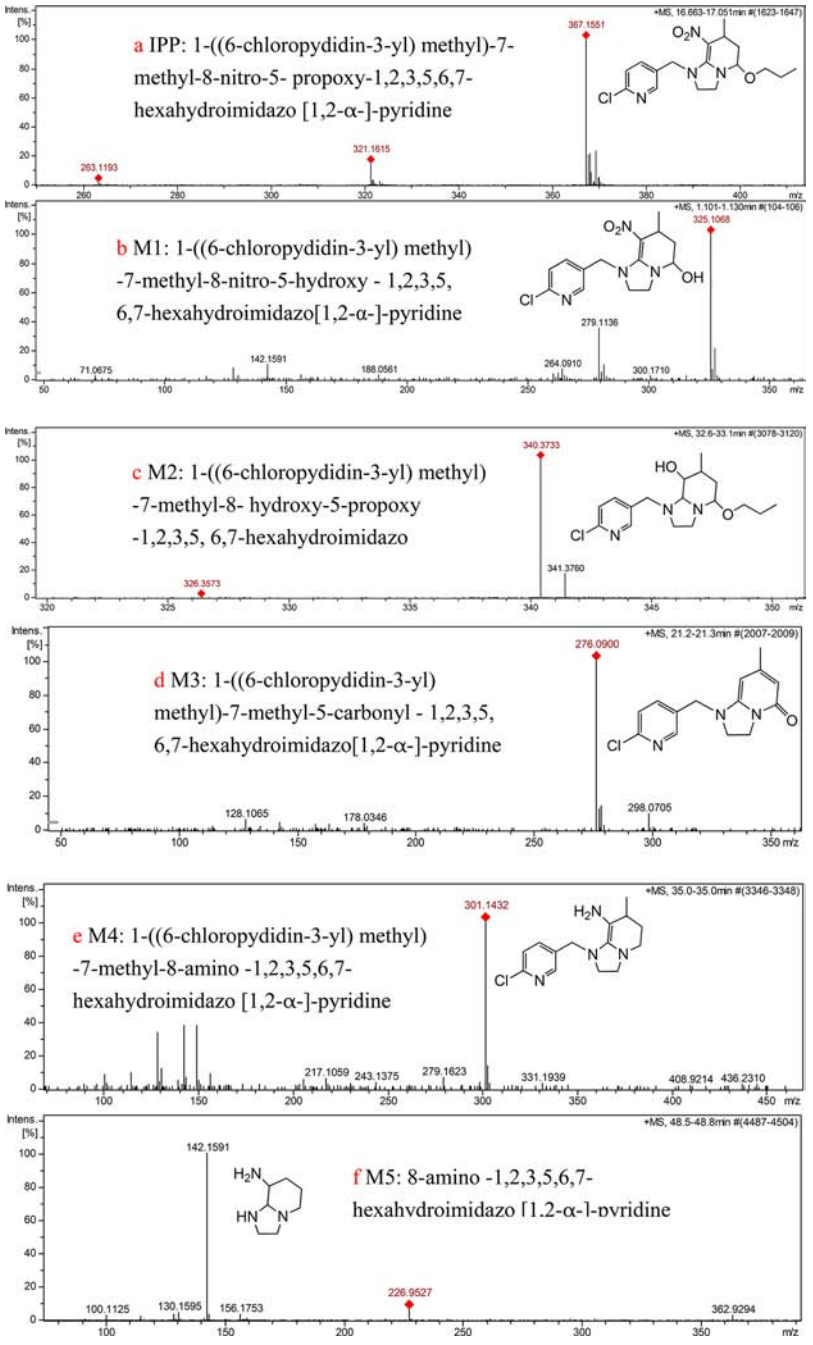

Figure 4. Mass spectra of metabolites formed during the degradation of IPP by *Sphingobacterium* sp. P1-3.

C═O and form carbonyl derivative M3. The nitro group of M1 could also be aminated to form amino product M4. Subsequently, the C−C bond between 1-(6-chloropydidin-3-yl)methyl and 7-methyl-8-amino-1,2,3,5,6,7-hexahydroimidazo-[1,2-α-]-pyridine of M4 was cleaved to form M5. M2, M3, and M5 should be used as carbon source by other microorganism and biodegradated in the environment.

As the proposed pathway described above, the results in this study and observations suggest that the proposed pathway is a major route for IPP degradation by *Sphingobacterium* sp. P1-3 in aquatic systems, which is significantly different from the previously reported pathway in soils and in aqueous systems.[1,2,5] Six metabolites were monitored and identified during the degradation of IPP in soils.[1,2] Zhao et al. reported IPP photodegradation pathway in aqueous solution. In the present study, two metabolites, M1 and M4, were in agreement with those previously studied in soils,[1,2] and M2, M3, and M5 were first monitored and identified in aqueous solution. It was also the first report on IPP biodegradation by a microorganism. The proposed IPP-degrading pathway by *Sphingobacterium* sp. P1-3 provides more information on biodegradation.[1,2]

In this study, *Sphingobacterium* sp. P1-3 with a higher IPP-degrading activity was successfully isolated from soil. The degradation rate by *Sphingobacterium* sp. P1-3 could reach 57.65% within 20 days in an aquatic system. The results indicated that IPP could ultimately be transformed to M5 through continuous biocatalyzed reactions, e.g., de-esterification, elimination of propyl and nitro, amination, hydroxylation, and demethyl reactions. The physicochemical properties of *Sphingobacterium* sp. P1-3 and the investigation of the IPP

DOI: 10.1021/acs.jafc.5b00706
J. Agric. Food Chem. 2015, 63, 3823−3829

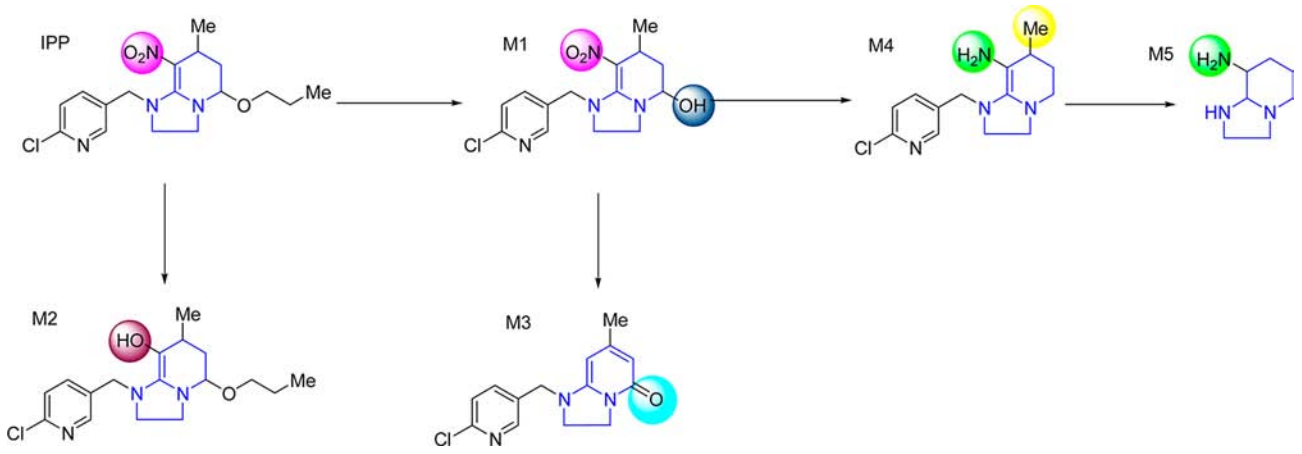

Figure 5. Proposed pathway of IPP biodegradation by *Sphingobacterium* sp. P1-3 in an aqueous system.

biodegradation pathway in aquatic systems open a new pathway for the bioremediation of IPP-contaminated environments.

AUTHOR INFORMATION

Corresponding Author

*Phone: 86-519-86330165. Fax: 86-519-86330165. E-mail: zhqcai@cczu.edu.cn.

Funding

This research was financially supported by grants from the National Natural Science Foundation (project no. 11275033) and the Talent Introduction Foundation of Changzhou University (no. ZMF13020003).

Notes

The authors declare no competing financial interest.

REFERENCES

(1) Fu, Q.; Wang, Y.; Zhang, J.; Zhang, H.; Bai, C.; Li, J.; Wang, W.; Wang, H.; Ye, Q.; Li, Z. Soil microbial effects on the stereoselective mineralization, extractable residue, bound residue and metabolism of a novel chiral cis neonicotinoid, paichongding. *J. Agric. Food Chem.* **2013**, *61*, 7689−7695.

(2) Fu, Q.; Zhang, J.; Xu, X.; Wang, H.; Wang, W.; Ye, Q.; Li, Z. Diastereoselective metabolism of a novel cis-nitromethylene neonicotinoid paichongding in aerobic soils. *Environ. Sci. Technol.* **2013**, *47*, 10389−10396.

(3) Li, J.; Zhang, J.; Li, C.; Wang, W.; Yang, Z.; Wang, H.; Gan, J.; Ye, Q.; Xu, X.; Li, Z. Stereoisomeric Isolation and Stereoselective Fate of Insecticide Paichongding in Flooded Paddy Soils. *Environ. Sci. Technol.* **2013**, *47*, 12768−12774.

(4) Wang, H.; Yang, Z.; Liu, R.; Fu, Q.; Zhang, S.; Cai, Z.; Li, J.; Zhao, X.; Ye, Q.; Wang, W.; Li, Z. Stereoselective uptake and distribution of the chiral neonicotinoidinsecticide, Paichongding, in Chinese pak choi (*Brassica campestris* ssp. *chinenesis*). *J. Hazard. Mater.* **2013**, *262*, 862−869.

(5) Zhao, X.; Shao, X.; Zou, Z.; Xu, X. Photodegradation of Novel Nitromethylene Neonicotinoids with Tetrahydropyridine-Fixed Cis Configuration in Aqueous Solution. *J. Agric. Food Chem.* **2010**, *58*, 2746−2754.

(6) Shao, X.; Zhang, W.; Peng, Y.; Li, Z.; Tian, Z.; Qian, X. *cis*-Nitromethylene neonicotinoids as new nicotinic family: synthesis, structural diversity, and insecticidal evaluation of hexahydroimidazo-[1,2-*α*] pyridine. *Bioorg. Med. Chem. Lett.* **2008**, *18*, 6513−6516.

(7) Tian, Z.; Shao, X.; Li, Z.; Qian, X.; Huang, Q. Synthesis, insecticidal activity, and QSAR of novel nitromethylene neonicotinoids with tetrahydropyridine fixed cis configuration and exo-ring ether modification. *J. Agric. Food Chem.* **2007**, *55*, 2288−2292.

(8) Zhang, J.; Fu, Q.; Wang, H.; Li, J.; Wang, W.; Yang, Z.; Zhang, S.; Ye, Q. Enantioselective Uptake and Translocation of a Novel Chiral Neonicotinoid Insecticide Cycloxaprid in Youdonger (*Brassica campestris* subsp. *Chinensis*). *Chirality* **2013**, *25* (11), 686−691.

(9) Matsuda, K.; Buckingham, S. D.; Kleier, D.; Rauh, J. J.; Grauso, M.; Sattelle, D. B. Neonicotinoids: insecticides acting on insect nicotinic acetylcholine receptors. *Trends Pharmacol. Sci.* **2001**, *22*, 573−580.

(10) Tomizawa, M.; Casida, J. E. Neonicotinoid insecticide toxicology: mechanisms of selective action. Annu. Rev. *Annu. Rev. Pharmacol. Toxicol.* **2005**, *45*, 247−268.

(11) Shao, X.; Lee, P. W.; Liu, Z.; Xu, X.; Li, Z.; Qian, X. *cis*-Configuration: a new tactic/rationale for neonicotinoid molecular design. *J. Agric. Food Chem.* **2011**, *59*, 2943−2949.

(12) Shao, X.; Ye, Z.; Bao, H.; Li, Z.; Xu, X.; Li, Z.; Qian, X. Advanced research on *cis*-Neonicotinoids. *Chimia* **2011**, *65*, 957−960.

(13) Shao, X.; Fu, H.; Xu, X.; Liu, Z.; Li, Z.; Qian, X. Divalent and oxabridged neonicotinoids constructed by dialdehydes and nitromethylene analogues of imidacloprid: design, synthesis, crystal structure, and insecticidal activities. *J. Agric. Food Chem.* **2010**, *58*, 2696−2702.

(14) Cai, Z. Q.; Chen, Q. L.; Wang, H. Y.; He, Y.; Wang, W.; Zhao, X.; Ye, Q. Degradation of the novel herbicide ZJ0273 by *Amycolatopsis* sp. M3−1 isolated from soil. *Appl. Microbiol. Biotechnol.* **2012**, *96* (5), 1371−1379.

(15) Cai, Z. Q.; Huang, L.; He, Y. C.; Shi, S.; Zhao, X. Y.; Wang, L. Enzyme Catalysis and Decolorization of Brilliant Reactive Red X-3B by Azoreductase From a Newly Isolated *Pseudomonas putida* WLY. *Biol. Environ.* **2012**, *112B*, 193−300.

(16) Cai, Z.; Shi, S.; Li, S.; Yang, B.; Chen, Q.; Zhao, X. Microbial degradation characteristics and kinetics of novel pyrimidynyloxybenzoic herbicide ZJ0273 by a newly isolated *Bacillus* sp. CY. *Environ. Sci. Pollut. Res.* **2013**, *20*, 8831−8838.

(17) Yang, G. H.; He, Y. C.; Cai, Z. Q.; Zhao, X. Y.; Wang, L. Q.; Wang, L. Isolation and characterization of *Pseudomonas putida* WLY for reactive brilliant red x-3b decolorization. *Afr. J. Biotechnol.* **2011**, *10*, 10456−10464.

(18) Mordaunt, C. J.; Gevao, B.; Jones, K. C.; Semple, K. T. Formation of non-extractable pesticide residues,observations on compound defferences, measurement and regulatory issues. *Environ. Pollut.* **2005**, *133*, 25−34.

(19) Yabuuchi, E.; Kaneko, T.; Yano, I.; Moss, C. W.; Miyoshi, N. *Sphingobacterium* gen. nov., *Sphingobacterium spiritivorum* comb. nov., *Sphingobacterium multivorum* comb. nov., *Sphingobacterium mizutae* sp. nov., and *Flavobacterium indologenes* sp. nov.: glucosenonfermenting Gram-negative rods in CDC groups IIK-2 and IIb. *Int. J. Syst. Bacteriol.* **1983**, *33*, 580−598.

DOI: 10.1021/acs.jafc.5b00706
J. Agric. Food Chem. 2015, 63, 3823−3829

(20) Janbandhu, A.; Fulekar, M. H. Biodegradation of phenanthrene using adapted microbial consortium isolated from petrochemical contaminated environment. *J. Hazard. Mater.* **2011**, *187*, 333−340.
(21) Ren, H.; Ji, S.; Cui, C.; Wang, D. Degradation pathway of 17α-ethynylestradiol by *Sphingobacterium* sp. JCR5. *Environ. Sci-China* **2006**, *27*, 1835−1840.
(22) Fang, H.; Dong, B.; Yan, H.; Tang, F.; Yu, Y. Characterization of a bacterial strain capable of degrading DDT congeners and its use in bioremediation of contaminated soil. *J. Hazard. Mater.* **2010**, *184*, 281−289.
(23) Fang, H.; Zhou, W.; Cao, Z.; Tang, F.; Wang, D.; Liu, K. Combined remediation of DDT congeners and cadmium in soil by *Sphingobacterium* sp. D-6 and *Sedum alfredi*i Hance. *J. Environ. Sci.* **2012**, *24* (6), 1036−1046.

DOI: 10.1021/acs.jafc.5b00706
J. Agric. Food Chem. 2015, 63, 3823−3829

with mineral matter in soil, could promote physical protection and therewith a high long-term stability.[16]

In this study, we performed four different composting experiments in order to verify the formation of oxygen-containing functional groups (carboxylic acids and phenols) at the biochar surface through composting. Additionally, we investigated original Terra Preta biochar particles and ancient charcoal pit biochars (CPB) to assess the results of the composting experiments.

2. MATERIAL AND METHODS

2.1. Biochar for Compost Experiments. In total, three different biochars were used in this experiment (Tables 1 and 3). First biochar was made from green cuttings, produced in a Pyreg reactor at ~800 °C (Dörth, Germany, www.pyreg.de). Second biochar was prepared from wood chips (a mixture of forestry residues) by CarbonTerra (Augsburg, Germany, www.carbon-terra.eu) at ~550 °C. A detailed description of the Pyreg and CarbonTerra production technologies are published in Wiedner et al.[5] Third biochar was produced from beech wood in a traditional charcoal pit at ~450 °C in Lower Austria (47°52′20.5″N 15°41′48.5″E).

Table 1. Composition of Composts I, II, II, and IV

	Application rate [Mg]			
Ingredients	Compost I	Compost II	Compost III	Compost IV
Green cutting biochar*	0.7			
Wood chips biochar*		0.7		
Beech biochar*			0.57	0.54
Straw*	1.1	1.1		
Draff*	5.3	5.3		
Horse manure*	1.1	1.1		
Chaffed lob* (grass, leaves twigs)			0.97	1.31
Maize silage*	5.3	5.3		
Sewage sludge*				
Biowaste*			1.21	1.64
Loam (Vol%)*	5.3	5.3		
Stone powder*	0.017	0.017		
Loamy sand*			0.24	0.33
EM	no	no	no	added
Duration of composting process in days	45	45	84	84
Fermentation process in days	no	no	no	32
Total mass of initial compost mixture	18.8	18.8	3	3.9
Turning times	7	7	14	8

*Application rates are based on dry matter.

2.2. Compost Experiments. Four different compost experiments were performed at industrial scale, outdoors and under practical field conditions with full exposure to weather conditions at professional composting facilities. The biochars were mixed into the fresh organic material prior to composting. Detailed information about the compost mixtures is given in Table 1. Biochar particles of all four composts were picked manually and cleaned for further analyses (see Section 2.3.3).

Composts I and II (Table 1) were produced within the ClimaCarbo Project (01LY1110B) near Gartow (Wendland region, Northern Germany) supported by the German Federal Ministry for Education and Science (BMBF). Composts III and IV were produced by "Sonnenerde" in Riedlingsdorf, Austria (47°20′33.5″N 16°08′28.0″E). The experiment aimed to evaluate the effects of ordinary composting occurring under aerobic conditions (Compost III) in comparison to possible effects of anaerobic lactic acid fermentation with effective microorganisms (EM; Compost IV).

Preparations with EM are composed of lactic acid producing bacteria, yeasts, phototropic bacteria, actinomycetes, and fungi. The following two products were used from Multikraft GmbH (Wels, Austria, www.multikraft.com): 0.5 L eMB-Starter and 5 L eMB-Aktiv were sprayed per m^3 related to the organic feedstock material for fermentation at the beginning of the experiment. Compost III was turned 6 times during the first 4 weeks in order to ensure enough oxygen supply. Compost IV was not turned within the first 4 weeks to maintain an anaerobic process. After 4 weeks, both piles were turned once a week for the remaining time (8 weeks) to promote better homogenization and stabilization. After the first 4 weeks, Compost IV was treated with both EM solutions again by applying 1 L m^{-3} and 5 L m^{-3} of eMB-Starter and eMB-aktiv, respectively.

Table 3. Chemical Characterization of Fresh and Ancient Biochars

	Black carbon [g C_{bc} kg^{-1} TOC]	pH [CaCl2]	EC [µS cm^{-1}]	Ash [g kg^{-1}]	Total N [g kg^{-1}]
Green cutting biochar[a]	409.9	8.6	1000	126	9.6
Wood chips biochar[b]	468.8	8.6	469	235	6.3
Beech biochar	725.7	8.1	200	117	3.1
Charcoal pit biochar 1[c]	403.2	n.d.	n.d.	n.d.	n.d.
Charcoal pit biochar 2[c]	424.9	n.d.	n.d.	n.d.	n.d.
Charcoal pit biochar 3[c]	382.2	n.d.	n.d.	n.d.	n.d.
Terra preta biochar 1[c]	534.5	n.d.	n.d.	n.d.	n.d.
Terra preta biochar 2[c]	447.6	n.d.	n.d.	n.d.	n.d.
Terra preta biochar 3[c]	507.5	n.d.	n.d.	n.d.	n.d.

[a]Data adopted from Wiedner et al.[5] [b]Data adopted from Glaser et al.[25] [c]Ancient biochars used for black carbon analysis were not the same used for SEM-EDS and FTIM but taken from same soil horizon.

2.3. Historical Charcoals. *2.3.1. Terra Preta Biochars (Brazil).* The Terra Preta biochars were collected from a Terra Preta near Manaus with an average age of about 2000 years.[17] Mean annual temperature (MAT) was 26 ± 3 °C and mean annual precipitation (MAP) was 2500 mm with a dry season between August and November. More details on the collected biochar are given in Table 2.

2.3.2. Historical Charcoal Pit Biochars (Northern Italy). Charcoal pit biochars were collected from 3 charcoal pits located in Val di Pejo (2050 to 2171 m a.s.l.), a lateral valley of Val di Sole, Trentino, in the

Table 2. Sampling Site and Depth (See also Glaser et al. 2000) as Well As Paleobotanical Analysis of Terra Preta Biochars

ID	Terra Preta Site Nr.*	Horizon	Depth [cm]	Characteristics	Taxonomic identification
Terra Preta biochar 1	1	Ah2	5-27	heterogenuous rays, 2-3 cellular; helical thickenings absent; simple perforation;	*LEGUMINOSAE PAPILIONOIDEAE Dalbergia spruceana Benth. (AMAZONAS PALISANDER, AMAZONAS ROSEWOOD)*
Terra Preta biochar 2	1	Ah3	27-50	difusse porous, helical thickenings; unicellular, heterogenuous rays;	*EUPHORBIACEAE Rhodothyrsus macrophyllus; MELASTOMATACEAE Brachyotum SPP.*
Terra Preta biochar 3	5	Ah2	27-40	same as TP site 1, Ah 3; very hard charcoal	*?*

*According the side description in Glaser et al. 2000.

DOI: 10.1021/acs.jafc.5b00846
J. Agric. Food Chem. 2015, 63, 3830−3837

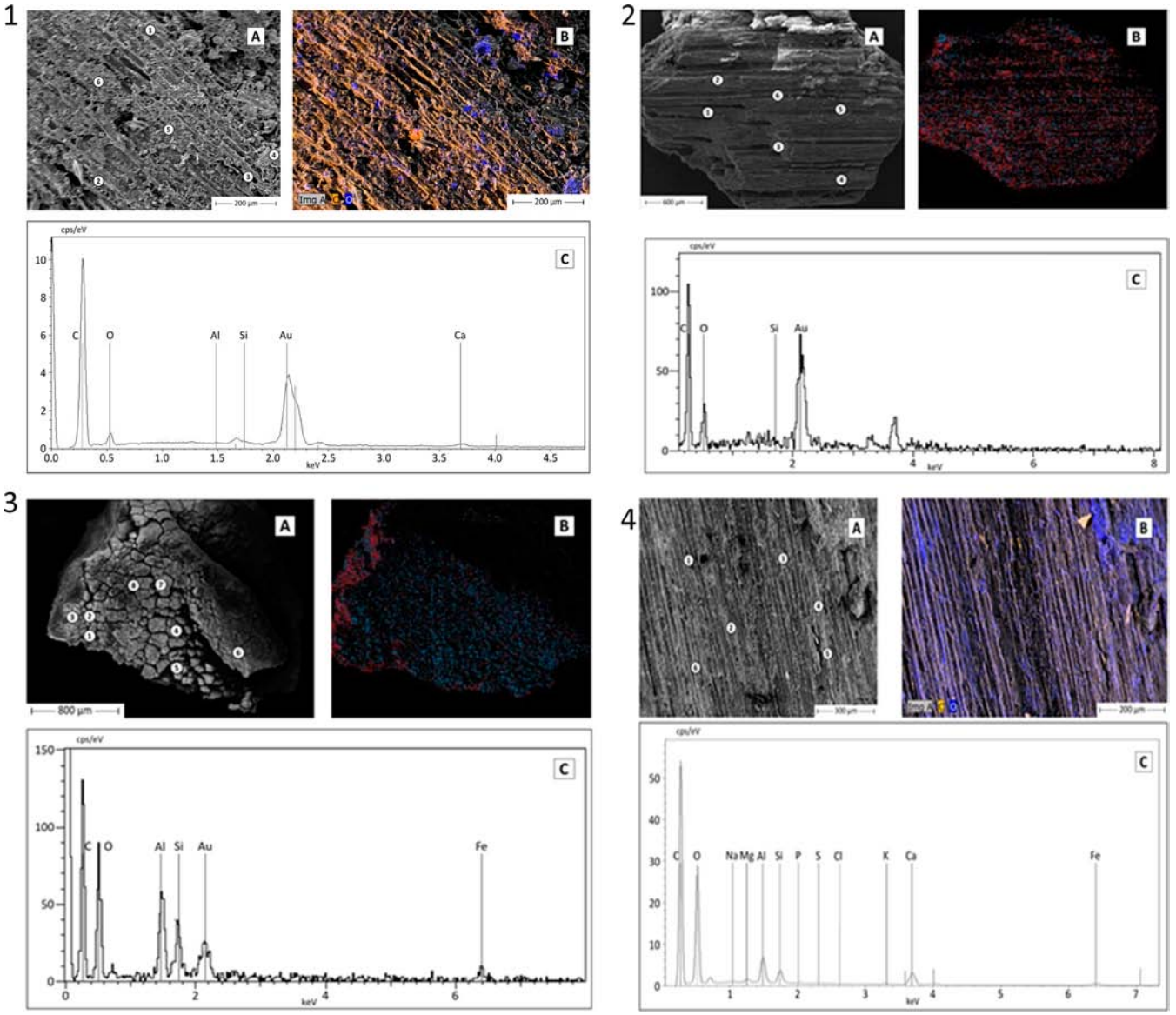

Figure 1. (A) Scanning electron microscope (SEM) picture and points of energy-dispersive X-ray spectroscopy (EDS) analysis; (B) element mapping of O (blue) and C (orange/red); and (C) exemplary EDS spectrum of analyzed points of (1) fresh biochar (green cutting), (2) Compost IV, (3) Terra Preta biochar, and (4) charcoal pit biochar.

southern Alpine belt of northern Italy. The charcoal pit biochars have an average ^{14}C age of 500 years. The climate of the valley ranges from temperate to alpine (above the tree line). MAT ranges from 8.2 °C (valley floor 800 m a.s.l.) to around 0 °C at 2400 m a.s.l. and MAP varies from about 800 to 1300 mm.[14] More detailed information about the Pejo Valley is published by Favilli et al.[18]

2.3.3. Preparation of Biochars for Analysis. Fresh biochars were dried to constant weight at 40 °C and stored at room temperature in plastic bags. Composted and ancient Terra Preta and charcoal pit biochars were cleaned carefully to remove adhesions. Ancient biochars were separately given in conventional bottles with snap-on caps and filled up with deionized water. The bottles were placed in an ultrasonic bath for 30 s. Subsequently, cleaned biochars were removed from water and dried to constant weight at 40 °C and stored in snap-on bottles. Investigated biochars had a particle size of averagely 0.6 × 0.6 mm^2.

2.3.4. Paleobotanical Analysis of Ancient Biochars. Biochars from Terra Preta were analyzed taxonomically (see Table 2) using a stereo lens (Nikon SMZ1500, magnifications ×7.5 to 112.5) and an episcopic microscope (Nikon ME600, ×100, ×200, and ×500). Wood anatomical features were observed on freshly broken surfaces on cross, tangential, and radial sections, according to Wheeler et al.[19] With the coding of the observable features, the InsideWood database was used.[20]

Charcoal pit biochars were analyzed microscopically as conifers with a stereomicroscope (magnification 6.4−40 × , Wild M3Z Leica, Germany).[21] The charcoal fragments from the coniferous trees were divided further at the genus level using a reflected-light microscope (objective 5× , 10×, and 20×, Olympus BX 51, Japan). The observations were compared with a histological wood-anatomical atlas, using an identification key.[22] The species identified are *Larix decidua* L. and *Picea abies* L. Analyzed charcoal pit biochars in this study are from *Larix decidua* L.

2.4. Characterization of Biochars. *2.4.1. pH, Electrical Conductivity and Ash.* Fresh biochar pH and electrical conductivity (EC) were measured using suspensions with 0.01 mol/L $CaCl_2$ and distilled H_2O (1:5). After shaking the suspensions for 1 h on a low speed shaker and sedimentation of solids for another hour at room temperature, EC and pH were determined in the supernatant.

For ash determination, samples were dried for 4 h at 105 °C in a drying oven and weighted after cooling. The dry combustion was

DOI: 10.1021/acs.jafc.5b00846
J. Agric. Food Chem. 2015, 63, 3830−3837

performed in a muffle furnace at 550 °C for 8 h and after cooling in a desiccator, samples were weighted again.

2.4.2. Black Carbon. Black carbon content and composition was determined using the benzene polycarboxylic acids (BPCAs) method of Glaser et al.[23] with the modification of Brodowski et al.[24] Separation and quantification of individual BPCAs was carried out with GC/FID using an HP5 column (30 m × 0.25 mm × 0.25 μm). The sum of individual BPCAs was taken as the black carbon content after multiplication with 2.27 (conversion factor for charcoal as suggested by Glaser et al.[23]).

2.4.3. Total N, Surface and Bulk O/C Ratios of Fresh and Ancient Biochars. Surface O/C ratio of fresh, composted, and ancient biochars were measured with scanning electron microscopy (SEM), a Jeol JSM 6300 SEM, which, for energy-dispersive X-ray spectroscopy (EDS), was coupled with a Bruker X-Flash 5010 detector having an energy resolution of 123 eV. The Quantax 200 Software was applied to evaluate the EDS data to characterize spatial distribution of oxygen on biochars surface differing in age and treatment. Samples were fixed on an object slide with conductive silver (Demetron L200) and coated with gold using a Bal-Tec SCD 050 sputter-coater in a low vacuum atmosphere.

Total N and C analysis was carried out with a "vario EL" analyzer by Elementar GmbH (Hanau, Germany) at the Institute of Chemistry of the Martin-Luther-University in Halle (Germany). The total O content was measured by using a EURO EA Elemental Analyzer (EuroVector, Hekatech, Germany) at the Soil Biogeochemistry Department of the Martin-Luther-University in Halle (Germany).

2.4.4. Fourier Transformation Infrared Microscopy (FTIM). In order to verify organically bound oxygen, FTIM was used as a suitable tool to visualize and quantify aromatic, carboxylic and phenolic functional groups at the biochar surface. In this study, a Nicolet Continuum FTIM coupled with a Nicolet iS50 FT-IR spectrometer (Thermo Fisher Scientific Inc., Waltham, U.S.A.) was used.

All samples were analyzed in the reflectance FTIM imaging mode while collecting all FTIM spectra in the mid-infrared range from 1585 to 1600 cm^{-1} (aromatics), 1700−1725 cm^{-1} (carboxylic acids), and 1190−1210 cm^{-1} (phenols) using 4 cm^{-1} spectral resolution and 64 scans for each single point collection. A XT-KBr beamsplitter was used during the analysis, autogain was enabled, and aperture was set to 100%. FTIM surface map areas comprised 16 × 16 spectra using a 10 μm step size resulting in a square map image of 150 × 150 μm^2. The data were preprocessed using the OMNIC Atlus software version 9.1.24 (Thermo Fisher Scientific Inc., Waltham, U.S.A.) by performing a conversion from reflectance to absorbance at first and, second, by undertaking an automatic baseline correction.

2.5. Statistics. The statistical software package SPSS Statistics 17.0[25] and R[26] for Windows was used for statistics. Kolmogorov−Smirnov test was used for testing data on normal distribution. Statistical differences among means were tested using ANOVA or a nonparametric Kruskal−Wallis test for the FTIM-mapping data, followed by a nonparametric multiple comparison test based on Holm−Bonferroni corrections. Tukey HSD post hoc test was applied for normal distributed data to compare means. The nonparametric Mann−Whitney U test was applied when normal distribution could not be achieved by logarithmic transformation. Significance levels were defined as highly significant ($p \leq 0.01$), significant ($0.01 < p < 0.05$), and not significant ($p > 0.05$). For statistical analysis of surface oxidation (O/C ratio), a minimum of 5 EDS spectra were measured on each biochar on three independent biochars per category.

3. RESULTS

3.1. General Characterization of Biochars. Chemical properties of fresh biochars such as pH, EC, ash, and total N are given in Table 3. Due to the small quantity of ancient biochars, general characterization could not be made.

The pH value ($CaCl_2$) of fresh biochar is between 8.1 and 8.6. EC show high variability with values ranging from 200 (beech biochar) to 1000 (green cutting biochar) μS cm^{-1}. Ash content of green cutting and beech biochar is more or less equal (126 and 117 g kg^{-1}, respectively) in contrast to wood chips biochar with an ash content of 235 g kg^{-1}. Total N content ranged between 3.1 (beech biochar) and 9.6 (green cutting biochar).

Black carbon contents (Table 3) were measured on fresh and ancient biochars. It should be noted that the black content of ancient biochars were not analyzed on the same biochars used for SEM-EDS and FTIM analysis. For fresh biochars, black carbon contents show high variations, ranging between 409.9 (green cutting biochar) and 725.7 (beech biochar) g C_{bc} kg^{-1} TOC. Black carbon content of charcoal pit biochars ranges between 382.2 and 403.2 g C_{bc} kg^{-1} TOC, whereas Terra Preta biochars show black carbon contents between 447.6 and 534.5 g C_{bc} kg^{-1} TOC (Table 3).

A more detailed description and discussion about green cutting and wood chips biochar is published in Wiedner et al.[5] Glaser et al.[28]

3.2. Surface and Bulk O/C Ratios of Fresh and Ancient Biochars. Images of Figure 1 show points of EDS analysis, elemental mapping, and an exemplarily EDS spectrum of analyzed points for fresh, composted, and ancient charcoals. Surface O/C ratios of fresh biochars increased significantly ($p < 0.05$) on average from 0.13 to 0.40 after composting (Figure 2).

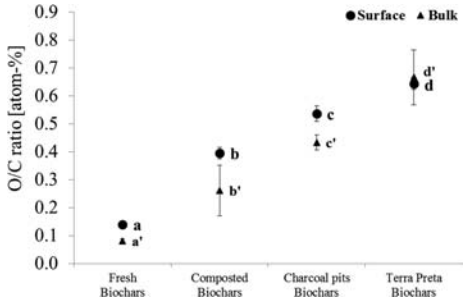

Figure 2. Mean surface (SEM-EDS) and bulk O/C ratios of fresh, composted, and historical biochars (charcoal pit and Terra Preta). Letters indicate significant differences (Tukey HSD test; $p < 0.05$; Error bars show SE).

In contrast, ancient biochars showed mean surface O/C ratios of 0.54 for charcoal pit and 0.64 for Terra Preta, being significantly higher compared to fresh and composted biochars (Figure 2).

The trend of bulk O/C ratios was similar as for surface O/C ratio. Lower bulk O/C ratios (Figure 2) could be observed for fresh, composted, and charcoal pit biochars of 0.08, 0.26, 0.43, and 0.67, respectively, indicating a higher aromaticity in the interior of the biochar particles. Terra Preta biochar particles showed similar surface and bulk O/C ratios of 0.64 and 0.67, respectively, indicating a high oxidation degree even in the interior of the biochar particle (Figure 2).

3.3. Surface Functional Groups. Energy-dispersive X-ray spectroscopy analysis displayed also the presence of Al, Si, and Fe on composted and ancient biochars (Figure 1). Organically bound oxygen is visualized by FTIM mapping (Figure 3) showing the relative distribution of phenols and carboxylic acids on the surface of Terra Preta, charcoal pit, and beech biochar prior and after composting (Compost III and IV). The images show that the ancient Terra Preta and charcoal pit biochars are dominated by carboxylic groups, whereas the proportion of carboxylic and phenolic groups on composted biochars are

DOI: 10.1021/acs.jafc.5b00846
J. Agric. Food Chem. 2015, 63, 3830−3837

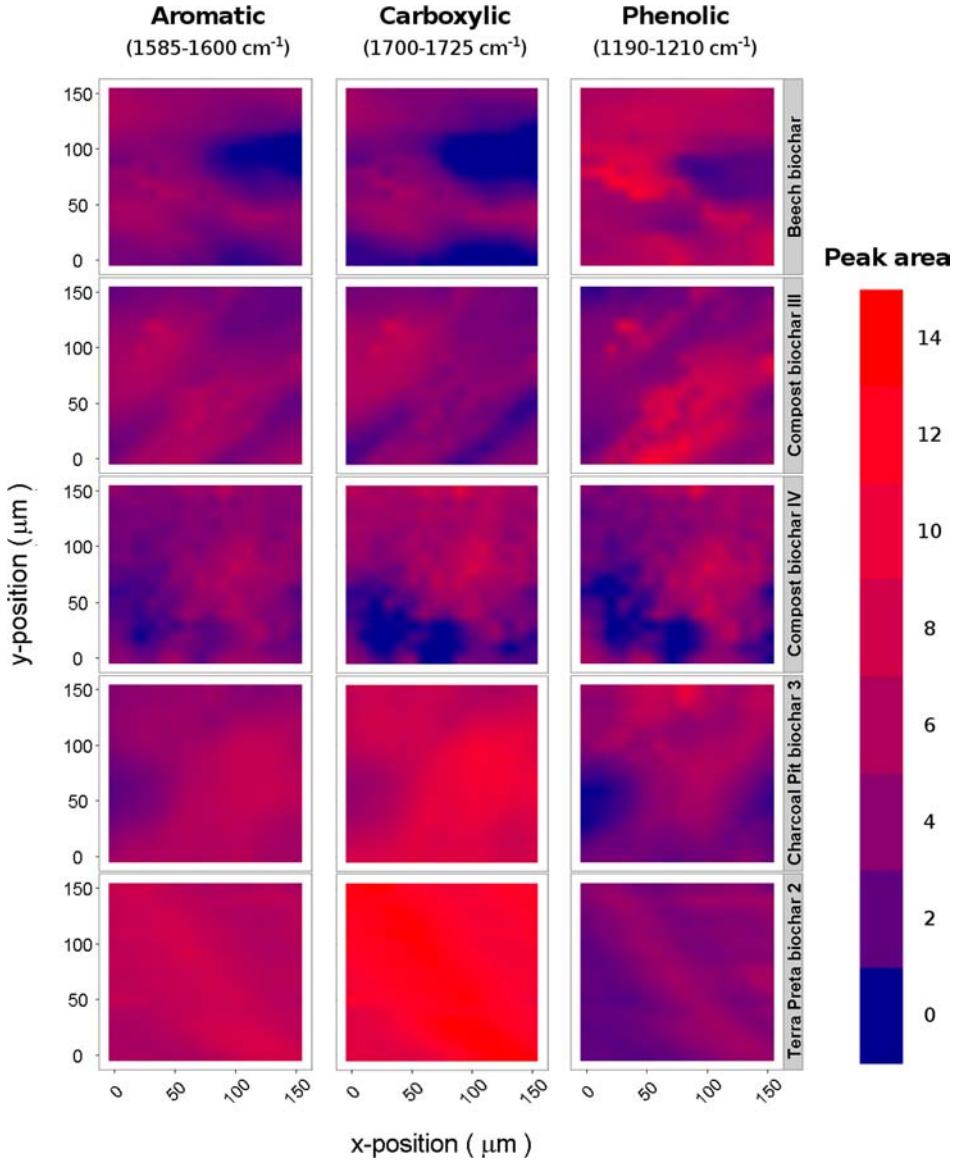

Figure 3. Fourier Transformation Infrared spectroscopy mapping of carboxyl and phenol groups on fresh (beech), composted (Compost III and IV)), charcoal pit biochar3, and Terra Preta biochar2.

equal. Fresh beech biochar is dominated by phenolic groups (Figure 3).

Data in Table 4 and Figure 4 show that the relative contribution of carboxylic acids on fresh biochars increased with increasing production temperature in the following order 20 ± 1% (beech biochar, ~450 °C) < 29 ± 1% (wood chips biochar, ~550 °C) < 41 ± 1% (green cutting biochar, ~800 °C). In contrast, the percentage of phenolic groups are highest at low production temperature (52 ± 1%, beech biochar, ~450 °C) decreasing to 33 ± 1% for wood chips biochar (~550 °C) and 22 ± 1% for green cutting biochar (~800 °C).

After composting, the percentage of carboxylic acids increased significantly ($p < 0.05$) for biochars produced at ~450 °C (beech) and ~550 °C (wood chips) whereas phenolic groups decreased significantly (Table 4). A reversed effect could be shown for composted green cutting biochar (produced at ~800 °C). The percentage of carboxylic acids significantly decreased and phenols significantly increased ($p < 0.05$) from 41 ± 1% to 20 ± 1% and 22 ± 1% to 45 ± 1%, respectively (see Table 4). The comparison of compost experiments III (aerobic) and IV (anaerobic) show that percentage of carboxylic acids increased significantly when composted with EM, whereas phenols significantly decreased (Table 4).

The carboxylic to aromatic ratios of ancient biochars (Table 4) were on average 1.7 and a lower phenolic to aromatic ratio of 0.7 (charcoal pit biochars) and 0.4 (Terra Preta biochars). In contrast, fresh and composted biochars exhibited an average carboxylic to aromatic ratio of 0.9, whereas the phenolic to aromatic ratio was higher (1.1 and 1.0 for fresh and composted biochar, respectively).

4. DISCUSSION

4.1. Properties of Ancient Biochar Particles. The question remains open whether the high surface oxidation of the ancient Terra Preta and charcoal pit biochars is the product of abiotic oxidation leading to the oxidation of exposed C rings with a high density of π-electrons and free radicals or biotic oxidation.[29] In the latter case, microorganisms incorporate O into the biochar structure.[30] Under natural conditions,

DOI: 10.1021/acs.jafc.5b00846
J. Agric. Food Chem. 2015, 63, 3830−3837

Table 4. Relative Contribution of Surface Functional Groups [%] and Ratios on Fresh, Composted, and Ancient Biochars

	Aromatic [%] 1585-1600	Carboxylic [%] 1700-1725	Phenolic [%] 1190-1210	Ratio carboxylic/ aromatic	Ratio phenolic/ aromatic
Wood chips biochar[1,a]	38 ± 1 b	29 ± 1 a'	33 ± 1 a"	0.8	0.9
Compost I[1,a]	31 ± 0 a	42 ± 0 b'	27 ± 0 b"	1.3	0.8
Green cutting biochar[2,a]	36 ± 1 a	41 ± 1 b'	22 ± 1 b"	1.1	0.6
Compost II[2,a]	36 ± 1 a	20 ± 1 a'	45 ± 1 a"	0.6	1.3
Beech biochar[3,b]	27 ± 0 a	20 ± 1 a'	52 ± 1 c"	0.7	1.9
Compost III[3,b]	33 ± 0 b	30 ± 1 b'	37 ± 1 b"	0.9	1.1
Compost IV[3,b]	36 ± 1 c	34 ± 1 c'	30 ± 1 a"	1.0	0.8
Charcoal pit biochar 1	31 ± 0 b	55 ± 0 e'	13 ± 1 g"	1.8	0.4
Charcoal pit biochar 2	25 ± 0 e	47 ± 0 f'	28 ± 0 h"	1.9	1.1
Charcoal pit biochar 3	30 ± 0 f	48 ± 0 g'	22 ± 1 c"	1.6	0.7
Terra Preta biochar 1	31 ± 0 f	53 ± 0 h'	15 ± 0 i"	1.7	0.5
Terra Preta biochar 2	36 ± 0 a	54 ± 0 i'	10 ± 0 j"	1.5	0.3
Terra Preta biochar 3	31 ± 0 f	57 ± 0 j'	12 ± 0 k"	1.8	0.4

[1,2,3]Biochars used for the composts with the same foodnote. [a]Statistical evaluation was performed with the Mann−Whitney U-test; $p < 0.05$. [b]Statistical evaluation was performed with a Kruskal−Wallis test followed by a multiple comparison; $p < 0.05$.

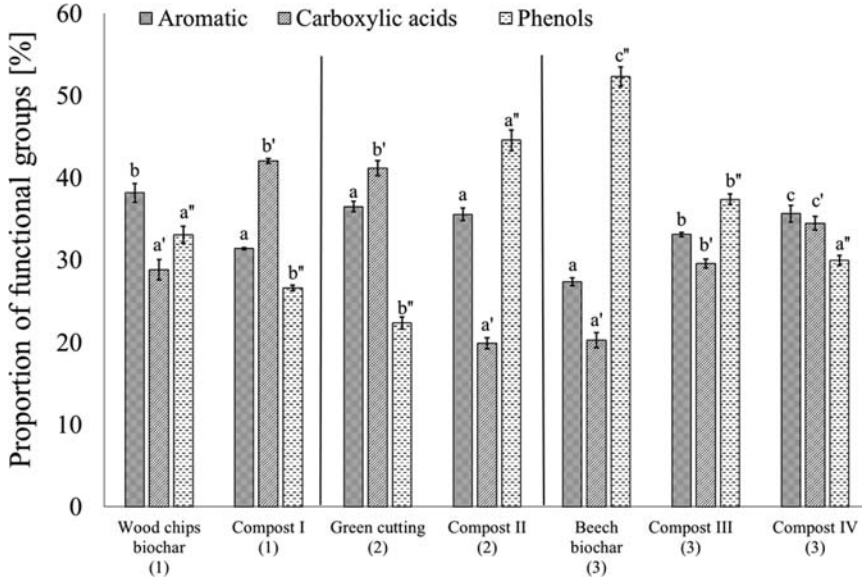

Figure 4. Proportion of functional groups (aromatic, carboxylic, and phenolic) on biochar before and after composting. Letters indicate significant differences (Mann-Withney U-test and Kruskal−Wallis test; $p < 0.05$; Error bars show SE; numbers in brackets indicate same biochar).

formation of O containing functional groups on biochar particles is a matter of time and strongly depends on soil environmental conditions such as moisture, temperature, soil C content or microbial community. For instance, Joseph et al.[27] used XPS to determine fresh and aged biochars after two years exposure in a Ferrosol in subtropical Australia. The authors observed an increase of surface O/C ratio from 0.2 (fresh biochar) to 0.75 (aged biochar). In comparison, Mao et al.[30] investigated biochar particles from a Terra Preta soil in Amazonia (>800 years old) and a Mollisol in Iowa in the U.S. (generated by presettlement fires) using two-dimensional NMR heteronuclear correlation spectroscopy. Terra Preta biochars investigated by Mao et al.[27] had an O/C ratio of ∼0.4, which is in comparison to the O/C ratios of Terra Preta biochars (∼0.64, see Figure 2) in this study rather low. Surface O/C ratios of the Iowa Mollisol biochar particles were only ∼0.2 which is negligible higher than the O/C ratios of fresh biochars determined in this study (Figure 2). The abundance of carboxyl groups on ancient biochar particles as shown by FTIM (Figure 3) was also detected by Mao et al.[30] NMR spectroscopy strongly indicate that carboxyl groups are directly bonded to the aromatic rings of biochar.[30] Joseph et al.[27] however, suggest that the increase of O containing functional groups on biochar surface is a combination of biochar oxidation and/or the absorption of natural organic matter (NOM) or microbial exudates. Liang et al.[31] compared ancient Terra Preta biochar particles from different soil depths applying scanning transmission X-ray microscopy (STXM)-near-edge X-ray absorption fine structure (NEXAFS) spectroscopy. Biochar particles from the A horizon were coated with NOM comparable to humic acids extracts and biofilm substances. In deeper soil horizons, biochar particles had only low proportions of NOM on its surface. Instead, the ratio of oxidized C to aromatic C increased from 2.9 to 3.1 with increasing soil depth showing an increased oxidation with aging.[31]

DOI: 10.1021/acs.jafc.5b00846
J. Agric. Food Chem. 2015, 63, 3830−3837

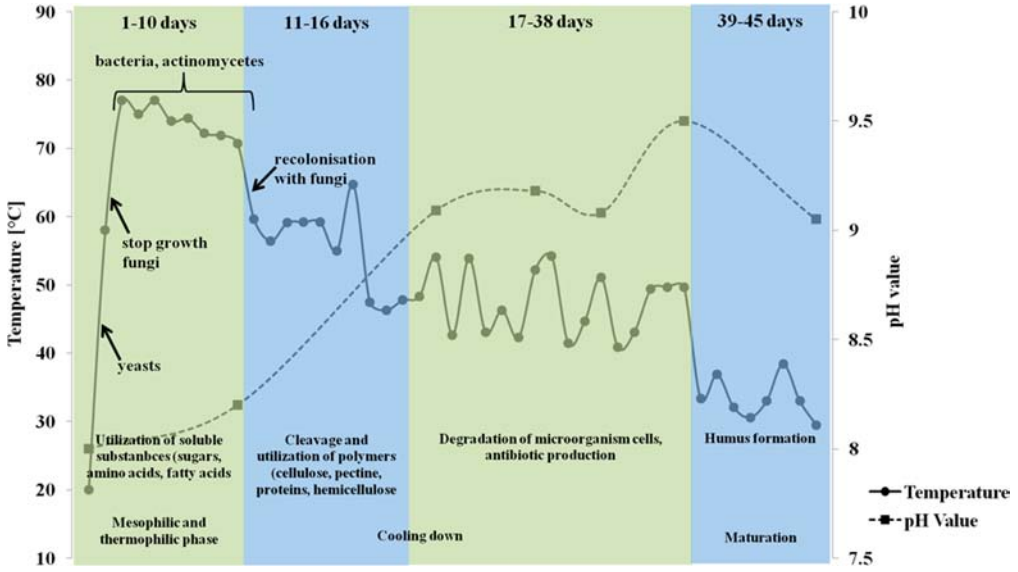

Figure 5. Temperature and pH during the composting process within 45 days of Compost I, complete with supporting information about the chemical and biological process during composting.

4.2. Composting As Driving Force for a Rapid and High Biochar Surface Modification? The compost experiments in this study showed that composting seems to be a suitable method to increase oxygen containing functional groups on biochar surface (Figure 4). However, the high proportion of oxygen as measured on ancient Terra Preta and charcoal pit biochars could not be achieved through composting, neither with ordinary composting (Compost I, II, and III) nor with anaerobic lactic acid fermentation with EM (Compost IV). The formation of carboxylic groups on beech biochar seem to be promoted when comparing compost experiment III and IV, which is not the case for phenols (Figure 4).

It is not clear whether O containing functional groups originated through biochar surface oxidation (abiotic or biotic) during composting or from the adsorption of NOM or microbial residues derived from compost. It is highly probable that the increase of O containing functionality during cocomposting of biochar is due to a complex interaction of both oxidation and adsorption.

O containing functional groups are derived from abiotic and biotic oxidation on biochar surface, resulting from highly complex interactions of temperature and pH, which in turn affect microbial activity and community (Figure 5). For instance, basic soil environments can accelerate self-humification of biochar as studied by Cohen-Ofri et al.[32] in archeological environments. In our biochar compost mixture, the typical acidification phase during the mesophilic phase does not occur (Figure 5). The initial pH value of 8 (first day) increased to 9.5 and slightly decreased to 9.1 on day 45. It is highly probable that biochar acts as buffer and prevents the acidification phase. This potential shift in pH value through biochar addition and the impact on microorganisms and in particular on biochar surface oxidation require further investigation. The incorporation of O into the biochar structure through microbial oxidation is still hard to document. Besides O incorporation, further effects such as cation exchange capacity, charge, or acidity are hard to distinguish from effects due to adsorption/desorption of nonbiochar components, such as microbial exudates or NOM.[29] Prost et al.[33] composted biochar with farmyard manure and observed a significant increase of biochar's potential CEC, but a declined surface area of biochar. The authors suggest that the interception and sorption of compost-derived organic materials clogged micropores, leading to a decreased surface area but adsorbed organic materials increased potential CEC of biochar.[33]

Although it could not be clarified in this study which mechanisms/interactions are responsible for the increase of carboxyl groups on biochar surface by an average of 12% (Compost I, III and IV), however, composting accelerates the development of carboxyl groups which have an important function to retain nutrients on biochar surface.[34] Under natural conditions, the development of carboxyl groups to a significant amount needs years (or even decades), as showed by a study of Singh et al.[35] The authors incubated biochar into four contrasting soils for up to 2 years, which did not lead to a significant increase of carboxyl groups on its surfaces as investigated with NEXAFS and X-ray photoelectron spectroscopy (XPS). In contrast, Hua et al.[8] cocomposted bamboo biochar (produced at 600 °C) and observed an increase of carboxylic groups by 2.4-fold after 42 days of composting, which is inherent with the results of our compost experiments (except Compost II, Table 4). The compost experiments from Hua et al.[8] also showed an increase of penolic groups by 1.5-fold, which is in contrast to our results where the proportion of phenolic groups decreased in extreme cases from 52% initially (beech biochar) to 30% (Compost IV) after composting (Table 4). Except biochar from the Compost II experiment doubled the percentage of phenolic groups (Table 4).

In conclusion, high surface oxidation of ancient biochar particles in Terra Preta is the key factor of increased CEC. The results indicate that composting seem to be a suitable method to accelerate the formation of organically bonded oxygen containing functional groups on the surface of fresh biochars. However, further research is necessary that examines the extent of biotic and abiotic processes during biochar oxidation and how to bring biochar surface properties into a state similar to ancient biochars within a short period of time under practical conditions.

DOI: 10.1021/acs.jafc.5b00846
J. Agric. Food Chem. 2015, 63, 3830−3837

AUTHOR INFORMATION

Corresponding Author

*Tel: 0345-55225540; e-mail: katja.wiedner@landw.uni-halle.de (K.W.).

Funding

We thank the European Community for financial support within the EuroChar project (FP7-ENV-2010ID-265179). We also kindly acknowledge the financial support of the German Federal Ministry for Education and Science (BMBF) within the ClimaCarbo project (01LY1110B).

Notes

The authors declare no competing financial interest.

ACKNOWLEDGMENTS

The authors gratefully acknowledge the producers Pyreg (Dörth, Germany, www.pyreg.de) and CarbonTerra (Augsburg, Germany, www.carbon-terra.eu). We thank all the helpers in the field for collecting the historical charcoals.

REFERENCES

(1) Glaser, B.; Balashov, E.; Haumaier, L.; Guggenberger, G.; Zech, W. Black carbon in density fractions of anthropogenic soils of the Brazilian Amazon region. *Org. Geochem.* **2000**, *31*, 669−678.

(2) Lehmann, J.; Liang, B.; Solomon, D.; Lerotic, M.; Luizão, F.; Kinyangi, J.; Schäfer, T.; Wirick, S.; Jacobsen, C. Near-edge X-ray absorption fine structure (NEXAFS) spectroscopy for mapping nano-scale distribution of organic carbon forms in soil: Application to black carbon particles. *Global Biogeochem. Cycles* **2005**, *19*, GB 1013.

(3) Glaser, B. Prehistorically modified soils of central Amazonia: a model for sustainable agriculture in the twenty-first century. *Philos. Trans. R. Soc. B* **2007**, *362*, 187−196.

(4) Cheng, C.-H.; Lehmann, J.; Thies, J. E.; Burton, S. D.; Engelhard, M. H. Oxidation of black carbon by biotic and abiotic processes. *Org. Geochem.* **2006**, *37*, 1477−1488.

(5) Wiedner, K.; Rumpel, C.; Steiner, C.; Pozzi, A.; Maas, R.; Glaser, B. Chemical evaluation of chars produced by thermochemical conversion (gasification, pyrolysis and hydrothermal carbonization) of agro-industrial biomass on a commercial scale. *Biomass Bioenerg.* **2013**, *59*, 264−278.

(6) Hina, K.; Bishop, P.; Arbestain, M. C.; Calvelo-Pereira, R.; Maciá-Agulló, J. A.; Hindmarsh, J.; Hanly, J. A.; Macías, F.; Hedley, M. J. Producing biochars with enhanced surface activity through alkaline pretreatment of feedstocks. *Aust. J. Soil Res.* **2010**, *48*, 606.

(7) Jindo, K.; Suto, K.; Matsumoto, K.; García, C.; Sonoki, T.; Sanchez-Monedero, M. A. Chemical and biochemical characterisation of biochar-blended composts prepared from poultry manure. *Bioresour. Technol.* **2012**, *110*, 396−404.

(8) Hua, L.; Wu, W.; Liu, Y.; McBride, M. B.; Chen, Y. Reduction of nitrogen loss and Cu and Zn mobility during sludge composting with bamboo charcoal amendment. *Energy Fuels* **2009**, *16*, 1−9.

(9) Bird, M. I.; Moyo, C.; Veenendaal, E. M.; Lloyd, J.; Frost, P. Stability of elemental carbon in a savanna soil. *Global Biogeochem. Cycles* **1999**, *13*, 923−932.

(10) Rumpel, C.; Chaplot, V.; Planchon, O.; Bernadou, J.; Valentin, C.; Mariotti, A. Preferential erosion of black carbon on steep slopes with slash and burn agriculture. *Catena* **2006**, *65*, 30−40.

(11) Liang, B.; Lehmann, J.; Solomon, D.; Kinyangi, J.; Grossman, J.; O'Neill, B.; Skjemstad, J. O.; Thies, J.; Luizão, F. J.; Petersen, J.; Neves, E. G. Black Carbon Increases Cation Exchange Capacity in Soils. *Soil Sci. Soc. Am. J.* **2006**, *70*, 1719.

(12) Czimczik, C. I.; Masiello, C. A. Controls on black carbon storage in soils, *Global Biogeochem. Cycles* **2007**, *21*.

(13) Uchimiya, M.; Wartelle, L. H.; Klasson, K. T.; Fortier, C. A.; Lima, I. M. Influence of pyrolysis temperature on biochar property and function as a heavy metal sorbent in soil. *J. Agric. Food Chem.* **2011**, *59*, 2501−2510.

(14) Trigo, C.; Spokas, K.; Cox, L.; Koskinen, W. C. Influence of soil biochar aging on sorption of the herbicides MCPA, Nicosulfuron, Terbuthylazine, Indaziflam, and Fluoroethyldiaminotriazine. *J. Agric. Food Chem.* **2014**, *62*, 10855−10860.

(15) Qian, L.; Chen, B. Interactions of aluminum with biochars and oxidized biochars: Implications for the biochar aging process. *J. Agric. Food Chem.* **2014**, *62*, 373−380.

(16) Brodowski, S.; John, B.; Flessa, H.; Amelung, W. Aggregate-occluded black carbon in soil. *Eur. J. Soil Science.* **2006**, *57*, 539−546.

(17) Servizio Idrografico. *Precipitazione medie mensili ed annue per il Trentino 1921−1950*; Istituto Poligrafico Dello Stato. Libreria Dello Stato: Roma, 1959.

(18) Favilli, F.; Cherubini, P.; Collenberg, M.; Egli, M.; Sartori, G.; Schoch, W.; Haeberli, W. Charcoal fragments of Alpine soils as an indicator of landscape evolution during the Holocene in Val di Sole (Trentino, Italy). *Holocene.* **2010**, *20*, 67−79.

(19) IAWA Committee. IAWA List of Microscopic Features for Hardwood Identification by an IAWA Committee. In: *IAWA Bulletin*; Wheeler, E. A., Baas, P., Gasson, P. E.; Eds., **1989**, n.s. *10*, 219−332.

(20) InsideWood Onwards. Published on the Internet, 2004. http://insidewood.lib.ncsu.edu/search. Thursday, September 6, 2012.

(21) Schoch, W. Wood and charcoal analysis. In *Handbook of Holocene Palaeoecology and Palaeohydrology*; Berglund, B. E., Ed.; John Wiley and Sons Ltd: Chichester, U.K., 1986; pp 619−626.

(22) Schweingruber, F. H. *Anatomy of European Woods. An Atlas for the Identification of European Trees, Shrubs and Dwarf Shrubs*; Verlag Paul Haupt: Bern, 1990.

(23) Glaser, B.; Haumaier, L.; Guggenberger, G.; Zech, W. Black carbon in soils: the use of benzenecarboxylic acids as specific markers. *Org. Geochem.* **1998**, *29*, 811−8119.

(24) Brodowski, S.; Rodinov, A.; Haumaier, L.; Glaser, B.; Amelung, W. Revised black carbon assessment using benzene polycarboxylic acids. *Org. Geochem.* **2005**, *36*, 1299−1310.

(25) SPSS Inc. Released 2008. *SPSS Statistics for Windows*, Version 17.0. SPSS Inc.: Chicago, 2008.

(26) R CORE TEAM. *R: A language and environment for statistical computing*. R Foundation for Statistical Computing: Vienna, Austria, 2012.

(27) Joseph, S. D.; Camps-Arbestain, M.; Lin, Y.; Munroe, P.; Chia, C. H.; Hook, J.; van Zwieten, L.; Kimber, S.; Cowie, A.; Singh, B. P.; Lehmann, J.; Foidl, N.; Smernik, R. J.; Amonette, J. E. An investigation into the reactions of biochar in soil. *Aust. J. Soil Res.* **2010**, *48*, 501.

(28) Glaser, B.; Wiedner, K.; Seelig, S.; Schmidt, H.-P.; Gerber, H. Biochar organic fertilizers from natural resources as substitute for mineral fertilizers. *Agron Sustain. Dev.* **2014**, 1−12.

(29) Pignatello, J. J.; Uchimiya, M., Abiven, S.; Schmidt, M. W. I. Evolution of biochar properties in soil. In *Biochar for Environmental Management*, 2nd ed.; Lehmann, J., Joseph, S., Eds.; Routledge: London, England, 2015; pp 195−234.

(30) Mao, J.-D.; Johnson, R. L.; Lehmann, J.; Olk, D. C.; Neves, E. G.; Thompson, M. L.; Schmidt-Rohr, K. Abundant and Stable Char Residues in Soils: Implications for Soil Fertility and Carbon Sequestration. *Environ. Sci. Technol.* **2012**, *46*, 9571−9576.

(31) Liang, B.; Wang, C.-H.; Solomon, D.; Kinyangi, J.; Luizao, F. J.; Wirick, S.; Skjemstad, J. O.; Lehmann, J. Oxidation is key for black carbon surface functionality and nutrient retention in Amazon anthrosols. *Br. J. Environ. Clim. Change* **2013**, 3 (no 1), 9−23.

(32) Cohen-Ofri, I.; Weiner, L.; Boaretto, E.; Mintz, G.; Weiner, S. Modern and fossil charcoal: aspects of structure and diagenesis. *J. Archaeol. Sci.* **2006**, *33*, 428−439.

(33) Prost, K.; Borchard, N.; Siemens, J.; Kautz, T.; Séquaris, J.-M.; Möller, A.; Amelung, W. Biochar Affected by Composting with Farmyard Manure. *J. Environ. Qual.* **2013**, *42*, 164.

(34) Glaser, B.; Haumaier, L.; Guggenberger, G.; Zech, W. The "Terra Preta" phenomenon: a model for sustainable agriculture in the humid tropics. *Naturwissenschaften* **2001**, *88*, 37−41.

(35) Singh, B.; Fang, Y.; Cowie, B. C.; Thomsen, L. NEXAFS and XPS characterisation of carbon functional groups of fresh and aged biochars. *Org. Geochem.* **2014**, *77*, 1.

DOI: 10.1021/acs.jafc.5b00846
J. Agric. Food Chem. 2015, 63, 3830−3837

volatile compounds analyzed in foods per se could undergo significant differences when the food is consumed and could lead to differences in the final aromatic perception. In fact, considerable physicochemical changes which affect the release of volatile compounds from emulsions occur in the mouth while eating. This is the reason the sensations of odor (the so-called nasal route) and aroma (retronasal route) could be perceived differently, even though the same olfactory sense is involved.[10,11] In fact, salivation, mouth size, shear forces from tongue compression, breathing, pH, and temperature are factors able to change the food matrix structure and sensory properties.[12] Among the physiological parameters, saliva has been described in the literature as the most important. Its first effect is to dilute the oil-in-water emulsion when this latter is tasted. Then, the activity of salivary proteins (mucins, albumin, and proteins rich in proline) and enzymes (amylase, lipase, and lysozymes) are responsible for the emulsion destabilization.[13,14] In addition, it was reported that phenolic compounds, in olive oil-in-water emulsions stabilized by β-lactoglobulin, affect the droplet size, improving the dispersion degree.[15] These changes in the structure of the emulsion could also have an effect on the final perception of the products.[16] Several studies have been aimed at understanding the aroma release of volatile compounds in vegetable oil model solutions and emulsions.[6,17−22] Only two published research papers reported the release of only one volatile compound after the interaction between whey proteins and saliva by *in vivo* analysis. The first one studied the release of ethyl butanoate in gel, while the latter reported on 2-nonanone in aqueous solution.[23,24] Another study reported the aroma release of emulsions obtained by soybean oil and β-lactoglobulin under simulated mouth conditions.[25] Moreover, the majority of *in vitro* studies employed artificial saliva.[20−23] This could be a limit because the effect of numerous enzymes and proteins present in human saliva were not considered.[4,12,26] So far, only one published study has investigated the interaction of phenolic compounds from olive oil with different food proteins, including β-lactoglobulin.[27] From a food technology point of view, the polyphenol−protein interaction is interesting as a possible means to reduce bitterness, whereas the effects of such an interaction on the release of flavor compounds has still to be investigated. Up to now, no study has reported on the aroma release of VOO after the interaction with whey proteins and human saliva. The effect of these interactions could be important in understanding oral mechanisms of the emulsion in relation to sensory perception. This piece of information will also be useful to deepen consumer attraction toward foods or dishes made by pairing olive oil with dairy products. Therefore, it could be the basis of further studies in sensory science about consumer preferences.

The present work aims to study the aroma release of volatile compounds in an oil-in-water model dispersion by adding refined olive oil spiked with VOO biophenols to a whey protein solution (1/5 v/v). In particular, this research aims to verify the changes in headspace release of target volatile compounds due to the interactions between virgin olive oil biophenol extract and whey proteins, in the presence of human saliva, simulating mouth conditions.

MATERIALS AND METHODS

Samples, Standards, and Reagents. Refined olive oil and extra virgin olive oil (EVOO) from the Coratina cultivar were supplied by the IOBM (Industria Olearia Biagio Mataluni, Montesarchio, Benevento, Italy). EVOO from the Ravece cultivar was provided by APOOAT Soc. Coop a.r.l. (Avellino, Italy) in 250 mL green glass bottles. EVOO samples were stored under suitable conditions, avoiding light exposure and high temperatures in order to prevent oxidation, and were used within 8 months from their production (November 2013). For the analysis of volatile compounds, ethyl isobutyrate (99%), ethyl butyrate (99%), ethyl 2-methylbutyrate (99%), hexyl acetate (99%), *cis*-3-hexenyl acetate (98%), *trans*-2-pentenal (95%), *trans*-2-hexenal (98%), 1-hexanol (99%), *cis*-3-hexen-1-ol (99%), linalool (97%), and 1-penten-3-one (97%) were supplied by Sigma-Aldrich (St. Louis, USA). For the analysis, the reagents hexane (95%), methanol (99.9%), glacial acetic acid, trifluoroacetic acid, acetonitrile, diethyl ether, and distilled water were supplied by Romil (Cambridge, England). Potassium iodide and sodium carbonate were provided by AppliChem (Darmstadt, Germany). Ammonium acetate, Folin−Ciocalteu solution, and sodium hydroxide were purchased from Sigma-Aldrich (Steinheim, Germany). Sodium hydroxide, phenolphthalein, and starch were provided by Titolchimica spa (Rovigo, Italy). Sodium thiosulfate was supplied by Fluka (Buchs, Switzerland), and chloroform was supplied by LabScan (Dublin, Ireland).

Sample Preparation. To study the effect of interactions between whey protein isolate and olive oil, added or absent, with biophenols from extra virgin olive oil on the aroma release, the experimental plan reported in the Supporting Information was applied. Six model systems were set up in order to obtain known initial concentrations of aroma compounds in olive oil added with phenolic compound extract and whey protein isolate. In order to verify our results, obtained by using model systems, a blank virgin olive oil was also analyzed. Human saliva was added to the model systems, and samples were subsequently analyzed by using a dynamic headspace simulating mouth conditions by a retronasal aroma simulator (RAS) device. In the systems without saliva, distilled water was added to obtain the same headspace volume in all of the samples, with the same pH of saliva.

Preparation of the Refined Olive Oil Sample with Added Virgin Olive Oil Biophenols (ROOP). The phenolic extract was obtained from extra virgin olive oil *cv.* Coratina, typically known for its high content of phenolic compounds. An aliquot of the oil sample (200 g) was dissolved in hexane (200 mL) and vigorously shaken for 10 s. A subsequent extraction was carried out using a water/methanol mixture (40/60 v/v) in a separatory funnel. This step was repeated three times by using a total of 420 mL of solvent. Subsequently, the obtained hydro-alcoholic extract was washed with hexane to remove any oil contamination and was centrifuged for 10 min at 3500 rpm (ALC International srl, PK-120, Milan, Italy). The organic phase was removed from the sample, and the hydro-alcoholic phase was collected in the flask and evaporated under vacuum in a rotary evaporator at 40 °C (Heidolph, VV 2000). The phenolic compounds were suspended using 40 mL of methanol. An aliquot of the extract was used for the HPLC and Folin−Ciocalteau analyses. A 2 mL amount of polyphenol extract was adjusted to volume using refined olive oil in a 100 mL volumetric flask, and the oil mixture was treated in an ultrasonic bath for 15 min. Then, methanol was evaporated in a vacuum evaporator (Heidolph VV 200) at 38 °C for 15 min.[28] The polyphenol extract was added to the refined oil all at once and stored in a refrigerated environment. Before the analyses were carried out, the solution was brought to room temperature. The amount of phenolic compounds (328 mg kg^{-1}) added to the refined olive oil was chosen on the basis of the average levels reported in the literature for extra virgin olive oil, equivalent to about 260 mg kg^{-1} of total phenolic compounds.[29] This level is between 220 and 340 mg kg^{-1}: i.e., it corresponds to the slightly bitter taste of VOO.[30]

Preparation of the Refined Olive Oil Sample (ROO). In the control sample the phenolic extract was not added; 2 mL of methanol was adjusted to volume using refined olive oil in a 100 mL volumetric flask. Then, the oil phase was submitted to the same protocol previously described for phenolic compound addition.

Preparation of the Oil Aroma Solution. The most abundant and significant volatile compounds of virgin olive oils were considered in our study for preparing the solutions of aroma compounds,

DOI: 10.1021/acs.jafc.5b00148
J. Agric. Food Chem. 2015, 63, 3838−3850

Table 1. Chemical Standards, Concentration Added, Odor Descriptor, Physical−Chemical Properties, and MS Fragments Used for Quantitative Analysis[a]

compound	level added (mg kg^{-1})	odor descriptor[b]	MW[c]	C[d]	log P[e] o/w	log P[e] o/a	log P[e] a/w	VP (Pa at 25 °C)[e]	IF[f] (m/z)	r^2	calibration curve (mg kg^{-1})	n
Ethyl Esters												
ethyl isobutyrate	0.141	fruity[51]	116	6	1.77	3.546	−1.78	3226	**71**−116−88	0.9998	0.0360−1.4061	5
ethyl butyrate	0.129	cheesy,[51] fruity,[51] sweet[45]	116	6	1.85	3.637	−1.79	1946	**71**−88	0.9995	0.0329−1.2840	5
ethyl 2-methylbutyrate	0.120	fruity[51]	130	7	2.26	3.912	−1.65	1071	**57**−102	0.9998	0.0306−1.1970	5
hexyl acetate	0.219	fruity[52]	144	8	2.83	4.494	−1.66	193	**43**−56−84	0.9996	0.0224−2.1807	6
cis-3-hexenyl acetate	1.536	banana-like,[5,51] green,[5,52] fruity,[5,52] floral,[5] ester[5]	142	8	2.61	4.195	−1.59	152	**43**−67−82	0.9991	0.0627−15.2965	7
Aldehydes												
hexanal	1.605	green,[5,51] green apple,[5,45] grassy,[45] cut grass[5,52]	100	6	1.8	3.84	−2.06	1276	**56**−57−72	0.9996	0.0655−15.9858	7
trans-2-pentenal	0.122	green,[5,45,52] apple,[45] grassy,[52] pleasant[5]	84	5	1.09	3.607	−2.52	2466	**55**−84−83	0.9993	0.0123−1.2155	6
trans-2-hexenal	6.112	green,[5,45,51,52] apple-like,[5,51] bitter almond,[5,45] cut grass[5,52]	98	6	1.58	4.279	−2.70	629	**55**−69−83	0.9992	0.2493−60.8713	7
C_6-Alcohols												
1-hexanol	0.207	fruit,[5] grass,[5,52] floral,[52] aromatic[5]	102	6	1.82	5.185	−3.16	117	**56**−55−69	0.9988	0.0084−2.0589	7
cis-3-hexen-1-ol	0.209	leaf-like,[5,51] green,[5,44] herbal,[52] cut grass,[52] banana,[5] pungent[5]	100	6	1.61	4.808	−3.20	125	**67**−82−55	0.9998	0.0213−2.0811	6
Others												
linalool	0.086	lilac,[52] lavender[52]	154	10	3.38	6.026	−3.06	11	**71**−93−121	0.9998	0.0220−0.8615	5
1-penten-3-one	0.114	green,[5,45,51] pungent,[5,51] sweet,[5] strawberry,[5] sharp,[5] metallic[5]	84	5	0.9	3.748	−2.85	5092	**55**−84	0.9983	0.0726−1.1340	4

[a] n = number of calibration points. r^2 = linear regression coefficient. [b] The odor descriptors were indicated as reported in the literature. [c] Molecular weight. [d] Number of carbon atoms. [e] The logarithms of octanol/water, octanol/air, and air/water partition coefficients (log P) and vapor pressures of the volatile compounds were calculated using EPI Suite v.4.1 software, U.S. Environmental Protection Agency and Syracuse Research Corp. [f] Bold numbers indicate quantifier ions.

according to the literature.[31] They included five esters, three aldehydes, two alcohols, one ketone and one terpene compound (Table 1). Volatile compounds were dissolved in 10 mL of refined olive oil and homogeneously mixed. The aroma solution was obtained by diluting 4 mL of each volatile compound in oil to 100 mL of refined oil. The aroma solution was added to the oil sample 1 h before the analysis, in order to allow its stabilization. The final concentration for each volatile compound in an oil sample is reported in Table 1. The concentrations were chosen to stay within the range typically found in extra virgin olive oil.[5,31]

Preparation of the Whey Protein Solution (WP). We considered the amount of whey proteins and the pH of the relative solution (11% and 5.8−6.6, respectively) to simulate a real food product commonly used in many food preparations: i.e., ricotta cheese (obtained from whey by adding sodium chloride and thermally treated to separate the upper phase). Whey protein isolate (95%) was supplied by ACEF s.p.a. (Fiorenzuola d'Arda, PC, Italy). Therefore, a water solution at 11% (WP) was prepared in an ammonium acetate buffer solution. The buffer solution was added to 27.5 g of whey protein isolate. The 0.4% ammonium acetate buffer solution (Sigma-Aldrich, Germany) was acidified to pH 6 by using acetic acid solution (Romil, U.K.) by using a few drops in 250 mL of the buffer solution. Whey protein isolate was characterized by 96.7% proteins, 2% ashes, 0.3% fat (dry weight), and 4.7% humidity.

Human Saliva Sampling. Mixed whole saliva (about 150 mL) was separately collected from 14 nonsmoking subjects (8 males and 6 females, 23−48 years of age) from the Department of Agriculture, University of Naples Federico II.[32] Saliva was separated into aliquots of 2 mL and frozen at −20 °C. Before being used, the samples were held in a thermal bath at 37 °C and shaken in order to dissolve any suspension.

Free Acidity, Peroxide Value, and Specific Ultraviolet Absorbances. Refined olive oil (ROO) and EVOO (from Ravece cultivar) were analyzed to determine their acidity levels, peroxide value, and K_{232}, K_{270} and ΔK values according to UE Reg. 2568/91. Acidity was expressed as oleic acid percentage (%), while the peroxide value (PV) was expressed as mequiv of O_2 per kg of oil. For the analysis of spectrophotometric indices a UV−visible Shimadzu UV-1601 spectrophotometer (Shimadzu, Kyoto, Japan) was used. All of the analyses were performed in triplicate.

Extraction and Analysis of Phenolic Compounds. The phenolic compounds were analyzed in both ROO and EVOO Ravece samples. The extraction of phenolic compounds was performed according to Vásquez-Roncero,[33] but slightly modified, in order to minimize the volume of solvent used. A 10 g portion of he sample was dissolved in 10 mL of hexane and vigorously shaken for 10 s. Then, the sample was extracted via a separating funnel by using three 7 mL portions of a water/methanol mixture (40/60 v/v). The obtained hydro-alcoholic extract was washed with hexane to remove any oil contamination and centrifuged (ALC International Ltd., mod. PK 120, Milan, Italy) for 10 min at 3500 rpm. The organic phase was removed from the extract. Thereafter, the lower phase was collected in a flask and evaporated under vacuum in a rotary evaporator (Heidolph, VV 2000) at 40 °C. The obtained residue was dissolved in 2 mL of methanol to obtain the final phenolic extract, and an aliquot of this solution was used for the analysis of phenolic compounds. All of the extractions were performed in duplicate. The quantification of total phenolic compounds was carried out by using the Folin−Ciocalteau colorimetric method according to Gutfinger.[34] The samples were diluted 1/50, and the solvent was completely removed by using a constant nitrogen flow. Distilled water (200 μL) was added to the polyphenol extract, and 800 μL of 7.5% sodium carbonate (Na_2CO_3)

DOI: 10.1021/acs.jafc.5b00148
J. Agric. Food Chem. 2015, 63, 3838−3850

Table 2. Quality Indices for Olive Oil and Total Phenolic Compounds by the Folin−Ciocalteau Method for Refined Olive Oil (ROO) and Extra Virgin Olive Oil (EVOO) from Ravece Cultivar[a]

	free acidity	peroxide value	K_{232}	K_{270}	ΔK	total phenolic compounds (mg kg^{-1})
ROO	0.09 ± 0.01	0.8 ± 0.0	1.82 ± 0.05	0.69 ± 0.02	0.08 ± 0.00	44.0 ± 7.1
Ravece EVOO	0.21 ± 0.03	11.8 ± 0.4	2.18 ± 0.01	0.16 ± 0.00	−0.07 ± 0.01	431.2 ± 93.2
ROO spiked with phenolic extract						328.0 ± 59.1
EVOO accepted values	≤0.80	20.0	≤2.50	≤0.22	≤0.01	
ROO accepted values	≤0.30	≤5.0		≤1.10	≤0.16	

[a]Acidity is expressed as oleic acid equivalent. Peroxide value is expressed as mequiv of O_2 per kg of oil. Values are the average of three replicates (n = 3).

and 1 mL of Folin−Ciocalteau (2 N) previously diluted by using distilled water (1/10) were finally added to the solution. The samples were left for 30 min in the dark at room temperature.[35] Absorbance was measured at 765 nm wavelength by using a UV-1601 spectrophotometer (Shimadzu, Kyoto, Japan). The blank samples consisted of 200 μL of distilled water and all of the other reagents previously described. The total phenolic content was determined by using a calibration curve constructed with caffeic acid and expressed as mg of caffeic acid per kg of oil. The analyses were performed in triplicate for each extraction.

Release of Aroma Compounds in Model Mouth System. The measurement of aroma compound headspace release was performed under dynamic conditions using an experimental RAS, as previously reported in the literature.[6,17,36,37] A 10 μL portion of aroma solution was added to 1.66 mL of the oil sample, and the solution was left to react for 50 min. Subsequently, 8.33 mL of buffer or whey protein solution was added to the system and gently mixed by using a magnetic stirrer (200 rpm) for 10 min. After 1 h, 10 mL of oil-in-water emulsion to which 10 μL of internal standard was previously added (500 mg L^{-1} isobutyl acetate, 99.8% purity, Fluka, Buchs, Switzerland) was transferred into a cylindrical glass jar (100 mL) of the model mouth system. Then, human saliva or distilled water (2 mL), at the same pH of saliva, was added to the system, which was kept in a water bath (Analitica De Mori, Milano, Italy) at 37 °C. The SPME fiber was inserted through the Teflon septum in the RAS and exposed to the sample headspace. Nitrogen flow (20 mL s^{-1}) was passed through the sample for 4 min. During this time, the volatile compounds were trapped on the fiber. The exposure time was chosen according to data previously reported by other authors.[6,38] In addition, this exposure time could represent a realistic application to study the retronasal aroma perception of a food during the simulation of its consumption, as longer times would represent an unrealistic situation.

Dynamic Headspace−Solid Phase Microextraction (SPME) and GC/MS Analysis. The SPME device (Supelco Co., Bellefonte, PA, USA) was equipped with a 50/30 μm thickness divinylbenzene/carboxen/polydimethylsiloxane (DVB/CAR/PDMS) fiber coated with a 2 cm length stationary phase. Volatile compounds were analyzed by GC coupled with a mass spectrometer using a GC/MS Shimadzu Model QP5050A instrument (Kyoto, Japan) equipped with a Supelcowax-10 capillary column (60 m × 0.32 mm i.d., with 0.5 μm thickness) (Supelco Co., Bellefonte, PA, USA). The temperature was set at 40 °C for 4 min followed by an increase of 3.5 °C min^{-1} up to 240 °C and was held at that temperature for 3 min. The injector was kept at 230 °C. Helium was used as the carrier gas (1.4 mL min^{-1}). Volatile compound thermal desorption was carried out by exposing the SPME fiber in the injector for 10 min. The compound identification was performed by comparing retention times and mass spectra obtained by analyzing pure reference compounds under the same conditions. Moreover, the identification was confirmed by comparing mass spectra with those of the NIST database. Mass spectra were recorded at 70 eV. The source temperature was 200 °C, and the interface temperature was 250 °C. Before it was used, the fiber was conditioned at 270 °C for 1 h for the analysis. A blank test was performed before each analysis to prevent the release of undesirable compounds. All of the analyses were performed in triplicate.

Quantitative Analysis. The quantitative analysis of olive oil volatile compounds was carried out by using selected ion monitoring (SIM). The selected ions for each volatile compound are given in Table 1. The peak areas of each compound were normalized with respect to the area of the internal standard peak and interpolated on the calibration curve. A calibration curve for each molecule was constructed by preparing a solution containing known amounts of analyte in the oil and the internal standard. The oil was diluted in order to obtain one to seven solutions with decreasing values of the concentration of analytes, and each of these solutions was analyzed by SPME-GC/MS in selected ion monitoring, by applying the same conditions previously reported. The concentration range considered for the calibration curve of each molecule (Table 1) was within the values typically found in virgin olive oil.[5,31] The peak areas were calculated by using a Lab solutions acquisition system (GCMS solutions version 1.20; Shimadzu, Kyoto, Japan). The linear regression coefficient (r^2) for the studied volatile compounds was satisfactory, resulting in a value higher than 0.9983 (Table 1).

Statistical Analysis of Data. Significant differences among the different model systems were determined for each compound by one-way ANOVA statistical analysis. Tukey's test was used to discriminate among the means of the variables. Differences with $p < 0.05$ were considered significant. In order to better understand the influence of saliva, biophenols, and WP presence in the food model system, as well as their interactions, on the volatile compound concentration, a multifactor analysis of variance (ANOVA) with second-order interactions was carried out. The data elaboration was carried out using XLStat (version 2009.3.02), an add-in software package for Microsoft Excel (Addinsoft Corp., Paris, France).

RESULTS AND DISCUSSION

Table 2 reports the free acidity, peroxide value, ultraviolet indices (K_{232}, K_{270}, ΔK), and total phenolic compounds in refined and extra virgin olive oils. Free acidity, peroxide value, K_{232}, K_{270}, and ΔK of all olive oil samples were within the legal limits of the category they belong to: i.e., extra virgin olive oil (EC 2568/91). VOO total phenolic compounds, quantified by the Folin−Ciocalteau colorimetric method, were 431 ± 93 mg kg^{-1}. With regard to the refined olive oil, the phenolic compounds were about 44 ± 7 mg kg^{-1}, while in the refined olive oil with an extract of VOO biophenols added their level was 328 ± 59 mg kg^{-1}.

Effect of WP Addition on VOO Aroma Release in the Presence of Biophenols. To verify the effect of the interaction between WP and VOO on aroma release, several model systems were added to VOO phenolic compounds, to reach a final concentration of 328 mg kg^{-1}. The aroma compounds were set up and were kept to interact with WP. In these systems, VOO aroma compounds are partitioned between the two liquid phases (water and oil) and liquid and gas phase (air). In addition, by its emulsion destabilization effect,[13,14] saliva could further affect the volatile compound partition. This complex balance could lead to a different aroma release in comparison to the initial level of volatile compounds in olive oil. In order to better detect these differences in headspace aroma release, a comparison was carried out by

DOI: 10.1021/acs.jafc.5b00148
J. Agric. Food Chem. 2015, 63, 3838−3850

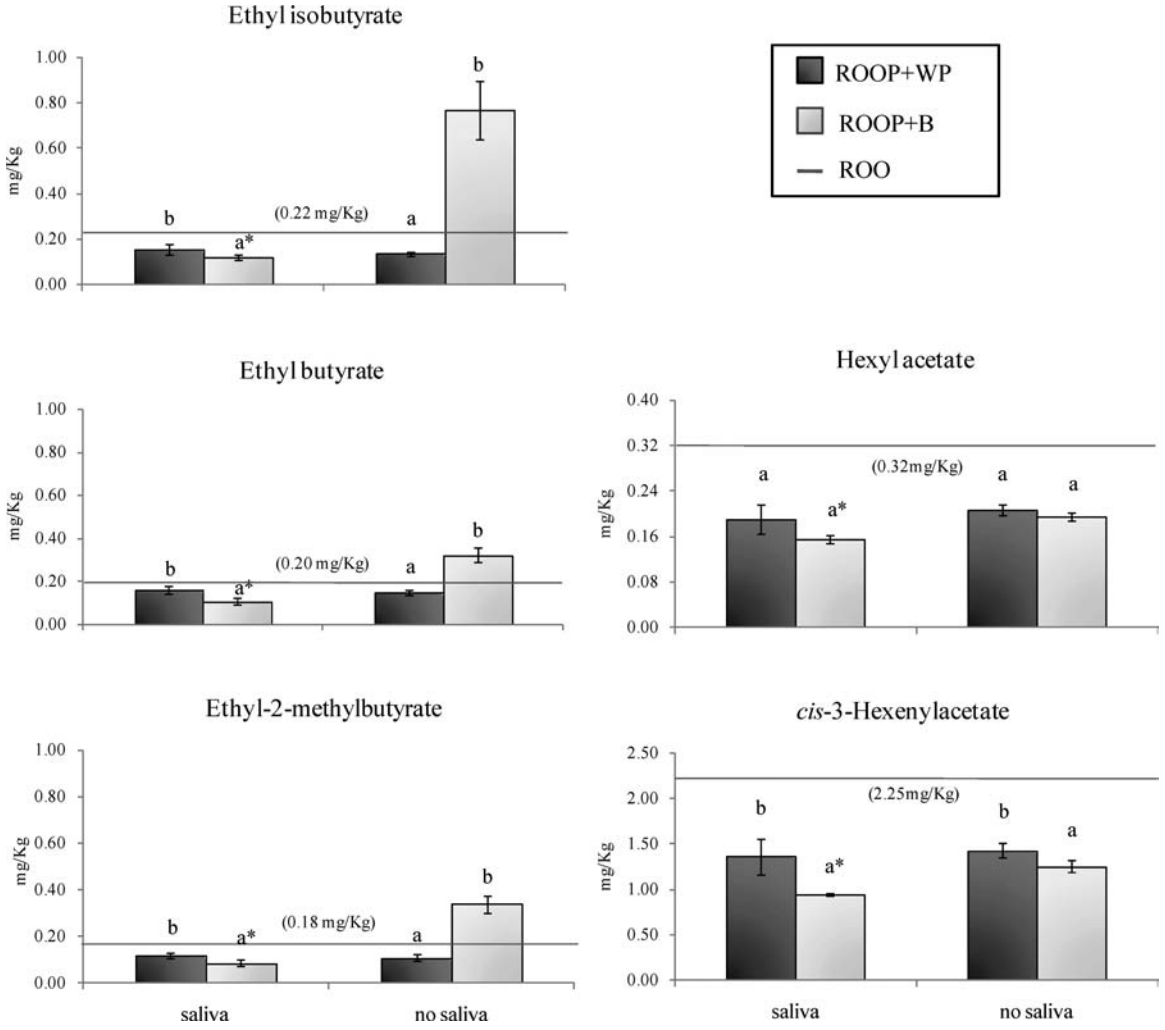

Figure 1. Headspace concentration of ethyl esters and acetates in the refined olive oil model system with the addition of VOO phenolic compounds (ROOP) in the presence (WP) and absence of whey proteins (B) and saliva. Lines indicate the level of volatile headspace release in refined olive oil (ROO) without interaction with WP and saliva. Different letters indicate significant differences ($p < 0.05$) between WP and blank samples. Asterisks indicate significant differences between saliva/no saliva runs.

analyzing the levels of added volatile compounds by using only refined olive oil (ROO): i.e., without interaction of WP and saliva (it is possible to refer to it as orthonasal odor). In the systems without whey proteins (WP) a buffer solution (B) was added to obtain the same headspace volume in all of the samples. The extent of simulated retronasal release of ethyl esters (Figure 1) was similar among the three molecules belonging to this chemical class (ethyl isobutyrate, ethyl butyrate, and ethyl 2-methylbutyrate). Saliva seems to cause a significant decrease in the release of the three esters analyzed without whey protein interaction (ROOP+B). This result could be explained by the binding effects of human saliva, as demonstrated by other researchers, who attributed it to both the chemical binding or hydrolysis and/or physical trapping of volatile compounds mainly caused by mucin.[17,32,36,39] In addition, in the whey protein system (ROOP+WP) a significant and considerable decrease in the release of the ethyl esters was obtained, and this result is in accordance with the literature,[9] but in the systems in which WP interacted with saliva, the decrease was lower. This behavior could be explained by a possible interaction between human salivary constituents and whey proteins, with the result that their action on these volatile compounds could be limited. In fact, it was shown that mucins form aggregates with β-lactoglobulin in aqueous and in oil-in-water emulsions.[40,41] These kinds of interactions, which occur *in vivo* during the consumption of dairy products, might be responsible for the sensory astringency.[42] In fact, in agreement with the well-accepted astringency model of wine polyphenols,[43] this sensation is due to the loss of lubrication of saliva when mucin and lactoglobulin interact to form an aggregate, which precipitates and leads to a dryness and roughness perception in the mouth. Therefore, as reported for red wine in the case of mucin and polyphenols,[36] in addition to sensory astringency, mucin and whey protein interaction affect the extent of ester release. A similar behavior was observed for acetates (hexyl acetate and *cis*-3-hexenyl acetate). In the case of this class of compounds, the level of aroma release was lower in the presence of saliva in the buffer system (ROOP+B) with respect to that of distilled water (no saliva), while in the systems with WP and saliva the lower decrease of aroma compounds was observed only for *cis*-3-hexenyl acetate (Figure 1). The result obtained for hexenyl acetate was in line with that for other acetates, whereas, in this case, statistical significance was not reached. In fact, it was demonstrated that, within one chemical class, the affinity for β-lactoglobulin increases with hydrophobic chain length or overall hydrophobicity (expressed

DOI: 10.1021/acs.jafc.5b00148
J. Agric. Food Chem. 2015, 63, 3838−3850

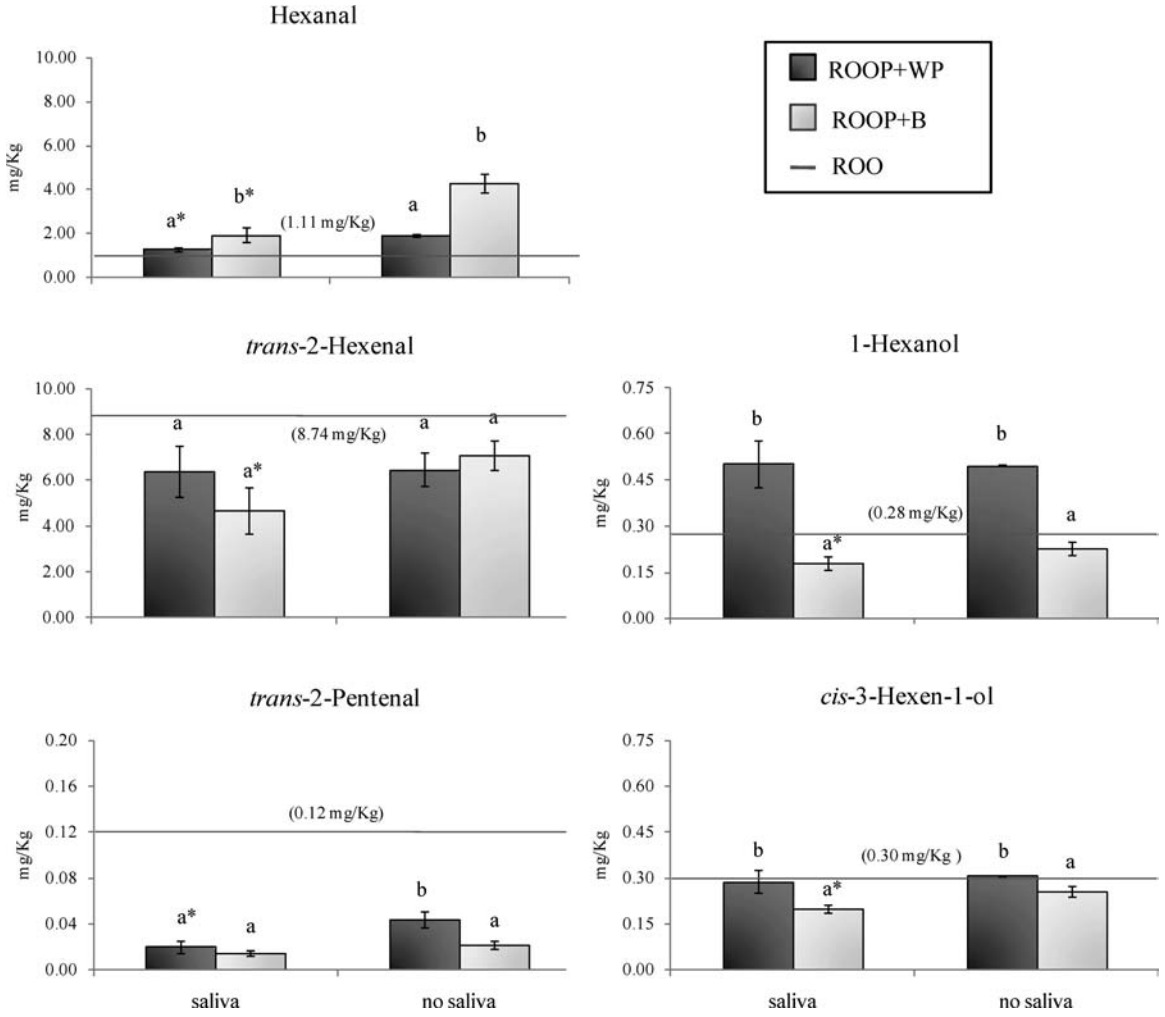

Figure 2. Headspace concentration of aldehydes and C_6-alcohols in the refined olive oil model system with the addition of VOO phenolic compounds (ROOP) in the presence (WP) and absence (B) of whey protein and saliva. Lines indicate the level of volatile headspace release in refined olive oil (ROO) without interaction with WP and saliva. Different letters indicate significant differences ($p < 0.05$) between WP and blank samples. Asterisks indicate significant differences between saliva/no saliva runs.

as log $P_{o/w}$ values).[9] Hexenyl acetate, which has a log $P_{o/w}$ value of 2.83, showed a higher affinity to whey proteins than the other volatile compounds. Therefore, this compound gave a lower release than *cis*-3-hexenyl acetate (log $P_{o/w}$ 2.61), which had lower affinity and higher headspace release.

In all of the systems in which saliva or whey proteins were added, a lower release of ethyl esters was obtained under simulated retronasal conditions with respect to the orthonasal simulation assay, only for refined olive oil (ROO without addition of saliva and whey proteins). In contrast, in the system without saliva and whey proteins, a higher release of ethyl esters was measured. This could indicate not only that aroma release is influenced by the phase separation but also that the increased viscosity of the emulsion could play an important role in the aroma release.

The behavior obtained for aldehydes (hexanal, *trans*-2-pentenal, *trans*-2-hexenal) was quite different (Figure 2). The addition of saliva clearly resulted in a decrease of hexanal headspace concentration with respect to distilled water. When WP was added to the systems, a significantly lower headspace concentration was observed, which indicates a possible further binding of hexanal by whey proteins. However, the behavior was different in comparison to those discussed for esters: i.e., when WP interacted with saliva there was not a significant increase with respect to whey protein or saliva alone, where a further decrease in headspace concentration was observed. Probably, this occurs because most of the aliphatic aldehydes are also linked to proteins by covalent irreversible bonds, as reported for β-lactoglobulin[8,9] and mucin,[7,39] to form Schiff bases. In contrast, in the case of esters and acetates, the interactions between protein and aroma compounds are reversible, involving only hydrophobic binding sites. In the first case, when the bonds to proteins are covalent, i.e. irreversible, a cumulative effect of the individual reaction occurs. Otherwise, in the latter case reversible hydrophobic or hydrogen bonds occur, resulting in an antagonistic and not a cumulative effect. Hexanal headspace concentration decreased in the presence of human saliva and WP, in accordance with Weel et al.,[44] who reported an *in vivo* study. A dissimilar phenomenon was observed in the case of *trans*-2-hexenal and *trans*-2-pentenal. The first showed a lower headspace concentration only in the buffer system with saliva, while the latter had a lower concentration in the presence of whey proteins. As discussed for acetates, this difference could be due to different hydrophobicities (expressed as log $P_{o/w}$ values) of aldehydes.[9] In fact, hexanal, which has a log P value of 1.8,

DOI: 10.1021/acs.jafc.5b00148
J. Agric. Food Chem. 2015, 63, 3838−3850

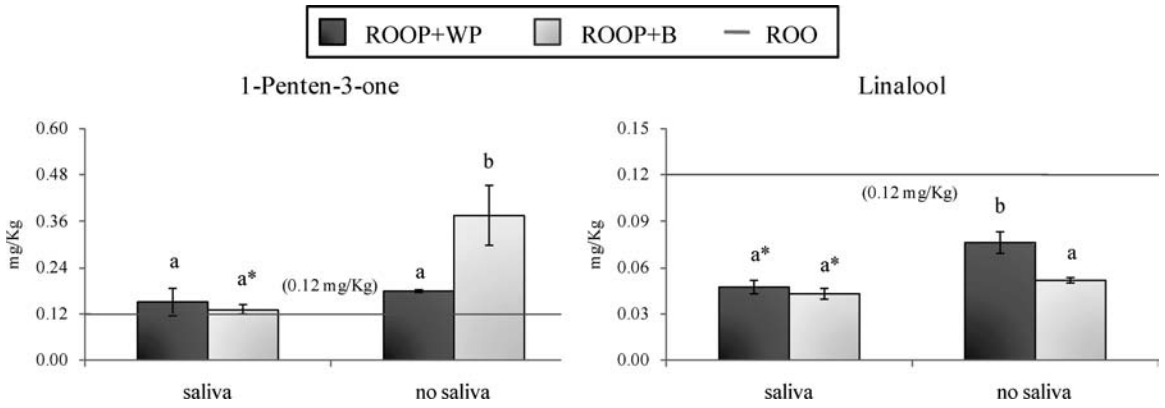

Figure 3. Headspace concentration of 1-penten-3-one and linalool in a refined olive oil model system with the addition of EVOO biophenols (ROOP) in the presence (WP) and absence (B) of whey protein and saliva. Lines indicate the level of volatile headspace release in refined olive oil (ROO) without interaction with WP and saliva. Different letters indicate significant differences ($p < 0.05$) between WP and blank samples. Asterisks indicate significant differences between saliva/no saliva runs.

Table 3. Results of Multifactor Analysis of Variance for Volatile Compounds of Olive Oil in Water Emulsion Differing in Whey Protein Addition and Saliva Treatments

	whey proteins			saliva			whey proteins × saliva		
compound	*F* ratio	*p* value	effect	*F* ratio	*p* value	effect	*F* ratio	*p* value	effect
				Esters					
ethyl isobutyrate	117.219	<0.0001	−	68.745	<0.0001	−	79.146	<0.0001	yes
ethyl butyrate	100.671	<0.0001	−	65.589	<0.0001	−	80.540	<0.0001	yes
ethyl 2-methylbutyrate	165.816	<0.0001	−	100.211	<0.0001	−	117.384	<0.0001	yes
hexyl acetate	0.243	0.635		11.016	0.011	−	2.127	0.183	
cis-3-hexenyl acetate	0.088	0.774		8.771	0.018	−	3.416	0.102	
				Aldehydes					
hexanal	63.465	<0.0001	−	84.982	<0.0001	−	27.894	0.0001	yes
trans-2-hexenal	5.130	0.053		7.883	0.023	−	7.096	0.029	yes
trans-2-pentenal	20.362	0.002	+	29.733	0.001	−	9.511	0.015	yes
				C_6-Alcohols					
1-hexanol	9.979	0.013	+	0.472	0.511		0.891	0.373	
cis-3-hexen-1-ol	0.002	0.962		11.613	0.009	−	3.090	0.117	
				Others					
linalool	28.796	0.001	+	53.019	<0.0001	−	14.292	0.005	yes
1-penten-3-one	28.731	0.001	−	30.581	0.001	−	19.805	0.002	yes

showed a lower release than *trans*-2-pentenal (log $P_{o/w}$ = 1.9), while *trans*-2-hexenal, characterized by an intermediate log $P_{o/w}$ value (1.58), showed an intermediate release. It is important to note that, among the aldehydes, only hexanal showed a higher retronasal release with respect to the orthonasal simulation assay of only refined olive oil (ROO without addition of saliva and WP). This behavior was also previously reported for fresh sunflower oil-in-water emulsions analyzed by a mouth model system and related to hexanal generation by lipid oxidation reactions.[17]

The two studied alcohols (1-hexenol and *cis*-3-hexen-1-ol) showed similar behavior: when WP was not added to the system, saliva caused a decrease in headspace release (Figure 2). When WP was present, no significant difference was observed in aroma release between the system with distilled water and those with human saliva. As discussed for ethyl esters, this phenomenon occurs because of the interaction between mucin and whey proteins which limits their action on alcohols. Therefore, this finally results in a higher release of these compounds. The retronasal release of 1-hexanol in the system with whey proteins was dramatically higher with respect to the orthonasal simulation assay of only refined olive oil (ROO) and significantly higher with respect to the buffer system. This so-called *salting-out* effect, accompanied by a decrease of about the same magnitude in hexanal headspace concentration, was reported by other authors[44] and was attributed to an enzymatic conversion of these two compounds. In Figure 3 the headspace release of 1-penten-3-one and linanool was shown. The retronasal concentration of 1-penten-3-one was significantly higher when distilled water was used instead of human saliva, but only in the buffer system solution. In fact, no statistical difference was observed between the buffer solution and saliva in the system with whey proteins. This result suggests that the presence of whey proteins has a strong effect over the headspace release of some aroma compounds, resulting in a retention effect similar to that caused by human saliva. Whey proteins seem to have stronger binding effects on retronasal concentration than 1-penten-3-one, due to possible chemical binding, as reported for 2-nonanone, a similar hydrophobic volatile compound.[45] In contrast, in the system with saliva, this phenomenon was not observed, probably because the binding sites of the volatile compound interacting with proteins are not available for further reaction with other proteins such as mucin. In fact, when whey proteins are added to such a system,

DOI: 10.1021/acs.jafc.5b00148
J. Agric. Food Chem. 2015, 63, 3838−3850

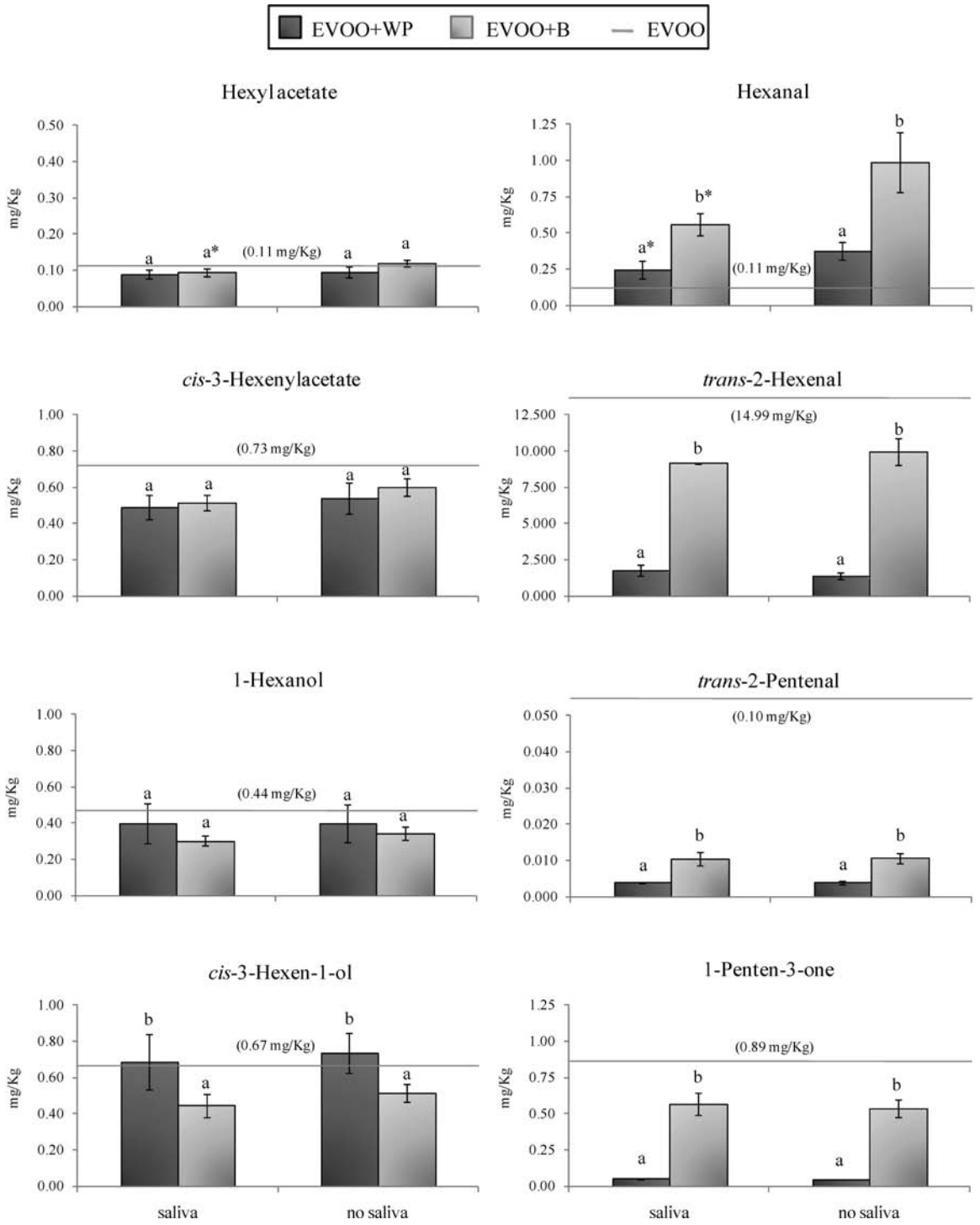

Figure 4. Headspace concentration of volatile compounds in the EVOO model system in the presence (WP) and absence (B) of whey protein and saliva. Lines indicate the level of volatile headspace release in refined olive oil (ROO) without interaction with WP and saliva. Different letters indicate significant differences ($p < 0.05$) between WP and blank samples. Asterisks indicate significant differences between saliva/no saliva runs.

covalent and irreversible interactions occur, as was also reported for aldehydes.[7,9]

In the case of linalool, its headspace concentration in simulated retronasal aroma was always lower than that of the orthonasal simulation assay of ROO. Particularly, in both the buffer and whey protein systems, saliva caused a significantly lower concentration of linalool with respect to distilled water. In systems without saliva, a higher release of linalool was measured in the headspace in comparison to that for the buffer system when WP was added. In other words, also in this case the salting-out effect was observed when whey proteins were added to the system with distilled water. This behavior was previously reported in the literature to be particularly affected at low pH values for other terpene compounds, such as limonene and myrcene.[46] These compounds have highly hydrophobic properties (log $P_{o/w}$ = 4.38 and 4.17, respectively, EPI Suite v.4.1 software, U.S. Environmental Protection Agency and Syracuse Research Corp.) close to those of linalool (log $P_{o/w}$ =

DOI: 10.1021/acs.jafc.5b00148
J. Agric. Food Chem. 2015, 63, 3838−3850

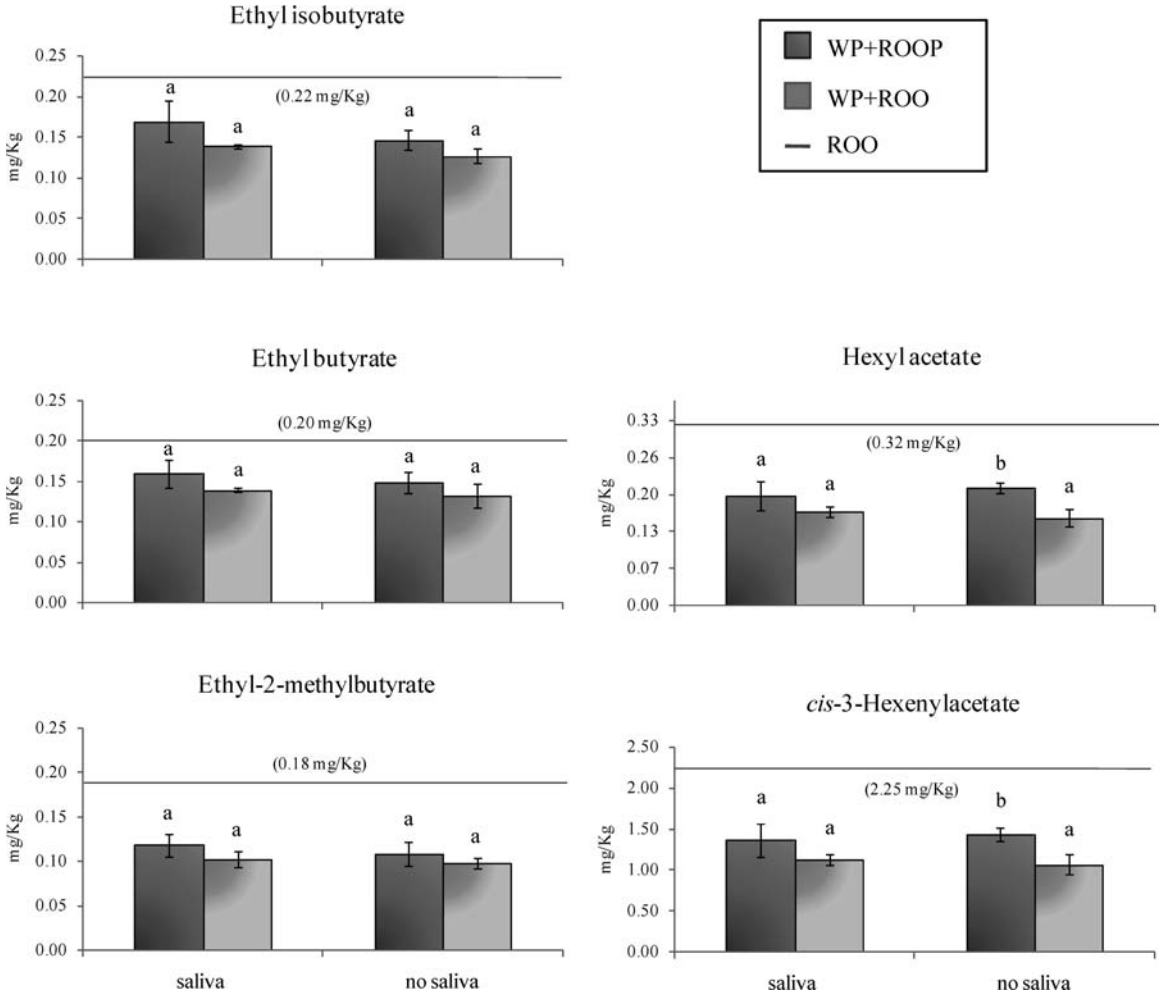

Figure 5. Headspace concentration of ethyl esters and acetates in the refined olive oil model system after interaction with whey protein (WP), in the presence (ROOP) and absence (ROO) of VOO phenolic compounds and saliva. Lines indicate the level of volatile headspace release in refined olive oil (ROO) without interaction with WP and saliva. Different letters indicate significant differences ($p < 0.05$) between ROOP and blank samples. Asterisks indicate significant differences between saliva/no saliva runs.

3.38). This difference was not detected when human saliva was used, and this result was explained by the interaction between salivary components and whey proteins, as previously discussed.

In order to better understand the influence of saliva and whey proteins, as well as the interactions among these factors on the retronasal aroma release in olive oil, a multifactorial ANOVA analysis was carried out. Table 3 shows the *F* ratio, *p* value, and direction of the effect of the factors on the average relative recoveries of the aroma compounds. The *F* ratio represents the quotient between the variability due to the effect considered and the residual variance. The higher the *F* ratio value, the more marked the effect of that factor with reference to a variable at $p < 0.05$. The sign of the effect shows the direction of the influence. Whey proteins seem to have a negative effect on the aroma release in the case of ethyl esters, hexanal, and 1-penten-3-one, responsible for fruit, green, and pungent odors, respectively (Table 1). In contrast, they showed a positive effect on *trans*-2-pentenal (green), 1-hexanol (fruit), and linalool (floral). Saliva showed a negative effect on all volatile compound concentrations, except for 1-hexanol. The interaction between the two factors took place for the majority of the volatile compounds, except for both acetates and alcohols. The results herein described suggest that whey proteins affect the aroma release of VOO but their interaction with saliva has an antagonistic effect on ester, acetate, and alcohol release while being synergistic for aldehydes and ketones. This different effect may imply a higher perception of fruity notes of VOO and a lower perception of green notes when VOO and dairy products are paired, if confirmed by further sensory studies.

Effect of Whey Protein Addition on EVOO Aroma Release. In the present section of our study a real sample of extra virgin olive oil was tested. In order to compare this system (EVOO cv. Ravece) and the model systems (refined olive oil added with selected aroma compounds), a quantification of volatile compounds was performed. EVOO (Figure 4) generally showed a slightly different behavior in comparison to the "simulated VOO" (Figures 1−3). Ethyl esters and linalool were not found in the EVOO headspace, mainly being present at a trace level. At low levels, ethyl esters contribute to the olive oil flavor,[31] while at higher levels they are associated with the fusty defect of virgin olive oil.[47] Linalool, as well as all terpene compounds, could depend on their variety.[48] Generally, headspace releases of volatile compounds were similar among their chemical classes: e.g., the releases of aldehydes and ketones were lowered by the presence of WP, with no effects or slight effects of saliva addition. For acetate compounds, no

DOI: 10.1021/acs.jafc.5b00148
J. Agric. Food Chem. 2015, 63, 3838−3850

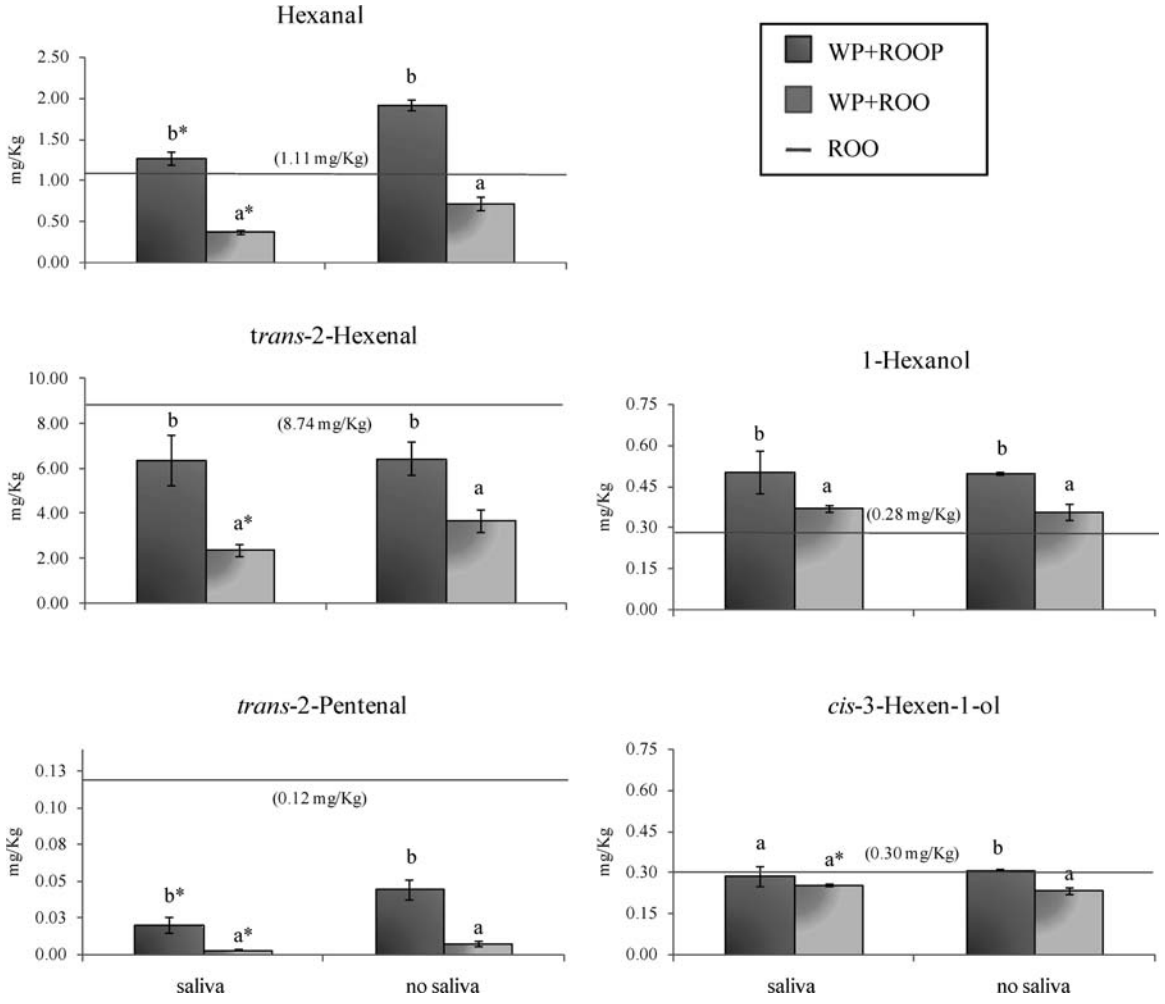

Figure 6. Headspace concentration of aldehydes and C_6-alcohols in the refined olive oil model system after interaction with whey protein (WP), in the presence (ROOP) and absence (ROO) of VOO phenolic compounds and saliva. Lines indicate the level of volatile headspace release in refined olive oil (ROO) without interaction with WP and saliva. Different letters indicate significant differences ($p < 0.05$) between ROOP and blank samples (ROO). Asterisks indicate significant differences between saliva/no saliva runs.

dramatic differences were observed. Alcohols had a slight tendency to higher headspace release when WP was added, and also in this case saliva showed no statistical differences. Therefore, it is possible to state that WP affects the VOO aroma release more than our model systems simulating VOO, while human saliva, in contrast, showed an opposite trend. In contrast to the model systems, the release of volatile compounds seems to be more in accordance with the chemical class they belong to. These differences are probably due to the chemical complexity of virgin olive oil in terms of both volatile and nonvolatile compounds. This complexity leads to a higher competition in the interaction among volatile compounds, human saliva, and WP which can affect their partition and release. In addition, the nature of the phenolic compounds and their physicochemical properties affect the dispersion properties and the oxidative stability of olive oil O/W emulsified systems.[49] Further studies to deepen the possible specific effect of individual phenolic compounds on aroma release are needed.

Effect of EVOO Biophenol Addition on Aroma Release in the Presence of Whey Proteins. In the previous section an oil-in-water emulsion was studied, by considering a pairing between VOO and WP. It is known that VOO is naturally rich in phenolic compounds, which are important for human health. They are probably also involved in the *in vivo* aroma release during consumption of this food paired with other food products. For this reason, the specific effect of VOO biophenol presence was studied by comparing a system with refined olive oil and refined olive oil added with olive oil biophenols. All of the model systems were made to interact with whey proteins. As shown in Figure 5, no statistical difference was obtained for ethyl esters between the system with phenolic compounds and the blank (absence of phenolics). Biophenols did not influence the release of either ethyl esters or acetate compounds in the presence of saliva. However, in the system with distilled water a significantly higher level of acetate compounds was found in ROOP in comparison to that for ROO. This phenomenon is probably due to a weak salting-out effect, as occurs for wine polyphenols.[50] In contrast, in the presence of saliva this level decreases due to the possible action of the carboxylesterases, which would be able to hydrolyze these aroma compounds.[32] In all of the systems, however, a lower release of volatile compounds was measured in simulated retronasal assays with respect to the orthonasal simulation assays of ROO.

More interesting results were obtained for aldehydes (Figure 6). In these systems higher release of 1-hexanol was measured in simulated retronasal assays with respect to the orthonasal simulation assay of only ROO. For hexanal, this occurs only for model systems with phenolic compound addition. A significant

DOI: 10.1021/acs.jafc.5b00148
J. Agric. Food Chem. 2015, 63, 3838−3850

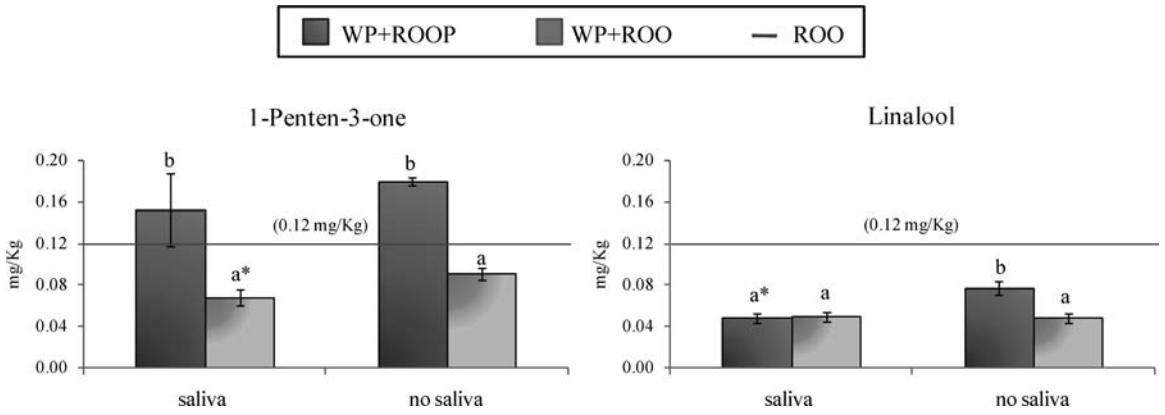

Figure 7. Headspace concentration of 1-penten-3-one and linalool in the refined olive oil model system after interaction with whey protein (WP), in the presence (ROOP) and absence (ROO) of VOO phenolic compounds and saliva addition. Lines indicate the level of volatile headspace release in refined olive oil (ROO) without interaction with WP and saliva. Different letters indicate significant differences ($p < 0.05$) between ROOP and blank samples (ROO). Asterisks indicate significant differences between saliva/no saliva runs.

Table 4. Results of Multifactor Analysis of Variance for Volatile Compounds of Olive Oil in Water Emulsion Differing in Phenolic Compound Addition and Saliva Treatments

	phenolic compound			saliva			phenolic compound × saliva		
compound	*F* ratio	*p* value	effect	*F* ratio	*p* value	effect	*F* ratio	*p* value	effect
				Esters					
ethyl isobutyrate	0.119	0.739		4.260	0.073		0.377	0.556	
ethyl butyrate	0.268	0.619		1.425	0.267		0.058	0.816	
ethyl 2-methylbutyrate	0.043	0.840		1.281	0.291		0.251	0.630	
hexyl acetate	7.068	0.029	+	0.065	0.805		1.960	0.199	
cis-3-hexenyl acetate	4.594	0.064	+	0.006	0.941		0.812	0.394	
				Aldehydes					
hexanal	146.648	<0.0001	+	161.752	<0.0001	−	14.387	0.005	yes
trans-2-hexenal	1.394	0.272		2.615	0.145		2.095	0.186	
trans-2-pentenal	47.657	0.000	+	30.042	0.001	−	14.633	0.005	yes
				C_6-Alcohols					
1-hexanol	3.759	0.088	+	0.159	0.701		0.022	0.885	
cis-3-hexen-1-ol	10.501	0.012	+	0.007	0.937		3.475	0.099	
				Others					
linalool	38.807	0.000	+	21.722	0.002	−	25.323	0.001	yes
1-penten-3-one	7.745	0.024	+	5.518	0.047	−	0.035	0.855	

effect of addition of both saliva and biophenols was observed. In particular, saliva seems to decrease the headspace release of aldehydes, while the presence of phenolic compounds seems to enhance their headspace release. For *trans*-2-hexenal, the concentration was always significantly higher when biophenols were added, but for this compound no difference was observed between distilled water and saliva, in the system with biophenols. This result strongly suggests that biophenols had a salting-out effect, for a possible interaction between phenolic compounds and WP. In fact, in these model systems the addition of WP is always responsible for both irreversible covalent and hydrophobic bonds with these volatile compounds,[8] as previously discussed. When VOO biophenols were added to the systems, they weakly interacted with whey proteins,[27] with the result that the binding sites may be much less available for hydrophobic interactions with aldehydes. In the model system with saliva addition the release was lower than that for distilled water due to the mucin interaction.[6,39]

A similar result was obtained for alcohols, which resulted in significantly higher headspace concentration in the system with phenolic compounds with no saliva addition. No difference was obtained between water and human saliva for 1-hexanol, while a significant but weak increase was observed for *cis*-3-hexen-1-ol (Figure 6). As previously discussed, this behavior could be due to a WP−mucin interaction, which leads to significantly higher concentration of alcohols because it limits their action in trapping alcohols, the hydrophobic binding sites no longer being available. Thus, for this class of compounds the presence of saliva seems to be of little or no effect, while the interaction with biophenols was significant, however. The behavior observed for 1-penten-3-one was similar to that reported for aldehydes and 1-hexanol, i.e. higher headspace release when biophenols were present, even more than the orthonasal simulation assay of only refined olive oil (ROO without the addition of saliva and whey proteins) (Figure 7). No significant difference was obtained between distilled water and the saliva system, due to the high variability obtained in this latter case. In general, the binding capacity of proteins increases from alcohols to ketones and to aldehydes.[8] For this reason the salting-out effect of VOO biophenols, inversely correlated to the binding capacity of whey proteins, was higher for aldehyde than for ketones and alcohols. Linalool headspace concentration was affected by the presence of phenolic compounds only with distilled water (Figure 7). This result could be due to a possible

DOI: 10.1021/acs.jafc.5b00148
J. Agric. Food Chem. 2015, 63, 3838−3850

linalool trapping during the interaction between biophenols and salivary constituents. In any case, its decrease was not due to mucin.[39] In order to better understand the influence of saliva and olive oil biophenols, as well as the interactions among these factors on the retronasal aroma release in olive oil, a multifactorial ANOVA analysis was carried out. Table 4 shows the *F* ratio, *p* value, and direction of the effect of the factors on the average relative recoveries of the aroma compounds. The VOO biophenols seem to have a strong positive effect on the aroma release in the case of both acetates and alcohols, hexanal, *trans*-2-pentenal, linalool, and 1-penten-3-one being responsible for fruit, green, floral, and pungent odors (Table 1). Saliva showed a negative effect on hexanal, *trans*-2-pentenal, linalool, and 1-penten-3-one concentrations; these compounds are responsible for green, floral, and pungent odors (Table 1). The interaction between the two factors took place only for hexanal, *trans*-2-pentenal, and linalool. Therefore, our results suggest that VOO biophenols could enhance the extent of VOO aroma release of volatiles related to green, floral, and pungent notes, while saliva negatively affects this release.

In conclusion, our results indicate that whey proteins negatively affected aroma release, whereas the interaction between proteins and human saliva led to a lower effect, particularly for some volatile compounds, such as acetates and alcohols. The presence of VOO biophenols positively affected the extent of aroma release, probably in competition with the binding of volatile compounds by whey proteins, for the polyphenol−protein interaction phenomenon. Therefore, it is suggested that, in the presence of a higher level of biophenols, VOO would probably have a higher retronasal release of green notes. Our results could be useful for the formulation of new functional foods to modulate flavor release and consumer acceptability, as well as in the design of new food products by using milk industry byproducts and olive mill biophenols. In fact, as these products considered to be waste and polluting substances, their use in functional foods could at least partially solve the problem of their disposal and could enhance the nutritional value of foods: for example, in the case of whey protein added to beverages as dietary supplements.

■ ASSOCIATED CONTENT

Supporting Information

Figure detailing the experimental plan applied for the retronasal aroma simulator (RAS) analysis of the refined olive oil model (A) and extra virgin olive oil (B) systems. This material is available free of charge via the Internet at http://pubs.acs.org.

■ AUTHOR INFORMATION

Corresponding Author

*A.G.: tel, +39 081 2539352; fax, +39 081 7762580; e-mail, alessandro.genovese@unina.it.

Notes

The authors declare no competing financial interest.

■ ACKNOWLEDGMENTS

Mariana D. Canela, MSc in Food Innovation and Products Design (FIPDes), is acknowledged for her support in sample preparation. Dr. Maria Savarese is acknowledged for providing olive oil samples. We thank Prof. Marco Genovese for proofreading the English manuscript. This work was partially supported by Regione Campania (SeSIRCA, Naples, Italy) with OMeGa Project.

■ ABBREVIATIONS USED

GC, gas chromatography; MS, mass spectrometry; HPLC, high performance liquid chromatography; SPME, solid-phase microextraction technique; VOO, virgin olive oil; RAS, retronasal aroma simulator; ROO, refined olive oil; ROOP, refined olive oil with added olive oil polyphenols; WP, whey proteins; B, buffer solution; EVOO, extra virgin olive oil

■ REFERENCES

(1) Estruch, R.; Ros, E.; Salas-Salvado, J.; Covas, M. I.; Corella, D.; Aros, F.; et al. Primary prevention of cardiovascular disease with a Mediterranean diet. *N. Engl. J. Med.* **2013**, *368*, 1279−1290.

(2) Tripoli, E.; Giammanco, M.; Tabacchi, G.; Di Majo, D.; Giammanco, S.; La Guardia, M. The phenolic compounds of olive oil: structure, biological activity and beneficial effects on human health. *Nutr. Res. Rev.* **2005**, *18*, 98−112.

(3) Frank, S.; Linder, K.; Fritsche, L.; Hege, M. A.; Kullmann, S.; Krzeminski, A.; et al. Olive oil aroma extract modulates cerebral blood flow in gustatory brain areas in humans. *Am. J. Clin. Nutr.* **2013**, *98*, 1360−1366.

(4) Salles, C.; Chagnon, M. C.; Feron, G.; Guichard, E.; Laboure, H.; Morzel, M.; Semon, E.; Tarrega, A.; Yven, C. In mouth mechanism leading to flavour release and perception. *Crit. Rev. Food Sci. Nutr.* **2011**, *51*, 67−90.

(5) Angerosa, F.; Servili, M.; Selvaggini, R.; Taticchi, A.; Esposto, S.; Montedoro, G. Volatile compounds in virgin olive oil: occurrence and their relationship with the quality. *J. Chromatogr. A* **2004**, *1054*, 17−31.

(6) van Ruth, S. M.; O'Connor, C. H.; Delahunty, C. M. Relationships between temporal release of aroma compounds in a model mouth system and their physico-chemical characteristics. *Food Chem.* **2000**, *71*, 393−399.

(7) Meynier, A.; Rampon, V.; Dalgalarrondo, M.; Genot, C. Hexanal and t-2-hexenal form covalent bonds with whey proteins and sodium caseinates in aqueous solutions. *Int. Dairy J.* **2004**, *14*, 681−690.

(8) Kuhn, J.; Considine, T.; Singh, H. Interactions of milk proteins and volatile flavor compounds: Implications in the development of protein foods. *J. Food Sci.* **2006**, *71*, 72−82.

(9) Guichard, E. Flavour retention and release from protein solutions. *Biotechnol. Adv.* **2006**, *24*, 226−229.

(10) Burdach, K. J.; Kroeze, J. H. A.; Koster, E. P. Nasal, retronasal, and gustatory perception: An experimental comparison. *Percept. Psychophys.* **1984**, *36*, 205−208.

(11) Linforth, R.; Martin, F.; Carey, M.; Davidson, J.; Taylor, A. J. Retronasal transport of aroma compounds. *J. Agric. Food Chem.* **2002**, *50*, 1111−1117.

(12) Chen, J. Food oral processing−A review. *Food Hydrocolloids* **2009**, *23*, 1−25.

(13) Vingerhoeds, M. H.; Blijdenstein, T. B. J.; Zoet, F. D.; Van Aken, G. A. Emulsion flocculation induced by saliva and mucin. *Food Hydrocolloids* **2005**, *19*, 915−922.

(14) Silletti, E.; Vingerhoeds, M. H.; Norde, W.; Van Aken, G. A. The role of electrostatics in saliva-induced emulsion flocculation. *Food Hydrocolloids* **2007**, *21*, 596−606.

(15) Di Mattia, C.; Paradiso, V. M.; Andrich, L.; Giarnetti, M.; Caponio, F.; Pittia, P. Effect of Olive Oil Phenolic Compounds and Maltodextrins on the Physical Properties and Oxidative Stability of Olive Oil O/W Emulsions. *Food Biophys.* **2014**, *9*, 396−405.

(16) Dalgleish, D. G. Food emulsions—their structures and structure-forming properties. *Food Hydrocolloids* **2006**, *20*, 415−422.

(17) van Ruth, S. M.; Roozen, J. P. Aroma compounds of oxidised sunflower oil and its oil-in-water emulsion: volatility and release under mouth conditions. *Eur. Food Res. Technol.* **2000**, *210*, 258−262.

(18) van Ruth, S. M.; Grossmann, I.; Geary, M.; Delahunty, C. M. Interactions between Artificial Saliva and 20 Aroma Compounds in Water and Oil Model Systems. *J. Agric. Food Chem.* **2001**, *49*, 2409−2413.

DOI: 10.1021/acs.jafc.5b00148
J. Agric. Food Chem. 2015, 63, 3838−3850

(19) van Ruth, S. M.; King, C.; Giannouli, P. Influence of lipid fraction, emulsifier fraction, and mean particle diameter of oil-in water emulsions on the release of 20 aroma compounds. *J. Agric. Food Chem.* **2002**, *50*, 2365−2371.
(20) Malone, M. E.; Appelqvist, I. A. M.; Norton, I. T. Oral behaviour of food hydrocolloids and emulsions. Part 2. Taste and aroma release. *Food Hydrocolloids* **2003**, *17*, 775−784.
(21) Arancibia, C.; Jublot, L.; Costell, E.; Bayarri, S. Flavor release and sensory characteristics of o/w emulsions. Influence of composition, microstructure and rheological behavior. *Food Res. Int.* **2011**, *44*, 1632−1641.
(22) Frank, D.; Appelqvist, I.; Piyasiri, U.; Wooster, T. J.; Delahunty, C. Proton Transfer Reaction Mass Spectrometry and Time Intensity Perceptual Measurement of Flavor Release from Lipid Emulsions Using Trained Human Subjects. *J. Agric. Food Chem.* **2011**, *59*, 4891−4903.
(23) Mestres, M.; Kieffer, R.; Buettener, A. Release and Perception of Ethyl Butanoate during and after Consumption of Whey Protein Gels: Relation between Textural and Physiological Parameters. *J. Agric. Food Chem.* **2006**, *54*, 1814−1821.
(24) Kuhn, J.; Delahunty, C. M.; Considine, T.; Singh, H. In-mouth flavour release from milk protein. *Int. Dairy J.* **2009**, *19*, 307−313.
(25) Benjamin, O.; Silcock, P.; Beauchamp, J.; Buettner, A.; Everett, D. W. Volatile release and structural stability of β-lactoglobulin primary and multilayer emulsions under simulated oral conditions. *Food Chem.* **2013**, *140*, 124−134.
(26) Humphrey, S. P.; Williamson, R. T. A review of saliva: Normal composition, flow, and function. *J. Prosthet. Dent.* **2001**, *85*, 162−169.
(27) Pripp, A. H.; Vreeker, R.; van Duynhoven, J. Binding of olive oil phenolics to food proteins. *J. Sci. Food Agric.* **2005**, *85*, 354−362.
(28) Garcia-Mesa, J. A.; Pereira-Caro, G.; Fernandez-Hernandez, A.; Garcia-Ortiz Civantos, C.; Mateos, R. Influence of lipid matrix in the bitterness perception of virgin olive oil. *Food Qual. Pref.* **2008**, *19*, 421−430.
(29) Bayram, B.; Esatbeyoglu, T.; Schulze, N.; Ozcelik, B.; Frank, J.; Rimbach, G. Comprehensive analysis of polyphenols in 55 extra virgin olive oils by HPLC-ECD and their correlation with antioxidant activities. *Plant Foods Hum. Nutr.* **2012**, *67*, 326−336.
(30) Beltrán, G.; Ruano, M. T.; Jiménez, A.; Uceda, M.; Aguilera, M. P. Evaluation of virgin olive oil bitterness by total phenol content analysis. *Eur. J. Lipid Sci. Technol.* **2007**, *108*, 193−197.
(31) Kalua, C. M.; Allen, M. S.; Bedgood, D. R., Jr.; Bishop, A. G.; Prenzler, P. D.; Robards, K. Olive oil volatile compounds, flavour development and quality: A critical review. *Food Chem.* **2007**, *100*, 273−286.
(32) Buettner, A. Influence of human salivary enzymes on odorant concentration changes occurring in vivo. 1. Esters and thiols. *J. Agric. Food Chem.* **2002**, *50*, 3283−3289.
(33) Vasquez-Roncero, A. Les polyphenols de l'huile d'olive et leur influence sur les characteristiques de l'huile (Polyphenols of olive oil and their influence on oil characteristics). *Rev. Fr. Corps Gras* **1978**, *25*, 21−26.
(34) Gutfinger, T. Polyphenols in olive oils. *J. Am. Oil Chem. Soc.* **1981**, *58*, 966−968.
(35) Sacchetti, G.; Di Mattia, C.; Pittia, P.; Mastrocola, D. Effect of roasting degree, equivalent thermal effect and coffee type on the radical scavenging activity of coffee brews and their phenolic fraction. *J. Food Eng.* **2009**, *90*, 74−80.
(36) Genovese, A.; Piombino, P.; Gambuti, A.; Moio, L. Simulation of retronasal aroma of white and red wine in a model mouth system. Investigating the influence of saliva on volatile compound concentrations. *Food Chem.* **2009**, *114*, 100−107.
(37) Genovese, A.; Caporaso, N.; Civitella, A.; Sacchi, R. Effect of human saliva and sip volume of coffee brews on the release of key volatile compounds by a retronasal aroma simulator. *Food Res. Int.* **2014**, *61*, 100−111.
(38) Mao, L.; Boiteux, L.; Roos, Y. H.; Miao, S. Evaluation of volatile characteristics in whey protein isolate−pectin mixed layer emulsions under different environmental conditions. *Food Hydrocolloids* **2014**, *41*, 79−85.
(39) Friel, E. N.; Taylor, A. J. Effect of salivary components on volatile partitioning from solution. *J. Agric. Food Chem.* **2001**, *49*, 3898−3905.
(40) Vardhanabhuti, B.; Cox, P. W.; Norton, I. T.; Foegeding, E. A. Lubricating properties of human whole saliva as affected by beta-lactoglobulin. *Food Hydrocolloids* **2011**, *25*, 1499−506.
(41) Sarkar, A.; Goh, K. K. T.; Singh, H. Colloidal stability and interactions of milk-protein-stabilized emulsions in an artificial saliva. *Food Hydrocolloids* **2009**, *23*, 1270−1278.
(42) Vardhanabhuti, B.; Kelly, M. A.; Luck, P. J.; Drake, M. A.; Foegeding, E. A. Roles of charge interactions on astringency of whey proteins at low pH. *J. Dairy Sci.* **2010**, *93*, 1890−1899.
(43) Kallithraka, S.; Bakker, J.; Clifford, M. N.; Vallis, L. Correlations between saliva protein composition and some T−I parameters of astringency. *Food Qual. Pref.* **2001**, *12*, 145−152.
(44) Weel, K. G. C.; Boelrijk, A. E. M.; Burger, J. J.; Claassen, N. E.; Gruppen, H.; Voragen, A. G. J.; Smit, G. Effect of whey protein on the in vivo release of aldehydes. *J. Agric. Food Chem.* **2003**, *51*, 4746−4752.
(45) Kuhn, J.; Zhu, X. Q.; Considine, T.; Singh, H. Binding of 2-nonanone and milk proteins in aqueous model systems. *J. Agric. Food Chem.* **2007**, *55*, 3599−3604.
(46) Jouenne, E.; Crouzet, J. Effect of pH on retention of aroma compounds by b-lactoglobulin. *J. Agric. Food Chem.* **2000**, *48*, 1273−1277.
(47) Morales, M. T.; Luna, G.; Aparicio, R. Comparative study of virgin olive oil sensory defects. *Food Chem.* **2005**, *91*, 293−301.
(48) Vichi, S.; Guadayol, J. M.; Caixach, J.; Lopez-Tamames, E.; Buxaderas, S. Monoterpene and sesquiterpene hydrocarbons of virgin olive oil by headspace solid-phase microextraction coupled to gas chromatography/mass spectrometry. *J. Chromatogr. A* **2006**, *1125*, 117−123.
(49) Di Mattia, C. D.; Sacchetti, G.; Mastrocola, D.; Sarker, D. K.; Pittia, P. Surface properties of phenolic compounds and their influence on the dispersion degree and oxidative stability of olive oil O/W emulsions. *Food Hydrocolloids* **2010**, *24*, 652−658.
(50) Lorrain, B.; Tempere, S.; Iturmendi, N.; Moine, V.; de Revel, G.; Teissedre, P. L. Influence of phenolic compounds on the sensorial perception and volatility of red wine esters in model solution: An insight at the molecular level. *Food Chem.* **2013**, *140*, 76−82.
(51) Reiners, J.; Grosch, W. Odorants of Virgin Olive Oils with Different Flavor Profiles. *J. Agric. Food Chem.* **1998**, *46*, 2754−2763.
(52) Kesen, S.; Kelebek, H.; Selli, S. Characterization of the key aroma compounds in Turkish olive oils from different geographic origins by application of aroma extract dilution analysis (AEDA). *J. Agric. Food Chem.* **2014**, *62*, 391−401.

DOI: 10.1021/acs.jafc.5b00148
J. Agric. Food Chem. 2015, 63, 3838−3850

Depending on the amount and availability of phosphatides, only parts of oilseed gums have the potential to be processed as lecithins. Common lecithin sources include cottonseed, corn, sunflower seed, and rapeseed. Due to the mass production of soybean oil, soybean gum obtained as a byproduct of the oil-refining process is the primary source of commercial lecithin. Recently, the demand for sunflower lecithin has grown because this lecithin is considered the product of a non genetically modified organism.[1,20−22] Moreover, the rheological and emulsifying properties of sunflower lecithin indicate that it is a desirable alternative to soybean lecithin.[20−22] However, little or no information is available regarding the composition of PC molecular species derived from sunflower lecithin. A previous study only focused on the fatty acid composition of lecithin, which was considered to be largely equivalent to that of the oil source.[1] Thus, analyzing PC species in conjunction with triacylglycerol (TAG) composition in crude lecithins may provide a more complete description of the deposition of fatty acids in plant lecithins.

In our previous study, TAG molecular species were successfully determined through HPLC-ELSD analysis by their retention times and theoretical carbon numbers (TCNs).[23] The retention times were found to correspond with their TCNs, which were calculated on the basis of the total carbon number, unsaturation degree, and types of unsaturated fatty acid. Nevertheless, these attempts to establish a correlation between the HPLC elution sequence of the PC molecular species and TCN with regard to the physical conformation of acyl chains remained inconclusive.

In this study, an RP-HPLC-ELSD method intended for the determination of the PC molecular species was introduced. L-α-PC from soybean origin was used to evaluate the chromatographic characteristics. Furthermore, the correlation between the TCNs of PC molecular species and their respective HPLC retention times was investigated. We revealed that, as for TAG, profiling could be achieved by comparison with TAG standards with reference to retention times to make a regression curve; by calculation of the TCN of respective peaks with reference to the regression analysis, PC peak profiling in the HPLC-ELSD chromatogram could be achieved by the regression curve that was made from the TCNs of known peaks with reference to retention times.

MATERIALS AND METHODS

Chemicals. L-α-PC (≥99%), L-α-PE (≥98%), five molecular species of PC, including LLPC, 1,2-dipalmitoyl-*sn*-glycero-3-phosphocholine (PPPC), 1,2-dioleoyl-*sn*-glycero-3-phosphocholine (OOPC), 1-oleoyl-2-palmitoyl-*sn*-glycero-3-phosphocholine (OPPC), and 1-palmitoyl-2-oleoyl-*sn*-glycero-3-phosphocholine (POPC), and 2,5-dihydroxybenzoic acid (2,5-DHB) were obtained from Sigma-Aldrich (St. Louis, MO, USA). All chromatographic-grade reagents used in HPLC and other analytical-grade solvents, as well as thin-layer chromatography (TLC) plates silica gel 60 (No. 5553), were obtained from Merck (Darmstadt, Germany). Silica gel (SiliaFlash G60, 70−230 mesh (60−200 μm), average pore size 25 Å) for column chromatography was obtained from SiliCycle (Quebec, Canada). Silica solid-phase extraction cartridges were obtained from J. T. Baker (Phillipsburg, NJ, USA).

Materials. The crude soybean lecithin was obtained as industrial soybean oil degummed residue from the Taiwan Sugar Corporation (Kaohsiung, Taiwan). Sunflower liquid lecithin was bought from Now Foods Company (Bloomingdale, IL, USA). The acetone-soluble fractions of crude soybean lecithin and sunflower liquid lecithin accounted for 43.6% and 61.7%, respectively.

PC Analysis by RP-HPLC-ELSD. The purity of commercially available L-α-PC was examined by TLC. Briefly, a silica gel 60 TLC plate and a mobile phase consisting of chloroform/methanol/acetic acid/water (75/40/8/3, v/v/v/v) were used for the separation of phospholipids. L-α-PC standard solution was prepared by dissolving 5 mg of L-α-PC in 1 mL of methanol, and then 10 μL of sample was applied by a microsyringe to the TLC plate prior to developing. The spot was visualized using iodine vapor and exposed in an oven set at 60 °C for 5 min. For HPLC analysis, a 20 μL aliquot of the PC sample was analyzed using an HPLC system (P1000, Thermo Fisher Scientific, Barrington, IL, USA) equipped with an ELSD (Alltech 2000, Deerfield, IL, USA) and a C30 analytical column (Develosil C30-UG-5, 4.6 × 250 mm, 5 μm; Nomura Chemical Co., Anada-cho Seto, Japan). The mobile phase was composed of acetonitrile, methanol, and triethylamine in a 40/58/2 ratio (v/v/v) at a flow rate of 1 mL/min. For the ELSD, the temperature of the drift tube was 80 °C and the air flow rate was 1.8 L/min. Each run lasted 40 min and required another 10 min to reach equilibrium. In addition, to quantitate the individual PC species, five species of pure PC molecules, namely LLPC, PPPC, OOPC, OPPC, and POPC, were analyzed at concentrations of 0.25, 0.5, 1, 2, and 5 g/L to prepare calibration curves.

Identification of PC Molecular Species by MALDI-TOF-MS. To identify the fatty acyl chains at the *sn*-1 and *sn*-2 positions, each PC molecular species eluted from HPLC was collected manually by using a flow splitter according to retention time and then analyzed by MALDI-TOF-MS. Aliquots of the PC samples were directly mixed (1/1, v/v) with the 2,5-DHB matrix solution (1 mL of 20 mg/mL 2,5-DHB in 70% acetonitrile with 0.1% trifluoroacetic acid). A 1 μL portion of the PC sample solution was used for MALDI-TOF-MS analysis. The sample/matrix solution was deposited onto the sample plate and vacuum-dried before being transferred into the ion source of a MALDI-TOF-MS (Autoflex III, Bruker Daltonics, Bremen, Germany). The sample spot was irradiated with a neodymium-doped yttrium aluminum garnet (Nd:YAG) laser (emitting at 355 nm; pulse duration, 3 ns; 100 Hz) for desorption and ionization. The extraction voltage was set to 2.5 kV, and gated matrix suppression was applied to prevent detector saturation. Positive ion mass spectra in the range m/z 400−1000 were acquired in reflectron mode under delayed extraction. In total, 300 laser shots were averaged for each sample analysis to obtain representative mass spectra, and three mass spectra were recorded from each sample.

Isolation of PC from Lecithins. The crude lecithins from soybean and sunflower seeds were fractionated by acetone prior to silica gel column chromatography. Briefly, 10 g of the crude lecithin was suspended with acetone (1/5, w/v), and then the insoluble fraction was separated from the solvent. This step was performed two or three times until the supernatant was colorless. The acetone-insoluble fraction was resuspended with 95% ethanol (1/4, w/v). The alcohol fraction was concentrated to approximately 20 mL under vacuum and then mixed with 10 g of Celite to obtain the preadsorbed sample for further silica gel chromatography. After the solvent was removed using a rotary evaporator, the dry powder was transferred to the top of the silica gel column (containing 40 g of silica gel, 2.2 cm i.d. × 28 cm) that had been previously equilibrated with ethyl acetate. Chromatography was performed by eluting the column with 180 mL of ethyl acetate to remove neutral lipids and impurities, and then eluting with 180 mL of ethanol, followed by 300 mL of methanol. The eluate was collected in 30 mL fractions and was monitored by TLC according to retention value (R_f). L-α-PE and L-α-PC standard solutions were used in TLC analysis as references. The fractions dominated by PC were combined, and the solvent was removed under reduced pressure for further analyses of PC content and molecular species.

The PC content of the sample was measured using a normal phase HPLC system equipped with a ConstraMetric 3200 solvent delivery pump and a SpectroMonitor 3200 UV−visible detector (Thermo Fisher Scientific, Barrington, IL, USA). Analysis was performed according to the American Oil Chemists' Society (AOCS) official method Ja 7b-91. The analytical column was a 250 × 4.6 mm i.d. 5 μm Reprosil 70 Si column (Dr. Maisch GmbH, Ammerbuch, Germany).

DOI: 10.1021/acs.jafc.5b01022
J. Agric. Food Chem. 2015, 63, 3851−3858

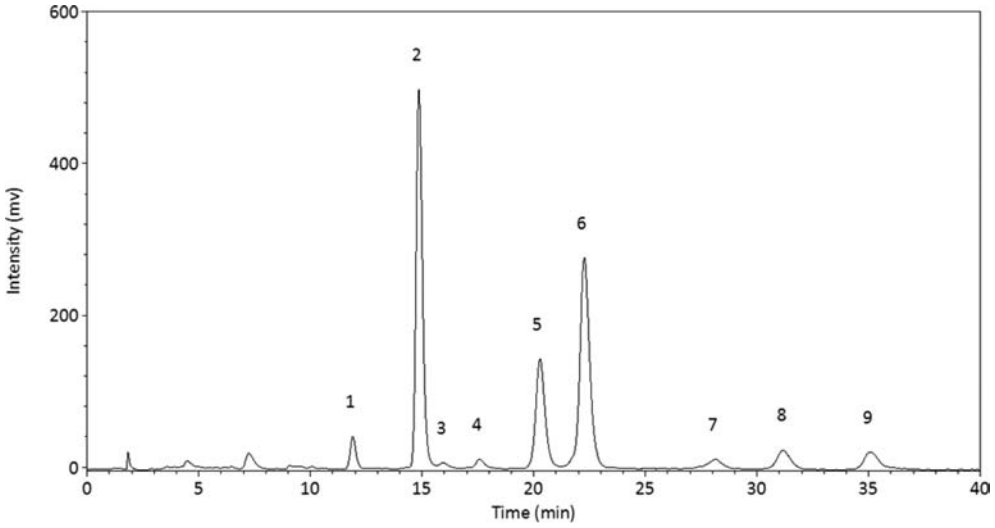

Figure 1. Chromatogram of L-α-PC by RP-HPLC-ELSD. Separation was performed using isocratic conditions: acetonitrile/methanol/triethylamine (40/58/2, v/v/v) at a flow rate of 1 mL/min on a C30 column (250 × 4.6 mm, 5 μm). Numbers were assigned to major identified peaks by MALDI-TOF-MS: (1) LLnPC; (2) LLPC; (3) OLnPC; (4) PLnPC; (5) OLPC; (6) PLPC; (7) SLPC; (8) PPPC; (9) SOPC.

The HPLC mobile phase was composed of *n*-hexane, isopropyl alcohol, and 0.2 M acetate buffer (pH 4.2) in a ratio of 8/8/1 (v/v/v) at a flow rate of 2 mL/min. The detection wavelength was set at 206 nm. The retention time of L-α-PC was used as a reference to determine the PC peak in lecithin profiles. The PC content was calculated from a linear calibrated curve derived from the corresponding peak areas of a serial dilution of authentic L-α-PC standard.

TAG Species Analysis by RP-HPLC-ELSD. The acetone-soluble fractions of crude lecithins were combined, and the solvent was removed under vacuum to obtain the oil. The TAG species of oils were analyzed on the basis of a previous study with some modifications.[23] Briefly, oil samples were dissolved in a small amount of *n*-hexane and pretreated using a silica solid-phase extraction cartridge to remove the potent polar constituents prior to HPLC analysis. The HPLC mobile phase was composed of acetonitrile (solvent A) and isopropyl alcohol (solvent B); the gradient elution started with 85% A, decreased to 30% over 55 min, was held at 30% for 10 min, and finally increased to 85% A over the next 5 min. The flow rate of the mobile phase was 1.2 mL/min. ELSD settings were 70 °C for the drift tube and a 2.0 L/min air flow rate. The peaks were determined by calculating the TCN and referencing the results with our previous study.[23] The percentage of TAG species was calculated using eq 1:

$$\%\ \text{of TAG} = \frac{A(\text{peak area of individual TAG species})}{\sum A(\text{total peak areas of TAG})} \times 100 \quad (1)$$

Data Analysis. The HPLC chromatograms were recorded and analyzed using SISC Chromatography Data Station v3.0 (SISC Inc., Taipei, Taiwan), and the results were calculated using Windows Excel 2010. The peak picking software used with MALDI-TOF-MS was FlexAnalysis 3.3 (Bruker Daltonics).

RESULTS AND DISCUSSION

PC Molecular Species Analysis by RP-HPLC-ELSD. L-α-PC was used as the reference to evaluate the separation of various species. L-α-PC was examined by TLC and presented as a single spot (R_f 0.41) on the silica-TLC plate, indicating that it was an assemblage of PC molecular species. Brouwers et al. reported that the separation was performed by connecting two C18 columns in series; the retention of PC molecular species decreased as the amount of triethylamine in the mobile phase increased, and the optimized solvent system varied with the different PC molecular species patterns of biological samples from animal origin.[11] We considered that triethylamine acted as an ion-pair reagent to reduce extensive peak tailing, because amines are known to prevent interactions between the stationary phase and the phospholipid headgroup moiety. Moreover, because of the repulsion between the positively charged choline of PC and triethylamine, the chromatographic time could be reduced by the addition of triethylamine. We obtained results similar to those of Brouwers et al.;[11] the content of triethylamine in the mobile phase affected the efficiency of separation greatly. Figure 1 revealed that nine molecular species of PC in L-α-PC were separated successfully through an isocratic mobile phase that was composed of acetonitrile/methanol/triethylamine (40/58/2, v/v/v); moreover, only one C30 column was used in the HPLC system, which could reduce excessive back pressure in the HPLC system.

Identification of PC Molecular Species by MALDI-TOF-MS. To identify the PC species corresponding with the individual peaks in the HPLC chromatogram, L-α-PC was analyzed using MALDI-TOF-MS in positive-ion mode. The identification of fatty acyl chains and the regiodistribution of individual PC species in these chains was achieved by verifying the fragment ions from the spectra. Parts A–E of Figure 2 shows the fragmentation patterns of the PC molecules associated with peak nos. 1, 2, 4, 6, and 7 in Figure 1. The mass signal at m/z 520.3 in Figure 2A refers to the molecular ion $[M + H]^+$ of lysophosphatidylcholine (LPC) esterified with linoleic acid. Furthermore, m/z 780.5 was identified as the molecular ion $[M + H]^+$ of linoleoyl-linolenoyl-glycerophosphocholine, whereas m/z 802.5 corresponded to the molecular ion of $[M + Na]^+$. Previous studies have reported that all PC molecular species normally occur in LPCs and fatty acids.[24] In addition, the *sn*-2 position of phospholipids contains unsaturated fatty acid, and the saturated fatty acids are most abundant at the *sn*-1 position.[25] Fuchs et al. reported that the resulting LPCs from diacyl-PCs possess a saturated fatty acid residue at the *sn*-1 position.[26] Therefore, the PC molecular species of peak no. 1 was identified as 1-linoleoyl-2-linolenoyl-*sn*-glycero-3-phosphocholine (LLnPC). Similar results can be observed in

DOI: 10.1021/acs.jafc.5b01022
J. Agric. Food Chem. 2015, 63, 3851−3858

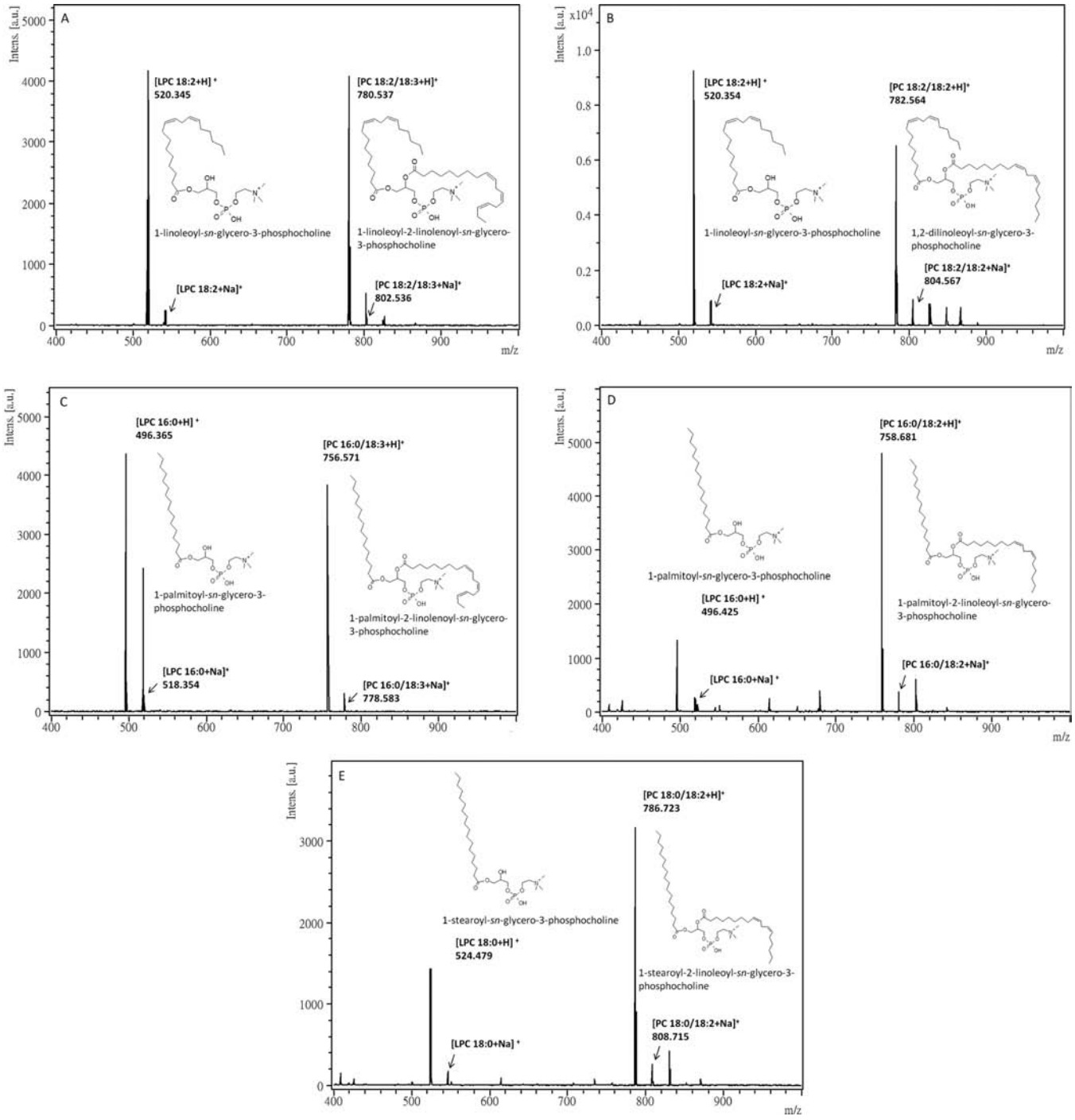

Figure 2. Ions obtained by MALDI-TOF-MS in positive-ion mode from m/z 400 to 1000 and corresponding structures of product nos. 1 (A), 2 (B), 4 (C), 6 (D), and 7 (E) in the L-α-PC profile. C16:0 refers to palmitic acid, C18:0 refers to stearic acid, C18:1 refers to oleic acid, C18:2 refers to linoleic acid, and C18:3 refers to linolenic acid.

Figure 2B–E. As far as L-α-PC was concerned, the major species were LLPC, 1-oleoyl-2-linoleoyl-*sn*-glycero-3-phosphocholine (OLPC), and 1-palmitoyl-2-linoleoyl-*sn*-glycero-3-phosphocholine (PLPC), with LLPC being the predominant species, whereas minor components included LLnPC, 1-oleoyl-2-linolenoyl-*sn*-glycero-3-phosphocholine (OLnPC), 1-palmitoyl-2-linolenoyl-*sn*-glycero-3-phosphocholine (PLnPC), 1-stearoyl-2-linoleoyl-*sn*-glycero-3-phosphocholine (SLPC), PPPC, and 1-stearoyl-2-oleoyl-*sn*-glycero-3-phosphocholine (SOPC). The PC composition was in good agreement with that in previous studies.[14,15]

PC Profiling: Relation between Retention Time and TCN. The TCN of PC (TCN_{PC}) was calculated according to the TCN of TAG (TCN_{TAG}) with some modification. The equivalent carbon numbers (ECNs), TCNs, and retention times of L-α-PC and soy TAG molecular species are shown in Table 1. According to El-Hamdy and Perkins, TAGs with the same ECN act as critical pairs, which means that these TAGs behaved similarly in response to RP chromatography in spite of the difference in chain lengths, number of double bonds, geometrical configuration, and their ability to be further

DOI: 10.1021/acs.jafc.5b01022
J. Agric. Food Chem. 2015, 63, 3851–3858

Table 1. ECNs, TCNs, and Retention Times of PC Molecular Species of L-α-PC and TAG Species of Soybean Oil

PC species	ECN_{PC}[a]	TCN_{PC}[a]	retention time	TAG species	ECN_{TAG}[a]	TCN_{TAG}[a]	retention time
LLnPC	26	24.42	11.89	LLnL	40	37.67	33.57
LLPC	28	26.50	14.85	LLL	42	39.75	37.03
OLnPC	28	26.55	15.98	OLnL	42	39.80	37.88
PLnPC	28	27.17	17.58	PLnL	42	40.42	39.69
OLPC	30	28.63	20.28	OLL	44	41.88	41.35
PLPC	30	29.25	22.26	OLnO	44	41.92	42.16
SLPC	32	31.25	28.13	PLL	44	42.50	43.18
PPPC	32	32.00	31.20	PLnO	44	42.55	44.08
SOPC	34	33.38	35.07	PLnP	44	43.17	44.83
				OLO	46	44.00	45.64
				PLO	46	44.63	47.50
				PLP	46	45.25	48.18
				OOO	48	46.13	49.78
				POO	48	46.75	51.71
				POP	48	47.38	52.34
				SOO	50	48.75	54.82
				SOP	50	49.38	56.41

[a] ECN_{TAG}, TCN_{TAG}, ECN_{PC}, and TCN_{PC} were calculated based on the basis of eqs 2, 3, 4. and 5, respectively.

separated in sequence with TCN.[27] The ECN of TAG (ECN_{TAG}) and TCN_{TAG} were calculated using eqs 2 and 3:

$$ECN_{TAG} = CN - 2n \quad (2)$$

$$TCN_{TAG} = ECN_{TAG} - \sum_{1}^{3} Ui \quad (3)$$

where CN is the total carbon number of the fatty acid residue per TAG molecule and n is the number of double bonds in the fatty acid residue per TAG molecule. The Ui value of unsaturated fatty acid was calculated from experimental data for known TAG species according to Elhamdy and Perkins.[27] In brief, a plot of retention times versus carbon numbers of several saturated TAG standards was used as a calibration curve. For any saturated TAG, the TCN value is equal to the actual carbon number of fatty acid residues while the Ui of unsaturated fatty acid was calculated from experimental data for the known fatty acyl chains of TAGs. For example, the triolein peak has ECN and TCN (which is calculated from the calibration curve) values of 48 and 46.125, respectively; then, $\sum_1^3 Ui = 48 - 46.125 = 1.875$. Consequently, the Ui factor for oleoyl is 0.625. The other Ui factors were obtained in the same way and are as follows: 0.75 for linoleyl, 0.83 for linolenyl groups, and 0.0 for saturated acyl groups.

As regards PC, only two fatty acids were taken into consideration to calculate their TCN_{PC} values. The ECN of PC (ECN_{PC}) and TCN_{PC} were calculated on the basis of eqs 4 and 5, respectively:

$$ECN_{PC} = CN - 2n \quad (4)$$

$$TCN_{PC} = ECN_{PC} - (U_1 + U_2) \quad (5)$$

where CN is the total carbon number of the fatty acid residue per PC molecule and n is the number of double bonds in the fatty acid residue per PC molecule. U_1 and U_2 are factors adapted from TAG for fatty acyl chains at the *sn*-1 and *sn*-2 positions, respectively.

As shown in Table 1, as the value of TCN increased, the relative retention time increased correspondingly. In addition, the TCNs and retention times of nine PC molecular species in the L-α-PC profile (Figure 1) were selected to construct a curve. The parameters appeared to fit a linear regression model, and the regression curve between the retention time and TCN_{PC} values of PC species showed good linearity (Figure S1A, Supporting Information). For the retention time and TCN_{TAG}, the linearity of the regression curve was also examined (Figure S1B, Supporting Information). The results suggested that, similar to the case for TAG species, L-α-PC could be separated into molecular species by a highly efficient C30 column, and the elution order paralleled TCN correspondingly. Therefore, we considered that linear regression curves from the TCN and retention time of individual molecular species can be used for the determination of molecular species in both PC and TAG.

Brouwers et al. suggested that a mathematical relationship exists between the retention time and ECN of each PE molecule, which was defined as $ECN = CN - 1.505n$ (where CN is the total carbon number of fatty acid residues per PE molecule and n is the number of double bonds in the fatty acid residue); this relationship has been used to assist in the identification of unknown PE species when mass spectrometry is not available.[12] The retention time of the PC molecule increases proportionally to the ECN coefficient ($ECN = CN - 2n$), which is a discriminating factor that can provide valuable information for PC separation.[15,28] Choi et al. developed a retention time index for PC profiling, which showed that the fatty acid chain length and the degree of unsaturation were linked, achieving linear curves between the relative retention time and mass over charge (m/z) of PC.[29] However, the relation between TCN and retention time of phospholipids has remained unclear to date. For those PC species with the same ECN_{PC} values, such as LLPC, OLnPC, and PLnPC, their TCN_{PC} values showed slight differences, enabling further discrimination (Table 1). Elhamdy and Perkins concluded the separate mechanism of TAGs was likely that the affinity between the stationary phase and fatty acids becomes stronger when the methylene groups in the chain increase or double bonds decrease, causing molecules to travel more slowly in a column, resulting in longer retention times.[27] Moreover, the TCN_{PC} and retention time of PC species were easily regressed as a linear curve ($R^2 > 0.98$) (Figure S1A, Supporting Information). Since TCN_{TG} has been widely used to predict

DOI: 10.1021/acs.jafc.5b01022
J. Agric. Food Chem. 2015, 63, 3851−3858

the unknown TG species in previous studies,[27,30] using the plot of the TCN_{PC} and retention time of known PC species to predict the fatty acid components of unknown PC peaks should be a promising alternative to specify the PC molecular species in HPLC-ELSD analysis. In addition, on the basis of the relation of TCN to retention time, we considered not only for TAG and PC species determination but also the molecular species of other phospholipids could be determined. Furthermore, we observed a disadvantage that the *sn* positional isomers, i.e., molecular species such as OPPC and POPC, have identical retention times and cannot be separated under the current HPLC separation conditions. The same situation also occurred in TAG analysis if their TCN_{TAG} values were near or identical. For instance, the TAG molecular species identified as POL represented a mixture of POL, PLO, and OPL. The detailed positional assignment of individual fatty acid residues is much more difficult or even impossible for TAG.

Quantitation of Individual PC Molecular Species. To prepare quantitative curves with this RP-HPLC-ELSD system, five pure PC species, including OOPC, POPC, OPPC, PPPC, and LLPC, were analyzed individually to determine their respective relationships between concentration and peak area. Regression analyses of these linear plots revealed that the correlations between ELSD responses to all analytes were almost identical (Figure S2, Supporting Information). The list of relative response ratio of their interception values showed that the relative response factor values were highly similar to one another (Figure S2, Supporting Information). Therefore, the contents of corresponding HPLC fractions could be determined on the basis of peak area percentage. The percentage of individual PC species was calculated by using eq 6.

$$\%\ \text{of PC species} = \frac{A(\text{peak area of individual PC species})}{\sum A(\text{total peak areas of PC species})} \times 100 \quad (6)$$

Determination of PC Contents in Lecithins and PC Profiling. The contents of PC in crude lecithins were determined according to AOCS method Ja 7b-91 to be 12.3 ± 2.6% (w/w) for crude soybean lecithin and 19.4 ± 1.5% (w/w) for sunflower liquid lecithin. The PC content in lecithin was quantitated by normal-phase HPLC-UV on the basis of the absorbance of the PC at 206 nm being proportional to the number of double bonds in PC from the same origin. Therefore, quantitation by normal-phase HPLC-UV is not appropriate when the PC molecular species of lecithin samples contain diverse fatty acyl chains.

PC profiles of isolated soybean PC and sunflower PC were analyzed by HPLC-ELSD (Figure S3A,B, Supporting Information). The compositions of isolated PC from soybean and sunflower lecithins are given in Table 2. Like the species L-α-PC, the isolated soybean PC was composed of nine PC species. The most abundant PC species was LLPC, accounting for 40.6%. The total amount of PC species with two polyunsaturated fatty acyl chains at the *sn*-1 and *sn*-2 positions, such as LLPC and LLnPC, were 44.4%. The major PC species in the sunflower PC profile were very similar to those in the soybean PC profile. The LLPC level was quite high (64.3%) in sunflower PC, but LLnPC, OLnPC, and PLnPC peaks were absent. Regarding of the fatty acid composition of lecithins, Nieuwenhuyzen and Tomas reported that soy lecithin contains 55% linoleic acid, 17% oleic acid, 16% palmitic acid, 7% linolenic acid, and 4% stearic acid and sunflower lecithin contains 63% linoleic acid, 18% oleic acid, 11% palmitic acid, and 4% stearic acid but no linolenic acid.[1] Our results were comparable with these data, and no linolenic acid was observed in isolated sunflower PC. In other words, sunflower PC lacks the linolenic acid-related PC molecular species, which significantly differentiates it from soybean PC.

Table 2. Distribution of the PC Molecular Species from Soybean Lecithin and Sunflower Lecithin

	area (%)[a]	
PC species	PC soybean	PC sunflower
LLnPC	3.77 ± 0.25	0.00 ± 0.00
LLPC	40.64 ± 0.28	64.25 ± 0.75
OLnPC	0.97 ± 0.01	0.00 ± 0.00
PLnPC	1.28 ± 0.01	0.00 ± 0.00
OLPC	15.18 ± 0.11	16.85 ± 0.37
PLPC	26.83 ± 0.19	13.02 ± 0.42
SLPC	2.42 ± 0.01	3.19 ± 0.25
PPPC	3.63 ± 0.01	2.32 ± 0.16
SOPC	5.29 ± 0.02	0.36 ± 0.19

[a]Data are mean ± SD of triplicate determinations. The contents of PC molecular species were determined according to eq 6.

Soybean oil and sunflower oil from their respective acetone-soluble fractions were analyzed by HPLC-ELSD (Figure S3C,D, Supporting Information). The TAG species were assigned by calculating the TCN_{TAG} value and comparing the results with TAG profiles of known TAG components.[23] The TAG compositions of soybean oil and sunflower oil samples are given in Table 3. The TAG species in soybean oil and sunflower oil were primarily trilinolein (LLL), dilinoleoyl oleoyl glycerol (OLL), and linoleoyl palmitoyl glycerol (PLL), accounting for 63.3% and 85.0%, respectively. Both soybean oil and sunflower oil contained minor amounts of dioleoyl linoleoyl (OLO), palmitoyl linoleoyl oleoyl glycerol (PLO), dipalmitoyl linoleoyl glycerol (PLP), OOO, dioleoyl palmitoyl glycerol (POO), dipalmitoyl oleoyl glycerol (POP), dioleoyl

Table 3. TAG Compositions of Soybean Oil and Sunflower Oil

	area (%)[a]	
TAG species	soybean oil	sunflower oil
LLnL	3.76 ± 0.11	0.00 ± 0.00
LLL	23.93 ± 0.11	40.94 ± 0.13
OLnL	2.59 ± 0.12	0.00 ± 0.00
PLnL	0.83 ± 0.19	0.00 ± 0.00
OLL	25.41 ± 0.11	37.26 ± 0.18
OLnO	0.47 ± 0.03	0.00 ± 0.00
PLL	13.95 ± 0.25	6.74 ± 0.03
PLnO	0.30 ± 0.02	0.00 ± 0.00
PLnP	0.18 ± 0.01	0.00 ± 0.00
OLO	9.91 ± 0.19	6.52 ± 0.15
PLO	8.34 ± 0.04	2.52 ± 0.03
PLP	2.37 ± 0.06	2.56 ± 0.07
OOO	4.20 ± 0.03	1.95 ± 0.08
POO	1.32 ± 0.15	0.41 ± 0.01
POP	1.76 ± 0.04	0.95 ± 0.02
SOO	0.42 ± 0.02	0.12 ± 0.00
SOP	0.27 ± 0.02[a]	0.05 ± 0.01[b]

[a]Data are mean ± SD of triplicate determinations. The contents of TAG species were determined according to eq 1.

DOI: 10.1021/acs.jafc.5b01022
J. Agric. Food Chem. 2015, 63, 3851−3858

stearoyl glycerol (SOO), and stearoyl oleoyl palmitoyl glycerol (SOP). Similarly, there were several TAGs containing linolenic acid in the soybean oil profile in comparison with the sunflower oil profile, such as dilinoleoyl linolenoyl glycerol (LLnL), oleoyl linolenoyl linoleoyl glycerol (OLnL), and palmitoyl linolenoyl linoleoyl glycerol (PLnL). The main TAGs in soybean oil and sunflower oil were consistent with those found in previous research.[31]

PCs are biologically active lipids and are the principal constituents of biological membranes. To date, publications regarding the characterization of PC molecular species in the food industry are still limited. Chen et al. screened the PC compositions of phospholipase-A_2-catalyzed enzymatic reaction products by LC ESI-tandem MS.[18] Hence, RP-HPLC-ELSD could be used to monitor the fatty acid composition of structured PCs during enzymatic interesterification. Recently, sunflower lecithin has been regarded as a promising replacement for soybean lecithin due to concerns about genetically modified products. As shown in Table 2, the major PC species of soybean lecithin and sunflower lecithin are quite similar. Moreover, sunflower lecithin was rich in the bioactive LLPC and may have the potential to replace soybean lecithin to produce LLPC from a non genetically modified source. Additionally, on the basis of the significant differences in minor PC species such as LLnPC, OLnPC, and PLnPC, determining the content of these PC molecular species was sufficient to differentiate soybean and sunflower lecithins. These various PC species could be viewed as prospective indicators to discriminate plant lecithins.

In conclusion, a method for PC molecular species profiling by RP-HPLC-ELSD was introduced. The PC molecular species were identified by positive-ion MALDI-TOF-MS. The relationship between the TCNs and retention times of standard PC species was developed alongside the RP-HPLC-ELSD analysis. The quantitation of PC molecular species was achieved on the basis of area normalization. This method can be used to characterize PC molecular species from crude lecithins, which would provide further information regarding the properties and functions of lecithins.

■ ASSOCIATED CONTENT

Supporting Information

Correlation between TCN and retention time (Figure S1), calibration curves (Figure S2), and chromatograms of isolated PCs (Figure S3). This material is available free of charge via the Internet at http://pubs.acs.org.

■ AUTHOR INFORMATION

Corresponding Author

*N.-W. Su: tel, +886-2-33664819; fax, +886-2-23632714; e-mail, snw@ntu.edu.tw.

Notes

The authors declare no competing financial interest.

■ ACKNOWLEDGMENTS

The MS spectra were obtained at the Joint Center for High Valued Instruments, National Sun Yat-Sen University, supported by the Ministry of Science and Technology, Taipei, Taiwan. The authors thank Prof. Jentaie Shiea and Dr. Hung Su for technical assistance with MS analysis.

■ ABBREVIATIONS USED

PC, phosphatidylcholine; PPC, polyenylphosphatidylcholine; RP, reverse phase; HPLC, high performance liquid chromatography; PE, phosphatidylethanolamine; ELSD, evaporative light scattering detector; UV, ultraviolet; GC, gas chromatography; FID, flame ionization detector; TAG, triacylglycerol; TCN, theoretical carbon number; 2,5-DHB, 2,5-dihydroxybenzoic acid; TLC, thin-layer chromatography; Nd:YAG, neodymium-doped yttrium aluminum garnet; R_f, retention value; AOCS, American Oil Chemists' Society; LPC, lysophosphatidylcholine; TCN_{PC}, TCN of PC; TCN_{TAG}, TCN of TAG; ECN, equivalent carbon number; ECN_{TAG}, ECN of TAG; TCN_{PC}, TCN of PC; LLnL, dilinoleoyl linolenoyl glycerol; LLL, trilinolein; OLnL, oleoyl linolenoyl linoleoyl glycerol; PLnL, palmitoyl linolenoyl linoleoyl glycerol; OLL, dilinoleoyl oleoyl glycerol; OLnO, dioleoyl linolenoyl glycerol; PLL, dilinoleoyl palmitoyl glycerol; PLnO palmitoyl linolenoyl oleoyl glycerol; PLnP, dipalmitoyl linolenoyl glycerol; OLO, dioleoyl linoleoyl glycerol; PLO, palmitoyl linoleoyl oleoyl glycerol; PLP, dipalmitoyl linoleoyl glycerol; OOO, triolein; POO, dioleoyl palmitoyl glycerol; POP, dipalmitoyl oleoyl glycerol; SOO, dioleoyl stearoyl glycerol; SOP, stearoyl oleoyl palmitoyl glycerol; LLPC, 1,2-dilinoleoyl-*sn*-glycero-3-phosphocholine; PPPC, 1,2-dipalmitoyl-*sn*-glycero-3-phosphocholine; OOPC, 1,2-dioleoyl-*sn*-glycero-3-phosphocholine; OPPC, 1-oleoyl-2-palmitoyl-*sn*-glycero-3-phosphocholine; POPC, 1-palmitoyl-2-oleoyl-*sn*-glycero-3-phosphocholine; LLnPC, 1-linoleoyl-2-linolenoyl-*sn*-glycero-glycero-3-phosphocholine; OLnPC, 1-oleoyl-2-linolenoyl-*sn*-glycero-3-phosphocholine; PLnPC, 1-palmitoyl-2-linolenoyl-*sn*-glycero-3-phosphocholine; OLPC, 1-oleoyl-2-linoleoyl-*sn*-glycero-3-phosphocholine; PLPC, 1-palmitoyl-2-linoleoyl-*sn*-glycero-3-phosphocholine; SLPC, 1-stearoyl-2-linoleoyl-*sn*-glycero-3-phosphocholine; SOPC, 1-stearoyl-2-oleoyl-*sn*-glycero-3-phosphocholine

■ REFERENCES

(1) van Nieuwenhuyzen, W.; Tomás, M. C. Update on vegetable lecithin and phospholipid technologies. *Eur. J. Lipid Sci. Technol.* **2008**, *110*, 472−486.

(2) Olthof, M. R.; Brink, E. J.; Katan, M. B.; Verhoef, P. Choline supplemented as phosphatidylcholine decreases fasting and post-methionine-loading plasma homocysteine concentrations in healthy men. *Am. J. Clin. Nutr.* **2005**, *82*, 111−117.

(3) Nishimoto, T.; Kanno, T.; Gotoh, A.; Nishizaki, T. DL−/PO− phosphatidylcholine serves as a memory enhancer for normal healthy subjects. *Personalized Medicine Universe* **2013**, *2*, 16−19.

(4) Gundermann, K. J.; Kuenker, A.; Kuntz, E.; Drozdzik, M. Activity of essential phospholipids (EPL) from soybean in liver diseases. *Pharmacol. Rep.* **2011**, *63*, 643−659.

(5) Duric, M.; Sivanesan, S.; Bakovic, M. Phosphatidylcholine functional foods and nutraceuticals: A potential approach to prevent non-alcoholic fatty liver disease. *Eur. J. Lipid Sci. Technol.* **2012**, *114*, 389−398.

(6) Guo, Z.; Vikbjerg, A. F.; Xu, X. B. Enzymatic modification of phospholipids for functional applications and human nutrition. *Biotechnol. Adv.* **2005**, *23*, 203−259.

(7) Kim, I. H.; Garcia, H. S.; Hill, C. G. Synthesis of structured phosphatidylcholine containing n-3 PUFA residues via acidolysis mediated by immobilized phospholipase A(1). *J. Am. Oil Chem. Soc.* **2010**, *87*, 1293−1299.

(8) Vikbjerg, A. F.; Rusig, J. Y.; Jonsson, G.; Mu, H. L.; Xu, X. B. Comparative evaluation of the emulsifying properties of phosphatidylcholine after enzymatic acyl modification. *J. Agric. Food Chem.* **2006**, *54*, 3310−3316.

DOI: 10.1021/acs.jafc.5b01022
J. Agric. Food Chem. 2015, 63, 3851−3858

(9) Maeba, R.; Yusufu, Y.; Shimasaki, H.; Ueta, N. Comparison of the oxidizability of various glycerophospholipids in bilayers by the oxygen uptake method. *Lipids* **2002**, *37*, 893−900.
(10) Peterson, B. L.; Cummings, B. S. A review of chromatographic methods for the assessment of phospholipids in biological samples. *Biomed. Chromatogr.* **2006**, *20*, 227−243.
(11) Brouwers, J. F. H. M.; Gadella, B. M.; van Golde, L. M. G.; Tielens, A. G. M. Quantitative analysis of phosphatidylcholine molecular species using HPLC and light scattering detection. *J. Lipid Res.* **1998**, *39*, 344−353.
(12) Brouwers, J. F. H. M.; Vernooij, E. A. A. M.; Tielens, A. G. M.; van Golde, L. M. G. Rapid separation and identification of phosphatidylethanolamine molecular species. *J. Lipid Res.* **1999**, *40*, 164−169.
(13) Du, J. M.; Hou, X. L.; Wu, D.; Feng, C. P. Rapid and efficient gas chromatographic method for measuring the kinetics of lipase-catalyzed transesterification of phosphatidylcholine. *J. Mol. Catal. B: Enzym.* **2011**, *69*, 103−106.
(14) Le Grandois, J.; Marchioni, E.; Zhao, M. J.; Giuffrida, F.; Ennahar, S.; Bindler, F. Investigation of natural phosphatidylcholine sources: separation and identification by liquid chromatography-electrospray ionization-tandem mass spectrometry (LC-ESI-MS2) of molecular species. *J. Agric. Food Chem.* **2009**, *57*, 6014−6020.
(15) Willmann, J.; Thiele, H.; Leibfritz, D. Combined reversed phase HPLC, mass spectrometry, and NMR spectroscopy for a fast separation and efficient identification of phosphatidylcholines. *J. Biomed. Biotechnol.* **2011**, DOI: 10.1155/2011/385786.
(16) Boselli, E.; Pacetti, D.; Lucci, P.; Frega, N. G. Characterization of phospholipid molecular species in the edible parts of bony fish and shellfish. *J. Agric. Food Chem.* **2012**, *60*, 3234−45.
(17) Montealegre, C.; Verardo, V.; Gomez-Caravaca, A. M.; Garcia-Ruiz, C.; Marina, M. L.; Caboni, M. F. Molecular characterization of phospholipids by high-performance liquid chromatography combined with an evaporative light scattering detector, high-performance liquid chromatography combined with mass spectrometry, and gas chromatography combined with a flame ionization detector in different oat varieties. *J. Agric. Food Chem.* **2012**, *60*, 10963−10969.
(18) Chen, S.; Subbaiah, P. V. Regioisomers of phosphatidylcholine containing DHA and their potential to deliver DHA to the brain: role of phospholipase specificities. *Lipids* **2013**, *48*, 675−686.
(19) Lucci, P.; Pacetti, D.; Calzuola, I.; Marsili, V.; Perni, S.; Giavarini, F.; Frega, N. G.; Gianfranceschi, G. L. Characterization of phospholipid molecular species and peptide molecules in wheat sprout hydroalcoholic extract. *J. Agric. Food Chem.* **2013**, *61*, 11453−9.
(20) Guiotto, E. N.; Cabezas, D. M.; Diehl, B. W. K.; Tomas, M. C. Characterization and emulsifying properties of different sunflower phosphatidylcholine enriched fractions. *Eur. J. Lipid Sci. Technol.* **2013**, *115*, 865−873.
(21) Krüger, S.; Bürmann, L.; Morlock, G. E. Comparison and characterization of soybean and sunflower lecithins used for chocolate production by high-performance thin-layer chromatography with fluorescence detection and electrospray mas spectrometry. *J. Agric. Food Chem.* **2015**, *63*, 2893−2901.
(22) Cabezas, D. M.; Diehl, B. W. K.; Tomas, M. C. Sunflower lecithin: application of a fractionation process with absolute ethanol. *J. Am. Oil Chem. Soc.* **2009**, *86*, 189−196.
(23) Lee, W. J.; Su, N. W.; Lee, M. H.; Lin, J. T. Assessment of authenticity of sesame oil by modified Villavecchia Test and HPLC-ELSD analysis of triacylglycerol profile. *Food Res. Int.* **2013**, *53*, 195−202.
(24) Zuidam, N. J.; Gouw, H. K. M. E.; Barenholz, Y.; Crommelin, D. J. A. Physical (in)stability of liposomes upon chemical hydrolysis - the role of lysophospholipids and fatty-acids. *Biochim. Biophys. Acta, Biomembr.* **1995**, *1240*, 101−110.
(25) Penci, M. C.; Constenla, D. T.; Carelli, A. A. Free-fatty acid profile obtained by enzymatic solvent-free hydrolysis of sunflower and soybean lecithins. *Food Chem.* **2010**, *120*, 332−338.
(26) Fuchs, B.; Müller, K.; Göritz, F.; Blottner, S.; Schiller, J. Characteristic oxidation products of choline plasmalogens are detectable in cattle and roe deer spermatozoa by MALDI-TOF mass spectrometry. *Lipids* **2007**, *42*, 991−998.
(27) Elhamdy, A. H.; Perkins, E. G. High-performance reversed phase chromatography of natural triglyceride mixtures - critical pair separation. *J. Am. Oil Chem. Soc.* **1981**, *58*, 867−872.
(28) Walczak, J.; Bocian, S.; Buszewski, B. Two-dimensional high performance liquid chromatography-mass spectrometry for phosphatidylcholine analysis in egg yolk. *Food Anal. Method* **2014**, 1−7 DOI: 10.1007/s12161-014-9942-3.
(29) Choi, J. M.; Kim, T. E.; Cho, J. Y.; Lee, H. J.; Jung, B. H. Development of lipidomic platform and phosphatidylcholine retention time index for lipid profiling of rosuvastatin treated human plasma. *J. Chromatogr. B: Anal. Technol. Biomed. Life Sci.* **2014**, *944*, 157−65.
(30) Sjovall, O.; Kuksis, A.; Marai, L.; Myher, J. J. Elution factors of synthetic oxotriacylglycerols as an aid in identification of peroxidized natural triacylglycerols by reverse-phase high-performance liquid chromatography with electrospray mass spectrometry. *Lipids* **1997**, *32*, 1211−8.
(31) Cunha, S. C.; Oliveira, M. B. P. P. Discrimination of vegetable oils by triacylglycerols evaluation of profile using HPLC/ELSD. *Food Chem.* **2006**, *95*, 518−524.

DOI: 10.1021/acs.jafc.5b01022
J. Agric. Food Chem. 2015, 63, 3851−3858

Table 1. Phenols Identified in Destoned Olive Fruits, Stones, Paste, Pomace, Wastewater, and Oil Using UPLC-DAD-ESI-QTOF-HRMS Analysis

N°[c]	Class / Phenolic compound	R_t	Formula *m/z* thr	De-stoned fruits			Stones			Paste			Pomace			Wastewater			Oil			Ref
				m/z exp	Δm	λ_{max}	*m/z* exp	Δm	λ_{max}	*m/z* exp	Δm	λ_{max}	*m/z* exp	Δm	λ_{max}	*m/z* exp	Δm	λ_{max}	*m/z* exp	Δm	λ_{max}	
Simple phenols																						
1	Hydroxytyrosol glucoside[a]	3.2	$C_{14}H_{20}O_8$ *315.1080*	315.1085	*1.6*	235 276	315.1090	*3.2*	230 276	315.1102	*7.0*	236 276	315.1076	*-1.3*	236 276	315.1059	*-6.7*	236 276	315.1079	*-0.3*	233 276	[1]
2	Hydroxytyrosol-1-β-glucoside[a]	3.3	$C_{14}H_{20}O_8$ *315.1080*	315.1074	*-1.9*	236 279	315.1102	*7.0*	235 277	315.1071	*-2.9*	236 279	315.1060	*-6.3*	236 279	315.1075	*-1.6*	236 279	315.1088	*2.5*	233 280	[1] [12]
3	Hydroxytyrosol[b]	3.5	$C_8H_{10}O_3$ *153.0552*	153.0547	*-3.3*	238 279	153.0550	*-1.3*	236 279	153.0559	*4.6*	236 280	153.0545	*-4.6*	236 280	153.0558	*3.9*	236 280	153.0550	*-1.3*	235 280	[18]
6	Tyrosol glucoside[a]	5.3	$C_{14}H_{20}O_7$ *299.1131*	299.1118	*-4.3*	238 275	299.1121	*-3.3*	233 275	299.1132	*0.3*	236 275	299.1124	*-2.3*	237 275	299.1130	*-0.3*	237 275	299.1131	*0.0*	237 275	[27]
8	Tyrosol[b]	5.8	$C_8H_{10}O_2$ *137.0603*	li[d]	–	236 277	Li	–	235 275	li	–	235 275	Li	–	234 275	li		237 275	li	–	234 275	[18]
19	Hydroxytyrosol acetate[a]	13.4	$C_{10}H_{12}O_4$ *195.0657*	195.0646	*-5.6*	235 281	nd[d]	–	nd	195.0651	*-3.1*	*[d]	195.0653	*-2.1*	*	195.0654	*-1.5*	*	195.0657	*0.0*	234 280	[24]
Benzoic acids																						
13	Vanillic acid[b]	10.3	$C_8H_8O_4$ *167.0344*	li	–	nd	Nd	–	nd	li	–	246 293	Li	–	250 293	li	–	245 293	li	–	258 293	[27]
15	Vanillin[b]	12.4	$C_8H_8O_3$ *151.0395*	nd	–	nd	151.0405	*6.6*	235 278 308	nd	–	nd	Nd	–	nd	nd	–	nd	151.0397	*1.3*	235 279 308	[24]
Cinnamic acids																						
16	*p*-Coumaric acid[b]	13.1	$C_9H_8O_3$ *163.0395*	163.0398	*1.8*	*	Nd	–	nd	163.0393	*-1.2*	235 309	163.0390	*-3.1*	236 310	163.0386	*-5.5*	236 310	163.0391	*-2.5*	236 308	[24]
	β-OH-verbascoside																					
17	isomer 1[a]	13.2	$C_{29}H_{36}O_{16}$ *639.1925*	639.1890	*-5.5*	251 281sh 329	639.1931	*0.9*	253 279sh 329	639.1900	*-3.9*	246 284sh 329	639.1929	*0.6*	246 285sh 329	639.1891	*-5.3*	245 285sh 329	nd	–	nd	[14]
18	isomer 2[a]	13.4	$C_{29}H_{36}O_{16}$ *639.1925*	639.1934	*1.4*	253 281sh 328	639.1902	*-3.6*	236 281sh 328	639.1888	*-5.8*	249 285sh 329	639.1909	*-2.5*	246 286sh 329	639.1926	*0.2*	246 285sh 329	nd	–	nd	[14]
26	Verbascoside[b]	17.1	$C_{29}H_{36}O_{15}$ *623.1976*	623.1976	*0.0*	245 284sh 330	623.2009	*5.3*	249 284sh 330	623.2003	*4.3*	248 285sh 330	623.1994	*2.9*	247 285sh 330	623.2017	*6.6*	245 285sh 330	nd	–	nd	[24]
Flavonoids																						
37	Rutin[b]	21.1	$C_{27}H_{30}O_{16}$ *609.1456*	609.1473	*2.8*	255 354	609.1442	*-2.3*	*	609.1446	*-1.6*	252 354	609.1459	*0.5*	252 355	609.1419	*-6.1*	248 353	609.1465	*1.5*	*	[24]
22	Luteolin-4',7-*O*-diglucoside[a]	15.9	$C_{27}H_{30}O_{16}$ *609.1456*	609.1425	*-5.1*	268 338	Nd	–	nd	609.1469	*2.1*	*	Nd	–	nd	nd	–	nd	nd	–	nd	[24]
41	Luteolin-7-*O*-glucoside[b]	24.1	$C_{21}H_{20}O_{11}$ *447.0927*	447.0942	*3.4*	254 349	Nd	–	nd	447.0948	*4.7*	254 350	447.0932	*1.1*	256 349	447.0913	*-3.1*	257 349	nd	–	nd	[24]
59	Luteolin-4'-*O*-glucoside[b]	36.6	$C_{21}H_{20}O_{11}$ *447.0927*	447.0931	*0.9*	268 338	nd	–	nd	447.0917	*-2.2*	268 339	447.0907	*-4.5*	270 339	447.0913	*-3.1*	*	nd	–	nd	[1]
61	Luteolin-3'-*O*-glucoside[a]	41.7	$C_{21}H_{20}O_{11}$ *447.0927*	447.0947	*4.5*	268 340	nd[d]	–	nd	447.0924	*-0.7*	269 340	447.0916	*-2.5*	270 340	447.0908	*-4.2*	268 340	nd	–	nd	[34]
	Luteolin rutinoside																					
42	isomer 1[a]	24.3	$C_{27}H_{30}O_{15}$ *593.1506*	593.1505	*-0.2*	254 343	Nd	–	nd	593.1469	*-6.2*	254 343	593.1505	*-0.2*	254 343	593.1486	*-3.4*	251 343	nd	–	nd	[12]
44	isomer 2[a]	25.5	$C_{27}H_{30}O_{15}$ *593.1506*	593.1487	*-3.2*	254 343	Nd	–	nd	593.1497	*-1.5*	253 342	593.1497	*-1.5*	251 342	593.1498	*-1.3*	250 342	nd	–	nd	[12]
VII	isomer 3[a]	26.6	$C_{27}H_{30}O_{15}$ *593.1506*	593.1473	*-5.6*	nd	Nd	–	nd	593.1519	*2.2*	nd	593.1527	*3.5*	nd	nd	–	nd	nd	–	nd	[12]
45	Quercitrin[b]	26.3	$C_{21}H_{20}O_{11}$ *447.0927*	447.0937	*2.2*	256 343	Nd	–	nd	447.0925	*-0.4*	255 342	447.0914	*-2.9*	254 342	447.0926	*-0.2*	251 342	nd	–	nd	[1]
	Apigenin glucoside																					
51	Apigenin-7-*O*-glucoside[b]	30.3	$C_{21}H_{20}O_{10}$ *431.0978*	431.0958	*-4.6*	234 266 337	Nd	–	nd	431.0988	*2.3*	236 267 340	431.0957	*-4.9*	237 267 340	431.0965	*-3.0*	231 268 340	nd	–	nd	[22]
VIII	isomer 1[a]	35.1	$C_{21}H_{20}O_{10}$ *431.0978*	431.0947	*-7.2*	nd	Nd	–	nd	431.0963	*-3.5*	nd	431.1013	*8.1*	nd	nd		nd	nd	–	nd	[22]
66	Luteolin[b]	51.4	$C_{15}H_{10}O_6$ *285.0399*	285.0418	*6.7*	nd	Nd	–	nd	285.0413	*4.9*	252 350	285.0410	*3.9*	255 353	285.0411	*4.2*	254 350	285.0406	*2.5*	254 349	[1]
69	Apigenin[b]	60.9	$C_{15}H_{10}O_5$ *269.0450*	nd	–	nd	Nd	–	nd	269.0459	*3.3*	242 267 339	269.0442	*-3.0*	235 268 339	269.0458	*3.0*	236 266 337	269.0444	*-2.2*	234 267 338	[21]
Lignans																						
55	Pinoresinol[b]	33.7	$C_{20}H_{22}O_6$ *357.1338*	li	–	nd	Li	–	nd	li	–	nd	Li	–	nd	li	–	nd	li	–	236 279	[21]
58	Acetoxy-pinoresinol[a]	35.9	$C_{22}H_{24}O_8$ *415.1393*	nd	–	nd	Nd	–	nd	nd	–	nd	Nd	–	nd	nd	–	nd	415.1375	*-4.3*	238 279	[18]
Secoiridoids																						
I	Oleoside[a]	3.5	$C_{16}H_{22}O_{11}$ *389.1084*	389.1091	*1.8*	*[d]	389.1061	*-5.9*	*	389.1071	*-3.3*	*	389.1076	*-2.1*	*	389.1081	*-0.8*	*	nd	–	nd	[22]
11	Secologanoside[a]	8.9	$C_{16}H_{22}O_{11}$ *389.1084*	389.1091	*1.8*	236	389.1100	*4.1*	236	389.1071	*-3.3*	236	389.1062	*-5.7*	236	389.1063	*-5.4*	237	389.1062	*-5.7*	236	[22]
	Elenolic acid glucoside																					
10	isomer 1[a]	8.6	$C_{17}H_{24}O_{11}$ *403.1240*	403.1240	*0.0*	237	403.1227	*-3.2*	236	403.1241	*0.2*	236	Nd	–	nd	nd	–	nd	nd	–	nd	[22]
12	isomer 2[a]	9.2	$C_{17}H_{24}O_{11}$ *403.1240*	403.1232	*-2.0*	244	403.1227	*-3.2*	240	403.1227	*-3.2*	*	403.1222	*-4.5*	*	403.1223	*-4.2*	*	403.1242	*0.5*	236	[22]
14	isomer 3[a]	10.2	$C_{17}H_{24}O_{11}$ *403.1240*	403.1236	*-1.0*	245	403.1244	*1.0*	242	403.1224	*-4.0*	nd	Nd	–	nd	nd	–	nd	nd	–	nd	[22]
II	isomer 4[a]	11.9	$C_{17}H_{24}O_{11}$ *403.1240*	403.1255	*3.7*	nd	403.1223	*-4.2*	nd	nd	–	nd	Nd	–	nd	nd	–	nd	nd	–	nd	[22]
20	Demethyl-oleuropein[a]	13.7	$C_{24}H_{30}O_{13}$ *525.1608*	525.1609	*0.2*	242 280	525.1605	*-0.6*	*	525.1605	*-0.6*	247 280	525.1584	*-4.6*	247 280	525.1583	*-4.8*	244 280	nd	–	nd	[22]

DOI: 10.1021/jf506345q
J. Agric. Food Chem. 2015, 63, 3859−3872

Table 1. continued

N°[c]	Class / Phenolic compound	R_t	Formula *m/z* thr	De-stoned fruits			Stones			Paste			Pomace			Wastewater			Oil			Ref
				m/z exp	Δm	λ_{max}	*m/z* exp	Δm	λ_{max}	*m/z* exp	Δm	λ_{max}	*m/z* exp	Δm	λ_{max}	*m/z* exp	Δm	λ_{max}	*m/z* exp	Δm	λ_{max}	
	Dihydro-oleuropein																					
21	isomer 1[a]	15.4	$C_{25}H_{36}O_{13}$ *543.2078*	543.2081	*0.6*	251 275	nd[d]	–	nd	543.2054	*-4.4*	250 278	543.2055	*-4.2*	249 278	543.2047	*-5.7*	247 278	nd	–	nd	[35]
27	isomer 2[a]	17.4	$C_{25}H_{36}O_{13}$ *543.2078*	543.2078	*0.0*	251 281	543.2087	*1.7*	248 276	543.2064	*-2.6*	251 277	543.2047	*-5.7*	250 276	543.2069	*-1.7*	248 277	nd	–	nd	[35]
	3,4-DHPEA-EDA[c]																					
23	isomer 1[a]	16.0	$C_{17}H_{20}O_6$ *319.1182*	nd	–	nd	Nd	–	nd	319.1182	*0.0*	250 280	319.1172	*-3.1*	246 280	nd		nd	nd	–	nd	[1]
34	isomer 2[a]	19.9	$C_{17}H_{20}O_6$ *319.1182*	nd	–	nd	Nd	–	nd	319.1199	*5.3*	243 280	319.1198	*5.0*	238 280	319.1201	*6.0*	242 280	319.1176	*-1.9*	243 281	[1]
	Oleuropein diglucoside																					
30	isomer 1[a]	18.5	$C_{31}H_{42}O_{18}$ *701.2293*	701.2281	*-1.7*	246 283	701.2309	*2.3*	251 276	701.2289	*-0.6*	250 276	701.2283	*-1.4*	*[d]	701.2260	*-4.7*	*	nd	–	nd	[22]
33	isomer 2[a]	19.5	$C_{31}H_{42}O_{18}$ *701.2293*	701.2260	*-4.7*	252 275	701.2280	*-1.9*	nd	701.2318	*3.6*	nd	701.2334	*5.8*	nd	701.2319	*3.7*	nd	nd	–	nd	[22]
V	isomer 3[a]	19.8	$C_{31}H_{42}O_{18}$ *701.2293*	701.2275	*-2.6*	nd	701.2244	*-7.0*	nd	nd	–	nd	Nd	–	nd	nd	–	nd	nd	–	nd	[22]
VI	isomer 4[a]	20.8	$C_{31}H_{42}O_{18}$ *701.2293*	701.2298	*0.7*	nd	701.2274	*-2.7*	nd	nd	–	nd	Nd	–	nd	nd	–	nd	nd	–	nd	[22]
	Nüzhenide																					
III	isomer 1[a]	16.7	$C_{31}H_{42}O_{17}$ *685.2344*	nd	–	nd	685.2344	*0.0*	*	nd	–	nd	Nd	–	nd	nd	–	nd	nd	–	nd	[16]
32	isomer 2[a]	18.8	$C_{31}H_{42}O_{17}$ *685.2344*	685.2305	*-5.7*	246 276	685.2354	*1.5*	247 275	685.2390	*6.7*	249 275	685.2346	*0.3*	249 275	685.2323	*-3.1*	245 281	nd	–	nd	[16]
35	isomer 3[a]	20.5	$C_{31}H_{42}O_{17}$ *685.2344*	685.2320	*-3.5*	nd	685.2352	*1.2*	253 275	nd	–	nd	Nd	–	nd	nd	–	nd	nd	–	nd	[16]
39	isomer 4[a]	21.7	$C_{31}H_{42}O_{17}$ *685.2344*	685.2308	*-5.3*	nd	685.2310	*-5.0*	250 275	nd	–	nd	Nd	–	nd	nd	–	nd	nd	–	nd	[16]
	Oleuropein aglycone																					
38	isomer 1[a]	21.5-22.8	$C_{19}H_{22}O_8$ *377.1236*	377.1247	*2.9*	nd	377.1247	*2.9*	nd	377.1255	*5.0*	244 280	377.1236	*0.0*	244 280	377.1221	*-4.0*	244 280	377.1235	*-0.3*	245 281	[17]
60	isomer 2[a]	37.5	$C_{19}H_{22}O_8$ *377.1236*	377.1241	*1.3*	nd	377.1213	*-6.1*	nd	377.1258	*5.8*	251 280	377.1244	*2.1*	250 280	377.1253	*4.5*	249 280	377.1237	*-0.3*	249 280	[17]
65	isomer 3[a]	47.3	$C_{19}H_{22}O_8$ *377.1236*	377.1248	*3.2*	nd	377.1245	*2.4*	nd	377.1249	*3.4*	258 276	377.1242	*1.6*	258 276	377.1234	*-0.5*	256 276	377.1227	*-2.4*	252 276	[17]
40	Oleuropein[b]	22.9	$C_{25}H_{32}O_{13}$ *539.1765*	539.1769	*0.7*	244 280	539.1780	*2.8*	244 280	539.1790	*4.6*	245 280	539.1752	*-2.4*	246 280	539.1763	*-0.4*	nd	nd	–	nd	[22]
47	Oleuroside[a]	27.0	$C_{25}H_{32}O_{13}$ *539.1765*	539.1758	*-1.3*	243 280	539.1749	*-3.0*	243 282	539.1742	*-4.3*	nd	Nd	–	nd	nd	–	nd	nd	–	nd	[22]
43	Caffeoyl-6'-secologanoside[a]	24.8	$C_{25}H_{28}O_{14}$ *551.1401*	551.1394	*-1.3*	237 327	nd[d]	–	nd	551.1370	*-5.6*	237 326	551.1387	*-2.5*	239 326	551.1419	*3.3*	238 326	nd	–	nd	[1]
46	*p*-HPEA-EDA[a,c]	26.4	$C_{17}H_{26}O_5$ 303.1232	nd	–	nd	Nd	–	nd	303.1237	*1.6*	nd	303.1248	*5.3*	nd	303.1213	*-6.3*	nd	303.1236	*1.3*	246 275	[1]
48	Oleuropein + Ligstroside aglycone 1[a]	28.5	$C_{19}H_{22}O_8$ *377.1236*	nd	–	nd	Nd	–	nd	nd	–	nd	nd	–	nd	nd	–	nd	377.1252	*4.2*	252 275	[19]
			$C_{19}H_{22}O_7$ *361.1287*	nd	–	nd	Nd	–	nd	nd	–	nd	nd	–	nd	nd	–	nd	361.1292	*1.4*		
49	Oleuropein + Ligstroside aglycone 2[a]	29.0	$C_{19}H_{22}O_8$ *377.1236*	nd	–	nd	Nd	–	nd	nd	–	nd	nd	–	nd	nd	–	nd	377.1238	*0.5*	251 275	[19]
			$C_{19}H_{22}O_7$ *361.1287*	nd	–	nd	Nd	–	nd	nd	–	nd	nd	–	nd	nd	–	nd	361.1276	*-3.0*		
52	Ligstroside[a]	30.5	$C_{25}H_{32}O_{12}$ *523.1816*	523.1831	*2.9*	246 275	523.1804	*-2.3*	249 275	523.1790	*-5.0*	nd	523.1812	*-0.8*	nd	523.1803	*-2.5*	nd	nd	–	nd	[24]
53	Comselogoside[a]	31.2	$C_{25}H_{28}O_{13}$ *535.1452*	535.1440	*-2.2*	236 313	Nd	–	nd	535.1461	*1.7*	236 313	535.1455	*0.6*	236 313	535.1462	*1.9*	236 313	nd	–	nd	[1]
57	Acetal of 3,4-DHPEA-EDA[a,c]	35.3	$C_{19}H_{26}O_7$ *365.1600*	nd	–	nd	365.1589	*-3.0*	nd	365.1611	*3.0*	nd	365.1585	*-4.1*	nd	365.1602	*0.5*	242 281	365.1597	*-0.8*	nd	[1]
	Ligstroside aglycone																					
X	isomer 1[a]	39.7	$C_{19}H_{22}O_7$ *361.1287*	nd	–	nd	Nd	–	nd	nd	–	nd	nd	–	nd	nd	–	nd	361.1284	*-0.8*	nd	[19]
64	isomer 2[a]	47.0	$C_{19}H_{22}O_7$ *361.1287*	nd	–	nd	Nd	–	nd	361.1281	*-1.7*	nd	361.1265	*-6.1*	nd	361.1280	*-1.9*	nd	361.1287	*0.0*	254 280	[19]
	Nüzhenide 11-methyl oleoside																					
54	isomer 1[a]	31.6	$C_{48}H_{64}O_{27}$ *1071.3557*	nd	–	nd	1071.3560	*0.3*	252 275	nd	–	nd	nd	–	nd	nd	–	nd	nd	–	nd	[16]
56	isomer 2[a]	35.1	$C_{48}H_{64}O_{27}$ *1071.3557*	nd	–	nd	1071.3546	*-1.0*	258 275	nd	–	nd	nd	–	nd	nd	–	nd	nd	–	nd	[16]
IX	isomer 3[a]	38.4	$C_{48}H_{64}O_{27}$ *1071.3557*	nd	–	nd	1071.3542	*-1.4*	nd	nd	–	nd	nd	–	nd	nd	–	nd	nd	–	nd	[16]
62	isomer 4[a]	41.8	$C_{48}H_{64}O_{27}$ *1071.3557*	nd	–	nd	1071.3563	*0.6*	246	1071.3571	*1.3*	251 276	1071.3558	*0.1*	252 276	1071.3549	*-0.7*	nd	nd	–	nd	[16]
	Nüzhenide di(11-methyl oleoside)																					
67	isomer 1[a]	51.5	$C_{65}H_{86}O_{37}$ *1457.4770*	nd	–	nd	1457.4796	*1.8*	253	1457.4722	*-3.3*	nd	1457.4760	*-0.7*	nd	nd	–	nd	nd	–	nd	[16]
68	isomer 2[a]	52.0	$C_{65}H_{86}O_{37}$ *1457.4770*	nd	–	nd	1457.4722	*0.1*	251	1457.4756	*-1.0*	nd	1457.4811	*2.8*	nd	1457.4836	*4.5*	nd	nd	–	nd	[16]
XI	isomer 3[a]	58.7	$C_{65}H_{86}O_{37}$ *1457.4770*	nd	–	nd	1457.4767	*-0.2*	nd	nd	–	nd	nd	–	nd	nd	–	nd	nd	–	nd	[16]

[a]Tentative identification based on accurate mass and literature data (tolerable range, 10 ppm). [b]Identification also confirmed by the use of standard. [c]N° = Arabic numbers refer to DAD and Romans to only MS-detected phenols; R_t = retention time (min); Formula = molecular formula; *m/z* thr = calculated monoisotopic mass $[M-H]^-$; *m/z* exp = detected mass; Δ*m* = calculated mass deviation, $[(m/z \text{ exp} - m/z \text{ thr})/m/z \text{ thr}] \times 10^6$ (ppm); λ_{max} = absorption maxima (nm); ref = reference. [d]Compound is described as (nd) not detected, (*) the evidence for its presence is inconclusive, and (li) not detected due to low ionization. [e]Abbreviations: decarboxymethyl elenolic acid linked to hydroxytyrosol (3,4-DHPEA-EDA) or tyrosol (*p*-HPEA-EDA).

DOI: 10.1021/jf506345q
J. Agric. Food Chem. 2015, 63, 3859−3872

Table 2. Unknown Compounds of Potent Phenolic Structure Detected in Olive Extracts Using UPLC-DAD-ESI-QTOF-HRMS Analysis

N°[a]	Compound	R_t	λ_{max}	Major ESI^- peaks	Major ESI^+ peaks	Proposed molecular formula / name / class	F / S / PS / PM / W / O (Δm)
4	A	3.7	236 313	409, 389, 355, 241, 209, 191	li[b]	– / – / secoiridoids	+ / + / + / + / + / +[b]
5	408 MW comp. 1	4.0	237 312	815[c], 407, 389, 377, 375, 357, 345, 313, 161, 151, 101	431[d], 415, 391, 247, 229, 211, 197, 169, 155	$C_{17}H_{28}O_{11}$ / – / secoiridoids	*0.5 / -3.4 / -0.7 / 3.7 / 3.2 / -2.0*
7	408 MW comp. 2	5.5	236 314	815[c], 407, 389, 375, 355, 191, 85	431[d], 415, 251, 211, 173, 132, 98	$C_{17}H_{28}O_{11}$ / – / secoiridoids	*-3.2 / -1.5 /-3.4 / -3.2 / -3.7 / –*
9	B	7.5	242 283	891, 673, 651, 403, 325, 163	*[b]	– / – /secoiridoids	+ / + / + / + / + / –
24	654 MW isomer 1[e]	16.2	249 284sh 331	653, 621, 459, 179, 161	li	$C_{30}H_{38}O_{16}$ / β-Methyl-OH-verbascoside isomer 1 / cinnamic acids	*-4.3 / -4.6 / -2.6 / -2.6 / -0.9 / –*
25	654 MW isomer 2[e]	16.6	247 285sh 331	653, 621, 459, 179, 161	li	$C_{30}H_{38}O_{16}$ / β-Methyl-OH-verbascoside isomer 2 / cinnamic acids	*0.3 / 4.7 / -4.0 / -4.1 / -1.2 / –*
IV	716 MW isomer 1[e]	17.1	–	1431[c], 715, 553, 483, 451, 329	739[d]	$C_{32}H_{44}O_{18}$ / Methoxynüzhenide isomer 1 / secoiridoids	*–/ 4.3 / -2.8 / -1.3 / –/ –*
28	484 MW isomer 1	17.8	242 280	967[c], 483, 347, 181, 139	507[d], 485, 429, 371, 250, 137	– / – / secoiridoids	–/ –/ –/ –/ + / –
29	484 MW isomer 2	18.1	246 278	967[c], 483, 347, 181, 139	507[d], 485, 429, 371, 250, 137	– / –/ secoiridoids	–/ –/ –/ –/ + / –
31	484 MW isomer 3	18.5	245 281	967[c], 483, 347, 181, 139	507[d], 485, 429, 371, 236 137	– / –/ secoiridoids	–/ –/ –/ –/ + / –
36	716 MW isomer 2[e]	20.9	250 277	1431[c], 715, 553, 483, 451, 329	739[d]	$C_{32}H_{44}O_{18}$ / Methoxynüzhenide isomer 2 / secoiridoids	*–/ -3.8 / 2.8 / –/ –/ –*
50	C	29.0	250 280sh	789, 539, 403, 275, 223	li	– / – / secoiridoids	+ / + / + / + / + / –
63	1102 MW[e]	43.2	255 276	1101, 715, 553, 329	1125[d]	$C_{49}H_{66}O_{28}$ / Methoxynüzhenide 11-methly oleoside / secoiridoids	*–/ 5.0 / 2.0 / 3.4 / -1.0 / –*

[a]N° = Arabic numbers refer to DAD and Roman numbers only to MS-detected phenols; R_t = retention time (min); λ_{max} = absorption maxima (nm); ESI^- = negative ion mode; ESI^+ = positive ion mode; *F* = fruit; S = stone; PS = paste; PM = pomace; W = wastewater; O = oil; Δ*m* = calculated mass deviation, $[(m/z \text{ exp} - m/z \text{ thr})/m/z \text{ thr}] \times 10^6$ (ppm). [b]Compound is described as (+) present, (−) not detected, (*) the evidence for its presence is inconclusive, and (li) low ionization. [c]$[2M-H]^-$. [d]$[M+Na]^+$. [e]Tentatively identified.

and oil), this study was carried out with a view to characterize their phenol constituents on the basis of HRMS and UV−vis spectroscopic data never collectively presented before. Moreover, simultaneous screening of all of the matrices from the same biological material provided us a basic insight into olive fruit phenols transfer, transformation, and the partition qualitative trail, rarely discussed in the literature to date. Nevertheless, this study also describes some of the new phenol constituents found in the extracts examined.

MATERIALS AND METHODS

Reagents and Standards. All solvents (acetic acid and methanol) were of HPLC grade and purchased from Sigma-Aldrich Co. (Darmstadt, Germany), as were vanillin and vanillic, caffeic, and *p*-coumaric acid standards. Others, hydroxytyrosol, tyrosol, oleuropein, luteolin, luteolin-7-*O*-glucoside, luteolin-4′-*O*-glucoside, apigenin, apigenin-7-*O*-glucoside, verbascoside, quercitrin, and rutin, were obtained from Extrasynthese (Genay, France), while pinoresinol was from ArboNova (Turku, Finland). Standard stock solutions were prepared by dissolving standards in pure methanol, which were rotary evaporated (35 °C) and in turn re-dissolved in a mixture of HPLC eluents (A:B = 90:10 (v/v)).

Sampling and Sample Preparation. Olive fruits of Istrska belica *cv.*, the most widely spread olive variety in Slovenia, were harvested in Gradno (Goriška Brda, Slovenia) at the end of maturation period, which was found to be optimal in terms of the oil content and sensorial characteristics, stored overnight and processed to olive oil the next day using a laboratory-scale Abencor olive mill (Seville, Spain). The fruits were ground to a paste using a hammer mill, and water (100 mL/kg of fruit) was added to improve the rheology. Then the paste was malaxed (30 min/(25 °C)) and centrifuged in order to obtain the three final products: oil and two types of waste (pomace and wastewater). All process-derived matrices were sampled at the end of processing, with the exception of paste, which was collected immediately after fruits crushing. The samples were prepared as previously described,[7,10,11] with destoned fruits, stones, paste, and pomace being frozen with liquid nitrogen, freeze-dried, homogenized, and stored at −25 °C until analysis, while the wastewater was primarily acidified (HCl, pH = 2.0) and defatted with *n*-hexane prior to freeze-drying and storage at −25 °C. The olive oil sample was stored in the dark at room temperature until extraction.

Extraction of Phenols from Destoned Fruits, Stones, Paste, Pomace, and Wastewater. Phenols were extracted according to a previously published ultrasound-assisted solid liquid extraction (USLE) method,[11] with which a freeze-dried sample (1.5 g) was sonicated (3 × 20 min) with 25 mL of methanol. The homogenates of

DOI: 10.1021/jf506345q
J. Agric. Food Chem. 2015, 63, 3859−3872

Table 3. MS Fragmentation Profiles, Chemical Structures, and UV−Vis Spectra of Detected Phenols

Class / Phenolic compound	ESI⁻ fragments[a]	Chemical structure / UV-Vis spectrum
Simple phenols		
Hydroxytyrosol glucoside; *Option* **I**; R_1 = H, R_2 = *O*-glucose, R_3 = OH *Option* **II**; R_1 = H, R_2 = OH, R_3 = *O*-glucose	315, 153, 123	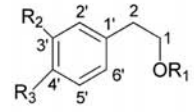 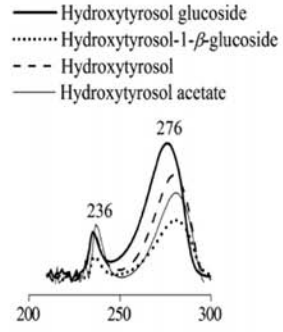
Hydroxytyrosol-1-*β*-glucoside; R_1 = glucose, R_2 = OH, R_3 = OH	315, 153, 123	
Hydroxytyrosol; R_1 = H, R_2 = OH, R_3 = OH	153, 123	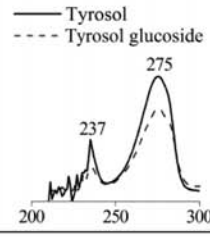
Hydroxytyrosol acetate; R_1 = CH_3CO_2, R_2 = OH, R_3 = OH	195	
Tyrosol; R_1 = H, R_2 = H, R_3 = OH	–	
Tyrosol glucoside; R_1 = glucose, R_2 = H, R_3 = OH	299, 137, 119	
Benzoic acids		
Vanillic acid; R_1 = COOH	–	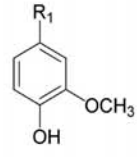 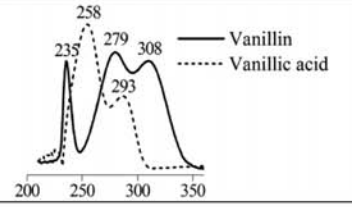
Vanillin R_1 = CHO	151, 136, 92	
Cinnamic acids		
p-Coumaric acid (**I**)	163, 119	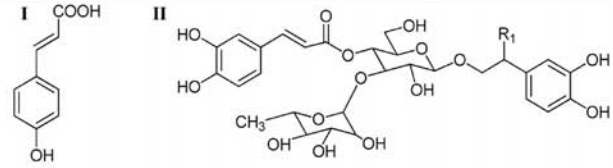 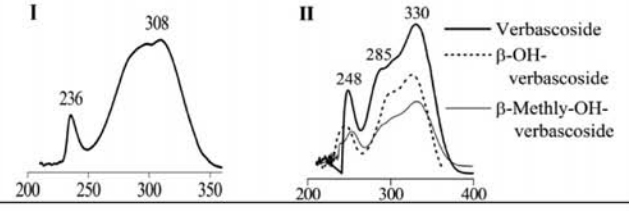
β-OH-verbascoside (**II**); R_1 = OH	639, 621, 459, 179, 161	
β-Methyl-OH-verbascoside (**II**); R_1 = OCH_3	653, 621, 459, 179, 161	
Verbascoside (**II**); R_1 = H	623, 461, 161	
Flavonoids		
Rutin; R_1 = OH, R_2 = OH, R_3 = OH, R_4 = *O*-rutinose	609, 300, 179	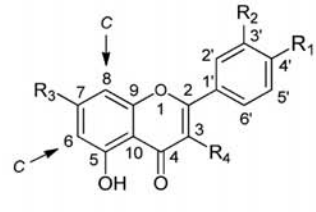 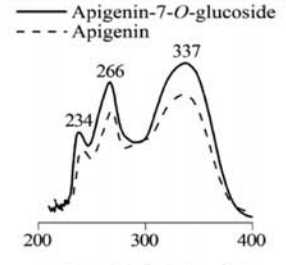
Luteolin-4',7-*O*-diglucoside; R_1=*O*-glucose, R_2 = OH, R_3 = *O*-glucose, R_4 = H	609, 447, 285	
Luteolin-7-*O*-glucoside; R_1 = OH, R_2 = OH, R_3 = *O*-glucose, R_4 = H	447, 285	
Luteolin-4'-*O*-glucoside; R_1 = *O*-glucose, R_2 = OH, R_3 = OH, R_4 = H	447, 285	
Luteolin-3'-*O*-glucoside; R_1 = OH, R_2 = *O*-glucose, R_3 = OH, R_4 = H	447, 285	
Luteolin rutinoside isomers; –	593, 447, 285	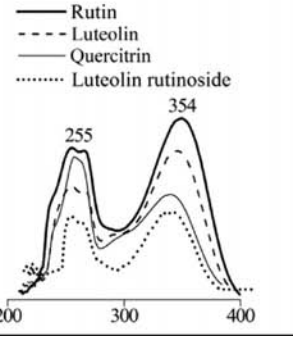 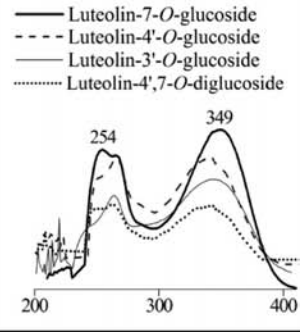
Luteolin; R_1 = OH, R_2 = OH, R_3 = OH, R_4 = H	285, 151, 133	
Quercitrin; R_1 = OH, R_2 = OH, R_3 = OH, R_4 = *O*-rhamnose	447, 301, 300	
Apigenin-7-*O*-glucoside; R_1 = OH, R_2 = H, R_3 = *O*-glucose, R_4 = H	431, 269	
Apigenin; R_1 = OH, R_2 = H, R_3 = OH, R_4 = H	269	

DOI: 10.1021/jf506345q
J. Agric. Food Chem. 2015, 63, 3859−3872

Table 3. continued

Class / Phenolic compound	ESI⁻ fragments[a]	Chemical structure / UV-Vis spectrum
Lignans		
Pinoresinol R_1 = H	–	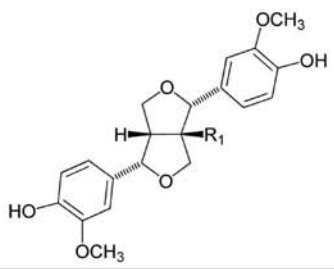 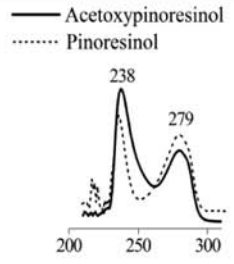
Acetoxypinoresinol R_1= $OCOCH_3$	415, 151	
Secoiridoids		
Oleoside (**I**); R_1 = H	779[b], 389, 345, 227, 209, 183	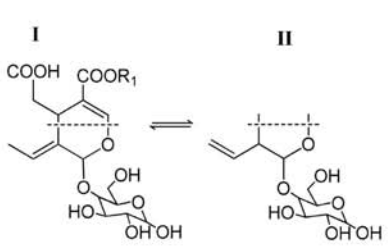 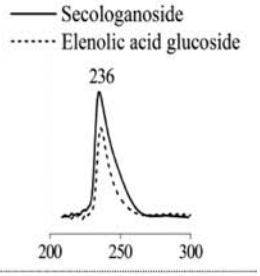
Secologanoside (**II**); R_1 = H	779[b], 389, 345, 209, 183	
Elenolic acid glucoside isomers (**I**, **II**); R_1 = CH_3	807[b], 403, 371, 223, 179	
Demethyloleuropein (**I**); R_1 = H, R_2 = OH, R_3 = OH	525, 389, 345, 319, 183	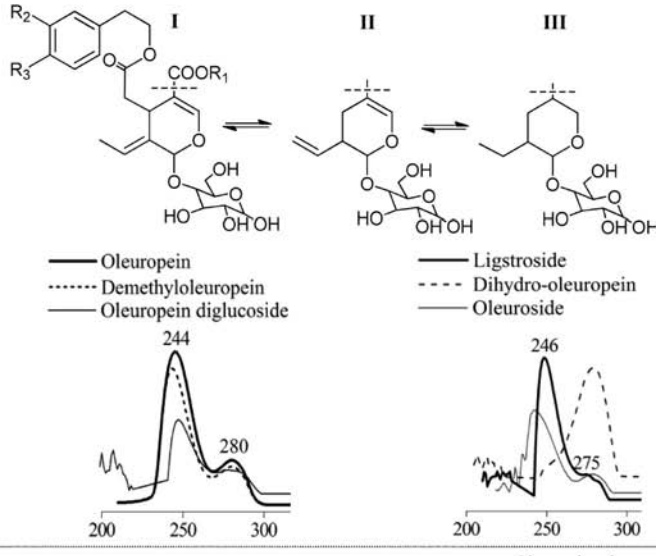
Oleuropein (**I**); R_1 = CH_3, R_2 = OH, R_3 = OH	539, 377, 307, 275, 223, 149, 139	
Oleuropein diglucoside isomers (**I**, **II**); R_1 = CH_3, R_2 = *O*-glucose/OH, R_3 = OH/*O*-glucose	701, 539, 377, 307, 275, 223	
Oleuroside (**II**); R_1 = CH_3, R_2 = OH, R_3 = OH	539, 377, 307, 275, 223, 149, 139	
Dihydro-oleuropein (**III**); R_1 = CH_3, R_2 = OH, R_3 = OH	543, 377	
Ligstroside (**I**); R_1 = CH_3, R_2 = H, R_3 = OH	523, 361, 291, 259, 223, 127, 101	
Oleuropein aglycone isomers (**I–XII**); R_1 = OH	755[b], 377, 345, 327, 307, 275, 149, 139	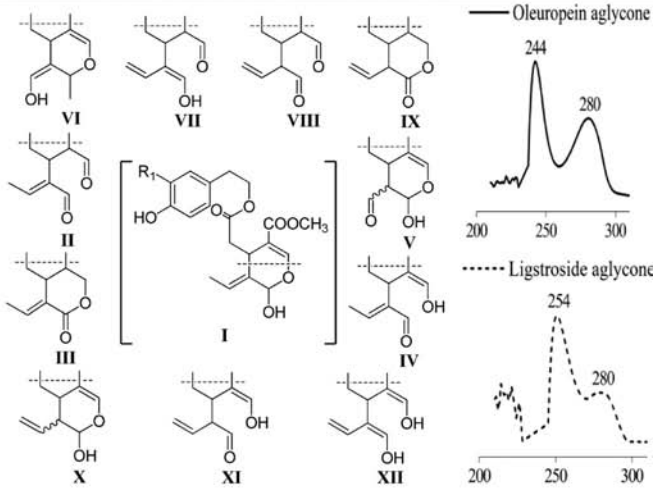
Ligstroside aglycone isomers (**I–XII**); R_1 = H	361, 329, 291, 259, 223, 139	

DOI: 10.1021/jf506345q
J. Agric. Food Chem. 2015, 63, 3859−3872

Table 3. continued

Class / Phenolic compound	ESI⁻ fragments[a]	Chemical structure / UV-Vis spectrum
3,4-DHPEA-EDA[c] (**I**); R_1 = OH	639[b], 319, 301, 195, 183, 165, 139	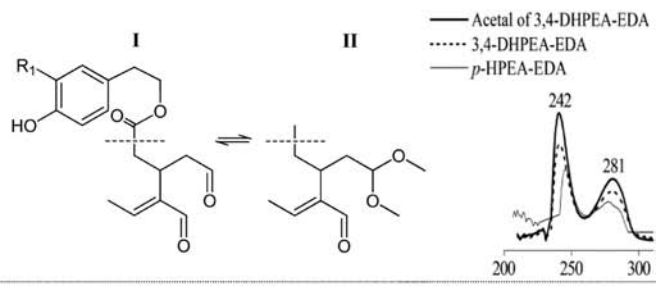
p-HPEA-EDA[c] (**I**); R_1 = H	607[b], 303, 285, 179, 165	
Acetal of 3,4-DHPEA-EDA (**II**); R_1 = OH	365, 229, 185, 153, 121, 95	
Comselogoside; R_1 = H	535, 491, 345, 265, 163, 145	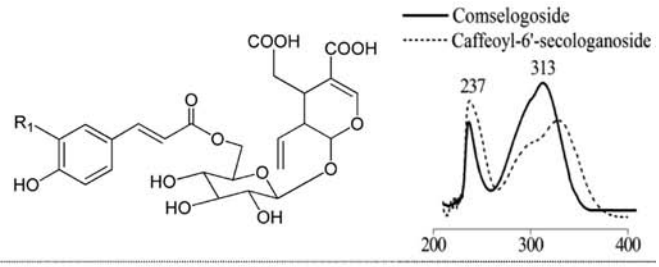
Caffeoyl-6'-secologanoside; R_1 = OH	551, 507, 393, 281, 251, 179, 161	
Nüzhenide; R_1 = OH, R_2 = H	685, 523, 453, 421, 299, 223	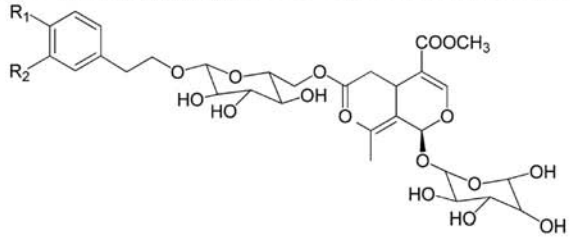
Nüzhenide 11-methyl oleoside; R_1 = 11-methyl oleoside, R_2 = H	1071, 909, 839, 771, 685, 523, 453, 403, 299, 223	
Nüzhenide di(11-methyl oleoside) R_1 = di(11-methyl oleoside), R_2 = H	1457, 1295, 1157, 1071, 909, 839, 771, 685, 523, 453, 299, 223	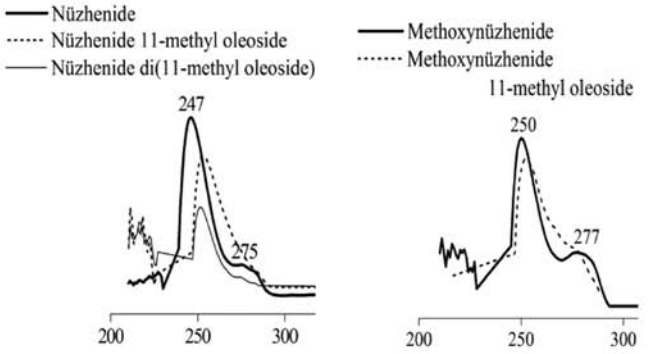
Methoxynüzhenide R_1 = OH, R_2 = OCH_3	1431[b], 715, 553, 483, 451, 329	
Methoxynüzhenide 11-methyl oleoside; R_1 = 11-methyl oleoside, R_2 = OCH_3	1101, 715, 553, 329	
Unknowns		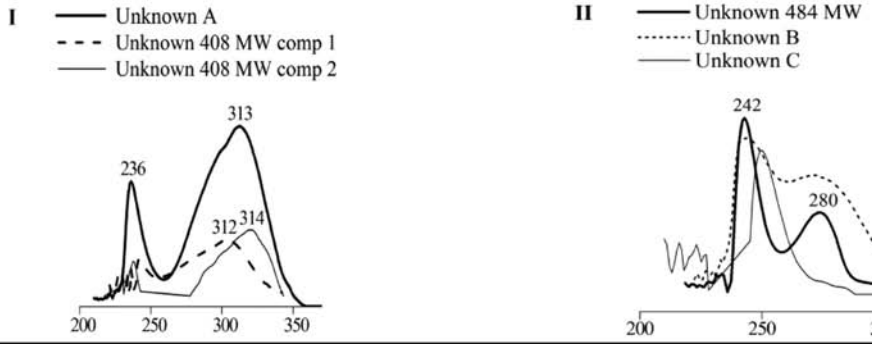

[a]ESI^- = negative ion mode. [b]$[2M-H]^-$. [c]Abbreviations: decarboxymethyl elenolic acid linked to hydroxytyrosol (3,4-DHPEA-EDA) or tyrosol (*p*-HPEA-EDA).

each extraction step were centrifuged (9000 rpm, 5 min) and combined supernatants diluted with pure methanol to 100 mL.

Extraction of Phenols from Olive Oil. Extraction was carried out using the ultrasound-assisted liquid liquid extraction (US-LLE) method previously described,[10] with 10 g of oil being dissolved in *n*-hexane (10 mL) and sonicated (3 × 10 min) with methanol (5 mL). The homogenates of each extraction step were centrifuged (9000 rpm, 2 min), combined, and defatted with a freeze-based fat precipitation

DOI: 10.1021/jf506345q
J. Agric. Food Chem. 2015, 63, 3859−3872

(20 min, −80 °C). Afterward, the remaining extract was reconstituted to 25 mL with pure methanol.

UPLC-DAD-ESI-QTOF-HRMS Analysis. Prior to analysis, the aliquots of extracts were rotary concentrated (10 times), the dry residue re-dissolved in a mixture of HPLC eluents (A(95:5 water−acetic acid (v/v)):B(methanol) = 90:10 (v/v)) and filtered through 0.22 μm/13 mm poly(vinylidene fluoride) (PVDF) filters from Carl Roth GmbH + Co. (Düren, Germany).

Phenols were characterized using a Waters UPLC system equipped with DAD and HRMS-QTOF Synapt MS with electrospray ionization (ESI) system from Waters Corp. (Milford, MA, USA). Separation was achieved on a Kinetex PFP column (2.6 μm, 100 mm × 4.6 mm) attached to a PFP security guard (2.1 mm × 4.6 mm), both from Phenomenex (Sydney, Australia) at a flow rate of 1 mL/min, using 10 μL of injection volume and a solvent system composed of water−acetic acid (95:5, v/v) (A) and methanol (B). The gradient elution for fruits, stones, paste, pomace, and wastewater analysis involved a nine-step program: 0−7 min, 1% B isocratic; 7−10 min, linear gradient from 1 to 25% B; 10−35 min, linear gradient from 25 to 36.2% B; 35−35.5 min, linear gradient from 36.2 to 36.5% B; 35.5−52 min, linear gradient from 36.5 to 43.7% B; 52−53 min, linear gradient from 43.7 to 45% B; 53−66 min, linear gradient from 45 to 50% B; 66−72 min, linear gradient from 50 to 100% B; 72−76 min, 100% B isocratic; 76−79 min, linear gradient from 100 to 1% B; and 79−88 min, 1% B isocratic. For the oil a 20-step solvent run was used as follows: 0−7 min, 1% B isocratic; 7−10 min, linear gradient from 1 to 25% B; 10−20 min, linear gradient from 25 to 29.4% B; 20−20.1 min, linear gradient from 29.4 to 29.9% B; 20.1−21.1 min, linear gradient from 29.9 to 40% B; 21.1−21.5, 40% B isocratic; 21.5−22.5 min, linear gradient from 40 to 30% B; 22.5−23 min, linear gradient from 30 to 28% B; 23−25 min, 28% B isocratic; 25−26 min, linear gradient from 28 to 30% B; 26−26.5 min, linear gradient from 30 to 31.8% B; 26.5−27 min, linear gradient from 31.8 to 32.8% B; 27−27.5 min, linear gradient from 32.8 to 40% B; 27.5−28 min, linear gradient from 40 to 41% B; 28−28.5 min, linear gradient from 41 to 33% B; 28.5−34 min, linear gradient from 33 to 36% B; 34−35 min, linear gradient from 36 to 36.8% B; 35−35.5 min, linear gradient from 36.8 to 40% B; 35.5−36 min, linear gradient from 40 to 36% B; 36−66 min, linear gradient from 36 to 50% B; 66−72 min, linear gradient from 50 to 100% B; 72−76 min, 100% B isocratic; 76−79 min, linear gradient from 100 to 1% B; and 79−88 min, 1% B isocratic.

The separated compounds were first monitored using DAD (280, 320, and 365 nm) and then MS scans were performed in both positive (PIM) and negative (NIM) ion modes, in the range m/z 50−3000 Da, in the following conditions: capillary voltage, 3 kV; sampling cone, 40 V; extraction cone, 3 V; source temperature, 100 °C; desolvation temperature, 350 °C; cone gas flow (N_2), 50 L/h; desolvation gas flow (N_2), 800 L/h. The MS was calibrated using sodium formate, and leucine encephalin was used as the lock mass. In these conditions the instrument is expected to provide experimental data with accuracy within ±3 ppm. All data were processed using MassLynx software 4.1 (Waters Corp.).

RESULTS AND DISCUSSION

UV−Vis and HRMS Spectroscopic Study of Olive Phenol Extracts. Two screening strategies were used in the phenol profiling study of extracts from the olive oil processing trial. The extracts were first screened for the range of phenols previously reported in *O. europaea* L. matrices and their identification confirmed, based on accurate mass and fragmentation profile comparison with literature data. In addition, the UV−vis spectra from DAD were generated, allowing classification and (if possible) structure/spectra relationship assessment. When the reference compounds were available, the phenols were also compared with standards in terms of R_t, UV−vis, and MS spectral characteristics. Using the strategy detailed earlier, 67 phenols of known identity were found in six olive matrices (Table 1), but the discussion focuses only on those best illustrating the innovative nature of the study (e.g., found for the first time, challenged to analytically characterize and/or detect). The second screening strategy was used for the new constituents and was based on the generation of UV−vis and MS spectra from DAD and TIC chromatograms scanned in both NIM and PIM ion modes, at soft and strong ionizations, obtaining major ESI^- and ESI^+ signals (Table 2).

Table 1 summarizes the MS and UV−vis spectral data of known phenolic compounds identified in extracts of destoned fruits, stones, and olive oil process-derived matrices (paste, pomace, wastewater, and oil). It also provides information about their elution time, molecular formula, theoretical and experimental m/z of deprotonated molecular ions in NIM mode, and calculated errors between them. Moreover, such data organization also allows one to infer the difference between the detectors' ability to assign the presence of individual phenolic compounds and/or to follow their origin, evolution, and disappearance during each operational step. Because data on UV−vis absorption maxima can sometimes vary due to matrix interference (which could lead to possible misinterpretation), the characteristic UV−vis spectral shapes of known and new phenol constituents were also presented in Table 3, along with their MS fragmentation profiles and chemical structures (if possible). The UPLC-DAD chromatograms of all matrices are presented in the Supporting Information (Figures S1−S6).

Simple Phenols. Among the simple phenols, it was possible to confirm the presence of hydroxytyrosol and tyrosol and their glucosides, in addition to hydroxytyrosol acetate eluting as last. All of them were equally well detected by both detectors, with the exception of tyrosol, which failed to ionize as already reported before,[1] but was easily confirmed with the use of the standard. While DAD alone did not permit unequivocal identification of hydroxytyrosol acetate in paste, pomace, and wastewater due to coelution problems, both detectors unambiguously confirmed the identity of two hydroxytyrosol glucosides. Their presence has rarely been reported in olive matrices, which could be a result of analytical issues[28] and/or their microlevels.[29] However, the EIC at m/z 315.1080 displayed the presence of two peaks (R_t 3.2 and 3.3 min) with the same fragmentation profile typical for this glucoside (m/z 153, 123). There are three possible isomers differing in the glycosidation position,[1] but only UV−vis spectra characterization allowed us to distinguish between them. The first eluting isomer had λ_{max} of the B-band at 276, suggesting that glycosidation occurred at 3′ or 4′ OH positions on the ring (Table 3), while the second isomer had its B-band shifted to a higher λ_{max} (~279 nm), indicating an attached glucose moiety in the OH group, outside the phenolic ring, which allowed us to tentatively identify it as hydroxytyrosol-1-β-glucoside.

Benzoic Acids. Two derivatives of benzoic acids were identified, namely, vanillin and vanillic acid, commonly found in olive matrices. However, only the former was well-detected by both detectors, while MS alone failed to confirm the identity of vanillic acid. Its MS ions were suppressed under the analytical conditions applied, increasing error outside the tolerable range of 10 ppm. However, the presence of both was unambiguously confirmed by the use of authentic standards. It is worth noting that vanillic acid was absent in the fruit, but nevertheless appeared in all of the process-derived matrices, unlike vanillin, whose presence was confirmed in the stone, from where it was apparently transferred to the oil.

DOI: 10.1021/jf506345q
J. Agric. Food Chem. 2015, 63, 3859−3872

Cinnamic Acids. Four known cinnamic acids were found in extracts, of which three were esters (verbascoside and its two β-hydroxylated derivatives) and one appeared in the form of a free acid, namely, *p*-coumaric acid. Their presence and/or absence was easily confirmed by both DAD and MS, with the exception of *p*-coumaric acid in destoned fruit, whose UV−vis spectra verification was hindered by coelution problems. However, none of the verbascosides were transferred to the oil but were instead all lost with the wastes. Moreover, the unexpected rise of two β-OH-verbascoside diastereoisomers was observed using DAD after crushing and malaxation, which could point to technologically induced formation and/or release. Indeed, their abundance has already been reported once in Italian solid olive mill waste.[15]

Lignans. One of the most interesting and analytically challenging groups was the class of lignans. Two derivatives were identified in extracts, however only in oil, while in other matrices it was not possible to detect them, despite several attempts. Similar difficulties were also described by López et al.[30] However, in our study, the low ionization of pinoresinol restricted accurate mass-based identification, confirmed instead by the UV−vis spectra and R_t match with the standard. In contrast, the same conditions were adequate for MS identity confirmation of acetoxypinoresinol, determined with an uncertainty of 4.3 ppm. However, it should be emphasized that the high background signal of the nearest eluting compounds (oleuropein and ligstroside aglycones) almost mis-assigned their presence, as DAD alone, due to great UV−vis spectra similarity with simple phenols (e.g., hydroxytyrosol; Table 3).

Flavonoids. MS and DAD had comparable efficiency in terms of the analysis of flavonoids, where seven out of 13 phenols found could be identified using standards, while others were tentatively assigned as follows.

Six peaks were detected when scanning TIC traces at m/z 447.0927 characteristic for luteolin glucosides, which eluted at R_t 4.6, 15.9, 24.1, 26.3, 36.6, and 41.7 min. The accurate mass of the first eluting peak was far above the tolerable level (>15 ppm), and the absence of the fragment at m/z 285 excluded the presence of luteolin glucoside. The identity of the second peak (R_t 15.9 min) was tentatively assigned as luteolin diglucoside, due to its relative short R_t, high mass accuracy (<6 ppm), and characteristic MS ions at m/z 609, 447, and 285. Its UV−vis spectra displayed two absorption maxima at 268 and 338 nm, which is identical to that of luteolin-4′-*O*-glucoside. According to the literature,[31] there are three glycosidation sites possible for luteolin diglucoside—at the 3′,4′-*O*, 3′,7-*O*, and 4′,7-*O* positions. The λ_{max} at 338 nm pointed to 4′-*O* substitution, while at 268 nm to additional 7-*O* glucosidation. The same rationale could also be established from its MS spectra, where the low intensity of aglycone ion at m/z 285 pointed to a loss of glucose from the 7-*O* rather than from the 3′-*O* position.[32] Overall, this indicated the presence of luteolin-4′,7-*O*-diglucoside, which to the best of the authors' knowledge has never been found in olives before, but instead once in the leaves.[24] The later eluting peaks were easily identified, based on the coelution of standards such as luteolin-7-*O*-glucoside (R_t 24.1 min), quercitrin (R_t 26.3 min), and luteolin-4′-*O*-glucoside (R_t 36.6 min), whereas the identity of the last peak was tentatively assigned as luteolin-3′-*O*-glucoside. In the structure of luteolin glucoside, the sugar residue may be either *C*-linked (at the 6 and 8 positions, corresponding to orientin and homoorientin) or *O*-linked at the 5, 3′, 4′, and 7 positions (Table 3). This compound had long R_t (41.7 min), which immediately excluded the presence of orientin, homoorientin, and 5-*O* glucoside, similarly as 4′-*O* and 7-*O*, due to standards availability. This left us only with the existence of luteolin-3′-*O*-glucoside, once indeed proved to elute after 4′-*O*-glucoside under reverse-phase liquid chromatography (RP-LC) conditions.[33] Its presence has already been confirmed once in the leaf,[34] sharing identical UV−vis maxima (λ_{max} 268, 340), which along with the abundance of m/z 285 in its MS spectrum strongly supports our decisive proof. Again, both detectors had an indispensable role in assigning identity with a higher degree of confidence.

Scanning for m/z 593.1506 corresponding to luteolin rutinoside revealed the presence of three peaks (R_t 24.3, 25.5, and 26.6 min), sharing identical fragment ions and relative abundance (m/z 593, 477, and 285). To date, only two isomers have been confirmed in *O. europaea* L. matrices, namely, luteolin 7-*O*-rutinoside and luteolin 4′-*O*-rutinoside, with the former having higher λ_{max} and a shorter R_t.[1,12] In our study, all three isomers eluted after luteolin-7-*O*-glucoside and prior to luteolin-4′-*O*-glucoside, suggesting that the nature of the sugar had no influence on elution order in RP-LC. Moreover, the first two isomers presented similar UV−vis spectra, with λ_{max} around 243 nm, indicating that glycosidation probably occurred away from the chromophore, whereas UV−vis spectra verification of a third isomer was not feasible due to the trace amounts present. These data suggest that these isomers could be either 7-*O*, 5-*O*, 6-*C*, or 8-*C* linked (Table 3); however, only the use of other analysis (e.g., NMR) could provide further structural assignment, and hence the peaks were only tentatively assigned as luteolin rutinoside isomers.

Apart from apigenin-7-*O*-glucoside (R_t 30.3 min), another peak with the same accurate mass, i.e., m/z 431.0978, was detected in fruit, paste, and pomace extracts. This compound, eluting at 35.1 min, showed no affinity for liquid matrices, and its trace levels were beyond DAD detection.

Secoiridoids. The combined use of DAD and ESI-QTOF-HRMS analysis permitted a facile identification of common secoiridoids such as oleuropein, ligstroside, demethyloleuropein, 3,4-DHPEA-EDA, *p*-HPEA-EDA, comselogoside, and caffeoyl-6′-secologanoside. Moreover, it also allowed the detection of others structurally correlated to oleuropein and/or other secoiridoidic derivatives, but the discussion focuses only on those detected in several isomeric forms and hence more challenging to characterize.

Oleoside. The EIC at m/z 389.1084 obtained by ESI-QTOF-MS displayed four peaks (R_t 2.7, 3.0, 3.5, and 8.9 min) with almost the same fragmentation profile characteristic for oleoside. The UV−vis spectra of the first two peaks exhibited two absorption maxima, which is not typical for oleoside and suggests that oleoside is only in their structures. However, their identities were not further investigated due to the trace concentrations present. In contrast, the third and fourth peaks (R_t 3.5 and 8.9 min) had one characteristic λ_{max} at 236 nm (Table 3), though the UV−vis of the former showed some deviation owing to coelution with hydroxytyrosol. This peak was tentatively identified as oleoside, based on high mass accuracy (<6 ppm) and a typical fragmentation profile (m/z 345, 227, 209, and 183), while the second was tentatively identified as secologanoside, owing to the absence of the fragment at m/z 227 and a strong signal at m/z 345 characteristic for this phenol.[19] In contrast, both isomers also displayed the ion species at m/z 779 corresponding to a

DOI: 10.1021/jf506345q
J. Agric. Food Chem. 2015, 63, 3859−3872

presence of dimers, which have sometimes overdominated molecular ions.

Elenolic Acid Glucosides. Five peaks (R_t 7.5, 8.6, 9.2 10.2, and 11.9 min) in EIC at m/z 403.1240 were detected in fruits with the same fragmentation pattern (m/z 371, 223, and 179) typical for elenolic acid glucoside, also described in the literature as 11-methyl oleoside.[13] The fragment at m/z 371 corresponds to a neutral loss of the methyl group, while the fragment at m/z 223 to the elimination of hexose, giving rise to m/z 179 by the neutral loss of CO_2. The presence of dimers was also detected at m/z 807.2559. However, of these peaks only four (nos. 10, 12, 14, and II) had the UV−vis spectra with one absorption maximum, which varied depending on the matrix and isomer investigated (λ_{max} 236−245 nm), but always retained the typical bell-shaped curve (Table 3), while the first eluting peak displayed two and presented a major signal at m/z 891. This could infer that 11-methyl oleoside is in its structure, but further assignment of identity was not feasible (presented elsewhere; Table 2; unknown no. 9). This compound was absent in olive stones but in addition displayed another isomer eluting at R_t 7.8 min. However, several isomers of elenolic acid glucosides have already been found in different olive tissues and olive oil process-derived matrices such as fruits, leaves, and wastes,[1,12,13,22,24,27] but their trail has never been followed during processing before. As evident from our results, only one, i.e., an isomer 2, was thoroughly sustained throughout all of the operational steps, while the others showed no or lower resistance; indeed the majority already diminished after crushing.

Oleuropein. The EIC at m/z 539.1765 in olive extracts showed the presence of three peaks eluting at R_t 22.9, 27.0, and 28.6 min. The first two peaks displayed the fragments at m/z 377, 307, 275, 223, 149, and 139, and presented similar UV−vis spectra characteristics (λ_{max} ∼244 and 280 nm; Table 3). The first eluting peak was identified as oleuropein using an authentic standard, and the second as oleuroside, known to elute afterward under RP-LC conditions.[13] Interestingly, the third peak (R_t 28.6 min) also displayed the predominant ion at m/z 539.1765, but only in the extract of destoned fruit, while in the stone the predominant ion was at m/z 789.2466. No fragment characteristic for oleuropein aglycone (m/z 377) was observed in its MS spectrum, which along with distinct UV−vis (λ_{max} 250, 280sh nm) excluded the presence of a third isomer (presented elsewhere; Table 2; unknown no. 50). However, as evident from our results, neither of the two recognized isomers was transferred to the oil, though representing a major phenolic fraction in fruit. On one hand this points to their relatively low lipophilic character, while on the other it indicates their fast and easy transformation during processing.

Oleuropein Diglucoside. Several peaks were detected in fruit at m/z 701.2293; however, only four (R_t 18.5, 19.5 19.8, and 20.8 min) exhibited the MS profile characteristic for oleuropein diglucoside (m/z 701, 539, 377, 307, 275, and 223). As previously demonstrated by Fu et al.,[22] there are five possible isomers of this diglucoside, but the absence of the fragment at m/z 341 suggested that none of them had the *O*-dihexosyl structure. As before, all eluted between demethyoleuropein and oleuropein, but no UV−vis spectra were provided for further data comparison. Once again, none of them were partitioned to the oily phase during processing, but two nevertheless appeared in the wastes.

Oleuropein Aglycone. Three major peaks with the same accurate mass (m/z 377.1236) and yielding fragments (m/z 345, 327, 307, 275, 149, and 139) were detected in extracts previously identified as oleuropein aglycone isomers in various tautomeric forms.[17] The peak of the first eluting isomer was broad (R_t 21.5−22.8 min) and also contained signals of residual oleuropein (m/z 539) and its diglucoside (m/z 701), while in the second peak (R_t 37.5 min) the presence of dimers (m/z 755) could also be observed. All three isomers appeared in all of the olive matrices, but the initial trace amounts in fruits prevented DAD detection. One significant fact is that crushing implied their rise to a level easily quantifiable using DAD in all process-derived matrices, where indeed they represented a major phenolic fraction. However, in spite of their minor absorption maxima deviations (λ_{max} 244−258 and 276−281; Table 2), they all kept the same spectral shape (Table 3) and could fit to any of the structures proposed by Fu et al.,[17] (Table 3, I−XII). Nonetheless, TIC traces in the oily phase also revealed the presence of other peaks with the same MS and similar UV−vis spectral characteristics; two of them were abundant and coeluted with ligstroside aglycones (peak nos. 48 and 49), whereas the identity of others could not be confirmed due to the ultratrace concentrations present.

Ligstroside Aglycone. Though analogous behavior was expected for ligstroside aglycones, these phenols displayed a distinct transfer/partition trail as compared to oleuropein aglycones. None of the detectors could assign their presence in fruits, while in their process-derived matrices, only one, an isomer 2, and yet only in the oil, was above the detection limit of DAD. Such tiny amounts suggest its fast and easy degradation, probably to *p*-HPEA-EDA, whose appearance in olive oil should be marked at the end of processing. However, the identity of all was unambiguously confirmed based on their high mass accuracy (≤6.1 ppm) and a fragmentation profile fitting well with a previous report,[19] but further distinction between them was not feasible and could hence fit any of the structures illustrated in Table 3 (I−XII).

3,4-DHPEA-EDA. The presence of two 3,4-DHPEA-EDA isomers (R_t 16.0 and 19.9 min) was confirmed based on accurate mass (m/z 319.1182) and characteristic fragment ions at m/z 301, 195, 183, 165, and 139, though a major signal in their MS spectra corresponded to a dimer (m/z 639.2442). In the literature several terms can be found for this compound, known as a dialdehydic form of decarboxymethyl elenolic acid linked to hydroxytyrosol (abbreviated as 3,4-DHPE-EDA),[3] though some others refer to it as 3,4-DHPEA-DEDA,[1] decarboxymethyl oleuropein aglycone[18] or deacetoxy oleuropein aglycon.[19] However, none of the two isomers were detected in olive fruits, whereas both of them appeared in their solid derived matrices, and one (isomer 2) also in the liquid ones, where it indeed represented one of the main phenol constituents. This points to its amphiphilic character, while their abundant evolution after brief crushing to a fast and efficient interconversion of fruit native phenols, probably of oleuropein and/or ligstroside, according to the mechanism previously proposed by Servili et al.[3]

Nüzhenide. Four isomers of nüzhenide were identified in olive stones based on mass accuracy and fragmentation profile (m/z 523, 453, 421, 299, and 223) matching with previous reports.[1,16] However, only three (isomers 2, 3, and 4) were present at levels quantifiable using DAD, of which two further diminished after crushing. In fact only one, namely, nüzhenide isomer 2, was maintained throughout all of the operational steps but showed no affinity for the oil matrix. However, in addition to nüzhenide isomers, the presence of their esters,

DOI: 10.1021/jf506345q
J. Agric. Food Chem. 2015, 63, 3859−3872

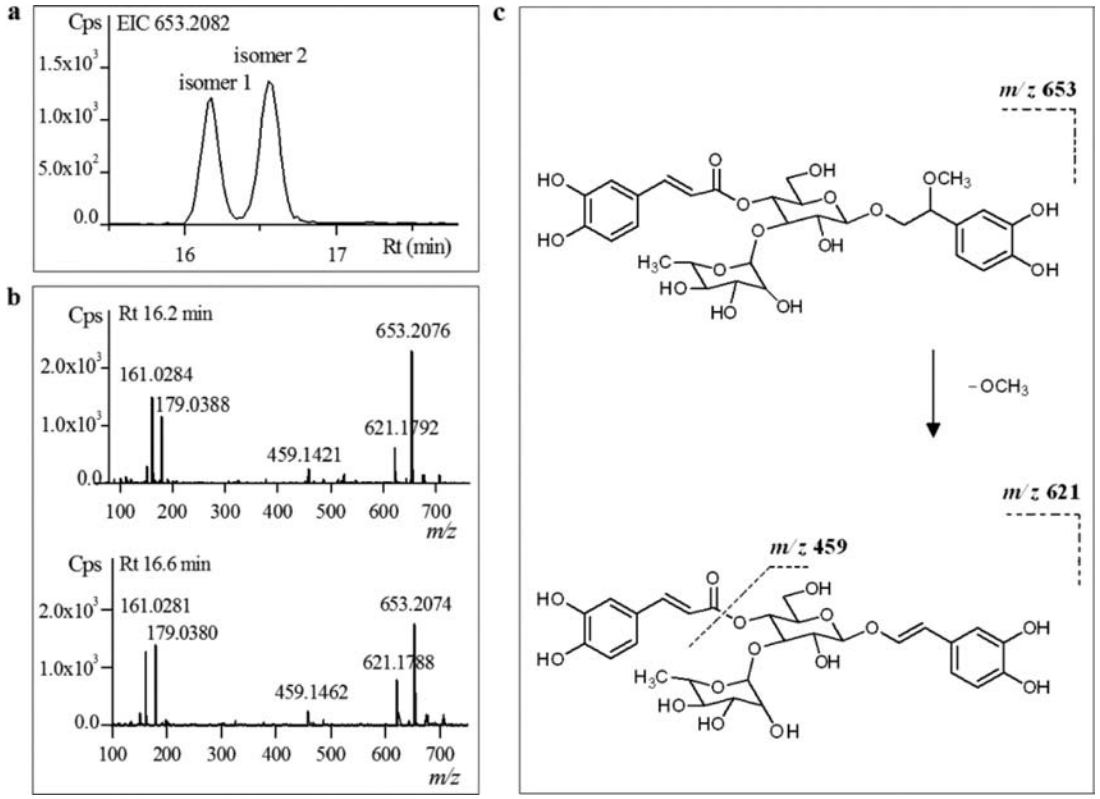

Figure 1. EIC of m/z 653.2082 (a), HRMS spectra (b), and fragmentation scheme (c) proposed for β-methyl-OH-verbascoside diastereoisomers.

namely, nüzhenide 11-methyl oleoside and nüzhenide bis(11-methyl oleoside), could also be confirmed in stones but not in other fruit compartments. While the former eluted as four peaks according to a previous report,[16] the second eluted as three at R_t 51.5, 52.0, and 58.7 min. Again, none of them were transferred to the oily phase, though some remained occluded in wastes.

Unknown Phenol Constituents. Apart from known phenols, the presence of other constituents could also be detected in olive extracts; however, only those for which spectroscopic evidence indicated a potent phenolic structure or which shared strong UV−vis or MS spectral similarities with already known phenols were included in Table 2. Three of them remained with an undefined MW (unknowns nos. 4, 9, and 50), while for four others new molecular formulas were assigned, of which three were also tentatively identified. Detailed MS and UV−vis spectra characterization is presented later for these, which could shed new light on the secondary metabolism of *O. europaea* L. plants.

Unknown A. The peak eluting at R_t 3.7 min was present in all olive matrices, presenting the same UV−vis spectra as a well-known secoiridoid, i.e., comselogoside (Table 3). Its MS spectrum in NIM mode showed the fragments at m/z 409, 389, 355, 241, 209, and 191, while in fruit extract the presence of an additional ion signal was detected at m/z 421. The latter was in fact the predominant ion, as already observed by Cardoso et al.,[12] in fruit and pomace extracts, however, due to its total absence in the other matrices, the MW of this compound was rather marked as undefined. This decision was further supported by the lack of sufficient evidence for its molecular ion in PIM. However, it is possible that the precursor ion signal was weak or absent due to fast dissociation, but the presence of two common fragments at m/z 389 and 241 and a similar elution order indicated that this compound is at least similar to that previously reported.[12] Unfortunately, no UV−vis spectrum characteristics were provided in the earlier study, and hence no further comparison was possible. Further research is undoubtedly needed to assign its identity, which is also interesting due to its widespread presence and apparent technological resistance.

Unknowns 408 MW. Two peaks (R_t 4.0 and 5.5 min) with the same exact mass (m/z 407.1553) and molecular formula $C_{17}H_{28}O_{11}$ generated by ESI-QTOF were detected in extracts, sharing similar UV−vis spectra (Table 3) but a different MS fragmentation profile (Table 2). The first eluting compound was more polar, had its B-band shifted to a lower λ_{max} (312 nm) and presented a similar MS spectrum, as previously reported.[1,12] The second eluting peak was less polar and had a slightly higher λ_{max} of the B-band at 314 nm but displayed many fewer MS fragment ions at lower intensities. Interestingly, both precursor ions corresponded to the same elemental formula ($C_{17}H_{28}O_{11}$) determined with high mass accuracy ($\leq$3.7 ppm), which could indicate the same chemical composition but probably a different structure. There are indeed several models possible for secoiridoid derivatives, differing in terms of the structure of elenolic ring; open or closed, aldehydic or nonaldehydic forms,[9] but beside the molecular formula proposed, no further structural assignment could be established. However, both of them again shared a strong UV−vis similarity with comselogoside, which along with the presence of diagnostic fragments of secoiridoids (m/z 389, 377, 375, and 345) allowed us to classify them among the secoiridoids.

Unknowns 654 MW. Two new diastereoisomers (R_t 16.2 and 16.6 min) of verbascoside derivatives were discovered in olive extracts that to the best of the authors' knowledge have

DOI: 10.1021/jf506345q
J. Agric. Food Chem. 2015, 63, 3859−3872

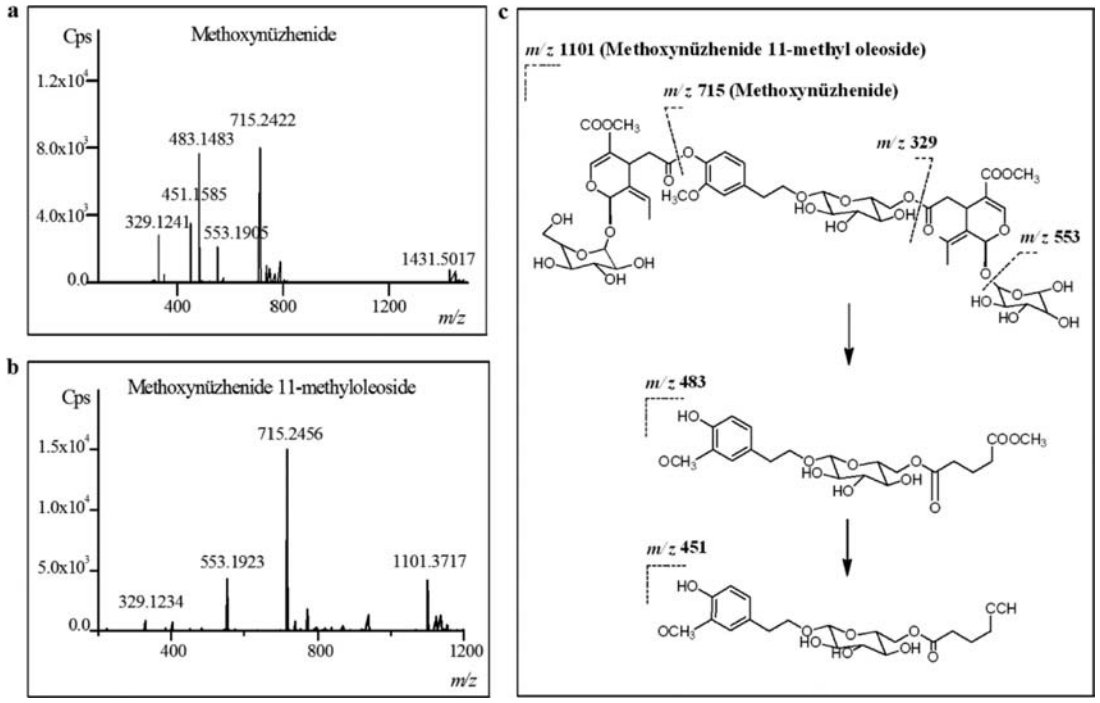

Figure 2. HRMS spectra (a) and fragmentation schemes (c) proposed for methoxynüzhenide and methoxynüzhenide 11-methyl oleoside.

Table 4. Accurate Mass Data for Methoxynüzhenide and Methoxynüzhenide 11-Methyl Oleoside and Their Proposed Fragment Ions

proposed fragment ions	m/z thr[a]	m/z exp	formula	Δm
methoxynüzhenide				
$[2M-H]^-$	1431.4977	1431.5017	$C_{64}H_{88}O_{36}$	2.8
$[M-H]^-$	715.2449	715.2422	$C_{32}H_{44}O_{18}$	−3.8
$[M-H-C_6H_{10}O_5]^-$	553.1921	553.1905	$C_{26}H_{34}O_{13}$	−2.9
$[M-H-C_6H_{10}O_5-C_4H_4O]^-$	483.1503	483.1483	$C_{22}H_{30}O_{12}$	−4.1
$[M-H-C_6H_{12}O_6-C_4H_6O_3]^-$	451.1604	451.1585	$C_{22}H_{28}O_{10}$	−4.2
$[M-H-C_6H_{10}O_5-C_{11}H_{12}O_5]^-$	329.1236	329.1241	$C_{15}H_{22}O_8$	1.5
methoxyünzhenide 11-methyl oleoside				
$[M-H]^-$	1101.3662	1101.3717	$C_{49}H_{66}O_{28}$	5.0
$[M-H-C_{17}H_{22}O_{10}]^-$	715.2449	715.2456	$C_{32}H_{44}O_{18}$	1.0
$[M-H-C_{17}H_{22}O_{10}-C_6H_{10}O_5]^-$	553.1921	553.1923	$C_{26}H_{34}O_{13}$	0.4
$[M-H-C_{17}H_{22}O_{10}-C_{11}H_{12}O_5]^-$	329.1236	329.1234	$C_{15}H_{22}O_8$	−0.6

[a] m/z thr = calculated monoisotopic mass $[M-H]^-$; m/z exp = detected mass; formula = molecular formula; Δm = calculated mass deviation, $[(m/z \text{ exp} - m/z \text{ thr})/m/z \text{ thr}] \times 10^6$ (ppm).

never been reported before. Their tentative identification was performed by calculating the possible molecular formula from experimental m/z and MS fragment data interpretation, yielding $C_{30}H_{38}O_{16}$ with a high mass accuracy (<5 ppm) for all matrices. Parts a and b of Figure 1 present the EIC at m/z 653.2082 and their corresponding HRMS spectra, showing an identical fragmentation profile (m/z 621, 459, 179, and 161) typical for verbascoside derivatives.[14] The ion at m/z 621 is formed by the loss of a methyl group and the formation of a double bond between α- and β- carbons, which subsequently form the fragment at m/z 459 due to loss of the caffeoyl group. The common ions at m/z 179 and 161 correspond to caffeic acid and its dehydrated ion. The structure and fragmentation pattern proposed for these two diastereoisomers is further presented in Figure 1c. As the latter is almost identical to an already known β-ethyl-OH verbascoside diastereoisomer previously found in pomace,[14] we analogously referred to the newly discovered compounds as β-methyl-OH-verbascoside isomers. Their structural correlation with verbascoside and β-OH-verbascoside is further apparent from UV−vis spectra comparison (Table 3) and supports their classification among cinnamic acids. What is of interest to add is their significant rise observed after fruits crushing, which kept increasing also during malaxation.

Unknowns 716 MW. This compound has already been detected before in stones, but not identified, though structurally correlated to nüzhenide having more than 30 mass units.[16] As before, it eluted as two peaks (R_t 17.1 and 20.9 min) and presented the same fragmentation profile (m/z 715, 553, 483, 451, and 329), suggesting the presence of isomers. HRMS analysis of both peaks provided the exact masses of 715.2449, corresponding to $C_{32}H_{44}O_{18}$, determined with less than 5 ppm uncertainty. Their product ion spectra showed a series of ions typical for nüzhenide, with m/z values increased by 30.0105 mass units (Figure 2a), which is probably due to a methoxy group attached to the tyrosol glucose moiety of nüzhenide. The

DOI: 10.1021/jf506345q
J. Agric. Food Chem. 2015, 63, 3859−3872

structure proposed for this compound is, along with the fragmentation scheme, presented in Figure 2c, where the ion at m/z 553 is formed by a neutral loss of glucose, while the ion at m/z 329 is formed by the consecutive loss of methoxytyrosol glucose. The common ions at m/z 483 and 451 originate from m/z 553, as previously demonstrated for nüzhenide.[16] Nevertheless, its UV−vis spectrum shares a strong similarity with nüzhenide (Table 3), which reasonably suggests the presence of methoxynüzhenide isomers. This decisive proof is further supported by the high mass accuracy of all of the characteristic fragment ions shown in Table 4. While their unique presence in the stone could point to a distinct biosynthetic metabolism of this fruit compartment, the traces present in process-derived matrices are probably a result of their transfer from the stone.

Unknown 1102 MW. Another compound found in stones, but never characterized using HRMS analysis, eluted at R_t 43.2 min. This compound is exactly 386.1213 mass units heavier than methoxynüzhenide and shares the same fragmentation pattern (m/z 715, 553, 329; Figure 2b) and similar UV−vis spectrum characteristics (λ_{max} 255 and 276; Table 3). Silva et al.,[16] already assigned its presence in the stone and surmised its structure as 11-methyl oleoside, linked to compound 716 MW. We in addition provide its molecular formula, namely, $C_{49}H_{66}O_{28}$, determined with a high mass accuracy of 5.0 ppm, its structure, and its proposed fragmentation scheme (Figure 2c). The accurate masses of detected fragment ions, their molecular formulas, and the calculated errors between them are also provided in Table 4, indicating that 11-methyl oleoside is indeed likely to be attached to methoxynüzhenide (716 MW). Collectively this information allowed us to tentatively identify the compound as methoxynüzhenide 11-methyl oleoside, with a high degree of confidence. Again, its presence was restricted solely to the stone, from where it was apparently transferred to the paste, pomace, and wastewater, however only in traces detectable by MS.

Olive Fruit Phenols Trail during Olive Oil Processing. The peel and pulp together (destoned fruits) represented a major phenolic fraction of the fruit's native constituents, while the stone represented only a minor fraction, being almost unique in the absence of flavonoids and the presence of nüzheonide-type phenols. While the appearance of these phenols in olive oil process-derived matrices, once released after crushing, is probably a result of their transfer from any of the fruit compartments, the presence of new phenolic compounds reasonably suggests their technologically induced formation and/or release. This is the case of vanillic acid, apigenin, 3,4-DHPEA-EDA, *p*-HPEA-EDA, and ligstroside aglycone found in the paste after crushing. Likewise, the unique presence of pinoresinol and acetoxypinoresinol in olive oil after malaxation, analogously as acetal of 3,4-DHPEA-EDA and unknown isomers of 484 MW in wastewater, could point to their artificial nature. Moreover, the DAD-detected rise observed in certain phenolic derivatives after crushing and/or malaxation could also highlight their transformative origin, probably from the fruit's native phenol constituents, whose disappearance was observed during processing. However, in qualitative terms, the behavior of olive fruit phenols followed a simple partitioning model, where the majority of them showed low or no affinity for the oil matrix, as with few minor exceptions only their aglycones were partitioned to the oil, while the fruit glycosides that yet reached the final products remained occluded in the wastes.

This study has made progress toward improved phenol profile characterization of olives and their olive oil process-derived matrices, as well as toward better understanding of phenols behavior during olive oil processing. In total, 80 different phenols were detected in six olive matrices and fully characterized based on HRMS and UV−vis spectroscopic data, which is far more extensive than previously reported for such matrices. Four new molecular formulas were proposed, and three new tentative identities were assigned to *β*-methyl-OH-verbascoside, methoxynüzhenide, and methoxynüzhenide 11-methly oleoside. However, only 66 were equally well-detected by both detectors; while DAD alone allowed the detection of sixty-nine phenols, ESI-QTOF-HRMS confirmed the presence of 77, due to trace detection outside the limits of DAD. MS was also more selective than DAD and provided elemental composition of known and new phenol constituents with a high mass accuracy below 10 ppm. Conversely, DAD allowed the identification of phenols which failed to ionize or whose ions were hindered by the matrix signal suppression effect. Moreover, it also provided valuable and complementary UV−vis spectra information that sometimes helped to distinguish between the phenols' isomeric forms and allowed one to specify the glycosidation site. Overall, this work demonstrated the power of a combined UPLC-DAD-ESI-QTOF-HRMS screening approach in phenol profile characterization of complex olive matrices.

■ ASSOCIATED CONTENT

Supporting Information

UPLC-DAD phenolic profile of olive destoned fruit, olive stone, olive paste, olive pomace, olive mill wastewater, and olive oil extracts monitored at 280, 320, and 365 nm. This material is available free of charge via the Internet at http://pubs.acs.org.

■ AUTHOR INFORMATION

Corresponding Author

*Tel.: + 38659099701. E-mail: branka.mozetic@ung.si.

Funding

This work was financially supported by the Slovenian Research Agency (ARRS), World Federation of Scientists (WFS), and the Slovenian L'OREAL-UNESCO program for "Women in Science", and partially performed within the Creative Core program (AHA-MOMENT) with Contract No. 3330-13-500031, cosupported by RS-MIZS and the European Regional Development Fund.

Notes

The authors declare no competing financial interest.

■ ACKNOWLEDGMENTS

We are grateful to Domenico Masuero for his technical assistance with mass spectrometry analysis.

■ REFERENCES

(1) Obied, H. K.; Bedgood, D. R., Jr.; Prenzier, P. D.; Robards, K. Chemical screening of olive biophenol extracts by hyphenated liquid chromatography. *Anal. Chim. Acta* **2007**, *603*, 176−189.

(2) Niaounakis, M.; Halvadakis, C. P. *Olive processing waste management: Literature review and patent survey*; Elsevier: Oxford, Great Britain, 2006.

(3) Servili, M.; Selvaggini, R.; Esposto, S.; Taticchi, A.; Montedoro, G.; Morozzi, G. Health and sensory properties of virgin olive oil hydrophilic phenols: Agronomic and technological aspects of

DOI: 10.1021/jf506345q
J. Agric. Food Chem. 2015, 63, 3859−3872

production that affect their occurrence in oil. *J. Chromatogr. A* **2004**, *1054*, 113−127.
(4) Servili, M.; Baldioli, M.; Mariotti, F.; Montedoro, G. Phenolic composition of olive fruit and virgin olive oil: Distribution in the constitutive parts of fruit and evolution during the oil mechanical extraction process. *Acta Hortic.* **1999**, *474*, 609−619.
(5) Gómez-Rico, A. M.; Inarejos-García, M.; Desamparados Salvador, G.; Fregapane, G. Effect of malaxation conditions on phenol and volatile profiles in olive paste and the corresponding virgin olive oils (*Olea europaea* L. Cv. Cornicabra). *J. Agric. Food Chem.* **2009**, *57*, 3587−3595.
(6) Jerman Klen, T.; Mozetič Vodopivec, B. The fate of olive fruit phenols during commercial olive oil processing: traditional press versus continuous two- and three-phase centrifuge. *LWT−Food Sci. Technol.* **2012**, *49*, 267−274.
(7) Jerman Klen, T.; Mozetič Vodopivec, B. Ultrasonic extraction of phenols from olive mill wastewater: Comparison with conventional methods. *J. Agric. Food Chem.* **2011**, *59*, 12725−12731.
(8) Bendini, A.; Cerretani, L.; Carrasco-Pancorbo, A.; Gómez-Caravaca, A. M.; Segura-Carretero, A.; Fernández-Gutiérrez, A.; Lercker, G. Phenolic molecules in virgin olive oils: A survey of their sensory properties, health effects, antioxidant activity and analytical methods. An overview of the last decade. *Molecules* **2007**, *12*, 1679−1719.
(9) De La Torre-Carbot, K.; Jauregui, O.; Gimeno, E.; Castellote, A. I.; Lamuela-Raventós, R. M.; López-Sabater, M. C. Characterisation and quantification of phenolic compounds in olive oils by solid phase extraction. *J. Agric. Food Chem.* **2005**, *53*, 4331−4340.
(10) Jerman Klen, T.; Mozetič Vodopivec, B. Optimisation of olive oil phenol extraction conditions using a high-power probe ultrasonication. *Food Chem.* **2012**, *134*, 248−2488.
(11) Jerman, T.; Trebše, P.; Mozetič Vodopivec, B. Ultrasound-assisted solid liquid extraction (USLE) of olive fruit (Olea europaea) phenolic compounds. *Food Chem.* **2010**, *123*, 175−182.
(12) Cardoso, S. M.; Guyot, S.; Marnet, N.; Lopes-da-Silva, J. A.; Renard, C. MGC.; Coimbra, M. A. Characterisation of phenolic extracts from olive pulp and olive pomace by electrospray mass spectrometry. *J. Sci. Food Agric.* **2005**, *85*, 21−32.
(13) Savarese, M.; De Marco, E.; Sacchi, R. Characterisation of phenolic extracts from olives (*Olea europaea cv.* Pisciottana) by electrospray ionization mass spectrometry. *Food Chem.* **2007**, *105*, 761−770.
(14) Innocenti, M.; la Marca, G.; Malvagia, S.; Giaccherini, G.; Vincieri, F. F.; Mulinacci, N. Electrospray ionisation tandem mass spectrometric investigation of phenylpropanoids and secoiridoids from solid olive residue. *Rapid Commun. Mass Spectrom.* **2006**, *20*, 2013−2020.
(15) Mulinacci, N.; Innocenti, M.; la Marca, G.; Mercalli, E.; Giaccherini, C.; Romani, A.; Erica, S.; Vincieri, F. F. Solid olive residues: Insight into their phenolic composition. *J. Agric. Food Chem.* **2005**, *53*, 8963−8969.
(16) Silva, S.; Gomes, L.; Leitão, F.; Bronze, M.; Coelho, A. V.; Boas, L. V. Secoiridoids in olive seed: Characterization of nüzhenide and 11-methyl oleosides by liquid chromatography with diode array and mass spectrometry. *Grasas Aceites (Sevilla, Spain)* **2010**, *61*, 157−164.
(17) Fu, S.; Arráez-Román, D.; Menéndez, J. A.; Segura-Carretero, A.; Fernández-Gutiérrez, A. Characterisation of oleuropein aglycon in olive oils by rapid-resolution liquid chromatography coupled to electrospray time-of-flight and ion trap tandem mass spectrometry. *Rapid Commun. Mass Spectrom.* **2009**, *23*, 51−59.
(18) Lozano-Sánchez, J.; Gambarelli, E.; Quirantes-Piné, R.; Cerretani, L.; Bendini, A.; Segura-Carretero, A.; Fernández-Gutiérrez, A. Wastes generated during the storage of extra virgin olive oil as a natural source of phenolic compounds. *J. Agric. Food Chem.* **2011**, *59*, 11491−11500.
(19) Fu, S.; Segura-Carretero, A.; Arráez-Román, D.; Menéndez, J. A.; De La Torre, A.; Fernández-Gutiérrez, A. Tentative characterisation of novel phenolic compounds in extra virgin olive oils by rapid-resolution liquid chromatography coupled with mass spectrometry. *J. Agric. Food Chem.* **2009**, *57*, 11140−11147.
(20) Dierkes, G.; Krieger, S.; Dück, R.; Bongartz, A.; Schmitz, O. J.; Hayen, H. High-performance liquid chromatography-mass spectrometry profiling of phenolic compounds for evaluation of olive oil bitterness and pungency. *J. Agric. Food Chem.* **2012**, *60*, 7597−7606.
(21) García-Villalba, R.; Carrasco-Pancorbo, A.; Oliveras-Ferraros, C.; Vázquez-Martín, A.; Menéndez, J. A.; Segura-Carretero, A.; Fernández-Gutiérrez, A. Characterisation and quantification of phenolic compounds of extra virgin olive oils with anticancer properties by a rapid and resolutive LC-ESI-TOF-MS. *J. Pharm. Biomed. Anal.* **2010**, *51*, 416−429.
(22) Fu, S.; Arráez-Román, D.; Segura-Carretero, A.; Menéndez, J. A.; Menéndez- Gutiérrez, M. P.; Micol, V.; Fernández-Gutiérrez, A. Qualitative screening of phenolic compounds in olive leaf extracts by hyphenated liquid chromatography and preliminary evaluation of cytotoxic activity against human breast cancer cells. *Anal. Bioanal. Chem.* **2010**, *397*, 643−654.
(23) Di Donna, L.; Mazzotti, F.; Salerno, R.; Tagarelli, A.; Taverna, D.; Sindona, G. Characterization of new phenolic compounds from leaves of Olea europaea L. by high-resolution tandem mass spectrometry. *Rapid Commun. Mass Spectrom.* **2007**, *21*, 3653−3657.
(24) Quirantes-Piné, R.; Lozano-Sánchez, J.; Herrero, M.; Ibáñez, E.; Segura-Carretero, A.; Fernández-Gutiérrez, A. HPLC-ESI-QTOF-MS as a powerful analytical tool for characterising phenolic compounds in olive-leaf extracts. *Phytochem. Anal.* **2013**, *24*, 213−223.
(25) Di Donna, L.; Mazzotti, F.; Napoli, A.; Salerno, R.; Sajjad, A.; Sindona, G. Secondary metabolism of olive secoiridoids. New microcomponents detected in drupes by electrospray ionisation and high-resolution tandem mass spectrometry. *Rapid Commun. Mass Spectrom.* **2007**, *21*, 273−278.
(26) Kanakis, P.; Termentzi, A.; Michael, T.; Gikas, E.; Halabalaki, M.; Skaltsounis, A.-L. From olive drupes to olive oil. An HPLC-orbitrap based qualitative and quantitative exploration of olive key metabolites. *Planta Med.* **2012**, *79*, 1576−1587.
(27) Peralbo-Molina, F.; Priego-Capote, M.; Luque de Castro, M. D. Tentative identification of phenolic compounds in olive pomace using liquid-chromatography-tandem mass spectrometry with a quadropole-quadropole-time-of-flight mass detector. *J. Agric. Food Chem.* **2012**, *60*, 11542−11550.
(28) Romero, C.; Brenes, M.; García, P.; Garrido, A. Hydroxytyrosol 4-β-D-glucoside, an important phenolic compound in olive fruits and derived products. *J. Agric. Food Chem.* **2002**, *50*, 3835−3839.
(29) Bianco, A.; Mazzei, R. A.; Melchioni, C.; Romeo, G.; Scarpati, M. L.; Soriero, A.; Uccella, N. Microcomponents of olive oil−III. Glucosides of 2(3,4-dihydroxy-phenyil)ethanol. *Food Chem.* **1998**, *63*, 461−464.
(30) Oliveras López, M. J.; Innocenti, M.; Ieri, F.; Giaccherini, C.; Romani, A.; Mulinacci, N. HPLC/DAD/ESI/MS detection of lignans from Spanish and Italian Olea europeaea L. fruits. *J. Food Compos. Anal.* **2008**, *21*, 62−70.
(31) Da Graça Campos, M.; Markham, K. R. *Structure information from HPLC and on-line measured absorption spectra: Flavones, flavonols and phenolic acids*. University of Coimbra: Coimbra, Portugal, 2007.
(32) Cuyckens, F.; Claeys, M. Mass spectrometry in the structural analysis of flavonoids. *J. Mass Spectrom.* **2004**, *39*, 1−15.
(33) Ko, J. H.; Kim, B. G.; Kim, H. J.; Kim, H.; Lim, C. E.; Lim, J.; Lee, C.; Lim, Y.; Ahn, J.-H. Four glucosyltransferases from rice: cDNA cloning, expression, and characterization. *J. Plant Physiol.* **2008**, *165*, 435−444.
(34) Mylonaki, S.; Kiassos, E.; Makris, D. P.; Kefalas, P. Optimisation of the extraction of olive (*Olea europaea*) leaf phenolics using water/ethanol-based solvent systems and response surface methodology. *Anal. Bioanal. Chem.* **2008**, *392*, 977−985.
(35) Obied, H. K.; Prenzler, P. D.; Ryan, D.; Servili, M.; Taticchi, A.; Esposto, S.; Robards, K. Biosynthesis and biotransformations of phenol-conjugated oleosidic secoiridoids from Olea europaea L. *Nat. Prod. Rep.* **2008**, *25*, 1167−1179.

DOI: 10.1021/jf506345q
J. Agric. Food Chem. 2015, 63, 3859−3872

selectively inhibit the most active α-glucosidases, Ct-MGAM and Ct-SI, causing slower digestion of the α-amylase degradation products of starch.[10] The inhibition of α-glucosidic activity of specific individual subunits of MGAM and SI can be considered as a key approach for controlling glucose release, because the α-glucosidase catalytic activities are responsible for producing virtually all of the free glucose available for intestinal absorption.

A variety of chemical compounds have been shown to have an inhibitory effect on mammalian intestinal α-glucosidases. These compounds are derived either from chemical synthesis[11,12] or from natural sources such as fruits[13,14] or plants.[15−17] Naturally occurring plant phenolic compounds are one group of chemical metabolites reported to have an inhibitory effect on the α-glucosidases. For instance, caffeic and chlorogenic acids are typical hydroxycinnamic acids found in high concentration in potatoes[18] and coffee beans.[19,20] Chlorogenic acids are esters of caffeic acids and quinic acids.[21] They were identified as the main α-glucosidase inhibitors found in the leaf extract of *Nerium indicum*, causing reduced postprandial rise in blood glucose after ingestion of 2 g of maltose or sucrose/kg body weight in rats administered either the leaf extract or pure chlorogenic acid (25 mg/kg body weight).[22] A single serving of coffee can have 70−350 mg of chlorogenic acid, and a regular coffee drinker can take up to 1 g of chlorogenic acids per day.[23] Caffeic acid was shown to be one of the most potent rat intestinal α-glucosidase inhibitors among different cinnamic acid derivatives.[24] The oxidized form of gallic acid caused nearly 40% inhibition of rat brush border sucrase and maltase activities.[25,26] (−)-Epigallocatechin gallate (EGCG), the main catechin found in green tea,[27] was also observed to be a potent inhibitor of maltase activity in rat brush border membrane vesicles,[28] rat intestinal acetone powder,[29] and recombinant human intestinal maltase.[30] It has been also shown that tea catechins, especially EGCG, may have potential for treating type 2 diabetes.[31,32] Subjects who consumed more than 6 cups of green tea daily were at less risk for type 2 diabetes compared to subjects who drank less than a cup per week.[33]

Overall, this information suggests that natural phenolic compounds present as normal dietary components may exert selective and differential inhibition of the individual subunits of MGAM and SI for the potential modulation of digestion of starchy and other glycemic carbohydrate-rich foods. Although there are multiple publications describing inhibition of α-glucosidases by phenolic compounds, the possibility of subunit selectivity for modulating glucose release has not been studied. In the present study, we analyzed the inhibitory properties and potential for the selective inhibition of the individual Ct and Nt subunits of MGAM and SI using five phenolic and polyphenolic compounds [chlorogenic acid, caffeic acid, gallic acid, (+)-catechin, EGCG] commonly found in Western diets and for which α-glucosidase inhibition has been previously described.

MATERIALS AND METHODS

Materials. All reagents including phenolic standards of chlorogenic acid [3-(3,4-dihydroxycinnamoyl)quinic acid], caffeic acid, gallic acid, (+)-catechin, and (−)- epigallocatechin gallate were purchased from Sigma-Aldrich (St. Louis, MO, USA).

Enzyme Preparation. Cloning, expression, and purification of recombinant mouse Ct-MGAM (glucoamylase subunit; spliceform N20), recombinant mouse Ct-SI (sucrase subunit),[4] recombinant human Nt-MGAM (maltase subunit),[34] and human recombinant Nt-SI[35] (isomaltase subunit) were reported previously. Mouse Ct-MGAM and Ct-SI were generated by recombinant expression in a baculovirus-Sf9 insect cell system.[4] Human Nt-MGAM and Nt-SI were expressed in *Drosophila* S2 cells.[34,35] Nickel-Sepharose resin was used to isolate the secreted proteins from the cell media that were further purified using anion exchange chromatography.

Determination of Protein Concentration. Protein concentration of solutions was determined with the Bio-Rad Protein Assay kit (Hercules, CA, USA), using 10 μL of the protein solution and 200 μL of Bradford dye reagent, and allowed to sit for at least 5 min. Absorbance was read at 595 nm using a Synergy HT microplate reader (BioTek, Winooski, VT, USA). Standards of bovine serum albumin were used in the concentration range of 31.25−500 μg/mL.

Enzyme and Inhibition Assays. Glucose release was measured according to the tris glucose oxidase (TGO) method[36] modified for microplate wells. Maltose solution (10 μL) at final concentrations ranging from 2.1 to 16.7 mM (approximately 1−8 times the K_m for maltose of Ct subunits and 0.3−3 times the K_m for maltose of Nt subunits) was mixed with 10 μL of the enzyme solution containing 0.2 mU of activity for Ct-MGAM, Ct-SI, and Nt-MGAM and 0.1 mU of activity for Nt-SI. One unit (U) of enzyme activity was defined as the activity that cleaves 1 μmol of maltose per minute. The mixtures were incubated for 1 h at 37 °C, and then TGO (180 μL) was added and incubated for an additional 45 min.[36] Absorbance was read at 450 nm in the microplate reader.

For inhibition assays, 10 μL of the phenolic inhibitor solutions was added to the above reaction mixtures to attain final concentrations ranging from 0 to 666.7 μM for the gallic acid, caffeic acid, and (+)-catechin, whereas chlorogenic acid and EGCG were used at final concentrations of 0−83.3 μM for C terminals of both MGAM and SI or 0−666.7 μM for N terminals of MGAM and SI. Analyses were conducted in triplicate. To correct for the scavenger effect of phenolics on the oxidative intermediates generated during the glucose oxidase−peroxidase reaction, which can lead to possible misleading readings of optical density (OD),[37] curves of glucose concentration versus OD in the presence of different concentrations of each individual phenolic compound were constructed and used to adjust the OD obtained during the assay of inhibition of the phenolics on the α-glucosidase enzymes. At the selected concentrations, phenolics caused <20% inhibition of the glucose oxidase−peroxidase developing reaction.

Determination of Inhibition Constant and Inhibition Mechanism. The inhibition mechanism and the respective inhibition constant (K_i) of each enzyme subunit−phenolic combination were determined by the best fit of nonlinear regression analysis with the Levenberg−Marquardt algorithm (Sigma Plot; Systat Software Inc., San Jose, CA, USA) and the standard mathematic equations describing the inhibition mechanisms for competitive, uncompetitive, noncompetitive homogeneous, and noncompetitive heterogeneous inhibition.[38] The mathematical fit with the best parameters of quality (highest r^2, lowest p, lowest residuals; $p \leq 0.05$ for the statistical significance) for each enzyme−inhibitor combination was chosen as the most probable inhibition mechanism in each case. For the calculations of kinetic parameters we chose nonlinear regression methods instead of linear transformations and linear regression, to avoid the additional error introduced by the latter procedures.[39,40]

Determination of IC_{50} Values. The concentration of each polyphenolic compound needed to cause 50% inhibition of the activity of the individual enzyme subunits was defined as the IC_{50} value. It was calculated by linear interpolation of the semilog plot of (log [I]) versus the relative activity (v/V_{max} = 0.5) at 16.67 mM maltose concentration (Minitab 14; State College, PA, USA).

RESULTS

Kinetics and Mechanism of Inhibition of the Recombinant Ct-MGAM, Nt-MGAM, Ct-SI, and Nt-SI. The inhibition capacity, the inhibition mechanism, and corresponding inhibition constants were determined for each

DOI: 10.1021/jf505425d
J. Agric. Food Chem. 2015, 63, 3873−3879

Table 1. Inhibition Mechanism and Inhibition Constant (K_i) for Each α-Glucosidase Subunit

		inhibition mechanism and inhibition constant (K_i, μM ± SD)			
		Ct-MGAM	Ct-SI	Nt-MGAM	Nt-SI
chlorogenic acid	type	noncompetitive homogeneous	noncompetitive heterogeneous	noncompetitive homogeneous	noncompetitive heterogeneous
	K_{i1}	3 ± 0.3	1.8 ± 0.3	43.2 ± 3.5	101.8 ± 36.6
	K_{i2}		28 ± 8.8		259.7 ± 114.5
	r^2	0.937	0.983	0.943	0.93
EGCG	type	noncompetitive heterogeneous	noncompetitive homogeneous	noncompetitive heterogeneous	noncompetitive heterogeneous
	K_{i1}	1.7 ± 0.7	15.1 ± 1.6	9 ± 1.5	76.3 ± 31.5
	K_{i2}	6.5 ± 2.1		97.6 ± 49.3	140.4 ± 53.5
	r^2	0.941	0.939	0.967	0.919
(+)-catechin	type	noncompetitive heterogeneous	noncompetitive heterogeneous	noncompetitive heterogeneous	noncompetitive homogeneous
	K_{i1}	20.4 ± 8.2	21.6 ± 8.1	20.4 ± 3.8	33.7 ± 4.1
	K_{i2}	96.7 ± 21.7	45.4 ± 5.9	97.2 ± 26.9	
	r^2	0.925	0.973	0.967	0.921
caffeic acid	type	noncompetitive heterogeneous	noncompetitive heterogeneous	noncompetitive heterogeneous	noncompetitive homogeneous
	K_{i1}	56.5 ± 25.4	58.2 ± 21.2	75.2 ± 13.3	103.3 ± 11.1
	K_{i2}	191.8 ± 39.6	323 ± 100.9	478.3 ± 167.1	
	r^2	0.918	0.902	0.968	0.909
gallic acid	type	noncompetitive heterogeneous	noncompetitive heterogeneous	noncompetitive heterogeneous	noncompetitive heterogeneous
	K_{i1}	24.9 ± 8.6	31.3 ± 7.2	85.7 ± 13.9	44.6 ± 14.4
	K_{i2}	50 ± 5.7	142.8 ± 24.7	460.6 ± 133.2	127.6 ± 28.7
	r^2	0.978	0.969	0.971	0.93

phenolic compound against each recombinant α-glucosidase subunit.

Chlorogenic Acid. Chlorogenic acid had higher inhibition binding affinities and correspondingly lower inhibition constants for Ct-MGAM (3 μM) and Ct-SI (1.8 and 28 μM) compared to caffeic acid, gallic acid, and (+)-catechin (Table 1). The binding affinities of chlorogenic acid were approximately 56 and 15 times greater for Ct-SI and Ct-MGAM than for Nt-SI and Nt-MGAM, respectively. Chlorogenic acid showed noncompetitive homogeneous inhibition for Ct-MGAM and Nt-MGAM, whereas Ct-SI and Nt-SI were inhibited in a noncompetitive heterogeneous way.

(−)-Epigallocatechin Gallate. Ct-MGAM was also the most strongly inhibited subunit by EGCG, with K_{i1} and K_{i2} values of 1.7 and 6.5 μM, respectively (Table 1). Figure 1 illustrates the change in the relative activities (v/V_{max}) of Ct-MGAM, Nt-MGAM, Ct-SI, and Nt-SI with the different concentrations (0−666.7 μM) of EGCG in the presence of different maltose concentrations (2.1, 4.2, 8.3, and 16.7 mM). The difference in the sensitivity to inhibition by EGCG observed between the Ct subunits and Nt subunits is notable, the former showing a K_i 2 orders of magnitude smaller than the latter. Thus, EGCG was a comparatively potent inhibitor for Ct-MGAM and Ct-SI (Figure 1a,b). EGCG inhibited Ct-MGAM, Nt-MGAM, and Nt-SI by a noncompetitive heterogeneous inhibition mechanism and caused noncompetitive homogeneous inhibition on Ct-SI.

(+)-Catechin. (+)-Catechin showed similar inhibition potency toward all four subunits (Figure 2). Affinities or inhibition constants of (+)-catechin for Ct-MGAM, Nt-MGAM, and Ct-SI were in the range of 20.4−97.2 μM (Table 1). The value of 33.7 μM (Table 1) for the K_i on Nt-SI indicated a higher inhibitory effect on this subunit compared to the other phenols. (+)-Catechin showed noncompetitive heterogeneous inhibition on Ct-MGAM, Nt-MGAM, and Ct-SI, whereas it showed noncompetitive homogeneous inhibition on Nt-SI.

Caffeic Acid. Caffeic acid had higher binding affinities (lower inhibition constant) for Ct-MGAM and Ct-SI than for the two N-terminal enzyme subunits tested. The inhibition constants, K_{i1} and K_{i2}, for Ct-MGAM were 56.5 and 191.8 μM, whereas they were 58.2 and 323 μM for Ct-SI (Table 1). Caffeic acid showed noncompetitive heterogeneous inhibition for Ct-MGAM, Nt-MGAM, and Ct-SI, whereas it inhibited Nt-SI in a noncompetitive homogeneous manner.

Gallic Acid. As with caffeic acid, Ct-MGAM and Ct-SI were the most sensitive to inhibition by gallic acid, with values for Ct-MGAM of 24.9 and 50 μM for K_{i1} and K_{i2} and 31.3 and 142.8 μM for Ct-SI K_{i1} and K_{i2}, respectively (Table 1). Gallic acid was inhibited by a noncompetitive heterogeneous mechanism for all four subunits.

Overall, inhibition by EGCG and chlorogenic acid showed a marked preference toward the C terminals of MGAM and SI than for N-terminals, but they displayed notable differences in their selectivity to the two enzymes. The greatest inhibition of Ct-MGAM was caused by EGCG and Ct-SI by chlorogenic acid. With the notable exception of (+)-catechin, which showed comparably higher inhibition of Nt-SI, there was a general trend toward higher binding affinities for Ct subunits over Nt.

IC_{50} Values of Inhibitors. IC_{50} values were also determined for the different phenolic compounds on the four individual α-glucosidase subunits. These values result from the overall inhibition effects of the different binding mechanisms that each compound may display and, therefore, are not necessarily expected to be of same ranking as the inhibition constants. In this context IC_{50} represents the required concentration to inhibit 50% of the enzymatic activity and is conducted at a single substrate concentration. The general trends observed

DOI: 10.1021/jf505425d
J. Agric. Food Chem. 2015, 63, 3873−3879

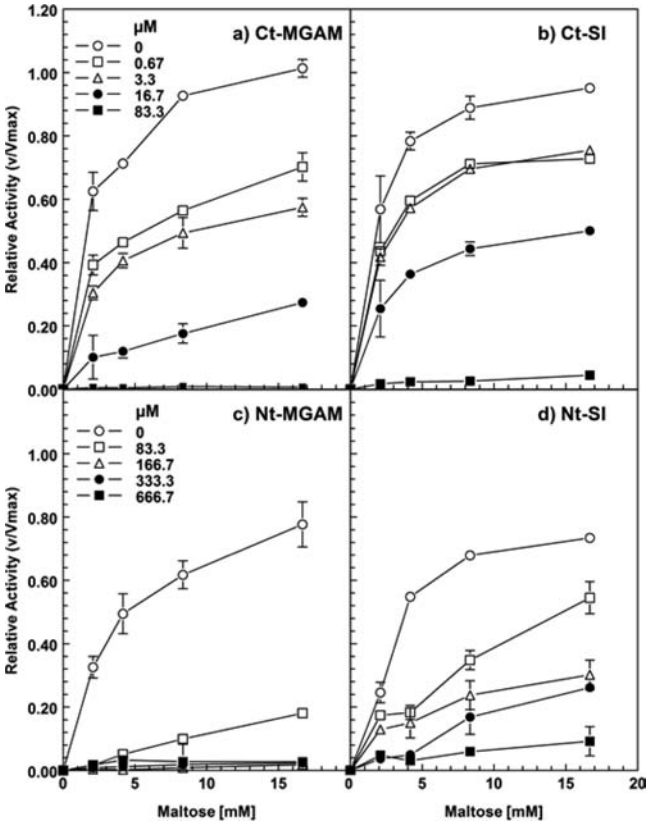

Figure 1. Relative activity (v/V_{max}) of (a) Ct-MGAM, (b) Ct-SI, (c) Nt-MGAM, and (d) Nt-SI at different maltose concentrations (2.1, 4.2, 8.3, and 16.7 mM) in the presence of EGCG at 0, 0.67, 3.3, 16.7, and 83.3 μM for Ct-MGAM and Ct-SI (panels a and b) and at 0, 83.3, 166.7, 333.3m and 666.7 μM for Nt-MGAM and Nt-SI (panels c and d).

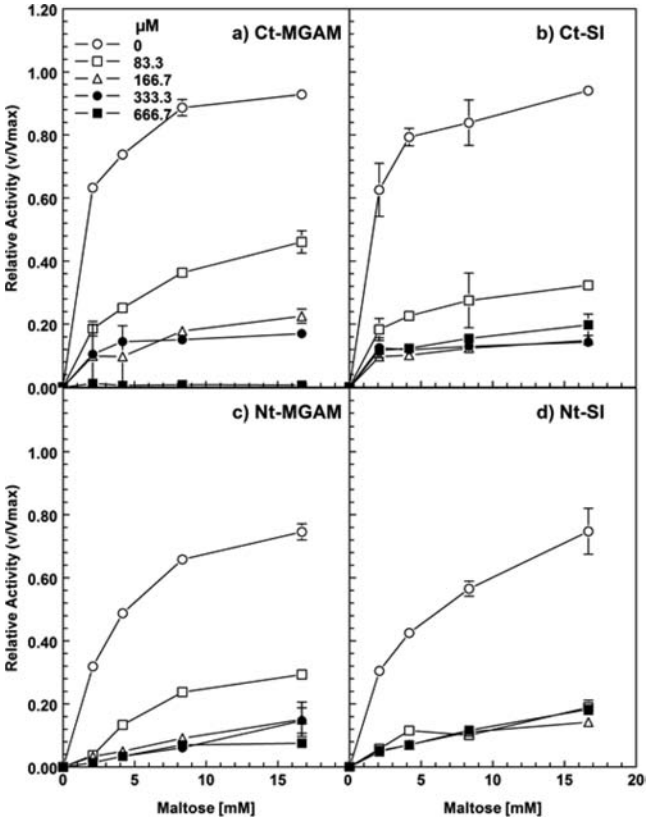

Figure 2. Relative activity (v/V_{max}) of (a) Ct-MGAM, (b) Ct-SI, (c) Nt-MGAM, and (d) Nt-SI at different maltose concentrations (2.1, 4.2, 8.3, and 16.7 mM) in the presence of (+)-catechin at 0, 83.3, 166.7, 333.3, and 666.7 μM.

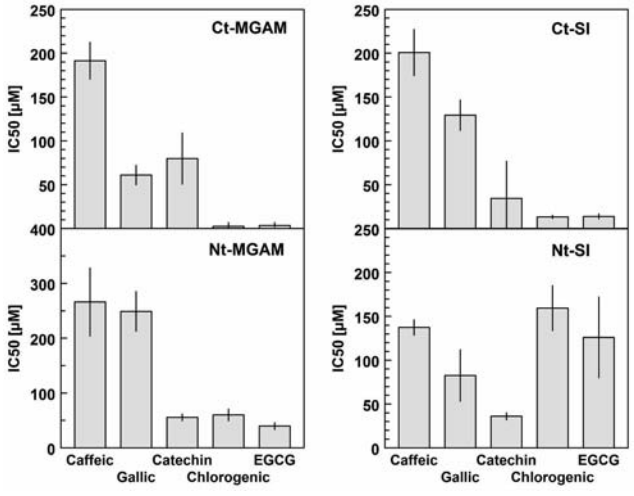

Figure 3. IC_{50} values (μM) of caffeic acid, gallic acid, (+)-catechin, chlorogenic acid, and EGCG for the inhibition of Ct-MGAM, Nt-MGAM, Ct-SI, and Nt-SI. Vertical lines represent the calculated 95% CI for the experimental data.

before for the inhibition constants held up. Among the compounds tested, chlorogenic acid and EGCG required the lowest concentration range (2.3−13.8 μM) to inhibit 50% of the activity of Ct-MGAM and Ct-SI, whereas a higher concentration range (39.6−159.4 μM) was required for Nt-MGAM and Nt-SI (Figure 3). (+)-Catechin showed 50% inhibition of Ct-SI and Nt-SI at comparably lower concentrations of 34.3 and 36 μM, respectively (Figure 3). Caffeic acid showed IC_{50} values in the range of 137.4−266 μM (Figure 3) for all of the α-glucosidase subunits; however, it did inhibit selectively Ct-MGAM and Nt-SI and with lower concentrations than required for the other two subunits (Figure 3). Gallic acid also showed stronger inhibition (lower IC_{50} values) on Ct-MGAM and Nt-SI than on the other two subunits.

DISCUSSION

Phenolic acids and polyphenols have been reported to inhibit the activities of the intestinal α-glucosidases, MGAM and SI.[24−30] The use of phenolic compounds as modulators of the rate of glucose release from starchy foods has been proposed for the treatment of metabolic diseases such as diabetes.[41] Although there are known strong inhibitors of α-glucosidases, such as acarbose,[41] they substantially reduce digestion of starch to glucose, resulting in dumping of starch and starch products into the large intestine to cause bloating and discomfort. The purpose of this study was to explore the selective inhibition by selected phenolic and polyphenolic compounds on individual MGAM and SI subunits. We propose partial inhibition of the highly active Ct-subunits or isomaltase for highly branched substrates could produce a slow, but still complete, digestion in the small intestine of the main glycemic carbohydrates, starch and sucrose. Additionally, slowly digested starch may trigger the ileal brake and gut−brain axis mechanisms that respectively control the stomach-emptying rate and influence hypothalamic

DOI: 10.1021/jf505425d
J. Agric. Food Chem. 2015, 63, 3873−3879

regulation of appetite, with potential impact on obesity and associated diseases.[9,42,43]

Our findings reveal that the four subunits of the intestinal α-glucosidases, SI and MGAM, can be selectively and differentially inhibited by certain plant-derived phenolics. This introduces the potential to induce different rates or profiles of digestion for starches, starch products, and sucrose. For instance, selective inhibition of the most active starch degrading subunit, Ct-MGAM (or glucoamylase), was achieved with EGCG and chlorogenic acid. This implies that the reducing activity of this enzyme could slow the rate of starch digestion and reduce particularly the glycemic spike, as was proposed in a recent paper by our group.[44] Chlorogenic acid had the highest binding affinity (K_{i1}) for Ct-SI (sucrase). This suggests the possibility of slowing the rate of digestion of sucrose-rich foods. Third, (+)-catechin showed higher inhibition for Nt-SI, the only subunit with endogenous α-1,6 branch hydrolyzing activity. The combination of (+)-catechin with a highly branched starch or starch products, such as a highly branched maltodextrin,[45] could obtain a slow glucose release effect. The results imply that the low inhibitory effect of phenolics on the slower acting Nt-MGAM and SI subunits may allow for the slow digestion of starch in diets containing such phenolics, but avoiding the inhibition of all four subunits caused by stronger inhibitors such as acarbose, which, although effectively reducing glycemic carbohydrate digestion, causes the delivery of large quantities of carbohydrates into the colon.

The tested phenolics were shown to affect the ability of the substrate to bind the active site of all enzyme subunits (K_{i1}); in some cases, phenolics may also bind an already formed enzyme−substrate complex, although this is with lesser affinity (K_{i2}). It has been reported that the catalytic pockets of Ct-MGAM, Nt-MGAM, and Nt-SI are surrounded by several aromatic amino acids, which may comprise the substrate binding motifs of these enzymes.[4] Therefore, it may be speculated that phenolic compounds could interact with or bind to these aromatic motifs in proximity to the active site, impairing the binding of the substrate with a correct orientation. The substantially higher values for K_{i1} of phenolics than those found for other competitive inhibitors[10] make unlikely the possibility for the existence of a typical competitive binding component in the interaction and therefore discards the possibility of the existence of classic mixed-type inhibition. Thus, the model of typical noncompetitive inhibition was the one that most closely described the effects of phenolics. Therefore, phenolic and polyphenolic inhibitors bind to at least a second additional site. Mathematical fittings of the experimental data indicated that only 5 (Nt-SI/caffeic acid; Nt-SI/(+)-catechin; Ct-MGAM/chlorogenic acid; Nt-MGAM/chlorogenic acid; and Ct-SI/EGCG) of the 20 different inhibitor-subunit combinations studied showed the same values for K_{i1} and K_{i2}. In these cases, therefore, the binding affinity of phenolic compounds to the free enzyme and enzyme−substrate complex was essentially the same, implying that there was a single binding site for phenolics, and the binding of substrate did not interfere with the binding of phenolics at their binding site. This also implies the occurrence of conformational changes in the enzyme after binding of these phenolics, with an effect on their substrate binding capability or catalytic mechanism.[38]

Another study, using rat intestinal powder, showed that chlorogenic acid has a noncompetitive inhibition behavior on maltase and sucrose activities, which agreed with our results.[22] However, the IC_{50} values of chlorogenic acid for maltase and sucrase were 2.99 and 2.18 mM, which are substantially higher than our calculated IC_{50} values (Figure 3).[22] This difference could be explained by binding multiple protein components present in the crude preparations of rat mucosal proteins. In another study, EGCG was shown as a competitive inhibitor and its IC_{50} was estimated as 20 μM for human intestinal maltase.[30] Also, results of an earlier study showed that caffeic acid had a very low inhibitory effect with IC_{50} values of 0.74 and 0.49 mM for maltase and sucrase, respectively.[24] In our study, caffeic and gallic acids were not nearly as strong inhibitors as chlorogenic acid and EGCG.

The stability of phenolic compounds must be considered for such a selective inhibition concept to be pursued in a practical sense. In one study, chlorogenic acid and caffeic acid were found to be stable after incubation with human gastric juice, duodenal fluid, and ileostomy effluent.[21] Another study showed that most (97.9−99.2%) of orally administered chlorogenic acid (700 μmol/kg) and a small amount of caffeic acid (0.8−2.1%) were found in the rat small intestine.[46] Record and Lane[47] tested the stability of gallic acid, caffeine, and EGCG in green tea at acidic pH and at a slightly alkaline pH. Caffeine concentration did not change under the exposure of either acidic (pH 2.0) or slightly alkaline pH (pH 7.5) conditions. Also, the concentration of gallic acid was only slightly reduced at pH of 2.0 and at pH 7.5. On the other hand, although EGCG concentration slightly declined at pH 2.0, its concentration was lower with incubation for 1 h at pH 7.5, decreasing from 1880 to 21 μmol/L in 1 g of green tea/50 mL of water. Several studies also reported that although acidic pH similar to that of the stomach slightly affected the concentration of catechins in green and black tea, the slightly alkaline pH (pH >7.4) caused a significant decrease in their concentration.[48−51] Those studies used alkaline pH (pH >7.4); however, it may not reflect the actual pH of the lumen of the entire small intestine because the pH measured in humans subjects was 6.4−6.6 in the duodenum or proximal small intestine and increased to 7.3−7.5 in the distal small intestine.[52,53] This difference could be important as the glycemic spike seen in the response profile arises from rapid proximal digestion of glycemic carbohydrates, and at this lower pH the catechins could be found with good qualities and high inhibition potential.

Of note, oxidative reactions in the gut lumen may lead to the formation of complex dimers including theasinesins.[54] The ability of these larger phenolic forms to interact with enzymes at the brush border is unknown.

In conclusion, the finding of selective inhibition by plant-derived phenolic compounds of the individual mucosal α-glucosidases implies that the digestion rate of starch, starch products, and sucrose can be differentially affected and modulated by these dietary components. The potential to control glycemic response profiles or sucrose hydrolysis rate using this selective inhibition concept with phenolic compounds warrants further study with an in vivo model.

■ ASSOCIATED CONTENT

Ⓢ Supporting Information

Reaction mechanisms for each of the different inhibition types and corresponding equations. This material is available free of charge via the Internet at http://pubs.acs.org.

DOI: 10.1021/jf505425d
J. Agric. Food Chem. 2015, 63, 3873−3879

AUTHOR INFORMATION

Corresponding Author

*(B.R.H.) Phone: (765) 494-5668. Fax: (765) 494-7953. E-mail: hamakerb@purdue.edu.

Funding

This work was funded by CONACYT, Mexico, Projects 80448 and 173965. We thank the Whistler Center for Carbohydrate Research at Purdue University for its partial support of the project.

Notes

The authors declare no competing financial interest.

ABBREVIATIONS USED

MGAM, maltase-glucoamylase; SI, sucrase-isomaltase; Ct, C-terminal end of proteins; Nt, N-terminal end of proteins; EGCG, (−)-epigallocatechin gallate; V_{max}, maximal rate of reaction; K_i, inhibition constant; IC_{50}, concentration required to inhibit 50% of the enzymatic activity; CI, confidence interval

REFERENCES

(1) Quezada-Calvillo, R.; Sim, L.; Ao, Z.; Hamaker, B. R.; Quaroni, A.; Brayer, G. D.; Sterchi, E. E.; Robayo-Torres, C. C.; Rose, D. R.; Nichols, B. L. Luminal starch substrate "brake" on maltase-glucoamylase activity is located within the glucoamylase subunit. *J. Nutr.* **2008**, *138*, 685−692.

(2) Quezada-Calvillo, R.; Robayo-Torres, C. C.; Ao, Z.; Hamaker, B. R.; Quaroni, A.; Brayer, G. D.; Sterchi, E. E.; Baker, S. S.; Nichols, B. L. Luminal substrate "brake" on mucosal maltase-glucoamylase activity regulates total rate of starch digestion to glucose. *J. Pediatr. Gastroenterol. Nutr.* **2007**, *45*, 32−43.

(3) Sim, L.; Quezada-Calvillo, R.; Sterchi, E. E.; Nichols, B. L.; Rose, D. R. Human intestinal maltase-glucoamylase: crystal structure of the N-terminal catalytic subunit and basis of inhibition and substrate specificity. *J. Mol. Biol.* **2008**, *375*, 782−792.

(4) Jones, K.; Sim, L.; Mohan, S.; Kumarasamy, J.; Liu, H.; Avery, S.; Naim, H. Y.; Quezada-Calvillo, R.; Nichols, B. L.; Pinto, B. M.; Rose, D. R. Mapping the intestinal α-glucogenic enzyme specificities of starch digesting maltase-glucoamylase and sucrase-isomaltase. *Bioorg. Med. Chem.* **2011**, *19*, 3929−3934.

(5) Auricchio, S.; Semenza, G.; Rubino, A. Multiplicity of human intestinal disaccharidases. II. Characterization of the individual maltases. *Biochim. Biophys. Acta, Nucleic Acids Protein Synth.* **1965**, *96*, 498−507.

(6) Lin, A. H.-M.; Lee, B.-H.; Nichols, B. L.; Quezada-Calvillo, R.; Rose, D. R.; Naim, H. Y.; Hamaker, B. R. Starch source influences dietary glucose generation at the mucosal α-glucosidase level. *J. Biol. Chem.* **2012**, *287*, 36917−36921.

(7) Lin, A. H.-M.; Nichols, B. L.; Quezada-Calvillo, R.; Avery, S. E.; Sim, L.; Rose, D. R.; Naim, H. Y.; Hamaker, B. R. Unexpected high digestion rate of cooked starch by the Ct-Maltase-Glucoamylase small intestine mucosal α-glucosidase subunit. *PLoS One* **2012**, *7*, No. e35473.

(8) Robayo-Torres, C. C.; Quezada-Calvillo, R.; Nichols, B. L. Disaccharide digestion: clinical and molecular aspects. *Clin. Gastroenterol. Hepatol.* **2006**, *4*, 276−287.

(9) Lee, B.-H.; Bello-Perez, L. A.; Lin, A. H.-M.; Kim, C. Y.; Hamaker, B. R. Importance of location of digestion and colonic fermentation of starch related to its quality. *Cereal Chem.* **2013**, *90*, 335−343.

(10) Lee, B.-H.; Eskandari, R.; Jones, K.; Reddy, K. R.; Quezada-Calvillo, R.; Nichols, B. L.; Rose, D. R.; Hamaker, B. R.; Pinto, B. M. Modulation of starch digestion for slow glucose release through "toggling" of activities of mucosal α-glucosidases. *J. Biol. Chem.* **2012**, *287*, 31929−31938.

(11) Eskandari, R.; Jones, K.; Reddy, K. R.; Jayakanthan, K.; Chaudet, M.; Rose, D. R.; Pinto, B. M. Probing the intestinal α-glucosidase enzyme specificities of starch-digesting maltase-glucoamylase and sucrase-isomaltase: synthesis and inhibitory properties of 3′- and 5′-maltose-extended de-*O*-sulfonated ponkoranol. *Chem.−Eur. J.* **2011**, *17*, 14817−14825.

(12) Eskandari, R.; Jones, K.; Rose, D. R.; Pinto, B. M. The effect of heteroatom substitution of sulfur for selenium in glucosidase inhibitors on intestinal α-glucosidase activities. *Chem. Commun.* **2011**, *47*, 9134−9136.

(13) McDougall, G. J.; Shpiro, F.; Dobson, P.; Smith, P.; Blake, A.; Stewart, D. Different polyphenolic components of soft fruits inhibit α-amylase and α-glucosidase. *J. Agric. Food Chem.* **2005**, *53*, 2760−2766.

(14) Kim, Y.-M.; Jeong, Y.-K.; Wang, M.-H.; Lee, W.-Y.; Rhee, H.-I. Inhibitory effect of pine extract on α-glucosidase activity and postprandial hyperglycemia. *Nutrition* **2005**, *21*, 756−761.

(15) Oku, T.; Yamada, M.; Nakamura, M.; Sadamori, N.; Nakamura, S. Inhibitory effects of extractives from leaves of *Morus alba* on human and rat small intestinal disaccharidase activity. *Br. J. Nutr.* **2006**, *95*, 933−938.

(16) Ryu, H. W.; Lee, B. W.; Curtis-Long, M. J.; Jung, S.; Ryu, Y. B.; Lee, W. S.; Park, K. H. Polyphenols from *Broussonetia papyrifera* displaying potent α-glucosidase inhibition. *J. Agric. Food Chem.* **2010**, *58*, 202−208.

(17) Ramkumar, K. M.; Thayumanavan, B.; Palvannan, T.; Rajaguru, P. Inhibitory effect of *Gymnema montanum* leaves on α-glucosidase activity and α-amylase activity and their relationship with polyphenolic content. *Med. Chem. Res.* **2010**, *19*, 948−961.

(18) Xu, X.; Li, W.; Lu, Z.; Beta, T.; Hydamaka, A. W. Phenolic content, composition, antioxidant activity, and their changes during domestic cooking of potatoes. *J. Agric. Food Chem.* **2009**, *57*, 10231−10238.

(19) Clifford, M. N.; Kazi, T. The influence of coffee bean maturity on the content of chlorogenic acids, caffeine and trigonelline. *Food Chem.* **1987**, *26*, 59−69.

(20) Clifford, M. N.; Knight, S.; Surucu, B.; Kuhnert, N. Characterization by LC-MSn of four new classes of chlorogenic acid in green coffee beans: Dimethoxycinnamoylquinic acids diferuloylquinic acids, and feruloyldimethoxycinnamoylquinic acids. *J. Agric. Food Chem.* **2006**, *54*, 1957−1969.

(21) Olthof, M. R.; Hollman, P. C. H.; Katan, M. B. Chlorogenic acid and caffeic acid are absorbed in humans. *J. Nutr.* **2001**, *131*, 66−71.

(22) Ishikawa, A.; Yamashita, H.; Hiemori, M.; Inagaki, E.; Kimoto, M.; Okamoto, M.; Tsuji, H.; Memon, A. N.; Mohammadi, A.; Natori, Y. Characterization of inhibitors of postprandial hyperglycemia from the leaves of *Nerium indicum*. *J. Nutr. Sci. Vitaminol.* **2007**, *53*, 166−173.

(23) Clifford, M. N. Chlorogenic acids and other cinnamates − nature, occurrence and dietary burden. *J. Sci. Food Agric.* **1999**, *79*, 362−372.

(24) Adisakwattana, S.; Chantarasinlapin, P.; Thammarat, H.; Yibchok-Anun, S. A series of cinnamic acid derivatives and their inhibitory activity on intestinal α-glucosidase. *J. Enzyme Inhib. Med. Chem.* **2009**, *24*, 1194−1200.

(25) Welsch, C. A.; Lachance, P. A.; Wasserman, B. P. Effects of native and oxidized phenolic compounds on sucrase activity in rat brush border membrane vesicles. *J. Nutr.* **1989**, *119*, 1737−1740.

(26) Gupta, N.; Gupta, S.; Mahmood, A. Gallic acid inhibits brush border disaccharidases in mammalian intestine. *Nutr. Res. (N. Y., NY, U. S.)* **2007**, *27*, 230−235.

(27) Forester, S. C.; Gu, Y.; Lambert, J. D. Inhibition of starch digestion by the green tea polyphenol, (−)-epigallocatechin-3-gallate. *Mol. Nutr. Food Res.* **2012**, *56*, 1647−1654.

(28) Kamiyama, O.; Sanae, F.; Ikeda, K.; Higashi, Y.; Minami, Y.; Asano, N.; Adachi, I.; Kato, A. *In vitro* inhibition of α-glucosidases and glycogen phosphorylase by catechin gallates in green tea. *Food Chem.* **2010**, *122*, 1061−1066.

(29) Matsui, T.; Tanaka, T.; Tamura, S.; Toshima, A.; Tamaya, K.; Miyata, Y.; Tanaka, K.; Matsumoto, K. α-Glucosidase inhibitory profile of catechins and theaflavins. *J. Agric. Food Chem.* **2007**, *55*, 99−105.

DOI: 10.1021/jf505425d
J. Agric. Food Chem. 2015, 63, 3873−3879

(30) Nguyen, T. T. H.; Jung, S.-H.; Lee, S.; Ryu, H.-J.; Kang, H.-K.; Moon, Y.-H.; Kim, Y.-M.; Kimura, A.; Kim, D. Inhibitory effects of epigallocatechin gallate and its glucoside on the human intestinal maltase inhibition. *Biotechnol. Bioprocess Eng.* **2012**, *17*, 966−971.
(31) Kao, Y. H.; Chang, H. H.; Lee, M. J.; Cheng, C. L. Tea, obesity, and diabetes. *Mol. Nutr. Food Res.* **2006**, *50*, 188−210.
(32) Thielecke, F.; Boschmann, M. The potential role of green tea catechins in the prevention of the metabolic syndrome − a review. *Phytochemistry* **2009**, *70*, 11−24.
(33) Iso, H.; Date, C.; Wakai, K.; Fukui, M.; Tamakoshi, A.; JACC Study Group. The relationship between green tea and total caffeine intake and risk for self-reported type-2 diabetes among Japanese adults. *Ann. Intern. Med.* **2006**, *144*, 554−562, DOI: 10.7326/0003-4819-144-8-200604180-00005.
(34) Rossi, E. J.; Sim, L.; Kuntz, D. A.; Hahn, D.; Johnston, B. D.; Ghavami, A.; Szczepina, M. G.; Kumar, N. S.; Sterchi, E. E.; Nichols, B. L.; Pinto, B. M.; Rose, D. R. Inhibition of recombinant human maltase glucoamylase by salacinol and derivatives. *FEBS J.* **2006**, *273*, 2673−2683.
(35) Sim, L.; Willemsma, C.; Mohan, S.; Naim, H. Y.; Pinto, B. M.; Rose, D. R. Structural basis for substrate selectivity in human maltase-glucoamylase and sucrase-isomaltase N-terminal domains. *J. Biol. Chem.* **2010**, *285*, 17763−17770.
(36) Quezada-Calvillo, R.; Markowitz, A. J.; Traber, P. G.; Underdown, B. J. Murine intestinal disaccharidases: identification of structural variants of sucrase-isomaltase complex. *Am. J. Physiol.* **1993**, *265*, G1141−G1149.
(37) Wong, A. I. C.; Huang, D. Assesment of the degree of interference of polyphenolic compounds on glucose oxidation/peroxidase assay. *J. Agric. Food Chem.* **2014**, *62*, 4571−4576.
(38) Segel, I. H. Simple inhibition systems. In *Enzyme Kinetics: Behavior and Analysis of Rapid Equilibrium and Steady-State Enzyme Systems, 1*; Wiley: New York, 1993; pp 100−136.
(39) Leatherbarrow, R. J. Use of nonlinear regression to analyze enzyme kinetic data: application to situations of substrate contamination and background subtraction. *Anal. Biochem.* **1990**, *184*, 274−278.
(40) Cornish-Bowden, A. Analysis and interpretation of enzyme kinetic data. *Perspect. Sci.* **2014**, *1*, 121−125.
(41) Hanhineva, K.; Törrönen, R.; Bondia-Pons, I.; Pekkinen, J.; Kolehmainen, M.; Mykkänen, H.; Poutanen, K. Impact of dietary polyphenols on carbohydrate metabolism. *Int. J. Mol. Sci.* **2010**, *11*, 1365−1402.
(42) Maljaars, P. W. J.; Peters, H. P. F.; Mela, D. J.; Masclee, A. A. M. Ileal brake: a sensible food target for appetite control. A review. *Physiol. Behav.* **2008**, *95*, 271−281.
(43) Strader, A. D.; Woods, S. C. Gastrointestinal hormones and food intake. *Gastroenterology* **2005**, *128*, 175−191.
(44) Lee, B.-H.; Lin, A. H.-M.; Nichols, B. L.; Jones, K.; Rose, D. R.; Quezada-Calvillo, R.; Hamaker, B. R. Mucosal C-terminal maltase-glucoamylase hydrolyzes large size starch digestion products that may contribute to rapid postprandial glucose generation. *Mol. Nutr. Food Res.* **2014**, *1*, 1−11.
(45) Lee, B.-H.; Yan, L.; Phillips, R. J.; Reuhs, B. L.; Jones, K.; Rose, D. R.; Nichols, B. L.; Quezada-Calvillo, R.; Yoo, S.-H.; Hamaker, B. R. Enzyme-synthesized highly branched maltodextrins have slow glucose generation at the mucosal α-glucosidase level and are slowly digestible in vivo. *PLoS One* **2013**, *8*, No. e59745.
(46) Azuma, K.; Ippoushi, K.; Nakayama, M.; Ito, H.; Higashio, H.; Terao, J. Absorption of chlorogenic acid and caffeic acid in rats after oral administration. *J. Agric. Food Chem.* **2000**, *48*, 5496−5500.
(47) Record, I. R.; Lane, J. M. Simulated intestinal digestion of green and black teas. *Food Chem.* **2001**, *73*, 481−486.
(48) Green, R. J.; Murphy, A. S.; Schulz, B.; Watkins, B. A.; Ferruzzi, M. G. Common tea formulations modulate in *vitro* digestive recovery of green tea catechins. *Mol. Nutr. Food Res.* **2007**, *51*, 1152−1162.
(49) Tenore, G. C.; Campiglia, P.; Giannetti, D.; Novellino, E. Simulated gastrointestinal digestion, intestinal permeation and plasma protein interaction of white, green, and black tea polyphenols. *Food Chem.* **2015**, *169*, 320−326.
(50) Zhu, Q. Y.; Zhang, A. Q.; Tsang, D.; Huang, Y.; Chen, Z. Y. Stability of green tea catechins. *J. Agric. Food Chem.* **1997**, *45*, 4624−4628.
(51) Yoshino, K.; Suzuki, M.; Sasaki, K.; Miyase, T.; Sano, M. Formation of antioxidants from (−)-epigallocatechin gallate in mild alkaline fluids, such as authentic intestinal juice and mouse plasma. *J. Nutr. Biochem.* **1999**, *10*, 223−229.
(52) Fallingborg, J.; Christensen, L. A.; Ingeman-Nielsen, M.; Jacobsen, B. A.; Abildgaard, K.; Rasmussen, H. H. pH-Profile and regional transit times of the normal gut measured by a radiotelemetry device. *Aliment. Pharmacol. Therap.* **1989**, *3*, 605−613.
(53) Evans, D. F.; Pye, G.; Bramley, R.; Clark, A. G.; Dyson, T. J.; Hardcastle, J. D. Measurement of gastrointestinal pH profiles in normal ambulat human subjects. *Gut* **1988**, *29*, 1035−1041.
(54) Neilson, A.; Bomser, J.; Periera, M.; Cooper, B.; Ferruzzi, M. G. Catechin degradation with concurrent formation of homo- and hetero-catechin dimers during in vitro digestion. *J. Agric. Food Chem.* **2007**, *55*, 8941−8949.

DOI: 10.1021/jf505425d
J. Agric. Food Chem. 2015, 63, 3873−3879

Further research focused on the regulation of the antioxidant-related gene by curcumin supplementation in experiment 2 was carried out to elucidate the possible mechanism by which supplemental curcumin protected the meat from oxidation under heat stress conditions.

MATERIALS AND METHODS

Ethics Statement. This experimental protocol was approved by the Ethical Committee and conducted under the supervision of the Institutional Animal Care and Use Committee of Nanjing Agricultural University, Nanjing, China.

Reagents and Chemicals. 2,2-Dipheny-l-picrylhydrazyl (DPPH), 2,2′-azinobis(3-ethylbenzothiazoline-6-sulfonic acid) diammonium salt (ABTS), and curcumin were purchased from Sigma Chemical Co., Ltd. All other chemicals used in the present study were obtained from Shanghai Chemical Agents Co., China, and were of analytical grade.

Animals and Diets. Two experiments were done to investigate the beneficial effects of curcumin on the meat quality and redox system of breast muscle in broilers.

In experiment 1, 320 1-day-old male broiler chicks (Arbor Acres, *Gallus gallus domesticus*) were obtained from a commercial hatchery (Hefei, Anhui, People's Republic of China) and randomly allotted to four treatments, in which there were eight replicates and 10 birds per replicate. All of the birds were placed in wire cages in a three-level battery and kept in an environmentally controlled room maintained at 34−36 °C until the birds reached 14 days of age and then gradually decreased to 26 ± 1 °C by 21 days of age, after which it was maintained at room temperature (24−26 °C) until the end of the experiment. The birds in the control group (C1) were fed a basal diet (Supporting Information, Table S1), and the other three groups (C2, C3, and C4) were offered the experimental diets based on the basal diet with an additional 50, 100, or 200 mg/kg curcumin, respectively. Feed and water were provided ad libitum to all the birds throughout the 42 day experiment period. At the end of the experiment, one bird per replicate was randomly selected and killed for the left breast muscle samples. One part of the left breast muscle was stored at 4 °C for meat quality measurement (pH, color, drop loss, and cooking loss), and the remainder was stored at −80 °C for biochemical assays.

In experiment 2, a total of 400 Arbor Acres broiler chickens were raised at a recommended environmental temperature from 1 to 20 days of age at the Qing Long Mountain Animal Center, Nanjing, China. At 21 days of age, broilers with similar body weight (BW) were randomly allocated into five treatment groups with eight replicate pens of 10 birds per pen, T1, T2, T3, T4, and T5. Birds in the T1 and T2 groups received the basal diet (Table S1), whereas birds in the T3, T4, and T5 groups received the basal diet containing 50, 100, or 200 mg/kg curcumin, respectively. Birds from the T1 group were housed at 24 °C for 24 h/day, whereas birds from the T2, T3, T4, and T5 groups were housed at 34 °C for 8 h/day (9:00 a.m.−5:00 p.m.) followed by 22 °C for 16 h/day. All of the broiler chickens had free access to water and feed and enjoyed a 12 h light−dark cycle of light regimen during the whole experiment. After 21 days of heat exposure, birds from each replicate were slaughtered and breast muscle examples were collected for homogenate preparation and real-time PCR analysis.

Meat Quality Measurement. The breast muscle pH was measured at 45 min (pH_{45}) and 24 h (pH_{24}) post-mortem using a pH meter (PH-STAR, Mattuas, Germany), as described by Zhen.[24] Three measurements were taken from each sample.

The color of the breast muscle was measured with a colorimeter (Minolta CR-10, Konica Minolta Sensing, Japan), based on the CIE $L^*a^*b^*$ system in which the L^*, a^*, and b^* values were determined as indicators of lightness, redness, and yellowness, respectively.[25] The average of the three measurements was recorded as color coordinate values of the sample.

For estimation of drip loss, breast muscle samples, size of 3 cm (length) × 2 cm (width) × 1 cm (thickness), were stored at 4 °C for 24 h post-mortem. The breast sample was placed in netting and suspended in a vacuumed bag for 24 and 48 h at 4 °C, respectively.[26] The drip loss of the breast muscle was calculated using the equation

$$\text{drip loss (\%)} = \frac{W_{\text{before}} - W_{\text{after}}}{W_{\text{before}}} \times 100$$

where W_{before} is the initial weight of breast muscle sample and W_{after} is the weight of breast muscle sample after 24 or 48 h of hanging.

About 15 g of each breast muscle sample was weighed, held in plastic bags, and immersed in a water bath at 80 °C until the internal temperature reached 75 °C. Then, the bags were cooled to approximately 25 °C, carefully wiped, and reweighed.[27] The cooking loss were calculated by applying the equation

$$\text{cooking loss (\%)} = \frac{W_{\text{before}} - W_{\text{after}}}{W_{\text{before}}} \times 100$$

where W_{before} is the initial weight of breast muscle sample and W_{after} is the weight of breast muscle sample after heating.

Preparation of Breast Muscle Homogenates. The minced breast muscle was homogenized in ice-cold 0.86% sodium chloride buffer (w/v, 1:9) and centrifuged at 3500*g* for 10 min at 4 °C. The supernatant was stored at −80 °C for further analysis. The protein concentrations of the 10% breast muscle homogenates were determined by using the bicinchoninic acid assay.[28]

Measurement of Antioxidant Potential. DPPH, $ABTS^+$, and superoxide radical (O_2^-) radical scavenging activities were estimated according to the methods described in our previous study.[12] Hydroxyl radical (OH^-) radical scavenging assay was determined according to the method by Noda.[29] The percentage inhibition of OH^- generation was calculated using the formula

$$OH^- \text{ radical scavenging effect (\%)} = \frac{A_{\text{control}} - A_{\text{sample}}}{A_{\text{control}}} \times 100$$

where A_{control} is the absorbance of the control reaction and A_{sample} is the absorbance of the test samples.

Determination of Protein Carbonyls (PC) and 8-Hydroxy-2′-deoxyguanosine (8-OHdG). The PC levels in the breast muscle were determined using 2,4-dinitrophenylhydrazine as described by Reiter.[30] The PC content was expressed as nanomoles per milligram of protein. The level of 8-OHdG in the breast muscle was determined by using an ELISA kit (Beijing North Institute of Biotechnology, Beijing, China) with a monoclonal antibody specific for broiler species. The procedure followed the manufacturer's protocols. The 8-OHdG content was calculated by a standard curve generated using 0.05−2 ng/mL 8-OHdG and corrected for the protein concentrations in each breast muscle homogenate sample. The final results were expressed in nanograms per milligram of protein.

Determination of Reactive Oxygen Species. Intracellular ROS production in breast muscle was measured by using 2,7-dichlorofluorescein diacetate as fluorescence probe, as previously described.[11] The fluorescence was measured at the excitation wavelength of 488 nm and an emission wavelength of 525 nm through a fluorescence spectrometer. The result was expressed as a percentage of the control group, which was taken as 100%.

Determination of Total Thiol Contents. The concentration of total thiol groups (T-SH) was determined according to the method of Tabassum.[31] The T-SH content was expressed as micromolers per milligram of protein.

Determination of Antioxidant Enzyme Activity. The activities of total SOD (T-SOD), glutathione peroxidase (GPx), glutathione *S*-transferase (GST), and catalase (CAT) and the contents of malondialdehyde (MDA) and reduced glutathione (GSH) were determined spectrophotometrically with the commercial kits purchased from Nanjing Jiancheng Insititute of Bioengineering (Nanjing, Jiangsu, People's Republic of China).[32] The results of T-SOD, Mn-SOD, GPx, GST, and CAT activities were expressed as units (U) per milligram of protein. The GSH content was expressed as micrograms per gram of protein, and MDA content was expressed as nanomoles per milligram of protein.

Real-Time Polymerase Chain Reaction (PCR) Analysis. Total RNA from the breast muscle was isolated using Trizol reagent (TaKaRa, Dalian, China). The RNA was quantified with a

DOI: 10.1021/jf505889b
J. Agric. Food Chem. 2015, 63, 3880−3886

Table 1. Effect of Curcumin on Meat Quality and Antioxidant Status of Breast Muscle in Broilers (Experiment 1)[a]

	curcumin treatment					p value	
	C1[b]	C2	C3	C4	SEM	linear[c]	quadratic
meat quality							
pH_{45}	6.05	6.04	6.11	6.15	0.023	0.057	0.146
pH_{24}	5.89	5.88	5.86	5.88	0.016	0.873	0.895
L^*	44.33	44.74	44.56	45.05	0.181	0.224	0.480
a^*	4.45 c	4.93 bc	5.69 ab	5.89 a	0.177	0.001	0.003
b^*	13.16	13.35	13.88	13.05	0.310	0.949	0.740
drip loss (%) at 24 h	5.33	4.63	4.13	4.92	0.182	0.287	0.062
drip loss (%) at 48 h	6.91 a	6.30 ab	5.36 b	6.22 ab	0.180	0.059	0.016
cooking loss (%)	13.95	13.49	13.40	13.68	0.367	0.789	0.859
antioxidant status							
CAT (U/mg protein)	2.46 b	3.04 ab	4.36 a	2.03 b	0.297	0.987	0.043
T-SOD (U/mg protein)	60.73	84.03	64.60	65.49	2.648	0.832	0.101
GPx (U/mg protein)	30.34	34.48	39.71	32.60	1.538	0.392	0.128
GST (U/mg protein)	31.78	37.45	34.09	32.78	1.481	0.977	0.515

[a]Values in the same row followed by different letters are significantly different ($n = 8$). [b]C1 group, basal diet; C2 group, basal diet containing 50 mg/kg curcumin; C3 group, basal diet containing 100 mg/kg curcumin; C4 group, basal diet containing 200 mg/kg curcumin. [c]Orthogonal polynomials were used to investigate linear and quadratic responses to the level of curcumin treatment.

Table 2. Effect of Curcumin on Free Radical Scavenging Activity of Breast Muscle in Broilers (Experiment 1)[a]

	curcumin treatment					p value	
	C1[b]	C2	C3	C4	SEM	linear[c]	quadratic
DPPH[d] (%)	22.22	25.96	31.40	26.22	0.603	0.907	0.745
ABTS (%)	31.37 c	36.45 b	42.04 a	32.93 c	0.246	0.035	0.004
O_2^- (%)	16.39	23.23	24.84	19.14	1.263	0.401	0.186
OH^- (%)	34.02	35.03	36.10	37.20	0.556	0.205	0.353

[a]Values in the same row followed by different letters are significantly different ($n = 8$). [b]C1 group, basal diet; C2 group, basal diet containing 50 mg/kg curcumin; C3 group, basal diet containing 100 mg/kg curcumin; C4 group, basal diet containing 200 mg/kg curcumin. [c]Orthogonal polynomials were used to investigate linear and quadratic responses to the level of curcumin treatment. [d]The free radical scavenging activity was calculated on the basis of the protein content (mg/mL) in breast muscle.

spectrophotometer (NanoDrop 2000c, Thermo Scientific, USA) and tested by agarose gel electrophoresis. Reverse transcription was performed immediately following the RNA isolation using the Perfect Real Time SYBR PrimeScriP kit (TaKaRa). Then the cDNA samples were amplified with the SYBR Premix Ex *Taq*II Tli RNaseH Plus kit (TaKaRa). Primer sequences are listed in Table S2. The relative amount of each target gene mRNA was calculated using the $2^{-\Delta\Delta Ct}$ method. The expression level of each target gene mRNA was normalized to the mRNA level of β-actin. In the present study, the results of gene expression were expressed as the fold changes between the treated and control groups.

Statistical Analysis. All data (experiments 1 and 2) were analyzed by using one-way analysis of variation (ANOVA) by SPSS 17.0. To evaluate the difference among groups, multiple comparisons were conducted using the Duncan test. Linear and quadratic contrasts were used to determine the effects for different dose levels (0, 50, 100, or 200 mg/kg) of supplemental curcumin in experiment 1. The significance level for difference was $p < 0.05$.

RESULTS AND DISCUSSION

Meat Quality and Antioxidant Status (Experiment 1). The effects of dietary curcumin on meat quality in breast muscle are presented in Table 1. Diet administered with curcumin had no difference on either the pH_{45} or pH_{24} of breast muscle in broilers. For meat color, the a^* value in breast muscle showed a linear and quadratic increase ($p < 0.05$) following the dietary curcumin supplementation ($p < 0.05$), but the L^* and b^* values showed no significant difference among the treatment groups. The water-holding capacity in the breast muscle of broilers was expressed by the drip loss at 24 and 48 h. The drip loss at 48 h of breast muscle was significantly influenced ($p < 0.05$) by dietary supplementation with curcumin and displayed a quadratic dose response. However, there was no significant effect on drip loss at 24 h and cooking loss of the breast muscle following the curcumin treatment.

Table 1 also shows the effects of dietary curcumin supplementation on the levels of antioxidant enzymes in breast muscle of broilers. The CAT activities of the breast muscle in curcumin-supplemented groups showed a quadratic dose response ($p < 0.05$). However, the breast muscle GPx, T-SOD, and GST activities of broilers fed the curcumin diet were not different ($p > 0.05$) from those of the broilers fed the basal diet. Minimal research has been conducted regarding the effect of various levels of curcumin on meat quality and oxidative status of breast muscle in broilers. Poultry meat contains a high concentration of polyunsaturated fatty acids, which makes it sensitive to free radical attack and oxidative deterioration.[33] The oxidant reaction initiated by free radicals destroyed the normal structure of the muscle and accumulated deleterious by-products, eventually influencing the meat quality.[34] On the other hand, the oxidation of myoglobin, which was mainly responsible for the meat color post-mortem, could lead to the discoloration of meat.[35] In the present study, curcumin, similar to fat-soluble antioxidant vitamin E, significantly improved the antioxidant capacity of the breast muscle. Similar beneficial effects of curcumin on enzyme activities were found in the literature.[10,34] It was suggested that curcumin improved the meat quality, especially the meat color, primarily due to its

DOI: 10.1021/jf505889b
J. Agric. Food Chem. 2015, 63, 3880−3886

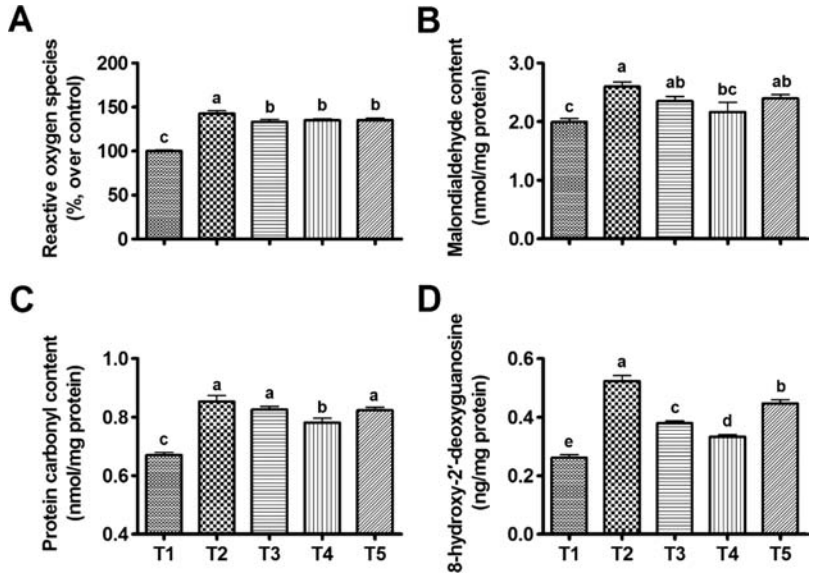

Figure 1. Effect of curcumin and heat treatment on (A) intracellular ROS levels and the concentrations of (B) MDA, (C) PC, and (D) 8-OHdG in breast muscle (experiment 2). Results are expressed as the mean ± SEM. Bars labeled with different letters are significantly different ($p < 0.05$). T1 group, basal diet + normal temperature; T2 group, basal diet + heat treatment; T3, 50 mg/kg curcumin + heat treatment; T4, 100 mg/kg curcumin + heat treatment; T5, 200 mg/kg curcumin + heat treatment.

ability to increase the antioxidant enzymatic activities in breast muscle.

Free Radical Scavenging Activity (Experiment 1). The DPPH radical is a stable nitrogen radical with yellow color and can be dissolved only in organic media.[36] The ABTS radical is a metastable radical with blue color and can be solubilized in both aqueous and organic media.[37] Both of them have been widely used to measure the antioxidant activity of biological materials and characterized by excellent reproducibility and stability under certain assay conditions.[38] O_2^- is one of the most representative free radicals, and its negative effects can be magnified because it produces other kinds of cell-damaging free radicals and oxidizing agents.[39] OH^- is well-known to be the most reactive of all the reduced forms of dioxygen and harmful to several cellular components such as DNA, lipid, and nucleus.[29] The antioxidant capacities of the breast muscle in broilers measured as DPPH, ABTS, O_2^-, and OH^- radical scavenging capacities are shown in Table 2. A linear and quadratic increase ($p < 0.05$) in the ABTS radical scavenging activities of breast meat was found with increasing dietary curcumin supplementation. The ABTS radical scavenging activities of breast meat in 50 and 100 mg/kg curcumin groups were significantly higher ($p < 0.05$) than that of the control group, whereas no difference was observed between the control group and the 200 mg/kg curcumin group. However, there was no significant variation ($p < 0.05$) in the percentage inhibition of DPPH, O_2^-, and OH^- radicals in the breast meat from the curcumin supplemental groups as compared to the control group. The high efficiency of antioxidants in the free radical scavenging assays could be attributed to either its direct capacity to neutralize stable free radicals or an indirect role as a hydrogen donor.[40] Our results suggested that curcumin, as a potential antioxidant, improved the antioxidant properties of breast muscle in broiler, possibly by the enhanced hydrogen-donating ability and free radical scavenging capacity.

Biomarkers of Oxidant Stress-Induced by Heat Treatment (Experiment 2). Studies on heat stress showed that its adverse effects are closely associated with the excessive ROS production.[23,41] A high level of free radicals caused oxidant stress and triggered oxidation of some critical cellular biomolecules, including lipid, protein, and DNA. In the present study, Figure 1 shows the increased ($p < 0.05$) intracellular ROS (Figure 1A), MDA (Figure 1B), PC (Figure 1C), and 8-OHdG (Figure 1D) levels in chickens reared under chronic heat treatment, suggesting the severe oxidant damage in breast muscle. When compared to the heat-stressed group, intracellular ROS levels in curcumin-administered groups (50, 100, or 200 mg/kg) were significantly decreased ($p < 0.05$) with the minimum level at 50 mg/kg. Compared with the heat-stressed group, administration with 100 mg/kg curcumin significantly decreased ($p < 0.05$) the breast muscle MDA and PC levels by 16.54 and 8.24%, respectively. In addition, curcumin supplementation (50, 100, or 200 mg/kg) significantly decreased the level of breast muscle 8-OHdG, which was a quantitative indicator for DNA damage occurring during oxidant stress.[42]

Curcumin had a strong capability of quenching free radicals, such as superoxide radicals and hydrogen peroxide.[12] Studies reported that Cr(VI) induced an increase in ROS level and severe oxidant damage, which were remarkably blocked by curcumin administration.[14] Besides, as a chain-breaking antioxidant, curcumin was proven to stop the reaction of chain propagation of lipid peroxidation through intercepting radical oxidation initiators.[14] A similar result was obtained from the recent work of Waseem et al., which suggested that the protective effects of curcumin against oxidant damage were partly attributed to its excellent free radical scavenging activity.[43]

Effect of Curcumin on Antioxidant Defense System Damaged by Heat Stress (Experiment 2). To evaluate whether dietary curcumin administration attenuated the oxidant damage induced by chronic heat treatment, we determined the capacity of the antioxidant defense system, consisting of the nonenzymatic and enzymatic antioxidant. Results showed that there existed significantly decreasing ($p < 0.05$) T-SH and GSH concentrations in breast muscle after

DOI: 10.1021/jf505889b
J. Agric. Food Chem. 2015, 63, 3880−3886

Table 3. Changes in Breast Muscle Antioxidant Enzyme Activity (Experiment 2)[a]

	T1[b]	T2	T3	T4	T5
T-SH (μmol/mg protein)	41.16 ± 0.54 a	33.26 ± 1.09 d	37.70 ± 0.67 b	36.47 ± 0.50 bc	35.10 ± 0.60 cd
GSH (μg/g protein)	24.18 ± 0.33 a	17.84 ± 0.25 c	20.66 ± 0.86 b	21.36 ± 0.79 b	19.92 ± 0.91 b
GPx (U/mg protein)	30.40 ± 0.50 a	23.79 ± 0.25 c	26.31 ± 0.34 b	26.36 ± 0.30 b	25.30 ± 0.71 b
GST (U/mg protein)	31.68 ± 1.34 a	23.04 ± 0.79 d	28.83 ± 0.60 b	26.88 ± 0.68 bc	24.66 ± 0.73 cd
CAT (U/mg protein)	2.49 ± 0.03 a	1.82 ± 0.02 d	2.06 ± 0.07 bc	2.15 ± 0.08 b	1.97 ± 0.06 cd
T-SOD (U/mg protein)	64.14 ± 0.83 a	47.77 ± 0.91 c	57.41 ± 3.53 b	58.81 ± 1.77 ab	50.14 ± 0.57 c

[a]Values are expressed as group mean values and SEM; mean values followed by different letters are significantly different. Test Duncan $p < 0.05$. [b]T1 group, basal diet + normal temperature; T2 group, basal diet + heat treatment; T3, 50 mg/kg curcumin + heat treatment; T4, 100 mg/kg curcumin + heat treatment; T5, 200 mg/kg curcumin + heat treatment.

exposure to heat treatment (Table 3). The T-SH level of chicken supplemented with 50 or 100 mg/kg curcumin was significantly increased by 13.35 and 9.65%, respectively, as compared with the heat-stressed group. The reduction of breast muscle GSH concentrations was attenuated to a significant extent upon curcumin supplementation (50, 100, or 200 mg/kg), but not dose-dependently ($p < 0.05$). Moreover, the weakened antioxidant defense system in breast muscle was also evidenced by the remarkable reductions ($p < 0.05$) of GPx, GST, CAT, and T-SOD activities following the exposure to heat treatment (Table 3). Dietary treatment with curcumin significantly attenuated ($p < 0.05$) heat stress-induced decrease of GPx activity; notably the greatest activities were found at 100 mg/kg curcumin. Chickens supplied with 50 or 100 mg/kg curcumin had 25.13 and 16.67% higher ($p < 0.05$) GST activities than those of the heat-stressed group, respectively. A similar observation ($p < 0.05$) was made regarding the breast muscle CAT and T-SOD activities.

The change of intracellular redox status is relevant to the ability of curcumin to cope with oxidative stress during heat exposure. To restore the balance of redox system caused by oxidant stress, cells facilitated the antioxidant defense system through enhancing activities of enzymatic antioxidants (CAT, T-SOD, and GSH-related enzymes) and elevating concentrations of nonenzymatic antioxidants (total thiols and GSH).[44] The present study showed that GPx, GST, CAT, and T-SOD activities were significantly increased in the breast muscle with the curcumin administration compared with the heat-stressed group. In cells, SOD served as the first line of defense against deleterious effects of ROS via catalyzing the dismutation of endogenous superoxide radicals to H_2O_2, which is further removed by CAT and GPx.[45] GST, a major group of GSH-related enzymes, was responsible for the detoxification of endogenous compounds to reduce the cytotoxicity of ROS.[46] Furthermore, T-SH and GSH levels were significantly increased in curcumin-supplemented groups. Generally, T-SH consists of nonprotein and protein-bound thiols, whereas GSH represents about 90% of the intracellular nonprotein thiols. Consistent with our results, numerous studies have confirmed that the depletion of GSH resulting from oxidant challenge was partially or even fully recovered with curcumin treatment.[11,18] These above results indicated that curcumin had prominent antioxidant activity not only through its enhancement of antioxidant enzyme activities but also through its effect on the redox status of intracellular thiols, especially GSH.

Gene Expression (Experiment 2). In the present study, birds reared in chronic heat stress showed typical characteristics of heat stress, including the overexpression of heat shock protein 70 (HSP70) and heat shock protein 90 (HSP90) mRNA in the breast muscle. As shown in Figure 2, curcumin

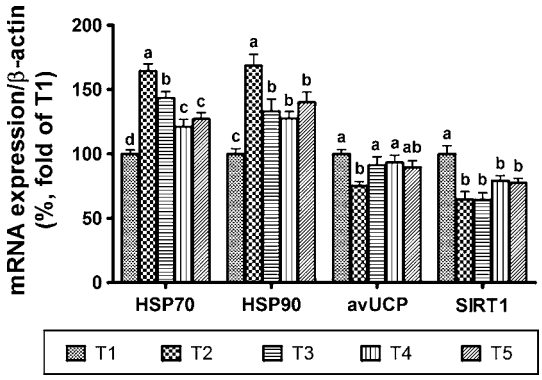

Figure 2. Effect of curcumin and heat treatment on gene expression in breast muscle (experiment 2). Results are expressed as the mean ± SEM. Bars labeled with different letters are significantly different ($p < 0.05$). T1 group, basal diet + normal temperature; T2 group, basal diet + heat treatment; T3, 50 mg/kg curcumin + heat treatment; T4, 100 mg/kg curcumin + heat treatment; T5, 200 mg/kg curcumin + heat treatment.

supplementation (50, 100, or 200 mg/kg) resulted in significant decreases in HSP70 and HSP90 expression levels. HSP70 and HSP90 are stress-defense proteins characterized by overexpression in response to many adverse environmental or physiological stimuli, including heat stress. Similar to our results, Hao et al. found a quick increase of HSP70 mRNA expression when chickens were exposed to heat stress for 2 h.[47] Parallel to the results of Sahin et al., our results have ascertained the protective role of curcumin by suppressing HSP expression in heat-stressed birds.[10] Furthermore, the mRNA expression of avUCP, an important regulator of mitochondrial ROS production,[48] was obviously depressed on exposure to chronic heat treatment while being markedly stimulated by curcumin supplementation (50, 100, or 200 mg/kg). The above data were consistent with the result of ROS level in breast muscle, indicating the inhibitory effect of curcumin on ROS production under heat stress. Moreover, we found that chronic heat treatment also significantly down-regulated sirtuin 1 (SIRT1) mRNA levels. SIRT1, an NAD^+-dependent protein deacetylase, plays an important role in the regulation of cellular oxidative stress burden.[49] Studies reported that the SIRT1 activation significantly decreases ROS levels, either directly or indirectly by deacetylation of the forkhead box class O 3 transcription factor and induction of manganese superoxide dismutase.[50] Recently, Yang et al. identified that SIRT1 activation by curcumin efficiently attenuated oxidant damage in the isolated heart.[15] In the present study, we found that the muscle mRNA expression of SIRT1 in heat-stressed groups, although not

DOI: 10.1021/jf505889b
J. Agric. Food Chem. 2015, 63, 3880−3886

significant, tended to increase in response to dietary curcumin treatment (100 or 200 mg/kg).

In conclusion, this study demonstrated that curcumin could be a potential feed additive that increased the oxidant stability of muscle and the meat quality in broiler chickens. Dietary curcumin supplementation could improve the meat color and increase water-holding capacity, free radical scavenging activity, and antioxidant enzymatic activity. The inclusion of 50 or 100 mg/kg curcumin was more effective in improving the meat quality and antioxidant system of breast muscle in broilers. The various levels of dietary curcumin had a positive effect on the redox status of breast muscle in broilers reared under chronic heat stress. Therefore, these results demonstrated that curcumin could serve as a potential promising antioxidant in poultry production that improved the redox status of breast muscle, in both normal and heat-stressed conditions, and benefit the resulting meat quality.

■ ASSOCIATED CONTENT

Supporting Information

Detailed table of ingredient composition and calculated nutrient content of the basal diets and detailed table of primers used for real-time PCR (experiment 2). This material is available free of charge via the Internet at http://pubs.acs.org.

■ AUTHOR INFORMATION

Corresponding Author

*(T.W.) E-mail: tianwangnjau@163.com. Phone: +86 025 84395156. Fax: +86 025 84395156.

Funding

This study was funded by the National Basic Research Program of China (2012CB124703) and Kehu Biotechnology Research Center, Guangzhou, People's Republic of China.

Notes

The authors declare no competing financial interest.

■ ACKNOWLEDGMENTS

We are grateful for the valuable comments made by anonymous reviewers and thank Yuxiang Yang and Chunlong Mu for assistance in the experiment and editing of the manuscript.

■ ABBREVIATIONS USED

ABTS, 2,2′-azinobis(3-ethylbenzothiazoline-6-sulfonic acid) diammonium salt; avUCP, avian uncoupling protein; CAT, catalase; DPPH, 2,2-dipheny-l-picrylhydrazyl; GPx, glutathione peroxidase; GSH, reduced glutathione; GST, glutathione *S*-transferase; HSP70, heat shock protein 70; HSP90, heat shock protein 90; MDA, malondialdehyde; PC, protein carbonyls; O_2^-, superoxide radical; OH^-, hydroxyl radical; ROS, reactive oxygen species; SIRT1, sirtuin 1; T-SH, total thiol groups; T-SOD, total superoxide dismutase; 8-OHdG, 8-hydroxy-2′-deoxyguanosine

■ REFERENCES

(1) Austic, R. E.; Mustafa, A.; Jung, B.; Gatrell, S.; Lei, X. G. Potential and limitation of a new defatted diatom microalgal biomass in replacing soybean meal and corn in diets for broiler chickens. *J. Agric. Food Chem.* **2013**, *61*, 7341−7348.

(2) Arshad, M. S.; Anjum, F. M.; Khan, M. I.; Shahid, M. Wheat germ oil and α-lipoic acid predominantly improve the lipid profile of broiler meat. *J. Agric. Food Chem.* **2013**, *61*, 11158−11165.

(3) Brettonnet, A.; Hewavitarana, A.; DeJong, S.; Lanari, M. C. Phenolic acids composition and antioxidant activity of canola extracts in cooked beef, chicken and pork. *Food Chem.* **2010**, *121*, 927−933.

(4) Luna, A.; Labaque, M. C.; Zygadlo, J. A.; Marin, R. H. Effects of thymol and carvacrol feed supplementation on lipid oxidation in broiler meat. *Poult. Sci.* **2010**, *89*, 366−370.

(5) Liu, D.-C.; Tsau, R.-T.; Lin, Y.-C.; Jan, S.-S.; Tan, F.-J. Effect of various levels of rosemary or Chinese mahogany on the quality of fresh chicken sausage during refrigerated storage. *Food Chem.* **2009**, *117*, 106−113.

(6) Goel, A.; Kunnumakkara, A. B.; Aggarwal, B. B. Curcumin as "curecumin': from kitchen to clinic. *Biochem. Pharmacol.* **2008**, *75*, 787−809.

(7) Jurenka, J. S. Anti-inflammatory properties of curcumin, a major constituent: a review of preclinical and clinical research. *Altern. Med. Rev.* **2009**, *14*, 277.

(8) Singh, S. From exotic spice to modern drug? *Cell* **2007**, *130*, 765−768.

(9) Maheshwari, R. K.; Singh, A. K.; Gaddipati, J.; Srimal, R. C. Multiple biological activities of curcumin: a short review. *Life Sci.* **2006**, *78*, 2081−2087.

(10) Sahin, K.; Orhan, C.; Tuzcu, Z.; Tuzcu, M.; Sahin, N. Curcumin ameloriates heat stress via inhibition of oxidative stress and modulation of Nrf2/HO-1 pathway in quail. *Food Chem. Toxicol.* **2012**, *50*, 4035−4041.

(11) Zhang, J.; Xu, L.; Zhang, L.; Ying, Z.; Su, W.; Wang, T. Curcumin attenuates D-galactosamine/lipopolysaccharide−induced liver injury and mitochondrial dysfunction in mice. *J. Nutr.* **2014**, *144*, 1211−1218.

(12) Zhang, J. F.; Hou, X.; Ahmad, H.; Zhang, H.; Zhang, L. L.; Wang, T. Assessment of free radicals scavenging activity of seven natural pigments and protective effects in AAPH-challenged chicken erythrocytes. *Food Chem.* **2014**, *145*, 57−65.

(13) Fu, Y.; Zheng, S.; Lin, J.; Ryerse, J.; Chen, A. Curcumin protects the rat liver from CCl4-caused injury and fibrogenesis by attenuating oxidative stress and suppressing inflammation. *Mol. Pharmacol.* **2008**, *73*, 399−409.

(14) Molina-Jijon, E.; Tapia, E.; Zazueta, C.; El Hafidi, M.; Zatarain-Barron, Z. L.; Hernandez-Pando, R.; Medina-Campos, O. N.; Zarco-Marquez, G.; Torres, I.; Pedraza-Chaverri, J. Curcumin prevents Cr(VI)-induced renal oxidant damage by a mitochondrial pathway. *Free Radical Biol. Med.* **2011**, *51*, 1543−1557.

(15) Yang, Y.; Duan, W. X.; Lin, Y.; Yi, W.; Liang, Z. X.; Yan, J. J.; Wang, N.; Deng, C.; Zhang, S.; Li, Y.; Chen, W. S.; Yu, S. Q.; Yi, D. H.; Jin, Z. X. SIRT1 activation by curcumin pretreatment attenuates mitochondrial oxidative damage induced by myocardial ischemia reperfusion injury. *Free Radical Biol. Med.* **2013**, *65C*, 667−679.

(16) Sharma, R. A.; Ireson, C. R.; Verschoyle, R. D.; Hill, K. A.; Williams, M. L.; Leuratti, C.; Manson, M. M.; Marnett, L. J.; Steward, W. P.; Gescher, A. Effects of dietary curcumin on glutathione S-transferase and malondialdehyde-DNA adducts in rat liver and colon mucosa: relationship with drug levels. *Clin. Cancer Res.* **2001**, *7*, 1452−1458.

(17) Vazeille, E.; Slimani, L.; Claustre, A.; Magne, H.; Labas, R.; Bechet, D.; Taillandier, D.; Dardevet, D.; Astruc, T.; Attaix, D.; Combaret, L. Curcumin treatment prevents increased proteasome and apoptosome activities in rat skeletal muscle during reloading and improves subsequent recovery. *J. Nutr. Biochem.* **2012**, *23*, 245−251.

(18) Sood, P. K.; Nahar, U.; Nehru, B. Curcumin attenuates aluminum-induced oxidative stress and mitochondrial dysfunction in rat brain. *Neurotoxic. Res.* **2011**, *20*, 351−361.

(19) Rajput, N.; Ali, S.; Naeem, M.; Khan, M.; Wang, T. The effect of dietary supplementation with the natural carotenoids curcumin and lutein on pigmentation, oxidative stability and quality of meat from broiler chickens affected by a coccidiosis challenge. *Br. Poult. Sci.* **2014**, *55*, 510−509 DOI: 10.1080/00071668.2014.925537.

(20) Kovats, R. S.; Hajat, S. Heat stress and public health: a critical review. *Annu. Rev. Public Health* **2008**, *29*, 41−55.

DOI: 10.1021/jf505889b
J. Agric. Food Chem. 2015, 63, 3880−3886

(21) Azad, M. A.; Kikusato, M.; Maekawa, T.; Shirakawa, H.; Toyomizu, M. Metabolic characteristics and oxidative damage to skeletal muscle in broiler chickens exposed to chronic heat stress. *Comp. Biochem. Physiol., Part A: Mol. Integr. Physiol.* **2010**, *155*, 401−406.
(22) Mujahid, A.; Sato, K.; Akiba, Y.; Toyomizu, M. Acute heat stress stimulates mitochondrial superoxide production in broiler skeletal muscle, possibly via downregulation of uncoupling protein content. *Poult. Sci.* **2006**, *85*, 1259−1265.
(23) Rhoads, R. P.; Baumgard, L. H.; Suagee, J. K.; Sanders, S. R. Nutritional interventions to alleviate the negative consequences of heat stress. *Adv. Nutr.* **2013**, *4*, 267−276.
(24) Zhen, S.; Liu, Y.; Li, X.; Ge, K.; Chen, H.; Li, C.; Ren, F. Effects of lairage time on welfare indicators, energy metabolism and meat quality of pigs in Beijing. *Meat Sci.* **2013**, *93*, 287−291.
(25) Li, K.; Zhang, Y.; Mao, Y.; Cornforth, D.; Dong, P.; Wang, R.; Zhu, H.; Luo, X. Effect of very fast chilling and aging time on ultrastructure and meat quality characteristics of Chinese Yellow cattle *M. Longissimus lumborum*. *Meat Sci.* **2012**, *92*, 795−804.
(26) Karami, M.; Alimon, A. R.; Sazili, A. Q.; Goh, Y. M.; Ivan, M. Effects of dietary antioxidants on the quality, fatty acid profile, and lipid oxidation of *longissimus* muscle in Kacang goat with aging time. *Meat Sci.* **2011**, *88*, 102−108.
(27) Kılıç, B.; Şimşek, A.; Claus, J.; Atılgan, E. Encapsulated phosphates reduce lipid oxidation in both ground chicken and ground beef during raw and cooked meat storage with some influence on color, pH, and cooking loss. *Meat Sci.* **2014**, *97*, 93−103.
(28) Bainor, A.; Chang, L.; McQuade, T. J.; Webb, B.; Gestwicki, J. E. Bicinchoninic acid (BCA) assay in low volume. *Anal. Biochem.* **2011**, *410*, 310−312.
(29) Noda, Y.; Kaneyuki, T.; Mori, A.; Packer, L. Antioxidant activities of pomegranate fruit extract and its anthocyanidins: delphinidin, cyanidin, and pelargonidin. *J. Agric. Food Chem.* **2002**, *50*, 166−171.
(30) Reiter, R. J.; Tan, D.-x.; Kim, S. J.; Manchester, L. C.; Qi, W.; Garcia, J. J.; Cabrera, J. C.; El-Sokkary, G.; Rouvier-Garay, V. Augmentation of indices of oxidative damage in life-long melatonin-deficient rats. *Mech. Ageing Dev.* **1999**, *110*, 157−173.
(31) Tabassum, H.; Parvez, S.; Pasha, S. T.; Banerjee, B. D.; Raisuddin, S. Protective effect of lipoic acid against methotrexate-induced oxidative stress in liver mitochondria. *Food Chem. Toxicol.* **2010**, *48*, 1973−1979.
(32) Ahmad, H.; Jinke, T.; Wang, J.; Khan, M. A.; Wang, Y.; Zhang, L.; Tian, W. Effect of dietary sodium selenite and selenium yeast on antioxidant enzymes activities and oxidative stability of chicken breast meat. *J. Agric. Food Chem.* **2012**, *60*, 7111−7120.
(33) Arshad, M. S.; Anjum, F. M.; Asghar, A.; Khan, M. I.; Yasin, M.; Shahid, M.; El-Ghorab, A. H. Lipid stability and antioxidant profile of microsomal fraction of broiler meat enriched with α-lipoic acid and α-tocopherol acetate. *J. Agric. Food Chem.* **2011**, *59*, 7346−7352.
(34) Brenes, A.; Viveros, A.; Goni, I.; Centeno, C.; Sayago-Ayerdy, S. G.; Arija, I.; Saura-Calixto, F. Effect of grape pomace concentrate and vitamin E on digestibility of polyphenols and antioxidant activity in chickens. *Poult. Sci.* **2008**, *87*, 307−316.
(35) Faustman, C.; Sun, Q.; Mancini, R.; Suman, S. P. Myoglobin and lipid oxidation interactions: mechanistic bases and control. *Meat Sci.* **2010**, *86*, 86−94.
(36) Kosińska, A.; Karamać, M.; Estrella, I.; Hernández, T.; Bartolome, B.; Dykes, G. A. Phenolic compound profiles and antioxidant capacity of *Persea americana* Mill. peels and seeds of two varieties. *J. Agric. Food Chem.* **2012**, *60*, 4613−4619.
(37) Re, R.; Pellegrini, N.; Proteggente, A.; Pannala, A.; Yang, M.; Rice-Evans, C. Antioxidant activity applying an improved ABTS radical cation decolorization assay. *Free Radical Biol. Med.* **1999**, *26*, 1231−1237.
(38) Arnao, M. B. Some methodological problems in the determination of antioxidant activity using chromogen radicals: a practical case. *Trends Food Sci. Technol.* **2000**, *11*, 419−421.
(39) Heo, S. J.; Park, E. J.; Lee, K. W.; Jeon, Y. J. Antioxidant activities of enzymatic extracts from brown seaweeds. *Bioresour. Technol.* **2005**, *96*, 1613−1623.
(40) Li, W.; Gao, Y.; Zhao, J.; Wang, Q. Phenolic, flavonoid, and lutein ester content and antioxidant activity of 11 cultivars of Chinese marigold. *J. Agric. Food Chem.* **2007**, *55*, 8478−8484.
(41) Mujahid, A.; Yoshiki, Y.; Akiba, Y.; Toyomizu, M. Superoxide radical production in chicken skeletal muscle induced by acute heat stress. *Poult. Sci.* **2005**, *84*, 307−314.
(42) Madsen-Bouterse, S. A.; Zhong, Q.; Mohammad, G.; Ho, Y. S.; Kowluru, R. A. Oxidative damage of mitochondrial DNA in diabetes and its protection by manganese superoxide dismutase. *Free Radical Res.* **2010**, *44*, 313−321.
(43) Waseem, M.; Parvez, S. Mitochondrial dysfunction mediated cisplatin induced toxicity: modulatory role of curcumin. *Food Chem. Toxicol.* **2013**, *53*, 334−342.
(44) Piantadosi, C. A.; Suliman, H. B. Redox regulation of mitochondrial biogenesis. *Free Radical Biol. Med.* **2012**, *53*, 2043−2053.
(45) Mittler, R. Oxidative stress, antioxidants and stress tolerance. *Trends Plant Sci.* **2002**, *7*, 405−410.
(46) Salinas, A. E.; Wong, M. G. Glutathione *S*-transferases − a review. *Curr. Med. Chem.* **1999**, *6*, 279−309.
(47) Hao, Y.; Gu, X. H.; Wang, X. L. Overexpression of heat shock protein 70 and its relationship to intestine under acute heat stress in broilers: 1. Intestinal structure and digestive function. *Poult. Sci.* **2012**, *91*, 781−789.
(48) Raimbault, S.; Dridi, S.; Denjean, F.; Lachuer, J.; Couplan, E.; Bouillaud, F.; Bordas, A.; Duchamp, C.; Taouis, M.; Ricquier, D. An uncoupling protein homologue putatively involved in facultative muscle thermogenesis in birds. *Biochem. J.* **2001**, *353*, 441−444.
(49) Williams, C. B.; Gurd, B. J. Skeletal muscle SIRT1 and the genetics of metabolic health: therapeutic activation by pharmaceuticals and exercise. *Appl. Clin. Genetics* **2012**, *5*, 81−91.
(50) Hori, Y. S.; Kuno, A.; Hosoda, R.; Horio, Y. Regulation of FOXOs and p53 by SIRT1 modulators under oxidative stress. *PLoS One* **2013**, *8*, No. e73875.

DOI: 10.1021/jf505889b
J. Agric. Food Chem. 2015, 63, 3880−3886

Table 1. Formulation of the Experimental Diets[a]

	FM-0	FM-2	FM-4	FM-6	FM-10	LP-0	LP-2	LP-4	LP-6	LP-10
Ingredients (g/kg)										
fishmeal[b]	587	587	587	587	587	235	235	235	235	235
lupin meal[c]						200	200	200	200	200
wheat gluten[d]						190	190	190	190	190
wheat meal	156	156	156	156	156	67	67	67	67	67
soya saponins[e]	0	2	4	6	10	0	2	4	6	10
wheat starch	10	8	6	4	0	10	8	6	4	0
fish oil[f]	221	221	221	221	221	242	242	242	242	242
vitamin mix[g]	20	20	20	20	20	20	20	20	20	20
mineral mix[g]	5	5	5	5	5	5	5	5	5	5
$Ca(H_2PO_4)\cdot 2H_2O$						10	10	10	10	10
carophyll pink	0.4	0.4	0.4	0.4	0.4	0.4	0.4	0.4	0.4	0.4
yttrium oxide	0.1	0.1	0.1	0.1	0.1	0.1	0.1	0.1	0.1	0.1
lysine hydrochloride						17	17	17	17	17
DL-methionine						3.6	3.6	3.6	3.6	3.6
Chemical Composition (%)										
crude protein	42.3	42.3	42.3	42.3	42.3	44.1	44.1	44.1	44.1	44.1
crude lipid	29.3	29.3	29.3	29.3	29.3	30.3	30.3	30.3	30.3	30.3
starch	10.3	10.3	10.3	10.3	10.3	7.5	7.5	7.5	7.5	7.5
gross energy (MJ/kg)	23.9	23.9	23.9	23.9	23.9	24.2	24.2	24.2	24.2	24.2

[a]Abbreviations: FM, fishmeal diet; LP, lupin meal diet; 0, 2, 4, 6, 10, levels of soya saponin inclusion in diets (g/kg). [b]Fishmeal 122/11, LTQ fishmeal, produced by Welcon AS, Norway. [c]Supplied by Holterman AS, Norway. [d]Wheat gluten 159/10, Amytex 100, produced by Syral, Belgium. [e]A 95% concentrate, supplied by Organic Technologies, United States. [f]Fish oil O5/10, NorSalmOil, produced by Norsildmel, Norway. [g]Supplemented to meet requirements.

such as lectins, protease inhibitors, oligosaccharides, phytate, alkaloids, and cyanogenic glycosides.[40,41] Despite the presence of these ANFs, lupin meals are considered highly digestible and good protein sources for salmonids.[42,43]

The purpose of this study was to investigate whether soya saponins alone may affect performance and induce enteritis in Atlantic salmon in the absence of other legume components in the diet, and to disclose the dietary threshold level. The recent introduction of a more purified soya saponin product (95% purity) allows for more conclusive data regarding this line of query. To assess threshold levels when other legume components are present, saponins were also supplemented to a legume-meal-containing diet. To this end, a dose–response design was employed using two basal diets without and with the presence of lupin meal, a diet ingredient that has previously been suggested to potentiate the effect of soya saponins.[16]

MATERIALS AND METHODS

Animal Husbandry. The experiment was conducted in compliance with laws regulating the experimentation with live animals in Norway as overseen by the Norwegian Animal Research Authority (FDU). The feeding trial was performed at Nofima's Aquaculture Research Station at Sunndalsøra, Norway. For each diet, duplicate, mixed-gender groups of 22 Atlantic salmon postsmolts of the Sunndalsøra strain with an initial mean body weight of 442 g (33 g SEM) were randomly distributed into 20 1 m^3 fiberglass tanks containing 250 L seawater replaced at a rate of 20 L/min. The temperature during the feeding trial decreased from 12 to 9 °C due to seasonal variation and affected all tanks equally. Oxygen saturation was above 85% throughout the experiment, whereas salinity varied between 32 and 33 g/L. Fish were fed continuously by automatic disk feeders. The economy and available facilities did not allow quantification of feed waste, but qualitative observations of appetite and waste accumulation in the tanks were made throughout the experiment. As the role of saponins in development of enteritis was the main goal of the study, this was considered an acceptable condition for the purpose of our study. A regimen of 24 h lighting was employed during the experimental period.

Diets. Diet formulations and their chemical compositions are shown in Table 1. Two basal diets were formulated, differing regarding protein sources. One was made with fishmeal supplying about 95% of the protein (FM). In the other, lupin meal and wheat gluten supplied about 25% and 35% of the protein, respectively, with fishmeal the remaining source (LP). Batches of each basal diet were subsequently supplemented with 0, 2, 4, 6, and 10 g/kg purified soya saponins (certified to be 95% pure, obtained from Organic Technologies, Coshocton, OH), replacing wheat starch. Accordingly, the diets were termed FM-0 and LP-0, FM-2 and LP-2, FM-4 and LP-4, FM-6 and LP-6, and FM-10 and LP-10. The basal diets were formulated to be isoenergetic (24 MJ GE/kg; GE = gross energy), and all diets were supplemented to fulfill the fishes' requirements for lysine, methionine, vitamins, and minerals. Fish oil and wheat meal were added as lipid and carbohydrate sources, respectively, to balance the nutrient composition of the diets. The fish were fed the experimental diets for 10 weeks.

Sampling. At the termination of the experiment, 10 randomly selected fish from each tank were sampled. All fish were fully anesthetized with tricaine methanesulfonate (MS222, Argent Chemical Laboratories) and subsequently euthanized by cervical dislocation prior to tissue sampling. Only fish with digesta throughout the intestinal tract were sampled to ensure intestinal exposure to the diets. Body weights and lengths were recorded for all fish. From five anesthetized fish per tank, blood was collected in heparinized vacutainers for plasma preparation. The abdominal cavities of all 10 euthanized fish per tank were opened, and the intestine was removed and cleared of any mesenteric and adipose tissue. Content from the proximal and distal halves of the proximal intestine (PI1 and PI2, respectively), the midintestine (MI), and the proximal and distal halves of the DI (DI1 and DI2, respectively) was collected into separate, preweighed tubes, frozen in liquid N_2, and then stored at −80 °C until further preparation and analyses could be conducted. The empty stomach, intestinal segments (PI, MI, and DI), liver, spleen, head kidney, and gall bladder were weighed. DI tissue samples for the histological evaluation were taken from six of the ten sampled fish per

DOI: 10.1021/jf506242t
J. Agric. Food Chem. 2015, 63, 3887–3902

tank, placed in 4% phosphate-buffered formaldehyde solution for 24 h, and subsequently stored in 70% ethanol until further processing. For mRNA extraction, DI samples from three of the six fish sampled for histology were placed in RNAlater (Ambion, Carlsbad, CA) at 4 °C for 24 h and subsequently stored at −20 °C. DI samples from the same three fish were taken for Western blots. These were frozen in liquid N_2 and then stored at −80 °C. For brush border membrane enzyme activity assessment, PI, MI, and the remaining DI tissues from all 10 fish per tank were frozen in liquid N_2 and stored at −80 °C.

Diet and Digesta Analyses. Feed and feces samples (from DI2) were analyzed for dry matter (EU 71/393), Kjeldahl nitrogen (N) (EU 93/28), lipid (HCl hydrolysis and diethyl ether extraction (EU 98/64)), and starch (AOAC enzymatic method 996.11). Gross energy was measured by bomb calorimetry (Parr 1271 bomb calorimeter, Parr, Moline, IL). Amino acid (except tryptophan) analysis of all samples was performed with a Biochrom 30 amino acid analyzer (Biochrom Ltd., Cambridge, U.K.) after hydrolysis, according to EC Commission Directive 98/64/EC. Tryptophan was analyzed on a Dionex Summit HPLC system, with a Shimadzu RF-535 fluorescence detector. Fatty acid composition of the feeds was determined by use of GC (gas chromatography) as previously described.[44] Yttrium oxide concentration in feed and feces was determined by inductively coupled plasma mass spectroscopy (ICPMS) as previously described by Refstie et al.[45]

Plasma Cholesterol, Total Bile Acids, and Other Metabolites. Analyses of plasma levels of cholesterol, total bile acids (conjugated and nonconjugated bile acids), total protein, glucose, triglycerides, free fatty acids, sodium, and phosphorus were performed by the Central Laboratory of the NMBU School of Veterinary Medicine (Oslo, Norway) according to standard protocols (Advia 1800, Siemens Healthcare Diagnostics, Erlangen, Germany).

Trypsin Activity and Total Bile Acids in the Digesta. Trypsin activity was determined colorimetrically as described by Kakade et al.[46] using the substrate benzoylarginine *p*-nitroanilide (Sigma no. B-4875, Sigma Chemical Co., St. Louis, MO) and a curve derived from standardized bovine trypsin solution. Total bile acid concentrations were determined using the Enzabile test kit (catalog no. 550101, BioStat Diagnostic Systems, Cheshire, U.K.) and a curve derived from standardized taurocholic acid solution.

Brush Border Membrane Enzyme Activity. The activity of the brush border membrane enzyme leucine aminopeptidase (LAP) was measured in PI and DI tissue homogenates diluted in ice cold Tris–mannitol buffer (1:20, w/v) containing 4-(2-aminoethyl)-benzenesulfonyl fluoride hydrochloride (Pefabloc SC, Pentapharm Ltd., Basel, Switzerland) as a serine proteinase inhibitor. The activity was determined colorimetrically using the substrate L-leucine β-naphthylamide hydrochloride as described by Krogdahl et al.[9] LAP specific activity was calculated following tissue protein concentration analysis using the BioRad protein assay (BioRad Laboratories, Munich, Germany).

Histology. Fixed DI tissue samples were processed according to standard histological techniques and stained with hematoxylin and eosin (H&E). Examination was conducted blindly with a light microscope using a continuous scoring scale from 0 to 10 as described elsewhere.[47] The following histological characteristics were evaluated: length and fusion of mucosal folds, cellular infiltration and width of the lamina propria and submucosa, enterocyte vacuolization, nucleus position within the enterocytes, and the relative number of goblet cells.

Immunohistochemistry. Detection of proliferating cell nuclear antigen (Pcna) in fixed sections of DI tissue was performed by immunohistochemistry. Sections were deparaffinized using xylene and subsequently rehydrated. Nonspecific antibody binding was reduced by incubating the sections for 20 min with 5% bovine serum albumin in Tris-buffered saline (BSA/TBS) containing normal horse serum diluted 1:50. This was followed by overnight incubation at 4 °C with the primary antibody (mouse monoclonal anti-Pcna, M0879, Dako Norge, Oslo, Norway) diluted 1:200 in 1% BSA/TBS. After being rinsed in PBS, sections were incubated with biotinylated horse antimouse secondary antibody at 1:200 in 1% BSA/TBS for 30 min. A Vectastain ABC-PO (mouse IgG) kit was used to visualize immunoreactivity. Sections were counterstained with Mayer's hematoxylin. Staining was evaluated by measuring the Pcna staining height as described elsewhere.[11]

Western Blot. Quantification of Pcna and fatty acid binding protein 2 (Fabp2) levels was performed in DI tissue samples from three fish from the control groups (FM-0 and LP-0) and from the 10 g/kg saponin groups (FM-10 and LP-10). Samples of 40 μg of protein were prepared, separated by SDS–PAGE, and blotted onto nitrocellulose membranes as previously described.[48] Membranes were incubated overnight at 4 °C with primary antibodies for the two target proteins: mouse monoclonal anti-Pcna (1:2000) and goat polyclonal anti-Fabp2 (1:4000, NB100-59746, Novus Biologicals, Littleton, CO). Primary antibodies for candidate reference proteins included rabbit polyclonal anti-glyceraldehyde-3-phosphate dehydrogenase (Gapdh; 1:250, PA1-987, Thermo Scientific, Waltham, MA) and rabbit polyclonal anti-actin (1:500, A5060, Sigma-Aldrich, St. Louis, MO). All antibodies were previously validated for use in Atlantic salmon.[48,49] After subsequent incubations with alkaline phosphatase-conjugated secondary antibodies, target and reference proteins were visualized with fluorescence by the ECF Western blotting reagent pack (GE Healthcare) and Typhoon 9200 imager system (Amersham Biosciences). ImageQuant software (Amersham Biosciences) was applied to quantify the band intensities. Both Gapdh and actin expression levels showed significant variation between diet groups and were therefore not suitable as reference proteins in the present study. Instead, total membrane protein content was visualized using a MemCode protein stain kit (Thermo Scientific) and used as a qualitative loading control.

Quantitative Real Time PCR (qPCR). RNA purification and quality control, DNase treatment, cDNA synthesis, and qPCR assays were performed as described by Kortner et al.[50] A selection of previously proposed marker genes for gut health and metabolism was profiled in DI tissue samples. Primer details are shown in the Supporting Information (Table SI 1). *gapdh*, *rnapolII* (RNA polymerase II), and *hprt1* (hypoxanthine phosphoribosyltransferase 1) were evaluated for use as reference genes as described by Kortner et al.[53] The geometric average expression of *gapdh* and *rnapolII* was used as the normalization factor. Mean normalized expression of the target genes was calculated from raw Cq values by relative quantification.[51]

Calculations. The specific growth rate (SGR) was calculated using the tank means for initial body weight (IBW) and final body weight (FBW) and calculated as follows:

$$\mathrm{SGR} = [(\ln \mathrm{FBW} - \ln \mathrm{IBW})/\text{number of days}] \times 100$$

The organosomatic index (OSI) was calculated as follows:

$$\mathrm{OSI}\ (\%) = [\text{organ weight (g)}/\text{body weight (g)}] \times 100$$

The apparent digestibility (AD) was estimated indirectly using Y_2O_3 and calculated as follows:

$$\mathrm{AD} = 100 - 100(M_{\mathrm{feed}}/M_{\mathrm{feces}})(N_{\mathrm{feed}}/N_{\mathrm{feces}})$$

where M_{feed} and M_{feces} are the concentrations (%) of marker (Y_2O_3) in the feed and feces and N_{feed} and N_{feces} are the concentrations (%) of a nutrient in the feed and feces.

The Pcna-positive proliferative compartment length (PCL) was corrected for body length (PCL_{BL}):

$$\mathrm{PCL_{BL}}\ (\mu\mathrm{m/m}) = [\mathrm{PCL}\ (\mu\mathrm{m})/\text{body length (cm)}] \times 100$$

Statistical Analysis. Data waere tested for normality and variance homogeneity using the Shapiro–Wilk *W* goodness of fit test and the Bartlett test, respectively. When necessary, data were transformed to achieve normal distribution (indicated by a superscript "†" in Table 10). Effects of the inclusion of levels of soya saponins were evaluated using regression analysis (GLM). The results were fit to polynomial models of first, second, and third degrees. The model considered to fit the results best on the basis of visual examination and the observed r^2 is reported. Comparison of basal diet effects was performed employing two-way analysis of variance (ANOVA) with the basal diet and saponin level as class variables. When interaction effects were

DOI: 10.1021/jf506242t
J. Agric. Food Chem. 2015, 63, 3887–3902

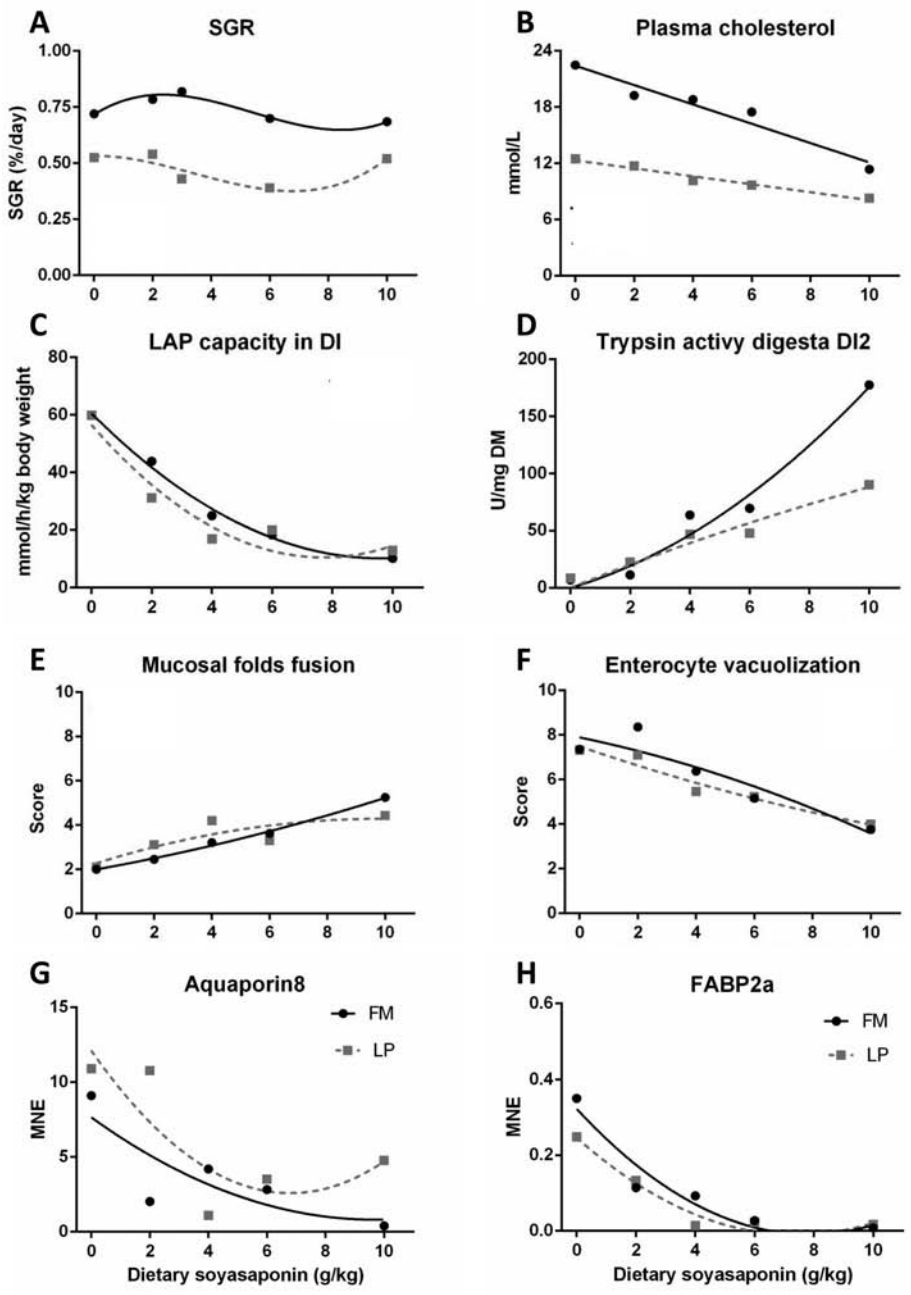

Figure 1. Illustration of relationships between level of dietary saponin supplementation (g/kg) and (A) specific growth rate (SGR; % per day), (B) plasma cholesterol level (mmol/L), (C) total capacity of leucine aminopeptidase (LAP) activity in the distal intestine (DI; mmol/h/kg of body weight), (D) trypsin activity of chyme from the DI (U/mg dry matter [DM]), (E) mucosal fold fusion in the distal intestine, (F) enterocyte vacuolization in the DI (score), (G) mean normalized expression (MNE) of *aqp8* in DI tissue, and (H) MNE of *fabp2a1* in DI tissue. The curves illustrate the regression that fits the results best for fish fed the fishmeal diet (FM; solid lines) and the diet with lupin meal (LP; dashed lines) according to the regressions shown in Tables 2, 4, and 7.

significant, one-way ANOVA and teh posthoc Tukey–Kramer HSD test were performed to aid in the interpretation of interactions.

Since histology and some qPCR data did not fulfill the requirement of normal distribution, the analysis was performed using the Wilcoxon/Kruskal–Wallis test followed by teh posthoc Steel–Dwass method to compare the means. Statistical analysis was performed using JMP statistical software (version 10, SAS Institute, United States), and graphs were made using GraphPad Prism, version 6.0 (GraphPad Software Inc., 2013). The level of significance for all analyses was set at $P < 0.05$. Results showing P values between 0.05 and 0.10 are discussed as results showing clear trends.

RESULTS

The presentation of the results is organized as follows: The response variables are grouped in subsections on the basis of their relationship regarding localization, function, and method of analysis. Within each subsection, the evaluation by regression analyses of saponin supplementation within the two basal diets is given first, followed by a comparison of the two basal diets based on the results of the two-way ANOVA. To allow interpretation of significant interaction effects, means and statistics resulting from a one-way ANOVA are also provided in the respective tables.

DOI: 10.1021/jf506242t
J. Agric. Food Chem. 2015, 63, 3887–3902

Table 2. Results of Regression Analysis of Increasing Doses of Soya Saponins on Specific Growth Rate (SGR), Nutrient Apparent Digestibility (AD), and Organosomatic Index (OSI) Data from Atlantic Salmon Fed the Experimental Diets[a]

	FM						LP					
	P (model)	R^2	intercept	X	X^2	X^3	P (model)	R^2	intercept	X	X^2	X^3
SGR	0.0277	0.76	0.71	0.087	−0.027	0.001	0.1137	0.60	0.529	0.026	−0.017	0.001
crude protein AD	0.0098	0.73	84.91	0.3201	−0.0652		0.9048	0.03	91.20	0.0288	−0.0053	
lipid AD	0.0040	0.79	95.29	−0.6398	0.0297		0.5167	0.17	96.38	0.1492	−0.021	
starch AD	0.4718	0.32	69.182	−2.093	0.624	−0.041	0.1261	0.58	66.771	1.900	−0.325	0.017
OSI stomach	0.5043	0.30	0.456	0.011	−0.003	0.0002	0.7432	0.17	0.41	0.007	−0.001	0.00006
OSI PI	0.1616	0.55	1.570	0.0649	−0.009	0.0004	0.1037	0.62	2.05	−0.192	0.0576	−0.0038
OSI MI	0.9587	0.05	0.23	0.0017	−0.0006	0.00005	0.1869	0.52	0.21	−0.029	0.0079	−0.0005
OSI DI	0.0002	0.84	0.48	−0.013			0.0143	0.54	0.45	−0.010		
OSI liver	0.0124	0.56	1.14	−0.019			0.2309	0.17	1.26	−0.008		
OSI spleen	0.2813	0.44	0.04	0.003	−0.0013	0.0001	0.4809	0.31	0.060	−0.004	0.0009	−0.00005
OSI head kidney	0.708	0.19	0.10	−0.0067	0.0013	−0.00006	0.7918	0.14	0.11	0.00407	−0.0013	0.00009
OSI gall bladder	0.0054	0.77	0.02	−0.0018	0.0001		0.8408	0.04	0.02	−0.0003	0.00004	

[a]Abbreviations: FM, fishmeal diet; LP, lupin meal diet.

Feed Acceptance and Growth Performance. During the course of the feeding trial, differences in feed acceptance of the basal diets regardless of saponin supplementation were observed visually. More feed waste was observed in the tanks of fish fed the LP diets compared to the FM diets, and this was reflected in differences in specific growth rates (Figure 1A). The regression analysis (Table 2) showed a significant cubic (third-degree) relationship between growth and soya saponin level for fish fed the FM basal diet, indicating a stimulating effect at the lower inclusion levels. Growth was similar in fish fed the FM-0 and FM-10 diets. The results did not indicate any negative effect of saponin inclusion within the investigated range of saponin inclusion. For LP-fed fish, the relationship between growth and saponin level was less clear and not significant, and no indication of a stimulating effect at low levels was observed. For fish fed the LP-0 diet, SGR was 0.53, which was 34% less than for fish fed the FM-0 diet with an SGR of 0.72 ($P < 0.0001$).

Apparent Nutrient Digestibilities (See Tables 2 and 3 and Supporting Information Tables SI 2−5). Regression analyses revealed a significant inverse relationship between the dietary saponin level and AD of crude protein and lipid, which followed a second-degree relationship; i.e., the effect became more pronounced at higher levels. The same picture was seen for amino acid ADs. For about half of the amino acids, the results fit a first-degree relationship best, while for the remainder a second-degree relationship was best. However, for crude protein and all amino acids, the effect depended on the basal diet and was clearly significant only for fish fed the FM diet. The LP diet showed significantly and substantially higher ADs for crude protein and all amino acids at all saponin supplementation levels compared to the respective FM diets. For the FM-0 and LP-0 diets the difference in AD of protein was 6%. The apparent digestibility of taurine also decreased with increasing saponin level, but again the effect was only seen in fish fed the FM basal diet. Significantly lower values were observed for fish fed the LP basal diet than those fed the FM diet. For crude lipid AD, an increasing saponin level generally decreased digestibility, but a clear effect was seen only for fish fed the FM diets. ADs of the individual fatty acids showed the same picture. In fish fed the LP diets, negative effects of saponins were observed for C16:0, with a similar trend for C18:0. Fish fed the LP diet generally showed the highest values for crude lipid and fatty acid ADs. ANOVA showed a significant interaction between basal diet and saponin level. For the FM-0 and LP-0 diets, the difference was 1%, whereas for FM-10 and LP-10 diets, the difference was 5%. No significant effect was observed for the AD of starch, either for saponin level or for basal diet. On the basis of the observed ADs of protein, lipid, and starch for diets FM-0 and LP-0, digestible energy values for the basal diets were estimated to be 20.7 and 21.8 MJ/kg, respectively. The values 23.6, 30.5, and 17.3 kJ/g were used, respectively, for the GE of protein (N × 6.25), lipid, and starch.

Table 3. Soya Saponin and Basal Diet Effects on the Apparent Digestibility (%) of Macronutrients in Atlantic Salmon Fed the Experimental Diets[a]

	crude protein	lipid	starch
Two-Way ANOVA Model			
P (model)	<0.0001	<0.0001	0.205
pooled SEM	0.55	0.46	1.28
P Values from Two-Way ANOVA			
saponin level	0.015	0.001	0.061
basal diet	<0.0001	<0.0001	0.473
interaction	0.026	0.021	0.476
Means of One-Way ANOVA			
FM-0	84.9 b	94.9 c	69
FM-2	85.4 b	94.8 c	68
FM-4	84.3 b	93.0 d	67
FM-6	85.1 b	92.1 d	70
FM-10	81.4 c	91.9 d	69
LP-0	91.0 a	96.0 abc	66
LP-2	91.8 a	97.0 ab	69
LP-4	90.4 a	97.2 a	71
LP-6	91.5 a	95.6 bc	69
LP-10	90.9 a	95.9 abc	70

[a]Abbreviations: FM, fishmeal diet; LP, lupin meal diet; 0, 2, 4, 6, 10, levels of soya saponin inclusion in diets (g/kg). Mean values with different online letters a, b, c, and d within a column are significantly different ($P < 0.05$).

Organosomatic Indices (See Table 2 and Supporting Information Table SI 6). Increasing soya saponin levels did not affect the OSI of the stomach, PI, or MI in fish fed either basal diet. The basal diet composition, on the other hand, affected these indices significantly. Fish fed the LP diet had a

DOI: 10.1021/jf506242t
J. Agric. Food Chem. 2015, 63, 3887−3902

Table 4. Results of Regression Analysis of Increasing Doses of Soya Saponins on Plasma Variables, Intestinal Mucosal Enzyme Activities, and Digesta Bile Acid Concentration and Trypsin Activity Data from Atlantic Salmon Fed the Experimental Diets[a]

	FM						LP					
	P (model)	R^2	intercept	X	X^2	X^3	P (model)	R^2	intercept	X	X^2	X^3
plasma total protein	0.090	0.31	43.68	−0.21			0.056	0.38	43.14	−0.55		
plasma total bile acids	0.009	0.59	24.80	−1.82			0.026	0.47	11.72	−066		
plasma cholesterol	<0.0001	0.91	22.40	−1.03			0.003	0.68	12.31	−0.42		
plasma triacylglycerides	0.572	0.14	3.242	0.387	−0.034		0.646	0.11	4.25	−0.09	0.002	
plasma free fatty acids	0.705	0.01	0.36	0.005			0.460	0.06	0.37	−0.003		
plasma glucose	0.256	0.46	5.723	−0.728	0.168	−0.01	0.383	0.37	4.624	0.377	−0.105	0.007
plasma phosphorus	0.860	0.11	3.996	0.090	−0.017	0.001	0.705	0.19	4.031	−0.114	0.042	−0.003
plasma sodium	0.352	0.25	164.06	−0.541	0.060		0.478	0.19	162.31	0.163	−0.051	
LAP PI capacity	0.079	0.33	209.93	2.88			0.0105	0.57	194.12	4.803		
LAP DI capacity	<0.0001	0.95	60.53	−10.468	0.543		0.0002	0.91	56.524	−11.955	0.775	
LAP PI activity	0.3201	0.41	431.68	39.131	−12.396	0.89	0.7608	0.16	361.83	16.683	−2.929	0.152
LAP DI activity	0.0002	0.84	352.8	−26.44			0.0013	0.74	345.22	−25.86		
TBA digesta-PI1	0.4588	0.33	279.14	136.22	−25.99	1.230	0.0104	0.82	533.30	−14.37	−4.266	0.455
TBA digesta-PI2	0.0048	0.78	382.99	−18.63	0.127		0.0974	0.48	366.40	−16.350	1.06	
TBA digesta-MI	0.0152	0.69	491.98	−12.825	−0.092		0.0737	0.52	461.65	−23.32	1.626	
TBA digesta-DI1	0.0041	0.66	257.83	−9.41			0.0597	0.37	234.37	−7.433		
TBA digesta-DI2	0.4163	0.22	71.055	−0.870	0.303		0.9159	0.02	69.184	0.587	−0.106	
trypsin digesta-PI1	0.2109	0.36	258.48	3.936	−0.970		0.4617	0.20	285.47	−14.567	1.066	
trypsin digesta-PI2	0.4348	0.34	160.33	−30.56	8.409	−0.576	0.2166	0.50	165.08	9.472	−3.577	0.233
trypsin digesta-MI	0.1499	0.42	108.89	−4.410	0.692		0.1898	0.38	107.81	−3.171	0.119	
trypsin digesta-DI1	0.0001	0.85	51.526	12.54			0.0384	0.43	61.315	3.690		
trypsin digesta-DI2	0.0001	0.92	5.144	5.767	1.13		0.0014	0.84	9.409	6.977	0.096	

[a]Abbreviations: FM, fishmeal diet; LP, lupin meal diet; LAP capacity, leucine aminopeptidase capacity in PI or DI; LAP activity, leucine aminopeptidase activity in PI or DI; PI, proximal intestine; DI, distal intestine; TBA digesta, total bile acid in the intestinal content in PI1, PI2, MI, DI1, or DI2; PI1, proximal section of proximal intestine; PI2, distal section of proximal intestine; MI, midintestine; DI1, proximal section of distal intestine; DI2, distal section of distal intestine; trypsin digesta, trypsin activity in the intestinal content in PI1, PI2, MI, DI1, or DI2; X, soya saponin level.

lower OSI of the stomach and MI and a higher OSI of the PI than fish fed the FM basal diet. For the DI, on the other hand, the basal diets did not affect the OSI differently, but for both, a clear negative effect of increasing soya saponin level was observed and the relationship fit a first-degree function best. The liver OSI decreased significantly for the FM fish with increasing soya saponin level, also fitting a first-degree function best. For the LP-fed fish, the relationship was not significant. The two-way ANOVA model did not show significant effects. The saponin level affected the gall bladder OSI significantly in fish fed the FM basal diet only, following a decreasing, second-degree relationship best, with a diminishing effect with increasing level. According to the results of the two-way ANOVA, there was no clear difference between the two basal diets in gall bladder OSI. Neither the spleen nor head kidney indices showed a significant relationship to soya saponin level or basal diet.

Plasma Values (see Table 4, Figure 1B, and Supporting Information Table SI 7). Increasing levels of soya saponins reduced plasma cholesterol following a first-order relationship. The magnitude of the effect, however, depended significantly on the basal diet. Fish fed the LP diet generally showed cholesterol levels 50% lower than those of fish fed the FM diet. Likewise and possibly related to the lower plasma values in general, the effect of saponin dose was less pronounced in fish fed the LP diet than fish fed the FM diet. Fish fed the FM-10 diet showed a reduction in plasma cholesterol of about 50% compared to those fed FM-0. For the LP fish the reduction was 23%. Plasma total bile acid concentrations showed a trend similar to that of the cholesterol results, but with somewhat greater variation. The effect depended on the basal diet. For fish fed the LP-0 diet, the total bile acid concentration was 35% lower than that for fish fed the FM-0 diet. The difference between fish fed the FM-0 and FM-10 diets was about 65%, whereas the decrease was 61% in fish fed the respective LP diets. The other plasma variables showed no significant effects either of soya saponin level or of basal diet.

Brush Border Membrane Leucine Aminopeptidase Activity (See Tables 4 and 5 and Figure 1C). Activities are presented as total capacity (mM/kg body weight) and specific activity (mM/mg of protein). In the PI, increasing levels of soya saponin inclusion significantly increased the total LAP capacity. The regression showed a significant first-order relationship for fish fed the LP diets, with the same trend for the FM-fed fish. In DI, the relationship was opposite and significant for both basal diets, fitting a second-degree relationship best with diminishing reductions with increasing saponin level. The specific activity was also affected by the saponin level, but only in the DI, fitting a first-order function best. Basal diet effects were also only observed on specific activity in the DI, whereas LAP capacity was not affected in any of the intestinal segments.

Total Bile Acid Concentration and Trypsin Activity in Intestinal Content (See Tables 4 and 6 and Figure 1D). Results reveal that increasing saponin levels decreased the chyme total bile acid concentration significantly in PI2, MI, and DI1 significantly for fish fed the FM diet, while a similar trend

DOI: 10.1021/jf506242t
J. Agric. Food Chem. 2015, 63, 3887−3902

Table 5. Soya Saponin and Basal Diet Effects on Leucine Aminopeptidase Total Capacity and Specific Activity in Intestinal Tissue Homogenate from the Proximal (PI) and Distal (DI) Intestine of Atlantic Salmon Fed the Experimental Diets[a]

	total capacity (mmol/h/kgfishweight)		specific activity (mmol/h/mg of tissue protein)	
	PI	DI	PI	DI
Two-Way ANOVA Model				
P (model)	0.009	<0.0001	0.005	<0.0001
pooled SEM	11.5	2.9	22.2	28.7
P Values from Two-Way ANOVA				
soya saponin level	0.001	<0.0001	0.354	<0.0001
basal diet	0.309	0.450	0.0007	0.828
interaction	0.361	0.493	0.999	0.931
Means of One-Way ANOVA				
FM-0	209	59 a	436	324 abc
FM-2	210	43 ab	449	338 ab
FM-4	236	24 cd	470	267 abcd
FM-6	217	18 cd	401	156 de
FM-10	239	10 d	477	95 e
LP-0	194	59 a	365	398 a
LP-2	200	31 bc	370	271 abcd
LP-4	224	16 cd	410	174 cde
LP-6	210	19 cd	379	201 bcde
LP-10	245	12 d	389	111 de

[a]Abbreviations: FM, fishmeal diet; LP, lupin meal diet; 0, 2, 4, 6, 10, levels of soya saponin inclusion in diets (g/kg); BW, body weight. Mean values with different online letters a, b, c, d, and e within a column are significantly different ($P < 0.05$).

was observed for the LP-fed fish. In PI2, the difference between the two basal diets was significant (significant interaction), with a more pronounced effect for fish fed the FM diet. For trypsin activity, significant effects of saponin level were observed only for the two most distal segments, DI1 and DI2, in which increasing dietary soya saponin levels increased the activity of trypsin markedly. The magnitude of the effect depended on the basal diet, with a greater effect for fish fed the FM diet. In DI1 the relationship followed a first-degree function, whereas in DI2 the effect seemed to accelerate with increasing saponin level; i.e., it fit a second-degree function better.

Morphology of the Distal Intestine (See Tables 7−9 and Figures 1E,F and 2A−C). The soya saponin level affected all the characteristics assessed and showed alterations typical for mucosal inflammation. The severity increased with increasing level of soya saponin inclusion. The effects seemed independent of the basal diet composition. The results showed decreased height and increased fusion of the mucosal folds, increased width and cellular (leucocyte) infiltration of the lamina propria and submucosa, reduced numbers of supranuclear absorptive vacuoles in enterocytes, displaced nuclei toward the apexes of the cells, and increased frequency of goblet cells in the mucosa. For all these characteristics, regression followed a second-degree relationship best, with increasing effect with increasing saponin level.

Immunohistochemical Examination of the Distal Intestine (See Table 9 and Figure 2D−F). Results of the Pcna staining indicate that increases in saponin levels significantly increased the height of the staining in the mucosal folds, regardless of the basal diet. The regression analyses showed that a second-degree function fit the results best. The height of Pcna staining did not differ for the two basal diets.

Western Blot (See Figure 3). Pcna protein levels in the DI were increased 2-fold by the 10 g/kg saponin dose, but the effect was only observed for fish fed the FM diet. In contrast, Fabp2a protein levels were significantly reduced and again only for fish fed the FM diet.

Table 6. Soya Saponin and Basal Diet Effects on Total Bile Acid Concentration and Trypsin Activity in the Digesta of Atlantic Salmon Fed the Experimental Diets[a]

	total bile acids (mg/g DM)					trypsin (U/mg DM)				
	PI1	PI2	MI	DI1	DI2	PI1	PI2	MI	DI1	DI2
Two-Way ANOVA Model										
P (model)	0.445	<0.0001	0.001	0.006	0.341	0.281	0.214	0.038	<0.0001	<0.0001
pooled SEM	87.2	21.2	24,7	17.5	13.1	29.3	17.2	8.7	14.9	12.3
P Values from Two-Way ANOVA										
saponin level	0.303	<0.0001	0.0004	0.0009	0.429	0.072	0.054	0.720	<0.0001	<0.0001
basal diet	0.239	0.134	0.172	0.315	0.272	0.604	0.150	0.050	0.002	0.017
interaction	0.670	0.012	0.154	0.638	0.217	0.667	0.739	0.025	0.001	0.001
Means of One-Way ANOVA										
FM-0	264	403 a	493 a	252 a	70	258	161	99 ab	59 b	6 c
FM-2	511	310 ab	475 ab	256 a	70	265	122	121 ab	73 b	11 c
FM-4	414	301 ab	405 ab	203 ab	74	248	143	102 ab	97 b	63 bc
FM-6	462	308 ab	438 ab	203 ab	74	255	151	95 ab	118 ab	69 bc
FM-10	269	200 b	349 b	165 ab	93	199	119	137 a	184 a	177 a
LP-0	533	362 a	456 ab	255 a	69	280	167	108 ab	64 b	8 c
LP-2	490	344 a	438 ab	231 ab	73	258	163	101 ab	74 b	22 bc
LP-4	437	321 a	376 ab	145 b	56	275	171	97 ab	67 b	46 bc
LP-6	391	298 ab	386 ab	202 ab	79	206	138	93 ab	76 b	47 bc
LP-10	417	311 ab	391 ab	173 ab	62	252	136	88 b	104 ab	90 b

[a]Abbreviations: FM, fishmeal diet; LP, lupin meal diet; 0, 2, 4, 6, 10, levels of soya saponin inclusion in diets (g/kg); DM, dry matter; PI1, proximal section of proximal intestine; PI2, distal section of proximal intestine; MI, midintestine; DI1, proximal section of distal intestine; DI2, distal section of distal intestine.

DOI: 10.1021/jf506242t
J. Agric. Food Chem. 2015, 63, 3887−3902

Table 7. Results of Increasing Doses of Soya Saponins on the Regression Analysis for Distal Intestine Histology and Gene Expression Data from Atlantic Salmon Fed the Experimental Diets[a]

	FM						LP					
	P (model)	R^2	intercept	*X*	X^2	X^3	*P* (model)	R^2	intercept	*X*	X^2	X^3
						Histology						
MF height	0.0005	0.89	8.185	−0.212	−0.018		0.0078	0.75	06.900	−0.337	0.015	
MF fusion	0.0003	0.92	2.001	0.233	0.009		0.027	0.64	2.275	0.408	−0.020	
LP width	0.0048	0.78	1.301	0.079	0.019		0.03	0.63	1.497	0.167	0.0006	
LP cellularity	0.006	0.76	1.244	0.031	0.023		0.01	0.67	1.398	0.214	−0.003	
SM width	0.007	0.76	1.092	0.072	0.018		0.026	0.65	1.368	0.184	−0.001	
SM cellularity	0.002	0.72	0.792	0.264			0.004	0.64	1.384	0.170		
ent vacuolization	0.001	0.84	7.893	−0.2711	−0.015		0.004	0.78	7.492	−0.448	0.009	
ent nucleus position	0.0006	0.88	1.672	0.410	−0.002		0.004	0.78	1.704	0.423	−0.015	
goblet cells	0.0009	0.87	1.582	0.372	−0.06		0.0005	0.88	1.559	0.397	−0.008	
						Gene Expression						
cd4α	0.08	0.51	0.0009	−0.0001	1.527×10^{-5}		0.42	0.22	0.0008	6.978×10^{-6}	−0.000007	
cd8ß	0.46	0.20	0.0312	0.0001	4.617×10^{-5}		0.37	0.24	0.0322	0.0017	−0.0001	
tcrγ	0.74	0.18	0.0072	−0.0004	0.00003	2.56×10^{-7}	0.06	0.67	0.0064	0.0013	−0.0003	−0.00002
mhcI	0.62	0.24	1.4474	0.0722	−0.027	0.0016	0.90	0.08	1.2925	0.1934	−0.0513	0.0033
il-1ß	0.051	0.57	0.0023	−0.001	0.0001		0.64	0.12	0.0019	4.984×10^{-5}	5.96×10^{-6}	
il-17a	0.071	0.53	0.0011	−0.0002	0.00019		0.56	0.15	0.0017	0.0017	−0.0001	
ifnγ	0.046	0.71	0.0008	0.0005	−0.0001	0.000007	0.24	0.48	0.0018	−0.0003	0.0002	−0.00002
gilt	0.005	0.78	25.556	1.7998	−0.279		0.46	0.20	27.667	−0.023	−0.0362	
par2a	0.41	0.36	0.2464	0.0197	−0.0019	0.00001	0.23	0.48	0.2609	0.0367	−0.0069	0.00034
par2b	0.58	0.14	0.0536	−0.0010	0.0001		0.84	0.05	0.0570	0.0004	-8.113×10^{-5}	
try	0.04	0.73	0.0002	0.0002	−0.00006	0.000004	0.64	0.23	0.0005	−0.0001	0.00002	−0.000001
myd88	0.006	0.76	0.0550	0.0002	0.0002		0.15	0.42	0.0603	0.0026	−0.0001	
pcna	0.32	0.42	0.2002	−0.0041	−0.0011	0.0001	0.63	0.24	0.1934	−0.0074	0.0033	−0.0002
mmp13	0.02	0.68	0.0158	−0.0057	0.0012		0.22	0.35	0.0101	0.0099	−0.0007	
muc2	0.08	0.52	8.1271	−0.7806	0.0819		0.63	0.12	11.407	−0.560	0.0479	
aqp8ab	0.19	0.37	7.6597	−1.413	0.0729		0.02	0.64	12.118	−2.805	0.2064	
fabp2a1	0.07	0.53	0.3218	−0.0843	0.0053		0.04	0.58	0.2460	−0.0694	0.0046	
fxr	0.70	0.19	0.0130	0.0006	−0.0002	0.00001	0.57	0.26	0.0144	0.0020	−0.0004	0.00002

[a]Abbreviations: FM, fishmeal diet; LP, lupin meal diet; MF, mucosal fold; LP, lamina propria; SM, submucosa; ent, enterocyte; *il-17A*, interleukin 17A; *ifnγ*, interferon *γ*; *il-1β*, interleukin 1*β*; *muc2*, mucin-2; *aqp8ab*, aquaporin 8ab; *fabp2a1*, fatty acid binding protein 2a1, *try*, trypsin; *cd4α*, cluster of differentiation 4*α*; *gilt*, interferon *γ*-inducible lysosomal thiol reductase; *pcna*, proliferating cell nuclear antigen; *cd8β*, cluster of differentiation 8*β*; *par2a*, proteinase-activated receptor 2a; *par2b*, proteinase-activated receptor 2b; *mhcI*, mhc class 1; *myd88*, myeloid differentiation factor 88; *tcrγ*, T-cell receptor *γ*; *fxr*; farnesoid x receptor; *mmp13*, matrix metallopeptidase 13; *X*, soya saponin level.

J. Agric. Food Chem. 2015, 63, 3887−3902

DOI: 10.1021/jf506242t

Table 8. Soya Saponin and Basal Diet Effects on Histological Evaluation of the Distal Intestine of Atlantic Salmon Fed the Experimental Diets[a]

	mucosal folds		lamina propria		submucosa		enterocytes		goblet cells
	height	fusion	width	cellular infiltration	width	cellular infiltration	vacuolization	nucleus position	relative nr
P value	<0.0001	<0.0001	<0.0001	<0.0001	<0.0001	<0.0001	<0.0001	<0.0001	<0.0001
pooled SEM	0.2	0.3	0.2	0.2	0.2	0.2	0.2	0.2	0.2
FM-0	8.0 a	2.0 de	1.3 e	1.3 e	1.2 d	1.1 d	7.4 ab	1.9 d	1.8 c
FM-2	8.1 a	2.5 cd	1.4 de	1.3 e	1.1 d	1.1 d	8.4 a	1.9 d	1.8 c
FM-4	7.2 a	3.2 bce	2.3 cd	2.0 bc	1.9 c	1.9 c	6.8 bc	3.7 bc	3.3 b
FM-6	5.8 c	3.6 abc	2.3 cd	2.1 cd	2.1 bc	2.0 bc	5.2 d	4.0 ab	3.6 b
FM-10	4.3 c	5.3 a	4.1 a	4.0 a	3.7 ab	3.7 ab	3.8 e	5.5 a	4.7 ab
LP-0	7.0 ab	2.1 d	1.4 de	1.3 de	1.3 d	1.3 d	7.3 ab	1.7 d	1.5 c
LP-2	7.0 ab	2.8 bcd	1.5 de	1.5 de	1.6 cd	1.6 cd	7.9 a	1.7 d	1.9 c
LP-4	5.3 cd	4.2 ab	2.7 abc	2.7 abc	2.7 abc	2.7 abc	5.5 cde	3.6 bc	3.4 b
LP-6	5.9 bc	3.3 abcd	1.9 cde	2.0 bcd	1.9 cd	1.9 bcd	5.2 cd	3.3 c	3.3 b
LP-10	4.9 cd	4.2 ab	3.4 ab	3.3 a	3.2 a	3.2 a	4.0 de	4.5 ab	4.8 a

[a]Abbreviations: FM, fishmeal diet; LP, lupin meal diet; 0, 2, 4, 6, 10, levels of soya saponin inclusion in diets (g/kg). Data were analyzed using the Wilcoxon/Kruskal–Wallis test followed by the posthoc Steel–Dwass method. Mean values with different online letters a, b, c, d, and e within a column are significantly different ($P < 0.05$).

Table 9. Soya Saponin and Basal Diet Effects on Pcna Staining Height Analysis of the Distal Intestine of Atlantic Salmon Fed the Experimental Diets[a]

	Pcna measurements	
	PCL (μm)	PCL_{BL} (μm/m)
Two-Way ANOVA Model		
P (model)	<0.0001	<0.0001
pooled SEM	14	31
P Values from Two-Way ANOVA		
saponin level	<0.0001	<0.0001
basal diet	0.136	0.106
interaction	0.612	0.31
Means of One-Way ANOVA		
FM-0	124 c	300 d
FM-2	137 c	336 cd
FM-4	133 c	336 cd
FM-6	186 abc	475 abc
FM-10	240 a	614 a
LP-0	126 c	320 d
LP-2	128 c	322 d
LP-4	132 c	334 cd
LP-6	162 bc	403 bcd
LP-10	205 ab	519 ab

[a]Abbreviations: FM, fishmeal diet; LP, lupin meal diet; 0, 2, 4, 6, 10, levels of soya saponin inclusion in diets (g/kg); PCL, Pcna-positive proliferative compartment length; PCL_{BL}, Pcna-positive proliferative compartment length corrected for body length. Mean values with different online letters a, b, c, and d within a column are significantly different ($P < 0.05$).

Gene Expression (See Tables 7, 10, and 11 and Figure 1G,H). Among the immune-related transcripts, interleukin 17a (*il-17a*), interferon γ (*ifnγ*), and myeloid differentiation factor 88 (*myd88*) were significantly increased with increasing saponin levels, and interleukin1β (*il-1β*) and matrix metalloproteinase 13 (*mmp13*) displayed a similar trend. For *il-17a*, the effect was apparent only in fish fed the FM diet as indicated by the significant interaction. The posthoc test based on the results of the one-way ANOVA showed that the effect became pronounced only at the highest saponin inclusion level, i.e., for fish fed FM-10. The FM-10 group also showed the numerically highest values for the other above-mentioned transcripts. Increasing saponin levels down-regulated the expression of *aqp8ab* (Figure 1G), *fabp2a1* (Figure 1H), and interferon γ-inducible lysosomal thiol reductase (*gilt*). For *aqp8ab* this effect seemed to depend on the basal diet with somewhat different dose–response curves for the two. Comparison of the two basal diets showed that fish fed the LP diets presented higher expression of *ifnγ* and mucin 2 (*muc2*) than fish fed the FM diets. For the other expression variables, no significant differences were observed.

DISCUSSION

The data reveal that 2–4 g/kg soya saponins in diets from a 95% purified source elicited signs of inflammation in the DI of Atlantic salmon without the presence of other legume components. Supplementation with 2 g/kg modified some functional characteristics, while a level between 2 and 4 g/kg appeared to be needed to induce signs of inflammatory changes. However, inclusion levels as low as 8% SBM have previously caused inflammation with concomitant digestive dysfunction,[9] which translates to a saponin level of ca. 0.4–0.6 g/kg in the diet. This is 70–80% lower than the lowest supplementation of 2 g/kg diet in the current study. Additionally, for several of the observed variables, such as enterocyte vacuolization, mucosal fold fusion, and Fabp2a, the dose–response effect did not clearly differ between the saponin-supplemented FM and LP diets, despite the apparent difference in feed intake and therefore saponin exposure. Thus, the saponin supplementation was more potent in the LP than the FM basal diet, most likely due to interactions with other lupin components. Therefore, the current study substantiates previous suggestions that the induction of inflammation by soya saponins is potentiated by other ANFs, antigens, or other components in SBM and other legumes such as peas and lupins.[16,19,20]

Effects of Basal Diet Composition. The observed, although not quantified, differences in feed intake, which are most likely the major cause of the differences in growth observed between fish fed the two basal diets along with the implicit underlying differences in digestive and metabolic

DOI: 10.1021/jf506242t
J. Agric. Food Chem. 2015, 63, 3887–3902

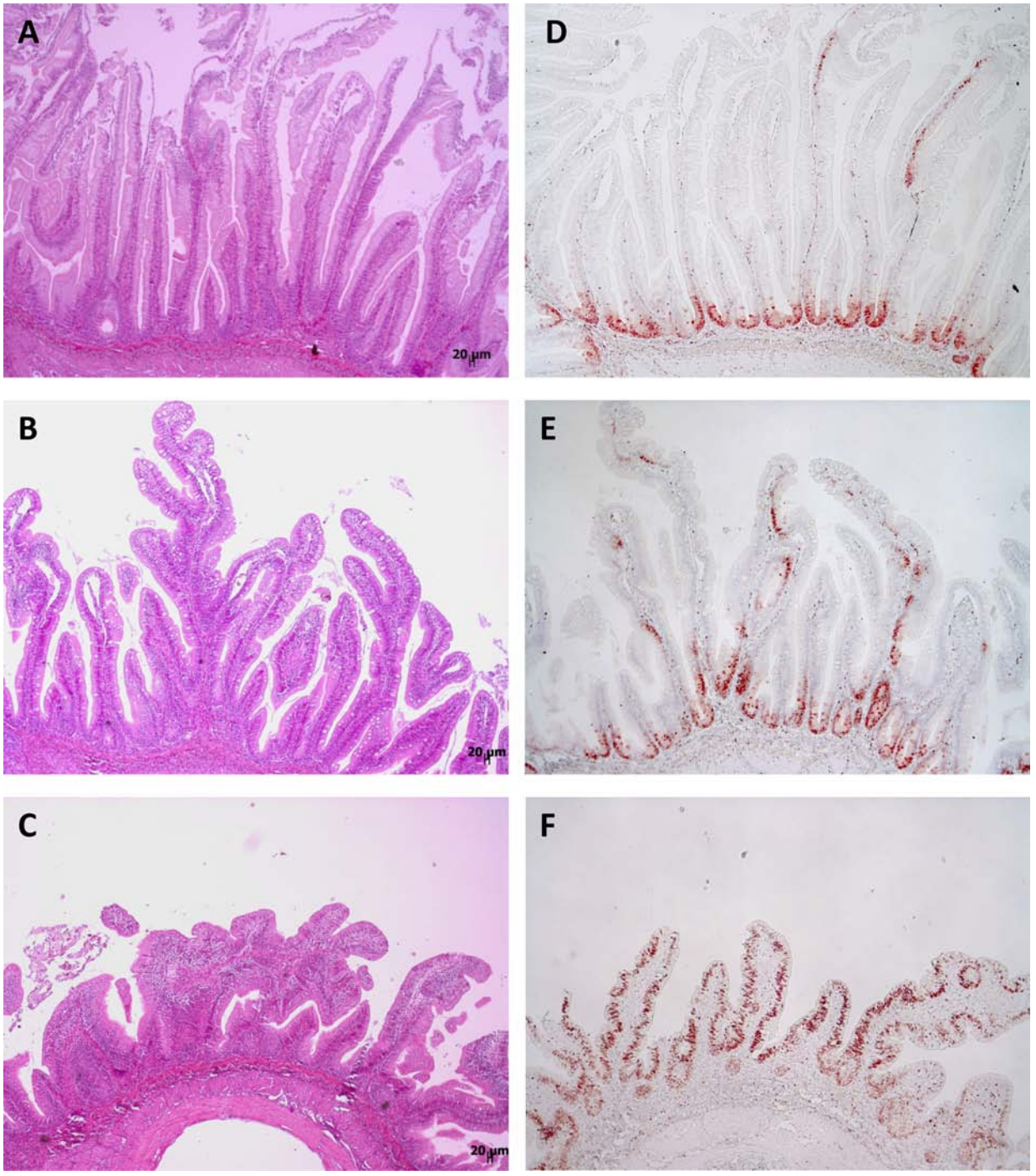

Figure 2. (A–C) Representative histomorphological images from hematoxylin and eosin-stained sections of the distal intestine of Atlantic salmon depicting the dose-dependent increase in the severity of the inflammatory changes with increasing soya saponin supplementation in fish fed the FM-0 (A), FM-6 (B), and FM-10 (C) diets. (D–F) Representative images of the localization and distribution of immunohistochemically labeled proliferating cell nuclear antigen (Pcna) protein in the epithelial cells of the distal intestine of Atlantic salmon depicting the dose-dependent increase in the relative number of proliferating cells with increasing soya saponin supplementation considered low for the FM-0 diet (D), moderately elevated for the FM-6 diet (E), and highly elevated for the FM-10 diet (F). FM = fishmeal diet, and 0, 6, and 10 indicate the levels of soya saponin inclusion in the diets (g/kg).

aspects, makes integration of results from the two groups challenging. The macronutrient digestibilities were generally higher for the LP than the FM diet. The estimates of digestible energy of the basal diets based on the ADs resulted in values of 20.7 and 21.8 MJ/kg for FM-0 and LP-0, respectively. Fish fed the LP-0 diet grew 32% less than those fed the FM-0 diet. Assuming their energy needs to be 17–19 MJ GE/kg of growth,[56] feed consumption is estimated at 230–250 g for the LP diet and 360–400 g for the FM diet. Thus, the LP-fed fish ate ca. 36% less. Lupins contain bitter alkaloids, which may be the cause of the low feed intake in the LP fed fish.[57,58] The lupin alkaloids, however, seem not to affect fish health importantly,[57−60] as supported by the present study.

DOI: 10.1021/jf506242t
J. Agric. Food Chem. 2015, 63, 3887−3902

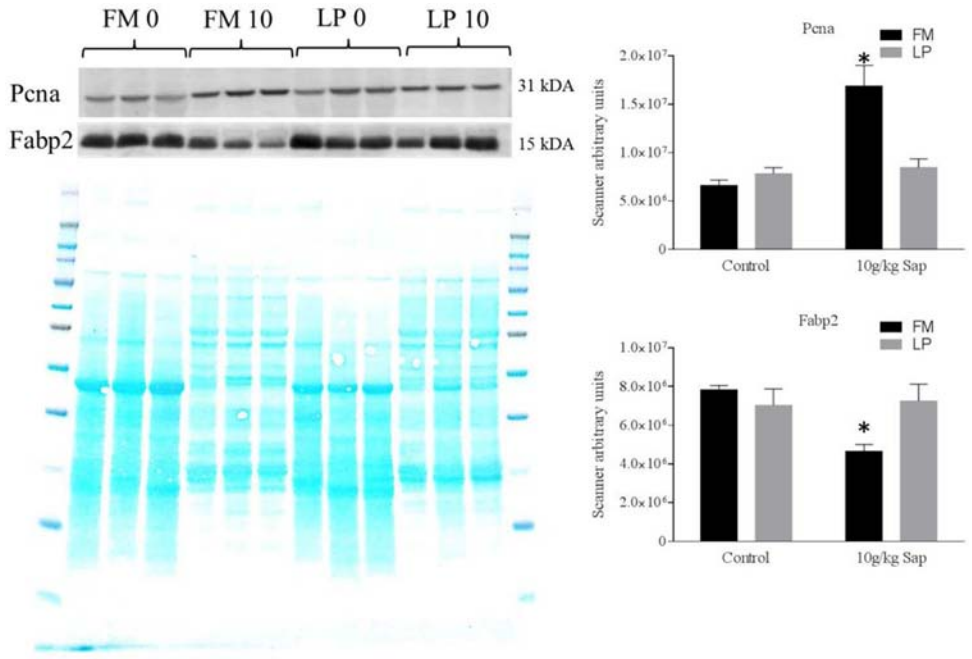

Figure 3. Western blot analysis of proliferating cell nuclear antigen (Pcna) and fatty acid binding protein 2 (Fabp2) proteins in the distal intestinal tissue of fish fed the four diets FM-0, FM-10, PM-0, and PM-10. Immunoblots are shown for $n = 3$ individual fish per diet group. The corresponding total protein stain is shown in blue below each individual blot. Relative staining intensity values in the columns of the graphs are means of the $n = 3$ fish per diet, with their standard errors represented by vertical bars. Asterisks denote saponin diet groups that are significantly different from their respective control diet groups.

The higher nutrient ADs for the LP-fed fish may at least partly be explained by the apparent difference in feed intake, which have been reported to decrease with increasing feed intake.[61,62] However, reported effects of feed intake are in general rather small. The 6% difference in protein AD in the present study was therefore remarkably high, and can only be explained by a higher protein digestibility of the plant meals in the LP diet, i.e., lupin and wheat gluten, compared to the fishmeal in the FM diet. Experience has indicated that protein digestibility may vary greatly among fishmeals, most likely due to differences in the quality of the raw materials, ash content, and processing conditions such as heat treatment.[63]

The lower relative weights of the stomach, MI, DI, and liver in the LP-fed fish were most likely also due to lower feed intake.[64] However, the higher PI weight, the section of the digestive tract that is responsible for the majority of nutrient absorption,[65] may be a result of (1) a higher concentration of digestible nutrients that can stimulate tissue growth and/or (2) a compensatory response to challenges to the digestive processes linked to fibers and possibly other ANFs in lupins. Fiber-rich diets have been shown to induce growth of intestinal tissues in Atlantic salmon[66] and cod,[67] possibly due to a need for a larger absorptive surface area when the volume of the chyme increases due to swelling of the fiber. Growth stimulation by fermentation products produced from the fibers in the digestive tract is another possible mechanism.[68,69] In any case, the effects on PI weight were clearly greater than any diminishing effect of reduced feed intake could be expected to be.

Plasma cholesterol and bile salt levels also differed markedly between the fish fed the two basal diets, with lower values in the LP-fed fish, which can again be explained by lower feed intake and lower diet cholesterol levels in this diet. However, this is also a commonly observed response to plant feed ingredients and foods, with their contents of fibers, phytosterols, phytoestrogens, and saponins all affecting cholesterol and bile salt absorption (reviewed by Krogdahl et al.[18]). In fish, low cholesterol and bile acid absorption and metabolism have been suggested to be a cause of the frequently observed reductions in lipid digestibility of plant ingredients, in particular standard SBM.[70] In the present experiment, however, lipid ADs did not significantly differ between the LP- and the FM-fed fish, although apparent lower feed intake in the LP-fed fish may have masked any negative effects.

Effects of Saponins. Under the condition that the difference in growth was due to a difference in feed intake, saponin exposure would have been lower in the LP fish. On the basis of feed intake estimates (see above), exposures of supplemented saponins were 0, 1.1, 1.7, 2.4, and 5.1 g/kg initial body weight for the fish fed the LP-0 to LP-10 diets and 0, 1.8, 3.8, 4.7, and 7.5 g/kg initial body weight for the FM-0 to FM-10 diets. For the LP diets the estimates are most likely lower than the actual values as the natural saponin contents of the lupins were not taken into account. However, the low levels reported in lupin seeds[36,37] can be considered negligible in this context, adding less than 0.1 g/kg to the LP diet, i.e., less than 5% of the supplementation level of the LP-2 diet. Since current tools used for saponin analysis lack accuracy,[39] saponin analysis was not performed.

On the basis of the above considerations, it might be argued that saponin effects should be evaluated on the basis of exposure, e.g., expressed per unit of fish weight, rather than level in the diet. Similarly, estimates of acceptable dose should also be based on exposure per unit of fish weight. However, the apparent difference in feed intake most likely interacted several ways with saponin effects, making a discussion based on saponin intake very difficult and its value questionable. The discussion on the effects of saponin exposure below is therefore

DOI: 10.1021/jf506242t
J. Agric. Food Chem. 2015, 63, 3887−3902

Table 10. Soya Saponin and Basal Diet Effects on Gene Expression Analysis of the Distal Intestine of Atlantic Salmon Fed the Experimental Diets[a]

	cd4α	*cd8ß*	*mhcI*	*il-1ß*†	*Il-17a*†	*ifnγ*†	*gilt*	*par2a*	*par2b*	*try*	*pcna*	*muc2*	*aqp8ab*†	*fabp2a1*†
						Two-Way ANOVA Model								
P (model)	0.369	0.423	0.529	0.082	0.003	0.005	0.035	0.530	0.679	0.515	0.862	0.004	0.005	<0.0001
pooled SEM	0.0001	0.003	0.222	0.002	0.004	0.0007	2.57	0.022	0.005	8.11×10^{-5}	0.018	0.916	2.100	0.091
						P Values from Two-Way ANOVA								
saponin level	0.232	0.215	0.388	0.027	0.001	0.026	0.011	0.564	0.992	0.885	0.689	0.922	0.003	<0.0001
basal diet	0.788	0.459	0.653	0.963	0.909	0.007	0.343	0.182	0.388	0.240	0.802	0.0005	0.057	0.787
interaction	0.204	0.405	0.269	0.162	0.042	0.188	0.212	0.973	0.398	0.364	0.485	0.560	0.120	0.333
						Means of One-Way ANOVA								
FM-0	0.0009	0.031	1.4	0.0017	0.0005 b	0.0008 b	26	0.25	0.055	0.0002	0.20	8.1 bc	9.1 a	0.34 a
FM-2	0.0008	0.031	1.5	0.0019	0.001 ab	0.0016 ab	26	0.26	0.047	0.0005	0.18	6.9 ab	2.0 ab	0.11 abc
FM-4	0.0008	0.032	1.3	0.0019	0.006 ab	0.0018 ab	28	0.31	0.055	0.0003	0.18	5.8 b	4.2 ab	0.09 abcd
FM-6	0.0007	0.034	1.2	0.0015	0.004 ab	0.0018 ab	27	0.28	0.051	0.0002	0.17	6.8 ab	2.8 ab	0.02 abcd
FM-10	0.001	0.037	1.1	0.010	0.018 a	0.002 ab	15	0.26	0.057	0.0004	0.22	8.4 ab	0.4 b	0.008 d
LP-0	0.0008	0.032	1.2	0.0021	0.001 ab	0.0017 ab	27	0.26	0.056	0.0005	0.19	11.9 a	10.9 a	0.24 ab
LP-2	0.0008	0.033	1.7	0.0016	0.003 ab	0.0023 ab	28	0.30	0.060	0.0003	0.19	8.8 ab	10.7 a	0.13 abc
LP-4	0.001	0.039	1.1	0.0029	0.008 ab	0.0027 ab	26	0.32	0.054	0.0004	0.19	11.8 a	1.1 ab	0.01 cd
LP-6	0.0009	0.035	1.4	0.0021	0.001 ab	0.004 a	25	0.30	0.057	0.0004	0.21	8.9 ab	3.5 ab	0.02 bcd
LP-10	0.0008	0.033	1.4	0.0031	0.003 ab	0.0026 ab	24	0.28	0.053	0.0004	0.18	10.6 ab	4.7 a	0.01 bcd

[a]Abbreviations: FM, fishmeal diet; LP, lupin meal diet; 0, 2, 4, 6, 10, levels of soya saponin inclusion in diets (g/kg); †, log-transformed data; *cd4α*, cluster of differentiation 4*α*; *cd8β*, cluster of differentiation 8*β*; *mhcI*, major histocompatibility class 1; *il-1β*, interleukin 1*β*; *il-17a*, interleukin 17a; *ifnγ*, interferon *γ*; *gilt*, interferon *γ*- inducible lysosomal thiol reductase; *par2a*, proteinase-activated receptor 2a; *par2b*, proteinase-activated receptor 2b; *try*, trypsinogen; *pcna*, proliferating cell nuclear antigen; *muc2*, mucin-2; *aqp8ab*, aquaporin 8ab; *fabp2a1*, fatty acid binding protein 2a. Mean values with different online letters a, b, c, d, and e within a column are significantly different ($P < 0.05$).

J. Agric. Food Chem. 2015, 63, 3887−3902 DOI: 10.1021/jf506242t

Table 11. Soya Saponin and Basal Diet Effects on Gene Expression Analysis of the Distal Intestine of Atlantic Salmon Fed the Experimental Diets[a]

	tcrγ	*myd88*	*mmp13*	*fxr*
	Wilcoxon/Kruskal–Wallis Test			
P value	0.193	0.036	0.060	0.445
pooled SEM	0.0007	0.004	0.015	0.001
	Mean Values			
FM-0	0.0070	0.054	0.012	0.0129
FM-2	0.0072	0.055	0.015	0.0138
FM-4	0.0052	0.065	0.016	0.0127
FM-6	0.0064	0.062	0.019	0.0128
FM-10	0.0066	0.086	0.083	0.0154
LP-0	0.0064	0.061	0.015	0.0143
LP-2	0.0078	0.059	0.017	0.0170
LP-4	0.0079	0.072	0.036	0.0165
LP-6	0.0070	0.068	0.048	0.0157
LP-10	0.0089	0.068	0.028	0.0155

[a]Abbreviations: FM, fishmeal diet; LP, lupin meal diet; 0, 2, 4, 6, 10, levels of soya saponin inclusion in diets (g/kg); *tcrγ*, T-cell receptor γ; *myd88*, myeloid differentiation factor 88; *mmp13*, matrix metallopeptidase 13; *fxr*; farnesoid x receptor. Data were analyzed using the Wilcoxon/Kruskal–Wallis test followed by the posthoc Steel–Dwass method.

mainly based on the responses seen for the FM-fed fish. Comments regarding effects in the fish fed the LP diet are reserved for response variables of particular importance. Absence of saponin effects in LP fish, as compared to FM fish, is not discussed when they were most likely a result of low saponin exposure.

Low levels of saponin exposure stimulated growth in the FM group, an effect which may have been due to increasing feed intake, or some metabolic or physiological effects. As for other toxins and stressors generally considered detrimental for health at higher doses, the apparently beneficial effects observed at low levels of saponin exposure can be considered a hormetic response. This may also be related to the immune-stimulating effects of saponin's adjuvant characteristics.[28−30,38] The apparent absence of such positive effects in LP-fed fish may be explained by antagonistic, possibly potentiating effects of other lupin components. The apparent lack of a significant effect of soya saponin exposure on growth for either basal diet group is in line with indications from other studies investigating similar saponin preparations in fish feed.[16,19]

The observed negative effects of higher saponin exposure on nutrient digestibilities are in agreement with the results of the work of Chikwati et al.[19] investigating the effect of adding 2 g/kg soya saponin to diets with different plant ingredients. However, in this earlier work, the saponin effects depended on the plant ingredient included in the diet and were significant for a diet containing pea protein concentrate, but not for the other diets with sunflower, horse beans, and rapeseed meal as alternative ingredients. The suggested explanation was differences in saponin level between the plant ingredients, as peas contain more saponins than the others, or other potentiating components in the pea meal.[19]

The mechanisms behind effects of saponin exposure on nutrient ADs may be related to reductions in cholesterol and bile salt levels in intestinal content and subsequently in plasma. Saponin binding to 3-β-hydroxysteroids such as cholesterol forms insoluble, nonabsorbable complexes and increases their excretion,[22,25,71] which alters the normal metabolic pathways of cholesterol and total bile acid production.[50] Thus, the current data support previous investigations suggesting that saponins are at least partially responsible for the drop in plasma cholesterol levels in several animal species fed plant meal diets.[23,25−27,50] Moreover, bile salts have the ability to stabilize pancreatic proteolytic enzymes (reviewed by Krogdahl et al.[18]). Accordingly, a reduction in chyme bile salt concentration may cause reduced protein digestibility, as observed at the highest level of saponin supplementation in the present study. The marked reduction in LAP activity in the DI may also have played a role in the saponin effect on protein and amino acid ADs.

The present study clearly demonstrated that soya saponins alone, supplemented at levels of 2−4 g/kg of diet and above, caused a dose-dependent increase in the severity of inflammatory changes in the DI tissue as described for SBMIE in salmonids,[6,8,9,13,19] strongly suggesting the involvement of saponins as a causatory agent. At the lowest saponin inclusion level, the effects were small, but trends were clearly observed for increased width and cellular infiltration in lamina propria and submucosa. The reductions in DI somatic index and digestive enzyme activities as well as marked reductions in gene expression for various functional proteins (see below) are signs of dysfunction caused by the inflammation and may be directly linked to the shortening of the mucosal folds, which has been suggested to be related to the increase in cell turnover with concomitant increases in proliferation, migration, and apoptosis observed in Atlantic salmon fed SBM.[11,13,72] These phenomena were apparent in the present study as well, as supported by data regarding mucosal fold height and Pcna protein expression in the DI tissue.

At the gene expression level in the DI, alterations observed at the higher saponin inclusion levels in the present study correspond well with the more convincingly up- or down-regulated genes reported for salmon with SBMIE.[52,54] Among these were genes related to recruitment and/or differentiation of inflammatory cells, i.e., *il-17a*, *ifnγ*, and *il-1β* in the FM-10 group and remodeling of the extracellular matrix as suggested by induction of *mmp13*. The cytokine *il-17a* has been suggested as a sensitive molecular marker for SBMIE[52] and may be a candidate marker for exposure to high levels of soya saponins as well, since transcript levels displayed a >30-fold induction in the FM-10 group. Other immune-related genes previously reported to be differentially regulated during SBMIE, but often less convincingly than those mentioned above,[10,52,54] were not significantly or dose-dependently affected in the current study. These include *par2a*, *par2b*, *tcrγ*, *cd4α*, *cd8β*, *gilt*, *mhcI*, *myd88*, *fxr*, and *muc2*. This may further support the theory that other SBM components may work synergistically with saponins to illicit a full inflammatory response.

Among functional transcript markers, *fabp2a1* for fatty acid binding protein and *aqp8ab* for one of the aquaporins were found to be strongly and dose-dependently down-regulated by soya saponin inclusion in both basal diets. A corresponding reduction in Fabp2 protein level was observed for the FM-10 group. These responses in Fabp2 protein and mRNA levels have also been observed during SBMIE[49,73] and inflammation caused by the combination of pea protein concentrate and 2 g/kg soya saponins.[20] Reduced Fabp2 levels could explain the decreased lipid ADs typically observed in fish fed SBM.[49] The transcriptional expression of *aqp8ab* also displayed marked suppression with increasing soya saponin levels for both basal

DOI: 10.1021/jf506242t
J. Agric. Food Chem. 2015, 63, 3887−3902

diets. This response has previously been observed in salmon with DI inflammation[20,73] and in mammals with intestinal inflammation.[74,75] In these latter studies, down-regulation of *aqp8* was concomitant with decreases in the absorption of water, suggesting a possible role of aquaporins in the pathogenesis of diarrhea accompanying intestinal inflammatory disease.

The observation of progressively increasing trypsin activity of the intestinal content supports earlier findings in salmonids,[9,55] as well as in other animals and humans,[76,77] and suggests that this variable is a good marker candidate for inflammation in the DI. In mammals, such increases in chyme trypsin activity of the distal compartments of the intestine have been shown to activate PAR-2, which mediates pro-inflammatory effects in the colon of mammals.[78,79] It may also be partly explained by decreased ability of the more immature or damaged epithelial cells to reabsorb pancreatic enzymes.[66,72]

■ ASSOCIATED CONTENT

Supporting Information

Primer pair sequence efficiency, amplicon size, and annealing temperature for the genes used for real-time PCR (Table SI 1), results of regression analysis of increasing doses of soya saponins on amino acid and fatty acid apparent digestibility (AD) data (Table SI 2), and soya saponin and basal diet effects on apparent digestibility (%) of essential amino acids (Table SI 3), nonessential amino acids and taurine (Table SI 4), and fatty acids (Table SI 5), on organosomatic indices (OSI) (Table SI 6), and on plasma parameters (Table SI 7). This material is available free of charge via the Internet at http://pubs.acs.org.

■ AUTHOR INFORMATION

Corresponding Author

*E-mail: ashild.krogdahl@nmbu.no. Phone: +47 2296 4534. Fax: +47 2259 7310.

Author Contributions

The contributions of the authors were as follows: Å.K., leadership, experimental design, data evaluation and interpretation, manuscript development; K.G., morphological evaluation, gene expression, statistical analysis, manuscript writing; M.P., experimental design, sampling, statistical analysis; T.M.K., gene expression analyses, Western blot; M.G., sampling, morphological evaluation, immunohistochemistry; G.M.B., feeding trial, sampling; A.M.B., experimental design, data evaluation and interpretation, manuscript development and review.

Notes

The authors declare no competing financial interest.

■ ACKNOWLEDGMENTS

We thank the animal technicians at Nofima's marine research station at Sunndalsøra, Norway, for their dedicated animal care and Ellen K. Hage at the NMBU School of Veterinary Medicine for organizing the sampling and skillful laboratory work.

■ REFERENCES

(1) Gatlin, D. M.; Barrows, F. T.; Brown, P.; Dabrowski, K.; Gaylord, T. G.; Hardy, R. W.; Herman, E.; Hu, G.; Krogdahl, Å.; Nelson, R.; Overturf, K.; Rust, M.; Sealey, W.; Skonberg, D.; Souza, E. J.; Stone, D.; Wilson, R.; Wurtele, E. Expanding the utilization of sustainable plant products in aquafeeds: a review. *Aquacult. Res.* **2007**, *38*, 551−579.

(2) Hardy, R. W. Alternate protein sources for salmon and trout diets. *Anim. Feed Sci. Technol.* **1996**, *59*, 71−80.

(3) Bureau, D. P.; Harris, A. M.; Cho, C. Y. The effects of purified alcohol extracts from soy products on feed intake and growth of chinook salmon (*Oncorhynchus tshawytscha*) and rainbow trout (*Oncorhynchus mykiss*). *Aquaculture* **1998**, *161*, 27−43.

(4) Kaushik, S. J.; Cravedi, J. P.; Lalles, J. P.; Sumpter, J.; Fauconneau, B.; Laroche, M. Partial or total replacement of fish meal by soybean protein on growth, protein utilization, potential estrogenic or antigenic effects, cholesterolemia and flesh quality in rainbow trout (*Oncorhynchus mykiss*). *Aquaculture* **1995**, *133*, 257−274.

(5) Olli, J. J.; Krogdahl, Å. Nutritive value of four soybean products as protein sources in diets for rainbow trout (*Oncorhynchus mykiss*, Walbaum) reared in fresh water. *Acta Agric. Scand., A: Anim. Sci.* **1994**, *44*, 185−192.

(6) Van den Ingh, T. S. G. A. M.; Krogdahl, Å.; Olli, J. J.; Hendriks, H. G. C. J. M.; Koninkx, J. G. J. F. Effects of soybean-containing diets on the proximal and distal intestine in Atlantic salmon (*Salmo salar*)—a morphological study. *Aquaculture* **1991**, *94*, 297−305.

(7) Van den Ingh, T. S. G. A. M.; Olli, J. J.; Krogdahl, Å. Alcohol-soluble components in soybeans cause morphological changes in the distal intestine of Atlantic salmon, *Salmo salar* L. *J. Fish Dis.* **1996**, *19*, 47−53.

(8) Baeverfjord, G.; Krogdahl, Å. Development and regression of soybean meal induced enteritis in Atlantic salmon, *Salmo salar* L., distal intestine: a comparison with the intestines of fasted fish. *J. Fish Dis.* **1996**, *19*, 375−387.

(9) Krogdahl, Å.; Bakke-McKellep, A. M.; Baeverfjord, G. Effects of graded levels of standard soybean meal on intestinal structure, mucosal enzyme activities, and pancreatic response in Atlantic salmon (*Salmo salar* L.). *Aquacult. Nutr.* **2003**, *9*, 361−371.

(10) Bakke-McKellep, A. M.; Frøystad, M. K.; Lilleeng, E.; Dapra, F.; Refstie, S.; Krogdahl, Å.; Landsverk, T. Response to soy: T-cell-like reactivity in the intestine of Atlantic salmon, *Salmo salar* L. *J. Fish Dis.* **2007**, *30*, 13−25.

(11) Bakke-McKellep, A. M.; Penn, M. H.; Salas, P. M.; Refstie, S.; Sperstad, S.; Landsverk, T.; Ringø, E.; Krogdahl, Å. Effects of dietary soyabean meal, inulin and oxytetracycline on intestinal microbiota and epithelial cell stress, apoptosis and proliferation in the teleost Atlantic salmon (*Salmo salar* L.). *Br. J. Nutr.* **2007**, *97*, 699−713.

(12) Bakke-McKellep, A. M.; Frøystad, M. K.; Koppang, E. O.; Krogdahl, Å. A soybean-induced enteritis: pathophysiological response of the salmon intestine. *FASEB J.* **2005**, *19*, A760.

(13) Bakke-McKellep, A. M.; Press, C. M.; Baeverfjord, G.; Krogdahl, Å.; Landsverk, T. Changes in immune and enzyme histochemical phenotypes of cells in the intestinal mucosa of Atlantic salmon, *Salmo salar* L., with soybean meal-induced enteritis. *J. Fish Dis.* **2000**, *23*, 115−127.

(14) Francis, G.; Makkar, H. P. S.; Becker, K. Antinutritional factors present in plant-derived alternate fish feed ingredients and their effects in fish. *Aquaculture* **2001**, *199*, 197−227.

(15) Knudsen, D.; Uran, P.; Arnous, A.; Koppe, W.; Frøkiær, H. Saponin-containing subfractions of soybean molasses induce enteritis in the distal intestine of Atlantic salmon. *J. Agric. Food Chem.* **2007**, *55*, 2261−2267.

(16) Knudsen, D.; Jutfelt, F.; Sundh, H.; Sundell, K.; Koppe, W.; Frøkiær, H. Dietary soya saponins increase gut permeability and play a key role in the onset of soyabean-induced enteritis in Atlantic salmon (*Salmo salar* L.). *Br. J. Nutr.* **2008**, *100*, 120−129.

(17) Iwashita, Y.; Yamamoto, T.; Furuita, H.; Sugita, T.; Suzuki, N. Influence of certain soybean antinutritional factors supplemented to a casein-based semipurified diet on intestinal and liver morphology in fingerling rainbow trout *Oncorhynchus mykiss*. *Fish. Sci.* **2008**, *74*, 1075−1082.

(18) Krogdahl, Å.; Penn, M. H.; Thorsen, J.; Refstie, S.; Bakke, A. M. Important antinutrients in plant feedstuffs for aquaculture: an update on recent findings regarding responses in salmonids. *Aquacult. Res.* **2010**, *41*, 333−344.

DOI: 10.1021/jf506242t
J. Agric. Food Chem. 2015, 63, 3887−3902

(19) Chikwati, E. M.; Venold, F. F.; Penn, M. H.; Rohloff, J.; Refstie, S.; Guttvik, A.; Hillestad, M.; Krogdahl, Å. Interaction of soyasaponins with plant ingredients in diets for Atlantic salmon, *Salmo salar* L. *Br. J. Nutr.* **2012**, *107*, 1570−1590.
(20) Kortner, T. M.; Skugor, S.; Penn, M. H.; Mydland, L. T.; Djordjevic, B.; Hillestad, M.; Krasnov, A.; Krogdahl, Å. Dietary soyasaponin supplementation to pea protein concentrate reveals nutrigenomic interactions underlying enteropathy in Atlantic salmon (*Salmo salar*). *BMC Vet. Res.* **2012**, *8*, 101.
(21) Shi, J.; Arunasalam, K.; Yeung, D.; Kakuda, Y.; Mittal, G.; Jiang, Y. M. Saponins from edible legumes: chemistry, processing, and health benefits. *J. Med. Food* **2004**, *7*, 67−78.
(22) Bangham, A. D.; Horne, R. W.; Glauert, A. M.; Dingle, J. T.; Lucy, J. A. Action of saponin on biological cell membranes. *Nature* **1962**, *196*, 952−953.
(23) Malinow, M. R.; McLaughlin, P.; Papworth, L.; Stafford, C.; Kohler, G. O.; Livingston, A. L.; Cheeke, P. R. Effect of alfalfa saponins on intestinal cholesterol absorption in rats. *Am. J. Clin. Nutr.* **1977**, *30*, 2061−2067.
(24) Johnson, I. T.; Gee, J. M.; Price, K.; Curl, C.; Fenwick, G. R. Influence of saponins on gut permeability and active nutrient transport invitro. *J. Nutr.* **1986**, *116*, 2270−2277.
(25) Francis, G.; Kerem, Z.; Makkar, H. P. S.; Becker, K. The biological action of saponins in animal systems: a review. *Br. J. Nutr.* **2002**, *88*, 587−605.
(26) Potter, S. M.; Jimenez-Flores, R.; Pollack, J.; Lone, T. A.; Berber-Jimenez, M. D. Protein−saponin interaction and its influence on blood lipids. *J. Agric. Food Chem.* **1993**, *41*, 1287−1291.
(27) Southon, S.; Johnson, I. T.; Gee, J. M.; Price, K. R. The effect of *Gypsophila* saponins in the diet on mineral status and plasma cholesterol concentration in the rat. *Br. J. Nutr.* **1988**, *59*, 49−55.
(28) Sparg, S. G.; Light, M. E.; Van Staden, J. Biological activities and distribution of plant saponins. *J. Ethnopharmacol.* **2004**, *94*, 219−243.
(29) Kensil, C. R. Saponins as vaccine adjuvants. *Crit. Rev. Ther. Drug Carrier Syst.* **1996**, *13*, 1−55.
(30) Oda, K.; Matsuda, H.; Murakami, T.; Katayama, S.; Ohgitani, T.; Yoshikawa, M. Adjuvant and haemolytic activities of 47 saponins derived from medicinal and food plants. *Biol. Chem.* **2000**, *381*, 67−74.
(31) Singh, M.; ÒHagan, D. T. Recent advances in veterinary vaccine adjuvants. *Int. J. Parasitol.* **2003**, *33*, 469−478.
(32) Song, X.; Hu, S. Adjuvant activities of saponins from traditional Chinese medicinal herbs. *Vaccine* **2009**, *27*, 4883−4890.
(33) Francis, G.; Makkar, H. P. S.; Becker, K. *Quillaja* saponins—a natural growth promoter for fish. *Anim. Feed Sci. Technol.* **2005**, *121*, 147−157.
(34) Ireland, P. A.; Dziedzic, S. Z.; Kearsley, M. W. Saponin content of soya and some commercial soya products by means of high-performance liquid chromatography of the sapogenins. *J. Sci. Food Agric.* **1986**, *37*, 694−698.
(35) Knudsen, D.; Røn, Ø.; Baardsen, G.; Smedsgaard, J.; Koppe, W.; Frøkiær, H. Soyasaponins resist extrusion cooking and are not degraded during gut passage in Atlantic salmon (*Salmo salar* L.). *J. Agric. Food Chem.* **2006**, *54*, 6428−6435.
(36) Muzquiz, M.; Ridout, C. L.; Price, K. R.; Fenwick, G. R. The saponin content and composition of sweet and bitter lupin seed. *J. Sci. Food Agric.* **1993**, *63*, 47−52.
(37) Ruiz, R. G.; Price, K. R.; Rose, M. E.; Rhodes, M. J. C.; Fenwick, G. R. Determination of saponins in lupin seed (*Lupinus angustifolius*) using high-performance liquid chromatography: comparison with a gas chromatographic method. *J. Liq. Chromatogr. Relat. Technol.* **1995**, *18*, 2843−2853.
(38) Refstie, S.; Glencross, B.; Landsverk, T.; Sørensen, M.; Lilleeng, E.; Hawkins, W.; Krogdahl, Å. Digestive function and intestinal integrity in Atlantic salmon (*Salmo salar*) fed kernel meals and protein concentrates made from yellow or narrow-leafed lupins. *Aquaculture* **2006**, *261*, 1382−1395.
(39) Anderson, R. L.; Wolf, W. J. Compositional changes in trypsin inhibitors, phytic acid, saponins and isoflavones related to soybean processing. *J. Nutr.* **1995**, *125*, S581−S588.
(40) Ruiz-Lopez, M. A.; Garcia-Lopez, P. M.; Castaneda-Vazquez, H.; Zamora, N. J. F.; Garzon-De la Mora, P.; Banuelos Pineda, J.; Burbano, C.; Pedrosa, M. M.; Cuadrado, C.; Muzquiz, M. Chemical composition and antinutrient content of three *Lupinus* species from Jalisco, Mexico. *J. Food Compos. Anal.* **2000**, *13*, 193−199.
(41) Sujak, A.; Kotlarz, A.; Strobel, W. Compositional and nutritional evaluation of several lupin seeds. *Food Chem.* **2006**, *98*, 711−719.
(42) De la Higuera, M.; Garcia-Gallego, M.; Sanz, A.; Cardenete, G.; Suarez, M. D.; Moyano, F. J. Evaluation of lupin seed meal as an alternative protein source in feeding of rainbow trout (*Salmo gairdneri*). *Aquaculture* **1988**, *71*, 37−50.
(43) Burel, C.; Boujard, T.; Tulli, F.; Kaushik, S. J. Digestibility of extruded peas, extruded lupin, and rapeseed meal in rainbow trout (*Oncorhynchus mykiss*) and turbot (*Psetta maxima*). *Aquaculture* **2000**, *188*, 285−298.
(44) Røsjø, C.; Berg, T.; Manum, K.; Gjøen, T.; Magnusson, S.; Thomassen, M. S. Effects of temperature and dietary n-3 and n-6 fatty acids on endocytic processes in isolated rainbow trout (*Oncorhynchus mykiss*, Walbaum) hepatocytes. *Fish Physiol. Biochem.* **1994**, *13*, 119−132.
(45) Refstie, S.; Helland, S.; Storebakken, T. Adaptation to soybean meal in diets for rainbow trout, *Oncorhynchus mykiss*. *Aquaculture* **1997**, *153*, 263−272.
(46) Kakade, M. L.; Hoffa, D. E.; Liener, I. E. Contribution of trypsin-inhibitors to deleterious effects of unheated soybeans fed to rats. *J. Nutr.* **1973**, *103*, 1772−1778.
(47) Penn, M. H.; Bendiksen, E. A.; Campbell, P.; Krogdahl, Å. High level of dietary pea protein concentrate induces enteropathy in Atlantic salmon (*Salmo salar* L.). *Aquaculture* **2011**, *310*, 267−273.
(48) Gu, J.; Krogdahl, Å.; Sissener, N. H.; Kortner, T. M.; Gelencser, E.; Hemre, G.-I.; Bakke, A. M. Effects of oral Bt-maize (MON810) exposure on growth and health parameters in normal and sensitised Atlantic salmon, *Salmo salar* L. *Br. J. Nutr.* **2013**, *109*, 1408−1423.
(49) Venold, F. F.; Penn, M. H.; Thorsen, J.; Gu, J.; Kortner, T. M.; Krogdahl, Å.; Bakke, A. M. Intestinal fatty acid binding protein (fabp2) in Atlantic salmon (*Salmo salar*): localization and alteration of expression during development of diet induced enteritis. *Comp. Biochem. Physiol., A: Mol. Integr. Physiol.* **2013**, *164*, 229−240.
(50) Kortner, T. M.; Gu, J.; Krogdahl, Å.; Bakke, A. M. Transcriptional regulation of cholesterol and bile acid metabolism after dietary soybean meal treatment in Atlantic salmon, *Salmo salar* L. *Br. J. Nutr.* **2013**, *109*, 593−604.
(51) Muller, P. Y.; Janovjak, H.; Miserez, A. R.; Dobbie, Z. Short technical report processing of gene expression data generated by quantitative Real-Time RT-PCR. *Biotechniques* **2002**, *32*, 1372−1379.
(52) Marjara, I. S.; Chikwati, E. M.; Valen, E. C.; Krogdahl, Å.; Bakke, A. M. Transcriptional regulation of IL-17A and other inflammatory markers during the development of soybean meal-induced enteropathy in the distal intestine of Atlantic salmon (*Salmo salar* L.). *Cytokine* **2012**, *60*, 186−196.
(53) Kortner, T. M.; Valen, E. C.; Kortner, H.; Marjara, I. S.; Krogdahl, Å.; Bakke, A. M. Candidate reference genes for quantitative real-time PCR (qPCR) assays during development of a diet-related enteropathy in Atlantic salmon (*Salmo salar* L.) and the potential pitfalls of uncritical use of normalization software tools. *Aquaculture* **2011**, *318*, 355−363.
(54) Sahlmann, C.; Sutherland, B. J. G.; Kortner, T. M.; Koop, B. F.; Krogdahl, Å.; Bakke, A. M. Early response of gene expression in the distal intestine of Atlantic salmon (*Salmo salar* L.) during the development of soybean meal induced enteritis. *Fish Shellfish Immunol.* **2013**, *34*, 599−609.
(55) Lilleeng, E.; Frøystad, M. K.; Østby, G. C.; Valen, E. C.; Krogdahl, Å. Effects of diets containing soybean meal on trypsin mRNA expression and activity in Atlantic salmon (*Salmo salar* L). *Comp. Biochem. Physiol., A: Mol. Integr. Physiol.* **2007**, *147*, 25−36.
(56) Helland, S. J.; Hatlen, B.; Grisdale-Helland, B. Energy, protein and amino acid requirements for maintenance and efficiency of utilization for growth of Atlantic salmon post-smolts determined using increasing ration levels. *Aquaculture* **2010**, *305*, 150−158.

DOI: 10.1021/jf506242t
J. Agric. Food Chem. 2015, 63, 3887−3902

(57) Serrano, E.; Storebakken, T.; Penn, M. H.; Øverland, M.; Hansen, J. Ø.; Mydland, L. T. Responses in rainbow trout (*Oncorhynchus mykiss*) to increasing dietary doses of lupinine, the main quinolizidine alkaloid found in yellow lupins (*Lupinus luteus*). *Aquaculture* **2011**, *318*, 122−127.
(58) Serrano, E.; Storebakken, T.; Borquez, A.; Penn, M. H.; Shearer, K. D.; Dantagnan, P.; Mydland, L. T. Histology and growth performance in rainbow trout (*Oncorhynchus mykiss*) in response to increasing dietary concentration of sparteine, a common alkaloid in lupins. *Aquacult. Nutr.* **2012**, *18*, 313−320.
(59) Borquez, A.; Serrano, E.; Dantagnan, P.; Carrasco, J.; Hernandez, A. Feeding high inclusion of whole grain white lupin (*Lupinus albus*) to rainbow trout (*Oncorhynchus mykiss*): effects on growth, nutrient digestibility, liver and intestine histology and muscle fatty acid composition. *Aquacult. Res.* **2011**, *42*, 1067−1078.
(60) Glencross, B.; Hawkins, W.; Evans, D.; Rutherford, N.; Dods, K.; Maas, R.; McCafferty, P.; Sipsas, S. Evaluation of the nutritional value of prototype lupin protein concentrates when fed to rainbow trout (*Oncorhynchus mykiss*). *Aquaculture* **2006**, *251*, 66−77.
(61) Grisdale-Helland, B.; Gatlin, D. M.; Helland, S. J. Optimization of dietary macronutrients for Atlantic salmon post-smolts using increasing ration levels. *Aquaculture* **2013**, *408*, 88−94.
(62) Grisdale-Helland, B.; Lemme, A.; Helland, S. J. Threonine requirement for maintenance and efficiency of utilization for threonine accretion in Atlantic salmon smolts determined using increasing ration levels. *Aquaculture* **2013**, *372*, 158−166.
(63) Ljøkjel, K.; Harstad, O. M.; Skrede, A. Effect of heat treatment of soybean meal and fish meal on amino acid digestibility in mink and dairy cows. *Anim. Feed Sci. Technol.* **2000**, *84*, 83−95.
(64) Bastrop, R.; Jürss, K.; Wacke, R. Biochemical parameters as a measure of food availability and growth in immature rainbow trout (*Oncorhynchus mykiss*). *Comp. Biochem. Physiol., A: Physiol.* **1992**, *102*, 151−161.
(65) Nordrum, S.; Krogdahl, Å.; Røsjø, C.; Olli, J. J.; Holm, H. Effects of methionine, cysteine and medium chain triglycerides on nutrient digestibility, absorption of amino acids along the intestinal tract and nutrient retention in Atlantic salmon (*Salmo salar* L.) under pair-feeding regime. *Aquaculture* **2000**, *186*, 341−360.
(66) Refstie, S.; Bakke-McKellep, A. M.; Penn, M. H.; Sundby, A.; Shearer, K. D.; Krogdahl, Å. Capacity for digestive hydrolysis and amino acid absorption in Atlantic salmon (*Salmo salar*) fed diets with soybean meal or inulin with or without addition of antibiotics. *Aquaculture* **2006**, *261*, 392−406.
(67) Refstie, S.; Førde-Skjærvik, O.; Rosenlund, G.; Rørvik, K. J. Feed intake, growth, and utilisation of macronutrients and amino acids by 1- and 2-year old Atlantic cod (*Gadus morhua*) fed standard or bioprocessed soybean meal. *Aquaculture* **2006**, *255*, 279−291.
(68) Kihara, M.; Sakata, T. Fermentation of dietary carbohydrates to short-chain fatty acids by gut microbes and its influence on intestinal morphology of a detritivorous teleost tilapia (*Oreochromis niloticus*). *Comp. Biochem. Physiol., A: Physiol.* **1997**, *118*, 1201−1207.
(69) Storebakken, T. Binders in fish feeds: I. Effect of alginate and guar gum on growth, digestibility, feed intake and passage through the gastrointestinal tract of rainbow trout. *Aquaculture* **1985**, *47*, 11−26.
(70) Romarheim, O. H.; Skrede, A.; Penn, M. H.; Mydland, L. T.; Krogdahl, Å.; Storebakken, T. Lipid digestibility, bile drainage and development of morphological intestinal changes in rainbow trout (*Oncorhynchus mykiss*) fed diets containing defatted soybean meal. *Aquaculture* **2008**, *274*, 329−338.
(71) Messina, M. J. Legumes and soybeans: overview of their nutritional profiles and health effects. *Am. J. Clin. Nutr.* **1999**, *70*, 439S−450S.
(72) Chikwati, E. M.; Gu, J.; Penn, M. H.; Bakke, A. M.; Krogdahl, Å.. Intestinal epithelial cell proliferation and migration in Atlantic salmon, *Salmo salar* L.: effects of temperature and inflammation. *Cell Tissue Res.* **2013**, *353*, 123−137.
(73) Grammes, F.; Reveco, F. E.; Romarheim, O. H.; Landsverk, T.; Mydland, L. T.; Øverland, M. *Candida utilis* and *Chlorella vulgaris* counteract intestinal inflammation in Atlantic salmon (*Salmo salar* L.). *PLoS One* **2013**, *8*, e83213.
(74) Fisher, H.; Stenling, R.; Rubio, C.; Lindblom, A. Differential expression of aquaporin 8 in human colonic epithelial cells and colorectal tumors. *BMC Physiol.* **2001**, *1*, 1.
(75) Hardin, J. A.; Wallace, L. E.; Wong, J. F. K.; O'Loughlin, E. V.; Urbanski, S. J.; Gall, D. G.; MacNaughton, W. K.; Beck, P. L. Aquaporin expression is downregulated in a murine model of colitis and in patients with ulcerative colitis, Crohn's disease and infectious colitis. *Cell Tissue Res.* **2004**, *318*, 313−323.
(76) Bustos, D. A. N. I.; Negri, G.; De Paula, J. A.; Di Carlo, M. A. R. I.; Yapur, V. I. V. I; Facente, A.; De Paula, A. L. D. O. Colonic proteinases: increased activity in patients with ulcerative colitis. *Medicina (Buenos Aires)* **1998**, *58*, 262−264.
(77) Hawkins, J. V.; Emmel, E. L.; Feuer, J. J.; Nedelman, M. A.; Harvey, C. J.; Klein, H. J.; Rozmiarek, H.; Kennedy, A. R.; Lichtenstein, G. R.; Billings, P. C. Protease activity in a hapten-induced model of ulcerative colitis in rats. *Dig. Dis. Sci.* **1997**, *42*, 1969−1980.
(78) Cenac, N.; Coelho, A. M.; Nguyen, C.; Compton, S.; Andrade-Gordon, P.; MacNaughton, W. K.; Wallace, J. L.; Hollenberg, M. D.; Bunnett, N. W.; Garcia-Villar, R. Induction of intestinal inflammation in mouse by activation of proteinase-activated receptor-2. *Am. J. Pathol.* **2002**, *161*, 1903−1915.
(79) Cenac, N.; Chin, A. C.; Garcia-Villar, R.; Salvador-Cartier, C.; Ferrier, L.; Vergnolle, N.; Buret, A. G.; Fioramonti, J.; Bueno, L. PAR2 activation alters colonic paracellular permeability in mice via IFN-g-dependent and -independent pathways. *J. Physiol.* **2004**, *558*, 913−925.

DOI: 10.1021/jf506242t
J. Agric. Food Chem. 2015, 63, 3887−3902

In the present study, a novel hemagglutinin was purified from the seeds of Northeast China black beans, and its biological properties and antitumor and immumoregulatory effects were characterized.

MATERIALS AND METHODS

Materials and Reagents. Northeast China black beans, a cultivar of *Phaseolus vulgaris,* were purchased from a local vender and authenticated by Professor Shiuying Hu, Honorary Professor of Chinese Medicine, The Chinese University of Hong Kong. Affi-Gel Blue gel, Mono Q 5/50 GL, Superdex 75 10/300 GL columns, and purifier were bought from GE Healthcare, UK. Human hepatocellular carcinoma HepG2 cell line, osteocarcinoma MG-63 cell line, and normal embryonic liver cell WRL 68 cell line were purchased from the American Type Culture Collection. All primary and secondary antibodies were purchased from Cell Signaling Technology (Danvers, MA). TRIZOL and the reverse transcriptase PCR kit were acquired from Invitrogen (Waltham, MA). Power SYBR Green PCR Master Mix was purchased from Applied Biosystems (Warrington, Cheshire, UK). FITC fluorescent dye was purchased from Thermo Scientific (Waltham, MA).

Purification of Hemagglutinin. Dried beans (60 g) were soaked in water overnight and then ground into a slurry. After centrifugation at 14000 rpm for 30 min at 4 °C and filtration through filter paper, the supernatant was adjusted with 2 M Tris−HCl buffer (pH 7.6) until the concentration of the buffer reached 20 mM, and it was then loaded on an Affi-Gel Blue gel column which was equilibrated with 20 mM Tris−HCl buffer (pH 7.6). Unadsorbed fraction and adsorbed fraction were, respectively, eluted with the starting buffer and 1 M NaCl in Tris−HCl buffer (20 mM, pH 7.6). Afterward, the bound fraction was dialyzed against water, lyophilized, dissolved in 20 mM NH_4HCO_3 buffer (pH 9.6), and chromatographed on a Mono Q column equilibrated with the same buffer. The bound fraction was eluted with three successive linear gradients of NaCl (0−0.2, 0.2−0.5, and 0.5−1 M, respectively, collected in 5, 20, and 5 mL of buffer) in the same buffer using fast protein liquid chromatography (FPLC). The active fraction was collected and processed as described in previous steps before loading on a Superdex 75 HR10/300 column attached to the FPLC system. The system was run with 0.1 M NaCl in 20 mM Tris−HCl buffer. Purified hemagglutinin from Northeast China black beans (NCBBH) was dialyzed and lyophilized before storage.

Characterization of NCBBH. To determine the molecular weight of NCBBH, sodium dodecyl sulfate-polyacrylamide gel electrophoresis (SDS-PAGE, 15% acrylamide gel) was performed in accordance with the procedure previously reported.[17] Besides, a standard curve was constructed by running three marker proteins on the same FPLC-gel filtration system to help further determine the molecular weight.

Amino acid sequence was analyzed by Edman degradation followed by HPLC system analysis or the protein was cleaved into small peptides and analyzed by mass spectrometry.

Hemagglutinating activity assay was conducted by incubating a serially 2-fold diluted hemagglutinin (50 μL) with 50 μL of rabbit blood (2% in phosphate-buffered saline) in microtiter U-plates. Agglutination status of the red blood cells was recorded when the blank had fully precipitated. The hemagglutination unit (HU) was defined as the reciprocal of the highest dilution of the sample which exhibited hemagglutination, and the number of hemaglutination units per milligram of protein was recorded as specific activity.[18]

The stability of hemagglutinin at different temperatures and pH values was determined by the following methods. Purified hemagglutinin was dissolved in phosphate-buffered saline (PBS) and incubated at different temperatures for 30 min. After the mixture was fully cooled to room temperature, the remaining hemagglutinating activity of the mixture was assayed. pH stability was tested by employing the following steps: NCBBH was first dissolved in water and then adjusted with NaOH and HCl to different pH values (0−14). After incubation at room temperature for 30 min, the mixture was neutralized to pH 7. Hemagglutinating activity was then determined.

Ethylenediaminetetraacetic acid (EDTA) at a final concentration of 10 mM was added to NCBBH dissolved in PBS. The mixture was incubated at 4 °C for 5 h with shaking to make sure the hemagglutinin had been fully demetalized. The residual hemagglutinating activity was determined after EDTA had been removed. If the activity decreased or was completely lost, one of the following cations (KCl, AgCl, $CuSO_4$, $MgSO_4$, $MnSO_4$, $CaCl_2$, $ZnSO_4$, $FeSO_4$, and $FeCl_3$ at a final concentration of 40 mM) was added, and after incubation for 3 h, hemagglutinating activity was assayed again to see whether it had been restored.

The inhibition of hemagglutinating activity by carbohydrates was determined. NCBBH was dissolved in PBS buffer which contained different concentrations of sugar (the highest concentration at 100 mM) and serially 2-fold diluted with the same buffer in microtiter U-plates. Wells with only PBS or PBS-containing sugars were taken as the control. The mixture was subsequently mixed with an equal volume of rabbit blood (2%). The changes of HU in the presence and absence of different sugars were recorded.

Labeling NCBBH with FITC. FITC labeled NCBBH was prepared by following the procedure provided by the manufacturer. Briefly, purified NCBBH was dissolved in 50 mM borate buffer at a concentration of 2 mg/mL. FITC dye (Thermo Scientific, Waltham, MA) dissolved in DMF at 10 mg/mL was slowly added to NCBBH solution with its final concentration 15-fold molar higher than that of NCBBH. The mixture was incubated in the dark at room temperature for 1 h. The excess FITC was removed by dialysis in ddH_2O overnight at 4 °C. The FITC-labeled NCBBH was lyophilized and stored at −20 °C.

Anticancer Activity of NCBBH. *Cell Viability Assay.* Osteosarcoma MG-63 cells, hepatoma HepG2 cells, and human embryonic liver WRL 68 cells were cultured in Dulbecco's modified Eagle's medium (DMEM) with 10% fetal bovine serum (FBS) and 1% penicillin/streptomycin (PS) at 37 °C. Cell viability after treatment with NCBBH was evaluated by the 3-(4,5-dimethylthiazol-2-yl)-2, 5-diphenyltetrazolium bromide (MTT) assay. Briefly, cells (5000 cells/100 μL/well) were seeded in a 96-well microtiter plate. Medium was discarded after 24 h, and cells were treated with 2-fold serially diluted NCBBH with a concentration varying from 15 to 0 μM for 24 or 48 h. MTT solution (25 μL 5 mg/mL) was added to each well after removal of the old medium and the solution incubated for another 4 h. Dimethyl sulfoxide (150 μL) was then added to each well to dissolve the crystal formazan. The absorbance at 570 nm was measured by using a BIO-RAD microplate reader.

Cells (5×10^3) were seeded on a 6-well culture plate for 24 h, followed by the treatment of different concentrations of NCBBH for 6 days. Medium was changed every 2 days. After being rinsed with PBS, cells were fixed in 4% formaldehyde and subsequently stained with crystal violet (0.4 g/L). The images were captured by using the Nikon Live Cell imaging System Ti-E. The number of cells was counted by using Image-Pro Plus 6.0. Cell density was compared between the wells treated with and without NCBBH.

Binding of NCBBH on Cells. 1×10^5 cells were seeded on 6-well culture plates overnight, followed by treatment of 20 μg/mL of FTIC-labeled NCBBH for 24 h. The cells were harvested and washed twice with PBS. The FITC signal was then measured by a flow cytometer.

Confocal Imaging Microscopy. 3×10^4 cells were seeded on the cover glass in 24-well culture plates overnight. Cells were then cultured with 0.2 mg/mL of FITC-labeled NCBBH for 3 or 24 h. After fixation in 4% formaldehyde for 15 min and washing three times with PBS, cells were then stained by 1 μM Hoechst 33342 for 20 min. The cover glass with cells were taken out from the culture plates and mounted in 50% glycerol on glass slide. The image was taken on the Olympus FV1000-ZCD laser scanning confocal system with a 60× oil immersion objective lens (Tokyo, Japan) and analyzed by Olympus Fluoview Version 2.0.

Assay of Changes in Nuclear Morphology of MG-63 Cells. MG-63 cells were incubated in the presence of 4.52 μM NCBBH for 24 h and stained with 1 μM Hoechst 33342 for 20 min after removal of the medium and rinsing with PBS. Nuclear morphology was observed under a Nikon Live Cell Imaging System Ti-E.

DOI: 10.1021/acs.jafc.5b00106
J. Agric. Food Chem. 2015, 63, 3903−3914

Flow Cytometry Assay for Apoptosis. Apoptosis-inducing activity of NCBBH was examined by using the Annexin-V (BD Pharmingen, San Jose, CA) and propidium iodide PI (Sigma-Aldrich, St. Louis, MO) staining methods. Briefly, MG-63 cells were treated with different concentrations of NCBBH for 48 h. Trypsinized cells were centrifuged (1500 rpm, 5 min), washed with PBS, and stained with 0.5 mg/mL Annexin V and PI (final concentration 5 μg/mL) in binding buffer (0.01 M HEPES, pH 7.4, containing 140 mM NaCl and 25 mM $CaCl_2$) in darkness at room temperature for 15 min. Cells were then applied to a flow cytometer (after filtration).

Assay of Mitochondrial Membrane Depolarization. The mitochondrial membrane potential of MG-63 cells was measured by JC-1 staining as previously reported, based on the principle that in healthy cells, JC-1 dye accumulates in the mitochondria and emits red fluorescence while JC-1 exists as a monomer in cytosol and emits green fluorescence when the mitochondrial membrane is depolarized.[19] After treatment with NCBBH (1.25, 0.625, and 0 μM) for 24 h, MG-63 cells were collected and stained with 2.5 μg/mL JC-19 dye for 15 min in darkness before analysis using a flow cytometer.

Western Blotting. After treatment of NCBBH for different durations, the MG-63 cells were lysed in ice-cold RIPA lysis buffer. The whole cell extracts were then added to the loading buffer and boiled for 5 min before loading on SDS-PAGE. After electrophoresis, the proteins on the gel were then transferred onto polyvinylidene fluoride membranes and blocked in 5% milk for 40 min. The membranes were subsequently incubated with the first antibody overnight at 4 °C and the second antibody for 2 h at room temperature. The bands were finally visualized by using ECL detection kits.

Effect of *N*-Acetylgalactosamine (GalNAc) on the Antiproliferative Activity of NCBBH. To determine whether GalNAc could partially inhibit the antiproliferation effect of NCBBH, MG-63 cells and HepG2 cells were cultured with different concentration of NCBBH in the presence and absence of GalNAc for 48 h. The highest concentration of GalNAc was 5 mM which is close to the plasma sugar level of human body. The toxicity of GalNAc itself on the cancer cells was also determined by culturing cells in the medium containing different concentrations of GalNAc for 48h.

Detection of Immunomodulatory Effect of NCBBH on Splenocytes. *Real-Time PCR.* The spleen was collected immediately after the mouse (C57BL/6J) was sacrificed and pressed gently through a sterile stainless steel sieve in PBS. The cell suspension was collected and centrifuged at 1500 rpm for 3 min, followed by the addition of lysis buffer (155 mM NH_4Cl, 12 mM $NaHCO_3$, 100 mM EDTA, pH 7.2) to lyse the blood cells. The splenocytes were collected by centrifugation at 1500 rpm and washed twice with PBS before culturing with different concentrations of NCBBH in DMEM for 4 h. The total RNA of splenocytes was extracted with TRIZOL and reverse-transcribed into cDNA with oligo-Dt primers using a Revert first strand cDNA synthesis kit. Real-time PCR was performed using SYBR Green. The target genes include IFN-γ, IL-2, IL-6-, IL-1β, TNF-α, and glyceraldehyde-3-phosphate dehydrogenase known as GAPDH as the standard (shown in Table 1).

Detection of Cytokine Secretion by Western Blotting. The splenocytes were prepared as described above and evenly separated into six cell culture dishes which contained different concentrations of NCBBH in the same final volume of FBS free DMEM. The cells were cultured for 24 h before the conditional medium was collected. The same volume of the conditional medium was taken for Western blotting by following the procedures described above.

Statistics. Results were taken from three independent experiments ($n = 3$), and data were expressed as means ± standard deviation (SD). Scatter diagram and histograms were drawn using GraphPad Prim 5 (Graphpad Software, La Jolla, CA). For PCR experiments, one-way ANOVA followed by a Bonferronni posthoc test was used for the comparisons between multiple groups. A P value <0.05 was considered as statistically significant, $p < 0.05$ (*), $p < 0.01$ (**), $p < 0.001$(***) versus respective control groups. All statistical analyses were performed using software GraphPad Prim 5.

Table 1. Primers Used for Analysis of Cytokine Expression

IFN-γ	
forward	TCAAGTGGCATAGATGTGGAAG
reverse	TGGCTCTGCAGGATTTTCATG
IL-2	
forward	CCTGAAACTCCCCAGGATGC
reverse	TCAAATCCAGAACATGCCGC
IL-6	
forward	TCCAGTTGCCTTCTTGGGAC
reverse	AGTCTCCTCTCCGGACTTGT
IL-1β	
forward	TGTAATGAAAGACGGCACACC
reverse	TCTTCTTTGGGTATTGCTTGG
TNF-α	
forward	CTGTAGCCCACGTCGTAGC
reverse	TTGAGATCCATGCCGTTG
GAPDH	
forward	GGTGAAGGTCGGTGTGAACG
reverse	CTCGCTCCTGGAAGATGGTG

RESULTS

Purification. The crude extract of NCBBH was first loaded on Affi-Gel Blue gel and eluted with 1 M NaCl. The bound fraction which contained hemagglutinating activity was then resolved on Mono Q 5/50 GL by employing an FPLC system. Hemagglutinating activity was confined to fraction M2, as shown in Figure 1A. This fraction was collected and subsequently subjected to size-exclusion chromatography on an FPLC-Superdex 75 column. A single sharp peak S1 was acquired as shown in Figure 1B.

Molecular Weight and N-Terminal Sequence. Purified NCBBH was loaded on SDS-PAGE, and a single band with a molecular weight around 36 kDa was observed (Figure 1C). A standard curve in Figure 1D was generated with three protein markers.

$$\log(\text{molecular weight}) = -0.099X + 2.779$$

$$R^2 = 0.974$$

$$\text{NCBBH elution volume} = 9.25\ \text{mL}$$

X in the equation indicates the elution volume of peaks in the FPLC-gel filtration system. According to the above formula, the molecular weight of NCBBH was estimated to be around 73 kDa. Combining the information from SDS-PAGE and gel filtration, it could be deduced that NCBBH was a dimer. Table 2 summarized the yields and hemagglutinating activities at each step of purification.

The N-terminal of NCBBH was found to be blocked. After the analysis of small peptides in the protein by mass spectrometry and comparison with those in green plant database, they were not found to be the same as with other proteins. Peptides of this hemagglutinin most closely resembled the hemagglutinin precursor peptide of *Phaseolus vulgaris*. Table 3 summarized the data of the three proteins that manifested the most pronounced similarities with NCBBH.

Chemical and Biological Characteristics. Parts A and B of Figure 2 displayed the thermal and pH stability of NCBBH. The hemagglutinating activity of NCBBH remained stable at temperatures from 20 to 60 °C and from pH 2 to 11. The activity decreased by half when temperature was raised to 70 °C or when pH was lowered to 1 and vanished completely at the

DOI: 10.1021/acs.jafc.5b00106
J. Agric. Food Chem. 2015, 63, 3903−3914

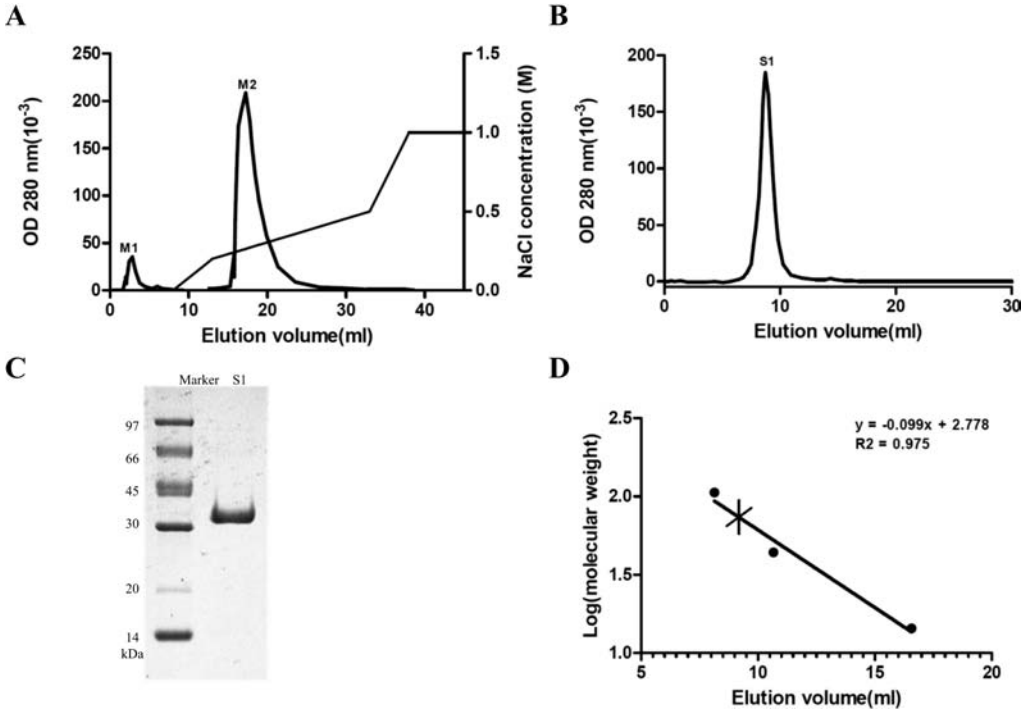

Figure 1. Purification of NCBBH by liquid chromatography techniques. (A) Adsorbed fraction from Affi-gel Blue gel was loaded on a Mono Q 5/50 column, generating two major peaks (M1 and M2). (B) Fraction M2 carrying hemagglutinating activity was collected and subsequently run on a Superdex 75 10/300 column, and a single peak S1 was observed. (C) SDS-PAGE: right lane contains molecular mass markers; band shown on left represents the purified hemagglutinin. (D) A standard curve was constructed by running three marker proteins on the FPLC-gel filtration system. They are, respectively, concanavalin A (106 kDa), albumin from chicken egg white (44 kDa), and lysozyme (14.4 kDa). The cross on the standard curve corresponds to NCBBH (elution volume = 9.7 mL).

Table 2. Yields and Hemagglutinating Activities at Various Steps of Purification (Starting Material: 60 g of Dried Beans)

chromatographic fraction with hemagglutinating activity	total protein (mg)	specific activity (HU/mg)	total activity (HU × 10^3)	purification fold	recovery of activity (%)
crude extract	8118	256	2078	1	100
after Affi-gel Blue gel	801.9	2000	1603	1.3	77
after Mono Q	270.4	4000	1082	15.6	52.1
after Superdex 75	110.6	4560	504	17.8	24.1

extreme pH values of 0 and 13 and at high temperatures above 80 °C.

The addition of EDTA could demolish the hemagglutinating activity of NCBBH, which may be attributed to demetalization. After the removal of EDTA, metal ions, KCl, AgCl, $CuSO_4$, $MgSO_4$, $MnSO_4$, $CaCl_2$, $ZnSO_4$, $FeSO_4$, and $FeCl_3$ were supplied in the NCBBH solution, and the activity was found to be reinstated in the presence of divalent cations (Cu^{2+}, Mg^{2+}, Mn^{2+}, Ca^{2+}, Zn^{2+}, and Fe^{2+}ions) and a trivalent cation (Fe^{3+}), which indicated that the hemagglutinating activity of NCBBH is ion-dependent.

Table 3. Three Proteins That Most Closely Resemble NCBBH

protein accession	coverage	peptides	description
P05088	69.82	SVLPEWVIVGFTATTGITK GENAEVLITYDSSTK YDSNAHTVAVEFDTLYNVHWDPKPR ... total no. of peptides: 16	erythroagglutinating phytohemagglutinin precursor (PHA-E) − *Phaseolus vulgaris* (kidney bean) (French bean) − [PHAE_PHAVU]
P05087	47.43	GNVETNDVLSWSFASK SVLPEWVSVGFSATTGINK TSFIVSDTVDLK ... total no. of peptides: 9	leucoagglutinating phytohemagglutinin precursor (PHA-L) − *Phaseolus vulgaris* (kidney bean) (French bean) − [PHAL_PHAVU]
P15231	27.47	GGFLGLFDGSNSNFHTVAVEFDTLYNK LLVASLVYPSLK DKGGFLGLFDGSNSNFHTVAVEFDTLYNK ... total no. of peptides: 7	leucoagglutinating phytohemagglutinin precursor (PHA-L) −- *Phaseolus vulgaris* (kidney bean) (French bean) − [PHAM_PHAVU]

DOI: 10.1021/acs.jafc.5b00106
J. Agric. Food Chem. 2015, 63, 3903−3914

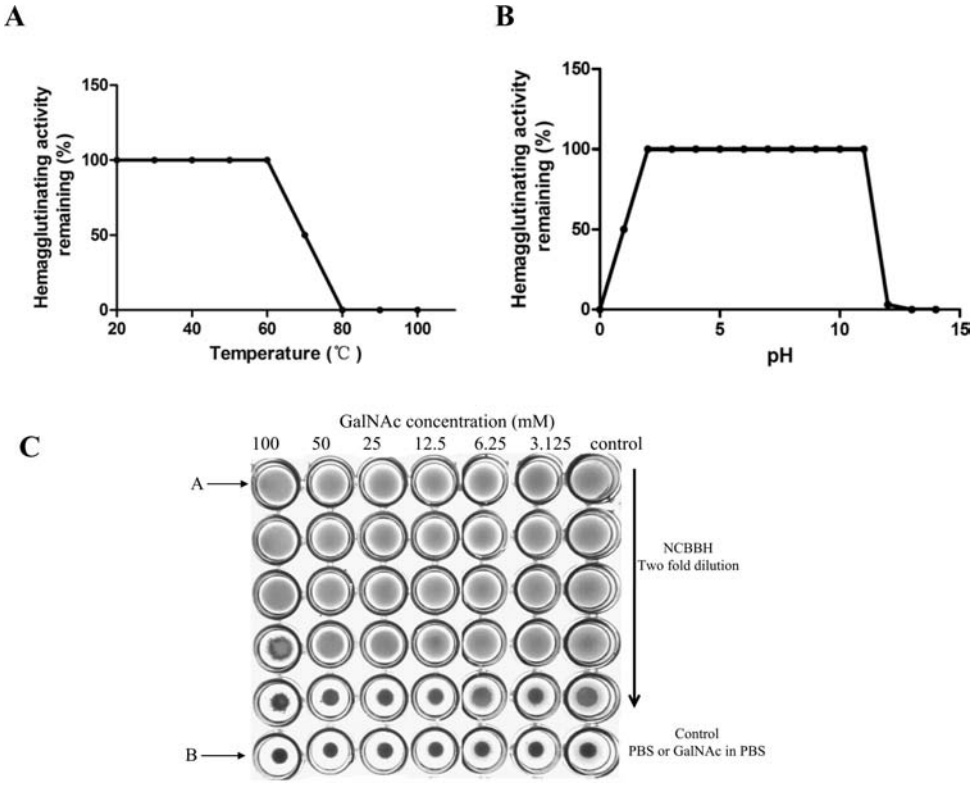

Figure 2. Influence of temperature, pH, and GalNAc on hemagglutinating activity of NCBBH. (A) NCBBH was stable at temperatures from 20 to 60 °C. (B) NCBBH was stable from pH 2 to 11. (C) GalNAc inhibited the hemaggluinating activity of NCBBH. NCBBH in PBS was taken as the control and it had 16 HU. When the cells were agglutinated by hemagglutinin, they appeared in a meshlike pattern and evenly spreaded on the button of microtiter U-plates (as shown with arrow A), while the unagglutinated cells precipitated in the lowest location of U-plants (as shown with arrow B).

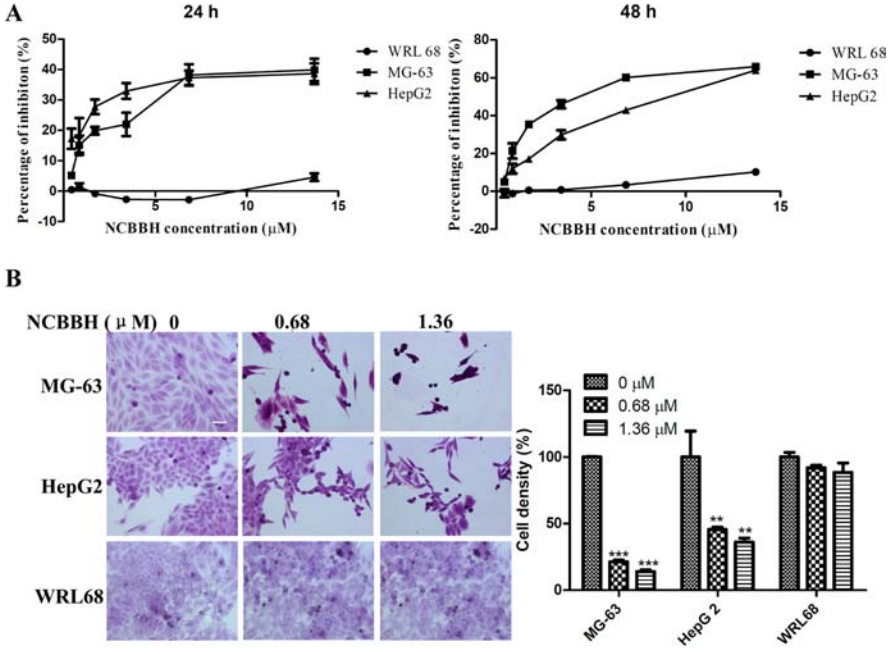

Figure 3. Antiproliferative activity by NCBBH on osteocarcinoma MG-63 cells and hepatoma HepG2 in vitro. (A) NCBBH induced an antiproliferative effect on MG 63 and HepG2 cells in a dose- and time-dependent manner with an IC_{50} of 4.5 and 9 μM at 48 h, but there was no antiproliferative activity on embryonic liver cell WRL68 cells. Results represent in mean ± SD (n = 3). (B) Low dosages of NCBBH suppressed the growth of MG-63 cells and HepG2 cells in a prolonged cell culture condition. Cells were cultured in the medium containing 0.68 and 1.36 μM NCBBH for 6 days. The density of cells was compared with that of control (no NCBBH treatment). $P < 0.05$ was taken as statistically significant; $p < 0.05$ (*), $p < 0.01$ (**), $p < 0.001$(***) versus, respectively, control groups.

DOI: 10.1021/acs.jafc.5b00106
J. Agric. Food Chem. 2015, 63, 3903−3914

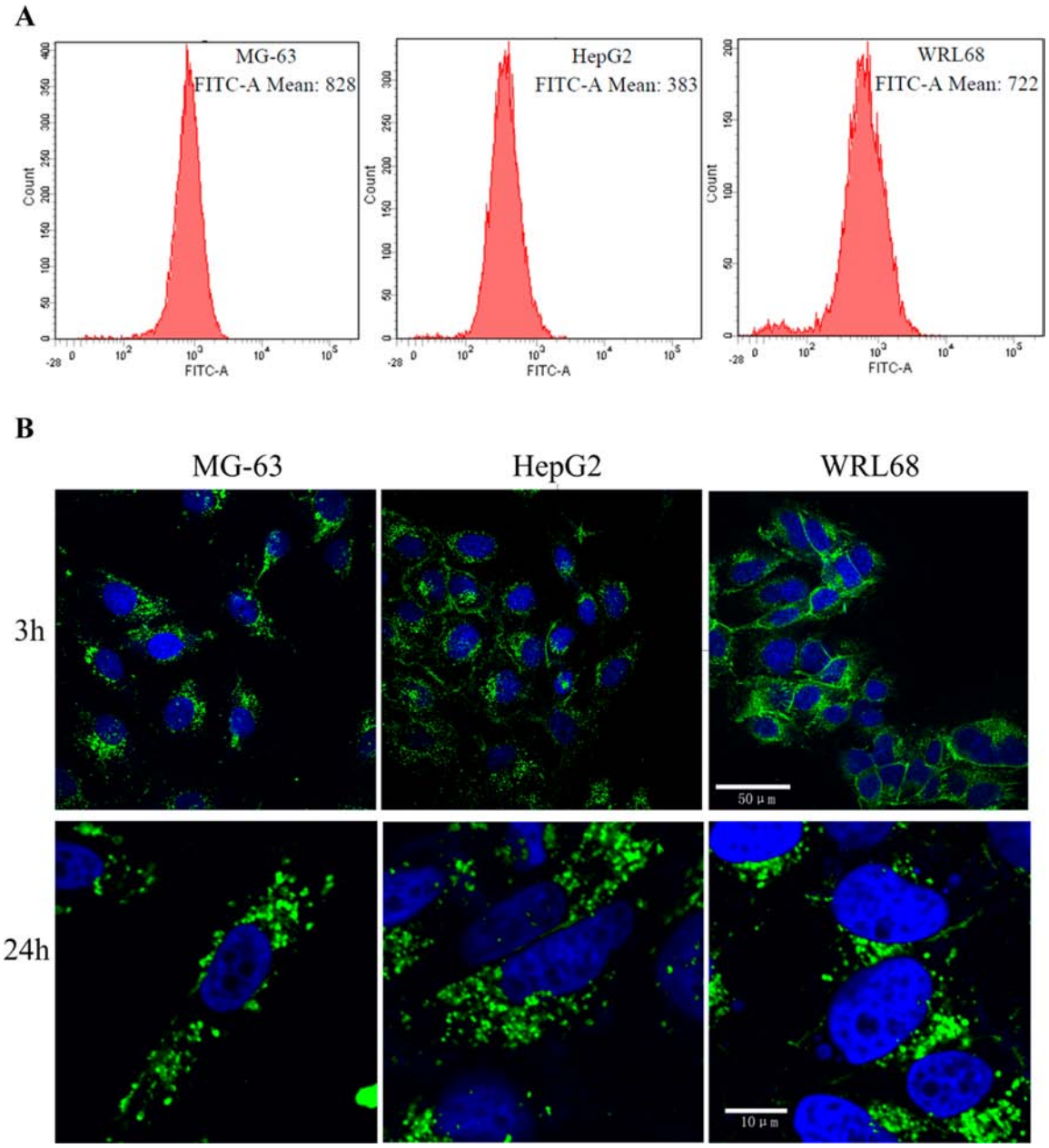

Figure 4. NCBBH detection on cells. (A) After the treatment of FITC-labeled NCBBH, the intake or binding of NCBBH on cells was monitored by use of a flow cytometer. (B) Confocal imaging of NCBBH localization in the cells. NCBBH tagged with FITC and nucleuses stained by Hoechst 33342 were, respectively, present in green and blue.

Among the 13 sugars tested in this experiment, only *N*-acetylgalactosamine (GalNAc) could partially suppress the hemagglutinating activity of NCBBH. In the presence of 100 mM GalNAc, the hemagglutin activity decreased from 16 to 8 HU, and the inhibitory effect faded with the decrease of the concentration of GalNAc as shown in Figure 2C. The remaining sugars tested had no effect on the hemagglutinating activity of NCBBH, and they comprised D-galactose, L-fucose, L-arabinose, D-fructose, D-mannose, D-manitol, D-xylose, D-glucose, maltose, α-lactose, raffinose, and L-rhamnose.

NCBBH Demonstrated Toxicity toward Tumor Cells. The antitumor activity of NCBBH was investigated by the MTT assay. As shown in Figure 3A, NCBBH inhibited the proliferation of MG-63 and HepG2 cells in a dose- and time-dependent manner. The IC_{50} values for MG-63 and HepG2 cells after treatment with NCBBH for 48 h were, respectively ,around 4.5 and 9 μM. After the same treatment, normal embryonic liver cells (WRL 68) were only slightly affected at both 24 and 48 h time points. Consistent with the results of the MTT assay, the density of MG-63 and HepG2 cells cultured in the medium containing 0.68 or 1.36 μM NCBBH was much lower than that of control, while no statistic difference of cell density was observed in WRL 68 cells treated in the presence and absence of NCBBH after 6 days as shown in Figure 3B.

Detection of NCBBH on Cells. After the same treatment with FITC-labeled NCBBH for 24 h, the signal of FITC detected by the flow cytometer on MG-63, WRL 68, and HepG2 cells varied from each other, among which the FITC signal on MG-63 cells was the highest, followed by WRL68 and HepG2 as shown in Figure 4A. NCBBH was observed both on

DOI: 10.1021/acs.jafc.5b00106
J. Agric. Food Chem. 2015, 63, 3903−3914

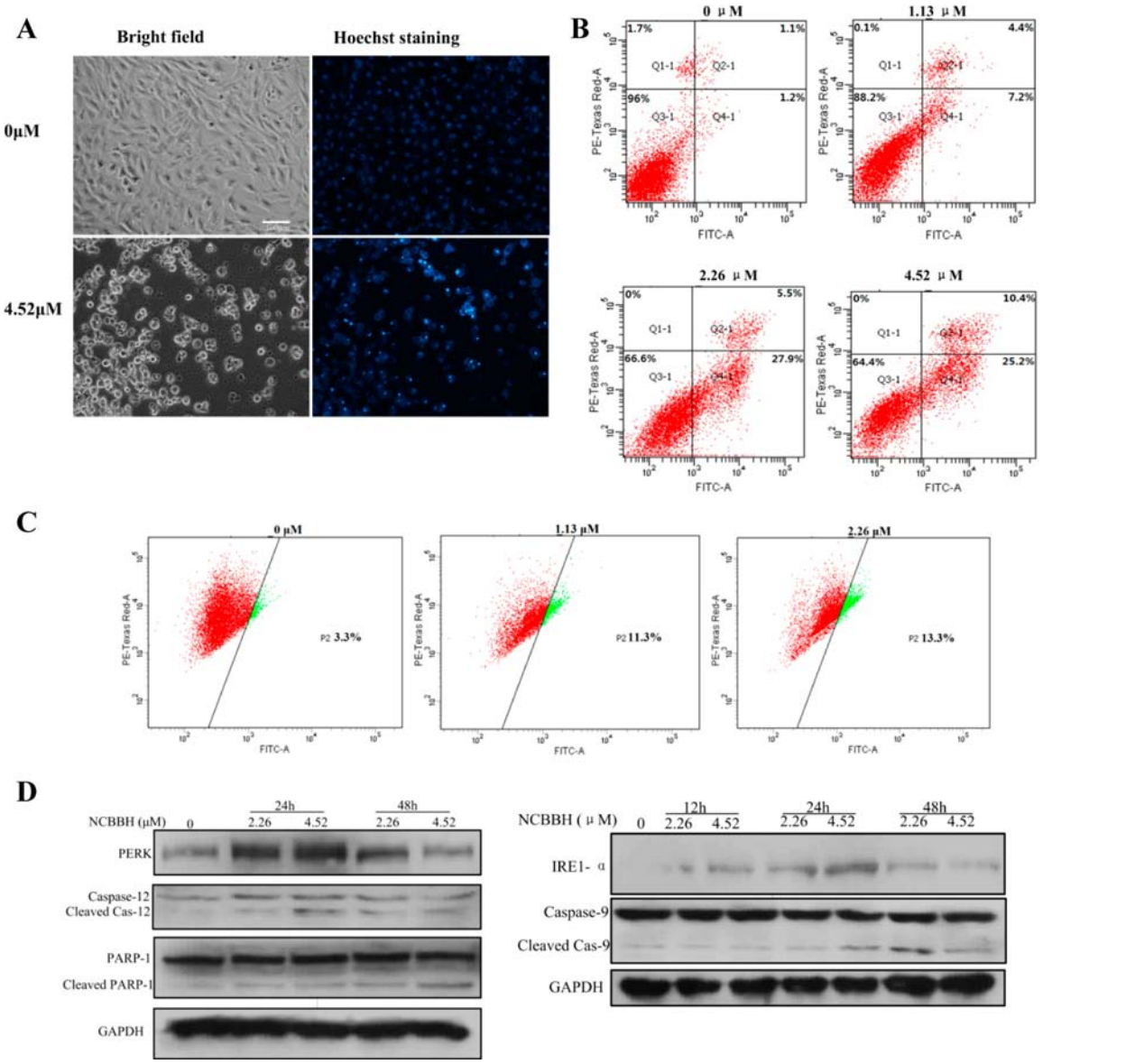

Figure 5. NCBBH-induced apoptosis in MG 63 cells. (A) NCBBH produced nuclear morphological changes in MG-63 cells. After the treatment with 4.52 μM NCBBH for 24 h, cells were stained with 1 μg/mL of Hoechst 33342 for 15 min. Nuclear morphological changes of MG-63 cells were observed with a Nikon Live Cell Imaging System Ti-E. (B) Cell apoptosis analysis by Annexin V-GFP/PI double staining. MG-63 cells were first treated with 0, 1.13, 2.26, and 4.52 μM NCBBH for 48 h. Cells were then harvested and washed with PBS, followed by staining with Annexin V-GFP/PI for 15 min. Apoptosis was then monitored by the flow cytometer. (C) Mitochondrial membrane potential detection by JC-1 staining. MG63 cells were cultured with 0, 1.13, and 2.26 μM NCBBH for 24 h. The mitochondrial membrane potential was then analyzed by a flow cytometer. (D) Treatment of MG 63 cells with NCBBH had initiated the activation of caspase-12 and caspase-9, cleavage of PARP, and up-regulation of IRE1-α and PERK.

the membrane and inside of the cells as early as 3 h. At 24 h, the majority of NCBBH was found in the cytoplasm of cells and discrepancy of NCBBH distribution was found in different cells that NCBBH tended to be evenly distributed in the cytoplasm of MG-63 cells and HepG2 cells, while NCBBH was found in part of the cytoplasm of WRL68 cells as shown in Figure 4B.

Apoptosis-Inducing Effect of NCBBH on MG-63 Cells. MG-63 underwent cellular and nuclear morphological changes after the treatment with NCBBH. Cell shrinkage and chromatin condensation were observed, characterized by bright staining as shown in Figure 5A, which may correspond to the features of apoptosis.

This apoptosis-inducing effect was then confirmed by flow cytometry. As shown in Figure 5B, with the increase of NCBBH dosage, the percentage of MG-63 cells undergoing apoptosis rose. At the concentration of 2.26 μM, apoptosis was detected in around 33% of the cells. In the group treated with 4.52 μM NCBBH, there were more cells found in the late apoptotic stage when compared with that in the group exposed to a lower dosage of NCBBH though the percentage of cells in the early apoptotic stage might be smaller. The loss of mitochondrial membrane potential after NCBBH treatment was also detected as shown in Figure 5C. The percentages of cells that were detected with mitochondrial depolarization in control, 0.165 μM, and 1.13 μM treatment groups were, respectively, 3.3%, 11.3%, and 13.3%.

DOI: 10.1021/acs.jafc.5b00106
J. Agric. Food Chem. 2015, 63, 3903−3914

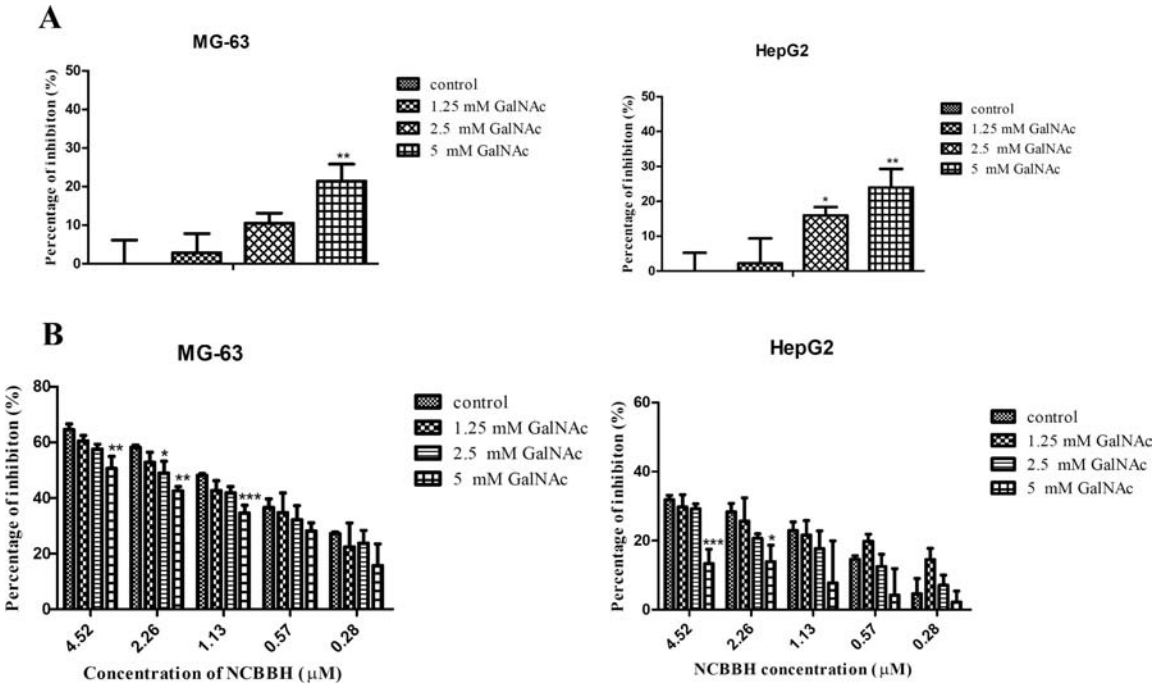

Figure 6. Effect of GalNAc on the anticancer efficiency of NCBBH. (A) GalNAc showed toxicity on tumor cells. Cancer cells were cultured with different concentrations of GalNAc for 48 h. Cells cultured without GalNAc were taken as the control. (B) The presence of GalNAc suppressed the antiproliferative effect of NCBBH. Cancer cells were cultured with different concentrations of NCBBH in the presence or absence of GalNAc for 48 h. To eliminate the antiproliferative effect of GalNAc on cancer cells, cells cultured in the presence of both GalNAc and NCBBH were compared with the cells cultured only in GalNAc to calculate the percentage of inhibition. The statistic analysis compared the inhibition rate of NCBBH (at a specific concentration) in the presence of different concentrations of GalNAc, taking the group cultured in the same concentration of NCBBH but without GalNAc as the control using one way ANOVAL. $P < 0.05$ was taken as statistically significant.

Western blotting assay with results presented in Figure 5D indicated that NCBBH treatment triggered the activation of mitochondrial pathway caspase-9 and apoptotic pathway related to endoplasmic reticulum stress (ERS), like PERK and IRE1-α, etc. The cleavage of PARP was also observed.

GalNAc Partially Inhibited the Antiproliferative Activity of NCBBH. GalNAc itself demonstrated toxicity on the cancer cells and with the increase of GalNAc concentration; there was a trend of a higher toxicity toward the cancer cells as shown in Figure 6A. However, the toxicity of GalNAc on MG-63 and HepG2 cells was only statistically significant at the concentrations of 5 and 2.5−5 mM, respectively. In order to eliminate the interference of GalNAc toxicity, cells cultured in the presence of both GalNAc and NCBBH were compared with the cells cultured at the same concentration of GalNAc to calculate the percentage of inhibition. The final statistical comparisons were made among the groups that were cultured in the same concentration of NCBBH but in different concentrations of GalNAc. From Figure 6B, an obvious trend was observed that with the increase of the concentration of NCBBH, the percentage of inhibition rates increased in both cell lines in the presence or absence of GalNAc and also confirmed that MG-63 cells was more sensitive to the treatment of NCBBH than HepG2 cells. When comparing groups cultured at the same concentrations of NCBBH but different concentrations of GalNAc, there was a trend showing that with the increase of the concentration of GalNAc, the antiproliferative activity of NCBBH decreased, but not all the groups were significantly different from the control which was cultured in the same concentration of NCBBH but without GalNAc.

Cytokine-Inducing Effect of NCBBH. NCBBH exerted an immunomodulatory function. The mRNA expression of IL-2, IFN-γ, and TNF-α were found to be more than 300-, 60-, and 10-fold higher after treatment with 1.37 μM NCBBH when compared with the control, and this augmenting effect was dose-dependent. The upregulation of IL-6 and IL-1β mRNA expression was not as striking as that of IL-2, IFN-γ, and TNF-α, but the differences between the NCBBH-treated groups and control were statistically significant as shown in Figure 7A. The secretion of some of the cytokines under the stimulation of NCBBH was detected by Western blotting as shown in Figure 7B. The secretion of IL-1β and IL-2 increased with the concentration of NCBBH. However, at a concentration of 1.37 μM, NCBBH exhibited an inhibitory effect on the secretion of IL-1β and TNF-α.

DISCUSSION

In the present study, a novel hemagglutinin with a molecular weight of 73 kDa was purified from Northeast China black beans and the similarities, and differences between this newly isolated hemagglutinin and previously reported lectin or hemmagglutinin are also discussed.

This hemagglutinin was found to be ion-dependent, which is in concordance with previous reports. The hemagglutinating activity of concanavalin A (Con A), the first lectin with its crystal structure elucidated, was also abolished after demetalization.[20] It had been pointed out that metal ions could affect the stability of its conformational structure and substrate binding capacity. Kaushik et al. conducted a more detailed investigation about the effect of metal ions on Con A by explicit solvent molecular dynamic simulations and pointed out that metal ions

DOI: 10.1021/acs.jafc.5b00106
J. Agric. Food Chem. 2015, 63, 3903−3914

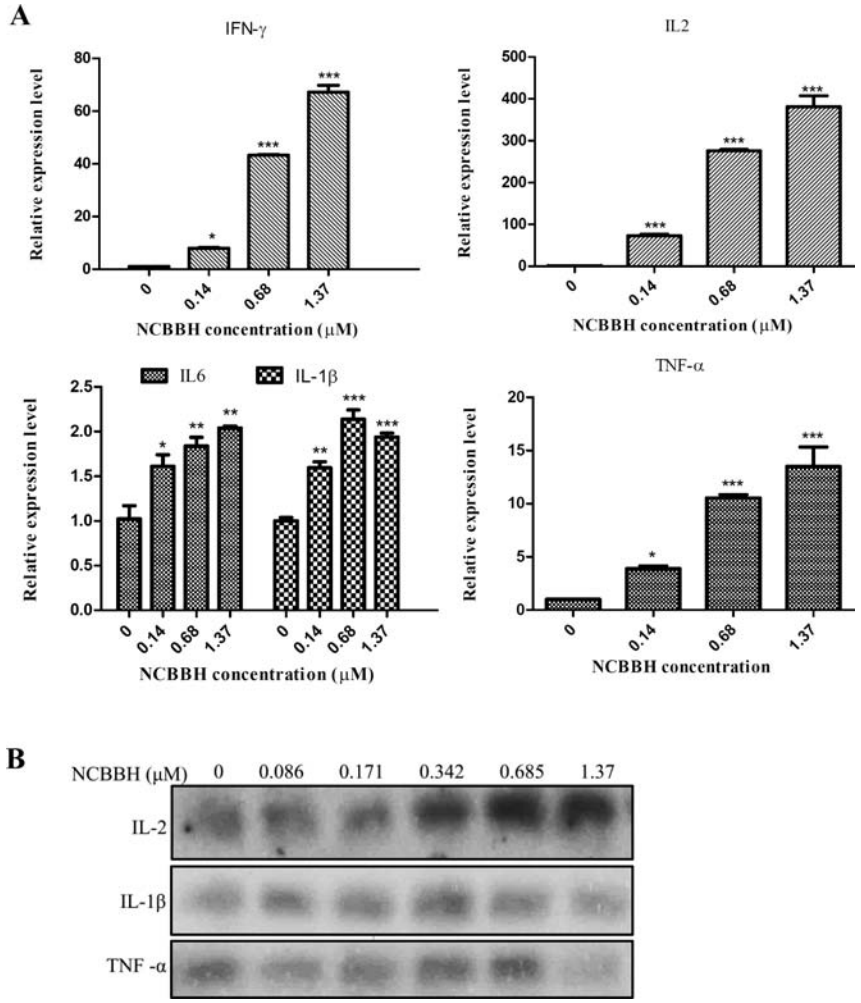

Figure 7. Modulation of the expression and secretion of cytokines by NCBBH. (A) NCBBH regulated the mRNA expression of cytokines. All of the treatment groups were compared with the control using one way ANOVAL. $P < 0.05$ was taken as statistic significant. (B) Splenocytes was cultured in FBS free medium with different concentrations of NCBBH for 24h. The same volume of supernatant from different groups was taken for Western blotting. The number of cells and final volume of medium were kept the same for all groups to make up the vacancy of standards.

Table 4. Comparison of Lectins/Hemagglutinins from Different Black Beans

characteristics	Korean large black soybean lectin[24] (kDa)	Chinese small glossy black soybean lectin[23]	Chinese little black soybean lectin[23]	NCBBH
mol wt (kDa)	48	50.2	62	73
N-terminal sequence	AETVSFSITKFVPDQ1	AETVSFSWNKFVPKQ15	1AETVSFSWNKFVPKQ15	Unavailable
pH stability	3−10	2−13	2−13	2−11
thermal stability (°C)	up to 60	up to 70	up to 40	up to 60
sugar specificity[a]	galactose (+)	galactose (+)	galactose (+)	galactose (−)
	arabinose (+)	arabinose (+)	arabinose (+)	arabinose (−)
	raffinose (+)	raffinose (+)	raffinose (+)	raffinose (−)
	melibiose (+)	melibiose (+)	melibiose (+)	galnac (+)
	lactose (+)	lactose (−)	lactose (−)	lactose (−)
antitumor activity	NPC (undetectable up to 20 μM)	HepG2 (72 h, IC_{50} = 4.1 μM)	not tested	HepG2 (48 h, IC_{50} = 9 μM)
		MCF-7 (72 h, IC_{50} 2.6 μM)		MG-63 (48 h, IC_{50} = 4.52 μM)

[a]+ or − indicates the sugar could or could not abolish the hemagglutinaing activity. NPC: the human nasopharyngeal carcinoma cell line. MCF-7: breast cancer cell line.

in Con A were originally coordinated by residues that carried negative charges; when metal ions were absent, the structure of the ion binding loop would undergo conformational deformation due to strong electrostatic repulsion, leading to the drifting of substrate sugars and abolition of hemagglutinating activity.[21] These studies provide us references on the explanations of the metal ion-dependence phenomenon of some plant lectins.

DOI: 10.1021/acs.jafc.5b00106
J. Agric. Food Chem. 2015, 63, 3903−3914

A comparison was made among lectins or hemagglutinins isolated from different black beans in the aspects of their thermal stability, molecular weight, and antitumor activity, etc., as shown in Table 4.[22,23] The most distinct difference between NCBBH and other black bean lectins is the carbohydrate specificity. Hemagglutinating activity of lectins isolated from Korean large black soybeans, Chinese small glossy black soybean, and Chinese little black soybeans could all be inhibited by galactose, arabinose, raffinose, and melibiose and only differed in lactose while none of these sugars inhibited the activity of NCBBH. Among the 13 sugars tested in the present study, GalNAc could partially inhibit the hemagglutinating activity of NCBBH at a very high concentration. It indicates that NCBBH is different from previously purified lectins of black beans and possesses complex carbohydrate specificity. One of the most interesting issues about lectin or hemagglutinin is whether their biological functions are dependent on their interactions with carbohydrates on the membrane of cells. According to the research of Wong et.al, both Con A and knife bean lectin manifested specify for glucose, but only the antiproliferative activity of Con A could be inhibited by glucose while the anti-HIV activity of both Con A and knife bean lectin could not be abolished by glucose.[24] The importance of lectin/hemagglutinin-carbohydrate interactions is still inexplicit or is case-specific. As we have illustrated previously, except for the specific carbohydrate binding property, structural specificity and other unique features may amplify the biological function.[25] The BH1(of Bcl-2 family)-like domain in gal-3 may contribute to its antiapoptotic function in cancer cells, and except for the B chain (a lectin chain), the A chain (an enzyme chain) in mistletoe lectin-II promoted its anticancer effect by inhibiting protein synthesis.[25]

In the present study, GalNAc partially inhibited the hemagglutinating activity of NCBBH, which indicates that this hemagglutinin may recognize several types of carbohydrate and initiate different biological reactions by binding to them. To determine whether GalNAc could also partially inhibit the antiproliferation effect of NCBBH, we cultured MG-63 cells and HepG2 cells with different concentrations of NCBBH in the presence and absence of GalNAc and made comparisons of their inhibition rates. The results revealed that, consistent with the hemagglutinating assay, GalNAc could also partially inhibit the antiproliferative activity of NCBBH on MG-63 and HepG2 cells, which indicated that this GalNAc binding sites on NCBBH may take a role in its antiproliferative function on these two cell lines.

When compared with lectins or hemagglutinin isolated from different cultivars of the same species, *Phaseolus vulgaris*, like "brown kidney bean", "French bean number 35", Hokkaido red bean, and another French bean, NCBBH differs from them in many aspects. Regarding antitumor activity, the IC_{50} of lectin from "brown kidney bean" and "French bean number 35" on HepG2 cells were, respectively, 32.85 and 100 μM, and lectins isolated from Hokkaido red bean and another French bean exhibited a very weak inhibitory effect on HepG2 cells, with IC_{50} too high to be determined.[10,12,26,27] Therefore, comparatively speaking, NCBBH demonstrated a potent antiproliferative effect on this tumor cell line.

It is interesting to find that NCBBH exhibited selective toxicity toward MG-63, HepG2, and WRL68 cells. This selective activity was thought to be caused by the difference of binding affinities of NCBBH on cells. In order to confirm it, NCBBH was labeled by FITC and allowed to bind cells in culture medium for 24 h. The signal of FITC in the cells was then measured by a flow cytometer. The results showed that MG-63 showed the highest FITC signal, followed by WRL68 and HepG2, which was not completely in consistent with the rank of NCBBH toxicity toward these three cell lines. This may help explain why MG-63 cells were more sensitive to the treatment of NCBBH than HepG2 cell, but it cannot explain why NCBBH was more toxic to HepG2 cells than to WRL68 cells. The difference of distribution of NCBBH in the cells were then monitored and compared. At 3 h, NCBBH was found both on the membrane and cytoplasm of HepG2 cells and WRL68 cells, while in MG-63 cells, NCBBH was mainly found in the cytoplasm, which may indicate that MG-63 was more efficient in the transportation of NCBBH from membrane to the cytoplasm. At 24 h, NCBBH was mainly found in the cytoplasm of cells in all cell lines. As observed in Figure 4B, NCBBH tended to be evenly and wide distributed in the cytoplasm of HepG2 and MG-63 cells. However, in WRL68 cells, NCBBH seemed to cluster in an area around the nucleus. The discrepancy may be caused by the divergence of glycoprotein expression on the organelle in different cell lines. However, further study was in need to elucidate the mechanisms of the selectivity of NCBBH toxicity on these three cell lines.

This novel hemagglutinin demonstrated antiproliferative and apoptosis inducing affects on MG-63 cells. In normal cells, phosphatidylserine (PS) is usually kept on the inner cell membrane. When cells undergo apoptosis, PS will be exposed on the surface to facilitate the recognition of apoptotic bodies by phagocytic cells; hence PS externalization is taken as a general marker of cell apoptosis.[28−30] Annexin V-PI staining suggested that treatment with NCBBH triggered PS externalization. DNA condensation and fragmentation which is another characteristic of cell apoptosis was observed using Hoechst 33342 staining. Mitochondria have been demonstrated to play a key role in cell apoptosis through control of mitochondrial membrane potential ($\Delta\Psi$m) and permeability. The mitochondrial permeability transition pore (PTP) is regulated by both pH and $\Delta\Psi$m. When $\Delta\Psi$m decreases, PTP opening increases and results in the swelling of mitochondrial matrix as well as the leakage of pro-apoptotic proteins.[30] The addition of NCBBH brought about dissipation of $\Delta\Psi$ and triggered the apoptosis of osteosarcoma cells. Besides, NCBBH could also trigger cell apoptosis by initiating endoplasmic reticulum stress (ERS) and unfolded protein response (UPR). This was evidenced by Western blot which disclosed enhanced expression of caspase-12, IRE1-α, and PERK.

Eradicating cancer through immune modulation has been proposed and explored with heightened efforts recently. Cytokines which are molecular messengers to evoke the immune system are demonstrated to directly stimulate immunocytes at the tumor site and facilitate the recognition of tumor cells by cytotoxic effector cells.[31] Animal studies have already demonstrated the effectiveness of cytokine-based approaches in cancer treatment. Two cytokines, IL-2 and IFN-α, have been approved by the FDA (Food and Drug Administration) as anticancer agents, while several other cytokines are undergoing clinical trials. Treatment with high-dose IL-2 can induce significant regression of metastatic melanoma and renal cell cancer in selective patients.[32] In our study, the IL-2 mRNA expression level was enhanced more than 300-fold after treatment with 1.37 μM NCBBH for 4 h when compared with the control, which together with the

DOI: 10.1021/acs.jafc.5b00106
J. Agric. Food Chem. 2015, 63, 3903−3914

apoptosis-triggering effect revealed the great potential of NCBBH as an anticancer agent.

In addition, the high pH and thermal stability of NCBBH make it possible to combine this protein with slow-release and point-insert biomaterials to make the treatment more specific. The application of proteins to the treatment of osteosarcoma has rarely been reported; the present report represents the first time that a lectin has been employed in the treatment of osteosarcoma, and the results are promising. We also found that this hemagglutinin exhibited different levels of toxicity on MG-63, HepG2, and WRL 68 cells. The difference may be attributed to the divergence of sugar or glycoprotein expression of cells, but it still needs further study. Such research may help reveal the functions of certain glycoprotein in cells and contributes to a more specific design of anticancer drugs.

AUTHOR INFORMATION

Corresponding Author

*E-mail: b021770@mailserv.cuhk.edu.hk. Tel.: (00852) 39438031. Fax.: (00852) 26035123.

Notes

The authors declare no competing financial interest.

ACKNOWLEDGMENTS

E.F.F. was supported by the Intramural Research Program of the NIH, National Institute of Aging.

ABBREVIATIONS USED

IL-2, interleukin-2; IL-6, interleukin-6; IL-1β, interleuin-1β; IFN-γ, interferon gamma; TNF-α, tumor necrosis factor alpha; NCBBH, purified hemagglutinin isolated from the Northeast China black beans; FPLC, fast protein liquid chromatography; EDTA, ethylenediaminetetraacetic acid; MG-63, human osteosarcoma cell line; HepG2, hepatoma cells; WRL 68, human embryonic liver; MTT, 3-(4,5-dimethylthiazol-2yl)-2,5-diphenyltetrazolium bromide

REFERENCES

(1) Gill, J.; Ahluwalia, M. K.; Geller, D.; Gorlick, R. New targets and approaches in osteosarcoma. *Pharmacol. Ther.* **2013**, *137*, 89−99.

(2) Marcove, R. C.; Mike, V.; Hajek, J. V.; Levin, A. G.; Hutter, R. V. Osteogenic sarcoma under the age of twenty-one. A review of one hundred and forty-five operative cases. *J. Bone Joint Surg Am.* **1970**, *52*, 411−23.

(3) Bielack, S. S.; Kempf-Bielack, B.; Delling, G.; Exner, G. U.; Flege, S.; Helmke, K.; Kotz, R.; Salzer-Kuntschik, M.; Werner, M.; Winkelmann, W.; Zoubek, A.; Jurgens, H.; Winkler, K. Prognostic factors in high-grade osteosarcoma of the extremities or trunk: an analysis of 1,702 patients treated on neoadjuvant cooperative osteosarcoma study group protocols. *J. Clin. Oncol.* **2002**, *20*, 776−90.

(4) Ayan, I.; Kebudi, R.; Ozger, H. Childhood osteosarcoma: multimodal therapy in a single-institution Turkish series. *Cancer Treat. Res.* **2009**, *152*, 319−38.

(5) Vijayan, M.; Chandra, N. Lectins. *Curr. Opin. Struct. Biol.* **1999**, *9*, 707−14.

(6) Lam, S. K.; Ng, T. B. Lectins: production and practical applications. *Appl. Microbiol. Biotechnol.* **2011**, *89*, 45−55.

(7) Vandenborre, G.; Smagghe, G.; Van Damme, E. J. Plant lectins as defense proteins against phytophagous insects. *Phytochemistry* **2011**, *72*, 1538−50.

(8) Garner, O. B.; Baum, L. G. Galectin-glycan lattices regulate cell-surface glycoprotein organization and signalling. *Biochem. Soc. Trans.* **2008**, *36*, 1472−1477.

(9) Guillot, J.; Konska, G. Lectins in higher fungi. *Biochem. Syst. Ecol.* **1997**, *25*, 203−230.

(10) Lam, S. K.; Ng, T. B. Isolation and characterization of a French bean hemagglutinin with antitumor, antifungal, and anti-HIV-1 reverse transcriptase activities and an exceptionally high yield. *Phytomedicine* **2010**, *17*, 457−62.

(11) Lei, H. Y.; Chang, C. P., Lectin of Concanavalin A as an anti-hepatoma therapeutic agent. *J. Biomed. Sci.* **2009**, *16*.10.1186/1423-0127-16-10

(12) Sharma, A.; Wong, J. H.; Lin, P.; Chan, Y. S.; Ng, T. B. Purification and characterization of a lectin from the Indian cultivar of French bean seeds. *Protein Pept. Lett.* **2010**, *17*, 221−7.

(13) Sharma, U.; Katre, U. V.; Suresh, C. G. Crystal structure of a plant albumin from Cicer arietinum (chickpea) possessing hemopexin fold and hemagglutination activity. *Planta* **2015**, DOI: 10.1007/s00425-014-2236-6.

(14) Rao, K. N.; Suresh, C. G.; Katre, U. V.; Gaikwad, S. M.; Khan, M. I. Two orthorhombic crystal structures of a galactose-specific lectin from Artocarpus hirsuta in complex with methyl-alpha-D-galactose. *Acta Crystallogr., Sect. D: Biol. Crystallogr.* **2004**, *60*, 1404−12.

(15) Hester, G.; Wright, C. S. The mannose-specific bulb lectin from Galanthus nivalis (snowdrop) binds mono- and dimannosides at distinct sites. Structure analysis of refined complexes at 2.3 and 3.0 A resolution. *J. Mol. Biol.* **1996**, *262*, 516−31.

(16) Barre, A.; Bourne, Y.; Van Damme, E. J.; Peumans, W. J.; Rouge, P. Mannose-binding plant lectins: different structural scaffolds for a common sugar-recognition process. *Biochimie* **2001**, *83*, 645−51.

(17) Lin, P.; Ng, T. B. Preparation and biological properties of a melibiose binding lectin from Bauhinia variegata seeds. *J. Agric. Food Chem.* **2008**, *56*, 10481−6.

(18) Wang, H.; Gao, J.; Ng, T. B. A new lectin with highly potent antihepatoma and antisarcoma activities from the oyster mushroom Pleurotus ostreatus. *Biochem. Biophys. Res. Commun.* **2000**, *275*, 810−6.

(19) Fang, E. F.; Zhang, C. Z.; Zhang, L.; Wong, J. H.; Chan, Y. S.; Pan, W. L.; Dan, X. L.; Yin, C. M.; Cho, C. H.; Ng, T. B. Trichosanthin inhibits breast cancer cell proliferation in both cell lines and nude mice by promotion of apoptosis. *PLoS One* **2012**, *7*, e41592.

(20) Edelman, G. M.; Cunningham, B. A.; Reeke, G. N., Jr.; Becker, J. W.; Waxdal, M. J.; Wang, J. L. The covalent and three-dimensional structure of concanavalin A. *Proc. Natl. Acad. Sci. U. S. A.* **1972**, *69*, 2580−4.

(21) Kaushik, S.; Mohanty, D.; Surolia, A. The role of metal ions in substrate recognition and stability of concanavalin A: a molecular dynamics study. *Biophys. J.* **2009**, *96*, 21−34.

(22) Lin, P.; Ye, X.; Ng, T. Purification of melibiose-binding lectins from two cultivars of Chinese black soybeans. *Acta Biochim. Biophys. Sin.* **2008**, *40*, 1029−38.

(23) Fang, E. F.; Wong, J. H.; Lin, P.; Ng, T. B. Biochemical and functional properties of a lectin purified from korean large black soybeans–a cultivar of glycine max. *Protein Pept. Lett.* **2010**, *17*, 690−8.

(24) Wong, J. H.; Ng, T. B. Isolation and characterization of a glucose/mannose/rhamnose-specific lectin from the knife bean Canavalia gladiata. *Arch. Biochem. Biophys.* **2005**, *439*, 91−8.

(25) Dan, X. L.; Ng, T. B. Lectins in human cancer: both a devil and an angel? *Curr. Protein Pept. Sci.* **2013**, *14*, 481−91.

(26) Chan, Y. S.; Wong, J. H.; Fang, E. F.; Pan, W.; Ng, T. B. Isolation of a glucosamine binding leguminous lectin with mitogenic activity towards splenocytes and anti-proliferative activity towards tumor cells. *PLoS One* **2012**, *7*, e38961.

(27) Wong, J. H.; Wan, C. T.; Ng, T. B. Characterisation of a haemagglutinin from Hokkaido red bean (Phaseolus vulgaris cv. Hokkaido red bean). *J. Sci. Food Agric.* **2010**, *90*, 70−7.

(28) Smrz, D.; Draberova, L.; Draber, P. Non-apoptotic phosphatidylserine externalization induced by engagement of glycosylphosphatidylinositol-anchored proteins. *J. Biol. Chem.* **2007**, *282*, 10487−97.

(29) Shiratsuchi, A.; Osada, S.; Kanazawa, S.; Nakanishi, Y. Essential role of phosphatidylserine externalization in apoptosing cell phagocytosis by macrophages. *Biochem. Biophys. Res. Commun.* **1998**, *246*, 549−55.

DOI: 10.1021/acs.jafc.5b00106
J. Agric. Food Chem. 2015, 63, 3903−3914

(30) Ly, J. D.; Grubb, D. R.; Lawen, A. The mitochondrial membrane potential (deltapsi(m)) in apoptosis; an update. *Apoptosis* **2003**, *8*, 115−28.
(31) Lee, S.; Margolin, K. Cytokines in cancer immunotherapy. *Cancers* **2011**, *3*, 3856−93.
(32) Rosenberg, S. A.; Yang, J. C.; Topalian, S. L.; Schwartzentruber, D. J.; Weber, J. S.; Parkinson, D. R.; Seipp, C. A.; Einhorn, J. H.; White, D. E. Treatment of 283 consecutive patients with metastatic melanoma or renal cell cancer using high-dose bolus interleukin 2. *JAMA* **1994**, *271*, 907−13.

DOI: 10.1021/acs.jafc.5b00106
J. Agric. Food Chem. 2015, 63, 3903−3914

the interaction of an amino group on a protein with a carbonyl group on a polysaccharide, leading to the formation of an N-substituted glycosylamine and then to an aldimine (Schiff base), which undergoes a rearrangement that results in an Amadori rearrangement product.[21] After these initial stages, a series of complex chemical reactions occurs, which eventually leads to degradation of the Amadori products and the formation of a wide variety of reaction products.[22] Some of these products have color and aroma characteristics that are undesirable for food quality. Therefore, it is often important to prevent the later stages of the Maillard reaction from occurring when using it to stabilize proteins.

As mentioned earlier, one of the main limitations to using resveratrol as a nutraceutical ingredient is its low oral bioavailability. Nanoparticles can often be designed to increase the bioavailability of the compounds encapsulated within them. The small size of the particles confers colloidal delivery systems with unique physicochemical characteristics that may enhance the bioavailability of lipophilic nutraceuticals.[23] This increase in bioavailability may occur for a number of different reasons: enhanced solubility in intestinal fluids; improved protection against chemical or metabolic transformations within the gastrointestinal tract; prolonged residence time due to mucoadhesion of the particles to the intestinal wall; or increased absorption by epithelium cells.[24] Studies have shown that the hydrolysis of Maillard conjugates by the digestive enzymes found in the gastrointestinal tract is lower than the hydrolysis of native proteins.[18,25] This could result in differences in the bioaccessibility of compounds encapsulated in conjugated or non-conjugated protein-based delivery systems.

The aim of the current study was to determine the effect of encapsulation on the physicochemical stability and bioaccessibility of resveratrol. Resveratrol was encapsulated using two different approaches: (i) within biopolymer complexes or (ii) within biopolymer nanoparticles. The biopolymer complexes were formed by binding the resveratrol to either caseinate or caseinate−dextran. The biopolymer nanoparticles were formed by coating a zein core with either a caseinate or a caseinate−dextran shell. The caseinate−dextran complexes were formed by heating the protein and carbohydrate together under appropriate conditions to induce the Maillard reaction. The physicochemical stability and bioaccessibility of the encapsulated resveratrol were determined to establish the potential efficacy of these two delivery systems. The results of this study will facilitate the rational design of effective encapsulation technologies that can enhance both the stability and effectiveness of hydrophobic nutraceuticals.

MATERIALS AND METHODS

Materials. Resveratrol standard (purity ≥ 99%) was purchased from Extrasynthese (Lyon, France). Sodium dodecylsufate (SDS), *o*-phthalaldehyde (OPA, ≥99%), leucine, and 2-mercaptoethanol were purchased from Merck (Madrid, Spain). Dextran (40 kDa), pepsin, pancreatin, and bile extract were purchased from Sigma-Aldrich Co. (Madrid, Spain). Ethanol 96% was purchased from OPPAC (Navarra, Spain). Sodium tetraborate analytical grade was purchased from Probus (Barcelona, Spain). Soy lecithin was purchased from Guinama (Valencia, Spain). Ammonium carbonate analytical grade was purchased from Alfa Aesar (Ward Hill, MA, USA). All other chemicals, reagents, and solvents were purchased from Panreac (Barcelona, Spain) and were of analytical grade unless otherwise stated. Resveratrol (99%) from grape skin extract was purchased from Changsha Organic Herb Inc. (Changsha, China). Food grade zein was purchased from Kobayashi Perfumery Co. (Tokyo, Japan). Sodium caseinate was kindly provided by VicorQuimia (Barcelona, Spain).

Maillard Conjugate Formation. Sodium caseinate (2% w/v) and dextran (3.5% w/v) were solubilized overnight at 5 °C in double-distilled water. The completely solubilized and hydrated samples were subsequently spray-dried (Mini Spray Drier B-191, Büchi, Flawil, Switzerland) using an inlet temperature of 180 °C, a feed rate of 7.5 mL/min, a compressed air pressure of 600 kPa, and an air flow rate of 35 m^3/h. Maillard conjugation reactions were performed by incubating the spray-dried mixture at 60 °C and 76% relative humidity for up to 48 h.[17,26] The relative humidity was maintained using a desiccator containing a saturated potassium bromide solution. After conjugation, the samples were allowed to cool to room temperature, ground using a mortar and pestle, and then stored in a desiccator prior to use.

Maillard Conjugate Characterization. *Conjugation Efficiency.* The conjugation efficiency was determined by measuring reduction in free amino groups using the OPA assay. OPA reagent was prepared freshly prior to use according to the method of Pan et al.[26] In short, 40 mg of OPA (dissolved in 1.0 mL of 95% ethanol v/v), 25 mL of 0.100 M sodium tetraborate buffer (pH 9.5), 2.5 mL of 20% SDS solution (w/v), and 0.10 mL of 2-mercaptoethanol were mixed together and brought to a final volume of 50 mL. After solubilization of the conjugates (5 mg mL^{-1}), 0.10 mL of the dispersion was mixed with 2.70 mL of OPA reagent and incubated for 1 min at room temperature. The absorbance at 340 nm was then measured immediately using a UV−vis spectrophotometer (Thermo Scientific Multiskan GO spectrophotometer, ThermoFisher Scientific, Vartaa, Finland). Calibration curves were constructed using L-leucine (0.2−5 mM) as a standard compound containing an amino group.[17,26] The conjugation efficiency was defined as follows:

$$\text{conjugation efficiency (\%)} = \left(1 - \frac{\text{amine groups after conjugation (M)}}{\text{amine groups before conjugation (M)}}\right) \times 100 \quad (1)$$

Stabilizing Effect of the Conjugation. The stabilizing effect of conjugation on casein was assessed by measuring the reduction in turbidity of conjugated samples around the isoelectric point of the protein (pH 4.6). Samples were dissolved in double-distilled water at concentrations of 5 mg mL^{-1} and subsequently acidified to pH 4.6 with HCl. Nephelometric turbidity units (NTU) of the samples were measured in a turbidimeter (Turbiquant 3000 IR, Merck, Darmstadt, Germany).

Browning. To assess browning caused by the Maillard reaction, the absorbance of conjugates was measured at 420 nm. Conjugates were dissolved in double-distilled water (5 mg mL^{-1}) and then diluted 5 times. The absorbance at 420 nm was measured using the UV−vis spectrophotometer with 1 cm polystyrene cuvettes.

Resveratrol Solubility. The solubility of resveratrol in the solvent was assessed by quantifying the amount of resveratrol dispersed in the antisolvent phase [1% (w/v) sodium caseinate solution, pH 7] after 120 h of storage at room temperature.[27] Different amounts of grape skin extract (25−1500 μg mL^{-1}) were dispersed in the antisolvent phase following the procedure described under Fabrication of Resveratrol-Loaded Core−Shell Nanoparticles without zein. After this storage period, samples were centrifuged for 10 min at 1000 rpm using an eppendorf centrifuge (Centrifuge 5415R, Eppendorf, Hamburg, Germany). An aliquot of supernatant was collected, diluted in DMSO, and measured as described under Resveratrol Quantification. The diluted antisolvent phase without grape skin extract was used as a blank.

Fabrication of Resveratrol-Loaded Core−Shell Nanoparticles. Zein (3% w/v) was dissolved in 85% (v/v) ethanol by stirring for 45 min followed by filtration using a filter paper. The filtered zein solution was subsequently added to the antisolvent at a 1:5 ratio under continuous stirring (440 rpm) at room temperature. The antisolvent phase consisted of aqueous sodium caseinate or Maillard conjugate solutions (pH 7.0, final protein concentration of 1% w/v). After addition, the particle suspensions were stirred for an additional 2 min.

DOI: 10.1021/acs.jafc.5b00777
J. Agric. Food Chem. 2015, 63, 3915−3923

Ethanol was removed from the mixtures using a vacuum oven (Binder, Binder GmbH, Tuttligen, Germany) at 30 °C for 1.5 h. For the nanoparticles loaded with resveratrol, 0.15% (w/v) of grape skin extract was dissolved in the solvent phase prior to particle formation. The final particle suspensions contained 0.5% (w/v) zein and 0.025% (w/v) resveratrol.

Fabrication of Resveratrol-Loaded Biopolymer Complexes. Resveratrol-loaded biopolymer complexes were prepared by mixing resveratrol (0.15% (w/v) of grape skin extract in 85% (v/v) ethanol) with an aqueous solution containing sodium caseinate or Maillard conjugates (Resveratrol Solubility). The final particle suspensions contained 1% (w/v) sodium caseinate and 0.025% (w/v) resveratrol.

Resveratrol Quantification. The resveratrol level contained in the nanoparticles was measured using a UV−visible spectrophotometer (Thermo Scientific Multiskan GO spectrophotometer) at a wavelength of 307 nm. Pure resveratrol was dissolved in dimethyl sulfoxide (DMSO) at 100 μg/mL and then diluted to create a calibration curve with concentrations ranging from 0.2 to 6.0 μg/mL.

Characterization of Nanoparticles. *Particle Size and ζ-Potential.* Mean particle diameter, polydispersity index, and particle size distribution based on number were obtained using a dynamic light scattering instrument (Zetasizer 3000, Malvern Instruments, Malvern, UK). The ζ-potential was determined by particle electrophoresis using the same instrument. Samples were diluted 20 times to avoid multiple scattering effects and equilibrated at 25 °C prior to analysis.

Retention Efficiency (RE). The capacity of the delivery systems to retain resveratrol was determined using the following equation:

$$\mathrm{RE}\,(\%) = \left(1 - \frac{C_F}{C_T}\right) \times 100 \tag{2}$$

Here, C_T is the resveratrol contained in the suspension and C_F is the amount of free resveratrol. The free resveratrol was determined as the amount of resveratrol that was collected in the filtrate receiver after being centrifuged at 4020*g* for 30 min using a benchtop centrifuge (Sigma 3K30, Sigma GmbH, Osterode am Harz, Germany). The sample was placed in a centrifugal filter (Amicon Ultracel-10 kDa 2 mL Millipore, Cork, Ireland).[28] The recovery yield of resveratrol after passing through the filter (92%) was taken into account to correct the actual amount of resveratrol in the filtrate. The resveratrol contained in the nanoparticles and the filtrate was assessed by diluting the suspension in DMSO[29] prior to quantification as described under Resveratrol Quantification. The suspensions without resveratrol were used as blank samples.

UV Light Stability. The stability of *trans*-resveratrol to light-induced isomerization was assessed using a UV light lamp and cabinet. An aliquot of 5 mL of each sample was poured into a Petri dish (60 mm diameter) and exposed to UV light at 365 nm for 1 h.[7] The remaining *trans*-resveratrol was measured as described under Resveratrol Quantification after the sample was diluted in DMSO. The suspensions without resveratrol were used as blanks.

In Vitro Digestion Model. A dynamic in vitro gastrointestinal model was used to study the influence of the biopolymer particle composition on resveratrol bioaccessibility. The gastrointestinal model was based on the work by Minekus et al.[30] with modifications. The mouth phase was not included in this work because most liquids do not require an oral phase, mainly due to the very short residence times in the oral cavity.[30]

Gastric Phase. The suspension (10 mL) was mixed with simulated gastric fluid (SGF, 10 mL) that had a composition shown in Table 1. The resulting mixture was readjusted to pH 3.0 using NaOH or HCl solution and then shaken continuously at 150 rpm and 37 °C in an incubator (Incubator Mini Shaker, VWR, Radnor, PA, USA) for 2 h to mimic the temperature and motility of the stomach. The samples were then transferred to the intestinal phase. An aliquot of the gastric phase was diluted 10 times in the simulated gastric buffer, and the particle size and ζ-potential were analyzed as described under Particle Size and ζ-Potential.

Intestinal Phase. The "chyme" sample collected from the gastric phase (15 mL) was mixed with simulated intestinal fluids (SIF, 15 mL) with a composition shown in Table 1. The resulting mixture was then readjusted to pH 7.0 using NaOH or HCl solution and then shaken continuously at 150 rpm and 37 °C in an incubator (Incubator Mini Shaker, VWR) for 2 h to mimic the temperature and movement of the intestine. The samples were then transferred to centrifugal tubes to determine the bioaccessibility of resveratrol. An aliquot of the intestinal phase was diluted 5 times in the simulated intestinal buffer, and the particle size and ζ-potential were analyzed as described under Particle Size and ζ-Potential.

Table 1. Final Concentrations of Constituents before Addition to the Sample of the Simulated Gastric and Intestinal Fluids

	simulated gastric fluid	simulated intestinal fluid
constituent	pH 3	pH 7
	mmol L^{-1}	
KCl	5.52	5.44
KH_2PO_4	0.72	0.64
$NaHCO_3$	20.00	68.00
NaCl	37.76	30.72
$MgCl_2(H_2O)_6$	0.08	0.26
$(NH_4)_2CO_3$	0.40	
NaOH		3.73
HCl	22.48	6.72
$CaCl_2(H_2O)_2$	0.07	0.30
lecithin[a]	0.17	
	U mL^{-1}	
pepsin[b]	2000.00	
pancreatin[c]		100.00
	mg mL^{-1}	
bile extract		6.25

[a]Based on the average molecular weight of lecithin (787 g mol^{-1}). [b]Made up in SGF. [c]Made up in SIF and based on the protolithic activity.

Bioaccessibility Determination. The bioaccessibility of resveratrol was evaluated after the samples had passed through the simulated small intestine phase of the gastrointestinal model. Aliquots of 10 mL of the samples were centrifuged (10000*g* for 40 min at 10 °C) using a benchtop centrifuge (Sigma 3K30, Sigma GmbH). After centrifugation, the samples separated into a sediment phase at the bottom and a clear micelle phase at the top. Aliquots (5 mL) were collected from the supernatant ("micelle phase") and filtered using a syringe filter (17 mm, 0.45 μm, PVDF, ThermoFisher Scientific, Rockwood, TN, USA). After filtration, the samples were diluted in DMSO and the resveratrol was measured as described under Resveratrol Quantification. The bioaccessibility (BA) was determined using the equation

$$\mathrm{BA}\,(\%) = \frac{C_M}{C_I} \times 100 \tag{3}$$

where C_M is the resveratrol concentration in the micelle phase and C_I is the initial concentration of resveratrol in the suspension.[27] The suspensions without resveratrol were used as blanks.

Data Analysis. All experiments were performed in triplicate, and the results are given as mean values ± standard deviation. Differences among the treatments were determined using an analysis of variance (ANOVA) and a post hoc Tukey test with a confidence level of 95%. The analyses were made using SPSS software (IBM Corp., Armonk NY, USA).

RESULTS AND DISCUSSION

Conjugation Characterization. Initially, we carried out a series of experiments to assess the time dependence of the formation of protein−carbohydrate conjugates through the

DOI: 10.1021/acs.jafc.5b00777
J. Agric. Food Chem. 2015, 63, 3915−3923

Maillard reaction (Figure 1). The conjugation efficiency of the reaction of sodium caseinate with dextran was analyzed using

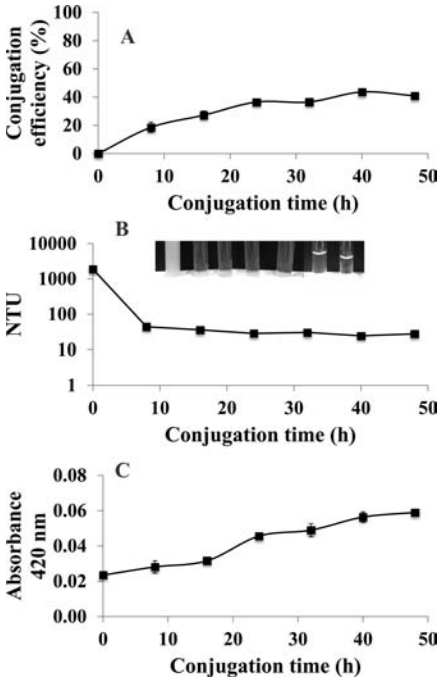

Figure 1. (A) Conjugation efficiency, (B) turbidity at pH 4.6, and (C) absorbance at 420 nm of the conjugates of sodium caseinate to dextran 40 kDa. (Inset) Appearance of the solutions (5 mg mL^{-1}) at pH 4.6: from left to right, 0, 8, 16, 24, 32, 40, and 48 h of conjugation. The conjugation was induced at 60 °C with 76% relative humidity for 48 h. The sampling was at intervals of 8 h. The ratio of dextran to sodium caseinate was 1.75 to 1.0 (w/w).

the OPA test, which quantifies the amount of unreacted amino groups remaining on the protein after conjugation (Figure 1A). The effect of conjugation on the aggregation stability of the sodium caseinate was assessed by measuring the turbidity of the conjugate solutions at the isoelectric point of the protein, that is, pH 4.6 (Figure 1B). The formation of brown colors in the samples as a result of the later stages of the Maillard reaction was determined by measuring the solution absorbance at 420 nm (Figure 1C).

The conjugation efficiency increased with increasing incubation time during the first 24 h and then reached a relatively constant level. The average number of amino groups per caseinate molecule available to react with reducing sugars of the polysaccharides has been reported to be 13.6.[17,26] This suggests that the number of dextran molecules attached per caseinate molecule were about 5.0 after 24 h of incubation (37% efficiency) and about 5.5 after 48 h of incubation (41% efficiency). The reduction in the conjugation rate with incubation time can be attributed to two effects: (i) a reduction in the number of amino groups available to react or (ii) steric hindrance caused by already attached dextran molecules.[17] The turbidity of the samples at pH 4.6 is related to the formation of protein aggregates near the isoelectric point of sodium caseinate. The absence of a net charge on the protein molecules reduces the electrostatic repulsion, which leads to the formation of protein aggregates.[31] Solutions containing aggregated caseinate appeared turbid because the protein aggregates were of a size that scattered light strongly (Figure 1B, inset).[32] The observed reduction in turbidity of the caseinate solutions after conjugation with dextran (Figure 1B), suggested that the carbohydrate chains inhibited protein aggregation near the isoelectric point. This stabilization can be attributed to an increase in the steric repulsion between the molecules after conjugation. The turbidity decreased sharply from 0 to 8 h of incubation, which indicated that this was sufficient time to form stable protein−carbohydrate conjugates. Finally, the presence of a brown color in the solutions due to the formation of secondary Maillard reaction products was determined by measuring changes in their absorbance at 420 nm.[22,33] This type of brown color is usually undesirable from a food quality perspective and should therefore be minimized. In addition, the appearance of color is the result of the degradation of the Amadori product,[22] which in advances stages of the Maillard reaction can lead to dissociation of the protein−carbohydrate conjugate. Therefore, it is important to keep the browning as low as possible. The absorbance of the samples continued to increase throughout the incubation period (Figure 1C), and therefore it is advantageous to use as short a conjugation time as possible.

Overall, our results suggest that a 24 h incubation period was an optimum compromise between increasing conjugation efficiency and decreasing browning reactions. Although there is a sharp increase in absorbance between 16 and 24 h, it is not until 24 that the conjugation efficiency and turbidity reached plateau values, with no changes observed between 24 and 36 h. We therefore used this time to fabricate the conjugates for the rest of the experiments described in this study.

Resveratrol Solubility. One of the factors that determine the efficacy of a delivery system is the maximum amount of the functional ingredient that can be incorporated into it. The amount of resveratrol that could be incorporated into aqueous solutions was therefore determined. Increasing amounts of grape skin extract were dispersed in a 1% (w/v) sodium caseinate solution (Figure 2). The dispersions were prepared

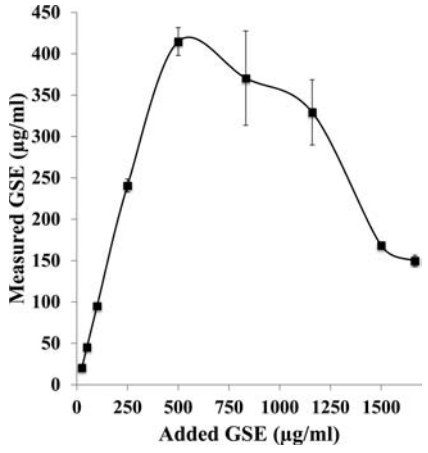

Figure 2. Dependence of the added and the dissolved grape skin extract in a 1% (w/v) of sodium caseinate solution. The dissolved resveratrol measurements were made at 307 nm after the samples had been centrifuged to remove any crystals.

using the same procedure as used to produce the nanoparticles by antisolvent precipitation (see Fabrication of Resveratrol-Loaded Core−Shell Nanoparticles), and then the mixtures were stored for 120 h at room temperature to allow the crystallization of any undissolved resveratrol.[34] The mixtures were then centrifuged, which caused the resveratrol crystals to

DOI: 10.1021/acs.jafc.5b00777
J. Agric. Food Chem. 2015, 63, 3915−3923

form a sediment at the bottom of the tubes, leaving a supernatant containing the dissolved resveratrol. The amount of dissolved resveratrol was then measured using a spectrophotometer. Adding up to 250 μg mL^{-1} of grape skin extract to the aqueous solution resulted in complete solubility of the resveratrol, indicated by the similarity of the added and measured resveratrol amounts. In this region the solution was either saturated or supersaturated with resveratrol. When 500 μg mL^{-1} of grape skin extract was added, the amount of measured resveratrol was only about 83% of the added resveratrol, which indicates that part of the resveratrol crystallized and precipitated. With a further increase in the amount of grape skin extract added, the measured resveratrol concentration actually decreased and the variability of the data became larger. This effect can be attributed to the fact that some of the supersaturated resveratrol crystallized, so that the amount of resveratrol remaining dissolved in the aqueous solution was equal to the equilibrium solubility.

The relatively high supersaturation of resveratrol in the aqueous solutions can be attributed to the presence of the sodium caseinate. It is known that proteins can act as nucleation and crystallization inhibitors by forming complexes with hydrophobic bioactive compounds, thus decreasing the nucleation rate.[34] In particular, resveratrol and sodium caseinate are known to form complexes through hydrophobic interactions and hydrogen bonding.[10] At 500 μg mL^{-1} of added grape skin extract, the amount of protein in the aqueous solution was insufficient to bind all of the resveratrol, leading to the formation of nuclei and crystals during the storage period.[34,35] From Figure 2 it can be deduced that the nucleation rate at grape skin extract concentrations >500 μg mL^{-1} was faster than the ability of the proteins to bind resveratrol, leading to sudden precipitation and lower amounts of resveratrol in the supernatant.

If a hydrophobic crystalline bioactive compound is going to be incorporated into an aqueous-based system, then it is important to ensure that it is present at a level below the loading capacity of the delivery system. Under these conditions, the saturation concentration will not be exceeded, and so bioactive precipitation during production, storage, or utilization will be avoided. For this reason, the grape skin extract concentration used in the remainder of this study was 250 μg mL^{-1}, that is, below the saturation level (Figure 2). Another important consideration when working with bioactive compounds is to reach the minimum concentration to promote a health benefit. In this case 250 μg mL^{-1} of grape skin extract in the colloidal dispersions represents 50 times the concentration typically found in wine (5 mg/L[36]).

Retention Efficiency. In this study, the retention efficiency means the amount of resveratrol associated within the biopolymer nanoparticles or complexes. The retention efficiency is important because it determines the fraction of the bioactive compound within a delivery system that is protected from degradation by external conditions, such as heat, light, or oxygen. The delivery systems could be classified into two groups according to their measured retention efficiencies (Figure 3), with the biopolymer nanoparticles (RE ≈ 83%) having a significantly higher retention efficiency (p < 0.05) than the biopolymer complexes (RE ≈ 68%). The retention efficiency of the biopolymer nanoparticles measured in this work was similar to that obtained in our previous study in which resveratrol was also encapsulated in zein nanoparticles formed by antisolvent precipitation.[8] All of the biopolymer

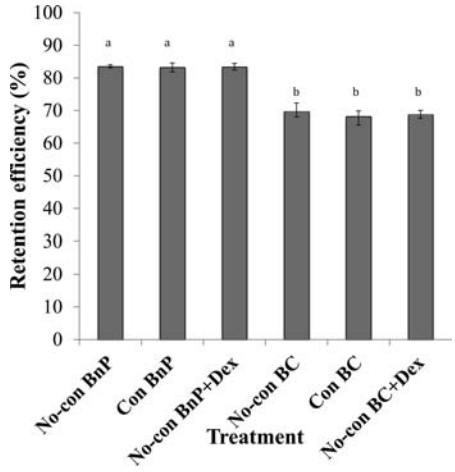

Figure 3. Retention efficiency of resveratrol in biopolymer nanoparticles (BnP) and biopolymer complexes (BC) loaded with grape skin extract prepared with conjugated (Con) and non-conjugated (No-con) sodium caseinate in the antisolvent [1.0% (w/v)]. The ratio of dextran to sodium caseinate was 1.75 to 1.0 (w/w). Zein and grape skin extract concentrations in the particle suspensions were 0.5 and 0.025% (w/v), respectively. Different letters (a, b) are significantly different for each treatment separately (p < 0.05).

nanoparticles formed in the current study had an inner core of zein surrounded by an outer layer of caseinate molecules. However, in some cases the caseinate molecules were covalently attached to dextran molecules through the Maillard reaction.

The retention efficiency was similar for protein nanoparticles, protein nanoparticles coated by Maillard conjugates, and a physical mixture of dextran and protein nanoparticles (p > 0.05). These results suggest that it was the protein core (zein and caseinate) that was primarily responsible for encapsulating the resveratrol, rather than the carbohydrate shell. Presumably, the nonpolar resveratrol molecules were trapped within the hydrophobic core formed by zein and caseinate. The retention efficiency of the biopolymer complexes was about 15% lower than that of biopolymer nanoparticles (Figure 3). For these systems, the retention efficiencies were similar for caseinate alone, caseinate conjugated to dextran, and a physical mixture of dextran and caseinate (p > 0.05), which suggested that it was the caseinate that was primarily responsible for resveratrol binding. Hydrophobic forces are known to play an important role in the binding of polyphenols to proteins.[10] This would account for the fact that dextran did not play an important role in determining the binding of the resveratrol to the caseinate molecules. In addition, the fact that the retention efficiency was higher for the biopolymer nanoparticles than for the biopolymer complexes may have been because zein has a higher hydrophobicity than caseinate.

UV Light Stability. UV light triggers the isomerization of *trans*-resveratrol to *cis*-resveratrol,[7] which results in a loss of biological activity.[37,38] The stability of the various delivery systems against isomerization was assessed by exposing them to UV light (365 nm) for 60 min in Petri dishes. Resveratrol dissolved in DMSO at the same concentration was used as a control. There was a significant difference (p < 0.05) in the amount of *trans*-resveratrol remaining among the different samples after exposure (Figure 4). Both the biopolymer nanoparticles and complexes were able to protect the resveratrol against isomerization, with the nanoparticles being

DOI: 10.1021/acs.jafc.5b00777
J. Agric. Food Chem. 2015, 63, 3915−3923

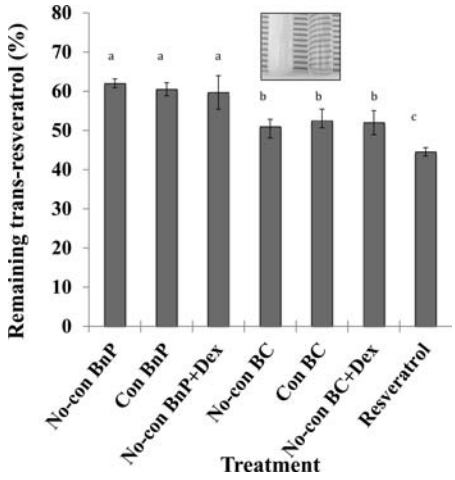

Figure 4. UV light stability of *trans*-resveratrol encapsulated in biopolymer nanoparticles (BnP) and biopolymer complexes (BC) loaded with grape skin extract prepared with conjugated (Con) and non-conjugated (No-con) sodium caseinate in the antisolvent [1.0% (w/v)]. The ratio of dextran to sodium caseinate was 1.75 to 1.0 (w/w). Zein and grape skin extract concentrations in the particle suspensions were 0.5 and 0.025% (w/v), respectively. (Inset) Left to right, appearance of one treatment containing zein and one without it. Different letters (a–c) are significantly different for each treatment separately ($p < 0.05$).

more effective. Conjugation of the caseinate with dextran, or the addition of free dextran, did not have a significant ($p > 0.05$) effect on the protection of resveratrol in either type of delivery system. The protection of resveratrol against exposure to light may have occurred through a number of different mechanisms. Proteins absorb UV light due to the presence of aromatic groups and double bonds,[39] which would reduce the intensity of light waves reaching the resveratrol. The suspensions of biopolymer nanoparticles contained 50% (w/w) more protein than the suspensions of biopolymer complexes, which may account for their better ability to inhibit isomerization. On the other hand, the higher protection of the nanoparticle systems might be because they scattered light more effectively and, thereby, allowed less light to reach the resveratrol.[32] This effect is seen in the inset of Figure 4, which compares the appearance of suspensions of biopolymer nanoparticles (turbid) and biopolymer complexes (clear). Finally, the retention efficiency of the systems (Figure 3) is closely related to the protection of resveratrol, the systems with higher retention efficiency being more protective. The treatments with lower retention efficiency have a higher amount of free resveratrol dispersed in the aqueous solution, which results in less protection from exposure to UV light.

In Vitro Digestion Model. The biopolymer nanoparticles and complexes were passed through the simulated gastrointestinal tract to assess resveratrol bioaccessibility. Changes in the size and charge of the biopolymer nanoparticles were measured throughout the simulated gastrointestinal tract, and the bioaccessibility of resveratrol for both types of biopolymer delivery systems was measured at the end.

Initial Biopolymer Nanoparticles. The non-conjugated biopolymer nanoparticles had similar diameters in the absence (238 nm) and presence (237 nm) of nonadsorbed dextran, which suggested that this carbohydrate did not directly influence their particle size (Figure 5A). In addition, the ζ-potential of the non-conjugated biopolymer nanoparticles was

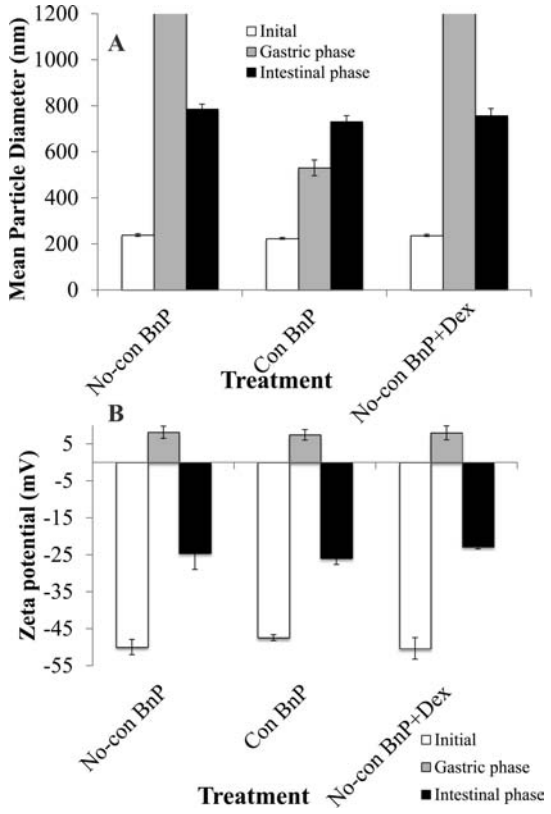

Figure 5. Effect of the in vitro digestion phase on the mean diameter (A) and ζ-potential (B) of grape skin extract loaded biopolymer nanoparticles (BnP) prepared with conjugated (Con) and non-conjugated (No-con) sodium caseinate in the antisolvent [1.0% (w/v)]. The ratio of dextran to sodium caseinate was 1.75 to 1.0 (w/w). Zein and grape skin extract concentrations in the particle suspensions were 0.5 and 0.025% (w/v), respectively.

similar in the absence (−50 mV) and presence (−50 mV) of nonadsorbed dextran (Figure 5B), which suggested that this carbohydrate did not appreciably modify interfacial properties. The conjugation of the caseinate with dextran did have an effect on particle size and charge, with the mean diameter falling to 224 nm and the ζ-potential falling to −47 mV. Particle size distribution measurements of the suspensions indicated that they had monomodal and narrow distributions (Figure 6). The slight reduction in particle size upon Maillard conjugation suggests that there is a change in the packing of the caseinate molecules at the nanoparticle interfaces due to the presence of the carbohydrate chains.[17] The slight reduction in the ζ-potential can be explained by a reduction of the number of ionizable amino groups on the protein after conjugation with dextran. In addition, the presence of the dextran may have increased the thickness of the hydration layer around the protein nanoparticles where the charge is measured, thereby leading to a decrease in surface potential.[18] Figure 7 shows that there were no flocs or aggregates in the initial conjugated or non-conjugated nanoparticle suspensions.

Gastric Phase. Samples were exposed directly to the gastric phase because liquids typically spend only a very short time in the oral cavity before swallowing.[30] The mean diameter of the non-conjugated nanoparticle suspensions increased greatly ($d > 1000$ nm) after exposure to the simulated gastric phase (Figure 5A). Conversely, the increase in particle size of the conjugated nanoparticle suspensions was much less ($d \approx 530$ nm). The ζ-

DOI: 10.1021/acs.jafc.5b00777
J. Agric. Food Chem. 2015, 63, 3915–3923

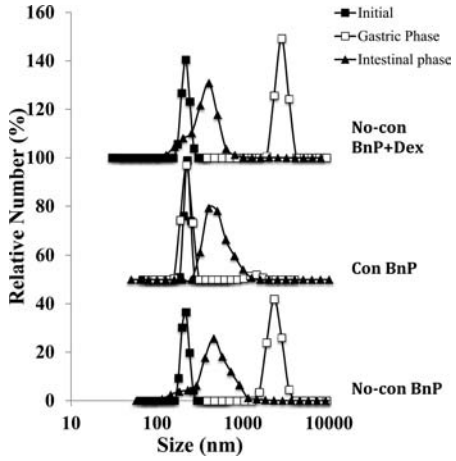

Figure 6. Effect of the in vitro digestion phase on the particle size distribution based on the number of grape skin extract loaded biopolymer nanoparticles (BnP) prepared with conjugated (Con) and non-conjugated (No-con) sodium caseinate in the antisolvent [1.0% (w/v)]. The ratio of dextran to sodium caseinate was 1.75 to 1.0. Zein and GSE concentrations in the particle suspensions were 0.5 and 0.025% (w/v), respectively. The distributions shown are representative ones for each treatment.

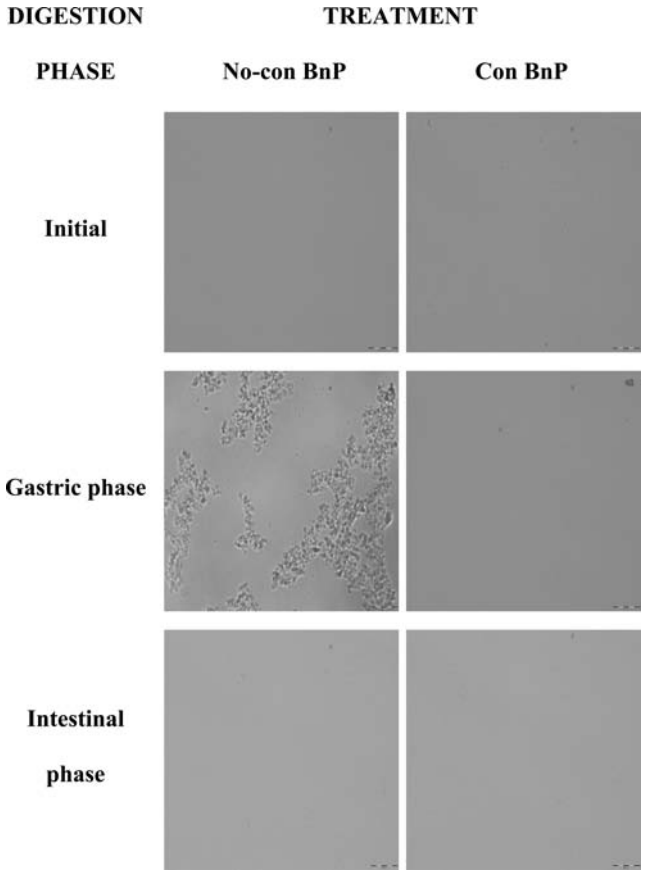

Figure 7. Microscopic images (40×) of grape skin extract loaded biopolymer nanoparticles (BnP) prepared with conjugated (Con) and non-conjugated (No-con) sodium caseinate in the antisolvent [1.0% (w/v)] after each phase of the in vitro digestion. The ratio of dextran to sodium caseinate was 1.75 to 1.0 (w/w). Zein and grape skin extract concentrations in the particle suspensions were 0.5 and 0.025% (w/v), respectively. Scale bar = 20 μm.

potential of the particles in the gastric "chyme" was slightly positive (Figure 5B), which can be attributed to the fact that both caseinate and zein were below their isoelectric point. The particle size distribution measurements show extensive aggregation of the non-conjugated nanoparticles, but only moderate aggregation of the conjugated ones after exposure to gastric fluids (Figure 6). The destabilization of protein-based colloidal delivery systems under simulated gastric conditions may occur for a number of reasons, including loss of charge due to pH changes, electrostatic screening due to an increased ionic strength, and proteolysis by pepsin.[18] Further information about the relative importance of pepsin on the stability of the nanoparticle systems was obtained by omitting pepsin from the gastric fluids. The particle diameter did not increase for the conjugated nanoparticles and increased by only about 50 nm for the non-conjugated ones (data not shown), suggesting that the hydrolysis of the proteins by pepsin was an important destabilizing factor during this phase.

The observed increase in particle size can be attributed to aggregation of the protein nanoparticles (Figure 7). The lower reactivity of digestive enzymes toward the conjugated nanoparticles can be attributed to the steric hindrance exerted by the dextran molecules attached to their exteriors.[40] Another possible explanation is the reduction of the proteolysis of certain amino acids due to glycation.[25]

Intestinal Phase. After the gastric phase, the resulting "chyme" was mixed with simulated intestinal fluids (SIF) and then incubated for 2 h. After exposure to simulated intestinal conditions, all of the nanoparticle systems had fairly similar size distributions and mean diameters ($d \approx 750$ nm) (Figures 5A and 6). Furthermore, the ζ-potential of all the samples became highly negative (Figure 5B), which can be attributed to the fact that the pH was above the isoelectric point of the proteins and due to the presence of anionic bile salts in the SIF. The fact that all of the samples had relatively similar particle sizes and charges suggests that they all contained fairly similar types of particle after digestion.[41] Presumably, these particles consisted of mixed micelles and liposome kinds of structures formed by bile salts and/or aggregated peptides remaining after digestion of the proteins by proteases. To confirm if the bile salts or the pancreatin were responsible for the changes in size and distribution, a digestion made with only pancreatin or bile extract was performed for the conjugated biopolymer nanoparticles (data not shown). The results indicated that the digestion with only bile salts resulted in the same size and distributions as the ones shown in Figures 5A and 6.

Bioaccessibility. Finally, the bioaccessibility of resveratrol encapsulated within the biopolymer nanoparticles or bound to the biopolymer complexes was determined by measuring the amount of resveratrol in the micelle phase after the intestinal step of the in vitro digestion model. It is assumed that only resveratrol incorporated within the mixed micelles is available for absorption within the small intestine, that is, is bioaccessible.[23] Figure 8 shows the percentage of resveratrol present in the micelle phase after the small intestine stage. In the absence of lipids, the mixed micelle phase will primarily be composed of micelles and liposomes formed by bile salts and phospholipids in the gastrointestinal fluids, as well as any undigested soluble proteins and peptides. Thus, the resveratrol measured in the mixed micelle phase could be present within micelles or liposomes[42,43] or bound to proteins or peptides.[10] It can be seen that there was a significant difference ($p < 0.05$) in the resveratrol contained in the mixed micelle phase between

DOI: 10.1021/acs.jafc.5b00777
J. Agric. Food Chem. 2015, 63, 3915−3923

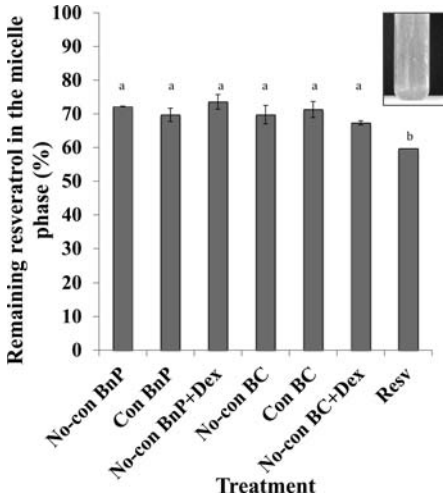

Figure 8. In vitro bioaccesability of resveratrol in biopolymer nanoparticles (BnP) and biopolymer complexes (BC) loaded with grape skin extract prepared with conjugated (Con) and non-conjugated (No-con) sodium caseinate in the antisolvent [1.0% (w/v)]. The ratio of dextran to sodium caseinate was 1.75 to 1.0 (w/w). Zein and grape skin extract concentrations in the particle suspensions were 0.5 and 0.025% (w/v), respectively. (Inset) Appearance of grape skin extract dispersed in water at 0.025% (w/v). Different letters (a, b) are significantly different for each treatment separately ($p < 0.05$).

the different delivery systems and the resveratrol dispersed in water at the same concentration. When resveratrol was directly added to water, it immediately formed crystals that could be seen by the naked eye (Figure 8, inset). Conversely, the resveratrol encapsulated within the biopolymer nanoparticles or complexes did not form any visible crystals. The crystallization and precipitation of resveratrol could explain the lower bioaccessibility of the free bioactive component compared to the encapsulated ones.[27] Nevertheless, the bioaccessibility of resveratrol was still >50%, and it has been demonstrated by fluorescence quenching studies that polyphenols can bind to the enzymes present in the gastric and intestinal fluids, increasing their solubility in the micelle phase.[44] The encapsulation of grape skin extract in the nanoparticles did not affect the bioaccessibility of resveratrol when compared to the ones bound to sodium caseinate. Neither the conjugation nor the presence of dextran had a significant effect ($p > 0.05$). Previous studies have shown that other types of caseinate-based and zein-based delivery systems are also able to retain hydrophobic nutraceuticals under simulated gastrointestinal conditions.[17,28,45,46] The fact that the resveratrol is retained within the colloidal particles in the gastrointestinal tract presumably accounts for the fact that it did not crystallize and was available to be solubilized within mixed micelles or to bind to peptides or proteins after digestion. The fact that all of the biopolymer nanoparticle samples had similar characteristics after the small intestine phase (Figures 5 and 6) can account for the lack of differences in the bioaccessibility among the different delivery systems. It is known from in vivo studies that resveratrol undergoes extensive metabolism within the gastrointestinal tract and liver, mainly due to glucorination and sulfonation, and that only traces reach the circulatory system in an active form.[1] One can speculate that these delivery systems may slow or prevent extensive metabolism and increase the bioactivity of resveratrol after consumption. Further research is clearly needed to test this hypothesis.

Both biopolymer nanoparticles (consisting of a zein core and a caseinate or caseinate−dextran shell) and biopolymer complexes (consisting of caseinate or caseinate−dextran) protected resveratrol against isomerization and increased its bioaccessibility, but the biopolymer particles were more effective. In conclusion, both delivery systems have the potential for application in functional food and beverage products. The biopolymer complexes are easier to form and can be incorporated into transparent products, whereas the biopolymer nanoparticles are more difficult to form and can be used only in turbid or opaque products, but are more effective.

AUTHOR INFORMATION

Corresponding Author

*(D.J.M.) E-mail: mcclements@foodsci.umass.edu. Mail: Department of Food Science, Chenoweth Lab, Room 228, University of Massachusetts, 102 Holdsworth Way, Amherst, MA 01002, USA. Phone: (413) 545-7157.

Funding

G.D.-P. is the recipient of a postdoctoral fellowship provided by the Secretaría de Ciencia Tecnología e Innovación del Distrito Federal (SECITI, Mexico City). This material is partly based upon work supported by the U.S. Department of Agriculture, NRI Grants (2011-03539, 2013-03795, 2011-67021, and 2014-67021).

Notes

The authors declare no competing financial interest.

REFERENCES

(1) Walle, T.; Hsieh, F.; DeLegge, M. H.; Oatis, J. E., , Jr.; Walle, U. K. High absorption but very low bioavailability of oral resveratrol in humans. *Drug Metab. Dispos.* **2004**, *32*, 1377−1382.

(2) Alves, N. E. G. Studies on mechanistic role of natural bioactive compounds in the management of obesity, an overview. *Open Nutraceuticals J.* **2012**, *5*, 193.

(3) Catalgol, B.; Batirel, S.; Taga, Y.; Ozer, N. K. Resveratrol: French paradox revisited. *Front. Pharmacol.* **2012**, *3* (July), DOI: 10.3389/fphar.2012.00141.

(4) Neves, A. R.; Lucio, M.; Martins, S.; Lima, J. L. C.; Reis, S. Novel resveratrol nanodelivery systems based on lipid nanoparticles to enhance its oral bioavailability. *Nanomedicine* **2013**, *8*, 177−187.

(5) Hung, C.-F.; Chen, J.-K.; Liao, M.-H.; Lo, H.-M.; Fang, J.-Y. Development and evaluation of emulsion-liposome blends for resveratrol delivery. *J. Nanosci. Nanotechnol.* **2006**, *6*, 2950−2958.

(6) Patel, K. R.; Scott, E.; Brown, V. A.; Gescher, A. J.; Steward, W. P.; Brown, K. Clinical trials of resveratrol. *Ann. N. Y. Acad. Sci.* **2011**, *1215*, 161−169, DOI: 10.1111/j.1749-6632.2010.05853.x.

(7) Trela, B. C.; Waterhouse, A. L. Resveratrol: isomeric molar absorptivities and stability. *J. Agric. Food Chem.* **1996**, *44*, 1253−1257.

(8) Davidov-Pardo, G.; Joye, I. J.; McClements, D. J. Encapsulation of resveratrol in biopolymer particles produced using liquid antisolvent precipitation. Part 1: Preparation and characterization. *Food Hydrocolloids* **2015**, *45*, 309−316.

(9) Joye, I. J.; McClements, D. J. Biopolymer-based nanoparticles and microparticles: fabrication, characterization, and application. *Curr. Opin. Colloid Interface Sci.* **2014**, *19*, 417−427.

(10) Acharya, D. P.; Sanguansri, L.; Augustin, M. A. Binding of resveratrol with sodium caseinate in aqueous solutions. *Food Chem.* **2013**, *141*, 1050−1054.

(11) Ye, J. H.; Thomas, E.; Sanguansri, L.; Liang, Y. R.; Augustin, M. A. Interaction between whole buttermilk and resveratrol. *J. Agric. Food Chem.* **2013**, *61*, 7096−7101.

DOI: 10.1021/acs.jafc.5b00777
J. Agric. Food Chem. 2015, 63, 3915−3923

(12) Liang, L.; Tajmir-Riahi, H. A.; Subirade, M. Interaction of β-lactoglobulin with resveratrol and its biological implications. *Biomacromolecules* **2008**, *9*, 50−56.
(13) Hemar, Y.; Gerbeaud, M.; Oliver, C. M.; Augustin, M. A. Investigation into the interaction between resveratrol and whey proteins using fluorescence spectroscopy. *Int. J. Food Sci. Technol.* **2011**, *46*, 2137−2144.
(14) Hu, K.; McClements, D. J. Fabrication of surfactant-stabilized zein nanoparticles: a pH modulated antisolvent precipitation method. *Food Res. Int.* **2014**, *64*, 329−335.
(15) Zhong, Q.; Jin, M. Zein nanoparticles produced by liquid−liquid dispersion. *Food Hydrocolloids* **2009**, *23*, 2380−2387.
(16) Oliver, C. M.; Melton, L. D.; Stanley, R. A. Creating proteins with novel functionality via the maillard reaction: a review. *Crit. Rev. Food Sci. Nutr.* **2006**, *46*, 337−350.
(17) Markman, G.; Livney, Y. D. Maillard-conjugate based core-shell co-assemblies for nanoencapsulation of hydrophobic nutraceuticals in clear beverages. *Food Funct.* **2012**, *3*, 262−270.
(18) Lesmes, U.; McClements, D. J. Controlling lipid digestibility: Response of lipid droplets coated by β-lactoglobulin-dextran Maillard conjugates to simulated gastrointestinal conditions. *Food Hydrocolloids* **2012**, *26*, 221−230.
(19) Wooster, T. J.; Augustin, M. A. β-Lactoglobulin-dextran Maillard conjugates: their effect on interfacial thickness and emulsion stability. *J. Colloid Interface Sci.* **2006**, *303*, 564−572.
(20) Davidov-Pardo, G.; Joye, I. J.; Espinal-Ruiz, M.; McClements, D. J. Encapsulation of resveratrol in biopolymer nanoparticles stabilized by Maillard conjugation. *Food Res. Int.* **2015**, submitted for publication.
(21) Ames, J. M. Control of the Maillard reaction in food systems. *Trends Food Sci. Technol.* **1990**, *1*, 150−154.
(22) Van Lancker, F.; Adams, A.; De Kimpe, N. Chemical modifications of peptides and their impact on food properties. *Chem. Rev.* **2011**, *111*, 7876−7903.
(23) Joye, I. J.; Davidov-Pardo, G.; McClements, D. J. Nanotechnology for increased micronutrient bioavailability. *Trends Food Sci. Technol.* **2014**, *40*, 168−182.
(24) Li, Z.; Jiang, H.; Xu, C.; Gu, L. A review: Using nanoparticles to enhance absorption and bioavailability of phenolic phytochemicals. *Food Hydrocolloids* **2015**, *43*, 153−164.
(25) Yi, J.; Lam, T. I.; Yokoyama, W.; Cheng, L. W.; Zhong, F. Controlled release of β-carotene in β-lactoglobulin−dextran-conjugated nanoparticles' in vitro digestion and transport with Caco-2 monolayers. *J. Agric. Food Chem.* **2014**, *62*, 8900−8907.
(26) Pan, X.; Mu, M.; Hu, B.; Yao, P.; Jiang, M. Micellization of casein-graft-dextran copolymer prepared through Maillard reaction. *Biopolymers* **2006**, *81*, 29−38.
(27) Pool, H.; Mendoza, S.; Xiao, H.; McClements, D. J. Encapsulation and release of hydrophobic bioactive components in nanoemulsion-based delivery systems: impact of physical form on quercetin bioaccessibility. *Food Funct.* **2013**, *4*, 162−174.
(28) Luo, Y. C.; Zhang, B. C.; Whent, M.; Yu, L. L.; Wang, Q. Preparation and characterization of zein/chitosan complex for encapsulation of alpha-tocopherol, and its in vitro controlled release study. *Colloids Surf., B* **2011**, *85*, 145−152.
(29) Podaralla, S.; Perumal, O. Influence of formulation factors on the preparation of zein nanoparticles. *AAPS PharmSciTech* **2012**, *13*, 919−927.
(30) Minekus, M.; Alminger, M.; Alvito, P.; Ballance, S.; Bohn, T.; Bourlieu, C.; Carriere, F.; Boutrou, R.; Corredig, M.; Dupont, D.; Dufour, C.; Egger, L.; Golding, M.; Karakaya, S.; Kirkhus, B.; Le Feunteun, S.; Lesmes, U.; Macierzanka, A.; Mackie, A.; Marze, S.; McClements, D. J.; Menard, O.; Recio, I.; Santos, C. N.; Singh, R. P.; Vegarud, G. E.; Wickham, M. S. J.; Weitschies, W.; Brodkorb, A. A standardised static in vitro digestion method suitable for food − an international consensus. *Food Funct.* **2014**, *5*, 1113−1124.
(31) Uskokovic, V. Dynamic light scattering based microelectrophoresis: main prospects and limitations. *J. Dispersion Sci. Technol.* **2012**, *33*, 1762−1786.
(32) McClements, D. J. *Food Emulsions: Principles, Practice, and Techniques*; CRC Press: Boca Raton, FL, USA, 2005; p 374.
(33) Moreno, F. J.; Molina, E.; Olano, A.; López-Fandiño, R. High-pressure effects on Maillard reaction between glucose and lysine. *J. Agric. Food Chem.* **2002**, *51*, 394−400.
(34) McClements, D. J. Crystals and crystallization in oil-in-water emulsions: implications for emulsion-based delivery systems. *Adv. Colloid Interface Sci.* **2012**, *174*, 1−30.
(35) Joye, I. J.; McClements, D. J. Production of nanoparticles by anti-solvent precipitation for use in food systems. *Trends Food Sci. Technol.* **2013**, *34*, 109−123.
(36) Baur, J. A.; Sinclair, D. A. Therapeutic potential of resveratrol: the in vivo evidence. *Nat. Rev. Drug Discovery* **2006**, *5*, 493−506.
(37) Fauconneau, B.; WaffoTeguo, P.; Huguet, F.; Barrier, L.; Decendit, A.; Merillon, J. M. Comparative study of radical scavenger and antioxidant properties of phenolic compounds from *Vitis vinifera* cell cultures using in vitro tests. *Life Sci.* **1997**, *61*, 2103−2110.
(38) Rius, C.; Abu-Taha, M.; Hermenegildo, C.; Piqueras, L.; Cerda-Nicolas, J. M.; Issekutz, A. C.; Estan, L.; Cortijo, J.; Morcillo, E. J.; Orallo, F.; Sanz, M. J. *trans*- but not *cis*-Resveratrol impairs angiotensin-II-mediated vascular inflammation through inhibition of NF-κB activation and peroxisome proliferator-activated receptor-γ upregulation. *J. Immunol.* **2010**, *185*, 3718−3727.
(39) Luo, Y. C.; Wang, T. T. Y.; Teng, Z.; Chen, P.; Sun, J. H.; Wang, Q. Encapsulation of indole-3-carbinol and 3,3′-diindolylmethane in zein/carboxymethyl chitosan nanoparticles with controlled release property and improved stability. *Food Chem.* **2013**, *139*, 224−230.
(40) Corzo-Martínez, M.; Soria, A. C.; Belloque, J.; Villamiel, M.; Moreno, F. J. Effect of glycation on the gastrointestinal digestibility and immunoreactivity of bovine β-lactoglobulin. *Int. Dairy J.* **2010**, *20*, 742−752.
(41) Sarkar, A.; Horne, D. S.; Singh, H. Interactions of milk protein-stabilized oil-in-water emulsions with bile salts in a simulated upper intestinal model. *Food Hydrocolloids* **2010**, *24*, 142−151.
(42) Wan, Z.-L.; Wang, J.-M.; Wang, L.-Y.; Yang, X.-Q.; Yuan, Y. Enhanced physical and oxidative stabilities of soy protein-based emulsions by incorporation of a water-soluble stevioside-resveratrol complex. *J. Agric. Food Chem.* **2013**, *61*, 4433−4440.
(43) Bonechi, C.; Martini, S.; Ciani, L.; Lamponi, S.; Rebmann, H.; Rossi, C.; Ristori, S. Using liposomes as carriers for polyphenolic compounds: the case of *trans*-resveratrol. *PLoS One* **2012**, *7*, 10.1371/journal.pone.0041438.
(44) Moser, S.; Chegeni, M.; Jones, O. G.; Liceaga, A.; Ferruzzi, M. G. The effect of milk proteins on the bioaccessibility of green tea flavan-3-ols. *Food Res. Int.* **2014**, *66*, 297−305.
(45) Patel, A. R.; Heussen, P. C. M.; Hazekamp, J.; Drost, E.; Velikov, K. P. Quercetin loaded biopolymeric colloidal particles prepared by simultaneous precipitation of quercetin with hydrophobic protein in aqueous medium. *Food Chem.* **2012**, *133*, 423−429.
(46) Pan, X.; Yao, P.; Jiang, M. Simultaneous nanoparticle formation and encapsulation driven by hydrophobic interaction of casein-graft-dextran and β-carotene. *J. Colloid Interface Sci.* **2007**, *315*, 456−463.

DOI: 10.1021/acs.jafc.5b00777
J. Agric. Food Chem. 2015, 63, 3915−3923

the plant's defense systems to protect it from insect attack, and many are known to have antimicrobial and antifungal properties.[22,23] Among the beneficial health properties attributed to saponins are hypocholesterolemic, anti-inflammatory, immunostimulant, antiobesity, and antiparasitic; all are proven on animal models.[23−27] Cell-based assays have also proven cytotoxic and antimicrobial effects.[28−30]

It has been suggested that the saponin content in agave species is affected by the ripening stage. The sapogenin structure and content are also affected by the agave species. Blunden et al.[19] evaluated 34 agave species and identified 12 sapogenins, with hecogenin and gentrogenin the most commonly found. In addition, hecogenin has been widely studied because of its use as a raw material to produce cortical hormones[31] and has been reported in dried leaves from 22 agave species.[19,28,32−34] Furthermore, Pinos-Rodriguez et al.[35,36] concluded in two studies with *A. salmiana*, that the total saponin content was lower in ripe plants compared with immature ones.

All these studies have been performed in agave leaves or rhizomes. To the best of our knowledge, there is no study performed to characterize the saponin content in aguamiel. Thus, the aim of this research was to identify and quantitate saponins in aguamiel from *A. americana* and *A. salmiana* at two ripening stages. It is important to evaluate the effect of species and maturity to standardize the sap and characterize the saponin content for further functional activity correlations. This would be a starting point for the development of functional foods derived from agave sap.

MATERIALS AND METHODS

Chemical Reagents. HPLC grade water, ethanol, and acetonitrile were obtained from BDH (Poole, UK). The reactive grade *n*-butanol solvent used for extraction was obtained from Desarrollo de Especialidades Químicas (Monterrey, Mexico). Hecogenin standard was purchased from Santa Cruz Biotechnology Inc. (Santa Cruz, CA), and protodioscin, from Sigma-Aldrich (St. Louis, MO).

Biological Material. Aguamiel samples were donated by AGMEL S.A de C.V. and collected at General Cepeda County, in Coahuila, Mexico (25° 22N, 101° 28W) at an altitude of 1410 m above sea level. The plant was identified by Dr. Marcela González Álvarez from the Universidad Autónoma de Nuevo León (UANL) in Mexico. A voucher specimen was deposited in the herbarium of the UANL under the numbers 025618 for *A. americana* and 025619 for *A. salmiana*. Eight-year-old plants from *A. americana* and *A. salmiana* were used in two ripeness stages: immature plants prior to entering into the reproductive stage and mature plants at the onset of reproductive stage. When the agave enters the reproductive stage, its shoot apex is thinned, displaying black, shiny spines.[11] Agaves were prepared following the traditional process to collect the aguamiel.[14] Aguamiel was collected during the month of May 2013. Samples were immediately placed on dry ice, transported to the laboratory, and stored at −20 °C until analysis. A pool of eight agaves per ripeness stage and species were used, for a total of 32 agaves. Dry matter (DM) was determined by gravimetric means (AOAC 425.45).[37] Sample (2 g) was mixed with 0.5 g of dry silicon dioxide (DEQ, Monterrey, Mexico) and dried at 60 °C for 24 h. Weight was recorded before and after drying to obtain the percentage of DM.

Saponin Extraction and Sapogenin Release. To obtain the saponin crude extract, 50 mL of aguamiel was added to 50 mL of *n*-butanol, and the mixture was shaken for 20 min at 250 rpm and 37 °C. Samples were then centrifuged for 5 min (3000 rpm and 4 °C). The organic phase was collected and dried under vacuum at 40 °C for 2 h. This extract was used to evaluate the saponin content.

To release the sapogenin, all the crude saponin extract was hydrolyzed by adding 5 mL of 2 N HCl and left for 60 min in a water bath at 100 °C. After hydrolysis, samples were neutralized (pH 7.0 ± 0.1) with 2 N NaOH. The neutralized samples were brought to a volume of 25 mL with distilled water, and this solution was added to 25 mL of *n*-butanol. The mixture was sonicated for 1 min and then centrifuged for 5 min (3000 rpm and 4 °C). The organic phase rich in sapogenins was collected and dried under vacuum (2 h at 40 °C). This extract was used to evaluate the sapogenin content.

Prior to analysis, all the samples were resuspended in 2 mL of methanol/water (1:1) HPLC grade and filtered through a syringe filter, pore size 0.45 μm, made of hydrophilic polypropylene (Pall Life Science, Ann Arbor, MI). All extractions were performed in triplicate.

Saponin and Sapogenin Analysis. Saponins and sapogenins were analyzed using a model 1100 high performance liquid chromatography coupled to electrospray ionization mass spectrometer equipped with a model G1969A time-of-flight (HPLC/ESI-MS/TOF) detector (Agilent Technologies, Santa Clara, CA). Conditions were adapted from a methodology to analyze steroidal saponins from Taiwanese yam with some modifications detailed below.[38]

Separation was performed at 25 °C. The column used was a 150 mm × 4.6 mm i.d., 5 μm, Zorbax Eclipse XDB-C18 with a 12.5 mm × 4.6 mm i.d. guard column of the same material (Agilent Technologies, Santa Clara, CA). The sample (20 μL) was eluted at 0.8 mL/min flow rate with a gradient consisting of solvent A, HPLC-grade water containing 0.1% formic acid; and solvent B, HPLC-grade acetonitrile containing 0.1% formic acid. The gradient used was as follows: 0→8 min isocratic at 28% B; 8→28 min, increased to 55% B; 28→31 min, increased to 100% B; 31→40 min, isocratic at 100% B. Mass spectra were collected using an electrospray source in positive mode (ESI^+) under the following conditions: m/z 300−1500 range; nitrogen gas at 350 °C and 9.0 L/min flow rate; 45 psig nebulizer pressure; 4000 V capillary voltage; fragment voltage 145 V; and skimmer at 40 V. Sapogenin identifications were based on the accurate mass previously reported for agave except for hecogenin, which was also confirmed with a commercial standard. For the identification of the glycosylated forms, ionization tests were performed to fragment the molecular ion and obtain the corresponding fragmentation pattern, which was compared with that previously reported for agave saponins. Extracted ion chromatograms were analyzed considering the saponins and sapogenin accurate mass (±0.05 units) using Analyst QS 1.1 software (Applied Biosystems, Carlsbad, CA).

Saponin and Sapogenin Quantitation. Quantitative analysis was performed with a 1200 Series HPLC coupled to an evaporative light scattering detector (HPLC/ELSD) (Agilent Technologies, Santa Clara, CA). Chromatographic conditions were the same as described above. ELSD conditions were adapted from a methodology to analyze steroidal saponins from Taiwanese yam.[38] Detection was accomplished using nitrogen as the drying gas, a pressure of 3.4 bar and tube temperature of 45 °C, gain of 9, and sampling time of 33 ms. All the saponins from the same aglycone were quantitated together. Sapogenin concentrations were obtained as hecogenin

DOI: 10.1021/acs.jafc.5b00883
J. Agric. Food Chem. 2015, 63, 3924−3930

Table 1. Sapogenin Quantitative Analysis in the Hydrolyzed Aguamiel from *A. americana* and *A. salmiana* at Two Ripening Stages and Total Dry Matter (DM)

	A. salmiana		*A. americana*	
sapogenin (HE μg/g aguamiel (DM))[a,b,c]	immature	mature	immature	mature
kammogenin	41.81 ± 12.83 a	16.37 ± 2.31 b	4.46 ± 0.39 c	2.14 ± 0.04 c
manogenin	7.14 ± 1.34 a	5.63 ± 0.50 b	3.77 ± 0.19 c	2.01 ± 0.03 d
gentrogenin	5.11 ± 0.14 a	4.87 ± 0.30 a	3.59 ± 0.20 b	1.95 ± 0.01 c
hecogenin	5.79 ± 0.27 a	5.39 ± 0.31 ab	3.75 ± 0.02 bc	1.99 ± 0.04 c
total sapogenin	59.85 ± 14.58 a	32.26 ± 3.42 b	15.57 ± 0.80 c	8.09 ± 0.12 c
fresh aguamiel dry matter	11.91 ± 0.04 a	11.73 ± 0.07 a	13.67 ± 1.77 a	11.57 ± 0.07 a

[a]HE, hecogenin equivalents μg/g aguamiel dry matter. [b]Data is expressed as mean ± SD of three independent extractions. [c]Mean values in each row with different letter are significantly different ($p < 0.05$).

Table 2. Saponin Quantitative Analysis in Aguamiel from *A. americana* and *A. salmiana* at Two Ripening Stages

	A. salmiana		*A. americana*	
saponin[a] (PE μg/g aguamiel (DM))[b,c,d]	immature	mature	immature	mature
kammogenin glycosides	321.9 ± 8.0 a	200.9 ± 11.8 b	97.9 ± 1.3 c	22.6 ± 0.8 d
manogenin glycosides	55.7 ± 0.7 a	50.2 ± 3.0 a	23.2 ± 0.8 b	12.2 ± 0.2 c
gentrogenin glycosides	51.4 ± 2.0 a	50.4 ± 0.9 a	29.5 ± 1.2 b	13.2 ± 0.2 c
hecogenin glycosides	49.3 ± 1.2 a	24.1 ± 0.5 b	28.3 ± 1.2 a	12.8 ± 0.3 c
total saponin content	478.4 ± 5.6 a	325.7 ± 15.7 b	179.0 ± 2.2 c	60.5 ± 1.1 d

[a]Saponins sharing the same aglycone were quantitated together. [b]PE, protodioscin equivalents μg/g aguamiel dry matter. [c]Data are expressed as mean ± SD of three independent extractions. [d]Mean values in each row with different letter are significantly different ($p < 0.01$).

equivalents (HE) using a standard curve from 10 to 125 ppm. Results were reported in HE μg/g aguamiel (DM). Saponin concentrations were obtained as protodioscin equivalents (PE) using a standard curve from 10 to 500 ppm. Results were reported in PE μg/g aguamiel (DM).

Statistical Analysis. All analyses were performed in triplicate, and results are expressed as mean ± standard deviation. Statistical analyses were conducted by one-way ANOVA, and differences among means were compared with the Tukey test using a level of significance of $p < 0.01$. The software used was GraphPad Prism version 5.0b.

RESULTS AND DISCUSSION

Aguamiel dry matter (DM) content ranged from 11.57 to 13.67%, and it was not affected by the agave species or ripening stage (Table 1). These results are in agreement with previous studies in aguamiel in which a DM of 11.5% was reported.[15]

Analysis and Quantitation of Sapogenins. Four sapogenins (kammogenin **1**, manogenin **2**, gentrogenin **3**, and hecogenin **4**) were released from their saponins by acid hydrolysis (Figures 1 and 2). These were detected across both agave species and ripening stages. These sapogenins have been previously reported in dried agave leaves after an acid hydrolysis treatment.[19,32] Kammogenin and manogenin have also been reported in callus cultures from *A. ameniensis*.[20] Even though kammogenin was the most abundant sapogenin found in aguamiel from both agave species, it has been previously quantitated as an aglycone only in callus cultures. These results also illustrate that the agave species and ripening stage did not affect the sapogenin diversity; however, the sapogenin content was, indeed, affected by both the species and the ripeness stage (Table 1). Aguamiel from immature *A. salmiana* contained more than twice the total amount of sapogenins compared with immature *A. americana* (59.85 ± 14.58 and 15.57 ± 0.80 μg HE/g aguamiel (DM), respectively). In both species, sapogenin content decreased almost half when the plant approached the reproductive stage. Among the four sapogenins identified,

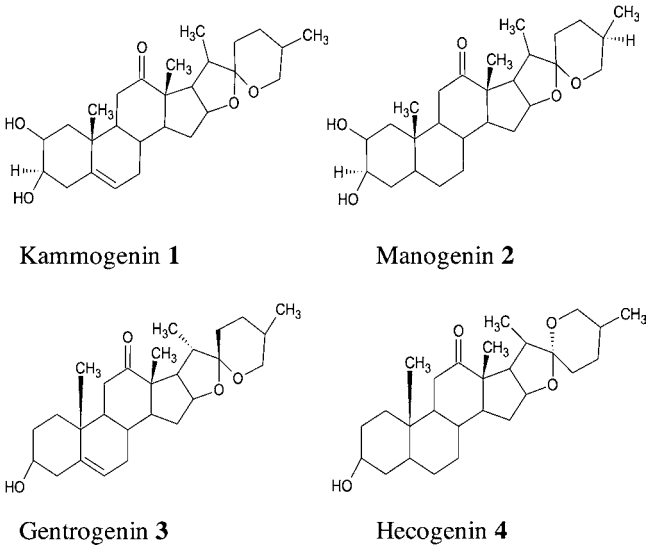

Figure 1. Chemical structures of the sapogenins kammogenin, manogenin, gentrogenin, and hecogenin detected in the hydrolyzed aguamiel extract from mature and immature *A. salmiana* and *A. americana*.

kammogenin was the most abundant, regardless the species and ripening stage. Contrary to what was observed in aguamiel, in callus cultures from *A. amaniensis*, kammogenin content (16 μg/g dry callus) was half the manogenin content (32 μg/g dry callus).[20]

According to a sapogenin screening in 34 agave species,[19] the species with the highest hecogenin content was *Agave franzosini* Nissen, with 0.46% leaf dry weight, in which *A. americana* and *A. salmiana* had 0.4% and 0.12%, respectively. These results differ from ours because *A. salmiana* was a better source of hecogenin as compared with *A. americana*. It is important to mention that in the above analysis, the agave ripeness stage was not standardized, and the plant age was not reported.

DOI: 10.1021/acs.jafc.5b00883
J. Agric. Food Chem. 2015, 63, 3924−3930

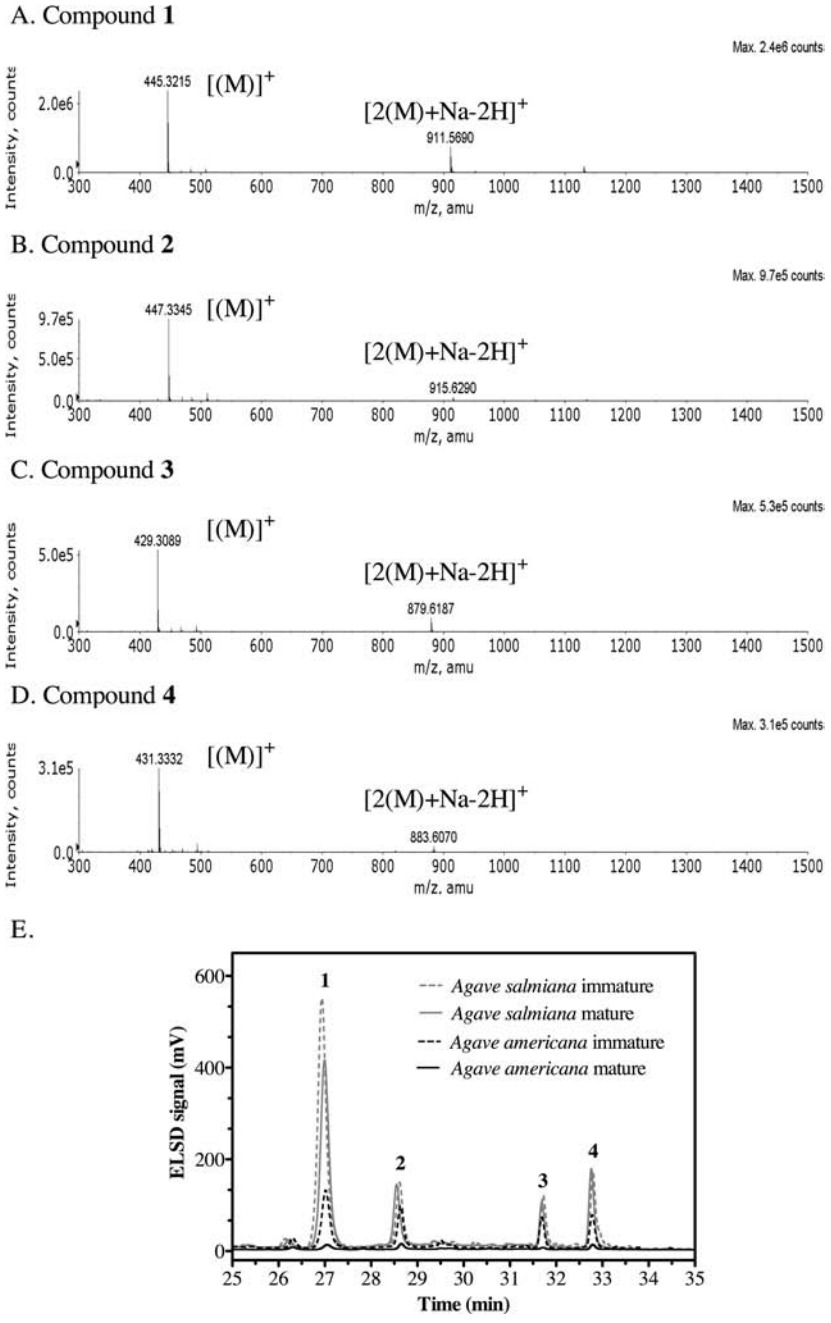

Figure 2. (A–D) Positive-ion mass spectra of kammogenin (**1**), manogenin (**2**), gentrogenin (**3**), and hecogenin (**4**) detected in the hydrolyzed aguamiel extract and (E) HPLC/ELSD chromatograms of the hydrolyzed aguamiel from *A. salmiana* an *A. americana* at two ripening stages.

Analysis and Quantitation of Saponins. Saponins from *A. americana* and *A. salmiana* were exhaustively extracted. A total of eight saponins derived from kammogenin (compounds **5** and **6**), manogenin (compounds **7** and **8**), gentrogenin (compounds **9** and **10**), and hecogenin (compounds **11** and **12**) were detected in aguamiel from both ripening stages of aguamiel (Figure 3A). Except for compounds **5**, **7**, and **10**, all the detected saponins had been previously reported.

Compound **5** mass spectra exhibited characteristic ions at m/z 1247.56 ($[M + Na]^+$), m/z 1115.51 ($[M - 1$ pentose + $Na]^+$), m/z 607.31 ($[M - 3$ hexose $- 1$ pentose$]^+$), and m/z 447.31 ($[M - 4$ hexose $- 1$ pentose$]^+$) (Figure 3B). Compound **6** exhibited the presence of ions at m/z 1217.56 ($[M + Na]^+$), m/z 1085.51 ($[M - 1$ pentose + $Na]^+$), m/z 607.31 ($[M - 2$ hexose $- 2$ pentose$]^+$), and m/z 447.31 ($[M - 3$ hexose -2 pentose$]^+$). This saponin has been recently isolated from the flowers and leaves of *Agave offoyana* and identified as magueyoside A.[39,40]

Compound **7** showed characteristic ion mass spectra at m/z 1249.54 ($[M + Na]^+$), m/z 1117.50 ($[M - 1$ pentose + $Na]^+$), m/z 609.36 ($[M - 3$ hexose -1 pentose$]^+$), and m/z 447.31 ($[M - 4$ hexose $- 1$ pentose$]^+$). Compound **8** exhibited the presence of ions at m/z 1219.56 ($[M + Na]^+$), m/z 1087.56 ($[M - 1$ pentose + $Na]^+$), m/z 609.36 ($[M - 2$ hexose -2 pentose$]^+$), and m/z 445.31 ($[M - 3$ hexose $- 2$ pentose$]^+$) and has also been found in the flowers from *A. offoyana* and was identified as magueyoside D.[40]

DOI: 10.1021/acs.jafc.5b00883
J. Agric. Food Chem. 2015, 63, 3924–3930

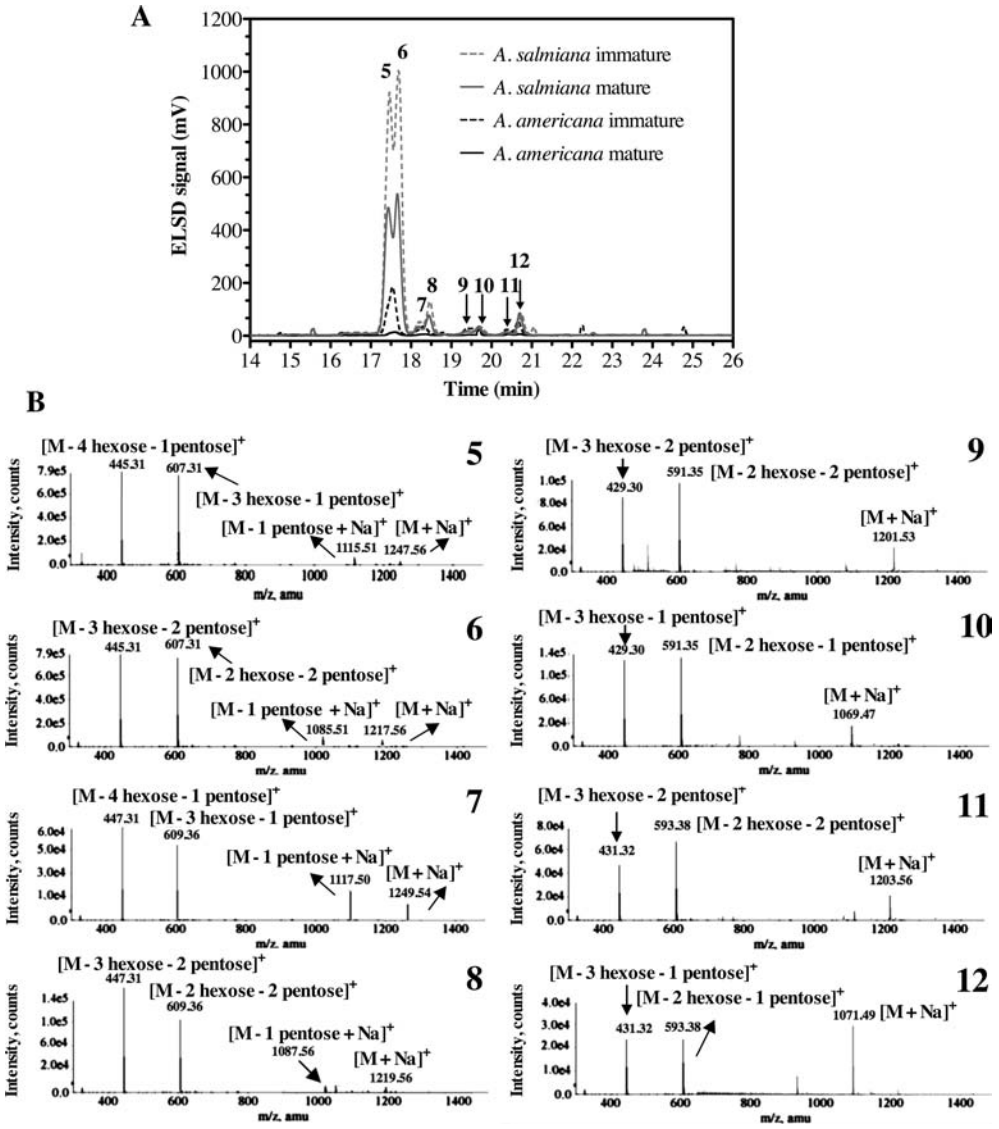

Figure 3. Positive ion mass spectra from compounds **1**−**8** and HPLC/ELSD chromatograms obtained from aguamiel from *A. salmiana* and *A. americana* at two ripening stages.

Compound **9** exhibited the presence of ions at *m*/*z* 1201.53 ([M + Na]$^+$), *m*/*z* 591.35 ([M − 2 hexose − 2 pentose]$^+$), and *m*/*z* 429.30 ([M − 3 hexose − 2 pentose]$^+$) as magueyoside H previously reported in *A. offoyana* leaves.[39] Compound **10** presented characteristic ion mass spectra with *m*/*z* 1069.47 ([M + Na]$^+$), *m*/*z* 591.35 ([M − 2 hexose − 1 pentose]$^+$), and *m*/*z* 429.30 ([M − 3 hexose − 1 pentose]$^+$), and therefore, it was tentatively similar to magueyoside H without a pentose.

Finally, both hecogenin glycosides have been identified in different agave species. Compound **11** presented ion mass at *m*/*z* 1203.56 ([M + Na]$^+$), *m*/*z* 593.38 ([M − 2 hexose − 2 pentose]$^+$), and *m*/*z* 431.32 ([M − 3 hexose − 2 pentose]$^+$) characteristic of those reported for cantalasaponin 4 in flowers from *A. offoyana* and in dried rhizomes from *A. cantalana*.[40,41] Compound **12** showed the presence of ions at *m*/*z* 1071.49 ([M+ Na]$^+$), *m*/*z* 593.38 ([M − 2 hexose −1 pentose]$^+$), and *m*/*z* 431.32 ([M − 3 hexose −1 pentose]$^+$) similar to those reported for a saponin identified in *A. americana* leaves,[42] *Agave cantala* rhizomes,[41] *Agave sisalana* leaves,[30] and *A. offoyana*.[40] This compound has been reported under different names: agavoside C′, agavesaponin C′, agaveside C′, and cantalasaponin 2.[41,42]

Among the aguamiel saponins that have been previously detected, many have shown beneficial properties. Compounds **6**, **8**, and **9** identified as magueyosides A, D, and H, respectively, showed greater phytotoxicity compared with the commercial herbicide Logran.[39,40] In addition, compound **8** extracted from *A. sisalana*, proved to be cytotoxic to human cell lines for gioblastoma, lung cancer, and breast cancer cell lines.[30]

The saponin content was affected by the plant ripening stage and species. When the plant evolved from immature vegetative to the reproductive stage, the saponin content significantly decreased in both species. This reduction was more pronounced in *A. americana* (66%) compared to *A. salmiana* (32%). These results concur with two previous studies with *A. salmiana* leaves in which total saponin content decreased significantly upon plant ripening.[35,36]

The correlation of the physiological phase and saponin content has been demonstrated in different plants.[43] In agreement with our results, the highest diosgenin concentration in the annual plant *Trigonella foenum-graecum* was observed in

DOI: 10.1021/acs.jafc.5b00883
J. Agric. Food Chem. 2015, 63, 3924−3930

young plants and decreased upon plant maturity.[44] In addition, in *Phytolacca dodecandra* berries, researchers found that young racemes contained the highest saponin concentration that decreased in the mature ones without changing the saponin proportion.[45]

It has also been suggested that saponin content and distribution may vary depending on the protection needed.[21] Decrease upon maturity may be explained by the fact that these compounds contribute to the plant's defense systems, because many saponins are known to be antimicrobial or antifungal, and to protect from insect attack.[22,23] A high saponin content in immature agave could serve as a protector to keep predators controlled, ensure full plant development, and guarantee the entrance to the reproductive stage. However, when the plant enters the reproductive stage, its pollination success is strongly correlated to nectar-feeding bats, birds, and insects.[46] This could explain the decrease in the saponin content to decrease pollinators deterrence and guarantee pollination.

Taking in total the presented information, the results of this investigation prove for the first time the presence of saponins in the edible sap or "aguamiel", which decreased with plant ripening. Moreover, *A. salmiana* yielded a greater amount of saponins compared with *A. americana*. Kammogenin saponins were the most abundant, regardless of the agave species and ripening stage. Aguamiel and its byproducts should be considered an edible source of saponins for further studies because these important phytochemicals have potential positive health implications.

■ ASSOCIATED CONTENT

Supporting Information

Further experiments were performed to compare tentatively new saponins with those previously identified in the literature. Figure S1 shows a chromatogram and mass spectrum of compounds **5** and **6**. Figure S2 includes a total ion chromatogram for the partially hydrolyzed kammogenin glycoside fraction with compound **5** and compound **6** and mass spectrum proposed for their glycosides and aglycone. Figure S3 includes a total ion chromatogram for 60 min hydrolyzed kammogenin glycoside fraction with compound **5** and compound **6** and mass spectrum proposed for their glycosides and aglycone. Figure S4 and Figure S5 show chromatograms of extracted ions, mass spectra, tentative structures, and fragmentation pattern for compounds **7** and **8** and for compounds **9** and **10**, respectively. This material is available free of charge via the Internet at http://pubs.acs.org.

■ AUTHOR INFORMATION

Corresponding Author

*Phone: 52-81-8328-4262. Fax: 52-81-8328-4262. E-mail: jagu@itesm.mx.

Funding

We would like to thank to the Nutrigenomic Research Chair Fund from Fundación FEMSA, CAT-005 and NutriOmics from Tecnológico de Monterrey, Monterrey Campus and CONACYT for financial support for graduate studies (CVU 388427).

Notes

The authors declare no competing financial interest.

■ ACKNOWLEDGMENTS

We are also grateful to AGMEL S.A. de C.V. for providing the aguamiel samples.

■ ABBREVIATIONS USED

DM, dry matter; ELSD, evaporative light scattering device; MS^2, tandem MS scan; HE, hecogenin equivalents; PE, protodioscin equivalents; UANL, Universidad Autónoma de Nuevo León

■ REFERENCES

(1) Jin, J.-M.; Zhang, Y.-J.; Yang, C.-R. Four new steroid constituents from the waste residue of fibre separation from *Agave americana* leaves. *Chem. Pharm. Bull.* **2004**, *52*, 654−658.

(2) Radding, C. The children of Mayahuel: agaves, human cultures, and desert. Landscapes in northern Mexico. *Environ. Hist.* **2012**, *17*, 84−115.

(3) Evans, T. S. The productivity of maguey terrace agriculture in central Mexico during the aztec period. *Lat. Am. Antiq.* **1990**, *1*, 117−132.

(4) Escalante, A.; Giles-Gómez, M.; Hernández, G.; Córdova-Aguilar, M. S.; López-Munguía, A.; Gosset, G.; Bolívar, F. Analysis of bacterial community during the fermentation of pulque, a traditional Mexican alcoholic beverage, using a polyphasic approach. *Int. J. Food Microbiol.* **2008**, *124*, 126−134.

(5) Linton, M. J.; Nobel, P. S. Hydraulic conductivity, xylem cavitation, and water potential for succulent leaves of *Agave deserti* and *Agave tequilana*. *Int. J. Plant Sci.* **2001**, *162*, 747−754.

(6) Anderies, J. M.; Nelson, B. A.; Kinzig, A. P. Analyzing the impact of agave cultivation on famine risk in arid pre-hispanic northern Mexico. *Hum. Ecol.* **2008**, *36*, 409−422.

(7) Santos-Zea, L.; Leal-Díaz, A.; Cortés-Ceballos, E.; Gutierrez-Uribe, J. Agave (*Agave* spp.) and its traditional products as a source of bioactive compounds. *Curr. Bioact. Compd.* **2012**, *8*, 218−231.

(8) Willems, J. L.; Low, N. H. Major carbohydrate, polyol, and oligosaccharide profiles of agave syrup. Application of this data to authenticity analysis. *J. Agric. Food Chem.* **2012**, *60*, 8745−8754.

(9) Secretaría de Economía. NMX-FF-110-SCFI-2008: Productos alimenticios-Jarabe de Agave-Especificaciones y Métodos de prueba. *Diario Oficial de la Federación*, 2008.

(10) García-Aguirre, M.; Sáenz-Álvaro, V. A.; Rodríguez-Soto, M. a; Vicente-Magueyal, F. J.; Botello-Alvarez, E.; Jimenez-Islas, H.; Cárdenas-Manríquez, M.; Rico-Martínez, R.; Navarrete-Bolaños, J. L. Strategy for biotechnological process design applied to the enzymatic hydrolysis of agave fructo-oligosaccharides to obtain fructose-rich syrups. *J. Agric. Food Chem.* **2009**, *57*, 10205−10210.

(11) Michel-Cuello, C.; Juárez-Flores, B. I.; Aguirre-Rivera, J. R.; Pinos-Rodríguez, J. M. Quantitative characterization of nonstructural carbohydrates of mezcal agave (*Agave salmiana* Otto ex Salm-Dick). *J. Agric. Food Chem.* **2008**, *56*, 5753−5757.

(12) Arrizon, J.; Morel, S.; Gschaedler, A.; Monsan, P. Comparison of the water-soluble carbohydrate composition and fructan structures of *Agave tequilana* plants of different ages. *Food Chem.* **2010**, *122*, 123−130.

(13) Lopez, M. G.; Mancilla-Margalli, N. A.; Mendoza-Diaz, G. Molecular structures of fructans from *Agave tequilana* Weber var. azul. *J. Agric. Food Chem.* **2003**, *51*, 7835−7840.

(14) Granados-Sanchez, D. *Los Agaves En México*, 1st ed.; Universidad Autónoma de Chapingo: Chapingo, México, 1991; pp 11−22.

(15) Ortiz-Basurto, R. I.; Pourcelly, G.; Doco, T.; Williams, P.; Dornier, M.; Belleville, M.-P. Analysis of the main components of the aguamiel produced by the maguey-pulquero (*Agave mapisaga*) throughout the harvest period. *J. Agric. Food Chem.* **2008**, *56*, 3682−3687.

(16) Albino Vargas from AGMEL. Personal communication, 2012.

DOI: 10.1021/acs.jafc.5b00883
J. Agric. Food Chem. 2015, 63, 3924−3930

(17) Wang, N.; Nobel, P. Phloem transport of fructans in the crassulacean acid metabolism species *Agave deserti*. *Plant Physiol.* **1998**, *116*, 709−714.
(18) Mellado-Mojica, E.; López, M. G. Fructan metabolism in *A. tequilana* Weber Blue variety along its developmental cycle in the field. *J. Agric. Food Chem.* **2012**, *60*, 11704−11713.
(19) Blunden, G.; Yi, Y.; Jewers, K. Steroidal sapogenins from leaves of agave species. *Phytochemistry* **1978**, *17*, 1923−1925.
(20) Indrayanto, G.; Studiawan, H.; Cholies, N. Isolation and quantitation of manogenin and kammogenin from callus cultures of *Agave amaniensis*. *Phytochem. Anal.* **1994**, *5*, 24−26.
(21) Augustin, J. M.; Kuzina, V.; Andersen, S. B.; Bak, S. Molecular activities, biosynthesis and evolution of triterpenoid saponins. *Phytochemistry* **2011**, *72*, 435−457.
(22) Osbourn, A. Saponins and plant defence - a soap story. *Trends Plant Sci.* **1996**, *1*, 4−9.
(23) Francis, G.; Kerem, Z.; Makkar, H. P. S.; Becker, K. The biological action of saponins in animal systems: a review. *Br. J. Nutr.* **2002**, *88*, 587−605.
(24) Silveira, R. X.; Chagas, A. C. S.; Botura, M. B.; Batatinha, M. J. M.; Katiki, L. M.; Carvalho, C. O.; Bevilaqua, C. M. L.; Branco, A.; Machado, E. A. A.; Borges, S. L.; Almeida, M. A. O. Action of sisal (*Agave sisalana*, Perrine) extract in the *in vitro* development of sheep and goat gastrointestinal nematodes. *Exp. Parasitol.* **2012**, *131*, 162−168.
(25) Han, L.; Zheng, Y.; Xu, B.; Okuda, H.; Kimura, Y. Saponins from *Platycodi radix* ameliorate high fat diet − induced obesity in mice. *J. Nutr.* **2002**, *132*, 2241−2245.
(26) Guang, C.; Chen, J.; Sang, S.; Cheng, S. Biological functionality of soyasaponins and soyasapogenols. *J. Agric. Food Chem.* **2014**, *62*, 8247−8255.
(27) Da Silva, B. P.; de Sousa, A. C.; Silva, G. M.; Mendes, T. P.; Parente, J. P. A new bioactive steroidal saponin from *Agave attenuata*. *Z. Naturforsch., C: J. Biosci.* **2002**, *57*, 423−428.
(28) Yokosuka, A.; Mimaki, Y. Steroidal saponins from the whole plants of *Agave utahensis* and their cytotoxic activity. *Phytochemistry* **2009**, *70*, 807−815.
(29) Killeen, G. F.; Madigan, C. A.; Connolly, C. R.; Walsh, G. A.; Clark, C.; Hynes, M. J.; Timmins, B. F.; James, P.; Headon, D. R.; Power, R. F. Antimicrobial saponins of *Yucca shidigera* and the implications of their in vitro properties for their in vivo impact. *J. Agric. Food Chem.* **1998**, *46*, 3178−3186.
(30) Chen, P.-Y.; Chen, C.-H.; Kuo, C.-C.; Lee, T.-H.; Kuo, Y.-H.; Lee, C.-K. Cytotoxic steroidal saponins from *Agave sisalana*. *Planta Med.* **2011**, *77*, 929−933.
(31) Djerassi, C.; Ringold, H. J.; Rosenkranz, G. Steroidal sapogenins. XXXVII. Experiments in the hecogenin series. (Part 6). Conversion to cortisone. *J. Am. Chem. Soc.* **1954**, *76*, 5533−5536.
(32) Marker, R. E.; Wagner, R. B.; Ulshafer, P. R.; Wittbecker, E. L.; Goldsmith, D. P. J.; Ruof, C. H. Isolation and structures of thirteen new steroidal sapogenins. New sources for known sapogenins. *J. Am. Chem. Soc.* **1943**, *65*, 1199−1209.
(33) Kartosentono, S.; Indrayanto, G.; Zaini, N. C. The uptake of copper ions by cell suspension cultures of *Agave amaniensis,* and its effect on the growth, amino acids and hecogenin content. *Plant Cell, Tissue Organ Cult.* **2002**, *68*, 287−292.
(34) Debnath, M.; Pandey, M.; Sharma, R.; Thakur, G. S.; Lal, P. Biotechnological intervention of *Agave sisalana*: A unique fiber yielding plant with medicinal property. *J. Med. Plants* **2010**, *4*, 177−187.
(35) Pinos-Rodríguez, J. M.; Zamudio, M.; González, S. S.; Mendoza, G. D. Effects of maturity and ensiling of *Agave salmiana* on nutritional quality for lambs. *Anim. Feed Sci. Technol.* **2009**, *152*, 298−306.
(36) Pinos-Rodríguez, J. M.; Zamudio, M.; González, S. S. The effect of plant age on the chemical composition of fresh and ensiled *Agave salmiana* leaves. *S. Afr. J. Anim. Sci.* **2008**, *38*, 43−50.
(37) Official Method 425.45. In *Official Methods of Analysis of AOAC International*; Horwitz, W., Ed.; AOAC International: Gaithersburg, MD, 2005.
(38) Lin, J.-T.; Liu, S.-C.; Chen, S.-L.; Chen, H.-Y.; Yang, D.-J. Effects of domestic processing on steroidal saponins in Taiwanese yam cultivar (*Dioscorea pseudojaponica* Yamamoto). *J. Agric. Food Chem.* **2006**, *54*, 9948−9954.
(39) Pérez, A. J.; Simonet, A. M.; Calle, J. M.; Pecio, Ł.; Guerra, J. O.; Stochmal, A.; Macías, F. A. Phytotoxic steroidal saponins from *Agave offoyana* leaves. *Phytochemistry* **2014**, *105*, 92−100.
(40) Pérez, A. J.; Calle, J. M.; Simonet, A. M.; Guerra, J. O.; Stochmal, A.; Macías, F. A. Bioactive steroidal saponins from *Agave offoyana* flowers. *Phytochemistry* **2013**, *95*, 298−307.
(41) Pant, G.; Sati, O. P.; Miyahara, K.; Kawasaki, T. Spirostanol glycosides from *Agave cantala*. *Phytochemistry* **1986**, *25*, 1491−1494.
(42) Bodeiko, V. A.; Kintya, P. K. Steroid Saponins VIII. The structure of Agave saponin C and D from the leaves of *Agave americana*. *Chem. Nat. Compd.* **1975**, *6*, 775−777.
(43) Szakiel, A.; Pączkowski, C.; Henry, M. Influence of environmental abiotic factors on the content of saponins in plants. *Phytochem. Rev.* **2011**, *10*, 471−491.
(44) Ortuño, A.; Oncina, R.; Botía, J. M.; Del Río, J. A. Distribution and changes of diosgenin during development of *Trigonella foenum-graecum* plants. Modulation by benzylaminopurine. *Food Chem.* **1998**, *63*, 51−54.
(45) Ndamba, J.; Lemmich, E.; Mølgaard, P. Investigation of the diurnal, ontogenetic and seasonal variation in the molluscicidal saponin content of *Phytolacca dodecandra* aqueous berry extracts. *Phytochemistry* **1994**, *35*, 95−99.
(46) Molina-Freaner, F.; Eguiarte, L. E. The pollination biology of two paniculate agaves (agavaceae) from northwestern Mexico: constrastig roles of bats as pollinators. *Am. J. Bot.* **2003**, *90*, 1016−1024.

DOI: 10.1021/acs.jafc.5b00883
J. Agric. Food Chem. 2015, 63, 3924−3930

ASE) to microwave-assisted[28] and ultrasound-assisted[26,27] organic solvent extraction and supercritical fluid extraction (SFE).[13,16,17] The majority of the methods use organic solvents, such as chloroform, pure alcohols (methanol, ethanol, isopropanol), hexane, dichloromethane, ethyl acetate, and so forth, or mixtures thereof. A combination of chloroform and methanol has been reported in the literature as the best option to recover total lipids from microalgae. These mixtures extract both neutral lipids by chloroform and polar lipids by methanol.[10,11,26] A chloroform/methanol mixture, for example, is used in the method of Folch et al.[29] for the extraction of total lipids from microalgae. This method, originally optimized for the isolation and purification of total lipids from animal tissues, uses 2:1 chloroform/methanol for lipid extraction and water to remove nonlipid substances from the extract.[29,30] Recently, 3:2 hexane/isopropanol has been suggested as an alternative to the chloroform/methanol system.[10,14,18] The mixture works in a similar fashion to the chloroform/methanol system with a higher selectivity toward neutral lipids compared to that of chloroform/methanol.[14,18]

However, these traditional extraction methods have some disadvantages, including the use of hazardous and flammable liquid organic solvents, costly high-purity solvents, and the presence of potentially toxic emissions during extraction. The extraction processes (e.g., Soxhlet) are often slow and time-consuming. Furthermore, an energy-intensive evaporation step is required for solvent removal. Additionally, these organic solvents can cause adverse health and environmental effects. To minimize these drawbacks, alternative, greener extraction techniques have been investigated[5,16] and have led to the development of other extraction methods that are considered to be more sustainable, such as PFE and SFE.

Despite the fact that PFE requires temperatures between 50 and 200 °C and pressures of 10−15 MPa, the associated increased lipid solubility, improved cell wall penetration by solvent, relatively low solvent use compared to other methods, and reduced emission of volatile organic compounds (VOC) due to the required pressure all add up to make this technique somewhat greener than the more traditional methods. Further advantages include its ability to be automated and a lack of light and oxygen within the process, which is beneficial when working with bioactive molecules.[4,5,31]

The vast majority of SFE applications use supercritical CO_2 ($scCO_2$) as the primary solvent. The low critical temperature (31.1 °C) and moderate critical pressure (7.4 MPa) make it particularly useful for extractions of thermolabile compounds.[5,14,16] Numerous literature examples of $scCO_2$ extractions on different natural sources have been reported.[7,8,17,32−34] A common practice in SFE, which has to be mentioned in relation to the physicochemical properties of supercritical fluids, is the use of modifiers (cosolvents). These cosolvents (e.g., methanol and ethanol) are added to the primary fluid to enhance extraction efficiency. For example, the addition of 1−10% methanol or ethanol to $scCO_2$ expands its extraction range to include more polar lipids. The addition of these modifiers is often required to assist $scCO_2$ in the extraction of highly polar compounds.[16] One disadvantage of $scCO_2$ extraction, however, is its high capital cost (CAPEX) due to its pressure-driven nature.

It has also been reported in the literature that differences in lipid extraction arise due to the method and solvent used.[15,35] Furthermore, the extraction efficiency of a particular solvent (system) cannot generally be extrapolated to microalgae species, as indicated in the study by Ryckebosch et al.[10] The main factor that determines recovery from different microalgae species seems to be the permeability of the cell wall.

The purpose of the present study was therefore to compare traditional (Soxhlet, Folch) and modern (PFE, $scCO_2$) extraction techniques for the extraction of lipids from *Nannochloropsis oculata*. Thus, the main focus was on the differences in the fatty acid profiles of the glyco- and phospholipids. The Soxhlet extraction method was included due to its simplicity in operation, relative safety, and potential for scaling up to an industrial plant level. Chloroform/methanol (2:1) was evaluated, as it is used as the extraction solvent in the Folch method, and hexane was selected as it is currently most commonly applied for both commercial extraction of food lipids and extraction of omega-3 LC-PUFA containing triglycerides from heterotrophic microalgae.[10] Ethanol was evaluated due to its low cost, its volatility and strong affinity for membrane-associated lipid complexes because of its ability to form hydrogen bonds.[14] On the basis of UPLC-MS data, the nature of glyco- and phospholipids present in the different extracts has been identified. Therefore, this study aims at providing new insights to the existing literature by giving a comprehensive view of the influence of the extraction method used on the lipid profile of the polar lipids at the molecular level.

MATERIALS AND METHODS

The microalgae species *Nannochloropsis oculata* was used in this study to perform the different extractions. Lyophilized algae were kindly provided by Proviron Industries NV (Hemiksem, Belgium; lot: CCAP 849/1). The algae were first concentrated in a microfiltration unit and subsequently centrifuged, resulting in approximately 9.44 L with a dry weight of ∼12.3%. They were then subjected to a freeze-drying process without delay by pouring concentrated microalgae mixtures onto 600 mL trays (∼1 cm thickness). The freeze-drying process was repeated once to completely dry the algae. Finally, the freeze-dried algae were vacuum packed. The analysis of Proviron Industries NV performed using the procedure described by Ryckebosch et al.[1] specified a total lipid fraction of *Nannochloropsis oculata* amounting to ∼31% with the following breakdown of the different lipid classes: 34% neutral lipids, 24% glycolipids, and 42% phospholipids. This data, obtained by the procedure of Ryckebosch et al.[1] (i.e., extraction with 1:1 chloroform/methanol), will be considered as the reference.

GC-grade chloroform, methanol, ethanol, and hexane were purchased from VWR International (Leuven, Belgium). All weight determinations were carried out on a calibrated analytical balance.

Extraction Conditions. All extractions were performed in triplicate using 7.5 g of freeze-dried *Nannochloropsis oculata* after homogenizing them with a mortar and pestle. For the Folch extraction, however, only 1 g of freeze-dried *Nannochloropsis oculata* was used. For the PFE and Soxhlet extraction, three solvents were selected: hexane, ethanol, and 2:1 chloroform/methanol. Conventional Folch extraction was performed with 2:1 chloroform/methanol, and the SFE extractions were performed with $scCO_2$ or $scCO_2$ plus 30% ethanol as a cosolvent.

More detailed description of the different extraction procedures is given below. After each replicate extraction experiment, with the exception of the Folch extraction, the extract was split into two fractions, and these fractions were accurately weighed. Both fractions were dried under nitrogen atmosphere until visibly dry and stored in a vacuum oven at 23 °C overnight.

Soxhlet Extraction. For Soxhlet extraction, the freeze-dried algae were placed in a 22 × 80 mm extraction thimble (Whatman, VWR, Leuven) and extracted with 80 mL of solvent (hexane, ethanol, 2:1 chloroform/methanol) for 6 h in a 30 mL Soxhlet apparatus.

Pressurized Fluid Extraction. Lipids were extracted from the lyophilized and homogenized algae using an automated Dionex

DOI: 10.1021/acs.jafc.5b00241
J. Agric. Food Chem. 2015, 63, 3931−3941

ASE200 Accelerated Solvent Extraction (ASE) system. The algae (60%) were mixed with Celite 545 (40%) (0.02−1 mm, Merck, VWR, Leuven) prior to being loaded into Dionex standard 33 mL stainless steel extraction thimbles. After a small amount of Celite was added to the extraction cell, the sample mix (12.5 g) was loaded. Sea sand (Merck, PA, USA; VWR, Leuven, Belgium) was finally used to fill any extra space in the cell. Extractions were performed with hexane, ethanol, and 2:1 chloroform/methanol as the extraction solvent. The same conditions were used for all of the solvents: 1500 psi (103 bar) and 125 °C with a 5 min static extraction (after 5 min preheating) and 4 static cycles. Upon completion of the extraction, the thimble was flushed with solvent (50%) and purged with nitrogen for 120 s. The solvent was collected in 60 mL vials with Teflon septa.

Conventional Folch Extraction. One gram of freeze-dried algae was weighed and put into glass vessels. One volume of chloroform, 1 volume of methanol, and 1 volume of chloroform were added in sequence to the algae sample. The mixture was shaken manually after each solvent addition. After addition of the three solvents, the mixture was shaken for 15−20 min at room temperature at high speed. Subsequently, phosphate buffered saline (PBS, pH 7−7.5, 0.8 volume) was added to obtain a final concentration of 1:20 (sample weight/solution volume; g/mL). This PBS was added to increase the ionic strength of the upper phase to improve phase separation.[29] The mixture was then centrifuged at 1000*g* for 1 min to allow the organic and aqueous layers to separate. After the organic layer was removed and collected, the aqueous layer was extracted twice more by adding only 2 volumes of chloroform followed by manual shaking and centrifugation to induce phase separation. The chloroform phases were collected in a tared glass vial. The extract was dried under nitrogen atmosphere until visibly dry and put in a vacuum oven at 23 °C overnight.

Supercritical Extraction. An ISCO SFX 220 Supercritical Fluid Extractor equipped with an ISCO Model 260 D Syringe pump, ISCO Restrictor Temperature Controller and an ISCO SFX 200 Controller (BRS) was used. Supercritical extraction with either CO_2 or CO_2/30% ethanol (cosolvent) was conducted at a pressure of 400 bar and a temperature of 40 °C with a 240 min dynamic extraction. The flow rate of $scCO_2$ and $scCO_2$/30% ethanol was set to 3 and 2.1 mL/min, respectively. The microalgae powder was placed in a high-pressure extraction cell. Carbon dioxide was liquefied by a cooler and pressurized to the preferred pressure using a high-pressure pump. Pressurized CO_2 was then pumped into the heated extraction cell during the SFE process. The extract was collected in a glass tube by venting $scCO_2$. The temperature of the restrictor (2 mL/min TCR 0.75) was set at 90 °C.

Analysis of Total Lipid Content in the Lipid Part of the Extract. With the exception of the Folch extraction, two fractions were obtained from each replicate extraction. One of these fractions was stored at −20 °C under nitrogen. Because it is known that some solvents (mixtures) may not only extract lipids but also nonlipid polar compounds, such as carbohydrates and proteins, the other half was treated with 10 mL 2:1 chloroform/methanol to separate the nonlipid and lipid fractions in the extract.[11,15] The redissolved extract was shaken for 2 min and then centrifuged for 5 min at 3000*g*. The supernatant was removed, and the residue was washed twice more with the chloroform/methanol mixture. The lipid fractions of the three washing steps were collected, dried under nitrogen atmosphere until visibly dry, and finally stored in a vacuum oven overnight. The residue was accurately weighed to determine the total lipid content. After weighing, the extract was resuspended in 10 mL 2:1 chloroform/methanol and divided into different fractions: one was used for analysis of the phosphorus content and the other for fractionation of the lipid classes. After being dried and weighed, the fraction for fractionation and the additional sample were stored at −20 °C under nitrogen to prevent lipid oxidation.

Separation of Lipid Classes. To determine the influence of the different extraction methods and conditions on the lipid class composition, the lipid class content of the extracts was determined using silica solid-phase extraction (SPE) performed according to the procedure described by Ryckebosch et al.[1]

Briefly, a 500 mg/6 mL Grace Pure SPE Silica column (Grace, Lokeren, Belgium) was first conditioned by elution with 10 mL of chloroform. Approximately 10−20 mg of lipids dissolved in 500 μL chloroform was brought onto the silica column. Elution with 10 mL of chloroform yielded the neutral lipids (NL), and 10 mL of acetone was used for elution of the glycolipids (GL). Finally, the phospholipids (PL) were eluted with 10 mL of methanol. The yield of each class was determined gravimetrically in triplicate.

Characterization of the Lipid Extracts and Fractions. The phosphorus concentration was determined in the total lipid extract after washing in 2:1 chloroform/methanol by means of inductively coupled plasma emission spectrometry following DIN EN 14107.

A known quantity of each fraction (NL, GL, and PL) was dissolved in 90:10 isopropanol/acetonitrile with 0.1% formic acid. Analysis was based on ultra performance liquid chromatography (UPLC)−mass spectrometry (MS). A Waters Acquity UPLC system (Waters, Milford, MA, USA) was used, equipped with an Acquity UPLC BEH300 C_{18} column (150 × 2.1 mm; 1.7 μm). The column temperature was maintained at 35 °C. Optimum separation was obtained with a binary mobile phase constituted of 50:50 acetonitrile/water (eluent A) and 90:10 isopropanol/acetonitrile (eluent B) with both solvent mixtures buffered with 0.1% formic acid. The gradient elution program was 0−1 min from 100% A to 45% A, 1−25 min from 45% A to 30% A, 25−26 min from 30% A to 0% A, 26−30 min with 100% B, 30−31 min from 0% A to 100% A, and 31−40 min with 100% A (returned to initial conditions and equilibration of the column). The flow rate of the mobile phase was 0.2 mL/min. Different injection volumes were used to be in the linear range for quantification.

The UPLC system was coupled to a Waters Single Quadrupole mass spectrometer (Waters, Milford, MA, USA), which was operated in the positive electrospray ionization mode (ESI+) in full scan acquisition. The parameters of the mass spectrometer were as follows: electrospray source block and desolvation temperatures of 150 and 300 °C, capillary voltage of 4.5 kV and cone voltage of 85 V.

Positive identification of the compounds was based on chromatographic retention times, molecular weights, and their characteristic m/z ions generated by in-source fragmentation. An overview of the retention times and m/z ions of the different compounds is given in the Supporting Information (Table S1). The ion chromatogram of each m/z ratio, corresponding to a particular compound, was derived from the total ion chromatogram using the MassLynx Mass Spectrometry Software (Waters). The area of the resulting single peak was then integrated.

Finally, quantitative determination of the phospholipids was made using an analytical standard. Thus, a phospholipid mixture for HPLC from Glycine max (soybean) in chloroform, containing phosphatidylcholine (PC), lyso-phosphatidylcholine, phospatidylethanolamine (PE), and phosphatidylinositol (PI), was purchased from Sigma-Aldrich (Bornem, Belgium). The phospholipid standard was dried under nitrogen to remove chloroform and reconstituted with 90:10 isopropanol/acetonitrile with 0.1% formic acid (eluent B). Five dilutions were made in duplicate to obtain the following PC concentrations: 25, 50, 100, 150, and 200 μg/mL. These calibration solutions were injected into the UPLC-MS system using the instrumental conditions described above. The calibration curve was made by plotting the total peak area of PC components in function of the total PC concentration reported on the certificate of analysis of the analytical standard. Linear calibration curves were constructed with a squared regression coefficient R^2 of 0.99. The limit of detection (LOD) and limit of quantification (LOQ) of the applied method were calculated considering the peak-to-peak signal-to-noise ratio in the chromatogram of the standard solution with the lowest concentration of PC (25 μg/mL). Because various PCs bearing different fatty acids were present in the analytical standard, the signal-to-noise ratio of the lowest chromatographic peak was determined (worst case scenario). The LOD and LOQ were defined as the concentration that would give a signal-to-noise ratio of 3 and 10, respectively. Extrapolating from the signal-to-noise ratio observed for the lowest peak, LOD and LOQ were calculated to be 4 and 13 μg/mL, respectively.

DOI: 10.1021/acs.jafc.5b00241
J. Agric. Food Chem. 2015, 63, 3931−3941

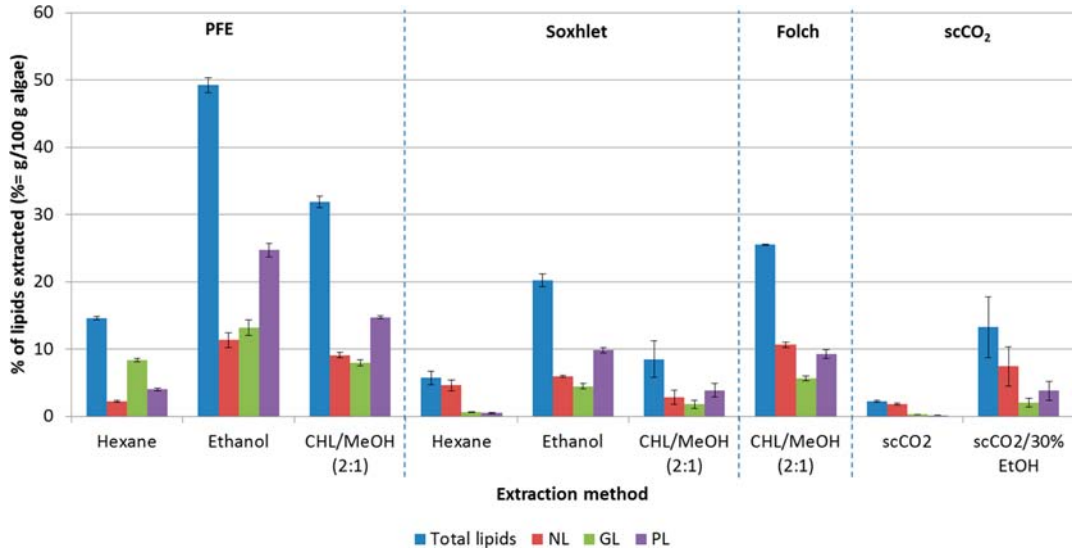

Figure 1. Total amount of lipids and lipid class composition obtained by the different extraction methods from *Nannochloropsis oculata* (mean ± SD; n = 3; CHL: chloroform; MeOH: methanol; EtOH: ethanol).

Calculations and Statistical Analysis. The presence of PC was assessed using the phosphorus content of the different lipid fractions. The phosphorus content was converted to a PC concentration expressed as g PC/100 g algae using the molecular weight of phosphorus (30.97 g/mol) and of oleoyl-palmitoyl-phosphatidylcholine (PC 16:0/18:1) (760 g/mol). PC 16:0/18:1 was used for this purpose because Wang et al. observed that C16:0 and C18:1 are the major fatty acids in PC in *Nannochloropsis* lipids.[15] The total lipid fraction, as well as the NL, GL, and PL fractions, were calculated on a weight basis as g/100 g algae, and the results are expressed as a percentage.

The chromatographic peak area of each compound belonging to a certain class was determined and related to the amount injected. This enabled the various extraction methods to be directly compared on the basis of their effects on each single component. An assessment of the total amount of the different lipid classes present was made by the sum of all chromatographic peak areas in the UPLC chromatogram belonging to the lipid class under consideration. The total peak area per mass algae extracted was then calculated by taking into account the relative contribution of that particular lipid class to the total lipid fraction. Finally, the peak area ratio of one specific compound relative to the total peak area of the lipid class under consideration yields the relative lipid composition (area in %). The PC concentration (μg/mL) was converted to w/w % (mass PC/mass algae) using the sample volume and the weight of the PL fraction. All results are an average of three replicate measurements. Each replicate measurement was obtained from an independent extraction and fractionation. In addition, standard deviations were calculated and are indicated by error bars.

RESULTS AND DISCUSSION

Total Lipid Fraction and Lipid Class Composition. The total lipid fractions were obtained after the washing step with 2:1 chloroform/methanol. Data on the influence of this washing step on the total lipid fraction are shown in the Supporting Information (Figure S1). In general, the total lipid fractions originating from extractions with more polar solvents (e.g., ethanol) were the most affected by the washing step with 2:1 chloroform/methanol, resulting in a larger mass loss compared to nonpolar extractions. The polar extractions are indeed more prone to the coextraction of nonlipid, more polar matrix materials (e.g., proteins and carbohydrates).

The final total lipid fractions after washing with 2:1 chloroform/methanol extracted by the different methods from *Nannochloropsis oculata* are shown in Figure 1. Chloroform/methanol (2:1) as the extraction solvent with PFE, Soxhlet, or Folch extraction resulted in comparable total lipid fractions in the range of 26−32%. These total lipid fractions correspond well with the reference value of 31% obtained by Ryckebosch et al.[1] via extraction with 1:1 chloroform/methanol. The 2:1 chloroform/methanol is the most frequently used solvent mixture for lipid extraction from any living tissue and is applied in methods such as Folch and Bligh and Dyer.[1,14,29,30] This mixture is able to extract both nonpolar lipids by chloroform and polar lipids by methanol. For this reason, mixtures of chloroform/methanol tend to be more efficient for the extraction of total lipids.[26]

The highest total lipid fraction is extracted from *Nannochloropsis oculata* using PFE extraction with ethanol (49%). It can be assumed that, even though a washing step has been performed, coextracted (polar) matrix components, such as phytochemicals, are still present in the extract as observed by Mulbry et al.[36]

On the basis of the total lipid fraction results, it can be concluded that the polarity of the extraction solvent clearly influences the crude lipid yield using both classical extraction methods (Soxhlet, Folch) and modern techniques (PFE, SFE). Nonpolar solvents can only extract very nonpolar lipids, whereas more polar solvents (mixtures) extract lipids of a broader polarity range, resulting in a higher lipid yield.

With either PFE or Soxhlet extractions, the following order of total lipid fraction was observed: ethanol > 2:1 chloroform/methanol > hexane. The addition of 30% ethanol as cosolvent to pure $scCO_2$ increased the total lipid yield relative to the extraction with pure $scCO_2$. Extractions that use only $scCO_2$ usually give good recoveries of nonpolar lipids. Polar lipids, however, have low solubility in $scCO_2$ and are thus not extracted. Adding ethanol expands the extraction range of $scCO_2$ to include the more polar lipids, resulting in a higher extraction yield.

These observations are in accordance with literature data on the influence of solvent polarity on the extraction of lipids from microalgae[10,11,20,34,36,37] For example, McNichol et al. observed

DOI: 10.1021/acs.jafc.5b00241
J. Agric. Food Chem. 2015, 63, 3931−3941

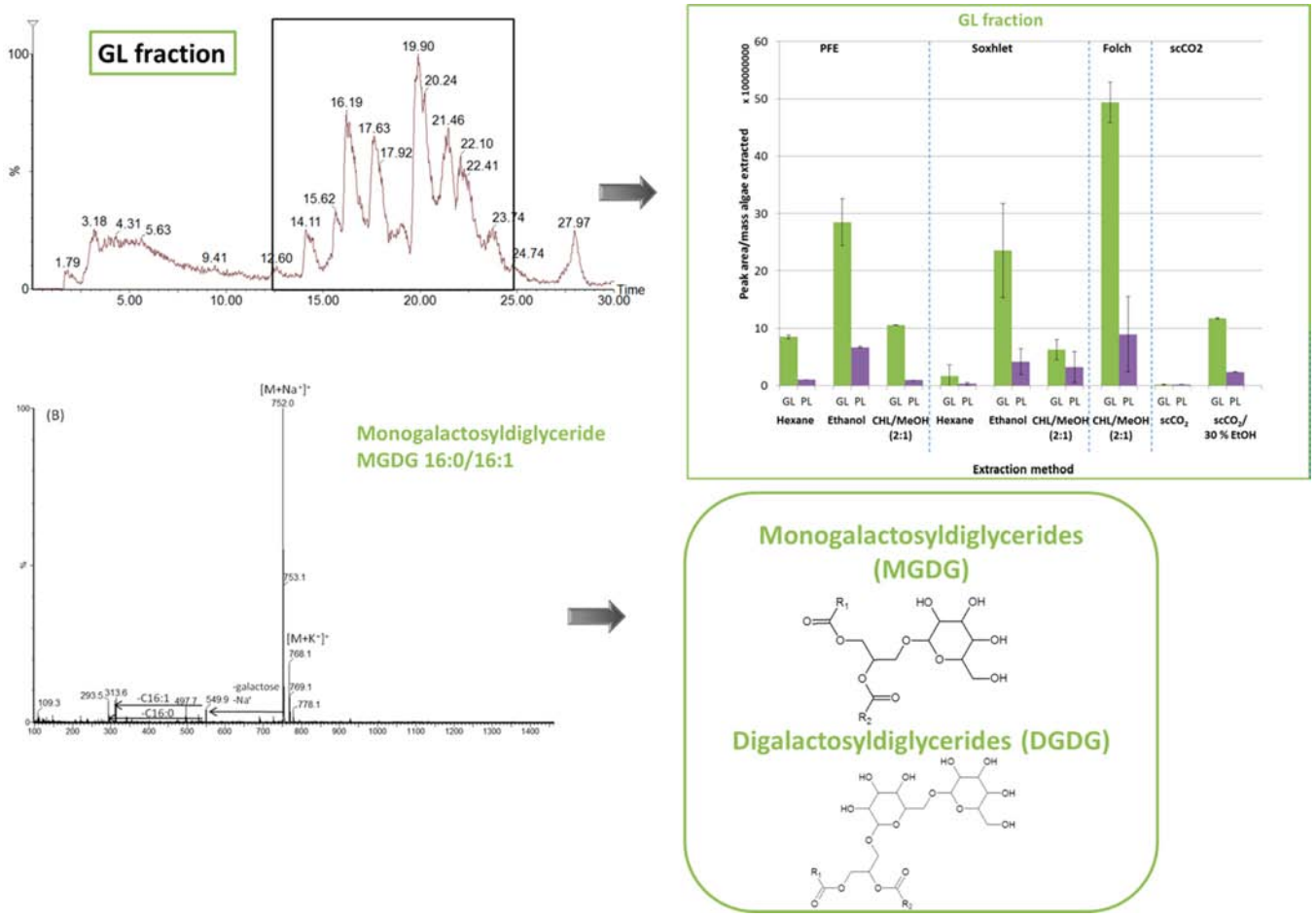

Figure 2. Total ion current (TIC) chromatogram of the GL fraction for PFE extraction with 2:1 chloroform/methanol. In the separate graph, the total chromatographic peak area is shown (mean ± SD; n = 3; CHL: chloroform; MeOH: methanol; EtOH: ethanol). The chemical structure of the compounds identified in the GL fractions is shown. The ESI+ mass spectrum of a compound is given as an example.

that hexane extracted ∼3% of lipids from *Nannochloropsis granulate*, whereas ethanol and 2:1 chloroform/methanol extracted >25% of lipids on a dry weight basis.[20] In a study by Balasubramanian et al., the use of hexane alone gave only 16% lipid yield whereas the addition of a polar solvent improved the yield.[37] Furthermore, no significant difference in the lipid extraction efficiency was observed between the different extraction methodologies (sonication, PFE, homogenization, Soxhlet) all using 2:1 chloroform/methanol as the extraction solvent.

To gain insight into the lipid class composition, we fractionated the different extracts into three portions using SPE to determine the percentages of NL, GL, and PL (Figure 1).[1] The lipid class composition of the 2:1 chloroform/methanol extracts obtained by Soxhlet, PFE, or Folch is in accordance with the specifications on *Nannochloropsis oculata* applying the reference method (1:1 chloroform/methanol). The distribution of the lipids among the different classes is as follows: phospholipids > neutral lipids > glycolipids. Phospholipids are predominantly present in these extracts in the range of 40−45% of total lipids.

Low polarity solvents are best for the extraction of neutral lipids, including waxes and pigments, which are characterized by a very low polarity. In contrast, lipids from the chloroplast and membrane, which contain GL and PL, respectively, are more effectively extracted by more polar organic solvents, such as ethanol or methanol.[10,37,38] The affinity of polar lipids (GL and PL) for more polar solvents (mixtures) is also observed in the present study. The PL fraction in the ethanol extracts is the most abundant, whereas the yield of PL using hexane is almost negligible due to the apolar character of the solvent. For SFE, the same trend is observed. Using pure $scCO_2$, the lipid fraction consists mainly of NL, which demonstrates the selectivity of $scCO_2$ toward nonpolar molecules.[16,39] Its nonpolar nature makes pure $scCO_2$ incapable of interacting with either polar lipids or neutral lipids that form complexes with polar lipids.[14] Through the addition of ethanol, the affinity toward GL and PL is enhanced, although the NL fraction is still predominant.

The findings in this study are consistent with literature data. In the study by Ryckebosch et al. comparing the extraction efficiency of 3:2 hexane/isopropanol and hexane for the extraction of lipids from different microalgae species, the NL content was higher in the hexane extract and lower in the 1:1 chloroform/methanol and 3:2 hexane/isopropanol extracts for each microalga.[10] Hence, the amount of polar lipids (GL and PL) was lowest in the hexane extract. Ryckebosch et al. also compared dichloromethane/ethanol with nonhalogenated solvent systems for the extraction of lipids from *Nannochloropsis gaditana*.[11] Dichloromethane/ethanol extracted the three lipid classes with essentially the same efficiency, whereas all nonhalogenated solvent mixtures more easily extracted NL than the polar lipids (GL and PL). Of the nonhalogenated

DOI: 10.1021/acs.jafc.5b00241
J. Agric. Food Chem. 2015, 63, 3931−3941

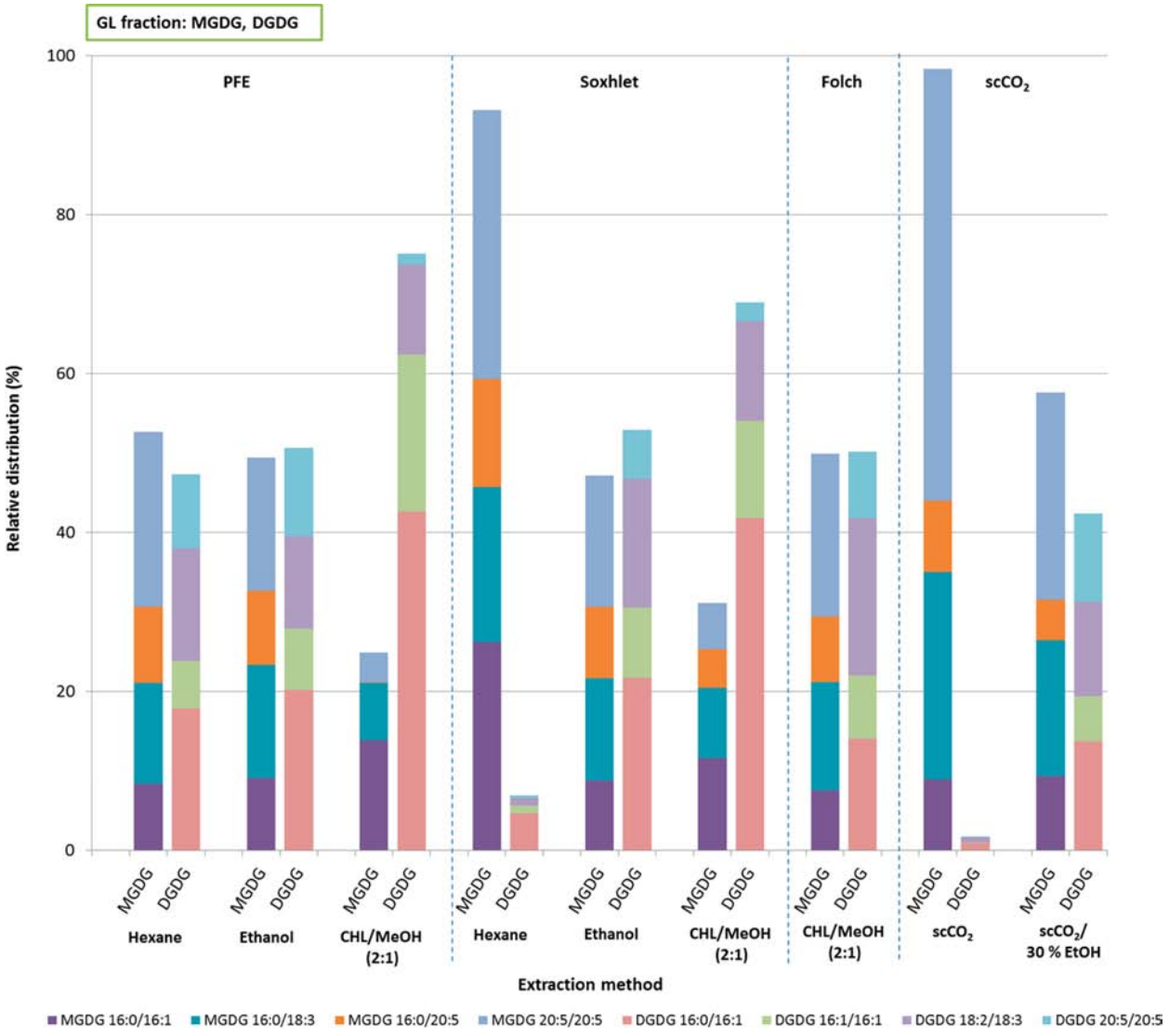

Figure 3. Relative distribution (% of total peak area) of the different MGDGs and DGDGs in the GL fraction. The results are the average of three replicate measurements (mean ± SD; CHL: chloroform; MeOH: methanol; EtOH: ethanol).

solvents, the highest recovery of NL was obtained with 3:2 hexane/isopropanol and ethyl acetate/hexane. Also for the GL, 3:2 hexane/isopropanol proved to be the most efficient solvent, whereas for PL, ethanol was best.[11] Similar results have also been observed by Balasubramanian et al.[37] and Mendes[34] and co-workers in which the latter uses solvent polarities to explain these observations.

The phosphorus content of the lipid extracts gives insight into the presence of phospholipids. According to the literature, PC was reported to be the major component of phospholipids in many microalgae, though its content might vary due to species-specificity or culture conditions.[8,11]

The phosphorus content of the different crude lipid extracts (Supporting Information, Figure S2) is in accordance with the lipid class composition. The extraction of PL is favored by a more polar extraction solvent. Indeed, the highest phosphorus content is observed for ethanol, followed by 2:1 chloroform/methanol, and then hexane. Furthermore, as pure $scCO_2$ is not polar enough to extract the phospholipids, none were detected above the LOQ in the $scCO_2$ extract. The increase in polarity by the addition of 30% ethanol, however, resulted in enhancement of the phosphorus concentration comparable to the content in the lipid extract of PFE with hexane.

Compound Identification in the Polar Lipid Fractions GL and PL. *GL Fractions.* An overview of the total chromatographic peak area integrated for the GLs in the different extracts is given in Figure 2. This data also indicates that by increasing the polarity of the solvent, more glycolipids are being extracted as indicated by the higher total chromatographic peak area. For all of the extraction methods used, the majority of the GLs (i.e., highest total peak area/mass algae extracted) is detected in the corresponding fractions. Analysis of the different PL fractions, however, revealed that quite a persistent proportion of GL is also present in these fractions (Figure 2). Thus, all extraction methodologies lead to higher yields of GL than the analysis of the GL fractions indicate. Similarities in chemical structure, and consequently polarity, between GL and PL lead to the observed incomplete separation, especially when using SPE.

Glycolipids and more specifically monoglycodiglycerides and diglycodiglycerides were detected as sodium adducts in the GL and PL fractions (Figure 2). Because galactolipids are the predominant lipids in photosynthetic membranes, they could

DOI: 10.1021/acs.jafc.5b00241
J. Agric. Food Chem. 2015, 63, 3931−3941

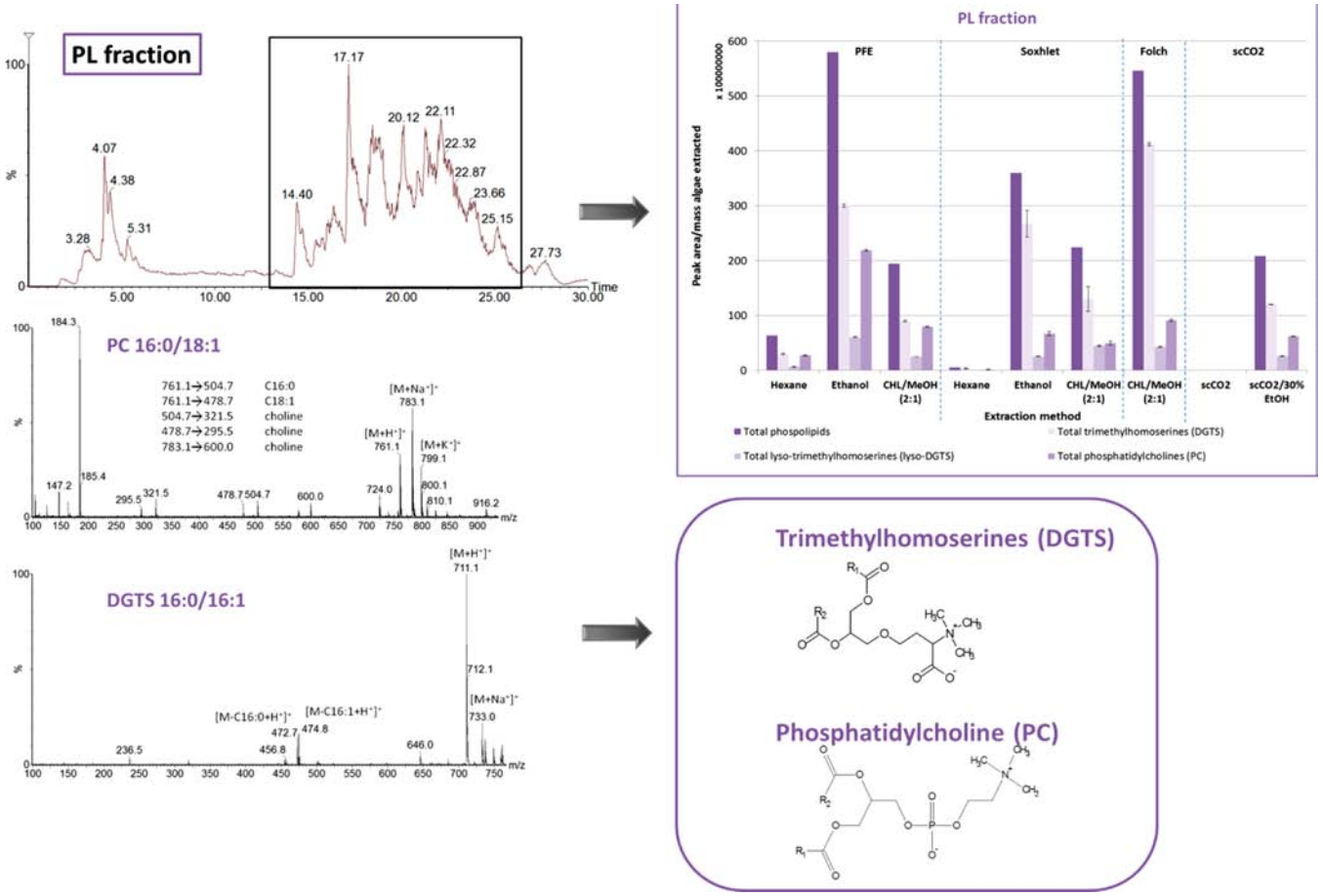

Figure 4. Total ion current (TIC) chromatogram of the PL fraction for PFE extraction with 2:1 chloroform/methanol. In the separate graph, the total chromatographic peak area is shown (mean ± SD; $n = 3$; CHL: chloroform; MeOH: methanol; EtOH: ethanol). The chemical structure of the compounds identified in the PL fractions is shown. The ESI+ mass spectrum of a compound is given as an example.

be assumed to be monogalactosyldiglycerides (MGDG) and digalactosyldiglycerides (DGDG). The structures of MGDG and DGDG are given in Figure 2. In these natural compounds, the galactopyranose moiety is linked to the glycerol backbone, bearing two long fatty acid chains.

As can be seen in Figure 3, the methodology used has a significant effect on the extraction yield of the galactolipids, shifting more toward MGDG or DGDG. SFE with pure $scCO_2$ and the Soxhlet extraction with hexane predominantly yield MGDGs with 98% and 92% of the total peak area, respectively, belonging to MGDG. The additional galactose moiety makes DGDG sufficiently polar to prevent its extraction with a nonpolar solvent. In contrast, the PFE extraction with hexane does extract DGDGs (53% MGDG and 47% DGDG), which can be explained by the higher extraction temperature and pressure. The extraction yield of DGDG is enhanced by increasing the solvent polarity with DGDG contributing >60% for the PFE or Soxhlet extraction with 2:1 chloroform/methanol.

Linked to MGDG and DGDG are different types of fatty acid (Figure 3). All of the galactolipids identified contain at least one site of unsaturation with a strong presence of C20:5. Among the saturated fatty acids, palmitic acid (C16:0) is the most abundant. PUFAs such as C20:5 are prone to oxidation,[30] and the incidence of C20:5 in the GL fractions indicates that the extraction methods used are able to preserve it intact. This occurrence of C20:5 is in accordance with literature data, where it is stated that PUFAs of microalgae are predominantly linked to polar lipids, especially glycolipids (MGDG, DGDG, and sulphoquinovosyldiacylglycerol (SQDG)).[4,10,11]

Also within every class, the abundance of one (or more) MGDG or DGDG compound(s) with a particular fatty acid is favored depending on the extraction method and solvent used (Figure 3). For example, DGDG 16:0/16:1 is the principle DGDG extracted with 2:1 chloroform/methanol as the solvent using either Soxhlet or PFE. The SFE-$scCO_2$ extraction, on the other hand, preferentially extracts MGDG 20:5/20:5. These observations again demonstrate that a more polar solvent mixture extracts more polar lipids (i.e., more sugars and shorter fatty acid chains), whereas the use of a less polar solvent yields less polar lipids (i.e., single sugars and longer fatty acid chains).

Wang et al. characterized the lipid profile of *Nannochloropsis oculata* extracted with ethanol (80 °C, 30 min) followed by separation of the lipid and nonlipid fractions using the Folch's procedure.[15] DGDG was the major GL class, accounting for 28.4% of all quantified polar lipids. The contribution of MGDG amounted to 2.1%. Hence, Wang et al. obtained an excess of DGDG in the ethanol extract, whereas MGDG and DGDG were more equally distributed in the ethanol extracts (PFE/Soxhlet) in the present study. According to Wang et al., the major fatty acids bound were C16:0 (52.3%), C14:0 (14.0%), and C18:1 (10.8%) in MGDG and C16:0 (51%) and C16:1 (19.1%) in DGDG.[15] In this study, however, different types of fatty acids are linked to MGDG and DGDG. Whereas C16:0

DOI: 10.1021/acs.jafc.5b00241
J. Agric. Food Chem. 2015, 63, 3931−3941

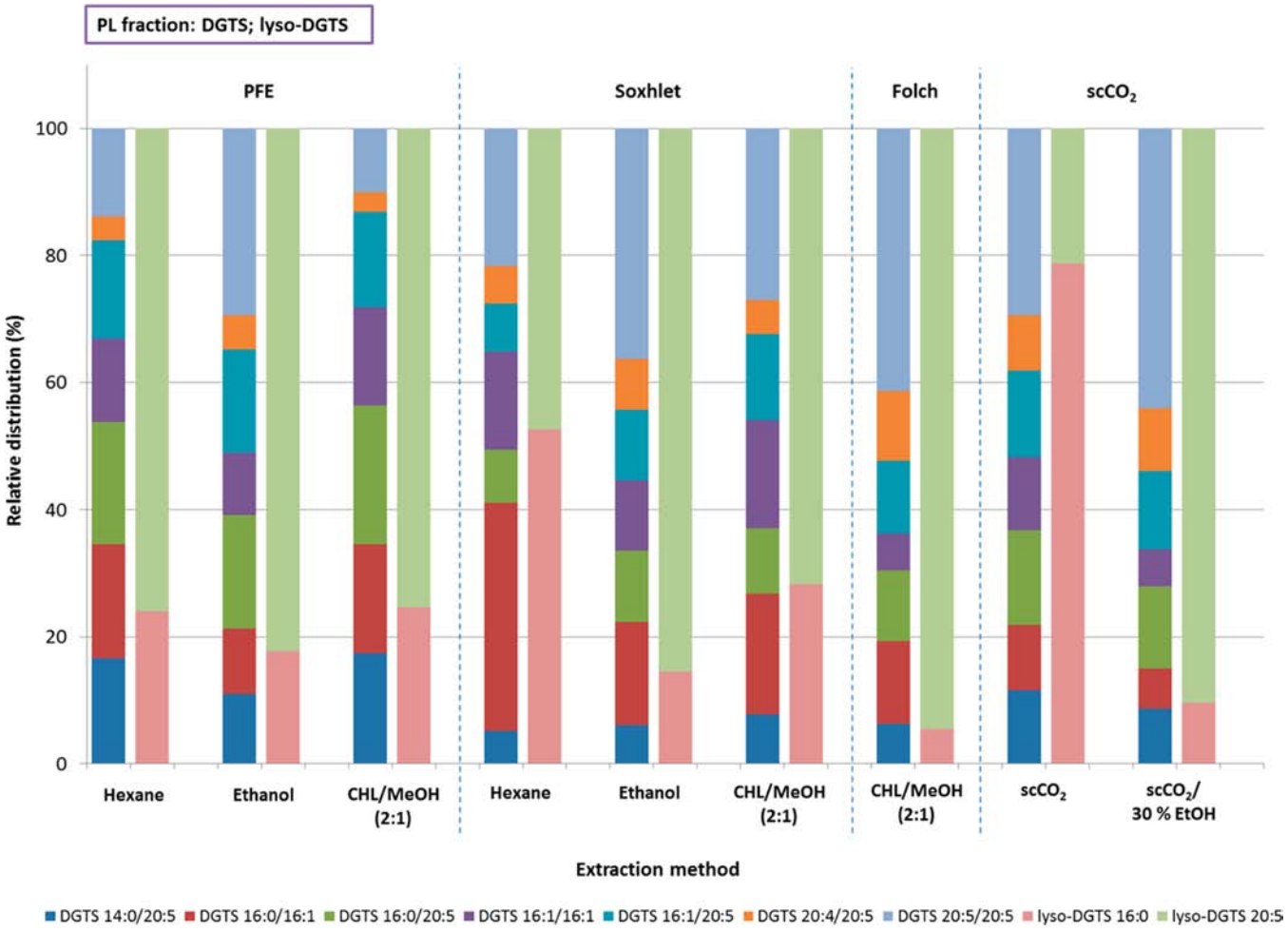

Figure 5. Relative distribution over different DGTS and lyso-DGTS expressed as % of total peak area of DGTS and lyso-DGTS, respectively. Results are the average of three replicate measurements (mean ± SD; CHL: chloroform; MeOH: methanol; EtOH: ethanol).

and C16:1 are common in both studies, the present study reveals the predominance of particular PUFAs, including C18:2, C18:3, and C20:5. This difference in fatty acid profile of the galactolipids can be explained by the cultivation, harvest (sedimentation, chemical flocculation, etc.), and storage (freeze, dry, freeze-dry, wet, etc.) conditions of the microalgae used. The extent of the production of biomass, lipids, carotenoids, and carbohydrates as well as the exact composition of the final products (e.g., fatty acid pattern of lipids) can vary considerably depending on the prevailing conditions in the cultivation medium.[5,6] In addition, differences in the fatty acid profile[15,35] of the extracts also arise due to the extraction methodology used (i.e., traditional vs PFE must also be taken into account), which can result in a different fatty acid profile.

PL Fractions. A typical chromatogram of a PL fraction is shown in Figure 4. In the PL fractions, two different classes of polar lipids were detected: trimethylhomoserines (DGTS; 1,2-diacylglyceryl-*O*-(*N*,*N*,*N*-trimethyl)-homoserine) and phoshatidylcholines (PC). The chemical structure of both classes is given in Figure 4. DGTS belongs to the betaine lipids, a recently discovered group of complex lipids primarily found in the plant kingdom.[40] Ether-linked glycerolipids containing a betaine moiety occur naturally in algae, bryophytes, fungi, and in some primitive protozoa and photosynthetic bacteria. These lipids contain a polar group linked by an ether bond in the *sn*-3 position of the glycerol moiety with the fatty acids esterified in the *sn*-1 and *sn*-2 positions (Figure 4). A positively charged trimethylammonium group and a negatively charged carboxyl group give them zwitterionic character at neutral pH. At least three types of betaine lipids have been described with differing permethylated hydroxyamino acids linked to diacylglycerols through an ether bond: DGTS, 1,2-diacylglyceryl-3-O-2′-(hydroxymethyl)-(*N*,*N*,*N*-trimethyl)-*β*-alanine and 1,2-diacylglyceryl-3-*O*-carboxy-(hydroxymethyl)choline. Of these, the first is by far the most common in nature.[40,41] There is evidence in the literature that supports betaine lipids (as well as glycolipids) being used to replace part of the membrane phospholipids in cases of phosphorus starvation as observed in the photosynthetic bacterium *Rhodobacter sphaeroides*[42] and plant *Arabidopsis thaliana*.[43]

DGTS can also be present in the lysated form due to the loss of a fatty acid residue, referred to as lyso-DGTS. The total peak area of polar lipids observed in the PL fractions of the different algae extracts is given in Figure 4 with a distinction between PC, DGTS, and lyso-DGTS. DGTS and PC are the major contribution to the total peak area of polar lipids. The highest total peak area was found for the PFE extraction with ethanol, followed by the conventional Folch extraction, with the highest affinity for DGTS. As for the GL fractions, a trend of increasing total peak area with increasing solvent polarity is observed, both for the traditional solvent systems and $scCO_2$.

DOI: 10.1021/acs.jafc.5b00241
J. Agric. Food Chem. 2015, 63, 3931−3941

Table 1. Total Concentration of Phosphatidylcholine (PC) and Relative Distribution among Different Combinations of Fatty Acid Chains in the Different Polar Lipid Fractions[a]

	PFE			Soxhlet			Folch	SFE	
extraction method	hexane	ethanol	2:1 CHL/MeOH	hexane	ethanol	2:1 CHL/MeOH	2:1 CHL/MeOH	$scCO_2$	$scCO_2$/30% EtOH
total PC (% w/w)	0.14	2.51	0.42	0.01	0.48	0.18	0.60	<LOQ[b]	0.33
relative distribution[c] (%) among PCs with different fatty acid chains									
PC 16:0/16:1	24.6	25.7	26.7	34.0	17.7	12.9	18.9		27.3
PC 16:0/18:1	19.0	15.3	19.0	4.2	9.0	5.5	10.6		17.6
PC 16:0/18:2				1.5	0.5	1.4			
PC 16:0/18:3	16.9	20.9	15.7	3.5	8.4	11.3	6.4		23.7
PC 16:0/20:5	6.6	8.3	7.2	9.1	7.8	6.8	11.1		8.7
PC 16:1/16:1	7.8	11.9	8.9	14.1	20.3	26.2	15.9		4.2
PC 16:1/18:0				1.2	1.6	4.7			
PC 16:1/20:5	5.6	5.7	4.5	8.2	14.8	10.8	15.9		7.3
PC 16:2/18:2				2.7	2.3	6.5			
PC 18:1/16:1	15.3	7.5	14.4	13.3	8.7	6.4	9.8		6.7
PC 20:3/16:0	4.1	4.8	3.7	8.3	8.9	7.6	11.5		4.6

[a]Results are the average of three replicate measurements (mean ± SD). [b]LOQ of PC analysis: 13 μg/mL. [c]Calculated using the relative peak area of each PC compound and the total PC concentration.

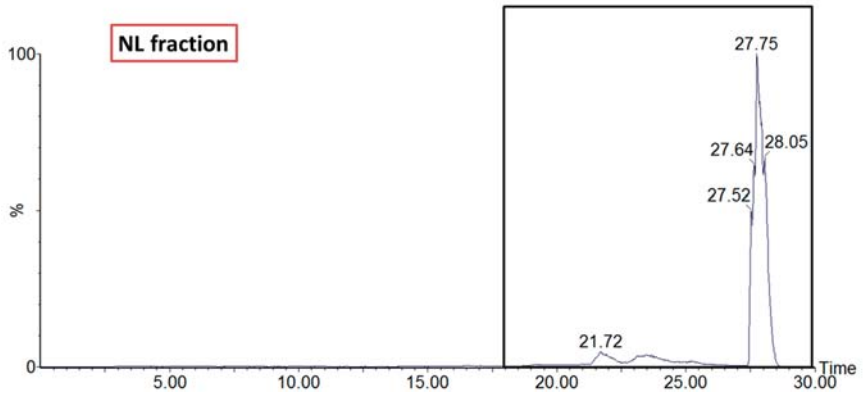

Figure 6. The total ion current (TIC) chromatogram of the NL fraction for PFE extraction with 2:1 chloroform/methanol.

Figure 5 shows the fatty acid profile of the DGTS, comprising large fractions of C20:5, C16:0, and C16:1. On the basis of these results, we can state that the various extraction methods under consideration are able to produce DGTS mixtures with slightly different compositions of fatty acids. However, in general, the methodology of extraction seems to affect the composition less than in the case of the galactolipids. This observation can possibly be explained by the amphiphilic structure of PC and DGTS, which both bear a positively charged group (quaternary ammonium), thus increasing their affinity for polar solvents, such as ethanol. On the other hand, sufficient solubility is maintained in more nonpolar solvents, such as chloroform/methanol mixtures, due to the presence of the two acyclic moieties. Hence, a very similar lipid distribution is generated among the different extraction methods. One exception is the extraction of DGTS 16:0/16:1 which is particularly favored by Soxhlet extraction with hexane.

In addition, two lysated forms of DGTS were identified in the different extracts (i.e., lyso-DGTS 16:0 and lyso-DGTS 20:5 with C16:0 and C20:5, respectively as the remaining fatty acids) (Figure 5). The majority of the extraction methods favor the extraction of lyso-DGTS 20:5. The trend is inverted, however, for Soxhlet extraction with hexane and $scCO_2$ extraction. The nonpolar character of the solvent used in the latter favors the extraction of lyso-DGTS bearing short chain fatty acids.

Because of the availability of a PC analytical standard, quantitative assessment of the PCs in the different extracts was carried out (Table 1). The highest PC concentration was observed in the PL fraction of the PFE extract with ethanol. No PCs were measured above LOQ (LOQ: 14 μg/mL) in the pure $scCO_2$ extract. The addition of 30% ethanol to $scCO_2$, however, results in increased extraction of PC at 0.33% (w/w).

A total concentration of PC in the range of only 1.5−10% (w/w) in the PL fractions, which corresponds to 0.1−2.5% in the algae, raises questions about the nature of other compounds present and their contribution to the total concentration of PLs. The presence of homoserines (DGTS, lyso-DGTS) can be stipulated with certainty, though due to the lack of an analytical standard their quantification was not possible. The presence of other PL classes (i.e., phosphatidylinositols and phosphatidylethanolamines) was investigated. However, these compounds were not detected in a quantifiable amount.

The chromatogram of the different PL fractions, indicating the considerable presence of polar compounds, combined with the low solubility of the PL samples even in a large volume of 90:10 isopropanol/acetonitrile with 0.1% formic acid, clearly suggests the presence of very polar compounds, possibly salts.

DOI: 10.1021/acs.jafc.5b00241
J. Agric. Food Chem. 2015, 63, 3931−3941

C16:0, C16:1, C20:5, and C18:3 are the dominant fatty acids linked to PCs in the different extracts (Table 1). The PL fractions of all PFE extractions and the $scCO_2$/30% ethanol extraction show a rather similar PC pattern dominated by PCs 16:0/16:1, 16:0/18:1, and 16:0/18:3. In contrast, the PL fraction originating from the conventional Folch extraction is rich in PC 16:0/20:5, PC 16:1/16:1, and PC 16:1/20:5. From the Soxhlet extract PC 16:0/16:1, PC 16:1/16:1, PC 16:1/20:5, and PC 18:1/16:1 are the most abundant, independent of the solvent used. Hence, in analogy to DGTS, it can be concluded that the different methodologies seem to be able to extract PCs with slightly different fatty acid profiles. Compared to the GL fractions, however, the fatty acid pattern seems to be less affected by the extraction methodology applied. Therefore, it can be stated that the different methods are able to extract PCs with similar fatty acid distribution.

Purity Control of NL Fractions. The UPLC-MS method applied here was specifically developed to assess the presence of GLs and PLs, which were the main focus of this study. Hence, TAGs could not be detected and identified. The NL fractions, however, were also analyzed using this method to establish the purity of these fractions. As expected, no polar lipids (GL and PL) were detected in the different NL fractions. The chromatogram of the NL fraction originating from the PFE extraction with 2:1 chloroform/methanol is given as an example in Figure 6, which clearly shows the absence of peaks belonging to GLs and PLs. Hence, the SPE fractionation of lipid classes results in complete separation of the neutral lipids from the more polar ones.

The peaks present in the chromatograms of the NL fractions can be attributed to pigments (i.e., oxygenated carotenoids, commonly known as xanthophylls). Because the presence of carotenoids in the different algae extracts are not the focus of the present study, no further attention has been paid to the detailed analysis of the carotenoids present.

Cultivation, harvesting, and storage conditions significantly influence the lipid and fatty acid profiles of microalgae species. This study clearly indicates that the extraction methodology also affects the composition of the lipid profile of *Nannochloropsis oculata*, affecting both the efficiency and selectivity of extraction. Nonpolar solvents show the highest affinity for neutral lipids, and the extraction of polar lipids is favored by increasing solvent polarity.

Special emphasis has been given to the identification of the polar lipids present in the GL and PL fractions. Within these lipid classes, the extraction methodology used affects the molecular composition of the extract, in both structure and fatty acid composition. This effect was more pronounced in the GL fractions. Thus, the extraction of lipids from microalgae is not only a matter of "how many", but also of "which ones", according to the different methodologies and solvents used.

■ ASSOCIATED CONTENT

Supporting Information

Phosphorus content of different extracts, influence of the 2:1 chloroform/methanol washing step, and details on instrumental analysis (i.e., retention time and m/z ions). This material is available free of charge via the Internet at http://pubs.acs.org.

■ AUTHOR INFORMATION

Corresponding Author

*E-mail: kathy.elst@vito.be. Phone: +32 14 33 56 17. Fax: +32 14 32 11 86.

Notes

The authors declare no competing financial interest.

■ ACKNOWLEDGMENTS

The authors acknowledge and thank Proviron NV for the *Nannochloropsis oculata* samples.

■ REFERENCES

(1) Ryckebosch, E.; Muylaert, K.; Foubert, I. Optimization of an analytical procedure for extraction of lipids from microalgae. *J. Am. Oil Chem. Soc.* **2012**, *89*, 189−198.

(2) Mercer, P.; Armenta, R. E. Developments in oil extraction from microalgae. *Eur. J. Lipid Sci. Technol.* **2011**, *113*, 539−547.

(3) Bong, S. C.; Loh, S. P. A study of fatty acid composition and tocopherol content of lipid extracted from marine microalgae, *Nannochloropsis oculata* and *Tetraselmis suecica*, using solvent extraction and supercritical fluid extraction. *Int. Food Res. J.* **2013**, *20*, 721−729.

(4) Pieber, S.; Schober, S.; Mittelbach, M. Pressurized fluid extraction of polyunsaturated fatty acids from the microalga *Nannochloropsis oculata*. *Biomass Bioenergy* **2012**, *47*, 474−482.

(5) Mubarak, M.; Shaija, A.; Suchithra, T. V. A review on the extraction of lipid from microalgae for biodiesel production. *Algal Res.* **2015**, *7*, 117−123.

(6) Koller, M.; Salerno, A.; Tuffner, P.; Koinigg, M.; Böchzelt, H.; Schober, S.; Pieber, S.; Schnitzer, H.; Mittelbach, M.; Braunegg, G. Characteristics and potential of micro algal cultivation strategies: a review. *J. Cleaner Prod.* **2012**, *37*, 377−388.

(7) Mouahid, A.; Crampon, C.; Toudji, S.-A. A.; Badens, E. Supercritical CO_2 extraction of neutral lipids from microalgae: Experiments and modelling. *J. Supercrit. Fluids* **2013**, *77*, 7−16.

(8) Andrich, G.; Nesti, U.; Venturi, F.; Zinnai, A.; Fiorentini, R. Supercritical fluid extraction of bioactive lipids from the microalga *Nannochloropsis* sp. *Eur. J. Lipid Sci. Technol.* **2005**, *107*, 381−386.

(9) Yen, H.-W.; Hu, I.-C.; Chen, C.-Y.; Ho, S.-H.; Lee, D.-J.; Chang, J.-S. Microalgae-based biorefinery − From biofuels to natural products. *Bioresour. Technol.* **2013**, *135*, 166−174.

(10) Ryckebosch, E.; Bruneel, C.; Termote-Verhalle, R.; Muylaert, K.; Foubert, I. Influence of extraction solvent system on extractability of lipid components from different microalgae species. *Algal Res.* **2014**, *3*, 36−43.

(11) Ryckebosch, E.; Cuéllar Bermúdez, S. P.; Termote-Verhalle, R.; Bruneel, C.; Muylaert, K.; Parra-Saldivar, R.; Foubert, I. Influence of extraction solvent system on the extractability of lipid components from the biomass of *Nannochloropsis gaditana*. *J. Appl. Phycol.* **2014**, *26*, 1501−1510.

(12) Chen, G.-Q.; Jiang, Y.; Chen, F. Fatty acid and lipid class composition of the eicopentaenoic acid-producing microalga *Nitzchia laevis*. *Food Chem.* **2007**, *104*, 1580−1585.

(13) Cheung, P. C. K.; Leung, A. Y. H.; Ang, P. O., Jr. Comparison of supercritical carbon dioxide and Soxhlet extraction of lipids from a brown seaweed, *Sargassum hemiphyllum* (Turn.) C. Ag. *J. Agric. Food Chem.* **1998**, *46*, 4228−4232.

(14) Halim, R.; Danquah, M. K.; Webley, P. A. Extraction of oil from microalgae for biodiesel production: A review. *Biotechnol. Adv.* **2012**, *30*, 709−732.

(15) Wang, G.; Wang, T. Characterization of lipid components in two microalgae for biofuel application. *J. Am. Oil Chem. Soc.* **2012**, *89*, 135−143.

(16) Sahena, F.; Zaidul, I. S. M.; Jinap, S.; Karim, A. A.; Abbas, K. A.; Norulaini, N. A. N.; Omar, A. K. M. Application of supercritical CO_2 in lipid extraction − A review. *J. Food Eng.* **2009**, *95*, 240−253.

(17) Cheng, C.-H.; Du, Tz.-B.; Pi, H.-C.; Jang, S.-M.; Lin, Y.-H.; Lee, H.-T. Comparative study of lipid extraction from microalgae by organic solvent and supercritical CO_2. *Bioresour. Technol.* **2011**, *102*, 10151−10153.

DOI: 10.1021/acs.jafc.5b00241
J. Agric. Food Chem. 2015, 63, 3931−3941

(18) Halim, R.; Gladman, B.; Danquah, M. K.; Webley, P. A. Oil extraction from microalgae for biodiesel production. *Bioresour. Technol.* **2011**, *102*, 178−185.
(19) Samburova, V.; Lemos, M. S.; Hiibel, S.; Hoekman, S. K.; Cushman, J. C.; Zielinska, B. Analysis of triacylglycerols and free fatty acids in algae using ultra-performance liquid chromatography mass spectrometry. *J. Am. Oil Chem. Soc.* **2013**, *90*, 53−64.
(20) McNichol, J.; MacDougall, K. M.; Melanson, J. E.; McGinn, P. J. Suitability of Soxhlet extraction to quantify microalgal fatty acids as determined by comparison with in situ transesterification. *Lipids* **2012**, *47*, 195−207.
(21) Olmstead, I. L. D.; Hill, D. R. A.; Dias, D. A.; Jayasinghe, N. S.; Callahan, D. L.; Kentish, S. E.; Scales, P. J.; Martin, G. J. O. A quantitative analysis of microalgal lipids for optimization of biodiesel and omega-3 production. *Biotechnol. Bioeng.* **2013**, *110*, 2096−2104.
(22) Olmstead, I. L. D.; Kentish, S. E.; Scales, P. J.; Martin, G. J. O. Low solvent, low temperature method for extracting biodiesel lipids from concentrated microalgal biomass. *Bioresour. Technol.* **2013**, *148*, 615−619.
(23) Guo, Z.; Vikbjerg, A. F.; Xu, X. Enzymatic modification of phospholipids for functional applications and human nutrition. *Biotechnol. Adv.* **2005**, *23*, 203−259.
(24) van Hoogevest, P.; Wendel, A. The use of natural and synthetic phospholipids as pharmaceutical excipients. *Eur. J. Lipid Sci. Technol.* **2014**, *116*, 1088−1107.
(25) Ramluckan, K.; Moodley, K. G.; Bux, F. An evaluation of the efficacy of using selected solvents for the extraction of lipids from algal biomass by the Soxhlet extraction method. *Fuel* **2014**, *116*, 103−108.
(26) dos Santos, R. R.; Moreira, D. M.; Kunigami, C. N.; Aranda, D. A. G.; Teixeira, C. M. L. L. Comparison between several methods for total lipid extraction from *Chlorella vulgaris* biomass. *Ultrason. Sonochem.* **2015**, *22*, 95−99.
(27) Montes D'Oca, M. G.; Viêgas, C. V.; Lemões, J. S.; Miyasaki, E. K.; Morón-Villarreyes, J. A.; Primel, E. G.; Abreu, P. C. Production of FAMEs from several microalgal lipidic extracts and direct esterification of the *Chlorella pyrenoidosa*. *Biomass Bioenergy* **2011**, *35*, 1533−1538.
(28) Balasubramanian, R. K.; Allen, J. D.; Kanitkar, A.; Boldor, D. Oil extraction from *Scenedesmus obliquus* using a continuous microwave system − design, optimization, and quality characterization. *Bioresour. Technol.* **2011**, *102*, 3396−3403.
(29) Folch, J.; Lees, M.; Stanley, G. H. S. A simple method for the isolation and purification of total lipids from animal tissues. *J. Biol. Chem.* **1957**, *226*, 497−509.
(30) Ryckebosch, E.; Muylaert, K.; Eeckhout, M.; Ruyssen, T.; Foubert, I. Influence of drying and storage on lipid and carotenoid stability of the microalga *Phaeodactylum tricornutum*. *J. Agric. Food Chem.* **2011**, *59*, 11063−11069.
(31) Plaza, M.; Santoyo, S.; Jaime, L.; García-Blairsy Reina, G.; Herrero, M.; Señoráns, F. J.; Ibáñez, E. Screening for bioactive compounds from algae. *J. Pharm. Biomed. Anal.* **2010**, *51*, 450−455.
(32) Herrero, M.; Cifuentes, A.; Ibañez, E. Sub- and supercritical fluid extraction of functional ingredients from different natural sources: Plants, food-by-products, algae and microalgae. *Food Chem.* **2006**, *98*, 136−148.
(33) Mendes, R. L.; Nobre, B. P.; Cardoso, M. T.; Pereira, A. P.; Palavra, A. F. Supercritical carbon dioxide extraction of compounds with pharmaceutical importance from microalgae. *Inorg. Chim. Acta* **2003**, *356*, 328−334.
(34) Mendes, R. L.; Reis, A. D.; Palavra, A. F. Supercritical CO_2 extraction of γ-linolenic acid and other lipids from *Arthrospira (Spirulina) maxima*: Comparison with organic solvent extraction. *Food Chem.* **2006**, *99*, 57−63.
(35) Guckert, J. B.; Cooksey, K. E.; Jackson, L. L. Lipid solvent systems are not equivalent for analysis of lipid classes in the microeukaryotic green alga *Chlorella*. *J. Microbiol. Methods* **1988**, *8*, 139−149.
(36) Mulbry, W.; Kondrad, S.; Buyer, J.; Luthria, D. L. Optimization of an oil extraction process for algae from the treatment of manure effluent. *J. Am. Oil Chem. Soc.* **2009**, *86*, 909−915.
(37) Balasubramanian, R. K.; Doan, T. T. Y.; Obbard, J. P. Factors affecting cellular lipid extraction from marine microalgae. *Chem. Eng. J.* **2013**, *215−216*, 929−936.
(38) Ferraz, T. P. L.; Fiúza, M. C.; dos Santos, M. L. A.; Pontes de Carvalho, L.; Soares, N. M. Comparison of six methods for the extraction of lipids from serum in terms of effectiveness and protein preservation. *J. Biochem. Biophys. Methods* **2004**, *58*, 187−193.
(39) Crampon, C.; Mouahid, A.; Toudji, S.-A. A.; Lépine, O.; Badens, E. Influence of pretreatment on supercritical CO_2 extraction from *Nannochloropsis oculata*. *J. Supercrit. Fluids* **2013**, *79*, 337−344.
(40) Dembitsky, V. M. Betaine ether-linked glycerolipids: Chemistry and biology. *Prog. Lipid Res.* **1996**, *35*, 1−51.
(41) Christie, W. W. Betaine lipids: occurrence, biochemistry and analysis. http://lipidlibrary.aocs.org/Lipids/betaine/index.htm (accessed July 2014).
(42) Benning, C.; Huang, Z. H.; Gage, D. A. Accumulation of a novel glycolipid and betaine lipid in cells of *Rhodobacter sphaeroides* grown under phosphate limitation. *Arch. Biochem. Biophys.* **1995**, *317*, 103−111.
(43) Li, M.; Welti, R.; Wang, X. Quantitative profiling of *Arabidopsis* polar glycerolipids in response to phosphorus starvation. Roles of phospholipases Dζ1 and Dζ2 in phosphatidylcholine hydrolysis and digalactosyldiacylglycerol accumulation in phosphorus-starved plants. *Plant Physiol.* **2006**, *142*, 750−761.

DOI: 10.1021/acs.jafc.5b00241
J. Agric. Food Chem. 2015, 63, 3931−3941

Arachidin-1 and arachidin-3 have been shown to modulate both cannabinoid receptors CB1 and CB2 in vitro. Molecular modeling studies with these compounds showed that the lipophilic side chain (3-methyl-1-butenyl group) in the structure of these stilbenoids was necessary for the high affinity attained to cannabinoid receptor CB2,[12] a therapeutic target in the treatment of neurodegenerative disorders such as Alzheimer's disease.[13] In addition, arachidin-3 and arachidin-1 are metabolized to fewer glucuronidated products than their nonprenylated analogues, resveratrol and piceatannol. This suggests that the lipophilic side chain might hinder the glucuronidation process and thereby enhance the bioavailability of arachidin-1 and arachidin-3 when compared to piceatannol or resveratrol.[12]

Despite the diverse bioactivities of peanut prenylated stilbenoids demonstrated in in vitro studies, in vivo studies have not been conducted due to their limited availability.[9,11,14,15] Furthermore, the biosynthetic pathways of these compounds have not been elucidated, which restricts potential metabolic engineering strategies for their bioproduction. To address these limitations, peanut hairy roots cultures have been developed as viable production platforms for stilbenoids.[16,17] Upon treatment with selected elicitors, the peanut hairy root cultures produce the same phytoalexins described in fungal-challenged peanut seeds. For instance, after 24 h of treatment with sodium acetate (NaOAc), peanut hairy roots secrete resveratrol, arachidin-1, and arachidin-3 into the culture medium.[16]

Different elicitors have been also used to induce the biosynthesis of stilbenoids in hairy roots of other species. For example, hydrogen peroxide (H_2O_2), a molecule in plants that mediates responses to stresses[18,19] and methyl jasmonate (MeJA), a key compound involved in defense-related signal transduction pathways in plants,[20] have been used as elicitors to induce the biosynthesis of resveratrol, piceatannol, and viniferins in hairy roots of *Vitis rotundifolia*.[21,22]

Previous studies have investigated the interaction between stilbenoids and cyclodextrins (CDs). The latter are torus-shaped oligosaccharides derived from starch that can form inclusion compounds with nonpolar molecules that fit into their hydrophobic cavity. For instance, resveratrol and CD were shown to form 1:1 inclusion complexes.[23] Interestingly, treatments with CD or CD plus MeJA were first used as an approach to increase the production of resveratrol in *Vitis vinifera* cell suspensions[24−26] and proved to be effective in enhancing the production of taxanes in cell suspension cultures of *Taxus* spp.[27] and inducing silymarin accumulation in *Silybum marianum* cell suspensions.[28]

In the current study, NaOAc, H_2O_2, MeJA, CD, and MeJA in combination with CD were tested as elicitors of stilbenoids in peanut hairy root cultures. The levels of stilbenoids in the culture medium were determined along a time course from 0 to 96 h. In addition, the effect of selected elicitor treatments on the expression of resveratrol synthase, the first committed metabolic step in stilbenoid biosynthesis, was investigated. Our results show that peanut hairy root cultures can be developed as controlled and sustainable high-level production systems for arachidin-1 and arachidin-3, two major peanut stilbenoids exhibiting a diversity of biological activities.

MATERIALS AND METHODS

Hairy Root Line and Growth Conditions. All experiments were conducted with hairy root cultures of peanut (*A. hypogaea*) cv. Hull line 3 established previously by the Medina-Bolivar laboratory.[16] Ten root tips (2−3 cm long) were inoculated into 250 mL flasks containing 50 mLof modified MS medium (MSV)[16] with 3% sucrose. The flask cultures were incubated on an orbital shaker (Innova 44R, New Brunswick Scientific) at 90 rpm and 28 °C and maintained under continuous darkness.

Elicitor Treatments. Nine-day-old hairy root cultures were treated under five different conditions to study stilbenoid production: 10.2 mM sodium acetate (NaOAc), 10 mM hydrogen peroxide (H_2O_2), 100 μM methyl jasmonate (MeJA), 9 g/L (6.87 mM) methyl-β-cyclodextrin (CD; Cavasol W7M), and 100 μM MeJA combined with 9 g/L CD. The concentration of NaOAc was established before,[16,17] whereas the concentration of MeJA was determined on the basis of previous studies with hairy root cultures of muscadine grape.[22] Preliminary studies with peanut hairy roots treated with different concentrations of H_2O_2 (Supporting Information, Figure S3) and MeJA combined with different concentrations CD (Figure S4) were used to determine the concentrations of H_2O_2 and CD used in the current study. Before elicitor treatment, the spent medium was removed and replaced with 50 mL of fresh MSV medium containing 3% sucrose and different elicitors. For the control group, the culture medium was replaced with MSV medium with 3% sucrose and 50 μL of absolute ethanol (EtOH; solvent of MeJA) (Sigma).

A 96 h time course per elicitor treatment was conducted including the following time points: 0, 0.5, 1, 3, 6, 9, 12, 15, 18, 21, 24, 30, 36, 40, 48, 72, and 96 h for the NaOAc-treated hairy roots; 0, 1, 2, 3, 6, 12, 18, 24, 48, 72, and 96 h for the H_2O_2-treated hairy roots; 0, 1, 3, 6, 12, 24, 48, 72, and 96 h for the MeJA-treated hairy roots; 0, 3, 9, 15, 24, 48, 72, and 96 h for the CD-treated hairy roots; and 0, 0.5, 1, 3, 6, 9, 12, 15, 18, 21, 24, 30, 36, 48, 60, 72, 84, and 96 h for the MeJA and CD co-treated hairy roots. All treatments were performed at 28 °C under continuous darkness with three biological replicates per time point per treatment.

Extraction and Analyses of Stilbenoids from the Culture Medium. Stilbenoids were extracted from the medium of NaOAc-, H_2O_2-, and MeJA-treated hairy roots as described before.[16] For the CD-treated and MeJA and CD-co-treated hairy roots, each medium sample (40 mL) was extracted twice with 50 mL of EtOAc in a separatory funnel. The organic phases were combined and evaporated to dryness under vacuum at 40 °C in a rotary evaporator (Büchi, rotavapor R-200). The extract was redissolved in 1.5 mL of MeOH and dried to completeness under a nitrogen stream using a Reacti-Vap III apparatus (Pierce). Extracts were redissolved in 1 mL of MeOH, filtered through a 0.2 μm nylon filter, and analyzed by reverse phase HPLC as detailed below.

HPLC analyses were performed in a Dionex Summit system equipped with a photodiode array detector. The separation was performed on a SunFire C_{18}, 5 μm, 4.6 × 250 mm column (Waters) at 40 °C with a flow rate at 1.0 mL/min. The mobile phase consisted of 2% formic acid in water (A) and MeOH (B). The column was initially equilibrated with 100% A for 1 min. Then a linear gradient was performed from 60% A and 40% B to 65% A and 35% B (1− 20 min), followed by a linear gradient from 65% A and 35% B to 100% B isocratic elution in 5 min (20−25 min). Reference compounds included commercially available *trans*-resveratrol (Biophysica) and *trans*-piceatannol (Axxora). *trans*-Arachidin-1 and *trans*-arachidin-3 standards were purified from elicited peanut seeds as described.[16] Dilutions of the standards were made in MeOH to obtain calibration curves for quantitative analysis. Calibration curves were established using absorbance at 320 nm for resveratrol and piceatannol and at 340 nm for arachidin-1 and arachidin-3.

Resveratrol Feeding Experiment. The spent media of 9-day-old hairy root cultures were removed and replaced with 50 mL of fresh MSV medium containing 3% sucrose. Resveratrol was fed into the hairy root culture at a concentration of 60 μM. A second experimental group included 60 μM resveratrol with 9 g/L CD. All cultures were maintained at 28 °C and 90 rpm under continuous darkness. A 1 mL aliquot was collected from each treatment at the following time points: 0, 0.5, 1, 3, 6, 12, and 24 h. Each aliquot was mixed thoroughly with 1 mL of EtOAc, and then the EtOAc phase was collected, dried under a

DOI: 10.1021/jf5050266
J. Agric. Food Chem. 2015, 63, 3942−3950

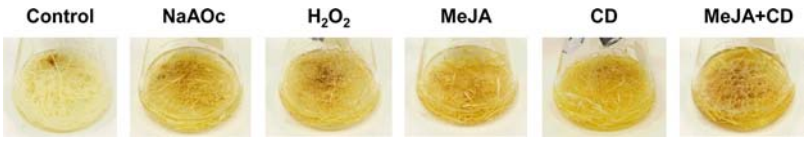

Figure 2. Phenotype of peanut cv. Hull hairy root line 3 after 48 h of treatment with different elicitors: sodium acetate (NaOAc, 10.2 mM); hydrogen peroxide (H_2O_2, 10 mM); methyl jasmonate (MeJA, 100 μM); methyl-β-cyclodextrin (CD, 9 g/L); and 100 μM MeJA with 9 g/L CD (MeJA+CD). Control represents nonelicited culture.

nitrogen stream, and dissolved in 500 μL of MeOH for HPLC analysis as described above. Three biological replicates were included per treatment.

RNA Extraction and Quantitative Real-Time PCR. Nine-day-old hairy root cultures were treated with 100 μM MeJA, 100 μM MeJA with additional 9 g/L CD, and 9 g/L CD alone to study the effect among these treatments on the expression of a previously described peanut resveratrol synthase gene, *JC1* (GenBank accession no. EU418492).[29] A 48 h time course per treatment was conducted including the following time points: 0, 0.5, 3, 9, 15, 24, and 48 h. Three biological replicates were performed at each time point per treatment.

Total RNA was isolated from 15 mg of lyophilized peanut hairy roots using TRIzol reagent (Life Technologies), according to the manufacturer's instructions. RNA concentration was estimated from absorbance readings at 260 nm, and the purity of the total RNA was estimated from the ratio of absorbance readings at 260 and 280 nm using a NanoDrop 800 spectrophotometer (Thermo Scientific). One microgram of total RNA was reversed transcribed in a 20 μL reaction mixture containing oligo (dt) primers using the iScript Select cDNA Synthesis Kit (Bio-Rad) following the manufacturer's instructions. The reaction mixture was incubated at 42 °C for 90 min, followed by an incubation at 85 °C for 5 min, after which the samples were cooled on ice or kept at −20 °C for later use. Quantitative real-time PCR (qPCR) reactions were carried out using iQ SYBR Green Supermix (Bio-Rad). The PCR reaction mixtures comprised 2× qPCR mix (5 μL), forward primer (0.4 μL, final concentration 0.8 μM), reverse primer (0.4 μL, final concentration 0.8 μM), water (0.2 μL), and 18 ng of cDNA template (4 μL) in a final volume of 10 μL. For target gene *JC1*, forward primer 5′-TATGTATTTAACAGAAGAAATAC-3′ and reverse primer 5′-AGTTGCAGCCTCTTTTCCAACT-3′ were used as specific primers as described previously.[29] Three reference genes, *ACT7* (encoding actin 7), *EFα1* (encoding elongation factor α1) and *TBP2* (encoding TATA box binding protein), were selected previously[30] and used to normalize the expression of resveratrol synthase in peanut hairy roots. All of the reactions were prepared using an automated pipetting system (epMotion 5075; Eppendorf) on Hard-Shell Thin-Wall 384-Well Skirted PCR plates (Bio-Rad). Technical replicates were run in triplicate, and the amplification program was followed as described previously.[30]

Statistical Analysis. Each treatment included three biological replicates. Two-way ANOVA with multiple-comparisons tests was conducted for the data in Figures 5 and 6 and analyzed with GraphPad Prism 6, version 6.02. Tukey's Studentized range (HSD) tests were done for the data in Tables S1−S6 of the Supporting Information and analyzed with SAS (Statistical Analysis Systems) statistics program version 9.2.

RESULTS AND DISCUSSION

Response of Peanut Hairy Root Cultures to Different Elicitors. A previously established hairy root culture of peanut cv. Hull line 3 was selected for elicitation studies on the basis of its vigorous growth in liquid MSV medium.[16] Accordingly, the best growth stage for producing the maximum level of arachidin-1 and arachidin-3 in the culture medium after 24 h of treatment with 10.2 mM NaOAc was 9-day-old hairy root cultures.[16] In preliminary studies, cultures at day 9 (mid-exponential growth stage as determined before[16]) showed the most reproducible levels of the different stilbenoids analyzed, independent of the elicitor used, when compared to 6-, 12-, and 15-day-old cultures. Therefore, we used 9-day-old cultures to compare the effects of the five treatments, namely, NaOAc, H_2O_2, MeJA, CD, and MeJA with CD, on production of stilbenoids along a time course from 0 to 96 h. In contrast to the white root tissue observed in nontreated control cultures, the peanut hairy root tissue showed a dark yellow color 48 h after elicitor treatment, the cultures treated with CD or co-treated with MeJA and CD being the ones with the darkest color (Figure 2). Because the hairy roots of peanut secrete most of stilbenoids into culture medium,[16] a slight yellow color that is the characteristic color of stilbenoids found in peanut root mucilage[8] was also observed in the medium of hairy root culture treated with NaOAc, H_2O_2, and MeJA alone. Strikingly, the medium of the cultures treated with CD or MeJA with CD turned a strong and bright yellow color (Figure S1), suggesting higher levels of arachidin-1, arachidin-3, and other stilbenoids in these cultures.

Effect of Different Elicitor Treatments on the Yield of Stilbenoids. The stilbenoids resveratrol, arachidin-1, and arachidin-3 have been described in fungal-challenged seeds[11,31] and elicited hairy roots of peanut.[16,17] Indeed, these stilbenoids accumulated in the culture medium of peanut hairy roots lines from different cultivars (i.e., Andru II and Hull) upon treatment with NaOAc as elicitor.[16,17] Interestingly, the prenylated stilbenoids arachidin-1 and arachidin-3 were not described in elicitor-treated peanut callus. Nonetheless, the nonprenylated analogue of arachidin-1, that is, piceatannol, was reported in these callus cultures upon elicitor treatment.[32−34]

Although resveratrol, arachidin-1, and arachidin-3 were described in peanut hairy root cultures upon 24 h of treatment with NaOAc,[16] detailed studies comparing distinct elicitor treatments over different periods have not been reported. Therefore, in this study a 96 h time course of accumulation of stilbenoids in the hairy root culture medium was conducted for each of the five elicitor treatments (NaOAc, H_2O_2, MeJA, CD, and MeJA with CD). In addition to the three stilbenoids described before (resveratrol, arachidin-1, and arachidin-3), piceatannol was also included in the study because it was previously described in callus cultures of peanut.[32−34] To study the potential molar contribution of the nonprenylated stilbenoids (resveratrol and piceatannol) to the formation of their prenylated analogues (arachidin-3 and arachidin-1), the yield of stilbenoids in culture medium was expressed as nanomoles and normalized per gram dry weight of hairy root tissue (nmol/g DW; Tables S1−S5). The levels of stilbenoids in the MeJA and CD co-treatment group are also reported in milligrams per liter of medium (Table S6). It is worth mentioning that in preliminary studies only trace levels of these stilbenoids were detected in the root tissue upon elicitor treatment; therefore, we report here the levels of stilbenoids in the culture medium.

The accumulation of resveratrol and arachidin-3 in the medium started at 3−6 h post elicitor treatment, whereas

DOI: 10.1021/jf5050266
J. Agric. Food Chem. 2015, 63, 3942−3950

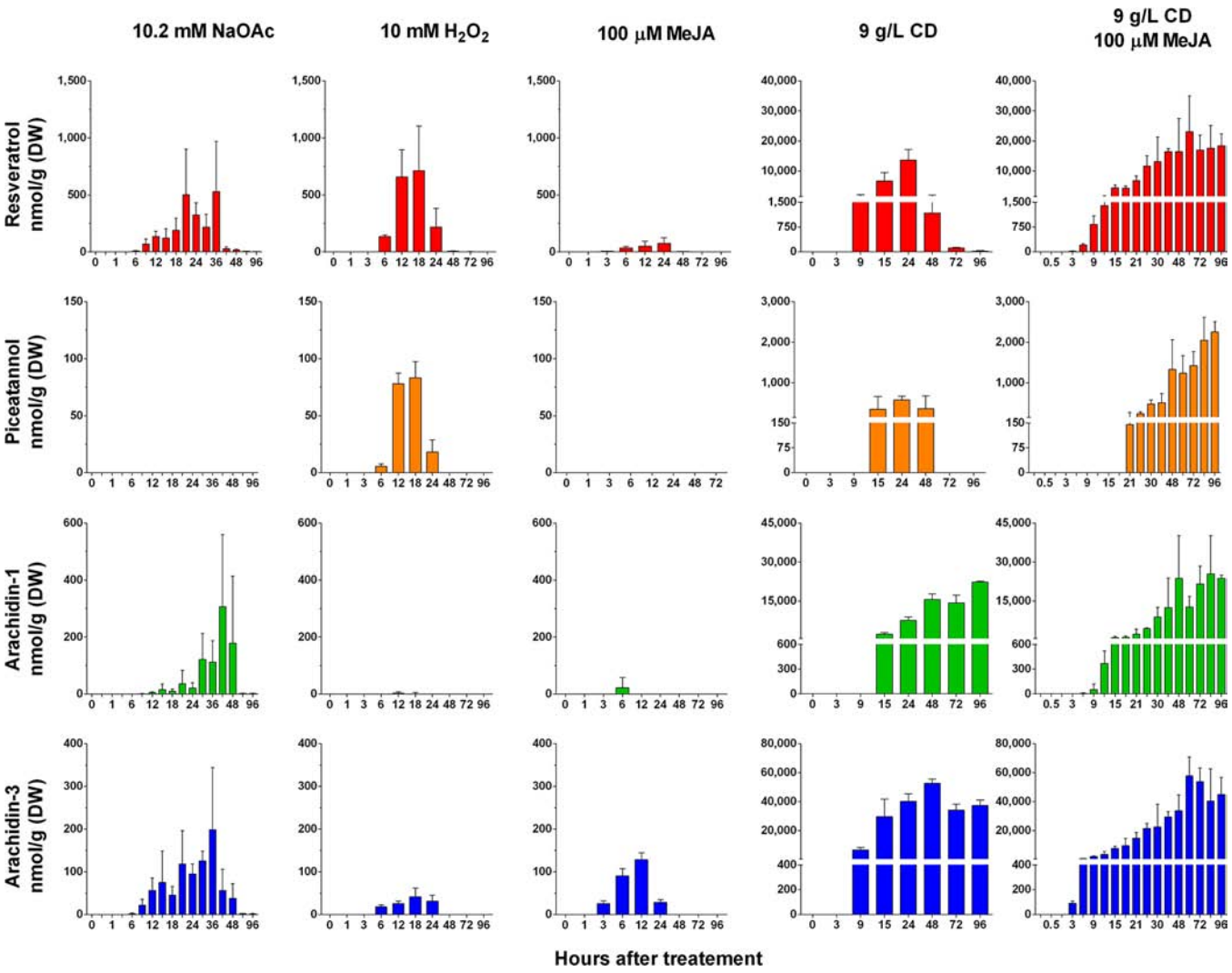

Figure 3. Time course of stilbenoid yield in the medium of peanut hairy roots culture after treatment with different elicitors. Values are the average of three replicates, and error bars represent standard deviation. Statistical analyses are shown in Tables S1−S5. DW, hairy root dry weight.

arachidin-1 was detected 3 h later. Among the five treatments, MeJA combined with CD led to the highest levels of resveratrol in the culture medium (Figure 3). No significant differences were observed in the levels of resveratrol between 24 and 96 h (Table S5), suggesting that resveratrol levels reached a plateau with an average yield of 16716 nmol/g DW. These levels corresponded to an average yield of 40.29 mg/L (24− 96 h time points, Table S6). Most interestingly, the levels of resveratrol remained at these high levels until the end of the time course (96 h). On the other hand, when the cultures were treated with NaOAc, H_2O_2, MeJA, or CD, the levels of resveratrol declined significantly toward the end of the time course (Figure 3 and Tables S1−S4). Remarkably, the yield of resveratrol in the elicited peanut hairy roots was much higher than that obtained from abiotic or biotic stimulated peanut callus[32−34] and sliced and fungi-challenged peanut kernels.[9,14,35] However, the highest yield of resveratrol (~17 μmol/g DW) in peanut hairy root cultures upon co-treatment with 9 g/L (6.87 mM) CD and 100 μM MeJA was still 94 times lower than the 1600 μmol/g DW concentration of resveratrol found in grape cell suspension cultures co-treated with 50 mM dimethyl-β-cyclodextrin (DIMEB) and 100 μM MeJA for >160 h.[25] This increased yield of resveratrol could be due to a higher concentration or different type of methylated cyclodextrin used in the grape study. In preliminary studies with peanut hairy root cultures, 15 mM was the highest concentration of CD used in combination with 100 μM MeJA (Figure S4). Higher concentrations of CD could be tested in peanut hairy root cultures to determine their effect on resveratrol production. Moreover, besides resveratrol, the stilbenoids piceatannol, arachidin-1, and arachidin-3 are also produced by peanut hairy roots, and these compounds may use resveratrol as a biosynthetic precursor. Additionally, the difference in the yield of resveratrol between the grape cell suspension and peanut hairy root cultures could be attributed to the distinct genetic and production capability of each of these systems.

Piceatannol was detected only in the hairy root cultures treated with H_2O_2, CD or MeJA with CD (Figure 3). Similarly to resveratrol, piceatannol levels remained high toward the end of the time course only in the cultures co-treated with MeJA and CD. Statistical analyses showed that the levels of this stilbenoid reached a maximum between 72 and 96 h with an average yield of 1909.92 nmol/g DW (Table S5). In the case of the CD-treated group, the highest yield was 582.13 at 24 h, which was significantly different from the 15 and 48 h elicitor treatments (Table S4), whereas, in the H_2O_2-treated group,

DOI: 10.1021/jf5050266
J. Agric. Food Chem. 2015, 63, 3942−3950

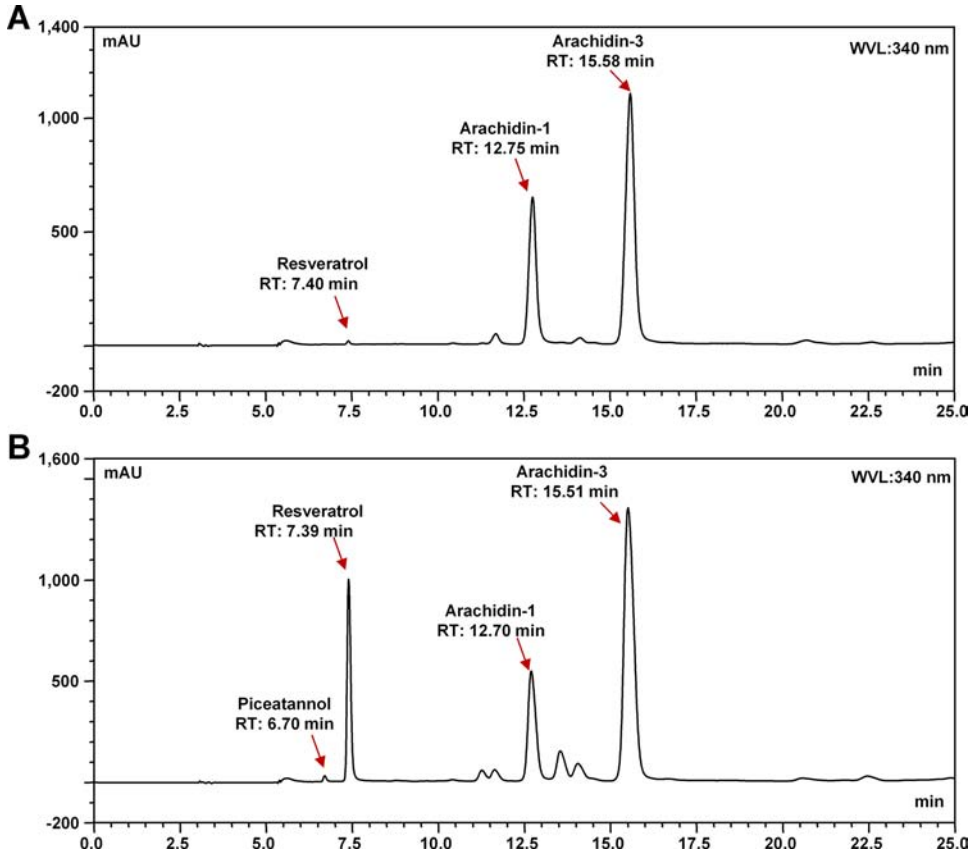

Figure 4. HPLC chromatogram (UV 340 nm) of ethyl acetate extract from the medium of peanut hairy root culture: (A) cultures were treated for 48 h treatment with 9 g/L methyl-β-cyclodextrin (CD); (B) cultures were co-treated for 48 with 100 μM methyl jasmonate and 9 g/L CD.

piceatannol yields reached their maximum at an average of 80.65 nmol/g DW (Table S2). Altogether, yields of piceatannol in the MeJA with CD-co-treated group were ~3-fold higher than in the CD-treated cultures and ~24-fold higher than in the H_2O_2-treated cultures. In the CD-treated and MeJA and CD-co-treated groups, piceatannol started to accumulate later than resveratrol. Similarly, piceatannol was also detected later than resveratrol in peanut callus exposed to fungi and chemicals elicitors,[34] suggesting that piceatannol was synthesized from resveratrol, which contains one fewer hydroxyl group. Meanwhile, in the H_2O_2-treated hairy root cultures, the accumulation of piceatannol was quite similar to the accumulation pattern of resveratrol. To date, the enzyme involved in piceatannol synthesis in peanut has not been described, although the biosynthesis of resveratrol has been elucidated in plants.[3] Interestingly, a cytochrome P450 enzyme capable of converting resveratrol to piceatannol has been identified in a human cancer cell line.[36]

The highest concentrations of arachidin-1 were obtained in the CD-treated and MeJA and CD-co-treated cultures. Under either treatment, the levels of arachidin-1 remained high until the end of the time course (96 h; Figure 3). In the CD-treated cultures, the 96 h treatment showed the highest yield of arachidin-1 (22316.80 nmol/g DW), and this time point was significantly higher than all other time points in the time course (Table S4), whereas in the MeJA and CD-co-treated cultures, the concentration of arachidin-1 reached a plateau at 30 h. The average yield of arachidin-1 from 30 to 96 h was 18396.70 nmol/g DW (Table S4). This yield was equivalent to 56 mg/L (30−96 h time points, Table S6). Arachidin-1 levels declined significantly after 48 h in the NaOAc-treated cultures. In these cultures, arachidin-1 levels were highest between 30 and 48 h with an average yield of 179.73 nmol/g DW. Very low amounts of arachidin-1 were detected at a few time points of the MeJA- or H_2O_2-treated cultures (Tables S2 and S3). Overall, the levels of arachidin-1 in the CD-treated and MeJA with CD-co-treated cultures were ~124- and ~102-fold higher than that in the NaOAc-treated cultures, respectively.

Similarly to arachidin-1, the highest yields of arachidin-3 were obtained in the cultures treated with CD or co-treated with MeJA with CD (Figure 3). In the CD-treated cultures, the highest levels of arachidin-3 were found from 24 to 48 h of treatment with an average yield of 46423.27 nmol/g DW (Table S4), whereas in the MeJA and CD-co-treated cultures, the levels of arachidin-3 reached a plateau after 48 h, because no significant differences in arachidin-3 yields among the different time points between 48 and 96 h were observed (Table S5). During this time period of 48−96 h the average yield of arachidin-3 was 46160.99 nmol/g DW. This yield represented ~148 mg/L of arachidin-3 (48−96 h time points, Table S6). In the NaOAc-treated cultures the levels arachidin-1 declined significantly after 48 h, whereas in the H_2O_2- and MeJA-treated cultures a significant decrease was observed after 24 h. The average maximum yield in the NaOAc-treated cultures was 122.78 nmol/g DW, which represented time points of 15 and 21−36 h. Overall, the yield in either the CD- or MeJA with CD-treated cultures was ~377-fold higher than that in the NaOAc-treated cultures.

As far as we know, arachidin-1 and arachidin-3 have been described only in peanut. Nonetheless, other prenylated

DOI: 10.1021/jf5050266
J. Agric. Food Chem. 2015, 63, 3942−3950

stilbenoids have been reported in a small number of plant species.[37−39] The maximum yields of these compounds in aerated and sliced peanut seeds have been 1586.53 nmol/g DW (495.7 μg/g DW) and 8158.11 nmol/g DW (2414.8 μg/g DW) peanut kernel for arachidin-1 and arachidin-3, respectively.[9] Herein we show that the hairy root cultures of peanut can be designed to produce much higher levels of arachidin-1 and arachidin-3. The accumulation of arachidin-1 was found 3 h later than that of resveratrol and arachidin-3 in any of the different treatments, much earlier than that of piceatannol, the nonprenylated analogue of arachidin-1. Whereas the highest yields of arachidin-1 and arachidin-3 were similar between the CD and MeJA with CD treatments, the levels of resveratrol and piceatannol were always higher under the MeJA with CD co-treatment. These differences could be appreciated by comparing the HPLC chromatograms of extracts from CD-treated versus MeJA and CD-co-treated groups (Figure 4). Therefore, the latter elicitation co-treatment is a preferred strategy to produce higher levels of diverse types of stilbenoids in peanut hairy root cultures.

The location and formation of phytoalexins induced by infection with soil fungal strains in peanut kernels were studied previously. Resveratrol could be found in deeper layers of the kernel slices, which were close to healthier tissue, whereas arachidin-1, arachidin-3, and other stilbenoids were detected near the infected area, suggesting that resveratrol might be the precursor of other stilbenoids in peanut.[40] In the MeJA and CD-co-treated group, the molar ratio of resveratrol to its prenylated analogue arachidin-3 was between 0.4 and 0.5, whereas that of piceatannol to its prenylated analogue arachidin-1 was only between 0.08 and 0.09. Meanwhile, piceatannol was not detected in the medium of the cultures upon treatment with NaOAc or MeJA alone, whereas arachidin-1 was found in these cultures. These results suggest that the main stilbenoids responding to the elicitor treatments are resveratrol, arachidin-3, and arachidin-1 in peanut hairy root cultures.

Effect of Methyl-β-cyclodextrin on the Levels of Resveratrol in the Medium of Peanut Hairy Root Cultures. The degradation of the stilbene-type phytoalexins resveratrol and pterostilbene have been reported during the interaction of grapevines with *Botrytis cinerea*,[41,42] whereas the catabolism of stilbenoids in non-pathogen-challenged plant tissues has not been studied. After treatment with NaOAc, H_2O_2, or MeJA alone, resveratrol and other stilbenoids accumulated in the medium of hairy root cultures of peanut and reached their maximum levels between 12 and 36 h. Thereafter, their concentrations decreased to barely detectable levels after 72 h of treatment (Figure 3). A similar decrease in resveratrol and piceatannol levels was reported when peanut callus was challenged with a fungal spore suspension as biotic elicitor[33] and UV irradiation as abiotic stress,[35] suggesting that peanut might have the ability to degrade these stilbene-type phytoalexins inside the root tissue or secrete specific enzymes to metabolize them after a temporal exposure to stress. However, the levels of resveratrol, piceatannol, arachidin-1, and arachidin-3 in the hairy root cultures co-treated with MeJA and CD remained high even up to 96 h. Interestingly, the levels of arachidin-1 and arachidin-3 also remained high in the medium over time in CD-treated peanut hairy root cultures, whereas resveratrol and piceatannol levels were not sustained over time. In grape cell suspension cultures co-treated with MeJA and CD, resveratrol levels were maintained at high levels in the medium up to 120 h, and this level was much higher than that of cultures treated with MeJA alone. In the latter cultures, no significant amounts of resveratrol were detected in the spent medium after 24 h.[25] These results could be due to CD's capability of forming inclusion complexes with stilbene compounds such as resveratrol,[23,43] piceatannol,[44] and pinosylvin,[45] which might protect stilbenoids from uptake or degradation by the host as suggested before.[23,24]

To study the effect of CD on the levels of resveratrol in the culture medium of peanut hairy roots, resveratrol alone or together with CD (9 g/L) was added to the peanut hairy root culture, and the concentration of resveratrol in the medium was determined at different time points. The 60 μM concentration of resveratrol used in this experiment represented the average level of this stilbenoid found in the culture medium upon co-treatment with MeJA and CD. In the control group containing resveratrol alone, the concentration of this stilbenoid declined dramatically to 27.04 ± 0.83 μM after 0.5 h and to 1.74 ± 1.29 μM after 1 h. These represented reductions of about 47 and 97% of the initial resveratrol concentration, respectively. Resveratrol was not detected after 3 h of incubation (Figure 5).

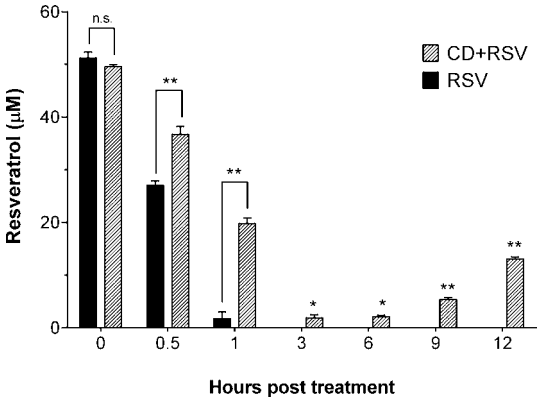

Figure 5. Effect of methyl-β-cyclodextrin (CD) on the levels of resveratrol (RSV) in the medium of hairy root cultures of peanut. Nine-day-old peanut hairy roots were co-inoculated with 60 μM RSV, and the concentration of RSV that remained in the medium was determined by HPLC. RSV, resveratrol alone; CD+RSV, RSV plus 9 g/L CD. Values are the average of three replicates, and error bars represent standard deviation. (*) $p < 0.05$; (**) $p < 0.001$; (n.s.) not significant by two-way ANOVA with Sidak's and Bonferroni's multiple-comparisons test.

Notably, resveratrol was stable in fresh culture medium and in culture medium from elicited cultures after 48 h of treatment with MeJA, in which no stilbenoid was detected (Figure S2). This suggests that peanut hairy roots do not secrete any enzymes that might metabolize resveratrol into the medium. However, resveratrol could have been converted into other metabolites by cell wall bound enzymes. Indeed, a cell wall bound peroxidase has been shown to dimerize resveratrol in grapevine cell suspension cultures.[46]

In the resveratrol and CD coculture group, the concentrations of resveratrol in the medium after 1 and 3 h of incubation were 19.78 ± 1.04 and 1.88 ± 0.61 μM, respectively. The rate at which the levels of resveratrol were reduced in the medium was statistically significantly lower than in control group (Figure 5). CD−stilbenoid inclusion complexes could promote an active biosynthesis and extracellular accumulation of stilbenoids by diminishing the usual feedback inhibition and/

DOI: 10.1021/jf5050266
J. Agric. Food Chem. 2015, 63, 3942−3950

or toxicity expected when a secondary metabolite is present at high levels in the cytoplasm, such as resveratrol in cell suspensions of *Vitis vinifera*[26] and taxol in cell suspensions of *Taxus baccata*.[47] Moreover, after 9 h of treatment with CD and resveratrol, the concentration of resveratrol rose to 5.35 ± 0.39 μM. Interestingly, arachidin-3 was also detected in medium (Table S4), confirming that CD also induces the biosynthesis of stilbenoids in peanut hairy root cultures as shown in Figure 3. Similarly, resveratrol biosynthesis was induced when grapevine cell suspension cultures were treated with CD alone, indicating that CD acts as elicitor.[23,24] Our results show that CD can stabilize resveratrol levels in the medium of peanut hairy root cultures, leading to several hundred-fold increases in the levels of these compounds in culture medium upon co-treatment with MeJA and CD.

Expression of Resveratrol Synthase Gene (*RS*) in Peanut Hairy Roots after Elicitor Treatment. MeJA and CD were reported to have a synergistic effect on the expression of the stilbene pathway in grape cell suspension cultures.[25] To this end, we studied the effect of CD and MeJA on the expression of resveratrol synthase (*RS*), a key gene involved in stilbenoid biosynthesis. In our previous study, a resveratrol synthase gene from peanut was cloned and functionally characterized in planta via transient expression in *Nicotiana benthamiana*. Therefore, the expression of this gene was studied by quantitative PCR in hairy roots of peanut treated with MeJA, CD, or MeJA combined with CD (Figures 6 and S5).

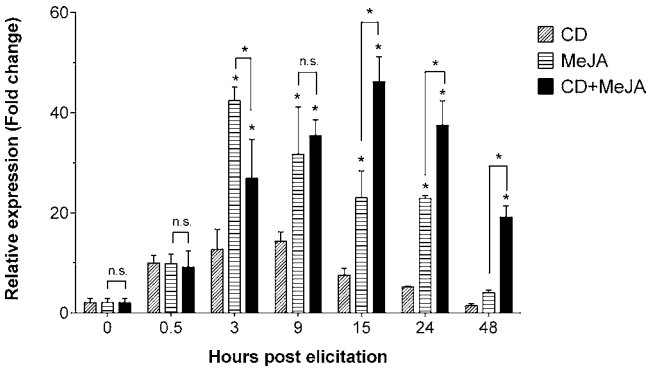

Figure 6. Relative expression of resveratrol synthase gene (*RS*) in peanut hairy roots after treatment with different elicitors. Nine-day-old peanut hairy roots were treated with 100 μM methyl jasmonate (MeJA), 100 μM methyl jasmonate with 9 g/L methyl-β-cyclodextrin (CD+MeJA), and 9 g/L methyl-β-cyclodextrin alone (CD). Relative expression of *RS* was normalized using *ACT7*, *EFα1*, and *TBP2* as reference genes. Values are the average of three replicates, and error bars represent standard deviation. Statistical analysis was performed by two-way ANOVA with Tukey's and Bonferroni's multiple-comparisons test. The asterisks above bars represent significant difference when compared to CD treatment group (*, $p < 0.001$; n.s., not significant), and the asterisks above the connecting line represent significant difference between MeJA and CD+MeJA groups (*, $p < 0.001$; n.s., not significant).

In the CD group, *RS* expression showed a peak at 9 h post treatment followed by a slight decrease during the next 6 h (Figure S5). When compared to the other two treatments, CD alone showed the lowest induction. After 3 h of treatment with MeJA alone, *RS* expression increased rapidly to (42.4 ± 2.7)-fold higher than the minimum *RS* expression value in the time course. This level of expression was significantly higher than the CD or CD with MeJA groups (Figure 6). Then the *RS* expression dropped quickly to (23.0 ± 5.4)-fold change at 15 h post treatment and finally to (4.0 ± 0.5)-fold change at 48 h post treatment, which was close to the *RS* expression at 0 h time point (Figures 6 and S5). This early induction of *RS* expression was also observed in peanut hairy roots treated with the elicitor NaOAc.[48]

In the hairy root cultures co-treated with CD and MeJA, the expression level of the *RS* increased gently to the highest point at 15 h post treatment with (46.2 ± 5.0)-fold change. Then it was followed by a slow decline, after it reached the peak. *RS* expression was maintained at (19.2 ± 1.2)-fold increase at 48 h post treatment, which was significantly higher that that of the CD or MeJA groups. These observations correlated to the highest levels of resveratrol observed in the cultures co-treated with MeJA and CD relative to cultures treated with CD alone (Figure 3). The relative expression level of resveratrol synthase (stilbene synthase) and central phenylpropanoid genes, phenylalanine ammonia-lyase, cinnamate 4-hydroxylase, and 4-coumarate CoA ligase, were also quantified through a time course in grapevine cell suspension culture incubated with MeJA, CD, or the combined treatment with MeJA and CD.[25] Compared to treatments with MeJA or CD alone, a sustainable expression of resveratrol synthase and phenylpropanoid-related genes was also observed in the MeJA and CD co-treated group. These results suggest that in grapevine cell suspension culture and peanut hairy root culture, MeJA and CD have a synergistic effect on stilbene biosynthesis pathway gene expression, which could be correlated with the increased yield of stilbenoids in the medium. Interestingly, a recent study has shown than CD is also capable of encapsulating MeJA to form MeJA−CD complexes with a 1:1 ratio in stoichiometry.[49] Further studies are necessary to evaluate a potential role of CD on the stability of MeJA in peanut hairy root cultures.

In conclusion, although prenylated stilbenoids isolated from treated peanut kernels show a diverse bioactivities in vitro, their production using these biological systems is limited. To address this issue, hairy root cultures of peanut co-treated with MeJA and CD have been developed as a controlled and sustainable system for the high-level production of the prenylated stilbenoids arachidin-1 and arachidin-3. Furthermore, peanut hairy root cultures also provide a viable platform to identify regulatory genes and key enzymatic steps in stilbenoid biosynthesis beyond resveratrol formation. For instance, these genes encode for enzymes involved in prenylation and hydroxylation reactions, which introduce the various functional groups that contribute to the structural and functional diversity of stilbenoids in peanut.

■ ASSOCIATED CONTENT

Supporting Information

Figures S1−S5 and Tables S1−S6. This material is available free of charge via the Internet at http://pubs.acs.org.

■ AUTHOR INFORMATION

Corresponding Author

*(F.M.-B.) Mail: Arkansas Biosciences Institute, Arkansas State University, P.O. Box 639, State University, AR 72467, USA. Phone: (870) 680-4319. Fax: (870) 680-4348. E-mail: fmedinabolivar@astate.edu.

Funding

This work was supported by USDA-NIFA Grant 2014-67014-21701, National Science Foundation−EPSCoR Grant EPS-

DOI: 10.1021/jf5050266
J. Agric. Food Chem. 2015, 63, 3942−3950

0701890 (Center for Plant-Powered Production-P3), the Arkansas ASSET Initiative, the Arkansas Science & Technology Authority, and the Arkansas Biosciences Institute.

Notes

The authors declare no competing financial interest.

■ ACKNOWLEDGMENTS

We thank Dr. Gaston Zolla for assistance with the preliminary elicitation experiments with hydrogen peroxide.

■ ABBREVIATIONS USED

CD, methyl-β-cyclodextrin; EtOAc, ethyl acetate; EtOH, ethanol; H_2O_2, hydrogen peroxide; HPLC, high-performance liquid chromatography; MeJA, methyl jasmonate; MeOH, methanol; NaOAc, sodium acetate; *RS*, resveratrol synthase; RT, retention time

■ REFERENCES

(1) Ahuja, I.; Kissen, R.; Bones, A. M. Phytoalexins in defense against pathogens. *Trends Plant Sci.* **2012**, *17*, 73−90.

(2) Hasan, M. M.; Cha, M.; Bajpai, V. K.; Baek, K.-H. Production of a major stilbene phytoalexin, resveratrol in peanut (*Arachis hypogaea*) and peanut products: a mini review. *Rev. Environ. Sci. Bio/Technol.* **2012**, *12*, 209−221.

(3) Chong, J.; Poutaraud, A.; Hugueney, P. Metabolism and roles of stilbenes in plants. *Plant Sci.* **2009**, *177*, 143−155.

(4) Baur, J. A.; Sinclair, D. A. Therapeutic potential of resveratrol: the in vivo evidence. *Nat. Rev. Drug Discovery* **2006**, *5*, 493−506.

(5) Vitaglione, P.; Sforza, S.; Galaverna, G. Bioavailability of *trans*-resveratrol from red wine in humans. *Mol. Nutr. Food Res.* **2005**, *49*, 495−504.

(6) Aguamaha, G. E.; Langcakeb, P.; Leworthyb, D. P.; Pageb, J. A.; Pryceb, R. J.; Strangea, R. N. Two novel stilbene phytoalexins from *Arachis hypogaea*. *Phytochemistry* **1981**, *20*, 1381−1383.

(7) Cooksey, C. J.; Garratt, P. J.; Richards, S. E.; Strange, R. N. A dienyl stilbene phytoalexin from *Arachis hypogaea*. *Phytochemistry* **1988**, *27*, 1015−1016.

(8) Sobolev, V. S.; Potter, T. L.; Horn, B. W. Prenylated stilbenes from peanut root mucilage. *Phytochem. Anal.* **2006**, *17*, 312−322.

(9) Chang, J. C.; Lai, Y. H.; Djoko, B.; Wu, P. L.; Liu, C. D.; Liu, Y. W.; Chiou, R. Y. Biosynthesis enhancement and antioxidant and anti-inflammatory activities of peanut (*Arachis hypogaea* L.) arachidin-1, arachidin-3, and isopentadienylresveratrol. *J. Agric. Food Chem.* **2006**, *54*, 10281−10287.

(10) Huang, C. P.; Au, L. C.; Chiou, R. Y.; Chung, P. C.; Chen, S. Y.; Tang, W. C.; Chang, C. L.; Fang, W. h.; Lin, S. B. Arachidin-1, a peanut stilbenoid, induces programmed cell death in human leukemia HL-60 cells. *J. Agric. Food Chem.* **2010**, *58*, 12123−12129.

(11) Liu, Z.; Wu, J.; Huang, D. New stilbenoids isolated from fungus-challenged black skin peanut seeds and their adipogenesis inhibitory activity in 3T3-L1 cells. *J. Agric. Food Chem.* **2013**, *61*, 4155−4161.

(12) Brents, L. K.; Medina-Bolivar, F.; Seely, K. A.; Nair, V.; Bratton, S. M.; Ñopo-Olazabal, L.; Patel, R. Y.; Liu, H.; Doerksen, R. J.; Prather, P. L.; Radominska-Pandya, A. Natural prenylated resveratrol analogs arachidin-1 and -3 demonstrate improved glucuronidation profiles and have affinity for cannabinoid receptors. *Xenobiotica* **2012**, *42*, 139−156.

(13) Velayudhan, L.; Van, D. E.; Marudkar, M.; Hands, O.; Suribhatla, S.; Prettyman, R.; Murray, J.; Baillon, S.; Bhattacharyya, S. Therapeutic potential of cannabinoids in neurodegenerative disorders: a selective review. *Curr. Pharm. Des.* **2014**, *20*, 2218−2230.

(14) Sobolev, V. S. Production of phytoalexins in peanut (*Arachis hypogaea*) seed elicited by selected microorganisms. *J. Agric. Food Chem.* **2013**, *61*, 1850−1858.

(15) Sobolev, V. S.; Khan, S. I.; Tabanca, N.; Wedge, D. E.; Manly, S. P.; Cutler, S. J.; Coy, M. R.; Becnel, J. J.; Neff, S. A.; Gloer, J. B. Biological activity of peanut (*Arachis hypogaea*) phytoalexins and selected natural and synthetic stilbenoids. *J. Agric. Food Chem.* **2011**, *59*, 1673−1682.

(16) Condori, J.; Sivakumar, G.; Hubstenberger, J.; Dolan, M. C.; Sobolev, V. S.; Medina-Bolivar, F. Induced biosynthesis of resveratrol and the prenylated stilbenoids arachidin-1 and arachidin-3 in hairy root cultures of peanut: effects of culture medium and growth stage. *Plant Physiol. Biochem.* **2010**, *48*, 310−318.

(17) Medina-Bolivar, F.; Condori, J.; Rimando, A. M.; Hubstenberger, J.; Shelton, K.; O'Keefe, S. F.; Bennett, S.; Dolan, M. C. Production and secretion of resveratrol in hairy root cultures of peanut. *Phytochemistry* **2007**, *68*, 1992−2003.

(18) Lamb, C.; Dixon, R. A. The oxidative burst in plant disease resistance. *Annu. Rev. Plant Physiol. Plant Mol. Biol.* **1997**, *48*, 251−275.

(19) Orozco-Cardenas, M. L. Hydrogen peroxide acts as a second messenger for the induction of defense genes in tomato plants in response to wounding, systemin, and methyl jasmonate. *Plant Cell* **2001**, *13*, 179−191.

(20) Xu, Y.; Chang, P.; Liu, D.; Narasimhan, M. L.; Raghothama, K. G.; Hasegawa, P. M.; Bressan, R. A. Plant defense genes are synergistically induced by ethylene and methyl jasmonate. *Plant Cell* **1994**, *6*, 1077−1085.

(21) Nopo-Olazabal, C.; Condori, J.; Nopo-Olazabal, L.; Medina-Bolivar, F. Differential induction of antioxidant stilbenoids in hairy roots of *Vitis rotundifolia* treated with methyl jasmonate and hydrogen peroxide. *Plant Physiol. Biochem.* **2014**, *74*, 50−69.

(22) Nopo-Olazabal, C.; Hubstenberger, J.; Nopo-Olazabal, L.; Medina-Bolivar, F. Antioxidant activity of selected stilbenoids and their bioproduction in hairy root cultures of muscadine grape (*Vitis rotundifolia* Michx.). *J. Agric. Food Chem.* **2013**, *61*, 11744−11758.

(23) Morales, M.; Bru, R.; Garcia-Carmona, F.; Ros Barcelo, A.; Pedreno, M. A. Effect of dimethyl-β-cyclodextrins on resveratrol metabolism in Gamay grapevine cell cultures before and after inoculation with shape *Xylophilus ampelinus*. *Plant Cell, Tissue Organ Cult.* **1998**, *53*, 179−187.

(24) Bru, R.; Sellés, S.; Casado-Vela, J.; Belchí-Navarro, S.; Pedreño, M. A. Modified cyclodextrins are chemically defined glucan inducers of defense responses in grapevine cell cultures. *J. Agric. Food Chem.* **2006**, *54*, 65−71.

(25) Lijavetzky, D.; Almagro, L.; Belchi-Navarro, S.; Martinez-Zapater, J. M.; Bru, R.; Pedreno, M. Synergistic effect of methyl jasmonate and cyclodextrin on stilbene biosynthesis pathway gene expression and resveratrol production in Monastrell grapevine cell cultures. *BMC Res. Notes* **2008**, *1*, 132.

(26) Belchí-Navarro, S.; Almagro, L.; Lijavetzky, D.; Bru, R.; Pedreño, M. A. Enhanced extracellular production of *trans*-resveratrol in *Vitis vinifera* suspension cultured cells by using cyclodextrins and methyl jasmonate. *Plant Cell Rep.* **2012**, *31*, 81−89.

(27) Cusido, R. M.; Onrubia, M.; Sabater-Jara, A. B.; Moyano, E.; Bonfill, M.; Goossens, A.; Pedreno, M. A.; Palazon, J. A rational approach to improving the biotechnological production of taxanes in plant cell cultures of *Taxus* spp. *Biotechnol. Adv.* **2014**, *32*, 1157−1167.

(28) Belchi-Navarro, S.; Pedreño, M. A.; Corchete, P. Methyl jasmonate increases silymarin production in *Silybum marianum* (L.) Gaernt cell cultures treated with β-cyclodextrins. *Biotechnol. Lett.* **2011**, *33*, 179−184.

(29) Condori, J.; Medrano, G.; Sivakumar, G.; Nair, V.; Cramer, C.; Medina-Bolivar, F. Functional characterization of a stilbene synthase gene using a transient expression system in planta. *Plant Cell Rep.* **2009**, *28*, 589−599.

(30) Condori, J.; Nopo-Olazabal, C.; Medrano, G.; Medina-Bolivar, F. Selection of reference genes for qPCR in hairy root cultures of peanut. *BMC Res. Notes* **2011**, *4*, 392.

(31) Sobolev, V. S. Production of phytoalexins in peanut (*Arachis hypogaea*) seed elicited by selected microorganisms. *J. Agric. Food Chem.* **2013**, *61*, 1850−1858.

(32) Ku, K. L.; Chang, P. S.; Cheng, Y. C.; Lien, C. Y. Production of stilbenoids from the callus of *Arachis hypogaea*: a novel source of the anticancer compound piceatannol. *J. Agric. Food Chem.* **2005**, *53*, 3877−3881.

DOI: 10.1021/jf5050266
J. Agric. Food Chem. 2015, 63, 3942−3950

(33) Yang, M. H.; Kuo, C. H.; Hsieh, W. C.; Ku, K. L. Investigation of microbial elicitation of *trans*-resveratrol and *trans*-piceatannol in peanut callus led to the application of chitin as a potential elicitor. *J. Agric. Food Chem.* **2010**, *58*, 9537−9541.
(34) Yang, M. H.; Lin, Y. J.; Kuo, C. H.; Ku, K. L. Medicinal mushroom *Ganoderma lucidum* as a potent elicitor in production of t-resveratrol and t-piceatannol in peanut calluses. *J. Agric. Food Chem.* **2010**, *58*, 9518−9522.
(35) Potrebko, I.; Resurreccion, A. V. A. Effect of ultraviolet doses in combined ultraviolet-ultrasound treatments on *trans*-resveratrol and *trans*-piceid contents in sliced peanut kernels. *J. Agric. Food Chem.* **2009**, *57*, 7750−7756.
(36) Potter, G. A.; Patterson, L. H.; Wanogho, E.; Perry, P. J.; Butler, P. C.; Ijaz, T.; Ruparelia, K. C.; Lamb, J. H.; Farmer, P. B.; Stanley, L. A.; Burker, M. D. The cancer preventative agent resveratrol is converted to the anticancer agent piceatannol by the cytochrome P450 enzyme CYP1B1. *Br. J. Cancer* **2002**, *86*, 774−778.
(37) Boonlansiri, C.; Oonanant, W.; Kongsaeree, P.; Kittakoop, P.; Tanticharoen, M.; Thebtaranonth, Y. An antimalarial stilbene from *Artocarpus integer*. *Phytochemistry* **2000**, *54*, 415−417.
(38) Ioset, J.-R.; Marston, A.; Gupta, M.; Hostettmann, K. Five new prenylated stilbenes from the root bark of *Lonchocarpus chiricanus*. *J. Nat. Prod.* **2001**, *64*, 710−715.
(39) Van der Kaaden, J.; Hemscheidt, T.; Mooberry, S. Mappain, a new cytotoxic prenylated stilbene from *Macaranga mappa*. *J. Nat. Prod.* **2001**, *64*, 103−105.
(40) Sobolev, V. S. Localized production of phytoalexins by peanut (*Arachis hypogaea*) kernels in response to invasion by *Aspergillus* species. *J. Agric. Food Chem.* **2008**, *56*, 1949−1954.
(41) Sbaghi, M.; Jeandet, P.; Bessis, R.; Leroux, P. Degradation of stilbene-type phytoalexins in relation to the pathogenicity of *Botrytis cinerea* to grapevines. *Plant Pathol.* **1996**, *45*, 139−144.
(42) Breuil, A. C.; Jeandet, P.; Adrian, M.; Chopin, F.; Pirio, N.; Meunier, P.; Bessis, R. Characterization of a pterostilbene dehydrodimer produced by laccase of *Botrytis cinerea*. *Phytopathology* **1999**, *89*, 298−302.
(43) Ansari, K. A.; Vavia, P. R.; Trotta, F.; Cavalli, R. Cyclodextrin-based nanosponges for delivery of resveratrol: in vitro characterization, stability, cytotoxicity and permeation study. *AAPS PharmSciTech* **2011**, *12*, 279−286.
(44) Messiad, H.; Amira-Guebailia, H.; Houache, O. Reversed phase high performance liquid chromatography used for the physicochemical and thermodynamic characterization of piceatannol/*β*-cyclodextrin complex. *J. Chromatogr., B: Anal. Technol. Biomed. Life Sci.* **2013**, *926*, 21−27.
(45) López-Nicolás, J. M.; Rodríguez-Bonilla, P.; García-Carmona, F. Complexation of pinosylvin, an analogue of resveratrol with high antifungal and antimicrobial activity, by different types of cyclodextrins. *J. Agric. Food Chem.* **2009**, *57*, 10175−10180.
(46) Calderón, A. A.; Zapata, J. M.; Ros Barceló, A. Peroxidase-mediated formation of resveratrol oxidation products during the hypersensitive-like reaction of grapevine cells to an elicitor from *Tricoderma viride*. *Physiol. Mol. Plant Pathol.* **1994**, *44*, 289−299.
(47) Expósito, O.; Bonfill, M.; Onrubia, M.; Jane, A.; Moyano, E.; Cusidó, R. M.; Palazon, J.; Pinol, M. T. Effect of taxol feeding on taxol and related taxane production in *Taxus baccata* suspension cultures. *New Biotechnol.* **2009**, *25*, 252−259.
(48) Condori, J. *Identification and Characterization of a Stilbene Synthase Gene Family in Peanut Hairy Roots*. Ph.D. dissertation, Arkansas State University, 2011; 231 pp.
(49) López-Nicolás, J. M.; Escorial Camps, M.; Pérez-Sánchez, H.; García-Carmona, F. Physicochemical and thermodynamic characterization of the encapsulation of methyl jasmonate by natural and modified cyclodextrins using reversed-phase high-pressure liquid chromatography. *J. Agric. Food Chem.* **2013**, *61*, 11347−11354.

DOI: 10.1021/jf5050266
J. Agric. Food Chem. 2015, 63, 3942−3950

reduction amount in cellulose and total hemicelluloses are observed at veraison and proceed throughout the subsequent phases.[18] In the pectic fraction, the total amount and neutral and acid sugars temporally increase form before veraison to veraison, decreasing rapidly in post veraison.[18,19] Conversely, the neutral sugar content of the hemicellulosic fraction decreases from before veraison to veraison. During veraison, the neutral sugar composition of each fraction changes little.[18] This result discloses a pattern of temporal modifications in grape berry softening from before veraison to veraison.[18]

Water is one of the most valued resources on the planet, and understanding the impact of water deficit on grape development is vital. Mechanisms to cope with drought such as stomata control or extensive root systems developed by the grapevine have been recognized.[20] It is well documented that water stress affects the variation of sugar and phenolic contents.[21−23] Although to a lower extent than shoot organs, berry growth is sensitive to water deficits, being arrested[24] mainly at the mesocarp level, so that the seed and skin mass account more significantly for berry weight,[25,26] leading to an irreversible reduction in berry size[27,28] often with thicker exocarps.

Under water deficit conditions occurring either before or postveraison, the anthocyanin content in the grape skin increases in a cultivar-dependent pattern.[29,30] In ripening Cabernet Sauvignon grapes, water deficit leads to an increase in sugar accumulation only if imposed before veraison,[29] while in the red cultivar Shiraz, water deficit applied at postveraison leads to a reduction in sugar concentration and an increase in phenolic compounds content, except for anthocyanins.[31] Despite that, moderate water stress may increase the extractability of the anthocyanins into wine;[32] therefore establishing a balanced water regime is vital to attaining a quality wine.

Functional genomic resources for *V. vinifera* have proliferated rapidly in the recent years after genome sequencing,[33,34] and such information has paved the way for large-scale studies of gene expression profiling during berry development. CW metabolism related genes were over-represented in gene clusters with significant differential expression in several development stages.[35−40]

In grapes, differences in CW composition[4] and transcriptome[41] were described between red wine varieties, advising investigating the behavior of different genetic backgrounds to understand physiological events and agronomic performances.

The goal of this research was to investigate the effect of nonirrigation versus irrigation practices on grape quality parameters, with emphasis on the berry skin CW in two Portuguese grape varieties, Touriga Nacional (TN) and Trincadeira (TR). Our hypothesis was to verify if the changes in berry composition due to water shortage were related with remodeling of skin CW. For that purpose, berry yield, chemical characteristics, and mechanical properties as well as skin CW composition and expression of key candidate genes associated with berry development and ripening were examined at two developmental moments, veraison and full maturation.

MATERIALS AND METHODS

Experimental Vineyard and Plant Material. The study was conducted in 2012, on a vineyard located at the Centro Experimental de Pegões, Portugal (38° 39′ 1″ N; 8° 38′ 42″ W). The climate in the vineyard is Mediterranean with Atlantic influence, summers with hot days and fresh nights, and mild winters (Figures S1 and S2). The soil is derived from podzols, with a sandy surface layer (0.6−1.0 m) and clay at 1 m depth. Mixed clones of Touriga Nacional and Trincadeira were established in 2002, both varieties grafted on 1103 Paulsen rootstock. The plants spaced 2.5 m between rows and 1 m within rows were trained on vertical trellis and uniformly pruned on a bilateral Royat Cordon, ca. 12 buds per vine. Two irrigation regimes were considered: rain fed, nonirrigation (NI), and full irrigation in which water was supplied according to the evapotranspiration (100% ETc; FI, control). ETc was estimated from the reference evapotranspiration (ET_0), obtained in an automatic weather station located within the experimental vineyard as described in Lopes et al.[42] Irrigation water was applied with drip emitters (4.0 L h^{-1} for FI) two per vine, positioned 30 cm from the vine trunk, and began on June 29. Relative soil humidity in the soil profile was measured with a Diviner 2000 capacitance probe (Sentek Environmental Technologies, Stepney, Australia) in vertical tubes at increments of 0.1 m from the soil surface to a depth of 1.0 m[43] and assessed at plant level by predawn leaf water potential on the preselected plants as described by Scholander et al.[44] Three plants in each treatment and plot were preselected for analysis in a total of six plants per water regime and variety. At veraison (50% colored berries) on July 27 for TR and August 10 for TN and full maturation, the berries were pooled per water regime and variety and development stages (Figure S2). Berries were kept frozen from arrival from the field until further analyses.

Grape Berry Composition. Three samples of 100 berries were used for berry composition analysis per treatment and variety. After detaching the pedicels and acquiring the sample fresh weight, must volume, pH, total soluble solids (TSS in °Brix) and total acidity, skin anthocyanin content and total phenol index were assessed.

The must pH was measured with a calibrated pH meter at room temperature. TSS were quantified using an Atago Brix pocket refractometer. Total acidity was measured via titration with sodium hydroxide and expressed in g dm^{-3} of tartaric acid. Color density is given as the sum of absorbances in a 1 cm pathway at 420, 520, and 620 nm.[45] For extracted anthocyanin content, the skins were treated by the method of Carbonneau and Champagnol.[46] The skins were suspended in 96% ethanol buffered with tartaric acid solution (pH 3.6), and after 24 h of maceration at 37 °C the solution was centrifuged at 5000*g* for 10 min for (1) the calculation of extracted anthocyanin concentration as quantified by the method of Ribereau-Gayon and Stonestreet[47] with the absorbances obtained at 520 nm converted from a standard curve prepared with malvidin 3-glucoside and (2) estimation of total phenol by absorbance in a 1 cm pathway at 280 nm.[48]

Texture Analyses. Two compression tests were employed to address texture attributes. Skin firmness was measured using a penetration test carried out on the detached skin of 50 mature berries trapped between two perforated acrylic plates. Measurements were made using a TA-XT Texture Analyser equipped with a HDP/90 platform and a cylinder flat probe of 2 mm Ø (ref.:P/2), using a 5 kg load cell.[49] Tests were performed at 1 mm s^{-1}, and berry skin breaking force is expressed in Newtons (N). Berry texture analysis was carried out in 50 uniform mature berries. Measurements were made using a TA-XT Texture Analyser (Stable Micro Systems Ltd., UK) equipped with a HDP/90 platform and compression platens of 75 mm Ø, using a 5 kg load cell. The force to deform 10% of the berry equatorial diameter was expressed in Newtons (N).[50]

Cell Wall Analysis. *Cell Wall Extraction.* Ten grams of fresh skins were lyophilized and homogenized in liquid nitrogen and the CW extracted according to the method described by Talmadge et al.[51] as per Fernandes et al.[52]

Cellulose and Lignin Quantification. Cellulose was quantified by the Updegraff[53] method, using the hydrolytic conditions described by Saeman et al.[54] and quantifying the released glucose by the anthrone method.[55] Klason lignin was determined using the method described by Hatfield et al.[56] The results are expressed as microgram per milligram of CW.

Cell Wall Fractionation and Monosaccharide Quantification. The fractionation of berry skin CW at maturation followed the method of Selvendran and O'Neill[57] with minor modifications as in Fernandes et al.[52] Total sugars and uronic acids were determined using the

DOI: 10.1021/jf505169z
J. Agric. Food Chem. 2015, 63, 3951−3961

Table 1. Berry Composition Parameters (Mean ± Standard Deviation) Measured at Veraison and Maturation for Touriga Nacional (TN) and Trincadeira (TR), under Fully Irrigated (FI) and Non Irrigated (NI) Conditions[a]

			berry weight (g) per 100 berries	must volume (mL) per 100 berries	pH	total soluble solids	total acidity (g L^{-1} of Ta)
Veraison	TN	FI	$126.83^{aA} \pm 5.95$	$78.83^{a} \pm 8.89$	$3.02^{A} \pm 0.16$	$13.33^{A*} \pm 0.51$	$13.00^{A} \pm 1.88$
		NI	$78.60^{A*} \pm 0.0$	$39.33^{A*} \pm 3.06$	$3.11^{A} \pm 0.13$	$12.67^{A*} \pm 0.12$	$11.55^{A*} \pm 0.91$
	TR	FI	$125.93^{A} \pm 12.17$	$80.33^{A} \pm 11.93$	$3.00^{A} \pm 0.21$	$11.30^{A} \pm 0.70$	$13.90^{aA} \pm 2.13$
		NI	$105.33^{A} \pm 6.35$	$61.00^{A} \pm 4.36$	$2.87^{A} \pm 0.08$	$10.53^{A} \pm 0.90$	$17.50^{A} \pm 0.74$
Maturation	TN	FI	$143.10^{a*} \pm 4.88$	$92.83^{a*} \pm 2.36$	4.16 ± 0.07	$22.20^{a*} \pm 0.26$	2.70 ± 0.15
		NI	113.28 ± 11.93	64.00 ± 11.03	4.29 ± 0.06	20.23 ± 0.84	2.55 ± 0.26
	TR	FI	$217.60^{a} \pm 11.46$	$134.33^{a} \pm 11.02$	4.20 ± 0.11	$20.60^{a} \pm 0.60$	3.05 ± 0.23
		NI	132.87 ± 4.54	83.67 ± 6.66	4.32 ± 0.45	19.33 ± 0.45	2.95 ± 0.31

[a]Lower case letter indicates significant differences between treatments, capital letter indicates significant differences between stages and asterisk indicates significant differences between varieties, at $p < 0.01$ significance.

phenol–sulfuric acid assay and the m-hydroxybiphenyl assay,[58] respectively. Glucose and galacturonic acid were the corresponding standards. Neutral sugars were quantified by Gas Chromatography (GC) according to Albersheim et al.[59] with minor adaptations[52] using a Supelco SP-2330 30 m × 0.25 mm × 0.20 μm Capillary Column in a Varian 450-GC fitted with flame-ionization detector. The temperature program consisted of 210 °C (6 min hold) increased to 230 at 20 °C/min (25 min hold). Helium (2 mL min^{-1}) was used as the carrier gas. Pure rhamnose, fucose, arabinose, xylose, mannose, galactose, and glucose were used as monosaccharide standards and inositol as an internal standard. For data acquisition, the Galaxie Chromatography Software (Agilent, USA) was used.

Quantification of Gene Expression. *RNA Extraction and cDNA Synthesis.* Total RNA was extracted from *V. vinifera* berries using the Spectrum Plant Total RNA Kit (Sigma-Aldrich) with some modifications. Samples were ground in liquid nitrogen, and 400 mg of the material was split into two eppendorf tubes, and 900 μL lysis buffer was added per tube.[60] After centrifugation (10 min), the combined supernatants were filtered using the necessary number of filtration columns. A total of 750 μL of binding solution was added to each filtrate and passed through a single binding column. The RNA was then eluted using Milli-Q water. RNA samples were further treated with RNase-free DNase I (Qiagen) according to the manufacturer protocol, and quantification was carried out in a Synergy HT Multiplate Reader, with Gene5 software, using a Take3Multi-Volume Plate (Bio-Tek Instruments Inc. Winooski, USA). For reverse transcription, the RevertAid reverse transcriptase priming with oligo-d(T) kit was used (Thermo Scientific) according to the manufacturer's recommendations.

Quantification of Gene Expression by Quantitative PCR (RT-qPCR). For each *V. vinifera* cDNA sequence retrieved from public databases (Genoscope 12X (http://www.genoscope.cns.fr/spip/)), a set of specific primers (Table S1) was designed and used to amplify grapevine skin cDNA resulting from the transcription of 2 μg of total RNA, using conventional PCR. When amplification confirmed the expression, the transcripts were quantified by real-time PCR (qPCR), performed in 20 μL reaction volumes composed of cDNA derived from 2 μg of RNA, 0.5 μM gene-specific primers (Table S1), and SsoFast EvaGreen Supermixes (Bio-Rad, Hercules, CA) using an iQ5 Real-Time Thermal Cycler (BioRad, Hercules, CA). Reaction conditions for cycling were 95 °C for 3 min followed by 40 cycles at 95 °C for 10 s, 61 °C for 25 s, and 72 °C for 30 s. Melting curves were generated in each case to confirm the amplification of single products and absence of primer dimerization. Each analysis was performed in triplicate reactions, each in three biologic replicates (n = 9, in which each replicate is the average of three technical measurements). The corresponding quantification cycles (Cq) obtained by the iQ5 optical system software (Bio-Rad, Hercules, CA) were exported to a MS Excel spreadsheet (Microsoft Inc.) for quantification. Cq values of each gene of interest were normalized with respect to actin (Act) and translation initiation factor eIF-3 subunit 4 (TIF) Cqs.[61] Relative gene expression values in NI conditions are presented in heat maps, performed using the MeV software,[62] as log2 fold-change values in relation to control conditions (FI).

Statistical and Principal Component Analysis. All data are presented as mean values ± standard deviation (SD) of at least three biological replicates in each assay. The results were statistically evaluated by variance analysis (ANOVA) and post hoc Bonferroni test with a $p < 0.01$ significance level to compare the meaning of each effect with the SigmaPlot (Systat Software Inc.) statistical package. The Pearson correlation coefficient was calculated to disclose correlations between texture and skin composition values.

Data from 50 individual attributes measured at maturation were standardized, and a pair-wised correlation matrix was calculated and subjected to eigenvalue decomposition to identify orthogonal components of the original matrix and generate a Principal Component Analysis (PCA) biplot, using the NTsys-PC version 2.20e software package.[63] The weight of each character in sample separation was determined by calculating eigenvectors using the mean values of each treatment.

RESULTS

Composition of Grape Berries. A first indication of the effect of stress imposition (rain fed, Non Irrigation (NI) compared with Full Irrigation (FI), control; Figure S1) on the *V. vinifera* berries was gained through the measurement of berry composition. NI treatment decreased berry weight and must volume in all cases and increased TSS at maturity in both varieties, as shown in Table 1, although it was more pronounced in TN at veraison and in TR at maturation. At veraison under a water deficit, total acidity was significantly different between varieties. However, TR was delayed comparing to TN in either sugar increase or acid decrease (Table 1). Furthermore, we observed that in TN, water shortage (TN-NI) induced anthocyanin accumulation, while in TR, higher anthocyanin content was observed at maturity in the absence of water shortage (Figure 1A). The total phenol index followed the same pattern except for a slight increase at veraison in TR-NI (Figure 1B). The color is one of the most important characteristics for a wine. At maturation the water shortage induces a more intense color in the berry skin, which was more intense in TN berries (Figure 1C).

Cellulose and Lignin Content. The cellulose content of TN berry skins was not affected by the water regime, whether in veraison or in maturation. However, in TR, a statistically significant decrease was observed in NI between veraison and maturation and, at maturation, between control and NI (Figure 2A). Following the same pattern, lignin decreased in TR-NI at maturation (Figure 2B).

Berry Texture. Alterations in berry firmness can be addressed by measuring changes in compression, while skin break force is

DOI: 10.1021/jf505169z
J. Agric. Food Chem. 2015, 63, 3951–3961

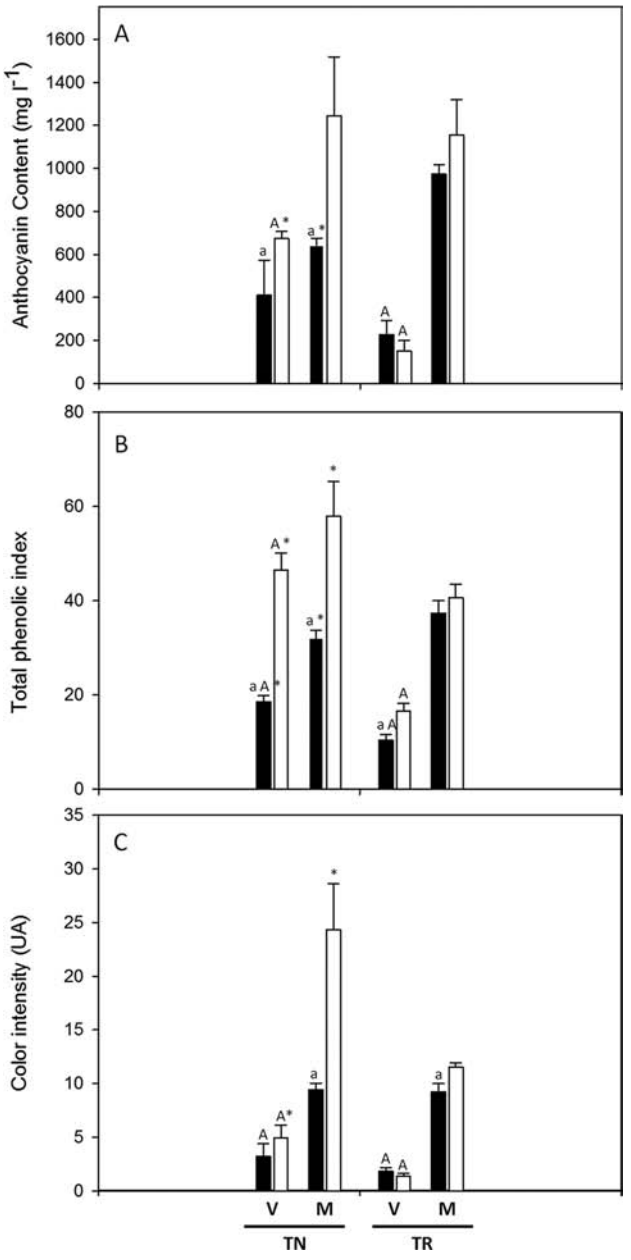

Figure 1. (A) Anthocyanin content, (B) total phenols and (C) color intensity of Touriga Nacional (TN) and Trincadeira (TR) berries at Veraison (V) and Maturation (M) grown in Full Irrigation (FI, black bars) or Non Irrigation (NI, white bars). Bars represent means ± SD of three samples of 100 berries. A lower case letter indicates significant differences between treatments; a capital letter indicates significant differences between stages. An asterisk indicates significant differences between varieties, at $p < 0.01$ significance.

given by the force rendered in penetration tests. In TN-NI, a higher force for berry deformation was necessary, while skin break force and energy were higher in TR-NI, decreasing from veraison to the maturation as expected (Table 2, see also Table S2). The Young modulus (E_{sk}) that represents the material resistance to axial deformation had the same trend as skin break force, revealing a decrease in the springiness of TR-NI berry skins (Table 2). Our results suggest that these specific properties may be influenced by the amount of phenolic compounds (Table S2).

The Pearson correlation between the berry texture attributes and CW composition showed significant negative correlations between skin break force and skin break energy with anthocyanin and total phenol contents. Noticeably, cellulose content was found to be positively correlated to the force needed to break the skin while lignin correlated to the energy applied to achieve rupture.

Sugar Composition in CW Fractions. Since major differences in cellulose and lignin between irrigation practices and varieties were observed at the maturation stage, only this stage was considered for berry skin CW fractionation. CDTA extracts polysaccharides that are less bound to the CW. The more tightly bound CW polysaccharides are extracted by increasing KOH molarity. The majority of polysaccharides were extracted in the alkaline fractions, particularly the 6 M KOH, with the exception of TR-FI. Considering the responses of the varieties to the irrigation regimes, in TN-NI, weakly bound polysaccharides were shown to be more extractable than under full water availability. In TR-NI, more polysaccharides were extracted in the 6 M KOH fraction, suggesting a more tight binding to the CW (Figure 3). The majority of uronic acids (reflecting the pectin content) was extracted in the CDTA and 0.1 M KOH fractions, with higher amounts in the latter (Figure 4A,B). No differences were observed between treatments or varieties. The analysis of the CW fractions by GC showed that the most abundant neutral monosaccharide present in all fractions was arabinose, followed by glucose, xylose, and galactose. The arabinose-, xylose-, and glucose-containing polysaccharides were in all cases higher in TR in all alkaline treatments, although in the 0.1 M KOH fraction, TR-NI samples showed decreased arabinose-containing polysaccharides when compared to the control (Figure 4B), which were shifted to the strong alkaline fraction (Figure 4C). For TN-NI, the 6 M KOH fraction showed a small but significant increase of arabinose-containing polysaccharides. The majority of xylose-containing polysaccharides were putatively tightly bonded to the CW since they only could be extracted by strong alkaline conditions. Conversely to TN, TR-NI was richer in xylose-containing polysaccharides (Figure 4C).

Changes in the Expression of Selected Key Genes Involved in Modification of the Berry CW. One way to access the effect of a stress on a given metabolic event is to understand the transcription of related genes. Figure 5 shows that water depletion gave rise to different gene expression patterns, some activated at veraison and others at maturation. As compared to TR, TN had more responsive genes, most of them down-regulated after water deficit in the two varieties. The expression of XTH genes was severely down-regulated at veraison on both varieties, with the exception of *VvXTH14* in TN. Conversely, at maturation, members of this family were not affected by the water shortage. At veraison, both PGs investigated were up-regulated in TN while *VvPG1* in TR showed a 3-fold down-regulation when compared to the control. In maturation, the majority of PGs were repressed, including *VvPG6*, which had a 7 fold repression compared to the control (Figure 5). The majority of EXPA gene expression had a similar down-regulation at veraison. EXPA genes were more repressed at maturation (Figure 5). The expression of PME genes unraveled a higher number of members showing down-regulation under water scarcity in both TN and TR. As in the case of EXPA, these genes were more repressed at maturation. Interestingly, under water shortage, PMEI gene expression was shown to be generally not affected at veraison. At maturation in TN, two

DOI: 10.1021/jf505169z
J. Agric. Food Chem. 2015, 63, 3951−3961

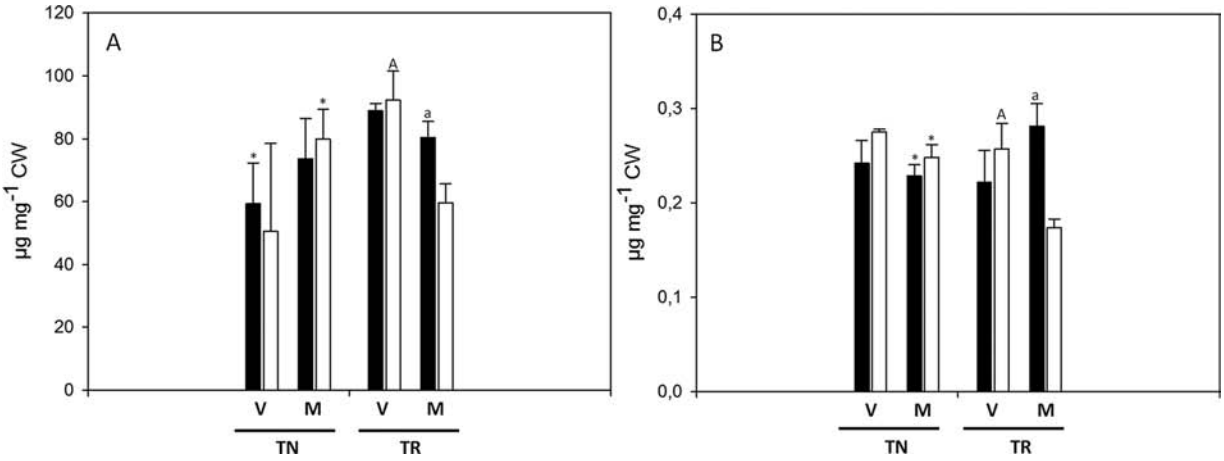

Figure 2. (A) Cellulose content and (B) lignin content of Touriga Nacional (TN) and Trincadeira (TR) berry skin CW at Veraison (V) and Maturation (M) grown in Full Irrigation (FI, black bars) or Non Irrigation (NI, white bars). Bars represent means of three samples ± SD. Lower case letters indicate significant differences between treatments. Capital letters indicate significant differences between stages, and asterisks indicate significant differences between varieties, at $p < 0.01$ significance.

Table 2. Berry Compression, Skin Break Force, Skin Break Energy, and Young's Modulus for Elasticity Parameters (Mean ± Standard Deviation) of Touriga Nacional (TN) and Trincadeira (TR) Berries at Veraison (V) and Maturation (M) Grown in Full Irrigation (FI) or Non Irrigation (NI)[a]

			berry firmness (N)	skin break force (N)	skin break energy (mJ)	Young's modulus for elasticity (N mm^{-1})
Veraison	TN	FI	2.07^{a*} ± 0.62	4.75^{a} ± 0.65	3.82^{a} ± 1.1	2.85 ± 0.62
		NI	4.46* ± 0.71	3.40* ± 0.73	2.14^{A*} ± 0.79	2.87* ± 0.82
	TR	FI	3.54 ± 0.39	5.08^{a} ± 0.79	4.85^{aA} ± 1.26	3.11^{aA} ± 0.83
		NI	2.99 ± 0.42	7.17^{A} ± 0.84	6.05^{A} ± 1.63	5.2^{A} ± 0.98
Maturation	TN	FI	1.03^{a*} ± 0.67	4.83 ± 0.78	3.58 ± 0.9	2.7^{a*} ± 0.43
		NI	4.19* ± 0.37	4.50 ± 0.75	3.58* ± 0.96	3.25* ± 0.64
	TR	FI	3.10 ± 0.36	3.54^{a} ± 0.60	3.73^{a} ± 0.99	1.93^{a} ± 0.37
		NI	2.49 ± 0.46	4.97 ± 0.60	4.85 ± 0.91	2.51 ± 0.31

[a]Lower case letters indicate significant differences between treatments. Capital letters indicate significant differences between stages, and asterisks indicate significant differences between varieties, at $p < 0.01$ significance.

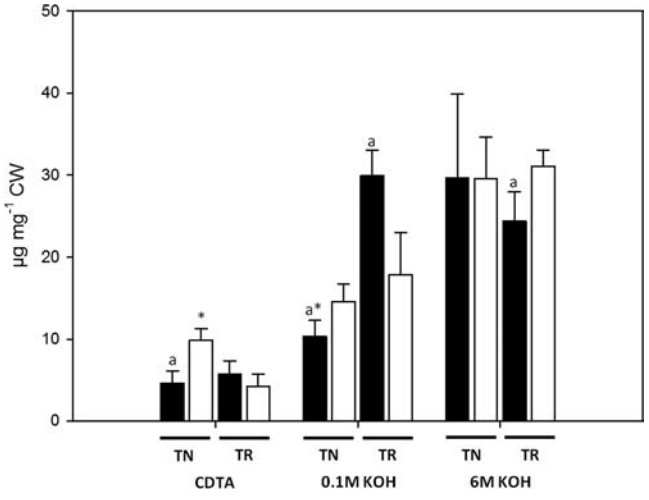

Figure 3. Total sugar quantification in CW fraction obtained from Touriga Nacional (TN) and Trincadeira (TR) berry skin CW at Maturation (M) grown in Full Irrigation (FI, black bars) or Non Irrigation (NI, white bars). Units are micrograms of glucose equivalents per millgram of CW. Bars represent means of three samples ± SD. Lower case letters indicate significant differences between treatments, and asterisks indicate significant differences between varieties, at $p < 0.01$ significance.

genes were down-regulated (*VvPMEI3* and *VvPMEI4*), but the same *VvPMEI3* in TR was up-regulated with a fold change of 6 (Figure 5).

Data Integration. To obtain a global representation of all data collected at maturation, samples were graphically plotted in a reduced number of axis after multivariate analysis (Principal Component Analysis; PCA). Principal components 1 and 2 (PC1 and PC2) in combination explain 58.8% of the total variation and could separate the samples according to the variety and water regime to which they were submitted. Replicates were generally closely clustered, demonstrating the accuracy of the analyses performed and the true biological basis of the measured dissimilarities. The results shown in Figure 6 reveal that PC1 clearly differentiates between varieties while PC2 separates the samples according to the treatments. According to the resultant eigenvectors calculated using the average values of the triplicates (Table S3), the variables that contributed more to PC1 separation were the higher amounts of arabinose- and galactose-containing polysaccharides extracted in the 0.1 M KOH fraction and xylose-containing polysaccharides collected in both alkaline solutions, and the lower relative transcription of *VvPMEI1*, *VvPMEI2*, *VvXTH31*, and *VvXTH15* in the TR variety. PC2 separation was mainly explained by lower amounts of glucose-containing polymers extracted by 0.1 M KOH solutions, by mannose- and fucose-containing polysaccharides present in the 6 M KOH solution

DOI: 10.1021/jf505169z
J. Agric. Food Chem. 2015, 63, 3951−3961

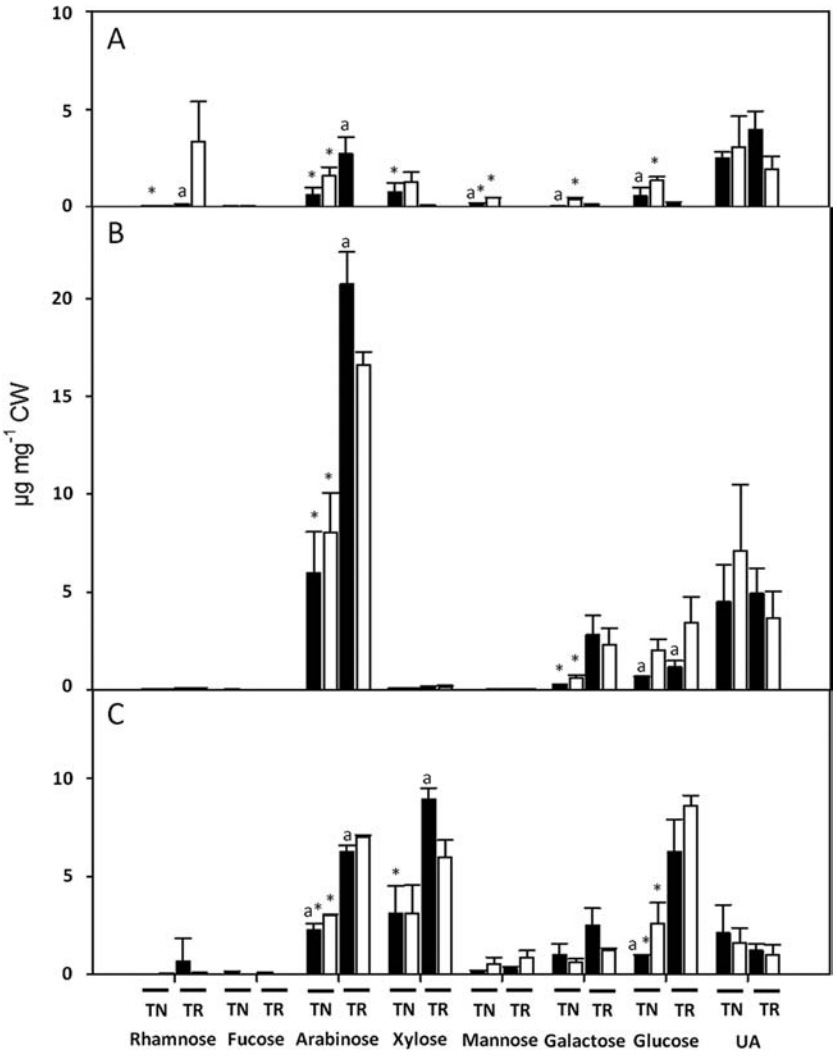

Figure 4. Monosaccharide composition of berry skin CW. (A) CDTA-soluble fraction, (B) 0.1 M KOH-soluble fraction, and (C) 6 M KOH-soluble fraction obtained by GC analysis and uronic acids levels measured by the m-hydroxybiphenyl assay in Touriga Nacional (TN) and Trincadeira (TR) berries at maturation grown in Full Irrigation (FI, black bars) or Non Irrigation (NI, white bars). Units are micrograms of each monosaccharide and galacturonic acid equivalents for uronic acids (UA) permilligram of CW. Bars represent means of three samples ± SD. Lower case letters indicate significant differences between treatments, and asterisks indicate significant differences between varieties, at $p < 0.01$ significance.

under the FI regime, and by the lower relative expression of two polygalacturonase genes, *VvPG2* and *VvPG4*, in the control.

DISCUSSION

Water deficit during *Vitis vinifera* L. growth, like other abiotic stresses, is known to decrease growth and yield,[64−66] impacting berry physical and chemical composition[67] and, ultimately, influencing the sensorial quality of the final product.[68] In this work, we assessed the influence of nonirrigation in comparison with water full conditions in berry characteristics, CW composition, and gene expression of two widespread Portuguese winegrape varieties, Touriga Nacional and Trincadeira, growing under Mediterranean conditions with Atlantic influence, to which some grapevines varieties are better adapted than others.[69] The clear effects exerted by water deficit on berry characteristics (Table 1) confirm previous results showing that water deficiency results in an increase in anthocyanin concentration,[70] and in total phenols (Figure 1).[29] It is unsure whether the increase in total polyphenol content is purely due to the fluctuations in anthocyanin content or by the increase of other phenolic compounds including flavanols and proanthocyanidins.[29] Moreover, the variety-specific amount of anthocyanin observed is also in agreement with previous studies.[71] The global CW results allowed an evident separation of both varieties and the imposed water regimes, as illustrated by the PCA plots (Figure 6). The separation in the two first components is mainly explained by the amount of monosaccharides extracted in distinct fractions, which suggest different polysaccharide linkages, and by CW-related gene expression (Table S3).

Among the effects on CW, the alterations mostly associated with changes in composition and architecture are the berry texture characteristics. Texture analysis is a rapid and low-cost analytical technique that can be applied in viticulture and enology as a routine tool for monitoring grape quality.[72] In our research, texture measurements were conducted with the objective of comparing the changes in mechanical properties of the berry and berry skin between the two cultivars under the water regimes imposed during grape development. Therefore, and since the assays were conducted with frozen/thawed grapes, the measurements do not describe fresh berries values

DOI: 10.1021/jf505169z
J. Agric. Food Chem. 2015, 63, 3951−3961

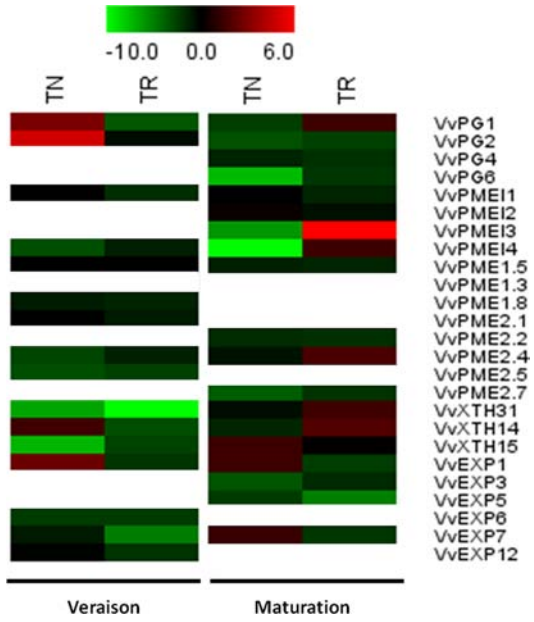

Figure 5. Heat-map of transcriptional responses to water shortage of CW modifying genes in TN and TR varieties at veraison and maturity. Color scale from green to red indicates log2 NI/FI expression ratio from 10-fold repression to 6-fold over transcription.

but clearly indicate that under our conditions the higher skin break force measured in TR-NI berries (Table 2) seems to be variety dependent, since TN break force was not affected by the water regime. Conversely, in TN-NI compression tests, higher forces were needed to attain the same berry deformation (Table 2). The increase in berry skin break force in TR-NI was also observed in stressed Mondeuse, Becuét, and Fumin grapes obtained during on-vine drying.[73,74] Recent observations by Zsófi et al.[67] in Kékfrankos grapes growing under greenhouse conditions suggest that skin break force increases significantly as a result of water deficit. Conversely, berry firmness measured as berry deformation by the compression test was decreased in TN-NI. As a whole, the skin break force and skin break energy correlated negatively with the amounts of berry secondary metabolites but positively with cellulose and lignin contents, respectively (Table S2). This suggests that the lower cellulose and lignin content verified after water deficiency contributes, although in different dimensions, to the alteration in the skin mechanical properties. The responses obtained so far corroborate the dependence on the variety and the environmental conditions.[75,76] However, and taking advantage of the aftermost results with fresh berries from an experimental water regime similar but not equivalent to the one reported here, for full clarification, the presented results might be confirmed with fresh berries from the cultivars and under the experimental setup as applied in the present study.

Aiming at gaining a further insight on the basis of water deficit on polysaccharide differences, general CW composition was investigated in all samples. In this work, TR-NI showed reduced amounts in cellulose and lignin at maturation (Figure 2), which was accompanied by a marked reduction in berry size (Table 1). In the Muscat Gordo Blanco variety, Nunan et al.[6] found that cellulose remained unaltered during ripening, putting forward the assumption that the decrease in TR may be a genotype-specific response to water availability. Conversely, the increased break force may be caused by CW polysaccharides besides cellulose since this polymer serves as a scaffold for the binding of other CW components.[77] The shift of arabinose-containing polysaccharides from the 0.1 M KOH to 6 M fraction in TR-NI (Figure 4) may indicate that

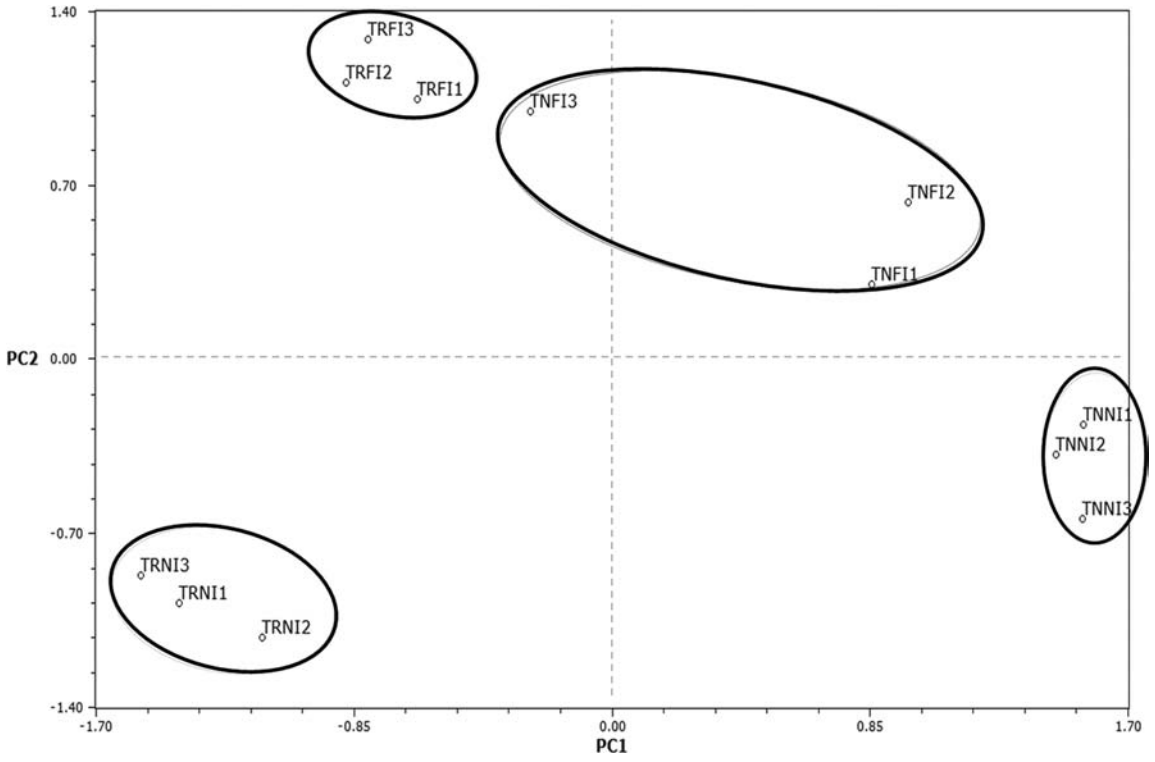

Figure 6. Principal component analysis (PCA) from 50 individual attributes measured at maturation. PC1 and PC2 explain, respectively, 35.3% and 25.6% of the total variation.

DOI: 10.1021/jf505169z
J. Agric. Food Chem. 2015, 63, 3951−3961

rhamnogalacturonan-I (RGI) arabinosyl residues became more tightly bound into CW with water shortage. The presence of RGI decorated with arabinose rich side chains in water deficient conditions can work as CW plasticizers.[78] Under water shortage, arabinose and also galactose rich polymers are known to retain relatively longer mobility than other CW polymers filling the cavities created upon physical rearrangement of the CW.[79] The unusually high arabinan content (approximately 38 mol %) observed in the resurrection plant *Myrothamnus flabellifolius*[80] further suggests an arabinose role for plants coping with water scarcity. Changes in pectin, break energy, and Young modulus (E_{sk}) showed similar patterns to break force, again with a variety dependent behavior, skins becoming less elastic in the absence of water. From the correlation of E_{sk} values with total phenols content (Table S2), it can be inferred that the stiffening of the CW may contribute to the extractability of the phenolic compounds, as observed by Rolle et al.[81] As referred to by other authors, Torchio et al.[82] and Zsófi et al.,[67] an increase in elasticity was observed from veraison to ripening.

Gene expression of key candidate genes was considered to be differential when above a log2 ± 2-fold change relative to the control and showed that all gene families investigated possess members that respond to water shortage (Figure 5). This complementary approach provided evidence that, although with a general pattern of down-regulation, responsive individual genes within each family were different depending on the stages. Exceptions were *VvPG1* and *VvPG2* at veraison in TN and *VvPMEI3* at maturation in TR that are up-regulated, both indicating changes in the pectic network of the CWs, which suggests different patterns of expression depending on the development stage, in accordance with Deluc et al.[36] findings. According to PCA, concerning gene expression, the observed differences between varieties are putatively associated with differences in the inhibition of pectin methylesterification and in the expression of members of the xyloglucan endotransglycosylase/hydrolase (XTH) family. Pectins are embedded within the cellulose/hemicellulose network, forming a hydrophilic gel that imposes mechanical features to the wall such as regulation of the hydration status or defining the porosity and stiffness of the wall.[83] PME activity can alter the degree and pattern of methyl esterification[84] and, therefore, change the biophysical properties of the CW. Under water scarcity, the PME expression decreased, as also observed for some members of Sangiovese grapes.[85] The maintenance in the degree of methyl esterification of pectins, as observed by Zoccatelli et al.[85] in Sangiovese grapes, may lead in our case to the preservation of the CW structure, especially in TR, which is further supported by the penetration tests. At the biochemical level, the activity of PMEs is also regulated by PMEIs. Grimplet et al.[37] reported modifications in the expression of a PMEI member, with downregulation at maturation, which is in agreement with the patter observed in this work in TN. Conversely, in TR its expression is upregulated, which contributes to the variety separation observed in the PCA analysis (Figure 6) This PME activity my change the pectin methyesterification degree. Changes in the degree of pectin methylation seem to be genotype-specific in *Vitis*, decreasing as ripening progresses in some cultivars like Cabernet Sauvignon, Merlot, and Monastrell, while it hardly changes in Syrah.[4] This observation is in accordance with the differences found between TN and TR. A total of 15−25% of the hemicelluloses present in dicot primary CW are constituted by xyloglucans.[12] The xyloglucan frame can be modified by XTHs, which can potentially have two distinct catalytic activities, namely transglycosylase (XET) or hydrolase (XEH).[86−88] These activities have been associated with the fruit softening that occurs during phase III of berry development and largely modulate CW loosening.[6] In the present study, the lowest *VvXTH* expression was observed at veraison, mainly in TR in result of water shortage. The low activity suggested by the down-regulation of XTH genes may lead to maintenance of the CW structure under water shortage. On the other hand, Deluc et al.[36] observed that XTH gene expression declined significantly along berry development.

The effect of distinct water regimes in gene expression was mainly due to the transcript abundance of polygalacturonases (PGs), which are CW-localized enzymes that cleave stretches of unesterified GalA residues and weaken the middle lamella.[89] PG activity is known to accompany fruit ripening.[90] The up-regulation of PG at veraison and subsequent down-regulation at maturation is in agreement with Grimplet et al.[37] under water deficit. In the pectin fraction of the grape mesocarp, both polysaccharide amounts and the neutral and acidic sugars of the water-soluble fraction temporally increase from before veraison to veraison stages, decreasing rapidly thereafter.[18,91] The maintenance of the pectin level in response to water shortage, especially in the 6 M KOH fraction, may be partially explained by the low transcription levels of PMEs and PGs strengthening the CW and increasing the force necessary to break the skin. In the mesocarp, pectin and xyloglucan solubilization seems to occur at later stages of ripening while depolymerization events occur at earlier stages (reviewed by Goulao et al.[92]).

Expansins (EXPA) play also an important role in the CW loosening phenomenon via nonenzymatic mechanisms.[93] Under water shortage, most expansin genes decreased expression during berry development, as observed by Grimplet et al.[37] Studies in postharvest Corvina withering berries, which can be considered as a water stress condition,[35] demonstrated the alteration in expression of several expansin genes, namely the downregulation of *VvEXPA1*, *VvEXPA14*, and *VvEXPA19* during withering. Some authors propose that expansins are associated with pectin turnover, probably by regulating the contact between pectins and pectin-degrading enzymes.[84] Brummell et al.[94] suggest the relation between different networks: the disassembly of the hemicellulosic network by expansin may be necessary for modifications in the pectins promoting physical accessibility of pectin substrates to PGs enzymes. From our results, it is possible to forward the hypothesis that water depletion has an indirect impact on pectins through the process proposed by Brummell et al.[94]

In summary, the overall results suggest differences in pectin metabolism between varieties in response to distinct water availability during growth under field conditions and support its involvement in distinct responses to environmental conditions. Water shortage affects grape berries by stiffening the CW, probably through alteration in PGs expression and pectin structure, in a way that significantly depends on the variety. Contrasting softening behaviors during ripening differs sufficiently between genotypes to allow discrimination regarding technological differences that can influence oenological practices.

■ ASSOCIATED CONTENT

Supporting Information

List of primers used for RT-qPCR (Table S1), Pearson correlation values between berry texture parameter and berry

DOI: 10.1021/jf505169z
J. Agric. Food Chem. 2015, 63, 3951−3961

CW components (Table S2), eigenvectors for each principal component (Table S3), fold change values of heat-map genes in Figure 5 (Table S4), precipitation at the vineyard throughout 2012 (Figure S1), and average soil humidity at different dates of the growing season (Figure S2) are available free of charge via the Internet at http://pubs.acs.org

AUTHOR INFORMATION

Corresponding Author

*Phone: 00351213653418. E-mail: samport@isa.ulisboa.pt.

Present Address

[§]Enotria Winecellars, London, UK.

Funding

The research was funded by Fundação para a Ciência e Tecnologia (FCT): project PTDC/AGR-GPL/099624/2008, the Ph.D. research grant SFRH/BD/64047/2009 to J.C.F. and CBAA PestOE/AGR/UI0240/2011. This work also benefited from European project KBBE InnoVine (ref 311775) and the European COST Action FA1106 "QualityFruit."

Notes

The authors declare no competing financial interest.

ACKNOWLEDGMENTS

The field work was performed at PORVID Experimental Station (Pegões, PT), and the authors thank the president of its executive board, Prof. Antero Martins. The authors also like to acknowledge Prof. Isabel Sousa and Prof. Margarida Moldão for excellent discussions on biophysical and chromatography experiments.

ABBREVIATIONS

Act, Actin; CDTA, cyclohexane−trans-1.2-diamine−N,N,N′,N′-tetraacetic acid sodium salt; CW, cell wall; EXPA, expansins; GC, gas chromatography; FI, full irrigation; N, Newton; NI, no irrigation; PCA, principal component analysis; PGs, polygalacturonases; PMEs, pectin methylesterases; PMEIs, pectin methylesterases inhibitors; qPCR, real-time PCR; TIF, translation initiation factor eIF-3 subunit 4; TSS, total soluble solids in °Brix; RGI, rhamnogalacturonan-I; TN, Touriga Nacional; TR, Trincadeira; XTH, xyloglucan endo-transglycosylase/hydrolase

REFERENCES

(1) Kammerer, D.; Claus, A.; Carle, R.; Schieber, A. Polyphenol screening of pomace from red and white grape varieties (Vitis vinifera L.) by HPLC-DAD-MS/MS. *J. Agric. Food Chem.* **2004**, *52*, 4360−4367.

(2) Pinelo, M.; Del Fabbro, P.; Manzocco, L.; Nunez, M. J.; Nicoli, M. C. Optimization of continuous phenol extraction from Vitis vinifera byproducts. *Food Chem.* **2005**, *92*, 109−117.

(3) Montealegre, R. R.; Peces, R. R.; Vozmediano, J. L. C.; Gascuena, J. M.; Romero, E. G. Phenolic compounds in skins and seeds of ten grape Vitis vinifera varieties grown in a warm climate. *J. Food Compos. Anal.* **2006**, *19*, 687−693.

(4) Ortega-Regules, A.; Romero-Cascales, I.; Ros Garcia, J. M.; Bautista-Ortin, A. B.; Lopez-Roca, J. M.; Fernandez-Fernandez, J. I.; Gomez- Plaza, E. Anthocyanins and tannins in four grape varieties (Vitis vinifera L.) - Evolution of their content and extractability. *J. Int. Sci. Vig. Vin.* **2008**, *42*, 147−156.

(5) Rolle, L.; Siret, R.; Río Segade, S.; Maury, C.; Gerbi, V.; Jourjon, F. Instrumental Texture Analysis Parameters as Markers of Table-Grape and Winegrape Quality: A Review. *Am. J. Enol. Vitic.* **2012**, *63*, 11−28.

(6) Nunan, K. J.; Sims, I. M.; Bacic, A.; Robinson, S. P.; Fincher, G. B. Changes in cell wall composition during ripening of grape berries. *Plant Physiol.* **1998**, *118*, 783−792.

(7) Brummell, D. A. Cell wall disassembly in ripening fruit. *Funct Plant Biol.* **2006**, *33*, 103.

(8) Dunlevy, J. D.; Kalua, C. M.; Keyzers, R. A.; Boss, P. K. The production of flavour & aroma compounds in grape berries. *Grapevine Molecular Physiology & Biotechnology*; Roubelakis-Angelakis, A. K., Ed.; Springer: Dordrecht, 2009; pp 293−340.

(9) Letaief, H.; Rolle, L.; Gerbi, V. Mechanical behavior of winegrapes under compression tests. *Am. J. Enol. Viticult.* **2008**, *59*, 323−329.

(10) Ortega-Regules, A.; Ros-García, J. M.; Bautista-Ortín, A. B.; López-Roca, J. M.; Gómez-Plaza, E. Changes in skin cell wall composition during the maturation of four premium wine grape varieties. *J. Sci. Food Agric.* **2008**, *88*, 420−428.

(11) Vicens, A.; Fournand, D.; Williams, P.; Sidhoum, L.; Moutounet, M.; Doco, T. Changes in polysaccharide and protein composition of cell walls in grape berry skin (Cv. Shiraz) during ripening and over-ripening. *J. Agric. Food Chem.* **2009**, *57*, 2955−2960.

(12) Carpita, N. C.; Gibeaut, D. M. Structural models of primary-cell walls in flowering plants - Consistency of molecular-structure with the physical-properties of the walls during growth. *Plant J.* **1993**, *3*, 1−30.

(13) Nunan, K. J.; Sims, I. M.; Bacic, A.; Robinson, S. P.; Fincher, G. B. Isolation and characterization of cell walls from the mesocarp of mature grape berries (Vitis vinifera). *Planta* **1997**, *203*, 93−100.

(14) Vidal, S. Polysaccharides from grape berry cell walls. Part I: tissue distribution and structural characterization of the pectic polysaccharides. *Carbohydr. Polym.* **2001**, *45*, 315−323.

(15) Lecas, M.; Brillouet, J. M. Cell-Wall composition of grape berry skins. *Phytochemistry* **1994**, *35*, 1241−1243.

(16) Saulnier, L.; Brillouet, J. M. An arabinogalactan protein from the pulp of grape berries. *Carbohydr. Res.* **1989**, *188*, 137−144.

(17) Bindon, K. A.; Smith, P. A.; Kennedy, J. A. Interaction between grape-derived proanthocyanidins and cell wall material. 1. effect on proanthocyanidin composition and molecular mass. *J. Agric. Food Chem.* **2010**, *58*, 2520−2528.

(18) Yakushiji, H.; Sakurai, N.; Morinaga, K. Changes in cell-wall polysaccharides from the mesocarp of grape berries during veraison. *Physiol. Plant.* **2001**, *111*, 188−195.

(19) Silacci, M. W.; Morrison, J. C. Changes in pectin content of cabernet-sauvignon grape berries during maturation. *Am. J. Enol. Viticult.* **1990**, *41*, 111−115.

(20) Chaves, M. M.; Maroco, J. P.; Pereira, J. S. Understanding plant responses to drought - from genes to the whole plant. *Funct. Plant Biol.* **2003**, *30*, 239−264.

(21) Matthews, M. A.; Nuzzo, V. Berry size and yield paradigms on grapes and wines quality. *Acta Hortic.* **2007**, 423−435.

(22) Deluc, L. G.; Decendit, A.; Papastamoulis, Y.; Mérillon, J.-M.; Cushman, J. C.; Cramer, G. R. Water deficit increases stilbene metabolism in Cabernet Sauvignon Berries. *J. Agric. Food Chem.* **2011**, *59*, 289−297.

(23) Zarrouk, O.; Francisco, R.; Pinto-Marijuan, M.; Brossa, R.; Santos, R. R.; Pinheiro, C.; Costa, J. M.; Lopes, C.; Chaves, M. M. Impact of irrigation regime on berry development and flavonoids composition in Aragonez (Syn. Tempranillo) grapevine. *Agr. Water Manage* **2012**, *114*, 18−29.

(24) Dai, Z. W.; Ollat, N.; Gomes, E.; Decroocq, S.; Tandonnet, J. P.; Bordenave, L.; Pieri, P.; Hilbert, G.; Kappel, C.; van Leeuwen, C.; Vivin, P.; Delrot, S. Ecophysiological, genetic, and molecular causes of variation in grape berry weight and composition: a review. *Am. J. Enol. Vitic.* **2011**, *62*, 413−425.

(25) Greenspan, M. D.; Shackel, K. A.; Matthews, M. A. Developmental-changes in the diurnal water-budget of the grape berry exposed to water deficits. *Plant, Cell Environ.* **1994**, *17*, 811−820.

(26) Roby, G.; Matthews, M. A. Relative proportions of seed, skin and flesh, in ripe berries from Cabernet Sauvignon grapevines grown in a vineyard either well irrigated or under water deficit. *Aust. J. Grape Wine Res.* **2004**, *10*, 74−82.

DOI: 10.1021/jf505169z
J. Agric. Food Chem. 2015, 63, 3951−3961

(27) Poni, S.; Lakso, A.; Turner, J.; Melious, R. Interactions of crop levels and late season water stress on growth and physiology of field-grown Concord grapevines. *Am. J. Enol. Viticult.* **1994**, *45*, 252−258.
(28) Ojeda, H.; Deloire, A.; Carbonneau, A. Influence of water deficits on grape berry growth. *Vitis* **2001**, *40*, 141−145.
(29) Castellarin, S. D.; Matthews, M. A.; Di Gaspero, G.; Gambetta, G. A. Water deficits accelerate ripening and induce changes in gene expression regulating flavonoid biosynthesis in grape berries. *Planta* **2007**, *227*, 101−12.
(30) Intrigliolo, D. S.; Castel, J. R. Interactive effects of deficit irrigation and shoot and cluster thinning on grapevine cv. Tempranillo. Water relations, vine performance and berry and wine composition. *Irrig. Sci.* **2011**, *29*, 443−454.
(31) Petrie, P. R.; Cooley, N. M.; Clingeleffer, P. R. The effect of post-veraison water deficit on yield components and maturation of irrigated Shiraz (Vitis vinifera L.) in the current and following season. *Aust. J. Grape Wine Res.* **2004**, *10*, 203−215.
(32) Koundouras, S.; Hatzidimitriou, E.; Karamolegkou, M.; Dimopoulou, E.; Kallithraka, S.; Tsialtas, J. T.; Zioziou, E.; Nikolaou, N.; Kotseridis, Y. Irrigation and rootstock effects on the phenolic concentration and aroma potential of Vitis vinifera L. cv. Cabernet Sauvignon grapes. *J. Agric. Food Chem.* **2009**, *57*, 7805−7813.
(33) Jaillon, O.; Aury, J. M.; Noel, B.; Policriti, A.; Clepet, C.; Casagrande, A.; Choisne, N.; Aubourg, S.; Vitulo, N.; Jubin, C.; Vezzi, A.; Legeai, F.; Hugueney, P.; Dasilva, C.; Horner, D.; Mica, E.; Jublot, D.; Poulain, J.; Bruyere, C.; Billault, A.; Segurens, B.; Gouyvenoux, M.; Ugarte, E.; Cattonaro, F.; Anthouard, V.; Vico, V.; Del Fabbro, C.; Alaux, M.; Di Gaspero, G.; Dumas, V.; Felice, N.; Paillard, S.; Juman, I.; Moroldo, M.; Scalabrin, S.; Canaguier, A.; Le Clainche, I.; Malacrida, G.; Durand, E.; Pesole, G.; Laucou, V.; Chatelet, P.; Merdinoglu, D.; Delledonne, M.; Pezzotti, M.; Lecharny, A.; Scarpelli, C.; Artiguenave, F.; Pe, M. E.; Valle, G.; Morgante, M.; Caboche, M.; Adam-Blondon, A. F.; Weissenbach, J.; Quetier, F.; Wincker, P.; Public, F.-I. The grapevine genome sequence suggests ancestral hexaploidization in major angiosperm phyla. *Nature* **2007**, *449*, 463−U5.
(34) Velasco, R.; Zharkikh, A.; Troggio, M.; Cartwright, D. A.; Cestaro, A.; Pruss, D.; Pindo, M.; FitzGerald, L. M.; Vezzulli, S.; Reid, J.; Malacarne, G.; Iliev, D.; Coppola, G.; Wardell, B.; Micheletti, D.; Macalma, T.; Facci, M.; Mitchell, J. T.; Perazzolli, M.; Eldredge, G.; Gatto, P.; Oyzerski, R.; Moretto, M.; Gutin, N.; Stefanini, M.; Chen, Y.; Segala, C.; Davenport, C.; Demattè, L.; Mraz, A.; Battilana, J.; Stormo, K.; Costa, F.; Tao, Q. Z.; Si-Ammour, A.; Harkins, T.; Lackey, A.; Perbost, C.; Taillon, B.; Stella, A.; Solovyev, V.; Fawcett, J. A.; Sterck, L.; Vandepoele, K.; Grando, S. M.; Toppo, S.; Moser, C.; Lanchbury, J.; Bogden, R.; Skolnick, M.; Sgaramella, V.; Bhatnagar, S. K.; Fontana, P.; Gutin, A.; Van de Peer, Y.; Salamini, F.; Viola, R. A High quality draft consensus sequence of the genome of a heterozygous grapevine variety. *PLoS One* **2007**, *2*.10.1371/journal.-pone.0001326
(35) Dal Santo, S.; Vannozzi, A.; Tornielli, G. B.; Fasoli, M.; Venturini, L.; Pezzotti, M.; Zenoni, S. Genome-wide analysis of the expansin gene superfamily reveals grapevine-specific structural and functional characteristics. *PLoS One* **2013**, *8*.10.1371/journal.-pone.0062206
(36) Deluc, L. G.; Grimplet, J.; Wheatley, M. D.; Tillett, R. L.; Quilici, D. R.; Osborne, C.; Schooley, D. A.; Schlauch, K. A.; Cushman, J. C.; Cramer, G. R. Transcriptomic and metabolite analyses of Cabernet Sauvignon grape berry development. *BMC Genomics* **2007**, *8*, 429.
(37) Grimplet, J.; Deluc, L. G.; Tillett, R. L.; Wheatley, M. D.; Schlauch, K. A.; Cramer, G. R.; Cushman, J. C. Tissue-specific mRNA expression profiling in grape berry tissues. *BMC Genomics* **2007**, *8*, 187.
(38) Blazquez, M. A.; Lijavetzky, D.; Carbonell-Bejerano, P.; Grimplet, J.; Bravo, G.; Flores, P.; Fenoll, J.; Hellín, P.; Oliveros, J. C.; Martínez-Zapater, J. M. Berry flesh and skin ripening features in vitis vinifera as assessed by transcriptional profiling. *PLoS One* **2012**, *7*, e39547.
(39) Terrier, N.; Glissant, D.; Grimplet, J.; Barrieu, F.; Abbal, P.; Couture, C.; Ageorges, A.; Atanassova, R.; Leon, C.; Renaudin, J. P.; Dedaldechamp, F.; Romieu, C.; Delrot, S.; Hamdi, S. Isogene specific oligo arrays reveal multifaceted changes in gene expression during grape berry (Vitis vinifera L.) development. *Planta* **2005**, *222*, 832−847.
(40) Waters, D. L. E.; Holton, T. A.; Ablett, E. M.; Lee, L. S.; Henry, R. J. cDNA microarray analysis of developing grape (Vitis vinifera cv. Shiraz) berry skin. *Funct. Integr. Genomics* **2005**, *5*, 40−58.
(41) Venturini, L.; Ferrarini, A.; Zenoni, S.; Tornielli, G. B.; Fasoli, M.; Dal Santo, S.; Minio, A.; Buson, G.; Tononi, P.; Zago, E. D.; Zamperin, G.; Bellin, D.; Pezzotti, M.; Delledonne, M. De novo transcriptome characterization of Vitis vinifera cv. Corvina unveils varietal diversity. *BMC Genomics* **2013**, *14*, 41.
(42) Lopes, C. M.; Santos, T. P.; Monteiro, A.; Rodrigues, M. L.; Costa, J. M.; Chaves, M. M. Combining cover cropping with deficit irrigation in a Mediterranean low vigor vineyard. *Sci. Hortic.* **2011**, *129*, 603−612.
(43) Santos, T. P.; Lopes, C. M.; Lucília, R. M.; de Souza, C. R.; Ricardo-da-Silva, J. M.; Maroco, J. P.; Pereira, J. S.; Manuela, C. M. Effects of deficit irrigation strategies on cluster microclimate for improving fruit composition of Moscatel field-grown grapevines. *Sci. Hortic.* **2007**, *112*, 321.
(44) Scholander, P.; Hammel, H.; Brandstreet, E.; Hemmingsen, E. Sap pressure in vascular plants. *Science* **1965**, *148*, 339−346.
(45) Dallas, C.; Laureano, O. Effects of pH, sulphur dioxide, alcohol content, temperature and storage time on colour composition of a young Portuguese red table wine. *J. Sci. Food Agric.* **1994**, *65*, 477−485.
(46) Carbonneau, A.; Champagnol, F. Nouveaux systemes de culture integré du vignoble. In *Programme AIR*; 1993.
(47) Ribereau-Gayon, P.; Stonestreet, E. Le dosage des anthocyanes dans le vin rouge. *Bull. Soc. Chim.* **1965**, *9*, 2649−2652.
(48) Ribéreau-Gayon, P. Le dosage des composés phénoliques totaux dans les vins rouges. *Chim. Anal.* **1970**, *52*, 627−631.
(49) Walker, T. L.; Morris, J. R.; Threlfall, R. T.; Main, G. L.; Lamikanra, O.; Leong, S. Density separation, storage, shelf life and sensory evaluation of 'Fry' muscadine grapes. *HortScience* **2001**, *36*, 941−945.
(50) Rolle, L.; Giacosa, S.; Gerbi, V.; Novello, V. Comparative study of texture properties, color characteristics, and chemical composition of ten white table-grape varieties. *Am. J. Enol. Vitic.* **2011**, *62*, 49−56.
(51) Talmadge, K. W.; Keegstra, K.; Bauer, W. D.; Albersheim, P. The structure of plant cell walls: I. The macromolecular components of the walls of suspension-cultured sycamore cells with a detailed analysis of the pectic polysaccharides. *Plant Physiol.* **1973**, *51*, 158−173.
(52) Fernandes, J. C.; García-Angulo, P.; Goulao, L. F.; Acebes, J. L.; Amâncio, S. Mineral stress affects the cell wall composition of grapevine (Vitis vinifera L.) callus. *Plant Sci.* **2013**, *205−206*, 111−120.
(53) Updegraff, D. M. Semimicro determination of cellulose inbiological materials. *Anal. Biochem.* **1969**, *32*, 420−424.
(54) Saeman, J. F.; Moore., W. E.; Millet, M. A. Sugar units present. Hydrolysis and quantitative paper chromatography. In CarbohydrateChemistry. *Cellulose*; Whistler, R. L., Ed.; Academic Press: New York, 1963; , Vol. 3, pp 54−69.
(55) Dische, Z. General color reactions. In *Carbohydrate chemistry*; Whistler, R. L., Ed. Academic: New York, 1962; pp 477−512.
(56) Hatfield, R. D.; Jung, H. J. G.; Ralph, J.; Buxton, D. R.; Weimer, P. J. A Comparison of the insoluble residues produced by the klason lignin and acid detergent lignin procedures. *J. Sci. Food Agric.* **1994**, *65*, 51−58.
(57) Selvendran, R. R.; Oneill, M. A. Isolation and analysis of cell-walls from plant-material. *Method Biochem Anal* **1987**, *32*, 25−153.
(58) Blumenkrantz, N.; Asboe-Hansen, G. New method for quantitative determination of uronic acids. *Anal. Biochem.* **1973**, *54*, 484−9.
(59) Albersheim, P.; Nevins, D. J.; English, P. D.; Karr, A. A method for the analysis of sugars in plant cell-wall polysaccharides by gas-liquid chromatography. *Carbohydr. Res.* **1967**, *5*, 340−345.

DOI: 10.1021/jf505169z
J. Agric. Food Chem. 2015, 63, 3951−3961

(60) Fasoli, M.; Dal Santo, S.; Zenoni, S.; Tornielli, G. B.; Farina, L.; Zamboni, A.; Porceddu, A.; Venturini, L.; Bicego, M.; Murino, V.; Ferrarini, A.; Delledonne, M.; Pezzotti, M. The grapevine expression atlas reveals a deep transcriptome shift driving the entire plant into a maturation program. *Plant Cell* **2012**, *24*, 3489−3505.
(61) Coito, J. L.; Rocheta, M.; Carvalho, L.; Amâncio, S. Microarray-based uncovering reference genes for quantitative real time PCR in grapevine under abiotic stress. *BMC Res. Notes* **2012**, *5*, 220.
(62) Saeed, A. I.; Sharov, V.; White, J.; Li, J.; Liang, W.; Bhagabati, N.; Braisted, J.; Klapa, M.; Currier, T.; Thiagarajan, M.; Sturn, A.; Snuffin, M.; Rezantsev, A.; Popov, D.; Ryltsov, A.; Kostukovich, E.; Borisovsky, I.; Liu, Z.; Vinsavich, A.; Trush, V.; Quackenbush, J. TM4: A free, open-source system for microarray data management and analysis. *Biotechniques* **2003**, *34*, 374.
(63) Rohlf, F. J. NTSYSpc: Numerical Taxonomy System, ver. 2.20; Exeter Publishing, Ltd: Setauket, NY, 2008.
(64) Chaves, M. M.; Santos, T. P.; Souza, C. R.; Ortuño, M. F.; Rodrigues, M. L.; Lopes, C. M.; Maroco, J. P.; Pereira, J. S. Deficit irrigation in grapevine improves water-use efficiency while controlling vigour and production quality. *Ann. Appl. Biol.* **2007**, *150*, 237−252.
(65) Chaves, M. M.; Zarrouk, O.; Francisco, R.; Costa, J. M.; Santos, T.; Regalado, A. P.; Rodrigues, M. L.; Lopes, C. M. Grapevine under deficit irrigation: hints from physiological and molecular data. *Ann. Bot.* **2010**, *105*, 661−676.
(66) Flexas, J.; Galmés, J.; Gallé, A.; Gulías, J.; Pou, A.; Ribas-Carbo, M.; Tomàs, M.; Medrano, H. Improving water use efficiency in grapevines: potential physiological targets for biotechnological improvement. *Aust. J. Grape Wine Res.* **2010**, *16*, 106−121.
(67) Zsófi, Z.; Villangó, S.; Pálfi, Z.; Tóth, E.; Bálo, B. Texture characteristics of the grape berry skin and seed (Vitis vinifera L. cv. Kékfrankos) under postveraison water deficit. *Sci. Hortic.* **2014**, *172*, 176−182.
(68) Bucchetti, B.; Matthews, M. A.; Falginella, L.; Peterlunger, E.; Castellarin, S. D. *Sci. Hortic.* **2011**, *128*, 297−305.
(69) Schultz, H. R.; Stoll, M. Some critical issues in environmental physiology of grapevines: future challenges and current limitations. *Aust. J. Grape Wine Res.* **2010**, *16*, 4−24.
(70) Olle, D.; Guiraud, J. L.; Souquet, J. M.; Terrier, N.; Ageorges, A.; Cheynier, V.; Verries, C. Effect of pre- and post-veraison water deficit on proanthocyanidin and anthocyanin accumulation during Shiraz berry development. *Aust. J. Grape Wine Res.* **2011**, *17*, 90−100.
(71) Mazza, G. Anthocyanins in grapes and grape products. *Crit. Rev. Food Sci. Nutr.* **1995**, *35*, 341−371.
(72) Rolle, L.; Torchio, F.; Ferrandino, A.; Guidoni, S. Influence of wine-grape skin hardness on the kinetics of anthocyanin extraction. *Int. J. Food Prop.* **2012**, *15*, 249−261.
(73) Rolle, L.; Torchio, F.; Zeppa, G.; Gerbi, V. Relationship between skin break force and anthocyanin extractability at different ripening stages. *Am. J. Enol. Viticult.* **2009**, *60*, 93−97.
(74) Rolle, L.; Torchio, F.; Cagnasso, E.; Gerbi, V. Evolution of mechanical variables of winegrapes for icewine production during on-vine drying. *Ital. J. Food Sci.* **2010**, *22*, 143−149.
(75) Rolle, L.; Gerbi, V.; Schneider, A.; Spanna, F.; Río Segade, S. Varietal Relationship between Instrumental Skin Hardness and Climate for Grapevines (Vitis vinifera L.). *J. Agric. Food Chem.* **2011**, *59*, 10624−10634.
(76) Río Segade, S.; Vázquez, E. S.; Orriols, I.; Giacosa, S.; Rolle, L. Possible use of texture characteristics of winegrapes as markers for zoning and their relationship with anthocyanin extractability index. *Int. J. Food Sci. Technol.* **2011**, *46*, 386−394.
(77) Lerouxel, O.; Cavalier, D. M.; Liepman, A. H.; Keegstra, K. Biosynthesis of plant cell wall polysaccharides — a complex process. *Curr. Opin. Plant Biol.* **2006**, *9*, 621−630.
(78) Harholt, J.; Suttangkakul, A.; Scheller, H. V. Biosynthesis of pectin. *Plant Physiol.* **2010**, *153*, 384−395.
(79) Tang, H. R.; Belton, P. S.; Ng, A.; Ryden, P. C-13 MAS NMR studies of the effects of hydration on the cell walls of potatoes and Chinese water chestnuts. *J. Agric. Food Chem.* **1999**, *47*, 510−517.
(80) Moore, J. P.; Nguema-Ona, E.; Chevalier, L.; Lindsey, G. G.; Brandt, W. F.; Lerouge, P.; Farrant, J. M.; Driouich, A. Response of the leaf cell wall to desiccation in the resurrection plant Myrothamnus flabellifolius. *Plant Physiol.* **2006**, *141*, 651−662.
(81) Rolle, L.; Río Segade, S.; Torchio, F.; Giacosa, S.; Cagnasso, E.; Marengo, F.; Gerbi, V. Influence of grape density and harvest date on changes in phenolic composition, phenol extractability indices, and instrumental texture properties during ripening. *J. Agric. Food Chem.* **2011**, *59*, 8796−8805.
(82) Torchio, F.; Cagnasso, E.; Gerbi, V.; Rolle, L. Mechanical properties, phenolic composition and extractability indices of Barbera grapes of different soluble solids contents from several growing areas. *Anal. Chim. Acta* **2010**, *660*, 183−189.
(83) Peaucelle, A.; Braybrook, S.; Höfte, H. Cell wall mechanics and growth control in plants: the role of pectins revisited. *Front. Plant Sci.* **2012**, 3.10.3389/fpls.2012.00121
(84) Jolie, R. P.; Duvetter, T.; Van Loey, A. M.; Hendrickx, M. E. Pectin methylesterase and its proteinaceous inhibitor: a review. *Carbohydr. Res.* **2010**, *345*, 2583−2595.
(85) Zoccatelli, G.; Zenoni, S.; Savoi, S.; Dal Santo, S.; Tononi, P.; Zandonà, V.; Dal Cin, A.; Guantieri, V.; Pezzotti, M.; Tornielli, G. B. Skin pectin metabolism during the postharvest dehydration of berries from three distinct grapevine cultivars. *Aust. J. Grape Wine Res.* **2013**, *19*, 171−179.
(86) Fry, S. C.; Smith, R. C.; Renwick, K. F.; Martin, D. J.; Hodge, S. K.; Matthews, K. J. Xyloglucan endotransglycosylase, a new wall-loosening enzyme-activity from plants. *Biochem. J.* **1992**, *282*, 821−828.
(87) Rose, J. K. C.; Braam, J.; Fry, S. C.; Nishitani, K. The XTH family of enzymes involved in xyloglucan endotransglucosylation and endohydrolysis: Current perspectives and a new unifying nomenclature. *Plant Cell Physiol.* **2002**, *43*, 1421−1435.
(88) Nishitani, K. T.; Tominaga, R. Endo-xyloglucan transferase, a novel class of glycosyltransferase that catalyses transfer of a segment of xyloglucan molecule to another xyloglucan molecule. *J. Biol. Chem.* **1992**, *267*, 21058−21064.
(89) Brummell, D. A.; Harpster, M. H. Cell wall metabolism in fruit softening and quality and its manipulation in transgenic plants. *Plant Mol. Biol.* **2001**, *47*, 311−40.
(90) Cabanne, C.; Doneche, B. Changes in polygalacturonase activity and calcium content during ripening of grape berries. *Am. J. Enol. Viticult.* **2001**, *52*, 331−335.
(91) Silacci, M. W.; Morrison, J. C. Changes in pectin content of Cabernet Sauvignon grape berries during maturation. *Am. J. Enol. Viticult.* **1990**, *41*, 111−115.
(92) Goulao, L. F.; Fernandes, J. C.; Lopes, P.; Amâncio, S. Tackling the Cell Wall of the Grape Berry. In *The biochemistry of the grape berry*; Gerós, H. C., Delrot, S., Eds.; Bentham Science Publishers: 2012; pp 172−193.
(93) Sampedro, J.; Cosgrove, D. J. The expansin superfamily. *Genome Biol.* **2005**, *6*.242 10.1186/gb-2005-6-12-242
(94) Brummell, D. A.; Harpster, M. H.; Civello, P. M.; Palys, J. M.; Bennett, A. B.; Dunsmuir, P. Modification of expansin protein abundance in tomato fruit alters softening and cell wall polymer metabolism during ripening. *Plant Cell* **1999**, *11*, 2203−2216.

DOI: 10.1021/jf505169z
J. Agric. Food Chem. 2015, 63, 3951−3961

used it as control because it underwent the same transformation steps as the PGIP plants. Neither PGIP nor NS plants show any significant difference in morphology and growth from the untransformed plants[11] (*T. aestivum* cv. Bobwhite).

Infection Experiments. Wheat seeds were surface-sterilized with sodium hypochlorite (0.5% v/v) for 20 min and then rinsed thoroughly in sterile water. Plants were grown in single pots at 18−23 °C, with a 14 h light/10 h dark photoperiod (300 μE m^{-2} s^{-1}).

At least 12 plants of each genotype (PGIP and NS plants) were subjected to five different infection experiments (corresponding to five biological replicates, hereafter named Fg-I−Fg-V) with *F. graminearum* using a point inoculation method. A 20 μL conidial suspension (5×10^4 conidia mL^{-1}) supplemented with 0.1% Tween-20 was pipetted directly through the glumes of two opposite central spikelets of a primary spike of flowering wheat plants (Zadoks stage 68). Infected spikes were covered with plastic bags for 2 days to maintain high humidity. Disease symptoms were assessed by counting the number of visually diseased spikelets over the following 18 days and by relating the diseased spikelets to the total number of spikelets of the respective head. These data were expressed as a percentage of symptomatic spikelets.

All seeds from the primary infected spikes of PGIP and NS plants and those from secondary mock-infected culms from each experiment were collected, and each group was pooled to obtain whole-grain flour corresponding to the four groups taken into consideration: PGIP seeds infected (PGIP-I) and not infected (PGIP-NI) and NS seeds infected (NS-I) and not infected (NS-NI).

Parameters Related to Yield, Fungal Biomass, DON Content, and Total Starch. Thousand kernel weight (TKW) was used as a yield indicator, along with kernel yield per spike (KYPS) and the number of kernels per spike (NKPS).

All mature kernels of each PGIP and NS plant obtained from each experiment were pooled to make whole wheat flour and used in the subsequent analyses.

Quantification of fungal biomass was performed by qPCR assay for the *Tri6* gene with the primers Tri6_10F and Tri6_4R.[12,13] Briefly, total DNA from whole flour was extracted with DNeasy plant mini kit (Qiagen) according to the manufacturer's instructions. qPCR experiments were performed using the iCycler (Bio-Rad Laboratories) and the master mix iQSYBR Green Supermix (Bio-Rad Laboratories) containing the fluorogenic SYBER Green I DNA binding dye. The actin wheat gene (accession no. AB181991) was used as housekeeping gene for the quantification of plant DNA, extracted from flour. The specificity of the primers was verified by nucleotide sequence of the amplicon.

DON was determined by immune-affinity cleanup and reverse phase HPLC. Briefly, 0.2 g aliquots of finely ground sample was extracted by shaking with 5 mL of 5% (w/v) solution of polyethylene glycol 8000/water for 30 min in the dark. Extracts were filtered by using Whatman no. 1 (Whatman International Ltd., Maidstone, UK) paper filters. A further filtration step was performed with glass fiber filters (VICAM, Watertown, MA, USA). For each sample, 250 μL of the filtrate was eluted in a DONtest (VICAM) immune-affinity column according to the manufacturer's instructions. DON was then eluted with 1.5 mL of HPLC grade methanol (Sigma-Aldrich, Milan, Italy) and collected in a 2 mL microcentrifuge tube. The solvent was evaporated under a gentle nitrogen stream at 40 °C in the dark; the dry residue was then recovered with 500 μL of mobile phase and transferred to an autosampler vial. The HPLC analysis was performed using a SpectraSystem (Thermo Separation Product, Riviera Beach, FL, USA) equipped with a reverse-phase column (Discovery C_{18} 4.6 mm i.d., 150 mm, 5 μm; Supelco, Bellefonte, PA, USA). Samples and standards were injected (100 μL) in duplicate, and the isocratic elution was performed at 30 °C. An acetonitrile/water (10:90) mixture pumped at 0.8 mL/min was used as mobile phase. DON was detected using a SpectraSystem UV6000 diode array detector (Thermo Separation Product) set at 218 nm. In those conditions, DON eluted at 6.1 ± 0.1 min. The area peak integration and data analyses were performed using the ChromQuestTM 3.0 software package (Thermo-Quest Inc., San Jose, CA, USA). The content of DON, expressed as micrograms per gram, was calculated by performing multiple six-point calibrations in the range of 0.016−1.024 ng/mL ($R^2 \geq 0.996$) using a commercial standard (Sigma-Aldrich) preliminarily diluted in HPLC grade acetonitrile. To check the accuracy of the method, recovery experiments were performed by analyzing spiked control flour ($n = 5$; from 0.1 to 2.5 μg DON/kg) as described above. Mean recovery of 91.1% was obtained. According to the 32645 Norma of the German institute for standardization,[14] the limit of detection (LOD) was estimated to be 0.017 μg DON/g.

Total starch content was determined using a Total Starch Amyloglucosidase/α-Amylase Assay Kit (Megazyme International Ireland Ltd., Bray, Ireland).

Gluten Proteins Analysis. Electrophoretic patterns of gliadins and glutenin subunits were analyzed by performing three technical replicates for each of the five biological replicates of the four groups: PGIP-I, PGIP-NI, NS-I, NS-NI.

Gliadins were extracted from whole-grain flour by keeping samples for 2 h at room temperature with a buffer containing 10% (v/v) dimethylformamide in a 1:10 (mg:μL) ratio. After centrifugation at 13000 rpm for 10 min, aliquots (5.5 μL) of the supernatants were loaded on acid PAGE (aluminum lactate buffer, pH 3.2), as reported in Khan et al.,[15] with minor modifications.

With regard to glutenin subunits, they were extracted from the pellets remaining after the previous gliadin extraction, by using 80 mM Tris-HCl, pH 8.5, 50%, 1-propanol, and 1% DTT, in a ratio of 1:5 (mg:μL), for 30 min at 65 °C. After a centrifuge step as above-described, the supernatants were alkylated with 1.4% (v/v) 4-vinylpirydine for 30 min at 65 °C. The proteins were successively precipitated overnight in 1 mL of cold acetone and centrifuged as above. The dried protein pellets were dissolved in a buffer containing 70 mM Tris-HCl, pH 6.8, 2% SDS, 10% glycerol, 0.02% pyronine Y, and 1% DTT, with the same volume used for extraction, centrifuged as above, and aliquots (5 μL) of the supernatant were separated by SDS-PAGE. The main gel was *T* (acrylamide concentration) 12, *C* (cross-linking concentration) 1.28, and the stacking gel was *T* 3.67, *C* 2.68. An SE 600 apparatus (Hoefer) was used. Run was performed at 30 mA per gel at 10 °C. The electrophoresis was stopped 45 min after the tracking dye reached the bottom of the gel. All of the gels were stained with Coomassie BBR 250 (Sigma). Densitometric analyses of total gliadins and of HMW-GS and of B-type LMW-GS were performed with the image software 1D (Kodak).

Total gluten proteins, replicated three times for each sample, were extracted from whole grain flour with 80 mM Tris-HCl, pH 8.5, in 50% 1-propanol and 1% DTT, in 1:20 (mg:μL) ratio for 30 min at 65 °C. After centrifugation at 13000 rpm for 10 min, supernatants were recovered, and with 1.4% 4-vinylpyridine was added for 30 min at 65 °C. The proteins were precipitated and dissolved as described above. Three aliquots of each extracted sample (5.0, 5.5, and 6 μL) were loaded to verify the appropriate loading amount, thus avoiding possible saturation problems. Separation was performed by SDS-PAGE as described above. Three independent SDS-PAGE experiments were run for each biological replicate. Densitometric analyses of HMW-GS (subunits A), LMW-GS (subunits B), and gliadins and gliadin-like LMW-GS (subunits C) were performed with image software Labimage (Kapelan Bio-Imaging, Germany). Outliers falling beside the range of linearity were excluded from the densitometric analysis. The ratios A/B and A/B + C were calculated, as well as the comparison among the sums A + B + C in the different samples.

Metabolic Proteins Analysis. Metabolic seed proteins were extracted according to the method of Hurkman et al.[16] Briefly, flour (150 mg) was suspended in 600 μL of cold KCl buffer (50 mM Tris-HCl, 100 mM KCl, 5 mM EDTA, pH 7.8). The suspension was incubated on ice for 5 min with intermittent mixing and centrifuged (14500*g*, 15 min, 4 °C). The KCl-soluble fraction was collected, and 5 volumes (v/v) of cold 0.1 M ammonium acetate in methanol were added. Following incubation overnight at −20 °C, the methanol-insoluble fraction was pelleted by centrifugation as above. The pellet (containing metabolic proteins) was rinsed with cold acetone, dried, and stored at −20 °C until further use. The 2-D quant Kit Assay (GE Healthcare) was used to have an accurate estimation of protein

DOI: 10.1021/jf506003t
J. Agric. Food Chem. 2015, 63, 3962−3969

amounts. The quality of extracted proteins was checked by SDS-PAGE and classical Coomassie staining,[17] as reported in Laino.[18]

DIGE was initially performed by the classical three-dye scheme, according to the procedure reported in Di Carli et al.,[19] and then we confirmed these data by applying a two-dye scheme, which leads to less noise in the protein analyses, which results in more reproducible results than the three-dye system.[20] In this latter case, metabolic proteins were dissolved in 500 μL of lysis buffer (8 M urea, 10 mM Tris-HCl, 5 mM magnesium acetate, pH 8.8), and the impurities were removed using a 2-D Clean-Up kit (GE Healthcare) following the manufacturer's procedures. Samples were eventually solubilized again in lysis buffer to a final protein concentration between 5.5 and 7.0 mg/mL. Samples were labeled using the fluorescent cyanine dyes developed for DIGE (GE Healthcare) following the manufacturer's recommended protocols. Fifty micrograms of protein was labeled with 400 pmol of amine reactive cyanine dyes, freshly dissolved in anhydrous dimethylformamide. The labeling reaction was incubated on ice in the dark for 30 min, and the reaction was terminated by the addition of 10 nmol of lysine. Equal volumes of 2× sample buffer (7 M urea, 2 M thiourea, 4% CHAPS, 20 mg/mL DTT, and 2% Pharmalytes IPG 3−10NL) were added to each of the labeled protein samples, and the two samples were mixed. Rehydration buffer (7 M urea, 2 M thiourea, 4% CHAPS, 2 mg/mL DTT, and 1% Pharmalytes IPG 3−10 NL) was added to make up the volume to 450 μL prior to IEF.

Nonlinear IPG strips (24 cm long), pH 3−10 (GE Healthcare), were rehydrated with CyDye-labeled samples for 12 h at 20 °C (room temperature). IEF was performed in a IPGphor II apparatus (GE Healthcare) for a total of 92 kVh (200 V for 8 h, 300 V for 3 h, 3500 V 30 min in gradient, 3500 V 3.5 h in gradient, 8000 V 2.30 h in gradient, 8000 V 8 h) at 20 °C. Prior to SDS-PAGE, the strips were equilibrated first for 15 min in 100 mM Tris, pH 6.8, 30% glycerol, 8 M urea, 1% SDS, 1% DTT, and 0.2 mg/mL bromophenol blue and then for a further 10 min in 100 mM Tris, pH 6.8, 30% glycerol, 8 M urea, 1% SDS, 2.5% IAA, and 0.2 mg/mL bromophenol blue on a rocking table. The strips were loaded onto 24 cm 15% polyacrylamide gel, pH 8.8, with about 1 cm of stacker gel (5% polyacrylamide, pH 6.8). The strips were overlaid with 1% agarose in SDS running buffer containing 5 mg of bromophenol blue. The gels were run in an Ettan Twelve apparatus (GE Healthcare) at 5 W/gel for 15 min and then at 20 W/gel at 15 °C. A running buffer of 25 mM Tris, pH 8.3, 192 mM glycine, and 0.1% SDS was used.

Labeled proteins were visualized using a Typhoon 9410 imager (GE Healthcare). The Cy3 images were scanned using a 532 nm laser and a 580 nm band-pass (BP) 30 emission filter. Cy5 images were scanned using a 633 nm laser and a 670 nm BP30 emission filter. All gels were scanned at 100 μm resolution. The PMT was set to ensure a maximum pixel intensity between 50000 and 80000 pixels.

The experimental design was performed to have an appropriate biological variation analysis (BVA) with a total of 20 maps in which both the samples (labeled with Cy3) and the pool or internal standard (a mixture of equal amounts of metabolic protein extracts from each sample) labeled with Cy5 were represented.

Gel analyses were performed using the software DeCyder BVA V5.0 (GE Healthcare). Data were normalized within the software using a ratiometric approach, and a $\log_{10}$ transformation was used on the standardized abundance to stabilize variance. The estimated number of spots for each codetection was set to 2500. Student's t test (p) was calculated, along with the q value, the latter via a point-and-click tool provided by Storey and Tibshirani.[21] Principal component analysis (PCA) of the $\log_{10}$ standard abundance of the spots matched on the 80% of the maps was performed using soft independent modeling of class analogy (SIMCA-P, Umetrics).

The spots of interest were selected according to the following criteria: t test (p) <0.01, fold change >1.2, and spot appearance on at least 80% of the total maps.

The gel spots were excided manually from two preparative silver-stained gels and identified by LC-ESI-ORBITRAP. In-gel reduction and alkylation were carried out using DTT and iodoacetamide, respectively.

Digestion with trypsin was performed according to the method of Coulthurst et al.[22] For LC-MS/MS experiments an Eksigent NanoLC-1D Plus (Eksigent Technologies, Dublin, CA, USA) an HPLC system coupled to an LTQ Orbitrap mass spectrometer (ThermoFisher, Waltham, MA, USA) was used. Separation of peptides was performed by reverse-phase chromatography employing a flow rate of 300 nL/min and an LC Packings (Dionex, Sunnyvale, CA, USA) PepMap 100 column (C_{18}, 75 μm i.d. × 150 mm, 3 μm particle size). Peptides were loaded onto a precolumn (Dionex Acclaim PepMap 100 C18, 5 μm particle size, 100A, 300 μm i.d. × 5 mm) with 0.1% formic acid for 5 min at a flow rate of 10 μL/min.

After elution of peptides from the precolumn onto the analytical column, an elution gradient of 5−50% B in 50 min was employed, where solvent A was 0.1% formic acid in water and solvent B was 0.1% formic acid in acetonitrile. The LC eluant was sprayed into the mass spectrometer by means of a New Objective nanospray source. All m/z values of eluting ions were measured in the Orbitrap mass analyzer, set at a resolution of 7500. Peptide ions with charge status of 2+ and 3+ were then isolated and fragmented in the LTQ linear ion trap by collision-induced dissociation, and MS/MS spectra were acquired. Postrun, the data were processed using Bioworks Browser (version 3.3.1 SP1, ThermoFisher). Briefly, all MS/MS data were converted to dta (text) files using the Sequest Batch Search tool (within Bioworks). The data files were converted to a single mgf file using a SSH script in the SSH Secure Shell Client program (version 3.2.9 Build 283, SSH Communications Corp.). These combined files were then submitted to the Mascot search algorithm (Matrix Science, London, UK) and searched against the NCBI-nr database (all entries, *Viridiplantae*, and human database), using a fixed modification of carbamidomethyl and a variable modification of oxidation (M).

RESULTS AND DISCUSSION

FHB Symptoms on Transgenic and Control Plants. Five independent infection tests were performed by using conidia of *F. graminearum*. FHB disease symptoms usually appeared 3 days post infection (dpi), and the spread of the disease was visually examined for 18 dpi. PGIP plants showed a significant reduction of FHB symptoms compared to control NS plants. In particular, at 18 dpi the average reduction of FHB symptoms in the five experiments was about 35% compared to control plants (Figure 1). Data relative to each experiment are reported in the Supporting Information (nr. 1).

One of the above experiments included also the untransformed cv. Bobwhite. At 18 dpi, statistical analysis revealed that the differences observed between NS-I and the untransformed cv. Bobwhite were not significant, whereas they

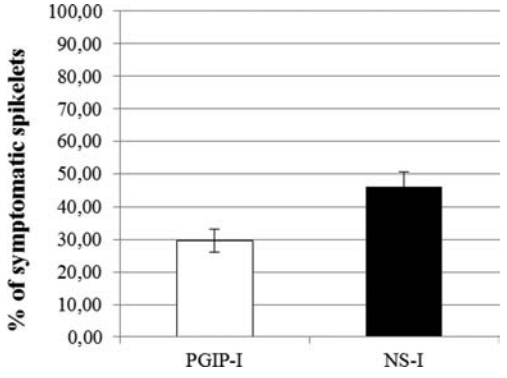

Figure 1. Evaluation of the spread of FHB symptoms in PGIP-I and NS-I plants relative to the five experiments, obtained by combining data collected at 18 dpi. Disease symptoms were evaluated as a percentage of visually diseased spikelets over the total number of spikelets.

DOI: 10.1021/jf506003t
J. Agric. Food Chem. 2015, 63, 3962−3969

were significant between PGIP-I and both NS-I and the untransformed cv. Bobwhite (data not shown).

Parameters Related to Yield. It is noteworthy that seed yield is strongly affected by *F. graminearum* infection. For this reason, we evaluated this aspect by analyzing kernels obtained from PGIP plants and NS plants, both infected and mock-inoculated (not infected). The parameters taken into consideration were the number of kernels per spike (NKPS), the kernel yield per spike (KYPS), and the thousand kernel weight (TKW). PGIP plants and NS plants, both infected and not infected, were not significantly different in regard to NKPS (Figure 2a). KYPS and TKW were significantly different only between infected and not infected NS plants (NS-I vs NS-NI), being higher in NS-NI plants (Figure 2b,c).

These data indicate that constitutive expression of PvPGIP2 in PGIP plants does not have any detrimental effect on parameters related to seed yield; conversely, their higher tolerance to *F. graminearum* infection has a positive effect on grain productivity.

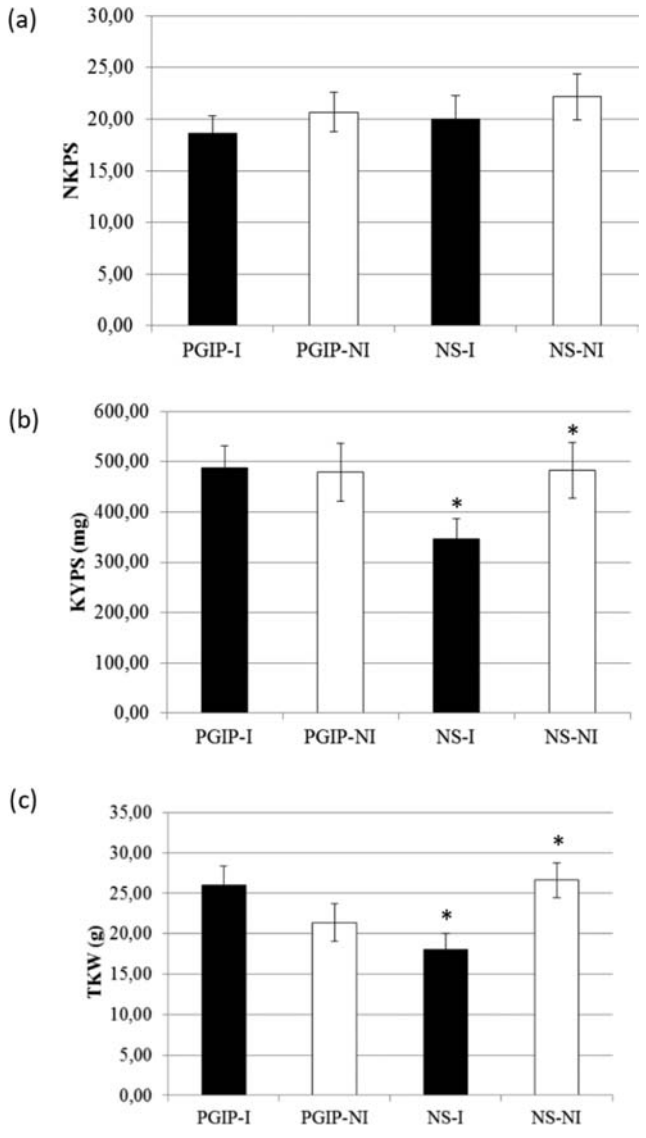

Figure 2. Parameters related to yield (a) NKPS, number of kernels per spike; (b) KYPS, kernel yield per spike (mg); and (c) TKW, thousand kernel weight (g). Data represent means ± standard error of five experiments. (*) In (b) and (c) the difference between NS-I and NS-NI plants is significantly different ($P \leq 0.01$).

Fungal Biomass, DON Content, and Total Starch Content. To verify whether the reduced FHB symptoms of the PGIP plants were associated with a reduced accumulation of fungal biomass in the caryopses of PGIP plants, we performed qPCR analyses with primers specific for the fungal *Tri6* gene,[11] on total DNA extracted from whole-grain flour. Because of limited material, these analyses were performed only on the biological replicates Fg-III and Fg-IV. The results revealed about 4-fold reduced fungal biomass in the flour of infected PGIP-I plants (average value = 0.245 ± 0.007) compared to the flour of infected control NS-I plants (Figure 3a).

The whole-grain flours of experiments Fg-III and Fg-IV were also used to evaluate the content of DON. Similarly to what was observed for the other parameters analyzed, DON accumulation was significantly lower ($p < 0.01$) in the whole-grain flour from PGIP plants as compared to that from NS plants. The results from both experiments showed about 57% reduction of DON content in the flour from infected PGIP-I plants (average = 23 μg/g ± 3.8) compared to the flour from infected control plants (NS-I) (average value = 54 μg/g ± 7.7) (Figure 3b).

Flour from experiments Fg-III and Fg-IV was also used to evaluate the total starch content. These analyses showed a significant difference ($p < 0.05$) between NS-NI and NS-I plants, with the latter sample showing a reduced total starch content. Similarly, a significant difference ($p < 0.05$) was observed between PGIP-I and NS-I plants, with the PGIP-I showing a higher total starch content. No significant difference was observed between NS-NI and PGIP-NI plants or between PGIP-NI and PGIP-I plants (Figure 3c).

Gluten Protein Analysis. Because gluten proteins are the main determinants of dough rheological properties, we verified whether FHB caused an altered pattern of protein accumulation in mature kernels.

Initially we analyzed separated protein fractions to detect better the possible differences in protein accumulation; however, densitometric analyses of gliadin and glutenin patterns did not show any significant difference between the four groups of samples (by comparison of either total amounts or the ratios among protein classes, Supporting Information (nr. 2)). Thus, we decided to analyze also total gluten proteins to avoid possible problems due to the fractionation procedures. In this latter case, only two biological replicates (Fg-III and Fg-IV) were used. Neither of these analyses revealed any significant difference among the four groups of samples by comparing total protein amounts and the ratios among the different protein classes (Supporting Information (nr. 3)).

Metabolic Protein Analysis. A first DIGE experiment was performed according to a three-dye scheme to investigate major protein changes involved during infection with *F. graminearum*. This analysis detected about 2000 protein spots, and any significant differential proteins resulted by considering the false discovery rate (FDR) adjustment of the probability value (data not shown). Thus, a second DIGE experiment based on a two-dye approach was carried out to reduce the higher noise typical of the three-dye approach. The results here reported are those relative to this latter approach.

A total of about 2000 protein spots were detected in this case also (Figure 4). The normalized volumes of the spots present in at least 80% of the total maps were used to perform PCA (Figure 5). The result did not discriminate any clusters among

DOI: 10.1021/jf506003t
J. Agric. Food Chem. 2015, 63, 3962−3969

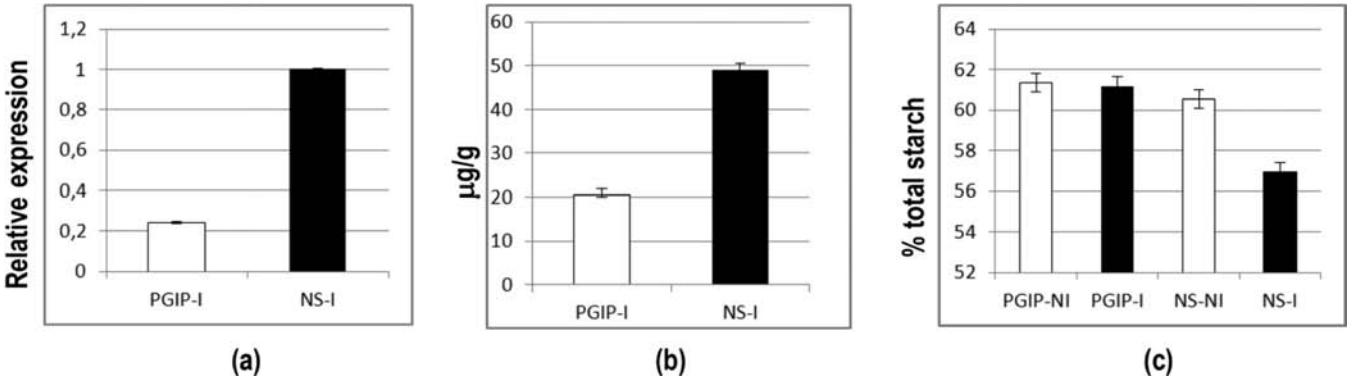

Figure 3. (a) Extent of pathogen contamination as assayed by qPCR; (b) DON content as assayed by RP-HPLC; (c) total starch content as assayed by a total starch amyloglucosidase/α-amylase assay.

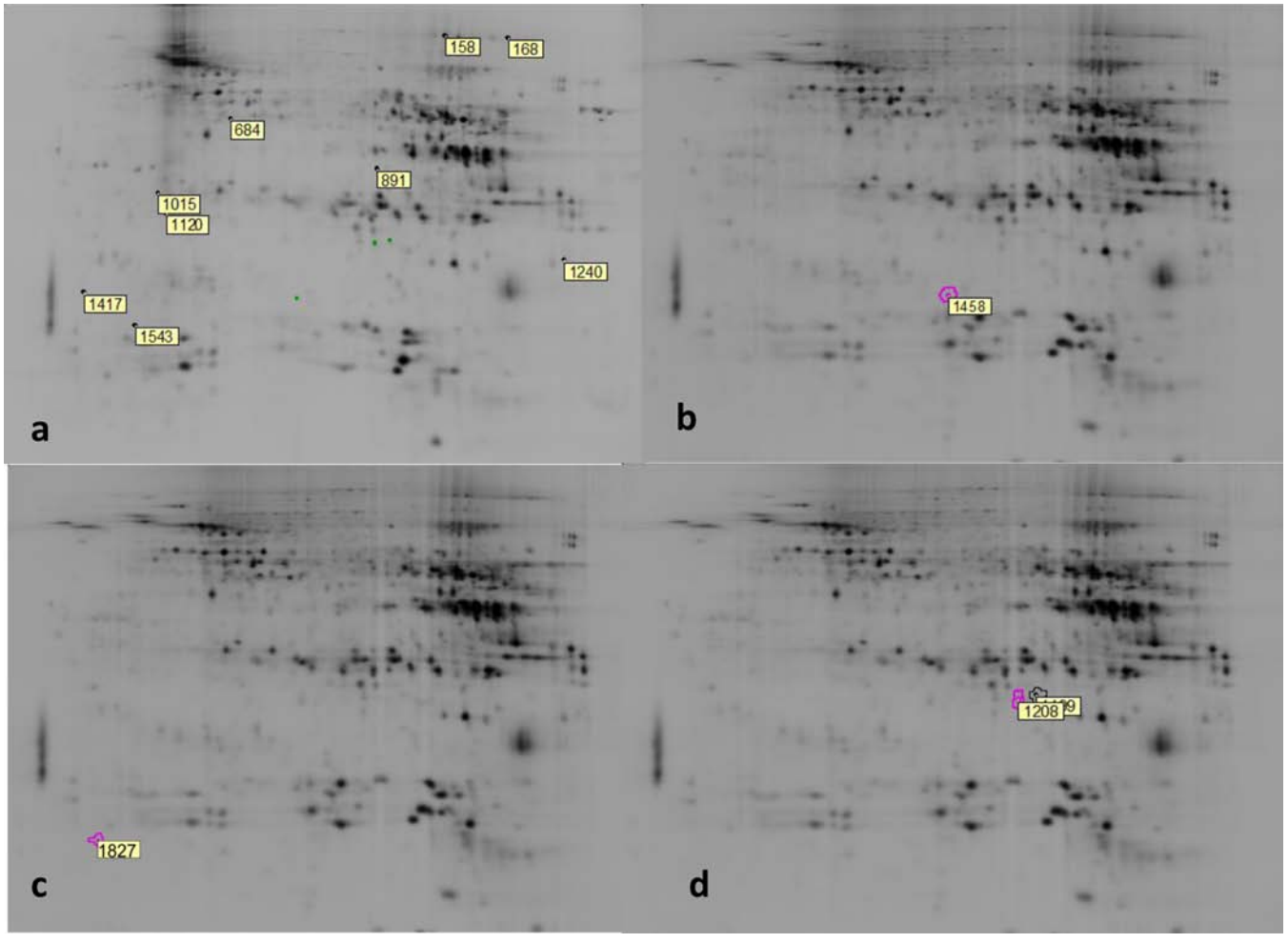

Figure 4. Spots identified as differentially accumulated by comparing NS-NI versus NS-I (a), NS-NI versus PGIP-NI (b), PGIP-NI versus PGIP-I (c), and NS-I versus PGIP-I (d). All of the differential spots represent minor polypeptides, because they are very faint.

the four groups (PGIP-I, PGIP-NI, NS-I, NS-NI), thus showing that they were not clearly differentiated at the protein accumulation level.

The biological variation analysis (BVA) revealed nine spots differentially accumulated in the comparison between NS-NI and NS-I (Figure 4a), one spot in each of the comparisons between NS-NI and PGIP-NI (Figure 4b) and between PGIP-NI and PGIP-I (Figure 4c), and two spots between NS-I and PGIP-I (Figure 4d; Table 1). All of these spots were very faint. The q values calculated for all of the spots were higher than the threshold of confidence (0.05), thus indicating that these spots, considered to be significantly different on the basis of the t test, could be false-positive identifications. However, they were recovered from the gels, digested with trypsin, and submitted to MS-MS analysis, but none of them produced any significant protein identification.

In conclusion, similarly to our previous paper,[9] the present results showed that PGIP-I plants have a significant reduction

DOI: 10.1021/jf506003t
J. Agric. Food Chem. 2015, 63, 3962−3969

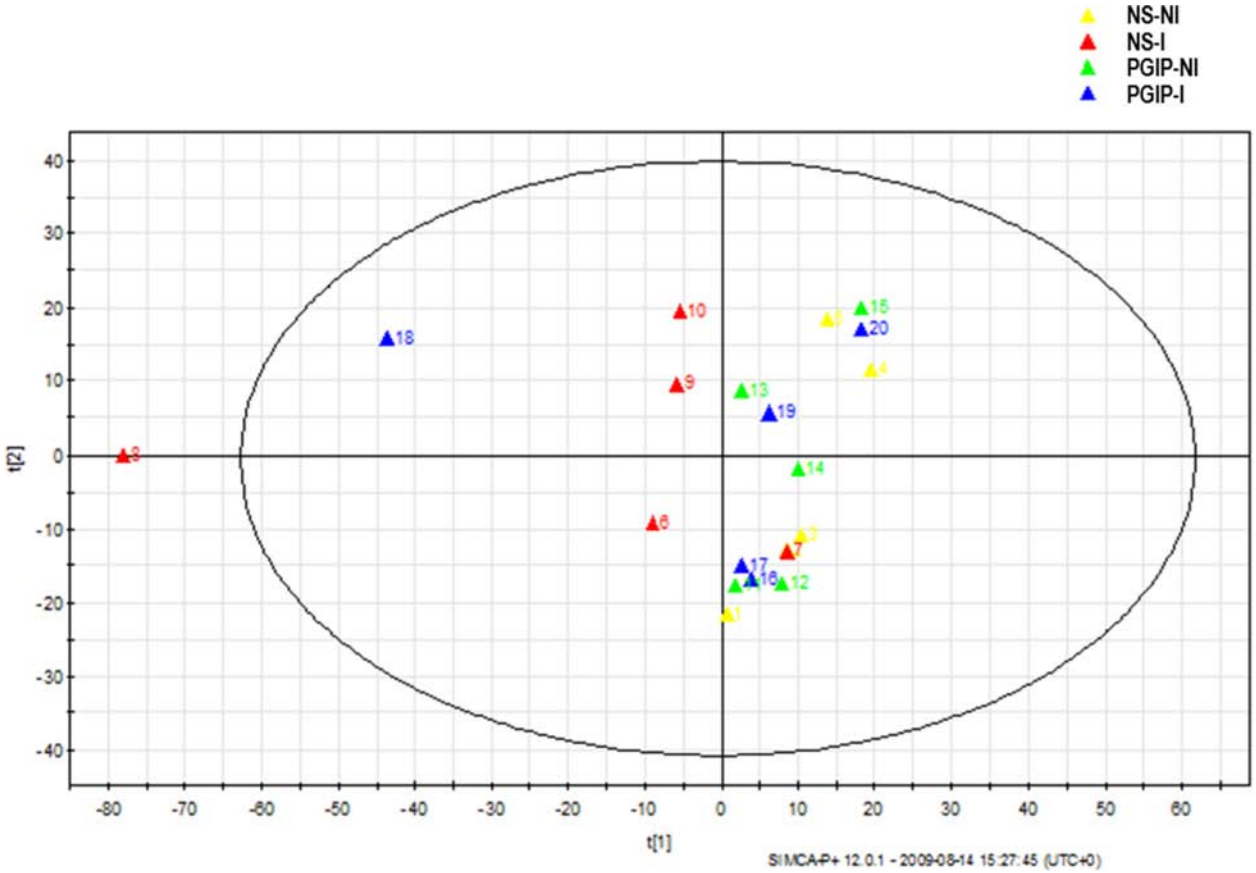

Figure 5. Principal component analysis plot of the log standard abundance of the spots present on 80% of the maps performed using SIMCA-P (soft independent modeling of class analogy, Umetrics). The four groups do not form any cluster, indicating no clear differentiation effects at protein expression level.

Table 1. Differentially Accumulated Polypeptides in the Four Comparisons Performed (Shown in Figure 4)[a]

comparison	spot ID	*t* test (*p*)	fold change	*q* value
NS-NI vs NS-I	1059	0.0049	−2.47	0.1103034
	1240	0.0051	1.84	0.1103034
	1120	0.0053	−1.35	0.1103034
	158	0.0058	1.66	0.1103034
	1417	0.0061	−1.53	0.1103034
	168	0.007	1.91	0.1103034
	684	0.0074	−1.38	0.1103034
	1015	0.0076	−1.44	0.1103034
	891	0.0094	−2.09	0.1103034
	1543	0.02	−4.63	0.1103034
NS-NI vs PGIP-NI	1458	0.0074	−1.21	0,9906046
PGIP-NI vs PGIP-I	1208	0.0083	1.38	0,7894998
	1199	0.014	1.5	0.7894998
NS-I vs PGIP-I	1827	0.0041	1.98	0.8366167

[a]Although the *t* test for these spots is significant, the relative *q* values are higher than the threshold of confidence, indicating possible false identifications.

of FHB symptoms, which was also correlated to a reduced accumulation of fungal biomass in wheat kernels, in comparison to control plants. This reduction had positive consequences on mycotoxin accumulation, because DON content was significantly lower in flour obtained from PGIP-I plants. Moreover, the parameter TKW, indicative of yield, was higher in infected PGIP-I plants, with respect to infected control plants. This difference is probably due to the higher starch content observed in infected PGIP-I plants as compared to NS-I plants. Indeed, the PGIP-I plants did not show any significant difference with the PGIP-NI plants; instead, control plants (NS-I) showed a significant reduction of total starch content. This finding is in agreement with previous studies[23,24] and probably is a consequence of damage to starch granules caused by fungal amylolytic enzymes, although endosperm damage can be quite variable.[25−27]

Interestingly, no significant difference was observed in protein accumulation in PGIP plants, both infected and not infected, in comparison with control plants, with regard to gluten proteins (measured as total gluten proteins and as purified gliadin and glutenin subunits fractions) and metabolic proteins. The latter were analyzed in more detail because this protein fraction is known to contain many allergenic polypeptides, which are usually induced after fungal infection and other stresses.[28]

This result is in agreement with Chetouhi et al.,[29] who made a proteomic survey of the bread wheat susceptible cultivar Recital after *F. graminearum* infection. These authors have taken into consideration three different stages after infection (3 dpi, corresponding to the cell division stage; 7 dpi, corresponding to cell differentiation stage; and 14 dpi, corresponding to grain-filling stage). They measured *F. graminearum* infection by using a RT-PCR approach and evaluated mycotoxin accumulation by measuring the activity of the *FgTrI5* gene (coding for trichodiene synthase, related to mycotoxins biosynthesis). Similarly to what was found in the

DOI: 10.1021/jf506003t
J. Agric. Food Chem. 2015, 63, 3962−3969

present work, they failed to identify any pathogen protein in their proteomic comparison, likely because their amount was not enough to be detected, although the pathogen presence was confirmed by the RT-PCR analysis, and observed that the grain protein pattern was not greatly affected by *F. graminearum* infection, in particular at the latest stage in which they mostly identified a down-regulation of some proteins involved in starch biosynthesis and up-regulation of a protein involved in starch degradation. Similar conclusions were made by Eggert et al.,[30] who, by analyzing the proteome of *Fusarium* infected emmers grown in the field in two different locations, identified only 10 polypeptides differentially accumulated, with a large variation due to the different environments. We made the proteomic comparison on mature dry kernels of a different wheat cultivar, but we also found that the wheat kernel proteome pattern is not severely affected by *F. graminearum* infection.

Taken all together, these results indicate that the expression of PGIP in wheat transgenic plants showing partially bleached spikes after infection with *F. graminearum* decreases the level of infection, as expected, and contributes to prevent yield and starch decreases and to reduce DON accumulation. Moreover, the wheat seed proteome, in both infected and not infected kernels, is not significantly altered by the transgenic PGIP expression.

■ ASSOCIATED CONTENT

Supporting Information

Nr. 1 Evaluation of the spread of FHB symptoms in PGIP-I and NS-I plants relative to each of the five experiments performed; Nr. 2 densitometric values of total gliadins and of total glutenin subunits, along with the ratios between HMW-GS and LMW-GS, calculated on separate gliadin and glutenin fractions, with the relative Student's *t* tests; Nr. 3 densitometric values of total kernel proteins, ratios between HMW-GS and LMW-GS and between HMW-GS and the sum of LMW-GS plus gliadins, calculated on total proteins, with the relative Student's *t* tests. This material is available free of charge via the Internet at http://pubs.acs.org.

■ AUTHOR INFORMATION

Corresponding Authors

(S.M.) Phone: +390761357255. E-mail: masci@unitus.it.
(R.D.) Phone: +390761357323. E-mail: dovidio@unitus.it.

Present Address

[Δ](P.L.) Consiglio per la Ricerca e la sperimentazione in Agricoltura, Genomics Research Centre, Fiorenzuola d'Arda (PC), Italy.

Funding

Research was supported by the Italian Ministry of University and Research (PRIN 2010−2011). P.L. was the recipient of an STMS award from the COST Action FA0603 Plant Proteomics.

Notes

The authors declare no competing financial interest.

■ ACKNOWLEDGMENTS

The "Centro Grandi Attrezzature (CGA)" of Tuscia University is acknowledged for the use of instrumentations.

■ ABBREVIATIONS USED

C, bis(acrylamide) concentration; CWDE, cell wall degrading enzymes; DON, deoxynivalenol; DTT, dithiothreitol; FHB, fusarium head blight; HMW-GS, high molecular weight glutenin subunits; KYPS, kernel yield per spike; LMW-GS, low molecular weight glutenin subunits; NKPS, number of kernels per spike; NS-I, seeds from null segregants (not expressing the PGIP transgene) wheat plants and infected with *F. graminearum*; NS-NI, seeds from null segregants (not expressing the PGIP transgene) wheat plants and NOT infected with *F. graminearum*; PG, polygalacturonase; PGIP, polygalacturonase inhibiting protein; PGIP-I, seeds from PGIP transformed wheat plants and infected with *F. graminearum*; PGIP-NI, seeds from PGIP transformed wheat plants and NOT infected with *F. graminearum*; SDS-PAGE, sodium dodecyl sulfate−polyacrylamide gel electrophoresis; *T*, total concentration of acrylamide and bis(acrylamide) monomer; TKW, thousand kernel weight

■ REFERENCES

(1) Bai, G.-H.; Plattner, R.; Desjardins, A.; Kolb, F. Resistance to fusarium head blight and deoxynivalenol accumulation in wheat. *Plant Breed.* **2001**, *120*, 1−6.

(2) Buerstmayr, H.; Ban, T.; Anderson, J. A. QTL mapping and marker-assisted selection for fusarium head blight resistance in wheat: a review. *Plant Breed.* **2009**, *128*, 1−26.

(3) Juge, N. Plant protein inhibitors of cell wall degrading enzymes. *Trends Plant Sci.* **2006**, *11*, 359−367.

(4) Kikot, G. E.; Hours, R. A.; Alconada, T. M. Contribution of cell wall degrading enzymes to pathogenesis of *Fusarium graminearum*: a review. *J. Basic Microbiol.* **2009**, *49*, 231−241.

(5) Tomassini, A.; Sella, L.; Raiola, A.; D'Ovidio, R.; Favaron, F. Characterization and expression of *Fusarium graminearum* endopolygalacturonases *in vitro* and during wheat infection. *Plant Pathol.* **2009**, *58* (3), 556−564.

(6) De Lorenzo, G.; D'Ovidio, R.; Cervone, F. The role of polygalacturonase-inhibiting proteins (PGIPS) in defense against pathogenic fungi. *Annu. Rev. Phytopathol.* **2001**, *39*, 313−335.

(7) D'Ovidio, R.; Mattei, B.; Roberti, S.; Bellincampi, D. Polygalacturonases, polygalacturonase-inhibiting proteins and pectic oligomers in plant-pathogen interactions. *Biochim. Biophys. Acta, Proteins Proteomics* **2004**, *1696*, 237−244.

(8) Protsenko, M. A.; Buza, N. L.; Krinitsyna, A. A.; Bulantseva, E. A.; Korableva, N. P. Polygalacturonase inhibiting protein is a structural component of plant cell wall. *Biochemistry* **2008**, *73*, 1053−1062.

(9) Ferrari, S.; Sella, L.; Janni, M.; De Lorenzo, G.; Favaron, F.; D'Ovidio, R. Transgenic expression of polygalacturonase-inhibiting proteins in Arabidopsis and wheat increases resistance to the flower pathogen *Fusarium graminearum*. *Plant Biol.* **2012**, *14* (Suppl. 1), 31−38.

(10) Tatham, A. S.; Shewry, P. R. Allergy to wheat and related cereals. *Clin. Exp. Allergy* **2008**, *38*, 1712−1726.

(11) Janni, M.; Sella, L.; Favaron, F.; Blechl, A. E.; De Lorenzo, G.; D'Ovidio, R. The expression of a bean polygalacturonase-inhibiting protein in transgenic wheat confers increased resistance to the fungal pathogen *Bipolaris sorokiniana*. *Mol. Plant−Microbe Interact.* **2008**, *21*, 171−177.

(12) Moscetti, I.; Tundo, S.; Janni, M.; Sella, L.; Gazzetti, K.; Tauzin, A.; Giardina, T.; Favaron, F.; Masci, S.; D'Ovidio, R. Constitutive expression of the xylanase inhibitor TAXI-III delays fusarium head blight symptoms in durum wheat transgenic plants. *Mol. Plant−Microbe Interact.* **2013**, *26* (12), 1464−1472.

(13) Horevaj, P.; Milus, E. A.; Bluhm, B. H. A real-time q PCR assay to quantify *Fusarium graminearum* biomass in wheat kernels. *J. Appl. Microbiol.* **2011**, *111*, 396−406.

(14) Deutsches Institut für Normung (DIN). 32645 Norma − Chemical analysis: Decision limit, detection limit and determination limit under repeatability conditions; Terms, methods, evaluation, 1994.

DOI: 10.1021/jf506003t
J. Agric. Food Chem. 2015, 63, 3962−3969

(15) Khan, K.; Hamada, A. S.; Patek, J. Polyacrylamide gel electrophoresis for wheat variety identification: effect of variables on gel properties. *Cereal Chem.* **1985**, *62*, 310−313.
(16) Hurkman, W. J.; Tanaka, C. K. Extraction of wheat endosperm proteins for proteome analysis. *J. Chromatogr., B: Anal. Technol. Biomed. Life Sci.* **2007**, *849*, 344−350.
(17) Neuhoff, V.; Arold, N.; Taube, D.; Ehrhardt, W. Improved staining of proteins in polyacrylamide gels including isoelectric focusing gels with clear background at nanogram sensitivity using Coomassie Brilliant Blue G-250 and R-250. *Electrophoresis* **1988**, *9*, 255−262.
(18) Laino, P. *Effects of the abiotic and biotic stresses on the wheat proteome*. Ph.D. thesis, Tuscia University, 2010, http://dspace.unitus.it/handle/2067/1007.
(19) Di Carli, M.; Villani, M. E.; Renzone, G.; Nardi, L.; Pasquo, A.; Franconi, R.; Scaloni, A.; Benvenuto, E.; Desiderio, A. Leaf proteome analysis of transgenic plants expressing antiviral antibodies. *J. Proteome Res.* **2009**, *8* (2), 838−848.
(20) Karp, N. A.; Lilley, K. S. Maximising sensitivity for detecting changes in protein expression: experimental design using minimal CyDyes. *Proteomics* **2005**, *5*, 3105−3115.
(21) Storey, J. D.; Tibshirani, R. Statistical significance for genome-wide studies. *Proc. Natl. Acad. Sci. U.S.A.* **2003**, *100* (16), 9440−9445.
(22) Coulthurst, S. J.; Lilley, K. S.; Hedley, P. E.; Liu, H.; Toth, I. K.; Salmond, G. P. DsbA plays a critical and multi-faceted role in the production of secreted virulence factors by the phytopathogen, *Erwinia carotovora* subsp. *atroseptica*. *J. Biol. Chem.* **2008**, *283*, 23739−23753.
(23) Matthaus, K.; Danicke, S.; Vahjen, W.; Simon, O.; Wang, J.; Valenta, H.; Meyer, K.; Strumpf, A.; Ziesenib, H.; Flachowsky, G. Progression of mycotoxin and nutrient concentrations in wheat after inoculation with *Fusarium culmorum*. *Arch. Anim. Nutr.* **2004**, *58*, 19−35.
(24) Siuda, R.; Grabowski, A.; Lenc, L.; Ralcewicz, M.; Spychaj-Fabisiak, E. Influence of the degree of Fusariosis on technological traits of wheat grain. *Int. J. Food Sci. Technol.* **2010**, *45*, 2596−2604.
(25) Dexter, J. E.; Clear, R. M.; Preston, K. R. Fusarium head blight: effect on the milling and baking of some Canadian wheats. *Cereal Chem.* **1996**, *73*, 695−701.
(26) Jackowiak, H.; Packa, D.; Wiwart, M.; Perkowski, J. Scanning electron microscopy of *Fusarium* damaged kernels of spring wheat. *Int. J. Food Microbiol.* **2005**, *98*, 113−123.
(27) Wang, J. H.; Pawelzik, E.; Weinert, J.; Wolf, G. A. Impact of *Fusarium culmorum* on the polysaccharides of wheat flour. *J. Agric. Food Chem.* **2005**, *53*, 5818−5823.
(28) Hoffmann-Sommergruber, K. Plant allergens and pathogenesis-related proteins: what do they have in common? *Int. Arch. Allergy Immunol.* **2000**, *122*, 155−166.
(29) Chetouhi, C.; Bonhomme, L.; Lecomte, P.; Cambon, F.; Merlino, M.; Biron, D. G.; Langin, T. A proteomics survey on wheat susceptibility to *Fusarium* head blight during grain development. *Eur. J. Plant Pathol.* **2015**, *141*, 407−418.
(30) Eggert, K. A.; Zörb, C. B.; Mühling, K. H. B.; Pawelzik, E. A. Proteome analysis of *Fusarium* infection in emmer grains (*Triticum dicoccum*). *Plant Pathol.* **2011**, *60*, 918−928.

DOI: 10.1021/jf506003t
J. Agric. Food Chem. 2015, 63, 3962−3969

min^{-1} in octyl/decyl glycerate.[21] In real matrix, Goula et al. found 0.0012 min^{-1} in tomato pulp at 90 °C[22] and Sharma et al. found 0.0048 min^{-1} in watermelon at the same temperature.[23] Colle et al. found a much higher degradation rate constant at 100 °C (0.095 min^{-1}), but in a formulated tomato and oil emulsion.[24] Activation energies found in model systems were 61 kJ mol^{-1} and 77 kJ mol^{-1}.[21] In real matrix, lycopene activation energies were 19.5 and 26.4 kJ mol^{-1} in tomato and watermelon, respectively.[22,23] Colle et al. found an activation energy of 28 kJ mol^{-1} in tomato pulp/olive oil emulsion. These results show that the kinetic parameters of lycopene degradation are also significantly different as a function of the food system, which could be due to the strong influence of the chemical environment and the inclusion of carotenes in complex structures. To overcome this matrix effect, some authors finally proposed to formulate a juicelike system with controlled composition, but which could be complexified progressively to gain greater insight into the effect of the chemical and structural environment and obtain better accuracy in the kinetic parameters. Zepka et al. designed a cashew apple juice model based on a water and ethanol mixture.[25] A more recent study by Hadjal et al.[34] assessed the degradation kinetics of xanthophylls from blood orange in both real and model matrices. They showed that the degradation rates were the lowest in real juice in comparison to the juicelike model. These authors suggested that phytochemical compounds of juice were able to protect xanthophylls, especially at high temperatures.

Kinetic uniresponse models mentioned above are commonly used because they are robust and useful to predict nutrient loss. Kinetic modeling studies of both carotenoid degradation (oxidation and cleavage) and production of neoformed compounds such as isomers are more limited. This approach implies the use of a more sophisticated kinetic model or mathematical tools such as multiresponse modeling.[26−28] However, knowledge of degradation and production rates could be of great interest to predict nutrient loss as well as neoformed compound production. Indeed, products generated during carotenoid degradation may have positive or negative biological activity. In addition, the knowledge of the impact of temperature on kinetic constants may help technologists improve thermal processes such as pasteurization. In addition to the prediction advantages, this approach could provide insight into the degradation reaction scheme. In particular, the use of multiresponse modeling was used to enhance the comprehension of β-carotene degradation in oils[27] or in orange-fleshed sweet potato.[28] The principle of such an approach is to enable the simultaneous study of analytical and literature results so as to be able to draw up possible observable degradation schemes that could be expressed mathematically. The most probable hypothesis can be chosen by discrimination of the best kinetic model: i.e., the model which presents the closest fit to the experimental data.

Consequently, the objectives of this study were to assess the degradation and isomerization kinetics of lycopene and β-carotene from pink grapefruit during heating, both in their natural matrix (juice) and in three different model systems (buffered water/ethanol basis) without or with the addition of ascorbic acid or naringin to simulate major antioxidant phytochemical compounds of pink grapefruit juice.[1] Moreover, multiresponse modeling has been applied to model simultaneous lycopene/β-carotene loss and isomerization during thermal treatment.

MATERIALS AND METHODS

Grapefruit Juice. South American pink grapefruits (*Citrus paradisi* Macf) purchased in a market were cut in half and squeezed using a domestic juicer (Moulinex Masterchef 470, France). The juice was then filtered through a stainless steel sieve (1 mm). The freshly pressed juice was placed in amber glass bottles under nitrogen and stored at −20 °C until analysis or heat treatment.

Preparation of Juicelike Model Systems. Juicelike model systems were formulated with grapefruit juice carotenoid extract to carry out a degradation test in controlled medium. This extract was formulated with three media, acidified aqueous medium (AM) and acidified aqueous medium supplemented with ascorbic acid (AM+AA) or naringin (AM+NAR); these latter supplements are major citrus juice phytochemicals that could have a protective effect.

Preparation of Carotenoid Extract. The first carotenoid extraction step was performed according to Dhuique-Mayer et al. by blending 80 g of grapefruit juice with an ethanol/hexane mixture (4/3, v/v, 0.1% BHT). The hexane fractions were collected, pooled, and evaporated for 15 min at 20 °C (GeneVac EZ-2 compatible, Suffolk, U.K.). The carotenoid extracts obtained were used to formulate the three model systems.[29]

Formulation of Model Systems. The model system was inspired from that of Zepka et al.[25] It first involved solubilization of carotenoid extracts in ethanol. A pH 3 citrate buffer mixture was added at an ethanol/buffer ratio of 25/75 (v/v). This was called the acid medium (AM). The resulting model system was a very homogeneous and stable cloudy liquid, even at high temperature. This mixture was assumed to be a spontaneous microemulsion, which is typically obtained when mixing hydrophobic molecules dissolved in ethanol with water. For AM+AA medium, the ethanolic carotenoid extract was mixed with citrate buffer supplemented with ascorbic acid in the same proportion (25/75, v/v). For AM+NAR medium, naringin was first dissolved in ethanol and mixed with 75% (v/v) citrate buffer. The amount of naringin and ascorbic acid added were calculated to obtain a content equivalent to that reported in the literature for pink grapefruit juice (300 mg L^{-1} for naringin and 400 mg L^{-1} for ascorbic acid).[1]

Heat Treatment. The kinetics of carotene thermal degradation were assessed at four temperatures: i.e. 60, 75, 90, and 95 °C. These temperatures cover the pasteurization treatment range involving low to high temperature (flash) treatments. For each temperature, 2 mL of grapefruit juice or model medium was heated in sealed 10 mL Pyrex tubes. The tubes were immersed in an oil bath with temperature control (Memmert, Legallais, France). A digital temperature probe (EKT 3001, Heidolph, Germany) fitted to a reference tube was used to measure the medium temperature during the thermal experiments. Five sampling points were selected from 5 to 300 min according to the temperature. Three replicates were done for each temperature. The time for juice to reach the set temperature was less than 4 min, and the cooling time was about 1 min in an ice/water bath. The thermal transient could thus be neglected, and the treatment could be considered isothermal. Each tube was stored under nitrogen at −20 °C until analysis.

HPLC Analysis of Carotenoids. *Sample Preparation.* A 2 mL sample of grapefruit juice was extracted with the ethanol/hexane mixture (4/3, v/v). A 20 μL portion of internal standard (apocarotenal) was added in order to estimate carotene losses during the manipulations. The mixture was shaken for 30 s and centrifuged for 7 min at 2400*g*. Four extractions were performed with 2 mL of hexane. The hexane fractions were pooled and then evaporated for 15 min (GeneVac EZ-2 compatible, Suffolk, U.K.). In the case of model systems (AM+AA and AM+NAR), 2 mL was extracted three times with 1 mL of hexane and the pooled hexane fraction was evaporated using the same procedure. All final extracts were solubilized in 500 μL of MTBE/methanol/dichloromethane (40/10/50, v/v/v) before HPLC injection.

HPLC Analysis. Carotenoids were analyzed by reverse-phase HPLC using an Agilent1100 system (Massy, France) according to Dhuique-Mayer et al.[14] The carotenoids were separated using a C30 column (250 mm × 4.6 mm, 5 μm YMC) (Europ GmbH, Germany), and the

DOI: 10.1021/acs.jafc.5b00509
J. Agric. Food Chem. 2015, 63, 3970−3979

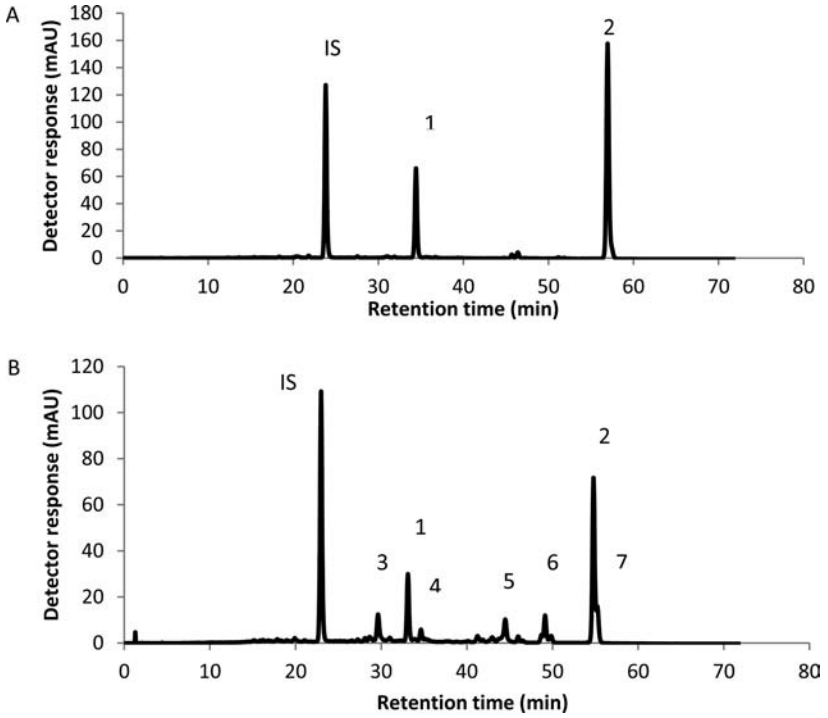

Figure 1. HPLC chromatogram: (A) fresh pink grapefruit juice, peaks 1 (β-carotene) and 2 (lycopene); (B) grapefruit juice heated for 5 h at 95 °C, peaks 3 and 4 (β-carotene isomers) and peaks 5−7 (lycopene isomers).

mobile phase was H_2O as eluent A, methanol as eluent B, and methyl *tert*-butyl ether as eluent C. The flow rate was set at 1 mL min^{-1}, the column was cooled to 15 °C, and the injection volume was 20 μL. A solvent gradient was programmed as follows: initial conditions, 40% A/60% B; 0−7 min, 20% A/80% B; 7−10 min, 4% A/81% B/15% C; 10−60 min, 4% A/11% B/85% C; 60−71 min, 100% B; 71−72 min, return to the initial conditions for rebalancing. β-Carotene and lycopene and their isomers were detected at 450 and 470 nm, respectively, using an Agilent photodiode array detector. Obvious carotenes were quantified on the basis of their calibration curve at the same wavelengths.

Determination of Ascorbic Acid in Real Juice and a Model System. Ascorbic acid was determined by HPLC according to Dhuique-Mayer et al.[29] Grapefruit juice or model juice (2 mL) was homogenized with 4 mL of a 4.5% metaphosphoric acid solution. Extractions were carried out in triplicate. After centrifugation, the supernatant was filtered through a 0.45 μm membrane and analyzed by HPLC using an Agilent Model 1100 system equipped with an RP 18e Licrospher 100 (5 μm) column (250 mm × 4.6 mm i.d.) (Merck KgaA, Darmstadt, Germany). The isocratic solvent system was a 0.01% solution of H_2SO_4, the flow rate was 1 mL min^{-1}, and detection was set at 245 nm. Ascorbic acid was quantified by the external standard method.

Determination of Naringin in Real Juice and a Model System. Naringin was determined by HPLC according to Dhuique-Mayer et al.[29] Briefly, 5 mL of juice was homogenized with 10 mL of dimethylformamide and 10 mL of ammonium oxalate (0.05 M). Then the mixture was heated for 10 min at 90 °C. After the mixture was cooled, the volume was completed with distilled water to 50 mL and centrifuged (1000*g*, 3 min) and the supernatant was filtered (0.45 μm). The HPLC analysis was carried out with an Agilent Model 1100 system (Massy, France) using an RP 18e Licrospher 100 (5 μm) column (250 mm × 4.6 mm i.d.) (Merck KgaA, Darmstadt, Germany). The isocratic solvent system was water/acetonitrile/THF/acetic acid (80/16/3/1, v/v/v/v). Quantification was carried out at 280 nm. The flow rate was set at 1 mL min^{-1}. Naringin concentrations were determined using an external calibration method.

Numerical Analysis of Kinetic Data. *Carotene Degradation in Real Juice and Model Media.* Carotene changes over time can be described by eq 1

$$\frac{d[X]}{dt} = -k[X]^{\alpha} \quad (1)$$

where [X] represents the carotene mass concentration (kg m^{-3}), t the time (s), k the reaction rate constant ($kg^{(1-\alpha)}$ $m^{3(\alpha-1)}$ s^{-1}), and α the apparent reaction order.

The rate constants k were assumed to vary with the temperature according to the Arrhenius equation

$$k = k_{ref} \exp\left(\frac{-E_a}{R}\left(\frac{1}{T} - \frac{1}{T_{ref}}\right)\right) \quad (2)$$

where k_{ref} is the rate constant at the reference temperature chosen in the middle of the studied temperature range (80 °C), with E_a, T, and R respectively denoting the activation energy (J mol^{-1}), medium temperature (K), and gas constant (8.314 J mol^{-1} K^{-1}).

The reaction order was determined by incrementing α in eq 1. Kinetic constants and activation energies were identified by nonlinear least-squares regression using the Levenberg−Marquardt least-squares minimization procedure with Matlab software (Mathworks Inc., Natick, MS, USA).

Multiresponse Modeling of the Thermal Degradation of Carotenes in Real Juice and Model Media. Carotenes and their isomers were monitored during heat treatments. Carotenoids were subjected to degradation, which could lead to other molecules that were not monitored by HPLC and were therefore missing species. These missing products were evaluated by mass balance.

Observable reaction schemes were proposed on the basis of experimental observations and literature data. When a reaction scheme was established, it was translated into a system of differential equations and the kinetic parameters were optimized with the Levenberg−Marquardt algorithm using Matlab software (Mathworks Inc., Natick, MS, USA).

Model Discrimination. To discriminate the appropriate kinetic model under monoresponse (reaction order) or multiresponse (most

DOI: 10.1021/acs.jafc.5b00509
J. Agric. Food Chem. 2015, 63, 3970−3979

Table 1. Second-Order Rate Constants in kg^{-1} m^3 s^{-1}, Arrhenius Parameters, Reference Constants in kg^{-1} m^3 s^{-1} at 80 °C, and Activation Energies in kJ mol^{-1} of *all-trans*-β-Carotene and *all-trans*-Lycopene Loss in Real Juice and Model Media

medium[a]	$k_{60\,°C}$	$k_{75\,°C}$	$k_{90\,°C}$	$k_{95\,°C}$	k_{ref}	E_a	R^2
			all-trans-β-Carotene				
real juice	8.83×10^{-3} (1.03×10^{-3})	2.35×10^{-2} (4.81×10^{-3})	5.62×10^{-2} (2.99×10^{-2})	5.14×10^{-2} (2.17×10^{-2})	3.08×10^{-2} (5.37×10^{-3})	45 (10)	0.97
AM	5.26×10^{-3} (2.32×10^{-3})	4.89×10^{-2} (1.46×10^{-2})	6.72×10^{-2} (1.27×10^{-2})	7.25×10^{-2} (2.27×10^{-2})	4.42×10^{-2} (7.17×10^{-3})	40 (10)	0.87
AM+AA	2.42×10^{-2} (3.93×10^{-3})	5.44×10^{-2} (3.38×10^{-3})	6.14×10^{-2} (1.03×10^{-3})	5.77×10^{-2} (1.03×10^{-3})	4.85×10^{-3} (5.56×10^{-2})	19 (6)	0.80
AM+NAR	3.59×10^{-3} (1.79×10^{-4})	1.71×10^{-2} (3.32×10^{-3})	8.63×10^{-2} (1.52×10^{-2})	1.68×10^{-1} (3.03×10^{-2})	2.42×10^{-2} (4.82×10^{-3})	138 (15)	0.99
			all-trans-Lycopene				
real juice	1.02×10^{-4} (2.73×10^{-5})	9.04×10^{-3} (4.10×10^{-3})	8.76×10^{-3} (4 32×10^{-3})	7.00×10^{-3} (3.21×10^{-3})	6.08×10^{-3} (2.11×10^{-3})	26 (10)	0.68
AM	8.90×10^{-4} (1.03×10^{-4})	1.65×10^{-2} (3.83×10^{-3})	9.23×10^{-2} (2.03×10^{-2})	1.04×10^{-1} (2.02×10^{-2})	3.25×10^{-2} (1.37×10^{-3})	89 (23)	0.99
AM+AA	1.48×10^{-2} (2.52×10^{-3})	1.07×10^{-2} (6.36×10^{-3})	7.17×10^{-2} (2.52×10^{-2})	8.86×10^{-2} (1.12×10^{-2})	3.06×10^{-2} (8.96×10^{-3})	79 (20)	0.67
AM+NAR	3.21×10^{-3} (5.05×10^{-4})	3.47×10^{-2} (1.77×10^{-3})	2.92×10^{-1} (3.15×10^{-2})	2.89×10^{-1} (4.84×10^{-2})	1.08×10^{-1} (4.91×10^{-3})	79 (23)	0.98

[a]Abbreviations: AM, citrate buffer/ethanol mixture; AM+AA, citrate buffer/ethanol mixture with added ascorbic acid; AM+NAR: citrate buffer/ethanol mixture with added naringin.

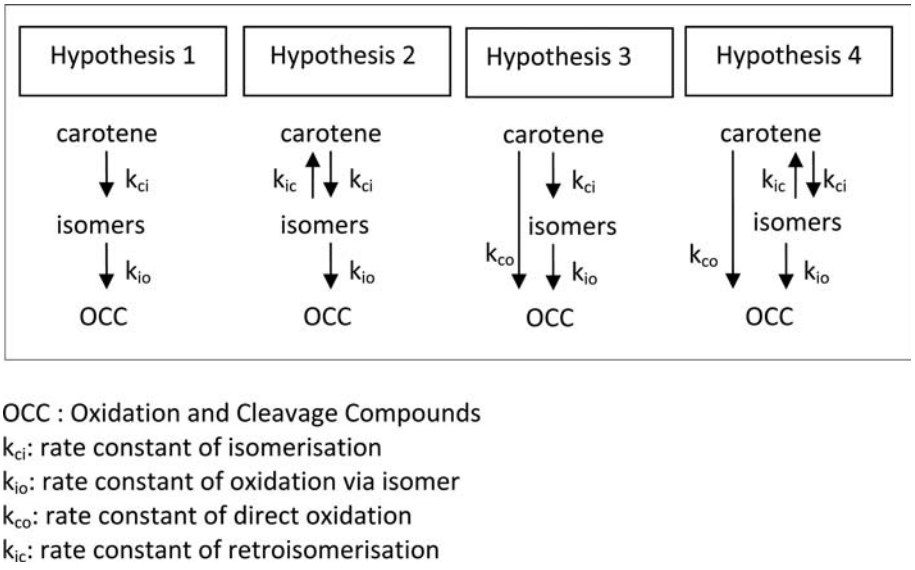

Figure 2. Presumed model of thermal degradation of lycopene and β-carotene (*all-trans*) and of their isomers in model systems.

probable reaction scheme) conditions, the residual sum of squares (RSS) was calculated according to eq 3

$$\mathrm{RSS} = \sum_{i=1}^{n} ([X_i] - [\hat{X}_i])^2 \tag{3}$$

where $[X_i]$ and $[\hat{X}_i]$ are respectively experimental and predicted concentrations of X and n is the number of experimental points. RSS measured the discrepancy between the experimental and simulated data. A small RSS indicated a suitable goodness of fit of the model to the data.

The coefficient of determination R^2 was calculated from the ratio of the explained variance to the total variance (TSS), with the explained variance being TSS minus RSS:

$$R^2 = \frac{\sum_{i=1}^{n} ([X_i] - [\bar{X}])^2 - \mathrm{RSS}}{\sum_{i=1}^{n} ([X_i] - [\bar{X}])^2}$$

where $[\bar{X}]$ is the mean concentration of X, and n is the number of experimental points.

For multiresponse models, RSS was also used to calculate the Akaike information criterion (AIC). AIC is a complementary measure of goodness of fit which was used by van Boekel[30] and which describes the tradeoff between the model accuracy (RSS) and complexity, i.e. the number of parameters (eq 4)

$$\mathrm{AIC} = n \ln\left(\frac{\mathrm{RSS}}{n}\right) + 2(p+1) \tag{4}$$

where n is the data number and p is the number of estimated parameters. AIC is an interesting criterion because it enables comparison of models having a different number of parameters. A small AIC indicates that the model presents a suitable goodness of fit to the experimental data while having a limited number of parameters.

Kinetic Parameter Uncertainty. The parameter uncertainty of the optimized parameters obtained with the Levenberg−Marquardt algorithm was calculated by nonlinear error propagation using Matlab software (Mathworks Inc., Natick, MS, USA).

DOI: 10.1021/acs.jafc.5b00509
J. Agric. Food Chem. 2015, 63, 3970−3979

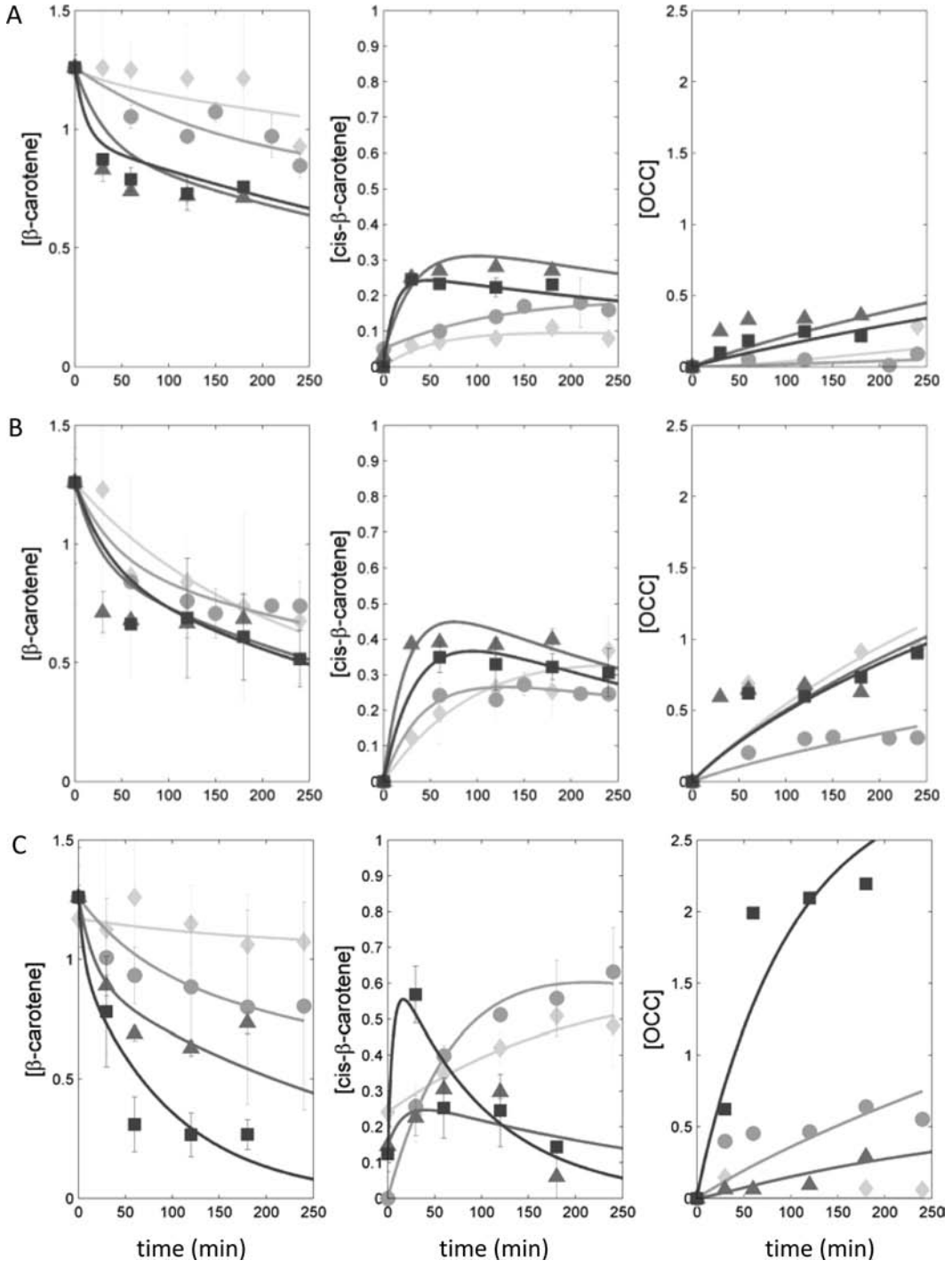

Figure 3. Experimental concentrations in mg L^{-1} over time during heat treatments at four temperatures (◆, 60 °C; ●, 75 °C; ▲, 95 °C; ■ 95 °C) of *β*-carotene, isomers, and other degradation products (OCC) (A) in a citrate buffer/ethanol mixture (AM), (B) with added ascorbic acid (AM +AA), and (C) with added naringin (AM+NAR). Error bars represent the standard deviation (n = 3), and lines represent the modeled data.

RESULTS AND DISCUSSION

Identification of Carotenoids from Fresh and Heated Grapefruit Juice. The two major carotenoids found in fresh grapefruit juice (*Citrus paradisi* Macf) were *all-trans-β*-carotene and *all-trans*-lycopene, at 1.25 ± 0.14 and 5.78 ± 0.58 mg L^{-1}, respectively, with the latter representing 80% of both (Figure 1A). The order of magnitude of the ratio lycopene/*β*-carotene found was close to that of the three found by Xu et al. in red grapefruit.[6] In heated grapefruit juice, *β*-carotene and lycopene isomerization was observed (Figure 1B). Thermal treatment led to a significant increase in 13-*cis*-*β*- and 9-*cis*-*β*-carotene. Heating also increased lycopene isomers: i.e., three *cis* isomers were tentatively identified, namely 5-*cis*-, 9-*cis*- and 13-*cis*-lycopene, according to their *cis* peak intensity and maximal absorption wavelength.[18,19,31] For 13-*cis*-lycopene, the *cis* peak intensity, expressed as percent AB/AII, was higher in comparison to that of 9-*cis*-lycopene because the *cis* double bond is closer to the center of the molecule. A hypsochromic shift of 6 nm occurred when the *cis* compound was compared

DOI: 10.1021/acs.jafc.5b00509
J. Agric. Food Chem. 2015, 63, 3970−3979

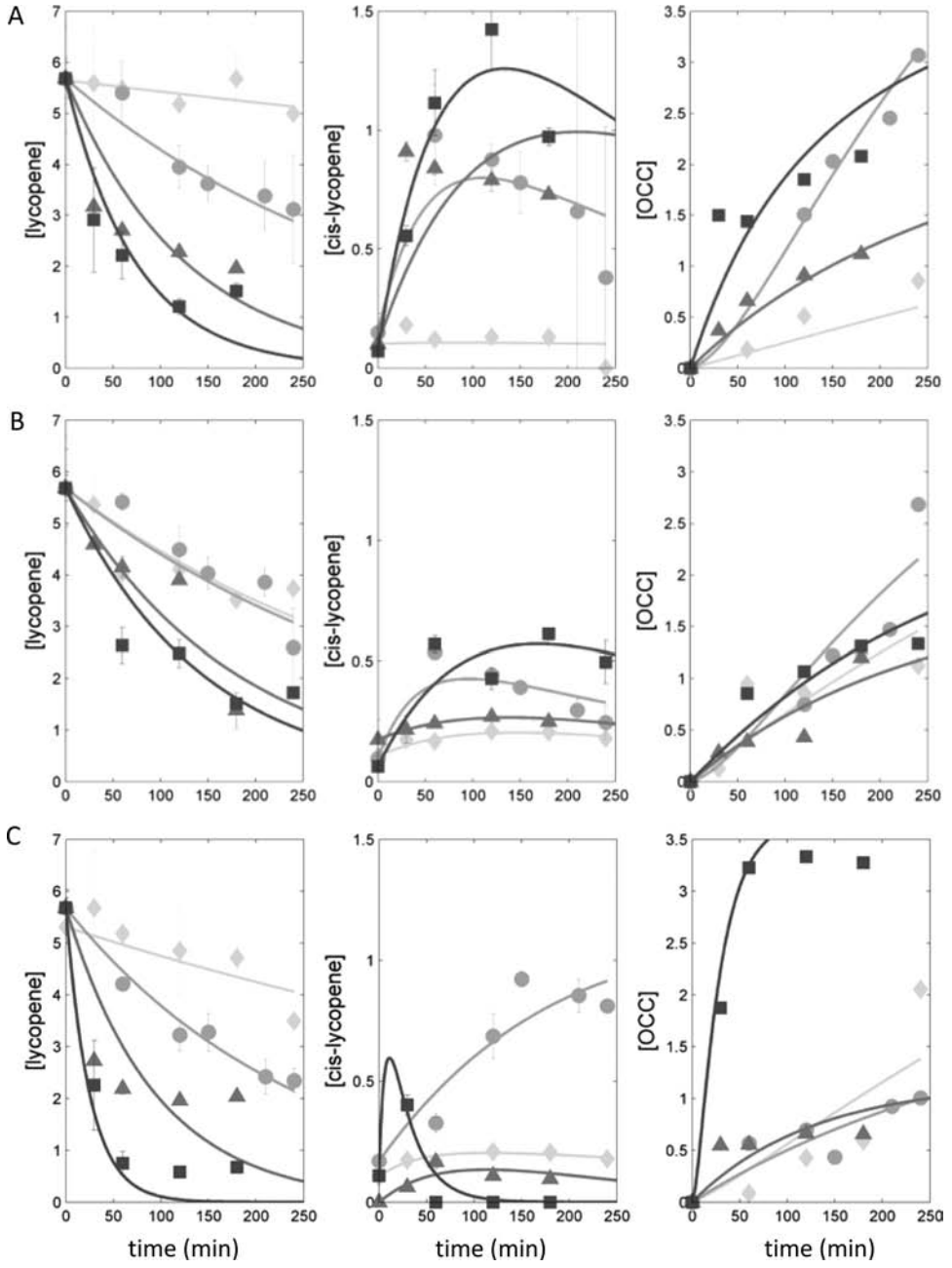

Figure 4. Experimental concentrations in mg L^{-1} over time during heat treatments at four temperatures (◆, 60 °C; ●, 75 °C; ▲, 95 °C; ■, 95 °C) of lycopene, isomers, and other degradation products (OCC) (A) in a citrate buffer/ethanol mixture (AM), (B) with added ascorbic acid (AM+AA), and (C) with added naringin (AM+NAR). Error bars represent the standard deviation (n = 3), and lines represent the modeled data.

to the *all-trans* compound, and this trend was similar to that reported in the literature.[24,27,31]

Carotene Degradation Kinetics in Real Juice and Model Media during Thermal Treatment. Kinetic models were drawn up on the basis of the analysis of experimental concentrations over the thermal treatment time for each carotene: i.e., β-carotene and lycopene. By incrementing α, the apparent order of the reaction in eq 1, and the calculation of the corresponding RSS (eq 3), second-order kinetics appeared to best fit the experimental data (minimal RSS). Most previously reported studies uses first-order kinetics to model carotene loss.[12] However, other orders have also been reported, especially in nonaqueous solvents.[32,33] Recently, Colle used a fractional conversion model to represent lycopene degradation in an olive oil/tomato emulsion. Indeed, they found that the carotene degradation pattern was that of an equilibrated reaction (nonzero plateau), which was also observed in real juice in our study.[31] However, a second-order kinetic model was preferred to compare all rate constants (in real juice and ethanol/water mixture).

The resulting rate constants and activation energies are presented in Table 1. All rate constants increased with temperature. The rate constants of β-carotene and lycopene were generally close. In similar matrices and under similar temperature conditions, their degradation rate was 2−10-fold lower than that of hydroxy-carotenoids (xanthophylls).[34] Therefore, carotenes are more stable because of the absence of hydroxyl groups. However, despite this structural similarity,

DOI: 10.1021/acs.jafc.5b00509
J. Agric. Food Chem. 2015, 63, 3970−3979

Table 2. Rate Constants of Lycopene and β-Carotene Thermal Degradation from Multiresponse Modeling in Model Media at the Reference Temperature (80 °C) According to Hypotheses 3 and 4, Respectively (Figure 2)[a]

	β-carotene rate constant k_{ref} (s^{-1}) of hypothesis 4 at 80 °C ref temp				lycopene rate constant k_{ref} (s^{-1}) of hypothesis 3 at 80 °C ref temp		
	AM	AM+AA	AM+NAR		AM	AM+AA	AM+NAR
k_{ci}	2.40×10^{-5} (6.3×10^{-6})	9.03×10^{-5} (1.2×10^{-5})	1.53×10^{-4} (2.2×10^{-5})	k_{ci}	4.88×10^{-5} (5.0×10^{-6})	3.25×10^{-5} (6.3×10^{-6})	1.75×10^{-6} (8.6×10^{-7})
k_{co}	1.18×10^{-5} (3.4×10^{-6})	4.30×10^{-5} (2.2×10^{-6})	6.09×10^{-8} (2.3×10^{-8})	k_{co}	1.05×10^{-5} (2.5×10^{-6})	3.02×10^{-5} (1.2×10^{-5})	4.17×10^{-5} (5.4×10^{-6})
k_{ic}	4.48×10^{-5} (2.4×10^{-5})	2.95×10^{-4} (6.5×10^{-5})	2.30×10^{-5} (1.0×10^{-5})				
k_{io}	7.67×10^{-6} (1.5×10^{-6})	4.66×10^{-7} (9.2×10^{-8})	2.60×10^{-5} (1.3×10^{-5})	k_{io}	1.68×10^{-4} (5.3×10^{-5})	1.75×10^{-4} (6.3×10^{-5})	2.39×10^{-6} (1.3×10^{-6})
RSS	0.88	2.78	2.73		7.19	3.57	4.07
R^2	0.95	0.90	0.96		0.92	0.65	0.98

[a]Abbreviations: AM, citrate buffer/ethanol mixture; AM+AA, citrate buffer/ethanol mixture with added ascorbic acid; AM+NAR, citrate buffer/ethanol mixture with added naringin.

the rate constants of the two carotenes varied differently as a function of the matrix. For instance, in real juice, the β-carotene rate constants ($(8.83 \pm 1.03) \times 10^{-3}$ to $(5.14 \pm 2.17) \times 10^{-2}$ kg^{-1} m^3 s^{-1}) were 3−80-fold superior to the values obtained for lycopene, in accordance with the findings of Abushita et al., D'Evoli et al., and Chanforan et al. Indeed, they all found a greater stability of lycopene in comparison to β-carotene in a vegetable matrix during heat treatment (tomato). They explained this difference in behavior by the fact that lycopene was more stable when it was bound to protein inside the vegetable matrix. However, when lycopene was not protein-bound, they showed that this pigment was less stable than β-carotene.[18,35,36] This is interesting, because we also noted an inversion of stability when carotenes were not in their initial matrix. Indeed, in all acid media (AM, AM+AA, AM+NAR), the reaction rates of lycopene at 90 and 95 °C were 1.2−3.6-fold higher than those of β-carotene. β-carotene was also less stable out of its original matrix, but to a lesser extent. In comparison to real grapefruit juice, the lycopene rate constant increased from 1- to 14-fold as a function of the temperature in the acid medium (AM), while it increased from 1- to 2-fold for β-carotene.

The activation energy of 45 ± 10 kJ mol^{-1} for β-carotene in grapefruit juice was in accordance with that found by Colle et al. in tomato emulsion (45 kJ mol^{-1}) but lower than that reported by Dhuique-Mayer et al. in orange juice (110 kJ mol^{-1}).[14,24] The activation energy of lycopene was 26 ± 10 kJ mol^{-1} in real juice. Lycopene was thus more sensitive to an increase of temperature than β-carotene, with an activation energy close to that reported for tomato pulp and watermelon juice (19.5 and 26.4 kJ mol^{-1}).[22,23]

Very few studies have compared the activation energies of lycopene and β-carotene in the same vegetal matrix. Demiray et al. found activation energies of 47 and 40 kJ mol^{-1} for lycopene and β-carotene, respectively, in tomato quarters during drying.[37] Colle et al. found activation energies of 28 and 45 kJ mol^{-1} for lycopene and β-carotene, respectively, in tomato emulsion during thermal treatment, which is out of line with the findings of Demiray et al.[24,37] Activation energies should therefore be considered very carefully because they highly depend on the matrix and temperature field studied.[12]

When carotenes were out of their matrix (i.e., in AM), the activation energies did not substantially change for β-carotene but increased from 26 ± 10 to 89 ± 23 kJ mol^{-1} for lycopene. The marked increase in the activation energy of lycopene (70%) showed that this carotene was particularly vulnerable and sensitive to an increase of temperature on isolation from the matrix. Therefore, the juice matrix affected both the rate constants and activation energies and had a protective role for carotenes, and especially lycopene. This was also demonstrated for xanthophylls in a previous study.[34] This protective role could have structural (by covalent or weak bonds or different matter state) or chemical origins. This latter hypothesis was tested by the addition to the acid medium of ascorbic acid (AM +AA) or naringin (AM+NAR), which are major phytochemicals of citrus juice that could have a protective effect. With regard to the rate constants, the addition of ascorbic acid did not significantly change the degradation trends from 75 to 95 °C for β-carotene and lycopene. Indeed, the degradation rate constant of β-carotene was $(6.14 \pm 1.03) \times 10^{-2}$ at 90 °C in AM+AA in comparison to $(6.72 \pm 1.27) \times 10^{-2}$ kg^{-1} m^3 s^{-1} in AM alone. Moreover, for lycopene, the degradation rate constant under the same conditions was $(7.17 \pm 2.52) \times 10^{-2}$ in AM+AA and $(9.23 \pm 2.03) \times 10^{-2}$ kg^{-1} m^3 s^{-1} in AM alone. Conversely, at 60 °C in AM+AA, the degradation rate was 5-fold higher for β-carotene and 17-fold higher for lycopene. This in turn decreased the activation energy from 40 ± 10 to 19 ± 6 kJ mol^{-1} for β-carotene and more slightly from 89 ± 23 to 79 ± 20 kJ mol^{-1} for lycopene. The interaction between ascorbic acid and carotenes has been questioned and is not well documented. Indeed, these molecules that have different polarities are supposed to interact at the interfaces in food matrices. Results reported by Sanchez et al. showed that vitamin C could preserve carotenoid compounds from oxidation in orange juice, but no mechanism was explained.[38] In contrast, Kanner et al. showed that ascorbic acid could have pro-oxidant effects with metal salts toward β-carotene in a linoleate system.[39] In an ethanol/water mixture, ascorbic acid and carotenes may interact as well. This interaction is only visible at 60 °C but no longer at 75 °C and higher temperatures. This may be partially explained by the thermolability of ascorbic acid in acid medium (AM+AA). Indeed, while 60% of ascorbic acid was retained at 300 min and 60 °C, degradation was almost total after 300 min and 95 °C. However, according to the study of Dhuique-Mayer et al., the retention of ascorbic acid after 150 min at 100 °C was 55% in citrus juice.[14] This therefore suggests that there was substantial retention of vitamin C throughout more than the half of the experiment conducted at 95 °C. Another explanation of this weak impact of ascorbic acid at high temperature could be the decrease in the dissolved oxygen concentration, which is known to be involved in ascorbic acid oxidation reactions. The

DOI: 10.1021/acs.jafc.5b00509
J. Agric. Food Chem. 2015, 63, 3970−3979

influence of ascorbic acid on the carotenoid degradation rate therefore decreases as the temperature increases. The addition of naringin affected the rate constants, but only at high temperatures. For β-carotene, the rate constants were slightly lower until 75 °C but 2-fold higher at 95 °C. This resulted in a strong 40 ± 10 to 138 ± 15 kJ mol^{-1} increase in activation energy. At moderate temperature (60 °C), the result was in accordance with a previous study that highlighted the protective effect of polyphenols on β-carotene at ambient temperature.[40] However, this protective role was not observed at higher temperature, and the addition of naringin even seemed to increase β-carotene degradation. For lycopene, the rate constants were on average 3-fold higher in AM+NAR. It is noteworthy that naringin, like other flavanone glycoside, is thermostable.[14] Interactions between polyphenols and carotene at different temperatures therefore need to be elucidated.

Rate constants and activation energies were higher in all model systems than in juice, especially for lycopene. The addition of ascorbic acid and naringin did not show a substantial improvement in stability in model systems. Indeed, ascorbic acid had no influence beyond 75 °C, while naringin seemed to increase its degradation from 75 °C. The protective effect of the juice matrix revealed in these experiments thus more have been due to structural protection than to phytochemicals. Indeed, in plant tissues, especially in citrus pulp, carotenoids are localized in chromoplasts within pulp particles. The particle sizes of citrus pulp are from 1 μm to 1 mm in juices.[41] During processing, carotenoids may be released from the matrix and undergo degradation because of the interaction with other fruit constituents (ascorbic acid, flavonoids, etc.). Therefore, the degradation rate is partially controlled by mass transfer from the pulp to the liquid fraction. In the model systems used in this study, carotenoids were homogeneously dispersed in a water/ethanol mixture with particles that were assumed to be very small due to this type of spontaneous microemulsion. Carotenoid degradation was thus less delayed by mass transfer, and surface contact was enhanced because of the emulsion. Despite these differences, the model systems were very convenient, as they enabled composition control and, even though they did not mimic the real juice exactly, the carotenoid reactivity did not differ markedly when comparing rate constants in PJ and AM, especially for β-carotene. The conclusions drawn in model systems concerning the interaction with microconstituents could therefore be transferable to real matrices. In addition to this model system approach, the role of structures surrounding carotenoids in the vegetable matrix, even destructured (juice), should be specified with further works based on microscopic observations, especially for lycopene.

Multiresponse Modeling of Carotene Thermal Degradation in Model Media. β-Carotene and lycopene degradation was limited in real juice (low rate constant), but it was significant in model media. In addition, high amounts of isomers could be measured in such media (dots in Figures 3 and 4). After 100 min and 95 °C, *cis* isomers could proportionally represent 40% and 60% of total β-carotene and lycopene, respectively. The amount of other degradation compounds—which were assumed to be oxidation and cleavage compounds (OCC)—was assessed at each time via mass balance calculations. From these data, we could represent both β-carotene degradation and the formation of neoformed isomers and other degradation compounds according to the different reaction schemes proposed in Figure 2, from the simplest (hypothesis 1) to the most complex (hypothesis 4). The four hypotheses represent different possibilities for carotenoid degradation. Isomer formation before oxidation and cleavage has been documented in many studies about carotenoids.[12] Hypothesis 1 is the simplest two-step reaction. Hypothesis 2 involves a reverse isomerization reaction which was also assumed to occur in previous studies.[27] Hypotheses 3 and 4 are the same as hypotheses 1 and 2, with the addition of direct cleavage from *trans*-carotenoids. Kinetic quantification of this direct reaction may provide evidence of the prevalence of oxidation reactions. Each hypothesis was transformed into an ordinary differential equation system including the different rate constants. As these schemes tend to describe each reaction step, the order for every reaction was assumed to be 1. A multiresponse modeling procedure enabled the identification of individual rate constants and the generation of modeled data (lines in Figures 3 and 4). The best hypothesis of Figure 2 was chosen by calculating the discrepancy between the experimental and simulated data (RSS) and the AIC criterion expressing the best tradeoff between accuracy and complexity. For β-carotene, substantially lower RSS and AIC values were found for hypothesis 4. Therefore, rate constants k_{ci} and k_{co} were the degradation constants of β-carotene in isomers and other oxidative and cleavage compounds (OCC), respectively.

Isomer rate constants were k_{ic} and k_{io} for retroisomerization in the trans form or degradation in OCC, respectively. β-Carotene retroisomerization was also demonstrated in oil medium by Achir et al.[27] All rates were identified at each temperature. The k_{ref} values extracted from eq 2 at a reference temperature of 80 °C are presented in Table 2. AA and NAR increased the k_{ci} isomerization constant from 3- to 7-fold, respectively. The k_{ic} retroisomerization constant only increased by 6.5-fold in the case of AA, while it decreased slightly with NAR. The k_{ci}/k_{ic} isomerization equilibrium constant could thus be calculated: 0.53 for AM, 0.32 for AM+AA, and 7 for AM +NAR. In the case of NAR, the equilibrium constant was thus higher, thus highlighting the importance of isomerization reactions. k_{co} increased by a 4-fold with AA addition. Direct β-carotene oxidation was thus promoted with this molecule. In contrast, k_{co} was very low with NAR, while k_{io} was 3-fold higher ($(2.60 \pm 1.3) \times 10^{-5}$ instead of $(7.67 \pm 1.5) \times 10^{-6}$ s^{-1}). Hence, with the addition of NAR, β-carotene was strongly isomerized and the formed isomers were very sensitive to oxidation and cleavage, giving rise to OCC.

In the case of lycopene, hypothesis 3 was sufficient to represent the experimental data (lowest RSS and AIC). The mechanisms therefore seemed to be different: no retroisomerization was identified with this approach. In this case, k_{ci} was the isomerization constant, k_{co} the direct oxidation constant, and k_{io} the isomer oxidation. With the addition of AA, k_{ci} and k_{io} remained the same. The only difference was the 3-fold increase in k_{co}, which was the direct oxidation rate. This confirmed that AA enhanced direct oxidation. With the addition of NAR, k_{ci} and k_{io} decreased by 27- and 70-fold, while k_{co} increased by 4-fold. With regard to lycopene, direct oxidation of this compound was also enhanced by NAR. Hence, designing a model system associated with multiresponse modeling may be useful to predict neoformation of compounds such as isomers during thermal processes, but it is also a way to quantify the kinetic importance of each reaction path as a function of the formulation and therefore gain insight into the microconsituent reaction mode. Further studies are now needed to better understand the interactions among

DOI: 10.1021/acs.jafc.5b00509
J. Agric. Food Chem. 2015, 63, 3970−3979

carotenoids, polyphenols, and ascorbic acid, which are very important phytochemicals in juice from nutritional and organoleptic standpoints.

AUTHOR INFORMATION

Corresponding Author

*N.A.: e-mail, nawel.achir@cirad.fr; tel, +33 (0) 4 67 87 40 89 or +33 (0) 4 67 61 55 47; fax, +33 (0) 4 67 61 70 55.

Notes

The authors declare no competing financial interest.

REFERENCES

(1) Uckoo, R. M.; Jayaprakasha, G. K.; Balasubramaniam, V. M.; Patil, B. S. Grapefruit (Citrus paradisi Macfad) phytochemicals composition is modulated by household processing techniques. *J. Food Sci.* **2012**, *77*, 921−926.

(2) Tanaka, T.; Tanaka, T.; Tanaka, M.; Kuno, T. Cancer Chemoprevention by Citrus Pulp and Juices Containing High Amounts of β-Cryptoxanthin and Hesperidin. *J. Biomed. Biotechnol.* **2012**, DOI: 10.1155/2012/516981.

(3) Gorinstein, S.; Caspi, A.; Libman, I.; Tzvi Lerner, H.; Huang, D.; Leontowicz, H.; Leontowicz, M.; Tashma, Z.; Katrich, E.; Shengbao, F.; Trakhtenberg, S. Red Grapefruit Positively Influences Serum Triglyceride Level in Patients Suffering from Coronary Atherosclerosis: Studies in Vitro and in Humans. *J. Agric. Food Chem.* **2006**, *54*, 1887−1892.

(4) Gorinstein, S.; Leontowicz, H.; Leontowicz, M.; Krzeminski, R.; Gralak, M.; Delgado-Licon, E.; Martinez Ayala, A. L.; Katrich, E.; Trakhtenberg, S. Changes in plasma lipid and antioxidant activity in rats as a result of naringin and red grapefruit supplementation. *J. Agric. Food Chem.* **2005**, *53*, 3223−3228.

(5) Poulaert, M.; Borel, P.; Caporiccio, B.; Gunata, Z.; Dhuique-Mayer, C. Grapefruit juices impair the bioaccessibility of β-carotene from orange-fleshed sweet potato but not its intestinal uptake by Caco-2 cells. *J. Agric. Food Chem.* **2012**, *60*, 685−691.

(6) Xu, J.; Tao, N.; Liu, Q.; Deng, X. Presence of diverse ratios of lycopene/β-carotene in five pink or red-fleshed citrus cultivars. *Sci. Hortic.* **2006**, *108*, 181−184.

(7) Honest, K. N.; Zhang, H. W.; Zhang, L. F. Lycopene: Isomerization Effects on Bioavailability and Bioactivity Properties. *Food Rev. Int.* **2011**, *27*, 248−258.

(8) Hiranvarachat, B.; Suvarnakuta, P.; Devahastin, S. Isomerisation kinetics and antioxidant activities of [beta]-carotene in carrots undergoing different drying techniques and conditions. *Food Chem.* **2008**, *107*, 1538−1546.

(9) Marx, M.; Stuparic, M.; Schieber, A.; Carle, R. Effects of thermal processing on trans-cis-isomerization of β-carotene in carrot juices and carotene-containing preparations. *Food Chem.* **2003**, *83*, 609−617.

(10) Rodriguez, E. B.; Rodriguez-Amaya, D. B. Formation of apocarotenals and epoxycarotenoids from [beta]-carotene by chemical reactions and by autoxidation in model systems and processed foods. *Food Chem.* **2007**, *101*, 563−572.

(11) Bechoff, A.; Dhuique-Mayer, C.; Dornier, M.; Tomlins, K. I.; Boulanger, R.; Dufour, D.; Westby, A. Relationship between the kinetics of [beta]-carotene degradation and formation of norisoprenoids in the storage of dried sweet potato chips. *Food Chem.* **2010**, *121*, 348−357.

(12) Penicaud, C.; Achir, N.; Dhuique-Mayer, C.; Dornier, M.; Bohuon, P. Degradation of β-carotene during fruits and vegetables processing or storage: reaction mechanisms and kinetics aspects. *Fruits* **2011**, *66*, 417−440.

(13) Vikram, V. B.; Ramesh, M. N.; Prapulla, S. G. Thermal degradation kinetics of nutrients in orange juice heated by electromagnetic and conventional methods. *J. Food Eng.* **2005**, *69*, 31−40.

(14) Dhuique-Mayer, C.; Tbatou, M.; Carail, M.; Caris-Veyrat, C.; Dornier, M.; Amiot, M. J. Thermal Degradation of Antioxidant Micronutrients in Citrus Juice: Kinetics and Newly Formed Compounds. *J. Agric. Food Chem.* **2007**, *55*, 4209−4216.

(15) Ahmed, J.; Shivhare, U. S.; Sandhu, K. S. Thermal Degradation Kinetics of Carotenoids and Visual Color of Papaya Puree. *J. Food Sci.* **2002**, *67*, 2692−2695.

(16) Lee, M. T.; Chen, B. H. Stability of lycopene during heating and illumination in a model system. *Food Chem.* **2002**, *78*, 425−432.

(17) Schierle, J.; Bretzel, W.; Buhler, I.; Faccin, N.; Hess, D.; Steiner, K.; Schuep, W. Content and isomeric ratio of lycopene in food and human blood plasma. *Food Chem.* **1997**, *59*, 459−465.

(18) Chanforan, C. l.; Loonis, M. l.; Mora, N.; Caris-Veyrat, C.; Dufour, C. The impact of industrial processing on health-beneficial tomato microconstituents. *Food Chem.* **2012**, *134*, 1786−1795.

(19) Xu, Y.; Pan, S. Effects of various factors of ultrasonic treatment on the extraction yield of all-trans-lycopene from red grapefruit (Citrus paradise Macf.). *Ultrason. Sonochem.* **2013**, *20*, 1026−1032.

(20) Lee, M. T.; Chen, B. H. Stability of lycopene during heating and illumination in a model system. *Food Chem.* **2002**, *78*, 425−432.

(21) Huawei, Z.; Xiaowen, W.; Elshareif, O.; Hong, L.; Qingrui, S.; Lianfu, Z. Isomerisation and degradation of lycopene during heat processing in simulated food system. *Int. Food Res. J.* **2014**, *21*, 45.

(22) Goula, A. M.; Adamopoulos, K. G.; Chatzitakis, P. C.; Nikas, V. A. Prediction of lycopene degradation during a drying process of tomato pulp. *J. Food Eng.* **2006**, *74*, 37−46.

(23) Sharma, R.; Kaur, D.; Oberoi, D. P. S.; Sogi, D. S. Thermal degradation kinetics of pigments and visual color in watermelon juice. *Int. J. Food Prop.* **2008**, *11*, 439−449.

(24) Colle, I. J. P.; Lemmens, L.; Van Buggenhout, S.; Van Loey, A. M.; Hendrickx, M. E. Modeling Lycopene Degradation and Isomerization in the Presence of Lipids. *Food Bioprocess Technol.* **2013**, *6*, 909−918.

(25) Zepka, L. Q.; Borsarelli, C. D.; Azevedo, M. A.; da Silva, P.; Mercadante, A. Z. Thermal Degradation Kinetics of Carotenoids in a Cashew Apple Juice Model and Its Impact on the System Color. *J. Agric. Food Chem.* **2009**, *57*, 7841−7845.

(26) Zepka, L. Q.; Mercadante, A. Z. Degradation compounds of carotenoids formed during heating of a simulated cashew apple juice. *Food Chem.* **2009**, *117*, 28−34.

(27) Achir, N.; Pénicaud, C.; Avallone, S.; Bohuon, P. Insight into β-carotene thermal degradation in oils with multiresponse modelling. *J. Am. Oil Chem. Soc.* **2011**, *88*, 2035−2045.

(28) Achir, N.; Pénicaud, C.; Bechoff, A.; Boulanger, R.; Dornier, M.; Dhuique-Mayer, C. Use of Multi-response Modelling to Investigate Mechanisms of β-Carotene Degradation in Dried Orange-Fleshed Sweet Potato During Storage: from Carotenoids to Aroma Compounds. *Food Bioprocess Technol.* **2014**, *7*, 1656−1669.

(29) Dhuique-Mayer, C.; Caris-Veyrat, C.; Ollitrault, P.; Curk, F.; Amiot, M. J. Varietal and Interspecific Influence on Micronutrient Contents in Citrus from the Mediterranean Area. *J. Agric. Food Chem.* **2005**, *53*, 2140−2145.

(30) van Boekel, M. A. J. S. *Kinetic Modeling of Reactions in Foods*; CRC Press: Boca Raton, FL, 2008.

(31) Colle, I.; Lemmens, L.; Tolesa, G.; Van Buggenhout, S.; De Vleeschouwer, K.; Van Loey, A.; Hendrickx, M. Lycopene degradation and isomerization kinetics during thermal processing of an olive oil/tomato emulsion. *J. Agric. Food Chem.* **2010**, *58*, 12784−12789.

(32) Shin, J. H.; Chung, H. L.; Seo, J. K.; Sim, J. H.; Huh, C. S.; Kil, S. K.; Baek, Y. J. Degradation Kinetics of Capsanthin in Paprika (Capsanthin annuum L.) as Affected by Heating. *J. Food Sci.* **2001**, *66*, 15−18.

(33) Achir, N.; Randrianatoandro, V. A.; Bohuon, P.; Laffargue, A.; Avallone, S. Kinetic study of beta-carotene and lutein degradation in oils during heat treatment. *Eur. J. Lipid Sci. Technol.* **2010**, *112*, 349−361.

(34) Hadjal, T.; Dhuique-Mayer, C.; Madani, K.; Dornier, M.; Achir, N. Thermal degradation kinetics of xanthophylls from blood orange in model and real food systems. *Food Chem.* **2013**, *138*, 2442−2450.

DOI: 10.1021/acs.jafc.5b00509
J. Agric. Food Chem. 2015, 63, 3970−3979

(35) Abushita, A. A.; Daood, H. G.; Biacs, P. A. Change in carotenoids and antioxidant vitamins in tomato as a function of varietal and technological factors. *J. Agric. Food Chem.* **2000**, *48*, 2075−2081.
(36) D'Evoli, L.; Lombardi-Boccia, G.; Lucarini, M. Influence of Heat Treatments on Carotenoid Content of Cherry Tomatoes. *Foods* **2013**, *2*, 352−363.
(37) Demiray, E.; Tulek, Y.; Yilmaz, Y. Degradation kinetics of lycopene, β-carotene and ascorbic acid in tomatoes during hot air drying. *LWT-Food Sci. Technol.* **2013**, *50*, 172−176.
(38) Sanchez-Moreno, C.; Plaza, L.; de Ancos, B.; Cano, M. P. Vitamin C, Provitamin A Carotenoids, and Other Carotenoids in High-Pressurized Orange Juice during Refrigerated Storage. *J. Agric. Food Chem.* **2002**, *51*, 647−653.
(39) Kanner, J.; Mendel, H.; Budomski, P. Prooxidant and antioxidant effects of ascorbic acid and metal salts in a β-carotene-linoleate model system. *J. Food Sci.* **1977**, *42*, 60−64.
(40) Unten, L.; Koketsu, M.; Kim, M. Antidiscoloring activity of green tea polyphenols on beta-carotene. *J. Agric. Food Chem.* **1997**, *45*, 2009−2012.
(41) Yuan, Q.; Yao, X. L.; Feng, G.; Huang, Q., Characteristic changes of naringin in grapefruit juice during heat treatment. *Food Sci. Technol.* **2012**, *7*.
(42) Buslig, B. S.; Carter, R. D. Particle size distribution in orange juices. *Fla. State Hortic. Soc.* **1974**, 302−305.

DOI: 10.1021/acs.jafc.5b00509
J. Agric. Food Chem. 2015, 63, 3970−3979

of lactations (two to three lactations). Each group was randomly assigned to one of the experimental diets: a control diet (CON), a diet including 300 g/day per head of grape seed (GS group), a diet including 220 g/day per head of linseed (LIN group), and a diet including both 300 g/day per head of grape seed and 220 g/day per head of linseed (MIX group). The ingredients, the chemical composition, and the fatty acid profile of the experimental diets are reported in Table 1. Diets included a common ration composed of commercial concentrate, beet pulp, mixed hay and alfalfa hay, and a mixed meal composed of pea, soybean, corn, grape seed, and linseed. Grape seed and linseed varied according to the different dietary treatments; the quantity of pea, soybean, and corn was calculated in order to make diets isoproteic and to supply the same level of metabolizable energy to each group. The linseed dose of 220 g/day was used to supply 70 g/day of fat per head. Considering that the total phenolic content of grape seed was 333.3 ± 10.1 mg of gallic acid equivalent (GAE)/100 g of dry matter (DM, mean ± S.E.), the grape seed dose of 300 g/day per head was used to provide approximately 1 g/day per head of total grape seed polyphenols. Details of feeding management and feed analysis and the results of feed intake and milk production traits have been previously reported.[16]

Table 1. Ingredients, Chemical Composition, and Fatty Acid Profile of Diets

	group[a]			
	CON	GS	LIN	MIX
Ingredients (kg/Day per Head, as Fed)				
Mixed Meal				
corn	0.15	0.17		
soybean	0.12	0.24	0.04	0.16
pea	0.25	0.09	0.15	0.02
grape seed		0.30		0.30
linseed			0.22	0.22
Beet Pulp	0.40	0.40	0.40	0.40
Commercial Concentrate[b]	0.50	0.50	0.50	0.50
Dehydrated Alfalfa Hay[c]	0.80	0.80	0.80	0.80
Mixed Hay[d]	0.20	0.20	0.20	0.20
Chemical Composition[e]				
dry matter (dm, %)	90.8	91.6	91.2	92.0
NDF (% DM)	41.8	42.8	43.7	44.5
NFC (% DM)	33.4	28.9	28.5	24.2
ADL (% DM)	4.6	8.9	5.0	9.4
CP (% DM)	18.0	17.9	17.9	17.9
ash (% DM)	7.8	7.4	8.1	7.6
EE (% DM)	2.0	3.2	5.1	5.8
ME supplied, Mcal/d	4.95	4.94	4.97	4.97
Major Fatty Acids (g/100 g of Total FA)				
C16:0	18.98	14.88	11.99	11.50
C18:0	3.33	4.47	4.39	4.68
C18:1 *cis*-9	22.79	23.52	21.78	21.91
C18:2 *n*-6 (LA)[f]	41.53	47.50	23.84	33.46
C18:3 *n*-3 (LNA)[f]	8.25	5.04	34.45	24.93
SFA[f]	24.24	20.88	17.75	17.42
MUFA[f]	25.84	26.02	23.70	23.94
PUFA[f]	49.92	53.11	58.55	58.64

[a]CON, control diet; GS, diet containing grape seed; LIN, diet containing linseed; MIX, diet containing both grape seed and linseed. [b]Commercial concentrate with the following ingredients: sunflower seed flour, wheat bran, dehydrated alfalfa meal, corn gluten, rice husks, corn flour, soybean hulls, sugar beet molasses, calcium carbonate from powdered calcium rocks, distilled wheat, sodium chloride, and plant oil (palm). Mineral supplement: ferrous sulfate monohydrate, 106 mg/kg; calcium diiodate, 1.7 mg/kg; manganese oxide, 90 mg/kg; sodium selenite, 0.46 mg/kg; zinc oxide, 87 mg/kg; and sodium molybdate, 2.5 mg/kg. Antioxidant E 310 propyl gallate, 4.3 mg/kg. Vitamin supplement: A, 17 971 UI/kg; D3, 3.494 UI/kg; and E, 60 mg/kg. [c]Dehydrated alfalfa hay: NFD, 387 g/kg DM; CP, 196 g/kg DM; and EE, 44 g/kg DM. [d]Mixed hay: NDF, 551 g/kg; DM, CP 116 g/kg; and DM, EE, 11 g/kg DM. [e]NDF, neutral detergent fiber; NFC, nonfiber carbohydrates; ADL, acid detergent lignin; CP, crude protein; EE, ether extract. [f]LA, linoleic acid; LNA, α-linolenic acid; SFA, total unsaturated fatty acids; MUFA, total monounsaturated fatty acids; PUFA, total polyunsaturated fatty acids.

Milk Samples. Individual morning milk samples were collected weekly (7:30 h) in the last 4 weeks of the trial and stored at −20 °C until analysis. The FA composition was determined on individual milk samples. For the analysis of riboflavin, tocopherols, hydroperoxides, and lipid oxidation of volatile compounds, the weekly milk samples were combined for each ewe.

Exposure of Milk to Fluorescent Light. To test the effect of light exposure on the milk oxidative stability, individual milk samples were transferred in a 30 mL capacity flask, previously cleaned with chloroform, stored in a working cooler at 4 °C, and placed under fluorescent light (400−600 nm) from a light source (TL-D 90 de Luxe Pro 18W/965 SLV, Philips, Frankfurt, Germany) with an intensity of 1500 lx and under continuous agitation by a rotator (Stuart rotator SB3, Bibby Sterilin, Stone, U.K.). Control samples were stored in parallel, under the same condition, and wrapped in an aluminum folium to protect the milk from light exposure. Samples were collected at time 0, after 6 and 24 h of light exposure.

Chemicals. Ascorbic acid (99.7%), α-, δ-, and γ-tocopherol (all >96%), citric acid monohydrate, ethylenediaminetetraacetic acid (99%), hexanal (98%), 1-hexanol (99.5%), heptanal (>92%), iron(III) chloride hexahydrate (97%), and riboflavin (>98%) were purchased from Sigma-Aldrich Chemie GmbH (Steinheim, Germany). Reagents such as HCl (37%), trichloroacetic acid (TCA, 99%), $BaCl_2$ (99%), iron(II) sulfate (99.5%), $NaH_2PO_4{\cdot}2H_2O$ (99.5%), $Na_2HPO_4{\cdot}2H_2O$, $CaCl_2{\cdot}2H_2O$ (99%), H_2O_2 (30%), and NaOH (>99%) were obtained from Merck (Darmstadt, Germany). NH_4SCN (99%) was from VWR BHD Prolabo (Leuven, Belgium). Sodium acetate, pentanal (97%), and 4-methyl-2-pentanone (99%) were purchased from Fluka Chemie GmbH (Buchs, Germany). All solvents of HPLC grade (acetonitrile, chloroform, hexane, 2-propanol, and methanol) and heptane (99%) were supplied by Rathburn Chemicals (Walkerburn, Scotland).

Milk Fatty Acid Profile. Milk fat extraction and fatty acid methyl ester (FAME) preparation were performed as described by Nudda et al.[17] A Turbo 3400 CX gas chromatograph (Varian Inc., Palo Alto, CA, USA), equipped with a flame ionization detector (FID) and an automatic injector 8200 (CX Varian Inc., Palo Alto, CA, USA) was used for the determination of FAME. The FAMEs were separated on a capillary column (CP-select CB for FAME; 100 m × 0.32 mm i.d., 0.25 μm film thickness, Varian Inc., Palo Alto, CA, USA) and quantified using pentanoic (C5:0) and nonadecanoic acid (C19:0) methyl esters (Sigma Chemical Co., St. Louis, MO, USA) as internal standards. The programmed temperature was 75 °C for 1 min, increased at 5 °C/min to 148 °C and at 8 °C/min to 165 °C, held for 35 min, increased at 5.5 °C/min to 210 °C, increased at 3 °C/min to 230 °C, and held for 14 min. Helium (1 mL/min flow rate) was used as the carrier gas with a pressure of 37 psi. The split ratio was 1:100. The injector and detector temperatures were held at 225 and 285 °C, respectively. Varian Star 3.4.1 software was used to compute the retention time and area of each individual FAME, identified by comparing their retention times with those of known standards and with published studies as detailed by Nudda et al.[17]

Riboflavin. Milk samples (1 mL) were added to 220 μL of 100% TCA to precipitate protein; after quick agitation they were placed on ice for 10 min and centrifuged (10 000 rpm, 10 min). About 1 mL of supernatant was transferred to a brown-colored vial through a microfilter (cellulose, 0.45 μm) and injected into an HPLC system equipped with a reverse-phase column (Zorbax SB-C8 4.6 mm × 150 mm, 5 μm; Agilent Technologies, USA). Fluorescence detection with excitation and emission at 450 and 530 nm, respectively, was used to measure the riboflavin according to Silva et al.[18] An external riboflavin

DOI: 10.1021/acs.jafc.5b01614
J. Agric. Food Chem. 2015, 63, 3980−3986

Table 2. Fatty Acid Composition of Milk from Different Groups

	group[a]					P values
fatty acid (g/100 g of FAME[f])	CON	GS	LIN	MIX	S.E.M.[b]	G[c]
C18:0	5.47[h]	8.73[g]	9.89[g]	10.03[g]	0.46	**
C18:1*cis*-9	13.39[h]	17.90[g]	19.66[g]	19.34[g]	0.64	**
C18:2 *n*-6 (LA)[d]	2.68[h]	4.65[g]	2.97[h]	4.86[g]	0.23	**
C18:3 *n*-3 (LNA)[d]	0.74[i]	0.58[i]	1.89[g]	1.43[h]	0.11	**
CLA *cis*-9,*trans*-11 (RA)[d]	0.70[i]	1.75[b,c]	2.18[a,b]	3.01[g]	0.01	**
total UFA[e]	25.11[i]	36.63[h]	41.14[b]	47.23[g]	1.81	**

[a]CON, control group; GS, group receiving grape seed; LIN, group receiving linseed; MIX, group receiving grape seed and linseed. [b]S.E.M., standard error of the mean. [c]G, group. [d]LA, linoleic acid; LNA, α-linolenic acid; RA, rumenic acid. [e]Total UFA, sum of all detected unsaturated fatty acids: C10:1, C14:1 *cis*-9, C16:1 *trans*-6 + *trans*-7, C16:1 *trans*-8, C16:1 *trans*-9, C16:1 *trans*-10, C16:1 *cis*-7, C16:1 *cis*-9, C16:1 *cis*-10, C17:1 *cis*-8, C17:1 *cis*-9, C18:1 *trans*-4, C18:1 *trans*-6 + *trans*-8, C18:1 *trans*-9, C18:1 *trans*-10, C18:1 *trans*-11, C18:1 *cis*-9 + *trans*-13 + *trans*-14, C18:1 *cis*-10 + *trans*-15, C18:1 *cis*-11, C18:1 *cis*-12, C18:1 *cis*-13, C18:1 *cis*-14 + *trans*-16, C18:2 *trans*-9,*trans*-12, C18:1 *cis*-15, C18:2 *trans*-8,*cis*-13, C18:2 *cis*-9,*trans*-12, C18:2 *trans*-9,*cis*-12, C18:2 *n*-6, C18:3 *n*-6, C18:3 *n*-3, CLA *cis*-9,*trans*-11, CLA *trans*-7,*cis*-9, C18:4 *n*-3, CLA *trans*-9,*cis*-11, CLA *trans*-10,*cis*-12, CLA *trans*-11,*cis*-13, CLA *trans*-11,*trans*-13, CLA *cis*-11,*cis*-13, CLA *trans*-9,*trans*-11 + C20:1 *n*-9, C20:2 *n*-6, C20:3 *n*-9, C20:3 *n*-6, C20:4 *n*-6, C20:3 *n*-3, C20:4 *n*-3, C22:1 *n*-11, C22:1 *n*-9, eicosapentaenoic acid, C22:2 *n*-6, C21:5 *n*-3, C22:4 *n*-6, C24:1 *cis*-15, docosapentaenoic acid, docosahexaenoic acid. [f]FAME, fatty acid methyl esters. [g]Means with different letters within a row are significantly different. $P < 0.05$; ** $P < 0.0001$. [h]Means with different letters within a row are significantly different. $P < 0.05$; ** $P < 0.0001$. [i]Means with different letters within a row are significantly different. $P < 0.05$; ** $P < 0.0001$.

standard curve was used for the quantification (5.0, 2.0, 1.0, 0.5, 0.250, 0.1, and 0.05 μg/mL) according to Dalsgaard et al.[19]

Tocopherols. Two milliliters of milk was added to an equal volume of ethanolic ascorbic acid (1%) and 0.3 mL of saturated potassium hydroxide solution and shaken for 10 s. The quantification of tocopherols was performed according to Dalsgaard et al.[19] Briefly, the samples were incubated at 70 °C for 30 min, shaken for 10 s after 15 min from the beginning of the incubation, and then cooled on ice. Then 1 mL of Milli-Q water and 3 mL of heptane were added to the samples, mixed for 1 min, and centrifuged at 1700*g* for 3 min. Thirty microliters of the upper phase was analyzed by HPLC to measure the concentration of α-, δ-, and γ-tocopherols. Chromatographic separation was performed using a Hypersil silica column (4.6 mm × 200 mm, 5 μm; Thermo Fisher Scientific Inc., Waltham, USA) and hexane/2-propanol (98:2) at a flow rate of 1 mL/min as the mobile phase. The elution was monitored by a fluorescence detector using excitation and emission wavelengths of 295 and 330 nm, respectively. An external standard curve was used for quantitative determination.

Lipid Hydroperoxides. Two milliliters of milk was transferred into a 10 mL glass tube and added to 2 mL of methanol and 4 mL of chloroform and shaken for 30 s, and quantification was performed according to Dalsgaard et al.[19] with a few modifications. Briefly, the sample was centrifuged at 3000*g* for 10 min before 1 mL of the chloroformic phase was mixed with 1 mL of iron(II) thiocyanate in a 10 mL glass tube that previously was cleaned with chloroform. Absorbance was measured at 500 nm after 5 min on a UV−vis spectrophotometer (Cary 60, Agilent Technologies, Palo Alto, CA, USA) using chloroform for the blank reading. Quantification was performed using an external standard curve made at concentrations 2, 5, 10, 15, 20, 40, and 60 μmol/L hydrogen peroxide in chloroform/methanol (50:50).

Secondary Lipid Oxidation Products. The volatile compounds (hexanal and heptanal) were identified and quantified by gas chromatography coupled with mass spectrometry headspace analysis, according to Dalsgaard et al.[19] with minor changes including the use of an isotopic internal hexanal standard according to Wold et al.[20] Briefly, 2 mL of milk was transferred to a 10 mL vial, added to deionized (18.2 MΩ) filtered water (0.22 μm) with an isotopic hexanal D12 (50 ng) from Fluka (Steinham, Germany). The samples were sealed with Teflon-coated lids before the headspace was analyzed for volatile compounds using a Carboxen/PDMS SPME fiber with a film thickness of 30 μm from Supelco (Bellefonte, PA, USA), which was incubated at 50 °C for 30 min in the headspace of each sample. Desorption of the sample from the fiber was performed in the inlet of a GC 7890A from Agilent Technologies (Waldbronn, Germany) equipped with an HP5-MS column from Agilent J&W Scientific (Folsom, CA, USA) and coated with a nonmetal 5% phenyl, 95% dimethylpolysiloxane phase with the following dimensions: 0.25 mm i.d., 0.25 μm, 30 m. Helium was used as the carrier gas with a constant flow of 1.2 mL/min. Quantification was performed relatively using an external standard curve with concentrations of 1−500 ng/mL milk of each compound, including isotopic hexanal to avoid in-between sample variation on individual compounds.

Statistical Analysis. A mixed model was used to analyze data for repeated measurements of fatty acids, riboflavin, tocopherols, hydroperoxides, and volatile compounds using the Proc Mixed procedure of SAS (2002, SAS Institute INC., Cary, NC, USA). The model included the diet and time and their interaction as fixed effects plus the random factor of ewes nested within the treatment. The mean values of fatty acids in milk of each animal were used to calculate the ratio between lipid oxidation products after 24 h of light exposure and the milk fatty acid composition; the data were analyzed with one-way ANOVA. Means were separated using the Tukey test ($P < 0.05$).

RESULTS

The BW of the animals was not affected by any of the treatments (CON, GS, LIN, or MIX) and increased with period (+5.9 ± 0.6 kg, mean ± SD). The fatty acid composition of milk was highly affected by the diet (Table 2). All groups receiving the experimental ingredients (GS and LIN alone or in combination (MIX)) showed higher levels of stearic acid (C18:0, SA) and oleic acid (C18:1 *cis*-9, OA) than the CON group ($P < 0.001$). The concentration of linoleic acid (C18:2 *n*-6, LA) increased ($P < 0.001$) in both groups fed grape seed (GS and MIX) compared to the CON and LIN groups. The level of α-linolenic acid (C18:3 *n*-3, LNA) increased ($P < 0.001$) in both groups receiving linseed compared to CON and GS groups, with the LIN group being the highest. The level of rumenic acid (CLA *cis*-9,*trans*-11, RA) was higher in the LIN and MIX groups than in the CON group ($P < 0.001$); the GS group showed a numerically higher concentration of RA than did the CON group, even though the differences did not reach the level statistical significance ($P < 0.10$). The concentration of total UFA increased in all groups receiving the experimental ingredients compared to the CON; the highest value was found in MIX, with GS and LIN being intermediate ($P < 0.001$).

The initial concentrations of riboflavin in milk from the four experimental groups (1.4 ± 0.4, 1.1 ± 0.4, 1.5 ± 0.3, and 1.1 ± 0.4 μg/mL for the CON, GS, LIN, and MIX groups,

DOI: 10.1021/acs.jafc.5b01614
J. Agric. Food Chem. 2015, 63, 3980−3986

respectively) did not show any significant difference ($P > 0.05$, Figure 1A). The level of riboflavin decreased ($P < 0.01$) by

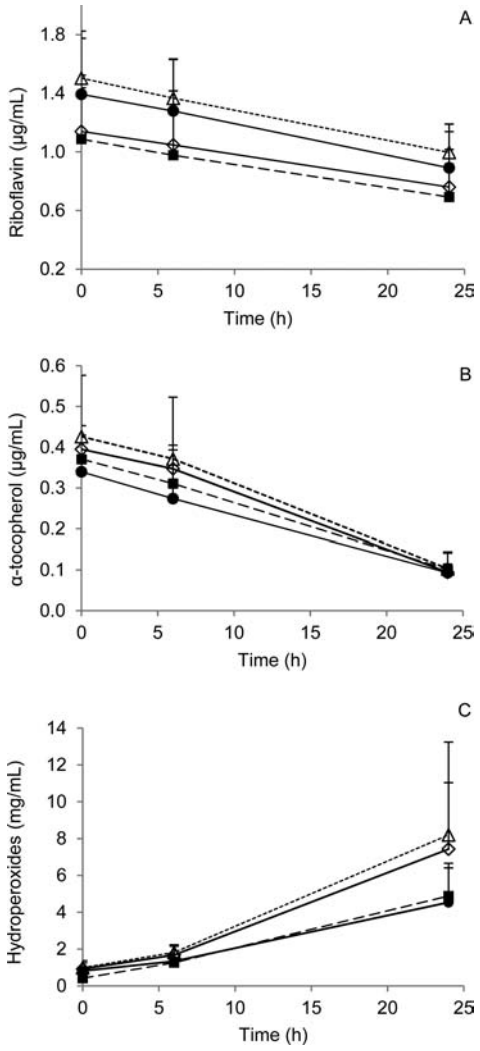

Figure 1. Decrease of riboflavin (A), degradation of α-tocopherol (B), and accumulation of lipid hydroperoxides (C) during illumination with fluorescent light (1500 lx) at 4 °C. Milk from sheep within the feeding groups: control (solid line, ●), grape seed (long-dashed line, ■), linseed (dotted line, △), and a group receiving both grape and linseed (solid line, ◊). Bars indicate standard deviations of the means of six individual animals in each treatment.

8.9% after 6 h of light exposure at 4 °C and by 35% after 24 h in all groups, independently of diets ($P > 0.05$), reaching a final concentration of 0.83 ± 0.1 μg/mL riboflavin. Dark samples of each group (data not shown) did not show any significant reduction of riboflavin after 24 h ($P > 0.05$).

The α-tocopherol was the only tocopherol detected in the milk of the four experimental groups (Figure 1B). No difference was found ($P > 0.05$) in the initial level of α-tocopherol between the groups (0.38 ± 0.09 μg/mL). The milk from all groups showed the same insignificant ($P > 0.05$) decreasing tendency (−14.9%) of α-tocopherol after 6 h. The loss (−74.4%) became significant ($P < 0.01$) after 24 h of light exposure but still without differences between groups ($P > 0.05$), with the α-tocopherol concentration being 0.1 ± 0.03 μg/mL (mean of all groups ± standard deviation).

The accumulation of lipid hydroperoxides in the milk from the four experimental groups during 24 h of fluorescent light exposure at 4 °C is shown in Figure 1C. The level of lipid hydroperoxides after 6 h of light exposition increased significantly ($P < 0.05$) in all experimental groups except for the CON ($P > 0.05$). The concentrations of lipid hydroperoxides after 6 h were 1.49, 1.37, 1.81, and 1.68 mg/mL for CON, GS, LIN, and MIX groups, respectively. After 24 h of light exposure the accumulation of lipid hydroperoxides increased significantly ($P < 0.05$) in both groups receiving linseed supplementation LIN and MIX (8.20 and 7.43 mg/mL, respectively); however, no significant differences ($P > 0.05$) were found in the accumulation of hydroperoxides in the CON and GS groups (4.53 and 4.88 mg/mL, respectively). The level of lipid hydroperoxides after 24 h was numerically greater in the milk of both groups fed linseed (mean, 7.81 mg/mL) compared to that from CON and GS groups (mean, 4.71 mg/mL) even if it did not reach a significant difference ($P > 0.05$). Dark samples of each group (data not shown) and the mean of all groups did not show any significant increase in lipid hydroperoxide accumulation after 24 h ($P > 0.05$).

Figure 2A shows the relationship between the accumulation of lipid hydroperoxides after 24 h of illumination with fluorescent light (1500 lx) at 4 °C and the concentration of UFA (g/100 g of total FAME) in milk samples from sheep of all groups. The level of hydroperoxides increased linearly ($P < 0.01$) with the concentration of total UFA in CON and LIN groups ($R^2 = 0.80$, $P < 0.01$). No correlation was found ($R^2 = 0.08$, $P > 0.05$) between the level of hydroperoxides and the concentration of total UFA in both groups fed grape seed (GS and MIX). Calculating the ratio between the concentration of lipid hydroperoxides in milk after 24 h and the concentration of total UFA (g/100 g of FAME) in the milk (Figure 2B) showed a significantly lower level of lipid hydroperoxides ($P < 0.05$) in GS and MIX (0.13 ± 0.05, mean ± SD) compared to the LIN group (0.26 ± 0.07, mean ± SD). The CON group showed an intermediate level (0.21 ± 0.06, mean ± SD) that is not significant different ($P > 0.05$) from any of the other groups.

As hexanal is accepted to be formed from LA, the ratio hexanal/LA was calculated in the same manner as for the hydroperoxide/UFA ratio (Figure 3A). The hexanal/LA ratio was lower ($P < 0.05$) in GS and MIX (5.26 ± 1.81, mean ± SD) than in the CON group (11.37 ± 1.18, mean ± SD), with LIN being intermediate (6.85 ± 1.47, mean ± SD).

Heptanal was significant higher in the MIX group than in the three others (data not shown). Heptanal has previously been correlated with OA, LA, and RA, and we obtained a good correlation between the concentration of these fatty acids and the accumulation of heptanal in milk samples after 24 h of light exposure ($R^2 = 0.85$, $P < 0.01$). When calculated as the ratio heptanal/(OA + LA + RA) there was no significant difference after 24 h of light exposure between any of the treatments (Figure 3B).

DISCUSSION

The effect of photooxidation on the lipid oxidation of sheep milk was investigated for the first time in the present study. Moreover, the effects of grape seed or linseed alone or in combination included in the sheep diet were studied with respect to the oxidative stability of sheep milk. In the present study the mean concentrations of riboflavin in ewe's milk was 1.3 μg/mL, and it was significantly reduced after 24 h of light exposure, independently of diets. The detected level of

DOI: 10.1021/acs.jafc.5b01614
J. Agric. Food Chem. 2015, 63, 3980−3986

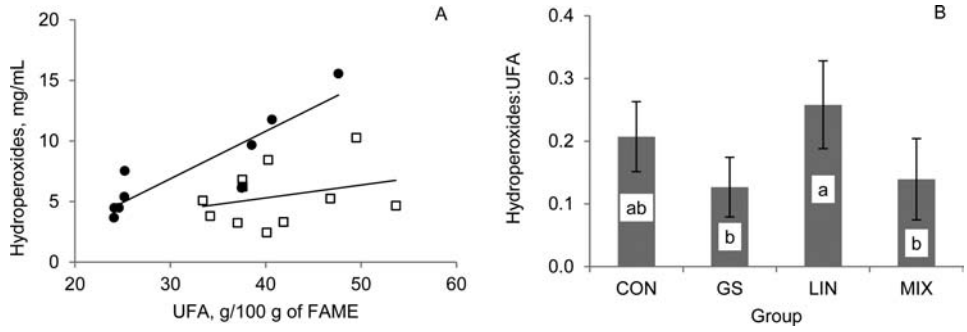

Figure 2. (A) Relationship between the accumulation of lipid hydroperoxides after 24 h of illumination with fluorescent light (1500 lx) at 4 °C and total UFA in milk samples from sheep fed grape seed (□, GS and MIX) and others groups (●, CON and LIN) ($y = 0.1062x + 1.0588$, $R^2 = 0.08$, and $P > 0.05$; $y = 0.3919x - 4.8692$, $R^2 = 0.80$, and $P < 0.01$, respectively). (B) Ratio between the accumulation of lipid hydroperoxides after 24 h of illumination at 4 °C and total UFA in milk samples from sheep of different experimental groups: CON, control group; GS, group receiving grape seed; LIN, group receiving linseed; MIX, group receiving both grape seed and linseed. Different letters (a, b) indicate significant differences ($P < 0.05$). Bars indicate standard deviations of the means of six individual animals in each treatment.

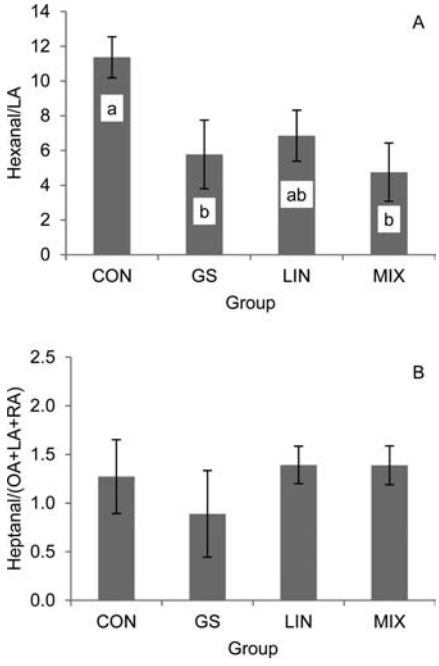

Figure 3. (A) Ratio between the accumulation of hexanal after 24 h of illumination with fluorescent light (1500 lx) at 4 °C and linoleic acid (LA) in a milk sample from sheep of different experimental groups. (B) Ratio between the accumulation of heptanal after 24 h of illumination with fluorescent light (1500 lx) at 4 °C and the sum oleic acid (OA), linoleic acid (LA), and rumenic acid (RA) in a milk sample from sheep of different experimental groups. CON, control group; GS, group receiving grape seed; LIN, group receiving linseed; MIX, group receiving both grape and linseed. Different letters (a, b) indicate significant differences ($P < 0.05$). Bars indicate standard deviations of the means of each treatment, $n = 6$.

riboflavin in sheep milk in our experiment was similar to those in previous reports (1.58 and 1.77 μg/mL),[21,22] and the bleaching of riboflavin has previously been shown upon illumination in other dairy systems as well.[19,23]

The degree of transfer of α-tocopherol from feed to the milk, in cows, has previously been positively correlated with the levels of LA and LNA in milk.[24,25] In our study the initial level of α-tocopherol seems to be independent of the concentration of LA and LNA; maybe the small differences in the levels of these fatty acids between groups were not enough to affect the transfer of α-tocopherol from feed to milk significantly. The pattern of degradation of α-tocopherol in the present study is in agreement with other studies showing a loss of α-tocopherol in bovine milk after fluorescent light exposure.[26,27] The loss of α-tocopherol did not affect the accumulation of lipid hydroperoxides within 24 h of light exposure; this finding disagrees with previous studies reporting the capacity of α-tocopherol to quench singlet oxygen.[28,29] When α-tocopherol was included in a cow's diet, reaching a concentration of 2.67 μg/mg in the milk, the oxidative stability of milk was improved.[25] This discrepancy could be due to the different concentrations of α-tocopherol in milk; in the present work the levels of α-tocopherol were 7 times lower than in the previously cited study.[25] Our result agrees with other studies where no relationship was found between the loss of α-tocopherol (at a level similar to our finding) and the accumulation of lipid hydroperoxides in cheese under light exposure.[19,30]

The accumulation of lipid hydroperoxides was used as a measurement of the light-induced lipid oxidation in milk. The high amount of UFA in milk samples with linseed made them more susceptible to the lipid oxidation as previously shown.[31] As UFA are logically more susceptible to oxidation,[32] a linear correlation between the concentration of these FAs and the level of lipid hydroperoxides could be hypotized, according to the findings of Havemose et al.,[26] who showed that higher concentrations of LNA were correlated with higher accumulations of lipid hydroperoxides in bovine milk after 24 h of fluorescent light exposure. Hence, the significantly higher level of UFA in the MIX group compared to those in the LIN and GS groups (MIX > LIN = GS > CON) would lead us to expect a higher level of hydroperoxides in the MIX group compared to those in the LIN and GS groups and also a higher level of hydroperoxides in the GS group compared to that in the CON group.

Although no statistical differences were observed among the four groups, it was evident that both groups receiving linseed tended to have higher accumulations of lipid hydroperoxides than the other groups. Biological variation and complex matrices may contribute to uncertainties in the obtained results. However, considering the level of total UFA found in milk, a good correlation was found between the accumulation of lipid hydroperoxides after 24 h of light exposure and the UFA (g/100g total FA) in the milk samples from the CON and LIN groups, whereas no correlation was found in milk from sheep fed grape seed (GS and MIX). The lower level of

DOI: 10.1021/acs.jafc.5b01614
J. Agric. Food Chem. 2015, 63, 3980−3986

hydroperoxides between the LIN and MIX groups indicates an antioxidative capacity of the grape seed that seems to protect UFA in the MIX group against type II photooxidation. This is also supported by a numerically lower level of the ratio hydroperoxides/UFA in the GS group compared to the CON, even though this was not found to be significantly different. The transfer of polyphenols from feed to the milk of ruminants[33−35] and their ability to quench singlet oxygen[36] could potentially explain the protection of the milk from the GS and MIX groups, both with grape seed in their diets. Furthermore, our finding agrees with Jung,[27] showing the protective activity of catechins in the accumulation of lipid hydroperoxides in milk after fluorescent light exposure. It has been proposed that the generation of lipid hydroperoxides in milk with fluorescent light can be a consequence of the reaction between singlet oxygen, resulting from the sensibilization of riboflavin and its reaction with unsaturated lipids,[37] but other photosensitizers may also play an important role in the generation of singlet oxygen.[23]

The secondary oxidation product, hexanal, has been reported to be a typical volatile product derived from LA oxidation.[38,39] It has previously been demonstrated that bovine milk with a high amount of LA was more susceptible to lipid oxidation compared to milk rich in RA, OA, and LNA, respectively.[40] The same authors demonstrated that milk containing a high amount of LA showed the highest production of secondary volatile compounds, compared to other milk models. In the present work, the lower ratio hexanal/LA calculated for milk from the GS group compared to the CON group (and the numerically lower value for MIX compared to that for LIN) supports the hypothesis that polyphenols from grape seed were able to reduce the formation of secondary oxidation product hexanal. This finding agrees with other studies reporting the antioxidant capacity of grape seed polyphenols[41,42] and is corroborated by other findings showing the capacity of catechins to reduce the accumulation of lipid volatile aldehydes in cheese and milk after light illumination.[43,27]

The higher accumulation of heptanal in MIX compared to that of the other groups could be explained with the high levels of OA, LA, and RA found in the milk of this group. In fact the formation of heptanal has been mainly associated with the oxidation of these fatty acids.[44,39,45] The ratio between the accumulation of heptanal after 24 h of illumination and the sum of OA, LA, and RA showed no difference between the experimental groups, supporting these previous finding. This result suggests that the grape seed byproduct may effectively reduce the formation of the secondary oxidation product heptanal, thus to a certain extent offering protection to the PUFA from the linseed. Moreover, the numerically lower value of the ratio heptanal/OA, LA, RA in the GS group compared to that for CON seems to confirm the ability of polyphenols from grape seed to reduce the formation of heptanal.

In conclusion, this study illustrated the differences in the milk's oxidative stability when sheep diets include a source of polyphenols (grape seed) and a source of PUFA (linseed), alone or in combination. The inclusion of linseed in the diet of sheep increased the amount of PUFA in the milk, which is advantageous for health effects, but the high levels of PUFA in milk made it vulnerable to oxidation. The addition of grape seed reduced the extent of oxidation of the total UFA when taking the ratio between lipid hydroperoxides after 24 h of light exposure and the milk fatty acid composition into account.

AUTHOR INFORMATION

Corresponding Author

*E-mail: trine.dalsgaard@food.au.dk. Phone: +458715 7998.

Funding

F.C. gratefully acknowledges the Sardinia Regional Government for the financial support of his Ph.D. scholarship (P.O.R. Sardegna F.S.E. Operational Programme of the Autonomous Region of Sardinia, European Social Fund 2007-2013 - Axis IV Human Resources, Objective l.3, Line of Activity l.3.1.).

Notes

The authors declare no competing financial interest.

ACKNOWLEDGMENTS

We thank Caroline Nebel and Rita Albrechtsen for their assistance in the laboratory.

ABBREVIATIONS USED

PUFA, polyunsaturated fatty acids; UFA, unsaturated fatty acids; LA, linoleic acid; LNA, α-linolenic acid; OA, oleic acid; RA, rumenic acid; CLA, conjugated linoleic acid; CON, control group; GS, group receiving grape seed; LIN, group receiving linseed; MIX, group receiving both grape seed and linseed

REFERENCES

(1) Nudda, A.; Battacone, G.; Boaventura Neto, O.; Cannas, A.; Francesconi, A. H. D.; Atzori, A. S.; Pulina, G. Feeding strategies to design the fatty acid profile of sheep milk and cheese. *R. Bras. Zootec.* **2014**, *43*, 445−456.

(2) Toral, P. G.; Frutos, P.; Hervás, G.; Gómez-Cortés, P.; Juárez, M.; De la Fuente, M. A. Changes in milk fatty acid profile and animal performance in response to fish oil supplementation, alone or in combination with sunflower oil, in dairy ewes. *J. Dairy Sci.* **2010**, *93*, 1604−1615.

(3) Østdal, H.; Bjerrum, M. J.; Pedersen, J. A.; Andersen, H. J. Lactoperoxidase-induced protein oxidation in milk. *J. Agric. Food Chem.* **2000**, *48*, 3939−3944.

(4) Juhlin, J.; Fikse, F.; Lundén, A.; Pickova, J.; Agenäs, S. Relative impact of α-tocopherol, copper and fatty acid composition on the occurrence of oxidized milk flavour. *J. Dairy Res.* **2010**, *77*, 302−309.

(5) O'Brien, N. M.; O'Connor, T. P. Lipid Oxidation. In *Encyclopedia of Dairy Sciences*, Roginski, H., Ed. Elsevier: Oxford, 2002; pp 1600−1604.

(6) Pikul, J.; Rudzińska, M.; Teichert, J.; Lasik, A.; Danków, R.; Przybylski, R. Cholesterol oxidation during storage of UHT-treated bovine and caprine milk. *Int. Dairy J.* **2013**, *30*, 29−32.

(7) Wisiiner, L. A. Light induced-oxidations in milk. *J. Dairy Sci.* **1964**, *47*, 216−221.

(8) Dalsgaard, T. K.; Sorensen, J.; Bakman, M.; Nebel, C.; Albrechtsen, R.; Vognsen, L.; Nielsen, J. H. Light-induced protein and lipid oxidation in low-fat cheeses: whey proteins as antioxidants. *Dairy Sci. Technol.* **2011**, *91*, 171−183.

(9) Bradley, D. G.; Min, D. B. Singlet oxygen oxidation of foods. *Crit. Rev. Food Sci. Nutr.* **1992**, *31*, 211−236.

(10) Foote, C. S. Photosensitized oxygenations and role of singlet oxygen. *Acc. Chem. Res.* **1968**, *1*, 104−110.

(11) Foote, C. S.; Denny, R. W. Chemistry of singlet oxygen.VII. Quenching by beta-carotene. *J. Am. Chem. Soc.* **1968**, *90*, 6233−6235.

(12) Bradley, D. G.; Kim, H. J.; Min, D. B. Effects, quenching mechanisms, and kinetics of water soluble compounds in riboflavin photosensitized oxidation of milk. *J. Agric. Food Chem.* **2006**, *54*, 6016−6020.

(13) Rawls, H. R.; van Santen, P. J. Singlet Oxygen: A possible source of original hydroperoxides in fatty acids. *Ann. N. Y. Acad. Sci.* **1970**, *171*, 135−137.

DOI: 10.1021/acs.jafc.5b01614
J. Agric. Food Chem. 2015, 63, 3980−3986

(14) O'Connell, J. E.; Fox, P. F. Significance and applications of phenolic compounds in the production and quality of milk and dairy products: a review. *Int. Dairy J.* **2001**, *11*, 103−120.
(15) Balasundram, N.; Sundram, K.; Samman, S. Phenolic compounds in plants and agri-industrial by-products: antioxidant activity, occurrence, and potential uses. *Food Chem.* **2006**, *99*, 191−203.
(16) Nudda, A.; Correddu, F.; Marzano, A.; Battacone, G.; Nicolussi, P.; Bonelli, P.; Pulina, G. Effects of diets containing grape seed, linseed or both on milk production traits, liver and kidney activities, and immunity of lactating dairy ewes. *J. Dairy Sci.* **2014**, *98*, 1157−1166.
(17) Nudda, A.; McGuire, M. A.; Battacone, G.; Pulina, G. Seasonal variation in conjugated linoleic acid and vaccenic acid in milk fat of sheep and its transfer to cheese and ricotta. *J. Dairy Sci.* **2005**, *88*, 1311−1319.
(18) Silva, L. S.; Trevisan, M. G.; Rath, S.; Poppi, R. J.; Reyes, F. G. R. Chromatographic determination of riboflavin in the presence of tetracyclines in skimmed and full cream milk using fluorescence detection. *J. Braz. Chem. Soc.* **2005**, *16*, 1174−1178.
(19) Dalsgaard, T. K.; Sorensen, J.; Bakman, M.; Vognsen, L.; Nebel, C.; Albrechtsen, R.; Nielsen, J. H. Light-induced protein and lipid oxidation in cheese: Dependence on fat content and packaging conditions. *Dairy Sci. Technol.* **2010**, *90*, 565−577.
(20) Wold, J. P.; Skaret, J.; Dalsgaard, T. K. The action spectrum for photooxidation versus the absorption spectrum of full fat bovine milk. *Food Chem.* **2015**, *179*, 68−75.
(21) Pearson, P. B.; Darnell, A. L.; Weir, J. The thiamine, riboflavin, nicotinic acid and pantothenic acid content of colostrum and milk of the cow and ewe. *J. Nutr.* **1946**, *31*, 51−57.
(22) Kneifel, W.; Mayer, H. K. Vitamin profiles of kefirs made from milks of different species. *Int. J. Food Sci. Techn.* **1991**, *26*, 423−428.
(23) Wold, J. P.; Jorgensen, K.; Lundby, F. Nondestructive measurement of light-induced oxidation in dairy products by fluorescence spectroscopy and imaging. *J. Dairy Sci.* **2002**, *85*, 1693−1704.
(24) Goering, H. K.; Gordon, C. H.; Wrenn, T. R.; Bitman, J.; King, R. L.; Douglas, F. W. Effect of feeding protected safflower oil on yield, composition, flavor, and oxidative stability of milk. *J. Dairy Sci.* **1976**, *59*, 416−425.
(25) Focant, M.; Mignolet, E.; Marique, M.; Clabots, F.; Breyne, T.; Dalemans, D.; Larondelle, Y. The effect of vitamin E supplementation of cow diets containing rapeseed and linseed on the prevention of milk fat oxidation. *J. Dairy Sci.* **1998**, *81*, 1095−1101.
(26) Havemose, M. S.; Weisbjerg, M. R.; Bredie, W. L. P.; Poulsen, H. D.; Nielsen, J. H. Oxidative stability of milk influenced by fatty acids, antioxidants, and copper derived from feed. *J. Dairy Sci.* **2006**, *89*, 1970−1980.
(27) Jung, M. Y. Effects of green tea catechin on the lipid oxidation, volatile compound formation, and losses of retinol and alpha-tocopherol in whole milk during light illumination as compared with ascorbic acid. *Food Sci. Biotechnol.* **2011**, *20*, 1425−1434.
(28) Di Mascio, P.; Devasagayam, T. P. A.; Kaiser, S.; Sies, H. Carotenoids, tocopherols and thiols as biological singlet molecular-oxygen quenchers. *Biochem. Soc. Trans.* **1990**, *18*, 1054−1056.
(29) Yang, W. T.; Lee, J. H.; Min, D. B. Quenching mechanisms and kinetics of alpha-tocopherol and beta-carotene on the photosensitizing effect of synthetic food colorant FD&C Red No. 3. *J. Food Sci.* **2002**, *67*, 507−510.
(30) Jensen, B. M.; Sorensen, J.; Mortensen, G.; Sorensen, M. B.; Dalsgaard, T. K. Effect of antioxidants on oxidation during the production of whey fat concentrate. *J. Agric. Food Chem.* **2011**, *59*, 13012−13017.
(31) Durand, D.; Scislowski, V.; Gruffat, D.; Chilliard, Y.; Bauchart, D. High-fat rations and lipid peroxidation in ruminants: consequences on the health of animals and quality of their products. In *Indicators of Milk and Beef Quality*; Hocquette, J. F., Gigli, S., Eds.; Wageningen Academic Publishers: Wageningen, 2005; pp 137−150.
(32) Roman, O.; Heyd, B.; Broyart, B.; Castillo, R.; Maillard, M. N. Oxidative reactivity of unsaturated fatty acids from sunflower, high oleic sunflower and rapeseed oils subjected to heat treatment, under controlled conditions. *Food Sci. Technol.* **2013**, *52*, 49−59.
(33) Di Trana, A.; Bonanno, A.; Cecchini, S.; Giorgio, D.; Di Grigoli, A.; Claps, S. Effects of Sulla forage (*Sulla coronarium* L.) on the oxidative status and milk polyphenol content in goats. *J. Dairy Sci.* **2015**, *98*, 37−46.
(34) Moñino, I.; Martínez, C.; Sotomayor, J. A.; Lafuente, A.; Jordán, M. J. Polyphenolic transmission to Segureño lamb meat from ewes' diet supplemented with the distillate from rosemary (Rosmarinus officinalis) leaves. *J. Agric. Food Chem.* **2008**, *56*, 3363−3367.
(35) De Feo, V.; Quaranta, E.; Fedele, V.; Claps, S.; Rubino, R.; Pizza, C. Flavonoids and terpenoids in goat milk in relation to forage intake. *Ital. J. Food Sci.* **2006**, *18*, 86−92.
(36) Mukai, K.; Nagai, S.; Ohara, K. Kinetic study of the quenching reaction of singlet oxygen by tea catechins in ethanol solution. *Free Radical Biol. Med.* **2005**, *39*, 752−761.
(37) Frankel, E. N. Antioxidants in lipid foods and their impact on food quality. *Food Chem.* **1996**, *57*, 51−55.
(38) Chavez-Servin, J. L.; Castellote, A. I.; Lopez-Sabater, M. C. Volatile compounds and fatty acid profiles in commercial milk-based infant formulae by static headspace gas chromatography: Evolution after opening the packet. *Food Chem.* **2008**, *107*, 558−569.
(39) García-Martínez, M. C.; Márquez-Ruiz, G.; Fontecha, J.; Gordon, M. H. Volatile oxidation compounds in a conjugated linoleic acid-rich oil. *Food Chem.* **2009**, *113*, 926−931.
(40) Timm-Heinrich, M.; Skall Nielsen, N.; Xu, X.; Jacobsen, C. Oxidative stability of structured lipids containing C18:0, C18:1, C18:2, C18:3 or CLA in sn2-position as bulk lipids and in milk drinks. *Innovative Food Sci. Emerging Technol.* **2004**, *5*, 249−261.
(41) Berradre, M.; Gonzalez, C.; Sulbaran, B.; Fernandez, V. Polyphenols content and antioxidant activity of grape seed extract (Vitis vinifera) malvasia and tempranillo variety. *Rev. Fac. Agron.* **2013**, *30*, 619−631.
(42) Chouchouli, V.; Kalogeropoulos, N.; Konteles, S. J.; Karvela, E.; Makris, D. P.; Karathanos, V. T. Fortification of yoghurts with grape (Vitis vinifera) seed extracts. *Food Sci. Technol.* **2013**, *53*, 522−529.
(43) Huvaere, K.; Nielsen, J. H.; Bakman, M.; Hammershoj, M.; Skibsted, L. H.; Sorensen, J.; Vognsen, L.; Dalsgaard, T. K. Antioxidant properties of green tea extract protect reduced fat soft cheese against oxidation induced by light exposure. *J. Agric. Food Chem.* **2011**, *59*, 8718−8723.
(44) Zanardi, E.; Novelli, E.; Nanni, N.; Ghiretti, G. P.; Delbono, G.; Campanini, G.; Dazzi, G.; Madarena, G.; Chizzolini, R. Oxidative stability and dietary treatment with vitamin E, oleic acid and copper of fresh and cooked pork chops. *Meat Sci.* **1998**, *49*, 309−320.
(45) Van Ba, H.; Amna, T.; Hwang, I. Significant influence of particular unsaturated fatty acids and pH on the volatile compounds in meat-like model systems. *Meat Sci.* **2013**, *94*, 480−488.

DOI: 10.1021/acs.jafc.5b01614
J. Agric. Food Chem. 2015, 63, 3980−3986

Table 1. Composition of Film-Forming Solutions[a]

film type	Gel (mL) (8% w/v)	Gly/Gel (% w/w)	TP (mg)	water (mL)	NS (mL)	TP/Gel (% w/w)	NP/Gel (% w/w, exclude TP)
			Without TP				
Gel	25	20		75			
Gel-0.5CSH	25	20			75		3.28
Gel-1CSH	25	20			75		6.45
Gel-2CSH	25	20			75		13.13
			With TP				
Gel-TP	25	20	18.75	75		0.93	
Gel-0.5CSH-TP	25	20	18.75		75	0.93	3.28
Gel-1CSH-TP	25	20	18.75		75	0.93	6.45
Gel-2CSH-TP	25	20	18.75		75	0.93	13.13

[a]Abbreviations: Gel, gelatin; Gly, glycerol; TP, tea polyphenol; NS, nanoparticle suspensions; NPs, nanoparticles; CSH, chitosan hydrochloride. Gel (or Gel-TP) and Gel-*x*CSH (or Gel-*x*CSH-TP), films prepared with gelatin + nonactive (or active) nanoparticles at the indicated CSH concentrations (mg/mL).

migration of some free TP to the film surface may be required in order to inhibit the initial oxidation, and perhaps both free TP and encapsulated TP within the film matrix are necessary to guarantee long-term oxidative stability. For TP chitosan nanoparticle incorporated films, it is still not known what differences in antioxidant properties would be presented when different free/nanoencapsulated active agent ratios are applied.

In addition to carrying and protecting bioactive compounds, nanoparticles such as blank chitosan nanoparticles can improve the barrier, thermal, and mechanical properties of films such as those based on hydroxypropyl methylcellulose (HPMC),[15] starch,[16] tara gum,[17] and gelatin.[18] Among them, the addition of chitosan nanoparticles with smaller particle sizes resulted in stronger mechanical properties and better barrier properties, as observed by de Moura et al.[15] in HPMC films. Therefore, the inclusion of antioxidants in chitosan nanoparticles into polymer matrices might bring a twofold advantage: the performance improvement of food packaging/edible film material and the provision of an additional antioxidant function.[19]

In this study, TP was encapsulated in the matrix of CSH and SBE-β-CD nanoparticles and the TP-containing nanoparticles were added into gelatin films. As a natural antioxidant, TP is subject to oxidation. In order to determine if encapsulation improved the antioxidative lifetime of TP and protected it from degradation, gelatin films were also prepared embedded with free TP. The objective of this study was to investigate the antioxidant activities of gelatin films incorporated with free TP and TP-loaded CSH-SBE-β-CD nanoparticle (CSN) suspensions with different encapsulation efficiencies.

MATERIALS AND METHODS

Materials. Gelatin (type B from bovine skin) and glycerol were purchased from China Medicine (Group) Shanghai Chemical Reagent Co. (Shanghai, People's Republic of China). CSH, molecular weight 100 kDa and degree of deacetylation 86%, derived from crab shells was obtained from Golden-Shell Biochemical Co., Ltd. (Hangzhou, People's Republic of China). SBE-β-CD (food grade), molecular weight 2.082 kDa and an average degree of substitution 6, was purchased from Kunshan Chemical Industries Co., Ltd. (Jiangsu, People's Republic of China). TP, polyphenol content ≥98% and catechins ≥90% (determined by manufacturer), was obtained from Qiangsheng Medicine Science Technology Co., Ltd. (Shanghai, People's Republic of China). 2,2-Diphenyl-1-picrylhydrazyl (DPPH) was purchased from Sigma Chemical Co. (St. Louis, MO, USA). All other reagents were analytical grade.

Preparation of CSNs. CSNs were prepared according to a previously reported method,[20] with minor modifications. Briefly, 24 mL of 2, 4, or 8 mg/mL SBE-β-CD in distilled water was added dropwise to 72 mL of 0.5, 1, or 2 mg/mL CSH aqueous solutions, respectively, with vigorous magnetic stirring, leading to the formation of nanoparticles via the ionic gelation mechanism. The CSH/SBE-β-CD mass ratios were controlled at 3/4 (w/w) in all cases. TP-loaded CSNs were prepared by adding an aqueous TP solution to the SBE-β-CD solution to obtain a concentration of 1 mg of TP/mL and stirred for 24 h at room temperature to promote inclusion complex formation. The TP-SBE-β-CD solution was combined with the CSH solution. The nanoparticle suspensions were immediately analyzed or used in film forming. All TP-loaded films contained the same total amount of TP.

Characterization of CSNs. The *z*-average particle size and size distribution of the nanoparticle suspensions were determined by dynamic light scattering (DLS, Zeta-PALS + BI-90Plus, Brookhaven Instrument Co., Holtsville, NY) at a fixed scattering angle of 90° at 25 ± 1 °C. All measurements were run in quadruplicate. The morphology of nanoparticles was examined by a high-performance digital imaging transmission electron microscope (TEM, JEOL 2100, Hitachi High-Technologies Corporation, Tokyo, Japan). The TEM samples were prepared by placing one drop of the suspension on a copper grid, staining with 2% (w/v) phosphotungstic acid, and air drying. Once dried, the sample was imaged by the microscope with an accelerating voltage of 100 kV.

Encapsulation Efficiency of TP-Loaded CSNs. The encapsulation efficiency (EE) of TP in CSNs was determined according to Hu et al.[21] Briefly, TP-loaded nanoparticles were carefully transferred into an AmiconUltra-4 centrifugal filter device (Millipore Co., Billerica, MA) with a 10000 MW cutoff Ultracel membrane. After centrifugation at 4000*g* for 10 min, the concentration of TP in the ultrafiltrate was determined by the Folin−Ciocalteu method. Prior to measurement, the filtrate was diluted fivefold with distilled water. The total content of TP was calculated from the TP concentration in the aqueous medium before CSN formation. The EE of TP was calculated using eq 1:

$$\mathrm{EE}\ (\%) = (((\text{total content of TP}) - (\text{content of TP in ultrafiltrate}))/(\text{total content of TP})) \times 100 \quad (1)$$

Preparation of Films. The gelatin films were prepared by our previously reported method with some modifications.[22] Briefly, 8% (w/v) gelatin solutions were prepared by hydrating gelatin powders in distilled water for 1 h at room temperature and then dissolved by heating at 65 °C with continuous stirring. Glycerol (1.6%) was added as a plasticizer in order to make the films less brittle and easier to handle. The composition of the gelatin films, including films with TP-loaded nanoparticle formulations, are shown in Table 1. The 8% gelatin−1.6% glycerol solutions (25 mL) were diluted with water (75 mL) or nanoparticle suspensions to 2% (w/v) gelatin in all film-forming solutions. A homogeneous solution was achieved after stirring for 1 h. Films were prepared by casting the 2% gelatin solutions (35

DOI: 10.1021/acs.jafc.5b00003
J. Agric. Food Chem. 2015, 63, 3987−3995

mL) in square Petri dishes (10 cm × 10 cm) and drying at 25 °C in an oven to a constant weight (approximately 36 h). The films were peeled off and conditioned at 25 °C and 53% relative humidity (RH) for at least 48 h in a controlled environmental chamber (Shengxing Experimental Equipment Co., Ltd. Shanghai, People's Republic of China) before testing.

Total Phenol Assay. The total phenolic content of films was estimated by the Folin−Ciocalteu method according to Jouki et al.[23] Initially cut conditioned films (2.5 cm × 2.5 cm) were weighed and redissolved in 10 mL of distilled water at 40 °C for 1 min and centrifuged (10000*g*, 10 min) at 20 °C. Supernatant (1 mL) and distilled water (1 mL) were thoroughly mixed with Folin−Ciocalteu reagent (5 mL, 10% v/v). After 6 min, 4 mL of 7.5% (w/v) sodium carbonate was added. The mixture was stirred thoroughly and allowed to stand at room temperature for 60 min prior to recording the absorbance at 765 nm with a spectrophotometer (Shimadzu UV-2450, Japan). The concentration of total phenol was expressed as (mg of gallic acid equivalent)/(g of film sample)according to eq 2

$$\text{total phenolic content} = (C \times V)/M \tag{2}$$

where C is the concentration of gallic acid obtained from the standard curve (mg/mL), V is the volume of the supernatant (mL), and M is the weight of film (g).

Characterization of Films. *Visual Appearance and Light Transmission.* The film-forming solutions and films were evaluated visually for uniform color and the presence of insoluble particles. The ultraviolet and visible light transmittance properties of the films were measured according to the method of Bitencourt et al.[9] Film samples of 10 × 25 mm were placed in the light path of a spectrophotometer (UV-2450, Shimadzu, Tokyo, Japan). Transmittance was recorded from 200 to 800 nm in triplicate.

Microstructure. The cross-section morphology of films was analyzed using a field emission scanning electron microscope (SEM, S-4800, Hitachi, Japan). Films were cryofractured by immersion in liquid nitrogen and conditioned in a desiccator at 25 °C before measurement. Samples were mounted on the specimen holder using double-sided adhesive tapes and then sputter coated with gold under vacuum. The samples were scanned with an accelerating voltage of 1 kV.

An atomic force microscope (AFM, Bruker Dimension Icon, Bruker Co., Germany) was used to observe the surface morphology of films in tapping mode, and 50 μm × 50 μm images under ambient conditions were obtained. All samples were analyzed in triplicate using a Bruker Nanoscope software (version 1.40) to calculate the roughness values. The obtained parameters were R_a, which is the arithmetic average of the absolute values of the surface height deviations (Z) measured from the mean plane, and R_q, which is the root-mean-square average of height deviations taken from the mean image data plane. R_a and R_q were calculated from eqs 3 and 4:

$$R_a = \frac{1}{N}\sum_{j=1}^{N} |Z_j| \tag{3}$$

$$R_q = \sqrt{\frac{\sum Z_i^2}{N}} \tag{4}$$

Determination of Antioxidant Activities in Vitro. The in vitro antioxidant properties of films were performed on the basis of the procedure reported by Wu et al.[10] The supernatant was prepared as stated in Total Phenol Assay and was collected for further analyses, including ferric reducing power and DPPH radical scavenging activity.

Ferric Reducing Power. The determination of reducing power was measured as described by Li et al.[24] with slight modifications. Briefly, 1.0 mL of redissolved film solution was mixed with 2.5 mL of phosphate buffer (0.2 M, pH 6.6) and 2.5 mL potassium ferricyanide (1%, w/v). After incubation at 50 °C for 20 min and rapid cooling, 2.5 mL of trichloroacetic acid (10%, w/v) was added to the mixture followed by centrifugation at 10000*g* for 10 min. The obtained supernatant (2.5 mL) was treated with 2.5 mL of distilled water and 0.5 mL of 0.1% ferric chloride (w/v). The absorbance of the reaction mixture was recorded at 700 nm (Shimadzu UV-2450, Japan) after 10 min of reaction. A higher absorbance indicates higher reducing power.

DPPH Radical Scavenging Activity. The method described by Yi et al.[25] was used to evaluate the DPPH radical scavenging activity, with slight modifications. A 2 mL portion of film supernatant was mixed with 2.5 mL (0.1 mM) of DPPH dissolved in ethanol. The mixture was kept in the dark for 30 min at room temperature followed by centrifugation at 8000*g* for 5 min. The absorbance was measured at 517 nm. The assay was carried out in triplicate. The DPPH radical scavenging activity was calculated as shown in eq 5

$$\text{DPPH scavenging (\%)} = 100 \times (1 - (A_s - A_b)/A_c) \tag{5}$$

where A_s represents the absorbance of sample after film supernatant was added, A_b the absorbance of film supernatant alone, and A_c the absorbance of the control as distilled water was mixed with the DPPH solution instead of the sample.

POV and TBARS of Sunflower Oil in Contact with or without Touching Films. Two methods were used to evaluate the antioxidant properties of films in contact with oil or above the headspace of the oil. The antioxidant properties of the films in contact with the oil was determined by the method of Bao et al.[13] The films were transformed into 4 cm × 4 cm bags by heat sealing, and 1 mL of fresh sunflower oil was added to the bags. The antioxidant properties of the films placed over the headspace of the oil were determined according to Jongjareonrak et al.[4] and Wu et al.[26] A 10 mL portion of fresh sunflower oil was poured into a glass cell (30 mm diameter × 50 mm height) and covered with the film (4 cm × 4 cm) sealed with glue and Parafilm. All samples were stored in a humidity-controlled chamber (53 ± 2% RH) at 28 °C. Samples for peroxide value (POV) and thiobarbituric acid reactive substance (TBARS) analysis were collected at intervals of 1 week over a period of 6 weeks. Samples without film packaging were also assessed as control.

POV Analysis. POV was determined by theAOCS Cd 8-53 Official Method.[27] The amount of oil sample analyzed varied and depended on its oxidation degree. The oil sample was dissolved in 50 mL of an acetic acid/chloroform mixture (3/2 v/v) within a 250 mL Erlenmeyer flask. Then saturated KI solution (0.5 mL) was added and the flask was allowed to stand for 1 min with occasional agitation. After addition of distilled water (50 mL), the mixture was titrated against sodium thiosulfate (0.01 M) with starch as an indicator. A blank titration was treated the same waybut without oil. POV (mequiv of oxygen/kg) was calculated using eq 6:

$$\text{POV} = 1000 \times S \times c/m \tag{6}$$

In this formula, S is the volume of sodium thiosulfate solution (blank corrected) in mL, c is the normality of the sodium thiosulfate solution, and m is the weight of the oil sample in grams.

TBARS Analysis. TBARS were detected using the AOCS Cd 19-90 method.[28] The oil sample (50−200 mg) was solubilized in 10 mL of 1-butanol, mixed with 10 mL of 0.2% TBA in 1-butanol, heated in a 95 °C water bath for 2 h, and rapidly cooled in an ice bath. The absorbance was measured at 532 nm against a corresponding blank (reaction with all the reagents and treatments except for the oil). The standard curve was calculated from the TBARS reaction of a series of aliquots (0.1−1 mL) of 0.2 mM 1,1,3,3-tetraethoxypropane (95%) prepared in 1-butanol. The results were expressed as μmol of malonaldehyde (MDA)/g of oil (n = 3).

Statistical Analysis. Data were presented as mean value ± standard deviation. The data were analyzed by one-way analysis of variance (ANOVA) using the SPSS 19.0 package (IBM, New York). Duncan's multiple range test was used to determine the significant differences of the mean values ($P < 0.05$).

RESULTS AND DISCUSSION

Impact of CSH Concentration on CSNs Size Distribution and Morphology. As observed from TEM in Figure 1a, regular spherical-shaped nanoparticles can be synthesized by ionic cross-linking between the positively charged amine of

DOI: 10.1021/acs.jafc.5b00003
J. Agric. Food Chem. 2015, 63, 3987−3995

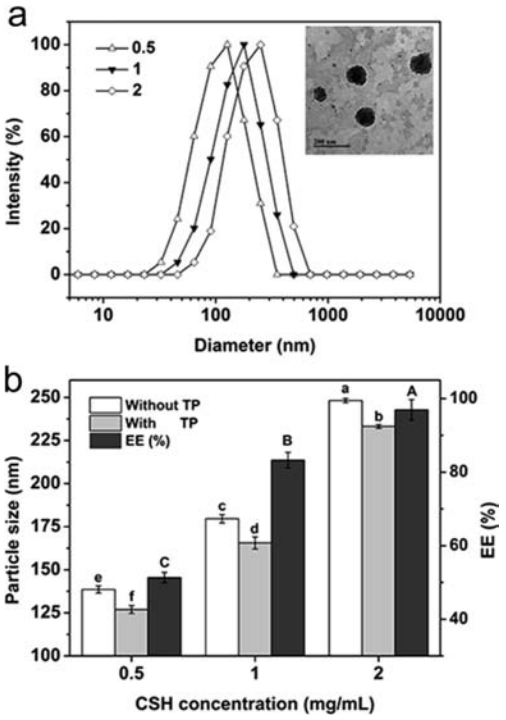

Figure 1. (a) Particle diameter distributions of TP-loaded chitosan nanoparticles prepared with different CSH concentrations (0.5, 1, and 2 mg/mL) and (inset) TEM of TP-CSNs prepared with 1 mg/mL of CSH (CSH/CSH-SBE-β-CD mass ratio is 3/4). The scale bar indicates 200 nm. (b) Particle size as a function of CSH concentration for nanoparticles with or without TP and encapsulation efficiency (EE) of related TP-loaded nanoparticles. Different lower-case or upper-case letters indicate significant differences ($P < 0.05$) for particle size and EE, respectively.

CSH and negatively charged sulfonate groups of SBE-β-CD. EE and release of TP may be related to particle size. Therefore, three particle size ranges were produced (Figure 1a) using three different concentrations of CSH (0.5, 1, and 2 mg/mL) to study the effect of EE and particle size on accessibility of free radicals to TP in gelatin films and/or nanoparticles embedded in gelatin films. Increased concentrations of the cationic and anionic components increase particle size and also entrap more TP, but in solution a larger particle size has been shown to lower TP release.[21] In this study particle size and EE increased as the nanoparticle mass concentration increased (Figure 1b). In a study of protein and peptide loading of nanoparticles, Grenha et al.[29] also reported that larger particles are produced by higher concentrations of chitosan. The mass ratios, salt concentration, and pH also affect particle size but were kept constant in this study.[30]

Incorporation of TP decreased the particle size of TP-CSNs in comparison to the corresponding blank CSNs (Figure 1b), and the smaller particle size may be attributed to a greater cross-linking density between the numerous OH groups of catechins, chitosan, and cyclodextran.[21] Vitamin C was also reported to decrease CSN size by a similar mechanism.[12] As the concentration of particle formers (CSH and SBE-β-CD) increased, the amount of nanoparticles available for encapsulation of TP increased. More TP-SBE-β-CD inclusion complexes were incorporated in the nanoparticles because more TP-SBE-β-CD inclusion complexes were formed as the concentration of SBE-β-CD increased simultaneously.[31]

Free TP Content in the Redissolved Film Solution. The free TP content of films was estimated by measuring the total phenolic content of the supernatant after dissolving the TP-CSN films and removing the CSNs particles by centrifugation. After dissolution in water no visible precipitates were observed and the resulting solutions were similar to the original film-forming solutions showing opacity. Li et al.[32] also reported similar results when sodium caseinate films incorporated with nanoparticles were redissolved. The total phenolic content of blank gelatin films and films with blank CSN nanoparticles were the same, 1.5 mg of gallic acid/g of film (Figure 2a). This value is similar to that reported for silver carp skin gelatin film[10] and may account for some of the antioxidant properties of the gelatin film alone. Total phenol content observed in the blank gelatin film might be attributed to the presence of amino acid residues, such as tyrosine and histidine, since these amino acids are able to reduce the Folin−Ciocalteu reagent.[33] The total phenolic content of the gelatin films increased after adding TP or TP-CSNs. Increasing the CSH concentration resulted in a significant ($P < 0.05$) decrease of the extractable phenols in the supernatant due to loss by entrapment of TP in the nanoparticles, which was related to EEs. The total phenolic content was inversely related to EE, revealing the stability of TP-loaded nanoparticles during the process of film forming.

Distribution of TP and CSNs in Films Analyzed by SEM and AFM. Because the TP and TP-CSNs are fixed in a solid film matrix, the accessibility of oxygen and lipid radicals to TP may depend on the proximity of the TP-CNS to the film surface. The cross-section morphology (by SEM) and surface morphology (by AFM) of gelatin films with nanoparticles with or without TP are shown in parts a and b of Figure 3, respectively. The cross-section of films containing TP appear more compact and smooth in comparison to the blank gelatin film (Figure 3a) and may be due to more hydrogen bonding because of protein−polyphenol interactions.[10] Cross sections of the films showed the disappearance of microvoids (granular appearance) in films containing CSNs or TP-CSNs, indicating that the nanoparticles were well dispersed throughout the film network.

Further support of the interaction between hydrophilic TP and gelatin proteins was suggested by the reduction of surface roughness (R_q and R_a in Figure 3b). Smaller CSNs had surface characteristics similar to that of the control (data not shown); however, larger particles increased the roughness of the surface microstructure from about 3.3 nm in Gel to 6.1 in Gel-2CSH films. Li et al.[32] reported similar results in the surface properties of sodium caseinate films upon adding thymol-loaded zein nanoparticles. The large accumulation of nanoparticles that formed enriched regions on the film surface also is the cause of the more smooth cross-sectional structure at higher CSN concentrations observed by SEM (Figure 3a).

Appearance and Light Transmission. The appearance of packaged food products, including transparency, directly affects consumer acceptability and assessment of quality.[14] The opaqueness of the gelatin solutions increased with increasing concentration of CSNs and corresponding increase in particle size (Figure 4a). However, unlike the case for the solutions, the films were transparent with smooth surfaces. All films had a homogeneous appearance without visible insoluble particles regardless of the CSH concentration, as shown in Figure 4b. Films containing free TP presented a stronger yellowish color due to the brown color of TP itself, which was reduced as the EE increased. The uniform distribution and stability of CSNs in

DOI: 10.1021/acs.jafc.5b00003
J. Agric. Food Chem. 2015, 63, 3987−3995

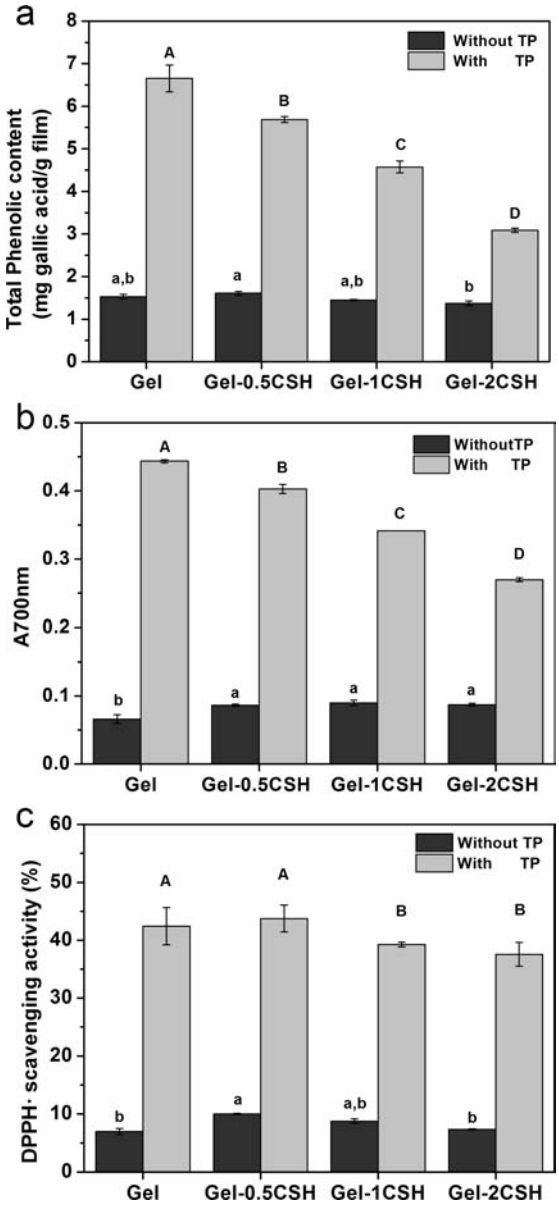

Figure 2. (a) Total phenolic content of gelatin-based films containing different nanoparticles. In vitro antioxidant antivities of gelatin-based films containing different nanoparticles: (b) reducing power; (c) DPPH radical scavenging activity. Different lower-case or upper-case letters indicate significant differences ($P < 0.05$) for nonactive (without TP) and active (with TP) gelatin-based films, respectively. Abbreviations: Gel, gelatin; TP, tea polyphenol; CSH, chitosan hydrochloride; Gel and Gel-*x*CSH, film-formation solutions or films prepared with gelatin + nonactive (or active) nanoparticles at the indicated CSH concentrations (mg/mL).

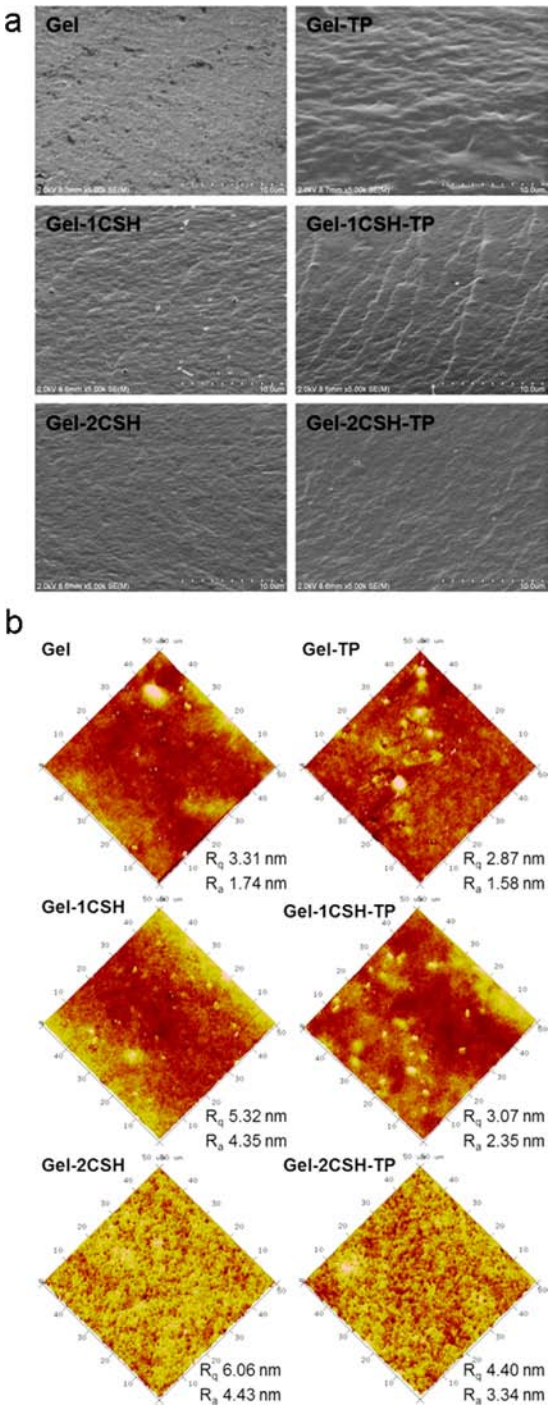

Figure 3. (a) SEM micrographs (magnification 5000×) of cross sections of gelatin films after cryofracturing containing different nanoparticles. (b) Surface micrographs and (inset) roughness values (R_q and R_a) obtained by AFM of gelatin films. Abbreviations: Gel, gelatin; TP, tea polyphenol; CSH, chitosan hydrochloride; Gel (or Gel-TP) and Gel-*x*CSH (or Gel-*x*CSH-TP), films prepared with gelatin + nonactive (or active) nanoparticles at the indicated CSH concentrations (mg/mL).

the film-forming solutions and resulting films (Figure 3) suggest that controlled release of TP by entrapment in nanoparticles may occur.[14]

Gelatin-based films have excellent UV barrier properties due to the UV absorption of peptide bonds in the polypeptide chains and aromatic residues of phenylalanine and tyrosine in gelatin.[34] Incorporation of TP into the gelatin films further decreased the values of light transmission in the near-UV range (250−400 nm) in comparison to the gelatin film alone (Figure 4c). TP in gelatin films also slightly decreased the percentage of transmittance in the visible range, below 500 nm, due to the brown coloration of TP. It is of interest to note that the blank CSN-included films showed no significant change in the light barrier properties in comparison to the blank film, and all TP incorporated nanoparticles showed similar light transmission despite the difference in EE or particle size in comparison to the film with free TP. These results may presumably be

DOI: 10.1021/acs.jafc.5b00003
J. Agric. Food Chem. 2015, 63, 3987−3995

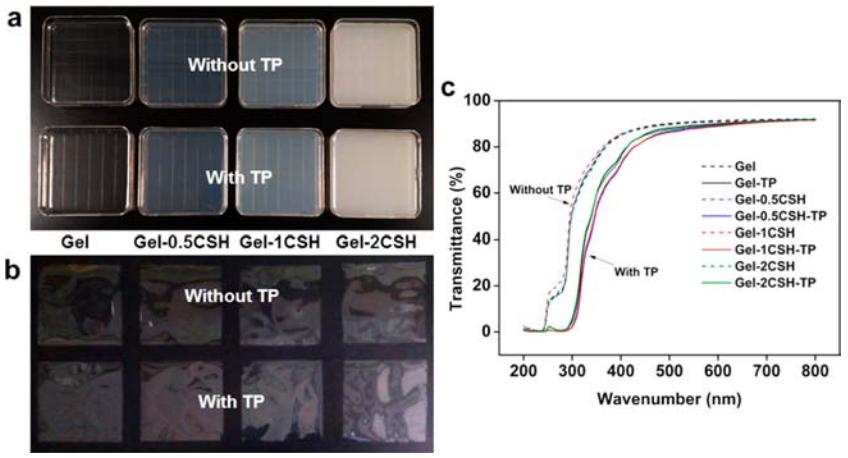

Figure 4. Visual aspects of various gelatin (a) film-forming solutions and (b) films. (c) Ultraviolet and visible light barrier properties of different gelatin films (wavelengths in the 200−800 nm range). In (c) the dashed lines are either Gel alone or Gel-*x*CSH (no TP) and the solid lines are Gel-TP-CSH. Abbreviations: Gel, gelatin; TP, tea polyphenol; CSH, chitosan hydrochloride; Gel and Gel-*x*CSH, film-formation solutions or films prepared with gelatin + nonactive (or active) nanoparticles at the indicated CSH concentrations (mg/mL).

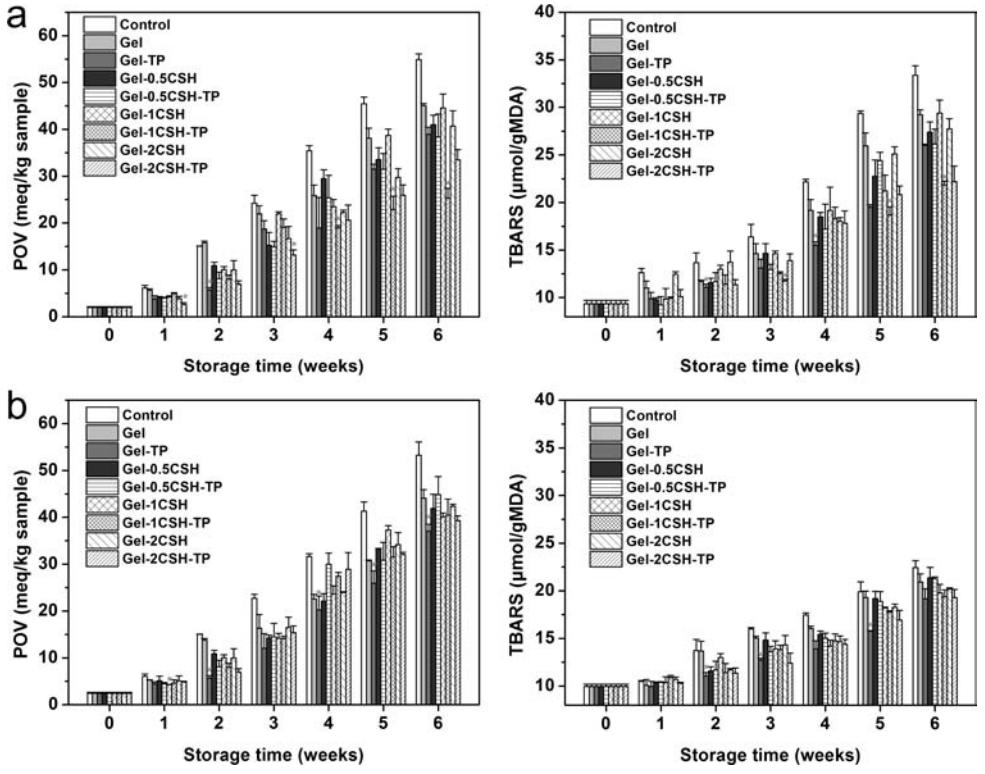

Figure 5. Antioxidant activities of gelatin-based films containing different nanoparticles on (a) oils in bags fabricated by films and (b) oils in cells covered by films. Formations of POV (left) and TBARS (right) were measured separately during storage. Asterisks indicate significant ($P < 0.05$) differences. Abbreviations: control, sunflower oil without film protection; Gel, gelatin; TP, tea polyphenol; CSH, chitosan hydrochloride; Gel (or Gel-TP) and Gel-*x*CSH (or Gel-*x*CSH-TP), films prepared with gelatin + nonactive (or active) nanoparticles at the indicated CSH concentrations (mg/mL).

attributed to the uniform dispersion of CSNs into the gelatin matrix. Films incorporated with TP with a higher UV/visible barrier can better prevent the lipid oxidation of the food product.

In Vitro Antioxidant Activities of Gelatin Films. The ferric reducing power assay is commonly used to study the antioxidant capacity of plant polyphenols.[35] Polyphenols, such as EGCG, are able to contribute a hydrogen atom ($H^{\bullet}$) to oxygen fatty acid radicals ($RO^{\bullet}$) to break the free radical chain reaction. Since the substrate for the ferric reducing power assay was the supernatant of the dissolved film, the assay had a profile (Figure 2b) very similar to that of the total phenolic content (Figure 2a), because the latter assay also used the film supernatant. These two assays verify the increasing antioxidant activity of the films as the EE of the nanoparticles decreased. An increase in the initial amount of free TP within the gelatin matrix led to a higher reducing capacity.

The DPPH radical scavenging activity, also associated with antioxidant activity, is shown in Figure 2c. The DPPH radical scavenging activity did not decrease with increasing EE. The

DOI: 10.1021/acs.jafc.5b00003
J. Agric. Food Chem. 2015, 63, 3987−3995

scavenging activity value of the TP-CSN films was reduced significantly ($P < 0.05$) only for CSH concentrations above 0.5 mg/mL and remained constant as the concentration increased. The concentration-independent fluctuation was primarily due to the antioxidant properties of chitosan.[35−37] The radical scavenging capacity of chitosan is believed to be related to the formation of stable radicals from the reaction between free radicals and residual free amino (NH_2) groups. The NH_2 groups could also form ammonium (NH^{3+}) groups by absorbing hydrogen ions from the solution.[35,37] The antioxidant properties of chitosan could also explain the slightly higher antioxidant activity (in the case of reducing power and DPPH) when blank CSN nanoparticles were added.

Antioxidant Activities of Gelatin Films on Sunflower Oil. Sunflower oil is sensitive to oxidation and rancidity because of its high content (~60%) of polyunsaturated linoleic acid. Analyses of POV and TBARS, corresponding to the primary and secondary lipid oxidation products, respectively, were performed to monitor the efficacy of films in inhibiting oil autoxidation.

Antioxidant Activities on Oils within Bags. The antioxidant proprieties of TP in liquid lipid systems such as bulk oil, oil on cellulose carrier, or emulsion have been determined.[38] In this study TP was immobilized in a solid matrix of protein, CSN, or cyclodextrin. As shown in Figure 5a, with increasing storage period the POV and TBARS of oils increased continuously with time regardless of the different packaging films. Lipid oxidation was lower in oils packaged in films in comparison to that in the control oil which was exposed to air. The difference in POV or TBARS inhibition was more pronounced after 3 weeks of storage ($P < 0.05$). This inhibitory effect may be dependent on the presence of antioxidants in the film. The oxygen barrier properties of the films may also play a role in inhibiting the POV and TBARS of oils.[13]

The film with the free homogeneously distributed TP exhibited the least oil oxidation in the first 4 weeks. There was a more conspicuous reduction in the antioxidant effect in comparison to that of 1CSH-TP and 2CSH-TP after 4 weeks, although the accumulated oxidation products (total TBARS) were significantly lower than that of the blank gelatin film ($P < 0.05$). TP in gelatin films is also subject to oxidation. The antioxidant activity of phenolic compounds such as TP is based on the quenching of free radicals of fatty acids; however, the antioxidant loses its activity at the same time.[38] Wu et al.[10] reported that the antioxidant activities of green tea extract in gelatin films decreased during storage due to the oxidation of TP. In this study the oil antioxidant ability of 1CSH-TP and 2CSH-TP remained high throughout the 6 week storage study in addition to 0.5CSH-TP.

No significant differences ($P > 0.05$) in TBARS or POV were observed between the blank gelatin films and those containing CSNs without TP. The protective effect of these films without TP in delaying the rancidity of sunflower oil is likely due to their oxygen barrier properties. The results also suggest that the DPPH scavenging ability of CS did not contribute to reducing fatty acid oxygen free radicals here. Encapsulation of TP in the CSNs greatly enhanced the oxidative protection of oils, especially when the EE of TP-loaded nanoparticles was high: 80% and 100% ($P < 0.05$). These results suggest that TP in contact with the oil is able to react with the reactive oxygen species at the package surface or diffuse from nanoparticles to the films and then into oil. TP-loaded nanoparticles with 50% EE did not show an inhibitory effect significantly higher than that of free TP. This result is not in agreement with the results reported by Imran et al.[14] in the control of food pathogens using nisin nanoliposome embedded films, showing that the POV or TBARS inhibition was not only dependent on the EE but also on the oxidation stability of active agents and other factors. In this study after 6 weeks oil oxidation control was lower for ~80% encapsulated than for ~100% encapsulated TP and free TP. This may be due to an optimum partition of free TP and encapsulated TP. The free TP reacts first to reduce the initial oxidative rancidity and later in the storage period TP released from nanoparticles continue to quench free radicals.

Antioxidant Activities of Gelatin Films Not in Contact with Oils. Containers or cells containing oil with a film over the headspace have been used to evaluate the antioxidant capacity of films[2,39] and also to measure the oxygen barrier properties of films.[26] POV and TBARS increased gradually with increasing storage time for all samples, with the uncovered oil having the highest values (Figure 5b). The film with free TP had the lowest POV and TBARS during all the storage times tested. Oxygen concentration in the headspace is one of the most important factors controlling the rate of lipid oxidation.[2] The homogeneous distribution of TP in the film may more efficiently scavenge singlet oxygen in comparison to the heterogeneous distribution of encapsulated TP.[40]

The incorporation of neither CSNs nor TP-CSN EEs had significant effects ($P > 0.05$) on oxidative rancidity. However, there was a slight decrease in POV and TBARS values (Figure 5b) with increasing CSN concentrations. This result suggests that the oxygen barrier was improved with increasing CSN concentration, possibly due to lower oxygen permeability of the nanoparticles and larger size of the aggregates at the surface (Figure 3b).[41] In addition, the reduction of moisture content (data not shown) would also reduce the film's permeability to oxygen.[2]

In summary, we prepared gelatin films incorporated with different free/encapsulated TP ratios through the fabrication of CSNs with three different EEs. The reduced oxidation of sunflower oil suggests that the incorporation of TP in chitosan nanoparticle form can improve the antioxidant effects of gelatin films. There may be an optimum partition of free and encapsulated TP to control oil oxidation over a long term (6 weeks) without compromising the basic physicochemical attributes of gelatin films. The results found in this study can be used in better designs of active edible film/packaging systems.

AUTHOR INFORMATION

Corresponding Author

*F.Z.: tel, +86-510-85197876; fax, +86-510-85197876; e-mail, fzhong@jiangnan.edu.cn.

Funding

This work was financially supported by National 863 Program 2011BAD23B02, 2013AA102207, National Natural Science Foundation of China 31171686, 31401532, the Natural Science Foundation of Jiangsu Province BK2012556, 111 project-B07029 and PCSIRT0627.

Notes

The authors declare no competing financial interest.

ABBREVIATIONS USED

TP, tea polyphenol; CSH, chitosan hydrochloride; SBE-β-CD, sulfobutyl ether-β-cyclodextrin sodium; CSN, CSH-SBE-β-CD

DOI: 10.1021/acs.jafc.5b00003
J. Agric. Food Chem. 2015, 63, 3987−3995

nanoparticle; BHA, butylated hydroxyanisole; BHT, butylated hydroxytoluene; TBHQ, *tert*-butylhydroquinone; PG, propyl gallate; EGCG, epigallocatechin gallate; EE, encapsulation efficiency; UV, ultraviolet; SEM, scanning electron microscope; AFM, atomic force microscope; POV, peroxide value; TBARS, thiobarbituric acid reactive substances

REFERENCES

(1) Gómez-Estaca, J.; López-de-Dicastillo, C.; Hernández-Muñoz, P.; Catalá, R.; Gavara, R. Advances in antioxidant active food packaging. *Trends Food Sci. Technol.* **2014**, *35*, 42−51.

(2) Osés, J.; Fernández-Pan, I.; Ziani, K.; Maté, J. I. Use of edible films based on whey protein isolate to protect foods rich in polyunsaturated fatty acids. *Eur. Food Res. Technol.* **2007**, *227*, 623−628.

(3) Colín-Chávez, C.; Soto-Valdez, H.; Peralta, E.; Lizardi-Mendoza, J.; Balandrán-Quintana, R. R. Fabrication and Properties of Antioxidant Polyethylene-based Films Containing Marigold (Tagetes erecta) Extract and Application on Soybean Oil Stability. *Packag. Technol. Sci.* **2013**, *26*, 267−280.

(4) Jongjareonrak, A.; Benjakul, S.; Visessanguan, W.; Tanaka, M. Antioxidative activity and properties of fish skin gelatin films incorporated with BHT and α-tocopherol. *Food Hydrocolloids* **2008**, *22*, 449−458.

(5) López-de-Dicastillo, C.; Pezo, D.; Nerín, C.; López-Carballo, G.; Catalá, R.; Gavara, R.; Hernández-Muñoz, P. Reducing Oxidation of Foods Through Antioxidant Active Packaging Based on Ethyl Vinyl Alcohol and Natural Flavonoids. *Packag. Technol. Sci.* **2012**, *25*, 457−466.

(6) Qin, Y. Y.; Yang, J. Y.; Lu, H. B.; Wang, S. S.; Yang, J.; Yang, X. C.; Chai, M.; Li, L.; Cao, J. X. Effect of chitosan film incorporated with tea polyphenol on quality and shelf life of pork meat patties. *Int. J. Biol. Macromol.* **2013**, *61*, 312−6.

(7) Sanches-Silva, A.; Costa, D.; Albuquerque, T. G.; Buonocore, G. G.; Ramos, F.; Castilho, M. C.; Machado, A. V.; Costa, H. S. Trends in the use of natural antioxidants in active food packaging: a review. *Food Addit. Contam., Part A* **2014**, *31*, 374−95.

(8) Pastor, C.; Sánchez-González, L.; Chiralt, A.; Cháfer, M.; González-Martínez, C. Physical and antioxidant properties of chitosan and methylcellulose based films containing resveratrol. *Food Hydrocolloids* **2013**, *30*, 272−280.

(9) Bitencourt, C. M.; Fávaro-Trindade, C. S.; Sobral, P. J. A.; Carvalho, R. A. Gelatin-based films additivated with curcuma ethanol extract: Antioxidant activity and physical properties of films. *Food Hydrocolloids* **2014**, *40*, 145−152.

(10) Wu, J.; Chen, S.; Ge, S.; Miao, J.; Li, J.; Zhang, Q. Preparation, properties and antioxidant activity of an active film from silver carp (Hypophthalmichthys molitrix) skin gelatin incorporated with green tea extract. *Food Hydrocolloids* **2013**, *32*, 42−51.

(11) Folch-Cano, C.; Jullian, C.; Speisky, H.; Olea-Azar, C. Antioxidant activity of inclusion complexes of tea catechins with β-cyclodextrins by ORAC assays. *Food Res. Int.* **2010**, *43*, 2039−2044.

(12) Aresta, A.; Calvano, C. D.; Trapani, A.; Cellamare, S.; Zambonin, C. G.; De Giglio, E. Development and analytical characterization of vitamin(s)-loaded chitosan nanoparticles for potential food packaging applications. *J. Nanopart. Res.* **2013**, *15*, 1592−11603.

(13) Bao, S.; Xu, S.; Wang, Z. Antioxidant activity and properties of gelatin films incorporated with tea polyphenol-loaded chitosan nanoparticles. *J. Sci. Food Agric.* **2009**, *89*, 2692−2700.

(14) Imran, M.; Revol-Junelles, A.-M.; René, N.; Jamshidian, M.; Akhtar, M. J.; Arab-Tehrany, E.; Jacquot, M.; Desobry, S. Microstructure and physico-chemical evaluation of nano-emulsion-based antimicrobial peptides embedded in bioactive packaging films. *Food Hydrocolloids* **2012**, *29*, 407−419.

(15) de Moura, M. R.; Aouada, F. A.; Avena-Bustillos, R. J.; McHugh, T. H.; Krochta, J. M.; Mattoso, L. H. C. Improved barrier and mechanical properties of novel hydroxypropyl methylcellulose edible films with chitosan/tripolyphosphate nanoparticles. *J. Food Eng.* **2009**, *92*, 448−453.

(16) Chang, P. R.; Jian, R.; Yu, J.; Ma, X. Fabrication and characterisation of chitosan nanoparticles/plasticised-starch composites. *Food Chem.* **2010**, *120*, 736−740.

(17) Antoniou, J.; Liu, F.; Majeed, H.; Zhong, F. Characterization of tara gum edible films incorporated with bulk chitosan and chitosan nanoparticles: A comparative study. *Food Hydrocolloids* **2015**, *44*, 309−319.

(18) Hosseini, S. F.; Rezaei, M.; Zandi, M.; Farahmandghavi, F. Fabrication of bio-nanocomposite films based on fish gelatin reinforced with chitosan nanoparticles. *Food Hydrocolloids* **2015**, *44*, 172−182.

(19) Noronha, C. M.; de Carvalho, S. M.; Lino, R. C.; Barreto, P. L. Characterization of antioxidant methylcellulose film incorporated with alpha-tocopherol nanocapsules. *Food Chem.* **2014**, *159*, 529−35.

(20) Aresta, A.; Calvano, C. D.; Trapani, A.; Zambonin, C. G.; De Giglio, E. α-Tocopherol/chitosan-based nanoparticles: characterization and preliminary investigations for emulsion systems application. *J. Nanopart. Res.* **2014**, *16*, 1−12.

(21) Hu, B.; Pan, C.; Sun, Y.; Hou, Z.; Ye, H.; Hu, B.; Zeng, X. Optimization of Fabrication Parameters To Produce Chitosan-Tripolyphosphate Nanoparticles for Delivery of Tea Catechins. *J. Agric. Food Chem.* **2008**, *56*, 7451−7458.

(22) Liu, F.; Antoniou, J.; Li, Y.; Ma, J.; Zhong, F. Effect of sodium acetate and drying temperature on physicochemical and thermomechanical properties of gelatin films. *Food Hydrocolloids* **2015**, *45*, 140−149.

(23) Jouki, M.; Mortazavi, S. A.; Yazdi, F. T.; Koocheki, A. Characterization of antioxidant−antibacterial quince seed mucilage films containing thyme essential oil. *Carbohydr. Polym.* **2014**, *99*, 537−546.

(24) Li, J.-H.; Miao, J.; Wu, J.-L.; Chen, S.-F.; Zhang, Q.-Q. Preparation and characterization of active gelatin-based films incorporated with natural antioxidants. *Food Hydrocolloids* **2014**, *37*, 166−173.

(25) Yi, J.; Lam, T. I.; Yokoyama, W.; Cheng, L. W.; Zhong, F. Beta-carotene encapsulated in food protein nanoparticles reduces peroxyl radical oxidation in Caco-2 cells. *Food Hydrocolloids* **2015**, *43*, 31−40.

(26) Wu, J.; Zhong, F.; Li, Y.; Shoemaker, C. F.; Xia, W. Preparation and characterization of pullulan−chitosan and pullulan−carboxymethyl chitosan blended films. *Food Hydrocolloids* **2013**, *30*, 82−91.

(27) AOCS. AOCS Official Method Cd 8-53: Peroxide value−acetic acid−chloroform method. *Official Methods and Recommended Practices of the American Oil Chemists' Society*, 5th ed.; AOCS: Champaign, IL, USA, 1998.

(28) AOCS. AOCS Official Method Cd 19-90:2-Thiobarbituric acid value method. . *Official Methods and Recommended Practices of the American Oil Chemists' Society*, 5th ed.; AOCS: Champaign, IL, USA, 1998.

(29) Grenha, A.; Seijo, B.; Remunan-Lopez, C. Microencapsulated chitosan nanoparticles for lung protein delivery. *Eur. J. Pharm. Sci.* **2005**, *25*, 427−37.

(30) Grenha, A. Chitosan nanoparticles: a survey of preparation methods. *J. Drug Targeting* **2012**, *20*, 291−300.

(31) Mahmoud, A. A.; El-Feky, G. S.; Kamel, R.; Awad, G. E. Chitosan/sulfobutylether-beta-cyclodextrin nanoparticles as a potential approach for ocular drug delivery. *Int. J. Pharm.* **2011**, *413*, 229−36.

(32) Li, K.-K.; Yin, S.-W.; Yang, X.-Q.; Tang, C.-H.; Wei, Z.-H. Fabrication and Characterization of Novel Antimicrobial Films Derived from Thymol-Loaded Zein−Sodium Caseinate (SC) Nanoparticles. *J. Agric. Food Chem.* **2012**, *60*, 11592−11600.

(33) Aewsiri, T.; Benjakul, S.; Visessanguan, W.; Eun, J. B.; Wierenga, P. A.; Gruppen, H. Antioxidative activity and emulsifying properties of cuttlefish skin gelatin modified by oxidised phenolic compounds. *Food Chem.* **2009**, *117*, 160−168.

(34) Wu, J.; Liu, H.; Ge, S.; Wang, S.; Qin, Z.; Chen, L.; Zheng, Q.; Liu, Q.; Zhang, Q. The preparation, characterization, antimicrobial stability and in vitro release evaluation of fish gelatin films

DOI: 10.1021/acs.jafc.5b00003
J. Agric. Food Chem. 2015, 63, 3987−3995

incorporated with cinnamon essential oil nanoliposomes. *Food Hydrocolloids* **2015**, *43*, 427−435.
(35) Ruiz-Navajas, Y.; Viuda-Martos, M.; Sendra, E.; Perez-Alvarez, J. A.; Fernández-López, J. In vitro antibacterial and antioxidant properties of chitosan edible films incorporated with Thymus moroderi or Thymus piperella essential oils. *Food Control* **2013**, *30*, 386−392.
(36) Wan, A.; Xu, Q.; Sun, Y.; Li, H. Antioxidant activity of high molecular weight chitosan and N,O-quaternized chitosans. *J. Agric. Food Chem.* **2013**, *61*, 6921−8.
(37) Yen, M.-T.; Yang, J.-H.; Mau, J.-L. Antioxidant properties of chitosan from crab shells. *Carbohydr. Polym.* **2008**, *74*, 840−844.
(38) Gramza, A.; Korczak, J. Tea constituents (Camellia sinensis L.) as antioxidants in lipid systems. *Trends Food Sci. Technol.* **2005**, *16*, 351−358.
(39) Atarés, L.; Bonilla, J.; Chiralt, A. Characterization of sodium caseinate-based edible films incorporated with cinnamon or ginger essential oils. *J. Food Eng.* **2010**, *100*, 678−687.
(40) Higdon, J. V.; Frei, B. Tea catechins and polyphenols: health effects, metabolism, and antioxidant functions. *Crit. Rev. Food Sci. Nutr.* **2003**, *43*, 89−143.
(41) Liang, J.; Ludescher, R. D. Antioxidants modulate molecular mobility, oxygen permeability, and microstructure in zein films. *J. Agric. Food Chem.* **2011**, *59*, 13173−80.

DOI: 10.1021/acs.jafc.5b00003
J. Agric. Food Chem. 2015, 63, 3987−3995

from non-milk protein samples. In addition, detailed differences between milk and non-milk proteins were demonstrated by PCA and partial least-squares-discriminant analysis (PLS-DA) using all 15 mole ratios of amino acids. This approach may provide a scientific foundation toward developing an effective nontargeted adulteration detection of foreign protein in milk and maybe other dairy products.

MATERIALS AND METHODS

Materials and Chemicals. Raw milk samples were respectively collected in local dairy farms from Shandong province (192 samples) and Shanghai suburbs (171 samples) during May 2012−May 2013. Between 0.3 and 1 L of milk was collected for each sample. All milking cows were of the Holstein breed. The samples were freeze-dried once transferred to the laboratory, and the dry milk powders were stored in zip-lock bags at −20 °C. Each dried milk powder weighed between 30 and 130 g. The dried milk powders were mixed by shaking the zip-lock bags. Other non-milk protein powders were byproducts from food-processing factories. Whey protein was purchased from Aocheng Trading (Zhuhai, Guangdong, China). Peanut protein was provided by Changshou Food (Qingdao, Shandong, China). Corn 1, corn 2, soy, fish, egg yolk, beef extract, collagen, and cattle bone proteins were provided by Yuantai Biotech (Shanghai, China). Among the non-milk protein powders, six (whey, fish, egg yolk, beef extract, collagen, and cattle bone) were made from animals and the other four (corn 1, corn 2, soy, and peanut) were from plants. The infant formula powder purchased from a local grocery store was used as a reference sample of processed milk product.

Water was purified using a Milli-Q Advantage A10 system (EMD Millipore, Darmstadt, Hesse, Germany). HPLC grade acetonitrile was purchased from Merck KGaA (Darmstadt, Hesse, Germany). The mixed amino acid standard AccQTag Ultra (ATU) eluent A and B and ATU derivatization kit were purchased from Waters Corp. (Milford, MA, USA). Other amino acid standards used in the recovery test were purchased from Sigma-Aldrich (St. Louis, MO, USA). Analytical grade hydrochloric acid was purchased from Linfeng Chemical Reagent (Shanghai, China). Other chemicals or solvents were of the highest commercial grade and used without further purification.

Sample Preparation. Each dried milk powder (30 mg) was hydrolyzed directly with 10 mL of 6 M hydrochloric acid by a Discover SP-D pressurized microwave digestion system (CEM, Matthews, NC, USA). The power was 200 W. The ramp time and the cooling time were 15 and 20 min, respectively. The high prestirring was 15 s, with a temperature of 160 °C and a pressure at 250 psi. After hydrolysis, the samples were mixed for 15 s using a vortexer. Then, 0.4 mL hydrolysates were evaporated using a Buchi R-215 rotary evaporator (Flawil, St. Gallen, Switzerland) and redissolved in 0.5 mL of water. The solution was filtered through a 0.22 μm membrane filter (ANPEL Scientific Instrument, Shanghai, China).

The Waters ATU derivatization kit was used for precolumn sample derivatization. The borate buffer (70 μL), the hydrolysates (10 μL), and the reconstituted reagent (20 μL) were sequentially added to a vial. The solution was mixed using a vortexer for 5 s and allowed to stand for 1 min at room temperature. Then, the solution was immediately transferred into an oven and heated at 55 °C for 10 min. The solution was stored at 4 °C and subjected to UPLC analysis.

UPLC Analysis. The concentrations of 17 amino acids, including histidine, serine, arginine, glycine, aspartic acid, glutamic acid, threonine, alanine, proline, cysteine, lysine, tyrosine, methionine, valine, isoleucine, leucine, and phenylalanine, were quantified. Three amino acids, tryptophan, asparagine, and glutamine, were not quantified. Tryptophan decomposed, and asparagine and glutamine were respectively converted to aspartic and glutamic acids under acidic conditions during hydrolysis. Cysteine, due to its low concentration, was excluded from further data analyses. The hydrolysates were analyzed by using a Waters Acquity H-class UPLC system equipped with a photodiode array (PDA) detector. A Waters ATU C18 column (2.1 mm i.d. × 100 mm, 1.7 μm) was used. The column temperature was 43 °C, and the sample manager temperature was 20 °C. A quaternary solvent system including ATU solvent A (A), 10% (v/v) ATU solvent B (B), water (C), and ATU solvent B (D) was applied. The gradient elution program is listed in Table 1. The flow rate was 0.5 mL/min. The injection volume was 1.0 μL. The PDA detection wavelength was 260 nm. All samples were analyzed in a random order. Triplicate measurements were performed for each hydrolysate, and the mean concentrations were used for further statistical and chemometric analyses. The concentrations of calibration standards were 0.03, 0.05, 0.10, 0.25, 0.50, and 1.00 mmol/L for all amino acids.

Table 1. UPLC Gradient Elution Program for Amino Acid Analysis[a]

time (min)	A (%)	B (%)	C (%)	D (%)	gradient curve
0.00	10.0	0.0	90.0	0.0	11
7.10	8.0	15.6	57.9	18.5	7
7.30	8.0	15.6	57.9	18.5	6
7.69	7.8	0.0	70.9	21.3	6
7.99	4.0	0.0	36.3	59.7	6
8.59	4.0	0.0	36.3	59.7	6
9.00	10.0	0.0	90.0	0.0	6
12.00	10.0	0.0	90.0	0.0	6

[a]A, AccQTag Ultra (ATU) solvent A; B, 10% (v/v) ATU solvent B; C, water; D, ATU solvent B.

Univariate Data Analysis. Univariate analysis classifies milk and non-milk protein powders using a single variable. The chromatographic peak areas were integrated by Empower 3 software (Waters) using a traditional integration algorithm with peak width at 10 and threshold at 300. Manual identification of amino acid peaks was performed after integration. The results were reported as millimoles of each amino acid per gram of dry milk powder. To reduce undesired variances introduced by protein concentration variances between samples, sample moisture, preprocessing, and injection, etc., the relative mole ratios were applied. Mole ratios of individual amino acids to glutamic acid, the most abundant amino acid in milk protein, were calculated for each sample. The sample was classified as a non-milk protein if the relative mole ratio of an amino acid to glutamic acid was outside the 99.7% confidence boundaries of the milk mean value. The boundaries represent the mean ratio ± 3 times the standard deviation.

Chemometric Data Analysis. The relative mole ratio data were processed with multivariate chemometric data analysis methods using a MATLAB R2013b (The MathWorks, Inc., Natick, MA, USA) in-house program. PCA and PLS-DA were performed by the "svd" and "plsregress" (available in statistics toolbox) MATLAB functions, respectively. The data were preprocessed by autoscaling (mean-centering and scaling to unit variance). Typically in PLS-DA, data are divided as training set for building the model and test set for quantitative validation of model. In this study, two-thirds of the samples were divided into a training set (249 samples), and the rest were put into an independent test set (124 samples). The test set included three non-milk samples, which were peanut, corn 2, and beef extract proteins. The milk and non-milk protein samples were coded "1" and "0" in the response variable, respectively.

RESULTS AND DISCUSSION

Method Development. A milk sample was selected randomly for method development. The hydrolysis is an important step that may influence the accuracy and precision when the amino acid concentration is quantified. The ramp time and the container used for hydrolysis were optimized. Three ramp times including 15, 30, and 40 min were compared. There is no significant difference between the hydrolysis effectiveness between 15 and 30 min of reaction, whereas 40 min of hydrolysis resulted in significantly lower amino acid contents, indicating a possible decomposition of amino acids with longer heating. A 15 min ramp time for hydrolysis was

DOI: 10.1021/acs.jafc.5b00702
J. Agric. Food Chem. 2015, 63, 3996−4002

selected for further study. In addition, the 10 and 25 mL hydrolysis vessels in the microwave digestion instrument were compared. There was no significant difference between the analysis results using both vessels, and the 25 mL vessel was employed for subsequent analyses.

The UPLC method was developed on the basis of the procedure recommended by Waters. The method was validated for linearity, repeatability, and stability. The correlation coefficients for all amino acids were >0.98 (Table 2). The limit of detection (LOD) and limit of quantification (LOQ) were determined using a chromatogram of amino acid standard at 12.5 μmol/L by comparing the peak height with the height of the surrounding baseline noise. LOD and LOQ were 0.63 and 2.50 μmol/L for all amino acids, respectively. The linearity ranges were 0.01−1.00 mmol/L for all amino acids. For intra- and interday precision evaluations, all samples were independently sampled and hydrolyzed. The intraday precision was calculated by four samples, and the interday precision was measured over two consecutive days with three samples each day. All intra- and interday variations were <25% other than that of aspartic acid (Table 2). The recovery test was performed at concentration levels of 80, 100, and 120%. The recoveries for all amino acids were >80% except that of histidine and lysine (Table 2).

Table 2. Calibration Parameters and UPLC Method Validation Results[a]

	RT (min)	R^2	intraday RSD (%)	interday RSD (%)	recovery (%)
His	2.67	0.997	7.6	7.6	74.9
Ser	3.87	0.997	6.4	4.5	84.6
Arg	4.10	0.998	6.2	6.9	112.8
Gly	4.29	0.997	6.4	5.5	135.8
Asp	4.70	0.988	5.5	25.3	89.9
Glu	5.23	0.989	5.5	5.0	86.6
Thr	5.66	0.997	6.2	5.9	97.3
Ala	6.12	0.990	6.7	5.5	104.4
Pro	6.73	0.997	6.4	4.7	93.3
Lys	7.69	0.984	6.6	22.6	72.8
Tyr	7.86	0.997	6.5	5.6	96.9
Met	7.98	0.998	23.0	19.4	93.7
Val	8.05	0.996	5.8	6.6	104.3
Ile	8.65	0.997	6.2	8.8	92.0
Leu	8.73	0.997	6.2	6.1	96.4
Phe	8.80	0.998	6.6	10.7	98.2

[a]RT, retention time; R^2, correlation coefficient; RSD, relative standard deviation. The calibrations were based on millimoles of each amino acid per gram of dry milk powder.

UPLC Chromatograms. The representative UPLC amino acid chromatograms are plotted in Figure 1. The chromatograms were plotted sequentially toward the top-right corner for better demonstration. 6-Aminoquinoline (AMQ) was a by-product of derivatization. All amino acid peaks were baseline separated and eluted within 9 min. Glutamic acid, proline, and leucine had the highest concentrations among the 16 quantified amino acids in the milk powders. The reported amino acid concentrations were in good agreement with that obtained from previous work using the conventional heating hydrolysis method.[12] The tested non-milk proteins had unique profiles of amino acids. For instance, there was a significantly higher amount of glycine in the collagen. Table 3 lists the relative mole amino acid ratios of the milk and non-milk proteins. Each protein material had a characteristic set of amino acid compositions. For example, beef extract, cattle bone, and collagen had a high concentration of glycine; egg yolk had high ratios of aspartic acid and serine. The amino acid ratios were different for proteins from different biological sources, consistent with previous findings in other food products such as in rice wines and liquors.[13,14] Due to the limited amount of non-milk proteins, these data alone may not be suitable for predicting other proteins outside the scope of this study. However, because these fingerprints exhibited significant dissimilarities from one another, it can be assumed that other

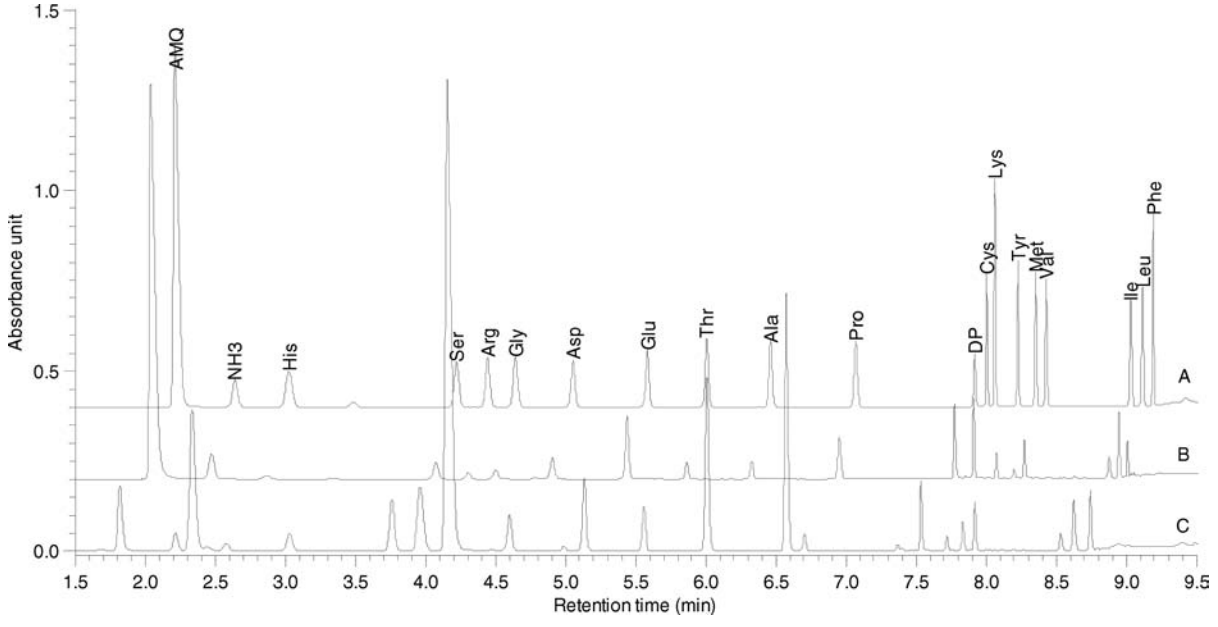

Figure 1. Representative UPLC amino acid chromatograms: (A) amino acid standard (0.50 mmol/L); (B) milk protein; (C) collagen. AMQ, 6-aminoquinoline; DP, derivatization peak. The chromatograms were plotted sequentially toward the top-right corner for better demonstration.

DOI: 10.1021/acs.jafc.5b00702
J. Agric. Food Chem. 2015, 63, 3996−4002

Table 3. Mole Ratios of Amino Acids in Protein Powders[a]

	milk	IM	whey	EY	BE	CB	CO	fish	soy	P	C1	C2
n	363	1	1	1	1	1	1	1	1	1	1	1
His	0.09 ± 0.06	0.09	0.08	0.16	0.21	0.29	0.16	0.06	0.12	0.11	0.17	0.16
Ser	0.34 ± 0.17	0.34	0.45	0.93	0.59	0.67	0.95	0.29	0.43	0.42	0.47	0.48
Arg	0.12 ± 0.08	0.11	0.11	0.46	0.41	0.87	1.56	0.48	0.35	0.57	0.35	0.40
Gly	0.17 ± 0.10	0.18	0.24	0.51	2.51	7.30	10.23	4.05	0.47	0.63	0.67	0.88
Asp	0.41 ± 0.06	0.43	0.71	0.92	0.64	0.59	0.60	0.53	0.64	0.65	0.59	0.37
Thr	0.23 ± 0.14	0.22	0.48	0.48	0.45	0.45	0.57	0.10	0.26	0.16	0.30	0.40
Ala	0.24 ± 0.04	0.24	0.55	0.80	1.10	1.67	2.50	1.59	0.39	0.37	0.63	1.32
Pro	0.58 ± 0.16	0.59	0.47	0.44	1.02	2.54	3.38	1.56	0.38	0.32	0.60	1.01
Lys	0.35 ± 0.09	0.37	0.60	0.66	0.49	0.26	0.31	0.32	0.37	0.20	0.31	0.25
Tyr	0.18 ± 0.12	0.15	0.12	0.26	0.29	0.20	0.10	0.05	0.15	0.17	0.18	0.10
Met	0.07 ± 0.07	0.01	0.10	0.13	0.19	0.15	0.21	0.00	0.02	0.01	0.05	0.17
Val	0.32 ± 0.10	0.32	0.35	0.58	0.63	0.58	0.37	0.28	0.27	0.26	0.42	0.61
Ile	0.20 ± 0.07	0.19	0.32	0.36	0.36	0.31	0.14	0.13	0.20	0.15	0.25	0.26
Leu	0.47 ± 0.15	0.47	0.66	0.78	0.80	0.68	0.50	0.37	0.43	0.39	0.58	0.73
Phe	0.20 ± 0.15	0.16	0.14	0.30	0.43	0.46	0.44	0.16	0.21	0.24	0.26	0.22

[a]IM, infant milk; EY, egg yolk; BE, beef extract; CB, cattle bone; CO, collagen; P, peanut; C1, corn 1; C2, corn 2; *n*, number of samples. Data were expressed as relative mole ratios to the glutamic acid. The data were reported as mean ± 3 times standard deviation for milk.

unknown proteins outside this study may also have unique amino acid fingerprints. To establish objective, quantitative, and detailed criteria for differentiation, both univariate and multivariate data modelings were performed.

Univariate Analysis of Milk and Non-milk Proteins. The confidence boundaries are reported in Table 3. The differentiation results by univariate analysis are reported in Table 4. Generally, confidence boundaries calculated from

Table 4. Univariate Analysis Results of Milk and Non-milk Proteins[a]

	milk (*n* = 363)		non-milk (*n* = 10)	
	pos	neg	pos	neg
His	353	10	6	4
Ser	352	11	4	6
Arg	352	11	9	1
Gly	352	11	9	1
Asp	361	2	9	1
Thr	352	11	6	4
Ala	358	5	10	0
Pro	353	10	7	3
Lys	357	6	5	5
Tyr	352	11	1	9
Met	358	5	4	6
Val	351	12	4	6
Ile	355	8	4	6
Leu	351	12	5	5
Phe	351	12	3	7

[a]*n*, total number of samples; pos, number of correctly differentiated samples; neg, number of incorrectly differentiated samples.

different amino acid ratios yielded significantly different correct identification rates for non-milk proteins. From the 15 confidence boundaries of amino acid ratios calculated, only the alanine to glutamic acid ratio correctly classifies all 10 non-milk proteins (Table 4). The confidence boundaries calculated by the mole ratio of arginine, glycine, or aspartic acid to glutamic acid yielded 90% correct identifications for non-milk protein samples. On the contrary, mole ratios of tyrosine, methionine, valine, isoleucine, and phenylalanine to glutamic acid yielded poor abilities in distinguishing milk and non-milk proteins (Table 4). In particular, only one non-milk protein was differentiated according to that of tyrosine. To conclude, the confidence bounds calculated from the mole ratios of alanine, arginine, glycine, and aspartic acid to glutamic acid were able to differentiate milk and non-milk proteins with at least 90% correct identification. However, other amino acid ratios, including histidine, serine, threonine, proline, lysine, tyrosine, methionine, valine, isoleucine, leucine, and phenylalanine to glutamic acid, were unable to be used alone as differentiation criteria. The selection of amino acid ratios greatly influenced the classification results in the univariate analysis approach. Therefore, the multivariate techniques PCA and PLS-DA were used in an attempt to better classify samples as milk or non-milk. The multivariate methods use latent variables constructed from combinations of the original variables (amino acid mole ratios) to extract additional information from the data set.

PCA of Milk and Non-milk Proteins. PCA is a mathematical approach that is able to transform the high-dimensional multivariate data into a lower number of dimensions. Figure 2 is the principal component (PC) scores and loading plots for milk and non-milk powders using all amino acid composition ratios. The first and second PCs that explain the top two largest percentages of total variances were plotted. The data points representing milk samples form a defined cluster, and the infant milk powder was inside this cluster (Figure 2A). Contrarily, data points representing non-milk proteins were positioned relatively outside the cluster of milk samples, suggesting that the amino acid compositions of milk samples measured by this method were unique compared to the non-milk proteins. In comparison with the univariate method, PCA could avoid the selection of amino acid ratios and yielded a direct plot for differentiation. The amino acid fingerprints contain much quantitative information on amino acid composition, and PCA conveniently combines and presents all of this information altogether.

Besides the differentiation of milk and non-milk proteins, the relationships between different non-milk proteins can also be studied by PCA to examine whether the sampling of the non-milk proteins was unbiased. All non-milk proteins were located in the lower region of Figure 2A. Although the model was

DOI: 10.1021/acs.jafc.5b00702
J. Agric. Food Chem. 2015, 63, 3996−4002

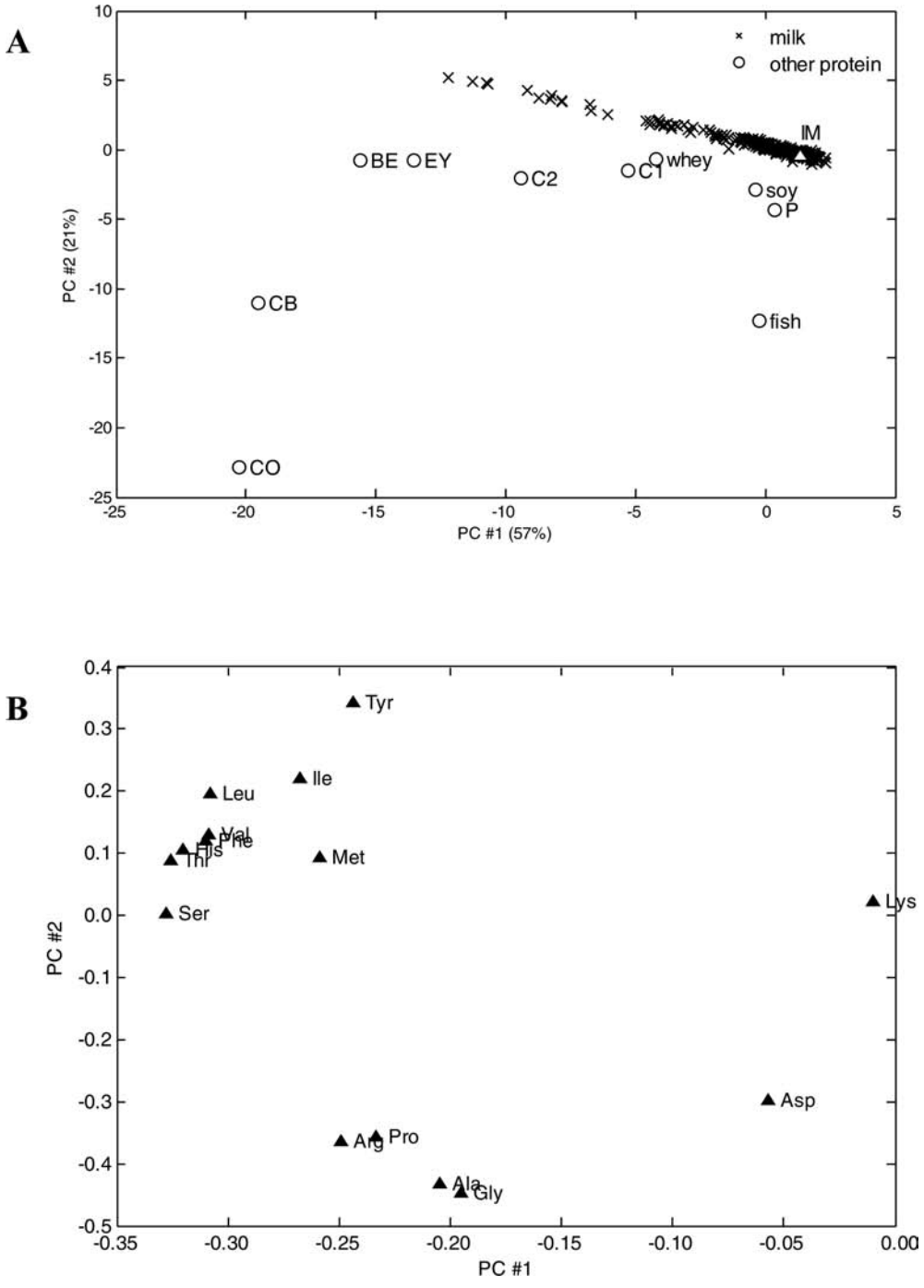

Figure 2. Principal component scores (A, top) and loading (B, bottom) plots for all milk and non-milk proteins. IM, infant milk; C1, corn 1; C2, corn 2; P, peanut; EY, egg yolk; BE, beef extract; CB, cattle bone; CO, collagen.

calculated from only 10 foreign protein samples, these samples spanned a much larger region than 363 milk samples, suggesting a large diversity in the amino acid compositions from different sources of proteins. The diversities in non-milk protein powders indicated that the sampling of the non-milk proteins was unbiased. Among these samples, whey protein was the nearest to milk, probably because whey is a major protein in milk. The plant proteins including corn, soy, and peanut proteins were clustered closely, in comparison with the animal proteins including beef, cattle bone, collagen, and egg yolk, which spanned a wider area. The fish protein was not located in either cluster. The tested animal proteins were generally farther away from the milk samples compared with the plant proteins.

The relative importance of each amino acid ratio for differentiation could be obtained from the loading plot (Figure 2B). According to the loading of the second PC, the mole ratios of tyrosine to glutamic acid were typically high in the milk samples, whereas the ratios of arginine, proline, alanine, glycine, and aspartic acid to glutamic acid were high in the non-milk samples, especially the animal proteins. The conclusion was consistent with the data in Table 4, which reported at least 70% correct prediction by any one of these amino acid ratios. It was also consistent with a previous study that reported aspartic acid,

DOI: 10.1021/acs.jafc.5b00702
J. Agric. Food Chem. 2015, 63, 3996−4002

proline, and alanine were marker amino acids to differentiate non-fat dry milk protein and whey protein.[15] Compared with previous IR spectroscopic studies with multivariate analysis,[6,7,10] spectroscopic methods are superior in analysis time and ease of application. However, the amino acid fingerprints furnish fewer variables and a compact data set, thus obtaining a simple differentiation model. Also, each coefficient in the amino acid fingerprint model can be clearly explained by the amounts of specific amino acid in the sample, in contrast with the IR spectroscopy where significant chemical variances appeared in different milk powders.[10,16] Consequently, the amino acid model might be less influenced by instrumental, environmental, or other sources of variances. In summary, PCA of UPLC amino acid fingerprints is able to demonstrate the differences of all milk and non-milk proteins, as well as to investigate the detailed relationships among non-milk proteins according to the PC scores plot without the selection of any particular amino acid.

PLS-DA of Milk and Non-milk Proteins. PLS-DA is a widely applied modeling technique.[17,18] It was applied to quantitatively evaluate the multivariate differentiation approach. Figure 3 demonstrated the percent of variance explained in the response variable of the training set with respect to PLS-DA models calculated by different numbers of latent variables. In this study, the minimum number of latent variables was determined to be the number required to reach >90% of variances explained in the response variable; meanwhile, the percent variances did not increase greatly with further addition of latent variables. From Figure 3, six latent variables that explained 91.1% of the variance in the response variable were chosen for PLS-DA modeling. All 124 samples in the test set were correctly differentiated as containing milk or non-milk proteins, consistent with the PCA result. Table S1 in the Supporting Information is the number of PLS-DA misclassifications in the test set with respect to different numbers of latent variables. It can be observed that the PLS-DA models built by 5−15 latent variables performed equally in prediction. The predicted and measured responses of the test set by PLS-DA with six latent variables are presented in Figure S1 in the Supporting Information.

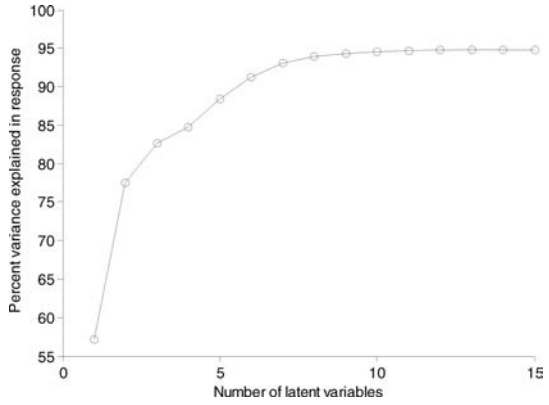

Figure 3. PLS-DA-explained variance plot.

Comparison of the uni- and multivariate approaches shows that the univariate approach offered intuitive confidence ranges. However, different amino acid ratios yielded different differentiation capabilities. Consequently, careful and thorough research about the selection of amino acids in a larger sample set in univariate approaches is necessary before actual application. The multivariate approaches such as PCA and PLS-DA build robust and informative models, although they depend on relatively complicated and specialized data-processing techniques. Both PCA and PLS-DA approaches were able to differentiate all non-milk protein samples from milk protein samples using the amino acid fingerprints. PCA was able to achieve a graphical overview of the relationships between different groups of samples. In PLS-DA, with the additional separation of data into training and test sets, the differentiation could be performed automatically and quantitatively.

In summary, amino acid fingerprinting combined with univariate or multivariate data analyses successfully differentiated milk protein from inexpensive non-milk protein powders. Amino acid fingerprints and chemometric techniques could be potentially developed as a nontargeted foreign protein detection technique for detecting milk adulteration.

■ ASSOCIATED CONTENT

Supporting Information

PLS-DA model prediction table and plot. This material is available free of charge via the Internet at http://pubs.acs.org.

■ AUTHOR INFORMATION

Corresponding Authors

*(H.S.) Phone: (86) 21-3420-4041. Fax: (86) 21-3420-4107. E-mail: hmshi@sjtu.edu.cn.

*(L.Y.) Phone: (301) 405-0761. Fax: (301) 314-3313. E-mail: lyu5@umd.edu.

Author Contributions

‖W.L. and X.L. contributed equally to this work.

Funding

This work was supported by the National High Technology Research and Development Program of China (Grants 2013AA102202 and 2013AA102207); a special fund for Agro-scientific Research in the Public Interest (Grant 201203069); SJTU startup fund for young talent (Grant 13X100040047); and SJTU 985-III disciplines platform and talent fund (Grants TS0414115001 and TS0320215001).

Notes

The authors declare no competing financial interest.

■ REFERENCES

(1) World Food and Agriculture. *FAO Statistical Yearbook 2013*; Food and Agriculture Organization of the United Nations: Rome, Italy, 2013.

(2) Moore, J. C.; Spink, J.; Lipp, M. Development and application of a database of food ingredient fraud and economically motivated adulteration from 1980 to 2010. *J. Food Sci.* **2012**, *77*, R118−R126.

(3) Sanchez-Monge, R.; Lopez-Torrejón, G.; Pascual, C. Y.; Varela, J.; Martin-Esteban, M.; Salcedo, G. Vicilin and convicilin are potential major allergens from pea. *Clin. Exp. Allergy* **2004**, *34*, 1747−1753.

(4) Caubet, J. C.; Ford, L. S.; Sickles, L.; Järvinen, K. M.; Sicherer, S. H.; Sampson, H. A.; Nowak-Węgrzyn, A. Clinical features and resolution of food protein-induced enterocolitis syndrome: 10-year experience. *J. Allergy Clin. Immunol.* **2014**, *134*, 382−389.

(5) Jaiswal, P.; Jha, S. N.; Borah, A.; Gautam, A.; Grewal, M. K.; Jindal, G. Detection and quantification of soymilk in cow−buffalo milk using attenuated total reflectance Fourier transform infrared spectroscopy (ATR−FTIR). *Food Chem.* **2015**, *168*, 41−47.

(6) Santos, P. M.; Pereira-Filho, E. R.; Rodriguez-Saona, L. E. Rapid detection and quantification of milk adulteration using infrared microspectroscopy and chemometrics analysis. *Food Chem.* **2013**, *138*, 19−24.

DOI: 10.1021/acs.jafc.5b00702
J. Agric. Food Chem. 2015, 63, 3996−4002

(7) Santos, P. M.; Pereira-Filho, E. R.; Rodriguez-Saona, L. E. Application of hand-held and portable infrared spectrometers in bovine milk analysis. *J. Agric. Food Chem.* **2013**, *61*, 1205−1211.
(8) Czerwenka, C.; Műller, L.; Lindner, W. Detection of the adulteration of water buffalo milk and mozzarella with cow's milk by liquid chromatography−mass spectrometry analysis of β-lactoglobulin variants. *Food Chem.* **2010**, *122*, 901−908.
(9) Scholl, P. F.; Farris, S. M.; Mossoba, M. M. Rapid turbidimetric detection of milk powder adulteration with plant proteins. *J. Agric. Food Chem.* **2014**, *62*, 1498−1505.
(10) Botros, L. L.; Jablonski, J.; Chang, C.; Bergana, M. M.; Wehling, P.; Harnly, J. M.; Downey, G.; Harrington, P.; Potts, A. R.; Moore, J. C. Exploring authentic skim and nonfat dry milk powder variance for the development of nontargeted adulterant detection methods using near-infrared spectroscopy and chemometrics. *J. Agric. Food Chem.* **2013**, *61*, 9810−9818.
(11) Jablonski, J. E.; Moore, J. C.; Harnly, J. M. Nontargeted detection of adulteration of skim milk powder with foreign proteins using UHPLC−UV. *J. Agric. Food Chem.* **2014**, *62*, 5198−5206.
(12) Marino, R.; Iammarino, M.; Santillo, A.; Muscarella, M.; Caroprese, M.; Albenzio, M. Technical note: Rapid method for determination of amino acids in milk. *J. Dairy Sci.* **2010**, *93*, 2367−2370.
(13) Shen, F.; Ying, Y.; Li, B.; Zheng, Y.; Zhuge, Q. Multivariate classification of rice wines according to ageing time and brand based on amino acid profiles. *Food Chem.* **2011**, *129*, 565−569.
(14) Xiao, X.; Hou, Y.; Liu, Y.; Liu, Y.; Zhao, H.; Dong, L.; Du, J.; Wang, Y.; Bai, G.; Luo, G. Classification and analysis of corn steep liquor by UPLC/Q-TOF MS and HPLC. *Talanta* **2013**, *107*, 344−348.
(15) Greenberg, R.; Dower, H. J. Detection of added whey protein concentrate in nonfat dry milk by amino acid analysis. *J. Agric. Food Chem.* **1986**, *34*, 30−32.
(16) Harnly, J. M.; Harrington, P. B.; Botros, L. L.; Jablonski, J.; Chang, C.; Bergana, M. M.; Wehling, P.; Downey, G.; Potts, A. R.; Moore, J. C. Characterization of near-infrared spectral variance in the authentication of skim and nonfat dry milk powder collection using ANOVA-PCA, pooled-ANOVA, and partial least-squares regression. *J. Agric. Food Chem.* **2014**, *62*, 8060−8067.
(17) Ellis, D. I.; Brewster, V. L.; Dunn, W. B.; Allwood, J. W.; Golovanov, A. P.; Goodacre, R. Fingerprinting food: current technologies for the detection of food adulteration and contamination. *Chem. Soc. Rev.* **2012**, *41*, 5706−5727.
(18) Lu, W.; Jiang, Q.; Shi, H.; Niu, Y.; Gao, B.; Yu, L. Partial least-squares-discriminant analysis differentiating Chinese wolfberries by UPLC−MS and flow injection mass spectrometric (FIMS) fingerprints. *J. Agric. Food Chem.* **2014**, *62*, 9073−9080.

DOI: 10.1021/acs.jafc.5b00702
J. Agric. Food Chem. 2015, 63, 3996−4002

JOURNAL OF AGRICULTURAL AND FOOD CHEMISTRY

Addition/Correction

pubs.acs.org/JAFC

Correction to Protocatechuic Acid Inhibits Oleic Acid-Induced Vascular Smooth Muscle Cell Proliferation through Activation of AMP-Activated Protein Kinase and Cell Cycle Arrest in G0/G1 Phase

Ming-Cheng Lin, Ting-Tsz Ou, Chun-Hua Chang, Kuei-Chuan Chan,* and Chau-Jong Wang*

J. Agric. Food Chem. **2015** (1), 235−241. DOI: 10.1021/jf505303s

Contact information was not complete for the corresponding authors. This is now provided.

AUTHOR INFORMATION

Corresponding Authors

*(K.-C.C.) Phone: 886-4-24739595, ext. 32527. Fax: 886-4-24739220. E-mail: chenkuei@ms16.hinet.net.

*(C.-J.W.) Phone: 886-4-24730022, ext. 11670. Fax: 886-4-23248167. E-mail: wcj@csmu.edu.tw.

Published: April 10, 2015

ACS Publications © 2015 American Chemical Society

DOI: 10.1021/acs.jafc.5b01741
J. Agric. Food Chem. 2015, 63, 4003−4003

Table 1. Main *n*-Alkane and Triterpenoid Components of Cuticular Waxes and Predominant Cutin Monomers Reported in Fruit Species According to Botanical Family

botanical family	fruit type	ripening type	predominant wax components		predominant cutin monomers	refs
Solanaceae						
tomato (*Solanum lycopersicum*)	berry	climacteric	*n*-hentriacontane (C_{31})	triterpenoid alcohols (*α*-, *β*-, and *δ*-amyrin)	C_{16} monomers (10,16-dihydroxy $C_{16:0}$)	69, 71−80, 134
pepper (*Capsicum* sp.)	berry	nonclimacteric	*n*-hentriacontane (C_{31})	triterpenoid alcohols (*α*- and *β*-amyrin)	C_{16} monomers (9(10),16-dihydroxy $C_{16:0}$)	81, 82, 84
eggplant (*Solanum melongena*)	berry	nonclimacteric	*n*-hentriacontane (C_{31})	triterpenoid alcohols (*α*- and *β*-amyrin)	not reported	82
wild tomato (*Solanum* Sect. *Lycopersicon*)	berry	climacteric	*n*-hentriacontane (C_{31}) (in most species studied)	triterpenoid alcohols (*α*-, *β*-, and *δ*-amyrin)	C_{16} monomers (10,16-dihydroxy $C_{16:0}$)	79
Rosaceae						
apple (*Malus* × *domestica*)	pome	climacteric	*n*-nonacosane (C_{29})	triterpenoid acids (ursolic acid)	C_{18} monomers (tetrahydroxy $C_{18:0}$)	60, 85−89
Asian pear (*Pyrus bretchneideri*)	pome	climacteric	*n*-nonacosane (C_{29})	triterpenoid alcohols (*α*-amyrin)	not reported	90
peach (*Prunus persica*)						
melting	drupe	climacteric	*n*-tricosane (C_{23}) *n*-pentacosane (C_{25}) *n*-heptacosane (C_{27})	triterpenoid acids (ursolic acid, oleanolic acid)	C_{18} monomers (*ω*-hydroxy $C_{18:1}$)	92
nonmelting	drupe	climacteric	*n*-pentacosane (C_{25})	triterpenoid acids (ursolic acid)	C_{18} monomers (*ω*-hydroxy $C_{18:1}$)	91, 92
plum (*Prunus domestica*)	drupe	climacteric	*n*-nonacosane (C_{29})	triterpenoid acids (oleanolic acid)	not reported	135
strawberry (*Fragaria* × *ananassa*)	etaerio	nonclimacteric	not reported	not reported	C_{16} monomers (9(10),16-dihydroxy $C_{16:0}$)	62
sweet cherry (*Prunus avium*)	drupe	nonclimacteric	*n*-nonacosane (C_{29})	triterpenoid acids (ursolic acid)	cultivar-dependent (dihydroxy $C_{16:0}$ or dihydroxy $C_{18:x}$ reported mainly)	3, 93, 94
black chokeberry (*Aronia melanocarpa*)	berry	nonclimacteric	not reported	not reported	C_{18} monomers (*ω*-hydroxy-9,10-epoxy $C_{18:1}$ and *ω*-hydroxy-9,10-epoxy $C_{18:0}$)	62
cloudberry (*Rubus chamaemorus*)	syncarp	nonclimacteric	not reported	not reported	C_{16} monomers (74% of 9(10),16-dihydroxy $C_{16:0}$)	62
raspberry (*Rubus idaeus*)	syncarp	climacteric	not reported	not reported	C_{16} monomers (9(10),16-dihydroxy $C_{16:0}$)	62
rosehip (*Rosa rugosa*)	etaerio	nonclimacteric	not reported	not reported	C_{16} monomers (79% of 9(10),16-dihydroxy $C_{16:0}$)	62
rowanberry (*Sorbus aucuparia*)	po*μ*e	nonclimacteric	not reported	not reported	C_{16} monomers (9(10),16-dihydroxy $C_{16:0}$)	62
Rutaceae						
grapefruit (*Citrus* × *paradisi*)	hesperidium	nonclimacteric	detailed composition not reported		C_{16} monomers (*ω*-hydroxy-10-oxo $C_{16:0}$)	61, 64, 96, 98
lemon (*Citrus limon*)	hesperidium	nonclimacteric	*n*-hentriacontane (C_{31}) *n*-nonacosane (C_{29})	not reported	C_{16} monomers (dihydroxy $C_{16:0}$ and *ω*-hydroxy-oxo $C_{16:0}$)	64, 98
mandarin (*Citrus reticulata*)	hesperidium	nonclimacteric	detailed composition not reported		C_{16} monomers (dihydroxy $C_{16:0}$ and *ω*-hydroxy-oxo $C_{16:0}$)	64, 97, 98
orange (*Citrus sinensis*)	hesperidium	nonclimacteric	*n*-hentriacontane (C_{31}) *n*-nonacosane (C_{29})	triterpenoid alcohols (*α*- and *β*-amyrin)	C_{16} monomers (dihydroxy $C_{16:0}$ and *ω*-hydroxy-oxo $C_{16:0}$)	64, 95, 98
Vitaceae						
grape (*Vitis vinifera*)	berry	nonclimacteric	*n*-pentacosane (C_{25}) *n*-heptacosane (C_{27}) *n*-nonacosane (C_{29})	triterpenoid acids (oleanolic acid)	not reported	65, 66, 99−102
Oleaceae						
olive (*Olea europaea*)	drupe	nonclimacteric	*n*-heptacosane (C_{27})	triterpenoid acids (oleanolic acid)	not reported	105
Ericaceae						
bilberry (*Vaccinium myrtillus*)	berry	nonclimacteric	not reported	not reported	C_{18} monomers (9,10,18-trihydroxy $C_{18:0}$ and *ω*-hydroxy-9,10-epoxy $C_{18:0}$)	106
cranberry (*Vaccinium oxycoccos*)	berry	nonclimacteric	not reported	not reported	C_{18} monomers (*ω*-hydroxy-9,10-epoxy $C_{18:0}$)	106
crowberry (*Empetrum nigrum*)	drupe	nonclimacteric	not reported	not reported	C_{16} monomers (9(10),16-dihydroxy $C_{16:0}$)	62

DOI: 10.1021/acs.jafc.5b00013
J. Agric. Food Chem. 2015, 63, 4005−4019

Table 1. continued

botanical family	fruit type	ripening type	predominant wax components		predominant cutin monomers	refs
Ericaceae						
lingonberry (*Vaccinium vitis-idaea*)	berry	nonclimacteric	not reported	not reported	C_{18} monomers (ω-hydroxy-9,10-epoxy $C_{18:0}$ and 9,10,18-trihydroxy $C_{18:0}$)	106
Grossulariaceae						
black currant (*Ribes nigrum*)	berry	nonclimacteric	not reported	not reported	C_{16} monomers (10(9,8),16-dihydroxy $C_{16:0}$)	106
Elaeagnaceae						
sea buckthorn (*Hippophaë rhamnoides*)	berry	nonclimacteric	not reported	not reported	C_{18} monomers (ω-hydroxy-9,10-epoxy $C_{18:1}$ and ω-hydroxy-9,10-epoxy $C_{18:0}$)	106

more elastic.[2] Some of these properties are also dependent, at least to some extent, upon the external conditions to which the plant organ is exposed, particularly temperature and humidity.[13−15]

The composition and biosynthesis of cutin[7,16] and cuticular waxes,[9,17−19] cuticle permeability properties,[20−22] and cuticle and cutin biomechanics[2,23,24] have been covered in published reviews and will not be addressed here in detail. However, because the majority of work investigating cuticle biosynthesis and composition has been conducted on vegetative plant tissues and, in contrast, little information is available in relation to the epidermis of fruits, this review adds a further perspective to the current knowledge of the roles of cuticle in plant development. The minimization of water loss has been generally considered the main function of the fruit cuticle, but there is ample experimental evidence that, in addition to water-proofing, it may also play a major role in modulating protection against biotic and abiotic factors, fruit appearance, and textural properties, thus significantly affecting major traits related to postharvest quality.[25] The preservation of all these functions requires structural integrity of the cuticle throughout fruit expansion and development, meaning that a finely tuned mechanism to control cuticular composition and structure must also be a part of the developmental program. Despite their physiological relevance in determining fruit quality attributes and the economic implications of their maintenance throughout the commercial production and distribution chain of fruit, significant questions remain to be answered, including the mechanisms of cuticle biosynthesis and the specific wax and cutin (Table 1) composition of fruit cuticles. This paper reviews currently available information on the specific composition and biochemical changes in cuticles during maturation and ripening of fruits. Such knowledge may help frame putative cuticle impacts when the developmental process of a given fruit is to be investigated.

PATHWAYS AND REGULATION OF CUTICLE BIOSYNTHESIS: A BRIEF OVERVIEW

Fatty acids are precursors for both cutin and wax biosynthesis. These fatty acid precursors are thought to be synthesized de novo in plastids as the result of fatty acid synthase (FAS) activity, which involves, sequentially, the condensation of acetyl CoA with malonyl-acyl carrier protein (ACP), the reduction of 3-ketoacyl-ACP, the dehydration of 3-hydroxyacyl-ACP, and finally the reduction of *trans*-Δ^2-enoyl-ACP.[19,26,27] This fatty acyl primer is further extended by repeated condensations, thus yielding long-chain fatty acids (C_{16} and C_{18}). The precursors for wax production are mainly saturated fatty acids (C_{16} and C_{18}), whereas cutin is a polymer of predominantly $C_{16:0}$ and $C_{18:x}$ hydroxy fatty acids,[6] and hence the partitioning of these long-chain fatty acid precursors into wax or cutin biosynthesis pathways is likely to be a key regulatory point controlling the amount and specific composition of these two types of cuticle lipids.

Whereas de novo fatty acid biosynthesis is ubiquitous, cutin is synthesized exclusively by epidermal cells. Current understanding of the specific pathway that leads to the production of cutin monomers was established essentially 40 years ago by Kolattukudy and co-workers through studies on apple and *Vicia faba* leaves,[6,28] but many remaining knowledge gaps[29,30] still preclude a comprehensive understanding of the biosynthesis and polymerization of cutin monomers including the polymerization site itself, the monomer transport mechanisms, and the enzymes involved in their assembly. Even so, two recent papers have shed some light on these aspects by identifying an acyltransferase responsible for cutin polymerization in fruit cuticles of a range of *Solanum* species.[31,32] The necessary hydroxylation (at both internal and terminal positions) and epoxydation reactions are catalyzed by enzymes showing typical characteristics of the cytochrome P450 (CYP) enzyme family, among which the CYP77A, CYP86A, and CYP94B subfamilies comprise members that catalyze the hydroxylation either at midchain positions or at the terminal methyl group (ω-hydroxylases) on aliphatic fatty acid chains.[33−37] An effective function in cutin biosynthesis has been confirmed for some fatty acid ω-hydroxylases through the physiological and biochemical characterization of the corresponding mutants.[38] Distinctive substrate specificities[39,40] and expression patterns in response to environmental conditions[41] have been revealed, too. Long-chain acyl-CoA synthetases (LACS) are also required for cutin production,[42] indicating that these precursors need to be activated (CoA-bound) prior to the establishment of the cutin network. The ω-hydroxyl groups in the monomers form ester bonds, whereas a variable portion of the midchain hydroxyl groups is involved in ester-type cross-links, thus giving rise to and holding together the final polymeric complex.[7,16] The establishment of these ester linkages is catalyzed by acyltransferases, which transfer the activated cutin monomers to the free hydroxyl groups present in the cutin polymer[28] in a reaction purported to require ATP and a cutin primer, and indeed two glycerol-3-phosphate acyltransferases, GPAT4 and GPAT8, have been proved necessary for cutin assembly.[43] Phenolic esters such as those of ferulic and *p*-coumaric acids also contribute, although to a minor extent, to the establishment of the cutin polymer.[44]

DOI: 10.1021/acs.jafc.5b00013
J. Agric. Food Chem. 2015, 63, 4005−4019

Because genetic and external factors are known to cause changes in the amount and composition of wax, a strict regulation of the underlying biosynthetic pathways is to be expected. The characterization of mutants with deficient or altered wax coatings has contributed to shedding light on wax biosynthesis,[9,45−47] which is likewise restricted to epidermal tissues.[19,48,49] Waxes are often rich in very long-chain fatty acids (VLCFA) esterified to very long-chain alcohols, and hence the elongation of C_{16} and C_{18} fatty acid precursors is required for the synthesis of these wax components. Further extension of C_{16} and C_{18} fatty acids requires ACP elimination by an acyl-ACP thioesterase and activation to fatty acyl-CoA esters, which is catalyzed by long-chain acyl-CoA synthetases.[19,26] Chain elongation is biochemically analogous to de novo synthesis, the four consecutive reactions being catalyzed by ATP-dependent fatty acid elongases (FAE),[18,50−52] which require malonyl-CoA rather than malonyl-ACP as the two-carbon donor. Because elongases catalyze the primary reaction characterizing wax biosynthesis, they have been assigned an essential role in the process and have thus been the object of considerable research effort. The biochemistry and genetics of these elongation systems have been reviewed elsewhere[9,17,19,50,53−55] and will not be considered herein.

In addition to lipids derived from fatty acids, cuticles are also composed of lipids derived from isoprene, which primarily include the triterpenoids present in cuticular waxes. Triterpenoid biosynthesis involves the joining of six isoprene units to yield the hydrocarbon precursor squalene, which is then activated into 2,3-epoxysqualene and then cyclized. The cyclization of 2,3-epoxysqualene represents the first committed step in triterpenoid biosynthesis, which is carried out by oxidosqualene cyclases (OSCs). The diversity of existing OSCs and the large range of possible rearrangements they can catalyze eventually result in a great diversity of triterpenoid structures even though they start from the same substrate.[56]

Wax and cutin secretion to organ surfaces is also a key aspect of cuticle formation, because these lipophilic compounds must be exported from the cytoplasm after biosynthesis, cross the hydrophilic apoplast, and finally be assembled. The delivery to the outer tissues apparently involves lipid transfer proteins (LTP), which are expressed in plant epidermal tissues and secreted to the outside of the cell wall and cuticle.[17,18,57,58] Some members of the ATP-binding cassette (ABC) transporter family have been actually demonstrated to be required for cuticular lipid secretion.[19,59]

THE FRUIT CUTICLE: ARE ALL SPECIES EQUAL?

Many studies on chemical composition of cuticles have been published taking as a model leaves and other plant vegetative tissues. The significant differences observed for over 40 years in cuticle composition of different organs of the same plant, regarding both cutin[60−63] and waxes,[64−66] provide clear evidence that the assumption that fruit cuticle composition can be inferred from that of leaves cannot be sustained.

Taking tomato as a model species, for example, published information on the composition of cuticular waxes and cutin monomers supports the existence of such differences. Noticeable differences in total wax and cutin loads have been observed between fruits and leaves of the 'Micro-Tom' cultivar.[67−69] Total cutin load was reported to amount to 2.5 μg cm^{-2} in leaves[68] and to as high as 586.1 μg cm^{-2} in fruits.[69] Such quantitative differences were found for cuticular waxes as well: total loads of 3.5 and 15 μg cm^{-2} were reported for leaves and fruits, respectively,[67] although total wax amount in fruits of the same cultivar has been recently shown to reach even higher values.[69] More importantly, substantial compositional differences have been also observed between leaves and fruits, in addition to differences in total wax and cutin loads. For waxes, the main compositional differences were found for the percentage of branched alkanes (approximately 22 vs. 8% of total cuticular waxes in leaves and fruit, respectively), whereas the percentages for *n*-alkanes and triterpenoids were similar in both cases,[67,69] and significant amounts of alcohols and fatty acids were found for fruit cuticles.[69] As to cutin monomers, the chief differences in composition between leaves and fruits referred to the amount and type of hydroxy-acids and to the percentage of dicarboxylic acids.[68,69]

Tomato fruit cuticles provide a valuable model for fruit cuticle research, as they are astomatous and comparatively thick, which means that it is possible to isolate considerable amounts of "unperforated" material for biochemical, physical, or structural characterization.[70] Albeit less intensively, cuticles of some other fruit species, mostly corresponding to crops of economic relevance, have also been investigated and revealed significant differences across genotypes in their properties. Because fruit cuticles modulate several traits of economic importance,[25,70] the understanding of the functions and impact of this outer layer on quality, storage potential, and shelf life of produce will require its characterization as a preliminary step.

To highlight interspecific differences in the chemical composition of fruit cuticles, the following subsections review published literature to reveal the variation in the main components of cutin and waxes that exists across different fruit types. With the purpose of revealing possible compositional similarities within fruits of species related taxonomically, this information has been organized according to botanical families. The many unknowns still existing in relation to fruit cuticle composition are highlighted in the summary of available information for each listed fruit species presented in Table 1.

Solanaceae. *Tomato (Solanum lycopersicon).* The cuticle composition of tomato, widely used as a model species for research related to different aspects of fruit development, has been investigated with considerably more intensity in comparison with other fruit species. Cuticular waxes of the 'Micro-Tom' cultivar consist predominantly of very long-chain alkanes and triterpenoids.[67,69,71] The C_{31} alkane *n*-hentriacontane was prevalent in the epicuticular wax film, whereas in the intracuticular wax compartment it was mixed with the pentacyclic triterpenoid alcohols α-, β-, and δ-amyrin. For the 'Ailsa Craig' cultivar, a similar composition of cuticular waxes was reported,[72] 55−60% of the total amount consisting of *n*-alkanes, among which *n*-hentriacontane was also shown as the most abundant, followed by *n*-nocacosane (C_{29}) and *n*-tritriacontane (C_{33}). Amyrins (α, β, and δ) together accounted for about 18% of wax components in this cultivar. When the cutin composition was analyzed, the C_{16} cutin monomer 10,16-dihydroxy $C_{16:0}$ acid was found to account for about 74% of total monomers. The prevalence of *n*-hentriacontane, amyrins, and 10,16-dihydroxy $C_{16:0}$ acid in the composition of tomato cuticles was confirmed in subsequent studies on 'Ailsa Craig',[73−77] 'M82',[76−79] and 'John Baer' and 'Pearson'.[80] However, when cuticles of seven different species of wild tomato were analyzed, substantial diversity in the microscopic morphology of the cuticle and the underlying epidermal cell layer, as well as in the content of cutin and waxes, was found.[79] The cuticular wax content of the wild species surpassed that of

DOI: 10.1021/acs.jafc.5b00013
J. Agric. Food Chem. 2015, 63, 4005−4019

cultivated tomato by up to 7-fold, and variability in the amount of wax esters and triterpenoid isomers was also found. It can be speculated that selection for this species has favored a particular cuticle composition that may be associated with more favorable agronomic characteristics.

Pepper (Capsicum sp.). Kissinger and co-workers[81] examined the cuticles of 10 *Capsicum* sp. cultivars differing in quality attributes such as pungency and fruit size. Globally, the cuticle was found to be particularly rich in C_{16} cutin monomers, the main component in quantitative terms being 9(10),16-dihydroxyhexadecanoic acid, whereas 9,10-epoxy-18-hydroxyoctadecanoic acid was the main representative of the C_{18} monomer type. The major aliphatic constituents of cuticular waxes were *n*-alkanes, in which *n*-hentriacontane was the predominant single compound. Significant amounts of methyl-branched alkanes and of the triterpenoids α- and β-amyrin were also detected. A concurrently published study on 12 bell pepper cultivars also identified *n*-hentriacontane and triterpenoid alcohols as the dominating wax components in these fruit.[82] A later work also disclosed that pepper fruit cuticles contain a cutan-like fraction.[83] More recently, the cuticle lipid composition in a near-isogenic backcross population (BC_2F_2) obtained between an inbred line of *C. annuum* and a wild line of *C. chinense*, which markedly differ in postharvest water loss rates, has been analyzed.[84] Interestingly, the major components of cuticular waxes and cutin were the same as mentioned above,[81] but significant differences in absolute and relative amounts within wax classes and cutin monomers were found between the parents and among the segregating BC_2F_2 population. Such approaches are needed for other fruit species, particularly when quality at harvest and during postharvest is affected by phenomena related with cuticle dynamics, such as water loss or microcracking. This would help identify metabolic signatures associated with particular physiological traits and quality attributes.

Eggplant (Solanum melongena). The surface waxes of eggplant fruit have been also examined in three cultivars.[82] In this study, waxes were extracted in *tert*-butylmethyl ether and chromatographed through a silica gel column, from which two fractions (termed fractions 1 and 2) were eluted using hexane/toluene and methanol, respectively. For all three cultivars, *n*-alkanes (C_{23}−C_{36}) predominated in fraction 1, which represented 77% of all waxes recovered. The dominating compound in this fraction (up to 18%) was *n*-hentriacontane, followed by *n*-tritriacontane. The triterpenoid components were eluted with fraction 2, amyrins and other triterpenols being the main compound detected, similar to the observations for other species within the Solanaceae family. No information was reported on cutin monomers.

Rosaceae. *Apple (Malus × domestica).* The first reports on cuticle composition of apple fruit date back to the 1970s. Three cultivars ('Dougherty', 'Granny Smith', and 'Sturmer') were studied in relation to the composition of their surface waxes,[85] and it was found that *n*-nonacosane and nonacosan-10-ol were prominent in all three cultivars among the constituent hydrocarbons and secondary alcohols, respectively. In contrast, the main primary alcohols differed among cultivars, with *n*-hexacosanol (C_{26}) predominating in 'Sturmer', whereas *n*-tetracosanol (C_{24}) was the most abundant in 'Dougherty' and 'Granny Smith' fruits. Waxes from 'Sturmer' also differed from the other two cultivars studied in regard to the main fatty acids present, showing a comparatively higher content of hexadecanoic and lower content of octadecadienoic acid. Subsequent studies on other cultivars[86,87] confirmed *n*-nonacosane as the main alkane in apple fruit cuticles, but also provided a broader overview of cultivar-specific variability in wax composition of apple cuticles. The analysis of cuticular waxes of 17 cultivars[86] showed triterpenoids as the dominating wax fraction, ursolic acid accounting for 30−72% of total waxes, and furthermore revealed that secondary alcohols were the most cultivar-specific compounds—more so than primary alcohols—contrasting with previous observations.[85] In addition to *n*-nonacosane, surface waxes of 'Red Fuji' apples included important amounts of nonacosan-10-ol and the ketone nonacosan-10-one.[87] Similar results indicative of cultivar-related variability were reported by other researchers as well.[88,89] In the latter case, the secondary alcohol nonacosan-10-ol was found to be the compound explaining the main differences in surface characteristics of 'Jonagold', 'Jonagored', and 'Elstar' fruit.

With respect to cutin monomers, the C_{18}-hydroxylated class of monomers was found to account for 73% of total cutin monomers in 'Golden Delicious',[60] which was much higher than the amounts in leaves and flower parts from this variety, and it was thus hypothesized that the content of C_{18} monomers was related to the rate of expansion of different organs. This finding emphasizes the need to assess compositional differences between particular tissues, as stated above. When the aliphatic components of apple fruit cuticles were characterized using elemental analysis, ^{13}C nuclear magnetic resonance (NMR), and Fourier transform infrared spectroscopy, they were shown to contain lower percentages of the cutan-like fraction than those of pepper fruit and to display slightly different chemical structure, too.[83]

Pear (Pyrus sp.). Despite the economic importance of the world trade of both European and Asian pears, only the latter have been investigated in relation to cuticle composition and uniquely in regard to their waxes. A total of 54 compounds were identified in the cuticular waxes of 'Pingguoli' Asian pear,[90] the main constituents observed being pentacyclic triterpene alcohols (32%), fatty acids (27.8%), and alkanes (25.9%). The composition of each of these three major compound families was dominated by α-amyrin, hexadecanoic acid, and C_{19}−C_{31} *n*-alkanes, respectively. To the best of our knowledge, there is no published information on the cutin composition of pear cuticles, thus also offering ample field for further research.

Peach (Prunus persica). Surprisingly, very limited research has been reported in regard to the cuticle composition of climacteric stone fruits such as peach, apricot, or plum, despite its potential relevance for water loss and decay susceptibility of these fruit species. Peach skin was taken as a model for studying properties of pubescent surfaces concerning water−plant surface interactions,[91] and cuticle composition was analyzed for the content of the main component types. Peach cuticles were found to be composed of 53% cutan, 27% waxes, 23% cutin, and 1% hydroxycinnamic acids, whereas trichomes contained 15% waxes and 19% cutin, filled with 63% polysaccharide material associated with hydroxycinnamic acid derivatives and flavonoids. Nevertheless, the detailed composition of each of these fractions was not described. We have recently analyzed the composition of waxes and cutin monomers in cuticles isolated enzymatically from melting- and non-melting-type peach fruit[92] and identified the $C_{18:1}$ derivative 18-hydroxyoctadecenoic acid as the most abundant cutin monomer (17−20% at harvest, depending on the cultivar), whereas the triterpenes ursolic acid and oleanolic

DOI: 10.1021/acs.jafc.5b00013
J. Agric. Food Chem. 2015, 63, 4005−4019

acid were prominent among the components of cuticular waxes, accounting together for 44−52% at harvest. In contrast to most published studies on fruit cuticles, in which *n*-nonacosane and *n*-hentriacontane were reported to be the main alkane components of cuticular waxes (Table 1), we identified *n*-tricosane (C_{23}), *n*-pentacosane (C_{25}), and *n*-heptacosane (C_{27}) as the predominant alkanes in peach fruit, with substantial cultivar-related differences in the total content of these compounds (10−24% at harvest).

Sweet Cherry (Prunus avium). Considerably more reports than for peach exist for sweet cherry cuticles, although most of them have been mainly concerned with its physical and mechanical properties as related to water permeability and disorders to which these fruit are particularly prone, such as cracking. An early study on ripe 'Bing' cherries[93] revealed ursolic acid and *n*-nonacosane as prominent components of cuticular waxes of fruit. This was confirmed when the composition of both cutin and waxes of four sweet cherry cultivars was studied during on-tree fruit development and maturation.[3] The most abundant constituents of waxes at fruit maturity were the triterpenes ursolic and oleanolic acids, which together accounted for 76% of total wax, followed by the alkanes *n*-nonacosane and *n*-heptacosane and the secondary alcohol nonacosan-10-ol. These data essentially agree with our own observations on 'Celeste' and 'Somerset' cherries, showing ursolic acid (roughly 50% of total waxes) to be the major triterpene, *n*-nonacosane and *n*-heptacosane the most abundant alkanes (7−11%), and *n*-tricosanol (C_{23}) and *n*-triacontanol (C_{30}) the main primary alcohols detected in cuticular wax.[94] Although these studies agree as to the major components of cuticular waxes in all of the cultivars assessed, they show discrepancies for other types of wax constituents. Specifically, cuticular waxes of 'Bing' cherries are rich in hexadecanoic, octadecanoic, octadecenoic, and octadecadienoic acids and contain significant amounts of sitosterol.[93] Because dehydrated fruit skins were used as the source of wax, when these compounds were not found in a later study,[3] it was concluded that their detection might have been an artifact derived from contamination with membrane lipids. However, the analysis of the cuticular waxes of 'Celeste' and 'Somerset' fruit also revealed significant contents of octadecadienoic acid and phytosterols,[94] despite the fact that enzymatically isolated cuticles were used as the source material for wax extraction. Therefore, these discrepancies are likely to reflect actual cultivar-related differences in cuticular wax composition.

Although published reports have shown only minor quantitative differences in wax composition among cherry cultivars, discrepancies have been found as to cutin monomer composition. The cutin fraction of mature 'Kordia' fruit consisted mainly of C_{16} (69.5%) and, to a much lesser extent, C_{18} (19.4%) monomers, the most abundant components being 9(10),16-dihydroxyhexadecanoic and 9,10,18-trihydroxyoctadecanoic acids.[3] However, we have found that the cutin fraction of 'Celeste' and 'Somerset' cherry fruit is composed mainly of C_{18} monomers (65.3 and 57.9%, respectively),[94] which contrasts with previous observations in this species and shows cultivar-related differences in cuticle composition.

Soft Fruit Species. The composition of the cutin fraction of some berries within the Rosaceae family has been investigated.[62] The cutin composition of strawberry (*Fragaria* × *ananassa*), raspberry (*Rubus idaeus*), and rowanberry (*Sorbus aucuparia*) fruit was shown to be dominated by 9(10),16-dihydroxyhexadecanoic acid, although all three species displayed wider variety of cutin monomers in comparison with non-Rosaceae berry fruits that were analyzed in the same work. A similar cutin composition was observed in rosehip (*Rosa rugosa*), black chokeberry (*Aronia melanocarpa*), and cloudberry (*Rubus chamaemorus*) fruits,[62] although additional compounds such as C_{15} monomers and α,ω-dicarboxylic acids with midchain hydroxyl groups were also found. Additionally, strawberry and raspberry cutin proved to be highly resistant to depolymerization, and this observation was suggested to arise from the presence of a particularly high amount of cutan-type compounds. The cutin/cutan ratio is likely to affect significantly the pre- and postharvest evolution of fruit quality attributes, including their value as a dietary fiber, and this topic is thus worthy of more detailed examination. Similarly, no published studies are available for cuticular wax composition of these species, thus offering ample opportunity for further research.

Rutaceae. *Citrus Fruit (Citrus sp.).* In orange, triterpenoids constitute the most abundant wax fraction found in mature fruits, mainly consisting of α-amyrin, β-amyrin, lupeol acetate, and friedelin.[95] Additionally, aldehydes are also major constituents of the cuticular waxes in orange and lemon fruit, together with alkanes, primary alcohols, and fatty acids. The predominant compounds are reportedly *n*-nonacosane and *n*-hentriacontane among the alkanes and *n*-tetracosanal (C_{24}), *n*-hexacosanal (C_{26}), and *n*-octacosanal (C_{28}) among the aldehydes.[64,95] Terpenoids and aldehydes were likewise reported to be the main compound families present in epicuticular waxes of grapefruit, with some differences observed according to the canopy position,[96] which supports the assumption that the environmental conditions cause cuticle modifications and affect fruit development. In contrast, mandarin fruit waxes are dominated by alkanes, followed by esters > ketones > aldehydes > fatty acids > primary alcohols > triterpenes.[97] The detailed compositions of each of these classes of component were not reported, but some differences were also found according to the canopy position of fruit.

We are aware of only two published studies on cutin components of citrus fruit. The fruit cuticles of four different species (orange, lemon, grapefruit, and mandarin) were reported to contain less cutin (59−67%) than those of their leaves (79−82%).[98] The major monomeric constituents detected were dihydroxy C_{16} (30−62%) and 16-hydroxy-oxo C_{16} acids. Similarly, when the cutin monomer composition was analyzed in different tissues of grapefruit, including fruit peel, leaf, juice sac, and inner seed coat, it was found that 16-hydroxy-10-oxo C_{16} acid was a major component in the fruit peel.[61] Substantial tissue-associated variation was observed, as 10,16-dihydroxy C_{16} acid and its positional isomers were the main cutin monomers in leaves, the composition of the juice sac cutin was dominated by dihydroxy C_{16}, hydroxy-oxo C_{16}, hydroxy-epoxy C_{18}, and trihydroxy C_{18} acids, and ω-hydroxy and dicarboxylic C_{16} and $C_{18:1}$, ω-hydroxy-epoxy C_{18} and trihydroxy C_{18} acids were the major components of the inner seed coat cutin.

Vitaceae. *Grape (Vitis vinifera).* Similarly to citrus fruit, aldehydes have also been found to be important constituents in waxes of grapes, where the straight-chain, even-chain length type predominates. Early in 1965, two published works[65,99] reported that the surface waxes of ripe sultana grapes consist largely of the triterpenoid oleanolic acid, with lesser amounts of *n*-alcohols (mainly C_{24}, C_{26}, and C_{28}), *n*-aldehydes (largely C_{28} and C_{30}), esters, free acids (predominantly C_{24}, C_{26}, and C_{28}), and *n*-hydrocarbons (mainly C_{25}, C_{27}, C_{29}, and C_{31}). A

DOI: 10.1021/acs.jafc.5b00013
J. Agric. Food Chem. 2015, 63, 4005−4019

considerable amount (around 30%) of oleanolic acid was also found in cuticle waxes of 'Palomino fino' grapes,[100] although surprisingly *n*-alkanes represented <5% of total mass and, remarkably, no aldehydes were identified. Oleanolic acid was also the dominant component in cuticular waxes of 'Pinot noir' grapes at all stages of fruit development,[101] as well as in eight different cultivars investigated in a recent study,[102] in which triterpenoid contents were found to range from 42% to as much as 80% of total cuticular waxes. Due to their relevance for fermentative processes and their health-promoting properties,[103] major triterpenes (oleanolic acid and β-sitosterol) in grape waxes have been targeted for study and suggested to be a suitable tool to characterize grape varieties.[104] When the cuticular wax of fruit of the European wild vine (*Vitis vinifera* ssp. *sylvestris*) was analyzed, only minor quantitative differences were found in some of the wax fractions in comparison with the cultivated vine (*V. vinifera* ssp. *vinifera*),[66] suggesting their conservation during evolution.

We are not aware of any published studies on the cutin composition of grape berry cuticles, although the evolution of total cutin amounts during fruit maturation has been reported.[101] Taking into account its commercial importance with regard to both fresh consumption of table grapes and winemaking, further studies addressing this topic are desirable.

Oleaceae. *Olive (Olea europaea).* Because the procedure for olive oil extraction may dissolve an important part of the surface waxes, and given its economic importance, a number of published studies have analyzed wax compounds present in the oil. In contrast, little information is available on the intact fruit. When chloroform-soluble waxes of 'Coratina' olives at the green and black maturity stages were extracted, substantial compositional differences were found in each case.[105] Triacylglycerols (17 and 25% in green and black fruit, respectively) and triterpene acids (38 and 26%, respectively) were the predominant families of wax compounds in the fruit. Triterpenols accounted for 14% of total waxes in green fruit, whereas only traces were detected in ripe samples. The major triterpene in both cases was oleanolic acid (70 and 83%, correspondingly). Similar to the observations in grape (see previous subsection), *n*-alkanes were only a small part of the total wax mass (3 and 7% in green and black fruit, respectively), dominated by C_{27} or C_{29}, depending on the maturity stage.

Ebenaceae. *Persimmon (Diospyros kaki).* The total amount of waxes and cutin in fruit cuticles isolated from 27 astringent and nonastringent cultivars of persimmon has been published recently,[12] although the chemical composition of each fraction was not analyzed in detail. The cuticles of these fruit were composed of 22−38% (337−770 μg cm^{-2}) of wax and 33−56% (578−1378 μg cm^{-2}) of cutin. Whereas significant cultivar-related differences in cuticle composition were found, in agreement with other fruit species, these differences were not related to fruit astringency. Additional studies should enable the determination of which are the quality traits, in each fruit species, that are modulated by cuticle subtleties as well as the mechanisms by which this regulation occurs.

Others: Grossulariaceae, Ericaceae, Elaeagnaceae. No published information is available regarding the cuticular wax composition of soft fruit species within these families, and only the composition of cutin monomers has been analyzed and reported. Studies on six non-Rosaceae berry types, namely, sea buckthorn (*Hippophaë rhamnoides*), black currant (*Ribes nigrum*), cranberry (*Vaccinium oxycoccos*), lingonberry (*Vaccinium vitis-idaea*), bilberry (*Vaccinium myrtillus*), and crowberry (*Empetrum nigrum*), have revealed notable differences in total cutin loads (6−47%) across species.[62,106] The predominant cutin monomers were C_{16} and C_{18} ω-hydroxy acids with midchain functionalities, among which epoxy groups were particularly frequent in sea buckthorn and cranberry (71 and 60% over total cutin monomers, respectively). Cuticles of these fruits also contained significant amounts of C_{15} monomers and α,ω-dicarboxylic acids.

Conclusion. This survey shows that fruit cuticles display considerable variability among species and illustrates the inappropriateness of generalizations on fruit cuticle properties. Yet a complete overview of cuticle constituents is available in only a few instances (Table 1). Although *n*-alkanes and triterpenoids are prominent components of cuticular waxes in all of the fruit species for which such information exists, fruit cuticle types seem to emerge according to their main alkane (C_{29} vs C_{31}) and triterpenoid (triterpenoid acids vs triterpenoid alcohols) components. Some grouping is also apparent according to the predominant cutin monomers (C_{16} vs C_{18}). On the basis of the scarce information currently available, these groupings do not seem to show any correspondence with fruit type (berries vs drupes) or with ripening pattern (climacteric vs nonclimacteric). However, this review reveals clear similarities in fruit cuticle composition among phylogenetically close species (Table 1). For example, the investigated species within the Solanaceae family display C_{31} and triterpenoid alcohols as the main *n*-alkane and triterpenoid components of cuticular waxes, respectively, with dihydroxy $C_{16:0}$ as the predominant cutin monomer. In contrast, C_{29} and triterpenoid acids have been reported as the main wax components in most of the species examined within the Rosaceae, with the predominant cutin monomers displaying wider variation. Cutin composition in the cuticles of citrus fruit is reportedly dominated by C_{16} monomers, whereas insufficient information is available to allow generalizations on predominant wax compounds within this botanical family (Table 1).

Recent studies conducted on *Arabidopsis* have identified proteins specifically involved in the elongation of compounds longer than C_{28} and C_{30}, which are moreover expressed differentially in an organ- and tissue-specific manner.[107−111] Although no similar information has been reported for edible fruits, the question arises whether potential differences in the expression of homologous fruit genes or proteins may be related to the dissimilarities in the chain length of the predominant cuticular alkanes across botanical families (Table 1). The potential relationship of these differences with cuticle structure and properties, and hence, with the horticultural attributes of each fruit type, requires intensive research. The implications of cuticle composition and structure for postharvest potential and for the design of handling strategies are huge.[25] In the absence of these studies, any careless generalization is likely to lead to oversimplification and to failure of any postharvest procedure designed on such a weak basis.

CUTICLE BIOSYNTHESIS IN FRUITS

Cuticle Biosynthesis during Fruit Maturation and Ripening. The process of cuticle, cutin, and cuticular wax formation during on-tree fruit development has been studied essentially from the ultrastructural,[101,112] biomechanical/biophysical,[113−116] and biochemical points of view.[3,73,86,87,95,102,117] It has frequently been observed that

DOI: 10.1021/acs.jafc.5b00013
J. Agric. Food Chem. 2015, 63, 4005−4019

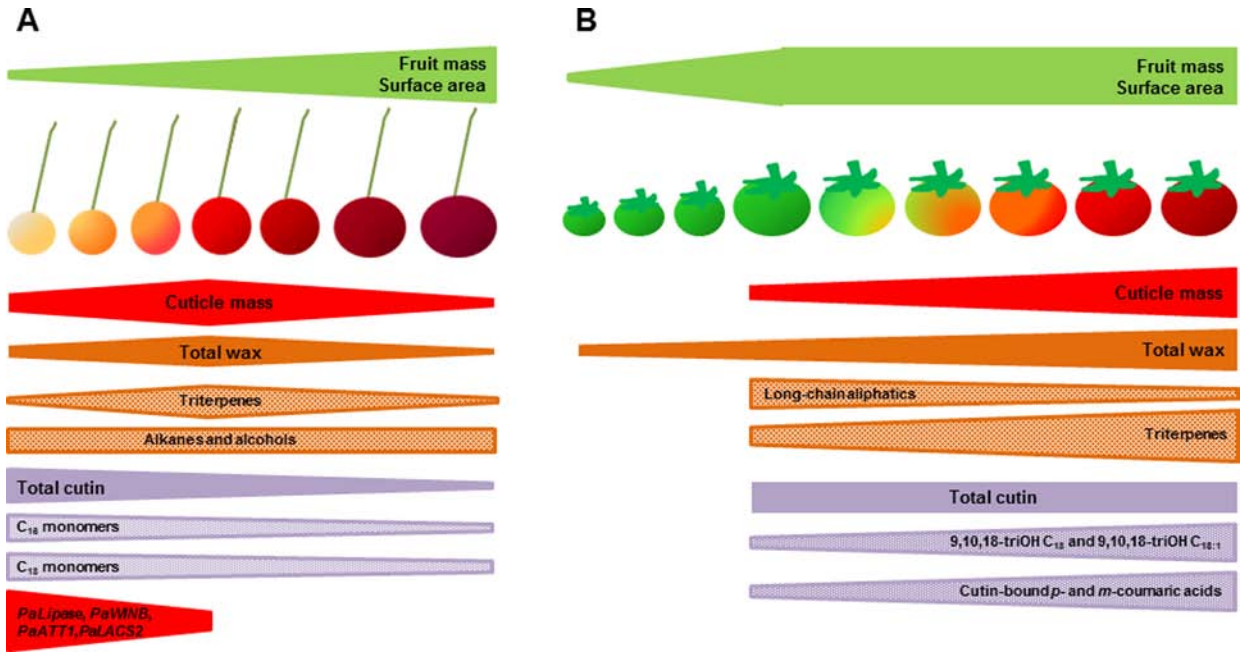

Figure 1. Changes in cuticle deposition and composition during the development of (A) sweet cherry and (B) tomato as an example of a nonclimacteric and a climacteric fruit species, respectively. The figure is intended uniquely as an illustration of the profound dissimilarities reported among different fruit species. The literature survey undertaken in this review indicates that the fate of cuticular compound families during fruit development differs noticeably among fruit species, and therefore these patterns should not be taken as representative of each ripening type. The figure was drawn from data reported in refs 3, 71−73, and 118−120. Changes are expressed per unit of surface area.

cuticle deposition ceases at a given developmental stage, generally corresponding to the transition between growth and ripening, giving rise to decreased amounts of cuticle per unit surface area. This favors increased surface strain as fruit expands, and thus the formation of micro- or macroscopic cracks, the latter having major economic consequences for some commercially important fruit crops. We are not aware of any cause/effect studies relating cuticle composition to the development of this disorder, but some genes are down-regulated concomitantly with arrested cuticle deposition in fruit species particularly prone to this disorder, such as sweet cherry,[118] which may provide the tools to investigate this aspect.

Generalizations on a particular biological event among different species should be treated with caution, as different genetic backgrounds often possess specific mechanisms to cope with environmental stimuli. For this reason, to tackle the compositional evolution of specific cuticular components during fruit development we inspected the available literature on those fruit species for which such information has been published. This survey indicates that any temptation to simplify or generalize the fate of different cuticular compound families during fruit development should be ruled out.

For instance, even the commonly observed trend of early cessation of cuticle deposition is not found in all cases, a notorious exception being tomato (Figure 1). Although long-chain aliphatics were actually found to decrease in developing tomato fruit, the extent of triterpene increases overcompensated for that reduction.[119] A continuous increase in the wax coverage during the developmental course from mature green to red ripe fruits in the 'Micro-Tom' cultivar has also been reported.[71] The total amount of wax and the proportion of alkadienes increased during ripening of 'Ailsa Craig' tomato from the mature green to the red ripe stages, whereas the total amount of cutin monomers per unit of surface area and the relative proportions of the corresponding constituents remained approximately constant during the same period, except for increases in 9,10,18-trihydroxyoctadecanoic and 9,10,18-trihydroxyoctadecenoic acids.[72] This continuous increase in total cuticular waxes during tomato maturation and ripening from as early as the small green stage was subsequently confirmed, with a progressive rise in the absolute content of all wax classes, with the exception of isoalkanes.[63] The amounts of most cutin monomers as well as that of *p*-coumaric and *m*-coumaric acids also increased throughout development. A substantial increase in the phenolic content of the cuticles of 'Ailsa Craig', 'Alicante', and 'Grower's pride' tomatoes was also observed in an earlier work,[120] the major part of the flavonoids detected in ripe fruit being bound to the cutin matrix.

A steady decrease in the proportion of primary alcohols and a progressive increase in esters in cuticular waxes were found during the maturation of grape berries, whereas the content in cutin per surface unit decreased sharply between berry set and véraison.[101] Total triterpenoid contents have also been observed to decline in grapes during fruit ripening.[102] In contrast, a survey on 17 different apple cultivars[86] disclosed increases in the percentage of primary alcohols in the epicuticular waxes as fruit development progressed. More recently, the alkanes *n*-nonacosane and *n*-heptacosane, the alkene *n*-nonacosene, and the secondary alcohol nonacosan-10-ol were observed to increase as fruit reached the mature stage, whereas nonacosan-10-one decreased during the same period.[87] For sweet cherry fruit, it was found that the amount of triterpenes per unit area decreased, with alkanes and alcohols remaining approximately constant throughout fruit development (Figure 1). On the other hand, the amounts of C_{16} and C_{18} cutin monomers per unit area declined, even though divergent trends were shown for different compounds within

DOI: 10.1021/acs.jafc.5b00013
J. Agric. Food Chem. 2015, 63, 4005−4019

Table 2. Tomato Fruit Genotypes Impaired or Altered in Cuticle-Related Genes

genotype	cuticle-related phenotype	refs
alcobaça	altered wax profiles (throughout development) and cuticle lipid compositions (early stages of development); higher relative amounts of C_{18} monomers	73
cutin deficient (*cd1*, *cd2*, *cd3*)	dramatic reduction in cutin content, altered cuticle architecture, increased stiffness of cuticle surface, enhanced water permeability	31, 77, 136
delayed fruit deterioration (*dfd*)	altered cuticle composition and architecture	72
GDSL1-silenced lines[a]	reduced thickness of fruit cuticle, decreased content of cutin monomers, decreased wax load	32
nonripening (*nor*)	altered wax profiles (throughout development) and cuticle lipid compositions (early stages of development); higher relative amounts of C_{18} monomers	73, 137
positional sterile (*ps*)	increased water loss, severe depletion of *n*-alkanes and aldehydes, increased triterpenoids and sterol derivatives, occurrence of alkyl esters not present in the wild-type fruit; similar wax load, unaffected cutin monomer composition	134
ripening inhibitor (*rin*)	altered wax profiles (throughout development) and cuticle lipid compositions (early stages of development); higher relative amounts of C_{18} monomers	73
slcer6 loss-of-function	deficiency in *n*-alkanes and aldehydes longer than C_{30}, increase in intracuticular triterpenoids	67, 71
SlSHN3-silenced lines	reduction in cuticular lipids, lower cutin content, and altered architecture of fruit surface	78
sticky peel (*pe*)[b]	severe reduction in cutin biosynthesis and altered wax deposition	75
sticky peel/light green double mutant (*pe lg*)	glossy soft fruit, severely reduced thickness of fruit cuticle, enhanced water permeability	134, 136
y	reduced thickness of fruit cuticle, lower cutin content, and decreased elasticity	138
16 glossy and 8 dull mutants	altered amount and/or composition of wax and cutin, cuticle thickness, and surface aspect of the fruit	69

[a]GDSL1 is allelic to CD1. [b]PE is allelic to CD2.

each monomer family.[3] The compositional changes in cuticular waxes during fruit development have also been investigated in 'Newhall' orange fruit, and it was found that waxes are secreted continuously during ripening and that decreases in the amount of all major wax fractions were related to the glossy fruit flavedo phenotype of the so-termed 'glossy Newhall' mutant.[95] The mutant fruits have dramatically reduced aldehyde and alkane contents associated with a severe loss of wax crystals. No information was reported on changes in the amount of total cutin or cutin monomers.

This handful of available studies exemplifies how modifications in cuticle composition during fruit maturation and ripening are variable among different fruits. Similar investigations, undertaken on a wide range of additional fruit species, may help identify putative common trends within particular fruit types.

Insights into the Molecular Aspects of Cuticle Biosynthesis in Fruits. Little information exists on the regulation of cuticle formation in fruits at the molecular level. In fact, only a few recent papers have reported the identification of genes related to cuticular wax or cutin biosynthesis in these organs, most of them conducted in tomato as the model species. Cuticle deposition involves a large number of steps and interconnected routes that determine its amount, composition, and correct structural assembly.[7,9,16−19] The identification of the key control points is rendered a difficult task by the multilevel regulation of these pathways, which may involve gene expression, protein modification, and cell environmental changes. A feasible way to tackle this subject is to use mutants altered in fruit cuticle attributes in comparison with the wild-type phenotype. Some of such cuticle mutants exist for tomato (Table 2), and their comprehensive analysis may help detect candidate key genes, proteins, metabolites, and pathways associated with cuticle biosynthesis and functions. The current availability and affordable cost of -omics technologies paves the way for such "systems biology" approaches.

Using this strategy, the gene *LeCER6* (currently referred to as *SlCER6*, owing to the renaming of tomato to *Solanum lycopersicum*), a homologue of *AtCER6*, which codes for a very long-chain fatty acid β-ketoacyl-CoA synthase, has been identified,[67] and a LeCER6 loss-of-function mutant was obtained by reverse genetic techniques. Associated functional characterization showed that waxes of the mutant fruit were deficient in *n*-alkanes and aldehydes longer than C_{30}, whereas hydrocarbons with shorter or branched chains were unaffected. Mutant waxes were also significantly richer in intracuticular terpenoids. Interestingly, these modifications were reflected in cuticle permeability, unquestionably demonstrating a major role of these compounds in the transpiration barrier properties of the cuticle.[67] When the developmental course of maturation and ripening was followed, both in the wild type and in the *LeCER6* mutant, the deficiency was discernible as early as the mature green stage.[71] Comparative transcriptome and metabolome analyses in tomato showed that 17% of 574 peel-associated transcripts were putatively related to cuticle component-generating metabolic pathways.[74] Among these, the expression of *LeCER6* in both fruit exocarp and endocarp was shown to increase progressively during maturation and ripening, supporting the putative association of this gene with cuticular wax formation.

More recently, a homology-based approach has been employed to isolate two oxidosqualene cyclases (OSC) involved in the biosynthesis of triterpene alcohols and expressed exclusively in fruit epidermis, one of which was demonstrated to be a product-specific β-amyrin synthase.[121] When the transcription ratios of these OSCs, designated SlTTS1 and SlTTS2, were compared among three tomato cultivars ('Micro-Tom', 'M82',"and 'Ailsa Craig') differing in their triterpenoid profile, it was found that transcriptional control of these two OSCs accounted only partially for these differences, suggesting the involvement of other factors such as differences in catalytic activity or the presence of additional OSCs.

A few fruit-expressed genes related to cutin deposition have been also identified taking advantage of altered genetic backgrounds (Table 2). The characterization of a tomato mutant designated *cutin deficient 1* (*cd1*), showing only 5−10% cutin content in comparison with the wild-type fruit,[77] revealed

DOI: 10.1021/acs.jafc.5b00013
J. Agric. Food Chem. 2015, 63, 4005−4019

that CD1 is an extracellular acyltransferase with polyester synthesis activity required for cutin accumulation in vivo, demonstrating it to be a cutin synthase directly involved in cutin polymerization.[31] The protein is localized in the cuticle, specifically at the interface with the cell wall, and the expression of its coding gene parallels spatial and temporal patterns of cuticle deposition in the fruit. Similarly, the characterization of the *sticky peel* (*pe*) tomato mutant, which suffers from severe reduction in cutin biosynthesis and alterations in wax deposition, allowed the identification and partial characterization of CD2, a putative transcription factor suggested to act upstream of several metabolic pathways involved in the biosynthesis of a range of surface tissue-associated molecules.[75] A tomato transcription factor (SlSHN3) that regulates fruit cuticle formation and epidermal patterning has also been characterized recently.[78] Silencing the *SlSHN3* gene resulted in remarkable morphological alterations of fruit epidermis and a significant reduction in cuticular lipids. Similarly, a mutation in *SlCYP86A69*, one of the SlSHN3 target genes, led to severe cutin deficiency and altered architecture of the fruit surface. SlCYP86A69 was characterized to possess NADPH-dependent ω-hydroxylation activity, with a preference for oleic acid ($C_{18:1}$) to yield the cutin monomer 18-hydroxyoctadecenoic acid.[78]

In this context, a recent work[69] has shown the potential of a simple phenotypic attribute such as fruit brightness for the identification of cuticle mutants, thus providing an additional tool for the discovery of new genes putatively involved in cuticle biosynthesis. A mutant collection of the 'Micro-Tom' cultivar was screened for altered fruit brightness, which led to the isolation of 16 glossy and 8 dull mutants displaying concomitant differences in cuticle composition, thickness, or structure. Whereas glossy mutants were altered in cutin load and/or composition, dull mutants differed from the wild-type fruit in the characteristics of the epidermis. Surprisingly, no relationship was found between fruit brightness and wax load variations.

Considerably less research effort at the molecular level has been focused on fruits other than tomato. The identification of several candidate genes putatively involved in cuticle formation during development and maturation of 'Regina' sweet cherry fruit revealed that 13 of 18 identified sequences showed expression patterns restricted to fruit exocarp and correlated with cuticle deposition rates.[118] This study recognized some genes that deserve further research as to a major role in cuticle formation, including two transcription factors, one lipase, one LTP, one ABC transporter, two CYP86A hydroxylases, two LACS, and one GPAT. More recently, two of these candidate genes, *PaLACS2* (a putative long-chain acyl-CoA synthetase) and *PaATT1* (a putative cytochrome P450 monooxygenase), were suggested to be major genes involved in cutin biosynthesis on the basis of the effects of their ectopic expression in *Arabidopsis thaliana*.[122]

A similar approach was adopted in apple (cv. 'Prima' and 'Florina') fruit, based on sequence homology studies and transcription profiling.[123] Expression patterns of the selected genes showed that they are active in, and in some cases specific to, fruit skin. The genes identified included some members involved in the FAE complex, wax and cutin modifications, one LTP, one ABC transporter, and one transcription factor. However, these apple and sweet cherry genes were identified on the basis of transcriptomic and homology data uniquely, and an actual involvement in cuticle formation remains to be confirmed. Even so, the proteins encoded by three full-length expressed sequence tag sequences identified in apple cDNA libraries as likely to encode triterpene synthases (*MdOSC1*, *MdOSC2*, and *MdOSC3*) have been actually demonstrated to possess triterpene synthase activity by transient expression in *Nicotiana benthamiana* leaves and by expression in *Pichia methanolica*.[124] Interestingly, MdOCS1 was shown to produce α- and β-amyrin in a 5:1 ratio and, thus, to be the only triterpene synthase identified to date for which α-amyrin accounts for >80% of the total product. This finding implies that MdOCS1 is primarily an α-amyrin synthase, and this is interesting in the light of earlier indications that the main component of the triterpene fraction in apple fruit cuticle is ursolic acid (Table 1), the precursor of which is α-amyrin. The expression levels for these *MdOSC* genes in 'Royal Gala' apple showed preferential expression in the fruit peel and also significantly dissimilar expression levels among tissues, which were reflected in different contents of ursolic and oleanolic acids. The increasing availability of genomic sequences for nonmodel fruit species will provide the basis for shedding light on the current knowledge of cuticle formation in these commodities.

METHODOLOGICAL FOOTPRINT IN CUTICLE COMPOSITION STUDIES

Cuticle components are usually extracted, identified, and quantified following similar methodologies, and therefore major compositional discrepancies found between fruit species are not likely to arise from technical variations across different research groups. This is particularly clear when a given team has found such dissimilarities after using the same methodology for the analysis of cuticles obtained from different fruit species. Even so, it is worth pointing out some methodological aspects that may have some influence on reported results. Indeed, many of the studies reviewed herein were conducted >30 years ago and used different technological solutions.

Waxes are usually extracted by dipping the starting material in an organic solvent such as chloroform, methanol, dichloromethane, hexane, petroleum ether, or toluene, at room temperature or at the boiling point of the solvent, in a single or in a two-step extraction to separate epi- and intracuticular waxes. However, although the sequential extraction with different organic solvents has often been used as an approach to differentiate between epi- and intracuticular waxes, such differential extraction procedures are not selective enough as the resulting extracts are cross-contaminated. For an accurate quantification of the components of both compartments, methods allowing the mechanical removal of epicuticular waxes have been demonstrated to be preferable for this separation, such as those involving the use of adhesives (glycerol, water, nitrocellulose, gum arabic), followed by the stripping off or brushing of the outer film so obtained.[125,126] The starting material, in turn, can involve intact fruit samples, dehydrated fruit skins, or enzymatically isolated cuticles, all of which methodologies have associated weaknesses. For instance, plant cuticles were shown to sorb large amounts of hexadecanoic and octadecanoic acids when incubated in cell slurries obtained through enzymatic digestion of fruits and leaves,[127] thus placing under suspicion the common method of estimating intracuticular wax composition from cuticles isolated enzymatically. Also, the remarkable differences in skin structure found across fruit types (such as those between apple and citrus fruit) may underlie a part of these discrepancies, together with chemical dissimilarities such as pH, which might influence the

DOI: 10.1021/acs.jafc.5b00013
J. Agric. Food Chem. 2015, 63, 4005−4019

extraction of individual compounds. Additional features of fruit skin structure that may prove problematic or account for detected interspecific differences include thickness, flexibility, or the presence of stomata, lenticels, or trichomes.

Gas chromatography (GC) separation of the extracted compounds has been employed since the early 1960s, but the subsequent introduction of capillary columns increased analysis robustness. Compounds in the extracts may be injected directly, with previous chemical derivatization of active functional groups, or with previous hydrolysis of high-molecular-weight esters to release moieties that are then detected. In addition, compound detection by flame ionization (FID) or by mass spectrometry (MS) can result in quantitative and qualitative differences and hence justify some discrepancies.

Effective compound identification can be achieved by the comparison of Kovats retention indices and mass spectral data between the analyses and appropriate standards processed under matching experimental conditions. As standards for cuticle components are not always available commercially, the identification may be impaired or biased with respect to results obtained by other researchers if the group has the possibility to produce them in house. On the other hand, GC-MS identification is not free from drawbacks. For instance, identification is done by comparing the recorded EI-MS spectra with those available in public databases or with those obtained from reference compounds and then interpreting the fragmentation patterns in terms of chemical structure. Yet the spectra of many wax and cutin constituents are not available in MS libraries. In addition, rearrangements and isomerization may occur in unsaturated hydrocarbons, which might lead to the obtained spectra not showing the expected characteristic fragmentation configurations.[128] Even so, chemical techniques such as stereospecific oxidation and trimethylsilylation followed by gas−liquid chromatography coupled to MS have been employed successfully for the determination of double-bond positions of unsaturated fatty acids.[129,130] The use of more sensitive and up-to-date methodologies, such as two-dimensional GC, tandem chromatography arrangements, high-temperature GC (HTGC), HTGC-MS, or infrared and Raman microspectroscopic analysis,[131,132] would provide a valuable complementary tool to add to the current chemical standard analytical methods employed in bulk composition of plant cuticle analyses and hence allow a more accurate comparison between different plant materials, at both the intra- and interspecific levels.

CONCLUDING REMARKS AND FUTURE PROSPECTS

Biological developmental processes in plants are strictly controlled at various levels by cell composition and architecture. Organ- and cell-surrounding structures, such as the cell wall and the cuticle, are now recognized as highly dynamic developmental controllers, at both the signaling and the metabolic levels, as they provide the first communication level in response to conditions imposed on the plant by the surrounding environment. Despite the enormous efforts and advances in understanding cell organization, some cell components have received less attention from the scientific community, even though they are of paramount importance for plant development. Cell walls have been intensively studied and shown to vary in their composition, metabolism, and dynamics among different fruit species and even genotypes of the same species.[133] In contrast, a large number of gaps in knowledge still exist for almost every step of the putative pathways for the biosynthesis of plant cuticle.[7,9,16−19] Differences in cuticle composition between vegetative organs and fruits have been reported, but it is unclear whether exactly the same biosynthetic pathways and regulating mechanisms operate in fruit tissues, and there are many unknowns in regard to cuticle composition of fruits themselves (Table 1).

In this review, we highlight the variability proven to exist across individual fruit species and even across different genotypes of the same species. Such observations raise questions on the precise role of cuticles and on how they act as factors determining organ development and in coping with environmental cues. Answering this challenge will entail further efforts of fundamental research aiming at devising a generalized model of cuticle structure, together with a comprehensive atlas of differences between organisms, organ and cell types, and a track of metabolic regulation, to translate this knowledge into a practical understanding of the resulting biophysical properties. Future perspectives include understanding their impact and a putative premise of manipulating biological features useful to human activity, such as growing rates, respiration and water dynamics, protection against pathogens, or quality preservation of agronomic products.

AUTHOR INFORMATION

Corresponding Author

*(I.L.) E-mail: lara@quimica.udl.cat. Phone: +34 973 702526.

Funding

B.B. is the recipient of a FI-DGR grant from AGAUR (Generalitat de Catalunya). Financial support through the AGL2010-14801/ALI project, granted by the Ministerio de Ciencia e Innovación (MICINN) of Spain, is gratefully acknowledged.

Notes

The authors declare no competing financial interest.

ABBREVIATIONS USED

ABC, ATP-binding cassette; ACP, acyl carrier protein; CD, cutin deficient; CYP, cytochrome P450; DFD, delayed fruit deterioration; EI, electron ionization; FAE, fatty acid elongase; FAS, fatty acid synthase; FID, flame ionization detector; GC, gas chromatography; GDSL-lipase, Gly-Asp-Ser-Leu esterase/acylhydrolase; GPAT, glycerol-3-phosphate:acyl-CoA acyltransferase; HTGC, high-temperature gas chromatography; LACS, long-chain acyl-CoA synthetase; LTP, lipid transfer protein; MS, mass spectrometry; OSC, oxidosqualene cyclase; VLCFA, very long-chain fatty acids

REFERENCES

(1) Guzmán, P.; Fernández, V.; Graça, J.; Cabral, V.; Kayali, N.; Khayet, M.; Gil, L. Chemical and structural analysis of *Eucalyptus globulus* and *E. camaldulensis* leaf cuticles: a lipidized cell wall region. *Front. Plant Sci.* **2014**, *5*, 481.

(2) Domínguez, E.; Cuartero, J.; Heredia, A. An overview of plant cuticle biomechanics. *Plant Sci.* **2011**, *181*, 77−84.

(3) Peschel, S.; Franke, R.; Schreiber, L.; Knoche, M. Composition of the cuticle of developing sweet cherry fruit. *Phytochemistry* **2007**, *68*, 1017−1025.

(4) Kolattukudy, P. E. Cutin, suberin, and waxes. In *The Biochemistry of Plants*; Stumpf, P. K., Conn, E. E., Eds.; Academic Press: New York, 1980; Vol. 4, pp 571−645.

(5) Kolattukudy, P. E. Biopolyester membranes of plants: cutin and suberin. *Science* **1980**, *208*, 990−1000.

DOI: 10.1021/acs.jafc.5b00013
J. Agric. Food Chem. 2015, 63, 4005−4019

(6) Kolattukudy, P. E. Polyesters in higher plants. *Adv. Biochem. Engin./Biotechnol.* **2001**, *71*, 1−49.
(7) Nawrath, C.; Poirier, Y. Pathways for the synthesis of polyesters in plants: cutin, suberin, and polyhydroxyalkanoates. In *Advances in Plant Biochemistry and Molecular Biology I. Bioengineering and Molecular Biology of Plant Pathways*; Bohnert, H. J., Nguyen, H., Lewis, N. G., Eds.; Elsevier: Amsterdam, The Netherlands, 2008; pp 201−239.
(8) Stark, R. E.; Tian, S. The cutin biopolymer matrix. In *Biology of the Plant Cuticle*; Riederer, M., Müller, C., Eds.; Blackwell Publishing: Oxford, UK, 2006; pp 126−144.
(9) Post-Beittenmiller, D. Biochemistry and molecular biology of wax production in plants. *Annu. Rev. Plant Physiol. Plant Mol. Biol.* **1996**, *47*, 405−430.
(10) Villena, J. F.; Domínguez, E.; Stewart, D.; Heredia, A. Characterization and biosynthesis of non-degradable polymers in plant cuticles. *Planta* **1999**, *208*, 181−187.
(11) López-Casado, G.; Matas, A. J.; Domínguez, E.; Cuartero, J.; Heredia, A. Biomechanics of isolated tomato (*Solanum lycopersicum* L.) fruit cuticles: the role of the cutin matrix and polysaccharides. *J. Exp. Bot.* **2007**, *58*, 3875−3883.
(12) Tsubaki, S.; Ozaki, Y.; Yonemori, K.; Azuma, J. Mechanical properties of fruit-cuticular membranes isolated from 27 cultivars of *Diospyros kaki* Thunb. *Food Chem.* **2012**, *132*, 2135−2139.
(13) Riederer, M.; Schreiber, L. Protecting against water loss: analysis of the barrier properties of plant cuticles. *J. Exp. Bot.* **2001**, *52*, 2023−2032.
(14) Edelmann, H. G.; Neinhuis, C.; Bargel, H. Influence of hydration and temperature on the rheological properties of plant cuticles and their impact on plant organ integrity. *J. Plant Growth Regul.* **2005**, *24*, 116−126.
(15) Matas, A. J.; López-Casado, G.; Cuartero, J.; Heredia, A. Relative humidity and temperature modify the mechanical properties of isolated tomato fruit cuticles. *Am. J. Bot.* **2005**, *92*, 462−468.
(16) Pollard, M.; Beisson, F.; Li, Y.; Ohlrogge, J. B. Building lipid barriers: biosynthesis of cutin and suberin. *Trends Plant Sci.* **2008**, *13*, 236−246.
(17) Kunst, L.; Samuels, A. L. Biosynthesis and secretion of plant cuticular wax. *Prog. Lipid Res.* **2003**, *42*, 51−80.
(18) Kunst, L.; Samuels, A. L. Plant cuticles shine: advances in wax biosynthesis and export. *Curr. Opin. Plant Biol.* **2009**, *12*, 721−727.
(19) Samuels, L.; Kunst, L.; Jetter, R. Sealing plant surfaces: cuticular wax formation by epidermal cells. *Annu. Rev. Plant Biol.* **2008**, *59*, 683−707.
(20) Kerstiens, G. Cuticular water permeability and its physiological significance. *J. Exp. Bot.* **1996**, *47*, 1813−1832.
(21) Kerstiens, G. In vivo manipulation of cuticular water permeance and its effect on stomatal response to air humidity. *New Phytol.* **1997**, *137*, 473−480.
(22) Kerstiens, G. Water transport in plant cuticles: an update. *J. Exp. Bot.* **2006**, *57*, 2493−2499.
(23) Domínguez, E.; Heredia-Guerrero, J. A.; Heredia, A. The biophysical design of plant cuticles: an overview. *New Phytol.* **2011**, *189*, 938−949.
(24) Heredia, A. Biophysical and biochemical properties of cutin, a plant barrier biopolymer. *Biochim. Biophys. Acta, Gen. Subj.* **2003**, *1620*, 1−7.
(25) Lara, I.; Belge, B.; Goulao, L. F. The fruit cuticle as a modulator of postharvest quality. *Postharvest Biol. Technol.* **2014**, *87*, 103−112.
(26) Li-Beisson, Y.; Shorrosh, B.; Beisson, F.; Andersson, M. X.; Arondel, V.; Bates, P. D.; Baud, S.; Bird, D.; DeBono, A.; Durrett, T. P.; Franke, R. B.; Graham, I. A.; Katayama, K.; Kelly, A. A.; Larson, T.; Markham, J. E.; Miquel, M.; Molina, I.; Nishida, I.; Rowland, O.; Samuels, L.; Schmid, K. M.; Wada, H.; Welti, R.; Xu, C.; Zallot, R.; Ohlrogge, J. Acyl-lipid metabolism. *Arabidopsis Book* **2013**, *8*, No. e0133, DOI: 10.1199/tab.0161.
(27) Yeats, T. H.; Rose, J. K. C. The formation and function of plant cuticles. *Plant Physiol.* **2013**, *163*, 5−20.
(28) Kolattukudy, P. E. Structure, biosynthesis, and biodegradation of cutin and suberin. *Annu. Rev. Plant Physiol.* **1981**, *32*, 539−567.
(29) Heredia, A.; Heredia-Guerrero, J. A.; Domínguez, E.; Benítez, J. J. Cutin synthesis: a slippery paradigm. *Biointerphases* **2009**, *4*, 1−3.
(30) Schreiber, L. Transport barriers made of cutin, suberin and associated waxes. *Trends Plant Sci.* **2010**, *15*, 546−553.
(31) Yeats, T. H.; Martin, L. B. B.; Viart, H. M. F.; Isaacson, T.; He, Y.; Zhao, L.; Matas, A. J.; Buda, G. J.; Domozych, D. S.; Clausen, M. H.; Rose, J. K. C. The identification of cutin synthase: formation of the plant polyester cutin. *Nat. Chem. Biol.* **2012**, *8*, 609−611.
(32) Girard, A. L.; Mounet, F.; Lemaire-Chamley, M.; Gaillard, C.; Elmorjani, K.; Vivancos, J.; Runavot, J. L.; Quemener, B.; Petit, J.; Germain, V.; Rothan, C.; Marion, D.; Bakan, B. Tomato GDSL1 is required for cutin deposition in the fruit cuticle. *Plant Cell* **2012**, *24*, 3119−3134.
(33) Li-Beisson, Y.; Pollard, M.; Sauveplane, V.; Pinot, F.; Ohlrogge, J.; Beisson, F. Nanoridges that characterize the surface morphology of flowers require the synthesis of cutin polyester. *Proc. Natl. Acad. Sci. U.S.A.* **2009**, *106*, 22008−22013.
(34) Bak, S.; Beisson, F.; Bishop, G.; Hamberger, B.; Höfer, R.; Paquette, S.; Werck-Reichhart, D. Cytochromes P450. *Arabidopsis Book* **2011**, *9*, No. e0144, DOI: 10.1199/tab.0144.
(35) Benveniste, I.; Tijet, N.; Adas, F.; Philipps, G.; Salaün, J.-P.; Durst, F. CYP86A1 from *Arabidopsis thaliana* encodes a cytochrome P450-dependent fatty acid omega-hydroxylase. *Biochem. Biophys. Res. Commun.* **1998**, *243*, 688−693.
(36) Pinot, F.; Beisson, F. Cytochrome P450 metabolizing fatty acids in plants: characterization and physiological roles. *FEBS J.* **2011**, *278*, 195−205.
(37) Wellesen, K.; Durst, F.; Pinot, F.; Benveniste, I.; Nettesheim, K.; Wisman, E.; Steiner-Lange, S.; Saedler, H.; Yephremov, A. Functional analysis of the LACERATA gene of *Arabidopsis* provides evidence for different roles of fatty acid omega-hydroxylation in development. *Proc. Natl. Acad. Sci. U.S.A.* **2001**, *98*, 9694−9699.
(38) Xiao, F.; Goodwin, S. M.; Xiao, Y.; Sun, Z.; Baker, D.; Tang, X.; Jenks, M. A.; Zhou, J. M. Arabidopsis CYP86A2 represses *Pseudomonas syringae* type III genes and is required for cuticle development. *EMBO J.* **2004**, *23*, 2903−2913.
(39) Pinot, F.; Benveniste, I.; Salaün, J. P.; Loreau, O.; Noël, J. P.; Schreiber, L.; Durst, F. Production *in vitro* by the cytochrome P450 CYP94A1 of major C_{18} cutin monomers and potential messengers in plant-pathogen interactions: enantioselectivity studies. *Biochem. J.* **1999**, *342*, 27−32.
(40) Tijet, N.; Helvig, C.; Pinot, F.; Le Bouquin, R.; Lesot, A.; Durst, F.; Salaün, J. P.; Benveniste, I. Functional expression in yeast and characterization of a clofibrate-inducible plant cytochrome P-450 (CYP94A1) involved in cutin monomers synthesis. *Biochem. J.* **1998**, *332*, 583−589.
(41) Duan, H.; Schuler, M. A. Differential expression and evolution of the *Arabidopsis* CYP86A subfamily. *Plant Physiol.* **2005**, *137*, 1067−1081.
(42) Schnurr, J.; Shockey, J.; Browse, J. The acyl-CoA synthetase encoded by *LACS2* is essential for normal cuticle development in Arabidopsis. *Plant Cell* **2004**, *16*, 629−642.
(43) Li, Y.; Beisson, F.; Koo, A. J. K.; Molina, I.; Pollanrd, M.; Ohlrogge, J. Identification of acyltransferases required for cutin biosynthesis and production of cutin with suberin-like monomers. *Proc. Natl. Acad. Sci. U.S.A.* **2007**, *104*, 18339−18344.
(44) Rautengarten, C.; Ebert, B.; Ouellet, M.; Nafisi, M.; Baidoo, E. E. K.; Benke, P.; Stranne, M.; Mukhopadhyay, A.; Keasling, J. D.; Sakuragi, Y.; Scheller, H. V. Arabidopsis *Deficient in Cutin Ferulate* encodes a transferase required for feruloylation of ω-hydroxy fatty acids in cutin polyester. *Plant Physiol.* **2012**, *158*, 654−665.
(45) Jenks, M. A.; Tuttle, H. A.; Eigenbrode, S. D.; Feldmann, K. A. Leaf epicuticular waxes of the *Eceriferum* mutants in *Arabidopsis*. *Plant Physiol.* **1995**, *108*, 369−377.
(46) Jenks, M. A.; Rashotte, A. M.; Tuttle, H. A.; Feldmann, K. A. Mutants in *Arabidopsis thaliana* altered in epicuticular wax and leaf morphology. *Plant Physiol.* **1996**, *110*, 377−385.

DOI: 10.1021/acs.jafc.5b00013
J. Agric. Food Chem. 2015, 63, 4005−4019

(47) Jenks, M. A.; Eigenbrode, S. D.; Lemieux, B. Cuticular waxes of *Arabidopsis*. *Arabidopsis Book* **2002**, *1*, No. e0016, DOI: 10.1199/tab.0016.
(48) Lessire, R.; Hartmann-Bouillon, M. A.; Cassagne, C. Very long chain fatty acids: occurrence and biosynthesis in membrane fractions from etiolated maize coleoptiles. *Phytochemistry* **1982**, *21*, 55−59.
(49) Suh, M. C.; Samuels, A. L.; Jetter, R.; Kunst, L.; Pollard, M.; Ohlrogge, J.; Beisson, F. Cuticular lipid composition, surface structure, and gene expression in *Arabidopsis* stem epidermis. *Plant Physiol.* **2005**, *139*, 1649−1665.
(50) von Wettstein-Knowles, P. M. Elongases and epicuticular wax biosynthesis. *Physiol. Veg.* **1982**, *20*, 797−809.
(51) Evenson, K. J.; Post-Beittenmiller, D. Fatty acid elongating activity in rapidly-expanding leek epidermis. *Plant Physiol.* **1995**, *109*, 707−716.
(52) Joubès, J.; Raffaele, S.; Bourdenx, B.; García, C.; Laroche-Traineau, J.; Moreau, P.; Domergue, F.; Lessire, R. The VLCFA elongase gene family in *Arabidopsis thaliana*: phylogenetic analysis, 3D modelling and expression profiling. *Plant Mol. Biol.* **2008**, *67*, 547−566.
(53) Serra, O.; Soler, M.; Hohn, C.; Franke, R.; Schreiber, L.; Prat, S.; Molinas, M.; Figueras, M. Silencing of *StKCS6* in potato periderm leads to reduced chain lengths of suberin and wax compounds and increased peridermal transpiration. *J. Exp. Bot.* **2009**, *60*, 697−707.
(54) von Wettstein-Knowles, P. M. Genes, elongases and associated enzyme systems in epicuticular wax synthesis. In *The Metabolism, Structure, and Function of Plant Lipids*; Stumpf, P. K., Mudd, J. B., Ness, W. D., Eds.; Plenum: New York, 1987; pp 489−498.
(55) von Wettstein-Knowles, P. M. Biosynthesis and genetics of waxes. In *Waxes: Chemistry, Molecular Biology and Functions*Hamilton, R. J., Ed.; Oily Press: Ayr, Scotland, 1995; Vol. 6, pp 91−130.
(56) Thimmappa, R.; Geisler, K.; Louveau, T.; O'Maille, P.; Osbourn, A. Triterpene biosynthesis in plants. *Annu. Rev. Plant Biol.* **2014**, *65*, 225−257.
(57) DeBono, A.; Yeats, T. H.; Rose, J. K. C.; Bird, D.; Jetter, R.; Kunst, L.; Samuels, L. *Arabidopsis* LTPG is a glycosylphosphatidylinositol-anchored lipid transfer protein required for export of lipids to the plant surface. *Plant Cell* **2009**, *21*, 1230−1238.
(58) Lee, S. B.; Go, Y. S.; Bae, H. J.; Park, J. H.; Cho, S. H.; Cho, H. J.; Lee, D. S.; Park, O. K.; Hwang, I.; Suh, M. C. Disruption of glycosylphosphatidylinositol-anchored lipid transfer protein gene altered cuticular lipid composition, increased plastoglobules, and enhanced susceptibility to infection by the fungal pathogen *Alternaria brassicicola*. *Plant Physiol.* **2009**, *150*, 42−54.
(59) Bird, D. A. The role of ABC transporters in cuticular lipid secretion. *Plant Sci.* **2008**, *174*, 563−569.
(60) Espelie, K. E.; Dean, B. B.; Kolattukudy, P. E. Composition of lipid-derived polymers from different anatomical regions of several plant species. *Plant Physiol.* **1979**, *64*, 1089−1093.
(61) Espelie, K. E.; Davis, R. W.; Kolattukudy, P. E. Composition, ultrastructure and function of the cutin- and suberin-containing layers in the leaf, fruit peel, juice-sac and inner seed coat of grapefruit (*Citrus paradisi* Macfed.). *Planta* **1980**, *149*, 498−511.
(62) Järvinen, R.; Kaimainen, M.; Kallio, H. Cutin composition of selected northern berries and seeds. *Food Chem.* **2010**, *122*, 137−144.
(63) Marga, F.; Pesacreta, T. C.; Hasenstein, K. H. Biochemical analysis of elastic and rigid cuticles of *Cirsium horridulum*. *Planta* **2001**, *213*, 841−848.
(64) Baker, E. A.; Procopiou, J.; Hunt, G. M. The cuticles of *Citrus* species. Composition of leaf and fruit waxes. *J. Sci. Food Agric.* **1975**, *26*, 1093−1101.
(65) Radler, F. The surface waxes of the sultana vine (*Vitis vinifera* cv. Thompson Seedless). *Aust. J. Biol. Sci.* **1965**, *18*, 1045−1056.
(66) Radler, F. Investigations on the cuticular wax of *Vitis vinifera* ssp. *sylvestris* and *Vitis vinifera* ssp. *vinifera*. *Angew. Bot.* **1970**, *44*, 187−195.
(67) Vogg, G.; Fischer, S.; Leide, J.; Emmanuel, E.; Jetter, R.; Levy, A. A.; Riederer, M. Tomato fruit cuticular waxes and their effect on transpiration barrier properties: functional characterization of a mutant deficient in a very-long-chain fatty acid β-ketoacyl-CoA synthase. *J. Exp. Bot.* **2004**, *55*, 1404−1410.
(68) Buxdorf, K.; Rubinsky, G.; Barda, O.; Burdman, S.; Aharoni, A.; Levy, M. The transcription factor *SlSHINE3* modulates defense responses in tomato plants. *Plant Mol. Biol.* **2014**, *84*, 37−47.
(69) Petit, J.; Bres, C.; Just, D.; García, V.; Mauxion, J. P.; Marion, D.; Bakan, B.; Joubès, J.; Domergue, F.; Rothan, C. Analyses of tomato fruit brightness mutants uncover both cutin-deficient and cutin-abundant mutants and a new hypomorphic allele of GDSL lipase. *Plant Physiol.* **2014**, *164*, 888−906.
(70) Martin, L. B. B.; Rose, J. K. C. There's more than one way to skin a fruit: formation and function of fruit cuticles. *J. Exp. Bot.* **2014**, *65*, 4639−4651.
(71) Leide, J.; Hildebrandt, U.; Reussing, K.; Riederer, M.; Vogg, G. The developmental pattern of tomato fruit wax accumulation and its impact on cuticular transpiration barrier properties: effects of a deficiency in a β-ketoacyl-coenzyme A synthase (LeCER6). *Plant Physiol.* **2007**, *144*, 1667−1679.
(72) Saladié, M.; Matas, A. J.; Isaacson, T.; Jenks, M. A.; Goodwin, S. M.; Niklas, K. J.; Xiaolin, R.; Labavitch, J. M.; Shackel, K. A.; Fernie, A. R.; Lytovchenko, A.; O'Neill, M. A.; Watkins, C. B.; Rose, J. K. C. A reevaluation of the key factors that influence tomato fruit softening and integrity. *Plant Physiol.* **2007**, *144*, 1012−1028.
(73) Kosma, D. K.; Parsons, E. P.; Isaacson, T.; Lü, S.; Rose, J. K. C.; Jenks, M. A. Fruit cuticle lipid composition during development in tomato ripening mutants. *Physiol. Plant.* **2010**, *139*, 107−117.
(74) Mintz-Oron, S.; Mandel, T.; Rogachev, I.; Feldberg, L.; Lotan, O.; Yativ, M.; Wang, Z.; Jetter, R.; Venger, I.; Adato, A.; Aharoni, A. Gene expression and metabolism in tomato fruit surface tissues. *Plant Physiol.* **2008**, *147*, 823−851.
(75) Nadakuduti, S. S.; Pollard, M.; Kosma, D. K.; Allen, C.; Ohlrogge, J. B.; Barry, C. S. Pleoiotropic phenotypes of the *sticky peel* mutant provide new insight into the role of *CUTIN DEFICIENT2* in epidermal cell function in tomato. *Plant Physiol.* **2012**, *159*, 945−960.
(76) Hovav, R.; Chehanovsky, N.; Moy, M.; Jetter, R.; Schaffer, A. A. The identification of a gene (*Cwp1*) silenced during *Solanum* evolution, which causes cuticle microfissuring and dehydration when expressed in tomato fruit. *Plant J.* **2007**, *52*, 627−639.
(77) Isaacson, T.; Kosma, D. K.; Matas, A. J.; Buda, G. J.; He, Y.; Yu, B.; Pravitasari, A.; Batteas, J. D.; Stark, R. E.; Jenks, M. A.; Rose, J. K. C. Cutin deficiency in the tomato fruit cuticle consistently affects resistance to microbial infection and biomechanical properties, but not transpirational water loss. *Plant J.* **2009**, *60*, 363−377.
(78) Shi, J. X.; Adato, A.; Alkan, N.; He, Y.; Lashbrooke, J.; Matas, A. J.; Meir, S.; Malitsky, S.; Isaacson, T.; Prusky, D.; Leshkowitz, D.; Schreiber, L.; Granell, A. R.; Widemann, E.; Grausem, B.; Pinot, F.; Rose, J. K. C.; Rogachev, I.; Rothan, C.; Aharoni, A. The tomato SlSHINE3 transcription factor regulates fruit cuticle formation and epidermal patterning. *New Phytol.* **2013**, *197*, 468−480.
(79) Yeats, T. H.; Buda, G. J.; Wang, Z.; Chehanovsky, N.; Moyle, L. C.; Jetter, R.; Schaffer, A. A.; Rose, J. K. C. The fruit cuticles of wild tomato species exhibit architectural and chemical diversity, providing a new model for studying the evolution of cuticle function. *Plant J.* **2012**, *69*, 655−666.
(80) Leide, J.; Hildebrandt, U.; Vogg, G.; Riederer, M. The *positional sterile* (*ps*) mutation affects cuticular transpiration and wax biosynthesis of tomato fruits. *J. Plant Physiol.* **2011**, *168*, 871−877.
(81) Kissinger, M.; Tuvia-Alkalai, S.; Shalom, Y.; Fallik, E.; Elkind, Y.; Jenks, M. A.; Goodwin, M. S. Characterization of physiological and biochemical factors associated with postharvest water loss in ripe pepper fruit during storage. *J. Am. Soc. Hortic. Sci.* **2005**, *130*, 735−741.
(82) Bauer, S.; Schulte, E.; Thier, H. P. Composition of the surface waxes from bell pepper and eggplant. *Eur. Food Res. Technol.* **2005**, *220*, 6−10.
(83) Johnson, E. J.; Dorot, O.; Liu, J. D.; Chefetz, B.; Xing, B. S. Spectroscopic characterization of apliphatic moieties in four plant cuticles. *Commun. Soil Sci. Plant Anal.* **2007**, *38*, 2461−2478.
(84) Parsons, E. P.; Popopvsky, S.; Lohrey, G. T.; Lü, S.; Alkalai-Tuvia, S.; Perzelan, Y.; Paran, I.; Fallik, E.; Jenks, M. A. Fruit cuticle

DOI: 10.1021/acs.jafc.5b00013
J. Agric. Food Chem. 2015, 63, 4005−4019

lipid composition and fruit post-harvest water loss in an advanced backcross generation of pepper (*Capsicum* sp.). *Physiol. Plant.* **2012**, *146*, 15−25.
(85) Morice, I. M.; Shortland, F. B. Composition of the surface waxes of apple fruits and changes during storage. *J. Sci. Food Agric.* **1973**, *24*, 1331−1339.
(86) Belding, R. D.; Blankenship, S. M.; Young, E.; Leidy, R. B. Composition and variability of epicuticular waxes in apples cultivars. *J. Am. Soc. Hortic. Sci.* **1998**, *123*, 348−356.
(87) Dong, X.; Rao, J.; Huber, D. J.; Chang, X.; Xin, F. Wax composition of 'Red Fuji' apple fruit during development and during storage after 1-methylcyclopropane treatment. *Hortic., Environ. Biotechnol.* **2012**, *53*, 288−297.
(88) Belding, R. D.; Sutton, T. B.; Blankenship, S. M.; Young, E. Relationship between apple fruit epicuticular wax and growth of *Peltaster fructicola* and *Leptodontidium elatius*, two fungi that cause sooty blotch disease. *Plant Dis.* **2000**, *84*, 767−772.
(89) Veraverbeke, E. A.; Lammertyn, J.; Saevels, S.; Nicolaï, B. M. Changes in chemical wax composition of three different apple (*Malus domestica* Borkh.) cultivars during storage. *Postharvest Biol. Technol.* **2001**, *23*, 197−208.
(90) Yin, Y.; Bi, Y.; Chen, S.; Li, Y.; Wang, Y.; Ge, Y.; Ding, B.; Li, Y.; Zhang, Z. Chemical composition and antifungal activity of cuticular wax isolated from Asian pear fruit (cv. Pingguoli). *Sci. Hortic.* **2011**, *129*, 577−582.
(91) Fernández, V.; Khayet, M.; Montero-Prado, P.; Heredia-Guerrero, J. A.; Liakopoulos, G.; Karabourniotis, G.; del Río, V.; Domínguez, E.; Tacchini, I.; Nerín, C.; Val, J.; Heredia, A. New insights into the properties of pubescent surfaces: peach fruit as a model. *Plant Physiol.* **2011**, *156*, 2098−2108.
(92) Belge, B.; Llovera, M.; Comabella, E.; Graell, J.; Lara, I. Fruit cuticle composition of a melting and a nonmelting peach cultivar. *J. Agric. Food Chem.* **2014**, *62*, 3488−3495.
(93) Markley, K. S.; Sando, C. E. The wax-like constituents of the cuticle of the cherry, *Prunus avium* L. *J. Biol. Chem.* **1937**, *119*, 641−645.
(94) Belge, B.; Llovera, M.; Comabella, E.; Gatius, F.; Guillén, P.; Graell, J.; Lara, I. Characterization of cuticle composition after cold storage of 'Celeste' and 'Somerset' sweet cherry fruit. *J. Agric. Food Chem.* **2014**, *62*, 8722−8729.
(95) Liu, D. C.; Zeng, Q.; Ji, Q. X.; Liu, C. F.; Liu, S. B.; Liu, Y. A comparison of the ultrastructure and composition of fruits' cuticular wax from the wild-type 'Newhall' navel orange (*Citrus sinensis* [L.] Osbeck cv. Newhall) and its glossy mutant. *Plant Cell Rep.* **2012**, *31*, 2239−2246.
(96) McDonald, R. E.; Nordby, H. E.; McCollum, T. G. Epicuticular wax morphology and composition are related to grapefruit chilling injury. *HortScience* **1993**, *28*, 311−312.
(97) Sala, J. M. Content, chemical composition and morphology of epicuticular wax of Fortune mandarin fruits in relation to peel pitting. *J. Sci. Food Agric.* **2000**, *80*, 1887−1894.
(98) Baker, E. A.; Procopiou, J. The cuticles of *Citrus* species. Composition of the intracuticular lipids of leaves and fruits. *J. Sci. Food Agric.* **1975**, *26*, 1347−1352.
(99) Radler, F.; Horn, D. H. S. The composition of grape cuticle wax. *Aust. J. Chem.* **1965**, *18*, 1059−1069.
(100) Casado, C. G.; Heredia, A. Structure and dynamics of reconstituted cuticular waxes of grape berry cuticle (*Vitis vinifera* L.). *J. Exp. Bot.* **1999**, *50*, 175−182.
(101) Comménil, P.; Brunet, L.; Audran, J. C. The development of the grape berry cuticle in relation to susceptibility to bunch rot disease. *J. Exp. Bot.* **1997**, *48*, 1599−1607.
(102) Pensec, F.; Pączkowski, C.; Grabarczyk, M.; Woźniak, A.; Bénard-Gellon, M.; Bertsch, C.; Chong, J.; Szakiel, A. Changes in the triterpenoid content of cuticular waxes during fruit ripening of eight grape (*Vitis vinifera*) cultivars grown in the upper Rhine valley. *J. Agric. Food Chem.* **2014**, *62*, 7998−8007.
(103) Szakiel, A.; Pączkowski, C.; Pensec, F.; Bertsch, C. Fruit cuticular waxes as a source of biologically active triterpenoids. *Phytochem. Rev.* **2012**, *11*, 263−284.
(104) Orbán, N.; Kozák, I. O.; Drávucz, M.; Kiss, A. LC-MS method development to evaluate major triterpenes in skins and cuticular waxes of grape berries. *Int. J. Food Sci. Technol.* **2009**, *44*, 869−873.
(105) Bianchi, G.; Murelli, C.; Vlahov, C. Surface waxes from olive fruits. *Phytochemistry* **1992**, *31*, 3503−3506.
(106) Kallio, H.; Nieminen, R.; Tuomasjukka, S.; Hakala, M. Cutin composition of five Finnish berries. *J. Agric. Food Chem.* **2006**, *54*, 457−462.
(107) Pascal, S.; Bernard, A.; Sorel, M.; Pervent, M.; Vile, D.; Haslam, R. P.; Napier, J. A.; Lessire, R.; Domergue, F.; Joubès, J. The *Arabidopsis cer26* mutant, like the *cer2* mutant, is specifically affected in the very long chain fatty acid elongation process. *Plant J.* **2013**, *73*, 733−746.
(108) Haslam, T. M.; Mañas-Fernández, A.; Zhao, L.; Kunst, L. Arabidopsis ECERIFERUM2 is a component of the fatty acid elongation machinery required for fatty acid extension to exceptional lengths. *Plant Physiol.* **2012**, *160*, 1164−1174.
(109) Haslam, T. M.; Haslam, R.; Thoraval, D.; Pascal, S.; Delude, C.; Domergue, F.; Mañas-Fernández, A.; Beaudoin, F.; Napier, J. A.; Kunst, L.; Joubès, J. ECERIFERUM2-LIKE proteins have unique biochemical and physiological functions in very-long-chain fatty acid elongation. *Plant Physiol.* **2015**, *167*, 682−692.
(110) Sakuradani, E.; Zhao, L.; Haslam, T. M.; Kunst, L. The *CER22* gene required for the synthesis of cuticular wax alkanes in *Arabidopsis thaliana* is allelic to *CER1*. *Planta* **2013**, *237*, 731−738.
(111) Haslam, T. M.; Kunst, L. Extending the story of very-long-chain fatty acid elongation. *Plant Sci.* **2013**, *210*, 93−107.
(112) Rosenquist, J. K.; Morrison, J. C. The development of the cuticle and epicuticular wax of the grape berry. *Vitis* **1988**, *27*, 63−70.
(113) Becker, T.; Knoche, M. Deposition, strain, and microcracking of the cuticle in the developing 'Riesling' grape berries. *Vitis* **2012**, *51*, 1−6.
(114) Khanal, B. P.; Grimm, E.; Knoche, M. Fruit growth, cuticle deposition, water uptake, and fruit cracking in jostaberry, gooseberry, and black currant. *Sci. Hortic.* **2011**, *128*, 289−296.
(115) Knoche, M.; Beyer, M.; Peschel, S.; Oparlakov, B.; Bukovac, M. J. Changes in strain and deposition of cuticle in developing sweet cherry fruit. *Physiol. Plant.* **2004**, *120*, 667−677.
(116) Knoche, M.; Peschel, S. Deposition and strain of the cuticle of developing European plum fruit. *J. Am. Soc. Hortic. Sci.* **2007**, *132*, 597−602.
(117) Sala, J. M.; Lafuente, T.; Cuñat, P. Content and chemical composition of epicuticular wax of 'Navelina' oranges and 'Satsuma' mandarins as related to rindstaining of fruit. *J. Sci. Food Agric.* **1992**, *59*, 489−495.
(118) Alkio, M.; Jonas, U.; Sprink, T.; van Nocker, S.; Knoche, M. Identification of putative candidate genes involved in cuticle formation in *Prunus avium* (sweet cherry) fruit. *Ann. Bot.* **2012**, *110*, 101−112.
(119) Baker, E. A.; Bukovac, M. J.; Hunt, G. M. Composition of tomato fruit cuticle as related to fruit growth and development. In *The Plant Cuticle*; Cutler, D. F., Alvin, K. L., Price, C. E., Eds.; Academic Press: London, UK, 1982; pp 33−44.
(120) Hunt, G. M.; Baker, E. A. Phenolic constituents of tomato fruit cuticles. *Phytochemistry* **1980**, *19*, 1415−1419.
(121) Wang, Z.; Guhling, O.; Yao, R.; Li, F.; Yeats, T. H.; Rose, J. K. C.; Jetter, R. Two oxidosqualene cyclases responsible for biosynthesis of tomato fruit cuticular triterpenoids. *Plant Physiol.* **2011**, *155*, 540−552.
(122) Declercq, M.; Alkio, M.; Sprink, T.; Schreiber, L.; Knoche, M. Effect of sweet cherry genes *PaLACS2* and *PaATT1* on cuticle deposition, composition and permeability in *Arabidopsis*. *Tree Genet. Genomes* **2014**, *10*, 1711−1721.
(123) Albert, Z.; Ivanics, B.; Molnár, A.; Miskó, A.; Tóth, M.; Papp, I. Candidate genes of cuticle formation show characteristic expression in the fruit skin of apple. *Plant Growth Regul.* **2013**, *70*, 71−78.

DOI: 10.1021/acs.jafc.5b00013
J. Agric. Food Chem. 2015, 63, 4005−4019

(124) Brendolise, C.; Yauk, Y. K.; Eberhard, E. D.; Wang, M.; Chagne, D.; Andre, C.; Greenwood, D. R.; Beuning, L. L. An unusual plant triterpene synthase with predomininat α-amyrin-producing activity identified by characterizing oxidosqualene cyclases from *Malus* × *domestica*. *FEBS J.* **2011**, *278*, 2485−2499.
(125) Jetter, R.; Schäffer, S.; Riederer, M. Leaf cuticular waxes are arranged in chemically and mechanically distinct layers: evidence from *Prunus laurocerasus* L. *Plant, Cell Environ.* **2000**, *23*, 619−628.
(126) Wen, M.; Buschhaus, C.; Jetter, R. Nanotubules on plant surfaces: chemical composition of epicuticular wax crystals on needles of *Taxus baccata* L. *Phytochemistry* **2006**, *67*, 1808−1817.
(127) Schönherr, J.; Riederer, M. Plant cuticles sorb lipophilic compounds during enzymatic isolation. *Plant, Cell Environ.* **1986**, *9*, 459−466.
(128) Jetter, J., Kunst, L., Samuels, A. L. Composition of plant cuticular waxes. In *Biology of the Plant Cuticle*; Riederer, M., Müller, C., Eds.; Blackwell Publishing: Oxford, UK, 2006; pp 145−181.
(129) Murata, T.; Ariga, T.; Araki, E. Determination of double bond positions of unsaturated fatty acids by a chemical ionization mass spectrometry computer system. *J. Lipid Res.* **1978**, *19*, 172−176.
(130) Murata, T. Analysis of fatty acid methyl esters by a gas-liquid chromatography-chemical ionization mass spectrometry computer system. *J. Lipid Res.* **1978**, *19*, 166−171.
(131) Yu, M. M. L.; Schulze, H. G.; Jetter, R.; Blades, M. W.; Tuner, R. F. B. Raman microspectroscopic analysis of triterpenoids found in plant cuticles. *Appl. Spectrosc.* **2007**, *61*, 32−37.
(132) Heredia-Guerrero, J. A.; Benítez, J. J.; Domínguez, E.; Bayer, I. S.; Cingolani, R.; Athanassiou, A.; Heredia, A. *Front. Plant Sci.* **2014**, *5*, 305.
(133) Goulao, L. F.; Oliveira, C. M. Cell wall modifications during fruit ripening: when a fruit is not the fruit. *Trends Food Sci. Technol.* **2008**, *19*, 4−25.
(134) Kimbara, J.; Yoshida, M.; Ito, H.; Hosoi, K.; Kusano, M.; Kobayashi, M.; Ariizumi, T.; Asamizu, E.; Ezura, H. A novel class of *sticky peel* and *light green* mutations causes cuticle deficiency in leaves and fruits of tomato (*Solanum lycopersicum*). *Planta* **2012**, *236*, 1559−1570.
(135) Ismail, H. M.; Brown, G. A.; Tucknott, O. G.; Holloway, P. J.; Williams, A. A. Nonanal in epicuticular wax of Golden Egg plums (*Prunus domestica*). *Phytochemistry* **1977**, *16*, 769−770.
(136) Kimbara, J.; Yoshida, M.; Ito, H.; Kitagawa, M.; Takada, W.; Hayashi, K.; Shibutani, Y.; Kusano, M.; Okazaki, Y.; Nakabayashi, R.; Mori, T.; Saito, K.; Ariizumi, T.; Ezura, H. Inhibition of *CUTIN DEFICIENT 2* causes defects in cuticle function and structure and metabolite changes in tomato fruit. *Plant Cell Physiol.* **2013**, *54*, 1535−1548.
(137) Bargel, H.; Neinhuis, C. Altered tomato (*Lycopersicon esculentum* Mill.) fruit cuticle biomechanics of a pleiotropic non ripening mutant. *J. Plant Growth Regul.* **2004**, *23*, 61−75.
(138) Adato, A.; Mandel, T.; Mintz-Oron, S.; Venger, I.; Levy, D.; Yativ, M.; Domínguez, E.; Wang, Z.; De Vos, R. C. H.; Jetter, R.; Schreiber, L.; Heredia, A.; Rogachev, I.; Aharoni, A. Fruit-surface flavonoid accumulation in tomato is controlled by a *SlMYB12*-regulated transcriptional network. *PLoS Genet.* **2009**, *5*, No. e1000777.

DOI: 10.1021/acs.jafc.5b00013
J. Agric. Food Chem. 2015, 63, 4005−4019

lees through processing using rotary drum vacuum filtration, specialized lees filtration equipment, or centrifugation—processes that are considered laborious and that can potentially degrade wine quality.[8−10] Quality degradation and loss of wine through bentonite usage has been estimated to cost the global wine industry around U.S.$1 billion per year.[11] Other issues and costs related to bentonite use include tank downtime for bentonite treatment, occupational health risks associated with inhalation of bentonite dust and slip hazards induced by bentonite slurry spills, the disposal of hazardous bentonite waste, and bentonite interference with increasingly common membrane-based winemaking technologies.[12] Consequently, winemakers aim to use the minimum amount of bentonite required for protein stability and would welcome the introduction of alternatives with fewer drawbacks than the current practice.

Since the last extensive review on the topic a decade ago,[8] research efforts have been equally divided into the elucidation of protein haze-forming mechanisms, in particular the effects of different wine components, as well as improving bentonite efficiency and finding alternative stabilization strategies. Significant attention has also been paid to developing methods for protein purification, quantification, and identification, as well as predicting wine haze potential (Figure 2).

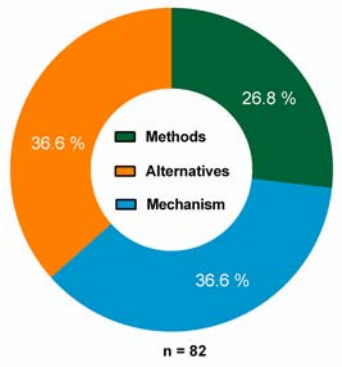

Figure 2. Distribution of peer-reviewed publications on wine protein haze, 2005−2013 (data from Scopus). Methods: papers on the development of methods for purification, quantification, and characterization of proteins, as well as on the prediction of haze potential. Alternatives: papers investigating possible alternatives to bentonite for wine protein stabilization. Mechanism: papers on the elucidation of the mechanism of haze formation in white wines.

This review summarizes recent advances in the knowledge of how protein haze forms in wine, as well as the latest alternatives to bentonite wine protein stabilization. The findings of recent research and the newly proposed mechanisms for haze will be discussed in part I. New alternatives to bentonite will be discussed in part II.

PART I. MECHANISMS OF PROTEIN HAZE FORMATION IN WHITE WINES

Current Model of Haze Formation. The mechanisms associated with haze formation in wines are not well understood and yet commonly cited as a two-stage process. In the first stage, wine proteins unfold in response to stimuli such as elevated storage temperatures. Once unfolded, the proteins aggregate and flocculate to form a visible haze.[13] Recent investigations of the proteins associated with haze formation, as well as the roles of other wine components, have enabled the proposed model to be revised into three separate stages described below. The steps include protein unfolding, protein self-aggregation, and aggregate cross-linking.

Haze-Forming Proteins. The isolation and characterization of proteins from white wines have traditionally been a difficult task due to the presence of grape and yeast proteins as well as their modified versions and degradation products caused by winemaking, which produces a complex protein mixture.[14,15] However, recent advances in techniques for wine protein purification,[16,17] as well as applications of newly developed proteomic techniques,[16,18−25] and the release of the grape genome[26] have significantly improved research capabilities in the identification and quantification of grape and wine proteins.

The most abundant classes of haze-forming proteins that occur in grape (*Vitis vinifera*) juice and white wines are chitinases and thaumatin-like proteins (TLPs).[14,27−29] These proteins are small (<35 kDa) and compact, have globular structures,[30] are positively charged at wine pH, and are tolerant of low pH in juice and wine.[8,31] Other proteins, such as *β*-glucanases, have also been shown to contribute to haze formation,[32,33] although they are much less abundant than chitinases and TLPs in wine and are not extensively studied. A typical electrophoretic profile of grape juice is shown in Figure 3, highlighting that pathogenesis-related (PR) proteins (*β*-1,3-glucanases, chitinases, TLPs, and lipid transfer proteins) are the major protein classes represented. However, haze-forming proteins vary in concentration and composition in ripe grapes and grape juice with cultivar,[34] vintage,[35] disease pressure,[36] and even harvest conditions.[37] The haze-forming proteins have been identified as those that are historically considered to be PR proteins, although they are constitutively expressed during berry ripening and can reach high concentrations regardless of pathogen exposure.[27,38,39] Both chitinases and TLPs have a high number of disulfide bonds that contribute to the highly stable globular structures of these proteins and make them inherently resistant to the enzymatic activity of pathogens.[30,40]

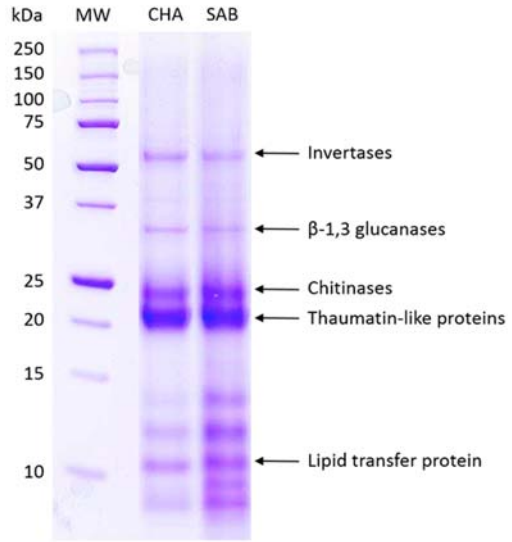

Figure 3. Typical electrophoretic profiles of two unfined grape juices (CHA, Chardonnay; SAB, Sauvignon blanc), with protein band identities assigned by proteomic analysis.[85]

DOI: 10.1021/acs.jafc.5b00047
J. Agric. Food Chem. 2015, 63, 4020−4030

Non-haze-forming proteins are also present in juice and white wine, including yeast mannoproteins,[41,42] grape invertase,[43,44] and grape cell wall glycoproteins and proteoglycans rich in arabinose and galactose (or arabinogalactan-proteins).[45,46] The presence of these non-haze-forming proteins can also affect white wine quality by stabilizing wine against heat-related protein instability,[47−49] influencing foaming properties in sparkling wines,[43,50] and possibly interacting with aroma compounds.[51,52]

The haze-forming tendencies of proteins isolated from white wines have been shown to depend on their aggregation behavior, and developments in the physical techniques used to characterize this behavior have improved the understanding of protein instability.[53−55]

In wines, different classes of haze-forming proteins have different thermal stabilities, as demonstrated by combinatorial peptide ligand libraries (CPLL) analyses[56] and differential scanning calorimetry (DSC).[57] Chitinases are generally less stable than TLPs and can denature within minutes at temperatures >40 °C, compared to weeks for TLPs under the same conditions[57] (Table 1).

Table 1. Predicted Half-Lives of Chitinases and TLPs in Artificial Wine (Based on Falconer et al.[57])

temperature (°C)	predicted half-lives for chitinases	predicted half-lives for TLPs
50	3 min	20 days
45	17 min	11 weeks
40	1.3 h	13 years
35	14 h	180 years
30	4.7 days	>1000 years
25	1.3 months	>1000 years
20	1 year	>1000 years
15	9 years	>1000 years
10	100 years	>1000 years

The temperature at which proteins unfold can also indicate stability, and recent experiments using differential scanning calorimetry (DSC) analyses have demonstrated differences in the melt temperature of chitinases and TLPs. The physical characteristics and aggregation tendencies of these proteins are given in Table 2. Chitinases unfold at a lower temperature than

Table 2. Summary of General Properties of Chitinases and TLPs

property	chitinases	stable TLPs	unstable TLPs
unfolding temperature	55 °C[57]	61−62 °C[57]	56 °C[57]
aggregate characteristics	visible aggregates (≥1 μm)[54]	microaggregates (<150 nm)[53,54]	visible aggregates (≥1 μm)[30,57]
aggregation tendency	self-aggregate[28,54]	cross-linked with other wine components[53,54]	self-aggregate[30]

TLPs, at 55 and 62 °C, respectively,[57] further indicating that they are less stable. As shown in Figure 4, once unfolded, chitinases did not regain their original structure (renature) after cooling, and this irreversible unfolding (denaturation) was shown to lead to protein aggregation and subsequent precipitation of chitinases.[57]

Results from DSC and dynamic light scattering (DLS) experiments have indicated that TLPs generally do not

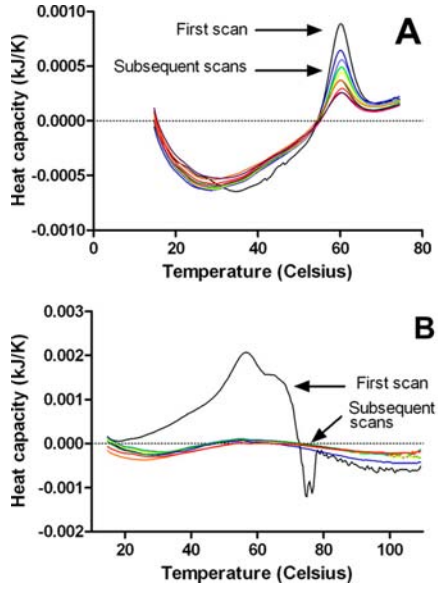

Figure 4. (A) Repeated DSC scans of thaumatin-like protein C from Semillon juice showing a melt temperature of 61 °C and reversibility of thermal unfolding. (B) Repeated DSC scans of chitinase F1 from Sauvignon blanc juice showing a melt temperature of 55 °C, no reversibility of thermal unfolding, and aggregation after unfolding. Reprinted from Falconer et al.[57]

contribute to the formation of visible aggregates,[28,54] although recent studies have indicated the presence of TLPs in wine hazes.[14,32] This apparent conflict of results most likely relates to the particular isoform of TLP that was used in the experiments. Recent studies have shown that some TLP isoforms will reversibly unfold/refold after heating and cooling, whereas other isoforms will irreversibly unfold (denature) and aggregate. Only the TLP isoforms that denature will participate in haze formation.[28,30,53,57,58]

Crystallography has been used to elucidate the 3D structures of three grape TLP isoforms displaying different hazing potentials and unfolding temperatures (Figure 5).[30] That study demonstrated a high degree of structural similarity among different TLP isoforms. However, a TLP isoform (4JRU) with lower unfolding temperature than the other two (56 vs 62 °C) showed the potential to aggregate upon unfolding in the presence of sulfate to form visible haze. The reason for this different hazing potential was attributed to small structural

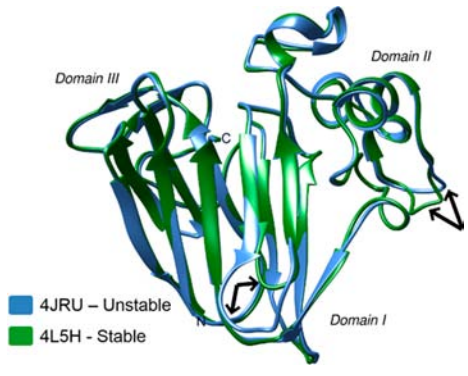

Figure 5. Superposition of the backbone representation of thaumatin-like proteins 4JRU (heat unstable) and 4L5H (heat stable).[30] Arrows indicate differing loops between the two protein isoforms.

DOI: 10.1021/acs.jafc.5b00047
J. Agric. Food Chem. 2015, 63, 4020−4030

differences related to the conformation of a single loop (located in domain 1) and the amino acid composition of its flanking regions, which could explain some of the variation of hazing potential among wines of similar total protein concentrations.

When proteins unfold and aggregate, the protein type can influence the characteristics of the resulting aggregates. TLPs tend to produce metastable microaggregates (<150 nm at normal wine ionic strength) that are invisible to the naked eye, whereas chitinases can rapidly flocculate and produce clearly visible large aggregates (≥1 μm).[13,54] Model studies have indicated that increasing the concentration of protein in solution will increase the amount of haze produced,[59,60] and yet no such correlation has been shown to exist in wine.[28,31] This is most likely due to other components in wine that can facilitate haze or prevent protein aggregation. For example, most TLP isoforms need to interact with other wine components such as salts or polyphenolics to contribute to visible haze.[53,54] Therefore, the size of TLP aggregates is wine-dependent.[13] The chitinases tested to date form aggregates by themselves after unfolding and cooling, assuming that there is sufficient solution ionic strength to suppress electrostatic repulsion.[54,55] This will be discussed in greater detail in the next section.

Other Wine Components That Contribute to Haze Formation. In addition to differing aggregation behaviors of different wine proteins, other components of wine can also contribute to haze formation. These components include polyphenols, sulfate, formerly indicated as the factor X required for protein haze formation,[61] and polysaccharides in particular, as well as characteristics of the wine matrix such as wine pH and organic acids.[28,52−55,58,62] In the two-stage model of haze formation, proteins first unfold and then aggregate to form a haze, and each of these mechanisms has different drivers. The mechanism of protein unfolding is largely influenced by temperature, with higher temperatures leading to more rapid protein unfolding.[13,28,53,54,57,58] However, this does not fully explain the gradual haze formation that can occur during wine storage, indicating that drivers in addition to temperature play a role.

The mechanism of protein aggregation differs for different protein classes,[28] is influenced by a number of factors, and is likely to be affected by other components present in the wine matrix.[54,58] When proteins unfold, they expose hydrophobic binding sites that are generally buried in the core of the proteins, and more hydrophobic proteins tend to cause hazes more easily. This suggests that the aggregation stage of haze formation is likely to be driven by hydrophobic interactions,[63] as recently confirmed by structural studies on TLPs.[30]

Haze-forming proteins also have a net positive charge at wine pH, and this can prevent protein aggregation and haze formation in model systems due to electrostatic repulsion. In white wines the presence of charged ions in solution increases the ionic strength, thus decreasing electrostatic repulsion among protein molecules, so that proteins aggregate upon unfolding and subsequent exposure of hydrophobic protein binding sites.[64] The presence of other charged molecules, particularly sulfates,[61] can also influence protein aggregation, as has been demonstrated with chitinases and, to a lesser extent, TLPs using DLS.[54] In that study model wine containing only chitinases did not form a haze upon heating, whereas increasing sulfate concentration in the matrix led to a dramatic increase in chitinases aggregation. The effect of sulfate on protein aggregation was beyond that which could be attributed to its contribution to ionic strength alone. It was therefore suggested that sulfate not only allows aggregation to occur by suppressing electrostatic repulsion but also allows, if not promotes, hydrophobic interaction-driven aggregation through kosmotropic effects; sulfate anions interact strongly with water, thus weakening hydrogen bonding between water and proteins and promoting salting-out and aggregation.[54]

In combination with ionic strength and temperature considerations, wine pH can prevent some wines from hazing while promoting haze in others.[55,65] Changes to wine pH have been shown to induce minor protein conformational changes that can change the temperature at which wine begins to show turbidity.[66] In that work, Erbaluce wines with lower pH (3.0) did not form a visible haze upon heating to 80 °C, whereas at higher pH (pH 3.30) the wine became hazy when heated to 60 °C.[66] Organic acids have also been attributed a stabilizing effect in wine protein stability.[65] The authors stated that at wine pH organic acids interact electrostatically with the wine proteins and speculated that this interaction would prevent wine compounds of phenolic nature to interact with the wine proteins and thus facilitate haze.[65]

The impact of wine pH on protein stability varies with protein type. Variations in wine pH from 2.5 to 4.0 at room temperature were sufficient to disrupt the native state of chitinases, resulting in the exposure of hydrophobic binding sites that eventually facilitated protein aggregation.[58] Conversely, TLPs and invertases were stable under the same conditions, further demonstrating the comparative instability and haze-forming potential of chitinases compared with stable TLP isoforms.

Polyphenols can also contribute to the aggregation and precipitation of wine proteins, and this can be due to the formation of hydrogen bonds or most likely to hydrophobic interactions.[65,67−69] A wide range of polyphenols have been identified from naturally precipitated proteins in Sauvignon blanc wines that were stored below 30 °C.[70] These include condensed tannins from grapes that are known to readily bind to proteins. Spiking experiments have indicated that polyphenols actively aggregate and precipitate wine proteins at room temperature,[63] most likely due to cross-linking protein aggregates forming larger aggregates that are visible to the naked eye. Cross-linking of proteins with nonprotein molecules includes both covalent and noncovalent interactions. However, because white wines are generally produced under nonoxidative conditions, there are probably few cases of phenolic compounds oxidizing to highly reactive quinones and covalently cross-linking proteins.

Therefore, the growth in size of protein self-aggregates seems also attributable to the cross-linking action of other matrix components. This will be discussed further in the next section. Elevated temperatures can increase polyphenol−protein interactions and aggregation because increased temperatures will increase the number of protein hydrophobic sites that are exposed, as well as the intensity of the hydrophobic interactions.[67] The exposure of hydrophobic sites also differs in magnitude and consequence depending on protein type.[63] Polysaccharides can also influence haze formation, although reports vary between stabilizing proteins against aggregation[41,47,49] to inducing haze formation.[59] This variation may be due to differences in the measured polysaccharide/protein ratio or in the type of protein, such as TLP isoform, used in the analysis.[53] Gazzola et al. showed that wine polysaccharides played a crucial role in haze formation of TLPs, whereas this

DOI: 10.1021/acs.jafc.5b00047
J. Agric. Food Chem. 2015, 63, 4020−4030

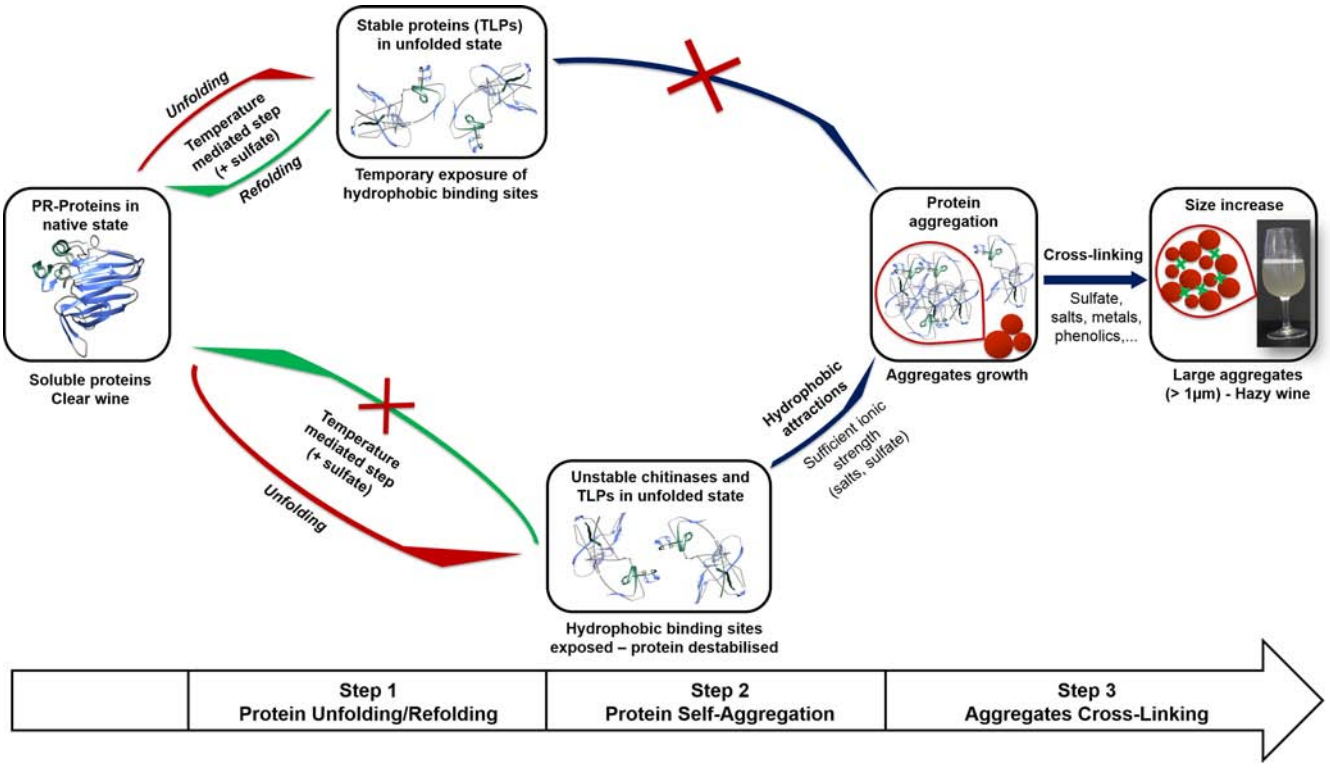

Figure 6. Revised unfolding and aggregation mechanisms of heat-unstable proteins in wine.

was not the case for chitinases. In general, it seemed that the type of protein was always more important than its interaction with polysaccharides.[53]

Another aspect investigated was the theory that denatured proteins (e.g., chitinases) could interact with otherwise soluble proteins (e.g., TLPs) in a coprecipitation mechanism (protein−protein interaction). Although this theory has not been comprehensively disproven in real wines, it has been shown to be insignificant in model wine and one Sauvignon blanc.[28]

Revised Mechanism of Protein Haze Formation. Haze formation is caused by the unfolding and aggregation of grape-derived wine proteins and can lead to precipitation. The current model of wine protein aggregation indicates that protein unfolding and aggregation are separate events, as demonstrated through DLS experiments.[13] Elucidating the mechanisms of haze formation has involved different analytical approaches characterizing naturally forming hazes from wine[28,70] as well as heat-induced haze from real wines.[14,71,72] Heat trials have indicated that proteins can unfold as wine is heated, although the wine becomes hazy only after cooling.[13] The fractionation of heat-unstable wines into their component parts, such as proteins, polysaccharides, and phenolics, and the heat aggregation behavior studied via reconstitution experiments in model or real wines have also improved the knowledge of the haze-forming mechanism.[28,53,54,61,63] Other significant advancements in understanding the mechanisms of wine haze include (i) the finding that sulfate plays an important role in hazing;[54,61] (ii) the explanation of the role of nonproteinaceous wine components, particularly ionic strength,[54,55] pH,[58,66] organic acids,[65] and phenolic compounds;[53,63,70] (iii) the development of an efficient protein purification method;[17] (iv) the release of the grape genome[26] and greater accessibility of proteomic techniques for protein characterization; (v) the discovery that TLPs and chitinases have different unfolding temperatures and unfolding/aggregation behavior;[57] and (vi) the solution of the crystal structure of thaumatin-like proteins.[30] On the basis of these advancements, a new model of haze formation has been proposed (Figure 6).

Immediately following winemaking and clarification, wine proteins are stable and folded in their native state, and the wine is clear. The first stage of haze formation involves the unfolding of these proteins in response to elevated storage temperatures, revealing the hydrophobic binding sites that are generally buried in the core of the proteins.[63] For TLPs this mechanism has recently been elucidated.[30] It appears that unstable TLPs have an exposed loop stabilized by a disulfide bridge that, if destabilized via heat, can expose the neighboring protein region (Figure 7).

In heat-unstable TLPs (e.g., 4JRU) the neighboring region that becomes exposed upon reduction of the disulfide bridge

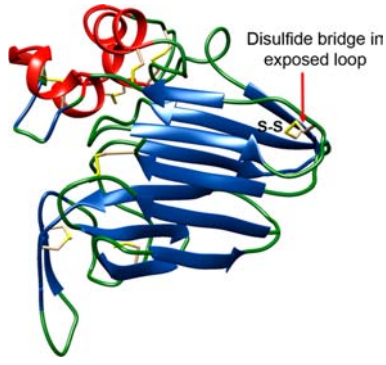

Figure 7. Backbone representation of the heat-unstable thaumatin-like protein 4JRU.[30] Disulfide bonds are yellow. The arrow indicates an exposed disulfide bond that could be susceptible to reduction by heat and sulfites.

DOI: 10.1021/acs.jafc.5b00047
J. Agric. Food Chem. 2015, 63, 4020−4030

located in the exposed loop is hydrophobic; thus, protein aggregation can occur under conditions that favor disulfide bond reduction, such as heating in the presence of sulfites.[30] Conversely, stable TLP does not precipitate due to the hydrophilic nature of exposed regions that prevent protein aggregation and allow refolding upon cooling.[30,57] In the second stage of haze formation unstable proteins begin to self-aggregate via hydrophobic interactions. At this stage wine components able to modify the ionic strength of the solution, such as salts and sulfate, can favor the bindingof the unfolded proteins, further promoting protein aggregation.[63] This is particularly the case with TLPs. In the third and final stage of aggregation the protein aggregates gradually become cross-linked due to the actions of sulfates and polyphenols. Proteins form increasingly larger aggregates until they reach a size that makes them visible to the naked eye ($\geq$1 μm) and eventually precipitate.[13,54,55] The presence of sulfate and salts can also neutralize protein net charges and reduce the natural electrostatic repulsion between similarly charged proteins, whereas polyphenols are more likely to cross-link protein aggregates via hydrophobic interactions. From this mechanism, the role of sulfate as a key wine matrix component for the formation of haze becomes apparent. Sulfate can potentially participate in each of the three stages of haze formation by modifying the melt temperature of proteins in stage 1, by screening the exposed protein charges in stage 2, thus favoring aggregation of unfolded proteins,[28,54] and by mediating the aggregation of small protein aggregates probably through a cross-linking action at stage 3 to modulate the final haze formed.[54]

Following the new insights into haze-forming mechanisms and protein stability, the next stage of research will focus on developing a new test for assessing the haze potential of white wines. The conditions used in the current test, known as the "heat test",[73] may overestimate the risk that a particular wine will haze by denaturing both haze-forming and non-haze-forming proteins. This can overpredict the amount of bentonite needed to stabilize the wine, leading to less cost-effective winemaking practices. Understanding the mechanisms of haze formation and the structures of the proteins involved can also lead to the development of new strategies for haze prevention in white wines.

PART II: BENTONITE ALTERNATIVES

Strategies for Wine Haze Prevention. Considering the mechanisms of wine protein haze formation, there are several possible strategies for preventing wine haze that would either reduce or eliminate the need for bentonite. These include (i) decreasing the ionic strength of the wine; (ii) decreasing the polyphenol concentrations in wine; (iii) stabilizing wine proteins against thermal unfolding; (iv) disrupting hydrophobic protein−protein interactions; (v) degrading wine proteins enzymatically; and (vi) using alternative adsorbents or ultrafiltration to remove proteins.

Strategies 1 and 2 are most likely impractical from a wine sensory quality perspective. Although it is possible to either decrease the ionic strength of wine or remove polyphenols using existing industrial-scale electrodialysis, ion exchange, and fining technologies, these techniques would dramatically change wine sensory attributes. Strategies 3 and 4 are potentially related in practice, as the promotion or addition of specific glycoproteins/proteoglycans/polysaccharides, including specific yeast mannoproteins, could both stabilize wine proteins and interfere with hydrophobic protein−protein interactions.[55] Protein stabilization with polysaccharides such as pectin and carrageenan is well established in other beverages such as milk[74] and beer, and the ability of a yeast mannoprotein to stabilize wine proteins was attributed specifically to the glycan portion of the proteoglycan.[49] However, in both cases, it is unclear at what point protection against haze formation by polysaccharides occurs: do the polysaccharides protect against denaturation or, once proteins are denatured, protect against aggregation? An unexplored alternative to polysaccharides that would implement strategy 4 would be the addition of surfactants to wines to prevent protein−protein interactions. Surfactants such as polysorbates are commonly used in processed foods and beverages to stabilize emulsions. However, their use in wine is not currently permitted, they might not be acceptable to consumers, and they could negatively affect foam properties in sparkling wines.

The most promising strategies for developing bentonite alternatives are strategy 5, the potential to degrade wine proteins with enzymes, and strategy 6, the potential for developing novel fining agents. The use of enzymes and novel fining agents as bentonite alternatives will be discussed in more detail in the following sections.

Protein Degradation Using Enzymes. Degrading haze-forming proteins in wine with enzymes is a particularly appealing alternative to bentonite because it minimizes wine volume loss and aroma stripping. Ideally, effective enzymes would be added to grape juice or ferment without the need for later removal, such as with pectinases and glucanases.[75] The degradation products of grape proteins may also be utilized by yeast as nitrogen sources, potentially reducing the frequent need for nitrogen additions (as diammonium phosphate) and improving wine aroma quality.[76,77] There are two types of enzymatic activity relevant to wine protein degradation: the hydrolysis of peptide bonds by proteases and the reduction of disulfide bonds by protein disulfide reductases. Proteases catalyze peptide bond hydrolysis through nucleophilic attack induced either by an amino acid side chain of the protease, such as for cysteine and serine proteases, or by an activated water molecule, such as for metalloproteases and aspartic proteases.[78] Proteolytic enzymes are routinely used in the beverage industry, for example, papain, a cysteine protease from papaya that is used in beermaking,[79] and are therefore a viable option for use in winemaking. Protein disulfide reductases could, theoretically, destabilize and precipitate haze-forming proteins during winemaking via the enzymatic reduction of disulfide bonds, because the chemical reduction of disulfide bonds has been shown to facilitate the unfolding of these proteins.[63] However, there have been no published examples of protein disulfide reductases being active under wine conditions. For this reason, the search for wine-relevant enzymes to degrade haze-forming proteins has focused on proteases and, at least since the 1950s, researchers have tried to find proteases that destroy haze-forming wine proteins under winemaking conditions.[80] The difficulty in using proteases for specifically degrading haze-forming proteins in wine is associated with the stability of the proteins in wine-like conditions. Chitinases and TLPs are characteristically highly resistant to proteases in their native state due to their rigid peptide backbone structure[72,81,82] and so can tolerate the endogenous proteases that degrade many grape proteins during crushing and pressing.[29] Grape TLPs, as with PR proteins from other plant species, have been found to be

DOI: 10.1021/acs.jafc.5b00047
J. Agric. Food Chem. 2015, 63, 4020−4030

resistant to many different types of proteases and may even inhibit the activity of some proteases.[83,84]

Marangon et al.[85] developed a promising new protease treatment that involves heating grape juice in the presence of a heat-tolerant protease prior to fermentation to produce wine that is free from haze-forming proteins. When juice is heated, the proteins unfold and thus become susceptible to enzymatic activity. The possible drawbacks of exposing grape juice or wine to elevated temperatures are the requirements of high energy inputs and the negative sensory implications,[86−89] even though it has been shown that when applied with care the potential negative sensory changes can be contained, as well as the energy requirements by optimizing the temperature and treatment time.[85] Previous research has focused on the ideal temperature and time of heating required to unfold haze-forming proteins without destroying flavor and aroma compounds.[90]

The method of Marangon et al.[85] involved rapidly heating grape juice to 75 °C for 1 min using flash pasteurization. This technique also required the addition of a protease that is active at the low pH of grape juice and white wines (pH 2.9−3.5) and at 75 °C. Aspergilloglutamic peptidase (AGP), known commercially as Proctase and formerly known as Aspergillopepsin II, was found to be active at 50−75 °C.[85] Adding AGP to clarified grape juice prior to flash pasteurization and fermentation resulted in wines that were heat stable and almost completely free from haze-forming proteins. Chemical and sensory results indicated that there were no significant changes to the main physicochemical parameters or wine preference.[85] This combination treatment of protease addition with flash pasteurization has been shown to be effective at industrial scale,[91] and the use of AGP in wine has recently been approved for Australian winemaking.[92] The cost of this treatment compared favorably to bentonite treatment,[85] making it a potentially cost-effective and commercially viable bentonite alternative.

Other proteases are also currently being investigated that are active at winemaking temperatures and are specific against grape haze-forming proteins. Recent investigations have focused on grape pathogens for specificity against PR grape proteins. Plant PR proteins continuously evolve ways to inhibit pathogen growth, and pathogens continuously evolve ways to counteract the inhibitory effects of PR proteins.[93] Elite grape cultivars have been clonally propagated for centuries; therefore, it is likely that pathogens have evolved proteases to destroy PR proteins encoded by ancient grape genes. The juice of grapes infected with *Botrytis cinerea* was found to have significantly lower concentrations of PR proteins than juice from healthy grapes,[36,94,95] whereas the opposite was true in grapes infected with other pathogens such as powdery mildew.[36] One particular protease from *B. cinerea*, BcAP8, has proven to be effective against grape chitinases during juice fermentation without the need for heating.[96] When BcAP8 was added to juice prior to fermentation, the resulting wines produced significantly less heat-induced protein haze than wines made without BcAP8.

Other potential sources of proteases that are active at wine pH include endogenous winemaking sources such as grapes, yeasts, and bacteria, because protein hydrolysis is known to occur during winemaking.[15,97,98] Endogenous grape (*V. vinifera*) proteases including both cysteine and serine proteases[99] have been found in berries and leaves,[88,100,101] although they are generally not well characterized.[102−106] Grape proteases are active at optima from pH 2 to 2.5 and from 60 to 70 °C,[99,107] and the protease activity is generally short-lived after pressing,[88,100] with few exceptions.[99]

Acid-tolerant yeasts and spoilage microbes have been found to secrete proteases at wine pH, although the secreted protease activity was not sufficient to stabilize wine.[108−114] An extracellular pepsin-like aspartic acid protease of 72 kDa was characterized from a *Saccharomyces cerevisiae* isolate,[115] one of the few isolates that secrete protease activity.[111,115] The secreted yeast protease activity discovered by Younes et al.[115,116] was active at wine pH during grape juice fermentation, although it did not affect grape PR proteins until after fermentation when the wine was incubated at 38 °C for prolonged periods. Nonetheless, the discovery of a secreted protease from a *S. cerevisiae* isolate demonstrates that proteolytic activity can occur prior to autolysis of the cell and the release of a vacuolar acid protease, which is a previously established mechanism of protease activity arising from yeast in wine.[117] The isolate that secretes protease activity is not currently used commercially in winemaking,[115] although it could be used as a tool to develop new industrial wine yeast strains that secrete protease.

Novel Fining Agents. Many novel fining agents and other protein removal techniques with the potential to replace bentonite have been explored in recent years. These include seaweed polysaccharides, chitin, zirconium dioxide, and packed-bed cation exchangers, as well as ultrafiltration techniques. Novel fining agents must meet several criteria to effectively compete with bentonite. They must be cost-effective and nontoxic and must not degrade wine quality.

Negatively charged polysaccharides extracted from seaweeds are a potential class of bentonite alternatives.[118] Carrageenan is a food grade polysaccharide that is extracted from red seaweed and is currently used for protein stabilization in the beer industry.[118] It has been shown to be effective in stabilizing white wines at low addition rates (125−250 mg/L), using only one-third or less of the bentonite concentration required.[119] Carrageenan has been found to produce no deleterious sensory impacts compared to bentonite-treated wines.[120] Although those results are promising, residual amounts of carrageenan in treated wines can potentially induce haze formation,[118,119] and this is likely to restrict commercial viability. Another potential protein-adsorbing polysaccharide is chitin. Chitin is a component of crustacean exoskeletons and, alongside its derivatives, such as chitosan, is widely used in industrial processes, including as a thickening agent for processed foods and in pharmaceuticals.[121] The structure of chitin also makes it selective for binding to chitinases, and in-line systems containing chitin can be effective in removing these particular PR proteins from wine,[122] even if its activity in stabilizing wine has been recently challenged.[123] Chitin could potentially have serious sensory impacts, however, by removing favorable wine components such as positive aroma compounds.[124]

The ultimate objective of novel fining agents and protein-adsorbing materials for the wine industry is to achieve wine stabilization using in-line applications with minimum wine loss and no extra processing steps. Zirconium dioxide (ZrO_2) is a readily available protein-adsorbing material that can be regenerated and thus reused.[125,126] ZrO_2 has shown the potential to remove haze-forming proteins when tested in continuous and batch-wise application both during and post fermentation.[12,127,128] However, despite ZrO_2 showing promise and the ability to be regenerated with a simple washing

DOI: 10.1021/acs.jafc.5b00047
J. Agric. Food Chem. 2015, 63, 4020−4030

procedure,[127] issues with the flow rates and high dosages required limit its commercial viability.

Ultrafiltration can also be effective in removing haze-causing proteins, although the process is not selective and can remove other, desirable, wine components including polysaccharides.[129] This application is not necessarily viable at winery-scale due the expense of equipment. Packed-bed cation-exchangers could improve process efficiency, and their effectiveness in removing wine proteins has been demonstrated,[130] but they have not as yet been adopted for protein removal.

The mechanisms of wine haze formation have been revised from the two-stage model to a three-stage model and now include protein unfolding, protein aggregation, and the cross-linking of aggregates to form a visible haze. Chitinases and TLPs are the most important proteins involved in wine haze formation, and other wine components such as sulfates and polyphenols, as well as wine pH, can influence protein aggregation in the second and third stages. This improved understanding of the mechanisms of haze formation will allow the development of better predictive tools for haze potential and more targeted techniques to prevent hazes forming in bottled white wines. Recent advances in the prevention of haze formation have led to the development of a new bentonite alternative that utilizes a heat-tolerant protease in combination with flash pasteurization. Further investigations into more efficient stabilization strategies, possibly by utilizing proteases that are active at winemaking temperature, will ultimately benefit winemakers worldwide.

AUTHOR INFORMATION

Corresponding Authors

*(S.C.V.S.) E-mail: steve.vansluyter@mq.edu.au. Phone: +61 (0)2 9850 6316. Fax: +61 (0)2 9850 8245.

*(M.M.) E-mail: matteo.marangon@plumpton.ac.uk. Phone: +44 (0)1273 890454. Fax: +44 (0) 1273 890071.

Funding

The work was funded by Australia's grapegrowers and winemakers through their investment body, the Australian Grape and Wine Authority, with matching funds from the Australian government.

Notes

The authors declare no competing financial interest.

REFERENCES

(1) FAOSTAT http://faostat.fao.org/.

(2) *OIV 2012 Statistical Report on Global Vitiviniculture*; 2013; pp 1–27.

(3) *Wine: Global Industry Almanac*; 2012.

(4) Butzke, C. E.; Vogt, E. E.; Chacón-Rodríguez, L. Effects of heat exposure on wine quality during transport and storage. *J. Wine Res.* **2012**, *23*, 15–25.

(5) Ribéreau-Gayon, P.; Glories, Y.; Maujean, A.; Dubourdieu, D. *Handbook of Enology: The Chemistry of Wine Stabilization and Treatments*, 2nd ed.; Wiley: Hoboken, NJ, USA, 2006; Vol. 2.

(6) Du Toit, M.; Pretorius, I. S. Microbial spoilage and preservation of wine: using weapons from nature's own arsenal – a review. *South African J. Enol. Vitic.* **2000**, *21*, 74–96.

(7) Lasanta, C.; Gomez, J. Tartrate stabilization of wines. *Trends Food Sci. Technol.* **2012**, *28*, 52–59.

(8) Waters, E. J.; Alexander, G.; Muhlack, R.; Pocock, K. F.; Colby, C.; O'Neill, B. K.; Høj, P. B.; Jones, P. Preventing protein haze in bottled white wine. *Aust. J. Grape Wine Res.* **2005**, *11*, 215–225.

(9) Miller, G. C.; Amon, J. M.; Gibson, R. L.; Simpson, R. F. Loss of wine aroma attributable to protein stabilization with bentonite or ultrafiltration. *Aust. Grapegrower Winemaker* **1985**, *256*, 49–50.

(10) Muhlack, R.; Nordestgaard, S.; Waters, E. J.; O'Neill, B. K.; Lim, A.; Colby, C. B. In-line dosing for bentonite fining of wine or juice: contact time, clarification, product recovery and sensory effects. *Aust. J. Grape Wine Res.* **2006**, *12*, 221–234.

(11) Majewski, P.; Barbalet, A.; Waters, E. J. $1 billion hidden cost of bentonite fining. *Aust. N. Z. Grapegrower Winemaker* **2011**, *569*, 58–62.

(12) Salazar, F. N.; de Bruijn, J. P. F.; Seminario, L.; Guell, C.; Lopez, F. Improvement of wine crossflow microfiltration by a new hybrid process. *J. Food Eng.* **2007**, *79*, 1329–1336.

(13) Dufrechou, M.; Sauvage, F.-X.; Bach, B.; Vernhet, A. Protein aggregation in white wines: influence of the temperature on aggregation kinetics and mechanisms. *J. Agric. Food Chem.* **2010**, *58*, 10209–10218.

(14) Vincenzi, S.; Marangon, M.; Tolin, S.; Curioni, A. Protein evolution during the early stages of white winemaking and its relations with wine stability. *Aust. J. Grape Wine Res.* **2011**, *17*, 20–27.

(15) Monteiro, S.; Piçarra-Pereira, M.; Mesquita, P. R.; Loureiro, V. B.; Teixeira, A.; Ferreira, R. B. The wide diversity of structurally similar wine proteins. *J. Agric. Food Chem.* **2001**, *49*, 3999–4010.

(16) Marangon, M.; Van Sluyter, S. C.; Haynes, P. A.; Waters, E. J. Grape and wine proteins: their fractionation by hydrophobic interaction chromatography and identification by chromatographic and proteomic analysis. *J. Agric. Food Chem.* **2009**, *57*, 4415–4425.

(17) Van Sluyter, S. C.; Marangon, M.; Stranks, S. D.; Neilson, K. A.; Hayasaka, Y.; Haynes, P. A.; Menz, R. I.; Waters, E. J. Two-step purification of pathogenesis-related proteins from grape juice and crystallization of thaumatin-like proteins. *J. Agric. Food Chem.* **2009**, *57*, 11376–11382.

(18) Kwon, S. W. Profiling of soluble proteins in wine by nano-high-performance liquid chromatography/tandem mass spectrometry. *J. Agric. Food Chem.* **2004**, *52*, 7258–7263.

(19) Sarry, J.-E.; Sommerer, N.; Sauvage, F.-X.; Bergoin, A.; Rossignol, M.; Albagnac, G.; Romieu, C. Grape berry biochemistry revisited upon proteomic analysis of the mesocarp. *Proteomics* **2004**, *4*, 201–215.

(20) Cilindre, C.; Jégou, S.; Hovasse, A.; Schaeffer, C.; Castro, A. J.; Clément, C.; Dorsselaer, A.; Van Jeandet, P.; Marchal, R. Proteomic approach to identify Champagne wine proteins as modified by *Botrytis cinerea* infection. *J. Proteome Res.* **2008**, 1199–1208.

(21) Palmisano, G.; Antonacci, D.; Larsen, M. R. Glycoproteomic profile in wine: a`sweet' molecular renaissance. *J. Proteome Res.* **2010**, *9*, 6148–6159.

(22) Le Bourse, D.; Conreux, A.; Villaume, S.; Lameiras, P.; Nuzillard, J.-M.; Jeandet, P. Quantification of chitinase and thaumatin-like proteins in grape juices and wines. *Anal. Bioanal. Chem.* **2011**, *401*, 1541–1549.

(23) Cilindre, C.; Fasoli, E.; D'Amato, A.; Liger-Belair, G.; Righetti, P. G. It's time to pop a cork on Champagne's proteome! *J. Proteomics* **2014**, *105*, 351–362.

(24) Le Bourse, D.; Jegou, S.; Conreux, A.; Villaume, S.; Jeandet, P. Review of preparative and analytical procedures for the study of proteins in grape juice and wine. *Anal. Chim. Acta* **2010**, *667*, 33–42.

(25) Giribaldi, M.; Giuffrida, M. G. Heard it through the grapevine: proteomic perspective on grape and wine. *J. Proteomics* **2010**, *73*, 1647–1655.

(26) Velasco, R.; Zharkikh, A.; Troggio, M.; Cartwright, D. A.; Cestaro, A.; Pruss, D.; Pindo, M.; FitzGerald, L. M.; Vezzulli, S.; Reid, J.; et al. A high quality draft consensus sequence of the genome of a heterozygous grapevine variety. *PLoS One* **2007**, *2*, No. e1326, DOI: 10.1371/journal.pone.0001326.

(27) Pocock, K. F.; Hayasaka, Y.; McCarthy, M. G.; Waters, E. J. Thaumatin-like proteins and chitinases, the haze-forming proteins of wine, accumulate during ripening of grape (*Vitis vinifera*) berries and drought stress does not affect the final levels per berry at maturity. *J. Agric. Food Chem.* **2000**, *48*, 1637–1643.

DOI: 10.1021/acs.jafc.5b00047
J. Agric. Food Chem. 2015, 63, 4020–4030

(28) Marangon, M.; Van Sluyter, S. C.; Neilson, K. A.; Chan, C.; Haynes, P. A.; Waters, E. J.; Falconer, R. J. Roles of grape thaumatin-like protein and chitinase in white wine haze formation. *J. Agric. Food Chem.* **2011**, *59*, 733−740.
(29) Waters, E. J.; Shirley, N. J.; Williams, P. J. Nuisance proteins of wine are grape pathogenesis-related proteins. *J. Agric. Food Chem.* **1996**, *44*, 3−5.
(30) Marangon, M.; Van Sluyter, S. C.; Waters, E. J.; Menz, R. I. Structure of haze forming proteins in white wines: *Vitis vinifera* thaumatin-like proteins. *PLoS One* **2014**, *9*, No. e113757, DOI: 10.1371/journal.pone.0113757.
(31) Ferreira, R. B.; Pic, M. A.; Monteiro, S.; Teixeira, A. R. The wine proteins. *Trends Food Sci. Technol.* **2001**, *12*, 230−239.
(32) Esteruelas, M.; Poinsaut, P.; Sieczkowski, N.; Manteau, S.; Fort, M. F.; Canals, J. M.; Zamora, F. Characterization of natural haze protein in Sauvignon white wine. *Food Chem.* **2009**, *113*, 28−35.
(33) Sauvage, F.-X.; Bach, B.; Moutounet, M.; Vernhet, A. Proteins in white wines: thermo-sensitivity and differential adsorbtion by bentonite. *Food Chem.* **2010**, *118*, 26−34.
(34) Hayasaka, Y.; Adams, K. S.; Pocock, K. F.; Baldock, G. A.; Waters, E. J.; Høj, P. B. Use of electrospray mass spectrometry for mass determination of grape (*Vitis vinifera*) juice pathogenesis-related proteins: a potential tool for varietal differentiation. *J. Agric. Food Chem.* **2001**, *49*, 1830−1839.
(35) Monteiro, S.; Piçarra-Pereira, M. A.; Teixeira, A. R.; Loureiro, V. B.; Ferreira, R. B. Environmental conditions during vegetative growth determine the major proteins that accumulate in mature grapes. *J. Agric. Food Chem.* **2003**, *51*, 4046−4053.
(36) Girbau, T.; Stummer, B. E.; Pocock, K. F.; Baldock, G. A.; Scott, E. S.; Waters, E. J. The effect of *Uncinula necator* (powdery mildew) and *Botrytis cinerea* infection of grapes on the levels of haze-forming pathogenesis-related proteins in grape juice and wine. *Aust. J. Grape Wine Res.* **2004**, *10*, 125−133.
(37) Pocock, K. F.; Hayasaka, Y.; Peng, Z.; Williams, P. J.; Waters, E. J. The effect of mechanical harvesting and long-distance transport on the concentration of haze-forming proteins in grape Juice. *Aust. J. Grape Wine Res.* **1998**, *4*, 23−29.
(38) Tattersall, D. B.; van Heeswijck, R.; Høj, P. B. Identification and characterization of a fruit-specific, thaumatin-like protein that accumulates at very high levels in conjunction with the onset of sugar accumulation and berry softening in grapes. *Plant Physiol.* **1997**, *114*, 759−769.
(39) Salzman, R. A.; Tikhonova, I.; Bordelon, B. P.; Hasegawa, P. M.; Bressan, R. A. Coordinate accumulation of antifungal proteins and hexoses constitutes a developmentally controlled defense response during fruit ripening in grape. *Plant Physiol.* **1998**, *117*, 465−472.
(40) Hamel, F.; Boivin, R.; Tremblay, C.; Bellemare, G. Structural and evolutionary relationships among chitinases of flowering plants. *J. Mol. Evol.* **1997**, *44*, 614−624.
(41) Waters, E. J.; Pellerin, P.; Brillouet, J.-M. A *Saccharomyces* mannoprotein that protects wine from protein haze. *Carbohydr. Polym.* **1994**, *23*, 185−191.
(42) Dupin, I. V.; McKinnon, B. M.; Ryan, C.; Boulay, M.; Markides, A. J.; Jones, G. P.; Williams, P. J.; Waters, E. J. *Saccharomyces cerevisiae* mannoproteins that protect wine from protein haze: their release during fermentation and lees contact and a proposal for their mechanism of action. *J. Agric. Food Chem.* **2000**, *48*, 3098−3105.
(43) Cilindre, C.; Liger-Belair, G.; Villaume, S.; Jeandet, P.; Marchal, R. Foaming properties of various champagne wines depending on several parameters: grape variety, aging, protein and CO_2 content. *Anal. Chim. Acta* **2010**, *660*, 164−170.
(44) Dambrouck, T.; Marchal, R.; Cilindre, C.; Parmentier, M.; Jeandet, P. Determination of the grape invertase content (using PTA-ELISA) following various fining treatments versus changes in the total protein content of wine. Relationships with wine foamability. *J. Agric. Food Chem.* **2005**, *53*, 8782−8789.
(45) Waters, E. J.; Pellerin, P.; Brillouet, J.-M. A wine arabinogalactan-protein that reduces heat-induced wine protein haze. *Biosci., Biotechnol., Biochem.* **1994**, *58*, 43−48.
(46) Pellerin, P.; Vidal, S.; Williams, P.; Brillouet, J. M. Characterization of 5-type-II arabinogalactan-protein fractions from red wine of increasing uronic-acid content. *Carbohydr. Res.* **1995**, *277*, 135−143.
(47) Brown, S. L.; Stockdale, V. J.; Pettolino, F.; Pocock, K. F.; De Barros Lopes, M.; Williams, P. J.; Bacic, A.; Fincher, G. B.; Høj, P. B.; Waters, E. J. Reducing haziness in white wine by overexpression of *Saccharomyces cerevisiae* genes YOL155c and YDR055w. *Appl. Microbiol. Biotechnol.* **2007**, *73*, 1363−1376.
(48) Ledoux, V.; Dulau, L.; Dubourdieu, D. Interprétation de l'amélioration de la stabilité protéique des vins au cours de l'élevage sur lies. *J. Int. Sci. Vigne Vin* **1992**, *26*, 239−251.
(49) Schmidt, S. A.; Tan, E. L.; Brown, S.; Nasution, U. J.; Pettolino, F.; Macintyre, O. J.; Lopes, M. D. B.; Waters, E. J.; Anderson, P. A. Hpf2 glycan structure is critical for protection against protein haze formation in white wine. *J. Agric. Food Chem.* **2009**, *57*, 3308−3315.
(50) Vincenzi, S.; Crapisi, A.; Curioni, A. Foamability of Prosecco wine: cooperative effects of high molecular weight glycocompounds and wine PR-proteins. *Food Hydrocolloids* **2014**, *34*, 202−207.
(51) Dufour, C.; Bayonove, C. L. Influence of wine structurally different polysaccharides on the volatility of aroma substances in a model system. *J. Agric. Food Chem.* **1999**, *47*, 671−677.
(52) Jones, P. R.; Gawel, R.; Francis, I. L.; Waters, E. J. The influence of interactions between major white wine components on the aroma, flavour and texture of model white wine. *Food Qual. Pref.* **2008**, *19*, 596−607.
(53) Gazzola, D.; Van Sluyter, S. C.; Curioni, A.; Waters, E. J.; Marangon, M. Roles of proteins, polysaccharides, and phenolics in haze formation in white wine via reconstitution experiments. *J. Agric. Food Chem.* **2012**, *60*, 10666−10673.
(54) Marangon, M.; Sauvage, F.-X.; Waters, E. J.; Vernhet, A. Effects of ionic strength and sulfate upon thermal aggregation of grape chitinases and thaumatin-like proteins in a model system. *J. Agric. Food Chem.* **2011**, *59*, 2652−2662.
(55) Dufrechou, M.; Poncet-Legrand, C.; Sauvage, F.-X.; Vernhet, A. Stability of white wine proteins: combined effect of pH, ionic strength, and temperature on their aggregation. *J. Agric. Food Chem.* **2012**, *60*, 1308−1319.
(56) D'Amato, A.; Fasoli, E.; Kravchuk, A. V.; Righetti, P. G. Mehercules, adhuc Bacchus! The debate on wine proteomics continues. *J. Proteome Res.* **2011**, *10*, 3789−3801.
(57) Falconer, R. J.; Marangon, M.; Van Sluyter, S. C.; Neilson, K. A.; Chan, C.; Waters, E. J. Thermal stability of thaumatin-like protein, chitinase, and invertase isolated from Sauvignon blanc and Semillon juice and their role in haze formation in wine. *J. Agric. Food Chem.* **2010**, *58*, 975−980.
(58) Dufrechou, M.; Vernhet, A.; Roblin, P.; Sauvage, F.-X.; Poncet-Legrand, C. White wine proteins: how does the pH affect their conformation at room temperature? *Langmuir* **2013**, *29*, 10475−10482.
(59) Mesquita, P. R.; Piçarra-Pereira, M. A.; Monteiro, S.; Loureiro, V. B.; Teixeira, A. R.; Ferreira, R. B. Effect of wine composition on protein stability. *Am. J. Enol. Vitic.* **2001**, *4*, 324−330.
(60) Bayly, F. C.; Berg, H. W. Grape and wine proteins of white wine varietals. *Am. J. Enol. Vitic.* **1967**, *18*, 18−32.
(61) Pocock, K. F.; Alexander, G. M.; Hayasaka, Y.; Jones, P. R.; Waters, E. J. Sulfate − a candidate for the missing essential factor that is required for the formation of protein haze in white wine. *J. Agric. Food Chem.* **2007**, *55*, 1799−1807.
(62) Batista, L.; Monteiro, S.; Loureiro, V. B.; Teixeira, A. R.; Ferreira, R. B. The complexity of protein haze formation in wines. *Food Chem.* **2009**, *112*, 169−177.
(63) Marangon, M.; Vincenzi, S.; Lucchetta, M.; Curioni, A. Heating and reduction affect the reaction with tannins of wine protein fractions differing in hydrophobicity. *Anal. Chim. Acta* **2010**, *660*, 110−118.
(64) Israelachvili, J. *Electrostatic Forces between Surfaces in Liquids*, 2nd ed.; Israelachvili, J., Ed.; Academic Press: New York, 1991; pp 213−259.

DOI: 10.1021/acs.jafc.5b00047
J. Agric. Food Chem. 2015, 63, 4020−4030

(65) Batista, L.; Monteiro, S.; Loureiro, V. B.; Teixeira, A. R.; Ferreira, R. B. Protein haze formation in wines revisited. The stabilising effect of organic acids. *Food Chem.* **2010**, *122*, 1067−1075.
(66) Lambri, M.; Dordoni, R.; Giribaldi, M.; Violetta, M. R.; Giuffrida, M. G. Effect of pH on the protein profile and heat stability of an Italian white wine. *Food Res. Int.* **2013**, *54*, 1781−1786.
(67) Siebert, K. J.; Troukhanova, N. V.; Lynn, P. Y. Nature of polyphenol-protein interactions. *J. Agric. Food Chem.* **1996**, *44*, 80−85.
(68) Siebert, K. J. Protein-polyphenol haze in beverages. *Food Technol.* **1999**, *53*, 54−57.
(69) Waters, E. J.; Peng, Z.; Pocock, K. F.; Williams, P. J. Proteins in white wine, I: procyanidin occurrence in soluble proteins and onsoluble protein hazes and its relationship to protein instability. *Aust. J. Grape Wine Res.* **1995**, *1*, 86−93.
(70) Esteruelas, M.; Kontoudakis, N.; Gil, M.; Fort, M. F.; Canals, J. M.; Zamora, F. Phenolic compounds present in natural haze protein of Sauvignon white wine. *Food Res. Int.* **2011**, *44*, 77−83.
(71) Dawes, H.; Boyes, S.; Keene, J.; Heatherbell, D. Protein instability of wines: influence of protein isolelectric point. *Am. J. Enol. Vitic.* **1994**, *45*, 319−326.
(72) Waters, E. J.; Wallace, W.; Williams, P. J. Identification of heat-unstable wine proteins and their resistance to peptidases. *J. Agric. Food Chem.* **1992**, *40*, 1514−1519.
(73) Pocock, K. F.; Waters, E. J. Protein haze in bottled white wines: how well do stability tests and bentonite fining trials predict haze formation during storage and transport? *Aust. J. Grape Wine Res.* **2006**, *12*, 212−220.
(74) Dickinson, E. Stability and rheological implications of electrostatic milk protein−polysaccharide interactions. *Trends Food Sci. Technol.* **1998**, *9*, 347−354.
(75) Moreno-Arribas, M. V.; Polo, M. C. Winemaking biochemistry and microbiology: current knowledge and future trends. *Crit. Rev. Food Sci. Nutr.* **2005**, *45*, 265−286.
(76) Pretorius, I. S. Tailoring wine yeast for the new millennium: novel approaches to the ancient art of winemaking. *Yeast* **2000**, *16*, 675−729.
(77) Guitart, A.; Orte, P. H.; Ferreira, V.; Peña, C.; Cacho, J. Some observations about the correlation between the amino acid content of musts and wines of the Chardonnay variety and their fermentation aromas. *Am. J. Enol. Vitic.* **1999**, *50*, 253−258.
(78) Van der Hoorn, R. A. L. Plant proteases: from phenotypes to molecular mechanisms. *Annu. Rev. Plant Biol.* **2008**, *59*, 191−223.
(79) Rehmanji, M.; Gopal, C.; Mola, A. Beer stabilization technology − clearly a matter of choice. *Master Brew. Assoc. Am. Technol. Q.* **2005**, *42*, 332−338.
(80) Pavlenko, N. M.; Datunashvili, E. N. Change of nitrogenous compounds in must and wine treated with proteolytic enzymes. *Prikl. Biokhimiya Mikrobiol.* **1969**, *5*, 337−342.
(81) Tattersall, D. B.; Pocock, K. F.; Hayasaka, Y.; Adams, K.; van Heeswijck, R.; Waters, E. J.; Høj, P. B. Pathogenesis related proteins − their accumulation in grapes during berry growth and their involvement in white wine heat instability. Current knowledge and future perspectives in relation to winemaking practices. In *Molecular Biology and Biotechnology of the Grapevine*; Roubelakis-Angelakis, K. A., Ed.; Academic: Dordrecht, The Netherlands, 2001; pp 183−201.
(82) Waters, E. J.; Peng, Z.; Pocock, K. F.; Williams, P. J. Proteins in white wine, II: their resistance to proteolysis is not due to either phenolic association or glycosylation. *Aust. J. Grape Wine Res.* **1995**, *1*, 94−99.
(83) Richardson, M.; Valdesrodriguez, S.; Blancolabra, A. A possible function for thaumatin and a TMW-induced protein suggested by homology to a maize inhibitor. *Nature* **1987**, *327*, 432−434.
(84) Linthorst, H. J. M.; Van Loon, L. C. Pathogenesis related proteins of plants. *Crit. Rev. Plant Sci.* **1991**, *10*, 123−150.
(85) Marangon, M.; Van Sluyter, S. C.; Robinson, E. M. C.; Muhlack, R. A.; Holt, H. E.; Haynes, P. A.; Godden, P. W.; Smith, P. A.; Waters, E. J. Degradation of white wine haze proteins by Aspergillopepsin I and II during juice flash pasteurization. *Food Chem.* **2012**, *135*, 1157−1165.
(86) Urlaub, R. Benefits of the combined use of a protease and a pctic enzyme in wine processing. In *Physical Stability of Wine: Proceedings of a Seminar*; Lee, T. H., Ed.; Reynella: Reynella, South Australia, 1986; pp 47−61.
(87) Heatherbell, D.; Ngaba, P.; Fombin, J.; Watson, B.; Garcia, Z.; Flores, J.; Hsu, J. Recent developments in the application of ultrafiltration and protease enzymes to grape juice and wine processing. In *The International Symposium on Cool Climate Viticulture and Enology*; Oregon State University: Corvallis, OR, USA, 1984; pp 418−445.
(88) Feuillat, M.; Ferrari, G. Hydrolyse enzymatique des protéines du raisin en vinification. *C R. Seances Acad. Agric. Fr.* **1982**, *68*, 1070−1075.
(89) Lloyd, F. K.; Colby, C. B.; O'Neill, B. K.; Waters, E. J. Combined heat/proteolytic enzyme treatment for the removal of protein haze in wine. In *Proceedings of Chemeca 2005*, 33rd Australasian Chemical Engineering Conference; The Institution of Engineers Australia: Brisbane (QLD), Australia, 2005.
(90) Pocock, K. F.; Høj, P. B.; Adams, K. S.; Kwiatkowski, M. J.; Waters, E. J. Combined heat and proteolytic enzyme treatment of white wines reduces haze forming protein content without detrimental effect. *Aust. J. Grape Wine Res.* **2003**, *9*, 56−63.
(91) Robinson, E. M. C.; Scrimgeour, N.; Marangon, M.; Muhlack, R. A.; Smith, P. A.; Godden, P. W.; Johnson, D. Beyond bentonite. *Wine Vitic. J.* **2012**, *27*, 24−30.
(92) Commonwealth of Australia. Application A1091 − Enzyme nomenclature change − Carboxyl proteinase to Aspergillopepsin I & II. In *Food Standards Gazette* **2014**, pp 1−5.
(93) Bishop, J. G.; Dean, A. M.; Mitchell-Olds, T. Rapid evolution in plant chitinases: molecular targets of selection in plant-pathogen coevolution. *Proc. Natl. Acad. Sci. U. S. A.* **2000**, *97*, 5322−5327.
(94) Marchal, R.; Berthier, L.; Legendre, L.; Marchal-Delahaut, L.; Jeandet, P.; Maujean, A. Effects of *Botrytis cinerea* infection on the must protein electrophoretic characteristics. *J. Agric. Food Chem.* **1998**, *46*, 4945−4949.
(95) Marchal, R.; Warchol, M.; Cilindre, C.; Jeandet, P. Evidence for protein degradation by *Botrytis cinerea* and relationships with alteration of synthetic wine foaming properties. *J. Agric. Food Chem.* **2006**, *54*, 5157−5165.
(96) Van Sluyter, S. C.; Warnock, N. I.; Schmidt, S.; Anderson, P.; van Kan, J. A. L.; Bacic, A.; Waters, E. J. Aspartic acid protease from *Botrytis cinerea* removes haze-forming proteins during white wine-making. *J. Agric. Food Chem.* **2013**, *61*, 9705−9711.
(97) Manteau, S.; Lambert, B.; Jeandet, P.; Legendre, L. Changes in chitinase and thaumatin-like pathogenesis-related proteins of grape berries during the Champagne winemaking process. *Am. J. Enol. Vitic.* **2003**, *54*, 267−272.
(98) Waters, E. J.; Hayasaka, Y.; Tattersall, D. B.; Adams, K. S.; Williams, P. J. Sequence analysis of grape (*Vitis vinifera*) berry chitinases that cause haze formation in wines. *J. Agric. Food Chem.* **1998**, *46*, 4950−4957.
(99) Exposito, J. M.; Gordillo, C. M.; Marino, J. I. M.; Iglesias, J. L. M. Purification and characterization of a cysteine protease in *Vitis vinifera* L grapes (Macabeo variety). *Nahrung* **1991**, *35*, 139−142.
(100) Feuillat, M.; Brillant, G.; Rochard, J. Mise en évidence d'une production de proteases exocellulaires par les levures au cours de la fermentation alcoolique du moût de raisin. *Connaiss. Vigne Vin* **1980**, *14*, 37−52.
(101) Repka, V. Evidence for the involvement of cysteine proteases in the regulation of methyl jasmonate-induced cell death in grapevine. *Vitis* **2002**, *41*, 115−121.
(102) Ferri, M.; Tassoni, A.; Franceschetti, M.; Righetti, L.; Naldrett, M. J.; Bagni, N. Chitosan treatment induces changes of protein expression profile and stilbene distribution in *Vitis vinifera* cell suspensions. *Proteomics* **2009**, 1−15.
(103) Martinez-Esteso, M. J.; Selles-Marchart, S.; Vera-Urbina, J. C.; Pedreno, M. A.; Bru-Martinez, R. Changes of defense proteins in the extracellular proteome of grapevine (*Vitis vinifera* cv. Gamay) cell cultures in response to elicitors. *J. Proteomics* **2009**, *73*, 331−341.

DOI: 10.1021/acs.jafc.5b00047
J. Agric. Food Chem. 2015, 63, 4020−4030

(104) Vincent, D.; Ergul, A.; Bohlman, M. C.; Tattersall, E. A. R.; Tillett, R. L.; Wheatley, M. D.; Woolsey, R.; Quilici, D. R.; Joets, J.; Schlauch, K.; et al. Proteomic analysis reveals differences between *Vitis vinifera* L. cv. Chardonnay and cv. Cabernet sauvignon and their responses to water deficit and salinity. *J. Exp. Bot.* **2007**, *58*, 1873−1892.
(105) Marsoni, M.; Bracale, M.; Espen, L.; Prinsi, B.; Negri, A. S.; Vannini, C. Proteomic analysis of somatic embryogenesis in *Vitis vinifera*. *Plant Cell Rep.* **2008**, *27*, 347−356.
(106) Sharathchandra, R. G.; Stander, C.; Jacobson, D.; Ndimba, B.; Vivier, M. A. Proteomic analysis of grape berry cell cultures reveals that developmentally regulated ripening related processes can be studied using cultured cells. *PLoS One* **2011**, *6*, No. e14708, DOI: 10.1371/journal.pone.0014708.
(107) Cordonnier, R.; Dugal, A. Les activités protéolytiques du rasin. *Ann. Technol. Agric.* **1968**, *17*, 189−206.
(108) Dizy, M.; Bisson, L. F. Proteolytic activity of yeast strains during grape juice fermentation. *Am. J. Enol. Vitic.* **2000**, *51*, 155−167.
(109) Charoenchai, C.; Fleet, G. H.; Henschke, P. A.; Todd, B. E. N. Screening of non-*Saccharomyces* wine yeasts for the presence of extracellular hydrolytic enzymes. *Aust. J. Grape Wine Res.* **1997**, *3*, 2−8.
(110) Lagace, L. S.; Bisson, L. F. Survey of yeast acid proteases for effectiveness of wine haze reduction. *Am. J. Enol. Vitic.* **1990**, *41*, 147−155.
(111) Rosi, I.; Costamagna, L.; Bertuccioli, M. Screening for extracellular acid protease(s) production by wine yeasts. *J. Inst. Brew.* **1987**, *93*, 322−324.
(112) Williams, P. J.; Strauss, C. R.; Wilson, B.; Massy-Westropp, R. A. Studies on the hydrolysis of *Vitis vinifera* monoterpene precursor compounds and model monoterpene β-D-glucosides rationalizing the monoterpene composition of grapes. *J. Agric. Food Chem.* **1982**, *30*, 1219−1223, 10.1021/jf00114a054.
(113) Strauss, M. L. A.; Jolly, N. P.; Lambrechts, M. G.; van Rensburg, P. Screening for the production of extracellular hydrolytic enzymes by non-*Saccharomyces* wine yeasts. *J. Appl. Microbiol.* **2001**, *91*, 182−190.
(114) Bossi, A.; Bonizzato, L.; Zapparoli, G. Acidic extracellular proteases from microrganisms of fairly acidic niche. *Protein Pept. Lett.* **2006**, *13*, 737−741.
(115) Younes, B.; Cilindre, C.; Villaume, S.; Parmentier, M.; Jeandet, P.; Vasserot, Y. Evidence for an extracellular acid proteolytic activity secreted by living cells of *Saccharomyces cerevisiae* PlR1: impact on grape proteins. *J. Agric. Food Chem.* **2011**, *59*, 6239−6246.
(116) Younes, B.; Cilindre, C.; Jeandet, P.; Vasserot, Y. Enzymatic hydrolysis of thermo-sensitive grape proteins by a yeast protease as revealed by a proteomic approach. *Food Res. Int.* **2013**, *54*, 1298−1301.
(117) Alexandre, H.; Heintz, D.; Chassagne, D.; Guilloux-Benatier, M.; Charpentier, C.; Feuillat, M. Protease A activity and nitrogen fractions released during alcoholic fermentation and autolysis in enological conditions. *J. Ind. Microbiol. Biotechnol.* **2001**, *26*, 235−240.
(118) Cabello-Pasini, A.; Victoria-Cota, N.; Macias-Carranza, V.; Hernandez-Garibay, E.; Muñiz-Salazar, R. Clarification of wines using polysaccharides extracted from seaweeds. *Am. J. Enol. Vitic.* **2005**, *56*, 52−59.
(119) Marangon, M.; Stockdale, V. J.; Munro, P.; Trethewey, T.; Schulkin, A.; Holt, H. E.; Smith, P. A. Addition of carrageenan at different stages of winemaking for white wine protein stabilization. *J. Agric. Food Chem.* **2013**, *61*, 6516−6524.
(120) Marangon, M.; Lucchetta, M.; Duan, D.; Stockdale, V. J.; Hart, A.; Rogers, P. J.; Waters, E. J. Protein removal from a Chardonnay juice by addition of carrageenan and pectin. *Aust. J. Grape Wine Res.* **2012**, *18*, 194−202.
(121) Shahidi, F.; Arachchi, J. K. V.; Jeon, Y.-J. Food applications of chitin and chitosans. *Trends Food Sci. Technol.* **1999**, *10*, 37−51.
(122) Vincenzi, S.; Polesani, M.; Curioni, A. Removal of specific protein components by chitin enhances protein stability in a white wine. *Am. J. Enol. Vitic.* **2005**, *56*, 246−254.
(123) Chagas, R.; Monteiro, S.; Boavida Ferreira, R. Assessment of potential effects of common fining agents used for white wine protein stabilization. *Am. J. Enol. Vitic.* **2012**, *63*, 574−578.
(124) Spagna, G.; Pifferi, P. G.; Rangoni, C.; Mattivi, F.; Nicolini, G.; Palmonari, R. The stabilization of white wines by adsorption of phenolic compounds on chitin and chitosan. *Food Res. Int.* **1996**, *29*, 241−248.
(125) Pashova, V.; Güell, C.; Pueyo, E.; López-Barajas, M.; Polo, M. C.; López, F. White wine protein stabilization by a continuous process using a packed column. *Am. J. Enol. Vitic.* **2004**, *55*, 195−198.
(126) Pashova, V.; Güell, C.; López, F. White wine continuous protein stabilization by packed column. *J. Agric. Food Chem.* **2004**, *52*, 1558−1563.
(127) Marangon, M.; Lucchetta, M.; Waters, E. J. Protein stabilisation of white wines using zirconium dioxide enclosed in a metallic cage. *Aust. J. Grape Wine Res.* **2011**, *17*, 28−35.
(128) Lucchetta, M.; Pocock, K. F.; Waters, E. J.; Marangon, M. Use of zirconium dioxide during fermentation as an alternative to protein fining with bentonite for white wines. *Am. J. Enol. Vitic.* **2013**, *64*, 400−404.
(129) Hsu, J. C.; Heatherbell, D. A.; Flores, J. H.; Watson, B. T. Heat-unstable proteins in grape juice and wine. II. Characterization and removal by ultrafiltration. *Am. J. Enol. Vitic.* **1987**, *38*, 17−22.
(130) Sarmento, M. R.; Oliveira, J. C.; Boulton, R. B. Selection of low swelling materials for protein adsorption from white wines. *Int. J. Food Sci. Technol.* **2000**, *35*, 41−47.

DOI: 10.1021/acs.jafc.5b00047
J. Agric. Food Chem. 2015, 63, 4020−4030

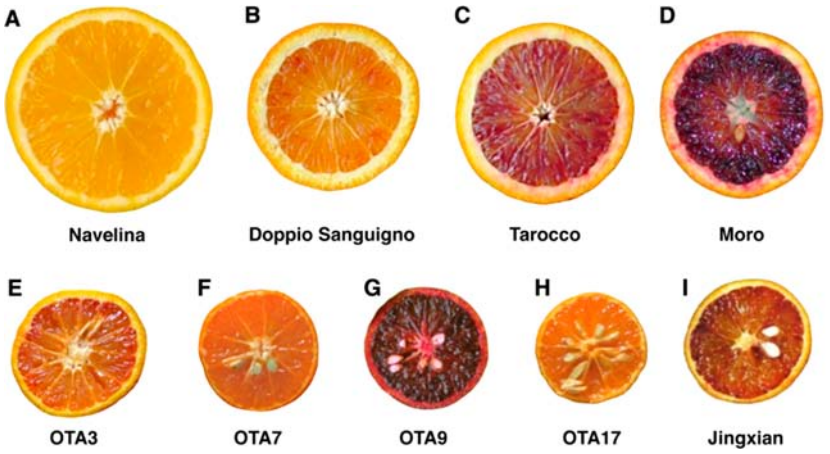

Figure 1. Phenotypes and genotypes of orange varieties and hybrids: Navelina (A); Doppio Sanguigno (B); Tarocco (CRA) (C); Moro (CRA) (D); OTA3 (E); OTA7 (F); OTA9 (G); OTA17 (H); Jingxian (I). Independent Blood Orange Accession, Jingxian, China. Reproduced with permission from ref 10. Copyright 2012 American Society of Plant Biologists.

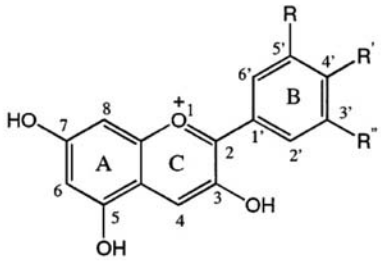

Anthocyanidin	R1	R2	R3
Delphinidin	OH	OH	OH
Cyanidin	OH	OH	H
Petunidin	OH	OH	OCH_3
Pelargonidin	H	OH	H
Peonidin	OCH_3	OH	H
Malvidin	OCH_3	OH	OCH_3

Figure 2. Structure of 3,5,7,4′-tetrahydroxylflavilium ion and of the six basic anthocyanins. Reproduced from ref 20.

are more sensitive to oxidation to produce *o*-diquinones, or even *o*-diphenol dimers.[17] Therefore, cyanidin, delphinidin, and petunidin, which contain the *o*-diphenol structure on the B ring, are more sensitive to oxidation. On the contrary, neither malvidin nor peonidin possesses the ortho-positioned hydroxyl groups, which results in their comparatively higher resistance to oxidation.[17] In most plants only O-glycosylation occurs for anthocyanins in which the sugar moiety is typically glucose, but it can be substituted by other sugars such as galactose, rhamnose, arabinose, or xylose.[18] In *Citrus* pigmented varieties, the glucose molecule can be linked to anthocyanidins through the glycosidic bonds at the C3 position to form the 3-*O*-monoglycoside anthocyanins. The junctions can also occur at both C3 and C5 positions to produce 3,5-*O*-diglycoside anthocyanins,[19] which seem to be more stable than their monoglucosidic counterparts. Blood orange [*C. sinensis* (L.) Osbeck] juices contain anthocyanins in differing concentrations depending on the variety, each showing a characteristic seasonal variation of the pigment content.[20] The two major anthocyanins of blood oranges (ca. 90%) have been identified as cyanidin 3-glucoside[19,21−23] and cyanidin 3-(6″-malonylglucoside)[23] in comparable concentrations, these data being confirmed in later studies.[20,24,25] The pioneering work of Maccarone et al.,[19,23] which was carried out by HPLC separation of pigments associated with their spectrophotometric detection, also led to the identification of minor anthocyanin components of blood orange juice [delphinidin 3-glucoside, petunidin 3-glucoside, pelargonidin 3-glucoside, cyanidin 3-(acetyl)glucoside], some of them found as hydroxycinnamic acids derivatives of cyanidin 3-glucoside [cyanidin 3-(feruloyl)glucoside, cyanidin 3- (coumarylferulyl)-glucoside, cyanidin 3-(sinapyl)glucoside, peonidin 3-(coumaryl)glucoside] as well as the diglucosylated forms (3,5) of delphinidin, cyanidin, petunidin, and pelargonidin. Dugo and co-workers[20] identified for the first time peonidin 3-glucoside, cyanidin 3-rutinoside, and the 6″-malonylglucose esters of delphinidin, peonidin, and petunidin as minor additional anthocyanins of blood orange juice by using microhigh-performance liquid chromatography (HPLC)−electrospray ionization mass spectrometry (ESI-MS) (Figure 3). Further investigations revealed the occurrence of cyanidin 3-(6″-dioxalylglucoside), as well as four other anthocyanin-derived pigments, which are formed through a direct reaction between anthocyanins and hydroxycinnamic acids only during prolonged storage of the juice.[25] These novel pyranoanthocyanins (i.e., anthocyanins that contain an additional pyran ring between the C-4 and the hydroxyl group attached to C-5) were identified as the 4-vinylphenol, 4-vinylcatechol, 4-vinylguaiacol, and 4-vinylsyringol adducts of cyanidin 3-glucoside.[25]

BIOSYNTHESIS OF ANTHOCYANINS IN RED ORANGES

Free anthocyanins are synthesized via the flavonoid pathway, which is a ubiquitous and well-described plant secondary metabolite pathway.[16] It has been found that at least two groups of genes are required for anthocyanin biosynthesis: the structural genes encoding the enzymes directly implicated in all of the metabolic reactions and the regulatory genes encoding the transcription factors that control the expression of the

DOI: 10.1021/acs.jafc.5b01123
J. Agric. Food Chem. 2015, 63, 4031−4041

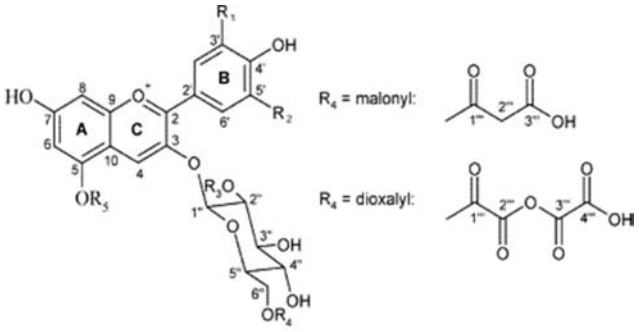

compd	R_1	R_2	R_3	R_4	R_5
1	OH	H	H	H	glucosyl
2	OH	OH	H	H	H
3	OH	H	glucosyl	H	H
4	OH	H	H	H	H
5	OH	OH	H	malonyl	H
6	OH	H	H	malonyl	H
7	OH	H	H	dioxalyl	H
8	OCH_3	H	H	malonyl	H

For compound labeling cf. Figure 1

Figure 3. Structures of the anthocyanins from blood orange juice: cyanidin 3,5-diglucoside (1), delphinidin 3-glucoside (2), cyanidin 3-sophoroside (3), cyanidin 3-glucoside (4), delphinidin 3-(6″-malonylglucoside) (5), cyanidin 3-(6″-malonylglucoside) (6), cyanidin 3-(6″-dioxalylglucoside) (7), and peonidin 3-(6″-malonylglucoside) (8). Reproduced from ref 25.

above-mentioned structural genes.[26−28] Most genes encoding the enzymes that biosynthesize the core structure have been cloned and characterized in various species.[1] Previous studies have revealed that the genes acting earlier in the flavonoid pathway are usually encoded by larger gene families, whereas the enzymes directly involved in later steps are encoded by single active genes.[29] This rule, probably resulting from the fact that the earlier acting genes are involved in diverse metabolic functions that require a specific control of gene expression, seems to be applicable to *C. sinensis* anthocyanin biosynthesis. In the *Citrus* genus the early studies on the genes encoding the key enzymes of anthocyanin biosynthesis and their expression analysis occurred more than 10 years ago,[30−32] and new information has since been released.[6,33−35] As shown below, anthocyanins are synthesized by an extremely complex network of all the structural enzymes in the pathway. Therefore, for an efficient production of anthocyanins at the different steps, it is speculated that all of the key enzymes involved in the anthocyanin biosynthesis are associated with each other to form a multienzyme complex.[36] Published evidence indicates the existence of such a complex in some model plants, such as *Arabidopsis thaliana*.[36] Phenylalanine is a direct precursor for the synthesis of anthocyanidins. The conversion of phenylalanine to anthocyanins requires a series of reactions: the first of them is represented by the transformation of phenylalanine to *trans*-cinnamic acid through the elimination of ammonia catalyzed by phenylalanine ammonia-lyase (PAL). PAL has been extensively studied because of its importance in plant stress responses and tissue wounding;[37] protection against UV radiation,[38] low temperature,[6,30] and levels of nitrogen, phosphate, and iron;[38] and pathogenic attack and ethylene response.[39] Two full-length cDNA clones (FPAL1 and FPAL2) were isolated from the flavedo tissue of the Fortune cultivar (*Citrus clementina* Hort. ex Tanaka × *Citrus reticulata* Blanco) library, and the deduced amino acid sequences showed a 75−85% similarity with PAL genes from other plant species.[30] A partial cDNA clone putatively coding for PAL was isolated from the Tarocco fruit juice vesicles [*C. sinensis* (L.) Osbeck] by RT-PCR. The partial nucleotide sequence (DQ088064.1) showed 98.0% identity with the available *C. clementina* sequence.[6] By browsing the *C. sinensis* genome using the BLASTP tool at Phytozome (http://www.phytozome.net/), four sequences matching the translated partial sequence of the Tarocco PAL have been found, and all of them were recognized as PAL (scaffold00201, position 117,512−120,607, *e* value $6.8^{e\text{-}117}$; scaffold00201, position 95,337−97,004, *e* value $2.8^{e\text{-}115}$; scaffold00349, position 92,401−96,606, *e* value $3.1^{e\text{-}111}$; scaffold08490, position 1,157−2,599, *e* value $2.4^{e\text{-}109}$), thus suggesting that the gene is present in four polymorphic forms in the *C. sinensis* genome as also emerged by the in silico analysis of CitEST database performed by Lucheta and co-workers.[40]

In the following steps, 4-hydroxylation of cinnamic acid by cinnamate 4-hydroxylase (C4H) generates *p*-coumaric acid, which is activated by the 4-coumarate:CoA ligase (4CL) to the respective CoA ester. In Valencia sweet orange (*C. sinensis*) two C4H genes were described coding a constitutively expressed C4H2 (AF255014) enzyme that plays an ordinary role in the phenylpropanoid pathway, in contrast to a wound-induced C4H1 (AF255013) isoform.[40,41] In silico studies revealed that the 4-coumarate:CoA ligase (4CL), which converts 4-coumarate (or *p*-coumaric acid) to 4-coumaroyl-CoA, is encoded by a multigene family in the *Citrus* genus.[40]

The first specific enzyme of the anthocyanin biosynthetic pathway is chalcone synthase (CHS) (Figure 4), which condenses three malonyl-CoA molecules and one *p*-coumaroyl-CoA to produce the naringenin chalcone, which is implicated not only in the anthocyanin biosynthesis but also in the creation of other phenolic compounds.[42] As a consequence, different CHS genes may act in different pathways producing distinct secondary metabolites. Two cDNA clones encoding CHS were isolated (CitCHS1, AB009350; and CitCHS2, AB009351) from the Valencia orange (*C. sinensis*) seed library. Southern blot analysis indicated that CitCHS1 (1481 bp long encoding a 389 amino acid protein) is present in a single copy, whereas some sequences related to CitCHS2 (1412 bp long encoding a 391 amino acid protein) are in the *C. sinensis* genome.[31] Furthermore, because hybridization patterns of CitCHS1 and CitCHS2 are different from each other, these cDNA clones have been likely originated from different loci. The expression analysis showed that CitCHS2 mRNA is notably induced by embryogenesis but CitCHS1 mRNA is not, thus indicating that two CHS genes are differentially expressed during citrus somatic embryogenesis and that CitCHS2 may regulate the accumulation of flavonoids in citrus cell cultures.[31]

The naringenin chalcone is isomerized by chalcone isomerase (CHI) to the flavanone naringenin, which is subsequently converted to dihydrokaempferol by flavanone 3′-hydroxylase (F3H). The gene active in the aforementioned stereospecific isomerization of naringenin chalcone into naringenin flavanone (CHI) and the one involved in the following naringen flavanone hydroxylation into dihydrokaempferol (F3H) were later isolated from a *Citrus unshiu* cDNA library, and their expression patterns were analyzed during citrus (Marc.) fruit development in relation to their flavonoid contents. The respective cDNA clones from chalcone isomerase (CHI, CitCHI, AB011794) and flavanone 3′-hydroxylase (F3H, CitF3H, AB011795) are 931 and 1360 bp long, encoding proteins of 222 and 362 amino acid residues, respectively. CitCHI seems to be a single-copy gene, as also confirmed by

DOI: 10.1021/acs.jafc.5b01123
J. Agric. Food Chem. 2015, 63, 4031−4041

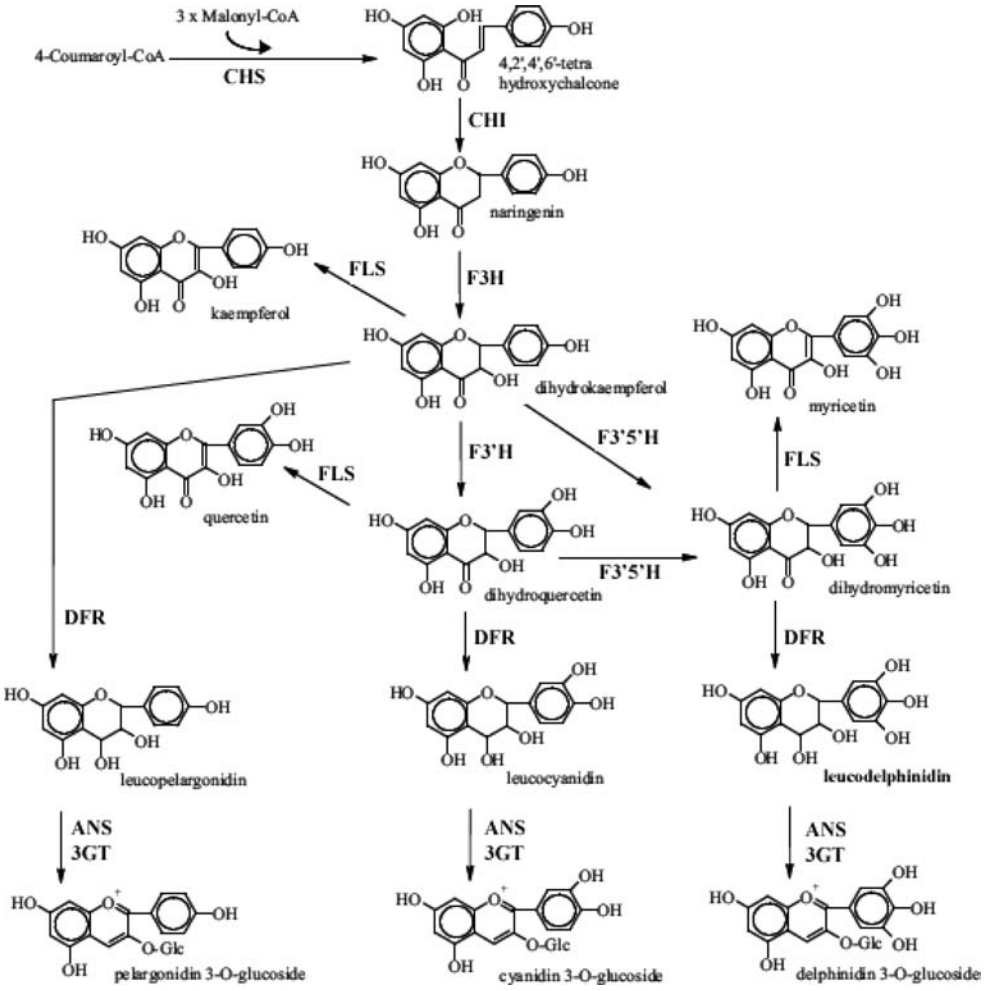

Figure 4. Outline of the biosynthetic pathway leading to the synthesis of anthocyanins. Enzyme names are abbreviated as follows: chalcone synthase (CHS); chalcone isomerize (CHI); flavanone 3′-hydroxylase (F3H), flavanoid 3′-hydroxylase (F3′H); flavanoid 3′,5′-hydroxylase (F3′5′H); flavonol synthase (FLS); dihydroflavonol 4-reductase (DFR); anthocyanidin synthase (ANS); UDP-glucose-flavonoid 3-*O*-glucosyltransferase (UFGT). Reproduced with permission from ref 7. Copyright 2006 American Society for Horticultural Science.

browsing the *C. sinensis* genome using the BLASTP tool at Phytozome (http://www.phytozome.net/) (scaffold00024, position 1,113,233−1,115,603, *e* value $2.9^{e\text{-}125}$), whereas a few CitF3H-related sequences are in the *C. unshiu* genome[32] as also found by the in silico analysis of the CitEST database.[40] Messenger RNA levels of the flavonoid biosynthetic genes CitCHI and CitF3H and two previously isolated chalcone synthases (CHS, CitCHS1, and CitCHS2) were analyzed in various tissues during Satsuma mandarin fruit development. Transcript levels for CitCHS1, CitCHS2, CitCHI, and CitF3H are generally high in young tissues that correspond to high accumulation of flavonoids.[32] However, the crucial role of both CitCHS and CitF3H in the development of anthocyanin pigmentation was confirmed by a later study regarding the analysis of the proteomic profile of two orange cultivars with different pigmentation (the blood orange Moro and the blond or common orange Cadenera), at ripening time.[43] Chalcone synthase as well as flavanone hydroxylase were identified as differentially expressed proteins among merely 55 proteins, suggesting that the activation of anthocyanin biosynthetic pathway in blood oranges is one of the major differences distinguishing blood and blond oranges.[43]

The dihydroflavonols, dihydroquercetin and dihydromyricetin, are synthesized from dihydrokaempferol by hydroxylation reactions catalyzed by flavonoid 3′-hydroxylase (F3′H)[44] and flavonoid 3′,5′-hydroxylase, respectively. Dihydroflavonol 4-reductase (DFR) can reduce the dihydroflavonols to their corresponding leucoanthocyanidins. The gene encoding dihydroflavonol 4-reductase was isolated from both a cDNA library (AY519363.1) and genomic DNA (DQ084722.1) (Tarocco and Navel varieties). The data revealed that the cDNA sequences of orange DFR belonging to the red and blond varieties were 100% homologous and contained a 1017 bp open reading frame that encodes a protein of 338 amino acid residues, corresponding to a molecular mass of 38010.76 Da, with a theoretical p*I* of 5.96. Southern blot analysis of genomic DNA indicated that *dfr* is a single-copy gene (as confirmed by browsing the *C. sinensis* genome using the BLASTP tool at Phytozome, http://www.phytozome.net/, scaffold00002, position 3,110,202−3,111,942) in both pigmented and nonpigmented orange varieties. The successful in vitro expression of orange DFR led to an active DFR enzyme that converts dihydroquercetin to leucoanthocyanidin, thus confirming the involvement of the isolated genes in the biosynthesis of anthocyanins.[34] Furthermore, the promoter of the DFR gene was cloned and analyzed.[34] The examination of the sweet orange *dfr* promoter sequence revealed a number of motifs that may be involved in the transcriptional activation of

DOI: 10.1021/acs.jafc.5b01123
J. Agric. Food Chem. 2015, 63, 4031−4041

the DFR genes: a putative unit I, which includes the homologous binding site for the G-box factor, and the downstream MYB homologous binding site were found.[45] Unit I was initially identified in the *chs* promoter and shown to be involved in light induction of the gene expression; it was shown to be necessary and sufficient to impart photoregulation through the phytochromes and the UV-A/blue and UV-B photoreceptors.[46] Two putative GA-myb (gibberellic acid activated myb) homologous binding sites are also located upstream of unit I. Several core elements for Dof3 (one zinc finger), which have been reported to be involved in tissue specificity and light regulation,[47] were observed in the *dfr* promoter. A sequence with homology to the TACpyAT box of the *chs* promoter,[48] which is responsible for organ-specific expression, was also identified immediately upstream of the TATA box. Moreover, three homologous SBF-1 transcription factor binding sites were also detected in the *dfr* promoter.[49] Finally, it was also found that there are no differences in the *dfr* coding and promoter sequences between red and blond oranges. Therefore, as the DFR transcripts are normally detected only in red oranges, its expression should be under extremely strict control of the transcriptional regulators.[34] Anthocyanidin synthase (ANS), an oxoglutarate-dependent Fe^{2+}/Fe^{3+} dioxygenase, converts the colorless leucoanthocyanidins into the colored anthocyanidins, that, once formed, must be immediately modified as they are inherently unstable under physiological conditions (Figure 4). Therefore, the UDP-glucose-flavonoid glucosyl transferase (UFGT) catalyzes the addition of one glucose moiety in the 3-OH positions of anthocyanidins, increasing their hydrophilicity and stability. The sweet orange [(*C. sinensis*) Osbeck, Tarocco] ANS and UFGT genes have been cloned by Lo Piero and co-workers (unpublished data), and their sequences are available at http://www.ncbi.nlm.nih.gov/ (ANS, AY581048; UFGT, AY519364). Both genes are likely in single copy in the *C. sinensis* genome as resulted by the BLASTP search tool at Phytozome (http://www.phytozome.net/) (ANS scaffold00074, position 275,559−279,543; UFGT scaffold00204, position 195,714−197,012). The presence of diglycosylated anthocyanins in blood orange juice[19−23] indicates that other glucosylating enzymes might be involved in anthocyanin modification as occurs in grape,[17] although a homologous gene has not yet been identified in *Citrus*. Acylation is one of the most common modifications of red orange anthocyanins, resulting in greatly increased structural diversity of anthocyanins from the addition of aromatic and/or aliphatic constituents linked to the C6″ positions of the glucosyl groups.[23] Anthocyanins, without the protection of acylation, can be easily and quickly decolorized in neutral or weakly acidic aqueous solutions. The acylation of anthocyanins in plants is catalyzed by the action of anthocyanin acyltransferases (ACT, also known as AAT), which have a really high substrate specificity for both the anthocyanin acceptors and the acyl group donors. In plants, there are mainly two types of ACTs that are classified on the basis of the acyl group donors: the BAHD family using acyl-CoA and the serine carboxypeptidase-like (SCPL) group using acyl-activated sugars.[50] Although in some important *C. sinensis* pigmented varieties the acylated anthocyanins can account for >40% of the total anthocyanin content (cyanidin 3-(6″-malonylglucoside),[23] until now there has been no report about the exact genes required for sweet orange anthocyanin acylation by ACTs.

ANTHOCYANIN TRANSPORTATION INTO THE VACUOLES

Anthocyanins are synthesized by multienzyme complexes that are localized at the cytoplasmic face of the endoplasmic reticulum (ER)[51,52] and then transported to the large vacuole,[53] this localization being necessary to prevent oxidation and for anthocyanins to function as pigments.[54] In some plants, anthocyanins are found in highly pigmented bodies located inside the vacuole; these vacuole-accumulating anthocyanins are also known as anthocyanic vacuolar inclusion (AVI) and contain a dense complex mix of anthocyanins concentrated above the levels that are possible in vacuolar solution.[55] The mechanism of anthocyanin transport to the vacuole has long been debated, with numerous models proposed such as membrane vesicle-mediated or membrane transporter-mediated transport.[56−58] To date, several molecular players involved in the sequestration of anthocyanins have been identified. The importance of glutathione-*S*-transferases (GSTs) for anthocyanin transport has been demonstrated in *Zea mays* (maize) BZ2,[54] petunia AN9,[59] and *Arabidopsis* TT19,[60] where mutations in the encoding genes lead to a reduction in anthocyanin accumulation and pigment mislocalization. A mechanism similar to the detoxification process was then proposed for anthocyanins, according to which they need to be transferred into the vacuoles as glutathione S-conjugates.[54] However, no anthocyanin−glutathione conjugate has been observed in vitro, so it has been suggested that anthocyanins could be transported via the noncovalent binding activity of glutathione *S*-transferase functioning as ligandin.[61,62] Two major transporter families, the multidrug resistance-associated protein (MRP) and the multidrug and toxic compound extrusion transporter (MATE) families, would also be involved in anthocyanin transport in maize[63] and grape.[64] However, the involvement of these different proteins in anthocyanin transport to the vacuole is still unclear. With regard to the anthocyanin transfer into the vacuole in blood oranges, a GST gene homologous to both the AN9 and BZ2 has been isolated from red orange fruit flesh.[35] Having considered gene organization and homology data, it has been suggested that the isolated GST gene is involved in the mechanism of vacuolar import of anthocyanins as confirmed by in vitro expression of orange GST, leading to an enzyme that is active against cyanidin-3-*O*-glucoside.[35] The comparison between colored and uncolored varieties reveals that blood and blond orange GST encoding genes share the same nucleotide sequences, but the GST expression in the nonpigmented orange cultivars (Navel and Ovale) was strongly reduced as compared to that of the pigmented orange (Tarocco). Interestingly, in the crude extracts of pigmented orange fruits, the GST activity is reproducibly detected by providing either 1-chloro-2,4 dinitrobenzene (CDNB) or cyanidin-3-*O*-glucoside as substrates; moreover, cyanidin-3-*O*-glucoside acts as a powerful competitive inhibitor of 1-chloro-2,4-dinitrobenzene conjugation to reduced glutathione (GSH) in the pigmented oranges, confirming that this molecule might easily bind to the active site of the enzyme and functions as a putative substrate.[35] Although the GST involved in anthocyanin conjugation to GSH has been unequivocally identified, it is obvious that the information to precisely understand the working mechanism of the entire complex in vivo is still lacking. As a consequence, more work is needed, and the just released *C. sinensis* genome sequence[65] will likely represent a valued source to recruit

DOI: 10.1021/acs.jafc.5b01123
J. Agric. Food Chem. 2015, 63, 4031−4041

orthologous sequences to provide additional insight into this metabolic pathway.

DEGRADATION OF RED ORANGE ANTHOCYANINS

In contrast to the detailed knowledge available on anthocyanin synthesis, very little is known about pigment stability and catabolism in plants. Transient anthocyanin accumulation and disappearance during plant development or changes in environmental conditions suggest that anthocyanin degradation is controlled and induced when beneficial to the plant.[66] Loss of red pigmentation can occur in young foliage as it matures, in developing flowers, or in response to changes in environmental conditions.[66] Anthocyanin degradation is also observed in Sicilian sweet orange varieties (Tarocco, Moro, and Sanguinello): the pigments accumulated at the late stages of ripening in both the rind and flesh may be degraded, leading to a commercially undesirable partial loss of this color.[67] Enzymatic studies of anthocyanin degradation in postharvest fruits and fruit juices have revealed several enzymes that degrade anthocyanins in these systems and may be candidates for the active in vivo degradation. Three enzyme groups that control degradation rates of anthocyanins in fruit extracts and juices are polyphenol oxidases, peroxidases, and β-glucosidases. Assuming that in planta anthocyanin degradation occurs in the cell vacuoles, the direct oxidation of anthocyanin with peroxidase, which is present in cell vacuoles unlike the oxidizing polyphenol oxidases, is more likely the candidate route for in planta anthocyanin degradation. Nevertheless, the possibility that anthocyanins are transferred out of the vacuoles before degradation exists, and further studies are needed to determine the site of degradation. Therefore, three alternative pathways for enzymatic anthocyanin degradation are presented: (1) direct oxidation of anthocyanin by peroxidase; (2) coupled oxidation, that is, reduction of quinones of phenolic compounds to the original phenolic compounds in parallel to oxidation of anthocyanin to anthocyanin quinine; (3) degradation in two steps, deglycosylation with anthocyanase (β-glucosidase) and then oxidation with polyphenol oxidase or peroxidase. The β-glucosidases may also be involved in the in planta degradation process, because they increase the degradation rate of anthocyanins in fruit extracts of both lychee and eggplant.[66] A specific β-glucosidase was isolated from the fruit juice of Tarocco blood oranges, and the anthocyanin degradation kinetic was followed physiochemically. This enzyme, mainly bound to pectin chains, turns out to be responsible for the degradation of anthocyanins in both the juice and the ripening fruits.[67] The yielded anthocyanidins may be a good substrate for oxidases such as polyphenol oxidase (PPO) in a successive step of the enzymatic degradation process.[66]

Many physical and chemical factors affect the stability of anthocyanins, including temperature, pH, the presence of oxygen, enzymes, the presence of copigments, metal ions, ascorbic acid, sulfur dioxide, sugars, and sugar degradation products. Both low and high temperatures might induce anthocyanin degradation. During cold storage (4 °C for 12 months), the anthocyanic pigments of blood orange juices undergo modifications that lead to the transformation of polycondensation compounds, the color of which changes from brick-red to brown. The process of polymerization is accompanied by the production of chemical indicators of sugar and ascorbic acid degradation (furfural and hydroxymethylfurfural).[68] Reactions between anthocyanic pigments and the aforementioned intermediates of degradation of sugar and ascorbic acid in an acidic environment are the main causes of the formation of these polymers.[69] Moreover, blood orange juice loses its color due to the anthocyanin degradation caused by the standard thermal treatment directed at pectinesterase inactivation, thus negatively influencing the commercial value of blood orange juice.[70] Studies on the thermal degradation of cyanidin 3-(6″-malonyl) glucoside and cyanidin 3-glucoside, which are the two major anthocyanins in blood orange juice,[19,23] as well as of cyanidin-3-glucoside-derived pyranoanthocyanins,[25] indicate that the cyanidin-3-(6′-malonyl)-glucoside is the most stable. Conversely, cyanidin-3-glucoside-derived pyranoanthocyanins show the highest degradation rates, suggesting that acylated anthocyanins could be very promising pigments contributing to the color of different products as stable and intense color molecules.[70] The major intrinsic factors such as ascorbic acid and sugars significantly accelerate the thermal degradation of blood orange anthocyanins, whereas flavonoids have a protective effect on the degradation of anthocyanins; the protective effect of flavonoids plays a more important role in the degradation of anthocyanins compared to the negative effect of ascorbic acid or sugars.[71] The effects of nonthermal preservation technologies including high hydrostatic pressure, pulsed electric field, ultrasound, irradiation, and ozone on the stability of anthocyanins in blood orange juice are reviewed in Tiwari et al.[72]

REGULATION OF ANTHOCYANIN BIOSYNTHESIS IN RED ORANGES

Sweet oranges can be easily divided into two groups based on color, red (or blood) and blond. The red varieties can synthesize and accumulate anthocyanins in both their rind and flesh to express their color, whereas the blond cultivars normally do not produce any anthocyanins in their fruits. The expression profiles of six anthocyanin biosynthetic genes (CHS, CHI, F3H, DFR, ANS, UFGT) were investigated in both blood and blond oranges and revealed that genes involved in the early steps of the anthocyanin biosynthetic pathway, such as CHS, CHI, and F3H, are expressed in juice vesicles of both uncolored and colored oranges. On the contrary, much lower expression levels were observed in the cases of DFR, ANS, and UFGT, the latter being barely detected or even totally unexpressed in blond cultivars (Navel and Ovale).[7,33] Moreover, in the pigmented varieties the anthocyanin content increases during red orange fruit ripening;[7] it is extremely variable among the sweet orange pigmented varieties[7,8] and also may vary due to genetic factors and environmental conditions such as temperature.[5,6,9,73,74]

Genetic Regulation of the Anthocyanin Biosynthesis in Pigmented Orange Fruit. As the secondary metabolites of the flavonoid pathway, anthocyanins are synthesized under the complex regulation of multiple regulatory genes at the transcriptional level. Generally, the spatial and temporal expression of structural genes is under the control of several different families of regulatory genes in plants, such as Myb, Myc (encoding basic helix−loop−helix proteins, bHLH), and WD40-like transcription factors, which also play crucial roles in the regulation of other flavonoid products, such as flavonols and proanthocyanidins.[17] These transcription factors are connected to form a ternary complex (MYB−bHLH−WD40, MBW complex) in a hierarchical network to regulate the expression of the structural genes involved in the flavonoid synthesis, such as CHI, CHS, F3H, and DFR.[17] As mentioned

DOI: 10.1021/acs.jafc.5b01123
J. Agric. Food Chem. 2015, 63, 4031−4041

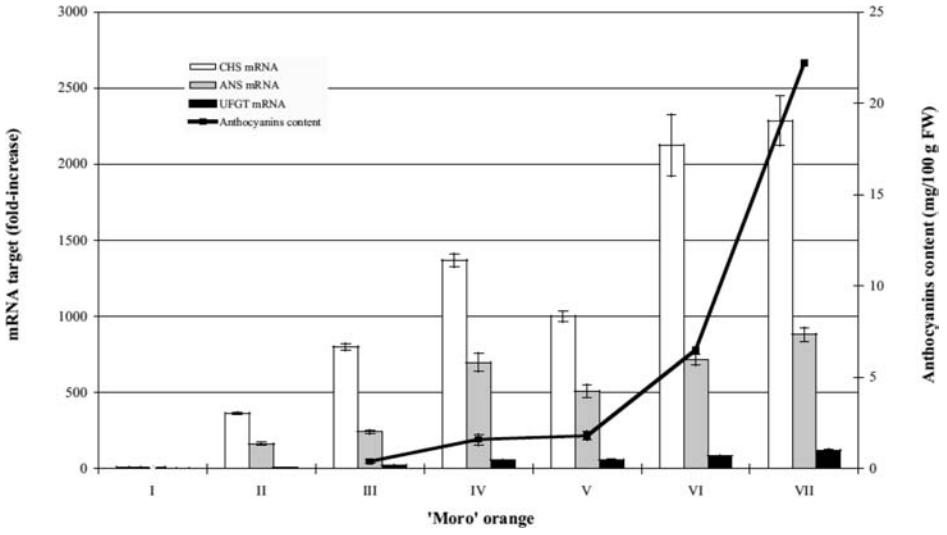

Figure 5. RT real-time PCR detection of anthocyanin biosynthetic genes and total anthocyanin content in the Moro orange flesh during fruit ripening. Fruits were collected at seven different stages, approximately every 3 weeks starting from October 19 and ending at February 21. CHS, chalcone synthase; ANS, anthocyanidin synthase; UFGT, UDP-glucose flavonid 3-*O*-glucosyl transferase. Reproduced with permission from ref 7. Copyright 2006 American Society for Horticultural Science.

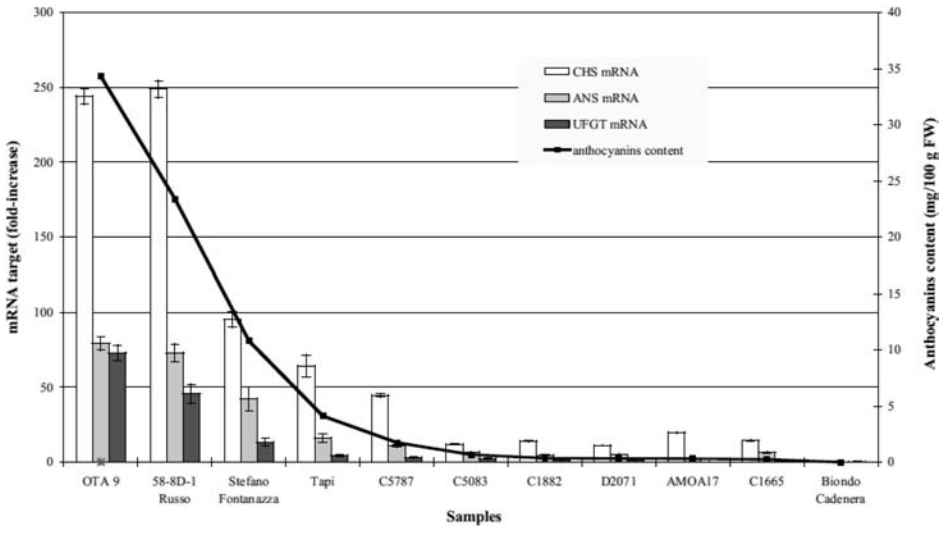

Figure 6. RT real-time PCR detection of anthocyanin biosynthetic genes and total anthocyanin content in the Tarocco Moro orange flesh in 11 genotypes harvested at the end of winter. OTA9, *C. reticulata* 'Oroval' Clementine × *C. sinensis* Tarocco; 58-8D-1-Russo, nucellar line of *C. sinensis* Moro; Stefano Fontanazza, old line of *C. sinensis* Tarocco; Tapi, nucellar line of *C. sinensis* Tarocco Arcimusa; C5787, nucellar line of *C. sinensis* Tarocco Lempso; C5083, nucellar line of *C. sinensis* Tarocco Giarretta; C1882, nucellar line of *C. sinensis* Tarocco Sciara, D2071, nucellar line of *C. sinensis* Tarocco Scirè; AMOA, poorly pigmented nucellar line of *C. sinensis* Moro; C1665, nucellar line of *C. sinensis* Tarocco Messina; Biondo Cadenera, *C. sinensis* blond orange; CHS, chalcone synthase; ANS, anthocyanidin synthase; UFGT, UDP-glucose flavonid 3-*O*-glucosyl transferase. Reproduced with permission from ref 7. Copyright 2006 American Society for Horticultural Science.

above, in blood oranges, several anthocyanin biosynthetic genes show increased expression compared with blond oranges.[33−35,73−76] Variation in pigment content or tissue specificity is largely governed by the activity of the R2R3Myb transcription factor in the complex, which has recently been isolated from blood orange and named *Ruby*.[10] The analysis of gene expression revealed that high levels of *Ruby* transcription are in the flesh and rind of blood oranges, whereas no *Ruby* expression is detectable in blond oranges, thus suggesting that a different regulatory mechanism occurs during *Ruby* transcription between blond and blood oranges.[10] The isolation and sequencing of the upstream regulatory regions of *Ruby* from both Moro (blood) and Cadenera (blond) highlighted an insertion of 501 nucleotides in Moro, 254 bp upstream of the initiating ATG in *Ruby*, compared with the otherwise identical *Ruby* promoter from the blond Cadenera orange. This insertion showed sequence similarity to the long terminal repeats (LTRs) of the Copia family of retrotransposons and included a 5 bp direct repeat, typical of LTR retroelement insertion sites.[77] The start of *Ruby* transcription mapped to an A, 551 nucleotides upstream of the initiating ATG of the *Ruby* gene. The insertion generates a TATA box 32 bp upstream of the start of transcription site within the LTR providing the regulatory sequences for initiating expression of the *Ruby* gene, whereas it is not possible to identify a TATA box in the sequence upstream of the *Ruby* gene from blond oranges.[10] The

DOI: 10.1021/acs.jafc.5b01123
J. Agric. Food Chem. 2015, 63, 4031−4041

finding that the *Cs*Myc, gene encoding the bHLH partner in the MWB complex[78] is expressed at detectable levels in both blond and blood oranges supports the hypothesis that the expression of the *Ruby* gene limits anthocyanin biosynthesis in citrus varieties.[10] Recently, a large number of *Citrus* genes belonging to a previously unidentified MYBA gene family were isolated, molecularly characterized, and functionally evaluated.[79] All of these genes were recovered by PCR amplification using primers corresponding to *Vv*MybA1 of grapevine. Transient transgene expression analysis using grapevine somatic embryos revealed that many members of two *Citrus* MYBA subgroups (named b and c) were fully functional and capable of activation anthocyanin biosynthesis in nonanthocyanic explants.[79] Noticeably, the null genes contained single-residue substitution mutations within the R2R3 repeat corresponding to the DNA binding domain. Most of these loss of function substitutions were associated with positively charged amino acids. The isolation of a large number of MYBA genes from *Citrus* suggests the existence of highly homologous regulatory genes involved in the anthocyanin pathway among taxonomically distant genera such as *Citrus* and *Vitis*.[79] Moreover, the identification of many paralogue genes able to turn on the anthocyanin biosynthesis needs to be further investigated to define their role in anthocyanin production likely related with developmental status, tissue specificity, or different color intensity.

Influence of Orange Fruit Ripening Stage and Genotype on Anthocyanin Accumulation. The amount of anthocyanins in blood oranges is strictly correlated with the fruit ripening stage as well as with transcriptional levels of the biosynthetic genes.[7] Figure 5 shows the expression profile of selected anthocyanin biosynthetic genes (CHS, ANS, and UFGT) as well as the total anthocyanin content during the Moro blood orange ripening period. The expression of CHS, ANS, and UFGT increases during the entire period, and the levels of all three transcripts appear to vary correspondingly. Total anthocyanins are undetectable at the beginning, but their levels rise from the third sampling (end of November) onward and show a sharp increase between the VI (late January) and VII samplings (mid-February). Further confirming results have been obtained by microarray analysis performed to study gene expression during blood orange ripening.[76] The custom array was hybridized using samples of the Moro (pigmented) and Cadenera (nonpigmented) cultivars, at three different ripening stages: immature phase, the halfway point of maturation (corresponding to the start of Moro pigmentation), and full ripe time. In Moro, the ripening process, which appears to be closely related to the accumulation of anthocyanins in the fruit flesh, is indeed associated with the induction of genes involved in the anthocyanin pathway.[76]

As shown in Figure 6, the anthocyanin levels might also vary depending on varieties or selections grown under the same environmental conditions ranging from 34 mg/100 g (OTA 9) to 0.25 mg/100g (Tarocco Messina). Generally, a relationship between biosynthetic gene expression and fruit flesh anthocyanin content is evident.[7]

Cold-Temperature Induction of Anthocyanin Content in Blood Orange Fruit. Activation of anthocyanin biosynthesis by cold has received more attention than other inducing environmental factors. In fact, the productivity of most commercially important *Citrus* varieties is severely affected by low temperature due to the induction of several metabolic alterations such as increased electrolyte leakage and decreased photosynthetic capacity and respiration rate.[80] The susceptibility to cold stress varies widely in the *Citrus* genus, ranging from very cold sensitive types, such as *Citrus grandis* (pummelo), to the cold-hardy *Citrus* relative *Poncirus trifoliata*. To complete the picture of the events taking place in cold-exposed *Citrus* fruits also including the pigmented varieties, Lo Piero and co-workers[33,35,74] have shown that postharvest exposure to cold induces an increase of the anthocyanin levels in the blood orange flesh. This enhancement, which may determine an 8-fold increase (from 0.5 to 7.46 mg/100g) depending on storage time, is accomplished by the up-regulation of the genes involved in the anthocyanin biosynthesis (PAL, CHS, DFR, ANS, UFGT, GST). Further transcriptome study based on the construction and analysis of a subtractive cDNA library was performed to address the overall activation of the gene expression in the blood orange [(*C. sinensis*) L. Osbeck, Tarocco Sciara] after exposure to cold stress conditions (4 °C for 77 days). Overall, the enhancement of transcripts involved in the defense mechanisms against oxidative damage, osmoregulating processes, and lipid desaturation as well as many ESTs implicated in both the primary and secondary metabolisms was observed. In particular, the results show that cold stress induces transcriptome modifications undoubtedly oriented toward the enhancement of the flavonoid biosynthesis pathway in blood oranges. They include the activation of genes directly involved in anthocyanin biosynthesis (CHS and ANS) as well as genes intervening in the metabolic pathways supplying it, such as the shikimate pathway, which yields phenylalanine.[9,74] Various functional genes and regulator genes with their target proteins play important roles in regulating low-temperature tolerance. Among low-temperature-induced genes, the dehydration responsive element binding protein (DREB)/C-repeat binding factor (CBF) genes encode key transcription factors implicated in the major transcriptional cascade that responds to cold.[81] Many abiotic-stress-inducible genes are controlled by abscisic acid (ABA), but CBFs are not, thus indicating that both ABA-dependent and ABA-independent regulatory systems are involved in cold stress responsive gene expression.[82] It is worthwhile to mention that in the cited study,[9] homologous cDNAs to CBFs have not been retrieved among the specifically cold-induced genes, suggesting that the blood orange response to cold might involve an ABA-dependent pathway.[9] Interestingly, several transcription factors have been identified for the first time as cold-responsive genes in plants.[9] In particular, a transcription factor belonging to the NAC transcription factor family was found specifically induced in blood oranges, but not in blond oranges, thus proposing it as a candidate gene involved in the signal cascade triggered in response to cold.[73] Recently, a gene encoding a NAC domain transcription factor (TF) was found to be highly up-regulated in blood-fleshed peaches when compared with non-red-fleshed peaches. This NAC transcription factor, designated BLOOD (BL), can activate the transcription of *Pp*MYB10.1, resulting in anthocyanin pigmentation in transgenic tobacco.[83] However, the cold dependency of anthocyanin production in blood oranges might also depend upon the cold induction of the retroelement controlling the *Ruby* gene expression (see Genetic Regulation of the Anthocyanin Biosynthesis in Pigmented Orange Fruit) as elevated levels of these transcripts are observed in Tarocco and Moro blood varieties following the storage of fruit in the cold.[10] Finally, by comparing the blood orange response to cold stress with those of other plant sources, such as grapefruit,[84] it seems to be similar to that of the chilling acclimated species.

DOI: 10.1021/acs.jafc.5b01123
J. Agric. Food Chem. 2015, 63, 4031−4041

Therefore, it is likely that the rise of anthocyanin levels occurring in the oranges subjected to cold stress might contribute to the control of cell osmotic potential, thus coping with the imposed stressful conditions.[9]

Other Anthocyanin Biosynthesis Induction Factors. An assortment of additional intrinsic and environmental factors has been linked to anthocyanin accumulation in several plant species as reviewed by Chalker-Scott[85] and more recently by de Pascual-Teresa and Sanchez-Ballesta.[86] Most research on anthocyanins has focused on their photoinduction by wavelengths in the UV, visible, and far-red regions. Nutrient deficiencies, especially of phosphorus (P) and nitrogen (N), commonly induce the accumulation of anthocyanin in many plant species. Also, exposure to lowered pH, methyl jasmonate, wounding, pathogen infection, and fungal elicitors may trigger a significant increase in the anthocyanin levels.[85,86] Both auxins and/or cytokinins have been shown to induce anthocyanins in cell cultures or whole plant systems, and some authors have linked gibberellins to anthocyanin production.[85] Plant hormones also affect anthocyanin biosynthesis: abscisic acid (ABA) promotes biosynthesis of anthocyanin, and poor coloration of fruit is improved by the application of ABA, which increases the anthocyanin content in both grape skin and cherry skin.[86] Ethylene has been shown to influence the biosynthesis of light-induced anthocyanin formation, improving color development and increasing anthocyanin content in apples.[86] Probably, the above-mentioned factors might have the same enhancing effect upon anthocyanin biosynthesis in pigmented orange but, as far as is known, there is no published experimental evidence confirming their role in activating the anthocyanin biosynthetic pathway. Invaluable personal observations of several researchers report that fruits on the same tree exposed to light in the top of the canopy produce more pigment than those located in a shady position of the canopy interior or that fruit that has fallen from the tree shows increased levels of these pigments. All of these observations leading to the consolidation of the physiological role of anthocyanin as a "defending molecule" in red orange fruit should be experimentally proven and lay the foundation for future work. In this respect, the antifungal activity of salicylic acid (SA) against the devastating pathogen *Penicillium digitatum*, the casual agent of green mold disease of blood oranges, has recently been investigated.[87] The authors showed that SA applications significantly decrease the postharvest decay of fruit as well as positively influence fruit quality parameters such as total soluble solid, titrable acidity, and anthocyanin content. These findings demonstrate that an increase of anthocyanin levels may be closely related to the antifungal activity triggered by SA in blood oranges.[87]

CONCLUSIONS

The importance of anthocyanins is due both to their impact on the organoleptic features of blood oranges, which may influence their technological behavior during juice extraction and processing, and to the beneficial effect on human health correlated with their consumption. The experimental work of several research groups led to greatly improved knowledge of how anthocyanins are synthesized in blood oranges as well as how this biosynthetic pathway is regulated at the transcriptional level by genetic and environmental factors, this being achieved with wide application of new biotechnological approaches such as "omics". However, there are still many aspects that need to be clarified, and it would be worthwhile to focus the next efforts on identifying the genes involved in anthocyanin modification, elucidating the mechanism of vacuole compartmentation of pigments, and defining the role of either phytohormones or biotic and abiotic factors in inducing anthocyanin accumulation.

AUTHOR INFORMATION

Corresponding Author

*E-mail: rlopiero@unict.it. Phone: +39-95-7580238.

Notes

The authors declare no competing financial interest.

ACKNOWLEDGMENTS

Thanks are due to all of the researchers who contributed to the enrichment of our knowledge on this topic.

REFERENCES

(1) Winkel-Shirley, B. Flavonoid biosynthesis. A colourful model for genetics, biochemistry, cell biology, and biotechnology. *Plant Physiol.* **2001**, *126*, 485−493.

(2) Ross, J. A.; Kasum, C. M. Dietary flavonoids: bioavailability, metabolic effects, and safety. *Annu. Rev. Nutr.* **2002**, *22*, 19−34.

(3) Amorini, A. M.; Lazzarino, G.; Galvano, F.; Tazzina, G.; Gavazzi, B.; Galvano, G. Cyanidin-3-*O*-*β*-glucopyranoside protects myocardium and erythrocytes from oxygen radical-mediated damages. *Free Radical Res.* **2003**, *37*, 453−460.

(4) Rapisarda, P.; Giuffrida, A. Anthocyanins level in Italian blood oranges. *Proc. Int. Soc. Citric.* **1992**, *3*, 1130−1133.

(5) Rapisarda, P.; Bellomo, S. E.; Intelisano, S. Storage temperature effects on blood orange fruit quality. *J. Agric. Food Chem.* **2001**, *49*, 3230−3235.

(6) Lo Piero, A. R.; Puglisi, I.; Rapisarda, P.; Petrone, G. Anthocyanins accumulation and related gene expression in red orange fruit induced by low temperature storage. *J. Agric. Food Chem.* **2005**, *53*, 9083−9088.

(7) Cotroneo, P. S.; Russo, M. P.; Ciuni, M.; Reforgiato Recupero, G.; Lo Piero, A. R. Quantitative real-time RT-PCR profiling of anthocyanin biosynthetic genes during orange fruit ripening. *J. Am. Soc. Hortic. Sci.* **2006**, *131*, 537−543.

(8) Rapisarda, P.; Lo Bianco, M.; Pannuzzo, P.; Timpanaro, N. Effect of cold storage on vitamin C, phenolic and antioxidant activity of five type orange genotypes [*Citrus sinensis* (L.) Osbeck]. *Postharvest Biol. Technol.* **2008**, *49*, 348−354.

(9) Crifò', T.; Puglisi, I.; Petrone, G.; Reforgiato Recupero, G.; Lo Piero, A. R. Expression analysis in response to low temperature stress in blood oranges: implication of the flavonoid biosynthetic pathway. *Gene* **2011**, *476*, 1−9.

(10) Butelli, E.; Licciardello, C.; Zhang, Y.; Liu, J.; Mackay, S.; Bailey, P.; Reforgiato Recupero, G.; Martin, C. Retrotransposons control fruit-specific, cold-dependent accumulation of anthocyanins in blood oranges. *Plant Cell* **2012**, *24*, 1242−1255.

(11) Zarbà, A. S.; Pulvirenti, G. The consumption of Sicilian red oranges: implications for firms involved in commercialization. *J. Bus. Chem.* **2006**, *3*, 22−41.

(12) Holmes, E. M. The origin of the Maltese blood orange. *Pharm. J. Citrus* **1924**, 614−615.

(13) Hodgson, R. W. History, world distribution, botany and varieties. In *The Citrus Industry*; Reuther, W., Webber, H. J., Batchelor, L. D., Eds.; University of California: Berkeley, CA, USA, 1967; Vol. I, pp 431−591.

(14) Mazza, G. Anthocyanins in grapes and grape products. *Crit. Rev. Food Sci. Nutr.* **1995**, *35*, 341−371.

(15) Bordignon-Luiz, M. T.; Gauche, C.; Gris, E. F.; Falcão, L. D. Colour stability of anthocyanins from Isabel grapes (*Vitis lambrusca* L.) in model systems. *Food Sci. Technol.* **2007**, *40*, 594−599.

(16) Dixon, R. A.; Steele, C. L. Flavonoids and isoflavonoids − a gold mine for metabolic engineering. *Trends Plant Sci.* **1999**, *4*, 394−400.

DOI: 10.1021/acs.jafc.5b01123
J. Agric. Food Chem. 2015, 63, 4031−4041

(17) He, F.; Mu, L.; Yan, G.; Liang, N.; Pan, Q.; Wang, J.; Reeves, M. J.; Duan, C. Biosynthesis of anthocyanins and their regulation in colored grapes. *Molecules* **2010**, *15*, 9057−9091.
(18) Andersen, Ø. M.; Jordheim, M. The anthocyanins. In *Flavonoids: Chemistry, Biochemistry, and Applications*; Anderson, Ø. M., Markham, K. R., Eds.; CRC Press: Boca Raton, FL, USA, 2006; pp 471−553.
(19) Maccarone, E.; Maccarone, A.; Perrini, G.; Rapisarda, P. Anthocyanins of the Moro orange juice. *Ann. Chim.* **1983**, *73*, 533−539.
(20) Dugo, P.; Mondello, L.; Morabito, D.; Dugo, G. Characterization of the anthocyanin fraction of sicilian blood orange juice by micro-HPLC-ESI/MS. *J. Agric. Food Chem.* **2003**, *51*, 1173−1176.
(21) Chandler, B. V. Anthocyanins of blood oranges. *Nature* **1958**, *182*, 933.
(22) Maccarone, E.; Maccarone, A.; Rapisarda, P. Acylated anthocyanins from oranges. *Ann. Chim.* **1985**, *75*, 79−86.
(23) Maccarone, E.; Rapisarda, P.; Fanella, F.; Arena, E.; Mondello, L. Cyanidin-3-(6″-malonyl)-*β*-glucoside. One of the major anthocyanins in blood orange juice. *Ital. J. Food Sci.* **1998**, *10*, 367−372.
(24) Lee, H. S. Characterization of major anthocyanins and the color of red-fleshed budd blood orange (*Citrus sinensis*). *J. Agric. Food Chem.* **2002**, *50*, 1243−1246.
(25) Hillebrand, S.; Schwarz, M.; Winterhalter, P. Characterization of anthocyanins and pyranoanthocyanins from blood orange [*Citrus sinensis* (L.) Osbeck] juice. *J. Agric. Food Chem.* **2004**, *52*, 7331−7338.
(26) Goodrich, J.; Carpenter, R.; Cohen, E. S. A common gene regulates pigmentation pattern in diverse plant species. *Cell* **1992**, *68*, 955−964.
(27) Dooner, H. K.; Robbins, T. P.; Jorgensen, R. A. Genetic and developmental control of anthocyanin biosynthesis. *Annu. Rev. Genet.* **1991**, *25*, 173−199.
(28) Quattrocchio, F.; Wing, J. F.; Leppen, H. T. C.; Mol, J. N. M.; Koes, R. E. Regulatory genes controlling anthocyanin pigmentation are functionally conserved among plant species and have distinct sets of target genes. *Plant Cell* **1993**, *5*, 1497−1512.
(29) Sparvoli, F.; Martin, C.; Scienza, A.; Gavazzi, G.; Tonelli, C. Cloning and molecular analysis of structural genes involved in flavonoid and stilbene biosynthesis in grape (*V. vinifera*). *Plant Mol. Biol.* **1994**, *24*, 743−755.
(30) Sanchez-Ballesta, M. T.; Lafuente, M. T.; Zacarias, L.; Granell, A. Involvement of phenylalanine ammonia-lyase in the response of Fortune mandarin fruits to cold temperature. *Physiol. Plant.* **2000**, *4*, 382−389.
(31) Moriguchi, T.; Kita, M.; Tomono, Y.; Endo-Inagaki, T.; Omura, M. One type of chalcone synthase gene expressed during embryogenesis regulates the flavonoid accumulation in citrus cell cultures. *Plant Cell Physiol.* **1999**, *40*, 651−655.
(32) Moriguchi, T.; Kita, M.; Tomono, Y.; Endo-Inagaki, T.; Omura, M. Gene expression in flavonoid biosynthesis: correlation with flavonoid accumulation in developing citrus fruit. *Physiol. Plant.* **2001**, *111*, 66−74.
(33) Lo Piero, A. R.; Consoli, A.; Puglisi, I.; Orestano, G.; Reforgiato Recupero, G.; Petrone, G. Anthocyaninless cultivars of sweet orange lack to express the UDP-glucose flavonoid 3-*O*-glucosyl transferase. *J. Plant Biochem. Biotechnol.* **2005**, *14*, 1−6.
(34) Lo Piero, A. R.; Puglisi, I.; Petrone, G. Gene characterization, analysis of expression and in vitro synthesis of dihydroflavonol 4-reductase from [*Citrus sinensis* (L.) Osbeck]. *Phytochemistry* **2006**, *67*, 684−695.
(35) Lo Piero, A. R.; Puglisi, I.; Petrone, G. Gene isolation, analysis of expression and in vitro synthesis of a glutathione *S*-transferase from orange fruit. [*Citrus sinensis* L. (Osbeck)]. *J. Agric. Food Chem.* **2006**, *54*, 9227−9233.
(36) Springob, K.; Nakajima, J.; Yamazaki, M.; Saito, K. Recent advances in the biosynthesis and accumulation of anthocyanins. *Nat. Prod. Rep.* **2003**, *20*, 288−303.
(37) Boava, L. P.; Cristofani-Yaly, M.; Stuart, R. M.; Machado, M. A. Expression of defence-related genes in response to mechanical wounding and *Phytophthora parasitica* infection in *Poncirus trifoliata* and *Citrus sunki*. *Physiol. Mol. Plant Pathol.* **2011**, *76*, 119−125.
(38) Dixon, R. A.; Palva, N. L. Stress-induced phenylpropanoid metabolism. *Plant Cell* **1995**, *7*, 1085−1097.
(39) Marcos, J. F.; González-Candelas, L.; Zacarías, L. Involvement of ethylene biosynthesis and perception in susceptibility of citrus fruits to *Penicillium digitatum* infection and the accumulation of defence-related mRNAs. *J. Exp. Bot.* **2005**, *56*, 2183−2193.
(40) Lucheta, A. R.; Silva-Pinhati, A. C. O.; Basílio-Palmieri, A. C.; Berger, I. J.; Freitas-Astúa, J.; Cristofani, M. An *in silico* analysis of the key genes involved in flavonoid biosynthesis in *Citrus sinensis*. *Genet. Mol. Biol.* **2007**, *30* (3 (Suppl.)), 819−831.
(41) Betz, C.; McCollum, T. G.; Mayer, R. T. Differential expression of two cinnamate 4-hydroxylase genes in 'Valencia' orange (*Citrus sinensis* Osbeck). *Plant Mol. Biol.* **2001**, *46*, 741−748.
(42) Holton, T. A.; Cornish, E. C. Genetics and biochemistry of anthocyanin biosynthesis. *Plant Cell* **1995**, *7*, 1071−1083.
(43) Muccilli, V.; Liccardello, C.; Fontanini, D.; Russo, M. P.; Cunsolo, V.; Saletti, R.; Reforgiato Recupero, G.; Foti, S. Proteome analysis of *Citrus sinensis* L. (Osbeck) flesh at ripening time. *J. Proteomics* **2009**, *73*, 134−152.
(44) Doostdar, H.; Shapiro, J. P.; Niedz, R.; Burke, M. D.; McCollum, T. G.; Mcdonald, R. E.; Mayer, R. T. A cytochrome p450 mediated naringenin 3′-hydroxylase from sweet orange cell cultures. *Plant Cell Physiol.* **1995**, *36*, 69−77.
(45) Grotewold, E.; Drummond, B. J.; Bowen, B.; Peterson, T. The myb homologous *p* gene controls phlobaphene pigmentation in maize floral organs by directly activating a flavonoid biosynthetic gene subset. *Cell* **1994**, *76*, 543−553.
(46) Gollop, R.; Even, S.; Colova-Tsolova, V.; Peri, A. Expression of the grape dihydroflavonol 4-reductase gene and analysis of its promoter region. *J. Exp. Bot.* **2002**, *53*, 1397−1409.
(47) Yanagisawa, S.; Schmidt, R. J. Diversity and similarity among recognition sequences of Dof transcription factors. *Plant J.* **1999**, *17*, 209−214.
(48) van der Meer, I. M.; Brouwer, M.; Spelt, C. E.; Mol, J. N. M.; Stuitje, A. R. The TACpyAT repeats in the chalcone synthase promoter of *Petunia hybrida* act as a dominant negative cis-acting module in the control of organ specific expression. *Plant J.* **1992**, *2*, 525−535.
(49) Lawton, M. A.; Dean, S. M.; Dron, M.; Kooter, J. M.; Kragh, K. M.; Harrison, M. J.; Yu, L.; Tanguay, L.; Dixon, R. A.; Lamb, C. J. Silencer region of a chalcone synthase promoter contains multiple binding sites for a factor, SBF-1, closely related to GT-1. *Plant Mol. Biol.* **1991**, *16*, 235−249.
(50) D'Auria, J. C. Acyltransferases in plants: a good time to be BAHD. *Curr. Opin. Plant Biol.* **2006**, *9*, 331−340.
(51) Winkel-Shirley, B. Evidence for enzyme complexes in the phenyl propanoid and flavonoid pathways. *Physiol. Plant.* **1999**, *107*, 142−149.
(52) Winkel, B. S. J. Metabolic channelling in plants. *Annu. Rev. Plant Biol.* **2004**, *55*, 85−107.
(53) Grotewold, E. The challenges of moving chemicals within and out of cells: insights into the transport of plant natural products. *Planta* **2004**, *219*, 906−909.
(54) Maars, K. A.; Alfenito, M. R.; Lloyd, A. M.; Walbot, V. A glutathione *S*-transferase involved in vacuolar transfer encoded by the maize gene bronze2. *Nature* **1995**, *375*, 397−400.
(55) Markham, K. R.; Gould, K. S.; Winefield, C. S.; Mitchell, K. A.; Bloor, S. J.; Boase, M. R. Anthocyanic vacuolar inclusions − their nature and significance in flower colouration. *Phytochemistry* **2000**, *55*, 327−336.
(56) Kitamura, S. Transport of flavonoids: from cytosolic synthesis to vacuolar accumulation. In *The Science of Flavonoids*; Grotewold, E., Ed.; Springer Science: New York, 2006; pp 123−146.
(57) Grotewold, E.; Davies, K. Trafficking and sequestration of anthocyanins. *Nat. Prod. Communs.* **2008**, *3*, 1251−1258.
(58) Zhao, J.; Dixon, R. The 'ns' and 'outs' of flavonoid transport. *Trends Plant Sci.* **2009**, *15*, 72−80.

DOI: 10.1021/acs.jafc.5b01123
J. Agric. Food Chem. 2015, 63, 4031−4041

(59) Alfenito, M.; Souer, E.; Goodman, C. D.; Buell, R.; Mol, J.; Koes, R.; Walbot, V. Functional complementation of anthocyanin sequestration in the vacuole by widely divergent glutathione *S*-transferase. *Plant Cell* **1998**, *10*, 1135−1149.
(60) Kitamura, S.; Shikazono, N.; Tanaka, A. TRANSPARENT TESTA 19 is involved in the accumulation of both anthocyanins and proanthocyanidins in *Arabidopsis*. *Plant J.* **2004**, *37*, 104−114.
(61) Mueller, L. A.; Goodman, C. D.; Silady, R. A.; Walbot, V. AN9, a petunia glutathione *S*-transferase required for anthocyanin sequestration, is a flavonoid binding protein. *Plant Physiol.* **2000**, *123*, 1561−1570.
(62) Mueller, L. A.; Walbot, V. Models for vacuolar sequestration of anthocyanins. In *Regulation of Phytochemicals by Molecular Techniques*; Romeo, J. T., Saunders, J. A., Matthews, B. F., Eds.; Pergamon: New York, 2001; Vol. 35, pp 297−312.
(63) Goodman, C. D.; Casati, P.; Walbot, V. A multidrug resistance associated protein involved in anthocyanin transport in *Zea mays*. *Plant Cell* **2004**, *16*, 1812−1826.
(64) Gomez, C.; Conejero, G.; Torregrosa, L.; Cheynier, V.; Terrier, N.; Ageorges, A. In vivo grapevine anthocyanin involves vesicle-mediated trafficking and the contribution of anthoMATE transporters and GST. *Plant J.* **2011**, *67*, 960−970.
(65) Xu, Q.; Chen, L.; Ruan, X.; Chen, D.; Zhu, A.; Chen, C.; Bertrand, D.; Jiao, W.; Hao, B.; Lyon, M. P.; Chen, J.; Gao, S.; Xing, F.; Lan, F.; Chang, J.; Ge, X.; Lei, Y.; Hu, Q.; Miao, Y.; Wang, L.; Xiao, X.; Biswas, M. K.; Zeng, W.; Guo, F.; Cao, H.; Yang, X.; Xu, X.; Cheng, Y.; Xu, J.; Liu, J.; Luo, O. J.; Tang, Z.; Guo, W.; Kuang, H.; Zhang, H.; Roose, M. L.; Nagarajan, N.; Deng, X.; Ruan, Y. The draft genome of sweet orange (*Citrus sinensis*). *Nat. Genet.* **2013**, *45*, 59−68.
(66) Oren-Shamir, M. Does anthocyanin degradation play a significant role in determining pigment concentration in plants? *Plant Sci.* **2009**, *177*, 310−316.
(67) Barbagallo, R. N.; Palmeri, R.; Fabiano, S.; Rapisarda, P.; Spagna, G. Characteristic of β-glucosidase from sicilian blood oranges in relation to anthocyanin degradation. *Enzyme Microb. Technol.* **2007**, *41*, 570−575.
(68) Arena, E.; Fallico, B.; Maccarone, E. Thermal damage in blood orange juice: kinetics of 5-hydroxymethyl-2-furancarboxaldehyde formation. *Int. J. Food Sci. Technol.* **2001**, *36*, 145−151.
(69) Krifi, B.; Chouteau, F.; Boudrant, J.; Metche, M. Degradation of anthocyanins from blood orange juices. *Int. J. Food Sci. Technol.* **2000**, *35*, 275−283.
(70) Liu, L.; Cao, S.; Pan, S. Thermal degradation kinetics of three kinds of representative anthocyanins obtained from blood orange. *Agric. Sci. China* **2011**, *10*, 642−649.
(71) Cao, S.; Liu, L.; Lu, Q.; Xu, Y.; Pan, S.; Wang, K. Integrated effects of ascorbic acid, flavonoids and sugars on thermal degradation of anthocyanins in blood orange juice. *Eur. Food Res. Technol.* **2009**, *228*, 975−983.
(72) Tiwari, B. K.; O'Donnell, C. P.; Cullen, P. J. Effect of non thermal processing technologies on the anthocyanin content of fruit juices. *Trends Food Sci. Technol.* **2009**, *20*, 137−145.
(73) Crifò', T.; Petrone, G.; Lo Cicero, L.; Lo Piero, A. R. Storage temperature and time influence the anthocyanin content and the level of transcript related to their biosynthesis in blood oranges. *J. Agric. Food Chem.* **2012**, *60*, 476−481.
(74) Lo Piero, A. R.; Lo Cicero, L.; Puglisi, I. The metabolic fate of citric acid as affected by cold storage in blood oranges. *J. Plant Biochem. Biotechnol.* **2014**, *23*, 161−166.
(75) Licciardello, C.; Russo, M. P.; Vale', G.; Reforgiato Recupero, G. Identification of differentially expressed genes in the flesh of blood and common oranges. *Tree Genet. Genomes* **2008**, *4*, 315−331.
(76) Bernardi, J.; Licciardello, C.; Russo, M. P.; Chiusano, M. L.; Carletti, G.; Reforgiato Recupero, G.; Marocco, A. Use of a custom array to study differentially expressed genes during blood orange (*Citrus sinensis* L. Osbeck) ripening. *J. Plant Physiol.* **2010**, *167*, 301−310.
(77) Kim, J. M.; Vanguri, S.; Boeke, J. D.; Gabriel, A.; Voytas, D. F. Transposable elements and genome organization: a comprehensive survey of retrotransposons revealed by the complete *Saccharomyces cerevisiae* genome sequence. *Genome Res.* **1998**, *8*, 464−478.
(78) Cultrone, A.; Controneo, P. S.; Reforgiato Recupero, G. Cloning and molecular characterisation of R2R3-MYB and bHLHMYC transcription factors from *Citrus sinensis*. *Tree Genet. Genomes* **2010**, *6*, 101−112.
(79) Li, Z. T.; Gmitter, F. G.; Grosser, J. W.; Chen, C.; Gray, D. J. Isolation and characterization of a novel anthocyanin-promoting MYBA gene family in Citrus. *Tree Genet. Genomes* **2012**, *8*, 675−685.
(80) Allen, D.; Ort, D. Impacts of chilling temperatures on photosynthesis in warm climate plants. *Trends Plant Sci.* **2001**, *6*, 36−42.
(81) Shinozaki, K.; Yamaguchi-Shinozaki, K. Molecular responses to dehydration and low temperature: differences and cross-talk between two stress signalling pathways. *Curr. Opin. Plant Biol.* **2000**, *3*, 217e223.
(82) Chinnusamy, V.; Zhu, J.; Zhu, J. K. Cold stress regulation of gene expression in plants. *Trends Plant Sci.* **2007**, *12*, 444−451.
(83) Zhou, H.; Lin-Wang, K.; Wang, H.; Gu, C.; Dare, A. P.; Espley, R. V.; He, H.; Allan, A. C.; Han, Y. Molecular genetics of blood-fleshed peach reveals activation of anthocyanin biosynthesis by NAC transcription factors. *Plant J.* **2015**, *82*, 105−121.
(84) Maul, P.; McCollum, G. T.; Popp, M.; Guy, C. L.; Porat, R. Transcriptome profiling of grapefruit flavedo following exposure to low temperature and conditioning treatments uncovers principal molecular components involved in chilling tolerance and susceptibility. *Plant, Cell Environ.* **2008**, *31*, 752−768.
(85) Chalker-Scott, L. Environmental significance of anthocyanins in plant stress responses. *Photochem. Photobiol.* **1999**, *70*, 1−9.
(86) de Pascual-Teresa, S.; Sanchez-Ballesta, M. T. Anthocyanins: from plant to health. *Phytochem. Rev.* **2008**, *7*, 281−299.
(87) Aminifard, M. H.; Mohammadi, S.; Fatemi, H. Inhibition of green mould in blood orange (*Citrus sinensis* var. Moro) with salicylic acid treatment. *Arch. Phytopathol. Plant Prot.* **2013**, *6*, 695−703.

DOI: 10.1021/acs.jafc.5b01123
J. Agric. Food Chem. 2015, 63, 4031−4041

and southern populations of *Helianthus maximiliani*.[13] For cultivated material, 30 publicly available inbreds were used, 15 each of maintainer (female) and restorer (male) sunflower lines. Although female lines used to produce hybrids differ from the maintainer lines by having male-sterile cytoplasm (CMS), they are considered equivalent in their nuclear genetic material. Furthermore, the use of CMS lines is likely problematic for sampling terpenoids in floral glandular trichomes, because cytoplasmic male sterility in sunflowers often produces significant deformities of florets. Finally, a group of 15 commercial sunflower hybrids was included. Commercial lines included five entries each from three commercial seed companies; the hybrids are not specifically identified to maintain anonymity of companies donating seed. However, the identities of the other 45 entries are available in Table 2. Seed of the identified entries may be obtained either from the USDA National Plant Germplasm System (for all wild entries) or the USDA Sunflower and Plant Biology Research Unit (for inbred lines) in Fargo, ND, USA.

Because pollinators may remove glandular trichomes from blooming sunflowers,[14] florets collected in 2012 were sampled just prior to anthesis. For each entry, five florets were carefully removed from each of three plants. After the corollas were removed from the florets (exposing the glandular trichomes), each group of five florets was stored and allowed to dry under refrigeration until analysis.

Sesquiterpene Lactone Identification and Quantification. To purify sesquiterpene lactones, air-dried wild or cultivated florets (2−6 g) were vortexed in dichloromethane (DCM, 10 mL/g). The solvent was filtered through a cotton plug and evaporated under a stream of nitrogen at 30 °C. Dried residue was dissolved in 1.0 mL of methanol (MeOH), vortexed, and centrifuged at 13000 rpm for 2 min. Distilled water (H_2O) was added to the supernatant to result in a MeOH/H_2O ratio of 25:75. Aliquots (1.0 mL) were injected onto a semipreparative HPLC column (10 × 250 mm Hypersil ODS, 5 μm) and eluted with acetonitrile (ACN)/H_2O (25:75) at 5 mL/min at 40 °C. Peaks were detected by UV at 225 nm. Individual peak fractions were collected and placed in a −80 °C freezer until lyophilized.

Compound identification was performed by means of NMR spectroscopic experiments and data comparison with authentic references. ^{1}H NMR measurements were conducted in a Varian Unity *Inova* spectrometer at 500 MHz. ^{1}H chemical shifts were referenced to residual solvent signals at $\delta_{H/C}$ 7.27 ($CDCl_3$) or 3.35 (CD_3OD), respectively. The following compounds were identified (numbered according to HPLC fractionation in order of decreasing polarity) according to signal identity with data previously reported in references noted:

1, argophyllin B, and **3**, argophyllin A[15]
2, 1,2-anhydrido-4,5-dihydroniveusin A[16]
4, 15-hydroxy-3-dehydrodesoxyfruticin[1]
6, argophyllone B[17]
7, niveusin B, and **8**, niveusin C[18]
9, haageanolide[19]
10, xanthomicrol (5, 4′-dihydroxy-6,7,8-trimethoxyflavone)[20]

An additional compound was identical in most ^{1}H NMR signals with argophyllone B, except for the side-chain signals (H-3′, H-4′, H-5′), which indicated an ester residue at C-8 with tiglic acid instead of angelic acid. This structure appears to be previously undescribed and is described here as *argophyllone B tiglate* (**5**): ^{1}H NMR (500 MHz, $CDCl_3$) δ 6.83 (1H q, H-3′), 6.36 (1H d, J = 1.0 Hz, H-13a), 5.83 (1H dd, J = 1.4 Hz, H-13b), 5.19 (1H t, J = 3.5 Hz, H-8), 4.60 (1H dd, J = 11.5, 3.1 Hz, H-6), 3.88 (1H dd, J = 9.5, 8.7 Hz, H-15a), 3.70 (1H dd, J = 9.5, 5.0 Hz, H-15b), 3.39 (1H dd, J = 9.6, 5.6 Hz, H-1), 3.30 (1H dd, J = 14.5, 9.6 Hz, H-2a), 3.21 (1H m, H-4), 3.06 (1H bs, H-7), 2.75 (1H dd, J = 15.2, 3.4 Hz, H-9a), 2.37 (1H dd, J = 14.4, 9.8 Hz, H-5a), 2.25 (1H dd, H-2b) 1.92 (1H m, H-5b), 1.80 (3H dq, H-4′), 1.79 (3H s, H-5′), 1.40 (3H s, H-14), 1.37 (1 H dd, J = 15.0, 3.2 Hz, H-9b).

Relative quantification of sesquiterpene lactones was accomplished by analyzing three replicate samples from each of the 60 germplasm entries. For each sample, five air-dried florets were vortexed in 0.5 mL of DCM. After 5 min, the samples were vortexed again, and the solvent was pipetted into a microcentrifuge tube and evaporated under a stream of nitrogen at 30 °C. The residue was dissolved by vortexing in 0.2 mL of MeOH. After centrifuging at 13000 rpm for 2 min, the sample was transferred to an autosampler vial for HPLC analysis. Before injection, 0.8 mL of water containing 0.010 mg/mL 2,5-dimethylphenol (2,5-DMP) internal standard was added to the sample vial and mixed using the autosampler. From the 1.0 mL mixed in each sample vial, 0.2 mL was injected onto an analytical column (4.6 × 250 mm Hypersil ODS, 5 μm) and eluted with ACN/H_2O (25:75) at 1 mL/min at 40 °C. Peaks were monitored at 225, 254, and 265 nm. A representative chromatogram showing UV absorbance at 225 nm for a wild *H. annuus* is included as Figure S1 of the Supporting Information.

Insect Assay. An assay with sunflower moth larvae was used to compare larval development upon exposure to mixed and pure extracts of sesquiterpene lactones found in *H. annuus*. Previous tests of biological activity of sesquiterpene lactones and diterpene acids have incorporated a known percentage of tested compounds into artificial diet on a dry mass basis.[4,7] However, because glandular trichomes are found on the outer surface of florets, applying sesquiterpene lactones onto the surface of an artificial diet may more closely resemble how sunflower moth larvae are normally exposed to the contents of glandular trichomes.

Florets from wild (PI 435430) and cultivated (HA 89) entries were collected from sunflower heads protected from pollinators by enclosure in mesh bags. Mixed extracts and pure sesquiterpene lactones were obtained from known numbers of florets as previously described. Each mixed extract or pure compound was dissolved in 600 μL of methanol, after which a 25 μL aliquot was applied to each of 24 wells containing 1.5 mL of a wheat germ-based artificial diet.[21] Treatments included mixed extracts of PI 435430 or HA 89, pure argophyllone B (**6**) or 15-hydroxy-3-dehydrodesoxyfruticin (**4**), and methanol or untreated controls. On the basis of scanning electron micrographs, the surface area of the wells used for the insect assay is approximately 60 times the area over which glands are present on a single *H. annuus* floret tip. Consequently, expressing the amount of sesquiterpene lactone in diet assays as floret-equivalents (60 floret-equivalents = estimated natural exposure) is an area-to-area conversion that incorporates the natural variation in *H. annuus* glandular trichome number.[9] At least 30 min after application of treatments, two newly hatched sunflower moth larvae were placed into each well, and clear adhesive lids were used to contain the larvae. After 7 days, each well was scored for larval mortality; for all larvae still alive at 7 days, mass was also measured.

Data Analysis. Analyses were performed using JMP and SAS software.[22,23] Because relationships between peak area (UV absorption) and concentration (or mass) are not established for any of the compounds, mean peak areas (a relative measure) for sesquiterpene lactones were used for statistical analyses. To assess possible relationships between the seven major sesquiterpene lactones, simple and partial correlations (accounting for glandular trichome density; from ref 9) were calculated. To determine whether significant differences in sesquiterpene lactone composition exist among *H. annuus* germplasm types, quadratic discriminant function analysis was used, which allowed for differing covariance among germplasm types. Variables for inclusion on the discriminant function analysis were chosen by forward stepwise selection ($P < 0.05$ for entry).

To test whether mixed or pure sesquiterpene lactone extracts influenced larval mass at 7 days, a single-factor analysis of variance was used for the seven treatments (five extracts and two controls); infestation date (occurring on two consecutive days) was used as a random blocking effect. Exclusion of outliers (mass more than three deviations above mean of treatment; <2% of observations) produced data with statistically equal variance over treatments, allowing analysis without need for transformation. Differences in larval mass among treatments were assessed using t tests incorporating a Bonferroni correction. The effect of extracts on larval mortality was tested using a Wald Chi-Square test; differences relative to the untreated control were established using 95% confidence limits for the odds ratio (= relative likelihood of mortality).

DOI: 10.1021/acs.jafc.5b00362
J. Agric. Food Chem. 2015, 63, 4042−4049

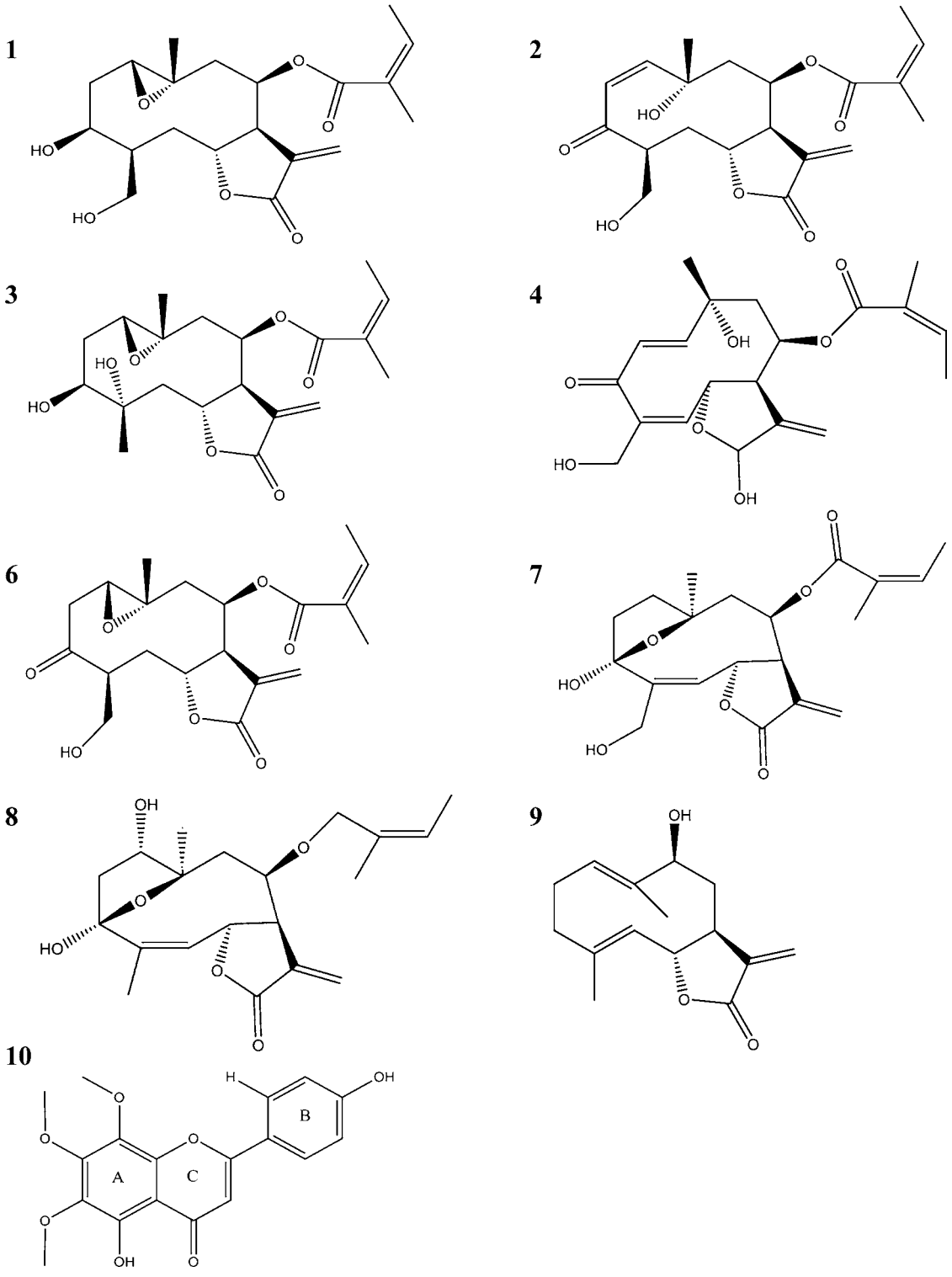

Figure 1. Structures of compounds **1**−**4** and **6**−**10** extracted from sunflower florets. All except **10** are sesquiterpene lactones.

RESULTS AND DISCUSSION

Correlations among Sesquiterpene Lactones and Number of Glandular Trichomes. Among the 10 peaks identified from *H. annuus* floret samples (Figure 1), seven previously identified sesquiterpene lactones were generally present in amounts sufficient for statistical comparison. Significant correlations among these compounds were common, but in some cases probably incidental, as all seven major peaks were also positively correlated with the estimated density of glandular trichomes. Using partial correlations to account for the effect of glandular trichome number, some strong associations remain; correlations with argophyllone B (**6**) (likely previously identified as 1-methoxy-4,5-dihydroniveusin A),[16] the most prominent peak in wild *H. annuus*, accounted for most of the variation in argophyllin B (**1**), 1,2-anhydrido-4,5-dihydro-niveusin A (**2**), and argophyllin A (**3**) (r = 0.77−0.97; Table 1). The remaining major peaks, 15-hydroxy-3-dehydrodesoxyfruticin (**4**), niveusin B (**7**), and

DOI: 10.1021/acs.jafc.5b00362
J. Agric. Food Chem. 2015, 63, 4042−4049

Table 1. Simple and Partial Correlation Coefficients (r) for Mean Peak Areas of Sesquiterpene Lactones from Wild and Cultivated *H. annuus* (n = 60)[a]

	argophyllin B	1,2-anhydrido-4,5-dihydro-niveusin A	argophyllin A	15-hydroxy-3-dehydrodesoxyfruticin	argophyllone B	niveusin B	haageanolide
glandular trichomes per floret (n)	0.62*	0.44*	0.42*	0.63*	0.48*	0.53*	0.33*
argophyllin B		0.85*	0.71*	0.32*	0.82*	0.45*	0.04
1,2-anhydrido-4,5-dihydro-niveusin A	0.82*		0.85*	0.19	0.97*	0.29*	−0.09
argophyllin A	0.63*	0.81*		0.11	0.84*	0.33*	−0.06
15-hydroxy-3-dehydrodesoxyfruticin	−0.11	−0.12	−0.22		0.28*	0.42*	0.17
argophyllone B	0.77*	0.97*	0.79*	−0.03		0.32*	−0.07
niveusin B	0.19	0.08	0.14	0.13	0.10		0.15
haageanolide	−0.22	−0.27*	−0.23	−0.05	−0.27*	−0.03	

[a]Correlations with estimated glandular trichome number (from Prasifka, 2014) also provided for comparison. Sesquiterpene lactone pairs below the diagonal show partial correlation coefficients where the effect of correlations with glandular trichome number is removed. Asterisks (*) indicate significant ($P < 0.05$) correlation.

haageanolide (**9**), showed low ($r < 0.30$) or no significant partial correlations with other sesquiterpene lactones. Also detected, but excluded because of their small, inconsistent peaks (at 225, 254, and 265 nm), were niveusin C (**8**) and argophyllone B tiglate (**5**). Xanthomicrol (**10**) (5,4′-dihydroxy-6,7,8-trimethoxyflavone)[20] and another unknown flavonoid were detected in samples but excluded as outside the intended scope of our investigation.

Differences in Sesquiterpene Lactone Composition among *H. annuus* Types. Discriminant function analysis showed that relative amounts of sesquiterpene lactones (Table 2) can be used to distinguish between wild and cultivated *H. annuus* and also between some groups of cultivated sunflower germplasm. The three latent variables used to distinguish among the sample types primarily represent argophyllone B (**6**) (standardized canonical loading = 0.99), niveusin B (**7**) (standardized canonical loading = 1.07), and 15-hydroxy-3-dehydrodesoxyfruticin (**4**) (standardized canonical loading = 0.85). Discrimination among the germplasm types based on the first two canonical variables is shown in Figure 2. Redundancy with argophyllone B (**6**) likely eliminated argophyllin B (**1**), 1,2-anhydrido-4,5-dihydro-niveusin A (**2**), and argophyllin A (**3**) from selection by the discriminant function analysis; a common precursor, possibly costunolide,[24] is one explanation for the strong correlations and is supported by the very similar structures of all four compounds. The final major peak, haageanolide (**9**), may not be useful for discrimination because of its consistency; it was present in all samples and showed relatively little variation across the 60 entries. The reason for the consistency of haageanolide (**9**) is unclear, but may be because it differs from the others in the presence of C-9 (rather than C-8) hydroxylation; whereas the C-8 hydroxylated derivatives of costunolide are subsequently processed by additional specific enzymes (e.g., formation of the side chain esters and P450 modulated oxidations at C-3, C-15) which can be regulated individually, haageanolide is not further processed and may accumulate as a side product of the early stages of sesquiterpene lactone biosynthesis.

On the basis of chemical composition, assignment to a germplasm group was correct for 75% of entries versus a random expectation of 25% over all 60 entries. Most errors in classification were in the maintainer group, for which 11 of 15 entries were incorrectly assigned to one of the other three groups (Table 3). The higher variability in sesquiterpene lactone composition for maintainer lines (used to produce female parents for hybrid sunflowers) could reflect a difference in the diversity of germplasm relative to the restorer group (male parents) or linkage of genes responsible for sesquiterpene lactone production to traits important in the restorer group (e.g., branching or fertility restoration).[25] Although wild *H. annuus* entries were generally distinct from cultivated entries (i.e., with much greater amounts of several compounds), the fact that some maintainer lines were incorrectly assigned to the wild group (and vice versa) indicates that some of the cultivated inbred lines may retain chemical defenses similar to those of wild sunflowers.

Variability in sesquiterpene lactone content has been assessed previously for some *Helianthus* spp. Sesquiterpene lactones extracted from both leaves and florets have been used to characterize intraspecific variation because the contents of capitate glandular trichomes on both tissue types are strongly correlated. Evaluations of leaves and flowers of the wild species, *H. maximiliani*, have shown considerable intraspecific variation, which has been characterized as the presence of distinct chemical races.[13,26,27] On the other hand, within *H. annuus*, an evaluation of sesquiterpene lactones from leaves and florets of 25 accessions of wild sunflowers found few qualitative differences, but significant quantitative variation.[11] Assessment of several ornamental *H. annuus* species showed a similar pattern of low qualitative and high quantitative variation in extracts from leaf tissue.[28] A recent evaluation of sesquiterpene lactones from leaves of one wild and one cultivated (HA 89) *H. annuus* entries showed primarily quantitative differences and was interpreted as evidence that reduced plant defense in sunflower is a trade-off produced by domestication.[10] Our data on sesquiterpene lactone composition from the broader range of 60 *H. annuus* entries both support and expand on previous results; differences between some germplasm types were based on primarily quantitative differences (e.g., wild versus cultivated hybrids; Table 2), whereas others (e.g., restorer group versus wild *H. annuus* or cultivated hybrids) showed strong qualitative differences in the occurrence of various compounds (Table 2; Figure 2).

Effects of Mixed and Pure Extracts on Sunflower Moth Larvae. Bioassays with sunflower moth larvae showed adverse effects from exposure to glandular trichome extracts. Larval mass was reduced at 7 days ($F_{(6;268)} = 10.61$, $P < 0.001$) relative to the untreated and solvent-only controls, although

DOI: 10.1021/acs.jafc.5b00362
J. Agric. Food Chem. 2015, 63, 4042−4049

Table 2. Sesquiterpene Lactone Content from Florets of Wild and Cultivated *H. annuus*[a]

	relative sesquiterpene lactone content (mean ± SD)						
germplasm	argophyllin B	1,2-anhydrido-4,5-dihydro-niveusin A	argophyllin A	15-hydroxy-3-dehydrodesoxyfruticin	argophyllone B	niveusin B	haageanolide
maintainer (female)							
HA 207	22 ± 9	2 ± 1	–	112 ± 28	17 ± 8	–	298 ± 56
HA 232	5 ± 2	17 ± 4	8 ± 1	7 ± 7	112 ± 29	11 ± 2	300 ± 33
HA 248	34 ± 17	70 ± 61	37 ± 38	180 ± 89	369 ± 320	39 ± 38	351 ± 78
HA 250	47 ± 22	30 ± 2	23 ± 2	64 ± 12	210 ± 25	49 ± 7	265 ± 36
HA 300	38 ± 14	50 ± 44	19 ± 26	365 ± 179	382 ± 341	22 ± 25	334 ± 106
HA 301	8 ± 2	3 ± 1	2 ± 3	8 ± 4	31 ± 5	3 ± 3	209 ± 36
HA 305	34 ± 11	29 ± 9	13 ± 4	275 ± 64	218 ± 54	81 ± 31	376 ± 76
HA 379	5 ± 2	–	–	–	–	–	228 ± 117
HA 404	17 ± 6	18 ± 3	4 ± 1	641 ± 110	137 ± 37	61 ± 20	307 ± 49
HA 441	15 ± 2	–	–	230 ± 41	–	–	510 ± 125
HA 445	–	9 ± 2	3 ± 1	50 ± 10	35 ± 7	5 ± 2	199 ± 40
HA 456	13 ± 6	3 ± 5	3 ± 1	–	–	–	278 ± 143
HA 467	10 ± 5	5 ± 3	–	190 ± 36	29 ± 17	–	294 ± 82
HA 821	26 ± 4	8 ± 1	–	484 ± 60	78 ± 20	–	278 ± 49
HA 89	15 ± 4	23 ± 5	9 ± 3	14 ± 6	99 ± 17	4 ± 4	312 ± 58
restorer (male)							
RHA 265	16 ± 3	0 ± 1	–	147 ± 27	11 ± 5	–	288 ± 20
RHA 266	6 ± 6	–	–	80 ± 45	3 ± 3	–	277 ± 10
RHA 270	13 ± 6	–	–	289 ± 107	9 ± 5	4 ± 7	260 ± 35
RHA 272	7 ± 1	–	–	33 ± 4	–	–	214 ± 32
RHA 274	6 ± 1	0 ± 1	–	30 ± 4	2 ± 2	–	247 ± 20
RHA 275	24 ± 2	15 ± 7	5 ± 2	66 ± 5	53 ± 23	11 ± 5	329 ± 85
RHA 278	32 ± 2	–	–	112 ± 12	–	–	376 ± 37
RHA 358	4 ± 3	1 ± 1	–	40 ± 12	9 ± 2	–	304 ± 13
RHA 377	8 ± 0	–	–	16 ± 3	1 ± 2	–	154 ± 14
RHA 386	4 ± 2	–	–	11 ± 5	–	–	264 ± 39
RHA 388	5 ± 3	–	–	5 ± 4	–	–	303 ± 100
RHA 400	16 ± 4	2 ± 2	–	121 ± 24	19 ± 10	.	265 ± 24
RHA 408	10 ± 4	–	–	16 ± 4	1 ± 2	–	325 ± 34
RHA 464	6 ± 1	–	–	–	–	–	219 ± 118
RHA 468	9 ± 5	2 ± 2	0 ± 1	39 ± 6	21 ± 9	8 ± 11	256 ± 135
commercial hybrids							
C1-E1	35 ± 4	74 ± 7	24 ± 0	53 ± 20	282 ± 24	33 ± 3	308 ± 17
C1-E2	28 ± 0	43 ± 2	10 ± 1	110 ± 16	225 ± 15	21 ± 12	309 ± 59
C1-E3	24 ± 2	19 ± 11	6 ± 5	86 ± 43	117 ± 45	11 ± 11	349 ± 51
C1-E4	26 ± 7	34 ± 6	10 ± 4	127 ± 37	211 ± 43	17 ± 5	467 ± 36
C1-E5	28 ± 4	50 ± 6	15 ± 2	80 ± 5	272 ± 59	30 ± 5	340 ± 41
C2-E1	11 ± 1	4 ± 3	–	137 ± 16	35 ± 14	24 ± 23	327 ± 41
C2-E2	20 ± 7	31 ± 26	10 ± 9	63 ± 64	152 ± 118	13 ± 12	282 ± 49
C2-E3	23 ± 7	11 ± 1	4 ± 1	8 ± 1	61 ± 8	7 ± 1	279 ± 90
C2-E4	43 ± 8	42 ± 3	18 ± 2	24 ± 3	218 ± 13	25 ± 3	255 ± 14
C2-E5	20 ± 10	17 ± 19	3 ± 4	99 ± 33	64 ± 58	5 ± 9	296 ± 47
C3-E1	31 ± 5	48 ± 15	28 ± 17	82 ± 27	209 ± 42	30 ± 4	284 ± 63
C3-E2	23 ± 5	40 ± 16	27 ± 10	40 ± 5	169 ± 27	20 ± 6	261 ± 45
C3-E3	31 ± 2	25 ± 4	11 ± 1	89 ± 27	158 ± 13	32 ± 10	361 ± 52
C3-E4	25 ± 2	27 ± 6	15 ± 3	46 ± 7	165 ± 44	35 ± 13	254 ± 117
C3-E5	20 ± 9	22 ± 17	7 ± 9	84 ± 3	134 ± 87	32 ± 16	295 ± 39
wild H. annuus							
PI 413030	39 ± 20	87 ± 60	23 ± 10	355 ± 132	505 ± 294	96 ± 59	291 ± 52
PI 413170	37 ± 6	115 ± 45	53 ± 36	237 ± 204	856 ± 212	18 ± 6	342 ± 184
PI 435413	34 ± 28	93 ± 92	57 ± 35	226 ± 174	464 ± 334	14 ± 14	350 ± 25
PI 435418	16 ± 3	47 ± 19	14 ± 13	140 ± 137	271 ± 89	12 ± 11	261 ± 52
PI 435430	87 ± 30	260 ± 54	61 ± 33	51 ± 12	1083 ± 40	13 ± 15	199 ± 22
PI 435485	71 ± 20	243 ± 109	88 ± 51	211 ± 213	1333 ± 415	29 ± 7	256 ± 80
PI 435556	48 ± 13	137 ± 40	16 ± 8	279 ± 126	924 ± 210	17 ± 16	271 ± 81
PI 468451	27 ± 3	100 ± 7	60 ± 22	79 ± 67	615 ± 81	10 ± 3	210 ± 50
PI 586807	31 ± 32	72 ± 59	7 ± 6	83 ± 59	348 ± 275	16 ± 14	345 ± 85
PI 586855	46 ± 34	40 ± 48	5 ± 7	479 ± 171	286 ± 370	27 ± 33	174 ± 163

DOI: 10.1021/acs.jafc.5b00362
J. Agric. Food Chem. 2015, 63, 4042−4049

Table 2. continued

germplasm	relative sesquiterpene lactone content (mean ± SD)						
	argophyllin B	1,2-anhydrido-4,5-dihydro-niveusin A	argophyllin A	15-hydroxy-3-dehydrodesoxyfruticin	argophyllone B	niveusin B	haageanolide
PI 586863	7 ± 5	17 ± 13	12 ± 11	82 ± 43	146 ± 109	–	269 ± 16
PI 613724	44 ± 11	116 ± 29	20 ± 4	85 ± 36	651 ± 183	24 ± 6	285 ± 3
PI 613743	35 ± 22	62 ± 30	13 ± 14	292 ± 149	385 ± 206	11 ± 9	253 ± 101
PI 613750	35 ± 6	101 ± 17	4 ± 4	244 ± 43	575 ± 24	–	355 ± 67
PI 613751	32 ± 3	99 ± 11	23 ± 9	158 ± 44	644 ± 117	23 ± 2	217 ± 11

[a]Values are expressed as mean (± SD) peak area (mAU·min) from HPLC analyses of replicate samples (n = 3). Entries without detectable amounts denoted with dash (–) as value. Commercial hybrids identified by code (i.e., C1-E1 = company 1, entry 1) for anonymity.

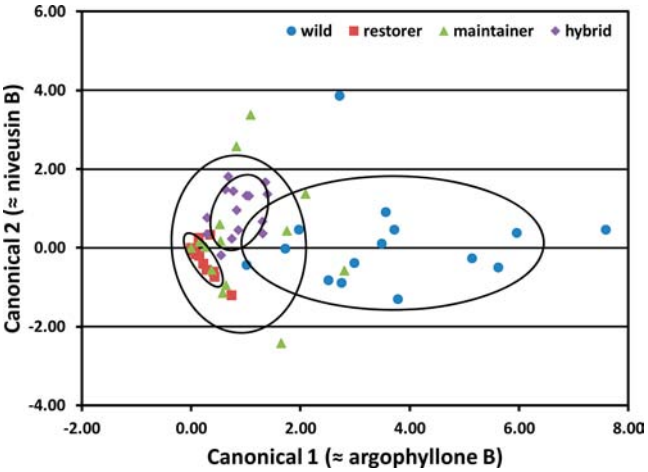

Figure 2. Plot of *H. annuus* entries by variables derived from discriminant function analysis. Canonical variables most closely corresponded to the two sesquiterpene lactones indicated (based upon loading of variables). Ellipses represent 95% confidence limits of means for each of the four groups of entries.

Table 3. Classification of Sunflower Entries to Group Based on Relative Abundance of Sesquiterpene Lactones Using Discriminant Function Analysis (Total of 15 Entries per Group)

actual group	predicted group				% misclassified
	wild	HA	RHA	hybrid	
wild *H. annuus*	12	2	0	1	20.00
maintainers (HA)	2	4	6	3	73.33
restorers (RHA)	0	0	14	1	6.67
commercial hybrids	0	0	0	15	0.00

only for one mixed extract (HA 89) and the higher dose of argophyllone B (**6**). For the treatments with significant effects, larval mass was ≈35% less relative to the solvent-only control (Table 4). Larval mortality was increased relative to the untreated control (Wald $\chi^2_{(6)}$ = 27.40), but only for the mixed extracts HA 89 (estimated odds ratio [OR] = 4.53) and PI 435430 (OR = 6.60), with one-third of larvae dying during the assay. Overall, the statistically similar results with mixed extracts from cultivated and wild entries suggest that cultivated sunflowers retain some significant chemical defenses against sunflower moth larvae. However, as observed for an unrelated insect (western corn rootworm), sunflower resistance to herbivory may manifest through behavioral or developmental changes, including reduced feeding, rather than high mortality.[8] The absence of effects from treatments that included single compounds, except the higher dose of argophyllone B (**6**),

Table 4. Effect of Mixed and Pure Sesquiterpene Lactone Extracts on Survival and Development of Sunflower Moth Larvae[a]

extract	floret-equivalents (dose)	larval mortality[b] (n of 48)	larval mass[c] (mg ± SE)
HA 89 (mixed)	25	14*	8.1 ± 1.1 c
PI 435430 (mixed)	25	18*	10.0 ± 1.2 bc
untreated	n/a	4	15.4 ± 1.0 a
methanol (solvent)	n/a	8	13.4 ± 1.1 ab
argophyllone B	60	5	12.8 ± 1.0 ab
argophyllone B	180	2	9.2 ± 1.0 c
15-hydroxy-3-dehydrodesoxyfruticin	60	4	13.2 ± 1.1 ab

[a]A dose of 60 floret-equivalents is approximately equal to the density of compounds on tips of florets. SE, standard error. [b]Asterisks (*) indicate increased mortality (P < 0.05) relative to untreated control based on 95% Wald confidence limits. [c]Different letters within the column indicate significant differences (P < 0.05) between least-squares estimated means using a Bonferroni adjustment.

suggests that sunflower sesquiterpene lactones are more effective in combinations of several compounds, as has been observed for other secondary metabolites that protect against pests.[29] An alternative, but biologically counterintuitive, explanation is that mixtures of sesquiterpene lactones may be effective only at doses that exceed the natural exposure for insect herbivores of sunflower. However, if the structurally related argophyllone B (**6**), argophyllin B (**1**), 1,2-anhydrido-4,5-dihydro-niveusin A (**2**), and argophyllin A (**3**) have similar effects on herbivores, the effective dose in nature may be similar to the higher tested dose of argophyllone B (**6**).

Results of the bioassays with pure compounds are difficult to compare to previous tests of the effects of sesquiterpene lactones against sunflower moth because of methodological differences; previous tests using sesquiterpene lactones from *Helianthus* spp. mixed a known percentage of compounds into artificial diet rather than applying them only to the surface (which mimics the distribution of glandular trichomes on florets). However, for *H. maximiliani*, significant effects on larval survival, feeding behavior, or development seemed to appear for the primary sesquiterpene lactone, 8β-sarracinoyloxycumambranolide, at concentrations between 1 and 5%.[6,7] Several pure compounds from *H. annuus* (and other species) at 1% delayed larval development and increased mortality for sunflower moth larvae.[4] Whereas previous studies support the role of sesquiterpene lactones as a defense against the sunflower moth, argophyllone B (**6**), one of the most abundant compounds in wild *H. annuus*, was recovered at only approximately 0.15% of floret dry mass; although the proportion of argophyllone B (**6**) recovered was not tested,

DOI: 10.1021/acs.jafc.5b00362
J. Agric. Food Chem. 2015, 63, 4042–4049

this observation suggests doses of 1% or more incorporated into artificial diet may exceed normal exposure for floret-feeding insects. Because several of the sesquiterpene lactones showed strong, positive correlations in their relative abundance, additional tests to understand the value of compounds (alone or in combination) would support further efforts to develop cultivated sunflowers with greater levels of sesquiterpene lactones.

Interest in using sesquiterpene lactones for resistance to insect herbivores of cultivated sunflower has persisted over the decades following their identification in wild *Helianthus* spp. An examination of a broad range of wild and cultivated *H. annuus* supports the potential for this host plant defense by finding some overlap between the sesquiterpene lactone composition of wild and cultivated sunflowers. Also, direct evidence for biological activity of argophyllone B (**6**) against sunflower moth larvae agrees with previous research showing antifeedant properties of similar compounds in cultivated sunflowers.[8] Efforts to understand the biological importance of sesquiterpene lactones are confounded; the presence of other compounds in florets with known antiherbivore properties (especially phenolics) likely obscures the effects of terpenoids and limits testing to studies in which sesquiterpene lactones are evaluated by addition to artificial diet.[30,31] However, the successful use of sesquiterpenes for enhanced insect resistance in other crops suggests that continued research is worthwhile.[32] Because sesquiterpene lactones in commercial sunflower hybrids appear qualitatively similar to those in wild sunflowers, future research should be directed to understanding the basis of clear quantitative differences to improve resistance to floret-feeding pests.

■ ASSOCIATED CONTENT

Supporting Information

HPLC chromatogram from wild sunflower (PI 435485) including eight of nine identified sesquiterpene lactones (Figure S1). This material is available free of charge via the Internet at http://pubs.acs.org.

■ AUTHOR INFORMATION

Corresponding Author

*(J.R.P.) Phone: (701) 239-1313. Fax: (701) 239-1346. E-mail: jarrad.prasifka@usda.ars.gov.

Notes

The authors declare no competing financial interest.

■ ACKNOWLEDGMENTS

We thank Reinhard Zipper (University of Hohenheim) for skillful sample processing for the spectroscopic analyses. Brent Hulke (USDA-ARS) provided helpful input on selection of lines and interpretation of results. Christopher Wallis (USDA-ARS) provided a constructive review of the manuscript. Mention of trade names or commercial products in the publication does not imply recommendation or endorsement by the U.S. Department of Agriculture.

■ REFERENCES

(1) Spring, O.; Albert, K.; Hager, A. Three biologically active heliangolides from *Helianthus annuus*. *Phytochemistry* **1982**, *21*, 2551–2553.

(2) Joel, D. M.; Chaudhuri, S. K.; Plakhine, D.; Ziadna, H.; Steffens, J. C. Dehydrocostus lactone is exuded from sunflower roots and stimulates germination of the root parasite *Orobanche cumana*. *Phytochemistry* **2011**, *72*, 624–634.

(3) Raupp, F. M.; Spring, O. New sesquiterpene lactones from sunflower root exudate as germination stimulants for *Orobanche cumana*. *J. Agric. Food Chem.* **2013**, *61*, 10481–10487.

(4) Rogers, C. E.; Gershenzon, J.; Ohno, N.; Mabry, T. J.; Stipanovic, R. D.; Kreitner, G. L. Terpenes of wild sunflowers (*Helianthus*): an effective mechanism against seed predation by larvae of the sunflower moth, *Homoeosoma electellum* (Lepidoptera: Pyralidae). *Environ. Entomol.* **1987**, *16*, 586–592.

(5) Spring, O.; Schilling, E. E. Chemosystematic investigation of the annual species of *Helianthus* (Asteraceae). *Biochem. Syst. Ecol.* **1989**, *17*, 519–528.

(6) Gershenzon, J.; Rossiter, M.; Mabry, T. J.; Rogers, C. E.; Blust, M. H.; Hopkins, T. L. Insect antifeedant terpenoids in wild sunflower: a possible source of resistance to the sunflower moth. In *Naturally Occurring Pest Bioregulators*; ACS Symposium Series 449; Hedin, P. A., Ed.; American Chemical Society: Washington, DC, USA, 1985; pp 278–292.

(7) Rossiter, M.; Gershenzon, J.; Mabry, T. J. Behavioral and growth responses of specialist herbivore, *Homoeosoma electellum*, to major terpenoid of its host, *Helianthus* spp. *J. Chem. Ecol.* **1986**, *12*, 1505–1521.

(8) Chou, J. C.; Mullin, C. A. Distribution and antifeedant associations of sesquiterpene lactones in cultivated sunflower (*Helianthus annuus* L.) on western corn rootworm (*Diabrotica virgifera virgifera* LeConte). *J. Chem. Ecol.* **1993**, *19*, 1439–1452.

(9) Prasifka, J. R. Variation in the number of capitate glandular trichomes in wild and cultivated sunflower germplasm and its potential for use in host plant resistance. *Plant Genet. Resour.* **2014**, *13*, 68–74.

(10) Rowe, H. C.; Ro, D.-K.; Rieseberg, L. H. Response of sunflower (*Helianthus annuus* L.) leaf surface defenses to exogenous methyl jasmonate. *PLoS One* **2012**, *7*, No. e37191.

(11) Spring, O. Microsampling: an alternative approach using sesquiterpene lactones for systematics. *Biochem. Syst. Ecol.* **1989**, *17*, 509–517.

(12) Spring, O.; Bienert, U. Capitate glandular hairs from sunflower leaves: development, distribution and sesquiterpene lactone content. *J. Plant Physiol.* **1987**, *130*, 441–448.

(13) Gershenzon, J.; Mabry, T. J. Sesquiterpene lactones from a Texas population of *Helianthus maximiliani*. *Phytochemistry* **1984**, *23*, 1959–1966.

(14) Griffiths, W. A.; Erickson, E. H.. Jr. Hybrid sunflowers. In *Handbook of Experimental Pollination Biology*; Jones, C. E., Little, R. J., Eds.; Scientific and Academic: New York, 1983; pp 522–535.

(15) Watanabe, K.; Ohno, N.; Yoshioka, H.; Gershenzon, J.; Mabry, T. J. Sesquiterpene lactones and diterpenoids from *Helianthus argophyllus*. *Phytochemistry* **1982**, *21*, 709–713.

(16) Spring, O.; Benz, T.; Ilg, M. Sesquiterpene lactones of the capitate glandular trichomes of *Helianthus annuus*. *Phytochemistry* **1989**, *28*, 745–749.

(17) Stipanovic, R. D.; Miller, R. B.; Hope, H. Argophyllone-B, a sesquiterpene lactone from *Helianthus argophyllus*. *Phytochemistry* **1985**, *24*, 358–359.

(18) Ohno, N.; Mabry, T. J. Sesquiterpene lactones and diterpene carboxylic acids in *Helianthus niveus* subspecies *canescens*. *Phytochemistry* **1980**, *19*, 609–614.

(19) Kisiel, W. A new germacranolide from *Zinnia haageana*. *Phytochemistry* **1978**, *17*, 1059–1060.

(20) Stout, G. H.; Stout, V. F. The structure and synthesis of xanthomicrol. *Tetrahedron* **1961**, *14*, 296–303.

(21) Wilson, R. L. Rearing the sunflower moth (Lepidoptera: Pyralidae) for use in field evaluation of sunflower germplasm. *J. Kans. Entomol. Soc.* **1990**, *63*, 208–210.

(22) SAS Institute Inc. *Using JMP 11*; SAS Institute Inc.: Cary, NC, USA, 2013.

(23) SAS Institute Inc. *SAS 9.1.3 Help and Documentation*; SAS Institute Inc.: Cary, NC, USA, 2007.

DOI: 10.1021/acs.jafc.5b00362
J. Agric. Food Chem. 2015, 63, 4042–4049

(24) Ikezawa, N.; Gopfert, J. C.; Nguyen, D. T.; Kim, S.-U.; O'Maille, P. E.; Spring, O.; Ro, D.-K. Lettuce costunolide synthase (CYP71BL2) and its homolog (CYP71BL1) from sunflower catalyze distinct regio- and stereoselective hydroxylations in sesquiterpene lactone metabolism. *J. Biol. Chem.* **2011**, *286*, 21601−21611.
(25) Mandel, J. R.; Nambeesan, S.; Bowers, J. E.; Marek, L. F.; Ebert, D.; Rieseberg, L. H.; Knapp, S. J.; Burke, J. M. Association mapping and the genomic consequences of selection in sunflower. *PLoS Genet.* **2013**, *9*, No. e1003378.
(26) Herz, W.; Kumar, N. Heliangolides from *Helianthus maximiliani*. *Phytochemistry* **1981**, *20*, 93−98.
(27) Stewart, E.; Mabry, T. J. Further sesquiterpene lactones from *Helianthus maximiliani*. *Phytochemistry* **1985**, *24*, 2733−2734.
(28) Spring, O.; Priester, T.; Stransky, H.; Hager, A. Sesquiterpene lactones in sunflower seedlings: distribution in the plant and occurrence in genetic varieties as determined by an isocratic HPLC technique. *J. Plant Physiol.* **1985**, *120*, 321−329.
(29) Wallis, C.; Eyles, A.; Chorbadjian, R.; McSpadden Gardener, B.; Hansen, R.; Cipollini, D.; Herms, D. A.; Bonello, P. Systemic induction of phloem secondary metabolism and its relationship to resistance to a canker pathogen in Austrian pine. *New Phytol.* **2008**, *177*, 767−778.
(30) Brewer, G. J.; Anderson, M. D. Modification of the effect of *Bacillus thuringiensis* on sunflower moth (Lepidoptera: Pyralidae) by dietary phenols. *J. Econ. Entomol.* **1990**, *83*, 2219−2224.
(31) Liang, Q.; Cui, J.; Li, H.; Liu, J.; Zhao, G. Florets of sunflower (*Helianthus annuus* L.): potential new sources of dietary fiber and phenolic acids. *J. Agric. Food Chem.* **2013**, *61*, 3435−3442.
(32) Bleeker, P. M.; Mirabella, R.; Diergaarde, P. J.; VanDoorn, A.; Tissier, A.; Kant, M. R.; Prins, M.; de Vos, M.; Haring, M. A.; Schuurink, R. C. Improved herbivore resistance in cultivated tomato with the sesquiterpene biosynthetic pathway from a wild relative. *Proc. Natl. Acad. Sci. U. S. A.* **2012**, *109*, 20124−20129.

DOI: 10.1021/acs.jafc.5b00362
J. Agric. Food Chem. 2015, 63, 4042−4049

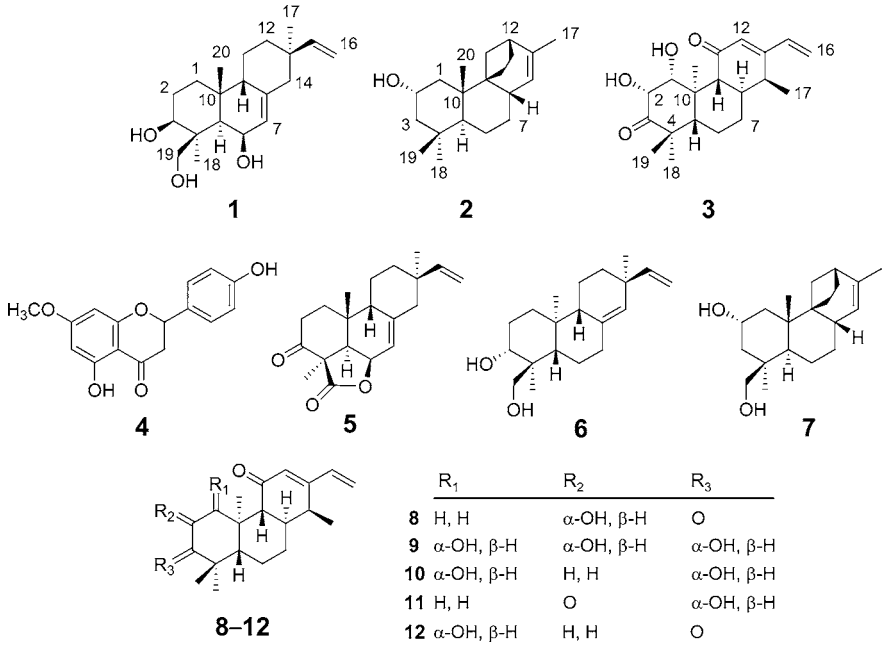

Figure 1. Structures of compounds.

complex mixture of biological origin, it is not suitable for analyzing heat-labile, highly polar, or nonvolatile compounds. In this context, LC/MS can be complementarily used for the analysis of such compounds. In this study, we used both the GC/MS and LC/MS techniques to find novel phytoalexins from UV-irradiated rice leaves, followed by complementary spectroscopic techniques to identify them.

MATERIALS AND METHODS

General Analytical Methods. ^{1}H NMR (400 MHz), ^{13}C NMR (100 MHz), and 2D-NMR spectra were acquired on an AVANCE III FT-NMR spectrometer (Bruker BioSpin, Rheinstetten, Germany) equipped with a 5 mm BBFO probe. The chemical shifts were referenced to TMS (δ_H 0.00; δ_C 0.00) or C_6D_6 (δ_H 7.16; δ_C 128.39) as an internal standard. The IR spectra were acquired using an FT/IR-4100 spectrometer (Jasco, Tokyo, Japan); the samples for IR were prepared as KBr disks. The UV spectra were acquired using a V-550 spectrometer (Jasco); the samples for UV spectroscopy were dissolved in MeOH. The specific rotations were measured using a P-2100 polarimeter equipped with a halogen lamp and a 589 nm filter (Jasco); the samples for polarimetry were dissolved in $CHCl_3$. The electron ionization (EI)-mass spectra (70 eV) were recorded with a JMS-BU25 mass spectrometer (Jeol, Tokyo, Japan) operated in direct inlet mode. GC/MS was performed with a JMS-BU25 mass spectrometer coupled with an HP6890 gas chromatograph (Agilent Technologies, Santa Clara, CA) under the following conditions: column, 30 m × 0.32 mm i.d., 0.25-μm film thickness, J&W Scientific HP-5 (Agilent Technologies); injection port temperature, 280 °C; carrier gas, He; flow rate, 1.0 mL/min; temperature program of column oven, 70 °C for 1 min before heating to 300 °C at 10 °C/min and then maintained at 300 °C for 3 min; ionization mode, EI (70 eV); ion chamber temperature, 200 °C; scan range, m/z 61−627; scan rate, 1 scan/s. LC/MS was performed with a 3200 QTRAP LC/MS/MS system (AB Sciex, Framingham, MA) coupled with a Prominence UFLC system (Shimadzu Co., Kyoto, Japan). The Turbo V ion source was operated in positive ESI mode. Preparative HPLC was carried out with a PU-980 HPLC pump and an MD-910 photodiode array detector (Jasco) under the following conditions; flow rate, 2.0 mL/min; detection, UV 210−350 nm.

Chemicals. Compound **4** was chemically synthesized from naringenin (Sigma-Aldrich, St. Louis, MO) according to the method reported by Aida et al.[27] Compound **5** was purified from rice husks according to the method reported by Kato et al.[28] with some modifications. Compounds **6** and **7** were purified from UV-irradiated rice leaves according to previously described methods with some modifications.[5,6] The standard solution for the quantitation of **8**−**12** was kindly gifted by Dr. Kazunori Okada at the University of Tokyo.

Plant Materials. Rice plants (*Oryza sativa* cv. Koshihikari) were grown in a phytotron at 27 °C under natural light conditions. The leaf blades of the seventh and eighth leaf stages were detached, and the middle regions of those leaf blades were used in the subsequent experiments.

Fungal Materials and Spore Preparation. The rice blast fungus (*Magnaporthe oryzae* strain P-2) had been maintained on a potato dextrose agar (PDA) (Nissui Pharmaceutical, Tokyo, Japan) medium as a stock culture in our laboratory. Spores of the fungus were prepared by the previously described method with some modifications.[29] The mycelia cultured on the oatmeal medium were transplanted to a vegetable-juice medium in a Petri dish and cultured for 2 weeks at 26 °C in the dark. For synchronously produced spores, aerial hyphae were removed by soft scratching with a paint brush in distilled water. The Petri dish was incubated for 48 h at 26 °C under a BLB 20 W near-UV light (Toshiba, Tokyo, Japan) in dry conditions. The produced spores were harvested with distilled water for a time course infection experiment or with a spore germination medium (4 g of glucose, 2 g of yeast extract, 7.4 g of $Na_2HPO_4 \cdot 12H_2O$ and 2 g of citric acid monohydrate dissolved in 1 L of distilled water) for an inhibition assay using a paint brush. The spore suspension was filtered through cheesecloth and stored on ice until use.

DOI: 10.1021/acs.jafc.5b00785
J. Agric. Food Chem. 2015, 63, 4050−4059

UV Irradiation of the Rice Leaves. UV irradiation was conducted by the previously described method.[9] UV-irradiated rice leaves were incubated at 26 °C under continuous light condition for 3 days for the screening and isolating of UV-inducible substances, and for 0, 1, 2, 3, 4, and 5 days for the quantitation of **1**−**12** in the UV irradiation time course experiment. The UV-irradiated leaves were stored at −20 °C before use.

Purification of 9β-Pimara-7,15-diene-3β,6β,19-triol, 1, and Stemar-13-en-2α-ol, 2, from UV-Irradiated Rice Leaves. The 400 g of UV-irradiated rice leaves were cut and shaken in 6 L of 80% (v/v) MeOH with a reciprocal shaker for 24 h. The homogenate was filtered to obtain an extract, and the residual leaves were then re-extracted with 4 L of 80% MeOH in the same manner. The combined extract was concentrated in vacuo to remove the MeOH. The resulting aqueous concentrate was extracted with EtOAc, and the organic layer was evaporated to dryness in vacuo. The EtOAc extract was subjected to column chromatography on 50 g of 63-210-μm particle size, silica gel 60N (Kanto Chemical Co., Tokyo, Japan) and eluted with a stepwise gradient of *n*-hexane/EtOAc (95:5, 80:20, 60:40, 20:80, 0:100; 300 mL of each). Each fraction was analyzed by GC/MS to detect the UV-induced substances. Compounds **1** and **2**, exhibiting plausible molecular ions at *m*/*z* 302 and 288, were detected in the fraction eluted with 80:20 and 0:100 *n*-hexane/EtOAc, respectively. Their MS and t_R did not correspond to those of known phytoalexins.

The fraction eluted with 0:100 *n*-hexane/EtOAc was applied to a 20 cm × 20 cm, 1.0 mm thick, silica gel 60 F_{254} preparative TLC plate (Merck Millipore, Billerica, MA) developed with 1:1 benzene/EtOAc. The R_f 0.10−0.40 TLC region, which contained **1**, was scraped off and extracted with EtOAc. The EtOAc extract was evaporated in vacuo to dryness to give a 127 mg of TLC-purified fraction. The fraction was dissolved in MeOH at a concentration of 4% (w/v) and separated by ODS-HPLC under the following conditions: column, 25 cm × 1 cm i.d., 5 μm particle size, COSMOSIL 5C18AR (Nacalai Tesque, Kyoto, Japan); solvent, 70% (v/v) MeOH; injection volume in a run, 200 μL. The peak containing **1** (t_R 30−35 min) was collected and evaporated to dryness in vacuo to afford 2.1 mg of purified **1**. Compound **1** was identified as 9β-pimara-7,15-diene-3β,6β,19-triol by spectroscopic methods. High-resolution electron ionization mass spectrum (HREIMS) (*m*/*z*): (M^+) calcd for $C_{20}H_{32}O_3$, 320.2352; found, 320.2377; ^{1}H NMR (400 MHz, $CDCl_3$, δ): 0.87 (3H, s, H-17), 1.26 (3H, s, H-20), 1.29 (3H, s, H-18), 1.91 (dd, *J* = 12.1, 2.3 Hz, 1H, H-14), 2.08 (d, *J* = 12.1 Hz, 1H, H-14), 3.32 (m, 1H, H-3), 4.03 (d, *J* = 11.6 Hz, 1H, H-19), 4.32 (d, *J* = 11.6 Hz, 1H, H-19), 4.46 (dd, *J* = 5.5, 3.8 Hz, 1H, H-6), 4.90 (dd, *J* = 10.7, 1.2, 1H, H-16), 4.94 (dd, *J* = 17.4, 1.2, 1H, H-16), 5.56 (br d, *J* = 5.5 Hz, 1H, H-7), 5.82 (dd, *J* = 17.4, 10.7 Hz, 1H, H-15); ^{13}C NMR (100 MHz, $CDCl_3$, δ): 21.77 (q, C-17), 21.85 (q, C-18), 24.81 (t, C-11), 26.39 (q, C-20), 27.25 (t, C-2), 35.00 (s, C-10), 35.61 (t, C-1), 37.54 (t, C-12), 39.35 (s, C-13), 44.15 (s, C-4), 47.88 (t, C-14), 48.42 (d, C-5), 53.49 (d, C-9), 62.77 (t, C-19), 65.01 (d, C-6), 80.59 (d, C-3), 109.68 (t, C-16), 121.66 (d, C-7), 141.14 (s, C-8), 149.61 (d, C-15); EIMS (70 eV) *m*/*z*: M^+ 320 (2), 302 (21), 287 (50), 269 (43), 149 (59), 105 (54), 91 (60), 81 (66), 61 (83), 55 (100); IR (KBr) $\tilde{\nu}_{max}$ (cm^{-1}): 3370, 1459, 1377, 1342, 1185, 959, 907; $[\alpha]^{20}_D$ −150 (*c* 0.16, $CHCl_3$).

The fraction eluted with 80:20 *n*-hexane/EtOAc was subjected to preparative TLC and developed with 3:1 benzene/EtOAc. The R_f 0.55−0.82 TLC region, which contained **2**, was scraped off and extracted with EtOAc. The EtOAc extract was evaporated in vacuo to dryness to give a 59 mg of TLC-purified fraction. The fraction was dissolved in MeOH at a concentration of 1% (w/v) and separated by ODS-HPLC under the following conditions: column, COSMOSIL 5C18AR; solvent, 70% (v/v) MeOH; injection volume in a run, 100 μL. A peak containing **2** (t_R 60−65 min) was collected and evaporated to dryness in vacuo to afford 1.3 mg of purified **2**. Compound **2** was identified as stemar-13-en-2α-ol by spectroscopic methods. HREIMS (*m*/*z*): (M^+) calcd for $C_{20}H_{32}O$, 288.2452; found, 288.2446; ^{1}H- and ^{13}C NMR (C_6D_6): see Table 1; EIMS (70 eV) *m*/*z*: M^+ 288 (33), 270 (57), 255 (100), 131 (43), 119 (48), 105 (92), 91 (83), 79 (55), 69 (53), 58 (86); IR (KBr) $\tilde{\nu}_{max}$ (cm^{-1}): 3348, 2954, 1459, 1389, 1317, 1255, 1162, 1039; $[\alpha]^{20}_D$ +60 (*c* 0.1, $CHCl_3$).

Table 1. ^{13}C and ^{1}H NMR Data for Stemar-13-en-2α-ol, 2, in C_6D_6

position	δ_C (multiplicity)	δ_H (multiplicity, *J* in Hz)
1	42.95 (t)	1.20 (m, overlapped, 1H)
		1.68 (m, overlapped, 1H)
2	65.23 (d)	3.74 (tt, 11.6, 3.9, 1H)
3	52.09 (t)	1.03 (t, 11.6, 1H)
		1.65 (m, overlapped, 1H)
4	35.29 (s)	-
5	49.11 (d)	1.00 (dd, 12.2, 2.6, 1H)
6	22.56 (t)	1.45 (m, overlapped, 1H)
		1.20 (m, overlapped, 1H)
7	32.33 (t)	1.64 (m, overlapped, 1H)
		1.28 (m, overlapped, 1H)
8	44.63 (d)	1.95 (ddd, 11.7, 4.5, 3.9, 1H)
9	51.53 (s)	-
10	41.07 (s)	-
11	30.52 (t)	1.63 (m, overlapped, 1H)
		1.36 (dd, 10.6, 4.3)
12	43.79 (d)	2.13 (br t, 4.3, 1H)
13	139.06 (s)	-
14	124.64 (d)	5.05 (dqd, 4.5, 1.5, 0.6, 1H)
15	33.92 (t)	1.66 (m, overlapped, 1H)
		1.47 (m, overlapped, 1H)
16	32.37 (t)	1.71 (m, overlapped, 1H)
		1.22 (m, overlapped, 1H)
17	22.59 (q)	1.63 (t, 1.5, 3H)
18	34.35 (q)	0.83 (s, 3H)
19	23.71 (q)	0.79 (s, 3H)
20	18.12 (q)	0.89 (br s, 3H)

Screening of UV-Inducible Substances with LC/MS. The control and UV-irradiated rice leaves were cut, weighed, and shaken in 80% (v/v) MeOH [5 mL/0.1 g fresh weight (FW)] using a reciprocal shaker. The homogenate was filtered through a cotton-plugged Pasteur pipet, and the extract was refiltered through a 13 mm diameter, 0.22-μm pore size, cellulose acetate membrane filter (Lab Lab Company, Tokyo, Japan). A 10 μL volume of the solution was subjected to LC/MS analysis. The liquid chromatographic separation of the analytes was achieved in a 150 mm × 2.1 mm i.d., 3.0-μm particle size, Atlantis T3 column (Waters, Milford, MA) with a binary gradient of 0.1% (v/v) aqueous formic acid (solvent A) and MeOH containing 0.1% (v/v) formic acid (solvent B) at flow rate of 0.2 mL/min and at a temperature of 40 °C. The solvent gradient elution was programmed as follows: initial,

DOI: 10.1021/acs.jafc.5b00785
J. Agric. Food Chem. 2015, 63, 4050−4059

20% B; 0−5 min, isocratic elution by 20% B; 5−35 min, a linear gradient from 20% B to 100% B; 35−40 min, isocratic elution by 100% B. The scan range of MS was set as m/z 100−711 (enhanced MS scan). Every extracted ion chromatogram obtained from the extracts of the control and UV-irradiated leaves were compared using LightSight 2.2 software (AB Sciex) in an attempt to discover novel UV-induced substances. An unknown compound exhibiting an m/z of 333, which was estimated as $[M + H]^+$, was detected at a t_R of 29.7 min in the chromatogram of the UV-treated leaves. Therefore, suspecting a novel phytoalexin candidate, we attempted to purify compound **3**.

Purification of 1α,2α-Dihydroxy-*ent*-12,15-cassadiene-3,11-dione, 3, from UV-Irradiated Rice Leaves. The LC/MS/MS analysis conditions were defined for a rapid monitoring of **3** during the purification procedure. The liquid chromatographic separation of the analytes was conducted using a 50 mm × 2.0 mm i.d., 3.0 μm particle size, TSKgel ODS-100V column (Tosoh, Tokyo, Japan) with a binary gradient of 0.1% (v/v) aqueous formic acid (solvent A) and MeOH containing 0.1% (v/v) formic acid (solvent B) at a flow rate of 0.2 mL/min and at a temperature of 40 °C. The solvent gradient elution was programmed as follows: initial, 20% B; 0−10 min, a linear gradient from 20% B to 100% B; 10−12 min, isocratic elution by 100% B. The scan range of MS was set as m/z 80−338 (enhanced MS scan). Compound **3** was detected at a t_R of 9.4 min under these conditions.

EtOAc extract was prepared from 400 g of UV-irradiated rice leaves in the same manner as the purification of **1** and **2**. The EtOAc extract was subjected to column chromatography on 60 g of silica gel and eluted with a stepwise gradient of *n*-hexane/EtOAc (95:5, 80:20, 60:40, 40:60, 20:80, 0:100; 300 mL of each). Each fraction was analyzed by LC/MS/MS under the previously described conditions to detect compound **3**. Compound **3** was detected in the fraction eluted with 20:80 *n*-hexane/EtOAc. The fraction was subjected to preparative TLC and developed with 10:1 chloroform/MeOH. The R_f 0.41−0.76 TLC region, which contained **3**, was scraped off and extracted with EtOAc. The EtOAc extract was evaporated in vacuo to dryness to give a 65 mg of TLC-purified fraction. The fraction was subjected to reversed-phase column chromatography using 6 g of 200−300 mesh, Chromatorex ODS (Fuji Silysia Chemical Ltd., Kasugai, Japan) and eluted with a stepwise gradient of MeOH/H_2O (20, 50, 80, 100% MeOH; 96 mL of each). Each fraction was also analyzed by LC/MS/MS in the same manner as the previous purification step. The fraction containing **3**, which was eluted with 80% MeOH, was then evaporated in vacuo to dryness to give a 26 mg of reversed-phase-chromatography-purified fraction. The fraction was dissolved in MeOH at a concentration of 2% (w/v) and separated by ODS-HPLC under the following conditions: column, 25 cm × 1 cm i.d., 5 μm particle size, Luna 5 μm C18(2) (Phenomenex, Torrance, CA); solvent, 60% (v/v) MeOH; injection volume in a run, 100 μL. A peak containing **3** (t_R 70−74 min) was collected and evaporated to dryness in vacuo to afford 1.9 mg of purified **3**. Compound **3** was identified as 1α,2α-dihydroxy-*ent*-12,15-cassadiene-3,11-dione by spectroscopic methods, as described in the Results and Discussion section. **3**. HREIMS (m/z): (M^+) calcd for $C_{20}H_{28}O_4$, 332.1988; found, 332.1955; ^{1}H- and ^{13}C NMR ($CDCl_3$): see Table 2; EIMS (70 eV) m/z: M^+ 332 (2), 315 (10), 279 (4), 229 (5), 203 (6), 167 (11), 149 (85), 83 (42), 57 (100); UV (MeOH) λ_{max} (log ε): 269 (4.0); IR (KBr) $\tilde{\nu}_{max}$ (cm^{-1}): 3453, 2963, 2857, 1726, 1634; $[\alpha]^{20}_D$ −147 (c 0.17, $CHCl_3$). During the purification of **3**, we also purified 2.6 mg of **8** from the 60:40 *n*-hexane/EtOAc-eluted silica gel column chromatography fraction, followed by reversed-phase chromatography and ODS-HPLC. The ^{1}H- and ^{13}C NMR data of **8** coincided with those previously reported.[7]

Table 2. ^{13}C and ^{1}H NMR Data for 1α,2α-Dihydroxy-*ent*-12,15-cassadiene-3,11-dione, 3, in $CDCl_3$

position	δ_C (multiplicity)	δ_H (multiplicity, J in Hz)
1	78.47 (d)	4.36 (dd, 8.0, 2.8, 1H)
2	70.57 (d)	4.74 (br d, 8.0, 1H)
3	214.58 (s)	-
4	47.02 (s)	-
5	48.27 (d)	1.91 (dd, 11.6, 3.3, 1H)
6	21.97 (t)	1.53 (m, overlapped, 1H)
		1.75 (m, overlapped, 1H)
7	30.32 (t)	1.54 (m, overlapped, 1H)
		1.75 (m, overlapped, 1H)
8	38.42 (d)	2.16 (m, 1H)
9	56.78 (d)	2.31 (d, 13.1, 1H)
10	42.49 (s)	-
11	202.67 (s)	-
12	127.91 (d)	5.86 (s, 1H)
13	163.37 (s)	-
14	33.38 (d)	2.72 (qd, 7.2, 4.2, 1H)
15	135.97 (d)	6.39 (dd, 17.6, 10.8, 1H)
16	122.09 (t)	5.57 (d, 10.8, 1H)
		5.76 (d, 17.6, 1H)
17	13.42 (q)	1.14 (d, 7.2, 3H)
18	18.79 (q)	1.10 (s, 3H)
19	29.25 (q)	1.17 (s, 3H)
20	11.49 (q)	0.74 (s, 3H)
1-OH	-	5.24 (d, 2.8, 1H)
2-OH	-	3.52 (br s, 1H)

Assay of the Antifungal Activity against the Rice Blast Fungus. For the fungal colony growth inhibition assay, each test compound was dissolved in an unsolidified PDA medium containing 1% (v/v) dimethyl sulfoxide at a concentration of 75 or 300 μM. The PDA medium was poured into a 9 cm Petri dish and solidified at room temperature. A PDA medium containing 1% (v/v) dimethyl sulfoxide was used as a control. Four 25 mm^2 pieces of the blast fungus, which had been cultured on a PDA medium, were transplanted to the PDA medium. The inoculated PDA medium was incubated at 26 °C in the dark. After 0, 1, 2, 3, 4, and 5 days of incubation, the distance between the front of the planted pieces and the front of the mycelium colony was measured using a ruler.

For the spore germination and germ tube growth inhibition assay, the concentration of spore suspension was adjusted to 6 × 10^4 spores/mL with a prechilled spore germination medium. The samples were dissolved in distilled water containing 0.2% (v/v) dimethyl sulfoxide and 0.1% (v/v) Tween 80. The 12.5 μL of spore suspension and the 12.5 μL of sample solution were mixed on a concavity slide and then incubated for 16 h at 26 °C in a highly humidified box in the dark. The germination rate and germ tube length of the *M. oryzae* spores were measured under a microscope. The inhibitory activity against spore germination and germ tube elongation was determined according to the previously reported method.[9]

Quantitative LC/MS/MS Analysis of 9β-Pimara-7,15-diene-3β,6β,19-triol, 1, Stemar-13-en-2α-ol, 2, 1α,2α-

DOI: 10.1021/acs.jafc.5b00785
J. Agric. Food Chem. 2015, 63, 4050−4059

Dihydroxy-*ent*-12,15-cassadiene-3,11-dione, 3, and Other Phytoalexins, 4−12. The liquid chromatographic separation of the analytes was achieved in an Atlantis T3 column with a binary gradient of 0.1% (v/v) aqueous formic acid (solvent A) and MeCN containing 0.1% (v/v) formic acid (solvent B) at a flow rate of 0.2 mL/min and at a temperature of 40 °C. The solvent gradient elution was programmed as follows: initial, 40% B; 0−3 min, isocratic elution by 40% B; 3−23 min, a linear gradient from 40% B to 100% B; 23−28 min, isocratic elution by 100% B. The selective reaction monitoring (SRM) transitions and the parameters of the mass spectrometer were optimized for detecting **1**−**12** using Analyst 1.5.1 software (AB Sciex). Calibration curves were obtained from the SRM peak areas of the standards for **1**−**12** in a concentration range of 1−1000 ng/mL. The concentrations of the analytes were calculated from their individual SRM peak area based on the calibration curves.

Quantitation of 9*β*-Pimara-7,15-diene-3*β*,6*β*,19-triol, 1, Stemar-13-en-2*α*-ol, 2, 1*α*,2*α*-Dihydroxy-*ent*-12,15-cassadiene-3,11-dione, 3, and Other Phytoalexins, 4−12, from UV-Irradiated and *M. oryzae*-Inoculated Rice Leaves. UV-irradiated rice leaves (ca. 3 leaves) were cut, weighed and shaken in 80% (v/v) MeOH (5 mL/0.1 g FW) using a reciprocal shaker. The extract was filtered through a cotton-plugged Pasteur pipet and was refiltered through a membrane filter.

The spore suspension of *M. oryzae* was diluted with water to a concentration of 2×10^5 spores/mL and 25 μL of the spore suspension was then applied to press-injured spots with a diameter of 1 mm on the rice leaves. The leaves were maintained in a highly humidified box and incubated for 1, 2, 3, 4, and 5 days at 26 °C under light irradiation. The leaf tissues around the injured spots were excised with a 4 mm i.d., cork borer. Approximately 45 pieces of the excised leaf tissues (ca. 100 mg) were collected and shaken in 5 mL of 80% MeOH using a reciprocal shaker. The homogenate was filtered through a cotton-plugged Pasteur pipet and a membrane filter.

A 5 μL volume of the sample solution was subjected to the aforementioned LC/MS/MS analysis to quantitate **1**−**12**.

RESULTS AND DISCUSSION

Purification and Structural Elucidation of 9*β*-Pimara-7,15-diene-3*β*,6*β*,19-triol, 1, Stemar-13-en-2*α*-ol, 2, and 1*α*,2*α*-Dihydroxy-*ent*-12,15-cassadiene-3,11-dione, 3, from UV-Irradiated Rice Leaves. We detected UV-induced compounds **1** and **2** in the silica gel column chromatography-purified fractions of UV-irradiated rice leaves by GC/MS analysis. Compounds **1** and **2** were detected at t_R 19.2 and 18.2 min and their mass spectra showed plausible molecular ions at m/z 302 and 288, respectively. These t_R and mass spectra did not correspond to those of known phytoalexins or to their biosynthetic precursors when compared to the t_R and mass spectra of authentic samples. Compounds **1** and **2** were not detected in healthy rice leaves that had not been UV-irradiated. Therefore, we isolated **1** and **2** to determine their structures. Compounds **1** (2.1 mg, a white solid) and **2** (1.3 mg, a colorless oil) were successfully purified from the 400 g of UV-irradiated rice leaves by chromatographic methods.

Although we estimated m/z 302 as the molecular ion of **1** in the GC/MS analysis, m/z 320 was detected as a more reasonable molecular ion in the MS analysis using the direct inlet mode, suggesting that m/z 302 should be $[M-H_2O]^+$. The HREIMS analysis of **1** suggested a molecular formula of $C_{20}H_{32}O_3$ and five degrees of unsaturation. The NMR spectra of **1** suggested that it contains two oxygenated methines and one oxygenated methylene. The acetylation of **1** using acetic anhydride gave a triacetylated compound, indicating that **1** has three hydroxyl groups (data not shown). The 1D- and 2D-NMR spectra indicated that the structure of **1** was 9*β*-pimara-7,15-diene-3*β*,6*β*,19-triol, which had been reported as a $LiAlH_4$-reduction product of **5**.[30] We also synthesized the compound from **5** using the method reported in the literature, and the ^{1}H- and ^{13}C NMR data of the synthetic **1** coincided with those of **1** obtained and purified from the UV-irradiated rice leaves (data not shown). Therefore, UV-induced compound **1** from rice leaves was identified as 9*β*-pimara-7,15-diene-3*β*,6*β*,19-triol.

The HREIMS analysis of **2** suggested a molecular formula $C_{20}H_{32}O$ and five degrees of unsaturation. The number of carbon atoms agreed with the ^{13}C NMR data (Table 1). IR data indicated the presence of a hydroxyl group, whose proton was not observed in the ^{1}H NMR spectrum. ^{13}C NMR and distortionless enhancement by polarization transfer (DEPT) spectra indicated the presence of one olefinic methine (C-14; δ_C 124.64 ppm) and one olefinic quaternary carbon (C-13; δ_C 139.06 ppm), suggesting that **2** has one C−C double bond. Five degrees of unsaturation and the presence of one C−C double bond indicated that **2** has four rings. ^{13}C NMR and DEPT data showed that **2** consists of four methyl, seven methylene, five methine, and four quaternary carbons. These results suggested that **2** should be a monohydroxylated tetracyclic diterpene. The ^{13}C chemical shifts of **2** were very similar to those of **7**, a rice stemarane-type phytoalexin, except that **2** lacks an oxymethylene signal corresponding to the C-19 of **7**.[31] Moreover, four methyl signals were observed in the ^{1}H- and ^{13}C NMR spectra of **2**, whereas three methyl signals were observed in those of **7**. Typical signals of a stemar-13-ene skeleton, such as δ_H 5.05 (H-14), 2.13 (H-12), 1.63 (H-17), 0.89 (H-20), 0.83 (H-18), and 0.79 (H-19), were observed in the ^{1}H NMR spectrum.[31−36] 2D-NMR correlations confirmed the stemar-13-ene skeleton (Figure 2). A methine carbon at δ_C 64.5 ppm (C-2) should be connected to a hydroxyl group. The coupling constants between H-2 and H-1/H-3 as well as nuclear Overhauser enhancement and exchange spectroscopy (NOESY) correlations between H-2 and H-19/H-20 indicated that the 2-hydroxyl group should be equatorial (α-orientation). These results suggested that the structure of **2** should be 19-deoxyoryzalexin S. Although the absolute stereochemistry of **2** was not determined experimentally, given its origin, it likely has the same stemarane skeleton as **7**. We thus concluded that **2** must be stemar-13-en-2*α*-ol.

UV-induced compounds **1** and **2** were successfully found using GC/MS analysis. We subsequently attempted to search for novel phytoalexins using LC/MS analysis. As a result, we discovered compound **3**, which showed an m/z 333 estimated as $[M + H]^+$ and a t_R of 29.7 min in the chromatogram of the UV-treated leaves. Its t_R and mass spectrum did not correspond to those of known phytoalexins or their biosynthetic precursors, as determined by a comparison with authentic samples and theoretical m/z values. Moreover, we estimated that the accumulated amount of **3** was as high as that of **5** based on the peak area, whose induction level was reported to be relatively high among known phytoalexins in UV-irradiated and *M. oryzae*-infected rice leaves.[9] Compound **3** was not detected in healthy rice leaves that had not been UV-irradiated. Therefore, we performed a large-scale isolation of **3** to determine its structure. Compound **3** (1.9 mg, a pale-yellow

DOI: 10.1021/acs.jafc.5b00785
J. Agric. Food Chem. 2015, 63, 4050−4059

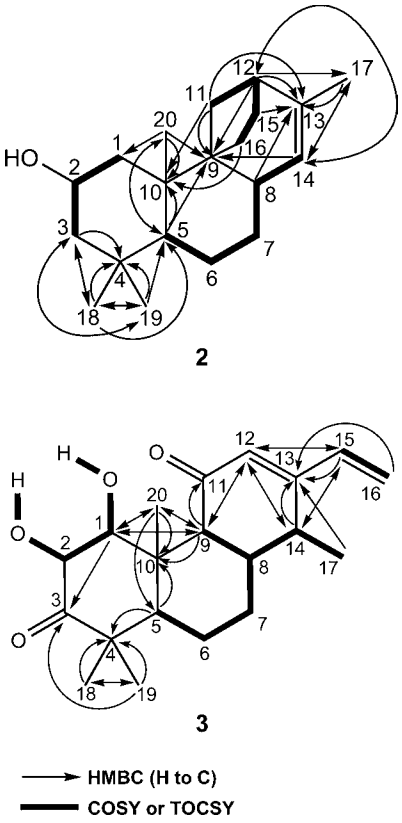

Figure 2. 2D-NMR correlations for stemar-13-en-2α-ol, **2**, and 1α,2α-dihydroxy-*ent*-12,15-cassadiene-3,11-dione, **3**.

oil) was successfully purified from the 400 g of UV-irradiated rice leaves by chromatographic methods. Compound **3** could not be detected by GC/MS, likely because of its high polarity or heat-labile property.

The HREIMS analysis of **3** suggested a molecular formula $C_{20}H_{28}O_4$ and seven degrees of unsaturation. The numbers of carbons and hydrogens agreed with the ^{1}H and ^{13}C NMR data (Table 2). ^{13}C NMR and IR data indicated that two of four oxygens belonged to two carbonyl groups and the two remaining oxygens belonged to two hydroxyl groups. ^{13}C NMR and DEPT data indicated the presence of two olefinic methines, one terminal olefinic methylene and one olefinic quaternary carbon, suggesting that **3** had two C−C double bonds. Seven degrees of unsaturation and the presence of two C−C double bonds and two carbonyl groups indicated that **3** had three rings. Correlated spectroscopy (COSY) and heteronuclear single quantum coherence (HSQC) correlations suggested OH-1/C-1/C-2/OH-2, C-15/C-16 and C-5/C-6/C-7/C-8/C-9/C-14/C-17 connectivities (Figure 2). Heteronuclear multiple bond correlation (HMBC) data (Figure 2), as well as UV (269 nm) and IR (1634 cm^{-1}) absorptions indicated the presence of an $\alpha,\beta,\gamma,\delta$-unsaturated ketone (C-11/C-12/C-13/C-15/C-16). The HMBC data suggested a quaternary carbon (C-4) bearing geminal methyls (C-18 and C-19) at the α-position of a ketone (C-3). The HMBC data were used to connect these fragment structures and the remaining fractions, including a quaternary carbon (C-10) and a methyl group (C-20). The skeleton of the deduced structure coincided with phytocassanes, the rice *ent*-cassadiene-type diterpene phytoalexins.[7,8,37] The ^{13}C chemical shifts of **3** were very similar to those of **12** except for the C-2, which bore a hydroxyl group in **3** but not in **12**. Moreover, NOESY correlations indicated that H-1/H-2/H-5/H-9/H-17/H-19 were located on the same side of the ring and that H-8/H-14/H-20/1-OH were located on the other side. These results suggested that **3** had the same relative configuration as phytocassanes. Although the absolute stereochemistry of **3** was not determined experimentally, given its origin, **3** likely has the same *ent*-cassadiene skeleton as phytocassanes. Therefore, the structure of **3** was determined as 1α,2α-dihydroxy-*ent*-12,15-cassadiene-3,11-dione.

Accumulation of 9β-Pimara-7,15-diene-3β,6β,19-triol, 1, Stemar-13-en-2α-ol, 2, and 1α,2α-Dihydroxy-*ent*-12,15-cassadiene-3,11-dione, 3, in UV-Irradiated and *M. oryzae*-Inoculated Rice Leaves. We subsequently developed a quantitation method for **1**, **2**, and **3**. The leaf extract was subjected to LC/MS/MS analysis, which resulted in the detection of these compounds in the SRM mode by positive ESI. The change in the accumulated levels of **1**−**12** after UV irradiation was analyzed using this method. We observed that brown spots dramatically increased in number and area 24−48 h after UV irradiation, and this change was not observed in the control leaves. Corresponding to this apparent change, the amounts of **1**, **2**, and **3** significantly increased after UV irradiation, reaching a maximum after 48 h and then slightly decreasing after 72−120 h (Figure 3). The leaves that had not been UV-irradiated did not show the presence of these compounds. In the case of *M. oryzae* infection, brown spots

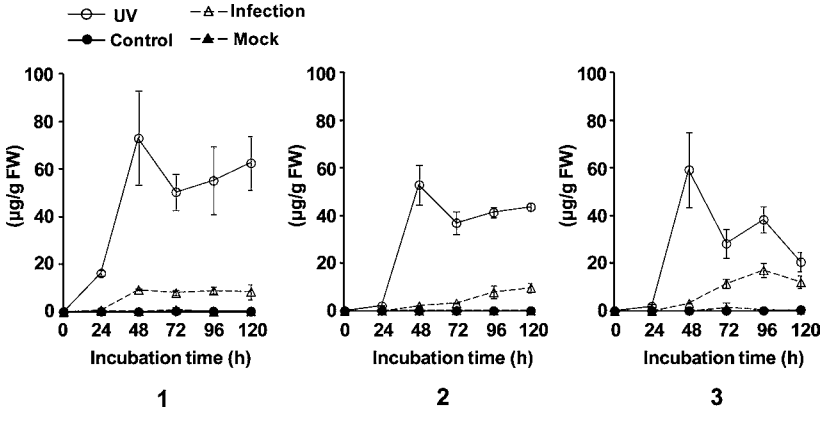

Figure 3. Time-dependent accumulation of 9β-pimara-7,15-diene-3β,6β,19-triol, **1**, stemar-13-en-2α-ol, **2**, and 1α,2α-dihydroxy-*ent*-12,15-cassadiene-3,11-dione, **3**, in UV-irradiated and rice blast fungus-inoculated rice leaves. Values are presented as the mean ± SD (n = 3).

DOI: 10.1021/acs.jafc.5b00785
J. Agric. Food Chem. 2015, 63, 4050−4059

emerged at the inoculated site 24 h after inoculation, and their areas gradually spread up to 120 h after inoculation. The brown spots were not observed in the mock-treated leaves. The amounts of **1**, **2**, and **3** also gradually increased up to 96 h after inoculation and were almost stable until 120 h after inoculation (Figure 3). The mock-treated leaves did not accumulate **1**, **2**, and **3**.

The contents of **1**−**12** in the UV-irradiated and *M. oryzae*-inoculated leaves are summarized in Table 3. A flavonoid-type phytoalexin, **4**, accumulated at the highest level in the UV-irradiated and *M. oryzae*-inoculated leaves. The levels of diterpenoid-type compounds in the UV-irradiated leaves were similar. The accumulation levels of **1**, **2**, and **3** in the *M. oryzae*-inoculated leaves were not substantially different from those of known phytoalexins, **6** and **8**−**12**, but were lower than those of **5** and **7**.

Table 3. Accumulation of Phytoalexins and 9β-Pimara-7,15-diene-3β,6β,19-triol, 1, Stemar-13-en-2α-ol, 2, and 1α,2α-Dihydroxy-*ent*-12,15-cassadiene-3,11-dione, 3, in UV-Irradiated Rice Leaves after 48 h of Incubation and in *M. oryzae*-Inoculated Rice Leaves after 120 h of Incubation[a]

	accumulation (μg/g FW)	
compd	UV irradiation	*M. oryzae* inoculation
1	73.0 ± 19.9	8.5 ± 3.2
2	52.9 ± 8.4	9.6 ± 1.8
3	59.2 ± 15.6	12.0 ± 2.7
4	352.9 ± 79.3	75.2 ± 30.7
5	96.1 ± 25.4	29.3 ± 6.8
6	60.9 ± 9.0	10.6 ± 5.5
7	53.4 ± 7.5	26.4 ± 3.5
8	75.9 ± 20.2	7.7 ± 2.4
9	23.0 ± 4.9	8.1 ± 1.9
10	12.8 ± 4.6	2.5 ± 0.4
11	10.8 ± 1.7	10.3 ± 1.9
12	15.9 ± 4.5	10.2 ± 2.3

[a]Values are presented as the mean ± SD (n = 3).

Antifungal Activities of 9β-Pimara-7,15-diene-3β,6β,19-triol, 1, Stemar-13-en-2α-ol, 2, and 1α,2α-Dihydroxy-*ent*-12,15-cassadiene-3,11-dione, 3. The antifungal activities of **1**, **2**, **3** and phytoalexins against *M. oryzae* were determined by a spore germination and germ tube growth assay. Initially, we tested the solubility of these compounds in an aqueous liquid medium and observed that **3** and **5** were insoluble at high concentrations. To ensure the effective concentration of insoluble compounds in the test, we attempted to add dimethyl sulfoxide and Tween 80 to the test solution in final concentrations of 0.1% and 0.05%, respectively. The additives did not affect the spore germination rate (95%) or germ tube growth of the control experiment. The spore germination was completely suppressed by the addition of **3** or **4** at a concentration of 300 μM. In the germ tube growth assay, **4**, **5**, **7**, and **3** exerted a dose-dependent inhibitory activity (Figure 4). The IC_{50} values of these compounds were calculated as 37, 74, 122, and 16 μM, respectively. Compounds **1** and **2** inhibited germ tube growth only in high doses, and their IC_{50} values were calculated to be approximately equal to or greater than 300 μM.

Furthermore, we investigated whether **3** inhibited the fungal mycelial colony growth of *M. oryzae* on a solid medium. Compound **3** showed dose-dependent inhibition of fungal colony growth, and the inhibition rate was calculated as 26% at 300 μM after 5 days of incubation (Figure 5). We also examined the inhibitory activity of known phytoalexins, **4**, **5**, and **8**. The inhibition rates of **4** and **8** were calculated as 51% and 22% at 300 μM after 5 days of incubation, respectively. However, **5** only slightly inhibited fungal growth. The inhibitory activities of **4** and **5** were approximately the same as that observed in previous reports.[12,13] Thus, the antifungal

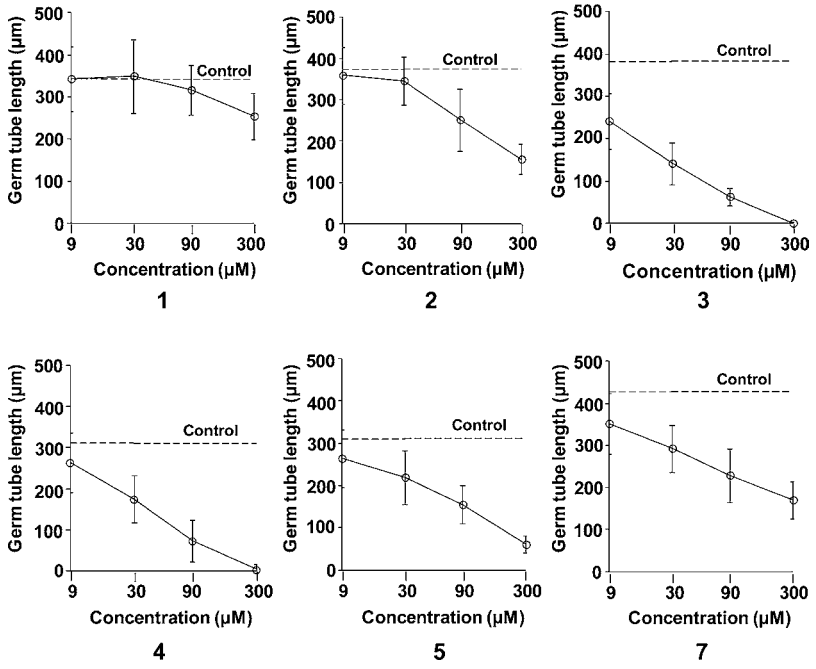

Figure 4. Antifungal activity of 9β-pimara-7,15-diene-3β,6β,19-triol, **1**, stemar-13-en-2α-ol, **2**, and 1α,2α-dihydroxy-*ent*-12,15-cassadiene-3,11-dione, **3**, against the germ tube growth of rice blast fungus. Values are presented as the mean ± SD (n = 100).

DOI: 10.1021/acs.jafc.5b00785
J. Agric. Food Chem. 2015, 63, 4050−4059

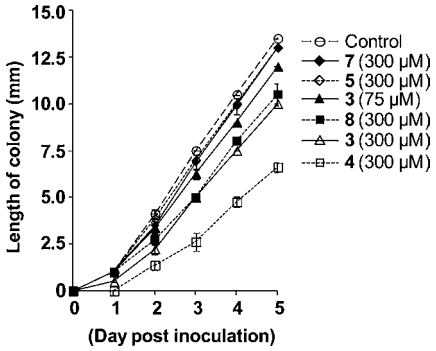

Figure 5. Antifungal activity of 1α,2α-dihydroxy-*ent*-12,15-cassadiene-3,11-dione, **3**, and phytoalexins against the mycelium growth of the rice blast fungus. Data are presented as means ± SD (n = 4) from four independent samples.

activity of **3** on mycelial growth was estimated to be approximately the same as that of **8** and lower than that of **4**.

The formation of compound **1** and **2** were induced by both UV irradiation and *M. oryzae* infection (Figure 3). However, **1** and **2** exhibited only slight antifungal activity on *M. oryzae* (Figure 4). Thus, these are not recognized as rice phytoalexins. Its structure clearly indicated that **1** should be biosynthesized by the oxidation of 9β-pimara-7,15-diene, which is a biosynthetic precursor of **5**. We speculated that **1** may be a biosynthetic intermediate of **5**. The structure of compound **2** suggested that **7** can be produced from **2** by the hydroxylation of the C-19. Kato et al.[20] identified a potential precursor of oryzalexins E and F, *ent*-isopimara-8(14),15-dien-3β-ol, from UV-irradiated rice leaves. They also confirmed that the enzymatic hydroxylation of each precursor was an important activation step for the antifungal activity of oryzalexins E and F.[19] In the case of **7**, C-19 oxidation is likely important for its antifungal activity.

The structure of **3** is regarded as 1-hydroxyphytocassane A, 3-dehydrophytocassane B, or 2-hydroxyphytocassane E. The accumulated level of **3** was approximately the same as that of **8** in the UV-irradiated and *M. oryzae*-inoculated leaves (Figure 3 and Table 3). Compound **8** has been reported to be the most abundant phytocassane in *M. oryzae*-inoculated rice leaves.[8] Thus, **3** is considered a major compound among rice cassane-type diterpenes. Phytocassanes A–D were isolated from *Rhizoctonia solani*-infected rice leaf stems,[7] and phytocassane E was isolated from elicitor-treated rice suspension cells.[8] We speculated that the difference between the materials may be critical to the isolation of **3** in this study. Moreover, compound **3** has a strong inhibitory activity on the spore germination and germ tube elongation of *M. oryzae*, to the same extent as **4** (Figure 4). The antifungal activity of **3** on fungal colony growth was greater than that of **5**, lower than that of **4** but approximately the same as that of **8** (Figure 5). Therefore, **3** is recognized as a phytoalexin with a *ent*-cassane-type diterpene skeleton and should be named phytocassane F.

Our study should contribute to greater understanding of the resistance of rice against *M. oryzae* and strengthen the foundation of phytoalexin biosynthetic pathways. In total, a flavanone **4** and 16 diterpene phytoalexins, including **3**, were identified from rice leaves.[2−11] Obara et al.[29] reported that many monoterpenes and sesquiterpenes were emitted from rice leaves in response to *M. oryzae* infection. Taniguchi et al.[38] also reported a volatile sesquiterpene, β-elemene, with an antifungal effect on *M. oryzae*. In addition to terpenoids, diverse antibacterial and antifungal components, such as oxidized fatty acids,[39] tryptophan-derived metabolites or phenylamides,[40,41] have been discovered in rice leaves. We found that **4** and **5** could be metabolized and detoxified by *M. oryzae*.[12,13,42] On the basis of these findings, we speculate that rice does not depend on only one or a few defensive compounds but rather divides its own resistant capacity among diverse compounds.

■ ASSOCIATED CONTENT

Supporting Information

Figure S1, Time-dependent accumulation of known phytoalexins in UV-irradiated and rice blast fungus-inoculated rice leaves; Figure S2, Representative images used for measuring the length of elongated germ tubes of rice blast fungus *M. oryzae*; Table S1, The ion source parameters for LC/MS/MS analyses; Table S2, LC/MS/MS conditions for quantitating **1**−**12** in the SRM mode. These materials are available free of charge via the Internet at http://pubs.acs.org.

■ AUTHOR INFORMATION

Corresponding Author

*E-mail: morifumi@mx.ibaraki.ac.jp. Tel.: +81-29-888-8660. Fax: +81-29-888-8525.

Present Address

[#](Q.Y.) Aikoku Gakuen University, 1532 Yotsukaido, Yotsukaido, Chiba 284-0005, Japan

Funding

This work was supported by JSPS KAKENHI Grant no. 22580113.

Notes

The authors declare no competing financial interest.

■ ACKNOWLEDGMENTS

Compounds **1** and **2** were discovered in our laboratory by Hideki Kato for the first time. Unfortunately, he passed away on May 13, 2010. We would like to express our respect for his pioneering work. We thank Shigeru Tamogami and Randeep Rakwal for critical reading of the manuscript. We thank Kazunori Okada for providing the standard solution of phytocassanes. We thank Hiroshi Kawaide for his helpful advice.

■ ABBREVIATIONS USED

COSY, correlated spectroscopy; DEPT, distortionless enhancement by polarization transfer; EI, electron ionization; FW, fresh weight; HMBC, heteronuclear multiple bond correlation; HSQC, heteronuclear single quantum coherence; HREIMS, high-resolution electron ionization mass spectrometry; NOESY, nuclear Overhauser enhancement and exchange spectroscopy; PDA, potato dextrose agar; SRM, selected reaction monitoring

■ REFERENCES

(1) Jwa, N.-S.; Agrawal, G. K.; Tamogami, S.; Yonekura, M.; Han, O.; Iwahashi, H.; Rakwal, R. Role of defense/stress-related marker genes, proteins and secondary metabolites in defining rice self-defense mechanisms. *Plant Physiol. Biochem. (Issy-les-Moulineaux, Fr.)* **2006**, *44*, 261−273.

(2) Akatsuka, T.; Kodama, O.; Sekido, H.; Kono, Y.; Takeuchi, S. Novel phytoalexins (oryzalexins A, B and C) isolated from rice blast leaves infected with *Pyricularia oryzae*. Part I: isolation, characterization

DOI: 10.1021/acs.jafc.5b00785
J. Agric. Food Chem. 2015, 63, 4050−4059

and biological activities of oryzalexins. *Agric. Biol. Chem.* **1985**, *49*, 1689−1694.
(3) Sekido, H.; Endo, T.; Suga, R.; Kodama, O.; Akatsuka, T.; Kono, Y.; Takeuchi, S. Oryzalexin D 3,7-dihydroxy-(+)-sandaracopimaradiene), a new phytoalexin isolated from blast-infected rice leaves. *J. Pestic. Sci. (Tokyo, Jpn.)* **1986**, *11*, 369−372.
(4) Kato, H.; Kodama, O.; Akatsuka, T. Oryzalexin E, a diterpene phytoalexin from UV-irradiated rice leaves. *Phytochemistry* **1993**, *33*, 79−81.
(5) Kato, H.; Kodama, O.; Akatsuka, T. Oryzalexin F, a diterpene phytoalexin from UV-irradiated rice leaves. *Phytochemistry* **1994**, *36*, 299−301.
(6) Kodama, O.; Li, W. X.; Tamogami, S.; Akatsuka, T. Oryzalexin S, a novel stemarane-type diterpene rice phytoalexin. *Biosci., Biotechnol., Biochem.* **1992**, *56*, 1002−1003.
(7) Koga, J.; Shimura, M.; Oshima, K.; Ogawa, N.; Yamauchi, T.; Ogasawara, N. Phytocassanes A, B, C and D, novel diterpene phytoalexins from rice, *Oryza sativa* L. *Tetrahedron* **1995**, *51*, 7907−7918.
(8) Koga, J.; Ogawa, N.; Yamauchi, T.; Kikuchi, M.; Ogasawara, N.; Shimura, M. Functional moiety for the antifungal activity of phytocassane E, a diterpene phytoalexin from rice. *Phytochemistry* **1997**, *44*, 249−253.
(9) Inoue, Y.; Sakai, M.; Yao, Q.; Tanimoto, Y.; Toshima, H.; Hasegawa, M. Identification of a novel casbane-type diterpene phytoalexin, *ent*-10-oxodepressin, from rice leaves. *Biosci., Biotechnol., Biochem.* **2013**, *77*, 760−765.
(10) Kodama, O.; Miyakawa, J.; Akatsuka, T.; Kiyosawa, S. Sakuranetin, a flavanone phytoalexin from ultraviolet-irradiated rice leaves. *Phytochemistry* **1992**, *31*, 3807−3809.
(11) Cartwright, D. W.; Langcake, P.; Pryce, R. J.; Leworthy, D. P.; Ride, J. P. Isolation and characterization of two phytoalexins from rice as momilactones A and B. *Phytochemistry* **1981**, *20*, 535−537.
(12) Hasegawa, M.; Mitsuhara, I.; Seo, S.; Imai, T.; Koga, J.; Okada, K.; Yamane, H.; Ohashi, Y. Phytoalexin accumulation in the interaction between rice and the blast fungus. *Mol. Plant-Microbe Interact.* **2010**, *23*, 1000−1011.
(13) Hasegawa, M.; Mitsuhara, I.; Seo, S.; Okada, K.; Yamane, H.; Iwai, T.; Ohashi, Y. Analysis on blast fungus-responsive characters of a flavonoid phytoalexin sakuranetin; accumulation in infected rice leaves, antifungal activity and detoxification by fungus. *Molecules* **2014**, *19*, 11404−11418.
(14) Toyomasu, T.; Usui, M.; Sugawara, C.; Otomo, K.; Hirose, Y.; Miyao, A.; Hirochika, H.; Okada, K.; Shimizu, T.; Koga, J.; Hasegawa, M.; Chuba, M.; Kawana, Y.; Kuroda, M.; Minami, E.; Mitsuhashi, W.; Yamane, H. Reverse genetic approach to verify physiological roles of rice phytoalexins: characterization of a knockdown mutant of *OsCPS4* phytoalexin biosynthetic gene in rice. *Physiol. Plant.* **2014**, *150*, 55−62.
(15) Peters, R. J. Uncovering the complex metabolic network underlying diterpenoid phytoalexin biosynthesis in rice and other cereal crop plants. *Phytochemistry* **2006**, *67*, 2307−2317.
(16) Toyomasu, T. Recent advances regarding diterpene cyclase genes in higher plants and fungi. *Biosci., Biotechnol., Biochem.* **2008**, *72*, 1168−1175.
(17) Yamane, H. Biosynthesis of phytoalexins and regulatory mechanisms of it in rice. *Biosci., Biotechnol., Biochem.* **2013**, *77*, 1141−1148.
(18) Mohan, R. S.; Yee, N. K. N.; Coates, R. M.; Ren, Y.-Y.; Stamenkovic, P.; Mendez, I.; West, C. A. Biosynthesis of cyclic diterpene hydrocarbons in rice cell suspensions: conversion of 9,10-*syn*-labda-8(17),13-dienyl diphosphate to 9β-pimara-7,15-diene and stemar-13-ene. *Arch. Biochem. Biophys.* **1996**, *330*, 33−47.
(19) Cho, E.-M.; Okada, A.; Kenmoku, H.; Otomo, K.; Toyomasu, T.; Mitsuhashi, W.; Sassa, T.; Yajima, A.; Yabuta, G.; Mori, K.; Oikawa, H.; Toshima, H.; Shibuya, N.; Nojiri, H.; Omori, T.; Nishiyama, M.; Yamane, H. Molecular cloning and characterization of a cDNA encoding *ent*-cassa-12,15-diene synthase, a putative diterpenoid phytoalexin biosynthetic enzyme, from suspension-cultured rice cells treated with a chitin elicitor. *Plant J.* **2004**, *37*, 1−8.
(20) Kato, H.; Kodama, O.; Akatsuka, T. Characterization of an inducible P450 hydroxylase involved in the rice diterpene phytoalexin biosynthetic pathway. *Arch. Biochem. Biophys.* **1995**, *316*, 707−712.
(21) Atawong, A.; Hasegawa, M.; Kodama, O. Biosynthesis of rice phytoalexin: enzymatic conversion of 3β-hydroxy-9β-pimara-7,15-dien-19,6β-olide to momilactone A. *Biosci., Biotechnol., Biochem.* **2002**, *66*, 566−570.
(22) Tamogami, S.; Rakwal, R.; Kodama, O. Phytoalexin production elicited by exogenously applied jasmonic acid in rice leaves (*Oryza sativa* L.) is under the control of cytokinins and ascorbic acid. *FEBS Lett.* **1997**, *412*, 61−64.
(23) Nakazato, Y.; Tamogami, S.; Kawai, H.; Hasegawa, M.; Kodama, O. Methionine-induced phytoalexin production in rice leaves. *Biosci., Biotechnol., Biochem.* **2000**, *64*, 577−583.
(24) Ko, K.-W.; Okada, K.; Koga, J.; Jikumaru, Y.; Nojiri, H.; Yamane, H. Effects of cytokinin on production of diterpenoid phytoalexins in rice. *J. Pestic. Sci. (Tokyo, Jpn.)* **2010**, *35*, 412−418.
(25) Kodama, O.; Yamada, A.; Yamamoto, A.; Takemoto, T.; Akatsuka, T. Induction of phytoalexins with heavy metal ions in rice leaves. *J. Pestic. Sci. (Tokyo, Jpn.)* **1988**, *13*, 615−617.
(26) Kodama, O.; Suzuki, T.; Miyakawa, J.; Akatsuka, T. Ultraviolet-induced accumulation of phytoalexins in rice leaves. *Agric. Biol. Chem.* **1988**, *52*, 2469−2473.
(27) Aida, Y.; Tamogami, S.; Kodama, O.; Tsukiboshi, T. Synthesis of 7-methoxyapigeninidin and its fungicidal activity against *Gloeocercospora sorghi*. *Biosci., Biotechnol., Biochem.* **1996**, *60*, 1495−1496.
(28) Kato, T.; Tsunakawa, M.; Sasaki, N.; Aizawa, H.; Fujita, K.; Kitahara, Y.; Takahashi, N. Growth and germination inhibitors in rice husks. *Phytochemistry* **1977**, *16*, 45−48.
(29) Obara, N.; Hasegawa, M.; Kodama, O. Induced volatiles in elicitor-treated and rice blast fungus-inoculated rice leaves. *Biosci., Biotechnol., Biochem.* **2002**, *66*, 2549−2559.
(30) Kato, T.; Aizawa, H.; Tsunakawa, M.; Sasaki, N.; Kitahara, Y.; Takahashi, N. Chemical transformation of the diterpene lactones momilactones A and B. *J. Chem. Soc., Perkin Trans. 1* **1977**, 250−254.
(31) Tamogami, S.; Mitani, M.; Kodama, O.; Akatsuka, T. Oryzalexin S structure: a new stemarane-type rice plant phytoalexin and its biogenesis. *Tetrahedron* **1993**, *49*, 2025−2032.
(32) Leonelli, F.; Latini, V.; Trombetta, A.; Bartoli, G.; Ceccacci, F.; La Bella, A.; Sferrazza, A.; Lamba, D.; Migneco, L. M.; Bettolo, R. M. Regio- and diastereoselective synthesis and X-ray structure determination of (+)-2-deoxyoryzalexin S from (+)-podocarpic acid. Structural nonidentity with its nominal natural isolated enantiomer. *J. Nat. Prod.* **2012**, *75*, 1944−1950.
(33) Chamy, M. C.; Piovano, M.; Garbarino, J. A.; Gambaro, V. Diterpenes from *Calceolaria polifolia*. *Phytochemistry* **1991**, *30*, 3365−3368.
(34) Garbarino, J. A.; Molinari, A. Diterpenes from *Calceolaria latifolia*. *Phytochemistry* **1990**, *29*, 3037−3039.
(35) Chamy, M. C.; Piovano, M.; Garbarino, J. A.; Miranda, C.; Gambaro, V. Diterpenes from *Calceolaria lepida*. *Phytochemistry* **1990**, *29*, 2943−2946.
(36) McCook, K. P.; Chen, A. R. M.; Reynolds, W. F.; Reese, P. B. The potential of *Cyathus africanus* for transformation of terpene substrates. *Phytochemistry* **2012**, *82*, 61−66.
(37) Yajima, A.; Mori, K. Absolute configuration of phytocassanes as proposed on the basis of the CD spectrum of synthetic (+)-2-deoxyphytocassane A. *Tetrahedron Lett.* **2000**, *41*, 351−354.
(38) Taniguchi, S.; Miyoshi, S.; Tamaoki, D.; Yamada, S.; Tanaka, K.; Uji, Y.; Tanaka, S.; Akimitsu, K.; Gomi, K. Isolation of jasmonate-induced sesquiterpene synthase of rice: product of which has an antifungal activity against *Magnaporthe oryzae*. *J. Plant Physiol.* **2014**, *171*, 625−632.
(39) Kato, T.; Yamaguchi, Y.; Uyehara, T.; Yokoyama, T.; Namai, T.; Yamanaka, S. Defense mechanism of the rice plant against rice blast disease. *Naturwissenschaften* **1983**, *70*, 200−201.
(40) Ishihara, A.; Hashimoto, Y.; Tanaka, C.; Dubouzet, J. G.; Nakao, T.; Matsuda, F.; Nishioka, T.; Miyagawa, H.; Wakasa, K. The tryptophan pathway is involved in the defense responses of rice against

DOI: 10.1021/acs.jafc.5b00785
J. Agric. Food Chem. 2015, 63, 4050−4059

pathogenic infection via serotonin production. *Plant J.* **2008**, *54*, 481−495.
(41) Park, H. L.; Yoo, Y.; Hahn, T.-R.; Bhoo, S. H.; Lee, S.-W.; Cho, M.-H. Antimicrobial activity of UV-induced phenylamides from rice leaves. *Molecules* **2014**, *19*, 18139−18151.
(42) Imai, T.; Ohashi, Y.; Mitsuhara, I.; Seo, S.; Toshima, H.; Hasegawa, M. Identification of a degradation intermediate of the momilactone A rice phytoalexin by the rice blast fungus. *Biosci., Biotechnol., Biochem.* **2012**, *76*, 414−416.

DOI: 10.1021/acs.jafc.5b00785
J. Agric. Food Chem. 2015, 63, 4050−4059

profile, some leaflets were crushed between fingertips and then orthonasally evaluated by experienced panelists familiar with authentic Sri Lankan cuisine.

Reference Odorants. **1**, **2**, (*R*)-**2**, (*S*)-**2**, **4**−**7**, **10**, **14**−**19**, (*R*)-**19**, **20**, **21**, and **23**−**27** were obtained from Sigma-Aldrich (Taufkirchen, Germany); **3**, **8**, **11**−**13**, (*R*)-**21**, and (*S*)-**26** were synthesized as detailed below.

Miscellaneous Chemicals and Reagents. 6-Methylheptanoic acid was purchased from Alfa Aesar (Karlsruhe, Germany). 7-Methyloctan-1-ol was from C/D/N Isotopes (Pointe-Claire, QC, Canada). Dess−Martin periodinane and (2*S*)-2-methylbutan-1-ol were from Sigma-Aldrich. Dichloromethane, diethyl ether, and pentane were freshly distilled before use. Silica gel 60 (0.040−0.063 mm) was purchased from VWR (Darmstadt, Germany) and purified as follows: After extraction with hydrochloric acid (32%; 3 h), the gel was washed with water until the eluate was acid free, dried at 120 °C until constant weight, and adjusted to 7% water content. Mercurated agarose gel was prepared from Affi-Gel 10 (Bio-Rad, Munich, Germany).[21]

Syntheses. The following reference odorants were synthesized using procedures detailed in the literature: **3**,[22] **11**,[23] **13**,[24] and (*S*)-**21**.[25] (*S*)-**26** was obtained from (2*S*)-2-methylbutan-1-ol by oxidation with Dess−Martin periodinane,[26] as detailed below for the synthesis of 6-methylheptanal.

6-Methylheptan-1-ol. In an argon atmosphere a solution of 6-methylheptanoic acid (288 mg, 2 mmol) in anhydrous diethyl ether (5 mL) was added to a suspension of lithium aluminum hydride (152 mg, 4 mmol) in anhydrous diethyl ether (10 mL) under stirring. The mixture was heated at reflux for 1 h. Under cooling (0 °C) a saturated aqueous ammonium chloride solution (10 mL) was added, followed by hydrochloric acid (2 mol/L; 10 mL). The phases were separated, and the aqueous phase was extracted with diethyl ether (10 mL). The combined organic phases were washed with saturated aqueous sodium hydrogen carbonate solution (5 mL) and dried over anhydrous sodium sulfate. The solvent was removed in vacuo to give 6-methylheptan-1-ol as a colorless oil (226 mg = 87%). RI FFAP, 1510; MS (EI, 70 eV), *m*/*z* (%) 39 (19), 40 (3), 41 (75), 42 (32), 43 (74), 44 (4), 45 (3), 53 (5), 54 (3), 55 (89), 56 (100), 57 (33), 67 (6), 68 (21), 69 (81), 70 (30), 71 (4), 83 (6), 84 (19), 97 (20), 98 (2).

*6-Methylheptanal (**8**).* 6-Methylheptan-1-ol (130 mg, 1 mmol) in dichloromethane (5 mL) was added to Dess−Martin periodinane (530 mg, 1.25 mmol) in dichloromethane (5 mL), and the mixture was stirred for 1 h at ambient temperature. Diethyl ether (80 mL) and a solution of sodium thiosulfate (1 mol/L; 100 mL) in saturated aqueous sodium hydrogen carbonate solution were added, and the mixture was intensely shaken until the initial opacity disappeared. The organic phase was washed with aqueous sodium hydrogen carbonate solution (0.5 mol/L; 100 mL) and dried over anhydrous sodium sulfate. The solvent was removed, and the raw product was purified by column chromatography with silica gel (6 g). After a washing with pentane (50 mL), the target compound was eluted with pentane/diethyl ether (45 mL + 5 mL) and its exact concentration in the eluate (50 mL) was determined by GC-FID using octanal as internal standard. Yield, 74.2 mg = 58%; purity, 90% (GC-FID); MS (EI, 70 eV), *m*/*z* (%) 39 (16), 41 (79), 42 (13), 43 (100), 44 (30), 45 (9), 53 (4), 55 (17), 56 (30), 57 (44), 67 (12), 68 (6), 69 (36), 71 (4), 82 (31), 83 (4), 84 (11), 85 (21), 93 (2), 95 (18), 100 (4), 109 (1), 110 (2); ^{1}H NMR (400 MHz, $CDCl_3$), δ 0.87 (d, 6H, J = 6.6 Hz, $CH(C\underline{H}_3)_2$), 1.15−1.26 (m, 2H, $CH_2C\underline{H}_2CH(CH_3)_2$), 1.28−1.37 (m, 2H, $CH_2C\underline{H}_2CH_2CH_2CHO$), 1.54 (nonet, 1H, J = 6.6 Hz, $CH_2C\underline{H}(CH_3)_2$), 1.61 (quint, 2H, J = 7.4 Hz, $CH_2C\underline{H}_2CH_2CHO$, 2.42 (td, 2H, J = 7.4, 1.9 Hz, $CH_2C\underline{H}_2CHO$), 9.76 (t, 1H, J = 1.9 Hz, $CH_2C\underline{H}O$); ^{13}C NMR (100 MHz, $CDCl_3$), δ 22.3 ($\underline{C}H_2CH_2CHO$), 22.5 ($CH(\underline{C}H_3)_2$), 26.9 ($\underline{C}H_2(CH_2)_2CHO$), 27.8 ($\underline{C}H(CH_3)_2$), 38.6 ($\underline{C}H_2CH(CH_3)_2$), 43.9 ($\underline{C}H_2CHO$), 203.0 (CHO).

*7-Methyloctanal (**12**).* Using the procedure detailed for **8**, **12** was obtained by oxidation of 7-methyloctan-1-ol (144 mg, 1 mmol) and purification by silica gel chromatography. The exact concentration of **12** in the eluate (50 mL) was determined by GC-FID using nonanal as internal standard. Yield, 64.4 mg = 45%; purity, 96% (GC-FID); MS (EI, 70 eV), *m*/*z* (%) 39 (16), 41 (73), 42 (16), 43 (78), 44 (32), 45 (7), 53 (4), 54 (6), 55 (63), 56 (68), 57 (100), 58 (5), 67 (24), 68 (18), 69 (24), 70 (15), 71 (9), 72 (3), 81 (27), 82 (16), 83 (9), 95 (7), 96 (11), 98 (5), 99 (4), 109 (19), 114 (3), 124 (3); ^{1}H NMR (400 MHz, $CDCl_3$), δ 0.87 (d, 6H, J = 6.6 Hz, $CH(C\underline{H}_3)_2$), 1.13−1.34 (m, 6H, $C\underline{H}_2C\underline{H}_2C\underline{H}_2CH(CH_3)_2$), 1.52 (nonet, 1H, J = 6.6 Hz, $CH_2C\underline{H}(CH_3)_2$), 1.58−1.67 (m, 2H, $CH_2C\underline{H}_2CH_2CHO$, 2.41 (td, 2H, J = 7.4, 1.9 Hz, $CH_2C\underline{H}_2CHO$), 9.75 (t, 1H, J = 1.9 Hz, $CH_2C\underline{H}O$); ^{13}C NMR (100 MHz, $CDCl_3$), δ 22.1 ($\underline{C}H_2CH_2CHO$), 22.5 ($CH(\underline{C}H_3)_2$), 27.1 ($\underline{C}H_2(CH_2)_3CHO$), 27.9 ($\underline{C}H(CH_3)_2$), 29.4 ($\underline{C}H_2(CH_2)_2CHO$), 38.7 ($\underline{C}H_2CH(CH_3)_2$), 43.9 ($\underline{C}H_2CHO$), 202.9 (CHO).

Isolation of Curry Leaf Volatiles. Curry leaves (10 g) and anhydrous sodium sulfate (50 g) were cryomilled at the temperature of liquid nitrogen. The obtained homogenate was added to dichloromethane (150 mL) and stirred for 30 min at ambient temperature. After filtration, nonvolatiles were removed by SAFE during 45 min at 40 °C. The distillate was concentrated to a final volume of 1 mL, first using a Vigreux column (50 × 1 cm) and subsequently a Bemelmans microdistillation device.[27] Separate curry leaf volatile isolates were prepared for screening by AEDA, fractionation by silica gel chromatography, and isolation of volatile curry leaf thiols.

Fractionation of Curry Leaf Volatiles. A curry leaf volatiles isolate prepared as detailed above was applied onto a slurry of purified silica gel (8 g) in pentane in a water-cooled (12 °C) glass column (1 cm i.d.). Elution was performed by pentane/diethyl ether mixtures of 100 + 0, 90 + 10, 70 + 30, 50 + 50, and 0 + 100 (v + v; 50 mL each), and the eluate was collected in 15 10 mL portions followed by two 50 mL portions. Each fraction was concentrated to 0.5 mL.

Isolation of Volatile Curry Leaf Thiols. From a curry leaf volatiles isolate prepared as detailed above, the thiols were isolated using a procedure published earlier[28] with some modifications. In detail, the isolate was initially applied onto mercurated agarose gel (1 g) in a glass column (0.5 cm i.d.). After the column had been rinsed with dichloromethane (50 mL), the thiols were eluted with dithiothreitol (10 mmol/L) in dichloromethane (50 mL). The excess of dithiothreitol was removed by SAFE distillation, and the distillate was concentrated to 0.5 mL.

GC-O and GC-FID Analyses. A Trace GC Ultra gas chromatograph (Thermo Scientific, Dreieich, Germany) was equipped with a cold-on-column injector, an FID, and a tailor-made sniffing port. The following fused silica columns were used: (1) DB-FFAP, 30 m × 0.32 mm i.d., 0.25 μm film; (2) DB-5, 30 m × 0.32 mm i.d., 0.25 μm film (both Agilent, Waldbronn, Germany); (3) BGB-176, 30 m × 0.25 mm i.d., 0.25 μm film; (4) BGB-174E, 30 m × 0.25 mm i.d., 0.25 μm film (both BGB Analytik, Rheinfelden, Germany). The carrier gas was helium at 70 kPa (DB-FFAP, DB-5) and 120 kPa (BGB-176, BGB-174E), respectively. The initial oven temperature was 40 °C (2 min). Gradients typically were 6 °C/min for DB-FFAP and DB-5 and 2 °C/min for BGB-176 and BGB-174E. For GC-O analyses, the column effluents were divided 1:1 using a deactivated Y-shaped glass splitter and two deactivated fused silica capillaries (50 cm × 0.25 mm i.d.) connecting the splitter to the FID and the sniffing port, respectively. The sniffing port consisted of a cylindrically shaped aluminum device (105 mm × 24 mm o.d.) with a beveled top and central drill hole (2 mm) housing the capillary. It was mounted on a heated (250 °C) detector base of the GC. During a GC-O run (35 min), the panelist placed her/his nose closely above the top of the device and sniffed the effluent. Whenever an odor was perceived, the retention time and the odor quality were noted in the FID chromatogram printed by a recorder. Linear retention indices (RI) of the odor-active compounds were calculated from their retention times and the retention times of adjacent *n*-alkanes by linear interpolation. GC-O analyses of the concentrated curry leaf volatiles isolate were performed by six trained panelists, and results were combined.

AEDA. The concentrated curry leaf volatiles isolate (1 mL) was stepwise diluted 1:2 with dichloromethane to obtain dilutions of 1:2, 1:4, 1:8, 1:16, etc. Each diluted sample was then analyzed by GC-O using the FFAP column. Odor-active compounds were assigned a flavor dilution (FD) factor, representing the dilution factor of the

DOI: 10.1021/acs.jafc.5b01174
J. Agric. Food Chem. 2015, 63, 4060−4067

Table 1. Odorants in the SAFE Distillate Obtained from Fresh Curry Leaves

no.	odorant[a]	odor[b]	RI[c] FFAP	RI[c] DB-5	FD factor[d]	first report[e]
1	butane-2,3-dione[f]	buttery	980	960	8	–
2	α-pinene	resinous, terpeny	1031	931	2048	3
3	3-methylbut-2-ene-1-thiol[f]	skunky	1112	820	16	–
4	(3*Z*)-hex-3-enal	green, grassy	1151	800	256	–
5	myrcene	terpeny, geranium leaf-like	1167	992	64	4
6	limonene	terpeny, citrusy	1181	1028	2	2
7	1,8-cineole	terpeny, eucalyptus-like	1222	1031	1024	7
8	6-methylheptanal	citrusy, soapy	1232	964	4	–
9	unknown	mushroom-like	1252	–	8	
10	octanal	citrusy, soapy	1278	1004	4	–
11	2-acetyl-1-pyrroline	roasty, popcorn-like	1335	915	8	–
12	7-methyloctanal	citrusy, soapy	1340	1068	4	–
13	(5*Z*)-octa-1,5-dien-3-one[f]	metallic, geranium leaf-like	1369	984	8	–
14	(3*Z*)-hex-3-en-1-ol	green, grassy	1378	854	32	4
15	nonanal	citrusy, soapy	1385	1104	1	8
16	(2*E*)-oct-2-enal	fatty, nutty	1425	1057	8	–
17	3-(methylsulfanyl)propanal	cooked potato-like	1458	917	128	–
18	3-isobutyl-2-methoxypyrazin[f]	bell pepper-like	1517	1185	4	–
19	linalool	citrusy	1546	1100	4096	4
20	(2*E*,6*Z*)-nona-2,6-dienal	cucumber-like	1580	1159	32	–
21	1-phenylethanethiol	sulfury, burnt	1601	1120	8192	–
22	calamenene[g]	clove-like	1818	1544	8	–
23	γ-heptalactone[f]	coconut-like	1822	1165	4	–

[a]Each odorant was identified by comparing its retention indices on two GC capillaries of different polarity (FFAP, DB-5) and its mass spectrum obtained by GC-MS, as well as its odor quality as perceived at the sniffing port during GC-O with data obtained from authentic reference compounds analyzed in parallel. [b]Odor quality as perceived at the sniffing port during GC-O. [c]Retention index; calculated from the retention time of the compound and the retention times of adjacent *n*-alkanes by linear interpolation. [d]Flavor dilution factor;[20] dilution factor of the highest dilution of the concentrated SAFE distillate in which the odorant was detected during GC-O by any of three panelists. [e]Reference reporting the compound for the first time as a curry leaf volatile. The dash (−) indicates compounds that have not been reported in curry leaves before. [f]A clear mass spectrum of the compound could not be obtained in the curry leaf isolates, identification was based on the remaining criteria detailed in footnote *a*. [g]No reference compound was available. The compound was tentatively identified on the basis of MS database[30] spectra and RI data in the literature.[34] Stereochemistry was not assigned.

highest dilution in which the respective odorant was detected by any of three trained panelists (two females, one male).

Gas Chromatography−Mass Spectrometry (GC-MS). Mass spectra were generated in the electron impact (EI) mode at 70 eV and a scan range of *m*/*z* 35−300 using a HP 5890 gas chromatograph (Hewlett-Packard, Heilbronn, Germany) connected to an MAT 95 sector field mass spectrometer (Finnigan, Bremen, Germany). Columns and further GC conditions were equivalent to those used in the GC-O analyses.

Static Headspace Gas Chromatography (SH-GC). Curry leaves (1 g) and anhydrous sodium sulfate (5 g) were cryomilled, and the homogenate was placed into a 20 mL septum-sealed vial. After 5 min at ambient temperature, 5 mL of the headspace was withdrawn using a gastight syringe and injected by means of a Combi PAL autosampler (CTC Analytics, Zwingen, Switzerland) via a cold-on-column injector (helium, 110 kPa) onto a deactivated fused silica precolumn (0.2 m × 0.53 mm i.d.) installed in a Trace GC Ultra gas chromatograph (Thermo). Volatiles were trapped on the precolumn using a cold trap 915 at −150 °C. The precolumn was connected to the main column and an outlet solenoid valve via a three-way connector. During trapping, the solenoid valve was open to maintain a flow of 20 mL/min through the precolumn. After injection had been finished, the solenoid valve was closed, and the trap was heated to 250 °C to transfer the trapped volatiles onto the main column, a DB-5, 30 m × 0.25 mm i.d., 1 μm film (Agilent). The oven start temperature was 0 °C maintained by liquid nitrogen oven cooling. After 2 min, the temperature was raised at 6 °C/min. The end of the main column was connected to a pressure-controlled stream switching system (S+H Analytik, Mönchengladbach, Germany), which transferred the eluate to an FID and a sniffing port and/or a Saturn 2100 mass spectrometer (Varian, Darmstadt, Germany).

Two-Dimensional Heart-Cut Gas Chromatography−Mass Spectrometry (GC-GC-MS). A Combi PAL autosampler (CTC) was mounted on a Trace GC Ultra equipped with a cold-on-column injector (Thermo) and an FFAP capillary, 30 m × 0.32 mm i.d., 0.25 μm film, or a DB-5 capillary, 30 m × 0.25 mm i.d., 1 μm film (Agilent). The column end was connected to a moving column stream switching system (MCSS) (Thermo), conveying the eluate time-programmed through deactivated fused silica capillaries (0.32 mm i.d.) either simultaneously to an FID and a sniffing port or via a heated (250 °C) transfer line to a cold trap localized in the oven of a CP 3800 GC (Varian). The tailor-made trap consisted of a piece of steel tubing housing the capillary and could be cooled by means of liquid nitrogen. Downstream, the capillary was connected to the BGB-176 or BGB-174E column described above. The end of this column was connected to a Saturn 2200 mass spectrometer (Varian) operated in the CI mode with methanol as reagent gas. For the determination of the enantiomeric distribution of **2**, **19**, and **21**, start temperatures were 40 °C (2 min) and gradients were 6 °C/min in the first dimension (FFAP) and 3 °C/min in the second dimension (BGB-176). For the determination of the enantiomeric distribution of **26**, start temperatures were 40 °C (2 min) and 35 °C (2 min) and gradients were 1 and 2 °C/min, in the first (DB-5) and second dimensions (BGB-174E), respectively. A heart-cut (0.5 min) of the eluate of the first column containing the respective target compound was transferred via the MCSS and the transfer line to the precooled trap. Then the trap cooling was turned off, and the second oven was started. The retention times of the target compounds in the first and second dimensions were previously determined using reference compounds.

NMR Spectroscopy. ^{1}H and ^{13}C NMR spectra were recorded at 25 °C using an Avance 400 NMR spectrometer (Bruker, Rheinstetten, Germany) and tetramethylsilane as the internal standard (δ = 0.00

DOI: 10.1021/acs.jafc.5b01174
J. Agric. Food Chem. 2015, 63, 4060−4067

ppm). Correct signal assignment was confirmed by 2D NMR spectroscopy using COSY, HMQC, and HMBC experiments (data not shown).

RESULTS AND DISCUSSION

Screening the Curry Leaf Volatiles for Odorants by AEDA. Freshly picked curry leaflets were cryomilled under addition of anhydrous sodium sulfate. The obtained powder was extracted by dichloromethane. Then, SAFE was applied on the extract to remove any nonvolatile material. The SAFE distillate, when placed on a fragrance test strip and sniffed after evaporation of the solvent, still fully reflected the characteristic aroma of fresh curry leaves. The SAFE distillate was gently concentrated, and the concentrate was submitted to AEDA.

AEDA resulted in 23 odorants in the FD factor range of 1−8192 (Table 1). The highest FD factor (8192) was found for sulfury- and burnt-smelling odorant **21**, clearly resembling the dominating aroma note in the overall sensory profile of the curry leaves. High FD factors were further determined for citrusy-smelling odorant **19** (FD 4096), resinous-smelling odorant **2** (FD 2048), eucalyptus-like-smelling odorant **7** (FD 1024), grassy-smelling odorant **4** (FD 256), and cooked potato-like-smelling odorant **17** (FD 128).

Structural Assignment of Odorants. As a first step, the RIs and odor descriptors of the odorants detected during AEDA were compared to previously published data of roughly 1600 odor-active compounds compiled in an in-house database. In the case of matching data, authentic reference compounds were obtained by purchase or synthesis and analyzed in an appropriate dilution by GC-O in parallel (i.e., same instrument, same day) to the curry leaf volatiles isolate. Because retention time and odor characteristics of the compound in the curry leaf volatiles isolate were in agreement with the retention time and odor characteristics of the reference compound on two GC-O systems of different separation phase polarities (DB-5, FFAP), the structures of 19 of the 23 curry leaf odorants (**1**−**7**, **10**, **11**, **13**−**21**, **23**) could be assigned. Final confirmation of these assignments was made by comparing the mass spectra of the curry leaf odorants and the reference compounds as obtained by GC-MS analysis. To avoid any overlay of mass spectra due to coelution, a particular problem with odor-active trace compounds, the curry leaf volatiles isolate was further fractionated before GC-MS analysis. Using silica gel as stationary phase and pentane/diethyl ether mixtures as eluents, the curry leaf volatiles were separated into 17 fractions according to their polarity. In a separate experiment, the thiols among the curry leaf volatiles were selectively isolated using mercurated agarose gel. Each fraction was then analyzed by GC-O to localize the odorants. Fractions containing any odorant detected during AEDA were subjected to GC-MS analysis (DB-5 and FFAP) in parallel with the reference compounds.

Using this approach, 14 of the 19 previously assigned structures were confirmed by mass spectral data, among them all odorants with high (≥32) FD factors (Figure 1). Sulfury- and burnt-smelling odorant **21**, exhibiting the highest FD factor (8192) in the AEDA, was recovered in the thiol fraction and finally identified as 1-phenylethanethiol. 1-Phenylethanethiol has not yet been reported in curry leaves and has rarely been found in nature before. Its only mention as an odor-active compound refers to Pontianak orange peel oil,[25] where it significantly contributes to the specific odor.[29] In that study, it was observed that 1-phenylethanethiol, when exposed to

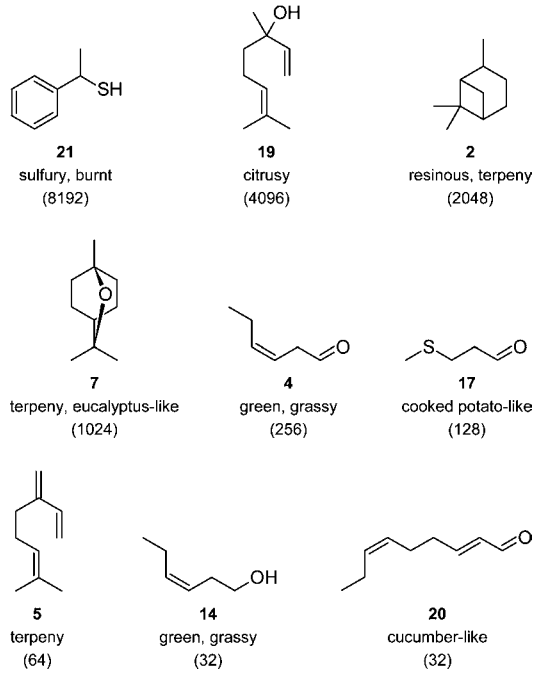

Figure 1. Most potent odorants (FD factor ≥ 32) in the SAFE distillate obtained from fresh curry leaves. FD factors are given in parentheses.

increased temperatures, readily undergoes 1,2-elimination to form H_2S and styrene.[25] This might explain why the compound has escaped discovery in curry leaves so far. The compound might have been destroyed by the high temperatures applied during hydrodistillation or in the hot GC injection port. This finding exemplifies the importance of avoiding elevated temperatures in aroma research, for example, by using mild isolation techniques such as SAFE and by using the cold-on-column injection technique in GC.

Odorants **19**, **2**, and **7**, assigned the second (4096), third (2048), and fourth highest FD factors (1024) in the AEDA, were identified as citrusy-smelling linalool, resinous-smelling *α*-pinene, and eucalyptus-like-smelling 1,8-cineole. All three have been identified in curry leaves before, but their high aroma potency has not been recognized yet. Further odorants with comparatively high FD factors were identified as (3*Z*)-hex-3-enal (green, grassy; FD 256; **4**), 3-(methylsulfanyl)propanal (cooked potato-like; FD 128; **17**), myrcene (terpeny, geranium leaf-like; FD 64; **5**), (3*Z*)-hex-3-en-1-ol (green, grassy; FD 32; **14**), and (2*E*,6*Z*)-nona-2,6-dienal (cucumber-like; FD 32; **20**). Of these, only myrcene has been reported as curry leaf constituent before. Mass spectral confirmation of the structural assignment was furthermore achieved for 2-acetyl-1-pyrroline (roasty, popcorn-like; FD 8; **11**), (2*E*)-oct-2-enal (fatty, nutty; FD 8; **16**), octanal (citrusy, soapy; FD 4; **10**), limonene (terpeny, citrusy; FD 2; **6**), and nonanal (citrusy, soapy; FD 1; **15**). No clear mass spectra were obtained for five trace odorants with low FD factors (**1**, **3**, **13**, **18**, **23**). However, their retention times and odor properties on the two GC-O systems (DB-5, FFAP) were identical to those of butane-2,3-dione (**1**), 3-methylbut-2-ene-1-thiol (**3**), (5*Z*)-octa-1,5-dien-3-one (**13**), 3-isobutyl-2-methoxypyrazin (**18**), and *γ*-heptalactone (**23**).

The retention indices and odor qualities of four odorants (**8**, **9**, **12**, **22**) did not match with any available database entries, but GC-MS analyses of the curry leaf fractions resulted in

DOI: 10.1021/acs.jafc.5b01174
J. Agric. Food Chem. 2015, 63, 4060−4067

congruent mass spectra on both separation systems (DB-5, FFAP) for odorants **8**, **12**, and **22**.

An MS database[30] library search applied on the mass spectra of odorants **8** and **12** (Figure 2) returned octanal and nonanal,

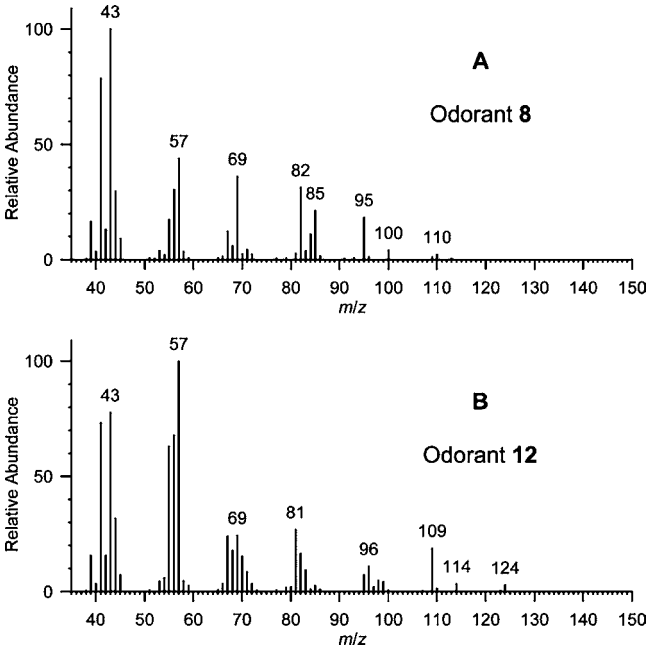

Figure 2. Mass spectra (EI) obtained for the citrusy-, soapy-smelling odorants **8** (A) and **12** (B) isolated from curry leaves.

respectively, with high matching factors. Octanal and nonanal, which had also been detected by AEDA of the curry leaf volatiles (odorants **10** and **15**), however, showed clearly different RIs. On the other hand, the similarities in the mass spectra were obvious. Similar to octanal (MS not shown), odorant **8** showed characteristic fragments of *m/z* 110, corresponding to a loss of water from the molecular ion *m/z* 128, and *m/z* 110, corresponding to a loss of carbon monoxide, thus suggesting the presence of an aldehyde group and a molecular mass of 128 u in analogy to octanal. Accordingly, odorant **12** showed fragments of *m/z* 124 and 114 in analogy to nonanal. Odorants **8** and **12** not only shared similar mass spectra with octanal and nonanal but also appeared in the same fraction after silica gel chromatography and exhibited virtually the same citrusy, soapy odor quality. In summary, the data suggested that odorants **8** and **12** were chain isomers of octanal and nonanal. A branched carbon skeleton would also correspond to the clearly lower RIs of odorants **8** (DB-5, 964; FFAP, 1232) and **12** (DB-5, 1068; FFAP, 1340) in comparison to octanal (DB-5, 1004; FFAP, 1278) and nonanal (DB-5, 1104; FFAP, 1385), respectively. Branched isomers typically show lower RIs than the corresponding straight-chain molecules due to their smaller surface and thus lower ability to interact with the GC stationary phase. Type and position of the branching, however, were difficult to predict. The similarity in the odor qualities at least suggested that the branching was rather distant from the odotope, that is, rather not too close to the aldehyde group.

Following the latter idea, we hypothesized that odorant **8** could be 6-methylheptanal. The compound was synthesized from commercially available 6-methylheptanoic acid by reduction with lithium aluminum hydride and subsequent reoxidation of the obtained alcohol to the aldehyde using Dess–Martin periodinane. Analysis of the synthesized compound by GC-O and GC-MS on the two separation systems (DB-5, FFAP) resulted in the same data as obtained for odorant **8**, which thus was finally identified as 6-methylheptanal. 6-Methylheptanal has not been reported from curry leaves yet, but has been found among the volatiles of other plants in the rue family.[31−33] In particular, it has been found as an aroma-active compound in mandarin peel oils[32] and orange essence oil.[31]

As odorant **12** exhibited RIs (DB-5, 1068; FFAP, 1340) that were approximately 100 units higher than those of 6-methylheptanal (DB-5, 964; FFAP, 1232), it was assumed to be its homologue, 7-methyloctanal. Synthesis of the compound by oxidation of the corresponding alcohol 7-methyloctan-1-ol confirmed this structural assignment, and odorant **12** was finally identified as 7-methyloctanal. This compound has rarely been reported from nature yet, and was also previously unknown as curry leaf constituent.

Clove-like-smelling odorant **22**, after silica gel fractionation, was recovered in the hydrocarbon fraction. Its mass spectrum matched the MS database[30] entry of calamenene, an aromatized sesquiterpene hydrocarbon, and its RI was in agreement with data from the literature.[34] However, no reference compound was available. For that reason, the identification of calamenene remained tentative.

No mass spectrum could be obtained for mushroom-like-smelling odorant **9**. Its odor quality, however, was clearly reminiscent of the odor of the button mushroom impact compound 1-octene-3-one. Taking into account that the RI of odorant **9** (FFAP, 1252) was lower than that of 1-octene-3-one (1293), and the difference was similar to that observed for the methyl-branched aldehydes **8** and **12** and their respective straight-chain isomers, it might be speculated that compound **9** could be a branched isomer of 1-octene-3-one such as 6-methyl-1-hepten-3-one. However, no attempt was made to prove this assumption, and odorant **9**, therefore, remained unidentified.

Screening for Highly Volatile Odorants by SH-GC-O. Very highly volatile odorants with boiling points below that of the extraction solvent are not covered by AEDA, because they are lost during the concentration of the SAFE distillate, so a static headspace GC-O analysis was performed as a complementary screening method. Four additional odorants were detected in the headspace above freshly cut curry leaves and structurally assigned by comparing their GC-O and GC-MS data with those of reference compounds. These odorants were fresh-, green-, and fruity-smelling acetaldehyde (**24**) and the malty-smelling compounds 2-methylpropanal (**25**), 2-methylbutanal (**26**), and 3-methylbutanal (**27**) (Table 2).

Enantiomeric Distribution of Chiral Curry Leaf Odorants. As enantiomers of chiral odorants may exhibit different odor thresholds or even different odor qualities, proper structure assignment of odor-active compounds must include the determination of the enantiomeric ratio. Seven of the total of 26 structurally assigned curry leaf odorants in this study were chiral. Among these were the three compounds with the highest FD factors in the AEDA, namely, 1-phenylethanethiol (**21**), linalool (**19**), and α-pinene (**2**), as well as highly volatile 2-methylbutanal (**26**) detected by SH-GC-O. To determine their enantiomeric ratios, a heart-cut GC-GC-MS system was equipped with a chiral cyclodextrin phase in the second dimension. Baseline separation of the enantiomers was achieved

DOI: 10.1021/acs.jafc.5b01174
J. Agric. Food Chem. 2015, 63, 4060−4067

Table 2. Odorants (RI DB-5 < 1000) in the Headspace above Fresh Curry Leaves

no.	odorant[a]	odor[b]	RI[c] DB-5	first report[d]
24	acetaldehyde	fresh, green, fruity	<500	–
25	2-methylpropanal	malty	550	–
1	butane-2,3-dione	buttery	580	–
26	2-methylbutanal[e]	malty	649	2
27	3-methylbutanal[e]	malty	649	–
4	(3*Z*)-hex-3-enal	green, grassy	800	–
2	α-pinene	resinous, terpeny	931	3
5	myrcene	terpeny, geranium leaf-like	992	4

[a]Each odorant was identified by comparing its retention index on capillary DB-5 and its mass spectrum obtained by GC-MS, as well as its odor quality as perceived at the sniffing port during GC-O, with data obtained from authentic reference compounds analyzed in parallel. [b]Odor quality as perceived at the sniffing port during GC-O. [c]Retention index; calculated from the retention time of the compound and the retention times of adjacent *n*-alkanes by linear interpolation. [d]Reference reporting the compound for the first time as a curry leaf volatile. The dash (−) indicates compounds that have not been reported in curry leaves before. [e]Methylbutanal isomers were not separated on the GC column used.

by using a 2,3-dimethyl-6-*tert*-butyldimethylsilyl-derivatized β-cyclodextrin-based phase for α-pinene (**2**), linalool (**19**), and 1-phenylethanethiol (**21**) and a 2,3-diacetyl-6-*tert*-butyldimethylsilyl-derivatized β-cyclodextrin-based phase for 2-methylbutanal (**26**). The elution order of the enantiomers was determined by analyzing enantiopure samples of the target compounds. Because of their comparatively low FD factors, no efforts were made to determine the enantiomeric ratios of limonene (**6**), calamenene (**22**), and γ-heptalactone (**23**).

Results showed enantiomeric ratios apparently different from racemic mixtures for all four compounds analyzed, but the odor qualities of the respective optical antipodes as perceived during GC-O analysis were virtually the same (Table 3). In α-pinene, the (1*S*,5*S*)-isomer clearly dominated with 93%. The threshold values reported in the literature, however, were in the same range for both enantiomers.[35] In linalool, an enantiomeric ratio of 62/38 was found in favor of the more odor-active[36] (3*R*)-form. The *R*-isomer also predominated in 1-phenylethanethiol. Its percentage in the curry leaves (67% *R*) was close to that recently reported in Pontianak orange peel oil (76% *R*).[25] As Pontianak oranges belong to the genus *Citrus* and thus also to the Rutaceae family, the similarity in the enantiomeric ratio may reflect a common biosynthetic pathway. The odor thresholds of (1*R*)- and (1*S*)-1-phenylethanethiol were reported to be in the same order of magnitude.[25]

In summary, gentle isolation of the volatile fraction from fresh curry leaves followed by systematic and nontargeted screening for odor-active compounds by application of an AEDA and a SH-GC-O analysis resulted in a total number of 27 odorants, among which, on the basis of their high FD factors, sulfury-smelling 1-phenylethanethiol, citrusy-smelling linalool, resinous-smelling α-pinene, eucalyptus-like-smelling 1,8-cineole, and grassy-smelling (3*Z*)-hex-3-enal most likely show a vital contribution to the overall aroma. To confirm this assumption and to unequivocally identify the key aroma compounds of fresh curry leaves, further experiments are currently under way. These will include exact quantitation of the most potent odorants detected in the screening experiments, the sensory evaluation of aroma reconstitution models based on the obtained concentration data as proof of success, and finally omission tests to assess the contribution of the individual odorants to the overall aroma of curry leaves.[37] The omission tests will particularly elucidate whether 1-phenylethanethiol can be considered as the character impact compound of fresh curry leaves. Its exceedingly high FD factor, its characteristic sulfury and burnt odor quality, and the absence of any other potent odorant with a sulfury odor note, however, support this assumption.

AUTHOR INFORMATION

Corresponding Author

*Phone: +49 8161 71 2991. Fax: +49 8161 71 2970. E-mail: martin.steinhaus@lrz.tum.de.

Notes

The authors declare no competing financial interest.

ACKNOWLEDGMENTS

We gratefully acknowledge the skillful technical assistance of Julia Bock, Anja Matern, and Vanessa Wehner.

ABBREVIATIONS USED

FD factor, flavor dilution factor; GC-O, gas chromatography−olfactometry; GC-GC-MS, two-dimensional heart-cut gas

Table 3. Enantiomeric Distribution of Important Chiral Curry Leaf Odorants

no.	odorant	odor[a]	column[b]	RI[c]	enantiomeric ratio in curry leaves[d]
(*R*)-**2**	(1*R*,5*R*)-α-pinene	resinous, terpeny	BGB-176	988	7
(*S*)-**2**	(1*S*,5*S*)-α-pinene	resinous, terpeny		982	93
(*R*)-**19**	(3*R*)-linalool	citrusy	BGB-176	1200	62
(*S*)-**19**	(3*S*)-linalool	citrusy		1209	38
(*R*)-**21**	(1*R*)-1-phenylethanethiol	sulfury, burnt	BGB-176	1245	67
(*S*)-**21**	(1*S*)-1-phenylethanethiol	sulfury, burnt		1241	33
(*R*)-**26**	(2*R*)-2-methylbutanal	malty	BGB-174E	972	7
(*S*)-**26**	(2*S*)-2-methylbutanal	malty		979	93

[a]Odor quality as perceived at the sniffing port during GC-O using the chiral column specified. [b]BGB-176, chiral column based on 2,3-dimethyl-6-*tert*-butyldimethylsilyl-β-cyclodextrin (30%); BGB-174E, chiral column based on 2,3-diacetyl-6-*tert*-butyldimethylsilyl-β-cyclodextrin. [c]Retention index; calculated from the retention time of the compound and the retention times of adjacent *n*-alkanes by linear interpolation using the chiral column specified. [d]Mean of duplicates.

DOI: 10.1021/acs.jafc.5b01174
J. Agric. Food Chem. 2015, 63, 4060−4067

chromatography−mass spectrometry; MCSS, moving column stream switching system; RI, retention index; SAFE, solvent-assisted flavor evaporation; SH-GC, static headspace gas chromatography

Nomenclature

2-acetyl-1-pyrroline, 1-(3,4-dihydro-2*H*-pyrrol-5-yl)ethanone; calamenene, 1,6-dimethyl-4-(propan-2-yl)-1,2,3,4-tetrahydronaphthalene; 1,8-cineole, 2,2,4-trimethyl-3-oxabicyclo[2.2.2]-octane; Dess−Martin periodinane, 1,1,1-tris(acetyloxy)-1,1-dihydro-1,2-benziodoxol-3-(1*H*)-one); γ-heptalactone, 5-propyldihydrofuran-2(3*H*)-one; limonene, 1-methyl-4-prop-1-en-2-ylcyclohexene; linalool, 3,7-dimethylocta-1,6-dien-3-ol; myrcene, 7-methyl-3-methylideneocta-1,6-diene

REFERENCES

(1) U.S. Department of Agriculture, Agricultural Research Service, National Genetic Resources Program. GRIN, Germplasm Resources Information Network, online database; National Germplasm Resources Laboratory, Beltsville, MD, USA; http://www.ars-grin.gov (accessed March 5, 2015).

(2) Macleod, A. J.; Pieris, N. M. Analysis of the volatile essential oils of *Murraya koenigii* and *Pandanus latifolius*. *Phytochemistry* **1982**, *21*, 1653−1657.

(3) Li, Q.; Zhu, L. F.; But, P. P. H.; Kong, Y. C.; Chang, H. T.; Waterman, P. G. Monoterpene and sesquiterpene rich oils from the leaves of *Murraya* species: chemotaxonomic significance. *Biochem. Syst. Ecol.* **1988**, *16*, 491−494.

(4) Wong, K. C.; Tie, D. Y. The essential oil of the leaves of *Murraya koenigii* Spreng. *J. Essent. Oil Res.* **1993**, *5*, 371−374.

(5) Mallavarapu, G. R.; Ramesh, S.; Syamasundar, K. V.; Chandrasekhara, R. S. Composition of Indian curry leaf oil. *J. Essent. Oil Res.* **1999**, *11*, 176−178.

(6) Mallavarapu, G. R.; Rao, L.; Ramesh, S. Volatile constituents of the leaf and fruit oils of *Murraya koenigii* Spreng. *J. Essent. Oil Res.* **2000**, *12*, 766−768.

(7) Onayade, O. A.; Adebajoa, A. C. Composition of the leaf volatile oil of *Murraya koenigii* growing in Nigeria. *J. Herbs, Spices Med. Plants* **2000**, *7*, 59−66.

(8) Raina, V. K.; Lal, R. K.; Tripathi, S.; Khan, M.; Syamasundar, K. V.; Srivastava, S. K. Essential oil composition of genetically diverse stocks of *Murraya koenigii* from India. *Flavour Fragrance J.* **2002**, *17*, 144−146.

(9) Walde, S. G.; Jyothirmayi, T.; Rao, P. G. P.; Shivaswamy, R.; Srinivas, P. Flavour volatiles of leaves, fruits and seed cotyledons of *Murraya koenigii* L. *Flavour Fragrance J.* **2005**, *20*, 169−172.

(10) Chowdhury, J. U.; Bhuiyan, M. N. I.; Yusuf, M. Chemical composition of the leaf essential oils of *Murraya koenigii* (L.) Spreng and *Murraya paniculata* (L.) Jack. *Bangladesh J. Pharmacol.* **2008**, *3*, 59−63.

(11) Padmakumari, K. P. Free and glycosidically bound volatiles in curry leaves (*Murraya koenigii*) (L) Spreng. *J. Essent. Oil Res.* **2008**, *20*, 479−481.

(12) Rajeswara Rao, B. R.; Rajput, D. K.; Mallavarapu, G. R. Chemotype characterization of curry leaf plants. *J. Essent. Oil-Bear. Plants* **2011**, *14*, 1−10 (review and meta-analysis). .

(13) Rao, B. R. R.; Rajput, D. K.; Mallavarapu, G. R. Chemical diversity in curry leaf (*Murraya koenigii*) essential oils. *Food Chem.* **2011**, *126*, 989−994.

(14) Nagappan, T.; Ramasamy, P.; Vairappan, C. S. Chemotaxonomical markers in essential oil of *Murraya koenigii*. *Nat. Prod. Commun.* **2012**, *7*, 1375−1378.

(15) Verma, R. S.; Padalia, R. C.; Arya, V.; Chauhan, A. Aroma profiles of the curry leaf, *Murraya koenigii* (L.) Spreng. chemotypes: variability in north India during the year. *Ind. Crops Prod.* **2012**, *36*, 343−348.

(16) Verma, R. S.; Chauhan, A.; Padalia, R. C.; Jat, S. K.; Thul, S.; Sundaresan, V. Phytochemical diversity of *Murraya koenigii* (L.) Spreng. from western Himalaya. *Chem. Biodiversity* **2013**, *10*, 628−641.

(17) Rajendran, M. P.; Pallaiyan, B. B.; Selvaraj, N. Chemical composition, antibacterial and antioxidant profile of essential oil from *Murraya koenigii* (L.) leaves. *Avicenna J. Phytomed.* **2014**, *4*, 200−214.

(18) Sukkaew, S.; Pripdeevech, P.; Thongpoon, C.; Machan, T.; Wongchuphan, R. Volatile constituents of *Murraya koenigii* fresh leaves using headspace solid phase microextraction−gas chromatography−mass spectrometry. *Nat. Prod. Commun.* **2014**, *9*, 1783−1786.

(19) Engel, W.; Bahr, W.; Schieberle, P. Solvent assisted flavour evaporation − a new and versatile technique for the careful and direct isolation of aroma compounds from complex food matrices. *Eur. Food Res. Technol.* **1999**, *209*, 237−241.

(20) Schieberle, P.; Grosch, W. Evaluation of the flavor of wheat and rye bread crusts by aroma extract dilution analysis. *Z. Lebensm.-Unters. Forsch.* **1987**, *185*, 111−113.

(21) Bio-Rad Laboratories, Munich, Germany; http://www.bio-rad.com/webroot/web/html/lsr/tech_support_faqs/FAQ268439460.html (accessed March 5, 2015).

(22) Holscher, W.; Vitzthum, O. G.; Steinhart, H. Prenyl alcohol source for odorants in roasted coffee. *J. Agric. Food Chem.* **1992**, *40*, 655−658.

(23) Buttery, R. G.; Ling, L. C.; Juliano, B. 2-Acetyl-1-pyrroline: an important aroma component of cooked rice. *Chem. Ind. (London)* **1982**, 958−959.

(24) Steinhaus, M.; Sinuco, D.; Polster, J.; Osorio, C.; Schieberle, P. Characterization of the aroma-active compounds in pink guava (*Psidium guajava*, L.) by application of the aroma extract dilution analysis. *J. Agric. Food Chem.* **2008**, *56*, 4120−4127.

(25) Fischer, A.; Grab, W.; Schieberle, P. Characterisation of the most odour-active compounds in a peel oil extract from Pontianak oranges (*Citrus nobilis* var. Lour. *microcarpa* Hassk.). *Eur. Food Res. Technol.* **2008**, *227*, 735−744.

(26) Dess, D. B.; Martin, J. C. Readily accessible 12-I-5 oxidant for the conversion of primary and secondary alcohols to aldehydes and ketones. *J. Org. Chem.* **1983**, *48*, 4155−4156.

(27) Bemelmans, J. M. H. Review of isolation and concentration techniques. In *Progress in Flavour Research*; Land, G. G., Nursten, H. E., Eds.; Applied Science: London, UK, 1979; pp 79−88.

(28) Full, G.; Schreier, P. Covalent chromatography. A valuable method for the aroma analysis of thiols at trace levels (in German). *Lebensmittelchemie* **1994**, *48*, 1−4.

(29) Fischer, A.; Schieberle, P. Characterisation of the key aroma compounds in the peel oil of Pontianak oranges (*Citrus nobilis* Lour. var. *microcarpa* Hassk.) by aroma reconstitution experiments. *Eur. Food Res. Technol.* **2009**, *229*, 319−328.

(30) U.S. Department of Commerce. *Mass Spectral Library NIST11*; National Institute of Standards and Technology, Gaithersburg, MD, USA.

(31) Widder, S.; Eggers, M.; Pickenhagen, W. New flavour compounds from orange essence oil. In *Flavour Research at the Dawn of the Twenty-First Century*; Le Quéré, J. L., Étiévant, P. X., Eds.; Intercept: London, UK, 2003; pp 745−748.

(32) Miyazawa, N.; Fujita, A.; Kubota, K. Aroma character impact compounds in Kinokuni mandarin orange (*Citrus kinokuni*) compared with Satsuma mandarin orange (*Citrus unshiu*). *Biosci., Biotechnol., Biochem.* **2010**, *74*, 835−842.

(33) Weyerstahl, P.; Marschall, H.; Splittgerber, U.; Son, P. T.; Giang, P. M.; Kaul, V. K. Constituents of the essential oil from the fruits of *Zanthoxylum rhetsoides* Drake from vietnam and from the aerial parts of *Zanthoxylum alatum* Roxb. from India. *Flavour Fragrance J.* **1999**, *14*, 225−229.

(34) Jirovetz, L.; Buchbauer, G.; Ngassoum, M. B.; Geissler, M. Aroma compound analysis of *Piper nigrum* and *Piper guineense* essential oils from Cameroon using solid-phase microextraction−gas chromatography, solid-phase microextraction−gas chromatography−mass spectrometry and olfactometry. *J. Chromatogr., A* **2002**, *976*, 265−275.

DOI: 10.1021/acs.jafc.5b01174
J. Agric. Food Chem. 2015, 63, 4060−4067

(35) Jagella, T.; Grosch, W. Flavour and off-flavour compounds of black and white pepper (*Piper nigrum* L.) II. Odour activity values of desirable and undesirable odorants of black pepper. *Eur. Food Res. Technol.* **1999**, *209*, 22−26.
(36) Steinhaus, M.; Fritsch, H. T.; Schieberle, P. Quantitation of (*R*)- and (*S*)-linalool in beer using solid phase microextraction (SPME) in combination with a stable isotope dilution assay (SIDA). *J. Agric. Food Chem.* **2003**, *51*, 7100−7105.
(37) Grosch, W. Evaluation of the key odorants of foods by dilution experiments, aroma models and omission. *Chem. Senses* **2001**, *26*, 533−545.

DOI: 10.1021/acs.jafc.5b01174
J. Agric. Food Chem. 2015, 63, 4060−4067

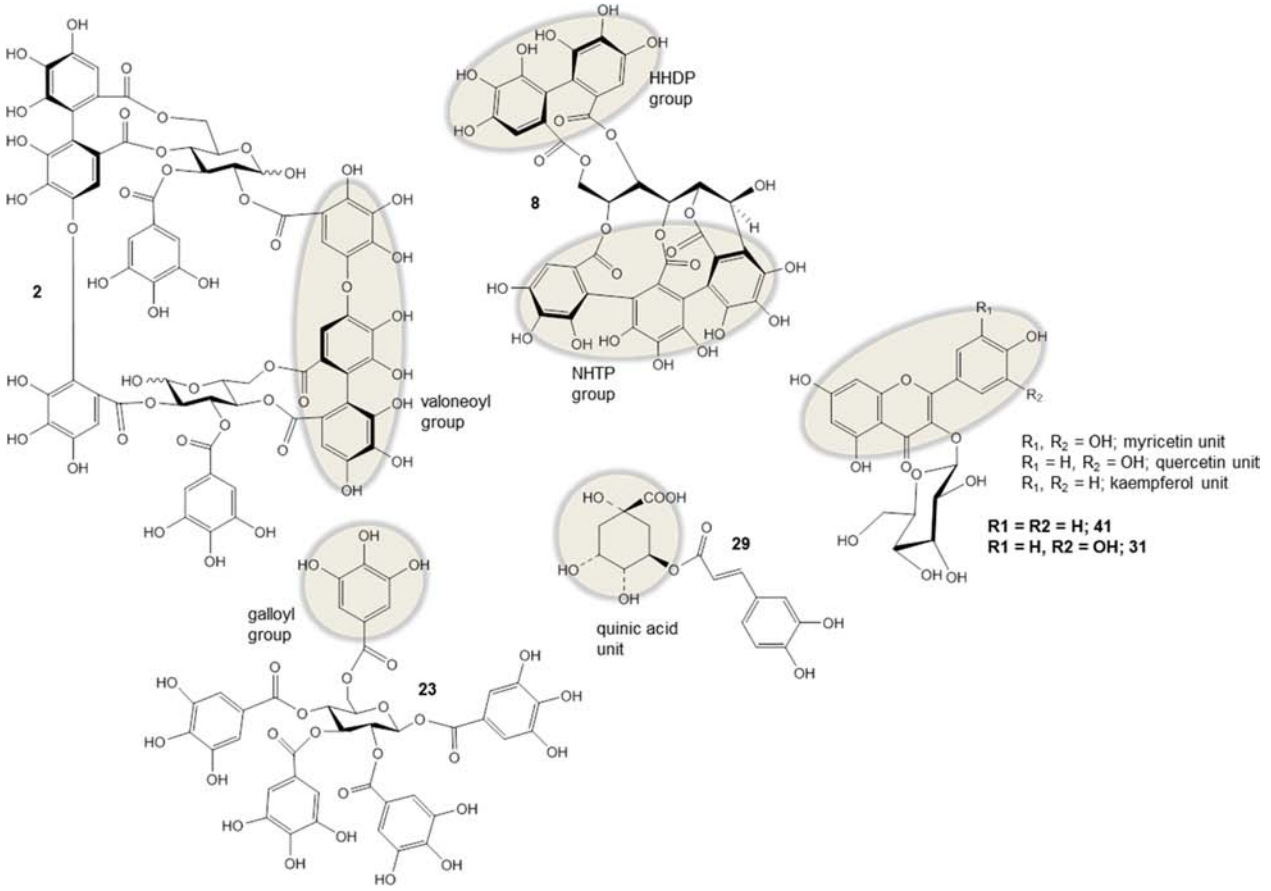

Figure 1. Example structures of the studied polyphenol subclasses. Compound identities: oenothein B (**2**), vescalagin (**8**), pentagalloyl glucose (**23**), 3-*O*-caffeoylquinic acid (**29**), quercetin-3-*O*-glucoside (**31**), and kaempferol-3-*O*-glucoside (**41**) (HHDP, hexahydroxydiphenoyl; NHTP, nonahydroxytriphenoyl).

quantitation impossible. If even more parent ion scans for different polyphenol groups are included, then also the measurement of qualitative group-specific fingerprints becomes impossible due to insufficient numbers of data points per single polyphenols. Therefore, more rapid nonscanning MS/MS methods are needed to enable more efficient quantitation and/or fingerprint detection of polyphenol groups. The speed of MRM technology would be especially suitable for this job as one MRM transition can be measured in 5 ms (vs 200 ms of the parent ion scan). However, to our knowledge, MRM-based LC-MS/MS methods for polyphenol subgroups have not been reported to be used for fingerprinting other than proanthocyanidins from plant extracts.[27]

To screen thousands of plant samples for their bioactive polyphenol content, rapid and specific methods are required. In these cases total concentrations of compounds belonging to different polyphenol subclasses are often of primary interest. If this is done by simultaneously recording the LC-MS/MS traces of many of the major polyphenol groups, overall views of sample-specific polyphenol fingerprints are achieved for every analyzed sample. The present study explored the potential of ultrahigh-performance liquid chromatography combined with a triple-quadrupole mass spectrometer for the rapid fingerprint analysis of different plant polyphenol subclasses from plant crude extracts. Our main interest was in establishing a fast, sensitive, and selective method for the simultaneous analysis of six common plant polyphenol subclasses: (1) ellagitannins, (2) gallic acid derivatives, (3) quinic acid derivatives, (4) quercetin-based flavonol glycosides, (5) kaempferol-based flavonol glycosides, and (6) myricetin-based flavonol glycosides (Figure 1).

MATERIALS AND METHODS

Chemicals and Reagents. Acetonitrile (LC-MS grade) used in the UPLC analyses was from Sigma-Aldrich (Steinheim, Germany). Formic acid was from VWR (Helsinki, Finland). Water was purified with a Millipore Synergy Water Purification System (Merck KGaA, Darmstadt, Germany). Flavonoids and quinic acids were from ExtraSynthese (Genay, France). Catechin was from Sigma (Sigma Chemical Co., St. Louis, MO, USA).

Materials. Pure compounds, simple galloylglucoses, ellagitannins, the less characterized flavonoids, quinic acids, and the gallotannin fractions used were isolated from different plant materials as described in Moilanen and Salminen.[28] The identities and purities of these compounds were established by UPLC-DAD-QqQ-MS and HPLC-ESI-Q-TOF-MS. The simple galloylglucoses and ellagitannins were additionally identified by NMR.[28,29] The compounds used are listed in Table 1. Plant materials used for plant extracts (Table 2) were collected from the Botanical Garden of the University of Turku and nearby forests in Turku, Finland. After collection, samples were freeze-dried and ground into powder. The plant powder was extracted with acetone/water (80:20, v/v) for 2 h, and the extraction was repeated two times. The acetone was evaporated from the extracts, and the extracts were frozen and freeze-dried. Freeze-dried samples were dissolved in 1 mL of water, filtered via 0.20 μm filters, and diluted 5 times with water before UPLC-MS/MS analyses.

UPLC-MS/MS Analysis. Sample analysis was carried out with an Acquity UPLC system (Waters Corp., Milford, MA, USA) coupled with a Xevo TQ triple-quadrupole mass spectrometer (Waters Corp.).

DOI: 10.1021/acs.jafc.5b00595
J. Agric. Food Chem. 2015, 63, 4068−4079

Table 1. Compounds and Fractions Used in the Present Work

no.	compound	MW	no.	compound	MW
1	tellimagrandin I	786.6	**28**	gallocatechin gallate	458.4
2	oenothein B	1569.1	**29**	3-*O*-caffeoylquinic acid	354.3
3	oenothein A	2353.6	**30**	3,4-*O*-dicaffeoylquinic acid	516.5
4	sanguiin H6	1871.3	**31**	quercetin-3-*O*-glucoside	464.4
5	lambertianin C	2805.9	**32**	quercetin-3-*O*-galactoside	464.4
6	agrimoniin	1871.3	**33**	quercetin-4′-*O*-glucoside	464.4
7	gemin A	1873.3	**34**	quercetin-7-*O*-glucoside	464.4
8	vescalagin	934.6	**35**	quercetin-3,4′-*O*-diglucoside	626.5
9	castalagin	934.6	**36**	quercetin-3-*O*-rhamnoside	448.4
10	vescavaloninic acid	1102.7	**37**	quercetin glycoside	874.7
11	castavaloninic acid	1102.7	**38**	quercetin glucuronide	478.4
12	cocciferin D2	1869.3	**39**	quercetin hexopentoside	596.5
13	sanguiin H10	1569.1	**40**	quercetin triglycoside	756.6
14	rugosin D	1875.3	**41**	kaempferol-3-*O*-glucoside	448.4
15	pedunculagin	784.5	**42**	kaempferol-7-*O*-glucoside	448.4
16	chebulagic acid	954.7	**43**	kaempferol-7-*O*-neohesperoside	594.5
17	punicalagin	1084.7	**44**	kaempferol glucuronide	462.4
18	geraniin	952.6	**45**	kaempferol rhamnoside	431.4
19	monogalloylglucose	332.3	**46**	kaempferol triglycoside	740.6
20	digalloylglucose	484.4	**47**	kaempferol malonylglucoside	534.4
21	trigalloylglucose	636.5	**48**	kaempferol diglycoside	594.5
22	tetragalloylglucose	788.6	**49**	myricetin 3-*O*-rhamnoside	464.4
23	pentagalloylglucose	940.7	**50**	myricetin glucoside	480.4
24	gallotannin fraction 1		**51**	myricetin arabinoside	450.4
25	gallotannin fraction 2		**52**	myricetin glucuronide	494.4
26	galloylquinic acid	344.3	**53**	myricetin glycoside	602.5
27	digalloylquinic acid	496.4			

Table 2. Plant Species Used in the Present Work

no.	plant
1	*Filipendula ulmaria* (meadow sweet), leaves
2	*Fumaria officinalis* (common fumitory), leaves
3	*Epilobium hirsutum* (great hairy willowherb), leaves
4	*Rosa pimpinellifolia* (burnet rose), leaves
5	*Lysimachia vulgaris* (yellow loosestrife), flowers
6	*Chamerion angustifolium* (fireweed), flowers
7	*Vicia cracca* (cow vetch), flowers
8	*Sorbus hybrida* (Swedish service tree), leaves
9	*Betula pubescens* (white birch), leaves
10	*Lythrum salicaria* (purple loosestrife), leaves
11	*Quercus robur* (English oak), leaves
12	*Geum urbanum* (wood avens), leaves
13	*Sorbus aucuparia* (rowan), leaves
14	*Vincetoxicum hirundinaria* (white swallow-wort), leaves
15	*Rubus saxatilis* (stone bramble), leaves

The UPLC system consisted of a sample manager, a binary solvent manager, a column, and a diode array detector. The column used was a 100 mm × 2.1 mm i.d., 1.7 μm, Acquity UPLC BEH Phenyl column (Waters Corp., Wexford, Ireland). The flow rate of the eluent was 0.5 mL min^{-1}. The elution profile used two solvents, acetonitrile (A) and 0.1% aqueous formic acid (B): 0−0.5 min, 0.1% A in B; 0.5−5.0 min, 0.1−30% A in B (linear gradient); 5.0−6.0 min, 30−35% A in B (linear gradient); 6.0−9.5 min, column wash and stabilization. UV and MS data were collected from 0 to 6 min. Negative ionization mode was used for MS analyzes. ESI conditions were as follows: capillary voltage, 2.4 kV; desolvation temperature, 650 °C; source temperature, 150 °C; desolvation and cone gas (N_2), 1000 and 100 L/h, respectively; and collision gas, argon. Catechin (1 μg mL^{-1}) was used to monitor the stability of the ionization efficiency of the mass spectrometer, and a mixture of different flavonoids (4 μg mL^{-1}) was used to monitor variations in retention time and m/z values.

Optimization of Cone Voltages and Collision Energies. When cone voltages and collision energies were optimized for the selected compounds, aqueous solutions of different compounds were directly infused into the ESI source with a syringe pump at a flow rate of 5−40 μL min^{-1}. The concentrations of the aqueous solutions were 40 μg mL^{-1} for pure compounds and 1 mg mL^{-1} for the gallotannin fractions. The ranges of cone voltage and collision energy varied between 10 and 170 V and between 5 and 50 eV, respectively.

Testing the UPLC-MS/MS Method with Plant Extracts and Polyphenol Mixtures. The method was first tested by three polyphenol mixtures made from pure compounds. This was necessary to avoid coelution of interfering substances with known compounds so that UV chromatograms could be directly compared with MRM chromatograms. The first mixture (1) contained compounds **1**, **2**, **6**, **8**, and **29**, the second mixture (2) compounds **30**, **32**, **33**, and **41**, and the third one (3) compounds **23**, **31**, **36**, **42**, **43**, and **49** (see Table 1 for compound identities). Mixture 1 was prepared in formic acid/acetonitrile/water (0.1:5:94.9, v/v/v), and mixtures 2 and 3 were prepared in formic acid/acetonitrile/water (0.1:10:89.9, v/v/v). The dilution range was from 20 μg mL^{-1} to 0.08 ng mL^{-1}. Three replicates of each sample were run. The mixtures were prepared fresh the same day as the analysis. Plant extracts were prepared as described under Materials, and samples of 1 mg mL^{-1} were prepared and diluted with water to the final test concentration of 0.2 mg mL^{-1}. The polyphenol mixtures mentioned above were utilized for quantification purposes in the present work. For estimating total concentrations, the responses of compounds belonging to the same polyphenol subgroup were combined and calibration curves prepared by using these values. For the comparison of group-specific and compound-specific methods with single compounds, calibration curves with corresponding compounds were prepared. The dilution range was from 0.08 ng mL^{-1} to 20 μg mL^{-1}, and only the linear parts of the calibration curves were used for quantification.

DOI: 10.1021/acs.jafc.5b00595
J. Agric. Food Chem. 2015, 63, 4068−4079

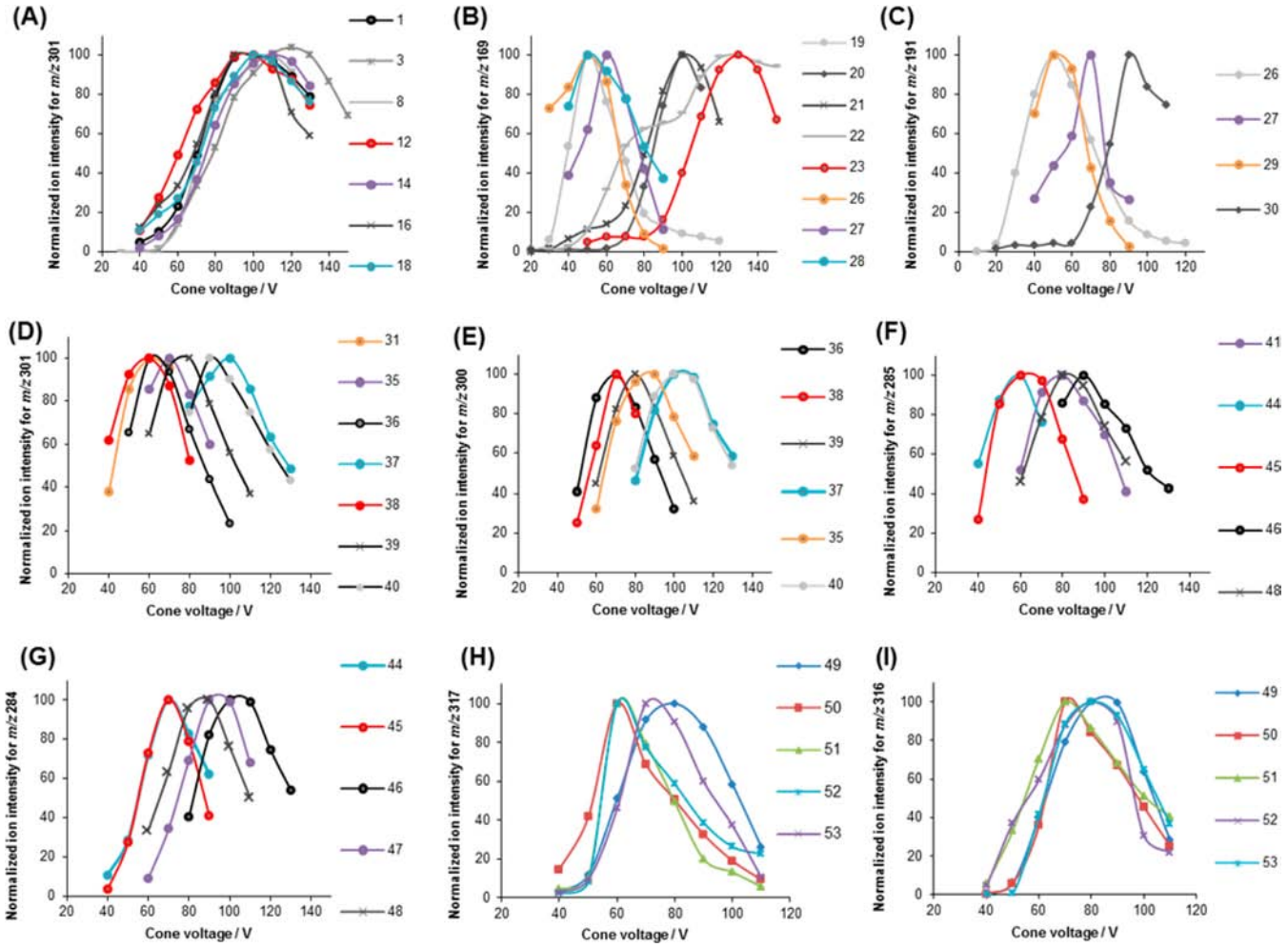

Figure 2. Optimization of cone voltages for the accumulation of precursor ions presenting ellagitannins (A), gallic acid derivatives (B), quinic acid derivatives (C), quercetin-based flavonoids (D, E), kaempferol-based flavonoids (F, G), and myricetin-based flavonoids (H, I). See Table 1 for compound identities.

Method Validation. Three mixtures containing different polyphenols (see Testing the UPLC-MS/MS Method with Plant Extracts and Polyphenol Mixtures) were used for the determination of the limit of detection (LOD), limit of quantitation (LOQ), linearity, repeatability, and sensitivity of the developed method. LOD and LOQ were determined as peak to peak values by the signal to noise process function in MassLynx software. Signal to noise ratios (S/N) were > 3 and >10 for LOD and LOQ, respectively. Dilution series were prepared from stock solutions of 40 μg mL^{-1} and diluted with formic acid/acetonitrile/water (0.1:5:94.9, v/v/v) (mixture 1) or formic acid/acetonitrile/water (0.1:10:89.9, v/v/v) (mixtures 2 and 3). The dilution range was from 0.08 ng mL^{-1} to 20 μg mL^{-1}. Three replicates of each sample were run for LOD, LOQ, and linearity and five replicates for repeatability.

RESULTS AND DISCUSSION

Optimization of the Cone Voltages. Because compounds that belong to the same polyphenol subgroup share similarities in their structural skeletons,[2,30,31] it was hypothesized that it would be possible to develop group-specific MRM methods for different polyphenol subclasses. To optimize MRM methods for ellagitannins, gallic acid derivatives, quinic acid derivatives, quercetin-based flavonol glycosides, kaempferol-based flavonol glycosides, and myricetin-based flavonol glycosides, direct flow injection experiments of the reference compounds (Table 1) were performed in both positive-ion and negative-ion modes. Negative mode was more sensitive than positive mode (data not shown) and, thus, negative-ion mode was selected to be used in the MRM methods. In addition, negative ion mode fragmented compounds less extensively and thus produced clearer fragmentation patterns.

As hypothesized, it was possible to find common precursor ions for fragments of compounds belonging to the same polyphenol subclass. For ellagitannins the selected precursor ion was m/z 301, which is in agreement with the earlier findings where m/z 301 has been reported as the main ellagitannin fragment.[32−36] This ion is formed when the hexahydroxydiphenoyl (HHDP) groups characteristic for ellagitannins fragment from the original structure to produce m/z 301.[37−39] The optimal cone voltage required for maximal accumulation of m/z 301 in the first quadrupole varied between 90 and 130 V (examples in Figure 2A), depending on the structural differences of the studied molecules: for example, the position of the HHDP group, additional galloyl groups attached to HHDP(s) (such as in valoneoyl and sanguisorboyl groups), size of the molecule, and rigidity of the structure. In general, HHDP groups located at the 2,3-position required higher cone voltages than HHDP groups at the 4,6- or 3,6-position for maximal accumulation of m/z 301. Valoneoyl, sanguisorboyl, and nonahydroxytriphenoyl groups either provided further stability to the ellagitannin structure or needed to be

DOI: 10.1021/acs.jafc.5b00595
J. Agric. Food Chem. 2015, 63, 4068−4079

fragmented before m/z 301 could be formed from the larger fragments. This was confirmed for ellagitannins with valoneoyl groups because these structures first yielded the valonic acid dilactone moiety and then ellagic acid when the cone voltage was further increased. Comparison of oligomeric series of ellagitannins with the same monomeric units suggested that the rigidity brought by the bonds between the monomeric units affected the required cone voltage more than the size of the molecule. For example, for the monomer tellimagrandin I and its dimeric and trimeric macrocyclic oligomers, oenothein B and oenothein A, the optimal cone voltages for the accumulation of m/z 301 were 90, 100, and 130 V, respectively. However, for both dimeric and trimeric sanguiin H-6 and lambertianin C the optimal cone voltage was the same, 120 V. In addition, the difference between the two dimers (oenothein B and sanguiin H-6; 100 vs 120 V) could be due to different types of linkages, DOG and GOD,[40] between the monomers. It is thus clear that a single cone voltage is not optimal for all types of ellagitannins and that the use of several cone voltages could produce different types of ellagitannin fingerprints, depending on the ellagitannin composition of the tested plant sample. Similar patterns have been earlier witnessed for other tannin fingerprints as well: large proanthocyanidins required higher cone voltages than their monomers to be witnessed in the crude extracts.[27]

For gallic acid derivatives the selected precursor ion was m/z 169, which is formed when galloyl groups fragment from the original gallic acid derivative.[38,41] Also for gallic acid derivatives, the size of the molecule along with the positions of the galloyl groups affected the required cone voltage for maximal accumulation of m/z 169. The optimal cone voltage varied between 50 and 130 V (examples in Figure 2B). Lowest, 50−70 V, cone voltages were optimal for simple gallic acid derivatives, such as galloyl quinic acids, gallocatechin gallate, and monogalloylglucose. For di-, tri-, tetra-, and pentagalloylglucoses the optimal cone voltages were between 100 and 130 V. Gallotannins have both galloyl groups attached to the core polyol and additional galloyls linked to the core galloyl groups via depside bond(s).[41,42] As a consequence, two cone voltages, 50 and 130 V, were obtained for the maximal accumulation of m/z 169. As previously reported,[31,41] the results indicated that depside bonds between two galloyls are less stable than ester bonds between the core polyol and galloyl groups.

For quinic acid derivatives the cone voltage optimization was straightforward. The tetraol moiety of quinic acid at m/z 191 was selected as the precursor ion.[43] The optimal cone voltage for accumulation of the precursor ion m/z 191 varied between 50 and 90 V (Figure 2C) and mainly depended on how easily the other functional groups of the studied compounds were fragmented from the quinic acid moiety. In some cases, these other functional groups could be detected separately as well. For example, galloylquinic acids can be detected by the galloyl-based MRM method. On the contrary, caffeoylquinic acids did not fragment into clearly detectable levels of caffeic acid, leaving these compounds to be detected by the quinic acid-based MRM method. Both digalloyl- and dicaffeoyl-substituted quinic acids required higher optimal cone voltages than the monogalloyl (50 → 70 V) or monocaffeoyl (50 → 90 V) derivatives (Figure 2C). This information could be used to screen plant samples for highly substituted quinic acid derivatives, because their quinic acid fingerprint is better visible by high than low cone voltages, whereas the opposite is true for monosubstituted quinic acids.

Formation of flavonol aglycone radical ions from flavonols during electrospray ionization mass spectrometry is a well-known phenomenon.[44−48] In the present study, the three flavonoid-based polyphenol groups studied, quercetins, kaempferols, and myricetins, formed two characteristic ions, the aglycone and the aglycone radical ions, in the cone voltage optimizations. These ions were m/z 301 and 300 for quercetin-based flavonoids, m/z 285 and 284 for kaempferol-based flavonoids, and m/z 317 and 316 for myricetin-based flavonoids. The optimal cone voltages for maximal accumulation of those ions varied depending on the structure of the original flavonol glycoside (examples in Figure 2D−I). The cone voltage experiments revealed that for some flavonol glycosides, ions at m/z 316, 284, and 300 derived from the ions at m/z 317, 285, and 301, respectively, by using higher cone voltages, whereas for other flavonol glycosides these ion pairs accumulated with the same cone voltages. Also, the ratio of the two adjacent ions depended on the exact structure of the studied molecule (Figure 3). Being in agreement with previous

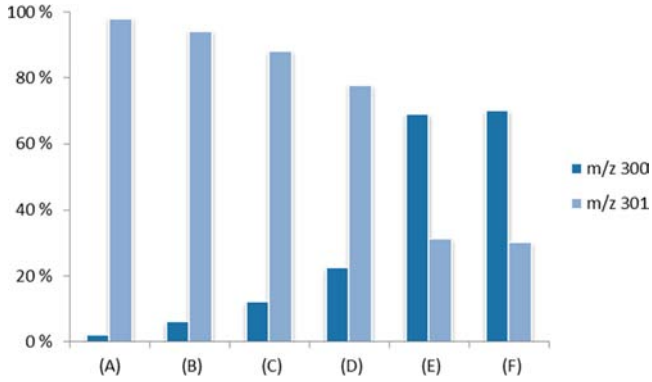

Figure 3. Ratio of quercetin aglycone and aglycone radical ions in (−)-ESI for quercetin aglycone (A), quercetin-4′-*O*-glucoside (B), quercetin-3,4′-*O*-diglucoside (C), quercetin-7-*O*-glucoside (D), quercetin-3-*O*-glucoside (E), and quercetin-3-*O*-galactoside (F).

studies,[44,48,49] the results suggested that 3-*O*-glycosylation favors formation of ions at m/z 300, 284, and 316, whereas 4′- and 7-glycosylations favor formation of ions at m/z 301, 285, and 317. This indicates that the comparison of ratios of different flavonol fingerprints (e.g., m/z 301 vs 300) of a given plant extract may yield information on the types of glycosylation patterns present in the flavonol glycosides (3-*O*-glycosides vs other types) in that plant.

Optimization of Collision Energies. Enhanced selectivity and sensitivity of the method are achieved by collision energies separately optimized for product ions of the specific precursor ions. Such an approach allows the accurate qualitative and quantitative analysis of different polyphenol subgroups directly from plant crude extracts. In contrast to identifying optimal cone voltages, the choice of optimal collision energy was straightforward. For ellagitannins, gallic acid and quinic acid derivatives, and quercetin, kaempferol, and myricetin glycosides, the selected product ions deriving from the selected precursor ions always had the same optimal collision energies. The optimal collision energies are presented in Table 3. Two transitions, one qualifier and one quantifier, were selected for the detection of each group of compounds to avoid detection of false positives. The ratios of the peak areas obtained by the qualitative and quantitative MRM transitions are shown in Table 3. These ratios are constant for true detections and

DOI: 10.1021/acs.jafc.5b00595
J. Agric. Food Chem. 2015, 63, 4068−4079

Table 3. Group-Specific and Compound-Specific MRM Methods Developed and Used in the Present Study

polyphenol class	precursor ion (m/z)	cone voltage (V)	product ion (quant) (m/z)	collision energy (eV)	product ion (qual) (m/z)	collision energy (eV)	qual/quant[a] (%)
ellagitannins	301	110 (90−120)	200	40	145	35	44 ± 3
gallic acid derivatives	169	80 (50−130)	125	15	107	20	32 ± 8
quinic acid derivatives	191	70 (50−90)	127	15	109	20	39 ± 3
quercetin derivatives	301	85 (60−110)	151	20	179	20	46 ± 2
	300	85 (60−110)	271	25	255	20	48 ± 3
kaempferol derivatives	285	80 (60−110)	229	20	257	25	27 ± 4
	284	80 (60−110)	255	25	227	25	99 ± 4
myricetin derivatives	317	75 (60−85)	271	20	287	25	14 ± 1
	316	75 (60−85)	271	20	287	25	61 ± 2
compound	precursor ion (m/z)	cone voltage (V)	product ion (m/z)	collision energy (eV)			
tellimagrandin I	785	55	301	40			
oenothein B	783	34	765	22			
agrimoniin	934	38	301	48			
vescalagin	933	46	301	64			
pentagalloylglucose	939	60	169	32			
3-*O*-caffeoylquinic acid	353	24	191	18			
3,4-*O*-dicaffeoylquinic acid	515	25	173	25			
	515	25	179	30			
quercetin-3-*O*-glucoside	463	40	300	35			
quercetin-3-*O*-galactoside	463	40	300	25			
	463	40	301	20			
quercetin-4′-*O*-glucoside	463	40	301	20			
quercetin-3-*O*-rhamnoside	447	45	301	20			
kaempferol-3-*O*-glucoside	447	35	284	25			
kaempferol-7-*O*-glucoside	447	40	285	25			
kaempferol-7-*O*-neohesperoside	593	50	285	30			
myricetin-3-*O*-rhamnoside	463	40	316	25			

[a]Ratio of the obtained peak areas with qualitative to quantitative MRM transitions (qual/quant × 100%).

change as a result of false positives. This was demonstrated with the total peak areas of the 15 plant extracts, the individual compounds of each extract, and the pure compounds presented in Table 3. These ratios should be used to verify that the correct polyphenol groups have been detected by the MRM methods.

Testing the UPLC-MS/MS Method with Plant Extracts and Polyphenol Mixtures. After optimization of MRMs, the new method was rigorously tested with 14 different plant extracts and 3 mixtures of different polyphenols and their dilution series. All samples were analyzed by using the developed group-specific MRM method and compound-specific MRM methods (Table 3). When the mixtures of pure compounds were analyzed, it was noted that the peak areas obtained with the group-specific MRM method depended both on the cone voltage used and on the number of the units in the studied polyphenol structure that yielded the precursor ions (Figure 4). As suggested already for cone voltage optimization, this indicated differences in the collision-induced dissociation of different molecules belonging to the same polyphenol subgroup. Due to this, the intensities of the peaks obtained, for example, for vescalagin (**8**) and agrimoniin (**6**) differed even if both molecules yielded maximum accumulation of m/z 301 when the cone voltage was 110 V (Figure 4B). In contrast, even though the change in applied cone voltage affected absolute peak areas, it did not affect the shape of the concentration versus peak area plots when dilution series were analyzed. This indicates that group-specific fingerprints can be detected even by using nonoptimal cone voltages, and fingerprints can be converted to quantitative data, if suitable standards of each detected polyphenol groups are available. Without proper standards, however, MRM fingerprints should not be converted into quantitative results, because this might result in severe over- or underestimation of the polyphenol groups, depending on the standards used.

Detection with the presented group-specific MRM method was also compared with compound-specific MRM methods (Figure 4) that were separately optimized for every quantified compound. The results indicated that for all but two compounds the compound-specific methods were more sensitive and yielded better responses than the group-specific methods. The two exceptions were tellimagrandin I and pentagalloyl glucose, which were better detected with the galloyl-specific MRM method than with the compound-specific MRM methods. In fact, tellimagrandin I, which contains one HHDP and two galloyl groups, was better detected by the galloyl than the ellagitannin method (**1** in Figure 4B,C). All in all, compound-specific MRM methods cannot be substituted by the developed group-specific methods, but both could be used parallel, depending on the need. For instance, Figure 5 shows how the UPLC-DAD chromatogram at 349 nm was able to reveal nine flavonoids from the crude extract of *Epilobium hirsutum* (characterization confirmed by UV spectra[28]). During the same UPLC run, group-specific MRM methods were able to classify three of these compounds as myricetin derivatives, three as quercetin derivatives, and the remaining three as kaempferol derivatives. Simultaneously acquired full scan MS revealed the molecular weights of these compounds, enabling their further characterization. It was found that all three sets of three flavonol glycosides presumably contained the same three

DOI: 10.1021/acs.jafc.5b00595
J. Agric. Food Chem. 2015, 63, 4068−4079

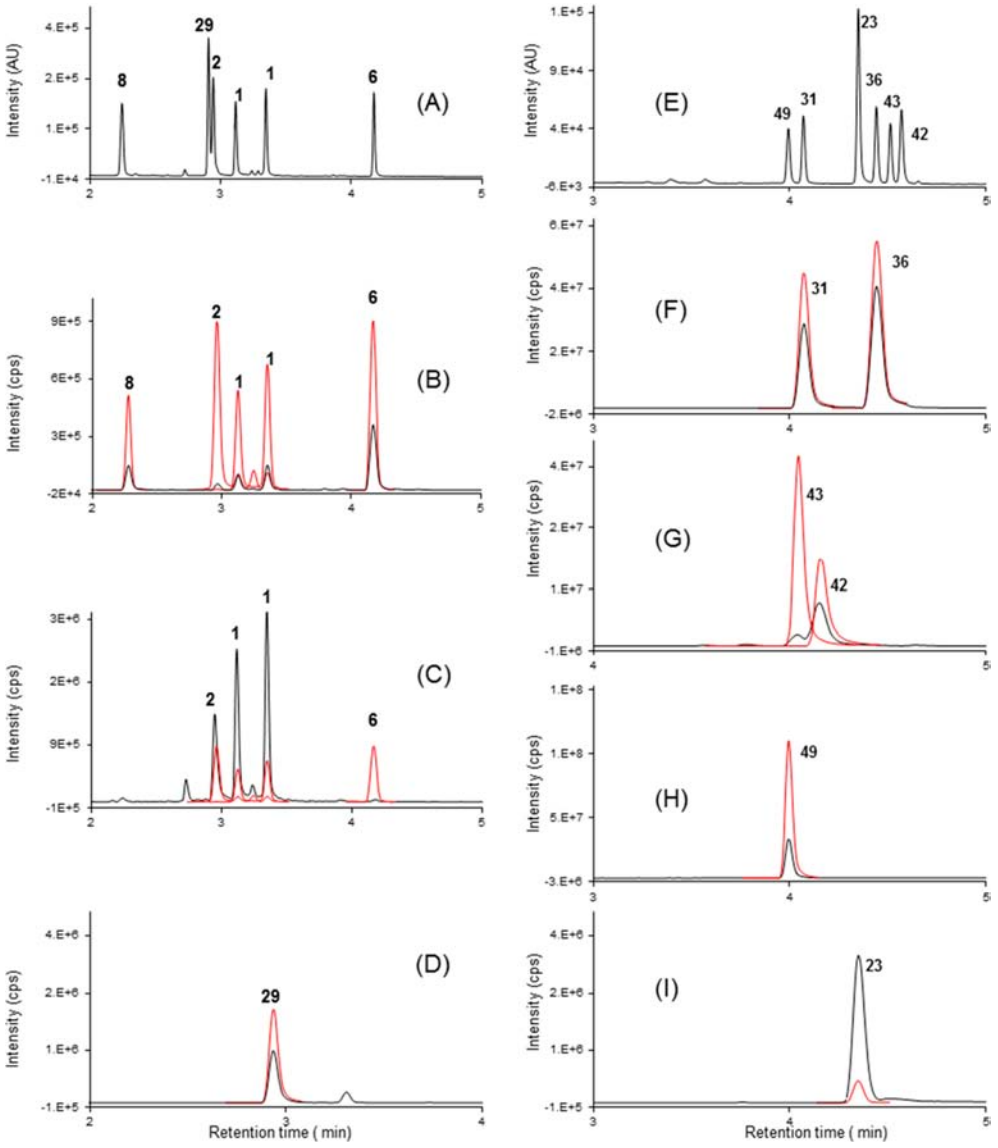

Figure 4. UPLC fingerprints of polyphenol mixtures 1 (A–D) and 3 (E–I) as detected by UV at 280 nm (A, E) and group-specific (black lines) and compound-specific (red lines) MRM methods for ellagitannins (B), gallic acid derivatives (C, I), quinic acid derivatives (D), quercetin-based flavonoids (F), kaempferol-based flavonoids (G), and myricetin-based flavonoids (H). See Table 1 for compound identities.

carbohydrates as building blocks: the first compound in the set of three peaks always gave the mass of 180 Da for the carbohydrate (possibly glucose or galactose), the second compound gave the mass of 132 Da (xylose/lyxose, but more presumably arabinose), and the third compound gave the mass of 146 Da (rhamnose) for the carbohydrate part of the glycoside. This could not have been achieved by full scan only as aglycone fragments are not always unequivocally witnessed. Furthermore, these findings were confirmed by compound-specific MRMs (see examples in Figure 5F–I). This illustrates the logic of how the created group-specific methods should be used to facilitate compound characterization and the measurement of group-specific fingerprints. For every species and polyphenol group analyzed, one should first reveal the percentage of the fingerprint produced by the qualifier MRM transition of that produced by the quantifier MRM transition. If the ratio deviates from values shown in Table 3, then further examination of the sample by UV and full scan MS is needed either to verify the results obtained by the fingerprint method or to reveal the causes for false positives. For instance, some flavonols and flavones share the same mass for their aglycone part (e.g., 286 Da for luteolin and kaempferol), but these two types of flavonoids are easily separated by both UV spectra and MS/MS spectra recorded for the aglycone part. The latter difference in MS/MS spectra explains why flavones produce variable ratios with the qualifier/quantifier transitions from those of flavonols.

In the present work, quantification was established by preparing calibration curves with pure compounds (polyphenol mixtures 1, 2, and 3). The results obtained by group- and compound-specific MRM methods (Table 3) for the 15 plant extracts are presented in Table 4. Results were expressed as milligrams per gram of plant dry weight. The developed group-specific MRM method was able to produce quantitative data comparable to the compound-specific MRM methods for all of the studied polyphenols. However, in some extracts detection of tellimagrandin I (**1**) with the compound- and group-specific methods yielded divergent results (see Table 4). Due to the

DOI: 10.1021/acs.jafc.5b00595
J. Agric. Food Chem. 2015, 63, 4068–4079

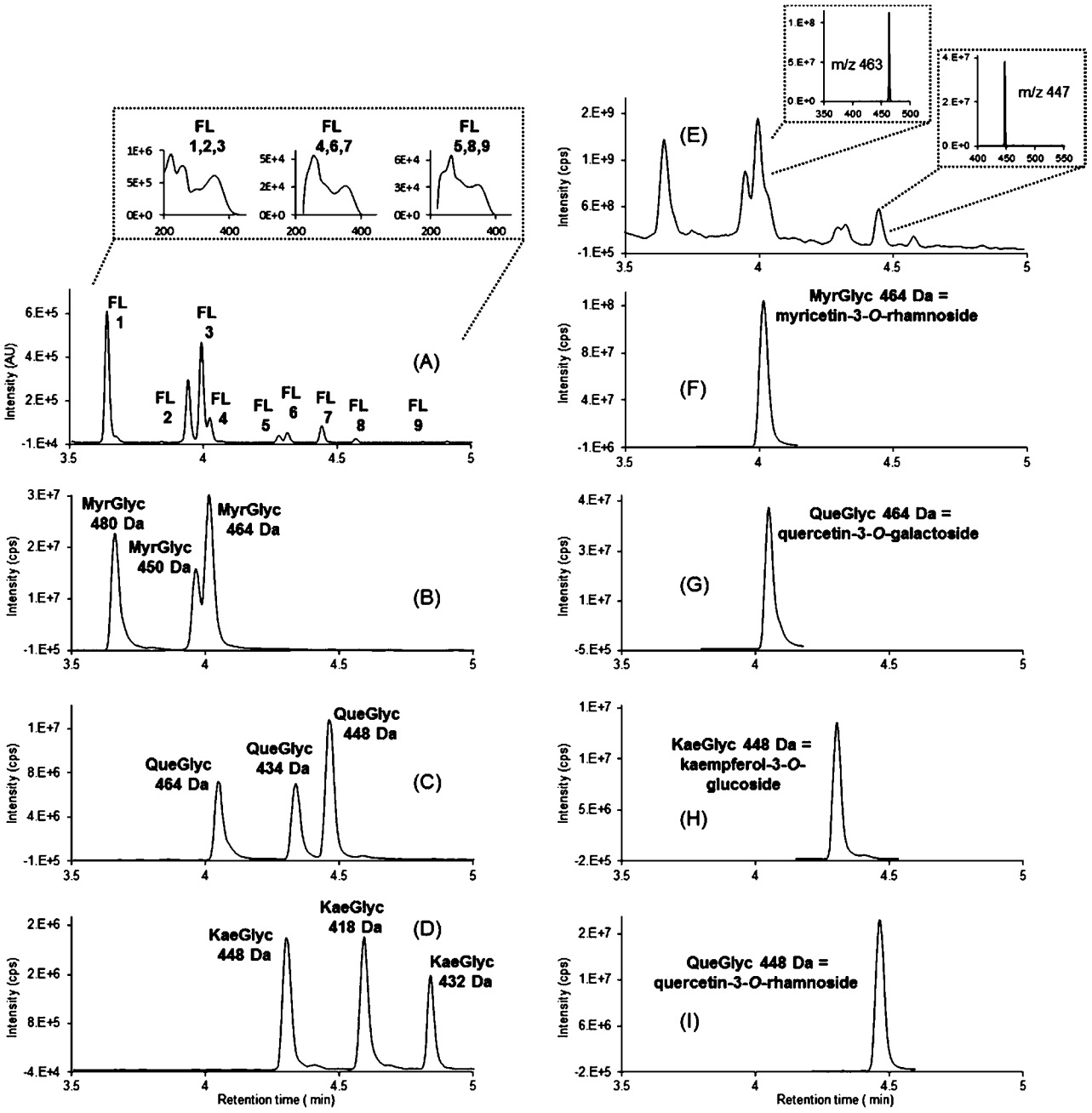

Figure 5. UPLC fingerprints of water-soluble flavonoids of *Epilobium hirsutum* (great hairy willowherb) leaves as detected by UV at 349 nm (A), full scan (E), and MRM methods for myricetin-based flavonoids (B), quercetin-based flavonoids (C), and kaempferol-based flavonoids (D). Panels F−I show detection with compound-specific MRM methods for myricetin-3-*O*-rhamnoside (F), quercetin-3-*O*-galactoside (G), kaempferol-3-*O*-glucoside (H), and quercetin-3-*O*-rhamnoside (I). Insets in (A) and (E) present UV and mass spectra for selected peaks. FL, flavonoid; MyrGlyc, myricetin glycoside; QueGlyc, quercetin glycoside; KaeGlyc, kaempferol glycoside.

coelution of compounds from the same polyphenol subgroup, tellimagrandin I could not be detected separately anymore by the developed group-specific MRM method, but instead a combined signal of several ellagitannins was detected. This resulted in overestimated quantification when compared to the results obtained by the compound-specific methods. This further demonstrated the purpose for which the method was developed: for fingerprint analysis and quantification of total concentrations of different polyphenol subgroups, not for quantification of individual compounds. The results indicated also that in the present work the matrix effect of the plant extracts was not remarkable, and calibration curves produced with pure compounds were sufficient for obtaining quantitative data. This highlights the importance of correct sample concentration: to minimize matrix effect, sample concentration should be preferably adjusted to such a level where no detection rises above the 1×10^6 limit. Also, compounds used for quantification must be carefully selected. In present work, compounds used in the standard mixtures were selected so that they would as well as possible resemble the range of polyphenols in the studied plant extracts. If this is not possible, the quantitation results should be treated as relative ones, not absolute, and expressed as equivalents of the compounds used as standards.

DOI: 10.1021/acs.jafc.5b00595
J. Agric. Food Chem. 2015, 63, 4068−4079

Table 4. Quantitative Results Obtained by the Developed Group-Specific MRM Method for the Different Polyphenol Subclasses in the Studied Plant Extracts and Comparison of Quantification of Single Compounds in the Studied Plant Extracts with the Developed Group-Specific MRM Method and Compound-Specific MRM Methods[a]

	plant extract														
quantitative results	1	2	3	4	5	6	7	8	9	10	11	12	13	14	15
total galloyl	6.7	4.3	1.4	0.4	0.5	3.3	0.4	0.4	1.4	2.2	3.2	1.0	0.4	0.1	4.0
totalellagitannin	41.3	147.4	69.7			30.9			2.7	142.7	151.9	127.3			55.3
total quinic acid	6.2	1.8			6.4	4.1		14.9	6.1	0.1		2.5	31.8	7.1	
total kaempferol	0.8	1.8	1.2	0.7	0.4	14.7	18.6	2.3	5.3	0.1	10.3	0.4	1.4	0.7	5.9
total quercetin	9.3	14.8	2.4	0.9	1.4	12.6	1.4	1.7	4.3	0.1	4.0	0.3	3.1	1.2	7.9
total myricetin			7.8		0.4	1.6	0.5		0.2		0.2				

	quantitative results (mg g^{-1})
compound	group-specific MRM/compound-specific MRM
1	7.6/8.1; 11.0/7.8; 5.5/2.5; 8.8/4.8; 0.9/0.2; 9.9/0.2; 25.2/0.8; 2.1/0.1
2	28.0/29.2; 26.2/27.4
6	27.9/21.2
8	2.2/3.4; 3.0/4.3
23	3.8/4.6; 1.4/0.9; 2.7/3.0
29	1.4/4.2; 0.5/1.8
31 + 32	2.8/2.6; 0.5/0.7; 0.3/0.3; 0.8/0.9; 0.2/0.1; 0.4/0.4; 1.0/1.3; 1.2/1.5
36	0.3/0.3; 0.1/0.1; 0.2/0.8; 4.6/5.3; 0.8/0.9; 0.4/0.3; 0.2/0.1
41	0.1/0.2; 0.3/0.3; 0.1/0.1; 0.1/0.1; 0.1/0.2; 0.4/0.6; 0.1/0.1; 0.3/0.4; 1.5/2.0; 0.1/0.2
49	3.9/3.6; 1.2/1.5; 0.5/0.6; 0.0/0.1; 0.0/0.1

[a]Results are expressed as mg g^{-1} of dry material. See Tables 1 and 2 for compound and plant extract identities, respectively.

One of the most common problems for the developed methods is related to both ellagitannins and quercetin-based flavonoids producing precursor ions with the very same m/z value (m/z 301), and therefore LC-MS/MS methods have been used in previous studies to distinguish their conjugates.[32,33] In the present study, it was noted that even if the ellagitannin and quercetin MRM transitions had different product ions (301 → 200/301 → 145 and 301 → 151/301 → 179 respectively), a small false-positive ellagitannin response (0.1−1%) was obtained from quercetin derivatives when their concentrations were >1 μg mL^{-1}. For qualitative analysis this will not cause any problems because the false-positive response of ellagitannins is easily distinguished directly from the MRM chromatograms: Figure 6C shows a false-positive detection of ellagitannins that is due to high levels of quercetin glycosides (panel B), and panel F shows the true ellagitannin detection that is not disturbed by the 0.1−1% false positive caused by the quercetin glycosides (panel E). As noted above, these findings can be confirmed by comparing peak areas obtained by quantifier versus qualifier MRM transitions as well. All in all, although the new MRM methods significantly aid in the mission of fingerprinting plant extracts for various polyphenol groups, they cannot be used as such without careful inspection of the data produced. Once the findings are confirmed for each studied species, the methods can be used to more routinely screen the differences of polyphenol fingerprints between individual plants of the selected species.

Method Validation. LOD, LOQ, and linearity were determined with the presented method for polyphenols present in the three mixtures containing different polyphenols. For both ellagitannins and gallic acid derivatives LOD and LOQ were 150 and 310 ng mL^{-1}, respectively. For quinic acid derivatives LOD was 20 ng mL^{-1} and LOQ, 80 ng mL^{-1}. The linear range was the same, 15−0.7 μg mL^{-1} for ellagitannins, gallic acid, and quinic acid derivatives. For the quercetin, kaempferol, and myricetin glycosides the linear ranges were 7.5−0.02, 7.5−0.08, and 10−0.3 μg mL^{-1}, respectively. For both quercetin and kaempferol glycosides LOD was 0.3 ng mL^{-1} and LOQ, 1.2 ng mL^{-1}. For myricetin-based flavonol glycosides LOD and LOQ were 40 and 80 ng mL^{-1}, respectively.

As witnessed in a previous section when the method was tested with polyphenol mixtures, these results further indicated that, in general, the developed UPLC-MS/MS method was more sensitive for the quercetin and kaempferol glycosides than for the other studied polyphenol subclasses. Also, the LOD, LOQ, and linear ranges varied slightly within each polyphenol subclass, depending on the exact structure of the studied molecule. The presented values were obtained with molecules for which the present method was most insensitive; that is, with other types of molecules the method would have performed better.

The repeatability of the method was determined using Student's t test at the 95% confidence interval. Five replicates in two different concentrations (20 and 5 μg mL^{-1}) were analyzed, and the results were presented as confidence intervals of the sums of peak areas obtained for ellagitannins, gallic acid and quinic acid derivatives, and quercetin-, kaempferol-, and myricetin-based flavonol glycosides. The relative standard deviation (RSD) for all six samples with five replicates was determined from these results. The RSD for peak areas was 2.4%, which demonstrates the pronounced reliability of the developed UPLC-MS/MS method. The results suggested that the quantitative determination of ellagitannins and quinic acid derivatives was slightly less accurate than for the other polyphenol classes (RSD, 3.1, 2.7, and 1.8−2.4%, respectively). Naturally, more accurate results were obtained when operating at the linear range than above the linear range.

In this study we created novel methods for the analysis of six common classes of plant polyphenols. UPLC enabled rapid chromatography of different kinds of polyphenols, whereas TQ-MS fragmented compounds into group-specific precursor and product ions for detection with MRM methods. With the

DOI: 10.1021/acs.jafc.5b00595
J. Agric. Food Chem. 2015, 63, 4068−4079

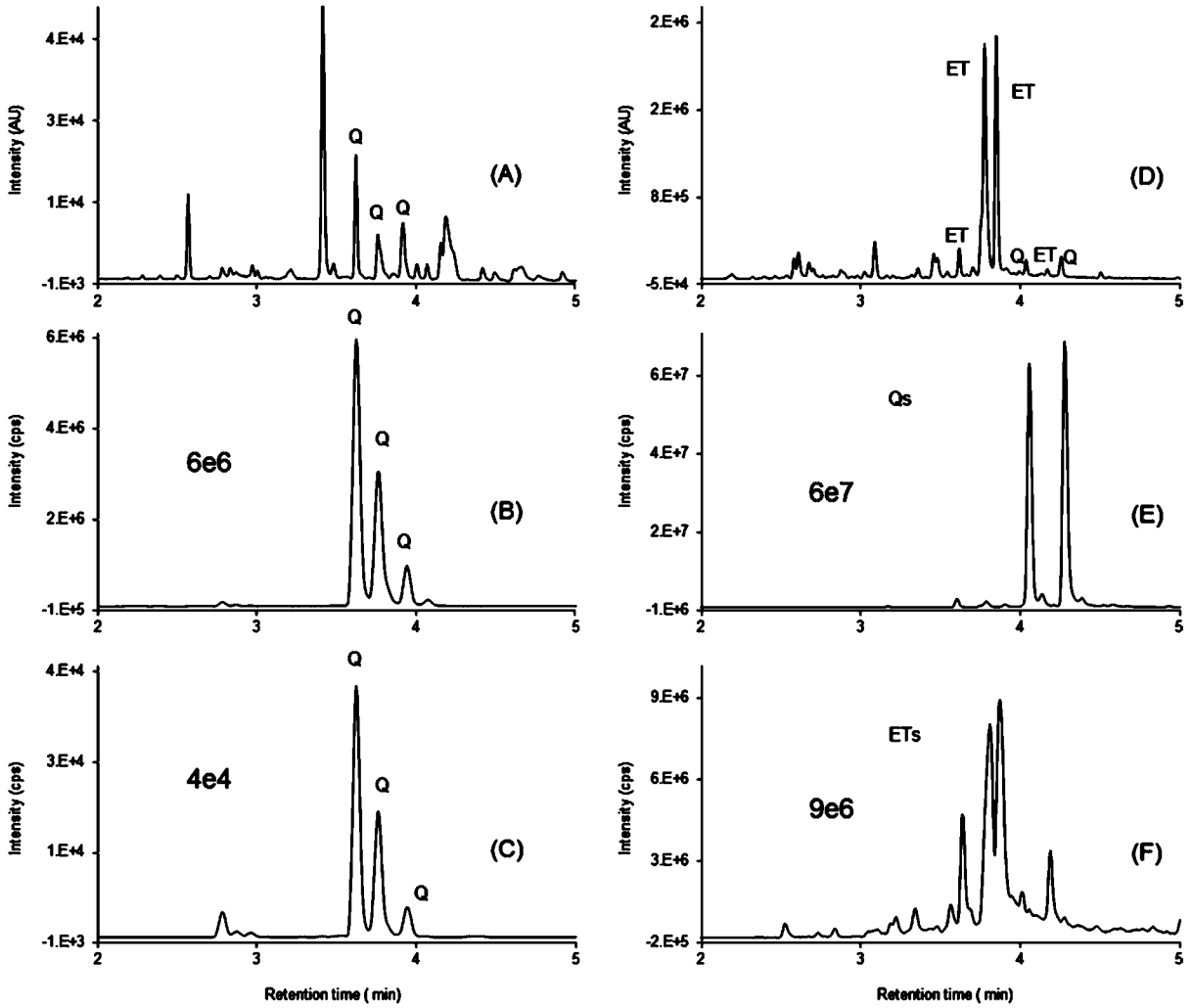

Figure 6. UPLC traces at 280 nm for polyphenol extracts of *Fumaria officinalis* flowers (A) and *Rubus saxatilis* leaves (D). Panels B and E show MRM fingerprints detected for quercetin-based flavonoids, and panels C and F show MRM fingerprints detected for ellagitannins. Quercetins produce <1% false-positive response with the ellagitannin method that can be verified by intensities of the matching fingerprints of panels B and C, because *F. officinalis* does not contain any ellagitannins. The true ellagitannin fingerprint of *R. saxatilis* (F) is not disturbed by the false positive of quercetins, because the ellagitannin detection is more than an order of magnitude higher than the false positive in the background. Q, quercetin-based flavonoid; ET, ellagitannin.

present methods, fingerprints of ellagitannins, gallic acid and quinic acid derivatives, and quercetin, kaempferol, and myricetin glycosides can be simultaneously recorded with UV and full scan mass spectra. The developed method is complementary for the UPLC-MS/MS method reported by Engström et al.[27] for the fingerprint analysis of procyanidin and prodelphinidin oligomers and polymers. By combining these two methods, a broad overview of fingerprints of eight common polyphenol classes can be achieved in relatively short time. The method is able to handle 140 extracts, produced from as little as 1 mg of plant powder, in a day, and it offers a user-friendly, robust, and fast addition to the chemistry tools currently used for the qualitative and quantitative screenings of large numbers of samples for their bioactive polyphenol types and contents. However, it must be remembered that the results of these types of semiautomatic fingerprint methods cannot be used without careful verification of the true presence of the detected polyphenol groups in tested samples. We offered tools for this by the use of quantifier and qualifier MRM transition for each polyphenol group and by using UV and MS spectra to verify the polyphenol groups of the main metabolites.

AUTHOR INFORMATION

Corresponding Author

*(M.T.E.) Phone: +358 2 333 6755. E-mail: marica.engstrom@utu.fi.

Funding

This study was supported by Turku University Foundation, Academy of Finland (Grant 258992 to J.-P.S.), the University of Turku Graduate School (UTUGS), Kone Foundation, and an EU Marie Curie Initial Training Network (PITN-GA-2011-289377, "LegumePlus"). A Strategic Research Grant (Ecological Interactions) enabled the use of the UPLC-MS/MS instrument.

Notes

The authors declare no competing financial interest.

ACKNOWLEDGMENTS

We thank Jussi Suvanto for help with sample analysis. We acknowledge Maarit Karonen, Nicolas Baert, Anne Koivuniemi, Jorma Kim, Jere Koira, and the entire Natural Chemistry Research Group for general help and discussion.

DOI: 10.1021/acs.jafc.5b00595
J. Agric. Food Chem. 2015, 63, 4068−4079

ABBREVIATIONS USED

HHDP, hexahydroxydiphenyl; UHPLC, ultrahigh-performance liquid chromatography; TQ-MS, triple-quadrupole mass spectrometer; MRM, multiple reaction monitoring; ESI, electrospray ionization; LOD, limit of detection; LOQ, limit of quantitation; S/N, signal-to-noise ratio; RSD, relative standard error

REFERENCES

(1) Mueller-Harvey, I. Unravelling the conundrum of tannins in animal nutrition and health. *J. Sci. Food Agric.* **2006**, *86*, 2010−2037.

(2) Quideau, S.; Deffieux, D.; Douat-Casassus, C.; Pouységu, L. Plant polyphenols: chemical properties, biological activities, and synthesis. *Angew. Chem., Int. Ed.* **2011**, *50*, 586−621.

(3) Li, M.; Hagerman, A. E. Interactions between plasma proteins and naturally occurring polyphenols. *Curr. Drug Metab.* **2013**, *14*, 432−445.

(4) Prasain, J. K.; Wang, C.-C.; Barnes, S. Mass spectrometric methods for the determination of flavonoids in biological samples. *Free Radical Biol. Med.* **2004**, *37*, 1324−1350.

(5) Ignat, I.; Volf, I.; Popa, V. I. A critical review of methods for characterisation of polyphenolic compounds in fruits and vegetables. *Food Chem.* **2011**, *126*, 1821−1835.

(6) Flamini, R. Recent applications of mass spectrometry in the study of grape and wine polyphenols. *ISRN Spectrosc.* **2013**, 1−45, 81356310.1155/2013/813563.

(7) Ciocalteu, F. O. On tyrosine and tryptophane determination in proteins. *J. Biol. Chem.* **1927**, *73*, 424−427.

(8) Bate-Smith, E. C. Detection and determination of ellagitannins. *Phytochemistry* **1972**, *11*, 1153−1156.

(9) Bate-Smith, E. C. Astringent tannins of *Acer* species. *Phytochemistry* **1977**, *16*, 1421−1426.

(10) Porter, L. J.; Hrstich, L. N.; Chan, B. G. The conversion of procyanidins and prodelphinidins to cyanidin and delphinidin. *Phytochemistry* **1986**, *25*, 223−230.

(11) Hagerman, A. E.; Butler, L. G. Choosing appropriate methods and standards for assaying tannin. *J. Chem. Ecol.* **1989**, *15*, 1795−1810.

(12) Wilson, T. C.; Hagerman, A. E. Quantitative determination of ellagic acid. *J. Agric. Food Chem.* **1990**, *38*, 1678−1683.

(13) Waterman, P. G., Mole, S. In *Analysis of Phenolic Plant Metabolites*; Blackwell Scientific Publications: Oxford, UK, 1994.

(14) Mueller-Harvey, I. Analysis of hydrolysable tannins. *Anim. Feed Sci. Technol.* **2001**, *91*, 3−20.

(15) Salminen, J.-P.; Karonen, M. Chemical ecology of tannins and other phenolics: we need a change in approach. *Funct. Ecol.* **2011**, *23*, 325−338.

(16) Arapitsas, P. Hydrolyzable tannin analysis in food. *Food Chem.* **2012**, *135*, 1708−1717.

(17) Valls, J.; Millán, S.; Martí, M. P.; Borràs, E.; Arola, L. Advanced separation methods of food anthocyanins, isoflavones and flavanols. *J. Chromatogr., A* **2009**, *1216*, 7143−7172.

(18) Motilva, M.-J.; Serra, A.; Macià, A. Analysis of food polyphenols by ultra high-performance liquid chromatography coupled to mass spectrometry: an overview. *J. Chromatogr., A* **2013**, *1292*, 66−82.

(19) Guillarme, D.; Schappler, J.; Rudaz, S.; Veuthey, J.-L. Coupling ultra-high-pressure liquid chromathography with mass spectrometry. *TrAC, Trends Anal. Chem.* **2010**, *29*, 15−27.

(20) Holčapek, M.; Jirásko, R.; Lísa, M. Recent developments in liquid chromatography-mass spectrometry and related techniques. *J. Chromatogr., A* **2012**, *1259*, 3−15.

(21) Rodriguez-Aller, M.; Gurny, R.; Veuthey, J.-L.; Guillarme, D. Coupling ultra high-pressure liquid chromatography with mass spectrometry: constraints and possible applications. *J. Chromatogr., A* **2013**, *1292*, 2−18.

(22) Xing, J.; Xie, C.; Lou, H. Recent applications of liquid chromatography−mass spectrometry in natural products bioanalysis. *J. Pharm. Biomed. Anal.* **2007**, *44*, 368−378.

(23) Bartolomé, B.; Monagas, M.; Garrido, I.; Gómez-Cordovés, C.; Martín-Álvarez, P. J.; Lebrón-Aguilar, R.; Urpí-Sardà, M.; Llorach, R.; Andrés-Lacueva, C. Almond (*Prunus dulcis* (Mill.) D.A. Webb) polyphenols: from chemical characterization to targeted analysis of phenolic metabolites in humans. *Arch. Biochem. Biophys.* **2010**, *501*, 124−133.

(24) Wu, H.; Guo, J.; Chen, S.; Liu, X.; Zhoud, Y.; Zhang, X.; Xu, X. Recent developments in qualitative and quantitative analysis of phytochemical constituents and their metabolites using liquid chromatography−mass spectrometry. *J. Pharm. Biomed. Anal.* **2013**, *72*, 267−291.

(25) Kårlund, A.; Salminen, J.-P.; Koskinen, P.; Ahern, J. R.; Karonen, M.; Tiilikkala, K.; Karjalainen, R. O. Polyphenols in strawberry (*Fragaria* × *ananassa*) leaves induced by plant activators. *J. Agric. Food Chem.* **2014**, *62*, 4592−4600.

(26) Sapozhnikova, Y. Development of liquid chromatography−tandem mass spectrometry method for analysis of polyphenolic compounds in liquid samples of grape juice, green tea and coffee. *Food Chem.* **2014**, *150*, 87−93.

(27) Engström, M. T.; Pälijärvi, M.; Fryganas, F.; Grabber, J.; Mueller-Harvey, I.; Salminen, J.-P. Rapid qualitative and quantitative analysis of proanthocyanidin oligomers and polymers by UPLC-MS/MS. *J. Agric. Food Chem.* **2014**, *62*, 3390−3399.

(28) Moilanen, J.; Salminen, J.-P. Ecologically neglected tannins and their biologically relevant activity: chemical structures of plant ellagitannins reveal their in vitro oxidative activity at high pH. *Chemoecology* **2008**, *18*, 73−83.

(29) Salminen, J.-P.; Ossipov, V.; Haukioja, E.; Pihlaja, K. Seasonal variation in the content of hydrolysable tannins in leaves of *Betula pubescens*. *Phytochemistry* **2001**, *57*, 15−22.

(30) Haslam, E. Proanthocyanidins. In *Plant Polyphenols: Vegetable Tannins Revisited*; Cambridge University Press: Cambridge, UK, 1989; pp 14−79.

(31) Vermerris, V.; Nicholson, R. In *Phenolic Compound Chemistry*; Springer: Dordrecht, The Netherlands, 2006; pp 3−34.

(32) Mullen, W.; Yokota, T.; Lean, M. E. J.; Crozier, A. Analysis of ellagitannins and conjugates of ellagic acid and quercetin in raspberry fruits by LC−MS^n. *Phytochemistry* **2003**, *64*, 617−624.

(33) Seeram, N. P.; Lee, R.; Scheuller, H. S.; Heber, D. Identification of phenolic compounds in strawberries by liquid chromatography electrospray ionization mass spectroscopy. *Food Chem.* **2006**, *97*, 1−11.

(34) Hager, T. J.; Howard, L. R.; Liyanage, R.; Lay, J. O.; Prior, R. L. Ellagitannin composition of blackberry as determined by HPLC-ESI-MS and MALDI-TOF-MS. *J. Agric. Food Chem.* **2008**, *56*, 661−669.

(35) Hanhineva, K.; Rogachev, I.; Kokko, H.; Mintz-Oron, S.; Venger, I.; Kärenlampi, S.; Aharoni, A. Non-targeted analysis of spatial metabolite composition in strawberry (*Fragaria* × *ananassa*) flowers. *Phytochemistry* **2008**, *63*, 2463−2481.

(36) Regueiro, J.; Sánchez-González, C.; Vallverdú-Queralt, A.; Simal-Gándara, J.; Lamuela-Raventós, R.; Izquierdo-Pulido, M. Comprehensive identification of walnut polyphenols by liquid chromatography coupled to linear ion trap−Orbitrap mass spectrometry. *Food Chem.* **2014**, *152*, 340−348.

(37) Kajdžanoska, M.; Gjamovski, V.; Stefova, M. HPLC-DAD-ESI-MS^n identification of phenolic compounds in cultivated strawberries from Macedonia. *Maced. J. Chem. Chem. Eng.* **2010**, *29*, 181−194.

(38) Mena, P.; Calani, L.; Dall'Asta, C.; Galaverna, G.; García-Viguera, C.; Bruni, R.; Crozier, A.; Del Rio, D. Rapid and comprehensive evaluation of (poly)phenolic compounds in pomegranate (*Punica granatum* L.) juice by UHPLC-MSn. *Molecules* **2012**, *17*, 14821−14840.

(39) Moilanen, J.; Sinkkonen, J.; Salminen, J.-P. Characterization of bioactive plant ellagitannins by chromatographic, spectroscopic and mass spectrometric methods. *Chemoecology* **2013**, *23*, 165−179.

(40) Okuda, Y.; Yoshida, T.; Hatano, T.; Ito, H. Ellagitannins renewed the concept of tannins. In *Chemistry and Biochemistry of Ellagitannins*; Quideau, S., Ed.; World Scientific Publishing: Singapore, 2009; pp 1−54.

DOI: 10.1021/acs.jafc.5b00595
J. Agric. Food Chem. 2015, 63, 4068−4079

(41) Salminen, J.-P.; Ossipov, V.; Loponen, J.; Haukioja, E.; Pihlaja, K. Characterization of hydrolysable tannins from leaves of *Betula pubescens* by means of high-performance liquid chromatography−mass spectrometry. *J. Chromatogr., A* **1999**, *564*, 283−291.
(42) Khanbabee, K.; van Ree, T. Tannins: classification and definition. *Nat. Prod. Rep.* **2001**, *18*, 641−649.
(43) Luo, C.; Wang, X.; Gao, G.; Wang, L.; Li, Y.; Sun, C. Identification and quantification of free, conjugate and total phenolic compounds in leaves of 20 sweetpotato cultivars by HPLC-DAD and HPLC-ESI-MS/MS. *Food Chem.* **2013**, *141*, 2697−2706.
(44) Hvattum, E.; Ekeberg, D. Study of the collision-induced radical cleavage of flavonoid glycosides using negative electrospray ionization tandem quadrupole mass spectrometry. *J. Mass Spectrom.* **2003**, *38*, 43−49.
(45) Cuyckens, F.; Clayes, M. Mass spectrometry in the structural analysis of flavonoids. *J. Mass Spectrom.* **2004**, *39*, 1−15.
(46) Cuyckens, F.; Claeys, M. Determination of the glycosylation site in flavonoid mono-*O*-glycosides by collision induced dissociation of electrospray-generated deprotonated and sodiated molecules. *J. Mass Spectrom.* **2005**, *40*, 364−372.
(47) Petsalo, A.; Jalonen, J.; Tolonen, A. Identification of flavonoids of *Rhodiola rosea* by liquid chromatography-tandem mass spectrometry. *J. Chromatogr., A* **2006**, *1112*, 224−231.
(48) Yang, W.-Z.; Qiao, X.; Bo, T.; Wang, Q.; Guo, D.-A.; Ye, M. Low energy induced homolytic fragmentation of flavonol 3-Oglycosides by negative electrospray ionization tandem mass spectrometry. *Rapid Commun. Mass Spectrom.* **2014**, *28*, 385−395.
(49) Vukics, V.; Guttman, A. Structural characterization of flavonoid glycosides by multi-stage mass spectrometry. *Mass Spectrom. Rev.* **2010**, *29*, 116.

DOI: 10.1021/acs.jafc.5b00595
J. Agric. Food Chem. 2015, 63, 4068−4079

has permitted researchers to solve a lot of ineresting problems unaddressed using other structural methods alone, has created significant impacts on structural characterization of macromolecules during the past several decades.[22] The combined studies via SAXS, circular dichroism (CD), fluorescence spectroscopy, and dynamic light scattering (DLS) have been conducted to investigate how the conformation and structure of BSA change as a function of the reaction time coexisting with dextran.

MATERIALS AND METHODS

Materials. BSA (fraction V) with a molecular weight of 66 kDa was obtained from Sigma Chemical Co. (St. Louis, MO). Technical-grade dextran (DT10) with an average molecular weight of 10 kDa was provided by Pharmacosmos (Danmark). The other chemicals, such as sodium chloride (NaCl), potassium chloride (KCl), $Na_2HPO_4{\cdot}7H_2O$, and $NaH_2PO_4{\cdot}H_2O$, were of analytical reagent grade and purchased from Sigma Chemical Co. (St. Louis, MO).

Preparation of BSA–Dextran Conjugates. The conjugates were synthesized through Maillard reaction by dry heating based on the method introduced by Kato et al.,[9] with minor modification. The BSA–dextran mixture in a 1:12 molar ratio was solubilized in phosphate buffer solution (PBS, pH 7.0, 0.1 M NaCl), followed by freezing dry. The freeze-dried mixtures were then put into a desiccator containing saturated KCl solution and incubated at 60 °C for different times (8, 19, and 26 h). The samples with BSA alone were also treated in the same way for comparison.

After incubation, the samples were solubilized in deionized water (0.25%, w/v) and then pre-filtered via a 0.45 μm pore membrane filter (Millipore Corp., Bedford, MA). A 20 mL Microsep advance centrifugal device (Pall Corporation, Port Washington, NY) was used for ultrafiltration with the molecular weight cut-off of 100 000. The samples were centrifuged at 1000 revolutions/min for 30 min to $^1/_8$ of the initial volume to maintain. The deionized water was added to complement the original volume. This procedure was repeated in triplicate to remove excess dextran and BSA. Afterward, the retentates (conjugates) were freeze-dried. It has been proven that the native or dry-heated BSA and 10 kDa dextran could penetrate through the cartridges.[4] The control samples containing pure protein or dextran were also treated accordingly.

SDS–PAGE. Electrophoresis analysis was conducted on the basis of the method provided by Jung et al.,[19] with minor modification. A 10% acrylamide separating gel and a 5% stacking gel containing 0.1% SDS were used. Samples were dissolved in phosphate buffer solution (pH 7.4, 10 mM). Afterward, samples were incubated for 3 min at 100 °C. Electrophoresis was conducted at about 10 mA until the dye front arrived at the bottom of the separating gel. The Coomassie Brilliant Blue R solution was used for gel staining to visualize protein. Later, it was discolored with a solution composed of 10% methanol and 10% acetic acid.

Binding Ratio of DT10 to BSA. Colorimetric methods for determing protein and polysaccharide concentrations were used to calculate the binding ratio of DT10 to BSA. The BSA content was assayed using the Bio-Rad Protein Assay Kit II (Bio-Rad Laboratories, Hercules, CA).[23] The dextran content was quantified by the phenol–sulfuric acid method.[24]

SAXS. BSA and BSA–dextran conjugate were dissolved in deionized water with 2 mg/mL BSA. The content of BSA in solustions was adjusted using the Bio-Rad Protein Assay Kit II for SAXS measurements. SAXS experiments were carried out at the BioCAT, 18-ID beamline of the Advanced Photon Source (Argonne National Laboratory) according to the way that we used previously.[25,26] A sample–detector distance of 3.5 m was taken to lay over a combined Q range from 0.006 to 0.37 Å^{-1}. The scattering data were obtained by a single exposure of 1 s, and 15 replicas were measured and averaged.

Fluorescence Spectroscopy. Fluorescence spectra were recorded with a Cary Eclipse fluorescence spectrophotometer (Varian Instruments, Walnut Creek, CA). A conjugate solution was prepared with 0.1 mg/mL BSA in deionized water. The quartz cuvette of a 1 cm path length was used for holding samples. The intrinsic fluorescence was detected at an excitation wavelength of 280 nm, and the emission wavelength ranged from 287 to 500 nm at 25 °C. The slit width of excitation and emission was 5 nm, respectively.

Far-ultraviolet (UV) CD Spectroscopy. CD of BSA and glycoconjugates was investigated by an Aviv model 420SF CD spectrometer (Biomedical, Inc., Lakewood, NJ). The spectral bandwidth was set at 1 nm. The glycoconjugate was solubilized in deionized water with the BSA concentration of 0.1 mg/mL and then added to the quartz cell of 0.1 cm light path length. CD spectra was obtained from 190 to 250 nm at 25 °C. Molar ellipticity (θ) was analyzed to obtain the α-helix content via the CDPro2 software.

DLS. The mean hydrodynamic diameters of protein and conjugates were determined with the methods described in our previous paper.[25] A dynamic-light-scattering-based BIC 90 plus particle size analyzer was used, fitted with a BI-9000AT digital correlator (Brookhaven Instrument Corporation, Holtsville, NY). Measurements were carried out in triplicate at room temperature.

RESULTS AND DISCUSSION

Binding of BSA with DT10. SDS–PAGE patterns of BSA–DT10 conjugates with different Maillard reaction times were used to prove the covalent binding between DT10 and BSA (Figure 1). It was found that the high-molecular-weight

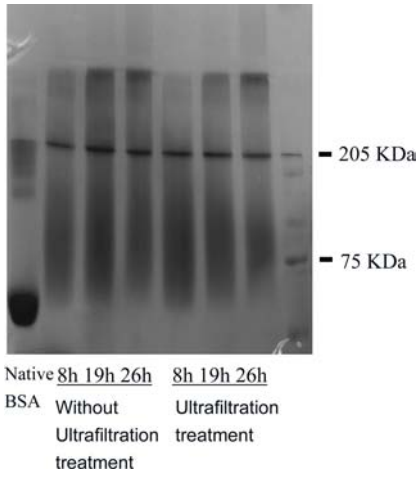

Figure 1. SDS–PAGE pattern of the BSA–DT10 mixture after Maillard reaction.

bands were broad using protein staining. There were bands (~205 kDa) at the head of the separating gel, implying the existence of high-molecular-weight product. Under the conditions of dry heating in this study, oligomers might first arise based on monomeric BSA; subsequently, Maillard reaction proceeded.[19] Therefore, larger oligomeric BSA–DT10 conjugates might exist in the product. In the electropherogram of the reactant (8 h), there was almost no band from the unreacted BSA. We also measured the composition of the conjugates with three reaction times. It was displayed that about 1.68 M DT10 was attached to 1 M BSA. With the reaction time prolonging to 19 and 26 h, about 2.50 and 3.12 M DT10 were bound to 1 M BSA, respectively.

SAXS Profiles. Heating of proteins may lead to conformational changes.[6] The scattering intensity profiles of pure BSA, dextran (DT10), and BSA–DT10 conjugate solutions were presented in Figure 2.

DOI: 10.1021/jf506267r
J. Agric. Food Chem. 2015, 63, 4080–4086

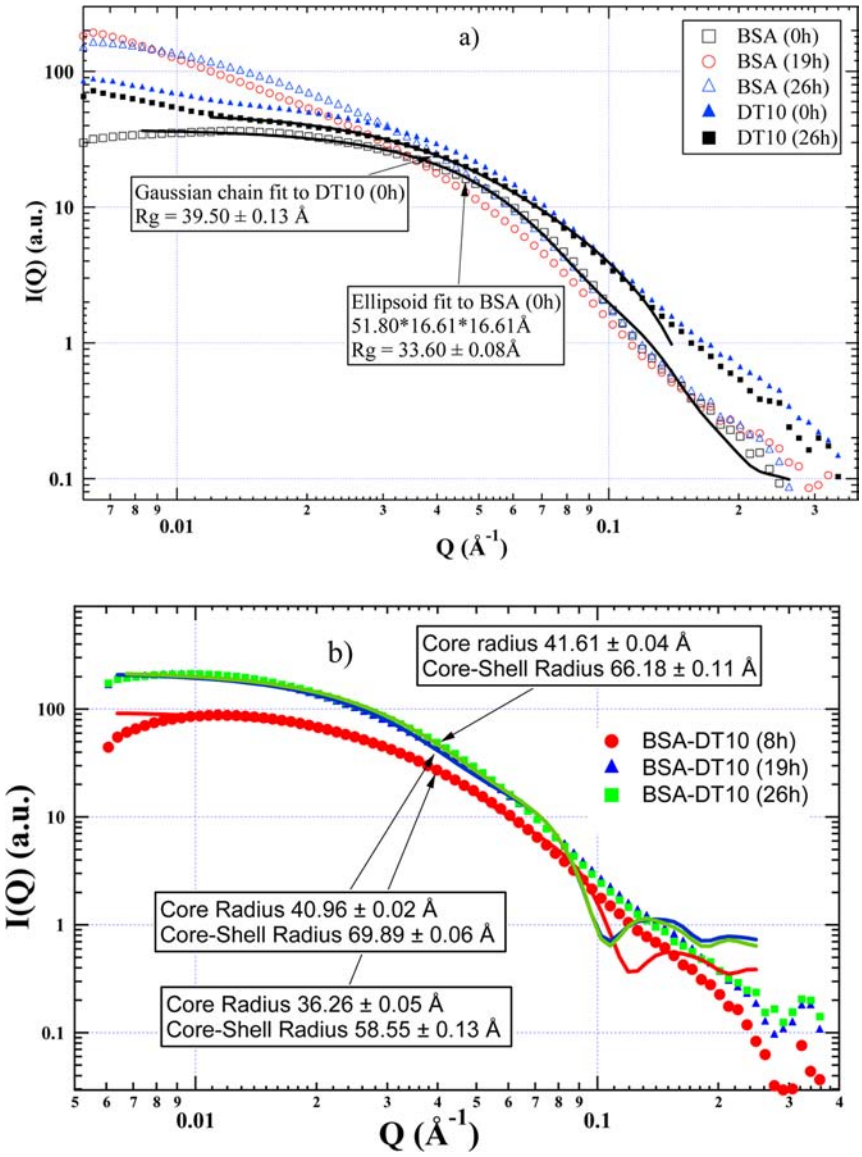

Figure 2. (a) Scattering intensity profiles of BSA and dextran (DT10) during the controlled dry heating period. (b) Spherical shell-fitting plots for scattering intensity profiles of BSA during the dry-heating period in the presence of dextran. Scaling exponents were obtained through the best fit in a log−log plot. The solid line is the fit to a Schultz polydisperse core spherical shell.

For the dry-heated BSA alone, the slopes in the large q range transformed little (Figure 2a). At small q range, the slopes increased sharply with the heating time prolonged. It changed from −0.23 to −1.19 in dilute solutions when the dry heating time prolonged up to 19 h, suggesting that large aggregates formed by interchain correlation of BSA. Such an obvious transformation also suggested that the aggregation of BSA during dry heating might undergo a rod-like shape (slope of −1).[26] However, at a longer heating time (26 h), the slope changed little, revealing that protein did not aggregate further. The 17 disulfide bridges inside BSA make the tertiary structure stable at room temperature, while they do not prevent changes of shape and size as a function of the temperature. Furthermore, a free thiol group (Cys34) is present in the BSA structure, which has been verified to be involved in heat-induced aggregation pathways of BSA. According to the literature, heat-induced aggregation of BSA takes place via two ways in solution. One is the formation of intermolecular disulfide bonds,[27−29] and the other is the formation of intermolecular β-sheet (i.e., β-amyloid).[30] The dry state may prefer β-amyloid because of the lower conformational relaxation freedom; this is also indicated from the CD results.

For BSA dry heated from 8 to 19 h in the presence of dextran (Figure 2b), the slopes also changed when the heating time prolonged in the small q range. It was noted that the slopes did not increase significantly, provided that the heating time prolonged to 26 h. This suggested that the conjugation reaction reached a steady state with the prolonging of the reaction time. The phenomenon was associated with the steric hindrance existing near ε-lysyl amino groups in BSA and branched structure in DT10.[19] Furthermore, the steric effect deriving from the attached dextran might bring an obstacle for further binding.

Guinier Analysis. The quantity radius of gyration (R_g) was commonly used to reflect the volume of solution occupied by the extended micromolecule.[20] Guinier analysis of the scattering curve gave an estimation of R_g. The R_g of particles in solutions was determined using the Guinier relationship.

DOI: 10.1021/jf506267r
J. Agric. Food Chem. 2015, 63, 4080−4086

$$\ln[I(Q)/(Q=0)] = -(QR_g)^2/3 \quad (1)$$

The data range for Guinier analysis was in accordance with $QR_g < 1.57$, which is appropriate to Guinier fitting.[26] Figure 3

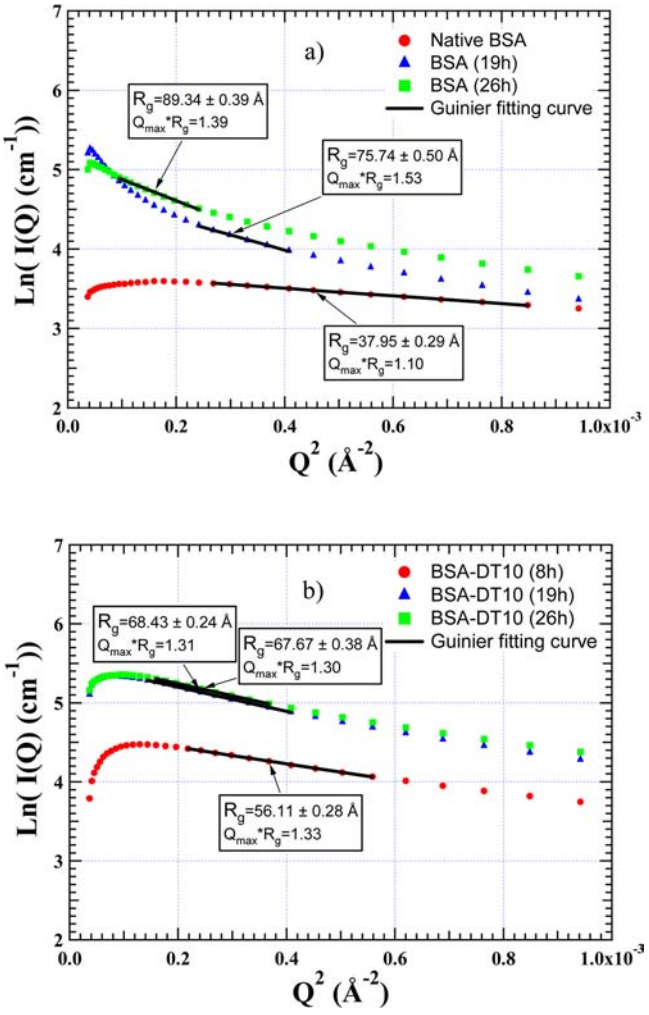

Figure 3. Guinier plots for scattering intensity profiles of BSA during the dry-heating period in the (a) absence and (b) presence of dextran (DT10, 10 kDa). Scaling exponents were obtained through the best fit in a log−log plot.

displayed the fitting line and the influence of heating time on R_g. With the prolonging of the reaction time, $I(Q)$ increased in a small Q range, which might be attributed to the aggregation of protein.[26]

The reaction time and dextran presence dependence of R_g are listed in Table 1. The R_g values of pure BSA increased from 3.8 nm (native) to 5.3 nm (8 h), 7.6 nm (19 h), and 8.9 nm (26 h) as the reaction time increased. However, the R_g values of conjugates just increased from 3.8 nm (native BSA) to 5.6 nm (8 h), 6.8 nm (19 h), and 6.8 nm (26 h). The R_g difference corresponding to the same reaction time may come from the competition between glycosylation and aggregation of BSA. It has already been found that free cysteine plays a notable role on the aggregate growth of BSA in the aqueous system via intermolecular disulfide bridges and S−S exchange.[31] The participation of the unique free cysteine in the aggregation pathway can be affected by the formation of glycosylated albumin. In fact, Maillard reaction of proteins generally involved amino groups (lysine and arginine residues) and thiol groups of the cysteine residue, owing to its powerful nucleophilic property.[32,33] Therefore, the adduction of dextran on the unique sulphydryl group could occur, which might prevent the cysteine residue from taking part in the formation of intermolecular bonds.[30]

The pure dextran was incubated in the same dry-heating condition too. The SAXS results indicated that the structure of DT10 was unchanged (Figure 2a). The dry heating has no significant impact on the conformation of dextran. The gyration radius is slightly changed from 3.6 to 3.8 nm with 26 h of heating.

Spherical Core−Shell Fitting. Conferred from the spherical core−shell fitting (Figure 2b), the core (BSA) has a radius of around 3.6−4.2 nm. When reaching a steady state, the conjugate has a shell with a thickness of around 6.8 nm. BSA conjugates with dextran are slightly smaller in shell thickness (~5.8 nm) for 8 h of dry heating compared to 19 h (~7.0 nm) and 26 h (~6.6 nm). The core radii (BSA) increased slightly with the increase of the dry-heating time. Hence, hydrophilic dextran was bound to the protein surface, followed by enclosing the protein, and the dextran reacted more extensively as the heating time increased. It might also be deduced that the conjugation between DT10 and BSA had no obvious influence on the BSA peptide backbone. In addition, because the steric effect depended upon the polymer chain density of the colloidal particle surface, the shell, owing to the attached dextran with a longer reaction time, agreed with the better stability against heat-induced aggregation of protein.

DLS Measurements. It was also found that the prolonging of the heating time was accompanied by the formation of larger molecules (Figure 4). This tendency could relate to the

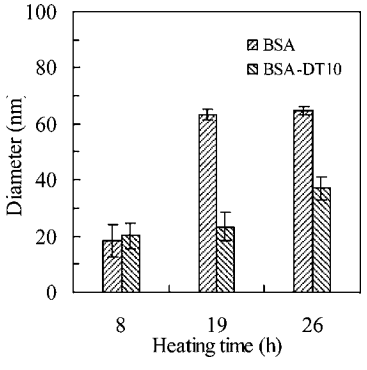

Figure 4. Average diameter of BSA for dry-heated [60 °C and 79% relative humidity (RH)] time periods in the absence and presence of dextran (DT10, 10 kDa).

Table 1. Variation of Radii of Gyration (R_g) during the Dry-Heating Period in the Absence and Presence of Dextran (DT10)

time (h)	0	8	19	26
R_g (Å) of BSA	38.0 ± 0.3	52.8 ± 0.1	75.7 ± 0.5	89.3 ± 0.4
R_g (Å) of BSA−DT10		56.1 ± 0.3	67.7 ± 0.4	68.4 ± 0.2

DOI: 10.1021/jf506267r
J. Agric. Food Chem. 2015, 63, 4080−4086

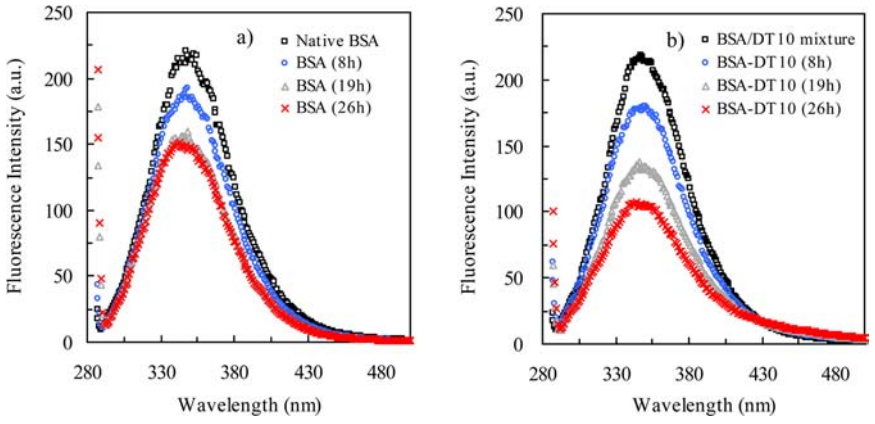

Figure 5. Intrinsic fluorescence spectra excited at 280 nm of BSA for dry-heated (60 °C and 79% RH) time periods in the (a) absence and (b) presence of dextran (DT10, 10 kDa). Fluorescence spectra of BSA samples were measured at 0.1 mg/mL.

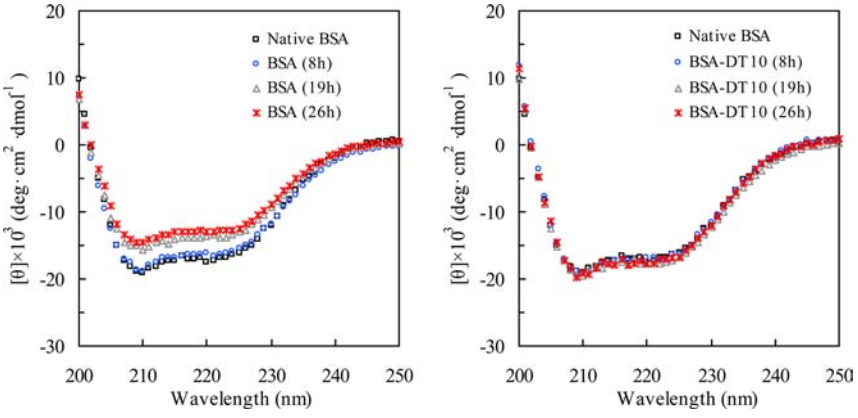

Figure 6. CD spectra of BSA for dry-heated (60 °C and 79% RH) time periods in the (a) absence and (b) presence of dextran (DT10, 10 kDa).

oligomerization of BSA.[19] Thermally induced denaturation and aggregation of BSA have been widely studied. The thiol groups and nonpolar amino acid residues are exposed because of denaturation, which results in the formation of irreversible aggregates via intermolecular disulfide bonds and hydrophobic attraction. This was the reason that the BSA formed aggregates when it was dry-heated alone. Whereas the aggregation and glysolation may occur simultaneously provided that there is dry heating in the presence of dextran, the shell by glycosylation may form a barrier to prevent BSA from aggregation further. This difference is in virtue of the introduction level of hydrophilic dextran to protein. The DLS results are in agreement with the SAXS experiments, in which the aggregation of BSA was concomitant with the reaction time and the extra aggregation was inhibited by the presence of dextran upon the increase of the dry-heating time.

Fluorescence Measurements. There are two tryptophan (Trp) residues possessing intrinsic fluorescence in BSA. Trp212 lies in a hydrophobic pocket of BSA, and Trp134 lies in a hydrophilic region of the molecule surface.[16] Moreover, tryptophan displays an emission maximum near 348 nm in water.[20] The intrinsic fluorescence spectra were used to elucidate the conformation change around the Trp microenvironment.

As shown in Figure 5, the fluorescence emission spectra of native BSA and BSA/DT10 mixture were compared to BSA dry heated alone and glycoconjugate. It was observed that native BSA presented fluorescence emission maxima at 350.92 nm. Once dry heating alone, the alternation of fluorescence intensity of BSA was significant, which came with an obvious shift of the emission maximum to 340.9 (19 h) and 343.9 (26 h), respectively. It is common knowledge that the protein aggregation produces a decrease of the fluorescence intensity, which is accompanied by a blue shift of the maximum emission intensity wavelength. Considering the results, it was implied that the protein underwent conformation change, resulting in the Trp residue exposure to a nonpolarity microenvironment when dry heating alone.

In contrast, there was little change in the emission maximum wavelength of glycoconjugates (λ_{max} = 347.81 nm at 19 and 26 h), suggesting that the conformation around the Trp microenvironment of glycoconjugates resembled with that of native BSA and BSA/DT10 mixture. Whereas in comparison to the controlled BSA by dry heating alone and BSA/DT10 mixture without the heating process, the fluorescence intensity in each glycoconjugate was lowered. Therefore, it could be postulated that the attachment of dextran to BSA took place on the surface of the protein molecule, which corresponded to the core−shell microstructure deduced from SAXS results. It might also be assumed that the binding between BSA and dextran had no significant influence on the conformation of BSA. A previous study of BSA−dextran conjugates with Maillard reaction time reaching 48 and 72 h showed little change in the fluorescence intensity when compared to the native protein.[4] On the contrary, the fluorescence intensity in native BSA alone increased upon dry heating at the same time period.

DOI: 10.1021/jf506267r
J. Agric. Food Chem. 2015, 63, 4080−4086

The reason for the discrepancy may be correlated with the long reaction time. As in our preliminary experiments, it was found that the solubility of the conjugates was very low and floccules formed in the aqueous dispersion when the reaction time reached 36 h or even higher. Jung et al. also characterized the structure of BSA−dextran (69 000 Da) conjugates after controlled dry heating for 7 days by fluorescence spectroscopy and found the similar fluorescence shielding effect by the dextran molecule bound to BSA.[19]

Far-UV CD Measurements. CD spectroscopy was used to investigate the influence of dextran on the characteristics of BSA at the secondary structure level during controlled dry heating. As shown in Figure 6, the helix presented two negative absorption bands at around 209 and 222 nm. Native BSA was reported to have a fraction of about 55% α-helix and 19% β-sheet at pH 7.[34] Herein, the α-helix content of native BSA was about 49% in deionized water, and it almost stayed constant in dry-heating BSA samples containing dextran (Table 2). In view of the minor difference in the CD spectra, the changes in the secondary structure of BSA upon the formation of the glycoconjugate were small. In contrast, the CD spectra changed significantly when the protein alone was dry-heated for 19 and 26 h (Figure 6a), and the α-helix content was found to decrease significantly (Table 2). This suggested that BSA underwent secondary structure changes because of thermal treatment and the presence of dextran might serve to maintain the structural integrity of BSA during dry-heat treatment. This behavior is consistent with the SAXS experimental finding, in which minor loss of secondary structure is accompanied with the prolonged reaction time upon glycosylation with dextran. Spectroscopic analysis by Kim et al. also found that the surface of glycoconjugate was covered with galactomannan and the hydrophobic interior conformation as well as the secondary structure were unchanged obviously.[20] In addition, alteration of the albumin tertiary structure with the glycation process by glucose in the aqueous system had no significant impact on the secondary structure of protein, which was probed after glycation for 7 weeks.[21,35]

Table 2. α-Helix Content of BSA by Dry Heating Alone and in the Presence of Dextran

		BSA			BSA−DT10		
dry-heating time	native BSA	8 h	19 h	26 h	8 h	19 h	26 h
α-helix (%)	48.9	46.5	38.2	34.9	50.8	50.5	49.9

In summary, SAXS, fluorescence, CD, and DLS were employed to investigate the structural change of BSA and BSA−dextran conjugate as a function of dry-heating time. Dextran was found to be able to protect BSA from denaturation and aggregation during dry heating. During incubation in controlled dry heating, BSA endures an obvious change in secondary structure, tertiary structure, and aggregation. Because of the protection from the conjugated dextran layer, the secondary structure of native BSA is well-preserved. The conjugate thickness after reaching a steady state is around 7 nm, with a core of 4 nm. It is necessary to study further to have good knowledge of the relationship between the glycoconjugate structure and functionality.

AUTHOR INFORMATION

Corresponding Author

*Telephone: 848-932-5514. Fax: 732-932-6776. E-mail: qhuang@aesop.rutgers.edu.

Funding

This work was supported by projects of the National Natural Science Foundation of China (31471624), the National 125 Program of China (2012BAD33B04), and 111 Project (B07029). This research used resources of the Advanced Photon Source by Argonne National Laboratory under Contract DE-AC02-06CH11357. This project was also supported by Grant 9 P41 GM103622 from the National Institute of General Medical Sciences of the National Institutes of Health.

Notes

The authors declare no competing financial interest.

REFERENCES

(1) Da Silva Pinto, M.; Bouhallab, S. D.; De Carvalho, A. F.; Henry, G.; Putaux, J.-L.; Leonil, J. Glucose slows down the heat-induced aggregation of β-lactoglobulin at neutral pH. *J. Agric. Food Chem.* **2012**, *60*, 214−219.

(2) Oliver, C. M.; Melton, L. D.; Stanley, R. A. Creating proteins with novel functionality via the Maillard reaction: A review. *Crit. Rev. Food Sci. Nutr.* **2006**, *46*, 337−350.

(3) Liu, J.; Ru, Q.; Ding, Y. Glycation a promising method for food protein modification: Physicochemical properties and structure, a review. *Food Res. Int.* **2012**, *49*, 170−183.

(4) Jiménez-Castaño, L.; Villamiel, M.; López-Fandiño, R. Glycosylation of individual whey proteins by Maillard reaction using dextran of different molecular mass. *Food Hydrocolloids* **2007**, *21*, 433−443.

(5) Wang, Q.; Ismail, B. Effect of Maillard-induced glycosylation on the nutritional quality, solubility, thermal stability and molecular configuration of whey protein. *Int. Dairy J.* **2012**, *25*, 112−122.

(6) Einhorn-Stoll, U.; Ulbrich, M.; Sever, S.; Kunzek, H. Formation of milk protein−pectin conjugates with improved emulsifying properties by controlled dry heating. *Food Hydrocolloids* **2005**, *19*, 329−340.

(7) Yadav, M. P.; Parris, N.; Johnston, D. B.; Onwulata, C. I.; Hicks, K. B. Corn fiber gum and milk protein conjugates with improved emulsion stability. *Carbohydr. Polym.* **2010**, *81*, 476−483.

(8) O'Regan, J.; Mulvihill, D. M. Heat stability and freeze−thaw stability of oil-in-water emulsions stabilised by sodium caseinate−maltodextrin conjugates. *Food Chem.* **2010**, *119*, 182−190.

(9) Kato, A.; Minaki, K.; Kobayashi, K. Improvement of emulsifying properties of egg white proteins by the attachment of polysaccharide through Maillard reaction in a dry state. *J. Agric. Food Chem.* **1993**, *41*, 540−543.

(10) Álvarez, C.; García, V.; Rendueles, M.; Díaz, M. Functional properties of isolated porcine blood proteins modified by Maillard's reaction. *Food Hydrocolloids* **2012**, *28*, 267−274.

(11) Sun, W.-W.; Yu, S.-J.; Yang, X.-Q.; Wang, J.-M.; Zhang, J.-B.; Zhang, Y.; Zheng, E.-L. Study on the rheological properties of heat-induced whey protein isolate−dextran conjugate gel. *Food Res. Int.* **2011**, *44*, 3259−3263.

(12) Matsudomi, N.; Nakano, K.; Soma, A.; Ochi, A. Improvement of gel properties of dried egg white by modification with galactomannan through the Maillard reaction. *J. Agric. Food Chem.* **2002**, *50*, 4113−4118.

(13) Xu, C.-h.; Yang, X.-q.; Yu, S.-j.; Qi, J.-r.; Guo, R.; Sun, W.-W.; Yao, Y.-J.; Zhao, M.-M. The effect of glycosylation with dextran chains of differing lengths on the thermal aggregation of β-conglycinin and glycinin. *Food Res. Int.* **2010**, *43*, 2270−2276.

(14) Enomoto, H.; Li, C.-P.; Morizane, K.; Ibrahim, H. R.; Sugimoto, Y.; Ohki, S.; Ohtomo, H.; Aoki, T. Glycation and phosphorylation of

DOI: 10.1021/jf506267r
J. Agric. Food Chem. 2015, 63, 4080−4086

β-lactoglobulin by dry-heating: Effect on protein structure and some properties. *J. Agric. Food Chem.* **2007**, *55*, 2392−2398.
(15) Li, Y.; Lee, J.; Lal, J.; An, L.; Huang, Q. Effects of pH on the Interactions and Conformation of Bovine Serum Albumin: Comparison between Chemical Force Microscopy and Small-Angle Neutron Scattering. *J. Phys. Chem. B* **2008**, *112*, 3797−3806.
(16) Bourassa, P.; Kanakis, C. D.; Tarantilis, P.; Pollissiou, M. G.; Tajmir-Riahi, H. A. Resveratrol, genistein, and curcumin bind bovine serum albumin. *J. Phys. Chem. B* **2010**, *114*, 3348−3354.
(17) Zhang, F.; Skoda, M. W. A.; Jacobs, R. M. J.; Martin, R. A.; Martin, C. M.; Schreiber, F. Protein interactions studied by SAXS: Effect of ionic strength and protein concentration for BSA in aqueous solutions. *J. Phys. Chem. B* **2007**, *111*, 251−259.
(18) Gospodarczyk, W.; Szutkowski, K.; Kozak, M. Interaction of Bovine Serum Albumin (BSA) with Novel Gemini Surfactants Studied by Synchrotron Radiation Scattering (SR-SAXS), Circular Dichroism (CD), and Nuclear Magnetic Resonance (NMR). *J. Phys. Chem. B* **2014**, *118*, 8652−8661.
(19) Jung, S. H.; Choi, S. J.; Kim, H. J.; Moon, T. W. Molecular characteristics of bovine serum albumin-dextran conjugates. *Biosci., Biotechnol., Biochem.* **2006**, *70*, 2064−2070.
(20) Kim, H. J.; Choi, S. J.; Shin, W.-S.; Moon, T. W. Emulsifying Properties of Bovine Serum Albumin−Galactomannan Conjugates. *J. Agric. Food Chem.* **2003**, *51*, 1049−1056.
(21) Rondeau, P.; Navarra, G.; Cacciabaudo, F.; Leone, M.; Bourdon, E.; Militello, V. Thermal aggregation of glycated bovine serum albumin. *Biochim. Biophys. Acta, Proteins Proteomics* **2010**, *1804*, 789−798.
(22) Graewert, M. A.; Svergun, D. I. Impact and progress in small and wide angle X-ray scattering (SAXS and WAXS). *Curr. Opin. Struct. Biol.* **2013**, *23*, 748−754.
(23) Bradford, M. M. A rapid and sensitive method for the quantitation of microgram quantities of protein utilizing the principle of protein-dye binding. *Anal. Biochem.* **1976**, *72*, 248−254.
(24) Dubois, M.; Gilles, K. A.; Hamilton, J. K.; Rebers, P. A.; Smith, F. Colorimetric method for determination of sugars and related substances. *Anal. Chem.* **1956**, *28*, 350−356.
(25) Huang, Y.; Yu, H.; Guo, L.; Huang, Q. Structure and self-assembly properties of a new chitosan-based amphiphile. *J. Phys. Chem. B* **2010**, *114*, 7719−7726.
(26) Li, Y.; Xia, Q.; Shi, K.; Huang, Q. Scaling behaviors of α-zein in acetic acid solutions. *J. Phys. Chem. B* **2011**, *115*, 9695−9702.
(27) Rondeau, P.; Armenta, S.; Caillens, H.; Chesne, S.; Bourdon, E. Assessment of temperature effects on β-aggregation of native and glycated albumin by FTIR spectroscopy and PAGE: Relations between structural changes and antioxidant properties. *Arch. Biochem. Biophys.* **2007**, *460*, 141−150.
(28) Rombouts, I.; Lagrain, B.; Delcour, J. A. Heat-Induced Cross-Linking and Degradation of Wheat Gluten, Serum Albumin, and Mixtures Thereof. *J. Agric. Food Chem.* **2012**, *60*, 10133−10140.
(29) Luthuli, S. D.; Chili, M. M.; Revaprasadu, N.; Shonhai, A. Cysteine-capped gold nanoparticles suppress aggregation of proteins exposed to heat stress. *IUBMB Life* **2013**, *65*, 454−461.
(30) Saguer, E.; Alvarez, P. A.; Sedman, J.; Ismail, A. A. Study of the denaturation/aggregation behaviour of whole porcine plasma and its protein fractions during heating under acidic pH by variable-temperature FTIR spectroscopy. *Food Hydrocolloids* **2013**, *33*, 402−414.
(31) Militello, V.; Vetri, V.; Leone, M. Conformational changes involved in thermal aggregation processes of bovine serum albumin. *Biophys. Chem.* **2003**, *105*, 133−141.
(32) Zeng, J.; Davies, M. J. Evidence for the Formation of sdducts and S-(Carboxymethyl)cysteine on reaction of α-dicarbonyl compounds with thiol groups on amino acids, peptides, and proteins. *Chem. Res. Toxicol.* **2005**, *18*, 1232−1241.
(33) Thorpe, S. R.; Baynes, J. W. Maillard reaction products in tissue proteins: New products and new perspectives. *Amino Acids* **2003**, *25*, 275−281.
(34) Quiming, N. S.; Vergel, R. B.; Nicolas, M. G.; Villanueva, J. A. Interaction of bovine serum albumin and metallothionein. *J. Health Sci.* **2005**, *51*, 8−15.
(35) Mendez, D. L.; Jensen, R. A.; McElroy, L. A.; Pena, J. M.; Esquerra, R. M. The effect of non-enzymatic glycation on the unfolding of human serum albumin. *Arch. Biochem. Biophys.* **2005**, *444*, 92−99.

DOI: 10.1021/jf506267r
J. Agric. Food Chem. 2015, 63, 4080−4086

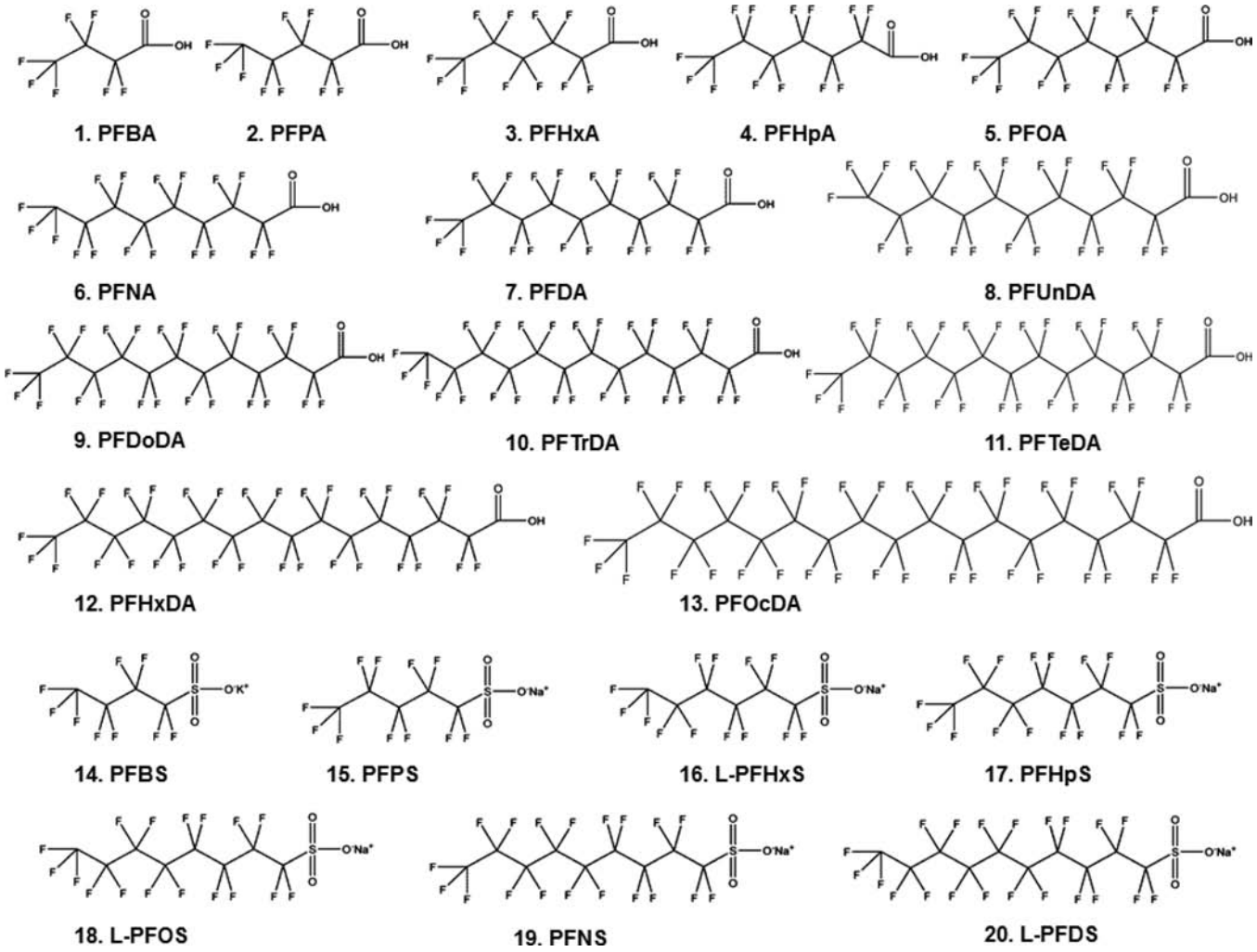

Figure 1. Molecular structures of the 20 PFASs.

Currently, PFASs have been found in cow milk and human milk in many countries including Germany,[22,23] Canada,[24] Italy,[25] China,[26,27] and the U.S.,[28] which is consistent with the persistence and bioaccumulative features of PFASs.[1,3] Furthermore, it was pointed out that the precision and LOD of most previously reported methods for PFASs measurement in the milk matrix varied largely, which might be caused by many factors including the background PFASs from solvents and the apparatus and different extraction efficiencies in milk.[22] With the decline in PFASs levels resulting from worldwide regulations and actions, a more sensitive and reliable method is highly demanded for monitoring PFASs in the complicated but representative milk matrix, which would enable a comprehensive survey and clarification of the exposure routes, particularly in rapidly developing industrialization regions such as China.

Currently available methods for the detection of PFASs in milk are mainly based on HPLC-MS/MS. The corresponding sample extraction methods include an ion-pairing technique,[29] alkaline digestion,[30] and direct methanol extraction.[31] The samples after extraction are normally loaded onto the SPE column for further cleanup.[32,33] However, SPE cleanup is often time-consuming, and not all compounds are retained in the SPE column efficiently, which may lead to low recovery. An alternative universal extraction and cleanup approach, QuEChERS, has been widely applied in pesticide residue screening in various food matrixes since it was first reported,[34] and it may be extended to the analysis of other contaminants such as PFASs in food. In addition, because of the ubiquitous presence of PFASs, the background level of PFASs from the entire analytical procedure has been paid particular attention by replacing the common laboratory apparatus and tubing with those made of glass and stainless steel as well as using an isolation column in the LC system,[8,22,32] which otherwise may lead to an overestimation of the PFASs levels in the measuring subjects and a decrease in the measurement precision. On the basis of the literature mentioned above and our laboratory practice, we are aiming at developing an approach to improve the PFASs measurement accuracy and reliability in milk by integrating the QuEChERS approach with an online trapping LC-MS/MS method and the least-biased quantitation using stable-isotope-labeled internal standards and further applying this method to the simultaneous screening of the common PFASs in dietary milk products.

MATERIALS AND METHODS

Reagents and Materials. The 20 PFASs are perfluoro-*n*-butanoic acid (PFBA), perfluoro-*n*-pentanoic acid (PFPA), perfluoro-*n*-hexanoic acid (PFHxA), perfluoro-*n*-heptanoic acid (PFHpA), perfluoro-*n*-octanoic acid (PFOA), perfluoro-*n*-nonanoic acid (PFNA), perfluoro-*n*-decanoic acid (PFDA), perfluoro-*n*-undecanoic

DOI: 10.1021/acs.jafc.5b00068
J. Agric. Food Chem. 2015, 63, 4087−4095

Table 1. List of Analytes and the Corresponding MRM Parameters for MS/MS Detection

no.	compounds[a,b]	molecular formula	precursor ion	product ion	fragment/V	CE/ev	internal standard
1	PFBA	C_3F_7COOH	213	169[c]	70	1	MPFBA
2	PFPA	C_4F_9COOH	263	219[c]	70	1	MPFBA
3	PFHxA	$C_5F_{11}COOH$	313	269[c]	70	1	MPFHxA
				119		9	
4	PFHpA	$C_6F_{13}COOH$	363	319[c]	90	1	MPFHxA
				169		8	
5	PFOA	$C_7F_{15}COOH$	413	369[c]	90	2	MPFOA
				169		9	
6	PFNA	$C_8F_{17}COOH$	463	419[c]	110	3	MPFNA
				219		9	
7	PFDA	$C_9F_{19}COOH$	513	469[c]	120	2	MPFDA
				269		10	
8	PFUnDA	$C_{10}F_{21}COOH$	563	519[c]	120	2	MPFUnDA
				319		11	
9	PFDoDA	$C_{11}F_{23}COOH$	613	569[c]	140	3	MPFDoDA
				169		15	
10	PFTrDA	$C_{12}F_{25}COOH$	663	619[c]	140	3	MPFDoDA
				169		14	
11	PFTeDA	$C_{13}F_{27}COOH$	713	669[c]	140	4	MPFDoDA
				269		18	
12	PFHxDA	$C_{15}F_{31}COOH$	813	769[c]	150	4	MPFDoDA
				169		19	
13	PFOcDA	$C_{17}F_{35}COOH$	913	869[c]	150	6	MPFDoDA
				219		23	
14	PFBS	$C_4F_7SO_3K$	299	99[c]	190	31	MPFHxS
				80		32	
15	PFPS	$C_5F_{11}SO_3Na$	349	99[c]	200	34	MPFHxS
				80		40	
16	L-PFHxS	$C_6F_{13}SO_3Na$	399	99[c]	230	33	MPFHxS
				80		38	
17	L-PFHpS	$C_7F_{15}SO_3Na$	449	99[c]	250	36	MPFHxS
				80		42	
18	L-PFOS	$C_8F_{17}SO_3Na$	499	99[c]	260	55	MPFOS
				80		59	
19	L-PFNS	$C_9F_{19}SO_3Na$	549	99[c]	280	49	MPFOS
				80		65	
20	L-PFDS	$C_{10}F_{21}SO_3Na$	599	99[c]	300	50	MPFOS
				80		65	
21	MPFBA	$^{13}C_4HF_7O_2$	217	172	70	1	
22	MPFHxA	$C_4{}^{13}C_2HF_{11}O_2$	315	270	70	2	
23	MPFOA	$C_4{}^{13}C_4HF_{15}O_2$	417	372	70	2	
24	MPFNA	$C_4{}^{13}C_5HF_{17}O_2$	468	423	100	1	
25	MPFDA	$C_8{}^{13}C_2HF_{19}O_2$	515	270	110	10	
26	MPFUnDA	$C_9{}^{13}C_2HF_{21}O_2$	565	520	110	3	
27	MPFDoDA	$C_{10}{}^{13}C_2HF_{23}O_2$	615	570	120	2	
28	MPFHxS	$C_6F_{13}S^{18}O_2Na$	403	103	220	33	
29	MPFOS	$C_4{}^{13}C_4F_{11}SO_3^-(Na^+)$	503	99	270	54	

[a] L to the left of compound names **16**−**20** means the levorotary isomer of the compounds. [b] M to the left of compound names **21**−**29** means monoisotope-labeled compounds, used as internal standards. [c] Qualitative MRM.

acid (PFUnDA), perfluoro-*n*-dodecanoic acid (PFDoDA), perfluoro-*n*-tridecanoic acid (PFTrDA), perfluoro-*n*-tetradecanoic acid (PFTeDA), perfluoro-*n*-hexadecanoic acid (PFHxDA), perfluoro-*n*-octadecanoic acid (PFOcDA), potassium perfluoro-1-butanesulfonate (PFBS), sodium perfluoro-1-pentanesulfonate (PFPS), sodium perfluoro-1-hexanesulfonate (PFHxS), sodium perfluoro-1-heptanesulfonate (PFHpS), sodium perfluoro-1-octanesulfonate (PFOS), sodium perfluoro-1-nonanesulfonate (PFNS), and sodium perfluoro-1-decanesulfonate (PFDS). The nine isotopically labeled internal standards are $^{13}C_4$−PFBA, $^{13}C_2$−PFHxA, $^{13}C_4$−PFOA, $^{13}C_5$−PFNA, $^{13}C_2$−PFDA, $^{13}C_2$−PFUnDA, $^{13}C_2$−PFDoDA, $^{18}O_2$−PFHxS, and $^{13}C_4$−PFOS. The molecular structures of these compounds are shown in Figure 1. All standard compounds were purchased from Wellington Laboratories (Guelph, Canada), with purity greater than 98%.

Methanol and acetonitrile were HPLC grade and were obtained from Merck (Darmstadt, Germany); ammonium acetate (HPLC grade) was from TEDIA (Fairfield, OH); hydrochloric acid (12 mol/L) and analytical grade sodium chloride were from National Chemical Groups (Beijing, China); sorbents such as primary and secondary amine (PSA), C18, and graphitized carbon black were obtained from Bonna-Agela Technologies Ltd. (Tianjin, China); water was purified with a Milli-Q system to yield a resistivity of 18.2 MΩ·cm.

DOI: 10.1021/acs.jafc.5b00068
J. Agric. Food Chem. 2015, 63, 4087−4095

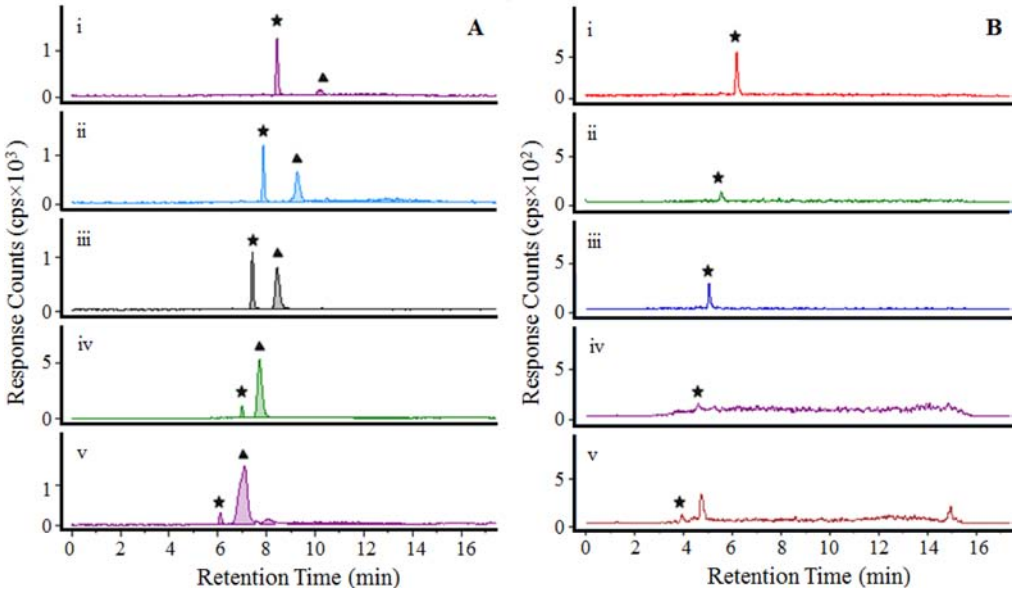

Figure 2. MRM chromatograms demonstrating the separation of target compounds from the background interference. (A) With the trapping column. (B) Without the trapping column. (i) PFOA, (ii) PFHpA, (iii) PFHxA, (iv) PFPA, and (v) PFBA. The spiking level of the analytes was 0.10 μg/L; ★ is the target compound, and ▲ is the interference compound. Note that the retention time for each compound is delayed 2.3 min by the increase in void volume introduced by the trapping column which delayed the gradient profile.

Instrumentations and Experimental Conditions. The separation was conducted using an Infinity UHPLC 1290 system consisting of a binary bump, an autosampler, and a column temperature control compartment (Agilent Technologies, Santa Clara, CA). The precolumn for interference trapping was a 50 mm × 4.6 mm i.d., 5 μm Zorbax Eclipse Plus C18 (Agilent Technologlies, Santa Clara, CA), and the analytical column was an 100 mm × 2.1 mm i.d., 2.7 μm Poroshell 120 Eclipse Plus C18 from the same manufacturer. The effluent from the analytical column was directed to an Agilent 6460 QQQ mass spectrometer fitted with a jetstream electrospray ionization source.

The chromatographic conditions were optimized to achieve high separation efficiency and selectivity. The column was maintained at 30 °C. A binary gradient elution was selected for separation of the 20 PFASs, with solvent A being 5 mmol/L ammonium acetate aqueous solution and solvent B being methanol containing 5 mmol/L ammonium acetate. The gradient profile was the following: %B increased from 10 to 70% within 3 min and then increased to 100% in the next 10 min. The %B was then reduced to 10% in 1 min and maintained at 10% for 6 min until the next analysis. The total LC analysis time was 20 min for each sample, and the flow rate was set at 0.2 mL/min. The injection volume was set at 5 μL.

All of the analytes were detected using triple quadrupole multiple reaction monitoring (MRM) mode under negative ionization; nitrogen was used as a nebulizer gas at 45 psi; the drying gas and flow rate were set at 300 °C and 6 L/min, respectively; those for the sheath gas were set at 260 °C and 11 L/min, respectively; the electrospray voltage (capillary voltage) was 3500 V. Each compound was detected using two MRM transitions: the one with the higher intensity was used for quantitation, and the other was used for qualitative confirmation. The detailed parameters for MRM transitions are listed in Table 1.

Sample Collection. A total of 46 cow milk samples from major brands were collected from 6 sampling sites in China in the provinces of Shandong, Anhui, Liaoning, Fujian, Jiangxi, and Guangdong. Samples were either collected in 50 mL low-density polyethylene (LDPE) (Linc-Bio, Shanghai, China) bottles directly and shipped frozen to the laboratory or left liquid and transported on ice to the laboratory, followed by transferring into 50 mL LDPE bottles upon receipt. The samples were then frozen at −20 °C until they were tested.

Sample Extraction and Cleanup. QuEChERS protocol was applied for PFAS extraction and cleanup. Briefly, a milk sample of 5.0 mL was transferred to a 50 mL LDPE centrifuge tube, and the mixture of internal standard compounds (1.0 ng each) and 5.0 mL of pure water were then added to the tube. After homogenization for 1 min, 10.0 mL of acetonitrile and 30 μL of concentrated hydrochloric acid were added, followed by vortex mixing for 1 min. Two grams of sodium chloride was then added to the tube, followed by 1 min of vortex mixing and sequential centrifugation at 5000 rpm for 10 min. The supernatant solution (acetonitrile layer) was transferred to a clean glass test tube and subjected to drying under nitrogen with a final volume of approximately 4 mL.

The extract from above was transferred to a 15 mL LDPE centrifuge tube containing 60 mg of PSA, 40 mg of C18, and 10 mg of graphitized carbon black. The tube was then vortex mixed for 5 min, followed by centrifugation at 5000 rpm for 10 min. The supernatant solution (approximately 4 mL) was transferred to another clean LDPE centrifuge tube and subjected to drying under nitrogen at 45 °C. The residue was dissolved in methanol to a final volume of 1.0 mL. The solution was then filtered through a 0.22 μm Whatman nylon membrane (GE Healthcare, Buckinghamshire, U.K.) and transferred to a 2 mL glass vial for LC-MS/MS analysis.

Quality Assurance and Quantitation. Because of the wide presence of PFASs in the environment, the experimental apparatus and the LC system such as the mobile phases, the tubing, and the other parts in the LC flow (e.g., seals) may introduce high level of background, which will lower the accuracy for the trace analysis of PFASs. To minimize quantitation bias, possible sources of contamination from both the instrument and sampling procedure were reduced by replacing fluoropolymer materials such as poly-(tetrafluoroethylene) (PTFE) tubing with stainless steel tubing and Teflon centrifuge tubes with LDPE tubes. Calibration solutions containing various amount of standard compounds (ranging from 0.010 to 20.0 μg/L for PFCAs and from 0.050 to 20.0 μg/L for PFSAs) and fixed amounts of isotope -labeled internal standards (1.0 μg/L for each) were prepared in pure methanol. The calibration curve was obtained by plotting the peak area ratios of standards to the corresponding isotope-labeled internal standards versus the amount of added standards. To ensure accurate measurement, quality control standards were measured every 10 injections to monitor the instrumental drift. When the quality control standard was outside

DOI: 10.1021/acs.jafc.5b00068
J. Agric. Food Chem. 2015, 63, 4087−4095

±20% of its theoretical value, a new calibration curve was established for the quantitation of the subsequent samples. The limit of detection (LOD) and limit of quantitation (LOQ) for method were estimated at the lowest spiking concentration at which an S/N could reach 3 and 10, respectively. A solvent blank, solvent standards, and a matrix-spiked standard subjected to the entire sample extraction and cleanup procedure were all analyzed during each set of samples to ensure accurate and precise measurement. When necessary, background subtraction was applied to further avoid the quantitation bias.

RESULTS AND DISCUSSION

Interference Trapping to Improve Detection Sensitivity and Accuracy. As stated above, care has been taken to reduce the interference resulting from the apparatus and tubing. In addition, common HPLC solvents including Milli-Q water and organic solvents often contain trace levels of PFASs, which may inevitably increase the background and result in low sensitivity as well as a quantitation bias for the real samples. To minimize the impact of interference from both mobile phases of the LC system, a precolumn was inserted between the mobile-phase mixer in the LC pump and the autosampler to trap the PFASs from the LC system.

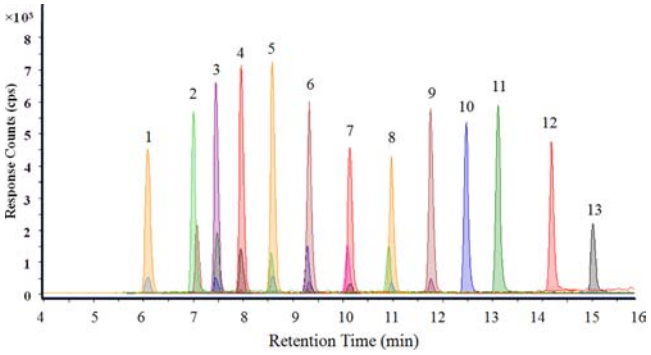

Figure 3. Overlapped MRM chromatograms for the 20 PFASs and 9 internal standard compounds under the optimized LC-MS/MS conditions. The concentration of each analyte was 10.0 μg/L, and the internal standard concentration was 1.0 μg/L. **1**, PFBA/MPFBA; **2**, PFPA/PFBS; **3**, PFHxA/PFPS/MPFHxA; **4**, PFHpA/PFHxS/MPFHxS; **5**, PFOA/PFHpS/MPFOA; **6**, PFNA/PFOS/MPFNA/MPFOS; **7**, PFDA/PFNS/MPFDA; **8**, PFUnDA/PFDS/MPFUnDA; **9**, PFDoDA/MPFUnDA; **10**, PFTrDA; **11**, PFTeDA; **12**, PFHxDA; **13**, PFOcDA.

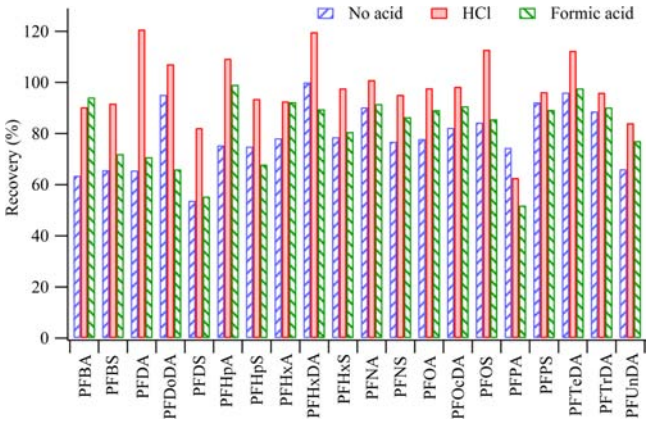

Figure 4. Comparison of the extraction efficiency using three different solvents.

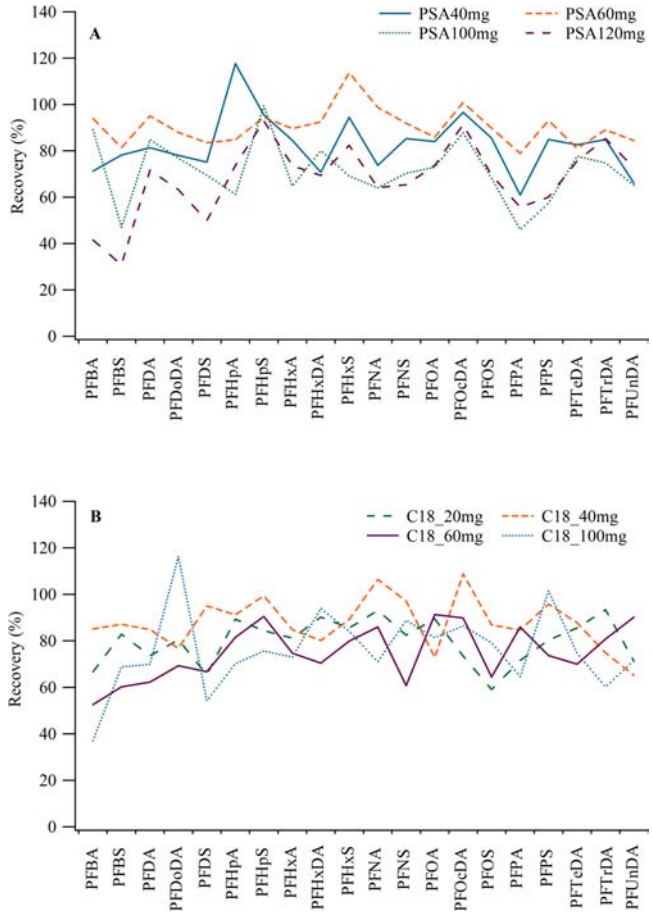

Figure 5. Cleanup efficiency using various amounts of (A) PSA and (B) C18.

With such a setup, during column equilibrium using the starting mobile phase with a low percentage of organic solvent, the interference from LC systems is trapped in the precolumn as a result of the hydrophobic properties of the interference. Upon sample injection, the analytes are transported to the analytical column. During LC gradient elution, with the increasing percentage of organic solvent, the interference trapped in the precolumn is eluted out and further loaded into the analytical column. Becasue the interference trapped in the precolumn is transported to the analytical column later than the analytes loaded through the autosampler, the background interference is delayed from eluting out of the analytical column. Through such a trapping-triggered delay elution, the background interference can be excluded from the elution time window of the analytes.

To efficiently trap the PFASs-related background interference, a high capacity of the precolumn should be selected for trapping. Considering the adsorption capacity, system equilibrium time, and system pressure, the column with a large diameter, large particle size, and shorter length should provide better trapping performance. In practice, it was found that the Zorbax Eclipse Plus-C18 column showed excellent trapping efficiency. As shown in Figure 2A, the majority of interfering species including PFOA, PFHpA, PFHxA, PFPA, and PFBA can be clearly separated from the target analytes by the baseline, and a trace level of the analytes can thus be accurately quantitated with much less bias and a lower background level. In contrast, the signal-to-noise ratio for the above compounds

DOI: 10.1021/acs.jafc.5b00068
J. Agric. Food Chem. 2015, 63, 4087−4095

Table 2. Recovery and Precision for the 20 PFASs at the Specified Spiking Levels[a]

	spiking concentrations					
	0.010 $\mu g \cdot L^{-1}$		0.50 $\mu g \cdot L^{-1}$		1.0 $\mu g \cdot L^{-1}$	
compound	recovery (%)	RSD (%)	recovery (%)	RSD (%)	recovery (%)	RSD (%)
PFBA	78.5	9.23	89.1	3.95	94.9	4.30
PFPA	89.2	13.1	86.4	4.50	91.5	2.91
PFHxA	84.2	2.64	92.2	1.23	100	1.77
PFHpA	79.6	10.1	85.6	3.52	111	3.97
PFOA	97.6	9.26	109	10.4	107	3.53
PFNA	85.4	6.96	91.6	7.19	91.9	9.00
PFDA	102	5.32	107	2.45	98.6	10.5
PFUnDA	85.9	3.78	98.2	3.97	92.4	3.64
PFDoDA	93.4	7.06	105	11.6	98.2	1.85
PFTrDA	92.4	8.04	92.3	9.48	89.9	5.99
PFTeDA	79.3	10.9	88.0	5.93	90.6	6.51
PFHxDA	89.5	4.88	98.7	2.18	98.9	4.74
PFOcDA	85.9	8.07	92.9	11.0	93.9	9.11
	spiking concentrations					
	0.050 $\mu g \cdot L^{-1}$		0.50 $\mu g \cdot L^{-1}$		2.0 $\mu g \cdot L^{-1}$	
compound	recovery (%)	RSD (%)	recovery (%)	RSD (%)	recovery (%)	RSD (%)
PFBS	72.9	8.00	89.3	10.0	90.9	7.78
PFPS	84.5	3.85	84.9	9.53	89.0	10.7
L-PFHxS	94.1	12.7	92.5	6.35	99.7	5.48
L-PFHpS	90.9	3.81	99.2	5.71	105	3.90
L-PFOS	93.1	6.96	101	13.1	98.6	3.53
L-PFNS	82.5	14.9	90.5	9.16	96.7	6.97
L-PFDS	72.8	8.64	88.1	7.96	92.9	5.06

[a] $n = 6$ for each level.

spiked at the same level is significantly lower in the absence of the precolumn (Figure 2B).

Optimization of HPLC-MS/MS Conditions. To monitor the PFASs with sufficient selectivity and sensitivity, MS scanning was initially acquired to find the precursor ions for all of the compounds. The fragmentor voltage was then optimized to achieve maximum intensity for the precursor ions. Product ion scanning was further applied to find the fragment ions and the corresponding optimized collision energy. It was found that perfluorinated carboxylic acids (PFCAs) are liable to lose the carboxyl group (COO^-) in the collision cell in the presence of nitrogen gas and generate $[M\text{-}H\text{-}44]^-$; perfluorinated sulfonic acids (PFSAs) can easily release the sulfonate group (SO_3^-) and the fluorinated sulfonate group (FSO_3^-) and produce fragments $[M\text{-}H\text{-}80]^-$ and $[M\text{-}H\text{-}99]^-$. The resultant fragments with high intensity and selectivity were selected for MRM detection and are listed in Table 1.

Because PFASs are substances with weak polarity, the C18 column could be selected for the separation of the 20 PFASs. With 5 mmol/L ammonium acetate/H_2O and 5 mmol/L ammonium acetate/MeOH as the binary mobile phases for gradient elution, 20 analytes can be separated with 13 major peaks (Figure 3). Those PFASs with similar carbon numbers cannot be separated completely by retention; nonetheless, the detection of these compounds is highly selective with the selection of the specific MRM transitions, which allow accurate quantitation of these compounds.

Optimization of the QuEChERS Procedure. The QuEChERS method has been widely used in the analysis of pesticide residues since 2003.[34] It involves two major steps: sample extraction and cleanup. Considering that PFASs contain acidic groups, it is expected that strongly acidic extraction solvents may extract more interference;[35] in addition, acetonitrile extraction was reported to have advantages over ion pair and formic acid extraction.[36] Hence, weakly acidic solvents including acidified acetonitrile using formic acid or hydrochloric acid (HCl) and pure acetonitrile were examined here. The recoveries of PFASs using different extraction solvents were then compared. As shown in Figure 4, nonacidified solvent showed the lowest recovery for most PFASs, formic acid/acetonitrile showed better recovery for PFBA compared to HCl/acetonitrile, and similar recoveries could be achieved using formic acid/acetonitrile or HCl/acetonitrile for other PFCAs. However, very low recovery was found for PFSAs using formic acid/acetonitrile compared to HCl/acetonitrile. Eventually, HCl/acetonitrile was selected as the extraction solvent. The amount of HCl in the extraction solvent was then examined, and the highest recoveries for PFASs were observed when 30 μL of HCl was added to 10 mL of acetonitrile. By further increasing the amount of acid, more interference compounds were coextracted, which can coelute with target analytes and affect the accuracy of the target quantitation. Hence, 0.3% HCl in the acetonitrile was selected as the extraction solvent.

During the QuEChERS cleanup step, conventional sorbents such as PSA, C18, and graphitized carbon black are often applied to remove organic/fatty acids, lipids, and pigments, respectively. Because of the large quantity of proteins and lipids in the milk matrix, the above sorbents were selected and the corresponding amount was further optimized. With the low selectivity of PSA for the acidic substances, it is necessary to control the adsorption of the target PFASs.[37] Examining the amount in the range of 40−120 mg, it was found that recoveries for PFASs were highest when using 60 mg of PSA (Figure 5A). As for C18, the recoveries for PFASs were highest when 40 mg of C18 was used (Figure 5B). In comparison, including graphitized carbon black did not clearly improve the recoveries for PFASs, which might be due to the low levels of pigment in milk. Hence, a very small amount of graphitized carbon black was added. In combination, a sorbent mixture containing 60 mg of PSA, 40 mg of C18, and 10 mg of graphitized carbon black was selected for cleanup.

Calibration Linearity and Detection Sensitivity. Initial laboratory practice demonstrated that the matrix effect could lead to low recovery when using an external standard calibration method for quantitation in LC-MS analysis. To better reduce the matrix effect and improve the accuracy of the measurement, here a stable-isotope-labeled internal standard was applied for quantitation. For the 20 PFASs, only 9 isotopic analogs were obtained. Hence, for those compounds without corresponding isotopic analogs, they were assigned an isotope-labeled standard with similar chemical structure, as shown in Table 1. By analyzing a series of calibration solutions containing various amounts of standard compounds and fixed amounts of isotope-labeled internal standards, the calibration curve for each analyte was then established by linearly plotting the peak area ratios of standards to the corresponding isotope-labeled standards versus the amount of added standards. It was found that all PFASs had very wide dynamic linear ranges, with PFCAs in the range of 0.010−20.0 μg/L and PFSAs in the range of 0.050−20.0 μg/L. The correlation coefficients of

DOI: 10.1021/acs.jafc.5b00068
J. Agric. Food Chem. 2015, 63, 4087−4095

Table 3. Average Concentration of PFASs in Milk Collected from Six Sites in China

sampling sites (n)[a]	average concentration ($\mu g \cdot L^{-1}$)[e]							
	PFBA	PFPA	PFHxA	PFHpA	PFOA	PFNA	PFDA	PFDoDA
site 1 (5)	0.11−0.34 (0.17)	ND	ND	ND	0.011−0.073 (0.058)	0.041−0.37 (0.16)	ND	<0.010−0.011 (<0.01)
site 2 (5)	0.010−0.18 (0.072)	ND	ND	0.016−0.041 (0.027)	ND	<0.010−0.10 (0.049)	<0.010−0.011 (<0.010)	<0.010−0.034 (0.011)
site 3 (12)	<0.010[b]−0.211 (0.094)	ND−0.029 (0.018)	ND	ND	ND−0.042 (0.034)	ND−0.038 (<0.010)	ND	ND−<0.010 (<0.010)
site 4 (8)	0.073−0.14 (0.089)	ND	ND−0.028 (0.010)	ND−0.034 (0.010)	ND	0.073−0.28 (0.17)	ND	ND
site 5 (11)	<0.010−0.13 (0.073)	ND−0.018 (<0.010)	ND	ND	ND−0.092 (0.027)	<0.010−0.082 (0.027)	ND−0.043 (0.012)	ND
site 6 (5)	ND[d]-0.092 (0.061)	ND−0.043 (0.012)	ND	ND	<0.01−0.11 (0.039)	ND−0.062 (0.018)	ND	ND

sampling sites[a]	average concentration ($\mu g \cdot L^{-1}$)[e]							
	PFTrDA	PFTeDA	PFHxDA	PFOcDA	PFPS	PFHxS	PFHpS	PFOS
site 1 (5)	0.048−0.11 (0.092)	ND−0.017 (<0.010)	<0.010−0.093 (0.063)	ND−0.037 (0.012)	ND−0.044 (0.020)	ND	ND	0.051−0.12 (<0.050)
site 2 (5)	<0.010−0.12 (0.081)	ND	<0.010−0.23 (0.012)	<0.010−0.33 (0.020)	ND	<0.050−0.092 (<0.050)	ND	<0.050−0.11 (0.086)
site 3 (12)	<0.010−0.018 (<0.010)	ND	0.021−0.065 (0.047)	ND	ND	ND	ND	ND
site 4 (8)	ND−0.024 (0.011)	ND−<0.010 (<0.010)	ND−<0.010 (<0.010)	ND−<0.010 (<0.010)	ND−<0.050[c] (<0.0150)	ND	<0.050−0.091 (<0.050)	<0.050−0.076 (<0.050)
site 5 (11)	<0.01−0.073 (0.046)	ND	<0.010−0.027 (0.010)	ND	ND	ND	ND	ND−0.081 (<0.050)
site 6 (5)	0.021−0.054 (0.029)	ND	<0.010−0.040 (0.010)	ND	ND	ND	ND−<0.050 (<0.050)	ND

[a]Number of samples from the corresponding sampling sites. [b]<0.010 represents the level below LOQ but higher than LOD for PFCAs. [c]<0.050 represents the level below LOQ but higher than LOD for PFSAs. [d]ND indicates under LOD and not detectable. [e]Each compound was reported with a concentration range of the tested samples from the corresponding region, and the average levels among the samples are listed in parentheses.

determination were all higher than 0.997, with most above 0.999.

In contrast to previous reports where the LOD and LOQ of the method are commonly obtained on the basis of the procedural blank and their deviation levels,[22] here seven concentrations of each PFAS (0.0010, 0.0030, 0.0050, 0.010, 0.030, 0.050, and 0.10 μg/L) were used to spike the blank milk matrix, and the levels which produced chromatographic peaks with S/N = 3 and 10 for the quantifier ions were set as the LOD and LOQ of the method, respectively. The LODs for PFCAs and PFSAs were 0.0030 and 0.010 μg/L, respectively, and LOQs for both groups were 0.010 and 0.050 μg/L, respectively. Such LOD and LOQ values are comparable to the currently reported method in milk;[10,22] moreover, they are adequately measurable.

Accuracy and Precision. Because the LOQs for PFSAs are 5- to 10-fold higher than those for PFCAs, the spiking levels for PFSAs were set at 0.050 (LOQ level), 0.50, and 2.0 μg/L and those for PFCAs were set at 0.010 (LOQ level), 0.50, and 1.0 μg/L. At each spiking level, six replicates were used with a blank matrix as the control. As shown in Table 2, the recoveries for PFCAs ranged from 78.5 to 111%, with RSD (n = 6) within 1.20−13.1%, and those for PFSAs were in the range of 72.8−105%, with RSD within 3.53−14.8% (n = 6). Even at a level as low as the LOQ, the recovery and precision for both groups of PFASs have no significant differences compared to those obtained at the higher spiking levels. This indicates that the method is very accurate and repeatable.

Real Sample Analysis. The developed method was applied to the real sample survey. Here, 46 milk samples randomly collected from various manufacturers in 6 provinces of China were analyzed. On the basis of the occurrence frequency, these 20 PFASs can be classified into 4 groups. PFUnDA, PFBS, PFHpS, and PFNS belong to the undetectable group in which the level of PFUnDA was under the detection limit of 0.0030 μg/L across all samples, and those of PFBS, PFHpS, and PFNS were undetectable at an LOD of 0.010 μg/L.

PFPA, PFOA, and PFOS were found to be the intermediate group with the occurrence frequency in approximately 50% of the total tested samples. As shown in Table 3, PFPA was more frequently detected at sites 3, 5, and 6, with the levels ranging from ND to 0.043 μg/L and the highest average of 0.018 μg/L at site 3. PFOA was detected primarily at sites 1, 3, 5, and 6, with the concentration across the whole sample within the range of ND−0.11 μg/L and the highest average of 0.058 μg/L at site 1. PFOS was detected within the range of ND−0.12 μg/L mainly in sites 1, 2, 4, and 5, with the highest average as 0.086 μg/L at site 2.

Furthermore, PFBA, PFNA, PFHxDA, and PFTrDA were classified as the high occurrence frequency group, found in 41 out of 46 (89%) milk samples (Table 3). PFBA was detected in the range from ND to 0.34 μg/L, with the highest average

DOI: 10.1021/acs.jafc.5b00068
J. Agric. Food Chem. 2015, 63, 4087−4095

levels found at site 1; PFNA was detected in the concentration range of ND−0.37 μg/L among the whole samples, and the average ones at sites 1 and 4 were particularly high. For PFHxDA and PFTrDA, the detected levels across the whole samples ranged from ND−0.12 μg/L and ND−0.23 μg/L, respectively, and the highest average levels for both were found at site 1.

The other nine PFASs consisting of PFHxA, PFHpA, PFDA, PFTeDA, PFOcDA, PFPS, PFHxS, PFHpS, and PFDoDA were occasionally detected in some samples, and the levels are relatively low, ranging from ND to 0.092 μg/L, except for PFOcDA, which was detected at a level as high as 0.33 μg/L in one sample at site 2. The average levels for these PFASs ranged from ND to 0.028 μg/L across all six sampling sites. In summary, the total concentration of PFASs in the 46 milk samples ranged from 0.19 to 0.66 μg/L.

A previous report from China has determined 13 PFASs in milk and its related products collected from 3 cities in China, and it was found that PFHpA, PFOA, PFOS, PFNA, PFDA, PFUnDA, and PFTA were positively detected.[26] Among them, the concentrations for PFDA were within <0.015−0.044 μg/kg with a mean value of 0.007 μg/kg, which is comparable to the current study. The maximum detected levels for PFOA, PFOS, PFNA, and PFUnDA in the aforementioned study are higher than those determined in the current study. However, most of the average values in the current study are slightly higher. Also, both the maximum level and the mean level of PFHpA found in the current study are relatively lower. In addition, 19 out of the 20 PFASs except PFNS were in the monitoring list of the 2012 EFSA report[6] in which comparable results were found for 13 PFASs belonging to the undetectable group and the occasionally detected group, with reported levels mostly under the LOQ of the method in milk and related products. For the remaining 6 PFASs, PFOS was reported with levels ranging from 0.005 to 1.2 μg/kg and an occurrence frequency of 3%; PFOA was found in 4 out of 319 samples, with the levels ranging from 0.007 to 3.7 μg/kg; PFNA was found in 3 milk and related products with a concentration range of 0.005−0.02 μg/kg; the levels of PFBA and PFHxDA were under the corresponding detection limits and those of PFTrDA were under the LOQ level.[6] In comparison, the maximum and average levels and the occurrence frequencies of PFPA, PFBA, PFHxDA, and PFTrDA in the present study are significantly higher. Although the maximum levels of PFOS and PFOA in the current study are lower, the occurrence frequency is much higher compared to the EFSA report.[6] It should be noted that the two PFASs with longer carbon chains, PFTrDA and PFHxDA, are particularly high at sites 1 and 2 where PFTrDA and PFHxDA ranged as high as 0.048−0.11 μg/L and <0.010−0.23 μg/L, respectively. Such high levels have not been reported previously. They may be related to the local industrial contamination and require further investigation.

Global industrialization has led to the ubiquitous presence of PFASs in the environment. Although the voluntary stewardship program has been making an effort to eliminate the new production of some PFASs,[3] the impact of PFASs already in the environment will continue be an issue in the food chain because of the persistent and bioaccumulative nature of these compounds. Knowledge and survey data on the level of PFASs through dietary exposure is essential to evaluating the impact of these compounds on human health. Compared to the previously reported methods, QuEChERS combined with the online interference trapping LC-MS/MS method developed here has the advantages of low background interference, high sensitivity, and high selectivity. It is also very rapid and can be applied for screening the trace level of PFASs in milk.

AUTHOR INFORMATION

Corresponding Author

*Tel: +86-592-3269935. Fax: +86-592-3269515. E-mail: xudm@xmciq.gov.cn.

Funding

We are grateful for financial support from the following programs: the Special Program of Fundamental Research of the Ministry of Science and Technology (no. 2013FY11310), the Natural Science Foundation of Fujian Province (no. 2012J01146), and the Xiamen City Science and Technology Project (no. 3502Z20124004).

Notes

The authors declare no competing financial interest.

ABBREVIATIONS USED

MRM, multiple reaction monitoring; PFASs, polyfluoroalkane substances; PFBA, perfluoro-*n*-butanoic acid; PFBS, potassium perfluoro-1-butanesulfonate; PFCAs, perfluorinated carboxylic acids; PFDA, perfluoro-*n*-decanoic acid; PFDoDA, perfluoro-*n*-dodecanoic acid; PFDS, sodium perfluoro-1-decanesulfonate; PFHpA, perfluoro-*n*-heptanoic acid; PFHpS, sodium perfluoro-1-heptanesulfonate; PFHxA, perfluoro-*n*-hexanoic acid; PFHxS, sodium perfluoro-1-hexanesulfonate; PFHxDA, perfluoro-*n*-hxadecanoic acid; PFNA, perfluoro-*n*-nonanoic acid; PFNS, sodium perfluoro-1-nonanesulfonate; PFOA, perfluoro-*n*-octanoic acid; PFOcDA, perfluoro-*n*-octadecanoic acid; PFOS, perfluorooctanesulfonic acid; PFPA, perfluoro-*n*-pentanoic acid; PFPS, sodium perfluoro-1-pentanesulfonate; PFSAs, perfluorinated sulfonic acids; PFTeDA, perfluoro-*n*-tetradecanoic acid; PFTrDA, perfluoro-*n*-tridecanoic acid; PFUnDA, perfluoro-*n*-undecanoic acid.

REFERENCES

(1) Ullah, S.; Alsberg, T.; Berger, U. Simultaneous determination of perfluoroalkyl phosphonates, carboxylates, and sulfonates in drinking water. *J. Chromatogr. A* **2011**, *1218*, 6388−6395.

(2) Giesy, J. P.; Kannan, K. Global distribution of perfluorooctane sulfonate in wildlife. *Environ. Sci. Technol.* **2001**, *35*, 1339−1342.

(3) http://www.epa.gov/oppt/pfoa/pubs/stewardship/pfoastewardshipbasics.html (access date: Dec. 20, 2014).

(4) Wang, T.; Wang, Y.; Liao, C.; Cai, Y.; Cai, Y.; Jiang, G. Perspectives on the inclusion of perfluorooctane sulfonate into the Stockholm convention on persistent organic pollutes. *Environ. Sci. Technol.* **2009**, *43*, 5171−5175.

(5) European Food Safety Authority (EFSA). Commission regulation (EC) No 2010 /161 /EU. *Official J. European Union* **2010**, *53*, 22−23.

(6) European Food Safety Authority (EFSA). Perfluoroalkylated substances in food: occurrence and dietary exposure. *EFSA J.* **2012**, *10* (2743), 1−55.

(7) Sepulvado, J. G.; Blaine, A. C.; Hundal, L. S.; Higgins, C. P. Occurrence and fate of perfluorochemicals in soil following the land application of municipal biosolids. *Environ. Sci. Technol.* **2011**, *45*, 8106−8112.

(8) Gulkowska, A.; Jiang, Q. T.; So, M. K.; Taniyasu, S.; Lam, P. K. S.; Yamashita, N. Persistent perfluorinated acids in seafood collected from two cities of China. *Environ. Sci. Technol.* **2006**, *40*, 3736−3741.

(9) Mak, Y. L.; Taniyasu, S.; Yeung, L. W. Y.; Lu, G.; Jin, L.; Yang, Y.; Lam, P. K. S.; Kannan, K.; Yamashita, N. Perfluorinated compounds in tap water from China and several other countries. *Environ. Sci. Technol.* **2009**, *43*, 4824−4829.

DOI: 10.1021/acs.jafc.5b00068
J. Agric. Food Chem. 2015, 63, 4087−4095

(10) Tao, L.; Ma, J.; Kunisue, T.; Libelo, E. L.; Tanabe, S.; Kannan, K. Perfluorinated compounds in human breast milk from several Asian countries, and in infant formula and dairy milk from the United States. *Environ. Sci. Technol.* **2008**, *42*, 8597−8602.
(11) Tittlemier, S. A.; Pepper, K.; Edwards, L. Concentrations of perfluorooctane -sulfonamides in Canadian total diet study composite food samples collected between 1992 and 2004. *J. Agric. Food Chem.* **2006**, *54*, 8385−8389.
(12) Ericson, I.; Martí-Cid, R.; Nadal, M.; Van Bavel, B.; Lindstrom, G.; Domingo, J. L. Human exposure to perfluorinated chemicals through the diet: intake of perfluorinated compounds in foods from the Catalan (Spain) market. *J. Agric. Food Chem.* **2008**, *56*, 1787−1794.
(13) Zhang, T.; Sun, H. W.; Wu, Q.; Zhang, X. Z.; Yun, S. H.; Kannan, K. Perfluorochemicals in meat, eggs and indoor dust in China: assessment of sources and pathways of human exposure to perfluorochemicals. *Environ. Sci. Technol.* **2010**, *44*, 3572−3579.
(14) Kuklenyik, Z.; Needham, L. L.; Calafat, A. M. Measurement of 18 perfluorinated organic acids and amides in human serum using on-line solid-phase extraction. *Anal. Chem.* **2005**, *77*, 6085−6091.
(15) Kennedy, G. L.; Butenhoff, J. L.; Olsen, G. W.; O'Connor, J. C.; Seacat, A. M.; Perkins, R. G.; Biegel, L. B.; Murphy, S. R.; Farrar, D. G. The toxicology of perfluorooctanoate. *Crit. Rev. Toxicol.* **2004**, *34*, 351−384.
(16) Harada, K.; Xu, F.; Ono, K.; Iijima, T.; Koizumi, A. Effects of PFOS and PFOA on L-type Ca^{2+} currents in guinea-pig ventricular myocytes. *Biochem. Biophys. Res. Commun.* **2005**, *329*, 487−494.
(17) Yang, Q.; Abedi-Valugerdi, M.; Xie, Y.; Zhao, X. Y.; Möller, G.; Nelson, B. D.; DePierre, J. W. Potent suppression of the adaptive immune response in mice upon dietary exposure to the potent peroxisome proliferator, perfluorooctanoic acid. *Int. Immunopharmacol.* **2002**, *2*, 389−397.
(18) Chang, S. C.; Ehresman, D. J.; Bjork, J. A.; Wallace, K. B.; Parker, G. A.; Stump, D. G.; Butenhoff, J. L. Gestational and lactational exposure to potassium perfluorooctanesulfonate (K+PFOS) in rats: Toxicokinetics, thyroid hormone status, and related gene expression. *Reprod. Toxicol.* **2009**, *27*, 387−399.
(19) Cui, L.; Zhou, Q.; Liao, C.; Fu, J. J.; Jiang, G. B. Studies on the toxicological effects of PFOA and PFOS on rats using histological observation and chemical analysis. *Arch. Environ. Contam. Toxicol.* **2009**, *56* (2), 338−349.
(20) Greaves, A. K.; Letcher, R. J.; Sonne, C.; Dietz, R. Brain region distribution and patterns of bioaccumulative perfluoroalkyl carboxylates and sulfonates in East Greenland polar bears (*Ursus maritimus*). *Environ. Toxicol. Chem.* **2013**, *32*, 713−722.
(21) EFSA. Perfluorooctane sulfonate (PFOS), perfluorooctanoic acid (PFOA) and their salts. *EFSA J.* **2008**, *653*, 1−131.
(22) Kärrman, A.; Lindström, G. Trends, analytical methods and precision in the determination of perfluoroalkyl acids in human milk. *TrAC, Trends Anal. Chem.* **2013**, *46*, 118−128.
(23) Kowalczyk, J.; Ehlers, S.; Oberhausen, A.; Tischer, M.; Fürst, P.; Schafft, H.; Lahrssen-Wiederholt, M. Absorption, distribution, and milk secretion of the perfluoroalkyl acids PFBS, PFHxS, PFOS, and PFOA by dairy cows fed naturally contaminated feed. *J. Agric. Food Chem.* **2013**, *61*, 2903−2912.
(24) Kubwabo, C.; Kosarac, I.; Lalonde, K. Determination of selected perfluorinated compounds and polyfluoroalkyl phosphate surfactants in human milk. *Chemosphere* **2013**, *91*, 771−777.
(25) Barbarossa, A.; Masetti, R.; Gazzotti, T.; Zama, D.; Astolfi, A.; Veyrand, B.; Pession, A.; Pagliuca, G. Perfluoroalkyl substances in human milk: A first survey in Italy. *Environ. Int.* **2013**, *51*, 27−30.
(26) Wang, J. M.; Shi, Y. L.; Pan, Y. Y.; Cai, Y. Q. Perfluorinated compounds in milk, milk powder and yoghurt purchased from markets in China. *Chin. Sci. Bull.* **2010**, *55*, 1020−1025.
(27) Liu, J.; Li, J.; Zhao, Y.; Wang, Y.; Zhang, L.; Wu, Y. The occurrence of perfluorinated alkyl compounds in human milk from different regions of China. *Environ. Int.* **2010**, *36*, 433−438.
(28) Young, W. M.; South, P.; Begley, T. H.; Diachenko, G. W.; Noonan, G. O. Determination of perfluorochemicals in cow's milk using liquid chromatography-tandem mass spectrometry. *J. Agric. Food Chem.* **2012**, *60*, 1652−1658.
(29) Kubwabo, C.; Kosarac, I.; Lalonde, K. Determination of selected perfluorinated compounds and polyfluoroalkyl phosphate surfactants in human milk. *Chemosphere* **2013**, *91*, 771−777.
(30) So, M. K.; Taniyasu, S.; Lam, P. K. S.; Zheng, G. J.; Giesy, J. P.; Yamashita, N. Alkaline digestion and solid phase extraction method for perfluorinated compounds in mussels and oysters from south China and Japan. *Arch. Environ. Contam. Toxicol.* **2006**, *50*, 240−248.
(31) Ostertag, S. K.; Tague, B. A.; Humphries, M. M.; Tittlemier, S. A.; Chan, H. M. Estimated dietary exposure to fluorinated compounds from traditional foods among Inuit in Nunavut, Canada. *Chemosphere* **2009**, *75*, 1165−1172.
(32) Haug, L. S.; Salihovic, S.; Thomsen, C.; Thomsen, C.; van Bavel, B.; LindstrÖm, G.; Becher, G. Levels in food and beverages and daily intake of perfluorinated compounds in Norway. *Chemosphere* **2010**, *80*, 1137−1143.
(33) Lin, Q. Determination of perfluorooctanoic acid and perfluorooctane sulphonic acid in foods of animal origin using polyamide solid-phase extraction. *Chin. J. Food Sci.* **2013**, *34*, 241−245.
(34) Anastassiades, M.; Lehotay, S. J.; Štajnbaher, D.; Schenck, F. J. Fast and easy multiresidue method employing acetonitrile extraction/partitioning and "dispersive solid-phase extraction" for the determination of pesticide residues in produce. *J. AOAC Int.* **2003**, *86*, 412−431.
(35) Guo, M. M.; Wu, H. Y.; Li, Z. X.; Tan, Z.-J.; Zhai, Y.-X. Determination of 23 perfluorinated alkyl substances in fishery products by ultra fast liquid chromatography -tandem mass spectrometry. *Chin. J. Anal. Chem.* **2013**, *41*, 1322−1327.
(36) Yeung, L. W. Y.; Taniyasu, S.; Kannan, K.; Xu, D. Z. Y.; Guruge, K. S.; Lam, P. K.S.; Yamashita, N. An analytical method for the determination of perfluorinated compounds in whole blood using acetonitrile and solid phase extraction methods. *J. Chromatogr. A* **2009**, *1216*, 4950−4956.
(37) Wang, M. L.; Yan, H. F.; Fu, S. L.; Zhang, F.; Yao, J.; Dai, H.; Li, Y. Rapid screening and confirmation of hormones in health foods by high performance liquid chromatography-ion trap-time of flight tandem mass spectrometry. *Chin. J. Chromatogr.* **2012**, *30*, 980−985.

DOI: 10.1021/acs.jafc.5b00068
J. Agric. Food Chem. 2015, 63, 4087−4095

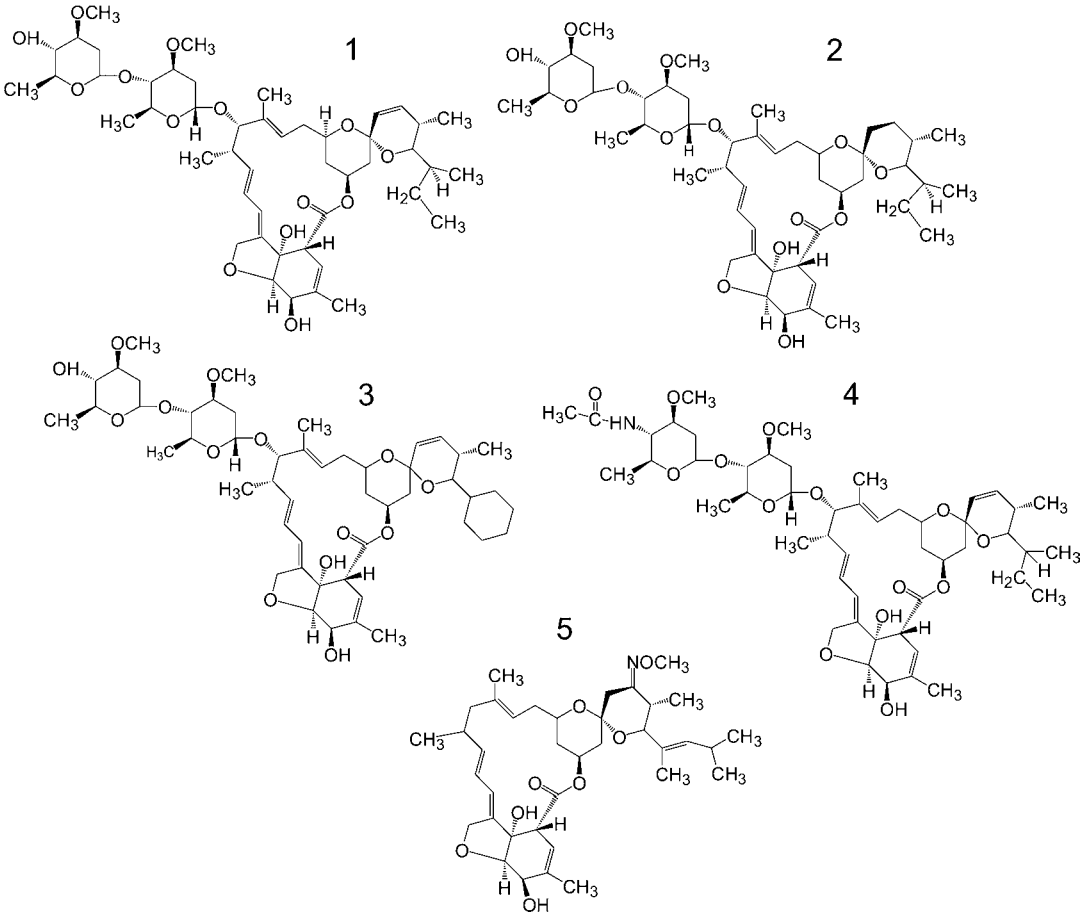

Figure 1. Chemical structures of five avermectins of interest.

matrices.[25−31] Polymeric monolithic materials possess obvious advantages including excellent biocompatibility, high permeability, and fast mass transfer, which are able to effectively extract trace target analytes from complicated food samples even at high flow velocities and under extreme pH conditions. Furthermore, organic polymer-based monoliths can be easily fabricated within the device, without the further packing steps required in the case of packed particulate adsorbents. Additionally, the porous structure and surface chemistry of the polymer are usually tunable and flexible. Therefore, several polymer-based monolithic columns have been shown to be promising tools for sample preparation.[32−35]

To further expand the application of monolithic sorbents, the present study focuses on the development of a robust and reusable polymeric monolithic sorbent capable of fast online SPE of five avermectins from both plant and animal origin food samples. In this work, a poly(butyl methacrylate-*co*-ethylene glycol dimethacrylate) (poly(BMA-*co*-EGDMA)) monolithic column was prepared and used as sorbent for online SPE of avermectins coupled with liquid chromatography tandem mass spectrometry (LC-MS/MS). The factors affecting the online SPE were studied in detail. A new method was established for the fast, automatic, and simultaneous determination of five avermectins in fresh pear, chili seed, bovine muscle, and milk samples.

MATERIALS AND METHODS

Reagents and Solutions. All chemicals and reagents used were at least of analytical grade or better. Purified water was obtained from a Waters Milli-Q system (Milford, MA, USA) and was used throughout all experiments. Butyl methacrylate (BMA) was purchased from Aladdin (Shanghai, China), and ethylene glycol dimethacrylate (EGDMA) was purchased from Alfa Aesar (Ward Hill, MA, USA). 1-Propanol and polyethylene glycol 400 were acquired from Tianjin Guangfu Fine Chemical Research Institute (Tianjin, China). Azobis(isobutyronitrile) (AIBN) was acquired from Tianjin Damao Chemical Reagent Factory (Tianjin, China) and was recrystallized with ethanol before use. HPLC-grade methanol (MeOH) and acetonitrile were provided by Fisher Scientific (Geel, Belgium). Ammonium acetate (NH_4OAc), acetic acid, formic acid, acetone, and isopropyl alcohol were purchased from Dikma (Beijing, China). Ammonium hydroxide (NH_4OH) was acquired from Chemical Reagent Factory (Shijiazhuang, China).

Abamectin (97%), ivermectin (96%), doramectin (96%), eprinomectin (91%), and moxidectin (87%) were purchased from Dr. Ehrenstorfer GmbH (Augsburg, Germany). Stock standard solutions of the avermectins were separately prepared at a concentration of 100 μg/mL in MeOH and stored at 4 °C in the dark. Working mixture solutions were freshly prepared from the stock solutions by stepwise dilution with MeOH. All solvents and solutions for LC analysis were filtered through a 0.45 μm Millipore filter.

Sample Preparation. The representative samples of plant origin (fresh pear and chili seed) and animal origin (bovine muscle and milk) were collected from supermarkets and local markets. Preliminary analysis showed that they were free of the analytes of interest. The samples including fresh pear, chili seed, and bovine muscle were first minced with a homogenizer, and the homogeneous samples were stored at −4 °C before use.

Plant origin samples (fresh pear and chili seeds): 2.0 g of pear and chili seed samples were weighed into a 50 mL centrifuge tube. Then, 10.0 mL of MeCN and 2.0 g of NaCl were added, and the samples

DOI: 10.1021/acs.jafc.5b00739
J. Agric. Food Chem. 2015, 63, 4096−4103

Table 1. Experimental Conditions Used for Online Clean-up on the Poly(BMA-*co*-EGDMA) Monolithic Extractor and LC-MS/MS Separation of the Avermectins from Various Samples

			loading pump[a]					eluting pump[b]			
step	start (s)	duration (s)	function	flow (mL/min)	A%	B%	C%	function	flow (mL/min)	D%	E%
1	0	60	loading	0.5	100			conditioning	0.5	10	90
2	60	90	washing	0.5		100		eluting	0.5	10	90
3	150	50	eluting	0.5		100		eluting	0.5	10	90
4	200	240	washing	0.5			100	eluting	0.5	95	5
5	440	130	washing	0.5			100	eluting	0.5	95	5
6	570	120	washing	0.5		100		eluting	0.5	95	5
7	690	210	conditioning	0.5	100			conditioning	0.5	10	90

[a]The mobile phases for the loading pump: (A) 10 mmol/L NH_4OAc solution, (B) MeCN, and (C) a mixture of MeCN, isopropyl alcohol, and acetone (1:1:1, v/v/v). [b]The mobile phases for the eluting pump: (D) MeCN, (E) 0.1% NH_4OH solution.

were blended with a homogenizer for 1 min. The samples were subsequently centrifuged at 0−4 °C for 5.0 min at 5000 rpm, and the supernatant was filtered through a 0.22 μm filter prior to the online extraction.

Animal origin samples (milk and bovine muscle): First, 2.0 g of previously minced bovine muscle was weighed into a centrifuge tube of 50 mL. After addition of 8.0 mL of MeCN, the sample was blended with a homogenizer for 1 min. Subsequently, the samples were extracted with MeCN twice. For the milk samples, 2.0 g of the sample was weighed into a 50 mL centrifuge tube. Next, 8.0 mL of MeCN, 1.0 g of NaCl, and 2.0 g of $MgSO_4$ were added. After being mixed with a vortex mixer for 2.0 min, the sample was centrifuged at 0−4 °C for 5.0 min at 5000 rpm. Subsequently, the supernatant was collected and the samples were extracted twice with MeCN. Finally, for the milk and bovine muscle samples, the supernatant was collected and diluted to 30.0 mL with MeCN. Three milliliters of each extraction solution was dried under flowing nitrogen gas at 40 °C. The residues were dissolved in 1.0 mL of MeCN and filtered through 0.22 μm filters prior to analysis.

Spiked samples were prepared in the same way with spiking required amounts of avermectins.

Fabrication of Poly(BMA-*co*-EGDMA) Monolithic Extractor. The poly(BMA-*co*-EGDMA) monolithic extractor was fabricated in a stainless steel chromatographic column (10 mm × 2.1 mm i.d.). Briefly, the polymerization mixture consisted of 0.5 mmol of BMA, 1.5 mmol of EGDMA, a mixture of 6.5 mmol of 1-propanol and 1.3 mmol of polyethylene glycol 400, and 4.0 mg of AIBN.[36−38] After sonication for 30 min, the solution was introduced into the column with both ends sealed and placed vertically in a water bath. The polymerization was performed for 2−24 h at 55 °C, and the temperature was 55, 60, or 65 °C; the reaction time was fixed at 4 h. The resulting column was connected to the LC system and washed with MeOH to remove the porogen and monomeric residues. Since the poly(BMA-*co*-EGDMA) monolithic extractor is a typical hydrophobic column, we chose a neutral compound, toluene, as the marker analyte. The retention factor (k) of toluene of each monolithic extractor was calculated to evaluate the corresponding hydrophobicity. The retention factor k was calculated from the equation $k = (t_R - t_0)/t_0$, where t_R and t_0 are the retention times of toluene and the void marker (MeOH), when MeOH/water (80:20, v/v) was used as the mobile phase. The scanning electron microscopy (SEM) images of the monoliths were obtained using an S-4800 scanning electron microscope (Hitachi, Tokyo, Japan).

Online Sample Extraction Based on the Poly(BMA-*co*-EGDMA) Monolithic Extractor. The online cleanup and separation was performed on an Aria TLX-2 system (Thermo Fisher Scientific, Franklin, MA, USA) equipped with a PAL autosampler (CTC Analytics, Zwingen, Switzerland) with a 200 μL sample injection loop, two high-pressure mixing quaternary pumps, one for online SPE (loading pump) and the other for analytical separation and elution (eluting pump), a multiple-column module, and a three-valve switching device unit with a six-port valve controlled by the Aria software, version 1.6.3. Automated SPE was achieved on the synthesized poly(BMA-*co*-EGDMA) monolithic column (10 mm × 2.1 mm i.d.). The online SPE procedure can be divided into four general steps: loading, washing, transfer, and conditioning. The mobile phases used for the loading pump were (A) 10 mmol/L NH_4OAc solution, (B) MeCN, and (C) the mixture of MeCN, isopropyl alsohol, and acetone (1:1:1, v/v/v). All of the parameters used for online cleanup on the poly(BMA-*co*-EGDMA) monolithic extractor and subsequent LC-MS/MS separation are listed in Table 1. In the loading step (step 1 in Table 1), 50 μL of the sample was injected into the poly(BMA-*co*-EGDMA) monolith. Then, during the washing step, the poly(BMA-*co*-EGDMA) monolithic column and the analytical column were not connected. The matrix components were washed out (waste) using solvent B, and the analytes were retained on the poly(BMA-*co*-EGDMA) monolith. For the transfer step (step 3 in Table 1), the poly(BMA-*co*-EGDMA) monolithic extractor was placed online with the LC-MS/MS system by switching the six-port valves, and the analytes were transferred from the poly(BMA-*co*-EGDMA) extractor into the analytical column. The last stage involved washing and conditioning of the poly(BMA-*co*-EGDMA) extractor (steps 4−7 in Table 1), while the analytes were being separated via LC-MS/MS. The poly(BMA-*co*-EGDMA) monolith was sequentially washed with solvents C and B to completely remove any residual contamination and to recondition the extractor for the next effective extraction. After that step, the entire online SPE procedure was completed. During the washing and conditioning steps, the poly(BMA-*co*-EGDMA) monolithic extractor and the analytical column were not connected.

LC-MS/MS Separation. Analytical separation was achieved using a 100 mm × 4.6 mm, 3 μm Hypersil Gold C_{18} column (Thermo Fisher Scientific, Pittsburgh, PA, USA). The mobile phase for separation consisted of (D) MeCN and (E) 0.1% NH_4OH solution. The parameters of LC-MS/MS separation (eluting pump) are shown in Table 1. The detection was performed by a triple-quadrupole Thermo Scientific TSQ Quantum Ultra mass spectrometer (Thermo Fisher Scientific, San Jose, CA, USA) equipped with an atmospheric-pressure chemical ionization probe that was maintained at 350 °C. All analyses were performed in the negative ionization mode. The sheath and auxiliary gases were nitrogen at 30 and 5 arbitrary units, respectively. The system was operated in multiple reaction monitoring (MRM) mode with argon as the collision gas at a pressure of 1.5 mTorr. The ion-transfer tube was maintained at 320 °C. The scan time and width were 0.02 s and m/z 0.01, respectively. The data were processed using the LC Quan software version 2.6. The retention time and mass spectrometer parameters for each analyte are given in Table 2. The total analytical run time for this method, including both SPE and separation, was 15.0 min.

RESULTS AND DISCUSSION

Characterization of the Poly(BMA-*co*-EGDMA) Monolithic Extractor. SPE sorbents based on hydrophobicity (reversed-phase retention) are most commonly used because of their versatility and ability to trap several compounds with weak polarity from a variety of food samples. Therefore, SPE

DOI: 10.1021/acs.jafc.5b00739
J. Agric. Food Chem. 2015, 63, 4096−4103

Table 2. Retention Time, Precursor Ion, Product Ion, and Collision Energy of the Five Avermectins

analyte	retention time (min)	precursor ion (m/z)	product ion (m/z)	collision energy (eV)
1	9.33	871.6	229.1	44
			565.5[a]	27
2	10.35	873.6	229.1	37
			567.4[a]	25
3	9.64	897.6	229.0	35
			591.3[a]	27
4	9.08	912.1	269.8	33
			565.4[a]	29
5	9.79	638.2	236.2	29
			528.5[a]	23

[a]Quantitative ion.

for avermectins is usually performed on a reversed-phase C_{18} or C_8 column depending on their polarities.[19,23] Thus, in the present experiment, since it is a widely accepted and convenient monomer, BMA was chosen to polymerize with EGDMA to prepare a miniature monolithic extractor with hydrophobicity provided by the butyl groups on the surface of the polymer skeletons. The monolithic extractor was fabricated via thermally initiated polymerization in the cartridge of a stainless steel column (10 mm × 2.1 mm i.d.). With the composition of the polymerization mixture fixed, the effects of the reaction time and reaction temperature on the performance of the extraction were investigated. The retention factor (k) of toluene on each monolith was calculated to evaluate the hydrophobicity of the extractors. The effects of reaction time over the range from 2 to 24 h and of the temperature in the range from 55 to 65 °C on k are shown in Figure 2A. No significant changes were observed when the reaction time exceeded 4 h and the temperature was higher than 55 °C. The procedure is easy, and the preparation conditions, including the reaction time and temperature, are controllable. A fast, robust and reproducible polymerization was established, offering the possibility for the facile fabrication of a hydrophobic monolithic sorbent. Thus, on the basis of these results, the monolithic column prepared at 55 °C for 4 h was chosen for further experiment. In addition, the mechanical stability of these monolithic columns is one of the most practical factors for SPE sorbent, especially for online operation. The relationship between the flow rate and the pressure in the synthesized columns was investigated when MeOH was used as the mobile phase. As shown in Figure 2B, a good linear (r = 0.999) dependence of the column pressure on

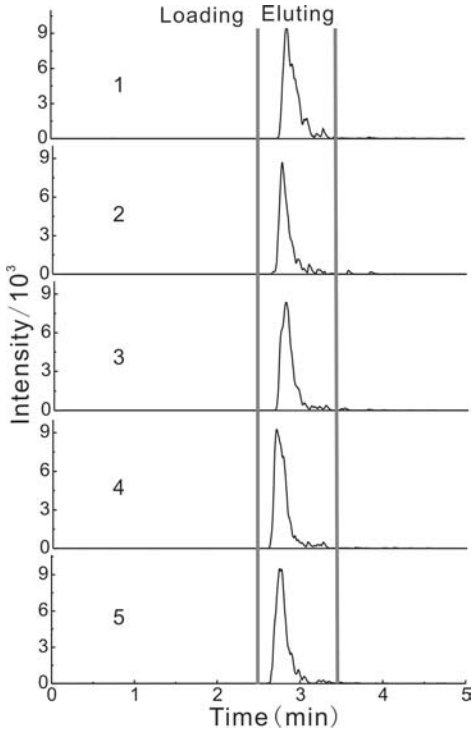

Figure 3. MRM chromatograms of the online SPE of the five avermectins with a 10 mmol/L NH_4OAc solution as loading solution and MeCN as eluting solution.

the flow rate was obtained. The pressure drop was lower than 1.0 bar at a flow rate of 0.5 mL min^{-1}, demonstrating the high permeability of the monolithic materials. The prepared monolith exhibited an adequate mechanical strength of up to 80 bar when it was operated in online mode. A SEM image of a poly(BMA-*co*-EGDMA) monolithic column further demonstrated the distinct continuous porous structure (Supporting Information, Figure S1). These results clearly indicate that the high mechanical strength and permeability allow the monolithic extractor to be available for online SPE, thus shortening the whole analysis time.

Online SPE and LC-MS/MS. The online analysis procedure includes loading, washing, transfer, conditioning, and LC-MS/MS separation. For the loading step, the loading solvent affects the efficiency of preconcentration and matrix elimination. The influence of the loading solvent was tested using 0.1% and 0.5% formic acid and 5 and 10 mmol/L NH_4OAc solution. To

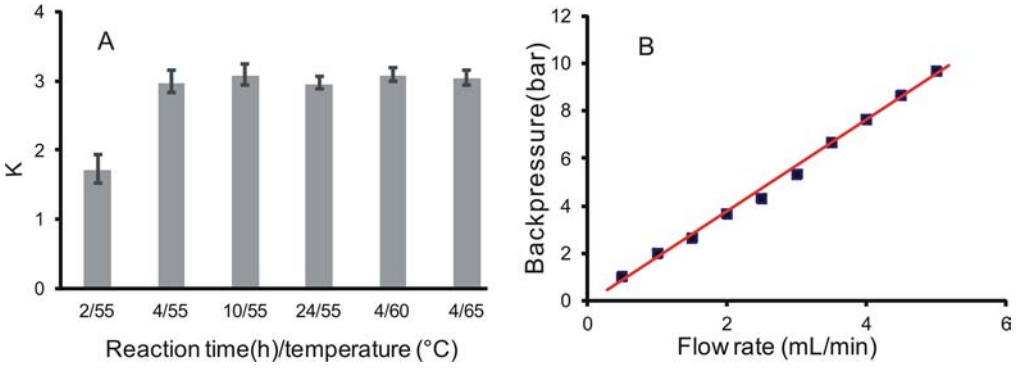

Figure 2. (A) Effect of the reaction time (h) and temperature (°C) on k. (B) Relationship between the flow rate and the back-pressure drop of the poly(BMA-*co*-EGDMA) monolithic extractor when MeOH was used as the mobile phase.

DOI: 10.1021/acs.jafc.5b00739
J. Agric. Food Chem. 2015, 63, 4096−4103

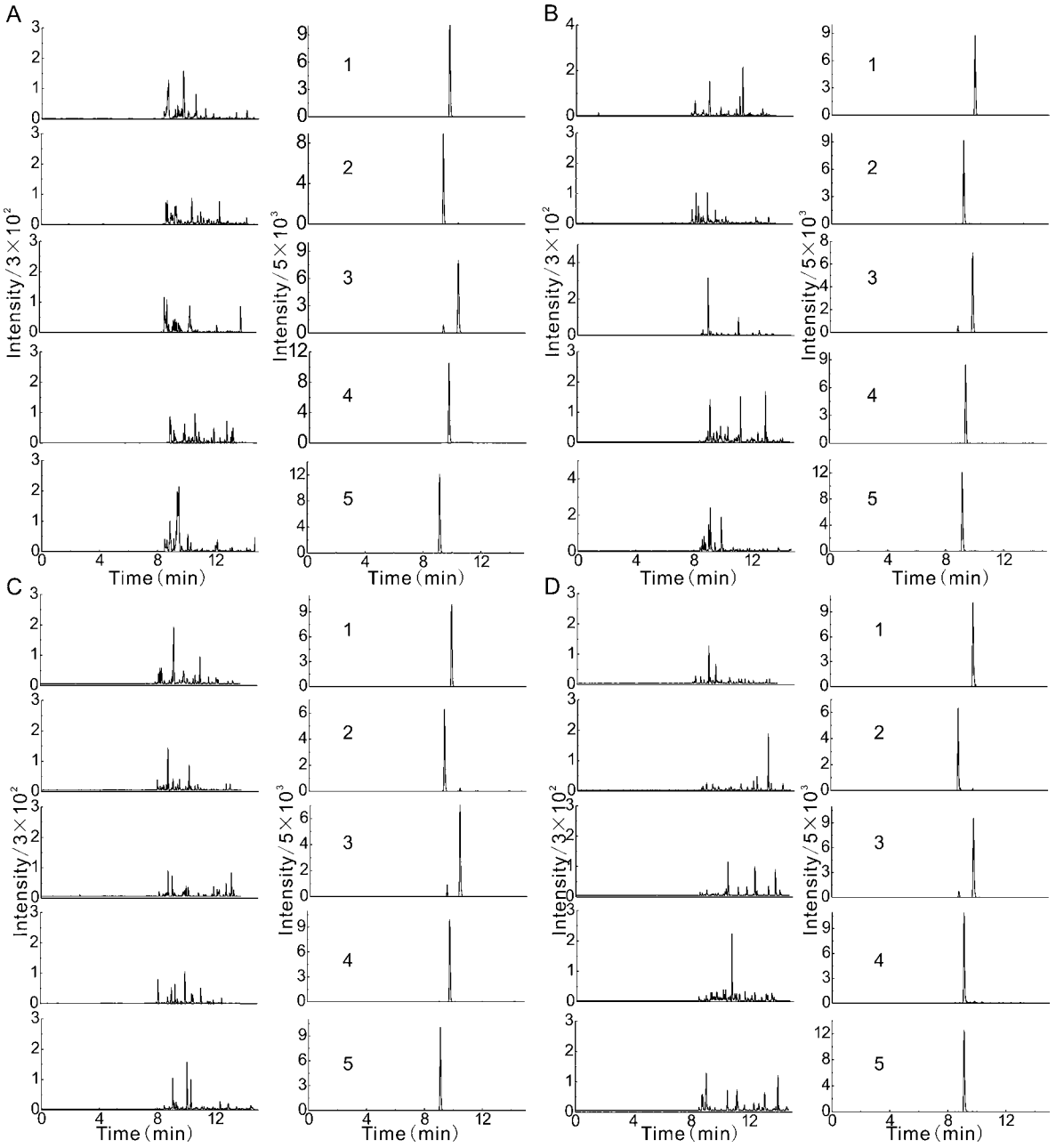

Figure 4. MRM mass chromatograms of blank samples and fortified samples: (A) chili seed, (B) fresh pear, (C) milk, and (D) bovine muscle.

evaluate the loading efficiency, the five extracted avermectins were eluted with MeCN and the chromatograms were compared. The most concentrated, sharp, and symmetric peaks with the maximum peak heights were obtained when 10 mmol/L NH_4OAc was used as the loading solution (Figure 3), providing the most efficient extraction for target compounds. After the loading and washing steps, the extracted analytes were transferred from the poly(BMA-*co*-EGDMA) monolithic extractor into a C_{18} analytical column for LC-MS/MS separation. MeCN and MeOH were each evaluated for use as the eluting solvent. The results showed that both MeCN and MeOH gave an effective eluting for the extracted avermectins. However, the peaks with MeCN as eluting solvent were more symmetrical and less broadened (Figure 3). Therefore, the adsorbed compounds may be quickly transferred into the subsequent LC-MS/MS without diffusion and any loss of the analytes. Considering peak broadening and tailoring in separation caused by the diffusion, MeCN was selected as the eluent.

The LC-MS/MS parameters were optimized to ensure proper resolution and symmetry and adequate separation of the analytes. In this work, to enhance ionization of the avermectins in the MS source, a mixture of MeCN and a 0.1% NH_4OH solution was found to be optimal for LC-MS/MS separation. The starting composition of MeCN for the gradient was investigated in the range 80−10%, and the final composition of MeCN was fixed at 95%. Baseline separation of five avermectins is achieved in all investigated mobile phases. However, different responses of the target compounds are found. Lower composition of MeCN may lead to better chromatographic resolutions and enhanced ionizations (Supporting Information, Figure S2). To reduce the retention time

DOI: 10.1021/acs.jafc.5b00739
J. Agric. Food Chem. 2015, 63, 4096−4103

Table 3. Recoveries of the Five Avermectins in Various Foodstuffs Determined by the Online SPE and LC-MS/MS

		recovery % (n = 6)			
analyte	added (μg/kg)	fresh pear	chili seed	bovine muscle	milk
1	5	71.8	80.5	77.4	84.5
	10	84.3	80.7	98.7	92.2
	50	97.6	98.6	81.3	87.0
2	5	79.9	80.3	86.5	80.3
	10	84.5	82.4	93.8	93.6
	50	97.6	92.8	101.3	89.5
3	5	77.6	75.9	77.8	92.6
	10	77.3	77.7	91.4	95.3
	50	99.5	94.1	92.5	90.8
4	5	90.9	76.3	89.4	81.3
	10	93.0	92.7	92.5	96.2
	50	98.0	98.4	95.1	93.4
5	5	76.9	75.2	74.0	88.9
	10	84.0	87.3	76.0	100.1
	50	83.2	91.5	97.1	84.9

and improve the sensitivity of the avermectins, the mobile phase consisting of MeCN/0.1% NH_4OH (10:90, v/v) was selected as starting mobile phase.

The proposed approach enabled us to enrich the analytes online from the sample matrix and accomplished the analysis in a very short time of less than 15 min. The online SPE procedure reduced manual handling to a minimum and thus saved both manpower and solvents. In addition, the use of LC-MS/MS ensured both highly sensitive and selective results.

Validation of the Method. A very generic sample extraction method is necessary to extract the compounds from a broad range of complicated matrices. The monolithic materials have been demonstrated to be available for plant[26] or animal origin[27,32,34] samples. In this work, the foodstuffs of both plant and animal origins including pear, chili seed, bovine muscle, and milk were pretreated using the poly(BMA-*co*-EGDMA) monolithic extractor. To evaluate the extraction efficiency and potential interfering compounds originating from the plant and animal origin matrices, blank samples, spiked samples, matrix effect, and recovery experiments were performed using the poly(BMA-*co*-EGDMA)-based SPE method.

Matrix Effect. The matrix effect was investigated by comparing the slopes of calibration curves obtained from a standard mixture of avermectins in solvent and the standards spiked with the samples. The matrix-matched calibration curves were constructed by spiking the avermectin standard solutions at seven concentration levels in the corresponding matrices. The solvent calibration curves were constructed in the same manner but without the addition of the matrix aliquots. For the bovine muscle sample, good linear relationships for five avermectins are achieved over the concentration range 0.5−100.0 ng/mL with a correlation coefficient (r) value higher than 0.995, and the matrix/solvent slope ratio for each avermectin in the bovine muscle sample ranged from 0.93 to 1.07 (Supporting Information, Table S1). The signal enhancement or suppression effect was considered acceptable if the ratio of the slope was in the range 0.8 to 1.2. Slope ratios with values higher than 1.2 or lower than 0.8 indicate a distinct matrix effect. Additionally, the matrix/solvent slope ratios in pear, chili seed, and milk samples were in the range 0.95−1.05, showing no significant matrix effect presented in the analysis of these real samples.

Specificity, Accuracy, and Precision. Figure 4 shows the MRM chromatograms of the blank samples and the corresponding blank samples spiked with 10 μg/kg of the standard avermectins. The results showed that the spiked samples were effectively purified by the poly(BMA-*co*-EGDMA) extractor. Compared with the blank samples, no interference peaks are observed in the chromatograms of any of the spiked samples. The results were further confirmed by the recovery experiments. The recovery of the proposed method was assayed on spiked real samples at three levels of five avermectins in four kinds of matrices, and the precision was described on the basis of the intraday and interday relative standard deviations (RSDs). As shown in Table 3, the recoveries of six replicate extractions ranged from 71.8% to 101.3%. The intraday and interday RSDs were in the range 4.38−8.62% and 5.49−8.94%, respectively (Table 4). These results indicate the suitability and the satisfactory reproduci-

Table 4. Precisions (RSDs) of the Five Avermectins in Foodstuffs Determined by the Online SPE and LC-MS/MS

		RSD % (n = 6)							
		fresh pear		chili seed		bovine muscle		milk	
analyte	added (μg/kg)	intraday	interday	intraday	interday	intraday	interday	intraday	interday
1	5	7.43	8.06	7.68	8.20	7.84	8.30	7.98	8.13
	10	7.44	7.76	6.42	7.26	6.36	8.14	7.18	8.07
	50	5.03	6.51	6.63	7.18	6.49	7.47	4.48	6.46
2	5	7.36	7.97	7.56	7.94	6.61	7.36	6.76	7.15
	10	7.11	7.65	6.88	7.25	6.49	6.61	6.88	7.25
	50	6.22	6.87	5.90	6.13	5.81	6.41	4.84	5.49
3	5	7.69	8.01	7.84	8.25	8.62	8.94	6.86	7.68
	10	7.36	7.89	7.21	8.07	8.04	7.96	6.49	6.94
	50	6.54	7.08	6.03	6.99	5.76	7.22	6.09	6.16
4	5	7.35	8.11	8.16	8.52	7.10	7.63	7.39	7.44
	10	6.80	7.67	8.06	7.64	6.70	6.78	7.10	7.75
	50	7.12	7.79	7.92	7.98	5.01	5.73	5.79	6.73
5	5	6.41	8.51	7.25	7.99	7.54	7.45	7.98	8.27
	10	5.97	6.09	6.69	7.36	7.60	7.57	7.56	7.38
	50	5.68	5.78	6.02	6.58	6.56	6.81	4.38	6.82

DOI: 10.1021/acs.jafc.5b00739
J. Agric. Food Chem. 2015, 63, 4096−4103

bility of the developed method for the determination of five avermectins in four matrices of both plant and animal origin.

LODs and LOQs. The limit of detection (LOD) was determined as the concentration that produced a peak with a height 3 times the level of the baseline noise, and the limit of quantitation (LOQ) was determined as the sample concentration that produced a peak 10 times greater than the baseline noise. The LODs and the LOQs of the proposed method were 2 μg/kg and 5 μg/kg for each analyte, which showed that the present method is sufficiently sensitive to measure avermectins at the MRLs[6−10] in various matrices.

Reusability and Reproducibility of the Poly(BMA-*co*-EGDMA) Monolithic Extractors. Traditional commercial SPE sorbents, such as C_{18}, C_8, and Al_2O_3 particles, are disposable. The reusability and reproducibility of the poly(BMA-*co*-EGDMA) monolithic sorbent trap were studied. Under the optimized conditions, at least 500 injections of pear sample were performed. Moreover, poly(BMA-*co*-EGDMA) monolithic extractors prepared from various batches were also used. No significant changes were observed in the extraction efficiency. The column-to-column reproducibility was assessed by calculating the RSDs of the extracted amount of abamectin while performing the online SPE. The intrabatch and interbatch RSDs were in the range 4.6−6.3% and 6.7−9.3%, respectively, indicating that the proposed sample preparation method is robust and practical.

Assay of Avermectins in Real Samples. The feasibility of the developed poly(BMA-*co*-EGDMA) monolithic column based on the online SPE method was further demonstrated for the analysis of real samples. Among the assayed samples from a local market, abamectin was detected in one bovine muscle sample with a concentration of 5.9 ± 0.6 μg/kg and ivermectin was detected in two chili seed samples with concentrations of 7.9 ± 0.9 and 8.2 ± 0.9 μg/kg. The present study focused on the development of a robust, simple, and practical method that is capable of quickly and simultaneously extracting and determining five avermectins in samples of both plant and animal origin. Although the poly(BMA-*co*-EGDMA) monolithic extractor gave better or comparable recovery and detection limits compared with other reported adsorbents,[15−21] this method gave more advantages by reducing analysis time and improving reusability of the sorbent. An offline cleaning and preconcentration process using a conventional SPE required several steps and took more than 2 h, while the time for online SPE and analysis of this work was only 15 min. In addition, the cost of the determination was also significantly reduced because the poly(BMA-*co*-EGDMA) monolithic extractor could be reused more than 500 times without any loss of extraction efficiency, even for different varieties of food samples. Since this kind of hydrophobic monolithic extractor could be easily obtained and showed good availability, we believe that the method was able to deal with a wide range of compounds with weak polarity from complicated samples.

■ ASSOCIATED CONTENT

Supporting Information

Detailed description of the SEM image of a poly(BMA-*co*-EGDMA) monolithic extractor prepared at 55 °C for 4 h, ×5000; response of the avermectins with different starting compositions of the mobile phase, and standard curves of avermectins in solvent and matrix and their slope ratios. This material is available free of charge via the Internet at http://pubs.acs.org.

■ AUTHOR INFORMATION

Corresponding Author

*Tel: +86-315-3725730. Fax: +86-315-2592281. E-mail: mmwangheuu@126.com.

Funding

This work was supported by the National Natural Science Foundation of China (No. 21305028), the Natural Science Foundation of Hebei Province, China (No. B2013209238), the Research Foundation of Education Bureau of Hebei Province, China (No. Q2012155), and the Research Foundation from General Administration of Quality Supervision, Inspection and Quarantine of China (Nos. 2013IK154 and 2014IK092).

Notes

The authors declare no competing financial interest.

■ REFERENCES

(1) Martin, D.; Wolfgang, R.; Lucija, K.; Jemma, K.; Vesna, C. F. Recent developments in the analysis of avermectin and milbemycin residues in food safety and the environment. *Curr. Pharm. Biotechnol.* **2012**, *13*, 936−951.

(2) Cabrera, J. A.; Menjivar, R. D.; Dababat, A. F. A.; Sikora, R. A. Properties and nematicide performance of avermectins. *J. Phytopathol.* **2013**, *161*, 65−69.

(3) Macdonald, N.; Gledhill, A. Potential impact of ABCB1 (*p*-glycoprotein) polymorphismson avermectin toxicity in humans. *Arch. Toxicol.* **2007**, *81*, 553−563.

(4) Sung, Y. F.; Huang, C. T.; Fan, C. K.; Lin, C. H.; Lin, S. P. Avermectin intoxication with coma, myoclonus, and polyneuropathy. *Clin. Toxicol.* **2009**, *47*, 686−688.

(5) EC Regulation (EU) No. 37/2010 of 22 December 2010 on pharmacologically active substances and their classification regarding maximum residue limits in foodstuffs of animal origin. *Off. J. Eur. Union* **2010**, *L15*, 1−17.

(6) European Medicines Agency, EMEA, Summary opinion of the committee for medicinal products for veterinary use on the establishment of MRL, doramectin, EMEA/CVMP/283233/2006, 21 July, 2006.

(7) European Medicines Agency, EMEA, Committee for medicinal products for veterinary use, ivermectin, EMEA/CVMP/915/04-FINAL, November 2004.

(8) European Medicines Agency, EMEA, Committee for medicinal products for veterinary use, emamectin, EMEA/CVMP/863/03-FINAL, February 2003.

(9) European Medicines Agency, EMEA, Committee for medicinal products for veterinary use, abamectin, EMEA/CVMP/838/02-FINAL, May 2002.

(10) National Standards of the People's Republic of China. National food safety standard maximum residue limits for 85 pesticides in food. GB 28260-2011.

(11) Wei, X. X.; Dou, C. Y.; Duan, Y. S.; Ma, Y. S. Determination of avermectin residues in dried chili by HPLC with fluorescence detection. *J. Food Saf. Qual.* **2013**, *1298*, 35−43.

(12) Giannetti, L.; Giorgi, A.; Necci, F.; Ferretti, G.; Buiarelli, F.; Neri, B. Validation study on avermectine residues in foodstuffs. *Anal. Chim. Acta* **2011**, *700*, 11−13.

(13) Rübensam, G.; Barreto, F.; Hoff, B. R.; Kist, L. T.; Pizzolato, M. T. A liquid-liquid extraction procedure followed by a low temperature purification step for the analysis of macrocyclic lactones in milk by liquid chromatography-tandem mass spectrometry and fluorescence detection. *Anal. Chim. Acta* **2011**, *705*, 24−29.

(14) Tao, Y. F.; Yu, G.; Chen, D. M.; Pan, Y. H.; Liu, Z. L.; Wei, H. M.; Peng, D. P.; Huang, L. L.; Wang, Y. L.; Yuan, Z. H. Determination of 17 macrolide antibiotics and avermectins residues in meat with accelerated solvent extraction by liquid chromatography-tandem mass spectrometry. *J. Chromatogr. B* **2012**, *897*, 64−71.

(15) Rübensam, G.; Barreto, F.; Hoff, R. B.; Pizzolato, T. M. Determination of avermectin and milbemycin residues in bovine

DOI: 10.1021/acs.jafc.5b00739
J. Agric. Food Chem. 2015, 63, 4096−4103

muscle by liquid chromatography-tandem mass spectrometry and fluorescence detection using solvent extraction and low temperature cleanup. *Food Contr.* **2013**, *29*, 55−60.
(16) Sannino, A. Determination of three natural pesticides in processed fruit and vegetables using high-performance liquid chromatography/tandem mass spectrometry. *Rapid Commun. Mass Spectrom.* **2007**, *21*, 2079−2086.
(17) Campillo, N.; Viñas, P.; Férez-Melgarejo, G.; Hernández-Córdoba, M. Dispersive liquid-liquid microextraction for the determination of macrocyclic lactones in milk by liquid chromatography with diode array detection and atmospheric pressure chemical ionization ion-trap tandem mass spectrometry. *J. Chromatogr. A* **2013**, *1282*, 20−26.
(18) Raich-Montiu, J.; Krogh, K. A.; Granados, M.; Jönsson, J. A.; Halling-Sørensen, B. Determination of ivermectin and transformation products in environmental waters using hollow fiber-supported liquid membrane extraction and liquid chromatography-mass spectrometry/mass spectrometry. *J. Chromatogr. A* **2008**, *1187*, 275−280.
(19) Berendsen, B. J. A.; Mulder, P. P. J.; Rhijn, V. H. (J.) A. The derivatisation of avermectins and milbemycins in milk: New insights and improvement of the procedure. *Anal. Chim. Acta* **2007**, *585*, 126−133.
(20) Cerkvenik-Flajs, V.; Milčinski, L.; Süssinger, A.; Hodošček, L.; Danaher, M.; Antonić, J. Trace analysis of endectocides in milk by high performance liquid chromatography with fluorescence detection. *Anal. Chim. Acta* **2010**, *663*, 165−171.
(21) Durden, D. A. Positive and negative electrospray LC-MS-MS methods for quantitation of the antiparasitic endectocide drugs, abamectin, doramectin, emamectin, eprinomectin, ivermectin, moxidectin and selamectin in milk. *J. Chromatogr. B* **2007**, *850*, 134−146.
(22) Tom, L. A.; Foster, N. Development of a molecularly imprinted polymer for the analysis of avermectin. *Anal. Chim. Acta* **2010**, *680*, 79−85.
(23) Wang, F. M.; Chen, J. H.; Cheng, H. Y.; Tang, Z. X.; Zhang, G.; Niu, Z. Y.; Pang, S. P.; Wang, X. R.; Lee, F. S. C. Multi-residue method for the confirmation of four avermectin residues in food products of animal origin by ultra-performance liquid chromatography-tandem mass spectrometry. *Food Addit. Contam. Part A* **2011**, *28*, 627−639.
(24) Krogh, K. A.; Björklund, E.; Loeffler, D.; Fink, G.; Halling-Sørensen, B.; Ternes, T. A. Development of an analytical method to determine avermectins in water, sediments and soils using liquid chromatography-tandem mass spectrometry. *J. Chromatogr. A* **2008**, *1211*, 60−69.
(25) Namera, A.; Nakamoto, A.; Saito, T.; Miyazaki, S. Monolith as a new sample preparation material: Recent devices and applications. *J. Sep. Sci.* **2011**, *34*, 901−924.
(26) Jandera, P. Advances in the development of organic polymer monolithic columns and their applications in food analysis-A review. *J. Chromatogr. A* **2013**, *1313*, 37−53.
(27) Wei, F.; Feng, Y. Q. Methods of sample preparation for determination of veterinary residues in food matrices by porous monolith microextraction-based techniques. *Anal. Methods* **2011**, *3*, 1246−1256.
(28) Arrua, R. D.; Causon, T. J.; Hilder, E. F. Recent developments and future possibilities for polymer monoliths in separation science. *Analyst* **2012**, *137*, 5179−5189.
(29) Zheng, M. M.; Gong, R.; Zhao, X.; Feng, Y. Q. Selective sample pretreatment by molecularly imprinted polymer monolith for the analysis of fluoroquinolones from milk samples. *J. Chromatogr. A* **2010**, *1217*, 2075−2081.
(30) Chienthavorn, O.; Ramnut, N.; Subprasert, P.; Sasook, A.; Insuan, W. Effective and reusable monolith capillary trap of nitrosamine extraction by superheated water from Frankfurter sausage. *J. Agric. Food Chem.* **2014**, *62*, 1240−1246.
(31) Regueiro, J.; Álvarez, G.; Mauriz, A.; Blanco, J. High throughput analysis of amnesic shellfish poisoning toxins in bivalve molluscs by dispersive solid-phase extraction and high-performance liquid chromatography using a monolithic column. *Food Chem.* **2011**, *127*, 1884−1891.
(32) Romanovskaya, A.; Sarin, L. P.; Bamford, D. H.; Poranen, M. M. High-throughput purification of double-stranded RNA molecules using convective interaction media monolithic anion exchange columns. *J. Chromatogr. A* **2013**, *1278*, 54−60.
(33) Javanbakht, M.; Moein, M. M.; Akbari-adergani, B. On-line clean-up and determination of tramadol in human plasma and urine samples using molecularly imprinted monolithic column coupling with HPLC. *J. Chromatogr. B* **2012**, *911*, 49−54.
(34) Hu, X. Z.; Wang, J. X.; Feng, Y. Q. Determination of benzimidazole residues in edible animal food by polymer monolith microextraction combined with liquid chromatography-mass spectrometry. *J. Agric. Food Chem.* **2010**, *58*, 112−119.
(35) Rogeberg, M.; Malerod, H.; Roberg-Larsen, H.; Aass, C.; Wilson, S. R. On-line solid phase extraction-liquid chromatography, with emphasis on modern bioanalysis and miniaturized systems. *J. Pharm. Biomed. Anal.* **2014**, *87*, 12−129.
(36) Liu, W.; Qi, J. R.; Yan, L. N.; Jia, Q.; Yu, C. Application of poly(butyl methacrylate-co-ethylene glycol dimethacrylate) monolith microextraction coupled with high performance liquid chromatography to the determination of polycyclic aromatic hydrocarbons in smoked meat products. *J. Chromatogr. B* **2011**, *879*, 3012−3016.
(37) Lin, S. L.; Wu, Y. R.; Lin, T. Y.; Fuh, M. R. Preparation and evaluation of 1,6-hexanediol ethoxylate diacrylate-based alkyl methacrylate monolithic capillary column for separating small molecules. *J. Chromatogr. A* **2013**, *1298*, 35−43.
(38) Liu, Y.; Wang, M. M.; Ai, L. F.; Zhang, C. K.; Li, X.; Wang, X. S. Determination of Sudan dyes in chili pepper powder by online solid-phase extraction with a butyl methacrylate monolithic column coupled to liquid chromatography with tandem mass spectrometry. *J. Sep. Sci.* **2014**, *37*, 1648−1655.

DOI: 10.1021/acs.jafc.5b00739
J. Agric. Food Chem. 2015, 63, 4096−4103

sensitive or allergic individuals. Regardless of the retrospective studies on plant lectins, they are still detected by hemadsorption, hemeagglutination, or bacterial agglutination assays.[21,22] These assays are qualitative and serve a common platform for all lectins; hence, they are not efficient in discriminating different lectins. Apart from classical agglutination assays, Con A detection in animal serum, plasma, cell culture supernatants, body fluid, and tissue homogenate is performed using ELISA and immunoelectrophoresis assays. However, these antibody-dependent assays are often costly due to the requirement of live hosts for antibody production. There is also a potential risk of antibody contamination with microorganisms or other immunologically active compounds. Contrary to this, aptamers are easy and rapid to produce with negligible batch-to-batch variability, are significantly cheap, and have higher thermal tolerance. Therefore, the aptamer-based assays are advantageous over antibody-based assays.

In this paper, we have identified an aptamer that selectively targets the Con A and has nanomolar affinity. As the developed aptamer is highly specific to Con A, it can be utilized as a valuable tool for the selective determination of Con A in food and agricultural products.

EXPERIMENTAL PROCEDURES

Materials. Concanavalin A (from jack bean), bovine serum albumin, acrylamide and bis-acrylamide solution (30%, w/v), TEMED, ammonium persulfate, nitrocellulose membrane, *o*-phenylenediamine dihydrochloride, 3,3′-diaminobenzidine, and 30% H_2O_2 were purchased from Sigma-Aldrich, USA. All PCR reagents were procured from New England BioLabs Inc., USA. Streptavidin-coated magnetic bead (Dynabeads M-280 Streptavidin, Invitrogen) was utilized to separate the biotinylated and non-biotinylated strands of PCR-amplified aptamer. *N*-Hydroxysuccinimide (NHS)-activated agarose columns were purchased from Pierce, Thermo Scientific, USA.

Oligonucleotide Synthesis. A oligonucleotide library of 77 nt length, comprising a central randomized region of 41-mer and 18-mer flanking sequences at both ends (5′-ATACCAGCTTATTCAATT-41nt -AGATAGTATGTGCAATCA-3′), was synthesized at 1.3 μmol scale on a Gene Assembler Special (Pharmacia LKB Biotechnology, Uppsala, Sweden) using standard phosphoramidite chemistry. Labeled primers were synthesized at 0.2 μmol scale. Synthesized sequences were deprotected and surface-cleaved using 30% ammonia and desalted on size exclusion columns (NAP-10, GE Healthcare, Sweden). The purity of synthesized oligonucleotides was checked on 15% polyacrylamide gel.

Preparation of Food Samples for Con A Detection. Seeds of jack bean, mung bean, kidney bean, and lentils and the wheat grains were crushed in a mixer grinder. A 10% meal was prepared for each sample by soaking their finely crushed powder in 0.5 M NaCl at 4 °C overnight (14−15 h). Homogenized meals were filtered through cheesecloth, and the homogenates were centrifuged at 10000 rpm for 10 min. Supernatants were collected and labeled separately as jack bean, mung bean, kidney bean, lentils, and wheat extracts.

Protein Preparation and SELEX Screening. NHS-treated agarose resin was used as solid support to carry out SELEX screening. For this, 330 mg of resin in a 5 mL column was charged with 1 g of Con A and incubated at room temperature (~27 °C) for 2 h with end-over-end mixings. The unreacted active ester groups on the resin were quenched with 1 M Tris buffer. The DNA library for SELEX screening was prepared by heat denaturing the library sequences at 95 °C for 10 min following a rapid cooling on ice. For the first round of selection, 10 nmol of prepared DNA library in 500 μL of aptamer binding buffer (20 mM Tris-HCl, pH 7.6, 120 mM NaCl, 5 mM KCl, 1 mM $MgCl_2$, and 1 mM $CaCl_2$) was added to the prepared agarose resin having 5 nmol (determined using BCA protein assay) of immobilized Con A. The column was incubated at room temperature for 2 h with end-over-end mixing. Thereafter, the unbound oligonucleotides were removed by washing with aptamer washing buffer (binding buffer with 0.2% Tween-20). Con A-bound DNA sequences were collected using high salt elutions (1.5 M NaCl in 10 mM Tris, pH 7.2) and PCR amplified with unlabeled forward and biotinylated reverse primers using the following thermal cycling: one hot start of 95 °C for 5 min and 15 thermal cycles of 95 °C for 30 s, 46 °C for 30 s, and 72 °C for 30 s and a final extension of 72 °C for 3 min. The PCR-amplified biotinylated double-stranded oligonucleotide sequences were converted to their respective single strands using the streptavidin magnetic beads. For this, PCR-amplified sequences were first immobilized over streptavidin beads followed by strand separation using alkaline denaturation (0.15 M NaOH). Separated non-biotinylated strands in the supernatant were collected and, after desalting, were utilized for the next round of screening. The mole ratio of immobilized Con A to oligonucleotides during subsequent SELEX screening was varied using a controlled number of Con A-coated agarose beads. Enrichment of Con A binding sequences was monitored by saturation binding assay. Upon adequate enrichment of Con A binding sequences, the entire enriched pool was PCR amplified and ligated to pCR2.1 TOPO TA vector. Transformation was carried out in competent *E. coli* cells (DH5α), and the transformed colonies were selected on the basis of blue-white screening. Positive colonies were picked and cultured overnight in 5 mL of LB broth. Plasmids were isolated from each culture via the mini prep plasmid isolation method, and the presence of insert in the isolated plasmid was checked using specific restriction digestion and PCR amplification. Subsequently, the plasmids were sequenced using Sangers Capillary sequencing, and the base sequences of enriched pool were obtained.

Activation of Microtiter Plates and Polypropylene Microtest Plates (PPμTP) by 1-Fluoro-2-nitro-4-azidobenzene (FNAB). Microtiter plates and polypropylene microtest plates were activated according to published procedures.[23−25] Briefly, the wells of a microtiter plate were loaded with 30 μL of methanolic solution of FNAB (1.82 mg/30 μL) and kept in the dark in a fume hood to evaporate the methanol. Thereafter, the FNAB-coated plates were exposed to UV light (365 nm) for 15 min in a UV Stratalinker (model 2400, Stratagene, USA). The plates were then washed thoroughly with methanol and dried. Wells of polypropylene microtest plate (PPμTP) were activated in the same way except that a lower amount of FNAB (0.125 mg/3 μL methanol per well) was used and the photoirradiation time was reduced to 12 min.

Enrichment Monitoring. Enriched sequences obtained during various rounds of SELEX screening were collected in their respective single-stranded biotinylated forms by making use of specific PCR amplification and strand separation over magnetic streptavidin beads. A fixed amount of these sequences (500 nM) was added to the wells of an activated polypropylene microtest plate (APPμTP) carrying the already immobilized Con A and incubated at room temperature for 2 h. After removal of the unbound sequences, retained DNA sequences in the microtiter plate were detected by probing the wells with streptavidin−HRP conjugate (1:1000 dilution; Sigma-Aldrich) and its substrate dye. Developed color was quantified as described earlier.[25]

In Silico Analysis of the Enriched Sequences. Secondary structure prediction and free energy of secondary structure formation were calculated using the Mfold Web server. Mean free energy ($\bar{E}$) and the standard deviation (SD) for enriched DNA sequences were calculated using a set of 1000 random sequences. The Quikfold Web server (Quikfold/mfold.rit.albany.edu) was used to predict the free energies of random sequences. Folding predictions for structural grouping were performed at default conditions of DNA folding (37 °C, 1 M NaCl, no divalent ions) on the Mfold server. Web-based QGRS Mapper was used to predict G-quadruplex forming abilities of the sequences.

Affinity and Specificity Measurement. Affinity and specificity measurements of the enriched sequences were carried out using the enzyme-linked aptamer assay. For affinity determination, 1.5 μg of Con A was coated to the activated wells of a 96-well microtiter plate by 4 h of incubation at 37 °C. After the unbound surface had been blocked with 2% BSA, the wells were titrated with 500 nM labeled sequences (seq-1−8) and incubated for 2 h at room temperature. After

DOI: 10.1021/acs.jafc.5b00784
J. Agric. Food Chem. 2015, 63, 4104−4111

the stipulated time, the wells were washed with aptamer washing buffer, probed with 100 μL of streptavidin−HRP conjugate (1:1500 dilution), and incubated at room temperature for 1 h. This followed the color development by the addition of 100 μL of substrate dye (*o*-phenylenediamine) to the wells of a microtiter plate and subsequent recording of absorbance at 490 nm. Nonspecific binding of DNA sequences to the microtiter plate was ruled out by performing a control experiment wherein aptamer was added to BSA-coated wells and the binding was measured.

For dissociation constant (K_d) measurement, 1−1000 nM biotinylated seq-1 was titrated against immobilized Con A in the wells of a microtiter plate. Con A-bound sequence was detected using the streptavidin−HRP colorimetric assay. The dissociation constant for aptamer−Con A interaction was determined by fitting the calculated absorbance values and aptamer concentrations to one-site specific binding (nonlinear) in GraphPad Prism (version 5.03 for Windows, GraphPad Software, San Diego, CA, USA), using the equation

$$Y = B_{max} \times X/(K_d + X)$$

For specificity measurements, an equivalent amount (1.5 μg) of Con A, jack bean meal extract, and bovine serum albumin was coated to the FNAB-activated wells of a microtiter plate and probed with 300 nM biotinylated seq-1. Binding was measured by recording absorbance values and were plotted against individual target protein.

Enzyme-Linked Aptamer Assay and Western Blot. For the enzyme-linked aptamer assay, pure Con A and two different dilutions of jack bean seed extracts were coated to the activated wells of a microtiter plate. After the wells had been blocked with 2% BSA, 300 nM biotinylated seq-1 was added to the wells, and the plate was incubated for 2 h at room temperature. Unbound sequences were removed by washing, and the bound seq-1 was detected by probing the wells with streptavidin−HRP and measuring the signal colorimetrically. In the control, the same set of samples was detected by enzyme-linked immunosorbent assay using Con A antibody.

For Western blot analysis, two different amounts of Con A (1 and 0.5 μg) were electrophoresed on 12% SDS-PAGE gel and blotted to nitrocellulose membrane. Thereafter, the membrane was incubated with 300 nM biotinylated seq-1 for 2 h at room temperature. After the stipulated time, the membrane was washed three times with 1× TBST, probed with HRP-conjugated streptavidin for 1 h at room temperature, and developed using DAB dye. In the control, the same proteins were detected using Con A-specific antibody.

RESULTS AND DISCUSSION

SELEX Enrichment of Con A-Binding DNA Sequences. To find the Con A aptamer, an oligonucleotide library of 77-mer with a central randomized region of 41 was used as the starting pool of oligonucleotides. Seven rounds of positive selections along with two negative screenings were carried out on NHS-activated agarose beads having Con A covalently attached to the bead surface (Scheme 1). The amount of oligonucleotides in the first round of SELEX screening was kept to 10 nmol to ensure a sufficient number of sequences during subsequent round of selections. Blocking the protein-bound surfaces prior to oligonucleotide binding is a common practice to counteract nonspecific enrichment. However, such practices also result in enrichment of "blocking agent-binding sequences". To overcome this, we omitted the BSA blocking and have introduced a negative selection step wherein the starting DNA library is incubated with agarose beads (without immobilized Con A) and the bead bound sequences were removed from the initial pool library. Any chance of enriching nonspecific sequences during the course of selection was additionally minimized by introducing two such negative selections before the fourth and sixth rounds of SELEX. Furthermore, a selection pressure was applied to SELEX

Scheme 1. Schematic Illustration of SELEX Screening over an Agarose Spin Column

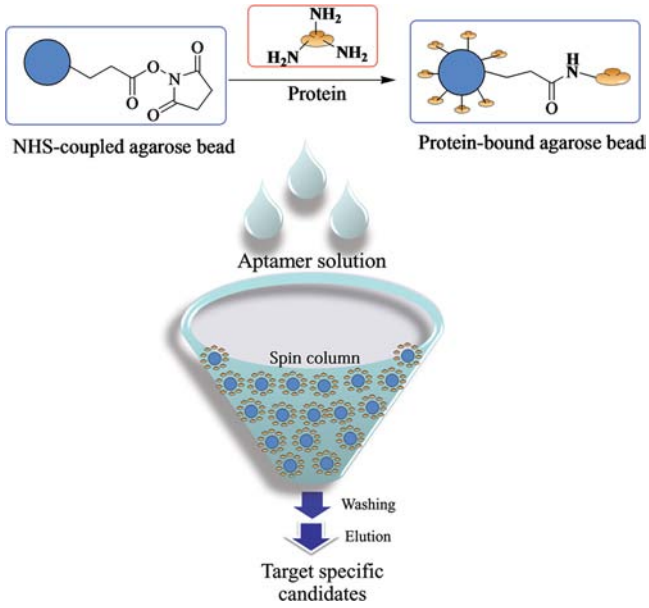

enrichment by decreasing the mole ratio of Con A to DNA from 1:1 to 1:10 during the fourth and fifth rounds and then to 1:20 during the sixth to seventh rounds of SELEX. The incubation time was also decreased concomitantly (Table 1).

Table 1. Summary of the SELEX Screenings Carried out on NHS-Activated Agarose Beads

SELEX round	protein (pmol)	aptamer (pmol)	incubation time (min)
1	5000	10000	120
2	500	500	60
3	500	500	60
4	10	100	30
5	10	100	30
6	5	100	15
7	5	100	15

Enrichment of potential aptamers during the SELEX run was monitored through our recently developed photocolorimetric method.[25] As shown in Figure 1, seven rounds of selections on NHS-activated agarose beads carrying the immobilized Con A has resulted in sufficient enrichment of Con A binding sequences. After satisfactory enrichment, the entire enriched pool of the last SELEX round was cloned and sequenced using Sangers' capillary sequencing. Analysis of the sequencing data showed the enrichment of eight different sequences, each having different sequence copy numbers (Table 2). Sequence 1 was found to have the highest copy number of 20, whereas other sequences showed varying sequence copy numbers between 1 and 5. This predominance of seq-1 over the remaining sequences indicated its superior binding propensities for Con A. Thus, SELEX enrichment over agarose spin columns was found to be an excellent approach as it resulted in enrichment of Con A binding DNA sequences in a mere seven to eight rounds of screening without having cumbersome binding and elution procedure.

Furthermore, we did in silico analysis of the enriched sequences to find the most potent Con A-aptamer. To figure out the most probable Con A-aptamer of the eight sequences,

DOI: 10.1021/acs.jafc.5b00784
J. Agric. Food Chem. 2015, 63, 4104−4111

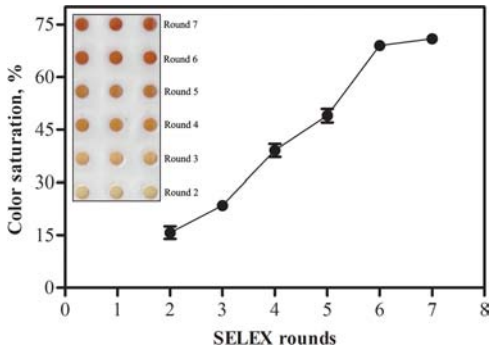

Figure 1. Aptamer enrichment monitoring during SELEX screening. A fixed amount of enriched ssDNA from different SELEX rounds was incubated with Con A followed by photocolorimetric quantification of Con A-bound sequences. A reasonable enrichment was attained by the seventh round of SELEX screening. (Inset) Image of developed color on APPμTP.

we carried out preliminary analyses such as free energy comparisons and structural stability and homology measurements. First, we folded these sequences to their secondary structures and divided them into three different groups based on secondary structure similarities (Figure 2). Group I included two sequences, seq-1 and seq-4, both forming dumbbell-shaped extended hairpin loops; group II had three sequences, seq-6, seq-7, and seq-8, each forming similar bihairpin loops; and group III also carried three sequences, seq-2, seq-3, and seq-5, each forming single hairpin loops. Consequently, the free energy of secondary structure formation was also calculated (Table 3). Free energy comparison was made by measuring the *Z*-score score of individual sequences. *Z*-score was calculated for each sequence using the equation

$$Z = (E_{apt} - \overline{E})/SD$$

where E_{apt} is the predicted affinity or score of individual solutions, $\overline{E}$ is the energy mean of random sequences, and SD is the standard deviation of random sequences. Here, the *Z*-score of a sequence/structure defines its specificity toward the observed or predicted conformation. A higher negative *Z*-score implies a more specific conformation and hence better structure prediction. As calculated in Table 3, seq-1 showed a minimum *Z*-score value of −1.51, demonstrating better structural folding of this sequence over same-length random sequences. Also, the observed free energy of secondary structure formation for seq-1 was found to be significantly lower than that of same-length random sequences, which indeed proves the better structural folding and selective enrichment of seq-1.

We also carried out homology measurements to find base similarities in the enriched sequences. However, no homology or pattern was observed. This shows that the observed homology in secondary structure formation was not due to the sequence similarities, rather an independent behavior. Conversely, few of the enriched sequences showed multiplicity of G stretches in their base sequences and therefore prompted us to analyze their G-quadruplex forming capability. To our surprise, one of the sequences, namely, seq-1, was predicted to have a quadruplex-forming G-rich sequence (GGAAGGCGG-AGGG; G-score = 20, length = 13 base; Table 4). Because quadruplex-forming sequences usually have better binding characteristics for their targets, seq-1 may represent the best ligand to Con A in the panel of selected sequences. Therefore, on the basis of structural analysis, free energy comparisons, and unique structural properties, we put forward seq-1 as the most probable aptamer for Con A.

Nanomolar Affinity of Selected Seq-1 for Purified Con A. To confirm the in silico predictions and subsequently determine the sequence with best binding credentials, we carried out saturation binding assays wherein each sequence was analyzed for its binding with the target Con A. Binding assays were carried out in a 96-well microtiter plate. Wells were coated with Con A and incubated with 500 nM biotinylated sequences (seq-1−8). Binding reaction was carried out for 2 h, after which the target-bound sequences were detected by probing the wells with streptavidin−HRP conjugate and its chromogenic substrate dye. Binding propensities were measured as color absorbance. As depicted in Figure 3A, seq-1 showed highest binding, followed by seq-4 and the remaining sequences, which showed almost equal and comparably lower bindings to Con A. These observations were in agreement with our in silico predictions that showed seq-1 to be the most probable aptamer. As a result, we selected seq-1 as the aptamer of Con A (Con A-aptabody) and subsequently measured the dissociation constant (K_d) and target specificity of the Con A-aptabody. For K_d determination, varying concentrations of aptabody (0−1000 nM) were titrated against a fixed amount of Con A. Binding was measured through color development assay using the streptavidin−HRP. A dissociation constant of 172.7 ± 29.7 nM was calculated by fitting the control subtracted values to one-site specific binding (nonlinear) in GraphPad Prism (Figure 3B).

We then measured the target specificity of aptabody for Con A. Three distinct samples, pure Con A, jack bean seed extract, and bovine serum albumin, were used as potential binding partners. As shown in Figure 4, the aptabody showed considerable binding to pure Con A and jack bean seed extract, but not to BSA. As jack bean is the major source of Con

Table 2. Enriched Sequences Obtained through Sanger's Sequencing[a]

sequence	length (base)	sequence	copy
1	41	CGAGTAACGCTGTCTCTTCCGAATCGGGGGAAGGCGGAGGG	22
2	42	AGGTACAGAAGGCGCGACAGAAACTGCGGTCCCAGGGCGTGT	5
3	41	GGGGATAACGTCGTCACGTCGTGTCATCATTGGTTCAGTCG	3
4	41	GCAGCAGTGTCATATGAGGGCGTTCGTCAAATGTGCAGGGT	2
5	41	CACTAATACTAGGCGGTCCACGCGCAGTTAAACCGGTCAAT	1
6	41	CACAGGGCTGTTTTTACGCAATGCTAGTGTTCGACTCAGTG	1
7	41	ACTACAGTGAATGTGTTGCGAAAGTGCGTTATATTAACATA	1
8	41	CGTTGCATTTAGGTGCATTACGGGGGTTATCCGCTCTCTCT	1

[a]Sequences are listed after trimming the priming sites.

DOI: 10.1021/acs.jafc.5b00784
J. Agric. Food Chem. 2015, 63, 4104−4111

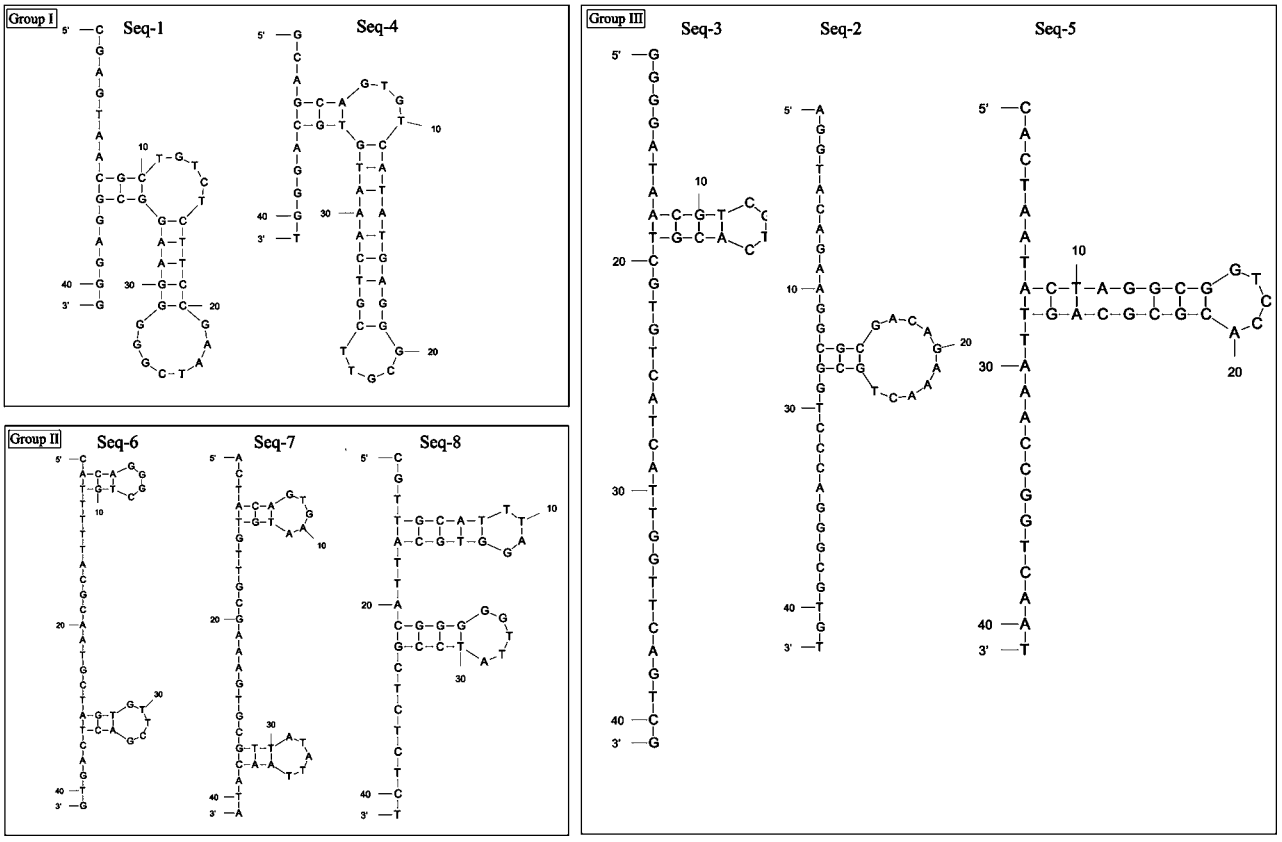

Figure 2. Grouping of the enriched sequences based on their secondary structure formations. Group I aptamers form dumbbell-shaped extended hairpin loops, group II aptamers form bihairpin loop structures, and group III aptamers form single hairpin loop structures.

Table 3. Free Energy Comparison of Enriched Sequences with Same-Length Random Sequences

sequence	length (base)	aptamer free energy (kcal/mol)	mean free energy (kcal/mol)	SD	*Z*-score
1	41	−4.53	−2.20	1.54	−1.51
2	42	−2.27	−2.37	1.57	0.06
3	41	−2.40	−2.20	1.54	−0.13
4	41	−3.36	−2.20	1.54	−0.75
5	41	−4.08	−2.20	1.54	−1.22
6	41	−1.72	−2.20	1.54	0.31
7	41	−2.25	−2.20	1.54	−0.03
8	41	−4.44	−2.20	1.54	−1.45

Table 4. G-Quadruplex Prediction in Sequence 1 Using QGRS Mapper

sequence	length of G-quadruplex forming region (base)	quadruplex forming G-rich sequence	*G*-score
1	13	GGAAGGCGGAGGG	20

A, the observed binding to seed extract of jack bean was obvious and also proves the target specificity of the aptabody. The absence of any binding to bovine serum albumin further confirmed the target specificity of identified aptabody. Here, we used the term "aptabody" to emphasize the unique recognition and binding properties of the developed aptamer of Con A, which were akin to those of Con A-antibodies.

In further assays, we checked the utility of this aptabody in Con A detection and method development of Con A quantification in food or agriculture products.

Development of Enzyme-Linked Aptamer Assays for Quantification of Con A in Jack Bean (*Canavalia ensiformis*). As aptamers offer substantial advantages over antibodies in terms of their production cost and time, production chemistry, and structural and functional stability, development of aptamer-based detection assays can provide an efficient and cost-effective substitute for immunoassays. To achieve the same, we utilized the ELISA concept to develop an aptamer-based detection methodology for Con A. For this, we coated the wells of a 96-well microtiter plate with an unknown quantity of pure Con A and jack bean seed extracts. Thereafter, 300 nM biotinylated aptabody was added to these wells and incubated for 2 h. Afterward, target-bound aptabody was detected by probing the wells with streptavidin−HRP and measuring the binding as color absorbance. Subsequently, the amount of Con A in all three samples was quantified from the Con A standards' curve prepared using specific-enzyme-linked aptamer assay (standard curve concentrations were 5−1000 ng/mL).

In the control, the same protein samples were detected using a conventional ELISA procedure employing Con A-antibody as a detection molecule. Furthermore, we determined the amount of Con A in all three samples, namely, an unknown Con A preparation, jack bean seed extract 1, and jack bean seed extract 2, by aptabody- and antibody-based assays. The results show that the values of the developed enzyme-linked aptamer assay are akin to those of the conventional ELISA assay (Figure 5A). As the methodology of the developed assay is similar to that of conventional ELISA, no specific training or instrumentation is required. However, the overall cost of the aptamer-based assay is comparably low and can be operated at ambient conditions.

DOI: 10.1021/acs.jafc.5b00784
J. Agric. Food Chem. 2015, 63, 4104−4111

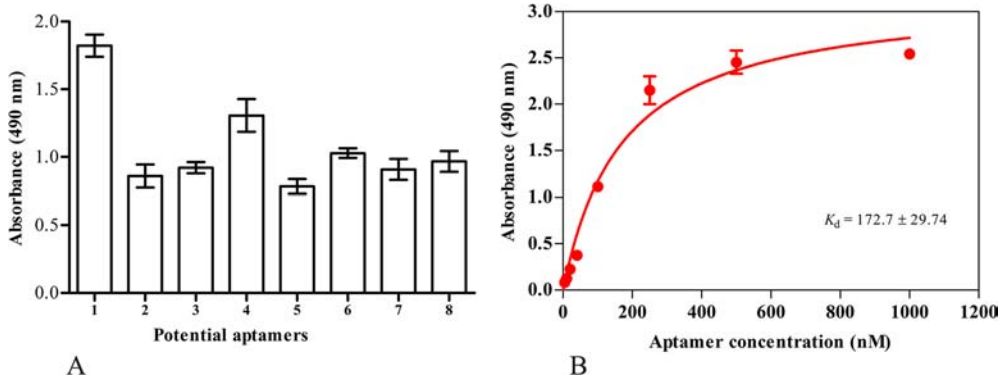

Figure 3. Affinity determination for enriched sequences. (A) Binding of enriched sequences (500 nM each) with immobilized Con A (1.5 μg) was measured by colorimetric saturation binding assays. (B) Equilibrium dissociation constant (K_d) is calculated by titrating 0−1000 nM seq-1 against a fixed amount of Con A (1.5 μg).

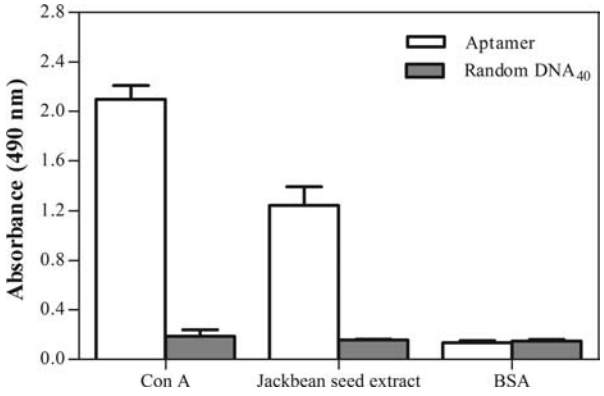

Figure 4. Specificity measurement for seq-1 as analyzed by binding reaction with pure Con A, extract of jack bean seed, and BSA. Target-bound seq-1 was detected colorimetrically.

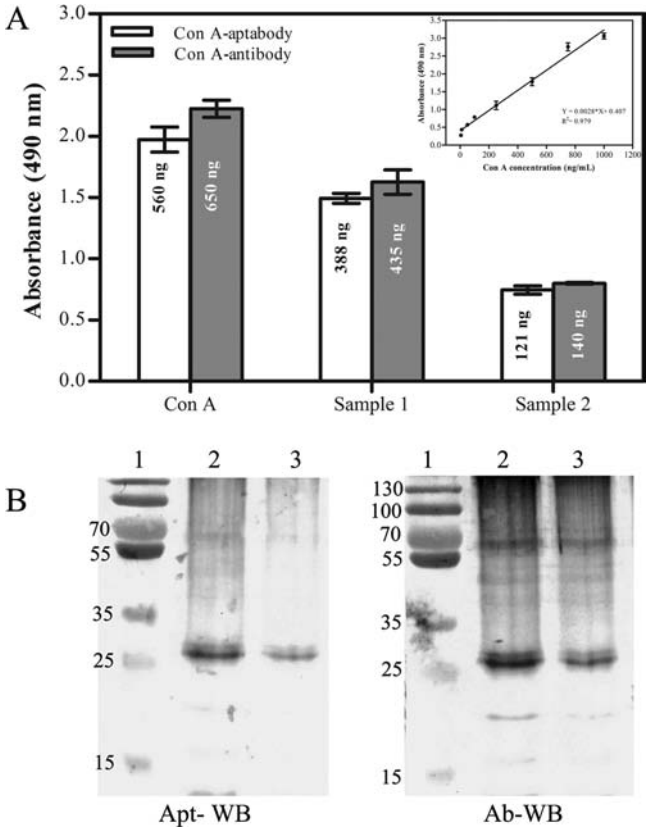

Figure 5. Enzyme-linked aptamer and Western blot assay. (A) Quantitation of Con A in three different samples, pure Con A, jack bean seed extract 1, and seed extract 2, was carried out using Con A-aptabody and -antibody in enzyme-linked aptamer and immunosorbent assays, respectively. The calculated amount of Con A in each sample is written in its corresponding bar. (Inset) Con A standard curve with concentrations of 5−1000 ng/mL. (B) Analysis of different amounts of Con A via aptamer-based Western blot and antibody-based Western blot assays: lane 1, protein marker; lanes 2 and 3, 1.0 and 5.0 μg of Con A, respectively.

Due to the ease in handling and storage and higher tolerance to thermal and environmental denaturation, Con A-aptabody provides a novel substitute for Con A-antibody. The detection range of the aptamer-based enzyme-linked aptamer assay was quantitated by plotting a standard curve for Con A in the working range of 5−1000 ng/mL (inset, Figure 5A). The enzyme-linked aptamer assay was performed in a sandwich format. The assay showed a linear rise in color absorbance in the dynamic range of 10−750 ng/mL Con A with a limit of detection of 13.229 ng/mL and a limit of quantification of 44.097 ng/mL. The precision of the assay is expressed as the coefficient of variation with intra-assay CV <12% (11.96, 5.18, and 2.87% for 5, 100, and 1000 ng/mL, respectively).

In another attempt to validate the utility of Con A-aptabody, we performed an aptamer-based Western blot assay for Con A detection. PAGE-separated dilutions of Con A (1 and 0.5 μg, respectively) were transferred to nitrocellulose membrane, and the membrane was probed with biotinylated Con A-aptabody. The blot was developed by probing with streptavidin−HRP conjugate and HRP substrate−dye. In the control, the same Con A samples were detected by antibody-based Western blot assay. The aptabody depicted an antibody-equivalent concentration-dependent detection of Con A (Figure 5B). This shows that the Con A-aptabody can efficiently be utilized to rival antibody-based affinity assays in Western blot and related applications.

Con A Determination in Food Samples. As lectins are abundantly present in common food products, such as plant seeds, raw legumes, and tubers, and most of them act as allergens, their determination is crucial for human health. Con A is one such lectin that causes toxicity to humans. In our most crucial effort to determine Con A using our developed Con A-aptabody, we analyzed five different food products—kidney bean (*Phaseolus vulgaris*), jack bean (*Canavalia ensiformis*),

DOI: 10.1021/acs.jafc.5b00784
J. Agric. Food Chem. 2015, 63, 4104−4111

wheat (*Triticum* spp.), mung bean (*Vigna radiata*), and lentil (*Lens culinaris*). Con A detection in these samples was carried out using the developed Con A-aptabody as well as the putative Con A-antibody. The results of this combined study are summarized in Figure 6. Seed extract of jack bean plant showed

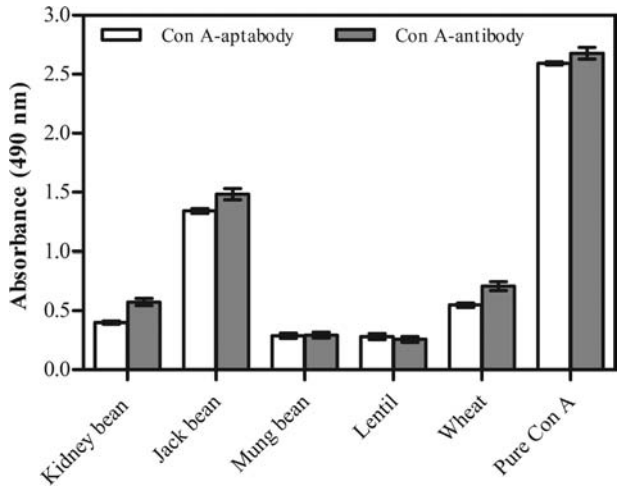

Figure 6. Con A determination in different food samples. Simultaneous analyses of five different samples by Con A-antibody and the aptabody showed similar trends.

the highest Con A, whereas kidney bean and wheat were calculated to contain low amounts of Con A. On the other hand, negligible amounts of Con A were detected in mung bean or lentils. Pure preparation of Con A was included as positive control. The results are in agreement with the literature, which reports jack bean as the major source of Con A.[26] Typical seeds of jack bean contain approximately 20−28 g (per 100 g dry seed mass) of protein, 60 g of carbohydrate, 10 g of ether extracts, and the remaining 10 g includes ash, crude fiber, and moisture contents. The protein contents of remaining food samples (*Phaseolus vulgaris*, *Vigna radiata*, *Lens culinaris*, and *Triticum* spp.) were also in the range of 20−26 g/100 g dry seed mass.[27] This means that irrespective of equivalent total proteins in the extracts of jack bean, mung bean, kidney beans, wheat, and lentils, the developed method and the aptabody are capable of determining the proportional Con A quantity specifically and precisely. At the same time, consecutive analysis of all five samples using putative Con A-antibody showed an almost similar pattern. From the results, it is clear that the developed aptabody of Con A is capable of detecting Con A in common food samples.

Taken together, we can conclude that the developed aptamer of Con A is highly specific, has a high binding affinity, and thus can rival antibodies in Con A detection. Its ability to detect Con A makes it a potentially useful molecule for lectin analysis in common food and agricultural products and research laboratories.

AUTHOR INFORMATION

Corresponding Author

*(P.N.) Mail: CSIR−Institute of Genomics and Integrative Biology, Mall Road, Delhi 110007, India. Phone: +91-11-27667439. E-mail: pnahar@igib.res.in.

Funding

R.A. thanks the Council of Scientific and Industrial Research, government of India, for the award of a senior research fellowship. This work is funded by CARDIOMED Project BSC0122 of the Council of Scientific and Industrial Research, government of India, New Delhi, India.

Notes

The authors declare no competing financial interest.

ABBREVIATIONS USED

Con A, concanavalin A; SELEX, systematic evolution of ligands by exponential enrichment; ELISA, enzyme-linked immunosorbent assay; TEMED, *N*,*N*,*N*′,*N*′-tetramethylethane-1,2-diamine; NHS, *N*-hydroxysuccinimide; TBST, Tris buffer saline Tween-20; DAB, 3,3′-diaminobenzidine; OPD, *o*-phenylenediamine dihydrochloride

REFERENCES

(1) Stoltenburg, R.; Reinemann, C.; Strehlitz, B. SELEX − a (r)evolutionary method to generate high-affinity nucleic acid ligands. *Biomol. Eng.* **2007**, *24*, 381−403.
(2) Kulbachinskiy, A. V. Methods for selection of aptamers to protein targets. *Biochemistry* **2007**, *72*, 1505−1518.
(3) Ni, X.; Castanares, M.; Mukherjee, A.; Lupold, S. E. Nucleic acid aptamers: clinical applications and promising new horizons. *Curr. Med. Chem.* **2011**, *18*, 4206−4214.
(4) Tombelli, S.; Minunni, M.; Mascini, M. Analytical applications of aptamers. *Biosens. Bioelectron.* **2005**, *20*, 2424−2434.
(5) Cho, E. J.; Lee, J.-W.; Ellington, A. D. Applications of aptamers as sensors. *Annu. Rev. Anal. Chem.* **2009**, *2*, 241−264.
(6) Pieve, C. D.; Williams, P.; Haddleton, D. M.; Palmer, R. M. J.; Missailidis, S. Modification of thiol functionalized aptamers by conjugation of synthetic polymers. *Bioconjugate Chem.* **2010**, *21*, 169−174.
(7) Jayasena, S. D. Aptamers: an emerging class of molecules that rival antibodies in diagnostics. *Clin. Chem.* **1999**, *45*, 1628−1650.
(8) McKeague, M.; DeRosa, M. C. Challenges and opportunities for small molecule aptamer development. *J. Nucleic Acids* **2012**, 748913.
(9) Cruz-Aguado, J. A.; Penner, G. Determination of ochratoxin A with a DNA aptamer. *J. Agric. Food Chem.* **2008**, *56*, 10456−10461.
(10) McKeague, M.; Giamberardino, A.; DeRosa, M. C. Advances in aptamer-based biosensors for food safety. In *Environmental Biosensors*; Somerset, V., Ed.; InTech: Rijeka, Croatia, 2011; ISBN 978-953-307-486- 3, pp 17−42.
(11) Sharon, N.; Lis, H. Detection, occurence and isolation. In *Lectins*, 2nd ed.; Sharon, N., Lis, H., Eds.; Kluwer Academic Publishers: Dordrecht, The Netherlands, 2003; pp 36−56.
(12) Freed, D. L. J. Do dietary lectins cause disease? The evidence is suggestive − and raises interesting possibilities for treatment. *BMJ* **1999**, *318*, 1023−1024.
(13) Nachbar, M. S.; Oppenheim, J. D. Lectins in the United States diet: a survey of lectins in commonly consumed foods and a review of the literature. *Am. J. Clin. Nutr.* **1980**, *33*, 2338−2345.
(14) Freed, D. L. J. Dietary lectins and the anti-nutritive effects of gut allergy. In *Protein Transmission Through Living Membranes*; Elsevier/North Holland Biomedical Press: Amsterdam, The Netherlands, 1979; pp 411−422.
(15) Liener, I. E. Nutritional significance of lectins in the diet. In *The Lectins*; Liener, I. E., Sharon, N., Goldstein, I. J., Eds.; Academic Press: Orlando, FL, USA, 1986; pp 529−552.
(16) Kumar, K. K.; Chandra, K. L.; Sumanthi, J.; Reddy, G. S.; Shekar, P. C.; Reddy, B. Biological role of lectins: a review. *J. Orofac Sci.* **2012**, *4*, 20−25.
(17) Magro, A. M.; Bennich, H. Concanavalin A induced histamine release from human basophils in vitro. *Immunology* **1977**, *33*, 51−58.
(18) Siraganian, R. P.; Siragania, P. A. Mechanism of action of concanavalin A on human basophils. *J. Immunol.* **1975**, *114*, 886−893.

DOI: 10.1021/acs.jafc.5b00784
J. Agric. Food Chem. 2015, 63, 4104−4111

(19) Sjolander, A.; Magnusson, K. E.; Latkovic, S. The effect of concanavalin A and wheat germ agglutinin on the ultrastructure and permeability of rat intestine. A possible model for an intestinal allergic reaction. *Int. Arch. Allergy Immunol.* **1984**, *75*, 230−236.
(20) Lorenzsonn, V.; Olsen, W. A. In vivo responses of rat intestinal epithelium to intraluminal dietary lectins. *Gastroenterology* **1982**, *82*, 838−848.
(21) Chuba, J. V.; Kuhns, W. J.; Oppenheim, J. D.; Nachbar, M. S.; Nigrelli, R. F. Multiple specificities of mammalian blood group substances comparatively studied with human isoagglutinins and fractionated anti-H lectins. *Immunology* **1975**, *29*, 17−30.
(22) Adamova, L.; Malinovska, L.; Wimmerova, M. New sensitive detection method for lectin hemagglutination using microscopy. *Microsc. Res. Tech.* **2014**, *77*, 841−849.
(23) Nahar, P.; Wali, N. M.; Gandhi, R. P. Light-induced activation of an inert surface for covalent immobilization of a protein ligand. *Anal. Biochem.* **2001**, *294*, 148−153.
(24) Parween, S.; Nahar, P. Image-based ELISA on an activated polypropylene microtest plate − a spectrophotometer-free low cost assay technique. *Biosens. Bioelectron.* **2013**, *48*, 287−292.
(25) Ahirwar, R.; Tanwar, S.; Parween, S.; Kumar, A.; Nahar, P. Image-based detection of oligonucleotides − a low cost alternative to spectrophotometric or fluorometric methods. *Analyst* **2014**, *139*, 2186−2192.
(26) Sumner, J. B. The globulins of the jack bean *Canavalia ensiformis*. *J. Biol. Chem.* **1919**, *37*, 137−142.
(27) Abitogun, A. S.; Olasehinde, E. F. Nutritional evaluation of seed and characterization of crude jack bean (*Canavalia ensiformis*) oil. *IOSR J. Appl. Chem.* **2012**, *1*, 36−40.

DOI: 10.1021/acs.jafc.5b00784
J. Agric. Food Chem. 2015, 63, 4104−4111

Table 1. Resonance Assignments and Integration Ranges for Egg Liqueurs and Calibration References of ^{1}H NMR Spectra (400 MHz)[a]

resonance assignment with δ in ppm	structural formula	integration ranges (δ in ppm) for egg liqueurs	integration ranges (δ in ppm) for calibration references
caffeine[13]: δ ≈ 7.8 (s, 1, C8H)	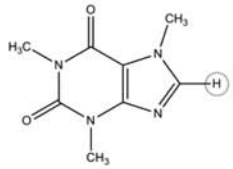	7.83 - 7.75	7.77 - 7.69
cholesterol[13] δ ≈ 0.7 (s, 3, C18H$_3$)	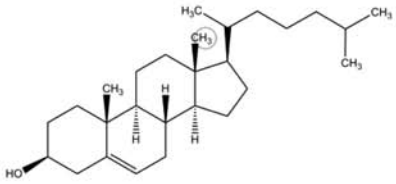	0.72 - 0.67	0.72 - 0.67
ethanol[13] δ ≈ 1.1 (t, 3, C2H$_3$)		1.25 - 1.10	1.06 - 0.99
α-D-fructofuranose/ β-D-fructofuranose[14] δ ≈ 4.1 (m, 1, C3H)/ δ ≈ 4.1 (m, 1, C3H), δ ≈ 4.1 (m, 1, C4H)	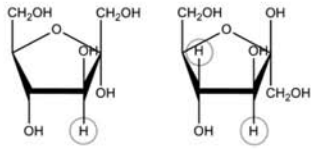	4.12 - 4.09	4.13 - 4.10
α-D-glucopyranose[15] δ ≈ 5.2 (d, 1, C1H)	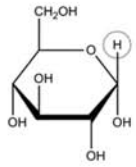	5.25 - 5.21	5.26 - 5.22
sucrose[13] δ ≈ 5.4 (d, 1, gluco-pyranosyl-C1H)	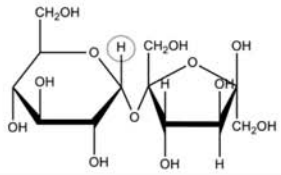	+/- 5 Hz from signal middle at about 5.40	

[a]MeOH-d_4/$CDCl_3$ (50:50, v/v) as solvent for caffeine and cholesterol and H_2O/D_2O (90:10, v/v) for ethanol, fructose, glucose, and sucrose.

(99%), glucose (99.5%), KI (99.5%), and sucrose (99.5%) were from Sigma (St. Louis, MO, USA), $CuSO_4 \cdot 5H_2O$ (99.5%), KOH (85%), $KNaC_4H_4O_6 \cdot 4H_2O$ (99%), $Na_2S_2O_3$ (99.5%), $ZnSO_4$ (99.5%), and MeOH-d_4 (99.8 atom % D) were from Carl Roth (Karlsruhe, Germany), MeOH (99.8%) was from Fisher Scientific (Pittsburgh, PA, USA), H_2SO_4 (96%) was from Fluka (Buchs, Switzerland), and isopropyl alcohol was from VWR Scientific Products (New York, NY, USA). A ready kit for enzymatic determination of cholesterol was purchased from r-biopharm (Boehringer Mannheim/r-biopharm, Darmstadt, Germany), and sea sand from Merck (Darmstadt, Germany).

TSP-d_4 solution consisted of 7 mM TSP-d_4 and 2 mM NaN_3 in D_2O, Carrez I solution of 15% $K_4[Fe(CN)_6] \cdot 3H_2O$ in demineralized water, Carrez II solution of 30% $ZnSO_4$ in demineralized water, and $CDCl_3$ solution of 7 mM TMS and 21.5 mM caffeine in $CDCl_3$.

^{1}H NMR Analysis of Egg Liqueurs. *Sample Preparation for Egg Liqueurs.* Fifteen different egg liqueurs were purchased from supermarkets in Germany. For analysis of alcoholic strength and total sugar content, about 2 g of egg liqueur was diluted to 10 mL with demineralized water, and 1000 μL of this dilution was mixed with 50 μL of Carrez I solution, 50 μL of Carrez II solution, and 100 μL of TSP-d_4 solution; subsequently this mixture was centrifuged at 6260*g* for 5 min, and 600 μL of clear supernatant was transferred to 5 mm NMR tubes. For analyzing cholesterol, about 200 mg of egg liqueur was mixed with 500 μL of MeOH-d_4 and 500 μL of $CDCl_3$ solution. After shaking for 30 min, samples were centrifuged at 1565*g* for 5 min, and 600 μL of clear supernatant was transferred to 5 mm NMR tubes.

Sample Preparation for Checking Recovery Rates. The increase in concentration by addition of reference solutions (ethanol/sucrose/egg yolk mixture) was divided by the theoretical increase in concentration in order to yield the percentage of recovery rates.

To check recovery rates of ethanol and total sugar content, five different egg liqueurs were analyzed. For ethanol, 5 g of egg liqueur was diluted to 50 mL with demineralized water, and 5 g of the same egg liqueur was mixed with 0.8 g of pure ethanol and diluted to 50 mL with demineralized water. A 1 mL amount of each dilution was mixed with 50 μL of Carrez I solution, 50 μL of Carrez II solution, and 100 μL of TSP-d_4 solution and centrifuged at 6260*g* for 5 min. For total

DOI: 10.1021/acs.jafc.5b00940
J. Agric. Food Chem. 2015, 63, 4112−4119

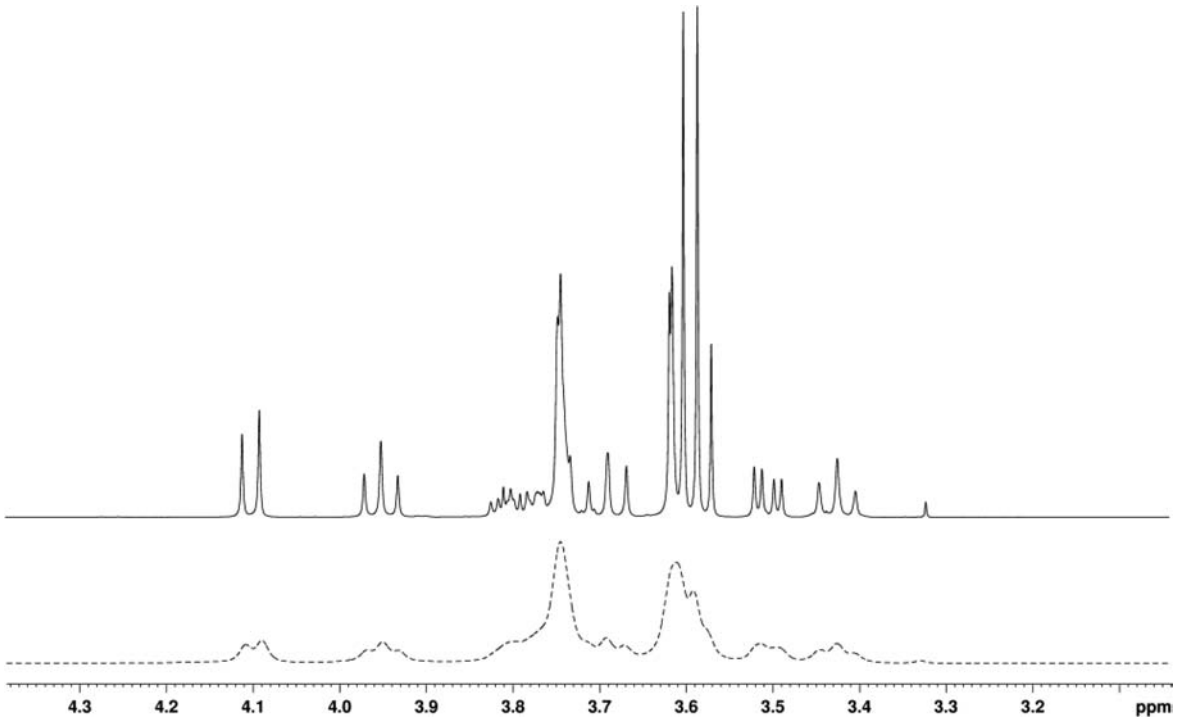

Figure 1. ^{1}H NMR spectrum of an egg liqueur without further preparation (1:2 diluted with demineralized water; dotted line) and after Carrez precipitation (1:5 diluted with demineralized water; constant line) at the spectral range from δ = 3.1 to 4.3 ppm, measured with a 400 MHz spectrometer.

sugar content, 2 g of egg liqueur was diluted to 10 mL with demineralized water. A 1 mL portion of this dilution was mixed with 100 μL of sucrose solution (containing 200 g/L sucrose), and 1 mL was mixed with 100 μL of demineralized water. Subsequently, the samples were mixed with 50 μL of Carrez I solution, 50 μL of Carrez II solution, and 100 μL of TSP-d_4 solution and centrifuged at 6260*g* for 5 min. Each 600 μL of clear supernatant was transferred to 5 mm NMR tubes, and the ethanol or sucrose content was determined by qNMR.

For checking cholesterol recovery rates, five egg liqueurs were prepared by adding different amounts (ranging between 6.6 and 25.9 g) of an egg yolk mixture (containing 335.3 g/L egg yolk and 4.2 g/L cholesterol on the assumption of 12.5 mg/g cholesterol in egg yolk[10]) to 50 g of an egg liqueur with a known content of cholesterol (calculated as the average value of five qNMR results). A 200 mg sample of this was mixed with 500 μL of MeOH-d_4 and 500 μL of $CDCl_3$ solution. After shaking for 30 min, samples were centrifuged at 1565*g* for 5 min, and 600 μL of clear supernatant was transferred to 5 mm NMR tubes.

^{1}H NMR Measurement. Hardware and software equipment for ^{1}H NMR measurement consisted of a Bruker Avance 400 spectrometer with a 5 mM SEI probe with Z-gradient coils, an automatic SampleChanger (SampleXpress), a BCU 05 temperature unit, and TopSpin 3.0 software.

Samples in aqueous solution were measured without rotation at 301.8 ± 0.1 K using 4 dummy scans prior to 16 scans. Acquisition parameters have been set as follows: size of FID = 64k, spectral width = 20.55 ppm, receiver gain = 16, acquisition time = 3.98 s, relaxation delay = 4 s, FID resolution = 0.25 Hz per point. Water suppression was achieved by an experiment using a 90° pulse with a NOESY-presaturation pulse sequence (Bruker 1D noesygppr1d) with irradiation of the water frequency during the recycle and mixing time delays. All spectra were automatically phased and manually baseline corrected.

Samples in MeOH-d_4/$CDCl_3$ solution were measured without rotation at 300 ± 0.1 K using 2 dummy scans prior to 256 scans. Acquisition parameters have been set as follows: size of FID = 64k, spectral width = 25.82 ppm, receiver gain was automatically set by *rga* command, acquisition time = 3.17 s, relaxation delay = 1 s, FID resolution = 0.32 Hz per point. A flip angle of 30° was used within the zg30 experiment. All spectra were manually phased and baseline corrected.

Quantification. Resonance assignments were based on spectral databases[13] and literature,[14,15] and integration ranges are displayed in Table 1. Quantification was performed by external calibration with concentration ranges from 12.5% to 22.5% by volume for ethanol, 100 to 500 g/L for sucrose, 20 to 80 g/L for glucose and fructose, and 1 to 3 g/L for cholesterol. For each calibration graph, linearity was verified by Mandel's fitting test (*F*-values were lower than reported values in *F*-tables with a confidence level of 95%). The limit of detection/limit of quantification values were determined according to DIN 32645[16] (significance level 5%; uncertainty of result 33%) and amounted to 0.80/2.78% by volume for ethanol, 6.79/26.11 g/L for sucrose, 0.56/2.23 g/L for glucose, 1.39/5.33 g/L for fructose, and 0.08/0.28 g/L for cholesterol, respectively.

To consider the influence of the pulse length on signal intensities, the signal areas of ethanol, sucrose, glucose, and fructose were converted into their theoretical values for an equal 90° pulse length of 11 μs. For this, each signal area was multiplied by the factual 90° pulse length (in μs) and divided by 11. To quantify cholesterol, the ratio of the signal area of cholesterol compared to the signal area of caffeine was used for examination of egg liqueurs as well as for calibration references.

Conventional Analytics of Egg Liqueurs. Alcoholic strength was determined pycnometrically after distillation,[3] total sugar content was determined as reducing sugars by a redox titration after reaction with Cu^{2+} as oxidizing agent (Luff–Schorl method),[4] and cholesterol was analyzed enzymatically subsequent to saponification (for saponification: 10 mL of 1 M KOH solution was added to 2 g of egg liqueur and 1 g of sea sand and heated under reflux for 25 min; the supernatant and two amounts each of 6 mL of isopropyl alcohol (used for washing solid residues) were diluted to 25.0 mL with isopropyl alcohol, and in case of turbid solutions, filtration was performed using a folded filter). Enzymatic determination of cholesterol was performed according to the instructions of a ready kit (purchased from Boehringer Mannheim/r-biopharm, Darmstadt, Germany).

DOI: 10.1021/acs.jafc.5b00940
J. Agric. Food Chem. 2015, 63, 4112–4119

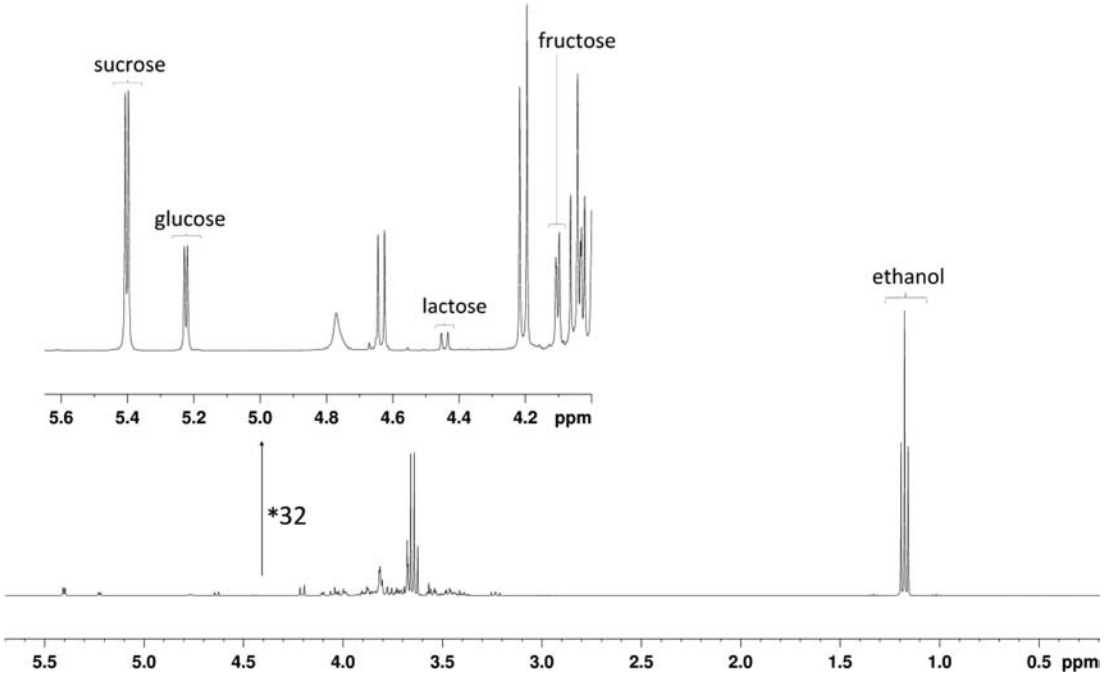

Figure 2. ^{1}H NMR spectrum of an egg liqueur after Carrez precipitation (1:5 diluted with demineralized water) at the spectral range from δ = 0.2 to 5.7 ppm with an enlarged view on the spectral range from δ = 4.1 to 5.6 ppm, measured with a 400 MHz spectrometer.

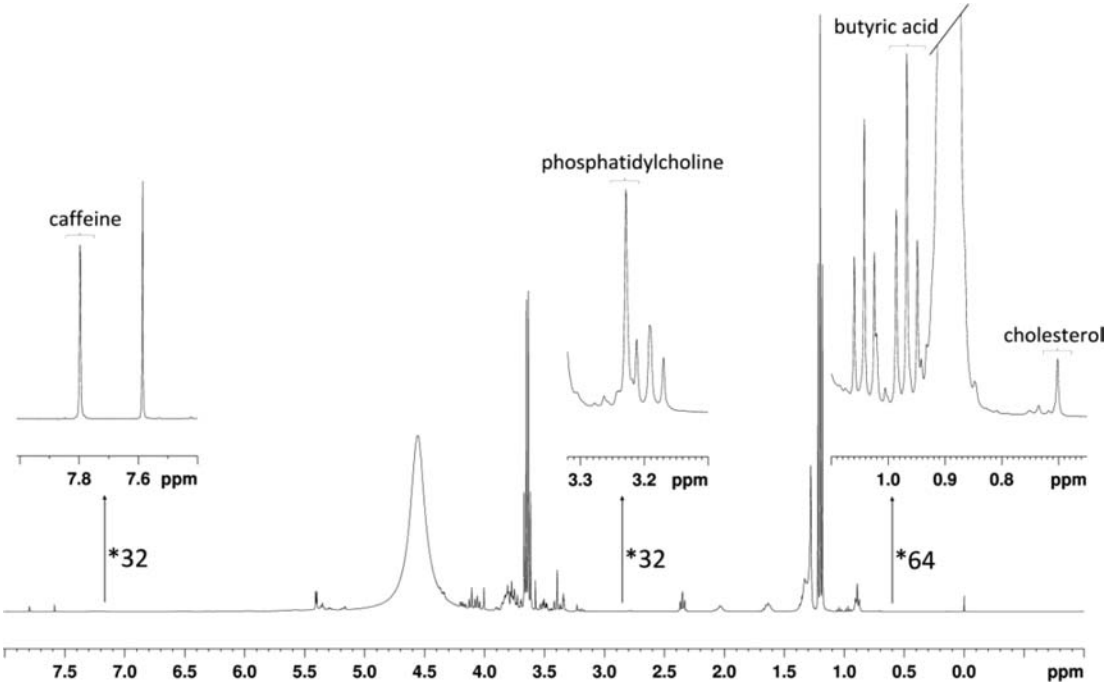

Figure 3. ^{1}H NMR spectrum of an egg liqueur extract (MeOH-d_4/$CDCl_3$ = 50:50 (v/v)) at the spectral range from δ = 0 to 8.0 ppm with an enlarged view of the spectral range from δ = 7.4 to 8.0 ppm, δ = 3.1 to 3.3 ppm, and δ = 0.7 to 1.1 ppm, measured with a 400 MHz spectrometer.

RESULTS AND DISCUSSION

Sample Preparation for ^{1}H NMR Measurement. Foremost, optimized conditions for sample preparation were developed. Considering the high viscosity of egg liqueurs, direct ^{1}H NMR measurements are not applicable. First, it is difficult to accurately fill viscous egg liqueurs into NMR tubes, and second, poor spectral resolution is obtained (Figure 1). By precipitation of proteins the viscosity of liqueurs is reduced, which increases spectral resolution. Figure 1 shows a ^{1}H NMR spectrum of an egg liqueur (1:2 diluted with water) without further preparation steps and of an egg liqueur (1:5 diluted) after Carrez precipitation. ^{1}H NMR spectra of the supernatant, obtained after Carrez precipitation of diluted egg liqueurs, revealed distinct resonance signals of ethanol, sucrose, glucose, and fructose (Figure 2), and the respective signal areas enabled the determination of alcoholic strength (as ethanol) and total sugar content (sum of sucrose, glucose, and fructose).

DOI: 10.1021/acs.jafc.5b00940
J. Agric. Food Chem. 2015, 63, 4112−4119

As cholesterol is difficult to dissolve in water, it was not detectable by use of this preparation process. Therefore, MeOH-d_4 and $CDCl_3$ (50:50, v/v) were added to a small amount of liqueur, and this solution was subsequently mixed for the extraction of cholesterol. Although this mixture contained nonpolar solvents and water (originating from liqueurs) at the same time, no layer separation occurred during extraction. Thus, it can be excluded that extraction losses of cholesterol are caused by partially dissolved cholesterol in different solvent phases. The appearance of a homogeneous solution can be attributed to the emulsifying effect of phospholipids from egg yolk. Aside from that, due to the precipitation of proteins by MeOH-d_4, a clear and nonviscous solution was available after centrifugation, and the supernatant was used for qNMR analysis of cholesterol (Figure 3).

Capabilities and Requirements of Quantitative ^{1}H NMR. As quantitative ^{1}H NMR spectroscopy (qNMR) presents a primary method,[17] the concentration of substances can be directly derived from the signal areas without the application of response factors or reference substances.[18] One major advantage of qNMR is the possibility for straightforward sample preparations, since every step of sample pretreatment implies a potential source of error. Furthermore, in contrast to analytical methods that are restricted in applicability by the selectivity of detectors, ^{1}H NMR spectroscopy enables simultaneous detection of all ^{1}H atoms and, thus, implements optimum conditions for multimethod approaches.

To gain benefit from these advantages, general prerequisites need to be fulfilled in order to yield accurate quantification results. In general, appropriate spectrometer configuration and measuring conditions as well as suitable processing parameters must be considered. Furthermore, distinct and well-separated resonance signals as well as sufficiently high concentrations are needed for proper integration, and the relaxation delay between consecutive pulses must be set adequate to ensure complete relaxation of the substances to be quantified.[19] Another effect to be considered is that the NMR signal strength is affected by the 90° pulse length that is inversely proportional to the signal intensity.[20,21]

When sample preparations were applied as previously described, distinct signals for ethanol, sucrose, glucose, fructose, and cholesterol were achieved (Figures 2 and 3) and integration ranges for qNMR were set adequate to eliminate nearby resonance signals from other components. With the exception of fructose and glucose, which were not contained in each egg liqueur, all concentrations were well above the respective limit of quantification. After integration, quantification was performed by external calibration with individual calibration graphs for each substance (ethanol, sucrose, glucose, fructose, and cholesterol). The sample preparation for qNMR of cholesterol included caffeine as an internal standard in the extraction solvents in order to avoid quantification errors caused by evaporation of volatile solvents. Thus, instead of the signal area of cholesterol, its ratio to the signal area of caffeine was used for examination.

To consider the influence of the 90° pulse length on signal intensities, the signal areas for ethanol, sucrose, glucose, and fructose were converted into their respective value for an equal 90° pulse length (11 μs; Materials and Methods). Since all resonance signals were affected by variations of the 90° pulse length, the signal areas of cholesterol and caffeine as internal standard were likewise influenced. Thus, the impact of the pulse length was already eliminated during examination of the cholesterol content, since the cholesterol signal areas were considered as their respective ratio to the signal areas of caffeine as internal standard.

The correctness and precision of qNMR were investigated by recovery rates (n = 5) and replicate measurements (n = 5). Accurate results were achieved for all quantified components (Table 2). Thus, the conditions for quantification were set adequately.

Table 2. Precision and Recovery Rates for qNMR of Ethanol, Total Sugar, and Cholesterol (n = 5)

component	precision	recovery rate
ethanol	0.5%	97.6 ± 2.0%
total sugar	3.2%	96.1 ± 7.6%
cholesterol	2.3%	106.6 ± 8.1%

Comparison of the Results of qNMR with Conventional Analysis. The direct comparison with the results of established conventional analysis is an important step in order to verify applicability and validity of qNMR as a rapid alternative method. Even if no factual concentrations for the egg liqueur samples were available, the methods accordance between established classical methods and qNMR gives a first impression of the suitability of NMR analysis. For comparison with qNMR, the following conventional analytical methods were applied: pycnometry after distillation for alcoholic strength, redox titration for sugar, and enzymatic analysis (after saponification of lipids) for cholesterol. However, the respective results are subject to individual uncertainties of measurement, and thus, they do not reflect real values but rather trusted estimations.

Correlations between data of qNMR and conventional methods were calculated for their comparability. Since correlation coefficients do not accommodate systematic differences, too optimistic results may be delivered, and thus, we additionally used the Bland−Altman plot to factor in eventual biases.[22] It is performed by plotting the differences between two methods against the respective mean value of both methods for each sample. For a better overview, three parallel lines for the mean deviation and mean deviation ± 1.96-fold standard deviation are indicated in the plot. This diagram offers information about systematic deviations between two methods, the variance around the mean deviation, and eventual dependencies between deviations and concentration range.[23] We analyzed overall 15 egg liqueurs by both quantitative ^{1}H NMR analysis and classical analytical techniques. The results are displayed in Table 3.

When qNMR results were plotted against results of customary analysis techniques, high correlations were achieved for alcoholic strength (R = 0.996, p < 0.001), content of total sugar (R = 0.989, p < 0.001), and content of cholesterol (R = 0.995 p < 0.001).

Regarding alcoholic strength, the absolute deviation between the methods averaged 0.2 ± 0.3% by volume and the relative deviation 1.0 ± 1.5% (with an average alcoholic strength of 19.0% by volume, determined by results of pycnometry). Thus, the results showed a tendency for marginally higher values for qNMR analysis. Besides a possible systematic error of qNMR, this may be due to a bias of the classical method (for instance caused by incomplete distillation processes prior to pycnometric analysis). The Bland−Altman plot shows no dependency between the concentration range and the deviation

DOI: 10.1021/acs.jafc.5b00940
J. Agric. Food Chem. 2015, 63, 4112−4119

Table 3. Results of qNMR and Respective Classical Analysis Methods for Quantification of Alcoholic Strength (Pynometry after Distillation as Classical Method), Total Sugar (Redox Titration as Classical Method), and Cholesterol (Enzymatic Analysis as Classical Method) in 15 Different Egg Liqueurs

	alcoholic strength in vol %			*c*(total sugar) in g/L			*c*(cholesterol) in g/L		
sample	NMR	classical	Δ	NMR	classical	Δ	NMR	classical	Δ
1	15.8	15.7	0.1	369	394	−26	1.5	1.6	−0.2
2	18.3	17.9	0.4	374	395	−22	1.0	1.2	−0.2
3	17.7	17.3	0.3	458	485	−27	2.5	2.6	−0.2
4	17.9	18.3	−0.4	363	390	−27	1.0	1.2	−0.2
5	19.9	19.8	0.1	370	395	−25	1.3	1.6	−0.3
6	17.9	17.7	0.2	372	408	−37	0.9	1.1	−0.2
7	26.2	25.9	0.3	316	329	−13	4.0	4.2	−0.2
8	19.9	20.2	−0.3	259	268	−10	3.0	3.4	−0.4
9	20.6	20.4	0.1	347	352	−4	2.6	2.9	−0.3
10	20.7	20.3	0.4	311	300	11	2.7	2.8	−0.1
11	14.2	13.4	0.8	327	340	−13	1.1	1.4	−0.4
12	20.2	19.9	0.4	301	297	5	2.4	2.8	−0.3
13	20.0	19.8	0.2	330	341	−11	1.7	1.8	−0.1
14	22.4	22.4	0.0	401	420	−19	3.5	3.7	−0.3
15	16.2	15.9	0.4	233	234	−1	2.5	2.7	−0.2
		Ø19.0			Ø357			Ø2.3	

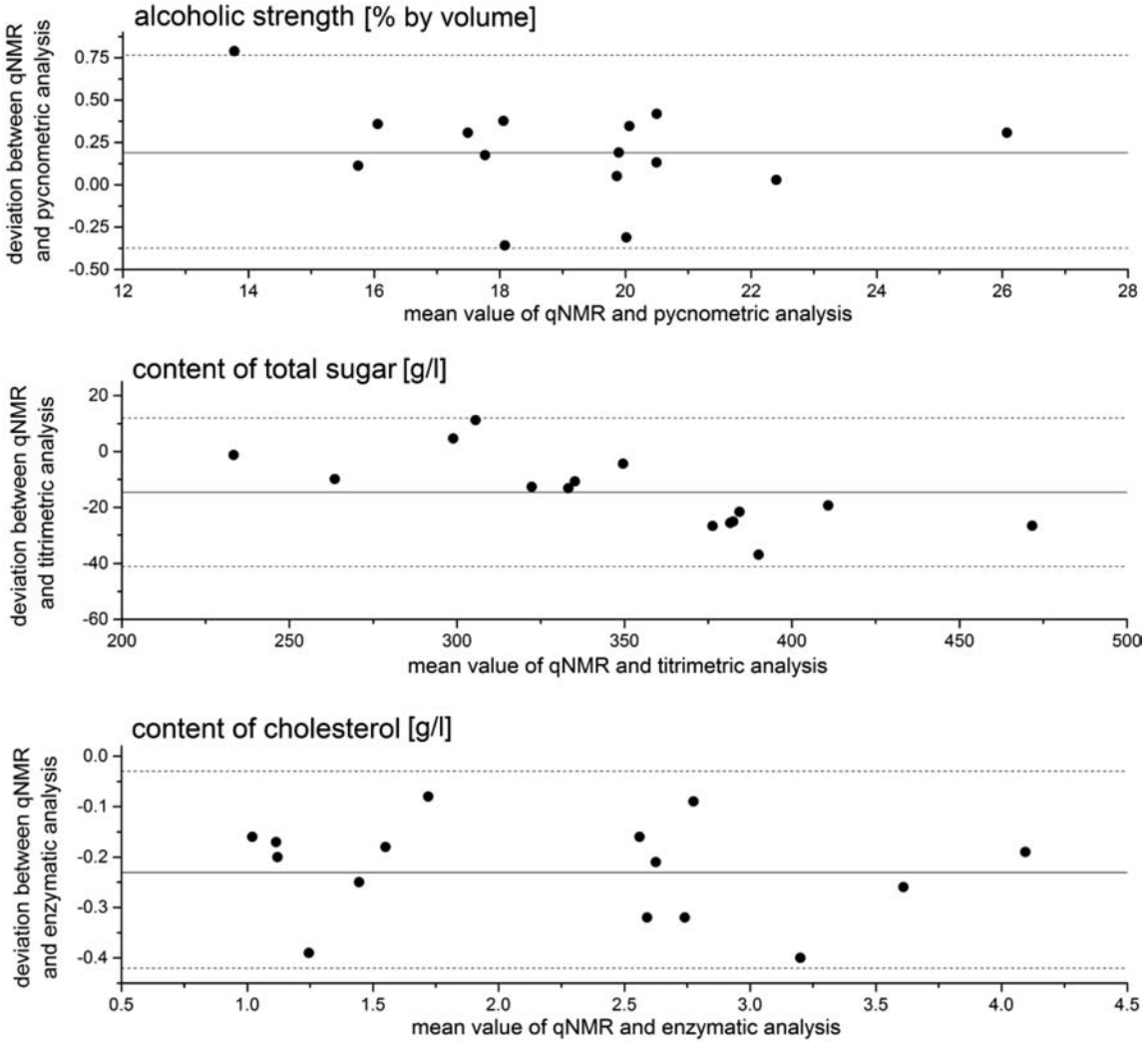

Figure 4. Bland−Altman plot for a comparison of the results of qNMR and classical analysis methods for the quantification of alcoholic strength, total sugar, and cholesterol in 15 different egg liqueurs; the mean deviation between the methods is plotted as a constant line, and the mean deviation ± 1.96-fold standard deviation as a dotted line.

DOI: 10.1021/acs.jafc.5b00940
J. Agric. Food Chem. 2015, 63, 4112−4119

between the methods (Figure 4). The deviations were rather symmetrically distributed between mean deviation ± 1.96-fold standard deviation (0.2 ± 0.6% by volume).

For total sugar, the absolute mean deviation between the methods amounted to −15 ± 13g/L, and the respective relative mean deviation to −4.1 ± 3.7% (with an average sugar content of 357 g/L, determined by results of titrimetry). Thus, the results of qNMR were found to be on average lower than the results of titrimetric analysis. The integral used for qNMR of total sugar derived from the same ^{1}H NMR spectrum that was used for quantification of ethanol. Since qNMR data of ethanol complied well with values of classical techniques for alcoholic strength, it is unlikely that the sample preparation of qNMR is responsible for the deviation between the methods in terms of total sugar content. Besides, lower results of qNMR may be due to the fact that only sucrose, fructose, and glucose were taken into account for examination, while titration involved all reducing sugars. For instance, egg liqueurs occasionally contain cream or condensed milk, and an addition of milk products implies an addition of lactose (on average 3.3 g/100 g cream or 10.2 g/100 g condensed milk[24]), which is analyzed as a reducing sugar during titrimetric analysis but not considered for qNMR. Thus, the average deviation between the methods was higher for egg liqueurs with lactose (−19 g/L; averaged by the results of nine egg liqueurs) than for egg liqueurs without lactose (−8 g/L; averaged by the results of six egg liqueurs). As the legal requirement for total sugar in egg liqueurs refers to invert sugar,[1] which is defined as the sum of sucrose, glucose, and fructose, this rather supports the approach of qNMR. Furthermore, performing classical titrimetry involved elaborate sample preparation as well as imprecise end points of titration, which can cause measurement errors and possibly resulted in deviations from qNMR data. The Bland−Altman plot demonstrates that the deviations between the methods tended to grow with increasing concentration (Figure 4). As titration of sugars was performed by means of a back-titration, high sugar concentrations resulted in small needs of titrant, which in turn means that the measurement error potentially increased with growing content of total sugar. This represents a possible explanation for the dependencies of deviations between the methods and the concentration range of total sugar. By all means, the aim of analyzing the total sugar content is simply to ensure that the minimum of 150 g/L[1] is exceeded. For this purpose qNMR is definitely suitable, especially as the absolute mean deviation between qNMR and classical analysis amounted to only −5 ± 10 g/L for egg liqueurs with sugar contents of less than 350 g/L.

The absolute mean deviation between qNMR and enzymatic analysis of cholesterol amounted to −0.2 ± 0.1 g/L, and the relative mean deviation to −9.7 ± 4.2% (with an average cholesterol content of 2.3 g/L, determined by results of enzymatic analysis), showing on average lower values for qNMR than for enzymatic investigations. As the Bland−Altman plot demonstrates (Figure 4), the deviations between the methods were independent from the measuring range. An overestimation of enzymatic results due to insufficient specificity of cholesterol oxidase[25] is unlikely, since egg liqueurs do not contain vegetable oils and structurally similar sterols are potentially also included in qNMR results. Comparing the sample preparations for both techniques, enzymatic determination is in general more elaborate and consequently more prone to errors than qNMR. However, since no factual data on cholesterol contents were available for the analyzed liqueurs, the reason for the observed deviations cannot be identified with certainty. Similar to the legislative background for total sugar, the purpose of cholesterol quantification is to control the egg yolk content with respect to the given minimum of 140 g/L[1] (1.75 g/L cholesterol, respectively, on the assumption of 12.5 mg/g cholesterol in egg yolk).[10] As a screening method for this, qNMR achieved absolutely appropriate results. In addition, since the deviation between enzymatic determination and qNMR was systematic, correction factors can be applied to adjust qNMR values to respective data of enzymatic analysis by use of the linear correlation between the methods' results ($\text{cholesterol}_{\text{qNMR}}(\text{g/L}) = 0.978\text{cholesterol}_{\text{enzymatic analysis}}(\text{g/L}) - 0.176$ g/L).

Taking the results together, the comparison of qNMR and classical data confirms NMR spectroscopy to be a suitable method to verify the accordance of egg liqueurs with the given legal limits. qNMR can be used as a screening tool, and in case of suspicious results the respective samples undergo additional analysis by reference methods. This enables risk-oriented sample management and high sample throughputs due to rapid determinations by qNMR. For the future, final assessment of the qNMR method should be achieved by analyzing egg liqueurs with a known alcoholic strength and known total sugar and cholesterol contents, for instance by participating in interlaboratory ring tests.

^{1}H NMR Spectrsocopic Fingerprint of the Basic Egg Liqueur Composition. Aside from the opportunity to use qNMR as a powerful innovative and economic analytical tool for simultaneous quantitative analysis of several components, ^{1}H NMR also provides further comprehensive information on egg liqueur composition, since each spectrum provides a fingerprint of all organic components.

For instance, a signal of phosphatidylcholine ($\delta \approx 3.20$ ppm, s, 9, choline-N($C\underline{H}_3$)$_3$; assignment according to the SDBS spectral database[13]) was detected in the ^{1}H NMR spectra after extraction with MeOH-d_4/$CDCl_3$, which is performed during cholesterol analysis (Figure 3). It is often claimed that the natural deviation of cholesterol in egg yolk is very high[5] (for instance due to breed[26] and age of hens[27]), and its validity as an indicator of the content of egg yolk is accordingly low. Thus, simultaneous analysis of phosphatidylcholine as a second marker substance of egg yolk ensures the results for the egg yolk content via cholesterol. As the chemical shift of this signal depends on the concentration level of phosphatidylcholine, integration ranges were adapted at 3 Hz to the left and right sides of the signal top for each spectrum. A comparison of the signal integrals for cholesterol (chol) and phosphatidylcholine (PC) showed a very high correlation with $R = 0.991$ ($p < 0.001$). The ratio of the integrals ($\text{signal area}_{\text{PC}}/\text{signal area}_{\text{chol}}$) averaged a value of 8.94 ± 0.78. Hence, it can serve as a value for the plausibility of the calculated egg yolk content by cholesterol quantification.

Additionally, a significant signal of lactose ($\delta \approx 4.46$ ppm; d, 1, C1$\underline{H}$; assignment according to the Bruker BBIOREFCODE database[28]) in the ^{1}H NMR spectrum after Carrez precipitation (Figure 2) as well as a characteristic signal of butyric acid ($\delta \approx 0.97$ ppm; t, 3, C4$\underline{H}_3$; assignment according to the SDBS spectral database[13]) in the ^{1}H NMR spectrum after extraction with MeOH-d_4/$CDCl_3$ (Figure 3) indicated an addition of milk products that has to be labeled to inform lactose-intolerant consumers.[2] The qualification of lactose or butyric acid by ^{1}H NMR spectroscopy compensates for an additional classical

DOI: 10.1021/acs.jafc.5b00940
J. Agric. Food Chem. 2015, 63, 4112−4119

analysis of lactose (e.g., by enzymatic analysis), to determine if milk products were added despite missing labeling.

Finally, ^{1}H NMR spectra generally indicate striking deviations from the typical composition of egg liqueurs. The example of melamine in milk powder[29] clearly demonstrated that it is of advantage to use analytical methods that also detect unsuspected adulterations. Thus, an increased use of methods such as qNMR (with nonselective detection and wide information) is beneficial for improved consumer protection.

AUTHOR INFORMATION

Corresponding Author

*Phone: +49 9131 68087159. Fax: +49 9131 68087210. E-mail: monika.hohmann@lgl.bayern.de.

Funding

This research was funded by the Bavarian State Ministry of the Environment and Consumer Protection.

Notes

The authors declare no competing financial interest.

ACKNOWLEDGMENTS

Special thanks are given to Carolin Psotta for performing classical analysis of egg liqueurs.

REFERENCES

(1) Regulation (EC) No. 110/2008 of the European Parliament and of the Council of 15 January 2008 on the definition, description, presentation, labelling and the protection of geographical indications of spirit drinks and repealing Council Regulation (EEC) No. 1576/89.

(2) Regulation (EU) No. 1169/2011 of the European Parliament and the Council of of 25 October 2011 on the provision of food information to consumers, amending Regulations (EC) No. 1924/2006 and (EC) No. 1925/2006 of the European Parliament and of the Council, and repealing Commission Directive 87/250/EEC, Council Directive 90/496/EEC, Commission Directive 1999/10/EC, Directive 2000/13/EC of the European Parliament and of the Council, Commission Directives 2002/67/EC and 2008/5/EC and Commission Regulation (EC) No. 608/2004.

(3) Commission Regulation (EC) No. 2870/2000 of 19 December 2000 laying down Community reference methods for the analysis of spirits drinks.

(4) Matissek, R.; Steiner, G.; Fischer, M. Kohlenhydrate. In *Lebensmittelanalytik*, 5th ed., Springer Verlag: Berlin, Germany, 2014.

(5) Čižková, H.; Voldřich, M.; Prokorátová, V.; Kvasnička, F. Determination of egg yolk content in egg liqueurs. *Czech J. Food Sci.* **2004**, *22*, 9−15.

(6) Bestimmung des Cholesteringehaltes in Eiern und Eiprodukten; Enzymatisches Verfahren (L 05.00-17). In *Amtl. Sammlung § 64 LFGB*; Beuth Verlag: Berlin, Germany, 1992.

(7) Brereton, P.; Hasnip, S.; Bertrand, A.; Wittkowski, R.; Guillou, C. Analytical methods for the determination of spirit drinks. *TrAC-Trends Analyt. Chem.* **2003**, *22*, 19−25.

(8) Pressi, G.; Curioni, A.; Peruffo, A. D. B.; Furegon, L.; Zamorani, A. Determination of egg content in egg pasta by an indirect ELISA procedure. *J. Sci. Food Agric.* **1994**, *64*, 163−169.

(9) Sajdok, J.; Rauch, P.; Paluska, E.; Káš, J. Determination of egg and egg white content of food products by means of immunochemical assessment of ovalbumin. *J. Sci. Food Agric.* **1990**, *53*, 253−259.

(10) Bauer-Christoph, C.; Christoph, N.; Rupp, M.; Schäfer, N. In *Spirituosenanalytik*, 1st ed.; Behr's Verlag: Hamburg, Germany, 2009.

(11) Ashurst, P. R.; Dennis, M. J. Enzymatic methods of food analysis. In *Analytical Methods of Food Authentication*, 1st ed.; Thomson Science: London, UK, 1998; p 149.

(12) Lachenmeier, D. W.; Burri, P. A.; Fauser, T.; Frank, W.; Walch, S. G. Rapid determination of alcoholic strength of egg liqueur using steam distillation and oscillation-type densimetry with peristaltic pumping. *Anal. Chim. Acta* **2005**, *537*, 377−384.

(13) Yamaji, T.; Saito, T.; Hayamizu, K.; Yanagisawa, M.; Yamamoto, O. SDBS - Spectral database for organic compounds. http://sdbs.db.aist.go.jp/sdbs/cgi-bin/cre_index.cgi (as from 09.02.2015).

(14) Barclaya, T.; Ginic-Markovica, M.; Johnstona, M. R.; Cooperb, P.; Petrovsky, N. Observation of the keto tautomer of D-fructose in D_2O using ^{1}H NMR spectroscopy. *Carbohydr. Res.* **2012**, *347*, 136−141.

(15) Cazor, A.; Deborde, C.; Moing, A.; Rolin, D.; This, H. Sucrose, glucose, and fructose extraction in aqueous carrot root extracts prepared at different temperatures by means of direct NMR measurements. *J. Agric. Food Chem.* **2006**, *54*, 4681−4686.

(16) DIN 32645: *Chemische Analytik: Nachweis-, Erfassungs- und Bestimmungsgrenze, Ermittlung unter Wiederholbedingungen. Begriffe, Verfahren, Auswertung*; Beuth-Verlag: Berlin, Germany, 2008.

(17) King, B. Metrology in chemistry: Part II. Future requirements in Europe. *Accredit. Qual. Assur.* **2000**, *5*, 266−271.

(18) Holzgrabe, U.; Deubner, R.; Schollmayer, C.; Waibel, B. Quantitative NMR spectroscopy - Applications in drug analysis. *J. Pharm. Biomed. Anal.* **2005**, *38*, 806−812.

(19) Holzgrabe, U. Quantitative NMR spectroscopy in pharmaceutical applications. *Prog. Nucl. Magn. Reson. Spectrosc.* **2010**, *57*, 229−240.

(20) Wider, G.; Dreier, L. Measuring protein concentrations by NMR spectroscopy. *J. Am. Chem. Soc.* **2006**, *128*, 2571−2576.

(21) Hoult, D. I.; Richards, R. E. The signal-to-noise ratio of the nuclear magnetic resonance experiment. *J. Magn. Reson.* **1976**, *24*, 71−85.

(22) Bland, J. M.; Altman, D. G. Statistical methods for assessing agreement between two methods of clinical measurement. *Lancet* **1986**, *1*, 307−10.

(23) Grouven, U.; Bender, R.; Ziegler, A.; Lange, S. Vergleich von messmethoden. *Dtsche. Med. Wochenschr.* **2007**, *132*, e69−e73.

(24) Souci, W.; Fachmann, W.; Kraut, H. In *Food Composition and Nutrition Tables*, 6th ed.; Medpharm Scientific Publishers Verlag: Stuttgart, Germany, 2000.

(25) Ulberth, F.; Reich, H. Gas-chromatographic determination of cholesterol in processed foods. *Food Chem.* **1992**, *43*, 387−391.

(26) Maurice, D. V.; Lightsey, S. F.; Hsu, K. T.; Gaylord, T. G.; Reddy, R. V. Cholesterol in eggs from different species of poultry determined by capillary GLC. *Food Chem.* **1994**, *50*, 367−372.

(27) Yang, P. K.; Tian, Y. D.; Sun, G. R.; Jiang, R. R.; Han, R. L.; Kang, X. T. Deposition rule of yolk cholesterol in two different breeds of laying hens. *Genet. Mol. Res.* **2013**, *12*, 5786−5792.

(28) BBIOREFCODE Database, pH3 Basic; Bruker BioSpin, Rheinstetten, Germany.

(29) Lachenmeier, D. W.; Humpfer, E.; Fang, F.; Schütz, B.; Dvortsak, P.; Sproll, C.; Spraul, M. NMR-spectroscopy for nontargeted screening and simultaneous quantification of health-relevant compounds in foods: the example of melamine. *J. Agric. Food Chem.* **2009**, *57*, 7194−7199.

DOI: 10.1021/acs.jafc.5b00940
J. Agric. Food Chem. 2015, 63, 4112−4119

Therefore, the present study has focused on the profile and content of bioactive lipophilic (carotenoids, phytosterols, fatty acids) and hydrophilic compounds (L-ascorbic acid, polyphenols) in chosen cultivated berries of *Hippophaë rhamnoides* subsp. *mongolica*.

MATERIALS AND METHODS

Reagents and Chemicals. Quercetin glycosides (3-*O*-glucoside, 3-*O*-galactoside, 3-*O*-rhamnoside, 3-*O*- rutinoside), kaempferol glycosides (3-*O*-glucoside, 3-*O*- rutinoside), isorhamnetin glycosides (3-*O*-glucoside, 3-*O*-rutinoside), *p*-coumaric acid, (+)-catechin, (−)-epicatechin, and procyanidins B1 and B2 were purchased from Extrasynthese (Lyon Nord, France). Acetic acid, phloroglucinol, methanol, sterol standards, and Sylon BTZ were purchased from Sigma-Aldrich (Steinheim, Germany, and St. Louis, MO, USA). Acetonitrile for UPLC (gradient grade) and ascorbic acid were from Merck (Darmstadt, Germany). UPLC grade water, prepared by using an HLP SMART 1000s system (Hydrolab, Gdańsk, Poland), was additionally filtered through a 0.22 μm membrane filter immediately before use.

Plant Material and Atmospheric Conditions in Harvesting Season. Ripe berries of eight Russian sea buckthorn (*H. rhamnoides* subsp. *mongolica*) cultivars (cv.), 'Aromatnaja', 'Avgustinka', 'Botaniczeskaja', 'Botaniczeskaja Ljubitelskaja', 'Luczistaja', 'Moskwiczanka', 'Podarok Sadu', and 'Porożrachnaja', were collected from the Institute of Horticulture in Skierniewice, Lodz province, Poland (51.59° N, 20.139° E) in September 2011. Manual harvesting fruits were picked, rinsed, and stored at −20 °C until analysis.

According to data from the meteorological station in Lodz, the average temperature in 2011 was 9 °C with total annual precipitation of 483 mm, insolation of 1966 h, and 5.1 octants of average cloudiness.

Lipophilic Compounds Analysis. Determination of Total Carotenoids Content. The content of total carotenoids in fruits was determined according to the spectrophotometric method described in Polish Standard (PN-90/A-75101/12: *Fruits and vegetables preserves. Preparation of samples and physicochemical test methods. Determination of total carotenoids and β-carotene)*.[10] All samples were analyzed in triplicate. Results were expressed in milligrams per 100 g of fresh weight (fw).

Sample Preparation of Phytosterols and Fatty Acids Content Analysis. Whole fruit pulp (±20 g) was quenched with 100 mL of a chloroform and methanol mixture (2:1) with the addition of BHT (0.1%), shaken in a separating funnel for 10 min, and allowed to separate. After phase separation, the extraction mixture was three times shaken in a separatory funnel with the addition of water. The chloroform layer was collected, centrifuged for 10 min at 15000*g* (MPW-380R, MPW Med. Instruments, Warszawa, Poland), and filtered through anhydrous sulfate(VI). The extracts were concentrated on a rotary evaporator (Rotavapor R-215, Büchi, Flawil, Switzerland) to 50% of the original volume.

Phytosterols Content Analysis. Sterol content and composition were determined according to AOCS Ch 6-91.[11] Fifty milligrams of extract (the procedure described above) with 100 g of 5-cholestanol as an internal standard were saponified with 2 mL of 1 mol of KOH in methanol, mixed, and placed for 18 h in the dark. Then 2 mL of distilled water and 5 mL of methyl *tert*-butyl ether (MTBE)/hexane (1:1, v/v) were added to extract the nonsaponifiable phase. The upper layer was transferred to a test tube, and the residue was washed twice by the addition of 3 and 2 mL of a mixture of MTBE/hexane. The solvent collected in the tube was evaporated to dryness under a nitrogen stream. Sterols were silylated with Sylon BTZ reagent for 4 h at 20 °C.

Chromatographic separation was performed on a Hewlett-Packard 6890 equipped with flame ionization detector (FID) and a capillary column DB-35 ms, 30 mm × 0.25 mm × 0.25 μm, in 30 min. The analysis was carried out without a split, and the temperature at the time of separation was programmed. In the initial phase (5 min) the temperature was 100 °C and then increased at 25 °C/min to 250 °C, which was maintained for 1 min and then increased at 3 °C/min to 290 °C. The temperature in the injection system and detector was 300 °C. All samples were analyzed in triplicate. Results were expressed in micrograms of phytosterols per 100 mL of lipid extract.

Determination of Fatty Acid Composition. Methyl esters of fatty acids (FAME) were prepared according to AOCS Method Ce 1k-07.[12] Diluted FAME were separated on a HP 5980 series II (Hewlett-Packard, Palo Alto, CA, USA) equipped with an Innowax capillary column (30 m × 0.20 mm × 0.20 μm) and flame ionization detector (FID). Hydrogen was used as the carrier gas at flow rate of 1.5 mL/min. The column temperature was programmed from 60 to 200 °C at 12 °C/min, and the final temperature was held for 25 min. Detector and injector temperatures were set at 250 °C. Fatty acids were identified by comparison of the retention times with authentic standards, and the results were reported as weight percentages after integration and calculation using ChemStation (Agilent Technologies). All samples were analyzed in triplicate. Results were expressed in percent.

Hydrophilic Compounds Analysis. Analysis of L-Ascorbic Acid Content. L-Ascorbic acid content analysis was based on the method previously described by Oszmiański and Wojdyło.[13] Seedless berries (ca. 5 g) were mixed with 50 mL of 0.1 M phosphoric acid and centrifuged at 14000*g* for 10 min at 4 °C. The estimation of L-ascorbic acid was carried out on the Waters liquid chromatograph with a tunable absorbance detector (Waters 486) and a quaternary pump with a Waters 600 Controller apparatus (Waters Associates). A 20 μL sample was injected into a Chromolith Performance RP-18e column (100 mm × 9 mm × 4.6 mm) (Merck). The elution was carried out using 0.1 M phosphoric acid, and the flow rate was 1 mL/ min. The absorbance was monitored at 254 nm. L-Ascorbic acid was identified by comparison with the standard. The calibration curve was prepared by plotting different concentrations of the standard versus the area measurements in HPLC. All samples were analyzed in triplicate. Results were expressed in milligrams per 100 g of fw of fruits.

Sample Preparation for Polyphenols Content Analysis. Extracts were prepared by mixing of 2 g of berries, 10 mL of HPLC grade methanol (30 mL/100 mL) with ascorbic acid (2 g/100 mL) and acetic acid (1 mL/100 mL), and 10 mL of hexane. Samples were sonicated for 15 min (Sonic 6D Polsonic, Warszawa, Poland), placed for 24 h at 4 °C, sonicated again for 15 min, and centrifuged (MPW-380R, MPW Med. Instruments, Warszawa, Poland) for 10 min (20000*g* at 4 °C). The hexane layer was removed. The methanol layer was purified with Merck Samplicity Filtration System (Merck Millipore, Ireland) and collected in 10 mL PE vials.

Determination of Polyphenols by UPLC Coupled to PDA and FL Detector. Conditions of quantitative polyphenols determination were previously described by Wojdyło et al.[14] Analysis was carried out on a UPLC system Acquity (Waters Corp., Milford, MA, USA) with a binary solvent manager, sample manager, PDA, and fluorescence detector (FL) (model λe). For chromatographic data collection and chromatograms integration Empower 3 software was used. The UPLC analyses were performed on a BEH Shield C18 analytical column (2.1 mm × 50 mm × 1.7 μm). The flow rate was 0.42 mL/min. A partial loop injection mode with a needle overfill was set up, enabling 5 μL injection volumes when a 10 μL injection loop was used. Acetonitrile (100%) was used as a strong wash solvent and acetonitrile in water (10%. v/v) as a weak wash solvent. Two milliliters of fruit extracts was centrifuged for 10 min at 15000*g* at 4 °C. The analytical column was kept at 30 °C by column oven, whereas the samples were kept at 4 °C. The mobile phase was composed of solvent A (4.5% formic acid) and solvent B (acetonitrile). Elution was as follows: 0−5 min, linear gradient from 1 to 25% B; 5.0−6.5 min, linear gradient from 25 to 100%; 6.5−7.5 min, column washing; and reconditioning for 0.5 min. PDA spectra were measured over the wavelength range of 200−600 nm in steps of 2 nm. The runs were monitored at the following wavelengths: flavan-3-ols at 280 nm, hydroxycinnamates at 320 nm, and flavonol glycosides at 360 nm. Retention times (t_R) and spectra were compared with those of pure standards. Calibration curves at concentrations ranging from 0.05 to 5 mg/mL (r^2 = 0.9998) were made from (−)-epicatechin, (+)-catechin,

DOI: 10.1021/acs.jafc.5b00564
J. Agric. Food Chem. 2015, 63, 4120−4129

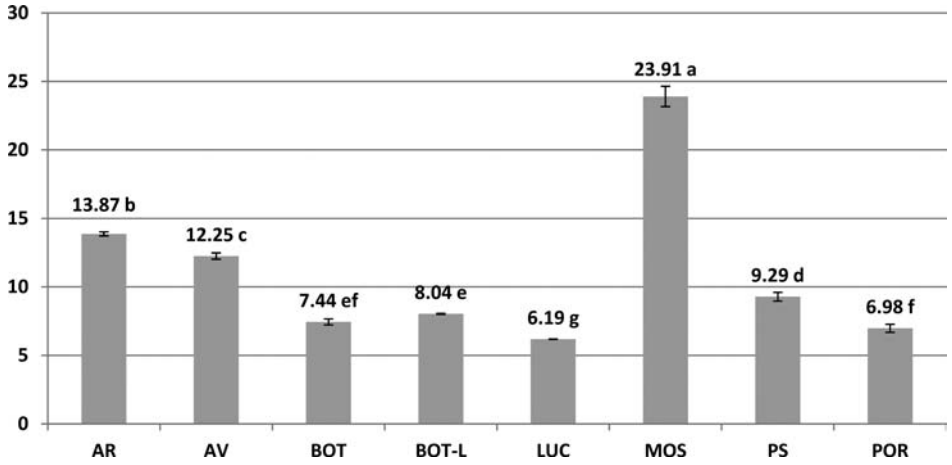

Figure 1. Total carotenoids content (mg/100 g fw) in berries of eight sea buckthorn cultivars.

procyanidin B1, *p*-coumaric acid, quercetin, isorhamnetin, and kaempferol 3-*O*-glucoside as standards.

All samples were analyzed in triplicate. Results were presented as total flavan-3-ols, hydroxycinnamates, and flavonol glycosides content and expressed in milligrams per 100 g of fw of fruits.

Analysis of Proanthocyanidins by Phloroglucinolysis. Polymeric proanthocyanidins content were determined in freeze-dried sea buckthorn berries (Alpha 1-4 LSC; Martin Christ GmbH, Osterode am Harz, Germany) according to a method described by Wojdyło et al.[14] Parameters of freeze-drying process were as follows: 18 h (time), 0.960 mbar (vacuum), 26 °C (shelf temperature). A 0.5 g portion of lyophilized seedless fruits was placed into 2 mL Eppendorf vials and mixed with 0.8 mL of methanolic solution containing phloroglucinol (75 g/L) and ascorbic acid (15 g/L) and then with 0.4 mL of methanol with HCl addition in a dose of 0.3 mol/L. The vials with reaction mixture were closed and incubated for 30 min at 50 °C with all time-vortexing by thermo shaker (TS-100, Biosan, Riga, Latvia). The reaction was stopped by placing the vials in an ice bath; 0.5 mL of the reaction medium was withdrawn and diluted with 0.5 mL of 0.2 mol/L sodium acetate buffer. Next the vials were cooled in ice water and centrifuged immediately at 20000*g* for 10 min at 4 °C. The temperatures in the column oven and sample manager were 15 and 4 °C, respectively. The mobile phase was composed of solvent A (2.5% acetic acid) and solvent B (acetonitrile). Elution was as follows: 0−0.6 min, isocratic 2% B; 0.6−2.17 min, linear gradient from 2 to 3% B; 2.17− 3.22 min, linear gradient from 3 to 10% B; 3.22−5.00 min, linear gradient from 10 to 15% B; 5.00−6.00 min, column washing and reconditioning for 1.50 min. The fluorescence detection was recorded at an excitation wavelength of 278 nm and an emission wavelength of 360 nm. The calibration curves, which were based on peak area, were established using (+)-catechin, (−)-epicatechin, and procyanidin B1 after phloroglucinol reaction as (+)-catechin and (−)-epicatechin-phloroglucinol adduct standards. The results were calculated as milligrams per 100 g of fw of fruits.

Identification of Polyphenols by the Ultraperformance Liquid Chromatography−Mass Spectrometry (UPLC-MS) Method. The method was previously described by Wojdyło et al.[14] Half a gram of freeze-dried powdered fruit (parameters of freeze-drying process described in the previous section) was extracted twice with 15 mL of 80% acetone acidified with 1% acetic acid. The extracts were sonicated for 15 min, centrifuged at 19000*g* for 10 min at 4 °C, and concentrated on a vacuum rotary evaporator to a volume of ca. 3 mL. The samples were applied to the Sep-Pak C18 cartridge (Waters, Milford, MA, USA) containing 1 g of the carrier, washed with distilled water to remove the sugar and organic acid (extract = 0 °Brix), and then collected into a vacuum flask with 15 mL of 80% methanol acidified with 1% HCl. The methanol extract was evaporated to dryness. The dry residue was dissolved in 4 mL of 4.5% formic acid, centrifuged for 5 min at 15000*g*, and then given to the analysis. Identification of sea buckthorn polyphenols was carried out using an ACQUITY Ultra Performance LC system (UPLC) with binary solvent manager (Waters, Milford, MA, USA) and a Micromass Q-Tof Micro mass spectrometer (Waters, Manchester, UK) equipped with an electrospray ionization (ESI) source operating in negative mode. For instrument control data acquisition and processing MassLynxTM software (version 4.1) was used. Separations of individual polyphenols were carried out using a UPLC BEH C18 column (1.7 μm, 2.1 mm × 50 mm; Waters, Milford, MA, USA) at 30 °C. Samples (10 μL) were injected and elution completed in 12 min with a sequence of linear gradients and isocratic flow rates of 0.45 mL/min. The mobile phase was composed of solvent A (0.1 mL/100 mL formic acid, v/v) and solvent B (100 mL/100 mL of acetonitrile). The program began with isocratic elution with 99% A (0−1 min), and then a linear gradient was used for 12 min, lowering A to 0%; from 12.5 to 13.5 min, the gradient returned to the initial composition (99% A) and then was held constant to reequilibrate the column. Analysis was carried out using full scan, data-dependent MS scanning from m/z 100 to 1000. The effluent was led directly to an electrospray source with a source block temperature of 130 °C, desolvation temperature of 350 °C, capillary voltage of 2.5 kV, and cone voltage of 30 V. Nitrogen was used as a desolvation gas at flow rate of 300 L/h.

Statistical Analysis. Statistical analysis (variance test and standard deviation values) was made using Statistica 10.0 (StatSoft, Kraków, Poland). Significant differences ($p \leq 0.05$) between means were evaluated by one-way ANOVA and Duncan's multiple-range test.

RESULTS AND DISCUSSION

Analysis of Lipophilic Bioactive Compounds. Total Carotenoids Content. In raw material total carotenoids (Figure 1), phytosterols, and fatty acids content (Tables 1 and 2) were examined.

The sea buckthorn fruits were characterized by a high concentration of carotenoids, 11.00 mg/100 g fw (mean value). The content of these compounds in berries was significantly correlated with cultivar and ranged from 6.19 to 23.91 mg/100 g fw (in 'Luczistaja' and 'Moskwiczanka', respectively). Similar values in nine cultivars of sea buckthorn were noted by Kruczek et al.[15] (from 8.85 in 'Botaniczeskaja Ljubitelskaja' to 43.06 mg/100 g fw in 'Botaniczeskaja'). It also should be emphasized that the content of these compounds in examined sea buckthorn fruits was comparable to that determined by Müller[16] in tomatoes, young carrots, and red peppers (12.69, 9.46, and 30.37 mg/100 g of edible part, respectively).

Carotenoids are located mainly in the soft parts of the fruit, giving them a characteristic orange-yellow color. In sea buckthorn berries 15−55% of all compounds of this group is β-carotene. In lower concentrations are also α-, γ-, and

DOI: 10.1021/acs.jafc.5b00564
J. Agric. Food Chem. 2015, 63, 4120−4129

Table 1. Phytosterols Content (Micrograms per 100 mL of Lipid Fraction) and Profile of Sea Buckthorn Berries

	cultivars[a]							
	AR	AV	BOT	BOT-L	LUC	MOS	PS	POR
squalene	1638.27 ± 25.97 c	1205.43 ± 0.60 e	2714.37 ± 7.72 a	1872.42 ± 106.12 b	885.71 ± 29.16 g	1110.10 ± 37.95ef	1516.27 ± 11.82 d	1026.05 ± 0.92 f
kampesterol	167.10 ± 1.25 b	139.22 ± 1.62 c	201.32 ± 12.67 a	95.71 ± 11.57 e	82.79 ± 2.63 e	44.37 ± 2.14 f	118.79 ± 1.39 d	127.68 ± 1.81 cd
stigmasterol	nd[b]	68.22 ± 2.03 a	nd	nd	nd	24.08 ± 0.06 b	nd	nd
β-sitosterol	6145.58 ± 41.11 a	4942.39 ± 4.91 b	3801.64 ± 10.69 f	4022.29 ± 47.14 e	2049.46 ± 32.23 g	2036.14 ± 59.47 g	4216.62 ± 20.01 d	4409.03 ± 14.80 c
sitostanol	217.29 ± 1.01 b	172.64 ± 4.31 c	217.80 ± 1.57 b	110.69 ± 1.19 e	97.77 ± 0.80 f	96.50 ± 0.94 f	254.67 ± 13.63 a	150.00 ± 0.90 d
Δ^5-avenasterol	274.08 ± 4.20 b	251.19 ± 4.05 c	377.56 ± 5.46 a	197.21 ± 1.64 d	198.22 ± 1.88 d	114.93 ± 1.27 e	249.42 ± 2.59 c	243.80 ± 0.31 c
α-amyrin	314.52 ± 2.82 a	110.48 ± 0.15 f	302.63 ± 13.83 a	130.68 ± 2.11 e	166.92 ± 4.82 d	112.86 ± 2.68 f	203.24 ± 5.52 c	228.35 ± 0.91 b
cycloartenol	441.78 ± 8.24 b	399.89 ± 10.50 c	462.48 ± 14.82 a	439.14 ± 5.54 b	299.14 ± 7.07 e	293.49 ± 3.12 e	474.38 ± 1.18a	360.94 ± 1.34 d
Δ^7-avenasterol	156.55 ± 0.65c	152.02 ± 3.63 cd	154.63 ± 1.62c	138.21 ± 0.53 e	147.61 ± 2.52 d	80.80 ± 0.08 f	186.73 ± 2.39 b	194.97 ± 1.01 a
28-methylobtusifoliol	249.39 ± 0.03 a	130.10 ± 3.94 d	251.85 ± 4.48 a	145.72 ± 1.56 c	152.03 ± 0.23 b	70.88 ± 1.40 f	89.96 ± 1.01 e	153.20 ± 0.72b
24-methylenecycloartanol	1554.42 ± 6.26f	4048.89 ± 87.92 a	2711.93 ± 36.19 c	2521.94 ± 14.64 d	1994.54 ± 19.38 e	1454.21 ± 10.62 g	3131.95 ± 3.58 b	2661.63 ± 32.09 c
erythrodiol	818.75 ± 2.61 a	680.91 ± 7.64 b	590.29 ± 2.88 c	367.19 ± 9.16 f	338.58 ± 2.33 g	284.02 ± 1.59 h	444.38 ± 1.55 d	407.97 ± 0.62 e
citrostadienol	663.22 ± 1.35 a	327.09 ± 8.61 d	417.42 ± 1.56 c	309.23 ± 4.35 e	244.82 ± 2.24 g	212.97 ± 6.52 h	444.95 ± 10.82 b	269.61 ± 1.39 f
friedelan-3-ol	737.28 ± 3.28 a	583.76 ± 2.16 c	606.44 ± 8.35 b	398.64 ± 6.30 d	257.16 ± 6.94 f	232.89 ± 3.42 g	260.73 ± 1.74 f	320.01 ± 1.77 e
total	13378.22 ± 61.82	13212.23 ± 89.29	12810.36 ± 40.90	10749.06 ± 16.55	6914.75 ± 10.64	6168.24 ± 9.04	11592.07 ± 12.96	10553.23 ± 11.76

[a]AR, 'Aromatnaja'; AV, 'Avgustinka'; BOT, 'Botaniczeskaja'; BOT-L, 'Botaniczeskaja Ljubitelskaja'; LUC, 'Luczistaja'; MOS, 'Moskwiczanka'; PS, 'Podarok Sadu'; POR, 'Porożrachnaja'. Entries followed by the same lower case letter constitute statistically homogeneous groups (Duncan test, $p \leq 0.05$). Values are expressed as the mean ± standard deviation ($n = 3$). [b]nd, not detected.

DOI: 10.1021/acs.jafc.5b00564
J. Agric. Food Chem. 2015, 63, 4120−4129

Table 2. Fatty Acids Content (Percent) and Profile in Lipid Fraction from Sea Buckthorn Berries

	cultivars[a]							
	AR	AV	BOT	BOT-L	LUC	MOS	PS	POR
C14:0 (myristic)	0.36 ± 0.00	0.24 ± 0.01	0.17 ± 0.00	0.36 ± 0.00	0.64 ± 0.01	0.29 ± 0.01	0.36 ± 0.01	0.18 ± 0.01
C16:0 (palmitic)	37.87 ± 0.03	34.47 ± 0.01	37.83 ± 0.02	38.25 ± 0.11	35.62 ± 0.17	37.62 ± 0.03	33.66 ± 0.01	39.65 ± 0.06
C16:1 n-7 (palmitoleic)	33.83 ± 0.11	38.01 ± 0.02	34.21 ± 0.08	34.54 ± 0.06	38.51 ± 0.11	36.03 ± 0.11	31.41 ± 0.17	32.98 ± 0.08
C16:2 n-7 (hexadecadienoic)	0.54 ± 0.00	0.51 ± 0.01	0.47 ± 0.01	0.81 ± 0.01	1.01 ± 0.01	0.63 ± 0.01	0.58 ± 0.00	0.50 ± 0.01
C18:0 (stearic)	0.91 ± 0.01	1.04 ± 0.02	1.04 ± 0.02	0.97 ± 0.01	0.64 ± 0.01	0.79 ± 0.01	0.85 ± 0.01	1.09 ± 0.01
C18:1 n-9 (oleic)	7.05 ± 0.01	6.67 ± 0.02	8.02 ± 0.04	5.25 ± 0.01	4.26 ± 0.02	6.27 ± 0.04	7.89 ± 0.01	7.82 ± 0.01
C18:1 n-7 (*cis*-vaccenic)	6.90 ± 0.01	7.92 ± 0.01	7.40 ± 0.01	6.66 ± 0.02	6.94 ± 0.01	7.11 ± 0.03	9.79 ± 0.01	7.33 ± 0.03
C18:2 n-6 (linoleic)	11.31 ± 0.02	10.32 ± 0.01	9.93 ± 0.04	12.20 ± 0.04	11.51 ± 0.06	10.29 ± 0.02	14.11 ± 0.04	9.69 ± 0.02
C18:3 n-3 (linolenic)	0.78 ± 0.00	0.52 ± 0.01	0.66 ± 0.00	0.69 ± 0.01	0.65 ± 0.01	0.69 ± 0.00	0.93 ± 0.01	0.58 ± 0.01
C20:0 (arachidic)	0.17 ± 0.01	0.14 ± 0.01	0.17 ± 0.00	0.17 ± 0.00	0.14 ± 0.01	0.16 ± 0.00	0.19 ± 0.01	0.13 ± 0.01
C20:1 n-9 (eicosenoic)	0.05 ± 0.00	0.04 ± 0.00	0.06 ± 0.01	0.05 ± 0.00	0.04 ± 0.00	0.06 ± 0.00	0.06 ± 0.01	0.04 ± 0.01
∑SFAs	39.31 ± 0.12 b	35.88 ± 0.04 b	39.21 ± 0.13 b	39.75 ± 0.01 b	37.03 ± 0.06 b	38.85 ± 0.03 b	35.05 ± 0.04 b	41.05 ± 0.05 b
∑MUFAs	47.82 ± 0.06 a	52.63 ± 0.10 a	49.68 ± 0.14 a	46.50 ± 0.04 a	49.75 ± 0.05 a	49.47 ± 0.16 a	49.14 ± 0.01 a	48.16 ± 0.11 a
∑PUFAs	12.62 ± 0.05 c	11.35 ± 0.40 c	11.06 ± 0.06 c	13.69 ± 0.03 c	13.16 ± 0.01 c	11.60 ± 0.03 c	15.61 ± 0.00 c	10.77 ± 0.02 c

[a]AR, 'Aromatnaja'; AV, 'Avgustinka'; BOT, 'Botaniczeskaja'; BOT-L, 'Botaniczeskaja Ljubitelskaja'; LUC, 'Luczistaja'; MOS, 'Moskwiczanka'; PS, 'Podarok Sadu'; POR, 'Porożrachnaja'. SFAs, saturated fatty acids; MUFAs, monounsaturated fatty acids; PUFAs, polyunsaturated fatty acids. Entries followed by the same lower case letter constitute statistically homogeneous groups (Duncan test, $p \leq 0.05$). Values are expressed as the mean ± standard deviation ($n = 3$).

DOI: 10.1021/acs.jafc.5b00564
J. Agric. Food Chem. 2015, 63, 4120−4129

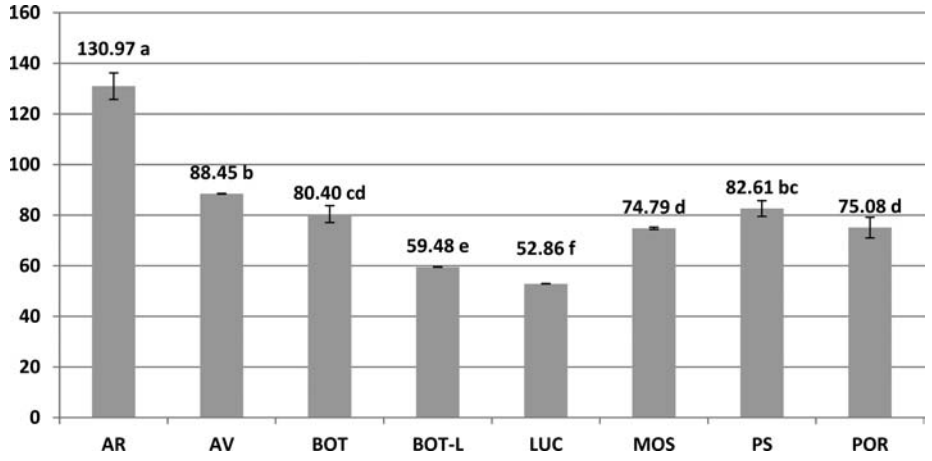

Figure 2. L-Ascorbic acid content (mg/100 g fw) in berries of eight sea buckthorn cultivars.

dihydroxy-β-carotene, lycopene, zeaxanthin, and cantha-xanthin.[17] The content of carotenoids in fruits is subject to extreme diversity. In the same population and species of the genus *Hippophaë* a 10-fold difference in the content of these components can be observed. As Yang's[18] study showed, the concentration of β-carotene ranged between 0.2 and 17 mg/100 g and that of total carotenoids from 1 to 120 mg/100 g fw of sea buckthorn berries.

Phytosterols Content. Bioactive substances of sea buckthorn include phytosterols characterized by a documented beneficial role in the prevention of cardiovascular diseases, mainly hypercholesterolemia[19,20] or cancer.[21] The results of qualitative and quantitative analyses of these compounds are presented in Table 1.

The total content of phytosterols in the lipid fraction from sea buckthorn pulp ranged from 6168.24 ('Moskwiczanka') to 13378.22 μg/100 mL ('Aromatnaja'). The results of GC analysis showed that in the examined extracts there occurred 14 compounds belonging to three subclasses of plant sterols, that is, 4-desmethyl sterols (cholestanol derivatives, including β-sitosterol, stigmasterol, campesterol, Δ^5-avenasterol), 4α-monomethyl sterols (e.g., citrostadienol), and 4,4-dimethyl sterols (e.g., 24-methylenecycloartanol). The predominant compound was β-sitosterol (26.64−42.57% of the total phytosterols in 'Luczistaja' and 'Aromatnaja', respectively). In the high concentration occurred also 24-methylenecycloartanol. This compound was determined in the range from 1454.21 to 4048.89 μg/100 mL in the lipid fraction from 'Moskwiczanka' and 'Avgustinka' berries.

Sea buckthorn can be considered as a valuable source of squalene. Depending on the cultivar, the lipid fraction isolated from berry pulp contained between 885.71 and 2714.37 μg/100 mL ('Luczistaja' and 'Botaniczeskaja'). Moreover, concentrations in a range from 300 to 800 μg of substances, such as erythrodiol > friedelan-3-ol > citrostadienol > or cycloartenol, were noted. In sea buckthorn trace amounts of stigmasterol were also detected. This compound was found only in two cultivars, 'Avgustinka' and 'Moskwiczanka', and its contents were 68.22 and 24.08 mg/100 mL ($p < 0.05$), respectively.

The results of the sterols profile analysis in sea buckthorn were confirmed by studies of other authors, such as Li et al.[22] or Cenkowski et al.[23] According to Bal et al.,[2] the major phytosterols in sea buckthorn oil are β-sitosterol and Δ^5-avenasterol. Other compounds are present in relatively minor quantities. The total quantity of phytosterol is quite high in sea buckthorn and may exceed soybean oil by 4−20 times. β-Sitosterol and β-sitosterol-β-D-glucoside in sea buckthorn oils are important for the antiulcerative activity. The efficacy of the two compounds may differ depending on the cause of ulcer formation.[24]

Fatty Acids Composition. The fatty acid (FA) compositions of sea buckthorn pulp oil are listed in Table 2. In the examined samples 11 fatty acids were identified, including 3 PUFAs, 4 MUFAs, and 4 SFAs. The FA profile was dominated by two compounds: palmitic acid (C16:0), which constituted from 33.66 to 39.65% of the total fatty acids content (in 'Podarok Sadu' and 'Porożrachnaja', respectively), and palmitoleic acid C16:1 n-7 (from 31.41% in 'Podarok Sadu' to 38.51% in 'Luczustaja'). In relatively high concentration occurred also 18-carbon unsaturated acids, that is, linoleic C18:2 n-6 (9.69−14.11% in 'Porożrachnaja' and 'Podarok Sadu', respectively), followed by *cis*-vaccenic C18:1 n-7 (6.66−9.79% in 'Botaniczeskaja Ljubitelskaja' and 'Podarok Sadu') and oleic C18:1 n-9 (4.26−8.02% in 'Luczistaja' and 'Botaniczeskaja'). Other compounds presented in concentrations between ∼0.5% in the case of eicosenoic acid (C20:1 n-9) and ∼1% for stearic acid (C18:0). From these results it can be concluded that MUFAs were the dominant fatty acid classes (46.50−52.63%), followed by SFAs (35.05−41.05%) and PUFAs (10.77−15.61%).

According to Dulf,[25] the dominating fatty acids in sea buckthorn berry pulp/peel oils were palmitic (23−40%), oleic (20−53%), and palmitoleic (11−27%). Small or trace amounts of vaccenic, linoleic, α-linolenic, stearic, myristic, pentadecanoic, *cis*-7-hexadecenoic, margaric, and two long-chain fatty acids, arachidic and eicosenoic acids, were observed in all analyzed oils. As the author showed, in two from six tested cultivars (C1 and C2), the proportions of oleic acid (32.76% for C1 and 53.08% for C2) exceeded that of palmitoleic acid (19.53% for C1 and 11.05% for C2). The fatty acid profile of sea buckthorn was presented also by Khabarovet al.[26] Oil samples from berry pulp and skin (species *H. rhamnoides*) contained the highest concentrations of palmitoleic > palmitic > and oleic acid. Our research showed that the quantified relationships between C16:1 and C16:0 acids noted by these authors occurred only in the oil fraction from 'Avgustinka' and 'Luczistaja' fruits. At the same time, a higher content of linoleic acid in all extracts was found. However, in the presented study fractions from whole berries (with skin and seeds) were examined, which could explain the observed differences. This is

DOI: 10.1021/acs.jafc.5b00564
J. Agric. Food Chem. 2015, 63, 4120−4129

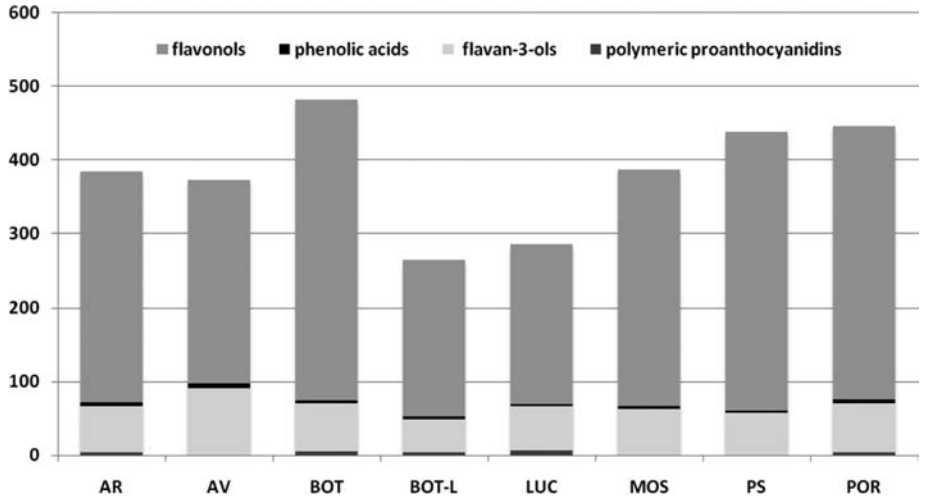

Figure 3. Polyphenols content (mg/100 g fw) and profile of sea buckthorn berries.

confirmed by George and Cenkowski.[27] They proved that three major fatty acids (palmitic, palmitoleic, oleic) accounted for approximately 32.2, 26.5, and 18.7% of the total fatty acids in the sea buckthorn fruit fraction, respectively. High levels of palmitoleic acid are present in only a few plants products, such as sea buckthorn pulp or macadamia nut oils. Because this fatty acid is a major constituent of skin fat, the pulp oil is used for cosmetic and healing purposes.[3]

Analysis of Hydrophilic Bioactive Compounds. L-Ascorbic Acid Content. Except for the lipophilic active compounds, such as carotenoids and phytosterols, sea buckthorn is also rich in hydrophilic substances known for health benefits properties, including L-ascorbic acid (Figure 2).

The mean content of ascorbic acid (AA) in the raw material was 80.58 mg/100 g. Likewise, as in the case of previously described compounds, the cultivar factor determined abundance of sea buckthorn in ascorbic acid ($p < 0.05$). The highest concentration of this compound were characterized in 'Aromatnaja' (130.97 mg/100 g fw) followed by 'Avgustinka' (88.45 mg) > 'Podarok Sadu' (82.61 mg) > 'Botaniczeskaja' (80.40 mg) > 'Moskwiczanka' and 'Porożrachnaja' (74.79 and 75.08 mg; $p > 0.05$) > 'Botaniczeskaja Ljubitelskaja' (59.48 mg) > 'Luczistaja' (52.86 mg). The presented results clearly showed that in terms of ascorbic acid content most of the examined sea buckthorn cultivars were definitely more valuable than many other popular fruit species including strawberries (65 mg/100 g fw), raspberries (29 mg), lemons (74.3 mg), mandarins (37.7 mg), or blackberry (21 mg).[28]

According to Tang,[29] the content of ascorbic acid in sea buckthorn (depending on the species, variety, region) was from 28 to 2500 mg/100 g. Berries of six cultivars examined by Rop et al.[30] contained between 398 and 573 mg AA/100 g fw (in 'Buchlovicky' and 'Ljubitelna', respectively). Kawecki et al.[31] determined the highest content of ascorbic acid in 'Trofimovskaja' (197 mg/100 g) > 'Otrodnaja' (191 mg) > 'Botaniczeskaja' (178 mg) > and 'Podarok Sadu' (161 mg). These values are therefore higher than in our study. However, the authors paid attention not only to varietal but also seasonal variation of ascorbic acid content in *H. rhamnoides* berries, which explains the observed differences.

Polyphenols Content and Profile. Interesting results were obtained indicating the content of polyphenols in sea buckthorn (Figure 3). Berries were characterized by a high concentration of flavonols (from 212.89 to 407.48 mg/100 g fw in 'Botaniczeskaja Ljubitelskaja' and 'Botaniczeskaja', respectively; $p < 0.05$). The structure of these compounds was investigated by qualitative analysis in LC-ESI/MS system performed in negative ionization mode (Table 3; Figure 4).

Table 3. LC-MS Identification of Sea Buckthorn Flavonols

no.	t_R[a] (min)	λ_{max}	$[M - H]^-$ (m/z)	MS-MS (m/z)	compound
1	5.56	352	639	315	isorhamnetin-3,7-diglucoside
2	5.90	354	785	639	isorhamnetin-3-sophoroside-7-rhamnoside
3	6.37	354	755	609	quercetin-glucoside-rhamnoside-7-rhamnoside
4	6.77	354	609	301	quercetin-3-rutinoside
5	7.33	352	609	301, 447	quercetin-3-glucoside-7-rhamnoside
6	7.51	354	771	625	quercetin-3-sophoroside-7-rhamnoside
7	7.59	355	623	315	isorhamnetin-3-rutinoside
8	8.49	348	593	285	kaempferol-3-rutinoside
9	8.78	353	623	315	isorhamnetin-3-rhamnosylglucoside
10	9.03	354	477	315	isorhamnetin-3-glucoside
11	11.28	356	869	723	isorhamnetin-3-acylo-glucoside-glucoside-7-rhamnoside

[a] t_R, retention time.

The examined sea buckthorn cultivars contained 11 flavonols, which were primarily derived of isorhamnetin (6 compounds), quercetin (4 compounds), and kaempferol (1 compound). The strongest signal in the obtained mass spectrum with a value of $[MH]^-$ at m/z 623 and a retention time of 8.78 min came from isorhamnetin-3-rhamnosylglucoside (compound **9**). The source of two successive intensity signals was compound **7** with a molecular weight $[M - H]^-$ at m/z 623 and **10** ($[MH]^-$ at m/z 477). In regard to the fragmentation direction of both compounds, that is, loss of the aglycone molecule with MS-MS (m/z) 315, UV−vis spectrum, and LC-MS standards analysis, as well as the literature data,[32] these compounds were identified as monoglycosides: isorhamnetin-3-rutinoside (compound **7**; t_R 7.59 min) and isorhamnetin-3-glucoside (compound **10**; t_R 9.03 min). Among the quercetin derivatives,

DOI: 10.1021/acs.jafc.5b00564
J. Agric. Food Chem. 2015, 63, 4120−4129

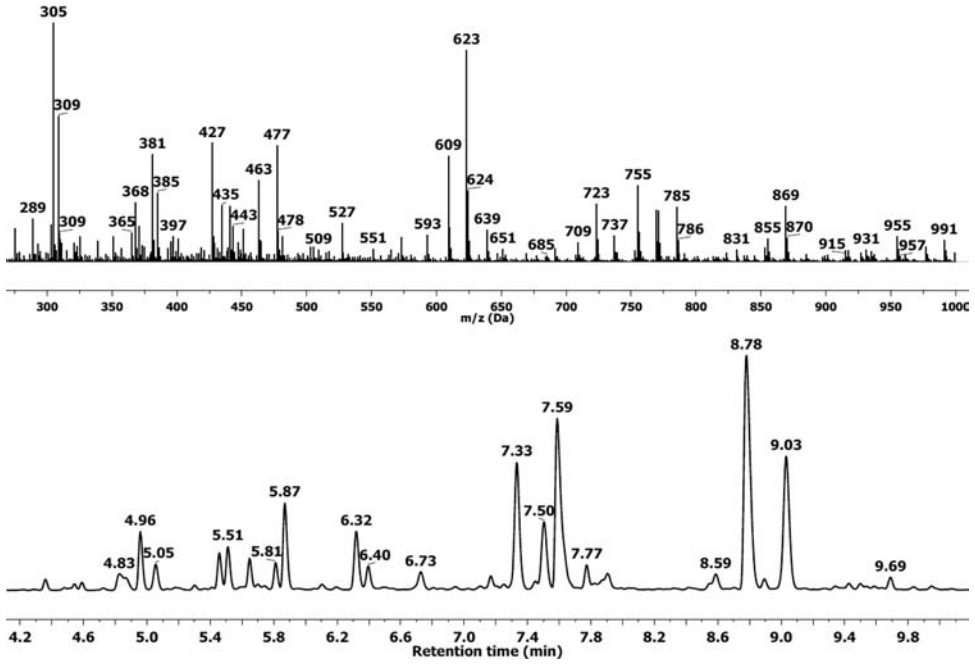

Figure 4. LC-ESI/MS spectrum and the chromatogram (360 nm) of sea buckthorn flavonols (cv. 'Porożrachnaja').

quercetin-3-glucoside-7-rhamnoside was dominant (compound **5**; $[MH]^-$ at m/z 609, t_R 7.33 min). After ion fragmentation, a strong, typical signal was registered from an ion with molecular mass MS-MS (m/z) 301. The signals from fission products of glucose ($[M - H^- 162]^-$ at m/z 447) and rhamnose ($[M - H^- 146]^-$ at m/z 463) were less abundant and characterized by a similar intensity.

According to Yang et al.[33] sea buckthorn berries of subsp. *mongolica* contain 80.6 mg flavonols/100 g fw, which is a significantly higher value than noted in chokeberry (23−40 mg/100 g fw),[34] cranberry (20−40 mg/100 g fw),[35] black currant (17−38 mg/100 g fw),[36] or bilberry (10−16 mg/100 g fw).[37,38] The results of our study also confirm this relationship;, however, in sea buckthorn we noted ca. a 4-fold higher content of flavonols.

The most common flavonols in sea buckthorn fruits are isorhamnetin derivatives with mono-, di-, and triglycoside structures.[33,39] As Pop et al.[40] research showed, in fruits and leaves of *H. rhamnoides* L. subsp. *carpatica* (cv. 'Serpenta', 'Serbanesti 4', 'Victoria', 'Sf. Gheorghe', 'Ovidiu', and 'Tiberiu') 17 and 19 flavonols occurred, respectively. Isorhamnetin-3-neohesperidoside, isorhamnetin-3-glucoside, isorhamnetin-3-rhamnosylglucoside, isorhamnetin-3-sophoroside-7-rhamnoside, and free isorhamnetin were predominant in the case of berries. In *rhamnoides* subspecies, the major compounds indicated by Kallio et al.[39] were isorhamnetin-3-sophoroside-7-rhamnoside > quercetin-3-glucoside > quercetin-3-rutinoside > isorhamnetin-3-rutinoside > isorhamnetin-3-glucoside. Chen et al.[41] isolated from the *n*-butanol fraction of sea buckthorn (subsp. *sinensis*) berries a novel acylated flavonol glycoside, isorhamnetin (3-*O*-[(6-*O*-*E*-sinapoyl)-*β*-D-glucopyranosyl-(1→2)]-*β*-D-glucopyranosyl-7-*O*-*α*-L-rhamnopyranoside), together with two known acylated flavonols glycosides, quercetin (3-*O*-[(6-*O*-*E*-sinapoyl)-*β*-D-glucopyranosyl-(1→2)]-*β*-D-glucopyranosyl-7-*O*-*α*-L-rhamnopyranoside) and kaempferol (3-*O*-[(6-*O*-*E*-sinapoyl)-*β*-D-glucopyranosyl-(1→2)]-*β*-D-glucopyranosyl-7-*O*-*α*-L-rhamnopyranoside). Due to such significant differences of sea buckthorn berries in terms of flavonol glycosides content, these compounds can be used as biomarkers for classification or recognition of sea buckthorn berries belonging to different species and varieties.[40]

Besides flavonols in sea buckthorn berries compounds belonging to three other groups of polyphenols, that is, polymeric proanthocyanidins, mono-, di-, and oligomers of flavan-3-ols, and phenolic acids, were determined. The highest contents of flavan-3-ols (88.04 mg/100 g fw) and phenolic acids (5.81 mg/100 g fw) were characterized by fruits of 'Avgustinka'. 'Luczistaja' was the richest in polymeric proanthocyanidins (5.76 mg/100 g fw), but contained the least value of phenolic acids (3.11 mg/100 g fw). Similarly to the flavonols determination, also flavan-3-ols concentration was the lowest in 'Botaniczeskaja Ljubitelskaja' (44.94 mg/100 g fw).

Compared to Hosseinian et al.[42] total proanthocyanidins content in examined samples was significantly different, especially in the case of polymeric form. In the whole fruit methanol fraction the authors noted 36.56 mg of polymeric proanthocyanidins per 100 g fw basis and 98.95 mg of mono-, di-, and oligomeric compounds. In our study a similar value of simple flavan-3-ols was determined only in 'Avgustinka' berries. This proves, however, that the content of polyphenols in plants is a result of many factors, such as cultivar, harvest year, or geographical origin. This correlation has been previously described in the literature.[43,44]

The proanthocyanidins profile in sea buckthorn is varied. According to Rösch et al.[45] the concentration of reaction products after acid-catalyzed cleavage (determined by HPLC) and calculated composition of sea buckthorn proanthocyanidins showed that major compounds were phloroglucinol adducts with (+)-gallocatechin, followed by (+)-catechin and (−)-epicatechin. The ratio between prodelphinidins (PD) and procyanidins (PC) was 2.1:1. On the basis of ESI-MS analysis, the authors detected compounds with different polymerization degrees, including pentameric, hexameric, heptameric, nonameric, and decameric proanthocyanidins.

DOI: 10.1021/acs.jafc.5b00564
J. Agric. Food Chem. 2015, 63, 4120−4129

With the phenolic acids structure taken into account, the compounds liberated from soluble esters are predominant in sea buckthorn berries (from 53.9 to 66.6%). Free phenolic acids are a minor fraction and constitute only 1.3−2.3%.[46] According to Arimboor et al.,[47] berry pulp contained a total of 1068 mg/kg phenolic acids, of which 58.8% was derived from phenolic glycosides. Free phenolic acids and phenolic acid esters constituted 20.0 and 21.2%, respectively. As the authors showed, gallic acid was identified as the predominant phenolic acid in both free and bound forms (66.0% of total phenolic acids in pulp). Considerable amounts of protocatechuic (136 mg/kg), ferulic (69 mg/kg), salicylic (54 mg/kg), *p*-hydroxybenzoic (40 mg/kg), and *p*-coumaric acid (37 mg/kg) were found to be present in berry pulp. The presence of vanillic (7 mg/kg), cinnamic (12 mg/kg), and caffeic acids (8 mg/kg) was also detected.

Sea buckthorn berries are a valuable source of compounds with beneficial effects for human health. The high concentrations of flavonols, L-ascorbic acid, but mostly lipophilic substances, namely, carotenoids, phytosterols, and fatty acids, determine the uniqueness of its chemical composition in comparison to other fruits. Our research confirms that the content of plant bioactives in the raw material significantly affects the cultivar factor. 'Aromatnaja' was characterized by the highest content of L-ascorbic acid and phytosterols, whereas 'Podarok Sadu' berries were rich in PUFAs. In 'Moskwiczanka' the highest carotenoids and in 'Botaniczeskaja' the highest polyphenol concentrations were noted.

Among the tested active compounds of sea buckthorn, the most diverse was the phytosterols profile, which consisted of 14 compounds, including 4-desmethyl sterols (e.g., β-sitosterol, stigmasterol, campesterol, Δ^5-avenasterol), 4α-monomethyl sterols (e.g., citrostadienol), and 4,4-dimethyl sterols (e.g., 24-methylenecycloartanol).

AUTHOR INFORMATION

Corresponding Author

*(A.W.) Phone: +48 71 320 77 06. Fax: +48 71 320 77 07. E-mail: aneta.wojdylo@up.wroc.pl

Funding

This work was supported by the European Union under Project POIG 01.01.02-00-061/09, acronym "Bioactive food".

Notes

The authors declare no competing financial interest.

ACKNOWLEDGMENTS

We thank Marii Bortkiewicz and Elżbiecie Buckiej for their technical assistance.

REFERENCES

(1) Rousi, A. The genus *Hippophaë* L. A taxonomic study. *Ann. Bot. Fenn.* **1971**, *8*, 177−227.

(2) Bal, L. M.; Meda, V.; Naik, S. N.; Satya, S. Sea buckthorn berries: a potential source of valuable nutrients for nutraceuticals and cosmoceuticals. *Food Res. Int.* **2011**, *44*, 1718−1727.

(3) Fatima, T.; Snyder, C. L.; Schroeder, W. R.; Cram, D.; Datla, R.; Wishart, D.; Weselake, R. J.; Krishna, P. Fatty acid composition of developing sea buckthorn (*Hippophaë rhamnoides* L.) berry and the transcriptome of the mature seed. *PLoS One* **2012**, *7*, 2−18.

(4) Patel, C. A.; Divakar, K.; Santani, D.; Solanki, H. K.; Thakkar, J. H. Remedial prospective of *Hippophaë rhamnoides* Linn. (sea buckthorn). *ISRN Pharmacol.* **2012**, *2012*, 1−6.

(5) Rongsen, L.; Ahani, H. The genetic resources of *Hippophae* genus and its utilization. *Int. J. Scholary Res. Gate* **2013**, *1*, 15−21.

(6) Szałkiewicz, M.; Zadernowski, R. Sea buckthorn: possibilities for the production and use of fruit (in polish). *Hasło Ogrodnicze*. **2006**, *02*, http://www.ho.haslo.pl/article.php?id=2601.

(7) Kallio, H.; Yang, B.; Peippo, P. Effects of different origins and harvesting time on vitamin C, tocopherols, and tocotrienols in sea buckthorn (*Hippophaë rhamnoides*) berries. *J. Agric. Food Chem.* **2002**, *50*, 6136−6142.

(8) Kalinina, I. P.; Panteleyeva, Y. I. Breeding of sea buckthorn in the Altai. In *Advances in Agricultural Science*; Nauk: Moscow, Russia, **1987**; pp 76−87.

(9) Hussain, M.; Ali, S.; Awan, S.; Hussain, M.; Hussain, I. Analysis of minerals and vitamins in sea buckthorn (*Hippophae rhamnoides*) pulp collected from Ghizer and Skardu districts of Gilgit-Baltistan. *Int. J. Biosci.* **2014**, *4*, 144−152.

(10) PN-90/A-75101/12: Fruits and vegetables preserves. Preparation of samples and physico-chemical test methods. Determination of total carotenoids and β-carotene,1990.

(11) AOCS Official Method Ch 6-91. Determination of the composition of the sterol fraction of animal and vegetable oils and fats by TLC and capillary GLC.

(12) AOCS Official Method Ce 1k-07. Direct methylation of lipids for the determination of total fat, saturated, *cis*-monounsaturated, *cis*-polyunsaturated, and *trans* fatty acids by chromatography.

(13) Oszmiański, J.; Wojdyło, A. Effects of black currant and apple pulp blended on phenolics, antioxidant capacity and colour of juices. *Czech J. Food Sci.* **2009**, *27*, 338−351.

(14) Wojdyło, A.; Teleszko, M.; Oszmiański, J. Antioxidant property and storage stability of quince juice phenolic compounds. *Food Chem.* **2014**, *152*, 261−270.

(15) Kruczek, M.; Świderski, A.; Mech-Nowak, A.; Król, K. Antioxidant capacity of crude extracts containing carotenoids from the berries of various cultivars of Sea buckthorn (*Hippophae rhamnoides* L.). *Acta Biochim. Pol.* **2012**, *59*, 135−137.

(16) Müller, H. Determination of the carotenoid content in selected vegetables and fruit by HPLC and photodiode array detection. *Z. Lebensm. Unters. Forsch. A* **1997**, *204*, 88−94.

(17) Yang, B.; Kallio, H. Composition and physiological effects of sea buckthorn (*Hippophaë*) lipids. *Trends Food Sci. Technol.* **2002**, *13* (5), 160−167.

(18) Yang, B. *Lipophilic Components in Seeds and Berries of Sea Buckthorn and Physiological Effects of Sea Buckthorn Oils*. Ph.D. thesis, University of Turku, Turku, Finland, 2001.

(19) Davidson, M. H.; Maki, K. C.; Umporowicz, D. M.; Ingram, K. A.; Dicklin, M. R.; Schaefer, E.; Lane, R. W.; McNamara, J. R.; Ribaya-Mercado, J. D.; Perrone, G.; Robins, S. J.; Franke, W. C. Safety and tolerability of esterified phytosterols administered in reduced-fat spread and salad dressing to healthy adult men and women. *J. Am. Coll. Nutr.* **2001**, *20*, 307−319.

(20) Neil, H. A.; Meijer, G. W.; Roe, L. S. Randomised controlled trial of use by hypercholesterolaemic patients of a vegetable oil sterol-enriched fat spread. *Atherosclerosis* **2001**, *156* (2), 329−337.

(21) Woyengo, T. A.; Ramprasath, V. R.; Jones, P. J. Anticancer effects of phytosterols. *Eur. J. Clin. Nutr.* **2009**, *63*, 813−820.

(22) Li, T. S. C.; Beveridge, T. H. J.; Drover, J. C. G. Phytosterol content of sea buckthorn *(Hippophaë rhamnoides* L.) seed oil: extraction and identification. *Food Chem.* **2007**, *101*, 1665−1671.

(23) Cenkowski, S.; Yakimishen, R.; Przybylski, R.; Muir, W. E. Quality of extracted sea buckthorn seed and pulp oil. *Can. Biosyst. Eng.* **2006**, *48*, 3.9−3.16.

(24) Erkkola, R.; Yang, B. Sea buckthorn oils: towards healthy mucous membranes. *Agro Food Ind. Hi-Tech.* **2003**, *May/June 2003*, 43−57.

(25) Dulf, F. V. Fatty acids in berry lipids of six sea buckthorn (*Hippophaë rhamnoides* L., subspecies carpatica) cultivars grown in Romania. *Chem. Cent. J.* **2012**, *6*, 1−12.

(26) Khabarov, S. N.; Vereshchagin, A. L.; Gur'yanov, G.; Goremykina, N. V.; Bychin, N. V. Identification of the origin of sea

DOI: 10.1021/acs.jafc.5b00564
J. Agric. Food Chem. 2015, 63, 4120−4129

buckthorn oil of the Altai Krai by differential scanning calorimetry. *Foods Raw Mater.* **2013**, *1*, 108−113.
(27) George, S. D. St.; Cenkowski, S. Influence of harvest time on the quality of oil-based compounds in sea buckthorn (*Hippophaë rhamnoides* L. ssp. sinensis) seed and fruit. *J. Agric. Food Chem.* **2007**, *55*, 8054−8061.
(28) Lee, S. K.; Kader, A. A. Preharvest and postharvest factors influencing vitamin C content of horticultural crops. *Postharvest Biol. Technol.* **2000**, *20*, 207−220.
(29) Tang, X. Intrinsic change of physical and chemical properties of sea buckthorn (*Hippophaë rhamnoides*) and implications for berry maturity and quality. *J. Hortic. Sci. Biotechnol.* **2002**, *77*, 177−185.
(30) Rop, O.; Ercişli, S.; Mlcek, J.; Jurikova, T.; Hoza, I. Antioxidant and radical scavenging activities in fruits of 6 sea buckthorn (*Hippophaë rhamnoides* L.) cultivars. *Turk. J. Agric. For.* **2014**, *38*, 224−232.
(31) Kawecki, Z.; Szałkiewicz, M.; Bieniek, A. The common sea buckthorn − a valuable fruit. *J. Fruit Ornam. Plant Res. Special Ed.* **2004**, *12*, 183−193.
(32) Rösch, D.; Krumbein, K.; Mügge, C.; Fogliano, V.; Kroh, L. W. Structural investigations of flavonol glycosides from sea buckthorn (*Hippophaë rhamnoides*) pomace by NMR spectroscopy and HPLC-ESI-MS^n. *J. Agric. Food Chem.* **2004**, *52*, 4039−4046.
(33) Yang, B.; Halttunen, T.; Raimo, O.; Price, K.; Kallio, H. Flavonol glycosides in wild and cultivated berries of three major subspecies of *Hippophaë rhamnoides* and changes during harvesting period. *Food Chem.* **2009**, *115*, 657−664.
(34) Jakobek, L.; Drenjančević, M.; Jukić, V.; Šeruga, M. Phenolic acids, flavonols, anthocyanins and antiradical activity of 'Nero', 'Viking', 'Galicjanka' and wild chokeberries. *Sci. Hortic.* **2012**, *147*, 56−63.
(35) Pappas, E.; Schaich, K. M. Phytochemicals of cranberries and cranberry products: characterization, potential health efects, and processing stability. *Crit. Rev. Food Sci. Nutr.* **2009**, *49*, 741−781.
(36) Mikkonen, T. P.; Määttä, K. R.; Hukkanen, A T.; Kokko, H. I.; Törrönen, A. R.; Kärenlampi, S. O.; Korjalajnen, R. O. Flavonol content varies among black currant cultivars. *J. Agric. Food Chem.* **2001**, *49*, 3274−3277.
(37) Laaksonen, O.; Sandell, M.; Kallio, H. Chemical factors contributing to orosensory profiles of bilberry (*Vaccinium myrtillus*) fractions. *Eur. Food Res. Technol.* **2010**, *231*, 271−285.
(38) Aherne, S. A.; O'Brien, N. M. Dietary flavonols: chemistry, food content, and metabolism. *Nutrition* **2002**, *18*, 75−81.
(39) Kallio, H.; Yang, B.; Halttunen, T. Flavonol glycosides of berries of three major sea buckthorn subspecies, *Hippophaë rhamnoides* ssp. *rhamnoides*, ssp. *sinensis* and ssp. *mongolica*. *Proceedings of Invited Speeches for the Second International Sea Buckthorn Association Conference*, Beijing, China, 2005; pp 29−35.
(40) Pop, R. M.; Socaciu, C.; Pintea, A.; Buzoianu, A. D.; Sanders, M. G.; Gruppen, H.; Vincken, J. P. UHPLC/PDA−ESI/MS analysis of the main berry and leaf flavonol glycosides from different Carpathian *Hippophaë rhamnoides* L. varieties. *Phytochem. Anal.* **2013**, *24*, 484−492.
(41) Chen, Ch.; Xu, X.-M.; Chen, Y.; Yu, M.-Y.; Wen, F.-Y.; Zhang, H. Identification, quantification and antioxidant activity of acylated flavonol glycosides from sea buckthorn (*Hippophaë rhamnoides* ssp. sinensis). *Food Chem.* **2013**, *141* (2013), 1573−1579.
(42) Hosseinian, F. S.; Li, W.; Hydamaka, A. W.; Tsopmo, A.; Lowry, L.; Friel, J.; Beta, T. Proanthocyanidin profile and ORAC values of manitoba berries, chokecherries, and seabuckthorn. *J. Agric. Food Chem.* **2007**, *55*, 6970−6976.
(43) Bolling, B. W.; Dolnikowski, G.; Blumberg, J. B.; Chen, C.-Y.O. Polyphenol content and antioxidant activity of California almonds depend on cultivar and harvest year. *Food Chem.* **2010**, *122*, 819−825.
(44) Jaakola, L.; Hohtola, A. Effect of latitude on flavonoid biosynthesis in plants. *Plant, Cell Environ.* **2010**, *33*, 1239−1247.
(45) Rösch, D.; Mügge, C.; Fogliano, V.; Kroh, L. W. Antioxidant oligomeric proanthocyanidins from sea buckthorn (*Hippophaë rhamnoides*) pomace. *J. Agric. Food Chem.* **2004**, *52*, 6712−6718.
(46) Zadernowski, R.; Naczk, M.; Czaplicki, S.; Rubinskiene, M.; Szałkiewicz, M. Composition of phenolic acids in sea buckthorn (*Hippophae rhamnoides* L.) berries. *J. Am. Oil Chem. Soc.* **2005**, *82*, 175−179.
(47) Arimboor, R.; Sarin Kumar, K.; Arumughan, C. Simultaneous estimation of phenolic acids in sea buckthorn (*Hippophaë rhamnoides*) using RP-HPLC with DAD. *J. Pharm. Biomed. Anal.* **2008**, *4*, 31−38.

DOI: 10.1021/acs.jafc.5b00564
J. Agric. Food Chem. 2015, 63, 4120−4129

content in rice was about 130 mg/100 g of grain. The content of proanthocyanidins in barley varied between 25 and 250 mg/100 g of grain.[4,10−12] Kamimura and Takahashi[13] demonstrated that procyanidin B-3 from barley can directly promote hair epithelial cell growth *in vitro*, counteract the growth-inhibiting effect caused by TGF-β1 *in vitro*, and stimulate anagen induction *in vivo*.

The analytical technique usually applied to determine the proanthocyanidins in cereal consist of high-performance liquid chromatography (HPLC) coupled to a diode array detector (DAD), fluorimetric detector (FLD), and mass spectrometer detector (MSD)[5,6,14] or matrix-assisted laser desorption/ionization time-of-flight (MALDI-TOF) analysis.[15] However, in the last few years, the use of infrared (IR) spectroscopy as a non-destructive method has been evaluated.[16−18]

Because of the large use of barley in food production, the aim of this work was to investigate the oligomeric proanthocyanidin content in different barley genotypes (waxy and non-waxy) using high-performance liquid chromatography−fluorescence detection−electrospray ionization−mass spectrometry (HPLC−FLD−ESI−MS). Moreover, Fourier transform near-infrared (FT-NIR) spectroscopy was performed to evaluate the possibility to discriminate between waxy and non-waxy samples and to estimate the proanthocyanidins in barley flours using a fast and non-destructive method.

MATERIALS AND METHODS

Samples. A total of 14 different varieties of barley grown under the same agronomic conditions in the same experimental field at the Department of Food Technology (DISTAAM), University of Molise (Italy) (41° 34′ 00″ N, 14° 40′ 00″ E) were analyzed.

The soil of the site is classified as a fine silty clay loam with 29% silt, 35% clay, 36% sand, 1.7% organic matter, total available P (6.1 mg kg^{-1}), total available K (78.3 mg kg^{-1}), and pH 7.3.

The trials were sown in a three-replication split-plot experimental scheme in October 2013 (sowing density was 300 seeds/m^2). Four of the barley varieties were waxy genotype (Canada, USA2, USA3, and USA7), and the other 10 were non-waxy genotype (Acquarelle, Bombay, Boreale, Margret, Messina, Metis, Naturelle, Otis, Rangoon, and Svenja). Harvest took place in June 2014 at grain full-ripening stage.

Whole grains were milled (particle size of 150−250 μm), and the flours were used for the analysis. The resulting flours reported moisture between 11.4 and 12.0%.

Chemicals. HPLC-grade acetonitrile, water, methanol, and acetone were purchased from Merck KGaA (Darmstadt, Germany). Catechin and procyanidin B2 were from Sigma-Aldrich (St. Louis, MO).

Extraction of Proanthocyanidins in Barley Samples. The protocol of Verardo et al.[11] was used to isolate the proanthocyanidin fraction. Briefly, barley flour (2 g) was extracted in an ultrasonic bath (20 min) with 20 mL of a solution of acetone/water (4:1, v/v). After centrifugation at 1000*g* for 10 min, the supernatant was removed and the extraction was repeated once more. The supernatants were collected, evaporated, and reconstituted in 2 mL of methanol/water (1:1, v/v). The final extracts were filtered through 0.2 μm polytetrafluoroethylene (PTFE) syringe filters and stored at −18 °C until the analyses.

Determination of Proanthocyanidin Compounds by HPLC−FLD−ESI−MS. Normal-phase (NP)-HPLC analysis was performed by an Agilent 1200 Series (Agilent Technologies, Santa Clara, CA), equipped with a binary pump delivery system, a degasser, an autosampler, a FLD, and a MSD.

A Develosil Diol 100 Å column, 5 μm, 250 × 4.6 mm inner diameter (Phenomenex, Torrance, CA), was used. All solvents were HPLC-grade and filtered through a 0.45 μm filter disk. The gradient elution was the same reported by Robbins et al.[19] Fluorescence detection was conducted with an excitation wavelength of 230 nm and an emission wavelength of 321 nm.

The injection volume was 5 μL. All of the analyses were carried out at 35 °C. Calibration curves of (+)-catechin and procyanidin B2 were arranged from 5 to 500 and from 1 to 500 μg/mL, respectively, at six concentration levels for each compound; correction factors suggested by Robbins and co-workers[19] were used for trimer, tetramer, and pentamer compounds.

The HPLC analysis was replicated 3 times for each extract and calibration point (n = 3).

Mass spectrometer analyses were carried out using an electrospray ionization (ESI) interface at the following conditions: drying gas flow (N_2), 9.0 L/min; nebulizer pressure, 50 psi; gas drying temperature, 350 °C; capillary voltage, 3500 V; and fragmentor voltage and scan range, variable. The fragmentor and m/z ranges used for HPLC−ESI/MSD analyses were as follows: 120 V and m/z 50−1000 and 140 V and m/z 1000−2000.

FT-NIR Spectroscopy. A spectrophotometer Vector 22/N (Bruker Optics, Ettlingen, Germany) in diffuse reflectance mode was used to obtain the NIR spectra. The instrument was equipped with a rotating integrating sphere that allows for a wide illumination of the sample and a better reduction of light scattering because of the irregularity of the particle surfaces. NIR spectra were obtained by an average of 32 scans of each sample. Three replicates for each individual sample (about 60 g of barley flours) were collected for a total of 42 spectra. The background was defined by acquiring the spectrum of the quartz support without the sample in the same instrumental conditions (25 °C). The speed of acquisitions was 10 kHz in a range from 800 to 2500 nm.

Statistical Analysis. The Pearson correlation coefficients (p < 0.05) were calculated to define a relation between the proanthocyanidins using Statistica 8.0 software (2007, StatSoft, Tulsa, OK).

Significant differences (at p < 0.05) between means of the proanthocyanidin compounds were explored using analysis of variance (ANOVA) combined with Tukey's post-hoc test using Statistica 8.0 software. Mean-centered data were subjected to principal component analysis (PCA) to find a possible discrimination between the sample as a function of barley genotypes (waxy and non-waxy) using The Unscrambler, version 9.7 (CAMO, Oslo, Norway).

With regard to the NIR spectra, to remove the effects of light scattering, NIR spectra were pretreated with multiplicative scattering correction (MSC). The first part of the spectra, until 1100 nm, was deleted before processing because it contained no useful chemical information but only instrumental noise. Data were also treated by applying the first derivative (Savitsky−Golay) to the absorbance data. Subsequently, the spectral data were subjected to PCA and partial least square (PLS) regression. The first one was applied as an exploratory analysis to define a possible discrimination between the sample as a function of barley genotypes (waxy and non-waxy), while the second one was applied to predict the proanthocyanidin compounds. The PLS models were validated using a full cross-validation and a test set validation technique. For the first validation, the same data set, characterized by an amount of 42 cases (three replicates for 14 samples), was used to calibrate and validate the model: a sample of total entire data set is removed one by one from the construction of the model and used to validate. For the test set validation, the data set was randomly divided into two sub-samples, one to calibrate the system (70% of the entire data set) and the other (30%) to validate it. Test set validation was repeated 5 times for each reference value (proanthocyanidin compounds), and the prediction indices [determination coefficient (R^2) and root mean square error (RMSE)] were averaged, because the PLS convergence is influenced by the data set.

All of the statistical elaborations were carried out using The Unscrambler, version 9.7 (CAMO, Oslo, Norway).

RESULTS AND DISCUSSION

Proanthocyanidin Identification by HPLC−ESI−MS. The method established by Robbins et al.[19] was used to

DOI: 10.1021/acs.jafc.5b01425
J. Agric. Food Chem. 2015, 63, 4130−4137

determine the proanthocyanidin oligomers in barley flours, and the resulted chromatogram is shown in Figure 1.

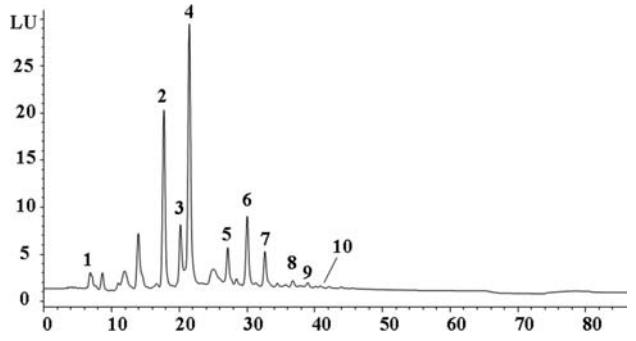

Figure 1. HPLC–FLD chromatogram of oligomeric proanthocyanidins in the barley sample. The number of the peaks are the same as reported in Table 1.

To identify the proanthocyanidins revealed by fluorimetric detection, mass spectrometry was used to confirm the peak identity (Table 1). As reported from several authors,[19,20] the compounds eluted according to their degree of polymerization, first eluting the monomers and then the different oligomers according to their degree of galoylation (for the same degree of polymerization).

Table 1. HPLC–ESI–MS Data of Proanthocyanidins in Barley Samples

	compound	Rt (min)	$[M - H]^-$	fragment (m/z)
1	catechin/epicatechin	7.13	289	245
2	procyanidin dimer	17.61	577	425, 289
3	prodelphinidin dimer I	20.30	593	467, 425, 289
4	prodelphinidin dimer II	21.66	593	467, 425, 289
5	procyanidin trimer	27.30	865	739, 713, 289
6	prodelphinidin trimer I (monogalloylated)	30.00	881	593, 577, 303
7	prodelphinidin trimer II (digalloylated)	32.87	897	771, 729, 593
8	procyanidin tetramer	36.65	1153	865
9	prodelphinidin tetramer (digalloylated)	38.81	1457	728
10	procyanidin pentamer	41.03	1441	

Catechin/epicatechin was the first compound that was identified. It provided a molecular ion at m/z 289; in addition, a fragment ion at m/z 245 ($[M - H - CO_2]^-$) was also shown.

Several oligomeric procyanidins (PCs) and prodelphinidins (PDs) were identified; many of them reported the fragmentation pathways for proanthocyanidins, such as (a) retro-Diels–Alder (RDA) cleavage and subsequent elimination of a water molecule, (b) interflavanic bond cleavage through the quinone–methine (QM) mechanism, and (c) heterocyclic ring fission (HRF).[5]

A procyanidin dimer with molecular ion at m/z 577 and two principal fragments at m/z 425 and 289 (corresponding to RDA and QM, respectively)[21] was detected at 17.6 min.

Two prodelphinidin dimers were also detected at 20 and 20.2 min; they showed a molecular ion at m/z 593 and three fragment ions at m/z 467, 425, and 289 corresponding to HRF, RDA, and QM, respectively.[5]

For procyanidin trimer (molecular ion at m/z 865), fragments at m/z 739, 713, and 289 were obtained as a result of HRF, RDA, and QM, respectively.

Two single peaks eluting at 30 and 30.2 min with m/z 881 and 897 ($[M - H]^-$) were detected. The first peak produced three fragment ions at m/z 593, 577, and 303. This compound was identified as prodelphinidin trimer monogallate; moreover, the presence of fragment ions at m/z 593 (corresponding to GC–C dimer) and m/z 577 (corresponding to C–C dimer) suggested that the peak was the sum of (epi)gallocatechin–(epi)catechin–(epi)catechin and (epi)catechin–(epi)-gallocatechin–(epi)catechin trimers.

The other peak at m/z 897 with fragment ions at m/z 771, 729, and 593 was identified as digalloylated prodelphinidin trimer according to Friedrich and co-workers.[22]

Two proanthocyanidin tetramers were detected. Procyanidin tetramer with molecular ion at m/z 1153 and a fragment ion at m/z 865 ($[M - H - \text{catechin}]^-$) was revealed at 36.7 min.

A prodelphinidin tetramer at 38.8 min was identified because of its molecular ion at m/z 1457; the fragment ion at m/z 728 permits identifying this compound as digalloylated oligomer, according to Lazarus et al.[23]

Finally, the compound at 41.0 min and m/z 1441 was identified as procyanidin pentamer according to Robbins et al.[19] As far as we are concerned, this is the first time that procyanidin pentamer has been detected in barley samples.

Proanthocyanidin Quantification by HPLC–FLD. To quantify the proanthocyanidins in barley samples, catechin and procyanidin B2 calibration curves were used. Moreover, the correction factors suggested by Robbins and co-workers[19] were chosen to calculate trimer, tetramer, and pentamer contents.

Barley samples exhibited ample variability of total proanthocyanidin content, with a range from 293.2 to 652.6 μg/g of flour (Table 2), and waxy and non-waxy genotypes reported statistical differences ($p < 0.05$). In fact, the mean of the total oligomeric content in waxy genotypes was about 1.6 times higher than that in non-waxy samples.

Monomers ranged between 10.9 and 48.3 μg/g of flour in non-waxy barley samples, whereas the content of monomers in waxy barley was significantly higher ($p < 0.05$), ranging from 44.1 to 87.1 μg/g of flour. Generally, these data are in the same order of magnitude of those reported by other authors.[12,24,25]

Dimer compounds were the principal proanthocyanidin constituents of barley samples. Total dimers content ranged between 116.8 and 214.6 μg/g of flour, and these amounts are in agreement with the results reported in the literature.[12,24,25] As seen for monomers, waxy samples showed a higher content of dimers (182.9–214.6 μg/g of flours) compared to non-waxy samples (116.8–173.8 μg/g of flour). Procyanidin dimers represented 35.4–51.2% of the total dimer class, and waxy samples contained a higher content (except for the Bombay sample), with an average of 89.6 μg/g of flour. Barley samples contained from 67.8 to 118.6 μg/g of flour of total prodelphinidin dimers, and waxy samples showed the highest content.

Proanthocyanidin trimers ranged between 149.8 and 317.4 μg/g of flour. Significant differences ($p < 0.05$) between waxy and non-waxy samples were found for procyanidin trimer: waxy samples showed an average of 127.4 μg/g of flour, while non-waxy barley had an average of 61.3 μg/g of flour. Similar amounts were determined by Holtekjølen and co-workers.[12]

DOI: 10.1021/acs.jafc.5b01425
J. Agric. Food Chem. 2015, 63, 4130–4137

Table 2. Proanthocyanidin Content in Barley Samples Obtained by HPLC−FLD (μg/g of Dry Weight of Flour)[a]

	monomers	PC dimer	PD dimer I	PD dimer II	PC trimer	PD trimer I	PD trimer II	PC tetramer	PD tetramer	PC pentamer	total
					Non-waxy Samples						
Acquarelle	32.9 ± 0.1 d	55.0 ± 0.8 b,c	16.1 ± 1.1 a,b	74.7 ± 3.3 c−e	64.7 ± 0.9 c,d	75.5 ± 0.7 b	49.8 ± 0.7 e,f	13.1 ± 0.6 c,d	21.8 ± 0.4 c,d	6.6 ± 0.7 b,c	410.5 ± 9.4 d
Bombay	27.7 ± 0.6 c,d	87.7 ± 0.8 g	16.5 ± 1.4 a,b	69.5 ± 3.2 c−e	65.1 ± 0.0 c,d	92.6 ± 0.8 d	40.2 ± 1.3 c,d	12.5 ± 0.2 b,c	23.8 ± 1.2 d,e	6.1 ± 0.7 b	442.0 ± 3.9 e
Boreale	22.5 ± 0.3 b,c	59.0 ± 1.9 c	15.5 ± 0.4 a	62.1 ± 1.4 b,c	43.7 ± 0.1 a,b	79.1 ± 1.4 b	46.8 ± 0.5 d,e	11.3 ± 0.4 b	25.8 ± 0.8 d,e	8.3 ± 0.5 d	374.2 ± 4.1 b,c
Margret	10.9 ± 1.0 a	60.0 ± 2.0 c	15.7 ± 0.3 a	58.3 ± 0.8 b	54.5 ± 1.4 b,c	81.4 ± 2.6 b	44.6 ± 1.3 d,e	10.1 ± 1.1 b	24.1 ± 0.8 d,e	6.7 ± 0.3 b,c	366.4 ± 2.8 b,c
Messina	16.7 ± 0.0 a,b	71.4 ± 2.0 d	19.3 ± 0.3 b,c	69.3 ± 0.3 c−e	66.0 ± 0.1 d,e	92.5 ± 0.1 d	51.3 ± 0.5 f	13.1 ± 0.4 c,d	30.8 ± 1.1 f	8.7 ± 0.1 d	439.2 ± 2.0 e
Metis	48.3 ± 1.0 e	48.8 ± 1.4 a,b	22.4 ± 0.3 d	49.3 ± 1.8 a	71.7 ± 0.7 e	54.2 ± 1.4 a	23.8 ± 0.5 a	8.0 ± 0.2 a	14.6 ± 0.9 a	4.5 ± 0.1 a	345.8 ± 7.9 b
Naturelle	23.5 ± 1.0 b,c	48.9 ± 0.8 a,b	17.1 ± 0.7 a,b	50.7 ± 1.0 a	36.7 ± 1.1 a	54.5 ± 1.4 a	31.7 ± 0.5 a	7.3 ± 0.8 a	16.1 ± 0.3 a,b	6.6 ± 0.1 b,c	293.2 ± 9.4 a
Otis	26.8 ± 0.2 c,d	75.2 ± 3.1 d,e	19.7 ± 0.2 b,c	66.0 ± 1.8 c,d	71.1 ± 0.4 e	89.5 ± 3.2 c	44.3 ± 1.2 d,e	12.7 ± 0.7 b,c	27.2 ± 1.1 e,f	6.6 ± 0.1 b,c	439.2 ± 5.4 e
Svenja	26.3 ± 0.9 c,d	76.2 ± 0.6 d,e	15.8 ± 0.7 a	56.8 ± 0.4 b	85.3 ± 4.4 f	84.7 ± 1.4 b	36.3 ± 0.3 b	12.1 ± 1.2 b	21.2 ± 0.7 c	6.4 ± 0.7 b,c	421.1 ± 5.3 d
Rangoon	17.0 ± 0.2 a,b	48.3 ± 1.5 a	16.7 ± 1.2 a,b	71.2 ± 1.9 c−e	54.2 ± 0.1 b,c	53.6 ± 2.4 a	43.1 ± 0.4 b,c	6.7 ± 0.9 a	14.1 ± 1.2 a	5.71 ± 0.5 b	330.6 ± 9.8 b
mean	25.27	63.06	17.50	62.80	61.32	75.77	41.19	10.71	21.96	6.63	386.21
CV (%)	40.9	21.8	13.0	14.0	23.3	21.0	20.6	23.6	25.4	18.0	13.5
					Waxy Samples						
Canada	87.1 ± 1.6 g	82.7 ± 1.4 f	35.0 ± 0.7 f	75.6 ± 1.1 d,e	137.2 ± i	86.9 ± 1.9 c	45.2 ± 1.5 d,e	14.1 ± 1.1 d	22.8 ± 0.6 c,d	12.1 ± 0.1 f	598.8 ± 6.1 f,g
USA2	72.1 ± 0.1 f	97.8 ± 0.1 h	37.6 ± 0.2 f	79.2 ± 0.7 f	118.5 ± 1.1 h	92.9 ± 0.6 d	44.8 ± 0.5 d,e	13.6 ± 0.3 d	24.9 ± 0.3 d,e	9.6 ± 0.2 e	591.0 ± 5.5 f,g
USA3	44.1 ± 0.7 e	90.6 ± 1.1 g	21.9 ± 0.1 d	96.7 ± 0.9 g	87.6 ± 1.2 g	105.3 ± 2.5 e	63.7 ± 1.9 g	15.1 ± 1.0 e	29.1 ± 0.6 e,f	12.9 ± 0.4 f	567.0 ± 6.5 f
USA7	74.1 ± 2.8 f	87.4 ± 2.9 g	30.9 ± 2.0 e	64.6 ± 1.6 c,d	166.5 ± 1.4 l	103.1 ± 2.0 e	48.0 ± 0.9 f	18.9 ± 0.5 f	36.3 ± 0.6 h	22.7 ± 1.1 g	652.6 ± 7.5 g,h
mean	69.37	89.63	31.38	79.02	127.45	97.04	50.42	15.43	28.26	14.35	602.35
CV (%)	26.1	7.1	22.0	16.9	26.0	9.0	17.7	15.7	21.0	40.0	6.0

[a]Different letters in the same column mean significantly different values ($p < 0.05$). PC, procyanidin; PD, prodelphinidin.

J. Agric. Food Chem. 2015, 63, 4130−4137
DOI: 10.1021/acs.jafc.5b01425

Table 3. Symmetric Matrix of Pearson Correlation Coefficients Obtained between the Proanthocyanidin Compounds ($p < 0.05$)

proanthocyanidins	monomers	PC dimer	PD dimer I	PD dimer II	PC trimer	PD trimer I	PD trimer II	PC tetramer	PD tetramer	PC pentamer	total
monomers	1										
PC dimer	0.61	1									
PD dimer I	0.93	0.64	1								
PD dimer II	0.41	0.66	0.4	1							
PC trimer I	0.91	0.69	0.84	0.46	1						
PC trimer I	0.43	0.89	0.41	0.68	0.61	1					
PD trimer II	0.15	0.49	0.16	0.88	0.31	0.69	1				
PC tetramer	0.66	0.66	0.54	0.57	0.8	0.77	0.55	1			
PD tetramer	0.43	0.71	0.41	0.5	0.62	0.9	0.64	0.78	1		
PC pentamer	0.74	0.62	0.65	0.53	0.85	0.69	0.55	0.76	0.8	1	
total	0.84	0.87	0.8	0.71	0.92	0.83	0.58	0.85	0.78	0.87	1

According to Holtekjølen and co-workers,[12] monogalloylated prodelphinidin trimers ranged between 53.6 and 105.3 μg/g of flour and represented 55.5−70.0% of total prodelphinidin trimers. Digalloylated prodelphinidin trimers were 31.7−63.7 μg/g of flour. No statistical differences ($p < 0.05$) between waxy and non-waxy samples were noticed for prodelphinidin trimer content.

Tetramers constituted 6.3−10.0% of total proanthocyanidin content, and their amounts varied from 20.8 to 55.2 μg/g of flour. Procyanidin tetramers ranged from 6.7 to 18.9 μg/g of flour, whereas digalloylated prodelphinidin was contained in the range of 14.1−36.3 μg/g of flour; no statistical differences ($p < 0.05$) were shown between waxy and non-waxy samples.

Pentamer oligomers were represented exclusively by one procyanidin that showed a total content from 4.5 to 22.7 μg/g of flour; waxy samples showed a higher content (average 14.3 μg/g of flour) compared to non-waxy samples (average 6.6 μg/g of flour).

The sum of tetramers and pentamers is in the same order of magnitude of the results reported by Hellström and co-workers.[6]

When the data obtained for barley to literature results[4,8] about other cereals are compared, it is evident that sorghum and rice are characterized by a higher content of total proanthocyanidins and a higher degree of polymerization of proanthocyanidins. As reported by several authors,[4,26] sorghum proanthocyanidins were represented by 68% of polymers, followed by oligomers from 4 to 10 monomeric units. A similar composition was reported by Min et al.[8] for rice. Instead, barley showed a low degree of polymerization, from monomers to pentamers, but reported a higher content of dimers and trimers compared to sorghum and rice and a higher content of monomers than rice and equal or higher than sorghum.

This aspect encourages the use of barley in functional food formulation as a cereal source of proanthocyanidins because, as reported by Ou and Gu,[1] proanthocyanidins with a degree of polymerization over 4 (DP > 4) are not absorbable because of their large molecular size and gut barrier.

The Pearson correlation matrix (Table 3) points out that all of the compounds are positively correlated; the correlation between PD trimer II and monomers or PD dimer I is not significant.

The score plot of the PCA performed to discriminate between samples with different barley genotypes is reported in Figure 2. The two first principal components accounted for 83% of total variance. PC1, explaining 66% of total variation, is clearly linked to proanthocyanidin composition. A clear separation between waxy (gray) and non-waxy (black) samples

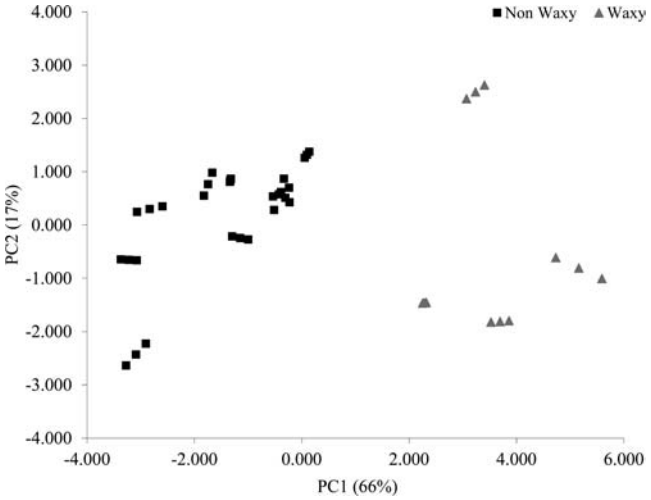

Figure 2. Score plot obtained by the PCA of the proanthocyanidin compounds determined by HPLC−FLD.

was observed. The waxy samples were grouped along the positive values of PC1 (x axis), while the non-waxy samples were grouped on the negative side of the axis.

The X-loadings plot shows how well a variable is taken into account by the model components, and it is used to understand how much each variable contributes to the meaningful variation in the data and to interpret variable relationships. Further, the comparison between score and loadings plot allows for interpretation of the relationships and dependence between variable and samples. In this case, the X-loadings plot (Figure 3) shows that all waxy samples are characterized by higher values of all proanthocyanidin compounds than non-waxy samples. Particularly, the USA3 sample, with respect to the other waxy samples, is characterized by a high content of PD trimer II, PD dimer II, and PD trimer I and by a low content of monomers, PD dimer I, and PC trimer.

NIR Spectroscopy. NIR spectra provided characteristic broad and overlapping peaks between 1100 and 2500 nm. The spectra of all of the samples and an example of first derivate are reported in Figure 4. All of the samples showed the main absorption bands. In particular, the overtones of the C−H bonds of the methylic and methylenic groups between 1170 and 1230 nm, the bands of the O−H bonds because of water and starch at about 1450 and 1940 nm, and the bands of the N−H bonds at about 1500−1570 and 2050−2070 nm were identified. The absorptions of constituents, such as starch, cellulose, and protein, are located at higher wavelengths. The flavonoid constituents can be observed in the regions from

DOI: 10.1021/acs.jafc.5b01425
J. Agric. Food Chem. 2015, 63, 4130−4137

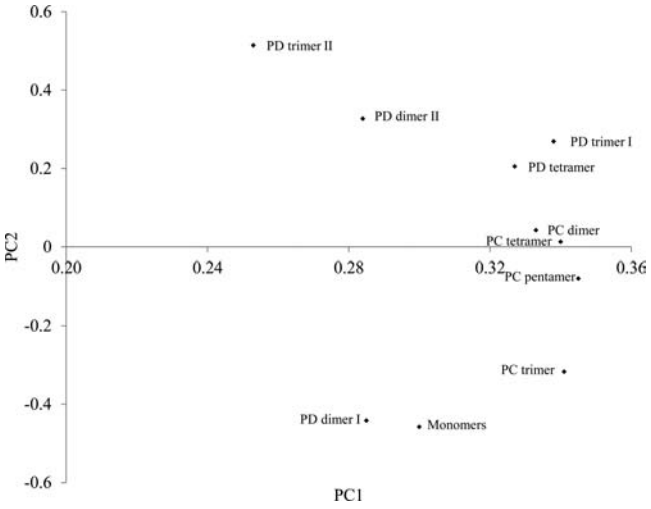

Figure 3. X-loadings of the PCA carried out with proanthocyanidin compound content.

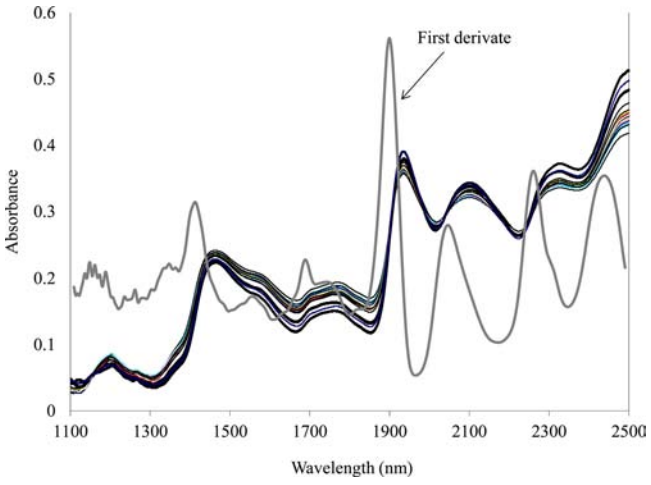

Figure 4. NIR spectra and first derivate.

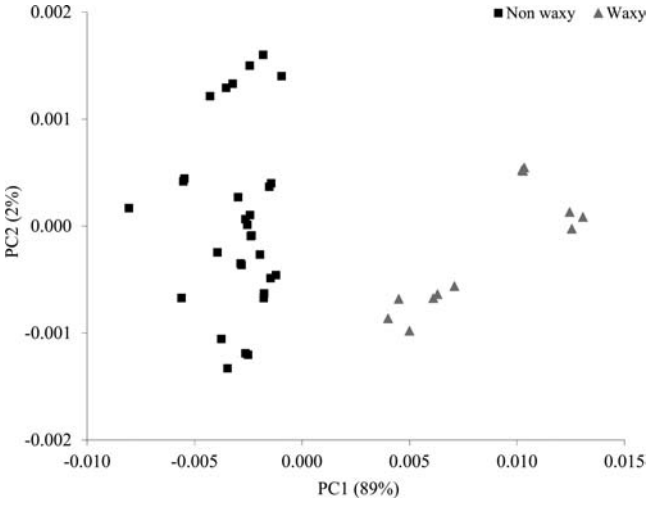

Figure 5. Score plot obtained by the PCA of the proanthocyanidin compounds determined by FT-NIR.

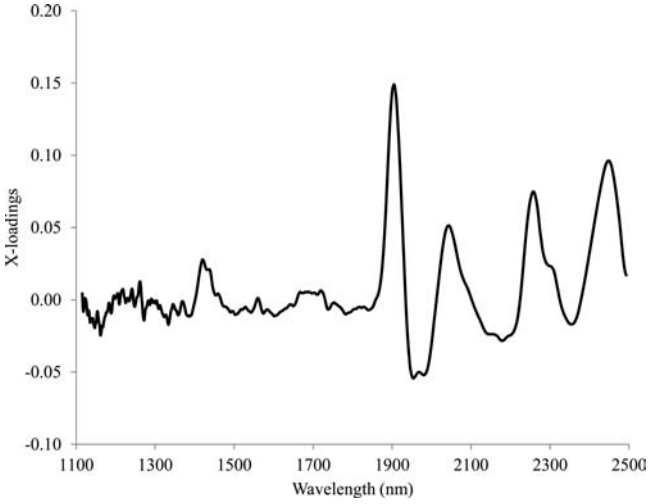

Figure 6. X-loadings for the PCA carried out with NIR spectra (from 1100 to 2500 nm).

1415 to 1512 nm, from 1650 to 1750 nm, and from 1955 to 2035 nm.[16,17,27]

The score plot of the PCA (in the 1100−2500 nm range, with MSC and first derivate treatments), performed to discriminate between waxy and non-waxy samples, is reported in Figure 5. A clear separation between waxy and non-waxy samples was observed along the PC1 (89%). The X-loadings plot (Figure 6) of the first component shows that maximum variance between spectra was identified from 1850 to 2500 nm; as a consequence, the discrimination might be attributed to flavonoid constituents, starch, cellulose, and protein.

The potential of NIR to determine proanthocyanidin oligomers in barley has been evaluated. Table 4 shows the results of PLS regressions in terms of R^2 and RMSE for calibration, full cross-validation, and test set validation. The models were built considering all of the spectrum points (from 1100 to 2500 nm) or the only absorption bands related to phenolic and flavonoid constituents (1415−1512, 1650−1750, and 1955−2035 nm). Generally, in full cross-validation and test set validation, the best results were obtained using the NIR regions associated with phenolic and flavonoid constituents. In full cross-validation, the R^2 values range from 0.94 (PC tetramers) to 0.98 (monomers), while in test set, the R^2 values range from 0.97 (PC trimer) to 0.92 (PD trimer II). However, the difference between the results obtained using all of the spectrum points and bands related to phenolic and flavonoid constituents is very low.

Because of that, the capability of FT-NIR spectroscopy technology as a rapid and non-destructive method to determine the proanthocyanidin oligomers in barley samples could be hypothesized.

In conclusion, the coupling of HPLC with FLD and MSD allows for the determination of proanthocyanidin oligomers in barley samples. Proanthocyanidins include procyanidins and prodelphinidins, and some of them are galloylated. The lower degree of polimerization of barley proanthocyanidins compared to other cereals encourages the use of barley in food formulation. Moreover, waxy barley genotype showed a higher proanthocyanidin content than non-waxy genotype.

In addition, the PLS results obtained by FT-NIR spectroscopy indicate that IR methodology has a good potential to predict proanthocyanidin compounds in barley samples. This aspect represents an advantage and proposes the use of this fast and non-destructive methodology for industry application. To confirm these preliminary results and the performance of NIR

DOI: 10.1021/acs.jafc.5b01425
J. Agric. Food Chem. 2015, 63, 4130−4137

Table 4. PLS Regression Results[a]

		NIR regions			
		1100−2500 nm		1415−1512, 1650−1750, and 1955−2035 nm	
constituent		R^2	RMSE	R^2	RMSE
monomers	C	0.99	2.54	0.99	2.16
	CV	0.97	4.04	0.98	3.58
	TSV	0.94	5.94	0.96	4.84
PC dimer	C	0.98	2.59	0.99	1.86
	CV	0.95	4.14	0.97	3.14
	TSV	0.96	3.53	0.95	3.48
PD dimer I	C	0.98	2.19	0.98	2.02
	CV	0.94	3.50	0.95	2.96
	TSV	0.92	3.91	0.93	3.62
PD dimer II	C	0.97	1.38	0.98	1.06
	CV	0.94	1.93	0.96	1.66
	TSV	0.87	2.38	0.93	1.93
PC trimer	C	0.99	4.12	0.99	4.07
	CV	0.97	6.69	0.97	6.05
	TSV	0.97	6.71	0.97	7.43
PD trimer I	C	0.98	2.31	0.99	1.94
	CV	0.96	3.94	0.97	3.09
	TSV	0.95	3.98	0.95	4.69
PD trimer II	C	0.98	1.56	0.98	1.30
	CV	0.94	2.47	0.96	1.97
	TSV	0.93	2.59	0.92	2.47
PC tetramer	C	0.97	0.81	0.98	0.59
	CV	0.94	1.17	0.94	1.17
	TSV	0.94	1.31	0.94	1.25
PD tetramer	C	0.98	1.02	0.98	0.78
	CV	0.94	1.65	0.96	1.36
	TSV	0.93	1.78	0.94	1.64
PC pentamer	C	0.97	0.65	0.98	0.64
	CV	0.94	1.03	0.96	0.97
	TSV	0.95	1.06	0.95	1.02
total	C	0.98	15.81	0.99	13.51
	CV	0.96	25.34	0.97	22.71
	TSV	0.96	25.64	0.95	22.00

[a]C, calibration; CV, cross-validation; and TSV, test set validation.

for proanthocyanidin determination in barley flours, the sampling should be improved in future investigations.

AUTHOR INFORMATION

Corresponding Author

*Telephone: +39-0-547-338117. Fax: +39-0-547-382348. E-mail: vito.verardo@unibo.it.

Funding

The research was supported by the Italian Ministry of Education, Universities and Research (MIUR), PRIN Project 2008E7HM44. Ana María Gómez-Caravaca is grateful for the postdoctoral contract Juan de la Cierva JCI-2012-12566.

Notes

The authors declare no competing financial interest.

REFERENCES

(1) Ou, K.; Gu, L. Absorption and metabolism of proanthocyanidins. *J. Funct. Foods* **2014**, *7*, 43−53.

(2) Manach, C.; Williamson, G.; Morand, C.; Scalbert, A.; Rémésy, C. Bioavailability and bioefficacy of polyphenols in humans. I. Review of 97 bioavailability studies. *Am. J. Clin. Nutr.* **2005**, *81*, 230S−242S.

(3) Ouédraogo, M.; Charles, C.; Ouédraogo, M.; Guissou, I. P.; Stévigny, C.; Duez, P. An overview of cancer chemopreventive potential and safety of proanthocyanidins. *Nutr. Cancer* **2011**, *63*, 1163−1173.

(4) Gu, L.; Kelm, M. A.; Hammerstone, J. F.; Beecher, G.; Holden, J.; Haytowitz, D.; Gebhardt, S.; Prior, R. L. Concentrations of proanthocyanidins in common foods and estimations of normal consumption. *J. Nutr.* **2004**, *134*, 613−617.

(5) Gu, L.; Kelm, M. A.; Hammerstone, J. F.; Beecher, G.; Holden, J.; Haytowitz, D.; Prior, R. L. Screening of foods containing proanthocyanidins and their structural characterization using LC-MS/MS and thiolytic degradation. *J. Agric. Food Chem.* **2003**, *51*, 7513−7521.

(6) Hellström, J. K.; Törrönen, A. R.; Mattila, P. H. Proanthocyanidins in common food products of plant origin. *J. Agric. Food Chem.* **2009**, *57*, 7899−7906.

(7) McCallum, J. A.; Walker, J. R. L. Proanthocyanidins in wheat bran. *Cereal Chem.* **1990**, *67*, 282−285.

(8) Min, B.; Gu, L.; McClung, A. M.; Bergman, C. J.; Chen, M. H. Free and bound total phenolic concentrations, antioxidant capacities, and profiles of proanthocyanidins and anthocyanins in whole grain rice (Oryza sativa L.) of different bran colours. *Food Chem.* **2012**, *133*, 715−722.

(9) Wu, L.; Huang, Z.; Qin, P.; Yao, Y.; Meng, X.; Zou, J.; Zhu, K.; Ren, G. Chemical characterization of a procyanidin-rich extract from sorghum bran and its effect on oxidative stress and tumor inhibition in vivo. *J. Agric. Food Chem.* **2011**, *59*, 8609−8615.

(10) Gómez-Caravaca, A. M.; Verardo, V.; Berardinelli, A.; Marconi, E.; Caboni, M. F. A chemometric approach to determine the phenolic compounds indifferent barley samples by two different stationary phases: A comparison between C18 and pentafluorophenyl core shell columns. *J. Chromatogr. A* **2014**, *1355*, 134−142.

(11) Verardo, V.; Gómez-Caravaca, A. M.; Marconi, E.; Caboni, M. F. Air classification of barley flours to produce phenolic enriched ingredients: Comparative study among MEKC-UV, RP-HPLC-DAD-MS and spectrophotometric determinations. *LWT - Food Sci. Technol.* **2011**, *44*, 1555−1561.

(12) Holtekjølen, A. K.; Kinitz, C.; Knutsen, S. H. Flavanol and bound phenolic acid contents in different barley varieties. *J. Agric. Food Chem.* **2006**, *54*, 2253−2260.

(13) Kamimura, A.; Takahashi, T. Procyanidin B-3, isolated from barley and identified as a hair-growth stimulant, has the potential to counteract inhibitory regulation by TGF-β1. *Exp. Dermatol.* **2002**, *11*, 532−541.

(14) Bittner, K.; Rzeppa, S.; Humpf, H. U. Distribution and quantification of flavan-3-ols and procyanidins with low degree of polymerization in nuts, cereals, and legumes. *J. Agric. Food Chem.* **2013**, *61*, 9148−9154.

(15) Monagas, M.; Quintanilla-López, J. E.; Gómez-Cordovés, C.; Bartolomé, B.; Lebrón-Aguilar, R. MALDI-TOF MS analysis of plant proanthocyanidins. *J. Pharm. Biomed. Anal.* **2010**, *51*, 358−372.

(16) Zhang, C.; Shen, Y.; Chen, J.; Peng, X.; Bao, J. Nondestructive prediction of total phenolics, flavonoid contents, and antioxidant capacity of rice grain using near-infrared spectroscopy. *J. Agric. Food Chem.* **2008**, *56*, 8268−8272.

(17) Dykes, L.; Hoffmann, L., Jr.; Portillo-Ridriguez, O.; Rooney, W. L.; Rooney, L. W. Prediction of total phenols, condensed tannins, and 3-deoxyanthocyanidins in sorghum grain using near-infrared (NIR) spectroscopy. *J. Cereal Sci.* **2014**, *60*, 138−142.

(18) Jantasee, A.; Thumanu, K.; Muangsan, N.; Leeanansaksiri, W.; Maensiri, D. Fourier transform infrared spectroscopy for antioxidant capacity determination in colored glutinous rice. *Food Anal. Methods* **2014**, *7*, 389−399.

(19) Robbins, R. J.; Leonczak, J.; Johnson, J. C.; Li, J.; Kwik-Uribe, C.; Prior, R. L.; Gu, L. Method performance and multi-laboratory assessment of a normal phase high pressure liquid chromatography−fluorescence detection method for the quantitation of flavanols and procyanidins in cocoa and chocolate containing samples. *J. Chromatogr. A* **2009**, *1216*, 4831−4840.

DOI: 10.1021/acs.jafc.5b01425
J. Agric. Food Chem. 2015, 63, 4130−4137

(20) Montero, L.; Herrero, M.; Prodanov, M.; Ibáñez, E.; Cifuentes, A. Characterization of grape seed procyanidins by comprehensive two-dimensional hydrophilic interaction×reversed phase liquid chromatography coupled to diode array detection and tandem mass spectrometry. *Anal. Bioanal. Chem.* **2013**, *405*, 4627−4638.
(21) Tomás-Barberán, F. A.; Gil, M. I.; Cremin, P.; Waterhouse, A. L.; Hess-Pierce, B.; Kader, A. A. HPLC-DAD-ESIMS analysis of phenolic compounds in nectarines, peaches, and plums. *J. Agric. Food Chem.* **2001**, *49*, 4748−4760.
(22) Friedrich, W.; Eberhardt, A.; Galensa, R. Investigation of proanthocyanidins by HPLC with electrospray ionization mass spectrometry. *Eur. Food Res. Technol.* **2000**, *211*, 56−64.
(23) Lazarus, S. A.; Adamson, G. E.; Hammerstone, J. F.; Schmitz, H. H. High-Performance Liquid Chromatography/Mass Spectrometry analysis of proanthocyanidins in foods and beverages. *J. Agric. Food Chem.* **1999**, *47*, 3693−3701.
(24) Goupy, P.; Hugues, M.; Boivin, P.; Amiot, M. J. Antioxidant composition and activity of barley (Hordeum vulgare) and malt extracts and of isolated phenolic compounds. *J. Sci. Food Agric.* **1999**, *79*, 1625−1634.
(25) Dvorakova, M.; Moreira, M. M.; Dostalek, P.; Skulilova, Z.; Guido, L. F.; Barros, A. A. Characterization of monomeric and oligomeric flavan-3-ols from barley and malt by liquid chromatography−ultraviolet detection−electrospray ionization mass spectrometry. *J. Chromatogr. A* **2008**, *1189*, 398−405.
(26) Prior, R. L.; Gu, L. Occurrence and biological significance of proanthocyanidins in the American diet. *Phytochemistry* **2005**, *66*, 2264−2280.
(27) Cozzolino, D.; Cynkar, W. U.; Dambergs, R. G.; Mercurio, M. D.; Smith, P. A. Measurement of condensed tannins and dry matter in red grape homogenates using near infrared spectroscopy and partial least squares. *J. Agric. Food Chem.* **2008**, *56*, 7631−7636.

DOI: 10.1021/acs.jafc.5b01425
J. Agric. Food Chem. 2015, 63, 4130−4137

digestive physiology as a functional dietary fiber, which escapes digestion before the colon but can be fermented by the colonic bacteria. Depending on this property, it has been reported from our group that RS3[12] and RSA (resistant starch acetate; one of RS4) can be used as potential carrier materials for oral colon-specific drug delivery.[13−16]

However, the bioadhesion of RS is nonspecific, which may limit the delivery efficacy (including targeting accuracy) and the bioavailability of bioactive peptides and proteins.[17,18] It has been found that the GI mucosa epithelial cells are covered with specific glycan moieties in different sites of the GI tract.[19,20] If RS is coupled by certain ligands that can bind to the surface of predetermined colonic mucosa epithelial cells, the specific bioadhesion of RS carriers could be achieved, with increased residence time and enhanced adsorption of bioactive peptides and proteins in the colon. Lectins are glycoproteins of nonimmune origins that are able to specifically recognize sugar molecules and bind to glycosylated membrane components. Lectin−sugar interactions play crucial roles in many cell recognition and adhesion processes.[21−24] It has been reported that lectin-conjugated particles were of benefit to bioactive ingredients absorption because of the interactions between lectin and cells.[25,26] Considering this, it is worth conjugating suitable lectin to RSA, which has proved to have good colonic targeting and controlled-release properties.[13] Using this method, a colon-specific bioadhesive delivery system might be achieved that will improve the oral bioavailability of bioactive peptides and proteins.

In this regard, the fluorescein-labeled lectins (wheat germ agglutinin, concanavalin-A, peanut agglutinin, *Lens culinaris*, *Dolichos biflorus* agglutinin, *Ulex europaeus* agglutinin I, *Pisum sativum* agglutinin, *Phaseolus vulgaris* agglutinin and *Galanthus nivalis* agglutinin) of different carbohydrate specificities were screened in our lab for binding to human colonic mucosa epithelial cells through three types of human GI mucosa epithelial carcinoma cells, namely, MGC803, Hic, and Caco-2 cell lines, which were derived from human stomach, small intestine, and colon carcinomas, respectively. In addition, the colon-bioadhesion of the screened lectins was confirmed further in vivo in the gastrointestinal epithelial tissues of rats by tissue immunocytochemistry. Our previous research indicated that concanavalin A (Con A), one of the most abundant lectins that could bind to the mannose of glycoprotein on the surface of cells,[27] showed better colon bioadhesion. Thus, this lectin was conjugated to the surface of RSA-film-coated microparticles. The structure of the Con A−RSA complex was investigated using Raman spectra and X-ray diffraction. On the basis of this, the insulin-loaded microparticles coated with this Con A−RSA complex film were prepared, and their colonic targeting and bioadhesion of the decorated microparticles were determined by in vivo optical imaging and tissue section tests. Furthermore, the in vivo hypoglycemic response of this kind of insulin-loaded microparticles was evaluated in streptozotocin (STZ)-induced diabetic rats.

MATERIALS AND METHODS

Materials. RSA was synthesized in our laboratory according to a previously published method.[13] 1,1′-Carbonyldiimidazole (CDI) was purchased from Alfa Aesar. (Shanghai, China). Commercial long-acting insulin glargine injection was supplied by Sanofi-Aventis Deutschland GmbH (Frankfurt am Main, Hessen, Germany). Microcrystalline cellulose was purchased from Anhui Shanhe Medicinal Accessary Material Co., Ltd. (Huainan, Anhui, China). Insulin was purchased from Newprobe Bioscience & Technology Co., Ltd. (Beijing, China). Native corn starch (medicinal grade) used for excipients in the preparation of insulin-loaded microparticles cores was supplied by Defeng Starch Sugar Co., Ltd. (Shunde District, Foshan, Guangdong, China). Con A, molecular weight 102 000, was purchased from Medicago (Quebec, Canada). Fluorescein isothiocyanate (FITC), glycine, and STZ were purchased from Sigma-Aldrich Co. LLC (Santa Clara, CA, USA). Acetone, ethanol, phosphate buffer solution, isoflurance, ether, and glucose were purchased from Sinopharm Chemical Reagent Co. Ltd. (Shanghai, China). The remaining chemical reagents were of analytical grade.

Synthesis of Con A-Conjugated RSA. Con A was introduced to the hydroxyl groups of RSA by the CDI activation method.[28] RSA was suspended in acetone, followed by the addition of CDI, and stirred at 30 °C for 8−26 h. The concentration of RSA was 10−35%. The weight ratio between CDI and RSA was 0.08−0.5. After reaction, the mixture was filtered and washed with ethanol to remove unreacted CDI. The product (N-resistant starch acetate imidazolyl carbamate) was dried at 45 °C and sieved. The nitrogen content was determined by a Kjeldahl meter (BÜCHI distillation unit B-324, Buchi, Flawil, Switzerland). Then 1−10 g of N-resistant starch acetate imidazolyl carbamate was suspended in phosphate buffer solution (10 mmol/L; pH 7.4), followed by addition of Con A (the weight ratio between N-resistant starch acetate imidazolyl carbamate and Con A was varied from 0.001 to 0.03) and kept at 37 °C for 8−28 h. After reaction, the products were filtered and washed several times in phosphate buffer solution to remove unreacted Con A and incubated for 1 h in 0.5% glycine (w/v) in phosphate buffer solution to quench activated sites to which Con-A was not bound. The filtrate and washing liquor after reaction were collected, and the leftover of Con A was analyzed using a Coomassie Brilliant Blue kit (G-250, Bio-Rad Corp., Hercules, California, America) at 595 nm by a UV spectrophotometer (Unico, UV-3802, Shanghai, China). The coupled Con A was the difference value of Con A between the amount added and that left without reaction.

Structures of Con A-Conjugated RSA. *Raman Spectrometry.* The Raman spectra were acquired using a micro-Raman spectroscopy system (LabRAM Aramis, Horiba Jobia Yvon Corp., Villeneuve d'Ascq, France) equipped with a 532 nm laser source and grating of 1200 g/mm. Data were collected over a range of 100−4000 cm^{-1} at an interval of 1 cm^{-1} using 2 scans per sample with an exposure time of 5 s.

X-ray Diffraction. Wide-angle X-ray powder diffraction analysis was performed using an X-ray diffractometer (X'Pert Prox, Panalytial, Eindhoven, Netherlands) operating at 40 kV and 40 mA with Cu−K radiation (λ = 0.1542 nm). The diffractograms of samples were acquired at an angular range of 2θ from 4° to 60° with a step size of 0.033° and a counting time of 4 s for each step. The samples were sieved through 0.180 mm and equilibrated at 25 °C for 24 h prior to the analysis.

Preparation of Con A−RSA Film-Coated Microparticles. The preparation of insulin-loaded microparticle cores were obtained via extrusion−spheronization.[13] The N-resistant starch acetate formate imidazole obtained above was dissolved in acetone at a concentration of 5% and used as the initial coating material. The 1% insulin-loaded microparticle cores (500 μm in diameter) were coated by a bottom-spray method in a fluidized bed coater (Mini-XYT, Xinyite Co., Ltd., Shenzhen, Guangdong, China) until a proper film coating thickness was achieved, which was represented by the dry weight gain of the microparticles.[13] The parameters for the film coating process were as followed: inlet temperature, 30−35 °C; product temperature, 23−27 °C; spray rate, 0.7−0.8 mL/min; atomization pressure, 0.125−0.2 MPa; and fluidization pressure at 0.1−0.15 MPa. Then the film-coated microparticles were conjugated with Con A according to the method mentioned above and dried at 26 °C.

In Vivo Colonic Targeting and Bioadhesion of the Con A−RSA Film-Coated Microparticles. *In Vivo Fluorescent Imaging.* Six 5- or 6-week-old SPF grade nude mice (half males and half females, Vital River Laboratory Animal Technology Co., Ltd., Beijing, China)

DOI: 10.1021/acs.jafc.5b00393
J. Agric. Food Chem. 2015, 63, 4138−4147

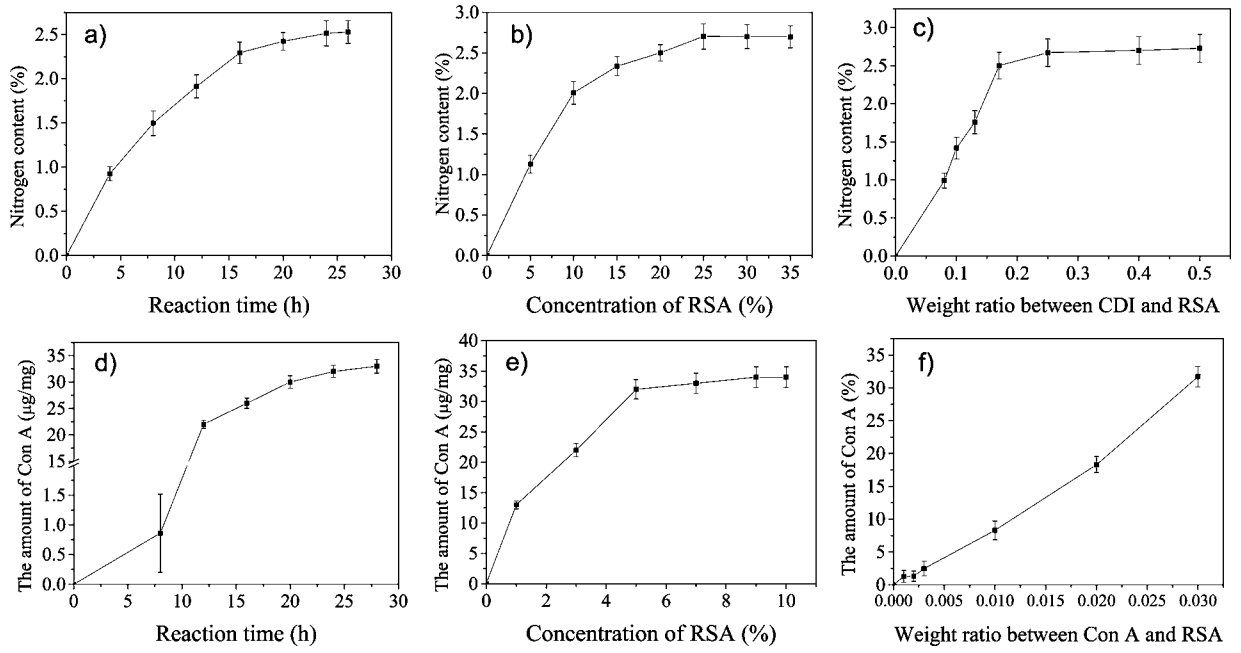

Figure 1. Effects of reaction time (a), concentration of RSA (b), weight ratio between 1,1′-carbonyldiimidazole and RSA (c) on the RSA activation by 1,1′-carbonyldiimidazole method; and the effects of reaction time (d), concentration of RSA (e), and weight ratio between Con A and RSA (f) on the reaction of Con A conjugated to RSA.

weighing approximately 12−14 g were fasted for 24 h before the study. The FITC-loaded microparticles coated with Con A−RSA film were orally administrated to the stomach via polyethylene tubing under light ether anesthesia. The microparticles were dosed at 0.2 mg per gram of body weight. At 2, 8, 14, and 44 min and at 24, 48, and 72 h after oral administration, the fluorescence intensity and transmission of the microparticles in the nude mice were observed by a whole-body small-animal in vivo imaging system (IVIS 200, Xenogen Corp., Alameda, CA, USA) at 445−490 nm of exciting light and 515−575 nm of emitted light with an exposure time of 5 s. The nude mice were anesthetized by isoflurance before being photographed.

Tissue Slices and Fluorescence Distribution. Six 5- or 6-week-old SPF grade KM mice (half males and half females, Vital River Laboratory Animal Technology Co., Ltd., Beijing, China) weighing approximately 18−22 g were fasted for 24 h before the study. The oral administration and dosage of FITC-loaded microparticles coated with Con A−RSA film was described in the previous section In Vivo Fluorescent Imaging". At 2, 4, 12, 24, 48, 72, and 144 h after oral administration, the mice were sacrificed by cervical dislocation, and the tissues of the stomach, small intestine, and colon were obtained. After washing the mucosal surface, the different parts of the mouse GI tract tissues were embedded with Optimum Cutting Temperature Compound and then cut on a cryostat microtome (Shandon cryotoZFE, ThermoFisher Scientific Inc., Waltham, MA USA) into 5 μm sections, and the tissue slices were thaw-mounted onto surface-treated glass slides. The FITC distribution in the different parts of the mouse GI tract and the fluorescence intensity were observed by a fluorescence microscope (BX51TRF, Olympus, Tokyo, Japan) at 445−490 nm of exciting light and 515−575 nm of emitted light.

In Vivo Hypoglycemic Response of Insulin-Loaded Microparticles Coated with Con A−RSA Film. The in vivo hypoglycemic response of the microparticles was evaluated using STZ-induced diabetic male Sprague-Dawley (SD) rats (Guangdong Animal Experimental Centre, Foshan, Guangdong, China).[12] The type II diabetic rats were randomly divided into five groups (n = 5 for each group, and the average plasma glucose concentrations of the different groups differed less than 2 mmol/L). The group that was subcutaneously injected with commercial long-acting insulin glargine injection at 35 IU/kg was the positive control group, and the diabetic group without insulin treatment was the negative control group. The other three groups are experimental groups. Before the tests, all the rats were fasted for 12 h with free access to water.

Effect of Con A Conjunction on the Surface of RSA Film on the Hypoglycemic Response after Single-Dose Oral Administration. The insulin-loaded microparticles coated by RSA film and Con A−RSA film were orally administered to the stomach via polyethylene tubing under light ether anesthesia. Insulin was dosed at different dosages: 60, 80, and 100 IU per kg body weight. After insulin administration, the rats in all the groups were allowed to diet freely. At predetermined time points, the plasma glucose concentrations of the rats were monitored by the glucose oxidase method.

Hypoglycemic Response after Successive Oral Administration. Current clinical use of long-acting insulin injections is generally subcutaneously injected at 19:00−21:00 every day. To coincide with the clinical use, the insulin-loaded microparticles coated with Con A−RSA film were orally administered at 19:00 on each of 5 consecutive days. On the first day, the insulin was dosed at 100 IU/kg; and from the second to the fifth days, the dose was 25, 40, 50 IU/kg, respectively. According to the predetermined time points for monitoring the plasma glucose concentrations of people with diabetes, the plasma glucose concentrations of the rats were monitored immediately before and 2 h after breakfast (8:00), lunch (12:00) and dinner (17:00) every day by the glucose oxidase method.

Oral Glucose Tolerance Test (OGTT). After oral administration for 5 successive days of the insulin-loaded microparticles coated with Con A−RSA film, all the rats from each group were fasted for 12 h with free access to water and orally administered with 20% glucose solution at 5.0 g/kg, and the rats of the negative control group received the same volume of distilled water. After glucose administration, the plasma glucose concentrations of the rats were measured at 30, 60, and 120 min.

Statistical Analysis. All data were subjected to statistical analysis using the SPASS 10.0 statistical package and were presented as mean ± standard deviation (± SD). Differences between groups were estimated by analysis of t test, and $P < 0.01$ was considered to indicate a statistically significant difference between two groups.

RESULTS AND DISCUSSION

Synthesis of Con A-Conjugated RSA. Con A was introduced to the hydroxyl groups of RSA by the conventional

DOI: 10.1021/acs.jafc.5b00393
J. Agric. Food Chem. 2015, 63, 4138−4147

CDI activation method.[28] The RSA with a DS of 1.94 and resistant starch content of ~90% was selected in this study. Its hydroxyl groups were activated by CDI and formed an imidazolyl carbamate complex that may be displaced by binding to the free amino group of Con A. The reaction is an N-nucleophilic substitution and results in a stable *N*-alkylcarbamate linkage of the ligand to the molecules of RSA. To investigate how the activation time, the RSA concentration, and the weight ratio between CDI and RSA will influence the level of activation, different amounts of RSA, activator and time periods were applied (shown in Figure 1). The optimized parameters for activating RSA were as follows: RSA concentration, 25% (w/v); weight ratio between CDI and RSA, 0.25; reaction temperature, 30 °C; and reaction time, 16 h. At these optimized conditions, the nitrogen content of RSA was at the highest value of 2.7%. This CDI-activated RSA was further treated with Con A. It can be seen from Figure 1b–d that the coupled Con A was at 0.86–34 μg/mg. The amount of coupled Con A could be 32 μg/mg when the concentration of RSA was 5% (w/v), the weight ratio between Con A and RSA was 0.03, and the reaction took place at 30 °C for 24 h.

The structural changes of RSA after conjugation with Con A were analyzed using Raman spectrometry and X-ray diffraction. The Raman spectrum of Con A had two bands at 620–640 cm^{-1} that indicated the stretching frequency associated with the C–S bond. The intense band at 1006 cm^{-1} presented in the spectra was the characteristic of the ring breathing of the benzene ring of phenylalanine. From Figure 2, the Raman spectrum of Con A–RSA possessed an absorption peak at 1006 cm^{-1}, indicating that the phenylalanine residue had been conjugated to RSA after reaction. In general, the presence of proteins can be noticed by amide I and amide III bands at about 1300 and 1655 cm^{-1}.[29,30] In the Raman spectrum of Con A, the absorption peaks at 1240 cm^{-1} were attributed to the N–H bending vibration band and the C–N stretching vibration band of amide III. The ν(C═O) stretch vibration band and N–H bending vibration of amide I caused an intense band at 1670 cm^{-1}.[31] The Raman spectrum of Con A-conjugated RSA had two bands at 1240 and 1670 cm^{-1}, which means the material has an O═C–NH group. The results of the Raman spectrum indicated that Con A had been successfully conjugated to RSA.

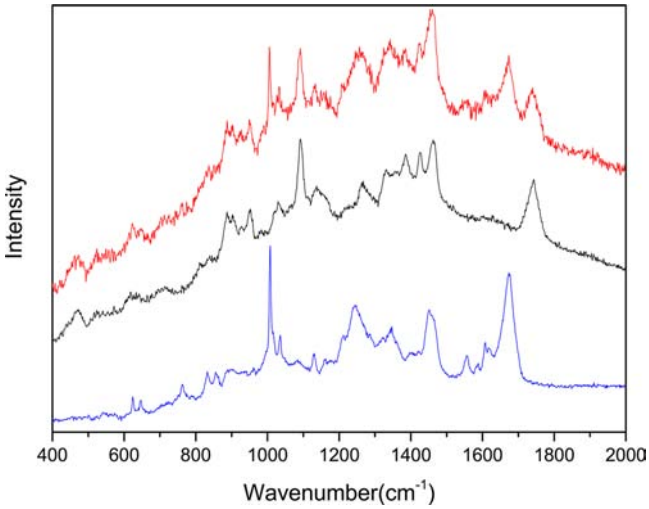

Figure 2. Effect of the conjugation of Con A on the molecular structure of RSA (from bottom to top are the Raman spectrum of Con A, RSA, and the Con A–RSA complex).

The XRD patterns of Con A and RSA coupled with different contents of Con A are shown in Figure 3. It can be seen that

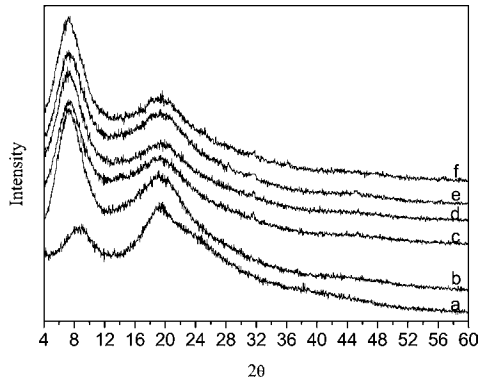

Figure 3. X-ray diffraction pattern of RSA with different contents of Con A (a, Con A; b, RSA; the contents of Con A are 8 (c), 18 (d), 32 (e), and 34 μg/mg (f)).

RSA had two humps on the XRD pattern at 7.2–7.3° and 19.0–19.7° that were related to the V-type starch crystalline structure. Thus, RSA presented a V-type diffraction pattern.[32] Con A had two humps on the XRD pattern at around 9° and 19° that were similar to that of RSA. After Con A was conjugated to RSA, the XRD pattern of Con A-conjugated RSA changed slightly. All the XRD patterns of Con A-conjugated RSA showed two humps on the diffraction pattern, suggesting that Con A-conjugated RSA was amorphous. The amorphous molecular chains of Con A-conjugated RSA could be easy to extend, which makes it possible to pass through mucosa and adhere to the surface of colonic epithelium cells.

Oral Colon-Targeting and Bioadhesive Property of the Con A–RSA Film-Coated Microparticles. *In Vivo Colonic Targeting in Mouse GI Tracts.* The size of Con A–RSA film-coated microparticles was ~500 μm in diameter (data not shown). Using in vivo fluorescent imaging observed by a whole-body small-animal in vivo imaging system, the oral colonic targeting capability of FITC-labeled microparticles coated with Con A–RSA film (the coupled Con A was 32 μg/mg) was studied. The images showing the microparticles distribution in different parts of the GI tract of nude mice at different times after oral administration of Con A–RSA film-coated microparticles are shown in Figure 4. Before administration, no fluorescence was shown in the nude mice (Figure 4a). With increased transit time after oral administration of Con A–RSA film-coated microparticles (from 2 to 44 min), the fluorescence spots moved from the stomach to the small intestine and then to the colon. The fluorescence intensity in the colon gradually increased. At 44 min after oral administration, all the fluorescence spots concentrated in the colon, indicating that the microparticles had been moved mainly to the colon (Figure 4b–e). As the transit time was prolonged further, the fluorescence intensity at the colon was gradually increased, and the fluorescence spots were enlarged, which suggested that FITC was released from the microparticles. When the transit time reached 72 h, the size of the fluorescence spot was smaller, but the intensity was still strong (Figure 4f–h). This indicated that Con A–RSA film-coated microparticles still existed in the colon. These results showed

DOI: 10.1021/acs.jafc.5b00393
J. Agric. Food Chem. 2015, 63, 4138–4147

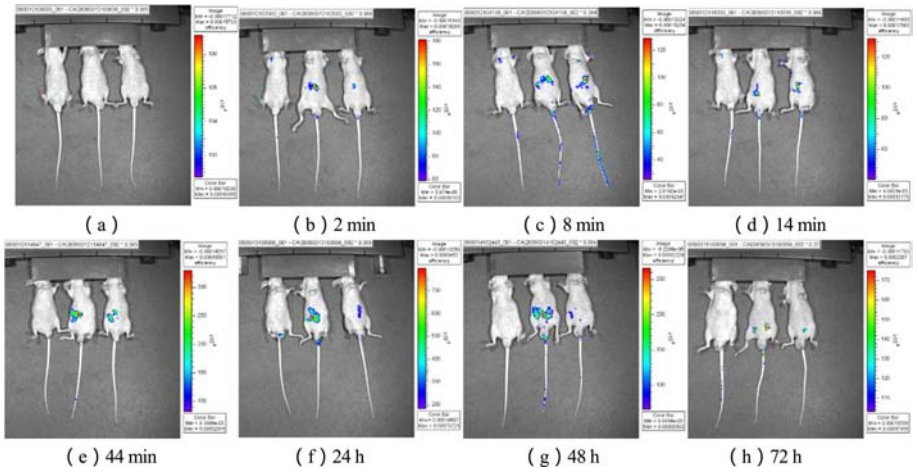

Figure 4. Microparticle transit after administration of fluorescein isothiocyanate loaded microparticles coated with Con A−RSA film in the gastrointestinal tract of nude mice at different time intervals (from left to right are the blank group and two Con A−RSA film-coated microparticle groups).

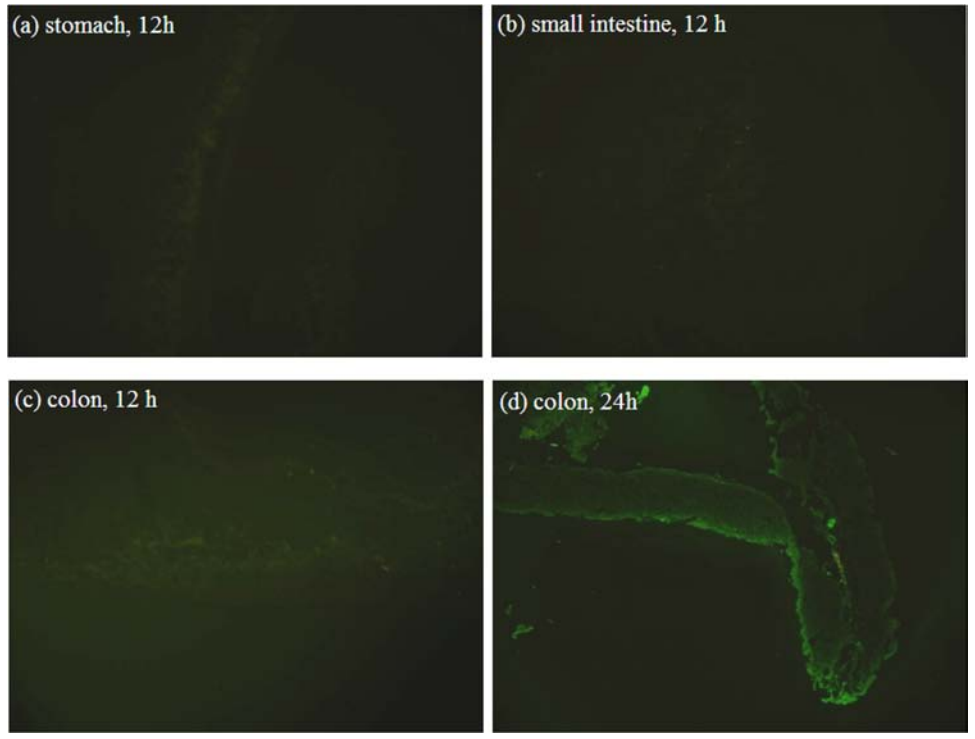

Figure 5. Fluorescence distribution after administration of fluorescein isothiocyanate-loaded microparticles coated with Con A−RSA film in the different regions of the gastrointestinal tract epithelial tissue of mice at different time intervals.

that Con A−RSA film-coated microparticles could not only target bioactive molecules to the colon but also stay in the colon for a longer time and continuously release bioactive molecules (FITC). This indicated good colonic targeting and bioadhesion abilities of Con A−RSA film-coated microparticles.

FITC Distribution in the Mouse GI Tract Epithelial Tissue. At 2 and 4 h after oral administration of Con A−RSA film-coated microparticles, no fluorescence was found in the GI tract epithelial tissue of mice because no FITC was released (the pictures are not shown). At 12 h after oral administration, very slight fluorescence was observed in the stomach and small intestine epithelial tissues (Figure 5a,b), meaning a very small amount of FITC was released in the stomach and small intestine. Meanwhile, minor green fluorescence was shown in the colon epithelial tissue (Figure 5c), suggesting that some of the FITC began to be released from the microparticles. When the administration time was prolonged to 24 h, the fluorescence intensity concentrated in the colon, indicating a large amount of FITC released in the colon (Figure 5d). These results showed that Con A−RSA film-coated microparticles could target and release the bioactive molecules to the colon.

To estimate the bioadhesion of Con A−RSA film-coated microparticles to the colon epithelial tissue, the difference in the FITC distribution in the mouse colon epithelial tissue was analyzed after prolonged administration of Con A−RSA film-coated microparticles and RSA film-coated microparticles, respectively. Figure 6 showed the FITC distribution in the mouse colon epithelial tissue at 24, 48, 72, and 144 h after oral

DOI: 10.1021/acs.jafc.5b00393
J. Agric. Food Chem. 2015, 63, 4138−4147

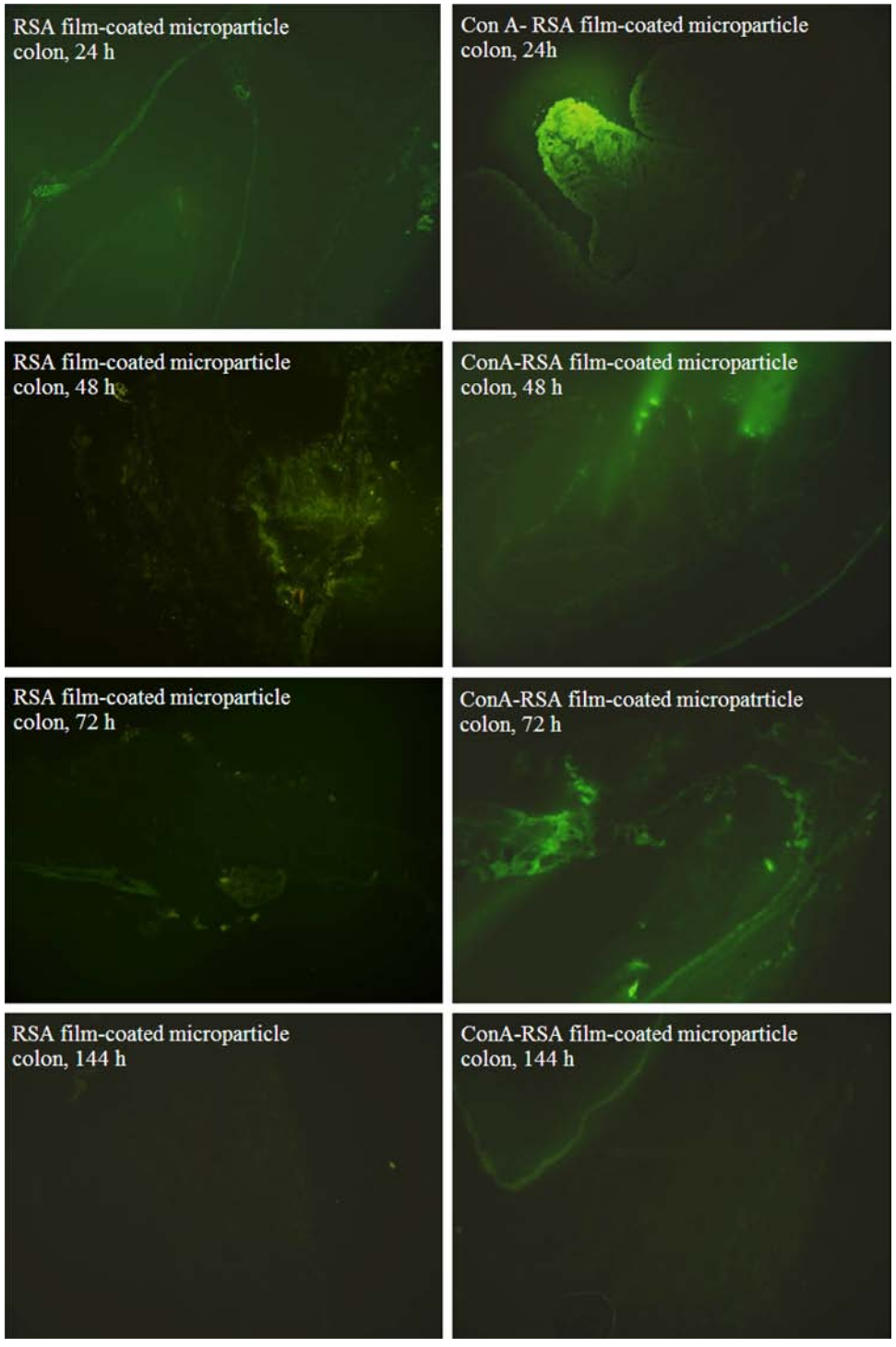

Figure 6. Fluorescence distribution after administration of fluorescein isothiocyanate-loaded microparticles coated with RSA film and Con A−RSA film in the colon epithelial tissue of mice at different time intervals (left, RSA film-coated microparticle group; right, Con A−RSA film-coated microparticles group).

administration of these two types of microparticles. By comparing the fluorescence intensity between images, the release behaviors of these two types of microparticles were shown to be different. It can be seen from Figure 6 that at the same time, the fluorescence intensity of the colon epithelial tissue slices after administration of Con A−RSA film-coated microparticles was stronger than that of the slices after administration of RSA film-coated microparticles. Moreover, at 24 h, the fluorescence intensity of the colon epithelial tissue slices after administration of RSA film-coated microparticles showed the highest value and then decreased as the time was further prolonged. This indicated that the microparticles could be easily eliminated from the body. When the time reached 144 h, the fluorescence had almost disappeared; however, for the colon epithelial tissue slices after administration of Con A−RSA film-coated microparticles, the fluorescence intensity still increased from 24 to 72 h and reached the highest value at 72 h. At 144 h, the fluorescence intensity was weaker but still

DOI: 10.1021/acs.jafc.5b00393
J. Agric. Food Chem. 2015, 63, 4138−4147

Table 1. Plasma Glucose Concentrations at Different Post-Administration Times in Diabetic Rats Following the Injected Insulin and Oral Administration of Rsa Film-Coated Microparticles with Different Insulin Dosages[a]

time, h	diabetic model group, (mmol/L)	insulin injected group, (mmol/L)	low-dose microparticles group, (mmol/L)	medium-dose microparticles group, (mmol/L)	high-dose microparticles group, (mmol/L)
0	17.9 ± 2.5	20.8 ± 4.3	17.7 ± 5.3	19.5 ± 3.2	19.0 ± 2.9
1	22.4 ± 2.6	11.6 ± 3.8[b]	29.7 ± 4.3[b,c]	30.3 ± 3.9[b,c]	32.5 ± 4.4[b,c]
2	25.1 ± 4.6	9.0 ± 3.9[b]	21.6 ± 5.2[c]	18.7 ± 4.0[c]	19.0 ± 3.4[c]
4	19.3 ± 3.7	5.6 ± 2.4[b]	13.0 ± 2.3[b,c]	9.7 ± 2.5[b]	11.1 ± 3.1[b,c]
6	16.4 ± 2.8	3.5 ± 0.6[b]	16.6 ± 3.5[c]	11.6 ± 2.8[d]	12.5 ± 2.8[c]
8	22.6 ± 3.0	6.5 ± 1.3[b]	11.3 ± 2.9[b,c]	7.5 ± 2.3[b]	5.9 ± 2.0[b,d]
10	17.9 ± 2.7	6.8 ± 0.9[b]	7.7 ± 2.2[b]	6.0 ± 1.3[b]	4.3 ± 1.5[b,d]
12	20.7 ± 3.4	6.4 ± 1.6[b]	9.7 ± 3.1[b]	5.2 ± 1.5[b,d]	5.0 ± 1.2[b,d]
24	17.9 ± 3.9	10.4 ± 2.9[b]	7.0 ± 1.9[b]	6.1 ± 1.8[b]	5.7 ± 0.8[b,c]
28	21.5 ± 4.4	14.5 ± 3.9[b]	6.3 ± 2.0[b,c]	6.0 ± 2.1[b,c]	6.2 ± 1.6[b,c]
30	18.7 ± 3.1	19.7 ± 3.9	6.9 ± 1.3[b,c]	6.8 ± 1.7[b,c]	7.0 ± 2.3[b,c]
36	19.4 ± 4.0	22.7 ± 4.7	7.8 ± 2.4[b,c]	6.9 ± 1.8[b,c]	8.3 ± 1.9[b,c]
48	18.0 ± 2.6	21.9 ± 3.6	15.1 ± 2.5[c]	16.3 ± 2.3[c]	15.7 ± 2.7[c]
52	20.0 ± 4.0	24.5 ± 4.6	17.6 ± 4.3	19.5 ± 3.7	19.5 ± 4.4
56	25.0 ± 3.3	26.5 ± 3.7	17.7 ± 3.5[b,c]	19.5 ± 4.5	19.0 ± 4.7[c]
60	23.1 ± 4.0	22.3 ± 4.0	29.7 ± 5.0	30.3 ± 4.2	32.5 ± 5.6[b,c]

[a] n=5 for each group. [b] Compared with those of the diabetic model group ($P < 0.01$). [c] Compared with those of the insulin injected group ($P < 0.01$). [d] Compared with those of the low-dose microparticles group ($P < 0.01$).

Table 2. Plasma Glucose Concentrations at Different Post-Administration Times in Diabetic Rats Following Injected Insulin and Oral Administration of Con A−RSA Film-Coated Microparticles with Different Insulin Dosages[a]

time, h	diabetic model group, (mmol/L)	insulin injected group, (mmol/L)	low-dose microparticles group, (mmol/L)	medium-dose microparticles group, (mmol/L)	high-dose microparticles group, (mmol/L)
0	19.9 ± 3.5	18.7 ± 2.4	18.1 ± 3.4	17.8 ± 3.0	21.6 ± 4.0
2	25.4 ± 3.7	10.6 ± 3.1[b]	30.9 ± 3.6[c]	30.0 ± 2.9[c]	28.1 ± 3.4[c]
6	23.3 ± 4.2	5.0 ± 1.5[b]	12.0 ± 2.8[b]	11.5 ± 2.2[b]	10.1 ± 2.7[b]
8	28.2 ± 3.3	3.6 ± 1.0[b]	12.9 ± 2.4[b,c]	12.1 ± 2.1[b,c]	9.4 ± 2.4[b]
10	26.6 ± 2.4	5.5 ± 0.9[b]	9.2 ± 1.5[b]	6.6 ± 1.4[b]	3.8 ± 1.8[b,d]
12	22.3 ± 2.9	6.5 ± 1.6[b]	6.4 ± 1.1[b]	4.7 ± 1.0[b]	4.2 ± 1.4[b]
24	18.7 ± 3.1	7.8 ± 2.1[b]	5.2 ± 0.9[b]	5.4 ± 1.4[b]	5.4 ± 1.6[b]
30	20.2 ± 3.4	12.4 ± 2.6[b]	6.9 ± 1.4[b,c]	6.5 ± 0.7[b,c]	6.3 ± 0.8[b,c]
36	22.6 ± 2.8	20.4 ± 3.4	7.6 ± 1.8[b,c]	7.1 ± 1.4[b,c]	6.7 ± 1.3[b,c]
48	21.5 ± 3.1	19.5 ± 2.9	7.3 ± 1.9[b,c]	7.1 ± 2.1[b,c]	6.2 ± 2.0[b,c]
54	18.5 ± 4.0	19.7 ± 3.7	7.5 ± 2.2[b,c]	6.5 ± 2.4[b,c]	6.4 ± 1.6[b,c]
60	21.2 ± 2.7	22.7 ± 4.0	11.7 ± 2.4[b,c]	10.5 ± 2.8[b,c]	9.7 ± 2.1[b,c]
72	19.4 ± 3.0	18.9 ± 2.9	18.0 ± 2.9	18.2 ± 3.4	18.5 ± 3.1
78	21.8 ± 3.7	24.5 ± 3.6	19.9 ± 3.4	19.3 ± 4.0	18.7 ± 3.2

[a] n = 5 for each group. [b] Compared with those of the diabetic model group ($P < 0.01$). [c] Compared with those of the insulin injected group ($P < 0.01$). [d] Compared with those of the low-dose microparticles group ($P < 0.01$).

stronger compared with that of slices after administration of RSA film-coated microparticles, indicating that Con A conjugated RSA film-coated microparticles can extend the residence time of the microparticles in the colon. These results showed that Con A conjugation to the surface of the RSA film could increase the microparticle residence time in the colon and enhance the bioactive molecules' (FITC) absorption effectively through bioadhesion to the surface of colonic mucosa cells.

In Vivo Hypoglycemic Response of Insulin-Loaded Microparticles Coated with Con A−RSA Film. *Hypoglycemic Response Improvement after Con A Conjunction on the Surface of RSA Film-Coated Microparticles.* After administration of the commercial long-acting insulin solution subcutaneously, the plasma glucose concentration decreased significantly within 1 h. A strong hypoglycemic response was observed between 4 and 12 h after injection; subsequently, the plasma glucose concentration increased with time and returned to the basal level at 30 h (Table 1). However, glycopenia (an abnormally low plasma glucose level of 3.5 ± 0.6 mmol/L) occurred at 6 h after injection. On the other hand, after RSA film-coated microparticles with different insulin dosages were orally administered, the hypoglycemic response was slowly but steadily maintained for a long time, and no glycopenia was observed between 8 and 36 h (total 28 h) (seen from Table 1). The hypoglycemic response was increased by an increase in the dosage of oral administration. It can be seen that the plasma glucose concentration declined into a lower range (6.3−9.7 mmol/L) at 10 h after oral administration of the low-dose microparticles and stayed within the lower range for 26 h. The medium-dose and the high-dose groups experienced a steady decrease in the plasma glucose concentration and stayed within the lower range for a total of 28 h, which was a little more rapid than that of the low-dose group. These results indicated that the plasma glucose concentration of the diabetic model rats was decreased steadily by using the RSA film-coated microparticles for the delivery of insulin; however, the plasma glucose

DOI: 10.1021/acs.jafc.5b00393
J. Agric. Food Chem. 2015, 63, 4138−4147

Table 3. Plasma Glucose Concentrations at Different Post-Administration Times in Diabetic Rats Following the Injected Insulin and Continuous Oral Administration of Con A−RSA Film-Coated Microparticles with Different Insulin Dosages[a]

time		diabetic model group, (mmol/L)	insulin injected group, (mmol/L)	low-dose microparticles group, (mmol/L)	medium-dose microparticles group, (mmol/L)	high-dose microparticles group, (mmol/L)
before administration		19.9 ± 2.5	20.0 ± 2.0	18.2 ± 2.1	17.9 ± 1.9	19.0 ± 2.5
first day	8:00	18.4 ± 2.7	6.7 ± 1.5[b]	4.3 ± 1.2[b]	4.3 ± 1.3[b]	4.1 ± 0.7[b]
	10:00	23.3 ± 3.2	9.5 ± 1.1[b]	9.2 ± 1.7[b]	8.6 ± 1.2[b]	8.6 ± 0.9[b]
	12:00	22.2 ± 3.4	6.8 ± 1.2[b]	5.7 ± 1.2[b]	5.4 ± 1.8[b]	6.2 ± 1.5[b]
	14:00	26.6 ± 2.8	10.7 ± 1.9[b]	10.9 ± 1.3[b]	11.0 ± 1.5[b]	9.9 ± 1.2[b]
	17:00	20.3 ± 2.9	7.1 ± 1.1[b]	5.1 ± 0.5[b]	5.6 ± 1.1[b]	5.7 ± 1.1[b]
	19:00	27.7 ± 3.1	11.4 ± 1.5[b]	9.2 ± 0.9[b]	10.4 ± 1.1[b]	10.3 ± 1.4[b]
second day	8:00	20.2 ± 2.9	6.1 ± 1.8[b]	6.6 ± 1.5[b]	5.6 ± 1.4[b]	5.3 ± 1.5[b]
	10:00	26.6 ± 2.7	10.7 ± 0.9[b]	12.4 ± 1.6[b]	9.7 ± 1.0[b]	10.9 ± 0.5[b]
	12:00	23.5 ± 3.1	5.6 ± 1.2[b]	7.0 ± 1.3[b]	6.1 ± 0.6[b]	5.8 ± 0.8[b]
	14:00	29.5 ± 3.2	11.1 ± 1.5[b]	12.8 ± 1.5[b]	11.2 ± 1.3[b]	10.9 ± 0.9[b]
	17:00	22.2 ± 2.7	6.0 ± 1.0[b]	7.8 ± 2.0[b]	6.3 ± 1.7[b]	5.9 ± 0.6[b]
	19:00	27.4 ± 3.0	11.6 ± 2.1[b]	14.2 ± 1.1[b]	11.4 ± 1.0[b]	10.8 ± 1.1[b]
third day	8:00	18.8 ± 2.6	6.0 ± 1.3[b]	7.7 ± 1.2[b]	5.7 ± 0.8[b]	5.4 ± 1.2[b]
	10:00	25.2 ± 3.1	10.7 ± 2.2[b]	13.3 ± 1.7[b]	11.1 ± 1.1[b]	10.2 ± 1.4[b]
	12:00	22.4 ± 3.1	5.9 ± 1.4[b]	9.5 ± 1.3[b]	6.2 ± 0.9[b]	5.7 ± 0.8[b]
	14:00	28.3 ± 2.6	10.6 ± 1.5[b]	13.8 ± 2.0[b]	11.3 ± 1.2[b]	10.8 ± 1.0[b]
	17:00	21.1 ± 2.7	6.0 ± 1.8[b]	9.6 ± 1.5[b]	6.7 ± 1.4[b]	6.1 ± 0.5[b]
	19:00	26.8 ± 3.0	11.3 ± 1.3[b]	14.5 ± 2.1[b]	11.4 ± 1.3[b]	10.9 ± 1.5[b]
fourth day	8:00	21.0 ± 3.5	6.2 ± 1.2[b]	7.9 ± 1.4[b]	5.7 ± 0.7[b]	5.3 ± 1.6[b]
	10:00	26.5 ± 2.5	10.4 ± 2.1[b]	13.4 ± 1.8[b]	11.2 ± 0.5[b]	10.4 ± 1.2[b]
	12:00	23.1 ± 2.6	6.1 ± 1.5[b]	9.8 ± 1.5[b]	6.6 ± 0.8[b]	6.0 ± 0.8[b]
	14:00	27.2 ± 2.9	10.3 ± 1.4[b]	14.4 ± 0.9[b]	11.1 ± 1.2[b]	10.8 ± 1.0[b]
	17:00	22.1 ± 3.0	5.8 ± 1.0[b]	9.8 ± 1.3[b]	6.7 ± 0.3[b]	6.0 ± 0.8[b]
	19:00	26.9 ± 3.1	10.2 ± 1.8[b]	16.3 ± 2.1[b,c]	11.8 ± 1.8[b]	10.2 ± 1.6[b,d]
fifth day	8:00	19.5 ± 2.8	5.5 ± 1.3[b]	13.0 ± 1.7[b,c]	6.8 ± 1.5[b,d]	5.5 ± 1.5[b,d]
	10:00	23.9 ± 3.0	10.1 ± 2.0[b]	16.8 ± 1.5[b,c]	11.6 ± 2.0[b]	10.3 ± 1.2[b,d]
	12:00	20.6 ± 3.2	6.1 ± 0.9[b]	13.4 ± 2.5[b,c]	7.0 ± 1.3[b,d]	6.1 ± 0.7[b,d]
	14:00	25.7 ± 3.1	10.2 ± 1.4[b]	17.5 ± 1.4[b,c]	12.9 ± 1.5[b]	10.6 ± 1.5[b,d]
	17:00	21.1 ± 3.8	6.0 ± 1.5[b]	13.3 ± 2.5[b,c]	7.0 ± 1.4[b,c]	5.8 ± 0.5[b,c]
	19:00	26.2 ± 3.3	10.2 ± 2.0[b]	16.6 ± 2.5[b,c]	12.3 ± 1.1[b]	10.3 ± 1.5[b,c]

[a] $n = 5$ for each group. [b] Compared with those of the diabetic model group ($P < 0.01$). [c] Compared with those of the insulin injected group ($P < 0.01$). [d] Compared with those of the low-dose microparticles group ($P < 0.01$).

concentration increased with time and returned to the basal level from 48 h after administration, suggesting that the RSA film-coated microparticles could be easily eliminated from the body.

The hypoglycemic response with different insulin dosages is shown in Table 2 for after Con A was conjugated to the surface of RSA film-coated microparticles. Comparing the data between Table 2 and Table 1, it is concluded that the time of the hypoglycemic response (when the plasma glucose concentration kept within a low range) was prolonged after the Con A−RSA film-coated microparticles with the same insulin dosage were orally administered. It can be seen that the plasma glucose concentration declined to a low range (5.2−9.2 mmol/L) from 10 to 54 h after administration of the low-dose and medium-dose microparticles and was kept within the lower range for 44 h. The high-dose group also showed the longest time of staying within a lower plasma glucose concentration from 8 to 60 h (for a total of 52 h). There was no glycopenia due to the steady release of insulin from the microparticles. In the treatment of diabetes mellitus, steadily decreasing the plasma glucose concentration is important to the patients.[33] Con A−RSA film-coated microparticles could adhere to the surface of colonic mucosa cells, increase the residence time in the colon, and steadily and sustainably release insulin. Thus, the plasma glucose concentration within the normal range could be maintained for a prolonged time (18−24 h with different insulin dosages), showing improved bioavailability of insulin.

Hypoglycemic Response after Successive Oral Administration. For investigating the continuous bioavailability of insulin delivered through Con A−RSA film-coated microparticles, the insulin-loaded microparticles were orally administered at 19:00 on each of 5 consecutive days. The plasma glucose concentration was assayed at 2 h before and after meals every day. Table 3 shows the blood glucose change by continuous administration of insulin-loaded Con A−RSA film-coated microparticles. After administration of microparticles, the plasma glucose concentration of experimental groups on the first day was at a low range, which was consistent with the results above. The differences among groups existed the following day. For the low-dose microparticles group, the plasma glucose concentration was at the upper level of the normal range on the second day. Then the plasma glucose concentration was out of the normal range, indicating that insulin for the low-dose microparticles group was not enough to decrease the plasma glucose. The plasma glucose concentration of the medium-dose microparticles group was within the normal range until the final day, but in the end, the plasma glucose concentration was higher than the normal level.

DOI: 10.1021/acs.jafc.5b00393
J. Agric. Food Chem. 2015, 63, 4138−4147

The plasma glucose concentration of the high-dose microparticles was steady during all the 5 days, which showed a hypoglycemic response similar to that of the group subcutaneously injected with commercial long-acting insulin.

OGTT mimics the physiological conditions of the glucose/insulin system closely and evaluates the insulin sensitivity and the β-cell function.[34,35] After 5 days of continuous administration with insulin-loaded Con A−RSA film-coated microparticles, the OGTTs were conducted; the results of different groups are shown in Figure 7. It can be seen from Figure 7 that

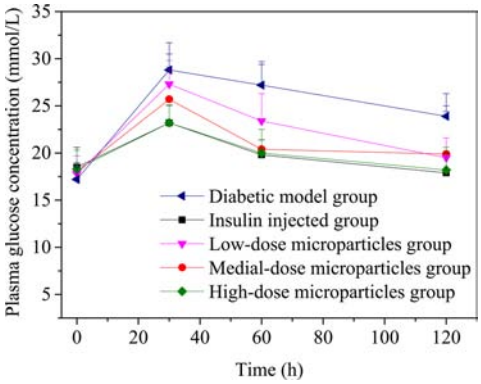

Figure 7. Results of oral glucose tolerance test in different rat groups.

the glucose tolerance of the type II diabetic rats after administration of the microparticles was gradually enhanced, with greater enhancement seen with increased insulin dosage. Compared with the diabetic model group, the high-dose microparticles group had a glucose tolerance similar to that of the insulin-injected group. In conclusion, Con A−RSA film-coated microparticles could adhere to the surface of colonic mucosa cells, prolonging the insulin release time and enhancing the hypoglycemic response. Thus, this study demonstrates the potential of Con A−RSA film-coated microparticles for oral colon-targeted delivery of polypeptide or protein ingredients with enhanced oral bioavailability.

Although the use of lectins as targeting ligands remains problematic because of their cytotoxic effects, which would preclude their use in targeting delivery systems,[36,37] the toxic effects of lectins are varied with different varieties. We did the toxicity tests when we screened the lectins of different carbohydrate specificities for binding to human colonic mucosa epithelial cells. The relative growth rate of Caco-2 cells was high (80%) when Caco-2 cells were exposed to Con A solutions in the microgram range (7.8−50 μg/cell) for 60 h (data not shown). This result indicated that the toxic effects of Con A would not be aggravated because the amounts of Con A conjugated to the microparticle surface were in the microgram range. Furthermore, the approach to overcome this limitation is to produce recombinant lectins with modified properties and to design and synthesize peptides or other organic molecules that mimic the function of the lectins.[38−40] Thus, better biocompatibility may result from the lectin-sugar interactions, which is applicable to the colon-specific bioadhesive delivery system.

AUTHOR INFORMATION

Corresponding Authors

*Phone: +86 20 8711 3252. Fax: +86 20 8711 3252. E-mail: xxlee@scut.edu.cn.

*E-mail: felchen@scut.edu.cn.

Funding

We acknowledge the National Natural Science Funds of China (No. 31271824); the National Science and Technology Supporting Program Projects (2012BAD33B04); the Ministry of Education Special R&D Funds for the Doctoral Disciplinary Stations in Universities (20120172110014); the Office of Education of Guangdong Province Science and Technology Innovation (Key) Projects in Universities (2012CXZD0006); the Ministry of Education Program for Supporting New Century Excellent Talents (NCET-12-0193); and the Fundamental Research Funds for the Central Universities, SCUT (2013ZG0009).

Notes

The authors declare no competing financial interest.

REFERENCES

(1) Day, L.; Seymour, R. B.; Pitts, K. F.; Konczak, I.; Lundin, L. Incorporation of functional ingredients into foods. *Trends Food Sci. Technol.* **2009**, *20*, 388−395.

(2) Mills, S.; Stanton, C.; Hill, C.; Ross, R. New developments and applications of bacteriocins and peptides in foods. *Annu. Rev. Food Sci. Technol.* **2011**, *2*, 299−329.

(3) Hartmann, R.; Meisel, H. Food-derived peptides with biological activity: from research to food applications. *Curr. Opin. Biotechnol.* **2007**, *18*, 163−169.

(4) McClements, D. J.; Decker, E. A.; Park, Y.; Weiss, J. Structural design principles for delivery of bioactive components in nutraceuticals and functional foods. *Crit. Rev. Food Sci. Nutr.* **2009**, *49*, 577−606.

(5) Maroni, A.; Zema, L.; Del Curto, M. D.; Foppoli, A.; Gazzaniga, A. Oral colon delivery of insulin with the aid of functional adjuvants. *Adv. Drug Delivery Rev.* **2012**, *64*, 540−56.

(6) Varum, F. J. O.; McConnell, E. L.; Sousa, J. J. S.; Veiga, F.; Basit, A. W. Mucoadhesion and the Gastrointestinal Tract. *Crit. Rev. Ther. Drug Carrier Syst.* **2008**, *25*, 207−258.

(7) Wittaya-areekul, S.; Kruenate, J.; Prahsarn, C. Preparation and in vitro evaluation of mucoadhesive properties of alginate/chitosan microparticles containing prednisolone. *Int. J. Pharm.* **2006**, *312*, 113−118.

(8) Haupt, S.; Zioni, T.; Gati, I.; Kleinstern, J.; Rubinstein, A. Luminal delivery and dosing considerations of local celecoxib administration to colorectal cancer. *Eur. J. Pharm. Sci.* **2006**, *28*, 204−211.

(9) Sharma, A.; Yadav, B. S.; Ritika. Resistant starch: Physiological roles and food applications. *Food Rev. Int.* **2008**, *24*, 193−234.

(10) McConnell, E. L.; Short, M. D.; Basit, A. W. An in vivo comparison of intestinal pH and bacteria as physiological trigger mechanisms for colonic targeting in man. *J. Controlled Release* **2008**, *130*, 154−60.

(11) Thompson, D. B. Strategies for the manufacture of resistant starch. *Trends Food Sci. Technol.* **2000**, *11*, 245−253.

(12) Situ, W.; Chen, L.; Wang, X.; Li, X. Resistant starch film-coated microparticles for an oral colon-specific polypeptide delivery system and its release behaviors. *J. Agric. Food Chem.* **2014**, *62*, 3599−609.

(13) Pu, H. Y.; Chen, L.; Li, X. X.; Xie, F. W.; Yu, L.; Li, L. An Oral Colon-Targeting Controlled Release System Based on Resistant Starch Acetate: Synthetization, Characterization, and Preparation of Film-Coating Pellets. *J. Agric. Food Chem.* **2011**, *59*, 5738−5745.

(14) Li, X.; Liu, P.; Chen, L.; Yu, L. Effect of resistant starch film properties on the colon-targeting release of drug from coated pellets. *J. Controlled Release* **2011**, *152*, e5−e7.

(15) Chen, L.; Pu, H. Y.; Li, X. X.; Yu, L. A novel oral colon-targeting drug delivery system based on resistant starch acetate. *J. Controlled Release* **2011**, *152*, E51−E52.

(16) Chen, L.; Li, X.; Li, L.; Guo, S. Acetylated starch-based biodegradable materials with potential biomedical applications as drug delivery systems. *Curr. Appl. Phys.* **2007**, *7*, e90−e93.

DOI: 10.1021/acs.jafc.5b00393
J. Agric. Food Chem. 2015, 63, 4138−4147

(17) Vasir, J. K.; Tambwekar, K.; Garg, S. Bioadhesive microspheres as a controlled drug delivery system. *Int. J. Pharm.* **2003**, *255*, 13−32.
(18) Smart, J. D. The basics and underlying mechanisms of mucoadhesion. *Adv. Drug Delivery Rev.* **2005**, *57*, 1556−1568.
(19) Gabius, H. J.; Andre, S.; Kaltner, H.; Siebert, H. C. The sugar code: functional lectinomics. *Biochim. Biophys. Acta, Gen. Subj.* **2002**, *1572*, 165−177.
(20) Gabius, H. J. The sugar code in drug delivery. *Adv. Drug Delivery Rev.* **2004**, *56*, 421−424.
(21) Ensign, L. M.; Cone, R.; Hanes, J. Oral drug delivery with polymeric nanoparticles: The gastrointestinal mucus barriers. *Adv. Drug Delivery Rev.* **2012**, *64*, 557−570.
(22) Gabor, F.; Bogner, E.; Weissenboeck, A.; Wirth, M. The lectin-cell interaction and its implications to intestinal lectin-mediated drug delivery. *Adv. Drug Delivery Rev.* **2004**, *56*, 459−480.
(23) Kilpatrick, D. C. Animal lectins: a historical introduction and overview. *Biochim. Biophys. Acta, Gen. Subj.* **2002**, *1572*, 187−197.
(24) Gajbhiye, V.; Gong, S. Lectin functionalized nanocarriers for gene delivery. *Biotechnol. Adv.* **2013**, *31*, 552−562.
(25) Jepson, M. A.; Clark, M. A.; Foster, N.; Mason, C. M.; Bennett, M. K.; Simmons, N. L.; Hirst, B. H. Targeting to intestinal M cells. *J. Anat.* **1996**, *189* (Pt 3), 507−16.
(26) Pusztai, A.; Ewen, S. W.; Grant, G.; Peumans, W. J.; Van Damme, E. J.; Coates, M. E.; Bardocz, S. Lectins and also bacteria modify the glycosylation of gut surface receptors in the rat. *Glycoconjugate J.* **1995**, *12*, 22−35.
(27) Rüdiger, H.; Gabius, H.-J. Plant lectins: occurrence, biochemistry, functions and applications. *Glycoconjugate J.* **2001**, *18*, 589−613.
(28) Stollner, D.; Scheller, F. W.; Warsinke, A. Activation of cellulose membranes with 1,1′-carbonyldiimidazole or 1-cyano-4-dimethylaminopyridinium tetrafluoroborate as a basis for the development of immunosensors. *Anal. Biochem.* **2002**, *304*, 157−65.
(29) De Gelder, J.; De Gussem, K.; Vandenabeele, P.; Moens, L. Reference database of Raman spectra of biological molecules. *J. Raman Spectrosc.* **2007**, *38*, 1133−1147.
(30) Zhu, G.; Zhu, X.; Fan, Q.; Wan, X. Raman spectra of amino acids and their aqueous solutions. *Spectrochim. Acta, Part A* **2011**, *78*, 1187−1195.
(31) Jaaskelainen, A.-S.; Holopainen-Mantila, U.; Tamminen, T.; Vuorinen, T. Endosperm and aleurone cell structure in barley and wheat as studied by optical and Raman microscopy. *J. Cereal Sci.* **2013**, *57*, 543−550.
(32) Rindlava, A.; Hulleman, S. H. D.; Gatenholm, P. Formation of starch films with varying crystallinity. *Carbohydr. Polym.* **1997**, *34*, 25−30.
(33) Monnier, L.; Mas, E.; Ginet, C.; Michel, F.; Villon, L.; Cristol, J. P.; Colette, C. Activation of oxidative stress by acute glucose fluctuations compared with sustained chronic hyperglycemia in patients with type 2 diabetes. *JAMA-J. Am. Med. Assoc.* **2006**, *295*, 1681−1687.
(34) Bartoli, E.; Fra, G. P.; Schianca, G. P. C. The oral glucose tolerance test (OGTT) revisited. *Eur. J. Intern. Med.* **2011**, *22*, 8−12.
(35) Palumbo, P.; Ditlevsen, S.; Bertuzzi, A.; De Gaetano, A. Mathematical modeling of the glucose-insulin system: A review. *Math. Biosci.* **2013**, *244*, 69−81.
(36) Smart, J. D. Lectin-mediated drug delivery in the oral cavity. *Adv. Drug Delivery Rev.* **2004**, *56*, 481−489.
(37) Yun, Y.; Cho, Y. W.; Park, K. Nanoparticles for oral delivery: targeted nanoparticles with peptidic ligands for oral protein delivery. *Adv. Drug Delivery Rev.* **2013**, *65*, 822−832.
(38) Eck, J.; Langer, M.; Möckel, B.; Witthohn, K.; Zinke, H.; Lentzen, H. Characterization of recombinant and plant-derived mistletoe lectin and their B-chains. *Eur. J. Biochem.* **1999**, *265*, 788−797.
(39) Lambkin, I.; Pinilla, C.; Hamashin, C.; Spindler, L.; Russell, S.; Schink, A.; Moya-Castro, R.; Allicotti, G.; Higgins, L.; Smith, M. Toward targeted oral vaccine delivery systems: selection of lectin mimetics from combinatorial libraries. *Pharm. Res.* **2003**, *20*, 1258−1266.
(40) des Rieux, A.; Pourcelle, V.; Cani, P. D.; Marchand-Brynaert, J.; Preat, V. Targeted nanoparticles with novel non-peptidic ligands for oral delivery. *Adv. Drug Delivery Rev.* **2013**, *65*, 833−844.

DOI: 10.1021/acs.jafc.5b00393
J. Agric. Food Chem. 2015, 63, 4138−4147

Flavonoids are abundant constituents of fruits, vegetables, and herbal beverages. Several food-derived flavonoids are associated with effects that prevent human disease, including protection from oxidative stress, inflammation, cardiovascular disease, neurodegeneration, and cancer.[10] Most of the beneficial effects of flavonoids have been demonstrated to involve the modulation of gene expression by activating or interacting with miRNAs. Recently, dietary flavonoids have been reported to regulate miRNA expression in animal and cell culture models. Flavonoids such as epigallocatechin-3-gallate (EGCG), quercetin, proanthocyanins, and citrus flavonoids have been shown to modulate miRNA transcription and, consequently, to control several biological functions in vitro or in vivo.[11,12]

Luteolin (3′,4′,5,7-tetrahydroxyflavone), a member of the flavone subgroup of flavonoids, is found in many vegetables, fruits, and herbs and is especially enriched in celery, parsley, orange, broccoli, cabbage, and green pepper. It exhibits antioxidant, anti-inflammatory, and anticancer activities.[13] Recently, several studies have shown that luteolin potentially exerts neuroprotective effects. Luteolin has been reported to reduce the neurotoxicity induced by neurotoxic agents in cell culture systems.[14,15] In addition to neuroprotection, luteolin has been shown to possess the neuritogenic activities in PC12 cells.[16,17] In animal studies, luteolin has been demonstrated to permeate the BBB to exert antiamnesic effects against amyloid toxicity in mice, protect against cognitive dysfunction induced by chronic cerebral hypoperfusion in rats and improve MPTP-induced Parkinsonism in mice.[18−20] In our previous studies, we have demonstrated that luteolin is a neurotrophic agent that promotes neurite outgrowth and neuronal differentiation via the activation of cell signaling cascades including the PKC-dependent and PKA- or ERK-dependent CREB/miR-132 pathways in PC12 cells.[21,22]

In the present study, we performed miRNA microarray analysis and identified luteolin-responsive miRNAs during neurite outgrowth of PC12 cells. Among the miRNAs up- or down-regulated by luteolin in PC12 cells, we focused on miR-34a, which was robustly and significantly upregulated in response to luteolin. We further elucidated in detailed mechanisms by which luteolin regulated miR-34a expression and examined the effects of miR-34a on the luteolin-mediated neurite outgrowth of PC12 cells.

MATERIALS AND METHODS

Materials. Luteolin, poly-L-lysine, dimethyl sulfoxide (DMSO), pifithrin-α (PFT-α), H-89, RPMI-1640 medium, nonessential amino acids (NEAA), and other chemicals, unless otherwise indicated, were purchased from Sigma-Aldrich Co. (St. Louis, MO, USA). The mouse 7S nerve growth factor (NGF) was purchased from Millipore (Billerica, MA, USA). Resveratrol was purchased from Tokyo Chemical Industry (Tokyo, Japan). The inhibitors U0126, SB203580, and LY294002 were purchased from Promega (Madison, WI, USA). SP600125 was purchased from Enzo Life Sciences (Ann Arbor, MI, USA). Bisindolylmaleimide I (BIM) was purchased from Cayman Chemical (Ann Arbor, MI, USA).

Cell Culture. PC12 cells were obtained from Bioresource Collection and Research Center (Hsinchu, Taiwan) and were maintained in RPMI-1640 medium supplemented with 10% heat-inactivated horse serum (HS), 5% fetal bovine serum (FBS) (Invitrogen, Carlsbad, CA, USA), and 1% NEAA in a 5% CO_2 incubator at 37 °C.

RNA Extraction and microRNA Microarray Analysis. Total cellular RNA was extracted from cells using Trizol reagent (Invitrogen) according to the manufacturer's protocol. Fluorescent targets were prepared from 2.5-μg total RNA samples using the miRNA ULSTM Labeling Kit (Kreatech Diagnostics, The Netherlands). The labeled miRNA targets enriched using NanoSep 100 K (Pall Corporation, NY, USA) were hybridized to the Mouse & Rat miRNA OneArray (Phalanx Biotech Group, Hsinchu, Taiwan), which contains triplicate unique miRNA probes from mouse and rat (miRBase Release 15.0). The fluorescence intensities of each spot were analyzed using GenePix 4.1 software (Molecular Devices, Sunnyvale, CA, USA). The normalized spot intensities were transformed to $\log_2$ ratios of gene expression between the control and treatment groups. The spots displaying a $\log_2$ ratio ≥ 0.7 or ≤ -0.7 and a p-value < 0.05 were selected for further analysis.

Analysis of Neurite Outgrowth in PC12 Cells. The quantification of neurite outgrowth in PC12 cells was performed as described previously.[4] Briefly, PC12 cells (2×10^5/ml) were seeded on poly-L-lysine-coated 6-well plates in standard serum-containing medium. After 24 h of incubation, the medium was replaced with low-serum (1% HS and 0.5% FBS) medium and treated with vehicle (0.1% DMSO) or luteolin for the indicated period. The cells were photographed using an inverted microscope (Olympus IX71), and the images were subsequently examined by counting the cells that were positive for neurites. The neurite-bearing cells were counted from ten randomly selected microscopic fields, which contained an average of 100 cells per field. The number of differentiated cells was measured by counting those cells that had at least one neurite with an length equal to the cell body diameter. The data are expressed as percentages of the total cells in the field. Each experiment was conducted in triplicate.

Reverse Transcription Quantitative PCR (RT-Q-PCR) Analysis of Pre-miR-34a and Mature miR-34a. PC12 cells were seeded on poly-L-lysine-coated 60 mm plates in standard serum-containing medium. After 24 h of incubation, the cells were incubated in low-serum medium and exposed to vehicle (0.1% DMSO) or the indicated compounds for the indicated period. Total cellular RNA was prepared using Trizol reagent (Invitrogen) according to the manufacturer's protocol. For the pre-miR-34a measurement, total cellular RNA was reverse-transcribed using a High Capacity cDNA reverse transcription kit (Applied Biosystems, Foster City, CA, USA). Quantitative real-time PCR was then performed using specific primers [pre-miR-34a, 5′-CGGCTGTGAGTAATTCTTTGG-3′ (forward) and 5′-CAACG-TGCAGCACTTCTAGG-3′ (reverse); β-actin, 5′-CCTCTGAAC-CCTAAGGCCAA-3′ (forward); and 5′-AGCCTGGATGGCTA-CGTACA-3′ (reverse)] and Maxima SYBR Green/ROX qPCR Master Mix (Fermentas, Burlington, ON, CA). Amplification was performed using an ABI Prism 7300 Real-Time PCR System. The PCR conditions used were as follows: 94 °C for 4 min followed by 40 cycles at 94 °C for 1 min, 58 °C for 1 min, and 72 °C for 1 min. The $\Delta\Delta C_t$ method was used for the data analysis of pre-miR-34a expression, which was estimated in triplicate samples and was normalized to the β-actin expression levels.

For the determination of mature miR-34a expression, RNA was reverse-transcribed using a TaqMan MicroRNA Reverse Transcription Kit (Applied Biosystems), and this product was subjected to a TaqMan miRNA assay (Applied Biosystems) using primers and probes specific for miR-34a or for the internal control U6 RNA according to the manufacturer's protocol. Amplification was performed using an ABI Prism 7300 Real-Time PCR System. The PCR conditions were as follows: 95 °C for 10 min followed by 40 cycles at 95 °C for 15 s and 60 °C for 1 min. The $\Delta\Delta C_t$ method was used for the data analysis of miR-34a expression, which was estimated in triplicate samples and was normalized to the U6 RNA expression levels.

Transfection of Anti-miR-34a Oligonucleotides. Transfection of anti-miR oligonucleotides was performed as described previously.[22] Briefly, PC12 cells were seeded on poly-L-lysine-coated 6-well plates in standard serum-containing medium for 24 h. The cells were then incubated in serum-free OPTI-MEM and transfected with antisense miR-34a (Ambion Anti-miR miRNA inhibitor) (Applied Biosystems) or a scrambled control miRNA (Ambion Anti-miR negative control #1) (Applied Biosystems) at a final concentration of 150 pmol/mL using the Lipofectamine 2000 reagent (Invitrogen) for 5 h. After

DOI: 10.1021/acs.jafc.5b01005
J. Agric. Food Chem. 2015, 63, 4148−4159

Table 1. MicroRNA expRession Profile of Luteolin-Treated PC12 Cells

	fold change[a]			
miRNAs	$\log_2$(8 h/0 h)	$\log_2$(24 h/0 h)	$\log_2$(48 h/0 h)	$\log_2$(72 h/0 h)
rno-miR-29a	0.76	1.07	0.84	0.76
rno-miR-29b	1.85	1.57	2.13	2.03
rno-miR-30a	1.10	1.21	1.50	1.38
rno-miR-30e	1.18	1.44	1.34	1.21
rno-miR-34a	1.20	1.52	2.42	2.57
rno-miR-192	1.48	1.47	0.74	0.84
rno-miR-210	0.98	1.24	1.13	0.79
rno-miR-322	1.03	1.64	1.67	1.49
rno-miR-324-5p	0.76	1.01	0.93	0.61
rno-miR-351	0.83	1.76	1.66	0.98
rno-miR-362	0.63	1.28	1.38	1.41
rno-miR-450a	0.87	1.76	1.66	0.98
rno-miR-483	0.61	0.71	0.90	1.17
rno-miR-500	0.60	0.87	1.39	1.18
rno-miR-501	0.80	1.25	1.40	0.89
rno-miR-532-5p	0.80	1.18	1.47	1.27
rno-miR-7a	−0.70	−0.81	−0.83	−1.02
rno-miR-10a-3p	−0.65	−1.81	−1.07	−0.77
rno-miR-668	−1.27	−1.92	−1.57	−0.63

[a]The fold change of mean normalized density of two replicates for each group. Only miRNAs ($p < 0.05$) with $\log_2$(ratio) ≥ 0.7 or ≤ -0.7 were presented.

transfection for 24 h, the cells were incubated in low-serum medium and treated with vehicle or luteolin for 72 h.

Western Blot Analysis. PC12 cells were seeded on poly-L-lysine-coated 100 mm dishes in standard serum-containing medium. After 24 h of incubation, the cells were then incubated in low-serum medium and exposed to vehicle or luteolin for the indicated period. Total cellular protein samples were prepared using RIPA buffer (Thermo Fisher Scientific, Inc., Rockford, IL, USA). The proteins were separated via 10% SDS-PAGE and were subsequently transferred to a PVDF membrane (PerkinElmer, Boston, MA, USA). The membranes were incubated in the following specific antibodies: anti-p53 (Santa Cruz Biotechnology, Santa Cruz, CA, USA), antiphospho-p53 (Ser15), anti-SirT1, anti-p38, antiphospho-p38 MAPK (Thr180/Tyr182), anti-JNK, antiphospho-JNK (Cell Signaling Technology, Danvers, MA, USA), anti-p53 (Acetyl K381) (Abcam, Cambridge, MA, USA), and monoclonal anti-β-actin (Sigma-Aldrich). Then, the membranes were incubated in the appropriate HRP-conjugated secondary antibodies (Santa Cruz Biotechnology, Santa Cruz, CA, USA) for 1 h. The proteins were detected using Amersham ECL Prime Western Blotting Detection Reagent (GE Healthcare, Buckinghamshire, UK), and the signal was visualized on Amersham Hyperfilm ECL (GE Healthcare).

Statistical Analysis. All experiments were repeated at least three times, and the values are expressed as the mean ± SD. Statistic calculations were performed using IBM SPSS Statistics 22.0 software. The results were analyzed using one-way ANOVA with Dunnett's posthoc test, and a p-value < 0.05 was considered statistically significant.

RESULTS

miR-34a: Highly Expressed during Luteolin-Induced Neurite Outgrowth in PC12 Cells. In our previous studies, we have demonstrated that luteolin (20 μM) significantly induced neurite outgrowth and neuronal differentiation in PC12 cells.[21] We first examined the differential expression of miRNAs during the luteolin-induced neuronal differentiation of PC12 cells via a genome-wide screen. To identify the miRNA expression profile of luteolin-mediated neurite outgrowth, the PC12 cells were treated with luteolin (20 μM) for 0, 8, 24, 48, or 72 h, and the miRNA levels were analyzed using Mouse & Rat miRNA OneArray expression profiling microarrays as described in the Materials and Methods section. A total of 16 and 3 miRNAs were robustly and significantly up-regulated ($\log_2$ ratio ≥ 0.7) and down-regulated ($\log_2$ ratio ≤ -0.7), respectively, in the PC12 cells treated with luteolin for 8−72 h compared to the 0 h-treated control cells (Table 1 and Figure S1, Supporting Information). Based on microarray analysis, among the 16 luteolin-induced miRNAs, the induction of miR-34a was the most pronounced, displaying increases of 2.3-, 2.9-, 5.3- and 6.0-fold after treatment of the cells with luteolin for 8, 24, 48, and 72 h, respectively (Figure 1).

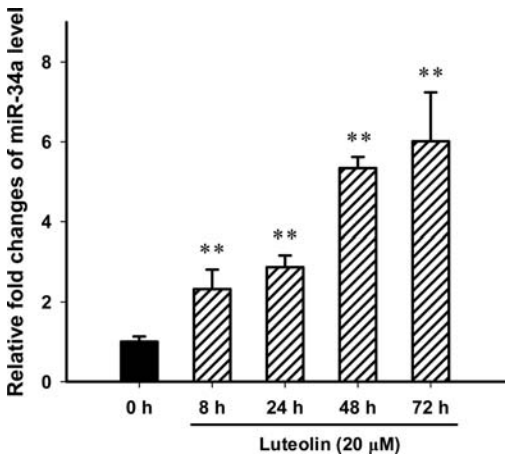

Figure 1. Fold-changes in miR-34a expression in luteolin-treated PC12 cells based on microarray analysis. The fluorescence intensities from the microarray data were analyzed as described in the Materials and Methods section. The fold-change in the expression level of miR-34a was measured and presented as the mean ± SD from the analysis of duplicate arrays. **$p < 0.01$ represents a significant difference compared to the 0 h group.

DOI: 10.1021/acs.jafc.5b01005
J. Agric. Food Chem. 2015, 63, 4148−4159

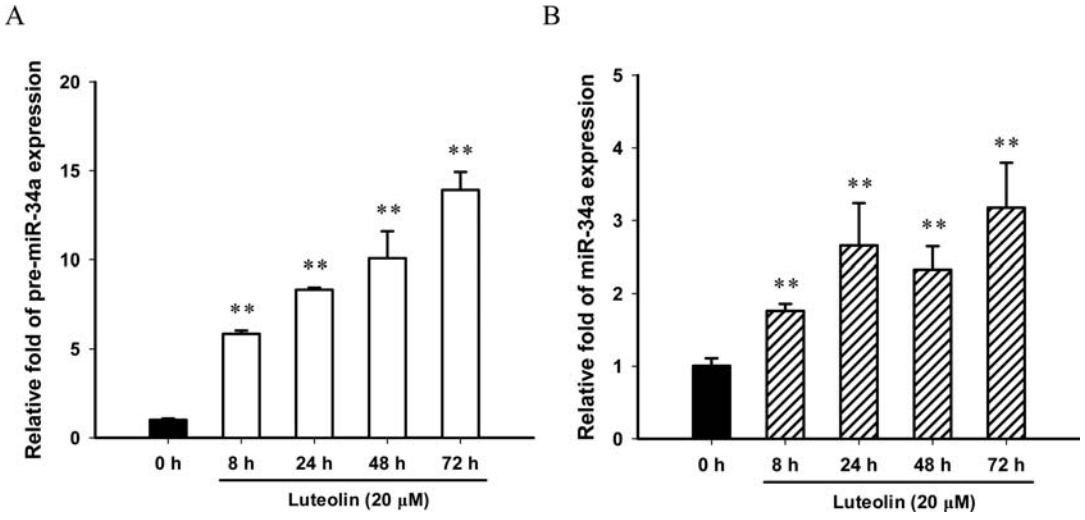

Figure 2. Luteolin induces miR-34a expression in PC12 cells. PC12 cells were treated with vehicle (0.1% DMSO) or luteolin (20 μM) for 8−72 h. Cellular RNA was prepared, and (A) the levels of pre-miR-34a and (B) mature miR-34a were determined via RT-Q-PCR as described in the Materials and Methods section. The data are presented as the means ± SD from three independent experiments. $^{**}p < 0.01$ represents a significant difference compared to the 0 h group.

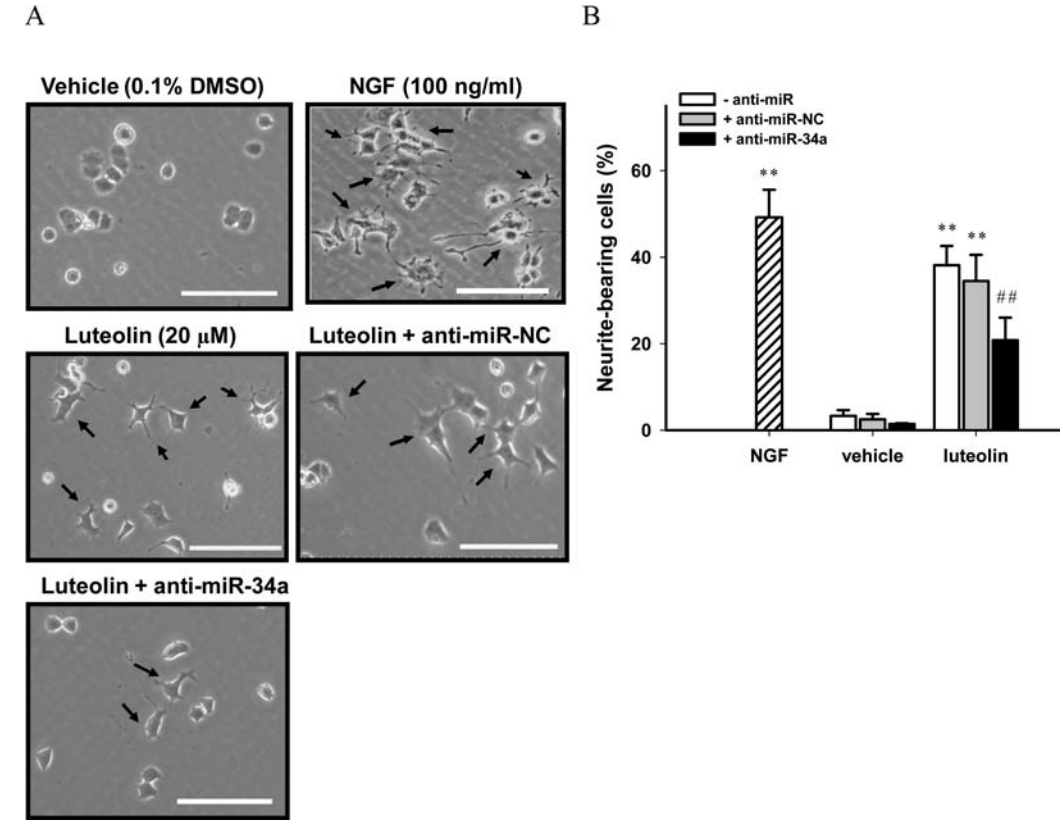

Figure 3. miR-34a is involved in the luteolin-induced neurite outgrowth of PC12 cells. (A) PC12 cells were transfected with antisense oligonucleotides targeting miR-34a (anti-miR-34a) or a scrambled negative control antisense miRNA (anti-miR-NC) for 24 h as described in the Materials and Methods section. After transfection, the PC12 cells were exposed to vehicle (0.1% DMSO) or luteolin (20 μM) for 72 h. The PC12 cells were treated with NGF (100 ng/mL) alone for 72 h as a positive control. Cell morphology was observed and photographed. The arrowheads indicate neurite-bearing cells; scale bar, 100 μm. (B) Neurite-bearing cells analyzed as described in the Materials and Methods section. The data are presented as the means ± SD from three independent experiments. $^{**}p < 0.01$ represents a significant difference compared to the vehicle-treated cells. $^{\#\#}p < 0.01$ represents a significant difference compared to the anti-miR-NC-treated cells.

To verify the effect of luteolin on miR-34a expression, PC12 cells were treated with luteolin (20 μM) for the indicated period. The RNA levels of precursor or mature miR-34a were determined via RT-Q-PCR as described in the Materials and Methods section. As shown in Figure 2A, the treatment of the cells with luteolin for 8 or 72 h markedly increased pre-miR-34a expression by 5.9- and 14.0-fold, respectively. Mature miR-34a expression was significantly elevated by 2.7-fold after 24 h-

DOI: 10.1021/acs.jafc.5b01005
J. Agric. Food Chem. 2015, 63, 4148−4159

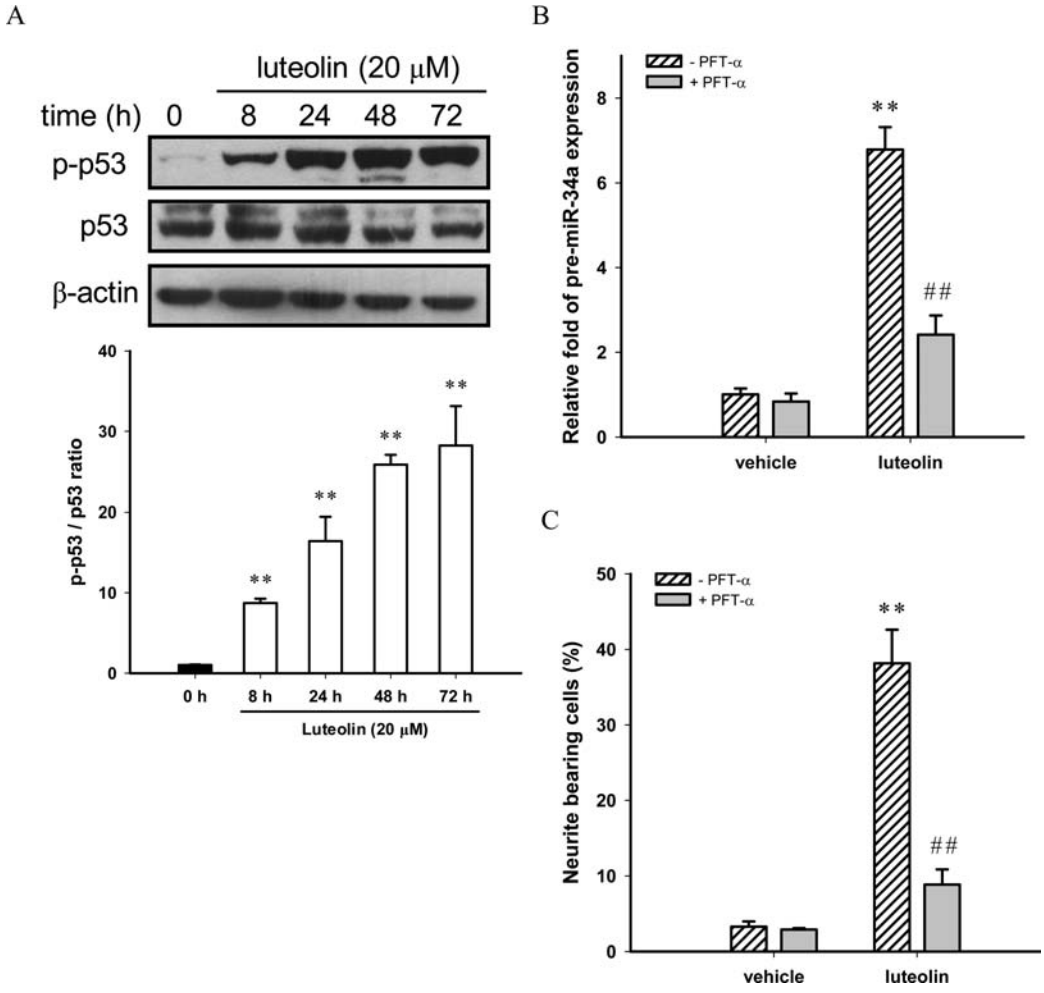

Figure 4. Contribution of p53 phosphorylation to luteolin-induced miR-34a expression and neurite outgrowth. (A) PC12 cells were treated with luteolin (20 μM) for 8−72 h, and the p53 and β-actin protein levels were analyzed via Western blot analysis. The immunoblot experiments were replicated at least three times, and a representative Western blot is shown. The intensity of phospho-p53-Ser15 (p-p53) normalized to that of p53 is presented as the means ± SD of three independent experiments. $^{**}p < 0.01$ represents a significant difference compared to the 0 h group. (B) PC12 cells were pretreated with the p53 inhibitor pifithrin-α (PFT-α, 20 μM) for 30 min and then exposed to vehicle (0.1% DMSO) or luteolin (20 μM) for 8 h. The levels of pre-miR-34a were determined via RT-Q-PCR. (C) PC12 cells were pretreated with pifithrin-α (PFT-α, 20 μM) for 30 min and then exposed to vehicle or luteolin (20 μM) for 72 h. Neurite-bearing cells were analyzed as described in the Materials and Methods section. The data are presented as the means ± SD from three independent experiments. $^{**}p < 0.01$ represents a significant difference compared to the vehicle-treated cells. $^{\#\#}p < 0.01$ represents a significant difference compared to the PFT-α-untreated cells.

treatment with luteolin (20 μM), and the miR-34a levels remained increased by 3.1-fold after 72 h of luteolin exposure ($p < 0.01$) (Figure 2B). This result indicated that luteolin exposure for 8−72 h highly up-regulates miR-34a expression in PC12 cells.

Effects of miR-34a Expression on the Luteolin-Induced Neurite Outgrowth of PC12 Cells. To investigate the effect of miR-34a expression on the luteolin-induced neurite outgrowth of PC12 cells, we used antisense miR-34a (anti-miR-34a) to knock down the levels of miR-34a. The PC12 cells were transfected with a negative control antisense miRNA (anti-miR-NC) or anti-miR-34a as described in the Materials and Methods section and then treated with vehicle or luteolin (20 μM) for 72 h; we achieved approximately a 92% knockdown of miR-34a in PC12 cells (Figure S2, Supporting Information). The percentage of neurite-bearing cells was further measured. Figure 3A and B shows that luteolin significantly increased the percentage of neurite outgrowth to 38.1 ± 4.5% relative to vehicle (3.3 ± 1.3%) ($p < 0.01$), as expected. The activity was comparable to those of the positive control, nerve growth factor (NGF). However, luteolin-mediated neurite outgrowth was significantly attenuated to 20.8 ± 5.2% in the cells transfected with anti-miR-34a; luteolin-induced neurite outgrowth remained unchanged in the anti-miR-NC-transfected cells (36.5 ± 6.1%). These results revealed that luteolin-induced miR-34a expression is involved in the neurite outgrowth of PC12 cells.

p53 Activation Involved in Luteolin-Mediated miR-34a Up-Regulation and Neurite Outgrowth. It has been reported that the primary miR-34a transcript is induced by p53 activation.[23] Ser15 of the p53 protein is a major target of primary phosphorylation, and its phosphorylation is required for p53 function in the physiological context of p53-responsive promoters.[24] Thus, to investigate whether luteolin-induced miR-34a up-regulation acts via p53 activation in PC12 cells, Western blot analysis was performed as described in the Materials and Methods section. As shown in Figure 4A, the treatment of PC12 cells with luteolin (20 μM) for 8 h markedly

DOI: 10.1021/acs.jafc.5b01005
J. Agric. Food Chem. 2015, 63, 4148−4159

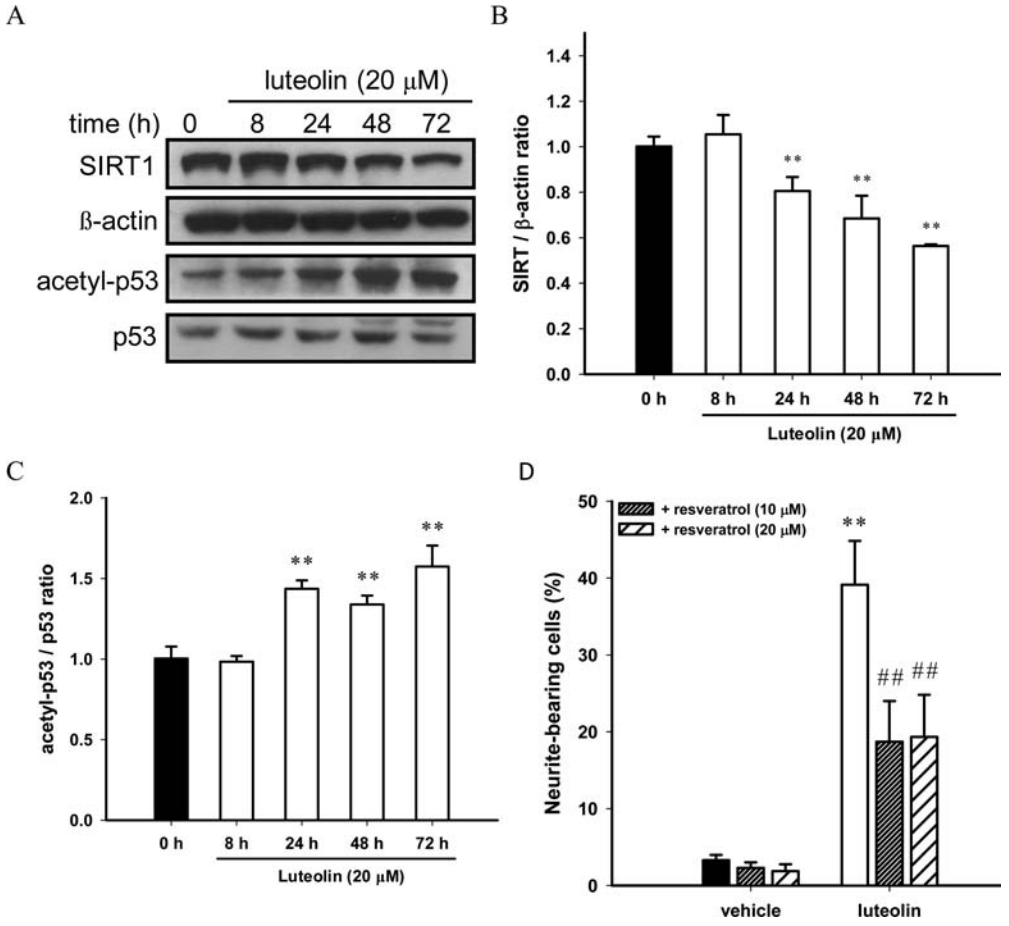

Figure 5. Effect of Luteolin on the Level of SIRT1 Protein. PC12 cells were treated with luteolin (20 μM) for 8−72 h. (A) SIRT1 and acetylated p53-Lys379 (acetyl-p53) proteins were analyzed via Western blot analysis. The immunoblot experiments were replicated at least three times, and a representative Western blot is shown. (B) Intensity of SIRT1 normalized to that of β-actin and (C) intensity of acetylated p53 normalized to that of p53 is presented as the means ± SD of three independent experiments. $^{**}p < 0.01$ represents a significant difference compared to the 0 h group. (D) PC12 cells were preincubated in resveratrol (10 or 20 μM) for 30 min and then exposed to vehicle or luteolin (20 μM) for 72 h. Neurite-bearing cells were analyzed as described in the Materials and Methods section. The data represent the means ± SD from three independent experiments. $^{**}p < 0.01$ represents a significant difference compared to the vehicle-treated cells. $\#\#p < 0.01$ represents a significant difference compared the resveratrol-untreated cells.

increased the phosphorylation of p53 at Ser15 by 8.7-fold, peaking at 48−72 h, compared to the 0 h treatment ($p < 0.01$).

The direct relationship between p53 phosphorylation and miR-34a up-regulation was further investigated by exposing the PC12 cells to pifithrin-α (PFT-α), a specific inhibitor that was shown to block the transcriptional activity of p53.[25] Luteolin-mediated pre-miR-34a expression was markedly attenuated by the treatment of PC12 cells with 20 μM PFT-α for 8 h (Figure 4B). Furthermore, the treatment of PC12 cells with PFT-α for 72 h significantly reduced the percentage of luteolin-induced neurite outgrowth from 38.1 ± 4.5% to 9.6 ± 1.9% ($p < 0.01$) (Figure 4C). These results suggested that luteolin induces neurite outgrowth via the p53-dependent up-regulation of miR-34a in PC12 cells.

Effect of Luteolin on Sirtuin 1 (SIRT1) Expression in PC12 Cells. It has been reported that overexpressed miR-34a targets the 3′-untranslated region (3′-UTR) of sirtuin 1 (SIRT1) and reduces its protein level, leading to enhanced levels of acetylated p53, elevated p53 binding activity, and promoted neuronal differentiation in embryonic cortical neuron and neuroblastoma cell lines.[26−28] Therefore, we further investigated the effect of luteolin exposure on the SIRT1 protein level in PC12 cells. As shown in Figure 5A and B, the protein level of SIRT1 was significantly reduced by treatment with luteolin (20 μM) for 24−72 h. Furthermore, we examined the effect of luteolin on the level of acetylated p53, a substrate of SIRT1-mediated deacetylation. As shown in Figure 5C, the level of acetylated p53 (K379) protein was significantly elevated by treatment with luteolin (20 μM) for 24−72 h. In addition, luteolin-induced neurite outgrowth was significantly attenuated by exposure to resveratrol, a SIRT1 activator,[29] compared to treatment with luteolin alone in PC12 cells (Figure 5D). These data indicated that the SIRT1 protein level is reduced, leading to increased acetylated p53 levels, during luteolin-mediated neuronal differentiation.

Signaling Pathways Involved in Luteolin-Mediated miR-34a Up-Regulation and Neurite Outgrowth in PC12 Cells. It has been known that the activation of signal transduction pathways, including MAPK, protein kinase C (PKC), protein kinase A (PKA), and PI3/Akt, is involved in the control of neuronal differentiation.[21,30,31] Thus, the possible involvement of these signaling pathways in luteolin-induced pre-miR-34a transcription and neurite outgrowth was investigated using kinase-specific inhibitors of these pathways. As shown in Figure 6A, luteolin-induced miR-34a transcription was markedly abolished by inhibitors of JNK (SP600125) or

DOI: 10.1021/acs.jafc.5b01005
J. Agric. Food Chem. 2015, 63, 4148−4159

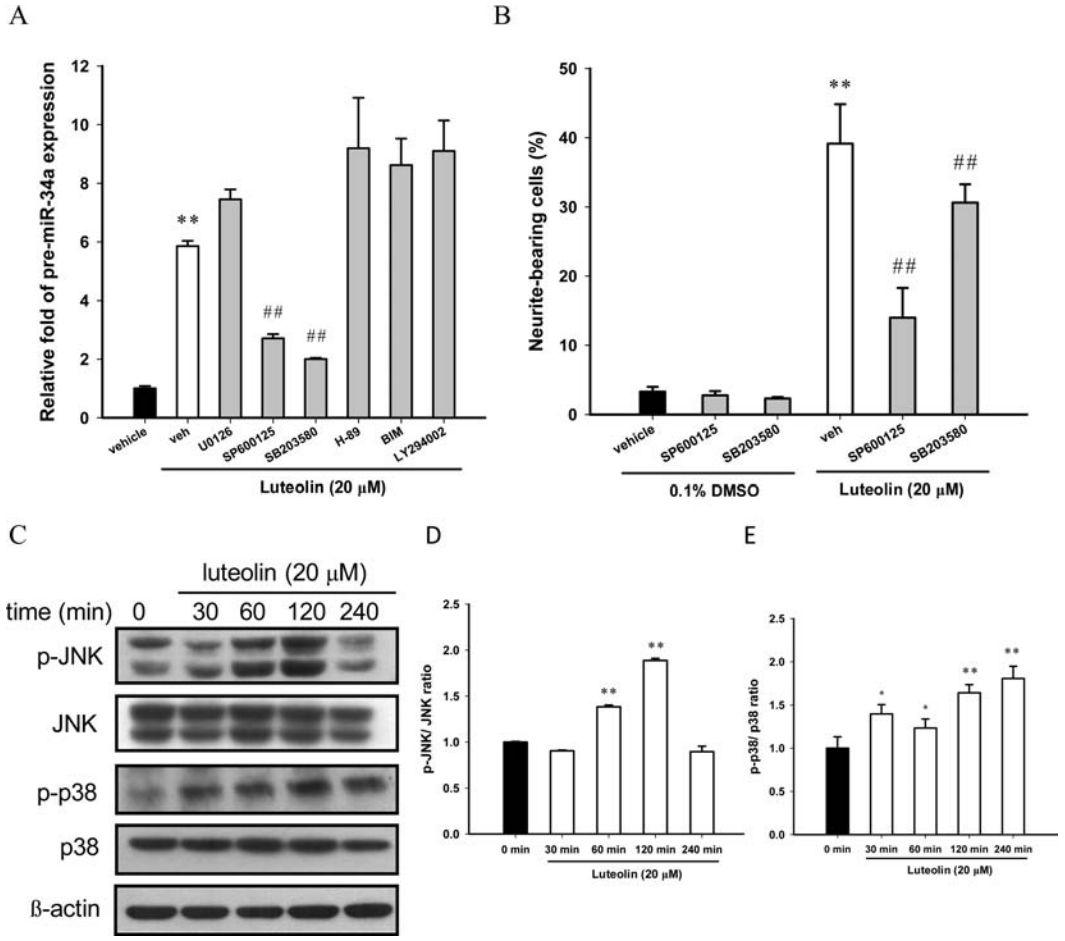

Figure 6. Involvement of JNK and p38 MAPK activation in luteolin-mediated miR-34a expression and neurite outgrowth. (A) PC12 cells were pretreated for 30 min with vehicle or one of the following inhibitors: U0126 (10 μM), SP600125 (10 μM), SB203580 (10 μM), H-89 (10 μM), BIM (2.5 μM), or LY294002 (40 μM). Then, the cells were exposed to luteolin (20 μM) for 8 h. The levels of pre-miR-34a were determined via RT-Q-PCR. $^{**}p < 0.01$ represents a significant difference compared to the vehicle-treated cells. $^{\#\#}p < 0.01$ represents a significant difference compared to the inhibitor-untreated (veh) group. (B) PC12 cells were pretreated for 30 min with vehicle, the inhibitor SP600125 (10 μM) or SB203580 (10 μM), followed by exposure to luteolin (20 μM) for 72 h. Neurite-bearing cells were analyzed, and the data are presented as the means ± SD from three independent experiments. $^{**}p < 0.01$ represents a significant difference compared to the vehicle-treated cells. $^{\#\#}p < 0.01$ represents a significant difference compared to the inhibitor-untreated (veh) group. (C) PC12 cells were treated with luteolin (20 μM) for 30, 60, 120, or 240 min. The phospho-JNK (p-JNK), JNK, phospho-p38 (p-p38), p38, and β-actin protein levels were analyzed via Western blot. The immunoblot experiments were replicated at least three times, and a representative Western blot is shown. (D) Intensity of p-JNK normalized to that of JNK and (E) intensity of p-p38 normalized to that of p38, respectively, presented as the means ± SD of three independent experiments. $^{*}p < 0.05$ and $^{**}p < 0.01$ represents a significant difference compared to the 0 min group.

p38 MAPK (SB203580) ($p < 0.01$). However, the inhibitors of MEK1/2 (U0126), PKC (BIM), PKA (H-89), and PI3/Akt (LY294002) did not reduce the level of miR-34a transcription in the luteolin-treated cells. Luteolin-induced neurite outgrowth was also attenuated by pretreatment of PC12 cells with the inhibitor SP600125 or SB203580 (Figure 6B). Next, we attempted to verify the signaling pathways activated by luteolin in PC12 cells. As shown in Figure 6C–E, the phosphorylation of JNK by luteolin (20 μM) treatment peaked at 120 min. Luteolin induced p38 MAPK activation at 30 min and peaked at 240 min after treatment ($p < 0.01$). These results confirmed the critical roles of the activation of the JNK and p38 MAPK pathways in the luteolin-mediated up-regulation of miR-34a and enhancement of neurite outgrowth. Furthermore, we examined whether these kinase-mediated signaling pathways are associated with luteolin-mediated p53 phosphorylation. As shown in Figure 7, the results showed that the inhibition of kinase activity using SP600125 or SB203580 did not block the luteolin-mediated phosphorylation of p53 at Ser15. Our findings demonstrated that luteolin induced miR-34a up-regulation and neurite outgrowth via p53-dependent and p53-independent pathways in PC12 cells.

DISCUSSION

High intake of fruits, vegetables, and beverages rich in polyphenolic phytochemicals may be associated with a decreased risk of several human chronic diseases, including neurodegenerative disorders. Emerging evidence supports that dietary flavonoids exert direct neuroprotective effects by interacting with cell signaling pathways, regulating transcription factors, and modulating gene expression. MicroRNAs are known as post-transcriptional modulators that regulate various biological activities, such as cell growth, differentiation, apoptosis, and metabolism. In the present study, we identified the changes in the miRNA expression profile caused by luteolin treatment in PC12 cells. The major finding of this study was

DOI: 10.1021/acs.jafc.5b01005
J. Agric. Food Chem. 2015, 63, 4148−4159

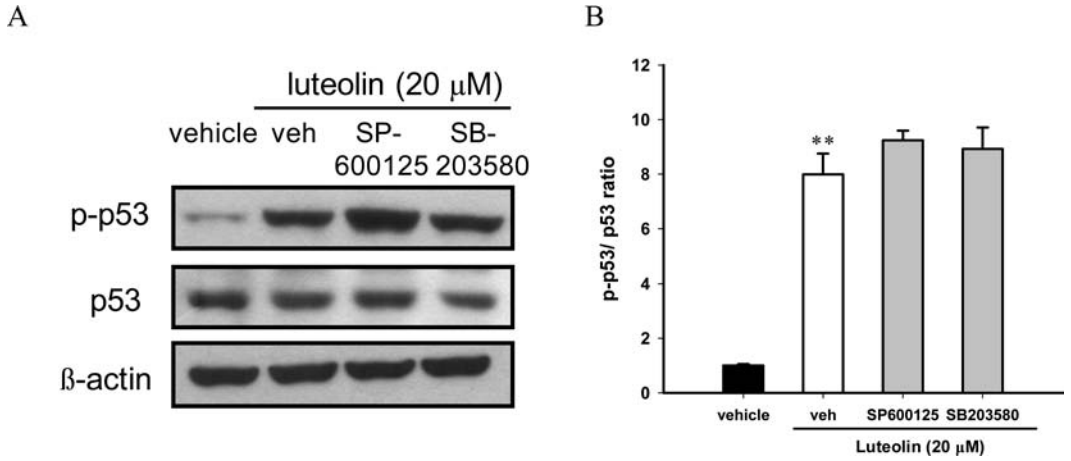

Figure 7. Activation of the JNK and p38 pathways did not affect luteolin-induced p53 phosphorylation. PC12 cells were treated with vehicle, the inhibitor SP600125 or SB203580 for 30 min prior to exposure to luteolin (20 μM) for 8 h. The levels of phospho-p53-Ser[15] (p-p53), p53, and β-actin were analyzed via Western blot. (A) Immunoblot experiments replicated at least three times. A representative Western blot is shown. (B) Intensity of p-p53 normalized to that of p53 presented as the means ± SD of three independent experiments. $^{**}p < 0.01$ represents a significant difference compared to the vehicle-treated group.

that luteolin induced a high level of miR-34a expression by increasing p53 phosphorylation and by activating the JNK and p38 MAPK p53-independent signaling pathways in response to luteolin-mediated neuronal differentiation in PC12 cells. Moreover, our findings revealed that luteolin attenuates the level of SIRT1, a known target gene of miR-34a, and induces an increase in the level of acetylated p53 (Figure 8). Our findings

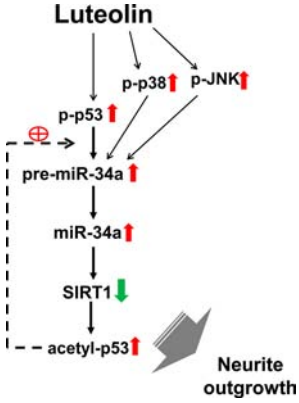

Figure 8. Hypothetical mechanism by which the miR-34a/SIRT1 axis is involved in the luteolin-mediated neurite outgrowth of PC12 cells. Luteolin induces the up-regulation of miR-34a via the activation of JNK-, p38-, and p53-dependent pathways. Thus, miR-34a may serve as a modulator of SIRT1 activity to increase p53 acetylation, potentially stimulating and maintaining neurite outgrowth in PC12 cells.

suggested the existence of a positive feedback loop in which p53 stimulates miR-34a expression, which modulates SIRT1 to increase p53 activity, potentially stimulating and maintaining neurite outgrowth in PC12 cells.

Several studies have demonstrated that luteolin has great potential to provide a neurotrophic or neuroprotective efficacy for prevention or treatment of neurodegenerative disorders. The bioavailability of luteolin is low because of its poorly soluble in water. Zhou et al. reported that oral administration of luteolin (14.3 mg/kg) in rats, it found that the plasma concentration of luteolin gradually increased and the maximal concentration (C_{max}) of luteolin was 1.97 ± 0.15 μg/mL (equivalent to 6.9 ± 0.5 μM).[32] Lin et al. demonstrated that the plasma concentration of luteolin was rapidly distributed and slowly decayed after luteolin administration via the femoral vein at a dose of 10 mg/kg in rats. The maximal concentrations (C_{max}) of luteolin could reach 7.47 ± 3.78 μg/mL (equivalent to 26.1 ± 13.2 μM) at 5 min and continually decreased up until 360 min after luteolin administration. During the oral administration of luteolin at 100 mg/kg in rats, the C_{max} of luteolin was 3.07 ± 0.72 μg/mL (equivalent to 10.7 ± 2.5 μM) and slowly decreased; it still could be detected up to 12 h after oral administration.[33] In the current study, we reported that the neurotrophic action and up-regulation of miR-34a by luteolin at a concentration of 20 μM, which is widely used in cell culture study, although it was higher than what can be reached in vivo. Several studies of flavonoids in foods have been reported to be permeable across the blood-brain barrier and provide good therapeutic efficacy.[34] Flavonoids could reach the peak plasma concentration of approximately 1−5 μM indicating that they are biologically active at low concentration.[35] To improve the bioavailability of luteolin in vivo, novel formulation or delivery systems such as nanoparticle delivery, nanostructured lipid carriers, and microemulsions may enhance its absorption and reach the concentration employed in this study.[36,37]

miR-34a belongs to the miR-34 family and is encoded by a gene located on chromosome 1p36.2. In mice, miR-34a expression is ubiquitous and is detected at the highest levels in the brain and the testes. The function of miR-34a has been shown to regulate genes involved in apoptosis and cell cycle control and to be an important mediator of tumor suppression in cancer.[26] Recently, specific roles of miR-34a in neuronal development and differentiation have been reported. In *Drosophila*, miR-34a up-regulation promotes neuronal survival and reduces neurodegeneration induced by polyglutamine-containing proteins.[38] In a mouse model, miR-34a has been demonstrated to regulate neuronal differentiation, synaptogenesis, and neuronal development.[39] miR-34a was shown to modulate mouse embryonic stem cell, neural stem cell, and neural differentiation.[27,40,41] These findings suggested that miR-34a expression may play a critical role in neuronal function. In the current study, we demonstrated that luteolin (20 μM) markedly increased the transcriptional levels of pre-miR-34a

DOI: 10.1021/acs.jafc.5b01005
J. Agric. Food Chem. 2015, 63, 4148−4159

and mature miR-34a during the neurite outgrowth of PC12 cells and verified the microarray analysis data showing miR-34a up-regulation. The silencing of miR-34a using antisense RNA oligonucleotides significantly attenuated the percentage of cells displaying neurite outgrowth, which was induced by luteolin. Our results indicated that luteolin-induced neurite outgrowth occurs, at least in part, via the up-regulation of miR-34a expression. In this study, we found that pre-miR-34a level changes do not correlate well with mature miR-34a after 24 h treatment of luteolin. It is unclear that luteolin continued to increase pre-miR-34a expression over time; however, in the mature form no further changes were detected by real-time PCR during 24−72 h treatment. Whether luteolin affects pre-miRNA stability, microprocessor activity, or mature miRNA turnover in PC12 cells remains to be further investigated.

The primary miR-34a transcript has been shown to be most strongly induced transcript by the tumor suppressor protein p53 among all identified microRNAs. The promoter of the miR-34a gene contains several p53-responsive elements, which have been shown to can directly bind to p53 to increase the transcriptional activity of miR-34a.[23,42] The p53 protein is known to display antiproliferative properties via the mediation of cell cycle arrest and apoptosis. However, high levels of p53 expression have been detected in areas of the developing brain in the absence of apoptosis. Hudson et al. reported that p53 expression was associated with cell differentiation and protection against apoptosis in neural progenitor cells.[43] Recent studies have demonstrated that p53 is required for axon regeneration, neurite outgrowth, neural precursor cell self-renewal, and neuronal differentiation.[44,45] Di Giovanni et al. reported that the early induction of nuclear p53 was observed in NGF-differentiated PC12 cells and that the transactivation of the actin-binding protein Coronin 1b and GTPase Rab13 was associated with neurite outgrowth.[44] In the current study, we clearly demonstrated that the treatment of PC12 cells with luteolin (20 μM) for 8−72 h markedly enhanced the levels of phosphorylated p53-Ser15, an active nuclear form of the p53 protein, and miR-34a transcriptional activation. The addition of the inhibitor pifithrin-α, which blocks p53 activity, significantly attenuated the luteolin-mediated induction of pre-miR-34a transcription and neurite outgrowth in PC12 cells. Our findings suggested that luteolin stimulates p53 phosphorylation, which, in turn, up-regulates miR-34a, a downstream target of p53, and other p53-responsive genes involved in the neurite outgrowth of PC12 cells. In addition, we found that at the concentration of luteolin (10 and 20 μM) used in the PC12 cell model did not induce apoptosis (data not shown). It has been reported that the phosphorylation of p53 at Ser15 can enhance the interaction of p53 with histone/lysine acetyltransferases (HATs), such as p300 and CBP.[46] Activated p53 coordinates a program of gene transcription that is dependent on the cell type and the growth status of the cells. The phosphorylation of p53 at Ser15 may play a central role in selectively regulating p53-dependent transcription in a cell type-specific manner. In mammary epithelial cells, p53-Ser15 phosphorylation and histone modification have been reported to contribute to ionizing radiation-induced miR-34a transcription.[47] Our current findings revealed that luteolin enhanced the phosphorylation of p53 at Ser15, which contributed to miR-34a expression and potentially played a critical role in the modulation of neuronal differentiation, but not apoptosis, in PC12 cells. The p53 protein may not be the only transcription factor that regulates miR-34a expression. The phosphorylation of p53 induced by luteolin may directly or indirectly control the expression of other transcription factors that may bind to the miR-34a promoter to modulate miR-34a transcription. In addition, luteolin-induced p53 activation may regulate neuronal differentiation-related gene expression to control neuronal function.

MicroRNAs are known to down-regulate the expression of several target genes in vivo and to mediate large-scale changes in the proteome to control cellular processes.[6] Many target genes of miR-34a have been identified and validated in various cellular processes.[26] One primary target of miR-34a is sirtuin 1 (SIRT1), a NAD^+-dependent lysine deacetylase that is involved in important biological functions, including energy metabolism, nutrient availability and neuroprotection.[48] SIRT1 is predominantly expressed in neurons of the adult brain, including the cortex, the hippocampus, the cerebellum, and the hypothalamus.[49] Recently, several substrates of STRT1-mediated deacetylation, such as p53, NF-κB, and PPARγ, were identified and shown to be involved in cell survival, stress responses, and neuronal differentiation.[50] Liu et al. reported that decreased SIRT1 expression was associated with the differentiation and maturation of embryonic cortical neurons and neural progenitor cells.[28] In mouse neural stem cells, miR-34a overexpression enhanced neurite outgrowth via the down-regulation of its target SIRT1, which increased the acetylation of p53 at Lys379 and the DNA-binding activity of p53, thus reinforcing the role of p53 in neural differentiation.[27] In the current study, we found that the level of SIRT1 protein was reduced during luteolin-mediated cell differentiation. However, the exposure of PC12 cells to resveratrol, a SIRT1 activator, markedly blocked luteolin-induced neuronal differentiation. These findings verified that SIRT1 activity may be involved in luteolin-induced neuronal differentiation. Our findings also showed that treatment of PC12 cells with luteolin increased the acetylation of the p53 at Lys379 protein. Several reports have been demonstrated that acetylated p53 may participate in regulating of genes involved in neuroprotection, neuritogenesis and neuronal differentiation.[27,51,52] In this study, our finding suggested that acetylated p53 may be involved in the maintenance and stimulation of p53 activity to further enhance pre-miR-34a and neuronal differentiation-related gene transcription in luteolin-treated PC12 cells.

In this study, we further demonstrated that inhibitors of JNK (SP600125) and p38 MAPK (SB203580) significantly blocked luteolin-induced miR-34a transcription and neurite outgrowth in PC12 cells. These results indicated that these signaling pathways may be involved in the induction of miR-34a transcription by luteolin. However, neither a MEK1/2 inhibitor (U0126), a PKA inhibitor (H-89), a PKC inhibitor (BIM), nor a PI3/Akt inhibitor (LY294002) attenuated luteolin-mediated pre-miR-34a expression. In our previous study, we identified the involvement of the PKA- and ERK-dependent CREB signaling pathways in luteolin-mediated miR-132 expression and neurite outgrowth in PC12 cells.[22] Treatment of PC12 cells with luteolin (20 μM) for 2 h significantly induced miR-132 expression and gradually reduced during 4−8 h exposure. miR-132 has been reported be involved in the regulation of neurite outgrowth, synaptic plasticity and neuroprotection. In this study, the microarray data showed that the induction of miR-132 displayed increases of 1.6-, 1.3-, 0.98-, and 0.96-fold after treatment of the cells with luteolin for 8, 24, 48, and 72 h, respectively (data not shown). These data indicated that miR-132 induced by luteolin may serve as an early response regulator to modulate neurite outgrowth in PC12 cells.

DOI: 10.1021/acs.jafc.5b01005
J. Agric. Food Chem. 2015, 63, 4148−4159

However, miR-34a up-regulation was sustained during 8−72 h treatment of luteolin. The miR-34a overexpression induced by luteolin may play a critical role to consistently augment p53 activation for promotion and maintenance of neurite outgrowth in PC12 cells. These findings revealed that different signaling cascades are involved in various types of luteolin-induced miRNAs expression, which, in turn, modulate different downstream targets affecting neuronal differentiation.

We further demonstrated that luteolin (20 μM) activated the phosphorylation of JNK and p38 in PC12 cells. The JNK and p38 MAPK pathways have been reported to regulate p53 phosphorylation at Ser15 in different cell types.[53,54] However, we found that the inhibition of JNK or p38 MAPK activation did not block luteolin-induced p53 phosphorylation in PC12 cells. No crosstalk was observed between these activated pathways and p53 phosphorylation at Ser15 in luteolin-treated PC12 cells. In this study, we found that pretreatment of cells with SP600125 (JNK inhibitor) or SB203580 (p38 MAPK inhibitor) significantly attenuated luteolin-mediated neurite outgrowth of PC12 cells. This data indicated that involvement of JNK and p38 phosphorylation during luteolin-induced neuronal differentiation. This finding is different from earlier study,[17] which showed that neurite outgrowth induced by high concentration of luteolin (100 μM) was significantly enhanced by treatment with inhibitor SB203580 in PC12 cells cultured in serum free medium. These results suggested that the inhibition of p38 activation may effectively enhance neurite outgrowth. It is plausible that the discrepancy effect of p38 activation on luteolin-mediated neurite outgrowth is due to the different luteolin dosage or experimental conditions. Several studies have been reported that activation of JNK and p38 is required for neuritogenesis and neuronal differentiation.[55,56] Our data supported that phosphorylation of JNK or p38 MAPK was involved in the luteolin-induced neuronal differentiation in PC12 cells. In addition to p53-mediated miR-34a transcription and neurite outgrowth, our findings suggested that JNK- and p38-mediated p53-independent cascades are involved in luteolin-induced miR-34a expression and neurite outgrowth in PC12 cells. Taken together, our findings provide evidence that the activation of p53-dependent and p53-independent miR-34a/SIRT1 pathways plays a critical role in the mechanisms underlying luteolin-induced neuronal differentiation.

■ ASSOCIATED CONTENT

Supporting Information

Figure S1. Expression profile of the luteolin-responsive miRNAs. Heat map comparing the miRNA expression of PC12 cells treated with luteolin (20 μM) for 0, 8, 24, 48, or 72 h. The color bar indicates relative miRNA expression in duplicate arrays; red and green indicate up-regulated and down-regulated expression, respectively. A total of 16 and three miRNAs shown in the heat map were robustly and significantly up-regulated ($\log_2$ ratio ≥ 0.7) and down-regulated ($\log_2$ ratio ≤ -0.7), respectively. Figure S2. Effects of miR-34a antisense on the mature miR-34a expression in PC12 cells. The cells were transfected with miRNA antisense negative control (anti-miR-NC) or miR-34a antisense oligonucleotides (anti-miR-34a) for 24 h as described in Materials and Methods. After transfection, PC12 cells were treated with vehicle (0.1% DMSO) or luteolin (20 μM). After 24 h treatment, the levels of mature miR-34a were detected by RT-Q-PCR as described in Materials and Methods. Data represent the mean ± SD from three independent experiments. $^{**}p < 0.01$ represents significant differences compared to vehicle-treated cells. $^{\#\#}p < 0.01$ represents significant differences compared to anti-miR-NC-transfected cells. This material is available free of charge via Internet at http://pubs.acs.org.

■ AUTHOR INFORMATION

Corresponding Author

*Tel.: +886-3-856-5301 ext 2683. Fax: +886-3-856-1422. E-mail: imyenjh@mail.tcu.edu.tw.

Funding

This research was supported by grant TCRD-103-17 (to P.-Y.C.) from Buddhist Tzu Chi General Hospital, Taiwan; grants MOST-102-2313-B-320-001-MY3 (to J.-H.Y.) and MOST-102-2320-B-041-003-MY3 (to M.-J.W.) from the Ministry of Science and Technology, Taiwan.

Notes

The authors declare no competing financial interest.

■ REFERENCES

(1) Spencer, J. P. Flavonoids and brain health: multiple effects underpinned by common mechanisms. *Genes Nutr.* **2009**, *4*, 243−50.

(2) Spencer, J. P. The interactions of flavonoids within neuronal signalling pathways. *Genes Nutr.* **2007**, *2*, 257−73.

(3) Lancon, A.; Michaille, J. J.; Latruffe, N. Effects of dietary phytophenols on the expression of microRNAs involved in mammalian cell homeostasis. *J. Sci. Food Agric.* **2013**, *93*, 3155−64.

(4) Chiu, S. P.; Wu, M. J.; Chen, P. Y.; Ho, Y. R.; Tai, M. H.; Ho, C. T.; Yen, J. H. Neurotrophic action of 5-hydroxylated polymethoxyflavones: 5-demethylnobiletin and gardenin A stimulate neuritogenesis in PC12 cells. *J. Agric. Food Chem.* **2013**, *61*, 9453−63.

(5) Ambros, V. The evolution of our thinking about microRNAs. *Nat. Med.* **2008**, *14*, 1036−40.

(6) Baek, D.; Villen, J.; Shin, C.; Camargo, F. D.; Gygi, S. P.; Bartel, D. P. The impact of microRNAs on protein output. *Nature* **2008**, *455*, 64−71.

(7) Friedman, R. C.; Farh, K. K.; Burge, C. B.; Bartel, D. P. Most mammalian mRNAs are conserved targets of microRNAs. *Genome Res.* **2009**, *19*, 92−105.

(8) Coolen, M.; Bally-Cuif, L. MicroRNAs in brain development and physiology. *Curr. Opin. Neurobiol.* **2009**, *19*, 461−70.

(9) Vo, N.; Klein, M. E.; Varlamova, O.; Keller, D. M.; Yamamoto, T.; Goodman, R. H.; Impey, S. A cAMP-response element binding protein-induced microRNA regulates neuronal morphogenesis. *Proc. Natl. Acad. Sci. U. S. A.* **2005**, *102*, 16426−31.

(10) Pan, M. H.; Lai, C. S.; Dushenkov, S.; Ho, C. T. Modulation of inflammatory genes by natural dietary bioactive compounds. *J. Agric. Food Chem.* **2009**, *57*, 4467−77.

(11) Chakrabarti, M.; Khandkar, M.; Banik, N. L.; Ray, S. K. Alterations in expression of specific microRNAs by combination of 4-HPR and EGCG inhibited growth of human malignant neuroblastoma cells. *Brain Res.* **2012**, *1454*, 1−13.

(12) Milenkovic, D.; Deval, C.; Gouranton, E.; Landrier, J. F.; Scalbert, A.; Morand, C.; Mazur, A. Modulation of miRNA expression by dietary polyphenols in apoE deficient mice: a new mechanism of the action of polyphenols. *PLoS One* **2012**, *7*, e29837.

(13) Pandurangan, A. K.; Esa, N. M. Luteolin, a bioflavonoid inhibits colorectal cancer through modulation of multiple signaling pathways: a review. *Asian Pac J. Cancer Prev* **2014**, *15*, 5501−8.

(14) Cheng, H. Y.; Hsieh, M. T.; Tsai, F. S.; Wu, C. R.; Chiu, C. S.; Lee, M. M.; Xu, H. X.; Zhao, Z. Z.; Peng, W. H. Neuroprotective effect of luteolin on amyloid beta protein (25−35)-induced toxicity in cultured rat cortical neurons. *Phytother. Res.* **2010**, *24* (Suppl 1), S102−8.

(15) Hu, L. W.; Yen, J. H.; Shen, Y. T.; Wu, K. Y.; Wu, M. J. Luteolin modulates 6-hydroxydopamine-induced transcriptional changes of stress response pathways in PC12 cells. *PLoS One* **2014**, *9*, e97880.

DOI: 10.1021/acs.jafc.5b01005
J. Agric. Food Chem. 2015, 63, 4148−4159

(16) El Omri, A.; Han, J.; Kawada, K.; Ben Abdrabbah, M.; Isoda, H. Luteolin enhances cholinergic activities in PC12 cells through ERK1/2 and PI3K/Akt pathways. *Brain Res.* **2012**, *1437*, 16−25.
(17) Nishina, A.; Kimura, H.; Tsukagoshi, H.; Kozawa, K.; Koketsu, M.; Ninomiya, M.; Furukawa, S. Neurite Outgrowth in PC12 Cells Stimulated by Components from Dendranthema x grandiflorum cv. "Mottenohoka" Is Enhanced by Suppressing Phosphorylation of p38MAPK. *Evid Based Complement Alternat Med.* **2013**, *2013*, 1.
(18) Liu, R.; Gao, M.; Qiang, G. F.; Zhang, T. T.; Lan, X.; Ying, J.; Du, G. H. The anti-amnesic effects of luteolin against amyloid beta(25−35) peptide-induced toxicity in mice involve the protection of neurovascular unit. *Neuroscience* **2009**, *162*, 1232−43.
(19) Fu, X.; Zhang, J.; Guo, L.; Xu, Y.; Sun, L.; Wang, S.; Feng, Y.; Gou, L.; Zhang, L.; Liu, Y. Protective role of luteolin against cognitive dysfunction induced by chronic cerebral hypoperfusion in rats. *Pharmacol., Biochem. Behav.* **2014**, *126*, 122−30.
(20) Patil, S. P.; Jain, P. D.; Sancheti, J. S.; Ghumatkar, P. J.; Tambe, R.; Sathaye, S. Neuroprotective and neurotrophic effects of Apigenin and Luteolin in MPTP induced parkinsonism in mice. *Neuropharmacology* **2014**, *86*, 192−202.
(21) Lin, C. W.; Wu, M. J.; Liu, I. Y.; Su, J. D.; Yen, J. H. Neurotrophic and cytoprotective action of luteolin in PC12 cells through ERK-dependent induction of Nrf2-driven HO-1 expression. *J. Agric. Food Chem.* **2010**, *58*, 4477−86.
(22) Lin, L. F.; Chiu, S. P.; Wu, M. J.; Chen, P. Y.; Yen, J. H. Luteolin induces microRNA-132 expression and modulates neurite outgrowth in PC12 cells. *PLoS One* **2012**, *7*, e43304.
(23) Tarasov, V.; Jung, P.; Verdoodt, B.; Lodygin, D.; Epanchintsev, A.; Menssen, A.; Meister, G.; Hermeking, H. Differential regulation of microRNAs by p53 revealed by massively parallel sequencing: miR-34a is a p53 target that induces apoptosis and G1-arrest. *Cell Cycle* **2007**, *6*, 1586−93.
(24) Loughery, J.; Cox, M.; Smith, L. M.; Meek, D. W. Critical role for p53-serine 15 phosphorylation in stimulating transactivation at p53-responsive promoters. *Nucleic Acids Res.* **2014**, *42*, 7666−80.
(25) Komarov, P. G.; Komarova, E. A.; Kondratov, R. V.; Christov-Tselkov, K.; Coon, J. S.; Chernov, M. V.; Gudkov, A. V. A chemical inhibitor of p53 that protects mice from the side effects of cancer therapy. *Science* **1999**, *285*, 1733−7.
(26) Rokavec, M.; Li, H.; Jiang, L.; Hermeking, H. The p53/miR-34 axis in development and disease. *J. Mol. Cell Biol.* **2014**, *6*, 214−30.
(27) Aranha, M. M.; Santos, D. M.; Sola, S.; Steer, C. J.; Rodrigues, C. M. miR-34a regulates mouse neural stem cell differentiation. *PLoS One* **2011**, *6*, e21396.
(28) Liu, D. J.; Hammer, D.; Komlos, D.; Chen, K. Y.; Firestein, B. L.; Liu, A. Y. SIRT1 knockdown promotes neural differentiation and attenuates the heat shock response. *J. Cell. Physiol.* **2014**, *229*, 1224−35.
(29) Sun, A. Y.; Wang, Q.; Simonyi, A.; Sun, G. Y. Resveratrol as a therapeutic agent for neurodegenerative diseases. *Mol. Neurobiol.* **2010**, *41*, 375−83.
(30) Vitolo, O. V.; Sant'Angelo, A.; Costanzo, V.; Battaglia, F.; Arancio, O.; Shelanski, M. Amyloid beta -peptide inhibition of the PKA/CREB pathway and long-term potentiation: reversibility by drugs that enhance cAMP signaling. *Proc. Natl. Acad. Sci. U. S. A.* **2002**, *99*, 13217−21.
(31) Liao, K. K.; Wu, M. J.; Chen, P. Y.; Huang, S. W.; Chiu, S. J.; Ho, C. T.; Yen, J. H. Curcuminoids promote neurite outgrowth in PC12 cells through MAPK/ERK- and PKC-dependent pathways. *J. Agric. Food Chem.* **2012**, *60*, 433−43.
(32) Zhou, P.; Li, L. P.; Luo, S. Q.; Jiang, H. D.; Zeng, S. Intestinal absorption of luteolin from peanut hull extract is more efficient than that from individual pure luteolin. *J. Agric. Food Chem.* **2008**, *56*, 296−300.
(33) Lin, L. C.; Pai, Y. F.; Tsai, T. H. Isolation of Luteolin and Luteolin-7-O-glucoside from Dendranthema morifolium Ramat Tzvel and Their Pharmacokinetics in Rats. *J. Agric. Food Chem.* **2015**, DOI: 10.1021/jf505848z.
(34) Youdim, K. A.; Dobbie, M. S.; Kuhnle, G.; Proteggente, A. R.; Abbott, N. J.; Rice-Evans, C. Interaction between flavonoids and the blood-brain barrier: in vitro studies. *J. Neurochem.* **2003**, *85*, 180−92.
(35) Manach, C.; Scalbert, A.; Morand, C.; Remesy, C.; Jimenez, L. Polyphenols: food sources and bioavailability. *Am. J. Clin. Nutr.* **2004**, *79*, 727−47.
(36) Majumdar, D.; Jung, K. H.; Zhang, H.; Nannapaneni, S.; Wang, X.; Amin, A. R.; Chen, Z.; Chen, Z. G.; Shin, D. M. Luteolin nanoparticle in chemoprevention: in vitro and in vivo anticancer activity. *Cancer Prev. Res.* **2014**, *7*, 65−73.
(37) Liu, Y.; Wang, L.; Zhao, Y.; He, M.; Zhang, X.; Niu, M.; Feng, N. Nanostructured lipid carriers versus microemulsions for delivery of the poorly water-soluble drug luteolin. *Int. J. Pharm.* **2014**, *476*, 169−77.
(38) Liu, N.; Landreh, M.; Cao, K.; Abe, M.; Hendriks, G. J.; Kennerdell, J. R.; Zhu, Y.; Wang, L. S.; Bonini, N. M. The microRNA miR-34 modulates ageing and neurodegeneration in Drosophila. *Nature* **2012**, *482*, 519−23.
(39) Agostini, M.; Tucci, P.; Killick, R.; Candi, E.; Sayan, B. S.; Rivetti di Val Cervo, P.; Nicotera, P.; McKeon, F.; Knight, R. A.; Mak, T. W.; Melino, G. Neuronal differentiation by TAp73 is mediated by microRNA-34a regulation of synaptic protein targets. *Proc. Natl. Acad. Sci. U. S. A.* **2011**, *108*, 21093−8.
(40) Tarantino, C.; Paolella, G.; Cozzuto, L.; Minopoli, G.; Pastore, L.; Parisi, S.; Russo, T. miRNA 34a, 100, and 137 modulate differentiation of mouse embryonic stem cells. *FASEB J.* **2010**, *24*, 3255−63.
(41) Aranha, M. M.; Santos, D. M.; Xavier, J. M.; Low, W. C.; Steer, C. J.; Sola, S.; Rodrigues, C. M. Apoptosis-associated microRNAs are modulated in mouse, rat and human neural differentiation. *BMC Genomics* **2010**, *11*, 514.
(42) Hermeking, H. MicroRNAs in the p53 network: micromanagement of tumour suppression. *Nat. Rev. Cancer* **2012**, *12*, 613−26.
(43) Hudson, C. D.; Podesta, J.; Henderson, D.; Latchman, D. S.; Budhram-Mahadeo, V. Coexpression of Brn-3a POU protein with p53 in a population of neuronal progenitor cells is associated with differentiation and protection against apoptosis. *J. Neurosci. Res.* **2004**, *78*, 803−14.
(44) Di Giovanni, S.; Knights, C. D.; Rao, M.; Yakovlev, A.; Beers, J.; Catania, J.; Avantaggiati, M. L.; Faden, A. I. The tumor suppressor protein p53 is required for neurite outgrowth and axon regeneration. *EMBO J.* **2006**, *25*, 4084−96.
(45) Mendrysa, S. M.; Ghassemifar, S.; Malek, R. p53 in the CNS: Perspectives on Development, Stem Cells, and Cancer. *Genes Cancer* **2011**, *2*, 431−42.
(46) Lambert, P. F.; Kashanchi, F.; Radonovich, M. F.; Shiekhattar, R.; Brady, J. N. Phosphorylation of p53 serine 15 increases interaction with CBP. *J. Biol. Chem.* **1998**, *273*, 33048−53.
(47) Wang, B.; Li, D.; Kovalchuk, O. p53 Ser15 phosphorylation and histone modifications contribute to IR-induced miR-34a transcription in mammary epithelial cells. *Cell Cycle* **2014**, *12*, 2073−83.
(48) Tang, B. L.; Chua, C. E. SIRT1 and neuronal diseases. *Mol. Aspects Med.* **2008**, *29*, 187−200.
(49) Ramadori, G.; Lee, C. E.; Bookout, A. L.; Lee, S.; Williams, K. W.; Anderson, J.; Elmquist, J. K.; Coppari, R. Brain SIRT1: anatomical distribution and regulation by energy availability. *J. Neurosci.* **2008**, *28*, 9989−96.
(50) Feige, J. N.; Auwerx, J. Transcriptional targets of sirtuins in the coordination of mammalian physiology. *Curr. Opin. Cell Biol.* **2008**, *20*, 303−9.
(51) Hasegawa, K.; Yoshikawa, K. Necdin regulates p53 acetylation via Sirtuin1 to modulate DNA damage response in cortical neurons. *J. Neurosci.* **2008**, *28*, 8772−84.
(52) Moriya, J.; Chen, R.; Yamakawa, J.; Sasaki, K.; Ishigaki, Y.; Takahashi, T. Resveratrol improves hippocampal atrophy in chronic fatigue mice by enhancing neurogenesis and inhibiting apoptosis of granular cells. *Biol. Pharm. Bull.* **2011**, *34*, 354−9.
(53) Ferreira, D. M.; Afonso, M. B.; Rodrigues, P. M.; Simao, A. L.; Pereira, D. M.; Borralho, P. M.; Rodrigues, C. M.; Castro, R. E. c-Jun

DOI: 10.1021/acs.jafc.5b01005
J. Agric. Food Chem. 2015, 63, 4148−4159

N-terminal kinase 1/c-Jun activation of the p53/microRNA 34a/sirtuin 1 pathway contributes to apoptosis induced by deoxycholic acid in rat liver. *Mol. Cell. Biol.* **2014**, *34*, 1100−20.
(54) Lin, T.; Mak, N. K.; Yang, M. S. MAPK regulate p53-dependent cell death induced by benzo[a]pyrene: involvement of p53 phosphorylation and acetylation. *Toxicology* **2008**, *247*, 145−53.
(55) Eriksson, M.; Taskinen, M.; Leppa, S. Mitogen activated protein kinase-dependent activation of c-Jun and c-Fos is required for neuronal differentiation but not for growth and stress response in PC12 cells. *J. Cell. Physiol.* **2007**, *210*, 538−48.
(56) Hansen, T. O.; Rehfeld, J. F.; Nielsen, F. C. Cyclic AMP-induced neuronal differentiation via activation of p38 mitogen-activated protein kinase. *J. Neurochem.* **2000**, *75*, 1870−7.

DOI: 10.1021/acs.jafc.5b01005
J. Agric. Food Chem. 2015, 63, 4148−4159

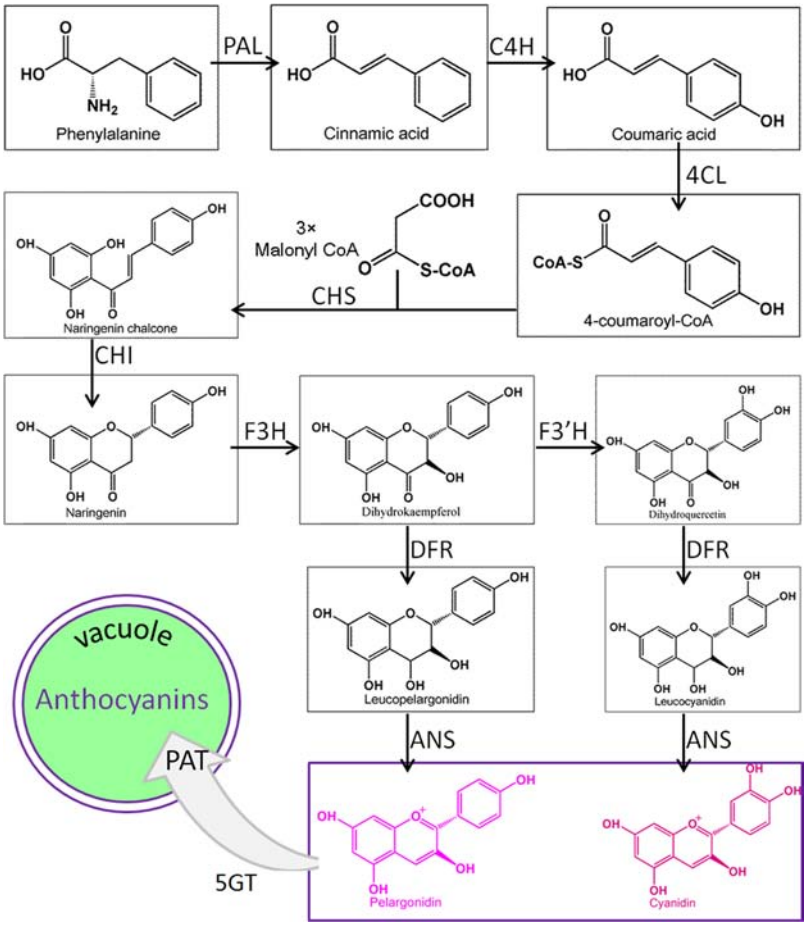

Figure 1. Schematic representation of the biosynthetic pathway of the anthocyanins. The names of the compounds in boxes are indicated. The enzyme names are as follows: PAL, phenylalanine ammonia lyase; C4H, cinnamate 4-hydroxylase; 4CL, 4-coumarateCoA ligase; CHS, chalcone synthase; CHI, chalcone isomerase; F3H, flavanone 3-hydroxylase; F3′H, flavanone 3′-hydroxylase; DFR, dihydroflavonol 4-reductase; ANS, anthocyanidin synthase; 5-GT, flavonoid-5-glucosyltransferase; PAT, putative anthocyanin transporter.

depending on pH, metal cations, copigmentation, and modifications of the backbone.[24]

Anthocyanins, as the metabolites of the flavonoid pathway, are synthesized under the complicated regulation of diverse regulatory genes mainly at the transcriptional level.[22,23,25] The flavonoid downstream pathway (from F3H to 5GT) of anthocyanin biosynthesis is regulated by several different families of regulatory genes, including MYB transcriptional factors, bHLH transcriptional factors, and WD40-like proteins.[26] By analysis of mutants of *Arabidopsis thaliana* with abnormal levels of anthocyanins and protein interaction assays, it has been proved that the transcription of anthocyanin biosynthetic genes is directly regulated by a transcriptional activation MYB-bHLH-WD40 complex (MBW) consisting of R2R3MYB, bHLH, and WD40 proteins.[27−29] Recent studies show that the variation in content of anthocyanins or tissue specificity in plants is governed mainly by the activity of the R2R3MYB transcription factors in the MBW complex.[30−36] However, the bHLH proteins always play essential roles in the synergistic regulation of anthocyanin accumulation.[29,37−39] In addition, heterogenous expression of bHLH genes individually greatly induced visible anthocyanin accumulation in the host plant.[40−42]

As a biennial plant native to northern Europe, kohlrabi (*Brassica oleracea* var. *gongylodes*) belongs to the Brassicaceae family and is grown widely for the round swollen stem at the base of the plant. Extensive studies show that cruciferous vegetables (including kohlrabi) supply human beings with a healthy diet due to the high levels of carotenoids, ascorbic acid, and tocopherols contained in the edible parts.[43,44] In addition to the natural antioxidants mentioned above, most of the antioxidative effects associated with food intake are largely due to the presence of phenolic compounds, including anthocyanins, flavones, flavonols, and so on.[45] In comparison with the green cultivars of kohlrabi, the purple cultivars which display abundant anthocyanin accumulation in the stems and leaves have attracted more attention from consumers due to their brilliant color and high levels of health-promoting ingredients. However, even though purple kohlrabi is consumed worldwide as a nutritious Brassica vegetable, the molecular mechanisms underlying its biosynthesis of anthocyanins in still remain unknown. In this paper, the components of anthocyanin production in a purple kohlrabi cultivar (Kolibri) were characterized with high-performance liquid chromatography−electrospray ionization tandem mass spectrometry (HPLC-ESI-MS/MS). In the following, the transcripts of anthocyanin biosynthetic and regulatory genes have been analyzed by quantitative real-time polymerase chain reaction (qRT-PCR) in different tissues of the purple and green cultivars (Kolibri and Winner). Furthermore, the influence of light on the development and anthocyanin accumulation of kohlrabi sprouts at different stages were analyzed. The consistent increase of the

DOI: 10.1021/acs.jafc.5b00473
J. Agric. Food Chem. 2015, 63, 4160−4169

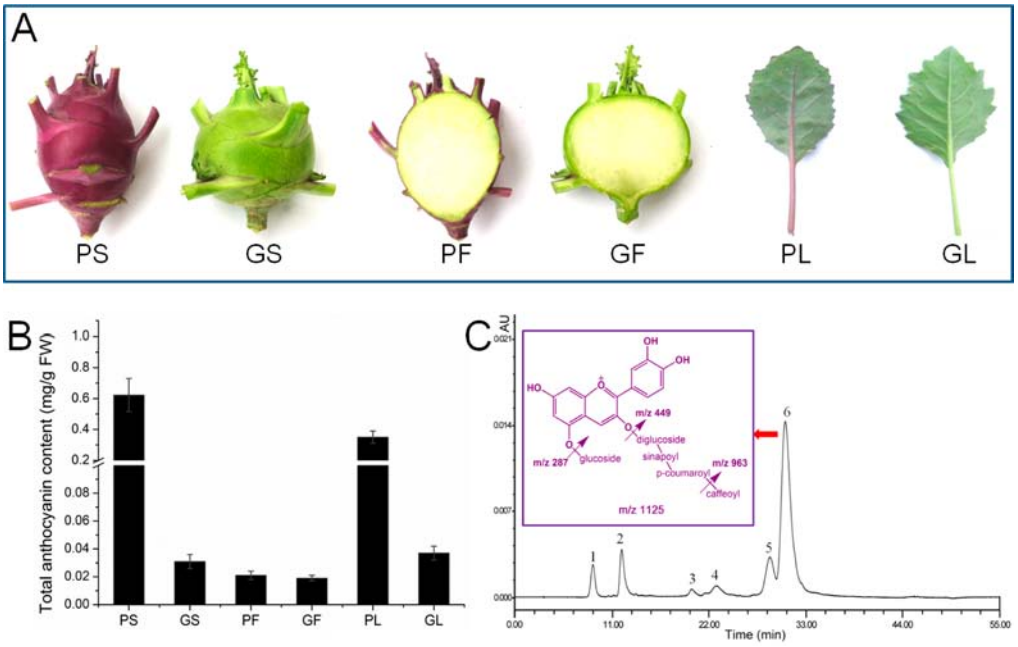

Figure 2. Anthocyanin analysis of different kohlrabi cultivars. (A) Photographs of the different tissues of two kohlrabi cultivars (Kolibri on the left and Winner on the right) used in this study. (B) Total anthocyanin content analysis of leaves, stem flesh, and skins in the two kohlrabi cultivars. Abbreviations: PS, purple skin of swollen stem; GS, green skin of swollen stem; PS, flesh of swollen stem in purple cultivar; GS, flesh of swollen stem in green cultivar; PL, purple leaf; GL, green leaf. Error bars represent the standard error of the mean (n = 3). (C) HPLC profiles of anthocyanins extracted from the skins of the purple swollen stem. Peak numbers refer to the anthocyanins given in Table 1. Structures and major cleavage of cyanidin 3-(caffeoyl)-*p*-coumaroyl (sinapoyl)-diglucoside-5-glucoside in reference to peak 6 are shown in the inset box.

anthocyanin biosynthetic genes with regulatory factors indicate that transcriptional activation of *BoPAP2* and *BoTT8* in a light-independent manner mainly accounts for the upregulation of anthocyanin structural genes and the onset of anthocyanin accumulation in purple kohlrabi. The results above enhanced our understanding about the mechanisms of anthocyanin biosynthesis in purple kohlrabi at both the metabolic and molecular levels.

MATERIALS AND METHODS

Chemicals and Solvents. Anthocyanin (cyanidin 3,5-diglucoside) for external standards was purchased from Phytolab (Germany). High-performance liquid chromatography (HPLC) grade formic acid and methanol (MeOH) were bought from Sigma. All other solvents were provided from Aldrich (St. Louis, MO).

Plant Materials and Culture Conditions. Kohlrabi (*Brassica oleracea* var. *gongylodes* L.) seeds of green cultivar (Winner) and purple cultivar (Kolibri) were obtained from the Chongqing Academy of Agriculture Sciences. The samples used for HPLC-ESI-MS/MS analysis were collected from the cuticles of swollen stems from two cultivars of kohlrabi which were grown in a greenhouse with a 16 h photoperiod at 22 °C. In addition, the mature leaves and the cuticles and fleshes of swollen stems were used for total anthocyanin and qRT-PCR analysis. The light- and darkness-treated samples used for total anthocyanin and qRT-PCR analysis were collected from the sprouts of green and purple cultivars which were generated by the following procedures. Kohlrabi seeds were surface-sterilized with 70% ethanol for 60 s and 2.5% (v/v) bleach solution for 5 min and rinsed six times in sterile water. These seeds were then placed on half-strength sterilized Murashige−Skoog medium (1/2 MS) solidified with 0.8% agar. The two cultivars were germinated in a growth chamber under light/dark (16/8 h) or dark conditions at 26 °C and approximately 60% humidity. Samples were harvested after 3, 6, 9, and 12 days, measured for their length and fresh weight, frozen in liquid nitrogen, and stored at −80 °C until further analysis.

RNA Extraction and qRT-PCR Analysis. The samples of the two kohlrabi cultivars were grounded into powder in liquid nitrogen. Total RNA was isolated from various tissues for three biological repeats using RNAiso reagent according to the manufacturer's instruction (Takara, Dalian, People's Republic of China). RNA samples (1 μg) were reverse transcripted into complementary DNA (cDNA) with an oligo(dT)20 primer and M-MLV reverse transcriptase (Promega, Madison, WI) following the manufacturer's protocol. The synthesized cDNAs were diluted five times in H_2O for qRT-PCR analysis. qRT-PCR was carried out using the CFX96 Real-Time System (C1000 thermal cycler). All reactions were performed using the GoTaq qPCR Master Mix according to the manufacturer's instructions. Reactions were performed in triplicate using 5 μL of Master Mix, 0.25 μM of each primer, 1 μL of diluted cDNA, and DNase-free water to a final volume of 10 μL. The PCR amplification was as follows: 1 cycle of 2 min at 95 °C, 40 cycles of denaturation for 5 s at 95 °C, annealing for 20 s at 60 °C, and elongation for 15 s at 72 °C. Amplification was followed by a melting curve analysis with continual fluorescence data acquisition during the 60−95 °C melt. A melt curve analysis of qPCR samples revealed that there was only one product for each gene primer reaction. The primers used for qPCR analysis of kohlrabi were designed by Primer Premier 5 and given in Supplementary Table 1 (Supporting Information). The PCR products were sequenced to confirm the specific amplifications. The gene expression was normalized to *BoApr* as a reference gene for kohlrabi. Values reported here were calculated from three biological repeats for each sample.

Anthocyanin Extraction and HPLC-ESI-MS/MS Analysis. Anthocyanin extraction of kohlrabi was carried out in the same way as described for radish.[46] The extract was filtered through a 0.2 μm PTFE syringe filter. The samples were then analyzed by an Agilent Technologies 1200 Series HPLC (Agilent Technologies, Palo Alto, CA), equipped with an Agilent 1200 HPLC variable-wavelength detector. The results were analyzed by Agilent 1200 HPLC ChemStation software. The chromatographic separation was performed on a Zorbax Stablebond Analytical SB-C18 column (4.6 mm × 250 mm, 5 μm, Agilent Technologies, Rising Sun, MD). The injection sling was 5 μL. Elution was performed using mobile phase A (aqueous

DOI: 10.1021/acs.jafc.5b00473
J. Agric. Food Chem. 2015, 63, 4160−4169

Table 1. Anthocyanin Levels in the Two Kohlrabi Cultivars (n = 3)

no.[a]	RT[b] (min)	$[M+M]^+$ (m/z)	MS/MS (m/z)	anthocyanin	anthocyanin level (mg/g dry weight) green[c]	purple[c]
1	8.83	979	449/287	cyanidin 3-(sinapoyl)-diglucoside-5-glucoside	nd[d]	0.16 ± 0.02
2	12.07	1141	449/287	cyanidin 3-(glycopyranosyl-sinapoyl)-diglucoside-5-glucoside	nd	0.29 ± 0.03
3	20.01	919	757/449/287	cyanidin 3- rutinose-5-glucoside	nd	0.04 ± 0.01
4	22.821	1185	1023/449/287	cyanidin 3- (caffeoyl)-disinapoyl (glucoside)-5-glucoside	nd	0.08 ± 0.01
5	28.890	1155	993/449/287	cyanidin 3-(caffeoyl)-feruloyl (sinapoyl)-glucoside-5-glucoside	nd	0.37 ± 0.04
6	30.625	1125	963/449/287	cyanidin 3-(caffeoyl) *p*-coumaroyl (sinapoyl)-diglucoside-5-glucoside	nd	2.08 ± 0.19
total					nd	3.02 ± 0.21

[a]The number corresponds to the elution order by HPLC analysis in Figure 1C. [b]RT stands for the retention time. [c]Green indicates the green kohlrabi cultivar (Winner) and purple the purple kohlrabi cultivar (Kolibri). [d]Nd, not detected.

2% formic acid solution) and mobile phase B (methanol). The detection was at 520 nm, and the column oven temperature was set at 40 °C. The flow rate was 0.6 mL/min. The gradient program is described as follows: 0−2 min, 10−20% B; 2−40 min, 20−55% B; 40−41 min, 55−80% B; 41−45 min, 80% B; 45−50 min, 80−10% B; 50−55 min, 10% B. Quantification of the different anthocyanins was based on peak areas and calculated as equivalents of the standard compounds. All contents were expressed as milligrams per gram of dry weight. Low-resolution electrospray mass spectrometry was performed with a solariX ion trap mass spectrometer (Bruker Daltonics, Billerica, MA). The experimental conditions were as follows: ESI interface, nebulizer, 50 psi; dry gas, 15.0 psi; dry temperature, 320 °C; MS/MS, scan from m/z 200 to 1500; ion trap, scan from m/z 200 to 1500; source accumulation, 50 ms; ion accumulation time, 300 ms; flight time to acquisition cell, 1 ms; smart parameter setting (SPS), compound stability, 50%; trap drive level, 60%.

Total Anthocyanin Analysis. Spectrophotometric differential pH methods were used for the total anthocyanin measurement of kohlrabi following the procedure of Yuan et al. with slight modifications.[25] The protocols are described as follows. Frozen samples (100 mg) were crushed into powder in liquid nitrogen and extracted separately with 2 mL of pH 1.0 buffer and 2 mL of pH 4.5 buffer. In addition, pH 1.0 buffer contains 50 mM KCl and 150 mM HCl, while pH 4.5 buffer contains 400 mM sodium acetate and 240 mM HCl. The mixtures were centrifuged at 14000*g* for 15 min at 4 °C. The supernatants were gathered for measurement of absorbance at 510 nm. The amount of total anthocyanin was calculated according to the equation

$$\text{amount (mg g}^{-1}\text{ FW)} = (\text{A1} - \text{A2}) \times 484.8/24.825 \times \text{dilution factor}$$

A1 represents the absorbance of supernatants gathered from pH 1.0 buffer solution at 510 nm, while A2 represents the other absorbance. The value 484.8 represents the molecular mass of cyanidin-3-glucoside chloride, while 24.825 reflects its molar absorptivity at 510 nm. The total anthocyanin of the sample was analyzed in triplicate.

Statistical Analyses. SPSS, version 17.0 (SPSS Inc., Chicago, IL), was used for the data analysis. One-way analysis of variance (ANOVA) followed by pairwise comparisons was performed with posthoc Tukey's honest significant difference (HSD) test, with significance set at $p < 0.05$ and $p < 0.01$.

RESULTS AND DISCUSSION

Phenotypic Characterization of Kolibri and Winner. To study the biosynthesis of pigments in kohlrabi, the purple cultivar Kolibri and green cultivar Winner were chosen to study. Visual inspection of the kohlrabi cultivars showed that Kolibri displays more purple pigments than Winner (Figure 2A and Figure 1S in the Supporting Information). The pigments extracted from purple tissues of Kolibri share the same spectral properties with anthocyanin standards (cyanidin-3,5-diglucoside) and were confirmed as anthocyanins in the following HPLC-ESI-MS/MS analysis (Figure 2C). In comparison with those of Winner, most of the organs of Kolibri contain a high amount of anthocyanins (Figure 2B). During all the developmental stages of vegetative growth, the Kolibri synthesizes and accumulates anthocyanins constantly (Figure 1S in the Supporting Information). Meanwhile, the young sprouts of Winner only show a faint purple color at the very beginning of germination but turn into green immediately as the elongation of hypocotyls. During the initial weeks of growth, all the leaves of Winner turn solid green, while those of Kolibri display dark purple pigments in the veins of leaves and a pale purple color in the mesophyll tissue (Figure 2A and Figure 1S in the Supporting Information). The purple pigments of Kolibri plants, especially in the round stems, become intense during the development. After 2 months of cultivation, Winner possesses green swollen stems, while Kolibri displays dark purple pigments at the skin of the swollen stems. The intense accumulation of anthocyanins in the purple cultivar indicates a high ability to synthesize and accumulate anthocyanins. The total anthocyanin content of the skin of the purple swollen stem is about 0.63 mg/g of fresh weight, while little is detected in the corresponding tissue of Winner. These results show that the drastic differences in anthocyanin accumulation arise from cultivar and genetic specificity.

Identification and Quantitative Analyses of Anthocyanins in Purple Kohlrabi. A total of six major anthocyanins were separated and characterized from the cuticle extracts of the purple swollen stem with the method of HPLC-ESI-MS/MS (Figure 2C). In order to verify the identity of anthocyanins in Kolibri, MS/MS fragmentation patterns (m/z) corresponding to the compounds emerging in HPLC profiles were analyzed according to the information on radical groups reported previously.[21] Consequently, six new kinds of modified cyanidin were identified as the major anthocyanins in the purple cultivar (Table 1). However, it is strange that pelargonidin-based anthocyanins were not detected in the purple kohlrabi. Furthermore, all of the anthocyanin modifications in Kolibri were found to be glycosylated cyanidin at the C5 position of anthocyanidins. Meanwhile, acylation at the C3 position of anthocyanidins seems like a common modification in this study.

The total anthocyanin content was found to be 3.02 mg/g of dry weight for the swollen stem skin of Kolibri with the application of HPLC, while there was no trace amount of anthocyanins detected in the corresponding tissue in Winner (Table 1). The content of anthocyanins in Kolibri is similar to those found in the head tissues of red cabbage reported

DOI: 10.1021/acs.jafc.5b00473
J. Agric. Food Chem. 2015, 63, 4160−4169

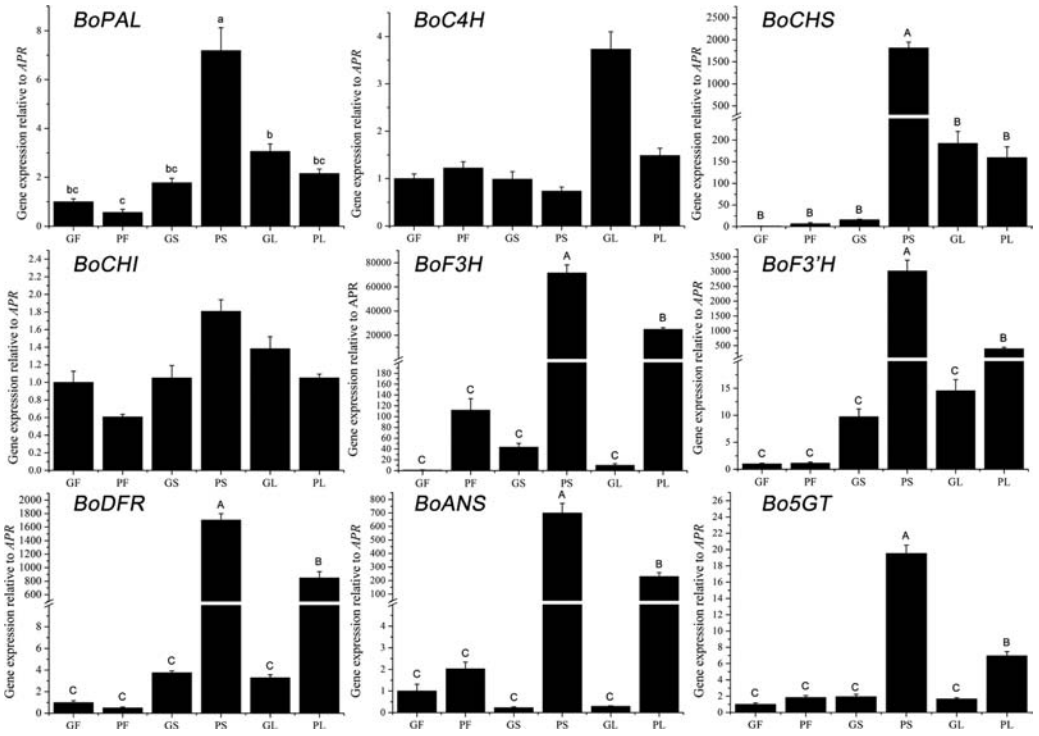

Figure 3. Expression analysis of anthocyanin biosynthetic genes in different tissues of the two kohlrabi cultivars. Abbreviations: PS, purple skin of swollen stem; GS, green skin of swollen stem; PS, flesh of swollen stem in purple cultivar; GS, flesh of swollen stem in green cultivar; PL, purple leaf; GL, green leaf. Error bars represent the standard error of the mean (n = 3). Error bars represent the standard error of the mean (n = 3). The statistical significance of the differences between samples was calculated with ANOVA by paired-group comparisons. Different uppercase letters indicate significance at $P < 0.01$. Different lowercase letters indicate significance at $P < 0.05$.

before.[25] Moreover, the anthocyanin cyanidin 3-(caffeoyl)-*p*-coumaroyl (sinapoyl)-diglucoside-5-glucoside shows the highest level (2.08 mg/g dry weight) in the stem skin of Kolibri (Table 1).

Transcriptional Analysis of Anthocyanin Biosynthetic and Regulatory Genes in Both Kohlrabi Cultivars. In order to investigate the mechanisms underlying the anthocyanin accumulation in purple kohlrabi, the transcripts of anthocyanin biosynthetic enzymes and regulatory genes were examined in the leaves, skins, and flesh of the two cultivars by qPCR. The expression of anthocyanin biosynthetic genes *BoPAL, BoC4H, BoCHS, BoCHI, RsF3H, BoF3′H, BoDFR, BoANS*, and *Bo5GT* are shown in Figure 3. In comparison with the pigmentless tissues, most of the anthocyanin pathway genes were significantly upregulated in the purple leaves and stem skins of Kolibri. In the leaves, the expression of anthocyanin structural genes from *BoF3H* was drastically increased in purple kohlrabi in comparison with the green cultivar. In the cuticles of swollen stems, the purple kohlrabi displayed increased expression of nearly all anthocyanin pathway genes except for *BoCHI* and *BoC4H*. Consistent with pigment production, the higher folds of expression changes happened in the skins of swollen stems, while the lower folds of expression changes happened in the leaves. Among the upregulated genes, *BoF3H* exhibited the highest fold increase (1000 folds at least) in both the leaves and skins of swollen stems. In the results shown in Figure 2, trace amounts of all the anthocyanin structural genes were detected by qPCR in different organs of Winner with the absence of visible anthocyanin production. These results indicate that a large amount of transcripts of structural genes is a prerequisite for abundant anthocyanin accumulation. Moreover, the constant upregulation of anthocyanin biosynthetic genes in certain colorful organs and/or tissues rich in anthocyanins was also found in red-fleshed apple, purple eggplant, purple tomato, red pear, and pap1-D *Arabidopsis*.[30,32,34−36] Collectively, purple kohlrabi shares similar mechanisms of transcriptional regulation in mediating anthocyanin accumulation with those high anthocyanin content plants mentioned above.

Here, the absence of pelargonidin-based pigments we have referred to in the anthocyanin profile analysis of the purple kohlrabi is worth discussing. First, the fact that the biosynthetic pathway for anthocyanin accumulation is intact should be admitted for the apparent anthocyanin accumulation in certain tissues in Kolibri. In addition, the substrate specificity of the *BoDFR* and *BoANS* is also relatively broad.[47] Then, the question seems to become more confused. However, the higher activity of *BoF3′H* due to the dramatically increased transcripts in purple kohlrabi might provide a reasonable answer to this question (Figure 3). In the anthocyanin biosynthetic pathway shown in Figure 1, most of the dihydrokaempferol has been applied to produce dihydroquercetin with two hydroxyl groups. Consequently, there is no doubt that most of the final products should be cyanindin-based anthocyanins. By the same token, the common glycosylated cyanidin at the C5 position of anthocyanidins in Kolibri might be due to the increased expression of *Bo5GT* in purple stem skins.

To verify whether any of the regulatory genes controlling the transcription of anthocyanin structural genes were upregulated in Kolibri, the transcripts of some vital anthocyanin biosynthesis regulatory orthologous genes of *Arabidopsis*, *BoPAP1*, *BoPAP2*, *BoMYB113*, *BoMYB114*, *BoTT8*, and *BoTTG1*, were examined. In *Arabidopsis*, four R2R3MYB genes (*AtPAP1*, *AtPAP2*, *AtMYB113*, and *AtMYB114*) are known to regulate

DOI: 10.1021/acs.jafc.5b00473
J. Agric. Food Chem. 2015, 63, 4160−4169

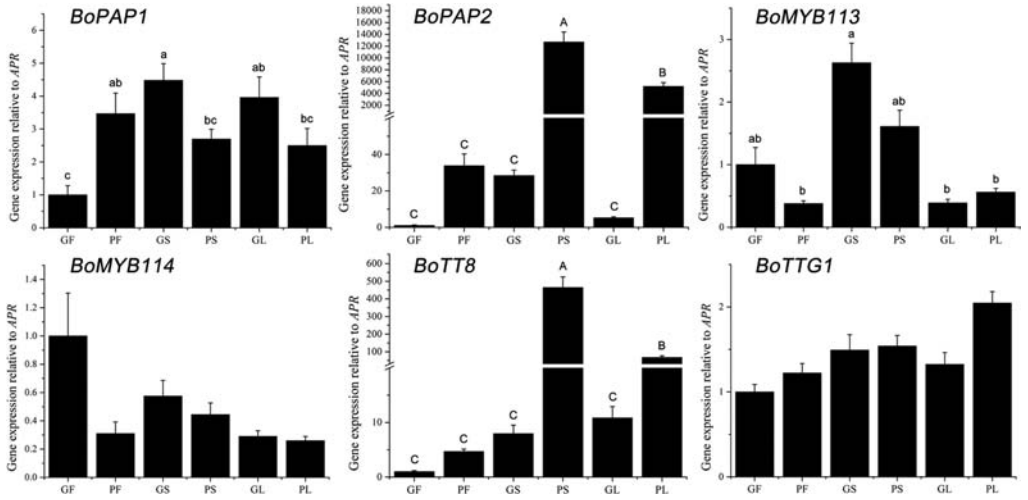

Figure 4. Expression analysis of anthocyanin biosynthesis regulatory genes in different tissues of the two kohlrabi cultivars. Abbreviations: PS, purple skin of swollen stem; GS, green skin of swollen stem; PS, flesh of swollen stem in purple cultivar; GS, flesh of swollen stem in green cultivar; PL, purple leaf; GL, green leaf. Error bars represent the standard error of the mean (n = 3). The statistical significance of the differences between samples was calculated with ANOVA by paired-group comparisons. Different uppercase letters indicate significance at $P < 0.01$. Different lowercase letters indicate significance at $P < 0.05$.

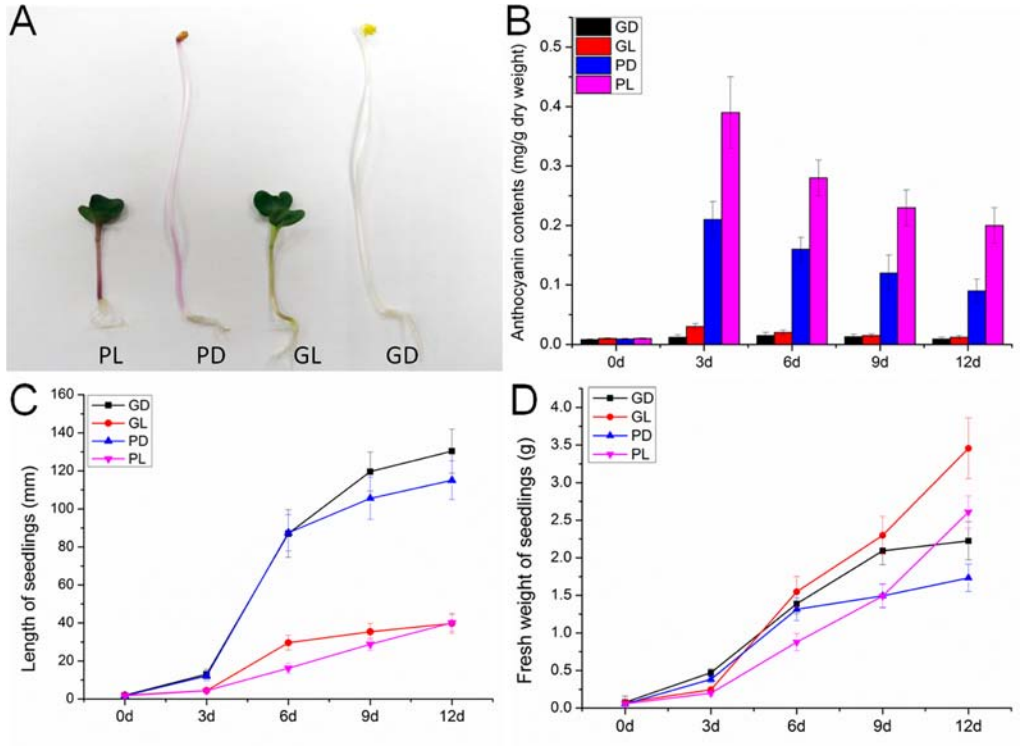

Figure 5. Phenotype of kohlrabi sprouts grown under dark and light conditions. (A) Photographs of kohlrabi sprouts of the two cultivars obtained at 6 days after sowing under dark and light conditions. (B) Anthocyanin contents (mg/g dry weight) during the development of kohlrabi sprouts under dark and light conditions. (C) Average length of sprouts of kohlrabi from 0 to 12 days after sowing (n = 30 per treatment). (D) Average fresh weight of sprouts of kohlrabi from 0 to 12 days after sowing (n = 30 per treatment). Abbreviations: PL, purple cultivar grown in the light; PD, purple cultivar grown in the dark; GL, green cultivar grown in the light; GD, green cultivar grown in the dark. Error bars represent the standard error of the mean (n = 3).

the biosynthesis of anthocyanins directly, while bHLH proteins *AtTT8* and *AtTTG1* play coordinate roles in the formation of a transcriptional regulation complex (MBW).[26] Thence, four MYB genes which shared high similarities with anthocyanin biosynthesis activators of *Arabidopsis* were cloned from the kohlrabi and designated as *BoPAP1*, *BoPAP2*, *BoMYB113*, and *BoMYB114*. Similarly, *BoTT8* and *BoTTG1*, as the orthologous genes of *AtTT8* and *AtTTG1*, respectively, were also cloned. In the results shown in Figure 4, *BoPAP2* and *BoTT8* were the only two regulatory genes greatly upregulated in tissues rich with anthocyanins. In the leaves, the expression levels of *BoPAP2* and *BoTT8* in Kolibri were about 990- and 6.8-fold higher than those in Winner, respectively. In the skins of swollen stems, the expression levels of *BoPAP2* and *BoTT8* in

DOI: 10.1021/acs.jafc.5b00473
J. Agric. Food Chem. 2015, 63, 4160−4169

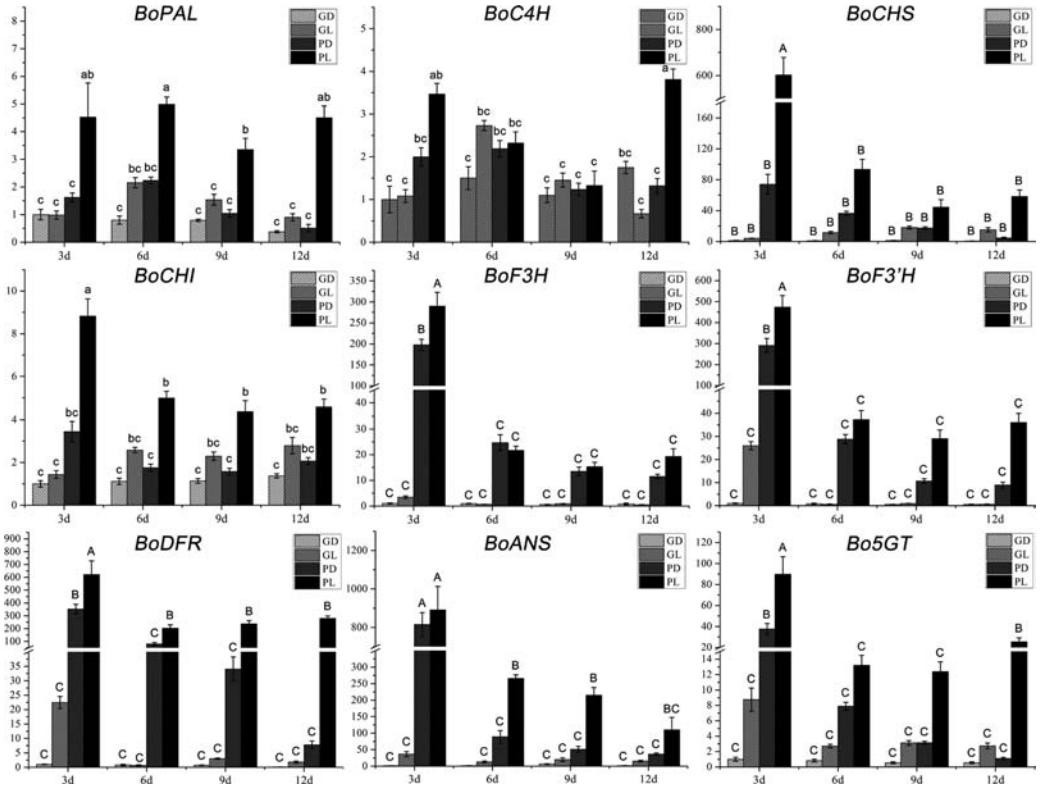

Figure 6. Expression profiles of anthocyanin biosynthetic genes during the development of kohlrabi sprouts under dark and light conditions. Abbreviations: PL, purple cultivar grown in the light; PD, purple cultivar grown in the dark; GL, green cultivar grown in the light; GD, green cultivar grown in the dark. The longitudinal axis indicates the expression levels of genes relative to the level of *BoApr*. Error bars represent the standard error of the mean (n = 3). The statistical significance of the differences between samples was calculated with ANOVA by paired-group comparisons. Different uppercase letters indicate significance at $P < 0.01$. Different lowercase letters indicate significance at $P < 0.05$.

Kolibri were about 452- and 57.7-fold higher than those in the green cultivar, respectively.

In the process of activating anthocyanin biosynthetic genes, the MYB and bHLH transcription factors make different contributions among plant species. In the anthocyanin biosynthesis regulatory complex of MBW, R2R3MYB transcription factors regulate anthocyanin biosynthesis specifically.[48] However, the functions of bHLH transcription factors and WD proteins are rather pleiotropic.[26] In addition, the increased expression of both MYB and bHLH is necessary for transcriptional activation of anthocyanin biosynthetic genes in petunia, cauliflower, and *Arabidopsis*.[26,31,49] Consequently, the dramatic increase of the pigment production and anthocyanin structural genes in purple kohlrabi should be due to the coordinated transcriptional activation of *BoPAP2* and *BoTT8*.

Light Sheds Evident Influence on the Growth and Anthocyanin Accumulation of Kohlrabi Sprouts. To study the effects of light on the development and pigment production of kohlrabi, sprouts of both cultivars grown under light and dark conditions were used as materials. The length, fresh weight, and total pigment content of sprouts were examined every 3 days until 12 days after sowing (DAS). As the results in Figure 5 show, the treated sprouts of Kolibri and Winner displayed completely different phenotypes in the production of anthocyanins. Kolibri showed apparent anthocyanin accumulation during all stages of development, regardless of light or dark conditions. However, the pigment intensity in sprouts of Kolibri cultured in the light is higher than that cultured in the dark. This phenomenon suggests that the production of pigments is not totally independent of light. In contrast, only a tiny amount of pigment was detected in the sprouts of Winner grown in the light and the production of pigments is totally dependent on light (Figure 5A,B). However, these two kohlrabi cultivars shared similar trends of growth (Figure 5C,D). The length increased with time during the entire process of the experiments. The sprouts cultured in the dark showed a much higher speed of elongation in comparison to those cultured in the light. The lengths of sprouts grown under dark conditions were 2-fold higher than those under light conditions after culturing in the medium for 9 days. In addition, the fresh weight of sprouts cultured for 12 days under dark conditions was not enhanced evidently in comparison with 9 day old sprouts. That is to say, the maximum biomass for kohlrabi sprouts cultured in the dark was reached at around 9 days. These results are concordant with the findings for buckwheat sprouts in a previous report.[50]

Expression Profiles of Anthocyanin Biosynthetic and Regulatory Genes in Sprouts of the Two Kohlrabi Cultivars Grown in Light and Dark Conditions. To investigate the molecular mechanism of anthocyanin accumulation under light and dark conditions, the expression profiles of the anthocyanin pathway and regulatory genes in the four groups of materials gathered at different stages were examined. The expression patterns of *BoPAL*, *BoC4H*, *BoCHS*, *BoCHI*, *BoF3H*, *BoF3′H*, *BoDFR*, *BoANS*, and *Bo5GT* are shown in Figure 6. During the different development stages in the light-treated sprouts of Kolibri, all of the anthocyanin structural genes exhibited the top expression level at 3 DAS. The expression patterns agree well with the amounts of pigment production in the corresponding tissues (Figure 5B). In

DOI: 10.1021/acs.jafc.5b00473
J. Agric. Food Chem. 2015, 63, 4160−4169

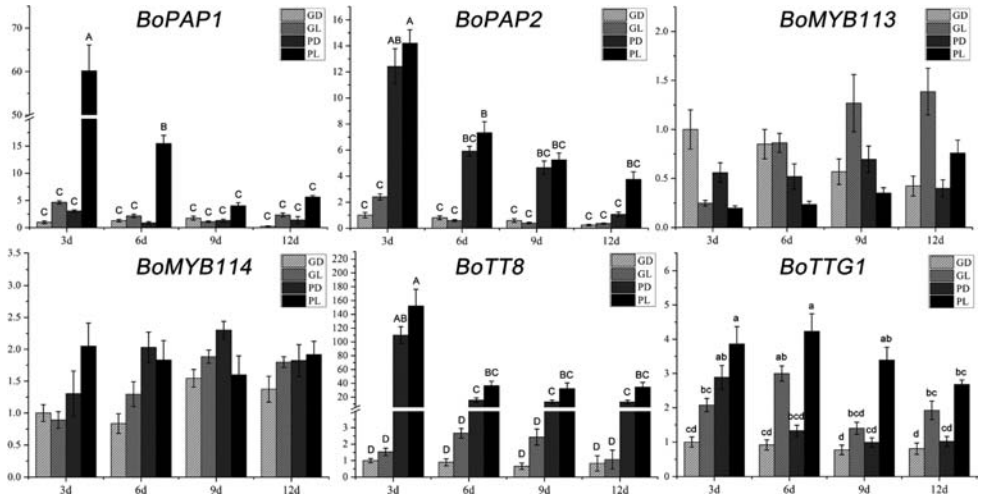

Figure 7. Expression profiles of anthocyanin biosynthesis regulatory genes during the development of kohlrabi sprouts under dark and light conditions. Abbreviations: PL, purple cultivar grown in the light; PD, purple cultivar grown in the dark; GL, green cultivar grown in the light; GD, green cultivar grown in the dark. The longitudinal axis indicates the expression levels of genes relative to the level of *BoApr*. Error bars represent the standard error of the mean (n = 3). The statistical significance of the differences between samples was calculated with ANOVA by paired-group comparisons. Different uppercase letters indicate significance at $P < 0.01$. Different lowercase letters indicate significance at $P < 0.05$.

comparison with the purple sprouts treated in the dark at 3 DAS, the expressions of *BoPAL*, *BoC4H*, *BoCHI*, *BoF3H*, *BoF3′H*, *BoDFR*, *BoANS*, and *Bo5GT* were all slightly raised in the purple sprouts treated in the light. In the same development stage, the expression of *BoCHS* in light-treated purple sprouts was significantly higher (8.2-fold) than that of purple sprouts in the dark. These results suggest that the expression of *BoCHS* in purple kohlrabi sprouts is strictly light dependent. Therefore, it is reasonable that the contents of anthocyanins in light-treated Kolibri sprouts are higher than those in dark-treated sprouts during all developmental stages. In combination with the expression analysis of anthocyanin biosynthetic genes at other developmental stages in purple sprouts, it can be concluded that light enhances the existing production of anthocyanins by strengthening the expression of structural genes, especially *BoCHS*, at the mRNA level. As we have mentioned that a trace amount of anthocyanins was detected in the light-treated sprouts of Winner, it is not astonishing that the transcripts of most anthocyanin pathway genes in the corresponding samples were significantly higher than those in dark-treated sprouts.

Expression profiles of anthocyanin biosynthesis regulatory genes in sprouts of the two kohlrabi cultivars grown under light and dark conditions are shown in Figure 7. In the light-treated sprouts of Kolibri at the stage of 3 DAS, the expression levels of *BoPAP1*, *BoPAP2*, and *BoTT8* were about 11-, 6-, and 101-fold higher than those in the light-treated green cultivar, respectively. It seems that the anthocyanin structural genes are coordinated regulated by *BoPAP1*, *BoPAP2*, and *BoTT8* in sprouts of Kolibri under light. Furthermore, *BoPAP1* was significantly raised at a transcriptional level under light conditions in purple sprouts during all stages of development and was about 23-fold higher than that in the dark-treated sprouts at 3 DAS. However, light did not have a significant influence on the transcription of *BoPAP2* and *BoTT8* in purple sprouts. In conclusion, the anthocyanin accumulation and upregulation of structural genes in the purple kohlrabi sprouts is mainly due to the transcriptional activation of *BoPAP2* and *BoTT8*. In addition, *BoPAP1* is the major regulatory gene responsible for the enhanced production of pigments in light-treated sprouts.

MYB genes associated with the regulation of anthocyanin accumulation are characterized by a conserved DNA-binding domain including two imperfect repeats (R2R3) with a specific motif for the interaction with the bHLH domain of bHLH proteins in the plant kingdom. The four MYB genes cloned from kohlrabi exhibited high sequence similarities with each other. The putative proteins contain conserved R2R3MYB domains and belong to the same subgroup 10 of MYB proteins as described by Allan et al. in anthocyanin production regulation.[48] In purple swollen stems of Kolibri, the upregulation of *BoTT8* and *BoPAP2* probably account for the accumulation of anthocyanins by transcriptional activation of the structural genes. Transcriptional factors of MYB or bHLH have been reported to be responsible for pigment production in many plant species. In certain anthocyanin-accumulating plants (such as red-fleshed apple, purple sweet potato, pap1-D *Arabidopsis*, and maize), the anthocyanin accumulation has been found to be due to an activation of a MYB transcriptional factor.[30,36,51−53] In contrast, white-skinned grapes arise from the mutations in a R2R3MYB protein.[54] In addition, the heterologous expression of bHLH transcriptional factors alter pigment production in the transgenic tomato.[40−42,55] In tissues rich with anthocyanins in Kolibri, both *BoPAP2* and *BoTT8* genes were constitutively upregulated. In the light-treated sprouts of Kolibri, *BoPAP1* was upregulated in large folds. A model illustrating that the transcriptional regulation complex consists of MYB, bHLH, and other proteins (*BoTTG1*) which regulate anthocyanin accumulation coordinatedly is presented in Figure 8. In the model, *BoTT8* and *BoPAP2* promote kohlrabi coloration in a light-independent manner, while the light-induced transcription factor *BoPAP1* (indicated by the dashed cycle) enhanced the existing production of pigments in the light-treated sprouts of Kolibri. In summary, the eye-catching purple kohlrabi not only supplies human beings with a healthy diet due to its high levels of carotenoids, ascorbic acid, and tocopherols contained in the edible parts but also contains large amounts of the natural antioxidants anthocyanins. The elucidations of anthocyanin accumulation at the molecular and metabolic levels in purple kohlrabi provide an important basis

DOI: 10.1021/acs.jafc.5b00473
J. Agric. Food Chem. 2015, 63, 4160−4169

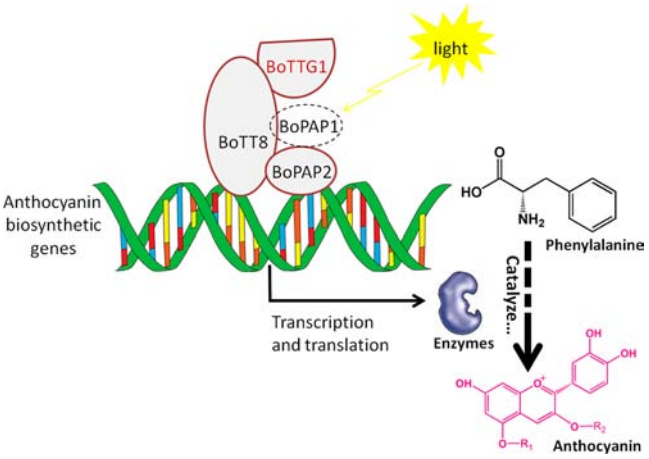

Figure 8. Model summarizing our findings that a transcriptional regulation complex consisting of MYB, bHLH, and WD40 proteins coordinatedly regulates anthocyanin accumulation by activating the transcription of anthocyanin strucural genes in response to light. The induced *BoPAP1*, which enhanced the production of anthocyanin in light-treated purple kohlrabi sprouts, is indicated in the dashed cycle.

for the breeding of new kohlrabi cultivars with even more excellent agronomic characters.

■ ASSOCIATED CONTENT

Supporting Information

A table of primers used for qPCR analysis of anthocyanin biosynthetic genes and associated regulatory genes in kohlrabi and a figure depicting phenotypic characterization of Kolibri and Winner during all developmental stages of vegetative growth. This material is available free of charge via the Internet at http://pubs.acs.org.

■ AUTHOR INFORMATION

Corresponding Author

*G.C.: tel, 00862365112674; fax, 0086 23 65112674; e-mail, chenguoping@cqu.edu.cn.

Funding

This work was supported by the National Natural Science Foundation of China (Nos. 30871709, 30600044, and 31171968) and the Technology System of National Bulk Vegetable Industry—Eggplant Breeding Position (CARS-25-A-06).

Notes

The authors declare no competing financial interest.

■ ABBREVIATIONS USED

PAL, phenylalanine ammonia lyase; C4H, cinnamate 4-hydroxylase; 4CL, 4-coumarateCoA ligase; CHS, chalcone synthase; CHI, chalcone isomerase; F3H, flavone 3-hydroxylase; F3′H, flavonoid 3′,-hydroxylase; DFR, dihydroflavonol reductase; ANS, anthocyanidin synthase; 5-GT, flavonoid-5-glucosyltransferase; GST, glutathione S-transferase; DHK, dihydrokaempferol; HPLC, high-performance liquid chromatography; ESI-MS/MS, elctrospray ionization tandem mass spectrometry; qRT-PCR, quantitative real-time PCR; DAS, days after sowing

■ REFERENCES

(1) Christie, P.; Alfenito, M.; Walbot, V. Impact of low-temperature stress on general phenylpropanoid and anthocyanin pathways: Enhancement of transcript abundance and anthocyanin pigmentation in maize seedlings. *Planta* **1994**, *194*, 541−549.

(2) Sarma, A. D.; Sharma, R. Anthocyanin-DNA copigmentation complex: mutual protection against oxidative damage. *Phytochemistry* **1999**, *52*, 1313−1318.

(3) Bradshaw, H. D.; Schemske, D. W. Allele substitution at a flower colour locus produces a pollinator shift in monkeyflowers. *Nature* **2003**, *426*, 176−8.

(4) Lorenc-Kukula, K.; Jafra, S.; Oszmianski, J.; Szopa, J. Ectopic expression of anthocyanin 5-o-glucosyltransferase in potato tuber causes increased resistance to bacteria. *J. Agric. Food Chem.* **2005**, *53*, 272−81.

(5) Castellarin, S. D.; Pfeiffer, A.; Sivilotti, P.; Degan, M.; Peterlunger, E.; G, D. I. G. Transcriptional regulation of anthocyanin biosynthesis in ripening fruits of grapevine under seasonal water deficit. *Plant, Cell Environ.* **2007**, *30*, 1381−99.

(6) Jin, H.; Cominelli, E.; Bailey, P.; Parr, A.; Mehrtens, F.; Jones, J.; Tonelli, C.; Weisshaar, B.; Martin, C. Transcriptional repression by AtMYB4 controls production of UV-protecting sunscreens in Arabidopsis. *EMBO journal* **2000**, *19*, 6150−61.

(7) Hannum, S. M. Potential impact of strawberries on human health: a review of the science. *Crit. Rev. Food Sci. Nutr.* **2004**, *44*, 1−17.

(8) Guarnieri, S.; Riso, P.; Porrini, M. Orange juice vs vitamin C: effect on hydrogen peroxide-induced DNA damage in mononuclear blood cells. *Br. J. Nutr.* **2007**, *97*, 639−43.

(9) Toufektsian, M. C.; de Lorgeril, M.; Nagy, N.; Salen, P.; Donati, M. B.; Giordano, L.; Mock, H. P.; Peterek, S.; Matros, A.; Petroni, K.; Pilu, R.; Rotilio, D.; Tonelli, C.; de Leiris, J.; Boucher, F.; Martin, C. Chronic dietary intake of plant-derived anthocyanins protects the rat heart against ischemia-reperfusion injury. *J. Nutr.* **2008**, *138*, 747−52.

(10) de Pascual-Teresa, S.; Moreno, D. A.; Garcia-Viguera, C. Flavanols and anthocyanins in cardiovascular health: a review of current evidence. *Int. J. Mol. Sci.* **2010**, *11*, 1679−703.

(11) Paredes-Lopez, O.; Cervantes-Ceja, M. L.; Vigna-Perez, M.; Hernandez-Perez, T. Berries: improving human health and healthy aging, and promoting quality life–a review. *Plant Foods Hum. Nutr.* **2010**, *65*, 299−308.

(12) Butelli, E.; Titta, L.; Giorgio, M.; Mock, H. P.; Matros, A.; Peterek, S.; Schijlen, E. G.; Hall, R. D.; Bovy, A. G.; Luo, J.; Martin, C. Enrichment of tomato fruit with health-promoting anthocyanins by expression of select transcription factors. *Nat. Biotechnol.* **2008**, *26*, 1301−8.

(13) Meiers, S.; Kemeny, M.; Weyand, U.; Gastpar, R.; von Angerer, E.; Marko, D. The anthocyanidins cyanidin and delphinidin are potent inhibitors of the epidermal growth-factor receptor. *J. Agric. Food Chem.* **2001**, *49*, 958−62.

(14) Williams, R. J.; Spencer, J. P.; Rice-Evans, C. Flavonoids: antioxidants or signalling molecules? *Free Radical Biol. Med.* **2004**, *36*, 838−49.

(15) Sparvoli, F.; Martin, C.; Scienza, A.; Gavazzi, G.; Tonelli, C. Cloning and molecular analysis of structural genes involved in flavonoid and stilbene biosynthesis in grape (Vitis vinifera L.). *Plant Mol. Biol.* **1994**, *24*, 743−755.

(16) Winkel-Shirley, B. Flavonoid biosynthesis. A colorful model for genetics, biochemistry, cell biology, and biotechnology. *Plant Physiol.* **2001**, *126*, 485−93.

(17) Harborne, J. B.; Williams, C. A. Advances in flavonoid research since 1992. *Phytochemistry* **2000**, *55*, 481−504.

(18) Guo, N.; Cheng, F.; Wu, J.; Liu, B.; Zheng, S.; Liang, J.; Wang, X. Anthocyanin biosynthetic genes in Brassica rapa. *BMC Genomics* **2014**, *15*, 426.

(19) Grotewold, E. The genetics and biochemistry of floral pigments. *Annu. Rev. Plant Biol.* **2006**, *57*, 761−80.

(20) Shirley, B. W. Flavonoid biosynthesis: 'new' functions for an 'old' pathway. *Trends Plant Sci.* **1996**, *1*, 377−382.

DOI: 10.1021/acs.jafc.5b00473
J. Agric. Food Chem. 2015, 63, 4160−4169

(21) Bogs, J.; Ebadi, A.; McDavid, D.; Robinson, S. P. Identification of the Flavonoid Hydroxylases from Grapevine and Their Regulation during Fruit Development. *Plant Physiol.* **2006**, *140*, 279−291.
(22) Springob, K.; Nakajima, J.; Yamazaki, M.; Saito, K. Recent advances in the biosynthesis and accumulation of anthocyanins. *Nat. Prod. Rep.* **2003**, *20*, 288−303.
(23) Boss, P. K.; Davies, C.; Robinson, S. P. Expression of anthocyanin biosynthesis pathway genes in red and white grapes. *Plant Mol. Biol.* **1996**, *32*, 565−9.
(24) Hichri, I.; Barrieu, F.; Bogs, J.; Kappel, C.; Delrot, S.; Lauvergeat, V. Recent advances in the transcriptional regulation of the flavonoid biosynthetic pathway. *J. Exp. Bot.* **2011**, *62*, 2465−83.
(25) Yuan, Y.; Chiu, L. W.; Li, L. Transcriptional regulation of anthocyanin biosynthesis in red cabbage. *Planta* **2009**, *230*, 1141−53.
(26) Gonzalez, A.; Zhao, M.; Leavitt, J. M.; Lloyd, A. M. Regulation of the anthocyanin biosynthetic pathway by the TTG1/bHLH/Myb transcriptional complex in Arabidopsis seedlings. *Plant J.* **2008**, *53*, 814−27.
(27) Nesi, N.; Debeaujon, I.; Jond, C.; Pelletier, G.; Caboche, M.; Lepiniec, L. The TT8 gene encodes a basic helix-loop-helix domain protein required for expression of DFR and BAN genes in Arabidopsis siliques. *Plant Cell* **2000**, *12*, 1863−78.
(28) Payne, C. T.; Zhang, F.; Lloyd, A. M. GL3 encodes a bHLH protein that regulates trichome development in arabidopsis through interaction with GL1 and TTG1. *Genetics* **2000**, *156*, 1349−62.
(29) Zhang, F.; Gonzalez, A.; Zhao, M.; Payne, C. T.; Lloyd, A. A network of redundant bHLH proteins functions in all TTG1-dependent pathways of Arabidopsis. *Development* **2003**, *130*, 4859−69.
(30) Espley, R. V.; Hellens, R. P.; Putterill, J.; Stevenson, D. E.; Kutty-Amma, S.; Allan, A. C. Red colouration in apple fruit is due to the activity of the MYB transcription factor, MdMYB10. *Plant J.* **2007**, *49*, 414−27.
(31) Chiu, L. W.; Zhou, X.; Burke, S.; Wu, X.; Prior, R. L.; Li, L. The purple cauliflower arises from activation of a MYB transcription factor. *Plant Physiol.* **2010**, *154*, 1470−80.
(32) Feng, S.; Wang, Y.; Yang, S.; Xu, Y.; Chen, X. Anthocyanin biosynthesis in pears is regulated by a R2R3-MYB transcription factor PyMYB10. *Planta* **2010**, *232*, 245−55.
(33) Butelli, E.; Licciardello, C.; Zhang, Y.; Liu, J.; Mackay, S.; Bailey, P.; Reforgiato-Recupero, G.; Martin, C. Retrotransposons control fruit-specific, cold-dependent accumulation of anthocyanins in blood oranges. *Plant Cell* **2012**, *24*, 1242−55.
(34) Zhang, Y.; Hu, Z.; Chu, G.; Huang, C.; Tian, S.; Zhao, Z.; Chen, G. Anthocyanin Accumulation and Molecular Analysis of Anthocyanin Biosynthesis-Associated Genes in Eggplant (Solanum melongena L.). *J. Agric. Food Chem.* **2014**, *62*, 2906−12.
(35) Mathews, H.; Clendennen, S. K.; Caldwell, C. G.; Liu, X. L.; Connors, K.; Matheis, N.; Schuster, D. K.; Menasco, D. J.; Wagoner, W.; Lightner, J.; Wagner, D. R. Activation tagging in tomato identifies a transcriptional regulator of anthocyanin biosynthesis, modification, and transport. *Plant Cell* **2003**, *15*, 1689−703.
(36) Borevitz, J. O.; Xia, Y.; Blount, J.; Dixon, R. A.; Lamb, C. Activation Tagging Identifies a Conserved MYB Regulator of Phenylpropanoid Biosynthesis. *Plant Cell* **2000**, *12*, 2383−2393.
(37) Park, K. I.; Ishikawa, N.; Morita, Y.; Choi, J. D.; Hoshino, A.; Iida, S. A bHLH regulatory gene in the common morning glory, Ipomoea purpurea, controls anthocyanin biosynthesis in flowers, proanthocyanidin and phytomelanin pigmentation in seeds, and seed trichome formation. *Plant J.* **2007**, *49*, 641−54.
(38) Feyissa, D. N.; Lovdal, T.; Olsen, K. M.; Slimestad, R.; Lillo, C. The endogenous GL3, but not EGL3, gene is necessary for anthocyanin accumulation as induced by nitrogen depletion in Arabidopsis rosette stage leaves. *Planta* **2009**, *230*, 747−54.
(39) Xie, X. B.; Li, S.; Zhang, R. F.; Zhao, J.; Chen, Y. C.; Zhao, Q.; Yao, Y. X.; You, C. X.; Zhang, X. S.; Hao, Y. J. The bHLH transcription factor MdbHLH3 promotes anthocyanin accumulation and fruit colouration in response to low temperature in apples. *Plant, Cell Environ.* **2012**, *35*, 1884−97.
(40) Goldsbrough, A. P.; Tong, Y.; Yoder, J. I. Lc as a non-destructive visual reporter and transposition excision marker gone for tomato. *Plant J.* **1996**, *9*, 927−933.
(41) Zhang, Y.; Chen, G.; Dong, T.; Pan, Y.; Zhao, Z.; Tian, S.; Hu, Z. Anthocyanin Accumulation and Transcriptional Regulation of Anthocyanin Biosynthesis in Purple Bok Choy (Brassica rapa var. chinensis). *J. Agric. Food Chem.* **2014**, *62*, 12366−12376.
(42) Mooney, M.; Desnos, T.; Harrison, K.; Jones, J.; Carpenter, R.; Coen, E. Altered regulation of tomato and tobacco pigmentation genes caused by the delila gene of Antirrhinum. *Plant J.* **1995**, *7*, 333−339.
(43) Jahangir, M.; Kim, H. K.; Choi, Y. H.; Verpoorte, R. Health-Affecting Compounds in Brassicaceae. *Compr. Rev. Food Sci. Food Saf.* **2009**, *8*, 31−43.
(44) Park, W. T.; Kim, J. K.; Park, S.; Lee, S. W.; Li, X.; Kim, Y. B.; Uddin, M. R.; Park, N. I.; Kim, S. J.; Park, S. U. Metabolic profiling of glucosinolates, anthocyanins, carotenoids, and other secondary metabolites in kohlrabi (Brassica oleracea var. gongylodes). *J. Agric. Food Chem.* **2012**, *60*, 8111−6.
(45) Cartea, M. E.; Francisco, M.; Soengas, P.; Velasco, P. Phenolic compounds in Brassica vegetables. *Molecules* **2011**, *16*, 251−80.
(46) Park, N. I.; Xu, H.; Li, X.; Jang, I. H.; Park, S.; Ahn, G. H.; Lim, Y. P.; Kim, S. J.; Park, S. U. Anthocyanin accumulation and expression of anthocyanin biosynthetic genes in radish (Raphanus sativus). *J. Agric. Food Chem.* **2011**, *59*, 6034−9.
(47) Boss, P. K.; Davies, C.; Robinson, S. P. Analysis of the Expression of Anthocyanin Pathway Genes in Developing Vitis vinifera L. cv Shiraz Grape Berries and the Implications for Pathway Regulation. *Plant physiology* **1996**, *111*, 1059−1066.
(48) Dubos, C.; Stracke, R.; Grotewold, E.; Weisshaar, B.; Martin, C.; Lepiniec, L. MYB transcription factors in Arabidopsis. *Trends Plant Sci.* **2010**, *15*, 573−81.
(49) Spelt, C.; Quattrocchio, F.; Mol, J. N.; Koes, R. anthocyanin1 of petunia encodes a basic helix-loop-helix protein that directly activates transcription of structural anthocyanin genes. *Plant Cell* **2000**, *12*, 1619−32.
(50) Li, X.; Thwe, A. A.; Park, N. I.; Suzuki, T.; Kim, S. J.; Park, S. U. Accumulation of phenylpropanoids and correlated gene expression during the development of tartary buckwheat sprouts. *J. Agric. Food Chem.* **2012**, *60*, 5629−35.
(51) Grotewold, E.; Sainz, M. B.; Tagliani, L.; Hernandez, J. M.; Bowen, B.; Chandler, V. L. Identification of the residues in the Myb domain of maize C1 that specify the interaction with the bHLH cofactor R. *Proc. Natl. Acad. Sci. U. S. A.* **2000**, *97*, 13579−84.
(52) Mano, H.; Ogasawara, F.; Sato, K.; Higo, H.; Minobe, Y. Isolation of a regulatory gene of anthocyanin biosynthesis in tuberous roots of purple-fleshed sweet potato. *Plant Physiol.* **2007**, *143*, 1252−68.
(53) Espley, R. V.; Brendolise, C.; Chagne, D.; Kutty-Amma, S.; Green, S.; Volz, R.; Putterill, J.; Schouten, H. J.; Gardiner, S. E.; Hellens, R. P.; Allan, A. C. Multiple repeats of a promoter segment causes transcription factor autoregulation in red apples. *Plant Cell* **2009**, *21*, 168−83.
(54) Walker, A. R.; Lee, E.; Bogs, J.; McDavid, D. A.; Thomas, M. R.; Robinson, S. P. White grapes arose through the mutation of two similar and adjacent regulatory genes. *Plant J.* **2007**, *49*, 772−85.
(55) Albert, N. W.; Lewis, D. H.; Zhang, H.; Irving, L. J.; Jameson, P. E.; Davies, K. M. Light-induced vegetative anthocyanin pigmentation in Petunia. *J. Exp. Bot.* **2009**, *60*, 2191−202.

DOI: 10.1021/acs.jafc.5b00473
J. Agric. Food Chem. 2015, 63, 4160−4169

(mainly histamine and tyramine) from different foods and foodstuffs: dry and raw sausages, cheese, fish slurry, Thai fish sauce, Myeolchi-jeot salted and fermented anchovy.[22−27] Some examples of these species are *Staphylococcus xylosus* (sausages), *Brevibacterium linens* (cheese), *Lactobacillus sakei* (fish slurry), and *Virgibacillus* sp. (Thai fish sauce). In contrast to García-Ruíz et al.,[28] who failed to show the ability of wine lactic acid bacteria (LAB) to reduce BA in wine, we have recently found that wine-associated strains of *L. plantarum*, as well as other LAB from sausages (*L. farciminis*) and beer (*P. acidilactici*) are competent to degrade histamine, tyramine, and putrescine in wine.[29]

In this work we show that cells of *K. varians* LTH 1540 are able to degrade putrescine in wine, providing the first report on putrescine degradation in wine by a species of *Micrococcus* genus. We also describe the purification, identification, and biochemical characterization of a novel amine oxidase enzyme responsible for putrescine degradation.

MATERIALS AND METHODS

Chemicals. Commercial standard proteins, reagents, and amines (putrescine, cadaverine, histamine, tyramine, methylamine, propylamine, ethanolamine, triethylamine, spermidine, and spermine) were obtained from Sigma-Aldrich (Steinheim, Germany).

HPLC analytical grade organic solvent methanol was supplied by Panreac. Reagent 6-aminoquinolyl-*N*-hydroxysuccinimidyl carbamate solution (AQC solution) was purchased from Waters (Milford, MA, USA). Horseradish peroxidase was purchased from Merck (Darmstadt, Germany). Ultrapure water was obtained from a Milli-Q Gradient water system (Millipore, Bedford, MA, USA).

Organism and Culture Conditions. The strain *K. varians* LTH 1540, formerly isolated from artisanal fermented sausage and deposited in Dr. Hammes' culture collection (Universität Hohenheim, Germany), was kindly provided by Professor Dr. Herbert Schmidt. Cells were cultured overnight at 30 °C in nutrient broth medium supplemented with putrescine at 10 mg/L under stirred aerobic conditions.

Assay for Putrescine Degradation by *K. varians* Cells. The ability of *K. varians* cells to degrade putrescine in buffer system, synthetic media, and wine was tested. Putrescine degradation assays in 50 mM sodium phosphate buffer, pH 7.4, were performed using cells from a 6 unit OD_{600} culture, collected by centrifugation, washed twice in that buffer, and resuspended in the same buffer supplemented with 100 or 1000 mg/L of putrescine. Reaction mixtures were incubated at 28 °C with shaking, aliquots were taken at different time periods, and their putrescine content was measured by LC-FLD according to a previously reported method[30] and described below. The ability of *K. varians* cells to degrade putrescine was also tested in modified Dapkevicius' medium.[23] To this end, 100 μL of an overnight culture grown on nutrient broth medium was added to 10 mL of the medium supplemented with 150 mg/L of putrescine (pH 5.5). After static incubation for 48 h at 28 °C, residual putrescine was measured by LC-FLD.

For the analysis of putrescine degradation in wine, cells from 20 mL of nutrient broth medium culture (OD_{600} around 1 unit) were collected by centrifugation, washed twice with 50 mM sodium phosphate buffer, pH 7.4, and finally resuspended in 2 mL of red wine containing 40 mg/L putrescine (pH 3.5). Cell suspension was incubated at 28 °C under shaking conditions for 1 week, and then putrescine concentration was determined by LC-FLD as described below. In addition, viable cell counts on nutrient agar plates at 0 and 7 days were performed to estimate survival of *K. varians* LTH 1540 in wine.

BA from synthetic medium and wine samples were extracted with Oasis MCX 1 cm^3 extraction cartridges (Waters) as described in Peña-Gallego et al.[31] An Agilent 1200SL LC-FLD system equipped with an in-line degasser, autosampler, column heater, and fluorescence detector was employed. Chromatographic separation was carried out on an LC-FLD Luna C18 silica Phenomenex column (250 × 4.6 mm) with a guard precolumn (20 × 4.6 mm) of the same type. A solution of 140 mM sodium acetate and 17 mM triethanolamine (TEA, pH 5.05) was used as mobile phase A, and methanol was used as mobile phase B. A volume of 10 μL of samples was mixed with 25 μL of a solution of 0.2 M sodium borate (pH 8.8) and 5 mM EDTA. The derivatization reaction was performed by adding 15 μL of AQC solution according to the optimized procedure described by Cohen and De Antonis.[32] A volume of 5 μL of the derivatized sample was injected for each analysis. Gradient conditions used for separation were described by Hernández-Orte et al.[30] Column temperature was kept at 65 °C, flow rate was 0.8 mL/min, and total elution time was 70 min. The excitation and emission wavelengths of the fluorescence detector were set at 250 and 395 nm, respectively. Quantification was performed by comparing integrated peak areas of the sample with the control.

Purification and Identification of Putrescine Oxidase (PuO) Enzyme. Resting cells from a 2 L culture grown overnight were harvested by centrifugation at 10000 rpm at 4 °C for 20 min (Beckman coulter Avanti J-E, JA 10 rotor) and washed with 50 mM sodium phosphate buffer, pH 7.4. Cells were then resuspended in 10 mL of the same buffer and disrupted in a Mikro-Dismembrator-S (Sartorius) with 1 g of 106 μm glass beads. Cell suspensions were subjected to 10 cycles of breakage at 3000 rpm for 40 s each, alternating with cooling periods of 5 min on ice. Cell homogenate was centrifuged at 10000 rpm for 15 min at 4 °C, and the supernatant was saved as whole-cell extract.

To isolate the putrescine-oxidizing enzyme, the whole-cell extract was further ultracentrifuged at 47000 rpm for 1 h in an SW55Ti rotor (Beckman L-70 Ultracentrifuge), and the resulting supernatant was subjected to fractionation by ammonium sulfate precipitation.[29] The fraction showing enzyme activity, as revealed by an in-gel assay (see later), was retained. After dialysis against equilibration buffer (50 mM Tris-HCl, pH 8.0, 0.1 M NaCl, 0.1% Tween 20), redissolved proteins were fractionated by anion-exchange chromatography on a Macro-Prep Q (Bio-Rad) column (0.9 × 6 cm) and eluted with a 0.1−0.6 M NaCl gradient as described previously.[29] Fractions containing the highest putrescine-degrading activity, as determined by the liquid PuO activity assay described below, were pooled and used for further purification by preparative gel electrophoresis. First, an 8% polyacrylamide nondenaturing gel electrophoresis was performed as described by Callejón et al.[29] After revealing in-gel PuO activity, the resulting brown bands were cut off, fragmented by passing them through a hole at the bottom of a microcentrifuge tube, and the resulting small gel fragments were resuspended in SDS-PAGE loading solution. The suspension, without boiling, was directly loaded on an 8% polyacrylamide gel containing SDS, and after running, PuO activity was also revealed by the in-gel assay (see later). Protein purity was checked by Coomassie blue staining of a parallel lane loaded with identical sample. The brown band corresponding to PuO enzyme was cut out and sent to the Experimental Research Support Centre (SCSIE, Universitat de València) for protein identification.

Tryptic digest of the protein from the excised gel fragment was analyzed by MALDI-TOF-TOF MS/MS on an Autoflex speed instrument (Bruker). Samples were prepared using 4-cyano-4-hydroxycinnamic acid (CHCA) as matrix on Prespotted Anchorchip targets (Bruker Daltonics). Calibration was performed by an external mode using a peptide calibration standard kit (Bruker Daltonics). Spectra were processed using Flex Analysis 3.3 software (Bruker Daltonics). In MS analysis, peak lists were generated using the signals in the m/z 800−4000 region, with a signal-to-noise threshold >3. The SNAP algorithm included in the software was used to select the monoisotopic peaks from the observed isotopic distributions. After removal of m/z values corresponding to usually observed matrix cluster ions, an internal statistical calibration was applied. The final list of the resulting peaks was used to identify the proteins by peptide mass fingerprint, once keratin and trypsin peptides were removed. For MS/MS analysis, the most significant peptides were analyzed. The Mascot 2.2 program (Matrix Science Ltd., London, UK) was used to search the NCBInr_20100430 database, limiting the search to actinobacterial

DOI: 10.1021/jf5026967
J. Agric. Food Chem. 2015, 63, 4170−4178

proteins. Searches were done with tryptic specificity allowing one or two missed cleavages and a tolerance on the mass measurement of 100 ppm in MS mode and 0.5 Da for MS/MS ions. Carbamidomethylation of Cys was used as a fixed modification and oxidation of Met as variable modification.

Putrescine Oxidase Assays. The amine oxidase activity assay on putrescine in a nondenaturing PAGE was carried out essentially as previously described.[29] Whole-cell extracts or fractions from the different purification steps were mixed with an equal volume of 2× loading buffer (100 mM Tris-HCl, pH 6.8, bromophenol blue 0.04%, and glycerol 10%), loaded on a stacking 4% polyacrylamide gel and resolved on a nondenaturing 8% polyacrylamide gel, using Tris−glycine as electrophoretic buffer (25 mM Tris, 192 mM glycine). These native gels were run at 30 mA for an hour. After electrophoresis, gels were soaked in sodium phosphate buffer (50 mM, pH 7.4) containing 1 mM putrescine and incubated at room temperature with gentle agitation for 15 min. Then, the solution was replaced by the same buffer containing horseradish peroxidase (HRP; 1000 U/L) and diaminobenzidine (DAB, 0.25 mM) as chromogenic substrate. The appearance of a brown band, due to the formation of a colored precipitated product from DAB oxidation, revealed putrescine-oxidizing activity. This brown color takes usually 10 min to appear. Control assays were carried out without putrescine.

As the enzyme PuO maintains activity after SDS treatment, the identity of the band corresponding to the PuO enzyme could be checked in SDS-PAGE. To do that, samples were dissolved in SDS-PAGE loading buffer (50 mM Tris-HCl, pH 6.8, 2% SDS, 1% β-mercaptoethanol, 10% glycerol, and 0.02% bromophenol blue), but not boiled, and then loaded onto standard SDS-8% polyacrylamide gels. Following electrophoresis, gels were washed in 50 mM sodium phosphate buffer, pH 7.4, and PuO activity was revealed by the same procedure described above for native gels.

To assess which fractions of the chromatographic purification process contained PuO activity, the liquid PuO assay described by Federico et al.,[33] but modified and adapted to microplates, was also employed. This kind of assay was likewise used for the biochemical characterization of the enzyme. Briefly, 2 μL from the chromatographic fractions was mixed with 198 μL of a peroxidase-coupled reaction solution containing 2 mM putrescine, 0.5 mM 4-amino-antipyrine (AAP), 5 mM 3,5-dichloro-2-hydroxybenzenesulfonic acid (DCHBS), and 1000 U/L of HRP in 50 mM sodium phosphate buffer, pH 7.4. Relative PuO activity was determined by registering absorption at 515 nm (ε_{515} = 26000 M^{-1} cm^{-1})[33] by a microplate reader, FLUOstar Optima (BMG Labtech), over a time period of 30 min.

Mass Spectrometry Analysis. Putrescine degradation assays by cells or by the partially purified enzyme, to detect Δ^1-pyrroline as PuO reaction product that forms spontaneously from 4-aminobutanal as described by DeSa and Richard,[34] were performed in 50 mM tetraborate buffer, pH 8.0. Cells at DO_{600} of 6 were incubated in the buffer cited containing 1 g/L putrescine for 6 h. After that, sample was centrifuged at 13500 rpm for 10 min, cells were discarded, and supernatant was directly injected into the mass spectrometry equipment for analysis. In the same way, partially purified enzyme was incubated for 1 h and then injected. Samples from the mixtures were taken at time 0 and processed for mass spectrometry examination as controls. Analyses were performed using the Turbo V source in an electrospray positive ion mode at an ionspray voltage of −4500 V on an AB SCIEX TripleTOF 5600 system (Applied Biosystems, Life Technologies, Canada). Curtain gas (CUR) was set at 25 psi, nebulizer gas (gas 1) at 35 psi, drying gas (gas 2) at 35 psi, and temperature at 650 °C, scan TOF MS. Data acquisition was performed using the software Analyst and was qualitatively evaluated using PeakView software (Applied Biosystems, Life Technologies, Canada).

Biochemical Characterization of the Enzyme PuO. Fractions from anion-exchange chromatography containing partially purified enzyme were used for biochemical characterization of *K. varians* PuO. Enzymatic activity was measured by liquid assay in microplates, as described previously.

The relative molecular mass of the catalytic polypeptide was estimated by comparison with molecular weight markers after a SDS-10% PAGE and subsequent in-gel assay to identify the protein with PuO activity. Molecular size determination of the native protein was performed by size exclusion chromatography and also by sucrose gradient ultracentrifugation. Chromatography was developed in a column (0.9 × 60 cm) of Sephacryl S-200 HR (GE Healthcare) equilibrated with 50 mM sodium phosphate buffer, pH 7.4, and operated at room temperature with a flow rate of 15 mL/h. Fractions of 0.5 mL were collected and analyzed for PuO activity by liquid assay. The column was calibrated using as standard molecular mass markers catalase (240 kDa), alcohol dehydrogenase (120 kDa), ovalbumin (47 kDa), and cytochrome *c* (12.5 kDa). For ultracentifugation experiments, linear sucrose gradients (7−18%) in 50 mM sodium phosphate buffer, pH 7.5, were used. Partially purified PuO was layered on the top of an 11 mL gradient and centrifuged in a Beckman SW41Ti rotor at 40000 rpm for 20 h. After centrifugation, tubes were bottom-punctured, and fractions of 0.45 mL were recovered and subjected to PuO activity liquid assay. In a parallel gradient, a mixture of the same molecular mass markers used in size exclusion chromatography was also ultracentrifuged and employed for gradient calibration.

To determine the optimal pH value of the enzyme, the following buffers (and their corresponding pH ranges) were employed at a concentration of 50 mM: acetic acid−sodium acetate buffer (for a pH range of 3.7−5.5), citric acid−Na_2HPO_4 (for pH values between 4.5 and 7.4), NaH_2PO_4−Na_2HPO_4 (pH 6.5−8.0), Tris-HCl (pH 7.2−9.0), and glycine−NaOH (pH 8.0−9.5). All samples were incubated at 28 °C. Immediately after starting the reaction by addition of 0.007 U of enzyme, absorbance at 515 nm was registered each minute for a total time of 10 min, and the initial slope of plots of A_{515} versus time, representing relative PuO activity, was calculated.

Temperature dependence was tested by an end point procedure in which the reaction mixtures were incubated at different temperatures between 4 and 75 °C. Tubes, containing 198 μL of 50 mM sodium phosphate buffer, pH 7.4, plus putrescine, and the components for the peroxidase-coupled reaction, were pre-incubated at the corresponding temperature for 5 min before the start of the reaction by adding 0.007 U of enzyme. Relative PuO activity was determined as absorbance at 515 nm. The maximum absorbance registered was considered as 100% relative activity.

For thermal stability tests, aliquots of enzyme solution were pre-incubated at different temperatures at 28, 30, 45, 55, 65, 75, 85, and 100 °C for 10 min and then were placed at 28 °C for 15 min and assayed by the PuO liquid assay. The activity obtained at 28 °C was considered as 100% relative activity.

To determine substrate specificity, different monoamines (histamine, tyramine, methylamine, propylamine, and ethanolamine), diamines (putrescine and cadaverine), and polyamines (spermine and spermidine) were used at concentrations of 2 and 50 mM, and enzyme activity was tested by liquid assay at 28 °C. In all cases reaction was initiated by the addition of 0.007 U of PuO enzyme. Absorption at 515 nm was regularly measured over 30 min in a microplate reader, and then amine oxidase activity was determined from the initial slope of plots of ΔA_{515} versus time. PuO activity on putrescine was considered as 100% relative activity. Enzyme activity on different amines was confirmed by in-gel activity assay, as previously described.

Kinetic parameters K_m and V_{max} were determined for putrescine and cadaverine by liquid assay, with various amine concentrations from 0.1 to 5 mM. Reactions were initiated by the addition of 0.007 U of PuO enzyme. Rate constants were deduced from the slope and intercept of double-reciprocal plots of initial velocity versus diamine concentration.

Bipyridyl, phenanthroline, *N*-(3-(dimethylamino)propyl)-*N*′-ethyl-carbodiimide (EDC), deprenyl, cyclopropilamine, rasagiline, pargyline, and semicarbazide were assessed as putative inhibitors of *K. varians* PuO. Inhibitor compounds were added to the reaction mixture to final concentrations of 0.1, 0.5, 1.0, and 5.0 mM. Enzyme (0.007 U) was pre-incubated at 28 °C for 5 min in the presence of each inhibitor before initiation of the reaction by adding putrescine. PuO activity measured in the absence of any inhibitor was considered as 100%

DOI: 10.1021/jf5026967
J. Agric. Food Chem. 2015, 63, 4170−4178

relative activity (control). As negative control a reaction mixture containing heat-denatured enzyme was used.

Given the potential use of the enzyme in wine, the effect of ethanol on enzyme activity was tested by adding it to the reaction mixture to a concentration between 0 and 15% (v/v). The PuO liquid assay with 0.007 U of enzyme was employed in these experiments. The volume of buffer solution was adjusted accordingly to maintain the final reaction volume. Enzyme activity in the absence of ethanol was taken as 100% relative activity (control).

To investigate the ability of PuO to degrade putrescine in wine, 10 μL of enzyme solution containing 2.8 mg/mL of partially purified enzyme was mixed with 10 volumes of red wine supplemented with 40 mg/L putrescine (pH adjusted to 3.5). Following incubation at 37 °C for 24 h, putrescine content was quantified by LC-FLD, as described above. Two controls were performed: one containing an identical non-incubated (time zero) reaction mixture and a second sample without enzyme but incubated in the same conditions as the test samples. The percentage of degradation in the test samples was calculated by comparison with those controls.

Statistical Analyses. All data are presented as the mean ± SE. Group means were compared using one-way ANOVA followed by Duncan's multiple-range tests to identify differences among groups when appropriate. Two-group comparisons of control and inhibitor-exposed groups were carried out using a two-tailed Student's *t* test. All analyses were carried out using IBM SPSS Statistics 19 (SPSS Inc., Chicago, IL, USA). Percentage data were normalized by arcsine transformation prior to the analysis.

RESULTS AND DISCUSSION

Ability of *K. varians* Cells To Degrade Putrescine. Previous experiments using different strains of this species isolated from fermented foods provided indications of their potential to degrade BA. We therefore started out by investigating the ability of *K. varians*, a microorganism initially obtained from dry sausages, to eliminate putrescine in different media: a defined buffered solution, Dapkevicius' medium, and wine. In the buffer solution, when the initial concentration was 100 mg/L, all putrescine was degraded by cells in <24 h. Under similar conditions, when the concentration of putrescine was 1000 mg/L, more than half of the amine was eliminated after only 4 h of incubation.

In Dapkevicius' medium, putrescine was completely removed after 48 h when the initial concentration was 150 mg/L. Furthermore, *K. varians* cells were able to degrade up to 30%, from an initial concentration of 40 mg/L in wine, after 7 days of incubation (Figure 1). At this time no viable *K. varians* cells were recovered from wine.

Purification and Identification of Putrescine Oxidase from *K. varians*. Twelve milliliters of cell-free extract with a protein concentration of 10.4 mg/mL (Table 1) was obtained after bead beating of *K. varians* LTH 1540 cells. Putrescine oxidase activity (5.6 U/mL) was recovered in the ammonium sulfate 70% saturation fraction (Table 1). PuO liquid assay of collected fractions from the Macro-Prep Q chromatography showed a single enzyme activity peak at fractions eluted around 300 mM NaCl. Table 1 summarizes the yield and purification of the *K. varians* putrescine oxidase in the first three steps of the procedure described under Materials and Methods. We performed a native gel electrophoresis as an additional purification step, which led us in the end to identify the protein with PuO activity. To do this, the Macro-Prep Q fraction showing the highest activity was loaded on a semipreparative 8% native polyacrylamide gel electrophoresis. PuO activity was revealed as a brown band by the in-gel assay. The native electrophoresis has not been included in the purification table (Table 1) because the in-gel activity assay, employed after this purification step, is neither quantitative nor comparable with the liquid assay used in the previous steps. Nonetheless, native electrophoresis generated the highest degree of purification of our protocol, given that the protein band corresponding to the enzyme accounts for >82% of total protein after this step (based on a densitometry analysis with ImageJ software of the gel after SDS-PAGE, see Figure 2, lane 5). Taking into account the protein amount (estimated also by densitometry) remaining after native-PAGE and supposing, as an upper limit, the absence of activity loss, a 4400-fold purification overall may be roughly estimated by our purification procedure. In any case, native electrophoresis was an essential step for the identification of *K. varians* PuO. When the PuO brown band from the native gel was cut out and subjected to an 8% PAGE in the presence of SDS, a single band was visualized after Coomassie blue staining, which moreover matched exactly with the brown band revealed by in-gel PuO assay on a parallel lane (Figure 2). Subjecting the brown band to a second SDS-10% PAGE, again, only one Coomassie blue stained band appeared and also coincident with a brown band resulting from the PuO in-gel assay (results not shown). Putrescine oxidase activity was recovered following exposure to, and subsequent removal of SDS, indicating that denaturation of the enzyme did not result in an irreversible loss of activity. This property of the enzyme together with the excellent resolution of proteins by SDS-PAGE enabled us to purify and identify the catalytically active polypeptide of the enzyme oxidizing putrescine. Figure 2 shows the protein analysis by SDS-PAGE corresponding to the different steps of PuO purification described under Materials and Methods. The single band with PuO activity, which appears as a homogeneous polypeptide, migrated to a position corresponding to a molecular mass of 43 kDa. Digestion of the excised brown band by trypsin gave eight internal peptides that were resolved

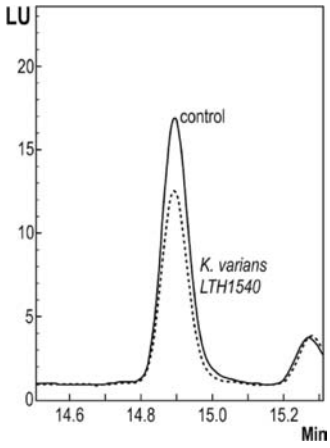

Figure 1. Degradation of putrescine in wine after incubation in the presence of *K. varians* LTH 1540 cells (equivalent to 10 OD_{600} units, approximately 7.6 × 10^{10} CFU/mL) (dotted line). Wine was supplemented with 40 mg/L of putrescine prior to inoculation of cells. Remaining putrescine in wine was quantified by LC-FLD. The graph shows the retention time on the *x*-axis versus fluorescence units (LU) recorded by the detector (*y*-axis). As negative controls, an identical mixture not incubated obtained at time zero (control 1) and wine supplemented with putrescine without the addition of cells incubated equally (control 2) were used. Because both controls gave the same peak area, only control 1 is shown. Only the chromatographic profile region corresponding to the putrescine peak is shown.

DOI: 10.1021/jf5026967
J. Agric. Food Chem. 2015, 63, 4170−4178

Table 1. Purification of *Kocuria varians* LTH 1540 Putrescine Oxidase[a]

step	volume (mL)	protein concentration (mg/mL)	enzyme activity[b] (units/mL)	specific activity (units/mg)	purification (-fold)
crude extract	12	10.4	1.22	0.12	1
$(NH_4)_2SO_4$ precipitation	2.4	7.4	5.60	0.76	6.4
Macro-Prep Q chromatography	1.0	2.8	6.70	2.40	20

[a]The table shows results of typical experiments starting from 2 L of a culture of cells grown overnight. [b]Enzyme activity is expressed in enzyme activity units (U), where 1 unit is defined as that amount of enzyme which oxides 1 μmol of substrate per minute, in the reaction mixture for the microplate PuO liquid assay as described under Materials and Methods.

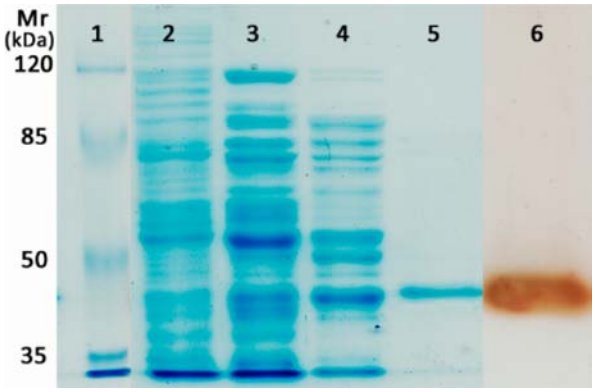

Figure 2. Electrophoretic analysis of proteins at different steps of the PuO purification in SDS-polyacrylamide gels. Lanes: 1, prestained molecular weight markers (Fermentas); 2, crude extract (~42 μg); 3, 70% saturation of ammonium sulfate precipitate (~42 μg); 4, Macro-Prep Q chromatography eluted fraction (34 μg); 5 and 6, proteins of the brown band resulting from native PAGE in which 250 μg of Macro-Prep Q partially purified protein was loaded. Lanes 1−5 were stained with Coomasie blue dye, and lane 6 was cut off and subjected to the in-gel PuO activity assay. Molecular masses of marker proteins are indicated on the left (kDa).

by mass spectrometry. Six of these peptides matched the putrescine oxidase enzyme of *K. rhizophila* (gil184199732) with a score of 321.4, covering 11.5% of protein sequence; 2 peptides matched the putrescine oxidase of *K. rosea* (gil730425) (syn. *M. rubens*) at a score of 229.3, which covers 8.2% of sequence; and 3 peptides were common to the two cited proteins (Supporting Information, Supplementary Figure 1). From this score value the putrescine degrading protein from *K. varians* LTH 1540 was unequivocally identified as a putrescine oxidase, because its score was >81, which is considered to be statistically significant for identification.[35] This protein is an ortholog of putrescine oxidase of *K. rhizophila* and belongs to the EC 1.4.3.10 class.

Supporting identification of the enzyme as PuO by mass spectrometry is the fact that Δ^1-pyrroline was detected by Mass qTOF as the product of putrescine degradation. Δ^1-Pyrroline is the product of the spontaneous condensation of 4-amino-butanal, which is the final product of putrescine oxidation by flavin-dependent PuO enzymes. A peak of m/z 70.06, corresponding to Δ^1-pyrroline, was obtained after incubation of putrescine with cells or partially purified enzyme in tetraborate buffer (Supporting Information, Supplementary Figure 2). The intensity of the Δ^1-pyrroline peak generated by the enzyme was 5-fold higher than that generated by cells.

Properties of the *K. varians* PuO. Partially purified enzyme from anion-exchange chromatography was employed to estimate the molecular mass of native PuO by size exclusion column chromatography and by sucrose density gradient ultracentrifugation. Analysis by size exclusion chromatography on Sephacryl S-200 HR yielded reproducibly an apparent PuO molecular mass of ~150 kDa. However, PuO molecular mass estimated by sucrose gradient centrifugation was around 87 kDa (results not shown). Because gel filtration and sedimentation should give similar values for globular macromolecules, our results strongly suggest that the shape of native *K. varians* PuO is elongated. Consequently, the actual molecular mass of the native enzyme probably lies somewhere between 87 and 150 kDa. Most importantly, these data demonstrate that the native form is notably higher than that of the catalytic single polypeptide obtained by SDS-PAGE (Figure 2), indicating that the *K. varians* native PuO must be a protein oligomer. The *K. varians* native enzyme is likely to be a dimer of identical subunits, given the homology with PuO from the nearby species *K. rosea*, which has been described in its native form as a homodimer with a molecular mass around 88 kDa,[34] similar to our ultracentrifugation results with *K. varians* PuO. To analyze the dependence of PuO enzyme activity on pH, different buffers with overlapping buffering capacities were used. *K. varians* PuO was found to be active over a relatively broad range of pH, which includes values from 5.5 to >9.5 (Figure 3A). No significant activity was detected below pH 5.0.

The optimal temperature for PuO activity was found to be 45 °C, although the enzyme retained activity in a rather wide temperature range, from 4 to 75 °C (Figure 3B). Moreover, temperature stability experiments revealed that *K. varians* PuO is a relatively thermostable enzyme compared to other amine oxidases. As deduced from the heat inactivation experiments (Figure 3C), the enzyme retained >50% of the activity after a pre-incubation treatment at 55 °C. In contrast, it was found that the putrescine oxidase from *K. rosea* suffered rapid inactivation at 50 °C.[20] Temperatures >65 °C completely inactivated the *K. varians* enzyme (Figure 3C).

Our substrate specificity analysis showed that none of the tested monoamines (histamine, tyramine, methylamine, propylamine, and ethanolamine) was oxidized by *K. varians* PuO (data not shown). The diamine putrescine was by far the best substrate for this enzyme, although the diamine cadaverine and, to a much lesser extent, the polyamine spermidine were also oxidized by the enzyme, as can be deduced from the relative activity data obtained from each substrate (Figure 4A). These results are consistent with previous data reported for known PuO enzymes from different species: *K. rosea*,[34,36] *M. luteus*,[16] and *R. erythropolis*.[37] Similarly to these enzymes, *K. varians* PuO apparently requires substrates with a minimum of two amino groups and, moreover, given that spermine cannot act as substrate (not shown) unlike spermidine, a free 4-aminobutyl moiety also seems to be essential for catalysis. Reactivity of *K. varians* PuO toward cadaverine and spermidine was verified by an in-gel assay after native 8% PAGE (Figure 4B), replacing putrescine with one of these other amines to reveal activities. In

DOI: 10.1021/jf5026967
J. Agric. Food Chem. 2015, 63, 4170−4178

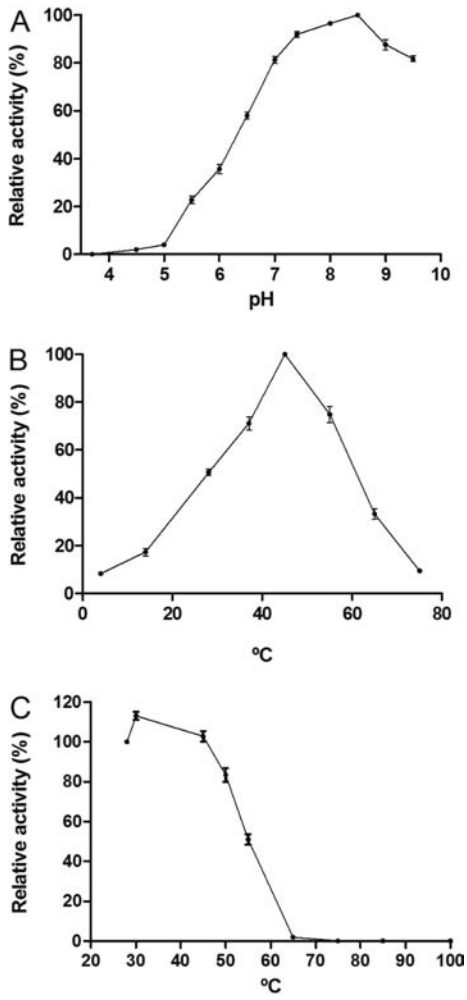

Figure 3. pH effect, temperature dependence, and thermal stability of the *K. varians* PuO. (A) pH effect. Reaction mixtures prepared with 50 mM of different buffers, at the shown pH, were assayed by the liquid procedure as described under Materials and Methods. The activity measures corresponding to the overlapping pH values were employed for normalization, and the resulting data expressed as percentage with respect to the maximum are plotted versus pH. (B) Temperature dependence. Liquid enzymatic reaction solutions were incubated at the indicated temperatures for 5 min. A_{515} was measured with a microplate reader and plotted as relative percentage to the maximum value. (C) Thermal stability. Equal aliquots of the enzyme solution were pre-incubated at the shown temperature for 10 min before being re-equilibrated to 28 °C. Putrescine was added to aliquots and degradation measured by the standard liquid assay. The residual enzymatic activity is represented as percentage relative to the value at 28 °C.

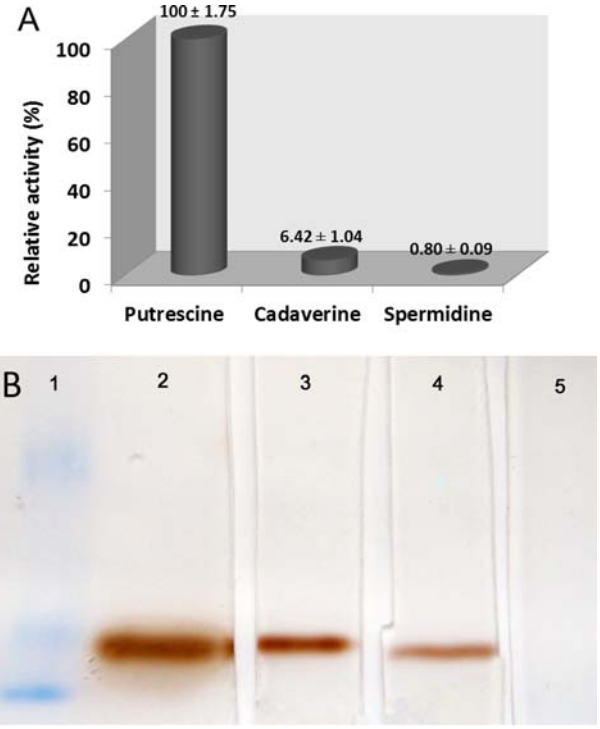

Figure 4. Substrate specificity analysis of partially purified *K. varians* LTH 1540 PuO. (A) Results from the liquid assay. Oxidation progression of the substrates, putrescine, cadaverine, and spermidine (2 mM), was determined as the absorption increase at 515 nm in a microplate reader. The initial slope of A_{515} versus time, expressing activity, was calculated and depicted as a percentage relative to that obtained with putrescine (100%). (B) Enzyme activity determined on a native−8% polyacrylamide gel and revealed by in-gel assay with 2 mM putrescine (lane 2), cadaverine (lane 3), or spermidine (lane 4). Lane 5 is a negative control without amine. Lane 1 was loaded with prestained protein markers (Fermentas) and used as reference during the electrophoresis progression.

all cases, a brown band was observed, but whereas it took only a few minutes to become visible when putrescine was the substrate, it lasted around 30 min with cadaverine and about 2 h with spermidine. No brown band was obtained in the absence of amine. These results evidence different preferences for substrate of *K. varians* LTH 1540 PuO enzyme.

We determined the steady state kinetic parameters for the diamine substrates, putrescine and cadaverine. The double-reciprocal plot of calculated initial velocities versus substrate concentrations was used to deduce K_m and V_{max}. The resulting kinetics parameters were as follows: $K_m = 94 \pm 10$ μM and $V_{max} = 2.30 \pm 0.1$ μmol/min·mg for putrescine; and $K_m = 75 \pm 5$ μM and $V_{max} = 0.15 \pm 0.02$ μmol/min·mg for cadaverine. *K. varians* PuO K_m for putrescine is in the same value range as that described for the homologue *K. rosea* PuO, slightly higher than that reported by DeSa[34] (38 μM), and a little lower than that reported by Okada et al.[36] (240 μM). It is, however, substantially higher than that for *R. erythropolis* (8.2 μM).[37] V_{max} values and results shown in Figure 4 clearly indicate that cadaverine (the five carbon analogue of putrescine) is worse than putrescine as substrate of *K. varians* PuO. However, the K_m value for cadaverine is slightly lower than that for putrescine, which suggests, as proposed for *K. rosea* PuO,[36] that hydrophobic interaction between the enzyme and the amine substrate must increase with methylene chain length.

Percentages of *K. varians* PuO enzymatic activity after the addition of different compounds, which are known inhibitors for amine oxidases from diverse origins, are shown in Table 2. In short, no inhibitor at a concentration of 100 μM showed any significant effect on enzyme activity (not shown). However, at concentration of 0.5 mM, EDC already revealed an important inhibitor effect, and at 1 mM rasagiline and pargyline also showed a decrease in putrescine oxidation. Deprenyl, cyclopropylamine, bipyridyl, phenanthroline, and semicarbazide did not affect PuO activity at the same concentration of 1 mM. When the concentration of inhibitors was 5 mM, PuO activity was diminished by deprenyl, semicarbazide, rasagiline, EDC, and pargyline, as can be seen in Table 2. EDC was described as

DOI: 10.1021/jf5026967
J. Agric. Food Chem. 2015, 63, 4170−4178

Table 2. Effect of Various Inhibitors on *K. varians* PuO[a]

	concentration (mM)	inhibition (%)
EDC	0.5	47 ± 1.63**
	1	70 ± 0.53**
	5	99 ± 0.02**
rasagiline	0.5	0
	1	10 ± 1.20*
	5	52 ± 1.46**
deprenyl	0.5	0
	1	0
	5	23 ± 0.50*
pargyline	0.5	2 ± 0.62
	1	14 ± 0.24*
	5	75 ± 1.14**
cyclopropylamine	0.5	0
	1	0
	5	0
bipyridyl	0.5	0
	1	0
	5	0
phenanthroline	0.5	0
	1	0
	5	0
semicarbazide	0.5	0
	1	0
	5	30 ± 0.43**

[a]Enzyme activity was measured by the 4-APP/DCHBS/HRP liquid assay as described under Materials and Methods. Results are expressed as percent inhibition related to the control in the absence of inhibitor. The negative control of the heat-denatured enzyme showed 100% inhibition. The experiments were done in triplicate. Asterisks indicate a *P* value of (*) <0.05 or (**) <0.01.

a carboxyl group modifying agent that affects the catalytic properties of PuO from *K. rosea*, which resulted in changes in substrate specificity and a ∼95% reduction of its catalytic potential.[38] As Table 2 shows, *K. varians* PuO was also inhibited by EDC, although to a lesser extent (∼70% reduction). It remains to be determined if modification by EDC causes the same alterations of properties in *K. varians* PuO as have already been described in *K. rosea*.

Rasagiline, deprenyl, and pargyline inhibit human monoamine oxidases (MAO)[39] through the formation of adducts with the FAD cofactor, and thus, unsurprisingly, the highest concentrations of these agents also inhibit the flavin-dependent PuO from *K. varians*. In contrast, cyclopropylamine, another MAO inhibitor, acts through alkylation of the active site.[40] Because the catalytic center of human MAOs differs from bacterial PuO as has been demonstrated by Van Hellemond et al.,[37] cyclopropylamine should act in a different way not exercising an inhibitory effect on *K. varians* PuO.

The fact that two metal chelating agents, bipyridyl and phenanthroline, did not affect the enzymatic activity of PuO suggests that no metallic cofactor is involved in catalytic activity, although both compounds significantly inhibit the activity of Cu-dependent amine oxidases.[41] Furthermore, phenanthroline at 1 mM did not affect enzymatic activity of the ortholog PuO enzyme from *K. rosea*.[42]

Semicarbazide is a carbonyl-modifying agent and a representative potent inhibitor of a specific group of amine oxidases, named semicarbazide-sensitive amine oxidases (SSAO). A high sensitivity to inhibition by semicarbazide, around 0.1 at 1 mM, distinguishes SSAOs from other amine oxidases, particularly from MAO.[43] *K. varians* PuO was not affected at all by 0.5 or 1 mM semicarbazide (Table 2) but was inhibited (by 30%) at the higher tested concentration of semicarbazide (at 5 mM), in contrast with *K. rosea* enzyme, which was not inhibited with up to 10 mM.[42]

Although the cofactor requirements of the enzyme have not been specifically analyzed in this work, MALDI-TOF identification and various physical properties including structure and substrate specificity similar to those of phylogenetically close species indicate that it is a flavin-dependent putrescine oxidase. The fact that it is inhibited by deprenyl, rasagiline, pargyline, and EDC, specific inhibitors of flavin-dependent amine oxidase, lends further support to this assumption. Likewise, the detection of Δ^1-pyrroline as product of putrescine degradation by Mass qTOF (Supporting Information, Supplementary Figure 2) confirms this idea.

Putrescine degradation in wine experiments showed that partially purified enzyme was able to degrade only 5% of putrescine after 24 h of incubation. Clearly wine conditions are not optimal for PuO activity; possible limiting factors could be ethanol and the low pH. Probably, ethanol is not the most limiting factor, as the enzyme maintains 82% activity in the presence of 15% ethanol (a higher concentration than normally found in wine). The most limiting factor should be thus the low pH of the wine (3.5 units in this case), a value at which PuO is almost completely devoid of activity (see Figure 3A). Higher reduction of putrescine in wine was achieved (30% approximately) using whole cells. Possibly inside cells, the enzyme may find a more appropriate environment for performing putrescine degradation, even if they are not growing.

Although the preferred methods for controlling BA in food are those involving prevention, it is not always possible to apply this kind of measure. Nowadays, the most widespread method for controlling BA in food is refrigeration. However, some bacteria can grow and produce BA below 5 °C, which demonstrates that refrigeration alone cannot always prevent the increase of BA and, thus, emerging control measures should be considered. New emerging control measures for delaying BA formation include high hydrostatic pressure, irradiation, packaging, microbial modeling, and the use of food additives or preservatives. These methods operate primarily through the inhibition of bacterial growth or the inhibition of the decarboxylase enzyme activity responsible for BA production.[21] In the case of wine, strategies that could be adopted to avoid BA formation are mainly reduction of precursor levels (amino acids) and prevention of growth of spoilage bacteria. Reduction can be achieved by avoiding practices such as long skin maceration, aging on lees, and amino acid addition for enhancing yeast growth during alcoholic fermentation, but these practices are not possible when full-bodied wines are intended. On the other hand, the prevention of bacterial growth is difficult due to the limited action of preservatives (lysozyme and SO_2) approved for enological use.[44]

DOI: 10.1021/jf5026967
J. Agric. Food Chem. 2015, 63, 4170−4178

Some authors have used BA-degrading bacteria to reduce BA content in several fermented products, either as starters for food fermentation or as additives. For instance, Leuschner and Hammes[22] used three different strains of *Brevibacterium linens* to eliminate tyramine and histamine in cheese. These authors also demonstrated the applicability of the strain *K. varians* LTH 1540 to degrade tyramine during sausage ripening.[17] Our results suggest that the use of this bacterium to eliminate putrescine in this process should be evaluated. Likewise, two different strains of *L. sakei* were applied to remove histamine in fish slurry by Dapkevicius et al.[23] Furthermore, Gardini et al.[24] achieved reduced concentrations of tyramine, spermine, and spermidine in dry sausages by inoculating a mixed starter consisting of *L. sakei* G20 and *S. xylosus* S8. Similarly, the inoculation of 10% (w/w) of *Virgibacillus* sp. SK33 in Thai fish sauce fermentation reduced histamine content by 50%.[26] More recently, Mah and Wang attained BA reduction in Myeolchi-jeot, a salted and fermented anchovy (*Engraulis japonicas*), by applying starter cultures of *S. xylosus* during ripening.[27] Finally, it is worth mentioning that multiple lactic acid bacteria strains are able to degrade amines in wine as described by Callejón et al.[29]

Purified enzyme amine oxidases have also been applied to reduce the BA content in food. With this aim, Dapkevicius et al.[23] utilized purified amine oxidase from porcine kidney to reduce histamine in ensiled fish slurry. Similarly, U.S. patent 4725540 describes the use of histaminases from *Lactobacillus* bacteria and from *Candida* yeast cells to eliminate BA from foodstuffs, beverages, and forages.[45] Therefore, cells containing amine oxidase activity or the direct use of the purified enzyme can be used to eliminate BA already generated in food. This strategy would be a potential measure of control when all other prevention practices have been ineffective.[21] In our case, the limited activity of the partially purified enzymatic fraction in wine does not support its use to decrease putrescine content. However, the fact that entire cells are able to degrade 30% of the amine opens the possibility of using them as an alternative to the enzyme. Because it has been shown that cells are unable to grow in wine, the use of high densities of nonproliferating cells is proposed. A similar strategy has been used to perform malolactic fermentation in wines in which very low pH values or high ethanol content prevented bacterial growth.[46]

In this work, we have demonstrated that *K. varians* LTH 1540 degrades diamines, mainly putrescine, in buffer, Dapkevicius' medium, and wine. We have identified the enzyme responsible for diamine degradation in this bacterium as a PuO; it has been biochemically characterized, and a strategy is proposed to degrade putrescine in wine. The applicability of *K. varians* LTH 1540 PuO in the food industry is a new challenge to be considered in the near future.

■ ASSOCIATED CONTENT

Ⓢ Supporting Information

Supplementary Figures 1 and 2. This material is available free of charge via the Internet at http://pubs.acs.org.

■ AUTHOR INFORMATION

Corresponding Author

*(I.P.) Phone: +34 96 354 43 90. Fax: +34 96 354 45 70. E-mail: Isabel.Pardo@uv.es.

Funding

We gratefully acknowledge financial support of this work from the Ministerio de Educación y Ciencia, Spain (Projects AGL2006-08495 and AGL2009-12167), European Regional Development Funds (ERDF), and the City Hall of Valencia.

Notes

The authors declare no competing financial interest.

■ ACKNOWLEDGMENTS

English text was revised by the English language reviewer Beverly Johnson.

■ REFERENCES

(1) Straub, B. W.; Tichaczek, P. S.; Kicherer, M.; Hammes, W. P. Formation of tyramine by *Lactobacillus curvatus* LTH 972. *Z. Lebensm.-Unters. Forsch.* **1994**, *199*, 9−12.

(2) Straub, B. W.; Kicherer, M.; Schilcher, S. M.; Hammes, W. P. The formation of biogenic amines by fermentation organisms. *Z. Lebensm.-Unters. Forsch.* **1995**, *201*, 79−82.

(3) Martin, W. H.; Pelczar, M. J.; Hansen, P. A. Putrescine as a growth requirement for *Neisseria*. *Science* **1952**, *116*, 483−484.

(4) Bauza, T.; Blaise, A.; Daumas, F.; Cabanis, J. C. Determination of biogenic amines and their precursor amino acids in wines of the Vallée du Rhône by high-performance liquid chromatography with precolumn derivatization and fluorimetric detection. *J. Chromatogr.* **1995**, *707*, 373−379.

(5) Silla Santos, M. H. Biogenic amines: their importance in foods. *Int. J. Food Microbiol.* **1996**, *29*, 213−231.

(6) Landete, J. M.; Arena, M. E.; Pardo, I.; Manca de Nadra, M. C.; Ferrer, S. The role of two families of bacterial enzymes in putrescine synthesis from agmatine via agmatine deiminase. *Int. Microbiol.* **2010**, *13*, 169−177.

(7) Eerola, S.; Roig Sagués, A. X.; Lilieberg, L.; Aalto, H. Biogenic amines in dry sausages during shelf-life storage. *Z. Lebensm. Unters. For.* **1997**, *205*, 351−355.

(8) Maintz, L.; Novak, N. Histamine and histamine intolerance. *Am. J. Clin. Nutr.* **2007**, *85*, 1185−1196.

(9) Landete, J. M.; Ferrer, S.; Polo, L.; Pardo, I. Biogenic amines in wines from three Spanish regions. *J. Agric. Food Chem.* **2005**, *53*, 1119−1124.

(10) Leitão, M. C.; Marques, A. P.; San Romão, M. V. A survey of biogenic amines in commercial Portuguese wines. *Food Control* **2005**, *16*, 199−204.

(11) Palacios, A.; Suárez, C.; Krieger, S.; Theodore, D.; Otaño, L.; Laucirica, A.; Peña, F. Influencia organoléptica de las aminas biógenas producidas durante la fermentación maloláctica del vino. *ACE Rev. Enol.* **2005**, *70*, 14−20.

(12) Levering, P.; van Dijken, J.; Veenhuis, M.; Harder, W. Arthrobacter P 1, a fast growing versatile methylotroph with amine oxidase as a key enzyme in the metabolism of methylated amines. *Arch. Microbiol.* **1981**, *129*, 72−80.

(13) Yagodina, O. V.; Nikol'skaya, E. B.; Khovanskikh, A. E.; Kormilitsyn, B. N. Amine oxidases of microorganisms. *J. Evol. Biochem. Physiol.* **2002**, *38*, 251−258.

(14) Yamada, H.; Tanaka, A.; Ogata, K. Putrescine oxidase of *Micrococcus rubens*. *Agric. Biol. Chem.* **1965**, *29*, 260−261.

(15) Stackebrandt, E.; Koch, C.; Gvozdiak, O.; Schumann, P. Taxonomic dissection of the genus *Micrococcus*: *Kocuria* gen. nov., *Nesterenkonia* gen. nov., *Kytococcus* gen. nov., *Dermacoccus* gen. nov., and *Micrococcus* Cohn 1872 gen. emend. *Int. J. Syst. Bacteriol.* **1995**, *45*, 682−692.

(16) Rokka, R.; Futamura, N.; Ishida, A. Role of putrescine oxidase in the generation of hydrogen peroxide by *Micrococcus luteus*. *J. Gen. Appl. Microbiol.* **1985**, *31*, 435−440.

(17) Leuschner, R. G. K.; Hammes, W. P. Tyramine degradation by micrococci during ripening of fermented sausage. *Meat Sci.* **1998**, *49*, 289−296.

DOI: 10.1021/jf5026967
J. Agric. Food Chem. 2015, 63, 4170−4178

(18) Coloretti, F.; Chiavari, C.; Armaforte, E.; Carri, S.; Castagnetti, G. B. Combined use of starter cultures and preservatives to control production of biogenic amines and improve sensorial profile in low-acid salami. *J. Agric. Food Chem.* **2008**, *56*, 11238−11244.
(19) Leuschner, R. G.; Heidel, M.; Hammes, W. P. Histamine and tyramine degradation by food fermenting microorganisms. *Int. J. Food Microbiol.* **1998**, *39*, 1−10.
(20) Yamada, H. Putrescine oxidase (*Micrococcus rubens*). In *Methods in Enzymology*; Tabor, H., Tabor, C. W., Eds.; Academic Press: New York, 1971; Vol. 17, Part B, pp 726−730.
(21) Naila, A.; Flint, S.; Fletcher, G.; Bremer, P.; Meerdink, G. Control of biogenic amines in food: existing and emerging approaches. *J. Food Sci.* **2010**, *75*, R139−R150.
(22) Leuschner, R. G.; Hammes, W. P. Degradation of histamine and tyramine by *Brevibacterium linens* during surface ripening of Munster cheese. *J. Food Prot.* **1998**, *61*, 874−878.
(23) Dapkevicius, M. L. N. E.; Nout, M. J. R.; Rombouts, F. M.; Houben, J. H.; Wymenga, W. Biogenic amine formation and degradation by potential fish silage starter microorganisms. *Int. J. Food Microbiol.* **2000**, *57*, 107−114.
(24) Gardini, F.; Martuscelli, M.; Crudele, M. A.; Paparella, A.; Suzzi, G. Use of *Staphylococcus xylosus* as a starter culture in dried sausages: effect on the biogenic amine content. *Meat Sci.* **2002**, *61*, 275−283.
(25) Swain, W. F.; Desa, R. J. Mechanism of action of putrescine oxidase: binding characteristics of the active site of putrescine oxidase from *Micrococcus rubens*. *Biochim. Biophys. Acta, Enzymol.* **1976**, *429*, 331−341.
(26) Yongsawatdigul, J.; Rodtong, S.; Raksakulthai, N. Acceleration of Thai fish sauce fermentation using proteinases and bacterial starter cultures. *J. Food Sci.* **2007**, *72*, 382−390.
(27) Mah, J.-H.; Hwang, H.-J. Inhibition of biogenic amine formation in a salted and fermented anchovy by *Staphylococcus xylosus* as a protective culture. *Food Control* **2009**, *20*, 796−801.
(28) García-Ruiz, A.; González-Rompinelli, E. M.; Bartolomé, B.; Moreno-Arribas, M. V. Potential of wine-associated lactic acid bacteria to degrade biogenic amines. *Int. J. Food Microbiol.* **2011**, *148*, 115−120.
(29) Callejón, S.; Sendra, R.; Ferrer, S.; Pardo, I. Identification of a novel enzymatic activity from lactic acid bacteria able to degrade biogenic amines in wine. *Appl. Microbiol. Biotechnol.* **2014**, *98*, 185−198.
(30) Hernández-Orte, P.; Peña-Gallego, A.; Ibarz, M. J.; Cacho, J.; Ferreira, V. Determination of the biogenic amines in musts and wines before and after malolactic fermentation using 6-aminoquinolyl-*N*-hydroxysuccinimidyl carbamate as the derivatizing agent. *J. Chromatogr., A* **2006**, *1129*, 160−164.
(31) Peña-Gallego, A.; Hernández-Orte, P.; Cacho, J.; Ferreira, V. Biogenic amine determination in wines using solid-phase extraction: a comparative study. *J. Chromatogr., A* **2009**, *1216*, 3398−3401.
(32) Cohen, S. A.; De Antonis, K. M. Applications of amino acid derivatization with 6-aminoquinolyl-N-hydroxysuccinimidyl carbamate. Analysis of feed grains, intravenous solutions and glycoproteins. *J. Chromatogr., A* **1994**, *661*, 25−34.
(33) Federico, R.; Angelini, R.; Ercolini, L.; Venturini, G.; Mattevi, A.; Ascenzi, P. Competitive inhibition of swine kidney copper amine oxidase by drugs: amiloride, clonidine, and gabexate mesylate. *Biochem. Biophys. Res. Commun.* **1997**, *240*, 150−152.
(34) DeSa, R. J. Putrescine oxidase from *Micrococcus rubens*. *J. Biol. Chem.* **1972**, *247*, 5527−5534.
(35) Shuai, Y.; Zhang, T.; Mu, W.; Jiang, B. Purification and characterization of γ-glutamyltranspeptidase from *Bacillus subtilis* SK11.004. *J. Agric. Food Chem.* **2011**, *59*, 6233−6238.
(36) Okada, M.; Kawashima, S.; Imahori, K. Substrate specificity and reaction mechanism of putrescine oxidase. *J. Biochem.* **1979**, *86*, 97−104.
(37) Van Hellemond, E.; van Dijk, M.; Heuts, D.; Janssen, D.; Fraaije, M. Discovery and characterization of a putrescine oxidase from *Rhodococcus erythropolis* NCIMB 11540. *Appl. Microbiol. Biotechnol.* **2008**, *78*, 455−463.
(38) Okada, M.; Kawashima, S.; Imahori, K. Mode of inactivation of putrescine oxidase by 1-ethyl-3-(3-dimethylaminopropylcarbodiimide) or metal ions. *J. Biochem.* **1980**, *88*, 481−488.
(39) Youdim, M. B. H.; Gross, A.; Finberg, J. P. M. Rasagiline [*N*-propargyl-1*R*(+)-aminoindan], a selective and potent inhibitor of mitochondrial monoamine oxidase B. *Br. J. Pharmacol.* **2001**, *132*, 500−506.
(40) Kim, J. M.; Bogdan, M. A.; Mariano, P. S. SET photochemistry of flavin-cyclopropylamine systems. Models for proposed monoamine oxidase inhibition mechanisms. *J. Am. Chem. Soc.* **1991**, *113*, 9251−9257.
(41) Hill, J. M.; Mann, P. J. G. The inhibition of pea-seedling diamine oxidase by chelating agents. *Biochem. J.* **1962**, *85*, 198−207.
(42) Yamada, H.; Tanaka, A.; Ogata, K. Putrescine oxidase of *Micrococcus rubens*. *Agric. Biol. Chem.* **1965**, *29*, 260−261.
(43) Kinemuchi, H.; Sugimoto, H.; Obata, T.; Satoh, N.; Ueda, S. Selective inhibitors of membrane bound semicarbazide-sensitive amine oxidase (SSAO) activity in mammalian tissues. *Neurotoxicology* **2004**, *25*, 325−335.
(44) Polo, L.; Ferrer, S.; Peña-Gallego, A.; Hernández-Orte, P.; Pardo, I. Biogenic amine synthesis in high quality Tempranillo wines. Relationship with lactic acid bacteria and vinification conditions. *Ann. Microbiol.* **2010**, 1−8.
(45) Underberg, E.; Lembke, A. Process for the preparation of amine-oxidase containing material, so produced amine-oxidase containing material. U.S. Patent 4725540, 1988.
(46) Maicas, S.; Natividad, A.; Ferrer, S.; Pardo, I. Malolactic fermentation in wine with high densities of non-proliferating *Oenococcus oeni*. *World J. Microbiol. Biotechnol.* **2000**, *16*, 805−810.

DOI: 10.1021/jf5026967
J. Agric. Food Chem. 2015, 63, 4170−4178

complex coacervates were expected to dissociate or precipitate. Nevertheless, the secondary aggregates of these biopolymer nanoparticles would possibly occur at a particular pH range such as physiological pH conditions. The stability problem of biopolymer nanoparticles formed by heating protein and polysaccharide electrostatic complexes has not yet been completely solved.

Whey protein isolate (WPI) is widely used as a food ingredient because of not only its high nutritional value but also its excellent functional properties, including emulsifying, foaming, and gelation. WPI consists mainly of several globular proteins, α-lactalbumin (α-la), β-lactoglobulin (β-lg), and bovine serum albumin (BSA). The functional properties of WPI are mainly dominated by β-lg, the major component of WPI. β-Lg is a suitable candidate for the preparation of drug delivery systems for lipophilic compounds because of its ability to bind hydrophobic constituents.[1,4] To the best of our knowledge, WPI and β-lg can form biopolymer nanoparticles with or without ionic polysaccharide through thermal treatment. However, these biopolymer nanoparticles are unstable at a pH range below their p*I* values with and without high salt concentrations, leading to the secondary aggregation. The stability problem of WPI-based nanoparticles under acidic pH conditions and high salt concentrations is greatly challenging.

The Maillard reaction is a complex series of reactions between reducing carbonyl groups of polysaccharide and free amino groups of protein, and it has become more and more popular for the preparation of glycosylated proteins compared with chemical glycosylation reagents. The covalent grafting of glycosyl residues to protein can significantly improve the solubility, thermal stability, and emulsifying properties of proteins.[22−26] Dextran is a neutral polysaccharide with high solubility, low viscosity, and no gelation. It has been widely used in the glycosylation of proteins to avoid the complication due to the formation of electrostatic complexes. Many studies have focused on the optimization process of the Maillard reaction and functional properties of protein−polysaccharide conjugates as well as their applications.[22−30] However, much less work has been reported on the influence of glycosyl residue introduction on the stability of biopolymer nanoparticles against pH and salt, which were formed by heating protein−polysaccharide conjugate and ionic polysaccharide electrostatic complexes.

Chondroitin sulfate (ChS) is a mucopolysaccharide extracted from animal cartilage as an important food grade material. ChS contains weakly acidic carbonyl groups and strongly acidic sulfate groups. Thus, ChS has a higher negative charge density and can form ionic complexes with positively charged substances. In addition, ChS has been investigated as a potential carrier for drug delivery due to its numerous appealing properties, including safety, biocompatibility, and biodegradability.[31,32]

Lutein, a non-provitamin A carotenoid, is widely distributed in fruits and vegetables and is one of the two carotenoids found in the macula and lens of the human eye, which is responsible for central vision and visual acuity. In addition, lutein is a powerful antioxidant, which plays an important role in the prevention of excessive ultraviolet light exposure, stroke, cardiovascular disease, and lung cancer.[33] Unfortunately, lutein is not synthesized in the human body. Therefore, dietary ingestion is the only source for the supplementation of lutein. However, the bioavailability of lutein is limited by its inherent poor water solubility.[33] Recent studies have demonstrated that nanoencapsulation is a promising approach to improve the bioavailability of poorly water-soluble compounds.[34,35]

The objective of the present study was to prepare stable nanoparticles against pH and salt by heating WPI−dextran conjugate/ChS electrostatic complexes and to elucidate the stability mechanism of the biopolymer nanoparticles over a wide pH range and at high salt concentration. The biopolymer nanoparticles were characterized by spectrophotometry, dynamic light scattering, zeta potential, transmission electron microscopy (TEM), atomic force microscopy (AFM), and scanning electron microscopy (SEM). As a nutrient model, lutein was used to evaluate the encapsulation efficacy of the biopolymer nanoparticles for hydrophobic compounds.

MATERIALS AND METHODS

Materials and Reagents. Whey protein isolate (WPI) was purchased from Hilmar Ingredients (Hilmar, CA, USA). WPI contained about 95.6% total solid, 88.7% protein, and 2.7% ash. Dextran with an average molecular weight of 40 kDa was obtained from Sinopharm Chemical Reagent Co., Ltd. (Shanghai, China). Chondroitin sulfate (ChS) was supplied by Shandong Yibao Biologics Co., Ltd. (Yanzhou, China). ChS was composed of 95.4% sodium ChS and 4.6% protein. Lutein (98% pure) was obtained from Zhejiang Medicine Co., Ltd. (Shaoxing, China). Hydrochloric acid, sodium hydroxide, anhydrous ethanol, phenol, sulfuric acid (98%), Coomassie brilliant blue G-250, and *o*-phthaldialdehyde (OPA) were purchased from Sinopharm Chemical Reagent Co., Ltd. All materials were used without further purification. All aqueous solutions were prepared with deionized water.

Preparation of WPI−Dextran Conjugates. WPI−dextran conjugates were prepared under macromolecular crowding conditions according to a method described previously with minor modifications.[23,36] Briefly, the conditions of pH 6.5 and 60 °C were used to maximize the extent of formation of Schiff base, which is the initial product of the Maillard reaction. The mixtures of WPI and dextran were dissolved in 10 mM sodium phosphate buffer solution (PBS) (pH 6.5) containing 0.02% (w/v) sodium azide to prevent bacterial growth. The degree of glycosylation (DG) increased with increasing protein concentration and mass ratio of dextran to WPI. However, protein concentration above 10% (w/w) would lead to the formation of WPI gelation during thermal treatment,[15,29,36] and dextran concentration above 30% could not significantly increase the DG of WPI.[36] In this work, the optimal concentrations of WPI and dextran were 7.5 and 22.5% (w/w), respectively. The solutions were carefully adjusted to pH 6.5 using 0.1 M HCl or 0.1 M NaOH and gently stirred for 6 h at room temperature to dissolve completely the mixtures. The mixed solutions were stored at 4 °C overnight for complete hydration. The following morning, 6 mL aliquots of the solutions were dispensed into 10 mL screw-top, glass vials sealed with Teflon tape to prevent evaporation and then incubated in a water bath at 60 °C for 24, 48, and 72 h (denoted WPI−dextran conjugates 1, 2, and 3, respectively). These reacted solutions were then removed from the water bath and immediately cooled in an ice−water bath. The reacted mixtures were diluted 4-fold with deionized water (pH 6.5, containing 0.02% NaN_3) and centrifuged at 10000*g* for 30 min. There were few white precipitates after centrifugation. The white precipitates were dissolved when resuspended in deionized water and heated at 100 °C for 30 min. After the redissolved solution was assayed by using the Coomassie brilliant blue and phenol−sulfuric acid methods, the white precipitates were identified as dextran self-associates due to its high concentration during thermal treatment.[36] The supernatant solutions were kept at −20 °C until use. WPI and dextran were separately incubated and centrifuged using the same treatment to serve as controls. All experiments were performed in triplicate.

Preparation of Biopolymer Nanoparticles from Mixtures of WPI/Polysaccharide. Biopolymer nanoparticles were prepared according to the method previously described.[12,13,37] Briefly, 1% (w/w) ChS stock solution was prepared by dissolving ChS in deionized

DOI: 10.1021/acs.jafc.5b00794
J. Agric. Food Chem. 2015, 63, 4179−4189

water and stirring for 2 h at room temperature. ChS stock solution was stored at 4 °C overnight for complete hydration. The stability of biopolymer nanoparticles prepared by the mixtures of protein and polysaccharide was investigated by the following experiments. (i) The WPI supernatant (WPI incubated at 60 °C for 48 h) and ChS stock solution were mixed and diluted with deionized water (WPI/ChS). (ii) The WPI and dextran supernatants (WPI and dextran separately incubated at 60 °C for 48 h) were mixed and diluted with deionized water (WPI/dextran). (iii) The WPI and dextran supernatants (WPI and dextran separately incubated at 60 °C for 48 h) and ChS stock solution were mixed and diluted with deionized water (WPI/dextran/ChS). WPI, dextran, and ChS concentrations were adjusted to fixed concentrations at 0.2, 0.55, and 0.008% (w/w), respectively (as discussed below). The concentrations of WPI and dextran in the supernatants were determined by using the Coomassie brilliant blue and phenol−sulfuric acid methods. After stirring for 2 h, the mixed solutions were adjusted to pH 5.2 (near the p*I* of WPI) with 0.1 M HCl and then heated at 85 °C for 15 min. The mixtures were finally cooled for 10 min in an ice−water bath. The nanoparticle suspensions obtained by the above process were kept at 4 °C before analysis.

Preparation of Biopolymer Nanoparticles from WPI−Dextran Conjugate and ChS. The WPI−dextran conjugate (*n*) supernatant and ChS stock solution (denoted WPI−dextran conjugate *n*/ChS, *n* = 1, 2, 3) were mixed and adjusted to the fixed final concentrations as described above. When WPI−dextran conjugate 2 (WPI and dextran mixtures incubated at 60 °C for 48 h) supernatant was adjusted to 0.2% (w/w) WPI, the dextran concentration was 0.55% (w/w). To keep experimental conditions as consistent as possible, the concentrations of WPI and dextran and ChS were fixed. All other procedures were the same as described above.

pH and Salt Stability. The stability of biopolymer nanoparticles against pH and salt was determined using spectrophotometry and dynamic light scattering. The nanoparticle suspensions were divided into two parts: one was adjusted to the desired pH values (1.0 to 8.0) using hydrochloric acid (2.0, 1.0, 0.1, and 0.01 M) or sodium hydroxide solution (0.1 and 0.01 M). The other portion was first added with NaCl stock solution (3 M NaCl) to reach a final concentration of 200 mM NaCl and then adjusted to the desired pH values as described above. In this study, the final NaCl concentration was 200 mM, slightly higher than physiological salt concentration, which was to verify salt stability of biopolymer nanoparticles in physiological concentration.

Lutein Loading. Lutein-loaded WPI−dextran conjugate/ChS nanoparticles were prepared according to the ethanol injection−ultrasonic method.[35] Lutein ethanol solution (0.2%, w/w) was obtained by dissolving lutein in anhydrous ethanol by sonication treatment (SK5210HP, Shanghai Kudos Ultrasonic Instrument Co., Ltd., China) for 1 min. Ten milliliters of lutein ethanol solution was rapidly injected into 100 mL of WPI−dextran conjugate/ChS nanoparticle suspension under agitation. After stirring for 1 h, the ethanol in the coarse suspension was removed by a rotary evaporator under reduced pressure at 40 °C. Then the lutein-loaded suspension was subjected to ultrasonic treatment in an ice bath for 4 min at 400 W with a pulse mode of 1 s of sonication and 1 s of rest using a probe sonicator (JY98-IIIDN, Ningbo Scientz Biotechnology Co., Ltd., China). The final suspension was kept at 4 °C in the dark before analysis.

Lutein was absorbed on the surface and entrapped in the lutein-loaded nanoparticles. To determine the amount and efficiency of lutein loading into the nanoparticles, the amount of lutein un-entrapped on the surface of nanoparticles was measured as follows: 0.5 mL of nanoparticle suspension was added to 2.5 mL of ethyl acetate, violently vortexed for 1 min, and then centrifuged at 1000*g* for 5 min. The resultant upper ethyl acetate layer was collected. The above treatment was repeated twice. The collected extracts were combined and concentrated to dryness under nitrogen conditions and redissolved in 10 mL of ethanol for spectral analysis. Lutein concentration was determined using a spectrophotometer (UV-1600; Mapada Instruments Co., Ltd., Shanghai, China) at 446 nm and calculated by the following equation: $C = 0.0322A - 0.0065$ (R^2 = 0.9992), where C and A were the concentration and absorbance of lutein in anhydrous ethanol, respectively. R^2 was the correlation coefficient of linear regression equation. The lutein loading content (LC, % w/w) and encapsulation efficiency (EE, %) were respectively calculated using the following equations:

$$\text{LC (\%w/w)} = \frac{\text{entrapped amount of lutein}}{\text{amount of WPI}} \times 100$$

$$\text{EE (\%)} = \frac{\text{total lutein} - \text{un-entrapped lutein}}{\text{total lutein}} \times 100$$

LC was defined as the content of lutein in the biopolymer nanoparticles measured by determining the ratio of entrapped amount of lutein to the total amount of WPI. The amount of lutein entrapped inside the biopolymer nanoparticles was calculated as the difference between the total amount of lutein added to the nanoparticle suspensions and that of lutein recovered by extraction. The amount of WPI in the biopolymer nanoparticles was obtained from the initial WPI concentration. EE was defined as the amount of lutein entrapped inside the biopolymer nanoparticles measured by determining the ratio of entrapped amount of lutein to the total amount of lutein.

Turbidity Measurements. Turbidity analysis of the biopolymer nanoparticle suspensions was carried out using an ultraviolet−visible spectrophotometer (UV-1600 spectrophotometer, Mapada Instruments Co., Ltd.) at 633 nm with a glass cuvette (1 cm path length).[37] Deionized water was used as blank for all solutions. All experiments were performed in triplicate.

Dynamic Laser Scattering (DLS) Measurements. The apparent *Z*-average hydrodynamic diameter (D_h) and polydispersity index (PDI) of biopolymer nanoparticles were measured by DLS using a Malvern Zetasizer Nano ZS analyzer (Malvern Instruments Ltd., Malvern, UK) fitted with a 633 nm He−Ne laser beam. Measurements were taken at 25 °C and 173° scattering angle. D_h and PDI were obtained by cumulant analysis (software of Zetasizer Nano ZS, Malvern Instruments Ltd.). The nanoparticle samples were measured directly without filtering or removing dust.

Zeta Potential Measurements. The zeta potential (ζ-potential) of nanoparticles was determined by laser Doppler electrophoresis at 25 °C using a Malvern Zetasizer Nano ZS analyzer (Malvern Instruments Ltd.). ζ-Potential was calculated by the Zetasizer Software (Malvern Instruments Ltd.) according to the Henry equation.[38] The nanoparticle samples were measured directly. Each sample was analyzed in triplicate.

Transmission Electron Microscopy Measurements. A drop of a 1000-fold dilution of the sample suspensions (approximately 7 μL) was deposited onto a carbon-coated copper grid. The samples were then allowed to dry for 72 h at ambient temperature. TEM images of biopolymer nanoparticles were recorded with a commercial TEM (JEM-2100, JEOL Ltd., Japan) operating at an accelerating voltage of 200 kV.

Atomic Force Microscopy Measurements. The nanoparticle suspensions for AFM measurement (Dimension icon, Bruker Co., USA) were diluted 400-fold with deionized water. AFM samples were prepared by dropping an aliquot (1 μL) of the diluted suspensions on a freshly cleaved mica surface and air-drying at room temperature for 72 h. The ScanAsyst mode was carried out using a silicon tip (TESP, Bruker, nom freq 320 kHz, nom spring constant of 42 N/m) with a scan resolution of 512 × 512 pixels in the dimension of 5 μm × 5 μm. Images were generated and processed using NanoScope software (Digital Instruments, version V614r1).

Scanning Electron Microscope Measurements. A drop of a 1000-fold dilution of the sample suspensions (approximately 7 μL) was deposited onto a carbon-coated copper grid. The samples were allowed to dry for 72 h at ambient temperature and then coated with gold palladium using a sputter coater. The morphology of biopolymer nanoparticles was observed at 40000× magnification with a field emission scanning electron microscope (S-4800, Hitachi Science Systems, Ltd., Japan) operating at an accelerating voltage of 5 kV.

Statistical Analysis. All experiments were performed in triplicate. Data were presented as a mean value with its standard deviation. The

DOI: 10.1021/acs.jafc.5b00794
J. Agric. Food Chem. 2015, 63, 4179−4189

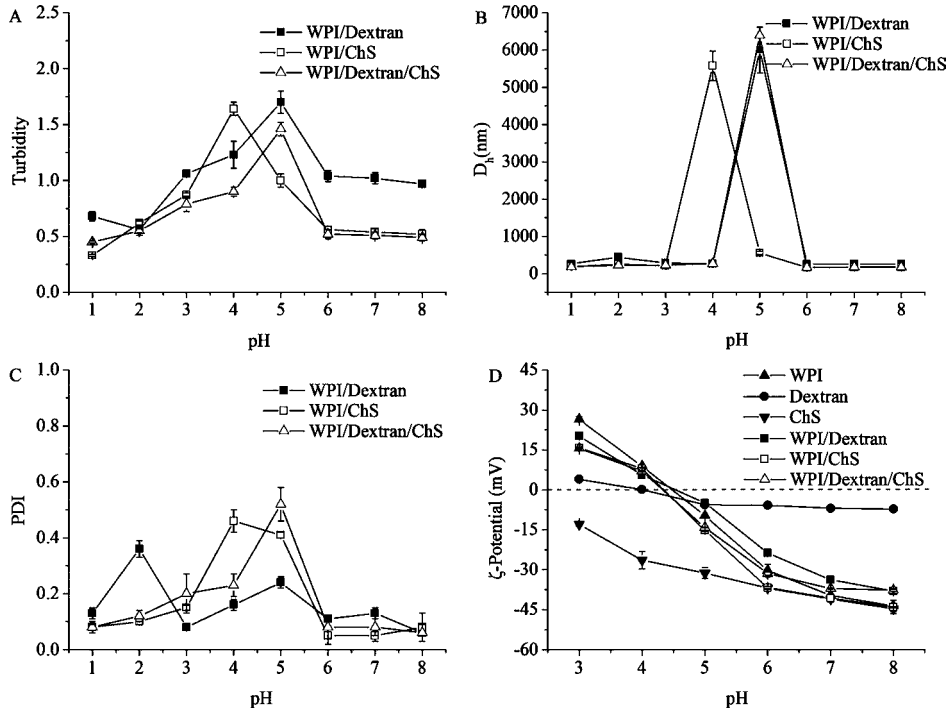

Figure 1. Effect of pH on turbidity (A), hydrodynamic diameter (D_h) (B), and polydispersity index (PDI) (C) of WPI/polysaccharide suspensions and effect of pH on ζ-potential (D) of WPI/polysaccharide suspensions and WPI or polysaccharide solutions. WPI/polysaccharide suspensions were prepared by heating WPI/polysaccharide mixtures at pH 5.2 and 85 °C for 15 min. WPI or polysaccharide solutions were prepared by dissolving WPI or polysaccharide in deionized water.

means were compared with one-way analysis of variance (ANOVA) followed by Duncan's multiple-range tests, and $p < 0.05$ was regarded as significant. Statistical analyses were conducted using SPSS 17.0 for Windows (SPSS Inc., Chicago, IL, USA).

RESULTS AND DISCUSSION

pH and Salt Stability of WPI/Polysaccharide Nanoparticles. *pH and Salt Effect on Turbidity of WPI/Polysaccharide Suspensions.* The effect of pH on the turbidity of protein/polysaccharide suspensions is shown in Figure 1A. All of the suspensions had a similar trend when the pH changed from pH 1.0 to 8.0. WPI solution (0.2%, w/w) rapidly coagulated, and the white precipitates were found at the bottom of the bottle during thermal treatment near its p*I*, whereas dextran did not form aggregates under the same experimental conditions (data not shown). Similar phenomena have previously been observed by other researchers. Jones and co-authors reported that solutions of β-lg alone at pH 4.0−5.5 became very turbid after heating at 83 °C for 15 min.[12] The reason may be related to the unfolding and self-association of protein through hydrophobic interactions and disulfide bonds, which led to the formation of irreversible particulate aggregates in the absence of interprotein charge repulsion and above its thermal denaturation temperature. Additionally, Jones and co-authors also found that when 0.5% (w/w) β-lg solution was heated at pH 5 in the absence of pectin, large protein aggregates (d > 6000 nm) were formed and remained large (d > 3000 nm) across the entire pH range.[20] The results suggested that the aggregation occurring near the p*I* of the globular protein was pH-irreversible.

Although the WPI/dextran solution did not rapidly form much white precipitates during thermal treatment, the turbidity of WPI/dextran suspensions remained relatively high and constant at high pH values (pH 6.0−8.0) and had a maximum turbidity at pH 5.0. In addition, the turbidity of WPI/dextran suspensions gradually decreased with pH values decreasing from 5.0 to 1.0. In most cases for biopolymer mixtures, WPI and dextran are cosoluble in very dilute solutions. Above WPI's denaturation temperature and near its p*I*, phase separation (aggregation) would take place, resulting in WPI-rich and dextran-rich domains. Due to the very low turbidity resulting from the dextran-rich domain, the turbidity of WPI/dextran suspensions was dominated by WPI self-association, which suggested that WPI was the core component of the nanoparticles. The results also indicated that dextran could only partly suppress the formation of large sediments during thermal treatment. It was possible that dextran could decrease the frequency of encounters between protein molecules and thereby reduce the magnitude and range of protein−protein interaction during thermal treatment. However, due to the lack of electrostatic repulsion and steric hindrance between dextran and WPI molecules, dextran could not completely prevent WPI self-association. Similar results were reported by Chakrabortee and co-authors.[39] They demonstrated that dextran behaved as a molecular shield polysaccharide and used physical interference to reduce protein aggregation caused by desiccation. These studies have shown that the neutral dextran could indeed partly affect the aggregation or gelation process of protein during thermal treatment.

As shown in Figure 1A, the turbidity of WPI/ChS suspensions significantly decreased at pH 5.0. This was due to the fact that ChS molecules could increase the electrostatic and steric forces between particles, but these forces were not sufficient to prevent the particle aggregation at pH 4.0. Similar results were reported in previous studies.[11,40] Pectin stabilized the β-lg/pectin particles against aggregation around the p*I* of β-lg, which was presumably due to an increase in the electrostatic

DOI: 10.1021/acs.jafc.5b00794
J. Agric. Food Chem. 2015, 63, 4179−4189

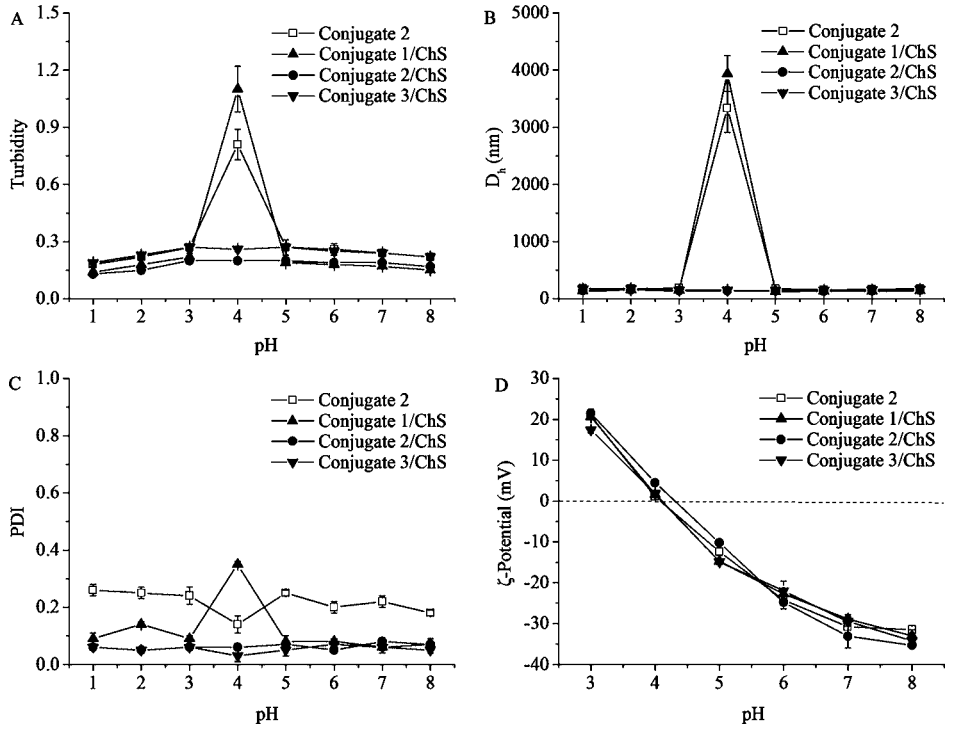

Figure 2. Effect of pH on turbidity (A), hydrodynamic diameter (D_h) (B), polydispersity index (PDI) (C), and ζ-potential (D) of WPI−dextran conjugate 2 (9.7% degree of glycosylation) and WPI−dextran conjugate/ChS suspensions. Suspensions were prepared by heating WPI−dextran conjugate 2 solutions or WPI−dextran conjugate/ChS electrostatic complexes at pH 5.2 and 85 °C for 15 min. Conjugate 1, WPI−dextran conjugate with 5.2% degree of glycosylation; conjugate 2, WPI−dextran conjugate with 9.7% degree of glycosylation; conjugate 3, WPI−dextran conjugate with 12.2% degree of glycosylation.

and steric repulsion between the biopolymer nanoparticles, whereas extensive aggregation was still observed at lower pH values.[11] In addition, the turbidity of WPI/ChS suspensions was relatively low in the pH ranges of 1.0−3.0 and 5.0−8.0, which was possible due to the lack of disulfide bond formation (pH 1.0−3.0) and the increase of repulsive electrostatic interaction (pH 1.0−3.0 and 5.0−8.0) between biopolymer nanoparticles.

The maximum turbidity of WPI/ChS and WPI/dextran/ChS suspensions was obtained at pH 4.0 and 5.0, respectively (Figure 1A). This was attributed to the fact that dextran could also decrease the collision frequency between WPI and ChS molecules as between WPI molecules. Therefore, dextran significantly weakened the suppressing effect of anionic ChS on WPI self-association. Similar results were reported in previous studies, demonstrating that the incompatibility between gelatin and pectin was attributed to the competitive interactions between dextran and the reactive groups of gelatin.[41] Additionally, it is well-known that high salt concentration can destabilize polyelectrolyte complexes due to the electrostatic screening effect. All suspensions in the presence of 200 mM NaCl had higher turbidity over a wider pH range compared with those in the absence of salt (Figure S1A and Figure 1A, respectively).

pH and Salt Effect on Particle Diameter of WPI/Polysaccharide Suspensions. The turbidity of the biopolymer suspensions was further supported by DLS measurements (Figure 1B,C and Figure S1B,C). As observed in Figure 1B, the *Z*-average particle diameter (160−250 nm) of WPI/ChS nanoparticles remained relatively stable in the pH ranges of 1.0−3.0 and 6.0−8.0. Figure 1C shows that the biopolymer nanoparticles had a small polydispersity index (PDI < 0.15) in the same pH ranges. However, the particle diameter significantly ($p < 0.05$) increased from 550 nm at pH 5.0 (PDI = 0.41) to 5600 nm at pH 4.0 (PDI = 0.46) (Figure 1B,C). The change trends of particle diameter of WPI/dextran and WPI/dextran/ChS suspensions were the same as that of WPI/ChS suspensions. In the presence of salt, the large aggregates in all suspensions occurred over a wider pH range compared with those in the absence of salt (Figure S1B and Figure 1B, respectively).

pH Effect on ζ-Potential of WPI and/or Polysaccharide Suspensions. The ζ-potential is directly related to the net charges on the surface of macromolecules and particles in solutions.[42] Figure 1D shows that the ζ-potentials of native WPI changed from negative at high pH values to positive at low pH values, with a zero charge point between pH 4.0 and 5.0. The pH value at the zero charge point was close to the p*I* of native WPI (4.8−5.2) reported in the literature.[14] ChS was negatively charged across the entire pH range of 3.0−8.0. Although dextran has no charges, its solution had a relatively low negative ζ-potential, which was attributed to the increased ionic strength when the solution was adjusted to various pH values by adding hydrochloric acid or sodium hydroxide. These results are in agreement with previous findings, which reported that the ζ-potential of dextran solution (phosphate buffer 0.01 M, pH 7.4) was −9.9 ± 0.5 mV.[43]

The absolute ζ-potential values of WPI/dextran suspensions, formed by heating at pH 5.2, were smaller than those of individual WPI solutions. The results confirmed that the principal component of the nanoparticles was composed of WPI, and dextran could affect the interactions between WPI molecules as discussed above. The ζ-potentials of WPI/ChS suspensions were between those of the individual WPI and ChS

DOI: 10.1021/acs.jafc.5b00794
J. Agric. Food Chem. 2015, 63, 4179−4189

solutions below pH 6.0, suggesting that there was electrostatic attraction between cationic patches on the protein surface and anionic groups on the polysaccharide backbone.[44] Therefore, ChS would influence the net surface charge of the outer periphery of WPI/ChS particles. It was important that the ζ-potentials could provide a good explanation for the turbidity and particle diameter of WPI/polysaccharide suspensions at different pH values. For example, the ζ-potentials of WPI/ChS suspensions went from negative (−36.8 mV) to positive (+15.8 mV) as pH values decreased from 8.0 to 3.0 (Figure 1D). The electrostatic repulsions between nanoparticles decreased with decreasing absolute ζ-potential values. Therefore, the turbidity and particle diameter of WPI/ChS suspensions increased.

Preparation of WPI−Dextran Conjugates. The Maillard reaction is a natural nontoxic process, which produces conjugates from the graft reaction between reducing end carbonyl groups of polysaccharide and free amino groups of protein. WPI−dextran conjugates prepared by the Maillard reaction have been reported in previous studies.[22,23,26,29,36] WPI−dextran conjugates exhibit higher solubility and thermal stability than those of the native WPI around its p*I*. In this study, WPI−dextran conjugates were prepared with the weight ratio of WPI to dextran 1:3 under macromolecular crowding conditions, which were previously reported by other researchers.[23,36] The formation of WPI−dextran conjugates was validated by the *o*-phthalaldehyde (OPA) method and Fourier transform infrared spectra (FT-IR) (Supporting Information, Figures S2 and S3, respectively). Meanwhile, the degree of glycosylation (DG) of the WPI−dextran conjugates was determined by the OPA assay from the loss of free amino groups of WPI.[29,45] The analysis revealed that DGs of WPI−dextran conjugate 1 (incubated for 24 h), conjugate 2 (incubated for 48 h), and conjugate 3 (incubated for 72 h) were 5.2, 9.7, and 12.2%, respectively (Supporting Information, Figure S2).

Stability of WPI−Dextran Conjugate/ChS Nanoparticles against pH and Salt. *Stability of WPI−Dextran Conjugate 1/ChS Nanoparticles against pH and Salt.* The stability of WPI−dextran conjugate/ChS nanoparticles against pH in the absence or presence of salt is shown in Figures 2 and 3, respectively. Compared with WPI/polysaccharide suspensions (Figure 1 and Figure S1), the turbidity and particle diameter of WPI−dextran conjugate or WPI−dextran conjugate/ChS suspensions significantly decreased ($p < 0.05$) at the same pH values in the absence or presence of salt, which illustrated that the dextran conjugated to WPI could significantly decrease the turbidity and particle diameter of the suspension systems. The results also suggested that the dextran conjugated to WPI could be extended to the periphery of the inner core of the nanoparticles and prevent their aggregation. The WPI−dextran conjugate 1/ChS suspensions had a relatively constant turbidity and smaller particle size diameter (about 150 nm, PDI < 0.15) at a low pH range of 1.0−3.0 and a high pH range of 5.0−8.0 (Figure 2A−C) and in the presence of 200 mM NaCl (Figure 3), indicating that the nanoparticles were fairly stable to association or dissociation. However, the turbidity and particle diameter of WPI−dextran conjugate 1/ChS were higher at the pH range of 3.0−5.0 regardless of salt. The results indicated that the steric hindrance provided by the dextran conjugated to WPI with only 5.2% DG could not effectively inhibit the aggregation of biopolymer nanoparticles in this pH range.

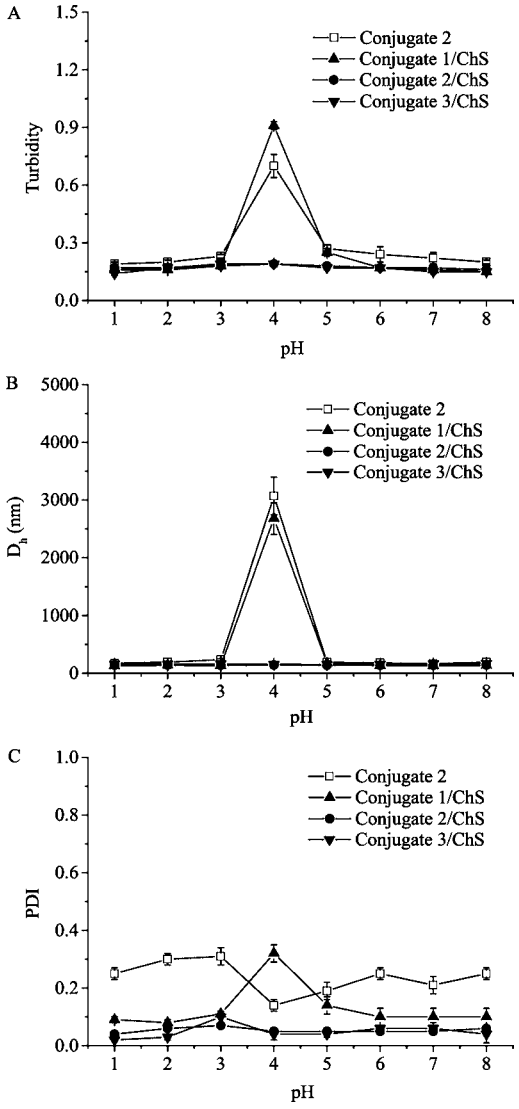

Figure 3. Effect of pH and 200 mM NaCl on turbidity (A), hydrodynamic diameter (D_h) (B), and polydispersity index (PDI) (C) of WPI−dextran conjugate 2 (9.7% degree of glycosylation) and WPI−dextran conjugate/ChS suspensions. Suspensions were prepared by heating WPI−dextran conjugate 2 solutions or WPI−dextran conjugate/ChS electrostatic complexes at pH 5.2 and 85 °C for 15 min. Conjugate 1, WPI−dextran conjugate with 5.2% degree of glycosylation; conjugate 2, WPI−dextran conjugate with 9.7% degree of glycosylation; conjugate 3, WPI−dextran conjugate with 12.2% degree of glycosylation.

Stability of WPI−Dextran Conjugate 2/ChS Nanoparticles against pH and Salt. It has been demonstrated that nanoparticles with 50−200 nm size acquire the best properties for cellular uptake.[46,47] The WPI−dextran conjugate 2/ChS nanoparticles (*Z*-average particle diameter about 150 nm and PDI 0.08) could remain stable in the entire pH range of 1.0−8.0 and in the absence or presence of salt (Figures 2 and 3, respectively), which was ideal for the encapsulation and transportation of nutraceuticals and drugs. Although the WPI/dextran/ChS nanoparticles had a smaller particle diameter (about 170−270 nm and PDI 0.08−0.23) at the pH ranges of 1.0−4.0 and 6.0−8.0, the secondary aggregates of the nanoparticles occurred in the pH range of 4.0−6.0 and in the presence of salt, and largest aggregates (about 6400 nm and

DOI: 10.1021/acs.jafc.5b00794
J. Agric. Food Chem. 2015, 63, 4179−4189

PDI 0.52) appeared at pH 5.0 (Figure 1B). Obviously, dextran conjugated to WPI could significantly improve the stability of WPI−dextran conjugate 2/ChS nanoparticles against pH and salt. However, the turbidity and particle diameter of WPI−dextran conjugate 2 suspensions were fairly similar to those of WPI−dextran conjugate 1/ChS suspensions (Figures 2 and 3, respectively). Only the introduction of dextran, from the WPI−dextran conjugate 2 with 9.7% DG, was not strong enough to stabilize the nanoparticles in the pH range from 3.0 to 5.0. This suggested that the combined action of the dextran conjugated to WPI with 9.7% DG and ChS could stabilize the nanoparticles against pH and salt.

Stability of WPI−Dextran Conjugate 3/ChS Nanoparticles against pH and Salt. There was no significant difference in the turbidity, particle diameter, and PDI between WPI−dextran conjugate 2/ChS and WPI−dextran conjugate 3/ChS suspensions over a wide pH range of 1.0−8.0 and in the absence or presence of salt (Figures 2A−C and 3A−C, respectively). The results illustrated that both dextran covalently conjugated to WPI with 9.7% DG and ChS electrostatically interacted with WPI were the minimum requirements to stabilize the nanoparticles. The WPI−dextran conjugate 2 was more economical than the WPI−dextran conjugate 3 because the latter required more preparation time. Therefore, the WPI−dextran conjugate 2/ChS complexes were used to further determine the characteristics of the stable nanoparticles.

ζ-Potentials of WPI−Dextran Conjugate 2 and WPI−Dextran Conjugate/ChS Suspensions. The ζ-potentials of biopolymer nanoparticle suspensions at different pH values are shown in Figure 2D. The ζ-potential values of all WPI−dextran conjugate or WPI−dextran conjugate/ChS suspensions were slightly lower than those of WPI/dextran or WPI/dextran/ChS suspensions (Figures 2D and 1D, respectively). For example, the ζ-potentials of WPI−dextran conjugate 2, conjugate 1/ChS, conjugate 2/ChS, and conjugate 3/ChS suspensions at pH 8.0 were −31.5, −33.0, −35.3, and −34.2 mV, respectively (Figure 2D), whereas the ζ-potentials of WPI/dextran and WPI/dextran/ChS suspensions at pH 8.0 were −38.1 and −37.7 mV, respectively (Figure 1D). The decrease of absolute ζ-potential values after protein glycosylation was probably related to the highly hydratable dextran lowering the electrophoretic mobility of the WPI−dextran conjugate and WPI−dextran conjugate/ChS suspensions. Similar results have been reported in previous studies.[25,27]

WPI−Dextran Conjugate 2/ChS Nanoparticle Formation Mechanism. As evidenced above, the stability of the nanoparticles was closely related to the degree of glycosylation of WPI. This indicated that the steric repulsions would stabilize the protein nanoparticles against aggregation, which were contributed by both dextran covalently conjugated to WPI and ChS electrostatically interacted with WPI. Therefore, the results suggested that the repulsive steric interactions were the major mechanism for the formation of the stable nanoparticles against pH and salt. It has been demonstrated that the steric hindrance of dextran conjugated to protein almost completely suppressed the protein aggregation during thermal treatment.[22−25,28] Combined with the present findings, it was further confirmed that the appropriate glycosylation of protein molecules was a crucial step to prepare the size-controlled nanoparticles. In addition, the ζ-potentials of WPI−dextran conjugate suspensions were slightly lower than those of WPI or WPI/dextran (Figures 2D and 1D, respectively), which indicated that dextran chains conjugated to WPI extended in the shell of the nanoparticle. Previous studies have also illuminated that steric hindrance was a function of polysaccharide chains on the colloidal particle surface to improve the heat stability of protein, which was supported by ζ-potentials of protein and glycosylated protein.[24,25,27,30]

Although the formation of the nanoparticles prepared by heating protein and ionic polysaccharide complexes undergoes a variety of interactions and processes, the electrostatic attraction and hydrophobic interaction primarily contribute to the initial structure development during gelation. Proteins might only electrostatically couple with a certain amount of ionic polysaccharides during thermal treatment. At the high mass ratio of WPI to ChS, most of the ChS chains could be partly or completely entrapped and fixed in the inner core of the nanoparticles during the process of denaturation and aggregation of WPI. It has been demonstrated that the β-lg/pectin nanoparticles prepared by thermal treatment were primarily composed of β-lg, but some pectin was still present.[12] In addition, Chakrabortee and co-authors have indicated that there was some association between proteins and neutral polysaccharides such as dextran during desiccation.[39]

The turbidity and particle diameter of WPI−dextran conjugate 2/ChS suspensions were stable in the pH range of 1.0−8.0 regardless of salt, but secondary aggregates occurred in the WPI−dextran conjugate 2 suspensions at pH 4.0 in the absence and presence of salt (Figures 2A,B and 3A,B, respectively). The results confirmed that not all ChS chains loosely distributed at the periphery of WPI−dextran conjugate 2/ChS nanoparticles after thermal treatment, but most of the ChS chains were incorporated into the nanoparticles to improve their stability, through the electrostatic interaction between the WPI−dextran conjugate or WPI and ChS molecules during thermal treatment. Although there was a slight difference in the ζ-potentials between WPI−dextran conjugate 2/ChS and WPI−dextran conjugate 2 suspensions in the pH range of 3.0−8.0, the ζ-potentials of the former and latter were from −24.8 to −35.3 mV and from −24.2 to −31.5 mV at the pH range of 6.0−8.0, respectively (Figure 2D), where the electrostatic repulsion between WPI−dextran conjugate and ChS was predominant. This suggested that some of the ChS chains extended in the shell of the nanoparticles. Therefore, the shell of the nanoparticles was composed of both ChS and dextran conjugated to WPI. Multiple interactions finally contributed to the stability of the nanoparticles against pH and salt. As discussed above, ChS, WPI, and WPI−dextran conjugate with an appropriate degree of glycosylation could be assembled into the stable nanoparticles with WPI-dextran conjugate/ChS shell and WPI/ChS core in a wide range of pH values and high salt concentration.

Lutein Loading of WPI−Dextran Conjugate 2/ChS Nanoparticles. There were no significant differences in the turbidity, particle diameter, and ζ-potential between lutein-unloaded and lutein-loaded nanoparticles in the absence or presence of salt (Figures 2, 3 and 4). The results illustrated that lutein loading did not impair the stability of the nanoparticles. The WPI−dextran conjugate 2/ChS suspension with light blue opalescence was obtained as shown in Figure 5A-1 (as inset), and the lutein-loaded nanoparticle suspension was uniformly stable as shown in Figure 5B-1 (as inset). Previous studies showed that the *Z*-average particle diameter of nanoemulsions decreased with sonication treatment.[48] This discrepancy was attributed to the good stability of the conjugate/polysaccharide nanoparticles formed by thermal treatment. On the contrary,

DOI: 10.1021/acs.jafc.5b00794
J. Agric. Food Chem. 2015, 63, 4179−4189

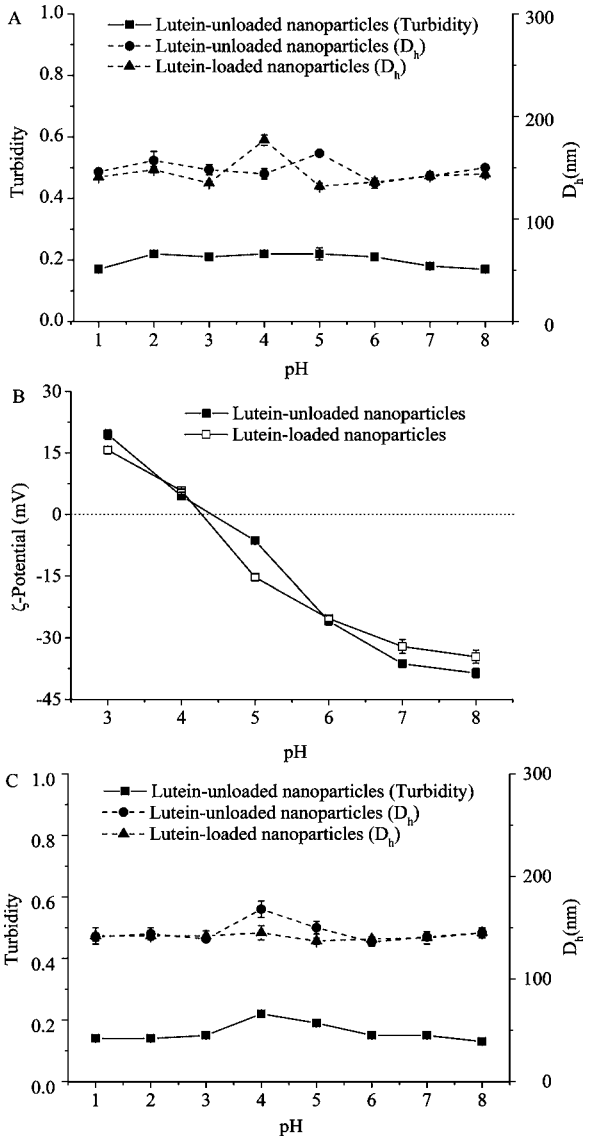

Figure 4. Effect of pH on turbidity and hydrodynamic diameter (D_h) of lutein-unloaded and lutein-loaded nanoparticle suspensions (A), effect of pH on ζ-potential of lutein-unloaded and lutein-loaded nanoparticle suspensions (B), and effect of pH and 200 mM NaCl on turbidity and hydrodynamic diameter (D_h) of lutein-unloaded and lutein-loaded nanoparticle suspensions (C). Suspensions were prepared by heating WPI–dextran conjugate 2 (9.7% DG)/ChS electrostatic complexes at pH 5.2 and 85 °C for 15 min, and then lutein-unloaded and lutein-loaded nanoparticle suspensions were evaporated by a rotary evaporator and subjected to ultrasonic treatment.

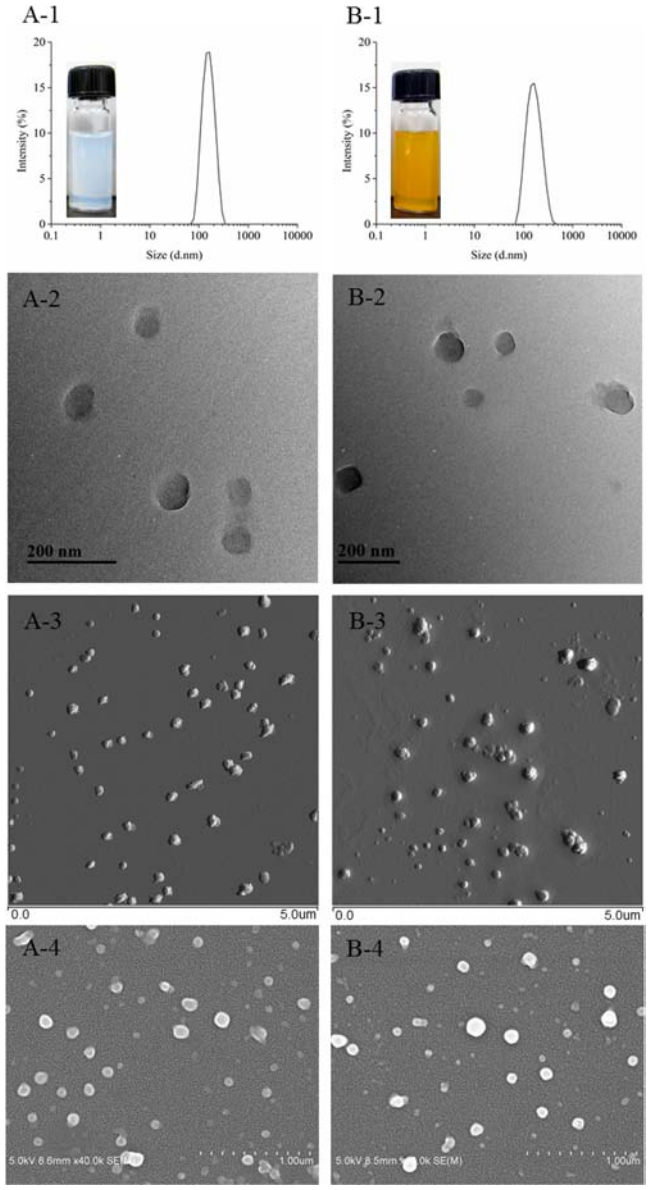

Figure 5. Particle size distribution of lutein-unloaded (A-1) and lutein-loaded (B-1) WPI–dextran conjugate 2 (9.7% DG)/ChS suspensions, TEM images of lutein-unloaded (A-2) and lutein-loaded (B-2) WPI–dextran conjugate 2 (9.7% DG)/ChS nanoparticles, AFM images of lutein-unloaded (A-3) and lutein-loaded (B-3) WPI–dextran conjugate 2 (9.7% DG)/ChS nanoparticles, and SEM images of lutein-unloaded (A-4) and lutein-loaded (B-4) WPI–dextran conjugate 2 (9.7% DG)/ChS nanoparticles. The insets are direct images of lutein-unloaded and lutein-loaded WPI–dextran conjugate 2 (9.7% DG)/ChS suspensions.

the ultrasonic cavitation could promote lutein molecules to migrate into the interior of the nanoparticles. Lutein molecules were trapped in the hydrophobic regions of the nanoparticle core, by hydrophobic interactions. In this study, the nanoparticles could effectively encapsulate lutein with the loading content and encapsulation efficiency of 8.03 and 94.07%, respectively. The ζ-potentials had no significant difference between lutein-unloaded and lutein-loaded nanoparticles (Figure 4B). Apparently, the neutral lutein could not influence the surface charge of the nanoparticles. The *Z*-average particle diameter of lutein-loaded nanoparticles remained almost unchanged over the entire pH range (1.0–8.0) regardless of salt (Figure 4A,C), indicating that lutein-loaded nanoparticles had good stability against pH and salt.

Morphology of WPI–Dextran Conjugate 2/ChS Nanoparticles. *TEM.* The morphology of lutein-unloaded and lutein-loaded nanoparticles was characterized using TEM, AFM, and SEM as shown in Figure 5. TEM images of the nanoparticles revealed a homogeneous size distribution and a spherical shape with smooth surface, as shown in Figure 5A-2,B-2. The particle diameters of lutein-unloaded and lutein-loaded nanoparticles in TEM images were approximately 70 and 90 nm, respectively, much smaller than the hydrodynamic diameter obtained from DLS (about 150 nm) (Figure 5A-1,B-

DOI: 10.1021/acs.jafc.5b00794
J. Agric. Food Chem. 2015, 63, 4179–4189

1). It is well-known that DLS determines the data for the particle swollen in solution, whereas the particle diameters in TEM images are obtained by spreading and drying the nanoparticles on a carbon-coated copper grid.[7,19] Meanwhile, Figure 5B-2 also shows that the lutein-loaded nanoparticles had greater density in the inner core of the nanoparticles compared with the lutein-unloaded nanoparticles because of the higher gray level in the former. Therefore, TEM images further confirmed that the lutein molecules were located in the core of the nanoparticles.

AFM. AFM and SEM are both powerful instruments to observe the three-dimensional morphology of the nanoparticles. AFM images of the nanoparticles are shown in Figure 5A-3,B-3. The images of all nanoparticles appeared to be fairly uniform and spherical in shape, indicating that the encapsulation of lutein did not greatly change the morphology of nanoparticles. Additionally, the dimensions of the lutein-loaded nanoparticles were slightly bigger than those of the unloaded nanoparticles, consistent with the results of TEM. The height of the nanoparticles in the AFM images was much smaller than their diameter, suggesting that the nanoparticles were very soft and collapsed on the mica surface during air-drying.[12,18,27]

SEM. SEM images showed that the nanoparticles had a fairly uniform spherical shape (Figure 5A-4,B-4) as observed by AFM. The diameters in SEM images exhibited a narrow size distribution from 50 to 100 nm, which was in good agreement with the dimensions obtained from TEM images. Our findings are consistent with previous studies.[34,46] The results confirmed the microstructure of the nanoparticles observed by AFM and TEM. It has been demonstrated that large amounts of water or biological fluids were imbibed into the three-dimensional networks of the hydrogel nanoparticles, and drugs could be entrapped into the mesh space between the hydrogel nanoparticle networks.[49] Li and co-authors have illuminated that lysozyme−dextran nanogels had a low-density structure and could contain a large amount of water by the swelling ratio of the nanogels estimated from the ratio of average volumes of DLS to AFM.[27] Therefore, the fact that the sizes observed by TEM, AFM, and SEM were smaller than those obtained by DLS was due to the syneresis of the nanoparticles during air-drying. These results also suggested that there were adequate mesh spaces between the nanoparticle networks, which could provide an opportunity to encapsulate other components within themselves.

Potential Application of WPI−Dextran Conjugate 2/ChS Nanoparticles. There has been great interest in applications of nanoparticles as biomaterials for delivering hydrophobic bioactive compounds such as nutraceuticals and drugs. Moreover, biopolymer nanoparticles can be easily prepared and scaled up during manufacture.[1,2] Several nanoparticles have been launched in the area of cancer treatment. For example, Abraxane (paclitaxel−albumin nanoparticle) with an approximate diameter of 130 nm is the first nanotechnology-based chemotherapeutic approved by the U.S. FDA and has shown significant benefit in treatment of metastatic breast cancer.[1,4] The commercial success of albumin-based nanoparticles has created a great interest in other proteins.[1,4,5] Whey protein has been used to prepare biopolymer-based nanoparticles using the bottom-up approach.[5,8] β-Lg, the major whey protein, is known to be stable at low pH and highly resistant to digestion by gastric proteases. β-Lg has been investigated for drug delivery applications.[1,4] Whey protein nanoparticles were successfully fabricated by pH-cycling treatment and thermal processing.[50] Jones and co-authors discussed the effect of polysaccharide charge on the formation and properties of biopolymer nanoparticles, which were created by heat treatment of β-lg/pectin complexes.[12] Chitosan/β-lg core−shell nanoparticles were prepared with the aim of developing a biocompatible carrier for the oral administration of nutraceuticals.[7]

However, the biopolymer nanoparticles were unstable over a wide pH range (especially the entire physiological pH range) and at high salt concentration. Glycosylation of whey protein with dextran increased protein solubility and thermal stability.[22] Liu and co-authors illustrated that the glycosylation of whey protein with maltodextrins prevented protein aggregation before and after heating, and steric hindrance was concluded to be the primary mechanism responsible for transparent dispersions with protein structures smaller than 12 nm after heating.[24] The results suggested that glycosylation of protein would offer an excellent opportunity to improve the stability of biopolymer nanoparticles. Therefore, the stable biopolymer nanoparticles against pH and salt, having spherical shapes with smooth surface, would be used as a promising delivery system for hydrophobic nutrients or drugs in physiological conditions. Additionally, it has been demonstrated that complexes of proteins and strong polyelectrolytes such as sulfated or phosphate polysaccharides tend to form precipitates or solid-like structures, and there is a narrow range of physicochemical conditions at which electrostatic complexes are formed and stay in solution.[9] Sulfated polysaccharides such as ChS may be suitable for delivering active compounds to target cells.[32] This method would provide an approach to prepare target nanoparticles from protein and sulfated polysaccharide.

■ ASSOCIATED CONTENT

Ⓢ Supporting Information

Additional experimental details. This material is available free of charge via the Internet at http://pubs.acs.org.

■ AUTHOR INFORMATION

Corresponding Author

*(X. Zhang) E-mail: xmzhang@jiangnan.edu.cn. Phone: +86 510 85197217. Fax: +86 510 85884496.

Funding

This research was financially supported by projects of the National 125 Program of China (2011BAD23B01, 2011BAD23B04, 2012BAD33B05, and 2013AA102204), projects of the National Natural Science Foundation of China (31471624), and open projects of The Key Laboratory of Carbohydrate Chemistry and Biotechnology, Ministry of Education (KLCCB-KF201202).

Notes

The authors declare no competing financial interest.

■ REFERENCES

(1) Elzoghby, A. O.; Samy, W. M.; Elgindy, N. A. Protein-based nanocarriers as promising drug and gene delivery systems. *J. Controlled Release* **2012**, *161*, 38−49.

(2) Nitta, S. K.; Numata, K. Biopolymer-based nanoparticles for drug/gene delivery and tissue engineering. *Int. J. Mol. Sci.* **2013**, *14*, 1629−1654.

(3) Liu, Z.; Jiao, Y.; Wang, Y.; Zhou, C.; Zhang, Z. Polysaccharides-based nanoparticles as drug delivery systems. *Adv. Drug Delivery Rev.* **2008**, *60*, 1650−1662.

DOI: 10.1021/acs.jafc.5b00794
J. Agric. Food Chem. 2015, 63, 4179−4189

(4) Lohcharoenkal, W.; Wang, L.; Chen, Y. C.; Rojanasakul, Y. Protein nanoparticles as drug delivery carriers for cancer therapy. *BioMed Res. Int.* **2014**, DOI: 10.1155/2014/180549.
(5) Chen, L.; Remondetto, G. E.; Subirade, M. Food protein-based materials as nutraceutical delivery systems. *Trends Food Sci. Technol.* **2006**, *17*, 272−283.
(6) Paillard, A.; Passirani, C.; Saulnier, P.; Kroubi, M.; Garcion, E.; Benoit, J. P.; Betbeder, D. Positively-charged, porous, polysaccharide nanoparticles loaded with anionic molecules behave as 'stealth' cationic nanocarriers. *Pharm. Res.* **2010**, *27*, 126−133.
(7) Chen, L.; Subirade, M. Chitosan/β-lactoglobulin core-shell nanoparticles as nutraceutical carriers. *Biomaterials* **2005**, *26*, 6041−6053.
(8) Gunasekaran, S.; Ko, S.; Xiao, L. Use of whey proteins for encapsulation and controlled delivery applications. *J. Food Eng.* **2007**, *83*, 31−40.
(9) de Kruif, C. G.; Weinbreck, F.; de Vries, R. Complex coacervation of proteins and anionic polysaccharides. *Curr. Opin. Colloid Interface Sci.* **2004**, *9*, 340−349.
(10) Shaw, K. L.; Grimsley, G. R.; Yakovlev, G. I.; Makarov, A. A.; Pace, C. N. The effect of net charge on the solubility, activity, and stability of ribonuclease Sa. *Protein Sci.* **2001**, *10*, 1206−1215.
(11) Jones, O. G.; Decker, E. A.; McClements, D. J. Comparison of protein-polysaccharide nanoparticle fabrication methods: impact of biopolymer complexation before or after particle formation. *J. Colloid Interface Sci.* **2010**, *344*, 21−29.
(12) Jones, O. G.; Lesmes, U.; Dubin, P.; McClements, D. J. Effect of polysaccharide charge on formation and properties of biopolymer nanoparticles created by heat treatment of β-lactoglobulin−pectin complexes. *Food Hydrocolloids* **2010**, *24*, 374−383.
(13) Jones, O. G.; McClements, D. J. Biopolymer nanoparticles from heat-treated electrostatic protein-polysaccharide complexes: factors affecting particle characteristics. *J. Food Sci.* **2010**, *75*, N36−N43.
(14) Damodaran, S. Food proteins: an overview. In *Food Proteins and Their Applications*; Damodaran, S., Paraf, A., Eds.; Dekker: New York, 1997; pp 1−24.
(15) Zhu, H.; Damodaran, S. Heat-induced conformational changes in whey protein isolate and its relation to foaming properties. *J. Agric. Food Chem.* **1994**, *42*, 846−855.
(16) Jones, O. G.; McClements, D. J. Stability of biopolymer particles formed by heat treatment of β-lactoglobulin/beet pectin electrostatic complexes. *Food Biophys.* **2008**, *3*, 191−197.
(17) Jones, O. G.; McClements, D. J. Recent progress in biopolymer nanoparticle and microparticle formation by heat-treating electrostatic protein-polysaccharide complexes. *Adv. Colloid Interface Sci.* **2011**, *167*, 49−62.
(18) Peinado, I.; Lesmes, U.; Andres, A.; McClements, J. D. Fabrication and morphological characterization of biopolymer particles formed by electrostatic complexation of heat treated lactoferrin and anionic polysaccharides. *Langmuir* **2010**, *26*, 9827−9834.
(19) Yu, S.; Hu, J.; Pan, X.; Yao, P.; Jiang, M. Stable and pH-sensitive nanogels prepared by self-assembly of chitosan and ovalbumin. *Langmuir* **2006**, *22*, 2754−2759.
(20) Jones, O. G.; Decker, E. A.; McClements, D. J. Formation of biopolymer particles by thermal treatment of β-lactoglobulin−pectin complexes. *Food Hydrocolloids* **2009**, *23*, 1312−1321.
(21) Sun, X. D.; Arntfield, S. D. Molecular forces involved in heat-induced pea protein gelation: effects of various reagents on the rheological properties of salt-extracted pea protein gels. *Food Hydrocolloids* **2012**, *28*, 325−332.
(22) Jiménez-Castaño, L.; Villamiel, M.; López-Fandiño, R. Glycosylation of individual whey proteins by Maillard reaction using dextran of different molecular mass. *Food Hydrocolloids* **2007**, *21*, 433−443.
(23) Zhu, D.; Damodaran, S.; Lucey, J. A. Physicochemical and emulsifying properties of whey protein isolate (WPI)-dextran conjugates produced in aqueous solution. *J. Agric. Food Chem.* **2010**, *58*, 2988−2994.
(24) Liu, G.; Zhong, Q. Glycation of whey protein to provide steric hindrance against thermal aggregation. *J. Agric. Food Chem.* **2012**, *60*, 9754−9762.
(25) Liu, G.; Zhong, Q. Thermal aggregation properties of whey protein glycated with various saccharides. *Food Hydrocolloids* **2013**, *32*, 87−96.
(26) Sun, W.; Yu, S.; Zeng, X.; Yang, X.; Jia, X. Properties of whey protein isolate−dextran conjugate prepared using pulsed electric field. *Food Res. Int.* **2011**, *44*, 1052−1058.
(27) Li, J.; Yu, S.; Yao, P.; Jiang, M. Lysozyme-dextran core-shell nanogels prepared via a green process. *Langmuir* **2008**, *24*, 3486−3492.
(28) Qi, J.; Yao, P.; He, F.; Yu, C.; Huang, C. Nanoparticles with dextran/chitosan shell and BSA/chitosan core-doxorubicin loading and delivery. *Int. J. Pharm.* **2010**, *393*, 176−184.
(29) Sun, W.; Yu, S.; Yang, X.; Wang, J.; Zhang, J.; Zhang, Y.; Zheng, E. Study on the rheological properties of heat-induced whey protein isolate−dextran conjugate gel. *Food Res. Int.* **2011**, *44*, 3259−3263.
(30) Pan, X.; Yao, P.; Jiang, M. Simultaneous nanoparticle formation and encapsulation driven by hydrophobic interaction of casein-*graft*-dextran and β-carotene. *J. Colloid Interface Sci.* **2007**, *315*, 456−463.
(31) Dawlee, S.; Sugandhi, A.; Balakrishnan, B.; Labarre, D.; Jayakrishnan, A. Oxidized chondroitin sulfate-cross-linked gelatin matrixes: a new class of hydrogels. *Biomacromolecules* **2005**, *6*, 2040−2048.
(32) Lee, C. M.; Tanaka, T.; Murai, T.; Kondo, M.; Kimura, J.; Su, W.; Kitagawa, T.; Ito, T.; Matsuda, H.; Miyasaka, M. Novel chondroitin sulfate-binding cationic liposomes loaded with cisplatin efficiently suppress the local growth and liver metastasis of tumor cells in vivo. *Cancer Res.* **2002**, *62*, 4282−4288.
(33) Johnson, E. J. A biological role of lutein. *Food Rev. Int.* **2004**, *20*, 1−16.
(34) Hu, D.; Lin, C.; Liu, L.; Li, S.; Zhao, Y. Preparation, characterization, and in vitro release investigation of lutein/zein nanoparticles via solution enhanced dispersion by supercritical fluids. *J. Food Eng.* **2012**, *109*, 545−552.
(35) Tan, C.; Xia, S.; Xue, J.; Xie, J.; Feng, B.; Zhang, X. Liposomes as vehicles for lutein: preparation, stability, liposomal membrane dynamics, and structure. *J. Agric. Food Chem.* **2013**, *61*, 8175−8184.
(36) Zhu, D.; Damodaran, S.; Lucey, J. A. Formation of whey protein isolate (WPI)-dextran conjugates in aqueous solutions. *J. Agric. Food Chem.* **2008**, *56*, 7113−7118.
(37) Zhang, S.; Zhang, Z.; Lin, M.; Vardhanabhuti, B. Raman spectroscopic characterization of structural changes in heated whey protein isolate upon soluble complex formation with pectin at near neutral pH. *J. Agric. Food Chem.* **2012**, *60*, 12029−12035.
(38) Deshiikan, S. R.; Papadopoulos, K. D. Modified Booth equation for the calculation of zeta potential. *Colloid Polym. Sci.* **1998**, *276*, 117−124.
(39) Chakrabortee, S.; Tripathi, R.; Watson, M.; Schierle, G. S.; Kurniawan, D. P.; Kaminski, C. F.; Wise, M. J.; Tunnacliffe, A. Intrinsically disordered proteins as molecular shields. *Mol. BioSyst.* **2012**, *8*, 210−219.
(40) Santipanichwong, R.; Suphantharika, M.; Weiss, J.; McClements, D. J. Core-shell biopolymer nanoparticles produced by electrostatic deposition of beet pectin onto heat-denatured β-lactoglobulin aggregates. *J. Food Sci.* **2008**, *73*, N23−N30.
(41) Antonov, Y. A.; Zubova, O. M. Phase state of aqueous gelatin-polysaccharide (1)-polysaccharide (2) systems. *Int. J. Biol. Macromol.* **2001**, *29*, 67−71.
(42) Murray, M. J.; Snowden, M. J. The preparation, characterization and applications of colloidal Microgels. *Adv. Colloid Interface Sci.* **1995**, *54*, 73−91.
(43) Morais, M.; Subramanian, S.; Pandey, U.; Samuel, G.; Venkatesh, M.; Martins, M.; Pereira, S.; Correia, J. D. G.; Santos, I. Mannosylated dextran derivatives labeled with *fac*-$[M(CO)_3]^+$ (M = ^{99m}Tc, Re) for specific targeting of sentinel lymph node. *Mol. Pharmaceutics* **2011**, *8*, 609−620.

DOI: 10.1021/acs.jafc.5b00794
J. Agric. Food Chem. 2015, 63, 4179−4189

(44) Chanasattru, W.; Jones, O. G.; Decker, E. A.; McClements, D. J. Impact of cosolvents on formation and properties of biopolymer nanoparticles formed by heat treatment of β-lactoglobulin−pectin complexes. *Food Hydrocolloids* **2009**, *23*, 2450−2457.
(45) Markman, G.; Livney, Y. D. Maillard-conjugate based core-shell co-assemblies for nanoencapsulation of hydrophobic nutraceuticals in clear beverages. *Food Funct.* **2012**, *3*, 262−270.
(46) Teng, Z.; Li, Y.; Luo, Y.; Zhang, B.; Wang, Q. Cationic β-lactoglobulin nanoparticles as a bioavailability enhancer: protein characterization and particle formation. *Biomacromolecules* **2013**, *14*, 2848−2856.
(47) Lerch, S.; Dass, M.; Musyanovych, A.; Landfester, K.; Mailander, V. Polymeric nanoparticles of different sizes overcome the cell membrane barrier. *Eur. J. Pharm. Biopharm.* **2013**, *84*, 265−274.
(48) Mishra, V.; Mahor, S.; Rawat, A.; Gupta, P. N.; Dubey, P.; Khatri, K.; Vyas, S. P. Targeted brain delivery of AZT via transferrin anchored pegylated albumin nanoparticles. *J. Drug Target* **2006**, *14*, 45−53.
(49) Hamidi, M.; Azadi, A.; Rafiei, P. Hydrogel nanoparticles in drug delivery. *Adv. Drug Delivery Rev.* **2008**, *60*, 1638−1649.
(50) Giroux, H. J.; Houde, J.; Britten, M. Preparation of nanoparticles from denatured whey protein by pH-cycling treatment. *Food Hydrocolloids* **2010**, *24*, 341−346.

DOI: 10.1021/acs.jafc.5b00794
J. Agric. Food Chem. 2015, 63, 4179−4189

and the European Union (EU Directive 110/2001).[28] Preliminary analyses on a number of fresh RJ samples showed that HMF concentrations were over the limit of quantification (LOQ) only in samples stored at room temperature. Hence, the principal aim of this study is to monitor the evolution of the concentration of HMF in fresh RJ stored for months at different temperatures in order to ascertain the potential suitability of HMF as a freshness marker for this foodstuff.

MATERIALS AND METHODS

Chemical and Reagents. The chromatographic solvents used were a 0.05 mol dm^{-3} H_2SO_4 aqueous solution and methanol (HPLC grade, Riedel de Haen, Milan, Italy). Before their use, all solvents were filtered through a 0.45 μm membrane from Millipore (Bedford, MA, USA) to remove any particulates. 5-Hydroxymethyl-2-furaldehyde was purchased from Lancaster (Milan, Italy). Trichloroacetic acid (TCA) was obtained from Sigma-Aldrich (Milan, Italy). All aqueous solutions were prepared using type I ultrapure water (New Human Power II Scholar UV, Human Corporation, Seoul, Korea).

Instrumentation. The HPLC equipment used for the experiments consisted of a Series 200 binary pump, a sampling valve, a 20 μL sample loop, a Series 200 LC column oven, and a Series 200 UV−vis variable wavelength detector, all from PerkinElmer, Milan, Italy. Separation was performed using a 250 mm × 4.6 mm Ascentis C18 column, 5 μm particle size (Supelco, Bellefonte, PA, USA), thermostated at 20 °C and fitted with a guard cartridge packed with the same stationary phase. Data were processed using Turbochrom Workstation Software (PerkinElmer, Milan, Italy).

Experimental Protocol. A freshly harvested RJ sample was obtained from "Organizzazione Produttori Apicoltori Sardi Terrantiga" (San Sperate, Sardinia, Italy). Once harvested, the RJ was homogenized, divided into 12 dark glass bottles (1−12), and kept at −18 °C until the beginning of the experimental protocol. The initial HMF content of RJ was determined within 5 days from delivery.

To study the evolution of the level of HMF in RJ stored under different conditions, the 12 bottles were divided into three groups of four samples. The groups were stored at −18, 4, and 25 ± 2 °C (room temperature), respectively. Each sample was analyzed in triplicate after 30, 90, 180, and 270 days from delivery. Samples stored at −18 and 4 °C were equilibrated at room temperature before analysis. Prior to each analysis, all of the samples were homogenized for 5 min.

Determination of HMF Content in Royal Jelly. The HMF concentration was determined using the same RP-HPLC procedure previously developed and validated for RJ by our research group.[26] Briefly, the analytical steps involved first a pretreatment of the sample with an aqueous solution of trichloroacetic acid followed by a gradient elution RP-HPLC analysis and analyte detection at 280 nm.

RESULTS

Review of the LOD and LOQ Values According to the Experimental Results of the Study. The calculation of the LOD in the method recently proposed by us was accomplished using the ULA1 approach.[29] This choice was supported both by the preliminary experience gained in the validation of HPLC methods devoted to measure HMF concentration in honey samples of different origin[19,21] and by the knowledge that the ULA1 method is optimal for reducing any decision error approach.[25] It is crucial, however, that the concentration of the most diluted standard solution used to evaluate LOD turns out to be close enough to the real LOD value. In this connection, the improved knowledge of the method acquired during this study has allowed us to observe that both the LOD and LOQ values previously measured were overestimated (i.e., the effective concentration of analyte associated with both qualitative and quantitative information was lower than that evaluated during the relevant validation step[26]). On the basis of these findings, we have repeated the evaluation of the LOD and LOQ with a better choice of the HMF standard solutions. Hence, four 4% TCA aqueous solutions containing respectively 4, 6, 8, and 10 μg L^{-1} of HMF have been analyzed in triplicate, now giving LOD and LOQ values of 0.13 and 0.39 mg kg^{-1}, respectively.

Figure 1 gives a comparison of selected portions of chromatograms (retention time between 5.5 and 6.5 min) of the blank solution (line 1), of the RJ sample 9 after 1 month of storage at 25 °C (line 2), and of the same RJ sample spiked with 50 μL of a freshly prepared 4 mg/L HMF aqueous solution (line 3).

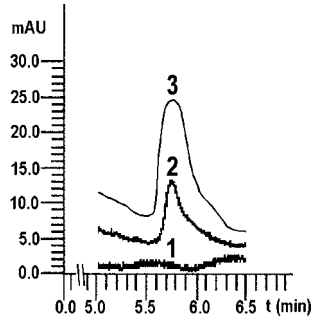

Figure 1. Overlapped chromatographic portions (retention time between 5.0 and 6.5 min) of a blank solution (line 1), sample 9 after 1 month of storage at 25 °C (line 2), and the same sample 9 spiked with 50 μL of a freshly prepared 4 mg/L HMF aqueous solution (line 3).

Monitoring of HMF in RJ on Variation of the Storage Temperature and Storage Time. In our previous study on the assessment and validation of the analytical method to measure the HMF concentration in RJ,[26] we observed proportionality between the amount of HMF measured and the age of RJ samples. In particular, whereas HMF was not quantifiable in any fresh samples, its concentration was higher than 9 mg kg^{-1} in the oldest RJ sample stored at room temperature. In this study, in order to verify the fitness of HMF as a potential marker of freshness of RJ, we carefully monitored the evolution of this analyte in RJ samples stored at different temperatures for the 9 months following their harvest. The RJ samples were always kept in dark glass bottles to prevent any degradation effect promoted by light. The initial concentration of HMF was under the LOD of the method for all samples, as shown in Table 1.

Samples stored at 4 and −18 °C showed only negligible levels of HMF for the entire duration of the study. On the other hand, in samples stored at room temperature we observed an exponential increase of the HMF concentration as a function of storage time. The dependence of the HMF concentration in RJ samples kept at room temperature and the storage time are shown in Figure 2.

DISCUSSION

The choice of a proper freshness marker for functional foods is a very complex problem that requires the careful and simultaneous consideration of a wide number of parameters, related to both the candidate marker and to the analytical method used to determine it. First, the optimal freshness marker should not be traceable in the fresh food product,[7,30] so that the mere presence of the marker is indicative of spoilage. If, on the other hand, the marker is present in the fresh matrix,

DOI: 10.1021/acs.jafc.5b00873
J. Agric. Food Chem. 2015, 63, 4190−4195

Table 1. Concentration of HMF in RJ at Varying Storage Temperatures and Times

		av HMF content (mg kg^{-1}), n = 3				
temp	sample	0 days	30 days	90 days	180 days	270 days
−18 °C	1−4[a]	<LOD[b]	<LOD[b]	<LOD[b]	<LOD[b]	<LOD[b]
4 °C	5−8[a]	<LOD[b]	<LOD[b]	<LOD[b]	<LOD[b]	<LOD[b]
room temp	9	<LOD[b]	0.39 ± 0.03	0.56 ± 0.01	1.30 ± 0.03	1.57 ± 0.07
	10	<LOD[b]	0.40 ± 0.03	0.60 ± 0.01	1.151 ± 0.002	1.69 ± 0.06
	11	<LOD[b]	0.58 ± 0.08	0.57 ± 0.03	0.93 ± 0.06	2.4 ± 0.4
	12	<LOD[b]	0.40 ± 0.06	0.60 ± 0.02	0.97 ± 0.02	2.1 ± 0.3
	av	<LOD	0.4 ± 0.1	0.58 ± 0.04	1.1 ± 0.7	1.9 ± 0.5

[a]The HMF content of each sample is below the LOD. [b]LOD = 0.13 mg kg^{-1}.

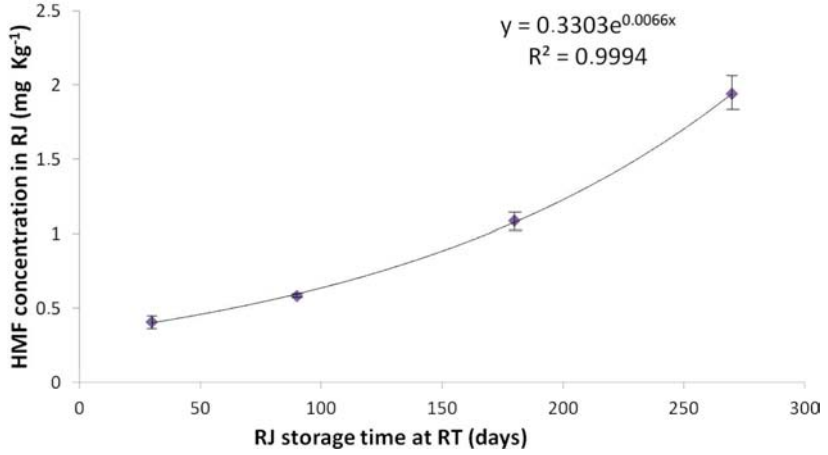

Figure 2. Dependence between HMF concentration and storage times of RJ held at room temperature (25 ± 2 °C).

slight variations in concentration with respect to the "expected" value for the unaltered matrix might be in principle ascribed not only to a loss of freshness but also to the natural variability of the analyte content. Hence, the only way to effectively apply this strategy is to evaluate the natural variability of the marker. However, such an effort has a high risk of being inconclusive, since the composition of RJ varies with seasonal and regional conditions.[9] In addition, the marker should be monitored in the matrix of interest for a period of time comparable to its expected shelf life.

Furthermore, the choice of the analytical method is critical to the effectiveness of the marker. The ideal analytical method must be simple to use and validated for the considered matrix and its chemical background must be completely known. In addition, the instrumentation required must be commonly available in any routine laboratory. Unfortunately, almost none of the RJ freshness markers proposed until now meet all these key requirements. The current situation is summarized in Table 2.

Most of the freshness markers proposed for RJ are traceable in the freshly harvested matrix. Even furosine, a promising index proposed by Marconi et al.,[7] is quantifiable in fresh samples, even if at low concentrations. Physical parameters—such as viscosity[9] and color[5,9,11]—are unreliable[1,7] and are characterized by an uncertain chemical background. On the other hand, protein-based candidate markers are usually measured with methods that require specific instruments and chemicals[5,8,9,14] and thus are unsuitable for routine applications. Finally, a complete validation protocol for the determination of a marker in a RJ matrix has rarely been provided,[13,15] meaning that the reliability of any conclusions based on the levels of those markers is questionable.

In this work, we suggest the use of HMF as a possible freshness marker for RJ. This molecule was found absent in the freshly harvested matrix in a preliminary study.[26] This is not surprising, HMF being a well-known neoformation intermediate in the Maillard reaction—i.e., in the process responsible for the most important alterations of RJ when it is improperly stored.[5,7,9] Our results clearly demonstrate that, when RJ is stored at low temperatures (equal to or less than 4 °C), even for long periods of time, the Maillard reaction is effectively slowed and the concentration of HMF remains under the LOD of the method. On the other hand, the storage of RJ at 25 °C for 1 month is sufficient to reach an HMF content that overcomes the LOQ, providing quantitative evidence of the alterations suffered by the matrix. These results are in excellent agreement with those reported earlier by Smith,[31,32] who observed no changes in the properties of the RJ stored at 5 °C for 1 year and in samples stored at −20 °C for years, while noting the deterioration of RJ's properties after only 1 month of storage at room temperature. This general behavior was more recently confirmed by results obtained by a number of different research groups.[7,8,13,14,16]

Interestingly, the growth of the HMF concentration in the RJ samples follows an exponential trend, representative of a pseudo-first-order kinetic model. Excellently correlated experimental data (the coefficient of the regression R^2 is 0.9994) substantiate the analogous exponential trend reported by Tosi, Ciappini, Rè, and Lucero[33] in a study on the effects of thermal treatments applied to honey samples on the amount of HMF. In spite of the deep and well-known differences between the chemical and physical properties of honey and royal jelly, it is evident that the heat-induced formation of HMF is active and measurable in both matrices and also that both formation

DOI: 10.1021/acs.jafc.5b00873
J. Agric. Food Chem. 2015, 63, 4190−4195

Table 2. Key Features of the Published Methods to Evaluate the Freshness of RJ

marker	analytical approach	validation	remarks	ref
color (+)[a]	spectrophotometry	no	*b*, *c*	9
viscosity (+)	viscosimetry	no	*b*, *c*	
color (+)	spectrophotometry	no	*d*	5
color (+)	colorimetry	no	*c*	11
water-soluble proteins (−)	gel filtration chromatography; SDS- PAGE; Kjeldahl method	no	*e*, *f*	9
glucose (+)		no		
fructose (+)	HPLC	no		
royalactin (−)	gel filtration chromatography	no	*f*, *g*	5
glucose oxidase (−)	colorimetry	no	*f*, *h*	10
D-proline (+−)	GC-MS	no	*i*	12
D-lysine (+−)				
total methionine (−), free glutamine (−)	ultraperformance liquid chromatography	yes[j]	*f*	13
furosine (+)	HPLC	no[k]	*f*	7
fraction of the major royal jelly proteins (MRJP4 in the study) (−)	2D-PAGE, MALDI-TOF-MS	no	*e*, *f*	8
glucose oxidase (−)	2D-PAGE, MALDI-TOF-MS	no	*e*, *f*, *l*	8
peroxiredoxin (−)				
glutathione (*S*)-transferase (−)				
fraction of the major royal jelly proteins (MRJP5 in the study) (−)	2D electrophoresis, MALDI-TOF/TOF MS	no	*e*, *f*	14
ATP, adenosine 5′-triphosphate (−)	ultraperformance liquid chromatography	yes[j]	*e*, *f*	15
pantothenic acid (−)	HPLC	no	*f*	6

[a]Definitions: +, the value of the parameter increases with storage time; −, the value of the parameter decreases with storage time; +−, the variation of marker concentration with increasing storage duration is not monotonic. [b]Semiquantitative parameter. [c]Unsuitable for the evaluation of storage periods longer than 1 month at room temperature. [d]Unsuitable for the evaluation of storage periods longer than 7 days at room temperature. [e]Method not widespread in control quality laboratories. [f]Analyte already present in RJ matrix; thus, a study to establish the "normal" concentration range of the analyte is needed before proposing it as a freshness marker. [g]Pure royalactin, needed as a standard, is not commercially available. [h]Study performed only for a short storage period (15 days). [i]Nonlinear behavior (maximum after 3 months of storage at room temperature) of the proposed markers. [j]LOD, LOQ, precision, recovery. [k]Validation protocol absent for this analyte in a RJ matrix. [l]Evaluation of analytes has only been performed on fresh and one-year-old samples.

processes roughly follow the same kinetic model. The value of the pseudo-first-order kinetic constant for HMF formation in RJ stored at room temperature in the period from 30 to 270 days (i.e. in the interval of time where the HMF concentration has been found over the LOQ of the method) is estimated at ca. 570 s^{-1}.

Finally, we remark on the fitness of the analytical method adopted for the purpose of this study. It appears completely validated and uses instrumentation commonly available in unspecialized laboratories. In addition, it has a consistent chemical background, since the generation of HMF by the Maillard reaction in foods containing both reducing sugars and amino acids (or their relevant precursors) has been thoroughly studied elsewhere.[34] Finally, it can be used to monitor RJ along its entire potential shelf life (in Europe: 18 months for refrigerated RJ; 24 months for RJ stored at −17 °C).[1]

In conclusion, the formation of HMF in fresh RJ as a function of storage temperature (from −18 °C to room temperature) and storage time (up to 270 days) was monitored by means of a RP-HPLC method, previously assessed in other work. While all the RJ samples stored at temperatures lower than room temperature did not show any detectable levels of HMF, those kept at 25 °C showed amounts of HMF which become quantifiable starting from the first month of storage. The exponential increase in HMF concentration as a function of the storage time at room temperature is representative of a pseudo-first-order kinetic model—already reported for honey. The results obtained in this study allow us to maintain that HMF can be taken into account as an eligible freshness marker for RJ, since the amount of sugars and proteins in this matrix is evidently adequate to provide an increase of the HMF concentration as a function of the storage time. Further studies may contribute to establish the dependence of the evolution of HMF in RJ as a function of intrinsic parameters (e.g., sugar and amino acidic composition, seasonality, geographic origin, botanical origin of the pollen fed by bees, race of the bees, harvesting time after grafting) and storage parameters (e.g., exposure to light, short exposure of RJ to heat).

DOI: 10.1021/acs.jafc.5b00873
J. Agric. Food Chem. 2015, 63, 4190−4195

AUTHOR INFORMATION

Corresponding Author

*G.S.: tel, +39 079 229500; fax, +39 079 229959: e-mail, sanna@uniss.it.

Notes

The authors declare no competing financial interest.

ACKNOWLEDGMENTS

The authors thank Francesco Caboni (Organizzazione Produttori Apicoltori Sardi TERRANTIGA, San Sperate, Sardinia, Italy) for generously donating the RJ samples used in this study.

REFERENCES

(1) Krell, R. Value-added products from beekeeping. FAO AGRICULTURAL SERVICE BULLETIN No 124. Food and Agriculture Organization of the United Nations Rome. 1996; available at: http://www.fao.org/docrep/w0076E/w0076E00.htm (last visited: 31/03/2015).

(2) Viuda-Martos, M.; Ruiz-Navajas, Y.; Fernàndez-Lopéz, J.; Pérez-Alvaréz, J. A. Functional properties of honey, propolis and royal jelly. *J. Food Sci.* **2008**, *73*, R117−R124.

(3) Bogdanov, S. Royal Jelly, Bee Brood: Composition, Health, Medicine: A Review. Bee Product Science, 2014; available at http://www.bee-hexagon.net/files/file/fileE/Health/RJBookReview.pdf (last visited: 31/03/2015).

(4) Sabatini, A. G.; Marcazzan, G. L.; Caboni, M. F.; Bogdanov, S.; de Almeida-Muradian, L. B. Quality and standardisation of royal jelly. *J. ApiProd. ApiMed. Sci.* **2009**, *1*, 16−6.

(5) Kamakura, M.; Fukuda, T.; Fukushima, M.; Yonekura, M. Storage-dependent degradation of 57-kDa Protein in royal jelly: a possible marker for freshness. *Biosci., Biotechnol., Biochem.* **2001**, *65*, 277−284.

(6) Kamakura, M. Royalactine induces queen differentiation in honey bees. *Nature* **2011**, *473*, 478−483.

(7) Marconi, E.; Caboni, M. F.; Messia, M. C.; Panfili, G. Furosine: a suitable marker for assessing the freshness of royal jelly. *J. Agric. Food Chem.* **2002**, *50*, 2825−2829.

(8) Li, J.; Feng, M.; Zhang, L.; Zhang, Z.; Pan, Y. Proteomics analysis of major royal jelly protein changes under different storage conditions. *J. Proteome Res.* **2008**, *7*, 3339−3353.

(9) Chen, C.; Chen, S. Changes in protein components and storage stability of royal jelly under various conditions. *Food Chem.* **1995**, *54*, 195−200.

(10) Baggio, A.; Dainese, N. Royal jelly quality during storage. *Ind. Aliment.-Italy* **1998**, *37*, 1290−1297. Available at http://www.ismea.it/flex/AppData/Redational/Normative/pubnaz/20000606000100073.pdf (last visited: 16/04/2015).

(11) Zheng, H.-Q.; Wei, W. T.; Wu, L. M.; Hu, F. L.; Dietmann, V. Fast determination of royal jelly freshness by a chromogenic reaction. *J. Food Sci.* **2012**, *77*, S247−S252.

(12) Boselli, E.; Caboni, M. F.; Sabatini, A. G.; Marcazzan, G. L.; Lercker, G. Determination and changes of free amino acids in royal jelly during storage. *Apidologie* **2003**, *34*, 129−137.

(13) Liming, W.; Jinhui, Z.; Xiaofeng, X.; Yi, L.; Jing, Z. Fast determination of 26 amino acids and their content changes in royal jelly during storage using ultra-performance liquid chromatography. *J. Food Compos. Anal.* **2009**, *22*, 242−249.

(14) Zhao, F.; Wu, Y.; Guo, L.; Li, X.; Han, J.; Chen, Y.; Ge, Y. Using proteomics platform to develop a potential immunoassay method of royal jelly freshness. *Eur. Food Res. Technol.* **2013**, *236*, 799−815.

(15) Zhou, L.; Xue, X.; Zhou, J.; Li, Y.; Zhao, J.; Wu, L. Fast determination of adenosine-5′-triphosphate (ATP) and its catabolites in royal jelly using ultraperformance liquid chromatography. *J. Agric. Food Chem.* **2012**, *60*, 8994−8999.

(16) Antinelli, J.; Zeggane, S.; Davico, R.; Rognone, C.; Faucon, J.; Lizzani, L. Evaluation of (E)-10-hydroxydec-2-enoic acid as a freshness parameter for royal jelly. *Food Chem.* **2003**, *80*, 85−89.

(17) Sanna, G.; Pilo, M. I.; Piu, P. C.; Tapparo, A.; Seeber, R. Determination of heavy metals in honey by anodic stripping voltammetry at microelectrodes. *Anal. Chim. Acta* **2000**, *415*, 165−173.

(18) Scanu, R.; Spano, N.; A. Panzanelli, A.; Pilo, M. I.; Piu, P. C.; Sanna, G.; Tapparo, A. Direct chromatographic methods for the rapid determination of homogentisic acid in strawberry-tree (Arbutus Unedo L.) honey. *J. Chromatogr. A* **2005**, *1090*, 76−80.

(19) Spano, N.; Casula, L.; Panzanelli, A.; Pilo, M. I.; Piu, P. C.; Scanu, R.; Tapparo, A.; Sanna, G. A RP-HPLC determination of 5-hydroxymethyl-2-furaldehyde in honey: the case of strawberry-tree honey. *Talanta* **2006**, *68*, 1390−1395.

(20) Spano, N.; Ciulu, M.; Floris, I.; Panzanelli, A.; Pilo, M. I.; Piu, P. C.; Scanu, R.; Sanna, G. Chemical characterization of a traditional honey-based Sardinian product: Abbamele. *Food Chem.* **2008**, *108*, 81−85.

(21) Spano, N.; Ciulu, M.; Floris, I.; Panzanelli, A.; Pilo, M. I.; Piu, P. C.; Salis, S.; Sanna, G. A direct RP-HPLC method for the determination of furanic aldehydes and acids in honey. *Talanta* **2009**, *78*, 310−314.

(22) Spano, N.; Piras, I.; Ciulu, M.; Floris, I.; Panzanelli, A.; Pilo, M. I.; Piu, P. C.; Sanna, G. Reversed-phase liquid chromatographic profile of free amino acids in strawberry-tree (*Arbutus Unedo L.*) honey. *J. AOAC Int.* **2009**, *92*, S1145−S1156.

(23) Ciulu, M.; Solinas, S.; Floris, I.; Panzanelli, A.; Pilo, M. I.; Piu, P. C.; Spano, N.; Sanna, G. RP-HPLC determination of water-soluble vitamins in honey. *Talanta* **2011**, *83*, 924−929.

(24) Ciulu, M.; Floris, I.; Nurchi, V. M.; Panzanelli, A.; Pilo, M. I.; Sanna, G. HPLC determination of pantothenic acid in royal jelly. *Anal. Methods* **2013**, *5*, 6682−6685.

(25) Ciulu, M., Spano, N., Salis, S., Pilo, M. I., Floris, I., Pireddu, L., Sanna, G. Assay of B vitamins and other water soluble vitamins in honey. In *B Vitamins and Folate: Chemistry, Analysis, Function and Effects*; Preedy, V. R., Ed.; Royal Society of Chemistry: London, 2013; Food and Nutritional Components in Focus No. 4, pp 173−194.

(26) Ciulu, M.; Farre, R.; Floris, I.; Nurchi, V. M.; Panzanelli, A.; Pilo, M. I.; Spano, N.; Sanna, G. Determination of 5-hydroxymethyl-2-furaldehyde in royal jelly by a rapid reversed phase HPLC method. *Anal. Methods* **2013**, *5*, 5010−5013.

(27) Codex Alimentarius Commission FAO-WHO. Alinorm 01/25, 2000; available in the web at the address: http://www.codexalimentarius.org/input/download/report/277/Al01_25e.pdf (last visited: 31/03/2015).

(28) Official Journal of the European Communities. Council Directive 2001/110/EC of 20 December 2001 relating to honey; available in the web at the address: http://eur-lex.europa.eu/legal-content/EN/TXT/PDF/?uri=CELEX:32001L0110&from=en (last visited: 31/03/2015).

(29) Mocak, J.; Bond, A. M.; Mitchell, S.; Schollary, G. A statistical overview of standard (IUPAC and ACS) and new procedures for determining the limits of detection and quantification: Application to voltammetric and stripping techniques (Technical Report). *Pure Appl. Chem.* **1997**, *69*, 297−328 IUPAC recommendation, document 550/35/87. .

(30) Pellegrino, L.; Resmini, P.; Luf, W. Assessment (indices) of heat treatment of milk. In *Heat-Induced Changes in Milk*, 2nd ed.; Fox, P. F., Ed.; IDF: Brussels, Belgium, 1995; pp 409−457.

(31) Smith, M. V. Some facts about royal jelly production. *Glean. Bee Cult.* **1954**, *82*, 713−715.

(32) Smith, M. V. The production of royal jelly. *Bee World* **1959**, *40*, 254−259.

(33) Tosi, E.; Ciappini, E.; Rè, E.; Lucero, H. Honey thermal treatment effects on hydroxymethylfurfural content. *Food Chem.* **2002**, *77*, 71−74.

DOI: 10.1021/acs.jafc.5b00873
J. Agric. Food Chem. 2015, 63, 4190−4195

(34) *Advances in Food Research*, Chichester, C. O., Ed.; Academic Press: Boston, MA, 1986; Vol. *30* (Advances in Food and Nutrition Research).

DOI: 10.1021/acs.jafc.5b00873
J. Agric. Food Chem. 2015, 63, 4190−4195

In this study, to understand how maltogenic α-amylase affects the retrogradation of AP, we subjected cooked waxy maize starch (WMS), which contained only AP, to different degrees of hydrolysis (DH) by maltogenic α-amylase and examined the structure and retrogradation properties of the resulting hydrolysates. We further related retrogradation properties to the chain length (CL) distributions of debranched starch hydrolysates. Our objective was to study the action of maltogenic α-amylase on AP, relate the structure of the hydrolysates to their retrogradation properties, and determine how much hydrolysis was needed to prevent the retrogradation of AP.

MATERIALS AND METHODS

Materials. WMS (Amioca) from National Starch LLC (Bridgewater, NJ, USA) was used for the study. Maltogenic α-amylase, Novamyl (BSuA, 3.2.122), was provided by Caravan Ingredients (Lenexa, KS, USA). Enzyme activity was assayed by quantifying the reducing sugars released from soluble starch (1.0% (w/v) solution) (St. Louis, MO, USA) according to the Somogyi–Nelson method[21] relative to a maltose standard curve. One enzyme unit is the amount of enzyme that releases 1 μmol of maltose/min at 62 °C and pH 5.0 (100 mM sodium acetate buffer containing 5 mM $CaCl_2$) for Novamyl. Isoamylase (EC 3.2.1.68) was obtained from Hayashibara Biochemical Laboratories, Inc. (Okayama, Japan) and had an enzyme activity of 1.41×10^6 isoamylase activity units (IAU)/g.[22] All chemicals and reagents were of analytical grade.

Enzymatic Starch Hydrolysis. Starch (1.8 g db) was mixed with 90 mL of 100 mM sodium acetate buffer containing 5 mM $CaCl_2$ (pH 5.0), heated at 120 °C for about 40 min in a pressure bottle (Ace Glass Inc., Vineland, NJ, USA), and cooled to the optimum temperature of 62 °C for Novamyl. Enzyme (9 EU/g starch db) was added to the starch slurry to initiate the enzyme reaction. This enzyme concentration was selected on the basis of previous studies.[20,23] Starch was hydrolyzed to ca. 5, 10, 20, 30, 40, and 50% by taking aliquots at different time intervals. Enzyme was denatured in a boiling water bath for 10 min. Starch hydrolysates were cooled to 25 °C and centrifuged at 8000*g* for 10 min. Part of the supernatant was further analyzed for saccharide composition, and the rest of the samples were freeze-dried for further study.

High-Performance Anion-Exchange Chromatography (HPAEC-PAD). Sacchaaride profile analysis of the supernatants from WMS hydrolysates was done using the procedure of Cai and Shi.[22] Eluents were (A) 500 mM NaOH and (B) 150 mM NaOH with 0.5 M sodium acetate. The gradient program was as follows: 85% eluent B for 0–0.4 min, 30% at 20 min, 25% at 30 min, 0% at 35 min, 0% at 40 min, 85% at 41 min, and 85% at 55 min. The separations were carried out at 25 °C with a flow rate of 1 mL/min. The concentration of the injected sample was 20 μg/mL in deionized (DI) water. Percentage DH was expressed as the total amount of saccharides released at any given time on the basis of initial dry weight of starch.

Size Exclusion Chromatography (SEC). After waxy maize starch (2%) was hydrolyzed by Novamyl, the mixture was heated at 95 °C for 30 min, cooled to 25 °C, and diluted with deionized water to a concentration of 10 mg/mL. Two drops of 0.25 M NaOH was added to further solubilize the sample. Samples were filtered with a 1 μm nylon syringe filter, and 100 μL was injected onto SEC columns. SEC separations were achieved using a HPLC (1200, Agilent, Santa Clara, CA, USA) equipped with OHpak SB-806 M HQ and OHpak SB-805 HQ columns in series with a OHpak SB-G guard column (Shodex, Showa Denko America, New York, NY, USA). The mobile phase, 0.1 M sodium nitrate, was pumped at a 0.5 mL/min flow rate and maintained at 55 °C. Elution was monitored using a multiangle light scattering detector (Dawn Heleos II, Wyatt Technology, Santa Barbara, CA, USA). A refractive index detector (1200, Agilent) was used to determine concentration (dn/dc = 0.147). Astra 6 software was used for data analysis.

Differential Scanning Calorimetry (DSC). Each starch hydrolysate and water (40% solid, w/w) were weighed in a DSC pan. The DSC pans were sealed, heated from 10 to 140 °C at 10 °C/min, and analyzed in duplicate using a Pyris-1 DSC (PerkinElmer, Norwalk, CT, USA). An empty pan was used as a reference. The first scan was done on day 0, and the second scan was done on day 7 after storage of the sample at 4 °C. The onset (T_o), peak (T_p), and conclusion (T_c) temperatures and enthalpy (ΔH) were obtained from the DSC endotherm with DSC software (TA Instruments, New Castle, DE, USA).

Debranching of Starch Hydrolysates. Freeze-dried starch samples were dissolved in 0.01 M acetic acid buffer (pH 4.0) with a starch/buffer ratio of 2:1. Starch solutions were cooked at 100 °C to ensure complete dissolution and then cooled to 50 °C. Isoamylase (1% based on dry weight of starch) was added. Debranching was done for 24 h, and the enzyme was denatured by boiling samples at 100 °C for 10 min. The samples were cooled to room temperature before further analysis.

CL Distribution Analysis. Debranched AP samples were further analyzed for CL distribution. Part of the samples was directly injected into HPAEC following debranching, and the remaining samples were freeze-dried for MS distribution analysis. For HPAEC, the sample was prepared at a concentration of 1.5 mg/mL in 150 mM sodium hydroxide. Analysis was performed according to the previously cited procedure.[22]

Statistical Analysis. Each experiment was performed in duplicate. Data were analyzed by analysis of variance (ANOVA) with Tukey's studentized range (HSD) test using SPSS version 20.0 (IBM Corp., Inc., Armonk, NY, USA). Mean values from the duplicated experiments were reported. The least significant differences (LSD) for comparison of means were computed at $p < 0.05$.

RESULTS AND DISCUSSION

Saccharide Composition of Starch Hydrolysates. WMS hydrolysates were analyzed for the saccharides produced and to

Table 1. Composition of Saccharides in Waxy Maize Starch Hydrolysates after Different Degrees of Hydrolysis (DH)

	degree of polymerization						
targeted %DH[a]	1	2	3	4	5	6	7
5	0.5	3.3	0.3	0.3	0.1	0.0	0.0
10	0.6	9.3	0.6	0.6	0.1	0.1	0.0
20	0.7	16.6	0.9	2.4	0.2	0.1	0.0
30	0.8	26.1	1.1	3.6	0.3	0.1	0.0
40	0.8	33.6	1.3	4.9	0.4	0.2	0.0
50	1.1	40.7	1.7	5.6	0.4	0.2	0.0

[a]Calculated as the total amount of saccharides released at any given time based on initial starch weight.

Table 2. Retrogradation Properties of Waxy Maize Starch Hydrolysates (After Storage at 4 °C for 7 Days) As Determined by Differential Scanning Calorimetry[a]

sample % DH[b]	T_o (°C)	T_p (°C)	T_c (°C)	ΔH (J/g)
control	38.7 ± 0.9c	54.8 ± 1.2a	79.9 ± 1.6a	9.1 ± 0.8a
5	38.4 ± 0.3c	56.6 ± 0.7a	78.8 ± 0.2a	7.1 ± 0.2b
10	41.6 ± 0.7b	57.4 ± 0.1a	73.1 ± 0.3b	3.2 ± 0.2c
20	46.0 ± 0.2a	59.8 ± 0.5a	73.6 ± 0.6b	0.8 ± 0.1d
30	no endothermic peak observed			
40	no endothermic peak observed			
50	no endothermic peak observed			

[a]Values with the same letter in the same column are not significantly different ($p < 0.05$). [b]DH, degree of hydrolysis.

DOI: 10.1021/jf506215s
J. Agric. Food Chem. 2015, 63, 4196–4201

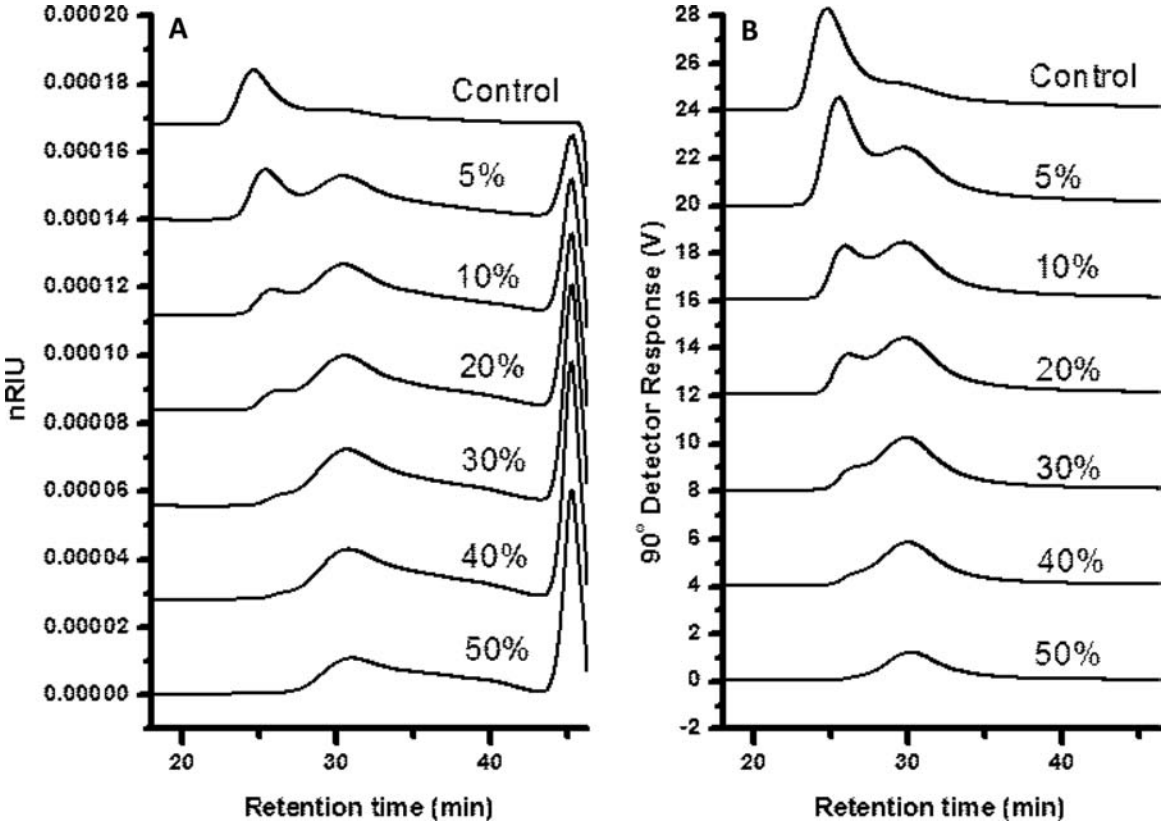

Figure 1. Molecular weight (M_w) distributions of waxy maize starch and its hydrolysates as determined by size exclusion chromatography: (A) response from refractive index (RI) detection; (B) response from light scattering detection.

Table 3. Average Molecular Weight (M_w) and *z*-Average Radius of Gyration (R_z) of Waxy Maize Starch (WMS) after Different Degrees of Hydrolysis (DH) As Determined by Size Exclusion Chromatography in Figure 1

	peak 1 (23−27.8 min)		peak 2 (27.8−35 min)	
	M_w (kg/mol)	R_z (nm)	M_w (kg/mol)	R_z (nm)
WMS control	473854	340.8	174075	220.1
5% DH	250818	247.2	37583	115.7
10% DH	159201	202.2	24316	93.1
20% DH	128655	175.1	20198	84.8
30% DH	93730	152.6	15981	75.3
40% DH	60499	141.2	13135	68.9
50% DH	33025	117.6	10435	58.5

determine %DH. Individual sugar percentages (based on initial starch weight) in the reaction mixture are given in Table 1. Saccharides up to degree of polymerization (DP) 6 were formed, and their concentrations continued to increase with increase in hydrolysis time. Maltose was the predominant sugar produced. The rate of formation of maltose was significantly higher than that of other saccharides. The maltose/glucose ratio increased with an increase in %DH, indicating the exoaction of enzyme producing maltose during earlier hydrolysis stages. A change in action pattern of maltogenic amylase from exo to endo with increase in hydrolysis time[18] and increase in temperature[4] was reported in earlier studies, as was the production of sugars up to DP 7−9, which were further hydrolyzed to maltose by this enzyme.[24,25]

Thermal and Retrogradation Properties. Retrogradation properties of starch hydrolysates after 7 days of storage at 4 °C are shown in Table 2. Starch hydrolysates produced no endothermic peak during the initial scan before storage (day 0) because the starch crystallinity was completely destroyed during cooking prior to hydrolysis. After 7 days of storage at 4 °C, WMS showed significant retrogradation. AP retrogradation enthalpy decreased to 0.8 J/g for 20% hydrolyzed starch. As the DH increased, the extent of retrogradation decreased, with no retrogradation observed for starches hydrolyzed to >20% DH. We suggest that the shortened outer chains inhibited formation of double helices and prevented AP recrystallization. Another reason for this result might be the increase in low molecular

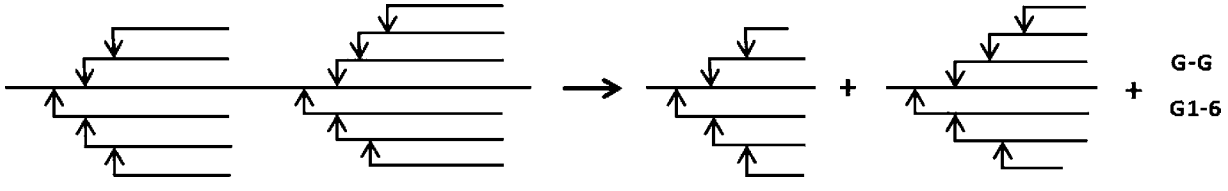

Figure 2. Schematic presentation of the action of maltogenic α-amylase on amylopectin: (−) 1,4-α-glucan; (→) α-1,6 linkage; (G-G) maltose; (G1−6) saccharides with 1−6 glucose units.

DOI: 10.1021/jf506215s
J. Agric. Food Chem. 2015, 63, 4196−4201

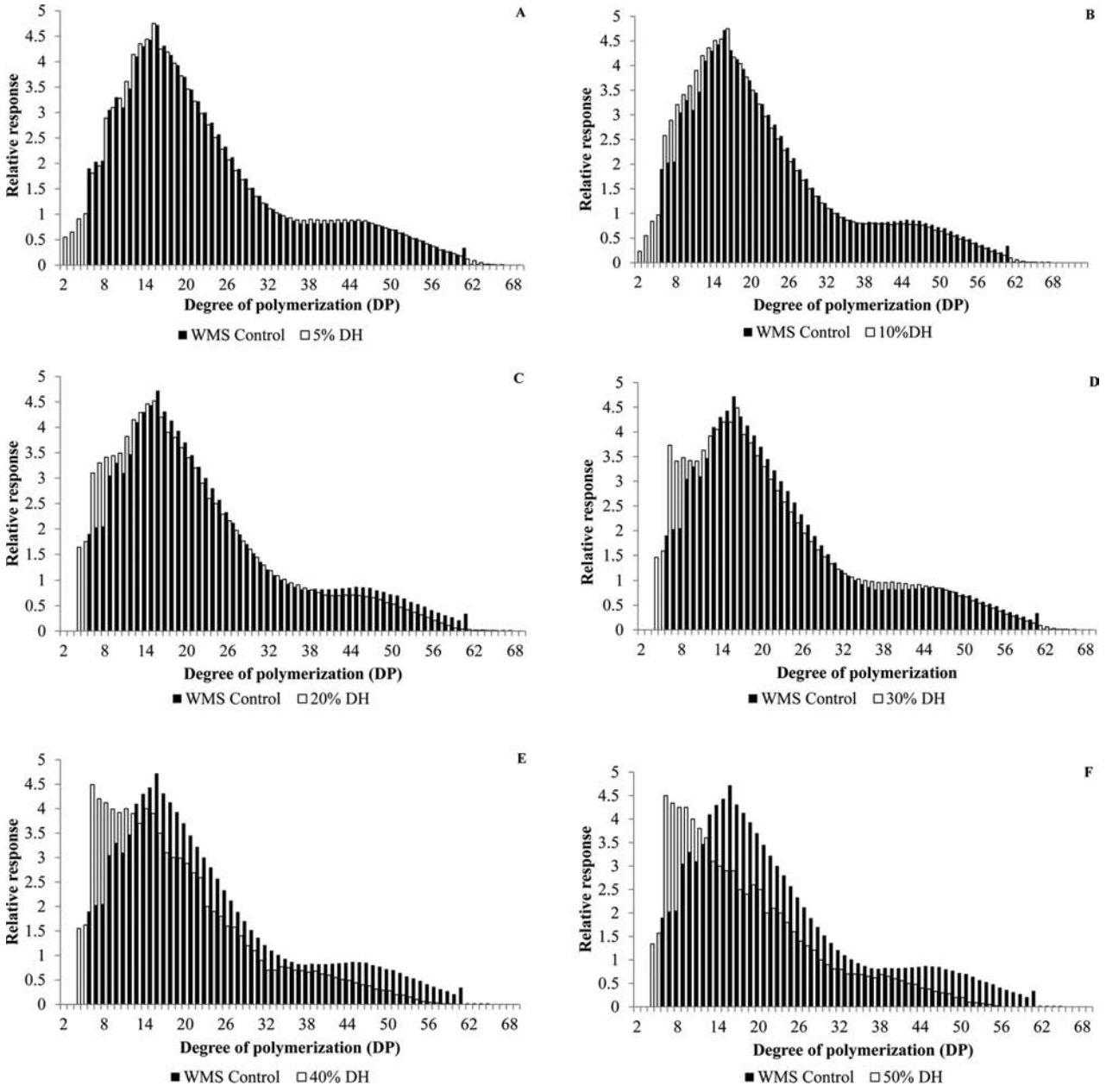

Figure 3. Chain length distributions of waxy maize starch compared to hydrolysates after (A) 5%, (B) 10%, (C) 20%, (D) 30%, (E) 40%, and (F) 50% hydrolysis as determined by high-performance anion-exchange chromatography.

Table 4. Level (Percent) of Unit Chains in Debranched Waxy Maize Starch Hydrolysates

sample %DH[a]	DP <9	DP 9−11	DP 12−16	DP 17−24	DP ≥25
0	5.98	9.45	21.02	28.54	35.04
5	9.68	10.01	22.00	26.81	33.04
10	10.27	10.90	22.36	26.32	30.15
20	12.20	10.75	21.62	25.9	29.92
30	13.67	10.46	20.86	25.36	29.72
40	17.98	16.91	20.00	21.15	22.89
50	20.45	18.78	18.65	19.99	20.28

[a]Calculated as total amount of saccharides released at any given time based on initial starch weight.

weight dextrins with an increase in DH, which interferes with AP recrystallization. These results are consistent with previous studies conducted on bread crumb.[4,11] The retrogradation tendency of AP depends on its CL distribution,[27−29] with retrogradation rate having a positive correlation with the mole fraction of unit chains of DP 14−24 and a negative correlation with mole fraction of unit chains of DP 6−11.[29,30] Using model compounds, other researchers observed no retrogradation when DP was <10;[31−33] however, in the presence of longer chains, chains as short as DP 6 can cocrystallize.[33]

Molecular Weight (M_w) Distributions of Starch Hydrolysates. To understand the reduced extent of retrogradation of starch hydrolysates, changes in the molecular structure of amylopectin during the enzymic hydrolysis were determined by SEC. Unique M_w distributions of the starch hydrolysates were observed (Figure 1). The proportion of the original AP in waxy maize starch (peak 1 with a peak retention time ca. 25 min) decreased, whereas a fraction with reduced M_w (peak 2 with peak retention time ca. 31 min) and low M_w saccharides (peak

DOI: 10.1021/jf506215s
J. Agric. Food Chem. 2015, 63, 4196−4201

3 with peak retention time ca. 45 min) increased with an increase in DH (Figure 1A). It is interesting to note that no peak or little hydrolyzed product was observed between peaks 2 and 3 (Figure 1A), indicating that few low M_w dextrins were produced during the hydrolysis. This unique M_w distribution suggests mostly exoaction during the early stage of hydrolysis. HPAEC results (Table 1) confirmed that only low M_w saccharides (DP 1−6) were detected and maltose was the predominant product.

Detailed M_w information (Figure 1B and Table 3) revealed that after 10% DH, M_w of the products increased at peak 2 was >10% of the original M_w of AP (peak 1), indicating that there was endoenzymic action on AP. However, few low M_w dextrins (DP 7−20) were detected between the low M_w saccharides (peak 3 with peak retention time ca. 45 min) and reduced AP (peak 2 with peak retention time ca. 31 min).

HPAEC (Table 1) and SEC (Figure 1 and Table 3) results suggest that the maltogenic α-amylase used in this study is unique and able to produce maltose through its exoaction, thus shortening outer CL of AP and reducing the M_w of AP through its endoaction but without producing excess low M_w dextrins. This unique action of the maltogenic α-amylase on amylopectin is schematically presented in Figure 2. The endoaction of the maltogenic α-amylase helps weaken the starch network by hydrolyzing the long polymer chains connecting the clusters, whereas the exoaction of the enzyme shortens the amylopectin side chains, making them too short to crystallize.[4]

CL Distributions of Debranched Waxy Maize Starch Hydrolysates. To further determine the fine structure of residual AP after the hydrolysis by maltogenic amylase, WMS hydrolysates were debranched with isoamylase and their unit chain length distributions were analyzed by HPAEC-PAD (Figure 3). At low DH, little difference was observed compared with the control, but with an increase in DH, the unit chains with DP <10 increased with a corresponding decrease in higher DP unit chains. These results concur with previous findings.[26] Higher relative amounts of CL with DP ≤9 support the complete suppression of retrogradation with a %DH >20 because of a decreased tendency of these short chains to participate in double-helix formation and give rise to crystalline lamellae.[34]

With an increase in hydrolysis, unit chains of DP 17−24 and DP 24 decreased, whereas unit chains of DP ≤9 increased (Table 4). Chains with DP 9−11 and DP 12−16 also increased, but only slightly compared with the control. Relating the retrogradation data with CL distributions, we can conclude that the higher the proportion of unit chains with DP ≤9, the lower the retrogradation rate. A minimum CL of DP 10 is required for the formation of stable double helices.[31,32] The short A chains with a DP of 5−10 cannot participate in stable double-helix formation, and they disrupt the formation of an ordered crystalline structure negatively affecting the perfection of AP crystalline structure.[35] Outer AP chains (mainly A and B1) greatly influence AP's molecular reorganization and aggregation during storage.[20] The net decrease in the proportion of unit chains with DP 14−24 could be another reason for reduced AP retrogradation.[29] The large decrease we observed for outer AP chains is in agreement with previous findings suggesting that the exo-like action of this enzyme[24,36] is similar to that of β-amylase, which removes the external chains from AP.[37] Compared with conventional α-amylase, which cleaves only internal starch chains and results in reduced MS without having much effect on the outer branches of AP, maltogenic α-amylase effectively shortens AP side chains and thus prevents crystalline junction zone formation.[4] High relative amounts of very short AP chains were correlated with reduced AP retrogradation.[8,27,29]

In conclusion, saccharide profile analysis of starch hydrolysates showed the formation of low DP saccharides during the course of hydrolysis with maltose constituting a major fraction in the reaction mixture. Maltogenic α-amylase was able to shorten the outer CL of AP and permanently prevent it from retrogradation after 20% hydrolysis. AP retrograded to one-third after 10% hydrolysis compared with unhydrolyzed AP. We found a positive correlation between the level of unit chains (DP ≤9) and retrogradation inhibition with an increase in % DH. These results illustrate the antistaling effect of this enzyme even at limited starch hydrolysis (20%).

AUTHOR INFORMATION

Corresponding Author

*(Y.-C.S.) Phone: (785) 532-6771. E-mail: ycshi@ksu.edu.

Funding

We thank Caravan Ingredients (Lenexa, KS, USA) for supporting the project via a grant from the Kansas Bioscience Authority.

Notes

The authors declare no competing financial interest.

ACKNOWLEDGMENTS

We thank Zhenhua Sun for drawing Figure 2 and Dr. Susan Sun for the use of the DSC. This is Contribution 12-435-J from the Kansas Agricultural Experiment Station.

REFERENCES

(1) Fadda, C.; Sanguinetti, M.; Del Caro, A.; Collar, C.; Piga, A. Bread staling: updating the view. *Compr. Rev. Food Sci. Food Saf.* **2014**, *13*, 473−492.

(2) Sargent, K. A softer approach to improving the quality of refrigerated bakery products. *Cereal Foods World* **2008**, *53*, 301−305.

(3) Gray, J. A.; Bemiller, J. N. Bread staling: molecular basis and control. *Compr. Rev. Food Sci. Food Saf.* **2003**, *2*, 1−21.

(4) Goesaert, H.; Slade, L.; Levine, H.; Delcour, J. Amylases and bread firming − an integrated view. *J. Cereal Sci.* **2009**, *50*, 345−352.

(5) Zobel, H. F.; Kulp, K. The staling mechanism. In *Baked Goods Freshness: Technology, Evaluation and Inhibition of Staling*; Hebeda, R. E., Zobel, H. F., Eds.; Dekker: New York, 1996; pp 1−64.

(6) Hizukuri, S. Polymodal distribution of the chain lengths of amylopectins, and its significance. *Carbohydr. Res.* **1986**, *147*, 342−347.

(7) Perez, S.; Bertoft, E. The molecular structure of starch components and their contribution to the architecture of starch granules: A comprehensive review. *Starch* **2010**, *62*, 389−420.

(8) Wursch, P.; Gumy, D. Inhibition of amylopectin retrogradation by partial β-amylolysis. *Carbohydr. Res.* **1994**, *256*, 129−137.

(9) Lundqvist, H.; Nilsson, G.; Eliasson, A.; Gorton, L. Changing the amylopectin-sodium dodecyl sulphate interaction by modifying the exterior chain length. *Stärke* **2002**, *54*, 100−107.

(10) Gerrard, J.; Every, D.; Sutton, K.; Gilpin, M. The role of maltodextrins in the staling of bread. *J. Cereal Sci.* **1997**, *26*, 201−209.

(11) Hug Iten, S.; Escher, F.; Conde Petit, B. Staling of bread: role of amylose and amylopectin and influence of starch-degrading enzymes. *Cereal Chem.* **2003**, *80*, 654−661.

(12) Martin, M.; Hoseney, R. A mechanism of bread firming. 2. Role of starch hydrolyzing enzymes. *Cereal Chem.* **1991**, *68*, 503−507.

(13) Defloor, I.; Delcour, J. Impact of maltodextrins and antistaling enzymes on the differential scanning calorimetry staling endotherm of baked bread doughs. *J. Agric. Food Chem.* **1999**, *47*, 737−741.

DOI: 10.1021/jf506215s
J. Agric. Food Chem. 2015, 63, 4196−4201

(14) Min, B.; Yoon, S.; Kim, J.; Lee, Y.; Kim, Y. Cloning of novel maltooligosaccharide-producing amylases as antistaling agents for bread. *J. Agric. Food Chem.* **1998**, *46*, 779−782.
(15) Slade, L.; Levine, H. Beyond water activity − recent advances based on an alternative approach to the assessment of food quality and safety. *Crit. Rev. Food Sci. Nutr.* **1991**, *30*, 115−360.
(16) Goesaert, H.; Gebruers, K.; Courtin, C. M.; Brijs, K.; Delcour, J. A. Enzymes in breadmaking. In *Bakery Products: Science and Technology 1*; Hui, Y. H., Ed.; Blackwell Publishing: Ames, IA, USA, 2006; pp 337−364.
(17) Delcour, J.; Goesaert, H.; Leman, P.; Bijttebier, A. Antifirming effects of starch degrading enzymes in bread crumb. *J. Agric. Food Chem.* **2009**, *57*, 2346−2355.
(18) Bijttebier, A.; Goesaert, H.; Delcour, J. Temperature impacts the multiple attack action of amylases. *Biomacromolecules* **2007**, *8*, 765−772.
(19) Leman, P.; Bijttebier, A.; Goesaert, H.; Vandeputte, G.; Delcour, J. Influence of amylases on the rheological and molecular properties of partially damaged wheat starch. *J. Sci. Food Agric.* **2006**, *86*, 1662−1669.
(20) Leman, P.; Goesaert, H.; Delcour, J. Residual amylopectin structures of amylase-treated wheat starch slurries reflect amylase mode of action. *Food Hydrocolloids* **2009**, *23*, 153−164.
(21) Somogyi, M. Notes on sugar determination. *J. Biol. Chem.* **1952**, *195*, 19−23.
(22) Cai, L.; Shi, Y. Structure and digestibility of crystalline short-chain amylose from debranched waxy wheat, waxy maize, and waxy potato starches. *Carbohydr. Polym.* **2010**, *79*, 1117−1123.
(23) Splender, T.; Nilsson, L.; Fugslang, C. C. Preparation of dough and baked products. Int. Patent Appl. WO 9953769, 1999.
(24) Christophersen, C.; Otzen, D.; Norman, B.; Christensen, S.; Schafer, T. Enzymatic characterisation of Novamyl (R), a thermostable α-amylase. *Stärke* **1998**, *50*, 39−45.
(25) Beier, L.; Svendsen, A.; Andersen, C.; Frandsen, T.; Borchert, T. Conversion of the maltogenic α-amylase novamyl into a CGTase. *Protein Eng., Des. Sel.* **2000**, *13*, 509−513.
(26) Bijttebier, A.; Goesaert, H.; Delcour, J. Hydrolysis of amylopectin by amylolytic enzymes: structural analysis of the residual amylopectin population. *Carbohydr. Res.* **2010**, *345*, 235−242.
(27) Yao, Y.; Zhang, J.; Ding, X. Partial beta-amylolysis retards starch retrogradation in rice product. *J. Agric. Food Chem.* **2003**, *51*, 4066−4071.
(28) Yuan, R.; Thompson, D.; Boyer, C. Fine structure of amylopectin in relation to gelatinization and retrogradation behavior of maize starches from 3 wx-containing genotypes in 2 inbred lines. *Cereal Chem.* **1993**, *70*, 81−89.
(29) Shi, Y.; Seib, P. The structure of 4 waxy starches related to gelatinization and retrogradation. *Carbohydr. Res.* **1992**, *227*, 131−145.
(30) Shi, Y.; Seib, P. Fine structure of maize starches from 4 wx-containing genotypes of the W64S inbred line in relation to gelatinization and retrogradation. *Carbohydr. Polym.* **1995**, *26*, 141−147.
(31) Gidley, M.; Bulpin, P. Aggregation of amylose in aqueous systems- the effect of chain length on phase behavior and aggregation kinetics. *Macromolecules* **1989**, *22*, 341−346.
(32) Pfannemuller, B. Influence of chain length of short monodisperse amylases on the formation of A type and B type X ray diffraction patterns. *Int. J. Biol. Macromol.* **1987**, *9*, 105−108.
(33) Gidley, M.; Bulpin, P. Crystallization of maltooligosaccharides as models of the crystalline forms of starch- minimum chail-length requirement for the formation of double helices. *Carbohydr. Res.* **1987**, *161*, 291−300.
(34) Srichuwong, S.; Jane, J. Physicochemical properties of starch affected by molecular composition and structures: a review. *Food Sci. Biotechnol.* **2007**, *16*, 663−674.
(35) Zhang, G.; Ao, Z.; Hamaker, B. Slow digestion property of native cereal starches. *Biomacromolecules* **2006**, *7*, 3252−3258.
(36) Outtrup, H.; Norman, B. Properties and use of a thermostable, maltose forming amylase from a *Bacillus* strain modified by a DNA recombination technique. *Zuckerindustrie* **1984**, *109*, 462−462.
(37) Perez, S.; Bertoft, E. The molecular structures of starch components and their contribution to the architecture of starch granules: a comprehensive review. *Stärke* **2010**, *62*, 389−420.

DOI: 10.1021/jf506215s
J. Agric. Food Chem. 2015, 63, 4196−4201

Enzymatic Modification of Starch: Debranching. Starch (15 g wet basis) was added to 400 mL of water (3.75% w/v) and gelatinized in a boiling water bath for 1 h with constant stirring. The temperature of the solution was equilibrated to 45 °C, and the pH was adjusted to 5.0 with 0.5 M HCl. To the starch solution, isoamylase and pullulanase, each at 1.33% (v/w, starch db), were added and then incubated at 50 °C with constant stirring for 48 h. The starch was recovered with a 4-fold volume of pure ethanol, centrifuged at 7000*g* for 10 min, dried at 40 °C for 48 h with a forced air oven (VWR, Cornelius, OR, USA) and milled using a UDY cyclone mill (UDY Corp., Ft. Collins, CO, USA) fitted with a 0.5 mm screen.

***β*-Amylase Treatment.** A portion of the debranched starch was further subjected to *β*-amylase hydrolysis to reduce the degree of polymerization (DP). After debranching for 48 h, the starch slurry pH was adjusted to 6.5 with 0.5 M NaOH and incubated with 0.5% (v/w, starch db) *β*-amylase at 40 °C for 4 h. The enzyme reaction was terminated by boiling for 15 min. The *β*-amylase-treated starch was recovered as previously described.

Characterization of Starch Structure. The molecular size distributions of debranched unacetylated and acetylated starch without or with the *β*-amylase treatment were recovered after complexation with oleic acid and characterized using a high-performance size-exclusion chromatography (HPSEC) system (Waters Corp., Milford, MA, USA). Starch (10 mg) was dissolved in 5 mL of 90% DMSO, boiled for 1 h, and filtered through a 5.0 μm filter prior to injection into the HPSEC system. The HPSEC system consisted of a guard column (OHpak SB-G, 6.0 × 500 mm^2 i.d. × length), two Shodex columns (OHpak KB-804 and KB-802, both 8.0 × 300 mm^2 i.d. × length), a 200 μL injector valve (model 7725i, Rheodyne, Cotati, CA, USA), an inline degasser, a model 515 HPLC pump, and a model 2414 refractive index detector. The mobile phase of 0.1 M sodium nitrate with 0.02% sodium azide was eluted at a flow rate of 0.6 mL/min. The temperature of the column was maintained at 60 °C, and that of the detector, at 40 °C. Dextran standards of molecular weight of 5200, 11 600, 23 800, 48 600, 273 000, and 410 000 g/mol from Waters Corp. (Milford, MA, USA) and 1 050 000 g/mol from Sigma-Aldrich (St. Louis, MO, USA) were used to establish the calibration curve.

The amylopectin chain-length distribution was characterized by high-performance anion-exchange chromatography equipped with pulsed-amperometric detection (HPAEC-PAD) according to the method of Wong and Jane.[27] The chains were divided into DP ranges and classified as follows: A chains (DP 6−12), B1 chains (DP 13−24), B2 chains (DP 25−36), and B3+ chains (DP 37+).[28] The average chain length was calculated as the cumulative sum of the product of DP and the percentage of relative areas for all of the identified peaks.

Complexation of Starch and Oleic Acid. All samples were prepared in replicates. The starch solution (3.75% w/v), debranched or debranched and *β*-amylase-treated, was adjusted to pH 7.0, equilibrated to 80 °C, and mixed with 1 g of oleic acid dissolved in warm 95% ethanol. The mixture was maintained at 80 °C for 30 min and stirred at 400 rpm continuously with a Barnstead supernuova stirring hot plate (model SP131825, Barnstead/Thermolyne, Dubuque, IA, USA) to ensure that there was sufficient interaction between starch and oleic acid, and then the temperature was maintained at 45 °C overnight with continuous stirring. The resulting mixture was centrifuged at 7000*g* for 10 min, from which the precipitate, that is, the insoluble complex, was obtained, whereas the soluble complex was recovered by precipitating the supernatant with a 4-fold volume of pure ethanol. Any uncomplexed oleic acid was removed from both the insoluble and soluble complexes by rinsing with excess 95% ethanol. Complexes were rotated in excess 95% ethanol using a labquake shaker rotisserie (Barnstead/Thermolyne, Dubuque, IA, USA) at room temperature for 2 h, centrifuged at 7000*g* for 10 min, dried at 40 °C for 48 h, milled using a mortar and pestle, sieved through a 250 μm sieve, and stored for further analysis.

Hydrolysis of Complexes and Oleic Acid Analysis. Soluble or insoluble complex (100 mg) was added with 10 mL of 1 M HCl and heated with continuous stirring in a boiling water bath for 1 h. After the complex mixture was cooled, 5 mL hexane was added, and the solution was rotated on the rotary shaker for 1 h. The hexane layer with the extracted oleic acid was recovered, and the extraction was repeated with another 5 mL of hexane for 1 h. To the recovered hexane phase, boron trifluoride methanol was added to convert oleic acid to oleic acid methyl esters. An internal standard of methyl heptadecanoate (~1 mg) was subsequently added to all samples. The oleic acid methyl ester was injected into a gas chromatographer (GC) (GC-2010, Shimadzu, Kyoto, Japan) equipped with a BP 21 capillary column (30 m × 0.25 mm^2 i.d.; SGE Inc., Austin, TX) with a flame ionization detector (FID), and responses were collected with a Shimadzu GCsolution Workstation 2.3 (Kyoto, Japan). The injection port and detector temperatures were set at 220 and 230 °C, respectively. The column oven temperature was equilibrated at 100 °C for 1 min, ramped up at 15 °C/min to 160 °C, again ramped up at 5 °C/min to 200 °C, and maintained at 200 °C for 10 min. The flow rate of the carrier gas (helium) was 30 mL/min. The concentration of oleic acid was determined from a standard curve prepared by using oleic acid methyl ester solution (0.1, 0.2, 0.4, 0.6, 0.8, and 1 mg/mL) containing a methyl heptadecanoate (0.5 mg/mL) internal standard.

Physicochemical Properties. A diffractometer (PW1830 MPD, Philips, Almelo, The Netherlands) was used to determine the powder X-ray diffraction (XRD) pattern of complexes. The generator voltage was set at 45 kV, and the current, at 40 mA. The sample was scanned over the 2θ angular range from 5 to 35° with a step size of 0.02° and a time of 1 s per step.

The thermal stability of all complexes was measured using a differential scanning calorimeter (DSC, Pyris-Diamond, PerkinElmer, Shelton, CT, USA). Approximately 8 mg of complex was weighed into a stainless steel pan, 16 μL of distilled water was added with the aid of a microsyringe, and the pan was hermetically sealed. The sample was equilibrated for 24 h at room temperature before scanning and was scanned from 25 to 180 °C at 10 °C/min, immediately cooled from 180 to 25 °C at 40 °C/min, and rescanned from 25 to 180 °C at 10 °C/min to confirm the formation of the starch−fatty acid complex. The onset temperature (T_o), peak temperature (T_p), conclusion temperature (T_c), and enthalpy (ΔH) of the endotherms were calculated using the Pyris data analysis software.

Statistical Analysis. All experiments were conducted in replicates, and data were analyzed using JMP software (SAS Institute Inc., Cary, NC, USA). The means were compared using Tukey's honestly significant differences (HSD) test.

RESULTS AND DISCUSSION

Degree of Substitution. The low- and high-acetylated starches used for complex formation with oleic acid had DS values of 0.041 and 0.091, respectively (Table 1). Acetylated starches were then debranched with isoamylase and treated with or without *β*-amylase prior to complexation. After

Table 1. Degree of Substitution (DS) of Acetylated Starches and Oleic Acid Complexes[a]

starch	*β*-amylase treatment	type of complex	DS
low-acetylated starch	N/A	N/A[b]	0.041 ± 0.001d
low-acetylated starch complex	no	soluble	0.045 ± 0.005d
		insoluble	0.036 ± 0.005d
	yes	soluble	0.071 ± 0.000c
		insoluble	0.045 ± 0.001d
high-acetylated starch	N/A	N/A	0.091 ± 0.001b
high-acetylated starch complex	no	soluble	0.077 ± 0.002b,c
		insoluble	0.062 ± 0.004c
	yes	soluble	0.119 ± 0.004a
		insoluble	0.072 ± 0.009c

[a]At least replicate samples were prepared for each complex. Data of two measurements with the standard deviation. Means in a column not sharing the same letter are significantly different based on Tukey's honestly significant difference test ($p < 0.05$). [b]N/A, not applicable.

DOI: 10.1021/acs.jafc.5b00125
J. Agric. Food Chem. 2015, 63, 4202−4210

complexation the soluble and insoluble complexes were recovered and analyzed for their DS of acetylation. Similar to the previous study,[23] the soluble complex fractions had a significantly higher DS than the insoluble ones for the same treatments. When β-amylase was combined with acetylation, an increase in DS was observed for all soluble and insoluble complexes. The lowest DS of acetylated starch to form a soluble complex with stearic acid was 0.063 in our previous study;[23] however, oleic acid formed soluble complexes at a lower DS of 0.045 in the present study. In addition, the difference in DS of acetylation between the soluble and insoluble complexes of oleic acid was significantly smaller than that of stearic acid. These differences in DS suggest that a lower DS of acetylation on starch was sufficient to encourage soluble complex formation with more polar molecules, such as oleic acid, compared to less polar molecules, such as stearic acid.

Complex Recovery and Complexation Yield. Complex recovery was determined by comparing the individual recovered complex weight against the initial material weight. The highest recovery for the insoluble complexes was 0.73 g/g from the unacetylated β-amylase-treated starches (Table 2),

Table 2. Complex Recovery and Percentage of Oleic Acid Content Recovered from All Complexes[a]

starch	type of complex	β-amylase treatment	recovery (g/g)	oleic acid in individual complex (mg/g)
unacetylated	soluble	no	0.34 ± 0.04c,d	3.0 ± 0.3g
	insoluble	no	0.61 ± 0.02a,b	3.3 ± 0.1g
	soluble	yes	0.12 ± 0.01e	10.9 ± 1.0e
	insoluble	yes	0.73 ± 0.01a	4.8 ± 0.0f
low acetylated	soluble	no	0.56 ± 0.03b	16.3 ± 0.1c,d
	insoluble	no	0.39 ± 0.03c,d	37.6 ± 3.6a
	soluble	yes	0.40 ± 0.04c	26.3 ± 0.3b
	insoluble	yes	0.56 ± 0.01b	42.9 ± 6.0a
high acetylated	soluble	no	0.66 ± 0.01a,b	38.0 ± 2.2a
	insoluble	no	0.27 ± 0.01d	20.1 ± 0.5b,c
	soluble	yes	0.57 ± 0.08b	12.5 ± 1.1d,e
	insoluble	yes	0.35 ± 0.01c,d	20.9 ± 1.0b,c

[a]Data of at least two measurements with standard deviation. Means in a column not sharing the same letter are significantly different based on Tukey's honestly significant difference test ($p < 0.05$).

which is similar to results from previous studies.[6,15,23] The total recovery when both soluble and insoluble complexes were included was 0.92−0.96 g/g, except for the unacetylated β-amylase-treated starch with a total recovery of 0.85 g/g. These results indicate that the modification of starch prior to complex formation did not change the total recovery but changed the proportions of the soluble and insoluble complexes for most complexes. The recovery of the insoluble complexes decreased with increasing DS of acetylation, whereas the opposite trend was observed for the soluble complexes. Acetylation increased the recovered soluble complexes by 65 and 94% for low- and high-acetylated starches, respectively, compared to that for the unacetylated one.

When an additional β-amylase treatment was incorporated, the recovery of the soluble complexes was decreased or unchanged, whereas that of the insoluble complexes was increased or unchanged. These results imply that the length of starch chains present in the debranched-only starches was more favorable to the formation of soluble complexes. The β-amylase treatment hydrolyzed some starch chains to a length that was too short to form complexes, thus resulting in a decrease in the proportion of recovered soluble complexes. Within the β-amylase-treated starches, the recovery of the soluble complexes was increased by 233−375% for low- and high-acetylated starches, respectively, when compared to that of the unacetylated starch.

The oleic acid content in all starch complexes was determined by GC (Table 2). Acetylated starches resulted in significantly higher amounts of complexed oleic acid per gram of complex in the recovered complexes compared to that for unacetylated starches for most treatments, suggesting that acetylation encouraged the formation of both soluble and insoluble complexes between starch and oleic acid. However, the amounts of complexed oleic acid were significantly lower than those of complexed stearic acid reported in the previous work.[23] This is attributed to the better stability of the complexes formed between starch and stearic acid, a saturated fatty acid, than oleic acid of an unsaturated fatty acid.[8,10,29,30]

For the insoluble complexes, the highest amount of oleic acid per gram of complex was recovered from the low-acetylated starch (37.6−42.9 mg), which also complexed the higher amounts of stearic acid (101.0 and 123.1 mg) in the previous study.[23] This indicates that the presence of a low level of acetylation (DS 0.036−0.045) hindered starch retrogradation and encouraged complexation with oleic acid. However, a high level of acetylation (DS 0.062−0.072) decreased not only the complex recovery but also the complexation yield with oleic acid. This indicates that the further increase in the number of acetyl groups on starch might destabilize the starch helices for complexation. In addition, when β-amylase treatment was combined with a high acetylation of starch, the amount of complexed oleic acid remained unchanged, suggesting that with the β-amylase treatment of high-acetylated starch there were still starch chains with favorable lengths that could participate in complexation with oleic acid.

For the soluble complexes, the highest amount of oleic acid was recovered from high-acetylated-only starch (38.0 mg), which was similar to the highest amount of complexed oleic acid in the insoluble complexes. In contrast, the highest amount of stearic acid was recovered from the high-acetylated and β-amylase-treated starch (61.2 mg).[23] It is hypothesized that the cis double-bond structure of oleic acid might require slightly longer starch chains than stearic acid to form soluble complexes with high-acetylated starch.

Molecular Size Distribution. Except for the high-acetylated-only starch (Figure 1E), all recovered starch in the starch complexes displayed an amylose peak at a retention time of 18.2−18.5 min, which corresponded to DP ∼7000 (Figure 1). The relative proportion of the amylose peak was greater in the insoluble complexes than in the soluble complexes and increased with increasing acetylation level. This increasing trend in the amylose peak was also noted in the previous study with stearic acid,[23] which was attributed to an increased hydrodynamic volume from higher acetyl contents.

The peak DP of soluble complexes shifted to a higher DP for unacetylated and acetylated starches after the β-amylase treatment, indicating that the β-amylolysis of starch hydrolyzed short chains and reduced the chain length of longer chains. For the insoluble complexes, the DP remained unchanged for unacetylated and low-acetylated starch and slightly increased for the high-acetylated starches after the β-amylase treatment.

DOI: 10.1021/acs.jafc.5b00125
J. Agric. Food Chem. 2015, 63, 4202−4210

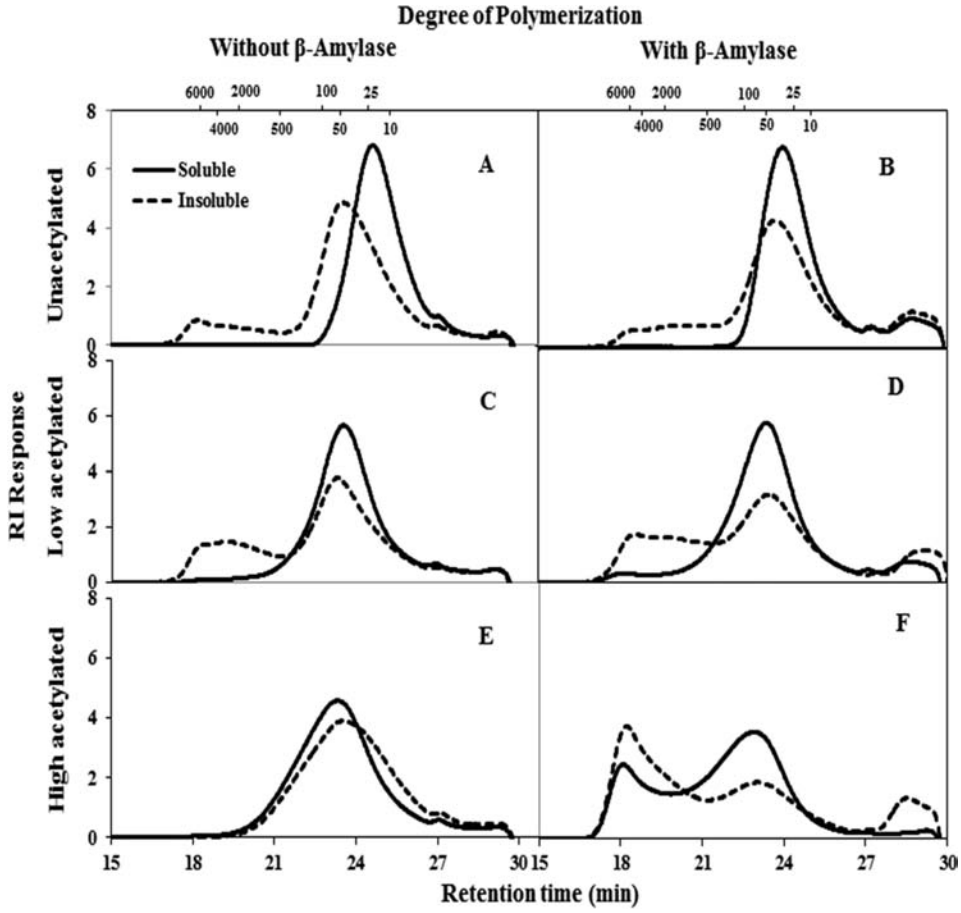

Figure 1. Normalized size-exclusion chromatograms of recovered soluble and insoluble starch complexes from unacetylated and acetylated potato starches after complexing with oleic acid: (A) potato starch, (B) β-amylase-treated potato starch, (C) low-acetylated potato starch, (D) low-acetylated β-amylase-treated potato starch, (E) high-acetylated potato starch, and (F) high-acetylated β-amylase-treated potato starch.

All complexes displayed a main peak at a retention time of between 23 and 24 min, which corresponded to DP 91 and 36, respectively, and were composed of mainly amylopectin long branched chains that were assumed to be involved in complex formation with oleic acid. The retention time of this peak shifted to a shorter time with increasing acetylation, which was similar to that of the amylose peak. The relative proportion of this main peak was greater in the soluble complex than in the insoluble complex for the same treatment. These results are similar to those in the previous stearic acid study, although a smaller amount of oleic acid was complexed in the present study. Although previous studies reported that the carbon atoms adjacent to the double bond in cis-unsaturated fatty acids may be capable of rotating freely to give rise to a relatively linear structure,[10,31] the complexation of starch with stearic acid was still more favored than with oleic acid. Overall, starch fractions with a DP of between 14 and 363 corresponding to retention times of 25 and 21.5 min, respectively, were observed in all starch complexes, indicating that these starch chain lengths were primarily responsible for complex formation with oleic acid. This agrees with Gelders et al.[32] that amylose chains with a DP of up to 400 were effective in forming complexes with glyceryl monostearate (GMS) and docosanoic acid (C22).

The chain-length distributions of starch chains of up to DP 60 of all starch complexes without and with the β-amylase treatment are displayed in Figures 2 and 3, respectively. For the soluble complexes, the additional β-amylase treatment resulted in an increase in the peak DP and the proportion of the higher DP peak, but it did not change the profiles of the insoluble complexes as much. The peak DPs for the soluble complexes of acetylated starches in the present work were slightly higher but not significantly different from those reported in the starch–stearic acid study,[23] although a larger amount of stearic acid versus oleic acid was complexed. Similar to the starch–stearic acid study,[23] the fraction of DP 6-17 was prominent in all starch complexes, but it represented the proportion of starch chains too short to form complexes. The proportion of DP 6-17 decreased with the β-amylase treatment for the soluble complexes but increased slightly for the insoluble complexes. These results indicate that when the amylopectin chains were considered, the favorable chain length for complexing with fatty acid, which was reported[9] to be DP >20, was longer for the soluble complexes than for the insoluble complexes.

Characterization of Starch–Oleic Acid Complexes. X-ray Diffraction Pattern. Most soluble and insoluble complexes of unacetylated starches displayed a mixture of the B-type and V-type X-ray diffraction patterns (Figure 4A,B) with peaks at 2θ = 17.0, 22, and 24° and 2θ = 12.9 and 20°, respectively. The only exception was the soluble complex from the unacetylated-only starch (Figure 4A), which displayed predominantly the A-type pattern with peaks at 2θ = 15.3, 17.2, 18.2, and 23.1° besides minor peaks at 2θ = 10, 11.5, 20, and 26.5° from the V-type pattern. The presence of the A-type polymorph may be ascribed to the high proportion of

DOI: 10.1021/acs.jafc.5b00125
J. Agric. Food Chem. 2015, 63, 4202–4210

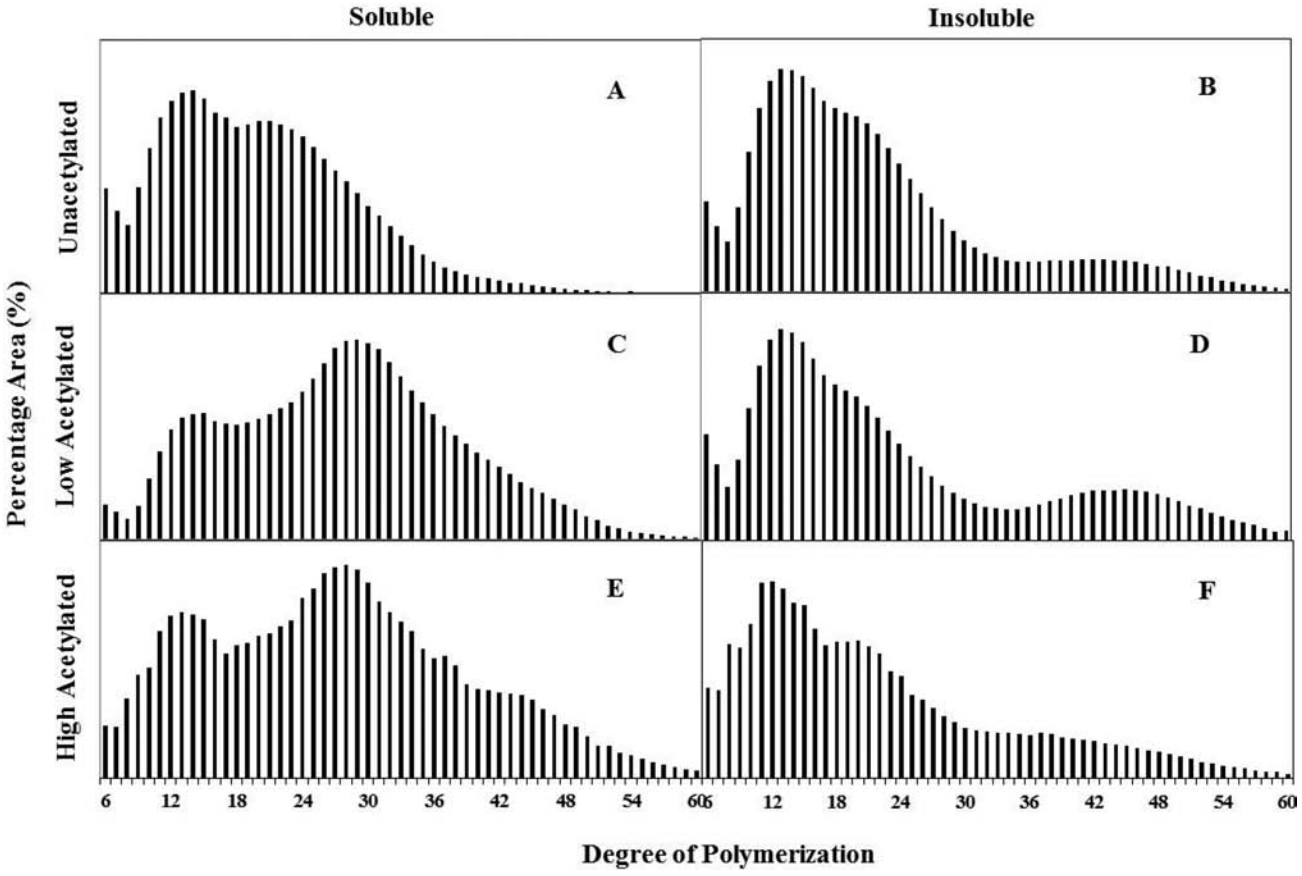

Figure 2. Normalized chain-length distributions of recovered soluble and insoluble starch complexes from unacetylated and acetylated potato starches without the β-amylase treatment after complexing with oleic acid using high-performance anion-exchange chromatography with pulsed amperometric detection (HPAEC-PAD): (A) potato starch, (B) β-amylase-treated potato starch, (C) low-acetylated potato starch, (D) low-acetylated β-amylase-treated potato starch, (E) high-acetylated potato starch, and (F) high-acetylated β-amylase-treated potato starch.

amylopectin short chains (Figure 2A) that were too short to complex with oleic acid but prone to reassociation to form a very ordered structure.[33] The additional β-amylase treatment on unacetylated starch decreased the intensity of the V-type pattern for the insoluble complexes, implying that the formation of insoluble starch−oleic acid complexes may require longer starch chains than would starch−stearic acid complexes.[23] The soluble complexes of the unacetylated starch changing from the A-type to B-type pattern after β-amylase treatment supports the HPSEC results that shorter chains have been hydrolyzed to result in predominantly longer chains. This is in agreement with previous works in which starches with shorter average chain lengths exhibited the A-type pattern (DP <19.7) and starches with a longer average chain lengths (DP >21.6) exhibited the B-type pattern.[34]

All soluble and insoluble acetylated complexes displayed the V-type pattern with peaks at 2θ = 7.4, 12.9, and 20° (Figure 4C−F). In previous work on starch−stearic acid complexes,[23] the V-type structure was not observed in the soluble complexes from acetylated debranched-only starches, even though a significant quantity of stearic acid was detected by GC. The XRD results imply that soluble starch−oleic acid complexes were formed, but when the GC results (Table 2) were considered, these complexes did not include as much oleic acid as did the soluble complexes of stearic acid from the previous work. The reason for the difference in the XRD patterns observed in the two studies may be due to the fact that stearic acid and oleic acid interacted differently with the acetylated starch helix because of their structural differences. The presence of the double bond in oleic acid may have created a different spatial arrangement which differed from that of stearic acid upon complexation with acetylated starch. However, limited information exists for inclusion complexes from chemically modified starch; therefore, more research is needed to explain the differences between XRD patterns and the complexed amount for acetylated starch complexes with stearic acid and oleic acid.

The acetylation of starch noticeably increased the intensity of the V-type pattern of the starch−oleic acid complex and reduced the starch retrogradation peak at 2θ = 17°. For the insoluble complexes, high-acetylated β-amylase-treated starch displayed the highest peak intensity (Figure 4F), which, however, did not contain the highest amount of complexed oleic acid by GC. This suggests that the intensity of the V-type pattern might not necessarily correlate with the quantity of complexed fatty acids, both soluble and insoluble complexes, such as oleic acid in this study and stearic acid in the previous study, but reflects only the level of organization and arrangement of the type of complex formed. When low-acetylated starches were treated with β-amylase, the peak intensity of the starch−oleic acid complex slightly increased for the soluble complexes but decreased for insoluble complexes (Figure 4C,D). Again, there was no correlation between the X-ray peak intensity and the amount of complexed oleic acid.

Melting Properties by Differential Scanning Calorimetry. All insoluble complexes and some soluble complexes

DOI: 10.1021/acs.jafc.5b00125
J. Agric. Food Chem. 2015, 63, 4202−4210

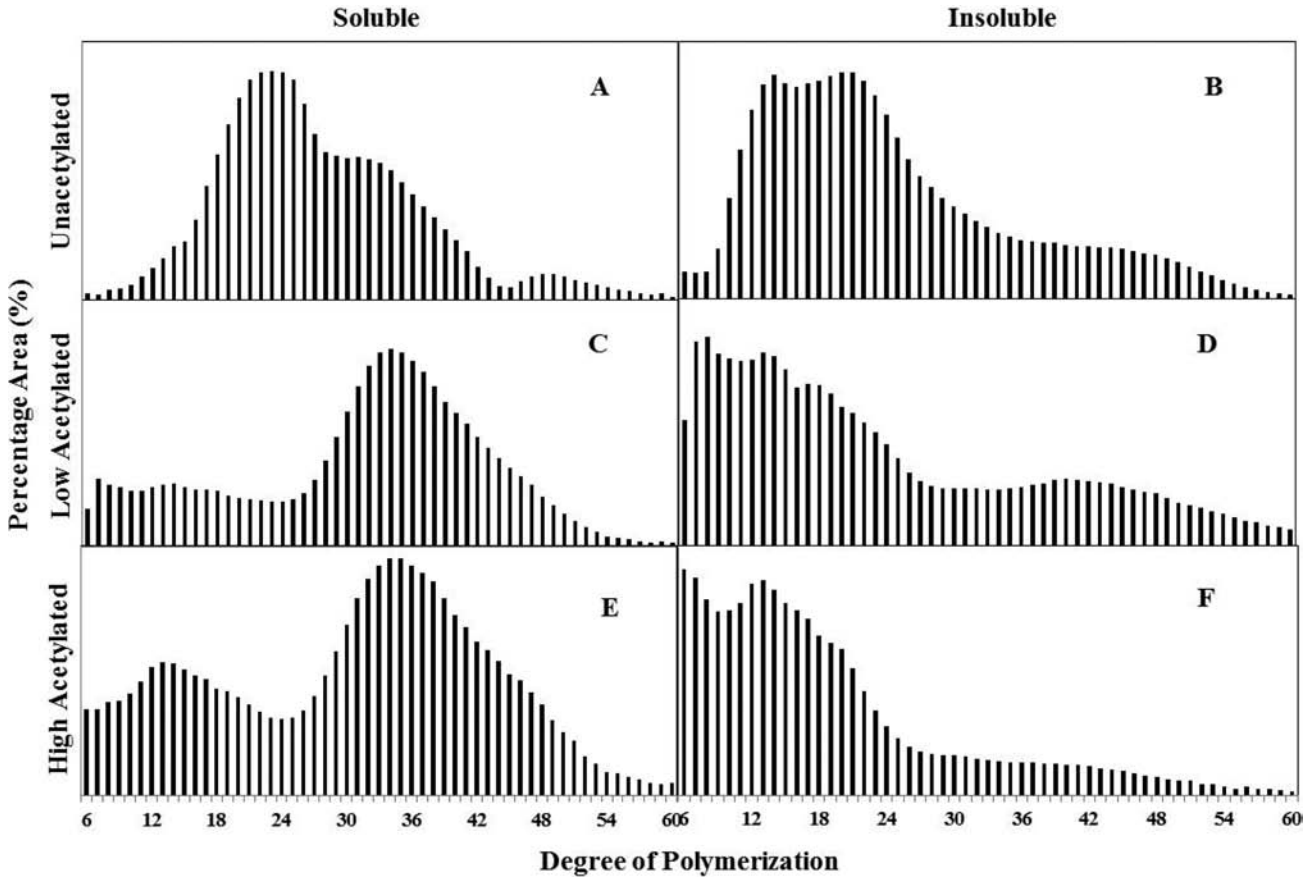

Figure 3. Normalized chain-length distributions of recovered soluble and insoluble starch complexes from unacetylated and acetylated potato starches with the β-amylase treatment after complexing with oleic acid using high-performance anion-exchange chromatography with pulsed amperometric detection (HPAEC-PAD): (A) potato starch, (B) β-amylase-treated potato starch, (C) low-acetylated potato starch, (D) low-acetylated β-amylase-treated potato starch, (E) high-acetylated potato starch, and (F) high-acetylated β-amylase treated potato starch.

displayed melting endotherms, but only the insoluble complexes exhibited the type II complex peak (Table 3). Within the unacetylated starches, the insoluble complexes of the debranched-only starch displayed a single melting endotherm with T_p at 106.7 °C, signifying the presence of the type II starch−fatty acid complex, whereas the soluble complex within the same treatment displayed only a type I complex with T_p at 94.8 °C. The type I complex has been reported to form at a lower temperature of ∼60 °C, leading to the production of randomly oriented helical segments,[35] whereas the type II complex is formed at temperatures of around 90 °C and produces well-defined crystallites.[36] Godet et al.[9,37] showed that longer starch chains can complex more lipids to produce crystals with higher melting temperatures.

When the unacetylated starch received the additional β-amylase treatment, two melting endotherms were observed for the insoluble complexes, including the type I and type II complex[38] with T_p at 94.9 and 102.9 °C, respectively. Lagendijk and Pennings[39] previously reported that amylose with DP 900 may contain between 10 and 12 helices, consisting of 6 glucose units per turn, and each helix can complex at least 1 glycerol monopalmitate. The bimodal distribution of the insoluble starch complexes consisting of both short and long starch chains (Figure 1B) may lead to the production of type I and type II complexs, respectively, which is in agreement with previous works.[37,39] However, although the type II complexes were formed for the unacetylated starch complexes, the amount of complexed oleic acid were still low, presumably because of the increased reassociation of starch chains as evidenced in the XRD results (Figure 4B). The additional β-amylase treatment of unacetylated starches had no significant effect on the T_p and the enthalpy of the soluble complexes, but it decreased that of the insoluble complexes slightly, indicating that the β-amylase treatment resulted in starch chains that formed insoluble complexes with a lower stability and required a lower energy to dissociate.

The introduction of acetyl groups to starch chains significantly decreased the T_o and T_p for all complexes. These findings are in agreement with previous works[22,23,40] in which the acetylation of starch was reported to decrease the complexing ability and dissociation temperature of amylose−lipid complexes, although the complexes referred to in these studies were only the insoluble complexes. In addition, acetylated starch complexes displayed only the type I complex melting peak, supporting the previous study in which the presence of the acetyl groups on starch may hinder the aggregation of the starch−oleic acid complexes.[23] However, there was no clear trend in melting enthalpy in terms of the β-amylase treatment. The enthalpy values also did not correlate with the amounts of complexed oleic acid as measured by GC (Table 2). This suggests that the enthalpy values might not necessarily represent the amount of oleic acid included in the starch complexes but might indicate the energy required to melt the starch−oleic acid complex due to the degree of order or level of organization existing within the complexes.

DOI: 10.1021/acs.jafc.5b00125
J. Agric. Food Chem. 2015, 63, 4202−4210

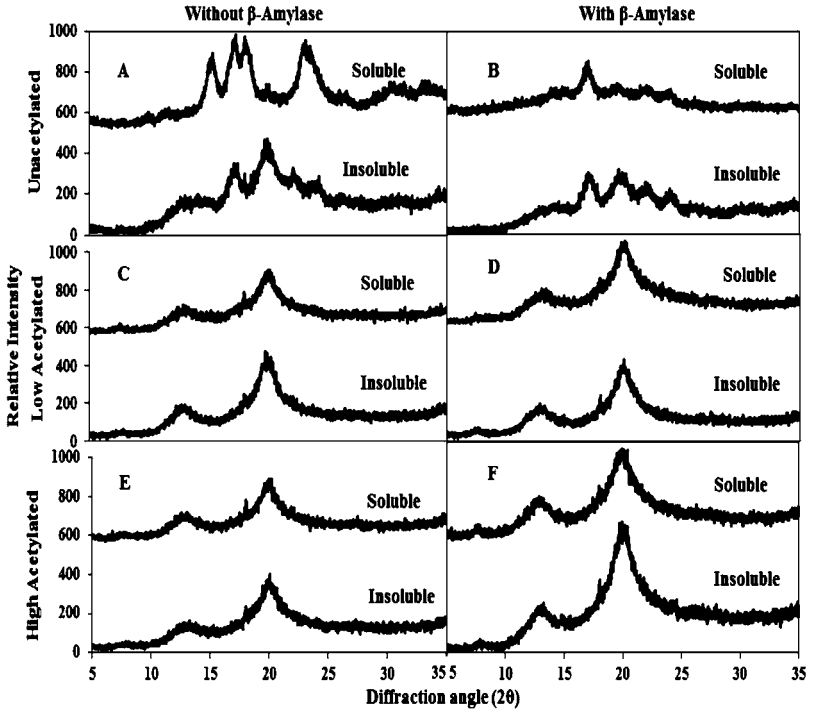

Figure 4. Normalized X-ray diffractograms of recovered soluble and insoluble starch complexes from unacetylated and acetylated potato starches after complexing with oleic acid: (A) potato starch, (B) *β*-amylase-treated potato starch, (C) low-acetylated potato starch, (D) low-acetylated *β*-amylase-treated potato starch, (E) high-acetylated potato starch, and (F) high-acetylated *β*-amylase-treated potato starch.

Table 3. Melting Temperatures and Enthalpies[a] of Recovered Soluble and Insoluble Fractions of Unacetylated and Acetylated Potato Starch−Oleic Acid Complexes[b]

			type I complex peak				type II complex peak			
starch	type of complex	*β*-amylase treatment	T_o (°C)	T_p (°C)	T_c (°C)	ΔH (J/g)	T_o (°C)	T_p (°C)	T_c (°C)	ΔH (J/g)
unacetylated	soluble	no	88.7a,b (0.1)	94.8a,b (0.9)	101.2a (0.6)	1.59b,c (0.13)				
	insoluble	no	ND	ND	ND	ND	92.1 (0.5)	106.7 (0.0)	114.7 (0.7)	1.89 (0.03)
	soluble	yes	90.5a (0.6)	96.1a (0.7)	102.1a (0.5)	1.84b (0.10)				
	insoluble	yes	91.6a (0.8)	94.9a,b (0.8)	98.0a (1.7)	0.44d (0.10)	101.0 (0.9)	102.9 (1.1)	109.0 (0.5)	0.76 (0.06)
low acetylated	soluble	no	ND[c]	ND	ND	ND				
	insoluble	no	79.8c (0.7)	91.4b (0.4)	100.8a (0.7)	2.84a (0.08)				
	soluble	yes	ND	ND	ND	ND				
	insoluble	yes	85.3b (2.4)	93.1a,b (1.9)	101.4a (1.9)	1.95b (0.08)				
high acetylated	soluble	no	79.8c (1.5)	86.1c (0.8)	99.9a (0.4)	1.86b (0.16)				
	insoluble	no	80.7c (0.8)	93.3a,b (0.7)	100.9a (0.7)	1.43c (0.04)				
	soluble	yes	ND	ND	ND	ND				
	insoluble	yes	80.7c (0.1)	91.6b (0.2)	98.6a (2.0)	1.73b,c (0.06)				

[a]Melting temperature and enthalpies of complexes scanned from 25 to 180 °C at 10 °C/min, immediately cooled from 180 to 25 °C at 40 °C/min and rescanned from 25 to 180 °C at 10 °C/min. Melting temperatures: onset, T_o; peak, T_p; conclusion, T_c; and enthalpy, ΔH. [b]Mean (standard deviation) of at least two measurements. Means in a column not sharing the same letter are significantly different based on Tukey's honestly significant difference test ($p < 0.05$). [c]ND, not detected.

Although no melting endotherm was observed for the soluble complexes from the low-acetylated without or with the *β*-amylase treatment and the high-acetylated *β*-amylase-treated starch, the presence of the starch−oleic acid complex was supported by the recovered oleic acid from the GC (Table 2) as well as by the presence of the V-type pattern displayed in the XRD results (Figure 4C,D,F). An opposite trend was observed in the soluble complexes of the low-acetylated-only starch from the previous study with stearic acid,[23] in which the presence of the starch−stearic acid complex was not observed in the XRD and DSC analyses, but stearic acid was recovered from the complexes as measured by GC. These results support the

DOI: 10.1021/acs.jafc.5b00125
J. Agric. Food Chem. 2015, 63, 4202−4210

hypothesis that acetylated starch complexes may exist in different polymorphic arrangements[21] because the presence of acetyl groups on starch rendered them more soluble and affected their structural characterization by DSC. Nevertheless, there may be other factors causing the absence of the melting endotherm in some of the soluble starch−oleic acid complexes in the present study. Therefore, further investigations such as different chemical modifications or analytical techniques such as FTIR may provide a better understanding of the various types of polymorphs that can be generated during the complexation of acetylated starch and oleic acid and their structural characteristics.

In conclusion, the present study demonstrates that the acetylation of starch alone can enhance the formation of both soluble and insoluble starch−oleic acid complexes compared with its unacetylated counterpart. Overall, high-acetylated-only starch and low-acetylated β-amylase-treated starch resulted in the highest complex formation with oleic acid for the soluble and insoluble complexes, respectively. All acetylated soluble and insoluble complexes displayed the V-type X-ray diffraction pattern regardless of the type of modification. The melting temperatures were reduced by acetylation for all complexes; however, little correlation was found among the melting enthalpy values, X-ray intensity, and amount of either the soluble or insoluble complex. The amount of complexed oleic acid in the present work was consistently lower than the amount of complexed stearic acid in the previous study for all treatments, confirming that the cis configuration in fatty acids is not favored to form stable soluble or insoluble complexes and longer starch chains were preferred for complexation with oleic acid than with stearic acid.

AUTHOR INFORMATION

Corresponding Author

*Tel: 479-575-3871. Fax: 479-575-6936. E-mail: yjwang@uark.edu.

Notes

The authors declare no competing financial interest.

ACKNOWLEDGMENTS

We are grateful to Dr. Steven Ricke and Dr. Sun-Ok Lee for access to the GC.

REFERENCES

(1) Colin, J. J.; de Claubry, H. G. Sur les combinaisons de l'iodie avec les substances végétales et animales. *Ann. Chim.* **1814**, *90*, 87−100.

(2) Schoch, T. J. Fractionation of starch by selective precipitation with butanol. *J. Am. Chem. Soc.* **1942**, *64*, 2957−2961.

(3) Hong, M.; Soini, H.; Baker, A.; Novotny, M. V. Complexation between amylodextrins oligomers and selected pharmaceuticals measured through capillary electrophoresis. *Anal. Chem.* **1998**, *70*, 3590−3597.

(4) Oguchi, T.; Yamasato, H.; Limmatvapirat, S.; Yonemochi, E.; Yamamoto, K. Structural change and complexation of strictly linear amylose induced by sealed-heating with salicylic acid. *J. Chem. Soc., Faraday Trans.* **1998**, *94* (7), 923−927.

(5) Cohen, R.; Orlova, Y.; Kovalev, M.; Ungar, Y.; Shimoni, E. Structural and functional properties of amylose complexes with genistein. *J. Agric. Food Chem.* **2008**, *56* (11), 4212−4218.

(6) Wulff, G.; Avgenaki, G.; Guzmann, M. S. P. Molecular encapsulation of flavors as helical inclusion complexes of amylose. *J. Cereal Sci.* **2005**, *41*, 239−249.

(7) Mikus, F. F.; Hixon, R. M.; Rundle, R. Complexes of fatty acids with amylose. *J. Am. Chem. Soc.* **1946**, *68*, 1115−1123.

(8) Eliasson, A. C.; Krog, N. Physical properties of amylose-monoglyceride complexes. *J. Cereal Sci.* **1985**, *3*, 239−248.

(9) Godet, M. C.; Bizot, H.; Buleon, A. Crystallization of amylose-fatty acid complexes prepared with different amylose chain lengths. *Carbohydr. Polym.* **1995**, *27*, 47−52.

(10) Karkalas, J.; Ma, S.; Morrison, W. R.; Pethrick, R. A. Some factors determining the thermal-properties of amylose inclusion complexes with fatty-acids. *Carbohydr. Res.* **1995**, *268*, 233−247.

(11) Tufvesson, F.; Wahlgren, M.; Eliasson, A. Formation of amylose-lipid complexes and effects of temperature treatment. Part 1. Monoglycerides. *Starch/Staerke* **2003a**, *55*, 61−71.

(12) Tufvesson, F.; Wahlgren, M.; Eliasson, A. Formation of amylose-lipid complexes and effects of temperature treatment. Part 2. Fatty acids. *Starch/Staerke* **2003b**, *55*, 138−149.

(13) Gelders, G. G.; Vanderstukken, T. C.; Goesaert, H.; Delcour, J. A. Amylose-lipid complexation: a new fractionation method. *Carbohydr. Polym.* **2004**, *56*, 447−458.

(14) Gelders, G. G.; Duyck, J. P.; Goesaert, H.; Delcour, J. A. Enzyme and acid resistance of the amylose-lipid complexes differing in the amylose chain length, lipid and complexation temperature. *Carbohydr. Polym.* **2005a**, *60*, 379−389.

(15) Lalush, I.; Bar, H.; Zakaria, I.; Eichler, S.; Shimoni, E. Utilization of amylose-lipid complexes as molecular nanocapsules for conjugated linoleic acid. *Biomacromolecules* **2005**, *6*, 121−130.

(16) Seneviratne, H. D.; Biliaderis, C. G. Action of alpha-amylases on amylose-lipid complex superstructures. *J. Cereal Sci.* **1991**, *13*, 129−143.

(17) Szejtli, J.; Banky-Elod, E. Inclusion complexes of unsaturated fatty acids with amylose and cyclodextrin. *Starch/Staerke* **1975**, *27*, 368−376.

(18) Yang, Y.; Gu, Z.; Zhang, G. Delivery of bioactive conjugated linoleic acid with self-assembled amylose-CLA complex. *J. Agric. Food Chem.* **2009**, *57*, 7125−7130.

(19) Gelders, G. G.; Goesaert, H.; Delcour, J. A. Amylose-Lipid complexes as controlled release agents during starch gelatinization and pasting. *J. Agric. Food Chem.* **2006**, *54*, 1493−149.

(20) Wulff, G.; Kubik, S. Helical amylose complexes with organic complex ands, 1 Microcalorimetric and circular dichroitic investigations. *Makromol. Chem.* **1992**, *193*, 1071−1080.

(21) Lui, H.; Arntfield, S. D.; Holley, R. A.; Aime, D. B. Amylose-lipid complex formation in acetylated pea starch-lipid systems. *Cereal Chem.* **1997**, *74*, 159−162.

(22) Eliasson, A. C.; Finstad, H.; Ljunger, L. A study of starch-lipid interactions for some native and modified maize starches. *Starch/Staerke* **1988**, *3*, 95−100.

(23) Arijaje, E. O.; Wang, Y.-J.; Shinn, S.; Shah, S.; Proctor, A. Effects of chemical and enzymatic modifications on starch-stearic acid complex formation. *J. Agric. Food Chem.* **2014**, *62*, 2963−2972.

(24) Wang, Y.-J.; Wang, L. Characterization of acetylated waxy maize starches prepared under catalysis by different alkali and alkaline-earth hydroxides. *Starch/ Staerke* **2002**, *54*, 25−30.

(25) McComb, E. A.; McCready, R. M. Determination of Acetyl in pectin and in acetylated carbohydrate polymers, hydroxamic acid reaction. *Anal. Chem.* **1957**, *29*, 819−820.

(26) Wurzburg, O. B. Crosslinked Starches. In *Modified Starches: Properties and Uses*; Wurzburg, O. B., Ed.; CRC Press: Boca Raton, FL, 1986; pp 41−53.

(27) Wong, K. S.; Jane, J. Effects of pushing agents on the separation and detection of debranched amylopectin by high performance anion-exchange chromatography with pulsed amperometric detection. *J. Liq. Chromatogr.* **1995**, *18*, 63−80.

(28) Hanashiro, I.; Abe, J. I.; Hizukuri, S. A periodic distribution of chain length of the amylopectin as revealed by high performance anion-exchange chromatography. *Carbohydr. Res.* **1996**, *147*, 342−347.

(29) Raphaelides, S.; Karkalas, J. Thermal−dissociation of amylose fatty-acid complexes. *Carbohydr. Res.* **1988**, *172*, 65−82.

(30) Zabar, S.; Lesmes, U.; Katz, I.; Shimoni, E.; Bianco-Peled, H. Structural characterization of amylose-long chain fatty acid complexes

DOI: 10.1021/acs.jafc.5b00125
J. Agric. Food Chem. 2015, 63, 4202−4210

produced via acidification method. *Food Hydrocolloids* **2010**, *24*, 347−357.
(31) Putseys, J. A.; Liesbeth, J. D.; Lamberts, L.; Goesaert, H.; Delcour, J. A. Production of tailor made short chain amylose-lipid complexes using varying reaction conditions. *Carbohydr. Polym.* **2009**, *78*, 854−861.
(32) Gelders, G. G.; Goesaert, H.; Delcour, J. A. Potato phosphorylase catalyzed synthesis of amylose-lipid complexes. *Biomacromolecules* **2005b**, *6*, 2622−2629.
(33) Luckett, C. R.; Wang, Y.-J. Effects of *β*-Amylolysis on the resistant starch formation of debranched corn starches. *J. Agric. Food Chem.* **2012**, *60*, 4751−4757.
(34) Hizukuri, S.; Kaneko, T.; Takeda, Y. Measurement of the chain length of amylopectin and its relevance to the origin of crystalline polymorphism of starch granules. *Biochim. Biophys. Acta, Gen. Subj.* **1983**, *760*, 188−191.
(35) Biliaderis, C. G.; Seneviratne, H. D. On the supermolecular structure and metastability of glycerol monostearate amylose complex. *Carbohydr. Polym.* **1990**, *13*, 185−206.
(36) Biliaderis, C. G.; Galloway, G. Crystallization behavior of amylose-V Complexes: Structure-property relationships. *Carbohydr. Res.* **1989**, *189*, 31−48.
(37) Godet, M. C.; Buleon, A.; Trans, V.; Colonna, P. Structural features of fatty acid-amylose complexes. *Carbohydr. Polym.* **1993**, *21*, 91−95.
(38) Biliaderis, C. G.; Page, C. M.; Maurice, T. J. On the multiple melting transitions of starch-monoglyceride systems. *Food Chem.* **1986**, *22*, 279−295.
(39) Lagendijk, J.; Pennings, H. J. Relation between complex formation of starch with monoglycerides and the firmness of bread. *Cereal Sci. Today* **1970**, *15*, 354−365.
(40) Zieba, T.; Kapelko, M.; Gryszkin, A. Selected properties of potato starch subjected to multiple physical and chemical modifications. *Pol. J. Food Nutr. Sci.* **2007**, *57*, 639−645.

DOI: 10.1021/acs.jafc.5b00125
J. Agric. Food Chem. 2015, 63, 4202−4210

the present study, non-network proteins, as with dextran[16,23,24] or PEG,[17−22] were used as "probes". The diffusion coefficients of non-network proteins with different molecular weights in heat-induced soy protein gels, in terms of the effect of the protein concentration and heating time, were investigated. Fick's diffusion law was used to analyze the release kinetics of the non-network proteins. The relationship between the release behavior of non-network proteins and the structure of the heat-induced soy protein gel in response to the protein concentration and heating time are discussed. The quantitative characterization of the diffusion behavior provides insight into the structure and properties of heat-induced soy protein gels.

MATERIALS AND METHODS

Materials. Low-temperature soy meals were kindly provided by Shandong Gushen Industrial & Commercial Co., Ltd. (Dongying, Shandong, People's Republic of China). The flakes had a protein content of 55.0% (N × 6.25, dry base) and a nitrogen solubility index of 87%. Defatted soy flakes were extracted with 85% aqueous alcohol at room temperature for 1 h with a ratio of 1/5 (w/v) flakes to solvent. The slurry was vacuum-filtered, and the filter cake was mixed with 95% (v/v) ethanol at room temperature for 1 h with a ratio of 1/2 (w/v). After it was dried for 2 days at room temperature, the meal was dispersed in distilled water (1/10, w/v) and adjusted to pH 7.0 by adding a small amount of 2 M NaOH. After it was stirred for 1 h at room temperature, the suspension was centrifuged (15800*g*, 30 min, 4 °C) to recover the supernatants. Soy protein was precipitated by adjusting the pH to 4.5 with 2 N HCl and centrifuged at 10000*g* for 30 min at 4 °C. After it was washed with distilled water, the protein precipitate was resuspended in distilled water and solubilized by adjusting the pH to 7.0. The protein dispersions were stirred overnight at 4 °C to enhance protein dissolution. The protein solution was lyophilized and stored at −18 °C. Proximate analysis showed that the dried powder had protein and ash contents of 91.65 ± 0.8% (*N* × 6.25) and 4.26 ± 0.04%, respectively, on a dry basis, and the 7S/11S ratio of native isolate was 0.79 ± 0.02 (determined by reducing-SDS-PAGE).[28] All other reagents were of analytical grade.

Preparation of the Protein Gels. Rehydration of the soy protein powder was performed by thorough magnetic stirring at room temperature with 0.1 M NaCl and 10 mM sodium phosphate buffer (pH 7.0) at the desired concentration (12%, 15%, and 18%, w/v) (soy gels with a protein concentration higher than 12% are easy to handle during the release process). In each case the pH was adjusted to 7.0 with 1 N HCl or 1 N NaOH. Sodium azide was added (0.02% w/v) to each solution to prevent bacterial development. The soy protein suspensions were centrifuged at 40000*g* for 30 min to remove gas and then carefully placed in SEBC bottles (special glass bottles with a tight screw-threaded blue cover and with high temperature, acid, and alkali resistance, Biocolor Co., Ltd., Shanghai, People's Republic of China). Gelation was then conducted by heating the soy protein dispersions in SEBC bottles at 95 °C, after the temperature of the solution reached the target value (95 °C), which occurred after approximately 3 min in a preliminary experiment. The solution was maintained in the water bath for exactly 30 min or for different time periods (30 min, 1 and 2 h). After heating, the bottles were immediately cooled in ice water for 5 min and stored at 4 °C overnight to ensure complete gelation before further use.

Release of Non-Network Proteins from Gels. The gels (approximate 20 g) generated under different conditions were cut into 1.5 mm thick slices with a razor and transferred to 10 mM sodium phosphate buffer (pH 7.0) (10 times excess w/v) in 500 mL SEBC bottles. NaN_3 (0.02% w/v) was added to each solution to inhibit bacteria growth. The SEBC bottles were gently rotated in a water bath at 25 °C. The non-network proteins in the gels were allowed to diffuse out of the gel slices for 56 h, which was sufficiently long to reach equilibrium on the basis of preliminary experiments. During diffusion, 0.5 mL samples were periodically collected and replaced with fresh buffer.

Determination of the Protein Concentration. The protein concentration of the samples (filtered through a cellulose acetate membrane with a pore size of 0.22 μm; Sartorius Co., Ltd., Gottingen, Germany) at different time points was determined using the bicinchoninic acid (BCA) method,[29] with bovine serum albumin as a standard. The BCA reagent was prepared by mixing 50 volumes of reagent A (containing 1% BCA, 2% Na_2CO_3, 0.16% $Na_2C_4H_4O_6$, 0.4% NaOH, 0.95% $NaHCO_3$) with 1 volume of reagent B (4% $CuSO_4$) immediately before use. Then, 100 μL of the sample and 2 mL of BCA reagent were pipetted into a test tube and mixed thoroughly. The mixture was allowed to stand for 30 min at 37 °C and then returned to room temperature, and the absorbance was monitored at 562 nm, using 100 μL of water as a control. All of the measurements were performed in triplicate.

Contents of Released Non-Network Proteins. The content (W_{rp}, g/100 g of total protein) of released proteins was calculated as

$$W_{rp} = \frac{C_{non}V_{buffer}}{1000C_pM_{gel}} \times 100$$

where C_{non}, V_{buffer}, C_p, and M_{gel} are the concentration (mg mL^{-1}) of non-network proteins in the buffer at equilibrium (48 h), the volume (mL) of buffer used, the protein concentration (g/g) in the gel, and the weight (g) of the gel in the buffer, respectively.

Contents of Released Undenatured 11S Proteins and Denatured Proteins. The contents of released proteins (W_{rp}, g/100 g of total protein) were divided into two parts. One part is the content of released undenatured 11S proteins. (The 7S component is completely denatured at 90 °C after 30 min according to Sorgentini et al.,[28] and therefore, the undenatured component in the released protein is native 11S-AB. Ruan et al.[30] found that the disruption of the interpolypeptide disulfide bond between A and B occurred even at 70−80 °C lower than the denaturation temperature (93.21 °C) of 11S. Therefore, the intact AB band in nonreducing SDS-PAGE can be identified as undenatured 11S.) The other part is the content of denatured proteins released from the protein gel. The content of undenatured 11S proteins ($W_{undenatured}$, g/100 g of total protein) released from the gel was calculated from the equation

$$W_{undenatured} = W_{rp}r_{AB} \quad (1)$$

where W_{rp} and r_{AB} are the content of released proteins (W_{rp}, g/100 g of total protein) and the ratio of the content of undenatured 11S proteins to that of released network proteins, obtained by comparing the AB band intensity with the total intensity of all of the bands in the same nonreducing SDS-PAGE lane.

The content of denatured proteins ($W_{denatured}$, g/100 g of total protein) in the released network proteins was calculated as

$$W_{denatured} = W_{rp}(1 - r_{AB}) \quad (2)$$

where $1 - r_{AB}$ represents the ratio of released denatured proteins to the content of released network proteins.

Network Protein Content per 100 g of Gel. The network protein content (W_{net}, g/100 g of gel) was calculated using the equation

$$W_{net} = C_p\left(1 - \frac{W_{rp}}{100}\right) \quad (3)$$

where C_p and W_{rp} are the protein concentration (g/g) in the gel and the content of released proteins (g/100 g of total protein).

High-Performance Size Exclusion Chromatography (SEC-HPLC). The molecular weight distribution of the samples was determined according to the method reported by Wu et al.[31] with some modifications. The samples were filtered through a cellulose acetate membrane with a pore size of 0.22 μm (Sartorius Co., Ltd., Gottingen, Germany). A Hitachi liquid chromatography system equipped with a Shodex protein KW-804 column (Shodex Separation and HPLC Group, Tokyo, Japan) was used. The elution was performed with 50 mM phosphate buffer (pH 7.0, including 0.3 M NaCl) at a flow rate of 1.0 mL/min. Each sample (20 μL) was injected

DOI: 10.1021/acs.jafc.5b00132
J. Agric. Food Chem. 2015, 63, 4211−4219

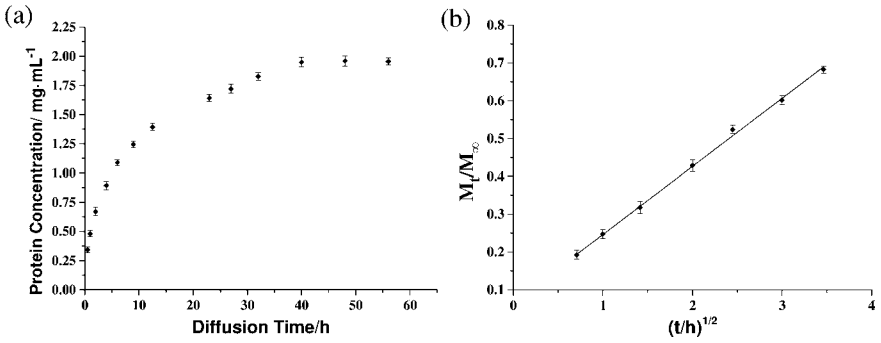

Figure 1. (a) Changes of protein concentration in the buffer after the gel slices (15% protein concentration) were placed in. (b) Relative non-network protein mass release as a function of the square root of the diffusion time.

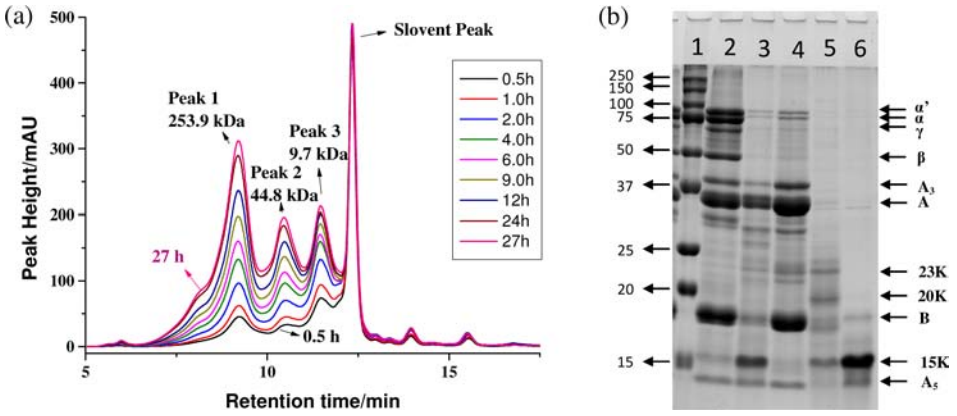

Figure 2. (a) SEC profiles of the samples released at different diffusion times from protein gels with a 15% protein concentration. (b) SDS-PAGE of eluates collected from the SEC-HPLC experiment. Reducing SDS-PAGE lanes 1−6: 1, marker (kDa); 2, gel; 3, diffusion sample; 4, peak 1; 5, peak 2; 6, peak 3.

into the column, and the effluent was monitored at 214 nm. The column was calibrated using standard proteins (Bio-Rad) between 1350 Da and 670 kDa (vitamin B_{12}, 1350 Da; horse myoglobulin, 17 kDa; chicken ovalbumin, 44 kDa; bovine gamma globulin, 158 kDa; thyroglobulin, 670 kDa). All of the samples were measured in triplicate, and an Agilent Chemistry Station was used to analyze the peak area.

Diffusion Coefficients of Non-Network Proteins in Gels and in Water. Non-network proteins with different molecular weights released from soy gel slices were characterized by calculating the apparent diffusion coefficient (D), which was estimated on the basis of the release kinetics curve, fitted using an analytical solution of Fick's second law:[32]

$$\frac{M_t}{M_\infty} = 4\left(\frac{Dt}{\pi\delta^2}\right)^{1/2} \quad (4)$$

where M_t and M_∞ are the amounts of protein released from the gel at time t and the protein in the buffer in the equilibrium state (48 h), respectively, while D and δ are the diffusion coefficient and the gel thickness, respectively. M_t/M_∞ can also be expressed as S_t/S_∞ (given that the volume of the diffusion buffer is almost constant), in which S_t and S_∞ are the SEC-HPLC peak areas at time t and at the time of equilibrium, respectively. Therefore, the diffusion coefficient of non-network proteins can be calculated as

$$D = \frac{k^2\delta^2\pi}{16} \quad (5)$$

where k is the slope of the relative solute release (S_t/S_∞) versus the square root of the time curve.

The diffusion coefficients in water (D_0) were calculated using the Stokes−Einstein equation, for different fractions:

$$D_0 = \frac{kT}{6\pi\eta R_h}$$

where T, k, and η are the kelvin constant (293.5 K), Boltzmann constant (1.38×10^{-23} J K^{-1}) and the viscosity of pure water (1.00×10^{-3} Pa s at 25 °C). The R_h values of peaks 1−3 used for calculations are 5.85 nm (Stokes radius of native 11S globulins),[33] 2.80 nm (ovalbumin, 45 kDa), and 2.01 nm (α-lactalbumin, 14 kDa), respectively.

SDS-PAGE. SDS-PAGE was performed to examine the protein compositions according to the method proposed by Laemmli.[34] Electrophoresis was performed with a continuous and dissociating buffer system: 0.375 M Tris-HC1 (pH 8.8) and 0.1% SDS for the separating gel and 0.025 M Tris-HC1 (pH 8.3), 0.192 M glycine, and 0.1% SDS for the run buffer. A 12.5% resolving gel overlaid with a 3% stacking gel was used. Aliquots of each sample were mixed with 1× sample dissolving buffer (4% SDS, 20% glycerol, 0.125 M Tris-HCl buffer, pH 6.8, 0.01% bromophenol blue) and divided into two parts: one part with 0.02% 2-mercaptoethanol (w/w) heated to 5 min at 100 °C and the other part without 2-mercaptoethanol. These two parts were centrifuged at 15000g for 10 min at room temperature. The two parts were loaded separately into SDS-PAGE gels and subjected to electrophoresis. The gel was then stained with Coomassie brilliant blue R250 and destained with deionized water that was changed two to three times. Finally, the gels were scanned using a computing densitometer (Molecular Imager Chemi Doc XRS+, Bio-Rad, USA). To investigate the protein compositions of the peak area of the SEC-HPLC curve, the eluates of the corresponding area were collected 50 times and then concentrated using an Amicon Ultra 15 mL centrifugal filter (Millipore Corporation, Germany) with a membrane NMWL (nominal molecular weight limit) of 3 kDa. The concentrated eluates were analyzed by SDS-PAGE. The intensities of the protein bands were analyzed using Image Lab software (Bio-Rad, USA). The content

DOI: 10.1021/acs.jafc.5b00132
J. Agric. Food Chem. 2015, 63, 4211−4219

of each component was determined as a percentage of the component in the sample by comparing the individual band intensities with the total intensity of all of the bands in the same lane.

Statistical Analysis. Experiment data were subjected to analysis of variance (ANOVA) using SAS 9.1. A least significant difference (LSD) test with a confidence interval of 95% was used to compare the means. All of the treatments were performed in triplicate. Data are expressed as the mean ± SD (n = 3).

RESULTS AND DISCUSSION

Release of Non-Network Proteins from 15% Soy Protein Gels. *Changes in the Released Non-Network Protein Concentration.* The protein concentrations after diffusion time of 0.5, 1, 2, 4, 6, 9, 12, 23, 27, 32, 40, 48, and 56 h were determined, and the results are displayed in Figure 1a. The concentration of released proteins increased steadily over the first 12 h, but there was essentially no change during the final 8 h. Therefore, the diffusion of non-network proteins reached an equilibrium state at approximately 48 h.

The diffusion of non-network proteins as a function of the diffusion time was fitted to Fick's second law by plotting the relative mass release of non-network proteins (M_t/M_{48}) against the square root of the diffusion time, as shown in Figure 1b. A linear relationship was observed during the first 12 h, indicating that the initial phase of the diffusion of non-network proteins could be described using the Fickian diffusion law.

Molecular Weight Distribution and Protein Composition of the Released Non-Network Proteins. Released proteins from the gel were sampled at different diffusion times, and the size distributions of the proteins were analyzed by SEC-HPLC (Figure 2a). Four peaks were observed, among which the last peak was attributed to solvent absorption. Peaks 1−3 were identified as proteins, with molecular weights of 253.9 ± 22.5, 44.8 ± 5.1, and 9.7 ± 1.6 kDa, respectively, as determined using a standard calibration curve. It is interesting to note that the areas with different protein peaks did not change synchronously during the diffusion period.

The protein compositions of peaks 1−3 on the basis fo SDS-PAGE are shown in Figure 2b. The protein gel per se (lane 2) contained all of the major components of soy proteins, including the 7S α', α, γ, and β subunits as well as the 11S A, B, A_3, and A_5 polypeptides,[35] in addition to a faint band with a size of 15 kDa protein (named 15K protein). Lane 3 shows the composition of the released proteins in the buffer. Only a very small amount of 7S α', α, and β subunits and a moderate amount of B polypeptides were detected, in comparison to the large amount of A and 15K band. Peak 1 (lane 4) contained almost all of the protein species found in the original diffusion sample (lane 3) in addition to a faint 15K band. A nonreducing SDS-PAGE analysis (data not shown) revealed that the A and B polypeptides in the diffused sample and peak 1 actually existed in the form of AB subunits. Peak 2 (lane 5) contained several unidentified proteins with molecular weights of 23 and 20 kDa as well as small amounts of B polypeptides. On the basis of the SDS-PAGE analysis, the 15K and small amount of A_5 polypeptides were eluted in peak 3 (lane 6). The SDS-PAGE analysis indicated that the proteins released from the 15% gel were composed of AB subunits of 11S and other small proteins. Because there was a very low content of 7S subunits in the diffusion buffer, it can be inferred that 7S contributed to the gel network, while a fraction of undenatured 11S and some small proteins were not involved in the formation of the gel network. Utsumi et al.[2,3] also discovered a difference in the contribution of soy protein components to the network structure of gels. Subunits that are weakly involved in the network should be relatively free and released from the gels by ultracentrifugation. Puppo et al.[9] reported that the 11S fractions remained in the native state after heating and would exist as soluble peptides in gel matrix interstices.

Diffusion Coefficients of Non-Network Proteins with Different Molecular Weights. Figure 3 shows the relative peak areas (S_t/S_∞) of peaks 1−3, respectively, as a function of the square root of the diffusion time ($t^{1/2}$). The cumulative release appeared to be proportional to the square root of the diffusion time up to approximately 70% protein release. This finding indicates that the release of peaks 1−3 was all controlled by Fickian diffusion processes in the initial stage (during the first 12 h). The diffusion coefficients (D) were calculated from the slope of the fitted lines according to eq 5. As shown in Table 1, the diffusion coefficients (D) increased from 2.90×10^{-12} to 1.64×10^{-11} m^2 s^{-1} as the protein molecular weight decreased from 253.9 ± 22.5 to 9.7 ± 1.6 kDa. Colsenet et al.[20] studied the diffusion of PEG in whey protein gels with a 75% protein denaturation ratio. They reported that the diffusion coefficient increased from 3.0×10^{-12} to 6.0×10^{-11} m^2 s^{-1} when the molecular weight of PEG decreased from 82.25 to 1.08 kDa. Moreover, the diffusion coefficients of PEG with molecular weights of 4, 12, 20, and 36 kDa were 8.9×10^{-11}, 3.8×10^{-11}, 2.0×10^{-11}, and 1.3×10^{-11} m^2 s^{-1}, respectively, in calcium alginate hydrogels with an alginate concentration of 16.5 g L^{-1}.[36]

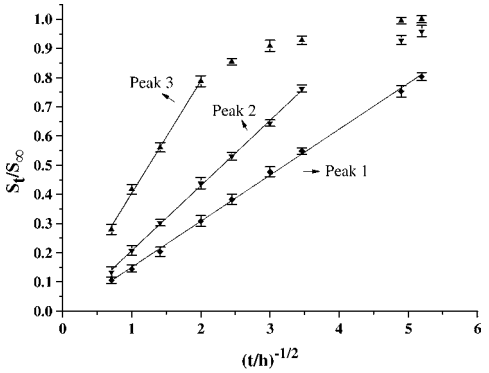

Figure 3. Cumulative release (%) of the proteins corresponding to peaks 1−3 (Figure 2a, SEC profiles) as a function of the square root of the diffusion time.

Table 1 also shows the diffusion coefficients in water (D_0). The results show that the gel matrix decreased the diffusion of non-network proteins by approximately 1 order of magnitude. This finding is in agreement with those reported by Schillemans et al.,[37] who demonstrated that the diffusion coefficients of myoglobin from chemically cross-linked dextran hydrogels decreased from 1.06×10^{-10} m^2 s^{-1} in pure water to $(0.9–1.3) \times 10^{-11}$ m^2 s^{-1} in hydrogels.

Moreover, Table 1 shows the theoretical values of D/D_0 using the predictive expression suggested by Davis[38] on the basis of studies of diffusion in polyacrylamide gels:

$$\frac{D}{D_0} = \exp(-(0.05 + 10^{-6}M)c_p) \quad (5)$$

where M and c_p are the molecular weight of the solute and the polymer gel mass fraction (expressed as a percent). According

DOI: 10.1021/acs.jafc.5b00132
J. Agric. Food Chem. 2015, 63, 4211−4219

Table 1. Diffusion Coefficients of Non-Network Proteins in 15% Gel and Water

peak	D	D_0	D/D_0	D/D_0 by Davis' model
1	$(2.90 \pm 0.16) \times 10^{-12}$a	$(35.78 \pm 3.1) \times 10^{-12}$d	0.074	0.009
2	$(6.43 \pm 0.17) \times 10^{-12}$b	$(76.74 \pm 5.3) \times 10^{-12}$e	0.085	0.256
3	$(1.64 \pm 0.46) \times 10^{-11}$c	$(10.69 \pm 0.6) \times 10^{-11}$f	0.153	0.408

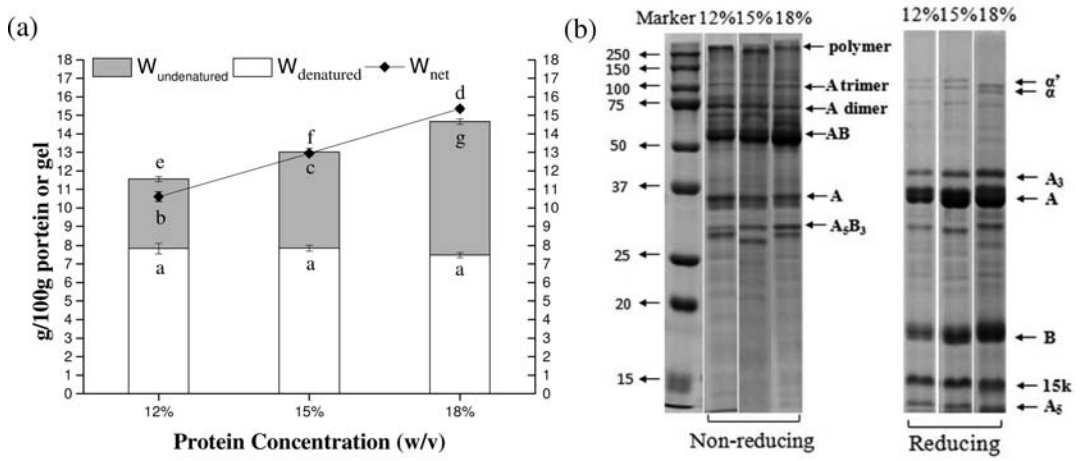

Figure 4. (a) Contents of undenatured 11S proteins ($W_{undenatured}$, g/100 g of total protein) and denatured proteins ($W_{denatured}$, g/100 g of total protein) released from the gels at different protein concentrations and the network protein content (W_{net}, g/100 g of gel). The three parameters are plotted as different protein concentrations. (b) SDS-PAGE of non-network proteins released from soy gels heating for 0.5 h at different protein concentrations.

Table 2. Diffusion Coefficients of Non-Network Proteins as a Function of the Soy Protein Concentration in the Gels

	D (m^2 s^{-1})		
protein concentration (% w/v)	peak 1	peak 2	peak 3
12	$(3.43 \pm 0.14) \times 10^{-12}$a	$(6.95 \pm 0.23) \times 10^{-12}$d	$(16.80 \pm 0.46) \times 10^{-12}$f
15	$(2.90 \pm 0.16) \times 10^{-12}$b	$(6.43 \pm 0.17) \times 10^{-12}$d	$(16.43 \pm 0.47) \times 10^{-12}$f
18	$(2.11 \pm 0.12) \times 10^{-12}$c	$(6.01 \pm 0.19) \times 10^{-12}$e	$(16.39 \pm 0.36) \times 10^{-12}$f

to eq 5, D/D_0 depended on the molecular weight of the solute and the polymer concentration of the gel. Although the calculated D/D_0 using Davis' model also increased with a decrease in molecular weight, the predictions of eq 5 are very different from the observed values, suggesting that the diffusion behavior of solutes in soy protein gels was substantially different from that in polyacrylamide gels. In fact, polyacrylamide gels behaved like a screen with homogeneous mesh size: peaks 2 and 3 with molecular weights of less than 44.8 kDa showed a much higher diffusion rate than that of peak 1 with a molecular weight of 253.9 kDa. On the other hand, soy protein gels were more heterogeneous in nature. Therefore, no clear-cut distinction between diffusion coefficients for high- and low-MW proteins was observed.

Effect of Protein Concentration on the Release of Non-Network Proteins. Heat-induced soy gels were made at 95 °C and 30 min using three protein concentrations: 12%, 15%, and 18% (w/v). With an increased protein concentration, more proteins were involved in the formation gel network as shown in Figure 4a. There were 10.61, 13.05, and 15.36 g of network proteins per 100 g of gel for the 12%, 15%, and 18% protein concentrations, respectively. However, the amount of released proteins, which was calculated on the basis of net protein mass rather than the gel mass, also increased. Figure 4a shows released undenatured 11S proteins ($W_{undenatured}$) and denatured proteins ($W_{denatured}$) calculated from eqs 1 and 2. When the protein concentration increased from 12% to 15% and finally to 18%, the corresponding released undenatured 11S proteins were 3.71, 5.17, and 7.18 g, respectively, per 100 g of gel proteins, which can also be explained by the increase in AB subunits (AB + A_3B_3) bands from 32.1 ± 0.4% to 39.7 ± 0.7% and 48.9 ± 0.5% in the released samples from gels with protein concentrations of 12%, 15%, and 18%, respectively, by nonreducing SDS-PAGE (Figure 4b). Concomitantly, the amounts of released denatured proteins were 7.85, 7.86, and 7.49 g, respectively, per 100 g of gel proteins. Thus, the increase in the total released non-network proteins (11.56, 13.03, and 14.67 g/100 g of total protein for protein concentrations of 12%, 15%, and 18%, respectively) was contributed mainly by the increase in the undenatured AB subunits. Several studies have reported that the degree of denaturation decreased with the increase in protein concentration. Zhang et al.[39] and Mills et al.[40] found that the onset temperature and peak temperature (in DSC curves) increased with an increasing content of crude soy protein. Mori et al.[41] also reported that the heat-induced association−dissociation of 11S globulin differs depending on the protein concentration, as evidenced by the finding that 11S-AB subunits did not dissociate into A and B polypeptides at a protein concentration of 5% to the extent they did at a protein concentration of 0.5%. At the same time, other studies have demonstrated the formation of higher molecular weight aggregates[1,40,41] and a decreased gelation temperature[26] when soy proteins are heated at higher concentrations. Thus, it is reasonable to postulate in our studies that, although the degree

DOI: 10.1021/acs.jafc.5b00132
J. Agric. Food Chem. 2015, 63, 4211−4219

of denaturation of 11S decreased, more proteins were involved in the gel network at higher protein concentrations.

The diffusion coefficients of non-network proteins with different molecular weights in the soy gels at different protein concentration are shown in Table 2. It is clear that the diffusion coefficients of the protein fractions with higher molecular weights were substantially more affected by the gel protein concentration. Gireeshkumar[23,24] found that the diffusion coefficients of dextran decreased strongly with the increase in the protein concentration of β-lactoglobulin gels and that the larger molecular size of dextran resulted in a greater decrease in the diffusion coefficient. For smaller molecular tracers (PEG) with MW values of 1 and 8.5 kDa, respectively, Colsenet[18] found that the structural changes of casein gels induced by different protein concentrations had essentially no effect on their diffusion in the gel, and the same effect was observed for the changes in the diffusion coefficients of peak 3.

For globular proteins, R_h is related to the cubic root of the molecular weight:

$$R_h = \sqrt[3]{\frac{3M_w}{4\pi N_a \rho}}$$

where M_w is the molecular weight, N_A is the Avogadro constant, and ρ is the density of a protein. From the Stokes−Einstein equation

$$D = \frac{kT}{6\pi\eta R_h}$$

the following power law dependence can be obtained:

$$D = AM_w^{-\alpha} \quad (6)$$

where A is a pre-exponential factor and α is the characteristic exponent. Equation 6 is often used to describe the self-diffusion of polymer chains in different systems with α ranging from 0.55 for dilute systems[42] to 2 in concentrated systems.[43] The diffusion coefficients determined for different protein fractions were plotted against MW on the double-logarithmic coordinate as shown in Figure 5. The exponent α yielded from the plot increased from 0.58 to 0.69 when the protein concentration increased from 12% to 18%. Favre et al.[36] determined the diffusion rate of PEG with a MW value from 4 to 35 kDa in calcium alginate hydrogels, and they reported that the exponent increased from 0.768 to 1.017 as the alginate concentration increased from 8.7 to 28.5 g mL^{-1}. On the other hand, in the study reported by Colsenet,[19] the diffusion of PEG in whey protein gels was determined by NMR. They found that α shifted from 0.59 to 0.84 as the protein concentration increased from 0.1 to 0.4 g/g. These authors[20] suggested that the diffusion of the probe was affected by the changes in the gel microstructure and that the increase in α occurred in accordance with a decrease in the interparticle distances in the gels. The power law exponent α would theoretically tend toward 1 for nonentangled polymer chains when the network mesh size of the gel decreases and approaches the solute radius.[44] For α equal to 2, eq 6 represents the reptation model first introduced by de Gennes.[42] The reptation model can be used to describe the dynamics of long polymer chain diffusion in a cross-linked gel, and according to this model, when the mesh size of the gel is less than the solute radius, the macromolecular solute would be forced to adopt a wormlike displacement behavior. The exponent determined in the present study was close to the theoretical value of 3/5 for a swollen coil in a good solvent.[42] Therefore, theoretically and practically, the pore size of the soy protein gel network is larger than the radius of non-network proteins. In addition, α gradually shifted toward higher values when the protein concentration or gel network density increased.

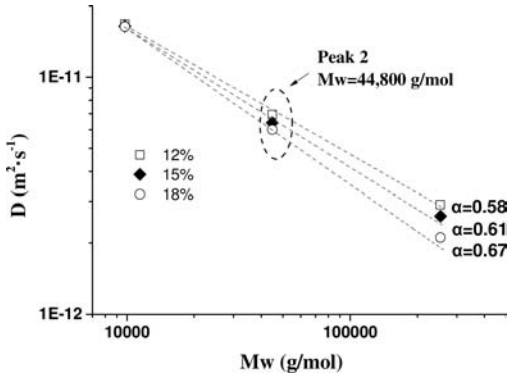

Figure 5. Power law representation of non-network protein diffusion coefficients in gels with different protein concentrations as a function of the non-network protein molecular mass.

Effect of Heating Time on the Release of Non-Network Proteins. The effect of heating time on the gel properties was investigated at 95 °C at a protein concentration of 18% (w/v) for 0.5, 1.0, and 2.0 h. Figure 6a shows that the amounts of undenatured 11S proteins released from the gels were 7.17, 3.92, and 1.54 g/100 g of total protein for heating times of 0.5, 1.0, and 2.0 h, respectively. Furthermore, the corresponding release of denatured proteins was of 7.49, 9.07, and 9.23 g/100 g of total protein, respectively. Moreover, the network protein content (W_{net}, g/100 g of gel) increased from 15.36 to 15.63 and 16.09 g/100 g of gel as the heating time increased.

As shown using nonreducing SDS-PAGE (Figure 6b), the intensity of the AB subunits decreased with an increase in heating time. Prolonging the heating time resulted in small increases in the contents of A polypeptides (17.1 ± 0.3%, 16.7 ± 0.5%, and 19.4 ± 0.6% for 0.5, 1.0, and 2.0 h, respectively; data not shown) and dimers of A polypeptides (2.3 ± 0.2%, 3.1 ± 0.3%, and 3.3 ± 0.2% for 0.5, 1.0, and 2.0 h, respectively; data not shown) but a slight decrease in trimers of A polypeptides from 3.2% to 0.5%. However, a remarkable increase in protein polymers was observed (7.8 ± 0.5% to 30.6 ± 0.7% for heating times from 0.5 to 2.0 h), in which A polypeptides were the main components on the basis of nonreducing/reducing diagonal electrophoresis (data not shown). Therefore, the increase in the amount of released denatured proteins ($W_{denatured}$ in Figure 6a) with an increase in heating time was probably contributed by the increase in polymers that were formed by the disassociated A polypeptides. The increase in network protein content (W_{net} in Figure 6a) can be explained by the increase in the amount of dissociated B polypeptides as a consequence of the preferential interaction between the β subunit of 7S and the B polypeptides of 11S, which has been reported to contribute to the gel network.[2,3] Marleen et al.[45] and Philippe et al.[16] also found that, upon prolonged heating of whey proteins or β-lactoglobulin, more proteins were incorporated into the gel network.

Diffusion coefficients (D) for different MW fractions from gels with different heating times are illustrated in Table 3. A higher molecular weight clearly resulted in greater sensitivity to

DOI: 10.1021/acs.jafc.5b00132
J. Agric. Food Chem. 2015, 63, 4211−4219

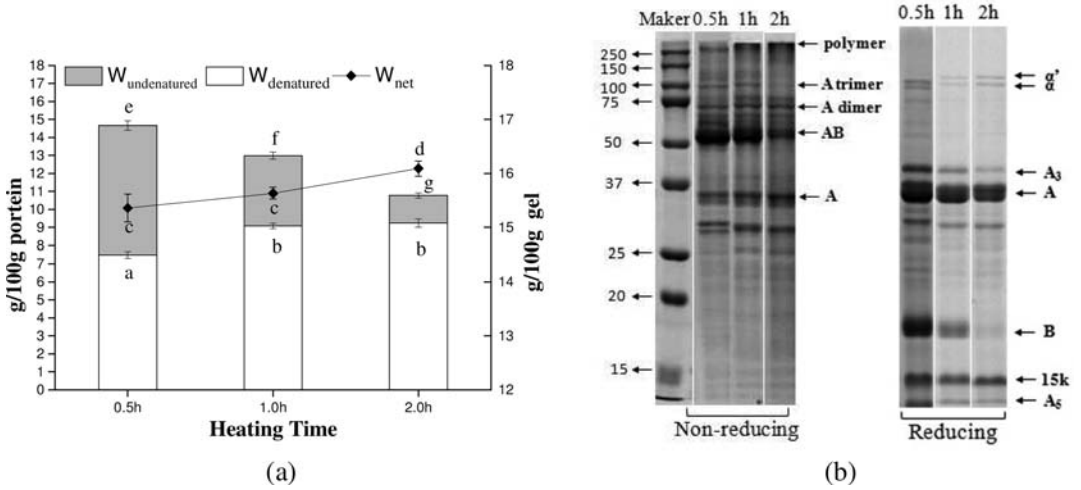

Figure 6. (a) Contents of undenatured 11S proteins ($W_{undenatured}$, g/100 g of total protein) and denatured proteins ($W_{denatured}$, g/100 g of total protein) released from the gels with a 18% protein concentration for heating for 0.5, 1.0, and 2.0 h, and the content of network protein content (W_{net}, g/100 g of gel). The three parameters are plotted as the heating time at a protein concentration of 18%. (b) SDS-PAGE of non-network proteins released from 18% soy gels at different heating times (h).

Table 3. Diffusion Coefficients of Non-Network Proteins in 18% Protein Gels as a Function of Heating Time

	D (m^2 s^{-1})		
heating time (h)	peak 1	peak 2	peak 3
0.5	$(2.11 \pm 0.12) \times 10^{-12}$a	$(6.01 \pm 0.23) \times 10^{-12}$c	$(16.39 \pm 0.46) \times 10^{-12}$e
1.0	$(2.06 \pm 0.14) \times 10^{-12}$a	$(5.75 \pm 0.17) \times 10^{-12}$cd	$(16.36 \pm 0.55) \times 10^{-12}$e
2.0	$(1.71 \pm 0.20) \times 10^{-12}$b	$(5.30 \pm 0.19) \times 10^{-12}$d	$(16.20 \pm 0.26) \times 10^{-12}$e

changes in diffusion with heating time. Good fits for the diffusion coefficients shown in Table 3 with eq 6 could also be obtained, yielding α values of 0.67, 0.69, and 0.75 for heating times of 0.5, 1.0, and 2.0 h, respectively. This finding suggested that a more compact gel network was obtained with a longer heating time. Lucey et al.[46] came to the same conclusion on the basis of a comparison of permeability measurements, demonstrating that the gels made from reconstituted skim milk heated at 80, 85, and 95 °C for 30 min had permeability coefficients lower than those that were heated for 15 min. Marleen et al.[45] also found that prolonged heating caused a decrease in pore size by studying the effect of the duration of heating on the properties of whey protein gels. Jacoba et al.[1] demonstrated that, after the onset of soy protein gelation, an increase in G' was observed upon further heating. They suggested that G' increased because more protein became incorporated into the network, leading to further accumulation of the network structure. Alternately, G' might have increased as a consequence of rearrangements in the network. A type of rearrangement that might occur is fusion of the protein aggregates in the strands, which results in an increase in protein−protein interactions per cross-section and thus in denser and stiffer strands.

In summary, this study demonstrated that the diffusion behavior of non-network proteins can be used to probe the structural characteristics of heat-induced soy protein gels. The major parts of the released non-network proteins were occupied by undenatured AB subunits, monomers, dimers, trimers, and polymers of A polypeptides, as well as the unidentified 15 kDa protein, while the amounts of 7S subunits and B polypeptides were very small among the released proteins. By SEC-HPLC, the released proteins could be classified into three fractions according to their size, with characteristic molecular weights of 253.9, 44.8, and 9.7 kDa. The release behavior of non-network proteins was fitted to Fick's second law. The increase in the gelling concentration resulted in a rise in non-network protein content in the gel, which was mainly contributed by undenatured AB subunits. A prolonged heating time reduced the amount of released non-network proteins and caused the composition to shift to more denatured proteins. In all of the cases, the diffusion coefficients of non-network proteins decreased with an increasing gel network density. An increase in the molecular weight of the protein fractions increased the sensitivity of the non-network protein diffusion coefficients to the structural changes in soy gels induced by different conditions. More proteins appeared to be involved in the gel network at elevated protein gelling concentrations to form a denser matrix, whereas the structural changes in the gels during prolonged heating might have been caused by rearrangements in the network structure and probably to some extent by further incorporation of protein into the network. Due to the elucidation of the relationship between the release behavior and structure of soy protein gels, further investigations are underway to reveal whether diffusion experiments can be affected by rheological properties and different proteins (7S and 11S).

AUTHOR INFORMATION

Corresponding Author

*Y.H.: tel, 0510-85917812; fax, 0510-85329091; e-mail, yfhua@jiangnan.edu.cn.

Funding

The work was financially supported received from the National Natural Science Foundation of China (No. 21276107), the National Great Project of Scientific and Technical Supporting

DOI: 10.1021/acs.jafc.5b00132
J. Agric. Food Chem. 2015, 63, 4211−4219

Programs funded by the Ministry of Science & Technology of China during the 12th five-year plan (No. 2012BAD34B04-1), and the 863 Program (Hi-tech research and development program of China, No. 2013AA102204-3).

Notes

The authors declare no competing financial interest.

REFERENCES

(1) Renkema, J. M.; Gruppen, H.; Van Vliet, T. Influence of pH and ionic strength on heat-induced formation and rheological properties of soy protein gels in relation to denaturation and their protein compositions. *J. Agric. Food Chem.* **2002**, *50* (21), 6064−6071.

(2) Utsumi, S.; Damodaran, S.; Kinsella, J. E. Heat-induced interactions between soybean proteins: Preferential association of 11S basic subunits and. Beta. Subunits of 7S. *J. Agric. Food Chem.* **1984**, *32* (6), 1406−1412.

(3) Utsumi, S.; Kinsella, J. E. Structure-function relationships in food proteins: subunit interactions in heat-induced gelation of 7S, 11S, and soy isolate proteins. *J. Agric. Food Chem.* **1985**, *33* (2), 297−303.

(4) Renkema, J. M.; van Vliet, T. Heat-induced gel formation by soy proteins at neutral pH. *J. Agric. Food Chem.* **2002**, *50* (6), 1569−1573.

(5) Bainy, E. M.; Tosh, S. M.; Corredig, M.; Woodrow, L.; Poysa, V. Protein subunit composition effects on the thermal denaturation at different stages during the soy protein isolate processing and gelation profiles of soy protein isolates. *J. Am. Oil Chem. Soc.* **2008**, *85* (6), 581−590.

(6) Nakamura, T.; Utsumi, S.; Mori, T. Network structure formation in thermally-induced gelation of glycinin. *J. Agric. Food Chem.* **1984**, *32* (2), 349−352.

(7) Nakamura, T.; Utsumi, S.; Mori, T. Effects of temperature on the different stages in thermal gelling of glycinin. *J. Agric. Food Chem.* **1985**, *33* (6), 1201−1203.

(8) Mori, T.; Nakamura, T.; Utsumi, S. Behavior of intermolecular bond formation in the late stage of heat-induced gelation of glycinin. *J. Agric. Food Chem.* **1986**, *34* (1), 33−36.

(9) Puppo, M. C.; Añón, M. C. Structural properties of heat-induced soy protein gels as affected by ionic strength and pH. *J. Agric. Food Chem.* **1998**, *46* (9), 3583−3589.

(10) Tay, S. L.; Kasapis, S.; Perera, C. O.; Barlow, P. J. Functional and structural properties of 2S soy protein in relation to other molecular protein fractions. *J. Agric. Food Chem.* **2006**, *54* (16), 6046−6053.

(11) Damodaran, S. Refolding of thermally unfolded soy proteins during the cooling regime of the gelation process: effect on gelation. *J. Agric. Food Chem.* **1988**, *36* (2), 262−269.

(12) Lakemond, C. M.; de Jongh, H. H.; Hessing, M.; Gruppen, H.; Voragen, A. G. Heat denaturation of soy glycinin: influence of pH and ionic strength on molecular structure. *J. Agric. Food Chem.* **2000**, *48* (6), 1991−1995.

(13) Wang, C. H.; Damodaran, S. Thermal gelation of globular proteins: influence of protein conformation on gel strength. *J. Agric. Food Chem.* **1991**, *39* (3), 433−438.

(14) Koutsopoulos, S.; Unsworth, L. D.; Nagai, Y.; Zhang, S. Controlled release of functional proteins through designer self-assembling peptide nanofiber hydrogel scaffold. *Proc. Natl. Acad. Sci. U. S. A.* **2009**, *106* (12), 4623−4628.

(15) Branco, M. C.; Pochan, D. J.; Wagner, N. J.; Schneider, J. P. The effect of protein structure on their controlled release from an injectable peptide hydrogel. *Biomaterials* **2010**, *31* (36), 9527−9534.

(16) Croguennoc, P.; Nicolai, T.; Kuil, M. E.; Hollander, J. G. Self-diffusion of native proteins and dextran in heat-set globular protein gels. *J. Phys. Chem. B* **2001**, *105* (24), 5782−5788.

(17) Colsenet, R.; Soderman, O.; Mariette, F. Diffusion of polyethyleneglycols in casein solutions and gels as studied by pulsed field gradient NMR. *Magn. Reson. Imaging* **2005**, *23* (2), 347−8.

(18) Colsenet, R.; Soderman, O.; Mariette, F. Effect of casein concentration in suspensions and gels on poly(ethylene glycol)s NMR self-diffusion measurements. *Macromolecules* **2005**, *38* (22), 9171−9179.

(19) Colsenet, R.; Söderman, O.; Mariette, F. Pulsed field gradient NMR study of poly(ethylene glycol) diffusion in whey protein solutions and gels. *Macromolecules* **2006**, *39* (3), 1053−1059.

(20) Colsenet, R.; Söderman, O.; Mariette, F. Effects of ionic strength and denaturation time on polyethyleneglycol self-diffusion in whey protein solutions and gels visualized by nuclear magnetic resonance. *J. Agric. Food Chem.* **2006**, *54* (14), 5105−5112.

(21) Le Feunteun, S.; Mariette, F. Impact of casein gel microstructure on self-diffusion coefficient of molecular probes measured by 1H PFG-NMR. *J. Agric. Food Chem.* **2007**, *55* (26), 10764−10772.

(22) Le Feunteun, S.; Mariette, F. Effects of acidification with and without rennet on a concentrated casein system: a kinetic NMR probe diffusion study. *Macromolecules* **2008**, *41* (6), 2079−2086.

(23) Balakrishnan, G.; Durand, D.; Nicolai, T. Particle diffusion in globular protein gels in relation to the gel structure. *Biomacromolecules* **2011**, *12* (2), 450−456.

(24) Balakrishnan, G.; Nicolai, T.; Durand, D. Relation between the gel structure and the mobility of tracers in globular protein gels. *J. Colloid Interface Sci.* **2012**, *388* (1), 293−299.

(25) Mohamad ramlan, B. M. S.; Maruyama, N.; Takahashi, K.; Yagasaki, K.; Higasa, T.; Matsumura, Y.; Utsumi, S. Gelling properties of soybean β-conglycinin having different subunit compositions. *Biosci., Biotechnol., Biochem.* **2004**, *68* (5), 1091−1096.

(26) Lakemond, C. M.; de Jongh, H. H.; Paques, M.; van Vliet, T.; Gruppen, H.; Voragen, A. G. Gelation of soy glycinin; influence of pH and ionic strength on network structure in relation to protein conformation. *Food Hydrocolloids* **2003**, *17* (3), 365−377.

(27) Renkema, J.; Lakemond, C. M.; de Jongh, H. H.; Gruppen, H.; van Vliet, T. The effect of pH on heat denaturation and gel forming properties of soy proteins. *J. Biotechnol.* **2000**, *79* (3), 223−230.

(28) Sorgentini, D. A.; Wagner, J. R.; Anon, M. C. Effects of thermal treatment of soy protein isolate on the characteristics and structure-function relationship of soluble and insoluble fractions. *J. Agric. Food Chem.* **1995**, *43* (9), 2471−2479.

(29) Smith, P.; Krohn, R. I.; Hermanson, G.; Mallia, A.; Gartner, F.; Provenzano, M.; Fujimoto, E.; Goeke, N.; Olson, B.; Klenk, D. Measurement of protein using bicinchoninic acid. *Anal. Biochem.* **1985**, *150* (1), 76−85.

(30) Ruan, Q.; Chen, Y.; Kong, X.; Hua, Y. Analysis of disulfide-mediated interactions of soy protein when heated using fluorescence labeling and mass spectrometry. *J. Agric. Food Chem.* **2015**, *63*, 3524−3533.

(31) Wu, W.; Wu, X.; Hua, Y. Structural modification of soy protein by the lipid peroxidation product acrolein. *LWT-Food Sci. Technol.* **2010**, *43* (1), 133−140.

(32) Ritger, P. L.; Peppas, N. A. A simple equation for description of solute release II. Fickian and anomalous release from swellable devices. *J. Controlled Release* **1987**, *5* (1), 37−42.

(33) Badley, R.; Atkinson, D.; Hauser, H.; Oldani, D.; Green, J.; Stubbs, J. The structure, physical and chemical properties of the soy bean protein glycinin. *Biochim. Biophys. Acta, Protein Struct.* **1975**, *412* (2), 214−228.

(34) Laemmli, U. K. Cleavage of structural proteins during the assembly of the head of bacteriophage T4. *Nature* **1970**, *227* (5259), 680−685.

(35) Poysa, V.; Woodrow, L.; Yu, K. Effect of soy protein subunit composition on tofu quality. *Food Res. Int.* **2006**, *39* (3), 309−317.

(36) Favre, E.; Leonard, M.; Laurent, A.; Dellacherie, E. Diffusion of polyethyleneglycols in calcium alginate hydrogels. *Colloids Surf., A* **2001**, *194* (1), 197−206.

(37) Schillemans, J. P.; Hennink, W. E.; van Nostrum, C. F. The effect of network charge on the immobilization and release of proteins from chemically crosslinked dextran hydrogels. *Eur. J. Pharm. Biopharm.* **2010**, *76* (3), 329−335.

(38) Davis, B. Diffusion in polymer gel implants. *Proc. Natl. Acad. Sci. U. S. A.* **1974**, *71* (8), 3120−3123.

DOI: 10.1021/acs.jafc.5b00132
J. Agric. Food Chem. 2015, 63, 4211−4219

(39) Zhang, H.; Takenaka, M.; Isobe, S. DSC and electrophoretic studies on soymilk protein denaturation. *J. Therm. Anal. Calorim.* **2004**, *75* (3), 719−726.
(40) Mills, E.; Huang, L.; Noel, T. R.; Gunning, A. P.; Morris, V. J. Formation of thermally induced aggregates of the soya globulin *β*-conglycinin. *Biochim. Biophys. Acta, Protein Struct. Mol. Enzymol.* **2001**, *1547* (2), 339−350.
(41) Mori, T.; Nakamura, T.; Utsumi, S. Gelation mechanism of soybean 11S globulin: Formation of soluble aggregates as transient intermediates. *J. Food Sci.* **1982**, *47* (1), 26−30.
(42) De Gennes, P. Brownian motions of flexible polymer chains. *Nature* **1979**, *282*, 367−370.
(43) Tao, H.; Lodge, T. P.; von Meerwall, E. D. Diffusivity and viscosity of concentrated hydrogenated polybutadiene solutions. *Macromolecules* **2000**, *33* (5), 1747−1758.
(44) Rouse, P. E., Jr A theory of the linear viscoelastic properties of dilute solutions of coiling polymers. *J. Chem. Phys.* **1953**, *21* (7), 1272−1280.
(45) Verheul, M.; Roefs, S. P.; Mellema, J.; de Kruif, K. G. Power law behavior of structural properties of protein gels. *Langmuir* **1998**, *14* (9), 2263−2268.
(46) Lucey, J. A.; Teo, C. T.; Munro, P. A.; Singh, H. Microstructure, permeability and appearance of acid gels made from heated skim milk. *Food Hydrocolloids* **1998**, *12* (2), 159−165.

DOI: 10.1021/acs.jafc.5b00132
J. Agric. Food Chem. 2015, 63, 4211−4219

Structural representation	R_1	R_2	R_3		Compound (number/name)	MS^2 Transition monitored
Glucosylated serotonin derivatives	H	H	H	1	Serotonin 5-*O*-*β*-glucoside	339.2→322
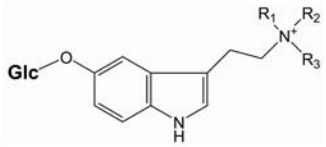	CH_3	H	H	2	*N*-methylserotonin 5-*O*-*β*-glucoside	353.2→322
	CH_3	CH_3	H	3	*N,N*-dimethylserotonin 5-*O*-*β*-glucoside	367.2→322
	CH_3	CH_3	CH_3	4	*N,N,N*-trimethylserotonin 5-*O*-*β*-glucoside	381.2→322
Serotonin derivatives	H	H	H	5	Serotonin (5-hydroxytryptamine)	177.1→160
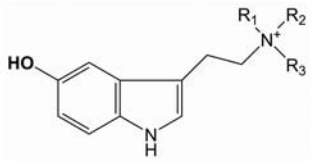	CH_3	H	H	6	5-Hydroxy-*N*-methyltryptamine	191.1→160
	CH_3	CH_3	H	7	5-Hydroxy-*N,N*-dimethyltryptamine	205.1→160
	CH_3	CH_3	CH_3	8	5-Hydroxy-*N,N,N*-trimethyltryptamine	219.1→160

Figure 1. Chemical structures and MS^2 transitions used for analyses of serotonin derivatives by LC−ESI−MS/MS.

receptors. 5-Hydroxy-*N,N,N*-trimethyltryptamine was found to be a cholinergic agent about 10-fold more powerful than *N,N,N*-trimethyltryptamine.[14] Considering their pharmacological properties, it was hypothesized that both compounds may represent the arrival point of a biosynthetic pathway aimed to provide *Citrus* plants with chemical defense against biotic agents. Our observation that leaves and seeds, more frequently attacked by biotic agents, are the plant parts where the highest levels of those compounds were found further suggests that possibility.[13] It is also well-known that many plants store their defense metabolites as inactive glycosides that can be hydrolyzed by specific glycosidases to release their toxic aglycones as a consequence of plant tissue damages caused by herbivores.[15] To date, the presence of this mechanism in *Citrus* is still unknown. Therefore, we sought to investigate the occurrence of glycosylated derivatives of serotonin and its N-methylated forms (Figure 1). To this aim, among *Citrus*, sweet orange, bitter orange, bergamot, citron, chinotto (*Citrus myrtifolia*), clementine, lemon, mandarin orange, and pomelo were investigated for the presence of glycosylated forms of serotonin and its N-methylated derivatives. Furthermore, for some species, the distribution of the glycosyl derivatives and their aglycones in flavedo, albedo, juice, and seeds was assessed.

MATERIALS AND METHODS

Reagents. Serotonin (5-hydroxytryptamine, **5**), *β*-glucosidase from almonds, and *β*-galactosidase from *Aspergillus oryzae* were purchased from Sigma-Aldrich (Milan, Italy). 5-Hydroxy-*N*-methyltryptamine (**6**), bufotenine (5-hydroxy-*N,N*-dimethyltryptamine, **7**), and bufotenidine (5-hydroxy-*N,N,N*-trymethyltryptamine, **8**) were synthesized and purified as reported.[16−18] Formic acid and 0.1% solution of formic acid in water used for the liquid chromatography−electrospray ionization−mass spectrometry (LC−ESI−MS) analyses were from Sigma-Aldrich. All other chemicals were of analytical reagent grade. Purified water was obtained from a Milli-Q system from Millipore (Milan, Italy).

***Citrus* Plant Materials.** *Leaf Extracts.* *Citrus* leaves of sweet orange, bitter orange, bergamot, citron, chinotto (*C. myrifolia*), clementine, lemon, mandarin, and pomelo were harvested in October and December 2013 from the Research Centre for Citrus Crops and Mediterranean (CRA-ACM), arboretum of Reggio Calabria (Italy). Leaves were washed with distilled water and dried with filter paper. For each species, 25 g of leaves, finely chopped, were homogenized in a blender with 100 mL of 0.1% formic acid in Milli-Q-grade water and then kept under stirring for 30 min. Homogenates were, finally, centrifuged at 18000*g* for 30 min, and the supernatant were stored in 20 mL vials at −20 °C.

Flavedo and Albedo Extracts. The preparations of flavedo and albedo extracts started by washing fruits, followed by manual scraping of the exocarp to remove the essential oils from the glands on the fruit surface, which is made by a continuous layer of epidermal cells with a thick cuticle containing stomata. The colored part just below the epidermis, called flavedo or epicarp, was obtained by manual scraping. Under the flavedo, the white spongy part of the fruit, called albedo, was also collected manually. Both flavedo and albedo were separately homogenized in a mixer with water in a 1:1 (w/w) ratio. The homogenates were kept for 2 h under constant agitation and then centrifuged at 18000*g* for 30 min. The supernatants were frozen at −20 °C until used for the subsequent determinations.

Endocarp Extracts (Juice). The endocarp (the edible part of the fruit constituted of carpels containing the juice cells) deprived of seeds was homogenized in a mixer and then centrifuged at 18000*g* for 30 min. The supernatant was frozen at −20 °C until used for the subsequent determinations.

Seed Extracts. The seeds were initially washed with water, drained, and dried on filter paper. Then, 4 g of seeds were homogenized in a mixer with 20 mL of Milli-Q water. The homogenate was kept under constant agitation for 3 h and then centrifuged at 18000*g* for 30 min. The supernatants were frozen at −20 °C until used for the subsequent determinations.

Extracts from Seeds of Zanthoxylum piperitum. The dried fruits were purchased in a local market. The seeds (1.0 g), freed from pericarps, were homogenized in a blender with 4.0 mL of 0.1% formic acid in Milli-Q water and stirred for 30 min. The homogenate was centrifuged at 18000*g* for 30 min, and the supernatant was stored in 20 mL vials at −20 °C.

Enzymatic Hydrolysis of Glycosyl Derivatives in Plant Tissue Extracts. The pH of the extracts from the different plant tissues was adjusted to 5.0, and then a solution of *β*-glucosidase from almonds or *β*-galactosidase from *A. oryzae* in 0.1 M sodium acetate buffer at pH 5.0 was added. The final enzyme concentration in the extracts was 1 unit/mL. After incubation at 37 °C for various times, the samples were centrifuged and analyzed by high-performance liquid chromatography−electrospray ionization−tandem mass spectrometry (HPLC−ESI−MS/MS).

Determination of Aglycones and Glucosides in Plant Tissue Parts. As the standards of serotonin and its N-methylated derivatives were available, the levels of such compounds in the extracts were determined by comparison of the areas of the respective peaks in the

DOI: 10.1021/acs.jafc.5b01031
J. Agric. Food Chem. 2015, 63, 4220−4227

tandem mass chromatograms to those in the chromatogram of the standard mixture. However, because the standards of the glucosides were not available, an estimate of their levels was indirectly obtained by subjecting the extracts to the action of β-glucosidase and then determining for each analyte the increases (in the case of aglycones) and the decreases (in the case of glucosides) of the peak areas in the tandem mass chromatograms with respect to the corresponding peaks in the extracts without enzyme. By comparison to standards, the production of each aglycone can be calculated from the increase of the respective peak area. The aglycone production, in terms of moles, is equal to the moles of glucoside that, because of hydrolysis, caused the decrease of the corresponding area of the chromatographic peak. This provides a value of the peak area per mole of the glucoside to be known and, consequently, converts into moles the area of the corresponding peak in the chromatogram of the extract without enzyme.

HPLC–ESI–MS/MS Analyses. Analyses were carried out using a 1100 series HPLC equipped with an autosampler coupled online with a LC–MSD SL quadrupole ion trap (Agilent Technologies, Milan, Italy). The liquid chromatography (LC) separation of all serotonin derivatives was carried out using a Discovery-C_8 column (Supelco, Milan, Italy), 250 × 3.0 mm inner diameter, 5 μm, with a 5 mm × 3 mm inner diameter guard column of the same material, eluted isocratically with 0.1% formic acid in water, at a constant flow rate of 0.1 mL/min. The injection volumes were 10–20 μL for each sample. Electrospray ionization (ESI) was performed in positive-ion mode, with nitrogen as the nebulizing and drying gas under the following conditions: nebulizer pressure, 30 psi; drying temperature, 350 °C; and drying gas, 7 L/min. The ion charge control (ICC) was applied with the target set a 30 000 and maximum accumulation time at 20 ms. Multiple reaction monitoring (MRM) was used for the detection of analytes in HPLC–ESI–MS/MS analyses. The retention times and peak areas of the monitored fragment ions were determined by Agilent Chemstation version 4.2 software. The chemical structures and the transitions used for monitoring in MRM mode the serotonin derivatives analyzed in this study by LC–ESI–MS/MS are reported in Figure 1.

RESULTS AND DISCUSSION

Identification and Characterization of the Glycosylated Forms of Serotonin and Its N-Methylated Derivatives. Our recent findings of the occurrence of serotonin (**5**) and all its N-methylated derivatives[12,13] in several *Citrus* genus plants prompted us to investigate the possibility that those compounds might also be stored in glycosyl derivative forms in the plant tissues. To this aim, we first subjected leaf extracts of various *Citrus* plants to HPLC–ESI tandem mass analysis. A representative HPLC–ESI–MS^2 chromatogram of a bergamot leaf extract is shown in Figure 2. The chromatogram was obtained by isolating the ion masses at m/z 339.2, 353.2, 367.2, and 381.2, which coincide with those of the protonated masses of glycosylated serotonin (**1**), *N*-methylserotonin (**2**), *N*,*N*-dimethylserotonin (**3**), and *N*,*N*,*N*-trimethylserotonin (**4**), respectively (Figure 2). In the same chromatographic analysis, the ion masses at m/z 177.1, 191.1, 205.1, and 219.1, which correspond to those of the protonated aglycones, were also monitored (Figure 2). The identity of the putative glycosides was first assessed by their MS^2 fragmentation patterns and, in successive analyses, by MS^3 fragmentation patterns of selected ions occurring in the MS^2 fragmentation patterns. Figures 3–6 report the fragmentation patterns of the four peaks of Figure 2 eluted at the retention times of 27.4, 33.2, 40.4, and 45.6 min, which correspond to the four putative glycosides. In the same chromatogram, serotonin (**5**), *N*-methylserotonin (**6**), *N*,*N*-dimethylserotonin (**7**), and *N*,*N*,*N*-trimethylserotonin (**8**) are seen to elute at retention

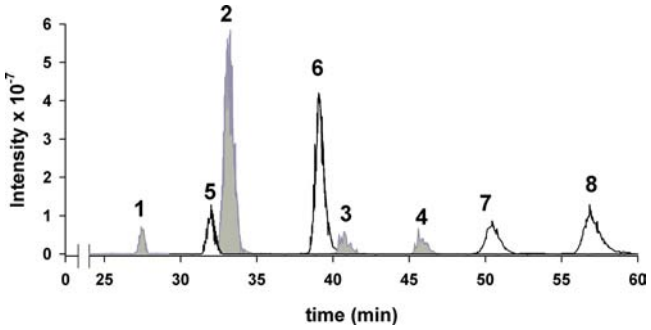

Figure 2. Representative MS^2 extracted ion chromatogram, in MRM mode, of a lemon leaf extract. Peaks in gray correspond to the glucosylated forms, and those in white correspond to the aglycones. The MS^2 transitions followed were 339.2 → 322 for serotonin 5-*O*-glucoside (**1**), 353.2 → 322 for *N*-methylserotonin 5-*O*-glucoside (**2**), 367.2 → 322 for *N*,*N*-dimethylserotonin 5-*O*-glucoside (**3**), 381.2 → 322 for *N*,*N*,*N*-trimethylserotonin 5-*O*-glucoside (**4**), 177.1 → 160 for serotonin (**5**), 191.1 → 160 for *N*-methylserotonin (**6**), 205.1 → 160 for *N*,*N*-dimethylserotonin (**7**), and 219.1 → 160 for *N*,*N*,*N*-trimethylserotonin (**8**). Retention times in minutes were 27.4 (**1**), 32.0 (**5**), 33.2 (**2**), 39.0 (**6**), 40.4 (**3**), 45.6 (**4**), 50.1 (**7**), and 56.8 (**8**).

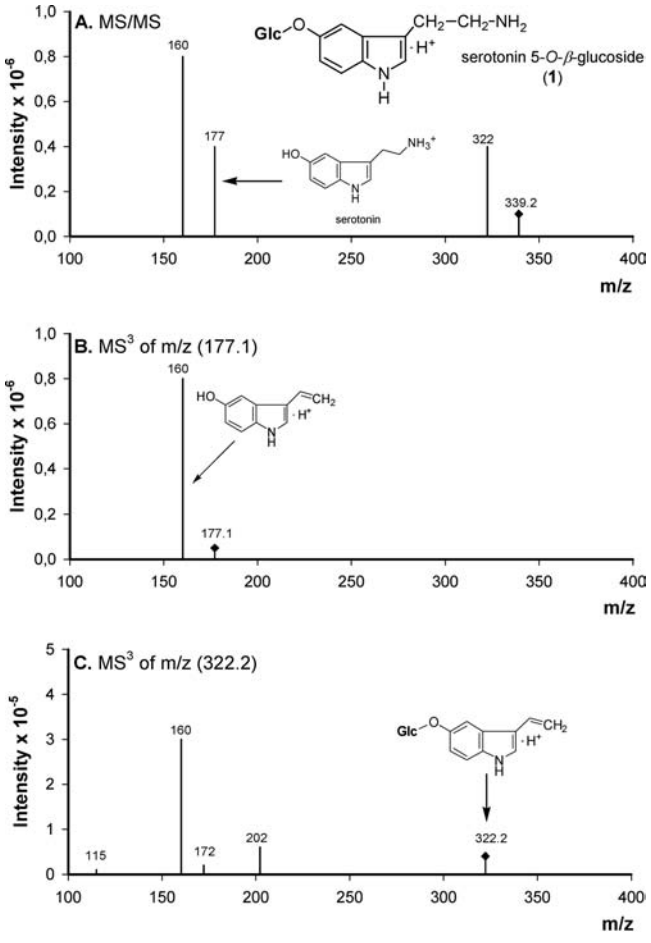

Figure 3. Mass spectra of serotonin 5-*O*-glucoside (**1**): (A) MS^2 fragmentation pattern, (B) MS^3 fragmentation pattern by isolating m/z 177.1, and (C) MS^3 fragmentation pattern by isolating m/z 322.2.

times of 32.0, 39.0, 50.1, and 56.8 min, respectively. The mass spectrometric behaviors of serotonin (**5**), *N*-methylserotonin (**6**), *N*,*N*-dimethylserotonin (**7**), and *N*,*N*,*N*-trimethylserotonin (**8**) were well-characterized by ESI–MS^n.[13,19,20] In particular,

DOI: 10.1021/acs.jafc.5b01031
J. Agric. Food Chem. 2015, 63, 4220–4227

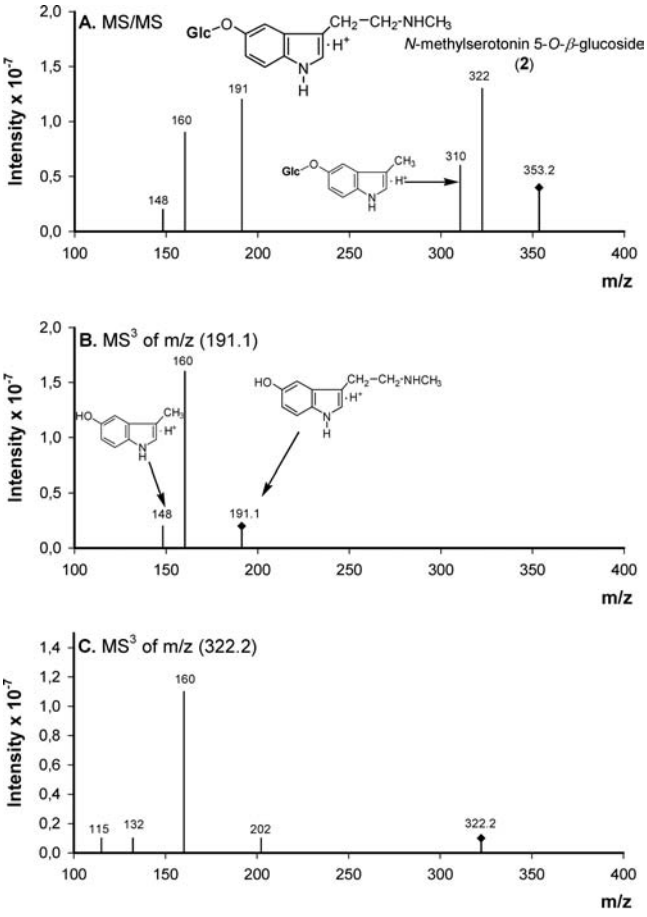

Figure 4. Mass spectra of *N*-methylserotonin 5-*O*-glucoside (**2**): (A) MS^2 fragmentation pattern, (B) MS^3 fragmentation pattern by isolating *m/z* 191.1, and (C) MS^3 fragmentation pattern by isolating *m/z* 322.2.

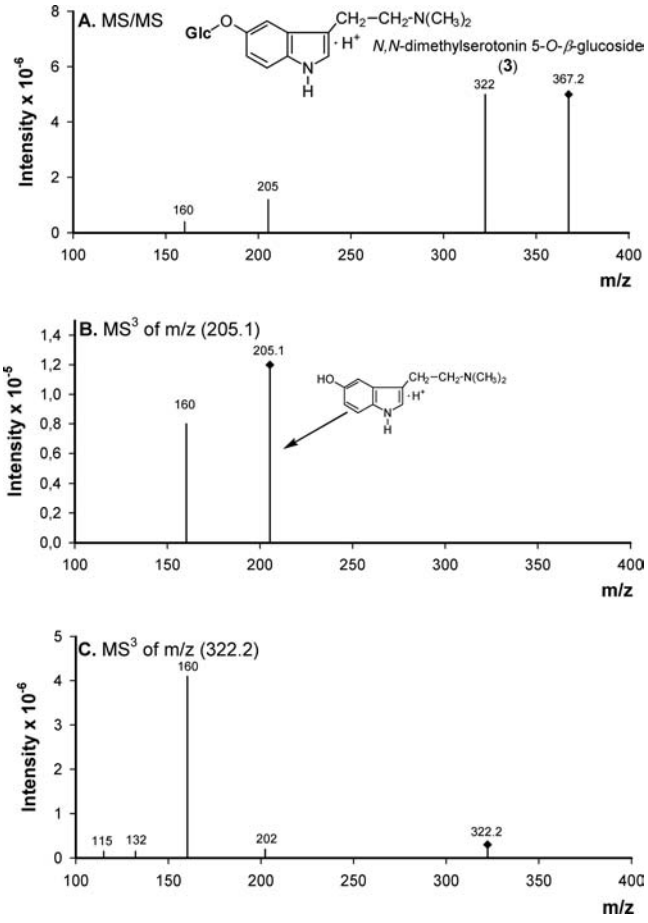

Figure 5. Mass spectra of *N*,*N*-dimethylserotonin 5-*O*-glucoside (**3**): (A) MS^2 fragmentation pattern, (B) MS^3 fragmentation pattern by isolating *m/z* 205.1, and (C) MS^3 fragmentation pattern by isolating *m/z* 322.2.

the MS^2 fragmentation patterns are in each case dominated by the ions at *m/z* 160, corresponding to protonated hydroxyvinylindole, which derives from the neutral loss of NH_3 for serotonin (**5**), CH_3NH_2 for *N*-methylserotonin (**6**), $(CH_3)_2NH$ for *N*,*N*-dimethylserotonin (**7**), and $(CH_3)_3N$ for *N*,*N*,*N*-dimethylserotonin (**8**).

As far as we know, the mass spectrometric features of the four glycosides of serotonin and its N-methylated derivatives have never been reported elsewhere, and therefore, it is of interest to address this issue. The MS^2 fragmentation pattern of all four peaks corresponding to the putative glycosides show an abundant fragment at *m/z* 322, which very likely derives from the neutral loss of NH_3, CH_3NH_2, $(CH_3)_2NH$, and $(CH_3)_3N$ from the ions at *m/z* 339.2, 353.2, 367.2, and 381.2, respectively, as it happens for aglycones. Furthermore, all four peaks in their MS^2 fragmentation pattern show ions at *m/z* corresponding to those of the protonated aglycone (that is *m/z* 177.1, 191.1, 205.1, and 219.1), which derive from the neutral loss of the glycosyl moiety from the parent ions to give the fragments at *m/z* $[M + H^+ - 162]$, specific for the loss of the precursor ion of a hexose residue (Figures 3A−6A).[21] Furthermore, the identical structure of the MS^2 fragments at *m/z* 322 deriving from each of four peaks is demonstrated by the identical MS^3 fragmentation patterns, in which, in all cases, the most abundant MS^3 fragment is that at *m/z* 160, likely corresponding to the protonated hydroxyvinylindole (Figures 3C−6C). Interestingly, when the ions at the *m/z* corresponding to each of the protonated aglycones are isolated from the MS^2 fragmentation pattern of each of the four glycoside peaks and fragmented, the most abundant MS^3 fragment is found at *m/z* 160 (Figures 3B−6B).

Glycosylated *N*-methylserotonin (**2**) deserves a separate discussion because it behaves quite differently from the other homologues, useful for its identification. In fact, the MS^2 fragmentation pattern of the peak at *m/z* 353, besides the expected fragments at *m/z* 322, 191, and 160, shows two unexpected fragments at *m/z* 310 and 148. The former is produced by the neutral loss of 43 Da ($CH_2{=}N{-}CH_3$) from the protonated parent molecule at *m/z* 353, and the latter is produced by the same neutral loss of 43 Da ($CH_2{=}N{-}CH_3$) from the fragment *m/z* 191 (protonated aglycone), as demonstrated by the MS^3 fragmentation pattern obtained by isolating the MS^2 fragment at *m/z* 191 (Figure 3B). On the other hand, the MS^2 fragmentation pattern of authentic *N*-methylserotonin (**6**) shows an identical fragmentation pattern.[13,19] All together, these results give strong evidence of the identity of the aglycone moieties.

An indication of the nature of the glycoside moiety in the compounds under study was obtained by subjecting *Citrus* leaf extracts to enzymatic hydrolysis by β-glucosidase from almonds, an enzyme specific for β-D-glucosides. The time course of the hydrolysis performed on a lemon leaf extract

DOI: 10.1021/acs.jafc.5b01031
J. Agric. Food Chem. 2015, 63, 4220−4227

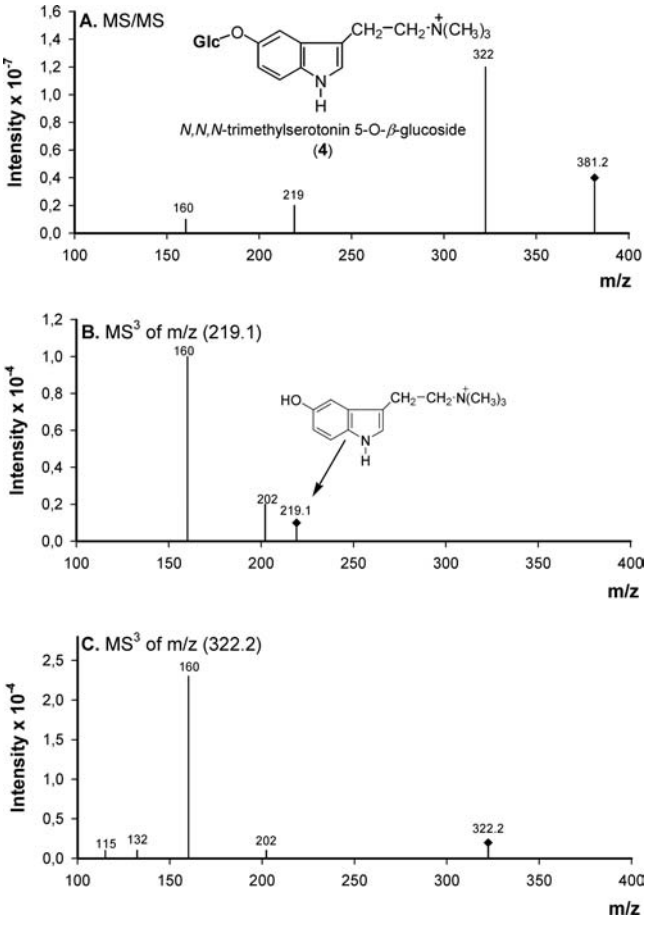

Figure 6. Mass spectra of *N,N,N*-trimethylserotonin 5-*O*-glucoside (**4**): (A) MS^2 fragmentation pattern, (B) MS^3 fragmentation pattern by isolating *m/z* 219.1, and (C) MS^3 fragmentation pattern by isolating *m/z* 322.2.

(Figure 7) clearly indicates the increase with time of the aglycone peaks and the decrease of those of the glycosides, thus showing that those compounds are substrates for the enzyme. Interestingly, the variations appear reduced when the N-methylation degree of the compound increases. As matter of fact, the putative 5-*O*-*β*-glucoside of serotonin (**1**) is the compound most affected by the enzymatic hydrolysis, while the

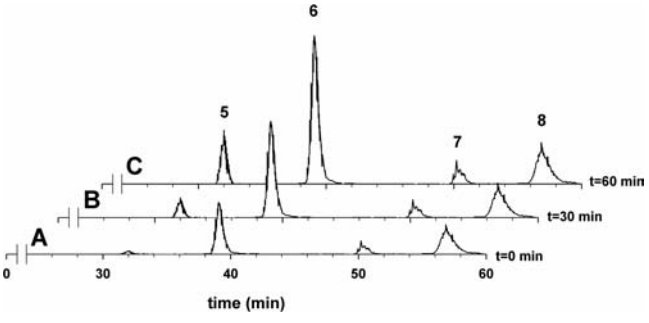

Figure 7. Time course of hydrolysis catalyzed by *β*-glucosidase from almonds of a lemon leaf extract: (A) 0 min, (B) 30 min, and (C) 60 min of incubation. The MS^2 extracted ion chromatograms in MRM mode show the production over time of serotonin (**5**), *N*-methylserotonin (**6**), *N,N*-dimethylserotonin (**7**), and *N,N,N*-trimethylserotonin (**8**). The *m/z* of the parent and extracted ions is the same as in the legend of Figure 3.

putative 5-*O*-*β*-glucoside of *N,N,N*-trimethylserotonin (**4**) appears almost unmodified after the same incubation time (Figure 7). Similar experiments were also conducted by performing the enzymatic hydrolysis with *β*-galactosidase from *A. oryzae*, but in this case, much slighter modifications were observed than those produced when using *β*-glucosidase (data not shown). Taken together, these experiments gave strong indications that the glycosidic moiety of the unknown compounds is represented by D-glucose. Conclusive evidence of the structures of at least two of the four substances under study comes from the comparison to the authentic 5-*O*-*β*-glucosides of *N*-methylserotonin (**2**) and *N,N*-dimethylserotonin (**3**). Actually, these two compounds were discovered in seeds of the plant *Z. piperitum* (Japanese pepper), and their structures were elucidated by nuclear magnetic resonance (NMR) studies.[22] We prepared extracts from seeds of this plant and compared their HPLC–ESI–MS^2 chromatograms to those of extracts from *Citrus* plant leaves. A complete superimposition of the two peaks from *Citrus* plants corresponding to the putative 5-*O*-*β*-glucosides of *N*-methylserotonin (**2**) and *N,N*-dimethylserotonin (**3**) was observed by comparison to those of the authentic substances present in the chromatogram of the *Z. piperitum* seed extracts. Moreover, the corresponding peaks showed identical MS^2 fragmentation patterns (data not shown).

Distribution of the Glucosylated Serotonin Derivatives in *Citrus* Plant Leaves. The distribution of the glucosylated forms of serotonin and its N-methylated derivatives in *Citrus* plant leaves indicates expression levels of the substances quite different among the species (Figure 8). The analysis of the distribution made it possible to divide the various species into three groups. The first group, represented by lemon, pomelo, and bergamot, expresses the highest levels of these compounds. The second group, represented by bitter orange, chinotto, and sweet orange, expresses levels of the four glucosides about one-half of the first group. Finally, the third group, represented by citron, mandarin, and clementine, shows very low expression levels of these metabolites, below 5% of those expressed by the richest species. The analysis of the levels of the four glucosides in the various *Citrus* species, reported relatively to the top species (first group), indicates that *N*-methylserotonin 5-*O*-*β*-glucoside (**2**) is the most expressed glucosylated form, followed by serotonin 5-*O*-*β*-glucoside (**1**), then *N,N*-dimethylserotonin 5-*O*-*β*-glucoside (**3**), and finally, *N,N,N*-trimethylserotonin 5-*O*-*β*-glucoside (**4**), which appears almost unexpressed in the third group (Figure 8).

Distribution of the Aglycones and Glucosylated Serotonin Derivatives in Bergamot and Bitter Orange Fruits. The distributions of glucosylated forms of serotonin derivatives and those of the corresponding aglycones were also estimated in the two *Citrus* plant species, bitter orange and bergamot, in various parts, that is, flavedo, albedo, juice, and seeds. The results showed that the aglycones are expressed at the highest levels in the seeds of both species (Table 1). *N*-Methylserotonin (**6**) and *N,N*-dimethylserotonin (**7**) resulted from being the more represented aglycones, with average values of 14 and 18 mg/kg, in bitter orange and bergamot seeds, respectively. In contrast, the level in seeds of *N,N,N*-trimethylserotonin (**8**) was about 4 mg/kg and even lower than that of serotonin (≤2 mg/kg). As for the glucoside fraction, it was distributed for both species in an almost uniform manner in flavedo (epicarp), albedo (the spongy white part under the epicarp), and fruit juice (Table 1). These results are similar to those found for other *Citrus* secondary metabolites,

DOI: 10.1021/acs.jafc.5b01031
J. Agric. Food Chem. 2015, 63, 4220–4227

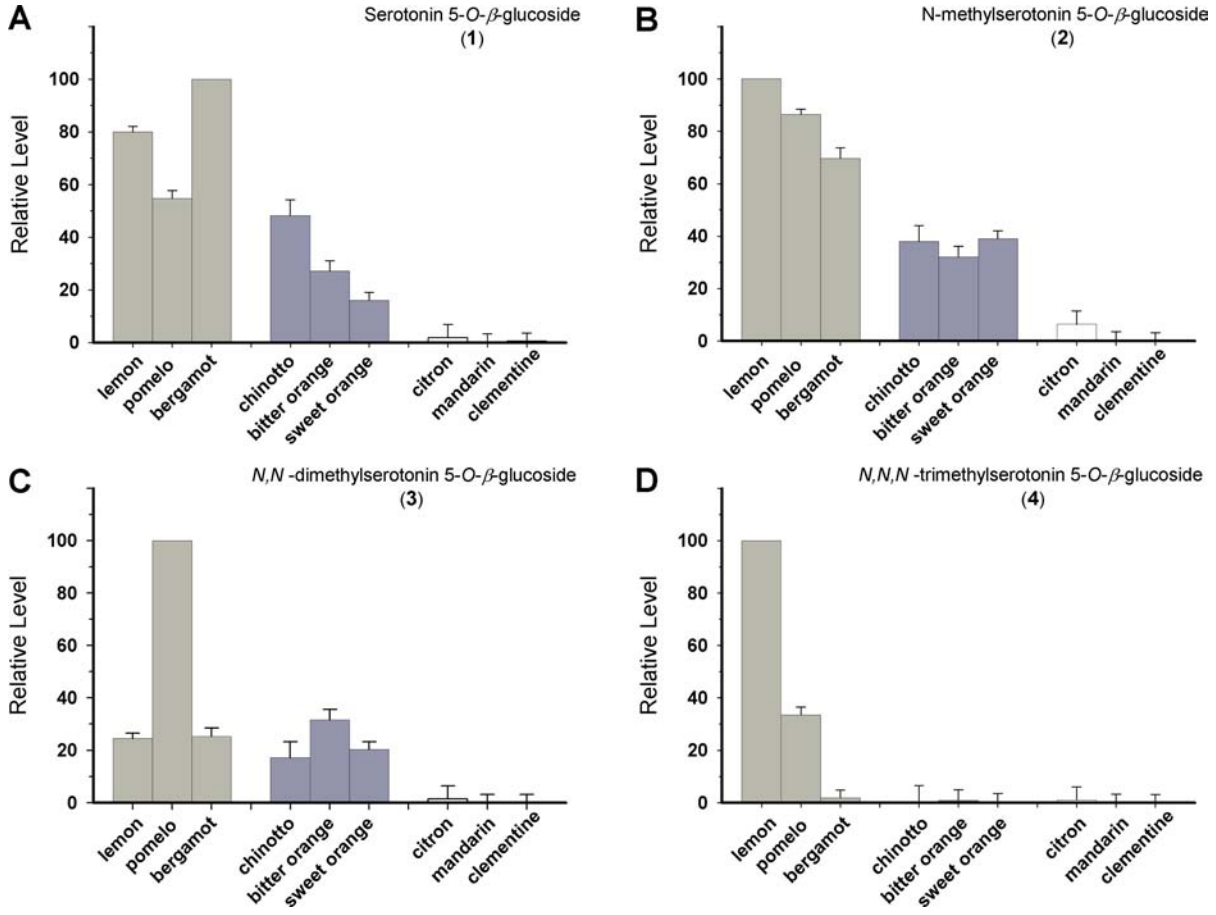

Figure 8. Relative levels in leaves of various *Citrus* species of serotonin 5-*O*-*β*-glucoside and its N-methylated forms: (A) serotonin 5-*O*-*β*-glucoside, (B) *N*-methylserotonin 5-*O*-*β*-glucoside, (C) *N*,*N*-dimethylserotonin 5-*O*-*β*-glucoside, and (D) *N*,*N*,*N*-trimethylserotonin 5-*O*-*β*-glucoside. The graphs are normalized to 100%, representing the level of the top productive species. The level of each compound is the average of three determinations. Bars represent the standard deviations.

Table 1. Percentage Distribution of Aglycones and Glucosylated Serotonin Derivatives in Tissue Parts of Bergamot and Bitter Orange Fruits

Citrus species	tissue	aglycones (%)	glucosides (%)
bergamot	flavedo	21	79
	albedo	30	70
	juice	13	87
	seeds	64	26
bitter orange	flavedo	13	87
	albedo	10	90
	juice	22	78
	seeds	66	34

such as flavanone and limonoids,[23−26] which play a key role in chemical defense and interaction with the environment.

Interrelationship of the Tryptamine Derivatives in *Citrus* Genus. In the genus *Citrus*, tryptamine is the biosynthetic precursor of a broad group of indole metabolites generated from biosynthetic steps of methylation and hydroxylation.[12,13] The results shown here indicate that an additional transformation of indole metabolites can occur through the biosynthetic step of glycosylation. The possible pathways that take into account these three steps, i.e., methylation, hydroxylation, and glycosylation, might involve a sequence of reactions starting with the formation of tryptamine from tryptophan, catalyzed by the enzyme tryptophan decarboxylase (Figure 9). Indeed, the absence of 5-hydroxytryptophan in the *Citrus* plants excludes that 5-hydroxytryptamine (serotonin) can be derived from decarboxylation of this amino acid. Once produced, tryptamine may be N-methylated by the action of the same or different methyltransferase(s) acting in a consecutive manner (Figure 9). Then, each methylated intermediate could be transformed in the corresponding hydroxylated form, or alternatively, tryptamine could be first hydroxylated to serotonin, which is successively N-methylated in a consecutive manner (Figure 9). Finally, in the last step, the transfer of the sugar residue occurs from the donor molecule, likely UDP-glucose, which is the most commonly used nucleotide sugar in plants,[27] to the acceptor molecule (Figure 9). In our case, the acceptor molecules are serotonin and its N-methylated derivatives. Alternatively, serotonin 5-*O*-*β*-glucoside (**1**) could also be N-methylated in a consecutive manner to produce forms at higher methylation degree. Of course, more in depth studies are required to support such hypothetical pathways.

The occurrence of the glucosylated serotonin derivatives in *Citrus* plants suggests a physiological role for these metabolites because it is well-known that glycosylation, by making many compounds less reactive and more water-soluble, represents a way adopted by plants to prevent cell damage and safely store toxic compounds important for their defense. When a plant is attacked, the toxic aglycones are released from the glycosylated compounds by action of glycosidases, which can occur in either

DOI: 10.1021/acs.jafc.5b01031
J. Agric. Food Chem. 2015, 63, 4220−4227

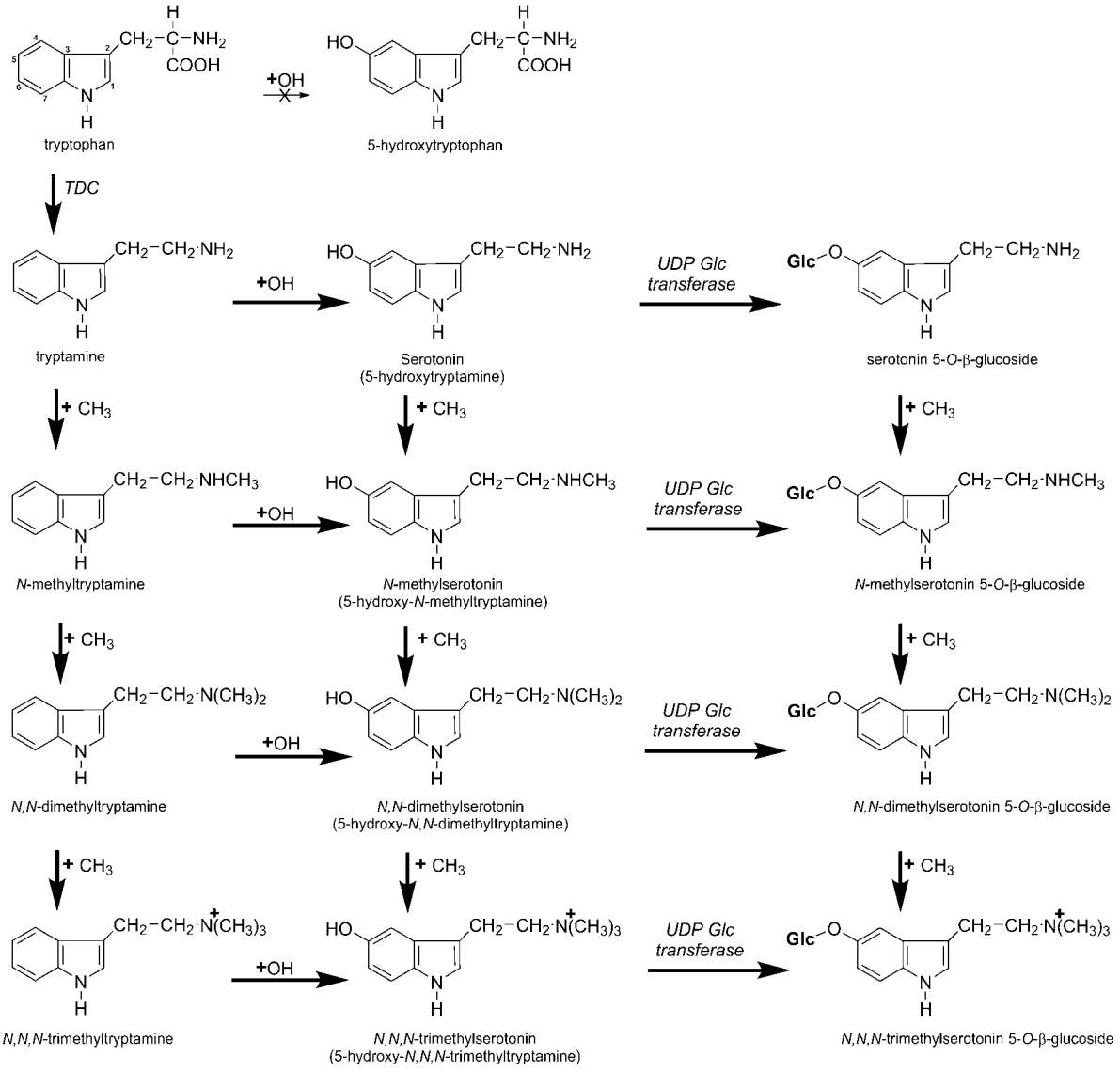

Figure 9. Hypothesized pathways for the biosynthesis of the tryptamine derivatives.

the plant or also aggressor tissues. In some cases, aglycone is also able to influence the behavior and physiology of insects and herbivores.[28,29] The distribution of the aglycone and glycosylated forms of serotonin derivatives found in various parts of the two *Citrus* species examined is consistent with the hypothesized defensive role (Table 1). In fact, in both bergamot and bitter orange, the aglycones are expressed mainly in the seeds, whose protection is crucial for plant diffusion. Conversely, the glycosylated derivatives are predominant in epicarp, albedo, and juice (Table 1). The distribution of glycosylated and aglycone forms of serotonin derivatives resembles that of other *Citrus* metabolites involved in defense and resistance mechanisms,[23−26] such as limonoids and flavanones, which act as powerful natural pesticides[30,31] and antifungal agents.[23,26] In fact, also for these compounds, the active forms are the aglycones, and their highest concentration is found in seeds.[23−25]

AUTHOR INFORMATION

Corresponding Author

*Telephone: +39-081-5665865. Fax: +39-081-5665863. E-mail: luigi.servillo@unina2.it.

Notes

The authors declare no competing financial interest.

REFERENCES

(1) Facchini, P. J.; Huber-Allanach, K. L.; Tari, L. W. Plant aromatic L-amino acid decarboxylase: evolution, biochemistry, regulation, and metabolic engineering applications. *Phytochemistry* **2000**, *54*, 121−138.

(2) De Luca, V.; Marineau, C.; Brisson, N. Molecular cloning and analysis of a cDNA encoding a plant tryptophan decarboxylase. *Proc. Natl. Acad. Sci. U. S. A.* **1989**, *86*, 2582−2586.

(3) O'Connor, S. E.; Maresh, J. Chemistry and biology of monoterpene indole alkaloids biosynthesis. *Nat. Prod. Rep.* **2006**, *23*, 532−547.

(4) Larsson, K. A.; Zetterlund, I.; Delp, G.; Jonsson, L. M. *N*-Methyltransferase involved in gramine biosynthesis in barley: cloning and characterization. *Phytochemistry* **2006**, *67*, 2002−8.

(5) Rogers, E. E.; Glazebrook, J.; Ausubel, F. M. Mode of action of the *Arabidopsis thaliana* phytoalexin camalexin and its role in Arabidopsis pathogen interactions. *Mol. Plant-Microbe Interact.* **1996**, *9*, 748−757.

(6) Ratzka, A.; Vogel, H.; Kliebenstein, D. J.; Mitchell-Olds, T.; Kroymann, J. Disarming the mustard oil bomb. *Proc. Natl. Acad. Sci. U. S. A.* **2002**, *99*, 11223−11228.

DOI: 10.1021/acs.jafc.5b01031
J. Agric. Food Chem. 2015, 63, 4220−4227

(7) Matsuo, H.; Taniguchi, K.; Hiramoto, T.; Yamada, T.; Ichinose, Y.; Toyoda, K.; Takeda, K.; Shiraishi, T. Gramine increase associated with rapid and transient systemic resistance in barley seedlings induced by mechanical and biological stresses. *Plant Cell Physiol.* **2001**, *42*, 1103−11.
(8) Ishihara, A.; Nakao, T.; Mashimo, Y.; Murai, M.; Ichimaru, N.; Tanaka, C.; Nakajima, H.; Wakasa, K.; Miyagawa, H. Probing the role of tryptophan-derived secondary metabolism in defense responses against *Bipolaris oryzae* infection in rice leaves by a suicide substrate of tryptophan decarboxylase. *Phytochemistry* **2011**, *72*, 7−13.
(9) Ishihara, A.; Hashimoto, Y.; Tanaka, C.; Dubouzet, J. G.; Nakao, T.; Matsuda, F.; Nishiaka, T.; Miyagawa, H.; Wakasa, K. The tryptophan pathway is involved in the defense responses of rice against pathogenic infection via serotonin production. *Plant J.* **2008**, *54*, 481−495.
(10) Ishihara, A.; Hashimoto, Y.; Miyagawa, H.; Wakasa, K. Induction of serotonin accumulation by feeling of rice striped stem borer in rice leaves. *Plant Signaling Behav.* **2008**, *3*, 714−716.
(11) Kang, K.; Kim, Y. S.; Park, S.; Back, K. Senescence-induced serotonin biosynthesis and its role in delaying senescence in rice leaves. *Plant Physiol.* **2009**, *150*, 1380−1393.
(12) Servillo, L.; Giovane, A.; Balestrieri, M. L.; Cautela, D.; Castaldo, D. N-Methylated tryptamine derivatives in *Citrus* genus plants: identification of *N*,*N*,*N*-trimethyltryptamine in bergamot. *J. Agric. Food Chem.* **2012**, *60*, 9512−9518.
(13) Servillo, L.; Giovane, A.; Balestrieri, M. L.; Casale, R.; Cautela, D.; Castaldo, D. *Citrus* genus plants contain N-methylated tryptamine derivatives and their 5-hydroxylated forms. *J. Agric. Food Chem.* **2013**, *61*, 5156−5162.
(14) Barlow, R. B.; Burston, K. N. A comparison of cinobufotenine (the quaternary derivative of 5-HT) and some related compounds with coryneine (the quaternary derivative of dopamine) on the frog rectus, guinea-pig ileum and rat fundus strip preparations. *Br. J. Pharmacol.* **1980**, *69*, 597−600.
(15) Pentzold, S.; Zagrobelny, M.; Rook, F.; Bak, S. How insects overcome two-component plant chemical defense: plant β-glucosidases as the main target for herbivore adaptation. *Biol. Rev. Cambridge Philos. Soc.* **2014**, *89*, 531−551.
(16) Chen, F. M. F.; Benoiton, N. L. A new method of quaternizing amines and its use in amino acid and peptide chemistry. *Can. J. Chem.* **1976**, *54*, 3310−3311.
(17) Servillo, L.; Giovane, A.; D'Onofrio, N.; Casale, R.; Cautela, D.; Ferrari, G.; Balestrieri, M. L.; Castaldo, D. N-Methylated derivatives of tyramine in *Citrus* genus plants: identification of *N*,*N*,*N*-trimethyltyramine (candicine). *J. Agric. Food Chem.* **2014**, *62*, 2679−2684.
(18) Servillo, L.; Giovane, A.; Balestrieri, M. L.; Ferrari, G.; Cautela, D.; Castaldo, D. Occurence of pipecolic acid and pipecolic acid betaine (homostachydrine) in *Citrus* genus plants. *J. Agric. Food Chem.* **2012**, *60*, 315−321.
(19) McClean, S.; Robinson, R. C.; Shaw, C.; Smyth, F. Characterisation and determination of indole alkaloids in frog-skin secretions by electrospray ionisation ion trap mass spectrometry. *Rapid Commun. Mass Spectrom.* **2002**, *16*, 346−354.
(20) Servillo, L.; Giovane, A.; Balestrieri, M. L.; Bata-Csere, A.; Cautela, D.; Castaldo, D. Betaines in fruits of *Citrus* genus plants. *J. Agric. Food Chem.* **2011**, *59*, 9410−9416.
(21) Ma, Y. L.; Vedernikova, I.; Van den Heuvel, H.; Claeys, M. Internal glucose residue loss in protonated *O*-diglycosyl flavonoids upon low-energy collision-induced dissociation. *J. Am. Soc. Mass Spectrom.* **2000**, *11*, 136−144.
(22) Yanase, E.; Ohno, M.; Harakawa, H.; Nakatsuka, S. Isolation of *N*,*N*-dimethyl and *N*-methylserotonin 5-*O*-β-glucosides from immature *Zanthoxylum piperitum* seeds. *Biosci., Biotechnol., Biochem.* **2010**, *74*, 1951−1952.
(23) Hasegawa, S.; Berhow, M. Analysis of limonoids by thin-layer chromatography. In *Citrus Limonoids: Functional Chemicals in Agriculture and Foods*; Berhow, M. A., Hasegawa, S., Manners, G., Eds.; American Chemical Society (ACS): Washington, D.C., 2000; ACS Symposium Series, Vol. *758*, Chapter 3, pp 31−39.
(24) Ozaki, Y.; Ayano, S.; Inaba, N.; Miyake, M.; Berhow, M. A.; Hasegawa, S. Limonoid glucosides in fruit, juice and processing by-products of satsuma mandarin (*Citrus unshiu* Marcov). *J. Food Sci.* **1995**, *60*, 186−189.
(25) Esposito, C.; Tridente, R. L.; Balestrieri, M. L.; Laratta, B.; De Masi, L.; Servillo, L.; Castaldo, D. Distribuzione dei limonoidi nelle diverse parti del frutto di bergamotto. *Essenze, Deriv. Agrum.* **2006**, *76*, 11−18.
(26) Del Rio, J. A.; Gomez, P.; Baidez, A. G.; Arcas, M. C.; Botia, J. M.; Ortuno, A. Changes in the levels of polymethoxyflavones and flavanones as part of the defense mechanism of *Citrus sinensis* (Cv.Valencia late) fruits against *Phytophthora citrophthora*. *J. Agric. Food Chem.* **2004**, *52*, 1913−1917.
(27) Ross, J.; Li, Y.; Lim, E.; Bowles, D. J. Higher plant glycosyltransferases. *Genome Biol.* **2001**, *2*, reviews3004.1−reviews3004.6.
(28) Thomas, J. C.; Adams, D. G.; Nessler, C. L.; Brown, J. K.; Bohnert, H. J. Tryptophan decarboxylase, tryptamine, and reproduction of the whitefly. *Plant Physiol.* **1995**, *109*, 717−720.
(29) Gill, R. I. S.; Ellis, B. E.; Isman, M. B. Tryptamine induced resistance in tryptophan decarboxylase transgenic poplar and tobacco plants against their specific herbivores. *J. Chem. Ecol.* **2003**, *29*, 779−793.
(30) Alford, A. R.; Cullen, J. A.; Storch, R. H.; Bentley, M. D. Antifeedant activity of limonin against the Colorado potato beetle (Coleopteran:Chrysomelidae). *J. Econ. Entomol.* **1987**, *80*, 575−578.
(31) Murray, K. D.; Groden, E.; Drummond, F. A.; Alford, A. R.; Conley, S.; Storch, R. H.; Bentley, M. D. Citrus limonoid effects on Colorado potato beetle (Coleopteran:Chrysomelidae) colonization and oviposition. *Environ. Entomol.* **1995**, *24*, 1275−1283.

DOI: 10.1021/acs.jafc.5b01031
J. Agric. Food Chem. 2015, 63, 4220−4227

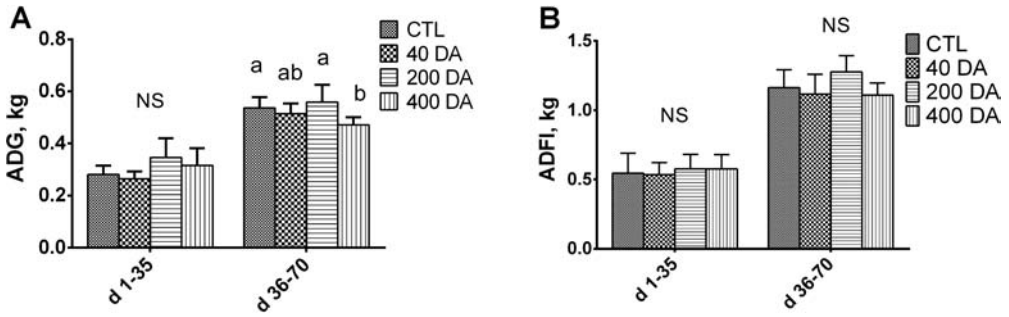

Figure 1. Effects of increasing concentrations of daidzein on performance of pigs in phase 1 (days 1−35) and 2 (days 36−70). (A) Average daily weight gain (ADG) of repeated dose daidzein-treated piglets with an initial average BW of 6.4 kg. (B) Average daily feed intake (ADFI) of repeated dose daidzein-treated piglets. Each bar represents the mean ± SD of six experimental units (pens). CTL, control group fed a basal diet. 40/200/400 DA, 40/200/400 mg/kg daidzein supplemented to CTL. *Significantly different from control at $P < 0.05$. NS, not significant ($P > 0.05$).

units/mL of glucuronidase activity and 775 units/mL of sulfatase activity) were obtained from Sigma-Aldrich Co. (St. Louis, Mo., USA). All other reagents used for residue measurement were of HPLC-grade. Deionized water was used throughout.

Experimental Design and Animal Management. Ninety-six crossbred [(Large White × Landrace) × Duroc] weaned pigs (23 ± 2 days postfarrowing; 48 males and 48 females) were sorted by body weight (BW) and sex and randomly allotted to dietary treatment in a 70 day experiment [phase 1 (days 1−35), 4 treatments; 6 replicates (pens) per treatment; 4 pigs per pen; phase 2 (days 36−70), 4 treatments; 6 replicates (pens) per treatment; 3 pigs per pen]. Average initial BW was 6.4 ± 0.1 kg. Diets were arranged as follows: (1) The NRC (1998) standard commercial feed without any soy source was used as the control group (CTL), (2) CTL + 40 mg/kg of daidzein (the manufacturer's recommended dose in young pigs), (3) CTL + 200 mg/kg of daidzein, and (4) CTL + 400 mg/kg of daidzein. Feed intake and BW measurements were obtained at the beginning of the experiment and weekly thereafter for the duration to determine average daily weight gain (ADG) and average daily feed intake (ADFI).

All pigs were housed in a temperature-controlled room with continuous lighting. Each pen contained a single nipple waterer and a single self-feeder to facilitate ad libitum access to water and feed.

Sample Collection. One pig was randomly selected from each pen to obtain blood samples collected from jugular veins on day 35 and day 70 before weighing (14 h after feeding); 10 mL of blood was collected into EDTA-coated pediatric Microvette tubes (Sarstedt AG and Co., Numbrecht, Germany) for hematological analysis. Another 10 mL of blood from each pig was centrifuged at 3000*g* for 15 min to obtain serum, which was stored at −20 °C until needed for the determination of blood markers and hormonal levels. Then the selected pigs were slaughtered by a lethal injection of sodium pentobarbital to obtain samples of small intestinal segment, mesenteric lymph, muscle, and organs (liver, heart, kidney, and spleen). The middle sections (4 cm) of duodenum, jejunum, and ileum were isolated and kept in 10% formalin for microscopic assessment of mucosal morphology. About 5 cm^3 of a regular shape sample from each organ was kept in the same way for morphological assessment. About 10 g of semitendinosus and liver samples was collected from each pig and kept at −20 °C for residue analysis of isoflavones.

Hormone Levels and Blood Parameters. Serum estradiol (E2), testosterone (T), growth hormone (GH), type-1 insulin-like growth factor (IGF-1), triiodothyronine (T3), and tetraiodothyronine (T4) were assayed using commercially available swine ELISA kits (BioSource International Inc., Camarillo, CA). The minimum detectable levels were 0.8 μg/L for GH, 10 μg/L for IGF-1, 1.8 pmol/L for estradiol, 20 ng/L for testosterone, 3 ng/mL for T3, and 10 ng/mL for T4. Heparinized whole blood was assayed for white blood cell count, red blood cell count, hemoglobin, hematocrit, mean corpuscular volume, mean corpuscular hemoglobin, hemoglobin concentration, and platelet count on an automated hematology analyzer (Sysmex XT 1800, Roche Diagnostics). Serum was assayed for the total protein, albumin, globulin, total bilirubin, alanine aminotransferase, aspartate aminotransferase, alkaline phosphatase, urea nitrogen, and glucose by an automatic biochemical analyzer (Hitachi 7180, Japan). Antioxidant indices, including glutathione peroxidase (GSH-PX), superoxide dismutase (SOD), malondialdehyde (MDA), and total antioxygenic capability (T-AOC), were determined with commercially available reagent kits (Nanjing Jiancheng Bioengineering Institute, China). All measurements were done in duplicate at minimum.

Intestinal Morphology and Organ/Tissue Histopathology. Organ (liver, heart, spleen, and kidney) samples, mesenteric lymph samples, and intestinal segments were embedded in paraffin wax. Cross sections (6 μm thick) of each sample were stained with hematoxylin and eosin. A biological microscope with a built-in digital camera was used (DM BA300, Motic, China). Organ and mesenteric lymph segments were observed at 100× to 400× magnifications to determine the morphological structures. The villus height and crypt depth of the intestinal segments were determined at 40× magnification to measure the lengths of 10 well-oriented intact villi and their associated crypt according to the methods of Touchette et al.[19] The villus height-to-crypt depth ratio (VCR) was calculated.

All sections were reviewed and graded in a blinded manner by a well-experienced vet from the pathology laboratory for histopathological analysis. For intestine, liver, kidney, heart, spleen, and lymphoglandulae mesentericae, qualitative scorings with respective scores and grading standards (see Table S1 in the Supporting Information for details) were used to evaluate the health status of the pigs. The highest score of the pathological change observed would be the score of the section. For example, if in a field a pathological change score of 1 and another score of 2 were observed at the same time, the score of this section is 2. The average value of the scores of all the sections in one group would be the viscera damage indices of the treatment, ranging from 0 to 3.

Distribution of Isoflavones in Body Tissues. Tissues from pigs (liver and semitendinosus muscle) were thawed at room temperature. Tissues (3−5 g depending on the type and amount of sample available) weighed with an electronic analytical balance (Hengping FA2004, Shanghai, China) with an accuracy of 1/10 000 g were diluted with 10 mL of ammonium acetate buffer solution (pH 5.0), homogenized with a Polytron System PET 2100 (Kinematica AG, Lucerne, Switzerland), and combined with 80 μL of hydrolytic enzyme (β-glucuronidase from *Helix pomatia*). The sample mixture solution was incubated at 37 °C for 8 h in a forma orbital shaker (Shanzhi TS-1102C, Shanghai, China). Then 10 mL of acetonitrile (Merck, Germany) and 10 mL of ethyl acetate (Merck, Germany) were added in sequence. After being sufficiently mixed with a vortex shaker (V-5, qilinbeier, Haimen, China), the samples were centrifuged at 10 000*g* for 10 min at 4 °C. All of the supernatant was transferred to clean Erlenmeyer flasks. The remaining isoflavones in the precipitate were extracted two more times with 20 mL of ethyl acetate each time to the same Erlenmeyer flasks. The extracts were concentrated to dry in a rotary evaporator at a negative pressure and then dissolved with 3 mL

DOI: 10.1021/acs.jafc.5b00677
J. Agric. Food Chem. 2015, 63, 4228−4235

Table 1. Serum Hormone Levels of Repeated Dose Daidzein-Treated Pigs on Day 35 and Day 70 ([a−c]Means in the Same Row with Different Superscripts Differ, $P < 0.05$)[a]

item[b]	control	dietary daidzein, mg/kg		
		40	200	400
		day 35		
T3	14.8 ± 0.13	15.0 ± 0.85	16.0 ± 3.18	14.7 ± 0.075
T4	121 ± 19.7	117 ± 21.9	132 ± 12.5	110 ± 10.0
IGF-1	150 ± 9.24	148 ± 27.7	157 ± 8.01	148 ± 36.9
GH	77.0 ± 14.0	88.8 ± 12.0	90.7 ± 18.0	81.9 ± 7.60
T-*m*	296 ± 72.8	346 ± 168	334 ± 167	320 ± 64.6
T-*f*	362 ± 47.7 a	324 ± 37.6 ab	246 ± 74.5 bc	224 ± 20.2 c
E2-*m*	38.4 ± 2.00	44.3 ± 6.43	42.3 ± 5.98	38.3 ± 2.46
E2-*f*	37.5 ± 0.53	39.1 ± 3.45	36.3 ± 2.10	40.8 ± 14.3
		day 70		
T3	15.1 ± 0.42	15.7 ± 2.54	15.4 ± 1.07	14.8 ± 0.23
T4	100 ± 13.0	101 ± 13.1	100 ± 23.5	85.0 ± 9.98
IGF-1	151 ± 38.4	150 ± 39.8	159 ± 24.3	148 ± 15.0
GH	80.8 ± 14.9	83.8 ± 20.5	91.8 ± 16.3	69.5 ± 21.0
T-*m*	272 ± 98.1	225 ± 13.8	245 ± 6.43	238 ± 57.4
T-*f*	374 ± 37.6 a	344 ± 43.8 ab	252 ± 37.6 bc	219 ± 76.6 c
E2-*m*	37.6 ± 3.17	39.9 ± 6.59	38.8 ± 0.61	38.2 ± 3.34
E2-*f*	36.2 ± 3.14	42.9 ± 3.28	40.6 ± 7.51	40.7 ± 1.55

[a]Values of T3, T4, GH, and IGF-1 are means ± SD ($n = 6$). Values of T-*m*, T-*f*, E2-*m*, and E2-*f* are means ± SD ($n = 3$). [b]T_3 = triiodothyronine, μg/L; T_4 = tetraiodothyronine, μg/L; IGF-1 = type-1 insulin-like growth factor, μg/L; GH = growth hormone, μg/L; T-*m* = testosterone level of male pigs, ng/L; T-*f* = testosterone level of female pigs, ng/L; E_2-*m* = estradiol level of male pigs, pmol/L; E_2-*f* = estradiol level of female pigs, pmol/L.

Table 2. Haematology and Clinical Biochemistry Analysis of Repeated Dose Daidzein-Treated Pigs on Day 35 and Day 70 ([a,b]Means in the Same Row with Different Superscripts Differ, $P < 0.05$)[a]

item[b]	control	dietary daidzein, mg/kg		
		40	200	400
		day 35		
WBC	14.5 ± 3.45	14.7 ± 2.12	17.4 ± 4.51	16.9 ± 3.22
RBC	6.01 ± 0.37	6.00 ± 0.50	6.38 ± 0.42	6.22 ± 0.48
HGB	96.2 ± 6.91	100 ± 10.4	105 ± 8.17	105 ± 19.2
HCT	0.350 ± 0.016 b	0.350 ± 0.036 b	0.390 ± 0.16 a	0.384 ± 0.0090 a
MCV	58.1 ± 2.10 b	58.4 ± 4.05 b	61.4 ± 3.21 ab	63.1 ± 2.73 a
MCH	15.3 ± 1.43 b	15.7 ± 1.41 b	16.8 ± 0.54 ab	17.3 ± 0.75 a
MCHC	274 ± 14.3	271 ± 6.98	274 ± 6.69	274 ± 8.18
PLT	438 ± 86.3	398 ± 46.4	440 ± 54.3	379 ± 62.5
		day 70		
WBC	15.4 ± 1.05	20.1 ± 5.78	19.6 ± 2.41	17.4 ± 1.78
RBC	6.85 ± 0.51	6.77 ± 0.73	6.72 ± 0.47	6.86 ± 0.51
HGB	106 ± 7.79	107 ± 8.41	113 ± 7.77	113 ± 8.52
HCT	0.398 ± 0.025	0.392 ± 0.028	0.420 ± 0.029	0.413 ± 0.023
MCV	57.8 ± 1.49	58.0 ± 5.03	62.0 ± 2.90	60.1 ± 2.65
MCH	15.4 ± 0.48	15.8 ± 1.40	16.9 ± 0.94	16.6 ± 0.72
MCHC	267 ± 7.42	273 ± 3.76	273 ± 8.26	275 ± 9.97
PLT	488 ± 178	469 ± 87.1	474 ± 133	532 ± 35.3

[a]Values are means ± SD ($n = 6$). [b]WBC = white blood count, 10^9/L; RBC = red blood cell count, 10^{12}/L; HGB = hemoglobin, g/L; HCT = hematocrit, %; MCV = mean corpuscular volume, fL; MCH = mean corpuscular hemoglobin, pg; MCHC = mean corpuscular hemoglobin concentration, g/L; PLT = blood platelet count, 10^9/L.

of 50% (v/v) methanol in deionized water. The solutions were centrifuged at 10 000*g* for 10 min at 4 °C and subsequently filtered through a 0.22 μm nylon membrane prior for analysis by UPLC/MS with the chromatographic conditions as follows: chromatographic column, thermoelectric C18.24 μm 2.4 × 50 mm (thermo); mobile phase, (A) water, (B) acetonitrile + methanol = 1 + 1; column temperature = 35 °C; sample size = 5 μL, using an electrospray ion source, negative ion mode (ESI−), and multiple reaction monitoring (MRM) mode. The synthetic standards (glycitein, genistein, daidzein, equol) were obtained from Sigma-Aldrich. Three linear calibration curves (low, medium, and high) with a minimum of four concentrations per curve were prepared according to the procedure of Gilani et al.[18] for glycitein, genistein, daidzein, and equol, and only calibration curves with high linearity from all analytes ($R^2 > 0.998$) in the expected calibration range were used.

Statistics. Data were compared between all of the four groups by subjecting them to ANOVA for a randomized complete block design by using the GLM procedure (SAS Inst. Inc., Cary, NC). Statistical differences among treatments were separated by Duncan's multiple range tests. Results were expressed as mean ± standard deviation

DOI: 10.1021/acs.jafc.5b00677
J. Agric. Food Chem. 2015, 63, 4228−4235

Table 3. Serum Antioxidant Levels of Repeated Dose Daidzein-Treated Pigs on Day 35 ([a,b]Means in the Same Row with Different Superscripts Differ, $P < 0.05$)[a]

		dietary daidzein, mg/kg		
item[b]	control	40	200	400
GSH-PX	729 ± 127	795 ± 172	1022 ± 361	845 ± 244
SOD	18.4 ± 1.39 b	18.8 ± 1.59 b	21.0 ± 0.78 a	19.6 ± 0.53 ab
MDA	7.94 ± 2.05 a	7.78 ± 1.83 a	5.42 ± 1.44 b	6.51 ± 0.95 ab
T-AOC	10.4 ± 2.26	10.2 ± 3.02	11.2 ± 2.21	11.2 ± 3.02

[a]Values are means ± SD ($n = 6$). [b]GSH-PX = glutathione peroxidase, U/mL; SOD = superoxide dismutase, U/mL; MDA = malondialdehyde, nmol/mL; T-AOC = total antioxygenic capability, U/mL.

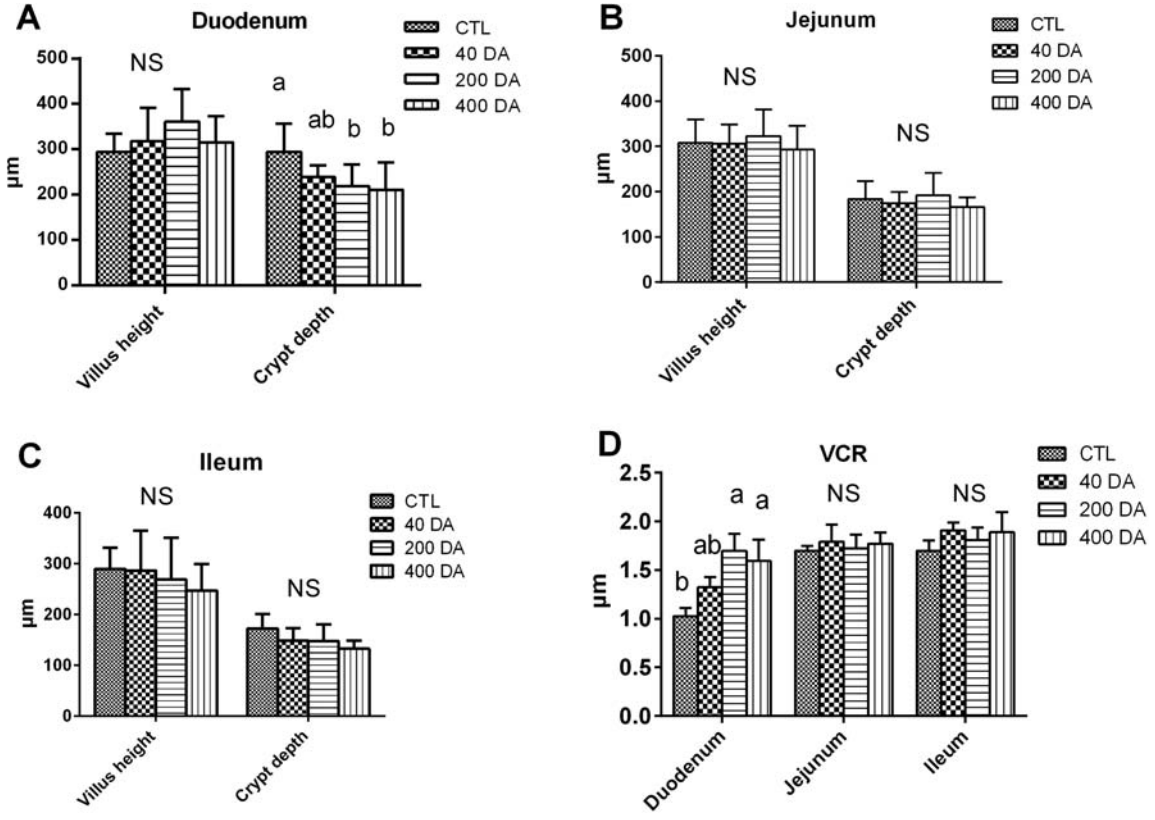

Figure 2. Intestinal morphology of repeated dose daidzein-treated piglets. (A–C) Villus height and crypt depth of duodenum, jejunum, and ileum, respectively on day 35. (D) Villus height-to-crypt depth ratio (VCR) of duodenum, jejunum, and ileum. Each bar represents the mean ± SD of six experimental units (pens) ($n = 6$). CTL, control group fed a basal diet. 40/200/400 DA, 40/200/400 mg/kg daidzein supplemented to CTL. Bars with different letters are significantly ($P < 0.05$) different from each other. NS, not significant ($P > 0.05$).

(SD). Probability values less than 0.05 were used as the criterion for statistical significance. The pen served as the experimental unit in the analyses.

RESULTS

Weight Gain and Feed Intake. In phase 1, there was no significant difference in average daily gain between the four groups. However, pigs fed 200 mg/kg of daidzein tended to have a greater ADG ($P = 0.082$) compared with those in CTL. In phase 2, ADG of pigs was decreased ($P = 0.03$) by 400 mg/kg of daidzein supplementation when compared with CTL. No differences were found in feed consumption (ADFI) throughout the whole experimental period (Figure 1). No gender differences were found in ADG or ADFI.

Hormone Levels and Blood Parameters. There were no effects ($P > 0.05$) of daidzein treatments on the content of triiodothyronine, tetraiodothyronine, IGF-1, GH, or estradiol in the serum of pigs in both phase 1 and phase 2 (Table 1). However, gilts receiving 200 and 400 mg/kg daidzein had a reduced ($P = 0.02$, phase 1; $P = 0.004$, phase 2) serum testosterone level compared with pigs in CTL.

Hematology analysis revealed that HCT, MCV, and MCH in pigs was significantly increased at the dose of 400 mg/kg of daidzein ($P < 0.05$), while other hematological parameters were not changed after 35 days of treatment (Table 2). It is shown that 200 mg/kg of daidzein supplementation also increased HCT ($P < 0.05$) of pigs compared with CTL. Beyond that, no significant differences in other tested hematological parameters were noted after a 35 day treatment. There was no significant differences between all the parameters in phase 2. We also investigated the effects of daidzein on some serum biochemical indices; however, there was no significant differences (data now shown). Gender differences were not found in any of the blood parameters.

Pigs receiving 200 mg/kg daidzein had greater ($P < 0.05$) SOD activity and lower ($P < 0.05$) MDA content in serum

DOI: 10.1021/acs.jafc.5b00677
J. Agric. Food Chem. 2015, 63, 4228–4235

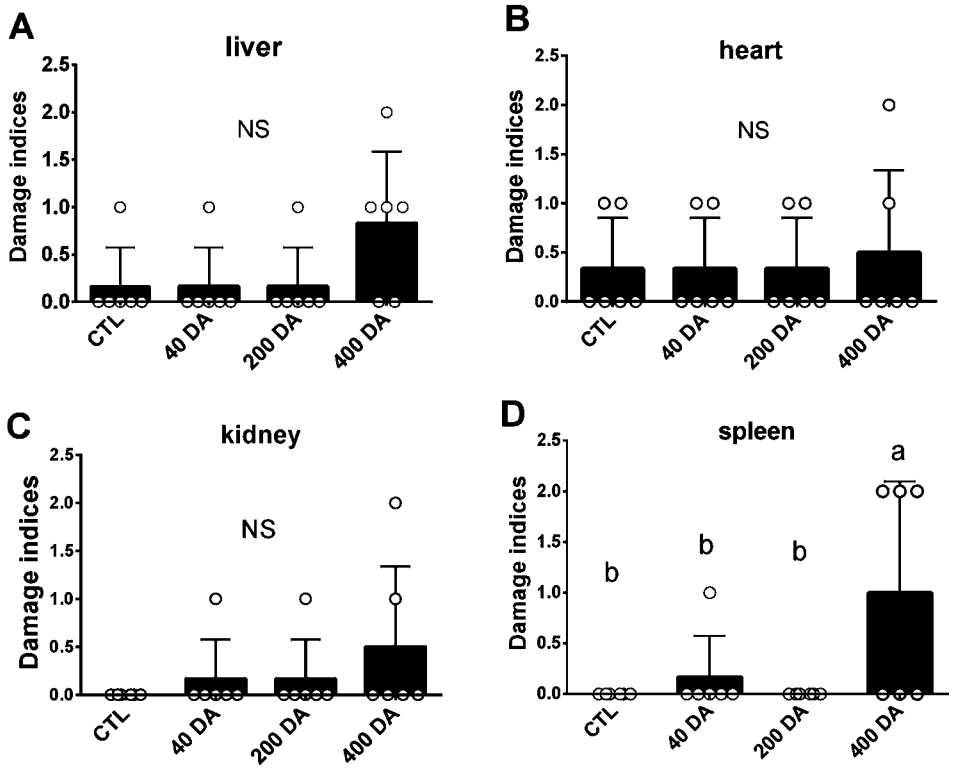

Figure 3. Organ damage indices of repeated dose daidzein-treated pigs on day 70. (A–D) Damage degree of liver, heart, kidney, and spleen of pigs in the four treatments, respectively. The damage indices ranges from 0 to 3 [0, completely healthy; 1, mild injury; 2, moderate injury; 3, severe injury (not shown in the graphs)]. Each dot represents the organ damage score of an individual pig (n = 6). Data are also expressed as mean ± SD. CTL, control group fed a basal diet. 40/200/400 DA, 40/200/400 mg/kg daidzein supplemented to CTL. Bars with different letters are significantly (P < 0.05) different from each other. NS, not significant (P > 0.05).

compared with CTL in phase 1 (Table 3). However, T-AOC and GSH-PX were not affected by treatments. There were no significant differences between treatments on antioxidant activities in phase 2 (data not shown). Besides, there were no gender differences found in the antioxidant indices tested.

Intestinal Morphology and Organ/Tissue Histopathology. Histological evaluation showed no effect of dietary supplementation of daidzein on villus height of the small intestine. However, pigs fed 200 and 400 mg/kg of daidzein had smaller (P < 0.05) crypt depth and greater (P < 0.05) VCR in the duodenum compared with that in CTL on day 35 (Figure 2). However, intestinal morphology was not effected by daidzein in phase 2 (data not shown). No gender differences were observed in villus height, crypt depth, or VCR.

According to the histology score (organ damage index), there were few observable effects of 40 and 200 mg/kg of dietary daidzein supplementation on the morphology of all the organs and tissues examined in both phases 1 and 2. However, 400 mg/kg of daidzein supplementation could cause mild damage (P < 0.05) to the spleens of weanling pigs by day 70 (Figure 3) (this effect was not obvious on day 35; data not shown). Meanwhile, 400 mg/kg of daidzein had a trend to increase (P = 0.08) the histology score of livers at the end of phase 2. Histology score shows no evident gender differences.

Distribution of Isoflavones in Body Tissues. The results (Figure 4) indicate that the amount of daidzein deposited in the liver and muscle of pigs was not affected (P > 0.05) by dietary daidzein supplementation for 35 days. In view of the fact that trace amounts of the soy isoflavones were detected in the diet (data not shown), we also monitored levels of glycitein and genistein in animal tissues. On day 35, the contents of glycitein and genistein in the liver were decreased by ingesting daidzein. Genistein level in the muscle (semitendinosus) was also decreased by 400 mg/kg dietary daidzein supplementation compared with CTL. On the 70th day of this experiment, dietary daidzein supplementation improved the content of daidzein (P < 0.05) in the pigs' livers compared with that in the control group. Similar to the result on the 35th day, the content of glycitein in the liver was decreased by 200 or 400 mg/kg of dietary daidzein supplementation compared with CTL on day 70. In addition, the contents of equol tended to be enhanced in livers (P = 0.09) and muscles (P = 0.1) of pigs by dietary daidzein supplementation in phase 2. It was shown that there were greater distributions of isoflavones in liver than in muscle in both phase 1 and phase 2. Meanwhile, in any of the four groups, the level of daidzein in the liver on day 70 was higher (P < 0.01) than on day 35. No gender differences were found in tissue residues of isoflavones.

■ DISCUSSION

Previous studies show that 20 or 40 mg/kg of dietary daidzein has no effect on the growth of mice,[20] but that 1000 mg/kg significantly decreases the body weight of female rats.[17] This suggests that there is a dose effect in terms of growth, regardless of gender. As mentioned above, the structure and function of daidzein resembles that of steroid estrogens. In many animals, including pigs, low concentration of daidzein binds weakly to estrogen receptors. However, daidzein at higher levels may act as anti-estrogen by antagonizing the binding of potent natural estrogens to its receptors.[21,22] Studies show that estrogen

DOI: 10.1021/acs.jafc.5b00677
J. Agric. Food Chem. 2015, 63, 4228–4235

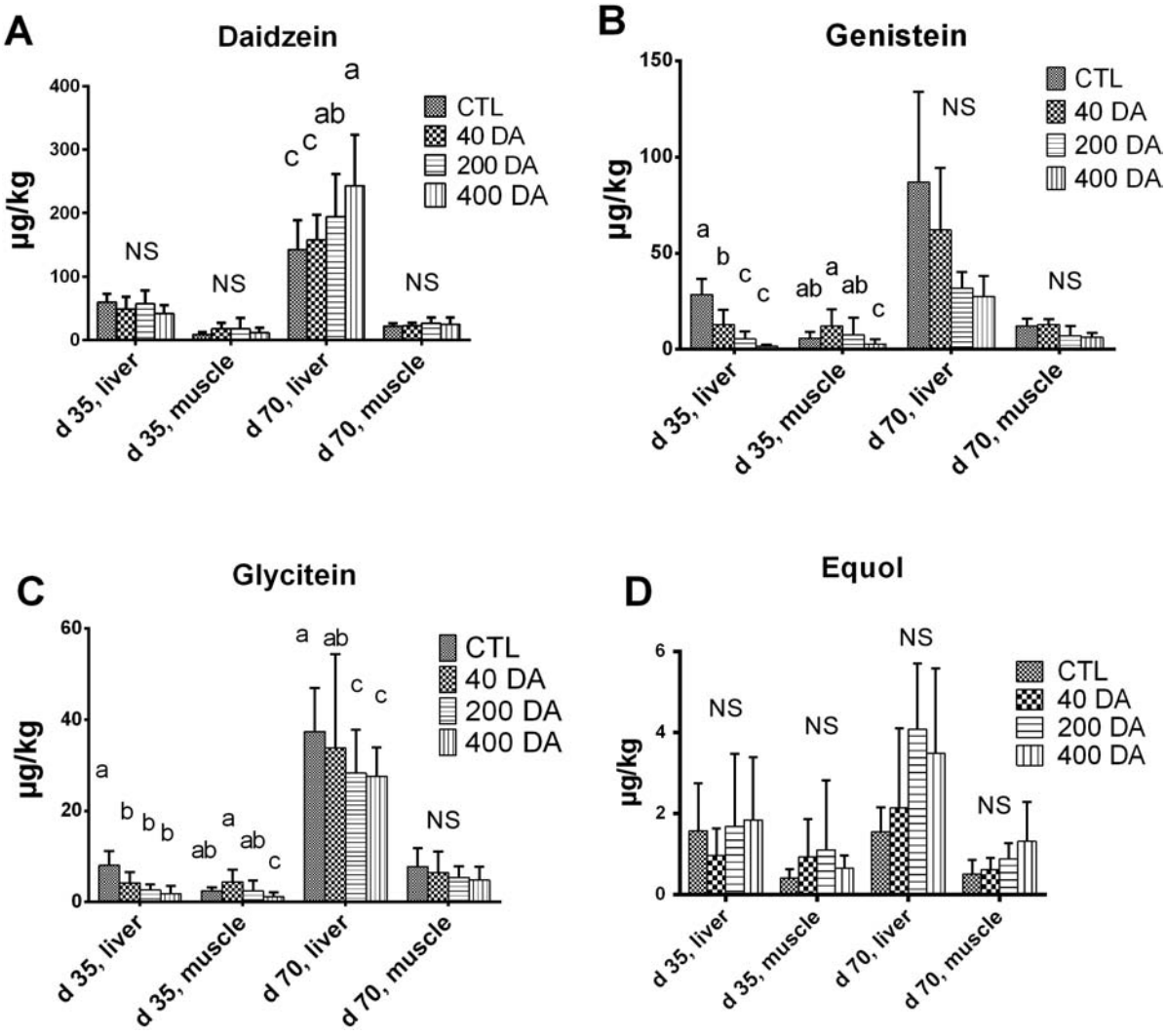

Figure 4. Concentrations of several isoflavones (μg/kg) in livers and muscles (semitendinosus) of repeated dose daidzein-treated pigs on day 35 and day 70. (A–D) Residual amount of daidzein, genistein, glycitein, and equol in tissues, respectively. Each bar represents the mean ± SD of six experimental units (pens) (n = 6). CTL, control group fed a basal diet. 40/200/400 DA, 40/200/400 mg/kg daidzein supplemented to CTL. Bars with different letters are significantly (P < 0.05) different from each other. NS, not significant (P > 0.05).

affects weight gain in human and murines.[23,24] Therefore, we speculate that the mechanism for daidzein's effects on pig growth relates to this feature. Further research is needed to elucidate the growth axis of daidzein/estrogen receptors.

Nevertheless, it is unclear whether other hormones related to growth are linked to daidzein's effects on regulating weight gain. Some studies show that daidzein promotes levels of growth-regulating hormones in breeding poultry (GH and tetraiodothyronine)[25,26] and intact male piglets (IGF-1).[27] Other research indicates the inhibitory effect of daidzein in vitro and in vivo.[14,28] Beyond these debates, our results show that daidzein is not effective enough to alter these hormones related to growth. This suggests that the function of daidzein in regulating growth is not through these hormones. Furthermore, studies show that endogenous estradiol is not affected by daidzein ingestion,[29] which accords with our results.

Other studies indicate that dietary genistein (20 mg/kg/day) decreases testosterone plasma levels of male rats, while the same doses of daidzein have no effect in this regard.[29] However, our results reveal the inhibitory effect of higher concentrations (200 and 400 mg/kg) of daidzein on the serum testosterone content for female pigs. This suggests that gender and dosage may be critical factors for daidzein in terms of regulating testosterone. This effect is also evident in porcine ovaries, suggesting that daidzein may disturb reproductive processes in pigs.[22] An in vitro study showed that daidzein increases StAR and 3β-HSD-1 mRNA levels, thereby increasing testosterone production in cultured mouse leydig cells in the presence of the chorionic gonadotropic hormone.[30] Alexa et al. reported that daidzein alone increases testosterone production in porcine ovarian cells, but that in the presence of follicle-stimulating hormone (FSH), daidzein prevents the FSH-stimulated release of testosterone.[31] In fact, the endocrine system is a complex regulatory system involving various interactions between hormones. Therefore, the mechanisms for the testosterone-reducing effect of daidzein in female piglets and how it plays a role in regulating steroid hormone metabolism in vivo warrant further study.

Numerous studies reveal daidzein's reactivity with active oxygen species. Therefore, it appears to have antioxidant potential via a radical-scavenging mechanism.[4,32] Our results indicate the efficacy of daidzein in piglets (day 35) in an oral

DOI: 10.1021/acs.jafc.5b00677
J. Agric. Food Chem. 2015, 63, 4228–4235

dose of 200 mg/kg, suggesting that the protective effects of daidzein against oxidation are more pronounced in piglets than growing pigs. A decrease in MDA suggests decreased lipid peroxidation, a process which is initiated by free radical reactions.[33] However, in our study, a decrease in MDA may also be associated with an increase in the activity of total SOD. It is not yet clear whether daidzein develops its antioxidant potential via a direct radical-scavenging mechanism or by improving the activity of other antioxidant enzymes such as SOD. Therefore, additional functional analyses are required to reveal how daidzein affects the free-radical-scavenging system.

In this study, we originally evaluated the effect of daidzein on intestinal morphology. Results show an increasing proliferation of duodenal mucosa with 200 mg/kg of daidzein. As previously noted, the same dose of daidzein tended to improve the ADG of pigs. This may be partially due to the increased VCR in the duodenum because the absorption capacity of the small intestine is affected by VCR.[34] Some studies show that increases in SOD lead to a decrease in intestinal crypt depth,[35] which accords with our results. Including soybean meal (5 g/day) in the diets of early weaned pigs has been found to decrease villus height and increase crypt depth, leading to transient hypersensitivity and subsequently poor growth performance.[36] However, there is no evidence to indicate that this effect mainly stems from soy isoflavones.

Previous studies on the effect of daidzein or isoflavones on organ development have mainly focused on reproductive issues. Findings show that daidzein or isoflavones at low concentrations have no significant effect on reproductive organs in hens (50 mg/kg daidzein) and mice (2 mg daidzein + 5 mg genistein/kg body weight/day).[37,38] To our knowledge, our study is the first to evaluate the long-term effects (35 and 70 days) of dietary daidzein at the high level of 400 mg/kg on pig organs. We employed histopathological scoring to identify the effects of dietary daidzein on pig organs. Our results suggest that ingesting high doses of daidzein for 70 days may increase spleen damage in pigs. This may compromise the ADG of pigs. However, the mechanisms involved are not clearly understood, and hence, the biochemical and toxic responses of daidzein deserve further study.

Previous studies on the tissue distribution of isoflavones in animals are limited. Urpi-Sarda et al. found that the major metabolites recovered in ewe tissues (liver and mammary glands) after consumption of red clover silage were equol and daidzein.[39] Gilani et al. studied tissue distribution of isoflavones in pigs following a daily dose of 2.3 g of total isoflavones. They found higher levels of daidzein, equol, genistein, and glycitein in livers compared with the CTL containing no isoflavones. The same effect was found in mammary gland extraparenchymal tissue of pigs for only daidzein and equol.[18] Our literature review found no studies on buildup in tissues when daidzein is added alone.

In our study, it was not surprising that daidzein was the metabolite found in the greatest amounts in pig livers. Unlike the findings of Urpi-Sarda and Gilani, we found that equal levels in both liver and muscle were low. The production of equol differs between species[40] and age stages (in a rat study).[41] These levels were not affected by the amount of daidzein ingested, which was possibly due to the pigs being too young to produce equol themselves.

Another notable finding from our study is that genistein and glycitein displayed an opposite distribution from that of daidzein in pig tissue when the level of dietary daidzein was increased. Reports had shown that the fraction of daidzein absorbed is greater than that of genistein.[42,43] Thus, we can speculate that daidzein acts as a competitive inhibitor against genistein and glycitein when they are deposited in animal tissue. Further studies will elucidate the absorption approach and deposition method of daidzein and other isoflavones, as well as the interaction between them in terms of buildup in animal tissue.

Another concern is that isoflavones may have a cumulative effect,[44] so that the biological effect is evident only after longer durations. Our findings indicate that daidzein may have a cumulative effect over time in terms of buildup in body tissues, as indicated by daidzein levels in pig livers on day 35 and day 70. This suggests a link between daidzein levels in animal products and the duration of ingestion.

In conclusion, this study on the biological activity of daidzein in pigs depends on dosage and the age of the pigs, as well as the duration of treatment. It may be a feasible option to give up to 200 mg/kg of daidzein to weanling pigs without negative consequences. As for the effects on consumer health, our findings reveal that the residual content of daidzein in pork products was not likely to raise safety concerns.

■ ASSOCIATED CONTENT

Supporting Information

Table S1. This material is available free of charge via the Internet at http://pubs.acs.org.

■ AUTHOR INFORMATION

Corresponding Author

*Tel.: +86 835 288 2088. Fax: +86 835 288 2088. E-mail: dwchen@sicau.edu.cn.

Funding

This work was financially supported by the Scientific and Technical Support Program of the "Twelfth Five-Year Plan", Feed Quality and Safety Supervision Project of Ministry of Agriculture (2012), PR China.

Notes

The authors declare no competing financial interest.

■ REFERENCES

(1) Larrosa, M.; González-Sarrías, A.; García-Conesa, M. T.; Tomás-Barberán, F. A.; Espín, J. C. Urolithins, ellagic acid-derived metabolites produced by human colonic microflora, exhibit estrogenic and antiestrogenic activities. *J. Agric. Food Chem.* **2006**, *54*, 1611−1620.

(2) Takashima, M.; Nara, K.; Niki, E.; Yoshida, Y.; Hagihara, Y.; Stowe, M.; Horie, M. Evaluation of biological activities of a groundnut (Apios americana Medik) extract containing a novel isoflavone. *Food Chem.* **2013**, *138*, 298−305.

(3) Adams, S. M.; Aksenova, M. V.; Aksenov, M. Y.; Mactutus, C. F.; Booze, R. M. Soy isoflavones genistein and daidzein exert anti-apoptotic actions via a selective ER-mediated mechanism in neurons following HIV-1 Tat1−86 exposure. *PLoS One* **2012**, *7*, e37540.

(4) Wijeratne, S. S.; Cuppett, S. L. Soy isoflavones protect the intestine from lipid hydroperoxide mediated oxidative damage. *J. Agric. Food Chem.* **2007**, *55*, 9811−9816.

(5) Murphy, P.; Farmakalidis, E.; Johnson, L. Isoflavone content of soya-based laboratory animal diets. *Food Chem. Toxicol.* **1982**, *20*, 315−317.

(6) Pediatrics, A. A. o., American Academy of Pediatrics. Committee on Nutrition. Soy protein-based formulas: recommendations for use in infant feeding. *Pediatrics* **1998**, *101*, 148.

DOI: 10.1021/acs.jafc.5b00677
J. Agric. Food Chem. 2015, 63, 4228−4235

(7) Badger, T. M.; Gilchrist, J. M.; Pivik, R. T.; Andres, A.; Shankar, K.; Chen, J.-R.; Ronis, M. J. The health implications of soy infant formula. *Am. J. Clin. Nutr.* **2009**, *89*, 1668S−1672S.
(8) Barrett, J. R. The science of soy: what do we really know? *Environ. Health Persp* **2006**, *114*, A352.
(9) Goldman, L. R.; Newbold, R.; Swan, S. H. Exposure to soy-based formula in infancy. *JAMA, J. Am. Med. Assoc.* **2001**, *286*, 2402−2403.
(10) Eldridge, A. C.; Kwolek, W. F. Soybean isoflavones: effect of environment and variety on composition. *J. Agric. Food Chem.* **1983**, *31*, 394−396.
(11) Kulling, S. E.; Honig, D. M.; Metzler, M. Oxidative metabolism of the soy isoflavones daidzein and genistein in humans in vitro and in vivo. *J. Agric. Food Chem.* **2001**, *49*, 3024−3033.
(12) Wähälä, K.; Hase, T.; Adlercreutz, H. Synthesis and labeling of isoflavone phytoestrogens, including daidzein and genistein. *Exp. Biol. Med.* **1995**, *208*, 27−32.
(13) Ni, Y.; Zhu, Q.; Zhou, Z.; Grossmann, R.; Chen, J.; Zhao, R. Effect of dietary daidzein on egg production, shell quality, and gene expression of ER-α, GH-R, and IGF-IR in shell glands of laying hens. *J. Agric. Food Chem.* **2007**, *55*, 6997−7001.
(14) Zhao, R.; Wang, Y.; Zhou, Y.; Ni, Y.; Lu, L.; Grossmann, R.; Chen, J. Dietary daidzein influences laying performance of ducks (Anas platyrhynchos) and early post-hatch growth of their hatchlings by modulating gene expression. *Comp. Biochem. Physiol., Part A: Mol. Integr. Physiol.* **2004**, *138*, 459−466.
(15) Rehfeldt, C.; Adamovic, I.; Kuhn, G. Effects of dietary daidzein supplementation of pregnant sows on carcass and meat quality and skeletal muscle cellularity of the progeny. *Meat Sci.* **2007**, *75*, 103−111.
(16) Strauch, T.; Carroll, J. A Daidzein and Weaned Pig Response to LPS. *Journal of Animal and Veterinary Advances* **2004**, *3*, 70−73.
(17) Lamartiniere, C. A.; Wang, J.; Smith-Johnson, M.; Eltoum, I.-E. Daidzein: bioavailability, potential for reproductive toxicity, and breast cancer chemoprevention in female rats. *Toxicol. Sci.* **2002**, *65*, 228−238.
(18) Gilani, G. S.; Farmer, C.; Dyck, M.; Robertson, P.; Dahiya, J.; Sepehr, E.; Fan, L.; Nicolidakis, H.; Curran, I.; Cooke, G. Distribution of isoflavones in samples of serum, liver and mammary glands of rats or pigs fed dietary isoflavones. *Ann. Nutr. Metab.* **2011**, *58*, 171−180.
(19) Touchette, K.; Carroll, J.; Allee, G.; Matteri, R.; Dyer, C.; Beausang, L.; Zannelli, M. Effect of spray-dried plasma and lipopolysaccharide exposure on weaned pigs: I. Effects on the immune axis of weaned pigs. *J. Anim. Sci.* **2002**, *80*, 494−501.
(20) Zhang, R.; Li, Y.; Wang, W. Enhancement of immune function in mice fed high doses of soy daidzein. *Nutr. Cancer* **1997**, *1*, 29.
(21) Kuiper, G. G.; Carlsson, B.; Grandien, K.; Enmark, E.; Haggblad, J.; Nilsson, S.; Gustafsson, J.-a. Comparison of the ligand binding specificity and transcript tissue distribution of estrogen receptors α and β. *Endocrinology* **1997**, *138*, 863−870.
(22) Nynca, A.; Słonina, D.; Jabłońska, O.; Kamińska, B.; Ciereszko, R. E. Daidzein affects steroidogenesis and oestrogen receptor expression in medium ovarian follicles of pigs. *Acta Vet. Hung.* **2013**, *61*, 85−98.
(23) Geary, N.; Asarian, L.; Korach, K. S.; Pfaff, D. W.; Ogawa, S. Deficits in E2-dependent control of feeding, weight gain, and cholecystokinin satiation in ER-α null mice. *Endocrinology* **2001**, *142*, 4751−4757.
(24) Wade, G. N. Sex hormones, regulatory behaviors, and body weight. *Adv. Stud. Behav.* **1976**, *6*, 201−279.
(25) Zhao, R.; Zhou, Y.; Ni, Y.; Lu, L.; Tao, Z.; Chen, W.; Chen, J. Effect of daidzein on egg-laying performance in Shaoxing duck breeders during different stages of the egg production cycle. *Br. Poult. Sci.* **2005**, *46*, 175−181.
(26) Zhao, X.; Shao, T.; Wang, Y.; Lu, X.; Luo, J.; Zhou, W. The phytoestrogen daidzein may affect reproductive performance of Zhedong White geese by regulating gene mRNA levels in the HPG axis. *Br. Poult. Sci.* **2013**, *54*, 252−258.
(27) Genlin, W.; Xiangying, Z.; Zhaoyu, H.; Zhaobin, L.; Weirong, L. Effects of daidzein on body weight gain, serum IGF-I level and cellular immune function in intact male piglets. *Asian-Australas. J. Anim. Sci.* **2002**, *15*, 1066−1070.
(28) Higashi, K.; Ogawara, H. Daidzein inhibits insulin-or insulin-like growth factor-1-mediated signaling in cell cycle progression of Swiss 3T3 cells. *Biochim. Biophys. Acta, Mol. Cell Res.* **1994**, *1221*, 29−35.
(29) Valeri, A.; Fiorenzani, P.; Rossi, R.; Aloisi, A.; Valoti, M.; Pessina, F. The soy phytoestrogens genistein and daidzein as neuroprotective agents against anoxia-glucopenia and reperfusion damage in rat urinary bladder. *Pharmacol. Res.* **2012**, *66*, 309−316.
(30) Zhang, L.; Cui, S. Effects of daidzein on testosterone synthesis and secretion in cultured mouse leydig cells. *Asian-Australas. J. Anim. Sci.* **2009**, *22*, 618−625.
(31) Alexa, R.; Stochmalova, A.; Kadasi, A.; Grossmann, R.; Kolesarova, A.; Sirotkin, A. The effect of soy phytoestrogen daidzein and fsh on porcine ovarian cell proliferation and steroidogenesis. *Anim. phys.* **2014**, 12.
(32) Liang, J.; Tian, Y.-X.; Fu, L.-M.; Wang, T.-H.; Li, H.-J.; Wang, P.; Han, R.-M.; Zhang, J.-P.; Skibsted, L. H. Daidzein as an antioxidant of lipid: Effects of the microenvironment in relation to chemical structure. *J. Agric. Food Chem.* **2008**, *56*, 10376−10383.
(33) Draper, H.; Hadley, M. Malondialdehyde determination as index of lipid Peroxidation. *Methods Enzymol.* **1990**, *186*, 421−431.
(34) Montagne, L.; Pluske, J.; Hampson, D. A review of interactions between dietary fibre and the intestinal mucosa, and their consequences on digestive health in young non-ruminant animals. *Anim. Feed Sci. Technol.* **2003**, *108*, 95−117.
(35) Ferencz, A.; Nedvig, K.; Fekecs, T.; Rácz, B.; Wéber, G.; Hashimoto, H.; Baba, A.; Helyes, Z.; Reglödi, D. Comparison of Intestinal Cold Preservation Injury on Pituitary Adenylate Cyclase−Activating Polypeptide in Knockout and Wild-Type Mice. *Transplant. Proc.* **2010**, *42*, 2290−2292.
(36) Li, D.; Nelssen, J.; Reddy, P.; Blecha, F.; Hancock, J.; Allee, G.; Goodband, R.; Klemm, R. Transient hypersensitivity to soybean meal in the early-weaned pig. *J. Anim. Sci.* **1990**, *68*, 1790−1799.
(37) Shi, S.; Gu, H.; Chang, L.; Wang, Z.; Tong, H.; Zou, J. Safety evaluation of daidzein in laying hens: Part I. Effects on laying performance, clinical blood parameters, and organs development. *Food Chem. Toxicol.* **2013**, *55*, 684−688.
(38) Kaludjerovic, J.; Chen, J.; Ward, W. E. Early life exposure to genistein and daidzein disrupts structural development of reproductive organs in female mice. *J. Toxicol. Environ. Health, Part A* **2012**, *75*, 649−660.
(39) Urpi-Sarda, M.; Morand, C.; Besson, C.; Kraft, G.; Viala, D.; Scalbert, A.; Besle, J.-M.; Manach, C. Tissue distribution of isoflavones in ewes after consumption of red clover silage. *Arch. Biochem. Biophys.* **2008**, *476*, 205−210.
(40) Gu, L.; House, S. E.; Prior, R. L.; Fang, N.; Ronis, M. J.; Clarkson, T. B.; Wilson, M. E.; Badger, T. M. Metabolic phenotype of isoflavones differ among female rats, pigs, monkeys, and women. *J. Nutr.* **2006**, *136*, 1215−1221.
(41) Sepehr, E.; Cooke, G. M.; Robertson, P.; Gilani, G. S. Effect of glycosidation of isoflavones on their bioavailability and pharmacokinetics in aged male rats. *Mol. Nutr. Food Res.* **2009**, *53*, S16−S26.
(42) King, R. A.; Bursill, D. B. Plasma and urinary kinetics of the isoflavones daidzein and genistein after a single soy meal in humans. *Am. J. Clin. Nutr.* **1998**, *67*, 867−872.
(43) Setchell, K. D.; Faughnan, M. S.; Avades, T.; Zimmer-Nechemias, L.; Brown, N. M.; Wolfe, B. E.; Brashear, W. T.; Desai, P.; Oldfield, M. F.; Botting, N. P. Comparing the pharmacokinetics of daidzein and genistein with the use of 13C-labeled tracers in premenopausal women. *Am. J. Clin. Nutr.* **2003**, *77*, 411−419.
(44) Murkies, A.; Lombard, C.; Strauss, B.; Wilcox, G.; Burger, H.; Morton, M. Dietary flour supplementation decreases post-menopausal hot flushes: effect of soy and wheat. *Maturitas* **1995**, *21*, 189−195.

DOI: 10.1021/acs.jafc.5b00677
J. Agric. Food Chem. 2015, 63, 4228−4235

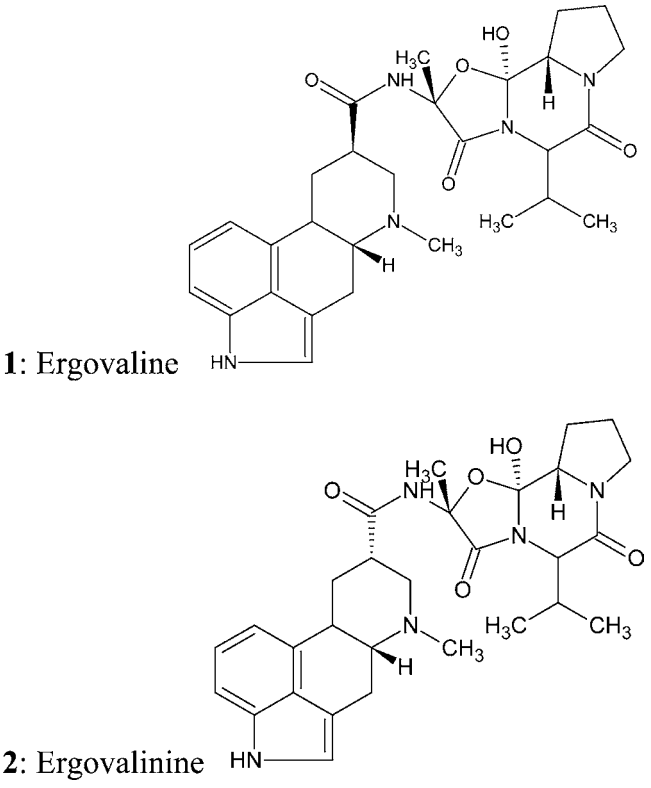

Figure 1. Chemical structures of ergovaline (**1**) and ergovalinine (**2**).

Sigma-Aldrich (St. Louis, MO). Anhydrous magnesium sulfate ($MgSO_4$), 99.5%, was purchased from UCT (Bristol, PA). Ammonium hydroxide, ACS grade, was purchased from VWR BDH Prolabo (West Chester, PA). Ultrapure water (18.2 MΩ cm^{-1}) was purified with a PURELAB Ultra Genetic system (Elga, Marlow, Buckinghamshire, U.K.).

Ergovaline tartrate was prepared by Dr. Forrest Smith, Department of Pharmacal Sciences, Auburn University, Auburn, AL. Chemical characterization and assessment of purity of the crystalline standard was established by nuclear magnetic resonance (NMR) and HPLC/mass spectrometry (HPLC/MS). It was established that the ergovaline tartrate was comprised of ergovaline/tartrate/water in the ratio 2/1/1. The **1** standard was weighed on an analytical balance, diluted in MeOH, dispensed in 10 μg aliquots, evaporated under nitrogen, and stored frozen at −20 °C. The working standard was prepared by dilution of a 10 μg aliquot in MeOH.

Sample Preparation. Tall fescue seed and straw samples were ground in a Cyclotec 1093 sample mill (Foss, Hilleroed, Denmark) to pass through a 0.5 mm screen and stored at −20 °C prior to analysis. Details on the collection of a representative straw or seed sample for forage testing can be found online.[20]

Optimization of Extraction Solvent. The first step of the extraction/partitioning process of the QuEChERS method was evaluated in a tall fescue seed sample with a known high **1** level (1998 μg/kg, n = 3/solvent). The extraction solutions were selected from published procedures that were used to extract mycotoxins via the QuEChERS method or used in the extraction of ergot alkaloids via other techniques and were as follows: extraction solvent 1, 1% acetic acid in MeCN (v/v);[11] extraction solvent 2, MeOH/MeCN (15/85, v/v);[11] extraction solvent 3, MeOH/MeCN (85/15, v/v);[11] extraction solvent 4, MeOH/water (60/40, v/v);[11] extraction solvent 5, MeOH/water (80/20, v/v);[11] extraction solvent 6, 2.1 mM ammonium carbonate/MeCN (16/84, v/v), modification from a method for the quantitation of ergot alkaloids in cereals and foodstuffs;[20] extraction solvent 7, isopropyl alcohol/1% lactic acid (50/50, v/v), method developed to quantitate **1** and peramine in grass tillers;[21] extraction solvent 8, MeCN/0.1% formic acid (57/43, v/v), modification of a method developed for detection of *Fusarium* mycotoxins in cereals;[13] extraction solvent 9, ethyl acetate/MeOH/4.1 mM ammonium carbonate (62.5/25/12.5, v/v), modification of a method for ergot alkaloid extraction from food and feed sources;[22] extraction solvent 10, water/0.5% acetic acid in MeCN (50/50, v/v), modification of a QuEChERS method developed for the analysis of 17 mycotoxins in cereals;[15] extraction solvent 11, ethyl acetate/MeOH/25% ammonium hydroxide solution (75/5/7, v/v), modification of a method developed for analysis of ergot alkaloids in rye and rye products;[23] extraction solvent 12, MeCN/1.0% acetic acid (80/20, v/v); extraction solvent 13, MeCN/1 mM ammonium carbonate (80/20, v/v); extraction solvent 14, MeOH/1% acetic acid (80/20, v/v).

For the initial survey of solvent systems, 1.0 g samples of ground tall fescue seed were placed into 16 × 125 mm glass screw top tubes in triplicate. A 5 mL portion of the solvent mixture was added; the tubes were capped and vortexed for 10 s. The tubes were placed on an end-over-end rotary mixer for 30 min, after which 0.5 g of $MgSO_4$ and NaCl (4/1, w/w)[9] was added. The tubes were capped and vortexed immediately to prevent agglomeration of the salts for 10 s, four times during a 10 min period. The samples were then centrifuged at 913*g* for 10 min. A 1 mL portion of the supernatant was evaporated to dryness at 50 °C under a gentle stream of nitrogen. The samples were reconstituted in 0.5 mL of MeOH and, after vortexing and sonication for 20 s each, transferred to a centrifugal filter tube with a 0.45 μm modified nylon membrane (VWR, Radnor, PA). The tubes were centrifuged at 8161*g* (10000 rpm) for 5 min; the filtrate was then transferred to an amber HPLC vial for analysis.

Final Extraction Procedure. A 5 mL portion of 2.1 mM ammonium carbonate/MeCN (50/50, v/v) extraction solvent was added to 0.5 g of ground plant material, mixed by vortexing for 30 s, and then placed on the rotary mixer for 30 min. Subsequently, 0.4 g of preweighed $MgSO_4$ and 0.1 g of NaCl was added and the tubes were capped and vortexed immediately for 10 s, four times during a 10 min period. Samples were centrifuged at 913*g* for 10 min. A 2.0 mL aliquot of the separated MeCN phase was evaporated to dryness at 50 °C under a gentle stream of nitrogen. The samples were reconstituted in 0.5 mL of MeOH and, after vortexing and sonication for 20 s each, were transferred to a centrifugal filter tube. The tubes were centrifuged at 8161*g* for 5 min, and the filtrate was transferred to an amber HPLC vial for analysis.

HPLC Analysis. A Series 200 HPLC system (PerkinElmer, Waltham, MA) was used throughout the experiment. This system consisted of an autosampler, binary pump, column oven, and fluorescence detector (λ_{ex} 250 nm, λ_{em} 420 nm). Chromatographic data were managed using TotalChrom Workstation Software version 6.3.2 (PerkinElmer). HPLC separations were performed with a 100 mm × 4.6 mm i.d., 2.7 μm Brownlee SPP C18 HPLC column (PerkinElmer), with a 4.6 mm i.d. SecurityGuard ULTRA C18 guard column (Phenomenex (Torrance, CA)) maintained at 35 °C. The mobile phase consisted of 30% MeCN in 200 mg/L ammonium carbonate in purified water (solvent A) and 100% MeCN (solvent B), run at a flow rate of 1.8 mL/min. Initial gradient conditions were 5% B held for 1.0 min, increasing linearly to 65% B over 0.8 min and held for 0.8 min. Finally, there was a linear return to initial conditions over 0.3 min, which was then held for 1.3 min for a total run time of 4.2 min. The injection volume was 10 μL.

Method Validation. Performance characteristics were evaluated using guidelines developed by the Food and Drug Administration for bioanalytical analysis.[24] Validation of the optimized extraction method included linearity, selectivity, recovery, limit of detection (LOD), limit of quantitation (LOQ), precision, accuracy, and stability. Linearity was assessed using matrix-matched calibration curves established using extracts of endophyte-free (E−) tall fescue seed and straw fortified with the working **1** standard at 50, 100, 500, 1000, 2500, and 3500 μg/kg. Selectivity was established using comparison of noninfected seed and straw sample chromatograms with **1**-fortified extracts. Interference (visual examination of the chromatogram for coelution of other peaks) at the retention times of **1** (1.75 min) and ergovalinine (**2**) (3.60 min) was checked.

For recovery investigations, the **1** standard was added to E− tall fescue seed and straw at fortification levels of 100, 1000, and 2500 μg/kg (n = 10/level). To avoid epimerization of **1**, the MeOH in the spiked sample was evaporated under a gentle steam of nitrogen, and then the

DOI: 10.1021/acs.jafc.5b01149
J. Agric. Food Chem. 2015, 63, 4236−4242

tube was capped and frozen at −20 °C until extraction. The LOD and LOQ were estimated by measurement of the peak-to-peak signal-to-noise ratio (S/N) and calculated at $S/N > 3$ and $S/N > 10$, respectively. LOQ values must meet an accuracy of ±20% and a precision of <20% relative standard deviation (RSD).

The accuracy and precision of the method was determined using in-house tall fescue seed and straw reference material. The **1** content of the reference material was established using the Ergosil silica gel solid phase extraction (SPE) method.[5,8] The intraday precision was established using five replicates at four levels of **1**. Interday precision and accuracy were evaluated over three separate days of analysis of five replicates at the four concentration levels. The stability of the sample extracts was investigated by repeat analysis of the samples ($n = 48$) after 24 h at room temperature.

Statistical Analysis. Statistical analyses (averages, standard deviations (SD), relative standard deviations (RSD), *t* tests (two-tailed, two-sample equal variance) and ANOVA) were performed in Excel (Microsoft Office 2010, Redmond WA) or GraphPad Prism (Version 5.01, La Jolla, CA). Results were considered significant when the p value was less than 0.05.

RESULTS

Optimization of Extraction Procedure. The 14 solvent mixtures were significantly different from each other in their ability to extract **1** (Kruskall-Wallis test, $P = 0.001$) (Figure 2).

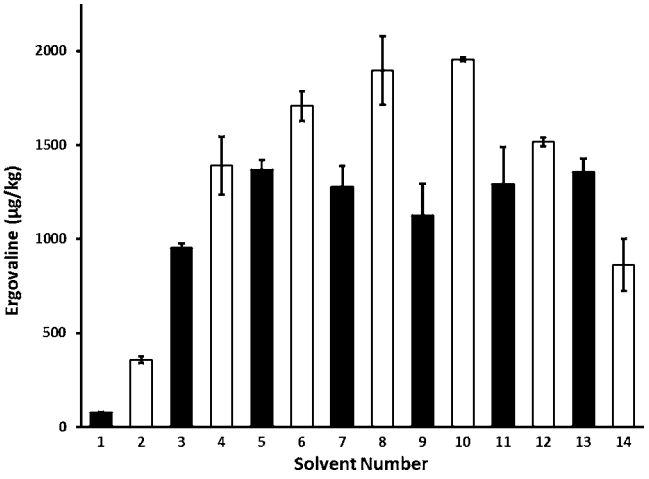

Figure 2. Evaluation of different solvent mixtures for extraction of **1** from endophyte-infected tall fescue seed containing 1998 µg of **1**/kg using the QuEChERS method ($n = 3$/solvent). For solvents tested refer to Materials and Methods.

The maximum amount of extracted **1** was obtained with water/0.5% acetic acid in MeCN (50/50), which extracted 98% of the 1998 µg of **1**/kg in the seed that was being used, with a low standard deviation of 12 µg/kg (RSD 0.6%). The MeCN/0.1% formic acid (57/43) mixture showed a similar ability to extract **1**, extracting 95% of the 1998 µg of **1**/kg in seed, but had a higher standard deviation of 182 µg/kg (RSD 9.6%). While the two solvent combinations were not statistically different from each other ($p = 0.611$), the water/0.5% acetic acid in MeCN (50/50) mixture was chosen for its lower standard deviation, which would ensure greater throughput under the rigorous quality control standards in a diagnostic laboratory setting. Once this was established, different types of aqueous solution, namely 0.5% and 1% acetic acid, 1% formic acid, 2.1 mM ammonium carbonate, and 1 mM ammonium carbonate, were studied in both seed (1998 µg of **1**/kg) and high **1** content straw (850 µg/kg). It was found that the highest and most consistent recoveries were achieved with 2.1 mM ammonium carbonate (Figure 3). This

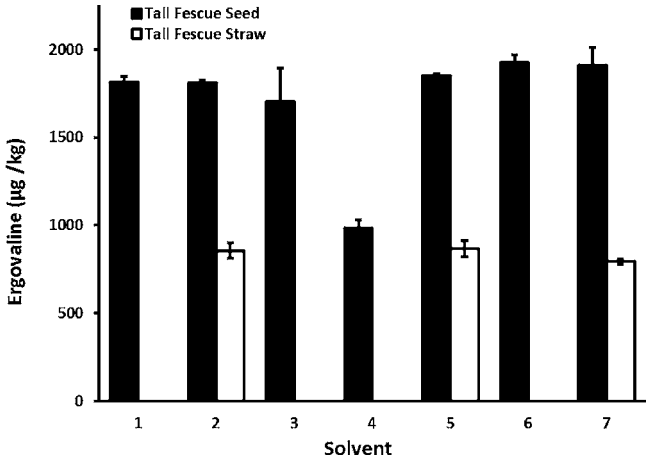

Figure 3. Additions to the aqueous component of the extraction solution evaluated for recovery of **1** from tall fescue seed (1998 µg of **1**/kg) and tall fescue straw (850 µg of **1**/kg) ($n = 3$/sample type/solvent mixture): (1) 1% acetic acid/MeCN (50/50); (2) 2.1 mM ammonium carbonate/MeCN (50/50); (3) 1 mM ammonium carbonate/MeCN (50/50); (4) 1% formic acid/MeCN (50/50); (5) 0.5% acetic acid/MeCN (50/50); (6) water/1% acetic acid in MeCN (50/50); (7) water/MeCN (50/50).

solvent mixture extracted 90.5 ± 1.0% of the **1** in the tall fescue seed (1998 µg/kg) and 100.5 ± 5.3% in the tall fescue straw (850 µg/kg) that were used. The addition of the 2.1 mM ammonium carbonate/MeCN extraction solution added as a mixture or separately as two components to tall fescue seed containing 1998 µg of **1**/kg was investigated; no statistical difference was found between either method ($n = 3$ replicates/method, *t* test $p = 0.656$). Thus, combining the 2.1 mM ammonium carbonate/MeCN (50:50, v/v) as one addition to the sample was chosen.

The optimum mixing time for the sample and extraction solvent was evaluated at 30, 60, 90, and 120 min in both seed and straw samples (Table 1). Thirty minutes was found to be a

Table 1. Comparison of Mixing Times for Solutions of 2.1 mM Ammonium Carbonate/MeCN (50/50, v/v) from Tall Fescue Seed and Straw for Extraction of Ergovaline (1) Using the QuEChERS Method

	amt of ergovaline (**1**), µg/kg[a]			
	30 min	60 min	90 min	120 min
tall fescue seed (1998 µg/kg)	1901(3)	1771(4)	1637(4)	1644(3)
tall fescue straw (776 µg/kg)	712(8)	675(8)	568(11)	620(9)

[a]RSD values are given in parentheses ($n = 5$).

sufficient amount of time for the sample and extraction solvent to mix to maximize the amount of **1** extracted, with low RSD values. Following addition of the 0.4 g of anhydrous $MgSO_4$ and 0.1 g NaCl, immediate vortexing and mixing four times during a 10 min period was required to give the most consistent mixing and to promote homogeneity.

Figure 4 shows representative HPLC-fluorescence chromatograms of the final, optimized QuEChERS procedure for tall fescue seed and straw, in comparison to the Ergosil SPE method currently used in our laboratory.[5]

Method Validation. *Linearity.* A calibration curve was constructed by plotting the peak area of **1** against the nominal concentrations of **1** at 50, 100, 500, 1000, 2500, and 3500 µg/kg. The correlation coefficient (R^2) generated from the calibration

DOI: 10.1021/acs.jafc.5b01149
J. Agric. Food Chem. 2015, 63, 4236−4242

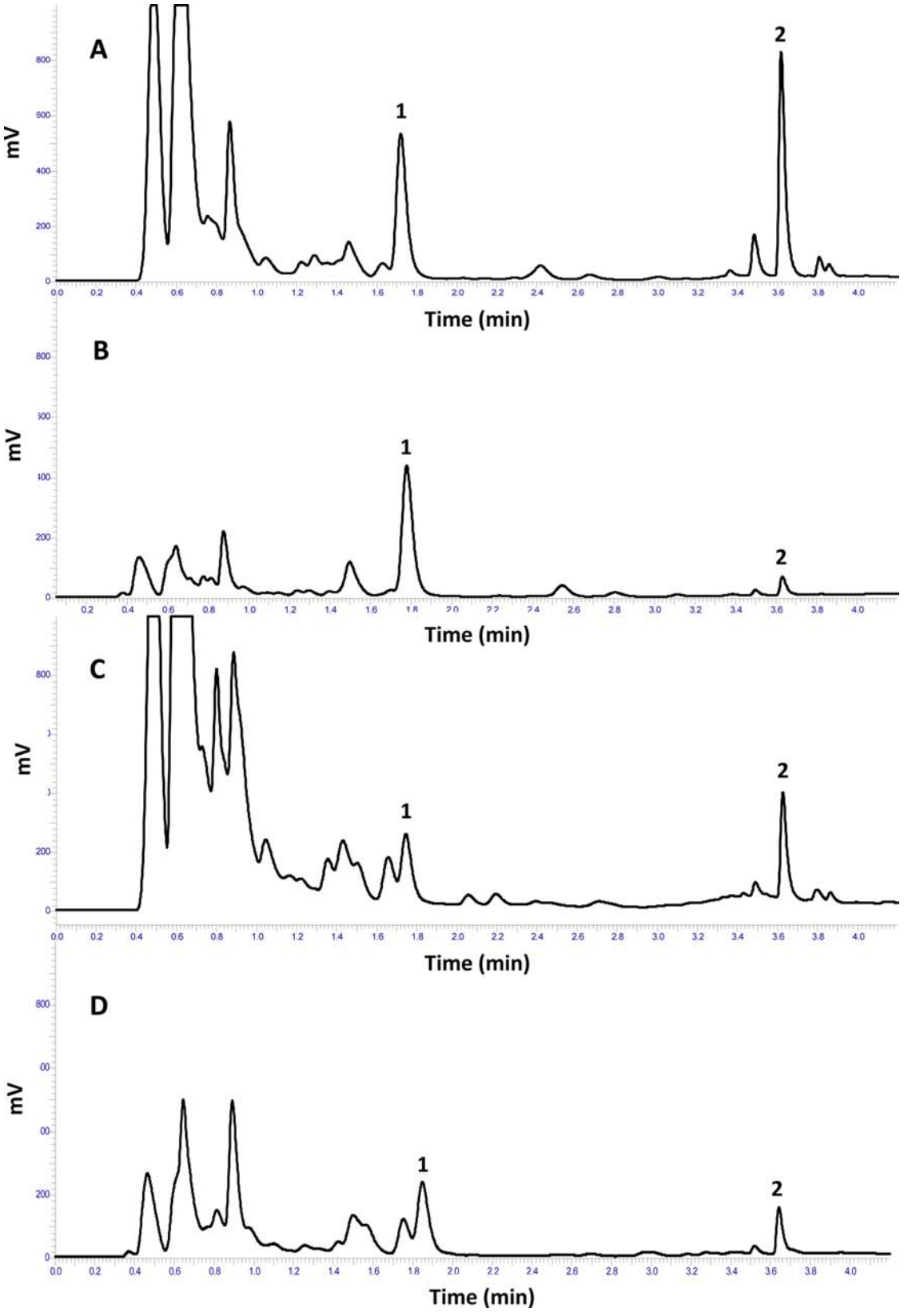

Figure 4. Representative HPLC-fluorescence chromatograms comparing extraction of tall fescue seed and straw between the optimized QuEChERS method and an Ergosil SPE method for **1** and its epimer **2**: (A) QuEChERS extract of tall fescue seed; (B) Ergosil SPE extract of tall fescue seed; (C) QuEChERS extract of tall fescue straw; (D) Ergosil SPE extract of tall fescue straw.

curve was >0.999 in both seed and straw from six replicate standard sets. The linear dynamic range was found to be 100−3500 μg/kg.

Selectivity. Noninfected seed and straw samples were extracted to verify that there were no peaks interfering with the fluorescent detection of **1** or its epimer **2** at

DOI: 10.1021/acs.jafc.5b01149
J. Agric. Food Chem. 2015, 63, 4236−4242

their expected retention times (1.75 and 3.60 min, respectively).

Recovery. **1** was spiked into E− seed and straw samples at three levels: 100, 1000, and 2500 μg/kg (n = 10/level). The mean recoveries varied from 91.3 to 97.2% in tall fescue seed and 89.6−98.1% in tall fescue straw.

LOD and LOQ. The LOD values were determined to be 37 and 30 μg/kg in tall fescue seed and straw, respectively. An LOQ level of 100 μg/kg was established in both seed and straw, with demonstrated accuracies of 98% and 91% and precision of 9% and 6%, respectively.

Precision and Accuracy. Precision and accuracy were determined by the extraction of **1** from tall fescue seed (143−1998 μg of **1**/kg) and straw (181−1061 μg/kg) reference material. The intraday precision, expressed in RSD, ranged from 1.8 to 5.8% in tall fescue seed and 0.5−3.4% in tall fescue straw. The interday precision ranged from 1.9 to 6.4% in seed and 0.7−4.8% in straw. The results from the experiments to establish accuracy ranged from 97.9 to 98.6% in tall fescue seed and 97.3−99.2% in tall fescue straw.

Stability. The extracted samples demonstrated stability comparable with that of the Ergosil SPE method upon repeat analysis after storage at room temperature for 24 h.

Application of the Method to Real Samples. The validated method was applied to 17 tall fescue straw samples which were previously analyzed using the Ergosil SPE method.[5,8] Including the standard reference material, controls, and samples run in duplicate, the run size was 48 individual extractions, which is a typical sample run in our laboratory. There was good agreement between the two different methods. Both methods found that 7 of the samples had less than a quantitative amount of **1** (<100 μg/kg). The results from the remaining 10 samples had a RSD of 10% or better agreement. **1** values for the QuEChERS/Ergosil SPE methods were 119/119, 156/173, 203/224, 237/244, 238/240, 339/318, 499/469, 523/530, 526/518, 535/482, and 632/603 μg/kg, respectively. Comparative statistics showed that application of the two extraction methods to the 17 samples gave results that were not different from each other (t test, p = 0.258) and that the methods were very well correlated (correlation coefficient 0.9978).

DISCUSSION

Endophyte (*Epichloë coenophiala*)-infected tall fescue (*Festuca arundinacea*) is used as forage for livestock in the form of pasture, straw, silage, and pellets. Some endophyte strains produce ergot alkaloids as a protective mechanism against herbivory which cause vasoconstrictive and reproductive abnormalities that present as the diseases known as "summer syndrome" and "fescue foot" in livestock.[2,3] **1** is the ergopeptide alkaloid produced in highest concentration in tall fescue[25] and is a potent vasoconstrictor with the potential to bioaccumulate in vascular tissue;[26,27] as such, it has been used to establish thresholds of toxicity for these diseases in relevant livestock species.[5] When it is used safely with these thresholds in mind, tall fescue can be fed as an important nutritional component in livestock feeding programs. To achieve this, accurate testing of **1** concentration in tall fescue material is vital. While we currently employ a robust SPE method for **1** quantitation,[5,8] we were interested in application of a QuEChERS method to make the assay more efficient and eliminate the use of chlorinated solvents.

Fourteen extraction solvents were examined, and 2.1 mM ammonium carbonate/MeCN (50/50, v/v) was found to have the highest and most consistent recovery (90.5 ± 1.0% and 100.5 ± 5.3% for tall fescue seed and straw, respectively) (Figures 2 and 3). Thirty minutes was found to be an adequate amount of time for mixing and produced the best recovery of **1** from tall fescue seed and straw (Table 1). Total extraction time was improved to 4.4 h, in comparison to 5.9 h using traditional SPE, giving a time savings of 1.5 h.

On validation of the method, performance characteristics were similar to existing extraction procedures using HPLC-fluorescence for detection. The QuEChERS procedure had an LOD of 37/30 μg/kg in tall fescue seed/straw, respectively, a LOQ level of 100 μg/kg in both seed and straw, a linear dynamic range of 100−3500 μg/kg, and recoveries of spiked **1** from 91.3 to 97.2% for seed and 89.6−98.1% for straw. The Ergosil SPE method[5,7] has an LOD value of 31 μg/kg, an LOQ value of 100 μg/kg, a linear dynamic range of 100−2000 μg/kg, and a recovery of 91% and is the method currently in use by the Endophyte Service Laboratory at Oregon State University. Previous extraction methods upon which the Ergosil SPE method was based also showed similar values with an LOD value of 50 μg/kg and a recovery of 85%[28] or 93%.[8] These parameters are in line with the ability to determine clinically relevant concentrations of **1** in feed, on the basis of the established thresholds of toxicity (300−800 μg of **1**/kg, depending on species and climatic conditions).[5] Another method using 2-propanol/lactic acid as an extraction solvent to examine **1** distribution throughout the plant established an LOQ value of 100 μg/kg, a linear dynamic range of 400−10000 μg/kg, and recoveries of 93−105% and had the advantage that small (2−5 mg) sample amounts could be used for quantitation.[21] More recently, an SPE method using sodium-neutralized strong cation exchange columns was developed which accounted for both the native toxicologically active *R* epimer of ergot alkaloids as well as their biologically inactive -inine *S* epimer forms in rye flour and wheat germ oil samples, while minimizing epimer formation during the extraction itself.[29] They achieved LOD values of 0.3−0.8 μg/kg, LOQs of 0.7−2.0 μg/kg, linear dynamic ranges of 8−200 μg/kg, and recoveries of 71−120%.

Advancements in LC-MS have made it increasingly common in diagnostic laboratories. Application of the QuEChERS extraction method to cleanup samples, particularly for those destined for screening of multiple ergot alkaloids via LC-MS/MS, is a logical next step, as this mode of detection will likely allow the limits of detection and quantitation to be lowered. Two methods using electrospray ionization (ESI) (+) for detection of **1** and other ergot alkaloids analyzed by selected reaction monitoring (SRM) laid out a robust framework which also allowed for elucidation of "unusual" ergot alkaloid compounds and metabolites.[30,31] Another LC-MS method, using extraction procedures developed by Spiering et al.,[21] employed SRM for the transition m/z 534−268 and found concentrations of 240−3480 μg of **1**/kg in five populations of tall fescue from Iran.[32] While **1** was not specifically included, LC-MS/MS determination of multiple ergot alkaloids in the following methods had performance characteristics of LOQs of 0.17−2.78 μg/kg (with LODs similar to LOQs), recoveries of 69−105%, concentration ranges of 0.5−200 μg/kg,[33] LODs of 0.04−0.29 μg/kg, LOQs of 0.1−1 μg/kg, and recoveries of 88−110%.[34] Finally, a method using saphenous vein tissue as a matrix gave an LOD value of 1 nM, an LOQ value of 2 nM, a linear dynamic range of 0.1−50 pmol, and a recovery of 86−90% for spiked **1**.[35]

We have observed epimerization of **1** to **2** in SPE-extracted samples at room temperature after approximately 12 h. On this basis, a complete batch of samples, validated reference materials, and controls are either always run immediately after extraction

DOI: 10.1021/acs.jafc.5b01149
J. Agric. Food Chem. 2015, 63, 4236−4242

via HPLC-fluorescence or stored in a freezer, which halts epimerization until samples can be analyzed.[36] For quantitation, only **1** and not **2** is analyzed for total concentration in this method, as the Ergosil silica material in the SPE appears limited in its ability to bind **2**. Further, the thresholds of toxicity for fescue toxicosis in livestock[5] were established using analysis of feed samples for **1** (and not its epimer) via the SPE method; thus, measurement of **1** in feed samples which will be used in livestock feeding programs to avert fescue toxicosis remains relevant. On the other hand, the QuEChERS method had a significant peak for **2** in both seed and straw samples (Figure 4A,C); this technique appears to be able to extract more of this stereoisomer than the SPE method and/or epimerization from the *R* to the *S* isomer configuration is occurring at a greater rate over the course of performing this method. However, quantitation was again performed using only **1**, to compare extractability of **1** alone between the two methods. When the QuEChERS extraction procedure was applied to 17 tall fescue straw samples that had also been quantitated for **1** using the Ergosil SPE method, a correlation coefficient of 0.9978 was obtained on comparison of the two methods. The concentrations tested ranged from 7 that were below the LOQ value (100 μg/kg) to an additional 10 from 119 to 632 μg/kg, giving a good representation of the **1** concentrations that are typically seen in samples submitted to the Endophyte Service Laboratory.

In summary, a method following the QuEChERS extraction procedure was developed for determination of **1** in tall fescue seed and straw material using HPLC-fluorescence for detection. The method has eliminated the need for halogenated/chlorinated solvents, is as fast and efficient as the Ergosil SPE method currently in use in our laboratory, and was validated to perform across a linear range of 100−3500 μg of **1**/kg in tall fescue seed and straw material. These features make it ideal for application in a high-throughput food safety laboratory.

■ ASSOCIATED CONTENT

Supporting Information

A figure giving additional chromatographic data and a table giving validation data. This material is available free of charge via the Internet at http://pubs.acs.org.

■ AUTHOR INFORMATION

Corresponding Author

*A.M.C.: tel, +1-541-737-3036; fax, +1-541-737-8160; e-mail, A.Morrie.Craig@oregonstate.edu.

Notes

The authors declare no competing financial interest.

Funding

Funding for this project was provided by the Oregon Agricultural Experiment Station (ORE00871) and the Oregon Export Straw Association.

■ REFERENCES

(1) Young III, W. *Oregon Grass Seed Crop Estimates*; Extension Economic Information Office, Oregon State University, Corvallis, OR; http://cropandsoil.oregonstate.edu/system/files/u1473/CDS11-13G.pdf; accessed 18 March 2015.

(2) Thompson, F. N.; Stuedemann, J. A. Pathophysiology of fescue toxicosis. *Agric., Ecosyst. Environ.* **1993**, *44*, 263−281.

(3) Strickland, J. R.; Aiken, G. E.; Spiers, D. E.; Fletcher, L.; Oliver, J. W. Physiological basis of fescue toxicosis. In *Tall Fescue for the Twenty-first Century*; Fribourg, H. A., Hannaway, D. B., West, C. P., Eds.; American Society of Agronomy, Crop Science Society of America, Soil Science Society of America: Madison, WI, 2009; pp 203−227.

(4) Blythe, L. L.; et al. Determination of the Toxic Threshold of Lolitrem B in Cattle Eating Endophyte-Infected Perennial Ryegrass. In *Fungal Endophytes of Grasses*, Proceedings of the 6th International Symposium on Fungal Endophytes of Grasses, Popay, A. J., Thom, E. R., ed.; New Zealand Grassland Association, 2007; pp 399−402.

(5) Craig, A. M.; Blythe, L. L.; Duringer, J. M. The role of the Oregon State University endophyte service laboratory in diagnosing clinical cases of endophyte toxicosis. *J. Agric. Food Chem.* **2014**, *62* (30), 7376−7381.

(6) Tor-Agbidye, J.; Blythe, L. L.; Craig, A. M. Correlation of endophyte toxins (ergovaline and lolitrem B) with clinical disease: fescue foot and perennial ryegrass staggers. *Vet. Hum. Toxicol.* **2001**, *43* (3), 140−146.

(7) Craig, A. M.; Bilich, D.; Hovermale, J. T.; Welty, R. E. Improved extraction and HPLC methods for ergovaline from plant material and rumen fluid. *J. Vet. Diagn. Invest.* **1994**, *6* (3), 348−352.

(8) Hill, N. S.; Rottinghaus, G. E.; Agee, C. S.; Schultz, L. M. Simplified sample preparation for HPLC analysis of ergovaline in tall fescue. *Crop Sci.* **1993**, *33* (2), 331.

(9) Anastassiades, M.; Lehotay, S. J.; Stajnbaher, D.; Schenck, F. J. Fast and easy multiresidue method employing acetonitrile extraction/partitioning and "dispersive solid-phase extraction" for the determination of pesticide residues in produce. *J. AOAC Int.* **2003**, *86*, 412−431.

(10) Anastassiades, M. *QuEChERS.*; http://quechers.cvua-stuttgart.de/; accessed 18 March 2015.

(11) Sirhan, A. Y.; Tan, G. H.; Wong, R. C. S. Method validation in the determination of aflatoxins in noodle samples using the QuEChERS method (quick, easy, cheap, effective, rugged and safe) and high performance liquid chromatography coupled to a fluorescence detector (HPLC-FLD). *Food Control* **2011**, *22*, 1807−1813.

(12) Sospedra, I.; Blesa, J.; Soriano, J. M.; Manes, J. Use of the modified quick easy cheap effective rugged and safe sample preparation approach for the simultaneous analysis of type A- and B-trichothecenes in wheat flour. *J. Chromatogr. A* **2010**, *1217*, 1437−1440.

(13) Zachariasova, M.; Lacina, O.; Malachova, A.; Kostelanska, M.; Poustka, J.; Godula, M.; Hajslova, J. Novel approaches in analysis of Fusarium mycotoxins in cereals employing ultra performance liquid chromatography coupled with high resolution mass spectrometry. *Anal. Chim. Acta* **2010**, *662*, 51−61.

(14) Rasmussen, R. R.; Storm, I. M. L. D.; Rasmussen, P. H.; Smedsgaard, J.; Nielsen, K. F. Multi-mycotoxin analysis of maize silage by LC-MS/MS. *Anal. Bioanal. Chem.* **2010**, *397* (2), 765−776.

(15) Desmarchelier, A.; Oberson, J. M.; Tella, P.; Gremaud, E.; Seefelder, W.; Mottier, P. Development and comparison of two multiresidue methods for the analysis of 17 mycotoxins in cereals by liquid chromatography electrospray ionization tandem mass spectrometry. *J. Agric. Food Chem.* **2010**, *58*, 7510−7519.

(16) Mol, H. G. J.; Plaza-Bolanos, P.; Zomer, P.; de Rijk, T. C.; Stolker, A. A. M.; Mulder, P. P. J. Toward a generic extraction method for simultaneous determination of pesticides, mycotoxins, plant toxins, and veterinary drugs in feed and food matrixes. *Anal. Chem.* **2008**, *80*, 9450−9459.

(17) Jia, W.; Chu, X.; Ling, Y.; Huang, J.; Chang, J. Multi-mycotoxin analysis in dairy products by liquid chromatography coupled to quadrupole orbitrap mass spectrometry. *J. Chromatogr. A* **2014**, *1345*, 107−114.

(18) Dzuman, Z.; Zachariasova, M.; Lacina, O.; Veprikova, Z.; Slavikova, P.; Hajslova, J. A rugged high-throughput analytical approach for the determination and quantification of multiple mycotoxins in complex feed matrices. *Talanta* **2014**, *121*, 263−272.

(19) Majors, R. E. *Application of existing sample preparation technologies to new areas*; http://www.chromatographyonline.com/lcgc/Column%3A+Sample+Prep+Perspectives/Application-of-Existing-Sample-Preparation-Technol/ArticleStandard/Article/detail/828413; accessed 21 Feb 2014.

DOI: 10.1021/acs.jafc.5b01149
J. Agric. Food Chem. 2015, 63, 4236−4242

(20) Craig, A. M. *How To Take a Sample: Sampling Tall Fescue and Perennial Ryegrass for Endophyte Toxin Analysis*; http://oregonstate.edu/endophyte-lab/public/howTo; accessed 18 March 2015.
(21) Spiering, M. J.; Davies, E.; Tapper, B. A.; Schmid, J.; Lane, G. A. Simplified extraction of ergovaline and peramine for analysis of tissue distribution in endophyte-infected grass tillers. *J. Agric. Food Chem.* **2002**, *50*, 5856−5862.
(22) De Boevre, M.; Di Mavungu, J. D.; Maene, P.; Audenaert, K.; Deforce, D.; Haesaert, G.; Eeckhout, M.; Callebaut, A.; Berthiller, F.; Van Peteghem, C.; De Saeger, S. Development and validation of an LC-MS/MS method for the simultaneous determination of deoxynivalenol, zearalenone, T-2-toxin and some masked metabolites in different cereals and cereal-derived food. *Food Addit. Contam., Part A* **2012**, *29* (1), 819−835.
(23) Müller, C.; Kemmlein, S.; Klaffke, H.; Krauthause, W.; Preiß-Weigert, A.; Wittkowski, R. A basic tool for risk assessment: a new method for the analysis of ergot alkaloids in rye and selected rye products. *Mol. Nutr. Food Res.* **2009**, *53* (4), 500−507.
(24) United States Food and Drug Administration. *Guidance for Industry Bioanalytical Method Validation*; http://www.fda.gov/downloads/Drugs/Guidances/ucm070107.pdf; accessed 18 March 2015.
(25) Lyons, P. C.; Plattner, R. D.; Bacon, C. W. Occurrence of peptide and clavine ergot alkaloids in tall fescue grass. *Science* **1986**, *232* (4749), 487−489.
(26) Klotz, J. L.; Kirch, B. H.; Aiken, G. E.; Bush, L. P.; Strickland, J. R. Bioaccumulation of ergovaline in bovine lateral saphenous veins in vitro. *J. Anim. Sci.* **2009**, *87* (7), 2437−2447.
(27) Klotz, J. L.; Bush, L. P.; Smith, D. L.; Shafer, W. D.; Smith, L. L.; Arrington, B. C.; Strickland, J. R. Ergovaline-induced vasoconstriction in an isolated bovine lateral saphenous vein bioassay. *J. Anim. Sci.* **2007**, *85* (9), 2330−2336.
(28) Rottinghaus, G. E.; Garner, G. B.; Cornell, C. N.; Ellis, J. L. HPLC method for quantitating ergovaline in endophyte-infested tall fescue: seasonal variation of ergovaline levels in stems with leaf sheaths, leaf blades, and seed heads. *J. Agric. Food Chem.* **1991**, *39* (1), 112−115.
(29) Köppen, R.; Rasenko, T.; Merkel, S.; Mönch, B.; Koch, M. Novel solid-phase extraction for epimer-specific quantitation of ergot alkaloids in rye flour and wheat germ oil. *J. Agric. Food Chem.* **2013**, *61* (45), 10699−10707.
(30) Hahn, I.; Thamhesl, M.; Apfelthaler, E.; Klingenbrunner, V.; Hametner, C.; Krska, R.; Schatzmayr, G.; Moll, W.-D.; Berthiller, F.; Schwartz-Zimmermann, H. E. Characterisation and determination of metabolites formed by microbial and enzymatic degradation of ergot alkaloids. *World Mycotoxin J.* **2015**, *1* (1), 1−12.
(31) Lehner, A. F.; Craig, M.; Fannin, N.; Bush, L.; Tobin, T. Electrospray[+] tandem quadrupole mass spectrometry in the elucidation of ergot alkaloids chromatographed by HPLC: screening of grass or forage samples for novel toxic compounds. *J. Mass Spectrom.* **2005**, *40*, 1484−1502.
(32) Najafabadi, A. S.; Mofid, M. R.; Mohammadi, R.; Moghim, S. Quantification of ergovaline using HPLC and mass spectrometry in Iranian *Neotyphodium* infected tall fescue. *Res. Pharm. Sci.* **2010**, *5* (2), 135−143.
(33) Krska, R.; Stubbings, G.; Macarthur, R.; Crews, C. Simultaneous determination of six major ergot alkaloids and their epimers in cereals and foodstuffs by LC-MS/MS. *Anal. Bioanal. Chem.* **2008**, *391* (2), 563−576.
(34) Diana Di Mavungu, J.; Malysheva, S. V.; Sanders, M.; Larionova, D.; Robbens, J.; Dubruel, P.; Van Peteghem, C.; De Saeger, S. Development and validation of a new LC-MS/MS method for the simultaneous determination of six major ergot alkaloids and their corresponding epimers. Application to some food and feed commodities. *Food Chem.* **2012**, *135* (1), 292−303.
(35) Smith, D.; Smith, L.; Shafer, W.; Klotz, J.; Strickland, J. Development and validation of an LC-MS method for quantitation of ergot alkaloids in lateral saphenous vein tissue. *J. Agric. Food Chem.* **2009**, *57* (16), 7213−7220.
(36) Smith, D.; Shappell, N. Technical note: Epimerization of ergopeptine alkaloids in organic and aqueous solvents. *J. Anim. Sci.* **2002**, *80*, 1616−1622.

DOI: 10.1021/acs.jafc.5b01149
J. Agric. Food Chem. 2015, 63, 4236−4242

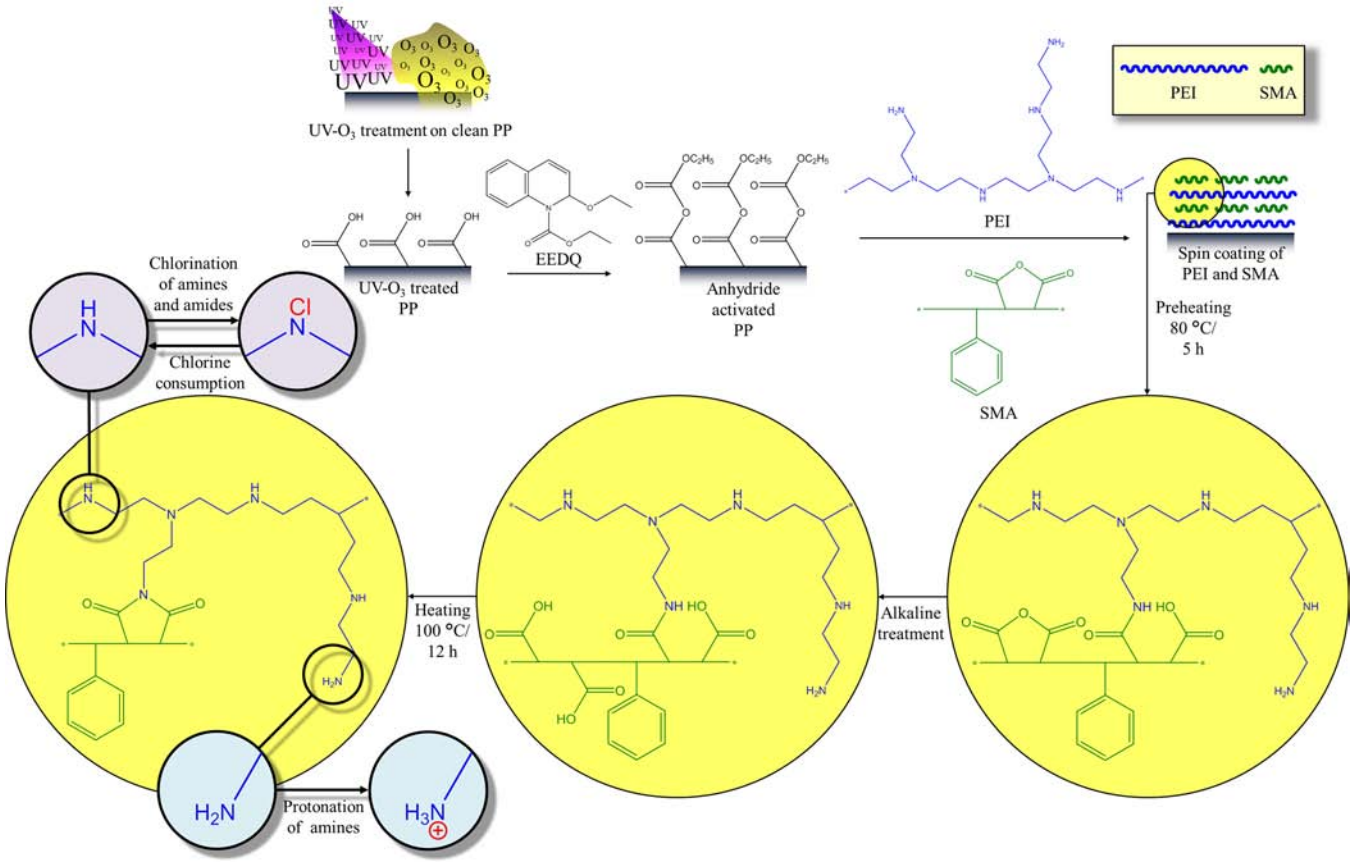

Figure 1. Process for application of the reported antimicrobial coating.

Polymer Products (Ontario, NY, USA). Isopropanol, acetone, methanol, and glycerol were from Fisher Scientific (Pittsburgh, PA, USA). Branched polyethylenimine (PEI, MW 25000), 2-ethoxy-1-ethoxycarbonyl-1,2-dihydroquinoline (EEDQ, MW 247.3), and 4-(2-hydroxyethyl)-1-piperazineethane-sulfonic acid (HEPES) were from Sigma-Aldrich (St. Louis, MO, USA). 2-(*N*-Morpholino)-ethanesulfonic acid sodium salt (MES, MW 217.2) was from GenScript Inc. (Piscataway, NJ, USA). The dye Orange (II) (Cert) (AO7), the sodium hypochlorite solution (5% chlorine), ethylene glycol, and absolute ethanol were from Acros Organics (Fair Lawn, NJ, USA). *N*,*N*-Diethyl-*p*-phenylenediamine DPD total chlorine reagent powder (DPD) was from Hach Co. (Loveland, CO, USA). Tryptic soy broth (TSB), tryptic soy agar (TSA), and neutralizing buffer were from Difco, Becton Dickinson (Sparks, MD, USA).

Antimicrobial Coating Application onto Polypropylene Coupons. *Preparation of PP Coupons.* PP pellets were cleaned by sonication first with isopropanol, then with acetone, and finally with deionized (DI) water (two cycles of 10 min were applied for each solvent). Cleaned PP pellets were left to dry overnight under anhydrous calcium sulfate (RH < 20%) and then hot pressed at 170 °C with a load force of 9000 lb. Coupons of 2 × 2 cm were cut from the obtained films (thickness = 0.5 ± 0.1 mm) and cleaned and dried under the same conditions applied to the PP pellets.

PP Surface Activation. The 2 × 2 cm coupons were UV-ozone-irradiated from one side with a Jelight Co. model 42 UVO Cleaner (Irvine, CA, USA) for 15 min to create carboxylic acid groups on their surfaces[28,29] (this step will be referred as UV-O_3). To create surface anhydride groups (and make the PP surface reactive toward the primary amines of PEI through nucleophilic attack), UV-O_3 coupons were shaken for 2 h at room temperature in a 0.1 mM solution of EEDQ in 50 mM MES buffer (pH 5.5).[30] Before mixing with the MES buffer, the necessary amount of EEDQ was dissolved in a volume of methanol equal to <1% of the final volume of the mix. This step will be referred to as EEDQ. EEDQ-treated coupons were rinsed with 1:100 methanol/DI water solution and dried under an air gun.

Assembly of Antimicrobial Coating. PEI and SMA were dissolved in acetone at a concentration of 60 and 43.2 mg mL^{-1} (respectively) by sonication for 20 min or until completely dissolved. This proportion of PEI and SMA was chosen so that there would be approximately three polymer chains of SMA for every polymer chain of PEI. Alternating volumes of the PEI and SMA solutions were spin-coated onto an anhydride-activated PP coupon (EEDQ-treated) for 1 min at 3000 rpm to produce two bilayers. PEI would covalently bind to the surface of anhydride-activated PP through amide bond formation between the anhydrides and the primary amines of PEI, and the alternating layers of PEI and SMA would cross-link through formation of the same type of bond (Figure 1). After spin-coating, a preheating step was applied to the coupons at 80 °C for 5 h to promote amide bond formation between the PEI and SMA layers.[31] Coupons were then subjected to an alkaline treatment (1 h at room temperature in a 50 mM, pH 10, MES buffer) to promote anhydride ring opening.[32] Coupons were then rinsed with DI water, dried under an air gun, and subjected to a final heating step of 12 h at 100 °C to promote imide ring closing[33] (Figure 1). Coupons were then kept in closed glass Petri dishes until use.

Antimicrobial Coating Surface Characterization. *Attenuated Total Reflectance Fourier Transform Infrared Spectroscopy (ATR-FTIR).* Changes in surface chemistry were analyzed by a diamond crystal ATR-FTIR (penetration depth ∼ 2 μm) after every step in the surface modification process with an IRPrestige 21 spectrometer (Shimadzu Corp., Tokyo, Japan). Coupons from three separately prepared sets were analyzed (three replicates), with at least one randomly chosen coupon from each preparation step. Three spots were analyzed per coupon using Happ−Genzel apodization with a resolution of 4 cm^{-1}, capturing 32 scans per spot. Spectra were obtained with the IR-solution software (Shimadzu Corp.) and interpreted with KnowItAll software (Bio-Rad Laboratories, Phila-

DOI: 10.1021/acs.jafc.5b00445
J. Agric. Food Chem. 2015, 63, 4243−4251

delphia, PA, USA). Average spectra from every step of the antimicrobial coating preparation were selected and combined for comparison after linear baseline correction. After the rechargeability evaluation (explained below), coupons were analyzed with the same criteria.[28,29]

X-ray Photoelectron Spectroscopy (XPS). As a complementary source of coating characterization, a 0.5 × 0.5 cm piece of modified PP cut from a randomly selected coupon at every step of the antimicrobial coating preparation was analyzed using a Physical Electronics Quantum 2000 (Physical Electronics, Chanhassen, MN, USA). A single 100 μm spot was analyzed from every coupon at an angle of 45° relative to the coupons' surface with Al Kα excitation (penetration depth of 2.5−3.0 nm). Survey scans were collected at a pass energy of 187.85 eV, and high-resolution spectra of C 1s, O 1s, and N 1s were collected at a pass energy of 46.95 eV. Atomic percentages and high-resolution spectra were analyzed with Multipak software version 6.1A (Physical Electronics). High-resolution bands of C 1s, O 1s, and N 1s were fitted using the Gaussian−Lorentzian model with 90% Gaussian. Three coupons from every surface modification step were analyzed, each taken from separately prepared sets (three replicates).[29,34]

Atomic Force Microscopy (AFM). Surface topographies were analyzed with a Dimension 3100 atomic force microscope (Digital Instruments, Santa Barbara, CA, USA) under tapping mode with a Si N-type tip (uncoated, f_0 = 200−400 kHz; Applied NanoStructures, Inc., Mountain View, CA, USA). Three measurements were taken from PP and as-prepared modified PP coupons. SPIP software version 6.0.6 (Scanning Probe Image Processor, Image Metrology, Hørsholm, Denmark) was used to calculate mean square roughness (R_q).

Primary Amine Quantification. The Acid Orange 7 (AO7) colorimetric assay[35] was followed to determine the primary amine content of the antimicrobial coating. At least two 1 × 1 cm coupons were taken from each of three separately prepared sets of samples (three replicates, at least two coupons per replicate) for analysis. Coupons were submerged in pH 3, 1 mM, solution (1 mL cm^{-2} of modified surface) of AO7 dye and shaken for 3 h. Then, coupons were rinsed with pH 3 DI water to remove unbound AO7 dye. Following rinsing, coupons were immersed in 5 mL of pH 12 DI water and shaken for 15 min to desorb dye. Absorbances of the solutions containing desorbed dye were read at 455 nm, and the concentrations were determined from a standard curve prepared with different AO7 concentrations in pH 12 DI water.

N-Halamine Quantification. To quantify the *N*-halamine content of the antimicrobial coating, a colorimetric assay published earlier was followed.[28,29,34] Coupons were first chlorinated by exposure to 200 ppm of chlorine (pH 9.7) prepared from sodium hypochlorite solution (5% chlorine), the chlorine content of which was previously confirmed through a standard procedure.[36] During chlorination, coupons were randomly taken at different points in time and rinsed with copious DI water to remove unbound chlorine. To quantify the *N*-halamine content of the chlorinated antimicrobial coatings, rinsed coupons were immersed in 2 mL of DI water, to which 50 μL of the DPD reagent was applied. DPD reagent was prepared by mixing one pack of DPD total chlorine reagent powder with 1 mL of DI water. The solutions containing the coupons were shaken for 5 min for color generation, and absorbances were read at 512 nm. *N*-Halamine content was determined from a standard curve prepared with multiple chlorine concentrations. Chlorination kinetics (and time of chlorine saturation) were determined by fitting data with the exponential association model using GraphPad Prism 5 version 5.04 (GraphPad Software Inc., La Jolla, CA, USA):

$$\mathrm{NH} = \mathrm{NH}_{\mathrm{asympt}}(1 - \mathrm{e}^{-Kt}) \quad (1)$$

NH is the *N*-halamine content in nmol cm^{-2}, $\mathrm{NH}_{\mathrm{asympt}}$ is the asymptotic *N*-halamine content (in nmol cm^{-2}, theoretical amount of *N*-halamines at saturation), K is the exponential rate constant (min^{-1}), and t is the time (min).

Surface pK_a Determination. Surface pK_a of the antimicrobial coating was quantified following a protocol reported in previous works.[37,38] Buffers (pH levels from 2 to 10) were prepared with 10 mM HEPES solutions. For every pH level evaluated, a 5 μL HEPES buffer drop was applied in at least two spots of the surface of a previously cut 1 × 2 cm PP and modified PP coupon. After 15 s, the static contact angle θ_S was measured with a drop shape analyzer DSA100 using its Drop Shape Analysis software version 1.91.0.2 (Krüss, Hamburg, Germany). Coupons from three sets prepared separately were analyzed (three replicates), with at least one coupon per replicate. To calculate surface pK_a, data from each replicate were fitted with the sigmoidal dose−response model through nonlinear regression using the GraphPad software:

$$\theta_S = \theta_{\min} + \frac{\theta_{\max} - \theta_{\min}}{(1 + 10^{(\mathrm{p}K_a - \mathrm{pH})})} \quad (2)$$

θ_S is the static contact angle (in degrees), $\theta_{\max}$ and $\theta_{\min}$ are the maximum and minimum angles obtained from the sigmoidal curve (respectively), and pH is the pH level of the buffer used.

Surface Energy Determination. The Zisman method was applied to calculate the surface energy[39] (surface tension, γ_{GS}, in mN m^{-1}) of the antimicrobial coating. Advancing contact angle (θ_A) was obtained with the same DSA100 Drop Shape Analyzer using liquids of different surface tensions:[40,41] DI water (72.8 mN m^{-1}), glycerol (63 mN m^{-1}), ethylene glycol (47.7 mN m^{-1}), and acetone (25.8 mN m^{-1}). A 5 μL drop of each liquid was applied in at least two spots of the surface of 1 × 2 cm coupons of PP and modified PP. For each liquid and each type of PP, at least one coupon was analyzed from each of three separately prepared sets (three replicates). The cosine of the values of θ_A (in radians) was plotted against the values of surface tension of the corresponding liquid (γ_{GL}) for each treatment (PP and modified PP). After linear regression analysis had been applied to the data with the GraphPad software, γ_{GS} values for PP and modified PP were obtained from the regression curves when $\cos(\theta_A) = 1$.

Antimicrobial Evaluation. The antimicrobial activity of native PP, as-prepared coated PP, and coated PP after exposure to dilute bleach was studied following a protocol published earlier.[28,29] Bacterial suspensions of *L. monocytogenes* Scott A (provided by Dr. Martin Wiedmann, Food Science Department, Cornell University, Ithaca, NY, USA) were prepared by streaking a loopful of stock culture kept at −80 °C in 25% glycerol onto TSA, which was incubated at 37 °C for 24 h. Then, a single colony was inoculated in 9 mL of TSB and incubated overnight for 14 h at the same temperature. A 1% dilution of this overnight broth was prepared with fresh and sterile TSB and incubated for 4 h at 37 °C. The bacterial suspension with approximately 6 log(CFU mL^{-1}) was obtained by preparing a 0.1% dilution of the broth incubated for 4 h in DI water. PP, chlorinated PP, modified PP, chlorinated modified PP, bacterial suspension alone, and bacterial suspension with chlorine added were tested. PP and modified PP 1 × 1 cm coupons were chlorinated for 45 min with a solution having 200 ppm of chlorine following the same procedure explained before. The chlorination time was chosen because (as will be explained later) that is the time required to reach chlorine saturation. A volume of 1 mL of bacterial suspension was put in contact with four 1 × 1 cm coupons of each treatment in individual test tubes and incubated for 2 h with rotation (60 rpm) at 32 °C.[28,29] For the case of bacterial suspension with chlorine added, the amount of chlorine was adjusted to mimic the amount of chlorine given by the four 1 × 1 cm coupons of chlorinated modified PP. After the 2 h of incubation, serial 10% dilutions were prepared from the bacterial suspensions. For the first dilution, neutralizing buffer was used to quench chlorine, and subsequent dilutions were prepared with 0.9% saline water. A volume of 100 μL of each dilution was inoculated onto TSA plates using an automated spiral plater (Autoplater 4000, Spiral Biotech Inc., Norwood, MA, USA) and incubated for 48 h at 37 °C. After incubation, colonies were counted with a plate reader Scan 500 (Interscience, Saint-Nonla-Brèteche, France). To lower the detection limit to 1 log(CFU mL^{-1}), the whole volume of the first dilution after incubation was inoculated manually onto three TSA plates (333 μL per plate). This antimicrobial evaluation was repeated three times using coupons from separately prepared sets (three replicates). For the chlorine rechargeability study (explained below) coupons were

DOI: 10.1021/acs.jafc.5b00445
J. Agric. Food Chem. 2015, 63, 4243−4251

challenged against *L. monocytogenes* at the 10th rechlorination under the same conditions explained for the antimicrobial evaluation.

The inactivation kinetics given by the antimicrobial coatings in cationic and *N*-halamine form was evaluated as follows.[28] Multiple test tubes with 1 mL of bacterial suspension with approximately 6 log(CFU mL^{-1}) containing four 1 × 1 cm coupons of either modified or chlorinated modified PP (chlorinated for 45 min as explained above) were incubated for up to 2 h under the same conditions described above. Test tubes were taken randomly over time and the corresponding dilutions prepared in the same way explained before and inoculated onto TSA plates to be incubated for 48 h at 37 °C. The number of survivors was quantified as in the preliminary evaluation. Data were fitted with the following models[42] using nonlinear regression with the software GraphPad:

$$\log\left(\frac{N}{N_0}\right) = -kt^n \tag{3}$$

$$\log\left(\frac{N}{N_0}\right) = -\frac{at}{(b+t)} - \frac{ct}{(d-t)} \tag{4}$$

Equation 3 corresponds to the Weibull model where $\log(N/N_0)$ is the survival ratio, k is the kinetic constant in min^{-1}, n is the shape factor, and t is the time in minutes. Equation 4 corresponds to a sigmoidal isothermal semilogarithmic model, where a, b (min), c, and d (min) are temperature-dependent coefficients. Two replicates were performed for the inactivation kinetics evaluation, with coupons from two independently prepared sets.

Scanning Electron Microscopy (SEM). To demonstrate that reductions in microbial populations were a result of the antimicrobial nature of the coating and not due to adhesion onto the surface, coupons were evaluated by electron microscopy following antimicrobial activity assays. Coupons were rinsed three times with sterile DI water and then immersed for 45 s in absolute ethanol to fix any attached bacteria.[43] Then, coupons were sputter-coated with gold for 20 s under argon with a Cressington Sputter Coater 108 Auto (Ted Pella, Inc., Redding, CA, USA). Surfaces of the coupons were extensively observed with a scanning electron microscope JCM-6000 NeoScope (JEOL, Japan) at 10 kV, and at least 10 images were taken from coupons of each treatment.

Chlorine Rechargeability. Modified PP coupons were subjected to 10 chlorination cycles to evaluate the ability of the antimicrobial coating to be rechlorinated. Each cycle consisted of 45 min of exposure to 200 ppm of chlorine. *N*-Halamine content was quantified through the DPD assay. Coupons were analyzed through ATR-FTIR as described before to evaluate changes in surface chemistry after the 10 rechlorinations.

Statistical Analysis. In addition to the regression analyses, significant differences between treatments were determined when appropriate through the general linear model followed by Tukey's pairwise comparisons with the software Minitab version 16.1.1 (Minitab Inc., State College, PA, USA), using a confidence interval of 95%. Unless otherwise stated in the corresponding section, three replicates were performed for each evaluation or analysis.

RESULTS AND DISCUSSION

Surface Characterization. An antimicrobial coating has been prepared that exhibits dual antimicrobial functionality by the presence of both cationic and *N*-halamine moieties (Figure 1). ATR-FTIR spectroscopy was performed at each step of the antimicrobial coating preparation to characterize changes in surface chemistry (Figure 2).

Figure 2 contains different regions of the infrared range in which the spectra corresponding to every step of the antimicrobial coating application are displayed: (a) PP, (b) UV−O_3, (c) EEDQ, (d) spin-coating, (e) preheating, (f) alkaline treatment, and (g) heating. The presence of the carbonyl group (C═O) from carboxylic acids can be observed

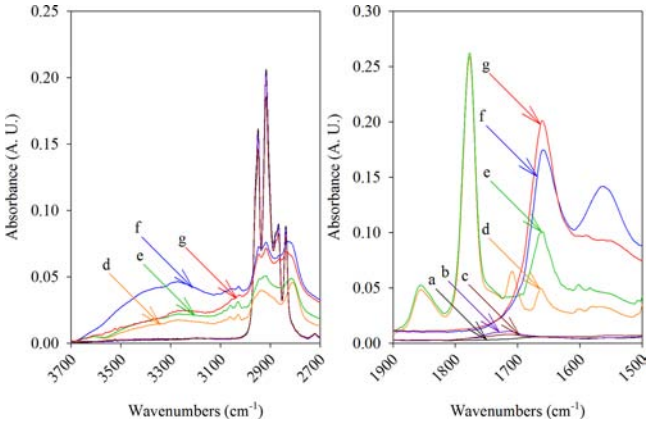

Figure 2. ATR-FTIR spectra showing characteristic bands throughout the antimicrobial coating preparation: PP (a), UV−O_3 (b), EEDQ (c), spin-coating (d), preheating (e), alkaline treatment (f), and heating (g).

in the 1740−1720 cm^{-1} range and confirms activation by the UV-O_3 (creating carboxylic acid groups) and EEDQ (creating anhydride groups) treatments (Figure 2, spectra b and c). After spin-coating, an increase of the carbonyl group of carboxylic acids is observed (1740−1720 cm^{-1} range, attributed to maleic anhydride units in SMA), as well as the formation of a band at ∼1650 cm^{-1} that corresponds to the carbonyl group of amides and imides (Figure 2, spectrum d). This confirms initial covalent cross-linking between the primary amine groups of PEI and the anhydrides from maleic anhydride units of SMA through nucleophilic attack. It can be observed from the increment in absorbance at ∼1650 cm^{-1} and the decrease in the carbonyl group of carboxylic acids (1740−1720 cm^{-1}) that the amide bond formation increases during the preheating step (Figure 2, spectrum e), which again confirms further cross-linking between PEI and SMA. After the alkaline treatment, the bands at ∼1780 and ∼1850 cm^{-1} that correspond to the vibration of C═O from anhydrides disappear (Figure 2, spectra d and e), which confirms the opening of the maleic anhydride rings of SMA, which makes them available for further covalent bond formation with the primary amines of PEI (Figure 1). Finally, after the heating step, the increase in absorbance from the carbonyl group of amides and imides at ∼1650 cm^{-1} (Figure 2, spectrum g) as well as the decrease in the absorbance of the O−H vibration from carboxylic acids in the 3400−3200 cm^{-1} range (Figure 2, spectra g, that confirms further condensation of the free carboxylic acids) and the decrease in absorbance at ∼1550 cm^{-1}, which belongs to the N−H bond in-plane bend of secondary amides (Figure 2, spectrum g), confirm the closing of the ring that results in imide formation through a ring-closing step that releases water (Figure 1).

X-ray photoelectron spectroscopy confirmed the anhydride surface activation of PP after the EEDQ treatment, as noted by the increase in the O—C═O deconvolution band from O 1s (Figure 3). The effect given by the preheating and heating steps was also confirmed from the increase in the amide bond formation exhibited by the increase in the N—C═O deconvolution band from O 1s and N 1s (Figure 3; Table S1 in the Supporting Information). A decrease in the band that encloses both O—C═O and N—C═O in O 1s[44] after the alkaline treatment and an increase in the deconvolution band

DOI: 10.1021/acs.jafc.5b00445
J. Agric. Food Chem. 2015, 63, 4243−4251

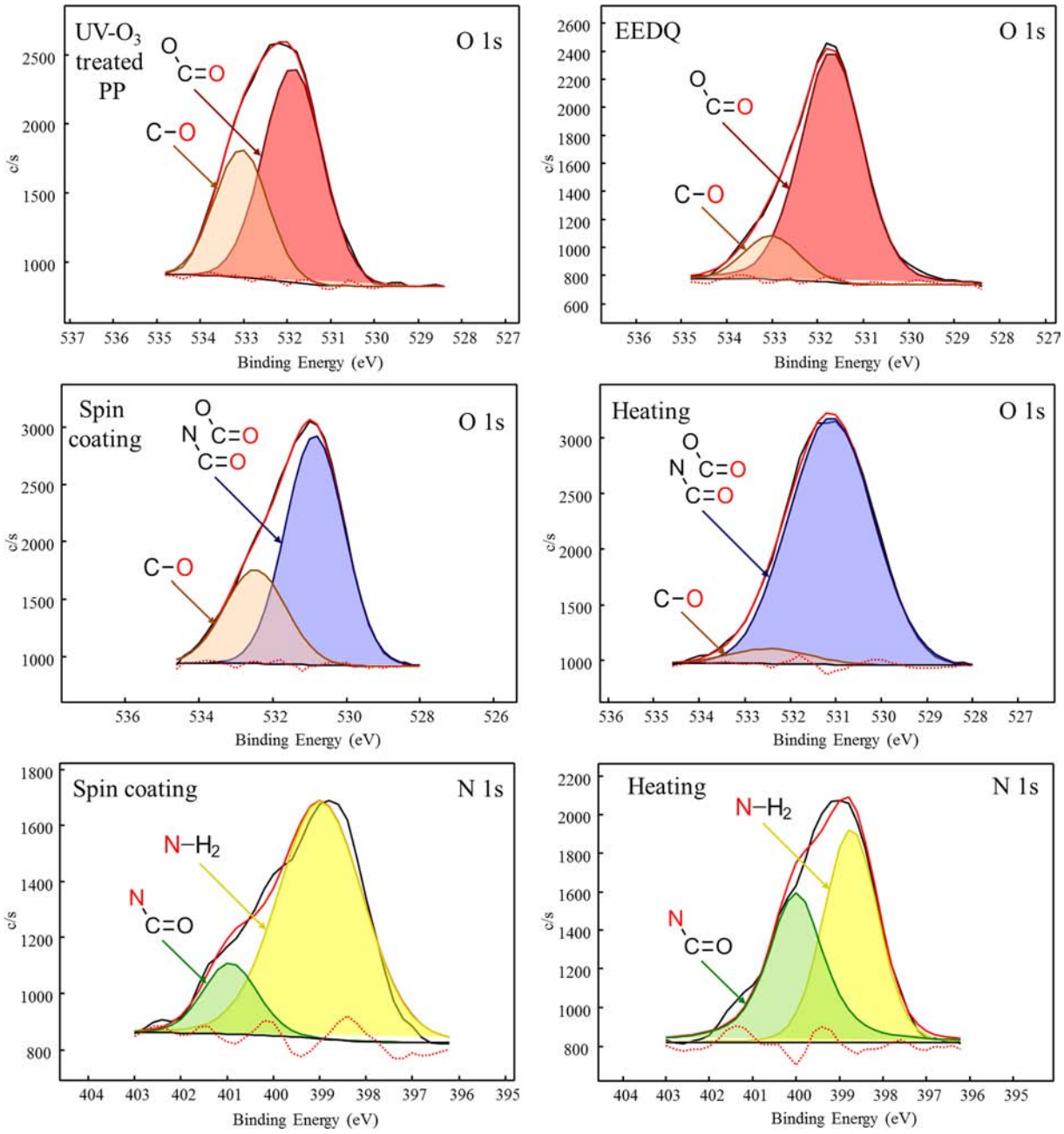

Figure 3. XPS high-resolution bands of O 1s and N 1s.

characteristic of the C—O bond confirms the resulting anhydride ring opening (Supporting Information, Table S1).

AFM images were obtained to characterize changes in surface morphology resulting from application of the antimicrobial coating (Figure 4). A significant ($P < 0.05$), although minor in terms of practical importance, increase in *Rq* was obtained after the application of the antimicrobial coating, going from 8.8 ± 2.6 to 18.3 ± 1.1 nm. A porous surface was observed from modified PP. This effect may be created by the evaporation of the solvent that contains PEI and SMA (acetone) during spin-coating and after heating. The scratches in PP may be originated by the hot pressing of the PP pellets. As can be observed, the antimicrobial coating possesses pores <1 μm in diameter, and electron microscopy confirmed that there was no evidence of bacterial adhesion in them.

Materials were further characterized by quantifying the number of primary amines and *N*-halamine-forming moieties, *N*-halamine chlorination kinetics, and surface pK_a. Application of the antimicrobial coating introduced approximately 500 nmol cm^{-2} of primary amines to the surface of the modified PP. Figure 5A shows the *N*-halamine content of the antimicrobial coating as a function of chlorination time according to eq 1 (NH_{asympt} = 151 ± 22 nmol cm^{-2}, K = 0.03 ± 0.01 min^{-1}, R^2 = 0.88 ± 0.1). As can be observed, the coating reaches chlorine saturation after 45 min, and this chlorination time was used for subsequent antimicrobial activity characterizations. Surface pK_a was determined by plotting static contact angles of dilute buffers on control and modified PP against their corresponding pH values (Figure 5B). Data were fitted with eq 2 (bold line, R^2 = 0.83 ± 0.04) and the data obtained from PP (dashed line represents the average θ_S value of PP in all of the pH range

DOI: 10.1021/acs.jafc.5b00445
J. Agric. Food Chem. 2015, 63, 4243−4251

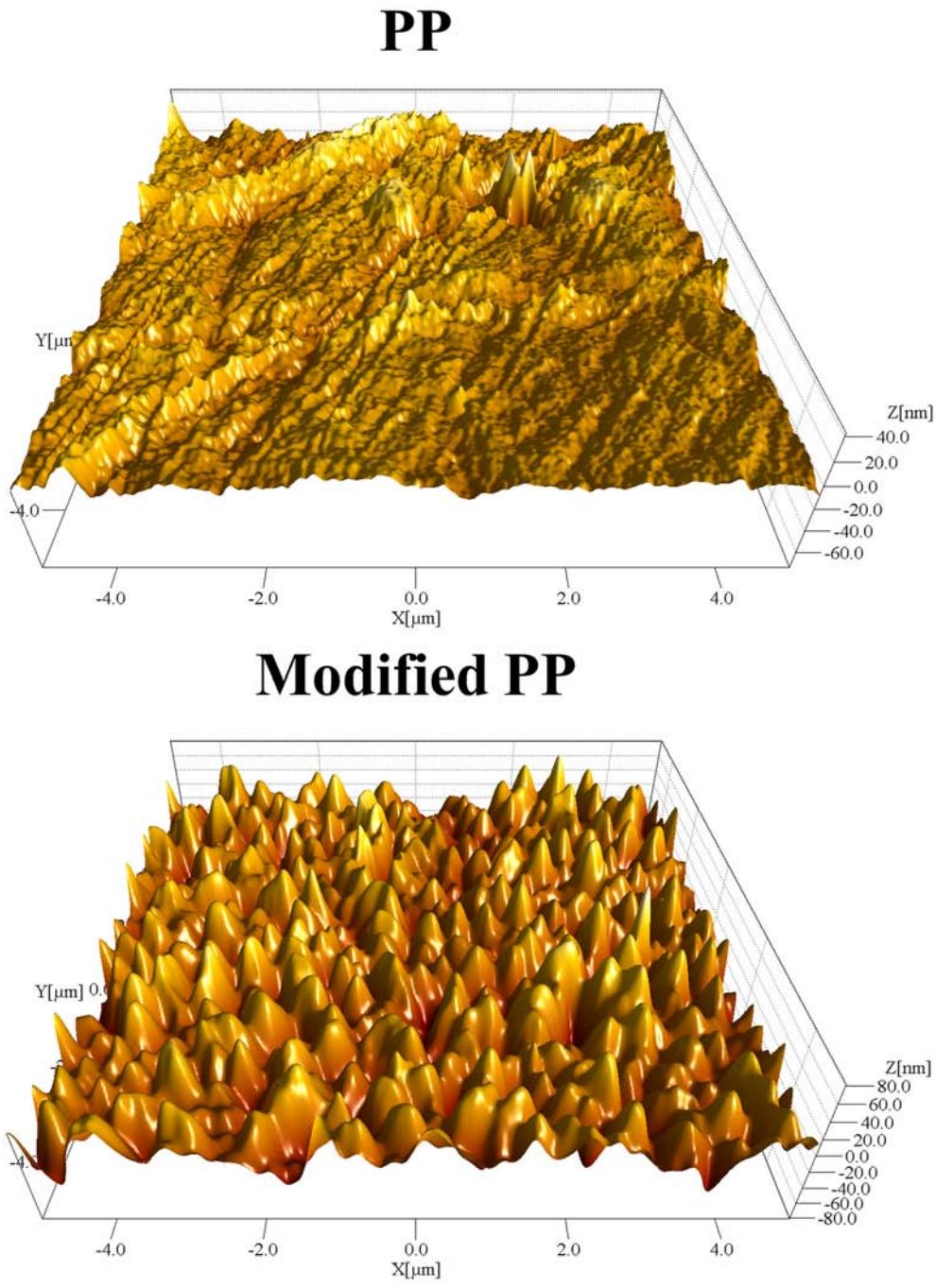

Figure 4. Atomic force micrographs of native and modified PP coupons.

evaluated). The shape of the sigmoidal curve obtained corresponds to that of a cationic surface (character given by the high amount of primary amines), and the obtained pK_a value (4.6 ± 1.4) is comparable to the ones reported in previous works involving similar surface chemistries.[38,45] A similar shift in pK_a values has been seen in previous works concerning attachment of basic (aminated) species on different substrates. The pK_a of the corresponding basic compounds when free in solution is substantially higher than after anchoring onto surfaces, and the reason is believed to be reorientation of the basic compounds toward the substrate, which prevents them from having the same behavior as a pure substance in solution.[46] In previous works in which surface pK_a has been evaluated through contact angle titration, surfaces containing carboxylic acids exhibit a *decrease* in contact angle as pH increases, whereas amine-containing surfaces exhibit an *increase* with increasing pH value. The transition of the sigmoidal curve for both types of ionizable groups can fall within an acidic, neutral, or alkaline pH range, depending on the chemical structure of the acid or amine moiety. In both cases, the surface pK_a values can differ substantially from those of the same chemical entities in solution. This phenomenon (also observed in the present study) can be attributed to a higher difficulty in creating a charged group at the surface

DOI: 10.1021/acs.jafc.5b00445
J. Agric. Food Chem. 2015, 63, 4243−4251

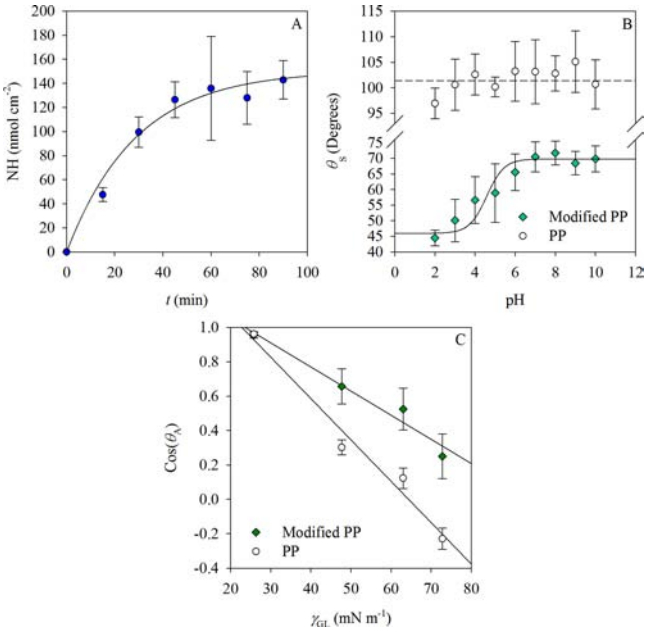

Figure 5. *N*-Halamine formation on the antimicrobial coating (A), contact angle titration curve for pK_a determination (B), and Zisman plot for surface energy determination (C).

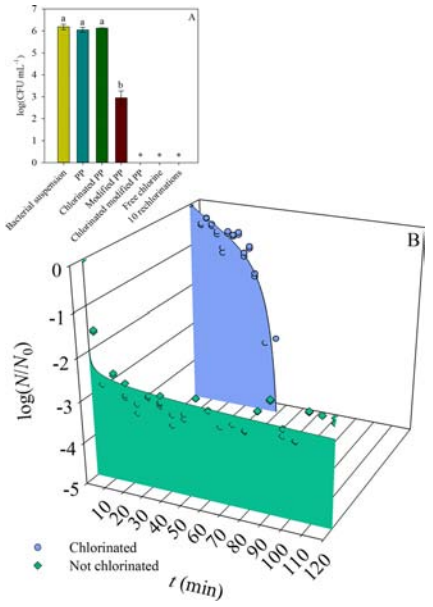

Figure 6. Antimicrobial evaluation (A, results after 2 h of incubation; treatments followed by the same letter are not significantly different, $P > 0.05$) and inactivation kinetics of modified PP and chlorinated modified PP (B; ∗ indicates inactivation below the limit of detection (<1 log(CFU mL^{-1}))).

interface (as compared to in solution), which in turn can be explained by a low local dielectric constant, as well as charge−charge interactions. Additionally, it is believed that as the pH increases, the amine moieties become deprotonated, which in turn decreases the polarity of the surface and increases the contact angle.[47] Even though a higher hydrophilicity was observed on coated PP compared to native PP, there was no significant difference ($P > 0.05$) in surface energy (Figure 5C). Values of γ_{GS} of PP and modified PP were 22.5 ± 0.5 and 23.9 ± 2.3 mN m^{-1}, respectively. Comparable results of surface energy for PP have been reported.[48] The low level of surface energy may have been given by the presence of styrene units in SMA, providing low polarity to the antimicrobial coating. Surfaces with surface energy values <30 mN m^{-1} can be considered as nonfouling.[49] The obtained value of surface energy (γ_{GS}) of modified PP is lower than those of other common food contact surfaces such as stainless steel 304 (39.2 mN m^{-1}), glass (33.8 mN m^{-1}), granite (46.2 mN m^{-1}), and marble (40.2 mN m^{-1}).[27]

Antimicrobial Evaluation. Antimicrobial activity of the cationic, *N*-halamine polymeric coating was characterized against *L. monocytogenes* by exposing coupons of control and modified PP to aqueous bacterial suspensions under rotation. As expected, no antimicrobial effect was observed from either PP or chlorinated PP, and after 2 h of incubation, approximately 3 logarithmic reductions were given by modified PP and >5 logarithmic reductions were given by both chlorinated modified PP and an equivalent concentration of free chlorine (Figure 6A). Because the pH of the bacterial suspension used was 6.0 ± 0.1, which falls in the range of the surface pK_a, the antimicrobial effect can be attributed to the positively charged nature of the surface. In addition, antimicrobial activity was preserved from modified PP coupons that had been subjected to 10 rechlorination cycles, providing also >5 logarithmic reductions. The inactivation kinetics showed a different behavior between modified PP and chlorinated modified PP (Figure 6B). The inactivation kinetics of unchlorinated modified PP exhibited a Weibullian behavior (the cationic form, eq 3, $R^2 = 0.84$), whereas chlorinated modified PP showed a sigmoidal behavior (*N*-halamine form, eq 4, $R^2 = 0.84$). Cationic polymers have been reported to inactivate microorganisms in previous studies, and the possible explanations provided for their action have been an ion exchange process between the positive charges of the polymers and the cell membrane (causing its deterioration), the generation of reactive oxygen species that can provoke oxidative stress and damage genetic information and other biomolecules, and interruption of the electron transport chain, vital for energy generation.[19−21] In previous works, *N*-halamines[11,28] and cationic polymers[50] have exhibited inactivation kinetics similar to the ones observed here. In the cited works, inactivation kinetics given by *N*-halamines exhibits an initially slow biocidal effect, which is followed by a drastic and abrupt reduction in the microbial population. In contrast, according to the cited reference in the case of cationic polymers, the inactivation kinetics shows initially a drastic and fast decrease in the microbial population, which is followed by a plateau or by an abrupt decrease in the speed of inactivation.

Scanning Electron Microscopy (SEM). To confirm that reductions in bacterial populations were due to inactivation by the antimicrobial coating and not a result of adhesion onto its surface due to its cationic nature, electron microscopy was performed on coupons following antimicrobial activity assays (Supporting Information, Figure S1). No visual evidence of attached bacteria was found on native or coated PP. Previous works have shown that PP exhibits a low level of surface attachment of *L. monocytogenes* as compared to other materials' surfaces. In the same mentioned studies, adhesion of *L. monocytogenes* cells on surfaces has not been possible to link with materials properties such as roughness and hydrophobicity,[27] which makes this phenomenon unpredictable on the basis of surface properties. The results obtained confirm that, under the test conditions and at the inoculum level used,

DOI: 10.1021/acs.jafc.5b00445
J. Agric. Food Chem. 2015, 63, 4243−4251

the reduction in microbial load exerted by modified PP and chlorinated modified PP is not caused by cell adhesion on the coupons' surfaces.

Chlorine Rechargeability of the Antimicrobial Coating. Modified PP was exposed to 10 cycles of chlorination to demonstrate the ability of the coating to regenerate *N*-halamines (Supporting Information, Figure S2). Some of the bonds that hold together the layers of PEI and SMA exhibited hydrolysis after the 10 rechlorinations according to the ATR-FTIR spectra. The absorbance increases in the 3400−3200 cm^{-1} range (Supporting Information, Figure S2A) and in the 1740−1720 cm^{-1} range (Supporting Information, Figure S2B), which are characteristic of the C—O and C═O vibrations of carboxylic acids, respectively, and an absorbance reduction at ∼1650 cm^{-1} (Supporting Information, Figure S2B, C═O vibration of amides) confirm the hydrolysis of amide and imide bonds. As can be observed (Supporting Information, Figure S2C), an initial increase in chlorine absorption is exhibited, followed by stabilization. From the SEM images (Supporting Information, Figure S1D), it can be seen that a single chlorination causes a change in the surface pattern. However, as the antimicrobial evaluation confirmed, the biocidal efficacy was retained after 10 rechlorinations (Figure 6A). Similar results have been reported in studies involving rechlorination of polymeric *N*-halamines.[29]

■ ASSOCIATED CONTENT

Ⓢ Supporting Information

A table of XPS analysis results, atomic percentages, and deconvolution of high-resolution bands of O 1s and N 1s; figures showing results from SEM analysis and the *N*-halamine content of the modified PP coupons during rechlorination and the ATR-FTIR spectra before and after the chlorine rechargeability evaluation. This material is available free of charge via the Internet at http://pubs.acs.org.

■ AUTHOR INFORMATION

Corresponding Author

*(J.M.G.) Phone: (413) 545-2275. Fax: (413) 545-1262. E-mail: goddard@foodsci.umass.edu.

Funding

This material is based upon work supported by the National Institute of Food and Agriculture, U.S. Department of Agriculture, under Project 2011-65210-20059.

Notes

The authors declare no competing financial interest.

■ ACKNOWLEDGMENTS

We thank Prof. Lynne A. McLandsborough for assistance in the antimicrobial evaluations, Prof. D. Julian McClements for the use of his Drop Shape Analyzer DSA100; Prof. Thomas McCarthy and Jacob Hirsch for use of their Physical Electronics Quantum 2000; and Dr. Sekar T. Dhanasekaran for training and assistance in the AFM analysis.

■ ABBREVIATIONS USED

PP, polypropylene; PEI, branched polypropylene; SMA, styrene maleic anhydride copolymer; DI, deionized; UV-O_3, ultraviolet-ozone; EEDQ, 2-ethoxy-1-ethoxycarbonyl-1,2-dihydroquioline; MES, 2-(*N*-morpholino)ethanesulfonic acid; ATR-FTIR, attenuated total reflectance Fourier transform infrared spectroscopy; XPS, X-ray photoelectron spectroscopy; AFM, atomic force microscopy; AO7, Acid Orange 7; DPD, *N*,*N*-diethyl-*p*-phenylenediamine; TSB, tryptic soy broth; TSA, tryptic soy agar; SEM, scanning electron microscopy

■ REFERENCES

(1) Cools, I.; Uyttendaele, M.; Cerpentier, J.; D'Haese, E.; Nelis, H. J.; Debevere, J. Persistence of *Campylobacter jejuni* on surfaces in a processing environment and on cutting boards. *Lett. Appl. Microbiol.* **2005**, *40*, 418−423.

(2) Vorst, K.; Todd, E.; Ryser, E. Transfer of *Listeria monocytogenes*during mechanical slicing of turkey breast, bologna, and salami. *J. Food Prot.* **2006**, *69*, 619−626.

(3) Wilks, S. A.; MichelS, H. T.; Keevil, C. W. Survival of *Listeria monocytogenes* Scott A on metal surfaces: implications for cross-contamination. *Int. J. Food Microbiol.* **2006**, *111*, 93−98.

(4) Jiang, H.; Manolache, S.; Wong, A.; Denes, F. Plasma-enhanced deposition of silver nanoparticles onto polymer and metal surfaces for the generation of antimicrobial characteristics. *J. Appl. Polym. Sci.* **2004**, *93*, 1411−1422.

(5) Asri, L. A. T. W.; Crismaru, M.; Roest, S.; Chen, Y.; Ivashenko, O.; Rudolf, P.; Tiller, J. C.; van der Mei, H. C.; Loontjens, T. J. A.; Busscher, H. J. A shape-adaptive, antibacterial-coating of immobilized quaternary-ammonium compounds tethered on hyperbranched polyurea and its mechanism of action. *Adv. Funct. Mater.* **2014**, *24*, 346−355.

(6) Jampala, S. N.; Sarmadi, M.; Somers, E. B.; Wong, A. C. L.; Denes, F. S. Plasma-enhanced synthesis of bactericidal quaternary ammonium thin layers on stainless steel and cellulose surfaces. *Langmuir* **2008**, *24*, 8583−8591.

(7) Chen, R.; Willcox, M. D. P.; Cole, N.; Ho, K. K. K.; Rasul, R.; Denman, J. A.; Kumar, N. Characterization of chemoselective surface attachment of the cationic peptide melimine and its effects on antimicrobial activity. *Acta Biomater.* **2012**, *8*, 4371−4379.

(8) Hequet, A.; Humblot, V.; Berjeaud, J.; Pradier, C. Optimized grafting of antimicrobial peptides on stainless steel surface and biofilm resistance Tests. *Colloids Surf., B* **2011**, *84*, 301−309.

(9) Kocer, H. B.; Akdag, A.; Worley, S. D.; Acevedo, O.; Broughton, R. M.; Wu, Y. Mechanism of photolytic decomposition of *N*-halamine antimicrobial siloxane coatings. *ACS Appl. Mater. Interfaces* **2010**, *2*, 2456−2464.

(10) Kenawy, E.; Worley, S. D.; Broughton, R. The chemistry and applications of antimicrobial polymers: a state-of-the-art review. *Biomacromolecules* **2007**, *8*, 1359−1384.

(11) Williams, D.; Worley, S.; Barnela, S.; Swango, L. Bactericidal activities of selected organic *N*-halamines. *Appl. Environ. Microbiol.* **1987**, *53*, 2082−2089.

(12) Lauten, S.; Sarvis, H.; Wheatley, W.; Williams, D.; Mora, E.; Worley, S. Efficacies of novel *N*-halamine disinfectants against *Salmonella* and *Pseudomonas* species. *Appl. Environ. Microbiol.* **1992**, *58*, 1240−1243.

(13) Worley, S.; Williams, D. Halamine water disinfectants. *Crit. Rev. Environ. Control* **1988**, *18*, 133−175.

(14) Goddard, J. M.; Hotchkiss, J. H. Rechargeable antimicrobial surface modification of polyethylene. *J. Food Prot.* **2008**, *71*, 2042−2047.

(15) Fang, B.; Jiang, Y.; Rotello, V. M.; Nuesslein, K.; Santore, M. M. Easy come easy go: surfaces containing immobilized nanoparticles or isolated polycation chains facilitate removal of captured *Staphylococcus aureus* by retarding bacterial bond maturation. *ACS Nano* **2014**, *8*, 1180−1190.

(16) Mansilla, A. Y.; Albertengo, L.; Rodriguez, M. S.; Debbaudt, A.; Zuniga, A.; Casalongue, C. A. Evidence on antimicrobial properties and mode of action of a chitosan obtained from crustacean exoskeletons on *Pseudomonas syringae* pv. Tomato DC3000. *Appl. Microbiol. Biotechnol.* **2013**, *97*, 6957−6966.

(17) Xia, B.; Dong, C.; Lu, Y.; Rong, M.; Lv, Y.; Shi, J. Preparation and characterization of chemically-crosslinked polyethyleneimine films

DOI: 10.1021/acs.jafc.5b00445
J. Agric. Food Chem. 2015, 63, 4243−4251

on hydroxylated surfaces for stable bactericidal coatings. *Thin Solid Films* **2011**, *520*, 1120−1124.
(18) Wang, B.; Navath, R. S.; Menjoge, A. R.; Balakrishnan, B.; Bellair, R.; Dai, H.; Romero, R.; Kannan, S.; Kannan, R. M. Inhibition of bacterial growth and intramniotic infection in a guinea pig model of chorioamnionitis using PAMAM dendrimers. *Int. J. Pharm.* **2010**, *395*, 298−308.
(19) Kugler, R.; Bouloussa, O.; Rondelez, F. Evidence of a charge-density threshold for optimum efficiency of biocidal cationic surfaces. *Microbiology* **2005**, *151*, 1341−1348.
(20) Lichter, J. A.; Rubner, M. F. Polyelectrolyte multilayers with intrinsic antimicrobial functionality: the importance of mobile polycations. *Langmuir* **2009**, *25*, 7686−7694.
(21) Chakraborti, S.; Bhattacharya, S.; Chowdhury, R.; Chakrabarti, P. The molecular basis of inactivation of metronidazole-resistant *Helicobacter pylori* using polyethyleneimine functionalized zinc oxide nanoparticles. *PLoS One* **2013**, *8*, No. e70776, DOI: 10.1371/journal.pone.0070776.
(22) Onnis-Hayden, A.; Hsu, B. B.; Klibanov, A. M.; Gu, A. Z. An antimicrobial polycationic sand filter for water disinfection. *Water Sci. Technol.* **2011**, *63*, 1997−2003.
(23) Liu, Y.; Liu, Y.; Ren, X.; Huang, T. S. Antimicrobial cotton containing *N*-halamine and quaternary ammonium groups by grafting copolymerization. *Appl. Surf. Sci.* **2014**, *296*, 231−236.
(24) Liang, J.; Chen, Y.; Barnes, K.; Wu, R.; Worley, S.; Huang, T. *N*-Halamine/quat siloxane copolymers for use in biocidal coatings. *Biomaterials* **2006**, *27*, 2495−2501.
(25) Li, L.; Pu, T.; Zhanel, G.; Zhao, N.; Ens, W.; Liu, S. New biocide with both *N*-chloramine and quaternary ammonium moieties exerts enhanced bactericidal activity. *Adv. Healthcare Mater.* **2012**, *1*, 609−620.
(26) Bastarrachea, L.; Dhawan, S.; Sablani, S. S. Engineering properties of polymeric-based antimicrobial films for food packaging. *Food Eng. Rev.* **2011**, *3*, 79−93.
(27) Silva, S.; Teixeira, P.; Oliveira, R.; Azeredo, J. Adhesion to and viability of *Listeria monocytogenes* on food contact surfaces. *J. Food Prot.* **2008**, *71*, 1379−1385.
(28) Bastarrachea, L. J.; Peleg, M.; McLandsborough, L. A.; Goddard, J. M. Inactivation of *Listeria monocytogenes* on a polyethylene surface modified by layer-by-layer deposition of the antimicrobial *N*-halamine. *J. Food Eng.* **2013**, *117*, 52−58.
(29) Bastarrachea, L. J.; McLandsborough, L. A.; Peleg, M.; Goddard, J. M. Antimicrobial *N*-halamine modified polyethylene: characterization, biocidal efficacy, regeneration, and stability. *J. Food Sci.* **2014**, *79*, E887−E897.
(30) Martin, J.; Mancheno, J.; Arche, R. Inactivation of penicillin acylase from *Kluyvera citrophila* by *N*-ethoxycarbonyl-2-ethoxy-1,2-dihydroquinoline − a case of time-dependent noncovalent enzyme-inhibition. *Biochem. J.* **1993**, *291*, 907−914.
(31) Karakus, G.; Polat, Z. A.; Yaglioglu, A. S.; Karahan, M.; Yenidunya, A. F. Synthesis, characterization, and assessment of cytotoxic, antiproliferative, and antiangiogenic effects of a novel procainamide hydrochloride-poly(maleic anhydride-*co*-styrene) conjugate. *J. Biomater. Sci., Polym. Ed.* **2013**, *24*, 1260−1276.
(32) Hermanson, G. In *Bioconjugate Techniques*; Academic Press: Boston, MA, USA, 2008; Vol. 381, pp 1202.
(33) Song, Z.; Baker, W. Chemical-reactions and reactivity of primary, secondary, and tertiary diamines with acid functionalized polymers. *J. Polym. Sci., Part A: Polym. Chem.* **1992**, *30*, 1589−1600.
(34) Bastarrachea, L. J.; Goddard, J. M. Development of antimicrobial stainless steel via surface modification with *N*-halamines: characterization of surface chemistry and *N*-halamine chlorination. *J. Appl. Polym. Sci.* **2013**, *127*, 821−831.
(35) Uchida, E.; Uyama, Y.; Ikada, Y. Sorption of low-molecular-weight anions into thin polycation layers grafted onto a film. *Langmuir* **1993**, *9*, 1121−1124.
(36) American Society for Testing and Materials. In *Standard Test Methods of Sampling and Chemical Analysis of Chlorine-Containing Bleaches, D 2022-89*; ASTM: Philadelphia, PA, USA, 2008.
(37) Holmes-Farley, S.; Reamey, R.; McCarthy, T.; Deuth, J.; Whitesides, G. Acid-base behavior of carboxylic-acid groups covalently attached at the surface of polyethylene − the usefulness of contact-angle in following the ionization of surface functionality. *Langmuir* **1985**, *1*, 725−740.
(38) Van der Maaden, K.; Sliedregt, K.; Kros, A.; Jiskoot, W.; Bouwstra, J. Fluorescent nanoparticle adhesion assay: a novel method for surface pK_a determination of self-assembled monolayers on silicon surfaces. *Langmuir* **2012**, *28*, 3403−3411.
(39) Combe, E.; Owen, B.; Hodges, J. A protocol for determining the surface free energy of dental materials. *Dent. Mater.* **2004**, *20*, 262−268.
(40) Costanzo, P.; Giese, R.; Vanoss, C. Determination of the acid-base characteristics of clay mineral surfaces by contact-angle measurements implications for the adsorption of organic solutes from aqueous-media. *J. Adhes. Sci. Technol.* **1990**, *4*, 267−275.
(41) Howard, K.; McAllister, R. Surface tension of acetone-water solutions up to their normal boiling points. *AIChE J.* **1957**, *3*, 325−329.
(42) Peleg, M. In *Advanced Quantitative Microbiology for Foods and Biosystems: Models for Predicting Growth and Inactivation*; Taylor & Francis: Boca Raton, FL, USA, 2006; pp 417.
(43) Djordjevic, D.; Wiedmann, M.; McLandsborough, L. Microtiter plate assay for assessment of *Listeria monocytogenes* biofilm formation. *Appl. Environ. Microbiol.* **2002**, *68*, 2950−2958.
(44) Lai, L.; Yang, Y.; Lin, Y.; Huang, L.; Hsieh, Y. Surface characterization of immunosensor conjugated with gold nanoparticles based on cyclic voltammetry and X-ray photoelectron spectroscopy. *Colloids Surf., B* **2009**, *68*, 130−135.
(45) Vezenov, D.; Noy, A.; Rozsnyai, L.; Lieber, C. Force titrations and ionization state sensitive imaging of functional groups in aqueous solutions by chemical force microscopy. *J. Am. Chem. Soc.* **1997**, *119*, 2006−2015.
(46) Abiman, P.; Wildgoose, G.; Crossley, A.; Jones, J.; Compton, R. Contrasting pK_a of protonated bis(3-aminopropyl)-terminated polyethylene glycol "jeffamine" and the associated thermodynamic parameters in solution and covalently attached to graphite surfaces. *Chem.−Eur. J.* **2007**, *13*, 9663−9667.
(47) Holmes-Farley, S.; Bain, C.; Whitesides, G. Wetting of functionalized polyethylene film having ionizable organic-acids and bases at the polymer water interface − relations between functional-group polarity, extent of ionization, and contact-angle with water. *Langmuir* **1988**, *4*, 921−937.
(48) Farris, S.; Pozzoli, S.; La Vecchia, S.; Biagioni, P.; Bianchi, C. L.; Piergiovanni, L. Mapping physicochemical surface modifications of flame-treated polypropylene. *eXPRESS Polym. Lett.* **2014**, *8*, 256−266.
(49) Kota, A. K.; Kwon, G.; Tuteja, A. The design and applications of superomniphobic surfaces. *NPG Asia Mater.* **2014**, *6*, e109.
(50) Milovic, N.; Wang, J.; Lewis, K.; Klibanov, A. Immobilized N-alkylated polyethylenimine avidly kills bacteria by rupturing cell membranes with no resistance developed. *Biotechnol. Bioeng.* **2005**, *90*, 715−722.

DOI: 10.1021/acs.jafc.5b00445
J. Agric. Food Chem. 2015, 63, 4243−4251

Table 1. Compilation of the Investigated Barley Cultivars

cultivar	origin	characteristics[a]
Argentinian Mutant 6519	Argentina; chemically induced mutant of Quilmes Paine (1993)	drought resistance; salt stress resistance
Mackay	Australia; Cameo × Coru (2001)	drought tolerance;[27] powdery mildew resistance; net blotch susceptibility; spot blotch susceptibility[28]
Palmella Blue (CIho 3609)	Ethiopian landrace	drought tolerance
IPZ 24727	Germany; Maresi × Omega	stress tolerance; ramularia tolerance; nonparasitic leaf spot tolerance; mildew susceptibility
Marnie	Germany; 6429f Havanna × (Prisma × Br 4714a) (2003)	mildew resistance; leaf rust resistance; net blotch resistance[26]
Iron	Germany; Marnie × LP 813.6.98 (2009)	leaf rust resistance
Barke	Germany; Libelle × Alexis (1996)	stress susceptibility; leaf disease resistances; mildew resistance
Steina	Germany; (Sultan × St.434/62) × (Voldagsen × Carlsberg × Volla) (1980)	leaf rust resistance
Streif	Germany; Pasadena × Aspen (2007)	mildew resistance; leaf rust resistance
Emperor	Canada; HB320 × Maresi	net blotch susceptibility; leaf rust moderate susceptibility; powdery mildew resistance
Polygena	Germany; 46401-80 × 45465-78 (1994)	leaf rust resistance

[a]According to descriptions provided by the plant breeders or in the literature.

studies on grain from plants grown under water limitation were performed to compare different hybrids.[9]

Additionally, there are some studies that investigated the cultivar-specific impact of drought stress on metabolites via targeted analyses. For example, Thakur and Rai studied the alterations of levels of amino acids in maize shoots from differently drought-resistant cultivars.[17] Singh et al. specifically analyzed the accumulation of proline in leaves of barley varieties with different adaptions to drought.[18]

The objective of the present study was to apply metabolite profiling to identify metabolites that might serve as markers for barley cultivars differently adapted to drought stress. Therefore, a set comprising both stress resistant/tolerant cultivars and cultivars, for which no drought resistance/tolerance had been described, were field-grown in three consecutive growing seasons under normal weather conditions as control and under induced drought stress using a rain-out shelter. The same barley cultivars were also grown under natural weather conditions in a second field trial at another location. Using metabolite profiling in combination with multivariate and univariate analyses, this setup should enable screening for cultivar-specific responses of barley grain to drought stress.

MATERIALS AND METHODS

Sample Material. Eleven two-row spring barley cultivars were field-grown under natural weather conditions at two control locations in Bavaria, Germany, and under drought stress induced by using a rain-out shelter in the growing seasons 2010−2012; information on the cultivars is provided in Table 1. The first control location (Freising, C1) was situated next to the rain-out shelter, whereas the second control location (Frankendorf, C2) was 30 km distant. GPS coordinates of the field sites were as follows: C1 and rain-out shelter, latitude 48.3924, longitude 11.7569, elevation 448 m above normal null (NN); C2, latitude 48.3667, longitude 12, elevation 455 m above NN. Two biological replicates were taken from field trials with totally randomized field plot design and analyzed in triplicate (laboratory replicate samples). For further information regarding growing periods, soil quality, and weather conditions, see Wenzel et al.[12]

Metabolite Profiling. *Preparation of Standard Solutions.* The following internal standards were used for nonpolar (fractions 1 and 2) and polar (fractions 3 and 4) extracts of barley (see later for fractionation protocol): 0.5 mg/mL heptacosane in hexane (fraction 1); 0.6 mg/mL 5α-cholestan-3β-ol in dichloromethane (fraction 2); 0.8 mg/mL phenyl-β-D-glucopyranoside in distilled water (fraction 3); 0.4 mg/mL *p*-chloro-L-phenylalanine in distilled water (fraction 4). The retention time mixture consisted of 1.5 mL of undecane (2 mg/mL in hexane), 2.5 mL of hexadecane (1.5 mg/mL in hexane), 4 mL of tetracosane (1.5 mg/mL), and 4 mL of triacontane (1.5 mg/mL) dissolved in 15 mg of octatriacontane. Internal standards and retention time mixture standards were purchased from Fluka (Buchs, Switzerland).

Sample Preparation. Barley plants were harvested and samples were prepared as previously described.[12] Barley kernels from each biological replicate were ground with a cyclone mill (Cyclotec 1093, Foss Tecator, Rellingen, Germany) using a 500 μm sieve and immediately freeze-dried for 48 h. Samples were transferred to LDPE bottles (Kautex Textron, Bonn, Germany) and stored at −18 °C until analysis.

Sample Workup. Freeze-dried barley samples were subjected to an extraction and fractionation scheme resulting in four fractions containing nonpolar (fractions 1 and 2) and polar constituents (fractions 3 and 4) as previously described in detail for maize.[19] Flour (200 mg) was weighed into a cartridge, and 100 μL of methanol was added for cell disruption. After 20 min, methanol was removed by application of vacuum (30 mbar, 30 min), and nonpolar and polar compounds were extracted. One hundred microliters of standard solutions 1 and 2 as well as 300 μL of standard solutions 3 and 4 was added to the nonpolar and polar extracts, respectively. The nonpolar extract was transesterified with sodium methoxide and separated by solid phase extraction (SPE) into fractions 1 and 2 containing fatty acid methyl esters (FAME) and hydrocarbons as well as phytosterols, free fatty acids (FFA), and fatty alcohols, respectively. An aliquot of the polar extract was silylated and purified by selective hydrolysis to obtain fraction 3 containing sugar and sugar alcohols. Fraction 4 containing acids, amino acids, and amines was obtained by subjecting a second aliquot of the polar extract to silylation, oximation, and selective hydrolysis. For gas chromatography−mass spectrometry (GC-MS) analysis, 1 μL of fractions 1 and 2 as well as 0.5 μL of fractions 3 and 4, respectively, was injected. In addition, 1 μL of a 1:10 dilution of fraction 1 was injected to quantitate constituents present in high concentrations. The GC-MS conditions were as previously described.[12]

Metabolite Identification. Metabolites were identified by comparison of mass spectra and retention indices with those of reference compounds, with data from the NIST08 mass spectra library, the GOLM metabolome database, and the literature.[20−22]

Quantitation of Free Amino Acids. Quantitation of proteinogenic free amino acids was based on the equation

DOI: 10.1021/acs.jafc.5b01114
J. Agric. Food Chem. 2015, 63, 4252−4261

$$c(\mathrm{A}) = \frac{\mathrm{height(A)} \times c(\mathrm{IS}) \times \mathrm{Rf} \times 100}{\mathrm{height(IS)} \times W} \times 5\ (\mathrm{mg/kg\ flour})$$

where c is the concentration (μg/g), height the average absolute peak height of three repetitions, IS the internal standard, A the analyte, Rf the response factor, W the recovery rate, and 5 the dilution factor. A mixture containing 0.1 mg/mL alanine, glycine, tyrosine, leucine, lysine, glutamine, isoleucine, proline, valine, phenylalanine, and tryptophan, 0.5 mg/mL serine, threonine, and asparagine, 0.3 mg/mL aspartic acid, and glutamic acid in MeOH/H_2O (80:20, v/v) was prepared for validation.

Response Factor. For calculating response factors (Rf), 1 mL of amino acid standard mixture was silylated and analyzed in triplicate. Response factors were calculated by using the equation

$$\mathrm{Rf} = \frac{\mathrm{height(IS)} \times c(\mathrm{A})}{\mathrm{height(A)} \times c(\mathrm{IS})}$$

where Rf is the response factor, height the averaged absolute peak height of three repetitions, IS the internal standard, A the analyte, and c the concentration.

Repeatability. Repeatability was determined by triplicate analysis of one barley sample. Relative standard deviations (RSD) of peak heights normalized to internal standard 4 were calculated for each amino acid.

Recovery. Recovery rates of amino acids were determined by analyzing nine aliquots of a polar extract. The first three aliquots of the extract were spiked with 50 μL of amino acid standard mixture at the beginning of the analytical workup, whereas three further aliquots were spiked at the end of the procedure prior to GC-MS measurement. The last three aliquots were analyzed to calculate peak heights of the amino acids naturally occurring in the unspiked flour. Recovery rates were calculated by using the equation

$$W = \frac{H_{\mathrm{P1}} - H_{\mathrm{P3}}}{H_{\mathrm{P2}} - H_{\mathrm{P3}}} \times 100\%$$

where W is the recovery rate, H_{P1} the average relative peak height from three aliquots of the extract spiked at the beginning of the analytical procedure, H_{P2} the average relative peak height from three aliquots of the extract spiked prior to GC-MS measurement, and H_{P3} the average relative peak height from three unspiked aliquots. Relative peak heights were normalized to the internal standard.

Linearity. Linearity was determined for each amino acid by analyzing different amounts of the amino acids standard mixture (corresponding to 10−2500 mg amino acid/kg barley flour) after silylation in triplicate. Calibration curves were plotted, and the respective regression coefficients were calculated.

Analysis of Protein. Analysis of protein contents was performed by near-infrared transmission spectroscopy (NIT) according to the method of Grausgruber and Vollmann and calculated as percent in grain.[23] Amino acid spectra of free and protein-derived amino acids were analyzed in duplicate according to Commission Regulation (EC) No. 152/2009, III, F and G.[24]

Quality Control. To ensure constant analysis conditions, reference material (commercially available barley kernels) was analyzed in triplicate at the beginning and end of each sample set (2 field replicates × 3 seasons) and regularly together within each batch. Data were considered acceptable when the variation coefficient of representatives of each compound class did not exceed 25%. The representatives were as follows: FAME (C16:0, C18:0, C20:0), hydrocarbons (squalene), free fatty acids (C16:0, C18:0), sterols (campesterol, β-sitosterol, β-sitostanol), monosaccharides (fructose, glucose, galactose), trisaccharides (raffinose), sugar alcohols (xylitol, *myo*-inositol), organic acids (citric acid, malic acid), and amines (γ-aminobutyric acid). Furthermore, data obtained by GC-MS analysis of the reference material were checked for additional peaks to control for potential laboratory contamination.

Data Processing and Statistical Analysis. Freeze-dried flour from each biological replicate was analyzed in triplicate. For analysis, the samples were grouped into randomized batches; each batch consisted of three biological replicates (C1, C2, rain-out shelter) analyzed in triplicate and one quality control. In total, there were 66 batches (11 cultivars × 2 field replicates × 3 seasons).

The GC-MS chromatograms were integrated by means of Xcalibur 2.1 (Thermo Fisher Scientific, Waltham, MA, USA). Standardization of peak heights and retention time matching were performed using Chrom*pare* 1.1.[25] For retention time matching characteristic compounds of the fractions 1−4 (fraction 1, myristic acid methyl ester, palmitic acid methyl ester, stearic acid methyl ester, arachidic acid methyl ester, and internal standard 1; fraction 2, silylated myristic acid, palmitic acid, stearic acid, internal standard 2, and β-sitosterol; fraction 3, silylated fructose, *myo*-inositol, internal standard 3, sucrose, and raffinose; fraction 4, silylated alanine, phosphoric acid, malic acid, internal standard 4, and citric acid) were used. Normalization of peak heights was done by using the internal standards 1−4. On the basis of noise levels of 1 and 2% peak heights relative to the internal standards in fractions 1/2 and 3/4, respectively, peaks below this threshold were discarded.

For multivariate data analysis, principal component analysis (PCA) was performed using XLSTAT version 2013.3.02 (Addinsoft, Paris, France).

Analysis of variance (ANOVA) was undertaken within GenStat 16 (VSN International Ltd., Hemel Hempstead, UK). The following described models were fit for each metabolite from polar fractions 3 and 4 across 11 cultivars, or for each cultivar, to evaluate the effect of growing across 11 cultivars or within each cultivar, respectively:

$$v_{ijkl} = \hat{i} + \hat{a}_i + s_j + n_k + t_l + (sn)_{jk} + (st)_{jl} + (nt)_{kl} + \mathring{a}_{ijkl} \quad \text{(i)}$$

$$v_{ijk} = \hat{i} + \hat{a}_i + s_j + n_k + (sn)_{jk} + \mathring{a}_{ijk} \quad \text{(ii)}$$

v_{ijkl} (or v_{ijk}, respectively) is the response for the ith block of the jth growing conditions/location and the kth season (and the lth cultivar for v_{ijkl}), μ is the overall mean, β_i is the random effect of the ith block, s_j is the effect of the jth growing conditions/location, n_k is the effect of the kth season, t_l is the effect of the lth cultivar, $(sn)_{jk}$ is the effect of the interaction between the jth growing conditions/location and the kth season, $(st)_{jl}$ is the effect of the interaction between the jth growing conditions/location and the lth cultivar, $(nt)_{kl}$ is the effect of the interaction between the kth season and the lth cultivar, and e_{ijkl} (or e_{ijk}, respectively) is the random error. Differences for the effect of growing conditions/location were considered to be statistically significant if the effect was significant by ANOVA, and changes were consistent for (i) each cultivar and season or (ii) for each season.

The effect of growing conditions/location was additionally statistically tested by Tukey's test. The significance level was set to $p < 0.01$ for all statistical comparisons.

RESULTS AND DISCUSSION

To reveal changes in the metabolite profiles reflecting the adaptation of cultivars to drought stress, the set of barley grain previously investigated by Wenzel et al. was further extended.[12] The material comprised two groups of spring barley assigned according to the descriptions provided by the plant breeders or in the literature.[26−28] The first consisted of three cultivars ('Argentinian Mutant 6519', 'Mackay', 'Palmella Blue') from countries with hot and dry summers reported to be drought resistant/tolerant and of one cultivar ('IPZ 24727') from Germany described to be generally stress tolerant. The second consisted of seven cultivars originating from countries with moderate climates being either stress susceptible ('Barke') or without specific reports on drought resistance/tolerance ('Marnie', 'Iron', 'Steina', 'Streif', 'Polygena', 'Emperor') (Table 1). PCA based on agronomic parameters (e.g., yield, grain size, thousand kernel weight) confirmed the different performances of the two groups upon drought stress in the three growing seasons.

DOI: 10.1021/acs.jafc.5b01114
J. Agric. Food Chem. 2015, 63, 4252−4261

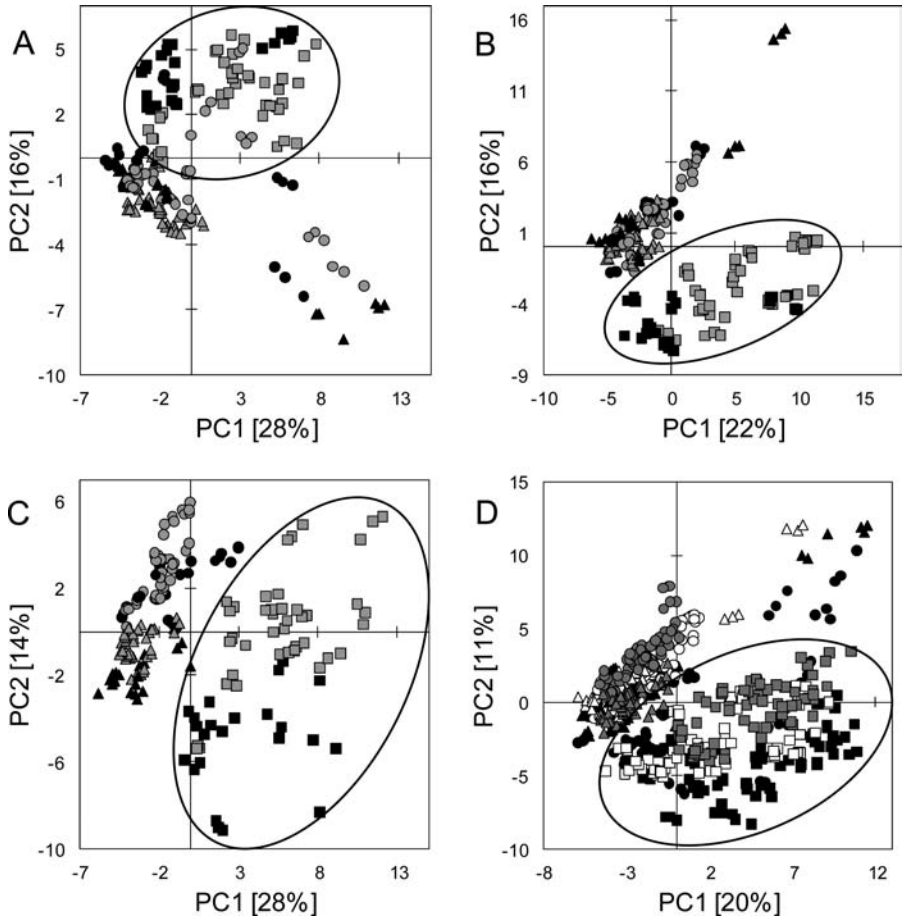

Figure 1. PCA of GC-MS metabolite profiling data of combined polar fractions 3 and 4 from stress resistant/tolerant barley cultivars (A–C, black symbols) and from cultivars reported to be either stress susceptible or without specific reports on drought resistance/tolerance (A–C, gray symbols) grown under drought stress in a rain-out shelter (squares) and under natural weather conditions at control location 1 (circles) and control location 2 (triangles) in (A) 2010, (B) 2011, and (C) 2012 and in (D) 2010 (black symbols), 2011 (white symbols), and 2012 (gray symbols). Circles encompass samples from the drought-stress conditions. Two field replicates were analyzed each in triplicate.

The 11 cultivars were field grown under induced drought stress using a rain-out shelter and under control, that is, natural weather conditions (C1 and C2), in three consecutive seasons. The GC/MS-based metabolite profiling was performed as previously described; the procedure results in four fractions containing FAME and hydrocarbons (fraction 1); FFA, sterols, and fatty alcohols (fraction 2); sugars and sugar alcohols (fraction 3); and amino acids, acids, and amines (fraction 4).[12,19] A total of 214 peaks (90 polar and 124 lipophilic) were detected; 60 polar and 77 lipophilic metabolites were identified by comparison of retention indices and mass spectra to those of reference compounds or from MS libraries.[12]

Changes Due to Drought Stress Irrespective of Cultivars. PCA of the GC-MS metabolite profiling data obtained for fractions 1 and 2 from the extended set of cultivars grown under induced drought stress and control conditions, respectively, confirmed the results from the previous study: Differences in lipophilic metabolites were mainly due to seasonal impact rather than to drought stress.[12]

In contrast, PCA of polar fractions 3 and 4 demonstrated that in each season samples subjected to drought stress were clearly separated from those grown under control conditions (Figure 1). The PCA plots are in agreement with those previously obtained for the smaller set of cultivars.[12] The best separation was observed in 2011 (Figure 1B). Again, the clustering in 2010 turned out to be influenced by a distinct aridity period in that season, and the clustering in 2012 also revealed separations according to growing location under the control conditions (Figure 1A,C). Importantly, the separation due to the factor growing conditions was still observed even when the data from all seasons were combined (Figure 1D).

These multivariate analyses revealed that the polar fractions are the most prominent metabolites contributing to a differentiation of barley grown under control conditions and induced drought, respectively. Therefore, the polar constituents were additionally subjected to univariate statistical analysis on the basis of the mean values of all cultivars. On the basis of the employed cutoff threshold, 49 components were assessed via ANOVA and Tukey's test. There were metabolites for which the responses were either significantly decreased or increased upon drought stress compared to C1 and C2, irrespective of the cultivar. They were the same 16 as those previously reported for the smaller set of cultivars;[12] the 13 identified metabolites including, for example, the monosaccharides fructose and glucose, the trisaccharide raffinose, the sugar alcohol mannitol, several organic acids, the biogenic amine γ-aminobutyric acid (GABA), and the amino acid glutamic acid are listed in Table 2.

They comprise many metabolites commonly reported to be involved in adjustment mechanisms to drought, such as

DOI: 10.1021/acs.jafc.5b01114
J. Agric. Food Chem. 2015, 63, 4252–4261

Table 2. Relative Mean Responses of Identified Metabolites from 11 Cultivars Found To Be Statistically Significant for the Factor Growing Conditions/Location across Three Consecutive Seasons

	relative mean response[a]		
metabolite	rain-out shelter	C1	C2
decreasing responses			
mannitol	0.026 (a)	0.215 (b)	0.165 (b)
2-glycerophosphoric acid	0.052 (a)	0.070 (b)	0.065 (b)
glutamic acid	0.465 (a)	0.692 (b)	0.574 (ab)
increasing responses			
glucose	0.674 (a)	0.386 (b)	0.353 (b)
fructose	0.775 (a)	0.417 (b)	0.428 (b)
raffinose	3.826 (a)	2.562 (b)	2.279 (b)
citric acid	1.000 (a)	0.681 (b)	0.626 (b)
isocitric acid	0.330 (a)	0.117 (b)	0.106 (b)
malic acid	4.378 (a)	3.361 (b)	3.396 (b)
succinic acid	0.176 (a)	0.077 (b)	0.066 (b)
threonic acid	0.070 (a)	0.031 (b)	0.021 (b)
GABA	0.358 (a)[b]	0.190 (b)[b]	0.160 (b)[b]
glycine	0.152 (a)	0.102 (b)	0.086 (b)[c]

[a]Relative mean response = response (metabolite)/response (internal standard) × 100. [b]Except for 'Palmella Blue'. [c]Rain-out shelter versus C2: not consistent across all growing seasons.

fructose, glucose, raffinose, mannitol, several organic acids, and the well-known stress marker GABA.[4,5,12,29−34]

The data demonstrate that responses to drought stress commonly known for plants and their vegetative tissues are not readily transferable to grain. For instance, levels of mannitol and glutamic acid decreased due to drought stress in barley grain, but have been described to be increased in vegetative tissues of several plants.[4,30,32] These differences in responses of metabolites to drought stress depending on the investigated tissue are in line with the results reported by Harrigan et al. in grain of maize hybrids grown under different water regimens.[9] Changes in the contents of raffinose, mannitol/sorbitol, and several organic acids observed in grain from drought-stressed maize were in accordance with those found in the present study.

For some of the constituents shown in Table 2, changes in concentrations upon stress have been reported to depend on the adaptation of the plant. For example, Sanchez et al. found species-specific differences for plant tissue of legumes with regard to their quantitative response to drought stress for fructose.[8] Levels of tricarboxylic acid cycle intermediates increased in leaves of a tolerant barley cultivar due to salinity stress, but were unchanged in a sensitive cultivar.[35] Analyzing drought-stressed rice grain, Nam et al. found increasing GABA, fructose, and glucose levels especially in the drought-tolerant genotypes.[10] For barley grain such correlations between the drought stress-induced responses of these metabolites and the degree of adaptation of the different cultivars could not be found.

Cultivar-Dependent Changes Due to Drought Stress. To reveal cultivar-specific changes in the responses of polar metabolites upon drought stress, statistical analysis (ANOVA, $p < 0.01$) of the polar metabolites was subsequently performed not on the basis of the mean values of all cultivars but for each individual cultivar. For 19 constituents the responses were not statistically significantly different; 30 metabolites including those from Table 2 showed significant results for at least one cultivar.

For two of the constituents presented in Table 2, mannitol and succinic acid, significant decreases and increases, respectively, were found for each cultivar. For the remaining metabolites, there were individual cultivars that did not show significant changes. However, despite these cultivar-specific results, the data of the 13 metabolites from Table 2 did not allow a correlation to be established between the number of significant differences and the degree of drought stress adaptation.

On the other hand, the components shown in Table 3 turned out to exhibit statistically significant differences corresponding to groups of cultivars. The stress-susceptible cultivar 'Barke' and the two cultivars 'Marnie' and 'Iron', for which no drought resistance/tolerance had been described, were characterized by significant changes, particularly for the branched-chain amino

Table 3. *p* Values of Identified Metabolites from Each Cultivar Found To Be Statistically Significant for the Factor Growing Conditions/Location across Three Consecutive Seasons

	p value										
metabolite	Arg. Mutant 6519	Mackay	Palmella Blue	IPZ 24727	Marnie	Iron	Barke	Steina	Streif	Emperor	Polygena
proteinogenic free amino acids											
alanine	–[a]	–	–	–	0.0016	<0.001	–	–	<0.001	–	–
valine	–	–	–	–	<0.001	–	0.0061	–	–	–	–
isoleucine	–	–	–	–	<0.001	<0.001	0.0011	–	–	–	–
leucine	–	–	–	–	0.0012	<0.001	0.0028	–	–	–	–
glutamine	–	–	–	0.0087	–	–	–	–	–	–	–
asparagine	–	–	0.0063	–	–	–	–	–	–	–	–
serine	–	<0.001[b,c]	0.0027	0.0025	–	–	–	–	–	–	–
threonine	–	–	–	–	<0.001	<0.001	0.0036	–	–	<0.001[b,c]	–
further metabolites											
pyroglutamic acid	–	0.0048	–	–	–	–	–	–	–	–	–
putrescine	–	0.0092	–	–	–	–	–	–	–	–	–
myo-inositol	–	–	–	–	–	0.0012[b]	<0.001[b,c]	–	–	–	–

[a]–, not statistically significant for factor growing conditions/location. [b]Statistically significant for factor growing condition/location × season. [c]Statistically significant for factor season.

DOI: 10.1021/acs.jafc.5b01114
J. Agric. Food Chem. 2015, 63, 4252−4261

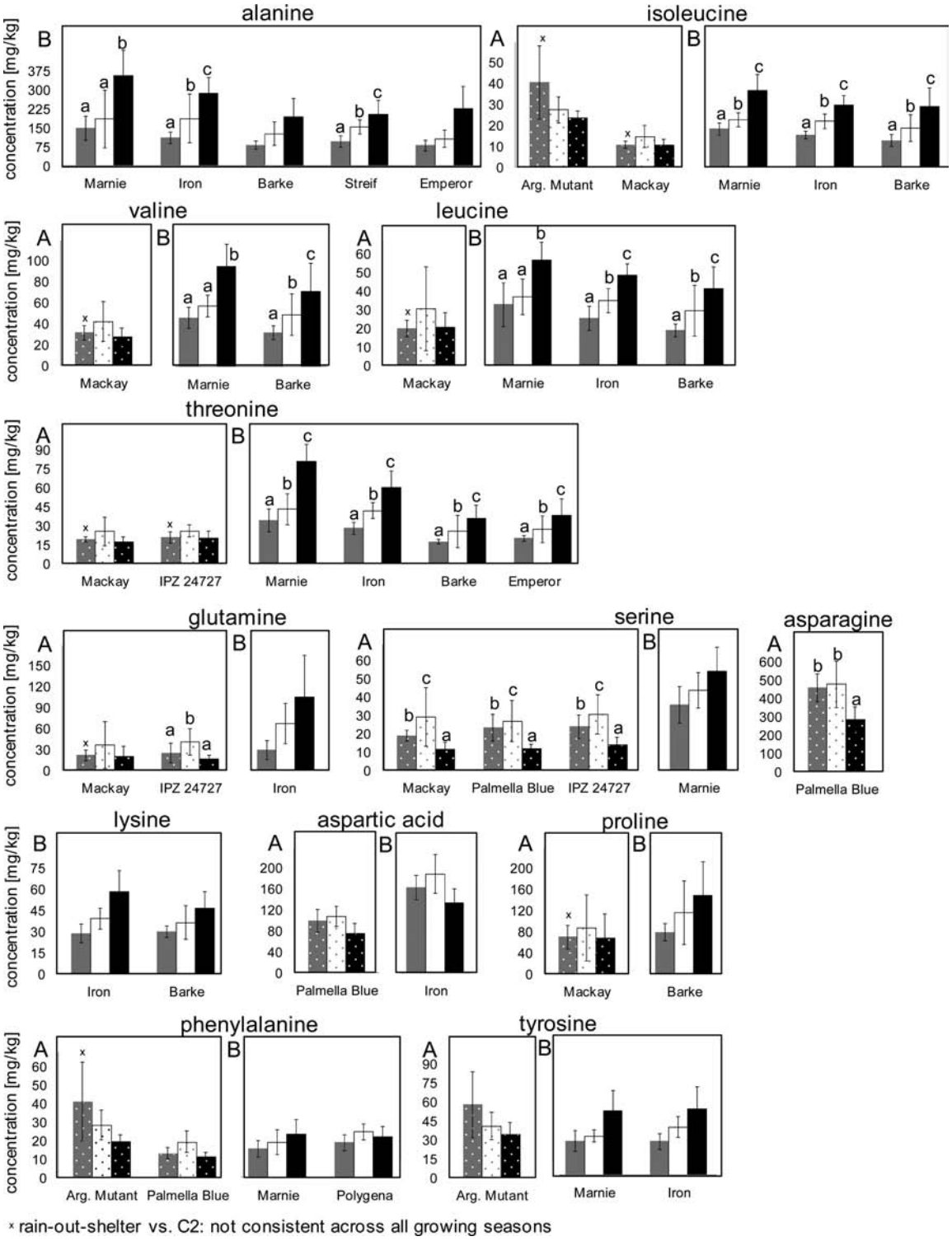

Figure 2. Concentrations of proteinogenic free amino acids found to be consistently changed across three consecutive growing seasons for the factor growing conditions/location. Dotted bars indicate (A) stress resistant/tolerant cultivars, and plain bars indicate (B) cultivars reported to be either stress susceptible or without specific reports on drought resistance/tolerance. Lower case letters display statistical significance for the factor growing conditions/location across three consecutive seasons by ANOVA ($p < 0.01$) and Tukey's test ($p < 0.01$). Two field replicates were analyzed each in triplicate. Gray bars, control location 2; white bars, control location 1; black bars, rain-out shelter.

acids (BCAAs) valine, leucine, and isoleucine, for alanine and threonine, and for *myo*-inositol. In the reportedly stress resistant/tolerant cultivars ('Mackay', 'Palmella Blue', 'IPZ 24727') these compounds were not significantly changed. This group of cultivars, in turn, showed significant differences for the amino acids glutamine, asparagine, and serine and, in addition, for pyroglutamic acid and putrescine. The drought-resistant cultivar 'Argentinian (Arg.) Mutant 6519' did not show significant differences at all. Among the remaining cultivars ('Steina', 'Streif', 'Emperor', 'Polygena'), for which no

DOI: 10.1021/acs.jafc.5b01114
J. Agric. Food Chem. 2015, 63, 4252−4261

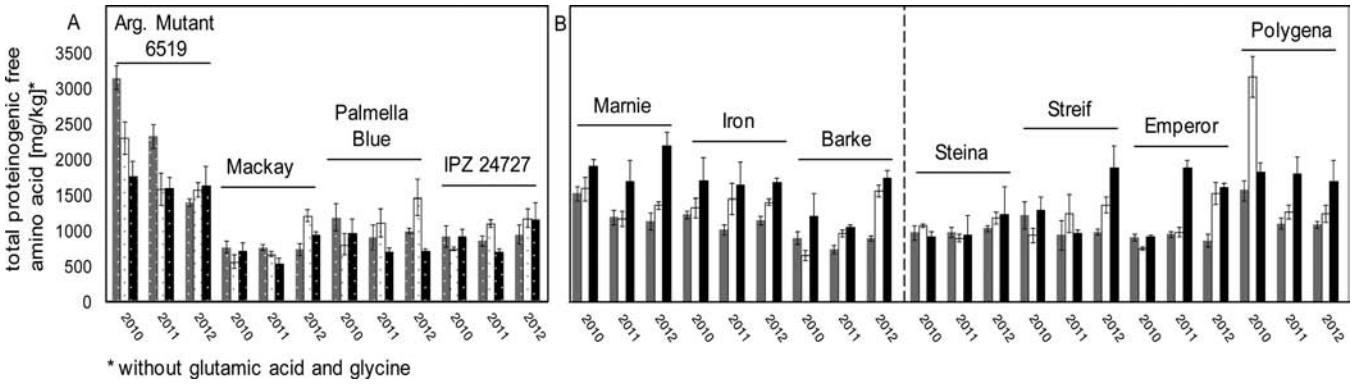

Figure 3. Sums of concentrations of free amino acids alanine, valine, leucine, isoleucine, proline, tryptophan, serine, threonine, aspartic acid, asparagine, glutamine, lysine, tyrosine, and phenylalanine. Dotted bars indicate (A) stress-resistant/tolerant cultivars, and plain bars indicate (B) cultivars reported to be either stress susceptible or without specific reports on drought resistance/tolerance. Two field replicates were analyzed each in triplicate. Gray bars, control location 2; white bars, control location 1; black bars, rain-out shelter.

drought resistance/tolerance had been described, only 'Streif' (alanine) and 'Emperor' (threonine) showed significant differences.

Quantitation of Proteinogenic Free Amino Acids. The data shown in Table 3 indicate that changes in the contents of proteinogenic free amino acids might be of importance as potential markers for the degree of drought stress adaptation in barley cultivars; therefore, these metabolites were quantitated. The mean values of the concentrations of proteinogenic free amino acids across 2010−2012 showed a high dependency on the growing season. Therefore, in a subsequent step only values that were consistently changed across the three consecutive growing seasons were assessed (Figure 2). In total, 44 consistent changes for single cultivars across three consecutive growing seasons were found; thereof, 20 changes were found to be significant. On the basis of the consistent changes, the following rule was observed: For stress-tolerant/resistant cultivars amino acid concentrations decreased, whereas for cultivars for which no drought resistance/tolerance had been described, levels of amino acid concentrations increased due to water deficit, except for the changes in concentrations of aspartic acid in 'Iron' and phenylalanine in 'Polygena'. This phenomenon of increasing concentrations of amino acids was particularly pronounced for BCAAs as well as for their precursor threonine in the stress-susceptible 'Barke' and in 'Marnie' and 'Iron', for which no drought resistance/tolerance had been described. In contrast, Bowne et al. reported BCAAs to be increased in leaves independent from the different tolerance levels of the investigated wheat plants as a response to water deficit treatment.[11] In leaves of drought-stressed *Arabidopsis* plants from one cultivar, levels of leucine and valine were increased, whereas levels of isoleucine were decreased.[7] In shoots of barley seedlings subjected to drought, the expression of a branched-chain amino transaminase (BCAT) was increased.[36] The authors suggested that increased BCAT expression protects cells from toxic BCAAs levels.[36] The fact that comparable changes (either decreased or increased) as observed for the concentrations of BCAAs have also been seen for threonine reflects their close biogenetic relation.

Proline is an amino acid commonly reported to show increasing levels in plants under drought conditions.[37,38] In the present study, either a consistent decrease or a consistent increase could be found for only one drought-tolerant ('Mackay') and one stress-susceptible ('Barke') cultivar, respectively. Proline accumulated upon drought in leaves of resistant and sensitive barley seedlings, even though many fold higher in drought-resistant than in drought-sensitive cultivars.[18] Similarly, Thakur and Rai found 4- or 3.5-fold increases in maize shoots of resistant or susceptible plants, respectively.[17] For salinity-tolerant barley genotypes, both increasing and decreasing levels of proline were observed in leaves of drought-stressed plants, whereas for one drought-tolerant barley genotype only increasing levels were reported.[39] The cited studies focused on the investigation of vegetative plant tissues and therefore cannot be readily extrapolated to the results found in grain.

Figure 3 shows the sums of the concentrations of proteinogenic free amino acids. In accordance with the results found for the individual amino acids, for the stress-susceptible 'Barke' and for 'Marnie' and 'Iron', for which no drought resistance/tolerance had been described, distinct increases of the sums of proteinogenic free amino acids were found for drought-stressed samples in the three consecutive growing seasons. In contrast, for the other cultivars for which no drought resistance/tolerance had been described and for stress tolerant/resistant cultivars, there were no consistent results for the investigated growing seasons.

Changes in the levels of free amino acids as a general response to stress and also specifically to drought have been described for several plants including barley; in most of the studies the concentrations of free amino acids have been shown to increase upon stress.[6,40−43] For leaves and roots/shoots of drought-stressed barley plants both increases and decreases of free amino acids have been reported.[13,44] However, only a few studies focused on the impact of water deficit in light of differences between cultivars regarding their adaptation to drought. Thakur and Rai demonstrated that in shoots of a resistant maize cultivar, concentrations of amino acids were much more increased than in a susceptible maize cultivar subjected to drought.[17] Similarly, in leaf blades of maize hybrids levels of amino acids increased due to drought stress except for one genotype, which was the only fully susceptible genotype.[45] In potato tubers from a drought-sensitive genotype free amino acids valine, leucine, and tyrosine increased, whereas in the drought-tolerant genotype they were decreased due to severe drought stress induced in a glasshouse experiment.[46] In leaves and roots of barley cultivars, it was shown that the more sensitive cultivar 'Clipper' had elevated levels of amino acids due to salinity stress.[35] In contrast, levels of free amino acids from leaves of wheat were all increased, although the

DOI: 10.1021/acs.jafc.5b01114
J. Agric. Food Chem. 2015, 63, 4252−4261

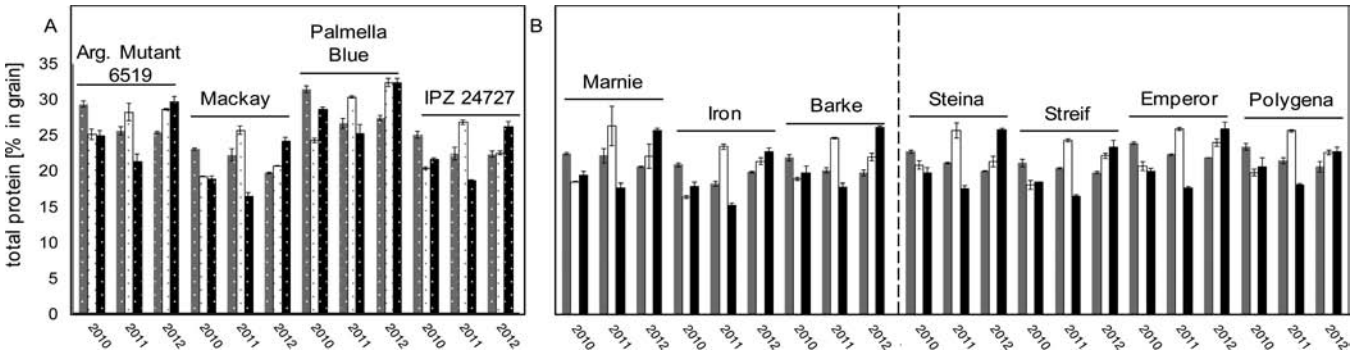

Figure 4. Concentrations of protein in grain (wt %) calculated as means of two field replicates. Dotted bars indicate (A) stress resistant/ tolerant cultivars, and plain bars indicate (B) cultivars reported to be either stress susceptible or without specific reports on drought resistance/tolerance. Gray bars, control location 2; white bars, control location 1; black bars, rain-out shelter.

investigated cultivars differed in their degree of drought tolerance.[11]

In the present study, increasing concentrations of proteinogenic free amino acids were observed only in cultivars for which no drought resistance/tolerance had been described. In contrast, decreasing levels upon drought stress were found only for stress-resistant/tolerant cultivars. However, this correlation was valid only if the results were consistent across all investigated growing seasons. This requirement of a strict restriction to consistent results is in accordance with the concerns expressed by Harrigan et al.;[9] they observed cultivar-specific differences in the changes of the concentrations of free amino acids in grain from maize hybrids, but did not consider them reliable because data were available from only one season.[9]

Another aspect that has to be considered is the dependency on the time interval during which drought treatment was induced. Harrigan et al. investigated grain from maize hybrids exposed to drought during the vegetative or the grain-filling developmental stages.[9] Taking into account the different points of treatment, they found opposite changes (decreases or increases) in the concentrations of some constituents.[9] Similarly, on the basis of targeted analyses of reducing sugar, starch, and protein, time-dependent compositional changes in grain from salinity-stressed rice plants have been observed.[47] The experimental setup employed in the present study does not allow the drought treatment to be assigned to one specific time point. Therefore, an interpretation of the data taking the plants' developmental stage into account is not possible.

Protein and Protein-Derived Amino Acids. Changes in proteinogenic free amino acids upon stress are frequently attributed to protein synthesis/degradation.[6,35] Therefore, it seemed reasonable to investigate not only the changes in the levels of free amino acids but also those of protein and protein-derived amino acids.

In 2011, the protein contents were decreased due to drought stress (rain-out shelter versus C1) in all cultivars, whereas in 2010 and 2012 the protein contents were increased in 64 and 77%, respectively, of the samples. Thus, the protein content is highly dependent on the growing season and less affected by drought (Figure 4).

The spectra of total (free and protein-derived) amino acids were analyzed in combined samples (field replicates 1 and 2) of the drought stress tolerant cultivar 'Mackay' and the stress-susceptible cultivar 'Barke' from 2011. The concentrations of all amino acids decreased due to water deficit, except for cysteine/cystine (sum calculated as cysteine) of cultivar 'Barke' (data not shown).

There are reports of increasing protein contents in kernels of barley plants subjected to drought.[48,49] Except for methionine, levels of total (free and protein-derived) amino acids were reported to be increased in grain of drought-stressed barley plants for each genotype, irrespective of the different adaptations to water deficit.[48] In the present study, the protein content was found to be highly dependent on the growing season. There was no correlation between the levels of protein or protein-derived amino acids, as determined by NIT or by amino acid analyzer, and the levels of free amino acids, as determined by GC-MS metabolite profiling, with regard to their responses to drought stress. This is in agreement with previously reported results that protein in barley grain is unaffected by water deficit.[50] Therefore, consistent changes of proteinogenic, free amino acids in correlation with the degree of drought stress adaptation of different cultivars cannot be attributed to an altered degradation/incorporation into protein.

In conclusion, this study, on the one hand, confirmed that there are metabolites which are significantly changed, either consistently increased or consistently decreased in all cultivars, in barley grain upon drought stress. On the other hand, responses of proteinogenic free amino acids were shown to be suitable for a classification of barley cultivars depending on their adaptation to drought. The well-known environmental variability of the concentrations of free amino acids was also observed under the experimental setup employed in this study; nevertheless, it could be demonstrated that changes which were consistently expressed for three growing seasons correlated with the degree of drought stress adaptation reported for the respective cultivar. Consistent increases of the concentrations of proteinogenic free amino acids were observed only in cultivars for which no drought resistance/tolerance had been found, whereas consistent decreases were seen only in the group of stress-tolerant/resistant cultivars. These cultivar-specific correlations were particularly pronounced for BCAAs; however, in principle they are valid for all amino acids, and the assignment of a cultivar is stronger the higher the number of amino acids exhibiting these consistent increases and decreases in concentrations, respectively.

The application of the described prediction model resulted in a correct assignment of all four stress-tolerant/resistant cultivars ('Arg. Mutant 6519', 'Mackay', 'Palmella Blue', 'IPZ 24727') investigated in the present study. Among the seven cultivars for which no drought resistance/tolerance had been described, five

DOI: 10.1021/acs.jafc.5b01114
J. Agric. Food Chem. 2015, 63, 4252−4261

('Marnie', 'Iron', 'Barke', 'Streif', 'Emperor') were correctly classified. Two cultivars could not be properly assigned because either no consistent change could be observed ('Steina') or the only observed consistent difference was based on a decrease rather than an increase of the amino acid ('Polygena').

Of course, the general validity of the observed consistent changes of the concentrations of free amino acids in grain as a parameter for the prediction of the adaptation of barley cultivars to drought stress needs confirmation in further field trials with additional cultivars. In particular, issues such as the responses of free amino acids depending on the developmental stage of the plant during which drought stress occurred would have to be investigated. Nevertheless, the data emphasize that metabolite profiling can serve as a tool supporting breeders to select cultivars that are able to cope with drought stress. To increase the usefulness of the described approach in breeding or for farmers, it should be investigated whether the potential markers are also confirmed under more time-saving experimental conditions, for example, in the glasshouse. This could pave the way to the use of metabolite profiling as a technique assisting in the screening of drought-tolerant barley cultivars at an early stage of the breeding process.

■ ASSOCIATED CONTENT

Supporting Information

Information on the plant breeders, p values of identified metabolites from each cultivar found to be statistically significant for the factor growing conditions/location, and validation data for the quantitation of free amino acids; PCA based on agronomic parameters of the 11 cultivars grown under drought stress and PCA of GC-MS metabolite profiling data of the combined lipophilic fractions; concentrations of proteinogenic, free amino acids. This material is available free of charge via the Internet at http://pubs.acs.org.

■ AUTHOR INFORMATION

Corresponding Author

*(K.-H.E.) Phone: +49 (0) 8161 71 4250. Fax: +49 (0) 8161 71 4259. E-mail: k.h.engel@wzw.tum.de.

Funding

The study was financially supported by the Bavarian State Ministry of Food, Agriculture and Forestry.

Notes

The authors declare no competing financial interest.

■ ACKNOWLEDGMENTS

Oxana Fastowski is gratefully acknowledged for technical support. Analyses of protein contents in barley grain were kindly done by the Quality lab (AQU 2) of the Bavarian State Research Center for Agriculture (LfL). We thank Bioanalytik Weihenstephan, Research Center for Nutrition and Food Sciences, Technische Universität München, Freising-Weihenstephan, Germany, for analyses of amino acid spectra.

■ ABBREVIATIONS USED

ANOVA, analysis of variance; Arg, Argentinian; BCAAs, branched-chain amino acids; BCAT, branched-chain amino transaminase; FAME, fatty acid methyl esters; FFA, free fatty acids; GABA, γ-aminobutyric acid; NN, normal null; PCA, principal component analysis; Rf, response factor; SPE, solid phase extraction

■ REFERENCES

(1) FAO. Food and Agriculture Organization of the United Nations 2014; http://faostat.fao, org/site/567/DesktopDefault.aspx?PageID=567#ancor (accessed Feb 26, 2015).

(2) Poehlman, J. M. Adaption and distribution. In *Barley*; Rasmusson, C. C., Ed.; American Society of Agronomy: Madison, WI, USA, 1985; pp 1−17.

(3) IPCC. Intergovernmental Panel on Climate Change. Climate Change 2007: The Physical Science Basis. Summary for Policymakers. Contributation of working group I to the fourth assessment report of the IPCC 2007, Paris, France.

(4) Seki, M.; Umezawa, T.; Urano, K.; Shinozaki, K. Regulatory metabolic networks in drought stress responses. *Curr. Opin. Plant Biol.* **2007**, *10*, 296−302.

(5) Rodziewicz, P.; Swarcewicz, B.; Chmielewska, K.; Wojakowska, A.; Stobiecki, M. Influence of abiotic stresses on plant proteome and metabolome changes. *Acta Physiol. Plant.* **2014**, *36*, 1−19.

(6) Rai, V. Role of amino acids in plants responses to stresses. *Biol. Plant.* **2002**, *45*, 481−487.

(7) Rizhsky, L.; Liang, H.; Shuman, J.; Shulaev, V.; Davletova, S.; Mittler, R. When defense pathways collide. The response of *Arabidopsis* to a combination of drought and heat stress. *Plant Physiol.* **2004**, *134*, 1683−1696.

(8) Sanchez, D. H.; Schwabe, F.; Erban, A.; Udvardi, M. K.; Kopka, J. Comparative metabolomics of drought acclimation in model and forage legumes. *Plant, Cell Environ.* **2012**, *35*, 136−149.

(9) Harrigan, G. G.; Stork, L. G.; Riordan, S. G.; Ridley, W. P.; Macisaac, S.; Halls, S. C.; Orth, R.; Rau, D.; Smith, R. G.; Wen, L.; Brown, W. E.; Riley, R.; Sun, D.; Modiano, S.; Pester, T.; Lund, A.; Nelson, D. Metabolite analyses of grain from maize hybrids grown in the United States under drought and watered conditions during the 2002 field season. *J. Agric. Food Chem.* **2007**, *55*, 6169−6176.

(10) Nam, K.-H.; Shin, H. J.; Pack, I.-S.; Park, J.-H.; Kim, H. B.; Kim, C.-G. Metabolomic changes in grains of well-watered and drought-stressed transgenic rice. *J. Sci. Food Agric.* **2015**, DOI: 10.1002/jsfa.7152.

(11) Bowne, J. B.; Erwin, T. A.; Juttner, J.; Schnurbusch, T.; Langridge, P.; Bacic, A.; Roessner, U. Drought response of leaf tissues from wheat cultivars of differing drought tolerance at the metabolite level. *Mol. Plant* **2012**, *5*, 418−429.

(12) Wenzel, A.; Frank, T.; Reichenberger, G.; Herz, M.; Engel, K.-H. Impact of induced drought stress on the metabolite profiles of barley grain. *Metabolomics* **2014**, *11*, 454−467.

(13) Sicher, R. C.; Timlin, D.; Bailey, B. Responses of growth and primary metabolism of water-stressed barley roots to rehydration. *J. Plant Physiol.* **2012**, *169*, 686−695.

(14) Silvente, S.; Sobolev, A. P.; Lara, M.; Yang, H. Metabolite adjustments in drought tolerant and sensitive soybean genotypes in response to water stress. *PLoS One* **2012**, *7*, 1−11.

(15) Semel, Y.; Schauer, N.; Roessner, U.; Zamir, D.; Fernie, A. R. Metabolite analysis for the comparison of irrigated and non-irrigated field grown tomato of varying genotype. *Metabolomics* **2007**, *3*, 289−295.

(16) Nam, K.-H.; Kim, D.-Y.; Shin, H. J.; Nam, K. J.; An, J. H.; Pack, I.-S.; Park, J.-H.; Jeong, S.-C.; Kim, H. B.; Kim, C.-G. Drought stress-induced compositional changes in tolerant transgenic rice and its wild type. *Food Chem.* **2014**, *153*, 145−150.

(17) Thakur, S. P.; Rai, V. K. Dynamics of amino acid accumulation of two differentially drought resistant *Zea mays* cultivars in response to osmotic stress. *Environ. Exp. Bot.* **1982**, *22*, 221−226.

(18) Singh, T.; Aspinall, D.; Paleg, L. G. Proline accumulation and varietal adaptability to drought in barleys: a potential metabolic measure of drought resistance. *Nature New Biol.* **1972**, *236*, 188−190.

(19) Röhlig, R. M.; Eder, J.; Engel, K.-H. Metabolite profiling of maize grain: differentiation due to genetics and environment. *Metabolomics* **2009**, *5*, 459−477.

(20) Kopka, J.; Schauer, N.; Krueger, S.; Birkemeyer, C.; Usadel, B.; Bergmüller, E.; Dörmann, P.; Weckwerth, W.; Gibon, Y.; Stitt, M.;

DOI: 10.1021/acs.jafc.5b01114
J. Agric. Food Chem. 2015, 63, 4252−4261

Willmitzer, L.; Fernie, A. R.; Steinhauser, D. GMD@CSB.DB: the Golm Metabolome Database. *Bioinformatics* **2005**, *21*, 1635−1638.
(21) Kamal-Eldin, A.; Appelqvist, L. A.; Yousif, G.; Iskander, G. M. Seed lipids of *Sesamum indicum* and related wild species in Sudan. The sterols. *J. Sci. Food Agric.* **1992**, *59*, 327−334.
(22) Xu, Z.; Godber, J. S. Purification and identification of components of γ-oryzanol in rice bran oil. *J. Agric. Food Chem.* **1999**, *47*, 2724−2728.
(23) Grausgruber, H.; Vollmann, J. Qualitätszüchtung bei Öl- und Eiweißpflanzen 2013; http://plantbreeding.boku.ac.at/957308/index.html (accessed Feb 26, 2015).
(24) Commission Regulation (EC) No. 152/2009 of 27 January 2009 laying down the methods of sampling and analysis for the official control of feed (text with EEA relevance) (L 54/1, 26.2.2009), Annex III, Part F and G.
(25) Frenzel, T.; Miller, A.; Engel, K.-H. A methodology for automated comparative analysis of metabolite profiling data. *Eur. Food Res. Technol.* **2003**, *216*, 335−342.
(26) Friedt, W. Barley breeding history, progress, objectives, and technology. In *Barley. Production, Improvement, and Uses*; Ullrich, S. E., Ed.; Wiley-Blackwell: Oxford, UK, 2011; pp 160−220.
(27) Manschadi, A. M.; Christopher, J.; deVoil, P.; Hammer, G. L. The role of root architectural traits in adaptation of wheat to water-limited environments. *Funct. Plant Biol.* **2006**, *33*, 823.
(28) Sturgess, J. Barley − planting and disease guide, 2014 (Queensland and NNSW); https://www.daff.qld.gov.au/__data/assets/pdf_file/0003/145587/Barley-Planting-Guide-2014.pdf (accessed Feb 26, 2015).
(29) Bartels, D.; Sunkar, R. Drought and salt tolerance in plants. *Crit. Rev. Plant Sci.* **2005**, *24*, 23−58.
(30) Bohnert, H. J.; Nelson, D. E.; Jensen, R. G. Adaptions to environmental stresses. *Plant Cell* **1995**, *7*, 1099−1111.
(31) Bouché, N.; Fromm, H. GABA in plants: just a metabolite? *Trends Plant Sci.* **2004**, *9*, 110−115.
(32) Bray, E. Molecular response to water deficit. *Plant Physiol.* **1993**, *103*, 1035−1040.
(33) Chaves, M. M. Effects of water deficits on carbon assimilation. *J. Exp. Bot.* **1991**, *234*, 1−16.
(34) Shanker, A. K.; Maheswari, M.; Yadav, S. K.; Desai, S.; Bhanu, D.; Attal, N. B.; Venkateswarlu, B. Drought stress responses in crops. *Funct. Integr. Genomics* **2014**, *14*, 11−22.
(35) Widodo; Patterson, J. H.; Newbigin, E.; Tester, M.; Bacic, A.; Roessner, U. Metabolic responses to salt stress of barley (*Hordeum vulgare* L.) cultivars, Sahara and Clipper, which differ in salinity tolerance. *J. Exp. Bot.* **2009**, *60*, 4089−4103.
(36) Malatrasi, M.; Corradi, M.; Svensson, J. T.; Close, T. J.; Gulli, M.; Marmiroli, N. A branched-chain amino acid aminotransferase gene isolated from *Hordeum vulgare* is differentially regulated by drought stress. *Theor. Appl. Genet.* **2006**, *113*, 965−976.
(37) Bandurska, H. Does proline accumulated in leaves of water deficit stressed barley plants confine cell membrane injury? I. Free proline accumulation and membrane injury index in drought and osmotically stressed plants. *Acta Physiol. Plant.* **2000**, *22*, 409−415.
(38) Heuer, B. Osmoregulatory role of proline in plants exposed to environmental stresses. In *Handbook of Plant and Crop Stress*; Pessarakli, M., Ed.; Dekker: New York, 1999; pp 409−415.
(39) Ahmed, I. M.; Dai, H.; Zheng, W.; Cao, F.; Zhang, G.; Sun, D.; Wu, F. Genotypic differences in physiological characteristics in the tolerance to drought and salinity combined stress between Tibetan wild and cultivated barley. *Plant Physiol. Biochem.* **2012**, *63*, 49−60.
(40) El-Tayeb, M. A. Response of barley grains to the interactive effect of salinity and salicylic acid. *Plant Growth Regul.* **2005**, *45*, 215−224.
(41) Good, A. G.; Zaplachinski, S. T. The effects of drought stress on free amino acid accumulation and protein synthesis in *Brassica napus*. *Physiol. Plant.* **1994**, *90*, 9−14.
(42) Krasensky, J.; Jonak, C. Drought, salt, and temperature stress-induced metabolic rearrangements and regulatory networks. *J. Exp. Bot.* **2012**, *63*, 1593−1608.
(43) Tully, R. E.; Hanson, A. D. Amino acids translocated from turgid and water-stressed barley leaves. *Plant Physiol.* **1979**, *64*, 460−466.
(44) Singh, T.; Paleg, L. G.; Aspinall, D. Stress metabolism 1. Nitrogen metabolism and growth in the barley plant during water stress. *Aust. J. Plant Physiol.* **1973**, *26*, 45−56.
(45) Witt, S.; Galicia, L.; Lisec, J.; Cairns, J.; Tiessen, A.; Araus, J. L.; Palacioa-Rojay, N.; Fernie, A. R. Metabolic and phenotypic responses of greenhouse-grown maize hybrids to experimentally controlled drought stress. *Mol. Plant* **2012**, *5*, 401−417.
(46) Muttucumaru, N.; Powers, S. J.; Elmore, S. J.; Mottram, D. S.; Halford, N. G. Effects of water availability on free amino acids, sugars and acrylamide-forming potential in potato. *J. Agric. Food Chem.* **2015**, *63*, 2566−2575.
(47) Thitisaksakul, M.; Tananuwong, K.; Shoemaker, C. F.; Chun, A.; Tanadul, O.-u.-m.; Labavitch, J. M.; Beckles, D. M. Effects of timing and severity of salinity stress on rice (*Oryza sativa* L.) yield, grain composition, and starch functionality. *J. Agric. Food Chem.* **2015**, *63*, 2296−2304.
(48) Ahmed, I. M.; Cao, F.; Han, Y.; Nadira, U. A.; Zhang, G.; Wu, F. Differential changes in grain ultrastructure, amylase, protein and amino acid profiles between Tibetan wild and cultivated barleys under drought and salinity alone and combined stress. *Food Chem.* **2013**, *141*, 2743−2750.
(49) Gous, P. W.; Hasjim, J.; Franckowiak, J.; Fox, G. P.; Gilbert, R. G. Barley genotype expressing "stay-green"-like characteristics maintains starch quality of the grain during water stress condition. *J. Cereal Sci.* **2013**, *58*, 414−419.
(50) Brooks, A.; Jenner, C.; Aspinall, D. Effects of water deficit on endosperm starch granules and on grain physiology of wheat and barley. *Aust. J. Plant Physiol.* **1982**, *9*, 423−436.

DOI: 10.1021/acs.jafc.5b01114
J. Agric. Food Chem. 2015, 63, 4252−4261

JOURNAL OF AGRICULTURAL AND FOOD CHEMISTRY

Addition/Correction

pubs.acs.org/JAFC

Correction to *N*-Glycome Profiling of Patatins from Different Potato Species of *Solanum* Genus

Erika Lattová, Adéla Brabcová, Veronika Bartová, David Potěšil, Jan Bárta, and Zbyněk Zdráhal*

J. Agric. Food Chem. **2015**, *63* (12), 3243−3250. DOI: 10.1021/acs.jafc.5b00426

The Funding statement should read as follows:

This work was carried out with the support of Proteomics Core Facility of CEITEC − Central European Institute of Technology (CZ.1.05/1.1.00/02.0068), financed from European Regional Development Fund; supported by the Czech Science Foundation (Project P206/12/G151) and by the Ministry of Agriculture of the Czech Republic (Project QI91A069).

Published: April 17, 2015

ACS Publications © 2015 American Chemical Society

DOI: 10.1021/acs.jafc.5b01760
J. Agric. Food Chem. 2015, 63, 4262−4262

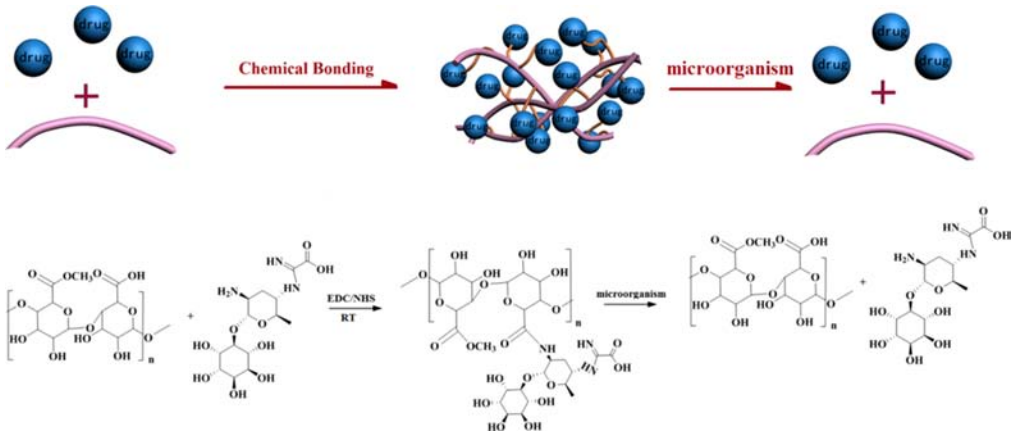

Figure 1. Reaction scheme of kasugamycin with pectin molecule.

(TGA). The stability of the conjugate under conditions of various pH, temperature, and UV irradiation and its release property triggered by Psl were investigated.

MATERIALS AND METHODS

Chemicals, Reagents, and Materials. Pectin (70 kDa, degree of esterification = 25%) was purchased from Quzhou Pectin Co., Ltd. (Zhejiang, China). Kasugamycin was obtained from the reference material service center of the National Institute for the Control of Pharmaceutical and Biological Products (Beijing, China). All other reagents were purchased from J. T. Baker (Phillipsburg, NJ, USA) and were of ACS grade or better. Milli-Q water used in all experiments was obtained in the laboratory using a Milli-Q water purification system (Millipore, Billerica, MA, USA). The 0.1 M phosphate-buffered solutions with pH 5.0, 7.0, and 8.5 were prepared by mixing 0.1 mol L^{-1} NaH_2PO_4 solution with 0.1 mol L^{-1} Na_2HPO_4 solution. The glycine buffers with pH 3.0 and 10.5 were prepared by mixing 0.05 mol L^{-1} glycine, 0.2 mol L^{-1} HCl solution, and 0.2 mol L^{-1} NaOH solution. Luria–Bertani (LB) medium was prepared with 0.5% NaCl, 0.5% yeast extract, and 1.0% peptone, and the pH was adjusted to 7.0 with 5 N NaOH before autoclaved sterilization. M9 minimal medium was prepared by mixing liquid A (0.05%NH_4Cl, 0.3% Na_2HPO_4, 0.15% KH_2PO_4, autoclaved sterilization) and liquid B (0.05% $MgSO_4 \cdot 7H_2O$, 0.0011% $CaCl_2$, 0.4% glucose, filter sterilization). Psl was obtained from the Laboratory of Seed Pathology and Fungicide Pharmacology, China Agricultural University.

Synthesis of Kasugamycin–Pectin. Due to the steric hindrance of the polysaccharide backbone and low reactivity of the carboxyl group, direct conjugation of kasugamycin to pectin is inefficient. Therefore, EDC and NHS were utilized to form the amide bond between the amino group in kasugamycin and the carboxyl group in pectin. The reaction scheme of kasugamycin with pectin molecule is presented in Figure 1. Briefly, pectin (1.0 g), EDC (1.15 g), and NHS (0.69 g) were dissolved in 20 mL of H_2O, stirring at 200 rpm for 30 min. Then kasugamycin (1.5 g) dissolved in 5 mL of H_2O was added dropwise into the reaction mixture under vigorous stirring at 1200 rpm. The whole solution was adjusted to pH 6 with 1 N HCl and kept at 4 °C for 24 h. Finally, the solution was precipitated and washed sufficiently with acetone, and the residue was filtered and then dried at 60 °C in an oven.

Characterization of Kasugamycin–Pectin. The product was sufficiently dialyzed against water using a dialysis membrane (MWCO 10 kDa; Spectrum Laboratories, Laguna Hills, CA, USA) for 3 days (water changed every 12 h), until the kasugamycin could not be detected in the water, and then vacuum-dried at 313 K for characterization.

Fourier Transform Infrared Spectroscopy. FT-IR spectra, recorded on a Jasco FT-IR 5300 spectrophotometer, were used to compare the structures of kasugamycin, pectin, and kasugamycin–pectin. Samples were prepared as KBr pellet and scanned against a blank KBr pellet background at wavenumbers ranging from 4000 to 450 cm^{-1} with a resolution of 4.0 cm^{-1}.

Ultraviolet Spectrophotometer. UV–vis experiments were performed with a UV-2100S spectrophotometer (Shimadzu, Tokyo, Japan) to compare the difference in UV absorption among kasugamycin, pectin, and kasugamycin–pectin.

Thermal Gravimetric Analysis. TGA was carried out with an SDT Q600 (TA Instruments-Waters LLC, New Castle, DE, USA) analyzer from 25 to 600 °C with a heating rate of 10 °C/min.

Determination of Kasugamycin. Kasugamycin was detected by using the HPLC method referenced from Ceshing Sheu with improvement.[31] Briefly, the mobile phase consisted of eluent A, acetonitrile, and eluent B, water with 0.1% H_3PO_4 and 0.1% sodium dodecyl sulfate (SDS) (40:60 v/v). An analytical C_{18} ODS column (250 mm × 4.6 mm, 5 μm; DIKMA, Beijing, China) was equipped with a guard column (4 mm × 3 mm) and pre-equilibrated with the mobile phase for about 40 min before analysis. The injection volume was 20 μL. The detection wavelength was 210 nm (LC-20ATvp, purchased from Shimadzu), and the flow rate was kept at 1.0 mL min^{-1}. Each sample was assayed in six replicates, and all of the assays were carried out at ambient temperature.

Substitution Degree for Kasugamycin–Pectin. The substitution degree for kasugamycin–pectin was defined as the ratio of the number of carboxyl groups coupled with kasugamycin to the number of total carboxyl groups of pectin, which can be determined by using the phenolphthalein method revised from the United States Pharmacopoeia.[32] One gram of pectin was acidized for 10 min by a mixture 5 mL of hydrochloric acid and 100 mL of 60% alcohol. Then it was filtered and washed until the filtrate was chloride free and then was dried. After cooling, the pectin was moistened by alcohol and dissolved in carbon dioxide-free water. Then phenolphthalein TS was added to the pectin solution, which was then titrated with 0.5 N sodium hydroxide. The consumed volume was recorded as the initial titer, V_i. The purified conjugate with same amount of pectin was tested in the same way, and the titer was defined as V_a.

The substitution degree for kasugamycin–pectin was calculated as

$$\text{substitution degree} = \frac{V_i - V_a}{V_i} \times 100\% \quad (1)$$

The mass ratio of kasugamycin in the conjugate was calculated as

$$\text{mass ratio of kasugamycin} = \frac{M_{r,k} \times (V_i - V_a) \times C_{NaOH}}{1 + M_{r,k} \times (V_i - V_a) \times C_{NaOH}} \times 100\% \quad (2)$$

C_{NaOH} is the concentration of sodium hydroxide, and $M_{r,k}$ is the relative molecular mass of kasugamycin.

Stability of Kasugamycin–Pectin. The stability of kasugamycin–pectin was measured as the release rate of kasugamycin from the conjugate under different conditions. Kasugamycin–pectin with a

DOI: 10.1021/jf5055062
J. Agric. Food Chem. 2015, 63, 4263–4268

kasugamycin concentration of 20 mg L^{-1} was dissolved in buffer at different pH values (3.0, 5.0, 7.0, 8.5, 10.5) and at different temperatures (25, 35, 45 °C) to study the hydrolysis property. The effect of UV irradiation (high-pressure mercury lamp; light intensity = 700 $\mu W/cm^2$ detected using ZDZ-1 UV irradiation photometer) on the release of kasugamycin−pectin was also investigated. The technical, a mixture of kasugamycin and pectin with equivalent amounts of kasugamycin and pectin, was set as control. Equal known aliquots of sample were sealed in dialysis tubing (10000 MWCO) and suspended in buffer solutions under different condition. The dialysis tubes were shaken in a shaking water bath and sampled at 2 mL at predetermined intervals. Each sample was evaporated under a stream of nitrogen at 25 °C for concentration, and then the residue was reconstituted to 0.5 mL with the same buffer and vortex-mixed for 1 min. The resulting solution was filtered through a 0.45 μm filter membrane and determined by HPLC to measure the amount of kasugamycin. Each sample was repeated in triplicate.

Kasugamycin Released by Psl from Kasugamycin−Pectin. *Pathogen Culture and Inoculum Preparation.* *Pseudomonas syringae* pv. *lachrymans* was streaked on a nutrient agar plate and cultured for 24 h and then incubated aerobically in 10 mL of CM medium at 28 °C in a water bath shaking at 150 rpm for 6 h to yield exponential-phase cells ($OD_{600\ nm}$ of 0.5), which used in all treatments.

Release of Kasugamycin during the Incubation. Two hundred microliters of Psl bacterial suspension was inoculated in 10 mL of CM liquid medium with kasugamycin−pectin at different concentrations (5, 10, 20 mg L^{-1} of kasugamycin), and kasugamycin with the same concentration was used as control. Psl was grown at 150 rpm for 24 h at 28 °C. Each concentration was sampled at 1.5, 3, 4.5, 6, 7.5, 9, and 24 h after inoculation, and the analysis was conducted in three replicates. In each sample, the medium was washed with buffer by centrifugation three times to separate medium from bacteria. Then each medium sample was evaporated under a stream of nitrogen at 25 °C for concentration, and the residue was reconstituted with the same buffer and vortex-mixed for 1 min, followed by filtration through a 0.45 μm filter membrane and analyzed by HPLC to measure the kasugamycin released in the medium. Each sample was repeated in triplicate.

RESULTS AND DISCUSSION

Structural Characterization of Kasugamycin−Pectin. *Fourier Transform Infrared Spectroscopy.* Figure 2 represents the FT-IR spectra of kasugamycin, pectin, and kasugamycin−pectin. Compared with pectin, the kasugamycin−pectin shows peaks at 1676 and 1536 cm^{-1}, which could be attributed to the newly formed amide bond (CO−NH stretch) (Figure 2B). In addition, another characteristic peak at 1725 cm^{-1} corresponding to the carboxyl group in pectin significantly decreases in the spectrum of kasugamycin−pectin (Figure 2A). These indicate that the $-NH_2$ of kasugamycin has reacted with the −COOH of pectin.

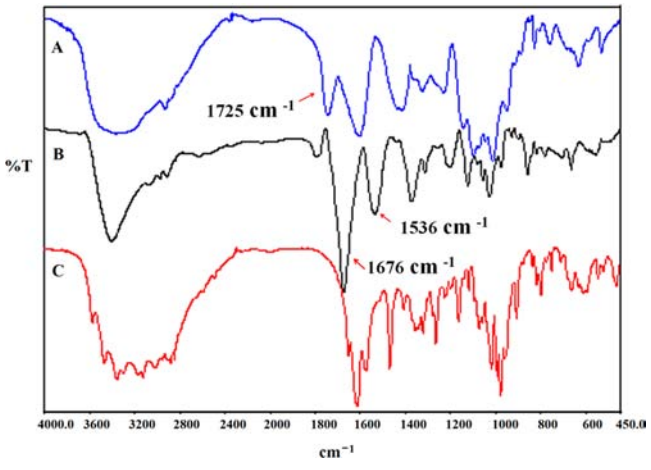

Figure 2. FT-IR spectra of pectin (A), kasugamycin−pectin (B), and kasugamycin (C).

Ultraviolet Spectrophotometer. UV−vis absorption spectra of kasugamycin, pectin, and kasugamycin−pectin from 200 to 450 nm with a magnified spectrum from 240 to 320 nm are analyzed (Figure 3). There are two characteristic peaks at 210 and 280 nm in kasugamycin−pectin, which are attributed to kasugamycin and pectin, respectively. Because the free kasugamycin was removed after dialysis, the absorption spectrum indicated that kasugamycin was assembled with the pectin successfully.

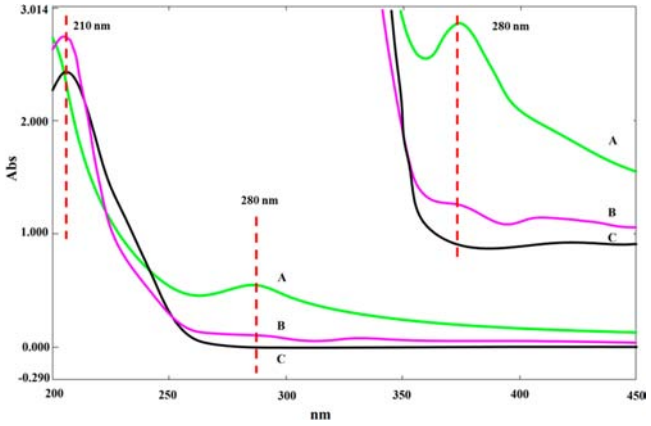

Figure 3. UV−vis spectrogram of pectin (A), kasugamycin−pectin (B), and kasugamycin (C).

Thermal Gravimetric Analysis. Figure 4 illustrates the TGA and DTG curves of kasugamycin, pectin, and kasugamycin−pectin. The results exhibited that about 8.4% weight of pectin and kasugamycin−pectin was lost around 120 °C, because of the water evaporation and decomposition of polymer into smaller molecules. However, the major decomposition of pectin happened around 236 °C, which could be attributed to the splitting of the saccharide rings, and reached about 70% weight loss at 600 °C, whereas kasugamycin−pectin showed this typical weight loss at a lower temperature, 226 °C, and about 85% weight was lost at 600 °C. Kasugamycin decomposed mainly at 197 and 263 °C. The thermal stability of

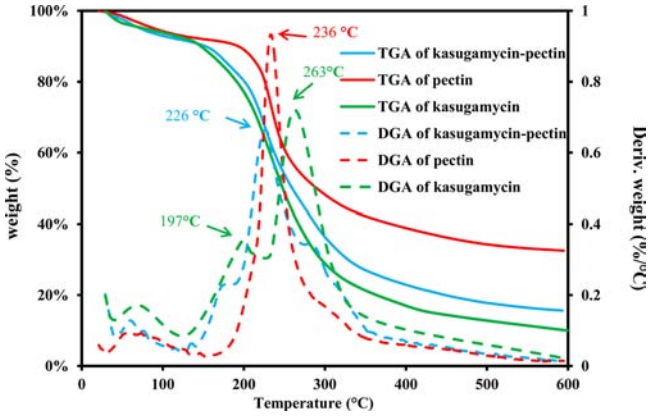

Figure 4. TGA and DTG curves of kasugamycin, pectin, and kasugamycin−pectin.

DOI: 10.1021/jf5055062
J. Agric. Food Chem. 2015, 63, 4263−4268

kasugamycin–pectin is not so strong as that of unmodified pectin because the introduction of the substituent groups decreases the crystallinity of pectin.

Substitution Degree for Kasugamycin–Pectin. According to eqs 1 and 2, the substitution degree of kasugamycin–pectin was 35.7 ± 0.7%. The mass ratio of kasugamycin in the conjugate was 40.5 ± 0.5%. Those results proved that the formation of amide between pectin and kasugamycin was effective. The formation of a new amide bond occurs easily between polymer and ingredient with EDC and NHS.[33,34]

Stability of Kasugamycin–Pectin. To study the hydrolysis property of kasugamycin–pectin, the effects of pH, temperature, and UV irradiation on this conjugate were investigated. The results showed that kasugamycin–pectin was stable at different conditions.

Effect of pH on the Stability of Kasugamycin–Pectin. Figure 5 shows the effects of different pH values (3.0, 5.0, 7.0, 8.5, 10.5) on the stability of kasugamycin–pectin at 25 °C. Technical was unstable in alkaline condition and degraded 22.5, 43.7, and 59.8% at 63 days at pH 7.0, 8.5, and 10.5, respectively. However, kasugamycin–pectin did not release any kasugamycin in the first 3 days and released little kasugamycin at all conditions during the 63 day evaluation. These results suggest that the kasugamycin can be stably kept within kasugamycin–pectin in aqueous conditions.

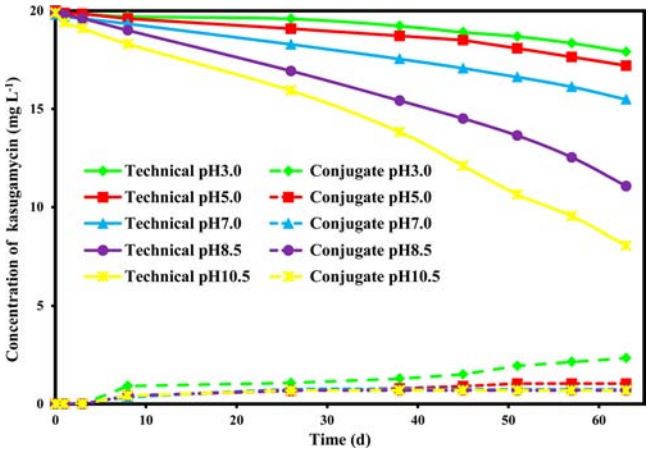

Figure 5. Effect of pH on the stability of kasugamycin–pectin, at 25 °C, without irradiation.

Effect of Temperature on the Stability of Kasugamycin–Pectin. Effects of different temperatures (25, 35, 45 °C) on the stability of kasugamycin–pectin at pH 7.0 are shown in Figure 6. In kasugamycin technical, there are about 11.5, 22.3, and 42.8% of kasugamycin degradation after 30 days at 25, 35, and 45 °C, respectively, but the release percent of the conjugate in all conditions was <9%. These results indicate that the kasugamycin–pectin has good stability against degradation within a wide range of temperatures. This property can be explained by the strong chemical bond between kasugamycin and pectin, and the phenomenon that the release percent of kasugamycin reduces with decreasing temperature indicates that the bond uncoupling can be accelerated by heat.

Effect of UV Irradiation on the Stability of Kasugamycin–Pectin. Kasugamycin–pectin and kasugamycin technical were irradiated under high-pressure mercury lamp (700 μW/cm^2) at pH 7.0 and 25 °C to investigate the effect of UV irradiation on the release of kasugamycin–pectin (Figure 7). The irradiated

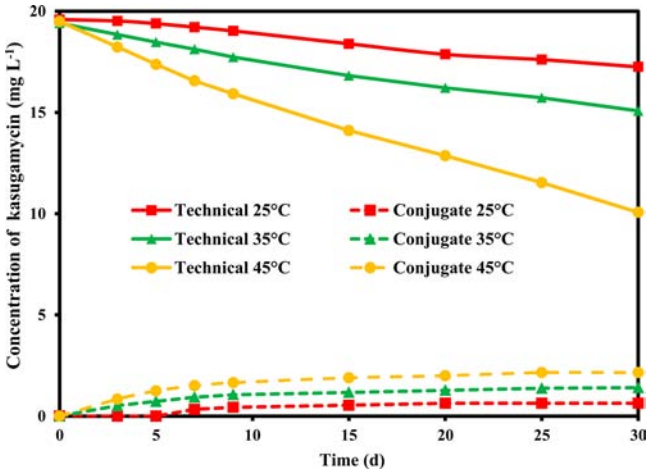

Figure 6. Effect of temperature on the stability of kasugamycin–pectin, at pH 7.0, without irradiation.

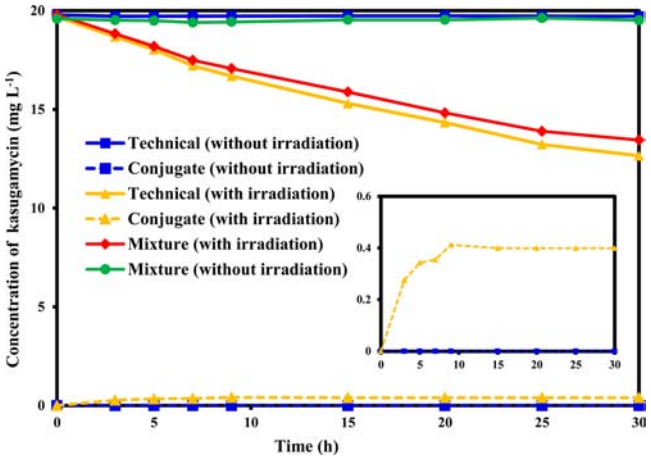

Figure 7. Effect of UV irradiation on the stability of kasugamycin–pectin, at 25 °C, pH 7.0.

kasugamycin technical samples had a 34.3% degradation after 30 h, which was far more than the nonirradiated one (1.95%). Nevertheless, the amount of kasugamycin in kasugamycin–pectin samples showed no significant difference between irradiation and non-irradiation conditions. The results indicate that the kasugamycin–pectin can provide further protection for kasugamycin against sunlight and offer a promising stability of kasugamycin, which guarantees the existence of kasugamycin in the environment for a long time. This fact shows that the concentration of kasugamycin in mixture is a little more than the technical on irradiation condition; therefore, the stability of kasugamycin–pectin relies not only on the chemical bond but also the protection of pectin.

Kasugamycin Released by Psl from Kasugamycin–Pectin. The release rate of kasugamycin from conjugate during the incubation at different concentrations is shown in Figure 8. The concentration of kasugamycin in the kasugamycin–pectin treatment keeps increasing during the incubation. Considering the conjugate exhibits a stable property under different conditions as above, the increased release of kasugamycin is attributed to bacteria. These results indicate that the release of the effective component from the conjugate can be triggered by the release of pathogenic bacteria. The potential underlying mechanism is that the pectin and the amide linkage in

DOI: 10.1021/jf5055062
J. Agric. Food Chem. 2015, 63, 4263–4268

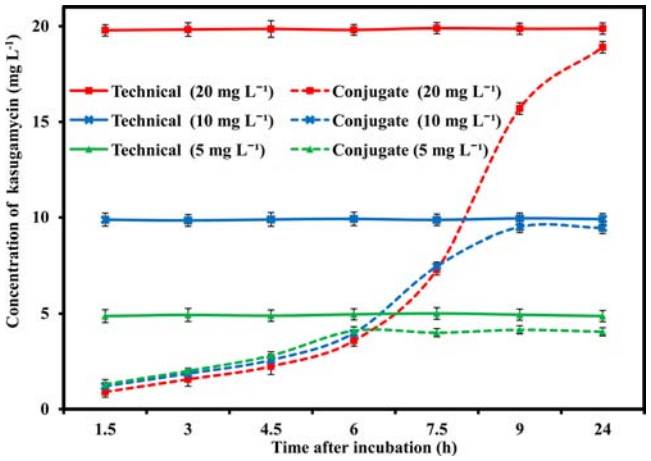

Figure 8. Concentration of kasugamycin in the medium at different times.

kasugamycin−pectin are degraded by enzymes such as pectinase and amidase secreted by Psl, which is a common process of bacterial infection in plant.[27] Noticeably, the release rate of kasugamycin also increased with time; the more enzymes were released during the propagation of bacteria, the more kasugamycin was freed.

In this research, kasugamycin was directly coupled with pectin to form a kasugamycin−pectin conjugate and the conjugate was characterized by FT-IR, UV−vis, and TGA. The results of controlled-release evaluation reveal that the pectin in the conjugate can effectively protect the active agent from degradation, and the conjugate exhibited a sustained release property. The conjugate was degraded by the pathogenic bacteria to release kasugamycin in the process of proliferation. Hence, with high stability and targeted release performance, kasugamycin−pectin can be a promising polymer conjugate in the application of kasugamycin and provide a new method to control plant disease.

AUTHOR INFORMATION

Corresponding Author

*(Y.C.) E-mail: caoysong@126.com.

Author Contributions

‖Y.L. and Y.S. contributed equally to this work.

Funding

This work was supported by the National Natural Science Foundation of China (31471799, 31171888) and the National Department Public Benefit Research Foundation (201003065).

Notes

The authors declare no competing financial interest.

REFERENCES

(1) Guzzella, L.; Pozzoni, F.; Giuliano, G. Herbicide contamination of surficial groundwater in northern Italy. *Environ. Pollut.* **2006**, *142*, 344−353.

(2) Lapworth, D. J.; Gooddy, D. C. Source and persistence of pesticides in a semi-confined chalk aquifer of southeast England. *Environ. Pollut.* **2006**, *144*, 1031−1044.

(3) Hildebrandt, A.; Lacorte, S.; Barceló, D. Assessment of priority pesticides, degradation products, and pesticide adjuvants in groundwaters and top soils from agricultural areas of the Ebro river basin. *Anal. Bioanal. Chem.* **2007**, *387*, 1459−1468.

(4) Palma, P.; Kuster, M.; Alvarenga, P.; Palma, V. L.; Fernandes, R. M.; Soares, A. M. V. M; López de Alda, M. J.; Barceló, D.; Barbosa, I. R. Risk assessment of representative and priority pesticides, in surface water of the Alqueva reservoir (south of Portugal) using on-line solid phase extraction-liquid chromatography-tandem mass spectrometry. *Environ. Int.* **2009**, *35*, 545−551.

(5) Pepperman, A. B.; Kuan, J. C. W.; McCombs, C. Alginate controlled release formulations of metribuzin. *J. Controlled Release* **1991**, *17*, 105−111.

(6) Alemzadeh, I.; Vossoughi, M. Controlled release of paraquat from poly vinyl alcohol hydrogel. *Chem. Eng. Process.* **2002**, *41*, 707−710.

(7) Cao, Y.; Huang, L.; Chen, J.; Liang, J.; Long, S.; Lu, Y. Development of a controlled release formulation based on a starch matrix system. *Int. J. Pharm.* **2005**, *298*, 108−116.

(8) Ziv, D.; Mishael, Y. G. Herbicide solubilization in micelle-clay composites as a basis for controlled release sulfentrazone and metolachlor formulations. *J. Agric. Food Chem.* **2008**, *56*, 9159−9165.

(9) Qian, K.; Shi, T.; Tang, T.; Zhang, S.; Liu, X.; Cao, Y. Preparation and characterization of nano-sized calcium carbonate as controlled release pesticide carrier for validamycin against *Rhizoctonia solani*. *Microchim. Acta* **2011**, *173*, 51−57.

(10) Lopez, M. D.; Maudhuit, A.; Pascual-Villalobos, M. J.; Poncelet, D. Development of formulations to improve the controlled-release of linalool to be applied as an insecticide. *J. Agric. Food Chem.* **2012**, *60*, 1187−1192.

(11) Grillo, R.; Pereira, A. d. E. S.; de Melo, N. F. S.; Porto, R. M.; Feitosa, L. O.; Tonello, P. S.; Filho, N. L. D.; Rosa, A. H.; Lima, R.; Fraceto, L. F. Controlled release system for ametryn using polymer microspheres: preparation, characterization and release kinetics in water. *J. Hazard. Mater.* **2011**, *186*, 1645−1651.

(12) Ma, Z.; Jia, X.; Zhang, G.; Hu, J.; Zhang, X.; Liu, Z.; Wang, H.; Zhou, F. pH-responsive controlled-release fertilizer with water retention via atom transfer radical polymerization of acrylic acid on mussel-inspired initiator. *J. Agric. Food Chem.* **2013**, *61*, 5474−5482.

(13) Kery, V.; Novotny, L.; Tihlarik, K.; Haplova, J.; Kacurakova, M.; Sandula, J.; Balazova, E. Preparation, properties and antileukemic activity of arabinosylcytosine polysaccharide conjugates. *Int. J. Biochem.* **1990**, *22*, 1203−1207.

(14) Palma, G.; Casals, P.; Cardenas, G. Synthesis and characterization of new chitosan-*O*-ethyl phosphonate. *J. Chil. Chem. Soc.* **2005**, *50*, 719−724.

(15) Josef, E.; Zilberman, M.; Bianco-Peled, H. Composite alginate hydrogels: an innovative approach for the controlled release of hydrophobic drugs. *Acta Biomater.* **2010**, *6*, 4642−4649.

(16) Ernsting, M. J.; Tang, W. L.; Maccallum, N.; Li, S. D. Synthetic modification of carboxymethylcellulose and use thereof to prepare a nanoparticle forming conjugate of docetaxel for enhanced cytotoxicity against cancer cells. *Bioconjugate Chem.* **2011**, *22*, 2474−2486.

(17) Liu, Y.; Sun, Y.; He, S.; Zhu, Y.; Ao, M.; Li, J.; Cao, Y. Synthesis and characterization of gibberellin-chitosan conjugate for controlled-release applications. *Int. J. Biol. Macromol.* **2013**, *57*, 213−217.

(18) Cai, S.; Thati, S.; Bagby, T. R.; Diab, H. M.; Davies, N. M.; Cohen, M. S.; Forrest, M.; Laird, M. L. Localized doxorubicin chemotherapy with a biopolymeric nanocarrier improves survival and reduces toxicity in xenografts of human breast cancer. *J. Controlled Release* **2010**, *146*, 212−218.

(19) BeMiller, J. N. An introduction to pectins. *Struct. Properties* **1986**, *310*, 2−12.

(20) Wakerly, Z.; Fell, J. T.; Attwood, D.; Parkins, D. A. In vitro evaluation of pectin-based colonic drug delivery systems. *Int. J. Pharm.* **1996**, *129*, 73−77.

(21) Giunchedi, P.; Conte, U.; Chetoni, P.; Saettone, M. F. Pectin microspheres as ophthalmic carriers for piroxicam: evaluation in vitro and in vivo in albino rabbits. *Eur. J. Pharm. Sci.* **1999**, *9*, 1−7.

(22) Liu, L.; Fishman, M. L.; Kost, J.; Hicks, K. B. Pectin-based systems for colon-specific drug delivery via oral route. *Biomaterials* **2003**, *24*, 3333−3343.

(23) Sande, S. A. Pectin-based oral drug delivery to the colon. *Expert Opin. Drug Delivery* **2005**, *2*, 441−450.

(24) Tang, X. H.; Xie, P.; Ding, Y.; Chu, L. Y.; Hou, J. P.; Yang, J. L.; Song, X.; Xie, Y. M. Synthesis, characterization, and in vitro and in vivo

DOI: 10.1021/jf5055062
J. Agric. Food Chem. 2015, 63, 4263−4268

evaluation of a novel pectin-adriamycin conjugate. *Bioorg. Med. Chem.* **2010**, *18*, 1599−1609.
(25) Perera, G.; Barthelmes, J.; Bernkop-Schnürch, A. Novel pectin-4-aminothiophenole conjugate microparticles for colon-specific drug delivery. *J. Controlled Release* **2010**, *145*, 240−246.
(26) Sriamornsak, P. Application of pectin in oral drug delivery. *Expert Opin. Drug Delivery* **2011**, *8*, 1009−1023.
(27) Collmer, A.; Keen, N. T. The role of pectic enzymes in plant pathogenesis. *Annu. Rev. Phytopathol.* **1986**, *24*, 383−409.
(28) Umezawa, H.; Okami, Y.; Hashimoto, T.; Suhara, Y.; Hamada, M.; Takeuchi, T. A new antibiotic, kasugamycin. *J. Antibiot.* **1965**, *18*, 101−103.
(29) Tomlin, C. D. S. *The Pesticide Manual: A World Compendium*, 14th ed.; British Crop Production Council: Norwich, UK, 2006.
(30) Suhara, Y.; Maeda, K.; Umezawa, H. Chemical studies on kasugamycin. V. The structure of kasugamycin. *Tetrahedron Lett.* **1966**, *7*, 1239−1244.
(31) Sheu, C.; Chen, S. C.; Lo, C. C. Analysis of antibiotic fungicide kasugamycin in irrigation water by high performance liquid chromatography. *J. Environ. Sci. Health, Part B* **2010**, *45*, 478−484.
(32) The United States Pharmacopeial Convention. *United States Pharmacopoeia*, 32nd ed.; The United States Pharmacopeial Convention: Rockville, MD USA, 2008.
(33) Hu, F. Q.; Liu, L. N.; Du, Y. Z.; Yuan, H. Synthesis and antitumor activity of doxorubicin conjugated stearic acid-g-chitosan oligosaccharide polymeric micelles. *Biomaterials* **2009**, *30*, 6955−6963.
(34) Kafedjiiski, K.; Föger, F.; Werle, M.; Bernkop-Schnürch, A. Synthesis and in vitro evaluation of a novel chitosan-glutathione conjugate. *Pharm. Res.* **2005**, *22*, 1480−1488.

DOI: 10.1021/jf5055062
J. Agric. Food Chem. 2015, 63, 4263−4268

Table 1. Optimized MRM Conditions for the Analyses of the Value-Added Compounds by UPLC−MS/MS

		quantitation (MRM_1)			confirmation (MRM_2)		
compound	precursor ion (m/z)	product ion	cone voltage (V)	collision energy (eV)	product ion	cone voltage (V)	collision energy (eV)
oleanolic acid (**1**)	455.54	407.65	90	40	389.71	90	45
maslinic acid (**2**)	471.48	393.36	80	40	405.21	80	50
ursolic acid (**3**)	455.49	407.45	85	40	166.47	85	45
erythrodiol + uvaol (**4** + **5**)	265.31	97.05	50	20	216.56	50	20
linoleic acid (**6**)	279.37	261.38	45	17	58.95	45	17
18β-glycyrrhetinic acid (**7**)	469.47	425.45	90	40	355.37	90	50

the basis of the literature available, this is the first attempt to determine the extraction efficiency of different samples of TPOMW (several types of drying and degreasing procedures, including the olive stones or not) on their triterpene content. This study is expected to provide researchers information on an efficient extraction method of triterpene compounds from TPOMW for industrial application.

MATERIALS AND METHODS

Materials and Reagents. Oleanolic (**1**) and linoleic (**6**) acid standards were purchased from Fluka (Steinheim, Germany) (Figure 1). Maslinic (**2**) and ursolic (**3**) acids standards were purchased from Sigma-Aldrich (St. Louis, MO, USA). Erythrodiol (**4**) and uvaol (**5**) were purchased from Extrasynthese (Genay, France). 18β-Glycyrrhetinic acid (**7**), also from Extrasynthese, was used as an internal standard. Methanolic-stock standard solutions in the range of 0.05−1.0 μg mL^{-1} were prepared for each analyte and stored at −20 °C. Standard solutions were analyzed by LC−MS daily. HPLC-grade ethyl acetate and methanol were purchased from Sigma-Aldrich (St. Louis, MO, USA). Analytical-grade hexane, from Panreac (Barcelona, Spain), was used for the oil extraction in samples with the Soxhlet method. Deionized water, acetonitrile, and methanol of LC−MS grade, from Waters (Barcelona, Spain), were used for the preparation of chromatographic mobile phases. Formic acid, from Waters (Barcelona, Spain), was used as an additive in the mobile phases to enhance ionization required for MS detection.

Sample Preparation. All samples of TPOMW were obtained from virgin olive-oil extraction using an Abencor laboratory oil mill (MC2 Ingeniería y Sistemas S.L. Sevilla, Spain), which kneaded the olive paste at 28 °C for 30 min. This system provided more homogeneous and representative samples with the control of two key variables, that is, temperature and extraction time, not an easy task in an industrial system.

(A) Fresh sample (FS). Original wet sample from the TPOMW.
(B) Dried sample (DS). The FS was dried in a forced-air oven at 105 °C until constant weight.
(C) Dried-extracted sample (DES). DS was placed in cellulose-extraction thimbles and extracted in a Soxhlet apparatus with 200 mL of hexane for 6−8 h. Then the solvent of the sample without oil was evaporated in a forced-air oven at 60 °C for 6 h. This type of oven has been used given the high stability of the compounds studied.
(D) Dried-sifted sample (DSS). DS was sifted sequentially with a 0.5 mm and a 0.1 mm pore size to separate the olive stones.

Extraction of Triterpene Compounds. The extraction procedure is similar to the method described by Guinda[31] and Romero,[30] with some modifications. That is, 1 g of each sample (FS, DS, DES, or DSS) was mixed, in a 15 mL centrifuge tube, with 10 mL of methanol or ethyl acetate. The mixture was stirred for 1 h and then centrifuged at 4000 rpm for 6 min. Finally, the extract was separated from the solid phase, and the solvent of this extract was removed under reduced pressure. The residue was dissolved in 2 mL of methanol or ethyl acetate and then was filtered through 0.45-μm pore size. This solution was diluted (1:20, v/v) in acetonitrile/water (75:25, v/v) (mobile phase). Finally, this solution was filtered through 0.2-μm pore size, and an aliquot (100 μL in methanol or ethyl acetate) together with 100 μL of a solution of 18β-glycyrrhetinic acid (**7**, 5 mg/L), as an internal standard, was injected into the liquid chromatograph.

UPLC−MS Analyses. The UPLC system consisted of an AcQuity ultra-performance liquid chromatographer equipped with a binary pump system, using an AcQuity UPLC BEH C18 column (100 mm × 2.1 mm, 1.7 μm), all from Waters (Milford, MA, USA). The mobile phase consisted of (A) acetonitrile and (B) water, containing 0.1% formic acid, 75:25 (v/v), and was kept isocratic for 10 min with a flow rate of 0.4 mL/min. During the analysis, the column was kept at 30 °C, and the injection volume was 10 μL.

The UPLC was coupled to a PDA detector AcQuity UPLC and a TQD mass spectrometer (Waters, Milford, MA, USA). The software used was Masslynx 4.1. The wavelength in the PDA detector was set at 205−215 nm. For ionization, an electrospray (ESI) interface was used, operating in the negative mode, and the data were collected in the selected reaction monitoring (MRM). The ionization source parameters were: capillary voltage 3 kV, source temperature 150 °C, and desolvation gas temperature 350 °C with a flow-rate of 650 L/h. Nitrogen (99.99% purity, N2 LC−MS nitrogen generator ZEFIRO 35, Strumenti Scientifici Cinel, Vigonza, Italy) and argon (>99.99% purity, Air−Liquide, Madrid, Spain) were used as cone and collision gases, respectively. The MRM transitions and the individual cone voltage and collision energy for each triterpene compound were evaluated by infusing 5 μg/mL to establish the best instrumental conditions. Two MRM transitions were studied to find the most abundant product ions, selecting the most sensitive transition for quantitation, and a second one for confirmation purposes. For the positive identification of the analytes in the sample, the chromatographic retention time of each analyte should not vary more than 2% compared to the standard, and the relative abundance of the two MRM transitions monitored had to be within 15% of the ratios calculated for the standards (Table 1).

Standards oleanolic, maslinic, ursolic, and linoleic acids, as well as uvaol and erythrodiol, were used to identify peaks. Stock solutions containing 10 μg/mL were prepared by dissolving the standards in methanol and diluted to a series of appropriate concentrations to construct the calibration curve. Triterpene compounds were quantified using a TargetLynx (Waters Inc.) system.

Statistical Analysis of Data. All data are presented as the means ± standard deviation from the independent experiments made in triplicates. The data were evaluated by one-way ANOVA with the Statistix 8 program for Windows, and the differences between means were assessed using the Fisher LSD test. Statistical significance was considered at $p < 0.05$.

RESULTS AND DISCUSSION

UPLC−MS/MS Method Validation. The development of the UPLC−MS/MS method was validated in terms of precision, accuracy, and linearity. The regression curve of the six compounds was drawn using the external-standard method. All of the correlation coefficient ($r > 0.9950$) values indicated appropriate correlations between the concentrations of the investigated compounds and their peak areas, within the test ranges. Assay precision was verified by using six independent tests. The accuracy of the assay method was evaluated in

DOI: 10.1021/jf506171y
J. Agric. Food Chem. 2015, 63, 4269−4275

Table 2. Retention Time, Regression Equation (r^2), Reproducibility (RSD, %), LOD, and LOQ, for the Analysis of the Triterpenic Compounds by UPLC−MS/MS, in Standard Solutions

compound	retention time (min)	regression equation	r^{2a}	RSD[b] (%)	LOD[c] (mg/kg)	LOQ[d] (mg/kg)
oleanolic acid (1)	4.54	$y = 0.0003x - 1.1388$	0.9999	3.87	0.35	0.97
maslinic acid (2)	1.78	$y = 0.0002x - 3.7261$	0.9966	3.39	0.72	1.97
ursolic acid (3)	4.28	$y = 0.0003x - 1.2226$	0.9998	3.57	0.37	1.03
erythrodiol + uvaol (4 + 5)	3.69	$y = 0.0005x - 5.1192$	0.9972	5.36	0.36	0.98
linoleic acid (6)	6.42	$y = 0.0013x + 1.5205$	0.9999	6.83	0.017	0.047
18β-glycyrrhetinic acid (7)	2.10	$y = 0.00002x + 0.3189$	0.9966	7.96	0.001	0.002

[a]Correlation coefficient. [b]RSD (%) = (SD/mean) × 100. [c]Limit of detection (S/N = 3). [d]Limit of quantitation (S/N = 10).

triplicate using low, middle, and high concentration levels. The limit of detection (LOD) and limit of quantitation (LOQ) were determined by injecting a series of diluted solutions with known concentrations. LOD and LOQ were defined as the signal-to-noise ratio equal to 3 and 10, respectively. These results are shown in Table 2. An internal standard, 18β-glycyrrhetinic acid (7), was added to the fresh TPOMW sample before any handling (extraction procedure, drying, and sifting) to gain information about the recovery of the compounds studied. This recovery was 96.3% for methanol and 99.5% for ethyl acetate.

Comparison of Extraction with Different Solvents. The selection of the most suitable solvent for extracting the analytes of interest from the sample matrix is not only a fundamental step for the development of an extraction method, but also for the solubility of the analytes in the solvent. Methanol, ethanol, ethyl acetate, and diethyl ether are the most frequently solvents used to extract the triterpene acids from plant material.[23,30−33] Ethanol and ethanol/water[29,33] are poor extractors for triterpenes, while better results were achieved with methanol and diethyl ether.

In this study, the solvents methanol and ethyl acetate, for their polarity, were selected for the extraction of the value-added compounds from the TPOMW samples (Table 3). These value-added compounds extracted from TPOMW samples (FS, DS, DES, and DSS) were triterpene acids (oleanolic, maslinic, and ursolic) and diols (erythrodiol and uvaol) (Figure 1). Also, the extract showed a large content in linoleic acid, a fatty acid of the olive oil saponifiable fraction. The extraction results (Table 3) showed that methanol was the most efficient solvent in extracting the value-added compounds from the FS, in agreement with several authors who consider methanol the best solvent,[23,29] probably because the sample contained water. By contrast, ethyl acetate, the best solvent for Romero et al.,[30] proved to be the best extracting solvent with the DSS. With the other samples (DS and DES), the results varied depending on the type of compound analyzed. Thus, ethyl acetate gave the best extraction results with oleanolic and linoleic acids, the less polar compounds, whereas methanol was the best for the more polar products, maslinic acid, and diols (erythrodiol and uvaol). Finally, ursolic acid had the same results of extraction with both solvents.

Effects of the Type of TPOMW Sample Preparation on Their Content of Each Compound. In this study, classic techniques such as drying (DS), drying and olive oil extraction with a Soxhlet (DES), and drying and sifting of the olive stones (DSS) were compared with the FS to analyze the influence of the type of sample on the content of each compound extracted from them.

The average content in oleanolic acid (1) was highly varied for the diverse TPOMW samples (FS, DS, DES, and DSS; Figure 2). The best results of extraction (Table 3) were achieved using the FS with both solvents (2.03 g kg^{-1} in methanol, and 1.81 g kg^{-1} in ethyl acetate) while using the DES with ethyl acetate (1.89 g kg^{-1}). Conversely, with the DS and DSS samples, the extraction of this compound (1) was clearly lower (between 0.82 and 0.55 g kg^{-1}).

Maslinic acid (2) is a more abundant compound in these olive-mill wastes (Figure 2). The average content of this triterpenic acid in the extraction of the diverse TPOMW samples was more regular (between 27.9 and 23.0 g kg^{-1}; Table 3), except for the DS, for which the extraction was considerably lower (15.6 g kg^{-1} in methanol, and 11.7 g kg^{-1} in ethyl acetate).

Table 3. Average Content of Several Value-Added Compounds Isolated from Different Preparations of Two-Phase Olive-Mill-Waste Samples[a]

		solvent extraction	
compound	sample	methanol	ethyl acetate
	FS[b]		
oleanolic acid (g/kg)		2.03 ± 0.25a	1.81 ± 0.43a
maslinic acid (g/kg)		25.5 ± 1.75a	23.7 ± 1.2b
ursolic acid (mg/kg)		287 ± 24a	181 ± 53b
erythrodiol + uvaol (mg/kg)		632 ± 91a	466 ± 61a
linoleic acid (mg/kg)		542 ± 94a	385 ± 31a
	DS[c]		
oleanolic acid (g/kg)		0.74 ± 0.13a	0.82 ± 0.15a
maslinic acid (g/kg)		15.6 ± 1.2 a	11.7 ± 0.8b
ursolic acid (mg/kg)		133 ± 17a	131 ± 14a
erythrodiol + uvaol (mg/kg)		523 ± 122a	400 ± 52a
linoleic acid (mg/kg)		403 ± 16a	449 ± 22a
	DES[d]		
oleanolic acid (g/kg)		1.47 ± 0.27b	1.89 ± 0.15a
maslinic acid (g/kg)		27.9 ± 1.20a	25.2 ± 0.93b
ursolic acid (mg/kg)		169 ± 29a	169 ± 22a
erythrodiol + uvaol (mg/kg)		509 ± 40a	378 ± 28b
linoleic acid (mg/kg)		323 ± 7a	324 ± 8a
	DSS[e]		
oleanolic acid (g/kg)		0.55 ± 0.08b	0.74 ± 0.08a
maslinic acid (g/kg)		23.0 ± 0.64b	25.4 ± 1.5a
ursolic acid (mg/kg)		240 ± 27a	242 ± 39a
erythrodiol + uvaol (mg/kg)		317 ± 28a	348 ± 39a
linoleic acid (mg/kg)		545 ± 63a	626 ± 33a

[a]The results are referenced to initial sample weight and expressed as mean ± standard deviation (n = 10). Results in a same row, not sharing a common letter, are significantly different ($P < 0.05$). [b]FS (fresh two-phase olive-mill-waste sample). [c]DS (dried two-phase olive-mill-waste sample). [d]DES (dried and extracted two-phase olive-mill-waste sample). [e]DSS (dried two-phase olive-mill-waste sample without olive stones).

DOI: 10.1021/jf506171y
J. Agric. Food Chem. 2015, 63, 4269−4275

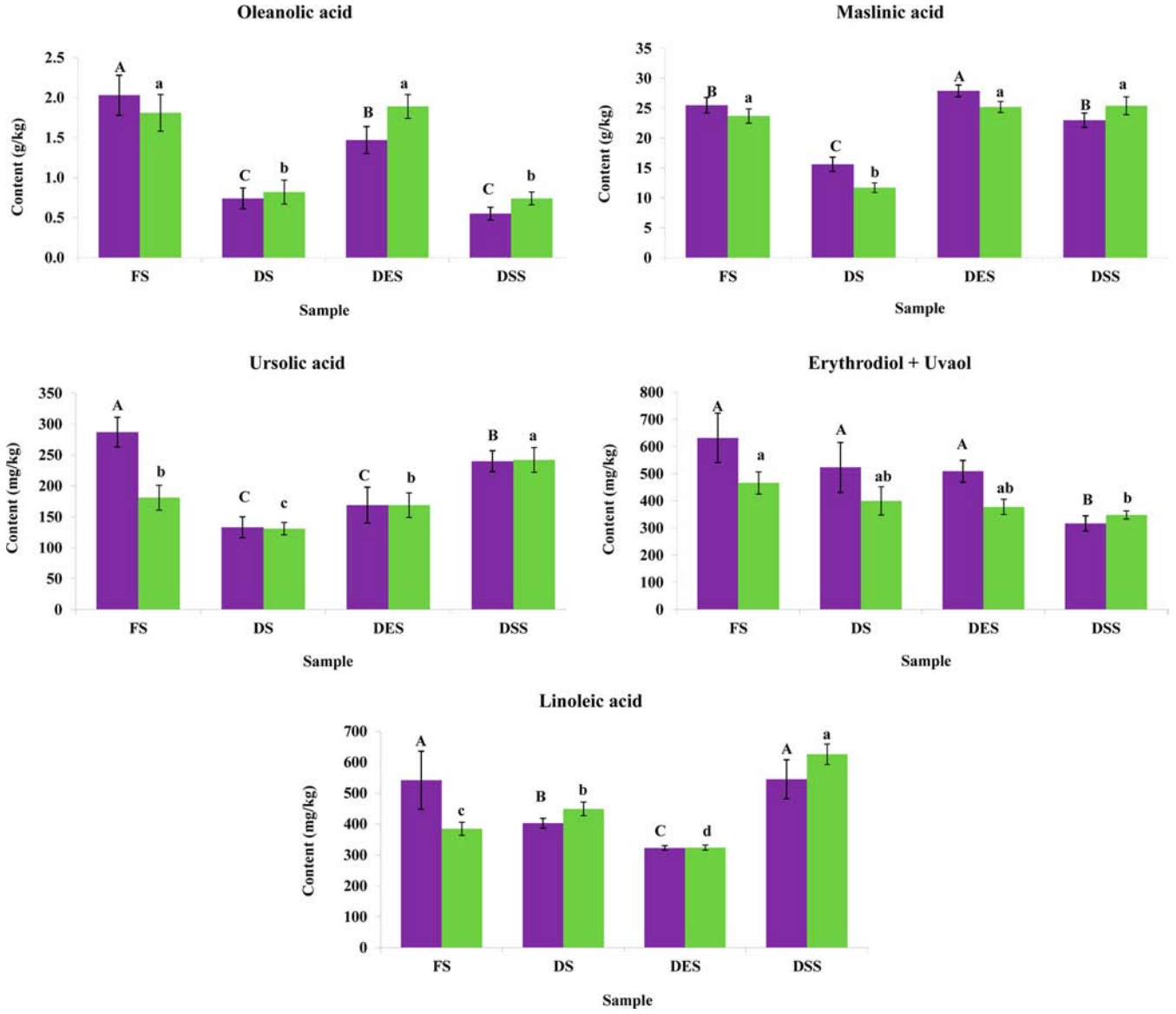

Figure 2. Content of triterpene compounds found using methanol (purple) or ethyl acetate (green) as solvent extraction from the different samples of TPOMW. The results are referenced to the sample weight and expressed as mean ± standard deviation (n = 10). Vertical bars with different capital letters (methanol) or small letters (ethyl acetate) indicate significant differences between the sample preparation process according to the Fisher LSD test at a $P < 0.05$ level of probability.

Ursolic acid (**3**) was the less abundant triterpene acid in these olive-mill wastes (Figure 2). The best extraction result (Table 3) was reached using the FS with methanol (287 mg kg^{-1}), which was clearly higher than with ethyl acetate (181 mg kg^{-1}). In the other TPOMW samples (DS, DES, and DSS), no differences were found between the two solvents, achieving the best extraction results (around 240 mg kg^{-1}) using the DSS.

In summary, the comparison of the average contents of the three triterpene acids (**1**–**3**) of the dried sample (DS) with those of the dried sample extracted in a Soxhlet (DES) suggests that the oil presence in the first sample seems to hinder the extraction of these triterpene acids (Table 3).

The average content of erythrodiol (**4**) and uvaol (**5**) of the diverse TPOMW samples (Figure 2) was higher when the corresponding sample was extracted with methanol (632–509 mg kg^{-1}) than with ethyl acetate (466–378 mg kg^{-1}), except for the DSS sample (Table 3). Therefore, it seems that the elimination of the olive stones from the DS by sifting techniques (DSS) hinders the extraction of the more polar fraction (triterpene diols).

The best results of extraction of linoleic acid (**6**) were achieved from the DSS with both solvents (626 mg kg^{-1} in ethyl acetate, and 545 mg kg^{-1} in methanol) and from the FS with methanol (542 mg kg^{-1}) (Figure 2). In this case, the removal of the olive stones from the DS seemed to help the extraction of the lipid fraction (linoleic acid, **6**) contrary to what happened with the triterpene diols (**4** and **5**).

In conclusion, the analysis of the average content of the different value-added compounds for all the TPOMW samples (FS, DS, DES, and DSS) indicated that for compounds **1**, **3**, **4**, and **5**, the best results were achieved by extraction with methanol from the FS. Furthermore, for compound **2**, the best results were reached also with methanol but from the DES. Finally, for linoleic acid (**6**), the best solvent was ethyl acetate on the DSS.

DOI: 10.1021/jf506171y
J. Agric. Food Chem. 2015, 63, 4269–4275

Study of the Type of TPOMW Sample on the Triterpenic Compound Contents by PCA. When the results of the extraction with methanol of the compounds with higher content (**1**, **2**, **4**, and **5**) on the TPOMW samples (FS, DS, DES, and DSS) were submitted to "principal component analysis" (PCA), we could see that maslinic acid (**2**) explained 98% of the data variance (PC1), whereas oleanolic acid (**1**) and the triterpene diols (**4** and **5**) accounted for only 1% (PC2). The visualization of the four sample types, as well as their distribution into groups according to principal-component scores, is displayed in Figure 3. The groups of

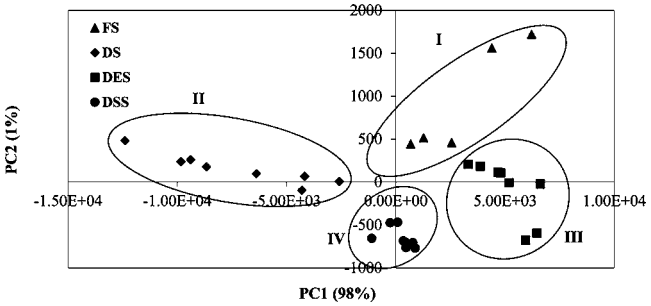

Figure 3. PCA plots for TPOMW samples using the oleanolic acid, maslinic acid, and erythrodiol + uvaol content with their methanol responses. FS (original fresh sample), DS (dried sample), DES (dried-extracted sample), and DSS (dried-sifted sample).

TPOMW samples established were as follows: Group I (FS), very high content of the triterpene compounds analyzed; Group II (DS), high content of erythrodiol + uvaol and low content of maslinic and oleanolic acids; Group III (DES): very high content of maslinic acids and intermediate content of oleanolic acid and erythrodiol + uvaol; and Group IV (DSS), high content of maslinic acid and low content of oleanolic acid and erythrodiol-uvaol.

Loading plot of array is displayed in Figure 4. Maslinic acid presented the highest value for the first principal component

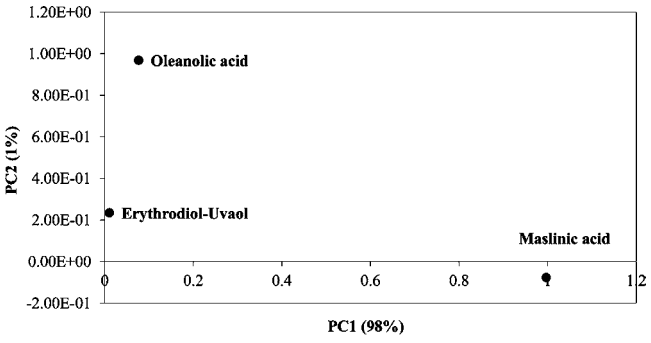

Figure 4. PCA loading plot for TPOMW samples using compounds **1**, **2**, and **3**−**4** content with their methanol responses.

(PC1), and the oleanolic acid had the highest one for PC2, while the triterpene diols (erythrodiol and uvaol) showed lower values for both components (PC1 and PC2).

When the extraction solvent was ethyl acetate and these data were submitted to the PCA (Figure 5), we found that maslinic acid (**2**) explained 99% of the data variance (PC1), while oleanolic acid (**1**) and triterpene diols (**4** and **5**) accounted for only 1% (PC2). Loading plot of array is displayed in Figure 6. Maslinic acid presented the highest value for PC1, and

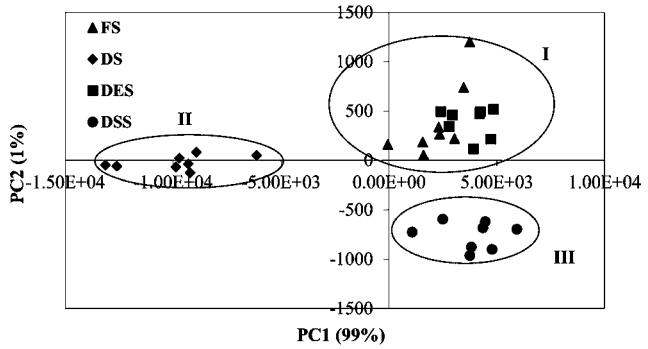

Figure 5. PCA plots for TPOMW samples using oleanolic acid, maslinic acid, and erythrodiol + uvaol content with their ethyl acetate responses. FS (original fresh sample), DS (dried sample), DES (dried-extracted sample) and DSS (dried-sifted sample).

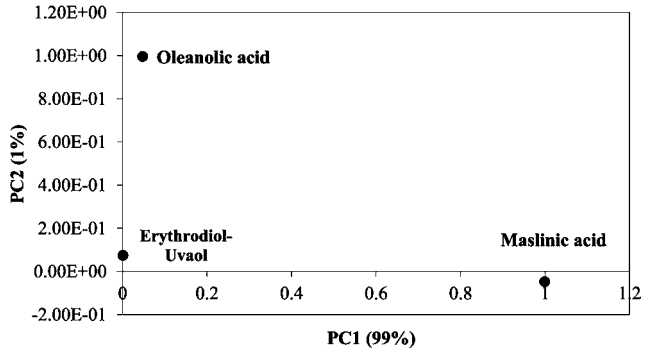

Figure 6. PCA loading plot for TPOMW samples using **1**, **2**, and **3**−**4** content with their ethyl acetate responses.

oleanolic acid had the highest one for PC2, while the triterpene diols (erythrodiol and uvaol) showed lower values for both components (PC1 and PC2). The groups of TPOMW samples established were as follows: Group I (FS and DES), very high content of maslinic and oleanolic acids; Group II (DS), high content of erythrodiol + uvaol and low content of maslinic and oleanolic acids; and Group III (DSS), very high content of maslinic acid and low content of oleanolic acid and erythrodiol + uvaol.

In summary, we describe and validate a UPLC−MS method for separating and quantitating five value-added compounds in several sample-preparation processes of TPOMW. Moreover, these extraction processes offer greater advantage for future applications due to the simplicity and relatively good extraction efficiency. For an industrial DES TPOMW sample, methanol should be used as the solvent for the highest extraction of maslinic acid, and ethyl acetate for oleanolic acid. For the industrial extraction of the highest content of triterpene diols (erythrodiol and uvaol), methanol should be used with a FS TPOMW sample. For the selective extraction of linoleic acid, industry should start from a DSS TPOMW sample and use ethyl acetate as solvent extraction.

In conclusion, the use of these processes for extracting the solid wastes of the olive-oil industry can reduce the environmental impact of these residues, since several bioactive compounds with high value-added can be isolated. These results may contribute to the revaluation of the TPOMW in view of the promising bioactivity properties of the natural triterpene acids.

DOI: 10.1021/jf506171y
J. Agric. Food Chem. 2015, 63, 4269−4275

AUTHOR INFORMATION

Corresponding Author

*Phone: +34671532209. Fax: +34953366380. E-mail: antonia.fernandez.he@juntadeandalucia.es.

Funding

A.F.-H. deeply appreciates the contract grant funded by the Agricultural Research Institute of Spain (INIA) and the European Social Fund. This work was also financially supported by grants from the "Consejería de Innovación, Ciencia y Empresa" of the "Junta de Andalucía" (FQM−7372), and the "Plan Propio" of the University of Granada.

Notes

The authors declare no competing financial interest.

ACKNOWLEDGMENTS

We thank David Nesbitt for reviewing the English in the manuscript.

ABBREVIATIONS USED

TPOMW, two-phase olive-mill-waste; UPLC−MS, ultraperformance liquid chromatography tandem mass spectrometry; FS, fresh sample; DS, dried sample; DES, dried-extracted sample; DSS, dried-sifted sample; PDA, photodiode array detector; TQD, tandem quadrupole detector; ESI, electrospray ionization; MRM, multiple reaction monitoring; LSD, least significant difference; LOD, limit of detection; LOQ, limit of quantitation; PCA, principal component analysis

REFERENCES

(1) *FAOSTAT Resource Statistics*; FAOSTAT: Rome, 2014. faostat3.fao.org (accessed December 2014).

(2) López-Piñeiro, A.; Albarrán, A.; Rato Nunes, J. M.; Peña, D.; Cabrera, D. Long-term impacts of de-oiled two-phase olive mill waste on soil chemical properties, enzyme activities, and productivity in an olive grove. *Soil Tillage Res.* **2011**, *114*, 175−182.

(3) Roig, A.; Cayuela, M. L.; Sánchez-Monedero, M. A. An overview on olive mil wastes and their valorisation methods. *Waste Manage.* **2006**, *26*, 960−969.

(4) Sabatini, N. Recent patents in olive oil industry: New technologies for the recovery of phenols compounds from olive oil, olive oil industrial byproducts, and waste waters. *Recent Pat. Food, Nutr. Agric.* **2010**, *2*, 154−159.

(5) Fernández-Bolaños, J.; Rodríguez, G.; Rodríguez, R.; Guillén, R.; Jiménez, A. Extraction of interesting organic compounds from olive oil waste. *Grasas Aceites* **2006**, *57*, 95−106.

(6) Bouzid, O.; Navarro, D.; Roche, M.; Asther, M.; Haon, M.; Delattre, M.; Lorquin, J.; Laba, M.; Asther, M.; Lesage-Meessen, L. Fungal enzymes as a powerful tool to release simple phenolic compounds from olive oil byproduct. *Process Biochem.* **2005**, *40*, 1855−1862.

(7) Fernández-Bolaños, J.; Rodríguez, G.; Gómez, E.; Guillén, R.; Jiménez, A.; Heredia, A.; Rodríguez, R. Total recovery of the waste of two-phase olive oil processing: Isolation of added-value compounds. *J. Agric. Food Chem.* **2004**, *52*, 5849−5855.

(8) Cardoso, A. M.; Coimbra, M. A.; Da Silva, J. A. L. Calcium-mediated gelation of an olive pomace pectic extract. *Carbohydr. Polym.* **2003**, *52*, 125−133.

(9) Garcia-Granados, A. *Preparation of mannitol and its derivatives from branches, leaves, juice, and peduncles of olives*. Spanish Patent 2056745, 1994.

(10) Calero, J.; Martínez, L.; Garcia-Granados, A. *Countercurrent extraction process for recovering acids, phenols, alcohols, and their derivatives, from olive-pressing waste*. Spanish Patent 2051238, 1994.

(11) Sanchez-Quesada, C.; Lopez-Biedma, A.; Warleta, F.; Campos, M.; Beltran, G.; Gaforio, J. J. Bioactive properties of the main triterpenes found in olives, virgin olive oil, and leaves of *Olea europaea*. *J. Agric. Food Chem.* **2013**, *61*, 12173−12182.

(12) Garcia-Granados, A. *Process for the industrial recovery of oleanolic and maslinic acids contained in the olive milling subproducts*. PCT Int. Appl. 9804331, 1998.

(13) Parra, A.; López, P. E.; Garcia-Granados, A. Bioactive compounds with added value prepared from terpenes contained in solid wastes from the olive-oil industry. *Chem. Biodivers.* **2010**, *7*, 421−439.

(14) Salvador, J. A. R.; Leal, A. S.; Alho, D. P. S.; Goncalves, B. M. F.; Valdeira, A. S.; Mendes, V. I. S.; Jing, Y. Highlights of pentacyclic triterpenoids in the cancer settings. *Stud. Nat. Prod. Chem.* **2014**, *41*, 33−73.

(15) Parikh, N. R.; Mandal, A.; Bhatia, D.; Siveen, K. S.; Sethi, G.; Bishayee, A. Oleanane triterpenoids in the prevention and therapy of breast cancer: Current evidence and future perspectives. *Phytochem. Rev.* **2014**, *13*, 793−810.

(16) Wolska, K. I.; Grudniak, A. M.; Fiecek, B.; Kraczkiewicz-Dowjat, A.; Kurek, A. Antibacterial activity of oleanolic and ursolic acids and their derivatives. *Cent. Eur. J. Biol.* **2010**, *5*, 543−553.

(17) Fernandez-Navarro, M.; Peragon, J.; Esteban, F. J.; Amores, V.; de la Higuera, M.; Lupianez, J. A. Maslinic acid: A component of olive oil on growth and protein-turnover rates. In *Olives and Olive Oil in Health and Disease Prevention*; Preedy, V. R., Watson, R. R., Eds.; Elsevier: London, 2010; pp 1415−1421.

(18) Rodriguez-Rodriguez, R.; Ruiz-Gutierrez, V. Vasorelaxant effects of oleanolic acid and erythrodiol in pomace olive oil. In *Olives and Olive Oil in Health and Disease Prevention*; Preedy, V. R., Watson, R. R., Eds.; Elsevier: London, 2010; pp 813−820.

(19) Ikeda, Y.; Murakami, A.; Ohigashi, H. Ursolic acid: An anti- and pro-inflammatory triterpenoid. *Mol. Nutr. Food Res.* **2008**, *52*, 26−42.

(20) Sultana, N.; Ata, A. Oleanolic acid and related derivatives as medicinally important compounds. *J. Enzyme Inhib. Med. Chem.* **2008**, *23*, 739−756.

(21) Zhang, S.; Sun, Y.; Sun, Z.; Wang, X.; You, J.; Suo, Y. Determination of triterpenic acids in fruits by a novel high performance liquid chromatography method with high sensitivity and specificity. *Food Chem.* **2014**, *146*, 264−269.

(22) Hao, Y.; Chen, X.; Hu, S.; Bai, X. Solvent bar microextraction with HPLC for determination and protein-binding characteristics of oleanolic acid and ursolic acid. *Chromatographia* **2014**, *77*, 359−363.

(23) Wójciak-Kosior, M.; Sowa, I.; Kocjan, R.; Nowak, R. Effect of different extraction techniques on quantification of oleanolic and ursolic acid in *Lamii albi flos*. *Ind. Crops Prod.* **2013**, *44*, 373−377.

(24) Xu, H.; Shi, X. W.; Ji, X.; Du, Y.; Zhu, H.; Zhang, L. A rapid method for simultaneous determination of triterpenoid saponins in *Pulsatilla turczaninovii* using microwave-assisted extraction and high performance liquid chromatography−tandem mass spectrometry. *Food Chem.* **2012**, *135*, 251−258.

(25) Pollier, J.; Goossens, A. Oleanolic acid. *Phytochem.* **2012**, *77*, 10−15.

(26) Li, G. L.; You, J. M.; Song, C. H.; Xia, L.; Zheng, J.; Suo, Y. R. Development of a new HPLC method with precolumn fluorescent derivatization for rapid, selective, and sensitive detection of triterpenic acids in fruits. *J. Agric. Food Chem.* **2011**, *59*, 2972−2979.

(27) Guo, S.; Duan, J.; Tang, Y.; Qian, Y.; Zhao, J.; Qian, D.; Su, S.; Shang, E. Simultaneous qualitative and quantitative analysis of triterpenic acids, saponins, and flavonoids in the leaves of two *Ziziphus* species by HPLC−PDA−MS/ELSD. *J. Pharm. Biomed. Anal.* **2011**, *56*, 264−270.

(28) Sánchez-Ávila, N.; Priego-Capote, F.; Ruiz-Jiménez, J.; Luque de Castro, M. D. Fast and selective determination of triterpenic compounds in olive leaves by liquid chromatography−tandem mass spectrometry with multiple reaction monitoring after microwave-assisted extraction. *Talanta* **2009**, *78*, 40−48.

(29) Goulas, V.; Manganaris, G. A. Towards an efficient protocol for the determination of triterpenic acids in olive fruit: A comparative study of drying and extraction methods. *Phytochem. Anal.* **2011**, *23*, 444−449.

DOI: 10.1021/jf506171y
J. Agric. Food Chem. 2015, 63, 4269−4275

(30) Romero, C.; García, A.; Medina, E.; Ruíz-Méndez, M. V.; de Castro, A.; Brenes, M. Triterpenic acids in table olives. *Food Chem.* **2010**, *118*, 670−674.
(31) Guinda, A.; Rada, M.; Delgado, T.; Gutierrez-Adánez, P.; Castellano, J. M. Pentacyclic triterpenoids from olive fruit and leaf. *J. Agric. Food Chem.* **2010**, *58*, 9658−9691.
(32) Parra, A.; Rivas, F.; López, P. E.; Garcia-Granados, A.; Martinez, A.; Albericio, F.; Marquez, N.; Muñoz, E. Solution- and solid-phase synthesis and anti-HIV activity of maslinic acid derivatives containing amino acids and peptides. *Bioorg. Med. Chem.* **2009**, *17*, 1139−1145.
(33) Tarvainen, M.; Suomela, J. P.; Kallio, H.; Yang, B. Triterpenic acids in *Plantago major*: Identification, quantification, and comparison of different extraction methods. *Chromatographia* **2010**, *71*, 279−284.

DOI: 10.1021/jf506171y
J. Agric. Food Chem. 2015, 63, 4269−4275

MATERIALS AND METHODS

Chemicals. Rotundone ((3*S*,5*R*,8*S*)-3,4,5,6,7,8-hexahydro-3,8-dimethyl-5-(prop-1-en-2-yl)-1(2*H*)-azulenone) and $^{2}H_{5}$-rotundone was synthesized as described previously.[2,3] Working solutions of standards were prepared volumetrically in ethanol and stored at 4 °C until required. High-performance liquid chromatography (HPLC)-gradient-grade ethyl acetate, *n*-pentane, methanol, and ethanol were obtained from Rowe Scientific (Doveton, Victoria, Australia). Analytical-reagent-grade potassium L-tartrate monobasic, tartaric acid, and other chemicals were obtained from Sigma-Aldrich (Castile Hill, New South Wales, Australia). Water was purified by the Milli-Q system (Millipore Australia, Bayswater, Victoria, Australia).

Vineyard Site. The study was conducted in a commercial vineyard (The Old Block, Mount Langi Ghiran, 37.31° S, 143.15° E) located in the Grampians wine region of Victoria, Australia. The vineyard is approximately 15.5 km east of the nearest Bureau of Meteorology (BOM) weather station at Ararat Prison (Australian BOM Station 089085), where the long-term mean January temperature is 18.9 °C and annual average rainfall is 587.9 mm, and is classified as a cool-climate production region.[13] The vineyard was planted in 1968 with *Vitis vinifera*, cv. Shiraz on its own roots at 3.0 m between rows and 1.8 m between vines, with rows oriented northeast to southwest. Grapevines are trained to a vertical shooting positioning trellis (VSP). Grapevines are irrigated using drip irrigation when required at a rate of 5.76 L h^{-1} $vine^{-1}$. Weather conditions and irrigation volume for both studied seasons are included in the Supporting Information. No significant pest or disease pressures were observed during the experimental seasons.

Experimental Design and Sampling. The experimental block has been previously divided into three vineyard zones based on plant cell density (PCD), electrical soil conductivity, and slope using the *k*-mean clustering tool. PCD is the ratio of reflected infrared to red light and has been used as a surrogate measure of vine vigor.[11] The values are provided for zone 1 (104, 63.5 mS/m, and 8.3%), zone 2 (174, 45.6 mS/m, and 5.9%), and zone 3 (134, 53.1 mS/m, and 3.4%) for mean PCD, electrical soil conductivity, and slope, respectively (Figure 1A).[11] The three identified zones have different aspects, with zone 1 having a northern aspect, most of zone 2 having a southern aspect, and zone 3 being located along the ridge, having all four aspects (Figure 1B). In the southern hemisphere, a northerly aspect has the highest amount of sunlight exposure. Separating the vineyard into these zones is important to assess the involvement of vine vigor, vineyard soil conductivity, and topography on rotundone accumulation in Shiraz grapes.

Within-Vineyard Variability of Rotundone. Five random field replicates were selected and georeferenced from each of the three vineyard zones (described previously in the study by Scarlett et al.[11]) as the sampling points for bunches (Figure 1A). Each replicate consisted of six vines each distributed in two adjacent rows (three vines in each row). Bunches were sampled from the northwest side of canopies at the time near commercial harvest in two continuous seasons (2011−2012 and 2012−2013) on April 5, 2012 and April 10, 2013, respectively. Commercial harvest was performed between April 11 and 18, 2012 and between April 9 and 16, 2013 with selective hand-harvest first, followed by machine harvest at the later dates. Three bunches of grapes were sampled from each selected grapevine in zip-lock plastic bags, frozen at −20 °C, transferred to the University of Melbourne laboratories in styrofoam boxes on dry ice, and stored at −20 °C before conducting bunch sectorization and laboratory analysis detailed in the within-bunch variability study below. The rotundone concentration in grapes has previously been reported to be stable under normal ambient temperature conditions.[4]

Within-Vine Variability of Rotundone. To assess within-vine variability, shading treatments were applied on three adjacent rows in zone 1 (Figure 1A). This design was chosen to minimize variation between vines because large within-vineyard variation in the berry rotundone concentration was previously reported for this experimental block by Scarlett et al.[11] Within these three rows, four replicates (blocks of six vines each) were separated by six vines as buffers and

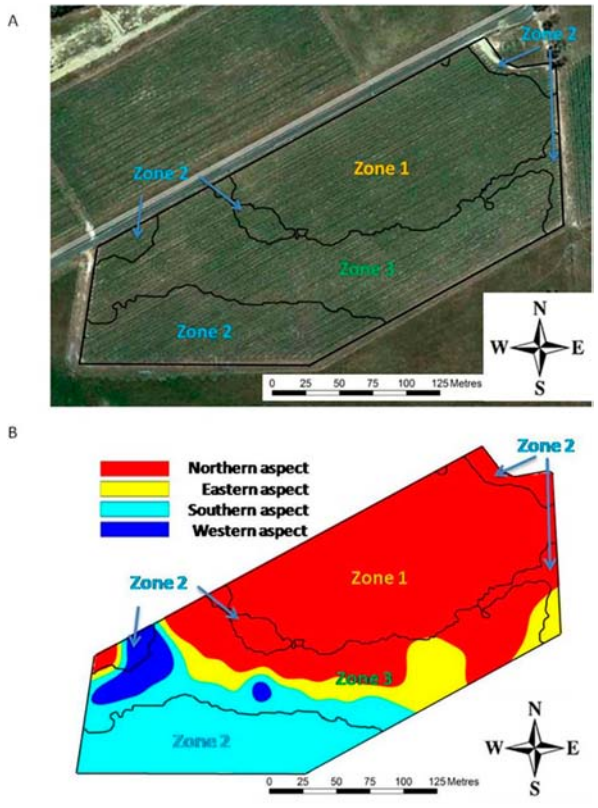

Figure 1. Vineyard zones of the experimental Shiraz block at Mount Langi Ghiran in the Grampians wine region of Victoria, Australia: (A) three vineyard zones previously established by Scarlett et al.[11] and (B) variation in the aspect of the experimental block, generated on the basis of the study by Scarlett et al.[11]

were randomly distributed for each of the following artificial shading treatments for the 2012−2013 growing season: (i) naturally occurring shade [control (Ctrl)], (ii) fruit zone shaded vines from veraison to harvest (FS), and (iii) whole vine shaded from veraison to harvest (WS). Artificial shading was achieved using commercial shade cloth, which is ultraviolet (UV)-stabilized high-density polyethylene (HDPE) shade cloth blocking 56.94% of light and 59.83% of UV (Coolaroo, Gale Pacific, Ltd., Australia).

Within individual vines, grape bunches on two sides of the vineyard row were considered as separated groups because of differing degrees of incident solar exposure. For the FS treatment, the shade cloth was cut into 0.4 m widths and placed on both sides of the fruit zone. For the WS treatment, the whole vine was shaded with the shading cloth (see panels A and B of Figure S1 of the Supporting Information). Sampling was performed at commercial harvest (April 10, 2013). Grape bunches from both sides of the canopy wall were sampled separately. Samples from the northwest-facing side of Ctrl, FS, and WS were labeled as Ctrl-NW, FS-NW, and WS-NW, while samples from the southeast-facing side were labeled as Ctrl-SE, FS-SE, and WS-SE. Three bunches of grapes were sampled from each selected grapevine in zip-lock plastic bags, frozen at −20 °C, transferred to the laboratory in styrofoam boxes on dry ice, and stored at −20 °C before analysis. Total soluble solids (TSS), titratable acidity (TA), and pH of the grape samples were analyzed using a refractometer, an alkaline titration, and a pH meter, following published protocols.[14]

To monitor the fruit zone temperature on both sides of the canopy walls, temperature loggers (Tinytag transit 2, Gemini Data Logger, Ltd., Chichester, U.K.) were placed next to grape bunches on both sides of the canopy for each treatment group, and six temperature loggers were used in total. The loggers were shaded by bunch zone leaves to minimize direct solar exposure. These loggers have an operational range from −40 to 70 °C, with a sensitivity of 0.01 °C.

DOI: 10.1021/acs.jafc.5b00590
J. Agric. Food Chem. 2015, 63, 4276−4283

The temperature was measured every 30 min from veraison (early February) to harvest, and the data recorded were analyzed with Tinytag Explorer software (version 4.7, Gemini Data Logger, Ltd., Chichester, U.K.), following the method described by Winter et al.[15] Fruit zone temperature overtime was calculated as degree hours and reflected the heat accumulated in the fruit zone. Degree hours in different temperature ranges and their percentage to the total degree hours were calculated and associated with the rotundone concentration of grape berries.

Within-Bunch Variability of Rotundone. Grape bunches from the within-vineyard variability study were also used for the within-bunch variability study. All berries from each representative bunch collected were divided into four sectors: top front (TF), top back (TB), bottom front (BF), and bottom back (BB), dependent upon their position in the bunch and bunch orientation in relation to incident solar radiation (Figure 2A). The *X* and *Y* axes in Figure 2A represented the direction of sunlight and vineyard row, respectively. TF and BF sectors were the directly exposed solar side of the bunch, while the TB and BB sectors were shaded. Grape bunches were divided into top and bottom parts with a length ratio of 4:6 to balance the weight of both parts (Figure 2B). Sectorized berry samples were collected in zip-lock plastic bags and stored at −20 °C before conducting laboratory analysis. TSS, TA, pH, total anthocyanins, and total phenolics of bunch samples were analyzed using a refractometer, an alkaline titration, a pH meter, and spectrophotometric measurements at $A_{520\ nm}$ and $A_{280\ nm}$, following published protocols.[14]

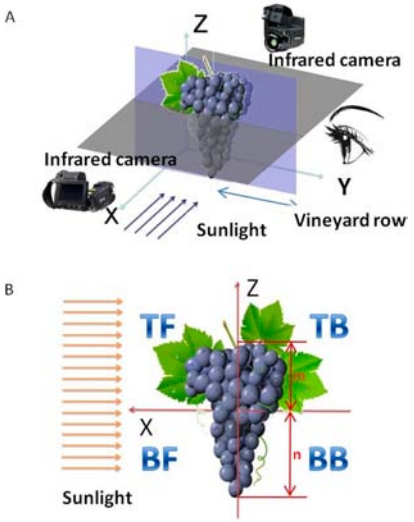

Figure 2. Illustration of grape bunch separation and surface temperature measurement of the within-bunch study: (A) separation of the grape bunch based on the direction of sunlight and vineyard row, with the grape bunch surface temperature being obtained by taking thermal images on both sides of the grape bunch, and (B) separation of the grape bunch into top and bottom parts based on the ratio of the distance between end points of the bunch to separating point (m/n = 4:6).

Infrared thermal images were obtained to assess the variability of berry surface temperatures and distribution within grape bunches from 24 randomly selected vines in the vineyard. The camera had a 0.3 megapixel (640 × 480) microbolometer sensor, sensitive in the temperature range from −40 to 2000 °C, with the thermal sensitivity of 0.04 °C, and a lens with an angular field of view of 25° (T640 model, FLIR System, Inc., Notting Hill, Australia). Thermal images were obtained between 15:30 and 16:00 h (Australian Eastern Daylight Time) on March 26, 2013 from both sides of the row with a distance of approximately 1 m between sampled bunches and the camera (Figure. 3A). Thermal images were processed using the FLIR ResearchIR software (FLIR System, Inc., Notting Hill, Australia). Maximum, minimum, and average surface temperatures of the top and bottom parts of the bunch were analyzed separately, selecting regions of interest manually using the FLIR software.

Preparation of Samples and Solid-Phase Microextraction–Gas Chromatography–Mass Spectrometry (SPME–GC–MS) Analysis of Rotundone. Grape samples were prepared for rotundone analysis based on the protocol described by Siebert et al.[2] Briefly, 100 g of destemmed grapes were sub-sampled before being homogenized using a hand-held blender. Sub-samples were centrifuged to separate the juice and solid parts. The solid parts were mixed with 30 mL of ethanol, 30 mL of water, and 100 μL of d_5-rotundone (516 ng/mL in ethanol) as the internal standard, then shaken for 24 h at 22 °C, and sonicated before adding the juice back. Sub-samples were then centrifuged (10 000 rpm for 20 min at 22 °C) and filtrated (1.6 μm glass fiber) to obtain berry extract filtrate, which was topped up to 200 mL with Milli-Q deionized water before subjected to solid-phase extraction (SPE), performed as reported previously.[2] The SPE residue supernatant collected was dried with nitrogen and reconstituted in 0.5 mL of ethanol and 9 mL of Milli-Q deionized water. The sample was then analyzed and quantified at the Australian Wine Research Institute using a published SPME–GC–MS protocol.[16]

Statistical Analysis. The rotundone concentration, TSS, pH, and TA of the within-vine study samples were analyzed using one-way analysis of variance (ANOVA) at $p < 0.05$ (CoStat, version 6.4, CoHort Software, Monterey, CA). The relationship between the percentage of degree hours under the canopy and the grape rotundone concentration was calculated using MatLab software 2014a (The MathWorks, Inc., Natick, MA). The berry surface temperature, rotundone concentration, TSS, pH, TA, total anthocyanins, and total phenolics of the within-bunch study samples were analyzed using one-way and two-way ANOVA at $p < 0.05$ (CoStat, version 6.4, CoHort Software, Monterey, CA). Data were graphed into a spider plot using MatLab software 2014a (The MathWorks, Inc., Natick, MA).

RESULTS AND DISCUSSION

In this study, we examined the berry rotundone concentration and other grape quality parameters as a function of the berry exposure and berry surface and bunch zone temperature over two growing seasons. Distinct within-vineyard, within-vine, and within-bunch variabilities have been observed in rotundone and other key grape quality attributes in this study. Dissection of the vineyard into distinctly different zones (as per Scarlett et al.[11]), vines into sides based on sunlight orientation, and grape bunches into sectors based on exposure to solar radiation has allowed for the influence of vine vigor, sunlight, and temperature to be considered for berry compositional parameters, including rotundone. Vineyard topography, vine vigor, vine orientation, and bunch orientation together influence grape berry surface/bunch zone temperature and, therefore, can influence grape quality parameters.

Within-Vineyard Variability of Rotundone. The differences in grape quality trait parameters and rotundone concentration between experimental vineyard zones in the 2011–2012 and 2012–2013 growing seasons were examined by two-way ANOVA ($p < 0.01$) (panels A and B of Figure 3). Overall, Shiraz grapes from zone 1 had a significantly lower concentration of rotundone (118.2 ng/kg) compared to zone 2 (196.9 ng/kg) and zone 3 (233.9 ng/kg), while the 2011–2012 growing season had a significantly higher concentration of rotundone overall (346.8 ng/kg) compared to the 2012–2013 growing season (19.2 ng/kg). In the 2011–2012 growing season, the rotundone concentration of Shiraz grapes from zone 2 (373.8 ng/kg) and zone 3 (447.3 ng/kg) was significantly higher compared to zone 1 (219.4 ng/kg) (Figure 3C). However, no statistical significant differences in rotundone were observed among vineyard zones in the 2012–2013 growing season (Figure 3D).

DOI: 10.1021/acs.jafc.5b00590
J. Agric. Food Chem. 2015, 63, 4276–4283

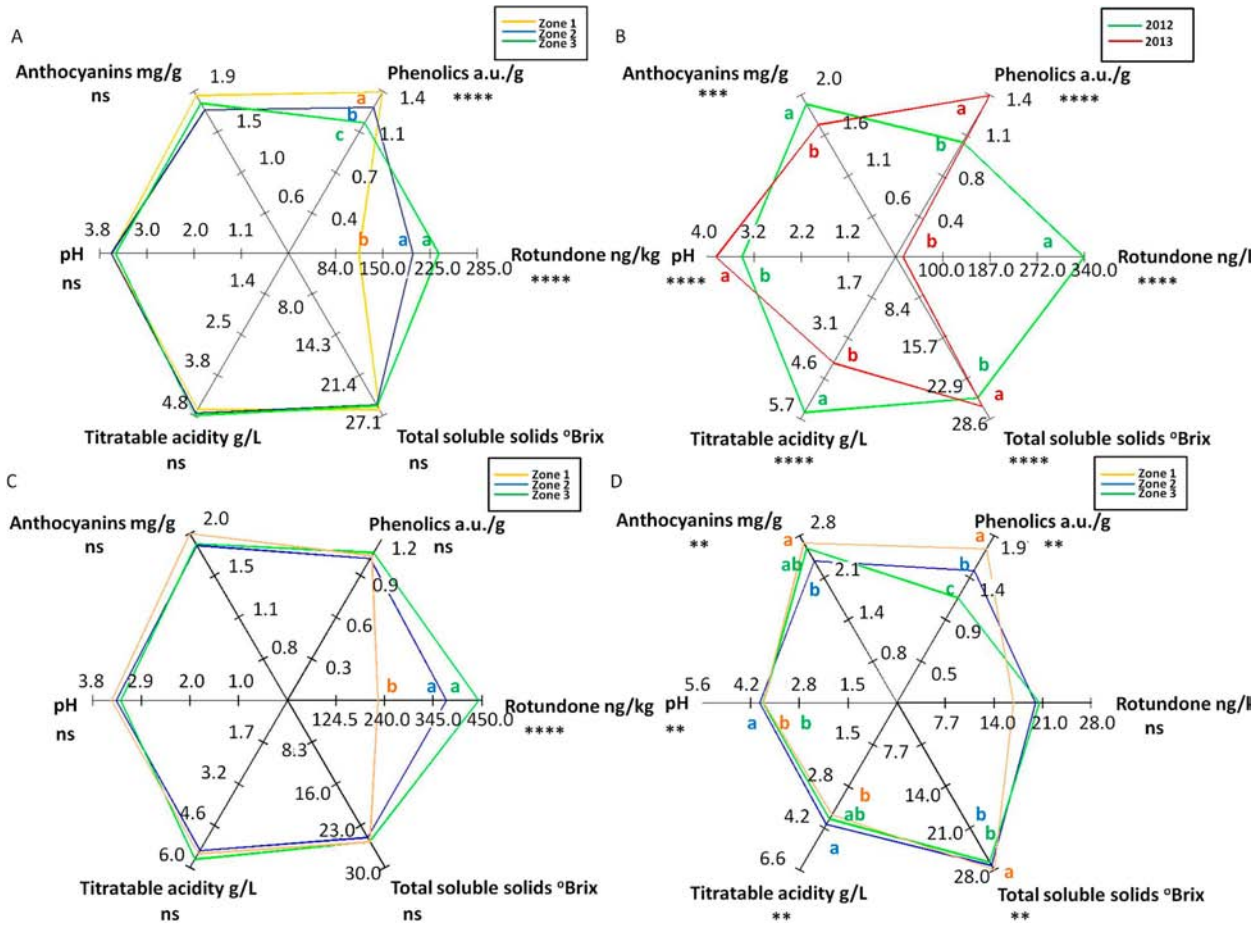

Figure 3. Comparison of the rotundone concentration and quality parameters among vineyard zones in the 2011−2012 and 2012−2013 growing seasons. Two-way ANOVA was conducted considering (A) vineyard zones and (B) growing seasons as two ANOVA independent variables for each quality parameter, while one-way ANOVA was conducted to compare each quality parameter among three zones in individual growing season (C) 2011−2012 and (D) 2012−2013, where ns, *, **, ***, and **** stand for no significant difference, no significant difference but $0.5 \leq p < 0.1$, $p < 0.05$, $p < 0.01$, and $p < 0.001$, respectively. a, b, and c were used to label the differences between experimental groups.

The differences in the grape rotundone concentration between three vineyard zones were associated with variations in vine vigor and, therefore, natural shading. Although vine vigor of the experimental block was measured in 2012, it has been proven to be relatively stable across different growing seasons.[17] The high vigor areas (zones 2 and 3) (Figure 1A, with a PCD index of zone 2 of 174 and zone 3 of 134) had more canopy coverage, mainly a southern, eastern, and western aspect (Figure 1B), and therefore, more natural bunch shading, receiving less direct solar radiation and, as a consequence, a relatively lower bunch zone/surface temperature compared to zone 1 (PCD index of zone 1 of 104), which were associated with the higher grape rotundone concentrations observed in zones 2 and 3, particularly in the 2011−2012 growing season (panels A and C of Figure 3). In the 2012−2013 growing season, where the temperature and solar exposure from veraison to harvest was high, the bunch zone temperature and surface temperatures under shading could still be too high for rotundone accumulation. As a result, no significant differences in the grape rotundone concentration were observed between grape samples from the three vineyard zones (zone 1, 17.0 ng/kg; zone 2, 20.5 ng/kg; and zone 3, 20.0 ng/kg) in the 2012−2013 growing season.

Large differences in the rotundone concentration were observed between the two studied growing seasons (2011−2012 and 2012−2013) (Figure 3B). The variation in the rotundone concentration between the two studied seasons (18-fold) is higher than the differences among vineyard zones (2-fold), the differences between shading treatments (1.7-fold), and the differences among bunch sectors (2-fold). This may be due to the large differences in weather patterns from veraison to harvest between the two studied seasons because rotundone mainly accumulates post-veraison.[16] The 2012−2013 growing season has a higher mean ambient temperature (18.9 °C) and mean solar exposure (18.1 MJ/m^2) from veraison to harvest but a lower total water precipitation (rainfall + irrigation) (208.4 mm) compared to the 2011−2012 growing season (16.7 °C, 16.1 MJ/m^2, and 259.8 mm). Higher temperatures in the 2012−2013 growing season led to higher evaporation and, therefore, more water loss.[18] As a result, higher water deficiency in the 2012−2013 growing season may have decreased vine vigor and natural shading and, therefore, increased the berry surface temperature to influence the grape rotundone concentration. Importantly, the zones and vines that showed high rotundone in the 2011−2012 growing season also show high rotundone in the (lower rotundone overall) 2012−2013 growing season. Thus, the factors contributing to the high or low rotundone accumulation between seasons is constant, despite the overall averages being different in the two seasons studied.

DOI: 10.1021/acs.jafc.5b00590
J. Agric. Food Chem. 2015, 63, 4276−4283

Table 1. Comparison of the Rotundone Concentration and Grape Quality Parameters within-Vines in the 2012−2013 Growing Season Using Two-Way ANOVA Analysis ($p < 0.05$)

two-way ANOVA	sample group	rotundone (ng/kg)	TSS[a] (°Brix)	pH	TA[b] (g/L)	Dh_{25}[c]
	Ctrl-NW[d]	22.5 ± 6.7	28.3 ± 1.7	3.86 ± 0.14	3.69 ± 0.11	13.7
	Ctrl-SE	34.6 ± 13.3	28.0 ± 2.1	3.87 ± 0.09	3.79 ± 0.11	8.8
	FS-NW	20.4 ± 1.6	27.9 ± 1.1	3.88 ± 0.09	3.85 ± 0.09	10.3
	FS-SE	33.0 ± 10.1	27.4 ± 1.5	3.80 ± 0.12	4.13 ± 0.21	6.6
	WS-NW	28.8 ± 7.8	26.0 ± 1.0	3.87 ± 0.08	3.90 ± 0.22	7.5
	WS-SE	37.9 ± 12.8	25.6 ± 0.3	3.83 ± 0.10	4.14 ± 0.19	6.9
factor 1 treatment groups	mean Ctrl	29.4 ± 12.0 ns[e]	28.1 ± 1.8 a[f]	3.86 ± 0.11 ns	3.74 ± 0.12 a	n/a[g]
	mean FS	26.7 ± 9.5 ns	27.6 ± 1.2 a	3.84 ± 0.10 ns	3.99 ± 0.21 b	n/a
	mean WS	33.3 ± 11.0 ns	25.8 ± 0.7 b	3.85 ± 0.09 ns	4.02 ± 0.23 b	n/a
factor 2 vine orientation	mean NW	24.4 ± 6.8 A	27.4 ± 1.5 ns	3.87 ± 0.10 ns	3.81 ± 0.17 A	n/a
	mean SE	35.4 ± 11.3 B	27.0 ± 1.7 ns	3.83 ± 0.10 ns	4.02 ± 0.23 B	n/a

[a]TSS = total soluble solids. [b]TA = titratable acidity as tartaric acid equivalents. [c]Dh_{25} = percentage of degree hours above 25 °C. [d]Ctrl, control; FS, fruit zone shading; WS, whole vine shading; NW, samples from the northwest side of the canopy; and SE, samples from the southeast side of the canopy. [e]ns = no significant difference ($p < 0.05$). [f]a, b, c, and d represent significant differences ($p < 0.05$) between treatment groups, while A and B represent significant differences ($p < 0.05$) between two sides of the vine. [g]n/a = not applicable.

Differences in grape quality trait parameters were observed among vineyard zones and between study seasons. Overall, significant differences were only observed in the total phenolics among the three zones (Figure 3A). Grapes from the 2012−2013 growing season had significantly higher total phenolics (1.45 au/g), pH (3.89), and TSS (27.0 °Brix) and lower total anthocyanins (1.68 mg/g) and TA (3.91 g/L) compared to the 2011−2012 growing season (1.06 au/g, 3.35, 25.6 °Brix, 1.93 mg/g, and 5.61 g/L) (Figure 3B). The differences in grape quality parameters between vineyard zones were further compared in individual seasons (panels C and D of Figure 3). In the 2011−2012 growing season, no significant differences in grape quality parameters were observed among the three zones (Figure 3C). In the 2012−2013 growing season, zone 1 had significantly higher total anthocyanins, total phenolics, and TSS and lower TA compared to zone 2, while grapes from zone 3 had intermediate levels of most grape quality parameters (Figure 3D).

Within-Vine Variability of Rotundone. A range of grape quality parameters and rotundone concentration were compared between the artificial shading treatments and two sides of the vine canopy (two-way ANOVA; $p < 0.05$) (Table 1). No significant differences were observed between shade treatment groups in the rotundone concentration, while berries from the SE side of the canopy had a significantly higher rotundone concentration compared to those from the NW side. WS treatments had significantly lower TSS (25.8 °Brix) compared to Ctrl (28.1 °Brix) and FS (27.6 °Brix) treatments, while no significant differences were observed between two sides of the canopy in TSS. Ctrl treatments had significantly lower TA (3.74) compared to the FS (3.99) and WS (4.02) treatments, while the NW side (3.81) of the canopy has significantly lower TA compared to the SE side (4.02). No significant differences were observed between artificial shading treatments and two sides of the canopy in pH.

The relationship between rotundone and the fruit zone temperature was explored. The fruit zone temperature over time was calculated as degree hours. Degree hours in different temperature ranges and their percentages to the total degree hours were calculated and associated with the rotundone concentration of grape berries. Percentages of degree hours in different temperature ranges higher than 25 °C (above 35 °C, between 30 and 35 °C, and between 25 and 30 °C) were found to have negative relationships with the grape rotundone concentration (details in the Supporting Information). Therefore, the percentage of degree hours above 25 °C (Dh_{25}) was used to analyze the relationship between the fruit zone temperature and the grape rotundone concentration (Table 1), which was explored in Figure 4. A power curve between the grape rotundone concentration and the percentage of degree hours above 25 °C [$y = 130.6x^{-0.696}$; $R^2 = 0.61$; root-mean-square error (RMSE) = 4.87; and $p = 0.065$] was established. Thus, a higher percentage of degree hours in a temperature range above 25 °C lead to a lower rotundone concentration in the berry.

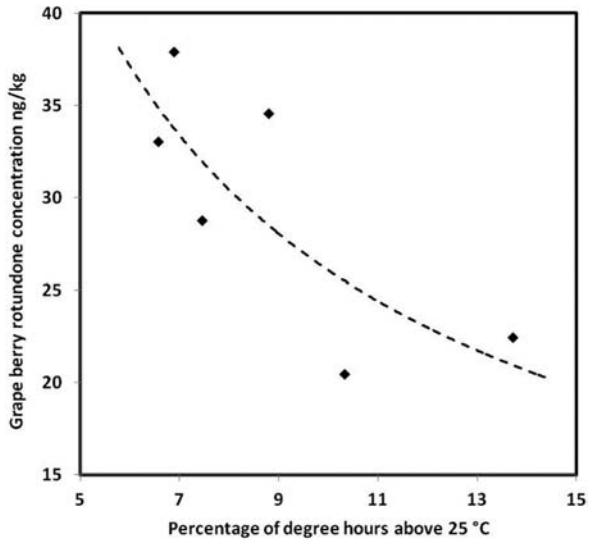

Figure 4. Relationship between the rotundone concentration and the percentage of degree hours above 25 °C in fruit zone from veraison to harvest in the 2012−2013 growing season. The equation for the trend lines is $y = 130.6x^{-0.696}$ ($R^2 = 0.61$; RMSE = 4.87; and $p = 0.065$).

The higher rotundone concentrations of berries located in the shaded side of the rows were associated with lower bunch zone/surface temperature. Because rotundone is found only in the skin of the Shiraz berries[9] and sesquiterpene biosynthesis occurs mainly in the berry skin,[8] this study indicates that the temperature/solar interception of grape berry skins is critical to

DOI: 10.1021/acs.jafc.5b00590
J. Agric. Food Chem. 2015, 63, 4276−4283

rotundone accumulation. No significant differences in the concentration of rotundone in grapes were observed among artificial shading treatments (Table 1), likely because of the large variation in the concentration of rotundone among vines. Another possible explanation is that the actual bunch zone solar radiation/temperature is determined not only by the artificial shading but also the natural canopy, which cause more variations in the actual light intensity in the canopy. Therefore, a better way to assess the impacts of shading is to directly study the relationship between the actual bunch zone temperature and the concentration of rotundone in grapes (Figure 4). While the relationship established in Figure 4 ($y = 130.6x^{-0.696}$; $R^2 = 0.61$; and RMSE = 4.87) was not statistically significant ($p = 0.065$), likely because of the small sample size ($n = 6$ shading levels) and large variation in the concentration of rotundone, the data nevertheless suggest the importance of the daytime bunch zone temperature on the concentration of rotundone in berries. Thus, increasing the duration of bunch zone temperatures higher than 25 °C will result in a lower concentration of rotundone in grapes. The impacts of sunlight on grapevine can be separated into direct illumination and indirect solar-radiation-induced temperature increases, which should be investigated separately to test their importance for the accumulation of rotundone in grapes.

Within-Bunch Variability of Rotundone. Grape berry surface temperature data of both the forward and backward sides of the bunch were obtained from thermal images (Figure 2A) taken on March 26, 2013 between 3:30 pm and 4:00 pm, with a mean bunch zone air temperature of 31.4 °C recorded in the vineyard during this period. Grape berry surface temperature data had a wide range, from 30.6 to 42.9 °C with a coefficient of variation (CV) of 8.09% for the maximum surface temperature, from 29.3 to 35.9 °C with CV of 4.57% for the minimum surface temperature, and from 30.05 to 39.05 °C with CV of 6.14% for the average surface temperature (Table 2). As expected, the sun-facing TF and BF sectors of the bunch had significantly higher maximum, minimum, and average surface temperatures than backward-orientated TB and BB sectors (Table 2).

Table 2. Comparison of the Grape Berry Surface Temperature among Four Bunch Sectors in the 2012−2013 Growing Season[a]

within-bunch sectors	grape surface temperature (°C)		
	average	maximum	minimum
TF[b]	34.74 ± 1.84 a[c]	37.11 ± 2.58 a	32.36 ± 1.38 a
TB	32.26 ± 1.44 b	33.27 ± 1.59 b	31.24 ± 1.37 b
BF	34.90 ± 1.88 a	37.13 ± 2.68 a	32.68 ± 1.26 a
BB	32.70 ± 1.64 b	33.79 ± 1.91 b	31.60 ± 1.42 b
overall range	30.05−39.05	30.60−42.90	29.30−35.90
mean (CV[d])	33.65 (6.14%)	35.32 (8.09%)	31.97 (4.57%)

[a]The average surface temperature was calculated by taking the average of maximum and minimum temperatures. [b]TF, top front sector of the bunch; TB, top back sector of the bunch; BF, bottom front sector of the bunch; and BB, bottom back sector of the bunch. [c]a, b, c, and d represent significant differences ($p < 0.05$) between bunch sectors. [d]CV = coefficient of variation.

In both seasons, the TB sector (2011−2012, 493.5 ng/kg; 2012−2013, 25.9 ng/kg) had a significantly higher concentration of rotundone compared to all other sectors ($p < 0.05$) (Table 3). In the 2011−2012 season, the TF sector (339.9 ng/kg) had a significantly higher concentration of rotundone compared to the BF sector (250.2 ng/kg) and the BB sector (303.7 ng/kg) tended to have a higher rotundone concentration compared to the BF sector ($p = 0.091$). No statistically significant differences were observed in the berry rotundone concentration between the TF and BB sectors. In the 2012−2013 growing season, the TF sector (19.2 ng/kg) had a higher concentration of rotundone compared to both BF (15.3 ng/kg) ($p = 0.068$) and BB (16.2 ng/kg) ($p = 0.057$). However, no differences were observed between the BB and BF sectors for berry rotundone concentration. The pattern of rotundone concentration distribution within bunch sectors was consistent across the two seasons.

Three possible reasons may explain the higher concentration of rotundone of berries from the top sectors of bunches (Table 3). First, the variation in the concentration of rotundone might reflect differences in grape surface temperatures because more shading from proximal leaves and/or the canopy and/or bunch architecture with a higher berry number within the top part of bunches could contribute to buffer the temperature of berries from these zones, lowering the surface temperature compared to fully exposed berries. On the contrary, the bottom part of bunches had less buffer capacity to maintain the temperature (in contact with fully exposed berries), which might explain higher temperatures in these sections (Table 2). Furthermore, the lower part of bunches is exposed to radiated transference of heat from the soil. Even though berry transpiration may lower the temperature of all berries, it cannot prevent the temperature increase caused by solar radiation. Therefore, the position of a berry in the bunch is crucial to its temperature, which is associated with its rotundone concentration. Notably, the position of a berry in the bunch might also result in increases in direct precursors to rotundone, such as guaiene, and increased concentrations in rotundone would then reflect the precursor concentrations. A second explanation is that the bottom sector of a bunch typically matures faster than the top sector.[19] The maximum rotundone concentration in grape berries is reached after veraison and slowly decreases afterward in the lead up to harvest.[16] As a result, a more mature bottom sector would have a lower rotundone concentration compared to the later ripening top sectors; i.e., rotundone concentrations would reflect the biochemical differences linked to a variation in maturity. A third possible explanation (the "transport theory") is that a shorter distance from berries to leaves and stems affects rotundone accumulation, because it has been reported that leaves and stems may contain higher concentrations of rotundone than berries and are potentially having a role as a source or storage.[7] This possibility requires an internal transportation mechanism for rotundone in grapevines. In other plant species, namely, *Asarina scandens* (Scrophulariaceae) and *Catalpa speciosa* (northern catalpa), it has been reported that monoterpene glycosides, antirrhinoside, and catalpol can be translocated via phloem transport.[20,21] However, translocation of aroma compounds has been studied in grapevines, with little evidence to show that it is a widespread phenomena. For example, translocation of monoterpene glycosides and their precursors from other parts of the vine into berries is unlikely in Muscat, unless an active transport mechanism exists for a specific compound.[22] In addition, the guaiacol glycosides can translocate between leaves and berries in Cabernet Sauvignon but to a very limited extent.[23] Therefore, there is a possibility that rotundone or a precursor,

DOI: 10.1021/acs.jafc.5b00590
J. Agric. Food Chem. 2015, 63, 4276−4283

Table 3. Comparison of the Rotundone Concentration and Grape Quality Parameters among Four Bunch Sectors in the 2011−2012 and 2012−2013 Growing Seasons Using One-Way ANOVA Analysis ($p < 0.05$)[a]

	2011−2012	2012−2013					
bunch sector	rotundone (ng/kg)	rotundone (ng/kg)	TSS[b] (°Brix)	pH	TA[c] (g/L)	anthocyanins (mg/g)	phenolics (au/g)
top front[d]	339.9 ± 149.5 b[e]	19.2 ± 6.5 b	27.0 ± 0.9 ab	3.94 ± 0.13 a	3.65 ± 0.37 a	1.64 ± 0.24 a	1.35 ± 0.30 a
top back	493.5 ± 186.2 a	25.9 ± 10.8 a	27.0 ± 1.0 ab	3.90 ± 0.11 b	3.98 ± 0.35 b	1.77 ± 0.27 b	1.58 ± 0.31 b
bottom front	250.2 ± 116.5 c	15.3 ± 5.6 b	26.8 ± 1.1 a	3.88 ± 0.13 b	3.89 ± 0.23 b	1.64 ± 0.25 a	1.40 ± 0.37 ab
bottom back	303.7 ± 120.3 bc	16.2 ± 4.7 b	27.1 ± 1.3 b	3.84 ± 0.13 c	4.14 ± 0.29 c	1.69 ± 0.24 ab	1.49 ± 0.37 ab

[a]Grape berry parameters were not collected in 2011−2012. [b]TSS = total soluble solids. [c]TA = titratable acidity. [d]Bunch sectors are illustrated in Figure 2. [e]a, b, c, and d represent significant differences ($p < 0.05$) between bunch sectors.

to some extent, may be formed elsewhere and is then translocated between berries, leaves, and stems, depending upon the availability of active transportation mechanisms, and this warrants further investigation.

In the 2012−2013 growing season, significant differences in grape quality parameters were observed (Table 3). Berries from the BF sector (26.8 °Brix) had slightly yet significantly lower TSS compared to the BB sector (27.1 °Brix). Berries from the solar exposed side of the bunch (TF and BF) had significantly lower TA and higher pH compared to their corresponding shaded side (TB and BB). In addition, berries from the TB sector had significantly higher total anthocyanins (1.77 mg/g) and total phenolics (1.58 au/g) compared to the bunch TF sector (1.64 mg/g and 1.35 au/g).

The differences in grape quality parameters between studied seasons and among vineyard zones, shading treatment groups, and bunch sectors are associated with berry surface temperature and solar radiation. Higher TSS has been shown with greater sunlight exposure and temperature and may explain the variances between studied seasons (Figure 3B), among vineyard zones (Figure 3D), shading treatments (Table 1), and bunch sectors (Table 3).[24,25] Higher temperatures stimulate respiration and modify organic acid metabolism, leading to decreased malate and citrate concentrations and, therefore, a likely decrease in TA and increase in pH.[26] As a result, berries from the warmer season (2012−2013) (Figure 3B) and the exposed sectors of bunch (Table 3) had higher pH and lower TA, while the unshaded treatment groups and the northwest side of the vine had lower TA (Table 1). A high temperature (>35 °C) has been shown to reduce the grape anthocyanin concentration, which explains the lower total anthocyanin concentration in the berries from the warmer season (2012−2013) (Figure 3B) and the exposed bunch sectors (Table 3).[27] However, moderate solar exposure increases anthocyanin concentration in grape berries, which explains the relatively higher concentration of total anthocyanins in berries from the low vigor zone (zone 1) (Figure 3D).[25,28] A previous study has demonstrated that the concentration of total phenolics increases gradually with increasing solar exposure and becomes relatively stable under higher solar exposure levels.[25] This is consistent with the higher total phenolics observed in the berries from the higher solar intensity season (2012−2013) and lower vigor zone (zone 1) (panels A, B, and D of Figure 3). However, the shaded bunch sectors tend to have higher total phenolics than the exposed sectors (Table 3), which may be due to degradation of certain phenolics under a higher temperature, such as anthocyanins.[27] In addition, grape quality parameters tend to be more sensitive at higher temperatures or solar exposure.[25,27] This could be the reason that differences in grape quality parameters among zones were only observed in the 2012−2013 growing season (panels C and D of Figure 3).

Fruit zone temperature and berry surface temperature are correlated with the concentration of rotundone in Shiraz grapes at this site. Vineyard topography, vine vigor, location of bunches within the vine, and bunch orientation to incident solar radiation also influence rotundone accumulation in Shiraz grapes. These factors affect the shading of grape berries and, therefore, adjust bunch surface and bunch zone temperatures. Sunlight interception and water availability may also influence rotundone production, which requires further investigation. Apart from climatic parameters, physiological parameters, such as the source−sink relationships between leave/stems and bunch in rotundone, may also influence its concentration in grape berries, which warrants further study. This study demonstrates the importance of the vine growing microenvironment and, specifically, the importance of the temperature on the formation of a key sesquiterpene compound responsible for wine aroma.

■ ASSOCIATED CONTENT

Ⓢ Supporting Information

Weather record of the vineyard in 2011−2012 and 2012−2013 seasons (Table S1), comparison of the grape berry rotundone concentration (ng/kg) and fruit zone temperature between two sides of the row with different degrees of shading (Table S2), illustrations of grapevine shading treatments in the 2012−2013 growing season (Figure S1), relationship between the percentage of degree hours in fruit zone from veraison to harvest and the mean rotundone concentration in grape samples from the within-vine variability study (Figure S2), and comparison of the rotundone concentration and quality parameters among within-bunch sectors in an individual vineyard zone in the 2012−2013 growing season (Figure S3). This material is available free of charge via the Internet at http://pubs.acs.org.

■ AUTHOR INFORMATION

Corresponding Author

*Telephone: +61-3-90353119. E-mail: khowell@unimelb.edu.au.

Funding

This work was jointly sponsored by the Rathbone Wine Group, the University of Melbourne, the Australian Wine Research Institute (AWRI), and the Australia Grape and Wine Authority. The work was performed at the University of Melbourne and AWRI and supported by Australia's grape growers and winemakers through their investment body, the Australia Grape and Wine Authority, with matching funds from the Australian Government. Funding was also received from the Faculty of Veterinary and Agricultural Sciences, University of Melbourne.

DOI: 10.1021/acs.jafc.5b00590
J. Agric. Food Chem. 2015, 63, 4276−4283

Notes

The authors declare no competing financial interest.

■ ACKNOWLEDGMENTS

The authors are most grateful to Dr. Tracey Siebert (AWRI) and Sheridan Barter (AWRI) for rotundone analysis and to Damien Sheehan (Rathbone Wine Group) for his support and assistance with the field trials.

■ ABBREVIATIONS USED

BOM, Bureau of Meteorology; VSP, vertical shooting positioning trellis; PCD, plant cell density; FS, fruit zone shaded; WS, whole vine shaded; NW, northwest facing side of the vine; SE, southeast facing side of the vine; TSS, total soluble solids; TA, titratable acidity; TF, top front sector of bunch; TB, top back sector of bunch; BF, bottom front sector of bunch; BB, bottom back sector of bunch; SPE, solid-phase extraction; au, absorbance units

■ REFERENCES

(1) Dunlevy, J. D.; Kalua, C. M.; Keyzers, R. A.; Boss, P. K. The production of flavour and aroma compounds in grape berries. In *Grapevine Molecular Physiology and Biotechnology*, 2nd ed.; Roubelakis-Angelakis, K. A., Eds.; Springer Science: New York, 2009; pp 293−340.

(2) Siebert, T. E.; Wood, C.; Elsey, G. M.; Pollnitz, A. P. Determination of rotundone, the pepper aroma impact compound, in grapes and wine. *J. Agric. Food Chem.* **2008**, *56*, 3745−3748.

(3) Wood, C.; Siebert, T. E.; Parker, M.; Capone, D. L.; Elsey, G. M.; Pollnitz, A. P.; Eggers, M.; Meier, M.; Vossing, T.; Widder, S.; Krammer, G.; Sefton, M. A.; Herderich, M. J. From wine to pepper: Rotundone, an obscure sesquiterpene, is a potent spicy aroma compound. *J. Agric. Food Chem.* **2008**, *56*, 3738−3744.

(4) Jeffery, D. W.; Siebert, T. E.; Capone, D. L.; Pardon, K. H.; Van Leeuwen, K. A.; Solomon, M. R. *Grape and Wine Pepper Aroma—Analytically Challenging but We Sniff It out in the End*; The Australian Wine Research Institute: Urrbrae, South Australia, Australia, 2009; Technical Review, Vol. *180*, pp 11−16.

(5) Willamson, P. O.; Robichaud, J.; Francis, I. L. Comparison of Chinese and Australian consumers' liking responses for red wines. *Aust. J. Grape Wine Res.* **2012**, *18*, 256−267.

(6) Herderich, M. J.; Siebert, T. E.; Parker, M.; Capone, D. L.; Jeffery, D. W.; Osidacz, P.; Francis, I. L. Spice up your life: Analysis of key aroma compounds in Shiraz. In *Flavor Chemistry of Wine and Other Alcoholic Beverages*; Qian, M. C., Shellhammer, T. H., Eds.; American Chemical Society (ACS): Washington, D.C., 2012; ACS Symposium Series, Vol. *1104*, Chapter 1, pp 3−13.

(7) Capone, D. L.; Jeffery, D. W.; Sefton, M. A. Vineyard and fermentation studies to elucidate the origin of 1,8-cineole in Australian red wine. *J. Agric. Food Chem.* **2012**, *60*, 2281−2287.

(8) May, B.; Lange, B. M.; Wüst, M. Biosynthesis of sesquiterpenes in grape berry exocarp of *Vitis vinifera* L.: Evidence for a transport of farnesyl diphosphate precursors from plastids to the cytosol. *Phytochemistry* **2013**, *95*, 135−144.

(9) Siebert, T. E.; Solomon, M. R. Rotundone: Development in the grape and extraction during fermentation. *Proceedings of the 14th Australian Wine Industry Technical Conference*; Adelaide, South Australia, Australia, July 3−8, 2010; pp 307−308.

(10) Huang, A.; Burrett, S.; Sefton, M. A.; Taylor, D. K. Production of the pepper aroma compound, (−)-rotundone, by aerial oxidation of α-guaiene. *J. Agric. Food Chem.* **2014**, *62*, 10809−10815.

(11) Scarlett, N. J.; Bramley, R. G. V.; Siebert, T. Within-vineyard variation in the 'pepper' compound rotundone is spatially structured and related to variation in the land underlying the vineyard. *Aust. J. Grape Wine Res.* **2014**, *20*, 214−222.

(12) Wilson, J. P.; Gallant, J. C. *Terrain Analysis—Principles and Applications*; John Wiley and Sons, Inc.: New York, 2000.

(13) Gladstones, J. S. Climate and Australian viticulture. In *Viticulture*, 2nd ed.; Dry, P. R., Coombe, B. G., Eds.; Winetitles: Adelaide, South Australia, Australia, 2004; Vol. *1*: Resources, Chapter 4, pp 90−118.

(14) Iland, P.; Bruer, N.; Edwards, G.; Weeks, S.; Wilkes, E. *Chemical Analysis of Grapes and Wine: Techniques and Concepts*; Patrick Iland Wine Promotions Pty Ltd: Campbelltown, New South Wales, Australia, 2004.

(15) Winter, E.; Lowe, S.; Bartrop, K. *Veraison to Harvest: Growers Guide for Riverina Vineyards*; Riverina Wine Grapes Marketing Board: Griffith, New South Wales, Australia, 2010.

(16) Geffroy, O.; Dufourq, T.; Carcenac, D.; Siebert, T.; Herderich, M.; Serrano, E. Effects of ripeness and viticultural techniques on the rotundone concentration in red wine made from *Vitis vinifera* L. cv. Duras. *Aust. J. Grape Wine Res.* **2014**, *20*, 401−408.

(17) Bramley, R. G. V. Understanding variability in winegrape production systems. 2. Within vineyard variation in quality over several vintages. *Aust. J. Grape Wine Res.* **2005**, *11*, 33−42.

(18) Linacre, E. D. A simple Formula for estimating evaporation rates in various climates, using temperature data alone. *Agr. Forest. Meteorol.* **1977**, *18*, 409−424.

(19) Pagay, V.; Cheng, L. Variability in berry maturation of Concord and Cabernet franc in a cool climate. *Am. J. Enol. Viticult.* **2010**, *61*, 61−67.

(20) Gowan, E.; Lewis, B. A.; Turgeon, R. Phloem transport of antirrhinoside, an iridoid glycoside, in *Asarina scandens* (Scrophulariaceae). *J. Chem. Ecol.* **1995**, *21*, 1781−1788.

(21) Turgeon, R.; Medville, R. Phloem loading. A reevaluation of the relationship between plasmodesmatal frequencies and loading strategies. *Plant Physiol.* **2004**, *136*, 3795−3803.

(22) Gholami, M.; Hayasaka, Y.; Coombe, B. G.; Jackson, J. F.; Robinson, S. P.; Williams, P. J. Biosynthesis of flavour compounds in Muscat Gordo Blanco grape berries. *Aust. J. Grape Wine Res.* **1995**, *1*, 19−24.

(23) Hayasaka, Y.; Baldock, G. A.; Pardon, K. H.; Jeffery, D. W.; Herderich, M. J. Investigation into the formation of guaiacol conjugates in berries and leaves of grapevine *Vitis vinifera* L. cv. Cabernet Sauvignon using stable isotope tracers combined with HPLC−MS and MS/MS analysis. *J. Agric. Food Chem.* **2010**, *58*, 2076−2081.

(24) Spayd, S. E.; Tarara, J. M.; Mee, D. L.; Ferguson, J. C. Separation of sunlight and temperature effects on the composition of *Vitis vinifera* cv. Merlot berries. *Am. J. Enol. Viticult.* **2002**, *53*, 171−182.

(25) Bergqvist, J.; Dokoozlian, N.; Ebisuda, N. Sunlight exposure and temperature effects on berry growth and composition of Cabernet Sauvignon and Grenache in the central San Joaquin Valley of California. *Am. J. Enol. Viticult.* **2001**, *52*, 1−7.

(26) Etienne, A.; Génard, M.; Lobit, P.; Mbeguié-A-Mbéguié, D.; Bugaud, C. What controls fleshy fruit acidity? A review of malate and citrate accumulation in fruit cells. *J. Exp. Bot.* **2013**, *64*, 1451−1469.

(27) Mori, K.; Goto-Yamanoto, N.; Kitayama, M.; Hashizume, K. Loss of anthocyanins in red-wine grape under high temperature. *J. Exp. Bot.* **2007**, *58*, 1935−1945.

(28) Cortell, J. M.; Halbleib, M.; Gallagher, A. V.; Righetti, T. L.; Kennedy, J. A. Influence of vine vigor on grape (*Vitis vinifera* L. cv. Pinot Noir) anthocyanins. 1. Anthocyanin concentration and composition in fruit. *J. Agric. Food Chem.* **2007**, *55*, 6575−6584.

DOI: 10.1021/acs.jafc.5b00590
J. Agric. Food Chem. 2015, 63, 4276−4283

However, other alternatives can be used to reduce the volume of data that hyperspectral imaging acquires. Characteristic vector analysis has been used to identify the most important wavelengths in the visible region by several authors. Then, these authors could reconstruct the visible spectra of other samples from these important wavelengths. In the visible region, characteristic vector analysis has been applied to the reflectance spectra of wines, brandies, vinegars, liquid honeys, and orange juices.[14−17] The aforesaid reflectance spectra were acquired by means of different spectroscopic tools (i.e., spectrophotometry and spectroradiometry). To check the accuracy of the reconstructed spectra, CIELAB coordinates were calculated from experimental and reconstructed spectra. Then, color differences were also calculated using the coordinates obtained from the experimental spectra as reference coordinates and the coordinates obtained after applying the characteristic vector method as recalculated coordinates.

However, to the best of our knowledge, characteristic vector analysis has not been applied to near-infrared spectra to identify the most important wavelengths and reconstruct the spectra. Nonetheless, characteristic vector analysis is an interesting tool to be applied to near-infrared spectra. By means of this tool, important wavelengths could be found and low-cost multispectral imaging systems could be developed. Thus, it would be possible to measure parameters of interest in food, reducing the total volume of data, using this method in a number of food fields, such as grape and wine industry.

Grape maturity is one of the most fundamental aspects that have influence on the future of wine quality. It is composed of technological and phenolic maturity, especially phenolic maturity of grape skin. Technological maturity is mainly related with the sugar concentration, titratable acidity, and pH. The sugar concentration determines the potential alcohol strength. The titratable acidity and pH help to control the wine quality and color. Phenolic maturity shows the ripening degree for the skins, pulp, and seeds, taking into account the phenolic composition.[18,19]

Nowadays, at wineries, maturity of grapes is usually controlled using classic physical and chemical analyses (e.g., refractometric, volumetric, chromatographic, or spectrophotometric analyses). As preliminary approaches, we have described some methods to screen grape maturity by means of near-infrared hyperspectral imaging.[20−22] These are useful and nondestructive hyperspectral methods. However, as described above, hyperspectral imaging involves high costs and achieves a high volume of data, while multi-spectral imaging reduces these problems considerably.

The main aim of this study is to check the feasibility of using characteristic vector analysis in the near-infrared spectral region. This method may provide the most important wavelengths to reconstruct the whole spectrum from discrete measurement. Furthermore, the spectra obtained using this simplified method are evaluated to screen technological maturity of red grape and total phenolic contents of red grape skin. To our knowledge, this is the first time that characteristic vector analysis has been applied to near-infrared spectra to face the aforementioned goals.

MATERIALS AND METHODS

Samples. *Vitis vinifera* L. cv. Tempranillo is the most often grown red grape cultivar in Spain for producing quality red wines, and *V. vinifera* L. cv. Syrah is a resistant cultivar to warm climatic conditions.[23,24] Tempranillo and Syrah samples were collected at different dates from mid-July to early September in the 2012 vintage. In this way, samples were collected at different stages of physiological maturity and from two vineyards located in the Condado de Huelva Designation of Origin D.O. (Andalusia, Spain) as previously described elsewhere by Nogales-Bueno et al.[21] Briefly, 16 and 17 dates were taken into account for Tempranillo and Syrah, respectively, and three groups of at least 150 berries were collected from several bunches for each date and vineyard. With the aim of achieving representative samples, the berries were collected from both sides (sunlight and shade) of vines located in different rows within the vineyard. Edge rows and the first two vines in a row were avoided. Berries were collected from the top, middle, and bottom of the cluster. A total of 99 samples were collected, 3 × 16 Tempranillo samples and 3 × 17 Syrah samples. From the three samples of each date, one (33%) was randomly allocated into the validation set and the other two (66%) were allocated to the calibration set.

Near-Infrared Hyperspectral Imaging. The hyperspectral imaging device (Infaimon S.L., Barcelona, Spain) comprised a Xenics XEVA-USB InGaAs camera (320 × 256 pixels, Xenics Infrared Solutions, Inc., Leuven, Belgium) and a spectrograph (Specim ImSpector N17E Enhanced, Spectral Imaging, Ltd., Oulu, Finland) covering the spectral range between 900 and 1700 nm (spectral resolution of 3.25 nm). The hyperspectral image of each sample was recorded. The equipment and procedure used for image recording are described in detail elsewhere by Hernández-Hierro et al.[20]

After the calibration and segmentation process, the average spectral profile for each sample was saved. Noisy wavebands at both extremes of the spectral range were removed. Thus, only spectral data in the resulting effective wavelength of 950−1650 nm regions were used in data analysis because of reduced efficiency outside this range in the used device. Finally, the average spectra were transformed into $\log(1/R)$ units, and 99 near-infrared absorbance spectra were obtained, with each of them composed of 215 wavelengths.

Reference Parameters. Reference parameters were total phenolic concentration in grape skins, sugar concentration, titratable acidity, and pH. The total phenolic concentration in grape skins was determined using the Folin−Ciocalteu method,[25] and it was expressed as gallic acid equivalents per gram of grape skin. This method was applied to an aqueous extract obtained from grape skin. Grape skins were separated manually from the whole grapes. Afterward, 1 g of grape skin was macerated in 10 mL of methanol containing 0.1% 12 M HCl. Methanolic phases were centrifuged (3000 rpm for 10 min) and successively pooled; approximately 2 mL of water was added; and the extract was concentrated under vacuum at 30 °C until methanol was removed and finally made up to 10 mL with ultrapure water. Technological maturity parameters were determined using the analytical methods recommended by the International Organisation of Vine and Wine (OIV)[26] as described elsewhere by Nogales-Bueno et al.[21]

Chemometrics Tools: Characteristic Vector Method. A mathematical statement of the characteristic vector analysis[27] might be given as follows:

Hyperspectral imaging spectra (HIS) are near-infrared absorbance spectra obtained from the hyperspectral device. An individual response data ρ_λ (absorbance spectrum between 950 and 1650 nm, at $\Delta\lambda = 3.25$ nm) is available for r (215) levels of the variable λ (wavelength) and can be plotted as a response curve. Therefore, for each sample, the r values of ρ_λ constitute a one-row r-column vector of response data. For n samples, the response vectors can be arrayed to form a data matrix of n rows and r columns.

If the variance−covariance matrix $\mathbf{S}$ from the original $(n \times r)$ data matrix is computed, characteristic vectors (or eigenvectors) are the solutions of the equation

$$\det(\mathbf{S} - \mathbf{LI}) = 0 \quad (1)$$

where $\mathbf{L}$ is the diagonal matrix $(r \times r)$ of the characteristic root and $\mathbf{I}$ is the $(r \times r)$ unit matrix.

It is possible to find a set of p characteristic vectors, $(p < r)$, which, added in the proper amounts, will adequately approximate any of the

DOI: 10.1021/jf505870s
J. Agric. Food Chem. 2015, 63, 4284−4290

original family of response vectors. The result is that the components of the generic vectors (i.e., the absorbance or reflectance spectra) can be expressed as

$$\rho_\lambda = M_1 V_{1\lambda} + M_2 V_{2\lambda} + ... + M_p V_{p\lambda}, \qquad p < r \tag{2}$$

where $V_{i\lambda}$ represents the components of the characteristic ith vector and M_i represents the specific coefficients, called scalar multiples, of each reconstructed vector. The M_i coefficients depend upon the absorbance values at as many wavelengths as characteristic vectors have been needed. These wavelengths are selected to maximize the accuracy of the characteristic vector reconstructed spectra (CVRS).

This analysis must be applied to a large number (n) of experimental curves. The iterative mathematical procedure calculates the characteristic vectors, the M_i coefficients to reconstruct each of these curves, and the percentage of variability among the family of homologous response curves explained for each characteristic vector.

The derivation of the vectors ensures that the first vector accounts for the largest amount of total response variability, the second vector accounts for the second-largest amount of variability, etc.

The inconvenience of this methodology is that it allows us to reconstruct the spectra of samples only from the calibration set (also called model group). If the results are to be applied to spectra of samples other than those used previously, it is necessary to calculate the corresponding M_i coefficients in a different way.

To solve this issue, characteristic vectors are calculated. Then, expressions to calculate the M_i coefficients are obtained. These expressions are functions of the absorbance or reflectance values at as many wavelengths as characteristic vectors have been needed. Therefore, these expressions allow us to calculate the M_i coefficients for the samples from the calibration set as well as for other samples from a different set called validation set. In this way, one of the requirements from the statistical methodology is completed that requires testing of a model with samples different from those used to obtain the model. Therefore, when the characteristic vector method is established, the absorbance or reflectance values at only a few wavelengths are necessary to reconstruct a spectrum.

Finally, to check the accuracy of the CVRS, root-mean-square error (RMSE) is calculated. This error measures the differences between CVRS and HIS for the calibration and validation sets. However, a small RMSE does not provide sufficient guarantee to conclude that the structural information offered by the near-infrared HIS may be kept.

Chemometrics Tools: Modified Partial Least-Squares (MPLS) Method. To check that CVRS keep the main structural information related to molecular bonds after the application of the characteristic vector method, a checking process has been purposed. Using the calibration models described in our previous study,[21] it was checked how, from CVRS, the aforementioned reference parameters were predicted. Then, the differences between the reference parameters predicted from the former data (HIS data) and the reference parameters predicted from the CVRS were checked.

Briefly, in our previous study,[21] it was established what spectral pretreatment was the best for each reference parameter. For red grapes, standard normal variate (SNV), detrend, or spectral derivative pretreatments were used to predict the different reference parameters. These pretreatments were shown to be the most effective tools to remove scattering effects. Then, calibration models were performed using MPLS regression, and the aforementioned reference parameters were predicted.

Consequently, these spectral pretreatments have been applied to the CVRS; quantitative calibrations have been developed by MPLS regression; and external validations have been carried out. Then, RSQ coefficients and SEP errors have been calculated and compared to the statistical parameters obtained from HIS.

To study the feasibility of the characteristic vector method to be used in the near-infrared region, this method has been developed from 3, 6, 9, and 12 characteristic vectors and the aforesaid process has been carried out from the different sets of CVRS.

RESULTS AND DISCUSSION

Reference Parameters. The total phenolic concentration ranged from 2.2 to 14.3 mg g^{-1} of grape skin expressed as gallic acid equivalents. The sugar concentration ranged from 4.1 to 25.4 °Brix. Titratable acidity ranged from 3.1 to 52.9 g L^{-1} expressed as tartaric acid equivalents. Finally, pH ranged from 2.5 to 3.8.

Spectral Samples and Spectral Reconstruction Process. After hyperspectral imaging acquisition, near-infrared HIS were combined into the spectral matrix (99 × 215), this spectral matrix was split into calibration (66 × 215) and validation (33 × 215) matrixes. Then, the characteristic vector method was applied to the calibration matrix, and the first 12 characteristic vectors were calculated. Both, calibration and validation matrixes were reconstructed using the first 3, 6, 9, and 12 characteristic vectors successively. The expressions and used wavelengths to calculate the M_i coefficients are available in the Supporting Information.

Figure 1 shows the first 12 characteristic vectors calculated from the HIS allocated into the calibration set. These vectors

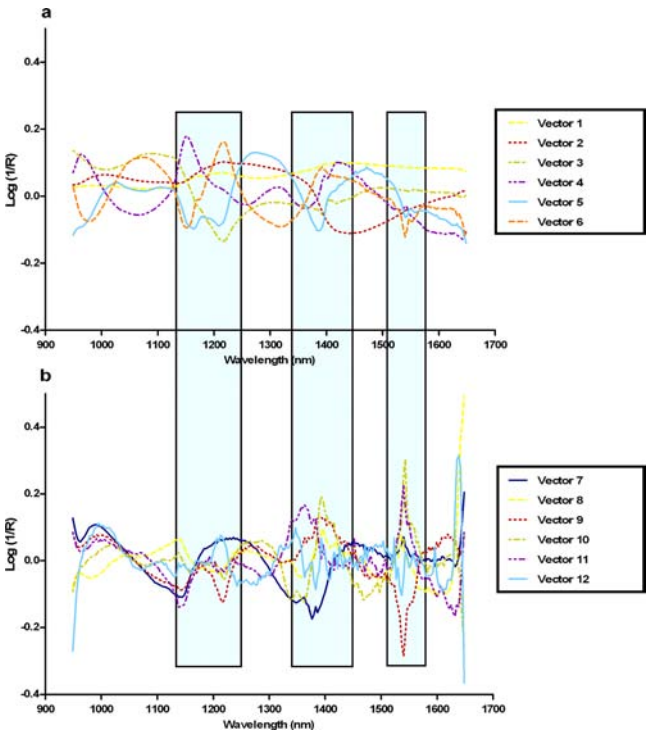

Figure 1. Characteristic vectors calculated from the spectra allocated into the calibration set. The first 6 characteristic vectors are shown in panel a, and the next 6 characteristic vectors are shown in panel b.

form the basis of a vector space, and thus, the HIS allocated into the calibration set belong to this vector space. The first 6 characteristic vectors are shown in Figure 1a, and the next 6 characteristic vectors are shown in Figure 1b. A strong feature of the characteristic vectors was the pattern around 1150, 1350, and 1550 nm wavelengths. The pattern around these wavelengths is mainly related to bands of the −CH and −OH functional groups.[28] Table 1 shows the RMSE values of the reconstruction of the calibration and validation matrixes. As expected, in all cases, the reconstruction of the calibration matrix is better than the reconstruction of the validation matrix. Nevertheless, all of these errors are really low; in fact, if a HIS is

DOI: 10.1021/jf505870s
J. Agric. Food Chem. 2015, 63, 4284−4290

Table 1. RMSE Obtained in the Reconstruction of the Calibration and Validation Matrixes from 3, 6, 9, and 12 Characteristic Vectors

RMSE[a]	3 vectors	6 vectors	9 vectors	12 vectors
calibration set (66 samples)	0.004778	0.001513	0.000819	0.000746
validation set (33 samples)	0.004873	0.001790	0.001149	0.001223

[a]RMSE = root-mean-square error [log(1/R) units].

plotted together with its respective CVRS, there are very few differences between them. However, it is not certain that CVRS keep all of the structural information related to molecular bonds. To check this, calibration models were developed from the different sets of CVRS.

Development of MPLS Calibrations. Table 2 resumes the calibration statistical descriptors for the different equations developed. Equations have been developed for each reference parameter using five different groups of spectra: the group of HIS and four groups of CVRS reconstructed from the first 3, 6, 9, and 12 characteristic vectors. In this table, it can be observed how models developed from CVRS achieve different results depending upon the number of characteristic vectors used to reconstruct them. Groups of CVRS reconstructed from 3 and 6 characteristic vectors show high values of error in the cross-validation process (SECV) and low correlation coefficients (RSQ). In addition, these equations have needed less PLS factors than the rest of spectral groups. This means that the spectral variability of the independent variable (X) related to the dependent variable (Y) is lower in groups of CVRS reconstructed from 3 and 6 vectors than in the rest of the groups of CVRS, and this spectral variability can be explained with a small number of PLS factors. In conclusion, these two reconstructions have not been able to reproduce all of the spectral variability of the HIS related to the dependent variable (Y).

The group of CVRS reconstructed from 9 and 12 characteristic vectors shows better results. In fact, the results obtained from the group reconstructed from 12 characteristic vectors are really close to the results obtained from HIS (Table 2).

For each model developed from the different calibration sets, its robustness was tested using its respective validation set (33 samples), which did not belong to the calibration set, as external validation. Using the characteristic vector analysis described above, these 33 HIS were reconstructed from 3, 6, 9, and 12 characteristic vectors and these matrixes were used in the different validation processes. As result of these external validations, standard errors of prediction (SEP) for each reference variable were obtained; these values were also included in Table 2. Figure 2 shows the SEP expressed as percentages. These errors follow the same pattern described for SECV: high errors for models developed from 3 and 6 characteristic vectors and lower errors for models developed from 9 and 12 vectors. For sugar, concentration errors obtained are not as low as expected; however, the model developed from 12 characteristic vectors predicts this parameter with sufficient precision. Furthermore, for total phenolic concentration and titratable acidity, SEP obtained in the model developed from 12 characteristic vectors is lower than SEP obtained in the model developed from HIS. This is perhaps due to the absence of noise in the CVRS. The characteristic vector method can reproduce the features of a spectrum linked to the chemical or physical properties of the sample. However, this method cannot reproduce the instrumental noise of a HIS, by its random nature. Consequently, in the CVRS, the instrumental noise cannot mask the features linked to the chemical or physical

Table 2. Calibration Statistical Descriptors for the Models Developed in the Near-Infrared Region Close to 950−1650 nm

parameters	spectra[a]	spectral pretreatments	T outliers	PLS factors	N[b]	estimated minimum	SD[c]	estimated maximum	SEC[d]	RSQ[e]	SECV[f]	SEP[g]
total phenols[h]	3 vectors	SNV and detrend 0, 0, 1, 1	4	1	62	0	2.95	16.95	2.00	0.54	2.07	1.86
	6 vectors		2	2	64	0	3.02	16.81	1.72	0.68	1.79	1.56
	9 vectors		0	4	66	0	3.13	17.30	1.29	0.82	1.42	1.35
	12 vectors		1	4	65	0	3.08	17.06	1.22	0.84	1.35	1.13
	HIS[i]		3	6	63	0	2.99	16.69	1.01	0.89	1.07	1.23
°Brix	3 vectors	none 2, 5, 5, 1	4	1	62	0.85	5.49	33.78	3.86	0.50	3.97	3.70
	6 vectors		2	3	64	0	6.00	34.60	2.65	0.80	2.90	2.62
	9 vectors		2	4	64	0	6.09	35.10	1.57	0.93	1.78	2.45
	12 vectors		3	5	63	0	6.04	34.76	1.61	0.93	1.78	2.26
	HIS[i]		4	6	62	0	5.98	34.61	0.73	0.99	1.04	1.37
titratable acidity[j]	3 vectors	SNV 0, 0, 1, 1	8	3	58	0	10.34	42.50	6.12	0.65	6.35	7.08
	6 vectors		6	4	60	0	13.69	54.25	3.24	0.94	3.33	4.58
	9 vectors		6	8	60	0	12.66	50.32	1.93	0.98	2.07	4.24
	12 vectors		5	6	61	0	13.49	53.79	2.38	0.97	2.62	3.87
	HIS[i]		5	8	61	0	13.39	53.08	1.72	0.98	2.24	3.88
pH	3 vectors	SNV and detrend 1, 5, 5, 1	6	2	60	2.16	0.33	4.17	0.19	0.67	0.20	0.21
	6 vectors		3	6	63	2.08	0.35	4.19	0.16	0.78	0.17	0.17
	9 vectors		0	6	66	2.08	0.36	4.23	0.13	0.87	0.14	0.15
	12 vectors		3	8	63	2.06	0.36	4.23	0.11	0.91	0.12	0.14
	HIS[i]		0	8	66	2.08	0.36	4.23	0.09	0.94	0.13	0.12

[a]Spectra = group of spectra used for develop the model. [b]N = number of samples (calibration set). [c]SD = standard deviation. [d]SEC = standard error of calibration. [e]RSQ = coefficient of determination. [f]SECV = standard error of cross-validation. [g]SEP = standard error of prediction (external validation). [h]Total phenols = mg g^{-1} of skin grape (expressed as gallic acid equivalents). [i]HIS = hyperspectral imaging spectra. [j]Titratable acidity = g L^{-1} (expressed as tartaric acid equivalents).

DOI: 10.1021/jf505870s
J. Agric. Food Chem. 2015, 63, 4284−4290

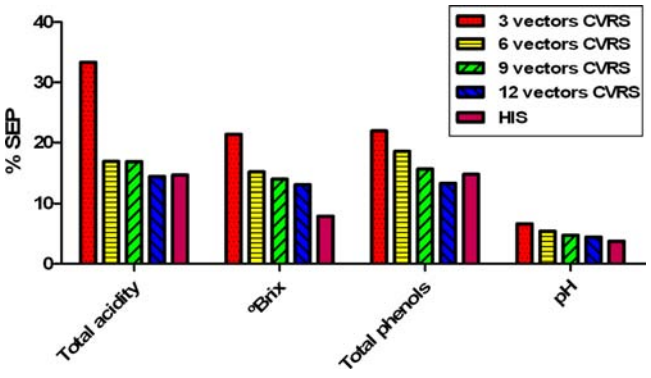

Figure 2. SEP for each reference parameter expressed as percentages, showing a comparison between the different calibration models developed.

properties of the sample, and the models developed from the CVRS reconstructed from 12 characteristic vectors can be more accurate than models developed from HIS.

To analyze the significance of differences between errors of prediction for the models developed from HIS and from the group of CVRS reconstructed from 12 characteristic vectors, a Student's *t* test for paired values was carried out. In each case, the level of significance was obtained. When this value was greater than 0.05 (chosen as the minimum level of significance), the null hypothesis was accepted (i.e., there were no differences among the different results). The levels of significance were 0.22 for total phenolic concentration, 0.76 for sugar concentration, 0.18 for titratable acidity, and 0.13 for pH. For all parameters, the level of significance was higher than 0.05. It may be concluded that the models developed from the group of CVRS reconstructed from 12 characteristic vectors provide significantly similar results to models developed from HIS.

Furthermore, the error of prediction (EP) of each sample was calculated to test the robustness of the developed models. For each developed model, differences between individual predicted and experimental reference parameters have been calculated and expressed as percentages. These percentages are plotted in Figure 3, which shows the distributions in error of predictions of samples allocated into the validation set. For all reference parameters, the number of samples with an error of prediction lower than 20% is very similar for the models developed from HIS and from the group of CVRS reconstructed from 12 characteristic vectors. This means that characteristic vector analysis reproduces, with only 6% of the spectral information that the hyperspectral device provides, the results reported in our previous study[21] in a very satisfactory way (RSQ between 0.84 and 0.97 units and SEP between 4 and 14%). In addition, Figure 3 also shows that pH could be predicted with an EP of lower than 20%, even using the model developed from the group of CVRS reconstructed from 3 characteristic vectors (Figure 3d).

In conclusion, simplified methods for the screening of technological maturity of red grape and total phenolic compounds of red grape skin have been described. These methods use characteristic vector analysis to reduce the volume of data that hyperspectral imaging acquires. This data reduction can, from a theoretical point of view, help to develop cheap spectral devices, such as multi-spectral systems.

The characteristic vector method allows us to reconstruct near-infrared spectra from a few characteristic vectors and wavelengths. To achieve good results, the correct number of characteristic vectors must be taken into account. The results reported here indicate that 12 characteristic vectors are sufficient to reconstruct near-infrared spectra and to develop from these spectra useful calibration models. Hence, this study is an important step to reduce the spectral information necessary for food evaluation and the cost of this technology.

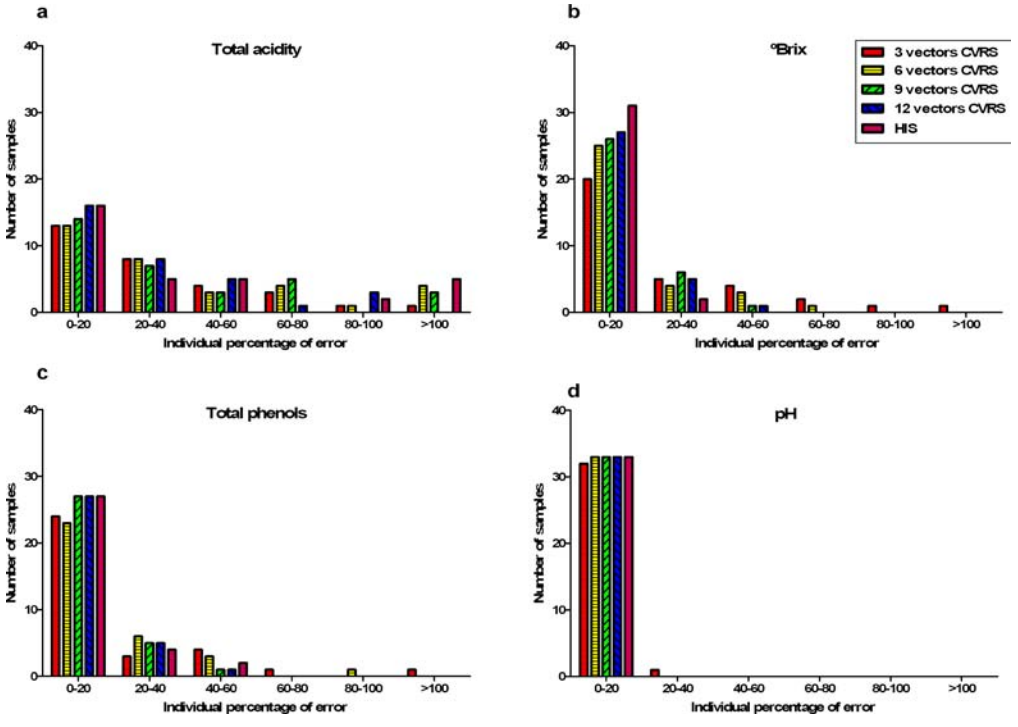

Figure 3. Frequency histograms of (a) total acidity, (b) sugar concentration, (c) total phenols, and (d) pH are represented.

DOI: 10.1021/jf505870s
J. Agric. Food Chem. 2015, 63, 4284−4290

■ ASSOCIATED CONTENT

Supporting Information

Expressions and used wavelengths to calculate the M_i coefficients (Appendix A: Spectral Reconstruction). The Supporting Information is available free of charge on the ACS Publications website at DOI: 10.1021/jf505870s.

■ AUTHOR INFORMATION

Corresponding Author

*Telephone: +34-9545-56495. Fax: +34-9545-56110. E-mail: heredia@us.es.

Funding

The Spanish Ministry of Economy and Competitiveness (MINECO) is thanked for the Formación de Personal Investigador (FPI) Grant (BES-2012-060192) to Julio Nogales-Bueno and Project AGL2014-58486-C2. José Miguel Hernández-Hierro thanks Universidad de Sevilla for the extension of the Juan de la Cierva postdoctoral contract. Francisco José Rodríguez-Pulido also thanks the Department of Financial Economics and Operations Management (VPPI-US), Universidad de Sevilla, for a postdoctoral grant. Junta de Andalucía is also thanked for financial support (Project P10-AGR6331).

Notes

The authors declare no competing financial interest.

■ ACKNOWLEDGMENTS

The authors thank the technical staff of Biology Service [Servicios Generales de Investigación (SGI), Universidad de Sevilla] for the technical assistance.

■ ABBREVIATIONS USED

2ndD, second derivative spectra; BR, band ratio; CVRS, characteristic vector reconstructed spectra; EP, error of prediction; HIS, hyperspectral imaging spectra; MPLS, modified partial least-squares; NIRS, near-infrared spectroscopy; PLSR, partial least-squares regression; RMSE, root-mean-square error; RSQ, coefficient of determination; SEC, standard error of calibration; SECV, standard error of cross-validation; SEP, standard error of prediction; SNV, standard normal variate; SPA, successive projections algorithm; SWR, stepwise regression; UVE, uninformative variable elimination

■ REFERENCES

(1) Qin, J.; Chao, K.; Kim, M. S.; Lu, R.; Burks, T. F. Hyperspectral and multispectral imaging for evaluating food safety and quality. *J. Food Eng.* **2013**, *118*, 157−171.

(2) Wu, D.; Sun, D. W. Advanced applications of hyperspectral imaging technology for food quality and safety analysis and assessment: A review—Part II: Applications. *Innovative Food Sci. Emerging Technol.* **2013**, *19*, 15−28.

(3) Gowen, A. A.; O'Donnell, C. P.; Cullen, P. J.; Downey, G.; Frias, J. M. Hyperspectral imaging—An emerging process analytical tool for food quality and safety control. *Trends Food Sci. Technol.* **2007**, *18*, 590−598.

(4) Garcia-Allende, P. B.; Conde, O. M.; Mirapeix, J.; Cobo, A.; Lopez-Higuera, J. M. Hyperspectral imaging for diagnosis and quality control in agri-food and industrial sectors. *Opt. Sens. Detect.* **2010**, *7726*, No. 77260E.

(5) Gou, P.; Santos-Garcés, E.; Høy, M.; Wold, J. P.; Liland, K. H.; Fulladosa, E. Feasibility of NIR interactance hyperspectral imaging for on-line measurement of crude composition in vacuum packed dry-cured ham slices. *Meat Sci.* **2013**, *95*, 250−255.

(6) Esquerre, C.; Gowen, A.; Downey, G.; O'Donnell, C. P. Wavelength selection for development of a near infrared imaging system for early detection of bruise damage in mushrooms (*Agaricus bisporus*). *J. Near Infrared Spectrosc.* **2012**, *20*, 537−546.

(7) Liu, D.; Sun, D. W.; Zeng, X. A. Recent advances in wavelength selection techniques for hyperspectral image processing in the food industry. *Food Bioprocess Technol.* **2014**, *7*, 307−323.

(8) Rajkumar, P.; Wang, N.; Eimasry, G.; Raghavan, G. S. V.; Gariepy, Y. Studies on banana fruit quality and maturity stages using hyperspectral imaging. *J. Food Eng.* **2012**, *108*, 194−200.

(9) Sugiyama, T.; Sugiyama, J.; Tsuta, M.; Fujita, K.; Shibata, M.; Kokawa, M.; Araki, T.; Nabetani, H.; Sagara, Y. NIR spectral imaging with discriminant analysis for detecting foreign materials among blueberries. *J. Food Eng.* **2010**, *101*, 244−252.

(10) Fang, H. Detection of activity of POD in tomato leaves based on hyperspectral imaging technology. *Spectrosc. Spect. Anal.* **2012**, *32*, 2228−2233.

(11) Wang, S.; Huang, M.; Zhu, Q. Model fusion for prediction of apple firmness using hyperspectral scattering image. *Comput. Electron. Agr.* **2012**, *80*, 1−7.

(12) Kamruzzaman, M.; Barbin, D.; Elmasry, G.; Sun, D. W.; Allen, P. Potential of hyperspectral imaging and pattern recognition for categorization and authentication of red meat. *Innovative Food Sci. Emerging Technol.* **2012**, *16*, 316−325.

(13) Li, J.; Rao, X.; Guo, J.; Ying, Y. Hyperspectral reflectance imaging for detecting citrus canker based on dual-band ratio image classification method. *Proceedings of the 5th International Symposium on Advanced Optical Manufacturing and Testing Technologies: Optical Test and Measurement Technology and Equipment*; Dalian, China, April 26−29, 2010; pp 76562C1−76562C10.

(14) Ayala, F.; Echávarri, J. F.; Negueruela, A. I. A new simplified method for measuring the color of wines. III. All wines and brandies. *Am. J. Enol. Vitic.* **1999**, *50*, 359−363.

(15) González-Miret, M. L.; Ayala, F.; Terrab, A.; Echávarri, J. F.; Negueruela, A. I.; Heredia, F. J. Simplified method for calculating colour of honey by application of the characteristic vector method. *Food Res. Int.* **2007**, *40*, 1080−1086.

(16) Meléndez-Martinez, A. J.; Ayala, F.; Echávarri, J. F.; Negueruela, A. I.; Escudero-Gilete, M. L.; González-Miret, M. L.; Vicario, I. M.; Heredia, F. J. A novel and enhanced approach for the assessment of the total carotenoid content of foods based on multipoint spectroscopic measurements. *Food Chem.* **2011**, *126*, 1862−1869.

(17) García-Parrilla, M. C.; Ayala, F.; Echávarri, J. F.; Troncoso, A. M.; Negueruela, A. I.; Heredia, F. J. Measurement of wine vinegars' color: Application of the characteristic vector method. *J. Agric. Food Chem.* **1998**, *46*, 4238−4241.

(18) Ferrer-Gallego, R.; Hernández-Hierro, J. M.; Rivas-Gonzalo, J. C.; Escribano-Bailón, M. T. Influence of climatic conditions on the phenolic composition of *Vitis vinifera* L. cv. Graciano. *Anal. Chim. Acta* **2012**, *732*, 73−77.

(19) Meléndez, E.; Ortiz, M. C.; Sarabia, L. A.; Íñiguez, M.; Puras, P. Modelling phenolic and technological maturities of grapes by means of the multivariate relation between organoleptic and physicochemical properties. *Anal. Chim. Acta* **2013**, *761*, 53−61.

(20) Hernández-Hierro, J. M.; Nogales-Bueno, J.; Rodríguez-Pulido, F. J.; Heredia, F. J. Feasibility study on the use of near-infrared hyperspectral imaging for the screening of anthocyanins in intact grapes during ripening. *J. Agric. Food Chem.* **2013**, *61*, 9804−9809.

(21) Nogales-Bueno, J.; Hernández-Hierro, J. M.; Rodríguez-Pulido, F. J.; Heredia, F. J. Determination of technological maturity of grapes and total phenolic compounds of grape skins in red and white cultivars during ripening by near infrared hyperspectral image: A preliminary approach. *Food Chem.* **2014**, *152*, 586−591.

(22) Nogales-Bueno, J.; Baca-Bocanegra, B.; Rodríguez-Pulido, F. J.; Heredia, F. J.; Hernández-Hierro, J. M. Use of near infrared hyperspectral tools for the screening of extractable polyphenols in red grape skins. *Food Chem.* **2015**, *172*, 559−564.

(23) España Exportación e Inversiones (ICEX). *Vinos de España*; www.winesfromspain.com/ (accessed May 2014).

DOI: 10.1021/jf505870s
J. Agric. Food Chem. 2015, 63, 4284−4290

(24) Gordillo, B.; Rodríguez-Pulido, F. J.; Mateus, N.; Escudero-Gilete, M. L.; González-Miret, M. L.; Heredia, F. J.; de Freitas, V. Application of LC−MS and tristimulus colorimetry to assess the ageing aptitude of Syrah wine in the Condado de Huelva D.O. (Spain), a typical warm climate region. *Anal. Chim. Acta* **2012**, *732*, 162−171.
(25) Singleton, V. L.; Rossi, J. A., Jr. Colorimetry of total phenolics with phosphomolybdic−phosphotungstic acid reagents. *Am. J. Enol. Vitic.* **1965**, *16*, 144−158.
(26) International Organisation of Vine and Wine (OIV). *Recuil de Methods Internationals d'Analyse des Vins*; OIV: Paris, France, 1990.
(27) Lebart, L.; Morineau, A.; Fénelon, J. P. *Tratamiento Estadístico de Datos: Métodos y Programas*; Marcombo S.A.: Barcelona, Spain, 1985.
(28) Siesler, H. W.; Ozaky, Y.; Kawata, S.; Heise, H. M. *Near Infrared Spectroscopy: Principles, Instruments, Applications*; Wiley-VCH: Weinheim, Germany, 2002.

DOI: 10.1021/jf505870s
J. Agric. Food Chem. 2015, 63, 4284−4290

Table 1. *Alicyclobacillus* spp., *Bacillus* spp., and *Clostridium* spp. Spores Used for Selectivity Determination of Real-Time PCR

Alicylobacillus spores	*Bacillus* spores	*Clostridium* spores
A. acidoterrestris (DSM 2498)	5× *B. cereus* (wild types)	2× *C. perfringens* (wild types)
A. acidoterrestris (DSM 3922)	*B. weihenstepanensis* (wild type)	
A. acidoterrestris (DSM 3929)	*B. thuringiensis* (ATCC 10792)	
A. acidoterrestris (DSM 3924)	*B. thuringiensis* (DSM 6029)	
A. cycloheptanicus (DSM 4005)	*B. licheniformis* (DSM 13)	
A. cycloheptanicus (DSM 4006)	*B. subtilis* (DSM 2109)	
A. cycloheptanicus (DSM 4007)	*B. coagulans* (ATCC 7050)	
A. acidocaldarius (DSM 446)	*B. circulans* (ATCC 9966)	
A. herbarius (DSM 13609)	*B. sphaericus* (ATCC 245)	
A. acidiphilus (DSM 14558)	*Paenibacillus polymyxa* (ATCC 10401)	
A. pomorum (DSM 14955)		
A. sacchari (DSM 17974)		
A. fastidiosus (DSM 17978)		
34× undefined wild types		

Table 2. 16S rDNA Primers and Corresponding PCR Product of the Real-Time PCR Assay

name	sequence (5′−3′)	position	length (bp)	T_m (°C)	GC (%)	PCR product (bp)
16S rDNA Fw	CGAAGGAAACCCAATAAGCAC	839−859	21	61.5	47.6	143
16S rDNA Rv	GGATGTCAAGCCCTGGTAAG	962−981	20	62.1	55.0	

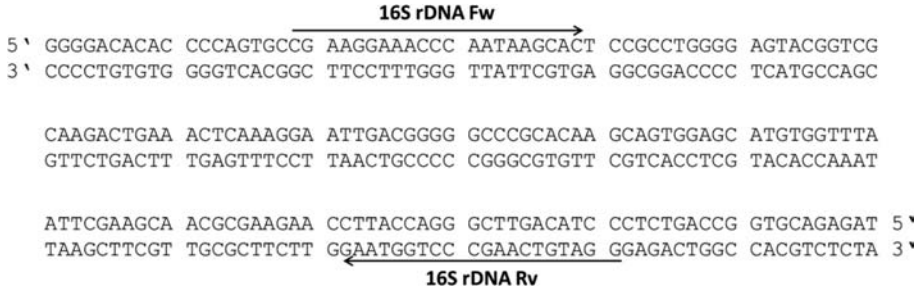

Figure 1. 16S rDNA gene sequence of *A. acidoterrestris* (DSM 2498; accession number AB059675.1; position 821−1000) with the designed primers (16S rDNA Fw and 16S rDNA Rv) marked by arrows.

to gain a maximum of reliability.[32] The assay was evaluated in terms of the correlation coefficient, slope of the regression line, amplification efficiency, dynamic range, relative repeatability standard deviation, limit of detection (LOD), and limit of quantification (LOQ).

MATERIALS AND METHODS

Spore Lysis. The spores used in the presented work (Table 1) were from our in-house collection and also provided by Dr. B. Schütze, LADR GmbH (Geesthacht, Germany). To obtain the 16S rDNA, spores were diluted in double-distilled water (ddH_2O) to a total volume of 400 μL and about 250 mg of glass beads (Ø = 0.5 mm, Sigma-Aldrich Chemie GmbH, Munich, Germany) were added and subsequently ground twice in a TissueLyser (Qiagen GmbH, Hilden, Germany) for 5 min at 30 Hz. The resulting fragmented spore mixtures were centrifuged for 5 min at 12000*g* to precipitate the glass beads and the spore fragments. The supernatant was used directly as a template for real-time PCR.

Real-Time PCR Design. To design primers, which are suitable for a wide variety of *Alicyclobacillus* spp. strains, the 16S rDNA sequences of various *Alicyclobacillus* spp. were collected from the National Center for Biotechnology Information (NCBI, Bethesda, MD). Suitable primers (Table 2) were designed using the PrimerQuest Tool (Integrated DNA Technologies, Inc., Leuven, Belgium).

The real-time PCR was performed in 96 well PCR plates (Sarstedt Inc. & Co., Nümbrecht, Germany) sealed with sealing tape (Sarstedt Inc. & Co., Nümbrecht, Germany) in a total volume of 20 μL. Each PCR reaction mix consisted of the following components: 1× DreamTaq buffer (10×, Fisher Scientific-Germany GmbH, Schwerte, Germany), 0.8 mM dNTPs (10 mM, Bioline GmbH, Luckenwalde, Germany), 0.25 unit DreamTaq polymerase (0.5 U/μL, Fisher Scientific-Germany GmbH, Schwerte, Germany), 0.2 μM of each primer (16S rDNA Fw and 16S rDNA Rv, Integrated DNA Technologies, Inc., Leuven, Belgium), 0.3125× SYBR Green I nucleic acid gel stain (10000×, Invitrogen GmbH, Karlsruhe, Germany), various concentrated spore lysates, and ddH_2O filled up to 20 μL. The PCR amplification was carried out in an iCycler iQ5 (BioRad Laboratories, Inc., Hercules, CA). The real-time PCR starts with a 5 min denaturation step at 95 °C, followed by 35 cycles of denaturation at 95 °C for 30 s, annealing at 58 °C for 30 s, elongation at 72 °C for 30 s, and detection at 84 °C after 30 s. The last step is a final elongation at 72 °C for 5 min. The fluorescence was excited at 485 nm, with the resulting emission measured at 530 nm, and the threshold cycle was calculated using the Optical System Software (version 2.0, BioRad Laboratories, Inc., Hercules, CA). Real-time PCR reaction curves with C_T values of >32 were defined as no amplification, and C_T values of ≤32 were defined as positive results, together with the expected amplicons. The calibration lines were obtained by plotting C_T values against the formed logarithm of diluted and prepared spore suspensions.

RESULTS AND DISCUSSION

Spore Lysis. For the DNA extraction from *Alicyclobacillus* spp. spores, several spore lysis methods were tested, e.g., (i) chemical lysis using surfactants, acids, and alkali, (ii) temperature treatment using liquid nitrogen, heat, and autoclaving,

DOI: 10.1021/acs.jafc.5b00874
J. Agric. Food Chem. 2015, 63, 4291−4296

(iii) various DNA extraction kits, (iv) mechanical spore treatment using glass beads or sonic waves, and (v) different combinations of the above-mentioned techniques.[28,33−38] The application of a TissueLyser with glass beads (0.5 mm diameter) and the subsequent centrifugation provide a very simple method for a rapid extraction of DNA from spores. Because of the fact that the spore lysis was performed in ddH_2O, the resulting supernatant is directly useable for the real-time PCR assay to quantify *Alicyclobacillus* spp. spores.[22]

Real-Time PCR Design. The 16S rDNA primers used in the presented work were designed regarding *A. acidoterrestris* DSM 2498 (accession number AB059675.1; Figure 1). This sequence was previously aligned with several *A. acidoterrestris* strains (e.g., DSM 3922, DSM 12489, ATCC 49025, NBRC 106291, NBRC 106287, and NBRC 106295) and other *Alicyclobacillus* spp., for example, *A. acidiphilus* (DSM 14558), and *A. herbarius* (DSM 13609). Sequences were obtained from the NCBI and aligned using GENtle (version 1.9.4, University of Cologne, Cologne, Germany). The 16S rDNA primers were designed by PrimerQuest Tool (Integrated DNA Technologies, Inc., Leuven, Belgium) and possess melting temperatures of 61.5 and 62.1 °C (Table 2). After optimization of the PCR assay, 58.0 °C seems to be the optimal annealing temperature, resulting in an amplicon with a length of 143 bp (Figure 1). To avoid detection of primer dimers and PCR artifacts, fluorescence monitoring was performed at 84 °C.[39] From this temperature, the detection of byproducts is suppressed, resulting in an overall increased sensitivity of the PCR assay (Figure 2).[40]

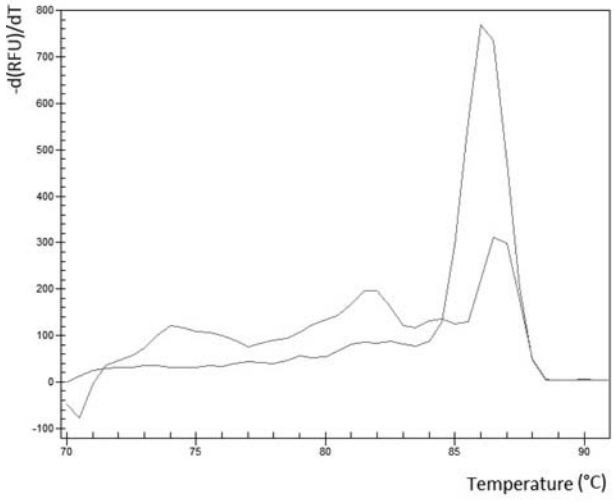

Figure 2. Melting temperature analysis of two different prepared spore concentrations [8.45 and 8.45 × 10^5 colony forming units (cfu)/mL].

The DNA amplification was monitored using the intercalating fluorescence dye SYBR Green I. These real-time PCR assays have various advantages, such as a high dynamic range for quantification and superior reproducibility.[24,41,42] Even though crude spore DNA was used as a template, SYBR Green I enables sensitive and precise quantification results (Figure 3 and Table 3).[43] Moreover, it is also useful for high throughput screening in incoming control of the fruit juice industry because of robustness, practicability, high standardization potential, and running expenses.[32,44]

Real-Time PCR Evaluation. The performance requirements of the ENGL were used to evaluate the real-time PCR for quantification of *Alicyclobacillus* spp. spores in terms of the correlation coefficient, slope of the regression line, amplification efficiency, dynamic range, relative repeatability standard deviation, limit of detection, and limit of quantification.[32,45]

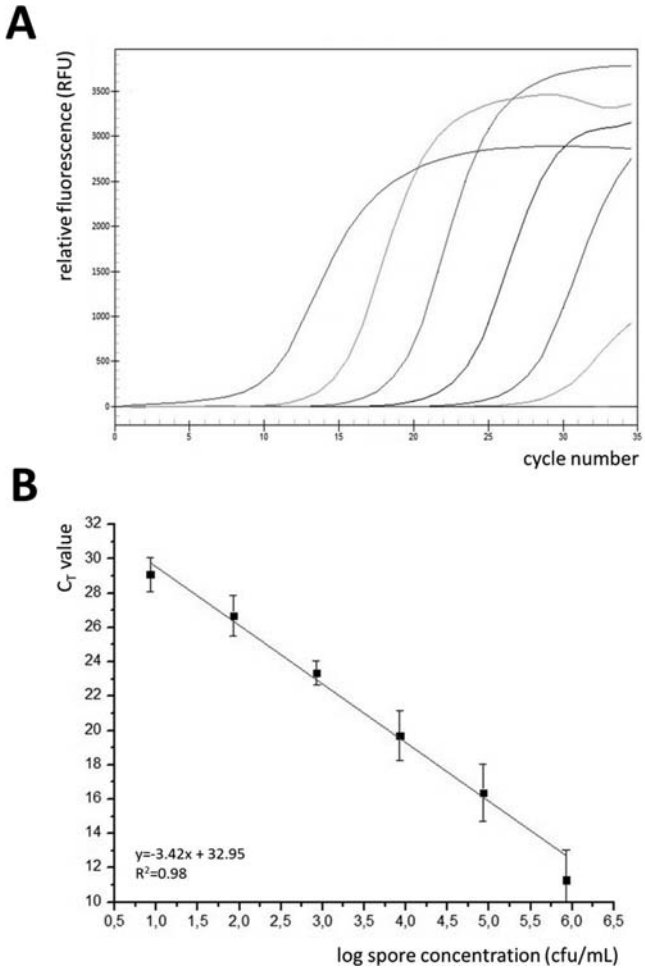

Figure 3. (A) Example of observed reaction curves during real-time PCR validation with different spore concentrations (cfu/mL). Spore concentrations from left to right: 8.45 × 10^5 cfu/mL, 8.45 × 10^4 cfu/mL, 8.45 × 10^3 cfu/mL, 8.45 × 10^2 cfu/mL, 8.45 × 10^1 cfu/mL, and 8.45 cfu/mL. (B) Resulting calibration line during real-time PCR validation with E = 96% (m = −3.42) and R^2 = 0.983. Spore concentrations from left to right: 8.45 cfu/mL, 8.45 × 10^1 cfu/mL, 8.45 ×10^2 cfu/mL, 8.45 × 10^3 cfu/mL, 8.45 × 10^4 cfu/mL, and 8.45 × 10^5 cfu/mL.

Table 3. Evaluation Parameters According to ENGL and Results of the Validation of Developed Real-Time PCR

evaluation parameters	ENGL criteria	results of developed real-time PCR
dynamic range (cfu/mL)		8.45−8.45 × 10^5
slope of the regression line	$-3.1 \geq m \geq -3.6$	−3.42
amplification efficiency (%)	110−90	96
correlation coefficient	≥0.98	0.983
relative repeatability standard deviation (%)	≤25	3.0−15.4
limit of quantification (LOQ) (cfu/mL)		8.45
limit of detection (LOD) (calculated by the regression line) (cfu/mL)		0.28

DOI: 10.1021/acs.jafc.5b00874
J. Agric. Food Chem. 2015, 63, 4291−4296

For the real-time PCR evaluation, spore concentrations from 8.45×10^2 to 8.45×10^6 cfu/mL of a strain mix (1:1, v/v, *A. acidoterrestris* DSM 2498/*A. acidoterrestris* wild type) were used. To increase the dynamic range of spore quantification, the lysed spore suspension of 8.45×10^2 cfu/mL was further diluted in 10-fold serial steps to a theoretical spore concentration of 0.845 cfu/mL. Mentioned dilutions of the applicable DNA templates were possible because of the high copy number of the 16S rDNA.[29−31]

During the extensive validation of the real-time PCR assay, a dynamic range of *Alicyclobacillus* spp. spore concentrations from 8.45 to 8.45×10^5 cfu/mL was established (Figure 3 and Table 3). The evaluation of a higher spore concentration than 8.45×10^5 cfu/mL is not necessary because it can be assumed that these concentration ranges never occur in orange juice samples or could be bypassed by dilution.

A correlation coefficient (R^2) of 0.983 was determined by linear regression analysis (Figure 3B and Table 3), which fulfills the performance requirements of the ENGL (according to ENGL, the correlation coefficient should be ≥0.98). Hence, this evaluation parameter confirms a linear correlation and, therefore, justifies the usage of a linear fit.[32] In addition, the slope of the regression line (m) of −3.42 (Figure 3 and Table 3) fulfills the performance requirements of the ENGL ($-3.1 \geq m \geq -3.6$) and is therefore considered as appropriate. Moreover, the amplification efficiency (E) was calculated by use of the regression line slope ($E = 10^{-1/m} - 1$). For the developed real-time PCR assay, an efficiency of approximately 96% was achieved, which is also within the requirements of ENGL (Figure 3 and Table 3).

The relative repeatability standard deviation (RSD_r) of the assay results indicates the reproducibility of the developed real-time PCR assay and should be ≤25% over the whole dynamic range of the developed method according to ENGL.[23] Moreover, the relative repeatability should be determined by a sufficient number of test results (at least 15), as indicated in ISO 5725-3.[32,46] During the whole assay development, the relative repeatability standard deviation was in the range of 3.0−15.4%. This is in accordance with the ENGL criteria and was obtained by considerably more than 15 approaches per amplification point (Figure 3 and Table 3).

Because of the above-mentioned aspect of unknown target concentrations after aptamer-based spore enrichment, one of the ENGL criteria [limit of detection (LOD) should be less than $^1/_{20}$ of the target concentration] is not determinable. However, according to ENGL, the LOD can also be determined by ensuring that ≥95% of false negative results are detectable. Under the assumption that C_T values of >32 are blank samples, this evaluation parameter could be fulfilled.[15] Therefore, the limit of detection of the present real-time PCR assay is below the dynamic range of quantification. A further equimolar dilution of spores would lead to a concentration of <1 cfu/mL, which is not relevant for the application. However, to indicate a theoretical detection limit, the LOD was calculated using a C_T of 32. Thus, the theoretical detection limit value is 0.28 cfu/mL.

According to ENGL, the limit of quantification (LOQ) should be less than $^1/_{10}$ of the target concentration, which is also not determinable because of the mentioned aspect of unknown target concentrations after spore enrichment. However, this spore concentration can be determined in consideration of the mentioned and defined performance requirements of the ENGL. Moreover, a further LOQ criterion (≤25% RSD_r) is achieved for the estimated spore concentration of 8.45 cfu/mL. Nevertheless, the statistical probability to receive precise results in a lower range of the spore concentration is significantly decreased and leads to C_T values beyond the RSD_r range of >25%.

In addition, the selectivity of the developed real-time PCR was assessed by an end-point PCR experiment and analysis by agarose gel electrophoresis (AGE). Because of the final application in conjunction with an aptamer-based spore enrichment for a rapid and direct proof and quantification of *Alicyclobacillus* spp. spores in orange juice, the selectivity toward several of the fruit juice industry relevant spores is especially important. In this context, 13 spores of various *Alicyclobacillus* spp. DSM strains, 34 *Alicyclobacillus* spp. wild types, 5 *Bacillus cereus*, 1 *Bacillus weihenstepanensis*, 2 *Bacillus thuringiensis*, 1 *Bacillus licheniformis*, 1 *Bacillus subtilis*, 1 *Bacillus coagulans*, 1 *Bacillus polymyxa*, 1 *Bacillus circulans*, 1 *Bacillus sphaericus*, and 2 *Clostridium perfringens* strains were analyzed (Table 1). All 47 *Alicyclobacillus* spp. spore strains yielded the calculated 143 bp amplicon, whereas neither *Bacillus* spp. nor *C. perfringens* spore strains were amplified.

In general, the developed method is suitable for spore quantification subsequent to an affinity enrichment procedure, for instance, from orange juice. Because of the intended spore elution with water after the enrichment process, the determination of spore suspensions in water is required. Moreover, this simple approach enables the variation of spore lysis volumes during the spore elution after the enrichment step. In summary, the aim of the whole technique includes (i) the aptamer-based enrichment step by magnetic spore separation with (ii) consecutive determination of *Alicyclobacillus* spp. spore concentration by real-time PCR.

As described by Hünniger et al., the selected aptamers possess a substantially high affinity to *Alicyclobacillus* spp. spores and a rather low affinity to *Bacillus* spp. or *Clostridium* spp. spores (see Figure S3 of the Supporting Information).[22] In the end, this given selectivity is substantially increased by the presented PCR, which allows for the distinction between *Alicyclobacillus* spp., *Bacillus* spp., and *Clostridium* spp. However, if further non-*Alicyclobacillus* spp. strains will be identified in orange juices in the future, their sequences have to be further characterized to assess the selectivity of the test system developed in this study.[47]

On the whole, the combination of the prior spore-collecting step by immobilized aptamers in combination with the very selective real-time PCR assay developed in this study appears as the scientific basis for the development of a rapid and reliable incoming control in the beverage plant. In an upcoming study, the whole system will be assembled, evaluated, and assessed using real and spiked orange juice samples of different origins.

■ ASSOCIATED CONTENT

Supporting Information

Alignment of non-*Alicyclobacillus* ssp. 16S rDNA sequences with *A. acidoterrestris* covered by this study (Figure S1), alignment of amplified 16S rDNA fragments (143 bp) (Figure S2), and summary of aptamer selectivity to several strains given in Table 1 (Figure S3). This material is available free of charge via the Internet at http://pubs.acs.org.

DOI: 10.1021/acs.jafc.5b00874
J. Agric. Food Chem. 2015, 63, 4291−4296

AUTHOR INFORMATION

Corresponding Author

*Telephone: +49-40-428384357. Fax: +49-40-428384342. E-mail: markus.fischer@chemie.uni-hamburg.de.

Funding

This research project was supported by the German Ministry of Economics and Technology (via AiF) and the Forschungskreis der Ernährungsindustrie e.V. (FEI, Bonn, Germany) (Project AiF 17245 N).

Notes

The authors declare no competing financial interest.

ACKNOWLEDGMENTS

The authors gratefully acknowledge Dr. Burkhard Schütze (LADR GmbH, Geesthacht, Germany) for the provision of various *Alicyclobacillus* spp. strains (spores and vegetative cells) and the Verband der deutschen Fruchtsaft-Industrie e.V. (Bonn, Germany) for support.

REFERENCES

(1) Merle, J.; Montville, T. J. *Alicyclobacillus acidoterrestris*: The organism, the challenge, potential interventions. *J. Food Process. Preserv.* **2014**, *38*, 153−158.

(2) Perez-Cacho, P. R.; Rouseff, R. Processing and storage effects on orange juice aroma: A review. *J. Agric. Food Chem.* **2008**, *56*, 9785−9796.

(3) Liu, T.; Zhang, X.; Zhu, W.; Liu, W.; Zhang, D.; Wang, J. A G-quadruplex DNAzyme-based colorimetric method for facile detection of *Alicyclobacillus acidoterrestris*. *Analyst* **2014**, *139*, 4315−4321.

(4) Chang, S. S.; Kang, D. H. *Alicyclobacillus* spp. in the fruit juice industry: History, characteristics, and current isolation/detection procedures. *Crit. Rev. Microbiol.* **2004**, *30*, 55−74.

(5) Smit, Y.; Cameron, M.; Venter, P.; Witthuhn, R. C. Alicyclobacillus spoilage and isolation—A review. *Food Microbiol.* **2011**, *28*, 331−349.

(6) Danyluk, M. D.; Friedrich, L. M.; Jouquand, C.; Goodrich-Schneider, R.; Parish, M.; Rouseff, R. L. Prevalence, concentration, spoilage, and mitigation of *Alicyclobacillus* spp. in tropical and subtropical fruit juice concentrates. *Food Microbiol.* **2011**, *28*, 472−477.

(7) Schroeder, M.; Pöllinger-Zierler, B.; Aichernig, N.; Siegmund, B.; Guebitz, G. Enzymatic removal of off-flavors from apple juice. *J. Agric. Food Chem.* **2008**, *56*, 2485−2489.

(8) Bevilacqua, A.; Sinigaglia, M.; Corbo, M. R. *Alicyclobacillus acidoterrestris*: New methods for inhibiting spore germination. *Int. J. Food Microbiol.* **2008**, *125*, 103−110.

(9) Walker, M.; Phillips, C. A. *Alicyclobacillus acidoterrestris*: An increasing threat to the fruit juice industry. *Int. J. Food Sci. Technol.* **2008**, *43*, 250−260.

(10) Zhang, J. B.; Yue, T. L.; Yuan, Y. H. *Alicyclobacillus* contamination in the production line of kiwi products in China. *PLoS One* **2013**, *8*, No. e67704.

(11) Steyn, C. E.; Cameron, M.; Witthuhn, R. C. Occurrence of *Alicyclobacillus* in the fruit processing environment—A review. *Int. J. Food Microbiol.* **2011**, *147*, 1−11.

(12) Lee, S. Y.; Dancer, G. I.; Chang, S. S.; Rhee, M. S.; Kang, D. H. Efficacy of chlorine dioxide gas against *Alicyclobacillus acidoterrestris* spores on apple surfaces. *Int. J. Food Microbiol.* **2006**, *108*, 364−368.

(13) Walls, I.; Chuyate, R. Isolation of *Alicyclobacillus acidoterrestris* from fruit juices. *J. AOAC Int.* **2000**, *83*, 1115−1120.

(14) Wang, Z.; Wang, J.; Yue, T.; Yuan, Y.; Cai, R.; Niu, C. Immunomagnetic separation combined with polymerase chain reaction for the detection of *Alicyclobacillus acidoterrestris* in apple juice. *PLoS One* **2013**, *8*, No. e82376.

(15) Wang, Z.; Cai, R.; Yuan, Y.; Niu, C.; Hu, Z.; Yue, T. An immunomagnetic separation-real-time PCR system for the detection of *Alicyclobacillus acidoterrestris* in fruit products. *Int. J. Food Microbiol.* **2014**, *175*, 30−35.

(16) Shields, M. J.; Hahn, K. R.; Janzen, T. W.; Goji, N.; Thomas, M. C.; Kingombe, C. B.; Paquet, C.; Kell, A. J.; Amoako, K. K. Immunomagnetic capture of *Bacillus anthracis* spores from food. *J. Food Prot.* **2012**, *75*, 1243−1248.

(17) Hünniger, T.; Wessels, H.; Fischer, C.; Paschke-Kratzin, A.; Fischer, M. Just in time-selection: A rapid semiautomated SELEX of DNA aptamers using magnetic separation and BEAMing. *Anal. Chem.* **2014**, *86*, 10940−10947.

(18) Wang, J.; Gong, Q.; Maheshwari, N.; Eisenstein, M.; Arcila, M. L.; Kosik, K. S.; Soh, H. T. Particle display: A quantitative screening method for generating high-affinity aptamers. *Angew. Chem., Int. Ed.* **2014**, *53*, 4796−4801.

(19) Freeman, R.; Girsh, J.; Jou, A. F.; Ho, J. A.; Hug, T.; Dernedde, J.; Willner, I. Optical aptasensors for the analysis of the vascular endothelial growth factor (VEGF). *Anal. Chem.* **2012**, *84*, 6192−6198.

(20) Bruno, J. G.; Kiel, J. L. In vitro selection of DNA aptamers to anthrax spores with electrochemiluminescence detection. *Biosens. Bioelectron.* **1999**, *14*, 457−464.

(21) Ellington, A. D.; Szostak, J. W. In vitro selection of RNA molecules that bind specific ligands. *Nature* **1990**, *346*, 818−822.

(22) Hünniger, T.; Fischer, C.; Wessels, H.; Hoffmann, A.; Paschke-Kratzin, A.; Haase, I.; Fischer, M. Food sensing: Selection and characterization of DNA aptamers to *Alicyclobacillus* spores for trapping and detection from orange juice. *J. Agric. Food Chem.* **2015**, *63*, 2189−2197.

(23) Hübner, P.; Waiblinger, H. U.; Pietsch, K.; Brodmann, P. Validation of PCR methods for quantitation of genetically modified plants in food. *J. AOAC Int.* **2001**, *84*, 1855−1864.

(24) Andersen, C. B.; Holst-Jensen, A.; Berdal, K. G.; Thorstensen, T.; Tengs, T. Equal performance of TaqMan, MGB, molecular beacon, and SYBR Green-based detection assays in detection and quantification of roundup ready soybean. *J. Agric. Food Chem.* **2006**, *54*, 9658−9663.

(25) Herrero, B.; Madrinán, M.; Vieites, J. M.; ESPINeira, M. Authentication of Atlantic cod (*Gadus morhua*) using real time PCR. *J. Agric. Food Chem.* **2010**, *58*, 4794−4799.

(26) Connor, C. J.; Luo, H.; Gardener, B. B.; Wang, H. H. Development of a real-time PCR-based system targeting the 16S rRNA gene sequence for rapid detection of *Alicyclobacillus* spp. in juice products. *Int. J. Food Microbiol.* **2005**, *99*, 229−235.

(27) Luo, H.; Yousef, A. E.; Wang, H. H. A real-time polymerase chain reaction-based method for rapid and specific detection of spoilage *Alicyclobacillus* spp. in apple juice. *Lett. Appl. Microbiol.* **2004**, *39*, 376−382.

(28) Dineen, S. M.; Aranda, R. t.; Anders, D. L.; Robertson, J. M. An evaluation of commercial DNA extraction kits for the isolation of bacterial spore DNA from soil. *J. Appl. Microbiol.* **2010**, *109*, 1886−1896.

(29) Haase, I.; Bruning, P.; Matissek, R.; Fischer, M. Real-time PCR assays for the quantitation of rDNA from apricot and other plant species in marzipan. *J. Agric. Food Chem.* **2013**, *61*, 3414−3418.

(30) Prokopowich, C. D.; Gregory, T. R.; Crease, T. J. The correlation between rDNA copy number and genome size in eukaryotes. *Genome* **2003**, *46*, 48−50.

(31) Gausterer, C.; Stein, C.; Stimpfl, T. Application of direct PCR in a forensic case of yew poisoning. *Int. J. Legal Med.* **2012**, *126*, 315−319.

(32) European Network of Genetically Modified Organisms (GMO) Laboratories (ENGL). *Definition of Minimum Performance Requirements for Analytical Methods of GMO Testing*; ENGL: Brussels, Belgium, 2009.

(33) Ryu, C.; Lee, K.; Yoo, C.; Seong, W. K.; Oh, H. B. Sensitive and rapid quantitative detection of anthrax spores isolated from soil samples by real-time PCR. *Microbiol. Immunol.* **2003**, *47*, 693−699.

(34) Martinez-Blanch, J. F.; Sanchez, G.; Garay, E.; Aznar, R. Evaluation of a real-time PCR assay for the detection and

DOI: 10.1021/acs.jafc.5b00874
J. Agric. Food Chem. 2015, 63, 4291−4296

quantification of *Bacillus cereus* group spores in food. *J. Food Prot.* **2010**, *73*, 1480−1485.
(35) Makino, S. I.; Cheun, H. I.; Watarai, M.; Uchida, I.; Takeshi, K. Detection of anthrax spores from the air by real-time PCR. *Lett. Appl. Microbiol.* **2001**, *33*, 237−240.
(36) Dugan, L.; Bearinger, J.; Hinckley, A.; Strout, C.; Souza, B. Detection of *Bacillus anthracis* from spores and cells by loop-mediated isothermal amplification without sample preparation. *J. Microbiol. Methods* **2012**, *90*, 280−284.
(37) Guidi, V.; De Respinis, S.; Benagli, C.; Luthy, P.; Tonolla, M. A real-time PCR method to quantify spores carrying the *Bacillus thuringiensis* var. *israelensis* cry4Aa and cry4Ba genes in soil. *J. Appl. Microbiol.* **2010**, *109*, 1209−1217.
(38) Marentis, T. C.; Kusler, B.; Yaralioglu, G. G.; Liu, S.; Haeggstrom, E. O.; Khuri-Yakub, B. T. Microfluidic sonicator for real-time disruption of eukaryotic cells and bacterial spores for DNA analysis. *Ultrasound Med. Biol.* **2005**, *31*, 1265−1277.
(39) Gudnason, H.; Dufva, M.; Bang, D. D.; Wolff, A. Comparison of multiple DNA dyes for real-time PCR: effects of dye concentration and sequence composition on DNA amplification and melting temperature. *Nucleic Acids Res.* **2007**, *35*, No. e127.
(40) Ginzinger, D. G. Gene quantification using real-time quantitative PCR: An emerging technology hits the mainstream. *Exp. Hematol.* **2002**, *30*, 503−12.
(41) Ponchel, F.; Toomes, C.; Bransfield, K.; Leong, F. T.; Douglas, S. H.; Field, S. L.; Bell, S. M.; Combaret, V.; Puisieux, A.; Mighell, A. J.; Robinson, P. A.; Inglehearn, C. F.; Isaacs, J. D.; Markham, A. F. Real-time PCR based on SYBR-Green I fluorescence: An alternative to the TaqMan assay for a relative quantification of gene rearrangements, gene amplifications and micro gene deletions. *BMC Biotechnol.* **2003**, *3*, 18.
(42) Yin, J. L.; Shackel, N. A.; Zekry, A.; McGuinness, P. H.; Richards, C.; Putten, K. V.; McCaughan, G. W.; Eris, J. M.; Bishop, G. A. Real-time reverse transcriptase-polymerase chain reaction (RT-PCR) for measurement of cytokine and growth factor mRNA expression with fluorogenic probes or SYBR Green I. *Immunol. Cell Biol.* **2001**, *79*, 213−221.
(43) Morrison, T. B.; Weis, J. J.; Wittwer, C. T. Quantification of low-copy transcripts by continuous SYBR Green I monitoring during amplification. *BioTechniques* **1998**, *24* (954−958), 960−962.
(44) Santhosh, S. R.; Parida, M. M.; Dash, P. K.; Pateriya, A.; Pattnaik, B.; Pradhan, H. K.; Tripathi, N. K.; Ambuj, S.; Gupta, N.; Saxena, P.; Lakshmana Rao, P. V. Development and evaluation of SYBR Green I-based one-step real-time RT-PCR assay for detection and quantification of Chikungunya virus. *J. Clin. Virol.* **2007**, *39*, 188−193.
(45) Mayer, F.; Haase, I.; Graubner, A.; Heising, F.; Paschke-Kratzin, A.; Fischer, M. Use of polymorphisms in the γ-gliadin gene of spelt and wheat as a tool for authenticity control. *J. Agric. Food Chem.* **2012**, *60*, 1350−1357.
(46) International Organization for Standardization (ISO) *ISO 5725, Accuracy (Trueness and Precision) of Measurement Methods and Results*; ISO: Geneva, Switzerland, 1994.
(47) Wisotzkey, J. D.; Jurtshuk, P., Jr.; Fox, G. E.; Deinhard, G.; Poralla, K. Comparative sequence analyses on the 16S rRNA (rDNA) of *Bacillus acidocaldarius*, *Bacillus acidoterrestris*, and *Bacillus cycloheptanicus* and proposal for creation of a new genus, *Alicyclobacillus* gen. nov. *Int. J. Syst. Bacteriol.* **1992**, *42*, 263−269.

DOI: 10.1021/acs.jafc.5b00874
J. Agric. Food Chem. 2015, 63, 4291−4296

and size of azoxymethane-induced distal tumors in Fisher 344 male rats as compared with controls.[22] In humans, a combination of supplements curcumin and quercetin regressed adenomas in patients with FAP.[3] DIM synergistically suppressed the proliferation of human colorectal cancer cells when combined with sulforaphane.[23] DIM in combination with genistein resulted in decreased proliferation by working on estrogen and androgen receptors in vitro LNCaP PCa cells.[24] These and others have shown the potential for synergistic activity of multiple phytochemicals to exert greater anticancer effects.

In this study, we aimed to elucidate the anticancer properties of the combined use of capsaicin and DIM with regard to cell growth inhibition and apoptosis in human colon cancer cells. Here we report that treating cells with the combination of capsaicin and DIM results in inhibition of cell proliferation and increased apoptosis through targeting transcriptional activation of p53 and NF-κB and activation of genes downstream of these transcription factors.

MATERIALS AND METHODS

Chemicals and Reagents. Cell culture media, Dulbecco's modified Eagle medium (DMEM), was purchased from Lonza (Walkersville, MD, USA), and Eagle's minimum essential medium (EMEM) was purchased from American Type Culture Collection (Manassas, VA, USA). Antibodies for p21, p27, CDK4, CDK6, Bak, Bid, Bax, Puma, Fas-L, Traf2, and Traf3 were purchased from Cell Signaling (Danvers, MA, USA). Antibodies for p53, TBP, and actin was purchased from Santa Cruz Biotechnology Inc. (Santa Cruz, CA, USA), and Bcl-2 antibody was purchased from BD Bioscience (San Jose, CA, USA). Capsaicin (catalog no. E2028) was purchased from Sigma-Aldrich (St. Louis, MO, USA), and DIM (catalog no. BML-GR207) was purchased from Enzo Life Science (Farmingdale, NY, USA). Capsaicin and DIM were dissolved in ethanol and dimethyl sulfoxide (DMSO), respectively. All chemicals were purchased from Fisher Scientific, unless otherwise specified.

Cell Culture and Treatment. Human colorectal cancer cell lines, HCT116, SW480, LoVo, Caco-2, and HT-29 were purchased from American Type Culture Collection and grown in DMEM supplemented with 10% fetal bovine serum (FBS), 100 U/mL penicillin, and 100 μg/mL streptomycin. Human normal colon cells, CCD112CoN, were purchased from ATCC and grown in EMEM supplemented with 10% FBS. The cells were maintained at 37 °C under a humidified atmosphere of 5% CO_2. Ethanol and DMSO were used as a vehicle and added into culture media at 0.1% (v/v).

Measurement of Apoptosis. Apoptosis of HCT116 cells was measured according to the manufacturer's instruction of propidium iodide/annexin V-FITC apoptosis detection kit (BD Biosciences) as described previously.[25] Early apoptosis and late apoptosis were quantified by flow cytometry in FACS facility at the University of Maryland. Apoptosis of other human colorectal cancer cells were tested using a Cell Death Detection ELISAPLUS Kit (Roche Diagnostics, Indianapolis, IN, USA) as we described previously.[26]

Measurement of Cell Proliferation. Cell proliferation was assessed by using the 4,5-dimethylthiazol-2-yl)-2,5-diphenyltetrazolium bromide (MTT) (Sigma, St. Louis, MO, USA) method. The optical density was recorded at 490 nm using an enzyme-linked immunosorbent assay plate reader (Bio-Tek Instruments Inc., Winooski, VT, USA). Briefly, cells were plated at the concentration of 1000−2000 cells/well in 96-well tissue culture plates and then treated with capsaicin, DIM, or a combination as described in the figure captions. After 0, 24, and 48 h, MTT was added to each well and the plate was incubated for 3 h at 37 °C; absorbance was measured in an ELISA plate reader (Bio-Tek Instruments).

Transient Transfection and Luciferase Assay. Transient transfection for *NF-κB Luc* and *p53 Luc* plasmid was performed using a Polyjet DNA transfection reagent (SignaGen Laboratories, Ijamsville, MD, USA) according to the manufacturer's instructions. HCT116 cells (2×10^5 cells/well) were plated in 12-well plates in three replicates and incubated overnight. The next day, plasmid mixtures containing 1 μg of *NF-κB Luc* or *p53 Luc* and 0.1 μg of *pRL-null* were transfected into the cells for 24 h. The transfected cells were treated in the compounds for 24 h. The cells were harvested in 1× luciferase lysis buffer. The luciferase activity was measured and normalized to the *pRL-null* luciferase activity using a dual-luciferase assay kit (Promega).

Reverse Transcription (RT) Polymerase Chain Reaction (PCR). Total RNA was isolated from cells using the RNeasy Micro Kit (QIAGEN, Valencia, CA, USA), and cDNA was synthesized using a VERSO cDNA SYN RT KIT (Thermo Scientific). PCR was performed using PCR master mix (Promega) with targeted primers for p21, Bak, and GAPDH. The PCR primers were synthesized from Sigma-Aldrich. Amplification was performed under conditions of 95 °C for 10 min, followed by 35 cycles of 94 °C for 30 s, 55 °C for 30 s, and 72 °C for 45 s. Primer sequences are following: p21, forward 5′-GAGCGATGGAACTTCGACTT-3′ and reverse 5′-CAGGTCCACATGGTCTTCCT-3′; Bak, forward 5′-TCTGGCCCTACACGTCTACC-3′ and reverse 5′-ACAAACTGGCCCAACAGAAC-3′; GAPDH, forward 5′-ACCCAGAAGACTGTGGATGG-3′ and reverse 5′-TTCTAGACGGCAGGTCAGGT-3′. Reaction products were analyzed on 1% agarose gel.

SDS-PAGE and Western Blot. Cells were washed with ice-cold 1× phosphate-buffered saline (PBS) and lysed in radioimmunoprecipitation assay (RIPA) buffer (Boston Bioproduct Inc., Ashland, MA, USA) supplemented with protease and phosphatase inhibitor cocktail (Sigma-Aldrich) and centrifuged at 12000*g* for 10 min at 4 °C. After protein concentration was determined by the bicinchoninic acid (BCA) protein assay (Pierce, Rockford, IL, USA), equal amounts of proteins were subjected to 10 or 12% SDS-PAGE, and the separated protein was transferred onto nitrocellulose membranes (Osmonics, Minnetonka, MN, USA). The membranes were blocked for nonspecific binding with 5% nonfat milk in Tris-buffered saline containing 0.05% Tween 20 (TBS-T) for 1 h at room temperature and then probed with primary antibodies overnight at 4 °C, followed by incubation with horseradish peroxidase (HRP)-conjugated immunoglobulin G (IgG) for 1 h at room temperature. Chemiluminescence was detected with Pierce ECL Western Blotting substrate (Thermo Scientific) and visualized by Chemidoc MP Imaging system (Bio-Rad, Hercules, CA, USA).

Isolation of Cytosol and Nucleus Fraction. Cytosol and nuclear fraction of cells were prepared according to the manufacturer's protocols of a nuclear extraction kit (Active Motif, Carlsbad, CA, USA). Briefly, after HCT116 cells were treated in the compounds for 24 h, the cells were washed twice with ice-cold PBS containing phosphatase inhibitors (Sigma-Aldrich). Cells were harvested with hypotonic buffer containing detergent and incubated at 4 °C for 15 min. The supernatants (cytoplasmic fraction) were collected after centrifugation at 14000*g* for 1 min at 4 °C and stored at −80 °C. For nuclear fractions, cell pellets were resuspended with lysis buffer and incubated at 4 °C for 30 min under shaking. After 30 min, nuclear suspensions was centrifuged at 14000*g* for 10 min at 4 °C, and the supernatants (nuclear fraction) were stored at −80 °C for further analysis

Statistics. Statistical analysis was performed with IBM SPSS, and the data were analyzed by one-way ANOVA with Duncan's multiple-comparison tests. Data are expressed as means ± SD, and differences were considered significant at $P < 0.05$.

RESULTS

Effect of Compounds on Apoptosis and Cell Proliferation. Previously we studied the anticancer activity of capsaicin in human colorectal cancer.[16] To further extend our understanding of the anticancer activity of capsaicin, we screened several phytochemicals including EGCG, ECG, apigenin, genistein, DIM, and resveratrol for potential synergistic activity with capsaicin, based on the expression of a newly identified pro-apoptotic gene, NSAIDs-activated gene 1 (NAG-1). As a result, we found that capsaicin and DIM synergistically induced expression of NAG-1 gene (data not shown). Therefore, in the

DOI: 10.1021/jf506098s
J. Agric. Food Chem. 2015, 63, 4297−4304

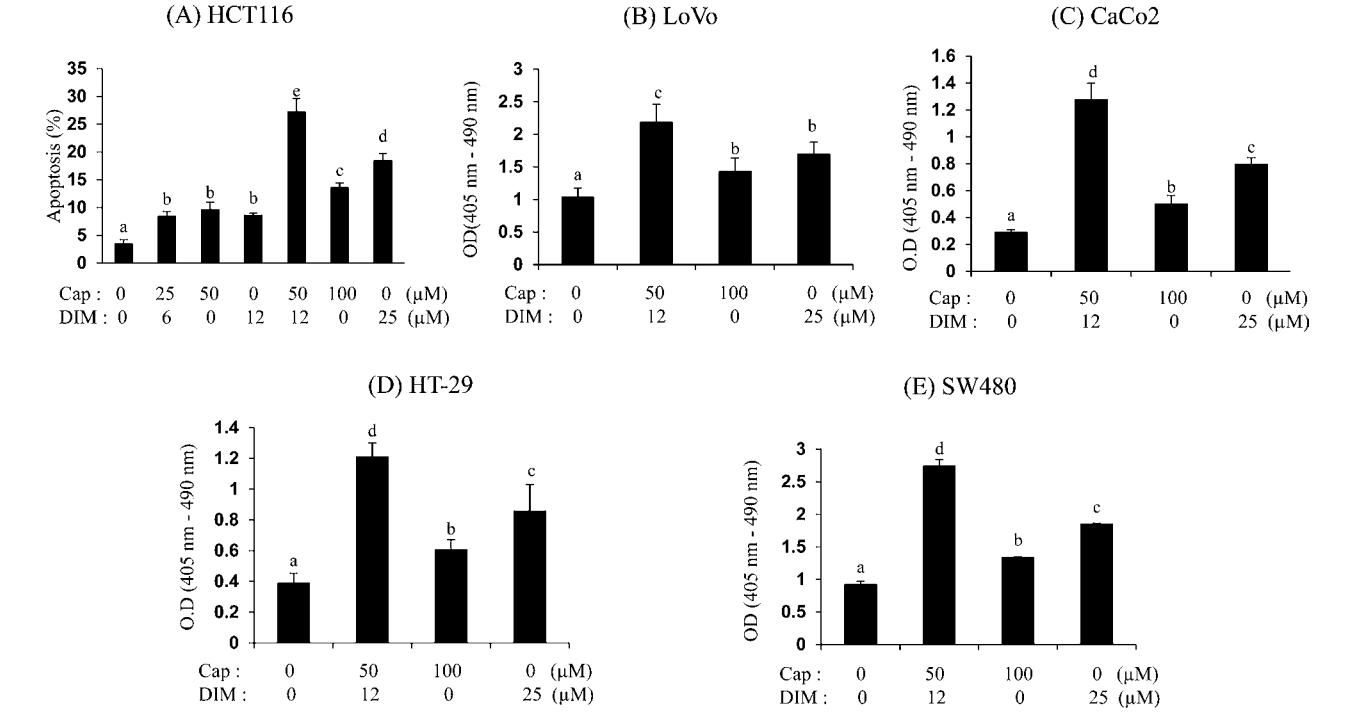

Figure 1. Synergistic effect of capsaicin and DIM on apoptosis of multiple human colorectal cancer cell lines. Apoptosis of different human colorectal cancer cells, HCT116 (A), LoVo (B), CaCo2 (C), HT-29 (D), and SW480 (E), was tested with FACS (HCT-116 cells) and a Cell Death Detection ELISA^{PLUS} Kit (Roche Diagnostics, Indianapolis, IN, USA) according to the manufacturer's instruction. Values are means ± SD, $n = 3$. Different letters indicate significant differences at $P < 0.05$.

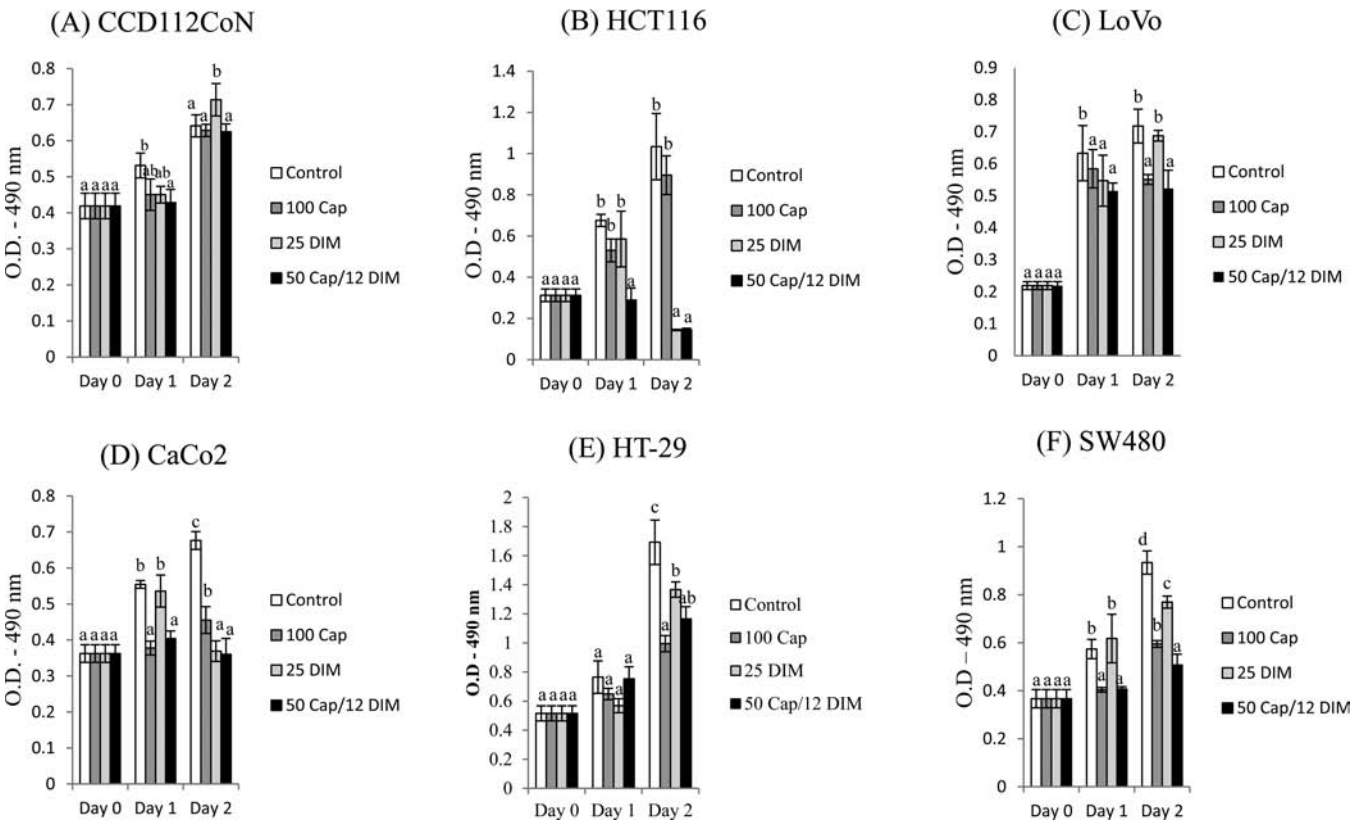

Figure 2. Combination treatment inhibits cell proliferation in multiple human colorectal cancer cell lines, but not normal colon cells. Normal human colon CCD112CoN (A) and human colorectal cancer cell lines HCT116 (B), LoVo (C), CaCo-2 (D), HT-29 (E), and SW480 (F) were plated onto a 96-well plate and grown overnight. The cells were treated with different concentrations of capsaicin (0 or 100 μM), DIM (0 or 25 μM), or a combination (50 μM capsaicin and 12 μM DIM) in media supplemented with 1% FBS for 24 and 48 h at 37 °C under 5% CO_2. Values are means ± SD, $n = 3$. Different letters indicate significant differences at $P < 0.05$.

DOI: 10.1021/jf506098s
J. Agric. Food Chem. 2015, 63, 4297−4304

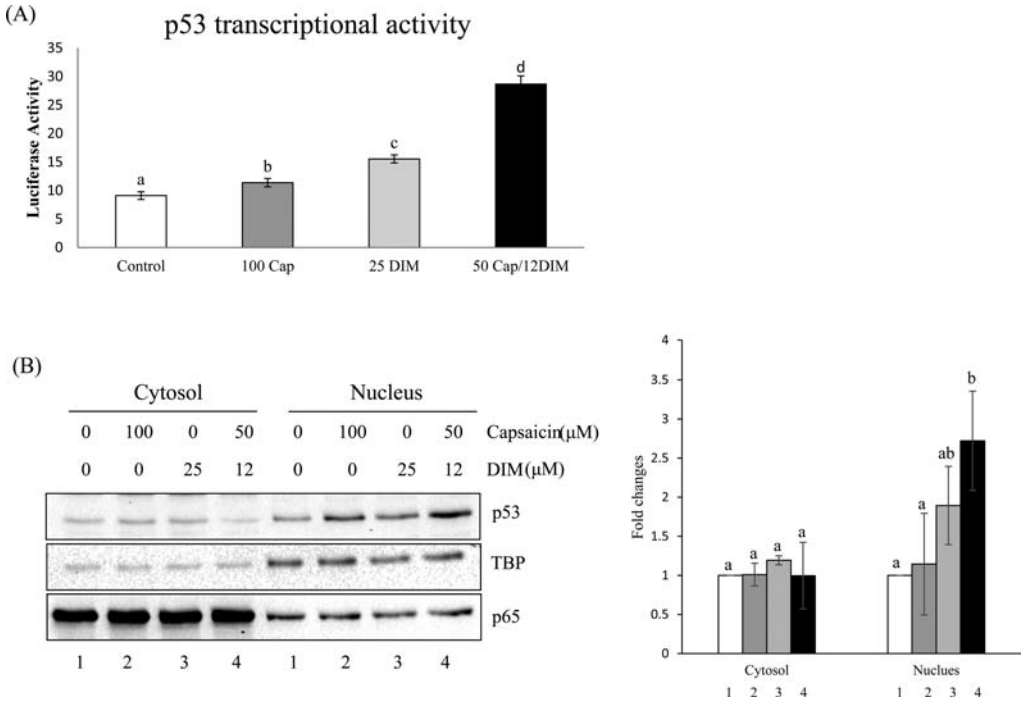

Figure 3. Combination treatment synergistically increases transcriptional activity of p53 and increases expression of p53 in nucleus. (A) HCT116 cells were transfected with plasmid containing 1 μg of p53 luciferase plasmid and 0.1 μg of pRL-null vector for 24 h at 37 °C. The transfected cells were then treated with the vehicle as the control or 100 μM capsaicin and 25 μM DIM individually or in combination for 24 h in serum-free media. The cells were harvested in 1× luciferase lysis buffer, and luciferase activity was measured. Values are means ± SD, $n = 3$. Different letters indicate significant differences at $P < 0.05$. (B) HCT116 cells were treated with 100 μM capsaicin and 25 μM DIM individually or combination for 24 h in serum-free media. Cells were washed with ice-cold PBS and harvested. The cytoplasm was separated from the nucleus and cell lysates were analyzed by Western blot for p53, TATA-binding protein (TBP), and p65. TBP was used as a nuclear loading control. The graph (right panel) indicates statistics of three independent experiments. Different letters indicate significant differences at $P < 0.05$ (1, control; 2, 100 μM capsaicin; 3, 25 μM DIM; 4, 50 μM capsaicin + 12 μM DIM combination).

present study, we hypothesize that capsaicin and DIM possess combinational anticancer activity.

To test this hypothesis, we treated HCT116 cells with different concentrations of the two compounds individually or combined and then measured apoptosis. As shown in Figure 1A, the combination of 50 μM capsaicin and 12 μM DIM resulted in a significant increase in the percentage of apoptotic cells. To assess if the compounds had the same effect in multiple colorectal cancer cell lines, LoVo, CaCo2, HT-29, and SW480 (Figure 1B–E) were all treated individually or in combination with the compounds. Interestingly, the combination of 50 μM capsaicin and 12 μM DIM significantly increased apoptosis in all of the cell lines. Thus, we chose this concentration for further study.

To assess the effect of treatment on normal colon cancer cells, CCD112CoN (Figure 2A) was treated with the compounds individually or in combination and cell proliferation was assessed. Whereas there was a small but significant decrease seen in cell proliferation following cotreatment for 24 h, this was not seen after 48 h of treatment. This is in agreement with others that have shown that capsaicin and DIM are nontoxic to normal cells.[10,27−29] However, when multiple colorectal cancer cell lines were treated with the compounds, significant inhibition of cell proliferation was noted in all cell lines (Figure 2B–F). Although the patterns of response of human colorectal cancer cells to capsaicin and DIM are different according to types of cells, the combination of low-dose capsaicin and DIM showed activity similar to that of high doses of single compounds in terms of suppressing cell proliferation. The synergistic antigrowth activity was also observed in non-colorectal cancer cell lines such as A549 and PC-3 (data not shown), indicating that antiproliferative activity by a combination of two dietary compounds might be common in human cancers.

Combination Treatment Increases Transcriptional Activity of p53 and Increases Expression in the Nucleus. The tumor suppressor gene p53 plays a major role in the regulation of apoptosis, cell cycle arrest, and DNA repair. Dysregulation of p53 leads to evasion of apoptosis and rapid growth of cancer cells;[30] many genes associated with cell cycle, senescence, DNA repair, and apoptosis are transcriptional targets of p53, and they are all essential barriers to tumor initiation and progression. Therefore, targeting p53 and the downstream transcriptional targets in cancer cells offers promising therapeutic interventions for cancer prevention and treatment.[31] For further study, we selected HCT116 cells, which is a p53 wild type, whereas other cell lines (CaCo-2, SW480, and HT-29) have truncated or point mutation of p53. To test if combination treatment targeted the p53 tumor suppressor, we measured the transcriptional activity of p53 in HCT116 cells transfected with the p53 luciferase plasmid. As shown in Figure 3A, treatment with the individual compounds resulted in increased transcriptional activity, but combination treatment was much more significant. To assess the level of p53 proteins in the cells, HCT116 cells were treated with the compounds for 24 h and harvested, and the cytoplasm and nucleus were separated. The fraction was analyzed by Western blotting for p53, and TATA-binding protein (TBP) and p65 were used as nuclear fraction marker and loading control, respectively. As seen in Figure 3B, there was an increase in the level of p53 in the nucleus of the cells

DOI: 10.1021/jf506098s
J. Agric. Food Chem. 2015, 63, 4297−4304

incubated with the combination of both capsaicin and DIM as compared to control and the individual compounds.

Combination Treatment Synergistically Increased Transcriptional Activity of NF-κB. The NF-κB family of transcription factors has been shown to play an important role in regulating apoptosis, in both inducing apoptosis and blocking it. It has also been shown to act on cell cycle regulation through sensitizing or desensitizing a cell to apoptotic signals. The dual roles of NF-κB transcription factors have led to much debate regarding its role in cancer initiation and progression.[32,33] Given that both p53 and NF-κB are transcription factors stimulated with cellular stress, and the compounds already have demonstrated the ability to increase p53 transcriptional activity, we tested if capsaicin and DIM affect the transcriptional activity of NF-κB. HCT116 cells were transfected with plasmid containing 1 μg of NF-κB luciferase plasmid and 0.1 μg of pRL-null vector for 24 h at 37 °C. The transfected cells were then treated with the vehicle as the control or capsaicin and DIM individually or in combination for 24 h. The cells were harvested in 1× luciferase lysis buffer, and luciferase activity was measured (Figure 4). Interestingly, the transcriptional activity of NF-κB significantly increased with combination treatment as compared with the individual compounds.

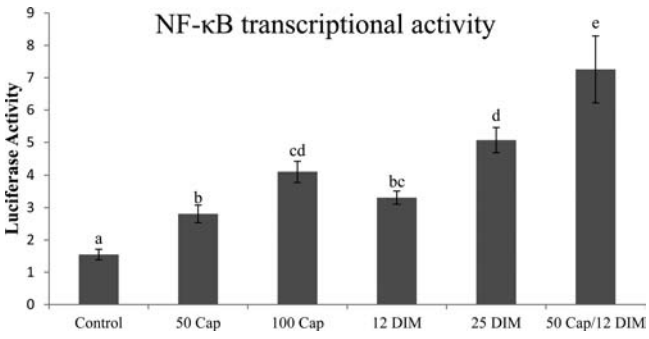

Figure 4. Combination treatment synergistically increases transcriptional activity of NF-κB. HCT116 cells were transfected with plasmid containing 1 μg of NF-κB luciferase plasmid and 0.1 μg of pRL-null vector for 24 h at 37 °C. The transfected cells were then treated with the vehicle as the control or 100 μM capsaicin and 25 μM DIM individually or combination for 24 h in serum-free media. The cells were harvested in 1× luciferase lysis buffer, and luciferase activity was measured. Values are means ± SD, $n = 3$. Different letters indicate significant differences at $P < 0.05$.

Effect of Combination Treatment on Expression of Genes Involved in Apoptosis and Cell Cycle. After observation of the effect of combination treatment on cell proliferation, apoptosis, p53, and NF-κB transcription, it was hypothesized that genes and proteins known to be regulated by p53 and NF-κB could be modulated through combination treatment. Western blot analysis was used to analyze target proteins that are involved in these processes, and RT-PCR was used to confirm mRNA levels of the target genes. As seen in Figure 5A, combination treatment resulted in increased expression of both p21 and 27 with subsequent inhibition of CDK4 and CDK 6. Treatment of HCT-116 cells with the combination of capsaicin and DIM significantly increased or tended to increase expression of multiple pro-apoptotic proteins (Figure 5B). Bak, BID, Bax, Puma, and Fas-L are all pro-apoptotic proteins that have been shown to be downstream of p53.[30,34,35]

Combination treatment resulted in down-regulation of pro-survival protein, Bcl-2 (Figure 5C). Bcl-2 inhibits apoptosis and has been shown to be overexpressed in many types of cancer cells.[36] Reduced Bcl-2 expression promotes apoptotic responses to anticancer drugs, whereas increased expression leads to resistance to chemotherapeutic drugs and radiation therapy and is a target to prevent drug resistance and increased apoptosis. Tumor necrosis factor receptor-associated factors 2 and 3 (Traf2 and Traf3) have also been shown to be oncogenes that regulate the noncanonical signaling of NF-κB. Previous groups have shown that suppression of Traf2 and Traf3 results in decreased proliferation and tumorigenesis.[37] Combination treatment resulted in down-regulation of these two oncogenes (Figure 5C).

Following treatment with capsaicin and DIM, cells were harvested, and RT-PCR was performed to analyze levels of mRNA for p21 and Bak (Figure 5D). Increased levels of p21 and Bak mRNA were identified following treatment with both capsaicin and DIM, although significantly so only in p21.

Modulation of Target Proteins in a p53-Dependent Manner. The p53 tumor suppressor protein performs a critical role in inducing apoptosis. Many of the pro-apoptotic Bcl-2 family members including Puma, Bax, and Bak have been reported to be transcriptional targets of p53.[34] Also, the cell cycle regulating proteins, p27 and p21, are also transcriptional targets of p53.[31] To test if the target genes modulated by combination treatment identified previously were dependent on p53, HCT116 p53 null cells were plated and treated with various concentrations of capsaicin individually (100 μM) and DIM individually (25 μM) as well as in combination (50 μM capsaicin and 12 μM DIM). The cells were harvested and the lysates subjected to analysis by Western blot. Interestingly, p21, p27, and Bak were all up-regulated in a p53-dependent manner (Figure 6).

DISCUSSION

There is growing evidence from in vitro and in vivo studies indicating that combinations of phytochemicals can result in significant activities at concentrations where any single agent is inactive. Here, we propose two mechanisms by which a combination of capsaicin and DIM increases apoptosis and changes expression of cell growth and apoptosis-related genes. First, we observed that the compounds increased transcriptional activity (Figure 3A) as well as p53 nuclear accumulation (Figure 3B). p53 accumulation in the nucleus seems to be associated with its protein stability. Ser15 phosphorylation of p53 suppresses ubiquitination of p53[38] and subsequent 26S proteasome-mediated degradation by reducing the interaction of p53 with E3 ligase and MDM2 and eventually promotes the accumulation and transactivation.[39] Most studies support that p53 degradation occurs exclusively on cytoplasmic proteasome by focusing on nuclear export of p53 via the CRM-1 pathway. However, proteasomes are abundant in both cytosol and nucleus, and many studies support proteosomal degradation of transcription factors in the nucleus. In addition, inhibition of proteasomal degradation using MG-132 leads to localization of p65 and p53 in nucleolus (fibrillar centers) compartments.[40]

Second, in the present study, we observed that combination of capsaicin and DIM synergistically increased the transcriptional activity of NF-κB. The transcription factor NF-κB is recognized as a key mediator of the cellular stress response upon anticancer therapy, and the activation of NF-κB can lead to a pro-death response. It is believed that increased NF-κB mediates apoptosis induced by anticancer agents.[41−44] Thus, further study is

DOI: 10.1021/jf506098s
J. Agric. Food Chem. 2015, 63, 4297−4304

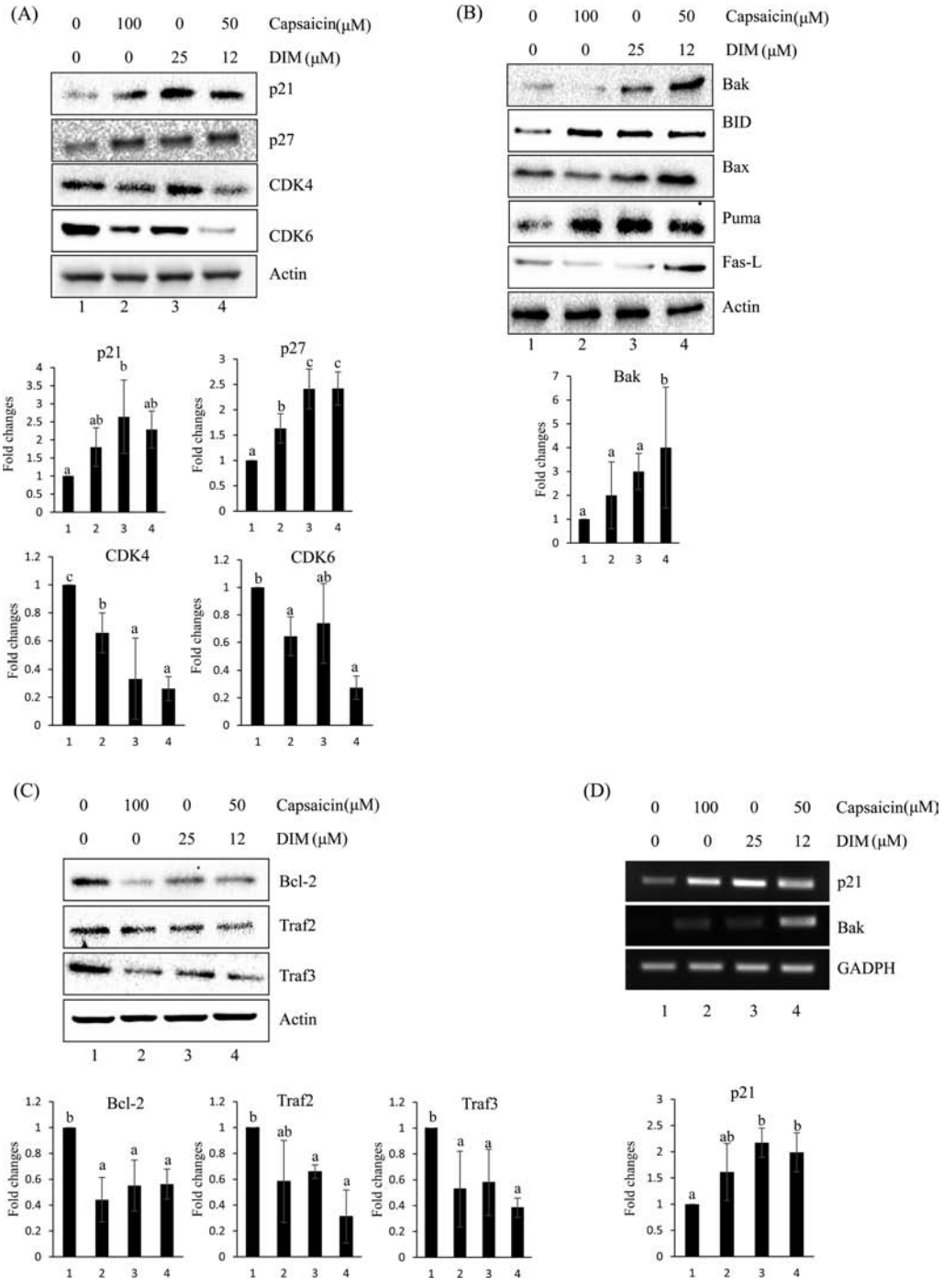

Figure 5. Analysis of protein and mRNA expressions in HCT116 cells treated with capsaicin and DIM. HCT116 cells were treated with different concentrations of capsaicin (0 or 100 μM), DIM (0 or 25 μM), or a combination (50 μM capsaicin and 12 μM DIM) for 24 h in serum-free media. The cells were harvested, and cell lysates were analyzed with Western blot for target proteins. (A) Expression of proteins regulating the cell cycle including p21, p27, CDK4, and CDK6. (B) Proteins with pro-apoptosis functions including Bak, BID, Bax, Puma, and Fas-L were analyzed. (C) Anti-apoptotic proteins including Bcl-2, Traf2, and Traf3 were analyzed. (D) HCT116 cells were treated with capsaicin (100 μM), DIM (25 μM), or a combination (50 μM capsaicin and 12 μM DIM) in serum-free media. Total mRNA was harvested and RT-PCR was performed. The graph indicates statistics of three independent experiments. Different letters indicate significant differences at $P < 0.05$ (1, control; 2, 100 μM capsaicin; 3, 25 μM DIM; 4, 50 μM capsaicin + 12 μM DIM combination).

required to investigate how compounds activate the transcriptional activity of NF-κB.

Although the main control of NF-κB activation is cytoplasmic IκB, recently many studies propose additional mechanisms that are required to activate or prevent activity of NF-κB protein. In fact, NF-κB recruitment is dynamically regulated by multiple signaling inputs, and NF-κB depends entirely on cooperative interactions with partner transcription factors for recruitment to some genes. NF-κB also can be regulated in the nucleus by complex mechanisms that are still obscure. They include post-translational modification and nuclear distribution of p65, which could determine cell fate, pro-apoptotic or anti-apoptotic, and

DOI: 10.1021/jf506098s
J. Agric. Food Chem. 2015, 63, 4297−4304

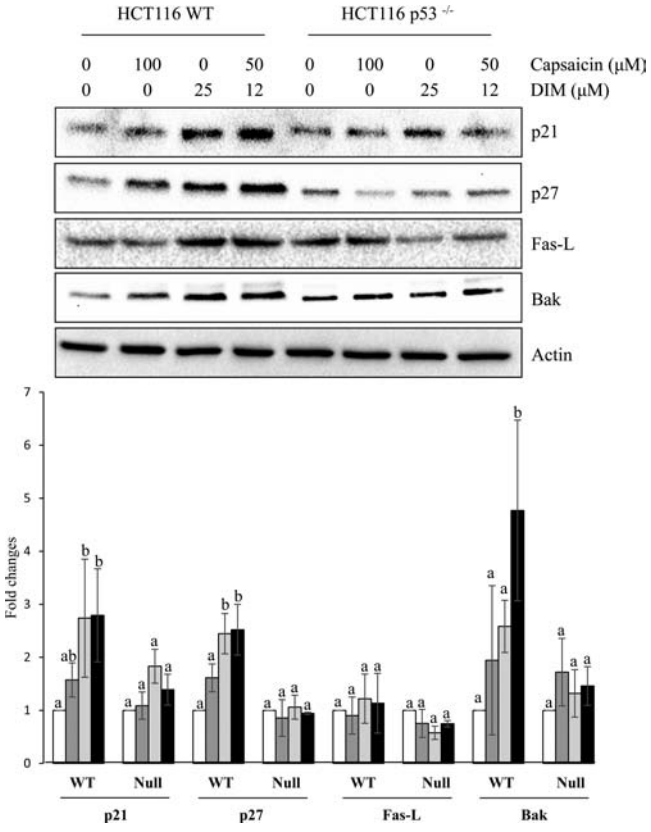

Figure 6. Modulation of target proteins in a p53-dependent manner. HCT116 wild type (WT) and HCT116 p53 null (−/−) cells were treated with capsaicin (100 μM), DIM (25 μM), or a combination (50 μM capsaicin and 12 μM DIM) for 24 h in serum-free media. The cells were harvested, and cell lysates were analyzed with Western blot for target proteins. The graph indicates statistics of three independent experiments. Different letters indicate significant differences at $P < 0.05$.

influence its transcriptional activity. For example, an increased accumulation of p65 in nucleoplasm results in apoptosis, whereas accumulation of p65 in nucleolus is a mechanism of apoptosis activation in response to apoptotic stimuli.[45]

Another interesting point is that p53 and NF-κB have shown an ability to interact with each other and coordinate induction of apoptosis. For example, many pro-apoptotic stimuli such as DNA-damaging agents lead to transcriptional coactivation of p53 and NF-κB. Ryan et al.[46] suggested that p53 directly activates transcriptional activity of NF-κB, which is required for p53-induced apoptosis. Other studies demonstrate that p53-dependent NF-κB activation could contribute to the apoptotic response,[47] and the loss of p53 could abrogate NF-κB-mediated apoptotic response.[48] p65 has been reported to promote apoptosis by actively repressing transcription of anti-apoptotic genes through association of p65 with histone deacetylase-containing complexes acting as co-repressor.[49] Overall, even though we did not study direct interaction between p53 and NF-κB, it is possible that both NF-κB and p53 may be essential for apoptosis induced by combination treatment. Fas ligand (FasL) is believed to be a common target for p53 and NF-κB, and induction of FasL is required for p53- and NF-κB-dependent apoptosis.[50−52] Therefore, FasL is a good target protein for studying p65- and p53-mediated apoptosis. Although we claim that p53 mediates capsaicin and DIM's effect, we do not exclude the possibility that this combination suppressed cell proliferation and induced apoptosis through a p53-independent mechanism because some cell lines such as SW480 and CaCo-2 are p53 mutants, and we showed in these cell lines increased apoptosis and inhibited cell proliferation with combinations (Figures 1 and 2).

In summary, the data presented here show that combination treatment is able to work synergistically to mediate inhibition of cell proliferation and induction of apoptosis. Interestingly, the compounds targeted p53 and NF-κB transcriptional factors and modulated known downstream target proteins. Dietary phytochemicals offer a safe colorectal cancer preventive alternative for targeting multiple pathways.

AUTHOR INFORMATION

Corresponding Author

*(S.-H.L.) Phone: (301) 405-4532. Fax: (301) 314-3313. E-mail: slee2000@umd.edu.

Funding

This work was supported by start-up funds from the University of Maryland to S.-H.L. This work is also supported in part by grant from the National Institutes of Health (R03CA137755) to S.-H.L.

Notes

The authors declare no competing financial interest.

ACKNOWLEDGMENTS

We thank Dr. Jin Boo Jeong for his technical support. We also thank Dr. Seung Joon Baek for providing p53 null HCT116 cells.

REFERENCES

(1) Glade, M. J., Food, nutrition, and the prevention of cancer: a global perspective. American Institute for Cancer Research/World Cancer Research Fund, American Institute for Cancer Research, 1997. *Nutrition* **1999**, *15*, 523−526.

(2) Riboli, E.; Norat, T. Epidemiologic evidence of the protective effect of fruit and vegetables on cancer risk. *Am. J. Clin. Nutr.* **2003**, *78*, 559s−569s.

(3) Cruz-Correa, M.; Shoskes, D. A.; Sanchez, P.; Zhao, R.; Hylind, L. M.; Wexner, S. D.; Giardiello, F. M. Combination treatment with curcumin and quercetin of adenomas in familial adenomatous polyposis. *Clin. Gastroenterol. Hepatol.* **2006**, *4*, 1035−1038.

(4) Lee, J. G.; Yon, J. M.; Lin, C.; Jung, A. Y.; Jung, K. Y.; Nam, S. Y. Combined treatment with capsaicin and resveratrol enhances neuroprotection against glutamate-induced toxicity in mouse cerebral cortical neurons. *Food Chem. Toxicol.* **2012**, *50*, 3877−3885.

(5) Shukla, Y.; George, J. Combinatorial strategies employing nutraceuticals for cancer development. *Ann. N. Y. Acad. Sci.* **2011**, *1229*, 162−175.

(6) de Kok, T. M.; van Breda, S. G.; Manson, M. M. Mechanisms of combined action of different chemopreventive dietary compounds: a review. *Eur. J. Nutr.* **2008**, *47* (Suppl. 2), 51−59.

(7) Liu, R. H. Potential synergy of phytochemicals in cancer prevention: mechanism of action. *J. Nutr.* **2004**, *134*, 3479S−3485S.

(8) Dragsted, L. O.; Strube, M.; Larsen, J. C. Cancer-protective factors in fruits and vegetables: biochemical and biological background. *Pharmacol. Toxicol.* **1993**, *72* (Suppl. 1), 116−35.

(9) Liu, R. H. Health benefits of fruit and vegetables are from additive and synergistic combinations of phytochemicals. *Am. J. Clin. Nutr.* **2003**, *78*, 517s−520s.

(10) Bley, K.; Boorman, G.; Mohammad, B.; McKenzie, D.; Babbar, S. A comprehensive review of the carcinogenic and anticarcinogenic potential of capsaicin. *Toxicol. Pathol.* **2012**, *40*, 847−873.

(11) Lee, J. S.; Chang, J. S.; Lee, J. Y.; Kim, J. A. Capsaicin-induced apoptosis and reduced release of reactive oxygen species in MBT-2 murine bladder tumor cells. *Arch. Pharmacal Res.* **2004**, *27*, 1147−1153.

DOI: 10.1021/jf506098s
J. Agric. Food Chem. 2015, 63, 4297−4304

(12) Surh, Y. J. More than spice: capsaicin in hot chili peppers makes tumor cells commit suicide. *J. Natl. Cancer Inst.* **2002**, *94*, 1263−1265.
(13) Srinivasan, K. Antioxidant potential of spices and their active constituents. *Crit. Rev. Food Sci. Nutr.* **2014**, *54*, 352−372.
(14) Iqbal, Q.; Amjad, M.; Asi, M. R.; Ariño, A. Characterization of capsaicinoids and antioxidants in hot peppers as influenced by hybrid and harvesting stage. *Plant Foods Hum. Nutr.* **2013**, *68*, 358−363.
(15) Jorge, L. L.; Feres, C. C.; Teles, V. E. Topical preparations for pain relief: efficacy and patient adherence. *J. Pain Res.* **2011**, *4*, 11−24.
(16) Lee, S. H.; Krisanapun, C.; Baek, S. J. NSAID-activated gene-1 as a molecular target for capsaicin-induced apoptosis through a novel molecular mechanism involving GSK3β, C/EBPβ and ATF3. *Carcinogenesis* **2010**, *31*, 719−728.
(17) Chang, X.; Tou, J. C.; Hong, C.; Kim, H. A.; Riby, J. E.; Firestone, G. L.; Bjeldanes, L. F. 3,3′-Diindolylmethane inhibits angiogenesis and the growth of transplantable human breast carcinoma in athymic mice. *Carcinogenesis* **2005**, *26*, 771−778.
(18) Beaver, L. M.; T, Y.; Sokolowski, E. I.; Williams, D. E.; Dashwood, R. H.; Ho, E. 3,3′-Diindolylmethane, but not indole-3-carbinol, inhibits histone deacetylase activity in prostate cancer cells. *Toxicol. Appl. Pharmacol.* **2012**, *263*, 345−351.
(19) Abdelrahim, M.; Newman, K.; Vanderlaag, K.; Samudio, I.; Safe, S. 3,3′-Diindolylmethane (DIM) and derivatives induce apoptosis in pancreatic cancer cells through endoplasmic reticulum stress-dependent upregulation of DR5. *Carcinogenesis* **2006**, *27*, 717−728.
(20) Kim, E. J.; S, P.; Shin, H. K.; Kwon, D. Y.; Surh, Y. J.; Park, J. H. Activation of caspase-8 contributes to 3,3′-diindolylmethane-induced apoptosis in colon cancer cells. *J. Nutr.* **2007**, *137*, 31−36.
(21) Manikandan, R.; B, M.; Arulvasu, C.; Sellamuthu, S.; Dinesh, D.; Prabhu, D.; Babu, G.; Vaseeharan, B.; Prabhu, N. M. Synergistic anticancer activity of curcumin and catechin: an in vitro study using human cancer cell lines. *Microsc. Res. Tech.* **2012**, *75*, 112−116.
(22) Khatiwada, J.; Verghese, M.; Davis, S.; Williams, L. L. Green tea, phytic acid, and inositol in combination reduced the incidence of azoxymethane-induced colon tumors in Fisher 344 male rats. *J. Med. Food* **2011**, *14*, 1313−1320.
(23) Pappa, G.; Strathmann, J.; Lowinger, M.; Bartsch, H.; Gerhauser, C. Quantitative combination effects between sulforaphane and 3,3′-diindolylmethane on proliferation of human colon cancer cells in vitro. *Carcinogenesis* **2007**, *28*, 1471−1477.
(24) Smith, S.; Sepkovic, D.; Bradlow, H. L.; Auborn, K. J. 3,3′-Diindolylmethane and genistein decrease the adverse effects of estrogen in LNCaP and PC-3 prostate cancer cells. *J. Nutr.* **2008**, *138*, 2379−2385.
(25) Choi, J.; Jiang, X.; Jeong, J. B.; Lee, S. H. Anticancer activity of protocatechualdehyde in human breast cancer cells. *J. Med. Food* **2014**, *17*, 842−848.
(26) Jeong, J. B.; Choi, J.; Lou, Z.; Jiang, X.; Lee, S. H. Patchouli alcohol, an essential oil of *Pogostemon cablin*, exhibits anti-tumorigenic activity in human colorectal cancer cells. *Int. Immunopharmacol.* **2013**, *16*, 184−190.
(27) Chanda, S.; Erexson, G.; Riach, C.; Innes, D.; Stevenson, F.; Murli, H.; Bley, K. Genotoxicity studies with pure *trans*-capsaicin. *Mutat. Res., Genet. Toxicol. Environ. Mutagen.* **2004**, *557*, 85−97.
(28) Proudlock, R.; Thompson, C.; Longstaff, E. Examination of the potential genotoxicity of pure capsaicin in bacterial mutation, chromosome aberration, and rodent micronucleus tests. *Environ. Mol. Mutagen.* **2004**, *44*, 441−447.
(29) Leibelt, D. A.; Hedstrom, O. R.; Fischer, K. A.; Pereira, C. B.; Williams, D. E. Evaluation of chronic dietary exposure to indole-3-carbinol and absorption-enhanced 3,3′-diindolylmethane in Sprague-Dawley rats. *Toxicol. Sci.* **2003**, *74*, 10−21.
(30) Fridman, J. S.; Lowe, S. W. Control of apoptosis by p53. *Oncogene* **2003**, *22*, 9030−40.
(31) Carr, A. M. Cell cycle. Piecing together the p53 puzzle. *Science* **2000**, *287*, 1765−1766.
(32) Hoesel, B.; Schmid, J. A. The complexity of NF-κB signaling in inflammation and cancer. *Mol. Cancer* **2013**, *12*, 86.
(33) Perkins, N. D. NF-κB: tumor promoter or suppressor? *Trends Cell Biol.* **2004**, *14*, 64−69.
(34) Chipuk, J. E.; Kuwana, T.; Bouchier-Hayes, L.; Droin, N. M.; Newmeyer, D. D.; Schuler, M.; Green, D. R. Direct activation of Bax by p53 mediates mitochondrial membrane permeabilization and apoptosis. *Science* **2004**, *303*, 1010−1014.
(35) Hemann, M. T.; Lowe, S. W. The p53-Bcl-2 connection. *Cell Death Differ.* **2006**, *13*, 1256−1259.
(36) Borner, C. The Bcl-2 protein family: sensors and checkpoints for life-or-death decisions. *Mol. Immunol.* **2003**, *39*, 615−647.
(37) Shen, R. R.; Zhou, A. Y.; Kim, E.; O'Connell, J. T.; Hagerstrand, D.; Beroukhim, R.; Hahn, W. C. TRAF2 is an NF-κB-activating oncogene in epithelial cancers. *Oncogene* **2013**, *34*, 209−216.
(38) She, Q. B.; Chen, N.; Dong, Z. ERKs and p38 kinase phosphorylate p53 protein at serine 15 in response to UV radiation. *J. Biol. Chem.* **2000**, *275*, 20444−20449.
(39) Kubbutat, M. H.; Jones, S. N.; Vousden, K. H. Regulation of p53 stability by Mdm2. *Nature* **1997**, *387*, 299−303.
(40) Karni-Schmidt, O.; Zupnick, A.; Castillo, M.; Ahmed, A.; Matos, T.; Bouvet, P.; Cordon-Cardo, C.; Prives, C. p53 is localized to a sub-nucleolar compartment after proteasomal inhibition in an energy-dependent manner. *J. Cell Sci.* **2008**, *121*, 4098−4105.
(41) Perkins, N. D.; Gilmore, T. D. Good cop, bad cop: the different faces of NF-κB. *Cell Death Differ.* **2006**, *13*, 759−772.
(42) Baud, V.; Karin, M. Is NF-κB a good target for cancer therapy? Hopes and pitfalls. *Nat. Rev. Drug Discovery* **2009**, *8*, 33−40.
(43) Jin, F.; Liu, X.; Zhou, Z.; Yue, P.; Lotan, R.; Khuri, F. R.; Chung, L. W.; Sun, S. Y. Activation of nuclear factor-κB contributes to induction of death receptors and apoptosis by the synthetic retinoid CD437 in DU145 human prostate cancer cells. *Cancer Res.* **2005**, *65*, 6354−6363.
(44) Farhana, L.; Dawson, M. I.; Fontana, J. A. Apoptosis induction by a novel retinoid-related molecule requires nuclear factor-κB activation. *Cancer Res.* **2005**, *65*, 4909−4917.
(45) Stark, L. A.; Dunlop, M. G. Nucleolar sequestration of RelA (p65) regulates NF-κB-driven transcription and apoptosis. *Mol. Cell. Biol.* **2005**, *25*, 5985−6004.
(46) Ryan, K. M.; Ernst, M. K.; Rice, N. R.; Vousden, K. H. Role of NF-κB in p53-mediated programmed cell death. *Nature* **2000**, *404*, 892−897.
(47) Bohuslav, J.; Chen, L. F.; Kwon, H.; Mu, Y.; Greene, W. C. p53 induces NF-κB activation by an IκB kinase-independent mechanism involving phosphorylation of p65 by ribosomal S6 kinase 1. *J. Biol. Chem.* **2004**, *279*, 26115−26125.
(48) Fujioka, S.; Schmidt, C.; Sclabas, G. M.; Li, Z. K.; Pelicano, H.; Peng, B.; Yao, A.; Niu, J. G.; Zhang, W.; Evans, D. B.; Abbruzzese, J. L.; Huang, P.; Chiao, P. J. Stabilization of p53 is a novel mechanism for proapoptotic function of NF-κB. *J. Biol. Chem.* **2004**, *279*, 27549−27559.
(49) Campbell, K. J.; Rocha, S.; Perkins, N. D. Active repression of antiapoptotic gene expression by RelA(p65) NF-κB. *Mol. Cell* **2004**, *13*, 853−965.
(50) Okazaki, T.; Sakamuro, D. Induction of Fas (CD95/APO-1) ligand is essential for p53-dependent apoptosis in an in vitro renal carcinoma model system. *J. Cancer Res. Clin. Oncol.* **2007**, *133*, 581−588.
(51) Muller, M.; Strand, S.; Hug, H.; Heinemann, E. M.; Walczak, H.; Hofmann, W. J.; Stremmel, W.; Krammer, P. H.; Galle, P. R. Drug-induced apoptosis in hepatoma cells is mediated by the CD95 (APO-1/Fas) receptor/ligand system and involves activation of wild-type p53. *J. Clin. Invest.* **1997**, *99*, 403−413.
(52) Kasibhatla, S.; Brunner, T.; Genestier, L.; Echeverri, F.; Mahboubi, A.; Green, D. R. DNA damaging agents induce expression of Fas ligand and subsequent apoptosis in T lymphocytes via the activation of NF-κB and AP-1. *Mol. Cell* **1998**, *1*, 543−551.

DOI: 10.1021/jf506098s
J. Agric. Food Chem. 2015, 63, 4297−4304

NASH. Therefore, in the present study, we investigated whether genistein alleviates NASH development in *db/db* mice fed an MCD diet.

MATERIAL AND METHODS

Animals and Diets. At 5 weeks of age, male C57BLKS/J-*db/db* mice were purchased from Japan SLC, Inc. (Hamamatsu, Japan). After a 2 week acclimation period, confirmed high-glucose *db/db* mice were randomly divided into three groups and fed a control MCS diet (no. 518811; Dyets Inc., Bethlehem, PA), an MCD diet (no. 518810), or an MCD diet supplemented with genistein (0.5 g/kg diet; ChromaDex Inc., Irvine, CA) for 6 weeks. A previous study reported that the serum genistein concentration of C57BL/6J mice fed a genistein-supplemented diet (0.6 g/kg diet) for 4 weeks was 3.97 μmol/L,[20] which is similar to that detected in women consuming soy products.[21] Body weight was recorded every week, and blood glucose levels were measured with a glucose meter (Accu-chekGo, Roche, Basel, Switzerland) after 6 h of fasting. All mice were maintained in a temperature-controlled (22 ± 3 °C), humidity-controlled (50 ± 10%) room with a 12 h dark−light cycle. All treatment protocols for this study were approved by the Seoul National University Institutional Animal Care and Use Committee (SNU-100524-5). At the end of the study, the mice fasted for 16 h, blood was collected by cardiac puncture, and tissues were removed, quickly frozen in liquid nitrogen, and stored at −80 °C until analysis.

Serum and Hepatic Biochemical Analyses. Serum was analyzed using commercial colorimetric assay kits (Asan Pharmaceutical Co., Seoul, Korea) for glucose, triglycerides, total cholesterol, and alanine aminotransferase (ALT) according to the manufacturer's protocol. Serum insulin levels were measured using an insulin ELISA kit (Millipore, Billerica, MA). Homeostasis model assessment-insulin resistance (HOMA-IR) was calculated using the following formula: HOMA-IR = [fasting glucose (mmol/L) × fasting insulin (μU/mL)]/22.5.

Hepatic total lipids were extracted according to the method of Folch et al.[22] Triglyceride and cholesterol concentrations were determined using the same commercial kits used in serum samples. Hepatic thiobarbituric acid reactive substances (TBARS) were measured according to the method of Ohkawa et al.[23] The absorbance of the butanol layer was measured at 532 nm using 1,1,3,3-tetraethoxypropane as a standard. The hepatic lipid peroxide level was expressed as malondialdehyde equivalents per milligram of protein. The protein content of the homogenate was measured with a protein assay kit (Bio-Rad, Hercules, CA).

Liver Histology Examination. Formalin-fixed liver tissue was processed into 4-μm-thick paraffin sections and stained with hematoxylin and eosin (H&E) for histological evaluation. Liver fibrosis was assessed with Masson's trichrome staining for collagen fibers. The morphology was observed under an Olympus BX50 microscope with a DP-72 digital camera (Olympus, Japan), and the image was captured using the Image-Pro Plus ver. 4.5 program (Media Cybernetics Inc., USA).

Immunoblotting. Liver tissues were homogenized in 10 volumes (w/v) of ice-cold protein lysis buffer. Thirty micrograms of protein was loaded into the lanes of an SDS-PAGE gel, separated, and blotted onto a PVDF membrane. After being blocked with 5% nonfat milk or bovine serum albumin in TTBS, membranes were probed with specific antibodies diluted in TTBS with 5% nonfat milk or bovine serum albumin as follows: anti-AMP kinase alpha (AMPKα; Cell Signaling, Danvers, MA), anti-p-AMPKα (Cell Signaling), anti-C/EBP homologous protein (CHOP; Santa Cruz Biotechnology, Santa Cruz, CA), anti-KDEL (Enzo Life Sciences, Farmingdale, NY), or anti-70-kDa heat shock cognate protein (HSC70; Santa Cruz Biotechnology). The membranes were then incubated with an IgG-peroxidase-conjugated secondary antibody for chemiluminescent detection. The band intensities were quantified using Quantity One software (Bio-Rad).

Semiquantitative and Quantitative PCR (qPCR) Analyses. The total RNA of the liver tissues was isolated using the RNAiso Plus (Takara Bio Inc., Otsu, Japan), and cDNA was synthesized with SuperscriptII Reverse Transcriptase (Invitrogen, Carlsbad, CA). Hepatic mRNA levels were analyzed by qPCR with a StepOne Real Time PCR System (Applied Biosystems, Carlsbad, CA) using the SYBR Green PCR Master Mix (Applied Biosystems). Mouse ribosomal protein L19 (RPL19) was used as a reference gene, and relative gene expression levels were analyzed using the $2^{-\Delta\Delta}$Ct method. To determine mRNA levels of spliced XBP-1, semi-quantitative PCR was used as previously described.[24] The expression of β-actin was examined as an internal control. The primer sequences are described in Supporting Information Table S1.

Statistical Analysis. All data were analyzed using SPSS software (ver. 21.0, SPSS Inc., Chicago, IL). For all experiments, one-way ANOVA followed by Duncan's multiple range test or the Student *t* test was employed to assess the statistical significance. Data were expressed as the mean ± SEM, and differences were considered to be statistically significant at $P < 0.05$.

RESULTS

Effects of Genistein on Body Weight and Serum Biochemical Parameters in *db/db* Mice Fed an MCD Diet. We observed a gradual body weight decrease in *db/db* mice fed an MCD diet (Supporting Information Figure S1). Blood glucose was also significantly reduced in mice fed an MCD diet within a week. Consistently, the epididymal fat mass weight was significantly lower in *db/db* mice fed an MCD diet than those fed an MCS diet (Table 1). Genistein supplementation significantly increased the relative epididymal fat mass weight. Although MCD feeding significantly reduced the relative liver weight, the effect of genistein on liver weight was not observed.

Table 1. Characteristics of *db/db* Mice Fed an MCS, MCD, or MCD with Genistein Diet[a]

	MCS	MCD	MCD + GEN
final body weight (g)	42.0 ± 1.4[b]	29.1 ± 1.2[a]	29.8 ± 1.1[a]
epididymal fat (g)	2.27 ± 0.10[b]	1.47 ± 0.08[a]	1.69 ± 0.08[a]
relative epididymal fat weight (% of body weight)	5.47 ± 0.21[ab]	5.01 ± 0.10[a]	5.67 ± 0.09[b]
liver weight (g)	3.47 ± 0.26[b]	1.62 ± 0.10[a]	1.69 ± 0.10[a]
relative liver weight (% of body weight)	8.19 ± 0.38[b]	5.55 ± 0.27[a]	5.64 ± 0.19[a]

[a]Results are given as the mean ± SEM ($n = 10$). Means that do not share the same superscript are significantly different by ANOVA ($P < 0.05$).

Table 2. Fasting Serum Biochemical Analyses of *db/db* Mice Fed an MCS, MCD, or MCD with Genistein Diet[a,*]

	MCS	MCD	MCD + GEN
glucose (mg/dL)	765.9 ± 74.7[b]	105.4 ± 7.1[a]	127.0 ± 14.4[a]
insulin (ng/mL)	1.59 ± 0.24[c]	0.92 ± 0.13[b]	0.39 ± 0.09[a]
HOMA-IR	67.86 ± 12.00[a]	5.63 ± 1.04[b]	2.48 ± 0.34[b]*
triglyceride (mg/dL)	122.8 ± 14.0	121.4 ± 12.8	108.4 ± 2.9
total cholesterol (mg/dL)	230.9 ± 21.9[b]	126.7 ± 4.7[a]	128.3 ± 10.7[a]
ALT (IU/L)	180.1 ± 23.6[a]	332.1 ± 43.9[b]	296.8 ± 9.8[b]

[a]Results are given as the mean ± SEM ($n = 7$). Means that do not share the same superscript are significantly different ($P < 0.05$). *MCD vs MCD + GEN by the *t* test ($P < 0.05$).

We observed significantly reduced serum glucose and insulin levels and HOMA-IR in mice fed an MCD diet compared to mice fed an MCS diet (Table 2). Supplementation of genistein

DOI: 10.1021/acs.jafc.5b00398
J. Agric. Food Chem. 2015, 63, 4305−4311

significantly reduced serum insulin levels and HOMA-IR (P = 0.014, t test). MCD feeding significantly reduced serum total cholesterol levels but not serum triglyceride levels. Serum ALT levels were significantly increased in *db*/*db* mice compared to those in mice fed an MCD diet, but there was no significant effect of genistein on serum ALT levels.

Effects of Genistein on Liver Steatosis in *db*/*db* Mice Fed an MCD Diet. The MCD diet significantly increased hepatic triglyceride levels in *db*/*db* mice (Figure 1A). The supplementation of an MCD diet with genistein did not alleviate the accumulation of hepatic triglyceride in *db*/*db* mice. There was no significant difference in hepatic cholesterol levels among the groups. The microscopic examination of H&E staining of liver tissues was consistent with hepatic lipid biochemical characteristics (Figure 1B). We observed the microvascular steatosis in *db*/*db* mice fed an MCS diet. Interestingly, the MCD diet induced macrovascular steatosis and inflammatory foci, which were less observed in *db*/*db* mice fed a genistein-supplemented diet.

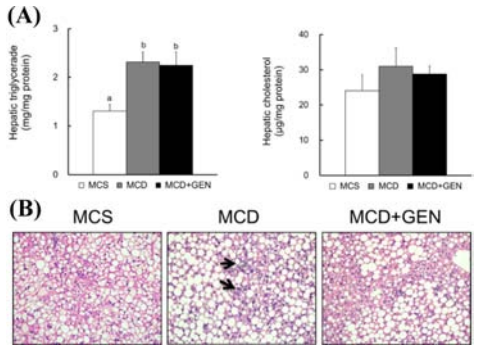

Figure 1. (A) Hepatic triglycerides and cholesterol contents in *db*/*db* mice fed an MCS diet, MCD diet, or MCD with genistein diet. Each bar represents the mean ± SEM (n = 7), and bars that do not share the same letter are significantly different by ANOVA (P < 0.05). (B) Representative H&E staining of liver tissue sections (n = 4). Black arrows indicate inflammatory foci.

Effects of Genistein on Oxidative Stress and ER Stress in *db*/*db* Mice Fed an MCD Diet. The increased generation of ROS by microsomal CYP2E1 enzyme has been proposed as an initiator of oxidative stress associated in MCD-diet-mediated steatohepatitis in mice.[25] To determine the oxidative stress, we measured hepatic malondialdehyde levels and hepatic enzyme levels involved in oxidative stress. Mice on an MCD diet exhibited significantly higher TBARS levels, which were alleviated by genistein supplementation (Figure 2A). Accordingly, the mRNA levels of heme oxygenase (HO-1) were significantly induced in mice fed an MCD diet (Figure 2B). Genistein supplementation significantly reduced the mRNA levels of HO-1.

In addition to oxidative stress, endoplasmic reticulum (ER) stress has been shown to be induced in an MCD-diet-induced NASH model. To determine the effects of genistein on ER stress, we examined the cellular markers of ER stress including glucose-regulated protein 78 (Grp78/BiP) and CHOP proteins

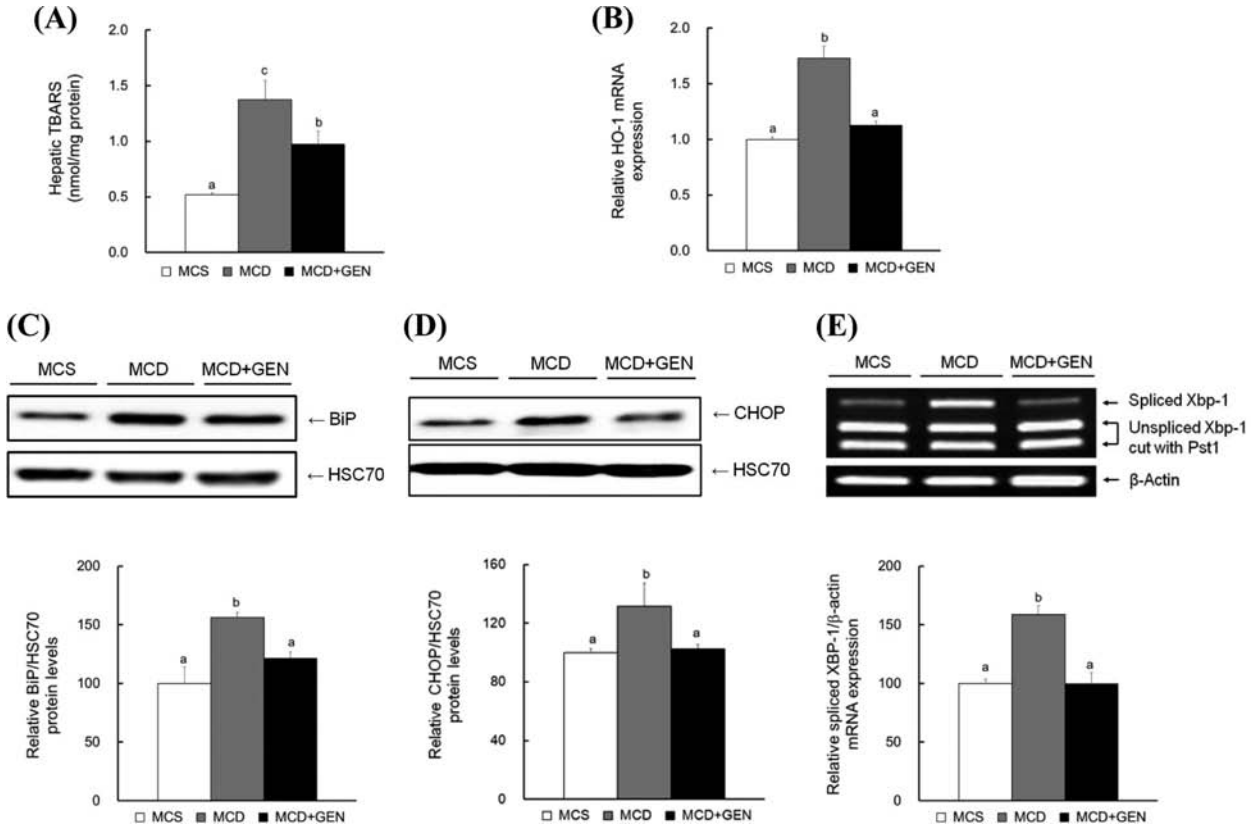

Figure 2. Oxidative stress and ER stress markers in *db*/*db* mice fed an MCS diet, MCD diet, or MCD with genistein diet. (A) Hepatic TBARS levels (n = 5). (B) Relative mRNA expression of HO-1/RPL19 determined by qPCR (n = 3–4). (C) Relative BiP/HSC70 and (D) CHOP/HSC70 protein levels determined by immunoblotting (n = 3). (E) Relative mRNA expression levels of the spliced form of XBP-1/β-actin determined by semiquantitative PCR (n = 3–4). Each bar represents the mean ± SEM, and bars that do not share the same letter are significantly different by ANOVA (P < 0.05).

DOI: 10.1021/acs.jafc.5b00398
J. Agric. Food Chem. 2015, 63, 4305–4311

and the spliced form of XBP-1 mRNA.[26] As shown in Figure 2C,D, protein expression levels of Grp78/BiP and CHOP were significantly increased in *db*/*db* mice fed an MCD diet compared to those in *db*/*db* mice fed an MCS diet. Genistein supplementation significantly alleviated Grp78/BiP and CHOP induced in mice fed an MCD diet. We also observed a significant induction of the spliced form of XBP-1 mRNA in mice fed an MCD diet. The suppressive effect of genistein on the induction of the spliced form of XBP-1 mRNA was significant (Figure 2E).

Effects of Genistein on Hepatic Inflammation in *db*/*db* Mice Fed an MCD Diet. Consistent with increased inflammatory foci, the MCD diet significantly induced the mRNA levels of tumor necrosis factor alpha (TNF-α), monocyte chemoattractant protein 1 (MCP-1), toll-like receptor 4 (TLR4), and interleukin 1 beta (IL-1β) (Figure 3A). These inflammatory gene expressions were significantly alleviated by genistein supplementation.

The hepatic adiponectin resistance has been suggested to be involved in steatohepatitis progression by changing peroxisome proliferator-activated receptor alpha (PPARα) activity and ROS accumulation.[27] Therefore, we determined whether genistein modulates the AMPK pathway in the MCD-mediated steatohepatitis model. Feeding an MCD diet significantly inhibited AMPK activation, which was alleviated by genistein supplementation (Figure 3B). Furthermore, mRNA levels of PPARα, a downstream transcription factor of adiponectin signaling, were significantly reduced in mice fed an MCD diet (Figure 3C). Although genistein supplementation tended to increase PPARα mRNA levels, the difference was not significant. As previously reported,[28] adiponectin resistance was not associated with an altered adiponectin receptor expression in the livers of MCD-diet-fed mice (data not shown).

Effects of Genistein on Liver Fibrosis in *db*/*db* Mice Fed an MCD Diet. To examine the effects of genistein supplementation on liver fibrosis, sections of liver were stained with Masson's trichrome. Mild periportal fibrosis in the absence of apparent hepatocellular ballooning was observed in MCD-diet-fed mice (Figure 4A). Genistein apparently reduced Masson's trichrome-stained fibrils induced by an MCD diet. Parallel to the changes in histological fibrosis, increased hepatic transforming growth factor β (TGF-β), procollagen, type I, alpha 1 type I (COL1A1), and tissue inhibitors of metalloproteinase 1 (TIMP1) mRNA levels in MCD-diet-fed *db*/*db* mice were significantly diminished by genistein treatment (Figure 4B).

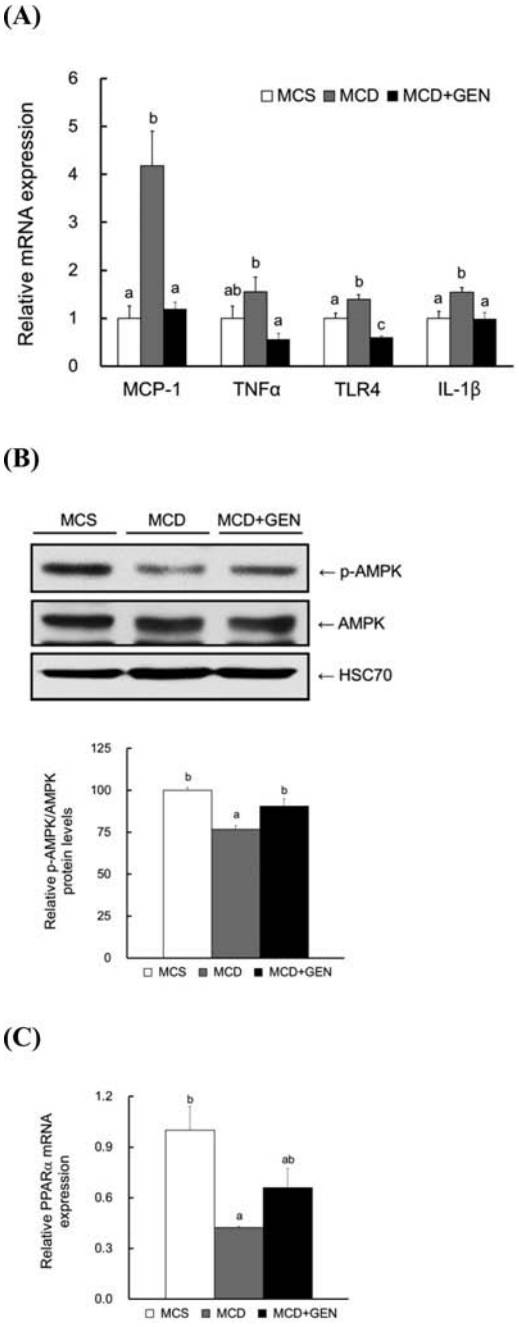

Figure 3. Hepatic inflammatory markers in *db*/*db* mice fed an MCS diet, MCD diet, or MCD with genistein diet. (A) Relative mRNA expression of genes involved in inflammation determined by qPCR and normalized to RPL19 (n = 3–4). (B) Relative p-AMPK/AMPK protein levels determined by immunoblotting (n = 3). (C) Relative mRNA expression of PPARα/RPL19 determined by qPCR (n = 3). Each bar represents the mean ± SEM, and bars that do not share the same letter are significantly different by ANOVA (P < 0.05).

DISCUSSION

We observed that genistein inhibited oxidative stress and ER stress, allowing for the alleviation of liver inflammation and fibrosis in the MCD-diet-mediated NASH model. Although this animal model has its own limitations, including the lack of obesity and peripheral insulin resistance,[29] it is a useful model for clarifying whether genistein could alleviate the progression of steatohepatitis to liver fibrosis, which is not easily induced in dietary NASH models. In addition, the present study allows us to clarify whether genistein could exhibit the anti-inflammatory effect in the NASH model which is not accompanied by obesity.

In the MCD model, the "first hit" is the impaired mitochondrial β-oxidation, and the "second hit" is increased oxidative stress and lipid peroxidation,[30] which induce proinflammatory gene expression, neutrophil chemotaxis, and hepatic stellate cell activation.[31−33] The protective action of genistein may be due to the inhibition of the pathway involved in the second hit because we did not observe a significant decrease in hepatic triglyceride levels by genistein supplementation. Indeed, genistein attenuated the oxidative stress in the liver of mice fed an MCD diet. In support of this view, we observed the antioxidative effect of genistein in the previous study, in which genistein supplementation (0.5 g/kg diet) in a

DOI: 10.1021/acs.jafc.5b00398
J. Agric. Food Chem. 2015, 63, 4305−4311

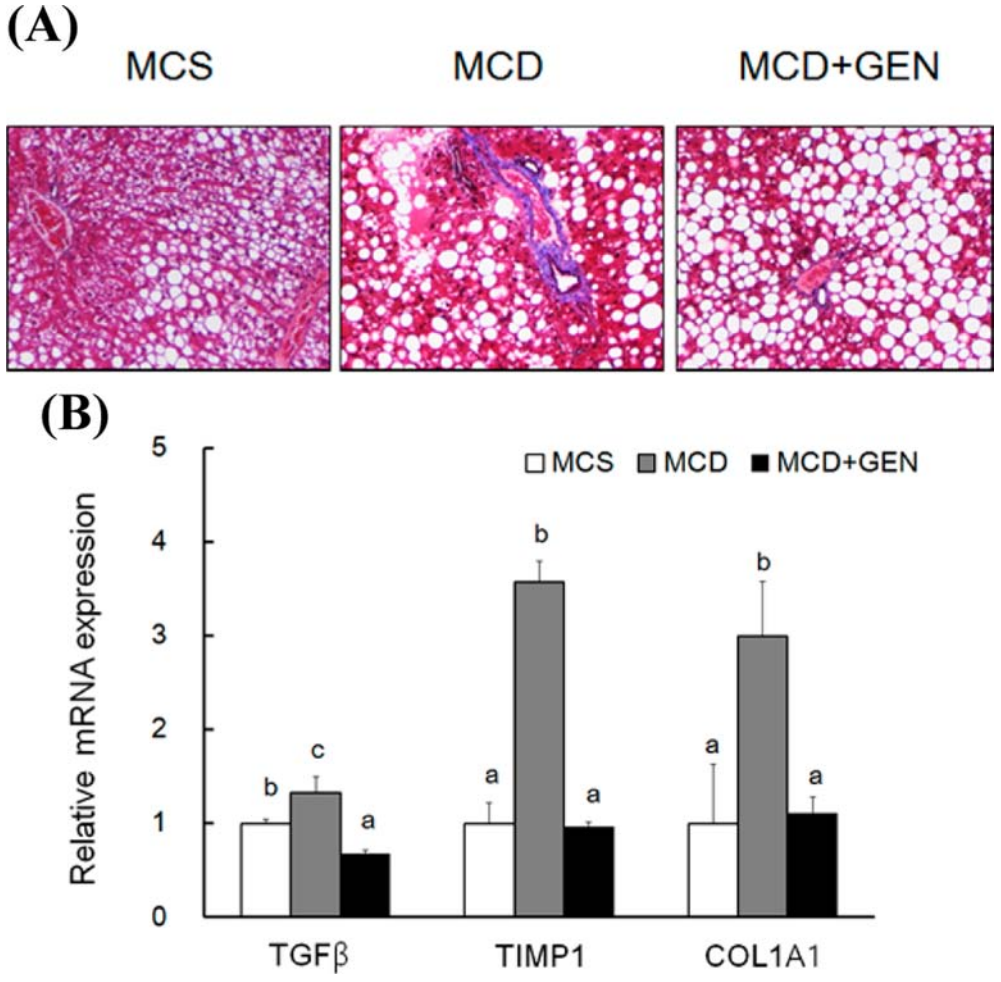

Figure 4. Hepatic fibrosis markers in *db*/*db* mice fed an MCS diet, MCD diet, or MCD with genistein diet. (A) Representative Masson's trichrome staining of liver tissue sections (n = 4). (B) Relative mRNA expression of genes involved in fibrosis determined by qPCR and normalized to RPL19 (n = 3–4). Each bar represents the mean ± SEM, and bars that do not share the same letter are significantly different by ANOVA (P < 0.05).

high-fat diet significantly lowered hepatic lipid peroxidation levels in ApoE knockout mice.[18] Antioxidants including vitamin E and α-lipoic acid have been shown to prevent the development and progression of NASH in mice fed an MCD diet.[34,35] ROS is shown to be involved in TLR4-mediated inflammasome activation in NASH,[36] which has been shown to be involved in hepatocyte pyroptosis, liver inflammation, and fibrosis.[37]

Furthermore, we observed that dietary supplementation of genistein attenuates liver fibrosis via the inhibition of collagen synthesis and the activation of extracellular matrix degradation. Several experimental studies have shown the protective effect of estrogen against liver fibrosis. Estradiol inactivated transcription processes involved in TGF-β1 expression by suppressing ROS generation and the mitogen-activated protein kinase pathways in hepatic stellate cells from rats,[13] suggesting that the estrogenic effect of genistein may be associated with the observed antifibrogenesis. Previous studies reported that genistein had positive effects on liver fibrosis induced by CCl_4 administration in rats[38,39] and by chronic alcohol administration in rats.[40] However, this is the first study to report the antifibrotic effect of genistein in dietary models of NASH.

We also demonstrated that genistein alleviated the impaired adiponectin signaling pathway. Previous studies reported that feeding an MCD diet induces hepatic adiponectin resistance, which fails to activate AMPK or PPARα,[28] and that the administration of a PPARα agonist reduces MCD-induced steatohepatitis in part by limiting lipid peroxidation.[31] Adiponectin has been shown to increase gene expressions of antioxidant enzymes and regulate the recruitment and phenotype polarization of Kupffer cells.[41] The anti-inflammatory effects of adiponectin in macrophages, although still not clearly understood, are likely to involve the inactivation of the TLR4 signaling pathway.[42] Additionally, the enhancement of adiponectin signaling reduced the hepatic expression of TGF-β1, a profibrotic factor involved in hepatic stellate cell activation in mice fed an MCD diet.[43]

Although some studies reported that hepatic steatosis is critical to the pathogenesis of liver injury in MCD-diet-fed mice,[32] we observed that hepatic inflammation and subsequent fibrosis could be regulated independently of hepatic steatosis in the MCD model. These data are in keeping with a previous study in which the treatment of MCD-diet-fed mice with a pan-caspase inhibitor decreased liver inflammation and fibrosis. However, serum ALT levels and hepatic triglyceride levels were comparable between the control and treated mice.[44] Polaprezinc, a zinc-carnosine chelate compound, also significantly alleviated MCD-mediated liver fibrosis without the inhibition of steatosis,[45] suggesting that liver steatosis is not

DOI: 10.1021/acs.jafc.5b00398
J. Agric. Food Chem. 2015, 63, 4305–4311

correlated with liver injury in the MCD model. In another setting, treating MCD-diet-fed mice with diacylglycerol O-acyltransferase 2 antisense oligonucleotide alleviated hepatic steatosis but increased lipid peroxidation, inflammation, and fibrosis.[25] Several biopsies in pediatric-type NASH (type 2 NASH) show prominent zone 3 steatosis and minimal zone 1 steatosis with the confined fibrosis in the portal area, suggesting that steatosis in the portal area may not be required for fibrogenesis.[46] Further studies are needed to investigate the molecular mechanism in the development of portal NASH in the MCD model.

Contradictory to the previous studies using obese animal models, the effects of genistein on either body weight change or serum profiles were not significant in the present study using the NASH model associated with lipodystophy. These minimal effects of genistein on metabolic profiles may be attributed to the overwhelming effect of the MCD diet per se. Previous observations reported that inhibitory effects of genistein on the development of NASH in obese mice are accompanied by a significant decrease in body weight. However, our present results clearly show that genistein could alleviate the development of NASH without reducing the adipose tissue and body weights of the subjects. Indeed, we observed that genistein activated adiponectin signaling in the liver of mice fed an MCD diet, suggesting that improved adiponectin resistance may be involved, at least in part, in alleviation of NASH progression.

When these results are taken together, our study shows that genistein supplementation alleviated liver inflammation and fibrosis in the MCD-diet-induced NASH model. The beneficial effects of genistein on NASH development seem to be mediated by its ability to inhibit oxidative stress and ER stress, to diminish proinflammatory cytokine expression, and to modulate impaired PPARα-mediated signaling even without affecting hepatic TG accumulation at least in the MCD model.

■ ASSOCIATED CONTENT

Supporting Information

Primer sequences for qPCR and semiquantitative PCR. Changes in body weight and fasting blood glucose levels of *db/db* mice fed an MCS diet, MCD diet, or MCD with genistein diet. MCS vs MCD and MCD + GEN ($P < 0.05$ by ANOVA). This material is available free of charge via the Internet at http://pubs.acs.org.

■ AUTHOR INFORMATION

Corresponding Author

*E-mail: hye0414@snu.ac.kr. Tel: +82-2-880-6833. Fax: +82-2-884-0305.

Funding

This research was supported by the Basic Science Research Program through the National Research Foundation of Korea (NRF) funded by the Ministry of Education, Science and Technology, Republic of Korea (no. 2009-0069120 and no. 2012-014736).

Notes

The authors declare no competing financial interest.

■ ABBREVIATIONS

ALT, alanine aminotransferase; AMPK, AMP-dependent kinase; CHOP, C/EBP homologous protein; COL1A1, collagen, type I, alpha 1; CYP2E1, cytochrome P450 2E1; ER, endoplasmic reticulum; HO-1, heme oxygenase 1; HOMA-IR, homeostasis model assessment-insulin resistance; IL-1β, interleukin-1 beta; MCD, methionine-choline deficient; MCP-1, monocyte chemoattractant protein 1; MCS, methionine-choline sufficient; NAFLD, nonalcoholic fatty liver disease; NASH, nonalcoholic steatohepatitis; PPARα, peroxisome proliferator-activated receptor alpha; ROS, reactive oxygen species; TBARS, thiobarbituric acid reactive substances; TGF-β, transforming growth factor beta; TIMP-1, tissue inhibitor of metalloproteinase 1; TLR4, toll-like receptor 4; TNFα, tumor necrosis factor alpha; XBP-1, X-box binding protein 1

■ REFERENCES

(1) Anderson, N.; Borlak, J. Molecular mechanisms and therapeutic targets in steatosis and steatohepatitis. *Pharmacol Rev.* **2008**, *60*, 311−57.

(2) Lazo, M.; Clark, J. M. The epidemiology of nonalcoholic fatty liver disease: a global perspective. *Semin. Liver Dis.* **2008**, *28*, 339−50.

(3) Day, C. P.; James, O. F. Steatohepatitis: a tale of two ″hits″? *Gastroenterology* **1998**, *114*, 842−5.

(4) Larter, C. Z.; Yeh, M. M. Animal models of NASH: getting both pathology and metabolic context right. *J. Gastroenterol. Hepatol.* **2008**, *23*, 1635−48.

(5) Varela-Rey, M.; Embade, N.; Ariz, U.; Lu, S. C.; Mato, J. M.; Martinez-Chantar, M. L. Non-alcoholic steatohepatitis and animal models: understanding the human disease. *Int. J. Biochem. Cell Biol.* **2009**, *41*, 969−76.

(6) Leclercq, I. A.; Farrell, G. C.; Field, J.; Bell, D. R.; Gonzalez, F. J.; Robertson, G. R. CYP2E1 and CYP4A as microsomal catalysts of lipid peroxides in murine nonalcoholic steatohepatitis. *J. Clin. Invest.* **2000**, *105*, 1067−75.

(7) Gao, D.; Wei, C.; Chen, L.; Huang, J.; Yang, S.; Diehl, A. M. Oxidative DNA damage and DNA repair enzyme expression are inversely related in murine models of fatty liver disease. *Am. J. Physiol Gastrointest Liver Physiol* **2004**, *287*, G1070−7.

(8) Sahai, A.; Malladi, P.; Pan, X.; Paul, R.; Melin-Aldana, H.; Green, R. M.; Whitington, P. F. Obese and diabetic db/db mice develop marked liver fibrosis in a model of nonalcoholic steatohepatitis: role of short-form leptin receptors and osteopontin. *Am. J. Physiol Gastrointest Liver Physiol* **2004**, *287*, G1035−43.

(9) Hashimoto, E.; Tokushige, K. Prevalence, gender, ethnic variations, and prognosis of NASH. *J. Gastroenterol.* **2011**, *46* (Suppl 1), 63−9.

(10) Jones, M. E.; Thorburn, A. W.; Britt, K. L.; Hewitt, K. N.; Wreford, N. G.; Proietto, J.; Oz, O. K.; Leury, B. J.; Robertson, K. M.; Yao, S.; Simpson, E. R. Aromatase-deficient (ArKO) mice have a phenotype of increased adiposity. *Proc. Natl. Acad. Sci. U. S. A.* **2000**, *97*, 12735−40.

(11) Helisten, H.; Hockerstedt, A.; Wahala, K.; Tiitinen, A.; Adlercreutz, H.; Jauhiainen, M.; Tikkanen, M. J. Accumulation of high-density lipoprotein-derived estradiol-17beta fatty acid esters in low-density lipoprotein particles. *J. Clin. Endocrinol. Metab.* **2001**, *86*, 1294−300.

(12) Uzui, H.; Sinha, S. K.; Rajavashisth, T. B. 17beta-estradiol inhibits oxidized low-density lipoprotein-induced increase in matrix metalloproteinase-9 expression in human macrophages. *J. Investig. Med.* **2011**, *59*, 1104−1108.

(13) Itagaki, T.; Shimizu, I.; Cheng, X.; Yuan, Y.; Oshio, A.; Tamaki, K.; Fukuno, H.; Honda, H.; Okamura, Y.; Ito, S. Opposing effects of oestradiol and progesterone on intracellular pathways and activation processes in the oxidative stress induced activation of cultured rat hepatic stellate cells. *Gut* **2005**, *54*, 1782−9.

(14) Omoni, A. O.; Aluko, R. E. Soybean foods and their benefits: potential mechanisms of action. *Nutr. Rev.* **2005**, *63*, 272−83.

(15) Messina, M.; Messina, V. The role of soy in vegetarian diets. *Nutrients* **2010**, *2*, 855−88.

(16) Fang, N.; Yu, S.; Badger, T. M. Comprehensive phytochemical profile of soy protein isolate. *J. Agric. Food Chem.* **2004**, *52*, 4012−20.

DOI: 10.1021/acs.jafc.5b00398
J. Agric. Food Chem. 2015, 63, 4305−4311

(17) Nagaraju, G. P.; Zafar, S. F.; El-Rayes, B. F. Pleiotropic effects of genistein in metabolic, inflammatory, and malignant diseases. *Nutr. Rev.* **2013**, *71*, 562−72.
(18) Jeon, S.; Park, Y. J.; Kwon, Y. H. Genistein alleviates the development of nonalcoholic steatohepatitis in ApoE(−/−) mice fed a high-fat diet. *Mol. Nutr. Food Res.* **2014**, *58*, 830−41.
(19) Ji, G.; Yang, Q.; Hao, J.; Guo, L.; Chen, X.; Hu, J.; Leng, L.; Jiang, Z. Anti-inflammatory effect of genistein on non-alcoholic steatohepatitis rats induced by high fat diet and its potential mechanisms. *Int. Immunopharmacol.* **2011**, *11*, 762−8.
(20) Al-Nakkash, L.; Clarke, L. L.; Rottinghaus, G. E.; Chen, Y. J.; Cooper, K.; Rubin, L. J. Dietary genistein stimulates anion secretion across female murine intestine. *J. Nutr.* **2006**, *136*, 2785−2790.
(21) Ju, Y. H.; Allred, C. D.; Allred, K. F.; Karko, K. L.; Doerge, D. R.; Helferich, W. G. Physiological concentrations of dietary genistein dose-dependently stimulate growth of estrogen-dependent human breast cancer (MCF-7) tumors implanted in athymic nude mice. *J. Nutr.* **2001**, *131*, 2957−2962.
(22) Folch, J.; Lees, M.; Stanley, G. H. S. A simple method for the isolation and purification of total lipids from animal tissues. *J. Biol. Chem.* **1957**, *226*, 497−509.
(23) Ohkawa, H.; Ohishi, N.; Yagi, K. Assay for lipid peroxides in animal tissues by thiobarbituric acid reaction. *Anal. Biochem.* **1979**, *95*, 351−8.
(24) Jung, G. Y.; Won, S. B.; Kim, J.; Jeon, S.; Han, A.; Kwon, Y. H. Betaine alleviates hypertriglycemia and tau hyperphosphorylation in db/db mice. *Toxicol. Res.* **2013**, *29*, 7−14.
(25) Yamaguchi, K.; Yang, L.; McCall, S.; Huang, J.; Yu, X. X.; Pandey, S. K.; Bhanot, S.; Monia, B. P.; Li, Y. X.; Diehl, A. M. Inhibiting triglyceride synthesis improves hepatic steatosis but exacerbates liver damage and fibrosis in obese mice with nonalcoholic steatohepatitis. *Hepatology* **2007**, *45*, 1366−74.
(26) Kaufman, R. J. Orchestrating the unfolded protein response in health and disease. *J. Clin. Invest.* **2002**, *110*, 1389−98.
(27) Tomita, K.; Oike, Y.; Teratani, T.; Taguchi, T.; Noguchi, M.; Suzuki, T.; Mizutani, A.; Yokoyama, H.; Irie, R.; Sumimoto, H.; Takayanagi, A.; Miyashita, K.; Akao, M.; Tabata, M.; Tamiya, G.; Ohkura, T.; Hibi, T. Hepatic AdipoR2 signaling plays a protective role against progression of nonalcoholic steatohepatitis in mice. *Hepatology* **2008**, *48*, 458−73.
(28) Larter, C. Z.; Yeh, M. M.; Williams, J.; Bell-Anderson, K. S.; Farrell, G. C. MCD-induced steatohepatitis is associated with hepatic adiponectin resistance and adipogenic transformation of hepatocytes. *J. Hepatol.* **2008**, *49*, 407−16.
(29) Schattenberg, J. M.; Singh, R.; Wang, Y.; Lefkowitch, J. H.; Rigoli, R. M.; Scherer, P. E.; Czaja, M. J. JNK1 but not JNK2 promotes the development of steatohepatitis in mice. *Hepatology* **2006**, *43*, 163−72.
(30) Anstee, Q. M.; Goldin, R. D. Mouse models in non-alcoholic fatty liver disease and steatohepatitis research. *Int. J. Exp. Pathol.* **2006**, *87*, 1−16.
(31) Ip, E.; Farrell, G. C.; Robertson, G.; Hall, P.; Kirsch, R.; Leclercq, I. Central role of PPARalpha-dependent hepatic lipid turnover in dietary steatohepatitis in mice. *Hepatology* **2003**, *38*, 123−32.
(32) Lee, G. S.; Yan, J. S.; Ng, R. K.; Kakar, S.; Maher, J. J. Polyunsaturated fat in the methionine-choline-deficient diet influences hepatic inflammation but not hepatocellular injury. *J. Lipid Res.* **2007**, *48*, 1885−96.
(33) George, J.; Pera, N.; Phung, N.; Leclercq, I.; Yun Hou, J.; Farrell, G. Lipid peroxidation, stellate cell activation and hepatic fibrogenesis in a rat model of chronic steatohepatitis. *J. Hepatol.* **2003**, *39*, 756−64.
(34) Phung, N.; Pera, N.; Farrell, G.; Leclercq, I.; Hou, J. Y.; George, J. Pro-oxidant-mediated hepatic fibrosis and effects of antioxidant intervention in murine dietary steatohepatitis. *Int. J. Mol. Med.* **2009**, *24*, 171−80.
(35) Min, A. K.; Kim, M. K.; Kim, H. S.; Seo, H. Y.; Lee, K. U.; Kim, J. G.; Park, K. G.; Lee, I. K. Alpha-lipoic acid attenuates methionine choline deficient diet-induced steatohepatitis in C57BL/6 mice. *Life Sci.* **2012**, *90*, 200−5.
(36) Wree, A.; Broderick, L.; Canbay, A.; Hoffman, H. M.; Feldstein, A. E. From NAFLD to NASH to cirrhosis-new insights into disease mechanisms. *Nat. Rev. Gastroenterol. Hepatol.* **2013**, *10*, 627−36.
(37) Wree, A.; Eguchi, A.; McGeough, M. D.; Pena, C. A.; Johnson, C. D.; Canbay, A.; Hoffman, H. M.; Feldstein, A. E. NLRP3 inflammasome activation results in hepatocyte pyroptosis, liver inflammation, and fibrosis in mice. *Hepatology* **2014**, *59*, 898−910.
(38) Demiroren, K.; Dogan, Y.; Kocamaz, H.; Ozercan, I. H.; Ilhan, S.; Ustundag, B.; Bahcecioglu, I. H. Protective effects of L-carnitine, N-acetylcysteine and genistein in an experimental model of liver fibrosis. *Clin. Res. Hepatol. Gastroenterol.* **2014**, *38*, 63−72.
(39) Salas, A. L.; Montezuma, T. D.; Farina, G. G.; Reyes-Esparza, J.; Rodriguez-Fragoso, L. Genistein modifies liver fibrosis and improves liver function by inducing uPA expression and proteolytic activity in CCl4-treated rats. *Pharmacology* **2008**, *81*, 41−9.
(40) Huang, Q.; Huang, R.; Zhang, S.; Lin, J.; Wei, L.; He, M.; Zhuo, L.; Lin, X. Protective effect of genistein isolated from Hydrocotyle sibthorpioides on hepatic injury and fibrosis induced by chronic alcohol in rats. *Toxicol. Lett.* **2013**, *217*, 102−10.
(41) Fukushima, J.; Kamada, Y.; Matsumoto, H.; Yoshida, Y.; Ezaki, H.; Takemura, T.; Saji, Y.; Igura, T.; Tsutsui, S.; Kihara, S.; Funahashi, T.; Shimomura, I.; Tamura, S.; Kiso, S.; Hayashi, N. Adiponectin prevents progression of steatohepatitis in mice by regulating oxidative stress and Kupffer cell phenotype polarization. *Hepatol. Res.* **2009**, *39*, 724−38.
(42) Wang, S. N.; Wang, S. T.; Lee, K. T. The potential interplay of adipokines with toll-like receptors in the development of hepatocellular carcinoma. *Gastroenterol Res. Pract* **2011**, *2011*, 215986.
(43) Finelli, C.; Tarantino, G. What is the role of adiponectin in obesity related non-alcoholic fatty liver disease? *World J. Gastroenterol* **2013**, *19*, 802−12.
(44) Witek, R. P.; Stone, W. C.; Karaca, F. G.; Syn, W. K.; Pereira, T. A.; Agboola, K. M.; Omenetti, A.; Jung, Y.; Teaberry, V.; Choi, S. S.; Guy, C. D.; Pollard, J.; Charlton, P.; Diehl, A. M. Pan-caspase inhibitor VX-166 reduces fibrosis in an animal model of nonalcoholic steatohepatitis. *Hepatology* **2009**, *50*, 1421−30.
(45) Sugino, H.; Kumagai, N.; Watanabe, S.; Toda, K.; Takeuchi, O.; Tsunematsu, S.; Morinaga, S.; Tsuchimoto, K. Polaprezinc attenuates liver fibrosis in a mouse model of non-alcoholic steatohepatitis. *J. Gastroenterol. Hepatol.* **2008**, *23*, 1909−16.
(46) Schwimmer, J. B.; Behling, C.; Newbury, R.; Deutsch, R.; Nievergelt, C.; Schork, N. J.; Lavine, J. E. Histopathology of pediatric nonalcoholic fatty liver disease. *Hepatology* **2005**, *42*, 641−9.

DOI: 10.1021/acs.jafc.5b00398
J. Agric. Food Chem. 2015, 63, 4305−4311

Study objectives were to (1) experimentally show the incorporation of 1-naphthol in the amylose lumen of the soluble nanoparticle and (2) evaluate the incorporation mechanism using MD simulation.

EXPERIMENTAL SECTION

Materials. High-amylose corn starch, AmyloGel, containing 50% amylose (w/w) was provided by Cargill, Inc. (Cedar Rapids, IA). β-Lactoglobulin, linoleic acid (C18:3), and 1-naphthol were purchased from Sigma Chemical Co. (St. Louis, MO).

Table 1. Amount of 1-Naphthol Incorporated into the Nanoparticle[a]

solution concentration (mM)	incorporated concentration (mM/M glucose)
	1-naphthol
1	28.4 ± 1.8
2.5	47.6 ± 9.4
5	79.9 ± 6.3
10	91.8 ± 3.1

[a]Values are the average value and standard error of the mean. Note that the "solution concentration" column in the table indicates the amount of 1-naphthol added in the nanoparticle suspension, whereas the "incorporated concentration" column indicates the actual quantity of 1-naphthol incorporated into the nanoparticles collected in the HPSEC fraction.

Preparation of the Nanoparticle. Dilute nanoparticle suspensions were prepared as described by Zhang et al.,[3] whereby a hot-water-extracted amylose-rich supernatant was mixed with a β-lactoglobulin solution (10 mg/mL) and linoleic acid, maintaining a weight ratio among the three components of 20:2:1. The mixture was then heated for 20 min in a boiling water bath with continuous stirring at 450 rpm, followed by cooling to room temperature for 4 h.

Incorporation of 1-Naphthol into the Nanoparticle. Different amounts of 1-naphthol powder were added to suspensions containing the nanoparticle to obtain concentrations of 1, 2.5, 5, and 10 mM 1-naphthol. The mixtures were then heated to 75 °C for 20 min with continuous stirring at 450 rpm to facilitate the 1-naphthol incorporation and then cooled to room temperature under stirring. The formation of the loaded nanoparticle was monitored using high-pressure size-exclusion chromatography (HPSEC) coupled with multi-angle light scattering (MALS) and refractive index (RI) detectors. The obtained suspension was passed through a 0.45 μm filter and injected (100 μL) into a Sephacryl HR-500 column (GE Healthcare, Piscataway, NJ) with 0.02% sodium azide in purified water as the mobile phase (flow rate of 1.3 mL/min). Light scattering was performed using a Dawn Heleos-II MALS detector equipped with a 658 nm GaAs laser diode and an Optilab rEx RI detector (Wyatt Technology Corporation, Santa Barbara, CA). Data collection and analysis were carried out using ASTRA software (version 5.3.4.10, Wyatt Technology Corporation). Light scattering data were analyzed by the Zimm method using a range of angles between 14.4° and 163.3° and a dn/dc value of 1.46 to obtain average molecular weight (M_w) and the radius of gyration (R_g). Samples were analyzed in triplicate.

For detection of 1-naphthol, samples were injected (500 μL) into the HR-500 SEC column attached to ultraviolet−visible (UV−vis) and RI detectors (Varian models 9040 and 9050, Walnut Creek, CA). Sodium azide (0.02%) in purified water was used as the mobile phase. A wavelength of maximum absorption for 1-naphthol (319 nm) was used to detect the presence of 1-naphthol in the nanoparticle. A nanoparticle solution was used as a control to assess potential interference of β-lactoglobulin at 319 nm. HPSEC fractions were collected to obtain purified nanoparticle with and without 1-naphthol, immediately frozen (−40 °C) by immersion in liquid nitrogen, and freeze-dried.

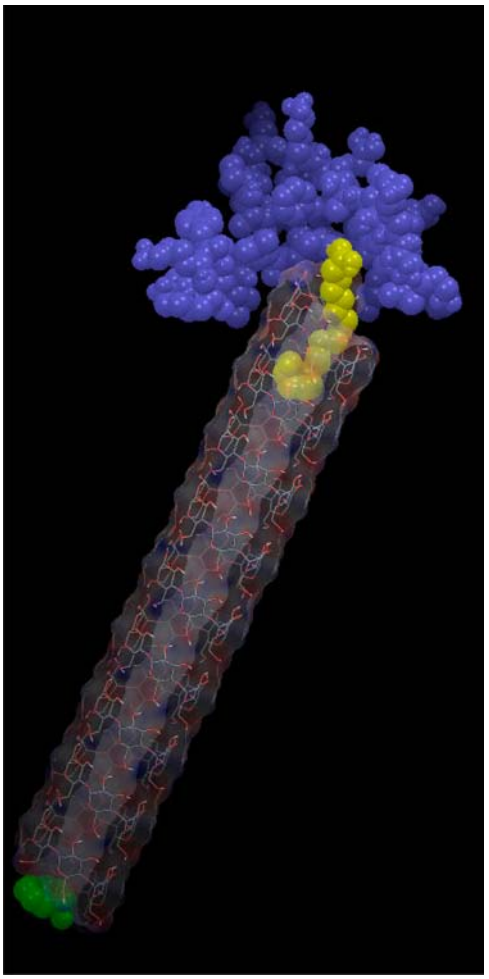

Figure 1. Initial configuration of the participating molecules at the start point of the four-component system, including the 55 glucose segment representing amylose [colored according to its three elements: oxygen (red), carbon (white), and hydrogen (blue)], α-linoleic acid (yellow), β-lactoglobulin-like peptide (blue), and 1-naphthol (green).

Potentiometric Titration. To assess 1-naphthol binding in the luminal space of the amylose molecule, potentiometric titration was used. A digital pH/mV meter (Corning pH/Ion Analyzer 350, Corning, NY) connected to a platinum redox combination electrode with a BNC connector (Corning, catalog number 476516, Big Flats, NY) was used. For the titrations, 5 mL solutions of amylose, amylose−fatty acid complex, nanoparticle, and 1-naphthol-loaded nanoparticle were mixed with 2.5 mL of 0.4 M potassium iodide. Mixtures were stirred at a constant rate, and the temperature was maintained at 25 °C. Potassium iodate (0.05 M) was added gradually to attain change in the voltage between 240 and 290 mV.[8] The volume of potassium iodate solution required to attain the voltage change provided information about the available space in the lumen of the amylose helix for binding of 1-naphthol. A blank containing 5 mL of purified water and 2.5 mL of 0.4 M potassium iodide was used as the control. Tests were conducted in triplicate.

Thermal Analysis. Thermal analysis was carried out on freeze-dried HPSEC-purified nanoparticle and 1-naphthol (5 mM)-loaded nanoparticle using a differential scanning calorimeter (DSC, Q2000, TA Instruments, New Castle, DE). Samples were mixed with water (1:3, w/w), placed in T-zero hermetically sealed pans (TA Instruments), and allowed to equilibrate overnight. The modulation mode of the DSC (MDSC) was used for the assay. A linear heating ramp from 20 to 120 °C at 3 °C/min was used, followed by cooling to

DOI: 10.1021/acs.jafc.5b00037
J. Agric. Food Chem. 2015, 63, 4312−4319

20 °C using the same rate. The modulation amplitude during the heating and cooling cycle was set to ±0.6 °C/min.

Dissociation of the 1-naphthol-loaded nanoparticle was detected by the endothermic peak in the heating cycle, whereas reassociation was detected by the exothermic peak in the cooling cycle. A similar methodology was applied to detect dissociation/reassociation in amylose inclusion complexes.[16] Controls were pure 1-naphthol and the nanoparticle. Tests were conducted in triplicate.

Quantification of the Amount of 1-Naphthol in the Nanoparticle. The amount of 1-naphthol in the HPSEC-isolated loaded nanoparticle was determined by its absorption at 319 nm using a UV−vis spectrophotometer (Beckman DU530, Danvers, MA). Different solution concentrations of 1-naphthol were used, and the amount of 1-naphthol incorporated into the nanoparticle is reported in Table 1. A standard curve for 1-naphthol in a concentration range of 1−5 mg/mL was prepared from a stock solution. Analyses were performed in triplicate.

MD Simulation. *Model Containing Amylose Segment, β-Lactoglobulin Peptide, α-Linoleic Acid, and 1-Naphthol.* An amylose segment of 55 glucose residues was used to form a 6-fold left-handed helix with inner and outer diameters of approximately 54 and 135 nm, and a length of 738 nm, as described by Tusch et al.[17]

A β-lactoglobulin peptide segment was used on the basis of the three-dimensional (3D) structure determined from a NMR analysis performed by Uhrinova et al.[18] This information was loaded into the Protein Data Bank (PDB; 1DV9). On the basis of a previous hypothesis of the role of lysyl residues in the nanoparticle formation,[4] a lysine-rich peptide segment of β-lactoglobulin was generated containing the following amino acid sequence from 67 to 101 (KKIIAEKTKIPAVFKIDALNENKVLVLDTDYKK) using the PRODRG server (http://davapc1.bioch.dundee.ac.uk/prodrg/).[19]

The PDB file for α-linoleic acid was obtained from the Hetero-compound Information Centre in Uppsala, Sweden.[20−23] The PDB file with ideal coordinates for 20 atoms was chosen using the Macromolecular Structure Database containing chemoinformatics (MSDchem database, http://www.ebi.ac.uk/pdbe/). The starting structure of α-linoleic acid was then generated using the same PRODRG server as in the case of the peptide segment above.

The PDB file of 1-naphthol was obtained from the Dictionary of Metabolites and Drug Binding Sites (SuperSite).[24] Similar to α-linoleic acid, the PDB file with ideal coordinates for 19 atoms was selected using the MSDchem database.

Force Field Details. The glucose force field was parametrized according to the method described by Damm et al.[25] and Kony et al.[26] All simulations for the amylose-like molecule were carried out using the glucose force field. The labels and corresponding charges of the atoms are shown in Table S1 and Figure S1 of the Supporting Information. The other three components were compatible with the glucose force field used.

MD Simulation Protocol. The Gromacs 4.6.1 MD package (Scala Life Competence Center, European Research Council) was used for the simulation. MD simulations were performed using the leapfrog motion routine with a 2 fs (1 fs = 10^{-15} s) time step. A total of 500 000 simulation steps (for a total simulation time of 500 ns) was performed to assess the progression of the self-assembly process. The LINCS algorithm was used to constrain all bond lengths with lincs_iter = 1 and lincs_order = 4. Because MD simulation is at the atomic level, our interest was how single molecules interact with each other. At a high temperature, the faster movement of the molecules facilitates their interaction and complexation by surpassing intrinsic energy barriers.[27,28] Therefore, even though the experimental work indicated that the exothermic event related to complex formation was lower, in the simulation, the temperature was set at 100 °C, necessary for initial formation of the complex. This was performed using the modified Berendsen thermostat coupling between the different groups, with a relaxation time of 0.1 ps, and pressure was maintained at 1.0 bar using the Parrinello−Rahman coupling to a pressure bath via an isotropic coordinate scaling, with a relaxation time of 2 ps, as described by Lopez et al.[29] Non-bonded interactions were handled using a neighboring grid cell cutoff scheme. Within a short-range neighbor list cutoff of 0.9 nm, the interactions were evaluated at every time step based on a pair list. A short-range electrostatic cutoff radius of 0.9 nm and a long-range van der Waals cutoff of 1.4 nm were evaluated simultaneously with each pair list update.

Simulations and Analysis. Because of limitation of computational capacity, as a beginning point, the amylose-like chain was pre-complexed with α-linoleic acid, the β-lactoglobulin-like peptide (blue) was located near α-linoleic acid (yellow), and 1-naphthol (green) was placed at the bottom of the amylose-like molecule (Figure 1). Because the whole system had for lysyl groups a net charge of +4, four chloride ions were added to neutralize the charges. The system was embedded in a rectangular box with a 10 × 5 × 5 nm^3 volume and filled with 7648 water molecules. The behavior of the water molecules was described by the TIP4P model.[30]

RESULTS AND DISCUSSION

Characterization of the Nanoparticle. As per previous work,[3,5] the nanoparticle was formed and identified by HPSEC−RI (Figure 2). UV absorbance at 280 nm at the same elution time confirmed the presence of protein in the nanoparticle. An average molar mass of the nanoparticle was 8−10 million Da, and radius of gyration was between 50 and 55

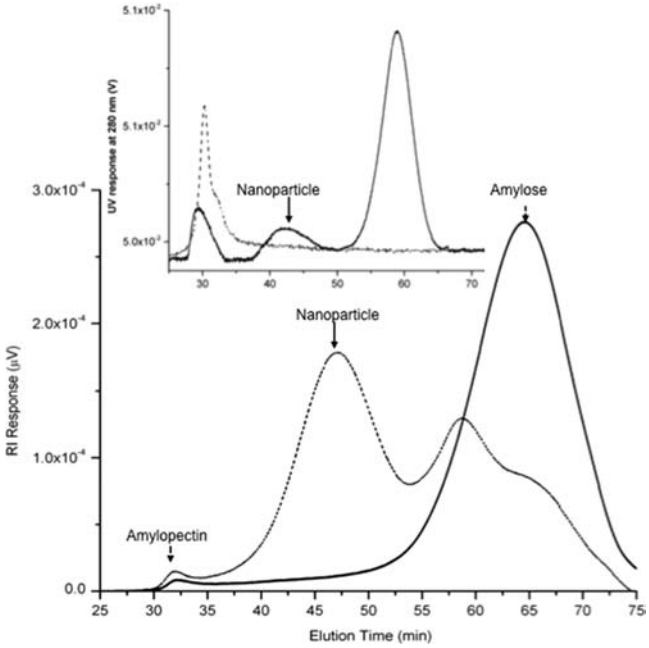

Figure 2. HPSEC−RI profile of the nanoparticle eluting between amylose and amylopectin. The inset illustrates the HPSEC−UV profile showing the presence of protein in the nanoparticle. The broken line trace is the HPSEC−UV profile of the starch supernatant.

Table 2. Changes in the Nanoparticle Structure Because of Mixing with Different Amounts of 1-Naphthol[a]

amount of 1-naphthol (mM)	M_w (Da)	R_z (nm)	M_w/M_n	slope of the conformation plot
control	8.1 × 10^6 (±8)	54.1 (±2)	2.9	0.68 (±6)
1	1.2 × 10^7 (±7)	50.4 (±7)	2.4	0.54 (±17)
2.5	1.6 × 10^7 (±3)	51.1 (±11)	2.1	0.47 (±13)
5	1.9 × 10^7 (±7)	48.6 (±8)	1.6	0.40 (±3)
10	2.7 × 10^7 (±6)	49.4 (±4)	1.5	0.38 (±3)

[a]Values are the average value. Values in parentheses indicate percent experimental error among the MALS detectors.

DOI: 10.1021/acs.jafc.5b00037
J. Agric. Food Chem. 2015, 63, 4312−4319

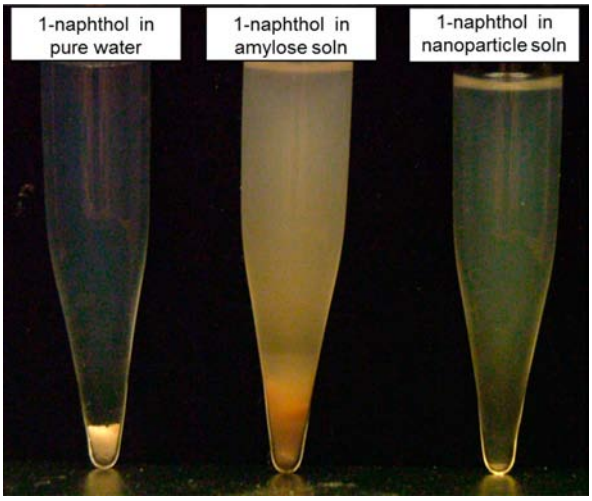

Figure 3. Photograph showing solubility of the 1-naphthol-loaded nanoparticle (right tube) compared to 1-naphthol in pure water (left tube) and incorporated with amylose (middle tube).

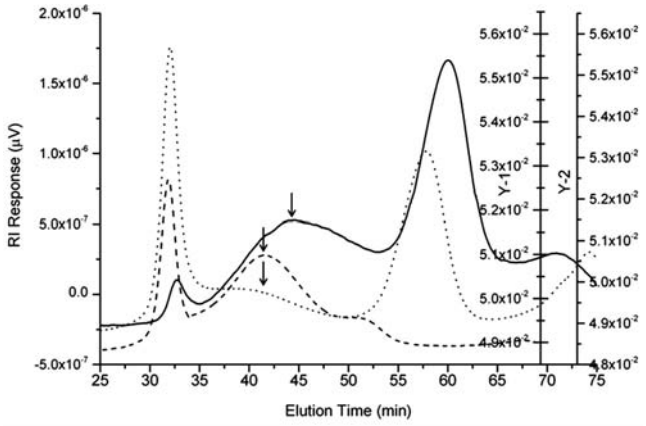

Figure 4. HPSEC profiles (RI and UV tracings) of the nanoparticle loaded with 5 mM 1-naphthol. The presence of the nanoparticle is indicated by the arrows. Solid line, RI response (left *y* axis); broken line, UV response at λ_{319} (Y-1, right axis); and dotted line, UV response at λ_{280} (Y-2, right axis).

nm (Table 2). These results are in general agreement with previous findings by Zhang et al.[4]

Characterization of the 1-Naphthol-Loaded Nanoparticle. 1-Naphthol has limited solubility in water (left tube in Figure 3). The addition of the same amount of 1-naphthol in an amylose-rich solution caused precipitation (center tube in Figure 3). This indicates complexation with amylose, and subsequent precipitation as has been reported by others for 1-naphthol[12] and other small hydrophobic flavor molecules.[31,32] When 1-naphthol was incorporated into the nanoparticle, it remained in solution (right tube in Figure 3).

1-Naphthol inclusion in the nanoparticle is shown in the HPSEC–UV chromatograms in Figure 4, where monitoring at 319 nm, the λ_{max} of 1-naphthol, resulted in a similar peak elution time as the nanoparticle RI and protein (280 nm) tracings. Incorporation of increasing amounts of 1-naphthol into the nanoparticle slightly increased its molecular size (Figure 5), which was quantitatively estimated by MALS analysis (Table 2). While addition of 1-naphthol (10 mM) increased the average molar mass of the nanoparticle from 8.1 $\times$ 10^6 to 2.7 $\times$ 10^7 Da, it did not change the radius of gyration.

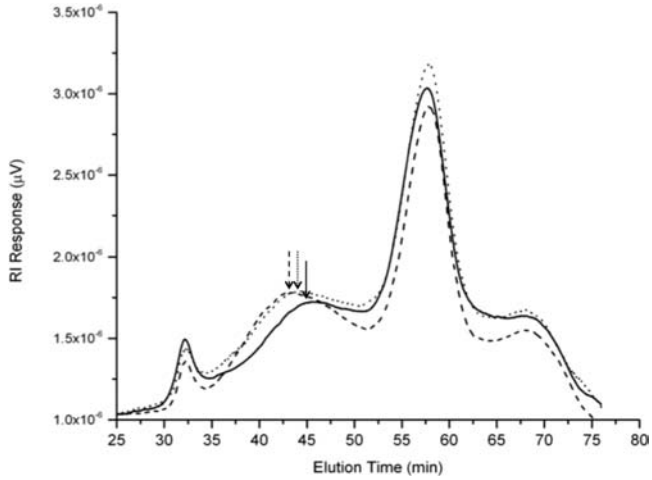

Figure 5. HPSEC–RI profiles of the nanoparticle mixed with different amounts of 1-naphthol. Peaks indicating the presence of the nanoparticles are indicated by the arrows. Solid line, pure nanoparticle; dotted line, nanoparticle mixed with 5 mM 1-naphthol; and broken line, nanoparticle mixed with 10 mM 1-naphthol.

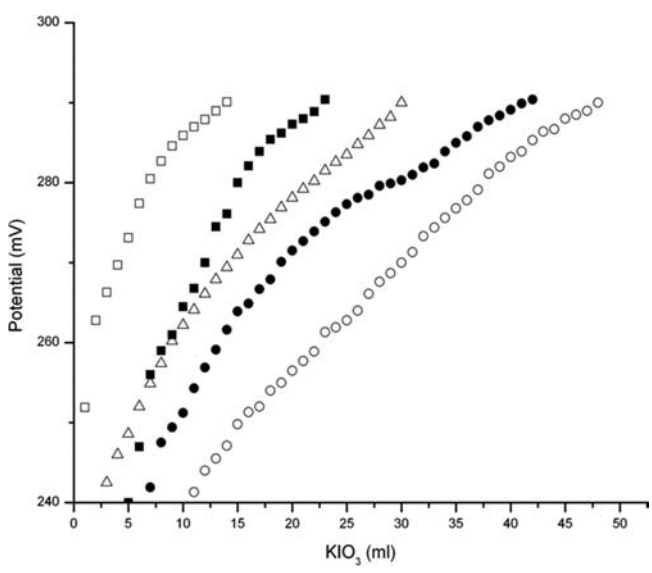

Figure 6. Iodine binding capacity of the 1-naphthol-loaded nanoparticle measured by potentiometric titration [□, blank; ○, amylose; ●, nanoparticle; △, amylose–fatty acid complex; and ■, 1-naphthol-loaded nanoparticle (mixed with 10 mM 1-naphthol)].

This suggested that inclusion of 1-naphthol changed the conformation of the nanoparticle, which was confirmed using a conformation plot (log–log plot of the root-mean-square radius as a function of the molar mass), showing a reduction in slope with increasing 1-naphthol concentration. The slope of the conformation plot is associated with shape of molecules in solution. For instance, a slope of 0.33 indicates a spherical arrangement, while a higher slope value (>0.6) is indicative of rod-like conformations.[33] Accordingly, the shape of the pure nanoparticle was rod-like, while the 1-naphthol-loaded nanoparticle was more spherical, and its spherical shape increased (decreasing slope) with higher concentrations of 1-naphthol (Table 2). Perhaps the explanation for the 3× increase in molar mass is a weak aggregation of a few nanoparticles that retain their individual nature.

DOI: 10.1021/acs.jafc.5b00037
J. Agric. Food Chem. 2015, 63, 4312–4319

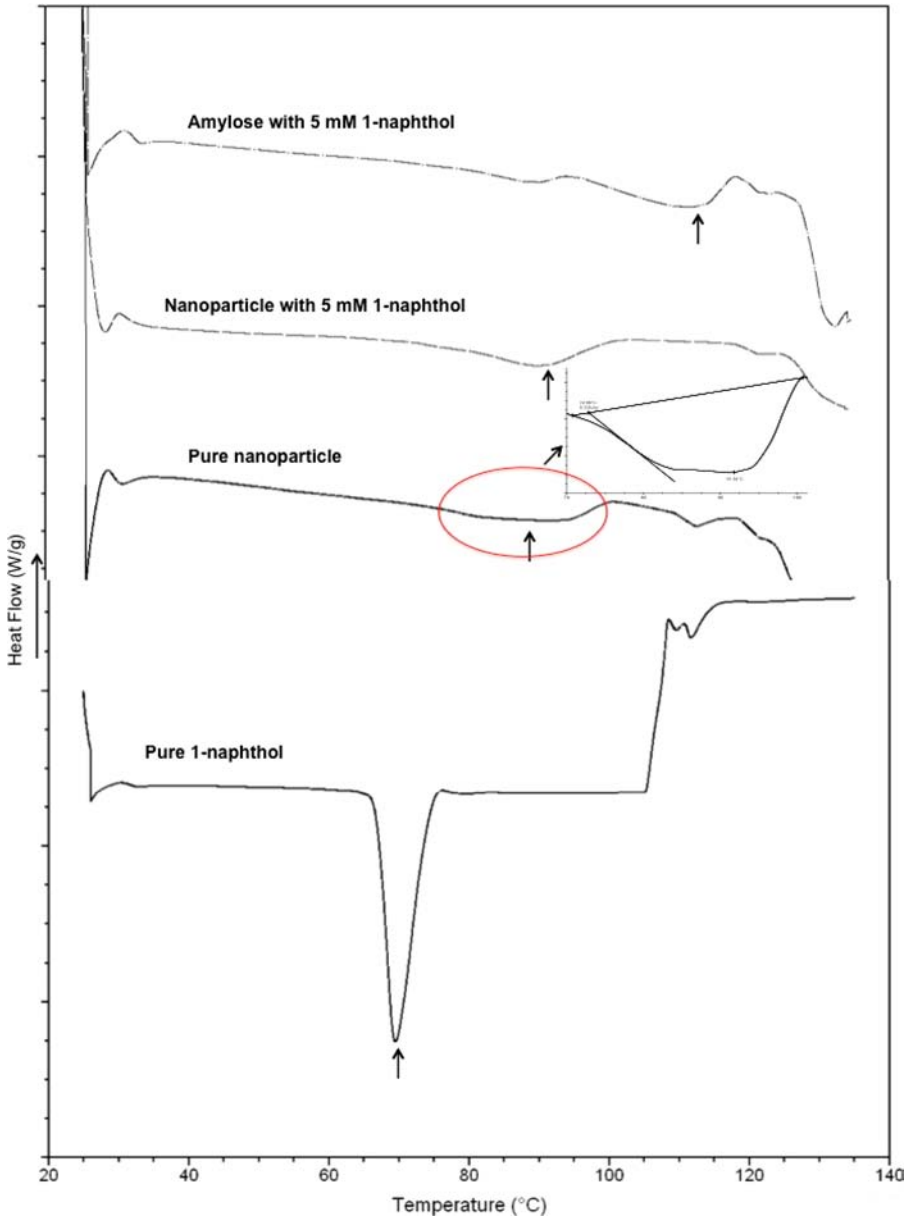

Figure 7. Thermal behaviors during heating of hydrated samples of amylose with 1-naphthol, nanoparticle with 1-naphthol, pure nanoparticle (with inset), and pure 1-naphthol.

Table 3. Melting Temperature and Enthalpy of Hydrated Samples of the Pure Nanoparticle, Pure 1-Naphthol, 1-Naphthol-Loaded Nanoparticle, and 1-Naphthol-Loaded Amylose[a]

	T_p (°C)	enthalpy (ΔH) (J/g)
nanoparticle	95.2 ± 0.9	7.3 ± 1.4
1-naphthol (pure)	69.5 ± 1.2	144.4 ± 5.9
1-naphthol (5 mM)-loaded nanoparticle	91.9 ± 0.2	12.2 ± 1.7
1-naphthol (5 mM)-loaded amylose	102.0 ± 2.9	10.0 ± 0.4

[a]Values are the average value and standard error of the mean.

Table 4. Reassociation Temperature and Enthalpy, after Heating and Cooling, of Hydrated Samples of the Pure Nanoparticle, Pure 1-Naphthol, 1-Naphthol-Loaded Nanoparticle, and 1-Naphthol-Loaded Amylose[a]

	$T_{reassociation}$ (°C)	enthalpy (ΔH) (J/g)
nanoparticle	80.1 ± 1.1	4.9 ± 0.1
1-naphthol (pure)	46.4 ± 2.9	1.2 ± 0.1
1-naphthol (5 mM)-loaded nanoparticle	62.8 ± 1.3	7.4 ± 1.2
1-naphthol (5 mM)-loaded amylose	77.5 ± 3.4	8.9 ± 1.8

[a]Values are the average value and standard error of the mean.

Evidence of 1-Naphthol in the Amylose Lumen of the Nanoparticle. Using the potentiometric titration technique, the nanoparticle was previously shown to have about 50% available space in the lumen of the amylose helix compared to about 15% for the amylose–fatty acid complex.[8] Here, potentiometric titration showed good binding of 1-naphthol in the amylose lumen of the nanoparticle (Figure 6). The amount of bound iodine of the pure nanoparticle was in between that of the uncomplexed amylose and the amylose–fatty acid inclusion complex, while for the 1-naphthol-loaded

DOI: 10.1021/acs.jafc.5b00037
J. Agric. Food Chem. 2015, 63, 4312–4319

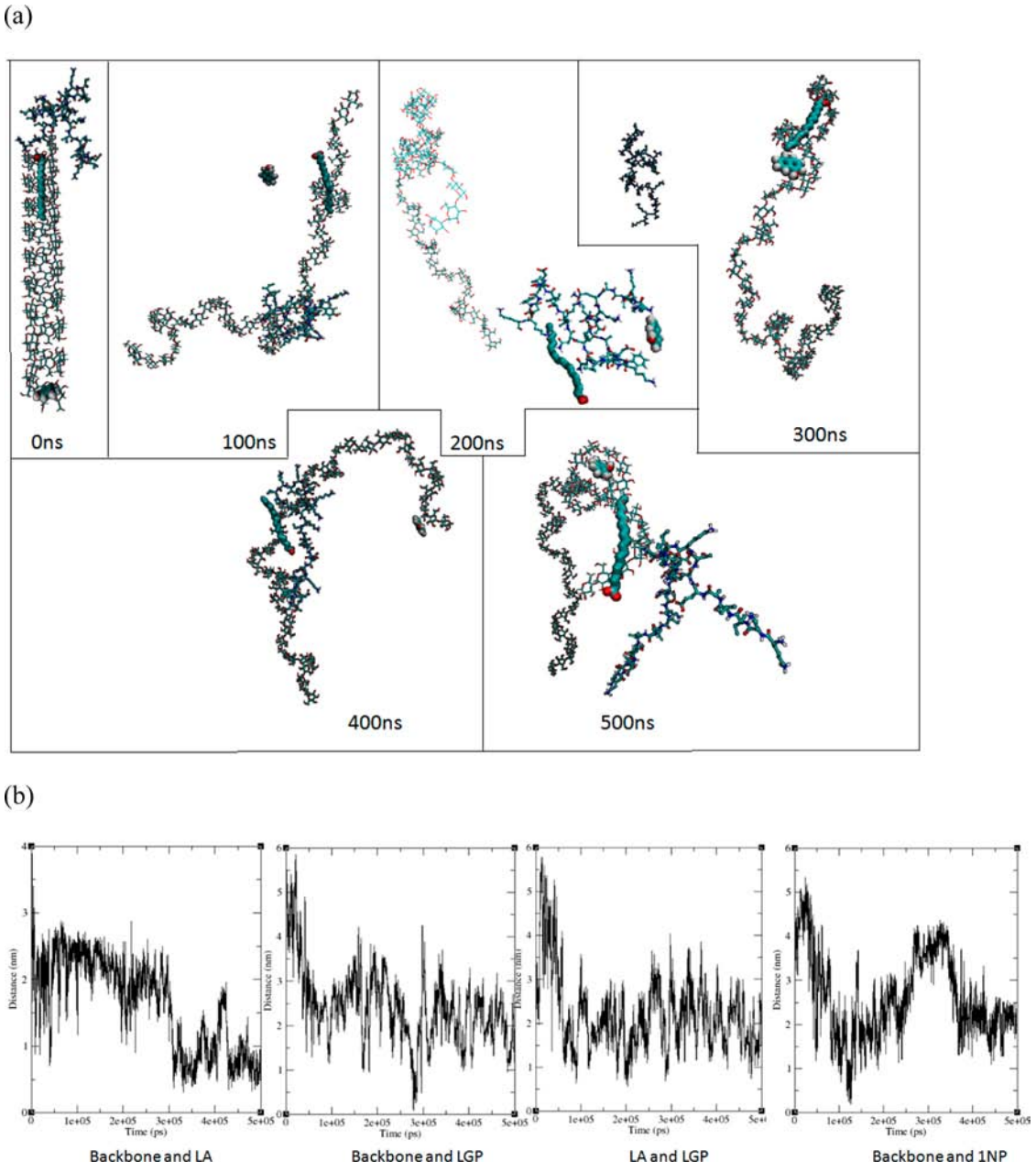

Figure 8. Time-dependent conformational transitions of a mixture of the amylose segment of 55 glucose residues (amylose backbone), β-lactoglobulin peptide (LGP), α-linoleic acid (LA), and 1-naphthol (1NP). (a) Snapshots from the simulations for the four-component system showing structural changes from the initial conformation to a final conformation at 500 ns. (b) Sequence of plots showing the distance between the amylose backbone and LA, amylose backbone and LPG, LA and LPG, and amylose backbone and 1NP.

nanoparticle, there was essentially no bound iodine, indicating that the amylose lumen of the nanoparticle was nearly fully occupied by 1-naphthol.

Thermal Behavior of the 1-Naphthol-Loaded Nanoparticle. Incorporation of 1-naphthol in the nanoparticle and amylose was further noted by thermal analysis, where a change in the melting endotherm was observed compared to hydrated pure 1-naphthol (Figure 7 and Table 3). The melting endotherm of hydrated pure 1-naphthol at 69.5 °C disappeared when the compound was incorporated. The pure nanoparticle melting endotherm occurred at 95.2 °C, while complexing 1-naphthol with the nanoparticle reduced it to 91.9 °C and significantly increased the melting enthalpy from 7.3 to 12.2 J/g (Table 3).

Reassociation after heating and cooling of the 1-naphthol-loaded nanoparticle occurred at a lower temperature (62.8 °C) and with higher enthalpy (6.4 J/g) than the pure nanoparticle (80.1 °C and 4.9 J/g) (Table 4). The large change in enthalpy suggests that additional non-covalent bonds were created during the formation of the 1-naphthol-loaded nanoparticle.

Quantification of 1-Naphthol Incorporation in the Nanoparticle. At the higher concentration of 10 mM 1-naphthol in the formation mixture, 91.8 mM 1-naphthol/mol of anhydroglucosyl unit (AGU) was found in the loaded nanoparticle (Table 1). This compares to previous studies showing the maximum binding capacity of 1-naphthol in the lumen of amylose of about 62−65 mM/mol of AGU.[31,34] Because potentiometric titration showed that only about 50%

DOI: 10.1021/acs.jafc.5b00037
J. Agric. Food Chem. 2015, 63, 4312−4319

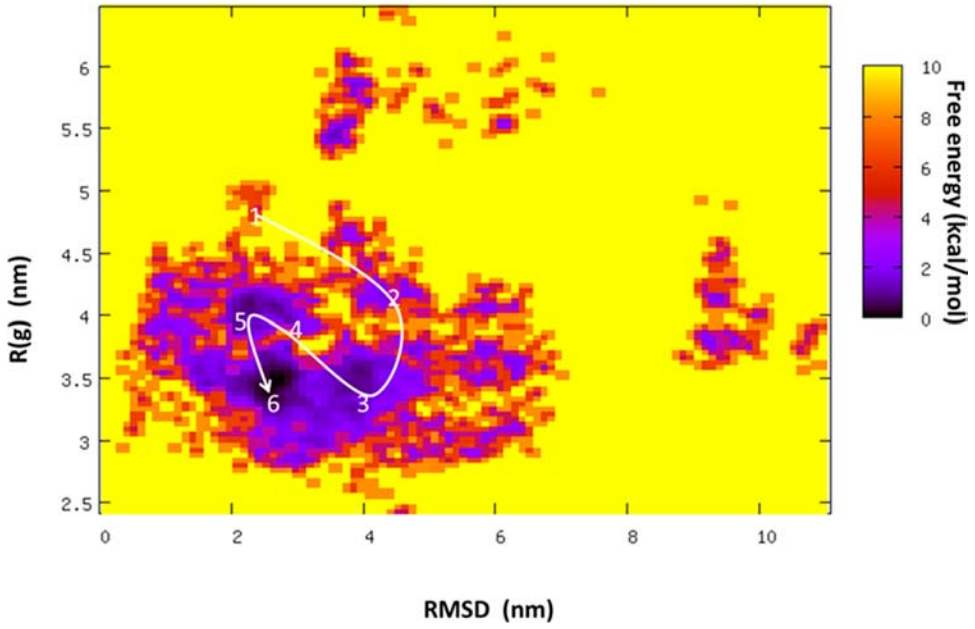

Figure 9. Free energy surface map of the four-component system composed of a mixture of the amylose segment of 55 glucose residues (amylose backbone), β-lactoglobulin peptide, α-linoleic acid, and 1-naphthol. Numbers correspond to snapshots at 100 ns intervals, as shown in Figure 8.

of the amylose inner helices was available for binding of 1-naphthol, the maximum inclusion capacity of the nanoparticle can be predicted to be only about 30 mM 1-naphthol. It is not clear where the remaining 1-naphthol is bound in the nanoparticle.

MD Simulation of the 1-Naphthol-Loaded Nanoparticle. *Structural Dynamics.* Figure 8 shows snapshots of the interaction of the four components in a 500 ns timeline, starting with the initial arrangement, as shown in Figure 1. Rearrangement of components over time shows a final structure with both the fatty acid and the 1-naphthol molecules residing in the lumen of the amylose helix with the 1-naphthol close to the hydrophobic tail of the fatty acid. The β-lactoglobulin peptide is found at the carboxyl head of the fatty acid. The sequence of interactions, as shown in Figure 8a, is as follows. In the first 100 ns, α-linoleic acid is included by the amylose-like segment, whereas the β-lactoglobulin peptide surrounds it and the 1-naphthol molecule is left out of the complex. At 200 ns, α-linoleic acid, β-lactoglobulin peptide, and 1-naphthol are close to each other, but all are separated from the amylose-like segment. At 300 ns, although the β-lactoglobulin peptide is still far from the amylose-like segment, both the α-linoleic acid and 1-naphthol molecules are incorporated into the amylose-like segment again. At 400 ns, α-linoleic acid is included in the middle of the amylose segment and the β-lactoglobulin peptide surrounds it; 1-naphthol remains out of the complex. Lastly, at 500 ns, both α-linoleic acid and 1-naphthol are included in the lumen of the amylose helix and the β-lactoglobulin peptide is associated with the carboxyl head of α-linoleic acid.

To analyze the conformational transitions quantitatively, the mutual distances between the interdomain backbone of the amylose-like segment, α-linoleic acid, β-lactoglobulin peptide, and 1-naphthol were calculated and are illustrated in Figure 8b. The shortest interdomain distance occurs between the amylose backbone and α-linoleic acid at 300 ns, which implies that these two molecules have a key role in stabilizing the system. The other three combinations of components show a rapid although more moderate decrease in interdomain distances, and corresponding distances were higher.

Free Energy Surface Map. Free energy changes from the initial time (0 ns) to the final time (500 ns) were calculated from the simulations and are presented as a free energy surface map tracing at 100 ns intervals during the assembly of the four components (Figure 9). With constituents placed initially as specified in Figure 1, the initial 0 ns state is thermodynamically unfavorable (region 1 in Figure 9), with a free energy of 6.3 kcal/mol. It then changes rapidly to a more stable second state (region 2 in Figure 9), with a free energy of 4.2 kcal/mol. At that moment, the complex separates into two parts, one being the amylose backbone and the other being the three components with an overall free energy decrease to 1.8 kcal/mol (region 3 in Figure 9). At a similar free energy state (1.5 kcal/mol), α-linoleic acid, 1-naphthol, and the amylose-like segment come together, while β-lactoglobulin peptide is set aside (region 4 in Figure 9). Then, a further lowering of free energy occurs as the constituents further assemble into a more compact macrostructure (regions 5 and 6 in Figure 9). Finally, a conformation was obtained with the lowest free energy of 0.05 kcal/mol, where both α-linoleic acid and 1-naphthol reside in the amylose helix and β-lactoglobulin peptide surrounds the amylose-like segment near the carboxyl group of α-linoleic acid. Such a process indicates a spontaneous self-assembling of the four components, which corresponds to the decrease in the estimated free energy and demonstrates that the self-assembling of these components comprises a thermodynamically favorable process.

Here, we have shown, experimentally and theoretically, that a previously identified soluble nanoparticle formed by the three macronutrients starch, protein, and fatty acid self-assembles with a sparingly soluble molecule (1-naphthol). 1-Naphthol occupies space in the amylose lumen and exists in a stable and soluble system. MD simulation of an amylose-like segment, β-lactoglobulin peptide, α-linoleic acid, and 1-naphthol confirmed that these molecules are thermodynamically driven into a four-component nanoparticle. 1-Naphthol was found to be included

DOI: 10.1021/acs.jafc.5b00037
J. Agric. Food Chem. 2015, 63, 4312−4319

in the lumen of the amylose helix and located in proximity to the hydrophobic tail of the fatty acid. The incorporation capacity of sparingly soluble small molecules in this soluble, safe, and soft nanoparticle suggests a number of potential applications, including the carrying and release of hydrophobic nutraceuticals and drugs.

■ ASSOCIATED CONTENT

Supporting Information

Charge of the atoms in glucose topology according to the glucose force field (Table S1) and atom labels in glucose topology according to the glucose force field (Figure S1). This material is available free of charge via the Internet at http://pubs.acs.org.

■ AUTHOR INFORMATION

Corresponding Authors

*Telephone: +1-765-494-6171. Fax: +1-765-494-7953. E-mail: campa@purdue.edu.

*Telephone: +1-765-494-6171. Fax: +1-765-494-7953. E-mail: hamakerb@purdue.edu.

Funding

The authors gratefully acknowledge partial financial support for this project from the United States Department of Agriculture (USDA)−Agriculture and Food Research Initiative (AFRI) program (Grant 07-35603-17741).

Notes

The authors declare no competing financial interest.

■ REFERENCES

(1) Savjani, K. T.; Gajjar, A. K.; Savjani, J. K. Drug solubility: Importance and enhancement techniques. *ISRN Pharm.* **2012**, *2012*, No. 195727.

(2) Merisko-Liversidge, E. M.; Liversidge, G. G. Drug nanoparticles: formulating poorly water-soluble compounds. *Toxicol. Pathol.* **2008**, *36*, 43−48.

(3) Zhang, G.; Maladen, M. D.; Hamaker, B. R. Detection of a novel three component complex consisting of starch, protein, and free fatty acids. *J. Agric. Food Chem.* **2003**, *51*, 2801−2805.

(4) Zhang, G.; Maladen, M.; Campanella, O. H.; Hamaker, B. R. Free fatty acids electronically bridge the self-assembly of a three-component nanocomplex consisting of amylose, protein, and free fatty acids. *J. Agric. Food Chem.* **2010**, *58*, 9164−9170.

(5) Zhang, G.; Hamaker, B. R. Starch-free fatty acid complexation in the presence of whey protein. *Carbohydr. Polym.* **2004**, *55*, 419−424.

(6) Zhang, G.; Hamaker, B. R. A three component interaction among starch, protein, and free fatty acids revealed by pasting profiles. *J. Agric. Food Chem.* **2003**, *51*, 2797−2800.

(7) Shah, A.; Zhang, G.; Hamaker, B. R.; Campanella, O. H. Rheological properties of a soluble self-assembled complex from starch, protein and free fatty acids. *J. Food Eng.* **2011**, *105*, 444−452.

(8) Liu, J.; Fei, L.; Maladen, M.; Hamaker, B. R.; Zhang, G. Iodine binding property of a ternary complex consisting of starch, protein, and free fatty acids. *Carbohydr. Polym.* **2009**, *75*, 351−355.

(9) Clays, K.; Olbrechts, G.; Munters, T.; Persoons, A.; Kim, O.-K.; Choi, L.-S. Enhancement of the molecular hyperpolarizability by a supramolecular amylose−dye inclusion complex, studied by hyper-Rayleigh scattering with fluorescence suppression. *Chem. Phys. Lett.* **1998**, *293*, 337−342.

(10) Conde-Petit, B.; Escher, F.; Nuessli, J. Structural features of starch-flavor complexation in food model systems. *Trends Food Sci. Technol.* **2006**, *17*, 227−235.

(11) Itthisoponkul, T.; Mitchell, J. R.; Taylor, A. J.; Farhat, I. A. Inclusion complexes of tapioca starch with flavour compounds. *Carbohydr. Polym.* **2007**, *69*, 106−115.

(12) Le Bail, P.; Rondeau, C.; Buléon, A. Structural investigation of amylose complexes with small ligands: helical conformation, crystalline structure and thermostability. *Int. J. Biol. Macromol.* **2005**, *35*, 1−7.

(13) Lopez, C. A.; de Vries, A. H.; Marrink, S. J. Molecular mechanism of cyclodextrin mediated cholesterol extraction. *PLoS Comput. Biol.* **2011**, *7*, e1002020.

(14) Zhang, H.; Feng, W.; Li, C.; Tan, T. *J.* Investigation of the inclusions of puerarin and daidzin with *β*-cyclodextrin by molecular dynamics simulation. *J. Phys. Chem. B* **2010**, *114*, 4876−83.

(15) Rodriguez, S. D.; Bernik, D. L.; Mereau, R.; Castet, F.; Champagne, B.; Botek, E. Amylose-vanillin complexation assessed by a joint experimental and theoretical analysis. *J. Phys. Chem. C* **2011**, *115*, 23315−22.

(16) Biliaderis, C. G.; Page, C. M.; Slade, L.; Sirett, R. R. Thermal behavior of amylose-lipid complexes. *Carbohydr. Polym.* **1985**, *5*, 367−89.

(17) Tusch, M.; Krüger, J.; Fels, G. Structural stability of V-amylose helices in water-DMSO mixtures analyzed by molecular dynamics. *J. Chem. Theory Comput.* **2011**, *7*, 2919−2928.

(18) Uhrinova, S.; Smith, M. H.; Jameson, G. B.; Uhrin, D.; Sawyer, L.; Barlow, P. N. Structural changes accompanying pH-induced dissociation of the *β*-lactoglobulin dimer. *Biochemistry* **2000**, *39*, 3565−74.

(19) Altaan, D. V. *PRODRG, a Program for Generating Molecular Topologies and Unique Molecular Descriptors from Coordinates of Small Molecules*; http://davapc1.bioch.dundee.ac.uk/prodrg/ (accessed 2013).

(20) *Hetero-compound Information Centre*; http://xray.bmc.uu.se/hicup/EIC/ (accessed 2013).

(21) Kleywegt, G. J.; Jones, T. A. Databases in protein crystallography. *Acta Crystallogr., Sect. D: Biol. Crystallogr.* **1998**, *54* (Pt 6 Pt 1), 1119−31.

(22) Kleywegt, G. J.; Henrick, K.; Dodson, E. J.; van Aalten, D. M. Pound-wise but penny-foolish: How well do micromolecules fare in macromolecular refinement? *Structure* **2003**, *11*, 1051−9.

(23) Kleywegt, G. J. Crystallographic refinement of ligand complexes. *Acta Crystallogr., Sect. D: Biol. Crystallogr.* **2007**, *63* (Part 1), 94−100.

(24) Bauer, R. A.; Gunther, S.; Jansen, D.; Heeger, C.; Thaben, P. F.; Preissner, R. *SuperSite: Dictionary of Metabolite and Drug Binding Sites in Proteins*; http://bioinf-tomcat.charite.de/supersite/resultHET.faces?hetid=1NP (accessed 2013).

(25) Damm, W.; Frontera, A.; Tirado−Rives, J.; Jorgensen, W. L. The OPLS all-atom force field for carbohydrates. *J. Comput. Chem.* **1997**, *18*, 1955−1970.

(26) Kony, D.; Damm, W.; Stoll, S.; Van Gunsteren, W. F. An improved OPLS−AA force field for carbohydrates. *J. Comput. Chem.* **2002**, *23*, 1416−29.

(27) Lawtrakul, L.; Viernstein, H.; Wolschann, P. Molecular dynamics simulations of *β*-cyclodextrin in aqueous solution. *Int. J. Pharm.* **2003**, *256*, 33−41.

(28) Lerbret, A.; Affouard, F.; Bordat, P.; Hédoux, A.; Guinet, Y.; Descamps, M. Molecular dynamics simulations of lysozyme in water/sugar solutions. *Chem. Phys.* **2008**, *345*, 267−274.

(29) Lopez, C. A.; de Vries, A. H.; Marrink, S. J. Amylose folding under the influence of lipids. *Carbohydr. Res.* **2012**, *364*, 1−7.

(30) Abascal, J. L. F.; Vega, C. A general purpose model for the condensed phases of water: TIP4P/2005. *J. Chem. Phys.* **2005**, *123*, 234505 http://dx.doi.org/10.1063/1.2121687,.

(31) Wulff, G.; Avgenaki, G.; Guzmann, M. S. P. Molecular encapsulation of flavours as helical inclusion complexes of amylose. *J. Cereal Sci.* **2005**, *41*, 239−249.

(32) Nuessli, J.; Conde-Petit, B.; Trommsdorff, U. R.; Escher, F. Characterization of amylose-flavour complexes by DSC and X-ray diffraction. *Carbohydr. Polym.* **1995**, *28*, 167−170.

(33) Wyatt, P. J. Light scattering and the absolute characterization of macromolecules. *Anal. Chim. Acta* **1993**, *272*, 1−40.

(34) Rutschmann, M. A.; Solms, J. Formation of inclusion complexes of starch in ternary model system with decanal, menthone, and 1-naphthol. *Lebensm.-Wiss. Technol.* **1990**, *23*, 457−464.

DOI: 10.1021/acs.jafc.5b00037
J. Agric. Food Chem. 2015, 63, 4312−4319

the properties of a protein, such as on stability, solubility, and metabolic energy.[2] Glycosylation of phytase has been shown to affect thermostability,[13,17,18] which would be a concern regarding enzyme activity loss due to heat such as that from feed pelleting. Phytases for commercial use have been isolated mainly from fungi and bacteria,[6,8,11] and selection for an efficacious product is greatly dependent on the source,[1] tolerance to processing factors, digestive resistance, and production costs.[6,8,19] Major feed crops have been genetically modified to increase phytase expression and are at various stages of product development.[20] For example, two separate studies on transgenic phytase barley have both reached an advanced developmental stage complete with field trials; however, only transgenic phytase corn (Event B23-3-1) has received approval status for commercial sale. Integration of such phytases as transgenes in agricultural products in a growing industry would benefit from inclusion of a means to verify transgenic phytase presence in food nutritional and environmental management strategies wherein concerns of phytate mineral availability and environmental issues need to be assessed. Development of a rapid diagnostic test (RDT), which is a qualitative immunoassay (consisting of target specific antibodies) used in point-of-care testing, for transgenic phytase would offer an efficient, convenient, and affordable method of detection.

Aspergillus niger phytase (*phy*A2), which has 10 potential N-glycosylation sites,[2] was cloned and expressed in a methylotrophic yeast, *Pichia pastoris*.[21] This same phytase was cloned into corn, yielding seeds with a maximal phytase activity of 125 FTU/g kernels, 1000-fold above that of the wild type, and with 1000 g of kernels containing up to 67 times the feed industry requirement.[22] Corn is a globally important animal feed crop; in China, corn occupies 30 million hectares of land from which much is used to feed 500 million pigs (approximately 50% of the global herd) and 13 billion chickens, ducks, and poultry.[23] As mentioned above, only transgenic phytase corn has been approved for commercialization; accessibility coupled with the ensuing demand for corn production, all make it an ideal product candidate for this project. Herein, two pairs of highly sensitive and specific monoclonal antibodies (MAbs) raised against *A. niger* recombinant phytase and generated through an extensive screening technique were described whereby each was found to detect a phytase protein of different sizes, possibly due to glycosylation. Using these MAbs, the transgenic corn was found to express lower levels of the larger-sized phytase than the recombinant phytase had expressed in yeast; however, the level of detection was predicated on the condition of the expressed phytase. Together, these findings provide important insight regarding the structural properties of phytase epitopes, suggesting a possible role of carbohydrates within antibody binding sites, and lead to the development of RDT strips coated with MAbs that can detect two differently sized proteins of transgenic phytase.

MATERIALS AND METHODS

Recombinant Phytase, Seeds, and Antibodies. *A. niger* 963 *phytase* (*phy*A2) expressed in *P. pastoris* was isolated by and donated from the Biotechnology Research Institute, Chinese Academy of Agricultural Sciences in Beijing, China. This recombinant protein was freeze-dried, reconstituted in PBS (at 200 μg/mL), and stored at 4 °C until required. This group also donated genetically modified (GM) phytase corn seeds, expressing this same *A. niger* phytase gene *phy*A2. Seeds from various plants [six varieties of GM corn, one variety of a GM soybean, corn (2733) from Pickseed, six corn varieties from West Coast Seeds (WCS; two of F1, two of P, one of DF1, and one unknown), green bean, white bean, and seven generic varieties of corn (purchased from local markets)] were used in characterization studies.

Phytase monoclonal antibodies (MAbs, EH10a, FA7, AF9a, and CC1) raised against a recombinant *A. niger* 963 (*phy*A2) phytase were donated by the Chinese Biotechnology Research Institute in Beijing and prepared in a manner similar to that described in Chen et al.[24]

Epitope Characterization. To characterize the epitopes recognized by the purified phytase MAbs, an ELISA and the additivity index (AI) described by Friguet et al.[25] were used. Briefly, wells of a 96-well plate were coated with 100 μL of 2 μg/mL recombinant phytase and incubated overnight at 4 °C. The following day, the wells were incubated with 100 μL of antibodies, EH10a, FA7, AF9a, CC1, individually or in paired combinations (50 μL each) of equivalent concentrations at 1:1000 overnight at 4 °C. The following day, the wells were incubated with 100 μL of a goat anti-mouse IgG−HRP secondary antibody at 1:1000 for 30 min at 37 °C. The absorbance value for each treatment was recorded at 450 nm. The AI was calculated using the following equation: $\{[2A_{1+2}/(A_1 + A_2)] - 1\} \times 100\%$, where A_1, A_2, and A_{1+2} are the absorbance values for the individual antibodies and the respective combined pairs. If the two antibodies are directed against different epitopes (no competition), A_{1+2} should be equal to the sum of A_1 and A_2 and the AI value should approach 100%. If the two antibodies are directed against the same epitope (competition), A_{1+2} should be equal to the mean value for A_1 and A_2 and AI should be close to 0%. The threshold was determined by AI $\geq$ 40%.

Protein Analysis. Protein and Western blot analyses on the specificity of the MAbs were evaluated by 15% SDS-PAGE using 1 μg of recombinant phytase and 50 mg of ground seeds from GM phytase corn, generic corn, green bean, white bean, Pickseed2733 corn, WCS F1 corn, four varieties of GM corn, and one GM soybean variety. The phytase could be released from the GM phytase corn only by homogenizing the corn seeds in a modified Tris buffer [50 mM Tris-HCl (pH 8.0), 10 mM KCl, 3 mM $MgCl_2$, 1 mM EDTA, 1 mM β-mercaptoethanol, 0.1% BSA, 13% sucrose, and SigmaFAST Protease inhibitor cocktail (Sigma-Aldrich, St. Louis, MO, USA)] at 400 μL per 100 mg tissue, after which the sample was centrifuged at 4500*g* for 10 min. Laemmli loading buffer[26] was then added to the supernatant and incubated at 65 °C for 20 min. The remaining seeds were ground, homogenized in 500 μL of Laemmli buffer, boiled for 10 min, and centrifuged for 2 min at 12000*g*. To improve Western blot detection, 5 μg of recombinant phytase and 100 mg of ground seeds were used. Twenty microliters of each prepared seed supernatant was used for protein and Western blot analysis. The recombinant phytase, 20 μL of water, and 10 mM Tris (the latter two as negative controls) were also boiled in Laemmli buffer as described above. The membrane blot was incubated overnight at 4 °C with a combined mixture of EH10a, FA7, AF9a, and CC1 MAbs (each at 1:400), whereas the SDS-PAGE protein gel was stained with Coomassie Brilliant Blue. The following day the membrane was incubated with horseradish peroxidise conjugated goat anti-mouse immunoglobulin (IgG−HRP at 1:1000) for 90 min at room temperature. Proteins on the blot were developed using the 3,3′-diaminobenzidine tetrahydrochloride (DAB; Sigma-Aldrich) method with 0.1% hydrogen peroxide.

To evaluate the nature of the MAbs directed to epitopes on phytase, an additional Western blot analysis was performed. Purified recombinant phytase protein isolated from yeast and ground seeds of GM phytase corn were both resuspended with PBS to a concentration of 200 μg/mL and stored at 4 °C until required. Every 2 weeks for a period of 10 weeks, 10 μL from each of the recombinant phytase and GM phytase corn was boiled with 10 μL of loading buffer for 5 min and loaded onto a 10% SDS-PAGE. Each transferred membrane blot was incubated overnight at 4 °C with a combined mixture of MAbs as described above. The subsequent steps are as described above, except the concentration of the IgG−HRP secondary antibody was 1:5000 with an incubation time of 30 min.

Construction and Evaluation along Immunolateral Flow Test Strips. The detection phytase antibody (the test line antibody, either FA7 or CC1) and the goat anti-mouse IgG (the control line

DOI: 10.1021/acs.jafc.5b00188
J. Agric. Food Chem. 2015, 63, 4320−4326

antibody) were diluted to a standard concentration of 1.5 mg/mL with 10 mM Tris-HCl (pH 8.0) and applied in a thin line onto a nitrocellulose membrane. The colloidal gold conjugated phytase capture antibody was prepared as described in Chen et al.[24] Briefly, 1.4 mL of 1% $Na_3C_6H_5O_7$ was first added to 100 mL of boiled 0.01% $HAuCl_4$. The colloidal gold solution was then allowed to cool gradually, after which the pH was adjusted to 8.4 with 1% K_2CO_3. The EH10a or AF9a antibodies were added dropwise into 10 mL of the colloidal gold solution and left to stabilize at 4 °C. After 30 min, BSA blocking agent was added, and the solution was placed at 4 °C for another 2 h. The mixture was centrifuged twice, the first time to recover the supernatant and the second to conjugate pellet, which was then suspended in 10 mM borax buffer (with 2% BSA and 0.05% NaN_3, pH 8.0). The conjugated antibody (i.e., EH10a if the detection antibody was FA7 or AF9a if the detection antibody was CC1) was sprayed twice onto a sheet of fiberglass and dried at 37 °C. The phytase lateral flow test strips were assembled as described in Chen et al.[24]

Two grams of each seed variety was ground in 10 mM Tris-HCl. The absorption pad end of a prepared test strip was immersed in seed supernatant. Test strips were also immersed in 200 μg/mL of recombinant phytase, 200 μg/mL of transgenic corn, distilled water, and 10 mM Tris-HCl (the latter two as negative controls). A response was observed within 5 min. The appearance of two bands, one each at the test and control sites, represents a positive test result; a single band at the control site represents a negative test result. The absence of a line at the control site indicates the test is invalid.

To determine the sensitivity of the antibodies to phytase along an immunolateral flow test strip, recombinant phytase was diluted in concentrations from 200 to 0.002 μg/mL by 10 mM Tris-HCl (pH 8.0) and tested using the EH10a−FA7 MAb match pair, whereas the transgenic phytase corn was tested in concentrations from 400 to 0.001 μg/mL using the AF9a−CC1 MAb match pair. The responses of the strips were evaluated as above.

The nature of the MAbs directed to epitopes on phytase was evaluated along an immunolateral flow test strip. Individual test strips consisting of either the EH10a−FA7 or the AF9a−CC1 MAb match pairs were immersed in the reconstituted recombinant or GM corn phytase samples every 2 weeks for a period of 10 weeks. The samples were stored at 4 °C until required. With the "MAX" line on the test strip positioned above the liquid level, a sample was allowed to migrate halfway up the strip, after which the strip was removed. The results were obtained within 30 min, and the strips were evaluated as above.

The stability of test strips was assessed when kept for 1 year at room temperature.

RESULTS AND DISCUSSION

Monoclonal Antibody Characterization. Phytase is considered the most prominent enzyme to hydrolyze phytate and release bound phosphorus in a form available to animals for growth and development. A recombinant *A. niger* phytase (*phy*A2) expressed in *P. pastoris*[21,22] was used to produce MAbs employing a very extensive and novel screening technique.[24] From a total of 976 hybridoma cell strains, 32 positive cell clones using repetitive ELISAs and cross-responsive screening of MAbs against *A. niger* (*phy*A2) phytase were generated (personal communication, Biotechnology Research Institute). Cell lines screened for the strongest positive signal in phytase-challenged cultures were selected, culminating in four MAbs candidates (EH10a, FA7, AF9a, and CC1). AI values were calculated to determine competition for the binding sites between the four MAbs. The following AI values were found for the following antibody pairs: FA7+AF9a (67.7%), FA7+CC1 (91.4%), AF9a+EH10a (57.7%), EH10a+CC1 (69.7%), FA7+EH10a (59.6%), and AF9a+CC1 (≥99%). These results indicate that any pair of these antibodies would result in the targeting of a different phytase epitope.

Evaluation of Monoclonal Antibody Pairs to Phytase Protein. *P. pastoris* is a methylotrophic yeast that, when under the control of a methanol-inducible alcohol oxidase (AOX1) promoter, has been successfully used to produce many proteins with varying degrees of success,[27−29] and these proteins are often glycosylated.[30] Protein analyses of various seed varieties (Figure 1A) were used to assess MAb specificity along with a

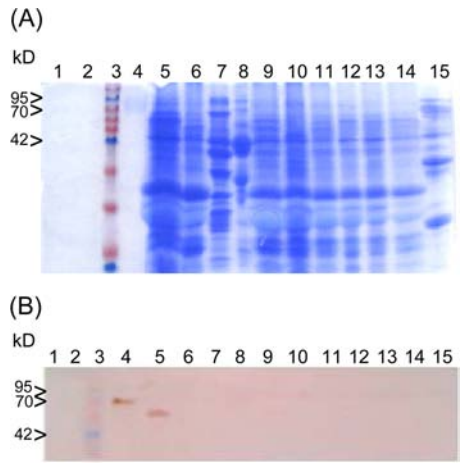

Figure 1. Monoclonal antibodies (MAbs) target phytase. (A) Fifty micrograms of plant seeds was ground in 500 μL of Laemmli buffer of which 20 μL was loaded into each lane. The lanes are as follows: (1) water; (2) 10 mM Tris-HCl, pH 8.0; (3) marker; (4) 1 μg of recombinant phytase; (5) GM phytase corn; (6) corn 1; (7) green bean; (8) white bean; (9) Pickseed2733 corn; (10) WCS F1 corn; (11) GM corn 1; (12) GM corn 2; (13) GM corn 3; (14) GM corn 4; (15) GM soybean. (B) Western blot analyses were conducted on the samples used in (A), except that 5 μg of recombinant phytase and 100 mg of ground plant seeds were used and probed with an equal mixture of MAbs EH10a, FA7, AF9a, and CC1. The protein marker sizes in kilodaltons (kD) are indicated on the left of the blot. GM, genetically modified; WCS, West Coast Seeds. Unless stipulated, GM corn samples are not GM phytase corn. Additional methods are described in the text.

recombinant *A. niger* phytase expressed from yeast and a genetically modified (GM) corn containing this same *A. niger* phytase. The samples were probed with a MAb mixture of EH10a, FA7, AF9a, and CC1 (in equal proportions). The recombinant *A. niger* phytase expressed from yeast shows a band of approximately 75 kDa (Figure 1B, lane 4), whereas the GM *A. niger* phytase corn reveals a band of about 60 kDa (Figure 1B, lane 5). Further, this MAb mixture did not cross-react with the other test seeds as shown from Western blot analysis (Figure 1B, lanes 6−15). The larger-sized protein from the yeast-expressed phytase may be due to the greater degree of glycosylation often observed in proteins expressed from yeast. Differences in glycosylation pattern expressed from different hosts may be attributed to the discrete processes found in their respective cellular environments. For example, *A. fumigates* was found to produce a phytase that can tolerate boiling at 100 °C for 20 min, retaining 90% of its initial activity.[31] Lucca et al.[32] found that when rice containing the *A. fumigates* phytase was boiled for 20 min, the enzyme had retained 50% of the enzyme activity. However, when rice seeds were cooked under the same conditions, only 8% of the phytase activity was retained. Similarly, these differences in thermotolerance may be attributed to the different glycosylation patterns in phytase expressed between diverse hosts. Phytases that have high

DOI: 10.1021/acs.jafc.5b00188
J. Agric. Food Chem. 2015, 63, 4320−4326

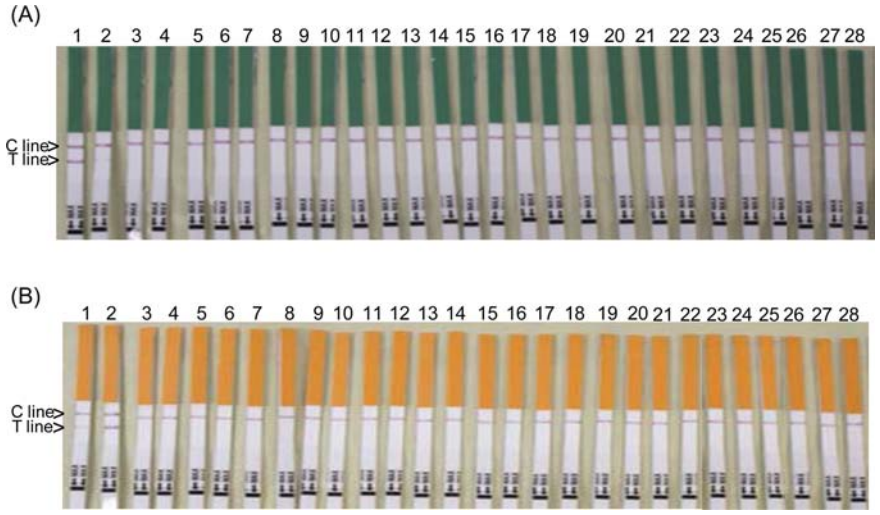

Figure 2. Both match pair EH10a−FA7 and AF9a−CC1antibodies show high specificity to phytase. (A) Phytase specificity analysis was conducted using lateral flow strips containing the EH10a conjugate antibody and the FA7 capture antibody. Strips 1−4 were immersed in a 10 mL solution consisting of (1) 200 μg/mL recombinant phytase, (2) 200 μg/mL transgenic phytase corn, (3) 10 mM Tris-HCl, and (4) distilled water. Strips 5−28 were immersed in the supernatant of 2 g of seeds ground in 10 mL of 10 mM Tris-HCl for 1−5 min. The strips were tested using the following seeds: (5) corn 1; (6) corn 2; (7) corn 3; (8) corn 4; (9) GM corn 1; (10) GM soybean; (11) Pickseed2733 corn; (12) GM corn 2; (13) GM corn 3; (14) GM corn 4; (15) WCS F1 corn 1; (16) WCS F1 corn 2; (17) WCS P corn 1; (18) WCS P corn 2; (19) WCS DF1 corn; (20) green soybean; (21) WCS corn; (22) green bean; (23) white bean; (24) corn 5; (25) corn 6; (26) corn 7; (27) GM corn 5; (28) GM corn 6. For each strip the upper line is the control (C) line containing antibodies to goat anti-mouse IgG and the lower line (if present) is the test (T) line with the FA7 capture antibody. The corn samples used in strips 5−8 and 24−26 were generic (non-GM) varieties. (B) Phytase specificity analysis was conducted using lateral flow strips containing the AF9a conjugate antibody and the CC1 capture antibody. Each strip was prepared and tested with the same samples as described in (A) except the lower T line (if present) contains the CC1 capture antibody.

tolerance to heat are advantageous not only for feed production due to temperatures associated with pelleting but for food processing activities such as cooking and baking.[6] Locations for new sources of thermotolerant as well as the engineer of technologically improved phytases to withstand increased temperatures and GM phytase crops are invaluable to industries that must deal with phytate and the challenges it represents.

Characterization of Phytase Monoclonal Antibody Pairs Using Lateral Strip Assays. The additive index results indicated that the four MAbs target different phytase epitopes; therefore, lateral flow strip comparison assays using all possible MAb pair combinations were conducted and showed that the EH10a−FA7 and AF9a−CC1 MAb pairs exhibited the strongest potential to be used in lateral flow strip products (data not shown). To determine the specificity of the phytase MAb pairs, immunoassays comprising of antibody-coated lateral strips were constructed and tested with different seed varieties of commercial plants. Lateral strips that consisted of the gold-conjugated EH10a antibody and the FA7 membrane capture antibody showed that this antibody pair was able to detect the *A. niger* recombinant (*phy*A2) phytase expressed in *P. pastoris* and, to a lesser extent, the GM (*phy*A2) phytase corn (Figure 2A, lanes 1 and 2). In contrast, strips that consisted of the gold-conjugated AF9a antibody and the CC1 membrane capture antibody showed that this antibody pair was able to detect the GM phytase corn more efficiently that the recombinant phytase (Figure 2B, lanes 1 and 2). Further, phytase could not be detected in any of the test seed varieties using either of the antibody pairs, indicating a high specificity to the *A. niger* recombinant protein that is used in GM phytase crops.

Antibody-coated lateral strips were also used to determine the sensitivity of the phytase MAb pairs. The EH10a−FA7 and AF9a−CC1 antibody pairs were able to efficiently detect the recombinant phytase and GM corn phytase, respectively. Therefore, serial dilutions were prepared with the recombinant phytase for the EH10a−FA7 antibody pair, with the GM phytase for the AF9a−CC1 antibody pair and tested on lateral flow strips. The detection limit to recombinant phytase using the EH10a−FA7 antibody pair was 5 ng/mL (Figure 3A), whereas the detection limit to GM phytase corn using the AF9a−CC1 antibody pair was as low as 2 ng/mL (Figure 3B). The strips were confirmed to be stable when kept at room temperature for 1 year.

Reactive Antibody Binding Sites May Involve Glycosylation. As stated earlier, the EH10a−FA7 antibody pair showed a greater ability to detect the yeast-expressed phytase, whereas the AF9a−CC1 antibody pair showed a greater ability to detect the GM corn phytase. Additionally, different-sized phytase proteins could be detected from these two sources. We wanted to further explore the nature of the epitopes between yeast- and plant-expressed phytases and assess whether glycosylation has a role that determines the responses to their respective antibody match pairs. Using Western blot analysis, phytases expressed from yeast and GM corn were probed with a combined MAb mixture of EH10a, FA7, AF9a, and CC1 and monitored over time. During the first 2 weeks, the 75 kDa band dominated with a lesser abundant 60 kDa band from the yeast-expressed phytase (Figure 4A, top row). By the fourth week, this 75 kDa band was progressively less detectable, whereas the 60 kDa band was progressively more detectable (Figure 4A, top row). In contrast, the 60 kDa band from the GM corn phytase was progressively less detectable over time (Figure 4A, bottom row) and the 75 kDa was not detectable at all (data not shown).

Phytase samples were prepared as above and tested over the same time periods using lateral flow strips consisting of either the EH10a−FA7 or the AF9a−CC1 antibody match pair. As

DOI: 10.1021/acs.jafc.5b00188
J. Agric. Food Chem. 2015, 63, 4320−4326

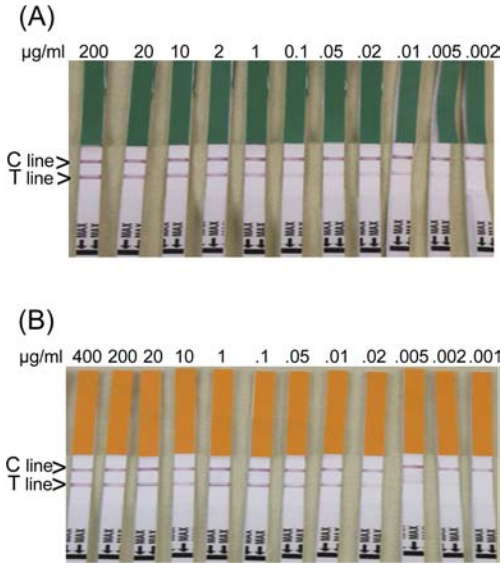

Figure 3. Match pair EH10a–FA7 and AF9a–CC1 antibodies were able to detect low concentrations of phytase. (A) To determine the sensitivity of the EH10a–FA7 antibodies, concentrations from 0.002 to 200 μg/mL of recombinant phytase were applied to lateral flow strips containing the EH10a conjugate antibody and the FA7 capture antibody. (B) To determine the sensitivity of the AF9a–CC1 antibodies, concentrations from 0.001 to 400 μg/mL of the GM phytase corn were applied to lateral flow strips containing the AF9a conjugate antibody and the CC1 capture antibody. The strips were immersed in a 10 mL solution of recombinant phytase (A) and GM phytase corn (B) at the various concentrations indicated above the strips. The arrangement of the control (C) and test (T) lines along the strips is as described in Figure 2.

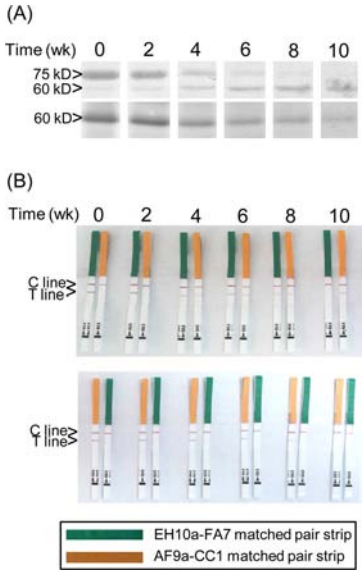

Figure 4. Nature of phytase epitopes affects detection by EH10a–FA7 and AF9a–CC1 match-pair MAbs over time. (A) Ten microliters of (200 μg/mL) purified recombinant phytase (phy2A) expressed from yeast (top row) and (200 μg/mL) phytase expressed from GM corn (bottom row) was prepared and evaluated every 2 weeks over a period of 10 weeks using Western blot analysis. Each blot was probed with a mixture of MAbs EH10a, FA7, AF9a, and CC1. Record dates are indicated above the blot with the protein marker sizes kilodaltons (kD) on the left. (B) Purified recombinant phytase (phy2A) expressed from yeast (top row) and phytase expressed from GM corn (bottom row) were prepared and tested along immunolateral flow strips. Test strips containing the EH10a conjugate antibody and FA7 capture antibody (green colored) and the AF9a conjugate antibody and CC1 capture antibody (brown colored) were immersed in a solution of their respectively prepared phytase, and detection was recorded on the dates indicated above the strips. The arrangement of the control (C) and test (T) lines along the strips are as described in Figure 2.

the yeast-expressed (75 kDa) phytase degrades, it becomes less detectable when using strips with the EH10a–FA7 antibody match pair (Figure 4B, top row, green strips) and becomes more detectable when using strips with the AF9a–CC1 antibody match pair over time (Figure 4B, top row, brown strips). This effect corresponds to the detection of the smaller-sized phytase protein, which is similar to that detected from the transgenic corn (60 kDa) phytase, which, too, becomes less detectable upon degradation using the AF9a and CC1 antibodies (Figure 4B, bottom row, brown strips) and was barely discernible on strips coated with the EH10a–FA7 antibody match pair (Figure 4B, bottom row, green strips). If the larger phytase size is indeed due to glycosylation and a loss of this glycosylation results in a change in antibody recognition, it may be tempting to assume that the epitope binding sites of one or both of the MAbs, EH10a and FA7, consists of a carbohydrate moiety. Guirakhoo et al.[33] demonstrated that a carbohydrate side chain was essential in stabilizing epitopes within the envelope protein of the tick-borne encephalitis (TBE) virus. Although little is known about the structure of phytase antibody binding sites, antibodies have been shown to recognize carbohydrate epitopes.[34] On the basis of our findings, one can assume that the epitope structural organization of the four MAbs is similar, albeit the carbohydrate group required for EH10a and FA7 MAbs and the antibody that prevails is dependent upon glycosylated sites and that glycosylation may be required to maintain site stability. Or one can assume that the epitopes are not similar in structure but lie near enough together so that the carbohydrate group is inhibiting or blocking the binding sites to antibodies that do not recognize glycosylation. Cryptic sites within the TBE virus envelope containing antigenic determinants when exposed allow cross-reactive antibodies to be efficiently recognized, which would not have been accessible in a native virus.[35] Further studies are required such as structural analysis of the antigenic sites of the phytase protein expressed from various sources to verify the contribution of carbohydrates to antibody binding.

The development of transgenic phytase plants and the call for greater awareness of the distribution of GM organisms brings about a need for accurate product verification. Further, the ability to correctly detect glycosylation within transgenic phytase plants may be beneficial when a product with a more thermostable enzyme is required. Methods to assess phytase activity usually involve detection of released inorganic phosphates by adding phytate as a substrate, requiring generation of a calibration curve and complex laboratory equipment.[36−38] In this study, MAbs were generated which are able to bind to different protein epitopes that were both highly sensitive and specific to transgenic phytase, efficiently so as to be differentiated from the yeast-expressed phytase. An RDT, which is an immunochromatographic capillary flow assay consisting of MAbs, one immobilized on the surface of the membrane and the other conjugated to particles near the sample pad, allows for an efficient and sensitive point-of-care testing method that would deliver immediate results, requiring little skill or additional equipment. Here we present the

DOI: 10.1021/acs.jafc.5b00188
J. Agric. Food Chem. 2015, 63, 4320−4326

development of such a RDT that is able to detect phytase from a GM crop.

AUTHOR INFORMATION

Corresponding Authors

*(Jian Zheng) E-mail: jian0102@hotmail.com. Phone: +86 13793183297. Fax: +86 2368486780.

*(Juan Zhang) Phone: +86 13793183297. Fax: +86 2368486780

Funding

This study was supported by a grant from the National Major Programs of the genetically modified organisms breeding during the 11th Five-Year Plan Period (Grant 2009ZX08012-008B).

Notes

The authors declare no competing financial interest.

ACKNOWLEDGMENTS

We thank Krystyna Pangilinan for graphical assistance.

ABBREVIATIONS USED

MAb, monoclonal antibody; *phy*A2, phytase A2 gene; GM, genetically modified; AI, additive index; RDT, rapid diagnostic test

REFERENCES

(1) Bohn, L.; Meyer, A. S.; Rasmussen, S. K. Phytate: impact on environment and human nutrition. A challenge for molecular breeding. *J. Zhejiang Univ., Sci., B* **2008**, *9*, 165−191.

(2) Wyss, M.; Pasamontes, L.; Friedlein, A.; Rémy, R.; Tessier, M.; Kronenberger, A.; Middendorf, A.; Lehmann, M.; Schnoebelen, L.; Röthlisberger, U.; Kusznir, E.; Wahl, G.; Müller, F.; Lahm, H.-W.; Vogel, K.; van Loon, A. P. G. M. Biophysical characterization of fungal phytases (*myo*-inositol hexakisphosphate phosphohydrolases): molecular size, glycosylation pattern, and engineering of proteolytic resistance. *Appl. Environ. Microbiol.* **1999**, *65*, 359−366.

(3) Kikunaga, S.; Takahashi, M.; Huzisige, H. Accurate and simple measurement of phytic acid contents in cereal grains. *Plant Cell Physiol.* **1985**, *26*, 1323−1330.

(4) Reddy, N. R.; Sathe, S. K.; Salunkhe, D. K. Phytates in legumes and cereals. *Adv. Food Res.* **1982**, *28*, 1−92.

(5) Ravindran, V.; Bryden, W. L.; Kornegay, E. T. Phytates: occurrence, bioavailability and implications in poultry nutrition. *Poult. Avian Biol. Rev.* **1995**, *6*, 125−143.

(6) Greiner, R.; Konietzny, U. Phytase for food application. *Food Technol. Biotechnol.* **2006**, *44*, 125−140.

(7) Lopez, H. W.; Leenhardt, F.; Coudray, C.; Remesy, C. Minerals and phytic acid interactions: is it a real problem for human nutrition? *Int. J. Food Sci. Technol.* **2002**, *37*, 727−739.

(8) Haefner, S.; Knietsch, A.; Scholten, E.; Braun, J.; Lohscheidt, M.; Zelder, O. Biotechnological production and applications of phytases. *Appl. Microbiol. Biotechnol.* **2005**, *68*, 588−597.

(9) Hoffmann, J.; Hoffmann, K.; Skut, J.; Huculak-Maczka, M. Modification of manufacturing process of feed phosphates. *CHEMIK* **2011**, *3*, 194−191.

(10) Lei, X. G.; Weaver, J. D.; Mullaney, E.; Ullah, A. H.; Azain, M. J. Phytase, a new life for an"old" enzyme. *Annu. Rev. Anim. Biosci.* **2013**, *1*, 283−309.

(11) Yao, M.-Z.; Zhang, Y.-H.; Lu, W.-L.; Hu, M.-Q.; Wang, W.; Liang, A.-H. Phytases: crystal structures, protein engineering and potential biotechnological applications. *J. Appl. Microbiol.* **2012**, *112*, 1−14.

(12) Greiner, R. *Update on Characteristics of Commercial Phytases*, presented at the International Phytase Symposium, Rome, Italy, Dec 11−13, 2012.

(13) Han, Y.; Lei, X. G. Role of glycosylation in the functional expression of an *Aspergillus niger* phytase (*phyA*) in *Pichia pastoris*. *Arch. Biochem. Biophys.* **1999**, *364*, 83−90.

(14) Panchal, T.; Wodzinski, R. J. Comparison of glycosylation patterns of phytase from *Aspergillus niger* (*A. ficuum*) NRRL 3135and recombinant phytase. *Prep. Biochem. Biotechnol.* **1998**, *28*, 201−217.

(15) Phillippy, B. Q.; Mullaney, E. J. Expression of an *Aspergillus niger* phytase (*phyA*) in *Escherichia coli*. *J. Agric. Food Chem.* **1997**, *45*, 3337−3342.

(16) Ullah, A. H. J.; Sethumadhavan, K.; Mullaney, E. J.; Ziegelhoffer, T.; Austin-Phillips, S. Fungal *phy*A gene expressed in potato leaves produces active and stable phytase. *Biochem. Biophys. Res. Commun.* **2003**, *306*, 603−609.

(17) Guo, M.; Hang, H.; Zhu, T.; Zhuang, Y.; Chu, J.; Zhang, S. Effect of glycosylation on biochemical characterization of recombinant phytase expressed in *Pichia pastori*. *Enzyme Microb. Technol.* **2008**, *42*, 340−345.

(18) Han, Y.; Wilson, D. B.; Lei, X. G. Expression of an *Aspergillus niger* phytase gene (*phyA*) in *Saccharomyces cerevisiae*. *Appl. Environ. Microbiol.* **1999**, *65*, 1915−1918.

(19) Lei, X. G.; Stahl, C. H. Biotechnological development of effective phytases for mineral nutrition and environmental protection. *Appl. Microbiol. Biotechnol.* **2001**, *57*, 474−481.

(20) Tillie, P.; Dillen, K.; Rodriguez-Cerezo, E. The pipeline of GM crops for improved animal feed. In *Animal Nutrition with Transgenic Plants*; CABI Biotechnology Series; Flachowsky, G., Ed.; CABI; Wallingford, UK, 2013; 231 pp.

(21) Yao, B.; Zhang, C.; Wang, J.; Fan, Y. Recombinant *Pichia pastoris* overexpressing bioactive phytase. *Sci. China, Ser. C: Life Sci.* **1998**, *41*, 330−336.

(22) Chen, R.; Zhang, C.; Yao, B.; Xue, G.; Yang, W.; Zhou, X.; Zhang, J.; Sun, C.; Chen, P.; Fan, Y. Corn seeds as bioreactors for the production of phytase in the feed industry. *J. Biotechnol.* **2013**, *165*, 120−126.

(23) ISAAA Brief 41-2009: Executive Summary ISAAA, 2009. Global status of commercialized Biotech/GM crops: 2009. The first fourteen years, 1996 to 2009; http://isaaa.org/resources/publications/briefs/41/executivesummary/ (accessed 2015).

(24) Chen, W.; Zhang, J.; Lu, G.; Yuan, Z.; Wu, Q.; Li, J.; Xu, G.; He, A.; Zheng, J.; Zhang, J. Development of an immunochromatographic lateral flow device for rapid diagnosis of *Vibrio cholera* 01 serotype Ogawa. *Clin. Biochem.* **2014**, *47*, 448−454.

(25) Friguet, B.; Djavadi-Ohaniance, L.; Pages, J.; Bussard, A.; Goldberg, M. A convenient enzyme-linked immunosorbent assay for testing whether monoclonal antibodies recognize the same antigenic site. Application to hybridomas specific for the β_2-subunit of *Escherichia coli* tryptophan synthase. *J. Immunol. Methods* **1983**, *60*, 351−358.

(26) Laemmli, U. K. Cleavage of structural proteins during the assembly of the head of bacteriophage T4. *Nature* **1970**, *227*, 680−685.

(27) Xuan, N. T.; Hang, M. T.; Thanh, V. N. Cloning and over expression of an *Aspergillus niger* XP phytase gene (phyA) in *Pichia pastoris*. *World Acad. Sci. Eng. Technol.* **2009**, *56*, 750−753.

(28) Xiong, A. S.; Yao, Q. H.; Peng, R. H.; Han, P. L.; Cheng, Z. M.; Li, Y. High level expression of a recombinant acid phytase gene in *Pichia pastoris*. *J. Appl. Microbiol.* **2005**, *98*, 418−28.

(29) Sreekrishna, K.; Brankamp, R. G.; Kropp, K. E.; Blankenship, D. T.; Tsay, J.-T.; Smith, P. L.; Wierschke, J. D.; Subramaniam, A.; Birkenberger, L. A. Strategies for optimal synthesis and secretion of heterologous proteins in the methylotrophic yeast *Pichia pastoris*. *Gene* **1997**, *190*, 55−62.

(30) Casey, A.; Walsh, G. Identification and characterization of a phytase of potential commercial interest. *J. Biotechnol.* **2004**, *110*, 313−322.

(31) Pasamontes, L.; Haiker, M.; Wyss, M.; Tessier, M.; van Loon, A. P. Gene cloning, purification, and characterization of a heat-stable phytase from the fungus *Aspergillus fumigates*. *Appl. Environ. Microbiol.* **1997**, *63*, 1696−1700.

DOI: 10.1021/acs.jafc.5b00188
J. Agric. Food Chem. 2015, 63, 4320−4326

(32) Lucca, P.; Hurrell, R.; Potrykus, I. Genetic engineering approaches to improve the bioavailability and the level of iron in rice grains. *Theor. Appl. Genet.* **2001**, *102*, 392−397.
(33) Guirakhoo, F.; Heinz, F. X.; Kunz, C. Epitope model of tick-borne encephalitis virus envelope glycoprotein E: analysis of structural properties, role of carbohydrate side chain, and conformational changes occurring at acidic pH. *Virology* **1989**, *169*, 90−99.
(34) Plum, M.; Michel, Y.; Wallach, K.; Raiber, T.; Blank, S.; Bantleon, F. I.; Diethers, A.; Greunke, K.; Braren, I.; Hackl, T.; Meyer, B.; Spillner, E. Close-up of the immunogenic α 1,3-galactose epitope as defined by a monoclonal chimeric immunoglobulin E and human serum using saturation transfer difference (STD) NMR. *J. Biol. Chem.* **2011**, *286*, 43103−43111.
(35) Stiasny, K.; Kiermayr, S.; Holzmann, H.; Heinz, F. X. Cryptic properties of a cluster of dominant Flavivirus cross-reactive antigenic sites. *J. Virol.* **2006**, *80*, 9557−9568.
(36) Abd-El Aziem, F.; Greiner, R. Recombinant bacterial phytases to reduce environmental phosphate pollution. In *Environmental Biotechnology: Advancement in Water and Wastewater Application in the Tropics*; Ujang, Z., Henze, M., Eds.; IWA Publishing: London, UK, 2004; pp 165−172.
(37) Berry, D. F.; Harich, K. Tetrachlorofluorescein $TInsP_5$ as a substrate analog probe for measuring phytase activity in surface water: proof of concept. *J. Environ. Qual.* **2012**, *42*, 56−64.
(38) Heinonen, J. K.; Lahti, R. J. A new and convenient colorimetric determination of inorganic orthophosphate and its application to the assay of inorganic phosphates. *Anal. Biochem.* **1981**, *113*, 313−317.

DOI: 10.1021/acs.jafc.5b00188
J. Agric. Food Chem. 2015, 63, 4320−4326

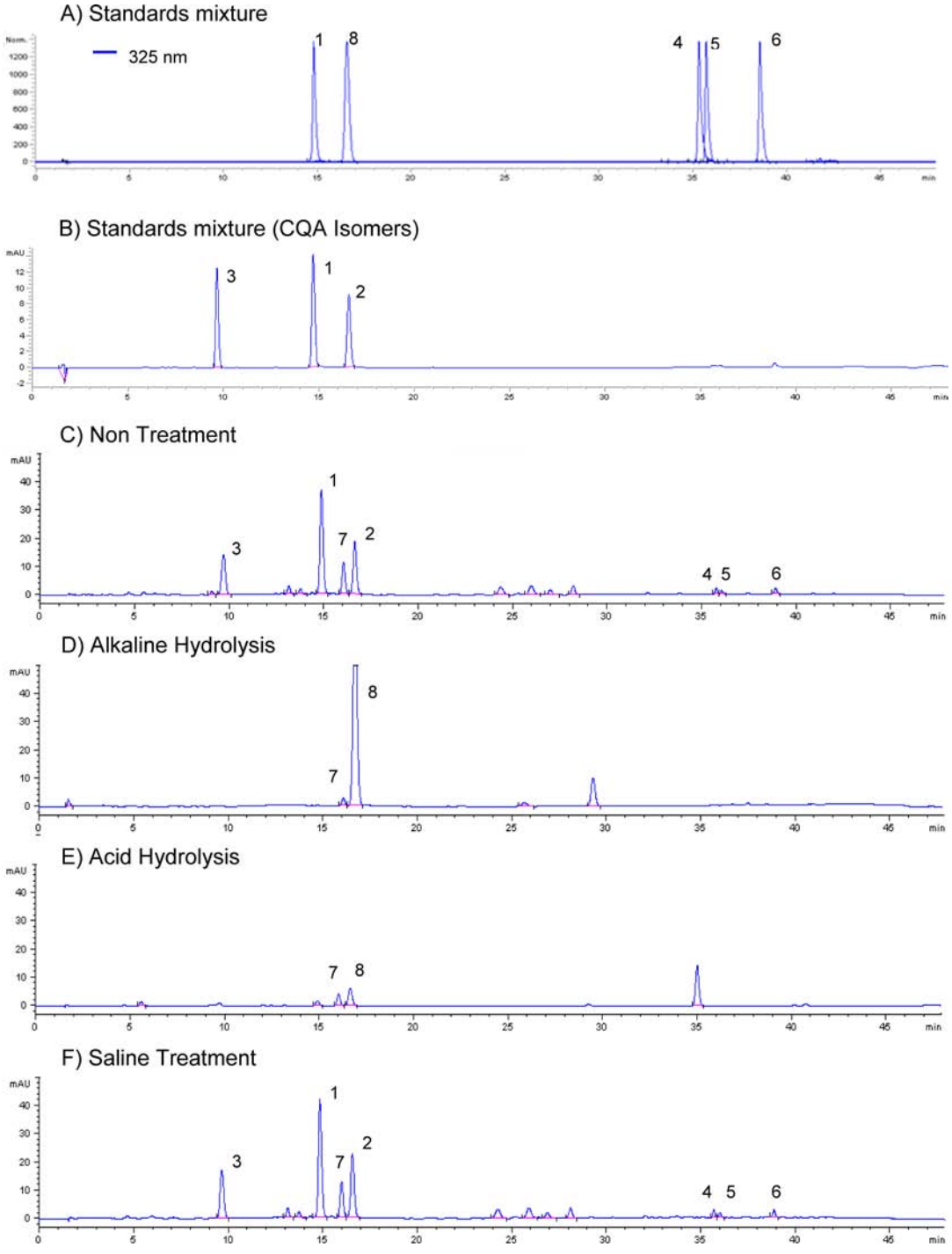

Figure 1. Chromatograms of (A) standards mixture, (B) standards mixture (CQA isomers), (C) nontreated coffee brew, (D) alkaline-hydrolyzed coffee brew, (E) acid-hydrolyzed coffee brew, and (F) saline-treated coffee brew. Peaks: (1) 5-CQA; (2) 4-CQA; (3) 3-CQA; (4) 3,4-diCQA; (5) 3,5-diCQA; (6) 4,5-diCQA; (7) caffeine; (8) caffeic acid.

bound compounds for the assessment of the total phenolic compounds content of spent coffee extracts and to determine the most accurate method for this purpose.

MATERIALS AND METHODS

Chemicals and Reagents. Methanol of HPLC grade, sodium chloride, ethylenediaminetetraacetic acid (EDTA), ascorbic acid, sodium hydroxide, and hydrochloric acid were obtained from Panreac (Barcelona, Spain). Pure reference standards of caffeic acid, ferulic acid, *p*-coumaric acid, 4-hydroxybenzoic acid, sinapic acid, and 5-caffeoylquinic acid were purchased from Sigma-Aldrich (Steinheim, Germany) and of 3,4-, 3,5-, and 4,5-dicaffeoylquinic acids from Phytolab (Vestenbergsgreuth, Germany).

Coffee Brew Preparation. Roasted coffee from Guatemala (*Coffea arabica*, 3.03% water content, $L^* = 24.69 \pm 0.74$, roasted at 219 °C for ca. 15 min) was provided by a local factory. The lightness value (L^*) indicates the coffee roasting degree, and it was analyzed by means of a tristimulus colorimeter (Chromameter-2 CR-200, Minolta, Osaka, Japan) using the D65 illuminant and CIE 1931 standard observer. The instrument was standardized against a white tile before sample measurements. Ground roasted coffee was spread in an l cm

DOI: 10.1021/acs.jafc.5b01619
J. Agric. Food Chem. 2015, 63, 4327−4334

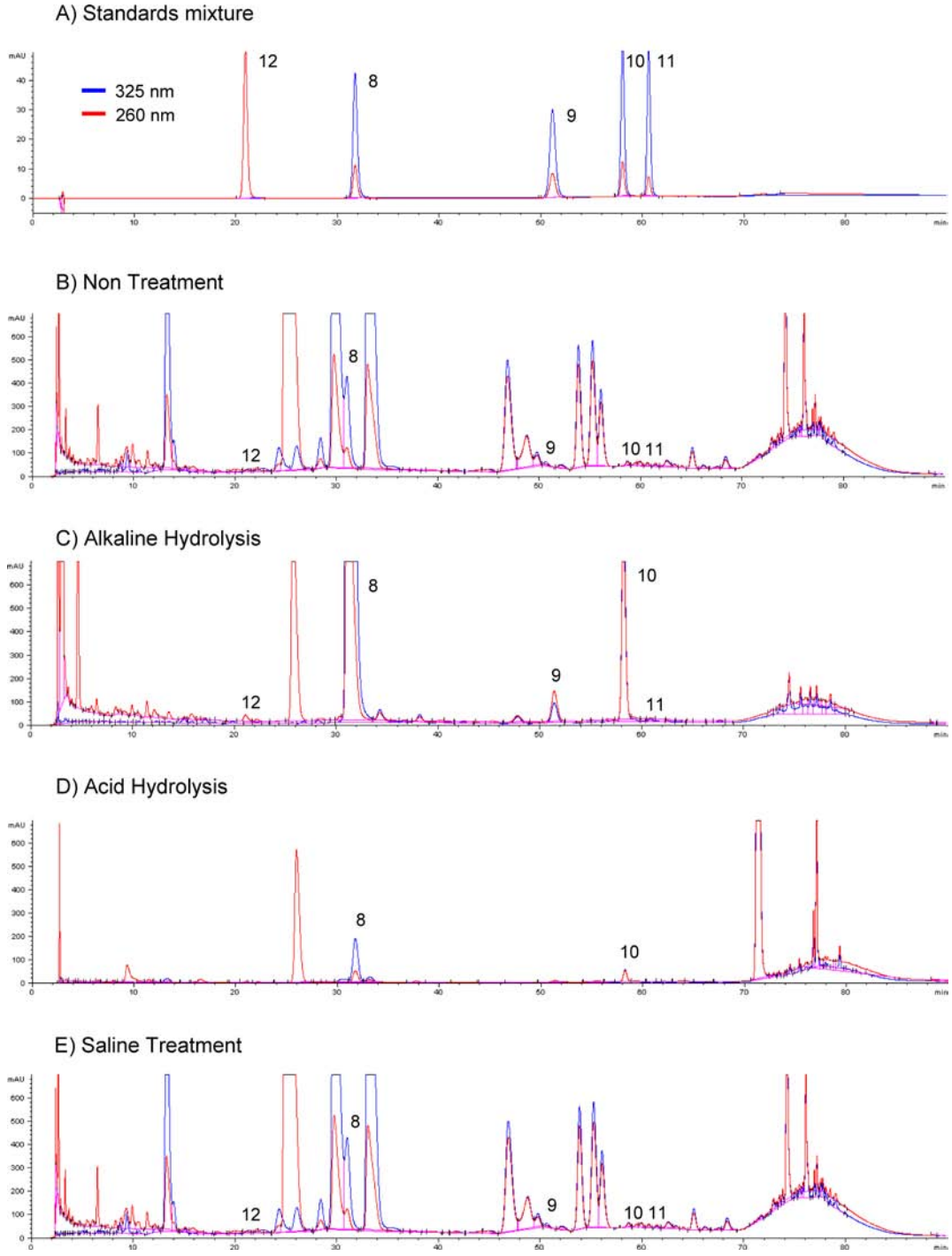

Figure 2. Chromatograms of (A) standards mixture, (B) nontreated coffee brew, (C) alkaline-hydrolyzed coffee brew, (D) acid-hydrolyzed coffee brew, and (E) saline-treated coffee brew. Peaks: (8) caffeic acid; (9) *p*-coumaric acid; (10) ferulic acid; (11) sinapic acid; (12) 4-hydroxybenzoic acid.

Petri plate, and the L^* value was measured in triplicate on the CIELab scale.

Roasted coffee beans were ground to a powder in a Moulinex coffee grinder (model Super Junior "s", Paris, France) for 20 s immediately before sample preparation. Filter coffee brew was prepared from 36 g of ground roasted coffee for a volume of 600 mL, using a filter coffee machine (model Avantis 70 Aroma plus, Ufesa, Spain). Extraction took approximately 6 min at 90 °C. Extraction as the percentage of total solids with respect to ground roasted coffee was 23.3%.

Spent Coffee Extract. Spent coffee extracts were prepared according to the method described by Bravo et al.[6] Briefly, first, spent coffee was defatted with petroleum ether (1:11, w/v) for 3 h at 60 °C in a Soxhlet extraction system (Extraction Unit B-811 Standard BUCHI, Flawil, 127 Switzerland). Then, 24 g of spent coffee was extracted with a volume of 400 mL of water using a filter coffeemaker (model AVANTIS 70 Inox, Ufesa, Spain). Extraction took approximately 6 min at 90 °C. Extraction as the percentage of total solids with respect to ground spent coffee was 11%.

Both coffee brew and spent coffee extract were lyophilized using a Cryodos Telstar (Terrassa, Spain).

Alkaline Hydrolysis. The procedure was performed according to the method of Nardini et al.,[16] with some modifications. A volume of 5

DOI: 10.1021/acs.jafc.5b01619
J. Agric. Food Chem. 2015, 63, 4327−4334

Table 1. Free and Total Phenolic Acid Content of Coffee Brew and Spent Coffee Extract[a]

	nontreated	alkaline hydrolysis	acid hydrolysis	saline treatment
3-CQA				
coffee brew	43.52 ± 0.87	nd	nd	50.89 ± 0.55***
spent coffee	27.36 ± 0.62	nd	nd	55.71 ± 0.31***
4-CQA				
coffee brew	49.27 ± 2.32	nd	nd	57.43 ± 1.01**
spent coffee	35.88 ± 0.88	nd	nd	62.92 ± 0.56***
5-CQA				
coffee brew	78.40 ± 1.09	nd	24.61 ± 0.34***	96.10 ± 2.40***
spent coffee	53.59 ± 2.15	nd	nd	112.87 ± 1.28***
total CQA				
coffee brew	171.19	nd	24.61	204.42
spent coffee	116.83	nd	nd	231.51
3,4-diCQA				
coffee brew	0.83 ± 0.03	nd	nd	1.14 ± 0.07**
spent coffee	1.39 ± 0.12	nd	nd	1.65 ± 0.00 ns
3,5-diCQA				
coffee brew	0.57 ± 0.02	nd	nd	0.79 ± 0.50**
spent coffee	0.99 ± 0.07	nd	nd	1.07 ± 0.00ns
4,5-diCQA				
coffee brew	0.90 ± 0.05	nd	nd	1.27 ± 0.09**
spent coffee	1.70 ± 0.13	nd	nd	1.88 ± 0.00 ns
total diCQA				
coffee brew	2.30	nd	nd	3.20
spent coffee	4.08	nd	nd	4.60
total CQA + diCQA				
coffee brew	173.49	nd	24.61	207.62
spent coffee	120.91	nd	nd	236.11
caffeic acid				
coffee brew	1.40 ± 0.04	136.53 ± 7.44***	2.01 ± 0.08**	2.24 ± 0.10***
spent coffee	2.00 ± 0.00	156.27 ± 15.53***	1.50 ± 0.01ns	2.51 ± 0.09**
ferulic acid				
coffee brew	0.09 ± 0.01	13.66 ± 1.49***	0.39 ± 0.01***	0.11 ± 0.03 ns
spent coffee	0.17 ± 0.01	17.49 ± 1.18***	nd	0.19 ± 0.03ns
p-coumaric acid				
coffee brew	0.19 ± 0.02	2.73 ± 0.25***	nd	0.50 ± 0.00***
spent coffee	0.24 ± 0.02	2.60 ± 0.14***	nd	0.67 ± 0.06***
sinapic acid				
coffee brew	0.07 ± 0.00	0.16 ± 0.02**	nd	0.10 ± 0.00***
spent coffee	0.12 ± 0.01	0.34 ± 0.04**	nd	0.15 ± 0.00ns
4-hydroxybenzoic acid				
coffee brew	0.16 ± 0.03	0.62 ± 0.04***	nd	0.22 ± 0.00*
spent coffee	0.17 ± 0.02	0.46 ± 0.02***	nd	0.26 ± 0.05ns

[a]Data are expressed as μmol/g of lyophilized coffee brew or spent coffee extract. All values are shown as means ± SD (n = 3). nd, not detected. In each row, asterisks indicate different significance: (*) $P > 0.05$; (**) $P > 0.01$; (***) $P > 0.001$ from nontreated sample; ns, $P < 0.05$.

mL of spent coffee extract (0.05 g) or coffee brew (0.08 g) was added to a 5 mL of 2 M NaOH solution containing 1% (w/w) ascorbic acid and 10 mM EDTA. The mixture was incubated for 30 min at 30 °C.

Acid Hydrolysis. The hydrolytic method was applied according to that of Alves et al.,[22] with some modifications. An aliquot (20 mL) of coffee brew (0.32 g) or spent coffee extract (0.2 g) was hydrolyzed by adding 20 mL of methanol, 4 mL of concentrated HCl (10.2 M), and 600 μL of antioxidant solution (1% BHT and 1% ascorbic acid). The mixtures were heated under reflux at 75 °C for 150 min. After the hydrolysis, samples were neutralized with 10 M NaOH.

Saline Treatment. Ionically bound phenolic compounds were obtained according to the method described by Delgado-Andrade and Morales.[14] Briefly, NaCl was added to an aliquot (50 mL) of coffee brew (0.8 g) or spent coffee extract (0.5 g) to have a 2 M concentration. Then, samples were maintained at 4 °C overnight.

After each treatment, samples were acidified to pH 3 with concentrated HCl and then were centrifuged, and the supernatant was stored at 4 °C for further analysis.

Chlorogenic Acids Analysis. Extraction of chlorogenic acids was carried out according to the method of Bicchi et al.[28] The compounds were analyzed by HPLC following the method described by Farah et al.[4] with some modifications.[5] HPLC analysis was achieved with an analytical HPLC unit model 1100 (Agilent Technologies, Palo Alto, CA, USA) equipped with a binary pump and an automated sample injector. A reversed-phase Poroshell 120 C-18 (2.7 μm particle size, 250 × 4.6 mm) column was used at 25 °C. Samples were properly diluted, and the sample injection volume was 100 μL. The chromatographic separation was performed using a gradient of methanol (solvent A) and Milli-Q water acidulated with phosphoric acid (pH 3.0, solvent B) at a constant flow of 0.8 mL/min. Elution was initiated at 10% A and maintained for 5 min; the percentage of solvent A was increased to 20% in 10 min and maintained for 10 min, then

DOI: 10.1021/acs.jafc.5b01619
J. Agric. Food Chem. 2015, 63, 4327−4334

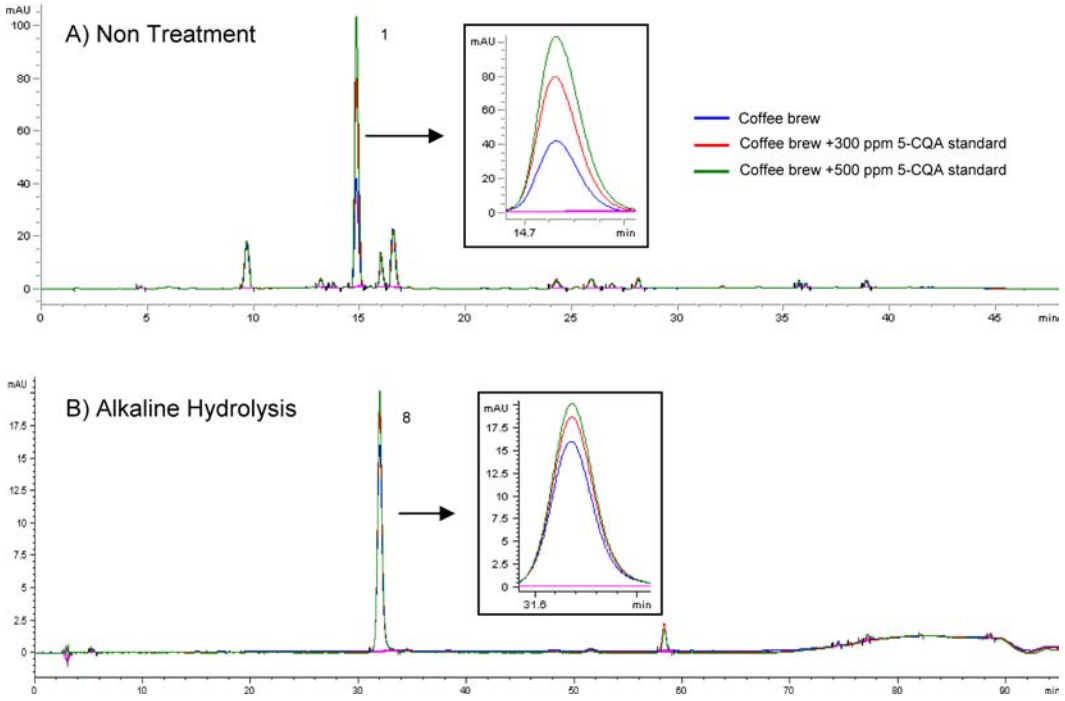

Figure 3. Chromatograms of (A) nontreated coffee brew spiked with 5-CQA standard and (B) alkaline-hydrolyzed coffee brew spiked with 5-CQA standard. Peaks: (1) 5-CQA; (8) caffeic acid.

increased to 50% in 20 min and maintained for 3 min, and finally increased to 80% for 15 min. Detection was accomplished with a diode array detector (DAD), and chromatograms were recorded at 325 nm. Identification of 5-CQA and diCQAs was performed by comparing the retention time and the photodiode array spectra with those of their reference standards compounds. 3-CQA and 4-CQA were identified by the isomerization of 5-CQA standard. Quantitation of 5-caffeoylquinic acid (5-CQA) was made by comparing the peak areas with those of the standards. Quantitation of the other CGAs was performed using the area of 5-CQA standard combined with their respective molar extinction coefficients as reported by Trugo and Macrae[29] and Farah et al.[4]

Other Phenolic Acids. The extraction of hydroxycinnamic acids and benzoic acid derivative was carried out according to the method of Alvarez-Vidaurre et al.[30] The HPLC analysis was performed following the method described by Nardini et al.,[16] with modifications. HPLC analysis was achieved with an analytical HPLC unit model 1200 (Agilent Technologies) equipped with a binary pump and an automated sample injector. The sample injection volume was 50 μL. Chromatographic separation was performed at 25 °C using a reversed-phase Gemini NX (5 μm particle size, 250 × 4.6 mm) column (Phenomenex, Torrence, CA, USA) and a mobile phase consisting methanol (solvent A) and Milli-Q water acidulated with phosphoric acid (pH 2.5, solvent B). The flow rate was 1 mL/min. Elution was initiated at 15% A and maintained for 20 min; the percentage of solvent A was increased to 20% in 10 min, to 45% in 5 min, to 55% in 10 min, then maintained for 10 min, and finally increased to 80% for 15 min. Detection was accomplished with a diode array detector at 325 nm for caffeic acid, ferulic acid, *p*-coumaric acid, and sinapic acid and at 260 nm for 4-hydroxybenzoic acid. Identification of phenolic acids was performed by comparing the retention time and the photodiode array spectra with those of their reference compounds. Calibration curves of standard were used to quantitate. Coefficients of linearity for the calibration curves were typically $R^2 > 0.99$.

Statistical Analysis. Each parameter was analyzed in triplicate. Results are shown as means ± standard deviations. A Student's *t* test was applied to determine differences of phenolic compounds between nontreated samples and each treatment. All statistical analyses were performed using the SPSS v.15.0 software package.

RESULTS AND DISCUSSION

Spent coffee is the byproduct generated after a brewing process and might be considered a valuable source of easily extracted phenolic compounds by the food industry. However, identification and quantitation of the total (free and bound) phenolic compounds should be a previous step before further applications. Therefore, spent coffee extracts were submitted to three treatments (alkaline, acid, and saline). Phenolic compounds were analyzed by HPLC-DAD and compared to those in their respective coffee brew. Figures 1 and 2 showed the chromatograms of phenolic compounds of coffee brews before and after each treatment. Similar chromatograms were obtained for spent coffee extract because samples were properly diluted before injection in HPLC to have areas ranged within calibration curves.

First, free chlorogenic acids (CGAs), the most abundant phenolic compounds in coffee, were identified and quantitated in nontreated samples. Figure 1C shows the CGAs peaks, which were identified as 3-caffeoylquinic acid (peak 3), 4-caffeoylquinic acid (peak 2), 5-caffeoylquinic acid (peak 1), 3,4-dicaffeoylquinic acid (peak 4), 3,5-dicaffeoylquinic acid (peak 5), and 4,5-di caffeoylquinic acid (peak 6), as compared with the standards mixtures (Figure 1A,B). Spent coffee extract showed less content of free CQAs than the coffee brew, whereas the concentration of free diCQAs was 1.8-fold higher in the byproducts (Table 1). Furthermore, the content of other phenolic compounds, such as hydroxycinnamic acids and benzoic acid derivative, was also measured by HPLC, and chromatograms are shown in Figure 2. The results (Table 1) showed low amounts of caffeic acid (peak 8), ferulic acid (peak 9), *p*-coumaric acid (peak 10), and sinapic acid (peak 11), as well as 4-hydroxybenzoic acid (peak 12), in both spent coffee extract and coffee brew (Figure 2B).

Alkaline Hydrolysis. Alkaline hydrolysis or saponification is applied to release compounds bound to polymers by covalent

DOI: 10.1021/acs.jafc.5b01619
J. Agric. Food Chem. 2015, 63, 4327−4334

interactions.[10] Spent coffee extract and coffee brew treated with alkaline solutions showed differences in the chromatographic phenolic acids profile compared with nontreated samples. The chromatogram (Figure 1D) showed the disappearance of the major CGAs, only one large peak (8) being detected. Even though the elution time of peak 8 was quite similar to that of 4-CQA (2), the spectral data confirmed that it was caffeic acid. Some authors have reported that phenolic compounds are susceptible to oxidation at pH 8 and higher, leading to degradation into their corresponding molecules derivatives.[9,31] Quantitation of the caffeic acid was carried out with the second chromatographic method (Figure 2C). It was also observed that ferulic acid, *p*-coumaric acid, sinapic acid, and 4-hydroxybenzoic acid peaks remained after the hydrolysis. Moreover, the numerical data showed a significant increase ($p < 0.01$) in the amounts of hydroxycinnamic acids in samples treated with alkaline conditions in comparison with nontreated spent coffee extract and coffee brew (Table 1). These results agree with previous studies, where high amounts of caffeic and ferulic acids were found in coffee brew or in the HMW melanoidins fraction after the application of alkaline hydrolysis.[16,17]

Chlorogenic acids are an ester formed between a quinic acid molecule and one or more hydroxycinnamic acid molecules. Alkaline medium can break not only the covalent bonds between melanoidins and phenolic compounds but also CGAs' internal bonds. Our findings suggest that the high concentration of caffeic, ferulic, and coumaric acids found in hydrolyzed samples were partially due to the cleavage of the ester linkages in free CGAs. In fact, an additional experiment showed that all 5-CQA from coffee brew and spiked standard (300 and 500 ppm of 5-CQA) has been hydrolyzed into caffeic acid, but only 50% of the expected caffeic acid was quantitated (Figure 3). With this loss taken into account, our results indicate that the amount of caffeic acid obtained after alkaline hydrolysis was approximately 58 and 35% higher than the expected in spent coffee extract and coffee brew, respectively. This fact could be partially explained by the presence of other chemical compounds with caffeic acid in their structure. A complete free phenolics profile of Arabica spent coffee extract and coffee brew (unpublished data) showed that CQLs were 18% of the total CQAs and diCQAs and as well an additional 8% of caffeoylquinic isomers were found. Then, the caffeic acid derived from overall free chlorogenic acids was deducted from the total caffeic acid, which included that obtained after alkaline hydrolysis and the estimated due to losses. Thus, the results suggest that around 47% (spent coffee extract) and 19% (coffee brew) of the caffeic acid found after the alkaline hydrolysis could come from CGAs or caffeic acids attached to other structures. In the case of coffee brew, this percentage of bound phenolic compounds is in the range of 1−29% proposed by Perrone et al.[19] depending on the roasting degree. The amount of bound phenolics in coffee might also be influenced by coffee variety because it has been reported that darker roasted Robusta coffees showed higher losses of chlorogenic acids, but an increase in bound compounds.[19,32]

Similarly, the increment of ferulic and coumaric acids concentration could be explained by the release of hydroxycinnamic acids from feruloylquinic and coumaroylquinic acids present in coffee brew and spent coffee extract. Unlike the caffeic acid, the other hydroxycinnamic acids do not suffer losses by the alkaline treatment. Moreover, the proportion of FQAs and FQLs in the samples was close to 9% of the total content of free CGAs (unpublished data). Thus, the percentage of extra ferulic acid found in hydrolyzed samples was similar, which indicates that a minor amount of this compound was released from melanoidins and other macromolecules. Even though the concentrations of sinapic and 4-hydroxybenzoic acids were lower than those of caffeic, ferulic, and coumaric acids, 2−3-fold significant increases ($p < 0.001$) were found in comparison to the values in the nontreated samples. There is scarce literature about the presence of sinapic acid in coffee. To our knowledge, sinapic acid linked to quinic, caffeoylquinic, and feruloylquinic acids has been reported only in Robusta green coffee.[33] Consequently, part of these chlorogenic acids could remain attached to melanoidins during roasting process. Finally, the increase of 4-hydroxybenzoic acid agrees with Nunes and Coimbra,[18] who found benzoic acid and derivatives as 4-hydroxybenzoic acid attached to the HMW melanoidins fraction of roasted coffee after applying alkaline fusion.

Acid Hydrolysis. Acid hydrolysis is also proposed to release bound compounds. The chemical basis is similar to alkaline hydrolysis, which is the rupture of covalent bonds using in this case a strong acid (HCl). Figure 1E shows a chromatogram of a hydrolyzed coffee brew, where four small peaks are observed. Two peaks were identified as 5-CQA and caffeine (peaks 1 and 7). Peak 8 eluted at the same time as 4-CQA, but it has been identified as caffeic acid by the spectrum data. The last peak (ca. 35 min) was the antioxidant used in the assay. Similarly, antioxidants used were detected in Figure 2 (ca. 71 and 77 min), as well as the caffeine (ca. 26 min). In spent coffee, caffeoylquinic and dicaffeoylquinic acids were completely lost after acid hydrolysis. Also, ferulic, coumaric, sinapic, and 4-hydroxybenzoic acids totally disappeared in both spent coffee extracts and coffee brews after acid treatment. Furthermore, minor changes in caffeic acid concentration were found in comparison to nontreated samples (1.50 μmol/g of spent coffee extract and 2.01 μmol/g of coffee brew). A previous study reported that this technique could be used to release and to quantitate phenolic compounds such as isoflavones from other coffee components.[22] However, our results strongly suggest that phenolic acids, such as CGAs and hydroxycinnamic acids, are very susceptible to acid hydrolysis. This in agreement with the study of Mattila et al.,[23] who found that phenolic compounds are affected by extreme pH conditions but that oxidation processes are more likely to occur in acid pH. Consequently, acid hydrolysis is an inadequate technique to release the main bound coffee phenolic compounds (phenolic acids), but it can be applied to evaluate others such as isoflavones.

Saline Treatment. This method has been used to release phenolic compounds ionically bound to proteins or melanoidins, using 2 M NaCl. Barbeau and Kinsella[24] reported that the chlorogenic acid carboxyl group is predominately ionized at neutral pH. Therefore, the increase of ionic strength tends to neutralize charge interaction between dissociated carboxylic groups of chlorogenic acid and positively charge side chain groups, like the amide carbonyls of the peptide bonds in proteins and melanoidins leading to the release of ionically bound phenolics. The chromatograms of CGAs (Figure 1F) and hydroxycinnamic acids (Figure 2E) after saline treatment show peak profiles similar to those of coffee samples without treatment. However, the results (Table 1) showed that samples treated with 2 M NaCl had higher concentrations of caffeoylquinic acids, with highly significant differences ($p < 0.001$). The amount of diCQAs was also higher ($p < 0.01$) in

DOI: 10.1021/acs.jafc.5b01619
J. Agric. Food Chem. 2015, 63, 4327−4334

comparison to nontreated samples, even though no statistical differences were detected for 3,5-diCQA in spent coffee extracts. The extra amounts of CQAs and diCQAs found after the saline treatment mean those compounds ionically attached to other structures. Thus, it should be highlighted that free and ionically bound CQAs were found in similar amounts in spent coffee extracts, whereas clearly lower amounts of bound CQAs (33.23 μmol/g) were in coffee brew. The addition of a caffeic acid moiety in the case of diCQAs increases the hydroxyl groups that can ionically interact with melanoidins, explaining the higher amount of bound diCQAs in coffee brews in comparison to spent coffee extracts. This is in agreement with previous works, which showed that a second extraction of ground coffee to obtain spent coffee extracts using a filter coffeemaker favors the extraction of bound CQAs, mainly diCQAs, probably due to the turbulences that facilitate contact of grounds and water.[5,34]

With regard to hydroxycinnamic acids, coumaric acid showed the largest increase, with values 3-fold higher than in nontreated samples. Sinapic acid and 4-hydrobenzoic acid raised their concentrations from 1.2- to 1.5-fold. However, caffeic acid and ferulic acid showed slight variations in the final content, with no significant differences ($p > 0.05$). Some authors did not find phenolic acid increases after applying high ionic strength treatment to the coffee brew HMW melanoidins fraction,[18,19] whereas others found caffeoylquinic acids ionically bound to the HMW melanoidins core contributing to the high antioxidant capacity of coffee.[14] Our data strongly suggest that the extra phenolic compounds found after the ionic treatment have been released from the melanoidins core or other medium and low molecular weight melanoidins or Maillard reaction products. In fact, our results support the theory of Bekedam et al.[20] that chlorogenic acids are also incorporated into the melanoidins through nonester linkages.

Total Phenolic Compounds. Free and estimated bound and total phenolic acids of spent coffee extracts are summarized in Table 2. Spent coffee extracts had around 2-fold higher content of total phenolics than those measured directly (without hydrolysis or saline treatment), showing an underestimation of phenolic acids. Phenolic compounds with one or more caffeic acid molecules were approximately 54% linked to macromolecules such as melanoidins, mainly by noncovalent interactions (up to 81% of bound phenolic compounds). The rest of the quantitated phenolic acids were mainly attached to other structures by covalent bonds (62−97% of total bound compounds).

Table 2. Free and Estimated Bound Phenolic Acids Content of Spent Coffee Extract[a]

	free	bound	ionically bound	total
total CQA	116.83	141.41	114.68	258.24
total diCQA	4.08	4.94	0.52	9.02
caffeic acid	2.00	2.42	0.51	4.42
ferulic acid	0.17	6.44	0.02	6.61
p-coumaric acid	0.24	2.36	0.43	2.60
sinapic acid	0.12	0.22	0.03	0.34
4-hydroxybenzoic acid	0.17	0.29	0.09	0.46

[a]Data are expressed as μmol per g of lyophilized spent coffee extract.

In conclusion, spent coffee extract is a rich source of phenolic acids with a high percentage of compounds linked to macromolecules such as melanoidins or other Maillard reaction products, mainly by noncovalent interactions. In contrast, coffee brew had only around 20% of attached phenolics. Moreover, caffeoylquinic acids are the most abundant and represent 70% of the total CGAs. With regard to the treatments, it could be said that two of the three methodologies provide accurate information about spent coffee extract and coffee brew bound phenolic compounds. The alkaline hydrolysis is a suitable method to know total phenolic compounds both free and bound. However, it cannot be used to directly quantitate total parent compounds, due to the susceptibility of coffee component internal linkage and oxidative losses at high pH conditions. On the other hand, saline treatment allowed ionically bound phenolic compounds to be quantitated. Thus, both methods increased the knowledge about the total content of phenolic compounds (free + bound) in spent coffee. All of the reported data must be taken into account for the characterization of this byproduct for use as a potential food ingredient by the food industry. Spent coffee phenolic compounds (free and bound) may add beneficial health properties to food, specifically in the prevention of oxidative stress related diseases, such as cancer and cardiovascular and neurodegenerative diseases.

AUTHOR INFORMATION

Corresponding Author

*(M.-P.D.P.) Phone: +34 948 425600 (806580). Fax: +34 948 425740. E-mail: mpdepena@unav.es.

Funding

This research was funded by the Spanish Ministry of Economy and Competitiveness (AGL2009-12052). We express our gratitude to the Association of Friends of the University of Navarra for the grant received. The Departamento de Educación, Cultura y Deporte of the Gobierno de Navarra is gratefully acknowledged for the grant given to I.A.L.

Notes

The authors declare no competing financial interest.

ACKNOWLEDGMENTS

C.M expresses her gratitude to the Unión Tostadora S.A. for providing the coffee.

REFERENCES

(1) Saura-Calixto, F.; Goñi, I. Antioxidant capacity of the Spanish Mediterranean diet. *Food Chem.* **2006**, *94*, 442−447.

(2) Pérez-Jiménez, J.; Fezeu, L.; Touvier, M.; Arnault, N.; Manach, C.; Hercberg, S.; Galan, P.; Scalbert, A. Dietary intake of 337 polyphenols in French adults. *Am. J. Clin. Nutr.* **2011**, *93*, 1220−1228.

(3) Clifford, M. N. Chlorogenic acids and other cinnamates − nature, occurrence and dietary burden. *J. Sci. Food Agric.* **1999**, *79*, 362−372.

(4) Farah, A.; De Paulis, T.; Trugo, L.; Martin, P. Effect of roasting on the formation of chlorogenic acid lactones in coffee. *J. Agric. Food Chem.* **2005**, *53*, 1505.

(5) Bravo, J.; Juaniz, I.; Monente, C.; Caemmerer, B.; Kroh, L.; De Peña, M. P.; Cid, C. Evaluation of spent coffee obtained from the most common coffeemakers as a source of hydrophilic bioactive compounds. *J. Agric. Food Chem.* **2012**, *60*, 12565−73.

(6) Bravo, J.; Monente, C.; Juániz, I.; De Peña, M. P.; Cid, C. Influence of extraction process on antioxidant capacity of spent coffee. *Food Res. Int.* **2013**, *50*, 610−616.

(7) Bravo, J.; Arbillaga, L.; de Peña, M. P.; Cid, C. Antioxidant and genoprotective effects of spent coffee extracts in human cells. *Food Chem. Toxicol.* **2013**, *60*, 397−403.

(8) Monente, C.; Bravo, J.; Vitas, A. I.; Arbillaga, L.; De Peña, M. P.; Cid, C. Coffee and spent coffee extracts protect against cell mutagens

DOI: 10.1021/acs.jafc.5b01619
J. Agric. Food Chem. 2015, 63, 4327−4334

and inhibit growth of food-borne pathogen microorganisms. *J. Funct. Foods* **2015**, *12*, 365−374.
(9) Kroll, J.; Rawel, H. M.; Rohn, S. Reactions of plant phenolics with food proteins and enzymes under special consideration of covalent bonds. *Food Sci. Technol. Res.* **2003**, *9*, 205−218.
(10) Pérez-Jiménez, J.; Torres, J. L. Analysis of nonextractable phenolic compounds in foods: the current state of the art. *J. Agric. Food Chem.* **2011**, *59*, 12713−12724.
(11) Andreasen, M. F.; Kroon, P. A.; Williamson, G.; Garcia-Conesa, M. Intestinal release and uptake of phenolic antioxidant diferulic acids. *Free Radical Biol. Med.* **2001**, *31*, 304−314.
(12) Manach, C.; Scalbert, A.; Morand, C.; Rémésy, C.; Jiménez, L. Polyphenols: food sources and bioavailability. *Am. J. Clin. Nutr.* **2004**, *79*, 727−747.
(13) Nunes, F. M.; Coimbra, M. A. Role of hydroxycinnamates in coffee melanoidin formation. *Phytochem. Rev.* **2010**, *9*, 171−185.
(14) Delgado-Andrade, C.; Morales, F. Unraveling the contribution of melanoidins to the antioxidant activity of coffee brews. *J. Agric. Food Chem.* **2005**, *53*, 1403.
(15) Ahn, J.; Grün, I. U.; Mustapha, A. Antimicrobial and antioxidant activities of natural extracts in vitro and in ground beef. *J. Food Prot.* **2004**, *67*, 148−155.
(16) Nardini, M.; Cirillo, E.; Natella, F.; Scaccini, C. Absorption of phenolic acids in humans after coffee consumption. *J. Agric. Food Chem.* **2002**, *50*, 5735.
(17) Bekedam, E. K.; Schols, H.; Van Boekel, M. A. J. S.; Smit, G. Incorporation of chlorogenic acids in coffee brew melanoidins. *J. Agric. Food Chem.* **2008**, *56*, 2055.
(18) Nunes, F.; Coimbra, M. Melanoidins from coffee infusions. Fractionation, chemical characterization, and effect of the degree of roast. *J. Agric. Food Chem.* **2007**, *55*, 3967.
(19) Perrone, D.; Farah, A.; Donangelo, C. M. Influence of coffee roasting on the incorporation of phenolic compounds into melanoidins and their relationship with antioxidant activity of the brew. *J. Agric. Food Chem.* **2012**, *60*, 4265−4275.
(20) Bekedam, E. K.; Loots, M.; Schols, H.; Van Boekel, M. A. J. S.; Smit, G. Roasting effects on formation mechanisms of coffee brew melanoidins. *J. Agric. Food Chem.* **2008**, *56*, 7138−7145.
(21) Coelho, C.; Ribeiro, M.; Cruz, A. C. S.; Domingues, M. R.; Coimbra, M. A.; Bunzel, M.; Nunes, F. M. Nature of phenolic compounds in coffee melanoidins. *J. Agric. Food Chem.* **2014**, *62*, 7843−7853.
(22) Alves, R. C.; Almeida, I. M. C.; Casal, S.; Oliveira, M. B. P. P. Method development and validation for isoflavones quantification in coffee. *Food Chem.* **2010**, *122*, 914−919.
(23) Mattila, P.; Hellstrom, J.; Torronen, R. Phenolic acids in berries, fruits, and beverages. *J. Agric. Food Chem.* **2006**, *54*, 7193−7199.
(24) Barbeau, W. E.; Kinsella, J. E. Factors affecting the binding of chlorogenic acid to fraction 1 leaf protein. *J. Agric. Food Chem.* **1983**, *31*, 993−998.
(25) Xu, L.; Diosady, L. L. Interactions between canola proteins and phenolic compounds in aqueous media. *Food Res. Int.* **2000**, *33*, 725−731.
(26) Borrelli, R.; Visconti, A.; Mennella, C.; Anese, M.; Fogliano, V. Chemical characterization and antioxidant properties of coffee melanoidins. *J. Agric. Food Chem.* **2002**, *50*, 6527.
(27) D'Agostina, A.; Boschin, G.; Bacchini, F.; Arnoldi, A. Investigations on the high molecular weight foaming fractions of espresso coffee. *J. Agric. Food Chem.* **2004**, *52*, 7118−7125.
(28) Bicchi, C.; Pinello, A.; Pellegrino, G.; Vanni, A. Characterization of green and roasted coffees through the chlorogenic acid fraction by HPLC-UV and principal component analysis. *J. Agric. Food Chem.* **1995**, *43*, 1549−1555.
(29) Trugo, L. C.; Macrae, R. A study of the effect of roasting on the chlorogenic acid composition of coffee using HPLC. *Food Chem.* **1984**, *15*, 219−227.
(30) Alvarez-Vidaurre, P.; Perez-Martinez, M.; de Peña, M. P.; Cid, C. Development, validation and application of a new analytical method of caffeic acid, ferulic acid and 4-vinylguaiacol in coffee brews. *Proc. 13th Euro Food Chem.* **2005**, 684−687.
(31) Cilliers, J. J. L.; Singleton, V. L. Nonenzymic autoxidative phenolic browning reactions in a caffeic acid model system. *J. Agric. Food Chem.* **1989**, *37*, 890−896.
(32) Perrone, D.; Donangelo, R.; Donangelo, C. M.; Farah, A. Modeling weight loss and chlorogenic acids content in coffee during roasting. *J. Agric. Food Chem.* **2010**, *58*, 12238−12243.
(33) Jaiswal, R.; Patras, M. A.; Eravuchira, P. J.; Kuhnert, N. Profile and characterization of the chlorogenic acids in green Robusta coffee beans by LC-MS n: identification of seven new classes of compounds. *J. Agric. Food Chem.* **2010**, *58*, 8722−8737.
(34) Ludwig, I. A.; Sanchez, L.; Caemmerer, B.; Kroh, L. W.; De Peña, M. P.; Cid, C. Extraction of coffee antioxidants: impact of brewing time and method. *Food Res. Int.* **2012**, *48*, 57−64.

DOI: 10.1021/acs.jafc.5b01619
J. Agric. Food Chem. 2015, 63, 4327−4334

ionic conditions all alter the aggregation process. Thus, there is a need to evaluate the colloidal stability of whey proteins in the context of consumer beverages under conditions that deliver a mixture of proteins and other compounds, in pH ranges that limit negative sensorial attributes, and after an industrially relevant thermal process.

Classical definitions of protein stability refer to maintaining secondary and tertiary structure and/or bioactivity after exposure to heat. In a beverage application, it is colloidal stability of a protein sol after thermal processing, which is commonly evaluated using indicators such as solubility[19] and turbidity.[20] Variations in protein solubility are due to physical and chemical properties of aggregates formed in thermal processing, including size, shape, density, and surface reactivity. Heating exposes free thiols and normally buried hydrophobic regions to initiate aggregation, and the balance of attractive and repulsive forces will determine the extent of aggregation. For example, heat treatment of β-Lg increases reactivity of the free thiol group, promoting aggregation and an increase in particle size[21,22] that potentially leads to decreased solubility and increased turbidity. Aggregation is more likely to occur in solution conditions producing weak electrostatic repulsion (pH close to the pI or high ionic strength)[17] but can potentially occur under strong electrostatic repulsive conditions.[23]

State diagrams have been used to represent the various physical states produced as a result of aggregation.[23−25] Unlike the traditional approach of showing treatment effects by selecting a limited set of conditions, state diagrams can be used to identify critical regions and transitions between sets of variables and can be tailored to specific parameters. Additionally, changes in experimental conditions can be evaluated via shifts in the critical transitions. This general approach has previously been used to evaluate β-Lg aggregation under steady state heating conditions by showing how pH, protein concentration, and salt concentration interrelate in forming a sol, precipitate, homogeneous gel, or microphase-separated gel.[23] Although this approach shows transitions between states, using extensive heating time at temperatures below 100 °C to achieve a steady state of aggregation is not valid for thermally processed beverages. The state diagram approach has also been used to evaluate WPI gelation[24] and changes in turbidity after thermal treatment.[25] In the context of whey protein beverages, this approach can be used to identify changes in colloidal stability such as sol−precipitate transitions or significant changes in turbidity or protein solubility. One of the limitations of this approach is that depending on the attributes that are desired (such as clarity or solubility), a single state diagram may not be the best representation of colloidal stability.

The goal of this investigation was to develop a state diagram approach to determine how whey proteins function in beverages after thermal treatments that mimic industrial ultrahigh-temperature (UHT) conditions. We chose to focus on the pH range in which beverages would typically be produced (pH 3−7). Additionally, instead of representing stability with one state diagram, we chose to depict three: protein solubility, turbidity, and macroscopic colloidal state. The combination of state diagrams provides a more complete view of colloidal stability over experimental conditions. To further explain state diagram trends and to identify key transitions, we developed pH−solubility curves for several protein concentrations. Gel electrophoresis and reverse phase chromatography were used to identify changes in the proportions of soluble β-Lg, α-La, GMP, and BSA after heating to elucidate the selectivity of the proteins toward heat-induced aggregation. The results of this study provide a framework for examining protein stability over a range of industrially relevant conditions and will assist in the formulation of beverages delivering higher levels of protein and potential health benefits.

MATERIALS AND METHODS

Preparation of Protein Solutions. Commercial WPI was provided by Glanbia Nutritionals (Twin Falls, ID, USA). Protein content was 92.13% as determined by Kjeldahl analysis (N × 6.38). The breakdown of whey proteins as determined by the manufacturer was 51.2% β-Lg, 21.3% α-La, 24.3% GMP, 1.6% immunoglobulins, 0.8% BSA, and 0.2% lactoferrin. Mineral composition as determined by inductively coupled plasma atomic emission spectroscopy was 14.44% N, 0.27% P, 0.42% K, 0.56% Ca, 1.05% S, and 0.23% Na. Chemical reagents were of analytical grade and supplied by Sigma-Aldrich (St. Louis, MO, USA). All subsequent calculations factor in purity and are expressed as protein concentration, not concentration of whey powder. All data are from three independent experimental replications unless stated otherwise.

Stock solutions (12% w/w protein) were made by solubilizing WPI in deionized water under magnetic agitation (400 rpm) for 3 h at 22 °C and storing overnight at 5 °C for maximum hydration. Solutions were diluted to the appropriate concentration (w/w protein) with deionized water. Sodium azide was added at a final concentration of 0.02% w/w to inhibit microbial growth. All pH adjustments were made with a combination of acids commonly used in commercial beverages (65:35 v/v phosphoric acid/citric acid) and 1 M sodium hydroxide. The volume added during pH adjustment was accounted for in determining final concentration of each protein solution.

Thermal Treatment. Two different heat treatments were used to mimic UHT thermal processing based on beverage pH: 109 °C for 3 s when pH ≤4.5 (LT) and 141 °C for 6 s when pH >4.5 (HT). A preliminary experiment was performed to determine the time required for solutions to reach the processing temperature in a Neslab EX7 silicon oil bath (Thermo Scientific, Waltham, MA, USA) set at 150 °C. Protein solutions were equilibrated to 20 °C, and 2 mL was placed in capped borosilicate test tubes (16 mm o.d.) before being processed in the 150 °C oil bath. Tubes were manually agitated during processing and remained quiescent in the bath for the respective hold time for total processing times of 29 + 3 and 62 + 6 s for LT and HT, respectively. At the conclusion of the hold time, test tubes were cooled in an ice slurry for 1 min and allowed to equilibrate overnight at 5 °C before analysis.

Nano Differential Scanning Calorimetry (nDSC). Samples of WPI were diluted to either 1.5 or 3.0 mg mL^{-1} with deionized water and adjusted to either pH 3.5 or 6.0 using the aforementioned acid blend. Both samples and reference deionized water were degassed at ∼1100 Torr for 1 h prior to analysis. Sample volumes of 300 μL were placed into a sample well with degassed water in the reference well, both under 3.0 atm of pressure to prevent gas bubble formation during heating. Thermograms were produced using a N-DSC II scanning calorimeter (TA Instruments, previously Calorimetry Sciences Corp., Provo, UT, USA) from 25 to 110 °C at a rate of 1 °C min^{-1}. Analysis of enthalpy and denaturation temperature was performed using NanoAnalyze software. Molar heat capacity was calculated using an average molecular weight of 16 kDa to reflect the main two proteins, β-Lg and α-La. A baseline scan of deionized water was subtracted from protein scans. A polynomial equation was fit to the scan and used to calculate enthalpy of unfolding (ΔH) and peak unfolding temperature (T_d).

Protein Solubility. Protein solubility after thermal treatment was determined using the method described by Morr et al.[26] with several modifications. After thermal processing, 2 mL samples were centrifuged at 17200g for 20 min at 15 °C, and the supernatant was removed and diluted 1:20 with deionized water. A Pierce bicinchoninic acid assay kit (Rockfold, IL, USA) was used to determine the concentration of protein in the supernatant per the manufacturer's instructions. The samples were combined with working reagent (1:8

DOI: 10.1021/acs.jafc.5b00633
J. Agric. Food Chem. 2015, 63, 4335−4344

ratio) in 96-well plates and incubated at 36 °C for 30 min. The absorbance of the plates was read at 562 nm on a Tecan Safire^2 (Männedorf, Switzerland) plate reader. The standard curve was developed using serial dilutions of centrifuged WPI to correct for the small amount of native insoluble protein. Solubility is expressed as the percentage of protein in the supernatant compared to the initial concentration of the solution.

Turbidity. The turbidity of the protein solutions after thermal treatment was determined using a Hach 21000AN Turbidimeter (Hach Co., Loveland, CO, USA). The solutions were analyzed in the 16 mm o.d. tubes in which they were thermally processed. Solutions were diluted by a factor of 5 with deionized water to fall within the range of the instrument, and reported values account for the dilution step. A preliminary test was performed to ensure that dilution did not cause disaggregation of particles (data not shown). The blank value for a test tube containing deionized water was subtracted from all values, which are given as nephelometric turbidity units (NTU).

Colloidal State Diagrams. State diagrams were developed for WPI solubility, turbidity, and macroscopic colloidal state after thermal processing. On the basis of pH, two different thermal treatments were used as described above. For ease of comparison across the entire pH range, these two treatments are shown on the same state diagram. For the macroscopic colloidal state diagram, each possible outcome (sol, precipitate, gel) was assigned a numeric value and averaged for each respective point. Definitions for states are as follows: sol, no visible aggregation; precipitate, visible aggregation; gel, solution does not flow when tilted 90°. All three state diagrams were plotted with triplicate values using the contour map function of Sigma Plot (Systat Software, San Jose, CA, USA).

Electrophoresis. Sodium dodecyl sulfate−polyacrylamide gel electrophoresis (SDS-PAGE) was performed under reducing conditions using a Novex NuPage gel system (Thermo Fisher Scientific, Waltham, MA, USA) per the manufacturer's instructions. After LT or HT heat treatment, solutions were centrifuged as described above; the supernatant was collected and diluted to 2 mg mL^{-1} with deionized water. Samples were mixed with Novex LDS sample buffer and Novex reducing agent and adjusted to a final protein concentration of 0.3 mg mL^{-1} with deionized water. Samples were heated to 70 °C for 10 min. In each gel, 5 μL of Novex Sharp prestained protein standard (Invitrogen Corp.) was used as a molecular weight reference in lane 1, and 3 μg of protein was added per lane to 4−12% mini Bis-Tris gels (Thermo Fisher Scientific). Gels were run with NuPage MES SDS running buffer (Thermo Fisher Scientific), and 500 μL of antioxidant was added to limit oxidation of disulfide bonds. The loaded gel received 200 V until the dye front reached the bottom of the gel. Gels were stained using SafeStain Coomassie stain (Thermo Fisher Scientific) for 1 h and destained with 100 mL of deionized water and 20 mL NaCl (20% w/v) for 3 h. Gel imaging was performed using a Gel Doc XR+ molecular imager (Bio-Rad Laboratories, Hercules, CA, USA), and bands were quantified with ImageLab software. Bands of β-Lg, α-La, and BSA were identified by comparison to known standards. Band intensities were determined and expressed as a percentage of the total band intensity in each respective lane, with unheated WPI used as a control. Data are average intensities of two independent replicates.

Reverse Phase High-Performance Liquid Chromatography (RP-HPLC). The percent loss of soluble GMP, α-La, and β-Lg after heat treatments was determined using RP-HPLC. After the heating, dilution, and centrifugation steps listed above, the supernatant was diluted 1:1 with the starting solvent blend and filtered through 0.1 μm Millipore filters. A gradient of solvent A (acetonitrile/water/TFA, 100:900:1 v/v/v) and solvent B (acetonitrile/water/TFA, 900:100:0.7 v/v/v) was applied using LC-20 AD pumps (Shimadzu Corp., Kyoto, Japan) at 0.8 mL min^{-1}. The ratio started with 74% solvent A and 26% solvent B, with iterative increases in solvent B percentage per the method described by Visser et al.[27] Chromatographic separations were performed using an Alltech Alltime 300 A 5 μm C_{18} column (Grace & Co., Columbia, MD, USA) at 30 °C and 1450 psi. Detection occurred at 220 nm using an SPD-M20-A photo diode array (Shimadzu Corp.). Peak areas were determined using LAB solutions software (Shimadzu Corp.) and were normalized against unheated WPI controls at each protein concentration to determine percent loss after heating. Average elution times were 6.9 and 11.9 min for GMP A and B, 38.1 min for α-La, and 52.3 and 53.6 min for β-Lg variants B and A, respectively.

Statistical Analysis. Statistical analysis of nDSC results was performed using the general linear model procedure in SAS v9.3 (Cary, NC, USA). Statistical significance was indicated at $p < 0.05$. Values for ΔH and T_d are shown plus/minus standard deviation. Differences between mean values were determined using Tukey's HSD comparison test.

RESULTS AND DISCUSSION

Thermal Properties of WPI Using nDSC. Thermal properties of native WPI were studied using nDSC (Figure 1) to determine the influence of pH on denaturation temperature (T_d) and enthalpy of unfolding (ΔH). The two pH values (3.5 and 6.0) were selected as values below and above the p*I* of whey proteins, respectively. Calorimetry cannot differentiate between denaturation and aggregation processes, so solutions were heated at dilute concentrations (1.5 and 3.0 mg mL^{-1}) to minimize the effects of aggregation. Additionally, the two concentrations served as a check to see if concentration affected the thermal properties of the proteins, which would most likely indicate aggregation.

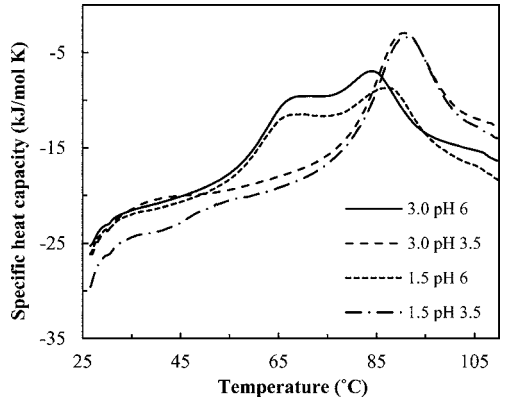

Figure 1. Calorimetric thermograms of WPI (1.5 and 3.0 mg mL^{-1}) at pH 3.5 and 6.0 heated from 25 to 110 °C at a rate of 1 °C min^{-1}.

Table 1. Denaturation Temperature (T_d) and Enthalpy (ΔH) of WPI at 1.5 and 3.0 mg mL^{-1} and pH 3.5 and 6.0[a]

protein (mg mL^{-1})	pH	ΔH (J g^{-1})	T_m (°C)
1.5	3.5	9.1 ± 0.1a	90.4 ± 0.1a
	6.0	11.7 ± 0.1b	87.4 ± 0.5b
3.0	3.5	9.2 ± 0.1a	90.2 ± 0.1a
	6.0	11.5 ± 0.2b	84.1 ± 0.9c

[a]Values listed are means of three replicates ± standard deviation. Lower case letters indicate significant differences in means within the column ($p < 0.05$).

At pH 3.5, WPI had a significantly ($p < 0.05$) greater T_d than at pH 6.0, suggesting greater thermal stability of protein structure. Both concentrations of WPI at pH 3.5 presented one large transition on the thermograph with a peak just above 90 °C. This is higher than reported T_d values of β-Lg (82 °C) and α-La (59 °C),[28] but α-La in particular has an increased T_d in the presence of β-Lg,[29] making it difficult to compare WPI with data from the individual proteins.

DOI: 10.1021/acs.jafc.5b00633
J. Agric. Food Chem. 2015, 63, 4335−4344

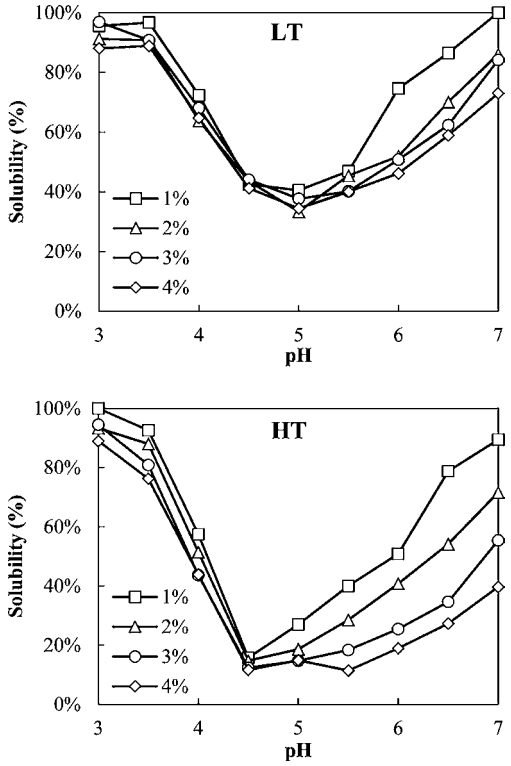

Figure 2. Solubility of WPI (1, 2, 3, and 4% protein w/w) after LT (top) or HT (bottom) heat treatments. Solubility is expressed as the amount of protein in the supernatant after centrifugation as a percentage of the initial protein prior to thermal treatment. Error bars are omitted for ease of viewing and were typically in the range of ±4%.

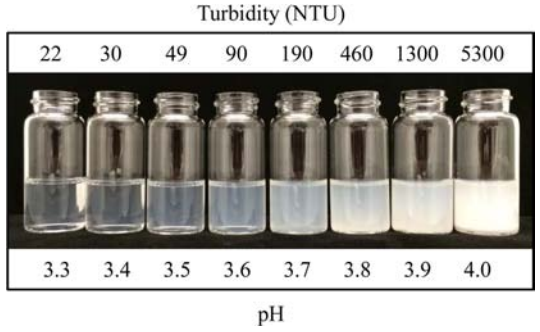

Figure 3. Turbidity of 1% w/w WPI solutions from pH 3.3 to 4.0 after heating to 109 °C for 3 s. The average turbidity (in NTU) of the solutions at each pH is shown above each sample.

At pH 6.0, one distinct peak was present near 85−87 °C, with a shoulder down to ∼65 °C. It has been shown that T_d is dependent on pH for individual whey proteins[28] and generally increases with a decrease in pH from 6.5 to 3.5, as seen in our experimental results. The lower shoulder of the pH 6.0 curve corresponds to the denaturation of α-La, which varies from 64 to 70 °C depending on calcium content.[30] The loss of calcium generally occurs at acidic pH[31] and converts α-La from the holo state to the apo state, with a T_d near 27 °C.[30] This explains the absence of an α-La peak on the pH 3.5 curve.

The enthalpy (ΔH) of unfolding was determined by analyzing the area between the endothermic curves and extrapolated baselines (Table 1). This represents the energy requirement to overcome noncovalent bonds during denaturation.[29] There was no difference in ΔH for each protein at

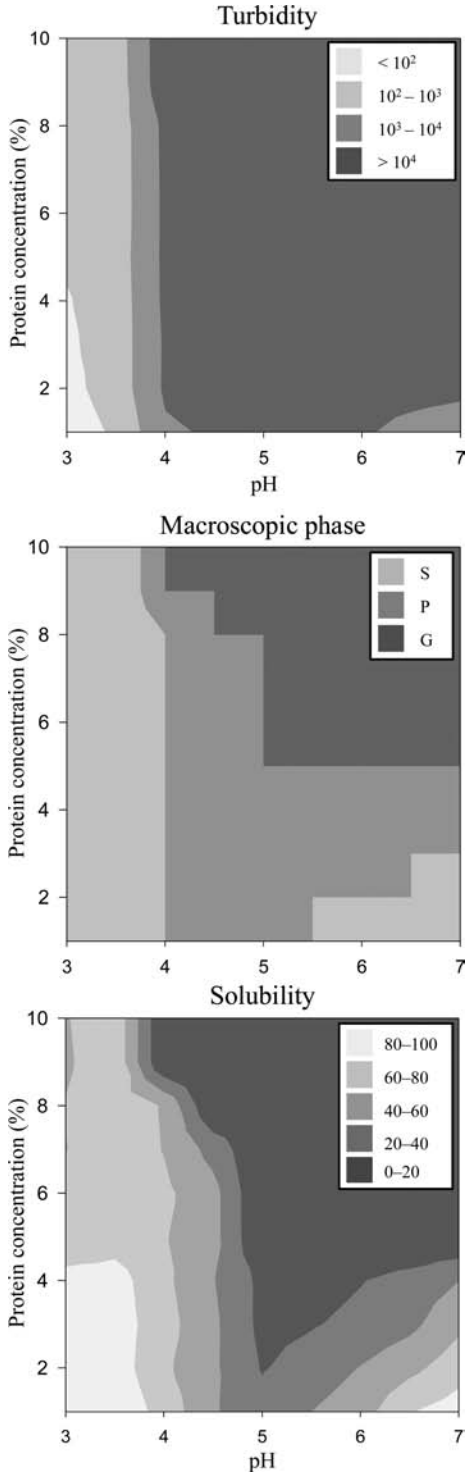

Figure 4. WPI (1−10% w/w, pH 3−7) state diagrams for turbidity (top), macroscopic colloidal state (middle), and solubility (bottom). Turbidity is presented as logarithmic NTU, with each iterative shade depicting a one $\log_{10}$ increase in solution turbidity after thermal treatment. Macroscopic colloidal state definitions are as follows: sol, no visible aggregation; precipitate, visible aggregation; gel, solution does not flow when turned on side. For the solubility diagram, different shaded regions represent 20% differences in solubility.

different concentrations, suggesting the major contribution was endothermic denaturation with minimal exothermic aggregation. Enthalpy at pH 6.0 is greater than at pH 3.5, but this value includes the peaks for both α-La and β-Lg, whereas ΔH for the

DOI: 10.1021/acs.jafc.5b00633
J. Agric. Food Chem. 2015, 63, 4335−4344

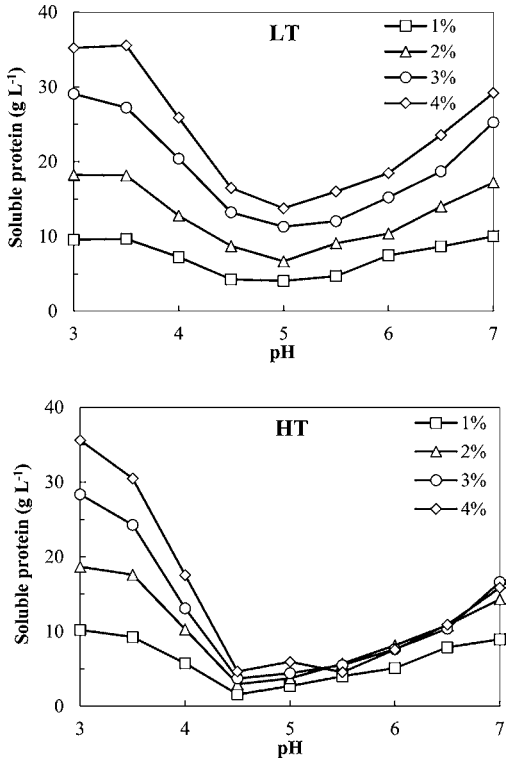

Figure 5. Solubility−pH profiles of 1, 2, 3, and 4% w/w WPI after LT (top) and HT (bottom) treatments. Values are expressed as protein concentration in the supernatant after centrifugation, instead of percent solubility. Error bars are omitted for ease of viewing and were typically in the range of ±4%.

pH 3.5 curves includes only β-Lg. The data generally agree with the literature, although one previous study found no change in enthalpy of WPC at pH 3.0 and 6.0 despite differences in T_d.[32]

Effects of Thermal Processing on Protein Solubility. Calorimetry was used to determine the thermal stability of individual proteins based on unfolding. In contrast, thermal stability in beverages is based on principles of colloidal stability. Protein solubility is often used as a marker for thermal stability of protein dispersions because loss of solubility is associated with decreased protein functionality.[33] Solubility−pH profiles were developed to determine the effects of the LT (109 °C for 3 s) and HT (141 °C for 6 s) processes on WPI solubility over a range of pH and protein concentrations (Figure 2). These thermal treatments mimic UHT thermal processing used to produce shelf-stable protein beverages.

For both thermal treatments, WPI solubility decreased as the pH approached the p*I* for all protein concentrations tested, in agreement with previous studies.[34−36] After the LT process, increased protein concentration from 1 to 4% was associated with decreased solubility at all pH values. Increasing concentration of β-Lg has been linked to the formation of higher molecular weight aggregates,[37,38] which settle at a faster rate during storage or centrifugation. Solubility was not significantly affected by increasing pH from 3.0 to 3.5, suggesting electrostatic repulsion at pH ≤3.5 is strong enough to limit further aggregation under the experimental conditions. Increasing pH from 3.5 to 5.0 decreased solubility for all concentrations. Above pH 5.0, solubility increased as pH increased, suggesting greater electrostatic repulsion. However, only 1% WPI had the same solubility at pH 7.0 that was seen at pH ≤3.5; all other concentrations had lower solubility at pH

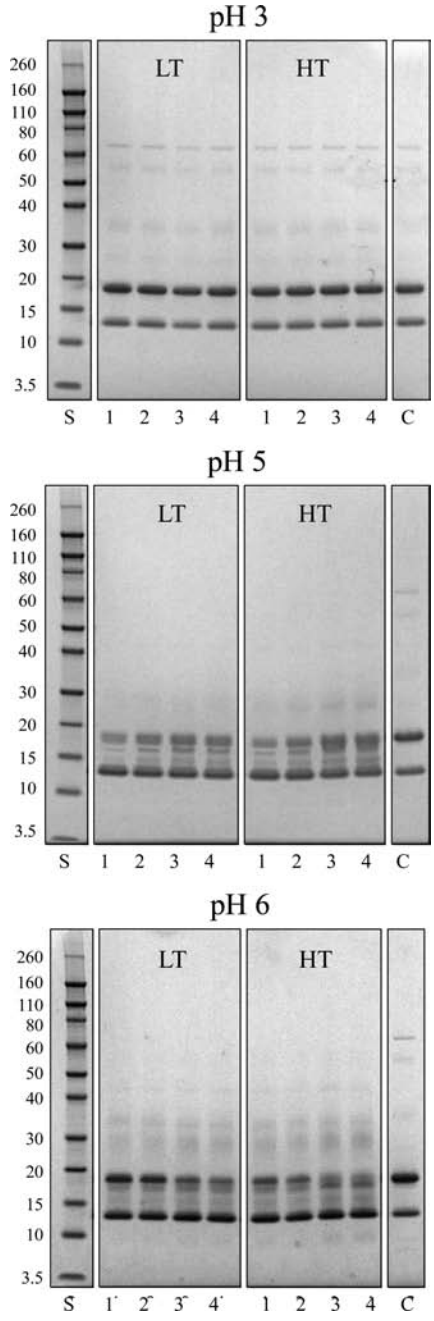

Figure 6. SDS-PAGE patterns of WPI supernatant after LT and HT treatments. The pH is shown at the top of each gel, and lane assignments are as follows: lane 1, molecular weight standards (S); lanes 2−5, initial starting protein concentration 1−4% w/w after LT; lanes 6−9, initial starting protein concentration 1−4% w/w after HT; lane 10, unheated WPI control (C).

7.0 than at pH 3.5. It is important to note that even at pH ≤3.5, solubility is not 100%, possibly due to the formation of insoluble protein aggregates during whey protein ingredient production.[39] These aggregates would be removed during centrifugation and thus not detected during analysis for solubility.

More severe drops in solubility were observed with the HT treatment. At pH 3.0, >80% solubility was retained for all concentrations regardless of thermal treatment, but dropped precipitously upon increasing pH to 4.5. All four concentrations retained only 12−16% solubility at pH 4.5. Above the p*I*,

DOI: 10.1021/acs.jafc.5b00633
J. Agric. Food Chem. 2015, 63, 4335−4344

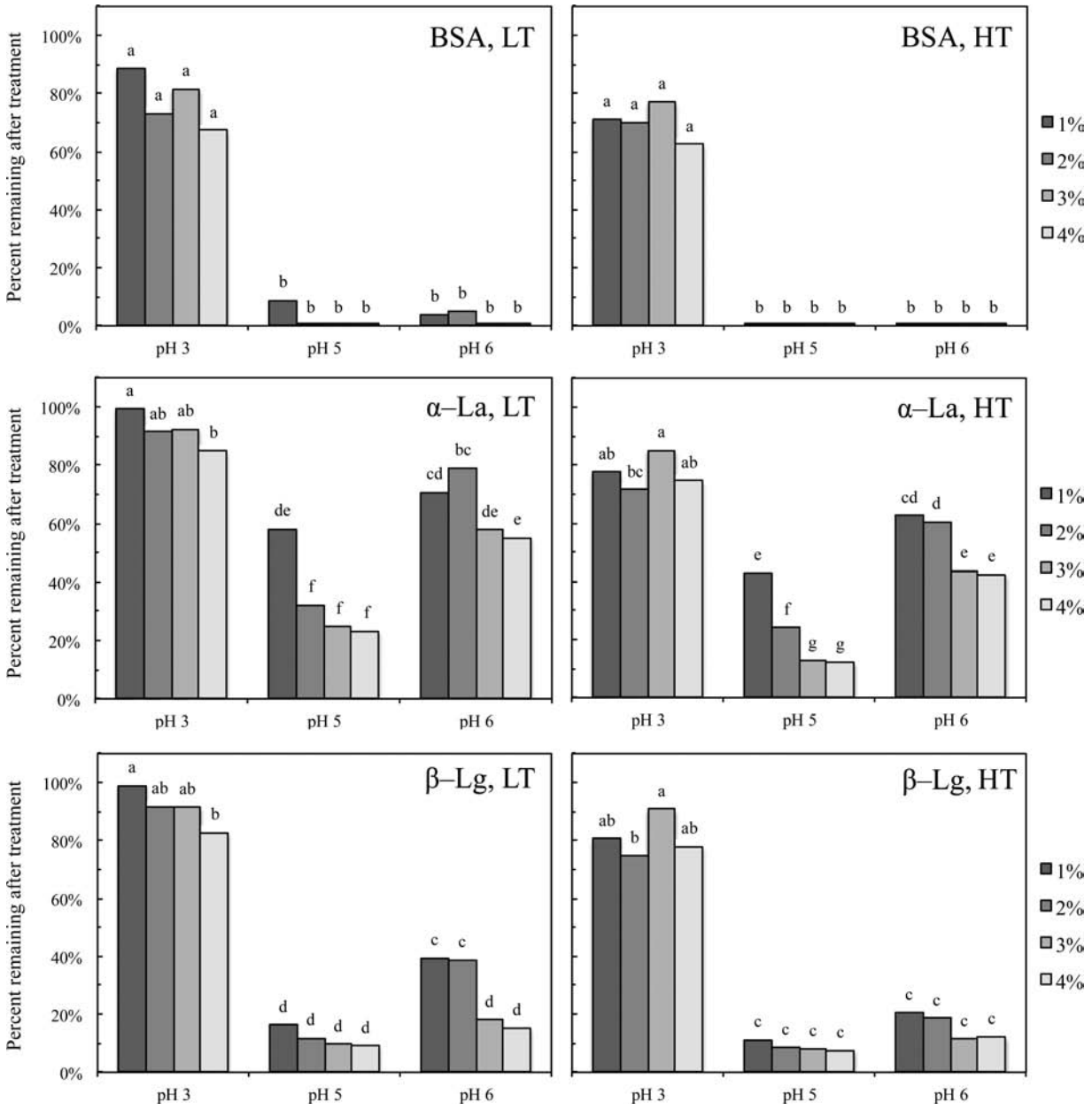

Figure 7. Percent soluble BSA, α-La, and β-Lg remaining after LT and HT compared to unheated controls as determined by band intensity after SDS-PAGE. Percentage (1−4%) indicates initial protein level. Lower case letters indicate significant differences between means within each individual treatment ($p < 0.05$).

increasing WPI concentration from 1 to 4% resulted in drops of solubility at pH 7.0 from 89 to 40%. Our nDSC results cover the temperature range of only the LT process, but it has been reported that β-Lg has a second transition peak just above 125 °C[40] that may be indicative of structural changes favoring aggregation. Increasing pH from 5.5 to 7.0 has been shown to increase onset temperature of WPI aggregation.[41] This would suggest decreased extent of aggregation and a higher degree of soluble protein, which our experimental data show. However, solubility is not as high above the p*I* as it is below. This may be explained by charge differences. Using the number of ionizable residues for calculations as an example, β-Lg has a net charge of approximately +16 at pH 3.6, but at pH 6.6 (∼equal pH units above the p*I*) the net charge is only −7.6.[42] Decreased net charge would favor aggregation and decreased solubility. Moreover, intermolecular disulfide interactions are favored more at pH > p*I* than below.[43] The pK_a of a cysteine thiol is ∼8.0, so thiol reactivity and disulfide bond formation are enhanced between pH 6.4 and 8.0.[37,44] Additionally, β-Lg undergoes a conformational change near pH 7 known as the Tanford transition,[18] associated with a marked increase in thiol reactivity.

Investigations on thermal denaturation and aggregation of whey proteins typically focus on temperatures below 100 °C. As such, very few studies have examined the effects of temperatures in excess of 100 °C, which is the temperature range for UHT processing. Noncovalent interactions may play a much more important role in aggregation at temperatures >90 °C.[45] Our results agree with a previous study showing significant drops in solubility after heating at temperatures ∼140 °C.[46]

DOI: 10.1021/acs.jafc.5b00633
J. Agric. Food Chem. 2015, 63, 4335−4344

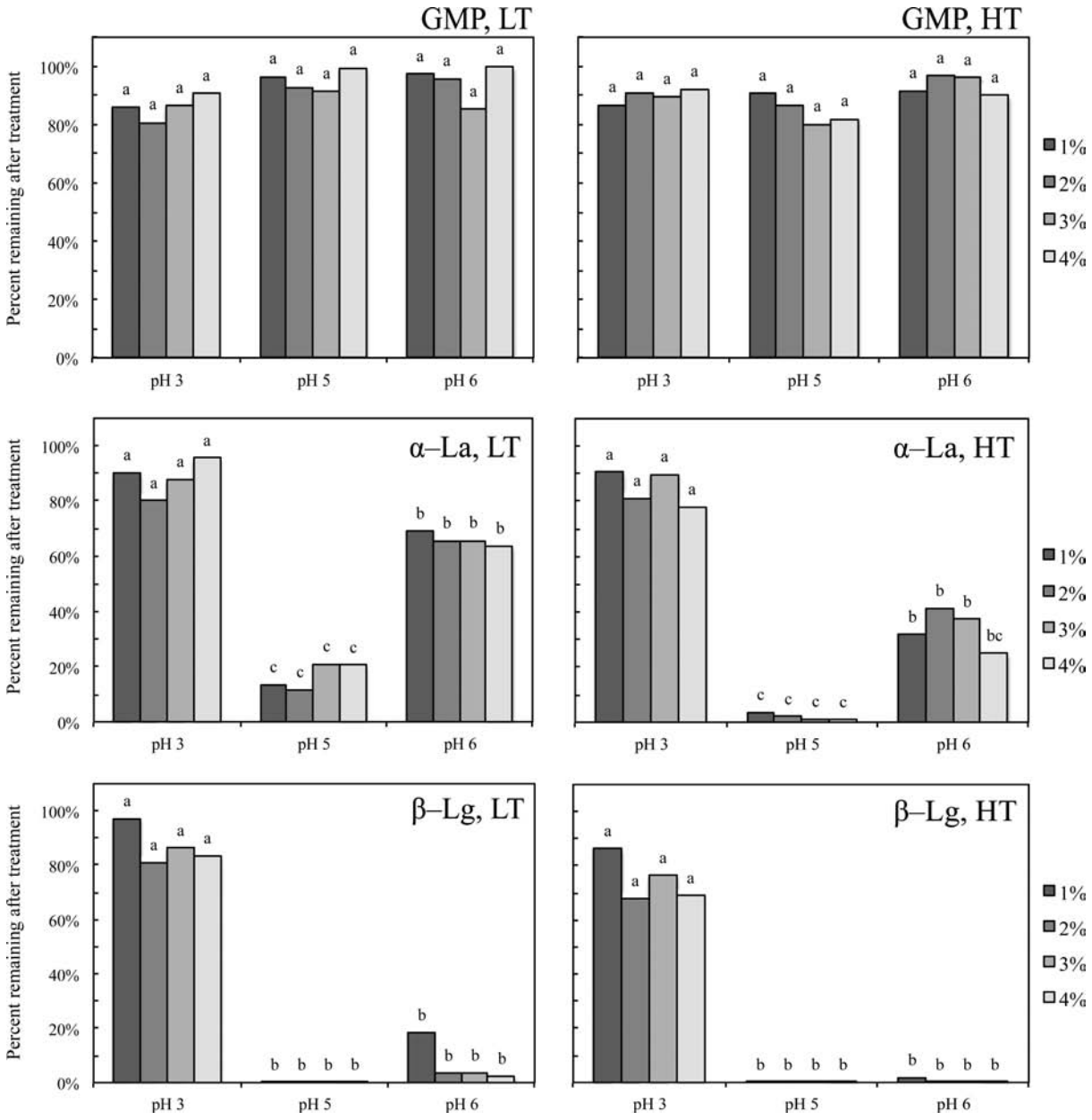

Figure 8. Percent soluble GMP (top), α-La (middle), and β-Lg (bottom) remaining after LT (left) and HT (right) as determined by HPLC. Percentage (1−4%) indicates initial protein level. Lower case letters indicate significant differences between means within each individual treatment ($p < 0.05$).

Effect of pH on Turbidity of Acidic Beverages. In the context of a whey protein beverage, turbidity is affected by many factors that influence aggregation, including protein concentration, thermal process time and temperature, pH, ionic strength, and other ingredients.[47] Turbidity is an important marker of stability in beverage applications due to consumer perception, as clear beverages are rated as more thirst quenching than turbid beverages.[48] Additionally, turbidity reflects size of dispersed particles, which is a predictor of colloidal stability per Stokes' law. We examined the turbidity of 1% WPI solutions over a pH range of 3.3−4.0 to provide a practical example of beverage turbidity (Figure 3). It is within this range that previous literature has reported a transition from clear to opaque beverages at pH 3.5,[25] 3.6,[49] and 3.7.[28] Beverages with turbidity below 50 NTU have been previously described as clear beverages.[49] However, as our state diagrams are represented on a logarithmic scale, we have designated 100 NTU as the cutoff for "clear" beverages. Our results show that at pH ≤3.6, solutions remained clear (90 NTU at pH 3.6) after thermal treatment. Beverages were no longer clear but only slightly turbid as pH increased to pH 3.7 (190 NTU) and 3.8 (460 NTU) and became completely opaque at pH 3.9 and 4.0 (>1300 NTU). This transition in turbidity is due to the formation of larger aggregates during thermal treatment, presumably because of diminished electrostatic repulsion close to the p*I*.

WPI State Diagrams as a Means To Represent Colloidal Stability. State diagrams were used to identify key regions of colloidal stability. We chose to depict three interrelated aspects of stability: turbidity, solubility, and the macroscopic colloidal state. Protein concentration (1−10% w/w) and pH (3−7) were varied over a range to depict conditions

DOI: 10.1021/acs.jafc.5b00633
J. Agric. Food Chem. 2015, 63, 4335−4344

suitable for whey protein beverages. Solution turbidity is expressed as log NTU values (Figure 4). Each iteratively darker region is a logarithmic increase in turbidity starting with clear beverages at <100 NTU. Solutions remained clear after heating, with a critical transition near pH 3.5 for 1% WPI or at pH 3.0 up to 4% WPI. At constant protein concentration, turbidity increased dramatically with increasing pH. Turbidity values began to decrease at pH > p*I*, but not by appreciable values except for low concentrations of WPI above pH 6.0. Thus, beverages in which clarity is desired require a pH below the critical transition, whereas clarity at neutral pH is not feasible under these conditions.

Similar trends are seen in the macroscopic colloidal state diagram (Figure 4). Solutions form stable sols at low pH independent of protein concentration due to the net positive charge on suspended protein particles. Near neutral pH, solutions with low protein concentration still form stable sols, but they are opaque instead of clear. The state diagram indicates a critical protein concentration required for gelation between 4 and 5% WPI for pH values from ∼4.8 to 7.0. Below the p*I*, higher protein levels are required for gelation. It should be noted that one limitation of the qualitative state diagram is the inexact demarcations between states. With only three possible numeric outcomes (sol, precipitate, or gel), the precision of the contour plot is somewhat limited without testing infinitesimally small increments of variables.

The solubility state diagram shows that at low pH (pH <3.5) and conditions of strong electrostatic repulsion, solubility after heating remained >80%, but decreased to 60−80% at protein concentrations >4% (Figure 4). Near the p*I*, solubility dropped below 40% for all protein concentrations. At a constant pH, increasing protein concentration also resulted in decreased solubility. Increasing β-Lg concentration has previously been associated with both the formation of larger aggregates[38] and increased rates and extent of β-Lg aggregation.[50] Even when heated to only 65 °C, higher concentrations of β-Lg shifted the fraction of aggregates toward higher molar mass aggregates.[37] Similar drops in solubility with WPI concentrations up to 10% have been reported.[36] In the context of colloidal stability, larger aggregates are more likely to be separated during centrifugation, resulting in decreased solubility.

Solubility−pH Profiles Based on Protein Concentration. The effects of the LT and HT thermal treatments on solubility are more apparent when expressing solubility as a concentration of protein in the supernatant after centrifugation rather than a percentage of the initial protein (Figure 5). After the LT treatment, the solubility−pH profiles for each protein concentration are similar. Solubility remains high at low pH, drops near the p*I*, and increases near neutral pH while remaining below the low pH levels. Beverages at pH 3 have approximately the same solubility after both LT and HT treatments. However, above pH 3, solubility drops more precipitously after the HT treatment, with higher initial protein concentration resulting in greater drops in solubility. Increased protein concentration has previously been associated with larger aggregate sizes,[38] decreased solubility,[36] and increased rates and extent of aggregation[50] while also affecting the morphological characteristics of protein aggregates.[4]

After the HT treatment, solubility gradually increased above the p*I*, but was lower than solubility levels after the LT treatment. The soluble protein concentration for 1% WPI (10 g L^{-1}) after heating was similar for the LT and HT treatments. For the other tested concentrations, the soluble protein concentration after HT treatment at pH 7 was 14, 17, and 16 g L^{-1} despite initial concentrations of 20, 30, and 40 g L^{-1}, respectively. This suggests that the protein remaining soluble is either a protein with limited participation in aggregation (i.e., GMP) or a combination of aggregating and nonaggregating proteins. We then chose to use complementary separation techniques to determine the aggregation selectivity of the individual proteins.

Electrophoretic Patterns of WPI Supernatant after Thermal Treatment. To determine aggregation selectivity of β-Lg, α-La, and BSA during heating, we used SDS-PAGE analysis. Samples were run under reducing conditions to compare the relative intensities of β-Lg, α-La, and BSA to that of native, unheated WPI. Several concentrations of WPI were compared at pH values above, near, and below the p*I*. Both thermal treatments (LT and HT) were also tested. Equal amounts of protein (not volume) were added to each lane, so changes in band intensity relative to the control indicate the participation of the proteins in forming insoluble aggregates and thus a change in the ratio of the proteins in the electrophoretic gel.

At pH 3.0, neither protein concentration nor heat treatment had a significant impact on the proportion of the major proteins in each lane (Figure 6). In the unheated control, the percentage of total protein in each lane was as follows: β-Lg, ∼54%; α-La, ∼30%; BSA, ∼4%. These values did not significantly change with increased protein content or heat treatment, suggesting limited aggregation and/or similar participation of individual proteins in aggregation across all concentrations. At pH 5.0, α-La comprises a greater percentage of total protein in each lane (43−52%) than the unheated control (30%), indicating that α-La was less involved in forming large aggregates than BSA and β-Lg. This is confirmed by the absence of BSA bands on the gels and the decreased intensity of the β-Lg bands compared to the control. Additionally, both LT and HT treatments at pH 5.0 resulted in a greater proportion of bands between α-La and β-Lg, between 20 and 30 kDa molar mass, and extending above 40 kDa.

The percentages of BSA, α-La, and β-Lg remaining after heating were also calculated (Figure 7). Solubility of BSA at pH 3 varied from ∼90% at 1% protein to ∼70% at 4% protein for the LT process and dropped slightly after the HT process. However, very little BSA remained at pH 5 and 6 for the LT process, with none remaining after the HT process, indicating a high propensity to aggregate. Both α-La and β-Lg generally trended toward lower solubility with increasing concentration, although the trends were not always statistically significant. Solubility was highest at pH 3 and lowest at pH 5 near the p*I*. Solubility at pH 6 was lower than at pH 3, which matches the trends in the pH−solubility profiles. β-Lg solubility was typically lower than that of α-La for all treatments.

Changes in Soluble GMP, α-La, and β-Lg after Heating As Determined by HPLC. Chromatography was used as a complementary method of comparing protein selectivity to heat-induced aggregation. Additionally, the HPLC method provided sensitivity for GMP detection, which SDS-PAGE could not provide. The same experimental variables (pH, initial protein concentration, and heat treatment) were explored (Figure 8). There were no significant losses in GMP solubility under all conditions tested. Heat stability at mildly acidic and near-neutral pH is in agreement with previous studies, but GMP heat stability has previously been shown to decrease at low pH.[51] This difference could be due to the different heat

DOI: 10.1021/acs.jafc.5b00633
J. Agric. Food Chem. 2015, 63, 4335−4344

treatments the authors used, but that remains to be established. At pH 3, there was no significant loss of α-La or β-Lg solubility after LT and HT treatments, which is in agreement with both the solubility state diagram and SDS-PAGE results. At pH 5, α-La and β-Lg solubility drops below 20% after LT, and negligible amounts of both proteins remain soluble after HT. Solubility of both proteins is higher at pH 6, suggesting greater thermal stability corroborated by increased solubility in the state diagrams. The decreased solubility of β-Lg as determined from both SDS-PAGE and HPLC suggests a higher propensity toward aggregation than that of α-La. β-Lg tends to form fewer small aggregates and more large aggregates in the presence of α-La.[52] It is also important to address the disparity between SDS-PAGE and HPLC results. Solubility for the same samples was lower per HPLC, likely due to the filtration step in HPLC that may have removed some of the medium-sized aggregates. Moreover, the small aggregates may have been broken up under reducing conditions for SDS-PAGE, allowing them to be quantified during image analysis.

Conclusions. Protein concentration, pH, and thermal treatment all influence the colloidal stability of whey protein beverages. Judicious selection of these variables is required to formulate stable protein beverages. Because of the complexity of protein beverages, state diagrams can be used to identify critical transition regions under set parameters to predict regions of thermal stability. This approach identified regions of colloidal stability at pH <3.5 (low turbidity and high solubility) and >6.5 (moderately high solubility). Thermal processing at higher temperatures and longer times resulted in a loss of protein solubility, even at pH 3.5. Closer to the p*I*, β-Lg and BSA were more likely to participate in aggregation reactions than α-La. The state diagram approach can also be used to elucidate the effects of alternate ingredients or formulations, gaining an understanding of how critical regions of the state diagrams are altered under different conditions.

AUTHOR INFORMATION

Funding

Support from the North Carolina Agricultural Research Service and Glanbia Nutritionals is gratefully acknowledged. The use of trade names in this publication does not imply endorsement by the North Carolina Agricultural Research Service of the products named or criticism of similar ones not mentioned.

Notes

The authors declare no competing financial interest.

ACKNOWLEDGMENTS

We are very grateful for the whey protein isolate donated by Glanbia Nutritionals and to Nathaniel Hentz and Brian Mosley for technical assistance in HPLC.

REFERENCES

(1) Smithers, G. W. Whey and whey proteins – from "gutter-to-gold". *Int. Dairy J.* **2008**, *18*, 695–704.

(2) Ha, E.; Zemel, M. B. Functional properties of whey, whey components, and essential amino acids: mechanisms underlying health benefits for active people. *J. Nutr. Biochem.* **2003**, *14*, 251–258.

(3) Dairy Products 2013 Summary; http://www.usda.gov/nass/pubs/todayrpt/daryan14.pdf (accessed July 8, 2014).

(4) Vardhanabhuti, B.; Yucel, U.; Coupland, J. N.; Foegeding, E. A. Interactions between β-lactoglobulin and dextran sulfate at near neutral pH and their effect on thermal stability. *Food Hydrocolloids* **2009**, *23*, 1511–1520.

(5) Kilara, A. Whey and whey products. In *Dairy Processing and Quality Assurance*; Chandan, R. C., Kilara, A., Shah, N., Eds.; Wiley-Blackwell: Hoboken, NJ, USA, 2008; Vol. 1, pp 337–355.

(6) Foegeding, E. A.; Luck, P.; Vardhanabhuti, B. Milk protein products: whey protein products. In *Encyclopedia of Dairy Sciences*; Fuquay, J. W., Ed.; Academic Press: San Diego, CA, USA, 2011; Vol. 1, pp 873–878.

(7) Fox, P. F.; McSweeney, P. L. H. *Advanced Dairy Chemistry*, 3rd ed.; Kluwer Academic/Plemum Publishers: University College: Cork, Ireland, 2003; Vol. 1.

(8) Farrell, H. M., Jr.; Jimenez-Flores, R.; Bleck, G. T.; Brown, E. M.; Butler, J. E.; Creamer, L. K.; Hicks, C. L.; Hollar, C. M.; Ng-Kwai-Hang, K. F.; Swaisgood, H. E. Nomenclature of the proteins of cows' milk – sixth revision. *J. Dairy Sci.* **2004**, *87*, 1641–1674.

(9) Huffman, L. M.; Harper, W. J. Maximizing the value of milk through separation technologies. *J. Dairy Sci.* **1999**, *82*, 2238–2244.

(10) Code of Federal Regulations. Title 21, sec. 114; http://www.access.gpo.gov/nara/cfr/waisidx_01/21cfr114_01.html (accessed June 25, 2014).

(11) Beecher, J. W.; Drake, M. A.; Luck, P. J.; Foegeding, E. A. Factors regulating astringency of whey protein beverages. *J. Dairy Sci.* **2008**, *91*, 2553–2560.

(12) Etzel, M. R. Manufacture and use of dairy protein fractions. *J. Nutr.* **2004**, *134*, 996S–1002S.

(13) Evans, J.; Zulewska, J.; Newbold, M.; Drake, M. A.; Barbano, D. M. Comparison of composition and sensory properties of 80% whey protein and milk serum protein concentrates. *J. Dairy Sci.* **2010**, *93*, 1824–1843.

(14) Park, C. W.; Bastian, E.; Farkas, B.; Drake, M. A. The effect of acidification of liquid whey protein concentrate on the flavor of spray-dried powder. *J. Dairy Sci.* **2014**, *97*, 4043–4051.

(15) McGarrahan, E. T. Considerations necessary to provide for sterilized milk and milk products in hermetically sealed, non-refrigerated containers. *J. Dairy Sci.* **1982**, *65*, 2023–2034.

(16) de Wit, J. N. Thermal behavior of bovine β-lactoglobulin at temperatures up to 150°C. A review. *Trends Food Sci. Technol.* **2009**, *20*, 27–34.

(17) Nicolai, T.; Britten, M.; Schmitt, C. β-Lactoglobulin and WPI aggregates: formation, structure and applications. *Food Hydrocolloids* **2011**, *25*, 1945–1962.

(18) De la Fuente, M. A.; Singh, H.; Hemar, Y. Recent advances in the characterisation of heat-induced aggregates and intermediates of whey proteins. *Trends Food Sci. Technol.* **2002**, *13*, 262–274.

(19) Foegeding, E. A.; Davis, J. P. Food protein functionality: a comprehensive approach. *Food Hydrocolloids* **2011**, *25*, 1853–1864.

(20) LaClair, C. E.; Etzel, M. R. Turbidity and protein aggregation in whey protein beverages. *J. Food Sci.* **2009**, *74*, 526–535.

(21) Iametti, S.; Cairoli, S.; De Gregori, B.; Bonomi, F. Modifications of high-order structures upon heating of β-lactoglobulin: dependence on the protein concentration. *J. Agric. Food Chem.* **1995**, *43*, 53–58.

(22) Anema, S. G.; McKenna, A. B. Reaction kinetics of thermal denaturation of whey proteins in heated reconstituted whole milk. *J. Agric. Food Chem.* **1996**, *44*, 422–428.

(23) Ako, K.; Nicolai, T.; Durand, D.; Brotons, G. Micro-phase separation explains the abrupt structural change of denatured globular protein gels on varying the ionic strength or the pH. *Soft Matter* **2009**, *5*, 4033–4041.

(24) Mehalebi, S.; Nicolai, T.; Durand, D. Light scattering study of heat-denatured globular protein aggregates. *Int. J. Biol. Macromol.* **2008**, *43*, 129–135.

(25) Kinekawa, Y.; Kitabatake, N. Turbidity and rheological properties of gels and sols prepared by heating process whey protein. *Biosci., Biotechnol., Biochem.* **1995**, *59*, 834–840.

(26) Morr, C. V.; German, B.; Kinsella, J. E.; Regenstein, J. M.; Buren, J. P. V.; Kilara, A.; Lewis, B. A.; Mangino, M. E. A collaborative study to develop a standardized food protein solubility procedure. *J. Food Sci.* **1985**, *50*, 1715–1718.

DOI: 10.1021/acs.jafc.5b00633
J. Agric. Food Chem. 2015, 63, 4335–4344

(27) Visser, S.; Slangen, C. J.; Rollema, H. S. Phenotyping of bovine milk proteins by reversed-phase high-performance liquid chromatography. *J. Chromatogr., A* **1991**, *548*, 361−370.
(28) Bernal, V.; Jelen, P. Thermal stability of whey proteins − a calorimetric study. *J. Dairy Sci.* **1985**, *68*, 2847−2852.
(29) Boye, J. I.; Alli, I. Thermal denaturation of mixtures of α-lactalbumin and β-lactoglobulin: a differential scanning calorimetric study. *Food Res. Int.* **2000**, *33*, 673−682.
(30) Hendrix, T.; Griko, Y. V.; Privalov, P. L. A calorimetric study of the influence of calcium on the stability of bovine α-lactalbumin. *Biophys. Chem.* **2000**, *84*, 27−34.
(31) Relkin, P.; Mulvihill, D. M. Thermal unfolding of β-lactoglobulin, α-lactalbumin, and bovine serum albumin. A thermodynamic approach. *Crit. Rev. Food Sci. Nutr.* **1996**, *36*, 565−601.
(32) de Wit, J. N.; Klarenbeek, G. Effects of various heat treatments on structure and solubility of whey proteins. *J. Dairy Sci.* **1984**, *67*, 2701−2710.
(33) de Wit, J. N.; van Kessel, T. Effects of ionic strength on the solubility of whey protein products. A colloid chemical approach. *Food Hydrocolloids* **1996**, *10*, 143−149.
(34) Zhu, H.; Damodaran, S. Heat-induced conformational changes in whey protein isolate and its relation to foaming properties. *J. Agric. Food Chem.* **1994**, *42*, 846−855.
(35) Pelegrine, D. H. G.; Gasparetto, C. A. Whey proteins solubility as function of temperature and pH. *LWT−Food Sci. Technol.* **2005**, *38*, 77−80.
(36) Cornacchia, L.; Forquenot de la Fortelle, C.; Venema, P. Heat-induced aggregation of whey proteins in aqueous solutions below their isoelectric point. *J. Agric. Food Chem.* **2014**, *62*, 733−741.
(37) Hoffmann, M. A. M.; van Mil, P. J. J. M. Heat-induced aggregation of β-lactoglobulin: role of the free thiol group and disulfide bonds. *J. Agric. Food Chem.* **1997**, *45*, 2942−2948.
(38) Le Bon, C.; Nicolai, T.; Durand, D. Growth and structure of aggregates of heat-denatured β-lactoglobulin. *Int. J. Food Sci. Technol.* **1999**, *34*, 451−465.
(39) Roufik, S.; Paquin, P.; Britten, M. Use of high-performance size exclusion chromatography to characterize protein aggregation in commercial whey protein concentrates. *Int. Dairy J.* **2005**, *15*, 231−241.
(40) de Wit, J. N.; Klarenbeek, G. A differential scanning calorimetric study of the thermal behaviour of bovine β-lactoglobulin at temperatures up to 160°C. *J. Dairy Res.* **1981**, *48*, 293−302.
(41) Xiong, Y. L. Influence of pH and ionic environment on thermal aggregation of whey proteins. *J. Agric. Food Chem.* **1992**, *40*, 380−384.
(42) Rhodes, G. Polypeptide charge calculation for β-lactoglobulin; http://spdbv.vital-it.ch/TheMolecularLevel/Goodies/PeptChg.xls (accessed Dec 29, 2014).
(43) Verheul, M.; Roefs, S. P. F. M.; de Kruif, K. G. Kinetics of heat-induced aggregation of β-lactoglobulin. *J. Agric. Food Chem.* **1998**, *46*, 896−903.
(44) Hoffmann, M. A. M.; van Mil, P. J. J. M. Heat-induced aggregation of β-lactoglobulin as a function of pH. *J. Agric. Food Chem.* **1999**, *47*, 1898−1905.
(45) Galani, D.; Apenten, R. K. O. Heat-induced denaturation and aggregation of β-lactoglobulin: kinetics of formation of hydrophobic and disulphide-linked aggregates. *Int. J. Food Sci. Technol.* **1999**, *34*, 467−476.
(46) Dissanayake, M.; Ramchandran, L.; Donkor, O. N.; Vasiljevic, T. Denaturation of whey proteins as a function of heat, pH and protein concentration. *Int. Dairy J.* **2013**, *31*, 93−99.
(47) Mahler, H. C.; Friess, W.; Grauschopf, U.; Kiese, S. Protein aggregation: pathways, induction factors and analysis. *J. Pharm. Sci.* **2009**, *98*, 2909−2934.
(48) Beucler, J.; Drake, M. A.; Foegeding, E. A. Design of a beverage from whey permeate. *J. Food Sci.* **2005**, *70*, 277−285.
(49) LaClair, C. E.; Etzel, M. R. Ingredients and pH are key to clear beverages that contain whey protein. *J. Food Sci.* **2010**, *75*, 21−27.
(50) Nielsen, B. T.; Singh, H.; Latham, J. M. Aggregation of bovine β-lactoglobulins A and B on heating at 75°C. *Int. Dairy J.* **1996**, *6*, 519−527.
(51) Siegert, N.; Tolkach, A.; Kulozik, U. The pH-dependent thermal and storage stability of glycosylated caseinomacropeptide. *LWT−Food Sci. Technol.* **2012**, *47*, 407−412.
(52) Schokker, E. P.; Singh, H.; Creamer, L. K. Heat-induced aggregation of β-lactoglobulin A and B with α-lactalbumin. *Int. Dairy J.* **2000**, *10*, 843−853.

DOI: 10.1021/acs.jafc.5b00633
J. Agric. Food Chem. 2015, 63, 4335−4344

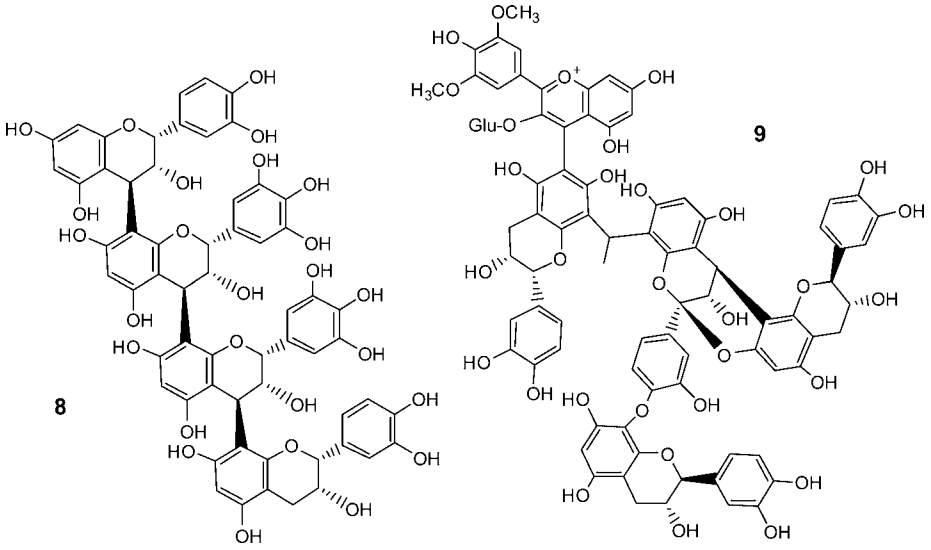

Figure 2. Examples of grape tannin (**8**) and wine tannin (**9**) structures showing B ring ether linkages, A-type linkages, and ethyl linkages.

in water were dominated by hydrogen bonding.[20] The structure of tannins also influences the extent of protein interaction, and larger tannins with more binding sites and flexible structures have been shown to interact more readily than smaller tannins.[18,21−25] Sensory studies have indicated that smaller wine tannins are less astringent than larger wine tannins,[26,27] which may relate to the extent of interaction between wine tannins and salivary proteins. Larger tannins bind proteins with a combination of hydrophobic interaction and hydrogen bonding, whereas flavan-3-ol monomer−protein interactions are driven by hydrogen bonding alone.[28] The strength of monomer interactions with poly(L-proline) (PLP) (**5**) are influenced by the relative hydrophobicity of the monomer, with the more hydrophobic epicatechin gallate (**3**) binding more strongly than the less hydrophobic epigallocatechin gallate (**4**) (Figure 1).[28] Conversely, comparatively hydrophilic grape tannins (**8**) have been shown to bind more strongly to PLP than the more hydrophobic wine tannins (**9**) (Figure 2).[29] The oxidation of grape tannins during crushing and fermentation, which form wine tannins, reduces the proportion of acid-labile interflavan bonds, thus creating a more rigid structure with potentially fewer binding sites than grape tannins due to intramolecular bonding and steric hindrances,[29−31] suggesting that overall tannin structure may be more important in protein interactions than hydrophobicity. Dimers and trimers with extended structures bind more readily to proteins than those with compact structures, where intramolecular interactions within the polyphenol dominate.[23] Proteins that are larger, such as gelatin, or have more extended structures, such as salivary PRPs, also bind more tannin due to the presence of more available binding sites, such as proline residues and amine groups,[11,14,18,24,32,33] compared with more globular proteins such as bovine serum albumin (BSA).[34−36] Binding of tannins and PRPs shows preference for available proline residues that are not obscured by stereochemistry or interfering structural moieties such as carbohydrate side chains of the protein,[37,38] and the residual structures of PRPs such as PPII helices promote tannin interactions due to the conformation of these structures.[39] The mechanism of interaction reportedly involves hydrophobic interactions and hydrogen bonding, although there are differences in the reported literature about which is the driving mechanism of the first stage of interaction.[15,23,29,40] Hydrophobic interactions involve $\pi-\pi$ bonding between the planar surfaces of the phenolic tannin structure and the proline ring of the PLP moiety,[15] whereas hydrogen bonding occurs between the carbonyl groups of the proline and the hydroxyl groups of the tannin.[1,23] Conversely, interactions between tannins and BSA have been found to be nonspecific and are likely to be driven by hydrogen bonding.[34,41]

Solvent composition, particularly ethanol concentration, can influence tannin solubility as well as tannin−protein interactions and astringency.[11,18,24] In the wine matrix, the ethanol concentration generally ranges from 10 to 15%, and this has been shown to influence the wine astringency,[42−44] with the intensity of overall astringency decreasing with increasing ethanol concentrations (from 0 to 15% ethanol).[44] The concentration of ethanol in wine can also alter the astringency subqualities, including "velvety" and "silkiness",[44] potentially by changing the extent of tannin−salivary protein interactions or via direct impact on the oral surfaces.[42,43] More research is also underway to decrease the concentration of ethanol in wine, such as the development of low-alcohol yeast strains,[45] which may also affect wine astringency. Wine tannin size and shape are not directly affected by ethanol concentration,[46] and therefore the changes in astringency with ethanol are more likely to be associated with the physicochemical properties of the different tannins in solvents with different ethanol concentrations.[16] Ethanol can disrupt tannin−cell wall binding of apple pulp at concentrations between 20 and 40%,[22] demonstrating the influence of ethanol on noncovalent tannin−protein binding. Storage of red wine can decrease the astringency of a wine as a result of decreased tannin concentrations as well as structural changes in wine tannins.[6,47] Tannin structures change over time as a result of gradual oxidation and structural rearrangement reactions that occur under the acidic conditions of wine (pH generally 3.0−4.0). Isothermal titration calorimetry (ITC) experiments have indicated that this can reduce the strength of the tannin−protein binding, potentially contributing to the decrease in astringency intensity.[29]

In this study, the binding strengths between PLP and a range of different wine tannins and tannin fractions were measured using ITC across a range of ethanol concentrations (5, 10, 15,

DOI: 10.1021/acs.jafc.5b00758
J. Agric. Food Chem. 2015, 63, 4345−4352

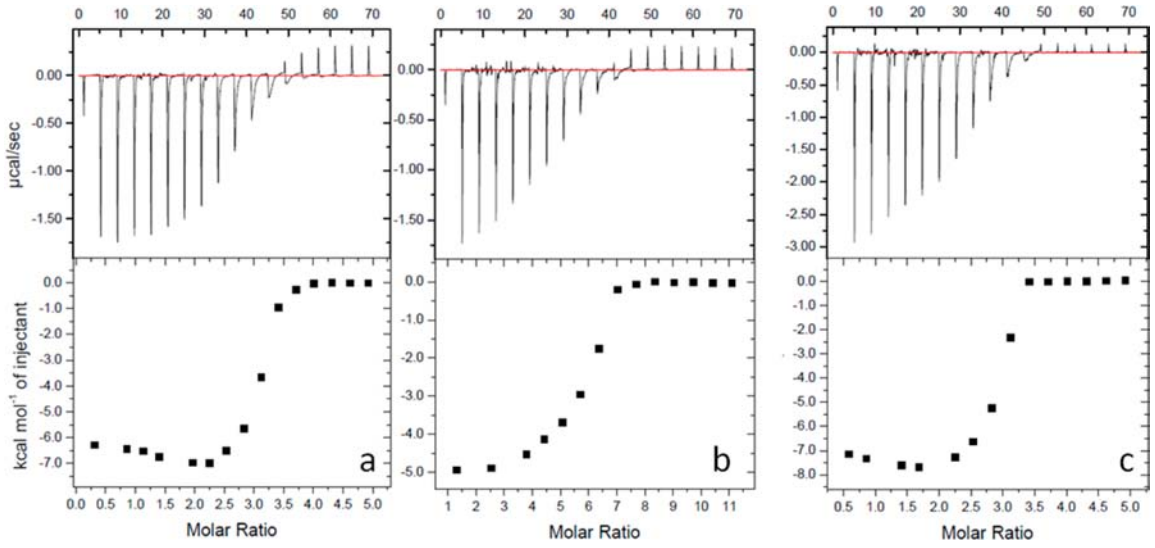

Figure 3. Thermograms and binding isotherms of wine tannin samples interacting with PLP (0.075 mM) in 10% ethanol: (a) TT3; (b) Bu3; (c) Aq3.

and 40% ethanol) to assess the impact of ethanol on tannin–peptide interactions for tannins with different structures.

MATERIALS AND METHODS

Chemicals. All solvents used were of high-performance liquid chromatography (HPLC) grade, all chemicals were of analytical reagent grade, and water was sourced from a Milli-Q purification system. Ethanol was purchased from Merck Australia (Kilsyth, VIC, Australia). Ammonium formate and poly(L-proline) (**5**, DPn 58, molecular weight 5600 Da) were purchased from Sigma-Aldrich (Castle Hill, NSW, Australia), and formic acid (99% w/w AR grade) was purchased from Chem-Supply.

Tannin Isolation and Composition. Wine tannin was isolated from 3- and 7-year-old Cabernet Sauvignon wines and fractionated as described previously[26] to give six tannin samples: total tannin (TT), aqueous (Aq) tannin, and butanol-soluble (Bu) tannin for each vintage wine. Fractionation of the TT tannins produced greater proportions of Aq tannin than Bu tannin for both wines with Aq/Bu mass ratios of 3.6:1 and 2.9:1 for the younger and older wines, respectively. The molar extinction coefficients (ε) of each tannin sample were determined as described previously[26,29] and used in calculating the concentration of tannin in the stock solutions for ITC analysis. Tannin analysis was performed in a previous study[26] using gel permeation chromatography for molecular size, phloroglucinolysis for percent yield (proportions of acid-labile interflavan bonds), and subunit composition and octanol–water coefficients (Log P). The percent yield of the young wine tannin samples was 30.2 ± 4.2% and for the aged wine tannin samples was 13.2 ± 2.3%, demonstrating the formation of non-acid-labile bonds in tannins as the wine ages. The percentages of epicatechin gallate subunits (**3**) were 3.4 ± 0.5 and 2.0 ± 0.2% for young and aged wines, respectively. There was no significant difference in the percent epigallocatechin between tannin samples of different ages.

Isothermal Titration Calorimetry. An auto-ITC 200 (GE life sciences) was used to measure the change in heat induced by tannin–PLP interactions, and data were analyzed using the MicroCal Origin version 7.0 software package adapted for auto-ITC data analysis. Tannin fractions were prepared for ITC and titrated using the method previously described.[29] Briefly, tannin samples (2 mM) in buffer solution (10 mM ammonium formate) were titrated into a cell containing 0.075, 0.050, or 0.033 mM PLP in the same buffer solution. The titration consisted of 17 × 2 µL injections at 25 °C. The concentration of ethanol was varied in the buffer solution (5, 10, 15, and 40% v/v ethanol), and this concentration was the same in both the titrant and PLP solutions for each experiment. Wine tannins were not soluble without ethanol; hence, 5% ethanol was considered the low-alcohol control sample. Solutions of 5–15% ethanol were at pH 3.5, and the 40% ethanol solution was at pH 4.0 due to the reduced proportion of the buffer solution. The influence of the different pH was considered to have a lesser impact than ethanol concentration on the basis of previous reports.[18,44,48] Experiments were replicated six times, and results were averaged. Thermograms and binding isotherms were used to determine the enthalpy (ΔH), binding constants (K), stoichiometry (N), and entropy ($T\Delta S$) using a single-site binding model. The change in standard Gibbs free energy (ΔG) was calculated using the Gibbs–Helmholz thermodynamic equation: $\Delta G = -RT \ln K$, where R is the ideal gas constant (1.985 cal mol^{-1} K^{-1}) and T is the temperature (298 K). Examples of the thermograms and binding isotherms for the different wine tannins are given in Figure 3.

Statistical Analysis. Differences in thermodynamic parameters between different tannins in each matrix and between the same tannin in different matrices were determined using ANOVAs and Tukey analyses with GraphPad Prism statistics software.

RESULTS AND DISCUSSION

Wine Tannin–Peptide Interactions. Tannins from 3- and 7-year-old Cabernet Sauvignon wines were isolated and fractionated in previous experiments[26] to produce a range of wine tannins with different structural properties: TT, Aq, and Bu tannins. The Bu tannins were consistently smaller with molecular weights of 1865 ± 92 g mol^{-1} compared with 3020 ± 182 g mol^{-1} for the TT and Aq tannins (Table 1).[26] The most notable difference between young and aged wine tannins was the proportion of acid-labile interflavan bonds at around 30 and

Table 1. Characteristics of Wine Tannins Used in This Study including the Molecular Weight (MW), Octanol/Water Partition Coefficient (Log P), and Extinction Coefficient (ε)

tannin sample	MW[a] (g mol^{-1})	Log P[a]	ε (×10^3) (M^{-1} cm^{-1})
TT3	2930	−0.61	44.3
Aq3	3030	−1.31	37.4
Bu3	1800	−0.7	27.1
TT7	2850	−0.55	36.3
Aq7	3270	−1.34	45.6
Bu7	1930	−0.72	29.2

[a]Results from McRae et al.[26]

DOI: 10.1021/acs.jafc.5b00758
J. Agric. Food Chem. 2015, 63, 4345–4352

Table 2. Thermodynamics Parameters for Interactions between Different Wine Tannins and PLP at 10% Ethanol including the Change in Enthalpy (ΔH), Change in Entropy ($T\Delta S$), Change in Gibbs Free Energy (ΔG), Stoichiometry (N), and Binding Association Constant (K)[a]

tannin fraction	ΔH (kcal mol^{-1})	$T\Delta S$ (kcal mol^{-1})	ΔG (kcal mol^{-1})	K (10^6 M^{-1})	N
TT3	−6.93 ± 0.09a	1.26 ± 0.20d	−8.19 ± 0.11bc	1.03 ± 0.20bc	3.06 ± 0.09d
Aq3	−7.09 ± 0.38a	1.59 ± 0.29d	−8.68 ± 0.09a	2.34 ± 0.35a	2.71 ± 0.11e
Bu3	−4.83 ± 0.08c	3.31 ± 0.07b	−8.14 ± 0.00c	0.93 ± 0.01c	5.50 ± 0.15b
TT7	−5.90 ± 0.18b	2.21 ± 0.16c	−8.11 ± 0.01d	0.89 ± 0.02d	3.41 ± 0.08c
Aq7	−6.04 ± 0.10b	2.22 ± 0.10c	−8.27 ± 0.02b	1.16 ± 0.03b	3.32 ± 0.10c
Bu7	−4.44 ± 0.13c	3.84 ± 0.10a	−8.28 ± 0.04b	1.18 ± 0.08b	5.68 ± 0.01a

[a]Values are shown as the average of six results ± one standard deviation, and letters indicate values in columns that are significantly different ($p < 0.05$).

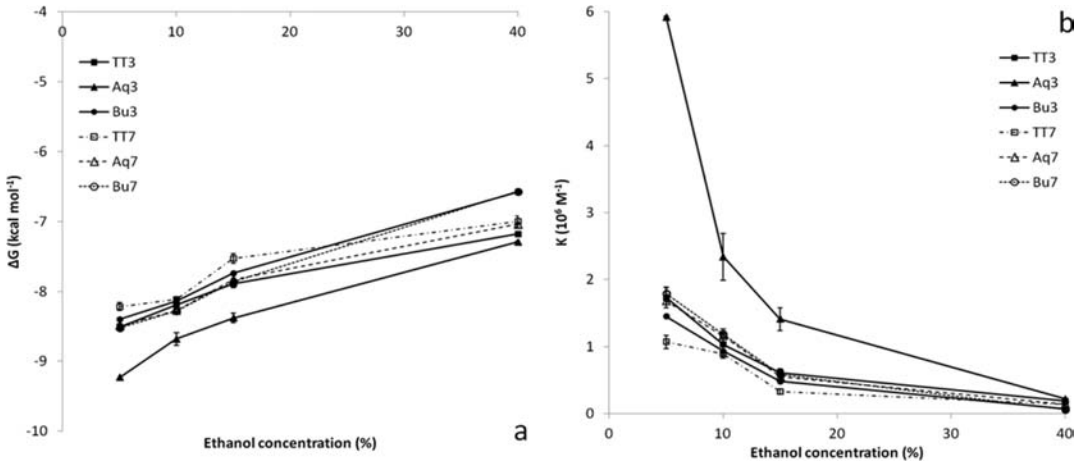

Figure 4. Overall binding strength of wine tannin samples and PLP across the range of ethanol concentrations as measured using (a) changes in Gibbs free energy (ΔG) and (b) binding association constants (K).

13%, respectively.[26] Gradual oxidation and structural rearrangement of tannin subunits over time have been shown to cause this reduction in acid-labile bonds.[30,47,49]

The strength of the interactions between wine tannins and the peptide, PLP (**5**), was measured across a range of ethanol concentrations, from 5 to 40% v/v, using ITC. Comparisons of the strength of tannin−peptide interactions for the different tannin samples were made at 10% ethanol (Table 2). The mechanisms of binding were assessed by comparing the change in enthalpy (ΔH), where a favorable change is indicated by a negative ΔH value and has been associated with hydrogen bonding, and the change in entropy ($T\Delta S$), where a favorable change is indicated by a positive $T\Delta S$ value and has been associated with hydrophobic interactions. Overall binding strength was assessed as a change in Gibbs free energy (ΔG), which is the sum of the changes in enthalpy and in entropy. The negative value of the change in Gibbs free energy indicates a spontaneous process. The binding constants (K) and stoichiometry (N) for each tannin sample were calculated on the basis of a single-site binding model. Greater K values indicated stronger PLP−tannin interactions, and greater N values indicated that more tannin molecules bound to each PLP molecule. For all tannin samples, binding with PLP was spontaneous and exothermic. At 10% ethanol, the changes in enthalpy and in entropy were favorable (Table 2), suggesting that PLP−wine tannin interactions involved both hydrophobic interactions and hydrogen bonding as previously reported.[28,29]

Hydrogen bonding contribution (ΔH) was greater in the young wine tannins when compared with the same type of tannin from the aged wine at 10% ethanol (Table 2), which is consistent with previous studies.[29] The contribution of hydrophobic interactions was greater in the Bu tannins and in the aged wine tannins compared with young wine tannins, as suggested by the greater $T\Delta S$ values. The combination of changes in enthalpy and entropy influenced the overall strength, ΔG, of the tannins. For the younger wine tannins, ΔG was greater for Aq3 and similar for TT3 and Bu3, whereas the ΔG values for the tannins from aged wines were similar for Aq7 and Bu7 and less for TT7. The binding association constant (K) for Aq3 tannin−peptide interactions at 10% ethanol was around double that of the other tannins. This may reflect a three-dimensional conformation of this tannin in this solution that was more favorable for peptide binding. Tannins that have more extended structures have been shown to interact more readily with proteins,[23,34] and Aq3 may have a more extended structure with more available binding sites. The molecular weight of the Aq tannin from the younger wine is slightly lower than that of the Aq tannin from the aged wine; however, changes in the tannin structure that are known to occur with wine aging result in tannins that have potentially more rigid structures with fewer acid-labile bonds.[6,30] Hence, Aq3 is likely to have a greater proportion of available binding sites than Aq7 despite a smaller molecular weight. The stoichiometry (N) of the interaction refers to the number of tannin molecules that bind to each PLP molecule. The number of tannins that can bind with each PLP molecule depends on the number of available binding sites, which relates to the molecular weight of the tannin as well as the structure. The calculated N was inversely proportional to the molecular weight of the tannin sample, indicating that the PLP molecules were

DOI: 10.1021/acs.jafc.5b00758
J. Agric. Food Chem. 2015, 63, 4345−4352

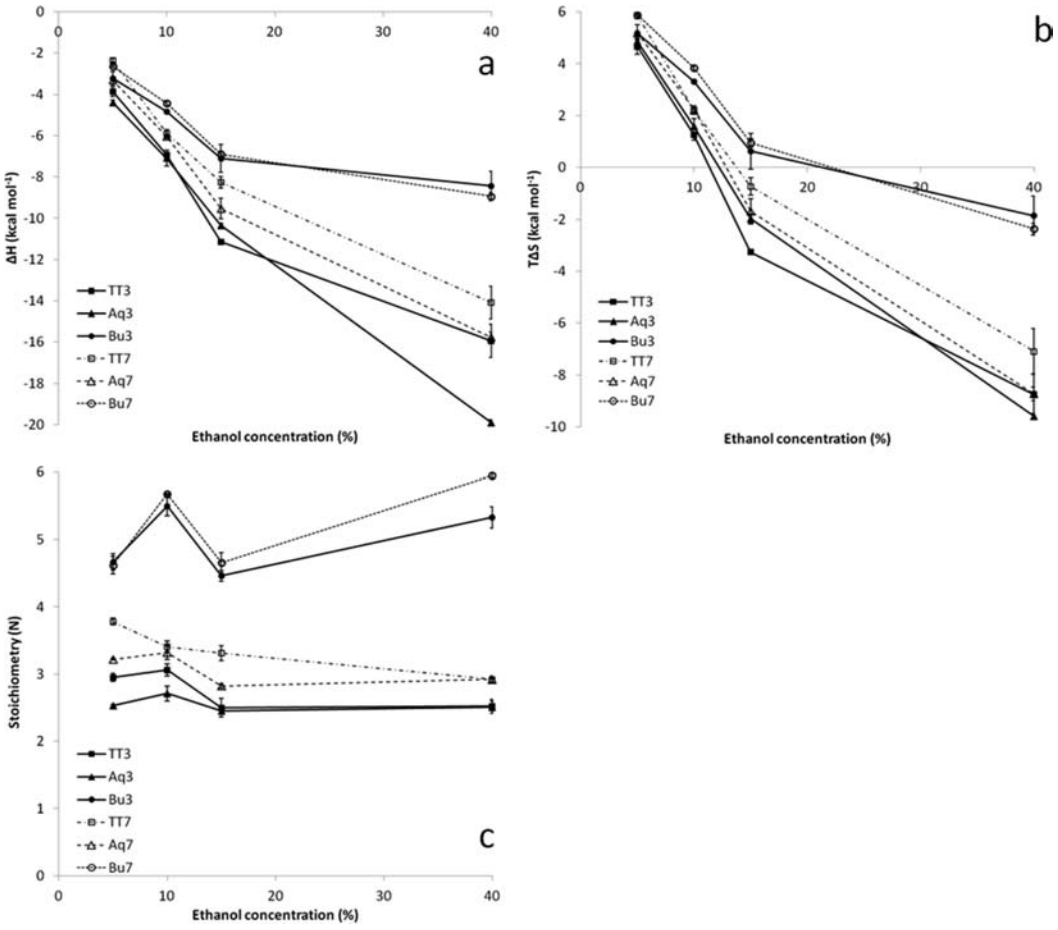

Figure 5. Impact of ethanol concentration on the interaction between wine tannin samples and PLP as measured with (a) change in enthalpy (ΔH), (b) change in entropy ($T\Delta S$), and the (c) the stoichiometry (N) of interaction (number of tannin molecules binding per PLP molecule).

able to bind more smaller tannins and fewer larger tannins (Tables 1 and 2). More aged wine tannins also bound to each PLP molecule compared with the younger wine counterparts, suggesting that these tannins have fewer available binding sites.[29] The structural changes of the tannins in wine over time form a more rigid structure as indicated by a reduction in the number of acid-labile interflavan bonds. Many more Bu tannins were able to bind to each PLP compared with either Aq or TT tannins, further suggesting that these tannins contained fewer available sites for peptide binding. The Aq tannin from the younger wine (Aq3) demonstrated the strongest peptide interactions of the measured tannins in 10% ethanol, and this is likely to relate to its 3D structure.[46]

Tannin−Peptide Interactions at Different Ethanol Concentrations. Tannin astringency reportedly decreases as ethanol concentration in model wines increases from 10 to 15%,[43] and the reason for this may relate to changes in the mechanisms of tannin−salivary protein interactions. In this study, ITC measurements were used to assess the strength of the interactions between wine tannins and PLP across a range of ethanol concentrations, from 5 to 40% v/v, as well as any differences in the changes in enthalpy and in entropy that may suggest differences in binding mechanisms. The binding strengths between the wine tannins and PLP as measured with changes in Gibbs free energy (ΔG) and binding constants (K) indicated that the wine tannin−PLP interactions were weaker at the greater ethanol concentrations (Figure 4). Ethanol has been shown to disrupt tannin−apple cell wall binding at higher concentrations such as 40% ethanol,[22] and the weak interaction between tannin and PLP at this higher ethanol concentration is also demonstrated here. The weaker tannin−peptide interactions at 15% ethanol compared with 10% ethanol may, at least in part, contribute to the previously observed reduction in wine astringency across this ethanol concentration range.[43,44]

The mechanism of binding of the tannin samples with PLP also changed over the wine-like ethanol range, and differences were observed in tannins with different solubilities. For the TT and Aq tannins, the change in entropy ($T\Delta S$) was favorable (positive) at 10% ethanol and unfavorable (negative) at 15% ethanol, whereas the Bu tannins also demonstrated slightly favorable entropy at 15% ethanol. The change in enthalpy (ΔH) was favorable for all tannin samples. A favorable ΔH value is associated with binding due to hydrogen bonding, whereas a favorable $T\Delta S$ value has been associated with hydrophobic interactions and the increased disorder due to the displacement of bulk water.[28] The favorable $T\Delta S$ at 10% ethanol and unfavorable $T\Delta S$ at 15% ethanol suggested that there were differences in the mechanism of tannin−peptide interactions across the wine-like ethanol range. Below 15% ethanol, there is evidence of hydrophobic interactions between tannins and PLP, and for solutions with ethanol concentrations ≥15%, peptide association appears to be driven only by hydrogen bonding. The combination of favorable ΔH (negative) and unfavorable $T\Delta S$ (negative) contributed to

DOI: 10.1021/acs.jafc.5b00758
J. Agric. Food Chem. 2015, 63, 4345−4352

the weaker overall binding (ΔG) in solutions containing 40% ethanol (Figure 4).

The different tannin samples varied in the strengths and mechanisms of peptide binding. The $T\Delta S$ was favorable for the Bu tannins at 15% ethanol, suggesting that the structure of these tannins promoted more hydrophobic interactions than the Aq and TT tannins, which showed unfavorable $T\Delta S$ at the same ethanol concentration. The differences between the changes in enthalpy and in entropy for the different tannin fractions were more pronounced at 40% ethanol compared with 5% ethanol, and this may relate to differences in tannin structure. Smaller tannins, such as Bu tannins, have fewer binding sites for peptide interactions than larger tannins such as TT and Aq, and therefore these interactions are more readily disrupted by higher ethanol concentrations. The number of TT and Aq tannin molecules that interacted with each PLP molecule (N) decreased slightly across the ethanol concentrations (Figure 5), whereas the number of Bu tannins that interacted with PLP ranged from around 4.6 to 5.6, independent of the ethanol concentration. This also may relate to the structure of these tannins and the limited number of available binding sites.

Different papers on the primary mechanism for tannin−protein interactions have indicated either hydrophobically driven interactions or hydrogen bond driven interactions,[15,23,40] and the reason for this discrepancy is likely to relate to the solvent system used as well as the particular tannin structure used in the analysis. Similarly, studies on the impacts of ethanol on sensory analysis have varied from ethanol increasing astringency to decreasing astringency,[43,50] and this again may relate to the structure and relative hydrophobicity of the tannins and the solvents used for analysis. More hydrophilic tannins such as grape skin tannins at higher ethanol concentrations are likely to interact with proteins primarily through hydrogen bonding, whereas more hydrophobic grape seed tannins may be driven by a combination of hydrophobic and hydrophilic interactions.[22,28] Similarly, the astringency of tannins in model wines will depend on the structure and physicochemical properties of the tannins in the study, particularly given the differences in binding strength and mechanisms of interaction for wine tannins over the wine-like ethanol concentration range. This demonstrates the need for reporting the hydrophobicity of the tannins used in structure−function experiments.

Impact of Wine Age on Tannin−Peptide Interactions. Red wine astringency reportedly decreases with wine age,[51] and this may relate to changes in the properties of the tannins, which subsequently affect the tannin binding capacity.[29,47] The tannin samples selected for this trial were isolated from red wines of 3 and 7 years of age, to compare the binding strength of wine tannin after different periods of aging. For Aq and TT tannins, those from the younger wine demonstrated slightly stronger binding (ΔG) across the different ethanol concentrations, even though the molecular weights were similar or smaller than those of the tannins from the aged wine (Table 1; Figure 4). The is in agreement with previous results.[29] During wine aging, wine tannin structures change due to gradual oxidation and structural rearrangement reactions, which can reduce the number of hydroxyl groups available for hydrogen bonding and potentially increase the proportion of hydrophobic binding sites[30,31] Differences in the ΔH and $T\Delta S$ for younger and aged wine tannins suggested differences in the mechanisms of interactions. Peptide interactions with aged wine tannins produced more favorable changes in entropy and smaller changes in enthalpy than with the younger wine tannins (Table 2), suggesting that the structures of these tannins promoted more hydrophobic interactions. The stoichiometry (N) indicated that more aged wine tannin molecules bind to PLP than the same fraction of young wine tannin molecules, suggesting that aged wine tannins may be more compact and have fewer binding sites for peptide interaction than younger wine tannins. The weaker binding of more aged wine tannins may, in part, contribute to the decrease in wine astringency with aging because protein interactions are associated with astringency.[14,52]

In summary, the strength of wine tannin−PLP binding was shown to decrease with increasing ethanol concentration, and the mechanisms of interaction changed between 10 and 15% ethanol. For the larger tannins, peptide interactions consisted of favorable changes in both entropy and enthalpy at 10% ethanol, but at 15% ethanol, interactions involved favorable changes in enthalpy and unfavorable changes in entropy. Peptide interactions with smaller tannins showed slightly favorable changes in entropy at 15% ethanol. This suggests that at lower ethanol concentrations, peptide interactions with wine tannin involve a combination of hydrophobic interactions and hydrogen bonding, whereas only hydrogen bonding occurred in the higher ethanol concentration. Tannins from aged wines also demonstrated more hydrophobic interactions than those from younger wines. These results indicate that the solvent composition and wine tannin structure can influence the mechanisms for tannin−protein interaction, which, in turn, may influence wine astringency. This may contribute to some of the differences observed in wine styles with different astringency qualities. Additionally, this work demonstrates the need for reporting the relative physical chemistry characteristics such as the hydrophobicity of the tannins used in structure−function experiments.

■ ASSOCIATED CONTENT

Supporting Information

Tables S1−S3: thermodynamics parameters for interactions between different wine tannins with PLP at 5, 15, and 40% ethanol. This material is available free of charge via the Internet at http://pubs.acs.org.

■ AUTHOR INFORMATION

Corresponding Author

*(J.M.M.) Phone: +61 8 8313 6600. Fax: +61 8 8313 6601.

Author Contributions

‖J.M.M. and Z.M.Z. contributed equally to this paper.

Funding

J.M.M., S.K., and P.A.S. from The Australian Wine Research Institute, a member of the Wine Innovation Cluster at the Waite Precinct in Adelaide, acknowledge the support of Australian grape growers and winemakers through their investment body, the Australian Grape and Wine Authority, with matching funds from the Australian government.

Notes

The authors declare no competing financial interest.

■ REFERENCES

(1) Haslam, E. Natural polyphenols (vegetable tannins) as drugs: possible modes of action. *J. Nat. Prod.* **1996**, *59*, 205−215.

DOI: 10.1021/acs.jafc.5b00758
J. Agric. Food Chem. 2015, 63, 4345−4352

(2) Vivas, N.; Glories, Y. Role of oak wood ellagitannins in the oxidation process of red wines during aging. *Am. J. Enol Vitic.* **1996**, *47*, 103−107.
(3) Vivas, N.; Nonier, M. F.; Gaulejac, N. V. d. Structural characterization and analytical differentiation of grape seeds, skins, stems and Quebracho tannins. *Bull. OIV* **2004**, *77*, 643−659.
(4) Herderich, M. J.; Smith, P. A. Analysis of grape and wine tannins: methods, applications and challenges. *Aust. J. Grape Wine Res.* **2005**, *11*, 1−10.
(5) Monagas, M.; Bartolome, B.; Gomez-Cordoves, C. Updated knowledge about the presence of phenolic compounds in wine. *Crit. Rev. Food Sci. Nutr.* **2005**, *45*, 85−118.
(6) Cheynier, V.; Duenas-Paton, M.; Salas, E.; Maury, C.; Souquet, J. M.; Sarni-Manchado, P.; Fulcrand, H. Structure and properties of wine pigments and tannins. *Am. J. Enol. Vitic.* **2006**, *57*, 298−305.
(7) Mercurio, M. D.; Dambergs, R. G.; Cozzolino, D.; Herderich, M. J.; Smith, P. A. Relationship between red wine grades and phenolics. 1. Tannin and total phenolics concentrations. *J. Agric. Food Chem.* **2010**, *58*, 12313−12319.
(8) Smith, P.; Mercurio, M.; Dambergs, R.; Francis, L.; Herderich, M. Red grape and wine quality − the roles and relevance of tannin. *Aust. N. Z. Wine Ind. J.* **2007**, 47−52.
(9) Vidal, S.; Courcoux, P.; Francis, L.; Kwiatkowski, M.; Gawel, R.; Williams, P.; Waters, E.; Cheynier, V. Use of an experimental design approach for evaluation of key wine components on mouth-feel perception. *Food Qual. Prefer.* **2004**, *15*, 209−217.
(10) Bajec, M. R.; Pickering, G. Astringency: mechanisms and perception. *Crit. Rev. Food Sci. Nutr.* **2008**, *48*, 858−875.
(11) Pascal, C.; Poncet-Legrand, C.; Cabane, B.; Vernhet, A. Aggregation of a proline-rich protein induced by epigallocatechin gallate and condensed tannins: effect of protein glycosylation. *J. Agric. Food Chem.* **2008**, *56*, 6724−6732.
(12) Tarascou, I.; Barathieu, K.; Simon, C.; Ducasse, M. A.; Andre, Y.; Fouquet, E.; Dufourc, E. J.; de Freitas, V.; Laguerre, M.; Pianet, I. A 3D structural and conformational study of procyanidin dimers in water and hydro-alcoholic media as viewed by NMR and molecular modeling. *Magn. Reson. Chem.* **2006**, *44*, 868−880.
(13) Payne, C.; Bowyer, P. K.; Herderich, M.; Bastian, S. E. P. Interaction of astringent grape seed procyanidins with oral epithelial cells. *Food Chem.* **2009**, *115*, 551−557.
(14) Jöbstl, E.; O'Connell, J.; Fairclough, J. P. A.; Williamson, M. P. Molecular model for astringency produced by polyphenol/protein interactions. *Biomacromolecules* **2004**, *5*, 942−949.
(15) Baxter, N. J.; Lilley, T. H.; Haslam, E.; Williamson, M. P. Multiple interactions between polyphenols and a salivary proline-rich protein repeat result in complexation and precipitation. *Biochemistry* **1997**, *36*, 5566−5577.
(16) Zanchi, D.; Poulain, C.; Konarev, P.; Tribet, C.; Svergun, D. I. Colloidal stability of tannins: astringency, wine tasting and beyond. *J. Phys.: Condens. Matter* **2008**, *20*, 494224.
(17) Dinnella, C.; Recchia, A.; Fia, G.; Bertuccioli, M.; Monteleone, E. Saliva characteristics and individual sensitivity to phenolic astringent stimuli. *Chem. Senses* **2009**, *34*, 295−304.
(18) Charlton, A.; Baxter, N.; Khan, M.; Moir, A.; Haslam, E.; Davies, A.; Williamson, M. Polyphenol/peptide binding and precipitation. *J. Agric. Food Chem.* **2002**, *50*, 1593−1601.
(19) Le Bourvellec, C.; Renard, C. M. G. C. Interactions between polyphenols and macromolecules: quantification methods and mechanisms. *Crit. Rev. Food Sci. Nutr.* **2012**, *52*, 213−248.
(20) Simon, C.; Barathieu, K.; Laguerre, M.; Schmitter, J.-M.; Fouquet, E.; Pianet, I.; Dufourc, E. J. Three-dimensional structure and dynamics of wine tannin-saliva protein complexes. A multitechnique approach. *Biochemistry* **2003**, *42*, 10385−10395.
(21) Bindon, K.; Smith, P.; Kennedy, J. A. Interaction between grape-derived proanthocyanidins and cell wall material. 1. Effect on proanthocyanidin composition and molecular mass. *J. Agric. Food Chem.* **2010**, *58*, 2520−2528.
(22) Le Bourvellec, C.; Guyot, S.; Renard, C. M. G. C. Non-covalent interaction between procyanidins and apple cell wall material: Part I. Effect of some environmental parameters. *Biochim. Biophys. Acta, Gen. Subj.* **2004**, *1672*, 192−202.
(23) Cala, O.; Pinaud, N.; Simon, C.; Fouquet, E.; Laguerre, M.; dufourc, E. J.; Pianet, I. NMR and molecular modeling of wine tannins binding to saliva proteins: revisiting astringency from molecular and colloidal prospects. *FASEB J.* **2010**, *24*, 4281−4290.
(24) Hagerman, A. E.; Rice, M. E.; Ritchard, N. T. Mechanisms of protein precipitation for two tannins, pentagalloyl glucose and epicatechin16 (4f8) catechin (procyanidin). *J. Agric. Food Chem.* **1998**, *46*, 2590−2595.
(25) Cheynier, V.; Prieur, C.; Guyot, S.; Rigaud, J.; Moutounet, M. The structures of tannins in grapes and wines and their interactions with proteins. In *Wine − Nutritional and Therapeutic Benefits*; Watkins, T. R., Ed.; American Chemical Society: Washington, DC, USA, 1997; pp 81−93.
(26) McRae, J. M.; Schulkin, A.; Kassara, S.; Holt, H.; Smith, P. A. Sensory properties of wine tannin fractions: Implications for in-mouth sensory properties. *J. Agric. Food Chem.* **2013**, *61*, 719−727.
(27) Vidal, S.; Francis, L.; Guyot, S.; Marnet, N.; Kwiatkowski, M.; Gawel, R.; Cheynier, V.; Waters, E. J. The mouth-feel properties of grape and apple proanthocyanidins in a wine-like medium. *J. Sci. Food Agric.* **2003**, *83*, 564−573.
(28) Poncet-Legrand, C.; Gautier, C.; Cheynier, V.; Imberty, A. Interactions between flavan-3-ols and poly(L-proline) studied by isothermal titration calorimetry: effect of the tannin structure. *J. Agric. Food Chem.* **2007**, *55*, 9235−9240.
(29) McRae, J. M.; Falconer, R. J.; Kennedy, J. A. Thermodynamics of grape and wine tannin interaction with polyproline: implications for red wine astringency. *J. Agric. Food Chem.* **2010**, *58*, 12510−12518.
(30) Poncet-Legrand, C.; Cabane, B.; Bautista-Ortín, A.; Carrillo, S.; Fulcrand, H.; Pérez, J.; Vernhet, A. Tannin oxidation: intra- versus intermolecular reactions. *Biomacromolecules* **2010**, *11*, 2376−2386.
(31) Vernhet, A.; Dubascoux, S.; Cabane, B.; Fulcrand, H.; Dubreucq, E.; Poncet-LeGrand, C. Characterization of oxidized tannins: comparison of depolymerization methods, assymetric flow field-flow fractionation and small-angle X-ray scattering. *Anal. Bioanal. Chem.* **2011**, *401*, 1559−1569.
(32) Boze, H.; Marlin, T.; Durand, D.; Pérez, J.; Vernhet, A.; Canon, F.; Sarni-Manchado, P.; Cheynier, V.; Cabane, B. Proline-rich salivary proteins have extended conformations. *Biophys. J.* **2010**, *99*, 656−665.
(33) Charlton, A. J.; Baxter, N. J.; Lilley, T. H.; Haslam, E.; McDonald, C. J.; Williamson, M. P. Tannin interactions with a full-length human salivary proline-rich protein display a stronger affinity than with single proline-rich repeats. *FEBS Lett.* **1996**, *382*, 289−292.
(34) Frazier, R. A.; Papadopoulou, A.; Mueller-Harvey, I.; Kissoon, D.; Green, R. J. Probing protein-tannin interactions by isothermal titration microcalorimetry. *J. Agric. Food Chem.* **2003**, *51*, 5189−5195.
(35) Deaville, E. R.; Green, R. J.; Mueller-Harvey, I.; Willoughby, I.; Frazier, R. A. Hydrolyzable tannin structures influence relative globular and random coil protein binding strengths. *J. Agric. Food Chem.* **2007**, *55*, 4554−4561.
(36) Frazier, R. A.; Deaville, E. R.; Green, R. J.; Stringanod, E.; Willoughbyd, I.; Plante, J.; Mueller-Harvey, I. Interactions of tea tannins and condensed tannins with proteins. *J. Pharm. Biomed. Anal.* **2010**, *51*, 490−495.
(37) Lu, Y.; Bennick, A. Interaction of tannin with human salivary proline-rich proteins. *Arch. Oral Biol.* **1998**, *43*, 717−728.
(38) Luck, G.; Liao, H.; Murray, N. J.; Grimmer, H. R.; Warminski, E. E.; Williamson, M. P.; Lilley, T. H.; Haslam, E. Polyphenols, astringency and proline-rich proteins. *Phytochemistry* **1994**, *37*, 357−371.
(39) Pascal, C.; Paté, F.; Cheynier, V.; Delsuc, M. Study of the interactions between a proline-rich protein and a flavan-3-ol by NMR: residual structures in the natively unfolded protein provides anchorage points for the ligands. *Biopolymers* **2009**, *91*, 745−756.
(40) Richard, T.; Lefeuvre, D.; Descendit, A.; Quideau, S.; Monti, J. P. Recognition characters in peptide-polyphenol complex formation. *Biochim. Biophys. Acta, Gen. Subj.* **2006**, *1760*, 951−958.

DOI: 10.1021/acs.jafc.5b00758
J. Agric. Food Chem. 2015, 63, 4345−4352

(41) Oh, H. I.; Hoff, J. E.; Armstrong, G. S.; Haff, L. A. Hydrophobic interaction in tannin-protein complexes. *J. Agric. Food Chem.* **1980**, *28*, 394−398.
(42) Kallithraka, S.; Bakker, J.; Clifford, M. N. Effect of pH on astringency in model solutions and wines. *J. Agric. Food Chem.* **1997**, *45*, 2211−2216.
(43) Fontoin, H.; Saucier, C.; Teissedre, P.-L.; Glories, Y. Effect of pH, ethanol and acidity on astringency and bitterness of grape seed tannin oligomers in model wine solution. *Food Qual. Prefer.* **2008**, *19*, 286−291.
(44) Demiglio, P.; Pickering, G. J. The influence of ethanol and pH on the taste and mouthfeel sensations elicited by red wine. *J. Food, Agric. Environ.* **2008**, *6*, 143−150.
(45) Carrau, F.; Gaggero, C.; Aguilar, P. S. Yeast diversity and native vigor for flavor phenotypes. *Trends Biotechnol.* **2015**, *33*, 148−154.
(46) McRae, J. M.; Kirby, N. M.; Mertens, H. D. T.; Kassara, S.; Smith, P. A. Measuring the molecular dimensions of wine tannins: comparison of small-angle X-ray scattering, gel-permeation chromatography and mean degree of polymerization. *J. Agric. Food Chem.* **2014**, *62*, 7216−7224.
(47) McRae, J. M.; Kassara, S.; Kennedy, J. A.; Waters, E. J.; Smith, P. A. Effect of wine pH and bottle closure on tannins. *J. Agric. Food Chem.* **2013**, *61*, 11618−11627.
(48) McManus, J. P.; Davis, K. G.; Beart, J. E.; Gaffney, S. H.; Lilley, T. H.; Haslam, E. Polyphenol interactions. Part 1. Introduction; some observations on the reversible complexation of polyphenols with proteins and polysaccharides. *J. Chem. Soc., Perkin Trans. 2* **1985**, 1429−1438.
(49) Vidal, S.; Cartalade, D.; Souquet, J.-M.; Fulcrand, H.; Cheynier, V. Changes in proanthocyanidin chain length in winelike model solutions. *J. Agric. Food Chem.* **2002**, *50*, 2261−2266.
(50) Obreque-Slíer, E.; Peña-Neira, A.; López-Solís, R. Enhancement of both salivary protein-enological tannin interactions and astringency perception by ethanol. *J. Agric. Food Chem.* **2010**, *58*, 3729−3735.
(51) Chira, K.; Pacella, N.; Jourdes, M.; Teissedre, P.-L. Chemical and sensory evaluation of Bordeaux wines (Cabernet-Sauvignon and Merlot) and correlation with wine age. *Food Chem.* **2011**, *126*, 1971−1977.
(52) Hofmann, T.; Glabasnia, A.; Schwarz, B.; Wisman, K. N.; Gangwer, K. A.; Hagerman, A. E. Protein binding and astringent taste of a polymeric procyanidin, 1,2,3,4,6-penta-*O*-galloyl-β-D-glucopyranose, castalagin, and grandinin. *J. Agric. Food Chem.* **2006**, *54*, 9503−9509.

DOI: 10.1021/acs.jafc.5b00758
J. Agric. Food Chem. 2015, 63, 4345−4352

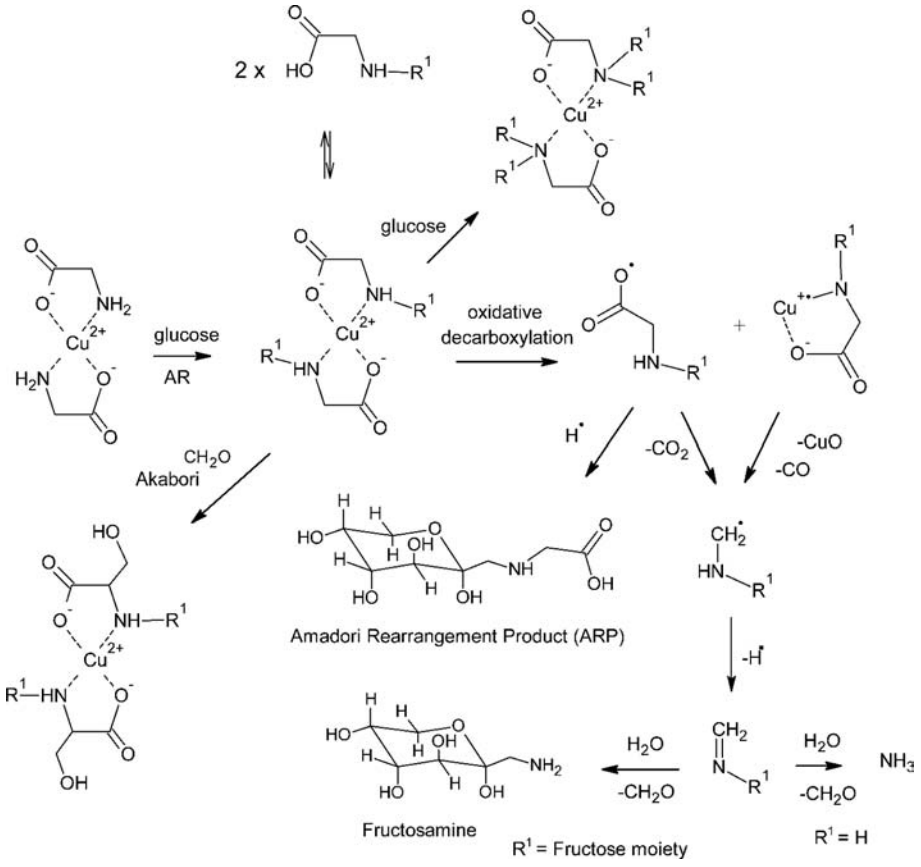

Figure 1. Mechanism of oxidative decarboxylation of free or sugar-conjugated amino acid copper complexes based on ref 8. ARP, Amadori rearrangement product; AR, Amadori rearrangement; and R^1, H or sugar moiety.

flight/mass spectrometry (ESI/qTOF/MS) analysis at m/z 233.9665 $[M + Na]^+$ (calculated for $C_4H_8CuN_2NaO_4$ with an error of 5.4 ppm). Isotope-labeled precursors were prepared similarly.

Sample Preparation. Model systems (10 mg) consisting of glycine/glucose (in a 2:1 relative molar ratio), glycine/glucose/$CuCl_2$ (in a 2:1:1 relative molar ratio), and $(Gly)_2Cu$/glucose (in a 1:1 relative molar ratio) with or without excess paraformaldehyde (20 mg) were dissolved in water (2 mL) and heated on a sand bath in an open vial (5 mL capacity) at 110 °C for 2 h until dry. During the reaction, the water evaporated and the sample was completely dried during the last 20 min of heating. To confirm the formation of some of the observed intermediates, commercial standards, such as glycine Amadori compound and 1-amino-1-deoxy-β-D-glucose, were used in appropriate model systems, as shown in Table 1. The reaction mixtures were subsequently analyzed by ESI/qTOF/MS, and some were analyzed by pyrolysis–gas chromatography/mass spectrometry (Py–GC/MS) for their volatile content. All of the samples were analyzed in duplicates.

Ninhydrin Test. Amino acid loss (glycine) was determined using the "ninhydrin reagent solution" test method by Sigma-Aldrich, Inc., using ninhydrin reagent (2% in DMSO and lithium acetate buffer). Model systems comprising glycine/glucose and $(Gly)_2Cu$/glucose, both containing 0.05 μmol/mL (50 μM) glycine in the final concentration, were dissolved in water (2 mL) and heated at 110 °C for 2 h in a sand bath until completely dry. After heating, the residues were dissolved in water (0.5 L) and 1 mL aliquots were pipetted into test tubes. To each aliquot, ninhydrin (1 mL) reagent was added, and the test tubes were placed in a sand bath at 100 °C for 10 min. After cooling to room temperature, 95% ethanol (5 mL) was added to each test tube. The absorbance was measured at 570 nm using distilled water as a blank on an Evolution 300 ultraviolet–visible (UV–vis) spectrophotometer (Thermo Fisher Scientific, Waltham, MA).

Table 1. Composition of the Model Systems

Model Systems Prepared under Akabori Reaction Conditions
glycine/glucose/paraformaldehyde[a,b] (2:1)
$(Gly)_2Cu$/glucose/paraformaldehyde[b]
Model Systems Prepared under Maillard Reaction Conditions
glycine/glucose[a,c] (2:1)
glycine/glucose/$CuCl_2$[a] (2:1:1)
$(Gly)_2Cu$/glucose[c]
N-(1-deoxy-D-fructos-1-yl)glycine[d] (glycine Amadori compound)
N-(1-deoxy-D-fructos-1-yl)glycine/$CuCl_2$
1-amino-1-deoxy-β-D-glucose[d]
glucose/1-amino-1-deoxy-β-D-glucose
glucose/1-amino-1-deoxy-β-D-glucose/$CuCl_2$

[a]Model systems that were prepared and analyzed in a 2:1 molar ratio. All other model systems in the table were prepared and analyzed in a 1:1 molar ratio. [b]Paraformaldehyde was added in excess in the Akabori reaction model systems. [c]Analyzed by Py–GC/MS in addition to ESI/qTOF/MS analysis. [d]Analyzed before and after heating at 110 °C for 2 h.

Spectrophotometric Measurements. Absorbance at 420 and 550 nm was used to estimate browning of the model systems heated on a sand bath in an open vial at 110 °C for 2 h until dry. Samples (10 mg) comprising glycine/glucose (in a 2:1 relative molar ratio), glycine/glucose/$CuCl_2$ (in a 2:1:1 relative molar ratio), and $(Gly)_2Cu$/glucose (in a 1:1 relative molar ratio) were dissolved in water (2 mL), and their absorbance was measured before and after heating, as indicated above. In both cases, the samples were diluted in distilled water (0.5 L) and 1 mL of each solution was used for the measurements. Absorbance of the samples were measured on an

DOI: 10.1021/acs.jafc.5b00932
J. Agric. Food Chem. 2015, 63, 4353–4360

Table 2. Elemental Composition[a] and Isotope Incorporation in the Products Originating from the $(Gly)_2Cu$/Glc Model System in the Absence and Presence of Paraformaldehyde (Akabori Reaction Conditions) and Shown in Figure 2

$[M + H]^+$ (m/z)[b]	elemental composition	[^{13}C−U$_6$]Glc	[^{13}C-1]Gly	[^{13}C-2]Gly	[^{15}N]Gly
180.0872	$C_6H_{14}NO_5$	6	0	0	1
192.0856	$C_7H_{14}NO_5$	6	0	1	1
202.0709	$C_8H_{12}NO_5$	6	1	1	1
220.0816	$C_8H_{14}NO_6$	6	1	1	1
238.0930	$C_8H_{16}NO_7$	6	1	1	1
268.1038[c]	$C_9H_{18}NO_8$	6	na[d]	na	na
299.0038/301.0028	$C_8H_{14}CuNO_7$	6	1	1	1
300.0079/302.0059	$C_8H_{15}CuNO_7$	6	1	1	1
324.1268	$C_{12}H_{22}NO_9$	12	0	0	1
329.0173/331.0163[c]	$C_9H_{16}CuNO_8$	6	na	na	na
330.0228/332.0281[c]	$C_9H_{17}CuNO_8$	6	na	na	na
342.1405	$C_{12}H_{24}NO_{10}$	12	0	0	1
374.0355/376.0313	$C_{10}H_{19}CuN_2O_9$	6	2	2	2
404.0508/406.0511[c]	$C_{11}H_{21}CuN_2O_{10}$	6	na	na	na
434.0611/436.0599[c]	$C_{12}H_{23}CuN_2O_{11}$	6	na	na	na
536.0925/538.0912	$C_{16}H_{29}CuN_2O_{14}$	12	2	2	2
566.1019/568.1027[c]	$C_{17}H_{31}CuN_2O_{15}$	12	na	na	na

[a]All of the ions listed in Figure 2 are included in this table. [b]The calculated error [in parts per million (ppm)] in all of the reported ions ranged between 0.02 and 22 ppm, and the two masses shown represent copper isotopes ^{63}Cu/^{65}Cu. [c]Products formed only in the model system containing CH_2O. [d]na = not analyzed.

Evolution 300 UV−vis spectrophotometer (Thermo Fisher Scientific, Waltham, MA) using distilled water as a blank.

ESI/qTOF/MS Analysis. The dry reaction mixtures were dissolved in liquid chromatography (LC)-grade water to a concentration of 1 mL/mg. The samples were then diluted 10-fold in 10% methanol prior to analysis by ESI/qTOF/MS. The ESI/qTOF/MS system was comprised of a Bruker Maxis Impact quadrupole-time-of-flight mass spectrometer (Bruker Daltonics, Bremen, Germany) operated in positive-ion mode. Samples (1 μL) were injected directly into ESI/qTOF/MS. Instrument calibration was performed using sodium formate clusters. The electrospray interface settings were the following: nebulizer pressure, 0.6 bar; drying gas, 4 L/min; temperature, 180 °C; and capillary voltage, 4500 V. The scan range was from m/z 100 to 1000. The data were analyzed using Bruker Compass DataAnalysis software, version 4.1. Tandem mass spectrometry (MS/MS) was carried out in multiple reaction monitoring (MRM) mode using 20.0 eV collision energy for the ions at m/z 180 and 342.

Thermal Desorption by Py−GC/MS. A Varian CP-3800 gas chromatograph coupled to a Saturn 2000 ion-trap detector interfaced to a CDS Pyroprobe 2000 unit through a valved interface (CDS 1500) was used for the desorption of the volatiles from glycine/glucose and $(Gly)_2Cu$/glucose model systems before and after heating in water (2 mL) at 110 °C for 2 h. For each analysis, approximately 0.5 mg of sample was weighed into a quartz tube, sealed with glass wool, inserted into the pyroprobe, and pyrolyzed for 20 s at 250 °C. The separation was performed using a fused silica DB-5MS column (50 m length × 0.2 mm inner diameter × 33 μm film thickness). The GC method used for the analysis of the volatiles was as follows: GC column flow rate was regulated by an electronic flow controller (EFC) and set at a pressure pulse of 55 psi for the first 3 min, then decreased to 32 psi at the rate of 300 psi/min, and finally, increased to 70 psi at a rate of 1.23 psi/min for the rest of the run. The GC oven temperature was set at −5 °C for the first 5 min using CO_2 as the cryogenic cooling source and then increased to 50 °C at a rate of 50 °C/min. Then, the oven temperature was again increased to 270 °C at a rate of 8 °C/min and kept at 270 °C for 5 min. The samples were detected using an ion-trap mass spectrometer. The MS transfer-line temperature was set at 250 °C; the manifold temperature was set at 50 °C; and the ion-trap temperature was set at 175 °C. The ionization voltage of 70 eV was used, and the electron multiplier voltage (EMV) was set at 1600 V. The generated data were analyzed using the AMDIS 32, version 2.69, computer software, and peak identification will be performed using the National Institute of Standards and Technology (NIST), version 2.0, mass spectral research program.

Structural Identification. Evidence for the proposed structures of non-volatile reaction intermediates was provided through ESI/qTOF/MS analysis of their elemental composition and the use of commercial or synthetic intermediates and isotope-labeling studies. Furthermore, MS/MS spectra of selected product ions were compared to those of commercial standards. The incorporation of copper in the identified complexes was confirmed by the isotopic signature of copper through detection of M + 2 peaks at 30% relative intensity.

RESULTS AND DISCUSSION

The development of color and aromas during the Maillard reaction is highly dependent upon the nature of amino acids and sugars used and the stability of the resultant Amadori products, in addition to other environmental factors that can either promote or hinder the reactivity of Amadori compounds, such as the transition metal ions. Such ions in their free form can accelerate oxidative degradation of sugars and Amadori products and enhance browning. On the other hand, amino acids can serve as potent ligands for metal ions not only to form strong complexes but also to provide stable backbones that can act as molecular scaffolds upon which up to four sugar molecules can be conjugated as Schiff bases or Amadori rearrangement products (see Figure 1). The buildup of such relatively stable intermediates can serve as a vehicle for their slow and steady release over the course of the reaction that in theory can affect the overall reaction profile. There are three possible pathways that allow for the release of the amino acids or their conjugates from the complexes; dissociation of the complex and ligand exchange[10,15] are considered as non-destructive mechanisms of release, and the third is through oxidative decarboxylation,[8] where one of the amino acid moieties in the complex is decomposed and the other is released intact, as shown in Figure 1. Previous experiments with glycine copper complexes[10] have demonstrated the enhanced ability of the amino groups in the complexes to undergo Schiff base formation with small aldehydes and their subsequent

DOI: 10.1021/acs.jafc.5b00932
J. Agric. Food Chem. 2015, 63, 4353−4360

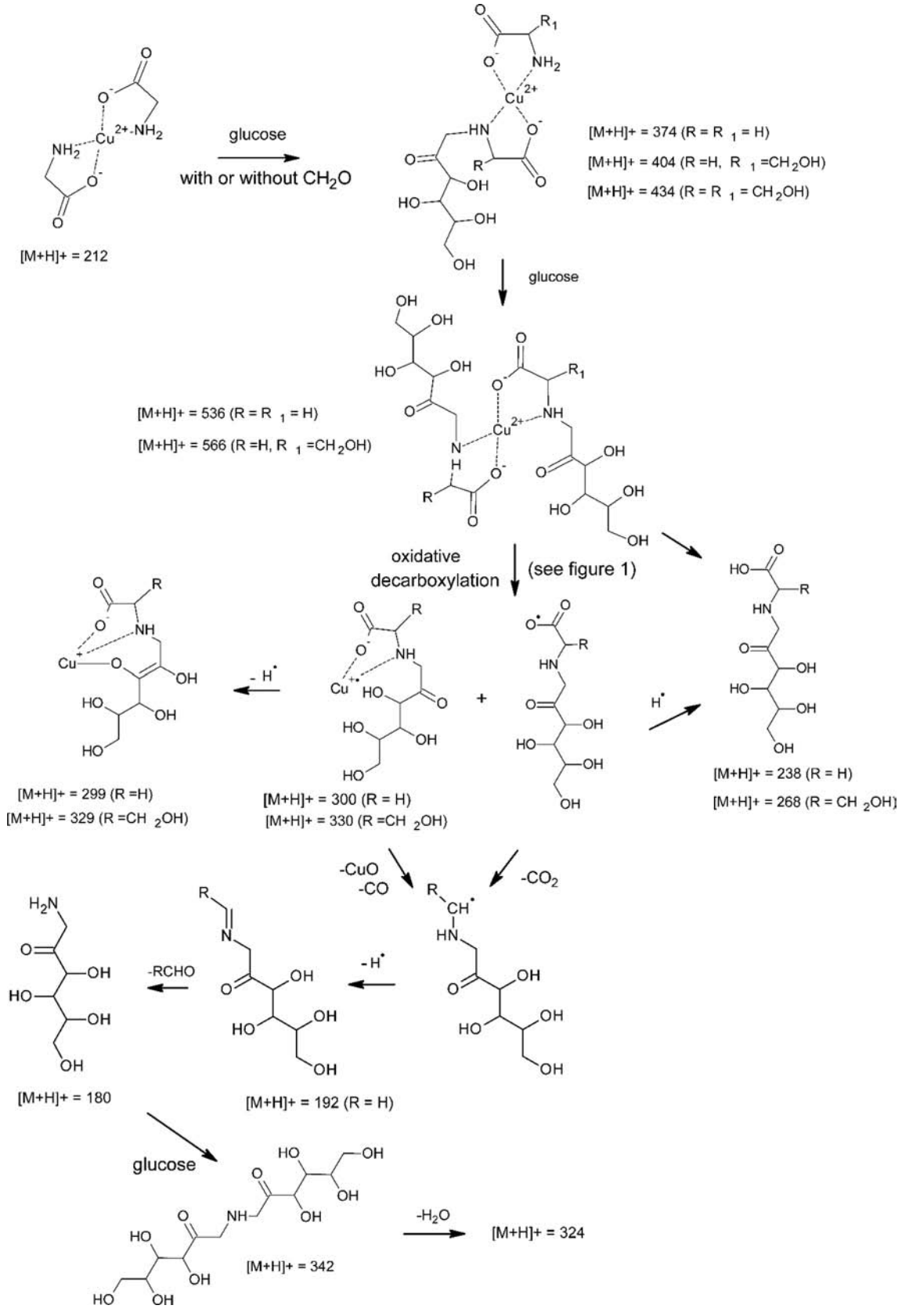

Figure 2. Proposed interaction of $(Gly)_2Cu$ with glucose in the presence or absence of formaldehyde.

Akabori reaction and/or oxidative decarboxylation[8] (see Figure 1). To take advantage of this enhanced reactivity of the amino groups of copper complexes of amino acids toward carbonyl compounds and to demonstrate the ability of glucose to conjugate with glycine copper complexes, model systems containing $(Gly)_2Cu$ and glucose were heated in aqueous

DOI: 10.1021/acs.jafc.5b00932
J. Agric. Food Chem. 2015, 63, 4353−4360

Table 3. MS/MS Fragmentation and the Elemental Composition of the Ions Observed at *m/z* 180 Generated in the Heated Model Systems

1-amino-1-deoxy-β-D-glucose[a] $[M + H]^+$ (*m/z*)	glucose/1-amino-1-deoxy-β-D-glucose $[M + H]^+$ (*m/z*)	glucose/1-amino-1-deoxy-β-D-glucose/$CuCl_2$ $[M + H]^+$ (*m/z*)	$(Gly)_2Cu$/glucose $[M + H]^+$ (*m/z*)
180.0863 ($C_6H_{14}NO_5$)	180.0865 ($C_6H_{14}NO_5$)	180.0861 ($C_6H_{14}NO_5$)	180.0866 ($C_6H_{14}NO_5$)
162.0756[b] ($C_6H_{12}NO_4$)	162.0766[b] ($C_6H_{12}NO_4$)	162.0768[b] ($C_6H_{12}NO_4$)	162.0762[b] ($C_6H_{12}NO_4$)
145.0430[c] ($C_6H_9O_4$)	144.0670 ($C_6H_{10}NO_3$)	144.0664 ($C_6H_{10}NO_3$)	144.0645 ($C_6H_{10}NO_3$)
144.0660 ($C_6H_{10}NO_3$)			
127.0428[c] ($C_6H_7O_3$)			
109.0257[c] ($C_6H_5O_2$)			
85.0247[c] ($C_4H_5O_2$)			

[a]Non-heated commercial standard. [b]Base peak. [c]The calculated error (in ppm) for the specified ions in the commercial standard was between 25 and 50 ppm. For all other ions, the calculated error (in ppm) ranged between 1 and 10 ppm.

Table 4. MS/MS Fragmentation and the Elemental Composition of the Ion Observed at *m/z* 342.1405 in the Heated Mixtures of Glucose/1-Amino-1-deoxy-β-D-glucose/$CuCl_2$ and $(Gly)_2Cu$/Glucose Model Systems

glucose/1-amino-1-deoxy-β-D-glucose/$CuCl_2$ $[M + H]^+$ (*m/z*)[a]	$(Gly)_2Cu$/glucose $[M + H]^+$ (*m/z*)[a]
342.1402 ($C_{12}H_{24}NO_{10}$)	342.1391 ($C_{12}H_{24}NO_{10}$)
324.1294 ($C_{12}H_{22}NO_9$)	324.1303 ($C_{12}H_{22}NO_9$)
306.1195[b] ($C_{12}H_{20}NO_8$)	306.1196[b] ($C_{12}H_{20}NO_8$)
288.1092 ($C_{12}H_{18}NO_7$)	288.1083 ($C_{12}H_{18}NO_7$)
240.0870 ($C_{11}H_{14}NO_5$)	240.0870 ($C_{11}H_{14}NO_5$)
204.0861 ($C_8H_{14}NO_5$)	204.0866 ($C_8H_{14}NO_5$)
174.0760 ($C_7H_{12}NO_4$)	174.0754 ($C_7H_{12}NO_4$)
162.0763 ($C_6H_{12}NO_4$)	162.0756 ($C_6H_{12}NO_4$)
144.0663 ($C_6H_{10}NO_3$)	144.0656 ($C_6H_{10}NO_3$)
127.0404 ($C_6H_7O_3$)	127.0401 ($C_6H_7O_3$)
109.0274 ($C_6H_5O_2$)	109.0282 ($C_6H_5O_2$)
97.0297 ($C_5H_5O_2$)	97.0299 ($C_5H_5O_2$)

[a]The calculated error (in ppm) in all of the reported ions ranged between 0.5 and 15 ppm. [b]Base peak.

solutions in the presence and absence of paraformaldehyde at 110 °C for 2 h and the dry residues were analyzed by ESI/qTOF/MS, with the major ions observed listed in Table 2. Control reactions conducted between free glycine and glucose indicated that the ions listed in Table 2 were not generated in the absence of the copper complexes. However, in the presence of free $CuCl_2$, the glycine/glucose mixture also generated the same peaks, although to a lesser extent. A logical sequence of reaction steps between $(Gly)_2Cu$ and glucose using the identified ions is shown in Figure 2. This figure also shows all of the corresponding ions generated through Akabori reaction[10] in the presence of formaldehyde. Interestingly, in the presence of glucose, formaldehyde Schiff bases of $(Gly)_2Cu$ complexes were not observed.

Glucose Conjugation with the Glycine Copper Complex. Much like the initial phase of the Maillard reaction, $(Gly)_2Cu$ can react with glucose via one of its amino groups to form Schiff bases or its Amadori rearrangement products. Theoretically, up to four sugar molecules can be conjugated with the complex. Mono- and diconjugated complexes were observed in the $(Gly)_2Cu$/glucose model system at *m/z* 374.0355 and 536.0925, respectively (see Figure 2). In the presence of formaldehyde, the Akabori reaction will transform glycine into a serine moiety;[10] consequently, in a $(Gly)_2Cu$/glucose/paraformaldehyde model system, monoconjugated complexes with either mixed amino acids observed at *m/z* 404.0508 or only serine at *m/z* 434.0611 and diconjugated complexes with mixed amino acids at *m/z* 566.1019 (Table 2 and Figure 2) were also detected. In Figure 2, diconjugated complexes are depicted as one of the two possible isomeric structures. Both mono- and diconjugated complexes can dissociate or undergo ligand exchange to release the sugar-conjugated amino acids at *m/z* 238.0930 (as glycine) or *m/z* 268.1038 (as serine). Furthermore, these complexes also underwent an oxidative decarboxylation reaction similar to the unreacted $(Gly)_2Cu$ complex,[8] as confirmed through observation of a series of ions consistent with the process shown in Figure 1. This process is capable of generating free (*m/z* 238.0930) and a monomeric copper complex of Amadori compound (*m/z* 300.0079) in addition to fructosamine (*m/z* 180.0872) through hydrolysis of the Schiff base observed at *m/z* 192.0856. Furthermore, the formation of a monomeric Amadori copper complex at *m/z* 300.0079 was further confirmed by observing the formation of the same ion in a control experiment, where the synthetic glycine Amadori compound and $CuCl_2$ mixtures were reacted under the same conditions. The detection of the Amadori copper complex at *m/z* 300.0079 represents the first evidence for the *in situ* formation of the complex from glucose and a $(Gly)_2Cu$ complex.

Release of Amadori Products. The conjugated Amadori products could be released from the mono- or dimeric complexes observed at *m/z* 374.0355 and 536.0925, respectively, through either dissociation or their oxidative decarboxylation and formation of the Amadori carboxyl radical, which can combine with a hydrogen radical to form the free Amadori compound. Ions associated with the free glycine Amadori product at *m/z* 238.0930 along with its dehydrated derivatives were observed at *m/z* 220.0816 and 202.0709 in the $(Gly)_2Cu$/glucose mixtures. The Amadori product incorporated six carbon atoms from glucose and two carbon atoms (C-1 and C-2) and one nitrogen atom from glycine. The serine Amadori compound observed at *m/z* 268.1038 was similarly identified in the $(Gly)_2Cu$/glucose/formaldehyde mixture incorporating six carbon atoms from glucose and two carbon and one nitrogen atom from glycine (see Table 2).

Formation of Fructosamine and Deoxy-fructosamine. In the process of oxidative decarboxylation of $(Gly)_2Cu$ complexes shown in Figures 1 and 2, two free radical species can be formed: one is the Amadori carboxyl radical, and the other is the copper-centered radical in the Amadori monocopper complex at *m/z* 300.0079. The former can decarboxylate, and the latter can lose CO and CuO molecules to form the same decarboxylated Amadori free radical, which can immediately lose a hydrogen atom to form the Schiff base

DOI: 10.1021/acs.jafc.5b00932
J. Agric. Food Chem. 2015, 63, 4353−4360

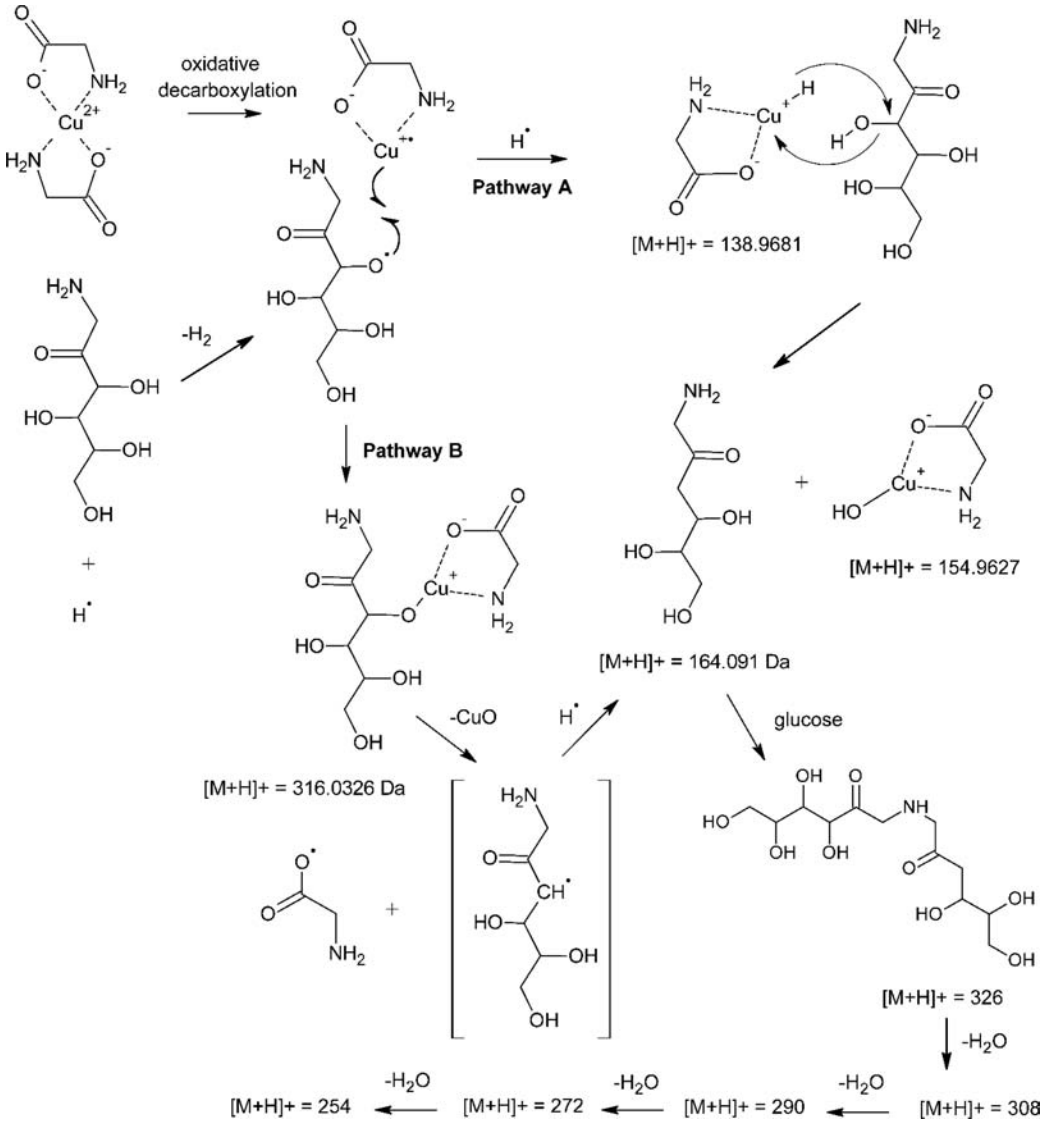

Figure 3. Proposed mechanism of carbon−oxygen bond cleavage in m/z 180. Pathway A is based on ref 19.

Table 5. Elemental Composition and Isotope Incorporation in the Reaction Products Originating from $(Gly)_2Cu$/Glc and Associated with the Ion Observed at m/z 164.0924 Shown in Figure 3

$[M + H]^+$ $(m/z)^a$	elemental composition	$[^{13}C-U_6]$Glc	$[^{13}C$-1]Gly	$[^{13}C$-2]Gly	$[^{15}N]$Gly
138.9681	$C_2H_6CuNO_2$	na[b]	na	na	na
154.9627	$C_2H_6CuNO_3$	na	na	na	na
164.0924	$C_6H_{14}NO_4$	6	0	0	1
254.1026	$C_{12}H_{16}NO_5$	12	0	0	1
272.1112	$C_{12}H_{18}NO_6$	12	0	0	1
290.1217	$C_{12}H_{20}NO_7$	12	0	0	1
308.1321	$C_{12}H_{22}NO_8$	12	0	0	1
326.1426	$C_{12}H_{24}NO_9$	12	0	0	1

[a]The calculated error (in ppm) in all of the reported ions ranged between 0.7 and 11 ppm. [b]na = not analyzed.

observed at m/z 192.0856 (see Figure 2). In this reaction mixture, an ion at m/z 180.0872 was also observed that was assigned to the fructosamine structure, the hydrolysis product of the above Schiff base through the loss of the Strecker aldehyde. This structure is expected to be formed from oxidative decarboxylation reactions of $(Gly)_2Cu$ complexes.[7,8] The tentative assignment of the fructosamine structure was based on its proposed mechanism of formation shown in Figure 2. In addition, the ion had a consistent elemental composition ($[M + H]^+$ $C_6H_{14}NO_5$) to that of fructosamine and showed incorporation of six carbon atoms from glucose and only one atom (nitrogen) from glycine (Table 2 and Figure 2). The structural information regarding the ion at m/z 180.0872 can also apply to its corresponding Schiff base, glycosylamine, which is typically synthesized by reacting glucose with highly reactive ammonia.[16,17] To further confirm the structure of the

DOI: 10.1021/acs.jafc.5b00932
J. Agric. Food Chem. 2015, 63, 4353−4360

Table 6. Comparison of Total Volatiles, Browning, and Ninhydrin-Active Amino Acid Content of Glycine/Glucose and $(Gly)_2Cu$/Glucose Model Systems before and after Heating for 2 h at 110 °C

Total Ion Current (TIC) ($\times 10^3$)			
model system[a]	before heating (%)	after heating (%)	relative decrease in volatiles
glycine/glucose	46.1 ± 10	7.9 ± 10	5.8
$(Gly)_2Cu$/glucose	20.6 ± 10	12.9 ± 10	1.6
Ninhydrin Assay absorbance (λ = 570 nm)			
model system	before heating	after heating	glycine loss (%)
glycine/glucose	0.275 ± 0.007	0.153 ± 0.005	44.85 ± 0.636
$(Gly)_2Cu$/glucose	0.239 ± 0.001	0.224 ± 0.001	5.9 ± 0.141
Browning Measurement			
model system	absorbance[b] (λ = 420 nm)	relative extent of browning[c]	absorbance (λ = 550 nm)	relative extent of browning[c]
glycine/glucose	0.166 ± 0.006	1	0.142 ± 0.006	1
$(Gly)_2Cu$/glucose	0.140 ± 0.001	0.84	0.130 ± 0.001	0.91
Gly/Glc/$CuCl_2$	0.182 ± 0.001	1.1	0.157 ± 0.002	1.11

[a]Samples were pyrolyzed (250 °C at 20 s) before and after heating. [b]The absorbance of the unheated model systems was the same as that of the blank. [c]The relative extent of browning is compared to the glycine/glucose model system.

ion observed at m/z 180.0872, the commercially available Schiff base precursor (1-amino-1-deoxy-glucose or glycosylamine) was heated alone or in the presence of glucose and $CuCl_2$ in water at 110 °C for 2 h and the MS/MS spectra of the ions at m/z 180 generated in the model systems were recorded (Table 3). The observed MS/MS fragmentation pattern of m/z 180.0865 in the heated standard matched exactly the ions generated from the ion at 180.0872 in the heated $(Gly)_2Cu$/glucose mixture and was different from the ions in the unheated sample of 1-amino-1-deoxy-glucose, indicating that, during heating in an aqueous solution, the standard Schiff base was rearranged into its observed Amadori form. Fructosamine and the associated ions at m/z 180.0872, 192.0856, and 330.0228 were similarly generated in the formaldehyde-containing model system. The assigned fructosamine structure was further supported by the observation of its glucose adduct observed at m/z 342.1405 and its further dehydration product at m/z 324.1268. The MS/MS fragmentation of m/z 342.1405 in the reaction mixture and that generated from the heated mixtures of glucose in the presence of 1-amino-1-deoxy-glucose was also compared and found to match (Table 4). To our knowledge, fructosamine thus far has not been identified in any Maillard model systems, except in synthetic preparations.[18] An ion related to fructosamine was also identified in the reaction mixture at m/z 164.0924; this ion, similar to fructosamine, consisted of six carbon atoms derived from glucose and one nitrogen and no carbon atoms from glycine and was predicted to originate from fructosamine (m/z 180.0872) through the loss of an oxygen atom (see Figure 3). Such a loss could be envisaged to occur through copper-catalyzed carbon−oxygen bond cleavage with a simultaneous hydride transfer, as suggested by Rao and Rao.[19] A proposed mechanism based on this suggestion is presented in Figure 3. In this proposal, the copper-centered free radical complex that forms as a result of oxidative decarboxylation of $(Gly)_2Cu$ shown in Figure 1 can either scavenge a hydrogen radical formed during oxidative decarboxylation and form copper hydride observed at m/z 138.9689 (pathway A) or combine with the oxygen-centered free radical on fructosamine (see Figure 3) and generate a new copper complex at m/z 316 (not observed, pathway B). In pathway A, fructosamine can undergo copper-catalyzed carbon−oxygen bond cleavage, preferably at the α position to carbonyl, with simultaneous hydride transfer[19] to from deoxy-fructosamine and the amino acid copper hydroxide complex observed at m/z 154.9627. Alternatively, the hypothetical ion at m/z 316 in pathway B can degrade into a 3-deoxy-fructosamine radical and an amino acid carboxyl radical with the loss of CuO. Both radicals can combine with hydrogen radicals formed during the process to generate glycine and the ion observed at m/z 164.0924. Similar to fructosamine, deoxy-fructosamine was also observed to react with glucose and form the ion at m/z 326.1426, shown in Figure 3. These ions at m/z 326.1426 and 342.1405, shown in Figure 2, along with their subsequent dehydration products (see Table 5 and Figure 3) constituted the major ions observed in the reaction mixture. All of the observed ions above had incorporated the expected number of labeled glucose atoms and labeled nitrogen atoms from glycine and, as expected, none of the labeled glycine carbon atoms (see Table 5). The above findings further support the importance of metal-catalyzed oxidative decarboxylation reactions of not only $(Gly)_2Cu$ complexes but also their corresponding sugar conjugates, generating simultaneously Amadori products, Strecker aldehydes, and fructosamine.

Consequences of Sugar Conjugation with Bis-(glycinato)copper(II) Complexes to Browning and Total Volatile Formation. As demonstrated above, glucose tends to form various conjugates with bis(glycinato)Cu(II) complexes, which can eventually undergo oxidative decarboxylation or dissociation to release the amino acid conjugates as Amadori products. It is expected that such complexes can serve as molecular scaffolds upon which different sugar moieties can accumulate and eventually be released over time, generating colors and aromas. This fact can create the opportunity for controlled release of aroma and flavor precursors. To demonstrate the role of amino acid metal complexes in aroma formation, the total volatiles generated from model systems of glycine/glucose and $(Gly)_2Cu$/glucose were analyzed using Py−GC/MS before and after heating in aqueous solutions at 100 °C for 2 h in open vials. Heating in open vials can lead to loss of volatiles but not loss of conjugated aroma precursors. The quantitation of the volatiles was performed through comparison of their total ion abundances after thermal desorption. As expected, the total ion current of both model systems decreased after heating in open vials (see Table 6). The

DOI: 10.1021/acs.jafc.5b00932
J. Agric. Food Chem. 2015, 63, 4353−4360

glucose/glycine model system exhibited a ~6-fold decrease in intensity, while the heated $(Gly)_2Cu$/glucose model system showed only a ~1.5-fold decrease relative to the unheated samples. These results indicated that, although heating in an open vial can lead to the loss of volatiles, however, as predicted, the $(Gly)_2Cu$ complex was able to retain the aroma precursors in the reaction medium and generate ~1.6-fold more volatiles upon reheating relative to the glucose/glycine model system. These results were also consistent with the measurement of the total content of ninhydrin-active[20] amino acid moieties (free amino acid, amino acid−metal complex, Amadori, and Amadori−metal complex) in glycine/glucose and $(Gly)_2Cu$/glucose model systems before and after heating (100 °C for 2 h) in aqueous solutions. Table 6 indicates that, at the end of the reaction, the $(Gly)_2Cu$/glucose model system retained almost 94% of its total ninhydrin-active amino acid content, whereas the glucose/glycine model showed only 55.2% retention. These changes in ninhydrin-active moieties indicate that, after 2 h of heating at 100 °C, the mixture containing $(Gly)_2Cu$ was still rich in aroma precursors, such as Amadori and Amadori−metal complexes, relative to the glycine/glucose sample, consistent with ESI/qTOF/MS studies reported above and shown in Figure 2. Furthermore, the role of metal ions in their free forms ($CuCl_2$/glycine) and as amino acid complexes, such as $(Gly)_2Cu$, in generating browning (heating at 100 °C for 2 h) in the presence of glucose was also investigated. Using the measurements from two different wavelengths (λ = 420 and 550 nm), the obtained data have indicated that the presence of free $CuCl_2$ in the glucose/glycine model system did not change the browning of the solution, whereas the $(Gly)_2Cu$ complex reduced the browning of the reaction mixture by 15% relative to the model system lacking a source of metal (see Table 6), indicating the dual role that metals can play as either free ions enhancing browning or part of complexes of amino acids inhibiting the browning.

AUTHOR INFORMATION

Corresponding Author

*Telephone: 514-398-7918. Fax: 514-398-7977. E-mail: varoujan.yaylayan@mcgill.ca.

Funding

The authors acknowledge funding for this research from the Natural Sciences and Engineering Research Council of Canada (NSERC).

Notes

The authors declare no competing financial interest.

REFERENCES

(1) Kwak, E. J.; Lim, S. I. The effect of sugar, amino acid, metal ion, and NaCl on model Maillard reaction under pH control. *Amino Acids* **2004**, *27*, 85−90.

(2) O'Brien, J.; Morrissey, P. A. Metal ion complexation by products of the Maillard reaction. *Food Chem.* **1997**, *58*, 17−27.

(3) Ramonaitytė, D. T.; Keršienė, M.; Adams, A.; Tehrani, K. A.; Kimpe, N. D. The interaction of metal ions with Maillard reaction products in a lactose−glycine model system. *Food Res. Int.* **2009**, *42*, 331−336.

(4) Rendleman, J. A., Jr; Inglett, G. E. The influence of Cu^{2+} in the Maillard reaction. *Carbohydr. Res.* **1990**, *201*, 311−326.

(5) Rizzi, G. P. Chemical structure of colored maillard reaction products. *Food Rev. Int.* **1997**, *13*, 1−28.

(6) (a) Beck, W. Metal complexes of biologically important ligands, CLXXVI.[1] Formation of peptides within the coordination sphere of metal ions and of classical and organometallic complexes and some aspects of prebiotic chemistry. *Z. Anorg. Allg. Chem.* **2011**, *637*, 1647−1672. (b) Beck, W. Metal complexes of biologically important ligands, CLXXII [1]. Metal ions and metal complexes as protective groups of amino acids and peptides—Reactions at coordinated amino acids. *Z. Naturforsch.* **2009**, *64b*, 1221−1245.

(7) Yablokov, V. A.; Smeltsova, I. L.; Faerman, V. I. Kinetics of heat-induced transformation of copper complexes with amino acids. *Russ. J. Gen. Chem.* **2014**, *84*, 568−570.

(8) Nashalian, O.; Yaylayan, V. A. Thermally induced oxidative decarboxylation of copper complexes of amino acids and formation of Strecker aldehyde. *J. Agric. Food Chem.* **2014**, *62*, 8518−8523.

(9) Akabori, S.; Otani, T. T.; Marshall, R.; Winitz, M.; Greenstein, J. P. A synthesis and resolution of DL-serine. *Arch. Biochem. Biophys.* **1959**, *83*, 1−9.

(10) Nashalian, O.; Yaylayan, V. A. De novo synthesis of amino acids during the Maillard reaction: qTOF/ESI mass spectrometric evidence for the mechanism of Akabori transformation. *J. Agric. Food Chem.* **2015**, *63*, 328−334.

(11) Horikawa, H.; Okada, M.; Nakamura, Y.; Sato, A.; Iwamoto, N. Production of hydroxyl radicals and α-dicarbonyl compounds associated with Amadori compound−Cu^{2+} complex degradation. *Free Radical Res.* **2002**, *36*, 1059−1065.

(12) Cheng, R.; Kawakishi, S. Novel decomposition of Amadori compound catalyzed by copper ion. *J. Agric. Food Chem.* **1994**, *42*, 700−703.

(13) Tonkovicc, M.; Jakas, A.; Horvat, S. Preparation and properties of an Fe(III)-complex with an Amadori compound derived from L-tyrosine. *BioMetals* **1997**, *10*, 55−59.

(14) Gyurcsik, B.; Gajda, T.; Nagy, L.; Burger, K.; Rockenbauer, A.; Korecz, L., Jr. Proton, copper(II) and nickel(II) complexes of some Amadori rearrangement products of D-glucose and amino acids. *Inorg. Chim. Acta* **1993**, *214*, 57−66.

(15) Pearson, R. G.; Lanier, R. D. Rates of rapid ligand exchange reactions by nuclear magnetic resonance line broadening studies. *J. Am. Chem. Soc.* **1964**, *86*, 765−771.

(16) Linek, K.; Alföldi, J.; Defaye, J. Structure of glycosylamines and diglycosylamines in the arabinose, mannose, and rhamnose series. *Carbohydr. Res.* **1993**, *247*, 329−335.

(17) Isbell, H. S.; Frush, H. L. Mutarotation, hydrolysis, and rearrangement reactions of glycosylamines. *J. Org. Chem.* **1958**, *23*, 1309−1319.

(18) Mossine, V. V.; Mawhinney, T. P. 1-Amino-1-deoxy-D-fructose ("fructosamine") and its derivatives. *Adv. Carbohydr. Chem. Biochem.* **2010**, *64*, 291−402.

(19) Rao, H. S. P.; Rao, A. V. B. Copper-catalyzed $C(sp^3)$−OH cleavage with concomitant C−C coupling: synthesis of 3-substituted isoindolinones. *J. Org. Chem.* **2015**, *80*, 1506−1516.

(20) Tomita, H.; Mitusaki, S.; Tamaki, E. Chemical studies on ninhydrin-positive compounds in cured tobacco leaves. *Agric. Biol. Chem.* **1964**, *28*, 451−455.

DOI: 10.1021/acs.jafc.5b00932
J. Agric. Food Chem. 2015, 63, 4353−4360

Table 1. Pasting Property Changes of Irradiated Brown Japonica Rice during 18 Months of Storage[a]

RVA pasting property	treatment (kGy)	storage time (months) 0	3	6	9	12	15	18
peak viscosity	0	2189.7 ± 71.3a(1)	2317.0 ± 27.7a(2)	2419.0 ± 16.9a(2,3)	2372.5 ± 35.7a(2,3)	2559.1 ± 8.7a(3)	2625.2 ± 28.3a(4)	2024.7 ± 68.5a(5)
	0.2	2081.5 ± 14.6a,b(1)	2280.1 ± 38.2a,b(2)	2363.7 ± 13.0a(2)	2356.7 ± 25.3a(2)	2581.1 ± 47.8b(3)	2493.2 ± 35.0b(3)	1970.0 ± 54.1a(4)
	0.5	1995.0 ± 47.1b,c(1)	2217.7 ± 24.4b(2,3)	2226.1 ± 17.3b(2,3)	2289.3 ± 29.5a(2)	2386.5 ± 35.1a(2)	2283.7 ± 17.3c(2)	2070.5 ± 139.5a(1,3)
	1	1906.5 ± 45.8c(1)	2030.2 ± 14.2c(2)	2176.3 ± 54.5b(3,4)	2092.7 ± 48.0b(2,3)	2128.5 ± 39.5c(2,3)	2275.0 ± 8.5c(4)	1729.0 ± 25.6b(5)
	2	1672.8 ± 47.9d(1)	1777.7 ± 24.1d(2)	1854.3 ± 4.6c(2)	1853.2 ± 11.7c(2)	1835.7 ± 21.1d(2)	1809.7 ± 20.2d(2)	1522.2 ± 14.9b(3)
through viscosity	0	941.3 ± 17.5a(1)	1013.1 ± 14.1a(1,2)	1060.7 ± 39.5a(2,3)	958.7 ± 23.1a(1)	1093.2 ± 17.0a,b(3,4)	1160.7 ± 37.8a(4)	750.5 ± 19.3a(5)
	0.2	913.8 ± 3.8a(1)	1012.6 ± 18.3a(2)	1051.0 ± 26.5a(2)	1049.5 ± 5.8b(2)	1136.2 ± 21.7a(3)	1129.2 ± 26.8a(3)	768.2 ± 19.2a(4)
	0.5	830.5 ± 16.5b(1)	926.3 ± 13.1b(2,3)	1003.2 ± 16.6a(2)	1036.2 ± 15.1b(3)	1053.5 ± 33.2b(3)	975.7 ± 9.9b(2,3)	817.7 ± 57.3a(1)
	1	717.7 ± 30.5c(1)	754.5 ± 17.7c(1,2)	866.7 ± 18.8b(3)	794.5 ± 14.3c(2,4)	824.5 ± 6.2c(3,4)	936.7 ± 10.4b(5)	632.7 ± 15.6b(6)
	2	564.7 ± 2.3d(1)	528.3 ± 5.8d(2)	571.1 ± 7.9c(1)	591.0 ± 2.5d(1)	605.7 ± 37.1d(1)	581.5 ± 16.1c(1)	421.5 ± 1.4c(3)
breakdown viscosity	0	1198.5 ± 54.8a(1)	1295.7 ± 14.3a(2)	1271.7 ± 4.6a(1,2)	1308.4 ± 2.5a(2)	1340.7 ± 11.4a(2)	1464.5 ± 13.2a(3)	1269.2 ± 48.8a(1,2)
	0.2	1171.1 ± 16.0a(1)	1268.5 ± 21.4a,b(2)	1287.7 ± 10.6a(2,3)	1280.2 ± 5.2a,b(2,3)	1367.2 ± 5.8a(3)	1364.0 ± 45.4b(3)	1201.7 ± 49.6a,b(1,2)
	0.5	1164.5 ± 34.3a(1)	1291.7 ± 28.1a(2)	1270.2 ± 6.0a(1,2)	1289.7 ± 3.9a,b(2)	1333.0 ± 24.2a(2)	1308.0 ± 15.7b(2)	1277.7 ± 82.1a(1,2)
	1	1188.7 ± 22.5a(1)	1276.0 ± 12.3a,b(2,3)	1234.2 ± 12.4b(1,2)	1260.0 ± 19.0b,c(2)	1304.0 ± 40.1a(2,3)	1338.2 ± 10.6b(3)	1096.2 ± 27.3b(4)
	2	1109.3 ± 49.3a(1)	1228.7 ± 11.8b(2)	1225.0 ± 5.6b(2)	1242.2 ± 7.1c(2)	1232.2 ± 6.9b(2)	1228.2 ± 18.6c(2)	1100.7 ± 13.5b(1)
final viscosity	0	2027.5 ± 39.7a(1)	2172.2 ± 26.8a(2)	2191.7 ± 16.9a(2)	2159.2 ± 29.6a(2)	2208.7 ± 39.8a(2)	2285.7 ± 39.6a(2)	1712.0 ± 68.5a(3)
	0.2	2048.2 ± 49.5a(1)	2102.5 ± 28.9b(1)	2082.5 ± 12.9b(1)	2105.7 ± 8.0b(1)	2206.5 ± 61.0a(2)	2115.5 ± 17.4b(1)	1666.2 ± 30.7a(3)
	0.5	1855.7 ± 55.1b(1)	1962.2 ± 9.3c(1,2)	1982.2 ± 1.5c(1,2)	2033.5 ± 14.6c(2)	2063.2 ± 38.1b(2)	1883.7 ± 14.5c(1)	1717.2 ± 94.5a(3)
	1	1561.1 ± 7.1c(1)	1704.2 ± 23.4d(2)	1714.6 ± 23.3d(2)	1780.2 ± 11.2d(3)	1736.5 ± 17.2c(2)	1820.7 ± 9.4c(3)	1343.0 ± 21.5b(4)
	2	1286.5 ± 22.6d(1,2)	1279.2 ± 15.4e(1,2)	1234.1 ± 9.1e(3)	1286.7 ± 2.4e(1,2)	1305.9 ± 24.8d(2)	1237.0 ± 11.9d(1,3)	1039.0 ± 13.1c(4)
setback viscosity	0	36.1 ± 8.7a(1)	−51.5 ± 11.0a(1)	−167.2 ± 7.8a(2)	−165.7 ± 4.6a(2)	−175.2 ± 6.3a(2)	−339.5 ± 13.3a(3)	−420.7 ± 79.7a,b(3)
	0.2	−74.5 ± 7.3b(1)	−132.7 ± 13.2b(1)	−279.5 ± 14.4b(2)	−278.5 ± 1.7b(2)	−274.5 ± 14.6b(2)	−377.7 ± 36.3a(3)	−303.7 ± 35.7a(2)
	0.5	−73.2 ± 9.9b(1)	−239.7 ± 12.6c(2)	−337.7 ± 7.9c(3,4,5)	−289.7 ± 15.5b(2,3)	−323.6 ± 26.0c(3,4)	−400.0 ± 12.6a,b(5)	−360.7 ± 45.2a,b(4,5)
	1	−202.5 ± 34.4c(1)	−332.2 ± 12.9d(2)	−443.2 ± 10.5d(3)	−444.7 ± 9.9c(3)	−442.5 ± 12.0d(3)	−454.2 ± 8.2b(3)	−386.0 ± 17.8a,b(4)
	2	−374.2 ± 27.6d(1)	−481.5 ± 9.1e(2)	−503.1 ± 7.5e(2,4)	−499.5 ± 7.0c(3)	−530.2 ± 11.8e(4)	−572.7 ± 15.2c(5)	−483.2 ± 6.9b(2)
pasting temp	0	72.2 ± 0.5a(1)	71.2 ± 0.4a(1,2)	69.8 ± 0.2a(2,3)	70.0 ± 0.0a(1,2)	70.1 ± 0.1a(1,2,3)	69.7 ± 1.5a(3)	70.3 ± 0.2a(1,2,3)
	0.2	72.7 ± 0.6a(1)	71.6 ± 0.2a(2)	70.0 ± 0.0a(3)	70.0 ± 0.0a(3)	70.2 ± 0.0a(3)	70.0 ± 0.2a(3)	70.4 ± 0.0a(3)
	0.5	72.6 ± 0.3a(1)	71.4 ± 0.4a(2)	71.0 ± 0.4a(2)	70.5 ± 0.5a(2,3)	70.2 ± 0.1a(2,3)	69.8 ± 0.0a(3)	70.5 ± 0.0a(2,3)
	1	73.9 ± 0.3b(1)	73.2 ± 0.2b(1)	70.5 ± 0.7a(2,3)	71.0 ± 0.4a(2)	70.4 ± 0.0a(2,3)	69.8 ± 0.0a(3)	70.2 ± 0.2a(2,3)
	2	75.5 ± 0.2c(1)	73.8 ± 0.2b(2)	73.8 ± 0.2b(2)	73.5 ± 0.3b(2)	71.1 ± 0.2b(3)	70.2 ± 0.2a(4)	70.3 ± 0.2a(4)

[a]In a column within one RVA pasting property, means followed by the same letter are not significantly different at $P < 0.05$ by LSD test. In a row, means followed by the same number are not significantly different at $P < 0.05$ by LSD test.

J. Agric. Food Chem. 2015, 63, 4361−4369
DOI: 10.1021/jf5047514

and dehulled after harvest. The initial moisture content of brown rice was 12.3 ± 0.5% (w.b.). Brown rice was irradiated using a Gammacell-220 ^{60}Co γ irradiator at the Jiangsu Academy of Agricultural Sciences (JAAS, Jiangsu province, People's Republic of China), with irradiation doses of 0, 0.2, 0.5, 1.0, and 2.0 kGy. The irradiation was conducted at room temperature (23 °C) with a dose rate of 5.0 Gy min^{-1}. After irradiation, brown japonica rice was sealed in polyethylene (PE) bags and stored at a temperature of 15.0 °C for 18 months.

Measurement of Physicochemical Parameters. Physicochemical parameters such as hardness, pasting viscosity, and lipid acidity were measured every 3 months. The hardness of cooked rice was measured using a Texture Analyzer (TA.XT2i, Stable Micro Systems, Godalming, U.K.). The cooked rice was placed in a cylindrical container and was compressed to 75% with a rod-type probe (2.5 cm diameter ×15 cm length) under the prespeed of 0.7 mm/s, a test speed of 0.5 mm/s, and a postspeed of 1.0 mm/s. The hardness was measured from the two-cycle curves using Texture Export for Windows (Stable Micro Systems, Godalming, U.K.). The pasting viscosity of rice flour was determined with a Rapid Visco Analyzer (RVA, Newport Scientific Instrument and Engineer, Warriewater, Australia). Brown rice was milled using a laboratory roller-type grinder (PQX) and then passed through an 80 mesh sieve. Flour samples were packed in polyethylene (PE) bags and stored at 4 °C until testing. The sample (3.5 g of rice flour) was dispersed in distilled water (25.0 mL) and stirred in an RVA container initially at 960 rpm for 10 s and finally at 160 rpm for the remaining test. The temperature profile was started at 50 °C, heating was carried out from 50 to 95 °C at a heating rate of 12 °C/min, the temperature was held for 2 min and 30 s at 95 °C, and cooling was carried out to 50 °C at the same rate. The pasting curves obtained were analyzed using an RVA Starch Master Software Setup Tool (SMST) to obtain the characteristic parameters. For lipid acidity analysis, lipid was extracted using ethanol and titrated with KOH using phenolphthalein as an indicator and then free fatty acid (FFA) content was measured by titration according to the method of Seibel;[33] the thiobarbituric acid (TBA) content assay was determined by the method described by Mariod et al.[34] The colormetry assay of brown rice was conducted in terms of L^* value (lightness) and b^* value (yellowness) using a spectrophotometer (Model CM-5, Konica Minolta, Inc. Japan).

Microstructure of Starch Granules in Brown Rice. The microstructures of kernels were measured at storage times of 0, 12, and 18 months. Brown rice samples were dried in a vacuum oven at 40 °C and cooled in a desiccator. Rice kernels were broken by a sharp blade. The treated samples were stuck on a specimen holder using a silver plate and coated with a thin film of gold (10 nm) in a vacuum evaporator. The obtained specimens were observed with a scanning electron microscope (SEM) (Model 27021-H, England) at a magnification of 1000× with an accelerating voltage of 7.0 kV.

Sensory Analysis. Sensory analysis was conducted after 18 months of storage. Milled rice samples (10 g each) were placed in aluminum cup, put into a rice cooker machine in which water boiled immediately, and then covered and heated for 40 min. Cooked rice then cooled naturally for sensory evaluation. A sensory panel consisting of 15 trained graduate students majoring in food science participated in this study. A hedonic scale (1 = extremely dislike and 9 = extremely like) was applied to determine consumer preference among cooked rice samples. The intensities of individual attributes of cooked rice were rated by the panelists, including appearance, color, odor, taste, and overall acceptability.

Data Analysis. The γ irradiation treatments and all analyses were performed at least three times. Mean values, standard deviation, and analysis of variance (ANOVA) were computed using the SPSS system (version 17.0, SPSS Inc.; Chicago, IL). These data were then compared using LSD tests. Correlation analysis was performed with the pooled data of irradiation dose, storage time, pasting viscosities, hardness, TBA content, FFA content, and rice color. Statistical significance was established at $P < 0.05$.

RESULTS AND DISCUSSION

Pasting Properties. The pasting curves of brown japonica rice flour were measured by RVA changed upon 18 months of storage (Table 1). Most of the pasting properties, including peak, through, breakdown, final, and setback viscosity, decreased ($P < 0.05$) considerably with irradiation dose increase. The peak viscosity (PV) decreased ($P < 0.05$) from 2,189 cP for the unirradiated sample to 1,672 cP for the 2 kGy sample without storage (0 month). PV was mainly related to swelling of starch granules.[14,35] The decrease in PV was mainly caused by reduction of the swelling index in rice starch due to its degradation upon irradiation.[12,36,37] The final viscosity (FV) was also decreased after γ irradiation, which showed that the starch gel became softer after γ irradiation. These results were

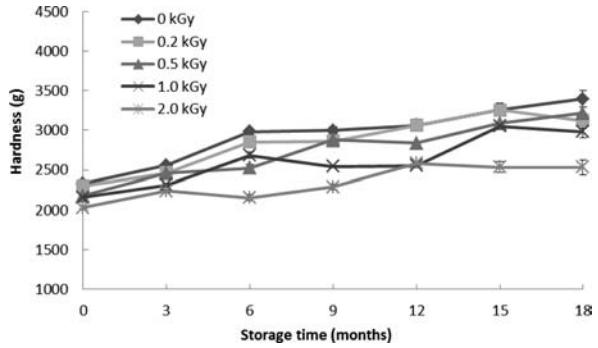

Figure 1. Cooked-grain hardness changes of irradiated brown japonica rice with 18 months of storage.

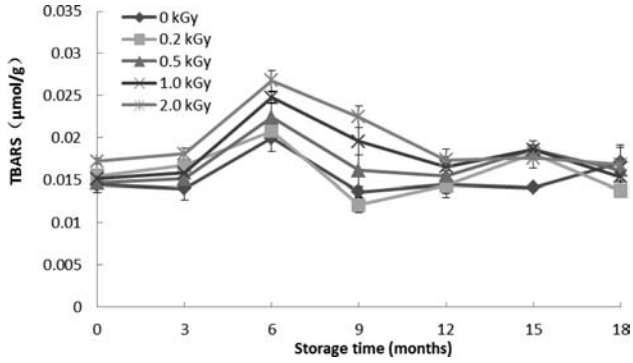

Figure 2. TBARS value changes of irradiated brown japonica rice with 18 months of storage.

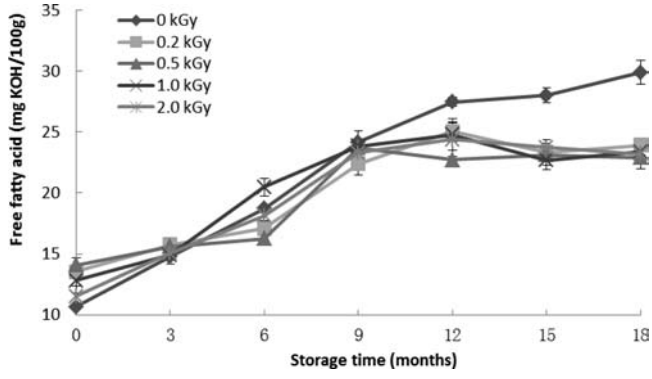

Figure 3. FFA content changes of irradiated brown japonica rice with 18 months of storage.

DOI: 10.1021/jf5047514
J. Agric. Food Chem. 2015, 63, 4361−4369

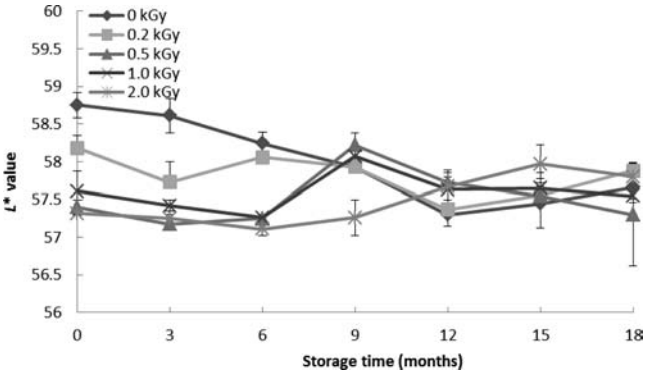

Figure 4. Brightness value (L^*) changes of irradiated brown japonica rice with 18 months of storage.

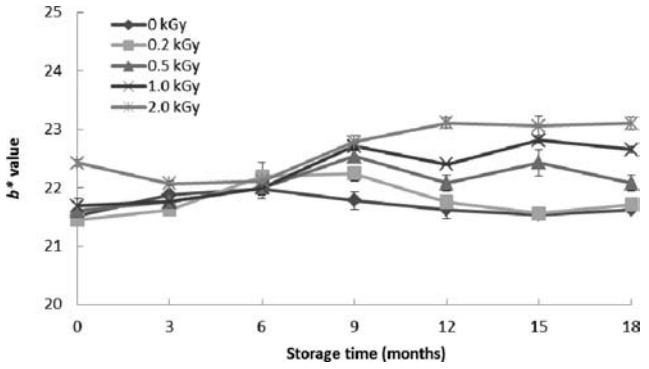

Figure 5. Yellowness value (b^*) changes of irradiated brown japonica rice with 18 months of storage.

consistent with the statement of Gani et al.[15] The lower breakdown viscosity (BD) of irradiated brown japonica rice was detected in comparison with that of nonirradiated brown japonica rice, which showed that starch might be broken in the irradiated rice as the viscosity breaks down, giving a measure of the fragility of the granules. Reports on changes in the viscosity breakdown of brown japonica rice after γ irradiation have been inconsistent.[36,37] Setback (SB) is an indicator of the firmness of cooked rice, a higher value of which indicates a firmer texture. A significantly lower SB value for irradiated brown japonica rice was exhibited in comparison with nonirradiated rice. The decrease in SB caused by γ irradiation was ascribed to the degradation of amylose and long linear amylopectin.[38] The higher pasting temperature (PT) of brown japonica rice meant that more water could be absorbed during the pasting process and the rice samples were more resistant to cooking.[39] It could be concluded that γ irradiation may improve the cooking quality. Also, it could be inferred that the starch gel was softer after an increased irradiation dose and the cooking quality was improved upon increasing doses of irradiation. Many studies have been conducted on the effect of γ irradiation on rice pasting viscosity.[7−9,30,40,41] γ irradiation caused starch polymer degradation, which resulted in a progressive reduction in the molecular weight of amylose and amylopectin and decreased viscosity while the solubility increased with increasing radiation dose.[8] It is commonly known that the chemical changes induced by ionizing radiation could be the result of "direct" or "indirect" action, depending on the radiation conditions.[42] In direct action, a sensitive target such as the DNA of a living organism was damaged directly by an ionizing particle or ray. This mechanism caused lethal effects in the microorganism. In indirect action, changes in the carbohydrate were caused mostly by the free radicals (i.e., radiolytic products) formed on dissociation of the excited molecules upon irradiation: in particular hydroxyl radicals (i.e., oxidizing agent) and hydrogen atoms (i.e., reducing agent) derived from water radiolysis. Ozone, a powerful oxidant, could also be formed from oxygen during irradiation. These free radicals substantially attacked the glycosidic bonding in the carbohydrate, causing depolymerization or degradation. The cleavage of glycosidic bonds subsequently caused the rupture of starch granules and gave rise to a reduction in viscosity; these might be the reason for viscosity changes in the current study. The same phenomena have been observed in wheat,[43] maize,[10,44] and legumes.[45]

Most parameters of pasting viscosity (i. e., peak, through, breakdown, final, and setback viscosity) increased within 12 months of storage, whereas these parameters decreased after 12−15 months of storage. γ irradiation fragmented the starch chain into short linear polymers, which might cause difficulty in the formation of helical structures with fatty acids during storage, and therefore passage of water might not be as restricted as that occurring naturally.[30] Storage could also decrease the rice flour pasting viscosity by increasing the disulfide bonds between protein networks.[46] Storage decreased the PT significantly ($P < 0.05$); this might be attributed to rice aging, which could form disulfide bonds between proteins.[47]

Table 2. Correlation Coefficients among Various Functional Properties of Irradiated Brown Japonica Rice[a]

	ST	dose	PV	TR	BD	FV	SB	PT	HD	TBA	FFA	L^*
dose	-											
PV	0.031	−0.796**										
TR	−0.036	−0.857**	0.972**									
BD	0.246	−0.493**	0.849**	0.740**								
FV	−0.136	−0.912**	0.941**	0.973**	0.679**							
SB	−0.542**	−0.722**	0.441**	0.549**	0.026	0.674**						
PT	−0.691**	0.504**	−0.555**	−0.533**	0.513**	−0.464**	0.050					
HD	0.721**	−0.580**	0.590**	0.549**	0.607**	0.484**	−0.045	−0.795**				
TBA	0.020	0.407*	−0.133	−0.192	0.013	−0.305	−0.542**	0.091	−0.119			
FFA	0.805**	−0.061	0.265	0.150	0.433**	0.070	−0.445**	−0.668**	0.659**	−0.005		
L^*	−0.120	−0.555**	−0.118	−0.034	−0.291	0.042	0.267	−0.363*	0.292	−0.372	−0.129	
b^*	0.176	0.624**	−0.318	−0.355*	−0.139	−0.451**	−0.579**	−0.036	−0.208	0.333	0.428**	0.005

[a]* and ** indicate significance at $P < 0.05$ and 0.01, respectively. Abbreviations: ST = storage time, PV = peak viscosity, TR = through viscosity, BD = breakdown, FV = final viscosity, SB = setback, PT = pasting temperature, HD = hardness, TBA = thiobarbituric acid content, FFA = free fatty acid content.

DOI: 10.1021/jf5047514
J. Agric. Food Chem. 2015, 63, 4361−4369

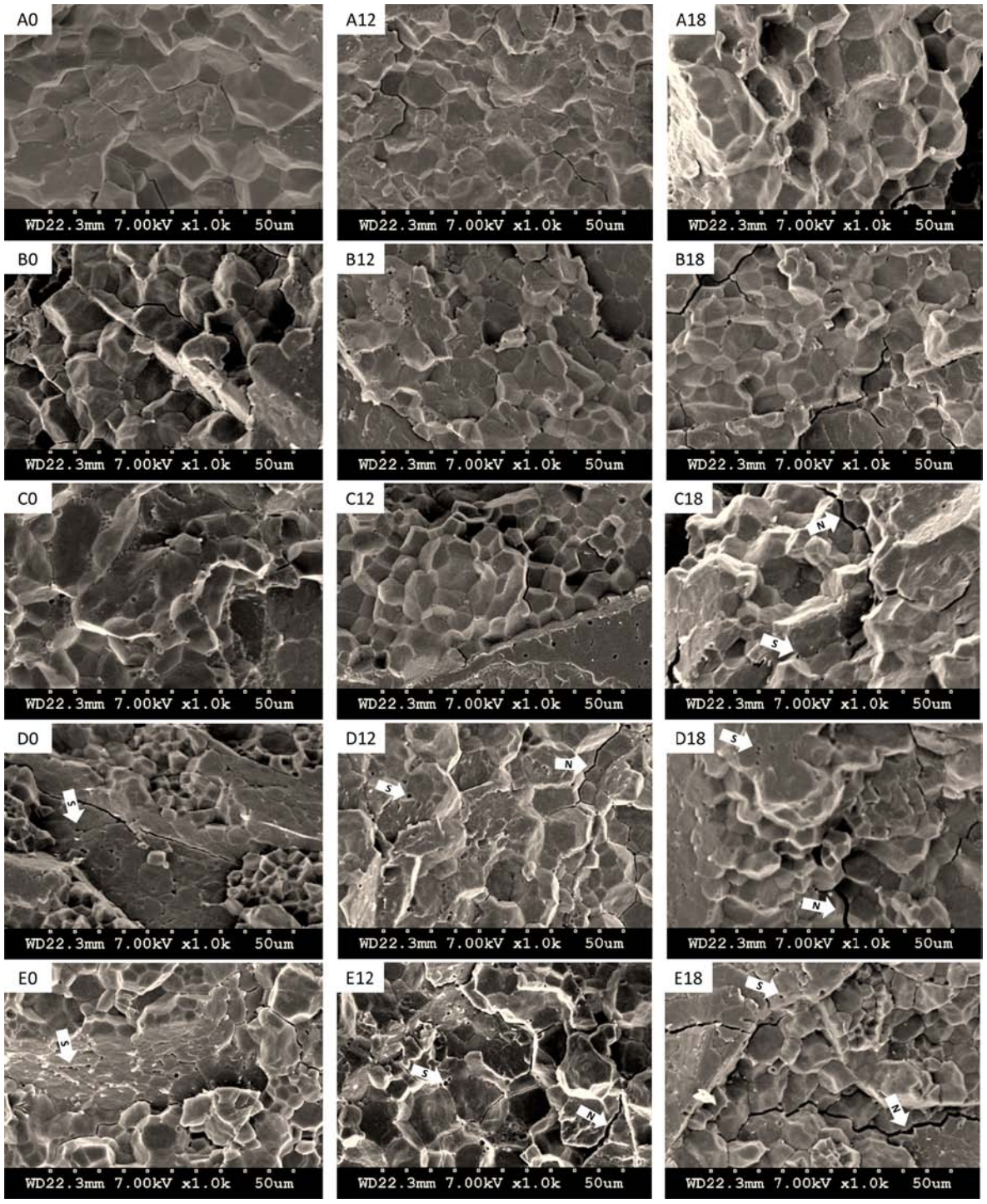

Figure 6. Scanning electron micrographs of exposed endosperm from irradiated brown japonica rice kernels with storage times of 0, 12, and 18 months (×1000 magnification): (A) 0 kGy; (B) 0.2 kGy; (C) 0.5 kGy; (D) 1.0 kGy; (E) 2.0 kGy. Arrows indicate the dark spots (S) and narrow cracks (N) among starch granules (distance between two adjacent scale points 5 μm).

The PT of nonirradiated and low-dose-irradiated brown japonica rice decreased significantly ($P < 0.05$) over 6 months of storage and remained almost constant until the end of storage (18 months). However, the PT of brown japonica rice irradiated at 2.0 kGy decreased throughout the period of storage. Studies that have analyzed pasting viscosities showed that protein had a major influence on flour pasting viscosity.[48] Aging significantly affected the pasting behavior of rice flour.[49] Thus, changes in protein content and disulfide bonds might control the differences in rice pasting viscosity during storage. As the main pasting viscosities of various starches were reduced by γ irradiation,[41,50] RVA measurement could be used as a potential method for analytical identification of irradiated grain.

Hardness of Cooked Rice. Overall, the hardness of irradiated or nonirradiated cooked rice showed an upward trend during storage (Figure 1). The hardness of cooked rice decreased ($P < 0.05$) significantly on treatment with irradiation doses of 0.5 kGy or more. After 18 months of storage, the

DOI: 10.1021/jf5047514
J. Agric. Food Chem. 2015, 63, 4361−4369

Table 3. Effect of γ Irradiation on the Sensory Qualities of Cooked Rice Stored for 18 Months[a]

	sensory quality				
treatment (kGy)	appearance	color	odor	taste	overall acceptability
0	6.5 ± 0.2a,b	6.4 ± 0.2a	6.3 ± 0.3a	6.6 ± 0.7a	6.4 ± 0.5a
0.2	6.7 ± 0.5a,b	6.6 ± 0.3a,b	6.0 ± 0.4a	6.7 ± 0.5a	6.6 ± 0.6a
0.5	6.6 ± 0.7a,b	6.3 ± 0.3a,b	5.9 ± 0.3a	6.5 ± 0.3a,b	6.7 ± 0.5a
1.0	5.8 ± 0.8b	6.1 ± 0.3b,c	4.3 ± 0.2b	6.1 ± 0.3b,c	5.5 ± 0.6b
2.0	5.0 ± 0.7c	5.9 ± 0.2c	3.3 ± 0.2c	5.9 ± 0.6c	4.6 ± 0.5c

[a]Sensory quality is defined as scores ranging from 1 (dislike extremely) to 9 (like extremely); means for each characteristic within a column followed by the same letter are not significantly different at $P > 0.05$ by LSD test.

differences in hardness between nonirradiated rice and low-dose irradiated rice (0.2 and 0.5 kGy) were not significant. Changes in cooked rice hardness might be due to γ-irradiation-induced structural degradation in starch granules,[51] which would enable water to penetrate relatively easily.[30,36,52] When rice starch was heated with steam or excess water, the crystalline structure was disrupted due to the breakage of hydrogen bonds, and molecules of water became linked by hydrogen bonding to the exposed hydroxyl group of amylose and amylopectin. This phenomenon causes an increase in granule swelling and solubility. The hardness of cooked rice in the current study increased in all samples with prolonged storage times. After 18 months of storage, nonirradiated brown rice had the highest increase in hardness (45.64%), whereas there were relatively small increases (35.75%, 39.42%, 37.89%, and 24.55%) for brown rice irradiated at 0.2, 0.5, 1.0, and 2.0 kGy, respectively. Thus, we consider that γ irradiation could improve the cooking quality induced by rice aging during long-term storage.

Lipid Properties. The lipid content of brown japonica rice obtained in this study was approximately 2.1−3.4% and did not change significantly during 18 months of storage. During storage, the surface lipids of brown japonica rice had undergone hydrolysis to form FFAs. These FFAs were particularly susceptible to oxidation and could form intermediate peroxides, followed by the decomposition of intermediate peroxides into various oxidation products. TBA reacted with oxidation products and produced a color pigment.[30] Initially, the TBA content obtained from irradiated brown japonica rice (2.0 kGy) was significantly higher ($P < 0.05$) than other samples (0, 0.2, 0.5, and 1.0 kGy) (Figure 2). During storage, the TBA content of brown japonica rice irradiated at doses of 0.2, 0.5, and 1.0 kGy had no significant difference ($P > 0.05$) from that of nonirradiated brown japonica rice, whereas the TBA increased significantly ($P < 0.05$) with irradiation doses up to 2.0 kGy. This might be due to the medium dose of 2.0 kGy having a marked function on lipids and accelerating lipid oxidation. A sharp increase of TBA content in all samples was observed after 3 months of storage, and this content then decreased significantly ($P < 0.05$) after 6 months of storage. At the end of storage (18 months), the TBA contents did not show significant differences in nonirradiated and irradiated brown japonica rice and were in the range of 0.014−0.018 μmol/g. During long-term storage, the TBA content of brown japonica rice had shown a dynamic change; this might be ascribed to changes in the duration of end products. These results were consistent with the research reported in the literature.[30] The FFA content in brown japonica rice is shown in Figure 3. Initially, the FFA content in nonirradiated brown japonica rice was 10.7 mg of KOH/100 g. After irradiation, the FFA content increased slightly (13.6, 14.1, 12.8, and 11.5 mg of KOH/100 g with doses of 0.2, 0.5, 1.0, and 2.0 kGy, respectively); however, no significant difference ($P > 0.05$) was observed among brown japonica rice samples with different irradiation doses (0.2, 0.5, 1.0, and 2.0 kGy). With 9 months of storage, the FFA contents of all irradiated brown japonica rice samples increased significantly ($P < 0.05$) in comparison with the values after short-term storage (0, 3, and 6 months). During storage from 12 to 18 months, the FFA content of irradiated brown rice remained constant within a range of 22.7−25.0 ($P > 0.05$). However, the FFA content of unirradiated brown rice increased steadily and reached a peak of 29.9 mg of KOH/100 g at 18 months of storage. Changes in lipids due to ionizing radiation could be brought about in two ways: (1) by catalyzing their reaction with molecular oxygen, i.e., autoxidation, or (2) by the action of high-energy radiation (direct or indirect) on lipid molecules.[53,54] In the presence of oxygen, both oxidative and radiolytic effects would occur and could be superimposed. The general mechanism of the radiolysis of lipids was thought to involve primary ionization, followed by migration of the positive charge toward the carboxyl group or double bonds. Cleavage occurred preferentially at the positions near carbonyl groups. As a result, the yield of hydrocarbon was increased. These effects subsequently brought about an increase in TBA content and FFA content.

Rice Color. Values of L^* (brightness) and b^* (yellowness) recorded for brown japonica rice are shown in Figures 4 and 5. After irradiation, in comparison to unirradiated rice (0 kGy), the L^* values of irradiated rice (0.2, 0.5, 1.0, and 2.0 kGy) decreased ($P < 0.05$) whereas the b^* values of irradiated rice (0.2, 0.5, 1.0, and 2.0 kGy) increased ($P < 0.05$). These results are consistent with research reported in the literature.[14,30,40] Brightness and yellowness changes might be explained by the breakdown of glycosidic and peptidic linkages promoted during irradiation. The free radicals, including hydroxyl radical, and hydrogen atoms derived from water radiolysis substantially attacked the glycosidic bonding in carbohydrates, causing depolymerization or degradation and the Maillard reaction. The cleavage of glycosidic bonds subsequently caused the rupture of starch granules and gave rise to browning. With prolonged storage time, the L^* and b^* values of brown rice varied differently. However, the lightness (L^*) values of brown rice irradiated with different doses began to converge and remained constant after 12 months of storage (varying within the range 57.3−58.0, $P > 0.05$). However, the yellowness (b^*) values of brown rice varied differently within 9 months of storage and then remained constant after 9 months. The yellowness values over 18 months were linearly dose dependent as follows: 21.62 for 0 kGy, 21.71 for 0.2 kGy, 22.08 for 0.5 kGy, 22.65 for 1.0 kGy, and 23.10 for 2.0 kGy. The changes in brightness and yellowness of brown rice after long-term storage might be explained by the fact that the cleavage of glycosidic bonds

DOI: 10.1021/jf5047514
J. Agric. Food Chem. 2015, 63, 4361−4369

carried out by free radicals became extremely weak after long-term storage. As the consumer favors rice with a low chroma value (i.e., yellowness) and a high lightness value, low-dose irradiation with short storage time is preferred for commercial storage.

Correlation among Properties of Irradiated Brown Japonica Rice. Pearson's correlation coefficients for the relationship among various functional properties of irradiated brown japonica rice during storage are shown in Table 2. Storage time had a positive correlation with hardness (r = 0.721, P < 0.01) and FFA content (r = 0.805, P < 0.01), whereas it had a negative correlation with SB (r = −0.542, P < 0.01) and PT (r = −0.691, P < 0.01). The irradiation dose had a positive correlation with PT (r = 0.504, P < 0.01), b^* value (r = 0.624, P < 0.01), and TBA content (r = 0.407, P < 0.05) and a negative correlation with L^* value and all pasting parameters except PT (r = 0.504, P < 0.01; these results were in agreement with the findings reported by Liu.[37] PV had a positive correlation with TR (r = 0.972, P < 0.01), BD (r = 0.849, P < 0.01), FV (r = 0.941, P < 0.01), and SB (r = 0.441, P < 0.01). Similar phenomena have been revealed in pasting properties on irradiation.[17,52]

Kernel Morphological Structure. The SEM photographs of starch granules showed an uneven surface with angular and polygonal shapes in all rice samples (Figure 6). After irradiation, dark spots developed among starch granules, especially in irradiated rice (1.0 or 2.0 kGy). These dark spots were probably the small spherical holes with diameters of about 1 μm. As the storage time was prolonged, these dark spots became rather dense and the narrow cracks became wider. However, the mean granule range and the shapes of starches did not vary significantly. The reason different levels of cracks and spots formed in irradiated rice samples and how they formed during storage were not clear and required further investigation. The isolated starches of irradiated rice grains (0.35 kGy) also showed similar morphology with respect to polygonal shape and size of starch granules but with few round starches.[50] However, with high-dose irradiation (maximum dose range from 10 to 50 kGy), microscopic observation of the starches indicated surface cracking of the starch samples with irradiation treatment, and the extent of surface cracking was dose-dependent and increased with increasing irradiation dose in rice,[9] corn,[10] potatoes,[12,14] and beans.[12,16] These changes were due to the cleavage of large starch molecules by free radicals generated from the treatment of γ irradiation;[55] the breakage or cleavage of long chains in amylopectin decreased the apparent amylose content, which might aid humans in digesting rice starch.[9,56,57] However, rice starch granules are the smallest granules known in cereal grains,[58] with sizes ranging from 4 to 8 μm in the current study; the granules were loosely packed and look like clusters. Wu et al.[51] observed the shape of the starch granule deformed by medium-dose γ irradiation (1 kGy) and considered that γ irradiation was capable of degrading starch through the cleavage of large molecules of starch into smaller fragments. However, in the current study, we did not observe any significant changes in starch granule shape except for the appearance of narrow cracks and dark spots among starch granules, even with medium-dose irradiation (1 and 2 kGy; Figure 6).

Panelist Acceptance of Cooked Rice. Sensory evaluation was one of the most important methods for shelf life determination in food products.[59] The results of sensory qualities of cooked rice stored for 18 months were presented in Table 3. Panelists did not report differences (P > 0.05) in appearance, color, odor, taste, and overall acceptability among samples after irradiation with 0, 0.2, and 0.5 kGy at the end of storage (18 months). However, very low scores for odor were obtained after γ irradiation, especially with medium-dose irradiated (1.0 and 2.0 kGy) brown japonica rice (P < 0.01). The disagreeable odor of brown japonica rice irradiated at 1.0 and 2.0 kGy might be ascribed to the increase in lipid degradation products (determined from an increase in TBA content) during 18 months of storage. The unsaturated fatty acids in brown japonica rice are easily oxidized to peroxides and change to carbonyl compounds,[53,54] which caused disagreeable odor and flavor of brown japonica rice stored long-term. Poor scores of appearance, color, and taste from cooked rice were obtained for irradiation doses up to 1.0 kGy (P < 0.05). For overall acceptability, scores given by panelists varied from 4.6 to 6.7. Irradiated rice at 0.5 and 0.2 kGy had significantly high scores ranging from 6.6 to 6.7 in comparison scores with irradiation doses of 1.0 and 2.0 kGy (P < 0.01). The unpleasant odor and color might be the main reason for the low scores. These results meant that, at the end of storage (stored for 18 months), panelists preferred irradiated rice with doses as follows: 0.5 kGy > 0.2 kGy > 0 kGy > 1.0 kGy > 2.0 kGy. Therefore, rice irradiated with relatively low doses was the most acceptable.

In conclusion, physicochemical, structural, and sensory properties of irradiated brown rice during long-term storage were characterized in the current work. A low or medium dose of γ irradiation (from 0.2 kGy to 2.0 kGy) increased the main pasting values and improved the storage performance of brown japonica rice. Irradiation decreased the FFA content of brown rice with long-term storage (from 12 to 18 months). Narrow cracks and dark spots developed among starch granules, especially in irradiated rice, which became wider and more dense with prolonged storage time. Extremely low scores for odor and overall acceptability were obtained from panelists on γ-irradiated brown rice especially with medium doses (1.0 or 2.0 kGy). On the basis of these observations, we considered that a dose of 0.5 kGy or below could be suitable for γ irradiation on brown japonica rice before long-term storage. These results could serve as a basis for developing an efficient method for grain storage.

AUTHOR INFORMATION

Funding

This research was supported by a project from the State Administration of Grain in China (201313010), a project from Jiangsu Education Department (13KJB550010), and a project from the Priority Academic Program Development of Jiangsu higher education institutions (PAPD).

Notes

The authors declare no competing financial interest.

ACKNOWLEDGMENTS

We wish to thank the JAAS for providing rice samples.

REFERENCES

(1) FAO, Seeking end to loss and waste of food along production chain. http://www.fao.org/docrep/018/i294-0c/i2940c02.pdf, 2014.

(2) Lacroix, M.; Ouattara, B. Combined industrial processes with irradiation to assure innocuity and preservation of food products — a review. *Food Res. Int.* **2000**, 33 (9), 719−724.

DOI: 10.1021/jf5047514
J. Agric. Food Chem. 2015, 63, 4361−4369

(3) Lado, B. H.; Yousef, A. E. Alternative food-preservation technologies: efficacy and mechanisms. *Microbes Infect.* **2002**, *4* (4), 433−40.
(4) Wang, J.; Yu, Y. Inactivation of mildew in rough rice and wheat by gamma irradiation. *Radiat. Phys. Chem.* **2010**, *79* (6), 740−743.
(5) El-Naggar, S. M.; Mikhaiel, A. A. Disinfestation of stored wheat grain and flour using gamma rays and microwave heating. *J. Stored Prod. Res.* **2011**, *47* (3), 191−196.
(6) Singh, B.; Datta, P. S. Effect of low dose gamma irradiation on plant and grain nutrition of wheat. *Radiat. Phys. Chem.* **2010**, *79* (8), 819−825.
(7) Bao, J.; Corke, H. Pasting Properties of γ-Irradiated Rice Starches as Affected by pH. *J. Agric. Food Chem.* **2002**, *50* (2), 336−341.
(8) Bao, J.; Ao, Z.; Jane, J.-l. Characterization of Physical Properties of Flour and Starch Obtained from Gamma-Irradiated White Rice. *Starch - Stärke* **2005**, *57* (10), 480−487.
(9) Yu, Y.; Wang, J. Effect of γ-ray irradiation on starch granule structure and physicochemical properties of rice. *Food Res. Int.* **2007**, *40* (2), 297−303.
(10) Chung, H. J.; Liu, Q. Effect of Gamma Irradiation on Molecular Structure and Physicochemical Properties of Corn Starch. *J. Food Sci.* **2009**, *74* (5), C353−C361.
(11) Ben Bettaïeb, N.; Jerbi, M. T.; Ghorbel, D. Gamma radiation influences pasting, thermal and structural properties of corn starch. *Radiat. Phys. Chem.* **2014**, *103* (0), 1−8.
(12) Chung, H.-J.; Liu, Q. Molecular structure and physicochemical properties of potato and bean starches as affected by gamma-irradiation. *Int. J. Biol. Macromol.* **2010**, *47* (2), 214−222.
(13) Singh, S.; Singh, N.; Ezekiel, R.; Kaur, A. Effects of gamma-irradiation on the morphological, structural, thermal and rheological properties of potato starches. *Carbohydr. Polym.* **2011**, *83* (4), 1521−1528.
(14) Gani, A.; Nazia, S.; Rather, S. A.; Wani, S. M.; Shah, A.; Bashir, M.; Masoodi, F. A.; Gani, A. Effect of γ-irradiation on granule structure and physicochemical properties of starch extracted from two types of potatoes grown in Jammu & Kashmir, India. *LWT - Food Science and Technology* **2014**, *58* (1), 239−246.
(15) Gani, A.; Bashir, M.; Wani, S. M.; Masoodi, F. A. Modification of bean starch by γ-irradiation: Effect on functional and morphological properties. *LWT - Food Science and Technology* **2012**, *49* (1), 162−169.
(16) Hussain, P. R.; Wani, I. A.; Suradkar, P. P.; Dar, M. A. Gamma irradiation induced modification of bean polysaccharides: Impact on physicochemical, morphological and antioxidant properties. *Carbohydr. Polym.* **2014**, *110* (0), 183−194.
(17) Sofi, B. A.; Wani, I. A.; Masoodi, F. A.; Saba, I.; Muzaffar, S. Effect of gamma irradiation on physicochemical properties of broad bean (Vicia faba L.) starch. *LWT - Food Science and Technology* **2013**, *54* (1), 63−72.
(18) Thayer, D. W. Food irradiation: benefits and concerns. *J. Food Qual.* **1990**, *13* (3), 147−169.
(19) Farkas, J. Irradiation for better foods. *Trends Food Sci. Technol.* **2006**, *17*, 148−152.
(20) Calado, T.; Venâncio, A.; Abrunhosa, L. Irradiation for Mold and Mycotoxin Control: A Review. *Compr. Rev. Food Sci. Food Saf.* **2014**, *13* (5), 1049−1061.
(21) Satin, M. *Food irradiation - a guidebook*, 2nd ed; Technomic Publishing: Lancaster, PA, 1996.
(22) Golding, J. B.; Blades, B. L.; Satyan, S.; Jessup, A. J.; Spohr, L. J.; Harris, A. M.; Banos, C.; Davies, J. B. Low dose gamma irradiation does not affect the quality, proximate or nutritional profile of 'Brigitta' blueberry and 'Maravilla' raspberry fruit. *Postharvest Biol. Technol.* **2014**, *96* (0), 49−52.
(23) Dogbevi, M. K.; Vachon, C.; Lacroix, M. Physicochemical Properties of Dry Red Kidney Bean Proteins and Natural Microflora as Affected by Gamma Irradiation. *J. Food Sci.* **1999**, *64* (3), 540−542.
(24) Kim, M. M.; Vanee, K., Irradiation of Food and Packaging: An Overview. In *Irradiation of Food and Packaging*; American Chemical Society: Washington, DC, 2004; Vol. *875*, pp 1−11.
(25) *Safety and Nutritional Adequacy of Irradiated Food*; World Health Organization: Geneva, Switzerland, 1994.
(26) FDA, Irradiation in the production, processing and handling of food. Final rule, *Fed. Reg.* **1986**, *51*, 13376−13399.
(27) Sung, W.-C.; Hong, M.-C.; Chang, T.-S. Effects of storage and gamma irradiation on (Japonica) waxy rice. *Radiat. Phys. Chem.* **2008**, *77* (1), 92−97.
(28) Zhou, Z.; Robards, K.; Helliwell, S.; Blanchard, C. Ageing of Stored Rice: Changes in Chemical and Physical Attributes. *J. Cereal Sci.* **2002**, *35* (1), 65−78.
(29) Park, C.-E.; Kim, Y.-S.; Park, K.-J.; Kim, B.-K. Changes in physicochemical characteristics of rice during storage at different temperatures. *J. Stored Prod. Res.* **2012**, *48* (0), 25−29.
(30) Sirisoontaralak, P.; Noomhorm, A. Changes in physicochemical and sensory-properties of irradiated rice during storage. *J. Stored Prod. Res.* **2007**, *43* (3), 282−289.
(31) Friedman, M. Rice Brans, Rice Bran Oils, and Rice Hulls: Composition, Food and Industrial Uses, and Bioactivities in Humans, Animals, and Cells. *J. Agric. Food Chem.* **2013**, *61* (45), 10626−10641.
(32) Ng, L.-T.; Huang, S.-H.; Chen, Y.-T.; Su, C.-H. Changes of Tocopherols, Tocotrienols, γ-Oryzanol, and γ-Aminobutyric Acid Levels in the Germinated Brown Rice of Pigmented and Non-pigmented Cultivars. *J. Agric. Food Chem.* **2013**, *61* (51), 12604−12611.
(33) Seibel, W. Approved Methods of the American Association of Cereal Chemists, 8th ed. (Standardmethoden der amerikanischen Gesellschaft für Getreidechemiker, 8. Ausgabe); Approved Methods Committee American Association of Cereal Chemists, Inc.: St. Paul, MN, USA. Seibel, W. *Starch - Stärke* **1989**, *41* (11), 443−443.
(34) Mariod, A. A.; Altine, A. H.; Maznah, I.; Norsharina, I. Antioxidative effects of stabilized and unstabilized defatted rice bran methanolic extracts on the stability of rice bran oil under accelerated conditions. *Grasas Aceites* **2010**, *61* (4), 409−415.
(35) Vandeputte, G. E.; Derycke, V.; Geeroms, J.; Delcour, J. A. Rice starches. II. Structural aspects provide insight into swelling and pasting properties. *J. Cereal Sci.* **2003**, *38* (1), 53−59.
(36) Ashwar, B. A.; Shah, A.; Gani, A.; Rather, S. A.; Wani, S. M.; Wani, I. A.; Masoodi, F. A.; Gani, A. Effect of gamma irradiation on the physicochemical properties of alkali-extracted rice starch. *Radiat. Phys. Chem.* **2014**, *99* (0), 37−44.
(37) Liu, T.; Ma, Y.; Xue, S.; Shi, J. Modifications of structure and physicochemical properties of maize starch by γ-irradiation treatments. *LWT - Food Science and Technology* **2012**, *46* (1), 156−163.
(38) Pimpa, B.; Muhammad, S. K. S.; Hassan, M. A.; Ghazali, Z.; Hashim, K.; Kanjanasopa, D. Effect of electron beam irradiation on physicochemical properties of sago starch. *Songklanakarin J. Sci. Technol.* **2007**, *29* (3), 759−768.
(39) Pitiphunpong, S.; Suwannaporn, P. Physicochemical properties of KDML 105 rice cultivar from different cultivated locations in Thailand. *J. Sci. Food Agric.* **2009**, *89* (13), 2186−2190.
(40) Sirisoontaralak, P.; Noomhorm, A. Changes to physicochemical properties and aroma of irradiated rice. *J. Stored Prod. Res.* **2006**, *42* (3), 264−276.
(41) Bao, J.; Shu, Q.; Xia, Y.; Bergman, C.; McClung, A. Effects of gamma irradiation on aspects of milled rice (oryza sativa) end-use quality1. *J. Food Qual.* **2001**, *24* (4), 327−336.
(42) *Food Irradiation Research and Technology*, 2nd ed.; Wiley: Somerset, NJ, USA, 2012; Institute of Food Technologists Series, Vol. *76*.
(43) MacArthur, L. A.; D'Appolonia, B. L. Gamma Radiation of Wheat. II. Effects of Low-Dosage Radiations on Starch Properties. *Cereal Chem.* **1984**, *61*, 321−326.
(44) Bra_oveanu, M.; Nemcanu, M. R.; Duc, D. Electron-beam processed corn starch: evaluation of physicochemical and structural properties and technical-economic aspects of the processing. *Brazilian Journal of Chemical Engineering* **2013**, *30*, 847−856.
(45) Oneh Abu, J.; Gyebi Duodu, K.; Minnaar, A. Effect of γ-irradiation on some physicochemical and thermal properties of cowpea

DOI: 10.1021/jf5047514
J. Agric. Food Chem. 2015, 63, 4361−4369

(Vigna unguiculata L. Walp) starch. *Food Chem.* **2006**, *95* (3), 386−393.
(46) Martin, M.; Fitzgerald, M. A. Proteins in Rice Grains Influence Cooking Properties! *J. Cereal Sci.* **2002**, *36* (3), 285−294.
(47) Sung, W.-C. Effect of gamma irradiation on rice and its food products. *Radiat. Phys. Chem.* **2005**, *73* (4), 224−228.
(48) Fitzgerald, M. A.; Martin, M.; Ward, R. M.; Park, W. D.; Shead, H. J. Viscosity of rice flour: a rheological and biological study. *J. Agric. Food Chem.* **2003**, *51* (8), 2295−9.
(49) Teo, C. H.; Abd. Karim, A.; Cheah, P. B.; Norziah, M. H.; Seow, C. C. On the roles of protein and starch in the aging of non-waxy rice flour. *Food Chem.* **2000**, *69* (3), 229−236.
(50) Kong, X.; Sun, X.; Xu, F.; Umemoto, T.; Chen, H.; Bao, J. Morphological and physicochemical properties of two starch mutants induced from a high amylose indica rice by gamma irradiation. *Starch - Stärke* **2014**, *66* (1−2), 157−165.
(51) Wu, D.; Shu, Q.; Wang, Z.; Xia, Y. Effect of gamma irradiation on starch viscosity and physicochemical properties of different rice. *Radiat. Phys. Chem.* **2002**, *65* (1), 79−86.
(52) Gani, A.; Gazanfar, T.; Jan, R.; Wani, S. M.; Masoodi, F. A. Effect of gamma irradiation on the physicochemical and morphological properties of starch extracted from lotus stem harvested from Dal lake of Jammu and Kashmir, India. *J. Saudi Soc. Agric. Sci.* **2013**, *12* (2), 109−115.
(53) Stark, G. The effect of ionizing radiation on lipid membranes. *Biochim. Biophys. Acta, Rev. Biomembr.* **1991**, *1071* (2), 103−122.
(54) Kiang, J. G.; Fukumoto, R.; Gorbunov, N. V. Lipid Peroxidation After Ionizing Irradiation Leads to Apoptosis and Autophagy. *Lipid Peroxidation*; Intech: Rijeka, Croatia, 2012.
(55) Grant, L. A.; D'Appolonia, B. L. Effects of Low-Level Gamma Radiation on Water-Soluble Nonstarchy Polysaccharides Isolated from Hard Red Spring Wheat Flour and Bran. *Cereal Chem.* **1991**, *68*, 651−652.
(56) Chiang, P. Y.; Yeh, A. I. Effect of Soaking on Wet-milling of Rice. *J. Cereal Sci.* **2002**, *35* (1), 85−94.
(57) Vandeputte, G. E.; Delcour, J. A. From sucrose to starch granule to starch physical behaviour: a focus on rice starch. *Carbohydr. Polym.* **2004**, *58* (3), 245−266.
(58) Eliasson, A.-C. *Starch in Food: Structure, Function and Applications*. CRC Press: Boca Raton, FL, 2004.
(59) Hough, G. *Sensory Shelf Life Estimation of Food Products*. CRC Press: Boca Raton, FL, 2010.

DOI: 10.1021/jf5047514
J. Agric. Food Chem. 2015, 63, 4361−4369

Next, Gray et al.[16] studied the efficacy of MON and SAL in the presence of sodium bentonite. The authors concluded that sodium bentonite could reduce the efficacy of MON and SAL but only at levels below the recommended dosages.

In vitro or in vivo literature data for other clays or other mycotoxin binders and for other veterinary medicinal products are not available despite the possible risk of binder−drug interactions and consequently the reduced efficacy of the drug. In the case of antibiotics, not only is the lack of efficacy of concern but also the possible increase of antimicrobial resistance due to exposure to subtherapeutic concentrations.[17−19] These concerns were also incorporated in the EFSA recommendations for this class of additives.[20] Besides macrolides, tetracycline antibiotics are frequently used in veterinary medicine, more specifically in feed or drinking water medication in pig and poultry farming. Doxycycline (DOX) is a broad-spectrum bacteriostatic tetracycline of the second generation. It is mainly used in broiler chickens to treat respiratory and systemic infections caused by *Mycoplasmata*, *Ornithobacterium rhinotracheale*, *Avibacterium paragallinarum*, *Pasteurella multocida*, and *Chlamydia* spp.[21−24]

Therefore, the aim of the present study was to evaluate the in vitro adsorption of DOX to four montmorillonite and one sepiolite clay, one leonardite-based binder, and including activated carbon (AC) as positive control. Next, to confirm and validate the in vitro model, an in vivo pharmacokinetic study was performed using oral bolus dosing of DOX and two of the in vitro studied mycotoxin binders in broiler chickens.

MATERIALS AND METHODS

Chemicals, Solutions, and Mycotoxin Binders. Sigma-Aldrich (Bornem, Belgium) supplied DOX hyclate, demethylchlortetracycline (DMCTC, used as internal standard), potassium chloride (KCl), and phosphoric acid (H_3PO_4). Water (H_2O), methanol (MeOH), and acetonitrile (ACN) used for the high-performance liquid chromatography (HPLC) analysis and preparation of stock solutions were of HPLC grade and provided by Fisher Scientific (Wijnegem, Belgium). Stock solutions of 10 mg/mL were made for DOX and DMCTC in, respectively, H_2O and MeOH/H_2O (50:50; v/v). Sodium chloride (NaCl), magnesium chloride ($MgCl_2{\cdot}6H_2O$), and calcium chloride ($CaCl_2{\cdot}2H_2O$) were supplied by VWR (Leuven, Belgium). Potassium dihydrogen phosphate (KH_2PO_4), disodiumhydrogen phosphate (Na_2HPO_4), formic acid (HCOOH), trifluoroacetic acid (TFA), and sodium hydroxide (NaOH) were obtained from Merck (Darmstadt, Germany). Six mycotoxin binders were evaluated and obtained from Sigma-Aldrich, Kemin (Herentals, Belgium) and Poortershaven (Rotterdam, The Netherlands)[7] and were identified as "montmorillonites 1, 2, 3 and 4", "leonardite", and "sepiolite". With regard to the composition of the evaluated binders, X-ray diffraction spectrometry (XRD) analysis of montmorillonite 1 indicated montmorillonite as the most prevalent mineral, but also the presence of mica, quartz, and kaolin was detected, and the mineral fraction was 97.0%. XRD analysis of montmorillonite 2 indicated mixed layered montmorillonite as the most prevalent mineral, but also trace amounts of quartz were detected, and the mineral fraction was 78.6%. XRD analysis of montmorillonite 3 indicated pure montmorillonite as the only mineral; the mineral fraction was 86.8%. Montmorillonite 4 contained montmorillonite, sepiolite, and a trace amount of calcite; the mineral fraction was 92.7%. XRD analysis of the leonardite indicated the presence of humic substance and small amounts of quartz; the mineral fraction was <16%. The sepiolite contained small amounts of a smectite clay; and the mineral fraction was 96%.[7] AC (Norit Carbomix), used as positive control, was obtained from Kela (Hoogstraten, Belgium) and was of pharmaceutical grade and applied in a granulated form. Doxycycline hyclate (Soludox 15%) used for the in vivo study was supplied by Dechravet (Heusden-Zolder, Belgium).

In Vitro Binding Assay. The protocol used for the in vitro binding assay was adapted from Sabater-Vilar et al.[25] The main adaptations were the use of phosphate-buffered saline (PBS) buffers of two different pH values instead of adjusting the pH during the conduct of the experiment. Also, the sample preparation, that is, centrifugation instead of filtering, and chromatographic sample analysis differed. PBS was prepared by adding first 24.0 g of NaCl, 0.3 g of $MgCl_2{\cdot}6H_2O$, 0.6 g of KCl, and 0.4 g of $CaCl_2{\cdot}2H_2O$ to 3 L of HPLC grade water. Next, a buffer system consisting of H_3PO_4 and KH_2PO_4, or KH_2PO_4 and Na_2HPO_4, was added to 1 L of salt solution to obtain a buffer solution of ±9.6 mM.[25] The pH was adjusted with H_3PO_4 or NaOH to obtain buffers of pH 2.5 and 6.5, respectively. Five milliliters of the respective PBS at pH 2.5 or 6.5 was added to a 60 mL flask containing 20 mg of the respective binder or AC. Finally, DOX hyclate was added to a concentration of 100 μg DOX/mL. All samples were prepared and analyzed in triplicate. The ratio DOX/binder of 1:40 (w/w) corresponds with a dose of 20 mg DOX/kg BW and a feed intake of 80 g/kg BW with inclusion of 1% binder.

The flask was shaken on a lateral shaker (IKA, Staufen, Germany) for 4 h at 37 °C and 180 rpm (New Brunswick Scientific, Rotselaar, Belgium). Next, samples were transferred to a 15 mL tube and centrifuged (10 min, 524*g*, 4 °C), and 100 μL of the supernatant was transferred to an Eppendorf cup, supplemented with 50 μL of a 50 μg/mL aqueous solution of DMCTC and diluted with HPLC grade H_2O to a volume of 1 mL. After thorough vortex mixing, 100 μL was transferred into an autosampler vial and diluted with ACN/H_2O 80:20 (v/v) to a final volume of 1 mL for further liquid chromatography−tandem mass spectrometric (LC-MS/MS) analysis. Negative control samples were included at 10 and 100 μg/mL DOX and were submitted to the same treatment as the other samples, but without addition of binder.

In Vivo Oral Bolus Pharmacokinetic Study. Montmorillonites 2 and 3 were selected for further research because montmorillonites are the most frequently used mycotoxin binders and because of the high purity of these two montmorillonites. Furthermore, montmorillonite 2 differs from montmorillonite 3 in terms of cation exchange capacity (CEC; 51.0 vs 111.7 $cmol_c/kg$),[7] type of montmorillonite, that is, mixed layered and normal layered, and mineral fraction. Thirty-two 14-day-old broiler chickens (Ross 308, as hatched) were randomly divided in four groups of eight birds, namely, DOX, DOX+AC, DOX +montmorillonite 2, and DOX+montmorillonite 3. The animals were housed and treated according to European guidelines for animal experiments.[26] Each group was housed in floor pens of 2 m^2 covered with wood shavings and equipped with a heating lamp. The animals had ad libitum access to feed and drinking water. Temperature and relative humidity were controlled between 15 and 25 °C and between 40 and 80% respectively. After 1 week of acclimatization, the animals were weighed and fasted 12 h before the onset of the experiment. According to their group, the birds received an oral intracrop bolus (2 mL) of tap water for the animals of the negative control group (DOX), AC dispersed in 2 mL of tap water for the positive control group (DOX+AC), and montmorillonite 2 or montmorillonite 3 also dispersed in 2 mL of tap water for the other two groups (DOX +montmorillonite 2 and 3, respectively). The montmorillonite and AC dose was equivalent to the expected daily intake when 1% (w/w) is included in the feed. Immediately after this bolus administration, an oral Soludox 15% bolus (1 mL) containing 20 mg DOX/kg BW in tap water was administered, followed by 1 mL of tap water to flush the tube. The ratio DOX/binder was with respect to the in vitro trial, namely, 1:40 (w/w). Next, blood samples were taken at 0 min (just before administration), 15, 30, and 45 min, and 1, 1.5, 2, 3, 4, 6, 8, 12, and 24 h postadministration (pa) of the binder and DOX. Blood samples were collected in heparinized tubes and centrifuged (524*g*, 10 min, 4 °C), and plasma was stored at ≤ −15 °C until analysis. This experiment was approved by the local Ethical Committee of the Faculty of Veterinary Medicine and Bioscience Engineering of Ghent University (Case EC 2014/08).

Quantification of Doxycycline in Buffer (in Vitro) and in Plasma (in Vivo). The sample preparation for the in vitro buffer samples is presented under In Vitro Binding Assay. Sample

DOI: 10.1021/acs.jafc.5b00832
J. Agric. Food Chem. 2015, 63, 4370−4375

preparation for plasma samples was as follows: 100 μL of plasma was supplemented with 15 μL of TFA, 50 μL of a 10 μg/mL aqueous DMCTC solution, and 50 μL of HPLC water. The sample was vortex mixed for 30 s before centrifuging at 10800*g* for 10 min at room temperature. The supernatant was diluted 5-fold in HPLC water before analysis. The HPLC system for all samples consisted of a Waters 2690 pump and an autosampler (Waters, Milford, MA, USA). Chromatographic separation was achieved on a Hypersil Gold column (100 mm × 2.1 mm, particle size = 5 μm) and corresponding guard column (Thermo Scientific, Erembodegem, Belgium). The mobile phases were (A) 0.1% HCOOH in H_2O and (B) 0.1% HCOOH in ACN. The following gradient elution program for the samples derived from the in vitro study was applied: 0−2 min, 98% A, 2% B; 2−5.5 min, 40% A, 60% B; 5.5−12 min, 98% A, 2% B. The flow rate was set at 0.30 mL/min, and 5 μL of sample was injected. For the analysis of plasma samples, the following gradient was applied: 0−0.3 min, 95% A, 5% B; 0.3−3.5 min, 10% A, 90% B; 3.5−8.5 min, 70% A, 30% B; 8.5−15 min, 95% A, 5% B. The flow rate was set at 0.45 mL/min, and a 5 μL aliquot of the sample extract was injected.

The HPLC effluent was interfaced to a Quattro Ultima tandem mass spectrometer (Micromass, Manchester, UK). The capillary and cone voltages were 3.0 kV and 40 V, respectively, the source temperature was set at 120 °C, and the desolvation temperature was set at 250 °C. Cone gas flow and desolvation gas flow were, respectively, 101 and 898 L/h. The positive electrospray ionization (ESI+) mode was applied, and collision energy was optimized to 25 eV for both DOX and DMCTC in plasma samples and to 25 and 20 eV for DOX and DMCTC in the samples from the in vitro study, respectively. The following selected reaction monitoring (SRM) transitions were monitored and used for quantification: m/z 445.0 → 428.2 for DOX and 465.0 → 448.1 for DMCTC.

The method was validated for DOX in plasma as well as samples from the in vitro study according to a validation protocol previously described by De Baere et al.,[27] using matrix-matched calibration curves. All parameters met the requirements and were in compliance with the recommendations and guidelines defined by the European Community[28,29] and with international criteria described in the literature,[30−32] except for carry-over of DOX on the instrument. A small interfering peak of 0.4−1% area relative to the area of the highest calibrator was detected when a solvent sample was injected directly after the highest calibrator; no peaks were detected when solvents were injected after the other calibrators. Because the majority of the samples fell below the concentration range in which carry-over was expected, no overestimation was present. The limit of quantification (LOQ) was 1 μg/mL for PBS at pH 6.5 and 2.5 and 50 ng/mL for plasma. Between-run recoveries ± standard deviation (SD, n = 6) of the quality control samples prepared in PBS at pH 2.5 were 10.9 ± 0.5 and 94.2 ± 2.2 μg/mL for blank samples spiked at 10 and 100 μg/mL, respectively. For pH 6.5 the recoveries were 10.4 ± 0.5 and 101.3 ± 3.9 μg/mL. Within-run recoveries (n = 6) in PBS at pH 2.5 were 10.7 ± 0.2 and 95.3 ± 0.2 μg/mL, whereas in PBS at pH 6.5 the recoveries were 10.1 ± 0.2 and 99.8 ± 1.8 μg/mL. Validation of the analytical method for the plasma samples included blank plasma samples spiked at 250 ng/mL (n = 6) and 2500 ng/mL (n = 6, both within- and between-run); between-run recoveries were 242.2 ± 4.6 and 2518.2 ± 59.8 ng/mL, respectively. For the within-run recovery, values of 243.8 ± 5.6 and 2460.4 ± 68.1 ng/mL were obtained.

Pharmacokinetic Analysis. A noncompartmental analysis of the DOX plasma concentration−time data was performed to determine the pharmacokinetic (PK) characteristics of DOX using WinNonlin 6.3 (Phoenix Pharsight, St. Louis, MO, USA). The following main PK variables were determined for each animal: C_{max}, T_{max}, area under the plasma concentration−time curve from time 0 to infinite and 24 h (AUC_{0-inf} and AUC_{0-24h}), elimination rate constant (k_{el}), elimination half-life ($T_{1/2el}$), volume of distribution relative to the absolute oral bioavailability (Vd/F), and clearance relative to the absolute oral bioavailability (Cl/F). The relative oral bioavailability (relative F) was calculated according to following formula:

$$\text{relative } F = \frac{AUC_{0-\text{inf, DOX + tested binder}}}{AUC_{0-\text{inf, DOX negative control}}} \times 100$$

Statistical Analysis. The free DOX concentrations in the in vitro trial were analyzed using a one-way analysis of variance (ANOVA) and executed using the statistical package SPSS for Windows (IBM, Brussels, Belgium). The PK values for each group in the in vivo study were compared using a one-way ANOVA; p values below 0.05 were considered as statistically significant.

RESULTS

Results of the in vitro binding assay are presented in Figure 1. The concentrations of DOX in the negative control samples at pH 2.5 were 10.6 ± 0.3 and 91.0 ± 1.8 μg/mL for the samples spiked at 10 and 100 μg/mL, respectively. For the samples at pH 6.5 the concentrations of DOX were 11.0 ± 6.8 and 100.3 ± 4.7 μg/mL, respectively. Low free concentrations of DOX after incubation are indicative of high adsorption and are seen in all of the tested binders. No significant differences were observed between the binders and AC; however, all of the tested binders differed significantly (p < 0.001) from the negative control samples.

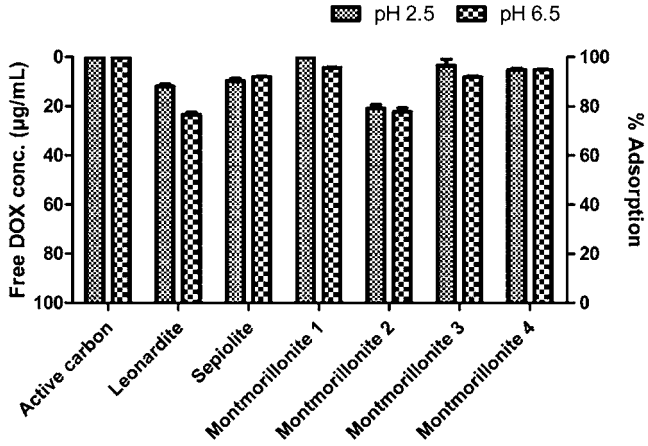

Figure 1. Doxycycline (DOX, 100 μg/mL) was incubated for 4 h at 37 °C with 20 mg of one of following binders in 5 mL of PBS buffer at pH 2.5 and 6.5: activated carbon (positive control), leonardite, sepiolite, and four different montmorillonites. The free DOX concentration (μg/mL) is presented on the left y-axis as the average of three independent measurements + standard deviation (SD). The percent adsorption is presented on the right y-axis. No significant differences were observed between the binders and activated carbon; however, all of the tested binders differed significantly (p < 0.001) from the negative control samples.

The plasma concentration−time profiles of DOX after a single oral bolus administration of the tetracycline whether or not combined with one of the binders are presented in Figure 2. Mean plasma concentration of DOX in the negative control group reached a first maximum at about 2.5 h and a second at 6 h. The area under the plasma concentration−time curves of the test groups are clearly lower compared to the control group, and the curves display only one maximum at the same time of the second maximum of the control group (at about 6 h). The PK parameters of DOX are presented in Table 1. Significant differences between the negative control group and test groups can be seen for the AUC_{0-inf}, AUC_{0-24h}, and C_{max} (p < 0.001). The absorption rate constant (k_a) was calculated using the curve-stripping method as described by Gabrielsson and

DOI: 10.1021/acs.jafc.5b00832
J. Agric. Food Chem. 2015, 63, 4370−4375

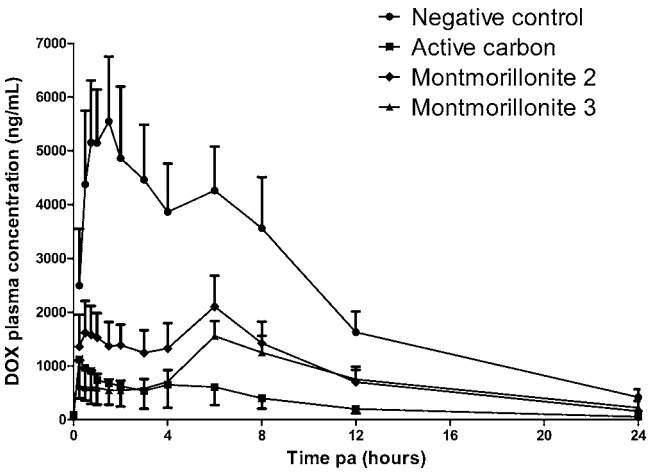

Figure 2. Four groups of eight broiler chickens were given an oral bolus containing water (negative control), activated carbon (positive control), montmorillonite 2, or montmorillonite 3 directly followed by an oral bolus containing doxycycline (DOX) at 20 mg/kg body weight. Plasma concentration−time profiles of DOX are presented as means of eight observations + standard deviation.

Weiner.[33] However, variance of the calculated k_a values did not allow meaningful comparison; therefore, this parameter was omitted from Table 1.

DISCUSSION

The aim of this study was to investigate the interactions between DOX and different feed additives used as mycotoxin binder. First, an in vitro adsorption screening study was performed. Therefore, an in vitro model as reported by De Mil et al.[7] and based on the model used by Sabater-Vilar et al.[25] was applied. This model uses PBS at pH values of 2.5 and 6.5, which represent, respectively, the gastric and duodenal pH conditions of monogastric animals. Less than 25% of the initial concentration could be detected as free DOX after 4 h of incubation at 37 °C in all groups, indicating that the majority of DOX is adsorbed by the additives. Deng et al.[10] described the binding mechanism between AFB1 and montmorillonite clays; the adsorption is facilitated by the exchangeable cations that form hydrogen bonds with AFB1. Along with the exchangeable cations, AFB1 can then be "trapped" between the silicate sheets of the montmorillonite and effectively bound. A similar mechanism might apply here because DOX has many sites suitable for hydrogen bonding.

When used as a mycotoxin binder, most recommendations mention an inclusion rate in the feed of 0.1−0.5% (w/w); however, when used as pelletizing, or binding, agent, inclusion rates up to 2% are recommended. A ratio of DOX/binder of 1:40 (w/w) is representative for the in vivo application of both substances when considering a clay inclusion rate of 1% (w/w); this ratio was the same in both the in vitro and in vivo trials.

The in vitro models used for the assessment of the efficacy include static[34,35] and dynamic[36,37] GI models, construction of adsorption isotherms,[38] and single-concentration studies.[25] Although the simple setup in this study cannot provide the same information as the complex dynamic and isotherm models, by using representative buffers and binder−drug ratios, this setup still can provide relevant information regarding the safety of the feed additives, which can be directly extrapolated to the in vivo situation. To verify the latter, in vivo experiments have to be carried out. An in vivo oral bolus model was applied to study the interactions from a PK perspective;[39] this is in accordance with EFSA guidelines for the safety testing of these group of additives.[12] Concerning the DOX PK parameters in the negative control group, the reported $T_{1/2,el}$ values are between 5.69 h[40] and 7.93 h[41] in broiler chickens, whereas this study found a $T_{1/2,el}$ of 8.22 h, which can be considered to be in the same range. The reported T_{max}, C_{max}, and AUC_{0-inf} values for most references are also in the same range as found for the control group in this study, namely, between 1.73 h[42] and 2.9 h[43] for T_{max}, between 3.18 μg/mL[40] and 7.84 μg/mL[41] for C_{max}, and between 39.84 μg·h/mL[40] and 97.6 μg·h/mL[41] for AUC_{0-inf}. The appearance of a second maximum in the plasma concentration−time profile is likely to be due to an enterohepatic recycling; this means excretion of DOX from the blood to the GI lumen by both hepatic/biliary or direct passive un-ionized diffusion from blood to gut, followed by reabsorption. This phenomenon, seen for most tetracyclines, has been described for many species such as pigs,[44] humans,[45] and sheep.[46] Pharmacokinetic analysis of DOX of the test groups clearly indicates that AUC_{0-inf} and C_{max} are decreased when AC or the tested montmorillonites are used simultaneously with DOX. Table 1 shows a somewhat delayed T_{max} of DOX in the montmorillonite test groups. However, this T_{max}

Table 1. Four Groups of Eight Broiler Chickens Were Given an Oral Bolus Containing Water (Negative Control), Activated Carbon (Positive Control), Montmorillonite 2, or Montmorillonite 3 Directly Followed by an Oral Bolus of Doxycycline (DOX) at 20 mg/kg Body Weight[a]

parameter	negative control	activated carbon	mont 2	mont 3
AUC^b_{0-inf} (h·μg/mL)	57.58 ± 16.37	7.91 ± 4.86 ‡[c]	23.01 ± 5.82 ‡	20.46 ± 6.22 ‡
AUC^b_{0-24h} (h·μg/mL)	54.70 ± 13.96	6.99 ± 4.77 ‡	21.73 ± 5.70 ‡	16.98 ± 4.35 ‡
relative F (%)	100.00 ± 28.42	13.74 ± 8.43 ‡	40.0 ± 10.10 ‡	35.52 ± 10.80 ‡
$T_{max}{}^d$ (h)	2.84 ± 2.73	0.88 ± 1.28	4.63 ± 2.55	6.00 ± 0.00 *
$C_{max}{}^e$ (μg/mL)	5.55 ± 1.40	1.16 ± 0.86 ‡	2.14 ± 0.53 ‡	1.56 ± 0.33 ‡
$k_{el}{}^f$ (1/h)	0.13 ± 0.02	0.14 ± 0.05	0.13 ± 0.02	0.11 ± 0.03
$T_{1/2el}{}^g$ (h)	8.22 ± 1.51	7.97 ± 2.64	7.82 ± 1.24	9.82 ± 3.20
Vd/F^h (L/kg)	3.05 ± 0.99	30.50 ± 24.21 *	7.20 ± 2.15	10.01 ± 3.06
Cl/F^i (L/h/kg)	0.38 ± 0.12	3.73 ± 2.48 ‡	0.91 ± 0.20	1.09 ± 0.47

[a]The pharmacokinetic parameters of DOX for the different test groups are presented as mean of the group ± standard deviation. [b]AUC, area under the curve from time 0 to infinity or 24 h. [c]*, †, and ‡ indicate significant difference compared to the control at the 0.05, 0.01, and 0.001 level, respectively. [d]T_{max}, time of maximum concentration. [e]C_{max}, maximum concentration. [f]k_{el}, elimination rate constant. [g]$T_{1/2el}$, elimination half-life. [h]Vd/F, distribution volume relative to the absolute oral bioavailability. [i]Cl/F, clearance relative to the absolute oral bioavailability.

DOI: 10.1021/acs.jafc.5b00832
J. Agric. Food Chem. 2015, 63, 4370−4375

coincides with the second absorption maximum of DOX in the control group (Figure 2), which indicates that this shift is rather due to the absence of the first maximum than a delayed absorption. Differences in Vd/F and Cl/F can be explained by a difference in bioavailability, although the latter cannot be calculated with the given data. As expected, no differences in elimination kinetics were seen, because k_{el} and $T_{1/2el}$ were similar in both control and test groups. The 60% decrease in AUC_{0-24h} in the test groups results in a lower AUC/minimal inhibitory concentration (MIC) ratio, which is of major importance for the clinical outcome.[47] Therefore, a decrease in treatment efficacy can be expected because a decrease in oral bioavailability F is linearly correlated to a decrease in AUC[48] and therefore also to the AUC/MIC ratio. Antimicrobials for which the efficacy depends on the time the plasma concentration is above the MIC, such as TYL, might even be more sensitive to a decrease in oral bioavailability because the time above MIC decreases in a logaritmic manner as a function of F. Moreover, subtherapeutic concentrations of tetracyclines can induce microbial resistance.[18] This interaction is in line with previously reported interactions of montmorillonite-based feed additives with the macrolides TIL[13] and TYL[15] in broiler chickens.

On the basis of the in vitro adsorption and in vivo pharmacokinetic results, it can be concluded that AC and the tested montmorillonite clays can substantially diminish the oral absorption of DOX in broiler chickens, and this is most likely due to the adsorption of DOX to the clay additives. Therefore, when DOX is orally administered to chickens that are also fed montmorillonite-based feed additives, a possible interaction needs to be carefully considered. Further research is needed to investigate the safety of other additives when used simultaneously with other veterinary medicinal products.

AUTHOR INFORMATION

Corresponding Author

*(T.D.M.) Phone: 0032 9 264 73 24. Fax: 0032 9 264 74 97. E-mail: thomas.demil@UGent.be.

Funding

This project (RF 11/6255 MYTOXBIND) was financed by the Federal Public Service of Health, Food chain Safety and Environment of the Belgian government.

Notes

The authors declare no competing financial interest.

ACKNOWLEDGMENTS

We gratefully acknowledge the assistance of Jelle Lambrecht, Joren De Smet, and Matteo Stecca.

ABBREVIATIONS USED

AC, activated carbon
ACN, acetonitrile
AFB1, aflatoxin B1
AUC, area under the curve
AUC_{0-24h}, AUC from time zero to the 24 h point
AUC_{0-inf}, AUC from time zero to infinity
BW, body weight
Cl/F, clearance relative to the absolute bioavailability
C_{max}, maximum plasma concentration
DMCTC, demethylchlortetracycline
EFSA, European Food Safety Authority
ESI+, electrospray ionization in the positive mode
F, bioavailability
GI, gastrointestinal
HPLC, high-performance liquid chromatography
k_{el}, elimination rate constant
LC-MS/MS, liquid chromatography−tandem mass spectrometry
LOQ, limit of quantification
MIC, minimal inhibitory concentration
MON, monensin
pa, post administration
PD, pharmacodynamic
PK, pharmacokinetic
relative F, relative bioavailability
SAL, salinomycin
SD, standard deviation
SRM, selected reaction monitoring
$T_{1/2,el}$, elimination half-life
TFA, trifluoroacetic acid
TIL, tilmicosin
T_{max}, time to reach C_{max}
TYL, tylosin
Vd/F, volume of distribution relative to the absolute bioavailability
XRD, X-ray diffraction

REFERENCES

(1) Streit, E.; Schatzmayr, G.; Tassis, P.; Tzika, E.; Marin, D.; Taranu, I.; Tabuc, C.; Nicolau, A.; Aprodu, I.; Puel, O.; Oswald, I. P. Current situation of mycotoxin contamination and co-occurrence in animal feed − focus on Europe. *Toxins* **2012**, *4*, 788−809.

(2) Binder, E. M.; Tan, L. M.; Chin, L. J.; Handl, J.; Richard, J. Worldwide occurrence of mycotoxins in commodities, feeds and feed ingredients. *Anim. Feed Sci. Technol.* **2007**, *137*, 265−282.

(3) Binder, E. M. Managing the risk of mycotoxins in modern feed production. *Anim. Feed Sci. Technol.* **2007**, *133*, 149−166.

(4) Jard, G.; Liboz, T.; Mathieu, F.; Guyonvarc'h, A.; Lebrihi, A. Review of mycotoxin reduction in food and feed: from prevention in the field to detoxification by adsorption or transformation. *Food Addit. Contam., Part A* **2011**, *28*, 1590−1609.

(5) Kolosova, A.; Stroka, J. Substances for reduction of the contamination of feed by mycotoxins: a review. *World Mycotoxin J.* **2011**, *4*, 225−256.

(6) Devreese, M.; De Backer, P.; Croubels, S. Different methods to counteract mycotoxin production and its impact on animal health. *Vlaams Diergen. Tijds.* **2013**, *82*, 181−190.

(7) De Mil, T.; Devreese, M.; De Baere, S.; Van Ranst, E.; Eeckhout, M.; De Backer, P.; Croubels, S. Characterization of 27 mycotoxin binders and the relation with in vitro zearalenone adsorption at a single concentration. *Toxins* **2015**, *7*, 21−33.

(8) Scientific Opinion on the safety and efficacy of bentonite as a technological feed additive for all species. *EFSA J.* **2012**, *10*, DOI: 10.2903/j.efsa.2012.2787.

(9) Desheng, Q.; Fan, L.; Yanhu, Y.; Niya, Z. Adsorption of aflatoxin B-1 on montmorillonite. *Poult. Sci.* **2005**, *84*, 959−961.

(10) Deng, Y. J.; Velazquez, A. L. B.; Billes, F.; Dixon, J. B. Bonding mechanisms between aflatoxin B-1 and smectite. *Appl. Clay Sci.* **2010**, *50*, 92−98.

(11) Phillips, T.; Afriyie-Gyawu, E.; Wang, J. S.; Williams, J.; Huebner, H. The potential of aflatoxin sequestering clay. In *The Mycotoxin Factbook, Food and Feed topics*; Barug, D., Bhatnagar, D., van Egmond, H. P., van der Kamp, J. W., van Osenbruggen, W. A., Visconti, A., Eds.; Wageningen Academic Publishers: Wageningen, The Netherlands, 2006; pp 329−346.

(12) Statement on the establishment of guidelines for the assessment of additives from the functional group 'substances for reduction of the

DOI: 10.1021/acs.jafc.5b00832
J. Agric. Food Chem. 2015, 63, 4370−4375

contamination of feed by mycotoxins'. *EFSA J.* **2010**, *8*, DOI: 10.2903/j.efsa.2010.1693.
(13) Shryock, T. R.; Klink, P. R.; Readnour, R. S.; Tonkinson, L. V. Effect of bentonite incorporated in a feed ration with tilmicosin in the prevention of induced mycoplasma gallisepticum airsacculitis in broiler chickens. *Avian Dis.* **1994**, *38*, 501−505.
(14) Canadian Bureau of Veterinary Drugs. Suspected drug adverse reactions reported to The Bureau of Veterinary Drugs. *Can. Vet. J.* **1992**, *33*, 237−244.
(15) Devreese, M.; Osselaere, A.; Goossens, J.; Vandenbroucke, V.; De Baere, S.; De Backer, P.; Croubels, S. Interaction between tylosin and bentonite clay from a pharmacokinetic perspective. *Vet. J.* **2012**, *194*, 437−439.
(16) Gray, S. J.; Ward, T. L.; Southern, L. L.; Ingram, D. R. Interactive effects of sodium bentonite and coccidiosis with monensin or salinomycin in chicks. *Poult. Sci.* **1998**, *77*, 600−604.
(17) Levy, S. B. Factors impacting on the problem of antibiotic resistance. *J. Antimicrob. Chemother.* **2002**, *49*, 25−30.
(18) Phillips, I.; Casewell, M.; Cox, T.; De Groot, B.; Friis, C.; Jones, R.; Nightingale, C.; Preston, R.; Waddell, J. Does the use of antibiotics in food animals pose a risk to human health? A critical review of published data. *J. Antimicrob. Chemother.* **2004**, *53*, 28−52.
(19) Kobland, J. D.; Gale, G. O.; Gustafson, R. H.; Simkins, K. L. Comparison of therapeutic versus subtherapeutic levels of chlortetracycline in the diet for selection of resistant salmonella in experimentally challenged chickens. *Poult. Sci.* **1987**, *66*, 1129−1137.
(20) AFSSA; CODA-CERVA; INRA; IRTA; ISPA. Review of Mycotoxin-Detoxifying Agents Used As Feed Additives: Mode of Action, Efficacy and Feed/Food Safety; Scientific Report submitted to EFSA, 2009.
(21) Avrain, L.; Humbert, F.; L'Hospitalier, R.; Sanders, P.; Vernozy-Rozand, C.; Kempf, I. Antimicrobial resistance in Campylobacter from broilers: association with production type and antimicrobial use. *Vet. Microbiol.* **2003**, *96*, 267−276.
(22) Cauwerts, K.; Decostere, A.; De Graef, E. M.; Haesebrouck, F.; Pasmans, F. High prevalence of tetracycline resistance in Enterococcus isolates from broilers carrying the erm(B) gene. *Avian Pathol.* **2007**, *36*, 395−399.
(23) Johansson, A.; Greko, C.; Engstrom, B. E.; Karlsson, M. Antimicrobial, susceptibility of Swedish, Norwegian and Danish isolates of *Clostridium perfringens* from poultry, and distribution of tetracycline resistance genes. *Vet. Microbiol.* **2004**, *99*, 251−257.
(24) Butaye, P.; Ducatelle, R.; De Backer, P.; Vermeersch, H.; Remon, J. P.; Haesebrouck, F. *In vitro* activities of doxycycline and enrofloxacin against European *Chlamydia psittaci* strains from turkeys. *Antimicrob. Agents Chemother.* **1997**, *41*, 2800−2801.
(25) Sabater-Vilar, M.; Malekinejad, H.; Selman, M. H. J.; van der Doelen, M. A. M.; Fink-Gremmels, J. In vitro assessment of adsorbents aiming to prevent deoxynivalenol and zearalenone mycotoxicoses. *Mycopathologia* **2007**, *163*, 81−90.
(26) European Council. *European Convention for the Protection of Vertebrate Animals used for Experimental and Other Scientific Purposes*; European Council: Strasbourg, France, 2009.
(27) De Baere, S.; Goossens, J.; Osselaere, A.; Devreese, M.; Vandenbroucke, V.; De Backer, P.; Croubels, S. Quantitative determination of T-2 toxin, HT-2 toxin, deoxynivalenol and deepoxy-deoxynivalenol in animal body fluids using LC-MS/MS detection. *J. Chromatogr. B: Anal. Technol. Biomed. Life Sci.* **2011**, *879*, 2403−2415.
(28) 96/23/EC, Implementing council directive 96/23/EC concerning the performances of analytical methods and interpretation of results. *Off. J. Eur. Communities* **2002**.
(29) 2002/657/EC, Commission decision 20028/657/EC implementing council directive 96/23/EC concerning the performances of analytical methods and interpretation of results. *Off. J. Eur. Communities* **2002**.
(30) VICH; GL49 *Guidance for Industry. Studies to Evaluate the Metabolism and Residue Kinetics of Veterinary Drugs in Food-Producing Animals: Validation of Analytical Methods used in Residue Depletion Studies*; U.S. Department of Health and Human Services, Food and Drug Administration, Center for Veterinary Medicine: Rockville, MD, USA, 2011.
(31) Knecht, J.; Stork, G. Percentage and logarithmic procedures for calculation of calibration curves. *Fresenius' Z. Anal. Chem.* **1974**, *270*, 97−99.
(32) Heitzman, R. J. *Veterinary Drug Residues*, Report Eur. 14126-EN; Commision of the EC: Brussels, Belgium, 1994; pp 399−415.
(33) Gabrielsson, J.; Weiner, D. Pharmacokinetic concepts, non compartmental analysis. In *Pharmacokinetic and Pharmacodynamic Data Analysis: Concepts and Application*, 4th ed.; Swedish Academy of Pharmaceutical Sciences: Stockholm, Sweden, 2000; pp 161−179.
(34) Vekiru, E.; Fruhauf, S.; Sahin, M.; Ottner, F.; Schatzmayr, G.; Krska, R. Investigation of various adsorbents for their ability to bind aflatoxin B1. *Mycotoxin Res.* **2007**, *23*, 27−33.
(35) Devreese, M.; Pasmans, F.; De Backer, P.; Croubels, S. An *in vitro* model using the IPEC-J2 cell line for efficacy and drug interaction testing of mycotoxin detoxifying agents. *Toxicol. In Vitro* **2013**, *27*, 157−63.
(36) Avantaggiato, G.; Havenaar, R.; Visconti, A. Assessing the zearalenone-binding activity of adsorbent materials during passage through a dynamic in vitro gastrointestinal model. *Food Chem. Toxicol.* **2003**, *41*, 1283−1290.
(37) Ramos, A. J.; Hernandez, E. *In situ* absorption of aflatoxins in rat small intestine. *Mycopathologia* **1996**, *134*, 27−30.
(38) Ramos, A. J.; Hernandez, E. *In vitro* aflatoxin adsorption by means of a montmorillonite silicate. A study of adsorption isotherms. *Anim. Feed Sci. Technol.* **1996**, *62*, 263−269.
(39) Devreese, M.; Osselaere, A.; Goossens, J.; Vandenbroucke, V.; De Baere, S.; Eeckhout, M.; De Backer, P.; Croubels, S. New bolus models for in vivo efficacy testing of mycotoxin-detoxifying agents in relation to EFSA guidelines, assessed using deoxynivalenol in broiler chickens. *Food Addit. Contam., Part A* **2012**, *29*, 1101−1107.
(40) El-Gendi, A. Y. I.; Atef, M.; Amer, A. M. M.; Kamel, G. M. Pharmacokinetic and tissue distribution of doxycycline in broiler chickens pretreated with either: diclazuril or halofuginone. *Food Chem. Toxicol.* **2010**, *48*, 3209−3214.
(41) Ismail, M. M.; El-Kattan, Y. A. Disposition kinetics of doxycycline in chickens naturally infected with *Mycoplasma gallisepticum*. *Br. Poult. Sci.* **2004**, *45*, 550−556.
(42) Laczay, P.; Semjen, G.; Lehel, J.; Nagy, G. Pharmacokinetics and bioavailability of doxycycline in fasted and nonfasted broiler chickens. *Acta Vet. Hung.* **2001**, *49*, 31−37.
(43) Gutierrez, L.; Vargas-Estrada, D.; Rosario, C.; Sumano, H. Serum and tissue concentrations of doxycycline in broilers after the subcutaneous injection of a long-acting formulation. *Br. Poult. Sci.* **2012**, *53*, 366−373.
(44) Riond, J. L.; Riviere, J. E. Pharmacokinetics and metabolic inertness of doxycycline in young pigs. *Am. J. Vet. Res.* **1990**, *51*, 1271−1275.
(45) Gibaldi, M. Pharmacokinetics of absorption and elimination of doxycycline in man. *Chemotherapy* **1967**, *12*, 265−271.
(46) Castro, L. J.; Sahagun, A. M.; Diez, M. J.; Fernandez, N.; Sierra, M.; Garcia, J. J. Pharmacokinetics of doxycycline in sheep after intravenous and oral administration. *Vet. J.* **2009**, *180*, 389−395.
(47) Hesje, C.; Tillotson, G.; Blondeau, J. MICs, MPCs and PK/PDs: a match (sometimes) made in hosts. *Expert Rev. Respir. Med.* **2007**, *1*, 7−16.
(48) Gabrielsson, J.; Weiner, D. Pharmacokinetic concepts. In *Pharmacokinetic and Pharmacodynamic Data Analysis: Concepts and Applications*, 4th ed.; Swedish Pharmaceutical Society: Stockholm, Sweden, 2006.

DOI: 10.1021/acs.jafc.5b00832
J. Agric. Food Chem. 2015, 63, 4370−4375

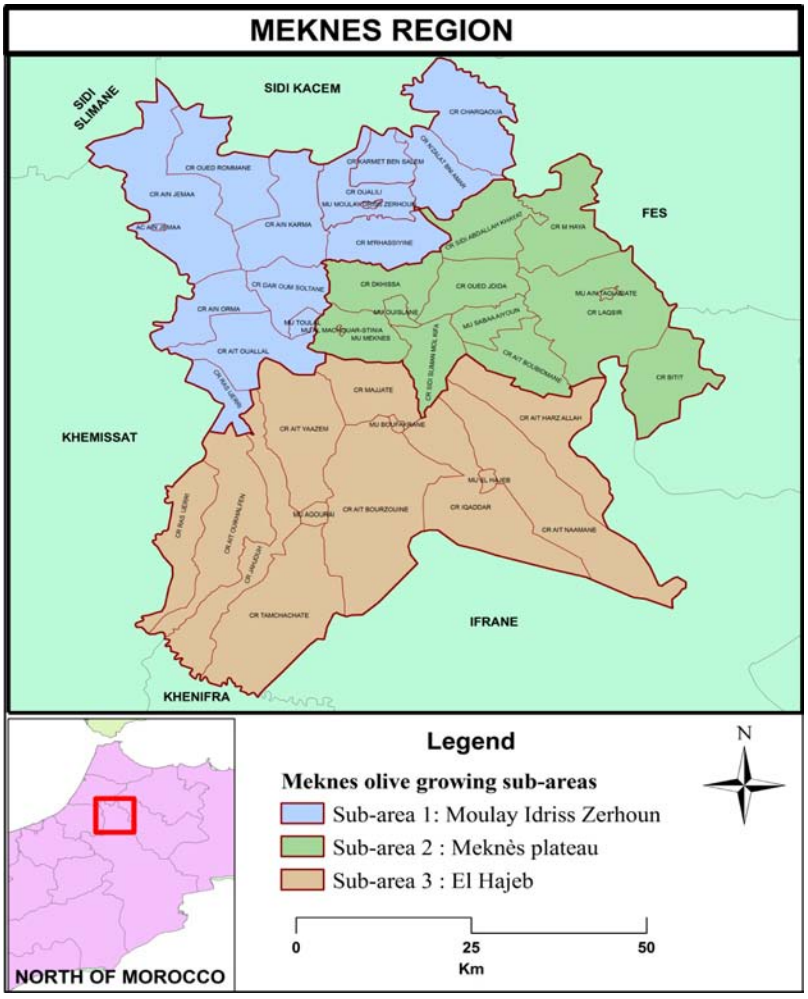

Figure 1. Map of the Meknès region showing the three subareas considered in the current study.

However, despite the importance of VOO production in the above-mentioned Meknès region, there is practically no detailed pluri-annual qualitative and quantitative characterization of the phenolic fraction of VOOs produced in this region.

Therefore, the aim of this work was to solve the lack of information in this regard by carrying out the comprehensive characterization and evolution of the phenolic fraction of Meknès VOOs over three consecutive seasons. A powerful LC-MS (using different analyzers) was used, and a total of 142 samples (from three diverse areas) were analyzed. The possible effect of interannual and intraregional variations on the content of the identified phenolic compounds was also evaluated. To our best knowledge, this work represents the first pluri-annual study reporting data on the phenolic fraction of VOOs from a Moroccan region.

MATERIALS AND METHODS

Olives Sampling. Monovarietal virgin olive oils from the most relevant Moroccan cultivar, Picholine marocaine, were considered. A total of 142 olive fruit samples were collected over three consecutive seasons (harvesting periods 2011−2013) from three subareas of the Meknès region (Figure 1). Sampling was carried out from the middle of October until the end of December. Olive samples (one sample is approximately 35 kg of olives) were handpicked in olive groves located in the three selected subareas belonging to the Meknès region. Only good-quality, fresh, and healthy fruits were selected. Ripening stage, being a parameter with great influence on olive oil characteristics, was evaluated by determining the ripening index following the method developed at the Agronomic Station of Jaén, based on the evaluation of the olive skin and pulp colors.[18] After harvesting, the olive fruit samples were immediately transported to the laboratory in ventilated rectangular plastic crates, and the oil was extracted within 24 h.

Oil Extraction. Oil extraction was carried out in a laboratory instrument, SPREMOLIVA C30 Oliomio (Oliomio, Italy) with a work capacity of 30 kg/h, and equipped with a knife crusher, a horizontal malaxator, and a two-phase decanter. Fruits were processed as follows: olives were washed to eliminate any foreign material and poured into the receiving hopper, where a screw feeds the crusher that is equipped with fix hole grid and grooved knife impeller at a temperature of 25−27 °C. The paste produced falls into the malaxing part; malaxing was carried out for 45 min at 28−30 °C. The resulting olive paste was decanted at a temperature of 23−27 °C without the addition of any water. All of the samples were subsequently filtered, placed in amber glass bottles, and stored in the dark at 4 °C.

Physicochemical Quality Indices. Determination of free fatty acids content (given as a percentage of oleic acid), peroxide value (expressed as milliequivalents of active oxygen per kilogram of olive oil (mequiv O_2/kg)) and K_{232} and K_{270} extinction coefficients calculated from absorption at 232 and 270 nm, respectively, was carried out by using the analytical methodologies described in the European Union Standard Methods Regulations 2568/91 and the subsequent amendments.[19] All of the parameters were determined in triplicate for each sample.

Phenolic Compound Analysis. *Chemicals and Reagents.* All of the reagents were of analytical grade and used as received. Methanol and *n*-hexane of HPLC grade supplied from Panreac (Barcelona, Spain)

DOI: 10.1021/jf506097u
J. Agric. Food Chem. 2015, 63, 4376−4385

were used for the extraction of the phenolic compounds from the olive oil samples. Acetonitrile from Lab-Scan (Dublin, Ireland) and acetic acid from Panreac were used for preparing the mobile phases. Water was deionized using a Milli-Q-system (Millipore, Bedford, MA, USA). Several phenolic standards were used for identification and quantification purposes, namely, hydroxytyrosol, tyrosol, luteolin, apigenin, and *p*-coumaric, quinic acid, ferulic, and caffeic acids supplied by Sigma-Aldrich (St. Louis, MO, USA), and (+)-pinoresinol was purchased from Arbo Nova (Turku, Finland). Oleuropein was acquired from Extrasynthese (Lyon, France). 3,4-Dihydroxyphenylacetic acid (DOPAC) was used as internal standard and supplied by Sigma-Aldrich.

Stock standard solutions of individual compounds at a concentration of 500 mg/L were prepared by exact weighing of the appropriate amount of the pure compound and dissolving it in methanol. These solutions were stored at −20 °C in the dark. Multianalyte working standard solutions at different concentration levels within the range of 0.5−250 ppm were prepared by appropriate dilutions of the stock solutions and stored in screw-capped glass tubes at −20 °C in the dark.

Phenolic Compound Extraction. The extraction of the phenolic compounds was carried out as previously described by Bajoub et al.,[16] with little modification. Briefly, 2 g of olive oil and 0.025 mL of internal standard solution (at a concentration of 500 mg/L) were extracted (repeating the same process three times in a row), adding every time 1 mL of *n*-hexane and 2 mL of methanol/water (60/40); the extract was centrifuged at 3500 rpm for 6 min. The combined extracts were evaporated to dryness using a rotary evaporator under reduced pressure and a temperature of about 30 °C. The residue was reconstituted up to 1 mL with methanol and filtered through 0.20 μm membrane (nylon) filters.

Chromatographic Separation. In a first step and for initial characterization purposes of the phenolic fraction of the studied samples, the analyses were carried out on a Waters LC Acquity system (LC, Acquity H-Class) (Milford, MA, USA) equipped with a Waters Acquity quaternary solvent manager (QSM), an Acquity sample manager (SM), a column heater, a degassing system, a diode array detector, and an ESI-time of flight MS detection system. Afterward, an Agilent 1260-LC system (Agilent Technologies, Waldbronn, Germany) equipped with an autosampler, degasser, quaternary pump, thermostated column compartment,diode array detector, and an ESI-ion trap MS detection system was used for further identification and quantification purposes. In both cases, the analysis of phenolic compounds was performed by following a previously reported methodology.[16] Separation was achieved on a Zorbax C18 analytical column (4.6 × 150 mm, 1.8 μm particle size), protected by a guard cartridge of the same packing. The injection volume was 10 μL in every case. The binary mobile phase consisted of water with acetic acid (0.5%) (phase A) and acetonitrile (phase B) and was delivered at a flow rate of 0.8 mL/min. Gradient elution was performed using the following solvent gradient: 0−10 min, 5% B; 10−12 min, 30% B; 12−17 min, 38% B; 17−20 min, 50% B; 20−23 min, 95% B. Finally, the B content was decreased to the initial conditions (5%) in 2 min and the column re-equilibrated for 2.5 min. As stated before, the separated compounds were monitored in sequence first with DAD (240, 280, and 330 nm) and then with a mass spectrometry detector (ESI-TOF MS or ESI-IT MS).

ESI-TOF MS and ESI-IT MS Conditions. To avoid the introduction of humidity into the system and achieve stable electrospray ionization and reproducible results, the flow delivered into the MS detectors from LC was reduced to 0.2 mL/min using a flow divisor 1:4. MS detection was first performed in a Synapt G2 time-of-flight (TOF) mass spectrometer (Milford, MA, USA) equipped with an electrospray interface. Spectra were recorded in negative mode, operating within the range of 50−1200 Da and at a scan speed of 240 ms. The source temperature was set at 100 °C with a cone gas flow of 800 L/h, a desolvation gas temperature of 500 °C, and a desolvation gas flow of 100 L/h. The capillary voltage was set at 2.2 kV. Internal calibration was performed using sodium formate cluster by using a solution containing 5 mM sodium hydroxide in the sheath liquid of 0.2% formic acid in water/isopropanol 1:1 v/v. The calibration solution was injected at the beginning of the run, and all of the spectra were calibrated prior to carrying out the compound identification. The accurate mass data of the molecular ions were processed through the software MassLynx 4.1 (Waters), which provided a list of possible elemental formulas, giving a Fit Conf (%) parameter that shows the prediction confidence.

After characterization of the phenolic fraction of the samples under study by TOF MS, a Bruker Daltonics Esquire 2000TM ion trap (Bruker Daltonik, Bremen, Germany) was used. The phenolic extracts were injected using the chromatographic conditions described above and both full scan (for quantitation purposes) and auto MS/MS (for further characterization purposes, in both negative and positive polarities). As far as MS/MS conditions are concerned, two methods were used: in the first one, the selected fragmentation energy (using nitrogen (N_2) as collision gas) was automatically applied to all of the ions that overtook the threshold intensity of 15000; in the second method, however, the analytical window was divided into two segments, and different threshold intensities were fixed for each one (the first one up to 12.5 min with an intensity threshold of 10000 and the second one, from 12.5 min until the end of the run, with a threshold intensity of 27000). Full scan mass spectra (m/z 50−800) were recorded in negative mode using a capillary voltage of 3.2 kV. The nebulizer gas was set at 30 psi, dry gas at 9 L/min, and drying gas (N_2) temperature at 300 °C. MS data were processed through Data Analysis 4.0 software (Bruker Daltonics, Bremen, Germany).

Phenolic Compound Identification and Quantification. Peak identification was done bearing in mind retention time, spectral data, and ESI-TOF MS and ESI-IT MS/MS information obtained from olive oil samples and pure standards. We also used the previously reported information.[12] The linearity of the detector response was verified with standard solutions at 11 different concentration levels over the range from the quantification limit to 250 ppm (0.5, 1, 5, 12.5, 25, 35, 50, 100, 150, 200, and 250 mg/L). Each point of the calibration graph corresponded to the mean value from three independent replicate injections. Calibration curves were obtained for each standard by plotting the standard concentration as a function of the peak area obtained from LC-ESI-IT MS analyses. The following equations were obtained for each calibration curve: apigenin ($y = 298095x + 53202$; $r^2 = 0.999$); caffeic acid ($y = 121649x + 45541$; $r^2 = 0.995$); ferulic acid ($y = 69884x + 26610$; $r^2 = 0.992$); hydroxytyrosol ($y = 117686x - 12928$; $r^2 = 0.998$); luteolin ($y = 259366x + 17767$; $r^2 = 0.999$); oleuropein ($y = 20535.20x + 5444.60$; $r^2 = 0.995$); *p*-coumaric acid ($y = 82728x + 23247$; $r^2 = 0.997$); pinoresinol ($y = 79815x + 44395$; $r^2 = 0.997$); quinic acid ($y = 77315x - 6950.41$; $r^2 = 0.997$); and tyrosol ($y = 33975x + 9524.70$; $r^2 = 0.995$). The compounds for which pure standards were not available were quantified on the basis of other analytes with similar chemical structures. In particular, secoiridoids were quantified in terms of oleuropein and lignans in terms of pinoresinol, and oxidized hydroxytyrosol was quantified by comparison with hydroxytyrosol.

Statistical Analysis. As the number of samples selected in the current study was considerably high (142 samples from different areas over three seasons), the quantitative data have been reported as mean ± standard deviation (SD) values of triplicate experiments and were analyzed using SPSS 20.0. One-way analysis of variance (ANOVA) and Tukey's test (with a significance level of 0.05) were used to determine the significance of the difference among the studied parameters regarding the subarea and crop season.

RESULTS AND DISCUSSION

Ripening and Quality Indices. Table 1 summarizes the mean ± standard deviation and maximum and minimum values of the ripening index and the regulated quality criteria (free fatty acids, peroxide value, K_{232}, and K_{270}) for all of the olive oil samples extracted from fruits of Picholine marocaine cultivar population grown in the areas considered within the current study. As can be seen, the ripening index values of the olive fruits used for the extraction of the olive oils were between a minimum value of 1.14 (crop season 2013) and a maximum

DOI: 10.1021/jf506097u
J. Agric. Food Chem. 2015, 63, 4376−4385

Table 1. Average Values and Intervals of Ripening Index and Quality Parameters (Free Fatty Acids (FAAs), Peroxide Values (PV), and Ultraviolet Absorbance at 232 nm (K_{232}) and 270 nm (K_{270})) Determined for Meknès Monovarietal Olive Oils Samples over the Three Crop Seasons Considered (2011, 2012, and 2013)

	subarea 1			subarea 2			subarea 3			category	
	mean[a] ± SD[b]	max	min	mean[a] ± SD[b]	max	min	mean[a] ± SD[b]	max	min	extra virgin	virgin
2011 (n = 43)											
ripening index	3.16Aa ± 1.25	4.85	1.67	2.99Aa ± 0.95	4.63	1.60	2.96Aa ± 1.19	5.60	1.44	41	2
FAAs (% oleic acid)	0.31Aa ± 0.07	0.41	0.21	0.31Aa ± 0.13	0.62	0.20	0.46Ba ± 0.20	0.86	0.22		
PV (mequiv O_2/kg)	8.18Aa ± 0.46	8.89	7.35	8.69Aa ± 0.69	9.50	7.46	8.11Aa ± 0.84	9.75	6.80		
K_{232}	1.28Aa ± 0.17	1.59	1.09	1.24Aa ± 0.16	1.54	1.02	1.28Aa ± 0.18	1.65	1.03		
K_{272}	0.13Aa ± 0.02	0.16	0.08	0.14Aa ± 0.03	0.16	0.08	0.13Aa ± 0.02	0.16	0.08		
2012 (n = 34)											
ripening index	3.52Aa ± 1.67	6.29	1.47	3.27Aa ± 1.43	6.78	1.40	3.43Aa ± 0.75	4.26	2.40	34	0
FAAs (% oleic acid)	0.20Ab ± 0.08	0.38	0.12	0.22Aa ± 0.06	0.35	0.11	0.18Ab ± 0.04	0.23	0.11		
PV (mequiv O_2/kg)	5.55Ab ± 1.13	8.00	4.50	7.53Ba ± 2.19	5.00	12.00	6.71ABa ± 3.40	12.50	3.50		
K_{232}	1.40Ab ± 0.23	1.74	1.03	1.49Ab ± 0.18	1.74	1.20	1.37Aab ± 0.23	1.73	1.08		
K_{272}	0.14Aa ± 0.04	0.21	0.09	0.15Aa ± 0.04	0.18	0.09	0.14Aa ± 0.02	0.16	0.11		
2013 (n = 65)											
ripening index	3.12Aa ± 0.93	5.45	1.14	2.56Aa ± 0.93	4.12	1.56	3.42Aa ± 1.37	6.72	1.75	63	2
FAAs (% oleic acid)	0.24Ab ± 0.11	0.51	0.11	0.26Aa ± 0.12	0.42	0.12	0.26Ac ± 0.15	0.89	0.12		
PV (mequiv O_2/kg)	9.17Aa ± 2.59	15.00	5.00	7.94Aa ± 2.48	12.50	5.00	7.73Aa ± 2.60	15.00	5.00		
K_{232}	1.60Ab ± 0.36	1.78	1.12	1.61Ab ± 0.36	1.85	1.12	1.52Ab ± 0.28	1.95	1.12		
K_{272}	0.15Aa ± 0.03	0.17	0.10	0.15Aa ± 0.03	0.18	0.09	0.14Aa ± 0.04	0.18	0.09		
									total	138 (97.18%)	4 (2.82%)

[a]Significant differences in the same row are indicated with different upper case letters (comparison between subareas at the same crop season, $p < 0.05$). Significant differences in the same column are indicated with different lower case letters (comparison among crop seasons, $p < 0.05$). [b]In this table and Table 3 the mean values are those calculated for all of the samples from the same area; therefore, SD gives to the reader an idea about only the variability of the olive oils in terms of composition and obviously not about the repeatability of the analytical methods used.

value of 6.78 (crop season 2012). This wide range allowed evaluation of the phenolic composition of the olive oil samples at three main maturation stages: green, spotted, and ripe. Furthermore, the ripening index was practically unaffected by the olive cultivation subarea or the crop season over the studied period. Therefore, the effect of the maturity stage on the differences found for the other studied parameters (in particular, for the phenolic composition) can be dismissed.

As far as the quality indices are concerned, and taking into account the limits set by the Commission of the European Community for olive oil classification,[19] 97.18% of the studied samples fell within the "extra virgin" category, and the rest (2.82%) were within the "virgin" category. This result is not surprising because the raw material was carefully selected, picked, and processed. Thus, as shown in Table 1, mean values for free fatty acid content (expressed as percentage of oleic acid) ranged from 0.18 to 0.46%. Only four olive oil samples showed a value >0.8%, which is the upper threshold limit established for the extra VOO category; none exceeded the limit of 2% for the VOO category.[19] The peroxide value was lower than the upper limit of 20 mequiv O_2/kg established for the extra virgin category for every sample, ranging from 5.55 to 9.17 mequiv O_2/kg. Likewise, all of the values of spectrophotometric UV absorption at 232 nm (K_{232}) and 270 nm (K_{270}) were below the limits of 0.22 and 2.25, respectively, established for the extra virgin category. Their mean values ranged from 1.24 to 1.61 and from 0.13 to 0.15 for K_{232} and K_{270}, respectively. Results of ANOVA test revealed that no statistically significant differences were observed for the quality indices according to production subarea. These results are in good agreement with the findings of other authors,[20,21] who claimed that these analytical parameters are mainly affected by factors causing damage to the fruits, such as olive fly attacks or inappropriate harvesting practices, transport, and storage of olives.

Phenolic Compound Profiling. *Qualitative Characterization.* Figure 2 shows a typical LC-ESI-TOF MS profile of a phenolic extract of Picholine marocaine, where the extract ion chromatograms (EICs) of the determined compounds are shown. The identification of these compounds was performed considering the information provided by the TOF MS detector, the information collected from MS/MS experiments in negative and positive modes, and the use of commercial pure standards (when available). The components were efficiently separated, and it was possible to identify 29 peaks, corresponding to a polar nonphenolic compound (quinic acid) and 28 phenolic substances (belonging to five different chemical categories) (see Table 2). The phenolic profile of Meknès olive oil samples was dominated by the presence of a high number of secoiridoids, mainly oleuropein aglycone (Ol Agl), ligstroside aglycone (Lig Agl), and six and three isomers of each one, respectively, decarboxymethyl oleuropein aglycone (DOA), dehydro oleuropein aglycone (Dehydro Ol Agl), methyl oleuropein aglycone (Methyl Ol Agl), methyl decarboxymethyl oleuropein aglycone (Methyl D-Ol Agl), decarboxymethyl ligstroside aglycone (D-Lig Agl), dialdehydic form of decarboxymethyl elenolic acid (D-Ald-D EA), desoxy elenolic acid (Desoxy-EA), and elenolic acid (EA). Besides, it was also possible to determine various simple phenols (hydroxytyrosol (Hyt), oxidized hydroxytyrosol (O-Hyt), and tyrosol (Ty)), lignans ((+)-pinoresinol (Pin), (+)-1-acetoxypinoresinol (Ac-Pin), and syringaresinol (Syr)), flavonoids (luteolin (Lut) and apigenin (Apig)), and a phenolic acid (*p*-coumaric acid).

Variation of the Phenolic Compounds Content over the Studied Period. It is well established that phenolic content in olive oil widely depends on intrinsic (genetic) and extrinsic

DOI: 10.1021/jf506097u
J. Agric. Food Chem. 2015, 63, 4376−4385

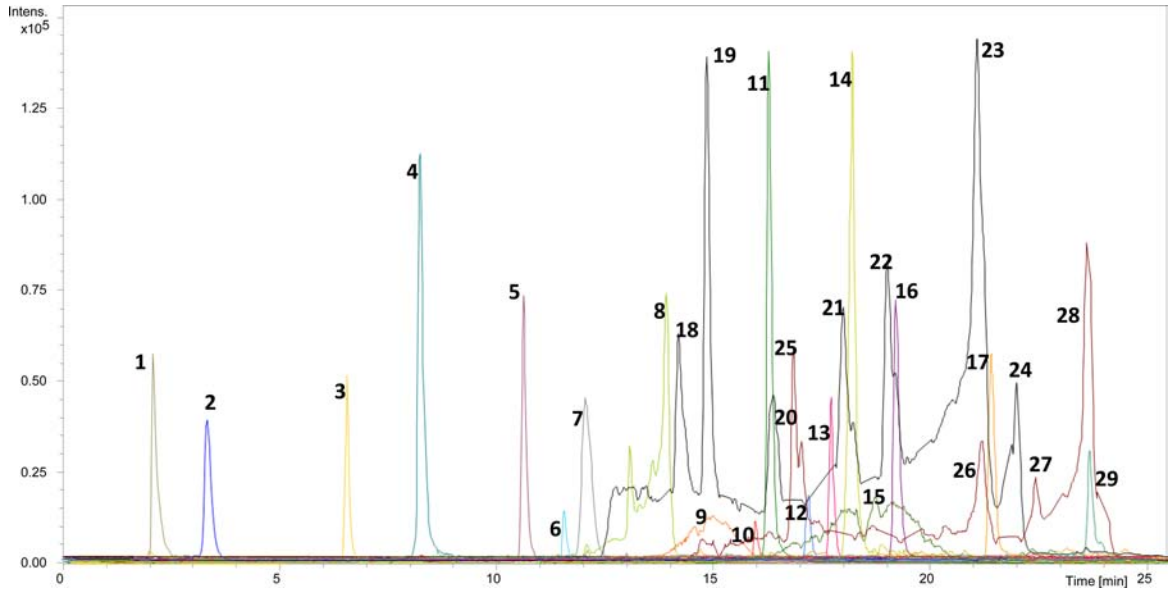

Figure 2. Extracted ion chromatograms (EICs) of the main phenolic compounds identified in Meknès VOOs. Peaks: 1, quinic acid; 2, O-Hyt; 3, Hyt; 4, Ty; 5, D-Ald-D EA; 6, *p*-cou; 7, Deoxy-EA; 8, EA; 9, DOA; 10, Syr; 11, Lut; 12, Pin; 13, Ac-Pin; 14, Methyl D-Ol Agl; 15, D-Lig Agl; 16, Apig; 17, Dehydro Ol Agl; 18, Ol Agl isomer 1; 19, Ol Agl isomer 2; 20, Ol Agl isomer 3; 21, Ol Agl isomer 4; 22, Ol Agl isomer 5; 23, Ol Agl; 24, Ol Agl isomer 6; 25, Lig Agl isomer 1; 26, Lig Agl isomer 2; 27, Lig Agl isomer 3; 28, Lig Agl; 29, Methyl Ol Agl.

Table 2. Phenolic Compounds (or Related Analytes) Found in the Extracts of Meknès VOOs, Identified by LC-TOF MS and LC-IT MS/MS Experiments

compound	retention time (min)	molecular formula	*m/z* exptl	*m/z* calcd	error (mDa)	fit conf (%)	fragments in MS/MS spectra
quinic acid	2.06	$C_7H_{12}O_6$	191.0568	191.0556	1.2	100	191; 127.0; 93.1
oxidized hydroxytyrosol	3.37	$C_8H_8O_3$	151.0384	151.0395	−1.1	100	151.1; 122.9; 169.9
hydroxytyrosol	6.74	$C_8H_{10}O_3$	153.0557	153.0552	0.5	100	153.0; 123
tyrosol	8.49	$C_8H_{10}O_2$	137.0591	137.0603	−1.2	100	137.0; 119.0; 105.9
decarboxymethylated form of elenolic acid	10.77	$C_9H_{12}O_4$	183.0654	183.0657	−0.3	100	183.0; 139.0; 95.1
p-coumaric acid	11.60	$C_9H_8O_3$	163.0378	163.0395	−1.7	100	163.1; 119
desoxy elenolic acid	12.13	$C_{11}H_{14}O_5$	225.0764	225.0763	0.1	100	225.0; 123.0; 101.0
elenolic acid	14.03	$C_{11}H_{14}O_6$	241.0709	241.0712	−0.3	88.11	241.0; 138.9; 127.0; 95.1; 110.1; 164.9
decarboxymethyl oleuropein aglycone	15.05	$C_{17}H_{20}O_6$	319.1158	319.1182	−2.4	99.69	319.1; 194.9; 165.0; 300.9
syringaresinol	16.13	$C_{22}H_{25}O_8$	417.1233	417.1251	−1.8	95.99	
luteolin	16.38	$C_{15}H_{10}O_6$	285.0409	285.0438	−2.9	92.74	285.0; 150.9; 164.9
pinoresinol	17.20	$C_{20}H_{22}O_6$	357.1279	357.1261	1.8	87.76	357.0; 151.0; 136.0; 311.0; 342.0
acetoxypinoresinol	17.85	$C_{22}H_{24}O_8$	415.1386	415.1393	−0.7	98.14	415.1; 325.0; 295.0; 371.0; 235.0
methyl decarboxymethyl oleuropein aglycone	18.04	$C_{11}H_{26}O_{11}$	333.1356	333.1397	−4.1	95.99	
decarboxymethyl ligstroside aglycone	18.64	$C_{17}H_{20}O_5$	303.1132	303.1126	0.6	98.86	303.0; 284.9; 165.0; 179.0
apigenin	19.27	$C_{15}H_{10}O_5$	269.0472	269.0451	2.1	99.51	269.0; 150.9; 183.5; 224.8; 201.0
dehydro oleuropein aglycone	21.43	$C_{19}H_{20}O_8$	375.1072	375.1068	0.4	95.99	375.0; 307.0; 275.2; 345.0; 139.2
oleuropein aglycone	21.50	$C_{19}H_{22}O_8$	377.1235	377.1236	−0.1	100	377.0; 307.0; 275.1; 345.0; 149.1
isomer 1	14.50	$C_{19}H_{22}O_8$	377.1256	377.1236	2	99.23	
isomer 2	15.20	$C_{19}H_{22}O_8$	377.1254	377.1236	1.8	99.88	
isomer 3	16.80	$C_{19}H_{22}O_8$	377.1263	377.1236	2.7	99.96	
isomer 4	18.00	$C_{19}H_{22}O_8$	377.1225	377.1236	−1.1	99.35	
isomer 5	19.50	$C_{19}H_{22}O_8$	377.1237	377.1236	0.1	100	
isomer 6	22.10	$C_{19}H_{22}O_8$	377.1248	377.1236	1.2	99.76	
methyl oleuropein aglycone	23.40	$C_{20}H_{24}O_8$	391.1403	391.1393	1.0	92.86	391.1; 321.0; 275.1; 209.1; 344.9
ligstroside aglycone	23.60	$C_{19}H_{22}O_7$	361.1263	361.1287	−2.4	99.96	361.1; 291.0; 259.1; 223.1
isomer 1	16.90	$C_{19}H_{22}O_7$	361.1288	361.1287	0.1	100	
isomer 2	21.30	$C_{19}H_{22}O_7$	361.1294	361.1287	0.7	100	
isomer 3	22.50	$C_{19}H_{22}O_7$	361.1282	361.1287	−0.5	100	

DOI: 10.1021/jf506097u
J. Agric. Food Chem. 2015, 63, 4376−4385

(geographical, seasonal, agronomic, environmental, maturation stage, processing and storage conditions) factors.[22−25] In the current study, the effect of the harvest season and production subarea on the composition of monovarietal olive oil from Meknès region (in terms of phenolic compounds) was evaluated (Table 3). Moreover, the total content for each chemical class (expressed in mg/kg) was calculated as the sum of the content of the individual phenols belonging to that chemical category (Table 3). It is possible to highlight the existence of an important intra-sub-zone variability, as attested by the wide range of obtained values. This variability can be the result of the genetic diversity of the cultivar Picholine marocaine. Indeed, several studies carried out to determine the comprehensive genetic characterization of this cultivar have reported that it includes several distinct clones and local genotypes, all known under the common name Picholine marocaine.[26,27]

Even if the qualitative phenolic compositions of all the analyzed olive oil samples from Meknès over the studied period were quite similar, the abundance of the analytes under study (in terms of both individual phenol concentration levels and global content by chemical categories) widely differed as illustrated by Figure 3 and Table 3. In general, *secoiridoids* were the most abundant group of phenolic compounds in every sample regardless of the subarea of origin and the harvest season, a fact that is in good agreement with the findings of other authors for various monovarietal olive oils.[12,28,29] This type of phenolic compound is of great importance because, for instance, it contributes to the organoleptic characteristics of VOO, by conferring bitterness and pungency.[10] The highest mean concentration value of secoiridoids (1106.96 mg/kg) was observed for olive oil samples from subarea 3 during crop season 2011, whereas the lowest mean concentration was found for samples from subarea 2 in crop season 2013, at 540.12 mg/kg. With regard to individual secoiridoids, the most abundant one over the evaluated period was DOA, with mean concentrations of 165.86, 168.34, and 101.39 mg/kg (for subarea 3), respectively, during the first, second, and third crop seasons. Other secoiridoids found at relatively high concentration levels were Ol Agl, with amounts ranging from 47.40 mg/kg in oils from subarea 2 for the third crop season to 155.45 mg/kg in olive oils from the same subarea for crop season 2011; Lig Agl, with mean values ranging from 70.42 to 111.23 mg/kg, respectively, in olive oils from subarea 1 (for the second crop season) and subarea 2 (for the third crop season); and EA, the lowest concentration of which was found in oils from subarea 3 at the third crop season (36.83 mg/kg) and the highest concentration value was registered in oils from subarea 2 during the first crop season (109.46 mg/kg). Isomers, of both Ol Agl and Lig Agl, were also determined at relatively high concentration levels. Indeed, in the case of Ol Agl, over the crop season 2011, isomers 5 and 2 showed the highest mean concentration level (60.79 and 55.95 mg/kg) in olive oils from subarea 3, whereas isomer 6 showed the highest mean concentration value (57.17 mg/kg) for samples from subarea 2. As far as Lig Agl isomers are concerned, isomer 1 remains the prevailing one in all of the analyzed samples over the three crop seasons with mean concentrations ranging from 33.20 mg/kg in oils from subarea 1 (for the first crop season) to 40.25 mg/kg in olive oils from the same subarea over the 2013 crop season. Besides the above-mentioned compounds, other secoiridoids were found at relatively lower amounts: Dehydro Ol Agl, which showed mean concentration values ranging between 3.06 mg/kg (found in oils from subarea 2 during the second crop season) and 15.02 mg/kg (found in oils from subarea 1 for crop season 2011); D-Ald-D EA, with mean concentration levels fluctuating from 0.39 mg/kg in oils from subarea 3 during the second crop season to 37.60 mg/kg in olive oils from subarea 1 over the crop season of 2011; Desoxy-EA, which was found at mean concentration levels between 8.23 mg/kg (in oils from subarea 1 in 2011) and 23.70 mg/kg (in olive oils from subarea 3 in 2012); D-Lig Agl, at concentrations ranging between 36.96 mg/kg (for oils from subarea 1 in 2012) and 157.90 mg/kg (in 2013, for oils from subarea 3); Methyl D-Ol Agl, in amounts between the following values, 15.80−27.27 mg/kg for oils from subarea 2 in 2012 and samples for subarea 1 over the first crop season, respectively, and Methyl Ol Agl, for which the lowest concentration was determined in oils from subarea 2 at the second crop season (1.28 mg/kg) and the highest one was registered in oils from the subarea in 2011 (4.15 mg/kg).

Simple phenols constitute the second group of phenols in terms of abundance in Meknès olive oil samples, with a total average amount that varies between 6.90 mg/kg (subarea 3, crop season 2013) and 13.07 mg/kg (subarea 2, crop season 2011). Within this group, Ty was the predominant substance, with levels found between 4.84 mg/kg, in oils from subarea 3 over the third crop season, and 7.80 mg/kg, in oils from subarea 1 during the second crop season. In terms of relative abundance, Ty was followed by Hyt, which showed mean concentration values oscillating between 1.07 mg/kg (subarea 3 for crop season 2013) and 5.62 mg/kg (subarea 2 afor crop season 2011); O-Hyt that was also found in relatively lower amounts, its mean values varying between 0.16 mg/kg (subareas 1 and 3, crop season 2013) and 1.02 mg/kg (subarea 3, crop season 2011). If these results are compared with those achieved in previous studies about the phenolic composition of monovarietal olive oils from different Mediterranean countries,[12,30] some particular characteristics can be highlighted for Meknès olive oils. The first feature is that Ty concentration levels in the evaluated oils are, in general, higher than Hyt concentration values; the second characteristic is that Hyt levels are lower than the previously published concentration values for other Mediterranean monovarietal olive oils. Both factors could be potentially considered as markers or discriminative characteristics of Meknès oils when compared with olive oils from other different Mediterranean locations.

Lignans were another relevant group of phenolic analytes determined in the selected samples; in terms of abundance, they were the third group, with average contents ranging from 1.43 to 5.34 mg/kg. The highest value was observed for oils from subarea 1 for the first crop season, whereas the lowest mean concentration level was found for oils from the same subarea over the 2013 crop season. When the concentration levels of individual compounds are taken into account within this group, we observe that Ac-pin levels were found between 0.91 mg/kg (subarea 1, crop season 2013) and 3.28 mg/kg (subarea 2, crop season 2012); Syr concentration values fell within the range between 0.17 mg/kg (subarea 1 and crop season 2013) and 2.42 mg/kg (subarea 1 and crop season 2011); and concentration values for Pin fluctuated within the range of 0.30−1.15 mg/kg, defined by the mean value obtained for the samples from subareas 1 and 3, respectively, over the 2011 season.

With regard to the *flavonoids* family, in terms of total content, average values were found within the range from 1.10 to 3.23 mg/kg, levels observed, respectively, in oils from subarea 3

DOI: 10.1021/jf506097u
J. Agric. Food Chem. 2015, 63, 4376−4385

Table 3. Mean ± Standard Deviation (Milligrams per Kilogram) of Phenolic Compounds Determined in Meknès Monovarietal VOOs[a,b]

		crop season 2011			crop season 2012			crop season 2013		
chemical category	phenolic compound	subarea 1 (n = 13)	subarea 2 (n = 15)	subarea 3 (n = 15)	subarea 1 (n = 11)	subarea 2 (n = 16)	subarea 3 (n = 7)	subarea 1 (n = 24)	subarea 2 (n = 9)	subarea 3 (n = 32)
simple phenols	O-Hyt	0.22Aa ± 0.11	0.65Ba ± 0.50	1.02Aa ± 1.56	0.40Bb ± 0.21	0.25Bb ± 0.06	0.26ABab ±0.11	0.16Aa ± 0.07	0.23Ab ± 0.32	0.16Ab ± 0.19
	Hyt	4.16Aa ± 4.90	5.62Aa ± 4.12	4.33Aa ± 3.75	2.01Ab ± 0.85	1.96Ab ± 0.99	1.46Ab ± 0.63	2.02Ab ± 2.72	1.31Ab ± 1.53	1.07Ab ± 0.94
	Ty	5.83Aa ± 3.11	6.79Aa ± 3.38	4.84Aa ± 2.62	7.80Aa ± 2.13	6.57Aa ± 2.47	5.92Aa ± 1.88	5.93Aa ± 2.34	5.98Aa ± 2.41	5.68Aa ± 2.51
	Total	10.22Aa ± 7.97	13.07Aa ± 6.98	11.19Aa ± 7.02	10.19Aa ± 2.63	8.77Aab ±2.98	7.64Aab ±1.78	8.11Aa ± 4.83	7.51Ab ± 3.95	6.90Ab ± 3.15
lignans	Syr	2.42Aa ± 1.78	1.18Ba ± 1.00	0.90Ba ± 0.46	0.23Ab ± 0.08	0.20Ab ± 0.06	0.20Ab ± 0.07	0.17Ab ± 0.04	0.21Ab ± 0.07	0.69Aab ±2.34
	Pin	0.30Aa ± 0.23	0.75ABa ± 0.97	1.15Ba ± 0.68	0.51Ab ± 0.19	0.61Aa ± 0.49	0.44Ab ± 0.16	0.35Aa ± 0.08	0.45Aa ± 0.1	0.47Ab ± 0.38
	Ac-pin	2.62Aa ± 1.16	2.16Aa ± 1.75	2.36Aa ± 2.79	2.25Aab ±3.04	3.28Aa ± 5.85	1.55Aa ± 1.96	0.91Ab ± 0.81	0.92Ab ± 0.35	1.91Aa ± 3.53
	total	5.34Aa ± 2.16	4.08Aa ± 2.23	4.41Aa ± 2.96	2.99Ab ± 3.25	4.09Aab ±5.83	2.19Aa ± 2.12	1.43Ab ± 0.87	1.58Ab ± 0.42	3.08Aa ± 4.77
flavonoids	Lut	1.22Aa ± 1.11	2.63Aa ± 2.19	2.50Aa ± 1.6	1.29Aa ± 0.23	1.39Ab ± 0.53	1.77Aab ±0.81	1.29Aa ± 0.45	1.02Ab ± 0.25	1.42Ab ± 0.53
	Apig	0.32Aa ± 0.12	0.59Aa ± 1.00	0.65Aa ± 1.01	0.11Ab ± 0.04	0.18Aa ± 0.24	0.33Aab ±0.30	0.09Ab ± 0.07	0.08Ab ± 0.06	0.21Ab ± 0.43
	total	1.55Aa ± 1.17	3.23Aa ± 3.18	3.15Aa ± 2.47	1.40Aa ± 0.24	1.57Aab ±0.76	2.10Aab ±1.1	1.38ABa ± 0.5	1.10Ab ± 0.29	1.63Bb ± 0.67
phenol acids	p-Cou	0.13Aa ± 0.09	0.22Aa ± 0.15	0.22Aa ± 0.27	0.18Aa ± 0.07	0.19Aa ± 0.14	0.22Aa ± 0.15	0.18Aa ± 0.09	0.17Aa ± 0.07	0.21Aa ± 0.15
secoiridoids	D-Ald-D EA	37.60Aa ± 44.96	30.90Aa ± 36.95	29.30Aa ± 49.79	2.76Ab ± 3.06	0.70Bb ± 0.70	0.39Bb ± 0.34	0.91Ab ± 1.42	6.57Bc ± 11.6	2.45ABb ± 4.82
	Deoxy-EA	8.23Aa ± 7.92	15.57Aab ±13.54	13.98Aa ± 23.6	12.89Ab ± 10.91	16.48Aa ± 8.98	23.70Aa ± 17.12	12.84Ab ± 8.69	8.48Ab ± 5.38	16.05Aa ± 14.36
	EA	83.22Aa ± 43.82	109.46Aa ± 64.90	92.66Aa ± 38.96	94.61Aa ± 50.69	51.74Bb ± 17.17	50.20Bb ± 10.94	45.35ABb ± 21.99	56.3Bb ± 17.82	36.83Ab ± 14
	DOA	32.84Aa ± 43.35	99.52ABa ± 96.64	165.86Ba ± 161.13	51.33Aab ±33.75	116.7ABa ± 76.38	168.34Ba ± 124.71	80.44ABb ± 59.23	49.51Bb ± 32.26	101.39Ab ± 70.18
	Methyl D-Ol Agl	27.27Aa ± 7.19	23.72Aa ± 12.44	18.85Aa ± 13.39	17.68Ab ± 9.21	15.80Aa ± 8.34	16.67Aa ± 7.73	20.94Ab ± 5.5	20.15Aa ± 6.47	17.36Aa ± 7.63
	D-Lig Agl	39.25Aab ±22.6	96.71ABa ± 80.47	157.9Ba ± 137.72	36.96Aa ± 20.56	67.20ABb ± 37.57	117.47Bab ±89.51	60.21Ab ± 30.39	61.71Ab ± 19.18	72.82Ab ± 35.59
	Dehydro Ol Agl	15.02Aa ± 6.94	8.61Aa ± 6.96	8.73Aa ± 10.23	5.23Ab ± 2.38	3.06Ab ± 2.53	3.24Ab ± 3.04	3.91Ab ± 2.47	5.50Aa ± 1.15	3.99Ab ± 2.84
	Ol Agl	109.01Aa ± 61.78	155.45Aa ± 73.37	152.29Aa ± 72.17	60.24Ab ± 16.68	77.83Ab ± 29.26	81.57Ab ± 31.64	75.13Ab ± 21.99	47.4Bc ± 14.25	70.60Ab ± 28.00
	Ol Agl-isomer 1	19.52Aa ± 26.59	31.99Aa ± 29.70	35.23Aa ± 39.44	27.35Aab ±20.78	31.71Aa ± 17.62	26.95Aa ± 14.30	39.77Ab ± 20.19	18.20Ba ± 11.32	37.10Aa ± 26.19
	Ol Agl-isomer 2	37.96Aa ± 43.32	54.68Aa ± 44.53	55.94Aa ± 53.73	38.70Aa ± 31.7	44.43Aa ± 21.95	39.69Aa ± 22.24	53.22Aa ± 23.11	28.51Bb ± 14.2	49.06Aa ± 30.98
	Ol Agl-Isomer 3	17.49Aab ± 14.86	27.34Aa ± 17.49	25.47Aa ± 20.08	14.57Aa ± 7.04	18.80Aab ±7.79	19.06Aa ± 8.31	21.99Ab ± 8.96	11.72Bb ± 5.94	19.74Aa ± 9.84
	Ol Agl-isomer 4	22.80Aa ± 20.32	39.66Aa ± 25.74	38.98Aa ± 28.55	20.84Aa ± 9.82	28.42Aa ± 12.56	30.22Aa ± 15.24	28.67Aa ± 10.79	17.27Bb ± 8.27	27.99Aa ± 16.17
	Ol Agl-isomer 5	34.80Aa ± 21.91	60.54Aa ± 34.12	60.79Aa ± 36.83	26.90Aa ± 9.62	35.67Ab ± 13.91	39.63Aab ±19.13	32.49Aa ± 9.89	18.79Bc ± 5.59	31.50Ab ± 13.72
	Ol Agl-isomer 6	44.23Aa ± 20.43	57.17Aa ± 25.77	53.42Aa ± 26.44	28.70Ab ± 8.18	31.98Ab ± 7.64	31.61Ab ± 5.32	32.49Ab ± 8.18	21.07Bc ± 7.59	33.16Ab ± 12.1
	Methyl Ol Agl	2.05Aa ± 1.19	4.15Aa ± 4.71	2.16Aa ± 1.58	1.61Aa ± 0.64	1.28Ab ± 0.58	1.67Aa ± 0.64	2.66ABa ± 2.22	3.67Ba ± 1.86	2.03Aa ± 1.33
	Lig Agl	93.01Aa ± 34.7	111.23Aa ± 64.32	108.27Aa ± 64.48	70.42Aa ± 29.71	84.65Aa ± 26.25	103.43Aa ± 51.85	83.75Aa ± 24.57	77.39Aa ± 32.8	85.67Aa ± 31.5
	Lig Agl-isomer 1	33.20Aa ± 17.97	39.44Aa ± 33.23	39.25Aa ± 35.86	33.71Aa ± 18.02	34.61Aa ± 16.45	33.53Aa ± 19.63	40.25Aa ± 12.69	38.88Aa ± 16.57	35.33Aa ± 17.41
	Lig Agl-isomer 2	29.58Aa ± 18.08	29.29Aa ± 22.36	25.87Aa ± 23.07	29.71Aa ± 12.53	27.42Aa ± 12.13	24.47Aa ± 11.67	32.19Aa ± 10.56	32.80Aa ± 15.07	28.50Aa ± 14.8
	Lig Agl-isomer 3	17.49Aa ± 5.90	22.55Aa ± 13.85	22.02Aa ± 13.22	20.31Aa ± 19.45	17.68Aa ± 6.10	19.64Aa ± 11.13	17.43Aa ± 5.37	16.21Aa ± 7.01	16.57Aa ± 7.37
	total	704.59Aa ± 361.56	1018.01Aa ± 524.23	1106.96Aa ± 553.85	594.50Aa ± 175.16	706.15Aab ±218.98	831.46Aab ±363.83	684.64Aa ± 177.52	540.12Ab ± 158.91	688.14Ab ± 253.54
other compounds	quinic acid	1.04Aa ± 1.05	12.87Ba ± 16.60	9.34Ba ± 15.2	2.80Aa ± 3.89	0.51Bb ± 0.53	1.32ABa ± 1.18	1.84Aa ± 2.35	5.48Aa ± 12.38	2.34Ab ± 3.83

[a]Significant differences in the same row are indicated with different lower case letters (comparison among crop seasons, $p < 0.05$) and with different uppercase letters (comparison among subareas at the same crop season, $p < 0.05$). [b]Quinic acid, Hyt, Ty, Pin, Lut, Apig, and p-Cou were quantified in terms of their commercial pure standards. O-Hyt was quantified in terms of Hyt. Lignans were quantified in terms of Pin. Secoiridoids were quantified in terms of oleuropein.

J. Agric. Food Chem. 2015, 63, 4376−4385

DOI: 10.1021/jf506097u

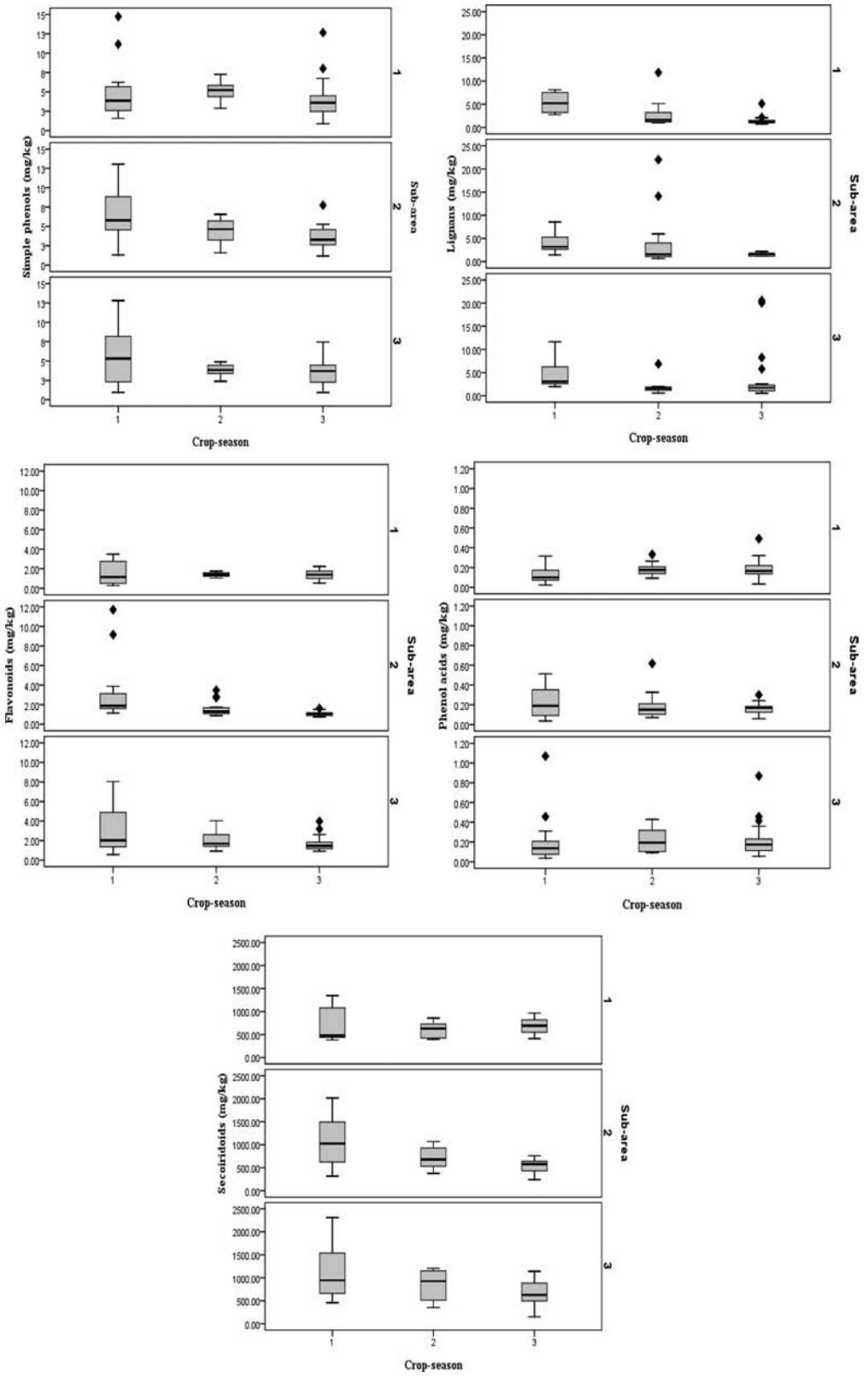

Figure 3. Box and whisker plots of total content of simple phenols, lignans, flavonoids, phenolic acids, and secoiridoids determined on Meknès VOOs. For box-plots, the line within the box indicates the median; the box boundary marks the 25th and 75th percentiles; percentiles and whiskers above and below the box indicate the 90th and 10th percentiles. Outlier data are shown as ♦.

during crop season 2013 and subarea 2 in 2011. Lut and Apig are the most relevant compounds within this group; Lut, which was the most abundant flavonoid occurring in the analyzed olive oil samples, was found at mean concentration levels ranging from 1.02 mg/kg (subarea 2, crop season 2013) to 2.63 mg/kg (subarea 2, crop season 2011), and Apig was found at lower concentration levels than those of Lut, with amounts oscillating between 0.08 and 0.65 mg/kg, observed for samples from

DOI: 10.1021/jf506097u
J. Agric. Food Chem. 2015, 63, 4376−4385

subarea 2 over the third crop season and olive oils from subarea 3 in 2011.

In the group composed by *phenolic acid*, p-Cou was the most abundant analyte. Its values (mean concentration) were found from 0.13 (in olive oils from the subarea 1 during the first crop season) to 0.22 mg/kg (which was a common concentration value for samples from subareas 2 and 3 in 2011 and those from subarea 3 in 2012).

The results obtained in this study are in good agreement with those achieved in a previous work in which the phenolic fractions of VOOs from seven north Moroccan olive growing areas were compared.[16] Also, some distinctive features of the phenolic fraction of Picholine marocaine VOOs, when compared to other Mediterranean VOOs, revealed by the mentioned work could be confirmed by the present study.

Furthermore, the study of intraregional and interannual variability of both the total and individual concentrations of the determined phenolic compounds in Meknès VOOs was carried out to evaluate the possible influence of the subarea and crop season factors on the phenolic fraction of the samples under study. Thus, an analysis of variance (ANOVA) was performed on the obtained quantitative data; the results are reported in Table 3.

Among the studied compounds, it should be pointed out that Ty, Lig Ag, and one of its isomers (isomer 3) were the analytes unaffected by both subarea and year of production factors. Furthermore, considering the influence of the subarea of origin, the examination of the results obtained by applying a post hoc test (Tukey's) showed that the total amount of the considered chemical classes seems to be unaffected by the subarea factor over the three crop seasons. However, as far as individual phenolic compounds content is concerned, we observed that in 2011, analytes such as O-Hyt, Syr, Pin, DOA, and D-Lig Agl were influenced by the subarea of origin. In 2012, the effect of subarea factor was observed for O-Hyt, D-Ald-D EA, EA, DOA, and D-Lig Agl. The third crop season, 2013, was the period with the highest number of compounds affected by the subarea factor, finding 10 compounds significantly affected ($p < 0.05$) by it, including O-Hyt, D-Ald-D EA, DOA, Methyl Ol Agl, and the six Ol Agl isomers. Despite these differences, there was no compound that could differentiate samples according to the subarea of origin, because the mean values for each variable were not significantly different ($p < 0.05$) at the same time for the three studied subareas (Table 3).

When the effect of crop season was evaluated, the ANOVA test revealed that this factor shows most pronounced influence in both the global amount of phenols (determined by families) and the content of individual phenolic analytes. Thus, olive oil samples from subarea 1 showed statistically significant differences ($p < 0.05$) for the following compounds: O-Hyt, Hyt, D-Ald-D EA, Desoxy-EA, EA, DOA, Syr, Pin, Ac-pin, Methyl D-Ol Agl, D-Lig Agl, Apig, Dehydro Ol Agl, Ol Agl, Ol Agl isomers 1, 3 and 6, and Methyl Ol Agl. When the same was made to evaluate the effect of harvest season factor on the samples from subarea 2, significant differences were found for O-Hyt, Hyt, D-Ald-EA, Desoxy-EA, EA, Syr, DOA, Lut, Ac-pin, Dehydro Ol Agl, Apig, D-Lig Agl, Ol Agl, Ol Agl isomers 2−6, and Methyl Ol Agl; in olive oils from subarea 3, crop season significantly affected O-Hyt, Hyt, D-Ald-EA, p-Cou, EA, DOA, Syr, Lut, Pin, Methyl D-Ol Agl, Dehydro Ol Agl, Apig, D-Lig Agl, Ol Agl, and Ol Agl isomer 5.

In conclusion, the work conducted here demonstrates that Picholine marocaine VOOs produced in the Meknès region could be considered as potential sources of phenolic bioactive compounds, because a total of 28 phenolic compounds (and quinic acid), belonging to five chemical classes, were identified and quantified in all of the analyzed samples. Differences were observed for the phenolic compounds under study as a function of the subarea of origin and harvest season, the latter being the most relevant variation factor. As a matter of fact, Picholine marocaine is the dominant olive cultivar in Moroccan olive-growing regions. We believe that our approach might be reasonably adopted in future studies for the comprehensive characterization of the selected variety (or any other), as well as for comparative studies of the composition of olive oils from a particular cultivar obtained in different growing areas.

AUTHOR INFORMATION

Corresponding Author

*(A.C.-P.) E-mail: alegriac@ugr.es. Phone: +34 958 248594. Fax: +34 958 243328.

Funding

We are grateful to the Andalusia regional government (Department of Economy, Innovation and Science, Project P09-FQM-5469), the Millennium Challenge Account Morocco, Fruit Tree Productivity Project (PAF)/Olive cultivation register Project/North Moroccan Regions, the Spanish Agency for International Development Cooperation (AECID) (Pre-doctoral grant), and the Vice-Rector's Office for International Relations and Development Cooperation of the University of Granada.

Notes

The authors declare no competing financial interest.

ACKNOWLEDGMENTS

We express our sincere gratitude to Meknès region olive farmers for their support in olive fruit sampling.

ABBREVIATIONS USED

Ac-Pin, (+)-1-acetoxypinoresinol; ANOVA, one-way analysis of variance; Apig, apigenin; DAD, diode array detector; D-Ald-D EA, dialdehydic form of decarboxymethyl elenolic acid; Dehydro Ol Agl, dehydro oleuropein aglycone; Deoxy-EA, desoxy elenolic acid; D-Lig Agl, decarboxymethyl ligstroside aglycone; DOA, decarboxymethyl oleuropein aglycone; DOPAC, 3,4-dihydroxyphenylacetic acid; EA, elenolic acid; EICs, extract ion chromatographs; ESI, electrospray ionization; FAAs, free fatty acids; HMR, high mass resolution; Hyt, hydroxytyrosol; IT, ion trap; MS, Lig Agl, ligstroside aglycone; LRM, low-resolution mass; Lut, luteolin; Methyl D-Ol Agl, methyl decarboxy oleuropein aglycone; Methyl Ol Agl, methyl oleuropein aglycone; MS, mass spectrometry; MS/MS, tandem mass spectrometry; O-Hyt, oxidized hydroxytyrosol; Ol Agl, oleuropein aglycone; *p*-cou, *p*-coumaric; Pin, (+)-pinoresinol; PV, peroxides value; Syr, syringaresinol; TIC, total ion current chromatogram; TOF, time-of-flight; Ty, tyrosol; VOOs, virgin olive oils

REFERENCES

(1) International Olive Council(IOC), Resolution No. No 3/Rev. 5 COI/T.15/NC. *International trade standard applying to olive oils and olive-pomace oils international trade standard applying to olive oils and olive-pomace oils*. 2010; p 17.

(2) De Carvalho, C. C. C. R.; Caramujo, M. J. Ancient procedures for the high-tech world: health benefits and antimicrobial compounds from the Mediterranean empires. *Open Biotechnol. J.* **2008**, *2*, 235−246.

DOI: 10.1021/jf506097u
J. Agric. Food Chem. 2015, 63, 4376−4385

(3) Owen, R. W.; Haubner, R.; Würtele, G.; Hull, W. E.; Spiegelhalder, B.; Bartsch, H. Olives and olive oil in cancer prevention. *Eur. J. Cancer Prev.* **2004**, *13*, 319−326.
(4) Covas, M. I. Olive oil and the cardiovascular system. *Pharmacol. Res.* **2007**, *55*, 175−186.
(5) Pérez-Martínez, P.; García-Ríos, A.; Delgado-Lista, J.; Pérez-Jiménez, F.; López-Miranda, J. Mediterranean diet rich in olive oil and obesity, metabolic syndrome and diabetes mellitus. *Curr. Pharm. Des.* **2011**, *17*, 769−777.
(6) European Commission Regulation.. EEC/432/2012 of 16 May 2012 establishing a list of permitted health claims made on foods, other than those referring to the reduction of disease risk and to child. *Off. J. Eur. Communities* **2012**, *L136*, 1−40.
(7) Visioli, F.; Galli, C. *Crit. Rev.* Biological properties of olive oil phytochemicals. *Crit. Rev. Food Sci. Nutr.* **2002**, *42*, 209−221.
(8) Aparicio, R.; Roda, L.; Albi, M. a; Gutiérrez, F. Effect of various compounds on virgin olive oil stability measured by Rancimat. *J. Agric. Food Chem.* **1999**, *47*, 4150−4155.
(9) Gallina-Toschi, T.; Cerretani, L.; Bendini, A.; Bonoli-Carbognin, M.; Lercker, G. Oxidative stability and phenolic content of virgin olive oil: an analytical approach by traditional and high resolution techniques. *J. Sep. Sci.* **2005**, *28*, 859−870.
(10) Bendini, A.; Cerretani, L.; Carrasco-Pancorbo, A.; Gómez-Caravaca, A. M.; Segura-Carretero, A.; Fernández-Gutiérrez, A.; Lercker, G. Phenolic molecules in virgin olive oils: a survey of their sensory properties, health effects, antioxidant activity and analytical methods. An overview of the last decade. *Molecules* **2007**, *12*, 1679−1719.
(11) Servili, M.; Esposto, S.; Fabiani, R.; Urbani, S.; Taticchi, a; Mariucci, F.; Selvaggini, R.; Montedoro, G. F. Phenolic compounds in olive oil: antioxidant, health and organoleptic activities according to their chemical structure. *Inflammopharmacology* **2009**, *17*, 76−84.
(12) García-Villalba, R.; Carrasco-Pancorbo, A.; Oliveras-Ferraros, C.; Vázquez-Martín, A.; Menéndez, J. A.; Segura-Carretero, A.; Fernández-Gutiérrez, A. Characterization and quantification of phenolic compounds of extra-virgin olive oils with anticancer properties by a rapid and resolutive LC-ESI-TOF MS method. *J. Pharm. Biomed. Anal.* **2010**, *51*, 416−429.
(13) Medina, E.; de Castro, A.; Romero, C.; Brenes, M. Comparison of the concentrations of phenolic compounds in olive oils and other plant oils: correlation with antimicrobial activity. *J. Agric. Food Chem.* **2006**, *54*, 4954−4961.
(14) Miles, E. A.; Zoubouli, P.; Calder, P. C. Differential anti-inflammatory effects of phenolic compounds from extra virgin olive oil identified in human whole blood cultures. *Nutrition* **2005**, *21*, 389−394.
(15) Rosignoli, P.; Fuccelli, R.; Fabiani, R.; Servili, M.; Morozzi, G. Effect of olive oil phenols on the production of inflammatory mediators in freshly isolated human monocytes. *J. Nutr. Biochem.* **2013**, *24*, 1513−1519.
(16) Bajoub, A.; Carrasco-Pancorbo, A.; Ajal, E. A.; Ouazzani, N.; Fernández-Gutiérrez, A. Potential of LC-MS phenolic profiling combined with multivariate analysis as an approach for the determination of the geographical origin of North Moroccan virgin olive oils. *Food Chem.* **2014**, *166*, 292−300.
(17) Direction Provinciale Agricole de Meknès(DPA). Données statistiques du secteur oléicole de Meknès; 2014.
(18) Uceda, M.; Frías, L. Harvest dates. Evolution of the fruit oil content, oil composition and oil quality. In Segundo Seminario Oleicola Internacional, Córdoba, Spain, 1975; pp 125−128.
(19) European Commission Regulation.. EEC/2568/91 of 11 July on the characteristics of olive and pomace oils and on their analytical methods. *Off. J. Eur. Communities* **1991**, *L248*, 1−82.
(20) Ben Temime, S.; Taamalli, W.; Baccouri, B.; Abaza, L.; Douja, D.; Zarrouk, M. Changes in olive oil quality of Chétoui variety according to origin of plantation. *J. Food Lipids* **2006**, *13*, 88−99.
(21) Guerfel, M.; Mansour, M.; Ben Boujnah, D. Compositional quality of virgin olive oils from cultivars introduced in two Tunisian locations. *Afr. J. Agric. Res.* **2012**, *7*, 2469−2474.
(22) Servili, M.; Esposto, S.; Lodolini, E.; Selvaggini, R.; Taticchi, A.; Urbani, S.; Montedoro, G.; Serravalle, M.; Gucci, R. Irrigation effects on quality, phenolic composition, and selected volatiles of virgin olive oils cv. Leccino. *J. Agric. Food Chem.* **2007**, *55*, 6609−6618.
(23) Ranalli, A.; Malfatti, A.; Lucera, L.; Contento, S.; Sotiriou, E. Effects of processing techniques on the natural colourings and the other functional constituents in virgin olive oil. *Food Res. Int.* **2005**, *38*, 873−878.
(24) Tura, D.; Gigliotti, C.; Pedò, S.; Failla, O.; Bassi, D.; Serraiocco, A. Influence of cultivar and site of cultivation on levels of lipophilic and hydrophilic antioxidants in virgin olive oils (*Olea europaea* L.) and correlations with oxidative stability. *Sci. Hortic.* **2007**, *112*, 108−119.
(25) Angerosa, F.; Mostallino, R.; Basti, C.; Vito, R. Influence of malaxation temperature and time on the quality of virgin olive oils. *Food Chem.* **2001**, *72*, 19−28.
(26) Ouazzani, N.; Villemur, R.; Lumaret, E. Genetic variation in the olive tree (*Olea europaea* L.) cultivated in Morocco. *Euphy.* **1996**, 9−20.
(27) Essadki, M.; Ouazzani, N.; Lumaret, R.; Moumni, M. ISSR variation in olive-tree cultivars from Morocco and other Western countries of the Mediterranean basin. *Genet. Resour. Crop Evol.* **2006**, *53*, 475−482.
(28) Taamalli, A.; Arráez Román, D.; Zarrouk, M.; Segura-Carretero, A.; Fernández-Gutiérrez, A. Classification of 'Chemlali' accessions according to the geographical area using chemometric methods of phenolic profiles analysed by HPLC-ESI-TOF-MS. *Food Chem.* **2012**, *132*, 561−566.
(29) Kesen, S.; Kelebek, H.; Selli, S. Characterization of the volatile, phenolic and antioxidant properties of monovarietal olive oil obtained from cv. Halhali. *J. Am. Oil Chem. Soc.* **2013**, *90*, 1685−1696.
(30) Ouni, Y.; Taamalli, A.; Gómez-Caravaca, A. M.; Segura-Carretero, A.; Fernández-Gutiérrez, A.; Zarrouk, M. Characterisation and quantification of phenolic compounds of extra-virgin olive oils according to their geographical origin by a rapid and resolutive LC-ESI-TOF MS method. *Food Chem.* **2011**, *127*, 1263−1267.

DOI: 10.1021/jf506097u
J. Agric. Food Chem. 2015, 63, 4376−4385

Table 1. Cheddar Cheese Production, Aging, And Flavor Profiles

aging period, flavor	batch	milk collection/cheese production date	cow herd feed
one year, sharp	1	14 Jul 2009	pasture, silage, grain
	2	17 Jul 2009	pasture, silage, grain
	3	03 Jun 2009	pasture, silage, grain
two years, extra sharp	1	18 Jul 2008	pasture, silage, grain
	2	14 Aug 2008	pasture, silage, grain
	3	15 Jul 2008	pasture, silage, grain
three years, extra extra sharp	1	24 Sep 2007	silage, grain
	2	23 Sep 2007	silage, grain

including blocks from three batches of one-year-aged, three batches of two-year-aged, and two batches of three-year-aged Cheddar. Table 1 provides the date each block was produced, which is also the date the aging process began for each batch of cheese, and the herd's feed at the time the milk was collected. The cheese blocks were stored in vacuum-sealed packaging shielded from light at 4 °C until testing. The cheese samples were prepared for analysis by cutting off ∼50 g of each 2-lb block and removing the exterior 1 cm of cheese. The remaining 30 g piece was cut into approximately 1 cm × 1 cm × 1 cm cubes (1 g each), which were stored at −20 °C until the day of analysis (3 days maximum). Five grams of Cheddar in a 100 mL sample bottle were used for each SESI-MS analysis. Two technical replicates of each block were tested per day over a period of three consecutive days for a total of six SESI-MS measurements for each block in positive-ion mode. Additional samples were prepared for negative-ion mode SESI-MS analysis following the same procedure. In total, 48 positive-ion and 48 negative-ion SESI-MS spectra were collected.

Secondary Electrospray Ionization-Mass Spectrometry (SESI-MS). *Tuning and Standardization.* SESI-MS fingerprints were collected as previously described on a modified SCIEX API 3000 triple quadrupole mass spectrometer (for a schematic of the SESI modifications and sampling apparatus, see ref 25). To control for potential fluctuations in ionization efficiency, we used mixtures of semivolatile compounds (Table 2) for tuning the SESI operation voltage to maximize the match score between replicate spectra of the standards mixtures at the beginning and periodically throughout sample testing. For instrument tuning only, the declustering potential (DP), focusing potential (FP), and entrance potential (EP) were set at 50, 375, and 10 V, respectively, in positive-ion mode, and −50, −300, and −10 V in negative-ion mode to induce in-source fragmentation of the standard molecules. Generating multiple fragment ions from the standards mixtures provided more coverage over the mass range that was tested and created overlapping groups of ions whose relative intensities were more dependent on the operation voltage and less dependent on the gas-phase concentration of any single compound to compensate for small changes in the relative concentrations of the three individual standards in each mixture. Table 2 provides the mass-to-charge ratios (m/z) for the molecular and fragment ions that were monitored for each component of the standards mixtures, which had a minimum of 10% relative intensity in positive-ion mode and 5% relative intensity in negative-ion mode. The intensities of these fragments, relative to each other and to background peaks (m/z = 129, 149, 185 in positive-ion mode, and m/z = 42, 61, 79, 123, 185 in negative-ion mode), were recorded to measure intraday and interday variability in the SESI-MS fingerprint. Interday replicates of the positive-ion mode standards spectra had an average match score of 964 (±20), which is statistically indistinguishable from the intraday variation (969 ± 24).

Cheddar SESI-MS Volatile Fingerprinting. Cheddar samples were allowed to warm to room temperature prior to analysis. The cheese volatiles were introduced into the mass spectrometer by displacing the sample bottle headspace with CO_2 (99.99%; 2 L/min) for 2 min. Formic acid (0.1% (v/v)) and methanol (5% (v/v)) in water were used as an electrospray solution in positive-ion mode, and ammonium hydroxide (0.03% (v/v)) and methanol (25% (v/v)) in water were used for negative-ion mode, which provided the optimal ionization efficiency and stability in our system. The electrospray solutions were delivered at a flow rate of 5 nL/s through a nonconductive silica capillary (40 μm ID) with a sharpened needle tip. The DP, FP, and EP were set at 5, 350, and 2 V, respectively, in positive-ion mode and −5, −300, and −2 V in negative-ion mode to minimize in-source fragmentation for volatile fingerprints of the Cheddar samples. The operation voltage of the electrospray was ∼2.2 kV in positive-ion mode, and approximately −2.2 kV in negative-ion mode. Spectra were collected over 2 min as an accumulation of 40 scans over 20−200 m/z in single quadrupole mode. Deionized water (30 mL) at room temperature was used as the blank. The system was flushed with CO_2 between samples to prevent carryover. Tandem mass spectrometry (MS/MS) fragmentation spectra were collected for a selection of positive-ion mode peaks as an accumulation of 10 scans using 50, 375, and 10 V for DP, FP, and EP, respectively, 25−40 eV collision energy, and N_2 collision gas.

Data Analysis. Analyst 1.4.2 software (Applied Biosystems) was used for data collection and raw data processing. SESI-MS spectra were blank-subtracted and normalized to the peak of highest intensity. Spectral matching was calculated using Spearman's rank correlation analyses for the Cheddar SESI-MS fingerprints, and with NIST MS search V 2.0 software (National Institute of Standards and Technology) for the standards mixtures and MS/MS fragmentation spectra. Presence/absence analyses on a year-by-year basis were performed with the criterion that a SESI-MS peak had to have a signal-to-noise (S/N) greater than 2 in at least 50% of all of the samples in an aging category (i.e., at least 9 replicates for 1- and 2-year-aged Cheddars, at least 6 replicates for 3-year-aged Cheddars) to be considered as present. Presence/absence analyses on a batch-to-batch basis was performed with the criterion that a SESI-MS peak had to have a S/N > 2 in at least 3 (50%) of the replicates for a batch.

JMP version 10, SAS version 10 (SAS Institute Inc., Cary, NC), and MATLAB version 8.2 (MathWorks Inc.) were used for statistical analyses in this study. Principal component analyses (PCA) were performed using all experimental replicates as observations, and the

Table 2. SESI-MS Tuning Mixtures

compound	CAS ID	conc. (v/v)	conc. (μM)	M_w (g/mol)	molecular and fragment ions (m/z)
Positive-Ion Mode Standards in Water					
pyrimidine	289-95-2	5×10^{-6}	63	80	81, 54
indole	120-72-9		17	117	118, 91
2-aminoacetophenone	551-93-9	1×10^{-5}	82	135	136, 118, 91
Negative-Ion Mode Standards in 1% (v/v) Methanol in Water					
hexanoic acid	142-62-1	1×10^{-4}	798	116	115
heptanoic acid	111-14-8	1×10^{-4}	705	130	129, 115
octanoic acid	124-07-2	1×10^{-4}	631	144	143, 129, 115

DOI: 10.1021/jf5063759
J. Agric. Food Chem. 2015, 63, 4386−4392

absolute intensities of the SESI-MS peaks 20−200 m/z with S/N > 2 as variables. The data were mean centered, and the range was scaled prior to PCA analysis; then, the statistical significance of the separations in PCA were calculated on a pairwise basis using two-sided Student's t tests of the principal component scores. The loading scores in principal components 1−3 were analyzed for each SESI-MS peak, and peaks with at least one loading score with an absolute intensity ≥0.7 (|LS| ≥ 0.7) were considered significant drivers of the PCA separation. To identify SESI-MS fingerprint peaks that can be used to predict the age classification of Cheddar cheeses, we performed partial least-squares-discriminant analysis (PLS-DA) of the normalized SESI-MS volatile fingerprints using all of the data for model building. In addition, PLS-DA leave-one-out cross validation was performed for the eight batch groups using all 48 samples. The correct classification rate was calculated by dividing the number of correctly classified samples by the total number of samples.

Two-sided nonparametric Mann−Whitney U-tests were carried out to identify SESI-MS fingerprint peaks that are significantly different between pairs of aging categories using a 5% significance level cutoff. The U-test z-scores were used as criteria for categorizing peaks as increasing or decreasing on a year-to-year basis. Increasing peaks have at least one z-score that exceeds the 5% cutoff (≤−1.96) for any two-year comparison, and all other z-scores for that peak must also be negative (i.e., must be less than zero; Table S2 in the Supporting Information). Decreasing peaks have at least one z-score that exceeds the 5% cutoff (≥1.96) for any two-year comparison and all other z-scores for that peak must also be positive (i.e., must be >0).

RESULTS AND DISCUSSION

SESI-MS Fingerprinting of Aged Artisanal Cheddar. *SESI-MS Volatile Fingerprints are Descriptive of Cheddar Cheese Aging.* The SESI-MS volatile fingerprints (m/z = 20−200) of one-, two-, and three-year-aged artisanal Cheddar cheeses were collected in both positive- and negative-ion modes (Figure 1) and were comprised of cheese volatiles that are Brønsted−Lowry bases and acids, respectively. Although there are volatile molecules that can be protonated or deprotonated depending on the electrospray solution, and therefore would be represented in both the positive- and negative-ion mode spectra, the information in these two spectra were considered to be complementary and have been combined into a single volatile fingerprint for each Cheddar sample. By visual inspection, the volatile fingerprints of aged Cheddar appear quite similar year-to-year, as the majority of the dominant SESI-MS peaks are present in all three ages. To quantify the similarity of the volatile fingerprints, the average Spearman's rank correlation coefficient (ρ) was calculated for the total SESI-MS fingerprint (positive- and negative-ion mode spectra) of all of the Cheddar samples. The fingerprints are well correlated within each aging period (ρ > 0.70; Table S1 in the Supporting Information), demonstrating that the SESI-MS fingerprints for the Cheddar samples are similar and reproducible.

It was hypothesized that the SESI-MS fingerprint of each aged Cheddar is unique and indicative of its aging period. A qualitative analysis of the spectral fingerprints indicates that 39% of the total peaks are uniquely present or uniquely absent in one of the aging categories (Figure 2a; Table S2 in the Supporting Information), and the unique peaks are consistently found in every batch of cheese tested in each category (Figure 2b-d; Table S2 in the Supporting Information). On the basis of these observations, it was posited that principal component analysis (PCA) could be used to cluster the Cheddar samples by their SESI-MS fingerprints (i.e., combined positive- and negative-ion mode spectra; Figure 3). Indeed, using all of the

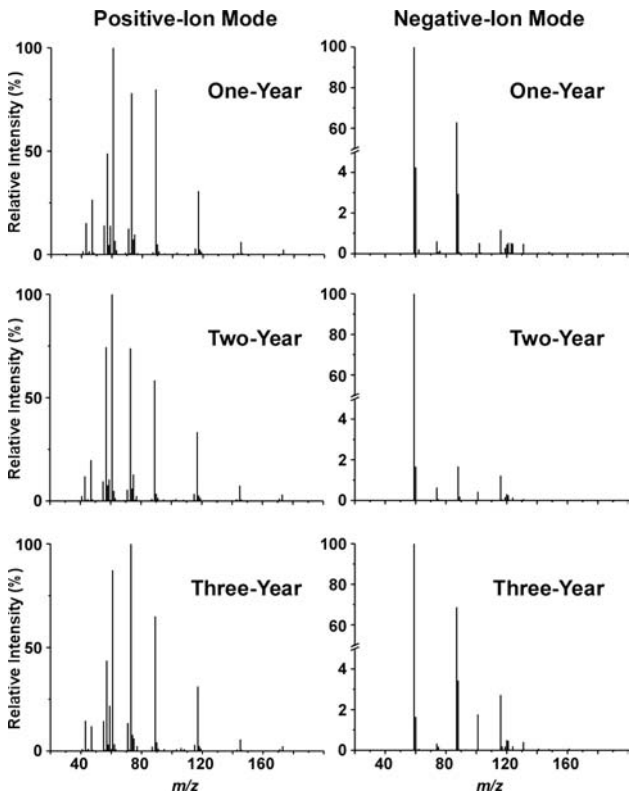

Figure 1. SESI-MS fingerprints from one-, two-, and three-year-aged Shelburne Farms Cheddar cheese in positive-ion mode (left column) and negative-ion mode (right column). The spectra are averages of 18 replicates for 1- and 2-year-aged Cheddar, and 12 replicates for 3-year-aged Cheddar, and normalized to the peak of greatest intensity in each spectrum.

SESI-MS peaks as variables and the 48 cheese samples as observations, it was found that all of the samples within an aging category clustered together and could be separated from the other aged Cheddars using the first three principal components (p < 0.0001; Table S3 in the Supporting Information). Partial least-squares discriminant analysis (PLS-DA) of the SESI-MS fingerprints was used to build a model for classifying the Cheddars by their aging periods and to identify any peaks that contributed significantly to the separation (i.e., VIP > 1.5; Table S2 in the Supporting Information). Surprisingly, it is not the peaks that are unique to an aging category that are responsible for the majority of the separation. Of the 35 peaks uniquely present or uniquely absent in the three aging groups, only 8 peaks (23%) have PCA loadings with an absolute value greater than 0.7, and 16 peaks (46%) have VIP scores greater than 1.5 (Table S2 in the Supporting Information). Looking at the data from the perspective of the 20 significant peaks in the PCA (loading absolute values ≥0.7) and the 27 peaks significant in the PLS-DA, 40% and 59% are uniquely present or uniquely absent in an aging category, respectively (Table S2 in the Supporting Information). Therefore, a large portion of the separation is generated by peaks that are shared by all of the aged Cheddars.

It was hypothesized that the shared SESI-MS peaks contribute to the statistical separation of the Cheddars due to nuances in peak intensity between the aging categories. The Mann−Whitney U-test was utilized on a peak-by-peak basis to identify SESI-MS peaks that are significantly different between each group (Figures S1 and S2 and Table S2 in the Supporting

DOI: 10.1021/jf5063759
J. Agric. Food Chem. 2015, 63, 4386−4392

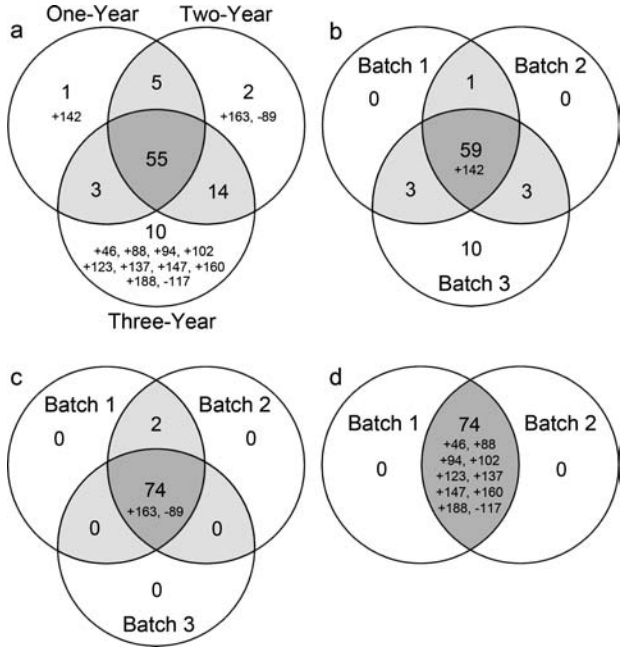

Figure 2. Number of SESI-MS peaks shared among artisanal Cheddar cheeses aged for 1−3 years. (a) Peaks shared by one-, two-, and three-year-aged Cheddars; (b) 1-year-aged Cheddar, batches 1, 2, and 3; (c) 2-year-aged Cheddar, batches 1, 2, and 3; and (d) 3-year-aged Cheddar, batches 1 and 2. Peaks were included if they were detected in at least half of the replicates for a given aging group. The mass-to-charge ratios (m/z) of peaks that are unique to a given age are listed.

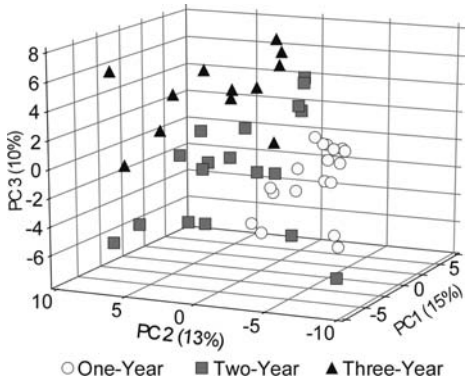

Figure 3. Principal component analysis of the SESI-MS volatile fingerprints of 1-, 2-, and 3-year-aged Cheddar cheeses. A total of 48 samples are included: 18 replicates of 1-, 18 replicates of 2-, and 12 replicates of 3-year-aged Cheddar.

Information). Of the 55 peaks in common with samples from all three Cheddar aging periods, 35 peaks (64%) have z-scores that exceed the 5% significance cutoff (≥1.96 or ≤−1.96) in at least one year-to-year comparison, eight of which also had significant loadings in the PCA and 11 of which have VIP > 1.5 in the PLS-DA (Table S2 in the Supporting Information). These data confirm that the presence and absence of SESI-MS peaks are not solely responsible for the characterization of aged Cheddars by their volatile profile. To utilize the differences in shared peaks, it is necessary to robustly measure the peak intensity (absolute or relative) in each sample day to day, and these data confirm that SESI-MS has this capability.

Peaks in the SESI-MS Volatile Fingerprint Correlate to Cheddar Cheese Aging. SESI-MS volatile fingerprints have utility beyond descriptively or predictively categorizing the Cheddar cheeses by aging period and can also be used to explore the impact of aging on the subtleties of the volatile profile. As Cheddars are aged, certain flavored components increase in intensity (e.g., sulfurous compounds) and others decrease (e.g., fresh milk-related flavor compounds);[28] therefore, it was hypothesized that a subset of SESI-MS peaks would trend over time. Of the 77 peaks in positive- or negative-ion modes that were different between any two ages of Cheddar (i.e., Mann−Whitney z-scores ≥1.96 or ≤−1.96; Figures S1 and S2 and Table S2 in the Supporting Information), we identified 26 peaks that were increased during the aging process and 11 peaks that were decreased (Table 3). For the majority of peaks, increasing intensity also correlated with increasing prevalence in the batches that were tested (or vice versa for decreasing peaks); that is, peaks that increase in intensity with age are also more likely to be measured in samples of three-year-aged Cheddars. One peak that increases with age, m/z = 95, may represent known aging-related flavor compounds in Cheddar (e.g., dimethyl disulfide (94 g/mol) and dimethyl sulfone (94 g/mol));[28] however, many of the aging-correlated SESI-MS peaks that were observed are likely not related to flavor. The flavorless compounds may still be valuable to cheesemakers, as they can be used as markers of the aging process.[29] All of the increasing and decreasing peaks that were observed contribute to the classification of Cheddars by aging period using PLS-DA (i.e., VIP > 0.8) and one-third of these peaks make very strong contributions to the classification (i.e., VIP > 1.5) and/or to the descriptive categorization of the Cheddars by PCA (i.e., |LS| ≥ 0.7; Table S2 in the Supporting Information).

There are an additional 40 peaks that have different intensities between two aging periods but do not demonstrate an increasing or decreasing trend (e.g., m/z = 101; Figure S1 and Table S2 in the Supporting Information). In some cases, the peak intensity variance is too great among these eight batches of Cheddar to confirm trends, and repeated longitudinal samples on several batches of Cheddar may be required to identify additional aging-related peaks. In other cases, it is postulated that several different compounds of the same nominal mass with unique aging-associated processes are being reported as a single peak in the SESI-MS fingerprints. MS/MS was performed on 29 positive-ion peaks (12% of the total peaks), and match scores between the fragmentation spectra indicate that the SESI-MS peaks represent the same compound(s) in >90% of the cases (Table S2 in the Supporting Information). However, the fragmentation spectra of the higher mass peaks do indicate mixtures of isobaric compounds (data not shown), and in two cases (m/z = 95 and 115), the relative abundances of the isobars appear to change year-to-year, which is reflected in the relatively low year-to-year match scores for m/z = 115 (Table S2 in the Supporting Information). Cheesemakers may find it beneficial to obtain additional information on isobaric compounds, as some will be flavored, and the nonflavored compounds may enhance or abrogate the sensory experience of the flavor volatiles of aged Cheddar.[30] Performing high resolution mass spectrometry (HRMS) or tandem mass spectrometry (MS/MS) will facilitate monitoring of additional aging-related compounds while preserving the nondestructive, rapid-analysis characteristics of SESI.[14,31]

Batches of Artisanal Cheddar Cheese Can Be Discriminated Using SESI-MS Fingerprints. The batches of aged Cheddars that were analyzed by SESI-MS are highly

DOI: 10.1021/jf5063759
J. Agric. Food Chem. 2015, 63, 4386−4392

Table 3. SESI-MS Peaks That Increase or Decrease in Intensity (+) or Prevalence (Shading) During Cheddar Aging

Increasing Trends

m/z [a]	1-Year	2-Year	3-Year
70	+	++	+++++
74	+++++	++++	+++++
77	++	+++++	+++++
95	+++	++++	+++++
106	+	+	+++++
107	++	+++	+++++
108	+	+++	+++++
-87	++++	++++	+++++
-88	++++	++++	+++++
-115	+++	++++	+++++
-116	++	++++	+++++
78		++++	+++++
88	++	++++	+++++
102		++++	+++++
120	++	+++	+++++
132		+++	+++++
134		+++	+++++
160		+++	+++++
162	+	+++	+++++
188		+++	+++++
190		+++	+++++
46		++	+++++
94		++	+++++
133		++	+++++
161			+++++
196		++	+++++

Decreasing Trends

m/z [a]	1-Year	2-Year	3-Year
47	+++++	++++	+++
48	+++++	++++	++++
63	+++++	++++	+++
69	+++++	+++	++
-124	+++++	+++	+++
29	+++++	+	
93	+++++	+++++	+
142	+++++	++	
187	+++++	+++++	
-102	+++++		
-103	+++++		

Peak Prevalence [b]
= 100% of batches
= ≥ 50% of batches
= < 50% of batches
= 0 batches

Normalized Peak Intensity [c]
+ 1-20%
++ 21-40%
+++ 41-60%
++++ 61-80%
+++++ 81-100%

[a]Peaks indicated in bold have statistically significant increases or decreases in all pairwise comparisons between years (Table S2, Supporting Information). [b]Peak prevalence was determined on a batch-by-batch basis using batch criteria described in the Materials and Methods. [c]Mean absolute peak intensities, normalized to 3-year peaks for increasing trends and 1-year peaks for decreasing trends.

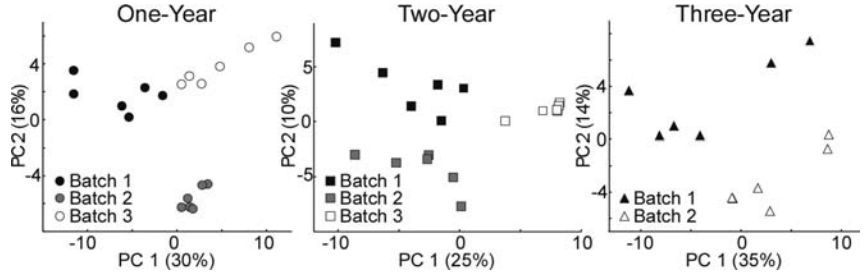

Figure 4. Principal component analysis (PCA) of the SESI-MS volatile fingerprints of batches of aged artisanal Cheddar cheeses. The two PCs providing the best separation for each age category are displayed. (a) Three batches of 1-year-aged Cheddar cheese ($p < 0.0001$). (b) Three batches of 2-year-aged Cheddar cheese ($p < 0.0001$). (c) Two batches of 3-year-aged Cheddar cheese ($p < 0.005$). Six replicates are included for each batch.

similar in their volatile fingerprint within each aging period (Figure 3; Table S1 in the Supporting Information) as well as in their flavor profiles, which met the age characteristics set forth by the cheesemakers (Table 1). However, subtle differences in the SESI-MS fingerprints of batches of the same age (Table S2 and Figure S3 in the Supporting Information) were observed, which were hypothesized to be statistically significant. Using PCA to evaluate the SESI-MS fingerprints within each age category, we observed that the six technical replicates of each batch cluster together and are statistically different from other batches of the same age (Figure 4; Table S4 in the Supporting Information). Whether the SESI-MS fingerprint could be used to identify the Cheddar samples by batch was also tested. PLS-DA leave-one-out cross validation was performed for all 48 samples in eight batch groups and obtained 100% correct batch assignments, confirming that the batches have unique volatile profiles and that SESI-MS fingerprints have the sensitivity and reproducibility necessary to discriminate highly similar samples with complex matrices. It must be noted that by testing only one sample per batch in this pilot study, it cannot be concluded whether the discrimination that was observed is on a batch-to-batch or sample-to-sample basis. However, other results from our lab indicate that SESI-MS volatile fingerprinting data can be used to correctly classify independent samples from closely related specimens.[32−35] From these previous studies and the observations presented here, it is posited that batch fingerprinting of Cheddar would be possible. Batch-to-batch variation is inherent to artisanal food production, and several variables in the milk and in the cheesemaking process impact the development of the Cheddar's flavor.[28] The cheesemakers at Shelburne Farms measure salinity, moisture, and pH and assess the overall milk quality and composition to predict the optimal aging time for each batch of Cheddar, balancing the time required to develop favorable flavor characteristics while diminishing less desirable ones. Prospectively monitoring volatile fingerprints for individual batches, and correlating early and final aging volatile fingerprints using rapid mass spectral fingerprinting techniques

DOI: 10.1021/jf5063759
J. Agric. Food Chem. 2015, 63, 4386−4392

such as SESI-MS may improve cheesemakers' ability to accurately forecast the aging time for every batch.

Through this pilot-scale study of the volatiles associated with aged artisanal Cheddar, it has been observed that SESI-MS is a robust and sensitive method for characterizing volatile mixtures arising from complex matrices. SESI-MS volatile fingerprints contain a wealth of data, and when coupled with chemometrics, the fingerprints can be mined for a variety of information on the samples' characteristics. The data suggest that SESI-MS can be employed to descriptively and predictively categorize artisanal Cheddar cheeses by their aging period, measure batch-to-batch differences in volatile profiles, and identify volatile components that are correlated with aging. Because SESI-MS is a rapid, nondestructive method for volatiles analysis, it is proposed that this technology is well-suited for quality analysis in food production and could be extended to the production of other artisanal aged products with complex flavor profiles, such as wines, spirits, and cured meats.

■ ASSOCIATED CONTENT

Supporting Information

Spearman's rank correlations, SESI-MS fingerprint peak table and summary of statistical analyses, principal component analyses t-tests, Mann-Whitney U-test z-score plots, and Venn diagrams for SESI-MS peaks shared among Cheddar batches. This material is available free of charge via the Internet at http://pubs.acs.org.

■ AUTHOR INFORMATION

Corresponding Author

*E-mail: jane.hill@dartmouth.edu. Telephone: 603-646-8656. Fax: 603-646-8778.

Author Contributions

§These authors contributed equally to this work.

Funding

This work was supported by funding from NASA EPSCoR (NNH09ZNE002C).

Notes

The authors declare no competing financial interest.

■ ACKNOWLEDGMENTS

The authors thank Shelburne Farms in Shelburne, Vermont, for providing us with the cheese samples used in this work as well as background information on artisanal Cheddar production and helpful comments on our results.

■ REFERENCES

(1) Paxson, H. *The life of cheese: Crafting food and value in America*. University of California Press: Berkeley, CA, 2012; Vol. *41*.

(2) United States Department of Agriculture Rural Development, In 2014; http://www.rurdev.usda.gov/bcp_vapg.html (accessed Feb 25, 2014).

(3) Delaney, C.; Kauppila, D. In *Start-up and operating costs of small farmstead cheese operations for dairy sheep*, 8th ed.; Thomas, D. L., Porter, S., Eds.; Great Lakes Diary Sheep Symposium, Cornell University, Ithica, NY, 2002; Cornell University: Ithica, NY, 2002; pp 127−140.

(4) Sakovitz-Dale, J. *Vermont Farmstead Cheese Marketing Study*; Vermont Housing and Conservation Board, 2006.

(5) Weston, D. J. Ambient ionization mass spectrometry: current understanding of mechanistic theory; analytical performance and application areas. *Analyst* **2010**, *135*, 661−668.

(6) Wang, X.; Wang, S.; Cai, Z. The latest developments and applications of mass spectrometry in food-safety and quality analysis. *TrAC, Trends Anal. Chem.* **2013**, *52*, 170−185.

(7) Nielen, M. W. F.; Hooijerink, H.; Zomer, P.; Mol, J. G. J. Desorption electrospray ionization mass spectrometry in the analysis of chemical food contaminants in food. *TrAC, Trends Anal. Chem.* **2011**, *30*, 165−180.

(8) Mohamed, R.; Guy, P. A. The pivotal role of mass spectrometry in determining the presence of chemical contaminants in food raw materials. *Mass Spectrom. Rev.* **2011**, *30*, 1073−1095.

(9) Ibáñez, C.; García-Cañas, V.; Valdés, A.; Simó, C. Novel MS-based approaches and applications in food metabolomics. *TrAC, Trends Anal. Chem.* **2013**, *52*, 100−111.

(10) Hajslova, J.; Cajka, T.; Vaclavik, L. Challenging applications offered by direct analysis in real time (DART) in food-quality and safety analysis. *TrAC, Trends Anal. Chem.* **2011**, *30*, 204−218.

(11) Biasioli, F.; Yeretzian, C.; Märk, T. D.; Dewulf, J.; Van Langenhove, H. Direct-injection mass spectrometry adds the time dimension to (B)VOC analysis. *TrAC, Trends Anal. Chem.* **2011**, *30*, 1003−1017.

(12) Cevallos-Cevallos, J. M.; Reyes-De-Corcuera, J. I.; Etxeberria, E.; Danyluk, M. D.; Rodrick, G. E. Metabolomic analysis in food science: a review. *Trends Food Sci. Technol.* **2009**, *20*, 557−566.

(13) Gu, H.; Xu, N.; Chen, H. Direct analysis of biological samples using extractive electrospray ionization mass spectrometry (EESI-MS). *Anal. Bioanal. Chem.* **2012**, *403*, 2145−2153.

(14) Hrbek, V.; Vaclavik, L.; Elich, O.; Hajslova, J. Authentication of milk and milk-based foods by direct analysis in real time ionization-high resolution mass spectrometry (DART-HRMS) technique: A critical assessment. *Food Control* **2014**, *36*, 138−145.

(15) Gasperi, F.; Gallerani, G.; Boschetti, A.; Biasioli, F.; Monetti, A.; Boscaini, E.; Jordan, A.; Lindinger, W.; Iannotta, S. The mozzarella cheese flavour profile: a comparison between judge panel analysis and proton transfer reaction mass spectrometry. *J. Sci. Food Agric.* **2001**, *81*, 357−363.

(16) Boscaini, E.; Van Ruth, S.; Biasioli, G.; Gasperi, F.; Mark, T. D. Gas chromatography-olfactometry (GC-O) and proton transfer reaction-mass spectrometry (PTR-MS) analysis of the flavor profile of Grana Padano, Parmigiano Reggiano, and Grana Trentino cheeses. *J. Agric. Food Chem.* **2003**, *51*, 1782−1790.

(17) Biasioli, F.; Gasperi, F.; Aprea, E.; Endrizzi, I.; Framondino, V.; Marini, F.; Mott, D.; Mark, T. D. Correlation of PTR-MS spectral fingerprints with sensory characterisation of flavour and odour profile of "Trentingrana" cheese. *Food Quality and Preference* **2006**, *17*, 63−75.

(18) Soukoulis, C.; Aprea, E.; Biasioli, F.; Cappellin, L.; Schuhfried, E.; Mark, T. D.; Gasperi, F. Proton transfer reaction time-of-flight mass spectrometry monitoring of the evolution of volatile compounds during lactic acid fermentation of milk. *Rapid Commun. Mass Spectrom.* **2010**, *24*, 2127−2134.

(19) Galle, S. A.; Koot, A.; Soukoulis, C.; Cappellin, L.; Biasioli, F.; Alewijn, M.; van Ruth, S. M. Typicality and geographical origin markers of protected origin cheese from The Netherlands revealed by PTR-MS. *J. Agric. Food Chem.* **2011**, *59*, 2554−2563.

(20) Fabris, A.; Biasioli, F.; Granitto, P. M.; Aprea, E.; Cappellin, L.; Schuhfried, E.; Soukoulis, C.; Mark, T. D.; Gasperi, F.; Endrizzi, I. PTR-TOF-MS and data-mining methods for rapid characterisation of agro-industrial samples: influence of milk storage conditions on the volatile compounds profile of Trentingrana cheese. *J. Mass Spectrom.* **2010**, *45*, 1065−1074.

(21) Aprea, E.; Biasioli, F.; Gasperi, F.; Mott, D.; Marini, F.; Märk, T. D. Assessment of Trentingrana cheese ageing by proton transfer reaction-mass spectrometry and chemometrics. *Int. Dairy J.* **2007**, *17*, 226−234.

(22) Li, X.; Hu, B.; Ding, J.; Chen, H. Rapid characterization of complex viscous samples at molecular levels by neutral desorption extractive electrospray ionization mass spectrometry. *Nat. Protoc.* **2011**, *6*, 1010−1025.

DOI: 10.1021/jf5063759
J. Agric. Food Chem. 2015, 63, 4386−4392

(23) Chen, H. W.; Zenobi, R. Neutral desorption sampling of biological surfaces for rapid chemical characterization by extractive electrospray ionization mass spectrometry. *Nat. Protoc.* **2008**, *3*, 1467−1475.
(24) Wu, Z.; Chingin, K.; Chen, H.; Zhu, L.; Jia, B.; Zenobi, R. Sampling analytes from cheese products for fast detection using neutral desorption extractive electrospray ionization mass spectrometry. *Anal. Bioanal. Chem.* **2010**, *397*, 1549−1556.
(25) Bean, H. D.; Zhu, J.; Hill, J. E., Characterizing bacterial volatiles using secondary electrospray ionization mass spectrometry (SESI-MS). *J. Visualized Exp.* **2011**, *52*, http://www.jove.com/details.php?id=2664. 10.3791/2664.
(26) Wu, C.; Siems, W. F.; Hill, H. H. Secondary electrospray ionization ion mobility spectrometry/mass spectrometry of illicit drugs. *Anal. Chem.* **2000**, *72*, 396−403.
(27) Martinez-Lozano, P.; Rus, J.; de la Mora, G. F.; Hernandez, M.; de la Mora, J. F. Secondary electrospray ionization (SESI) of ambient vapors for explosive detection at concentrations below parts per trillion. *J. Am. Soc. Mass Spectrom.* **2009**, *20*, 287−294.
(28) Burbank, H. M.; Qian, M. C. Volatile sulfur compounds in Cheddar cheese determined by headspace solid-phase microextraction and gas chromatograph-pulsed flame photometric detection. *J. Chromatogr. A* **2005**, *1066*, 149−157.
(29) Marsili, R. Monitoring chemical changes in Cheddar cheese during aging by high performance liquid chromatography and gas chromatography techniques. *J. Dairy Sci.* **1985**, *68*, 3155−3161.
(30) Drake, M. A. Invited review: Sensory analysis of dairy foods. *J. Dairy Sci.* **2007**, *90*, 4925−4937.
(31) Chen, H. W.; Wortmann, A.; Zenobi, R. Neutral desorption sampling coupled to extractive electrospray ionization mass spectrometry for rapid differentiation of biosamples by metabolomic fingerprinting. *J. Mass Spectrom.* **2007**, *42*, 1123−1135.
(32) Bean, H. D.; Zhu, J.; Sengle, J. C.; Hill, J. E. Identifying methicillin-resistant *Staphylococcus aureus* (MRSA) lung infections in mice via breath analysis using secondary electrospray ionization-mass spectrometry (SESI-MS). *J. Breath Res.* **2014**, *8*, 041001.
(33) Zhu, J.; Hill, J. E. Detection of *Escherichia coli* via VOC profiling using secondary electrospray ionization-mass spectrometry (SESI-MS). *Food Microbiol.* **2013**, *34*, 412−417.
(34) Zhu, J.; Bean, H. D.; Kuo, Y.-M.; Hill, J. E. Fast detection of volatile organic compounds from bacterial cultures by SESI-MS. *J. Clin. Microbiol.* **2010**, *48*, 4426−4431.
(35) Zhu, J.; Bean, H. D.; Wargo, M. J.; Leclair, L. W.; Hill, J. E. Detecting bacterial lung infections: *in vivo* evaluation of *in vitro* volatile fingerprints. *J. Breath Res.* **2013**, *7*, 016003.

DOI: 10.1021/jf5063759
J. Agric. Food Chem. 2015, 63, 4386−4392

Marie Cook of FDACS. She described how to improve sampling quality and accuracy and elaborated on the techniques used to obtain good representative samples for analysis. After the symposium, she was invited to give a webinar for ACS-AGRO, which can be found at www.agrodiv.org/webinars/nov2014/1.html. Robert Gooding from BASF presented results from the use of microtechnology in high-throughput analysis of soil and plant samples. He emphasized factors of particle size, matrix, and analyte when choosing sample size for analysis. Kari Lynn from Dow AgroSciences presented the results from a round-robin study to assess the feasibility of a two-stage homogenization process that maintains homogeneity down to milligram level subsamples. This was independently performed by four laboratories, including Monsanto. The results demonstrated that each subsampling process (from kg to g and from g to mg) retained a comparable accuracy and precision, demonstrating 75 mg subsamples that adequately represented the original field samples processed using the advanced protocol for four analytes in six matrices tested.

The symposium concluded with a very interactive open question and discussion period, and several experts from the audience described their diverse range of experiences and findings. A main conclusion was that all milling approaches, including microtechnologies in residue analysis, should be evaluated for a given application to demonstrate acceptable performance before the protocol is applied in practice. The posters on sampling and combined uncertainties presented by Zsuzsa Farkas, who won a poster award in the IUPAC Congress, were prominently mentioned during the discussion, as were practical sample processing approaches used in regulatory monitoring laboratories in The Netherlands, United Kingdom, United States, China, India, and elsewhere.

Although the presentation rooms and poster floor were filled to capacity during the presentations, the compilation of the submitted papers published in this special section can benefit a great many residue chemists and other interested parties for years to come. The reader may not feel the same excitement from the lively discussions at both symposia, but the information in the papers should still benefit those in the pesticide analytical field who are interested in improving quality of results while saving time and cutting operating costs in the process.

Steven J. Lehotay[*,†]
Leah S. Riter[§]
Manasi Saha[#]

[†]Eastern Regional Research Center, Agricultural Research Service, U.S. Department of Agriculture, Wyndmoor, Pennsylvania 19038, United States

[§]Environmental Sciences Technology Center, Monsanto Company, St. Louis, Missouri 63167, United States

[#]Consumer and Environmental Safety, BASF Crop Protection, Research Triangle Park, North Carolina 27709, United States

AUTHOR INFORMATION

Corresponding Author

*(S.J.L.) E-mail: Steven.Lehotay@ars.usda.gov.

Notes

The authors declare no competing financial interest.

DOI: 10.1021/jf5059599
J. Agric. Food Chem. 2015, 63, 4393−4394

needs in an efficient manner, but great caution and care are required to ensure that sample processing is properly done to provide meaningful results that lead to better conclusions and decisions.

SAMPLING

Why should laboratories care about sampling? It is easy for laboratory personnel to justify that sample collection is not their concern, but the quality of work suffers if expensive analyses are blindly conducted with no regard for the correctness of the sample and how it was obtained. Too often the sampling plan and its manner of execution are thought to be of no importance to laboratory personnel, but the final reports are often signed by laboratory staff who become liable for the quality of the findings. Just as an analyst cannot hide from the quality of his/her results when confronted with quality control (QC) findings, laboratory chemists should take ownership of their results with a holistic perspective. They should test the validity and determine uncertainties of all aspects in the process, and those responsible for sampling plans and sample collection should be held accountable to the same degree of oversight and verification to which the analysts are held accountable for their results. The tide of importance in pesticide residue analysis is rising, and analytical practices that can be likened to sand castles on the beach will not last long.

As food safety becomes increasingly complex due to far-reaching global food supplies, pesticide manufacturers are seeking to register pesticides in multiple countries and have their residue data accepted by regulators in the European Union, United States, Japan, Australia, Brazil, and many other countries. To demonstrate environmental and human health impacts, as well as the anticipated food residues, expensive field trials must be conducted. It is important that residue data generated from these studies yields acceptable trueness and precision for use in complex risk assessment calculations and statistical analyses. Regulators who enforce maximum residue levels (MRLs) must have confidence that the reported analytical results represent the true residue concentrations. Millions of dollars of perishable food shipments may be needlessly lost, causing much economic hardship to farmers and importers/exporters, if sampling leads to a false violation, or environmental and consumer safety may be compromised if actual violations are missed.

Due to the high stakes involved, food safety regulatory agencies can no longer afford to ignore the contribution of sampling to total analytical uncertainty. When data are shared between far-reaching organizations, there should be transparency and understanding of what, when, where, and how the sample was taken, and the degree of uncertainty in the analytical findings needs to be known when making inferences about the population from which the sample was taken.

CURRENT SAMPLING PRACTICES

Actually, studies involving pesticide application field trials have shown current practices to be acceptably precise (<25% RSD) if carried out according to common regulatory standards (e.g., EPA, OECD, FAO/WHO, Codex).[26−29] Similarly, sampling studies for regulatory monitoring have shown similarly good precision if enough replicate samples (≥6 from 8−12 lots) are taken, but this has been shown to depend significantly on analyte/commodity pairs.[30−33] Ambrus has recommended collecting 10−25 increments per sample, which has been shown to yield 16−25% uncertainty.[29] For a typical field trial of fruit trees, this translates into collecting samples from at least half of the trees dispersed randomly within a given plot and compositing 24 fruits per sample.[34] Sample weight can be reduced to 2−3 kg (or 4−6 lb) by taking alternate or single quarters from each fruit. Sample reduction is already taking place in the field, which makes sample transport, storage, and processing much easier in the laboratory. However, further reports in the scientific literature involving additional analytes/commodities to evaluate sample correctness and integrity would provide more confidence in whether this convenience should be followed more widely or not.

When sampling a crop from the field, U.S. Food and Drug Administration (FDA) recommends superimposing an imaginary grid on the field, dividing it into approximately 100 areas, randomly selecting 10 areas, and collecting 1 lb portions from each section. This yields 10 increments in the composite, which is typical for medium-sized crops.[35] Would it be better to take 30 increments of one-third pound each? In many cases, more increments are more representative, but this requires more effort and may or may not provide significant benefit depending on the crop and pesticide analytes. Ambrus and Soboleva found in a study of medium-size crops that increments of 5, 10, and 25 yielded RSDs of 37, 25, and 16%, respectively.[29]

Recommendations in monitoring programs for collection of fruits and vegetables range from 2 to 5 lb composites in accordance with FDA, Codex, European Commission, and Pesticide Data Program guidelines.[35−38] FDA recommends collection of 1 kg (10 units) for tomatoes, 2 kg (5 units) for cabbage, 0.5 kg for herbs, and 0.1 kg for spices. Whereas spices and herbs may warrant smaller masses, should the mass of the vegetable determine the number of increments collected (i.e., only 5 units of cabbage)? In the case of aflatoxin, FDA recommends sampling collection of twenty 1 lb units if the lot consists of fewer than 200 bags of grain, 40 units if fewer than 800 bags, and 60 units if fewer than 2000 bags. Should the size of the lot determine the number of increments, or should the number of needed increments be determined by the heterogeneity of the food being sampled and the error that can be tolerated?

Currently, most sampling plans/collections are assumed to be acceptable on the basis of theory and only a few studies, but little is done to verify the validity of the procedures in practice. At a minimum, laboratory personnel and sample collectors should meet each other and learn about their roles in the overall sampling/analysis chain and open lines of communication. Laboratories should also include the collection of replicates in their sampling protocols and periodically send a QC officer to the field to observe collection technique and collect duplicate (or more) samples of the same lots in the same way as the sample collector. The results from the duplicates can be compared to empirically measure sampling error. Just as proficiency testing results were quite poor to start (e.g., 50% RSD), current sampling practices may lead to embarrassingly high variability at first. However, recent interlaboratory proficiency test results often yield <25% RSD,[39] and the same motivations to instill better practices and performance due to peer pressure and personal responsibilities will take root with respect to sampling. Data quality improvement incentives can blossom only if the plan designers and sample collectors are held accountable in a similar way that laboratories have been held accountable for their operations.

DOI: 10.1021/jf5056985
J. Agric. Food Chem. 2015, 63, 4395−4404

RECENT DEVELOPMENTS INVOLVING SAMPLING

In 2011, the United States passed new food safety legislation known as the Food Safety Modernization Act (FSMA).[40] This law mandates the creation of an integrated food safety system to both prevent food safety problems (Title 1) and determine and respond to food safety problems (Title 2). Such an integrated system would require U.S. federal, state, territorial, and local food safety agencies, as well as food producers, to share information and analytical data. The law includes emphasis on the importance of sampling. The guidance to laboratories encourages laboratory accreditation, including standards for both sampling and testing (Section 202). For sampling, it mandates sampling procedures, QC systems, and trained, qualified sample collectors (Section 202 (a) (6)). The writers of the legislation recognized the need for scientifically defensible sampling as part of the goal to achieve a truly integrated food safety system.

In 2010, the FDA convened the Partnership for Food Protection to provide guidance on the many different sections of the new law. Drafted by members of federal, state, and local food and feed safety agencies across the country, the Laboratory Task Group drafted the Food and Feed Laboratories Best Practices Manual, which was published on the FDA Web site in 2013.[41] Sampling is discussed in Chapter 4, which states "Uniformity in sample collection is essential to achieve consistent laboratory analytical results between multiple federal, state and local food/feed safety agencies." The authors identified four critical elements about sampling: (1) the sampler must have policies, procedures, and records in place to ensure sample integrity security, accountability, and chain of custody; (2) the sampler must have a statistically appropriate sampling plan; (3) the sampler must undergo a training program; and (4) the sampler must be prepared to develop "incident specific" sampling plans prior to beginning collection. Note that the guidance recommends documented policies and procedures that would be consistent with any accredited program. But how are agencies to develop such plans?

In short, greater care must be taken than currently applied to sampling. Current practices are largely unchecked and lead to no guarantees. Much care is taken to collect samples that yield statistically valid results for risk assessment purposes in the Pesticide Data Program, which is conducted by several states in the United States and managed by the USDA Agricultural Marketing Service.[42] However, monitoring programs conducted by the FDA and USDA Food Safety and Inspection Service have recently been criticized by the U.S. Government Accountability Office for inadequate sampling plans and execution.[43] The USDA and FDA agreed with the report findings and will seek to address the limitations in their pesticide monitoring programs in the future. To provide more guidance and foster implementation of FSMA mandates, FDA awarded a cooperative agreement[44] jointly to three professional organizations: Association of Public Health Laboratories (APHL); Association of Food and Drug Officials (AFDO); and American Association of Feed Control Officials (AAFCO). One of 14 working groups is preparing a document, "Guidance on Obtaining Defensible Samples" (GOOD Samples), to address issues of sampling and sample processing.

GY'S THEORY OF SAMPLING

Just as a chain is only as strong as its weakest link, accuracy in sampling and laboratory sample processing is equally essential as all other aspects in the overall analytical workflow. Pierre Gy developed an extensive theory of sampling in his work with mining ores, and he literally wrote the book on the subject.[45] Pitard further explained Gy's theories and their application in practice.[46] The concepts Gy developed are universal when it comes to sampling and sample comminution for any application. Gy's theories have been applied in the cases of relatively dry food samples, such as grains and feeds, but less work has been done in other food types such as fruits, vegetables, and animal tissues. The general tenants that Gy developed apply to collections of primary samples from the agricultural fields as well as laboratory processing to produce an analytical test sample. Pitard tells us that "Sampling is correct when it gives all elements, in the batch to be sampled, a uniform probability of being selected".[46] Incorrect sampling may be responsible for large, undetected biases. Sampling theory describes the sources of variability (heterogeneity) that must be considered in the development of sampling and sample processing plans to ensure that the test portion analyzed is representative of the lot sampled and sources of error and uncertainty are reduced.

Gy asserted that both constitutional (compositional) and distributional heterogeneity are important in sampling. The greater the chemical and/or physical differences (such as density, proportion, reactivity, stability, bound state, particle shape, and range of sizes) between each fragment making up a particular analyte/matrix lot of interest, the greater the potential sample heterogeneity (both types), whether it be for the primary sample collected from the lot or the sample processed in the laboratory. Compositional (or constitutional) heterogeneity is due to the difference in composition of each fragment of the lot. Distributional heterogeneity is the manner in which separate and distinct particles or units are scattered or segregated within the lot. Distributional heterogeneity is the difference in composition of the increments (groups of particles). The greater the difference in composition of each fragment (the compositional heterogeneity), the greater is the possible distributional heterogeneity. The error that results from the compositional heterogeneity is called fundamental error (FE). Gy states that FE may be small but only zero "if the material is composed of one completely pure constituent",[45] which the residue chemist knows is rarely, if ever, true. The error that results from the distributional heterogeneity includes grouping and segregation error (GSE). One of the main components of GSE is segregation due to gravity. In residue chemistry, large compositional (relativity small test aliquot mass) and large distributional heterogeneity (segregation due to density differences) leads to large errors that must be measured and controlled.

To express the variance of FE as s^2, Gy derived the equation $s^2 = Cd^3/m$, in which d is the diameter of the largest particles (in cm), m is mass (in g) of the sample collected (or comminuted), and C is a constant (in g/cm^3) that is specific to the nature of the analyte/matrix in the lot.[45] Gy's constant is fixed by the nature of the material in the lot and refers to the compositional characteristics that cannot always be easily measured in food and feed samples but can be empirically estimated for particular analyte/matrix sample types. In practice, Gy's equation tells us that, for a particular analyte/matrix lot with a fixed C, the variance of FE due to sampling may be reduced by decreasing the size of the units (particles) within the sample and/or by increasing the mass of the sample collected. Laboratory sample reduction processes (such as

DOI: 10.1021/jf5056985
J. Agric. Food Chem. 2015, 63, 4395−4404

cutting, blending, chopping, and/or cryogenic grinding/cryomilling) all fall under the umbrella of "sample comminution".[35] Comminution is the process of reducing the particle size of a sample by grinding, blending, or other forms of pulverizing and is also commonly, but inaccurately, referred to as homogenization. We make this distinction because sampling theory states that "A set of units is homogeneous when all its units are strictly identical to each other."[46] The essence of comminution is to yield test sample portions of smaller particle size and reduce the FE. Comminution of laboratory samples never results in an entirely homogeneous sample and may, in fact, increase the distributional heterogeneity of the sample. In chemical residue analyses, the goal of the sample comminution process and the selection of a test portion is to reduce FE and provide an analytical test portion that accurately represents the original sample, composed of multiple increments, collected from a defined portion of product such as a lot of food or feed in commerce (e.g., store, slaughterhouse, warehouse, shipping container, field, crop).[16−25]

However, the relationship of density and mass changes with respect to matrix, analyte, and other sample characteristics such as analyte concentration and size/shape of fragments that are expressed by *C* in Gy's equation. Uncertainty also depends on the variability of the analyte(s) between the different fragments of the original sample. For example, aflatoxin in corn is typically less evenly distributed than common pesticides because it is more common that only a few kernels of corn are contaminated with aflatoxin, whereas applied systemic or nonsystemic pesticides tend to be present in many kernels. Thus, there must always be sufficient sample mass collected for comminution and subsampled for analysis to adequately represent the varying composition of analytes of interest in the sample.

Gy also described distributional heterogeneity, which corresponds to GSE. As an example, this can be likened to granola. Pesticides are not typically distributed evenly between the oatmeal, pecans, and crispy honey clusters (compositional heterogeneity). The small grains of crushed cereal and peanut dust also drop to the bottom. Distributional heterogeneity is changed by mixing (i.e., when you shake a cereal box, the crumbs fall to the bottom, but when you mix applesauce, the apples and liquid are more evenly dispersed.) GSE from distributional heterogeneity is reduced by correctly sampling multiple increments and combining into a single sample. An increment is the group of particles collected with one operation of a sampling tool. Each of the increments (groups) within the lot should have the same probability of being selected, and multiple increments should be taken from randomly chosen portions of the lot. The role of sampling tools is very critical to avoid sampling bias. The sampling tool must be capable of choosing all of the different fragments/particles of the lot without excluding particular particles such as clusters too large to be sampled or introducing additional bias such as missing the smaller particles or denser materials in a product sinking to the bottom or the oil on top of water being pushed to the side by a scoop. Thus, each sample should have the same relative amounts of each component (oatmeal, pecans, clusters, and crumbs) as in the lot.

Just as smaller particles settle to the bottom in a silo of grain, test samples may have differently sized particles dispersed in a container. For example, a blended slurry of tomatoes may contain liquid with more dense fragments of skin (containing the pesticide of interest), pulp, and seed in various sizes, shapes, composition and densities, resulting in a mixture of units that are more unalike than the whole tomatoes from which they were derived. The test portion that has very uniform particle size, such as may be achieved with cryomilling, may have less distributional heterogeneity and less GSE. How often do we just mix and scoop to take a test portion from a blended material? Mixing may or may not reduce distributional heterogeneity, but Gy's theory indicates that taking several smaller increments would yield a more representative test portion.

Thus, Gy's theories urge us to learn more about the physical characteristics and analyte distribution of our collected and comminuted samples. Reducing particle size and increasing mass reduce FE, and increasing the number of increments reduces GSE, but only if we have tools and techniques that allow us to achieve sample correctness.

EVALUATING SAMPLING ERROR

In multiclass, multiresidue methods for diverse commodity types, representative pesticides and matrices can be used in spiking experiments, but incurred residues in real samples provide more realistic results to validate appropriate sampling/processing standard operating procedures. To evaluate the degree of uncertainty in the overall analytical process, Lyn et al.[24] described a nested replicate design in which replicate strawberry samples were collected, each processed in duplicate, and each replicate was analyzed in duplicate. This enabled the use of analysis of variance (ANOVA) statistics to estimate the error due to sampling, sample processing, and analytical testing. This work not only demonstrated the significant contributions of sampling (38−99%) and processing (7−50%) to overall analytical uncertainty but also showed that these errors varied with respect to analyte and the source of strawberries.

Just as we conduct routine QC of our analytical methods, we can also determine the error contributed by our laboratory methods by analyzing a replicate test portion with each batch of 10−20 samples, reanalyzing samples with positive findings or analyzing multiple replicates of an incurred residue using different processing methods and analytical sample sizes during validation. Over time, these QC procedures will provide us with valuable information about the uncertainty in our procedures and help us to minimize the errors due to the sampling steps prior to our instrumental analyses.

In his chapter "Sampling for Trace Constituents", Pitard pointed out that when measuring trace level analytes, both constitutional and thus distributional heterogeneity are often very high. He stated that "analytical subsamples may be affected by a fundamental sampling error that is so high that data often show only the fraction of a constituent of interest that is finely disseminated everywhere within the product".[46] In determining whether we have achieved appropriate sample mass to control FE, Pitard describes an experiment in which 50 samples of at least 10 increments each are collected from a lot and analyzed using their whole mass. This same experiment is repeated with 50 samples of at least 10 increments each but totaling at least 10 times greater mass. If the variance is acceptably small (16−25%) when either the small or large mass is analyzed, then we have more confidence that the appropriate sample mass was collected. This same type of experiment may be performed to evaluate the appropriate mass for new processing and analysis methods. Whereas these very large experiments may be outside the capacity of many individual laboratories, it is hoped that, over time, more work will be conducted and reported in the

DOI: 10.1021/jf5056985
J. Agric. Food Chem. 2015, 63, 4395−4404

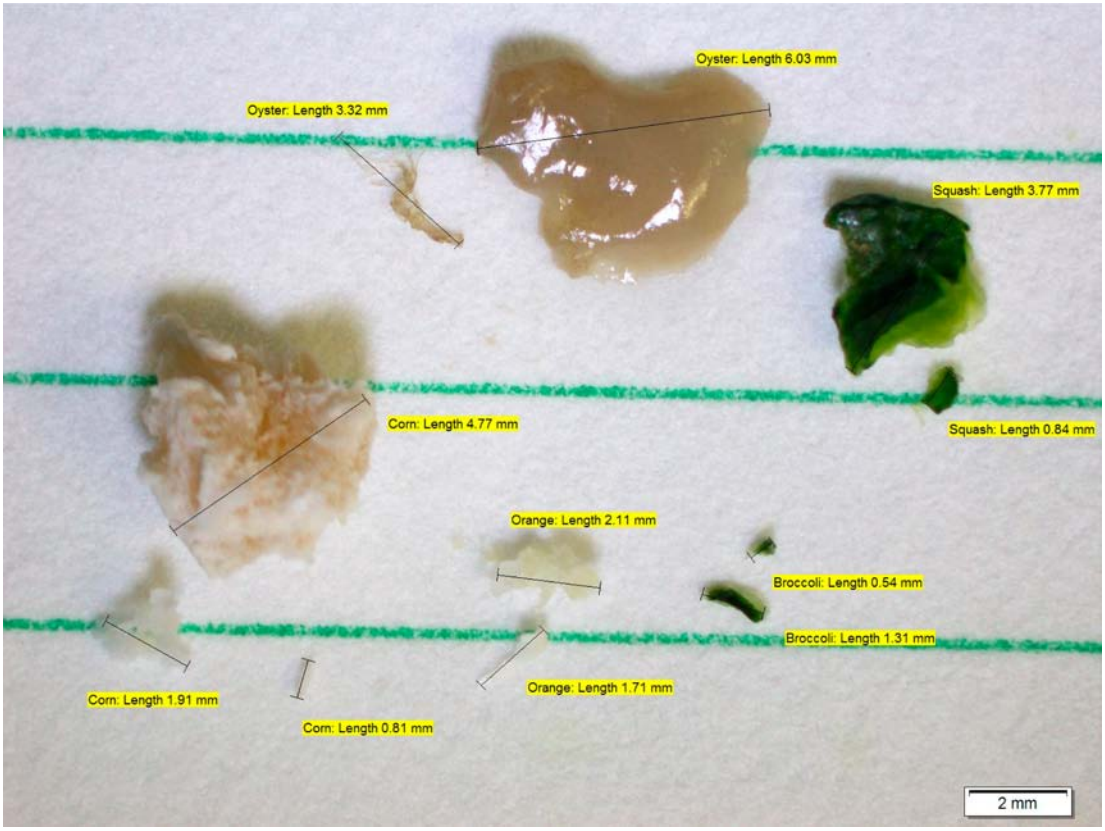

Figure 1. Example particle sizes of broccoli, corn, zucchini, squash, oranges, and oysters after room temperature blending.

literature that will inform residue chemists of sampling errors and how they may be minimized. The reader is encouraged to become more familiar with the Theory of Sampling[2,3,45,46] and incorporate it into the development of their sampling plans and comminution procedures.

■ COMMINUTION PROCEDURES IN PRACTICE

What is the smallest analytical test portion that can achieve results that represent the original sample? Before the quick, easy, cheap, effective, rugged, and safe (QuEChERS) approach to residue analysis,[48] most laboratories analyzed subsamples of 50−100 g.[47,49,50] Young et al.[23] demonstrated that ≈25 g subsamples can be representative of typical composite samples using standard FDA practices at the time.[40] On the basis of additional studies,[16,17,21] Ambrus has recommended that 30 g test samples are acceptable if traditional single-step comminution is conducted using common choppers. However, de Kok et al.[51] in the Dutch pesticide monitoring program have been using 15 g test samples since the 1980s in the mini-Luke method, a modification of the FDA PAM 302 method.[47] They still use this process and method, in which a simple two-step comminution procedure is followed: the 1−2 kg composite sample is comminuted at room temperature as in common practices,[16,17,21,23,47] and then a ≈200 g subsample is taken and thoroughly comminuted with a probe blender (e.g., Ultra-Turrax). A 15 g test portion is easily representative of the ≈200 g subsample, which is easily representative of the original 1−2 kg collected sample from the field. Meanwhile, the ≈200 g subsample is stored frozen for further analysis if needed for confirmation of a violative finding.

Similarly, QuEChERS calls for 10−15 g test samples for wet samples, and 2−5 g portions for dry samples to which water (e.g., 10 mL) is added. From the beginning, the developers have emphasized the importance of proper sample comminution when QuEChERS is employed, not only to obtain meaningful results from representative test samples but also to generate fine particles to allow better access of the extraction solvent to the pesticide analytes in the test sample.[43] For these reasons, some laboratories that use QuEChERS conduct comminution of frozen samples integrated with dry ice using vertical, s-blade choppers (e.g., Robot Coupe). Fussell et al.[19−21] evaluated cryogenic comminution for different pesticides/matrices, and their results show that in some cases, 2 g samples are sufficiently representative in a one-step process, but 10−15 g test portions are more appropriate to cover the gamut of common pesticides/matrices analyzed.

Pesticide monitoring programs in the United Kingdom and Germany have adopted the cryogenic comminution procedure and QuEChERS sample preparation. Another advantage of using frozen sample conditions is that fewer losses of analytes occur through degradation and volatilization.[18−20] However, cryogenic comminution also has disadvantages. For one, composite samples need to be frozen in chunks before comminution with dry ice, or else an eruption of CO_2 gas will occur when the dry ice is exposed to the sample at room temperature. It often takes an extra day to cut and freeze the composite samples for cryogenic processing and much freezer space depending on sample-throughput needs. Samples comminuted at room temperature in the FDA and Dutch approaches can be processed within the same day. In the case of cryogenic sample processing, there is an art in finding the right balance in the amounts of dry ice and sample, as well as the size of frozen sample chunks, in the chopper container. The amount of time given is also critical to achieve a flowing, homogeneous

DOI: 10.1021/jf5056985
J. Agric. Food Chem. 2015, 63, 4395−4404

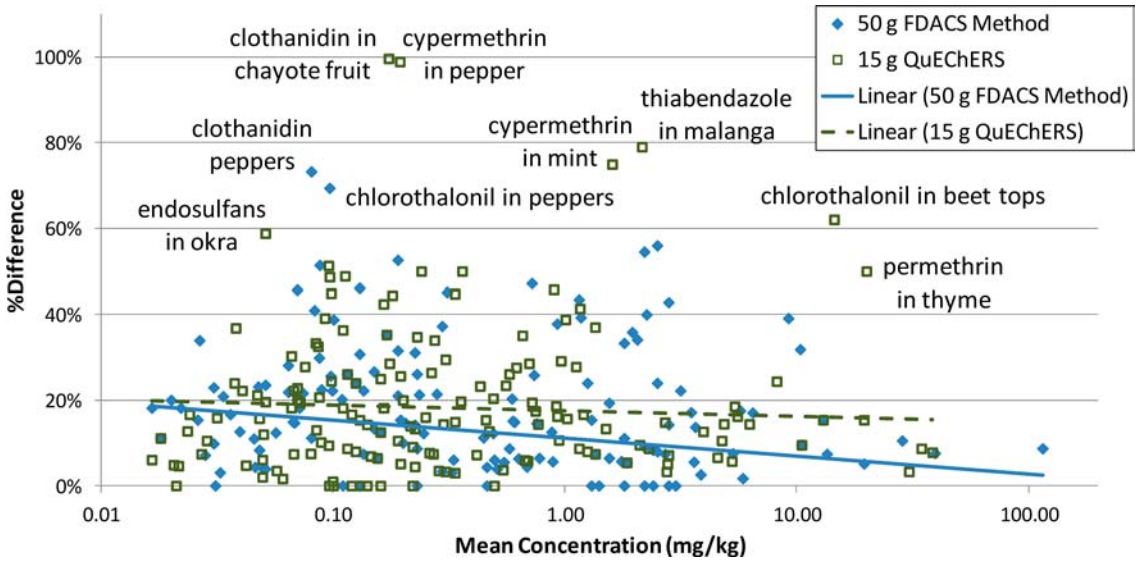

Figure 2. Absolute percent difference in results versus mean concentrations in reanalyses of 15−50 g duplicate test samples that were subsampled from ≈1 kg samples comminuted at room temperature and stored frozen until confirmatory reanalysis of potentially violative samples on a different date.

sample powder in the chopper. In a humid environment, the moisture from the atmosphere will condense in the sample to cause a low bias in the results due to added sample weight. Similarly, enough time must be given for all of the dry ice to sublime, which is typically done by placing the samples in a freezer in another time- and space-consuming step. Finally, frozen samples should be thawed prior to extraction, which allows greater access and solubility of the analytes in the extraction solvent, but to allow thawing during a longer extraction is also possible.

Disadvantages of the Dutch two-step method also include the need for worker skill/experience, particularly during the probe blender step. Cleaning of the blender and containers is more difficult when using wet samples, and care must be taken to avoid cross-contamination or introduction of water/solvent if the surfaces are not dry. Worker safety is a concern in either approach, but use of the probe blender is very noisy and requires ear protection, as well as care to avoid cut fingers, broken glass containers, and spraying of sample.

REAL-WORLD RESULTS

The aspects to consider in laboratory "sampling" (comminution) are the same as described for the field sample: more mass, smaller particle sizes, and more increments lead to less uncertainty. Unfortunately, the type of food and the analyte greatly affect the uncertainty. For example, a systemic pesticide distributed in oranges may allow 10 g highly representative test portions, but using the same comminution procedure for nonsystemic pesticides in tomatoes may need 30 g to yield the same degree of accuracy. We propose that the comminution protocol should be validated in the laboratory in a similar manner as the analytical method via replicate analyses of spiked and incurred precomminuted samples to determine pesticide recoveries and repeatabilities of test portions.

In the Florida Chemical Residue Laboratories, fresh fruits and vegetables are blended at room temperature in one step akin to the FDA protocol.[23,47] Microscopic examination of broccoli, corn, oranges, zucchini, and oysters (from Gulf Oil Spill samples) demonstrated that the particle sizes ranged from 0.5 to 6.0 mm (see Figure 1). Each sample type was quite different in consistency. For example, zucchini had two distinct layers of skin and pulp. Corn was very spongy, broccoli gave small oblong pieces, and oyster was a mixture of slimy gelatin and fibrous strings.

When screening >300 pesticides in 30 or more different types of samples in a single batch, are 10−15 g test portions adequate? Without replicate analyses of subsamples from the processed samples, the degree of uncertainty from the comminution step is unknown, but this issue is largely ignored in quality assurance programs and laboratory operations. Routine addition of replicates to a laboratory sampling, processing, and analytical scheme would allow the regulatory agency to estimate the total uncertainty in their measurement and make better decisions.

In regulatory analyses, samples indicated to be violative in the first analysis need to be reanalyzed for confirmation purposes. For indicated violative samples in the Florida laboratory, reanalyses were conducted of stored, frozen, duplicate test portions taken from the same processed samples after a period of days to weeks. Using the equation to calculate percent difference from the mean $|A - B|/[(A + B)/2] \times 100\%$, where A and B are the determined concentrations of the same analyte in the duplicate test portions, the reanalyses can be used to estimate uncertainty of the processing step in the laboratory (for the diverse range of analytes and samples monitored). Unfortunately, possible analyte degradation over time or changes in the matrix (cell disruptions, moisture gain/loss, freeze/thaw factors) also affect the consistency of results. Furthermore, the duplicate analyses were conducted on different days potentially by different analysts using different instruments. On the basis of proficiency testing results,[39] we assume that reproducibility is ≈25% RSD due to analytical and storage factors.

In all, 309 samples covering 70 different foods and 79 different analytes were reanalyzed, and determined concentrations ranged from 0.017 to 110 mg/kg. During the time period evaluated, the laboratory switched from analyzing 50 g subsamples by the Florida Department of Agriculture and

DOI: 10.1021/jf5056985
J. Agric. Food Chem. 2015, 63, 4395−4404

Consumer Services (FDACS) method[49] to their modified version of the QuEChERS method using 15 g test portions.[48] All together, 147 pesticide/matrix pair 50 g duplicates were analyzed by the FDACS method, which yielded 18 ± 15% differences, and 15 g test portions using the QuEChERS approach gave 20 ± 18% differences in the reanalyses. Figure 2 shows all percent difference results versus mean concentration in the duplicate analyses for each method. The 2% observed difference in precision did not significantly affect overall quality of results, but it reinforces the previous findings on sample comminution.[16−25]

Overall, the average percent difference was 19 ± 16% (n = 309), which can be compared with results for specific pesticides and commodities shown in Tables 1 and 2, respectively. The pesticide/matrix pairs that gave particularly variable results are listed in Figure 2, and the trend lines show the typical relationship of increasing precision versus concentration. In any case, the average 19% difference is less than the expected 25% RSD observed in interlaboratory trials for replicate analyses of proficiency test samples.[34] In general, the overall findings for many fruits and vegetables indicate that sample comminution at room temperature using common choppers to generate as little as 15 g test portions does not significantly contribute to overall uncertainty in pesticide residue analyses at violative levels. However, instances of higher variability can be observed in Figure 2 and Tables 1 and 2, which are due to a variety of factors including sample comminution.

Table 1. Absolute Percent Difference in Results for Pesticides (with $n \geq 3$) in the Reanalyses of 15−50 g Duplicate Test Samples That Were Subsampled from ≈1 kg Samples of Diverse Commodites That Were Comminuted at Room Temperature and Stored Frozen until Confirmatory Reanalysis of Potentially Violative Samples on a Different Date

pesticide	av % diff	SD (%)	n
acephate	13	9	6
atrazine	19	6	3
azoxystrobin	10	5	4
benomyl (carbendazim)	17	12	26
captan	11	15	6
carbaryl	17	13	3
chlorfenapyr	17	9	3
chlorothalonil	24	17	27
chlorpyrifos	18	15	6
clothianidin	72	23	3
cyhalothrin	17	7	4
cypermethrin	29	29	15
dimethoate	15	13	14
dinotefuran	26	13	5
diphenylamine	7	3	4
endosulfans	17	16	15
fludioxonil	13	6	3
imazalil	11	3	4
iprodione	22	15	10
methamidophos	14	9	6
methomyl	9	8	12
omethoate	27	3	3
o-phenylphenol	17	7	3
oxamyl	29	16	4
permethrin	16	16	6
prochloraz	15	11	14
propamocarb HCl	22	10	5
pyrimethanil	11	6	5
thiabendazole	26	25	7
thiacloprid	24	9	3
thiamethoxam	23	8	3
thiophanate-methyl	18	17	15
triadimefon	16	6	5

Table 2. Absolute Percent Difference in Results for Commodities (with $n \geq 3$) in the Reanalyses of 15−50 g Duplicate Test Samples That Were Subsampled from ≈1 kg Samples That Were Comminuted at Room Temperature and Stored Frozen until Confirmatory Reanalysis of Potentially Violative Samples on a Different Date

commodity	av % diff	SD (%)	n
asparagus	10	10	5
basil	14	11	11
beet (tops)	30	23	4
cabbage	22	15	6
chayote fruit	48	32	4
cilantro	16	11	13
collard greens	10	4	3
cucumber	21	15	7
eggplant	21	8	5
ginger	23	13	7
green bean	21	14	13
lettuce	10	7	3
malanga	20	18	29
mango	10	5	4
orange	16	8	4
papaya	17	10	15
pear	7	3	3
peas (snow)	16	12	14
peppers (diverse)	29	17	15
potato/yam	14	12	20
rosemary	30	17	14
squash	9	8	7
strawberry	11	10	15
thyme	16	12	17
tomato	19	13	6
zucchini	12	9	4

EVALUATION OF COMMINUTION VIA QUALITY CONTROL SPIKES

In other assessments that included sample processing, Lehotay has led two successful AOAC International Collaborative Studies (interlaboratory trials) for multiclass, multiresidue analysis of pesticide residues in fruits and vegetables.[47,48] In the first study involving supercritical fluid extraction (AOAC International Official Method 2002.03), cryogenic processing of 1−3 kg frozen chunks of apple, green bean, and carrot was conducted with dry ice, and test samples of 10 g were sent to collaborators, who further mixed the test portions with Hydromatrix for extraction and analysis of 1.9−2.6 g equivalent subsamples.[47] Similar sample processing with dry ice was conducted for AOAC International Official Method 2007.01 (QuEChERS) for grapes, lettuces, and oranges, which were subsampled into 15 g test portions.[52] In each case, Lehotay added a QC spike to determine the uncertainty of the sample processing (and subsequent) steps.

DOI: 10.1021/jf5056985
J. Agric. Food Chem. 2015, 63, 4395−4404

The sum of squares equation was used to calculate total and individual uncertainties for each step in the methods for each collaborating laboratory and matrix: $RSD_{total} = \sqrt{(RSD^2_{processing} + RSD^2_{extraction} + RSD^2_{cleanup} + RSD^2_{analysis})}$, or $RSD_{processing} = \sqrt{(RSD^2_{total} - RSD^2_{extraction} - RSD^2_{cleanup} - RSD^2_{analysis})}$. This empirical approach using QC spikes added to each step in the method can be used routinely by any laboratory to assess measurement uncertainties in method performance and pinpoint the source of problems leading to poor results. In both collaborative studies, the sample comminution step with dry ice and subsampling of 10−15 g test samples did not measurably contribute to the overall uncertainty in the methods (average $RSD_{processing} \approx 0\%$) for the given matrices and QC spikes (and incurred pesticides). In AOAC International Official Method 2002.03, average $RSD_{analysis} \approx 7\%$, $RSD_{extraction} \approx 8\%$, and $RSD_{mixing} \approx 10\%$ for average overall method RSD ≈ 15% for 16 laboratories.[47] In AOAC International Official Method 2007.01, average $RSD_{analysis} \approx 11\%$, and $RSD_{QuEChERS} \approx 9\%$ for average overall method RSD ≈ 14% for 13 laboratories.[53]

CRYOMILLING TO MINIMIZE SIZE OF TEST SAMPLES

At the IUPAC symposium, Gooding presented three case studies to demonstrate "How to verify that your comminution technique is adequate for your demands."[54] Miniaturization of test sample sizes in the laboratory eases sample preparation and analysis. In particular, agrochemical companies are striving for improved overall efficiency of operations without suffering loss of analytical quality in field trials by implementing high-throughput microextraction methods using analytical test portions of ≈0.1 g, thus enabling automation in the 96-well plate format, reduced solvent use, and reduction in time, costs, and labor.

In Gooding's Case Study 1, comminution to produce soil sample particles <350 μm was essential to microextract pesticides at 10 ng/g from three soil types. When using dry ice, it was necessary to first blend and then mill the samples to obtain a uniformly fine particle size. Milling the same original soil sample size with liquid nitrogen reduced the processing procedure to a single step. For triplicate analyses of ≈0.1 g subsamples, the %RSD values for the pesticide in sandy loam and loamy sand soils were about 25−35%, but silty loam gave RSD >100%. A small difference in matrix made a big difference in the test sample repeatability. These findings stress how important it is to validate miniaturized methods with incurred samples and validate the sample processing method as well as the analytical method. Results for microsamples should be compared with results from proven macro-sampling methods to demonstrate validity before implementation. Furthermore, we believe this should be done for every analyte/matrix pair to be analyzed.

In Case Study 2, Gooding demonstrated that when cryomilling high water content foods such as oranges, if the homogenate is warmed to room temperature before weighing, the 0.1 g test portion's measured pesticide concentration repeatability was 35−50% RSD. For cryomilled subsamples of peaches, blueberries, grapes, and plums weighed while still frozen, determined repeatabilities were <15% RSD. He cautioned that a fine and uniform particle size was not the only criteria for good results, and analyte/matrix dependency was observed.

In Case Study 3, Gooding noted the drawback when extracting microsamples that highly sensitive and precise instruments are needed to detect the concomitantly lower amount of analyte present at a given concentration. Smaller test samples translate to less analyte and greater difficulties in manipulating microvolumes. He gave an example of soil extracted in the 96-well plate format that required additional concentration of the extracts to achieve 1 μg/kg detection limits in liquid chromatography−tandem mass spectrometry (LC-MS/MS). Gooding concluded that microextraction methods increased throughput from 120 to 280 samples per person per week, but processing to a uniformly fine particle size was essential, and not all analytes/matrices met validation criteria for 0.1 g test sample sizes.

INTERLABORATORY ASSESSMENT OF CRYOMILLING

In the symposium's next presentation, Lynn detailed how three independent laboratories prepared samples using a two-step comminution procedure first entailing conventional blending of large composite samples followed by secondary cryomilling of 20 g subsamples for six matrices (soybean grain, cotton seed, whole oranges, and corn grain, stover, and forage).[55] High-throughput LC-MS/MS analysis involved 96-well plates for four different analytes (spinosyns A and D, glyphosate, and its AMPA metabolite) spiked ($n = 6$ for each laboratory) into the 20 g subsamples for each matrix. Replicate cryomilled samples were shipped to the source laboratory on dry ice for analysis of 75 mg test portions. The mean recoveries for spinosyns A and D in corn and soybean grains ranged from 87 to 123% with 6.1−7.6% RSD. Recoveries for oranges were 93−102% with 11−12% RSD. The accuracy of results was similar to analytical QC results for method spikes. Recoveries for glyphosate and AMPA ranged from 76 to 105% (6−14% RSD) for cotton seed and corn forage and stover, except for high recoveries of glyphosate in cotton seed (304 ± 24% SD) and stover (122 ± 10% SD) in cryomilled subsamples from one laboratory. Recoveries of incurred glyphosate and AMPA in corn forage ranged from 93 to 115% (8−13% RSD). In conclusion, cryomilling was reproducible across three laboratories, enabling the automation of microextraction using 96-well plates with an estimated 3−10-fold reduction in overall costs.

Pesticide registrants and contract laboratories have shown that new, 96-well plate analyses may be used in the analysis of pesticide residues in field trials, but only when validated to meet regulatory acceptability standards. To be acceptable for risk assessment and regulatory monitoring purposes, it must be demonstrated that the small test samples correctly represent the real situation in the sampled lot.

SUMMARY OF RECOMMENDATIONS

To summarize, we urge scientists conducting pesticide residue analyses to engage their samplers and include QC measures in their sampling protocols. Analysts should ensure that they are fully aware of parameters of sample heterogeneity with the goal to avoid incorrect sampling and comminution and reduce the uncertainty introduced to test samples. Validation of sampling and sample processing protocols and ongoing QC should be implemented in monitoring programs, just as such data quality assurances are required for analytical methods. If the state-of-the-art two-step comminution process using cryomilling can be demonstrated to yield acceptably accurate results for given

DOI: 10.1021/jf5056985
J. Agric. Food Chem. 2015, 63, 4395−4404

analytes/matrices of interest, then the automated high-throughput methods involving microsubsampling may be used just as any other validated protocols. The reports described above have shown this to be possible in some cases, but not in others. In any case, the dearth of publications in the scientific literature on the subject does not instill confidence among residue chemists and regulators that the described practices are ready for wider implementation. Just as the agrochemical industry led the way when LC-MS/MS was first introduced to help convince others of its attributes and validity, the analytical chemists conducting field trials for pesticide registrations are the early adopters to assess the new cryomilling and automated high-throughput approaches. For ongoing evaluations, we suggest that laboratories add QC spikes to samples prior to each step in the analytical process (comminution, cryomilling, sample preparation, and analysis) and thereby isolate these steps to assess the degree of uncertainties and help with troubleshooting if problems occur. The expenditure of so much time, effort, and expense in residue monitoring programs warrant assurances that the analytical results are meaningful for the intended purposes of regulatory registrations, enforcement, risk assessment, and other needs.

AUTHOR INFORMATION

Corresponding Author

*(J.M.C.) Phone: (850) 617-7505. Fax: (850) 922-9110. E-mail: JoMarie.Cook@freshfromflorida.com.

Notes

The use of trade, firm, or corporation names does not constitute an official endorsement or approval by the USDA of any product or service to the exclusion of others that may be suitable.

The authors declare no competing financial interest.

ACKNOWLEDGMENTS

We thank Chuck Ramsey for his help in the explanation and discussion of sampling theory. We also thank Arlene Kirkland and Elfren Noche for providing microscopy images and particle size measurements.

REFERENCES

(1) van 't Klooster, H. The weakest link. *Anal. Sci.* **2014**, article 305, https://theanalyticalscientist.com/issues/0914/the-weakest-link/.

(2) Esbensen, K. H.; Wagner, C. Why we need the theory of sampling. *Anal. Sci.* **2014**, article 402, https://theanalyticalscientist.com/issues/1014/why-we-need-the-theory-of-sampling/.

(3) Esbensen, K. H.; Wagner, C. Theory of sampling (TOS) vs. measurement uncertainty (MU) – a call for integration. *Trends Anal. Chem.* **2014**, *57*, 93–106.

(4) Barnes, R. M.; Junior, D. S.; Krug, F. J. Introduction to sample preparation for trace element determination. In *Microwave-Assisted Sample Preparation for Trace Element Determination*; de Moraes Flores, E. M., Ed.; Elsevier: Oxford, UK, 2014; pp 1–58.

(5) Makert, B. Sample preparation (cleaning, drying, comminution) for trace element analysis in plant matrices. *Sci. Total Environ.* **1995**, *176*, 45–61.

(6) Cunningham, W. C. Study of cryogenic procedures for preparation of food for element analysis. *J. Food Compos. Anal.* **2008**, *21*, 35–44.

(7) Pettinati, J. D.; Ackerman, S. A.; Jenkins, R. K.; Happich, M. L.; Phillips, J. G. Comparative analysis of meat samples prepared with food chopper and bowl cutter. *J. Assoc. Off. Anal. Chem.* **1983**, *66*, 759–765.

(8) Romanik, G.; Gilgenast, E.; Przjazny, A.; Kaminksi, M. Techniques of preparing plant material for chromatographic separation and analysis. *J. Biochem. Biophys. Methods* **2007**, *70*, 253–261.

(9) Gouveia, S. T.; Lopes, G. S.; Fatibello-Filho, O.; Nogueira, A. R. A.; Nobrega, J. A. Homogenization of breakfast cereals using cryogenic grinding. *J. Food Eng.* **2002**, *51*, 59–63.

(10) Poster, D. L.; Schantz, M. M.; Wise, S. A.; Vangel, M. G. Analysis of urban particulate standard reference materials for the determination of chlorinated organic contaminants and additional chemical and physical properties. *Fresenius' J. Anal. Chem.* **1999**, *363*, 380–390.

(11) Sykes, M.; Thompson, M.; Reynolds, S. Pesticide residues in food-based proficiency test materials, spiking values versus consensus assigned values. *J. Agric. Food Chem.* **2013**, *61*, 4205–4209.

(12) Tittlemier, S. A.; Roscoe, M.; Kobialka, C.; Blagden, R. Considerations in the preparation of laboratory samples for the analysis of ochratoxin A in wheat. *World Mycotox. J.* **2012**, *5*, 107–116.

(13) Tittlemier, S. A.; Varga, E.; Scott, P. M.; Krska, R. Sampling of cereals and cereal-based foods for the determination of ochratoxin A: an overview. *Food Addit. Contam. A* **2011**, *28*, 775–785.

(14) Whitaker, T. B. Sampling foods for mycotoxins. *Food Addit. Contam.* **2006**, *23*, 50–61.

(15) Whitaker, T. B. Standardisation of mycotoxin sampling procedures: an urgent necessity. *Food Control* **2003**, *14*, 233–237.

(16) Hill, A. R. C.; Harris, C. A.; Warburton, A. G. Effects of sample processing on pesticide residues in fruits and vegetables. In *Principles and Practices of Method Validation*; Fajgelj, A., Ambrus, A., Eds.; Royal Society of Chemistry: Cambridge, UK, 2000; pp 41–48.

(17) Maestroni, B.; Ghods, A.; El-Bidaoui, M.; Rathor, T.; Ton, T.; Jarju, O. P.; Ambrus, A. Testing the efficiency and uncertainty of sample processing using ^{14}C-labelled chlorpyrifos, parts I and II. In *Principles and Practices of Method Validation*; Fajgelj, A., Ambrus, A., Eds.; Royal Society of Chemistry: Cambridge, UK, 2000; pp 49–74.

(18) El-Bidaoui, M.; Jarju, O. P.; Maestroni, B.; Phakaeiw, Y.; Ambrus, A. Testing the effect of sample processing and storage on the stability of residues. In *Principles and Practices of Method Validation*; Fajgelj, A., Ambrus, A., Eds.; Royal Society of Chemistry: Cambridge, UK, 2000; pp 75–88.

(19) Fussell, R. J.; Addie, K. J.; Reynolds, S. L.; Wilson, M. F. Assessment of the stability of pesticides during cryogenic sample processing. 1. Apples. *J. Agric. Food Chem.* **2002**, *50*, 441–448.

(20) Fussell, R. J.; Hetmanski, M. T.; Colyer, A.; Caldow, M.; Smith, F.; Findlay, D. Assessment of the stability of pesticides during the cryogenic processing of fruits and vegetables. *Food Addit. Contam.* **2007**, *24*, 1247–1256.

(21) Fussell, R. J.; Hetmanski, M. T.; Macarthur, R.; Findlay, D.; Smith, F.; Ambrus, A.; Brodesser, P. J. Measurement uncertainty associated with sample processing of oranges and tomatoes for pesticide residue analysis. *J. Agric. Food Chem.* **2007**, *55*, 1062–1070.

(22) Reynolds, S. L. Sample handling and clean-up procedures I. *Compr. Anal. Chem.* **2005**, *43*, 75–111.

(23) Young, S. J. V.; Parfitt, C. H., Jr.; Newell, R. F.; Spittler, T. D. Homogeneity of fruits and vegetables comminuted in a vertical cutter mixer. *J. AOAC Int.* **1996**, *79*, 976–980.

(24) Lyn, J. A.; Ramsey, M. H.; Fussell, R. J.; Wood, R. Measurement uncertainty from physical sample preparation: estimation including systematic error. *Analyst* **2003**, *128*, 1391–1398.

(25) Suszter, G.; Ambrus, A.; Turcu, M.; Klaus, P. Estimation of efficiency of processing soil samples for pesticide residues analysis. *J. Environ. Sci. Health B* **2006**, *41*, 531–552.

(26) Ambrus, A. Within and between field variability of residue data and sampling implications. *Food Addit. Contam. A* **2000**, *17*, 519–537.

(27) Nanita, S. C.; Ziegler, M.; Giammarrusti, L.; Huber, A.; Astor, A.; Ruhl, J. C. Error propagation in pesticide residue measurements estimated by computational simulations and interlaboratory sample analysis. *J. Environ. Sci. Health B* **2009**, *44*, 640–648.

(28) Ambrus, A. Variability of pesticide residues in crop units. *Pest Manage. Sci.* **2006**, *62*, 693–714.

DOI: 10.1021/jf5056985
J. Agric. Food Chem. 2015, 63, 4395–4404

(29) Ambrus, A.; Soboleva, E. Contribution of sampling to the variability of pesticide residue data. *J. AOAC Int.* **2004**, *87*, 1368−1379.
(30) Fujita, M.; Yajima, T.; Iijima, K.; Sato, K. Effect of sampling size on the determination of accurate pesticide residue levels in Japanese agricultural commodities. *J. Agric. Food Chem.* **2012**, *60*, 4457−4464.
(31) Fujita, M.; Yajima, T.; Iijima, K.; Sato, K. Comparison of the variability levels of pesticide residue observed in Japanese cabbage and grape units. *J. Agric. Food Chem.* **2012**, *60*, 1516−1521.
(32) Horvath, Z.; Ambrus, A.; Meszaros, L.; Braun, S. Characterization of distribution of pesticide residues in crop units. *J. Environ. Contam. Health B* **2013**, *48*, 615−625.
(33) Xu, X. M.; Huo, R.; Salazar, J. D.; Hyder, K. Investigating factors affecting unit-unit variability in non-systemic pesticide residues by stochastic simulation modeling. *Hum. Ecol. Risk Assess.* **2008**, *14*, 992−1006.
(34) U.S Environmental Protection Agency. Residue Chemistry Test Guidelines, OPPTS 860.1500 Crop Field Trials, EPA-HQ-OPPT-2009-0155, 1996; http://www.regulations.gov/ (accessed Jan 31, 2015).
(35) U.S. Food and Drug Administration. Investigation Operations Manual, Sample Schedule 3: Pesticide Samples; http://www.fda.gov/iceci/inspections/iom (accessed Jan 31, 2015).
(36) Codex Alimentarius Commission. CAC/GL 33-1999. Recommended Methods of Sampling for the Determination of Pesticide Residues for Compliance with MRLs, 1999; http://www.fao.org/home/en/ (accessed Jan 31, 2015).
(37) European Commission Directive 2002/63/EC Establishing Community Methods of Sampling for the Official Control of Pesticide Residues in and on Products of Plant and Animal Origin and repealing Directive 79/700/EEC, 2002; http://ec.europa.eu/food/plant/plant_protection_products/index_en.htm (accessed Jan 31, 2015).
(38) U.S. Department of Agriculture. Pesticide Data Program, Sampling SOPs and Commodity Specific Fact Sheets; http://www.ams.usda.gov/AMSv1.0/ (4th quarter 2014).
(39) Medina-Pastor, P.; Mezcua, M.; Rodriguez-Torreblanca, C.; Fernandez-Alba, A. R. Laboratory assessment by combined z score values in proficiency tests: experience gained through the European Union proficiency tests for pesticide residues in fruits and vegetables. *Anal. Bioanal. Chem.* **2010**, *397*, 3061−3070.
(40) U.S Public Law 111-353, Food Safety Modernization Act, 111th Congress, p 124 STAT, 3885, Jan 4, 2011; www.gpo.gov/fdsys/pkg/PLAW-111publ353/pdf/PLAW-111publ353.pdf.
(41) FDA Partnership for Food Protection. *Food and Feed Laboratories Best Practices Manual*; U.S. Food and Drug Administration, Nov 1, 2013; www.fda.gov/downloads/ForFederalStateandLocalOfficials/FoodSafetySystem/PartnershipforFoodProtectionPFP/UCM404716.pdf.
(42) USDA Agricultural Marketing Service. Pesticide Data Program Annual Summary Calendar Year 2012, Washington, DC, Feb 2014; www.ams.usda.gov/AMSv1.0/PDP.
(43) U.S. Government Accountability Office. Food Safety − FDA and USDA should strengthen pesticide residue monitoring programs and further disclose monitoring limitations; report GAO-15-38, Oct 2014; www.gao.gov/products/GAO-15-38.
(44) Association of Public Health Laboratories. *Cooperative agreement with FDA's Office of Partnerships*, Sept 2012; www.aphl.org/aphlprograms/food/laboratory-accrediation/Pages/Associations-Cooperative-Agreement-with-FDA.aspx.
(45) Gy, P. *Sampling for Analytical Purposes*; Wiley: Chichester, UK, 1998.
(46) Pitard, F. F. *Pierre Gy's Sampling Theory and Sampling Practice*, 2nd ed.; CRC Press: Boca Raton, FL, USA, 1993.
(47) U.S. Food and Drug Administration. *Pesticide Analytical Manual*, 3rd ed.; Department of Health and Human Services: Washington, DC, USA, 1996.
(48) Anastassiades, M.; Lehotay, S. J.; Stajnbaher, D.; Schenck, F. J. Fast and easy multiresidue method employing acetonitrile extraction/partitioning and dispersive solid-phase extraction for the determination of pesticide residues in produce. *J. AOAC Int.* **2003**, *86*, 412−431.
(49) Cook, J.; Beckett, M.; Reliford, B.; Hammack, W.; Engel, M. Multi-residue analysis in fresh fruits and vegetables using procedures developed by the Florida Department of Agriculture. *J. AOAC Int.* **1999**, *82*, 1419−1435.
(50) Lee, S. M.; Papathakis, M. L.; Feng, H. M. C.; Hunter, G. F.; Carr, J. E. Multipesticide residue method for fruits and vegetables − California Department of Food and Agriculture. *Fresenius' J. Anal. Chem.* **1991**, *339*, 376−383.
(51) de Kok, A.; Hiemstra, M.; Vreeker, C. P. Improved cleanup method for the multiresidue analysis of N-methylcarbamates in grains, fruits and vegetables by means of HPLC with postcolumn reaction and fluorescence detection. *Chromatographia* **1987**, *24*, 469−476.
(52) Lehotay, S. J. Determination of pesticide residues in nonfatty foods by supercritical fluid extraction and gas chromatography/mass spectrometry: collaborative study. *J. AOAC Int.* **2002**, *85*, 1148−1165.
(53) Lehotay, S. J. Determination of pesticide residues in foods by acetonitrile extraction and partitioning with magnesium sulfate: collaborative study. *J. AOAC Int.* **2007**, *90*, 485−520.
(54) Gooding, R.; Saha, M.; Horowitz, M.; Gordon, B.; Finch, A.; Downs, C.; Jones, J. 248th ACS National Meeting and 13th IUPAC Congress on Pesticide Chemistry, Aug 10−14, 2014, San Francisco, CA, USA; Abstract Agro586.
(55) Lynn, K.; Buchholz, L.; Riter, L. S. 248th ACS National Meeting and 13th IUPAC Congress on Pesticide Chemistry, Aug 10−14, 2014, San Francisco, CA, USA; Abstract Agro587.

DOI: 10.1021/jf5056985
J. Agric. Food Chem. 2015, 63, 4395−4404

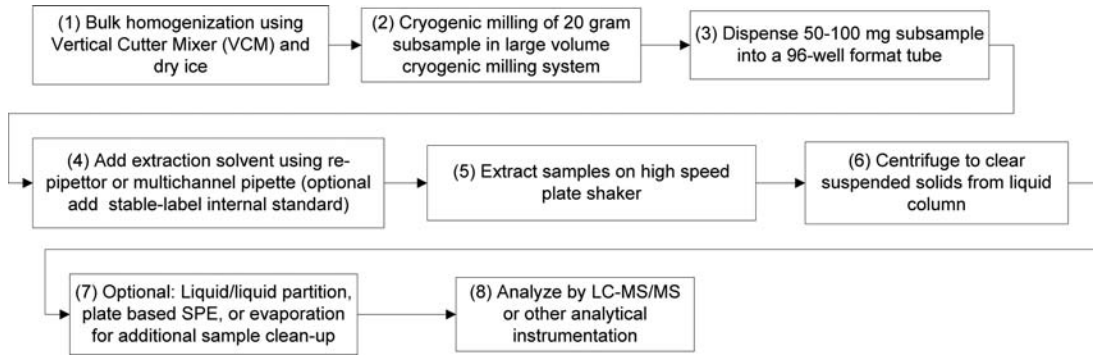

Figure 1. High-throughput plate-based workflow.

Table 1. Accuracy and Variability in Field-Treated Samples

		Monsanto		laboratory A		laboratory B	
matrix	analyte	concn ratio[a] (N = 6)	% RSD	concn ratio (N = 6)	% RSD	concn ratio (N = 6)	% RSD
corn forage	glyphosate	100	11.5	93	12.7	95	11.3
	AMPA	99	8.1	115	9.3	98	9.7

[a]Concentration determined by new high-throughput method divided by concentration determined by the previous method (10 g), expressed as a percentage.

Table 2. Accuracy and Variability in Fortified Samples Comparing Laboratories, Matrices, and Analytes Tested

		Monsanto		laboratory A		laboratory B	
matrix	analyte	av recovery (N = 36)	% RSD	av recovery (N = 36)	% RSD	av recovery (N = 36)	% RSD
corn forage	glyphosate	96	10.1	90	13.6	98	8.7
	AMPA	85	10.9	79	9.4	98	12.9
cotton seed	glyphosate	92	5.8	88	5.8	304[a]	8.0
	AMPA	76	9.1	105	9.1	97	8.9
corn stover	glyphosate	94	10.3	92	10.3	122[b]	7.8
	AMPA	92	10.2	92	10.2	91	11.4
		Dow AgroSciences		laboratory A		laboratory B	
matrix	analyte	av recovery (N = 36)	% RSD	av recovery (N = 36)	% RSD	av recovery (N = 36)	% RSD
corn grain	spinosad A	93	6.9	99	6.7	122[b]	6.7
	spinosad D	87	7.1	92	7.4	123[b]	6.9
soybean grain	spinosad A	94	6.1	99	6.2	90	6.4
	spinosad D	92	7.6	98	7.2	89	7.6
whole oranges	spinosad A	93	12.4	101	11.1	95	11.7
	spinosad D	96	11.4	102	11.7	97	10.5

		Dow AgroScience 10 g data[c] − LOQ (10 ppb)		Dow AgroScience 10 g data[c] − 100X LOQ	
		av recovery (N = 6)	% RSD	av recovery (N = 6)	% RSD
soybean grain	spinosad A	95.0	4.30	98.0	2.89
	spinosad D	94.3	5.15	95.5	8.14
whole oranges	spinosad A	94.8	9.61	94.7	11.0
	spinosad D	95.7	9.09	96.2	10.8

[a]This set of samples has a significantly high bias in recovery. This anomalous result was repeated across all subsamples of the site with consistent precision, and therefore it was concluded that this result is not an artifact of poor homogenization, but is more likely an error in fortification. [b]Average recovery is not within 70−120%. [c]Concentration determined by using a low-throughput method that uses 10 g of sample.

various models). Ten 20 ± 1 g aliquots of each of the primary milled tissues were weighed into plastic tubes. Four of these tubes were retained by the company laboratory, and three were sent to each of two external laboratories along with fortification solutions prepared by the company laboratory. The subsamples were fortified and secondary milled by the procedure described above and then returned to the company laboratory. A single subsample of each matrix was fine-milled without fortification to serve as batch quality controls.

For field-treated residue samples, a primary milled corn forage sample with known levels of glyphosate and AMPA was aliquoted into nine 20 ± 1 g subsamples. Three subsamples were retained by the company laboratory, and three were sent to each of two external laboratories.

After the secondary milling procedure was completed by each study site, the samples were returned to the company laboratory (either Monsanto or DowAgroSciences) for analysis by LC-MS/MS. Multiple 75−100 mg subsamples of each fine-milled sample were dispensed for analysis.

Dispensing Secondary Milled Samples. Samples that have undergone fine-milling were maintained in a frozen state to ensure homogeneity and prevent stratification. This was particularly important for higher water content samples such as forage and

DOI: 10.1021/jf505249y
J. Agric. Food Chem. 2015, 63, 4405−4408

Table 3. Physicochemical Properties of Analytes

Matrix	Glyphosate	AMPA	Spinosad A	Spinosad D
Structure	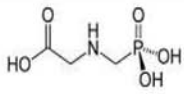	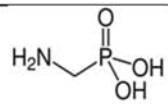	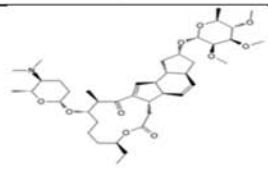	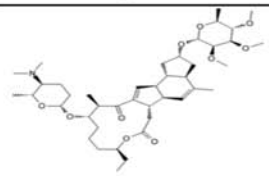
Molecular Weight	169	111	732	746
H_2O Solubility, mg/L	10000	5800	235	333
K_{ow}	-3.2	-1.6	55	90

oranges. Sets of samples were placed at the dispensing station on dry ice. Plastic disposable spatulas (VWR, Radnor, PA, USA) used for transferring were also chilled on dry ice prior to use. Subsamples of 75 ± 10 mg (for glyphosate/AMPA) or 100 ± 5 mg for spinosyn A/D were transferred to tared 1.4 mL polypropylene Matrix tubes (Thermo Scientific, Waltham, MA, USA). The exact sample mass was recorded and used to apply the appropriate factor for correcting sample concentration.

Analytical Methods. After homogenization and dispensing into 96-well format tubes, matrix samples were extracted and processed using validated methods. An overview of the workflow is shown in Figure 1. Within-set quality control samples assured the performance of the methods. Samples were analyzed by LC-MS/MS using electrospray ionization (ESI), and the mass spectrometer was operated in multiple reaction monitoring mode using two transitions for each analyte. Glyphosate and AMPA were analyzed in negative ionization mode, whereas spinosads A and D were analyzed in positive mode.

RESULTS AND DISCUSSION

The capability of the two-stage milling process to provide milligram scale subsamples that are representative of the field was tested by examining replicate subsamples in three phases of this round-robin study: (1) field-treated residue samples; (2) fortified samples; and (3) comparison with large-scale (5 g) samples.

The field-treated residue sample phase utilized corn forage as model RAC with field-applied glyphosate. Glyphosate and AMPA residues were previously determined at a 10 g scale using a validated analytical method. These same samples were bulk homogenized, and replicate 20 g subsamples were fine-milled using the secondary process by three independent laboratories. Six 75 mg subsamples of the fine-milled product were analyzed from each independent laboratory preparation. The results from the scaled-down assay are summarized in Table 1. The glyphosate and AMPA concentrations determined according to the new method were compared to those of the previous assay and were nearly identical (91−115%) In addition, the variability obtained using the scaled-down method ranged from 8 to 13%, well within SANCO's acceptable margin of <20%. These results demonstrate that 20 g subsamples are suitable for the secondary fine-milling to represent original primary milled bulk taken from the field in this RAC.

The fortification experiment enabled systematic examination of additional matrices across crop grouping categories using analytes that ranged in molecular weight, polarity, and charge (Table 3) to determine the effectiveness of sample comminution. The fortification approach represents the worst-case scenario, where all of the residue of the 20 g sample is fortified within a very small region, creating a "hotspot". The even distribution of this hotspot is performed solely by the secondary fine-milling process. Precision and recovery data from this interlaboratory study are summarized in Table 2.

Precision for glyphosate and AMPA ranged from 8.7 to 13.6% in corn forage, from 5.8 to 9.1% in cottonseed, and from 7.8 to 11.4% in corn stover across the three laboratories (Table 2). The recoveries of glyphosate and AMPA in cottonseed (oily matrix), corn forage (wet matrix), and corn stover (dry matrix) were mostly within the acceptable range of 70−120%. One result, the glyphosate data from the cottonseed samples prepared by laboratory B, had a significantly high bias in recovery. This anomalous result was repeated across all subsamples from that site with consistent precision (8% CV), and therefore it was concluded that this high result is not an artifact of poor homogenization.

A second pair of analytes, spinosads A and D, were chosen for testing on the basis of their dissimilarity to glyphosate and AMPA (Table 3). The fortification and milling processes were identical to those used for glyphosate and AMPA. The resulting mean recoveries of spinosads A and D in corn grain (dry matrix), soybean grain (oily matrix). and oranges (acidic matrix) were mostly within the acceptable range of 70−120%. There was a small amount of positive bias in the recoveries observed for spinosads A and D in the corn grain samples prepared by laboratory B. However, the precision values for spinosads A and D across all of the matrices tested were all <13%.

Low variability was observed in samples evaluated across laboratory sites, matrices, and analytes. Fortifying a hotspot is a worst-case scenario, yet uniformity in the sample results was still observed when a 75 or 100 mg aliquot was analyzed. Across laboratories, the % RSDs were very consistent, demonstrating the robustness of the technique across laboratories with varying degrees of experience.

The spinosad A and D recoveries and RSDs from samples analyzed in 10 g or 75 mg aliquots were compared to determine if additional variability was observed with the scaled-down assay. The 10 g aliquot samples were prepared by fortification of spinosads A and D into a 10 g aliquot of control matrix that had been primary-milled only. The 75 mg aliquot samples were prepared as described above with primary milling of the control matrix, followed by fortification of a 20 g aliquot of the matrix prior to the secondary milling step. The % RSD obtained at the 10 g scale ranged from 2.9 to 8.1 for spinosads A and D in soybean grain and was comparable to the % RSD obtained from

DOI: 10.1021/jf505249y
J. Agric. Food Chem. 2015, 63, 4405−4408

the 75 mg scale assay of 6.1−7.6%. In addition, the % RSD obtained at the 10 g scale ranged from 9.1 to 11.0% for spinosads A and D in oranges, which, again, was comparable to the % RSD obtained from the 75 mg scale assay of 10.5−12.4%. This similarity in RSD values across sampling size and milling procedure demonstrates that additional variability was not observed in the 75 mg samples beyond the innate inconsistency of the assay.

The advantages of the fine-milling and scaled-down sample size methods are a significant increase in throughput, improved quality due to a reduced risk of contamination and reduced variability, and a decrease in costs due to fewer FTE hours required due to automating the extraction, reduced reagent use, and reduced reagent disposal. The increase in throughput observed with the milligram-scale sample methods was 10 times for glyphosate and AMPA and 3 times for spinosads A and D when compared to the traditional gram-scale methods. Thus, there is a significant increase in the number of samples that can be processed in the same time interval utilizing the milligram-scale methods.

In conclusion, analysis of the field-treated samples demonstrated that the 10 g scale method and the 75 mg scale method that included a second processing step, fine-milling, gave comparable results in terms of calculated concentrations and variability. The fortified samples were prepared using analytes chosen for their dissimilar physicochemical properties, matrices that encompass the four main crop groupings (wet, dry, oily, and acidic), and laboratories with various degrees of experience with the secondary fine-milling technique. When the resulting concentration data were compared across these variables, excellent agreement in the recovery and variability values obtained was observed. Additionally, the fine-milling technique has significant advantages in increasing throughput, decreasing cost, and increasing assay quality.

Leah S. Riter[*,†]
Kari J. Lynn[§]
Chad E. Wujcik[†]
Lisa M. Buchholz[§]

[†]Monsanto Company, 800 North Lindbergh Boulevard, St. Louis, Missouri 63167, United States

[§]Dow AgroSciences, 9330 Zionsville Road, Indianapolis, Indiana 46268, United States

AUTHOR INFORMATION

Corresponding Author

*(L.S.R.) Mail: Monsanto Co., 800 N. Lindbergh Blvd., St. Louis, MO 63167, USA. E-mail: lsriter@monsanto.com.

Notes

The authors declare no competing financial interest.

ACKNOWLEDGMENTS

We thank Albert White at Monsanto, Joe Warnick at EPL, Joe Hesting at Syntech, and Jordan Marckel and Mike Hastings at Dow AgroSciences for performing milling or analytical assays.

ABBREVIATIONS USED

VCM, vertical cutter-mixer; RAC, raw agricultural commodities; RSD, relative standard deviation; LC-MS/MS, liquid chromatography−tandem mass spectrometry

REFERENCES

(1) Fussell, R. J.; Hetmanski, M. T.; Macarthur, R.; Findlay, D.; Smith, F.; Ambrus, Á.; Brodesser, P. J. Measurement uncertainty associated with sample processing of oranges and tomatoes for pesticide residue analysis. *J. Agric. Food Chem.* **2007**, *55* (4), 1062−1070.

(2) (a) Bidari, A.; Ganjali, M. R.; Norouzi, P.; Hosseini, M. R. M.; Assadi, Y. Sample preparation method for the analysis of some organophosphorus pesticides residues in tomato by ultrasound-assisted solvent extraction followed by dispersive liquid−liquid microextraction. *Food Chem.* **2011**, *126* (4), 1840−1844. (b) Eble, J. E.; Orth, A.; Champion, W. Analysis of residue samples: Effect of homogenization and sample size in extractions. Presented at the 236th National Meeting of the American Chemical Society, Philadelphia, PA, 2008. (c) Hengel, M. J.; Miller, M. Analysis of flonicamid and its metabolites in dried hops by liquid chromatography−tandem mass spectrometry. *J. Agric. Food Chem.* **2007**, *55* (20), 8033−8039. (d) Lyn, J. A.; Ramsey, M. H.; Fussell, R. J.; Wood, R. Measurement uncertainty from physical sample preparation: estimation including systematic error. *Analyst* **2003**, *128* (11), 1391−1398. (e) Peng, C.; Kuang, H.; Li, X.; Xu, C. Evaluation and interlaboratory validation of a GC-MS method for analysis of pesticide residues in teas. *Chem. Pap.* **2007**, *61* (1), 1−5.

(3) European Commission. Guidance Document on Pesticide Residue Analytical Methods. Document SANCO/825/00/rev. 8.1/16/11/2010, 2010.

DOI: 10.1021/jf505249y
J. Agric. Food Chem. 2015, 63, 4405−4408

Table 1. Examples for Different Crops, Sprayers, Plot Sizes, and Field Sample Sizes in the Supervised Trials

crop	place	year	sprayer	plot size	sample size
alfalfa	Australia	1988−1989	precision plot sprayer	60−240 m^2	
apple	Australia	1991	LPG-powered hand lance	2 trees	
apple	New Zealand	1986	precision plot sprayer	9 m^2	2 kg, 15 fruits
apple	USA	1987	CO_2-powered backpack, tractor-mounted CO_2 sprayer	1 tree, 37−46 m^2	
banana	Australia	1991	precision plot sprayer		25 fruits
bean	Costa Rica	1998	CO_2-powered backpack sprayer	32 m^2	2 kg
bean	Europe	2000−2001	3 m boom, knapsack sprayer, compressed air sprayer	45−90 m^2	1−2 kg
coffee	Colombia	1984	CO_2-powered backpack	3 trees	
cotton	Brazil	1997	CO_2-powered backpack	24 m^2	1−2 kg
cotton	Brazil	2001	CO_2-powered backpack	60−500 m^2	2 kg
grapefruit	New Zealand	1985	precision backpack	10 m^2	2 kg, >8 fruits
grape	Australia	1990	precision plot sprayer	1 vine	
grape	Italy	1989	crystal sprayer, motor pump, and teejet	10−40 m^2	1 kg
lemon	Australia	1990	precision plot sprayer	1 tree	
onion	Europe	1999−2000	3 m boom, boom sprayers	42−93 m^2	1−2.3 kg
onions	New Zealand	1987	precision plot sprayer	12 m^2	2 kg, 12 onions
orange	Italy	1991	knapsack	3 trees	24 fruits
peach	Australia	1991	LPG-powered hand lance	2 trees	
peanut	Argentina	1992	CO_2 powered backpack	11 m^2	
peanut	Australia	1997	precision plot sprayers	120 m^2	
pea	Europe	1999−2000	hand-carried boom sprayer, motorized backpack, plot sprayer, 3 m boom, knapsack	44−90 m^2	1−6 kg
peas	Europe	2004	AUK plot sprayer	39−60 m^2	0.3−1 kg
rice	USA	1987−1988	aircraft, CO_2 -powered backpack, small plot sprayers, 4-wheeled CO_2-powered sprayer	37−3300 m^2	
soybean	Brazil	2000−2002	CO_2-powered handboom	64−184 m^2	2 kg
soybean	Europe	2000−2001	AUK plot sprayer, plot boom sprayer	30−60 m^2	1−3 kg
sugar beet	Europe	1988	knapsack with teejet, flat nozzle sprayer	22−144 m^2	5 plants
sugar beet	Europe	2000	boom sprayers	42−45 m^2	1−6 kg
sunflower	Europe	2000	boom sprayers	42−60 m^2	1−1.3 kg

sampled commodity, which indicates that the results of modeling are applicable regardless of the characteristics of the residue distribution in the sampled population. Knowledge of the uncertainty of sampling enables the calculation of combined uncertainty of residue concentrations measured in composite samples, which then can be used to test compliance with maximum residue limits as part of the premarketing self-control program of the producers.

The objective of this study is to utilize the extensive pesticide residue data obtained from supervised trials for estimation of average sampling uncertainty for all groups of fresh fruits and vegetables, primary feed commodities, and semiprocessed plant products included in the Codex Commodity Classification,[16] as well as for some individual crops for which sufficient residue data were available.

MATERIALS AND METHODS

Selection of Residue Database. For the evaluation of the within-field variability of pesticide residues of different crops and crop groups, supervised residue trials reported by the JMPR between 1997 and 2010 [8] were considered. In some of the trials, replicate samples were taken (duplicate samples in >99.95% of the cases) from the single-trial plots to get more accurate information on the average residue concentration of the treated field, according to the requirements of U.S. EPA.[17] These residue data were collected and used in our study. The selected data set contained altogether 12087 replicate sample sets (25876 individual ones), comprising 706 pesticide−crop combinations formed from 66 different pesticides and 106 commodities, referred to as "crops" in the study.

The Codex Classification of Foods and Animal Feeds,[16] developed within the framework of the Codex Committee on Pesticide Residues (CCPR), was primarily used for grouping the various crops. It takes into account, among other things, the nature of the crops and expectable level of pesticide residues; therefore, fresh and dry foods and semiprocessed foods and feeds were classified into different groups. It is intended to ensure the use of unambiguous description of various crops and to classify food commodities into groups for the purpose of establishing group maximum residue limits based on the

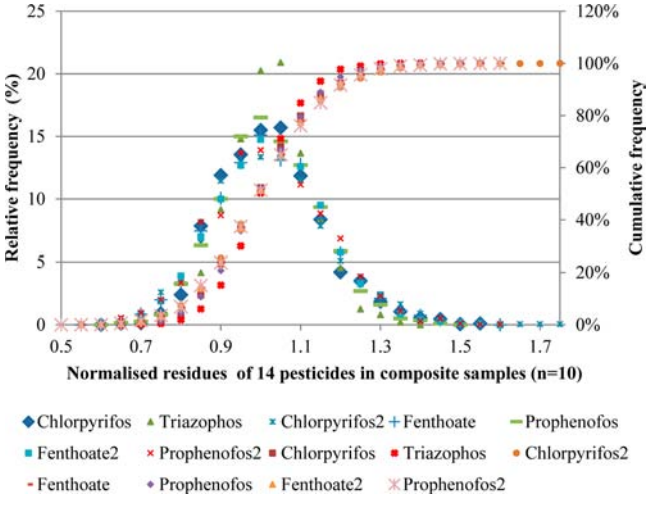

Figure 1. Relative frequency distribution of different pesticide residues measured in composite samples of size 10 taken from different cabbage fields treated with different pesticides independently. Reprinted with permission from ref 18. Copyright 2014 WESSLING Beneficial Nonprofit Ltd.

DOI: 10.1021/jf5055112
J. Agric. Food Chem. 2015, 63, 4409−4417

Table 2. Summary of Average CV_A Values Obtained from Recovery Studies

commodity group[a]	typical commodity category	no.[b]	spike range[c]	no.[d]	CV_{Aw}%[e]
1	pome fruit	2	0.01−2.0	115	7.75
	stone fruit	3	0.02−4.0	149	9.62
	bulb vegetables	1	0.02−0.3	24	8.70
	Brassica vegetables	3	0.01−5.0	223	11.86
	fruiting vegetables/cucurbits	5	0.01−11.4	723	8.77
	leafy vegetables and fresh herbs	4	0.01−5.0	227	10.30
	stem and stalk vegetables	2	0.02−10.0	32	14.13
	forage crops	9	0.01−40.0	623	9.35
	fodder crops	6	0.01−20.0	632	9.01
	fresh legume vegetables	4	0.01−5.0	474	8.18
	root and tuber vegetables or feed	4	0.01−2.0	225	8.70
	citrus fruit	3	0.01−5.0	526	7.00
	small fruits and berries	5	0.01−2.0	446	7.56
	other	1	0.02−0.5	28	10.94
2	tree nuts	2	0.01−1.0	12	11.88
	oilseeds	6	0.01−3.0	672	8.08
3	oily fruits and products	2	0.01−5.0	42	9.25
4	dry legume vegetables, pulses	2	0.01−1.0	362	7.04
	cereal grain and products thereof	5	0.01−20	691	7.45
	almond hull, cotton hull, peanut shell	3	0.01−7.5	81	10.68
5	hops, dried, tea, coffee, sugar cane	4	0.01−20.0	160	7.38
	sum			6467	
	grand weighted average				8.56

[a]1, high water content; 2, high oil content and very low water content; 3, high oil content and intermediate water content; 4, high starch and/or protein content and low water and fat content; 5, difficult or unique commodities. [b]Number of commodities. [c]Range of spike concentration, mg/kg. [d]Number of recovery tests. [e]CV_{Aw}%, weighted average CV_A value.

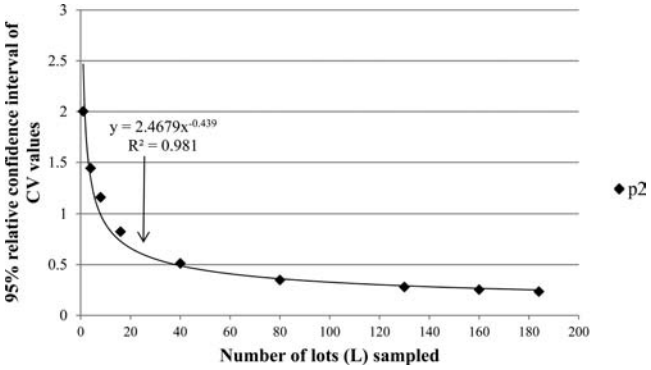

Figure 2. Relationship of relative difference of the 95% range of estimated relative standard deviations based on duplicate samples (p2) of size 10 taken from *L* lots.

residues in/on representative commodities, which then can be extrapolated to the so-called minor commodities belonging to the group. In addition, we also took into account the sampling aspects in grouping of crops: for example, small-, medium-, and large-sized fresh fruits and vegetables.

The crops included in the supervised trial residue database belonged to 24 groups having similar characteristics. In addition to the determination of sampling uncertainties for individual crops, the typical sampling uncertainty was also calculated for crop groups aiming to provide initial estimates for the expectable sampling uncertainties for minor commodities, belonging to the given group, for which supervised trial residue data are not available.

Estimation of Sampling Uncertainty. The characteristic within-field variation of the residues in/on a crop is expressed as the relative standard deviation, CV. The use of CV values is more suitable than the standard deviation of the residues because the variability of pesticide residues in different data sets, expressed with their CV value, is comparable regardless of their average concentration. Previous studies revealed that the relative frequency distributions of pesticide residues are very similar and independent from the type of the pesticide (Figure 1); therefore, the average of the CV values of different data sets is considered to be the best estimate for the uncertainty of the measured residues.[18]

From the combined uncertainty of the measured residues (CV_R) and the uncertainty of the laboratory phase of the determination of residues[19] (CV_L), the uncertainty of sampling (CV_S) can be calculated as

$$CV_R = \sqrt{CV_S^2 + CV_L^2} \rightarrow CV_S = \sqrt{CV_R^2 - CV_L^2} \quad (1)$$

As the database used contained replicate samples, range statistics[20] was applied to calculate the relative standard deviation of the measured residues in one replicate sample set (CV_1), and their average was considered as the characteristic uncertainty of measured residue values in a given crop (CV_{R1}).

For replicate samples from one trial

$$CV_{R1} = \left(\frac{R_{max} - R_{min}}{\overline{R}}\right)/d_2 \quad (2)$$

where R_{max}, R_{min}, and $\overline{R}$ are the maximum, minimum, and mean residue values in replicate samples taken from one trial site and d_2 is the corresponding factor of 1.128, 1.693, or 2.059, for two, three, or four replicate samples, respectively.[21] Because the d_2 values are different, the CV values were calculated separately for replicate sample sets consisting of two, three, or four residue values, and their average was calculated afterward.

For a single *i*th commodity from k_i trials

DOI: 10.1021/jf5055112
J. Agric. Food Chem. 2015, 63, 4409−4417

$$CV_{Ri} = \frac{\sum_i CV_{R1}}{k_i} \quad (3)$$

The supervised trial reports include the validation data, but the details of concurrent recoveries obtained during the analysis of samples are usually not included in the FAO evaluations. Therefore, we collected the recovery data obtained during the validation of the methods used for analyzing samples from supervised trials by the specialized laboratories reported in the FAO evaluations.[8] The recovery studies were generally conducted at spike levels from 0.01 to 10 mg/kg with three to eight replicates. The CV_A obtained from the recovery studies generally ranged between 2 and 12%, with higher values up to 20% occurring in very few cases. There was no observable correlation between the spike level and the CV_A values of recoveries of various pesticide residues of different chemical structures and physicochemical properties from different sample matrices. Therefore, the weighted average of reported CV_A values was considered as the best practical estimate for the expectable variability of the results derived from the analysis phase. The results are summarized in Table 2. The grand weighted average (CV_{Aw}) of CV_A of recoveries obtained from various pesticide−crop combinations was calculated as

$$CV_{Aw} = \sqrt{\frac{\sum (df_i \times CV_{Ai}^2)}{\sum df_i}} \quad (4)$$

where df_i is the degree of freedom for the CV_{Ai} of the ith pesticide residue−crop combination.

The chopping and grinding of sample materials and their homogenization are generally carried out very carefully in the presence of dry ice, and the consequent sample processing error is usually negligible compared to CV_A.

The uncertainty of the analytical results varied from trial to trial; therefore, on the basis of the typical performance characteristic of analytical methods applied, we assumed an average value of 0.1 for the uncertainty of the laboratory phase (CV_L) and used eq 1 to get the uncertainty of sampling (CV_{S1}) from each calculated CV_{R1} value of a crop. In cases when the uncertainty of the measured residues (CV_{R1}) was lower than the assumed CV_L of 0.1, as a conservative approach, 0.1 was considered as the uncertainty of sampling. Because the sampling uncertainty was usually much larger, this assumption did not practically affect the results of our calculations.

The sample sizes (number of individual crop units or sample increments) making up a composite sample) were not systematically reported by the JMPR (Table 1). The mass of the sample is often indicated instead of the number of primary samples making up a composite sample. We assumed that the protocols of pesticide manufacturers, specifying typically large samples (24 units for small- and medium-sized and 12 for large-sized crops), were generally followed, but at least the minimum sample sizes recommended by the FAO guidelines were satisfied.[22] For official control, taking a minimum of 10 primary samples for small- and medium-sized and 5 for large-sized crops, respectively, is recommended according to the relevant Codex standards;[14] therefore, the CV_{S1} values calculated for each crop in supervised residue trials were adjusted with a factor of 1.55 ($f = \sqrt{24}/\sqrt{10} = \sqrt{12}/\sqrt{5} = 1.55$) based on the central limit theorem (eq 5), which is applicable for the far from normal distributions of residues in primary crop units (CV_{prim}) according to the study of Horváth et al.[23]

$$CV_n = \frac{CV_{prim}}{\sqrt{n}} \quad (5)$$

The adjusted CV_{S1} values (CV_{S1adj}) were calculated as

$$CV_{S1adj} = CV_{S1} \times f \quad (6)$$

The characteristic sampling uncertainty, CV_S, of a crop group consisting of i crops is calculated from the pooled variances of the CV_{S1adj} values of the crops belonging to one group, without excluding any $CV_{S1adj,i}$ values. For instance, for the group of small fruits (sf)

$$CV_{Ssf} = \sqrt{\frac{\sum (df_i \times CV_{S1adj,i}^2)}{\sum df_i}} \quad (7)$$

Calculation of Confidence Limits with Chi² Distribution. The confidence intervals of the sampling uncertainties, the upper and lower confidence limits of CV_S and CV_{S1adj} values were calculated by applying the Chi^2 distribution:

$$LCL = \sqrt{(df \times CV_S^2/\chi_{0.975})} \quad (8)$$

$$UCL = \sqrt{(df \times CV_S^2/\chi_{0.025})} \quad (9)$$

df, the degree of freedom, is the number of replicate sample pairs of a crop or a crop group, and $\chi_{0.975}$ and $\chi_{0.025}$ are the tabulated values for the 97.5th and 2.5th percentiles of the χ^2, distribution, respectively. The χ^2 values were calculated with linear interpolation in cases where they were not available to the corresponding df. [24]

Calculation of Confidence Limits by Using the Results of Modeling Experimental Data. According to the results of our previous study,[15] the 95% relative confidence interval of the sampling uncertainty is independent from the relative standard deviation of the measured residues in the sampled commodity, and it decreases with the increasing number of lots sampled. The modeling was carried out with only up to 20 independent lots to determine the confidence intervals of the CV_{S1adj} values. However, in the case of supervised residue trials, the number of trial sites from which replicate samples were taken amounted to over several hundred; therefore, the modeling has been performed again with the same methodology utilizing 182 primary residue data sets obtained from commercial lots[12] or specifically designed field trials: (1) 19 residue data sets,[15] each consisting of 104−120 residue values, comprising the combinations of 7 different pesticide active ingredients present in carrot or parsley leaves. (2) 68 lots, assumed to contain crops of the same origin, imported from various countries or grown locally in the United Kingdom were selected in logistic centers, and 100−100 individual fruits were randomly taken from each lot. The fruits were analyzed with multiresidue methods to detect all residues present in the fruits. The 68 data sets comprised apple, banana, kiwi, orange, peach, plum, potato, and tomato.[12] 24 different pesticide residues were detected in the samples. (3) 95 data sets were obtained from a coordinated research program, including field studies, to determine residues in individual items of leafy vegetables, small and large crops in 13 countries, representing the actual agricultural practice worldwide. Twenty-five pesticide active ingredients were analyzed from black currant, cherry, cabbage, chicory, kale, cucumber, grape, lettuce, mango, papaya, strawberry, and zucchini samples.[13]

10−10 residue values were selected with random sampling procedure with replacement 1000 times from each of the 182 primary residue data set. The average of the 10 randomly selected residue values were calculated and considered as the residue concentration in one composite sample. The procedure was repeated two times to obtain two databases for assessing the effect of taking duplicate samples to reflect the situation of the supervised trials database, containing mostly duplicate samples. The CV values were calculated from the composite samples with eq 2, applying the corresponding factor of 1.128.

Calculation of 95% Confidence Limits. The P0.025 and P0.975 percentiles of ranked CV values calculated from 1000 duplicate samples drawn from each of the 182 individual primary residue populations and the corresponding average CV values were taken to calculate the relative confidence intervals from one data set:

$$CI_{rel,i} = \frac{CV_{P0.975} - CV_{P0.025}}{\overline{CV_i}} \quad (10)$$

As shown in our previous study, the calculated confidence intervals are independent from the CV value of the parent population.[15] Figure 2 shows the fitted curve for the 95% relative difference of the CV values obtained from the 1000 duplicate composite samples generated from the 182 lots. The regression equation obtained was ($R^2 = 0.981$)

DOI: 10.1021/jf5055112
J. Agric. Food Chem. 2015, 63, 4409−4417

Table 3. Estimated CV Values of Individual Crops and Upper Confidence Limits Calculated with the New Approach

crop group	crop name	k^a	CV_{R1}	CV_{S1}	$CV_{S1adj}{}^b$	UCL^c
small fruits	plum	344	0.25	0.23	0.35	0.38
	strawberry	215	0.24	0.22	0.33	0.38
	cherry	189	0.18	0.15	0.23	0.27
bush berries	blueberry	74	0.16	0.12	0.19	0.23
	cranberry	55	0.14	0.09	0.14	0.18
	raspberry	22	0.16	0.13	0.20	0.29
	blackberry	15	0.15	0.11	0.17	0.26
medium fruits	apple	636	0.17	0.14	0.22	0.24
	peach	409	0.24	0.22	0.34	0.37
	orange	328	0.18	0.15	0.23	0.26
	pear	316	0.18	0.14	0.22	0.25
	lemon	195	0.19	0.16	0.25	0.29
	grapefruit	99	0.23	0.20	0.31	0.37
	banana	47	0.21	0.18	0.28	0.35
	mandarin	36	0.27	0.25	0.39	0.51
	avocado	10	0.35	0.34	0.52	0.85
	nectarine	9	0.15	0.11	0.17	0.29
	Japanese apricot (pitted fruit)	8	0.13	0.08	0.13	0.22
large fruits	grape	494	0.22	0.19	0.30	0.32
	mango	32	0.16	0.13	0.20	0.27
	pineapple	21	0.25	0.22	0.35	0.49
	papaya	13	0.32	0.30	0.46	0.72
legume vegetables	bean	72	0.20	0.18	0.27	0.33
	bean (green) plant	40	0.29	0.27	0.42	0.55
	pea (succulent seeds)	36	0.23	0.20	0.32	0.41
	pea (edible podded)	18	0.28	0.26	0.41	0.59
	hops (fresh)	17	0.21	0.19	0.29	0.43
	bean (lima)	15	0.27	0.25	0.38	0.58
	soybean	13	0.20	0.17	0.27	0.42
medium vegetables	tomato	624	0.25	0.23	0.36	0.38
	pepper	503	0.26	0.23	0.36	0.39
	onion (green)	29	0.25	0.23	0.35	0.48
	onion (bulb)	44	0.30	0.28	0.44	0.56
Brassica vegetables	cabbage (head only)	398	0.25	0.23	0.35	0.39
	broccoli	205	0.20	0.17	0.27	0.30
	cauliflower	73	0.22	0.20	0.31	0.37
	Brussels sprout	22	0.24	0.22	0.34	0.47
cucurbits	cucumber	111	0.24	0.21	0.33	0.39
	squash	77	0.29	0.27	0.42	0.51
	melon	74	0.25	0.23	0.35	0.42
	cantaloupe	64	0.27	0.25	0.39	0.48
	eggplant (whole fruit)	11	0.09	0.10	0.15	0.25
leafy vegetables	leaf lettuce	769	0.23	0.20	0.31	0.34
	mustard green	345	0.14	0.10	0.16	0.17
	spinach	304	0.20	0.18	0.27	0.30
	sugar beet (top)	261	0.21	0.19	0.29	0.32
	radish	61	0.19	0.16	0.25	0.31
	tea (fresh)	52	0.48	0.47	0.73	0.92
	mint leaves (intended for processing)	18	0.16	0.12	0.19	0.28
	endive	16	0.12	0.06	0.09	0.13
	rape greens	16	0.17	0.14	0.21	0.32
	basil (fresh)	12	0.11	0.05	0.07	0.12
	beetroot (top)	8	0.12	0.07	0.12	0.20

DOI: 10.1021/jf5055112
J. Agric. Food Chem. 2015, 63, 4409−4417

Table 3. continued

crop group	crop name	k^a	CV_{R1}	CV_{S1}	CV_{S1adj} [b]	UCL[c]
root and tuber vegetables	potato	104	0.16	0.12	0.19	0.22
	sugar beet root	51	0.28	0.26	0.40	0.51
	carrot	39	0.30	0.28	0.43	0.56
	radish (root)	28	0.21	0.18	0.28	0.39
	turnip	9	0.16	0.13	0.20	0.34
	beetroot (root)	8	0.19	0.17	0.26	0.44
stalk and stem	celery	267	0.16	0.13	0.20	0.23
	artichoke	8	0.11	0.04	0.07	0.12
pulses	bean (dry)	137	0.33	0.31	0.48	0.56
	soybean (dry)	128	0.26	0.24	0.37	0.43
	pea (dry)	68	0.21	0.18	0.28	0.35
	lima bean (dry)	13	0.26	0.24	0.37	0.57
cereal grains	wheat (grain)	86	0.21	0.19	0.29	0.35
	rice (grain)	64	0.13	0.09	0.14	0.17
	barley (grain)	63	0.16	0.13	0.20	0.25
	paddy rice (husked grain)	62	0.15	0.12	0.18	0.23
	sorghum (grain)	27	0.15	0.11	0.17	0.23
grasses, for sugar or syrup production	sugar cane	15	0.46	0.44	0.69	1.04
tree nuts	almond	60	0.15	0.11	0.17	0.21
	pecan	39	0.17	0.14	0.22	0.29
oilseeds	cotton seed	130	0.25	0.22	0.35	0.40
	peanut	52	0.15	0.11	0.17	0.22
	rape (seed)	23	0.18	0.14	0.22	0.31
	cotton (undelinted seed)	21	0.38	0.36	0.56	0.80
	sunflower seed	21	0.25	0.22	0.35	0.50
seeds for beverages and sweets	coffee (dry bean)	18	0.38	0.37	0.57	0.84
legume forage and fodder	soybean (forage)	184	0.17	0.13	0.21	0.24
	alfalfa (forage)	48	0.33	0.31	0.49	0.62
	bean forage	31	0.13	0.08	0.13	0.17
	peanut fodder	13	0.20	0.17	0.26	0.41
straw, hay (of legume feeds	soybean (hay)	199	0.18	0.15	0.24	0.27
	peanut (hay)	133	0.27	0.25	0.39	0.45
	barley straw	85	0.18	0.15	0.23	0.28
	alfalfa (hay)	64	0.25	0.23	0.36	0.45
	pea hay	28	0.18	0.15	0.23	0.31
	bean hay	14	0.26	0.24	0.37	0.56
cereal forage, fodder and straw	wheat (straw)	353	0.18	0.15	0.24	0.26
	corn forage	247	0.25	0.22	0.35	0.39
	wheat (forage)	191	0.18	0.15	0.23	0.26
	maize straw	110	0.25	0.23	0.36	0.42
	barley fodder (hay and straw)	93	0.21	0.19	0.29	0.35
	sorghum (fodder)	72	0.24	0.22	0.33	0.41
	rice (straw)	66	0.26	0.24	0.37	0.45
	rice (shoot panicle)	16	0.12	0.06	0.10	0.15
	rye straw	12	0.25	0.23	0.35	0.55
	oat foliage	9	0.05	0.10	0.15	0.26
grass forage	Bermuda grass (forage)	8	0.09	0.10	0.15	0.27
grass hay	Bermuda grass (hay)	8	0.09	0.10	0.15	0.27

DOI: 10.1021/jf5055112
J. Agric. Food Chem. 2015, 63, 4409−4417

Table 3. continued

crop group	crop name	k^a	CV_{R1}	CV_{S1}	$CV_{S1adj}{}^b$	UCL^c
dried herbs	hop (cones, dried)	87	0.18	0.15	0.23	0.28
	basil (dry)	9	0.07	0.10	0.15	0.26
byproducts for animal feed and miscellaneous products	almond (hull)	238	0.19	0.16	0.25	0.28
	peanut hulls	89	0.14	0.09	0.15	0.18
	cotton gin trash	58	0.18	0.15	0.24	0.30

[a]k, number of replicate sample pairs used for estimation of CV_{R1}. [b]CV_{S1adj}, relative standard deviation of residues in composite samples adjusted to the minimum sample size requirements of the Codex sampling procedure. [c]UCL, upper 95% confidence limit of CV_{S1adj} calculated with the new approach.

Table 4. Estimated CV_S Values of Crop Groups and Confidence Limits Calculated with Different Methods

				calculated from chi^2 distribution			new approach		
N^a	crop group	k^b	$CV_S{}^c$	LCL	UCL	CI	LCL	$UCL_{mod}{}^d$	CI
4	small-sized fruits	768	0.33	0.31	0.34	0.03	0.30	0.35	0.04
12	medium-sized fruits	2139	0.27	0.26	0.28	0.02	0.25	0.28	0.02
4	large-sized fruits	560	0.30	0.28	0.32	0.03	0.28	0.32	0.05
4	medium-sized vegetables	1211	0.36	0.35	0.38	0.03	0.34	0.38	0.04
4	bush berries	171	0.18	0.16	0.20	0.04	0.16	0.20	0.05
7	legume vegetables	211	0.33	0.31	0.37	0.06	0.30	0.38	0.08
4	*Brassica* vegetables	698	0.32	0.31	0.34	0.03	0.30	0.35	0.05
5	cucurbits	337	0.37	0.34	0.40	0.06	0.33	0.40	0.07
11	leafy vegetables	1872	0.29	0.28	0.31	0.02	0.28	0.31	0.03
6	root and tuber vegetables	256	0.30	0.28	0.33	0.06	0.27	0.34	0.07
2	stalk and stem vegetables	276	0.20	0.18	0.22	0.04	0.18	0.22	0.04
4	pulses	346	0.40	0.38	0.44	0.06	0.37	0.45	0.08
6	cereal grains	340	0.21	0.20	0.23	0.03	0.19	0.23	0.04
1	grasses, for sugar or syrup production	15	0.71	0.52	1.09	0.57	0.53	1.06	0.53
2	tree nuts	101	0.19	0.17	0.23	0.05	0.17	0.23	0.06
5	oilseeds	247	0.33	0.30	0.36	0.06	0.30	0.37	0.07
1	seeds for beverages and sweets	22	0.55	0.42	0.78	0.35	0.43	0.77	0.35
4	legume forage and fodder	288	0.28	0.26	0.31	0.05	0.26	0.31	0.06
6	straw, hay (of legume feeds)	523	0.30	0.27	0.30	0.03	0.26	0.31	0.05
10	cereal forage, fodder, and straw	1176	0.29	0.28	0.30	0.02	0.27	0.32	0.05
2	grass forage	19	0.22	0.17	0.32	0.15	0.17	0.32	0.15
1	grass hay	18	0.15	0.12	0.23	0.11	0.12	0.23	0.11
2	dried herbs	99	0.23	0.20	0.26	0.06	0.20	0.27	0.07
3	byproducts for animal feed	391	0.23	0.21	0.24	0.03	0.21	0.25	0.04

[a]N, number of commodities considered. [b]k, number of replicate sample sets used for estimation of CV_S. [c]CV_S, relative standard deviation of residues in composite samples meeting the minimum sample size requirements of the Codex sampling procedure. [d]UCL_{mod}, upper 95% confidence limit of the estimated sampling uncertainty (CV_S) calculated with the new approach.

$$CI_{rel,i} = 2.4679k^{-0.439} \quad (11)$$

Equation 10 was used for the estimation of the relative confidence intervals for the calculated CV_{S1adj} and CV_S values taking into account the number of trial sites (number of replicate sets, k). The absolute confidence intervals, CI_{na}, were calculated by multiplying the relative confidence limit values with the estimated average CV_{S1adj} and CV_S values. The estimated relative confidence intervals, obtained from the modeling experiment, were somewhat larger than those calculated with eqs 8 and 9. The upper confidence limit based on modeling (UCL_{mod}) was calculated proportionally to that obtained from Chi^2 distribution to take into account that CV_S-LCL < UCL-CV_S due to the asymmetrical nature of Chi^2 distribution. The calculation of UCL described above is called the "new approach".

To evaluate the effect of the number of lots randomly selected for estimation of the sampling uncertainty and its upper confidence limit as well as to assess the reliability of the estimated relative confidence intervals, an additional modeling has been made. From the 182 primary sample data sets, 4, 8, 16, and 20 were chosen independently 15 times, and the CV_S values and their relative confidence intervals were calculated from each of the duplicate composite samples drawn from them. In the cases of 16 and 20 lots, when the 182 data sets of CV values were not enough to get 15 repetitions, the 16 and 20 lots were selected following a random order of the data sets.

RESULTS AND DISCUSSION

The grand average of 8.56% calculated from 6467 recovery studies (Table 2) covering the most frequently occurring residue ranges of 0.01−10 mg/kg and the five typical commodity categories recommended for performing recovery studies as part of the method validation[25] can be considered as a good estimate for the expectable uncertainty of the analysis (CV_A) of residues. The average CV_L of 10% used for the calculation of CV_S from CV_R (eq 1) includes an allowance for sample processing CV_{SP} of 5.17%, which generally covers the contribution of sample homogenization procedures applied by the specialized laboratories analyzing samples from supervised trials.

The uncertainty of sampling was determined for 106 individual crops (Table 3) and 24 different crop groups

DOI: 10.1021/jf5055112
J. Agric. Food Chem. 2015, 63, 4409−4417

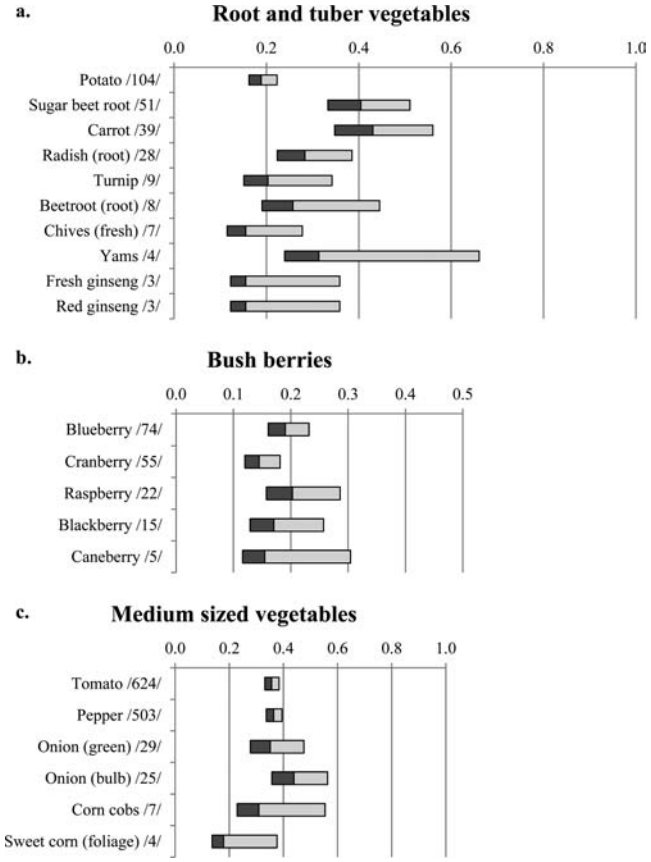

Figure 3. Confidence intervals of CV_{S1corr} values calculated with the new approach of crops belonging to root and tuber vegetables, bush berries, and medium-sized vegetable crop groups. (Number of samples sets is given within slashes.)

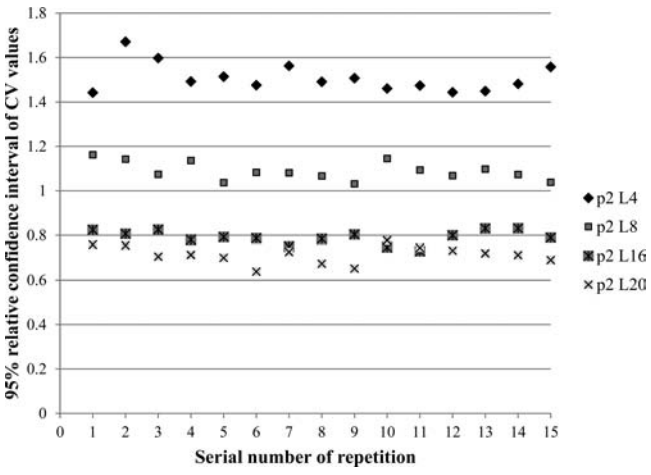

Figure 4. Variation of relative confidence intervals of the CV values calculated from two replicate samples (p2) from 4, 8, 16, or 20 lots independently selected up to 15 times.

(Table 4) based on the supervised residue trial data by applying the methods described above. The lower and upper confidence limits calculated on the basis of Chi^2 distribution and with modeling using 182 independent primary residue data sets are very similar, but the confidence intervals obtained with the new approach are somewhat larger as can be seen in Table 4. Examples of CV_{S1adj} values and confidence intervals of crops belonging to various crop groups calculated with the new approach can be seen in Figure 3. The range of the confidence intervals depends on the number of replicate sample sets, and it is increasing with decreasing number of sample sets used for calculation of CV_S (Figure 3).

The modeling experiments carried out for assessing the effect of data sets on the estimated sampling uncertainty and their confidence limits revealed (Figure 4) that they are robust and only minimally affected by the concentration level and distribution of residues in the lots from which the samples were taken. The relative standard deviations of the calculated confidence intervals from 15 repetitions were 4.3, 3.8, 3.9, and 5.5% in the cases of 4, 8, 16, and 20 lots, respectively, with an average value of 4.4%. This finding is in agreement with the previous experiments[15] showing that the relative confidence interval is practically independent from the variability of the parent population.

Taking into account the potentially serious consequences of an underestimated sampling uncertainty, as the largest contributor to the combined uncertainty, and to get reliable results when testing the compliance of a product in at least 95% of the cases, we recommend using the upper confidence limit of the estimated sampling uncertainties calculated with the new approach in practical applications.

Previous studies[15,26] indicated that sampling uncertainty values calculated from a minimum of eight lots can be considered as a borderline for acceptable estimate, as below that the confidence interval is getting very large. Therefore, where the number of sampled lots was <8, the estimated CV_S values are not indicated in Table 3; however, they were taken into account in the calculation of CV_S value of the corresponding crop group (Table 4). It is noted that, due to the small value of k, they practically do not affect the weighted average CV_S value.

In view of the large confidence intervals in cases when the number of tested lots is between 8 and 20, the sampling uncertainty results should be considered as temporary estimates, and they should be refined and revised when more information is available. In such borderline cases, the risk manager or other responsible person may decide whether to use the sampling uncertainty value belonging to an individual crop (Table 3) or a crop group (Table 4), but taking the UCL as the sampling uncertainty is recommended in all cases.

AUTHOR INFORMATION

Corresponding Author

*(Zs.F.) E-mail: farkas.zsuzsa13@gmail.com.

Notes

The authors declare no competing financial interest.

†(A.A.) Retired.

ACKNOWLEDGMENTS

We greatly appreciate the invitation of S. Lehotay, M. Krolski, J. Sandahl, J. Jenkins, and C. Harris, organizers of the *Poster Session on Residues in Food and Feed Monitoring Results and Dietary Risk Assessment* of the 13th IUPAC International Congress of Pesticide Chemistry, to publish the detailed results of our work in this special issue.

ABBREVIATIONS USED

CV, coefficient of variation (relative standard deviation); CV_R, combined relative uncertainty of the measured residues (in general); CV_L, relative uncertainty of the laboratory phase of the determination of residues including subsampling, sample

DOI: 10.1021/jf5055112
J. Agric. Food Chem. 2015, 63, 4409−4417

processing and the analysis phase of the determination [16]; CV_A, relative uncertainty of the analysis phase of the determination of residues including, for instance, extraction, cleanup and quantitative determination; CV_{Aw}, weighted average of relatives standard deviations of replicate recovery sets; CV_S, relative uncertainty of sampling (in general and in case of crop groups); CV_1, relative uncertainty of the measured residue values calculated from replicate samples from one trial; CV_{R1}, combined relative uncertainty of the measured residue values regarding one crop; CV_{S1}, relative uncertainty of sampling regarding one crop; CV_{S1adj}, relative uncertainty of sampling in case of composite samples meeting the minimum sample size requirements of the Codex sampling procedure; CV_{Sprim}, relative sampling uncertainty of residues in primary (incremental samples); CI, confidence interval; CI_{rel}, 95% relative confidence interval; CI_{na}, confidence interval calculated from the results of modeling experiments (called "new approach"); *k*, number of replicate sample pairs; LCL, lower confidence limit (2.5th percentile); UCL, upper confidence limit (97.5th percentile); UCL_{mod}, upper confidence limit calculated from the results of modeling experiments ("new approach")

REFERENCES

(1) Ambrus, A. Within and between field variability of residue data and sampling implications. *Food Addit. Contam.* **2000**, *17*, 519−537.

(2) Huo, R.; Salazar, J. D.; Hyder, K.; Xu, X. M. Modelling non-systemic pesticide residues in fruits with initial deposit variability and weather effects. *Food Addit. Contam.* **2007**, *24*, 1257−1267.

(3) Xu, X. M.; Murray, R. A.; Salazar, J. D.; Hyder, K. The effects of temperature, humidity and rainfall on captan decline on apple leaves and fruit in controlled environment conditions. *Pest Manage. Sci.* **2008**, *64*, 296−307.

(4) Hall, F. R.; Downer, R. A.; Cooper, J. A.; Ebert, T. A.; Ferree, D. Changes in spray retention by apple leaves during growing season. *HortScience* **1997**, *32*, 858−860.

(5) Linders, J.; Mensink, H.; Stephenson, G.; Wauchope, D.; Racke, K. Foliar interception and retention values after pesticide application. A proposal for standardized values for environmental risk assessment (technical report). *Pure Appl. Chem.* **2000**, *72*, 2199−2218.

(6) MacLachlan, D. J.; Hamilton, D. A new tool for the evaluation of crop residue trial data (day-zero-plus decline). *Food Addit. Contam., Part A* **2010**, *27*, 347−364.

(7) World Trade Organisation. Sanitary and phytosanitary measures. http://www.wto.org/english/tratop_e/sps_e/sps_e.htm (accessed Oct 30, 2014).

(8) Food and Agriculture Organization, Pesticide residues in food 1997−2011 Evaluations Part I − Residues, FAO Plant Production and Protection Paper series, Nos: 146, 152/1, 152/2, 157, 165, 171, 175/1, 175/2, 177, 82/1, 182/2, 184/1, 184/2, 189/1, 189/2, 192, 193, 198, 206, 2012; http://www.fao, org/agriculture/crops/core-themes/theme/pests/jmpr/jmpr-rep/en/ (accessed Sept 3, 2014).

(9) OECD Guideline for testing chemicals Test No. 504: Residues in Rotational Crops (limited field studies), 2007; http://www.oecd-ilibrary.org/content/book/9789264013384-en (accessed 23 Aug 2013).

(10) Ambrus, A.; Zentai, A.; Sali, J.; Ficzere, I. Hidden contributors to uncertainty and accuracy of results of residue analysis. *Accred. Qual. Assur.* **2011**, *16*, 3−11.

(11) Ambrus, Á.; Soboleva, E. Contribution of sampling to the variability of pesticide residue data. *J. AOAC Int.* **2004**, *87*, 1368−1379.

(12) Hill, A. R. C.; Reynolds, S. L. Unit to unit variability of pesticide residues in fruits and vegetables. *Food Addit. Contam., Part A* **2002**, *19*, 733−747.

(13) Ambrus, Á. Estimation of sampling uncertainty for determination of pesticide residues in plant commodities. *J. Environ. Sci. Health, Part B* **2009**, *44*, 1−13.

(14) Codex Secretariat. Recommended method of sampling for the determination of pesticide residues for compliance with MRLs, 2002; www.codexalimentarius.org/input/download/standards/361/CXG_033e.pdf (accessed Oct 30, 2014).

(15) Farkas, Zs.; Horváth, Zs.; Kerekes, K.; Ambrus, Á.; Hámos, A.; Szeitzné Szabó, M. Estimation of sampling uncertainty for pesticide residues in root vegetable crops. *J. Environ. Sci. Health, Part B* **2014**, *49* (1), 1−14.

(16) Codex Alimentarius Commission. Codex Alimentarius Volume 2. Pesticide Residues in Food, Codex Classification of Foods and Animal Feeds; FAO, Rome, Italy, 1993; http://www.codexalimentarius.org/search-results/?cx=018170620143701104933%3Ai-zresgmxec&cof=FORID%3A11&q=CODEX+CLASSIFICATION+OF+FOODS+AND+ANIMAL+FEEDS&sa.x=10&sa.y=3&siteurl=http%3A%2F%2Fwww.codexalimentarius.org%2F&siteurl=www.codexalimentarius.org%2F&ref=&ss=55j3025j2 (accessed Oct 30, 2014). Ambrus, A. Reliability of measurement of pesticide residues in food. *Accred. Qual. Assur.* **2004**, *9*, 288−304.

(17) U.S. Environmental Protection Agency. Pesticides: Regulation of pesticides; http://www.epa.gov/opp00001/regulating/registering/ (accessed Oct 30, 2014).

(18) Ambrus, A.; Farkas, Zs.; Horváth, Zs.; Kötelesné, S. G. Principles and practices of control of pesticide residues in food. *J. Food Invest.* **2014**, *60*, 8−32.

(19) Ambrus, A. Reliability of measurement of pesticide residues in food. *Accred. Qual. Assur.* **2004**, *9*, 288−304.

(20) Eurachem; EUROLAB; CITAC; Nordtest; RSC Analytical Methods Committee. *Measurement Uncertainty Arising from Sampling: A Guide to Methods and Approaches*; Ramsey, M. H., Ellison, S. L. R., Eds.; Eurachem: Leoben, Austria, 2007; ISBN 978 0 948926 26 6.

(21) Anderson, L. R. *Practical Statistics for Analytical Chemists*; Van Nostrand Reinhold: New York, 1987; Appendix D12.

(22) Food and Agriculture Organization. Submission and evaluation of pesticide residues data for the estimation of maximum residue levels in food and feed, FAO Plant Production and Protection Paper 197, FAO, Rome, 2009; http://www.fao.org/fileadmin/templates/agphome/documents/Pests_Pesticides/JMPR/FAO_manual2nded_Oct07.pdf (accessed Oct 30, 2014).

(23) Horváth, Zs.; Ambrus, A.; Mészáros, L.; Braun, S. Characterization of distribution of pesticide residues in crop units. *Environ. Sci. Health, Part B* **2013**, *48*, 615−625.

(24) MedCalc. Statistical tables: values of the Chi-squared distribution; http://www.medcalc.org/manual/chi-square-table.php (accessed Sept 7, 2014).

(25) European Commission. Guidance document on analytical quality control and validation procedures for pesticide residues analysis in food and feed. SANCO/12571/2013, 2013, rev. 0; http://ec.europa.eu/food/plant/plant_protection_products/guidance_documents/docs/qualcontrol_en.pdf (accessed Nov 4, 2014).

(26) Lyn, J. A.; Ramsey, M. H.; Coad, D. S.; Damant, A. P.; Wood, R.; Boon, K. A. The duplicate method of uncertainty estimation: are eight targets enough? *Analyst* **2007**, *132*, 1147−1152.

DOI: 10.1021/jf5055112
J. Agric. Food Chem. 2015, 63, 4409−4417

authorities are generally the same or very similar to those given in the relevant Codex Standards, such as for pesticide residues.[6]

The objective of this paper is to show that available data on the uncertainty (variability) of pesticide residue measurement results may be used in the process of certification of compliance with MRLs. The principles described are also applicable for other chemical contaminants.

EXPERIMENTAL METHODS

Estimation of Combined Uncertainty of the Measured Residues. The combined relative standard uncertainty (expressed as relative standard deviation or coefficient of variation) of the residues measured in composite samples (CV_R) can be expressed as[25]

$$CV_R = \sqrt{CV_S^2 + CV_{SS}^2 + CV_{SP}^2 + CV_A^2} \quad (1)$$

It incorporates the uncertainties of sampling (CV_S), subsampling (CV_{SS}), sample processing (CV_{SP}) (chopping, mincing, and homogenization of analytical sample), and analysis (CV_A). The methods for estimation of sampling uncertainty have been described in detail in previous publications;[7,8,26] therefore, they are not repeated here. When the contribution of uncertainty of subsampling and sample processing is included in the estimated uncertainty of the laboratory phase of measurement (CV_L), the two phases of the process can be distinguished as

$$CV_R = \sqrt{CV_S^2 + CV_L^2} \quad (2)$$

$$CV_L = \sqrt{CV_{SS}^2 + CV_{SP}^2 + CV_A^2} \quad (3)$$

It is noted that the CV_L should always be determined either from retained test portions of the laboratory samples that contain incurred residues[10] or after treatment of the surface of the individual crop units with the test compound.[14] Furthermore, the results of collaborative studies or proficiency tests can provide information only on the uncertainty of the analytical procedure (CV_A) from the point of extraction and not for the combined uncertainty of the analytical results (CV_L), as the appropriate homogeneity of those samples had been carefully checked before distribution to the participants.

Principles of Control of Compliance of Food Commodities with the Legal Limits. As the consequence of the definition of MRLs, there are two distinctly different situations in the control of compliance of food commodities with the legal limits. Different sampling plans are required for testing compliance with MRLs of pesticide residues in commodities before and after marketing.

Control of Commodities on the Market (Enforcement or Monitoring Program). As the permissible maximum concentrations of residues and chemical contaminants apply to the average concentration of the substances in the bulk/laboratory sample, the combined uncertainty of the laboratory phase of the determination of the residue concentration (CV_L) shall be taken into account in deciding on the compliance or noncompliance of the sampled product. If the samples taken satisfy the minimum requirements for the number of primary samples and the mass of the laboratory/bulk sample,[6] the average residue determined in the sample provides the basis for deciding on the acceptability of the sampled lot. To make regulatory action in accordance with the relevant ISO and Codex guidelines,[27,28] among other regulatory agencies, the European Commission (EC) regulations clearly indicate that a lot is considered noncompliant if the measured analyte concentration corrected for recovery, when it should specifically be considered, minus 2 times the expanded uncertainty of the results is above the legal limit. For pesticide residues the default combined relative uncertainty reflecting the CV_L value (eq 3) is defined as 25%.[29] This means that a lot could be rejected if the residue measured in the composite sample taken from the lot would be >2 × MRL. We call this concentration the decision limit (DL). Figure 1 illustrates the situation when the MRL is 0.2 mg/kg and the apple lot (mean of 0.1 mg/kg and CV_R of 0.35) would be tested on the market applying the decision limit of 0.4 mg/kg (0.4−2 × 0.25 × 0.4 = 0.2 mg/kg) as defined by the EC. Under this condition a testing laboratory would reject a lot containing residues ≤0.2 mg/kg in 2.3% of the cases, because the dispersion of analytical measurement results can be considered normal.[30]

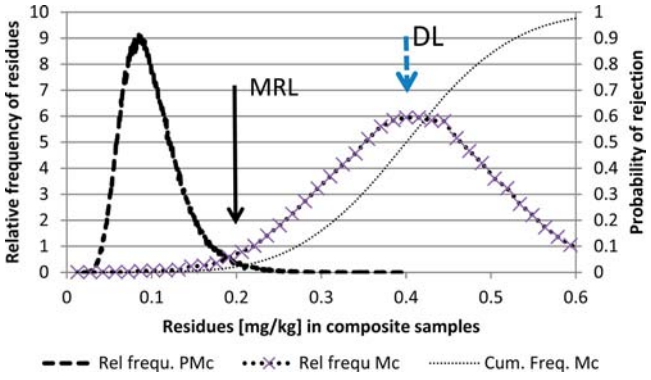

Figure 1. Distribution of residues in composite samples taken as part of the premarketing self-control (PMc) and distribution of analytical measurement results assuming a CV_L of 0.25 and measured residue of 0.4 mg/kg (decision limit, DL). The cumulative frequency of analytical measurements (Cum. Freq. Mc) indicates the probability of rejection of the lot based on the random error of the analysis.

Premarketing Self-Control. When the product is tested before it is placed on the market, it should be certified that at least a specified proportion of the product in terms of the minimum size and mass of bulk/laboratory sample complies with the legal limit. In this case the combined uncertainty (CV_R) including sampling uncertainty shall be taken into account, and the measured value should not be directly compared to the MRL as it may allow a product to be placed on the market with a substantial proportion containing the contaminant above the permitted limit. Let us assume that the MRL is 0.1 mg/kg and the average concentration of a pesticide residue is also 0.1 mg/kg in the sampled lot. If the measured residue in the sample taken from the given lot is <0.1 mg/kg, the sampled lot would be declared to be compliant. However, the decision would be correct only in about 56% and would be wrong in 44% of the cases as indicated by the cumulative frequency distribution curve in Figure 2. Therefore, a lower concentration must be selected as the action limit (AL), which should not be exceeded by the residue measured in the sample. The AL can be calculated by taking into account the combined relative uncertainty of the measured value (CV_R) (eq 1) and the targeted level of compliance.

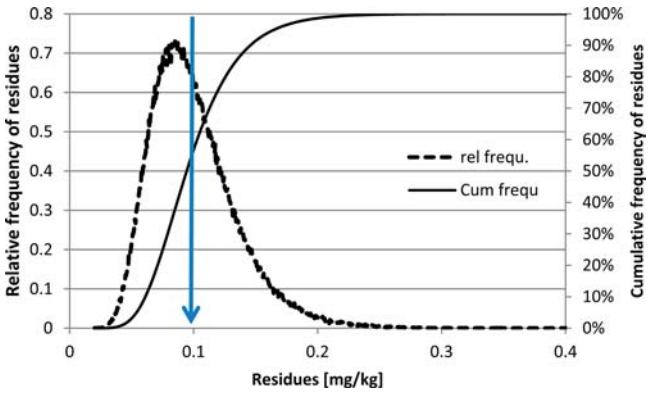

Figure 2. Distribution of residues in apple composite samples with a true mean of 0.1 mg/kg and CV_R of 0.35. MRL = 0.1 mg/kg.

The relationship of AL and MRL can be described with the following equations:

$$AL + k \times CV_R \times AL = MRL \quad (4)$$

DOI: 10.1021/jf505512h
J. Agric. Food Chem. 2015, 63, 4418−4428

$$AL = \frac{MRL}{1 + k \times CV_R} \quad (5)$$

The value of k depends on the agreed acceptable violation rate (P_V) or the compliant proportion of the lot, P_C, relative to the minimum sample size specified in the corresponding regulation ($1 - P_V = P_C$). For normal distribution, which may approximately be assumed with samples of size ≥25 for fruits and vegetables, k is equal to the corresponding standard normal variate, Z. A normal distribution may also be assumed for liquid materials and processed products, such as tomato puree. It is pointed out that in other cases the relative frequency distribution of pesticide residues can be best described with a log-normal distribution.[1]

Calculation of AL for Given Acceptance Probability at MRL. If the distribution of x_i can be described by the log-normal function, then the transformed variable $y_i = \mathrm{Ln}(x_i)$ is normally distributed. If the distribution of x_i has a mean (m) and standard deviation (s), then the distribution of the transformed variable y_i has a mean (M) and standard deviation (S). M and S can be calculated from m and s using the equations

$$M = \mathrm{Ln}\left(\frac{m^2}{\sqrt{(s^2 + m^2)}}\right) \quad (6)$$

$$S^2 = \mathrm{Ln}\left(\frac{s^2}{m^2} + 1\right) \quad (7)$$

Because y_i is normally distributed, the probability P_i (0.0−1.0) for any value y_i occurring from a distribution with mean M and standard deviation S can be calculated from normal distribution tables using the standardized equation

$$Z = \frac{(y_i - M)}{S} \quad (8)$$

$$y_i = M + Z \times S \quad (9)$$

In the sampling domain, m takes on the value of the legal limit MRL and x_i takes on the value of the AL. Typically $x_i \leq m$ (AL ≤ MRL); therefore Z will vary from zero to a negative value usually between 0.0 and −3.5 based upon the specified acceptance probability (acceptable violation rate), P_V. Once m and s are transformed into M and S and the acceptance probability (that will define Z) is specified, y_i can be determined from eq 9. Then x_i can be calculated by transforming y_i back to x_i.

$$x_i = \exp(y_i) \quad (10)$$

x_i is the AL in the linear scale.

RESULTS AND DISCUSSION

Comparison of Sampling Uncertainties Estimated from Supervised Trials and Commercial Field Samples. On the basis of the limited data available, the average sampling uncertainty for primary samples, CV_{Sprim} of 0.78, 0.81, 0.74, and 0.45, were estimated for residues in crop units of a small-, medium-, and large-size crops and *Brassica* leafy vegetables, respectively.[7] Additional residue data measured in carrot and parsley enabled the estimation of CV_{Sprim} values of 0.59 and 0.60, respectively.[8] Duplicate samples taken from 12087 supervised trials carried out in 106 different crops treated with 66 different pesticides provided the best available database for estimation of uncertainty of sampling.[31] The supervised trials are carried out usually on small scale with strictly controlled conditions for the application of pesticides. They aim to provide information on the maximum residues that can occur on treated crops under the critical use conditions [shortest interval between last application and harvest (preharvest interval), highest permitted dose, and application frequency] specified in the registration or use permit documents.[32] Consequently, these trials may not reflect the within-field residue distribution that occurs when the pesticides are applied according to the general agricultural practice. Table 1 summarizes the estimated sampling uncertainties obtained from the databases consisting of residues in/on primary samples, which were taken from fields treated according to normal farming practice and from supervised trials. The CV_S values were calculated for the minimum size of composite samples (12) specified by the Codex Standard for sampling plant products.[6] In Table 2 the sampling uncertainties calculated from residues in samples taken from commercial fields and from supervised trials are compared. The relative sampling uncertainty of residues in field composite samples (CV_{CS}) was calculated from four replicate samples and for supervised trials mostly from duplicate samples with range statistics.[8] The same tendency was observed in both cases. As the number of data sets from which the CV values were calculated greatly varies and the sample sizes in supervised trials had only sometimes been reported, precise comparison of the variability of residues in supervised trial and field samples could not be done. Therefore, the averages of CV ratios (1.15 and 1.19) are considered to be the best indicator of the difference in the variability of residues. Exceptions are papaya, strawberry,

Table 1. Comparison of Estimated Sampling Uncertainties from Resides Measured in Primary Samples Taken from Commercial Fields and Composite Samples Derived from Supervised Trials[a]

	primary field samples			supervised field trials		
crop	no.[b]	CV_{Sprim}	CV_{CS}	no.[b]	CV_{Stcs}	CV_{CS}/CV_{Stcs}
apple	19	0.82	0.26	636	0.22	1.17
pear	4	0.88	0.28	316	0.22	1.25
orange	15	0.90	0.28	328	0.23	1.21
peach	7	1.08	0.34	409	0.34	1.01
plum	8	0.91	0.29	344	0.35	0.82
potato	8	1.06	0.33	104	0.19	1.78
tomato	4	1.45	0.46	624	0.36	1.29
medium size crops		1.01	0.32		0.27	1.19
mango	14	0.73	0.33	494	0.30	1.10
papaya	4	0.60	0.27	13	0.46	0.58
squash	4	0.87	0.39	77	0.42	0.92
grape	14	0.75	0.33	494	0.30	1.13
cucumber	14	0.80	0.36	111	0.33	1.07
banana	2	1.03	0.46	47	0.28	1.66
large crops		0.76	0.34		0.30	1.13
strawberry	9	0.66	0.21	215	0.33	0.62
black currant	2	0.80	0.25	171	0.18	1.40
cherry	7	0.94	0.30	189	0.23	1.28
small fruits		0.80	0.25		0.33	0.76
lettuce	10	0.75	0.34	769	0.31	1.07
cabbage	7	0.41	0.18	398	0.35	0.52
carrot	10	0.60	0.19	39	0.43	0.44
parsley	9	0.65	0.20	2	0.29	0.70
av						1.15

[a]The sample size of the samples has been recalculated to match the criteria of the minimum requirements of Codex Sampling procedure.[6] [b]Number of residue data sets used for the calculation of sampling uncertainty.

DOI: 10.1021/jf505512h
J. Agric. Food Chem. 2015, 63, 4418−4428

Table 2. Comparison of Estimated Sampling Uncertainties from Resides Measured in Composite Samples Taken from Commercial Fields and Supervised Trials

	samples taken from commercial fields				samples taken from supervised trials				
crop	no.[a]	CV_{CS}	LCL	UCL	no.[b]	CV_{Stcs}[c]	LCL	UCL	CV_{CS}/CV_{Stcs}
apple	137	0.34	0.17	0.77	636	0.22	0.20	0.24	1.52
gooseberry	104	0.32	0.11	0.73	171	0.18			1.78
lettuce	42	0.28	0.00	1.21	769	0.31	0.29	0.34	0.90
carrot	29	0.44	0.20	0.67	36	0.43	0.35	0.55	1.03
parsley	24	0.21	0.02	0.40	2	0.29	0.15	1.83	0.70
av									1.19

[a]Number of crop−pesticide combinations (in each case four replicate samples were taken from one field). [b]Number of replicate residue data sets. [c]The relative standard deviations of residues in composite samples were adjusted to the minimum sample size requirements of the Codex sampling procedure.[6]

Table 3. Descriptive Statistical Parameters of Data Sets Used for Modeling the Effect of LOQ Values[a]

	data sets with original residue values										
	1	2	3	4	5	6	7	8	9	10	11
count	106	78	85	36	36	64	111	121	1000	1000	1000
LOQ	0.02	0.02	0.01	0.02	0.01	0.05	0.05	0.01	0.01	0.01	0.01
<LOQ %	0	0	0	0	0	0	0	0	0	0	0
min	0.03	0.03	0.01	0.02	0.27	0.70	0.09	0.01	20.46	0.10	0.03
av	1.66	0.26	0.66	0.10	2.73	15.52	7.56	0.18	50.41	1.01	1.03
P0.95	5.0	0.7	1.4	0.3	7.5	47.0	20.0	0.5	77.7	2.4	3.3
max	6.90	0.85	4.80	0.45	17.00	86.00	30.00	1.20	112.52	4.86	18.42
CV	0.94	0.75	0.97	1.06	1.25	1.06	0.75	1.12	0.29	0.69	1.39
$LOQ/\bar{R}$	0.012	0.076	0.015	0.207	0.004	0.003	0.007	0.055	0.001	0.010	0.010
	data sets with normalized residue values										
	1	2	3	4	5	6	7	8	9	10	11
min	0.02	0.11	0.01	0.21	0.10	0.05	0.15	0.04	0.41	0.09	0.03
av	1.00	1.00	1.00	1.00	1.00	1.00	1.04	1.00	1.00	1.00	1.00
P0.95	3.0	2.8	2.1	3.0	2.7	3.0	2.6	2.9	1.5	2.3	3.2
max	4.15	3.24	7.29	4.66	6.22	5.54	3.97	6.63	2.23	4.83	17.86
CV	0.94	0.75	0.97	1.06	1.25	1.06	0.71	1.12	0.29	0.69	1.39
$LOQ/\bar{R}$	0.01	0.01	0.01	0.01	0.01	0.01	0.01	0.01	0.000	0.010	0.010

[a]Data sets: 1, wheat, barley straw pyraclostrobin; 2, tomato endosulfan; 3, cucurbits propamocarb; 4, potato aldicarb; 5, soybean glyphosate; 6, propamocarb lettuce; 7, cereal grains prochloraz; 8, MLE fitted prochloraz in wheat and barley straw; 9, synthetic log-normal distribution with mean of 50.41 and CV of 0.29; 10, synthetic log-normal distribution with mean of 1.01 and CV of 0.69; 11, synthetic log-normal distribution with mean of 1.03 and CV of 1.39. The selected data sets contained no residue below the LOQ value, except data set 8 in which the 27 values below the varying LOQs of 0.1 mg/kg (6), 0.05 mg/kg (19), and 0.02 mg/kg (2) were replaced with the maximum likelihood procedure assuming log-normal distribution provided by Villanueva.[34]

cabbage, carrot, and parsley for which the ratios of relative sampling uncertainty of composite samples taken from supervised trials and relative sampling uncertainty of residues in field composite samples (CV_{CS}/CV_{Stcs}) are within the range of 0.44 and 0.70. The low variability in field trials cannot be explained on the basis of the available information. As it is quite unlikely that supervised trials lead to higher variability of residues than field trials, these values were disregarded.

Taking into account the uncertainties of the estimations, a rounded correction factor of 1.2 is used to account for the larger variability of residues in field samples.

Effect of Number of Residue Values below the LOQ on the Estimated Sampling Uncertainty. The range of residues in primary samples taken from a single field is typically hundred-fold. Depending on the average residue and the limit of quantification (LOQ) of the analytical method, various proportions of the primary samples may not contain detectable residues. The proportion of residues below LOQ is not known. The effect of the LOQ values in relation to the average of residue data population was studied with experimental supervised trial data[1] and synthetic log-normal distributions, as it was found that the within-field distribution of residues in crop units (primary samples) can be best described with log-normal distribution.[2] Of the supervised trial residue data sets, compiled by the FAO WHO Joint Meeting on Pesticide Residues for estimation of MRLs, those were selected that contained a relatively large number of data points. The descriptive statistical parameters of the selected data sets are summarized in Table 3. The selected data sets contained no residue below the LOQ value, except data set 8, in which the 27 values below the varying LOQs were replaced with the maximum likelihood estimation (MLE) procedure assuming log-normal distribution provided by Villanueva.[33] The residue values were also normalized by dividing them with the corresponding average residues of their data set to assist comparison of the spread of residues in the data sets with different mean residues.

For studying the effect of LOQ (mg/kg) values on the CV of the data population, the selected data sets were arranged in increasing order. The lowest number of residue values

DOI: 10.1021/jf505512h
J. Agric. Food Chem. 2015, 63, 4418−4428

corresponding to the selected percentage of the original data population (10−90%) was replaced with various LOQ values ranging from 2 times the reported LOQ to 0.7 average residues in the data set. These data sets are called adjusted data sets. For instance, in the case of data set 1, the lowest 11 values (0.03, 0.06, 0.07, 0.09, 0.09, 0.1, 0.1, 0.11, 0.12,0.12, and 0.12) were replaced with 0.04, 0.2, ..., 1.16) and then the descriptive statistical parameters were recalculated for each adjusted data set. The process was repeated with 20% of the residue values in the original data set and so on.

The percentage of residue values below the LOQ and the value of LOQ affect the average and the relative standard deviation of the original residue population (CV_O). The relationships of the corresponding CV and average residue of the adjusted data sets are complex, and they are best illustrated graphically. Figure 3 shows the ratios of the CVs of adjusted

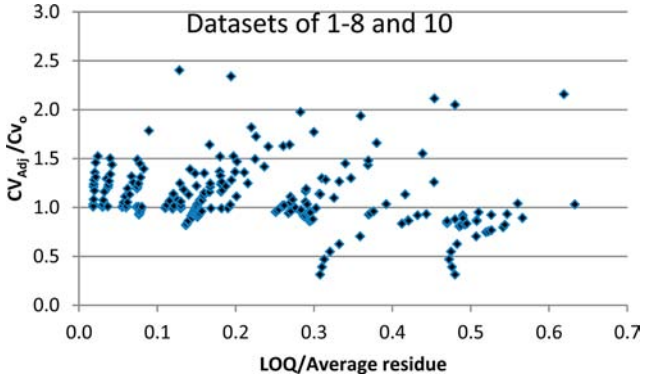

Figure 3. Relationship of the ratio of the CV values of adjusted (CV_{Adj}) and original (CV_O) data sets and the LOQ/average residue in the adjusted data sets 1−8 and 10.

data set (CV_{Adj}) and the original data set (CV_O) as the function of the ratio of LOQ and the average residue ($\overline{R}$) of adjusted data set ($LOQ/\overline{R}$). Figure 4 illustrates the CV_{Adj}/CV_O relationship as the function of the $LOQ/\overline{R}$ residues and the percentage of residues at or below the LOQ obtained from the data set 8 (Table 3, MLE fitted prochloraz residues). As similar $LOQ/\overline{R}$ residues could be obtained from various combinations of LOQ values (Figure 4) and their percentage proportion in the adjusted data sets, the CV_{Adj} values corresponding to $LOQ/\overline{R}$ ranges from ≤0.03 to ≤0.7 were grouped and the averages of $LOQ/\overline{R}$ and the CV_{Adj}/CV_O values being in the given ranges were calculated. The results obtained from the supervised trials and synthetic data sets are shown in Table 4. The results

Table 4. Relationship of Average $LOQ/\overline{R}$ and Average CV_{Adj}/CV_O Values

$LOQ/\overline{R}$		av of CV_{Adj}/CV_O values in data sets	
range	av	1−8 and 10	11
<0.03	0.02	1.17	
0.031−0.06	0.04	1.24	
0.060−0.083	0.07	1.12	
<0.1	0.10		1.02
0.11−0.2	0.16	1.07	1.24
0.21−0.3	0.26		1.07
0.21−0.3	0.27	1.10	
0.31−0.4	0.36		1.07
0.31−0.4	0.39	0.99	
0.41−0.5	0.43		1.30
0.41−0.5	0.46	0.92	
0.51−0.6	0.53	0.83	
0.51−0.6	0.55		0.87
0.61−0.7	0.64		0.93
grand av		1.08	1.12

indicate certain variation among data sets, which is attributed to the distribution of residues within the individual data sets and sampling uncertainty. As the typical sampling uncertainties were obtained from data sets with detectable residues, they do not represent the situations where the various proportions of the treated crops may contain residues below the LOQ. The probability of finding primary samples with nondetectable residues increases as the $LOQ/\overline{R}$ increases. However, no general tendency in the relationship between the $LOQ/\overline{R}$ and CV_{Adj}/CV_O could be established. The grand averages of CV_{Adj}/CV_O up to $LOQ/\overline{R}$ < 0.45 and <0.7 were 1.08 and 1.12, respectively (Table 4). Therefore, it is recommended that an adjusting factor of 1.1 be applied to account for the potential nondetects in the primary units of the sampled crop.

Effect of Mixing Commodities with Different Average Residues. Mixing commodities containing contamination above the legal limits with lots containing no or low level of contamination is not permitted by law.[34] However, it often

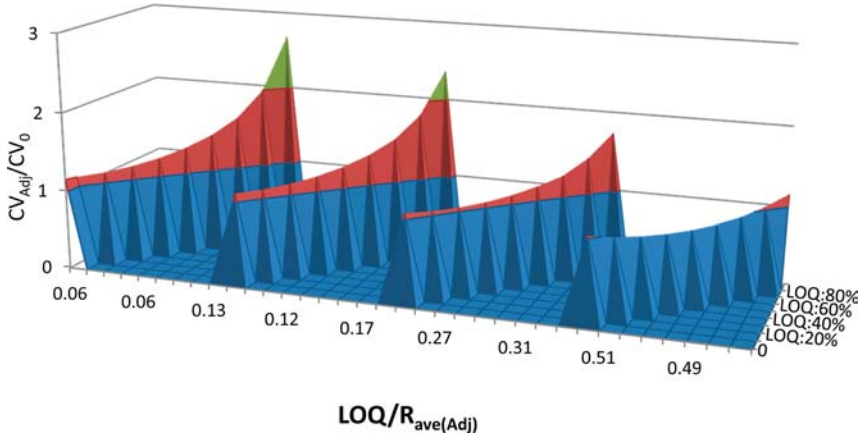

Figure 4. Relationship of CV_A/CV_O as a function of $LOQ/R_{av(A)}$ and percent of residues at LOQ in the case of data set 8 (prochloraz residue in cereal grains).

DOI: 10.1021/jf505512h
J. Agric. Food Chem. 2015, 63, 4418−4428

occurs or might occur in practice. Figure 5 illustrates the residue distribution in mixed and not-mixed products. It can be clearly seen that mixing substantially increases the spread of residues.

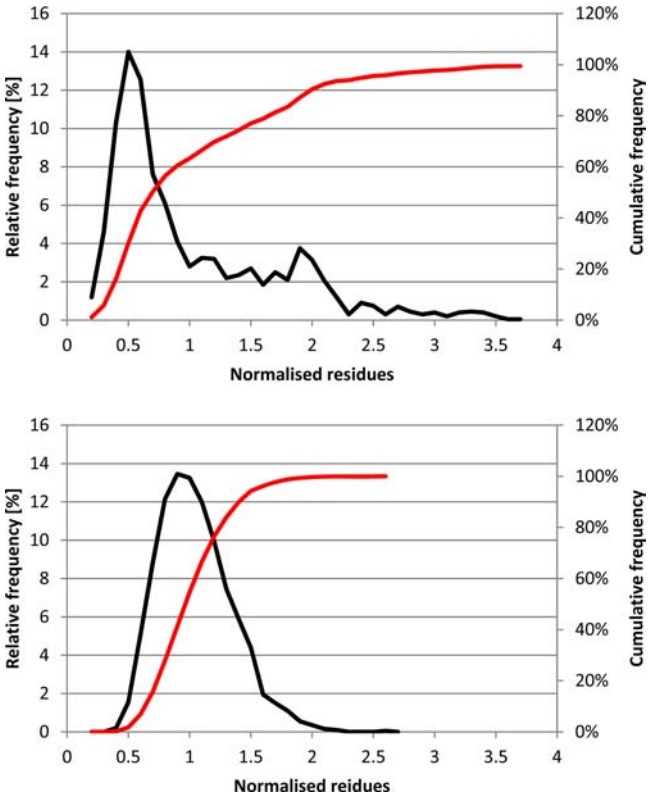

Figure 5. Relative and cumulative frequency distributions of phosalone residues in plum fruit samples taken from mixed (upper chart) and not mixed (lower chart) lots.

To examine the effect of mixing of commodities with substantially different average residues, model experiments were carried out with data set 9 (Table 3) in its original form (average residue 50.41 mg/kg, CV = 0.29) and its normalized version having an average of 1 and the same CV as the original data set. Random samples of 100, 200, 300, 400, and 500 were drawn from the normalized residue data population (representing the low-contaminated lot) and 900, 800, 700, 600, and 500 samples were drawn randomly from the original population (representing the contaminated lot). The residue values obtained from the two data sets were mixed, and the descriptive statistical parameters of the mixed data sets are summarized in Table 5. The same procedure was repeated with data set 8 and the normalized data set 9 to model the effect of the different average and CV values of the lots to be mixed. The results are shown in Tables 6 and 7.

The mixing reduced the average residue in the mixed lot but at the same time substantially increased its CV value. The change of the ratios of the average residues of the "contaminated" and "noncontaminated" data sets from 50.4 to 278 did not change the tendency of increase of CV values in the mixed data set. The large difference of the CV values (1.12 for the noncontaminated data set and 0.29 for the contaminated data set, Table 6) did not affect either the dependence on mixing ratio or the increase of CV_M/CV_O values shown in Tables 6 and 7, where CV_M is the relative standard deviation of residues in the mixed data set. The percentage of the noncontaminated samples (x%) in the mixed data set and the ratio of the CV_M of the mixed lot and the CV_O of the contaminated lot have a linear relationship, and the linear regression lines practically overlap for the two combinations:

original and normalized data set 9:

$$CV_M/CV_O = 0.0518x + 0.9874;\ R^2 = 0.9973 \quad (11)$$

original data set 8 and original data set 9:

$$CV_M/CV_O = 0.05413x + 0.9734;\ R^2 = 0.9967 \quad (12)$$

average regression equation:

$$CV_M/CV_O = 0.05527x + 0.9803;\ R^2 = 0.995 \quad (13)$$

In practice, the effect of mixing a contaminated lot with a noncontaminated one can be taken into account in compliance assessment only if the producer reveals the mixing ratio. In this case, the appropriate adjusting factor can be calculated with eq 13, and it should be used to multiply the recommended practical sampling uncertainties given in Tables 8 and 9. It should be emphasized that the presented principle is valid and applicable only if the effective mixing of the two lots is possible and it has been done. In practice, only liquid products and small grains can be properly mixed, other commodities cannot. Furthermore, it is re-emphasized that mixing a contaminated lot with a noncontaminated one is illegal in many countries.

Recommended Sampling Uncertainties for Control of Pesticide Residues in Food. Due to the large variability of residues in raw agricultural commodities (e.g., fresh fruits and vegetables), the sampling uncertainty cannot be determined reliably from a few measurements. Therefore, to ensure that the calculated AL values are correct in at least in 95% of the cases, it is recommended that the upper 95% confidence limits of the

Table 5. Descriptive Statistical Parameters of the Mixed Dataset Obtained from the Commingled Dataset 9 (D9) and Its Normalized Version (ND9)[a]

	count	min	av	P0.95	max	CV	LOQ/$\bar{R}$	CV_M/CV_O
D9	1000	20.5	50.4	77.7	112.5	0.29	0.000	
ND9	1000	0.41	1	1.54	2.2	0.29	0.01	
ND9_1:D9_9	1000	0.49	45.8	77.0	111.4	0.447	0.0002	1.54
ND9_2:D9_8	1000	0.48	40.9	77.2	112.5	0.584	0.0002	2.01
ND9_3:D9_7	1000	0.45	35.8	73.8	111.4	0.727	0.0003	2.51
ND9_4:D9_6	1000	0.47	30.6	72.8	111.4	0.874	0.0003	3.01
ND9_5:D9_5	1000	0.41	25.5	71.5	112.5	1.053	0.0004	3.63

[a]D9, identification of data set (see Table 3); ND9, normalized form of D9 data set; ND9_1:D9_9 indicates a mixture containing 10% of ND9 and 90% of D9.

DOI: 10.1021/jf505512h
J. Agric. Food Chem. 2015, 63, 4418−4428

Table 6. Descriptive Statistical Parameters of the Mixed Dataset Obtained from the Commingled Dataset D8 and the Original Version of Dataset D9[a]

	count	min	av	P0.95	max	CV	LOQ/av	CV_M/CV_O
D9	1000	20.5	50.4	77.7	112.5	0.29	0.0	
D8	121	0.0	0.18	0.5	1.2	1.12	5.6	
D8_1:D9_9	1000	0.0	45.7	77.0	111.4	0.45	0.0	1.56
D8_2:D9_8	1000	0.0	40.8	77.2	112.5	0.59	0.1	2.04
D8_3:D9_7	1000	0.0	35.6	73.8	111.4	0.74	0.1	2.56
D8_4:D9_6	1000	0.0	30.3	72.8	111.4	0.90	0.2	3.09
D8_5:D9_5	1000	0.0	25.0	71.5	112.5	1.08	0.2	3.74

[a]D8_1:D9_9 indicates a mixture containing 10% of D8 and 90% of D9.

Table 7. Descriptive Statistical Parameters of the Mixed Dataset Obtained from the Commingled Datasets D8 and Its Normalized Version (ND8)[a]

	count	min	av	P0.95	max	CV	LOQ/av	CV_M/CV_O
D8	121	0.01	0.18	0.53	1.2	1.12	0.055	
ND8	1000	0.04	1.00	2.93	6.63	1.12	0.010	
D8_1:ND8_9	1000	0.01	0.94	3.26	6.63	1.20	0.011	1.08
D8_2:ND8_8	1000	0.01	0.85	2.93	6.63	1.31	0.012	1.19
D8_3:ND8_7	1000	0.01	0.77	2.76	6.63	1.30	0.013	1.18
D8_4:ND8_6	1000	0.01	0.65	2.6	6.63	1.41	0.015	1.28
D8_5:ND8_5	1000	0.01	0.65	2.76	6.63	1.54	0.015	1.40

[a]D8_1:ND8_9 indicates a mixture containing 10% of D8 and 90% of ND8.

Table 8. Summary of Sampling Uncertainties of Pesticide Residues in Individual Crop Units or Primary Sample Increments Recommended for Practical Use

crop name	k^a	CV_{Sprim}	crop name	k^a	CV_{Sprim}	crop name	k^a	CV_{Sprim}	crop name	k^a	CV_{Sprim}
Foods						**Foods**					
almond	60	0.85	melon	74	1.74	eggplant	11	1.02	soybean	13	1.72
apple	636	0.98	mint leaves	18	1.15	endive	16	0.55	soybean (dry)	128	1.75
artichoke	8	0.49	mustard green	345	0.72	grape	494	1.32	spinach	304	1.24
avocado	10	3.51	nectarine	9	1.18	grapefruit	99	1.53	squash	77	2.11
banana	47	1.46	onion (bulb)	44	2.32	hop (cones, dried)	87	1.15	strawberry	215	1.55
barley (grain)	63	1.02	onion (green)	29	1.96	hop (fresh)	17	1.76	sugar beet root	51	2.10
basil (dry)	9	1.07	orange	328	1.06	Japanese apricot	8	0.90	sugar cane	15	4.27
basil (fresh)	12	0.47	paddy rice (husked grain)	62	0.93	leaf lettuce	769	1.38	sunflower seed	21	2.04
bean	72	1.38	papaya	13	2.96	lemon	195	1.19	tea (fresh)	52	3.76
bean (dry)	137	2.30	pea (dry)	68	1.43	lima beans	15	2.38	tomato	624	1.58
beetroot (root)	8	1.83	pea (edible podded)	18	2.43	lima beans (dry)	13	2.35	turnip	9	1.41
blackberry	15	1.06	pea (succulent seeds)	36	1.70	mandarin	36	2.10	wheat (grain)	86	1.45
blueberry	74	0.95	peach	409	1.52	mango	32	1.11			
broccoli	205	1.24	peanut	52	0.91	**Animal Feeds**					
Brussels sprout	22	1.95	pear	316	1.02	alfalfa (forage)	48	2.54	pea hay	28	1.28
cabbage, head	398	1.59	pecan	39	1.17	alfalfa (hay)	64	1.84	peanut fodder	13	1.67
cantaloupe	64	1.96	pepper	503	1.62	almond (hull)	238	1.14	peanut hulls	89	0.72
carrot	39	2.30	pineapple	21	2.03	barley fodder (hay and straw)	93	1.42	rice (shoot panicle)	16	0.62
cauliflower	73	1.53	plum	344	1.58	barley straw	85	1.14	rice (straw)	66	1.86
celery	267	0.93	potato	104	0.92	bean (green) plant	40	2.25	rye straw	12	2.28
cherry	189	1.09	radish	61	1.28	bean forage	31	0.69	sorghum (fodder)	72	1.67
coffee (dry bean)	18	3.44	radish (root)	28	1.58	bean hay	14	2.32	soybean (forage)	184	0.97
cotton (undelinted seed)	21	3.28	rape greens	39	1.30	beetroot (top)	8	0.82	soybean (hay)	199	1.10
cotton seed	130	1.66	raspberry	22	1.18	cotton gin trash	58	1.22	sugar beet (top)	261	1.33
cranberry	55	0.75	rice (grain)	64	0.69	maize straw	110	1.74	wheat (forage)	191	1.08
cucumber	111	1.61	sorghum (grain)	27	0.95	oat foliage	9	1.07	wheat (straw)	353	1.08

[a]Number of residue data sets used for the estimation of sampling uncertainty.

estimated average sampling uncertainties calculated from residue data obtained from 12087 independent supervised residue trials[31] be used (Tables 8 and 9). Taking into account the larger variability expected under field conditions than in

DOI: 10.1021/jf505512h
J. Agric. Food Chem. 2015, 63, 4418−4428

Table 9. Summary of Estimated Sampling Uncertainties for Crop Groups Recommended for Practical Use

crop group	no.[a]	UCL of CV_{Stcs}	practical CV_{Sprim}
small fruits[b]	768	0.35	1.43
medium-sized fruits[b]	2139	0.28	1.14
large-sized fruits[b]	560	0.32	1.32
medium-sized vegetables[b]	1211	0.38	1.57
bush berries	171	0.20	0.83
legume vegetables[c]	211	0.38	1.55
brassica vegetables[c]	698	0.35	1.43
fruiting vegetables, cucurbits[c]	337	0.40	1.66
leafy vegetables[c]	1872	0.31	1.27
root and tuber vegetables[c]	256	0.34	1.39
stalk and stem vegetables[c]	276	0.22	0.92
pulses[c]	346	0.45	1.83
cereal grains[c]	340	0.23	0.96
grasses, for sugar or syrup production[c]	15	1.06	4.37
tree nuts[c]	101	0.23	0.95
oilseeds[c]	247	0.37	1.52
seeds for beverages and sweets	22	0.77	3.18
legume forage and fodder	288	0.31	1.29
straw, hay (of legume feeds)	523	0.31	1.26
cereal forage, fodder, and straw	1176	0.32	1.30
grass forage	19	0.32	1.32
grass hay	18	0.23	0.93
dried herbs	99	0.27	1.11
byproducts for animal feed[c]	391	0.25	1.02

[a]Number of replicate sample sets used for estimation of CV_{Stcs}. [b]Crops are grouped according to the size of crop units specified by the Codex Sampling procedure[6] or [c] by the Codex Commodity Classification.[40]

supervised trials and the potential effect of nondetectable residues on the relative standard deviation of residues, a combined multiplying factor of 1.3 is incorporated in the CV_{Sprim} values recommended for use under practical conditions. The CV_{Sprim} values are given to enable convenient determination of the expectable sampling uncertainty for various sample sizes (n) with eq 14, when sampling plans are designed for premarket self-control.

$$CV_n = \frac{CV_{prim}}{\sqrt{n}} \quad (14)$$

Farkas and co-workers demonstrated that the relative range of the 95% confidence limits around the sampling uncertainty, estimated from duplicate samples taken from different lots, rapidly decreases up to eight lots and the range gradually decreases with increasing number of lots. The gain above 20 lots is marginal.[8] This finding is in line with the ISO Standard,[35] which recommends a minimum of 20 lots to be tested for determination of sampling uncertainty of bulk materials with as many replicate samples as feasible. Therefore, when the number of trials providing the basis for the calculation of sampling uncertainty is <20 but ≥8, the estimated CV_S values should be used with caution. In case of doubt, it is recommended to use the typical sampling uncertainties estimated for the corresponding crop group. Likewise, CV_S values estimated for crop groups (Table 9) should be used when the database consists of <8 trials to concord with the conclusions of Lyn and co-workers.[36]

Optimization of Sampling and Testing Plan. *Consideration of the Uncertainty of the Laboratory Phase (CV_L) for Determination of Pesticide Residues.* Although the combined relative uncertainty of subsampling and sample homogenization can be at the same magnitude as that of the uncertainty of sampling,[11,15] laboratories generally pay very little attention to controlling the variability of these two steps, and the repeatability and reproducibility of the measurements are usually reported on the basis of the recoveries obtained with spiked samples.[37−39] The determination of CV_L is especially important when only 1−2 g portions are analyzed from the laboratory sample, which may amount to 1−>15 kg for small- and medium-size and large-size fruits (e.g., cabbage, watermelon), respectively. As the variability resulting from the test portion and particle size reduction depends on the laboratory equipment used and the sample materials analyzed, no typical values can be estimated. Therefore, the CV_L should be determined by each laboratory regularly as part of the routine operation by reanalysis of retained test portions[25] taken from samples containing incurred residues at well detectable concentration. An alternative option is the surface treatment method suggested by Maestroni and co-workers[11,12] and applied successfully in other studies.[13,14] It is especially important when the test portion size is reduced below 15 g.

Table 10. Examples for the Contribution of the Individual Steps of the Analytical Procedure to the Combined Uncertainty (CV_R) of the Results

									percentage contribution to total variance of results			
CV_{Sprim}	n	no.[a]	CV_{SP}	M_{TP}	no.[b]	CV_A	CV_L	CV_R	V_S	V_{SP}	V_A	V_L
1.43	10	1	0.1	15	1	0.12	0.16	0.477	89%	4%	6%	11%
1.43	10	1	1.5	1	1	0.12	1.50	1.571	8%	91%	1%	92%
1.43	10	2	1.5	1	1	0.12	1.06	0.877	15%	84%	1%	85%
1.43	10	3	1.5	1	1	0.12	0.87	0.675	21%	77%	1%	79%
1.43	10	3	1.5	1	2	0.12	0.87	0.674	21%	78%	1%	79%
1.43	25	3	1.5	1	1	0.06	0.87	0.576	10%	90%	0%	90%
1.43	25	3	0.3	5	1	0.06	0.18	0.304	71%	26%	3%	29%
0.81	10	1	0.1	15	1	0.12	0.16	0.300	73%	11%	16%	27%
0.81	10	1	0.3	5	1	0.12	0.32	0.412	39%	53%	8%	61%
0.81	10	2	0.3	5	1	0.12	0.23	0.303	52%	36%	12%	48%
0.81	10	2	0.3	5	2	0.12	0.22	0.300	56%	38%	6%	44%

[a]Number of test portions withdrawn from the homogenized laboratory sample for extraction. [b]Number of replicate analyses performed from the extract of the test portion.

DOI: 10.1021/jf505512h
J. Agric. Food Chem. 2015, 63, 4418−4428

It should be noted that simple recovery studies with spiked test portions before extraction do not provide any information on the efficiency of sample processing and its consequences on the CV_L. Furthermore, neither proficiency test nor collaborative study results provide information on CV_L.

Minimizing Combined Uncertainty of the Measured Residues. Applying eqs 1 or 2, the combined uncertainty of the measured result can be simply calculated with an Excel spreadsheet taking into account the best estimates for the sampling uncertainty (Tables 8 and 9) and the reproducibility CV values of the individual steps of the determination of the residues, which had been obtained from the method validation. The analysts can test the effect of various combinations in advance and select those that fit the purpose of the analyses. As a first step, the largest contributors to the total variance of the results should be reduced if possible. On the other hand, practically no improvement can be achieved by improving the procedure which contributes to the total variance with <30% of the largest contributor. Table 10 provides some examples to illustrate the application of the principle.

If the task of the laboratory is to test the compliance of the marketed products with the MRL, then only the CV_L value should be taken into consideration. It should be noted that the default CV_L of 25% specified by the EC[29] can be comfortably achieved with a CV_A of <20% determined with recovery studies, provided that the CV_{SP} of ≤10% can be maintained. It is pointed out that if a 1 g test portion is extracted instead of 15 g, applying the same sample processing (homogenization) procedure, which is increasingly getting into practice, the CV_L can be as large as 150% and the EC requirement cannot be met.[29] It should also be noted that the relevant minimum mass and sample size requirements must be met for market control. With smaller samples justified legal actions cannot be made.

For premarketing control, the sampling uncertainty should always be taken into account. The sampling uncertainty can be reduced with increasing sample size, provided that the sample processing equipment is suitable for efficiently handling and comminuting a large quantity of materials. Alternately, a sample size reduction step to obtain a sample mass that then can be further processed shall be included in the determination process, and its uncertainty shall be determined and taken into account for the calculation of CV_L. The latter option is not shown in Table 10.

Calculation of Action Limits and Operation Characteristic Curves. Using the combined uncertainty calculated from the recommended practical sampling uncertainties, CV_{Sprim} listed in Tables 8 and 9, and the actual CV_L of the laboratory phase of the residue analysis, the AL and the operation characteristic (OC) curves can be calculated on the basis of the underlying theory described with eqs 8−10. To facilitate premarketing control of pesticide residues, an MS Excel template was developed following the basic principles elaborated by Whitaker and co-workers.[41,42] The template calculates the AL, which should not be exceeded by the measured residues to achieve the desired compliance level. If replicate samples are taken, the residues measured in each sample should be below the calculated AL.

Figure 6 illustrates the calculated OC curves assuming CV_{Sprim} = 0.985, CV_L = 0.16 (15 g test portion), and CV_L = 1.5 (1 g test portion; one and three replicate extractions) and 2% acceptable violation rates. The corresponding AL concentrations of <0.065, <0.011, and <0.025 mg/kg clearly show the disadvantage of indiscriminate reduction of test portion size

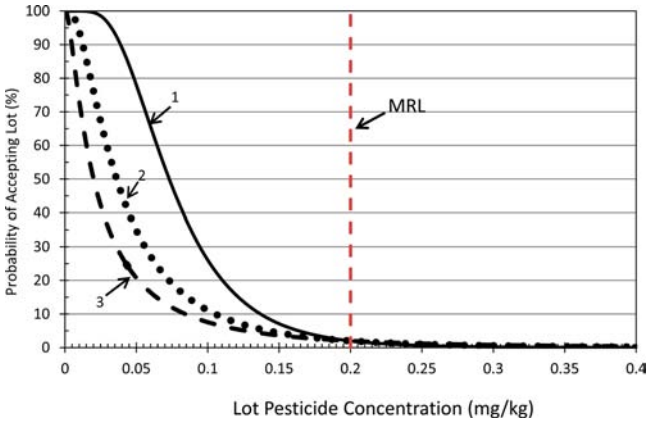

Figure 6. Operation characteristic curves indicating 2% violation rate at the MRL if the residue concentration in the sampled lot was ≤ALs of 0.065, 0.011, and 0.025. The CV_L values and number of test portions in parentheses for curves 1, 2, and 3 were 0.16 (1), 1.5 (1), and 1.5 (3), respectively.

(the residue concentration measured in a 1 g test portion should not be larger than 0.011 and 0.025 mg/kg when the MRL is 0.2 mg/kg) for the sake of reduction of the amount of chemicals required. Figure 7 illustrates the relationship of

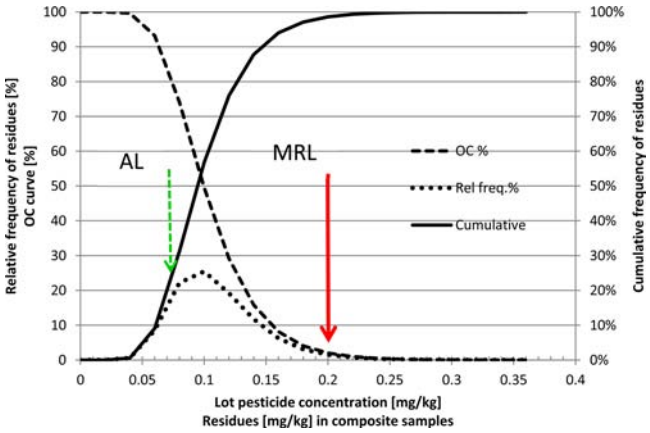

Figure 7. Relationship of relative and cumulative frequencies of residues in samples taken from a lot and the calculated operation characteristic curve assuming 98% compliance of the sampled lot.

relative and cumulative frequencies of residues in samples taken from a lot and the calculated OC curve. It can be seen that in the given case 98% of the samples contain residues below the MRL and the residues in 2% of the samples would exceed it.

It is emphasized that if a crop has been treated with a pesticide, 100% compliance cannot be certified. At present, there is no information available on an officially acceptable violation rate from any country. To enable the design of a sampling plan, which specifies the number and size of samples to be taken and the corresponding AL, an acceptable violation rate should be declared by the responsible national agencies. The BASELINE project carried out within the EU seventh research framework program recommended 98% compliance with the MRLs with 95% probability,[9] as performance objective for chemical contaminants if they do not impose any health risk to consumers. This criterion might be considered as a starting point to establish official acceptable violation rates.

DOI: 10.1021/jf505512h
J. Agric. Food Chem. 2015, 63, 4418−4428

AUTHOR INFORMATION

Corresponding Author

*(Zs.F.) E-mail: farkas.zsuzsa13@gmail.com.

Notes

The authors declare no competing financial interest.

[⊥]Retired Scientific Adviser.

ACKNOWLEDGMENTS

We greatly appreciate the invitation of S. Lehotay, M. Krolski, J. Sandahl, J. Jenkins, and C. Harris, organizers of the Poster Session on Residues in Food and Feed Monitoring Results and Dietary Risk Assessment of the 13th IUPAC International Congress of Pesticide Chemistry, to publish the detailed results of our work in this special issue.

ABBREVIATIONS USED

CV	coefficient of variation (relative standard deviation)
CV_A	relative uncertainty of the analysis phase of the determination of residues including, for instance, extraction, cleanup, ..., and quantitative determination
CV_{Adj}	relative standard deviation of residues in data sets in which the original residue data were replaced with various LOQ values
CV_L	relative uncertainty of the laboratory phase of the determination of residues including subsampling, sample processing and the analysis phase of the determination
CV_R	combined relative uncertainty of the measured residues (in general)
CV_O	relative standard deviation of residues in the original data set
CV_S	relative uncertainty of sampling in general
CV_{SS}	relative uncertainty of the subsampling of a large crop or a large bulk (aggregate) sample
CV_{SP}	relative uncertainty of sample processing including chopping, grinding, mincing, mixing the laboratory sample or part of it
CV_{Sprim}	relative sampling uncertainty of residues in primary (incremental samples)
CV_{CS}	relative sampling uncertainty in the case of composite samples
CV_{S1corr}	relative uncertainty of sampling in case of composite samples meeting the minimum sample size requirements of the Codex sampling procedure;[5]
CV_{Stcs}	relative sampling uncertainty of composite samples taken from supervised trials
CV_M	relative standard deviation of residues in mixed data set
LCL	lower confidence limit (2.5th percentile)
UCL	upper confidence limit (97.5th percentile)
LOQ	limit of quantification of an analyte in a sample matrix
MLE	maximum likely hood estimation procedure
MRL (ML)	maximum concentration of pesticide residues (contaminants) which is legally permitted in/on food and feed
n	sample size (number of primary samples in a composite sample)
$\bar{R}$	average of residues in a data set
M_{TP}	mass of portion of sampled material removed for extraction
DL	decision limit, the concentration of pesticide residue in a sample above which the sampled lot can be considered noncompliant
AL	action limit, also called accept/reject limit; the maximum residue concentration in a random sample satisfying the minimum requirements of laboratory sample, which can be present if the sampled lot is expected to comply with the MRL at specified probability level
P_V	violation rate; the percentage of the sampled lot that does not comply with the MRL; it is also called acceptance probability
P_C	proportion of the sampled crop complying with MRL

REFERENCES

(1) Ambrus, Á.; Horváth, Zs.; Farkas, Zs.; Szabó, I. J.; Dorogházi, E.; Szeitzné-Szabó, M. Nature of the field-to-field distribution of pesticide residues. *J. Environ. Sci. Health, Part B* **2014**, *49*, 229−244.

(2) Horváth, Zs.; Ambrus, Á.; Mészáros, L.; Braun, S. Characterization of distribution of pesticide residues in crop units. *J. Environ. Sci. Health, Part B* **2013**, *48*, 615−625.

(3) European Food Safety Authority. Opinion of the Scientific Panel on Plant health, Plant protection products and their Residues on a request from Commission related to the appropriate variability factor (s) to be used for acute dietary exposure assessment of pesticide residues in fruit and vegetables. *EFSA J.* **2005**, *177*, 1−61. http://www.efsa.europa.eu/en/efsajournal/doc/177.pdf (accessed Oct 30, 2014).

(4) Ambrus, Á. Variability of pesticide residues in crop units. *Pest Manage. Sci.* **2006**, *62*, 693−714.

(5) Ambrus, Á. Estimation of sampling uncertainty for determination of pesticide residues in plant commodities. *J. Environ. Sci. Health, Part B* **2009**, *44*, 1−13.

(6) Codex Secretariat. Recommended method of sampling for the determination of pesticide residues for compliance with MRLs, 2002; www.codexalimentarius.org/input/download/standards/361/CXG_033e.pdf (accessed Oct 30, 2014).

(7) Ambrus, Á.; Soboleva, E. Contribution of sampling to the variability of pesticide residue data. *J. AOAC Int.* **2004**, *87*, 1368−1379.

(8) Farkas, Zs.; Horváth, Zs.; Kerekes, K.; Ambrus, Á.; Hámos, A.; Szeitzné Szabó, M. Estimation of sampling uncertainty for pesticide residues in root vegetable crops. *J. Environ. Sci. Health, Part B* **2014**, *49*, 1−14.

(9) Farkas, Zs.; Ambrus, Á.; Szabó, I. J. Validation of targeted sampling with the new data and development of quantitative indices on reliability and precision, accounting for on food risk factor information. Deliverable 7.2 of BASELINE Project 2013; https://secure.baselineeurope.eu/gest/documentspublic/docup/D7.2_Validation%20of%20targeted%20sampling.pdf (accessed Oct 30, 2014).

(10) Ambrus, Á.; Solymosné, M. E.; Korsós, I. Estimation of uncertainty of sample preparation for the analysis of pesticide residues. *J. Environ. Sci. Health, Part B* **1996**, *31*, 443−450.

(11) Maestroni, B.; Ghods, A.; El-Bidaoui, M.; Rathor, N.; Jarju, O. P.; Ton, T.; Ambrus, Á. Testing the efficiency and uncertainty of sample processing using ^{14}C labelled chlorpyrifos. Part I. In *Principles of Method Validation*; Fajgelj, A., Ambrus, A., Eds.; Royal Society of Chemistry: Cambridge, UK, 2000; pp 49−58.

(12) Maestroni, B.; Ghods, A.; El-Bidaoui, M.; Rathor, N.; Ton, T.; Ambrus, A. Testing the efficiency and uncertainty of sample processing using ^{14}C labelled chlorpyrifos. Part II. In *Principles of Method Validation*; Fajgelj, A., Ambrus, A., Eds.; Royal Society of Chemistry: Cambridge UK, 2000; pp 59−74.

DOI: 10.1021/jf505512h
J. Agric. Food Chem. 2015, 63, 4418−4428

(13) Tiryaki, O.; Baysoyu, D. Estimation of sample processing uncertainty for chlorpyrifos residue in cucumber. *Accred. Qual. Assur.* **2006**, *10*, 550−553.
(14) Fussell, R. J.; Hetmanski, M. T.; Macarthur, R.; Findlay, D.; Smith, F.; Ambrus, Á.; Brodesser, J. P. Measurement uncertainty associated with sample processing of oranges and tomatoes for pesticide residue analysis. *J. Agric. Food Chem.* **2007**, *55*, 1062−1070.
(15) Omeroglu, P. Y.; Ambrus, Á.; Boyacioglu, D.; Majzik, E. S. Uncertainty of the sample size reduction step in pesticide residue analysis of large-sized crops. *Food Addit. Contam.: Part A* **2013**, *30*, 116−126.
(16) Regulation (EC) No. 299/2008 of the European parliament and of the council of 11 March 2008 amending Regulation (EC) No. 396/2005 on maximum residue levels of pesticides in or on food and feed of plant and animal origin, as regards the implementing powers conferred on the Commission. *Off. J. Eur. Union* **2008**, *L97*, 67−71.
(17) Australian Pesticides and Veterinary Medicines Authority (APVMA). Maximum Residue Limits (MRL) in Food and Animal Feedstuff; http://apvma.gov.au/search/node?search=Maximum+residue+limits+for+pesticides (accessed Oct 30, 2014).
(18) Food and Agricultural Materials Inspection Center (Japan), Data Requirements for Supporting Registration of Pesticides; http://www.acis.famic.go.jp/eng/shinsei/index.htm (accessed Oct 30, 2014).
(19) U.S. Environmental Protection Agency. Pesticides: Regulation of pesticides; http://www.epa.gov/opp00001/regulating/registering/ (accessed Oct 30, 2014).
(20) Commission Regulation (EU) No. 420/2011 of 29 April 2011 amending Regulation (EC) No. 1881/2006 setting maximum levels for certain contaminants in foodstuffs. *Off. J. Eur. Union* **2011**, *L111*, 3−6.
(21) Commission Regulation (EC) No. 199/2006 of 3 February 2006 amending Regulation (EC) No. 466/2001 setting maximum levels for certain contaminants in foodstuffs as regards dioxins and dioxin-like PCBs. *Off. J. Eur. Union*. **2006**, *L32*, 34−38.
(22) Codex Alimentarius Commission. Codex Pesticides Residues in Food (online database); http://www.codexalimentarius.org/standards/pesticide-mrls/ (accessed Oct 30, 2014).
(23) Codex Alimentarius Commission. Codex Veterinary Drug Residue in Food (online database) http://www.codexalimentarius.org/standards/veterinary-drugs-mrls/en/ (accessed Oct 30, 2014).
(24) Codex Alimentarius Commission. Codex General Standard for Food Additives (GSFA) (online database). http://www.codexalimentarius.org/standards/gsfa/ (accessed Oct 30, 2014).
(25) Ambrus, A. Reliability of measurement of pesticide residues in food. *Accred. Qual. Assur.* **2004**, *9*, 288−304.
(26) Ramsey, M. H., Ellison, S. L. R., Eds. Eurachem/EUROLAB/CITAC/Nordtest/AMC Guide: Measurement uncertainty arising from sampling: a guide to methods and approaches. *Eurachem*; 2007; ISBN 978 0 948926 26 6.
(27) Joint Committee for Guides in Metrology (JCGM/WG 1). Evaluation of measurement data − guide to the expression of uncertainty in measurement; http://www.bipm.org/utils/common/documents/jcgm/JCGM_100_2008_E.pdf (accessed Oct 30, 2014).
(28) Codex Alimentarius Commission. Guidelines on Measurement Uncertainty; CAC/GL 54-2004; http://www.codexalimentarius.org/search-results/?cx=018170620143701104933%3Ai-zresgmxec&cof=FORID%3A11&q=CAC%2FGL+54-2004&siteurl=http%3A%2F%2Fwww.codexalimentarius.org%2F&sa.x=16&sa.y=5 (accessed Oct 30, 2014).
(29) Europen Commission. Guidance document on analytical quality control and validation procedures for pesticide residues analysis in food and feed. SANCO/12571/2013. 19 November 2013; rev. 0; http://ec.europa.eu/food/plant/plant_protection_products/guidance_documents/docs/qualcontrol_en.pdf.
(30) Thompson, M.; Howarth, R. J. The frequency distribution of analytical error. *Analyst* **2008**, *105*, 1188−1195.
(31) Farkas, Zs.; Horváth, Zs.; Szabó, I. J.; Ambrus, Á. Estimation of sampling uncertainty of pesticide residues based on supervised residue trial data. *J. Agric. Food Chem.* **2014**, DOI: 10.1021/jf5055112.
(32) Food and Agriculture Organization. Submission and evaluation of pesticide residues data for the estimation of maximum residue levels in food and feed. *FAO Plant Production and Protection Paper 197*; FAO: Rome, Italy, 2009 http://www.fao.org/fileadmin/templates/agphome/documents/Pests_Pesticides/JMPR/FAO_manual2nded_Oct07.pdf (accessed Oct 30, 2014).
(33) Villanueva, P. U.S. EPA's Office of Pesticide Programs, Washingon DC, personal communication, 2006.
(34) Regulation (EC) No. 396/2005 of the European parliament and of the council of 23 February 2005 on maximum residue levels of pesticides in or on food and feed of plant and animal origin and amending Council Directive 91/414/EEC. *Off. J. Eur. Union* **2005**, *70*, 1−16.
(35) International Standard Organization, Agricultural Products. Layout for standard method of sampling from a lot. ISO 7002-1, 1986.
(36) Lyn, J. A.; Ramsey, M. H.; Coad, D. S.; Damant, A. P.; Wood, R.; Boon, K. A. The duplicate method of uncertainty estimation: are eight targets enough? *Analyst* **2007**, *132*, 1147−1152.
(37) Cuadros-Rodríguez, L.; Hernández Torres, M. E.; Almansa López, E.; Egea González, F. J.; Arrebola Liébanas, F. J.; Martínez Vidal, J. L. Assessment of uncertainty in pesticide multiresidue analytical methods: main sources and estimation. *Anal. Chim. Acta* **2002**, *454*, 297−314.
(38) da Silva, R. J.; Lino, M. J.; Santos, J. R.; Camões, M. F. Estimation of precision and efficiency mass transfer steps for the determination of pesticides in vegetables aiming at the expression of results with reliable uncertainty. *Analyst* **2000**, *125*, 1459−1464.
(39) Kmellár, B.; Fodor, P.; Pareja, L.; Ferrer, C.; Martínez-Uroz, M. A.; Valverde, A.; Fernandez-Alba, A. R. Validation and uncertainty study of a comprehensive list of 160 pesticide residues in multi-class vegetables by liquid chromatography-tandem mass spectrometry. *J. Chromatogr., A* **2008**, *1215*, 37−50.
(40) Codex Alimentarius Commission. *Codex Alimentarius Vol. 2. Pesticide Residues in Food, Codex Classification of Foods and Animal Feeds*; FAO: Rome, Italy, 1993; http://www.codexalimentarius.org/search-results/?cx=018170620143701104933%3Ai-zresgmxec&cof=FORID%3A11&q=CODEX+CLASSIFICATION+OF+FOODS+AND+ANIMAL+FEEDS&sa.x=10&sa.y=3&siteurl=http%3A%2F%2Fwww.codexalimentarius.org%2F&siteurl=www.codexalimentarius.org%2F&ref=&ss=55j3025j2 (accessed Oct 30, 2014).
(41) Whitaker, T. B.; Slate, A. B.; Giesbrecht, F. G. Designing sampling plans to detect foreign material in bulk lots of shelled peanuts. *Peanut Sci.* **2008**, *35*, 159−164.
(42) Food and Agriculture Organization of the United Nations. *Mycotoxin Sampling Tool, User Guide*; 2013; http://www.fstools.org/mycotoxins/Documents/UserGuide.pdf (accessed Oct 30, 2014).

DOI: 10.1021/jf505512h
J. Agric. Food Chem. 2015, 63, 4418−4428

followed by gel permeation chromatography (GPC) or column chromatography with sorbents to remove lipids and other interfering components from fish extracts.[9] Nonpolar solvents, such as hexane, acetone, dichloromethane, and ethyl acetate, are commonly used for extraction. Similar techniques may be used to prepare fish samples for ELISA. For example, PLE with hexane and dichloromethane was used for extraction of fish tissues, followed either by cleaning with sulfuric acid or an acidified silica gel column to prepare fish samples for ELISA.[10,11]

PBDEs and DDTs are lipophilic and therefore accumulate in fatty tissues, such as in fish. In most method development studies, laboratory-spiked samples are used to assess method performance, but analytes are not internally integrated into the fat; thus, spiking is not necessarily acceptable to determine true extractability of the analytes from within fatty tissues. In incurred samples, contaminants are bound into cells and absorbed by fat and may not be readily available to the extraction solvent compared to spiked samples. The extractability of incurred contaminants is an important topic, but it is not given enough attention in method validation guidelines or in the scientific literature. A previous report on sample preparation for many POPs and pesticides in incurred fish with lipid content 3−10% showed acceptable total extractability and method performance using analysis by low-pressure gas chromatography−tandem mass spectrometry (LPGC-MS/MS).[12] This method should also be applicable to ELISA and provide superior ease, lower cost, and other benefits compared to PLE and GPC as described in the literature.[9,11,13]

The goal of this study was to evaluate a simple, rapid, and cost-effective sample preparation method, previously developed and validated for the analysis of diverse POPs in various fish tissues using LPGC-MS/MS, for the analysis of PBDEs and DDTs by commercial ELISA kits using incurred fish samples with various lipid content. Additionally, we sought to estimate matrix effects affecting the accuracy of measurements in the ELISAs for both contaminant groups. Comparison of ELISA and LPGC-MS/MS was also possible for the same samples, taking cross-reactivities of the ELISAs for individual analytes into account.

MATERIALS AND METHODS

Samples of Pacific white croaker (*Genyonemus lineatus*) and salmon (unknown species) were received from the National Institute of Standard and Technology (NIST) Marine Environmental Specimen Bank in Charleston, SC, USA. The croaker was collected in 2002 from Palos Verdes Shelf Los Angeles Sanitation District Zone 1 EPA Superfund site in Palos Verdes, CA, USA. Croaker samples were received as a frozen, homogenized powder. The salmon was contributed to the specimen bank by Axys Analytical, Sidney, BC, Canada (collection location was unknown). The salmon was received frozen as a whole-body fish and was thawed, filleted into skinless and boneless chunks, refrozen, and then homogenized with dry ice using a Robot Coupe (Ridgeland, MS, USA) RSI 2Y1 chopper. It was stored in glass containers at −18 °C until portions were thawed for analysis. The measured moisture content was 63% for salmon and 79% for croaker, respectively. Reported average lipid levels were 3−4 and 5−10% for croaker and salmon, respectively.[14] Standard Reference Material (SRM) 1947 (Lake Michigan Fish Tissue) was purchased from NIST (Gaithersburg, MD, USA), and contained 73% moisture and 10% fat content. SRM 1947 contains PBDE congeners and DDT pesticides with certified/reference concentrations. In addition, samples of Pacific white croaker and salmon were purchased from local grocery stores as "clean" matrices for use in matrix-matched calibration. They were homogenized with dry ice as described above and stored in glass containers in a −18 °C freezer.

Standards of PBDE congeners (28, 47, 99, 100, 153, 154, and 183) and DDT pesticides (*o,p′*-DDE, *p,p′*-DDE, *o,p′*-DDD, *p,p′*-DDD, *o,p′*-DDT, and *p,p′*-DDT) were purchased from AccuStandard (New Haven, CT, USA). All standards were ≥98% purity, and all solvents were of HPLC grade. Acetonitrile (MeCN), ethyl acetate, and hexane were from Fisher Scientific (Pittsburgh, PA, USA) and methanol (MeOH) was from VWR International (Radnor, PA, USA). Deionized water of 18.2 Ω-cm was prepared with an E-Pure model D4641 from Barnstead/Thermolyne (Dubuque, IA, USA). Primary−secondary amine (PSA) and C18 sorbents were purchased from UCT (Bristol, PA, USA). Z-Sep sorbent, which incorporated zirconium dioxide, was from Supelco (Bellefonte, PA, USA). Ammonium formate was from Sigma-Aldrich (St. Louis, MO, USA). PVDF 0.2 μm filter vials were from Thomson Instrument Co. (Oceanside, CA, USA). ELISA kits, 96-well microliter plates for PBDE and DDE/DDT, were from Abraxis (Warminster, PA, USA).

Sample Preparation. The sample preparation procedure was based on the quick, easy, cheap, rugged, effective, and safe (QuEChERS) approach including the recently reported filter-vial d-SPE cleanup technique.[15] Homogenized fish samples (4 g) were placed into 50 mL polypropylene tubes, and after the addition of 4 mL of MeCN, the tubes were shaken for 10 min on a pulsed-vortexer (Glas-Col, Terre Haute, IN, USA) at 80% setting with maximum pulsing. Water (4 mL) was used as a reagent blank. After extraction, 2 g of ammonium formate was added to induce the phase separation,[16] and the samples were shaken for 1 min on the pulsed-vortexer and centrifuged for 2 min at 3700 rcf. Extracts (0.5 mL) were transferred into the shell (bottom) portions of 0.2 μm PVDF filter-vials containing 75 mg of anhydrous $MgSO_4$, 25 mg of PSA, 25 mg of C18, and 25 mg of Z-Sep sorbents. The filter-vial plungers (top pieces) were partially depressed, and the extracts were shaken by hand for 30 s in an autosampler vial tray. Then the plungers were fully depressed into the filter-vial shells, forcing the cleaned-up extract through the filter membrane. Filtered extracts (200 μL) were transferred to glass autosampler vials containing inserts for LPGC-MS/MS analysis. Another set of filtered extracts (200 μL) was transferred to glass tubes for ELISA analysis. These extracts were evaporated to dryness with nitrogen and reconstituted in 200 μL of 1:1 (v/v) MeOH/water for ELISA analysis. Different fish extracts were prepared in four replicates (except for SRM 1947) on different days for separate ELISA and LPGC-MS/MS analysis. The equivalent fish tissue concentration was 1 g/mL in all final extracts.

Determination of Coextractives. Four types of fish tissues (croaker and salmon each from the specimen bank and from grocery stores) were extracted with MeCN, hexane, and ethyl acetate. Each solvent (15 mL) was added to 15.0 g each of the four fish tissues in 50 mL polypropylene tubes, and the tubes were shaken on the pulsed-vortex shaker for 10 min as described above. In the case of MeCN, two replicate extracts were prepared (one was used to determine coextractives, and the other was to estimate d-SPE cleanup efficiency). Additional MeCN extracts were prepared in the same manner for store-purchased salmon and croaker to generate matrix-matched (MM) calibration standards. For MeCN extracts, 7.5 g of ammonium formate was added to induce phase separation. The tubes were then centrifuged for 2 min at 3700 rcf, and 10 mL of each corresponding solvent extract was transferred into a preweighed glass tube, evaporated to dryness, and dried in an oven at 120 °C, after which the glass tubes with residues were reweighed.

d-SPE Removal Efficiency. Aliquots (10 mL) of MeCN extract for each fish type were placed into 50 mL tubes, to which 1500 mg of anhydrous $MgSO_4$ and 500 mg each of PSA, C18, and Z-sep were added for d-SPE cleanup. The tubes were shaken for 30 s and centrifuged for 2 min at 3700 rcf. The treated extracts (5 mL) were placed into preweighed glass tubes and evaporated to dryness. After drying in the oven at 120 °C, the glass tubes with residues were weighed again.

To prepare MM calibration curves for the ELISA procedure, another set of MeCN extracts after d-SPE of store-bought salmon and

DOI: 10.1021/jf505651g
J. Agric. Food Chem. 2015, 63, 4429−4434

croaker (5 mL of each fish extract) were transferred into glass tubes, evaporated to dryness, and reconstituted in 5 mL of 1:1 (v/v) MeOH/water. Aliquots of 0.45 mL of the corresponding fish extracts were placed into autosampler vials, and PBDE 47 standard solution was added to yield concentrations of 0, 0.1, 0.25, 0.5, 1, 2, and 4 ng/g, as was *p,p′*-DDE standard solution to yield concentrations of 0, 0.625, 1.25, 2.5, 5, 10, and 25 ng/g in a final volume of 0.5 mL.

LPGC-MS/MS. Low-pressure vacuum outlet GC was carried out using an Agilent 7890 GC system with a multimode inlet (MMI) interfaced to a 7000B triple-quadrupole MS/MS. The GC instrument was upgraded with a 220 V rapid heating oven device. A capillary column (15 m × 0.53 mm i.d. × 1 μm film thickness) Rti-5 ms (Restek, Bellefonte, PA, USA) was coupled to a restriction capillary (5 m × 0.18 mm i.d.) (Restek HydroGuard). High-purity He was the carrier gas at a constant flow rate of 2 mL/min. The MMI was initially set at 80 °C for 0.31 min with vent at 50 mL/min, then ramped at 420 °C/min to 320 °C, and held until 9.5 min. Injection volume was 5 μL. The oven temperature started at 70 °C for a 1.5 min hold, followed by a ramp at 80 °C/min to 180 °C, then at 40 °C/min to 250 °C, and then at 70 °C/min to 290 °C, at which it was held until 9.5 min. The transfer line and ion source were set at 280 and 320 °C, respectively, and the quadrupole was at 150 °C. Two MRMs per each analyte were used with a dwell time of 2.5 ms.

Calibration curves for PBDE congeners 28, 47, 99, 100, 153, 154, and 183 and *p,p′*-DDD, *o,p′*-DDT, *o,p′*-DDD, and *p,p′*-DDT were constructed at 0, 0.1, 1, 5, 10, 50, 100, 250, and 500 ng/g in MeCN. To quantify the high concentrations of DDE in the croaker, an additional calibration point of 1000 ng/g was added for *o,p′*-DDE. For *p,p*-DDE, the least intense MRM transitions were selected to avoid detector saturation and still achieve linear calibration with additional calibration points at 500, 1000, 2500, 5000, 7500, 10000, and 15000 ng/g of *p,p′*-DDE.[12]

ELISA Procedure. Because the analyte concentrations in the incurred samples were known, croaker and SRM 1947 extracts were diluted 1:50, 1:100, and 1:1000 times with MeOH/water (1:1 v/v) to fall within the calibration curve range.

The ELISA procedure described in the commercial kit instructions was followed.[17] For PBDE analysis, 50 μL of the final extracts and MM and solvent calibration standards (in MeOH/water (1:1 v/v) were placed into the wells, and 50 μL of PBDE antibody solution was added. After careful mixing and 30 min of incubation time at room temperature, 50 μL of PBDE enzyme conjugate solution was added. After further mixing, the solutions in the wells were incubated for another 30 min at room temperature. Then, the solutions were removed from the wells, which were rinsed with the washing buffer (provided with the commercial kit) four times. Afterward, 100 μL of color solution (hydrogen peroxide and 3,3′,5,5′-tetramethylbenzidine) was added, mixed, and allowed to incubate again for 30 min. Finally, 100 μL of stopping solution (0.5% of sulfuric acid) was added, and the optical density (OD) was read at 450 nm using the 96-well plate reader Synergy HT from Bio-Tek Instruments (Winooski, VT, USA). Quantification was based on MM calibration curves for croaker and salmon.

For the DDE/DDT pesticide assay,[18] 25 μL of final extracts and MM and solvent calibration standards were incubated in wells with 50 μL of DDE/DDT antibody solution at room temperature for 30 min, after which 50 μL of enzyme conjugate solution was added, mixed, and incubated again for 30 min. After the incubation, all wells were emptied, rinsed four times with washing buffer, and 150 μL of color solution was added. Following another 30 min of incubation, 100 μL of stopping solution was added, and the OD was measured as before. Measured OD was converted to ng/g concentrations using semilog calibration curves after normalization to the OD control values (%B/B_0). In initial experiments, measured ODs from replicated wells were within 1% RSD; thus, only one well per sample was used for subsequent analyses.

RESULTS AND DISCUSSION

Sample Preparation. In our sample preparation method, MeCN was used as an extraction solvent, providing acceptable recoveries for relatively nonpolar and polar organic contaminants from fish tissues without extracting significant amounts of lipids and other possible interferences. For instance, hexane and ethyl acetate are commonly used for extraction of lipophilic POPs from fish and other fatty tissues.[19,20] On the basis of studies using spiked samples, both solvents were shown to provide excellent recoveries. However, because hexane and ethyl acetate are rather nonpolar, they tend to extract significant amounts of lipids and similar coextractive components, creating a need for extensive cleanup to remove interfering coextractive components prior to analysis. Figure 1A demonstrates the

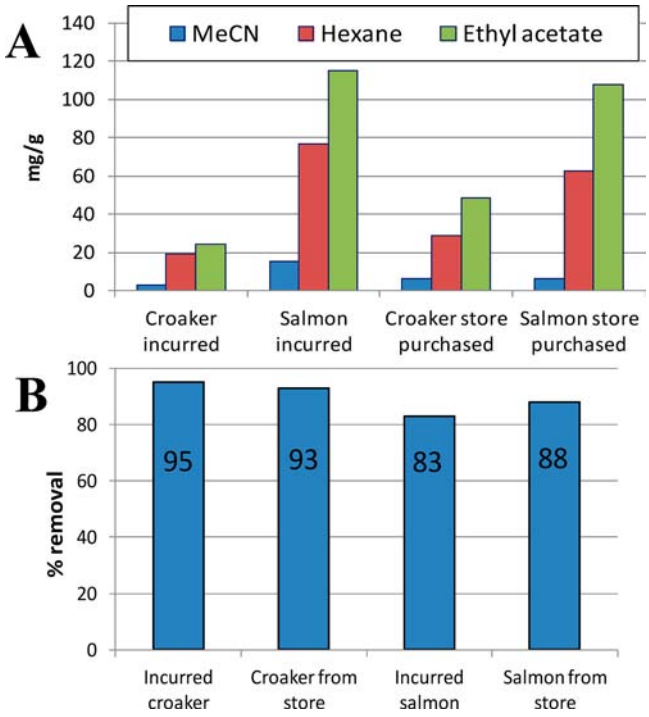

Figure 1. Comparison of matrix coextractive amounts (mg/g): (A) initial extraction; (B) coextractive removal efficiency (%) of MeCN extracts by d-SPE in the method.

difference in amounts of coextracted materials in four fish types in this study using hexane, ethyl acetate, and MeCN as extraction solvents. Hexane and ethyl acetate extracts contained up to 11 and 18 times, respectively, more coextractives compared to MeCN extracts. Furthermore, the filter-vial d-SPE approach with the selected combination of sorbents (C18, PSA, and Z-Sep) removed 83−95% of coextracted matrix from the salmon and croaker extracts (Figure 1B), providing relatively clean extracts for analysis. This new QuEChERS-based sample preparation method is simple and rapid, enabling preparation of a batch of 10 prehomogenized fish in 1 h by one analyst, and it can be implemented in any laboratory or even in the field if shaking is done vigorously by hand and time is given for the salted-out MeCN layer to separate from the water. The cost per sample is approximately $3 for materials.

The final MeCN extracts could be directly injected in GC-MS. However, MeCN is not typically suitable for ELISA, and our experiments using 10, 25, and 50% MeCN in aqueous solutions for final extracts in analysis of PBDEs by ELISA failed

DOI: 10.1021/jf505651g
J. Agric. Food Chem. 2015, 63, 4429−4434

Table 1. Average Measured Concentrations of Incurred PBDEs and DDT Pesticides in Croaker and Salmon by LPGC-MS/MS, Measured Concentrations of Contaminants in SRM 1947, and Accuracy of Measurements versus Certified/Reference Concentrations

	av ± SD (ng/g) (n = 4)		SRM 1947	
analyte	croaker	salmon	ng/g	accuracy (%)
p,p'-DDD + o,p'-DDT	457 ± 63	1.64 ± 0.15	57.7	94
o,p'-DDD	26 ± 2		3.9	119
o,p'-DDE	1210 ± 110		2.9	87
p,p'-DDE	10200 ± 670	9.8 ± 1.1	753	105
p,p'-DDT	23 ± 2		57.5	97
PBDE 28	1.9 ± 0.2		1.95	86
PBDE 47	173 ± 8	1.9 ± 0.1	68.3	93
PBDE 99	7.8 ± 0.9		14.5	76
PBDE 100	34.7 ± 1.7		11.9	70
PBDE 153	4.0 ± 0.6		3.8	100
PBDE 154	6.5 ± 0.2		8.3	122

Table 2. Comparison PBDEs and DDTs Concentrations between LPGC-MS/MS and ELISA Methods

	PBDE 47 equivalents, av ± SD (ng/g)		p,p'-DDE equivalents, av ± SD (ng/g)	
	calcd from LPGC-MS/MS data	measured by ELISA, (n = 4)	calcd from LPGC-MS/MS data	measured by ELISA, (n = 4)
croaker	181 ± 8	195 ± 28	10450 ± 670	6800 ± 2400
salmon	1.9 ± 0.1	2.1 ± 1.0	11 ± 1	9 ± 2
SRM 1947	82	89	786	560

to produce a dose−response curve, which is consistent with findings from a previous study.[21] Therefore, the fish extracts had to be evaporated to dryness and reconstituted in 50% aqueous MeOH solution prior to ELISA. When aqueous solutions containing <50% MeOH were tested, the amounts of measured contaminants were orders of magnitude lower compared to LPGC-MS/MS results, most likely because highly aqueous solutions failed to dissolve DDTs and PBDEs, which have rather high log K_{ow} values.

Comparison of LPGC-MS/MS and ELISA Results. The results of LPGC-MS/MS analyses of incurred PBDE congeners and DDT pesticides are presented in Table 1. PBDE 183 was not detected. Large amounts of PBDEs and DDTs in croaker tissues may be attributed to its origination to the Palos Verdes location, an EPA Superfund site.

To compare the results of PBDEs measured by both methods, equivalent amounts of PBDE 47 (analyte by which cross-reactivity in the ELISA is measured) were calculated from LPGC-MS/MS data. The cross-reactivity values for PBDE congeners 28, 47, 99, 100, and 153 were 0.15, 1, 0.9, 0.025, and 0.014, respectively.[10] Calculated PBDE 47 equivalents were 2.1 ng/g in salmon, 181 ng/g in croaker, and 82 ng/g in SRM 1947 (Table 2). Similarly, p,p'-DDE equivalents were calculated on the basis of cross-reactivity coefficients reported for its metabolites in the kit instructions. Concentrations were 10500, 11, and 786 ng/g p,p'-DDE equivalents for croaker, salmon, and SRM 1947, respectively, on the basis of concentrations measured by LPGC-MS/MS, as shown in Table 2. ELISA calibration curves ranged from 0.04 to 4 ng/g for PBDEs and from 0.625 to 25 ng/g for DDTs; thus, fish extracts prepared for ELISA underwent appropriate dilution factors to fall within the calibration curves.

The results by both methods agreed well (see Table 2) for the three types of fish and both contaminant groups, despite fundamental differences in the chemical nature of the analyses. ELISA is susceptible to altered responses due to indirect and direct matrix effects from chemicals in the extracts. PBDE 47 equivalent concentration calculated from LPGC-MS/MS data was 181 ng/g compared to 195 ng/g PBDE in croaker measured by ELISA. Croaker was the leanest fish with a lipid content of 3−4%. Repeatability, expressed in RSD for four replicates, was 14% for the PBDE assay, which was comparable to 3−15% RSDs for individual PBDE congeners measured by LPGC-MS/MS. DDT pesticides were measured at high concentrations in croaker samples. p,p'-DDE equivalent concentration measured by ELISA was 65% of the concentration measured by LPGC-MS/MS with RSD = 39%. In contrast, LPGC-MS/MS RSDs were 7−14% for individual DDT pesticides. For salmon, with 5−10% lipid content, the average of both techniques agreed within 11% for PBDEs (1.9 vs 2.1 ng/g) and 19% for DDTs (11 vs 9 ng/g), but the results were rather variable for the replicates. For SRM 1947, the results agreed within 9% (82 vs 89 ng/g) for PBDEs and within 29% for (786 vs 560 ng/g) for DDT pesticides.

To estimate the limit of detection by ELISA, average OD and standard deviation (SD) for salmon and croaker control samples (B_0) were calculated. $\%B/B_0$ corresponding to the LOD was calculated as previously described:[21] $\%B/B_{0\,LOD} = [B_0 - (3 \times SD)]/B_0$ (converted to ng/g using semilog calibration curves). LOD for both salmon and croaker was 1 ng/g PBDE equivalent. To compare this with LPGC-MS/MS, PBDE congeners 28, 47, 99, and 100 gave a method detection limit (MDL) of 1 ng/g each, whereas PBDEs 153 and 154 had MDL of 2 ng/g each. LODs for DDT pesticides calculated in the same manner yielded 0.4 ng/g p,p'-DDE equivalent in fish, which are quite similar to the MDLs for individual DDT pesticides measured by LPGC-MS/MS (0.5 ng/g). The LODs for each individual PBDE congener and DDT-type analyte are proportional to their cross-reactivities in ELISA. A significant advantage of the LPGC-MS/MS approach is the ability to identify and quantify each analyte individually.

Matrix Effects (MEs). It is well documented that coextractives from complex biological samples may cause MEs and inaccurate quantification in instrumental analysis,

DOI: 10.1021/jf505651g
J. Agric. Food Chem. 2015, 63, 4429−4434

including GC-MS.[22] However, MEs in ELISA are not as commonly characterized. A study on PBDEs in fish and comparison with GC-MS results suggested that higher concentrations of PBDEs in fish measured by ELISA in comparison to GC-MS may be explained by MEs.[10]

To compare the effect of coextracted matrix components for analysis of PBDEs and DDTs by ELISA, two sets of MM calibration standards (croaker and salmon) were prepared for each ELISA experiment. Figure 2 shows solvent-only (50% aqueous MeOH) and MM calibration curves for croaker and salmon in the PBDE ELISA. Both MM curves have similar slopes, which are different from the solvent-only calibration. Calculated MEs were −53 and −60% for salmon and croaker, respectively. These findings are similar to a study investigating MEs for microcystins in catfish with ELISA, in which −63% MEs were obtained.[21] This finding emphasizes a need for MM calibration in ELISA to obtain accurate results.

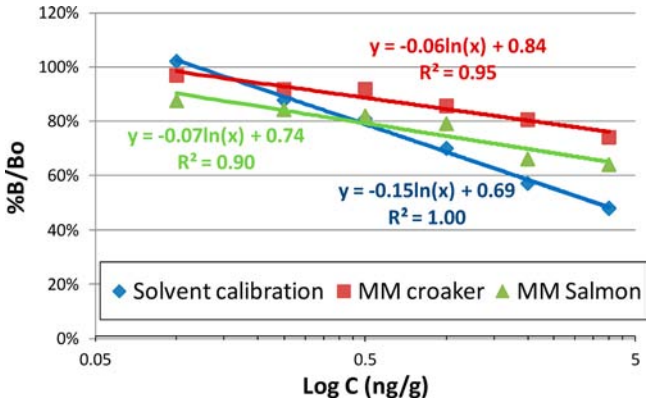

Figure 2. ELISA calibration curves for PBDE 47 in solvent only (50% aqueous MeOH) and matrix-matched (MM) fish extracts.

In the case of DDTs in ELISA, there was no difference for solvent versus MM calibration curves for croaker, nor in the case of salmon (Figure 3). Three calibration curves were identical, suggesting no direct/indirect interfering components in the extracts affecting the ELISA measurement for DDTs.

In conclusion, a simple and fast method for sample preparation of fish tissues previously developed for LPGC-MS/MS was evaluated for use in ELISAs of PBDEs and DDTs employing incurred fish with lipid content of 3−10%. In ELISA sample preparation, an additional solvent exchange step is needed prior to analysis. This method can be adopted in any typical laboratory and probably in the field. Matrix effects were estimated for croaker and salmon and were significant (up to −60%) in the PBDE ELISA, suggesting that MM calibration is essential for accurate quantification of PBDEs in fish extracts. Conversely, MEs in the DDTs assay were not observed. The method proved to work well for the three diverse fish matrices, and the results obtained by both measurement techniques were within reasonable agreement. Orthogonal confirmation is often required in many applications, and results of initial ELISA screening may be confirmed by the developed LPGC-MS/MS method using an alternative chemical mechanism.

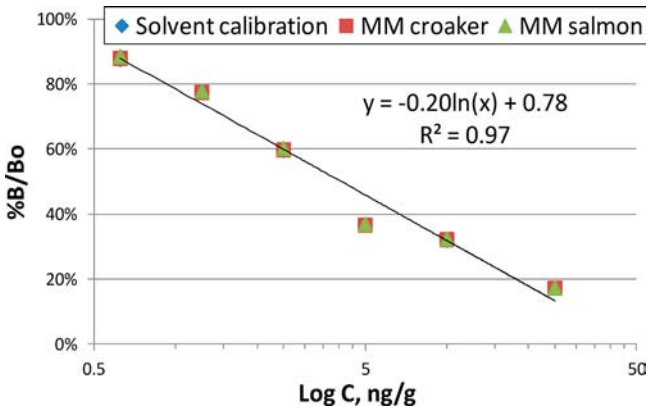

Figure 3. ELISA calibration curves for *p,p′*-DDE in solvent only (50% aqueous MeOH) and matrix-matched (MM) fish extracts.

AUTHOR INFORMATION

Corresponding Author

*(Y.S.) Phone: (215) 233-6655. Fax: (215) 233-6581. E-mail: yelena.sapozhnikova@ars.usda.gov.

Notes

Mention of brand or firm names does not constitute an endorsement by the U.S. Department of Agriculture above others of a similar nature not mentioned.

The authors declare no competing financial interest.

ACKNOWLEDGMENTS

We thank Rebecca Pugh, NIST Marine Environmental Specimen Bank in Charleston, SC, USA, for providing the croaker and salmon samples; Sam Ellis, Thomson Instrument Co., Oceanside, CA, USA, for the filter-vial d-SPE supplies, and Fernando Rubio, Abraxis, for providing ELISA kits for this study.

REFERENCES

(1) Birnbaum, L. S.; Staskal, D. F. Brominated flame retardants: cause for concern? *Environ. Health Perspect.* **2004**, *112*, 9−17.

(2) The Stockholm Convention on Persistent Organic Pollutants. United Nations Environmental Programme; http://chm.pops.int/Convention/tabid/54/Default.aspx (accessed Oct 31, 2014).

(3) Renner, R. Government Watch: In U.S., flame retardants will be voluntarily phased out. *Environ. Sci. Technol.* **2004**, *38*, 14A.

(4) Grier, J. W. Ban of DDT and subsequent recovery of reproduction in bald eagles. *Science* **1982**, *218*, 1232−1235.

(5) Hanberg, A. Toxicology of environmentally persistent chlorinated organic compounds. *Pure Appl. Chem.* **1996**, *68*, 1791−1799.

(6) Covaci, A.; Harrad, S.; Abdallah, M. A. E.; Ali, N.; Law, R. J.; Herzke, D.; de Wit, C. A. Novel brominated flame retardants: a review of their analysis, environmental fate and behaviour. *Environ. Int.* **2011**, *37*, 532−556.

(7) Sapozhnikova, Y. Evaluation of low-pressure gas chromatography-tandem mass spectrometry method for the analysis of >140 pesticides in fish. *J. Agric. Food Chem.* **2014**, *62*, 3684−3689.

(8) Shelver, W. L.; Keum, Y. S.; Kim, H. J.; Rutherford, D.; Hakk, H. H.; Bergman, A.; Li, Q. X. Hapten syntheses and antibody generation for the development of a polybrominated flame retardant ELISA. *J. Agric. Food Chem.* **2005**, *53*, 3840−3847.

(9) Stapleton, H. M.; Keller, J. M.; Schantz, M. M.; Kucklick, J. R.; Leigh, S. D.; Wise, S. A. Determination of polybrominated diphenyl ethers in environmental standard reference materials. *Anal. Bioanal. Chem.* **2007**, *387*, 2365−2379.

(10) Xu, T.; Cho, I. K.; Wang, D.; Rubio, F. M.; Shelver, W. L.; Gasc, A. M.; Li, J.; Li, Q. X. Suitability of a magnetic particle immunoassay for the analysis of PBDEs in Hawaiian euryhaline fish and crabs in comparison with gas chromatography/electron capture detection-ion trap mass spectrometry. *Environ. Pollut.* **2009**, *157*, 417−22.

(11) Shelver, W. L.; Parrotta, C. D.; Slawecki, R.; Li, Q. X.; Ikonomou, M. G.; Barcelo, D.; Lacorte, S.; Rubio, F. M. Development

DOI: 10.1021/jf505651g
J. Agric. Food Chem. 2015, 63, 4429−4434

of a magnetic particle immunoassay for polybrominated diphenyl ethers and application to environmental and food matrices. *Chemosphere* **2008**, *73*, S18−S23.
(12) Sapozhnikova, Y.; Lehotay, S. J. Evaluation of different parameters in the extraction of incurred pesticides and environmental contaminants in fish. *J. Agric. Food Chem.* **2015**, DOI: 10.1021/jf506256q.
(13) Sapozhnikova, Y.; Liebert, D.; Wirth, E.; Fulton, M. Polycyclic musk fragrances in sediments and shrimp tissues. *Polycyclic Aromat. Compd.* **2010**, *30*, 298−308.
(14) USDA National Nutrient Database for Standard Reference; http://ndb.nal.usda.gov.
(15) Han, L.; Sapozhnikova, Y.; Lehotay, S. J. Streamlined sample cleanup using combined dispersive solid-phase extraction and in-vial filtration for analysis of pesticides and environmental pollutants in shrimp. *Anal. Chim. Acta* **2014**, *827*, 40−46.
(16) Gonzalez-Curbelo, M. A.; Lehotay, S. J.; Hernandez-Borges, J.; Rodriguez-Delgado, M. A. Use of ammonium formate in QuEChERS for high-throughput analysis of pesticides in food by fast, low-pressure gas chromatography and liquid chromatography tandem mass spectrometry. *J. Chromatogr., A* **2014**, *1358*, 75−84.
(17) http://www.abraxiskits.com/wp-content/uploads/2014/03/PBDE-PL-Users-Guide.pdf (accessed Jan 22, 2015).
(18) http://www.abraxiskits.com/moreinfo/PN540041info.pdf (accessed Jan 22, 2015).
(19) Kalachova, K.; Pulkrabova, J.; Drabova, L.; Cajka, T.; Kocourek, V.; Hajslova, J. Simplified and rapid determination of polychlorinated biphenyls, polybrominated diphenyl ethers, and polycyclic aromatic hydrocarbons in fish and shrimps integrated into a single method. *Anal. Chim. Acta* **2011**, *707*, 84−91.
(20) Sapozhnikova, Y.; Zubcov, N.; Hungerford, S.; Roy, L. A.; Boicenco, N.; Zubcov, E.; Schlenk, D. Evaluation of pesticides and metals in fish of the Dniester River, Moldova. *Chemosphere* **2005**, *60*, 196−205.
(21) Geis-Asteggiante, L.; Lehotay, S. J.; Fortis, L. L.; Paoli, G.; Wijey, C.; Heinzen, H. Development and validation of a rapid method for microcystins in fish and comparing LC-MS/MS results with ELISA. *Anal. Bioanal. Chem.* **2011**, *401*, 2617−2630.
(22) Sapozhnikova, Y. Rapid sample preparation and fast GC-MS/MS for the analysis of pesticides and environmental contaminants in fish. *LCGC North Am.* **2014**, *32*, 878−886.

DOI: 10.1021/jf505651g
J. Agric. Food Chem. 2015, 63, 4429−4434

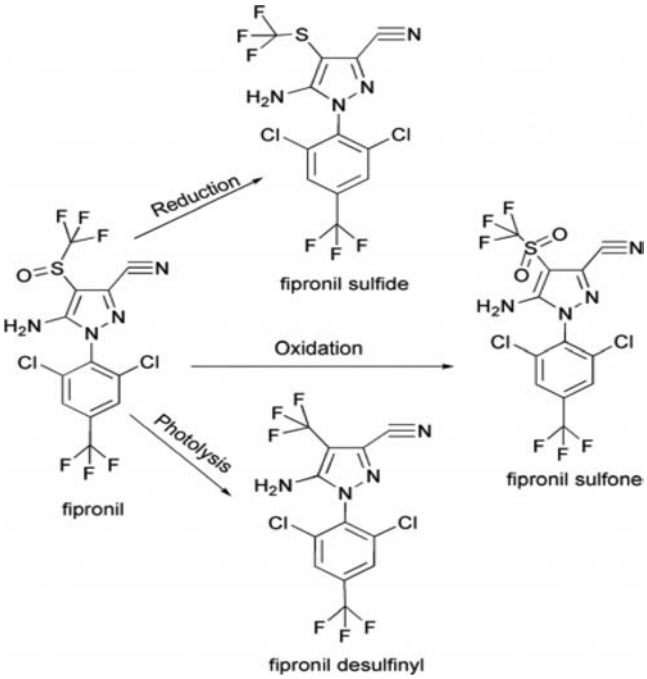

Figure 1. Degradation process of fipronil in the environment.[7]

peanut products and the environment. However, no studies are described in the literature about residue analysis and dissipation dynamics of fipronil and its metabolites in peanuts.

Due to the high toxicity and extensive use of fipronil in agriculture, a few scientific studies on the determination of fipronil in water, soil, and food samples have been reported. Fipronil was detected in soil and water samples by gas chromatography with mass spectrometric detection (GC-MS),[12] liquid chromatography (LC)−UV,[13] and GC with electron-capture detection (ECD).[14] Due to its toxicity to bees, there are also studies about its residue determination in honeybees, honey, and pollen samples by GC with nitrogen−phosphorus detection (NPD),[15] LC with tandem mass spectrometry (MS/MS),[16] GC-ECD/MS,[17] and LC-UV.[18] Methods to determine fipronil in cabbage,[19] tomato,[20] pepper, and Chinese cabbage[21] using GC-ECD were also reported.

Other papers describe the simultaneous determination of fipronil and its metabolites in environmental samples such as soil and water. In the study of Sunayana et al.,[22] soil samples were extracted using matrix solid-phase dispersion (MSPD) and analyzed by GC-MS. Dang et al.[23] detected paddy water samples by solid-phase extraction (SPE) and LC. Recently, the quick, easy, cheap, effective, rugged, and safe (QuEChERS) method was used for the determination of fipronil and its metabolites in cabbage, cauliflower, okra, tomato, grapes, and soil samples;[24] the samples were extracted with ethyl acetate and cleaned up by dispersive-SPE and then were quantified and identified by GC-MS.

A few papers appear concerning the residues and dissipation of fipronil and its metabolites in maize. Wang et al.[25] used a three-step method that consisted of liquid−solid extraction followed by liquid−liquid partitioning and florisil SPE for cleanup and, finally, detection with GC-ECD. Cheng et al.[26] applied the QuEChERS method for extraction and C_{18}, C_{18}/PSA, and PSA/GCB absorbents for cleanup for soil, maize grain, and straw, respectively; samples were detected by ultrahigh-performance (UHP)LC-MS/MS. There are other reports involving the residues and dissipation of fipronil and its metabolites on sugar cane leaves and juice[27] and grape leaves and berries,[28] but the methods used were time-consuming and solvent-intensive.

Because no paper has yet reported on the dissipation and residues of fipronil and its three metabolites (fipronil-sulfone, fipronil-sulfide, and fipronil-desulfinyl) in peanut, the overall aim of this project was to establish a simple and effective residue analysis method for fipronil and its three metabolites in peanut matrices and soil and then to investigate the dissipation trend and final residue levels in peanut plant and soil under field conditions.

MATERIALS AND METHODS

Chemicals and Standards. The fipronil (98.5%), fipronil-sulfone (99%), fipronil-sulfide (99.5%), and fipronil-desulfinyl (10 mg/L) standards were purchased from Dr. Ehrenstorfer GmbH Company (Augsburg, Germany), and the formulation (seed treatment microcapsule suspension containing 3% fipronil) was obtained from Beijing Yanhua Yongle Pesticide Ltd. (Beijing, China). High-performance (HP)LC-grade acetonitrile was supplied by Fisher Scientific (Pittsburgh, PA, USA). Ultrapure water was obtained from Aquapro Ultrapure Water System (Chongqing, China). Analytical grade NaCl and Cleanert florisil were purchased from the Beijing Reagent Co. (Beijing, China). PSA (primary−secondary amine), GCB (graphitized carbon black), C_{18}, and MWCNT (multiple-walled carbon nanotubes) were purchased from Agela Ltd. (Tianjin, China).

Fipronil, fipronil-sulfone, and fipronil-sulfide stock standard solutions of 1000 mg/L were prepared in acetonitrile, and the working standard solutions required for fortification and quantification were prepared from stock solution by dilution with acetonitrile. All standard solutions were stored at −20 °C before use. The stability of the four compounds in acetonitrile was reported to be stable at −20 °C for >15 months.[29]

Field Experiments. In normal agricultural practice, a 3% fipronil seed dressing formulation was recommended to be used on peanuts at a ratio of 1:50 (formulation weight/seed weight). In this study, field experiments (including the dissipation and terminal residue experiments) were conducted in 2012−2013 at three places that have different climate conditions, namely, Hebei province (in northern China, 116.51 E, 39.32 N), Hubei province (southern China, 113.45 E, 30.36 N), and Shandong province (eastern China, 117.07 E, 36.68 N). Each treatment field consisted of three replicate plots, and each plot had an area of 30 m^2 and was separated by irrigation channels. The organic matter contents of soil at Hebei, Hubei, and Shandong province were 15.7, 16.7, and 15.8 g/kg, and the pH values were 5.8, 6.2, and 7.5, respectively.

For the dissipation experiments, the peanut seeds were mixed evenly with fipronil formulation before sowing. To get the residue data during the growing process of the peanut seedlings, the treatment dosage was set as 1:25 (formulation weight/seed weight), which was 2 times the recommended dosage. When the peanut seedling reached 10−15 cm, the peanut seedling samples (about 1 kg) were randomly collected at 0, 1, 3, 5, 7, 14, 21, 28, 35, and 40 days (the first day of the sample collection was recorded as day 0). All collected samples were stored in a freezer at −20 °C until analysis.

To investigate the residue levels of the target pesticides in harvested peanut products, the terminal residue experiments were performed at the 1:50 recommended dosage as well as a higher dosage of 1:33 (1.5 times of the recommended dosage). The growth season of peanut was about 100−150 days (from June to October) at the experimental sites. At harvest time, samples of peanut, peanut shell, peanut straw, and soil (all about 1 kg) were randomly collected from each plot. Then the samples were shattered and analyzed to get the final residue data.

For the purpose of getting the dissipation curves of fipronil and its metabolites in soil, an experiment was applied in loam soil (organic matter content of 2.2%) with different pH values of acidic (pH 5), neutral (pH 7), and alkaline (pH 8) conditions. The soil samples were

DOI: 10.1021/jf5054589
J. Agric. Food Chem. 2015, 63, 4435−4443

Table 1. Parameters for Analysis of Fipronil and Its Metabolites

analyte	retention time (min)	qualitative ion transition (m/z)	quantification ion transition (m/z)	fragmentor (V)	collision energy (V)
fipronil	0.64	435/330	435/330	120	8
		435/250			25
fipronil-sulfide	0.67	419/382	419/382	130	8
		419/314			15
fipronil-sulfone	0.66	451/415	451/415	130	8
		451/282			25
fipronil-desulfinyl	0.64	387/350	387/350	100	8
		387/282			25

treated with fipronil standard solution to yield the concentration of 1.5 mg/kg. Then, the individually mixed samples (100 g in each container) were exposed to natural sunlight and were watered every day to keep the water content relatively constant at ≈15% in the soil. Then, the soil sample boxes were randomly collected at 0, 1, 3, 5, 7, 14, 21, 35, and 60 days. All collected samples were stored in a freezer at −20 °C until analysis.

Sample Preparation. Harvested peanut samples were separated into peanut kernels and peanut shell and were comminuted with an IKA (Staufen, Germany) grinder. Peanut seedling and peanut straw were also comminuted in the same way before analysis. All samples (including soil) were placed in polyethylene bags and stored at −20 °C until analyzed.

Samples (10 g of soil, 5 g of peanut kernels, 5 g of peanut shell, 5 g of peanut straw, 5 g of peanut seedling) were put into 50 mL centrifuge tubes, and then 5 mL of aqueous solution of formic acid (0.1%) and 20 mL of acetonitrile were added (except 10 mL of acetonitrile for soil samples). After the tubes were vortexed for 2 min, NaCl (3 g) was put into each tube. Then, the samples were vortexed again for 1 min and centrifuged at 3800 rpm (2260 rcf) for 5 min.

For the peanut straw samples, the extract (supernatant) was filtered through a 0.22 μm nylon filter into an autosampler vial for LC-MS/MS analysis. For the other samples (soil, peanut kernel, shell, and seedling), 1 mL of extract was transferred into a 2 mL centrifuge tube with 50 mg of PSA, and the tube was vortexed for 1 min. Afterward, each tube was centrifuged at 10000 rpm (4472 rcf) for 1 min, and the extract was filtered through a 0.22 μm nylon filter into an autosampler vial for LC-MS/MS analysis.

Analytical Procedure. All samples were detected with an Agilent 1200 HPLC and an Agilent 6410 B triple-quadrupole MS/MS. The separation was performed using a reverse-phase C_{18} HPLC column (50 mm × 2.1 mm × 3.5 μm particle size), which contains a dense monolayer of dimethyl-*n*-octadecylsilane stationary phase and an ultra-high purity ZORBAX Rx-SIL porous silica support. The mobile phase was isocratic and consisted of acetonitrile/water (90:10 by volume, containing 0.1% formic acid), with a flow rate of 0.3 mL/min. The MS/MS system gas was nitrogen at a constant flow of 8.0 L/min, and the source temperature was 350 °C. The nebulizer was 35.0 psi, and the injection volume was set at 5 μL.

The spectral acquisition was conducted using the mode of negative electrospray ionization for all four analytes, and multiple reaction monitoring (MRM) was utilized. The data acquisition parameters are listed in Table 1.

Statistical Analysis. The dissipation curves of fipronil were analyzed using nonlinear regression with Microsoft Excel software. The degradation kinetics followed first-order kinetics, $C = C_0e^{-kt}$, where C is chemical concentration (mg/kg) at time t (days), C_0 is initial concentration (mg/kg), and k is the first-order rate constant (day^{-1}) independent of C and C_0. The correlation coefficient (R^2) is used to represent the congruence between the data and the first-order dynamic equation. The dissipation of those compounds has been generally expressed in terms of DT_{50}, that is, the time after which 50% of the pesticide has disappeared, which can be calculated using Hoskins formula ($DT_{50} = (\ln 2)/k$). In this work, the curves from the simulation experiment on soil were fit to the best-fit first-order kinetics equation, but the curves for peanut seedling did not fit to the first-order kinetics very well, so the DT_{50} in seedling was estimated by measuring the time when fipronil degraded to half of the initial concentration. The terminal residue level was the total residues (the sum of fipronil, fipronil-desulfinyl, fipronil-sulfone, and fipronil-sulfide, expressed as fipronil), and the highest total residues (HR) in each matrix were calculated, which could be used for the dietary intake risk assessment of fipronil in peanut.[29]

RESULTS AND DISCUSSION

Optimization of the LC-MS/MS Conditions. GC analysis with various detectors (ECD, NPD, MS, and MS/MS) are usually used for the detection of fipronil and its metabolites. However, the analysis time in GC is normally longer than in LC methods. In this study, LC-MS/MS detection parameters for the four compounds were investigated, and sensitive responses were achieved using negative electrospray ionization (ESI−) mode. Mobile phases with different proportions of acetonitrile/water containing 0.1% formic acid were compared to obtain optimal instrument response, better peak shapes, and satisfactory separation efficiency. When the mobile phase was isocratic and consisted of acetonitrile/water (90:10 by volume, containing 0.1% formic acid), with a flow rate of 0.3 mL/min, we obtained optimal responses and peak shapes.

MS/MS conditions of the four target compounds were first optimized in both positive and negative ESI modes. The ionization efficiency was obviously higher in ESI− than in ESI+ for the analytes. Two product ions with the highest sensitivity and optimal selectivity were selected for each compound for establishment of the multiple reaction monitoring (MRM) parameters. The ion with higher response was used for quantification, whereas the less intense one as well as the retention time were used for qualification. The optimal MRM parameters including precursor ions, cone energies, product ions, and collision energies are shown in Table 1.

Development of the Residue Analysis Methods. Taking advantage of the high selectivity and sensitivity of the LC-MS/MS detection, we applied and modified the QuEChERS method[30] for sample preparation. Acidic aqueous acetonitrile was used as the extraction solvent, and the recoveries of 66−116% were satisfactory at four spiking levels for all of the matrices.

As a fast and efficient cleanup procedure in the QuEChERS method, dispersive SPE was also used in this study. Different sorbents such as 50 mg of florisil, 50 mg of PSA, 30 mg of GCB, 50 mg of C18, and 15 mg of multiwalled carbon nanotubes (MWCNT) were compared in the dispersive SPE

DOI: 10.1021/jf5054589
J. Agric. Food Chem. 2015, 63, 4435−4443

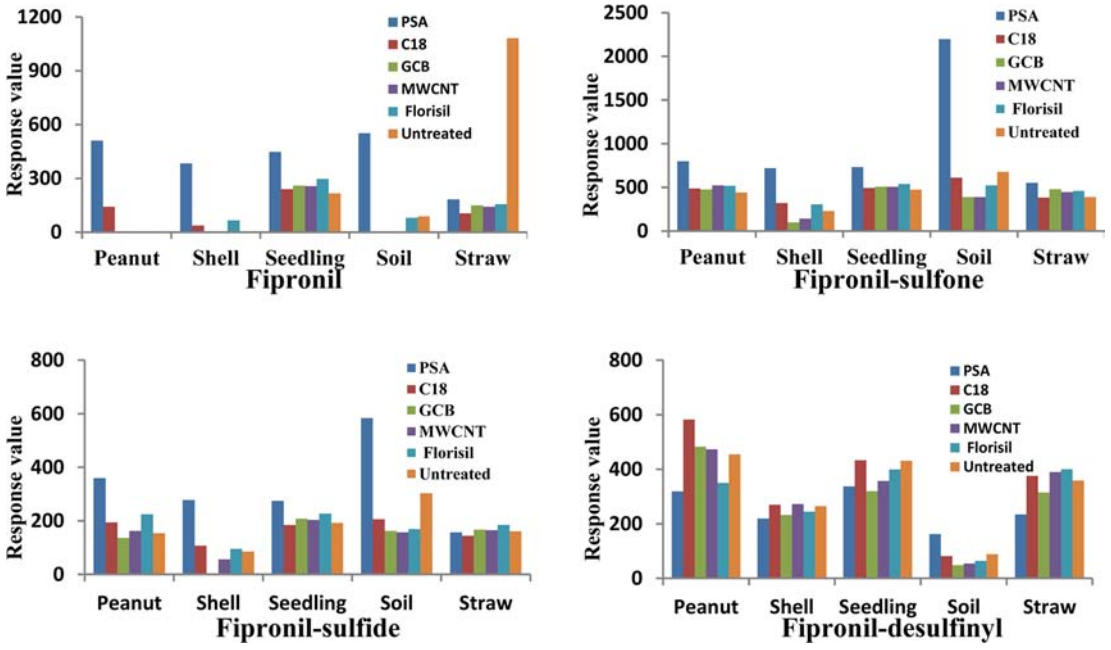

Figure 2. Response (peak area) of the four compounds in the peanut matrices and soil.

Table 2. Recoveries of Fipronil and Its Metabolites in Peanut and Soil Samples

		av[a] recovery ± SD (%)			
matrix	fortification level (mg/kg)	fipronil	fipronil-sulfone	fipronil-sulfide	fipronil-desulfinyl
peanut kernels	0.001	66 ± 8	92 ± 5	92 ± 15	106 ± 9
	0.005	89 ± 3	97 ± 4	98 ± 5	96 ± 4
	0.01	90 ± 2	96 ± 3	96 ± 3	87 ± 3
	0.1	92 ± 4	91 ± 4	91 ± 4	95 ± 2
peanut shell	0.001	77 ± 8	94 ± 3	87 ± 4	98 ± 9
	0.005	98 ± 6	107 ± 3	100 ± 4	76 ± 3
	0.01	95 ± 2	100 ± 6	105 ± 4	76 ± 6
	0.1	96 ± 9	100 ± 8	97 ± 7	96 ± 7
peanut seedling	0.001	67 ± 14	71 ± 7	68 ± 9	88 ± 6
	0.005	102 ± 5	98 ± 3	103 ± 1	99 ± 5
	0.01	100 ± 1	98 ± 1	101 ± 1	101 ± 1
	0.1	99 ± 5	99 ± 5	100 ± 5	98 ± 6
peanut straw	0.001	74 ± 19	78 ± 10	89 ± 3	102 ± 2
	0.005	115 ± 3	101 ± 4	112 ± 5	116 ± 3
	0.01	98 ± 4	97 ± 2	98 ± 3	102 ± 6
	0.1	98 ± 4	93 ± 3	100 ± 3	99 ± 4
soil	0.001	77 ± 9	88 ± 13	91 ± 11	101 ± 4
	0.005	101 ± 2	100 ± 1	91 ± 6	101 ± 6
	0.01	98 ± 4	97 ± 4	103 ± 1	99 ± 1
	0.1	99 ± 3	103 ± 3	99 ± 2	98 ± 3

[a]Average of five replicates.

procedure at a spiking level of 0.01 mg/kg. Although the recoveries were consistent when the different sorbents were used, different response levels (peak areas) were obtained. The responses of the target compounds cleaned up by different sorbents are shown in Figure 2. From the histogram, we can observe that PSA achieved the highest response in most cases, except for fipronil-desulfinyl and fipronil in peanut straw. For peanut straw samples, there was no significant difference between the five sorbents and no-cleanup samples, except that fipronil got a much higher response without cleanup. To get high sensitivity for fipronil, no cleanup was chosen for the peanut straw samples. For the other four matrices (peanut kernel, shell, seedling, and soil), although PSA did not get the highest response for fipronil-desulfinyl, it achieved the best responses for the other three compounds, so PSA was chosen

DOI: 10.1021/jf5054589
J. Agric. Food Chem. 2015, 63, 4435−4443

as the cleanup sorbent for the determination of the four compounds in the four matrices.

MWCNTs constitute a new carbon-based nanomaterial that has been widely used in the analysis of metals, veterinary drugs, and other pollutants.[31] However, the performance of MWCNTs in this study was not outstanding (almost the same as GCB) and did not improve the response of fipronil and its metabolites.

Method Validation. To evaluate the repeatability and trueness of the method, the fortification experiment was carried out at levels of 0.001, 0.005, 0.01, and 0.1 mg/kg with five replicates at each level. Recovery and precision tests were performed by spiking the standard solutions into the noncontaminated samples. After being set aside for 30 min at room temperature, the samples were analyzed as described under Sample Preparation. The fortification recoveries were calculated by using the equation

$$\%R = [\text{residue found } (\mu g/g)/\text{added concn } (\mu g/g)] \times 100\%$$

All quantitative analyses were conducted using matrix-matched calibration curves. The recoveries are listed in Table 2, and the data show that the average recoveries of fipronil and its three metabolites in all five matrices (peanut kernel, shell, straw, seedling, and soil) range from 66−116% with relative standard deviations (RSDs) of 1−19%, which illustrates that the proposed method meets typical validation requirements for pesticide residue analysis.[32]

For the LC-MS/MS analysis, the presence of matrix components may result in a matrix-induced enhancement or suppression effect. With the aim of evaluating the matrix effects of the method, both reagent-only and matrix-matched calibration curves were produced. The calibration curves were linear in the concentration range of 0.001−0.5 mg/kg for the four compounds in different peanut matrices with correlation coefficient above 0.99. The matrix effect was evaluated by the equation:

$$\%ME = [(\text{slope of matrix-matched calibration curve} - \text{slope of reagent-only calibration curve}) / \text{slope of reagent-only calibration curve}] \times 100\%$$

If the %ME fell in the range of ±10%, the matrix effect was considered negligible.[33] As shown in Table 3, the %ME data are

Table 3. Matrix Effect (%ME) of the Different Matrices in LC-MS/MS Analysis

compound	peanut	shell	seedling	straw	soil
fipronil	−86	−84	−91	−92	−95
fipronil-sulfone	−71	−73	−88	−81	−80
fipronil-sulfide	−91	−91	−95	−96	−96
fipronil-desulfinyl	−96	−86	−98	−98	−97

in the range from −98 to −71%, which indicates a strong matrix suppression for the four compounds in the five matrices, without noticeable difference among the peanut matrices. Consequently, matrix-matched calibration standards were necessary for accurate quantification of fipronil and its metabolites in all samples in this study.

The limits of detection (LODs) were calculated at 3 times the signal/noise ratio at the retention time of the peak of interest, and the limit of quantification (LOQ) was taken as the minimum concentration of a substance that can be quantitatively measured in the specific matrix with acceptable precision. The LOD of fipronil and its three metabolites was 0.3 ng/g, and the LOQ of these four compounds was 0.001 mg/kg in all matrices.

Residue Dynamics of Fipronil and Its Metabolites in Soil. The fipronil active ingredient in the seed dressing formulation was poorly mobile in soil, and at the end of the cultivation period, it was mostly concentrated in the soil layer close to the seed.[3] Due to the unique application approach, we did not get the normal dissipation curve in soil under field conditions. There are many factors influencing the degradation fate of fipronil in soil, such as mineral clay content[34] and organic matter.[35] Understanding how pH influences the dissipation of fipronil in the soil is important for ensuring the safe use of fipronil. Therefore, the degradation dynamics of fipronil in soil of different pH values were investigated in a simulation experiment in the laboratory.

The dissipation trends of fipronil and its metabolites in acidic, neutral, and alkaline soil are illustrated in Figure 3. The dissipation curves show that the degradation of fipronil in soil

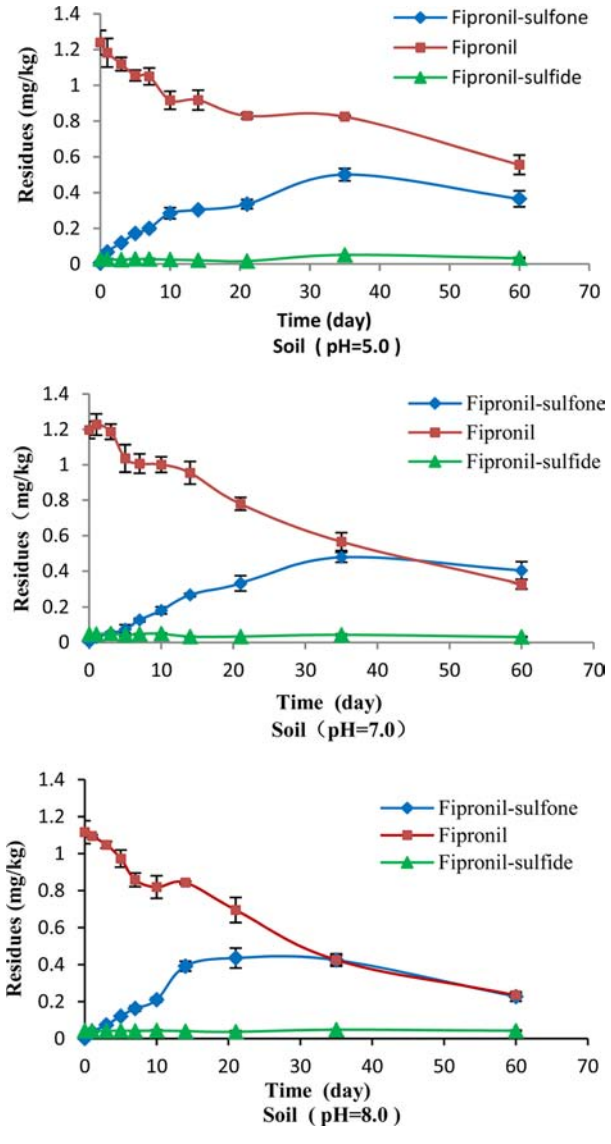

Figure 3. Dissipation curves of fipronil and its metabolites in soils of different pH values.

DOI: 10.1021/jf5054589
J. Agric. Food Chem. 2015, 63, 4435−4443

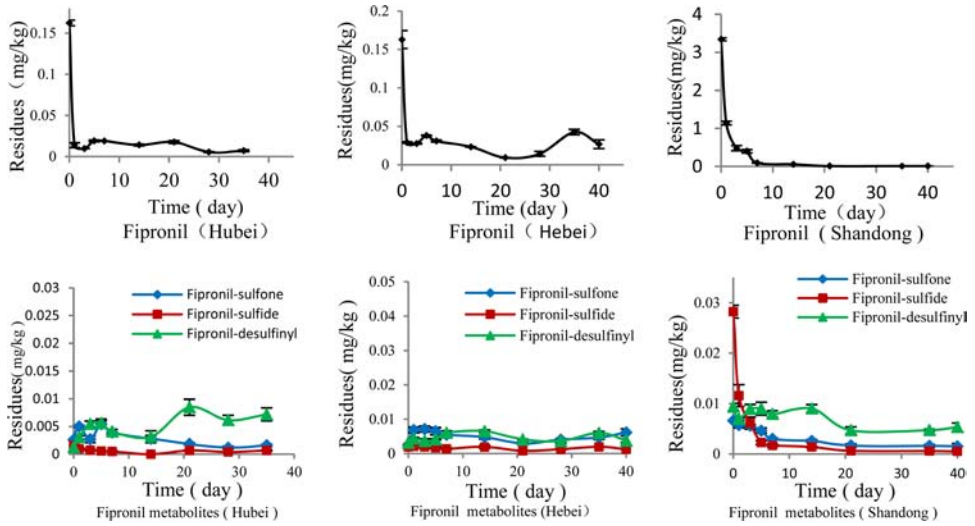

Figure 4. Dissipation curves of fipronil and its metabolites in peanut seedling at each trial site.

under different pH values (5, 7, 8) had a similar tendency. The residue of the parent fipronil gradually decreased, whereas the concentration of fipronil-sulfone increased gradually at first and then decreased over time. Fipronil-sulfide was also detected, but remained at a very low concentration (<0.04 mg/kg) during the entire dissipation process. Almost no photolysis product (fipronil-desulfinyl) was detected in the experiment, which was likely due to the total absence of light in the soil compartment. Therefore, the presence of fipronil-sulfone in a significantly higher amount compared to the other metabolites clearly demonstrates that the oxidation process played the major role in the metabolism of fipronil in the soil.

Considering the first-order kinetics equations, the half-lives of fipronil in acidic, neutral, and alkaline soils were calculated as 57, 32, and 27 days, respectively, which indicated that fipronil dissipated more rapidly in alkaline than in acidic soil. The degradation of fipronil in soil was also studied by Zhu et al.,[36] who found that the half-lives of fipronil in nonsterile clay loam soil were 9.7 and 8.8 days at 25 and 35 °C, respectively, whereas they were 3 times longer (about 33 days) in sterile soil. This means that microbial degradation had a significant influence on the half-life of fipronil in soil. In our work, the soil was almost sterile due to the pretreatment with acid or alkaline solutions, which might be the main reason for the relatively long half-lives of fipronil in the soil.

Dissipation of Fipronil in Peanut Seedling. The dissipation curves of fipronil and its metabolites in peanut seedling in Hebei, Hubei, and Shandong are illustrated in Figure 4. The dissipation curves show that fipronil dissipated rapidly in peanut seedling with estimated half-lives of <1 day at all three sites. The residues of fipronil dropped quickly and were <0.05 mg/kg in about 1−5 days. However, fipronil was still the highest residue compound versus the metabolites during all stages of dissipation.

From the dissipation curves of the three metabolites in peanut seedling (Figure 4), all three metabolites were detected during the dissipation of fipronil, although the concentrations were very low (all <0.01 mg/kg). Among the three metabolites, fipronil-desulfinyl had the highest concentration overall, especially at Hubei and Shandong, and fipronil-sulfide had the lowest. Fipronil-desulfinyl was found to be the major photodegradation product after the application of fipronil to corn, pea, and pear crops and, thus, is proposed to be the primary persistent residue on foliage-treated crops.[8] In our work, although peanut was treated with seed-dressing formulation, photolysis was also the relatively main degradation route in peanut crop other than oxidation and reduction.

Terminal Residue Analysis. After the peanut seeds were treated with the seed-dressing formulation at two dosages (1:50 and 1:33 formulation/seeds, in weight), the peanut and soil samples were collected at harvest time. Table S1 (see the Supporting Information) lists the terminal residue data of fipronil and its three metabolites in the harvested peanut and soil samples. For the purpose of dietary intake risk assessment, the total residue (the sum of fipronil and its three metabolites, expressed as fipronil) was calculated, and the total residue ranges are listed in Table 4. The results show that the final total residues in peanut shell and straw were relatively high, with the highest total residues of 0.99 and 0.30 mg/kg, respectively, whereas the residues were much lower in peanut kernels (<0.02 mg/kg) and in soil (0.003−0.15 mg/kg).

Table 4. Final Total Residues of Fipronil in Harvested Peanut and Soil Samples

	final residue (mg/kg)		
matrix	low dosage	high dosage	final total residue (mg/kg)
peanut kernel	0.003−0.014	0.003−0.020	0.003−0.020[a]
peanut shell	0.009−0.91	0.011−0.99	0.009−0.99[a]
peanut straw	0.061−0.30	0.055−0.20	0.055−0.30[a]
soil	0.014−0.15	ND[b]−0.011	0.003−0.15[a]

[a]Highest residue (HR) data. [b]ND means <0.0005 mg/kg.

The residues of the high-application experiment were a little higher than in the low-application experiment for peanut kernels and shells. Residues of the low-dosage experiment were even higher than in the high-dosage experiment in peanut straw and soil, which is likely due to the inhomogeneous distribution of the seed-dressing formulation in soil.

To demonstrate the residue distribution of fipronil and its three metabolites in harvested peanut samples, the final residues (see Table S1) are illustrated in Figure 5. In general, the parent compound fipronil had the highest residues in

DOI: 10.1021/jf5054589
J. Agric. Food Chem. 2015, 63, 4435−4443

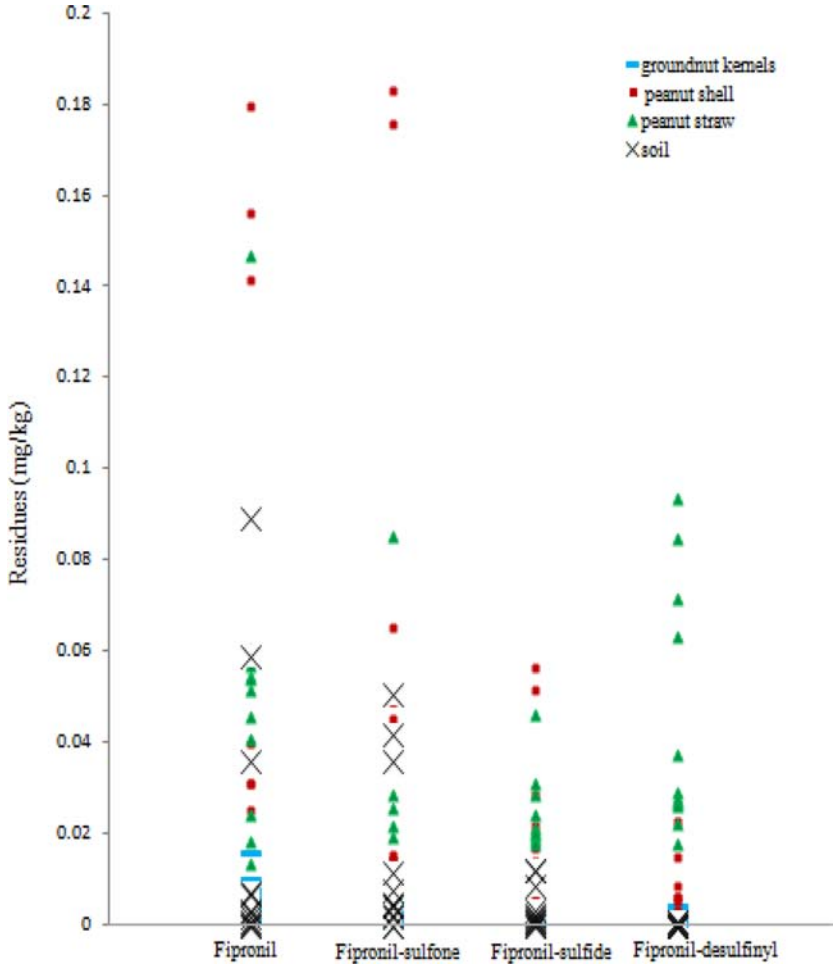

Figure 5. Distribution of the final residue data of fipronil and metabolites.

almost all four matrices (peanut kernel, shell, straw, and soil), whereas the residues of the three metabolites were a little different. The oxidation product (fipronil-sulfone) was the main metabolite found in peanut kernels, whereas in peanut straw, residue of photolysis metabolite (fipronil-desulfinyl) was the highest one and almost higher than fipronil. In the soil samples, fipronil-sulfone was also the highest, and there was also no detectable fipronil-desulfinyl in the terminal soil samples. This result is consistent with the residue distribution of the three metabolites in peanut seedling and soil in the dissipation experiment.

Until now, no MRL has been established for fipronil in peanut in other countries except for Japan, which set the MRL of fipronil in dried peanut as 0.01 mg/kg. Compared with the highest total residue data of 0.02 mg/kg in peanut kernels in our study, there would be some potential risks in the use of fipronil in peanut crops. However, the dietary intake risk assessment of fipronil leads to an acceptable daily intake (ADI) of fipronil as 0.0002 mg/kg body weight.[37] In China, assuming that the average adult body weight is 60 kg, then the ADI of fipronil for each person is 0.012 mg (0.0002 mg/kg bw ×60 kg bw). According to the dietary guideline in China,[38] the dietary intake of nut (including peanut) is 0.0039 kg each day, and based on the highest total residue of 0.02 mg/kg fipronil in harvested peanut kernels, the dietary intake of fipronil for each person would be <0.000078 mg (0.0039 kg × 0.02 mg/kg). Therefore, compared with the ADI of 0.012 mg, the acute risk quotient of fipronil was only 0.65%. This result indicates that the recommend dosage of fipronil would be safe in peanut for human health. The terminal residue data provides a basic evaluation for the safe use of fipronil as a seed-dressing formulation in peanut crops.

In conclusion, a residue analysis method for the simultaneous determination of fipronil and its three metabolites in peanut kernel, shell, straw, seedling, and soil samples was established using a modified QuEChERS sample preparation and LC-MS/MS analysis. The method was simple and fast, and the recoveries and LOQs were satisfactory for all matrices tested. The results of experiments demonstrated that fipronil dissipated rapidly in peanut seedling with a half-life of <1 day and degraded slowly in soil with half-lives of 27−57 days depending on soil pH values. The simulation experiment showed that fipronil degraded more rapidly in alkaline than in acidic soil, and oxidation was the main degradation route in soil samples, whereas no photolysis product fipronil-desulfinyl was detected. The final residues at harvest peanut kernels were all <0.02 mg/kg, whereas in peanut shell and straw the total residues were up to 0.99 and 0.30 mg/kg, respectively. Among the three metabolites, fipronil-sulfone was the highest residue compound in peanut kernels and soil samples, whereas fipronil-desulfinyl was the highest in peanut straw. The residue distribution of the metabolites is consistent with the results in dissipation experiments, which means that the photolysis metabolite fipronil-desulfinyl and the oxidation product

DOI: 10.1021/jf5054589
J. Agric. Food Chem. 2015, 63, 4435−4443

fipronil-sulfone were the highest residue metabolites in peanut plant (seedling and straw) and soil samples, respectively. The final total residue data in peanut kernels were used to evaluate the dietary intake risk of fipronil in peanut consumption, and results showed that the acute risk quotient of fipronil was only 0.65%, which provides an evaluation for the safe use of fipronil as a seed-dressing formulation in peanut crops. The data would also be helpful for the establishment of MRLs of fipronil in peanut.

■ ASSOCIATED CONTENT

Supporting Information

Table S1. This material is available free of charge via the Internet at http://pubs.acs.org.

■ AUTHOR INFORMATION

Corresponding Author

*(L.H.) E-mail: hanlijun2000@163.com. Phone: 086-10-62733219. Fax: 086-10-62733620.

Funding

We acknowledge the National Natural Science Foundation of China (No. 21177155), and the National Instrumentation Program of China (No. 2013YQ510391) from the Chinese Ministry of Science and Technology for financial support.

Notes

The authors declare no competing financial interest.

■ ACKNOWLEDGMENTS

We are grateful to Yanjun Xu and Shuaigang Liu for their excellent technical assistance in laboratory experiments and field trials.

■ REFERENCES

(1) Tian, C. Y.; Guo, X. Y. Analysis of peanut production development and competitive in China. *Cereals Oil* **2004**, *4*, 41−43.

(2) Sun, F. W.; Zhang, Q.; Li, Z. F. Research progress on the comprehensive utilization of peanut hull. *Shandong For. Sci. Technol.* **2008**, *179* (6), 84−88.

(3) Turnblad, K. M.; Chen, Y. A. Insecticidal seed coating. US005849320A[P], 1998.

(4) Balanca, G.; Visscher, M. N. D. Effect of very low doses of fipronil on grasshoppers and non target insects following field trials for grasshopper control. *Crop Prot.* **1997**, *16*, 553−564.

(5) Margarido, T. C. S.; Felicio, A. A.; Rossa-Feres, D. D. C.; Almeida, E. A. D. Biochemical biomarkers in scinax fuscovarius tadpoles exposed to a commercial formulation of the pesticide fipronil. *Mar. Environ. Res.* **2013**, *91*, 61−67.

(6) Pesticide Action Network-UK (PAN). Active ingredient fact sheet: fipronil. *Pestic. News London* **2000**, *48*, 20−22.

(7) Tingle, C. C. D.; Rother, J. A.; Dewhurst, C. F.; Lauer, S.; King, W. J. Briefing AI 1. Pesticide Action Network UK, London, UK, 2000; http://www.pan-uk.org-.pan-uk.org/archive/Publications/Briefing/fipronil.pdf.

(8) Hainzl, D.; Cole, L. M.; Casida, J. E. Mechanisms for selective toxicity of fipronil insecticide and its sulfone metabolite and desulfinyl photoproduct. *Chem. Res. Toxicol.* **1998**, *11* (12), 1529−1535.

(9) Hainzl, D.; Casida, J. E. Fipronil insecticide: novel photochemical desulfinylation with retention of neurotoxicity. *Proc. Natl. Acad. Sci. U.S.A.* **1996**, *93*, 12764−12767.

(10) Gunasekara, A. S.; Truong, T.; Goh, K. S.; Spurlock, F.; Tjeerdema, R. S. Environmental fate and toxicology of fipronil. *J. Pestic. Sci.* **2007**, *32*, 189−199.

(11) The General Office of the Ministry of Agriculture of China. The Fourth Plenary Meeting of the Vetting Committee of the Eighth National Pesticide Registration, Beijing, China, 2008.

(12) Aajoud, A.; Ravanel, P.; Tissut, M. Fipronil metabolism and dissipation in a simplified aquatic ecosystem. *J. Agric. Food Chem.* **2003**, *51*, 1347−1352.

(13) Hadjmohammadi, M. R.; Nikou, S. M.; Kamel, K. Determination of fipronil residue in soil and water in the rice fields in north of Iran by RP-HPLC method. *Acta Chim. Slov.* **2006**, *53*, 517−520.

(14) Brennan, A. A.; Harwood, A. D.; You, J.; Landrum, P. F.; Lydy, M. J. Degradation of fipronil in anaerobic sediments and the effect on porewater concentrations. *Chemosphere* **2009**, *77*, 22−28.

(15) Morzycka, B. Simple method for the determination of trace levels of pesticides in honeybees using matrix solid-phase dispersion and gas chromatography. *J. Chromatogr., A* **2002**, *982* (2), 267−273.

(16) Kadar, A.; Faucon, J. P. Determination of traces of fipronil and its metabolites in pollen by liquid chromatography with electrospray ionization-tandem mass spectrometry. *J. Agric. Food Chem.* **2006**, *54* (26), 9741−9746.

(17) Jimenez, J. J.; Bernal, J. L.; Nozal, M.; Martin, M. T.; Mayo, R. J. Sample preparation methods to analyze fipronil in honey by gas chromatography with electron-capture and mass spectrometric detection. *J. Chromatogr., A* **2008**, *1187* (1/2), 40−45.

(18) Tomasini, D.; Sampaio, M. R. F.; Cardoso, L. V.; Caldas, S. S.; Primel, E. G. Comparison of dispersive liquid-liquid microextraction and the modified QuEChERS method for the determination of fipronil in honey by high performance liquid chromatography with diode-array detection. *Anal. Methods* **2011**, *3* (8), 1893−1900.

(19) Wu, F.; Zhang, H.; Liu, F.; Han, L.; Jiang, S. Dissipation of fipronil in cabbage and soil at different sites. *J. Agro-environ. Sci.* **2006**, *25*, 265−268.

(20) Cao, H.; Shi, Y.; Hua, T.; Tang, F.; Yue, Y. Study of analytical method of fipronil residue in tomato and soil. *J. Anhui Agric. Univ.* **2005**, *32* (1), 31−35.

(21) Cao, H.; Shi, Y.; Hua, R.; Tang, F.; Yue, Y. Study on analytical method on fipronil residue in pepper and Chinese cabbage. *Food Sci.* **2005**, *26* (9), 377−379.

(22) Sunayana, S.; Mamta, R.; Beena, K. Persistence of fipronil and its metabolites in soil under field conditions. *Environ. Monit. Assess.* **2014**, *186*, 69−75.

(23) Dang, Q. T.; Hirozumi, W.; Junghun, O. Effect of pH on the degradation of imidacloprid and fipronil in paddy water. *J. Pestic. Sci.* **2013**, *38* (4), 223−227.

(24) Mariappan, P.; Chandrasekaran, S. Determination of fipronil and its major metabolites in vegetables, fruit and soil using QuEChERS and gas chromatography-mass spectrometry. *Int. J. Environ. Anal. Chem.* **2013**, *93* (11), 1203−1211.

(25) Wang, T.; Hu, J.; Liu, C. Simultaneous determination of insecticide fipronil and its metabolites in maize and soil by gas chromatography with electron capture detection. *Environ. Monit. Assess.* **2014**, *186*, 2767−2774.

(26) Cheng, Y.; Dong, F.; Liu, X.; Xu, J.; Meng, W.; Liu, N.; Chen, Z.; Tao, Y.; Zheng, Y. Simultaneous determination of fipronil and its major metabolites in corn and soil by ultra-performance liquid chromatography-tandem mass spectrometry. *Anal. Methods* **2014**, *6*, 1788−1795.

(27) Kousik, M.; Balwinder, S. Persistence and metabolism of fipronil in sugarcane leaves and juice. *Bull. Environ. Contam. Toxicol.* **2014**, *92*, 220−224.

(28) Mohapatra, S.; Deepa, M.; Jagdish, G. K.; Rashmi, N.; Kumar, S.; Prakash, G. S. Fate of fipronil and its metabolites in/on grape leaves, berries and soil under semi arid tropical climatic conditions. *Bull. Environ. Contam. Toxicol.* **2010**, *84*, 587−591.

(29) Pesticide residues in food. Evaluation of the 2001 Joint Meeting of the FAO Committee on Pesticides in Agriculture and the WHO Expert Committee on Pesticide Residues, Geneva, Switzerland, 2001.

(30) Lehotay, S. J. Determination of pesticide residues in foods by acetonitrile extraction and partitioning with magnesium sulfate: collaborative study. *J. AOAC Int.* **2007**, *90*, 485−520.

(31) Zhao, P.; Huang, B.; Han, Y.; Zhou, N.; Gu, K.; Li, X.; Pan, C. Rapid multi-plug filtration cleanup with multiple-walled carbon nanotubes and gas chromatography-triple-quadrupole mass spectrom-

DOI: 10.1021/jf5054589
J. Agric. Food Chem. 2015, 63, 4435−4443

etry detection for 186 pesticide residues in tomato and tomato products. *J. Agric. Food Chem.* **2014**, *62*, 3710−3725.
(32) European Commission Directorate General Health and Consumer Protection, Guidance Document on Method Validation and Quality Control Procedures for Pesticide Residues Analyses in Food and Feed, SANCO/12571/2013, 01.01.2014; http://ec.europa.eu/food/plant/pesticides/guidance_documents/docs/qualcontrol_en.pdf.
(33) Li, M.; Liu, X.; Dong, F.; Xu, J.; Kong, Z.; Li, Y.; Zheng, Y. Simultaneous determination of cyflumetofen and its main metabolite residues in samples of plant and animal origin using multi-walled carbon nanotubes in dispersive solid-phase extraction and ultrahigh performance liquid chromatography-tandem mass spectrometry. *J. Chromatogr., A* **2013**, *1300*, 95−103.
(34) Sanchez-Martin, M. J.; Sanchez-Camazano, M. Relationship between the structure of organophosphorus pesticides and adsorption by soil components. *Soil Sci.* **1991**, *152* (4), 283−288.
(35) Bobe, A.; Coste, C. M.; Cooper, J. F. Factors influencing the adsorption of fipronil on soil. *J. Agric. Food Chem.* **1997**, *45*, 4861−4865.
(36) Zhu, G.; Wu, H.; Guo, J.; Kimaro, F. M. E. Microbial degradation of fipronil in clay loam soils. *Water, Air Soil Pollut.* **2004**, *153*, 35−44.
(37) GB/T 2763-2014. Maximum residue limits for pesticides in food, National Food Safety Standard of China.
(38) Keyou, G.; Jia, J. B.; Liu, H. Food-based dietary guidelines in China practices and problems. *Ann. Nutr. Metab.* **2007**, *51*, 26−31.

DOI: 10.1021/jf5054589
J. Agric. Food Chem. 2015, 63, 4435−4443

Table 1. Treatments Performed in the Trial

control (C)	without application of agrochemicals
glyphosate (GL)	3 L ha^{-1} of glyphosate, commercial product
phosphorus (P)	100 kg ha^{-1} of calcium triple superphosphate
phosphorus + glyphosate (P+GL)	100 kg ha^{-1} of calcium triple superphosphate + 3 L ha^{-1} of glyphosate, commercial product

Table 2. Rainfall Simulation Dates

1 (Nov 7, 2012)	24 h after application
2 (Nov 11, 2012)	5 days after application
3 (Nov 14, 2012)	8 days after application

(phosphonomethyl)glycine potassium salt), 66.2 g, + inert ingredients and adjuvants, csp 100 cm^3) and phosphate fertilizers (calcium triple superphosphate, dissolved in distilled water; composition: 0−46−0, with 14% of calcium) were applied with manual spraying over the ground and without incorporation. Although glyphosate as foliar systemic herbicide in normal use is not applied on the soil, in this experiment we tried to generate conditions to analyze directly the interaction with P in the soil surface, avoiding crop canopy and residue interception by removing them before starting the treatment. The trial plots were preserved with nylon until the last simulation date to avoid possible variations in soil moisture.

Rainfall simulations at the field were performed using a small portable simulator designed by Irurtia and Mon.[17,18] The microsimulator consists of a metallic angle iron square prism. It is 1.5 m high and 0.25 m per side, holding clear acrylic walls that act as windbreaks (Figure 1). At the top there is a box holder with 49 plastic tubes that produce droplets. This box has a water feed from a reservoir placed in one of the edges of the structure. The reservoir is graduated in millimeters (laminar) of water applied to the microplots. In turn, the reservoir base can be varied in height, providing different pressures to form drops. The droplets formed have average diameters of approximately 4.7 mm. For a 1.5 m drop height the calculated kinetic energy of the microsimulator is 12.7 kJ m^{-2} m^{-1}, representing approximately 32.6% of the energy of natural rainfall.[18] In working position the device is attached to an iron frame, previously driven into the ground. This framework defines the microplot of 0.25 × 0.25 m where the measurements are made. The runoff is received through a funnel into a graduated (mm) container on one side of the bottom framework. With this device constant rainfall intensity is applied between 10 and 130 mm h^{-1} for each test site.

Measurements. Once the simulation process was initiated, sampling started when runoff began, collecting runoff water at the graduated reservoir at 5 min intervals, until constant runoff was verified, when three consecutive constant measurements were obtained (approximately 1 h), meaning that the basic infiltration rate was achieved. The total water volumes collected through the experience ranged from 1.5 to 2.5 L and were used to calculate infiltration and runoff rates. Samples were filtered and chemically analyzed for soluble phosphorus, glyphosate, and AMPA. The soluble phosphorus in the runoff water was determined using a colorimetric method.[19]

Glyphosate and AMPA Analyses.[20,21] Glyphosate (98%), AMPA (98%), glyphosate-FMOC (98.5%), AMPA-FMOC (97%), and isotopically labeled standards (ILS) [1,2-$^{13}C_2{}^{15}N$]glyphosate (98%) and [$^{13}C^{15}N$]AMPA were obtained from Dr. Ehrenstorfer (Augsburg, Germany). All other supplies used were of the best commercially available analytical grade.

Water sample aliquots of 3 mL, previously homogenized and filtered with 0.45 μm regenerated cellulose membrane filters, were placed in 15 mL Teflon centrifuge tubes and acidified with 6 M HCl to pH 1 (to maximize the dissociation of possible analyte−cation complexes). The samples were then spiked with internal standard (40 μL of ILS 1 mg L^{-1}) and neutralized to pH 6−7 with 6 M KOH. The derivatization

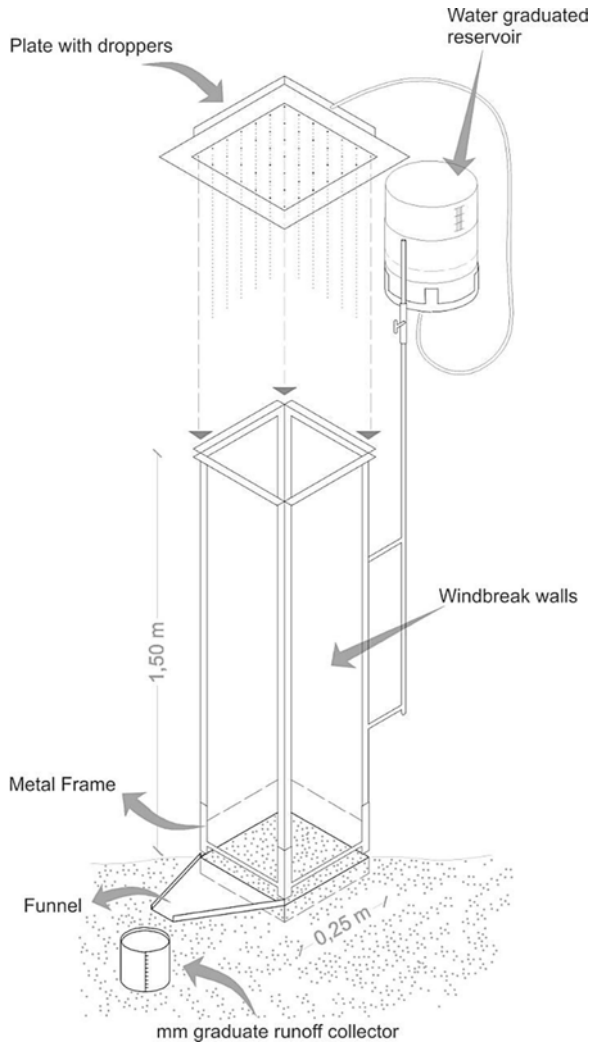

Figure 1. Scheme of portable rainfall simulator.

step was initiated with the addition of 0.5 mL of borate buffer (pH 9), FMOC-Cl (6 g L^{-1}), and acetonitrile. After overnight reaction at room temperature, the derivatization step was quenched by acidification to pH 3 with formic acid (FA).

After filtering with 0.45 μm regenerated cellulose filters, the derivatized extracts were passed through Oasis HLB (200 mg, Waters, Milford, MA, USA) cartridges. Cartridges were conditioned with 5 mL of MeOH, followed by 5 mL of 0.1% FA. Eluates were discarded, and the cartridges were washed with 3.5 mL of dichloromethane. The analytes were eluted with 9 mL of MeOH. The methanol aliquots were evaporated and reconstituted with the mobile phase (H_2O/MeCN 98:2 + 0.1% FA). Following 0.2 μm nylon syringe filtering, the extracts were ready for injection.

Liquid chromatography−tandem mass spectrometry (LC-MS/MS) analyses were performed using an Acquity UPLC liquid chromatograph (Waters) coupled to a triple-quadrupole mass spectrometer equipped with an ESI source (TQD, Waters Micromass, UK). Separations were performed at 40 °C using an Acquity UPLC HSS C18 column (1.8 μm particle size, 2.1 × 100 mm) at a flow rate of 0.35 mL min^{-1}. Standard and/or sample extract aliquots of 10 μL were introduced by means of an autosampler (Waters). The mobile phase consisted of H_2O/MeCN (98:2 + 0.1% FA; A1) and MeCN (+ 0.1% FA, B1), operated with a 10 min gradient run time.

Ionization was performed in positive-ion mode using nitrogen as the desolvation and cone gas at 600 and 15 L h^{-1}, respectively. A 1 kV capillary voltage was applied, and the source temperature was set at 140 °C. The desolvation temperature was 500 °C. Argon (1.32 × 10^{-5} mbar) was used at the collision cell to produce the respective ion

DOI: 10.1021/jf505533r
J. Agric. Food Chem. 2015, 63, 4444−4448

fragments, and acquisition was performed in MRM mode. The precursor and fragment m/z values for each specific compound, along with their respective cone voltages, collision energies, and dwell values, were optimized (Table 3). Chromatography and mass spectrometry data management was performed using MassLynx software v 4.1 (Waters).

Table 3. Optimized MS/MS Parameters for the FMOC Derivatives of Glyphosate, AMPA, and ILS

compound	precursor ion (m/z)	product ion[a] (m/z)	cone voltage (V)	collision energy (eV)
glyphosate-FMOC	392.0	Q 88.1	20	30
		q 214.1		10
AMPA-FMOC	334.0	Q 179.1	20	15
		q 112.1		20
GLI-1,2-[$^{13}C_2$,^{15}N]FMOC	395.0	Q 91.1	20	30
		q 217.1		10
AMPA-[^{13}C,^{15}]NFMOC	336.0	Q 114.1	20	15
		q 181.1		20

[a]Q, transition used for quantification; q, transition used for confirmation. Dwell time (s): 0.01.

The main parameters from our validation studies are shown in Table 4. Calibration curves from spiked nanopure water standards with concentration levels of 0.1, 0.5, 1, 10, 100, and 500 $\mu g\ L^{-1}$ were used for quantification purposes.[22]

Concentrations of glyphosate + AMPA ($\mu g\ L^{-1}$) and phosphorus (mg L^{-1}) were multiplied by the total volume of runoff water in 60 min to obtain the amount of glyphosate + AMPA and phosphorus lost in grams per hectare and kilograms per hectare, respectively.

Statistical Analyses. Data statistical analyses were realized through sampling variance and Tukey's test at a 5% significance level.[23]

RESULTS AND DISCUSSION

Runoff Analyses. The treatments applied had no influence on water dynamics. Thus, no significant differences were observed between either the runoff of different treatments or between the dates of simulation.

Phosphorus (P) in Runoff Water. *P Concentration.* The concentration of P in runoff water ranged between 0.3 and 5.9 mg L^{-1}. These values are similar to those obtained in runoff plots in fallow periods of a no-till Aquic Argiudoll.[24] Statistical analysis indicated that no significant interaction between treatment and date ($p < 0.05$) was observed, but significant differences between treatments and simulation dates were observed.

On the first simulation date, the P concentration in water was higher than and different from the third date (Table 5), indicating that nearby rainfall 1 day after the application of fertilizer favors the loss of P by superficial runoff to a representative dose of that used in the region.

With regard to treatment (Figure 2), no significant differences were found between the fertilized treatments, but there were differences with the treatments not fertilized with P. This behavior demonstrates that the higher P concentrations observed in runoff water were influenced by the practice of fertilization and not by the effect of the herbicide.

Table 5. Variance Analysis of Phosphorus Concentrations from Different Simulation Dates

date	concentration of P[a] (mg L^{-1})
1	2.6 a
2	2.1 ab
3	1.6 b

[a]Different letters indicate significant differences (Tukey $\alpha = 0.05$).

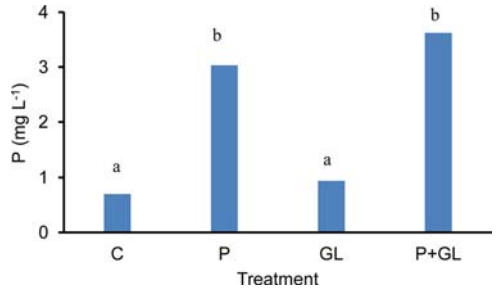

Figure 2. Variance analysis for phosphorus concentration (mg L^{-1}). Different letters indicate significant differences (Tukey $\alpha = 0.05$).

Amount of P in Runoff Water. The amount of P in runoff water ranged between 0.02 and 1.9 kg ha^{-1}. A significant interaction between treatment and date was found. Greater losses of P were observed with phosphate fertilizer treatment.

Treatments with P after a rainfall of approximately 1 h with 60 mm h^{-1} intensity lost 4% of the P applied by fertilization. These losses reduced the efficiency of the fertilization and consequently increased the pollution risk. Austin et al.[25] and Gaynor and Findlay[26] also reported on superficial phosphate transport and the eventual losses of the system under the dissolved or particulate shapes produced by rainfall or irrigation.

Glyphosate and AMPA in Runoff Water. *Glyphosate and AMPA Concentrations.* The glyphosate concentration in runoff water ranged between 18.6 and 1552.9 $\mu g\ L^{-1}$. This finding highlights the presence of glyphosate in all treatments, including the control, most likely because 2 months before the installation of our trial, the plot was sprayed for weed control in fallow with a 3 L ha^{-1} dose of the same commercial product used in the present trial.

A significant interaction was observed between the simulation dates and different treatments (Table 6). Treatment with P+GL on the first simulation date presented a higher concentration of glyphosate in water (19 times that of the control). On the same date, treatment with the same dose of herbicide without P exhibited approximately half the concentration of glyphosate in runoff water. The concentration was

Table 4. Validation Parameters of the Optimized Methodology

compd	LOD[a] ($\mu g\ L^{-1}$)	LOQ[b] ($\mu g\ L^{-1}$)	recovery (1 $\mu g\ L^{-1}$) (RSD[c] %); $n = 6$	recovery (100 $\mu g\ L^{-1}$) (RSD %); $n = 6$	linearity (0.1−500 $\mu g\ L^{-1}$)
GL	0.2	0.6	96−102 (3%)	89−101 (6%)	$y = 82.521x - 761.41$ $R = 0.989$
AMPA	0.2	0.6	105−107 (5%)	121−126 (8%)	$y = 78.581x - 748.57$ $R = 0.987$

[a]Limit of detection. [b]Limit of quantification. [c]Relative standard deviation.

DOI: 10.1021/jf505533r
J. Agric. Food Chem. 2015, 63, 4444−4448

Table 6. Variance Analysis of Glyphosate Concentration

	treatment[a] (μg L^{-1})			
date	P+GL	GL	P	C
1	1417.6 a	767.2 b	40.1 d	74.1 d
2	277.9 c	168.8 cd	26.9 d	39.4 d
3	133.1 cd	65.5 d	29.8 d	32.6 d

[a]Different letters indicate significant differences (Tukey α = 0.05).

diminished during the days after application, and the treatments without glyphosate were not different on any of the dates.

The concentration of AMPA also presented a significant interaction between treatment and date (Table 7). With P+GL

Table 7. Variance Analysis of AMPA Concentration

	treatments[a] (μg L^{-1})			
date	P+GL	GL	P	C
1	453.7 a	561.5 a	144.6 b	199.6 b
2	478.4 a	127.7 b	184.6 b	160.4 b
3	543.3 a	262.2 b	175.1 b	171.8 b

[a]Different letters indicate significant differences (Tukey α = 0.05).

treatment, no significant differences between dates were observed, implying that the degradation of the glyphosate molecule was immediate upon application, presenting no differences between the first and eighth days after application. With GL treatment, the first simulation date presented higher concentrations with respect to the others, and no significant difference was observed compared to P+GL.

Glyphosate + AMPA Concentration. Analysis of glyphosate + AMPA concentration presented a significant interaction between treatment and date. In Figure 3, P+GL

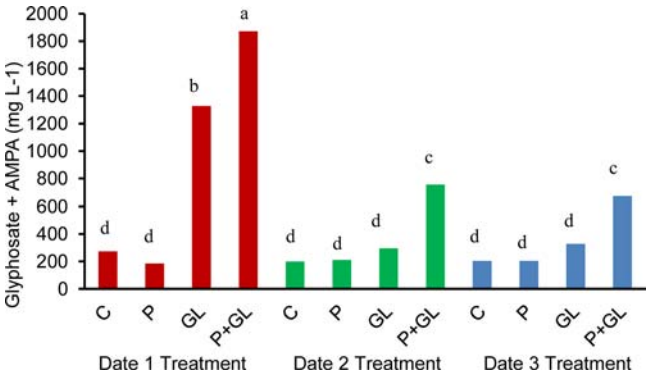

Figure 3. Variance analysis for glyphosate + AMPA concentration (μg L^{-1}). Different letters indicate significant differences (Tukey α = 0.05).

treatment presented a higher concentration on the first date, which was significantly different from GL treatment on the same date. For the other simulation dates, P+GL treatment was different from the other treatments.

Amount of Glyphosate + AMPA. Table 8 represents the analysis of the amount of glyphosate + AMPA lost in 1 h of rainfall simulation, 60 mm h^{-1} above bare soil. There were significant differences for the interaction between date and treatment; treatment with P+GL on the first simulation date was significantly higher than the other treatments.

The analysis of the first 5 cm of soil prior to the rainfall simulation indicated that no significant differences were

Table 8. Variance Analysis for the Amount of Glyphosate + AMPA[a]

	treatments (g ha^{-1})			
date	P+GL	GL	P	C
1	607.8 a	236.5 b	60.9 b	56.1 b
2	88.6 b	53.5 b	58.8 b	24.7 b
3	117.9 b	53.3 b	31.1 b	51.2 b

[a]Different letters indicate significant differences (Tukey α = 0.05).

observed in the total P concentration between treatments (data not shown). Nevertheless, differences in glyphosate concentration were evident (Figure 4). No difference was

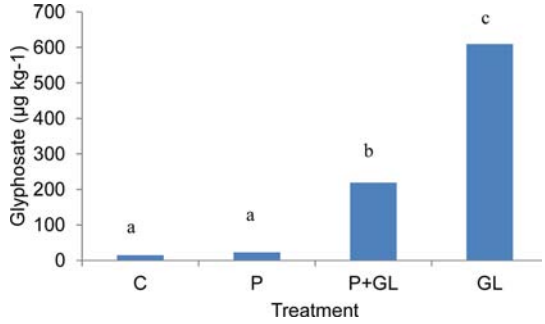

Figure 4. Variance analysis for glyphosate concentration (μg kg^{-1}) in the first 5 cm of the soil prior to each rainfall simulation. Different letters indicate significant differences (Tukey α = 0.05).

observed between the treatments that were not sprayed with glyphosate, and GL treatment had the highest concentration, confirming that 24 h after spraying, P occupied the exchanging sites in P+GL.

After P+GL treatment, 28% of the applied glyphosate was lost in the runoff water. In the case of GL treatment at the same dose, the losses were 2.5-fold less than those of the P+GL treatment, indicating that the practice of phosphate fertilization and the application of glyphosate significantly increase the loss of glyphosate by runoff.

Morillo et al.[27] reported that glyphosate can act in the soil in a similar way to phosphate, possibly through the phosphate group. According to the results obtained by Zhao et al.,[28] the effect of the phosphate application on glyphosate mobility in different soils is due to the combination of reduced pH produced by the addition of acidic phosphate solution and the repulsion between the glyphosate and preabsorbed phosphate.

A significant interaction between P and glyphosate in common sorption sites of no-till Aquic Argiudoll soil was verified in the field conditions. The application of phosphate fertilizer increased the loss of glyphosate with the runoff caused by rain a day after its application.

The rain simulators were useful for analyzing the effect of the time elapsed between application and rainfall, demonstrating competitive adsorption and transport of P and glyphosate on soil exchange sites.

The relationship between the application of glyphosate and phosphate fertilizers and their contribution to pollution by runoff had not been identified using field conditions before this work. Some authors have studied this subject under laboratory conditions and in other parts of the world where the lack of tillage does not have the same importance as in the Argentinean Humid Pampa. As a consequence, the environmental impact of

DOI: 10.1021/jf505533r
J. Agric. Food Chem. 2015, 63, 4444−4448

the interaction of those two practices, the most commonly used under no-tillage conditions, was unknown. As such, our results strengthen the necessity to pursue further studies aimed at understanding phosphorus−glyphosate interactions in soils under real conditions to establish an optimized time and conditions in current practice to reduce the risks of pollution by runoff. These results are of great importance for minimizing the environmental impact in the Argentinean setting, where no-tillage practices are extended to >20 Mha.

AUTHOR INFORMATION

Corresponding Author

*(H.B.) E-mail: hbeldo@fiq.unl.edu.ar or hbeldomenico@fibertel.com.ar.

Funding

This work was funded by the PNNAT 1128041, PNNAT 1128043 and PRET ERIO 102 Projects.

Notes

The authors declare no competing financial interest.

ACKNOWLEDGMENTS

We are thankful for assistance from the technical and support personnel of the Natural Resources Group of EEA Parana, INTA.

REFERENCES

(1) Borggaard, O. K.; Gimsing, A. L. Fate of glyphosate in soil and the possibility of leaching to ground and surface waters: a review. *Pest Manage. Sci.* **2008**, *64*, 441−456.

(2) Sprankle, P.; Meggit, W.; Penner, D. Rapid inactivation of glyphosate in the soil. *Weed Sci.* **1975**, *23*, 224−228.

(3) Sprankle, P.; Meggit, W. F.; Penner, D. Adsorption, mobility and microbial. *Weed Biol. Manage.* **1975**, *3*, 228−232.

(4) Petersen, C.; Holm, J.; Koch, C. B.; Jensen, H. E.; Hansen, S. Movement of pendimethalin, ioxynil and soil particles to field drainage tiles. *Pest Manage. Sci.* **2002**, *59*, 85−96.

(5) Jaynes, D. B.; Ahmed, S. I.; Kung, K. J. S.; Kanwar, R. S. Temporal dynamics for preferential flow to a subsurface drain. *Soil Sci. Soc. Am. J.* **2001**, *65*, 1368−1376.

(6) Elliott, J. A.; Cesna, A. J.; Best, K. B.; Nicholaichuk, W.; Tollefson, L. C. Leaching ratesand preferential flow of selected herbicides through tilled and untilled soil. *J. Environ. Qual.* **2002**, *29*, 1650−1656.

(7) Villholth, K. G.; Jarvis, N. J.; Jabobson, O. H.; de Jonge, H. Field investigations and modelling of particle-facilitated pesticide transport in macroporous soil. *J. Environ. Qual.* **2000**, *29*, 1298−1309.

(8) Flury, M. Experimental evidence of transport of pesticides through field soil. A review. *J. Environ. Qual.* **1996**, *25*, 25−45.

(9) Sasal, M. C.; Andriulo, A. E.; Wilson, M. G.; Portela, S. I. Pérdidas de glifosato por drenaje y escurrimiento en molisoles bajo siembra directa [Glyphosate loss by drainage and runoff in mollisols under no tillage cropping]. *Inf. Tecnol.* **2010**, *5*, 135−142.

(10) Sasal, M. C.; Marcelo, G. W.; Andriulo, A. E.; Oszust, J. D.; Gabioud, E. A. Estudios del impacto de la agricultura sobre la calidad del agua [Studies on the impact of agriculture on water quality]. Presented at Symposium Fertility 2013, Nutrition for sustainable crop production intensification (Engl. Transl.), Rosario, Santa Fe, Argentina, May 22−23, 2013.

(11) Primost, J. *Estudio de niveles ambientales de glifosato y AMPA en una zona modelo de intensa actividad agrícola en los alrededores de Urdinarrain [Study of environmental levels of glyphosate and AMPA in a model zone of intense agriculture activity in the surroundings of Urdinarrain]*. Graduate thesis, National University of Entre Ríos, Argentina, Environment Research Center (CIMA), Faculty of Exact Sciences, National University of La Plata, Argentina, 2013.

(12) Gimsing, A. L.; Borggaard, O. K. Effect of KCl and $CaCl_2$ as background electrolytes on the competitive adsorption of glyphosate and phosphate on goethite. *Clay Miner.* **2001**, *49*, 270−275.

(13) Nicholls, P. H.; Evans, A. A. Sorption of ionisable organic compounds by field soils. Part 2: Cations, bases and zwitterions. *Pestic. Sci.* **1991**, *33*, 331−345.

(14) Mcbride, M.; Kung, K. H. Complexation of glyphosate and related ligands with iron(III). *Soil Sci. Soc. Am. J.* **1989**, *53*, 1668−1673.

(15) Hance, R. J. Adsorption of glyphosate by soils. *Pestic. Sci.* **1976**, *7*, 363−366.

(16) Soil Map Plan. Soil Chart of the Argentinean Republic (1998); Department of Paraná, Entre Ríos Province (1998), Natural Resources Survey Series 17, EEA Paraná, Entre Ríos, Argentina, 1998; 114 pp, ISSN-0325-9099.

(17) Irurtia, C. B.; Mon, R. *Microsimulador de lluvia para determinar infiltración a campo [Rainfall micro-simulator to determinate soil infiltration at field conditions]*; Technical Publication 176; Soil Institute, National Institute of Agricultural Technology (INTA)-Castelar: Buenos Aires, Argentina, 1994; pp 1−18.

(18) Aoki, A. M.; Sereno, R. Evaluación de la infiltración como indicador de calidad de suelo mediante un microsimulador de lluvias [Evaluation of infiltration as soil quality indicator using a rainfall micro-simulator]. *Agriscientia* **2006**, *23* (1), 23−31.

(19) *Standard Methods for the Examination of Water and Wastewater*, 20th ed.; American Public Health Association: Washington, DC, USA, 1998; Standard Method 4500-P E, pp 4−146.

(20) Ibánez, M.; Pozo, O. J.; Sancho, J. V.; López, F. J.; Hernández, F. Re-evaluation of glyphosate determination in water by liquid chromatography coupled to electrospray tandem mass spectrometry. *J. Chromatogr., A* **2006**, *1134*, 51−55.

(21) Hanke, I.; Singer, H.; Hollender, J. Ultratrace-level determination of glyphosate, aminomethylphosphonic acid and glufosinate in natural waters by solid-phase extraction followed by liquid chromatography-tandem mass spectrometry: performance tuning of derivatization, enrichment and detection. *Anal. Bioanal. Chem.* **2008**, *391*, 2265−2276.

(22) European Commission Health & Consumer Protection Directorate-General. Guidance document on analytical quality control and validation procedures for pesticide residues analysis in food and feed; SANCO/12571/2013. Safety of the food chain. Chemicals, contaminants, pesticides; 19 November 2013, rev. 0; http://ec.europa.eu/food/plant/pesticides/guidance_documents/docs/qualcontrol_en.pdf (accessed Nov 3, 2014).

(23) Infostat Group. INFOSTAT, version 1.1; National University of Córdoba, Faculty of Agricultural Sciences, Córdoba, Argentina, 2002.

(24) Sasal, M. C.; Castiglioni, M. G.; Wilson, M. G. Effect of crop sequences on soil properties and runoff on natural rainfall erosion plots under no tillage. *Soil Tillage Res.* **2010**, *108*, 24−29.

(25) Austin, N. R.; Prendergast, J. B.; Collins, M. D. Phosphorus losses in irrigation runoff from fertilized pasture. *J. Environ. Qual.* **1996**, *25*, 63−68.

(26) Gaynor, J. D.; Findlay, W. I. Soil and phosphorus loss from conservation and conventional tillage in corn production. *J. Environ. Qual.* **1995**, *24*, 734−741.

(27) Morillo, E.; Undabeytia, T.; Maqueda, C. Adsorption of glyphosate on the clay mineral montmorillonite: effect of Cu(II) in solution and adsorbed on the mineral. *Environ. Sci. Technol.* **1997**, *31*, 3588−3592.

(28) Zhao, B.; Zhang, J.; Gong, J.; Zhang, H.; Zhang, C. Glyphosate mobility in soils by phosphate application: laboratory column experiments. *Geoderma* **2009**, *149*, 290−297.

DOI: 10.1021/jf505533r
J. Agric. Food Chem. 2015, 63, 4444−4448

MATERIALS AND METHODS

Chemicals. Certified reference standards of all test compounds were of >97% purity and purchased from Ehrenstorfer GmbH (Augsburg, Germany) and Sigma-Aldrich (Steinheim, Germany). All of the solvents were of analytical reagent (AR) or ultragradient HPLC grade and obtained from J. T. Baker (Center Valley, PA, USA). All other reagents were of AR grade and purchased from Thomas Baker (Mumbai, India) and Merck India Ltd. (Mumbai, India). The dispersive solid phase extraction (dSPE) sorbent, namely, primary−secondary amine (PSA), was received from Agilent Technologies (Santa Clara, CA, USA). Ultipor Nylon-6,6 membrane filters (0.2 μm pore size and 13 mm diameter) were purchased from Pall Life Sciences (Ann Arbor, MI, USA). HPLC grade water was obtained through Sartorius water purification system (Göttingen, Germany).

Apparatus. For sample preparation a mixer with grinder (0.5 and 2 L capacity, model GX7, Bajaj India Ltd., Mumbai, India), vortex mixer (Genie 2T, Imperial Biomedicals, Mumbai, India), ultrasonic bath (Oscar Electronics, Mumbai, India), low-volume concentrator (TurboVap LV; Caliper Life Sciences, Russelsheim, Germany), high-speed refrigerated centrifuge (Kubota 6500, Kubota Corp., Tokyo, Japan), and a microcentrifuge (Microfuge Pico, Kendro D-37520, Osterode, Germany) were used. A pH meter (Thermo Orion, Chelmsford, MA, USA) was used after calibration using buffer solutions of pH 4 and 7. Residue analysis was performed using an LC-MS/MS [Shimadzu UFLC XR connected to API 5500 QTrap (AB Sciex, Toronto, Canada) mass spectrometer], supplied by Labindia Instruments Pvt. Ltd. (Mumbai, India).

Selection of Matrices and Sample Homogenization. Fruit and vegetable matrices were selected considering their importance for export and domestic consumption. The selected matrices were grape (*Vitis vinifera* L.), mango (*Mangifera indica* L.), capsicum (*Capsicum annuum* L.), okra (*Abelmoschus esculentus* L.), curry leaf (*Murraya koenigii* L.), drumstick (*Moringa oleifera* L.), and bitter gourd (*Mormordica charantia* L.). The method was initially optimized in grape and then extended to other commodities. The control matrices were obtained from the organically grown local farms and used after ensuring absence of any of the target incurred residues. About 0.5−2 kg sample sizes of different matrices were selected (0.5 kg for curry leaf, 1 kg for other vegetables, and 2 kg for grape and mango) to obtain a homogenized representative sample. The samples were chopped (except grape) after removal of stalks, caps in the case of vegetables, and stone in the case of mango, followed by crushing in a mixer−grinder. In the following step, about 0.1−0.4 kg of this crushed material (0.1 kg for curry leaf; 0.2 kg for bitter gourd, drumstick, and okra; 0.4 kg for grape, mango, and capsicum) was again homogenized in a smaller jar (0.5 L capacity) to obtain a finely crushed homogeneous sample with or without addition of water. In the case of bitter gourd, okra, and drumstick, water was added in the proportion of 1:1 w/w, and for curry leaf, the ratio was 1:3 w/w. The proportion of water added was based on the inherent moisture content of the matrices and was optimized through separately conducted experiments to achieve the desired level of homogeneity (RSD < 10% when analyzed in six replicates).

Selection of Agrochemicals. The study included 296 multiclass agrochemicals (including selective metabolites) with different biological activities such as insecticides, acaricides, fungicides, herbicides, and plant growth regulators, which were either neutral, acidic, or basic by chemical nature. The compounds were selected considering the MRL database of the European Union[2] and Food Safety Standards Authority of India.[3] Details of the test analytes are presented in Supplementary Table 1 of the Supporting Information.

Preparation of Standard Solutions. The stock solutions of individual certified reference standards (CRS) were prepared by accurately weighing 10−20 mg of each analyte in volumetric flasks (certified A class) and dissolving in 10 mL of methanol (stored at −20 °C). Intermediate standard mixtures of 10 μg/mL and a working standard mixture of 1 μg/mL were prepared by diluting the stock solutions in methanol. From this, the calibration standards within the range of 0.2−40.0 ng/mL were prepared by serial dilution with methanol/20 mM ammonium formate in water (1:1 v/v) or control matrix extracts.

Existing Method. Homogenized samples (10 g) were extracted with ethyl acetate (10 mL) per the procedure reported earlier.[4]

Optimization of Buffer Concentration. Homogenized grape (10 g) spiked at 10 ng/g was extracted with 10 mL of ethyl acetate either using no buffer or in the presence of acetic acid (1% v/v) plus variable amounts of sodium acetate (0, 0.1, 0.5, 1, and 2 g; $n = 6$) along with 10 g of sodium sulfate. No PSA cleanup was employed to avoid resultant pH-dependent effects on the recovered analytes. The average recoveries were compared against the respective matrix-matched standards employing single-point calibration.

Effect of Dispersive SPE Cleanup Using PSA. For this, two sets of homogenized control grape samples (10 g) were extracted with the existing method[4] and optimized sodium acetate buffer method, each in six replicates. The resultant extracts were spiked at 10 ng/g level and treated as (1) no cleanup, (2) cleanup with 25 mg of PSA per 5 mL of extract, and (3) cleanup with 125 mg of PSA per 5 mL of extract. The cleanup efficiencies in each case were evaluated by gravimetric comparison of the residual matter. At each variable amount of PSA, the pH of the corresponding ethyl acetate extract was measured after dilution with water and under continuous stirring with a magnetic stirrer. The average concentration of the analytes at different treatments were estimated as accuracy (%) against solvent standards and compared.

Optimization of DEG Quantity. Two milliliters of ethyl acetate extract of control grape and pure ethyl acetate solvent were taken in six different sets of 10 mL evaporation tubes and spiked with a mixture of pesticides at 10 ng/mL. DEG (10% in methanol) was then added in each tube at different volumes of 0, 10, 25, 50, 100, and 200 μL, respectively. After evaporation under a gentle stream of nitrogen at 35 °C, the residues were reconstituted in methanol/water (50:50) and injected into LC-MS/MS after passing through a Nylon-6,6 membrane filter (0.2 μm). The area (%) responses of the test analytes were compared. Full-scan analysis of selective samples was done using information dependent acquisition (IDA) functionalities of a QTrap LC-MS/MS system.

Proposed Method. The sample (10 g) was extracted with 10 mL of ethyl acetate (+ 1% acetic acid) in the presence of sodium acetate (0.5 g) and anhydrous sodium sulfate (10 g) by means of vortexing (2 min) and subsequent centrifugation at 5000 rpm for 5 min. An aliquot of the upper ethyl acetate extract (5 mL) was drawn and treated with PSA (25 mg) by means of vortexing for 30 s. The cleaned supernatant extract (2 mL) was placed in a 10 mL test tube, and to it 10% DEG (10 μL) was added. This mixture was subsequently evaporated to dryness under a gentle stream of nitrogen (in a low-volume concentrator) at 35 °C. The residue was dissolved in 1:1 methanol plus 20 mM ammonium formate in water (2 mL) by ultrasonication (1 min) followed by vortexing (30 s). This solution was centrifuged at 10000 rpm for 5 min. The extracts were analyzed by LC-MS/MS after passing through a Nylon-6,6 membrane filter (0.2 μm).

LC-MS/MS Analyses. Chromatographic separation of the test compounds was achieved on an Ultra AQ C18 column (3 μm, 100 mm length, 2.1 mm i.d.; Restek Corp., Bellefonte, PA, USA). The mobile phase composition was (A) water with 10 mM ammonium formate and (B) methanol with 10 mM ammonium formate, each with 0.1% formic acid, at flow rate of 0.5 mL/min with a gradient profile.[15] The column oven temperature was maintained at 40 (±1) °C. The injection volume was 10 μL. Measurements were done with electrospray ionization (ESI) in positive polarity with optimized multiple reaction monitoring (MRM) transitions. The source parameters, namely, ion source voltage (5500 V), nebulizer gas (30 psi), heater gas (60 psi), ion source temperature (550 °C), and curtain gas (40 psi), were maintained throughout the analysis.

Residue estimation was performed by retention time dependent "scheduled multiple reaction monitoring" (sMRM) with two mass transitions for each test molecule, one for quantification and the other for confirmation. The MRM detection window (MRM DW) was 90 s with the target scan time of 1 s. The ion ratio for the two mass transitions was used for unambiguous identification of each pesticide

DOI: 10.1021/jf505221e
J. Agric. Food Chem. 2015, 63, 4449−4456

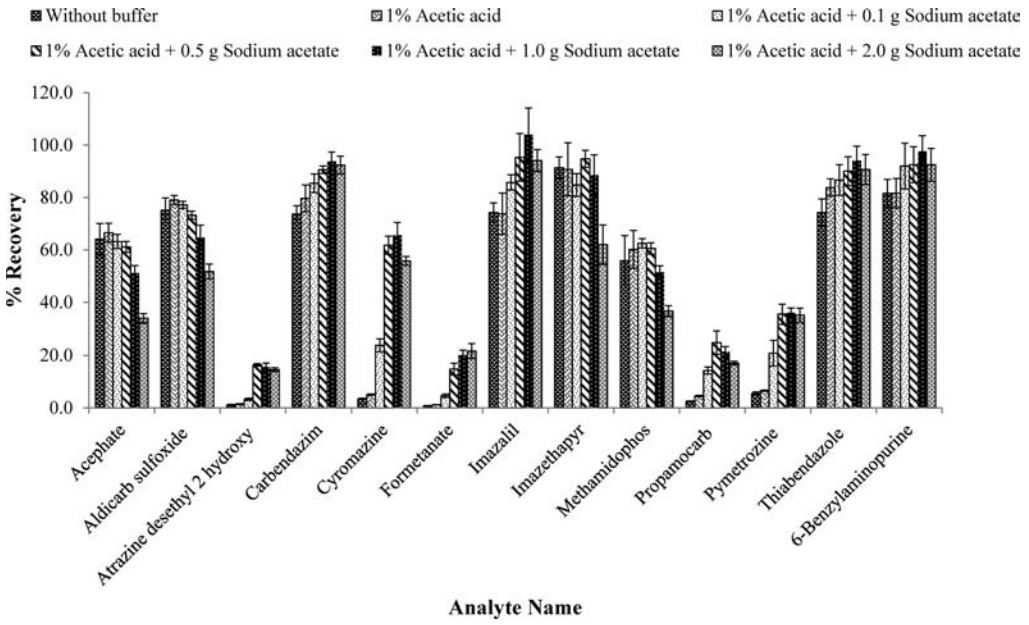

Figure 1. Effect of buffering on recovery of analytes.

per the criteria of the SANCO guideline.[14] A representative LC-MS/MS chromatogram is given in Supplementary Figure S1 in the Supporting Information.

Method Validation. The performance of the analytical method was assessed per the SANCO guideline.[14] Standard calibration was established on the basis of solvent and matrix-matched standards in the concentration range of 0.2−40 ng/mL. Limits of detection (LOD) and quantification (LOQ) were determined by considering signal-to-noise ratios (S/N) of 3 and 10, respectively, for the quantifier MRM ensuring that the qualifier MRM has S/N of ≥3:1 at LOQ. For the recovery experiment, at first the samples were spiked at the desired level from a standard working solution of 1 μg/mL and then thoroughly homogenized. Ten grams of homogenized mass was weighed in a 50 mL polypropylene tube and then extracted per the proposed method. The recovery experiments were carried out in grape at five spiking levels, that is, 1, 2.5, 5, 10, and 40 ng/g (n = 6). For all other matrices three spiking levels were selected, which were equivalent to 1, 5, and 10 ng/g for mango and capsicum; 2, 10, and 20 ng/g for bitter gourd, okra, and drumstick; and 4, 10, and 40 ng/g for curry leaf on an actual weight basis. Recoveries (%) were calculated against the respective matrix-matched calibrations. The precision in terms of repeatability in recovery was estimated as % RSD. The results were summarized in different categories, namley, I, recovery (70−120%), RSD ≤ 20%; II, recovery (60−140%), RSD ≤ 20%; III, recovery (60−140%), RSD > 20%; IV, recovery (<60%), RSD ≤ 20%; V, recovery (<60%), RSD >20%; VI, other (include the compounds below LOQ or those suffering from matrix-specific degradation and thus not included in categories I−V).

Dilution and Matrix Effect. Cleaned ethyl acetate extracts (control) of all test commodities were aspirated in evaporation tubes in the volumes of 2, 0.4, 0.2, and 0.1 mL (n = 6) and made up to 2 mL with appropriate quantities of ethyl acetate, which resulted into corresponding dilution of 0, 5, 10, and 20 times (v/v). After fortification (at the level of 10 ng/mL), they were evaporated to near dryness under a gentle stream of nitrogen in the presence of DEG solution (10 μL, 10%). The residue was dissolved in 1:1 methanol plus 20 mM ammonium formate in water (2 mL). The percent accuracy of each analyte response in undiluted or diluted matrix was compared to that of solvent standard, and the results are summarized in distinct groups: I, accuracy 0−30% (very high matrix induced signal suppression); II, accuracy 30−60% (high signal suppression); III, accuracy 60−80% (moderate signal suppression); and IV, accuracy 80−130% (low or no signal suppression or enhancement).

Comparison of Proposed Method with Existing Ethyl Acetate[4] and Buffered QuEChERS[10] Method. The proposed method was compared against the existing ethyl acetate[4] and buffered QuEChERS[10] methods (n = 6), and the method performances were evaluated in terms of recovery (%).

RESULTS AND DISCUSSION

In a highly acidic matrix suc as grape (pH ∼4), with the existing ethyl acetate method[4] the recoveries of certain basic pesticides (such as cyromazine, pymetrozine, atrazine desethyl 2-hydroxy, and propamocarb) were poor (<6%) as against the matrices with relatively higher pH such as okra (pH >5). Similar poor recoveries were also recorded in other acidic matrices, for example, plum (pH ∼3). Poor recoveries of such pesticides in highly acidic matrices could be attributed to their poor partitioning into the ethyl acetate phase, which might have occurred due to their ionization in acidic pH (in grape and plum) and the greater affinity of the ionized forms toward the aqueous phase.[16,17] Considering the role of pH adjustment explained in the buffered QuEChERS method[10] and with the optimized quantities of acetate buffer (i.e., 1% acetic acid + 1 g of sodium acetate per 10 g of sample), the pH of grape and plum matrix was adjusted to 5−6. Use of acetate buffer was cost-effective and easy to handle, and being in solid form, it avoided efforts for preparing and maintaining buffers in solution forms. With this approach, the recoveries of the above-mentioned compounds could be improved significantly. However, at the same time, the recoveries of certain compounds such as acephate, aldicarb sulfoxide, and methamidophos were decreased substantially as against the non-buffered method. Therefore, we decided to evaluate the best concentration of acetate buffer to obtain overall acceptable recoveries for the entire range of the test compounds.

Optimization of Buffer Concentration. With the addition of acidified ethyl acetate (1% acetic acid) and 0, 0.1, 0.5, 1, and 2 g of sodium acetate, the initial pH of the lower aqueous layer was changed from 3.9 (without buffer) to about 3.8 (1% acetic acid), 4.9, 5.7, 5.9, and 6.3, respectively. Recoveries of weakly acidic pesticides such as acephate and aldicarb sulfoxide showed about 15% loss in recovery when the

DOI: 10.1021/jf505221e
J. Agric. Food Chem. 2015, 63, 4449−4456

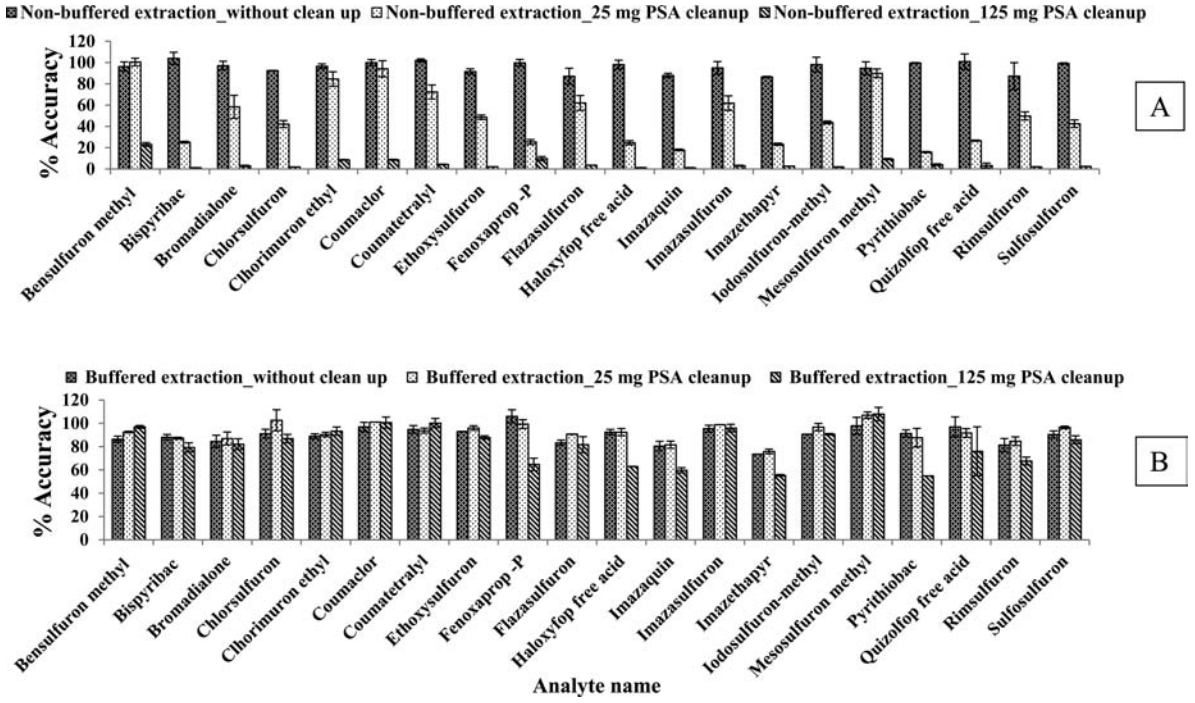

Figure 2. Effect of PSA cleanup in nonbuffered (A) and buffered (B) ethyl acetate extraction.

quantity of sodium acetate was increased from 0.5 to 1 g. A decreasing trend in recoveries (up to 28% loss in recovery) was observed with further addition (2 g) of sodium acetate for these compounds. For imazethapyr (acidic in nature) with increase in pH above 6, the recovery loss was about 30% (Figure 1). These acidic pesticides tend to form negatively charged ions as the pH increases with corresponding increase in water solubility and reduced partitioning into the ethyl acetate phase. In the case of methamidophos (basic in nature), a similar decreasing trend in recoveries was observed probably due to its hydrolysis with increase in pH toward neutral. In contrast to this, in the case of basic analytes, namely, atrazine desethyl 2-hydroxy, propamocarb, formetanate, cyromazine, and pymetrozine, the recoveries were enhanced by 10−25 times after adjustment of the pH above 5 as against the nonbuffered method. Although the recoveries of these compounds were comparatively low (15−65%) due to their highly polar nature and low extractability into ethyl acetate, buffering enhanced their extractability and facilitated accurate quantification. Other basic compounds such as carbendazim, thiabendazole, imazalil, and 6-benzylaminopurine (6-BA) also showed improved recoveries with buffering at pH >5 due to better partitioning into ethyl acetate.

To achieve the best compromise for optimum extraction of acidic and basic analytes, for the final method, 0.5 g of sodium acetate + 1% acetic acid was selected as the optimized quantity for buffering. The pH of all the test commodities was effectively adjusted within the range of 5−6 irrespective of the initial matrix pH (Supporting Inforamtion, Supplementary Figure S2).

Effect of Dispersive SPE Cleanup Using PSA. In the existing ethyl acetate method[4] 25 mg of PSA per 5 mL of extract had been used for dispersive cleanup to remove matrix coextractives such as fatty acids and sugars. In the initial studies, with this unbuffered method, we found that the PSA cleanup resulted in severe losses of certain acidic pesticides in all test matrices. Therefore, we decided to evaluate the effect of PSA cleanup in the optimized buffered ethyl acetate extraction. The quantities of PSA were selected per the existing ethyl acetate method,[4] that is, 25 mg/5 mL of extract, and per the original version of the QuEChERS method,[18] that is, 125 mg/5 mL extract (equivalent to 25 mg/mL).

Gravimetric estimation of the residual matrix showed that, in the existing method,[4] 56% residual matrix was removed as against 38% in buffered method using 25 mg of PSA; that is, the efficiency of PSA cleanup was reduced to 66% in the buffered extraction. This was attributed to partitioning of acetic acid (used during buffering) in the organic layer (ethyl acetate), which probably saturated the binding sites of PSA and was indicated by acidic pH of the ethyl acetate extract. The reduced cleanup efficiency of PSA due to transfer of acetic acid in the organic phase was also reported earlier in the buffered QuEChERS method.[10] It was observed that there was no significant difference in the residual matrix using 25 or 125 mg PSA and, therefore, 25 mg was chosen as the optimum quantity for cleanup.

The percent accuracy of test analytes against solvent standards in the existing and buffered methods without and with PSA cleanup (25 and 125 mg PSA/5 mL extract) revealed interesting results. In the unbuffered method, after PSA cleanup, many acidic urea herbicides (pyrimidinylsulfonylurea, triazinylsulfonylurea, aryloxyphenoxypropionic acid, imidazolinone, pyrimidinyloxybenzoic acid compounds) had significant recovery losses, which ranged between 25 and 83% with the cleanup using 25 mg of PSA and 73−98% with the cleanup using 125 mg of PSA per 5 mL of extract (Figure 2). Similar observations were reported in the literature recommending no PSA cleanup during extraction of acidic compounds to protect against recovery loss.[19,20] In buffered extraction, practically there were no losses with respect to the treatment with 25 mg of PSA, although 13−41% losses in recovery were recorded in the case of 125 mg of PSA. The probable reasons for this result could be related to the presence of acetic acid in the ethyl

DOI: 10.1021/jf505221e
J. Agric. Food Chem. 2015, 63, 4449−4456

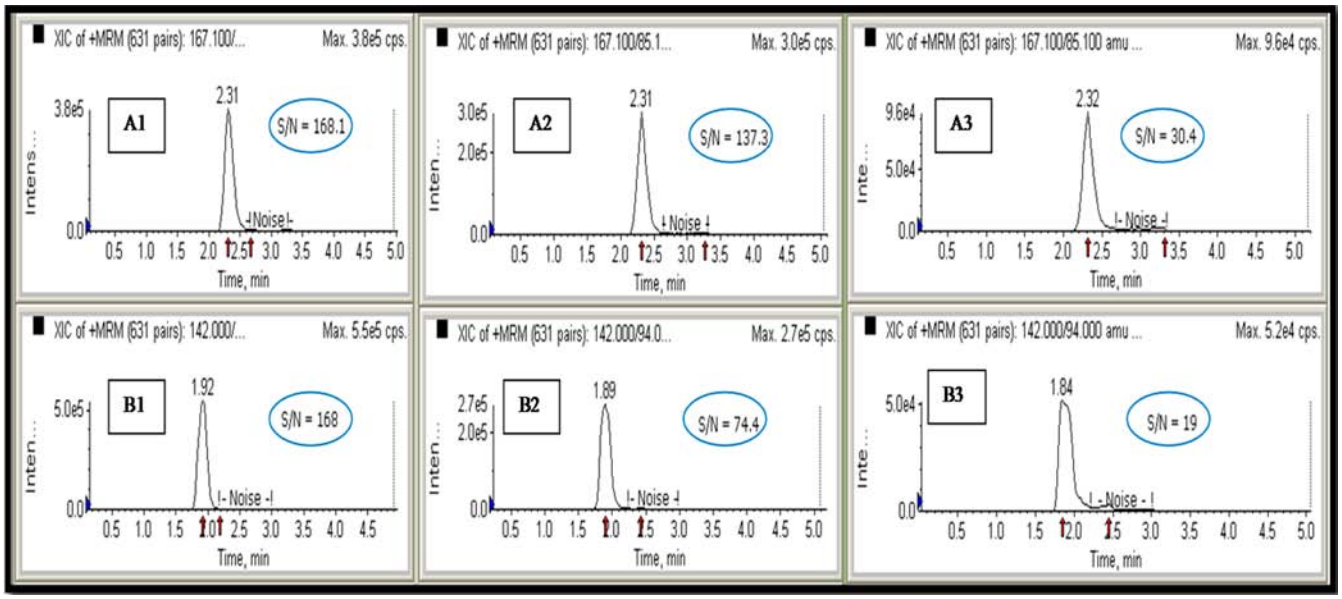

Figure 3. Signal suppression of (A) cyromazine and (B) methamidophos (10 ng/mL) corresponding to (1) no DEG, (2) 10 μL of DEG, and (3) 200 μL of DEG.

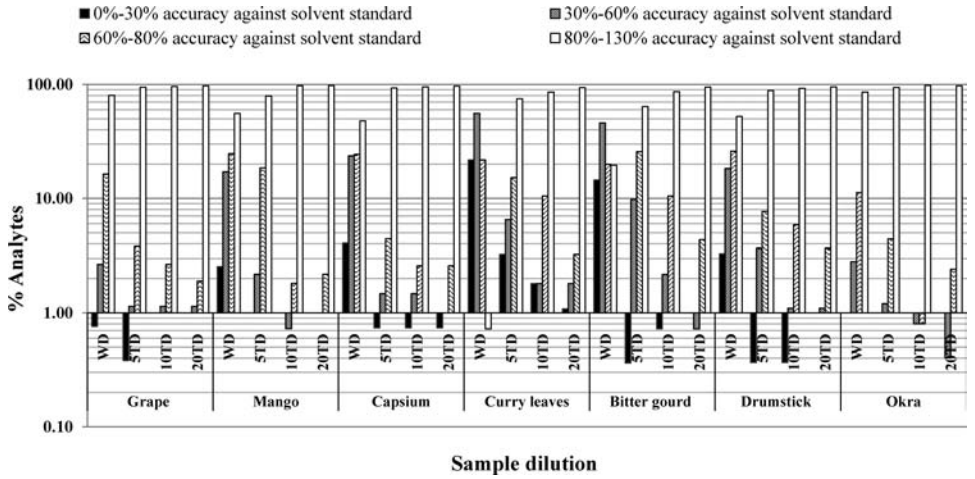

Figure 4. Demonstration of dilution approach for reducing matrix effect in different commodities.

acetate phase, which reduced direct interaction of PSA with the acidic analytes. This was another important and favorable aspect of buffering, and thus there was no need to omit PSA cleanup; good recoveries of acidic compounds could still be achieved. Furthermore, with this optimum quantity, signal suppression was significantly reduced by 20−50% for compounds, namely, dodine, bupirimate, fenpropimorph, imazalil, mexacarbate, methoprotryne, pirimicarb, prometon, prometryne, spiroxamine, and 6-BA.

Optimization of DEG Quantity. In the existing ethyl acetate based extraction method,[4] 200 μL of DEG (10% solution in methanol) for 2 mL of final extract is employed as a keeper during the solvent evaporation step. The significance of the use of DEG solution is explained by Mol et al.[21] In brief, addition of this high boiling, viscous liquid in the extract protects against loss of analytes during evaporation and avoids hard drying of the residual matrix, which otherwise may trap analytes and make their solubilization difficult. In our routine analysis, it was observed that the early-eluting compounds (t_R 2−5 min) suffer serious signal suppressions (>50%) irrespective of the matrix examined. Considering its polar nature and early elution, we assumed that DEG might be contributing to matrix effect, and hence its impact was investigated further. During the DEG optimization experiment, it was observed that the early-eluting compounds such as methamidophos, acephate, atrazine desethyl, atrazine desethyl 2-hydroxy, cyromazine, and dinotefuran showed significant signal suppressions (30−80%) as the quantity of DEG was increased from 0 to 200 μL (Supporting Information, Supplementary Figure S3). The trend in signal suppression of these analytes was similar in the case of pure solvent and matrix, which demonstrated that DEG rather than the matrix coextractives was responsible for signal suppressions. The effect was most prominent in the case of methamidophos, the earliest eluting compound (t_R 1.9 min), which had almost 40% signal suppression with 10 μL of DEG and almost 80% suppression after the addition of 200 μL of DEG. Figure 3 shows how signal suppression due to the addition of DEG resulted in lower signal-to-noise ratios (S/N) and, thus, increased LOQs of cyromazine (by 5 times) and methamidophos (by 8 times).

DOI: 10.1021/jf505221e
J. Agric. Food Chem. 2015, 63, 4449−4456

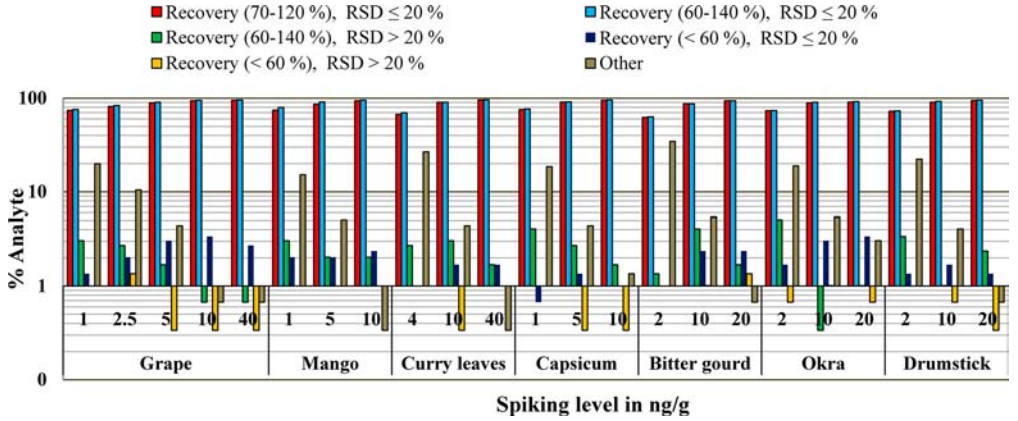

Figure 5. Summarized data on the performance of the buffered ethyl acetate method for 296 compounds in all test matrices.

To evaluate this further, DEG solution (equivalent to 200 μL of 10% DEG solution/2 mL) along with methamidophos (10 ng/mL) in methanol was injected in the same chromatographic system and analyzed in full-scan mode using QTrap functionalities. Analysis was performed using enhanced mass spectra (EMS) as "survey scan" and enhanced product ion (EPI) as "dependent scan". The extracted ion chromatogram of DEG (m/z 107.0) and enhanced product ion spectra revealed prolonged elution of DEG within 1−5 min (Supporting Information, Supplementary Figure S4), which could be the main reason for signal suppression of early-eluting compounds. The spectral confirmation was obtained by comparing the same with the earlier reported spectrum of DEG.[22] Due to relatively higher viscosity and boiling point (245 °C) DEG might be incompletely evaporated and reduce ionization of early-eluting compounds. Volatile or semivolatile compounds such as dichlorvos, molinate, and isoprocarb suffered higher recovery losses (20−60%) in the case when no DEG was used in the evaporation step, which could be avoided when 10 μL of DEG solution was added. Therefore, considering the role of DEG to avoid hard drying of residues, instead of completely omitting its use, its volume was optimized to 10 μL in place of 200 μL[4]

Dilution and Matrix Effect. In Figure 4, the results corresponding to "without dilution" (WD) indicate matrix effect of the respective test matrix. In the case of grape, mango, capsicum, okra, and drumstick, 72−97% of the test compounds had moderate to low matrix effect (groups III and IV). In the case of bitter gourd and curry leaf, 40 and 23% of the compounds suffered from moderate to low matrix effects, whereas 46−56 and 15−22% of compounds belonged to the high (group II) and very high (group I) matrix effect categories, respectively, in terms of signal suppressions. Hence, quantification of the residues of these compounds was performed on the basis of matrix-matched calibration standards.

Dilution led to cleaner extracts, reducing signal suppressions significantly.[9] In recent publications,[23,24] a similar approach has been demonstrated with reference to QuEChERS extraction. From the comparative study (Figure 4), it was concluded that 5−10 times dilution of the final extract effectively reduced matrix-induced signal suppression for most of the compounds. After dilution of the bitter gourd extract by 5 and 10 times, the percentage of compounds falling into groups I (very high matrix effect) and II (high matrix effect) came down from 60 to 10 and 3%, respectively. Similarly, for curry leaf, the dilution of extract by 5 and 10 times reduced the proportion of compounds falling into groups I and II from 77 to 10 and 3%, respectively. This study will thus help employ appropriate dilution for quantification against solvent standard and nullify the requirement of control matrix for preparation of matrix-matched standards.

Method Validation. Calibration linearity employing linear or quadratic regression equation was established with $r^2 \geq 0.995$ for all of the test analytes in solvent and matrix-matched standards within the range of 0.2−40 ng/mL with a weighting factor of $1/x$. The method LOD and LOQ values of all the analytes were determined in grape matrix based on S/N ratio and specified in Supplementary Table 2 in the Supporting Information. Results showed that, of 296 test compounds, 79.3% of the compounds had LOQs in the range of 0.2−1 ng/g whereas for 16.2 and 3.7% compounds, the LOQs were in the ranges of 1−5 and 5−10 ng/g, respectively. As about 80% of compounds could be easily quantified at the 1 ng/g level, it was selected as the lowest spiking level (LOQ) for recovery study in grape matrix. Per the SANCO guideline,[14] recovery study at minimum two levels (at LOQ and another higher level) need to be performed and thus, considering the entire range of LOQs, that is, 1−10 ng/g, the recovery study was performed at five spiking levels, 1, 2.5, 5, 10, and 40 ng/g in grape matrix. Once the method was validated for grape matrix, it was extended to other matrices and corresponding LOQs were estimated. Recoveries at LOQ were estimated for all matrix−chemical combinations, and the lowest level at which recovery is reported is the method LOQ for that particular matrix (Supplementary Table 2).

Figure 5 shows summarized method performance data classified into categories I−VI for all of the matrices. Of the 296 test compounds, 61.2−75.7% had recoveries in the range of 70−120 (±20)% at the lowest spiking level across the commodity matrices. At the regulatory default LOQ level of 10 ng/g, the recoveries for 87.1−94.9% of the compounds were within 70−120 (±20)%. Only 1−3.7% of the total compounds had recoveries <60 (±20)% at the 10 ng/g level, which could, however, be correctly quantified after the application of a recovery correction. Around 0.33−4% of compounds had good recoveries (60−140%) but with high RSDs (>20%) and about 0−1% of compounds had lower recoveries (<60%) with higher RSDs (>20%) at the 10 ng/g level. Of the 296 test analytes, 15−34% at the lowest spiking level and 0.33−3% at the highest spiking level (in all matrices) fell into category VI, which included the compounds below the LOQ or compounds that suffered matrix-specific degradation. Low recoveries were observed for compounds such as propamocarb and atrazine

DOI: 10.1021/jf505221e
J. Agric. Food Chem. 2015, 63, 4449−4456

desethyl 2-hydroxy due to poor extraction in ethyl acetate as discussed earlier, although their RSD (%) values were acceptable. Lower and variable recoveries were recorded for alanycarb in grape, mango, drumstick, and okra; cycloxydim in grape, bitter gourd, capsicum, and okra; thiophanate methyl in all of the matrices except okra and bitter gourd; bifenazate in all of the matrices except mango, capsicum, and drumstick; benfuracarb and formetanate in all of the matrices except capsicum and bitter gourd; and ethoxyquin in all the matrices except drumstick, okra, and mango, probably due to their degradation in matrix. Some compounds showed matrix-specific recovery problems, which could be due to different reasons, including metaflumizone degradation in bitter gourd, low recoveries (50−69%) of bromadiolone and quinoxyfen, conversion of quizalofop-*p*-ethyl, haloxyfop, and fenoxaprop-*p*-ethyl into their metabolites, namely, quizalofop free acid, haloxyfop free acid, and fenoxaprop-P, respectively, in okra matrix. However, it was possible to achieve sufficiently low LOQs for most of these compounds for effective screening and quantification at or less than the regulatory MRLs. In the case of bitter gourd and curry leaf, the lowest numbers of compounds falling within the acceptable performance criteria (recovery = 70−120 ± 20%, at the lowest spiking level) were mainly due to very high matrix-induced signal suppressions.

Comparison of the Proposed Method with the Buffered QuEChERS Method[10] and the Existing Ethyl Acetate Method.[4] The comparative method performances of the proposed method vis-a-vis the buffered QuEChERS method[10] are shown in Supplementary Figure S5 in the Supporting Information for the grape matrix. For the basic compounds such as imazalil, thiabendazole, and cyromazine, the performances of both methods were comparable. For atrazine desethyl 2-hydroxy, formetanate, propamocarb, and pymetrozine, the recoveries for the proposed method were less as compared to acetonitrile extraction because of the comparatively less polar nature of ethyl acetate, but they showed acceptable RSDs (<20%). For acidic pesticides such as imazethapyr and imazosulfuron, the results for the proposed method were superior as compared to the buffered QuEChERS method,[10] probably due to the lower quantity of PSA (25 mg/5 mL) required in the ethyl acetate method as against the buffered QuEChERS method (50 mg/mL), which is mainly responsible for the adsorption losses of these compounds. For most of the other analytes, the proposed method showed comparable results with the buffered QuEChERS methodology. In view of the lower unit price of ethyl acetate as compared to acetonitrile and the lower amount of cleanup sorbents used, the proposed method offers a cheaper alternative to the buffered QuEChERS method with comparable proficiency.

As shown in Supplementary Figure S6 in the Supporting Information, the recoveries of acidic and basic compounds were much improved after buffering at the time of extraction as compared to the unbuffered ethyl acetate method.[4] The basic compounds, namely, cyromazine, atrazine desethyl 2-hydroxy, propamocarb, and pymetrozine, and the acidic compounds, namely, bispyribac, imazaquin, and imazosulfuron, which were pH dependent, showed improved recoveries due to optimum extraction conditions in the buffered method as compared to the earlier one.

The improved method is a common platform for the analysis of a large number of agrochemicals including acidic, basic, and neutral compounds with polar or midpolar nature. The buffered approach has improved the multiresidue analytical performance by offering stability and extractability to a wide range of compounds, especially those the stability of which is dependent on matrix pH. Use of a single extraction protocol for multiple matrices with minimum cleanup makes the method suitable for routine analysis in a commercial testing laboratory setup. The LC-MS/MS method enabled quantitative screening of a large number of target analytes at 1 ng/g and lower traces. Even the pesticides with problematic nature could be satisfactorily screened with sufficiently low LOQs (≤10 ng/g). The method has a good potential for implementation as a regulatory generic method for quantitative screening of residues in fruits and vegetables.

■ ASSOCIATED CONTENT

Ⓢ Supporting Information

Supplementary Figure S1: LC-MS/MS chromatogram of 296 agrochemicals in solvent standard at 10 ng/mL. Supplementary Figure S2: pH adjustment of matrices with diverse pH using optimized quantity of buffer. Supplementary Figure S3: effect on analyte response with respect to addition of variable volumes of diethylene glycol (DEG) solution (10%) during evaporation. Supplementary Figure S4: full scan analysis of standard methamidophos and DEG indicating coelution of DEG. Supplementary Figure S5: comparison of buffered QuEChERS and buffered ethyl acetate extraction methodologies. Supplementary Figure S6: comparative method performance for acidic and basic compounds in nonbuffered and buffered ethyl acetate extraction (I, recovery in grape, nonbuffered; II, recovery in grape, buffered; III, recovery in bitter gourd, nonbuffered; IV, recovery in bitter gourd, buffered; A, bispyribac; B, pymetrozine; C, cyromazine; D, atrazine desethyl 2-hydroxy). Supplementary Table S1: LC-MS/MS parameters of the test compoundsand. Supplementary Table S2. This material is available free of charge via the Internet at http://pubs.acs.org.

■ AUTHOR INFORMATION

Corresponding Author

*(K.B.) Phone: +91 20 2695 6091. Fax: +91 20 2695 6099. E-mail: kbgrape@yahoo.com.

Funding

We acknowledge funding support from the ICAR National Fellow project and APEDA, Ministry of Commerce, Government of India.

Notes

The authors declare no competing financial interest.

■ ACKNOWLEDGMENTS

We thank Dr. D. G. Naik from Agharkar Research Institute, Pune, India, for technical advice.

■ ABBREVIATIONS USED

QuEChERS, Quick, Easy, Cheap, Effective, Rugged, Safe, an acetonitrile-based sample preparation method used worldwide for pesticide residue analysis in foods; AOAC, Association of Analytical Communities; DG-SANCO, Directorate General for Health and Consumer Affairs

■ REFERENCES

(1) Insecticides registered under section 9 (3) of the Insecticides Act, 1968 as on 20/01/2012, New Delhi, India; http://www.cibrc.nic.in/reg_products.htm (accessed Aug 10, 2014).

DOI: 10.1021/jf505221e
J. Agric. Food Chem. 2015, 63, 4449−4456

(2) Pesticide EU-MRLs, Regulation (EC) No. 396/2005; http://ec.europa.eu/sanco_pesticides/public/index.cfm (accessed Aug 10, 2014).
(3) Food Safety and Standards (Contaminants, Toxins and Residues) Regulations, 2011; http://www.fssai.gov.in/Portals/0/Pdf/Food%20safety%20and%20standards%20(contaminats,%20toxins%20and%20residues)%20regulation,%202011.pdf (accessed Oct 14, 2014).
(4) Banerjee, K.; Oulkar, D. P.; Dasgupta, S.; Patil, S. B.; Patil, S. H.; Savant, R.; Adsule, P. G. Validation and uncertainty analysis of a multi-residue method for pesticides in grape using ethyl acetate extraction and liquid chromatography−tandem mass spectrometry. *J. Chromatogr., A* **2007**, *1173*, 98−109.
(5) Banerjee, K.; Oulkar, D. P.; Patil, S. B.; Jadhav, M. R.; Patil, S. H.; Dasgupta, S.; Bal, S.; Adsule, P. G. Multiresidue determination and uncertainty analysis of 87 pesticides in mango by liquid chromatography-tandem mass spectrometry. *J. Agric. Food Chem.* **2009**, *57*, 4068−4078.
(6) Banerjee, K.; Oulkar, D. P.; Patil, S. B.; Patil, S. H.; Dasgupta, S.; Savant, R.; Adsule, P. G. Single-laboratory validation and uncertainty analysis of 82 pesticides determined in pomegranate, apple, and orange by ethyl acetate extraction and liquid chromatography/tandem mass spectrometry. *J. AOAC Int.* **2008**, *91* (6), 1435−1445.
(7) Banerjee, K.; Utture, S.; Dasgupta, S.; Kandaswamy, C.; Pradhan, S.; Kulkarni, S.; Adsule, P. G. Multiresidue determination of 375 organic contaminants including pesticides, polychlorinated biphenyls and polyaromatic hydrocarbons in fruits and vegetables by gas chromatography-triple quadrupole mass spectrometry with introduction of semi-quantification approach. *J. Chromatogr., A* **2012**, *1270*, 283−295.
(8) Food and Feed Safety Alerts, European Commission; https://webgate.ec.europa.eu/rasff-window/portal (accessed Oct 10, 2014).
(9) Mol, H. G. J.; Rooseboom, A.; Van Dam, R.; Roding, M.; Arondeus, K.; Sunarto, S. Modification and re-validation of the ethyl acetate-based multi-residue method for pesticides in produce. *Anal. Bioanal. Chem.* **2007**, *389*, 1715−1454.
(10) Lehotay, S. J.; Mastovská, K.; Lightfield, A. Use of buffering and other means to improve results of problematic pesticides in a fast and easy method for residue analysis of fruits and vegetables. *J. AOAC Int.* **2005**, *88* (2), 615−629.
(11) Multiresidue method using QuEChERS followed by GC-QqQ/MS/MS and LC-QqQ/MS/MS for fruits and vegetables; http://www.crl-pesticides.eu/library/docs/fv/CRLFV_Multiresidue_methods.pdf (accessed Oct 14, 2014).
(12) Lehotay, S. J. Determination of pesticide residues in foods by acetonitrile extraction and partitioning with magnesium sulfate: collaborative study. *J. AOAC Int.* **2007**, *90*, 485−520.
(13) AOAC official method 2007.01, Pesticide residues in foods by acetonitrile extraction and partitioning with magnesium sulphate; http://www.weber.hu/PDFs/QuEChERS/AOAC_2007_01.pdf (accessed Oct 14, 2014).
(14) Guidance document on analytical quality control and validation procedures for pesticide residues analysis in food and feed SANCO/12571/2013; http://ec.europa.eu/food/plant/pesticides/guidance_documents/docs/qualcontrol_en.pdf (accessed Oct 14, 2014).
(15) Zhang, K.; Wong, J. W.; Yang, P.; Hayward, D. G.; Sakuma, T.; Zou, Y.; Schreiber, A.; Borton, C.; Nguyen, T.; Banerjee, K.; Oulkar, D. P. Protocol for an electrospray ionization tandem mass spectral product ion library: development and application for identification of 240 pesticides in foods. *Anal. Chem.* **2012**, *84* (13), 5677−5684.
(16) Anastassiades, M.; Scherbaum, E.; Taşdelen, B.; Štajnbaher, D. Recent developments in QuEChERS methodology for pesticide multiresidue analysis. In *Pesticide Chemistry: Crop Protection, Public Health, Environmental Safety*; Ohkawa, H., Miyagawa, H., Lee, P. W., Eds.; Wiley-VCH Verlag: Weinheim, Germany, 2007; pp 439−458.
(17) Wells, M. J. M. Principles of extraction and the extraction of semivolatile organics from liquids. In *Sample Preparation Techniques in Analytical Chemistry*; Mitra, S., Ed.; Wiley: Hoboken, NJ, USA, 2003; pp 37−138.
(18) Anastassiades, M.; Lehotay, S. J.; Štajnbaher, D.; Schenck, F. J. Fast and easy multiresidue method employing acetonitrile extraction/partitioning and "dispersive solid-phase extraction" for the determination of pesticide residues in produce. *J. AOAC Int.* **2003**, *86* (2), 412−431.
(19) Kostelac, D.; Anastassiades, M. QuEChERS validation method for acidic pesticides; http://www.eurl-pesticides.eu/library/docs/fv/2ndtr2007_AcidicKostelac.pdf (accessed Oct 10, 2014).
(20) Akiyama, Y.; Matsuoka, T.; Mitsuhashi, T. Multi-residue screening method of acidic pesticides in agricultural products by liquid chromatography/ time of flight mass spectrometry. *J. Pestic. Sci.* **2009**, *34* (4), 265−272.
(21) Mol, H. G. J.; Ruud, C. J.; Van Dam, R.; Steijger, O. M. Determination of polar organophosphorus pesticides in vegetables and fruits using liquid chromatography with tandem mass spectrometry: selection of extraction solvent. *J. Chromatogr., A* **2003**, *1015*, 119−127.
(22) Barr, D. B.; Barr, J. R.; Weerasekera, G.; Wamsley, J.; Kalb, S. R. Identification and quantification of diethylene glycol in pharmaceuticals implicated in poisoning epidemics: an historical laboratory perspective. *J. Anal. Toxicol.* **2007**, *31* (6), 295−303.
(23) Ferrer, C.; Lozano, A.; Agüera, A.; Girón, A. J.; Fernández-Alba, A. R. Overcoming matrix effects using the dilution approach in multiresidue methods for fruits and vegetables. *J. Chromatogr., A* **2011**, *1218*, 7634−7639.
(24) Stahnke, H.; Kittlaus, S.; Kempe, G. N.; Alder, L. Reduction of matrix effects in liquid chromatography-electrospray ionization mass spectrometry by dilution of the sample extracts: how much dilution is needed? *Anal. Chem.* **2012**, *84*, 1474−1482.

DOI: 10.1021/jf505221e
J. Agric. Food Chem. 2015, 63, 4449−4456

agricultural products in terms of more than 400 pesticides has not been validated (e.g., analytical sensitivity of the pesticides, evaluation of sample matrix effect for multiple pesticides, and recovery of the multiple pesticides from sample matrix). Moreover, high-polarity pesticides such as diquat dibromide ($\log P_{ow}$ = −4.6) need a special analytical method using hydrophilic interaction chromatography (HILIC)[13] or ion-pair LC.[14] Therefore, it is difficult to analyze both high-polarity and low-polarity pesticides simultaneously under the same LC conditions. In addition, because analytical times for multiresidue pesticide analysis by LC/MS or LC/MS/MS are longer than 30 min, an improved throughput without reduction in chromatographic resolution is one of the technical issues that must be overcome.

Supercritical fluid chromatography (SFC) is a chromatographic technique that uses a supercritical fluid (SF) as a mobile phase. Because the temperature and pressure of a SF exceed the critical point, the SF also has certain physicochemical properties such as low viscosity and high diffusivity. By using SFC, one can achieve a high-throughput analysis without reduction in chromatographic resolution.[15,16] Supercritical carbon dioxide ($SCCO_2$) is the most frequently used mobile phase for SFC, because carbon dioxide can be easily converted to its supercritical state (critical temperature, 31.1 °C; and critical pressure, 7.38 MPa). $SCCO_2$ also exhibits favorable properties because it is chemically inert, nonflammable, relatively nontoxic, easy to handle, and inexpensive. Although $SCCO_2$ has relatively low polarity, the polarity of the mobile phase in SFC can be changed considerably by adding a polar organic solvent such as methanol as a modifier.[17] Therefore, SFC can be used in the analysis of chemical compounds with a wide range of polarities.[18,19] In previous works, we presented the potential of SFC coupled to triple-quadrupole mass spectrometry (QqQMS) under MRM for the high-throughput and simultaneous analysis of pesticides using 17 selected pesticides with a wide range of molecular weights (112.1−888.6) and polarities ($\log P_{ow}$ = −4.6 to 6.9).[20] A column screening study determined that the GL Sciences Inertsil ODS-EP column, containing polar embedded reverse phase particles, was suitable for the simultaneous SFC analysis of a wide variety of pesticides. Consequently, high-polarity pesticides (e.g., fosetyl, $\log P_{ow}$ = −2.7, and diquat dibromide), and low-polarity pesticides (e.g., cypermethrin, $\log P_{ow}$ = 6.6, and tralomethrin, $\log P_{ow}$ = 5.5) could be analyzed simultaneously by performing a single-run SFC/MS/MS method with a 20 min run time. However, our previous analytical system was composed of an SFC and a QqQMS. Although QqQMS-based methods provide highly sensitive and robust quantitative measurements, this approach has drawbacks and limitations, which are inherent to the targeted acquisition involved in the MS measurement: (i) usage limited only to targeted pesticide analysis; (ii) requirement of a complicated setup for the determination of the optimized MRM transition settings for every individual pesticide; and (iii) limitation in terms of the number of pesticides detected in a single-run experiment due to limitations regarding instrument performance (i.e., scanning speed).[21] Meanwhile, high-resolution mass spectrometry (HRMS) has attracted attention as a new promising tool for multiresidue pesticide analysis.[12,21]

The objective of the present research was to develop a practical and high-throughput simultaneous analytical system for multiple pesticides using SFC coupled to HRMS, (i.e., Q Exactive, a high-performance benchtop quadrupole Orbitrap mass spectrometer) (SFC/Q Exactive) and an automated library-based detection. The SFC/Q Exactive system provides high chromatographic separation, high mass resolution (a value of $m/\Delta m$ = 70000), and high mass accuracy (<5 ppm) with positive/negative polarity switching. The SFC/Q Exactive system was used in the screening of 508 pesticides, which have been previously analyzed by a combination of GC/MS and LC/MS. Together with the evaluation of the effect of the biological matrix on multiple pesticide analysis using a QuEChERS-based spinach extract without dispersive solid phase extraction (d-SPE), we have also addressed the performance of the recently developed automated HRMS software (ExactFinder) in multiresidue pesticide analysis.

MATERIALS AND METHODS

Chemicals, Reagents, and Materials. Ammonium formate was obtained from Sigma-Aldrich Co. (St. Louis, MO, USA). MS grade methanol was purchased from Kanto Chemical Co., Ltd. (Tokyo, Japan). All other chemicals and reagents were of the highest analytical grade available. Carbon dioxide (99.99% grade, Nerikigasu, Osaka, Japan) was used as the SFC mobile phase. All standards of pesticides (pesticide mix solutions for food analysis) were purchased from Hayashi Pure Chemical Ind., Ltd. (Osaka, Japan) and are listed in Table S1 of the Supporting Information. A total of 17 standard mixtures with 7−56 targeted substances were used for the development of an analytical method for multiresidue pesticides using SFC/Q Exactive (see Table S1). Each standard mix solution was diluted with methanol to 0.02, 0.05, 0.1, 0.2, 0.5, 1, 2, 5, 10, 20, 50, 100, 200, 500, and 1000 $\mu g\ L^{-1}$, and these mixture solutions were used to validate the performance of our analytical system. Spinach was purchased from the local markets in Miyazaki, Japan, and used for sample purposes.

Sample Preparation. The extraction method for spinach used the QuEChERS procedure (without d-SPE protocol) using an Agilent Bond Elut QuEChERS EN 15662 kit (Agilent Technologies, Santa Clara, CA, USA).[22] Spinach was homogenized using a Retsch Grindomix GM200 (Retsch, Haan, Germany). Homogenized spinach (10 g) was placed in a 50 mL centrifugation tube, and 10 mL of acetonitrile was added. The tube was shaken manually for 1 min. Anhydrous NaCl (1 g), anhydrous $MgSO_4$ (4 g), sodium citrate (1 g), and disodium citrate sesquihydrate (0.5 g) were added in the tube. The tube was shaken using a vortex mixer for 30 s. Subsequently, the mixture was centrifuged for 5 min at 1500*g* using an LX-120 (Tomy Seiko Co., Ltd., Tokyo, Japan). The supernatant (the final spinach extract) contained the equivalent of 1 kg sample L^{-1}. For the evaluation of sample matrix effect, 7 standard mixture solutions with 47−106 targeted substances (see Table S2) were added individually to the extract. The final concentration of each standard mixture was adjusted to 1, 10, and 100 $\mu g\ kg^{-1}$. The prepared mixtures were used as samples to validate the system sensitivity and selectivity in the presence of contaminants.

SFC/MS Analysis. The SFC/MS analysis was performed using an Analytical SFC Method Station (Waters, Milford, MA, USA) coupled with a Q Exactive, a high-performance benchtop quadrupole Orbitrap mass spectrometer (Thermo Fisher Scientific, Waltham, MA, USA). The SFC system was equipped with a binary pump, a temperature-controlled column component, an autosampler, and a refrigerator. The mass spectrometer was equipped with an electron spray ionization (ESI) source. The SFC conditions were as follows: mobile phase, $SCCO_2$ (solvent A) and methanol with 0.1% ammonium formate (solvent B); injection volume, 5 μL; flow rate, 3 mL min^{-1}; column temperature, 35 °C; and column, Inertsil ODS-EP (250 × 4.6 mm i.d., particle size = 5 μm, GL Sciences, Tokyo, Japan). The gradient conditions were as follows: 5% B, 0−1 min; 5−10% B, 1−2 min; 10−20% B, 2−12 min; 20−30% B, 12−14 min; 30% B, 14−18 min; 30−5% B, 18−19 min; and 5% B, 19−20 min. The MS analysis conditions were as follows: polarity, positive and negative ionization; sheath gas flow rate, 20 arb; auxiliary (Aux) gas flow rate, 5 arb; spray voltage, 3600 V for both positive and negative ionization; capillary temper-

DOI: 10.1021/jf5056248
J. Agric. Food Chem. 2015, 63, 4457−4463

ature, 360 °C; S-lens level, 50; heater temperature, 200 °C; mass resolution, 70000; automatic gain control (AGC) target, 1,000,000; maximum IT, 250 ms; and scan range, 100−1500 (m/z). The SFC and MS analyses were controlled using the software SuperCrom (Waters) and Xcalibur 1.4 (Thermo Fisher Scientific), respectively.

Data Analysis. ExactFinder ver. 2.0 software (Thermo Fisher Scientific) was used for acquisition and data processing. Using this software, we developed a components database, searched for compound peaks, and calculated the peak area for each compound. The optimized automatic filter criteria for peak picking and compound identification were as follows: allowed mass deviation, 5 ppm; allowed intensity deviation of all expected isotopic ions, 10%; isotopic pattern matching score, >70%; retention time (RT) width, <30 s; and response threshold, 5000. The main criteria are that the mass deviation for each ion should be <5 ppm between the measured m/z and the theoretical m/z and that the relative intensity deviation should be <10% between the measured and theoretical values. However, the experimental and theoretical intensities are different for each ion. The spectral noise threshold is used to decide which peaks will be monitored in the experimental data. The theoretical noise threshold is calculated using the noise label, the theoretical intensity, and the experimental intensity of the monoisotopic ions. The ions having intensities are above the theoretical noise threshold are expected to be identified in the measured spectrum. These are the ions the program focuses on afterward, during the calculation of the isotopic score. The number of these ions indicates the number of expected isotopic pattern peaks based on the Fourier transform noise in the spectrum. However, the actual number of expected ions in the measured spectrum can be different from the theoretical one, due to variations in concentration or ionization efficiency. Therefore, ExactFinder uses the isotopic pattern to obtain a score value from a combination of the mass and intensity deviations between the theoretical and experimental spectra. The score is calculated using each ion's expected fit and the individual fit score weighted by its expected intensity. The normalized difference in mass and intensity between the theoretical and experimental spectra of each ion is summed by vector addition. The weighting contribution of each individual ion to the final isotopic pattern score is proportional to its intensity. The weighting factor of each ion is shown as the ratio between the intensity of each ion and the sum of the intensities of all the expected ions. The weighted deviation for each individual ion is computed by multiplying the vector form deviation by the weighting factor. The final isotopic pattern matching score is calculated as the percentage of the weighted deviation of each individual ion minus the sum of all weighted deviation value (ExactFinder ver. 2.0). All processing data were saved in CSV format, and then Microsoft Excel 2007 was used to calculate the average and relative standard deviation values of RT or peak area and linearity.

RESULTS AND DISCUSSION

Optimization of SFC and Q Exactive Conditions. To develop a practical and high-throughput simultaneous analytical method for multiple pesticides using a full-scan SFC/Q Exactive system, we used 508 agricultural chemicals covering a wide polarity range (logP_{ow} from −4.2 to 7.7) and a wide molecular weight range (from 99.0 to 872.5) as analytes. For the separation of multiple pesticides using SFC, we selected an Inertsil ODS-EP column, which contained polar embedded reverse phase particles. This column offered an effective separation of pesticides with a wide range of chemical properties in our previous investigation.[20] The modifier concentrations were changed from the 5% customary in SFC analyses to 30% to adjust to the various degrees of solubility of the targeted pesticides. Several compounds that were expected to exhibit weak retention on the stationary phase were also included in the target components. Therefore, the modifier percentage was increased slowly from 5 to 10%, stepwise from 10 to 20%, and dramatically from 20 to 30% and was maintained at 30% for 4 min to wash out any remaining hydrophilic compounds.

The Q Exactive operating parameters including sheath gas flow rate, Aux gas flow rate, spray voltage, capillary temperature, and heater temperature were optimized to separate a set of selected pesticides with a wide molecular weight range (i.e., aldicarb, MW 190.3; acibenzolar *S*-methyl, MW 210.3; clothianidin, MW 249.7; carpropamid, MW 334.7; indanofan, MW 340.8; tebufenozide, MW 352.5; and novaluron, MW 492.7). The variations in peak area for each of the seven pesticides was monitored using different parameter settings, which were as follows: sheath gas flow rate, from 20 to 50 arb; Aux gas flow rate, from 5 to 10 arb; spray voltage, from 1 to 5 kV; capillary temperature, from 200 to 400 °C; and heater temperature, from 200 to 350 °C. Accordingly, the operating conditions for Q Exactive were set as follows: sheath gas flow rate, 20 arb; Aux gas flow rate, 5 arb; spray voltage, 3,600 V; capillary temperature, 360 °C; and heater temperature, 200 °C.

Finally, we evaluated the effective mass resolving power (a value of $m/\Delta m$ = 70000) and mass accuracy (<5 ppm) under the optimized SFC and MS conditions using two sets of isobaric pesticides with a mass difference of <0.01 Da (group 1, tolyfluanid metabolite, m/z 215.0848, and metribuzin, m/z 215.0960; group 2, isoxathion m/z 314.0607, triazophos, m/z 314.0710, and hexaconazol m/z 314.0827). Our optimized full-scan SFC/Q Exactive system achieved discrimination among very similar isobaric pesticides through a combination of high mass resolution, high mass accuracy, and highly efficient separation by SFC (Figure 1).

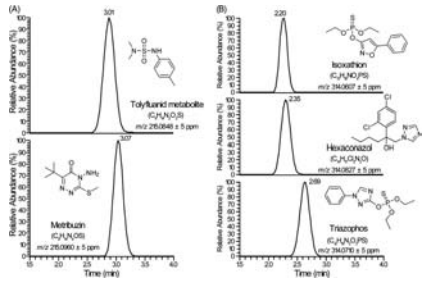

Figure 1. Separation of two sets of isobaric pesticide standards using the optimized full-scan SFC/Q Exactive system: (A) extracted ion chromatograms of tolyfluanid metabolite $(M + H)^+$ (m/z 215.0848 ± 5 ppm, RT 3.01 min) and metribuzin $(M + H)^+$ (m/z 215.0960 ± 5 ppm, RT 3.07 min); (B) extracted ion chromatograms of isoxathion $(M + H)^+$ (m/z 314.0607 ± 5 ppm, 2.20 min), hexaconazol $(M + H)^+$ (m/z 314.0827 ± 5 ppm, 2.35 min), and triazophos $(M + H)^+$ (m/z 314.0710 ± 5 ppm, 2.69 min).

Development of a Multiresidue Pesticide Database Using the SFC/Q Exactive System and ExactFinder Software. The workflow for the development of the pesticide database using the SFC/Q Exactive system and ExactFinder software is shown in Figure 2. To create the pesticide database, the compound name, the molecular formula, and all expected molecular ions [i.e., $(M + H)^+$, $(M + NH_4)^+$, $(M + Na)^+$, $(M - H)^-$, $(M + HCOO)^-$, and $(M + CH_3COO)^-$] of the targeted 508 psticides were stored in the ExactFinder database. Subsequently, 17 kinds of standard mixture solutions at a concentration of 1 mg L^{-1} were analyzed individually using the optimized full-scan SFC/Q Exactive method with high-throughput performance (20 min run time). Peak picking

DOI: 10.1021/jf5056248
J. Agric. Food Chem. 2015, 63, 4457−4463

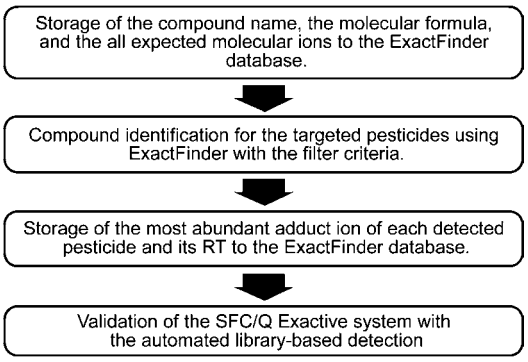

Figure 2. Workflow for the development of the pesticide database using the SFC/Q Exactive system and ExactFinder software in the present study.

and compound identification for the targeted 508 pesticides were carried out using ExactFinder with the filter criteria (i.e., allowed mass deviation, 5 ppm; allowed intensity deviation of all expected isotopic ions, 10%; isotopic pattern matching score, >70%). The main criteria are that the mass deviation for each ion should be <5 ppm between the measured m/z and the theoretical m/z and that the relative intensity deviation should be <10% between the measured and theoretical values. The isotopic pattern matching score, which is a vector sum approach based on a combination of the exact mass and the predicted intensity of each expected isotopic ion, was also used to determine the targeted pesticides (see Materials and Methods for details). In total, 444 pesticides were identified and the information on their RT and the most abundant adduct ion of each detected pesticide were added to the database; 64 chemicals were not confirmed by ExactFinder (see Table S1). We considered that this was due to the fact that either those chemicals were not solvated in $SCCO_2$ or methanol or were not efficiently ionized by electrospray ionization (ESI). Also, three sets of structural isomers, butachlor and pretilachlor, iprodione and iprodion metabolite, and promecarb and fenobucarb, coeluted. However, the separation of a large number of geometric isomers (i.e., fenpyroximate, phenothrin, cypermethrin, cyfluthrin, permethrin, bitertanol, pyriminobac methyl, metominostrobin, diclobutrazol, ferimzone, triadimenol, pyrifenox, and bromoconazole) and structural isomers (i.e., aldicarb and butocarboxim; esfenvalerate and fenvalerate; bioresmethrin and resmethrin; phenmedipham and desmedipham; haloxyfop and oxyfluorfen; acetochlor and alachlor; trifluralin and benfluralin; phoxim and quinalphos; ethiofencarb and methiocarb; 2,3,5-trimethacarb, 3,4,5-trimethacarb, and isoprocarb; bendiocarb and dioxacarb; prometryn and terbutryn; and MPMC and XMC) was enhanced by using high resolution in SFC (Figure 3). Our SFC/Q Exactive system also allowed simultaneous detection of both cationic (positive ion) and anionic (negative ion) species owing to their positive/negative fast polarity switching function.

A validation test for the 444 pesticides was performed to evaluate the system. Diluted stock solutions (0.02−1000 μg L^{-1}) were used to estimate the limit of detection (LOD), the linear dynamic range, its linearity (R^2 values), and repeatability. All of the experiments were repeated five times. The Q Exactive system removes the low-intensity regions, which are regarded as noise during the storage of raw data, to reduce the huge amount of data obtained from Fourier transform. Therefore, noise intensity was very low, and the signal-to-noise (S/N) ratio cannot be calculated in many cases. An S/N = 3 or 10 as a reference for the calculation of LOD or limit of quantification (LOQ), respectively, was not available. In this study, the LOD was defined as the actual detected concentration with the repeatability of peak area value. The threshold of the repeatability was set at a relative standard deviation (RSD) <25%. The linear range was calculated as that interval where the R^2 was >0.99. All data including pesticide name, molecular formula, polarity, adduct ion, RT, RSD for RT and peak area at LOD, linear range, and R^2 are presented in Table S1. The LOD for 391 pesticides (88.1% of the 444 pesticides investigated) was <10 μg L^{-1} (as shown in Table 1). The peak intensities for 53 chemicals were too low, even when their concentrations in the sample were high. This was due to the fact that almost all of these chemicals are usually analyzed using GC/electron ionization (EI)-MS^{2-5} because ESI is not considered as a suitable ionization technique for these compounds. However, the results above showed anew the wide coverage that SFC has and its usefulness in the rapid analysis of a wide variety of chemicals with logP_{ow} ranging from −4.2 to 7.7. The number of analytes was increased from the 17 chemicals analyzed in our

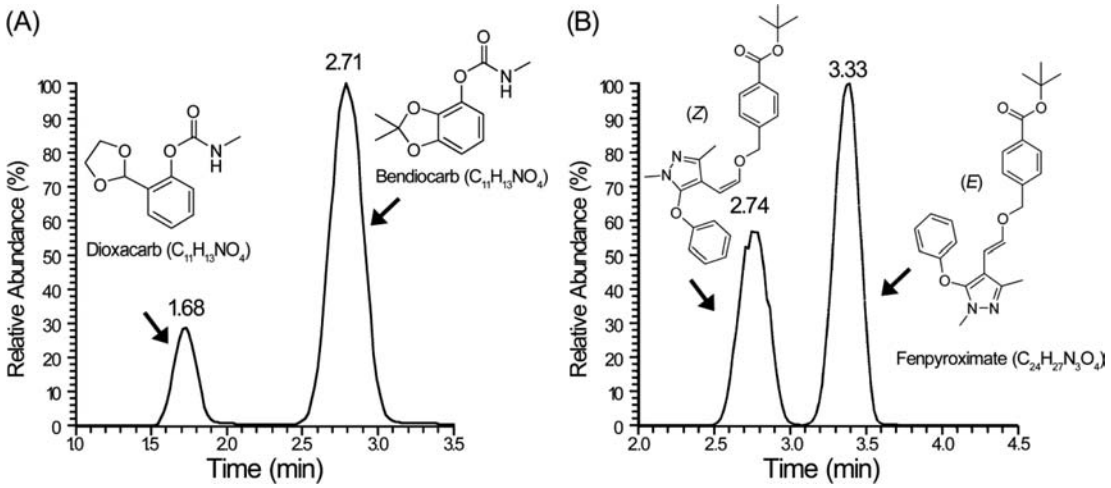

Figure 3. Representative chromatograms of isomeric pesticides obtained by the optimized SFC/Q Exactive system: (A) structural isomers, dioxacarb (1.68 min) and bendocarb (2.71 min); (B) geometrical isomers, (*Z*)-fenpyroximate (2.74 min) and (*E*)-fenpyroximate (3.33 min).

DOI: 10.1021/jf5056248
J. Agric. Food Chem. 2015, 63, 4457−4463

Table 1. Analytical Sensitivity of SFC/Q Exactive System for Multiresidue Pesticide Screening

LOD (μg L^{-1})	0.02	0.05	0.1	0.2	0.5	1	2	5	10	20	50	100	200	500	1000
no. of pesticides	44	84	59	45	43	41	39	22	14	17	12	11	7	4	2

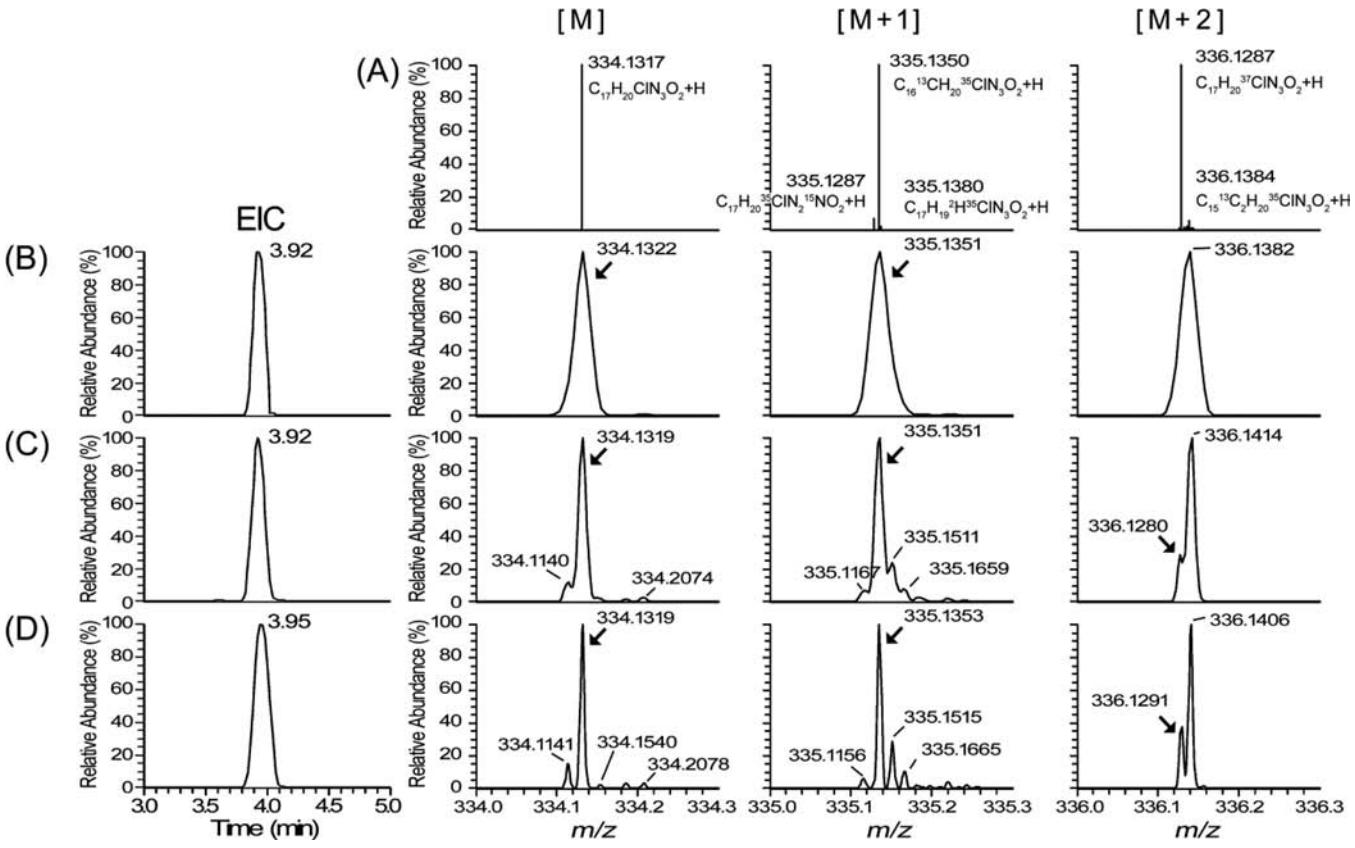

Figure 4. Influence of mass resolution on pesticide screening in the presence of contaminants: (A) theoretical monoisotopic ion and isotopic ions derived from furametpyr; extracted ion chromatograms and spectrum of furametpyr in spinach extract at different mass resolutions of 17500 (B), 35000 (C), and 70000 (D).

previous study to 444. Furthermore, these results indicated that not only the separation technique but also the ionization technique must be improved to construct a simultaneous analytical system for agricultural chemicals.

Validation of the SFC/Q Exactive System and ExactFinder Software Using Spinach Extracts Spiked with Pesticide Standards. The use of isotopic ions with both high mass accuracy and high mass resolution was considered useful to reduce the number of false positives in compound identification using the HRMS full-scan data.[12,23] However, too strict criteria may result in analytes going undetected (false negatives) if mass assignment obtained during the measurement proves to be insufficient or unreliable. For this reason, a thorough evaluation of mass assignment errors in complex samples and understanding of the parameters causing them is essential for automated wider scope screening methods.[21] Thus, we considered the influence of mass resolution on pesticide screening in the presence of contaminants (i.e., false-negative response). QuEChERS spinach extracts without d-SPE spiked with the seven different standard mixtures at the 10 μg kg^{-1} level were used as samples. The SFC/Q Exactive analyses were performed at different mass resolutions, that is, 17500, 35000, and 70000, and the raw data were analyzed using ExactFinder with the optimized automatic filter criteria (see Materials and Methods). The presence of 308, 349, and 373 chemicals was confirmed when using 17500, 35000, and 70000 mass resolutions, respectively (Table S2). These differences were caused by insufficient resolution, which made the contaminants hard to separate. For example, the extracted ion chromatogram and the spectra of the proton adduct of furametpyr (theoretical monoisotopic mass, m/z 334.1317) in spinach extract are shown in Figure 4. Furametpyr was not confirmed by ExactFinder at mass resolutions of 17500 and 30000. However, a peak derived from the monoisotopic ion of furametpyr was present in the case of both mass resolution settings (Figure 4B,C). The reason furametpyr could not be confirmed at mass resolutions of 17500 and 30000 was that its isotopic pattern matching score was not above the threshold value. In Figure 4D, the experimentally observed isotopic mass (M + 2, m/z 336.1291) could be discerned for the contaminant (m/z 336.1406) near the target mass, when using a mass resolution of 70000. The separation of target and contaminant in the spectrum becomes more difficult with a decrease in mass resolution. These results suggested that an analytical system with high mass resolution (a value of $m/\Delta m$ = 70000) and high mass accuracy (<5 ppm) must be used to distinguish between the target and the noise spectrum in the full-scan analysis to reduce false positives and negatives.

Figure 5 shows the number of confirmed pesticides at 1, 10, and 100 μg kg^{-1} using the optimized SFC/Q Exactive system

DOI: 10.1021/jf5056248
J. Agric. Food Chem. 2015, 63, 4457−4463

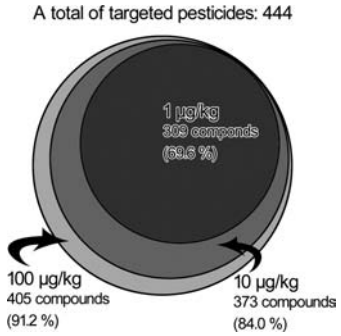

Figure 5. Comparison of the number of confirmed pesticides in QuEChERS spinach extracts at 1, 10, and 100 μg kg^{-1} using the SFC/Q Exactive system and ExactFinder software.

with a mass resolution of 70000 and the automated library-based detection (see Table S2 for details). The overall detection rate was 1 μg kg^{-1} for 69.6%, 10 μg kg^{-1} for 84.0%, and 100 μg kg^{-1} for 91.2% of the 444 pesticides investigated. In the range of 1−100 μg kg^{-1} levels, a large number of pesticides was detected, despite the lack of solid-phase purification; 39 pesticides were not identified regardless of their concentration. These included 24 chemicals considered to have poor sensitivity even when analyzed only in the absence of contaminants. Other pesticides (i.e., 15 chemicals) were easy to detect even at concentrations below 10 μg L^{-1}. Therefore, strong ion-suppressing effects of the biological matrices were considered as the main reason these chemicals were not found. This indicated that there could be other reasons, such as a decrease in the isotopic pattern score caused by contaminants. However, reducing the threshold of the isotopic pattern score may carry a significant risk of increasing the false positives because the threshold of the isotopic pattern score is an important criterion in the screening of target chemical ions from the full-scan analysis data. Fragment ion information is expected to be effective in solving this problem.

These results indicated that it is possible to get an accurate result rapidly in the presence of contaminants by using the SFC/Q Exactive (time for data acquisition, 72 samples per day) and ExactFinder software for data processing (time for data processing of 72 samples, approximately 45 min). On the other hand, the purification procedure is unavoidable to reduce the ionization suppression. Therefore, it might be a new challenge to attempt to optimize the purification conditions to purify more agriculture chemicals simultaneously.

In conclusion, the SFC/Q Exactive system developed in this study has sufficient sensitivity and accuracy for the practical analysis of multiresidue pesticides. The advantage of SFC is that it can achieve a high-throughput multiple pesticide analysis without reduction in chromatographic resolution, because a total of 444 chemicals including isomers were analyzed simultaneously by performing the single-run SFC/Q Exactive method with a 20 min run time. In addition, the effect of the biological matrix on multiple pesticide analysis using a QuEChERS-based spinach extract without d-SPE was evaluated using the SFC/Q Exactive system and ExactFinder software with the optimized automatic filter criteria. Using this system, we demonstrated that the use of both monoisotopic ion and isotopic ions with high mass accuracy (a value of $m/\Delta m$ = 70000) and high mass resolution (<5 ppm) was considered useful to reduce the number of false positives and negatives in compound identification using the HRMS full-scan data. Finally, we demonstrated that a total of 373 pesticides were confirmed in QuEChERS spinach extracts at 10 μg kg^{-1} levels (provisional MRLs in Japan), despite the lack of solid-phase purification. Taking all of the present results into account, our developed analytical system is a promising new tool for the accurate multiresidue pesticide screening with high throughput (time for data acquisition, 72 samples per day, and time for data processing of 72 samples, approximately 45 min).

■ ASSOCIATED CONTENT

Ⓢ Supporting Information

Additional tables (S1 and S2) as discussed in the text. This material is available free of charge via the Internet at http://pubs.acs.org.

■ AUTHOR INFORMATION

Corresponding Author

*(T.B.) Phone/fax: +81-(0)6-6879-7418. E-mail: bamba@bio.eng.osaka-u.ac.jp.

Funding

This work was supported by the Development of Systems and Technology for Advanced Measurement and Analysis Project of The Japan Science and Technology Agency (JST).

Notes

The study represents a portion of the dissertation submitted by M. Ishibashi to Osaka University in partial fulfillment of the requirement for his Ph.D. degree.

The authors declare no competing financial interest.

■ ACKNOWLEDGMENTS

We are grateful to T. Hamasaka of Thermo Fisher Scientific (Yokohama, Japan) for the technical support of ExactFinder software.

■ ABBREVIATIONS USED

MRLs, maximum residue limits; GC/MS, gas chromatography/mass spectrometry; LC/MS, liquid chromatography/mass spectrometry; SFC/MS, supercritical fluid chromatography/mass spectrometry; $SCCO_2$, supercritical carbon dioxide; QqQMS, triple-quadrupole mass spectrometry; HRMS, high-resolution mass spectrometry; SFC/Q Exactive, supercritical fluid chromatography/quadrupole Orbitrap mass spectrometery; d-SPE, dispersive solid phase extraction

■ REFERENCES

(1) Tomlin, C. D. S. *The Pesticide Manual − A World Compendium*, 16th ed.; British Crop Protection Council (BCPC) Publications: Hampshire, UK, 2009.

(2) Alder, L.; Greulich, K.; Kempe, G.; Vieth, B. Residue analysis of 500 high priority pesticides: better by GC-MS or LC-MS? *Mass Spectrom. Rev.* **2006**, *25*, 838−865.

(3) Pihlström, T.; Blomkvist, G.; Friman, P.; Pagard, U.; Österdahl, B.-G. Analysis of pesticide residues in fruit and vegetables with ethyl acetate extraction using gas and liquid chromatography with tandem mass spectrometric detection. *Anal. Bioanal. Chem.* **2007**, *389*, 1773−1789.

(4) Lehotay, S. J.; Koesukwiwat, U.; van der Kamp, H.; Mol, H. G.; Leepipatpiboon, N. Qualitative aspects in the analysis of pesticide residues in fruits and vegetables using fast, low-pressure gas chromatography-time-of-flight mass spectrometry. *J. Agric. Food Chem.* **2011**, *59*, 7544−7556.

(5) Hayward, D. G.; Wong, J. W.; Shi, F.; Zhang, K.; Lee, N. S.; DiBenedetto, A. L.; Hengel, M. J. Multiresidue pesticide analysis of botanical dietary supplements using salt-out acetonitrile extraction,

DOI: 10.1021/jf5056248
J. Agric. Food Chem. 2015, 63, 4457−4463

solid-phase extraction cleanup column, and gas chromatography-triple quadrupole mass spectrometry. *Anal. Chem.* **2013**, *85*, 4686−4693.
(6) Stalikas, C. D.; Pilidis, G. A. Development of a method for the simultaneous determination of phosphoric and amino acid group containing pesticides by gas chromatography with mass-selective detection. Optimization of the derivatization procedure using an experimental design approach. *J. Chromatogr., A* **2000**, *872*, 215−225.
(7) Soler, C.; Picó, Y. Recent trends in liquid chromatography-tandem mass spectrometry to determine pesticides and their metabolites in food. *Trends Anal. Chem.* **2007**, *26*, 103−115.
(8) Gómez-Ramos, M. M.; Ferrer, C.; Malato, O.; Agüera, A.; Fernández-Alba, A. R. Liquid chromatography-high-resolution mass spectrometry for pesticide residue analysis in fruit and vegetables: screening and quantitative studies. *J. Chromatogr., A* **2013**, *1287*, 24−37.
(9) Wong, J.; Leung, D.; Chow, W. Applications of LC/ESI-MS/MS and UHPLC QqTOF MS for the determination of 148 pesticides in berries. *J. Agric. Food Chem.* **2010**, *58*, 5904−5925.
(10) Zhang, K.; Wong, J. W.; Yang, P.; Tech, K.; DiBenedetto, A. L.; Lee, N. S.; Hayward, D. G.; Makovi, C. M.; Krynitsky, A. J.; Banerjee, K.; Jao, L.; Dasgupta, S.; Smoker, M. S.; Simonds, R.; Schreiber, A. Multiresidue pesticide analysis of agricultural commodities using acetonitrile salt-out extraction, dispersive solid-phase sample clean-up, and high-performance liquid chromatography-tandem mass spectrometry. *J. Agric. Food Chem.* **2011**, *59*, 7636−7646.
(11) Gilbert-López, B.; García-Reyes, J. F.; Fernández-Alba, A. R.; Molina-Díaz, A. Evaluation of two sample treatment methodologies for large-scale pesticide residue analysis in olive oil by fast liquid chromatography−electrospray mass spectrometry. *J. Chromatogr., A* **2010**, *1217*, 3736−3747.
(12) Mol, H. G. L.; Zomer, P.; de Koning, M. Qualitative aspects and validation of a screening method for pesticides in vegetables and fruits based on liquid chromatography coupled to full scan high resolution (Orbitrap) mass spectrometry. *Anal. Bioanal. Chem.* **2012**, *403*, 2891−2908.
(13) Hao, C.; Zhao, X.; Morse, D.; Yang, P.; Taguchi, V.; Morra, F. Optimized liquid chromatography tandem mass spectrometry approach for the determination of diquat and paraquat herbicides. *J. Chromatogr., A* **2013**, *1304*, 169−176.
(14) Oh, J.-A.; Lee, J.-B.; Lee, S.-H.; Shin, H.-S. Ultra-trace level determination of diquat and paraquat residues in surface and drinking water using ion-pair liquid chromatography with tandem mass spectrometry: a comparison of direct injection and solid-phase extraction methods. *J. Sep. Sci.* **2014**, *37*, 2900−2910.
(15) Bamba, T.; Shimonishi, N.; Matsubara, A.; Hirata, K.; Nakazawa, Y.; Kobayashi, A.; Fukusaki, E. High throughput and exhaustive analysis of diverse lipids by using supercritical fluid chromatography-mass spectrometry for metabolomics. *J. Biosci. Bioeng.* **2008**, *105*, 460−469.
(16) Matsubara, A.; Bamba, T.; Ishida, H.; Fukusaki, E.; Hirata, K. Highly sensitive and accurate profiling of carotenoids by supercritical fluid chromatography coupled with mass spectrometry. *J. Sep. Sci.* **2009**, *32*, 1459−1464.
(17) Bamba, T.; Lee, J. W.; Matsubara, A.; Fukusaki, E. Metabolic profiling of lipids by supercritical fluid chromatography/mass spectrometry. *J. Chromatogr., A* **2013**, *1250*, 212−219.
(18) Taguchi, K.; Fukusaki, E.; Bamba, T. Simultaneous and rapid analysis of bile acids including conjugates by supercritical fluid chromatography coupled to tandem mass spectrometry. *J. Chromatogr., A* **2013**, *1299*, 103−109.
(19) Taguchi, K.; Fukusaki, E.; Bamba, T. Simultaneous analysis for water- and fat-soluble vitamins by a novel single chromatography technique unifying supercritical fluid chromatography and liquid chromatography. *J. Chromatogr., A* **2014**, *1362*, 270−277.
(20) Ishibashi, M.; Ando, T.; Sakai, M.; Matsubara, A.; Uchikata, T.; Fukusaki, E.; Bamba, T. High-throughput simultaneous analysis of pesticides by supercritical fluid chromatography/tandem mass spectrometry. *J. Chromatogr., A* **2012**, *1266*, 143−148.
(21) Kellmann, M.; Muenster, H.; Zomer, P.; Mol, H. Full scan MS in comprehensive qualitative and quantitative residue analysis in food and feed matrices: how much resolving power is required? *J. Am. Soc. Mass Spectrom.* **2009**, *20*, 1464−1476.
(22) Anastassiades, M.; Lehotay, S. J.; Štajnbaher, D.; Schenck, F. J. Fast and easy multiresidue method employing acetonitrile extraction/partitioning and "dispersive solid-phase extraction" for the determination of pesticide residues in produce. *J. AOAC Int.* **2003**, *86*, 412−431.
(23) Moschet, C.; Piazzoli, A.; Singer, H.; Hollender, J. Alleviating the reference standard dilemma using a systematic exact mass suspect screening approach with liquid chromatography−high resolution mass spectrometry. *Anal. Chem.* **2013**, *85*, 10312−10320.

DOI: 10.1021/jf5056248
J. Agric. Food Chem. 2015, 63, 4457−4463

Table 1. Noncoded Levels of the Factors Screened by Plackett−Burman Design

run order	salt (%)	pH	temperature (°C)	pre-incubation time (min)	stirring rate (rpm)	extraction time (min)	solvent (% v/v)	dilution (%, w/w)
5	10.0	9.0	30.0	15.0	750.0	15.0	10.0	0.0
2	10.0	9.0	30.0	15.0	250.0	15.0	0.0	50.0
12	0.0	4.0	30.0	5.0	250.0	15.0	0.0	0.0
11	0.0	9.0	30.0	5.0	250.0	60.0	10.0	50.0
3	0.0	9.0	60.0	5.0	750.0	15.0	0.0	0.0
1	10.0	4.0	60.0	5.0	250.0	15.0	10.0	50.0
9	0.0	4.0	30.0	15.0	750.0	60.0	0.0	50.0
13 (C)	5.0	6.5	45.0	10.0	500.0	37.5	5.0	25.0
14 (C)	5.0	6.5	45.0	10.0	500.0	37.5	5.0	25.0
8	0.0	4.0	60.0	15.0	750.0	15.0	10.0	50.0
4	10.0	4.0	60.0	15.0	250.0	60.0	0.0	0.0
15 (C)	5.0	6.5	45.0	10.0	500.0	37.5	5.0	25.0
7	0.0	9.0	60.0	15.0	250.0	60.0	10.0	0.0
10	10.0	4.0	30.0	5.0	750.0	60.0	10.0	0.0
6	10.0	9.0	60.0	5.0	750.0	60.0	0.0	50.0

The aforementioned facts and limitations led to the development of a matrix-compatible SPME fiber coating.[18] The same authors have employed the matrix-compatible coating to develop and validate an automated direct immersion−solid-phase microextraction−gas chromatography−time-of-flight mass spectrometry (DI-SPME-GC-ToFMS) method for the determination of triazole pesticides in grapes and strawberries. Rewarding results were achieved, as LOQs ranged from 0.25 to 5 ng/g for both matrices.[19]

To date, the application of SPME has not been considerably established for multiclass analysis of contaminants in food samples, given the limitations and challenges encountered concerning coating suitability toward complex matrices. In light of the good performance achieved by the developed matrix compatible coating, in this work, a DI-SPME-GC-ToFMS method for multiresidue analysis of pesticides in grapes is presented. The main goal was to develop a detailed protocol for the analysis of multiple pesticides comprising several different classes in grapes based on direct SPME extraction of grape sample matrix by employing a matrix-compatible SPME coating. Several factors that could influence method efficiency were carefully evaluated, from GC-ToFMS (GC oven program rate, MS acquisition rate, and ion source temperature) to parameters such as choice of internal standard, matrix modifications (salt addition, dilution factor), and extraction conditions (temperature and time). It is important to emphasize that the acquisition of high-quality analytical methods in combination with SPME requires optimization of the parameters that affect the extraction efficiency, namely, extraction phase chemistry, extraction mode, agitation method, sample modification (pH, ionic strength, organic solvent content), sample temperature, extraction time, and desorption conditions. Therefore, multivariate approaches such as Plackett−Burman and Central Composite Design (CCD) were employed to screen the most important parameters affecting extraction efficiency and to find optimum values for the most important parameters, respectively. To the best of our knowledge, this is the first time that the matrix compatible SPME coating has been used in a multiresidue pesticide determination.

MATERIALS AND METHODS

Solvents and Materials. All solvents used were of HPLC grade. Acetonitrile (MeCN), acetone, methanol (MeOH), dichloromethane (DCM), and isopropyl alcohol were purchased from Fisher Scientific. Glacial acetic acid, sodium sulfate, and sodium chloride were purchased from Supelco (Bellefonte, PA, USA). PDMS/DVB 65 μm Stableflex fibers were purchased from Supelco. Sylgard 184 (PDMS prepolymer and curing agent) was purchased from Dow Corning (Midland, MI, USA). Green seedless grapes were purchased at local markets in Waterloo (ON, Canada). Deionized water was obtained from a Barnstead/Thermodyne NANO-pure ultrawater system (Dubuque, IA, USA).

Standards. Pesticide standards (see Table S-1 in the Supporting Information for a list of all analytes) of purity of 95% or higher were purchased from Supelco, Accustandard, C/D/N Isotopes, and Restek. Details pertaining to the chemical structures and physicochemical properties of each analyte used in this work are described in the Supporting Information (Figure S-1 and Table S-1).

Individual solutions of standards were prepared in acetone, methanol, dichloromethane, and acetonitrile at 10 mg/mL (except chlorothalonil, which was prepared in dichloromethane, and folpet, which was prepared in toluene). A composite mixture was prepared, containing each contaminant at 100 μg/mL in acetonitrile (0.1% acetic acid).

Internal standard (quintozene, triphenylphosphate, trifluralin-d_{14}, terphenyl-d_{14}, 2-fluorobiphenyl, 2,4-dichlorophenol, phenol-d_5, and nitrobenzene-d_5) solutions were prepared at 1 mg/mL, except for parathion-d_{10} and α-HCH-d_6, which were purchased from Restek as 40 μg/mL solutions in acetonitrile. All standard solutions were stored in a freezer at −30 °C.

During method development, spiking standard mixtures were prepared containing target analytes at either 20 or 100 μg/mL, and internal standards were prepared at 50 μg/mL. The concentration of each analyte was carefully chosen to guarantee enough sensitivity for all analytes (final sample concentrations of 20, 100, and 50 ng/g).

To calculate the amount extracted by SPME for each analyte, a stock standard mixture containing all analytes of interest was prepared at 100 ng/μL in acetonitrile. This stock solution was used for successive dilutions to obtain calibration solutions ranging from 0.25 to 50 ng/μL (eight levels). Liquid injections of calibration solutions were carried out in quadruplicates.

Preparation of PDMS-Modified Coating. PDMS-modified coatings were prepared in-house employing a procedure described elsewhere.[18] All coatings were prepared at least in triplicate. Prior to their use, each coating was conditioned at 250 °C for 1 h and visually evaluated for uniformity and smooth surface coverage. If any defect was noted, coatings were discarded and new coatings were prepared.

SPME Procedure. Green seedless grapes, purchased at local markets in Waterloo (ON, Canada), were manually stemmed, washed with nanopure water, and dried. Next, grapes were crushed, homogenized using a blender, transferred to 200 mL amber glass flasks, and then stored in a freezer at −30 °C until analysis. Organically

DOI: 10.1021/jf506212j
J. Agric. Food Chem. 2015, 63, 4464−4477

Table 2. Noncoded Levels of the Factors Analyzed by CCD

run order	temperature (°C)	extraction time (min)	dilution (%)	salt (%)	mass, water (g)	mass, grapes (g)	mass, salt (g)
25 (C)	45.0	37.5	25.0	15.0	2.0	6.0	1.2
10	52.5	26.3	12.5	22.5	1.0	7.0	1.8
12	52.5	26.3	37.5	22.5	3.0	5.0	1.8
22	45.0	37.5	50.0	15.0	4.0	4.0	1.2
20	45.0	60.0	25.0	15.0	2.0	6.0	1.2
5	37.5	48.8	12.5	7.5	1.0	7.0	0.6
9	52.5	26.3	12.5	7.5	1.0	7.0	0.6
17	30.0	37.5	25.0	15.0	2.0	6.0	1.2
14	52.5	48.8	12.5	22.5	1.0	7.0	1.8
8	37.5	48.8	37.5	22.5	3.0	5.0	1.8
11	52.5	26.3	37.5	7.5	3.0	5.0	0.6
15	52.5	48.8	37.5	7.5	3.0	5.0	0.6
7	37.5	48.8	37.5	7.5	3.0	5.0	0.6
23	45.0	37.5	25.0	0.0	2.0	6.0	0.0
21	45.0	37.5	0.0	15.0	0.0	8.0	1.2
13	52.5	48.8	12.5	7.5	1.0	7.0	0.6
18	60.0	37.5	25.0	15.0	2.0	6.0	1.2
24	45.0	37.5	25.0	30.0	2.0	6.0	2.4
26 (C)	45.0	37.5	25.0	15.0	2.0	6.0	1.2
3	37.5	26.3	37.5	7.5	3.0	5.0	0.6
1	37.5	26.3	12.5	7.5	1.0	7.0	0.6
19	45.0	15.0	25.0	15.0	2.0	6.0	1.2
4	37.5	26.3	37.5	22.5	3.0	5.0	1.8
27 (C)	45.0	37.5	25.0	15.0	2.0	6.0	1.2
16	52.5	48.8	37.5	22.5	3.0	5.0	1.8
2	37.5	26.3	12.5	22.5	1.0	7.0	1.8
6	37.5	48.8	12.5	22.5	1.0	7.0	1.8

grown fruits were obtained for method development and validation steps (previously analyzed for the absence of the target pesticides), whereas conventionally grown fruits were obtained for real sample analysis.

During initial SPME method development, 8 g of whole fruit pulp was weighed in a 10 mL vial, fortified with 8 μL of a spiking standard mixture to achieve the appropriate analyte concentration, and pre-incubated for at least 60 min prior to extraction to allow for the binding of the analyte to the matrix to occur. Once dilution occurred, the samples were thoroughly vortexed and allowed to stand for 1 h prior to extraction. A 5 min pre-extraction incubation of the sample was performed in the agitation unit at 500 rpm and at 30 °C, followed by a 30 min extraction in direct immersion mode at 30 °C while stirring at 500 rpm. Following extraction, the fiber was rinsed in deionized water and then desorbed for 10 min at 260 °C.

For Plackett−Burman experiments, 200 g of grape pulp was weighed into a 250 mL jar and spiked with an appropriate amount of standard mix. The sample was then allowed to stand in the agitation table for 1 h. Subsequently, appropriate amounts of salt (Na_2SO_4), followed by spiked grape pulp amounts, were weighed into each vial. Next, appropriate amounts of DI water and isopropyl alcohol were added to each vial, corresponding to each experiment, as defined by the Plackett−Burman design matrix.

For the CCD experiments, sample preparation was similar to that performed for Plackett−Burman, except that no isopropyl alcohol was added.

The levels tested for each factor during Plackett−Burman and CCD are presented in Tables 1 and 2, respectively. For the final SPME method, 4 g of whole fruit pulp was weighed in a 10 mL vial, followed by 4 mL of a Na_2SO_4 aqueous solution at 15% (w/w) (1.2 g of Na_2SO_4/vial). The mixture was thoroughly vortexed to ensure homogeneity. A 5 min pre-extraction incubation of the sample was performed in the agitation unit at 750 rpm and at 55 °C, followed by a 30 min extraction in direct immersion mode at 55 °C while stirring at 750 rpm. Following extraction, the fiber was rinsed in deionized water and then desorbed for 10 min at 260 °C.

SPME matrix-matched calibration curves were obtained in grape matrix to establish the linear dynamic range, LOQs, and method precision and accuracy.

Instrumentation. Sample pH was measured by a Metter Toledo MP220 (Schwerzenbach, Switzerland) pH meter. For centrifugation of samples, a Thermo Jouan BR4i (Waltham, MA, USA) centrifuge was used.

GC-ToFMS analyses were carried out using a Pegasus 4D instrument consisting of an Agilent 6890N gas chromatograph equipped with a split/splitless injector (Agilent Technologies, Palo Alto, CA, USA), an MPS2 autosampler for automated SPME (Gerstel, Mülheim and der Ruhr, Germany), and a Pegasus III high-speed time-of-flight mass spectrometer (Leco Corp., St. Joseph, MI, USA). Chromatographic separation was performed in a Restek Rxi-5Sil MS capillary (30 m, 0.25 mm i.d., 0.25 μm film thickness) with a 5 m integra-guard column. Helium was used as carrier gas at 1.2 mL/min. Oven temperature was initially set at 70 °C for 1.5 min, ramped at 40 °C/min to 210 °C for 1 min, and then ramped at 10 °C/min to 280 °C, at which it was held for 10 min, resulting in a total run time of 23 min. The injector was maintained at 260 °C (0.75 mm i.d. insert used for SPME and 4 mm i.d. insert packed with glass wool at the bottom used for liquid injections) in splitless mode (split was opened for SPME method after 10 min; for liquid injections, the split was opened after 1.5 min). MS operational conditions were as follows: electron ionization (EI) at 70 eV; ion source temperature, 240 °C; transfer line temperature, 280 °C; mass range, m/z 35−550; acquisition rate, 50 Hz; detector voltage, −1700 V. Retention times, as well as the selected quantifier and qualifier ions, are presented in Table S-2.

Data Processing. ChromaTOF (Leco Corp.) software (v. 4.24) was used for GC-ToFMS instrument control, data acquisition, peak deconvolution, and data preprocessing. Library searching was performed using the commercial NIST library. Data were further processed using Microsoft Excel (2010) and GraphPad Prism 5 (version 5.01, 2007, GraphPad Softwate, San Diego, CA, USA). The Statistica 8.0 (2007, StatSoft, Tulsa, OK, USA) program was used to construct experimental design matrices and for evaluation of results.

DOI: 10.1021/jf506212j
J. Agric. Food Chem. 2015, 63, 4464−4477

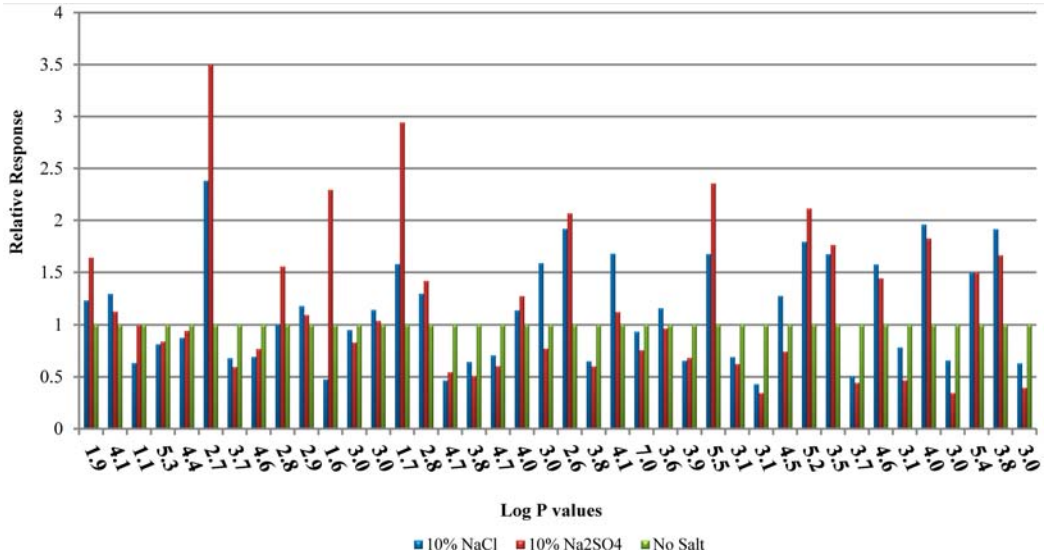

Figure 1. Influence of salt addition on extraction efficiency. Results are normalized for the response obtained without salt addition.

RESULTS AND DISCUSSION

The GC-ToFMS method was optimized to achieve chromatographic separation of the target pesticides with good peak shape, minimum matrix interferences, and increased sensitivity (S/N) within the shortest possible run time. Detailed discussion regarding the GC-ToFMS method optimization is presentated in the Supporting Information (section S-1).

SPME Method Development. *Preliminary Tests.* Once the GC-ToFMS method was developed, some preliminary DI-SPME studies in spiked water and grapes were carried out. Due to the addition of new analytes to the method, the time used for rinsing the fiber in water before desorption was reassessed. The predetermined time of 10 s[19] did not cause any statistically significant loss of analytes as compared to nonrinsing (data not shown).

Next, preliminary extractions in spiked grape pulp were performed to assess the optimum concentration level to be used during SPME method development. To establish such a level (analyte-dependent) the following factors were taken into account: (i) instrument response; (ii) SPME extraction efficiency; (iii) MRLs in grapes; and (iv) solubility of analytes. According to this assessment, pesticides were divided by low, medium, and high levels (10, 50, and 100 ng/g). Internal standards were kept at 50 ng/g. Regardless of the increased sample concentration of 100 ng/g, more polar pesticides such as acephate (log P = −0.85), omethoate (log P = −0.74), and dimethoate (log P = 0.704) could not be detected.

Because a multiresidue method should competently analyze both polar and nonpolar pesticides, different strategies were assessed to improve method sensitivity toward polar analytes (salting-out and water dilution).

A preassessment of the salting-out effect on extraction efficiency, determined by literature review, together with this author's previous findings, was carried out for two salts, NaCl and Na_2SO_4, at 10% (w/w). In agreement with our previous study,[19] the addition of NaCl did not yield satisfactory results. Interestingly, Na_2SO_4 not only provided better extraction efficiencies as compared to NaCl but also provided better repeatability of the data (assessed as RSD%, n = 3). Figure 1 shows the obtained results for selected pesticides (assigned according to their log P values). As expected, extraction efficiencies for pesticides bearing log P < 3 were positively affected by the addition of salt. It is important to note, however, that the addition of salt also improved the extraction of endogenous matrix compounds, such as organic acids (Figure S-5).

Screening of Influential Factors: Plackett−Burman. Plackett−Burman designs are used to obtain qualitative information, such as to detect which factors have the greatest influence on extraction efficiency in SPME. However, this saturated design assumes that there are no interactions between the different extraction variables, with each variable being tested at two experimental levels: a high level (+) and a low level (−).[21,22]

As presented in Table 1, in the current study, eight factors were studied, namely, (1) extraction time (15 and 60 min), (2) sample temperature (30 and 60 °C), (3) incubation time (5 and 15 min), (4) Na_2SO_4 addition (0 and 10%, w/w), (5) isopropyl alcohol addition (0 and 10%, v/v), (6) sample dilution (0 and 50%, w/w), (7) stirring rate (250 and 750 rpm), and (8) pH (natural grape pulp pH levels of 3.8 and 9). The ranges of the considered factors were chosen according to preliminary tests.

The rationale behind the selection of these factors was (1) extraction time affects the extraction efficiency; when extraction time increases, extraction efficiency also increases, until a maximum is reached (equilibrium). (2) An increase in sample temperature decreases sample viscosity, increasing analyte diffusivity in the medium, which in turn increases the amounts extracted in pre-equilibrium conditions. Increasing sample temperature may also favor the release of matrix-bound analytes into their free form in aqueous media. Conversely, an increase in temperature negatively affects the K_{fs}; however, this will be an issue only for equilibrium extractions. (3) Sample pre-incubation is closely related to sample temperature, although this parameter is more relevant in HS extraction than in DI; in DI mode, to avoid reproducibility problems, pre-incubation time must be sufficient to ensure uniform temperature throughout the whole sample. (4) The addition of salt modifies the ionic strength of the medium and can improve the extraction of more polar analytes via the salting-out effect. However, as a possible adverse effect of salt addition,

DOI: 10.1021/jf506212j
J. Agric. Food Chem. 2015, 63, 4464−4477

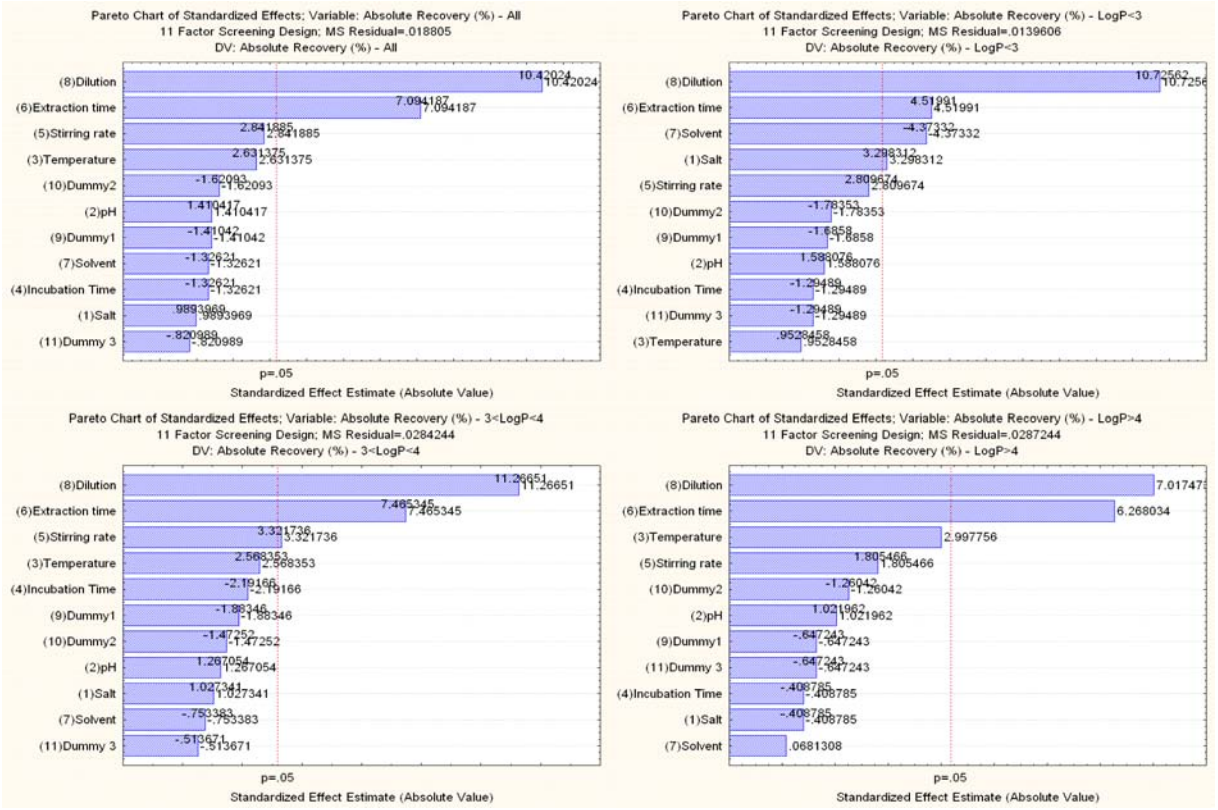

Figure 2. Pareto chart showing significant variables obtained in the Plackett–Burman design as a function of the average absolute recovery of pesticides studied: for all pesticides, dilution and extraction time were significant variables ($P < 0.05$); for the most polar pesticides (log $P < 3$), dilution, extraction time, solvent addition (negative), and salt were significant variables ($P < 0.05$); for the midpolarity pesticides ($3 < \log P < 4$), dilution, extraction time, and stirring rate were significant variables ($P < 0.05$); for the most hydrophobic pesticides (log $P > 4$), dilution and extraction time were significant variables ($P < 0.05$).

free-form analytes may be driven into matrix binding. When biological matrices are used, the addition of salt may aid in the natural normalization of occurring variations in salt content. (5) An addition of modifier (organic solvent) should be avoided, or kept at minimum, not exceeding 1–5%.[23] However, in some cases, the addition of organic solvent may help release matrix-bound analytes. (6) In general, dilution with water improves method performance in several ways, such as by minimizing the effect of the matrix and augmenting the release of analytes bound to matrix components to the aqueous phase (free concentration). Water addition may also minimize the attachment of matrix macromolecules onto the coating and decrease matrix viscosity, which increases the diffusion coefficients of the analytes, allowing higher extraction efficiencies in pre-equilibrium conditions. (7) Increasing the stirring rate, that is, agitation, assists the mass transport of the analytes between the sample and the fiber coating, which improves pre-equilibrium extraction and can shorten equilibration time. (8) Sample pH is important for analytes possessing pH-dependent ionizable groups, as only the nonionized form of the analyte is extracted by the coating.

Three "dummy" factors were also added to the design. These were fictitious factors, representing no procedural changes, and were used as a quality control measure for the design. If these factors appeared to influence the results, then the method was affected by variables other than the defined experimental parameters. The use of three central points also effectively accounted for experimental errors that could be associated with instrumental drifts.

Results were evaluated by calculating the amounts extracted and then calculating the absolute recovery for each analyte in each experiment. Analysis of variance (ANOVA) was used to evaluate results, and effects were deemed statistically significant at a 95% confidence level ($P < 0.05$). Because of the physical–chemical diversity of the analytes, results were analyzed as the average absolute recovery for all analytes, as well as per range of log P values. Absolute recovery (%) was selected to evaluate the processes, because analytes were present in different concentrations, and different amounts of spiked matrix were used for the experiments.

The results presented in Figure 2 showed that responses obtained for all three "dummy" factors, representing no procedural changes, showed no significant effect on the recovery of analytes. If these factors had appeared to influence the outcome, the method would be affected by variables other than the defined experimental parameters and should have been redesigned. The obtained data confirmed that this was not the case, indicating that all appropriate factors were considered.

As can be seen in Figure 2, when the average absolute recoveries for all pesticides were taken into account, the factors dilution and extraction time were significant, in a positive direction. This means that increasing sample dilution from 0 to 50% (4 mL of water) caused an increase in the amount extracted. In SPME, when additional phases are present in the sample, partitioning of the analytes in complex matrices occurs among all of the phases present in the system. Therefore, in the case of complex matrices, such as grapes, sample dilution may improve the partitioning of analytes between the sample and

DOI: 10.1021/jf506212j
J. Agric. Food Chem. 2015, 63, 4464–4477

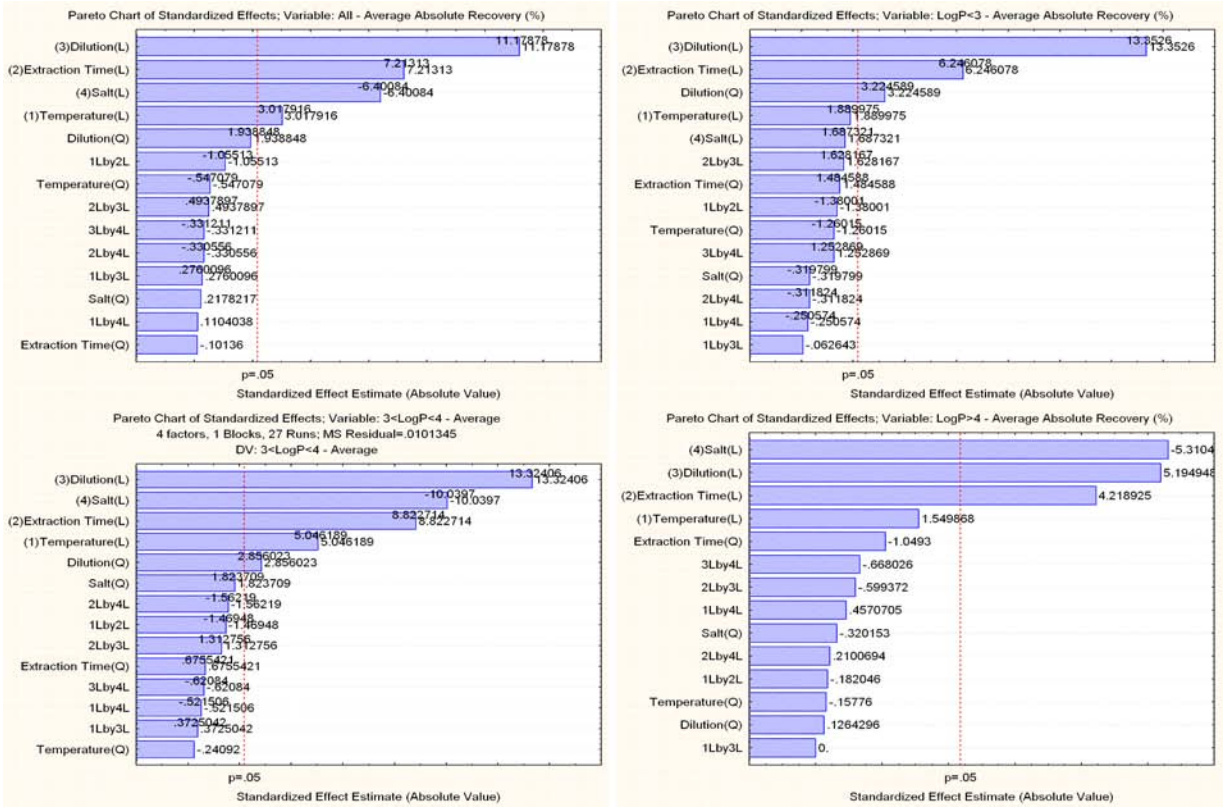

Figure 3. Pareto chart of effects showing significant variables obtained for central composite design as a function of the average absolute recovery of pesticides studied.

the coating as analyte competition between the other phases is diminished.[23−25] Extraction time and sample dilution were positively significant factors in the examination of all subgroups. The addition of organic solvent was negatively significant for most polar analytes (log P < 3). The addition of isopropyl alcohol decreased the polarity of the aqueous medium, causing the equilibrium between free-form and matrix-bound analytes to be shifted toward matrix binding, which in turn decreased the extraction efficiency. The addition of salt was shown to be significant (positively) only for more polar analytes, as the salting-out effect increased their extraction efficiency. Stirring rate was significant (positively) only for midpolarity pesticides (3 < log P < 4), possibly due to the improved extraction efficiency obtained as a function of the enhanced mass transfer through a thinner boundary layer. It is important to note that this is significant only for this group of analytes, taking note of their molecular size together with diffusion their through the PDMS overcoating. For more polar analytes, diffusion through the PDMS layer would still be the major limiting step in mass transfer, which explains why stirring rate does not play a significant role for these analytes. Conversely, stirring rate would be expected to play a significant role in the pre-equilibrium extraction efficiency of more hydrophobic pesticides. A possible explanation for the result herein obtained could be associated with the high matrix binding of these compounds, as well as the inherent limitation of a Plackett−Burman design that evaluates only main factors, with all interactions being cofounded. Therefore, keeping in mind that faster agitations lead to enhanced mass transfers, 750 rpm was chosen for all subsequent experiments. Surprisingly, extraction temperature did not have a significant effect on any subgroup assessed, because it is known that an increase in sample temperature may lead to improved extraction efficiency, as explained before. Even though sample temperature presented no effect on the outcome, it was still chosen for the following optimization step due to another limitation of the Plackett−Burman design; it evaluates only two levels, and no information regarding the behavior of a given factor in small increments comprising the range between these two levels can be acquired. To summarize, the factors chosen for optimization via surface response were extraction time, sample temperature, salt addition, and dilution.

Optimization of Factors: Central Composite Design. Once the significant variables were identified, an optimization of these variables was conducted to find the optimum values that can lead to a maximum signal. For this purpose, a CCD was employed for optimization of dilution ratio (% of water added), extraction time (min), extraction temperature (°C), and salt addition (% of Na_2SO_4). All other parameters were kept constant, as follows: stirring rate at 750 rpm; pre-incubation time of 5 min; and no pH modification (natural pH of ∼3.8).

In short, a CCD for k factors has three groups of design points: (1) two-level full factorial design points, containing a total of $n_{factors} = 2^k$ with coordinates $x_i = -1$ or $x_i = 1$, for $i = 1, ..., k$; (2) axial points ("star" points), formed by $n_{axial} = 2k$, with all factors set to coded level 0 (the midpoint) and the value $+\alpha$; and (3) central points, which are points with all levels set to coded level 0, the midpoint for each factor range. These points at the center serve two purposes: they provide an estimate of experimental error and determine the precision of an estimated response at and in the proximity of the central point.[21,26]

In the present study, the CCD consisted of four factors, with rotatability $\alpha = 2$ (the choice of α value will determine the predictability of the model) and three central points. To

DOI: 10.1021/jf506212j
J. Agric. Food Chem. 2015, 63, 4464−4477

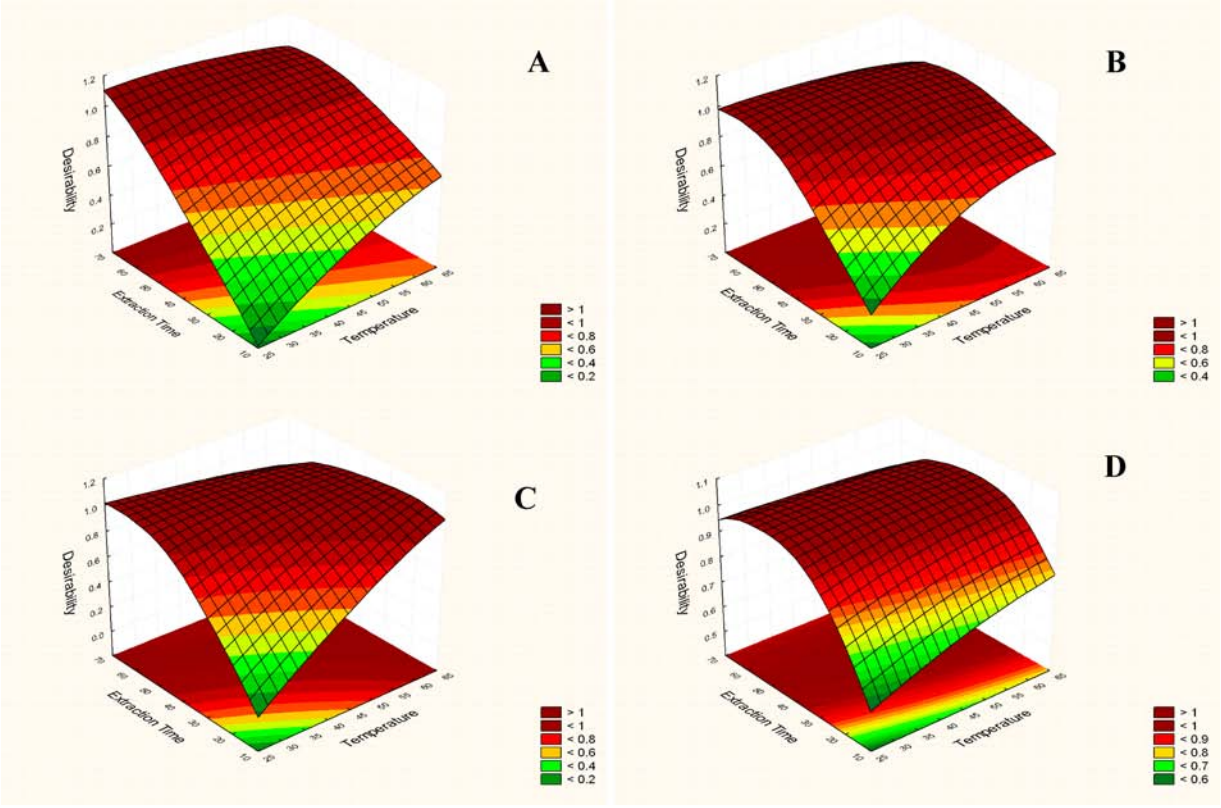

Figure 4. Response surface plot for desirability versus extraction time (min) and sample temperature (°C) for all analytes (A), for more polar analytes (B), for midpolarity analytes (C), and for most hydrophobic analytes (D).

summarize, all four factors were evaluated at five levels ($-\alpha$, −1, 0, +1, $+\alpha$), resulting in 27 experiments. The summarized conditions utilized for each experiment are presented in Table 2.

The data obtained for CCD experiments were also calculated as absolute recoveries (%). The Pareto charts of effects for all pesticides, as well as for subgroups, are presented in Figure 3.

By investigating the Pareto charts of effects in Figure 3 together with the profiles for predicted values and desirability, it could be seen that, overall, the most important factor leading to improved extraction efficiencies is the dilution of the matrix with water, with optimum results obtained at dilution percentages as high as 50%. Similarly, the effect of extraction time also led to improved extraction efficiencies, as expected.

Sample temperature effects were observed only for midpolarity analytes, and the temperature effect in the extraction efficiencies for these analytes have already been discussed. However, a closer inspection at surface responses generated between extraction time and sample temperature (Figure 4) shows that for a given extraction time, an improved extraction efficiency should be expected with an increase in sample temperature. Obviously, the effect varies among the subgroups, but in general, to differing extents, analyte recovery increases as temperature is increased (within the scope of the present study). Possible reasons are likely associated with decreased sample viscosity, as well as unbinding of analytes from the matrix.

The addition of salt seems to worsen analyte extraction, especially for midpolarity and more hydrophobic pesticides. This result was expected; as previously stated, the addition of salt might drive these analytes into matrix binding. However, the most surprising outcome of salt addition was obtained for the most polar pesticides: according to the Pareto chart of effects, salt addition had no significant effect in the recovery of these pesticides. Nonetheless, the surface responses generated between salt addition and sample temperature for these most polar analytes show that for a given sample temperature, improved extraction efficiency should be expected when salt is added to the sample (Figure 5). Accordingly, due to the salting-

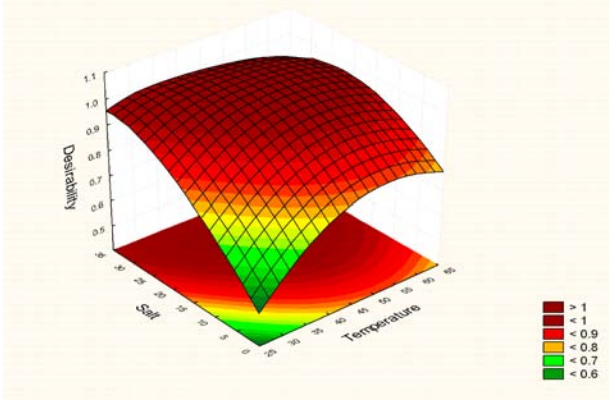

Figure 5. Response surface plot for desirability versus salt addition (%, w/w) and sample temperature (°C) for most polar analytes.

out effect, water molecules would form hydration spheres around the ionic salt molecules, reducing the concentration of water available, thus driving analytes into the fiber coating. However, if the salt concentration is increased past a certain extent, then a concurrent effect that reduces the ability of the analytes to move into the coating takes place, where the

DOI: 10.1021/jf506212j
J. Agric. Food Chem. 2015, 63, 4464−4477

Table 3. Internal Standard Selection[a]

	internal standard						
analyte	none	parathion-d_{10}	TPP	terphenyl-d_{14}	trifluralin-d_{14}	quintozene	α-BHC-d_6
trifluralin	1−1000	50−500	50−500	1−100	1−1000	1−1000	1−1000
	R^2 = 0.9964	R^2 = 0.9986	R^2 = 0.9977	R^2 = 0.9958	R^2 = 0.9986	R^2 = 0.9995	R^2 = 0.9985
dimethoate	50−500	50−500	50−500	50−500	50−1000	50−1000	50−1000
	R^2 = 0.9977	R^2 = 0.9993	R^2 = 0.9982	R^2 = 1	R^2 = 0.9997	R^2 = 0.9979	R^2 = 0.9957
Atrazine	1−500	1−1000	1−1000	1−250	1−500	1−500	1−500
	R^2 = 0.9955	R^2 = 0.9993	R^2 = 0.9982	R^2 = 0.9964	R^2 = 0.9957	R^2 = 0.9991	R^2 = 0.9992
diazinon	1−500	1−1000	1−1000	1−250	1−250	1−500	1−500
	R^2 = 0.9981	R^2 = 0.9964	R^2 = 0.9963	R^2 = 0.9957	R^2 = 0.9976	R^2 = 0.9982	R^2 = 0.9992
pyrimethanil	1−250	1−500	1−100	1−250	1−500	1−500	1−500
	R^2 = 0.9971	R^2 = 0.9954	R^2 = 0.9999	R^2 = 0.9962	R^2 = 0.9989	R^2 = 0.9997	R^2 = 0.9985
chlorothalonil	25−500	1−1000	1−1000	1−250	50−500	1−500	50−500
	R^2 = 0.9962	R^2 = 0.9996	R^2 = 0.9991	R^2 = 0.9968	R^2 = 0.997	R^2 = 0.9968	R^2 = 1
pirimicarb	1−500	1−1000	1−1000	1−250	50−500	1−500	1−500
	R^2 = 0.9988	R^2 = 0.9991	R^2 = 0.9980	R^2 = 0.9981	R^2 = 0.9984	R^2 = 0.9982	R^2 = 0.9981
vinclozoline	1−500	1−1000	1−1000	1−250	50−500	1−500	1−500
	R^2 = 0.9965	R^2 = 0.9988	R^2 = 0.9979	R^2 = 0.9984	R^2 = 0.9972	R^2 = 0.998	R^2 = 0.9985
parathion-methyl	1−500	1−1000	1−500	1−250	1−50	1−500	1−500
	R^2 = 0.9954	R^2 = 0.9953	R^2 = 0.9985	R^2 = 0.9967	R^2 = 0.9981	R^2 = 0.9977	R^2 = 0.9979
metalaxyl	1−500	1−1000	1−1000	1−250	50−500	1−500	50−500
	R^2 = 0.9968	R^2 = 0.9997	R^2 = 1	R^2 = 0.9979	R^2 = 0.9958	R^2 = 0.9954	R^2 = 0.9998
malathion[b]	1−250	1−500	1−100	1−250	1−50	1−500	1−100
	R^2 = 0.9982	R^2 = 0.9935	R^2 = 0.9970	R^2 = 0.9946	R^2 = 0.9972	R^2 = 0.9989	R^2 = 0.9970
chlorpyrifos	5−1000	5−500	5−500	5−250	5−500	5−1000	5−1000
	R^2 = 0.9967	R^2 = 0.9996	R^2 = 0.9971	R^2 = 0.9992	R^2 = 0.9957	R^2 = 0.9991	R^2 = 0.996
parathion	5−500	5−1000	5−1000	5−250	5−50	5−500	5−500
	R^2 = 0.9976	R^2 = 0.9995	R^2 = 0.999	R^2 = 0.9986	R^2 = 0.996	R^2 = 0.9952	R^2 = 0.9966
cyprodinil	1−500	1−1000	1−500	1−250	50−500	1−500	1−500
	R^2 = 0.9951	R^2 = 0.9957	R^2 = 0.9976	R^2 = 0.998	R^2 = 0.9984	R^2 = 0.9987	R^2 = 0.9987
methidathion	5−500	5−1000	5−1000	5−250	5−50	5−500	5−500
	R^2 = 0.9963	R^2 = 0.9988	R^2 = 0.9984	R^2 = 0.996	R^2 = 0.9959	R^2 = 0.9948	R^2 = 0.9958
endosulfan I	5−1000	5−500	5−500	5−100	5−1000	5−1000	5−1000
	R^2 = 0.9983	R^2 = 0.993	**R^2 = 0.9853**	R^2 = 0.9969	R^2 = 0.9941	R^2 = 0.9977	R^2 = 0.9998
fludioxonil	1−500	1−1000	1−1000	1−250	5−100	1−500	1−500
	R^2 = 0.9967	R^2 = 0.9997	R^2 = 0.9996	R^2 = 0.9988	R^2 = 0.9953	R^2 = 0.9955	R^2 = 0.9963
4,4′-DDE	1−100	1−50	1−50	1−100	1−1000	1−1000	1−500
	R^2 = 0.9996	R^2 = 0.9995	R^2 = 0.9970	R^2 = 0.997	R^2 = 0.9959	**R^2 = 0.9931**	R^2 = 0.9988
myclobutanil	1−500	1−1000	1−1000	1−250	50−500	1−500	1−500
	R^2 = 0.997	R^2 = 0.9995	R^2 = 0.9992	R^2 = 0.9978	R^2 = 0.9952	R^2 = 0.9954	R^2 = 0.9966
kresoxim-methyl	1−500	1−1000	1−1000	1−250	50−500	1−500	1−500
	R^2 = 0.997	R^2 = 0.9974	R^2 = 0.9963	R^2 = 0.9983	R^2 = 0.9961	R^2 = 0.9966	R^2 = 0.9974
flusilazole	1−500	1−1000	1−1000	1−250	50−500	1−500	1−500
	R^2 = 0.9972	R^2 = 0.9993	R^2 = 0.9989	R^2 = 0.9983	R^2 = 0.995	R^2 = 0.9952	R^2 = 0.9963
cyproconazole	5−500	5−1000	5−1000	5−250	50−500	5−500	5−500
	R^2 = 0.9967	R^2 = 0.9999	R^2 = 1	R^2 = 0.9981	R^2 = 0.9957	R^2 = 0.9958	R^2 = 0.9969
endosulfan II	5−500	5−1000	5−1000	5−250	50−500	5−500	5−500
	R^2 = 0.997	R^2 = 0.9967	R^2 = 0.9973	R^2 = 0.9995	R^2 = 0.9958	R^2 = 0.9969	R^2 = 0.9979
trifloxystrobin	5−500	5−1000	5−1000	5−250	5−500	5−500	5−500
	R^2 = 0.9939	R^2 = 0.9993	R^2 = 0.9991	R^2 = 0.999	R^2 = 0.9959	R^2 = 0.999	R^2 = 0.9988
quinoxyfen	5−500	5−1000	5−1000	5−250	5−500	50−500	5−500
	R^2 = 0.9956	R^2 = 0.9989	R^2 = 0.9993	R^2 = 0.9978	R^2 = 0.9971	R^2 = 0.9986	R^2 = 0.9973
fenhexamide	5−500	5−1000	5−1000	5−250	50−500	50−500	5−500
	R^2 = 0.9967	R^2 = 0.9999	R^2 = 0.9997	R^2 = 0.9985	R^2 = 0.9958	R^2 = 0.9989	R^2 = 0.9971
tebuconazole	5−500	5−1000	5−1000	5−250	5−500	5−500	5−500
	R^2 = 0.9972	R^2 = 0.9997	R^2 = 1	R^2 = 0.9982	R^2 = 0.9952	R^2 = 0.9956	R^2 = 0.9969
iprodione	5−500	5−1000	5−1000	5−250	5−500	5−500	5−500
	R^2 = 0.9969	R^2 = 0.9997	R^2 = 1	R^2 = 0.997	R^2 = 0.9954	R^2 = 0.9954	R^2 = 0.9961
fenpropathrin	10−250	10−1000	10−1000	**R^2 < 0.9**	10−1000	25−1000	10−1000
	R^2 = 0.998	R^2 = 0.9707	R^2 = 0.9707		R^2 = 0.9999	R^2 = 0.9989	R^2 = 0.9976

DOI: 10.1021/jf506212j
J. Agric. Food Chem. 2015, 63, 4464−4477

Table 3. continued

	internal standard						
analyte	none	parathion-d_{10}	TPP	terphenyl-d_{14}	trifluralin-d_{14}	quintozene	α-BHC-d_6
phosalone	10−500	10−1000	10−1000	10−1000	50−500	10−500	10−500
	R^2 = 0.9956	R^2 = 0.9998	R^2 = 0.9999	R^2 = 0.9999	R^2 = 0.9967	R^2 = 0.9967	R^2 = 0.9973
azinphos-methyl	5−500	5−1000	5−1000	5−1000	5−500	5−500	5−500
	R^2 = 0.9961	R^2 = 0.9993	R^2 = 0.998	R^2 = 0.998	R^2 = 0.9963	R^2 = 0.999	R^2 = 0.9994
pyriproxyfen	5−500	5−1000	5−1000	5−1000	10−500	5−500	5−500
	R^2 = 0.9977	R^2 = 0.9967	R^2 = 0.9974	R^2 = 0.9974	R^2 = 0.9975	R^2 = 0.998	R^2 = 0.9989
pyridaben	25−1000	50−1000	25−1000	25−1000	50−1000	50−1000	25−1000
	R^2 = 0.9973	R^2 = 0.9855	R^2 = 0.9852	R^2 = 0.9852	R^2 = 0.9956	R^2 = 0.9981	R^2 = 0.9988
fenbuconazole	10−500	5−1000	5−1000	5−1000	5−500	5−500	5−500
	R^2 = 0.9985	R^2 = 0.9994	R^2 = 0.9997	R^2 = 0.9997	R^2 = 0.9904	R^2 = 0.996	R^2 = 0.9977
boscalid	1−500	1−1000	1−1000	1−1000	50−500	1−500	50−500
	R^2 = 0.9956	R^2 = 0.9993	R^2 = 0.9997	R^2 = 0.9997	R^2 = 0.9965	R^2 = 0.9952	R^2 = 0.9996
pyraclostrobin	10−500	10−1000	10−1000	10−1000	10−250	10−500	10−500
	R^2 = 0.9891	R^2 = 0.9992	R^2 = 0.9981	R^2 = 0.9981	R^2 = 0.9975	R^2 = 0.999	R^2 = 0.9979
es/fenvalerate[c]	**R^2 < 0.9**	**R^2 < 0.9**	**R^2 < 0.9**	**R^2 < 0.9**	**R^2 < 0.9**	**R^2 < 0.9**	**R^2 < 0.9**
azoxystrobin	25−500	5−1000	5−1000	5−250	50−500	5−500	5−500
	R^2 = 0.999	R^2 = 0.9984	R^2 = 0.9989	R^2 = 0.9983	**R^2 = 0.9929**	**R^2 = 0.9948**	R^2 = 0.9967
dicofol[d]	10−1000	10−500	10−500	10−100	10−1000	10−1000	10−1000
	R^2 = 0.999	R^2 = 0.9977	R^2 = 0.9958	R^2 = 0.9984	R^2 = 0.9954	R^2 = 0.9984	R^2 = 0.9997
folpet[e]	10−500	10−500	10−500	10−100	10−500	10−500	10−500
	R^2 = 0.9994	R^2 = 0.9986	R^2 = 0.9951	R^2 = 0.9962	**R^2 = 0.9845**	**R^2 = 0.9907**	**R^2 = 0.9942**
λ-cyhalothrin[f]	**R^2 < 0.9**	**R^2 < 0.9**	**R^2 < 0.9**	**R^2 < 0.9**	**R^2 < 0.9**	**R^2 < 0.9**	**R^2 < 0.9**
cyfluthrin[g]	**R^2 < 0.9**	**R^2 < 0.9**	**R^2 < 0.9**	**R^2 < 0.9**	**R^2 < 0.9**	**R^2 < 0.9**	**R^2 < 0.9**
difenoconazole[h]	10−500	10−1000	10−1000	10−250	10−500	10−500	10−500
	R^2 = 0.9956	R^2 = 0.9999	R^2 = 0.9995	R^2 = 0.9976	R^2 = 0.9958	R^2 = 0.9991	R^2 = 0.9994
deltamethrin[i]	**R^2 < 0.9**	**R^2 < 0.9**	**R^2 < 0.9**	**R^2 < 0.9**	**R^2 < 0.9**	**R^2 < 0.9**	**R^2 < 0.9**

[a]In black boldface font: R^2 < 0.995. [b]Sum of malathion and malaoxon (DP). [c]Sum of esfenvalerate and fenvalerate. [d]Sum of dicofol and 4,4′-dichlorobenzophenone (DP). [e]Sum of folpet and phthalimide (DP). [f]Sum of two isomers. [g]Sum of four isomers. [h]Sum of two isomers. [i]Sum of two isomers.

analytes participate in electrostatic interactions with the salt ions in solution. To further investigate this effect, a closer look was taken at individual data for most polar analytes, which at this point may be considered the weak link in developing such a multianalyte SPME method. Dimethoate (log P = 0.704) displayed optimum results for sample temperatures above 43.5 °C and salt (%, w/w) above 20%. Similarly, pirimicarb (log P = 1.55) displayed little sample temperature effect and optimum extraction efficiency at values above 19.5% of salt added.

In summary, the effect of each factor in the extraction efficiency seen for each subgroup of analytes is as follows:

- For compounds characterized by log P < 3, sample temperature and extraction time had little effect; salt addition (%, w/w) yielded optimum results above 18%; sample dilution with water (%, w/w) yielded optimum results above 48%.
- For compounds characterized by 3 < log P < 4, extraction time had little effect; sample temperature yielded optimum results above 54 °C; salt addition (%, w/w) yielded optimum results below 4.5%; sample dilution with water (%, w/w) yielded optimum results above 42.5%.
- For compounds characterized by log P > 4, sample temperature and extraction time had little effect; salt addition (%, w/w) yielded optimum results below 7.5%; sample dilution with water (%, w/w) yielded optimum results above 45%.

The development of an SPME method aiming at simultaneous extraction of numerous analytes covering a broad range of polarities cannot succeed without a compromise in "optimum" values. Indeed, a multiresidue pesticide method, such as the one proposed here, must focus on the overall quality of data, keeping in mind method sensitivity. Therefore, rather than choosing the "optimum" values proposed by the CCD computation of all pesticide recoveries, the "optimized" method has the following conditions:

- An extraction time of 30 min represents a good compromise between good sample throughput with the GC run time and method sensitivity.
- A sample temperature of 55 °C provides enhanced mass transfer.
- Fifty percent dilution (4 mL of water) also improves mass transfer, increases coating lifetime, and broadens method linear dynamic range.
- The 15% of Na_2SO_4 (1.2 g) represents the main compromise of this method. Even though it does not help the extraction efficiency of most hydrophobic analytes, it does provide better results for the most polar analytes. Because more hydrophobic analytes display good extraction efficiency by SPME, a sacrifice was made here to improve the extraction efficiency of the more polar analytes (which typically yield low GC responses, together with a low affinity by the SPME coating) while keeping the response for all other analyte groups ≥75% of the optimum value.
- Other parameters already defined are a stirring rate of 750 rpm, a pre-incubation time of 5 min, a desorption temperature of 260 °C, and a desorption time of 10 min.

DOI: 10.1021/jf506212j
J. Agric. Food Chem. 2015, 63, 4464−4477

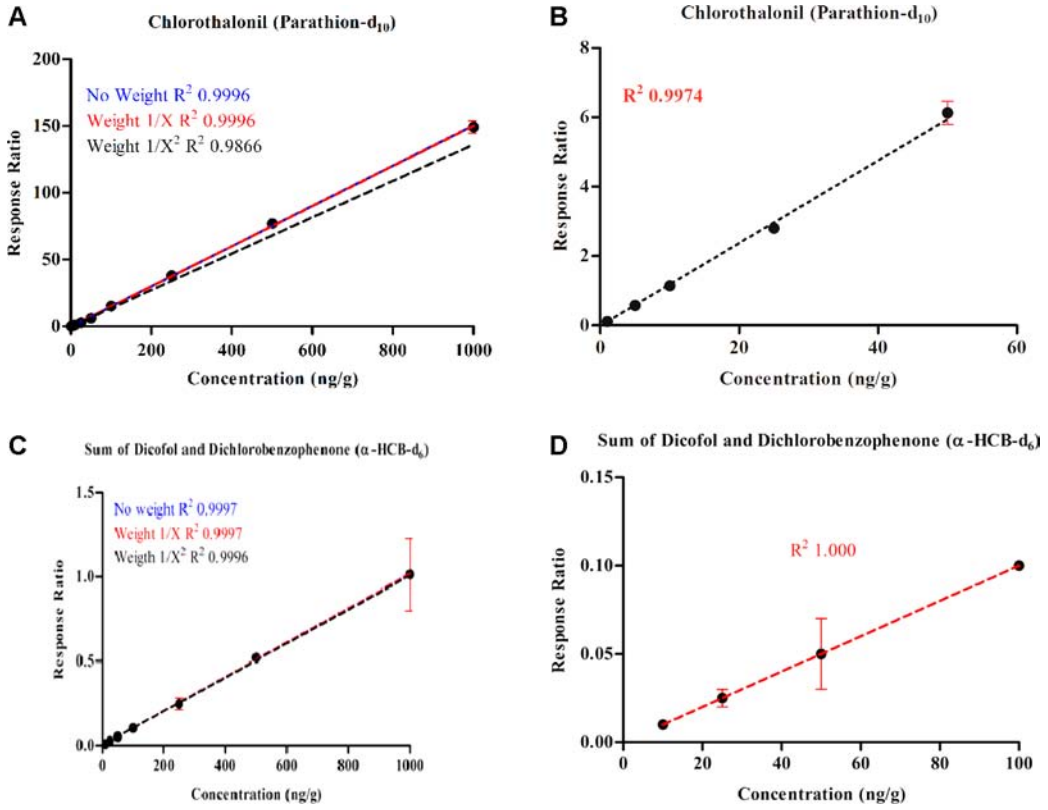

Figure 6. Representative calibration plots comparing different weights for regression curve (A, C) and inspection at lower concentration levels using weight $1/X$ (B, D), for chlorothalonil using parathion-d_{10} as internal standard (A, B) and for dicofol using α-HCH-d_6 as internal standard (C, D).

Internal Standard (IS) Selection. In quantitative determinations of multiresidue pesticides in food, the utilization of internal standards is of utmost importance, as they are used to correct for possible drifts in instrumental responses, as well as to account for losses during sample preparation steps.

A literature review of the most recent publications regarding GC-based multiresidue analysis in food shows that the vast majority of methods employ a solvent extraction step, as is the case for QuEChERS and its modifications.[2,4,27−32] In such cases, most of the published work reports an addition of internal standards (surrogates), such as parathion-d_{10} and α-HCH-d_6, before extraction to account for losses during sample preparation steps. Triphenylphospate (TPP) is then added to the final extract to correct for any instrumental drift. In short, given the exhaustive nature of such extraction methods, these three internal standards are successful in ensuring adequate quantitative data.

Because of the nonexhaustive nature of SPME, the application of these widely employed internal standards, generally used for exhaustive methods, would not be advisible without a previous investigation of their applicability. In SPME, internal standards should resemble, as closely as possible, the behavior of the analyte in the system matrix/coating; in other words, the IS should be able to mimic the partition of the analyte for the extraction phase and any competing phase.

For this reason, 10 compounds (Figure S-6), widely used as internal standards and surrogates in pesticide determinations by various methods, were investigated for their applicability as internal standards in the SPME method. Employing the previously optimized conditions, a matrix-matched calibration curve ranging from 1 to 1000 ng/g (eight points, quadruplicate) was performed with the addition of the mixture of internal standard (each IS at 50 ng/g).

The obtained data were processed by computing the ratio between the peak area of the analyte and that obtained for the internal standard (A_{an}/A_{IS}). This process was accomplished for each analyte and each IS candidate. For each analyte/IS pair, the data were analyzed according to a linear range that yielded a correlation coefficient (R^2) ≥0.995. The data are summarized in Table 3. Tribromophenol was excluded from the evaluation at the data processing stage due to its poor ionization in EI. Nitrobenzene-d_5 and 2,4-dichlorophenol were also eliminated from the IS selection because their extraction efficiencies were far superior to those displayed by the targeted pesticides. These small polar molecules are less prone to matrix binding and, as such, are more available in their free form in the aqueous phase of the matrix. Due to a mismatched extraction efficiency, 2-fluorobiphenyl was also eliminated from further assessment. The areas obtained by this IS were 1 order of magnitude higher than those obtained by the target analytes (at the same concentration of 50 ng/g).

In the analysis of complex matrices, where a significant and variable competing phase is present in the sample, the selection of internal standard is critical. If the internal standard has a different affinity for the competing phases from that of the analyte of interest, the amounts of internal standard and analyte bound to the matrix may not correlate linearly, and peak ratio analysis will not yield an adequate quantification.

The internal standards most used in the QuEChERS methods, parathion-d_{10} and TPP, resulted in very similar performances, as they both corrected well for approximately 70% of the analytes. Trifluralin-d_{14}, quintozene, and α-HCH-d_6 exhibited similar behaviors among themselves and were able to

DOI: 10.1021/jf506212j
J. Agric. Food Chem. 2015, 63, 4464−4477

correct well for approximately 20% of the analytes. Interestingly, these three IS candidates corrected analytes that were not corrected well by parathion-d_{10} and TPP. Most importantly, it has been determined that using only one pair of internal standards (parathion-d_{10} or TPP + quintozene or α-HCH-d_6) is sufficient to ensure reliable correction not only for instrumental drifts but also for variations that could occur when one is dealing with natural matrices. Moreover, the choice of TPP/quintozene as internal standards would render significant economic savings, because these compounds are significantly less expensive than the isotopically labeled ones.

Whereas terphenyl-d_{14} showed good correlation, the linear range was significantly shortened for all corrected analytes. Terphenyl-d_{14} presented the lowest extraction efficiencies among all tested IS candidates, as it was expected to be more strongly bound to the matrix. One hypothesis is that as the concentration of more hydrophobic compounds increased (in the calibration), more competition took place for adsorption onto the solid matrix. As such, more terphenyl-d_{14} would be available in its free form, which could account for the loss of linearity analyte/IS. This explanation is in line with the plot of instrumental response for terphenyl-d_{14} as a function of calibration level. For comparison, and to ensure that no mistakes were made during the spiking of the IS mixture, quintozene is also plotted in Figure S-7.

The more hydrophobic pyrethroid pesticides did not yield linear responses throughout the evaluation. It is possible that due to their low solubility in water and high hydrophobicity, these compounds adsorbed onto the vial walls during the duration of the sequence run. However, this hypothesis must be further investigated. At this point, the proposed method moves forward to the validation steps without the inclusion of these troublesome pesticides.

Method Validation. After establishment of the extraction conditions, the method obtained was validated in fortified samples by evaluating linearity, sensitivity, accuracy, and precision.

Linearity and Limit of Quantification. Method linearity was studied by means of matrix-matched calibration curves, using relative area versus adequate IS. Calibration levels were prepared at 1, 5, 10, 25, 50, 100, 250, 500, and 1000 ng/g. Linearity was assumed when the correlation coefficient (R^2) was >0.995 with randomly distributed residuals lower than 20%.

For each pesticide, the results were analyzed for hetero- or homoscedasticity using no weight, weight $1/X$, and weight $1/X^2$ (X = concentration). In addition, as shown in Figure 6, the obtained curves were also inspected at the lower range to ensure the validity of the regression model.

The results for method validation are summarized in Table 4. As can be seen, the method showed good linearity for all 40 pesticides in the entire calibration range selected for each analyte, with $R^2 > 0.995$. Even though calibration ranges were chosen to include concentration levels bracketing the EU MRL, when "relatively high", the proposed method did not meet the linearity requirement at the MRL concentration. For example, as the MRL for boscalid was 5000 μg/kg, the present method was validated and linear for boscalid in the range of 1−1000 μg/kg. In effect, the greatest strength of the proposed method also leads to one disadvantage. On the one hand, owing to the preconcentration capabilities of this method, admirably low limits of quantitation can be attained. On the other hand, the same preconcentration power causes the proposed SPME method to have a "relatively low" upper limit of linearity. For example, for the QuEChERS method, without solvent exchange or large volume injection, 1 g of sample will generate 1 mL of extract, of which only 1−3 μL will be injected in the GC. Conversely, in the present method, the totality of analytes extracted by the coating will be transferred to the GC. In the QuEChERS method, if the analyte is present in the sample in concentrations above the upper limit of linearity, the sample can be simply diluted so that a concentration within the linearity range is attained. In SPME, as discussed previously, the analyte will partition between the coating and all competing phases present in the sample. Dilution of the sample may cause significant differences in the content of these competing phases, which could lead to the unsuitability of the calibration data for the diluted sample. Matrix effects caused by further dilution of samples were not investigated in this work; however, it is an important point to be validated in future work.

In the present study, the LOQ objective is defined according to SANCO guidelines (SANCO/12571/2013) as the lowest assessed concentration of an analyte that yields a reproducible response that is both accurate (according to the expected value using the linear regression equation) and precise (≤20% RSD). Excellent LOQs were achieved for 38 pesticides (LOQ ≤ 10 ng/g, except dimethoate (LOQ = 50 ng/g), and pyridaben (LOQ = 25 ng/g)). By comparison of the LOQ values obtained with the proposed method with recent publications reported for GC-based multiresidue pesticide analysis in grapes, it is evident that the LOQs obtained in this study are in a similar range or better than those reported.[30,33−38] Furthermore, the LOQ values validated in this study are far below the MRL set for grapes.[39] The only exception is dimethoate, which has the MRL set as 20 ng/g and a presented LOQ value of 50 ng/g.

Precision and Accuracy. Precision as intraday repeatability was determined for grape samples spiked at three concentrations, 10, 50, and 500 ng/g. Data from five analyses for each concentration level performed in the same day were used for calculations (n = 5), with the data expressed as relative standard deviations (RSD, %). As presented in Table 4, good results were obtained for nearly all pesticides (RSD ≤ 20%).

Intermediate precision as interday reproducibility was also determined for grape samples spiked at three concentrations, 10, 50, and 500 ng/g. Data obtained from three analyses for each concentration level performed on three nonconsecutive days (n = 9) was used for calculations, with the data expressed as RSD (%). As in the case of repeatability, good results were obtained for nearly all pesticides (RSD ≤ 20%).

Accuracy was assessed by fortifying blank samples of grapes at three concentration levels (n = 5 intraday, and n = 9 interday). Results obtained were back-calculated by means of "estimated concentration values" to estimate accuracy.[40] For all pesticides, accuracy ranged from 82 to 120%.

It is worth highlighting the excellent performance obtained by the proposed method for pesticides such as chlorothalonil, dicofol, and folpet, which are considered the weak link in QuEChERS-based multiresidue methods.[5,20]

Commercial Samples. The validated method was applied for the analysis of six commercial samples of conventionally grown green seedless grapes purchased at local markets in Waterloo (ON, Canada).

Twelve pesticides, all pertaining to the so-called new generation of pesticides, were detected in the commercial samples (Table 5). These pesticides are preferred for applications in grape crops because they are considered

DOI: 10.1021/jf506212j
J. Agric. Food Chem. 2015, 63, 4464−4477

Table 4. Method Validation Parameters for Grape Analysis at Optimized SPME Conditions

					intraday accuracy[b]			intraday precision[c]			interday accuracy[d]			interday precision[e]		
analyte	MRL[a] (ng/g)	LOQ (ng/g)	linearity (ng/g)	R^2	10 ng/g	50 ng/g	100 ng/g	10 ng/g	50 ng/g	100 ng/g	10 ng/g	50 ng/g	100 ng/g	10 ng/g	50 ng/g	100 ng/g
trifluralin	10	1	1–1000	0.9986	94	90	113	14	19	12	100	113	91	15	12	8
dimethoate[f]	20	50	50–500	0.9993		102	85		20	2		117	82		13	8
atrazine	50	1	1–1000	0.9993	111	109	109	16	20	12	109	120	120	15	20	12
diazinon	10	1	1–1000	0.9964	102	114	95	19	17	2	83	117	109	17	17	11
pyrimethanil	5000	1	1–500	0.9985	94	111	111	21	10	2	91	82	104	12	18	4
chlorothalonil	1000	1	1–1000	0.9996	94	99	87	11	17	4	82	112	89	8	18	4
pirimicarb	1000	1	1–1000	0.9991	91	97	105	20	5	4	99	115	82	20	13	9
vinclozoline	50	1	1–1000	0.9988	105	105	108	9	7	7	85	110	100	18	18	8
parathion-methyl	20	1	1–1000	0.9953	85	95	93	22	13	3	83	113	112	22	11	11
metalaxyl	2000	1	1–1000	0.9997	101	100	99	17	7	9	97	86	90	20	7	11
malathion	20	1	1–500	0.9989	101	94	103	10	15	9	91	112	115	20	15	3
chlorpyrifos	500	5	5–1000	0.9991	115	109	113	21	12	6	110	97	92	15	19	11
parathion	50	5	5–1000	0.9995	96	115	109	14	7	10	98	86	110	10	13	4
cyprodinil	5000	1	1–1000	0.9957	106	91	93	14	15	5	103	91	94	19	18	7
methidathion	20	5	5–1000	0.9988	108	109	103	9	9	12	94	110	112	21	17	11
endosulfan I[g]	50	5	5–1000	0.9998	89	113	94	17	9	4	81	86	110	12	8	5
fludioxonil	2000	1	1–1000	0.9997	104	112	112	13	8	12	81	94	105	19	5	2
4,4′-DDE	50	1	1–500	0.9988	102	95	87	16	20	5	112	89	107	15	7	9
myclobutanil	1000	1	1–1000	0.9995	111	108	109	20	7	6	119	83	100	21	13	7
kresoxim-methyl	1000	1	1–1000	0.9974	85	110	111	13	8	10	101	100	103	9	7	2
flusilazole	50	1	1–1000	0.9993	107	112	103	14	13	2	116	111	102	20	18	8
cyproconazole	200	5	5–1000	0.9999	110	94	98	12	12	8	98	113	86	13	15	6
endosulfan II[g]	50	5	5–1000	0.9967	88	100	105	11	12	11	105	88	115	19	17	11
trifloxystrobin	5000	5	5–1000	0.9993	102	115	91	11	7	9	97	94	115	11	15	11
quinoxyfen	1000	5	5–1000	0.9989	102	106	96	22	18	4	91	86	103	12	8	7
fenhexamide	5000	5	5–1000	0.9999	108	87	104	8	19	12	95	115	86	11	16	9
tebuconazole	2000	5	5–1000	0.9997	90	96	110	10	5	9	107	83	120	19	17	7
iprodione	10	5	5–1000	0.9997	86	94	86	16	11	2	87	112	92	15	11	12
fenpropathrin	10	**10**	10–1000	0.9989	90	114	112	19	6	5	122	102	103	22	14	6
phosalone	50	10	10–1000	0.9998	113	85	91	21	19	9	80	119	108	19	19	7
azinphos-methyl	50	5	5–1000	0.9993	100	103	97	12	19	6	120	114	80	16	7	2
pyriproxyfen	50	5	5–1000	0.9967	114	114	91	12	7	6	83	111	115	22	16	6
pyridaben	500	25	25–1000	0.9988		99	96		19	8		102	102		16	12
fenbuconazole	1000	10	5–1000	0.9994	117	90	103	16	8	3	82	89	96	17	18	10
boscalid	5000	1	1–1000	0.9993	97	94	114	11	5	7	114	83	119	18	11	12
pyraclostrobin	1000	10	10–1000	0.9992	82	106	110	20	9	11	119	93	111	17	20	7
azoxystrobin	2000	5	5–1000	0.9984	86	102	108	19	12	7	120	107	113	15	16	2
dicofol	20	10	10–1000	0.9997	112	115	85	21	20	7	83	102	96	20	6	6
folpet	20	10	10–500	0.9986	111	97	93	19	13	10	106	118	112	23	7	11
difenoconazole	500	10	10–1000	0.9999	94	95	97	17	17	2	83	83	97	21	8	4

[a]EU MRL ref 39. [b]n = 5. [c]RSD, % (n = 5). [d]n = 9. [e]RSD, % (n = 9). [f]LOQ > MRL. [g]For mixture of both isomers.

J. Agric. Food Chem. 2015, 63, 4464−4477 DOI: 10.1021/jf506212j

Table 5. Target Pesticides Found in Analyzed Commercial Grape Samples

	concentration found (ng/g, ±CV) (n = 3, each)					
analyte	sample 1	sample 2	sample 3	sample 4	sample 5	sample 6
boscalid	62 ± 2	nd[a]	nd	19 ± 1	161 ± 12	nd
cyprodinil	nd	83 ± 8	nd	73 ± 1	nd	<1
fenbuconazole	nd	nd	nd	<10	nd	nd
fenhexamide	nd	269 ± 51	nd	nd	nd	nd
fludioxonil	nd	47 ± 8	nd	nd	nd	nd
kresoxim-methyl	nd	nd	nd	<1	<1	1.4 ± 0.2
myclobutanil	nd	1.1 ± 0.1	nd	nd	nd	<1
pyraclostrobin	12 ± 7	nd	<10	nd	75 ± 4	nd
pyrimethanil	<1	192 ± 12	<1	nd	nd	<1
quinoxyfen	nd	36 ± 3	53 ± 19	nd	nd	nd
tebuconazole	nd	6.4 ± 0.1	5.8 ± 0.3	17 ± 1	nd	nd
trifloxystrobin	nd	nd	nd	nd	nd	nd

[a]nd, not detected.

somehow more innocuous than, but just as effective as, the older pesticides.[41] Pyrimethanil was detected in four of the six samples analyzed. The highest concentration was found for fenhexamide. Despite these findings, all pesticides were present at concentrations much lower than their respective MRLs.

In summary, the validated method yielded good accuracy, precision, and sensitivity. Taking into account the method's performance by using an environmentally friendly and automated technique, the proposed method is considered appropriate for the determination of 40 pesticides, comprising 21 different classes, in grapes, with a performance similar or superior to that of exhaustive extraction methods based on solvent extraction. Furthermore, the method was successfully applied for multiresidue determination of pesticides in the incurred samples. Therefore, the present method could be satisfactorily applied in routine monitoring of pesticides in agricultural commodities, provided that proper optimization is carried out.

With regard to the limitations of the proposed method, the DI-SPME method did not meet a satisfactory performance toward more polar pesticides (e.g., acephate, omethoate, dimethoate) due to the low affinity of these compounds toward the fiber coating in conjunction with their impaired GC responses. Another limitation of this method was its inability to provide reliable results for highly hydrophobic pesticides, such as pyrethroids. In this case, further investigation is currently underway to avoid losses due to the interaction of these compounds with labware.

Despite the challenges and limitations encountered by this method, the practical aspects of the PDMS-modified coating demonstrated here create new opportunities for the application of SPME in food analysis.

■ ASSOCIATED CONTENT

Supporting Information

Additional structures, physicochemical properties of target analytes, and experimental details. This material is available free of charge via the Internet at http://pubs.acs.org.

■ AUTHOR INFORMATION

Corresponding Author

*(J.P.) Phone: (519) 888-4567, ext. 84641. Fax: (519) 746-0435. E-mail: janusz@sciborg.uwaterloo.ca.

Funding

We thank the Natural Sciences and Engineering Research Council of Canada (NSERC), Agilent Technologies Foundation, and Sigma-Aldrich Corp. for financial support.

Notes

The authors declare no competing financial interest.

■ ACKNOWLEDGMENTS

We thank Olivier Niquette for all of his help troubleshooting the GC-ToFMS system.

■ REFERENCES

(1) Wong, J.; Hao, C.; Zhang, K.; Yang, P.; Banerjee, K.; Hayward, D.; Iftakhar, I.; Schreiber, A.; Tech, K.; Sack, C.; Smoker, M.; Chen, X.; Utture, S. C.; Oulkar, D. P. *J. Agric. Food Chem.* **2010**, *58*, 5897−5903.

(2) Koesukwiwat, U.; Lehotay, S. J.; Miao, S.; Leepipatpiboon, N. *J. Chromatogr., A* **2010**, *1217*, 6692−6703.

(3) Nguyen, T. D.; Han, E. M.; Seo, M. S.; Kim, S. R.; Yun, M. Y.; Lee, D. M.; Lee, G.-H. *Anal. Chim. Acta* **2008**, *619*, 67−74.

(4) Mastovska, K.; Dorweiler, K. J.; Lehotay, S. J.; Wegscheid, J. S.; Szpylka, K. a. *J. Agric. Food Chem.* **2010**, *58*, 5959−5972.

(5) Lehotay, S. J.; Mastovská, K.; Yun, S. J. *J. AOAC Int.* **2005**, *88*, 630−638.

(6) Blasco, C.; Vazquez-Roig, P.; Onghena, M.; Masia, A.; Picó, Y. *Sel. Pap., 28th Int. Symp. Chromatogr.* **2011**, *1218*, 4892−4901.

(7) Guillet, V.; Fave, C.; Montury, M. *J. Environ. Sci. Health, Part B* **2009**, *44*, 415−422.

(8) Cai, L. S.; Gong, S. L.; Chen, M.; Wu, C. Y. *Anal. Chim. Acta* **2006**, *559*, 89−96.

(9) Saraji, M.; Rezaei, B.; Boroujeni, M. K.; Bidgoli, A. A. H. *J. Chromatogr., A* **2013**, *1279*, 20−26.

(10) Abdulra'uf, L. B.; Hammed, W. A.; Tan, G. H.; Abdulra'uf, L. B. *Crit. Rev. Anal. Chem.* **2012**, *42*, 152−161.

(11) Viñas, P.; Campillo, N.; Martínez-Castillo, N.; Hernández-Córdoba, M. *J. Chromatogr., A* **2009**, *1216*, 140−146.

(12) Schurek, J.; Portolés, T.; Hajslova, J.; Riddellova, K.; Hernández, F. *Anal. Chim. Acta* **2008**, *611*, 163−172.

(13) Chai, M. K.; Tan, G. H. *Food Chem.* **2009**, *117*, 561−567.

(14) Cortés-Aguado, S.; Sánchez-Morito, N.; Arrebola, F. J.; Frenich, A. G.; Vidal, J. L. M.; Cortesaguado, S.; Sanchezmorito, N. *Food Chem.* **2008**, *107*, 1314−1325.

(15) Martins, J.; Esteves, C.; Simoes, T.; Correia, M.; Delerue-Matos, C. *J. Agric. Food Chem.* **2011**, *59*, 6847−6855.

(16) Balasubramanian, S.; Panigrahi, S. *Food Bioprocess Technol.* **2010**, *4*, 1−26.

(17) Abdulra'uf, L. B.; Hammed, W. A.; Tan, G. H. *Crit. Rev. Anal. Chem.* **2012**, *42*, 152−161.

DOI: 10.1021/jf506212j
J. Agric. Food Chem. 2015, 63, 4464−4477

(18) Souza-Silva, É. A.; Pawliszyn, J. *Anal. Chem.* **2012**, *84*, 6933−6938.
(19) Souza-Silva, É. A.; Lopez-Avila, V.; Pawliszyn, J. *J. Chromatogr., A* **2013**, *1313*, 139−146.
(20) Maštovská, K.; Lehotay, S. J. *J. Chromatogr., A* **2004**, *1040*, 259−272.
(21) Stalikas, C.; Fiamegos, Y.; Sakkas, V.; Albanis, T. *J. Chromatogr., A* **2009**, *1216*, 175−189.
(22) Callao, M. P. *TrAC, Trends Anal. Chem.* **2014**, *62*, 86−92.
(23) Pawliszyn, J. *Handbook of Solid Phase Microextraction*; Pawliszyn, J., Ed.; Chemical Industry Press: Beijing, China, 2009; p 410.
(24) Simplício, a L.; Boas, L. V. *J. Chromatogr., A* **1999**, *833*, 35−42.
(25) Perestrelo, R.; Barros, A. S.; Rocha, S. M.; Câmara, J. S. *Talanta* **2011**, *85*, 1483−1493.
(26) Leardi, R. *Anal. Chim. Acta* **2009**, *652*, 161−172.
(27) Kolberg, D. I.; Prestes, O. D.; Adaime, M. B.; Zanella, R. *Food Chem.* **2011**, *125*, 1436−1442.
(28) Wilkowska, A.; Biziuk, M. *Food Chem.* **2011**, *125*, 803−812.
(29) Yang, X.; Zhang, H.; Liu, Y.; Wang, J.; Zhang, Y. C.; Dong, a J.; Zhao, H. T.; Sun, C. H.; Cui, J. *Food Chem.* **2011**, *127*, 855−865.
(30) Banerjee, K.; Mujawar, S.; Utture, S. C.; Dasgupta, S.; Adsule, P. G. *Food Chem.* **2013**, *138*, 600−607.
(31) Cunha, S. C.; Fernandes, J. O. *J. Chromatogr., A* **2011**, *1218*, 7748−7757.
(32) Dasgupta, S.; Banerjee, K.; Patil, S. H.; Ghaste, M.; Dhumal, K. N.; Adsule, P. G. *J. Chromatogr., A* **2010**, *1217*, 3881−3889.
(33) Lehotay, S. J.; O'Neil, M.; Tully, J.; García, A. V.; Contreras, M.; Mol, H.; Heinke, V.; Anspach, T.; Lach, G.; Fussell, R.; Mastovska, K.; Poulsen, M. E.; Brown, A.; Hammack, W.; Cook, J. M.; Alder, L.; Lindtner, K.; Vila, M. G.; Hopper, M.; De Kok, A.; Hiemstra, M.; Schenck, F.; Williams, A.; Parker, A. *J. AOAC Int.* **2007**, *90*, 485−520.
(34) Cunha, S. C.; Fernandes, J. O.; Alves, A.; Oliveira, M. B. P. P. *J. Chromatogr., A* **2009**, *1216*, 119−126.
(35) Rial Otero, R.; Cancho Grande, B.; Simal Gándara, J. *J. Chromatogr., A* **2003**, *992*, 121−131.
(36) Banerjee, K.; Patil, S. H.; Dasgupta, S.; Oulkar, D. P.; Patil, S. B.; Savant, R.; Adsule, P. G. *J. Chromatogr., A* **2008**, *1190*, 350−357.
(37) Banerjee, K.; Oulkar, D. P.; Dasgupta, S.; Patil, S. H. S. B. S. H. S. H. B.; Savant, R.; Adsule, P. G. *J. Chromatogr., A* **2007**, *1173*, 98−109.
(38) Payá, P.; Anastassiades, M.; Mack, D.; Sigalova, I.; Tasdelen, B.; Oliva, J.; Barba, A. *Anal. Bioanal. Chem.* **2007**, *389*, 1697−1714.
(39) SANCO, D. EU Pesticides Database, http://ec.europa.eu/sanco_pesticides/public/?event=commodity.resultat (accessed Dec 1, 2014).
(40) Martins, J.; Esteves, C.; Limpo-Faria, A.; Barros, P.; Ribeiro, N.; Simões, T.; Correia, M.; Delerue-Matos, C. *Food Chem.* **2012**, *132*, 630−636.
(41) Sannino, A. Food contaminants and residue analysis. In *Comprehensive Analytical Chemistry*, 1st ed.; Picó, Y., Ed.; Elsevier: Amsterdam, The Netherlands, 2008; Vol. 51, p 821.

DOI: 10.1021/jf506212j
J. Agric. Food Chem. 2015, 63, 4464−4477

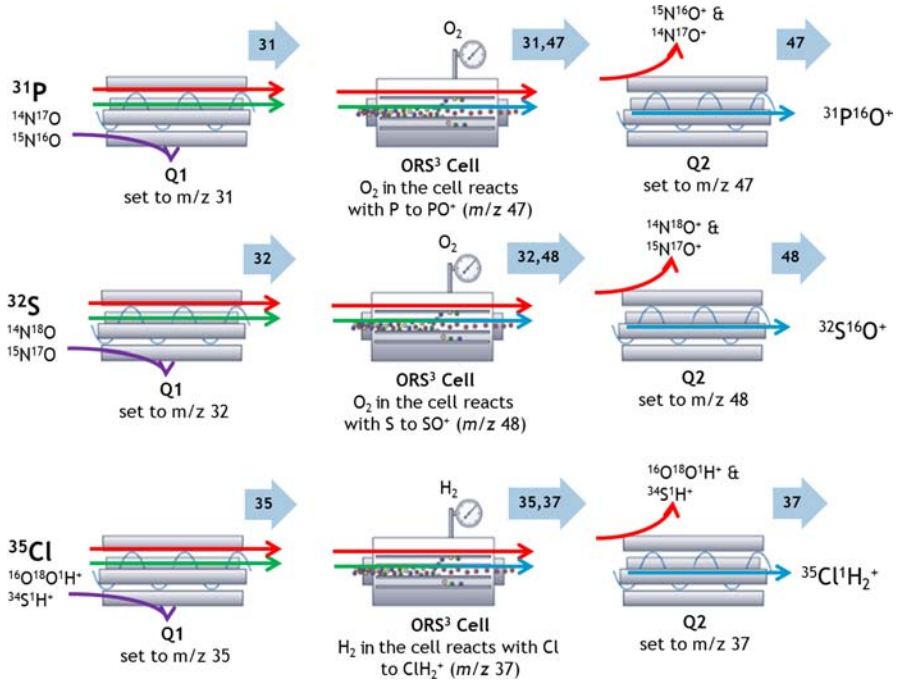

Figure 1. MS/MS mass shift mode using oxygen cell gas for the measurement of P and S. Q1 is set to m/z 31 and 32, allowing $^{31}P^+$ and $^{32}S^+$ and any other ions at m/z 31 and 32 to enter the CRC. All other ions are rejected. In the cell, P and S react with oxygen to form PO^+ at m/z 47 and SO^+ at m/z 48. Q2 is set to m/z 47 and 48, allowing PO^+ and SO^+ to pass to the detector. Because no NO^+ ions react with oxygen, they are rejected by Q2.

However, if these elemental interferences could be overcome, element-specific detection has the potential to further improve the pesticide detection limits by lowering the background chemical noise. The recent combination of tandem MS detection with inductively coupled plasma (ICP-MS/MS or ICP-QQQ) is a way to address this challenge. Similar to GC or LC-MS/MS, in ICP-MS/MS the first quadrupole (Q1) acts as a mass filter. In the collision reaction cell (CRC) that follows, analytes or interferences react with various gases in a very selective way to produce a product ion, which is then accepted (analyte) or rejected (interference) by the second quadrupole (Q2) prior to detection (Figure 1). Using this approach, background levels are dramatically reduced, thus increasing the sensitivity of the detection.

Presented here is the first application of a GC-ICP-MS/MS method for the selective and sensitive detection of heteroatom-containing pesticides in various food matrices. For the detection of organophosphorus pesticides, oxygen was used in the reaction cell to convert P (m/z 31) to PO^+ (m/z 47). Similarly, SO^+ (m/z 48) was monitored after the reaction of S (m/z 32) with oxygen for the detection of organosulfur pesticides. To detect chlorine pesticides, Cl (m/z 35) was reacted in the CRC with H_2 to form ClH_2 (m/z 37).

The developed method is an attractive alternative to existing highly sensitive and selective organophosphorus detection methods, with detection limits comparable to, or even slightly lower than, those of GC-MS/MS. The GC-ICP-MS/MS method is easy to set up and does not require retention time based acquisition conditions such as selected ion monitoring windows or the development of multiple reaction monitoring (MRM) settings. Due to the detection of heteroatoms instead of compounds, GC-ICP-MS/MS allows the quantification of unknown peaks by compound-independent calibration (CIC). The use of the MS/MS mode dramatically reduces background levels for interference-prone elements such as P, S, and Cl, thereby increasing the sensitivity of the method significantly compared to single-quadrupole ICP-MS detection.

Although this paper focuses on the analysis of pesticides by GC-ICP-MS/MS, it is understood that this system is unlikely to replace conventional GC-MS/MS approaches for the analysis of pesticide residues. Most pesticide residue laboratories have already invested in GC-MS/MS and LC-MS/MS equipment and, in most cases, these instruments provide more than adequate sensitivity. Furthermore, such methods have already been validated by the laboratory, a process that can be time-consuming. However, pesticides are a good model for other organophosphorus compounds (e.g., fire retardants and polymer additives) and sulfur compounds that can have a significant influence on flavor and aromas at trace levels. This GC-ICP-MS/MS approach may be useful when extremely low detection limits are desirable, such as for the analysis of pesticides in drinking water or baby food.

MATERIALS AND METHODS

Materials. A variety of food matrices were tested for their pesticide content including baby food fruit purees, green onions, tea (three types), green peppers, and yellow onion. The baby food purees were purchased in São Paulo, Brazil; the fresh vegetables were purchased at various produce markets in San Francisco, CA, USA; and the loose tea was purchased in various locations in China. All food matrices were extracted in triplicate using the AOAC 2007.1 QuEChERS method before analysis by GC-ICP-MS/MS. HPLC grade acetonitrile was purchased from J. T. Baker (Center Valley, PA, USA). Calibration was performed using three standard pesticide mixes obtained from Ultra Scientific (Kingstown, RI, USA) and Agilent Technologies (Santa Clara, CA, USA). The three mixed standard solutions were diluted with acetonitrile to form intermediate solutions, which were then used to prepare calibration standard solutions following serial dilutions in acetonitrile. QuEChERS kits were obtained from Agilent.

Sample Preparation. Apart from the prehomogenized baby food purees, all samples were ground in a food processor to obtain a homogeneous sample (NutriBullet, LLC, Porcomia, CA, USA).

DOI: 10.1021/jf506372e
J. Agric. Food Chem. 2015, 63, 4478−4483

Approximately 15 ± 0.1 g of sample (5 ± 0.1 g in the case of the tea samples due to their low density) were weighed into 50 mL centrifuge tubes, and then 15 mL of acetonitrile and two ceramic bars were added. This mixture was homogenized for 1 min on a vortex mixer. Then, prepackaged amounts of $MgSO_4$ and NaCl were added, and the system was agitated for 1 min again. The mixture was centrifuged at 2600*g* for 5 min. An 8 mL aliquot of the upper acetonitrile layer was transferred to 15 mL centrifuge tubes containing the dispersive and cleanup agents (PSA, $MgSO_4$). The tube was homogenized for 1 min and centrifuged at 2600*g* for 5 min. The resultant upper layer was transferred to an amber glass vial (Agilent Technologies) for analysis.

Instrument Setup. All measurements were carried out using an Agilent 7890 GC (Agilent Technologies, USA) coupled via an Agilent GC-ICP-MS transfer line (Agilent Technologies, Japan) to an Agilent 8800 ICP-QQQ instrument (Agilent Technologies, Japan). The chromatographic separation parameters were used as previously published.[12] The GC system was equipped with fast oven heating (240 V), a split/splitless inlet, a 7693A autosampler, auxiliary electronic pressure control (aux EPC), and a column backflushing system based on a purged union. Two columns were configured in an arrangement that allowed the first column to be backflushed shortly before the run had ended or during a postrun period.[13] The first column was a 5 m × 0.25 mm i.d. × 0.25 μm film thickness DB-5MS UI capillary column (cut from a 30-m DB-5MS UI column obtained from Agilent), which was installed between the inlet and one end of the purged union. The second column was a 15 m × 0.25 mm i.d. × 0.25 μm film thickness DB-5MS UI capillary column (Agilent Technologies) installed between the other end of the purged union and the transfer line connection inside the GC oven. Injections (1 μL) were made under splitless conditions with the inlet held at 280 °C. The GC oven temperature program started at 60 °C (held for 1.5 min), followed by a 50 °C/min ramp to 150 °C, then 8 °C/min to 240 °C, then 50 °C/min to 280 °C (2.5 min), and finally 100 °C/min to 290 °C (held for 2.05 min). The helium carrier gas was controlled in constant flow mode. The flow rate settings for analysis and backflushing mode were used as described previously.[12] Helium makeup gas (0.7 mL/min, controlled by an aux EPC module on the ICP-MS/MS) was passed through a metal tube placed in the GC oven and connected to the transfer line interface. The preheated makeup gas was used to sweep the GC column effluent efficiently into the plasma.

During ICP-MS/MS tuning, the helium carrier gas supplying the GC inlet and aux EPC module was replaced by argon containing H_2S at 100 ppm. The oxygen flow rates in the reaction cell and the quadrupole energy settings of the ICP-MS/MS were optimized by manually following the $^{32}S^+$ signal from the H_2S-spiked Ar gas. As discussed below, this resulted in a high sulfur background for several days after the switch back to pure helium, so an alternative position to feed the tuning gas into the ICP-MS/MS is recommended. The optimal operating conditions for the ICP-MS/MS are shown in Table 1.

The ICP-MS/MS includes an octopole reaction system (ORS^3) that is positioned between two quadrupole analyzers, as shown in Figure 1. The width of the bandpass of the first quadrupole analyzer can be varied from "fully open" to a unit mass filter, restricting the ions entering the CRC to a single mass to charge ratio (m/z) at any given time. For this study, two separate time-resolved analysis (TRA) methods were run simultaneously. P and S were analyzed using the same method as they both react spontaneously ($\Delta H_{reaction} < 0$) with oxygen:

$$^{31}P^+ + {}^{16}O_2 \rightarrow {}^{31}P^{16}O^+ + {}^{16}O \quad \Delta H_{reaction} = -3.17 \text{ eV}$$

$$^{32}S^+ + {}^{16}O_2 \rightarrow {}^{32}S^{16}O^+ + {}^{16}O \quad \Delta H_{reaction} = -0.34 \text{ eV}$$

For the determination of P and S, Q1 was set to transmit m/z 31 (for ^{31}P) and m/z 32 (for ^{32}S). O_2 was used as a reaction gas in the CRC. Q2 was set to monitor m/z 47 and 48 so that the product ions $^{31}P^{16}O^+$ and $^{32}S^{16}O^+$ could be detected free of any interferences. Besides the single oxides, the PO_2^+ and SO_2^+ masses at m/z 63 and 64 were monitored. Both P and S show high isotope purity (P, 31 (100%); S, 32 (94.99%), 33 (0.75%), 34 (4.25%), 36 (0.01%)[14]); thus, only the major isotope of each element was monitored.

Table 1. ICP-MS/MS Settings for the Two Different Detection Modes (Oxygen for P and S and Hydrogen for Cl Detection)

cell mode	O_2	H_2
scan mode	MS/MS	MS/MS
RF Power	1600	900
sampling depth (mm)	3	3
dilution gas (L/min)	0.6	0.5
octopole bias (V)	−0.5	−0.5
octopole RF (V)	150	150
KED (V)	−13	−13
cell gas	O_2	H_2
cell gas flow rate (%)	20	7
cell entrance (V)	−50	−30
cell exit (V)	−70	−70
deflect (V)	10	10
plate bias (V)	−60	−60
monitored masses	Q1 ≫ Q2	Q1 ≫ Q2
	31 ≫ 47	35 ≫ 37
	32 ≫ 48	

An illustration of the theory of the mass shift method using oxygen reaction gas is shown in Figure 1.

Even though the reaction between Cl^+ and O_2 is exothermic ($\Delta H_{reaction} = -0.91$ eV), the dominant process in the CRC under the conditions used is charge transfer ($Cl^+ + O_2 \rightarrow Cl + O_2^+$). Consequently, H_2 was used as the cell gas for the analysis of the Cl based pesticides based on the following theoretical reactions:

$$^{35}Cl^+ + {}^1H_2 \rightarrow {}^{35}Cl^1H^+ + {}^1H \quad \Delta H_{reaction} = -0.17 \text{ eV}$$

$$^{35}Cl^1H^+ + {}^1H_2 \rightarrow {}^{35}Cl^1H^1H^+ + {}^1H \quad \Delta H_{reaction} = -0.39 \text{ eV}$$

Q1 was set to m/z 35, where ^{35}Cl reacts with H_2 in the CRC to form $^{35}Cl^1H^1H^+$.[15] The Q2 was set to m/z 37, allowing the product ion ClH_2^+ to pass to the detector. Chlorine shows high isotopic purity (Cl, 35 (75.78%), 37 (24.22%)[14]); thus, only the major isotope was monitored.

RESULTS AND DISCUSSION

It has been shown previously that GC is an excellent sample introduction system for the ICP-MS detection of organophosphorus compounds.[10,16−21] Compared to liquid sample introduction into the ICP-MS, the GC delivers dry helium carrier gas containing relatively little matrix. However, GC-ICP-MS is limited to the determination of heteroatom-containing compounds that are volatile and thermally stable or can be converted to a volatile form by derivatizaton before injection into the GC-ICP-MS. Tuning of the GC-ICP-MS/MS was done by substituting the helium carrier gas with 100 ppm of H_2S spiked in Ar. As has already been discussed in the literature,[16] the optimal instrumental parameters for GC-ICP-MS are different from those required under wet plasma conditions. Thus, tuning for optimal parameter settings is required. For this study, optimization of the GC-ICP-MS/MS instrumental settings was carried out manually following the $^{32}S^+$ signal from the Ar gas spiked with 100 ppm of H_2S. The optimized plasma parameters are shown in Table 1.

In retrospect, introducing the Ar/H_2S tuning mixture through the EPC modules and carrier gas lines of the GC was problematic. H_2S contaminated the flow system and

DOI: 10.1021/jf506372e
J. Agric. Food Chem. 2015, 63, 4478−4483

Table 2. Retention Times (RT), Detection Limits for Compounds and for Elements, and Background-Equivalent Concentrations (BEC)

		P			S			Cl		
		compd	element		compd	element		compd	element	
compd	RT ± 0.3 (min)	LOD ($\mu g\ L^{-1}$)	LOD ($\mu g\ L^{-1}$)	BEC ($\mu g\ L^{-1}$)	LOD ($\mu g\ L^{-1}$)	LOD ($\mu g\ L^{-1}$)	BEC ($\mu g\ L^{-1}$)	LOD ($\mu g\ L^{-1}$)	LOD ($\mu g\ L^{-1}$)	BEC ($\mu g\ L^{-1}$)
trichlorfon	4.103			0.013						4.038
thionazin	5.926	0.028	0.004	0.009	1.236	0.159	0.741			
dicrotophos										
terbufos	7.071	0.019	0.002	0.005	1.298	0.432	−0.382			
fonofos	7.185	0.047	0.006	0.045	0.649	0.169	0.282			
phosphamidon	7.299	0.015	0.002							−0.191
dichlofenthion	7.858	0.010	0.001	0.005	0.666	0.068	−0.336	0.671	0.149	0.166
chloropyrifos-methyl	7.973	0.015	0.001	0.019	1.710	0.170	−0.287	1.478	0.481	−4.103
fenitrothion	8.440	0.005	0.001	0.011	3.032	0.350	0.282			
aspon	8.705	0.009	0.002	0.007	0.885	0.150	0.366			
chlorfenvinphos	9.486	0.033	0.003	0.005				1.746	0.510	−4.415
crotoxyphos	9.541	0.033	0.003	0.037						
carbophenothion	11.158	0.004	0.000	0.008	0.980	0.274	0.649	1.868	0.191	2.678
ethion	11.527	0.024	0.004	0.054	2.830	0.942				
famphur	12.547	0.036	0.003	0.083	2.162	0.425	1.965			
phosmet	12.851	0.258	0.025	0.111						
leptophos	13.263	0.032	0.002	0.019	6.077	0.472	0.377	1.327	0.225	2.592
azinphos-ethyl	13.827	0.103	0.009	0.004	2.802	0.519	2.056			
dioxathion	14.587	0.265	0.036	0.027	34.000	9.533				

Table 3. Elemental Detection Limits Comparison among Some GC-ICP-MS Methods

analysis	LOD for P ($\mu g\ L^{-1}$)	LOD for S ($\mu g\ L^{-1}$)	LOD for Cl ($\mu g\ L^{-1}$)	instrumental details	ref
volatile S compounds in human breath		8.0−33.0		GC-ICP-HRMS (resolution 3000)	26
total homocysteine in human serum		22		GC-ICP-HRMS (resolution 3000)	27
petroleum products	0.2−0.3	3.0−11	1.0−3.0	GC-ICP-MS collision cell with He	24
petroleum products		0.6		GC-ICP-MS modified interface and Ar purification to reduce the O_2 interference	28
organophosphorus fire retardants and plasticizers in wastewater	3.2−4.2			GC-ICP-MS collision cell with He	19
trihalomethanes in drinking water			0.35	GC-ICP-MS	29
organophosphorus nerve agent degradation products in pesticide mixtures	5000 (working range)			GC-ICP-MS no gas cell, monitoring $^{31}P^+$ and $^{31}P^{16}O^+$	30
thiophene derivates in petroleum products		7		GC-ICP-MS no cell isotopic dilution	31
organopesticides in food	0.0004−0.0359	0.07−9.5	0.15−0.51	GC-ICP-MS/MS with mass shift for P ($^{31}P^+ \rightarrow {}^{31}P^{16}O^+$), S ($^{32}S^+ \rightarrow {}^{32}S^{16}O^+$), and Cl ($^{35}Cl^+ \rightarrow {}^{35}Cl^1H^1H^+$)	this work

continued to bleed out for the duration of these experiments. A better choice would be to introduce the H_2S/argon mixture as close to the ICP torch as possible, thereby minimizing the contact area for H_2S adsorption. This approach will be tested in future studies.

Once the GC-ICP-MS/MS was optimized for S sensitivity, the same instrument conditions were used for both S and P. The limits of detection were calculated on the basis of the standard deviations ($3 \times \sigma$, where σ is the standard deviation) from seven replicate blank samples, as shown in Table 2. Compound LODs and element specific LODs results are summarized in Table 2.

Careful optimization of the GC-ICP-MS/MS instrumental setup provides improved elemental detection limits compared to previously published GC-ICP-MS methods shown in Table 3.

Currently, one of the best ways to analyze GC-amenable pesticides is by GC-MS/MS with electron impact ionization.[29] This approach has largely replaced the use of traditional element-selective detectors such as the NPD, ECD, and FPD. GC-MS/MS offers high selectivity based on molecular fragmentation and the ability to detect any pesticide using a single detector. Detection limits for pesticides using current GC-MS/MS instrumentation typically vary from about 0.1 to 10 $\mu g\ kg^{-1}$ depending on the pesticide and instrument used.[22,23] The data in Table 2 would suggest that the GC-ICP-MS/MS is about an order of magnitude more sensitive than GC-MS/MS for organophosphorus pesticides. Using S or Cl, detection limits are similar to those achieved by GC-MS/MS. It is likely that detection limits using S will improve if the instrument can be tuned without contaminating the GC with H_2S. With one exception (dioxathion using S), all of the

DOI: 10.1021/jf506372e
J. Agric. Food Chem. 2015, 63, 4478−4483

pesticides in Table 2 could be detected well below 10 μg L^{-1}, which is the LOQ required by most food safety laboratories.

After instrumental conditions were optimized, mixtures of the three Ultra Scientific standard solutions were diluted with acetonitrile. Figure 2 shows chromatograms showing the heteroatom traces for P, S, and Cl of the calibration standard with identified pesticide compounds. The chromatogram for P and S was run in the same TRA run, and the Cl chromatogram trace was run in a separate TRA run and overlaid.

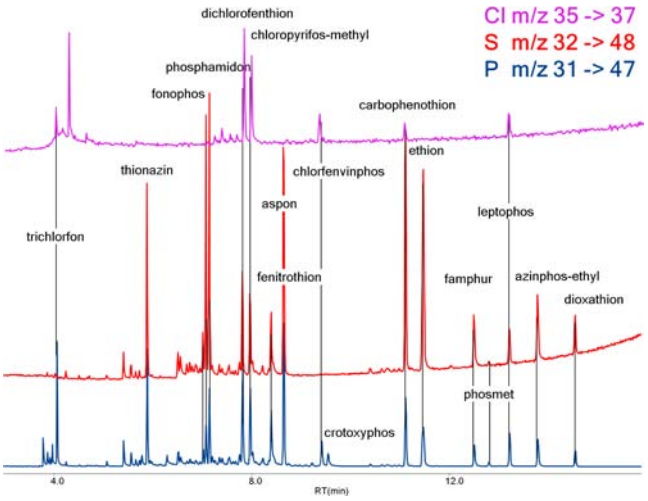

Figure 2. Chromatograms showing the heteroatom traces for P, S, and Cl of the calibration standard with identified pesticide compounds.

For a real-world application, real food samples (baby food purees, fresh vegetables, loose tea) were screened for their pesticide content. Every real-world food sample that was tested showed positive traces of pesticides in the chromatograms. Figure 3 shows an example of the P chromatogram of some of the analyzed food samples, together with a 200 ppb calibration standard.

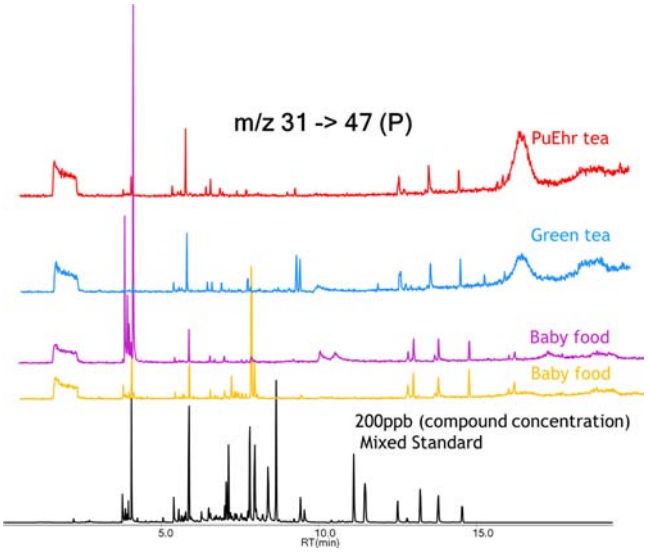

Figure 3. Example chromatogram showing the P trace of the analyzed food samples, together with a 200 ppb calibration standard. Baby food purple line or baby food 1, papaya + orange purée; baby food yellow line or baby food 3, grape purée.

This work clearly shows the potential of GC-ICP-MS/MS to be used for the ultratrace analysis of P-, S-, and Cl-containing compounds such as the pesticides in our test samples. GC-ICP-MS/MS optimization is essential to achieve the ultratrace LODs achieved in this study. There is also the possibility of using a CIC heteroatom method for quantification without the need for individual pesticide standards as shown by Bouyssiere et al.[24] and González-Gago et al.[25] Calibrating with pesticide mixes containing all analytes in the method is both time-consuming and expensive, especially as the analyte lists grow. In theory, one could calibrate for a long list of pesticides using a single compound containing the heteroatoms common to the target pesticides. However, this approach does not account for the behavior of individual pesticides (adsorption, degradation, etc.) during the chromatographic analysis. Future investigations will also target the application of GC-ICP-MS/MS for other matrices that would benefit from ultratrace detection limits and will look at ways of tuning the GC-ICP-MS/MS instrument that do not result in sulfur contamination.

AUTHOR INFORMATION

Corresponding Author

*(J.N.) E-mail: jenny_nelson@agilent.com. Phone: (517) 510-6475. Fax: (302) 636-1584.

Notes

The authors declare no competing financial interest.

ACKNOWLEDGMENTS

We thank Harry Prest, Dan Manuto, and Charles Thomson for the use of the GC and assistance in its setup. Harry Prest also donated standards for the method development. We also thank Craig Jones and Emmett Soffey for the use of the 8800 ICP-MS/MS and their advice for setting up the ICP-MS/MS.

REFERENCES

(1) Weiss, B.; Amler, S.; Amler, R. W. *Pediatrics* **2004**, *113*, 1030–1036.
(2) Sadowska-Rociek, A.; Surma, M.; Cieślik, E. *Bull. Environ. Contam. Toxicol.* **2013**, *90*, 508–513.
(3) Casals-Casas, C.; Desvergne, B. *Annu. Rev. Physiol.* **2011**, *73*, 135–162.
(4) Mnif, W.; Hassine, A. I. H.; Bouaziz, A.; Bartegi, A.; Thomas, O.; Roig, B. *Int. J. Environ. Res. Public Health* **2011**, *8*, 2265–2303.
(5) Anastassiades, M.; Lehotay, S. J. *J. AOAC Int.* **2003**, *86*, 412–431.
(6) Ramírez Restrepo, A.; Gallo Ortiz, A. F.; Hoyos Ossa, D. E.; Peñuela Mesa, G. A. *Food Chem.* **2014**, *158*, 153–161.
(7) Hou, X.; Han, M.; Dai, X.; Yang, X.; Yi, S. *Food Chem.* **2013**, *138*, 1198–1205.
(8) Al-Taher, F.; Chen, Y.; Wylie, P.; Cappozzo, J. *J. Food Prot.* **2013**, *76*, 510–515.
(9) Chen, Y.; Al-Taher, F.; Juskelis, R.; Wong, J. W.; Zhang, K.; Hayward, D. G.; Zweigenbaum, J.; Stevens, J.; Cappozzo, J. *J. Agric. Food Chem.* **2012**, *60*, 9991–9999.
(10) Frenich, A. G.; Vidal, J. L. M.; Frías, M. M.; Rodriguez, L. C. *Chromatographia* **2003**, *57*, 213–220.
(11) Words, K. *Chromatographia* **2000**, *52*, 614–620.
(12) Wylie, P. L.; Meng, C. A method for the trace analysis of 175 pesticides using the Agilent triple quadrupole GC/MS/MS. Agilent Application Note, Feb 25, 2009.
(13) Mastovska, K.; Wylie, P. L. *J. Chromatogr., A* **2012**, *1265*, 155–164.
(14) Coursey, J. S.; Schwab, D. J.; Tsai, J. J.; Dragoset, R. A. *Atomic Weights and Isotopic Compositions*, version 3.0; NIST: Gaithersburg, MD, USA, 1999.

DOI: 10.1021/jf506372e
J. Agric. Food Chem. 2015, 63, 4478–4483

(15) Linstrom, P. J.; Mallard, W. G. *NIST Chemistry WebBook, NIST Standard Reference Database Number 69*; NIST: Gaithersburg, MD, USA, 2000.
(16) González-Gago, A.; Pröfrock, D.; Prange, A. *J. Anal. At. Spectrom.* **2015**, *30*, 180−190.
(17) Easter, R. N.; Caruso, J. A.; Vonderheide, A. P. *J. Anal. At. Spectrom.* **2010**, *25*, 493.
(18) Fidalgo-Used, N.; Montes-Bayón, M.; Blanco-González, E.; Sanz-Medel, A. *J. Anal. At. Spectrom.* **2005**, *20*, 876.
(19) Ellis, J.; Shah, M.; Kubachka, K. M.; Caruso, J. A. *J. Environ. Monit.* **2007**, *9*, 1329−1336.
(20) García-López, M.; Rodríguez, I.; Cela, R.; Kroening, K. K.; Caruso, J. A. *Talanta* **2009**, *79*, 824−829.
(21) Wuilloud, J. C. .; Wuilloud, R. G.; Vonderheide, A. P.; Caruso, J. A. *Spectrochim. Acta Part B: At. Spectrosc.* **2004**, *59*, 755−792.
(22) Churley, M. *Agilent Technolgies Application Note 5991-4131EN*, 2014; pp 1−10
(23) Hernández, F.; Cervera, M. I.; Portolés, T.; Beltrán, J.; Pitarch, E. *Anal. Methods* **2013**, *5*, 5875−5894.
(24) Bouyssiere, B.; Leonhard, P.; Pröfrock, D.; Baco, F.; Lopez Garcia, C.; Wilbur, S.; Prange, A. *J. Anal. At. Spectrom.* **2004**, *19*, 700.
(25) González-Gago, A.; Marchante-Gayón, J. M.; García Alonso, J. I. *J. Anal. At. Spectrom.* **2007**, *22*, 1138.
(26) Rodriguez-Fernandez, J.; Montes-Bayon, M.; Pereiro, R.; Sanz-Medel, A. *J. Anal. At. Spectrom.* **2001**, *16*, 1051−1056.
(27) De la Flor St Rèmy, R. R.; Montes-Bayón, M.; Sanz-Medel, A. *Anal. Bioanal. Chem.* **2003**, *377*, 299−305.
(28) Tao, H.; Nakazato, T.; Akaska, M.; Satoh, S. *Bunseki Kagaku* **2007**, *56*, 333−347.
(29) González-Gago, A.; Marchante-Gayón, J. M.; García Alonso, J. I. *J. Anal. At. Spectrom.* **2007**, *22*, 1138.
(30) Richardson, D. D.; Caruso, J. A. *Anal. Bioanal. Chem.* **2007**, *389*, 679−682.
(31) Heilmann, J.; Heumann, K. G. *Anal. Bioanal. Chem.* **2008**, *390*, 643−653.

DOI: 10.1021/jf506372e
J. Agric. Food Chem. 2015, 63, 4478−4483

honey.[2,7,10−13] The methods comprise the use of different strategies for the elimination of coextractives; for example, in the case of bees a hexane partition of the acetonitrile (MeCN) extraction solution is used to remove lipids from the extract.[11] Recently, our group reported an optimized combination of sample amount, extraction temperature, and cleanup methodology using freeze out, PSA, C18, and GCB as sorbents for beeswax pesticide residues analysis.[14] This approach was more effective than matrix solid phase dispersion (MSPD), which gave a high load of coextractives that spoiled the chromatographic system after a few injections. Pesticide residues in bees were analyzed using the MeCN-based extraction followed by different combinations of sorbents that optimized the performance of the method for the investigated analytes.[10,14] Compared with pollen, bees, and wax, honey is a simpler matrix, and due to its importance as food, it has been widely analyzed following different protocols. CEN 15662 QuEChERS has been smoothly applied to pesticide residue analysis in honey by our group.[15] As pointed out above, extensive surveys of pesticide residues in bees and beehives in North America and other parts of the world, looking for possible causes of bee decline,[2−8] have shown the presence of important amounts of pesticide residues in beehives. The major pesticide classes found were insecticides and fungicides, the latter being the most ubiquitous among North American apiaries. Chlorothalonil and strobilurins as well as some azoles accounted for the more frequent findings. The relationship of these pesticide cocktails to bee health is an open question that deserves a multiple-faceted approach to solve it, but at the same time, the vast array of residue findings in beehives supports the idea that bees collect what is in the environment, an ideal characteristic for an environmental monitor.[3,16−24]

In the present paper, the application of QuEChERS protocols for pesticide residue analysis in bees and bee products is reported. After the data gathered had been studied, a novel, first approach to check the recording of season variations in pesticide residues profiles in beehives within an agroecosystem is explored along with other statistical analysis to check the viability of beehives as environmental monitors.

MATERIALS AND METHODS

Chemicals and Standards. MeCN and *n*-hexane of HPLC quality were from Pharmco Products Inc. (Brookfield, CT, USA). Water was deionized in the laboratory using a Thermo Scientific (Marietta, OH, USA) EASYpure RoDi Ultrapure water purification system. Magnesium sulfate anhydrous, reagent grade, was from J. T. Mallinckrodt Baker Inc. (Phillipsburg, NJ, USA), and formic acid p.a. 88% was purchased from Macron Chemicals (Deventer, The Netherlands). A solution of 5% formic acid (v/v) was prepared in MeCN. The bulk amino sorbent (PSA, 40−60 μm), RP-C18, and graphitized carbon black (GCB) were from Scharlab (Barcelona, Spain). Analytical standards, of purity ≥95%, were from Dr. Ehrenstorfer (Augsburg, Germany).

Stock standard solutions of 1 mg/mL were prepared in MeCN, and working standard mixtures were prepared by appropriately diluting multiple stock solutions with MeCN. The pesticides studied were all LC amenable pesticides; no GC amenable pesticides were included. They were selected among the most used in extensive plantations in Uruguay aiming to check the model suitability. All working solutions were stored in the dark at 4 °C.

Apparatus. LC-MS/MS was performed with an Agilent 1200 LC system coupled to a 4000 QTRAP LC-MS/MS System from AB SCIEX run in the Scheduled MS/MS mode. LC separation was performed on a ZORBAX Eclipse XDB-C18 (150 mm × 4.6 mm, 5 μm) column. The operation of the LC gradient involved the following elution program: (A) water/HCOOH 0.1% (V/V); (B) MeCN. It was run at 600 μL min^{-1} starting with 10% component B at injection time during 1 min and gradually changing to 100% B over 15 min. This mobile phase was kept for 10 min and then shifted back to the starting conditions (10% component B) and kept there until 35 min after injection. The injection volume was 5 μL. MS/MS detection was performed in the multiple reaction monitoring (MRM) mode using an ESI interface in the positive ion mode. The ionization voltage was 4500 V, the nebulizer gas was synthetic air at 70 psi, and the curtain gas was nitrogen at 30 psi. The solvent evaporation in the source was assisted by a drying gas (heated synthetic air at 425 °C/50 psi). The optimal MRM transitions, collision energies, and declustering potentials for each investigated compound were determined by directly infusing with a syringe the standard solutions to the instrument at a constant flow. The MS/MS settings used in this study are listed in the Supporting Information.

Methodology. *Sampling Design.* Seven apiaries located in different production zones of Uruguay were selected on the basis of their health history and management. All of the apiaries have at least 20 beehives. From each apiary, samples of bees and honeycombs were taken randomly from five beehives in fall, winter, and spring. Then the samples were driven to the laboratory where they were joined, obtaining one composed sample per beehive product representing each apiary. The beehive matrices were obtained by allowing honey to drain. Once the wax was honey free, the pollen inside the cells was collected by digging into them one by one.

Sample Preparation. (a) Pesticide Residue Analysis in Beeswax. The methodology employed for the pesticide residue analysis in beeswax was that already described in a previous work by our group.[8] Briefly, 2 g of beeswax is extracted with 10 mL of MeCN at ∼80 °C. Then, the extract is frozen-out and cleaned up with 25 mg of primary−secondary amine (PSA) and 25 mg of C18 sorbent per milliliter of extract. Finally, the extract is acidified with 5% formic acid solution in MeCN (v/v) (10 μL/mL extract) and injected in LC-MS/MS.

(b) Pesticide Residue Analysis in Honey. The methodology employed for the pesticide residue analysis in honey was that already described in a previous work by our group.[9] Briefly, 5 g of honey is extracted with 10 mL of water and 10 mL of MeCN. Then the mixture of citrate buffer salts is added. The extract is cleaned up with PSA, 25 mg/mL, and $MgSO_4$, 150 mg/mL. Finally, the extract is acidified with 5% formic acid solution in MeCN (v/v) (10 μL/mL extract) and injected in LC-MS/MS.

(c) Pesticide Residue Analysis in Bees. Fifty grams of frozen honeybees weas thoroughly comminuted and homogeneized with a hand blender, and then 2 g was weighed in a 50 mL centrifuge tube and 5 mL of water; 10 mL of MeCN was added and shaken vigorously for 1 min; 0.5 g of disodium hydrogencitrate sesquehydrate, 1 g of trisodium citrate dihydrate, 4 g of anhydrous magnesium sulfate, and 1 g of sodium chloride were added and the mixture was shaken again; then the tube was centrifuged for 5 min at 3000 U/min. The extract was frozen out overnight and cleaned up by dispersive solid phase extraction: PSA and C18, 25 mg/mL, and $MgSO_4$/GCB (59:1), 150 mg/mL; vortexed for 30 s; and centrifuged for 5 min, 3000 U/min. The aliquot for LC-MS/MS analysis was acidified with 5% HCOOH in 10 μL/mL MeCN.

(d) Pesticide Residue Analysis in Pollen. Pollen isolated from the sampled portions of honeycomb was thoroughly comminuted and homogeneized with a hand blender, and then 5 g was weighed in a 50 mL centrifuge tube, and 5 mL of water and 10 mL of MeCN were added and shaken vigorously for 1 min; 1 g of sodium acetate, 4 g of anhydrous magnesium sulfate, and 100 μL of acetic acid were added, and the mixture was shaken again; then the tube was centrifuged for 5 min at 3000 U/min. The extract was cleaned up with dispersive solid phase extraction: PSA and C18, 25 mg/mL, and $MgSO_4$, 150 mg/mL; vortexed for 30 s; and centrifuged for 5 min, 3000 U/min. Finally, the cleaned extract was transferred into a screw-cap vial and injected in LC-MS/MS.

Statistical Analysis. Statistical analysis were performed using R, which is a free software environment for statistical computing and graphics.[25]

DOI: 10.1021/acs.jafc.5b00795
J. Agric. Food Chem. 2015, 63, 4484−4492

Table 1. Percentage Recoveries (% rec), Relative Standard Deviations (RSDs), Limits of Quantification (LOQs), and Lethal Doses (LD_{50} Values) of the Pesticides Analyzed in Bees (n = 5 Replicates)

	0.2 mg/kg		0.1 mg/kg		0.05 mg/kg		0.01 mg/kg		0.001 mg/kg		0.0001 mg/kg						
pesticide	% rec	RSD (%)	% rec	RSD (%)	% rec	RSD (%)	% rec	RSD (%)	% rec	RSD (%)	% rec	RSD (%)	LOQ (mg/kg)	LD_{50} (μg/bee)	linear range (mg/L)	linear correlation coefficient (r^2)	matrix effect (%)
acetamiprid	93	7	96	4	92	3	102	6	87	14	nd[a]	nd	0.0010	8	0.002−0.1	0.999	−1
azoxystrobin	104	14	109	4	95	6	102	2	102	6	118	16	0.0001	25	0.002−0.1	0.999	−3
boscalid	80	5	85	5	92	2	99	2	119	11	nd	nd	0.0010	100	0.002−0.1	0.998	−6
carbaryl	94	5	98	4	92	4	94	4	96	0	nd	nd	0.0010	0.14	0.002−0.1	0.999	28
carbendazim	73	4	73	6	46	7	69	19	80	8	nd	nd	0.0010	50	0.002−0.1	0.999	3
chlorpyrifos ethyl	104	1	111	10	93	10	90	14	94	28	75	32	0.0100	0.024	0.002−0.1	0.999	−12
clothianidin	92	6	94	4	99	6	118	24	92	20	nd	nd	0.0010	0.004	0.002−0.1	0.999	6
coumaphos	98	3	102	8	77	7	71	4	128	31	nd	nd	0.0100		0.002−0.1	0.998	−12
dimethoate	95	6	99	4	97	3	97	3	94	3	84	12	0.0001	0.12	0.002−0.1	0.999	7
haloxifop-methyl	102	6	106	5	94	8	97	7	103	5	113	9	0.0001		0.002−0.1	0.999	−2
hexythiazox	114	10	119	8	90	5	104	12	103	12	nd	nd	0.0010	112	0.002−0.1	0.998	−26
imazalil	101	6	111	5	92	6	94	30	nd	nd	nd	nd	0.0500	35.1	0.002−0.1	0.999	1
imidacloprid	94	5	103	4	88	5	105	14	nd	nd	nd	nd	0.0100	0.0037	0.002−0.1	0.999	2
iprodione	71	2	74	6	84	5	102	10	nd	nd	nd	nd	0.0100	25	0.002−0.1	0.998	−4
methomyl	96	6	96	4	94	3	98	7	102	3	89	14	0.0001	0.16	0.002−0.1	0.999	−3
pyraclostrobin	103	4	107	5	90	11	97	3	74	3	nd	nd	0.0010	73.1	0.002−0.1	0.999	1
tebuconazole	92	4	94	6	87	2	96	6	99	8	nd	nd	0.0010	83	0.002−0.1	0.999	−6
thiacloprid	92	5	96	5	97	5	101	7	75	8	nd	nd	0.0010	17.3	0.002−0.1	0.999	−2
thiamethoxam	97	8	106	7	91	10	106	10	114	22	nd	nd	0.0010	0.005	0.002−0.1	0.999	2

[a]nd, not detected.

DOI: 10.1021/acs.jafc.5b00795
J. Agric. Food Chem. 2015, 63, 4484−4492

Table 2. Percentage Recoveries (% rec), Relative Standard Deviations (RSDs), and Limits of Quantification (LOQs) of the Pesticides Analyzed in Pollen (n = 5 Replicates)

	0.05 mg/kg		0.01 mg/kg		0.001 mg/kg		0.0001 mg/kg					
pesticide	% rec	% RSD	% rec	% RSD	% rec	% RSD	% rec	% RSD	LOQ (mg/kg)	linear range (mg/L)	linear correlation coefficient (r^2)	matrix effect (%)
acetamiprid	86	3	88	4	119	8	nd[a]	nd	0.0010	0.005−0.1	0.999	−44
azoxystrobin	84	5	98	5	198	19	85	17	0.0001	0.005−0.1	0.999	43
boscalid	89	7	82	19	127	13	nd	nd	0.0100	0.005−0.1	0.991	−1
carbaryl	87	4	87	7	138	3	92	12	0.0001	0.005−0.1	0.999	−45
carbendazim	80	2	86	5	126	16	121	7	0.0001	0.005−0.1	0.998	29
clothianidin	90	5	82	6	104	14	nd	nd	0.0010	0.005−0.1	0.997	−26
coumaphos	94	3	96	3	175	8	100	10	0.0001	0.005−0.1	0.998	−41
dimethoate	84	3	87	5	115	7	84	8	0.0001	0.005−0.1	0.998	−44
haloxifop-methyl	87	2	95	4	163	3	78	24	0.0100	0.005−0.1	0.999	−14
hexythiazox	98	11	116	4	373	19	nd	nd	0.0100	0.005−0.1	0.994	−58
imazalil	87	5	72	12	nd	nd	nd	nd	0.0100	0.005−0.1	0.998	−44
imidacloprid	84	6	73	7	97	17	nd	nd	0.0010	0.005−0.1	0.997	−50
iprodione	92	7	104	6	139	8	92	20	0.0001	0.005−0.1	0.995	−36
methomyl	87	3	83	6	111	6	66	11	0.0010	0.005−0.1	0.999	−23
metsulfuron methyl	79	3	84	3	125	2	105	7	0.0001	0.005−0.1	0.998	11
pyraclostrobin	86	11	95	1	193	5	95	27	0.0100	0.005−0.1	0.999	−38
tebuconazole	86	4	89	6	160	20	124	24	0.0100	0.005−0.1	0.998	13
thiacloprid	87	2	91	3	131	14	nd	nd	0.0100	0.005−0.1	0.999	−46
thiamethoxam	96	4	90	7	nd	nd	nd	nd	0.0100	0.005−0.1	0.998	−15

[a]nd, not detected.

Besides the statistical description by average values and standard errors, two kinds of statistical analysis were done: a multiple factorial analysis (MFA, Escofier and Pages)[26,27] and the calculation of the Gower[28] distance. The MFA is done in two steps: first, a principal components analysis (PCA) is made per group of variables (groups being bees, wax, pollen, and honey), and the original values are standardized by the square root of the first eigenvalue from each group analysis; second, a new global PCA is made using the standardized values. That kind of analysis allows the relationship between concentration of products per group to be shown in a two-dimensional figure in such a way that the groups near one another in the figure are more similar in concentration of products.

The Gower distance is a distance based on the absolute values of differences between statistical samples,; in this case the samples are the apiaries in each season, and what is compared is the pesticide residues profile obtained in the four matrices analyzed. Calculus: (value − minimum)/range.

This distance allows the presence of missing values in some comparisons, and results are in the 0−1 interval, allowing an easy interpretation.

For all of the calculations, the concentration of coumaphos found for the different apiaries was not considered as the acaricide is an agrochemical commonly employed in apiculture and has no meaning in the consideration of the agroecosystem under study.

RESULTS AND DISCUSSION

The extracts produced had a significant load of coextractives. To overcome this difficulty and obtain low LODs, an LC-MS/MS using the scheduled option in the MRM mode with optimized transitions, collision energies, and declustering potentials for the 19 LC-amenable currently employed pesticides in Uruguayan agroecosystems was used, as continuous scanning of the whole mass range led to higher LODs and LOQs.

Methods Validation. In agreement with the analytical quality control procedures document by DG-SANCO,[29] five replicates of spiked blanks of bees at different levels (0.2, 0.1, 0.05, 0.01, 0.001, 0.0001 mg/kg) and of pollen (0.05, 0.01, 0.001, 0.0001 mg/kg) were analyzed to assess accuracy (% recovery) and repeatability (% RSD) of the procedure (Tables 2 and 3). Limits of quantification (LOQs) were considered as the lowest successfully validated levels, that is, the levels at which acceptable recoveries (70−120%) and RSDs (<20%) were achieved. For every pesticide, its LOQ is lower than the corresponding reported LD_{50}.[30] If we consider the weight of a bee is approximately 100 mg, a factor of 10 is needed to convert μg/bee to mg/kg. Very low LOQs (0.0001 mg/kg) were obtained for several pesticides, particularly azoxystrobin and dimethoate in both matrices, which is important if we consider that the concentrations found in the real samples were around this level.

Calibration curves were constructed using both solvent-based and matrix-matched standards at five concentration levels: 0.002, 0.01, 0.02, 0.05, and 0.1 mg/L for bees and 0.005, 0.01, 0.025, 0.05, and 0.1 mg/L for pollen. Linear correlation coefficients were >0.999 for bees and >0.991 in pollen for all of the studied analytes. Linear ranges were fit for purpose considering the concentrations found in real samples.

Matrix effects were calculated as the percentage difference in the best-fit slopes of the matrix-matched calibration curves versus the respective best-fit slopes of the solvent calibration curves.

Matrix effects were quite pronounced and variable from analyte to analyte (Tables 1 and 2), particularly in the case of pollen analysis. This is explained by the fact that matrix effects depend on whether a target analyte coelutes with coextracted matrix components, affecting the yield of free analyte ions generated within the ESI-ion source and thus the detection signals.

Where matrix effects remain strong, the use of matrix-matched calibration standards (prepared from extracts of blank matrix so far available) or the method of standard additions are

DOI: 10.1021/acs.jafc.5b00795
J. Agric. Food Chem. 2015, 63, 4484−4492

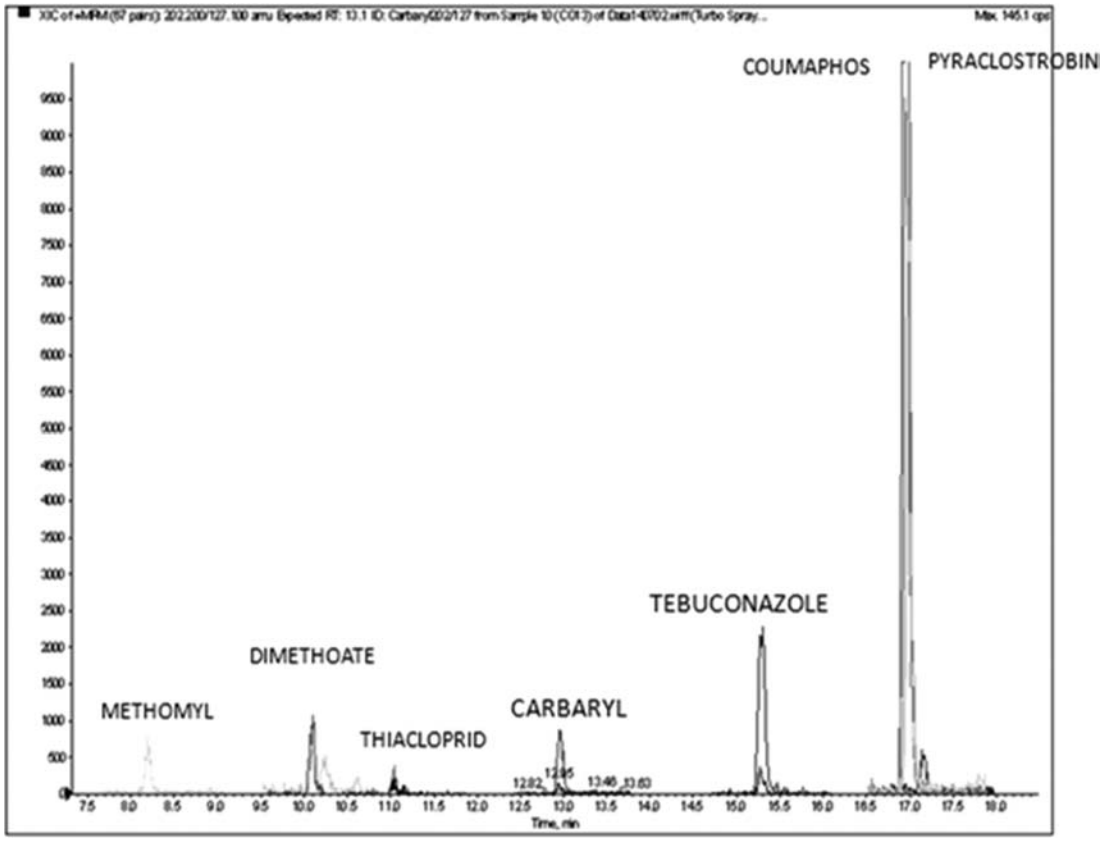

Figure 1. LC-MS/MS chromatogram showing multiple positive findings in a real beeswax sample.

recommended to obtain reliable quantification. Matrix-matched calibration was used during this study.

Beehive Samples Analysis. Pesticide residue analysis of the different samples of bees, pollen, beeswax, and honey yielded results similar to those found in North America and Europe.[5,10,19] Multiple findings in a single sample were frequent as shown in Figure 1, particularly in beeswax and pollen. Figure 2 shows a detailed graph of the frequency of positive findings

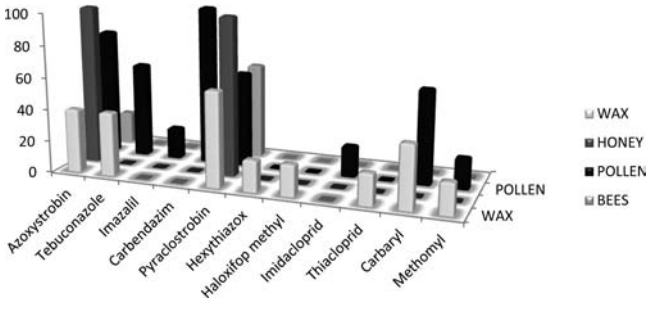

Figure 2. Frequency of positive findings in the four analyzed hive matrices.

for each matrix where the prevalence of fungicides is observed. However, the concentrations found were low, within the range of 0.0001−0.01 mg/kg. Mullin et al.[5] found a high occurrence of chlorothalonil in North American apiaries. In our case, all of the samples contained strobilurins as azoxystrobin and pyraclostrobin. The peculiarity of the high occurrence of fungicides in bee products has not been properly explained yet. Fungicides have intermediate pK_a and pK_{ow} on which the basis to understand their ubiquity in the different bee matrices, wax, pollen, and honey, could be built. The occurrence of pesticides in pollen is originated directly from what was applied over the crops. Depending on their physicochemical properties, residues can diffuse to other beehive compartments; the most remarkable ones are wax and honey. Either due to a dilution effect or slow solubility in them, their detection is hampered. Pesticide residues in honey are less frequent, probably because honey is an aqueous matrix, whereas most pesticides are lipophilic. Diffusion from a lipophilic matrix such as pollen to an aqueous one is not favored. Pesticides found in bees are those that they were directly exposed to; therefore, residue findings in bees could vary with time.

Taking advantage of the plasticity of the QuEChERS template coupled to modern analytical instrumentation, the validated analytical methodologies described, developed specifically for pesticide residue analysis in bees, honey, beeswax, and pollen, were applied to real sample analysis from beehives placed in Uruguayan agroecosystems: Insecticides (e.g., thiacloprid, imidacloprid, methomyl, carbaryl), fungicides (e.g., azoxystrobin, pyraclostrobin, tebuconazole, hexythiazox), and herbicides (e.g., haloxyfop-methyl) have been detected at 0.0001−0.01 mg/kg levels (Table 3).

Beehives as Environmental Monitors of the Application of Pesticides in Agroecosystems. The type of pesticide residues could be relatively similar within each matrix (bees, wax, honey, and pollen), independent of the agroecosystem due to its intrinsic chemical composition. Therefore, different residue profiles are expected per matrix. To check this assumption, a MFA of pesticide residue findings from all analyzed samples in bees, honey, pollen, and beeswax was performed. None of the four matrices is too close (Figure 3). This indicates that each matrix gives different information. If we

DOI: 10.1021/acs.jafc.5b00795
J. Agric. Food Chem. 2015, 63, 4484−4492

Table 3. Positive Findings of Pesticide Residues in Beehive Matrices Ordered per Apiary and Season

matrix	season	azoxystrobin (mg/kg)	carbendazim (mg/kg)	carbaryl (mg/kg)	pyraclostrobin (mg/kg)	imidacloprid (mg/kg)	tebuconazole (mg/kg)	methomyl (mg/kg)	thiacloprid (mg/kg)	boscalid (mg/kg)	dimethoate (mg/kg)	hexythiazox (mg/kg)	haloxifop-methyl (mg/kg)
Apiary A													
beeswax	autumn	0.0002	nd[a]	nd	nd	nd	nd	nd	nd	nd	nd	nd	nd
honey	autumn	0.0012	nd	nd	0.0015	nd	nd	nd	nd	nd	nd	nd	nd
pollen	autumn	0.0006	0.0014	0.0008	<LOQ	nd	nd	nd	nd	nd	nd	nd	nd
bees	autumn	nd	nd	nd	<LOQ	nd	nd	nd	nd	nd	nd	nd	nd
beeswax	spring	nd	nd	nd	nd	nd	nd	nd	nd	nd	nd	nd	nd
honey	spring	0.0007	nd	nd	0.0034	nd	nd	nd	nd	nd	nd	nd	nd
pollen	spring	0.0011	0.0013	0.0004	nd	nd	<LOQ	nd	<LOQ	nd	nd	nd	nd
bees	spring	nd	nd	nd	0.003	nd	nd	nd	nd	nd	nd	nd	nd
Apiary B													
beeswax	autumn	nd	nd	0.0004	nd	nd	nd	nd	nd	nd	nd	nd	nd
honey	autumn	0.0008	nd	nd	0.0021	nd	nd	nd	nd	nd	nd	nd	nd
pollen	autumn	0.0003	0.0008	0.0003	<LOQ	nd	nd	nd	nd	nd	nd	nd	nd
bees	autumn	nd	nd	nd	nd	nd	nd	nd	nd	nd	nd	nd	nd
beeswax	spring	nd	nd	0.0004	0.001	nd	nd	<LOQ	nd	nd	nd	nd	0.001
honey	spring	0.0007	nd	nd	0.0011	nd	nd	nd	nd	0.001	nd	nd	nd
pollen	spring	0.0010	0.0038	0.0003	<LOQ	nd	<LOQ	nd	nd	nd	nd	nd	nd
bees	spring	0.0001	nd	nd	0.004	nd	nd	nd	nd	nd	nd	nd	nd
Apiary C													
beeswax	autumn	0.0100	nd	0.0009	0.002	nd	0.0031	0.001	<LOQ	nd	<LOQ	nd	0.001
honey	autumn	0.0010	nd	nd	0.0013	nd	nd	nd	nd	nd	nd	nd	nd
pollen	autumn	0.0009	0.0009	0.0002	<LOQ	nd	<LOQ	nd	nd	nd	nd	nd	nd
bees	autumn	nd	nd	nd	nd	nd	nd	nd	nd	nd	nd	nd	nd
beeswax	winter	0.0062	nd	nd	nd	nd	nd	nd	nd	nd	nd	nd	nd
honey	winter	0.0009	nd	nd	0.0015	nd	nd	nd	nd	nd	nd	nd	nd
pollen	winter	0.0003	nd	0.0003	nd	nd	nd	nd	nd	nd	nd	nd	nd
bees	winter	nd	nd	nd	nd	nd	nd	nd	nd	nd	nd	nd	nd
Apiary D													
beeswax	winter	0.0025	0.002	nd	nd	nd	nd	nd	nd	nd	nd	nd	nd
honey	winter	0.0008	nd	nd	0.0010	nd	nd	nd	nd	nd	nd	nd	nd
pollen	winter	0.0030	0.0024	nd	<LOQ	nd	<LOQ	nd	nd	nd	nd	nd	nd
bees	winter	0.0001	nd	nd	nd	nd	nd	nd	nd	nd	nd	nd	nd
beeswax	spring	0.0002	nd	0.0007	nd	nd	nd	nd	nd	nd	nd	nd	nd
honey	spring	0.0007	nd	nd	0.0010	nd	nd	nd	nd	nd	nd	nd	nd
pollen	spring	0.0110	0.0029	0.0005	<LOQ	nd	<LOQ	nd	nd	nd	nd	nd	nd
bees	spring	0.0032	nd	nd	nd	nd	nd	nd	nd	nd	nd	nd	nd
Apiary E													
beeswax	autumn	nd	nd	nd	<LOQ	nd	nd	nd	nd	nd	nd	0.01	nd
honey	autumn	0.0009	nd	nd	0.0013	nd	nd	nd	nd	nd	nd	nd	nd
pollen	autumn	0.0007	0.0023	nd	nd	nd	<LOQ	nd	nd	nd	nd	nd	nd
bees	autumn	nd	nd	nd	0.002	nd	nd	nd	nd	nd	nd	nd	nd
beeswax	spring	0.0002	nd	nd	<LOQ	nd	nd	nd	nd	nd	nd	nd	nd

DOI: 10.1021/acs.jafc.5b00795
J. Agric. Food Chem. 2015, 63, 4484−4492

Table 3. continued

matrix	season	azoxystrobin (mg/kg)	carbendazim (mg/kg)	carbaryl (mg/kg)	pyraclostrobin (mg/kg)	imidacloprid (mg/kg)	tebuconazole (mg/kg)	methomyl (mg/kg)	thiacloprid (mg/kg)	boscalid (mg/kg)	dimethoate (mg/kg)	hexythiazox (mg/kg)	haloxifop-methyl (mg/kg)
							Apiary E						
honey	spring	0.0007	nd	nd	0.0010	nd	nd	nd	nd	nd	nd	nd	nd
pollen	spring	0.0020	0.0020	0.0003	<LOQ	nd	<LOQ	nd	nd	nd	nd	nd	nd
bees	spring	0.0003	nd	nd	0.001	nd	0.001	nd	nd	nd	nd	nd	nd
							Apiary F						
beeswax	autumn	0.0003	nd	nd	0.001	nd	0.0017	nd	nd	nd	nd	nd	nd
honey	autumn	0.0010	nd	nd	0.0012	nd	nd	nd	nd	nd	nd	nd	nd
pollen	autumn	0.0055	0.0090	nd	<LOQ	0.003	<LOQ	<LOQ	nd	nd	nd	nd	nd
bees	autumn	0.0005	nd	nd	0.001	nd	nd	nd	nd	nd	nd	nd	nd
							Apiary G						
beeswax	spring	nd	nd	0.0003	nd	nd	nd	nd	nd	nd	nd	nd	nd
honey	spring	0.0007	nd	nd	0.0010	nd	nd	nd	nd	nd	nd	nd	nd
pollen	spring	0.0003	0.0014	0.0004	nd	nd	<LOQ	nd	nd	nd	nd	nd	nd
bees	spring	nd	nd	nd	0.001	nd	nd	nd	nd	nd	nd	nd	nd

[a]nd, not detected.

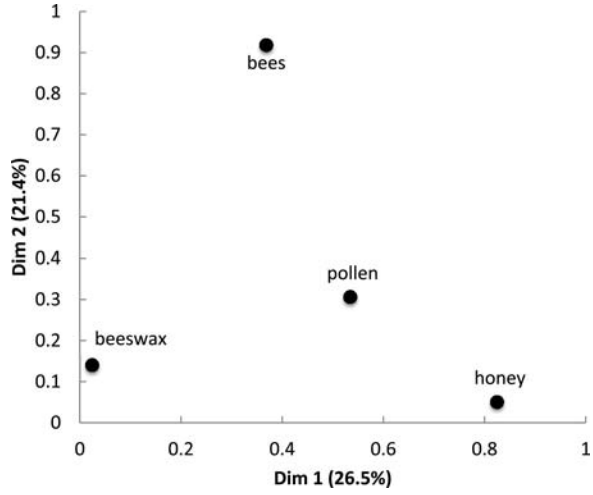

Figure 3. Multiple factorial analysis of pesticide residue findings from all analyzed samples in bees, honey, pollen, and beeswax.

consider how the residues reach the hive, more valuable information is gathered when each matrix is analyzed separately. Whereas the wax is an historic reservoir of the collected pesticides, residues in pollen are more diverse and represent what has been directly sprayed over the crops. A higher number of insecticides were detected in it: imidacloprid, carbaryl, and dimethoate. On the other hand, pesticide residues in bees tell us about the latest pesticide applications to which bees were exposed. In samples from the apiaries under study, bees carried mostly fungicides and the only herbicide detected, haloxyfop-methyl. Honey is a hydrophilic matrix, and lipophilic pesticides are expected to occur at low concentrations if at all, and more hydrophilic pesticides should be present. In our case, only the strobilurins were detected in this matrix.

An agroecosystem's monitor should be stable but capable of recording the baseline variations that occur in a definite environment. To assay the usefulness of the beehive as a monitor, we have to check the range of variability of the load of residues within the hive in an agroecosystem and if the differences found have some significance. Table 4 shows the evaluation of the Gower distances (G-distances) for five of the apiaries between two sampling seasons. For the other two, samples of only one season were taken, making the comparison impossible. The first conclusion is that the values of pesticide residues have to be compared within the same apiary. The lowest value was for apiary E, located near forestation and native wood, meaning that the change in pesticide residues content between the two seasons was low. This result could be explained as no pesticide is applied over the native crop and pesticide residues came from the forestry activities. Going up in

Table 4. Comparison of Apiaries Placed in Different Environments in Two Seasons According to Their Total Pesticide Residues Profile

apiary	season compared	environment	G-distance
A	autumn and spring	dairy basin	0.24
B	autumn and spring	forest	0.24
C	autumn and winter	cattle breeding and rice culture	0.35
D	winter and spring	dairy basin, natural prairie	0.18
E	autumn and spring	forest and native forest	0.15

DOI: 10.1021/acs.jafc.5b00795
J. Agric. Food Chem. 2015, 63, 4484−4492

Table 5. Gower Distances between All Pairs of Apiaries−Seasons Sampled

	A−autumn	F−autumn	B−autumn	E−autumn	C−autumn	C−winter	D−winter	G−spring	B−spring	E−spring	A−spring
F−autumn	0.38										
B−autumn	0.18	0.34									
E−autumn	0.23	0.30	0.14								
C−autumn	0.41	0.48	0.31	0.36							
C−winter	0.18	0.34	0.09	0.15	0.35						
D−winter	0.24	0.26	0.15	0.14	0.37	0.13					
G−spring	0.20	0.29	0.09	0.12	0.33	0.12	0.10				
B−spring	0.35	0.41	0.24	0.26	0.34	0.29	0.26	0.19			
E−spring	0.23	0.30	0.15	0.15	0.37	0.16	0.13	0.09	0.23		
A−spring	0.24	0.36	0.17	0.15	0.40	0.17	0.17	0.10	0.23	0.14	
D−spring	0.28	0.35	0.17	0.23	0.37	0.22	0.18	0.14	0.27	0.18	0.21

G-distances, apiary D, near a natural prairie, has a slightly higher G-distance as no pesticide is applied over the natural field. On the other hand, for apiary A, located also in a dairy basin where lotus and clover prairies, two very visited species by foraging bees, were planted, a higher G-distance was obtained, showing that the monitor is also capable to distinguish between different agricultural practices, although the same production activity is being developed in the hive surroundings. The G-distance found between apiaries A and D, bred in different dairy basin environments in spring, is 0.21 (Table 5), proving that the hive detected the different managements of the agricultural environment. Apiary B, located in the middle of eucalyptus forest plantations, showed the same G-distance as apiary A, which indicates that both apiaries were able to record the same change in their pesticide residues profile between autumn and spring. These findings confirm also the beekepers' observation that bees prefer to visit the natural forest due to its diversity rather than the cultivated one, usually a monospecies, either eucalyptus or pines. The highest G-distances were obtained for a complex environment where mixed production activities were being developed. The rotation from rice to cattle breeding is characteristic of the Uruguayan rice production, and apiary C located in such environment registered this variation. The differences in the pesticide residue loads observed between the two seasons in the apiaries located in all of the environments studied sustain the idea of the beehive as an environmental monitor. They are the first objective observations that the incorporation of pesticide residues, although low, is characteristic of each agroecosystem and the cropping practices developed in it. The apiaries in the different environments showed significant seasonal variations in the load of pesticide residues, which were characteristic for these environments. Figure 4 shows the change in the pesticide residues profile of an apiary located near soybean plantations, before and after the cropping season. The amount and type of residues found are higher at the end of the agricultural period, showing again that the beehive is sensitive to the seasonal changes that occur in the environment.

The data presented show that the work hypothesis is valid. However, more work is needed to understand the dynamics of bees' pesticide collection and residue storage in the beehive compartments to properly evaluate the hive as a monitor of an agroecosystem. The separate study of the different bee matrices gives richer insights into this problem. The information yielded by the pesticide residues profile of each matrix contributes to a wider picture of the situation. The analytical methodologies described allow gathering an enormous amount of information in a fast and effective way that makes feasible the idea of monitoring agroecosystems through the analysis of complex bee products.

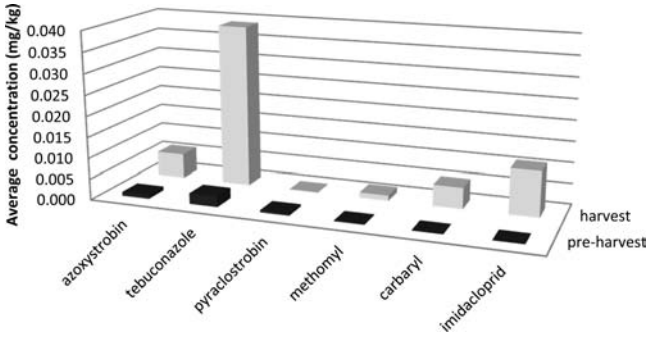

Figure 4. Average concentrations of the residues found in an apiary located in a soybean plantation sampled at pre- and postharvest.

■ ASSOCIATED CONTENT

Ⓢ Supporting Information

Table of mass spectrometry settings for the LC-MS/MS system used. This material is available free of charge via the Internet at http://pubs.acs.org.

■ AUTHOR INFORMATION

Corresponding Author

*(H.H.) E-mail: heinzen@fq.edu.uy.

Notes

The authors declare no competing financial interest.

■ ACKNOWLEDGMENTS

Instituto Nacional de Investigaciones Agropecuarias (INIA) for FPTA 320, PEDECIBA Química, Comisión Sectorial de Investigación Científica and Facultad de Química (Universidad de la República), Dirección General de la Granja, DiGeGra, are greatly acknowledged.

■ ABBREVIATIONS USED

QuEChERS, quick, easy, cheap, effective, rugged, and safe; dSPE, dispersive solid phase extraction; LC-MS/MS, liquid chromatography−tandem mass spectrometry; RSD, relative standard deviation; MRM, multiple reaction monitoring; ESI, electrospray ionization; PSA, primary and secondary amine

■ REFERENCES

(1) Genthon, P. Blue and green honey makes French beekeepers see red; http://www.reuters.com/article/2012/10/04/us-france-bees-dUSBRE8930MQ20121004 (accessed Feb 6, 2015).

DOI: 10.1021/acs.jafc.5b00795
J. Agric. Food Chem. 2015, 63, 4484−4492

(2) Mullin, C. A.; Frazier, M.; Frazier, J. L.; Ashcraft, S.; Simonds, R.; vanEngelsdorp, D.; Pettis, J. S. High levels of miticides and agrochemicals in North American apiaries: implications for honey bee health. *PLoS One* **2010**, *5*, No. e9754, DOI: 10.1371/journal.pone.0009754.
(3) Chauzat, M.; Martel, A.; Cougoule, N.; Porta, P.; Lachaize, J.; Zeggane, S.; Aubert, M.; Carpentier, P.; Faucon, J. An assessment of honeybee colony matrices, *Apis mellifera* (Hymenoptera: Apidae) to monitor pesticide presence in continental France. *Environ. Toxicol. Chem.* **2011**, *30*, 103−111.
(4) Orantes-Bermejo, F. J.; Pajuelo, A. G.; Megías, M. M.; Fernández-Píñar, C. T. Pesticide residues in beeswax and beebread samples collected from honey bee colonies (*Apis mellifera* L.) in Spain. Possible implications for bee losses. *J. Apic. Res.* **2010**, *49*, 243−250.
(5) Chauzat, M. P.; Carpentier, P.; Martel, A. C.; Bougeard, S.; Cougoule, N.; Porta, P.; Lachaize, J.; Madec, F.; Aubert, M.; Faucon, J. P. Influence of pesticide residues on honey bee (Hymenoptera: Apidae) colony health in France. *Environ. Entomol.* **2009**, *38*, 514−523.
(6) Kasiotis, K. M.; Anagnostopoulos, C.; Anastasiadou, P.; Machera, K. Pesticide residues in honeybees, honey and bee pollen by LC−MS/MS screening: reported death incidents in honeybees. *Sci. Total Environ.* **2014**, *485*−*486*, 633−642.
(7) Lambert, O.; Piroux, M.; Puyo, S.; Thorin, C.; L'Hostis, M.; Wiest, L.; Buleté, A.; Delbac, F.; Pouliquen, H. Widespread occurrence of chemical residues in beehive matrices from apiaries located in different landscapes of western France. *PLoS One* **2013**, *8*, DOI: 10.1371/journal.pone.0067007.
(8) Pareja, L.; Colazzo, M.; Pérez-Parada, A.; Niell, S.; Carrasco-Letelier, L.; Besil, N.; Cesio, M. V.; Heinzen, H. Detection of pesticides in active and depopulated beehives in Uruguay. *Int. J. Environ. Res. Public Health* **2011**, *8*, 3844−3858.
(9) Anastassiades, M.; Lehotay, S. J.; Štajnbaher, D.; Schenck, F. J. Fast and easy multiresidue method employing acetonitrile extraction/partitioning and "dispersive solid-phase extraction" for the determination of pesticide residues in produce. *J. AOAC Int.* **2003**, *86*, 412−431.
(10) Walorczyk, S.; Gnusowski, B. Development and validation of a multi-residue method for the determination of pesticides in honeybees using acetonitrile-based extraction and gas chromatography−tandem quadrupole mass spectrometry. *J. Chromatogr., A* **2009**, *1216*, 6522−6531.
(11) Wiest, L.; Buleté, A.; Giroud, B.; Fratta, C.; Amic, S.; Lambert, O.; Pouliquen, H.; Arnaudguilhem, C. Multi-residue analysis of 80 environmental contaminants in honeys, honeybees and pollens by one extraction procedure followed by liquid and gas chromatography coupled with mass spectrometric detection. *J. Chromatogr., A* **2011**, *1218*, 5743−5756.
(12) Anastassiades, M.; Tasdelen, B.; Scherbaum, E.; Stajnbaher, D. Recent developments in QuEChERS methodology for pesticide multiresidue analysis. In *Pesticide Chemistry: Crop Protection, Public Health, Environmental Safety*; Ohkawa, H., Miyagawa, H., Lee, P. W., Eds.; Wiley-VCH: Weinheim, Germany, 2007.
(13) Stoner, K. A.; Eitzer, B. D. Using a hazard quotient to evaluate pesticide residues detected in pollen trapped from honey bees (*Apis mellifera*) in Connecticut. *PLoS One* **2013**, *8*, No. e77550, DOI: 10.1371/journal.pone.0077550.
(14) Niell, S.; Cesio, V.; Hepperle, J.; Doerk, D.; Kirsch, L.; Kolberg, D.; Scherbaum, E.; Anastassiades, M.; Heinzen, H. QuEChERS-based method for the multiresidue analysis of pesticides in beeswax by LC-MS/MS and GC×GC-TOF. *J. Agric. Food Chem.* **2014**, *62*, 3675−3683.
(15) Niell, S.; Cesio, V.; Hepperle, J.; Roux, D.; Kirsch, L.; Kolberg, D.; Anastassiades, M.; Heinzen, H. Análisis multiresiduo de 41 pesticidas en miel por LC-MS/MS: evaluación de dos métodos de clean-up. *Agrociencia Uruguay* **2013**, *17*, 101−107.
(16) Balayiannis, G.; Balayiannis, P. Bee honey as an environmental bioindicator of pesticides' occurrence in six agricultural areas of Greece. *Arch. Environ. Contam. Toxicol.* **2008**, *55*, 462−470.
(17) Celli, G.; Maccagnani, B. Honey bees as bioindicators of environmental pollution. *Bull. Insectol.* **2003**, *56*, 137−139.
(18) Ghini, S.; Fernández, M.; Picó, Y.; Marín, R.; Fini, F.; Mañes, J.; Girotti, S. Occurrence and distribution of pesticides in the province of Bologna, Italy, using honeybees as bioindicators. *Arch. Environ. Contam. Toxicol.* **2004**, *47*, 479−488.
(19) Porrini, C.; Caprio, E.; Tesoriero, D.; Prisco, G. D. Using honey bee as bioindicator of chemicals in Campanian agroecosystems (south Italy). *Bull. Insectol.* **2014**, *67*, 137−146.
(20) Porrini, C.; Ghini, S.; Girotti, S.; Sabatini, A.; Celli, G.; Gattavecchia, E. Use of honey bees as bioindicators of environmental pollution in Italy. In *Honey Bees: Estimating the Environmental Impact of Chemicals*; CRC Press: Boca Raton, FL, USA, 2002; pp 186−247.
(21) Porrini, C.; Sabatini, A. G.; Girotti, S.; Ghini, S.; Medrzycki, P.; Grillenzoni, F.; Bortolotti, L.; Gattavecchia, E.; Celli, G. Honey bees and bee products as monitors of the environmental contamination. *Apiacta* **2003**, *38*, 63−70.
(22) Kezic, N.; Barisic, D.; Bromenshenk, J.; Vertacnik, A. The role of honey bees in environmental monitoring in Croatia. In *Honey Bees: Estimating the Environmental Impact of Chemicals*; CRC Press: Boca Raton, FL, USA, 2002; pp 160−185.
(23) Porrini, C.; Celli, G.; Radeghieri, P. Monitoring of pesticides through the use of honeybees as bioindicators of the Emilia-Romagna coastline (1995−1996). *Ann. Chim.* **1998**, *88*, 243−252.
(24) Raeymaekers, B. A prospective biomonitoring campaign with honey bees in a district of Upper-Bavaria (Germany). *Environ. Monit. Assess.* **2006**, *116*, 233−243.
(25) R Core Team. *R: A Language and Environment for Statistical Computing*; R Foundation for Statistical Computing: Vienna, Austria; http://www.R-project.org/.
(26) Escofier, B.; Pagès, J. *Analyses factorielles Simples et Multiples*, 3rd ed.; Dunod: Paris, France, 1998.
(27) Lê, S.; Josse, J.; Husson, F. FactoMineR: An R package for multivariate analysis. *J. Stat. Softw.* **2008**, 25.
(28) Gower, J. C. A general coefficient of similarity and some of its properties. *Biometrics* **1971**, *27*, 857−874.
(29) European Commission Health & Consumer Protection Directorate-General. Guidance document on analytical quality control and validation procedures for pesticide residues analysis in food and feed. In SANCO/12571/2013, 2013.
(30) University of Hertfordshire. *The Pesticide Properties DataBase (PPDB)*, developed by the Agriculture and Environment Research Unit (AERU), 2006−2014.

DOI: 10.1021/acs.jafc.5b00795
J. Agric. Food Chem. 2015, 63, 4484−4492

Several methods using LC-TOF-MS that monitor veterinary drug and pharmaceutical residues in food products have been published.[19−23] However, having MS data only for the precursor ions is not considered sufficient for residue identity confirmation, even with high mass accuracy. In some methods in-source fragmentation was performed (in-source CID) to generate fragment ions that could provide additional data for compound identification.[22] However, the in-source CID fragmentation has significant drawbacks compared to tandem mass spectrometry. Matrix interferences could preclude its use, and large amounts of impurities can significantly complicate the analysis process.[24] A hybrid quadrupole TOF (QTOF) has the additional ability to obtain MS/MS spectra that can be used to further characterize drug residues. QTOF MS allows working under broad-band collision-induced dissociation (bbCID) (or MS^E) mode, switching alternately between low (LE) and high collision energy (HE) in the collision cell Q2, at the same run. The low-energy data set provides information for molecular (precursor) ions corresponding to a given retention time, whereas the second set contains their fragment ions.[25] The information provided, along with the isotopic distribution observed in the spectra, allows the reliable identification of the compounds detected in the samples.

In multiresidue analysis the LC part is responsible for some limitation as well, mainly due to the large number of target analytes that need to be separated simultaneously. Ultrahigh-performance liquid chromatography (UHPLC) can eliminate these limitations, providing additional chromatographic resolution and significantly lowering analysis times using sub-2-μm particulate column packing material.[21]

With the demand for high-throughput analysis constantly increasing, the development and application of generic extraction procedures, able to extract a wide range of compounds with different physical/chemical properties, have become essential. A wide array of the proposed methodologies for analyzing veterinary drug residues in food products employs liquid−liquid extraction (LLE) or solid−liquid extraction (SE), with solid-phase extraction (SPE) being the most widely used technique for the cleanup of the extracts.[26] The combination of solid−liquid extraction or liquid−liquid extraction followed by the SPE cleanup step has been satisfactorily applied to the analysis of several antibacterials in milk,[19] meat,[20,23] and eggs and fish.[23] An effort was made to omit cleanup steps by performing a single-solvent extraction in fish and feed matrices,[27] but matrix effects proved to be problematic leading to reduced sensitivity in some cases. To conclude, for an accurate and efficient multiresidue screening method, both a sensitive full scan technique and a comprehensive sample preparation are required.

So far, the number of applications of LC-QTOF MS determination of veterinary drug residues in food and feed matrices is quite limited.[5,27−35] Some of these studies cover a single class of drugs such as macrolides and quinolones in fish[29,30] or fewer than 30 compounds in milk[28,31] and aquaculture species.[32] Two of them cope with feed matrices: Boix et al. presented a qualitative screening of 116 veterinary drugs, validated on the basis of a previously reported validation protocol,[5] and Aguilera-Luiz et al. developed a wide-scope multiresidue method able to cover the analysis of >200 pesticide and veterinary residues.[33] As Aguilera-Luiz et al. stated in the conclusions of their study,[33] the developed method showed some limitations because some families of drugs, such as tetracyclines, quinolones, and penicillins, were not properly extracted, and low sensitivity made the detection of some compounds and fragments at low concentrations unfeasible. Deng et al. presented a multiresidue/multiclass quantitative screening approach for 105 veterinary drugs in meat, milk, and egg with UHPLC-QTOF MS/MS,[34] and Nácher-Mestre et al. described the development, qualitative validation, and application of a screening method for the detection and identification of about 70 organic compounds, including antibiotics, pesticides, and mycotoxins, in fish feed and fish fillets.[27] Most recently, Turnipseed et al. presented an LC-QTOF MS/MS method for the screening of about 200 veterinary drugs in milk, providing experimental retention time and product ion information.[35]

The objective of this work is the development of a reliable, sensitive, and modern screening methodology for the detection and identification of 143 veterinary drugs and pharmaceuticals in milk and fish samples based on the use of an advanced UHPLC-QTOF MS technique. Generic sample extraction procedures were used, and their efficiency was evaluated. A qualitative validation of the screening method was performed, and levels of detection and identification were specified for all target analytes in both matrices. Subsequently, the method was applied to the analysis of different milk and fish samples to test its applicability. Experimental data including retention times, product ion spectra, and precursor and product ion mass accuracy as well as precursor−product ion ratios were obtained and presented for all target compounds.

MATERIALS AND METHODS

Reagents and Chemicals. All veterinary drug and pharmaceutical standards were of high-purity grade (>90%). The majority of them were purchased from Sigma-Aldrich (Steinheim, Germany). Sulfadoxine (SDX) and sulfaclozine (SClZ) were donated by the National Laboratory of Residue Analysis of Food of Animal Origin of the Hellenic Ministry of Rural Development and Food. Bacitracin, halofuginone, arprinocid, salinomycin, semduramicin, manduramycin, nigericin, narasin, albendazole sulfone, carprofen, diclofenac, flunixin, mefenamic acid, meloxicam, niflumic acid, and tolfenamic acid were donated by the Veterinary Drug Residues Laboratory of the State General Laboratory of Cyprus.

Acetonitrile (ACN) and methanol (MeOH) of LC-MS grade were purchased from Merck (Darmstadt, Germany), whereas 2-propanol of LC-MS grade was from Fisher Scientific (Geel, Belgium). Sodium hydroxide monohydrate (NaOH) for trace analysis ≥99.9995% and formic acid 99% were purchased from Fluka (Buchs, Switzerland). Hexane (pesticide analysis grade, 95%) was purchased from Carlo Erba (Milan, Italy), and distilled water was provided by a Milli-Q purification apparatus (Millipore Direct-Q UV, Bedford, MA, USA). The ethylenediaminetetraacetic acid disodium salt (EDTA) and the trichloroacetic acid (TCA) were of analytical grade and were purchased from Panreac (Barcelona, Spain) and Fisher Scientific (Loughborough, UK), respectively. Regenerated cellulose (RC) syringe filters (15 mm diameter, 0.22 μm pore size) were provided from Phenomenex (Torrance, CA, USA). Solid phase extraction cartridges were Oasis HLB 3 cc (60 mg) from Waters (Milford, MA, USA).

Stock standard solutions of individual compounds (1000 μg mL^{-1}) were prepared in methanol and stored at −20 °C in brown glass to prevent photodegradation. Penicillins, cefalosporines, and metformin were dissolved in Milli-Q water and stored at 4 °C. In quinolone standard solutions, 100 μL of formic acid was added to enhance solubility. Four intermediate standard solutions containing the analytes were prepared by dilution of the stock solutions with methanol. The final concentration of these multicomponent solutions was 10 μg mL^{-1}, and they were also stored at −20 °C. New intermediate standard solutions were prepared every month. Working solutions and

DOI: 10.1021/acs.jafc.5b00962
J. Agric. Food Chem. 2015, 63, 4493−4508

calibration standards, containing all of the target analytes, were obtained by gradient dilution of the intermediate solutions, in concentrations varying from 1 μg mL^{-1} to 1 ng mL^{-1}. The working solutions were kept at −20 °C and renewed weekly.

Instrumentation. An ultrahigh-performance liquid chromatography (UHPLC) system (Dionex UltiMate 3000 RSLC, Thermo Fisher Scientific, Germany) interfaced to a QTOF mass spectrometer (Maxis Impact, Bruker Daltonics, Bremen, Germany) was used for the screening analysis.

The chromatographic separation was performed on an ACQUITY UHPLC BEH C18 column (2.1 × 50 mm, 1.7 μm) from Waters (Ireland), thermostated at 30 °C. The mobile phases were (A) MeOH and (B) an aqueous solution with 0.01% formic acid. The flow rate was 0.1 mL min^{-1} despite the fact that UHPLC allows higher flow rates (<0.2 mL min^{-1}) because electrospray ionization is more compatible with low flow rates and thus sensitivity of the detection is increased. The gradient elution program started with 5% MeOH (A), increased to 100% in 7 min, and kept constant for 3 min. Then, the initial conditions were restored, and the system was allowed to re-equilibrate for the next injection for 7 min (17 min total run time). Although the re-equilibration step is rather extended for a 50 mm length column, it is necessary to ensure retention time stability, which is indispensable for the adequate detection of target compounds. The injection volume was set to 5 μL.

The QTOF MS system was equipped with an electrospray ionization interface (ESI), operating in positive mode, with the following operation parameters: capillary voltage, 2500 V; end plate offset, 500 V; nebulizer pressure, 2 bar (N_2); drying gas, 8 L min^{-1} (N_2); and drying temperature, 200 °C.

The QTOF MS system was operating in broadband collision-induced dissociation (bbCID) acquisition mode and recorded spectra over the range m/z 40−1000 with a scan rate of 2 Hz. The Bruker bbCID mode provides MS and MS/MS spectra at the same time (as MS^E mode described in a previous study[5]). It works at two different collision energies; at low collision energy (4 eV), MS spectra were acquired, where all of the ions from the preselected mass range m/z 40−1000 are heading toward the flight tube without isolation at the quadrupole and there is no collision-induced dissociation at the collision cell. At high collision energy (25 eV), no isolation is taking place at the quadrupole, and the ions from the preselected mass range m/z 40−1000 are fragmented at the collision cell.

A QTOF external calibration was daily performed with a sodium formate solution, and a segment (0.1−0.25 min) in every chromatogram was used for internal calibration, using a calibrant injection at the beginning of each run. The sodium formate calibration mixture consists of 10 mM sodium formate in a mixture of water/isopropanol (1:1). The theoretical exact masses of calibration ions with formulas $Na(NaCOOH)_{1-14}$ in the range of 40−1000 Da were used for calibration. The instrument provided a typical resolving power of 36000−40000 during calibration (39274 at m/z 226.1593, 36923 at m/z 430.9137, and 36274 at m/z 702.8636).

Samples. Pasteurized whole bovine and ovine milk samples were purchased from local retail food outlets and supermarkets. Samples were stored at 4 °C before analysis (within 10 days). Cultured fish samples, consisting of gilthead sea bream (*Sparus aurata*) and sea bass (*Dicentrarchus labrax*) samples, were obtained from aquaculture and local fish markets. The fillets were homogenized with a high-speed blender and stored at −23 °C until analysis. One sample of each matrix was tested to ensure that it did not contain any analytes, and it was used for negative control and fortified with target compounds. Milk and fish samples contain different amounts of fat (2−3.5% for milk and 5−10% for fish tissue), so the method can be used to analyze different categories of food products with different fat contents.

Sample Preparation. Two different sample preparation protocols were developed and used for the extraction of veterinary drugs and pharmaceuticals from fish and milk samples. A schematic representation of the extraction and cleanup procedures is presented in the Supporting Information (Figure S1).

The sample preparation method for the fish tissue samples has been developed in a previous study from our group. It consists of a generic extraction of the analytes from the tissue using a mixture of analytes and further low-temperature and hexane cleanup. A 1 g portion of fish tissue sample is weighed and placed into a 15 mL polypropylene centrifuge tube. For fortified fish tissue samples, aliquots of 20 and 200 μL of a working solution standard containing all of the analytes at a concentration of 1 μg mL^{-1} were added. Spiked levels obtained were 20 and 200 μg kg^{-1}, respectively. When fortified, the samples are vortex-mixed for 30 s and allowed to stand for 10−15 min. Two milliliters of H_2O containing 0.1% formic acid (v/v) and 0.1% EDTA (w/v), 2 mL of MeOH, and 2 mL of ACN are added in all samples, subsequently. After the addition of each solvent, the tube is vortex-mixed for 30 s. The sample set is placed in an ultrasonic bath at 60 °C for 20 min, the samples are centrifuged at 4300g for 10 min, and the supernatant is decanted into a new polypropylene centrifuge tube. The tubes are placed in −20 °C for 12 h to precipitate the lipids and remaining proteins. After centrifuging and discarding the precipitate, defatting with hexane completes the sample cleanup. The extracts are evaporated to dryness under a nitrogen stream and reconstituted in 0.5 mL of methanol/aqueous solution of formic acid, 0.05% (25:75 v/v), achieving a two-time preconcentration of the analytes in the samples. Finally, the extracts are filtered through a 0.22 μm pore size RC filter (to remove matrix interferences).

Milk samples are allowed to thaw, and a quick homogenization of the fat is performed by shaking before taking up the test portion of 2 g for the analysis. The samples were extracted with a mixture of aqueous TCA 5% (w/v)−ACN (3:1, v/v) and were then subjected to cleanup with hydrophilic−lipophilic balance (HLB) SPE cartridges. In particular, 2 mL of whole milk is transferred in a 50 mL polypropylene centrifuge tube. For fortified milk samples, aliquots of 30 and 300 μL of a working solution standard containing all of the analytes at a concentration of 1 μg mL^{-1} were added to 2 mL milk samples. Spiked levels obtained were 15 and 150 ng mL^{-1}, respectively. When fortified, the samples are vortex-mixed for 30 s and allowed to stand for 10−15 min. After the addition of 12 mL of aqueous TCA solution 5% (w/v) and 4 mL of ACN, the samples are vortexed for 1 min and shaken for 60 min using a mechanical shaker in medium speed (approximately 1000 rpm). Then, the sample tube is centrifuged at 4000g for 5 min, and the supernatant is decanted in a new polypropylene tube and diluted to 50 mL with Milli-Q water. The diluted sample extract is adjusted to pH 5.5 by dropwise addition of ammonia hydroxide 15% (w/v) and measurement of the pH value with a pH meter. Afterward, the extract is loaded onto an Oasis HLB cartridge (60 mg, 3 mL) previously conditioned sequentially with 6 mL of MeOH and 6 mL of H_2O. The sample is passed through the cartridge at a flow no faster than 1 drop/2 s, and then it is vacuum-dried for 30 min. No washing step was applied to minimize analyte loss. The elution is carried out with 2 × 3 mL of MeOH, and the eluent is collected and evaporated to dryness under a stream of nitrogen at 40 °C. The residue is redissolved in 0.5 mL of MeOH/aqueous solution of formic acid, 0.05% (25:75 v/v), and filtered through a 0.22 μm RC filter. The preconcentration factor achieved with this method is 4-fold.

Qualitative Validation. Validation of the screening method was performed for qualitative purposes following the strategy described in the literature,[5,27,36] which is in part based on the SANCO/12571/2013 guideline.[37] Two sets of six fish samples (2 × 3 sea bream and 2 × 3 sea bass) and two sets of six milk samples (2 × 3 bovine milk and 2 × 3 ovine milk samples) were spiked at two concentration levels (20 and 200 μg kg^{-1} for fish samples and 15 and 150 ng mL^{-1} for milk samples). The samples were analyzed in four sets during four different laboratory days. Each set of samples consisted of seven samples of each matrix (six spiked samples, three at the low concentration level and three at the high concentration level, together with their respective nonspiked blanks) and one reagent blank to ensure that no laboratory contamination was held during the analysis.

The main validation parameters investigated were the screening detection limit (SDL) and the limit of identification (LOI). The lowest concentration level in which a target compound was detected in all samples is defined as the SDL, whereas the lowest concentration in which a target compound was satisfactorily identified in all spiked samples is defined as the LOI. The detection criterion was the

DOI: 10.1021/acs.jafc.5b00962
J. Agric. Food Chem. 2015, 63, 4493−4508

Table 1. Average |dRT|, Mass Accuracy, and Ion Intensity Ratios (IIR) of Target Compounds in Fish and Milk Samples in Two Concentration Levels[a]

	milk								fish							
	low concn level (15 ng mL^{-1}, n = 6)				high concn level (150 ng mL^{-1}, n = 6)				low concn level (20 μg kg^{-1}, n = 6)				high concn level (200 μg kg^{-1}, n = 6)			
		av mass accuracy				av mass accuracy				av mass accuracy				av mass accuracy		
compound	|dRT| (min)	prec ion (mDa)	prod ion 1 (mDa)	IIR	|dRT| (min)	prec ion (mDa)	prod ion 1 (mDa)	IIR	|dRT| (min)	prec ion (mDa)	prod ion 1 (mDa)	IIR	|dRT| (min)	prec ion (mDa)	prod ion 1 (mDa)	IIR
quinolones																
ciprofloxacin	0.14	0.3	0.6	0.92	0.13	0.5	0.5	0.84	0.12	1.0	NI	NI	0.08	0.4	0.4	1.14
danofloxacin	0.10	0.5	0.3	0.69	0.11	0.7	0.6	0.57	ND	ND	NI	NI	0.05	0.8	0.5	0.69
difloxacin	0.10	0.5	0.6	0.44	0.11	0.8	0.5	0.39	0.11	0.6	NI	NI	0.10	1.0	0.5	0.67
enrofloxacin	0.09	0.4	0.5	0.63	0.09	0.6	0.5	0.55	0.09	0.5	0.5	2.07	0.12	0.7	0.4	0.62
flumequine	0.01	0.2	0.2	0.99	0.01	0.4	0.2	0.96	0.02	0.3	0.5	1.18	0.00	0.3	0.3	1.03
marbofloxacin	0.10	0.8	0.5	0.19	0.08	0.6	0.6	0.19	0.04	0.9	1.2	1.12	0.09	0.4	0.6	0.34
norfloxacin	0.11	0.4	0.5	0.98	0.10	0.6	0.6	0.83	0.09	1.2	0.5	2.12	0.09	0.3	0.3	1.15
ofloxacin	0.02	0.5	0.4	1.03	0.03	0.7	0.6	1.01	0.11	0.6	0.8	2.69	0.09	0.7	0.8	1.30
oxolinic acid	0.01	0.4	0.3	9.44	0.02	0.4	0.5	2.60	0.03	0.5	0.5	0.50	0.02	0.3	0.3	0.37
sarafloxacin	0.01	0.3	0.5	0.74	0.04	0.7	0.6	0.72	0.13	0.7	0.7	1.68	0.09	0.7	0.4	0.86
tetracyclines																
chlortetracycline	0.04	0.7	0.8	1.14	0.04	0.5	1.0	1.11	0.09	1.1	NI	NI	0.08	0.5	0.6	1.33
doxycycline	0.13	0.6	0.8	2.09	0.13	0.7	0.4	2.08	0.01	1.0	0.8	1.69	0.06	0.6	0.8	2.26
minocycline	0.08	1.0	0.9	2.07	0.11	0.7	0.3	2.31	0.05	1.3	NI	NI	0.06	1.1	NI	NI
oxytetracycline	0.04	0.7	NI	NI	0.04	0.5	0.6	1.47	ND	ND	NI	NI	0.06	0.7	0.8	1.59
tetracycline	0.11	0.5	0.5	1.93	0.11	0.8	0.5	1.50	0.09	1.0	NI	NI	0.08	0.9	0.7	2.72
cefalosporines																
cefaclor	ND	ND	NI	NI	ND	ND	NI	NI	ND	ND	NI	NI	ND	ND	NI	NI
cefadroxil	ND	ND	NI	NI	0.08	0.4	0.5	3.09	ND	ND	NI	NI	0.04	0.5	0.5	5.56
cefalexin	ND	ND	NI	NI	0.03	0.4	1.1	3.02	ND	ND	NI	NI	0.07	0.8	0.8	4.98
cefapirin	ND	ND	NI	NI	ND	ND	NI	NI	ND	ND	NI	NI	ND	ND	NI	NI
cefazolin	ND	ND	NI	NI	ND	ND	NI	NI	ND	ND	NI	NI	ND	ND	NI	NI
ceftiofur	ND	ND	NI	NI	0.13	1.1	0.6	0.78	ND	ND	NI	NI	0.11	0.8	NI	NI
penicillins																
amoxicillin	ND	ND	ND	ND	ND	ND	ND	ND	ND	ND	NI	NI	0.08	0.7	0.7	11.84
ampicillin	ND	ND	ND	ND	ND	ND	ND	ND	ND	ND	NI	NI	0.05	0.9	NI	NI
cloxacillin	0.04	0.6	0.2	1.96	0.04	0.9	0.3	1.46	0.04	0.9	0.7	5.58	0.02	0.5	0.3	2.03
dicloxacillin	0.09	1.1	0.3	2.74	0.09	0.8	0.1	1.84	0.08	1.2	0.3	10.93	0.11	0.6	0.1	2.77
oxacillin	0.05	0.4	NI	NI	0.05	0.5	0.3	0.07	ND	ND	NI	NI	ND	ND	NI	NI
penicillin G	0.01	0.5	0.4	2.58	0.01	0.4	0.5	1.84	0.02	0.6	0.7	3.13	0.02	0.4	0.3	2.32
penicillin V	0.10	0.5	0.5	0.42	0.06	0.5	0.3	0.31	0.02	0.9	0.7	3.49	0.02	0.4	0.5	0.34
macrolides																
azithromycin	ND	ND	ND	ND	ND	ND	ND	ND	0.06	1.3	0.2	7.80	1.40	1.2	0.3	5.07

DOI: 10.1021/acs.jafc.5b00962
J. Agric. Food Chem. 2015, 63, 4493−4508

Table 1. continued

	milk								fish							
	low concn level (15 ng mL^{-1}, n = 6)				high concn level (150 ng mL^{-1}, n = 6)				low concn level (20 μg kg^{-1}, n = 6)				high concn level (200 μg kg^{-1}, n = 6)			
		av mass accuracy				av mass accuracy				av mass accuracy				av mass accuracy		
compound	|dRT| (min)	prec ion (mDa)	prod ion 1 (mDa)	IIR	|dRT| (min)	prec ion (mDa)	prod ion 1 (mDa)	IIR	|dRT| (min)	prec ion (mDa)	prod ion 1 (mDa)	IIR	|dRT| (min)	prec ion (mDa)	prod ion 1 (mDa)	IIR
clarithromycin	ND	ND	NI	NI	ND	ND	NI	NI	0.07	0.9	0.2	2.44	0.03	1.4	0.1	1.30
erythromycin−H_2O	ND	ND	NI	NI	0.06	1.2	0.6	3.57	0.10	1.1	0.8	1.84	0.09	1.1	0.6	1.61
tiamulin	0.10	0.6	0.1	2.71	0.09	1.2	0.5	2.42	0.04	0.9	0.5	3.80	0.05	0.8	0.4	2.22
tilmicosin	0.10	0.6	1.2	0.16	0.14	0.5	1.3	0.22	0.07	0.7	0.4	0.68	0.12	0.2	0.8	0.16
sulfonamides																
dapsone	ND	ND	NI	NI	0.02	0.2	0.4	4.52	ND	ND	NI	NI	0.07	0.5	0.2	7.40
sulfachloropyridazine	0.09	0.4	0.2	4.35	0.06	0.2	0.3	2.94	0.07	0.7	0.4	14.53	0.07	0.5	0.2	5.54
sulfaclozine	0.07	0.5	0.1	8.08	0.06	0.3	0.3	5.26	ND	ND	NI	NI	0.04	0.6	0.3	9.12
sulfadiazine	0.03	0.6	0.7	1.77	0.04	0.2	0.7	0.83	0.06	0.6	1.0	2.56	0.03	0.5	0.3	1.40
sulfadimethoxine	0.02	0.4	0.2	1.28	0.02	0.6	0.4	0.84	0.06	0.5	0.3	1.87	0.04	0.4	0.2	1.64
sulfadimidine	0.05	0.3	0.2	5.76	0.04	0.5	0.1	1.92	0.04	0.8	0.6	19.31	0.06	0.6	0.3	2.98
sulfadoxine	0.02	0.3	0.2	3.60	0.02	0.5	0.3	2.30	0.04	0.7	0.2	5.11	0.03	0.5	0.2	3.39
sulfaguanidine	0.05	0.7	0.4	1.72	0.05	0.3	0.1	0.49	0.06	0.6	0.6	0.15	0.05	0.5	0.5	0.14
sulfamerazine	0.03	0.5	0.3	1.01	0.10	0.3	0.5	0.78	ND	ND	NI	NI	0.07	0.5	0.2	7.39
sulfameter	0.03	0.6	0.2	4.17	0.02	0.4	0.4	3.11	ND	ND	NI	NI	0.03	0.5	0.3	4.67
sulfamethizole	0.04	0.5	0.2	3.86	0.03	0.3	0.4	3.48	ND	ND	NI	NI	0.06	0.8	0.2	5.84
sulfamethoxazole	0.05	0.4	0.2	3.15	0.03	0.2	0.3	1.89	0.07	0.5	0.3	9.19	0.08	0.3	0.2	3.35
sulfamethoxypyridazine	0.04	0.6	0.2	1.78	0.05	0.2	0.3	1.44	0.06	0.7	0.3	6.98	0.08	0.8	0.3	3.56
sulfamonomethoxine	0.06	0.4	0.2	5.39	0.06	0.3	0.3	3.79	0.06	1.2	0.4	10.19	0.03	1.0	0.2	6.05
sulfamoxole	0.01	0.4	0.1	8.59	0.02	0.2	0.3	6.61	0.05	0.3	0.4	14.49	0.05	0.4	0.2	6.00
sulfapyridine	0.01	0.5	0.5	0.77	0.02	0.2	0.7	0.76	0.06	0.8	0.2	2.05	0.03	0.4	0.2	1.19
sulfaquinoxaline	0.05	0.4	0.1	2.23	0.04	0.6	0.3	1.49	0.02	0.6	0.4	3.64	0.01	0.5	0.2	2.10
sulfathiazole	0.02	0.6	0.5	1.24	0.03	0.2	0.6	0.99	0.04	0.8	0.3	3.73	0.03	0.3	0.3	1.51
sulfisoxazole	0.04	0.5	0.2	2.57	0.05	0.3	0.3	1.85	0.10	1.1	0.3	8.32	0.08	0.7	0.2	8.29
quinoxalines																
carbadox	0.02	0.4	0.7	0.29	0.01	0.2	0.2	0.18	0.06	0.8	NI	NI	0.01	0.7	NI	NI
olaquindox	0.03	0.5	0.7	0.19	0.02	0.2	0.3	0.07	ND	ND	NI	NI	ND	ND	NI	NI
amphenicols																
florfenicol	0.04	0.4	0.3	1.28	0.06	0.5	0.3	1.09	ND	ND	NI	NI	0.04	0.9	0.3	1.54
thiampenicol	0.02	0.8	NI	NI	0.02	0.4	NI	NI	ND	ND	NI	NI	ND	ND	NI	NI
diaminopyrimidines																
baquiloprin	0.12	0.3	0.4	0.38	0.10	0.4	0.4	0.38	0.04	0.3	NI	NI	0.09	0.3	0.3	0.40
trimethoprim	0.07	0.3	0.3	0.43	0.04	0.5	1.4	0.20	0.11	0.6	0.9	1.08	0.08	0.7	1.4	0.33

DOI: 10.1021/acs.jafc.5b00962
J. Agric. Food Chem. 2015, 63, 4493−4508

Table 1. continued

	milk								fish							
	low concn level (15 ng mL^{-1}, n = 6)				high concn level (150 ng mL^{-1}, n = 6)				low concn level (20 μg kg^{-1}, n = 6)				high concn level (200 μg kg^{-1}, n = 6)			
		av mass accuracy				av mass accuracy				av mass accuracy				av mass accuracy		
compound	|dRT| (min)	prec ion (mDa)	prod ion 1 (mDa)	IIR	|dRT| (min)	prec ion (mDa)	prod ion 1 (mDa)	IIR	|dRT| (min)	prec ion (mDa)	prod ion 1 (mDa)	IIR	|dRT| (min)	prec ion (mDa)	prod ion 1 (mDa)	IIR
other antibiotics																
lincomycin	0.09	0.4	0.1	2.94	0.07	1.0	0.2	2.79	0.08	0.9	0.2	9.19	0.07	1.0	0.2	6.01
novobiocin	ND	ND	NI	NI	0.04	1.0	0.3	2.10	ND	ND	NI	NI	0.01	0.9	0.7	2.04
rifaximin	0.04	0.9	1.4	0.88	0.05	1.3	1.6	0.75	0.02	0.9	1.2	1.52	0.05	1.2	1.4	0.88
anthelmintics																
albendazole	0.01	0.3	0.2	1.25	0.01	0.5	0.3	1.22	0.13	0.3	0.2	1.51	0.10	0.3	0.2	1.52
albendazole oxide	0.05	0.4	0.4	0.45	0.04	0.5	0.2	0.43	0.03	0.7	0.5	0.70	0.03	0.5	0.2	0.49
albendazole sulfone	ND	ND	ND	ND	ND	ND	ND	ND	0.01	0.6	1.0	1.31	0.02	0.5	0.2	1.22
dimetridazole	0.01	0.1	0.2	0.50	0.02	0.2	0.1	0.48	0.11	0.2	0.4	1.18	0.05	0.2	0.3	0.38
febantel	ND	ND	NI	NI	0.03	0.9	NI	NI	ND	ND	NI	NI	ND	ND	NI	NI
fenbendazole	0.06	0.3	0.3	1.58	0.06	0.5	0.4	1.48	0.10	0.5	0.7	1.96	0.06	0.3	0.2	1.78
flubendazole	0.04	0.4	0.4	1.48	0.04	0.6	0.6	1.42	0.02	0.4	0.7	1.63	0.01	0.6	0.5	1.63
levamisole	0.14	0.4	0.6	0.40	0.15	0.2	0.3	0.66	0.13	0.6	0.5	0.72	0.09	0.3	0.6	0.52
mebendazole	0.05	0.2	0.3	1.70	0.05	0.7	0.4	1.48	0.02	0.4	0.4	1.89	0.03	0.4	0.4	1.63
metronidazole	0.02	0.7	0.1	0.52	0.03	0.3	0.2	0.53	0.07	0.2	0.3	1.07	0.05	0.4	0.4	0.90
morantel	0.01	0.3	0.2	0.29	0.04	0.2	0.2	0.22	0.11	0.6	0.4	0.77	0.09	0.4	0.3	0.48
oxfendazole	0.05	0.3	1.3	0.78	0.05	0.7	1.1	0.67	0.02	0.4	0.9	1.24	0.03	0.5	1.2	0.81
piperazine	ND	ND	NI	NI	ND	ND	NI	NI	ND	ND	NI	NI	ND	ND	NI	NI
ronidazole	0.04	0.7	0.2	0.73	0.06	0.4	0.2	0.57	ND	ND	NI	NI	ND	ND	NI	NI
ternidazole	0.05	0.4	0.1	1.23	0.03	0.2	0.2	1.12	0.12	0.4	0.4	3.29	0.05	0.3	0.2	1.40
thiabendazole	0.02	0.3	0.2	0.47	0.02	0.3	0.3	0.48	0.11	0.4	0.4	0.80	0.05	0.5	0.3	0.48
triclabendazole	0.02	0.4	1.1	0.36	0.02	0.5	0.9	0.22	0.01	0.6	0.7	0.27	0.00	0.5	0.5	0.16
coccidiostats																
arprinocid	0.03	0.2	0.2	4.01	0.03	0.4	0.2	3.27	0.05	0.4	0.5	7.57	0.04	0.3	0.2	4.11
clopidol	0.08	0.6	0.2	0.37	0.07	0.1	0.1	0.27	0.06	0.7	NI	NI	0.06	0.5	NI	NI
decoquinate	ND	ND	NI	NI	0.04	0.9	NI	NI	ND	ND	NI	NI	0.02	0.5	0.4	0.69
diaveridine	0.01	0.3	0.5	0.52	0.02	0.3	0.3	0.46	0.13	0.8	0.9	0.68	0.10	0.4	0.3	0.52
ethopabate	0.00	0.2	0.2	1.67	0.00	0.2	0.1	1.27	0.02	0.3	0.4	2.17	0.02	0.3	0.4	1.49
halofuginone	0.12	0.9	0.2	0.55	0.10	0.4	0.1	11.1	ND	ND	NI	NI	0.07	1.0	0.8	0.79
imidocarb	0.05	0.4	1.2	2.92	0.06	0.5	0.3	4.54	0.03	0.8	NI	NI	0.05	0.6	NI	NI
lasalocid	0.06	0.2	0.3	0.46	0.07	1.0	0.1	0.61	0.02	0.1	NI	NI	0.05	0.9	1.0	0.71
monensin	0.06	1.4	0.9	0.75	0.11	1.5	1.5	0.48	ND	ND	NI	NI	ND	ND	NI	NI
narasin	ND	ND	NI	NI	0.02	1.4	NI	NI	ND	ND	NI	NI	0.04	1.5	1.1	1.6
nigericin	ND	ND	NI	NI	0.08	1.2	NI	NI	ND	ND	NI	NI	0.06	1.1	NI	NI
robenidine	ND	ND	NI	NI	0.12	1.1	0.8	1.22	ND	ND	NI	NI	ND	ND	NI	NI
salinomycin	ND	ND	NI	NI	0.04	1.5	NI	NI	ND	ND	NI	NI	0.06	1.2	NI	NI

DOI: 10.1021/acs.jafc.5b00962
J. Agric. Food Chem. 2015, 63, 4493−4508

Table 1. continued

	milk								fish							
	low concn level (15 ng mL^{-1}, n = 6)				high concn level (150 ng mL^{-1}, n = 6)				low concn level (20 μg kg^{-1}, n = 6)				high concn level (200 μg kg^{-1}, n = 6)			
		av mass accuracy				av mass accuracy				av mass accuracy				av mass accuracy		
compound	|dRT| (min)	prec ion (mDa)	prod ion 1 (mDa)	IIR	|dRT| (min)	prec ion (mDa)	prod ion 1 (mDa)	IIR	|dRT| (min)	prec ion (mDa)	prod ion 1 (mDa)	IIR	|dRT| (min)	prec ion (mDa)	prod ion 1 (mDa)	IIR
NSAIDs																
5-hydroxyflunixin	0.11	0.4	0.3	1.06	0.10	0.6	0.5	0.96	0.04	0.6	0.4	1.14	0.01	0.2	0.4	0.99
aceclofenac	0.10	1.0	1.1	3.95	0.12	0.4	1.8	2.05	ND	ND	NI	NI	0.10	0.4	1.5	1.94
diclofenac	ND	ND	NI	NI	0.01	0.6	0.5	2.43	0.04	0.7	0.8	2.83	0.04	0.4	0.7	2.25
flunixin	0.09	0.3	0.9	1.41	0.07	0.5	0.5	1.25	0.06	0.7	1.2	1.18	0.06	0.4	0.9	1.15
ketoprofen	0.04	0.3	0.2	3.76	0.04	0.3	0.4	2.51	0.02	0.7	0.2	5.27	0.05	0.2	0.2	3.32
mefenamic acid	ND	ND	0.2	2.49	0.06	0.4	0.4	2.03	ND	ND	NI	NI	0.04	0.7	0.7	1.46
meloxicam	0.07	0.3	0.4	11.8	0.07	0.8	0.4	4.20	0.06	0.4	0.2	19.11	0.04	0.6	0.2	5.94
naproxen	0.04	0.2	0.5	2.03	0.04	0.1	0.2	1.30	0.03	0.7	0.5	3.88	0.04	0.6	0.4	1.51
niflumic acid	0.03	0.3	0.4	1.63	0.05	0.5	0.5	1.68	0.02	0.5	0.6	1.48	0.02	0.2	0.3	1.37
phenylbuntazone	0.01	1.3	0.5	1.28	0.02	0.6	0.1	0.53	0.02	1.6	0.2	1.07	0.01	0.7	0.3	0.68
tolfenamic acid	0.07	1.4	NI	NI	0.06	1.8	NI	NI	0.10	0.5	NI	NI	ND	ND	NI	NI
vedaprofen	ND	ND	NI	NI	0.07	0.4	NI	NI	ND	ND	NI	NI	ND	ND	NI	NI
β-agonists																
cimaterol	0.02	0.6	0.6	1.01	0.03	0.2	0.4	0.89	0.10	0.5	0.4	1.24	0.09	0.3	0.4	1.06
clenbuterol	0.02	0.3	0.2	1.26	0.05	0.4	0.1	1.12	0.09	0.5	0.5	2.51	0.08	0.5	0.2	2.08
clenpenterol	0.10	0.3	0.3	1.35	0.09	0.3	0.4	1.23	0.06	0.6	0.4	1.69	0.05	0.6	0.3	1.49
mabuterol	0.13	0.3	0.2	1.25	0.13	0.6	0.1	1.23	0.02	0.7	0.4	1.42	0.05	0.7	0.3	1.57
ractopamine	0.11	0.3	0.2	1.74	0.09	0.4	0.1	1.23	0.05	1.0	0.4	5.92	0.07	0.5	0.3	2.55
salbutamol	0.03	0.3	0.4	1.11	0.03	0.2	0.2	1.25	0.06	0.6	0.3	1.90	0.04	0.1	0.2	1.49
terbutaline	0.02	0.3	0.5	0.79	0.02	0.1	0.2	0.76	0.10	0.7	0.4	1.30	0.08	0.3	0.3	1.00
steroids																
betamethasone	0.04	0.6	NI	NI	0.03	0.8	0.5	0.13	ND	ND	NI	NI	0.01	0.3	0.4	0.25
cortisol	0.02	1.0	0.2	5.72	0.01	0.3	0.1	1.83	ND	ND	NI	NI	0.01	0.5	0.5	2.56
cortison	0.02	0.7	0.2	6.81	0.02	0.7	0.2	0.79	ND	ND	NI	NI	0.04	0.5	0.3	1.42
dexamethazone	ND	ND	NI	NI	0.04	1.1	NI	NI	ND	ND	NI	NI	ND	ND	NI	NI
methylprednisolone	0.00	0.4	NI	NI	0.01	0.9	0.3	0.05	ND	ND	NI	NI	ND	ND	NI	NI
progesteron	ND	ND	NI	NI	0.02	0.6	0.3	0.05	ND	ND	NI	NI	0.03	0.3	0.1	1.73
thyreostats																
methyl-thiouracil	ND	ND	NI	NI	ND	ND	NI	NI	0.02	0.7	NI	NI	0.02	0.3	0.4	15.71
phenyl-thiouracil	ND	ND	NI	NI	0.04	0.6	0.5	0.75	0.08	0.7	0.5	9.28	0.06	0.3	0.4	1.23
propyl-thiouracil	ND	ND	NI	NI	0.05	0.3	0.2	3.51	0.09	0.7	1.0	5.23	0.10	0.3	0.5	1.05

DOI: 10.1021/acs.jafc.5b00962
J. Agric. Food Chem. 2015, 63, 4493−4508

Table 1. continued

	milk								fish							
	low concn level (15 ng mL^{-1}, n = 6)				high concn level (150 ng mL^{-1}, n = 6)				low concn level (20 μg kg^{-1}, n = 6)				high concn level (200 μg kg^{-1}, n = 6)			
		av mass accuracy				av mass accuracy				av mass accuracy				av mass accuracy		
compound	|dRT| (min)	prec ion (mDa)	prod ion 1 (mDa)	IIR	|dRT| (min)	prec ion (mDa)	prod ion 1 (mDa)	IIR	|dRT| (min)	prec ion (mDa)	prod ion 1 (mDa)	IIR	|dRT| (min)	prec ion (mDa)	prod ion 1 (mDa)	IIR
pharmaceuticals																
ambroxol	0.14	0.9	0.4	4.81	0.14	0.2	0.3	5.14	0.04	1.2	0.3	4.30	0.05	0.5	0.3	4.98
atenolol	0.13	0.3	0.7	0.15	0.14	0.2	0.4	0.15	0.10	0.5	0.8	0.19	0.07	0.3	0.6	0.17
atorvastatin	0.05	1.0	0.7	3.63	0.05	1.0	0.7	1.95	0.03	1.1	0.7	2.35	0.02	0.5	0.4	1.81
caffeine	0.01	0.2	0.9	0.04	0.02	0.2	1.7	0.04	0.11	0.7	0.8	4.35	0.04	0.5	0.9	0.67
carbamazepine	0.04	0.1	0.1	1.43	0.05	0.2	0.2	1.24	0.02	0.4	0.5	1.83	0.02	0.3	0.4	1.58
cimetidine	0.05	0.3	0.2	1.57	0.06	0.2	0.2	1.63	0.06	0.7	0.2	3.41	0.05	0.1	0.1	2.10
gemfibrozil	0.06	0.8	0.2	8.96	0.06	0.1	0.3	1.95	ND	ND	NI	NI	0.02	0.6	0.3	2.09
haloperidol	0.13	0.4	0.3	4.12	0.12	1.0	0.5	3.38	0.05	0.6	0.5	5.78	0.04	0.5	0.3	4.03
indapamide	0.05	0.4	0.3	15.75	0.04	0.5	0.2	12.9	0.03	0.6	NI	NI	0.01	0.4	0.9	15.30
metformin	0.03	0.2	0.6	0.09	0.05	0.1	0.3	0.04	ND	ND	NI	NI	0.10	0.3	1.9	2.07
metoprolol	0.08	0.3	0.1	0.32	0.08	0.6	0.2	0.32	0.04	0.5	0.2	0.48	0.04	0.7	0.2	0.33
paracetamol	0.03	0.5	0.8	1.08	0.03	0.3	1.2	0.90	0.02	0.9	0.4	0.77	0.03	0.2	0.2	1.01
propranolol	0.15	0.2	0.4	0.09	0.12	0.5	0.1	0.01	0.07	0.3	0.4	1.08	0.05	0.4	0.2	0.79
ranitidine	0.14	0.4	0.6	0.35	0.15	0.5	0.4	0.39	0.13	0.5	0.7	0.46	0.10	0.4	0.6	0.41
simvastatin	0.12	1.3	0.8	0.04	0.02	0.7	0.3	0.51	ND	ND	NI	NI	0.11	1.1	0.9	3.63
theophyline	0.05	0.4	0.2	1.84	0.03	0.2	0.2	1.37	ND	ND	NI	NI	0.08	0.4	0.3	2.37
tramadol	0.04	0.3	0.1	1.53	0.05	0.6	0.3	1.27	0.11	0.6	0.2	2.42	0.10	0.8	0.2	1.35
triamterene	0.02	0.3	0.3	0.21	0.02	0.3	0.1	0.18	0.08	0.5	0.6	0.58	0.03	0.3	0.3	0.27
valsartan	0.13	0.3	0.6	0.88	0.13	1.0	0.1	0.67	0.07	1.0	0.5	1.52	0.05	0.5	0.6	0.69
others																
bromhexine	0.10	0.3	0.5	0.52	0.11	0.5	0.2	0.48	0.08	0.7	0.7	0.70	0.06	0.5	0.5	0.60
chlorpromazine	0.07	0.3	0.1	6.02	0.07	0.8	0.3	2.81	0.04	0.7	0.2	4.56	0.08	0.7	0.5	1.93
colchicine	0.01	0.5	0.3	0.16	0.01	1.1	0.4	0.10	0.02	0.6	1.2	0.25	0.04	0.7	0.4	0.18
coumaphos	ND	ND	NI	NI	0.01	0.4	0.4	0.61	0.05	0.7	NI	NI	0.05	0.4	0.5	0.50
melamine	0.12	0.3	0.6	0.60	0.15	0.2	0.2	0.64	ND	ND	NI	NI	ND	ND	NI	NI

[a]ND, compound not detected; NI, compound not identified.

DOI: 10.1021/acs.jafc.5b00962
J. Agric. Food Chem. 2015, 63, 4493−4508

presence of the most abundant ion (most frequently, the protonated molecule) in the LE function at the expected retention time (±2.5% tolerance) measured at its exact mass with a maximum mass error of 2 mDa. For identification at least two m/z ions (for example, the precursor and one product ion) are required (in either the LE or HE function).

According to Commission Decision 2002/657/EC, a minimum of three identification points (IPs) is required for authorized substances and four for banned compounds.[38] For HRMS, 2 IPs are earned for the precursor and 2.5 IPs for each product ion. Consequently, when a compound is successfully identified (at LOI) 4.5 IPs are earned, in agreement with the EU requirements.

RESULTS AND DISCUSSION

UHPLC-QTOF MS Method Development. Data analysis and evaluation were processed with Data Analysis 4.1 and Target Analysis 1.3 (Bruker Daltonics). An in-house database of 143 pharmaceutical compounds and veterinary drugs was built including information on the analytes' retention time, molecular formula (to extract the accurate mass of the corresponding pseudomolecular ion and adducts $[M + H]^+$, $[M + Na]^+$, and $[M + NH_4]^+$), isotopic fit, and qualifier ions. All aforementioned data were obtained after injection into the UHPLC-QTOF MS of solvent standard solutions for all target analytes in a concentration of 0.5 μg mL^{-1}. From the LE and HE operation modes, two chromatograms were acquired, a MS and MS/MS chromatogram. LE provided the MS spectra and chromatograms, and thus it was used for the retention time and the molecular formula and mass accuracy of the precursor ions and adducts. From the HE operation the MS/MS spectra and chromatograms were obtained and, thus, information on the molecular formula and mass accuracy of the fragment ions used for the identification of the analytes. Mass spectra obtained from the injection of a standard solution of sulfamethoxazole, in both LE and HE modes, are presented in Figure S2. All TOF data obtained were evaluated against this database.

The addition of retention time and product ion data for target compounds in the database renders the analysis of samples much more efficient as many false-positive detects are precluded. Elemental compositions of the product ions were investigated, and the proposed formulas have arisen using the experimental m/z and Bruker's Data Analysis Smart Formula Tool, which proposes formulas based on the number and type of atoms found in the precursor ion. Many of these structures have been previously reported in the literature.[35,39,40] Table S1 shows the compound name, retention time (minutes), elemental compositions, and theoretical exact mass for precursor and main fragment ion.

For some compounds, the $[M + H]^+$ did not appear to be the most abundant ion. Ionophores, such as monensin, narasin, nigericin, and salinomycin, formed ammonium adducts; the same applied for amphenicols and some nonsteroidal anti-inflammatory drugs (tolfenamic acid and vedaprofen). Erythromycin presented a very abundant $[M - H_2O + H]^+$ ion, because it is very unstable in acidic conditions and is rapidly subjected to a loss of H_2O.[29] Finally, some penicillins were monitored as their $[(M + H_2 - CO) + H]^+$ degradation products. Penicillin G, penicillin V, cloxacillin, dicloxacillin, and oxacillin are subjected to a β-lactam ring-opening that leads to the formation of these products. Amoxicillin and ampicillin, due to their structure ($-NH_2$ at the R ring), are stable even in very acidic conditions.[41]

After internal calibration, specific criteria thresholds were set to screen the chromatograms for identified compounds and optimized to prevent false-negative results, but also with an acceptable percentage of false-positive results. Initially, retention time tolerance threshold was set at 0.15 min, which is lower than 2.5% RT deviation tolerance for all of the compounds eluting after 6 min. As can be seen in Table S1 only 5 of 143 compounds elute in a RT< 6 min (amoxicillin, melamine, metformin, sulfaguanidine, and piperazine). Thus, the EU requirements that set <2.5% RT deviation tolerance are practically fulfilled. All dRT are presented in Table 1.

The mass accuracy of the precursor ion, as well as of the qualifiers, should be <2 mDa compared to standard solutions for the compound to be considered as positively detected and identified. This threshold is quite strict, but it contributes significantly to reduce the number of false-positive results. Average mass accuracy values obtained in fortified milk and fish samples in both concentration levels examined are presented in Table 1. Ion intensity ratios (IIRs) were also calculated for all samples, and the average values in each matrix and each spike concentration level are presented in Table 1. However, the compliance of IIRs was not used as a criterion for identification.[36]

The isotopic fit is an additional criterion for the identification of a compound.[23] The isotope pattern matching algorithm (SigmaFit) is a feature of Bruker Daltonics software. Smaller values show better isotopic fit; however, in less abundant peaks, the mSigma values are relatively high, and thus no filtering is carried out for this parameter. Moreover, thresholds for the area and the intensity of the chromatographic peak are set, according to validated experiments, at levels of 2000 and 500, respectively. These thresholds were set, as a compromise of false-positive and false-negative results, bearing in mind the total number of features of a full scan chromatogram. These optimization results will be presented in detail in a future study from our group.

Sample Preparation Optimization. Finding suitable extraction conditions for a large range of target analytes displaying different chemical properties (lipophilicity, hydrophilicity, alkaline and acidic characteristics, etc.), along with keeping the procedure as short and simple as possible is a great challenge. Having a look at the literature in the field of veterinary drug residue analysis, it becomes apparent that acetonitrile extraction is the most common extraction route used for many veterinary drugs including antibiotics, anthelmintics, and coccidiostats.[9,11,14,42] Acidic extraction with trichloroacetic acid was found to be suitable for quinolones, lincomycin, and tetracyclines.[10,43,44]

Two different sample preparation procedures were followed in this study for the simultaneous extraction of 143 veterinary drugs and pharmaceuticals from fish and milk samples. The first method involves a simple generic solid−liquid extraction step of the analytes from fish tissue. The extraction is performed with 0.1% formic acid in an aqueous solution of EDTA 0.1% (w/v −ACN−MeOH (1:1:1, v/v), and additional ultrasonic-assisted extraction ensures the effective release of the analytes from the matrix. Precipitation of lipids and proteins was promoted by subjecting the extracts at very low temperature (−23 °C) for 12 h, and further cleanup with hexane ensures fat removal from the matrix. This method was developed, optimized, and validated in a previous study by our group and proved to be suitable for the efficacious extraction of veterinary drugs and pharmaceuticals from fish tissue. The second protocol consists of a generic extraction of the analytes from milk samples with a combination of ACN/5% aqueous

DOI: 10.1021/acs.jafc.5b00962
J. Agric. Food Chem. 2015, 63, 4493−4508

Table 2. SDLs, LOIs, and MRLs Established for All Target Compounds in the Matrices Examined[a]

	milk samples (n = 12)			fish samples (n = 12)		
compound	SDL (ng mL^{-1})	LOI (ng mL^{-1})	MRL (ng mL^{-1})	SDL (μg kg^{-1})	LOI (μg kg^{-1})	MRL (μg kg^{-1})
quinolones						
ciprofloxacin	15	15	100	20	200	100
danofloxacin	15	15	30	200	200	100
difloxacin	15	15	prohibited	20	200	300
enrofloxacin	15	15	100	20	20	100
flumequine	15	15	50	20	20	600
marbofloxacin	15	15	75	20	20	
norfloxacin	15	15		20	20	
ofloxacin	15	15		20	20	
oxolinic acid	15	15	prohibited	20	20	100
sarafloxacin	15	15		20	20	
tetracyclines						
chlortetracycline	15	15	100	20	200	100
doxycycline	15	15	prohibited	20	20	
minocycline	15	15		20	NI	
oxytetracycline	15	150	100	200	200	100
tetracycline	15	15	100	20	200	100
cefalosporines						
cefaclor	ND	NI		ND	NI	
cefadroxil	150	150		200	200	
cefalexin	150	150	100	200	200	
cefapirin	ND	NI	60	ND	NI	
cefazolin	ND	NI	50	ND	NI	
ceftiofur	150	150	100	200	NI	
penicillins						
amoxicillin	ND	NI	4	200	200	50
ampicillin	ND	NI	4	200	NI	50
cloxacillin	15	15	30	20	20	300
dicloxacillin	15	15	30	20	20	300
oxacillin	15	150	30	ND	NI	300
penicillin G	15	15	4	20	20	50
penicillin V	15	15		20	20	
macrolides						
azithromycin	ND	NI		20	20	
clarithromycin	ND	NI		20	20	
erythromycin−H_2O	150	150	40	20	20	200
tiamulin	15	15		20	20	
tilmicosin	15	15	50	20	20	50
sulfonamides						
dapsone	150	150	prohibited	200	200	prohibited
sulfachloropyridazine	15	15	100	20	20	100
sulfaclozine	15	15	100	200	200	100
sulfadiazine	15	15	100	20	20	100
sulfadimethoxine	15	15	100	20	20	100
sulfadimidine	15	15	100	20	20	100
sulfadoxine	15	15	100	20	20	100
sulfaguanidine	15	15	100	20	20	100
sulfamerazine	15	15	100	200	200	100
sulfameter	15	15	100	200	200	100
sulfamethizole	15	15	100	200	200	100
sulfamethoxazole	15	15	100	20	20	100
sulfamethoxypyridazine	15	15	100	20	20	100
sulfamonomethoxine	15	15	100	20	20	100
sulfamoxole	15	15	100	20	20	100

DOI: 10.1021/acs.jafc.5b00962
J. Agric. Food Chem. 2015, 63, 4493−4508

Table 2. continued

	milk samples (n = 12)			fish samples (n = 12)		
compound	SDL (ng mL^{-1})	LOI (ng mL^{-1})	MRL (ng mL^{-1})	SDL (μg kg^{-1})	LOI (μg kg^{-1})	MRL (μg kg^{-1})
sulfapyridine	15	15	100	20	20	100
sulfaquinoxaline	15	15	100	20	20	100
sulfathiazole	15	15	100	20	20	100
sulfisoxazole	15	15	100	20	20	100
quinoxalines						
carbadox	15	15		200	NI	
olaquindox	15	15		ND	NI	
amphenicols						
florfenicol	15	15	prohibited	200	200	1000
thiampenicol	15	NI	50	ND	NI	50
diaminopyrimidines						
baquiloprin	15	15	30	200	200	
trimethoprim	15	15	50	20	20	50
other antibiotics						
lincomycin	15	15	150	20	20	100
novobiocin	150	150	50	200	200	
rifaximin	15	15	60	20	20	
anthelmintics						
albendazole	15	15	100	20	20	
albendazole oxide	15	15	100	20	20	
albendazole sulfone	ND	NI	100	20	20	
dimetridazole	15	15	prohibited	20	20	prohibited
febantel	150	NI	10	ND	NI	
fenbendazole	15	15	10	20	20	
flubendazole	15	15		20	20	
levamisole	15	15	prohibited	20	20	
mebendazole	15	15	prohibited	20	20	
metronidazole	15	15	prohibited	20	20	prohibited
morantel	15	15	50	20	20	
oxfendazole	15	15	10	20	20	
piperazine	ND	NI		ND	NI	
ronidazole	15	15	prohibited	ND	NI	prohibited
ternidazole	15	15		20	20	
thiabendazole	15	15	100	20	20	
triclabendazole	15	15	prohibited	20	20	
coccidiostats						
arprinocid	15	15		20	20	
clopidol	15	15		20	NI	
decoquinate[b]	150	NI	20	200	200	20
diaveridine	15	15		20	20	
ethopabate	15	15		20	20	
halofuginone	15	15	prohibited	200	200	
imidocarb[c]	15	15	50/prohibited	20	NI	
lasalocid	15	15	prohibited	20	20	2
monensin[b]	15	15	2	ND	NI	5
narasin[b]	150	NI	1	200	200	5
nigericin	150	NI		200	NI	
robenidine[b]	150	150	5	ND	NI	5
salinomycin[b]	150	NI	2	200	NI	2
NSAIDs						
5-hydroxy-flunixin	15	15	40	20	20	
aceclofenac	15	15		200	200	

DOI: 10.1021/acs.jafc.5b00962
J. Agric. Food Chem. 2015, 63, 4493−4508

Table 2. continued

	milk samples (n = 12)			fish samples (n = 12)		
compound	SDL (ng mL^{-1})	LOI (ng mL^{-1})	MRL (ng mL^{-1})	SDL (μg kg^{-1})	LOI (μg kg^{-1})	MRL (μg kg^{-1})
diclofenac	150	150	0.1	20	20	
flunixin	15	15		20	20	
ketoprofen	15	15		20	20	
mefenamic acid	150	150		200	200	
meloxicam	15	15	15	20	20	
naproxen	15	15		20	20	
niflumic acid	15	15		20	20	
phenylbuntazone	15	15		20	20	
tolfenamic acid	15	NI	50	ND	NI	
vedaprofen	150	NI		ND	NI	
β-agonists						
cimaterol	15	15		20	20	
clenbuterol	15	15	0.05	20	20	
clenpenterol	15	15		20	20	
mabuterol	15	15		20	20	
ractopamine	15	15		20	20	
salbutamol	15	15		20	20	
terbutaline	15	15		20	20	
steroids						
betamethasone	15	150	0.3	200	200	
cortisol	15	15		200	200	
cortison	15	15		200	200	
dexamethazone	150	NI	0.3	ND	NI	
methylprednisolone	15	150	prohibited	ND	NI	
progesteron	150	150		200	200	
thyreostats						
methyl-thiouracil	ND	NI		20	200	
phenyl-thiouracil	150	150		20	20	
propyl-thiouracil	150	150		20	20	
pharmaceuticals						
ambroxol	15	15		20	20	
atenolol	15	15		20	20	
atorvastatin	15	15		20	20	
caffeine	15	15		20	20	
carbamazepine	15	15		20	20	
cimetidine	15	15		20	20	
gemfibrozil	15	15		200	200	
haloperidol	15	15		20	20	
indapamide	15	15		20	200	
metformin	15	15		200	200	
metoprolol	15	15		20	20	
paracetamol	15	15		20	20	
propranolol	15	15		20	20	
ranitidine	15	15		20	20	
simvastatin	15	15		200	200	
theophyline	15	15		200	200	
tramadol	15	15		20	20	
triamterene	15	15		20	20	
valsartan	15	15		20	20	
others						
bromhexine	15	15	prohibited	20	20	prohibited
chlorpromazine	15	15	prohibited	20	20	prohibited
colchicine	15	15	prohibited	20	20	prohibited
coumaphos	150	150		20	20	

DOI: 10.1021/acs.jafc.5b00962
J. Agric. Food Chem. 2015, 63, 4493−4508

Table 2. continued

	milk samples (n = 12)			fish samples (n = 12)		
compound	SDL (ng mL^{-1})	LOI (ng mL^{-1})	MRL (ng mL^{-1})	SDL (μg kg^{-1})	LOI (μg kg^{-1})	MRL (μg kg^{-1})
melamine	15	15	2500	ND	NI	

[a]ND, not detected; NI, not identified. [b]Maximum levels (MLs) according to Commission Regulation (EC) 124/2009. [c]Different MRLs in bovine/ovine milk.

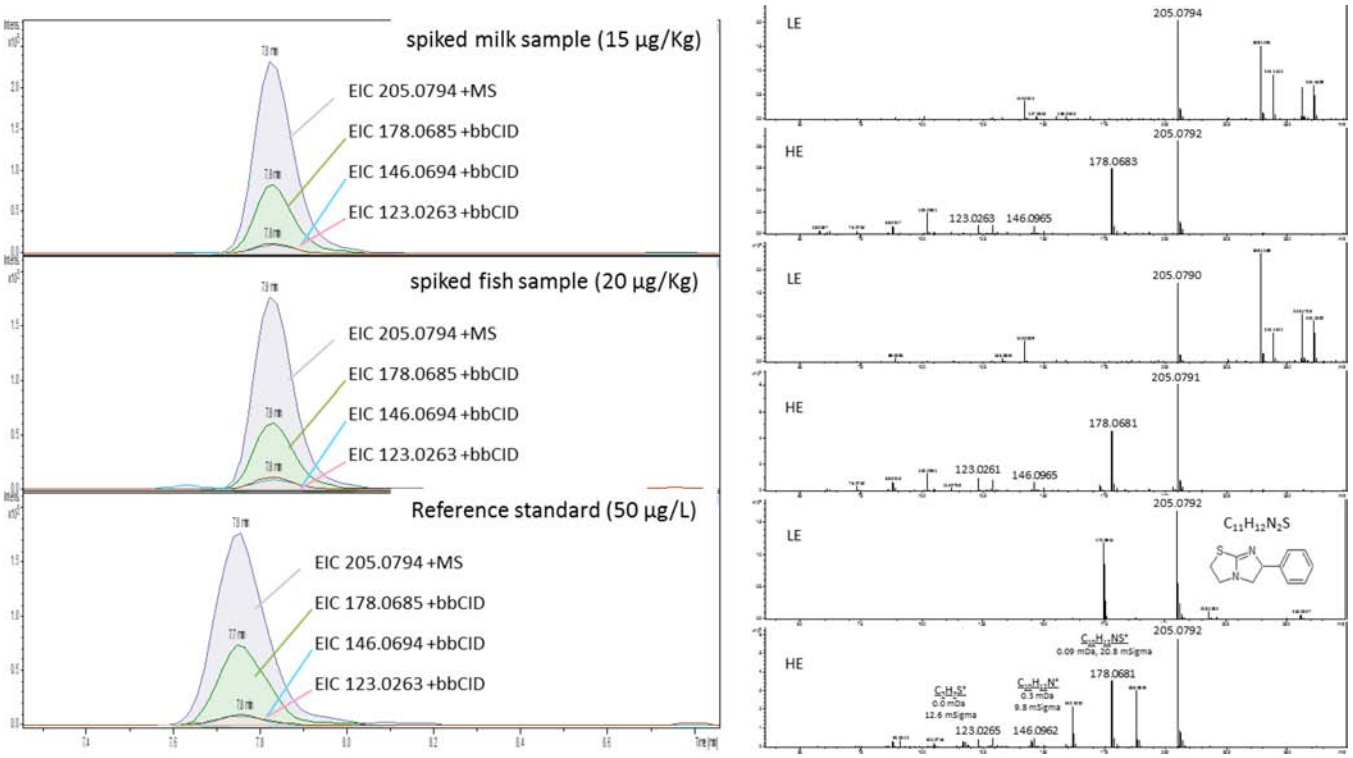

Figure 1. nw-XICs of levamisole corresponding to the protonated molecule at LE and to its fragment ions at HE for 50 ng mL^{-1} reference standard, 15 ng mL^{-1} spiked milk sample, and 20 ng g^{-1} spiked fish sample.

TCA solution 5% (1:3, v/v). Further cleanup with SPE (Oasis HLB cartridges) was performed to remove interfering proteins and provide clean and stable extracts. Extraction with ACN−TCA is a well-established sample preparation approach for food samples.[9,43] Because the screening method is intended to be used only as a qualitative method, there were no requirements with regard to recovery of the analytes.

The development of a generic SPE procedure can present some difficulties. If carefully designed, reversed phase SPE can recover most analytes from polar extraction solutions but may lead to losses of some (very polar) analytes.[4,21,23] Mixed-mode materials exhibiting both hydrophobic and ion-exchange properties have become a valuable alternative. One of the most widely used sorbents is a copolymer of divinylbenzene and vinylpyrrolidone, which has been commercialized under the trade name Oasis HLB by Waters. It has become the prime sorbent for multiresidue methods of veterinary drugs and pharmaceuticals due to its broad applicability spectra.[4,19,21,23,34]

The primary extracts had to be diluted in water to decrease the percent content of ACN (<10%) in the sample that will be loaded in the SPE. This is a practice that many researchers employ to avoid breakthrough of analytes during the SPE step due to a moderate amount of ACN in the extracting solution.[19,23,44] Proper adjustment of sample pH is necessary to avoid deprotonation of acidic compounds and protonation of basic compounds as well as to enhance extraction efficiency.[4] As analytes belong to different classes with different pK_a values, it is extremely difficult to establish a SPE protocol that is efficient for all of the target compounds. The extract pH was adjusted to 5.5 with ammonium hydroxide solution, according to the method of Kaufmann et al.,[25] who clearly state that this value constitutes a compromise and might not be the optimum for some very acidic and strongly basic analytes. Neutral pH values of the extract loaded in the SPE have been reported in cases when the extraction was held with water,[19,23] whereas a pH value of 4 was selected by Bohm et al.,[45] who used McIlvaine buffer as the extraction solvent.

Finally, the effectiveness of MeOH and ACN as elution solvents was evaluated. Elution with MeOH achieved higher responses of β-lactams and tetracyclines from the milk samples, because MeOH is a more polar solvent than ACN. On the contrary, less polar compounds, like some macrolides (tiamulin, tylosin) and some ionophore coccidiostats (semduramycin, narasin), presented better results when the elution was performed with ACN. However, MeOH was deemed to be the most suitable elution solvent because it revealed satisfactory results for the majority of the target analytes.

Qualitative Validation. The aim of a qualitative validation is to verify the presence of an analyte in a sample at a certain concentration level. As no quantitation is necessary, method recovery, accuracy, and precision were not examined.[36] Two different milk matrices (ovine and bovine milk) and two

DOI: 10.1021/acs.jafc.5b00962
J. Agric. Food Chem. 2015, 63, 4493−4508

different fish matrices (sea bream and sea bass) were tested at method validation at two concentration levels, 20 and 200 ng g^{-1} for fish samples and 15 and 150 ng mL^{-1} for milk samples. To consider the method fully validated for a given compound, the compound should be detected and identified according to the established criteria in all of the samples tested at a certain concentration level (6 of 6 for each matrix). Table 2 summarizes the SDLs and LOIs obtained for each analyte in milk and fish samples.

More compounds could be detected and identified in milk samples as compared to fish, although milk samples were prepared at lower concentration levels. This could be due to the higher preconcentration achieved with the sample preparation protocol used for milk, which succeeds in an increase in sensitivity. The more effective cleanup of milk samples, using SPE, could also lead to reduced matrix effects and enhanced sensitivity.

The majority of the compounds in both milk and fish samples were detected at the lowest concentration level (78% in milk samples and 60% in fish samples). What is of great significance is that, practically, the same number of compounds was also identified at this level: 74% in milk samples and 60% in fish samples, indicating the wide effectiveness and applicability of the proposed methodology. In relation to MRLs, as can be seen in Table 2, several of the target compounds are regulated in milk and fish tissue. On average, the method can be considered suitable for screening veterinary drug residues in milk and fish samples because both the SDLs and LOIs were below the established MRLs in most of the cases. More than 85% of the target analytes are identified in concentration lower than their MRLs in both matrices. Oxytetracycline, oxacillin, and tolfenamic acid could only be detected at regulatory levels in milk samples. For some compounds, the lowest concentrations tested were above their established MRLs, mainly in milk samples. However, according to our results, for some of these compounds, such as penicillin G, fenbendazole, oxfendazole, monensin, and clembuterol in milk samples and lasalocid in fish samples, their detection at the MRL levels would be quite probable considering their signal observed at the lowest concentration level examined.

Overall, for milk samples, the reliable identification using two accurate-mass ions was feasible for 74% of compounds at 15 ng mL^{-1} and for 87% at 150 ng mL^{-1}. For the remaining 13% of the compounds, LOIs could not be calculated with this method due to unsatisfactory fragmentation or insufficient sensitivity of fragment ions. Only 8% of the compounds could not be detected at 150 ng mL^{-1}. For fish samples, as mentioned above, 60% of the compounds were detected and identified at 20 ng g^{-1}. SDLs for the 29% of the compounds and LOIs for the 24% were calculated at 200 ng g^{-1}, whereas 11% of the compounds could not be detected and 16% could not be identified at the concentrations examined. The identification of the anthelmintic levamisole in a spiked milk sample (15 ng mL^{-1}) and in a spiked fish sample (20 ng g^{-1}) is shown in Figure 1.

Two compounds (tolfenamic acid and febantel) presented poor or no fragmentation as a result of the collision energy value applied, which was the result of a compromise for all compounds. For these compounds no fragments could be obtained and, therefore, the screening method was limited for detection, because no identification could be performed. Cefaclor, amoxicillin, and clarithromycin were not detected or identified in any of the spiked milk samples, whereas in fish, cefapirin, cefazolin, and febantel could be neither detected nor identified at the levels tested. This could be due to ineffective ionization of the compounds in the selected conditions, especially for cephalosporins. Another reason is that these compounds might not be stable under the extraction conditions assayed and that they are metabolized.[29,46] Matrix effects could also highly affect the determination.

Application to Milk and Fish Samples. To evaluate the applicability of the proposed method in routine analysis, five milk samples (four bovine and one ovine) and five fish samples (three sea bream and two sea bass) were tested. No positive results were found in any of these samples. The results reported by QTOF MS were confirmed by LC-MS/MS analysis in MRM mode, monitoring two transitions per compound, revealing the absence of any of the target analytes in the samples examined. The absence of false-positive results, even in this quite limited set of samples, is indicative of the adequate selectivity of the proposed methodology.

In conclusion, the qualitative validation of a wide-scope screening method including 143 veterinary drugs and pharmaceuticals has been carried out in two types of milk and two types of fish samples. Using this method, data including retention times, as well as accurate mass measurements for precursor and product ions, have been collected for all analytes. Detection, based mainly on the presence of the protonated molecule, as well as identification using a second accurate-mass fragment ion, was feasible in many cases at the lowest level tested (20 ng g^{-1} for fish samples and 15 ng mL^{-1} for milk samples). Finally, the applicability of the method was examined, and no false-positive results were revealed in a limited number of blank samples.

■ ASSOCIATED CONTENT

Supporting Information

Schematic of the screening methodology along with chromatograms and MS and MS/MS spectra of standard solutions; also an extended database of veterinary drugs and pharmaceuticals, including retention times, elemental formulas, and theoretical exact masses for precursor and fragment ions of the analytes. This material is available free of charge via the Internet at http://pubs.acs.org.

■ AUTHOR INFORMATION

Corresponding Author

*(N.S.T.) Phone: +30 210 7274317. Fax: +30 210 7274750. E-mail: ntho@chem.uoa.gr.

Funding

This research has been cofinanced by the European Union (European Social Fund − ESF) and Greek national funds through the Operational Program "Education and Lifelong Learning" of the National Strategic Reference Framework (NSRF) − Research Funding Program: Heracleitus II. Investing in knowledge society through the European Social Fund.

Notes

The authors declare no competing financial interest.

■ REFERENCES

(1) Van den Bogaard, A. E.; Stobberingh, E. E. Antibiotic usage in animals: impact on bacterial resistance and public health. *Drugs* **1999**, *58*, 589−607.

(2) Lathers, C. M. Clinical pharmacology of antimicrobial use in humans and animals. *J. Clin. Pharmacol.* **2002**, *42*, 587−600.

DOI: 10.1021/acs.jafc.5b00962
J. Agric. Food Chem. 2015, 63, 4493−4508

(3) Mompelat, S.; Le Bot, B.; Thomas, O. Occurrence and fate of pharmaceutical products and by-products, from resource to drinking water. *Environ. Int.* **2009**, *35*, 803−814.
(4) Buchberger, W. W. Current approaches to trace analysis of pharmaceuticals and personal care products in the environment. *J. Chromatogr., A* **2011**, *1218*, 603−618.
(5) Boix, C.; Ibáñez, M.; Sancho, J. V.; León, N.; Yusá, V.; Hernández, F. Qualitative screening of 116 veterinary drugs in feed by liquid chromatography−high resolution mass spectrometry: potential application to quantitative analysis. *Food Chem.* **2014**, *160*, 313−320.
(6) Codex Guidelines for the Establishment of a Regulatory Program for Control of Veterinary Drug Residues in Foods; Food and Agricultural Organization of the United Nations, Rome, Italy, 1993.
(7) Commission Regulation (EU) 37/2010, on pharmacologically active substances and their classification regarding maximum residue limits in foodstuffs of animal origin. *Off. J. Eur. Communities.* **2010**, *L 15*, 1−72.
(8) The Code of Federal Regulations, Title 21, Food and Drugs, PART 556, revised April 1, 2014 (http://www.accessdata.fda.gov/scripts/cdrh/cfdocs/cfCFR/CFRSearch.cfm?CFRPart=556&showFR=1) (accessed Jan 26, 2015).
(9) Gaugain-Juhel, M.; Delépine, B.; Gautier, S.; Fourmond, M. P.; Gaudin, V.; Hurtaud-Pessel, D.; Verdon, E.; Sanders, P. Validation of a liquid chromatography-tandem mass spectrometry screening method to monitor 58 antibiotics in milk: a qualitative approach. *Food Addit. Contam., Part A* **2009**, *26*, 1459−1471.
(10) Garrido Frenich, A.; Aguilera-Luiz, M. M.; Martínez Vidal, J. L.; Romero-González, R. Comparison of several extraction techniques for multiclass analysis of veterinary drugs in eggs using ultra-high pressure liquid chromatography−tandem mass spectrometry. *Anal. Chim. Acta* **2010**, *661*, 150−160.
(11) Schneider, M. J.; Lehotay, S. J.; Lightfield, A. R. Evaluation of a multi-class, multi-residue liquid chromatography-tandem mass spectrometry method for analysis of 120 veterinary drugs in bovine kidney. *Drug Test. Anal.* **2012**, *4*, 91−102.
(12) Zhan, J.; Yu, X.-J.; Zhong, Y.-Y.; Zhang, Z.-T.; Cui, X.-M.; Peng, J.-F.; Feng, R.; Liu, X.-T.; Zhu, Y. Generic and rapid determination of veterinary drug residues and other contaminants in raw milk by ultra performance liquid chromatography−tandem mass spectrometry. *J. Chromatogr., B: Anal. Technol. Biomed. Life Sci.* **2012**, *906*, 48−57.
(13) Biselli, S.; Schwalb, U.; Meyer, A.; Hartig, L. A multi-class, multi-analyte method for routine analysis of 84 veterinary drugs in chicken muscle using simple extraction and LC-MS/MS. *Food Addit. Contam., Part A* **2013**, *30*, 921−939.
(14) Zhan, J.; Zhong, Y.-Y.; Yu, X.-J.; Peng, J.-F.; Chen, S.; Yin, J.-Y.; Zhang, J.-J.; Zhu, Y. Multi-class method for determination of veterinary drug residues and other contaminants in infant formula by ultra performance liquid chromatography-tandem mass spectrometry. *Food Chem.* **2013**, *138*, 827−834.
(15) Kaufmann, A. The current role of high-resolution mass spectrometry in food analysis. *Anal. Bioanal. Chem.* **2012**, *403*, 1233−1249.
(16) Ibáñez, M.; Portolés, T.; Rúbies, A.; Muñoz, E.; Muñoz, G.; Pineda, L.; Serrahima, E.; Sancho, J. V.; Centrich, F.; Hernández, F. The power of hyphenated chromatography/time-of-flight mass spectrometry in public health laboratories. *J. Agric. Food Chem.* **2012**, *60*, 5311−5323.
(17) García-Reyes, J. F.; Hernando, M. D.; Molina-Díaz, A.; Fernández-Alba, A. R. Comprehensive screening of target, non-target and unknown pesticides in food by LC-TOF-MS. *TrAC, Trends Anal. Chem.* **2007**, *26*, 828−841.
(18) Krauss, M.; Singer, H.; Hollender, J. LC-high resolution MS in environmental analysis from target screening to the identification of unknowns. *Anal. Bioanal. Chem.* **2010**, *397*, 943−951.
(19) Stolker, A. A. M.; Rutgers, P.; Oosterink, E.; Lasaroms, J. J. P.; Peters, R. J. B.; van Rhijn, J. A.; Nielen, M. W. F. Comprehensive screening and quantification of veterinary drugs in milk using UPLC-ToF-MS. *Anal. Bioanal. Chem.* **2008**, *391*, 2309−2322.
(20) Villar-Pulido, M.; Gilbert-López, B.; García-Reyes, J. F.; Martos, N. R.; Molina-Díaz, A. Multiclass detection and quantitation of antibiotics and veterinary drugs in shrimps by fast liquid chromatography time-of-flight mass spectrometry. *Talanta* **2011**, *85*, 1419−1427.
(21) Kaufmann, A.; Butcher, P.; Maden, K.; Widmer, M. Quantitative multiresidue method for about 100 veterinary drugs in different meat matrices by sub 2-μm particulate high-performance liquid chromatography coupled to time of flight mass spectrometry. *J. Chromatogr., A* **2008**, *1194*, 66−79.
(22) Ortelli, D.; Cognard, E.; Jan, P.; Edder, P. Comprehensive fast multiresidue screening of 150 veterinary drugs in milk by ultra-performance liquid chromatography coupled to time of flight mass spectrometry. *J. Chromatogr., B: Anal. Technol. Biomed. Life Sci.* **2009**, *877*, 2363−2374.
(23) Peters, R. J. B.; Bolck, Y. J. C.; Rutgers, P.; Stolker, A. A. M.; Nielen, M. W. F. Multi-residue screening of veterinary drugs in egg, fish and meat using high-resolution liquid chromatography accurate mass time-of-flight mass spectrometry. *J. Chromatogr., A* **2009**, *1216*, 8206−8216.
(24) Lee, S. H.; Choi, D. W. Comparison between source-induced dissociation and collision-induced dissociation of ampicillin, chloramphenicol, ciprofloxacin and oxytetracycline via mass spectrometry. *Toxicol. Res.* **2013**, *29*, 107−114.
(25) Chernushevich, I. V.; Loboda, A. V.; Thomson, B. A. An introduction to quadrupole−time-of-flight mass spectrometry. *J. Mass Spectrom.* **2001**, *36*, 849−865.
(26) Dasenaki, M. E.; Bletsou, A. A.; Thomaidis, N. S. Antibacterials (Chapter 38). In *Handbook of Food Analysis*, 3rd ed.; Nollet, L. M. L., Toldra, F., Eds.; CRC Press: Boca Raton, FL, USA, 2014; ISBN 13:978-1466556546.
(27) Nácher-Mestre, J.; Ibáñez, M.; Serrano, R.; Pérez-Sánchez, J.; Hernández, F. Qualitative screening of undesirable compounds from feeds to fish by liquid chromatography coupled to mass spectrometry. *J. Agric. Food Chem.* **2013**, *61*, 2077−2087.
(28) Turnipseed, S. B.; Storey, J. M.; Clark, S. B.; Miller, K. E. Analysis of veterinary drugs and metabolites in milk using quadrupole time-of-flight liquid chromatography-mass spectrometry. *J. Agric. Food Chem.* **2011**, *59*, 7569−7581.
(29) Sismotto, M.; Paschoal, J. A. R.; Teles, J. A.; de Rezende, R. A. E.; Reyes, F. G. R. A simple liquid chromatography coupled to quadrupole time of flight mass spectrometry method for macrolide determination in tilapia fillets. *J. Food Compos. Anal.* **2014**, *34*, 153−162.
(30) Paschoal, J. A. R.; Reyes, F. G. R.; Rath, S. Quantitation and identity confirmation of residues of quinolones in tilapia fillets by LC-ESI-MS-MS QToF. *Anal. Bioanal. Chem.* **2009**, *394*, 2213−2221.
(31) Freitas, S. K. B.; Paim, A. P. S.; Silva, P. T. S. Development of a lc-it-tof ms procedure to quantify veterinary drug residues in milk employing a quechers approach. *Food Anal. Methods* **2014**, *7*, 39−46.
(32) Turnipseed, S. B.; Clark, S. B.; Storey, J. M.; Carr, J. R. Analysis of veterinary drug residues in frog legs and other aquacultured species using liquid chromatography quadrupole time-of-flight mass spectrometry. *J. Agric. Food Chem.* **2012**, *60*, 4430−4439.
(33) Aguilera-Luiz, M. M.; Romero-González, R.; Plaza-Bolaños, P.; Martínez Vidal, J. L.; Garrido Frenich, A. Wide-scope analysis of veterinary drug and pesticide residues in animal feed by liquid chromatography coupled to quadrupole-time-of-flight mass spectrometry. *Anal. Bioanal. Chem.* **2013**, *405*, 6543−6553.
(34) Deng, X.-J.; Yang, H.-Q.; Li, J.-Z.; Song, Y.; Guo, D.-H.; Luo, Y.; Du, X.-N.; Bo, T. Multiclass residues screening of 105 veterinary drugs in meat, milk, and egg using ultra high performance liquid chromatography tandem quadrupole time-of-flight mass spectrometry. *J. Liq. Chromatogr. Relat. Technol.* **2011**, *34*, 2286−2303.
(35) Turnipseed, S. B.; Lohne, J. J.; Storey, J. M.; Andersen, W. C.; Young, S. L.; Carr, J. R.; Madson, M. R. Challenges in implementing a screening method for veterinary drugs in milk using liquid chromatography quadrupole time-of-flight mass spectrometry. *J. Agric. Food Chem.* **2014**, *62*, 3660−3674.

DOI: 10.1021/acs.jafc.5b00962
J. Agric. Food Chem. 2015, 63, 4493−4508

(36) Diaz, R.; Ibáñez, M.; Sancho, J. V.; Hernández, F. Qualitative validation of a liquid chromatography−quadrupole-time of flight mass spectrometry screening method for organic pollutants in waters. *J. Chromatogr., A* **2013**, *1276*, 47−57.
(37) SANCO/12571/2013. Method Validation and Quality Control Procedures for Pesticide Residue Analysis in Food and Feed, Implemented by 01/01/2014 (http://www.eurl-pesticides.eu/docs/public/tmplt_article.asp?CntID=727) (accessed Jan 27, 2015).
(38) Commission Decision 2002/657/EC, implementing Council Directive 96/23/EC concerning the performance of analytical methods and the interpretation of results. *Off. J. Eur. Communities* **2002**, *L 221*, 8−36.
(39) Geis-Asteggiante, L.; Nuñez, A.; Lehotay, S. J.; Lightfield, A. R. Structural characterization of product ions by electrospray ionization and quadrupole time-of-flight mass spectrometry to support regulatory analysis of veterinary drug residues in foods. *Rapid Commun. Mass Spectrom.* **2014**, *28*, 1061−1081.
(40) Gomez Perez, M. L.; Romero-Gonzalez, R.; Plaza-Bolanos, P.; Genin, E.; Vidal, J. L.; Frenich, A. G. Wide-scope analysis of pesticide and veterinary drug residues in meat matrices by high resolution MS: detection and identification using Exactive-Orbitrap. *J. Mass Spectrom.* **2014**, *49*, 27−36.
(41) Grunwald, L.; Petz, M. Food processing effects on residues: penicillins in milk and yoghurt. *Anal. Chim. Acta* **2003**, *483*, 73−79.
(42) Kinsella, B.; Lehotay, S. J.; Mastovska, K.; Lightfield, A. R.; Furey, A.; Danahe, M. New method for the analysis of flukicide and other anthelmintic residues in bovine milk and liver using liquid chromatography−tandem mass spectrometry. *Anal. Chim. Acta* **2009**, *637*, 196−207.
(43) Bousova, K.; Senyuva, H.; Mittendorf, K. Quantitative multi-residue method for determination antibiotics in chicken meat using turbulent flow chromatography coupled to liquid chromatography−tandem mass spectrometry. *J. Chromatogr., A* **2013**, *1274*, 19−27.
(44) Li, H.; Kijak, P. J.; Turnipseed, S. B.; Cui, W. Analysis of veterinary drug residues in shrimp: A multi-class method by liquid chromatography−quadrupole ion trap mass spectrometry. *J. Chromatogr., B: Anal. Technol. Biomed. Life Sci.* **2006**, *837*, 22−38.
(45) Bohm, D. A.; Stachel, C. S.; Gowik, P. Multi-method for the determination of antibiotics of different substance groups in milk and validation in accordance with Commission Decision 2002/657/EC. *J. Chromatogr., A* **2009**, *1216*, 8217−8223.
(46) Junza, A.; Montané, A.; Barbosa, J.; Minguillón, C.; Barrón, D. High resolution mass spectrometry in the identification of transformation products and metabolites from β-lactam antibiotics in thermally treated milk. *J. Chromatogr., A* **2014**, *1368*, 89−99.

DOI: 10.1021/acs.jafc.5b00962
J. Agric. Food Chem. 2015, 63, 4493−4508

Table 1. Three Monovarietal Olive Oils from Cultivars Arbequina (Spain), Coratina (Italy), and Koroneiki (Greece) Characterized by Fatty Acids (Percent), 4-Demethylsterols (Milligrams per Kilogram), Diols (Milligrams per Kilogram), and Aliphatic Alcohols (Milligrams per Kilogram)[a]

compound	Arbequina	Coratina	Koroneiki
C16:0	12.54 ± 3.76	9.13 ± 0.28	11.21 ± 0.57
C16:1	1.36 ± 0.30	0.44 ± 0.06	0.95 ± 0.07
C17:0	0.12 ± 0.01	0.06 ± 0.01	0.25 ± 0.1
C17:1n-8	0.20 ± 0.04	0.11 ± 0.02	0.15 ± 0.05
C18:0	1.40 ± 0.36	2.36 ± 0.14	2.59 ± 0.24
C18:1	72.12 ± 3.44	80.8 ± 1.00	77.75 ± 1.76
C18:2n-6	11.38 ± 0.17	6.07 ± 0.66	5.63 ± 1.10
C18:3n-3	0.69 ± 0.11	0.68 ± 0.02	0.55 ± 0.13
C20:0	0.40 ± 0.07	0.37 ± 0.01	0.5 ± 0.09
C20:1n-9	0.35 ± 0.05	0.42 ± 0.02	0.55 ± 0.07
C22:0	0.12 ± 0.00	0.12 ± 0.00	0.27 ± 0.10
campesterol	61.01 ± 8.89	46.76 ± 0.68	43.25 ± 0.68
stigmasterol	14.85 ± 6.94	10.99 ± 0.96	6.95 ± 0.79
β-sitosterol	1269.10 ± 195.73	1157.60 ± 5.86	831.1 ± 6.11
Δ^5-avenasterol	289.02 ± 60.25	98.20 ± 5.27	187.1 ± 8.74
cholesterol	2.17 ± 0.54	3.60 ± 0.80	3.59 ± 0.16
24-methylenecholesterol	6.84 ± 0.73	4.05 ± 1.20	4.71 ± 0.22
campestanol	7.24 ± 0.28	5.89 ± 0.42	5.49 ± 1.23
Δ^7-campesterol	1.99 ± 0.35	4.73 ± 0.57	1.10 ± 0.05
chlerosterol	1.99 ± 0.19	14.06 ± 1.04	12.77 ± 0.94
sitostanol	18.29 ± 0.83	18.87 ± 5.25	8.63 ± 1.89
$\Delta^{5,24}$-stigmastadienol	12.13 ± 0.19	6.79 ± 1.26	6.39 ± 0.48
Δ^7-stigmastenol	2.72 ± 0.23	3.18 ± 0.32	2.91 ± 0.29
Δ^7-avenasterol	6.88 ± 0.47	4.26 ± 0.55	4.37 ± 0.31
erythrodiol + uvaol	17.92 ± 4.78	26.80 ± 5.40	27.67 ± 3.29
docosanol	11.36 ± 2.23	23.52 ± 3.05	13.16 ± 3.98
tetracosanol	17.79 ± 1.85	33.17 ± 4.70	35.69 ± 6.23
hexacosanol	40.60 ± 4.19	52.52 ± 9.54	73.48 ± 9.96
octacosanol	30.67 ± 1.98	26.77 ± 4.55	26.71 ± 5.28

[a]C16:1 is the sum of C16:1n-9 and C16:1n-7, and C18:1 is the sum of C18:1n-9 and C18:1n-7.

esters, and fatty acid ethyl esters by capillary gas chromatography.[6] This wide range of possible standard methods is sometimes perceived as a disadvantage by newcomers to the olive oil sector instead of an advantage when selecting a method for their own needs. As there are several standard methods to solve the same problem (i.e., to detect the same adulterant or to identify and quantify the same chemical compounds), the analysts often have difficulties establishing which standard method is the most suitable for their purposes. The extensive collection of standard methods is partially due to the fact that the regulatory bodies add the new methods to the list of the standard methods, keeping the previous ones. This additive—instead of substitutive—policy seems to imply that not all of the standard methods satisfy completely the requested expectations. Consequently, a considerable investment in optimizing current methods and developing new ones is important to keep pace with changing technologies and sophisticated adulterations. These new methods should be easy to implement and robust, have an adequate precision, be amenable to being validated, and be capable of detecting any fraud and malpractices in olive oil production.

In addition to the difficulties of analysts in choosing the most adequate standard method, they may have problems in applying the methods due to lack of experience. For example, they may have problems in the identification of the chemical compounds, due to possible shifts in the retention time, small changes in column composition, temperature program, or low resolution of peaks. Thus, in the particular case of analysts that work with olive oil for the first time, they often need to discuss their results with other analysts, expert in the field, to identify any problem and to confirm that they are working properly.

Not only is the expertise of the analyst a critical issue but there are also other factors such as the quality of equipment, reagents, environment (e.g., temperature, humidity, air pollution), among others, that can make the results difficult to reproduce. Validated analytical methods are thus essential for the quality performance of analytical laboratories. Today, analysts must be aware of the important role of quality assurance of their laboratories. The results of the laboratories are directly related to the use of validated and accredited methods. With regard to laboratory accreditation, the complexity of the standard methods is again a problem. A better justification for the existing methods through a detailed description of their application and the avoidance of any overlap between them is desirable to facilitate the accreditation of laboratories.

Understanding all of the drawbacks associated with the considerable complexity of standard methods, the olive oil sector is demanding the development of a rapid and universal method that can be used for all of the determinations required to confirm olive oil authenticity and/or quality. Despite the difficulties implementing the current standard methods, certain improvements have been achieved. For example, the compilation of information about the validation of the standard

DOI: 10.1021/jf5062265
J. Agric. Food Chem. 2015, 63, 4509−4526

Table 2. Utility of Some Chemical Parameters in Olive Oil Authenticity and Approximate Percentage of Detection of Adulterant Oils[a]

chemical parameter	related regulations	informing variables	adulterant oil	approx % detection
sterols	COI/T.20/Doc. No. 30[58]	brassicasterol; apparent β-sitosterol	rapeseed oil	1.0−1.5
		apparent β-sitosterol; campesterol	mustard seed oil	1.0−1.5
sterols + ΔECN42	COI/T.20/Doc. No. 30[58]	apparent β-sitosterol; ΔECN42; campesterol; stigmasterol	corn oil	1.0−1.5
	COI/T.20/Doc. No. 20[16]	apparent β-sitosterol; ΔECN42	safflower oil; sesame oil; soybean oil	1.0−4.0
		campesterol; stigmasterol; ΔECN42	cotton oil	3.5−5.0
		apparent β-sitosterol; ΔECN42; Δ^7-stigmastenol	sunflower oil	0.5−2.5
FAMEs + sterols	COI/T.20/Doc. No. 24[19]	behenic acid; stigmasterol	peanut oil	3.0−5.0
	COI/T.20/Doc. No. 30[58]	myristic acid;	palm oil	3.5−10.0
		stigmasterol	palm kernel oil	
FAMEs + TAGs	COI/T.20/Doc. No. 25[17]	results from applying GM	hazelnut oil[115]	>8%

[a]GM, global method;[17] FAMEs, fatty acid methyl esters.

methods[7] has allowed a better monitoring of the reproducibility and robustness of the methods. Additionally, the optimization of some standard methods has been carried out by improving columns, using different solvents, changing chromatographic conditions, and reducing the pretreatment of samples.

The improvement of the standard methods requires time, and the alternative to the current situation could be the design of a global procedure that allows the detection of different adulterations. Thus, the strategy of some current research studies is to combine standard methods and emerging technologies—including fingerprinting approaches—into a single comprehensive analytical strategy. The analytical techniques that have been suggested to achieve this aim are spectroscopic techniques—near-infrared (NIR) spectroscopy,[8] Fourier transform mid-infrared spectroscopy (FTIR),[9] FT-Raman spectroscopy,[10] fluorescence spectroscopy[11] nuclear magnetic resonance (NMR) spectroscopy[13]—spectrometric techniques—isotope ratio mass spectrometry[12]—and "omic" techniques.[14] In these areas, the fraudsters do not have much information on how to avoid being detected, but analysts may have problems in interpreting the information with plausible chemical explanations. These techniques can be helpful if they are combined with multivariate statistical techniques. Even then, the conclusions obtained from the analysis ideally should be supported by chemical or biochemical explanations. These new techniques, which provide a wide range of information about different chemical compounds in only one analysis, need to be validated with blind samples prior to being proposed as standards.

In this paper the standard methods have been analyzed from a point of view of the analysts and the potential problems that they may have when applying them. The practical aspects and the possible alternatives (nonstandard methods) for each determination have been discussed as well. A critical review of the chemical compounds analyzed by these methods and the concentration range of these compounds in olive oil is presented, together with the utility of these determinations in the characterization and authentication of olive oil.

METHODS FOR THE CONTROL OF OLIVE OIL PURITY AND AUTHENTICITY

The chemical compounds used for determining olive oil authenticity are numerous, and to explain their analytical methods, the compounds have been clustered into the sets of major and minor compounds. The group of major compounds is primarily made up of triacylglycerols (TAGs) or glycerol esters of fatty acids (FAs); fatty acids account for 94−95% of the total weight of TAGs. Table 2 shows some examples of applications of these major and minor compounds in detecting adulterations.

The broad and heterogeneous set of minor compounds includes several series of chemical compounds with a lipid structure (e.g., waxes), compounds that are not related to lipids from a chemical structure viewpoint (e.g., pigments, volatiles), and compounds that have the common characteristic of being obtained from unsaponifiable matter. The compounds that are present in unsaponifiable matter, which rarely represent >2% by weight of total olive oil, are regarded as the olive oil fingerprint. Thus, this fingerprint is very useful in authentication and geographical identification of olive oil, among other applications.

Olive Oil Major Compounds. *Fatty Acid Methyl Esters and Trans Fatty Acids.* Fatty acids (FAs) are the main components of olive oil. They are not generally present, however, as free fatty acids; when they are, they occur only in small amounts. Fatty acids are usually forming part of glycerides (mono-, di-, and triacylglycerols) and phospholipids through ester bonds. FAs present in olive oil are linear chains of 16−24 carbon atoms. FAs, which were some of the very early compounds to be analyzed by gas chromatography (GC), were of maximum importance in the detection of adulterants until the end of the 1960s. At that time seed oils with a modified fatty acid composition similar to that of olive oil appeared. The analytical performance, however, was improved and made the method suitable to determine *trans* isomers of fatty acids (TFAs) because TFAs appears as a result of certain manipulations, for instance, isomerization reactions that occur during the heating processes of olive oil.[15] The interest in determining the TFAs is explained by the fact that their determination allows the detection of refining oils in VOO.

DOI: 10.1021/jf5062265
J. Agric. Food Chem. 2015, 63, 4509−4526

Table 3. Most Common Methods for Quantifying Fatty Acids and Derived Acyl Lipids

compound	technique	sample pretreatment	reference	method details
fatty acids; *trans* fatty acids	GC-FID[a]	purification with silica gel extraction cartridge; cold methylation with KOH	COI/T.20/Doc No. 17.[113]	column: capillary 50−100 m × 0.25−0.32 mm ×0.1−0.3 μm stationary phase: cross-linked cyanopropylsilicone carrier gas: hydrogen or helium temperature program: 165 °C (15 min) to 200 °C at 5 °C/min injection mode: split
triacyglycerols	HPLC-RI[b]	0.12 g of oil in 0.5 mL of hexane is charged into column (SPE[c] cartridge: 1 g of Si) and solution pulled through then, eluted with 10 mL of hexane/diethyl ether (87:13 v/v); the purified oil is dissolved in acetone at 5%	COI/T.20/Doc No. 20.[16]	oven temperature: 25 °C mobile phase: acetone/acetonitrile (1:1 v/v) or propionitrile (flow rate = 0.6−1.0 mL/min) column: RP-18 (25 cm × 4 mm i.d.) (5 μm) with 22−23% carbon in the form of octadecylsilane detector: RI
	HPLC-RI	purification by SPE (IUPAC method 2507);[29] the purified oil is dissolved in acetone at (5%)	COI/T.20/Doc No. 25.[17]	oven temperature: 20 °C mobile phase: propionitrile (flow rate = 0.6 mL/min) column: RP-18 (25 cm × 4.5 mm i.d.) (4 μm) detector: RI
triacylglycerols; diacylglycerols	GC-FID	requires silylation; gives information clustered into their carbon numbers	COI/T.20/Doc No. 32.[39]	capillary column: 3−7 m × 0.25−0.32 mm ×0.10−0.15 μm; C58 and C60 loss by thermal degradation can be avoided by short column, 5 m should be enough phase: SE52, SE54 (5% diphenyl-dimethyl polyxilosane) carrier gas: hydrogen or helium temperature program: 80 °C, 1 min; to 220 °C at 20 °C/min to 340 °C, 10 min, at 5 °C/min injection mode: on-column
2-glyceryl monopalmitate (%)	GC-FID	GLC or SPE separation after hydrolytic reaction with pancreatic lipase; silylation should be applied	COI/T.20/Doc No. 23.[26]	capillary column: 12 m × 0.32 mm ×0.10−0.30 μm phase: methylpolisiloxane or 5% phenyl-methyl-polysiloxane carrier gas: hydrogen or helium temperature program: e.g., 60 °C, 1 min to 180 °C at 15 °C/min, to 340 °C, 13 min, at 5 °C/min injection mode: on-column
waxes	GC-FID	fractionation by LC on hydrated silica gel column (15 g of silica)	COI/T.20/Doc No. 18.[5]	capillary column: 8−15 m × 0.25−0.32 mm × 0.1 −0.3 μm phase: 5% phenyl-methyl-polysiloxane, liquid phase SE52, SE54 carrier gas: hydrogen or helium temperature program: e.g., 80 °C, 1 min, to 240 °C at 20 °C/min to 325 °C, 6 min, at 5 °C/min to 340 °C, 10 min, at 20 °C/min injection mode: on-column

[a]Gas chromatograph−flame ionization detector. [b]High-performance liquid chromatography−refractive index. [c]Solid phase extraction.

J. Agric. Food Chem. 2015, 63, 4509−4526

DOI: 10.1021/jf5062265

Furthermore, GC analysis of FAs is also carried out as a tool for the calculation of the theoretical composition of TAGs with the final objective of determining the value of the theoretical ECN42 (equivalent carbon number)[16] and for the detection of the presence of hazelnut oil by means of the global method.[17]

The first step of FA analysis is derivatization by forming methyl esters (FAMEs), because they are more volatile and nonpolar than free fatty acids, and this makes them easier to elute through chromatographic columns. Among the methods for preparing FAMEs[18] the transesterification with methanolic solution of potassium hydroxide at room temperature[19,20] is the most commonly used. However, another method is suggested for VOOs with acidity >3.3% and crude olive pomace, which is based on the esterification and transesterification with sodium methylate in methanol in acid conditions at high temperature.[18] Perhaps the first method can be also suggested for the determination of *trans* fatty acid and the determination of ECN42 if samples are always first purified through a silica gel solid-phase extraction cartridge, and the sample spiked with hexane—olive oil/hexane (1:4); for example, 0.15 g of olive oil in 0.6 mL of hexane—is pulled down with hexane/diethyl ether (87:13) as in other standards.[18]

GC analysis can be undertaken with chromatographic columns with diverse characteristics. For instance, phases with the highest polarity allow excellent separations of polyunsaturated FAs. Phases with lower polarity are used for the separation of saturated and monoenoic compounds with the same chain length, although it may produce peaks that interfere in the determination of *trans* isomers of linolenic acid. An HP-88 capillary column, coated with 88% cyanopropyl aryl siloxane (100 m × 0.2 mm i.d. × 0.2 μm film thickness), or a Varian Chrompack CP-Sil 88 column, coated with cyanopropyl polysiloxane (100 m × 0.25 mm i.d. × 0.2 μm film thickness), can provide an accurate quantification of TFAs previously derivatized as methylesters. These columns are too long for FAs and can be substituted by others of 50 m × 0.20−0.32 mm i.d. 0.1 × 0.2 μm film thickness with a cross-linked stationary phase of cyanopropylsiloxane allowing also the *trans* fatty acid determination (Table 3). However, columns shorter than 50 m allow determining FAs but with loss of *trans* fatty acids.

The stationary phase polymerizes in aged columns, and the variation of retention times for the esters of FAs is observed. Better peak resolution is obtained if the carrier gas is hydrogen instead of helium. Furthermore, no silver ion prefractionation of TFA (by TLC, SPE, or HPLC) is required prior to the GC analysis.[21]

The use of WCOT columns of fused silica introduced remarkable improvements in separations with higher resolution, higher precision in analysis in both quality and quantity, higher sensitivity, a shorter analysis time, reduction in the preparation of analysis procedures, etc. Most phases are now chemically bonded to tube walls, which decreases loss in the column and, in turn, increases duration and temperature resistance and improves the resolution.

The determination of *trans* fatty acids can present a problem of overestimation. Small quantities of *trans* oleic acid could be formed when the sample is introduced into the gas chromatographic injector. This problem is more pronounced when automatic samplers with packing materials are used. To minimize this problem, it is necessary to replace the injector insert by a clean insert, deactivate the inset, lower the injector temperature from 250 to 30−50 °C, or remove the packing materials if the injection is manual.

Alternative methods based on spectroscopic techniques have been developed to analyze FAs and *trans* fatty acids, although they cannot determine individual FAs and TFAs as the GC method does. Thus, ^{1}H NMR methodology shows a good performance for FA quantification despite the fact that results for individual saturated compounds often deviate from GC results because of the sensitivity of ^{1}H NMR (400 MHz) integration; total amounts of saturates are, however, accurately determined.[22] Quantification of the sum of saturated fatty acids (SFAs), the monounsaturated oleic acid (MUFA), and the polyunsaturated linoleic and linolenic acids (PUFAs) can be obtained by means of mathematical equations using appropriate signal intensities as variables.[22] Additionally, linolenic acid can be quantified from the signal of the methyl protons of the linolenyl chain at δ 0.96.

TFAs can also be determined by IR spectroscopy, which is a rapid tool for detecting isomers.[23] The intensities of Raman spectroscopy bands near 1656 and 1670 cm^{-1} have also been related to the content of *cis* and *trans* isomers.[24]

Triacyglycerols (TAGs). TAGs consist of a glycerol moiety with each hydroxyl group esterified to a fatty acid. Each individual TAG species has three characteristics: (i) the total carbon number (CN), which is the sum of the alkyl chain lengths of each of the three FAs; (ii) the degree of unsaturation in each FA; and (iii) the position and configuration of the double bonds in each FA.[25] Twenty TAGs have been identified and independently quantified in olive oil, but only five are present in significant proportions.[18]

One of the main aims of TAG analysis is identifying TAGs that are biosynthesized and those that are synthesized by means of FFA esterification with glycerol. The analytical approach is based on the use of pancreatic lipase, an enzyme that has the ability to hydrolyze the 1- and 3-positions of natural TAGs, thereby producing 2-monoacylglycerols. The initial determination of palmitic and stearic acids at the 2-position has been currently substituted by determination of the content of 2-glyceryl monopalmitate.[26,27]

Thus, the possible combinations of FA molecules and their positions on the glycerol backbone of TAGs make the analysis of the TAG composition a very challenging task with either gas−liquid chromatography (GLC) or reversed phase liquid chromatography (RP-HPLC). Table 3 summarizes the RP-HPLC conditions (column dimension, stationary and mobile phases, kind of detector, and flow rate) and GLC conditions (columns, detectors, and chromatographic conditions) used for the determination of olive oil TAG profiles.

TAG separation is based on the number of carbon atoms and their unsaturation when RP-HPLC is used because of the good resolution of the RP-18 column. In the case of the presence of oxidized compounds, which interfere in the trilinolein (LLL) determination, samples should be purified by means of silica gel. Thus, in the case of olive pomace oil, the EC recommends using the SEP-PAK silica cartridge (Waters).[28] The IOC recommends making the purification by SPE according to IUPAC 2.507.[29]

This procedure, however, implies checking FA compositions in the oil after its purification in a long and tedious process during which mistakes can occur. This test is recommended by the EC in the case of the olive pomace oil and the IOC recommends this test in the determination of the 2-glyceryl monopalmitate.[26]

The purified oil is resolved in acetone, but sometimes the impurities of acetone can produce disturbances in the baseline

DOI: 10.1021/jf5062265
J. Agric. Food Chem. 2015, 63, 4509−4526

of the chromatogram (region 12−15 min); if this happens, a good solution is using another source of acetone or a mixture of propionitrile/acetone (25:75 v/v).

The RP-18 column resolution depends on the particle diameter. Experience shows that columns with 3 μm have no loss of resolution while saving time and solvents. Another empirical aspect concerns samples of raw olive pomace oils, which should be resolved in acetone and then filtered, with 0.2 μm pore size, to remove precipitates that would shorten the column life.

With regard to the mobile phase, critical peaks are effectively separated with acetone/acetonitrile in isocratic elution, although with this phase, saturated long-chain TAGs are not sufficiently resolved. As a consequence, some researchers[30,31] carried out experiments on isocratic elution with propionitrile as previously investigated.[32] Although propionitrile (HPLC grade) is expensive and highly toxic, it reduces dramatically the baseline drift when compared with the methods based on an acetone/acetonitrile mixture. The result is a better separation of TAGs clustered as ECN42, and it is used for the detection of the admixture of hazelnut oil to olive oil.[33]

The refractive index (RI) is the most appropriate detector, despite its drawbacks of low sensitivity and different responses toward saturated and highly unsaturated TAGs and the numerous external variables that affect baseline stability.[34] In comparison to other detectors, the UV detector, which has not been very widely used because it presents problems with isomerization and conjugation of double bonds, has good sensitivity and allows the use of elution gradients that improve the resolution.

The alternative of using GLC (Table 3) is scarcely applied today despite the fact that it also offers attractive possibilities as an efficient separation method, good quantitative recovery and reproducibility, an adequate time for analysis, and the availability of a flame ionization detector (FID), a simple but universal linear response detector. However, the GLC technique is not free of problems such as, for example, the injection system and the column deterioration. Selectivity in GLC depends on the length and chemical nature of the column stationary phase. For example, columns with phenyl-methyl-silicone phase are capable of reaching temperatures of about 360−370 °C for a long time and of separating TAGs by carbon atom number; unsaturated positional isomers cannot be separated by this phase unless sample derivatization followed by a reduction had previously been done.[18]

Another alternative is the analysis by HPLC-MS because MS can identify partially resolved HPLC peaks,[35] giving much more information on the position of the three fatty acid molecules at TAGs. Although few ionization techniques can be coupled to HPLC, the identification of positional isomers[36] can be carried out by atmospheric pressure chemical ionization (APCI) coupled to HPLC, whereas the identification of individual acyls can be done without electrospray ionization (ESI) without reference materials. A rapid and simple sample preparation—no analyte purification, chemical modification, or derivatization is required[37]—has increased the interest in applying matrix-assisted laser desorption ionization time-of-flight mass spectrometry (MALDI-TOF-MS), LDI-TOF-MS being proposed for detecting the presence of sunflower oils in olive oil.[38]

Olive Oil Minor Compounds. As already mentioned, the set of minor components, which are used for the determination of purity and authenticity of olive oil designations, consists of compounds that derive from TAGs and other liposoluble compounds and the compounds that derive from the unsaponifiable matter.

Diacylglycerols (DAGs) and Monoacylglycerols. DAGs, which are present in a range of 1−3% in olive oils, are found as 1,2- and 1,3-isomers, 1,2-isomers being attributed to the incomplete biosynthesis of TAGs (Kennedy pathway), whereas 1,3-isomers are attributed to enzymatic or chemical hydrolysis of TAGs.

The official method[39] allows the determination of DAGs and TAGs together. TAGs are clustered on the basis of their carbon atom number, whereas in the case of DAGs the peaks are resolved according to their carbon atom number and their structure, the 1,2-isomers having lower retention time than 1,3-isomers. The method does not require particular experience of the analyst. Thus, 1 mL of the internal standard (dinonadecanoine 0.1% w/v in methyl *tert*-butyl ether) is added to a sample of 100 mg. Later, a dried aliquot of 20−30 μL is silylated with 200 μL of the silylation reagent, consisting of a 9:3:1 (v/v/v) mixture of anhydre pyridine/hexamethyl disilazane/trimethylchlorosilane. After a complete silylation, 2 mL of *n*-heptane is added, and 0.5−1.0 μL is injected into a GC instrument equipped with a capillary column of 3−7 m length × 0.25−0.32 mm i.d. (coated with SE52 or SE54 stationary phase). Experience has taught that it is advisible to purify the sample by column chromatography or SPE prior to addition of the internal standard that could also be 1,3-dipalmitoyl *rac*-glycerol. The silylation process can be critical. The solution of silylation reagent should be freshly made. It is not easy to detect the end of the reaction; it takes about 20 min. If a slight opalescence is observed after the silylation, it does not mean any anomaly. However, the formation of a white floc or the appearance of a pink color is indicative of the presence of moisture. A rapid warming applied to the bottom of the conical flask to the GC detector can eliminate the moisture. If the floc is not eliminated, the silylation reagent is deteriorated and the test must be repeated.

The method for the determination of the percentage of 2-glyceryl monopalmitate (Table 3) has some drawbacks such as the fact that it is a lengthy and tedious method (e.g., when sample acidity is >3%, it has to be previously neutralized). The neutralization of the oil is necessary because the activity of the pancreatic lipase depends on the pH, which should be adjusted to 8.3. Furthermore, the separation between phases after lipase pancreatic digestion is not automatic; it should be taken into account that lipase pancreatic is not stable and may lose activity easily. The thick interface between phases (diethyl ether and aqueous phase), after the centrifugation step, makes it difficult to collect an aliquot of the organic phase for preparing the silanized derivatives. Moreover, on-column injection shows well-known problems such as a large broad solvent front, low repeatability, and tailing peaks.

Waxes. The waxes, which are usually referred to wax esters because they are fatty acids esterified to long-chain alcohols,[20] contain even numbers of carbon atoms from C36 to C46 in olive oil. Because waxes are in the epidermal cells of olives,[40] their concentration characterizes olive oil pomace categories.

The official method for determining waxes[5] uses lauryl arachidate in hexane as internal standard and on-column GC injection. The standard method also suggests using palmityl palmitate or myristyl stearate as internal standards. Aragón et al.[41] propose to use these internal standards in heptane to avoid the impurities that can be present in some commercial hexane and to increase the time of its evaporation. With regard to

DOI: 10.1021/jf5062265
J. Agric. Food Chem. 2015, 63, 4509−4526

Table 4. Most Common Methods for Determining Minor Compounds

chemical series	technique	sample pretreatment	reference	method details
stigmastadienes	GC-FID[a]	fractionation of unsaponifiable matter on LC Si-column	COI/T.20/ Doc No. 11.[45]	capillary column: 25−30 m × 0.25−0.32 mm ×0.15−0.30 μm phase: 5% methylpolysiloxane carrier gas: hydrogen with quality N-50 or helium operation conditions: 235 °C, 6 min, to 285 °C at 2 °C/min injection mode: split (ratio 1:15) or on column
aliphatic hydrocarbons and sterenes	GC-FID	fractionation of unsaponifiable matter on LC Si-column impregnated with silver nitrate	COI/T.20/ Doc No. 16.[47]	column: capillary (25−30 m × 0.25−0.32 mm ×0.15−0.30 μm) phase: 5% phenyl-methyl-polysiloxane (see section 2.2.3.1) carrier gas: hydrogen or helium temperature program: 235 °C, 6 min, to 285 °C at 2 °C/min injection mode: split (ratio 1:15) or on column
sterols[b] and triterpene dialcohols (erythrodiol + uvaol)	GC-FID	fractionation of unsaponifiable matter on TLC[c] or HPLC; silylation should be applied	COI/T.20/ Doc No. 30.[58]	capillary column: 20−30 m × 0.25−0.32 mm ×0.15−0.30 μm phase: 5% diphenyl−95% dimethylpolysiloxane (SE-52 or SE-54) carrier gas: hydrogen or helium operation conditions: isothermal 260 ± 5 °C injection mode: split (ratio from 1:50 to 1:100)
aliphatic and triterpenic alcohols	GC-FID	fractionation of unsaponifiable matter on TLC or HPLC; silylation should be applied	COI/T.20/ Doc No. 26.[60]	capillary column: 20−30 m × 0.25−0.32 mm ×0.10−0.30 μm phase: SE-52, SE-54 carrier gas: hydrogen or helium temperature program: 180 °C, 8 min, to 260 °C, 15 min, at 5 °C/min injection mode: split (ratio from 1:50 to 1:100)
tocopherols	HPLC[d]-F (Si column)	0.10 g of oil in 10 mL of *n*-heptane	ISO 9936.[66]	oven temperature: 20 °C mobile phase: *n*-hexane/isopropanol (99:1 v/v) (flow rate = 1.0 mL/min) detector: fluorescence λ_{ex}, 295 nm; λ_{em}, 330 nm detector: ultraviolet λ_{ex}, 292 nm (not recommended)
waxes, fatty acid methyl esters, fatty acid ethyl esters	GC-FID	fractionation by LC on hydrated silica gel column 15 g of silica;[6] fractionation by LC on hydrated silica gel column 3 g of silica[43]	COI/T.20/ Doc No. 28.[28]	capillary column: 8−12 m × 0.25−0.32 mm × 0.1 −0.3 μm
			COI/T.20/ Doc No. 31.[43]	phase: liquid phase SE52, SE54 carrier gas: hydrogen or helium temperature program: e.g., 80 °C, 1 min, to 140 °C at 20 °C/min to 335 °C, 20 min, at 5 °C/min injection mode: on-column
free fatty alcohols, free tocopherols, free sterols, free triterpenic alcohols, methyl sterols, sterols, triterpenic esters	GC-FID	silylation reaction. fractionation by LC on silica gel column	Mariani et al.[114]	capillary column: 15 m × 0.32 mm ×0.1 μm phase: methylsilicone at 5% diphenyl carrier gas: hydrogen temperature program: e.g., 80 °C, 1 min, to 180 °C at 20 °C/min to 330 °C at 6.5 °C/min injection mode: on-column

[a]Gas chromatograph−flame ionization detector. [b]See ref 56 for the methodology of free and esterified sterols. [c]Thin layer chromatography. [d]High-performance liquid chromatography. .

J. Agric. Food Chem. 2015, 63, 4509−4526
DOI: 10.1021/jf5062265

sample purification, SPE cartridges have replaced silica gel columns because the former requires smaller amounts of sample that reduce the elution solvent volume. SPE cartridges, however, need much more attention from the analyst. On the basis of this change, new methods have been proposed as alternatives to the standard method.[42] They are more rapid with lower consumption of organic solvents and no difference concerning the recovery factors. However, there is not much information about the precision and limits of quantification yet. With respect to the chromatographic column, the standard method suggests using semipolar columns with phenyl-methyl-silicone because this allows for a high resolution but is resistant at high temperatures. Columns, however, should be conditioned, prior to being used, with a gradual heat until a temperature of 350 °C is reached. It is important to note that in the last standard method[43] the sum of the contents of waxes is computed from C42 to C46, excluding C40, unlike previous norms.[5,6]

Unsaponifiable Fraction. As mentioned earlier, the unsaponifiable matter fails to react with sodium hydroxide and potassium hydroxide to produce soaps but remains soluble in classic solvents (e.g., hexane, petroleum ether, diethyl ether) after saponification. Thus, any method for determining unsaponifiable matter involves olive oil saponification and unsaponifiable matter separation by means of extraction with an appropriate solvent, such as diethyl or petroleum ether. Although the determination of unsaponifiable matter seems simple, this type of analysis still presents problems because of the lack of accuracy and precision in the results. Some difficulties are the impossibility of extracting all of the unsaponifiable matter and the formation of emulsions due to a too vigorous shaking. These emulsions can be destroyed by adding small quantities of ethanol. Other problems are soap hydrolysis, loss of unsaponifiable matter during solvent drying, evaporation, and incomplete saponification.

Although diethyl ether is the preferred solvent, it has a number of limitations. For example, if soaps pass into the solvent together with the unsaponifiable matter, it is wise to separate the soaps by washing the ether extract with an aqueous solution of sodium hydroxide, which can provoke soap hydrolysis and liberate acids. After solvent evaporation at a low temperature and reduced pressure, it is necessary to dry the unsaponifiable residue to ensure the elimination of any traces of solvent and water. A drying process should be carried out to avoid possible volatile compounds being present in the unsaponifiable fraction. Water elimination is usually performed by treating the unsaponifiable extract with water-free sodium sulfate followed by filtration. Finally, any remaining moisture traces are eliminated by vacuum drying with acetone or benzene. Sometimes incomplete saponification may occur,[44] in which case, error can be introduced due to the saponifiable portion of TAGs soluble in ether and hexane. When incomplete saponification is thought to have happened, the unsaponifiable residue containing the nonsaponified segment has to be saponified and extracted again following the same procedure.

Fractionation of the unsaponifiable components into several groups of constituents (e.g., hydrocarbons, tocopherols, and sterols) can be carried out by several procedures, most of them being chromatographic such as column chromatography and thin layer chromatography (TLC) with two different supports, alumina and silica gel (Table 4). The latter, which has traditionally been the method chosen for the complete fractionation of the unsaponifiable matter, can be applied to unsaponifiables extracted from petroleum ether and containing FFAs. In this case, first the silica gel must be treated with diluted potassium hydroxide to retain the FFAs and avoid interference with the other fractions. In the separation by TLC, the temperature is an important factor to have a good separation; the optimum temperature is 20−25 °C.

Currently HPLC has been described to carry out the fractionation of the unsaponifiable components, as described in the section focused on Sterols.

Hydrocarbons. The hydrocarbons, which are present in olive oils, include from high amounts of squalene ($C_{30}H_{50}$), an unsaturated linear triterpenic polymer of isoprene, to small quantities of saturated, linear (from C-15 to C-35), branching and terpenic compounds. Steroidal hydrocarbons (sterenes or steradienes) with two double bonds in the ring system are present in refined olive oils (ROOs), whereas small quantities of polycyclic aromatic hydrocarbons (PAHs) have been quantified in olive pomace oils.

The need to detect the presence of refined edible oils in VOOs resulted in a standard,[45] Lanzón[46] being the pioneer in suggesting stigmasta-3,5-diene (derived from β-sitosterol) as a marker for detecting admixtures of VOOs with refined vegetable oils. The method is based on the isolation of unsaponifiable matter, separation of steroidal hydrocarbon fraction with a 15 g silica gel chromatography column, and analysis by on-column GC with a column of 25 m coated with 5% phenyl-methyl silicone phase, as first proposed by Lanzón.[46] The separation by silica gel chromatographic can result in chromatograms with interfering peaks because the silica has low acidity. If this occurs, the silica gel should be treated by heating for a minimum of 4 h at 550 °C, or extra pure silica gel 60 (Merck, ref 7754) could be used.

Technological advancements have allowed for the preparation of fraudulent mixtures of desterolized vegetable oils in refined olive oil. In 2001 the IOC published the method to determine sterenes (campestadienes and stigmastadienes)[47] to detect desterolized seed oils in refined oils. This determination is based on the isolation of unsaponifiable matter, separation of sterene fraction with silica gel chromatographic column impregnated with silver nitrate, and analysis by capillary GC. The critical part of this determination is the optimization of the volumes used to extract each fraction (three different fractions are extracted from the silica gel column). The chromatograms obtained from each fraction can be used for identification if the volumes have been optimized correctly. Another problem with this determination is that in some cases 2,4- and 3,5-diene isomers are separated into two different peaks, which entails the computation of the sum of area to know the total concentration. In these cases the column should be changed with another that is less polar or has bigger internal diameter. This method can be applied to the quantification of stigmastadiene only if the concentration is >4 mg/kg. If the concentration of stigmastadiene is within 0.01 and 4 mg/kg, the IOC method[45] should be used. The presence of PAHs in olive pomace oils—arising from pyrolysis processes and environmental and natural sources—compelled IOC[48] to set up an analytical method with suitably sensitive, selective, and accurate analytical parameters for routine analysis to determine the PAHs concentration, expressed as benzo(*a*)pyrene on wet weight. It consists of an extraction step (e.g., saponification with alcoholic KOH and liquid−liquid partitioning) followed by one or more purification procedures (column chromatography, TLC, SPE) to end with the analytical determination by GC

DOI: 10.1021/jf5062265
J. Agric. Food Chem. 2015, 63, 4509−4526

coupled to flame ionization detection (FID) or mass spectrometry (MS), or by HPLC with spectrofluorometric detection. The last has proven to successfully separating PAHs from the other hydrocarbons (PAHs coelute with other hydrocarbons in silica TLC) with a good quantitative response.[49,50]

Sterols. The major chemical series of the olive oil unsaponifiable matter is that of sterols, which are usually grouped into 4-demethylsterols or phytosterols, 4,4-dimethylsterols or triterpenic alcohols, and 4-monomethylsterols or methylsterols; all of them have analogous chemical structures.

The fact that the concentrations of some sterols are characteristic of the genuineness of vegetable oils made them of interest for purity and authenticity control olive oil designations. Thus, for example, brassica seed oils have a high content of brassicasterol, whereas olive oils are characterized by a high concentration of Δ^5-avenasterol. These differences induced IOC to set up a method that allowed for their quantification. Results are expressed as percent of the total area of sterols, although the illegal process of removing sterols without forming fatty acid *trans* isomers[51] suggests giving the information in absolute concentration. In addition to qualitative differences in the sterol profiles of vegetable oils, some researchers[52,53] have pointed out that the pedoclimate (soil, climate, etc.) of the orchards and the cultivars affects the olive oil sterolic composition up to the point that some authentic olive oils can be qualified as nongenuine. The current proposal of decision trees[2,54] has been approved to be applied in those anomalous oils to overcome the number of wrong classifications by means of the implementation of equations that combine values of several chemical parameters.

The chromatographic methods are mostly devoted to determining the composition of 4-demethylsterols or phytosterols. Generally speaking, the determination of sterols comprises the sum of both possible forms (free and esterified) as their sterol acetates[55] as shown in Figure 1. Nevertheless, there is a method for determining the individual concentration of free and esterified sterols independently with the particular objective of detecting the presence of hazelnut oil.[56] For the determination of both forms together, the unsaponifiable material is usually purified by TLC on silica gel with hexane/diethyl ether (65:35 v/v). The experience has demonstrated that two developments must take place to obtain a satisfactory separation. The plate can be impregnated with alcoholic KOH for the purpose of retaining the FFAs in the unsaponifiable fraction. Three large bands would appear on the TLC plate. The first one contains 4,4-dimethylsterols or triterpenic alcohols, some phytols, and aliphatic alcohols. The second is composed of the remaining phytols and methyl sterols, and the third band contains sterols, erythrodiol, and uvaol. However, the individual separation of sterols is not exempt from difficulties as the amount of the unsaponifiable fraction in diethyl ether to be deposited on TLC exceeds 200 μL. An inadequate development of TLC and defective scraping on TLC of the sterol band are other habitual problems the analysts deal with.

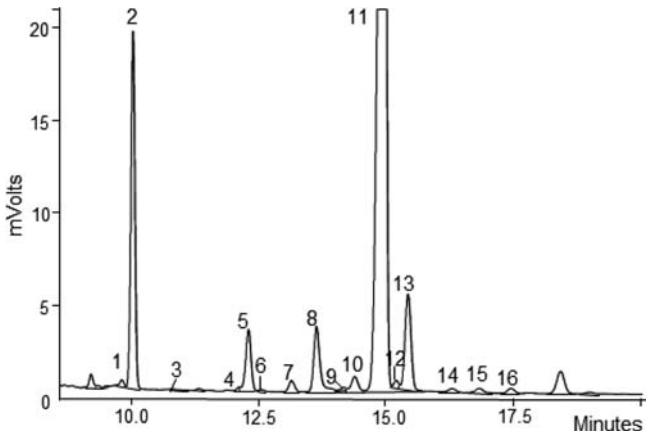

Figure 1. Chromatogram of 4-demethylsterols of a sample of virgin olive oil. Peaks: 1, cholesterol; 2, internal standard; 3, brassicasterol; 4, 24-methylenecholesterol; 5, campesterol; 6, campestanol; 7, stigmasterol; 8, Δ^7-campesterol; 9, $\Delta^{5,23}$-stigmastadienol; 10, chlerosterol; 11, β-sitosterol; 12, sitostanol; 13, Δ^5-avenasterol; 14, $\Delta^{5,24}$-stigmastadienol; 15, Δ^7-stigmastenol; 16, Δ^7-avenasterol.

4,4-Dimethylsterols or triterpenic alcohols, the first fraction, are analyzed by saponifying olive oil with KOH after the addition of an internal standard such as C-20 or C-21 and by extracting the unsaponifiable matter with diethyl ether and later purifying it on a plate. No analytical problems have been observed for their GC determination in a nonpolar column (100% dimethylpolysiloxane or a 5% phenyl−95% dimethylpolysiloxane).[57]

The methyl sterols, the second fraction, are separated on TLC with a mobile phase of cyclohexane/ethylic acetate (85:15, v/v). GC analysis of methyl sterols can be carried out under the same conditions as for 4-demethylsterols or phytosterols (EC 1991[1] and henceforth). These compounds are quantified together with triterpenic alcohols in the same chromatogram.[57]

Erythrodiol and uvaol (triterpene dialcohols) are determined by scraping their TLC band with the band of 4-demethylsterols or phytosterols,[58] the third fraction, and subsequent GC analysis. The use of capillary columns yields a significant chromatographic resolution of those diols. Results are still given in percentages, whereas absolute values (concentrations) are preferred as they would diminish substantially the current high number of false positives (genuine VOO classified as adulterated).

Analysts, however, have simplified the analysis because of the problems of using TLC. Thus, the most reliable and widely used technique is the off-line HPLC-GC coupling that comprises separation of the fractions of sterols or other unsaponifiable components (e.g., branching and terpenic hydrocarbons) by HPLC with a silica gel column, collection of the fraction, elimination of the solvent, further derivation, and injection onto GC. Figure 2 shows a typical HPLC chromatogram in which the peaks assigned to the different sterol fractions are shown.[59] Figures 3 and 4 display the correct separation and peak resolution of the compounds named 4,4-dimethylsterols and 4-monomethylsterols after application of the described HPLC-GC-based method.

Aliphatic Alcohols. Free and esterified aliphatic alcohols are a linear chain made of even and odd numbers of 20−32 carbon atoms. It is important to note that phytol (present in VOOs at low concentrations) is an artifact generated from chlorophyll decomposition by alkaline treatment during saponification. The standard method[60] begins by adding the internal standard (1-eicosanol) to 5 g of the sample prior to the saponification with ethanolic KOH and then extraction with ethyl ether. The alcoholic fraction is separated from the unsaponifiable matter by depositing it on a silica gel plate, or in a column of the same

DOI: 10.1021/jf5062265
J. Agric. Food Chem. 2015, 63, 4509−4526

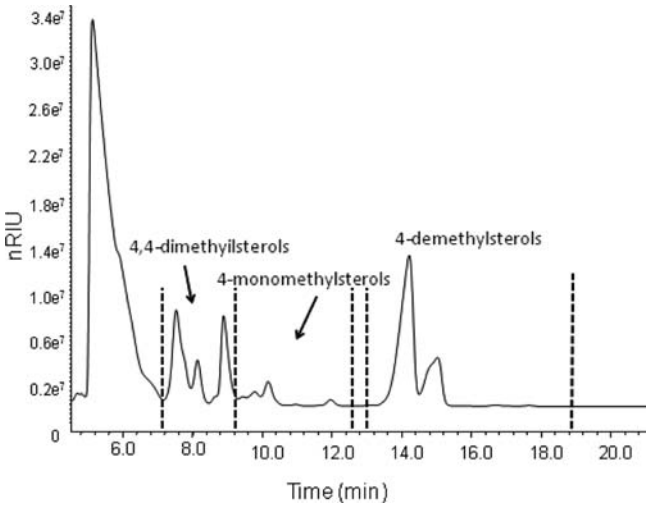

Figure 2. Sterols obtained in fractionation of the unsaponifiable matter by HPLC.[59]

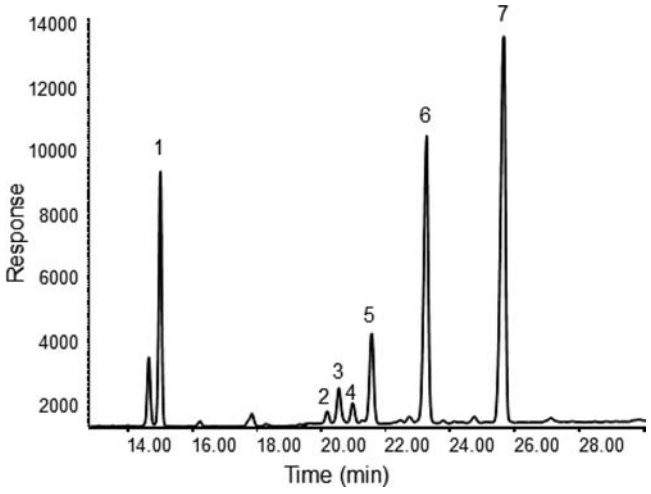

Figure 3. Chromatogram of 4,4-dimethylsterols of a sample of virgin olive oil. Peaks: 1, internal standard (5-α-cholestanol); 2, taraxerol; 3, dammaradienol; 4, β-amyrin; 5, butyrospermol; 6, cycloartenol; 7, 24-methylenecycloartanol.

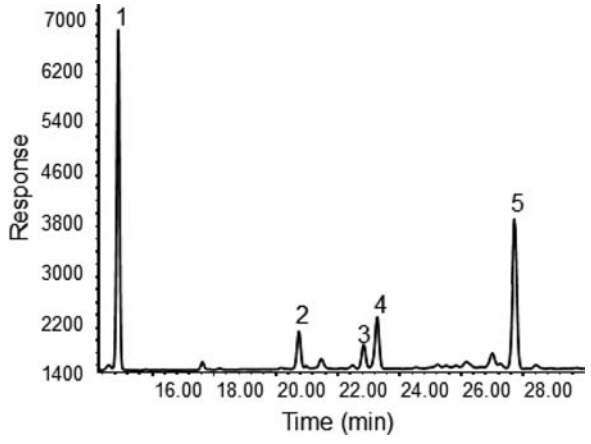

Figure 4. Chromatogram of 4-monomethylsterols of a sample of virgin olive oil. Peaks: 1, internal standard (5-α-cholestanol); 2, obtusifoliol; 3, gramisterol, 4, cycloeucalenol; 5, citrostadienol.

material, and eluting with hexane/diethyl ether (60:40 or 70:30, v/v). The silylized derivatives can be analyzed with SE-30 or SE-54 or SE-52 capillary nonpolar columns. Because EU regulations[61] (and followings) proposed the determination of wax content as an alternative to the quantification of aliphatic alcohols, the analytical method has not been modified since it became a standard method.

Tocopherols. Tocopherols (heteroaromatic acid compounds with high molecular weight) are lipid-soluble compounds easily oxidized in the presence of light, oxygen, alkaline pH, or traces of transition metal ions. The detection method[62] employs the direct analysis using normal-phase HPLC and fluorescence or UV detection. Tocopherols are directly analyzed through olive oil injection, dissolved in a hexane/isopropanol (99.8:0.2, v/v) mobile phase, in a Si-60 5 μm LiChrosorb column with a length of 250 mm and an internal diameter of 4 mm. The fluorescence detector characteristics are λ_{ext} = 290 nm and λ_{em} = 330 nm.[63] SPE has also been reported as an adequate procedure for sample preparation prior to HPLC analysis of tocopherols in VOO.[64] Luminescent methods have also been used for the determination of total tocopherols in VOO without prior separation.[65] IOC[2] recommends using the ISO 9936 method[66] to determine α-tocopherol. A portion of oil is dissolved in *n*-heptane, and the individual tocopherols are separated by HPLC-fluorescence or HPLC-UV. The content of each tocopherol is calculated by using calibration curves.

METHODS FOR OLIVE OIL SENSORY QUALITY CONTROL

Virgin olive oil stands out as a gourmet product because of its rich flavor, and its classification into quality categories basically relies on the sensory assessment, together with some chemical indices that do not provide information about aroma or taste. The sensory assessment by panel test is not, obviously, a chemical method, but some analytical techniques attempt to analyze the chemical compounds actually responsible for flavor and give objective chemical information that can explain the sensory perception.

Numerous problems make the sensory interpretation of instrumental analysis difficult to accomplish. This sensory interpretation can be even harder if those analyses do not provide information on the compounds that cause a particular attribute. Thus, instrumental approaches can be grouped as those that have a casual relationship with sensory quality (henceforth, apparently causal relationship) and those that have a causal relationship. The former methods do not analyze flavor compounds that are responsible for attributes, but compounds whose concentrations are, or seem to be, mathematically correlated with some sensory parameters. Mathematical correlation, however, can fail under certain circumstances, and in those cases, the relationship between sensory and chemical information would be dissociated.

Apparently Causal Methods for Sensory Quality Control. Although methods are validated prior to being proposed as standards, the validation step is not always carried out under the strictest conditions, which can result in overstated and overly optimistic analytical parameters (e.g., reproducibility, robustness) that usually present many exceptions when the method is widely applied by analysts. The problem is circumscribed not only to methods based on multivariate information but also to methods based on parameters with a weak or casual relationship with sensory quality. The fact is that a successful control of olive oil

DOI: 10.1021/jf5062265
J. Agric. Food Chem. 2015, 63, 4509−4526

adulteration by means of statistical procedures encouraged some analysts to think that a strong mathematical relationship can prevail over the lack of any scientific evidence explaining the relationship between sensory assessment and chemical compounds (e.g., pyropheophytins, ethyl esters).

Pigments. Although pigments are related to VOO color,[67] the determination of some of their compounds has been proposed as a method for determining VOO quality and adulteration,[68,69] although its fundamentals in this application are not quite clear.

In analytical terms, the method can be focused on determining a particular compound (pyropheophytin *a*) in a rapid way[69,70] or the maximum number of pigments.[71] In the first case, the analyst can use two methods,[69,70] although one is more focused on the determination of pheophytins[70] than pyropheophytins,[69] because both methods use a reverse-phase solid-phase extraction (RP-SPE). The first, however, elutes with petroleum ether (65−95 °C) and the second with petroleum ether (40−60 °C)/ethyl ether (9:1) for removing lipids. Acetone is used in both methods to collect the pigments. The critical point in both methods is the collection of the analytes in 0.2−0.3 mL of acetone and later the injection in the HPLC instrument because the high volatility of acetone suggests making this step as rapid as possible.

When the objective is to have information on a complete profile of pigments, SPE packs can be responsible for the degradation of some pigments—mostly carotenoids—despite their well-known ability in cleanliness and free acidity removal. In that case, it is suggested to employ a method that is lengthy and tedious but excellent and well-tested: liquid−liquid extraction, with hexane and dimethylformamide (DMF).[71]

Diacylglycerols. The difference in the formation of DAG isomers has not only been proposed for olive oil authenticity but also for distinguishing VOOs from extra-VOOs (EVOOs),[72] despite the fact that the relationship of DAGs with sensory quality is merely a result of casual with the apparent causal relationship in the case of VOO defects resulting from hydrolytic processes, for example, before processing of olives (e.g., fusty) or when vertical containers are used for decanting, among others.

The method proposed by Gertz and Fiebig[72] uses a silica gel column chromatograph to which 100 mg of the olive oil spiked with 1 mL of toluene is transferred, and then the column is washed with isooctane/diisopropyl ether (0.85:0.15) in a first step. In a second step the DAGs are eluted with diethyl ether and the solvent is removed with a rotary evaporator prior to being silylated at room temperature. Then 1 mL of acetone is added to the solution, and 1−2 μL is injected into a gas chromatograph. Pérez-Camino et al.,[73] however, suggested using SPE to which an aliquot of 500 μL of the dehydrated olive oil solution in hexane (0.2 mg/mL) and 200 μL of the internal standard are transferred. The method provided by IOC[39] allows separating the 1,2-isomer from the 1,3-isomer of diacylglycerols although saturated and unsaturated DAGs are eluted together.[74] This method suggests analyzing the olive oil sample by GC once it is purified. The suggested chromatographic conditions consist in a direct on-column injection with a capillary column fused silica 3−7 m coated with SE 52 or SE 54 liquid phase (5% diphenyl-dimethyl polysiloxane) (Table 3).

Fatty Acid Alkyl Esters. Alkyl esters are made up of methyl and ethyl esters of fatty acids previously present in their free form. They are a consequence of inappropriate practices in the harvesting and storing of the olives prior to olive oil extraction because of the rupture of the olive drupe and its contact with microorganisms (yeasts) and lipolytic and pectolytic enzymes. Consequently, it seems that the presence of the ethyl esters of fatty acids (FAEEs), which are present in the waxy fraction of olive oils,[75] indicates that olive oil could have been obtained from unhealthy olives when harvested or because of inadequate processing of the olives. However, the relationship of fatty acid alkyl esters with soft-deodorized oil[76] is casual as well as its relationship with sensory quality.

The method COI/T.20/DOC. No. 31,[43] which allows the determination of waxes as well (Table 3), is based on solid−liquid chromatography (LC) by traditional glass column for isolating the fraction containing alkyl esters and waxes. The method, although very simple—it requires only the addition of a suitable amount of internal standard to 500 mg of the sample prior to transfer into LC—may pose problems in its implementation because of the difficulty in having similar packing of the silica gel columns in repeatability studies. The difficulty becomes greater with the change of LC packed with 15 g of silica gel[6] to 3 g of silica gel,[43] which reduces the sample preconcentration. Furthermore, the flow rate of hexane/diethyl ether (99:1) of about 15 drops every 10 s is not an easy matter for inexperienced analysts. Experience also suggests that 15−20 mL of hexane should be added instead of 10 mL immediately after the sample is transferred into the column, which helps to achieve a better chromatogram resolution. Furthermore, in samples with low concentration of alkyl esters, they can be masked by the peak tail of the solvent (*n*-heptane or isooctane), which suggests using *n*-hexane, which is much more volatile.

An interesting alternative is the use of a method based on GC-(EI)MS/[77] in which there is no sample preparation and FAAEs are directly thermo-desorbed and cryo-focused in the cooled injector of a GC-MS (EI) instrument. The detection limit of the method competes with the standard, but the new one is faster and simpler, requires a lower amount of organic solvents, and significantly enhances method repeatability. However, it is a new method that requires further studies to fully understand its performance parameters and potential problems.

Free Fatty Acids (FFAs). FFAs arise from of the separation of fatty acids from TAGs in the olive because of the action of enzymes, further stimulated by light, water, and heat. Thus, FFA content is a marker of TAG hydrolysis, and hence it indicates how fresh and how well handled the olives were before being milled. The content of FFAs or free acidity is usually determined by titration following well-established standards,[78,79] although the amount of sample[1] seems to be high (i.e., 20 g when acidity is <1.0%) and could be reduced to half. There is also the alternative of substituting the solvents for others that are much more amicable, such as ethanol/water (1:1).[80]

Determination can be carried out by GC as FAMEs as well. FFA methyl esters are prepared by derivatization with trimethylsilyldiazomethane because methylation enhances the volatility and reduces the activity of FFAs, although methylation can be omitted if a highly polar capillary column (e.g., coated with 88% cyanopropyl-aryl-siloxane or 100% cyanopropyl polysiloxane) is used. The procedure also requires the addition of an internal standard (e.g., tridecanoic or nonadecanoic FAs) and a purification step by SPE filled with an amino stationary phase. Medium-polarity thermostable columns (e.g., coated 65% phenyl−35% dimethyl-polysiloxane) have also been used with success.

DOI: 10.1021/jf5062265
J. Agric. Food Chem. 2015, 63, 4509−4526

Although FFA determinations can be easily and rapidly achieved by FTIR, this approach is not an official method yet. Lanser et al.[81] used peaks near 1745 and 1711 cm^{-1} to construct a model allowing the determination of the free fatty acid content in crude oils. The C═O carbonyl groups of esters absorb at ∼1746 cm^{-1}, whereas the carboxylic acid group of FFAs has its characteristic band at 1711 cm^{-1}. Later, an FTIR instrument and ATR accessory were successfully used to determine FFA content in oils and fats.[82] However, it is FTIR with transmission cells that has been much more successful.[83] In this procedure the FFAs that are present in the sample are derivatized to the corresponding free fatty acid salt after reacting with sodium carbodiimide (a weak base) in methanol. The resulting salt presents a measurable spectroscopic band in a region without interference, and consequently this band is very easy to measure and calibrate.[84,85]

Oxidation Products. The peroxide value (PV) is an indicator of the primary oxidation status of olive oil, mainly because of the presence of hydroperoxides.[86] Despite the importance of PV as a quality index, the standard method (ISO 2009)[78] is laborious and time-consuming and requires the use of organic solvents and, even more importantly, its accuracy depends strongly on the experience of the analyst.[88] Its relevance justifies the need for reliable methods that use amicable solvents (i.e., isooctane) that do not perturb the interpretation of the results and can also be fast and nondestructive, with a high degree of automation to provide near-real-time measurements for assessing olive oil quality. In this context, vibrational spectroscopy offers alternative analytical tools;[87] for example, disposable IR cards have successfully been applied to determine PV of edible oils.[89,90]

A shift in double-bond configuration occurs during the formation of peroxy radicals and hydroperoxides because the normal methylene-interrupted configuration is transformed into a conjugated form. The absorbance in ultraviolet light of secondary oxidative compounds (conjugated dienes and trienes) is determined according to standard methods,[91] which can be easily implemented by analysts. New instrumentation, however, has better characterized the exact wavelengths at which the conjugated dienes and trienes absorb, 232 and 268 nm when using isooctane and 232 nm and 270 when cyclohexane is the solvent.

Causal Methods for Sensory Quality Control. The sensations perceived when a VOO is consumed are evaluated by sensory assessment implemented in the so-called panel test.[92] The official method, however, is questioned by numerous VOO sectors, because the difference between virgin and extra-virgin olive oils depends on the presence of defects, whatever their level of perception. It is there where the method fails: when the panel test analyzes oils that could not have any defect for some panel tests whereas others have been able to detect defects at very low intensity of the sensory perception, which is enough to qualify olive oils as virgin instead of extra-virgin. Reasons can be found in many aspects—limit of detection, subjectivity, inadequate training, too high sensitivity of some assessors for some odors—but none of them is convincing by itself to explain the errors in the analysis. Therefore, an objective measurement of VOO sensory quality should follow another strategy based on analytical chemistry.

From a chemical perspective, the flavor of VOO is explained by the occurrence of a series of minor chemical compounds that have a significant sensory impact. Thus, "I smell, therefore there are volatiles" is the sentence, which, emulating Descartes' phrase, summarizes the scientific support explaining that there is a causal relationship between volatile compounds and aroma, and, for a similar reason, between phenols and VOO taste. The methods for quantifying those chemical compounds have as their main objective to contribute to the explanation of what the assessors perceive when they smell and taste VOOs.

Phenols. The prevalent classes of phenols found in VOOs are phenolic alcohols, phenolic acids, flavonoids, lignans, and secoiridoids, some of them having antioxidant properties.[93] However, and despite, the interest of these compounds from sensory and health viewpoints, no harmonized and widely accepted analytical method exists today because their results are not comparable.[94] There are several approaches, one of them being supported by IOC,[95] whereas another[96] is still under evaluation. The first one is based on the individual separation of phenols by HPLC, and the second one provides the total content of *o*-diphenols by a more rapid and cost-effective colorimetric method. Their results, however, do not seem to be comparable. The colorimetric method has a low specificity, as the color reaction can occur with any oxidizable phenolic hydroxyl group.[97] However, it could be a valid method to determine the concentration of total phenols as required in the recent health claim on polyphenols[98] once the method is improved and corrected.

Regardless of the method applied, the first step is the extraction of the phenol fraction from the oil matrix removing the interfering components (e.g., lipids, pigments). The extraction of the phenol fraction can be carried out by SPE (e.g., C18 or diol) or liquid−liquid extraction (LLE). If SPE is used, the addition of hexane or other organic solvents to the oil before extraction[99] makes the sample flow through the SPE cartridge more easily with no effect on the recovery of phenols. However, the IOC method[95] uses a LLE with methanol/water (80:20, v/v). Some authors[100,101] have pointed out that the recovery of "bitter" phenolic compounds increases as follows: SPE C18 (with methanol) < SPE diol (with methanol) < LLE (60% aqueous methanol). LLE also seems to be more appropriate for the extraction of oxidized phenolic compounds.[102]

In the separation step, reversed-phase HPLC has been the most successful approach despite the fact that the elution time is generally long, >40 min. Separation is carried out using a column RP C18 (250 × 4 or 4.6 mm i.d.) with water/methanol or water/acetonitrile mixtures enriched with acetic, phosphoric, or sulfuric acid (up to 3%, pH <2) to suppress phenol dissociation and improve peak asymmetry. Analysts, however, should pay attention to the various pK_a values of individual phenols. Furthermore, degassing should be constant to avoid bubbles that disrupt the long runs. The starting composition of eluent should use a small amount of organic phase (approximately 5%). By the end of the run, this amount is usually rather high, although it should never reach 100%. The water quality used for the analysis is essential for avoiding higher backpressures expected at certain ratios. The conditioning times from run to run that are needed to ensure reproducible retention data are long.

Ultrahigh-performance liquid chromatography (UHPLC), with columns packed with 1.7 μm particles, coupled to MS/MS (LLE-UPLC-MS/MS) has been applied with success up to the point that its analytical parameters, as LOD and LOQ, are better than HPLC-DAD and HPLC-FLD with the exception of vanillic acid and pinoresinol.[103] Although it is much more rapid (18 min) than the IOC standard method and methodologies

DOI: 10.1021/jf5062265
J. Agric. Food Chem. 2015, 63, 4509−4526

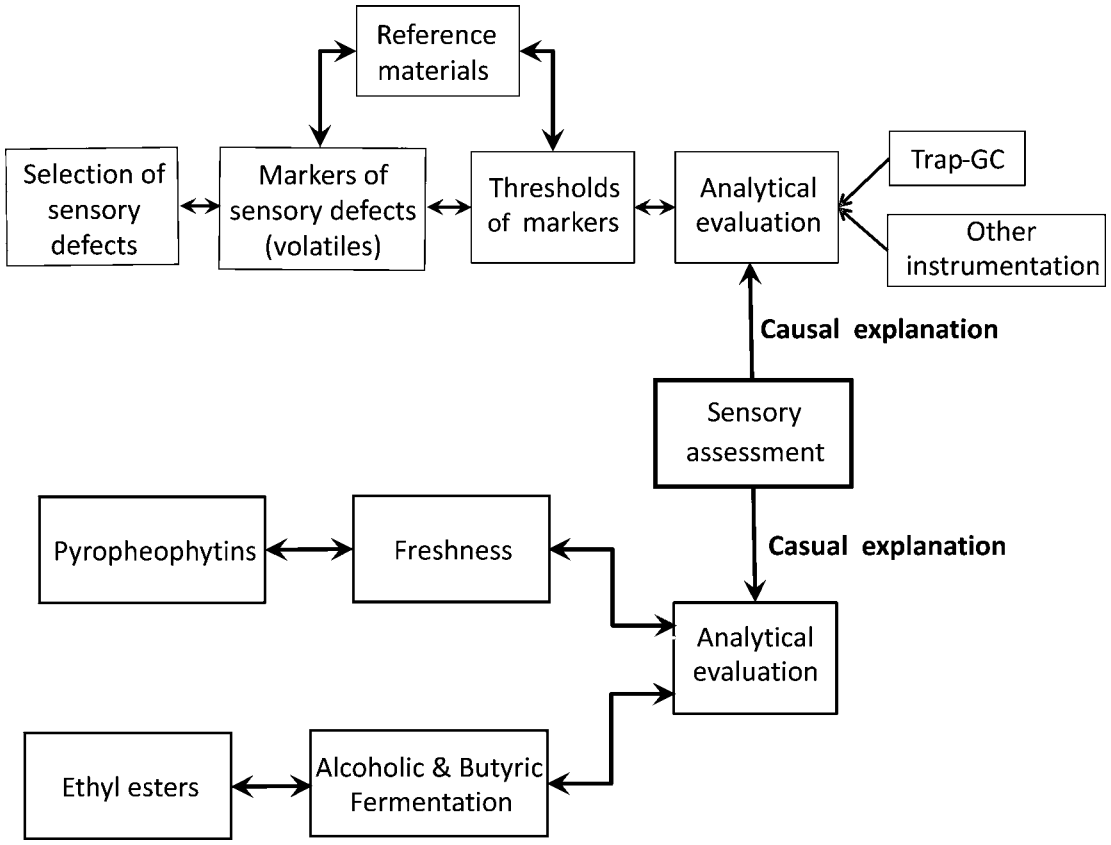

Figure 5. Different approaches to explain the sensory assessment from chemical compounds.

under evaluation by IOC, the instrumentation is not affordable for most laboratories.

The identification and quantification techniques depend on the aim of the study and available facilities. In the past decade LC-MS techniques have found extended application, although routine analysis is still less demanding regarding instrumentation. Thus, a good detection system can be an in-tandem diode array detector (DAD) with fluorescence detector (FLD). It is well-known that UV detection at 280 nm is the standard wavelength, although others (225, 240, and254 nm) are also useful for constituents of olive oil polar fractions, whereas flavonoids are detected at higher wavelengths (340 nm).

UV spectrophotometry (spectrum region between 200 and 290 nm) is extremely helpful in the identification of phenols and monitoring the purity of HPLC peaks, although hydroxycinnamic acids have a characteristic maximum at 310−332 nm. Differences in maximum wavelength and molar absorption values among the various phenols affect quantification.[93] Spectrofluorometry, in-tandem or not with DAD, is a valuable tool as it is more specific and sensitive than spectrophotometric detection.[104,105] However, there is a certain interest in modifying the IOC standard by adding a step of hydrolysis prior to the quantification with HPLC-DAD and suggesting the colorimetric method under revision[96] as a routine method for determining the phenolic content for verifying health claims.[98] This, once again, increases confusion among analysts because it does not produce comparable results and it is contrary to the current demand of analysts for a reduced number of standard methods.

Other alternatives to quantify the phenolic fractions have been studied. Mass spectrometry (MS), for its part, offers a high volume of data on fragments derived from phenolic compounds. Thus, MS can be also used to perform quantitative analysis of phenol composition on the basis of fragment abundance. Finally, nuclear magnetic resonance (NMR) and NMR-MS are powerful tools for the structural elucidation of isolated phenolic compounds that are not detectable by other means,[106] although NMR cannot yet be used in routine analysis.

Volatile Compounds. Any proposal to replace sensory assessment with an analytical procedure presently has two challenges. The first is the determination of the chemical compounds responsible for VOO aroma from the large set of currently identified compounds.[107,108] The second challenge is to explain those important VOO sensory attributes that are described with considerable vagueness such as fruitiness and green. Therefore, the establishment of the relationship between VOO chemical compounds and sensory attributes is the most complex aspect of the global study of olive oil flavor. However, the relationship between volatile compounds and sensory defects is already well-established.[109] Once the markers for a sensory defect are identified, a series of tasks should be implemented: (i) calculate the thresholds of the markers; (ii) select the better analytical evaluation (e.g., Trap, SPME); (iii) produce reference materials to facilitate the implementation of the method for analytical evaluation. All of these tasks (Figure 5) should be carried out to develop an analytical method for aroma authentication.

The separation and quantification of volatiles is usually carried out by GC, although aroma sensors,[110] which do not require a sample preparation step, are gaining in popularity. The sensors are applicable within a screening context, because aroma sensors do not supply individual information on volatiles but instead produce a response curve resulting from all of the

DOI: 10.1021/jf5062265
J. Agric. Food Chem. 2015, 63, 4509−4526

Table 5. Advantages and Disadvantages of Most Common Analytical Techniques, Chemical Phases, and Sensors Used To Study the Sensory Attribute of VOO

technique	description	advantages	disadvantages
dynamic headspace gas chromatography with Tenax	inert gas (e.g., N_2) sweeps headspace of sample, which is stirred or bubbled	high adsorption capacity	less sensitive to some acids
	volatiles are trapped in Tenax	useful for almost all kinds of volatiles	temperature and flow rate must be controlled
	trap is thermally desorbed in GC; heating the trap to a high temperature while passing a current of inert gas through it	good recovery factors	possible impurities of the adsorbent
		good repeatability	analysis per sample
		no artifacts	
static headspace gas chromatography with SPME	SPME fiber is exposed to sample vapor phase; volatiles adsorbed on fiber are desorbed in GC injection port	rapid, cheap, easy to use all steps in a single process when using automatic injector various kinds of fibers good repeatability	differences in quantification of low molecular weight molecules
			lower number of volatiles at low concentrations
			some of the disadvantages of the static headspace
			competitive effect between volatiles in SPME absorption
metal oxide semiconductor (MOS)	ceramic former heated by wire and coated with a metal oxide semiconducting film	robust	sensitivity affected by humidity
n-type (oxidizing compounds)		quite good sensitivity	temporary blinding effect
p-type (reducing compounds)		simple signal processing	sensor drifts
		low cost	poor specificity and selectivity with compounds with high molecular weight
		can be doped with metals to improve sensitivity and selectivity and diminish humidity and temperature dependence	nonlinear response to some chemical compounds
conducting polymer (CPSs)	based on a measurable change in electrical conductivity when are exposed to volatile compounds	easy to manufacture	nonreproducible
polypyrroles		low power consumption	too long response time (20−40 s)
polyanilines		robust	drift over time or changes in temperature
		can work at room temperature	extremely sensitive to moisture
		can be doped, producing sensors to specific series of volatiles or to a particular application	
acoustic sensors	based on the propagation of acoustic waves produced by piezoelectric materials in a multilayer structure	high sensitivity	temperature and humidity dependence
surface acoustic wave (SAW)		short response time	poor reproducibility in the deposition of the coating material
bulk acoustic wave (BAW)		low power consumption	certain level of noise because of the oscillator high frequency
		small size	
		robustness	

J. Agric. Food Chem. 2015, 63, 4509−4526
DOI: 10.1021/jf5062265

volatiles present in a static headspace.[111] Table 5 describes the analytical techniques, chemical phases, and sensors that are commonly used in the analysis of volatiles. In addition to the described methods, in-tandem GC-olfactometry (GC-O) is a valuable tool for the selection of aroma-active components. In GC-O human subjects (assessors) assign the sensory properties of the different peaks/zones of the chromatogram when sniffing GC effluents. Many key aroma compounds occur at very low concentrations but still have sensory relevance due to low odor thresholds,[108] and they are perceived by panelists and consumers.[112,113]

UNIFYING METHODS

Researchers have always looked for unifying methods that allow reduction of the tremendous laboratory workload, given that the current methods offer partial solution for determining the presence of adulterants in olive oil. A difference between theoretical and empirical TAGs is an indication of a mixture of different oils and hence of the presence of an extraneous edible oil in olive oil. The practical implementation of this theory is the so-called global method, in which an analytical step for determining FAMEs and TAGs is followed by a mathematical procedure that makes this standard[17] different from the other previously approved methods to date.

Another proposal of a unifying method was provided by Mariani and co-workers in 1991,[114] in which sterols, triterpenic alcohols, squalene, and tocopherols are quantified simultaneously. This method is based on the concurrent determination of these compounds, avoiding the use ofTLC for separating the unsaponifiable fraction, which is tedious. The procedure is something similar to that already described for the simultaneous determinations of waxes, FAMEs, and FA ethyl esters.[6]

With regard to the unifying method for the sensory quality assessment, a recent method based on the quantification of ethyl esters has been proposed. However, the relationship between ethyl esters and VOO quality is casual. Furthermore, there is no kinetic equation that explains the formation of ethyl esters in VOO. This method has also raised the interest in quantifying ethanol, which is involved in the formation of ethyl esters but it is important to note that the odor threshold of ethanol is so high in a lipidic matrix that it does not contribute to VOO aroma.

The aforementioned unifying methods satisfy one of the requirements of analysts working on olive oil control, that is, to obtain complete chemical information from an oil without use of extensive resources. Therefore, such methods will presumably be welcomed by control laboratories. However, these methods still need to be fully validated, and experience is currently insufficient to propose amendments or detect potential problems. It is also unclear whether these methods should be proposed as alternatives to the current standard methods or as additional options for more experienced analysts.

FURTHER RESEARCH IN PERFECTING METHODS

The described methods have solved many problems and have made olive oil one of the most protected foodstuffs, although they still need to be improved with further research. The required improvements need to take into account current problems, which are somewhat different from those encountered in the past, and to be stricter in repeatability and reproducibility considering the recent technical advances. The greater ability of current techniques for identifying compounds in olive oil also sets the stage for the evaluation of new purity and quality parameters in addition to validating the current ones. Searching new parameters is of particular interest in quality assessment, where the development of alternative methods based on volatile compounds for the assessment of sensory characteristics is required. New research based on chemical and sensory approaches would make the current sensory assessment dispensable to some extent, alleviating the workload associated with panel tests. Researchers also strive to develop methods for assessing health benefits of virgin olive oil (e.g., analyzing phenols) to respond to the current demands of industry and consumers. Another challenge is to develop rapid approaches that may serve as alternatives to lengthy chromatographic methods. Thus, spectroscopic techniques may provide effective solutions in cases of complex analytical tasks such as identification of geographical origins. The establishment of open databank and data-sharing platforms fed with spectroscopic and chromatographic data is also being pursued to facilitate the implementation of practical and standardized applications. This task is arduous, requires time, and needs to keep pace with the development of new accurate methods and the rise of new challenges.

AUTHOR INFORMATION

Corresponding Author

*(R.A.) Phone: +34 954611550. Fax: +34 954616790. E-mail: aparicio@cica.es.

Notes

The authors declare no competing financial interest.

REFERENCES

(1) EC Commission Regulation (EEC) 2568/91 on the characteristics of olive oil and olive-residue oil and on the relevant methods of analysis. *Off. J. Eur. Communities* **1991**, *L248*, No. 2568/91.

(2) International Olive Council (IOC) T.15/Doc. No. 3/Rev. 7. Trade standard applying to olive oils and olive-pomace oils, Madrid, Spain, 2013.

(3) Codex Alimentarius Commission (CODEX STAN) 33-1981. Codex standard for olive oils and olive pomace oils, 1981.

(4) Aparicio, R.; Conte, L. S.; Fiebig, H. J. Olive oil authentication. In *Handbook of Olive Oil*; Aparicio, R., Harwood, J., Eds.; Springer Science: New York, 2013; pp 589−653.

(5) International Olive Council (IOC) T.20/doc. No. 18/Rev. 2. Determination of wax content by capillary column gas chromatography, Madrid, Spain, 2003.

(6) International Olive Council (IOC) COI/T.20/DOC. 28 Determination of the content of waxes, fatty acid methyl esters and fatty acid ethyl esters by capillary gas chromatography, Madrid, Spain, 2010.

(7) International Olive Council (IOC) T.20/DOC. NO 42-2/Rev. 1. Precision values of the methods of analysis adopted by the international olive council, Madrid, Spain, 2011.

(8) Laroussi-Mezghani, S.; Vanloot, P.; Molinet, J.; Dupuy, N.; Hammamib, M.; Grati-Kamoun, N.; Artaud, J. Authentication of Tunisian virgin olive oils by chemometric analysis of fatty acid compositions and NIR spectra. Comparison with Maghrebian and French virgin olive oils. *Food Chem.* **2015**, *173*, 122−132.

(9) Rohman, A.; Man, Y. B. C.; Yusof, F. M. The use of FTIR spectroscopy and chemometrics for rapid authentication of extra virgin olive oil. *J. Am. Oil Chem. Soc.* **2014**, *91*, 207−213.

(10) Zhang, X.; Qi, X.; Zou, M.; Liu, F. Rapid authentication of olive oil by Raman spectroscopy using principal component analysis. *Anal. Lett.* **2011**, *44*, 2209−2220.

(11) Guzmán, E.; Baeten, V.; Fernández Pierna, J.; García-Mesa, J. A. Evaluation of the overall quality of olive oil using fluorescence

DOI: 10.1021/jf5062265
J. Agric. Food Chem. 2015, 63, 4509−4526

spectroscopy. *Food Chem.* **2014**, DOI: 10.1016/j.foodchem.2014.10.041.
(12) Faberi, A.; Marianella, R. M.; Fuselli, F.; La Mantia, A.; Ciardiello, F.; Montesano, C.; Mascini, M.; Sergic, M.; Compagnonec, D. Fatty acid composition and $\delta^{13}C$ of bulk and individual fatty acids as marker for authenticating Italian PDO/PGI extra virgin olive oils by means of isotopic ratio mass spectrometry. *J. Mass Spectrom.* **2014**, *49*, 840−849.
(13) Xu, Z.; Morris, R. H.; Bencsik, M.; Newton, M. I. Detection of virgin olive oil adulteration using low field unilateral NMR. *Sensors* **2014**, *14*, 2028−2035.
(14) Agrimonti, C.; Vietina, M.; Pafundo, S.; Marmiroli, N. The use of food genomics to ensure the traceability of olive oil. *Trends Food Sci. Technol.* **2011**, *22*, 237−244.
(15) Tena, N.; Aparicio, R.; García-González, D. L. Thermal deterioration of virgin olive oil monitored by ATR-FTIR analysis of *trans* content. *J. Agric. Food Chem.* **2009**, *57*, 9997−10003.
(16) International Olive Council (IOC) T.20/Doc. No. 20 /Rev. 3. Determination of the difference between actual and theorical content of triacyglycerols with ECN 42, Madrid, Spain, 2010.
(17) International Olive Council (IOC) T.20/Doc. No. 25/Rev. 1. Global method for the detection of extraneous oils in olive oils, Madrid, Spain, 2013.
(18) León-Camacho, M.; Morales, M. T.; Aparicio, R. Chromatographic methodologies: compounds for olive oil traceability issues. In *Handbook of Olive Oil: Analysis and Properties*, 2nd ed.; Aparicio, R., Harwood, J. L., Eds.; Springer: New York, 2013; pp 163−218.
(19) International Olive Council (IOC) T.20/Doc. No. 24. Preparation of the fatty acids methyl esters from olive oil and olive-pomace oil, Madrid, Spain, 2001.
(20) Christie, W. W. Preparation of ester derivatives of fatty acids for chromatographic analysis. In *The AOCS Lipid Library*; Christie, W. W., Ed.; AOCS Press: Champaign, IL, USA, 2011; available from http://lipidlibrary.aocs.org/topics/ester_93/index.htm.
(21) Nimal Ratnayake, W. M.; Hansen, S. L.; Kennedy, M. P. Evaluation of the CP-Sil 88 and SP-2560 GC columns used in the recently approved AOCS official method Ce 1h-05: determination of *cis-*, *trans-*, saturated, monounsaturated, and polyunsaturated fatty acids in vegetable of non-ruminant animal oils and fats by capillary GLC method. *J. Am. Oil Chem. Soc.* **2006**, *83*, 475−488.
(22) Knother, G.; Kenar, J. A. Determination of fatty acid profile by ^{1}H-NMR spectroscopy. *Eur. J. Lipid Sci. Technol.* **2004**, *106*, 88−96.
(23) van de Voort, F. R.; Ismail, A. A.; Sedman, J. A rapid automated method for the determination of cis and trans content of fats and oils by Fourier transform infrared spectroscopy. *J. Am. Oil Chem. Soc.* **1995**, *72*, 873−880.
(24) Bailey, G. F.; Horvat, R. J. Raman spectroscopic analysis of the cis trans isomer composition of edible vegetable oils. *J. Am. Oil Chem. Soc.* **1972**, *49*, 494−498.
(25) Buchgraber, M.; Ulberth, F.; Emons, H.; Anklam, E. Triacylglycerol profiling by using chromatographic techniques. *Eur. J. Lipid Sci. Technol.* **2004**, *106*, 621−648.
(26) International Olive Council (IOC) T.20/Doc No. 23. Method for the determination of the percentage of 2-glyceryl-monopalmitate, Madrid, Spain, 2006.
(27) EC. European Communities (EC) Regulation No. 702/2007. *Off. J. Eur. Communities* **2007**.
(28) EC. European Communities (EC) Regulation No. 1996/92, L199. *Off. J. Eur. Communities* **1992**.
(29) International Union of Pure and Applied Chemistry (IUPAC) Method 2.507, Determination of polar compounds in frying fats. In *Standard Methods for the Analysis of Oils, Fats and Derivatives*, 7th ed.; Paquot, C., Haufenne, A., Eds.; Blackwell Scientific Publications: Oxford, UK, 1987.
(30) Moreda, W.; Pérez-Camino, M. C.; Cert, A. Improved method for the determination of triacylglycerols in olive oils by high performance liquid chromatography. *Grasas Aceites* **2003**, *54*, 175−179.
(31) Ollivier, D.; Artaud, J.; Pinatel, C.; Durbec, J. P.; Guérère, M. Triacylglycerol and fatty acid compositions of French virgin olive oils. Characterization by chemometrics. *J. Agric. Food Chem.* **2003**, *51*, 5723−5731.
(32) Fiebig, H. J. HPLC-Trennung von triglyceriden. *Fette, Seifen, Anstrichm.* **1985**, *87*, 53−57.
(33) García-González, D. L.; Viera-Macías, M.; Aparicio-Ruiz, R.; Morales, M. T.; Aparicio, R. Validation of a method based on triglycerides for the detection of low percentages of hazelnut oil in olive oil by column liquid chromatography. *J. AOAC Int.* **2007**, *90*, 1346−1353.
(34) Christie, W. W. Detectors for high-performance liquid chromatography of lipids with special reference to evaporative light-scattering detection. In *Advances in Lipid Methodology − One*; Christie, W. W., Ed.; Oily Press: Ayr, UK, 1992; pp 239−271.
(35) Cozzolino, R.; De Giulio, B. Application of ESI and MALDI-TOF MS for triacylglycerols analysis in edible oils. *Eur. J. Lipid Sci. Technol.* **2011**, *113*, 160−167.
(36) Holčapek, M.; Jandera, P.; Zderadička, P.; Hrubá, L. Characterization of triacylglycerol and diacylglycerol composition of plant oils using high-performance liquid chromatography atmospheric pressure chemical ionization mass spectrometry. *J. Chromatogr., A* **2003**, *1010*, 195−215.
(37) Chapagain, B. P.; Wiesman, Z. MALDI-TOF/MS fingerprinting of triacylglycerols (TAGs) in olive oils produced in the Israeli Negev Desert. *J. Agric. Food Chem.* **2009**, *57*, 1135−1142.
(38) Calvano, C. D.; Palmisano, F.; Zambonin, C. G. Laser desorption/ionization time-of-flight mass spectrometry of triacylglycerols in oils. *Rapid Commun. Mass Spectrom.* **2005**, *19*, 1315.
(39) International Olive Council (IOC) T.20/Doc. No. 32. Determination of composition of triacylglycerols and composition and content of di-acylglycerols by capillary gas chromatography in vegetable oils, Madrid, Spain, 2013.
(40) Marsilio, V.; Lanza, B.; De Angelis, M. Olive cell wall components: physical and biochemical changes during processing. *J. Sci. Food Agric.* **1996**, *70*, 35−43.
(41) Aragón, A.; Toledano, R. M.; Cortes, J. M.; Villén, J.; Vázquez, A. Wax ester composition of monovarietal olive oils from designation of origin (DO) "Campos de Hellin". *Food Chem.* **2011**, *129*, 71−76.
(42) Nota, G.; Naviglio, D.; Romano, R.; Sabia, V.; Spagna-Musso, S.; et al. Determination of the wax ester content in olive oils. Improvement in the method proposed by EEC regulation 183/93. *J. Agric. Food Chem.* **1999**, *47*, 202−205.
(43) International Olive Council (IOC) T.20/Doc. No. 31. Determination of the content of waxes, fatty acid methyl esters and fatty acid ethyl esters by capillary gas chromatography using 3 grams of silica, Madrid, Spain, 2012.
(44) Mehlenbacher, V. C. *The Analysis of Fats and Oils*; Garrard Press: Champaign, IL, USA, 1960.
(45) International Olive Council (IOC) T.20/Doc. No. 11/Rev. 2. Determination of stigmastadienes in vegetable oils, Madrid, Spain, 2001.
(46) Lanzón, A. *Changes Produced in the Components of the Unsaponifiable of Olive Oil As Consequence of the Refining Process.* Ph.D. thesis, University of Seville, Spain, 1990.
(47) International Olive Council (IOC) T.20/Doc. no. 16/Rev. 1. Determination of sterenes in in refined vegetable oils, Madrid, Sevilla, 2001.
(48) International Olive Council (IOC) RES-1/93-IV/05. Detection of polycyclic aromatic hydrocarbons in edible olive oils and olive-pomace oils, Madrid, Spain, 2005.
(49) Moret, S.; Conte, L. Off-line LC-LC determination of PAHs in edible oils and lipidic extracts. *J. High Resolut. Chromatogr.* **1998**, *21*, 253−257.
(50) Moret, S.; Conte, L. Polycyclic aromatic hydrocarbons in edible fats and oils: occurrence and analytical methods. *J. Chromatogr., A* **2000**, *882*, 245−253.

DOI: 10.1021/jf5062265
J. Agric. Food Chem. 2015, 63, 4509−4526

(51) Grob, K.; Giuffré, M. A.; Biedermann, M.; Bronz, M. The detection of adulteration with desterolized oils. *Fat Sci. Technol.* **1994**, *9*, 341−345.
(52) Aparicio, R.; Ferreiro, L.; Alonso, V. Effect of climate on the chemical composition of virgin olive oil. *Anal. Chim. Acta* **1994**, *292*, 235−241.
(53) Aparicio, R.; García González, D. L. Olive oil characterization and traceability. In *Handbook of Olive Oil*; Aparicio, R., Harwood, J., Eds.; Springer Science: New York, 2013; pp 431−478.
(54) European Communities (EC) Regulation No. 1348/2013. *Off. J. Eur. Communities* **2013**, *L338*.
(55) International Olive Council (IOC) T.20/Doc. No. 10/Rev. 1. Determination of the composition and content of sterols by capillary-column gas chromatography, Madrid, Spain, 2001.
(56) Mariani, C.; Bellan, G.; Lestini, E.; Aparicio, R. The detection of the presence of hazelnut oil in olive oil by free and esterified sterols. *Eur. Food Res. Technol.* **2006**, *223*, 655−661.
(57) Aparicio, R.; Alonso, V. Characterization of virgin olive oils by SEXIA expert system. *Prog. Lipid Res.* **1994**, *33*, 29−38.
(58) International Olive Council (IOC) T.20/Doc. No. 30/Rev. 1. Determination of the composition and content of sterols and triterpene dialcohols by capillary column gas chromatography, Madrid, Spain, 2013.
(59) Arjona, J. *Oral communication: Caracterización de aceites de oliva vírgenes monovarietales: incidencia del origen geográfico*. Master's thesis, Universidad de Sevilla, 2013.
(60) International Olive Council (IOC) T.20/Doc. No. 26. Determination of aliphatic alcohols content by capillary gas chromatography, Madrid, Spain 2003.
(61) European Communities (EC) Regulation No. 656/95. *Off. J. Eur. Communities* **1995**.
(62) International Union of Pure and Applied Chemistry (IUPAC) Method 2.411, identification and determination of tocopherols. In *Standard Methods for the Analysis of Oils, Fats and Derivatives*, 7th ed.; Paquot, C., Haufenne, A., Eds.; Blackwell Scientific Publications: Oxford, UK, 1987; pp 174−182.
(63) International Union of Pure and Applied Chemistry (IUPAC) Method 2.432, determination of tocopherols and tocotrienols in vegetable oils and fats by HPLC. In *Standard Methods for the Analysis of Oils, Fats and Derivatives*, 7th ed.; Paquot, C.;, Haufenne, A., Eds.; Blackwell Scientific Publications: Oxford, UK, 1987; pp 2432/1−2432/7.
(64) Grigoriadou, D.; Androulaki, A.; Psomiadou, E.; Tsimidou, M. Z. Solid phase extraction in the analysis of squalene and tocopherols in olive oil. *Food Chem.* **2007**, *105*, 675−680.
(65) Escuderos, M. E.; Sayago, A.; Morales, M. T.; Aparicio, R. Evaluation of α-tocopherol in virgin olive oil by a luminiscent method. *Grasas Aceites* **2009**, *60*, 336−342.
(66) International Organization for Standardization (ISO) 9936. *Animal and vegetable fat and oils. Determination of tocopherol and tocotrienol contents by high-performance liquid chromatography*; Ethiopia, 2012.
(67) Gandul-Rojas, B.; Gallardo-Guerrero, L.; Roca, M.; Aparicio-Ruiz, R. Chromatographic methodologies: compounds for olive oil color issues. In *Handbook of Olive Oil: Analysis and Properties*, 2nd ed.; Aparicio, R., Harwood, J. L., Eds.; Springer: New York, 2013; pp 219−260.
(68) Gandul-Rojas, B.; Roca, M.; Minguez-Mosquera, M. I. Chlorophyll and carotenoid pattern invirgin olive oil. Adulteration control. In *Proceeding of the 1st International Congress on Pigments in Food Technology (PFI)*; Minguez-Mosquera, M. I., Jaren-Galan, M., Hornero-Mendez, H., Eds.; PFT Press: Sevilla, Spain, 1999; pp 381−386.
(69) Gertz, C.; Fiebig, H.-J. Pyropheophytin a − determination of thermal degradation products of chlorophyll a in virgin olive oil. *Eur. J. Lipid Sci. Technol.* **2006**, *108*, 1062−1065.
(70) Hornero-Méndez, D.; Gandul-Rojas, B.; Mínguez-Mosquera, M. I. Routine and sensitive SPE-HPLC method for quantitative determination of pheophytin a and pyropheophytin *a* in olive oils. *Food Res. Int.* **2005**, *38*, 1067−1072.
(71) Mínguez-Mosquera, M. I.; Gandul-Rojas, B.; Gallardo-Guerrero, M. L. Rapid method of quantification of chlorophylls and carotenoids in virgin olive oil by high-performance liquid chromatography. *J. Agric. Food Chem.* **1992**, *40*, 60−63.
(72) Gertz, C.; Fiebig, H.-J. Isomeric diacylglycerols − determination of 1,2- and 1,3-diacylglycerols in virgin olive oil. *Eur. J. Lipid Sci. Technol.* **2006**, *108*, 1066−1069.
(73) Pérez-Camino, M. C.; Moreda, W.; Cert, A. Effects of olive fruit quality and oil storage practices on the diacylglycerol content of virgin olive oils. *J. Agric. Food Chem.* **2001**, *49*, 699−704.
(74) Frega, N.; Bocci, F.; Lercker, G. High-resolution gas-chromatographic determination of diacylglycerols in common vegetable oils. *J. Am. Oil Chem. Soc.* **1993**, *70*, 175−177.
(75) Mariani, C.; Bellan, G. Detection of low quality oils in extra virgin olive oils. *Riv. Ital. Sostanze Gras.* **2008**, *85*, 3−20.
(76) Pérez-Camino, M. C.; Cert, A.; Romero-Segura, A.; Cert-Trujillo, R.; Moreda, W. Alkyl esters of fatty acids a useful tool to detect soft deodorized olive oils. *J. Agric. Food Chem.* **2008**, *56*, 6740−6744.
(77) Boggia, R.; Borgogni, C.; Hysenaj, V.; Leardi, R.; Zunin, P. Direct GC-(EI) MS determination of fatty acid alkyl esters in olive oil. *Talanta* **2014**, *119*, 60−67.
(78) International Organization of Standardization (ISO) 660. Animal and vegetable fats and oils − Determination of acid value and acidity, Geneva, Switzerland, 2009.
(79) American Oil Chemists Society (AOCS). Official method Cd 3d-63. Acid value; AOCS Press, Champaign, IL, USA, 1999.
(80) Aricetti, J. A.; Tubino, M. A. Visual titration method for the determination of the acid number of oils and fats: a green alternative. *J. Am. Oil Chem. Soc.* **2012**, *89*, 113−2115.
(81) Lanser, A. C.; List, G. R.; Holloway, R. K.; Mounts, T. L. FTIR estimation of free fatty acid content in crude oils extracted from damaged soybeans. *J. Am. Oil Chem. Soc.* **1991**, *68*, 448−449.
(82) Ismail, A. A.; van de Voort, F. R.; Emo, G.; Sedman, J. Rapid quantitative determination of free fatty acids in fats and oils by Fourier transform infrared spectroscopy. *J. Am. Oil Chem. Soc.* **1993**, *70*, 335−341.
(83) Li, D.; Sedman, J.; García-González, D. L.; van De Voort, F. R. Automated acid content determination in lubricants by FTIR spectroscopy as an alternative to acid number determination. *J. ASTM Int.* **2009**, *6*, 1−12.
(84) Li, Y.; García-González, D. L.; Yu, X.; van de Voort, F. R. Determination of free fatty acids in edible oils with the use of a variable filter array IR spectrometer. *J. Am. Oil Chem. Soc.* **2008**, *85*, 599−604.
(85) Yu, X.; Du, S.; van de Voort, F. R.; Yue, T.; Li, Z. Automated and simultaneous determination of free fatty acids and peroxide values in edible oils by FTIR spectroscopy using spectral reconstitution. *Anal. Sci.* **2009**, *25*, 627−632.
(86) Choe, E.; Min, D. B. Mechanisms and factors for edible oil oxidation. *Compr. Rev. Food Sci. Food Saf.* **2006**, *5*, 169−186.
(87) Guillén, M. D.; Cabo, N. Some of the most significant changes in the Fourier transform infrared spectra of edible oils under oxidative conditions. *J. Sci. Food Agric.* **2000**, *80*, 2028−2036.
(88) Van de Voort, F. R.; Ismail, A. A.; Sedman, J.; Dubois, J.; Nicodemo, T. The determination of peroxide value by Fourier transform infrared spectroscopy. *J. Am. Oil Chem. Soc.* **1994**, *71*, 921−926.
(89) Ma, K.; van de Voort, F. R.; Ismail, A. A.; Sedman, J. Quantitative determination of hydroperoxides by FTIR spectroscopy using a disposable IR card. *J. Am. Oil Chem. Soc.* **1998**, *75*, 1095−1101.
(90) Pizarro, C.; Esteban-Díez, I.; Rodríguez-Tecedor, S.; González-Sáiz, J. M. Determination of the peroxide value in extra virgin olive oils through the application of the stepwise orthogonalisation of predictors to mid-infrared spectra. *Food Control* **2013**, *34*, 158−167.
(91) International Olive Council (IOC) T20/Doc. No. 19/Rev. 3. Method of analysis spectrophotometric investigation in the ultraviolet, Madrid, Spain, 2010.

DOI: 10.1021/jf5062265
J. Agric. Food Chem. 2015, 63, 4509−4526

(92) International Olive Council (IOC) T.20/Doc. No. 15/Rev. 6. Sensory analysis of olive oil: method for the organoleptic assessment of virgin olive oil, Madrid, Spain, 2013.
(93) Tsimidou, M. Z. Analytical methodologies: phenolic compounds related to olive oil taste issues. In *Handbook of Olive Oil: Analysis and Properties*, 2nd ed.; Aparicio, R., Harwood, J. L., Eds.; Springer: New York, 2013; pp 311−334.
(94) Romero, C.; Brenes, M. Comment on addressing analytical requirements to support health claims on "Olive oil polyphenols" (EC Regulation 432/212). *J. Agric. Food Chem.* **2014**, *62*, 10210−10211.
(95) International Olive Council (IOC) T.20/Doc No. 29. Determination of biophenols in olive oils by HPLC, Madrid, Spain, 2009.
(96) International Olive Council (IOC) Decision No. DEC-17/97-V/2009. Identification and quantification of the phenolics in olive oil, Madrid, Spain, 2009.
(97) Carrasco-Pancorbo, A.; Cerretani, L.; Bendini, A.; Segura-Carretero, A.; Gallina-Toschi, T.; Fernandez-Gutierrez, A. Analytical determination of polyphenols in olive oils. *J. Sep. Sci.* **2005**, *28*, 837−858.
(98) European Comunities (EC) No. 432/2012 L 136/1-40. Establishing a list of permitted health claims made on foods, other than those referring to the reduction of disease risk and to children's development and health. *Off. J. Eur. Communities* **2012**.
(99) Papoti, V. T.; Tsimidou, M. Z. Looking through the qualities of a fluorimetric assay for the total phenol content estimation in virgin olive oil, olive fruit or leaf polar extract. *Food Chem.* **2009**, *112*, 246−252.
(100) Pirisi, F. M.; Cabras, P.; Falqui, C. C.; Migliorini, M.; Muggelli, M. Phenolic compounds in virgin olive oil. 2. Reappraisal of the extraction, HPLC separation, and quantification procedures. *J. Agric. Food Chem.* **2000**, *48*, 1191−1196.
(101) Hrncirik, K.; Fritsche, S. Comparability and reliability of different techniques for the determination of phenolic compounds in virgin olive oil. *Eur. J. Lipid Sci. Technol.* **2004**, *106*, 540−549.
(102) Armaforte, E.; Mancebo-Campos, V.; Bendini, A.; Salvador, M. D.; Fregapane, G.; et al. Retention effects of oxidized polyphenols during analytical extraction of phenolic compounds of virgin olive oil. *J. Sep. Sci.* **2007**, *30*, 2401−2406.
(103) Suárez, M.; Macià, A.; Romero, M. P.; Motilva, M. J. Improved liquid chromatography tandem mass spectrometry method for the determination of phenolic compounds in virgin olive oil. *J. Chromatogr., A* **2008**, *1214*, 90−99.
(104) Brenes, M.; García, A.; Ríos, J. J.; García, P.; Garrido, A. Use of 1-acetoxypinoresinol to authenticate Picual olive oils. *Int. J. Food Sci. Technol.* **2002**, *37*, 615−625.
(105) Selvaggini, R.; Servili, M.; Urbani, S.; Esposto, S.; Taticchi, A.; et al. Evaluation of phenolic compounds in virgin olive oil by direct injection in high-performance liquid chromatography with fluorometric detection. *J. Agric. Food Chem.* **2006**, *54*, 2832−2838.
(106) Pérez-Trujillo, M.; Gómez-Caravaca, A. M.; Segura-Carretero, A.; Fernández-Gutiérrez, A.; Parella, A. T. Separation and identification of phenolic compounds of extra virgin olive oil from Olea europaea L by HPLC-DAD-SPE-NMR/MS. Identification of a new diastereoisomer of the adehydic form of oleuropein aglycone. *J. Agric. Food Chem.* **2010**, *58*, 9129−9136.
(107) Aparicio, R.; Morales, M. T.; García-González, D. L. Towards new analyses of aroma and volatiles to understand sensory perception of olive oil. *Eur. J. Lipid Sci. Technol.* **2012**, *114*, 1114−1125.
(108) Morales, M. T.; Aparicio-Ruiz, R.; Aparicio, R. Chromatographic methodologies: compounds for olive oil odor issues. In *Handbook of Olive Oil: Analysis and Properties*, 2nd ed.; Aparicio, R., Harwood, J. L., Eds.; Springer: New York, 2013; pp 261−310; DOI: 10.1007/978-1-4614-7777-8_8.
(109) Morales, M. T.; Luna, G.; Aparicio, R. Comparative study of virgin olive oil sensory defects. *Food Chem.* **2005**, *91*, 293−301.
(110) García-González, D. L.; Aparicio, R. Sensors: from biosensors to the electronic nose. *Grasas Aceites* **2002**, *53*, 96−114.
(111) García-González, D. L.; Aparicio, R. Coupling MOS sensors and gas chromatography to interpret the sensor responses to complex food aroma: application to virgin olive oil. *Food Chem.* **2010**, *120*, 572−579.
(112) García-González, D. L.; Vivancos, J.; Aparicio, R. Mapping brain activity induced by olfaction of virgin olive oil aroma. *J. Agric. Food Chem.* **2011**, *59*, 10200−10210.
(113) International Olive Council (IOC) T.20/Doc. No. 17/Rev. 1. Determination of *trans* unsaturated fatty acids by capillary column gas chromatography, Madrid, Spain, 2001.
(114) Mariani, C.; Fedeli, E.; Grob, K. Valutazione dei componenti minori liberi ed esterificati nelle sostanze grasse. *Riv. Ital. Sostanze Gras.* **1991**, *68*, 233−242.
(115) Aparicio, R. Final report project G6RD-CT2000-00440 (MEDEO). Commission of the European Communities (Growth Program), Brussels, Belgium, 2004.

DOI: 10.1021/jf5062265
J. Agric. Food Chem. 2015, 63, 4509−4526

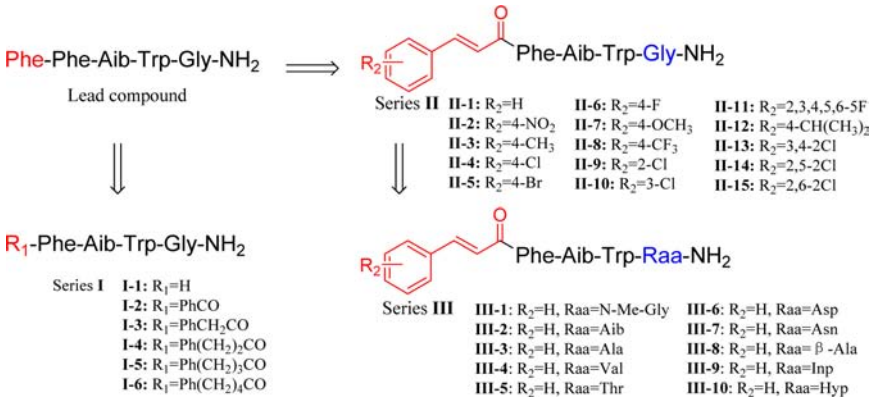

Figure 1. Design strategy of the insect kinin analogues using the peptidomimetic approach.

insect kinin sequence. These analogues not only maintain their activity *in vitro* in *A. domesticus* and *A. aegypti* Malpighian tubule fluid secretion assays and activity *in vivo* in *M. domestica* diuretic assay but also retain their resistance to hydrolysis of ACE and NEP endopeptidases. In addition, these analogues showed a response in receptor-expressing systems of tick *Boophilus microplus* and *A. aegypti*.[10,18,19,28] Among these analogues, the double Aib-containing kinin analogue (**K-Aib-1**: Aib-Phe-Phe-Aib-Trp-Gly-NH_2) was first reported to exhibit good aphicidal activity against pea aphid *Acyrthosiphon pisum*.[13] However, this analogue is still not suitable for use as an insecticide as a result of its longer peptide chain, higher molecular weight, and lower aphicidal activity. Further studies need to be undertaken to discover better kinin analogues with simpler structure and higher activity.

In our previous work, we designed and synthesized a series of analogues using **K-Aib-1** as the lead compound, modifying the N-terminal by replacing the N-terminal Aib with different substitutes or completely removing the N-terminal Aib. The sequence-simplified pentapeptide analogue Phe-Phe-[Aib]-Trp-Gly-NH_2, which was first synthesized and reported by Nachman et al.[18] to show resistance to an insect angiotensin converting enzyme and potent diuretic activity, also showed higher aphicidal activity than the **K-Aib-1**.[29] In the present work, we used the structure-simplified pentapeptide analogue Phe-Phe-[Aib]-Trp-Gly-NH_2 as the lead compound, and we further incorporated peptidomimetics to this structure, in an attempt to find (a) new analogue(s) with higher activity to employ as (a) new lead(s) for novel eco-insecticide candidates (Figure 1). Three series, comprising 31 analogues, were designed and synthesized by replacing/modifying the positions that played an important role in bioactivities.

MATERIALS AND METHODS

Synthesis. *Materials.* Rink Amide-AM resin (0.56 mmol/g), *O*-benzotriazole-*N*,*N*,*N*′,*N*′-tertramethyl uronium hexafluorophosphate (HOBt), 1-hydroxybenzotriazole anhydrate (HBTU), *N*,*N*′-diisopropylethylamine (DIEA), *N*,*N*′-dissoprophlcarbodiimide (Dic), trifluoroacetic acid (TFA), Fmoc-protected amino acids, Fmoc-Gly-OH, Fmoc-*N*-Me-Gly-OH, Fmoc-*L*-Phe-OH, Fmoc-*L*-Trp(Boc)−OH, Fmoc-*L*-Aib−OH, Fmoc-*L*-Ala-OH, Fmoc-*L*-Val-OH, Fmoc-*L*-Thr-OH, Fmoc-*L*-Asp(OtBu)-OH, Fmoc-*L*-Asn-OH, Fmoc-Inp-OH, and Fmoc-*L*-Hyp(tBu)-OH were purchased from GL Biochem, Ltd. (Shanghai, China). High-performance liquid chromatography (HPLC)-grade *N*,*N*-dimethylformamide (DMF), dichloromethane (DCM) and methanol were purchased from Dima Technology, Inc. (Richmond Hill, Ontario, Canada). Thioanisole, phenol, (substituted) cinnamic acids, phenylacetic acid, hydrocinnamic acid, 4-phenylbutyrilc acid, and 5-phenylpentanoic acid were purchased from Alfa Aesar, U.S.A.

General Synthesis Procedure. F[Aib]WG and F[Aib]W-[Raa] with Resin was synthesized from Rink Amide-AM resin (536 mg, 0.3 mmol) using the standard Fmoc/*t*Bu chemistry and HBTU/HOBt protocol.[30] Incoming amino acids were activated with HOBt (164 mg, 1.2 mmol), HBTU (456 mg, 1.2 mmol), and DIEA (210 μL, 1.2 mmol) in DMF (5 mL) for 5 min, and the couplings were run for 2 h. Removal of the N-terminal Fmoc group from the residues was accomplished with 20% piperidine in DMF (5 mL) for 20 min.

The lead compound and analogues were cleaved from the resin with TFA (9 mL) containing 5% phenol, 2.5% thioanisole (0.5 mL), and 5% water (0.5 mL) for 2 h after the mimic acids were coupled to the F[Aib]WG with resin (0.3 mmol) with HOBt (164 mg, 1.2 mmol), HBTU(456 mg, 1.2 mmol), and DIEA (210 μL, 1.2 mmol) in DMF (5 mL) for 3 h at room temperature. Removal of the protective group Boc and tBu was also accomplished in the cleavage procedure. To avoid the generation of OBt esters, some analogues containing a carboxylic acid group were synthesized using Dic as the coupling reagent instead of HBTU/HOBt. The general synthesis procedure is shown in Figure 2.

Purification and Characterization. The crude compounds were purified on a C_{18} reversed-phase semipreparative column with a flow rate of 10 mL/min using different ratio of acetonitrile/water (v/v) from 30/70 to 70/40 containing 0.1% TFA as an ion-pairing reagent. The wavelength of UV detection was set at 214 nm. The purified compounds were run again on HPLC to ensure that the purity was higher than 95%. The structures of the analogues were confirmed by high-resolution mass spectrometry (HRMS) using an Agilent Accurate-Mass-Q-TOF MS 6520 system equipped with an Electro Spray Ionization (ESI) source. All the MS experiments were detected in the positive ionization mode. For Q-TOF/MS conditions, fragment and capillary voltages were kept at 130 and 3500 V, respectively. Nitrogen was supplied as the nebulizing and drying gas. The temperature of the drying gas was set at 300 °C. The flow rate of the drying gas and the pressure of the nebulizer were 10 L/min and 25 psi, respectively. Full-scan spectra were acquired over a scan range of m/z 80−1200 at 1.03 spectra s^{-1}.

DOI: 10.1021/acs.jafc.5b01225
J. Agric. Food Chem. 2015, 63, 4527−4532

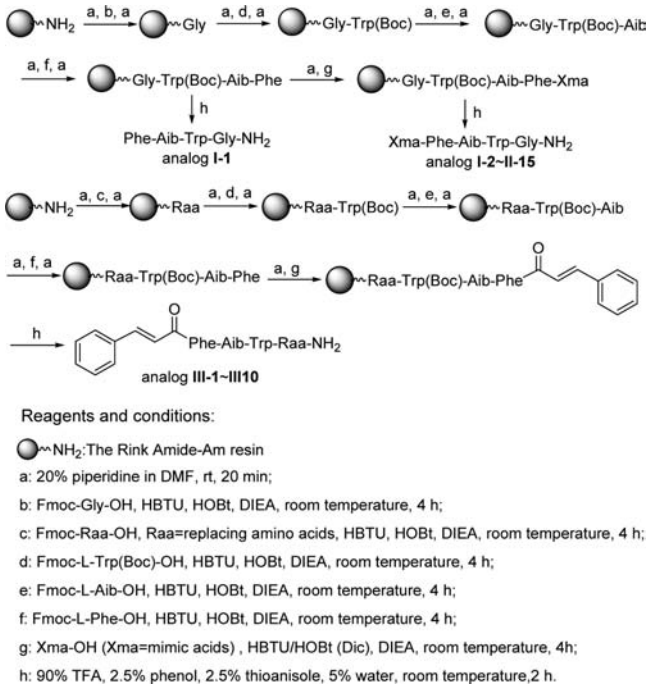

Figure 2. General synthesis procedure.

Aphicidal Bioassay. The aphicidal activity of the insect kinin analogues against *Aphis glycines* was determined using the reported procedure.[31]

Compounds were dissolved to a concentration of 2000 mg/L and then diluted to lower concentrations with 0.05% Triton X-100. Soybean leaf discs of about 3 cm diameter were dipped into the test solution for 15 s. The discs dipped into 0.05% Triton X-100 were set as the negative control. After air-drying, the treated leaf discs were placed individually into bioassay plates with 1% agar to keep moist. The discs were infested with 20 ± 3 3-day old aphids and kept in an incubator with constant temperature (25 ± 1 °C) for 48 h. The number of dead aphids was then counted, and the mortality rates were corrected using Abbott's formula.[32] Each experiment was performed three times. The standard deviations of the tested aphicidal values were ≤10%. The LC_{50} values were calculated using the SAS 9.0 (SAS Institute Inc., U.S.A.).

RESULTS AND DISCUSSION

Design and Synthesis of Analogues. Members of the insect kinin family are inactive *in vivo* as a consequence of hydrolysis by both hemolymph and tissue-bound peptidases in insects.[16,33,34] The two susceptible hydrolytic sites of the kinin core pentapeptide have been reported.[10] Analogues with modification and replacement of amino acids at the hydrolysis sites not only showed resistance to peptidases but also retained their bioactivities.[7,14,20,27,28] Our previous work demonstrated that the N-terminal Aib of the secondary hydrolysis site of analogue **K-Aib-1** did not play an important role in aphicidal activity.[29] Removing the N-terminal protective group might not only simplifies the structure but also maintains or even increases the aphicidal activity of analogues. Thus, the simplified analogue Phe-Phe-[Aib]-Trp-Gly-NH_2 could be a good lead compound. In this work, we replaced the terminal Phe of the lead compound with different mimics, which was also modified by Nachman et al.[35,36] in the N-terminal region of the insect kinin core pentapeptide to discover active diuretic analogues, expecting to find (a) new analogue(s) with higher aphicidal activity. As shown in Figure 1, the first step of the strategy is replacing the N-terminal Phe with H, aromatic carboxylic acids with different carbon chain lengths (Series **I**) and substituted phenyl cinnamic acids (Series **II**), which have been demonstrated to be good mimics of Phe in our previous work to obtain the optimal mimic of Phe. The result of aphicidal bioassay showed that the optional carbon chain length was 3-C and analogue containing the cinnamic acid group exhibited improved bioactivity. We subsequently used the optimal analogue (**II-1**) as the second lead, and we performed modifications at the C-terminal Gly, the site shown to enhance inhibition of weight gain and induce significant mortality in *Helicoverpa zea* larvae when modified with terminal aldehyde or with hydrophilic/hydrophobic natural/unnatural amino acids to assess its importance to bioactivity (Series **III**). The aphicidal activity against the soybean aphid *Aphis glycines* of all analogues was evaluated.

The analogues were synthesized using the solid-phase peptide synthesis (SPPS) employing the Fmoc protecting group strategy. For avoiding the generation of OBt esters, some analogues containing (substituted) cinnamic acid group were synthesized using Dic as the coupling reagent instead of HBTU/HOBt.[37] The purity and high-resolution mass spectrometry (HRMS) data of all target compounds are shown in Table 1.

Aphicidal Activity. The aphicidal activity of the lead compound, the analogues, and pymetrozine against *A. glycines* are shown in Table 1. The preliminary bioassay results (at a concentration of 200 mg/L, 48 h) indicated that all the analogues exhibited aphicidal activity. The aphicidal activity of analogue **I-4**, **I-5**, **I-6**, **II-1**, **II-3**, **II-10**, **III-2**, **III-3**, **III-6**, and **III-9** are comparable to or even better than that of the lead compound Phe-Phe-[Aib]-Trp-Gly-NH_2. On the basis of the primary experimental results, analogues showing a mortality rate higher than 70% were chosen to determine the LC_{50} values. As shown in Table 1, **I-4**, **II-1**, and **III-9** exhibited higher aphicidal activity against soybean aphid with LC_{50} values of 0.039, 0.019, and 0.034 mmol/L, respectively, compared to the lead compound (LC_{50} = 0.045 mmol/L). In particular, **II-1** was the most toxic compound to the soybean aphid with an LC_{50} of 0.019 mmol/L, even higher than the commercial insecticide pymetrozine with an LC_{50} of 0.034 mmol/L. However, the aphicidal activity of analogue **II-1** is not statistically significant and still needs to be improved in the further work.

Removing the terminal Phe (**I-1**) significantly decreased the ahpicidal activity, indicating that the N-terminal Phe group was important to maintain the bioactivity of the analogues. Thus, we retained the hydrolysis site Phe, but we modified it with other mimics. Analogues **I-4** and **II-1**, with 3-carbon mimetic aromatic carboxylic acids on the Phe[1] position, exhibited higher aphicidal activity than other analogues, suggesting that the optimal carbon chain length of mimetic aromatic carboxylic acids was 3-carbon, whereas the optimal mimic of Phe was the cinnamic acid. We surmised that the C═C bond of cinnamic acid might play an important role, such as forming a $\pi-\pi$ stacking effect, in the interaction of the mimetic insect kinin analogues with target receptors.

Recently, the widely accepted active conformation of an insect kinin C-terminal pentapeptide core region in the interaction of the analogue with the receptor is a 1-4 β-turn. The aromatic side chains of the critical residues Phe[1] and Trp[4]

DOI: 10.1021/acs.jafc.5b01225
J. Agric. Food Chem. 2015, 63, 4527−4532

Table 1. HRMS Results, Purity, and Aphicidal Activity against *Aphis glycines* of Target Compounds

	HRMS			aphicidal activity	
compd	calcd (m/z)	measured (m/z)	purity (%)	mortality (%) (200 mg/L,48h)	LC_{50} (95% FL) (mmol/L, 48 h)
lead	$[M + H]^+$ 640.3242	$[M + H]^+$ 640.3246	98	78.56 ± 3.04	0.045 (0.026−0.074)
I-1	$[M + H]^+$ 493.2558	$[M + H]^+$ 493.2556	98	40.80 ± 4.96	nt
I-2	$[M + H]^+$ 597.2820	$[M + H]^+$ 597.2819	97	54.93 ± 2.73	nt
I-3	$[M + Na]^+$ 633.2796	$[M + Na]^+$ 633.2802	98	62.56 ± 4.24	nt
I-4	$[M + Na]^+$ 647.2952	$[M + Na]^+$ 647.2955	98	83.23 ± 5.48	0.039 (0.032−0.062)
I-5	$[M + Na]^+$ 661.3109	$[M + Na]^+$ 661.3101	96	73.71 ± 2.95	0.170 (0.067−0.22)
I-6	$[M + Na]^+$ 675.3265	$[M + Na]^+$ 675.3273	98	74.93 ± 3.94	0.120 (0.070−0.30)
II-1	$[M + Na]^+$ 645.2796	$[M + Na]^+$ 645.2800	98	89.66 ± 4.23	0.019 (0.0035−0.039)
II-2	$[M + Na]^+$ 690.2647	$[M + Na]^+$ 690.2649	98	58.53 ± 4.86	nt
II-3	$[M + Na]^+$ 659.2952	$[M + Na]^+$ 659.2954	97	77.04 ± 7.16	0.140 (0.074−0.44)
II-4	$[M + Na]^+$ 679.2406	$[M + Na]^+$ 679.2412	96	54.27 ± 33.23	nt
II-5	$[M + Na]^+$ 723.2901	$[M + Na]^+$ 723.2982	96	56.41 ± 4.75	nt
II-6	$[M + Na]^+$ 663.2702	$[M + Na]^+$ 663.2708	96	37.98 ± 5.00	nt
II-7	$[M + H]^+$ 653.3082	$[M + H]^+$ 653.3079	96	62.88 ± 6.29	nt
II-8	$[M + Na]^+$ 713.2670	$[M + Na]^+$ 713.2683	98	37.47 ± 2.45	nt
II-9	$[M + Na]^+$ 679.2406	$[M + Na]^+$ 679.2408	98	57.56 ± 4.62	nt
II-10	$[M + Na]^+$ 679.2406	$[M + Na]^+$ 679.2403	97	75.08 ± 0.61	0.065 (0.041−0.10)
II-11	$[M + Na]^+$ 735.2325	$[M + Na]^+$ 735.2332	97	50.16 ± 5.40	nt
II-12	$[M + Na]^+$ 687.3265	$[M + Na]^+$ 687.3270	98	35.03 ± 3.43	nt
II-13	$[M + Na]^+$ 713.2016	$[M + Na]^+$ 713.2019	98	44.05 ± 5.22	nt
II-14	$[M + Na]^+$ 713.2016	$[M + Na]^+$ 713.2024	97	36.16 ± 4.11	nt
II-15	$[M + Na]^+$ 713.2016	$[M + Na]^+$ 713.2016	96	53.67 ± 2.64	nt
III-1	$[M + Na]^+$ 659.2952	$[M + Na]^+$ 659.2955	98	64.60 ± 3.58	nt
III-2	$[M + Na]^+$ 673.3109	$[M + Na]^+$ 673.3114	97	68.98 ± 7.85	nt
III-3	$[M + Na]^+$ 659.2952	$[M + Na]^+$ 659.2957	99	67.16 ± 9.87	nt
III-4	$[M + Na]^+$ 687.3265	$[M + Na]^+$ 687.3261	98	46.05 ± 5.01	nt
III-5	$[M + Na]^+$ 689.3058	$[M + Na]^+$ 689.3064	97	63.07 ± 7.80	nt
III-6	$[M + H]^+$ 681.3031	$[M + H]^+$ 681.3028	98	67.18 ± 2.75	nt
III-7	$[M + H]^+$ 680.3191	$[M + H]^+$ 680.3189	98	49.01 ± 1.20	nt
III-8	$[M + H]^+$ 637.3133	$[M + H]^+$ 637.3132	98	63.25 ± 3.85	nt
III-9	$[M + H]^+$ 677.3446	$[M + H]^+$ 677.3450	99	75.99 ± 4.67	0.034 (0.020−0.063)
III-10	$[M + H]^+$ 679.3239	$[M + H]^+$ 679.3242	98	63.10 ± 6.70	nt
pymetrozine	\	\	99	90.37 ± 2.50	0.034 (0.012−0.083)

nt: LC_{50} value was not tested when screening mortality was lower than 70% at the concentration of 200 mg/L, 48 h. 95% FL: 95% fiducial interval.

interact to form a selective aromatic surface that interacts with the receptor site.[38] Analogues of series **II** were designed to determine the substituent effect of the benzene ring of cinnamic acid with different substitutes and they exhibited decreased aphicidal activity to varying degrees compared with **II-1**. We speculate that substitutions in the benzene ring affected the formation of the aromatic surface and thus interfered with interaction of analogues with the receptor site as a result of their steric stabilization, which led to the decreased bioactivity. Therefore, the side aromatic group without substitution of Phe played a critical role in bioactivity. Further studies on the effect of different side heterocyclic groups without substitution will also be useful to assess. In series **III**, analogues were designed based on **II-1** to assess the importance of the C-terminal Gly. The bioassay result showed that all the analogues were less toxic to the soybean aphid than **II-1**, which demonstrated that the C-terminal Gly site should be conserved.

In summary, three series of novel insect kinin analogues were designed and synthesized. The aphicidal bioassay results showed that most analogues exhibited considerable aphicidal activity against *A. glycines*, especially analogue **II-1** with an LC_{50} of 0.019 mmol/L, which exhibited improved aphicidal activity compared with the lead compound (LC_{50} = 0.045 mmol/L), and comparable activity to the commercial insecticide pymetrozine with an LC_{50} of 0.034 mmol/L. Therefore, analogue **II-1** could be used as a new lead for further chemical modifications and simplifications to discover eco-friendly insecticides.

AUTHOR INFORMATION

Corresponding Author

*E-mail: yangxl@cau.edu.cn. Tel: +86-10-62732223.

Author Contributions

C.-L.Z., Y.L., and X.-L.Y. designed the analogues and experiments. C.-L.Z. and X.-Q.W. performed the synthesis and purification of analogues. C.-L.Z., Y.-Y.Q., and D.-L.S. conducted the aphicidal bioassay. C.-L.Z., D.-L.S., Y.L., and X.-L.Y. analyzed the data. C.-L.Z. and X.-L.Y. wrote the manuscript. All authors read and approved the final manuscript.

Funding

This study was financially supported by the National Natural Science Foundation of China (No. 21132003) and the National "Twelfth Five-Year" Plan for Science and Technology (No. 2011BAE06B05-5).

Notes

The authors declare no competing financial interest.

DOI: 10.1021/acs.jafc.5b01225
J. Agric. Food Chem. 2015, 63, 4527−4532

■ ACKNOWLEDGMENTS

We are grateful to Professor Stephen Tobe and Dr. Juan Huang for their kind help on this manuscript writing.

■ REFERENCES

(1) Holman, G. M.; Nachman, R. J.; Wright, M. S. Comparative aspects of insect myotropic peptides. *Prog. Clin. Biol. Res.* **1990**, *342*, 35.

(2) Holman, G. M.; Nachman, R.; Wright, M. Insect neuropeptides. *Annu. Rev. Entomol.* **1990**, *35*, 201−217.

(3) Holman, G.; Cook, B.; Nachman, R. Primary structure and synthesis of a blocked myotropic neuropeptide isolated from the cockroach, *Leucophaea maderae*. *Comp. Biochem. Physiol., C: Comp. Pharmacol.* **1986**, *85*, 219−224.

(4) Nachman, R. J.; Holman, G. M. Myotropic insect neuropeptide families from the cockroach *Leucophaea maderae*. Structure-activity relationships. *ACS Symp. Ser.* **1991**, *453*, 194−214.

(5) Holman, G. M.; Nachman, R. J.; Coast, G. M. Isolation, characterization and biological activity of a diuretic myokinin neuropeptide from the housefly, *Musca domestica*. *Peptides* **1999**, *20*, 1−10.

(6) Torfs, P.; Nieto, J.; Veelaert, D.; Boon, D.; Van de Water, G.; Waelkens, E.; Derua, R.; Calderon, J.; De Loof, A.; Schoofs, L. The kinin peptide family in invertebrates. *Ann. N. Y. Acad. Sci.* **1999**, *897*, 361−373.

(7) Sajjaya, P.; Chandran, D.; Sreekumar, S.; Nachman, R. *In vitro* regulation of gut pH by neuropeptide analogues in the larvae of red palm weevil *Rhynchophorus ferrugineus*. *J. Adv. Zool.* **2001**, *22*, 26−30.

(8) Harshini, S.; Manchu, V.; Sunitha, V.; Sreekumar, S.; Nachman, R. *In vitro* release of amylase by culekinins in two insects: *Opsinia arenosella* (Lepidoptera) and *Rhynchophorus ferrugineus* (Coleoptera). *Trends. Life. Sci.* **2003**, *17*, 61−64.

(9) Harshini, S.; Nachman, R.; Sreekumar, S. Inhibition of digestive enzyme release by neuropeptides in larvae of *Opisina arenosella* (Lepidoptera: Cryptophasidae). *Comp. Biochem. Physiol., Part B: Biochem. Mol. Biol.* **2002**, *132*, 353−358.

(10) Nachman, R. J.; Strey, A.; Isaac, E.; Pryor, N.; Lopez, J. D.; Deng, J.-G.; Coast, G. M. Enhanced *in vivo* activity of peptidase-resistant analogs of the insect kinin neuropeptide family. *Peptides* **2002**, *23*, 735−745.

(11) Coast, G. M.; Holman, G. M.; Nachman, R. J. The diuretic activity of a series of cephalomyotropic neuropeptides, the achetakinins, on isolated Malpighian tubules of the house cricket. *J. Insect Physiol.* **1990**, *36*, 481−488.

(12) Nachman, R. J. Neuropeptides and receptors as targets for bioinsecticides. *Abstracts of Papers, 246th ACS National Meeting and Exposition*, Indianapolis, IN, United States, September 8−12, 2013, AGRO-137.

(13) Smagghe, G.; Mahdian, K.; Zubrzak, P.; Nachman, R. J. Antifeedant activity and high mortality in the pea aphid *Acyrthosiphon pisum* (Hemiptera: Aphidae) induced by biostable insect kinin analogs. *Peptides* **2010**, *31*, 498−505.

(14) Nachman, R. J.; Coast, G. M.; Douat, C.; Fehrentz, J.-A.; Kaczmarek, K.; Zabrocki, J.; Pryor, N. W.; Martinez, J. A C-terminal aldehyde insect kinin analog enhances inhibition of weight gain and induces significant mortality in *Helicoverpa zea* larvae. *Peptides* **2003**, *24*, 1615−1621.

(15) Seinsche, A.; Dyker, H.; Lösel, P.; Backhaus, D.; Scherkenbeck, J. Effect of helicokinins and ACE inhibitors on water balance and development of *Heliothis virescens* larvae. *J. Insect Physiol.* **2000**, *46*, 1423−1431.

(16) Cornell, M. J.; Williams, T. A.; Lamango, N. S.; Coates, D.; Corvol, P.; Soubrier, F.; Hoheisel, J.; Lehrach, H.; Isaac, R. E. Cloning and expression of an evolutionary conserved single-domain angiotensin converting enzyme from *Drosophila melanogaster*. *J. Biol. Chem.* **1995**, *270*, 13613−13619.

(17) Lamango, N.; Nachman, R.; Hayes, T.; Strey, A.; Isaac, R. Hydrolysis of insect neuropeptides by an angiotensin-converting enzyme from the housefly, *Musca domestica*. *Peptides* **1997**, *18*, 47−52.

(18) Nachman, R. J.; Isaac, R. E.; Coast, G. M.; Holman, G. M. Aib-containing analogues of the insect kinin neuropeptide family demonstrate resistance to an insect angiotensin-converting enzyme and potent diuretic activity. *Peptides* **1997**, *18*, 53−57.

(19) Taneja-Bageshwar, S.; Strey, A.; Zubrzak, P.; Pietrantonio, P. V.; Nachman, R. J. Comparative structure-activity analysis of insect kinin core analogs on recombinant kinin receptors from Southern cattle tick *Boophilus microplus* (Acari: Ixodidae) and mosquito *Aedes aegypti* (Diptera: Culicidae). *Arch. Insect Biochem. Physiol.* **2006**, *62*, 128−40.

(20) Pietrantonio, P.; Jagge, C.; Taneja-Bageshwar, S.; Nachman, R.; Barhoumi, R. The mosquito *Aedes aegypti* (L.) leucokinin receptor is a multiligand receptor for the three Aedes kinins. *Insect Mol. Biol.* **2005**, *14*, 55−67.

(21) Nachman, R. J.; Coast, G. M.; Holman, G. M.; Beier, R. C. Diuretic activity of C-terminal group analogues of the insect kinins in *Acheta domesticus*. *Peptides* **1995**, *16*, 809−813.

(22) Holmes, S.; Barhoumi, R.; Nachman, R.; Pietrantonio, P. Functional analysis of a G protein-coupled receptor from the Southern cattle tick *Boophilus microplus* (Acari: Ixodidae) identifies it as the first arthropod myokinin receptor. *Insect Mol. Biol.* **2003**, *12*, 27−38.

(23) Roberts, V. A.; Nachman, R. J.; Coast, G. M.; Hariharan, M.; Chung, J. S.; Holman, G. M.; Williams, H.; Tainer, J. A. Consensus chemistry and β-turn conformation of the active core of the insect kinin neuropeptide family. *Chem. Biol.* **1997**, *4*, 105−117.

(24) Giannis, A.; Rübsam, F. Peptidomimetics in drug design. *Adv. Drug Res.* **1997**, *29*, 1−78.

(25) Hruby, V. J.; Li, G.; Haskell-Luevano, C.; Shenderovich, M. Design of peptides, proteins, and peptidomimetics in chi space. *Biopolymers* **1997**, *43*, 219−266.

(26) Hruby, V. J.; Qiu, W.; Okayama, T.; Soloshonok, V. A. Design of nonpeptides from peptide ligands for peptide receptors. *Methods Enzymol.* **2002**, *343*, 91−123.

(27) Kai, Z.-P.; Xie, Y.; Huang, J.; Tobe, S. S.; Zhang, J.-R.; Ling, Y.; Zhang, L.; Zhao, Y.-C.; Yang, X.-L. Peptidomimetics in the discovery of new insect growth regulators: studies on the structure−activity relationships of the core pentapeptide region of allatostatins. *J. Agric. Food Chem.* **2011**, *59*, 2478−2485.

(28) Taneja-Bageshwar, S.; Strey, A.; Isaac, R. E.; Coast, G. M.; Zubrzak, P.; Pietrantonio, P. V.; Nachman, R. J. Biostable agonists that match or exceed activity of native insect kinins on recombinant arthropod GPCRs. *Gen. Comp. Endocrinol.* **2009**, *162*, 122−128.

(29) Zhang, C.; Qu, Y.; Wu, X.; Song, D.; Ling, Y.; Yang, X. Design, synthesis and aphicidal activity of N-terminal modified insect kinin analogs. *Peptides* **2014**. 10.1016/j.peptides.2014.07.028

(30) Ripka, A. S.; Rich, D. H. Peptidomimetic design. *Curr. Opin. Chem. Biol.* **1998**, *2*, 441−452.

(31) Busvine, J. R. *Recommended methods for measurement of pest resistance to pesticides*. FAO Plants Production Paper No. 21; Food and Agricultural Organization: Rome, Italy, 1980.

(32) Abbott, W. A method of computing the effectiveness of an insecticide. *J. Econ. Entomol.* **1925**, *18*, 265−267.

(33) Gäde, G.; Goldsworthy, G. J. Insect peptide hormones: a selective review of their physiology and potential application for pest control. *Pest Manage. Sci.* **2003**, *59*, 1063−1075.

(34) Lamango, N.; Sajid, M.; Isaac, R. The endopeptidase activity and the activation by Cl^- of angiotensin-converting enzyme is evolutionarily conserved: purification and properties of an angiotensin-converting enzyme from the housefly. *Musca domestica. Biochem. J.* **1996**, *314*, 639−646.

(35) Nachman, R. J.; Holman, G. M.; Hayes, T. K.; Beier, R. C. Acyl, pseudotetra-, tri- and dipeptide active-core analogs of insect neuropeptides. *Int. J. Pept. Protein Res.* **1993**, *42*, 372−377.

(36) Nachman, R. J.; Kaczmarek, K.; Zabrocki, J.; Coast, G. M. Active diuretic peptidomimetic insect kinin analogs that contain β-turn mimetic motif 4-aminopyroglutamate and lack native peptide bonds. *Peptides* **2012**, *34*, 262−265.

DOI: 10.1021/acs.jafc.5b01225
J. Agric. Food Chem. 2015, 63, 4527−4532

(37) Chan, W. C.; White, P. D., Eds.; *Fmoc solid phase peptide synthesis*; Oxford University Press: Oxford, U.K., 2000.
(38) Nachman, R. J.; Zabrocki, J.; Olczak, J.; Williams, H. J.; Moyna, G.; Scott, A. I.; Coast, G. M. cis-Peptide bond mimetic tetrazole analogs of the insect kinins identify the active conformation. *Peptides* **2002**, *23*, 709−716.

DOI: 10.1021/acs.jafc.5b01225
J. Agric. Food Chem. 2015, 63, 4527−4532

the resulting glycoconjugates were then hydrolyzed during winemaking, that is, in a manner analogous to that observed in smoke-affected grapes and wine.[14]

Oak lactone, that is, the *cis*- and *trans*-isomers of 5-*n*-butyl-4-methyl-4,5-dihydro-2(3*H*)-furanone **1a** and **1b** (Figure 1), is an

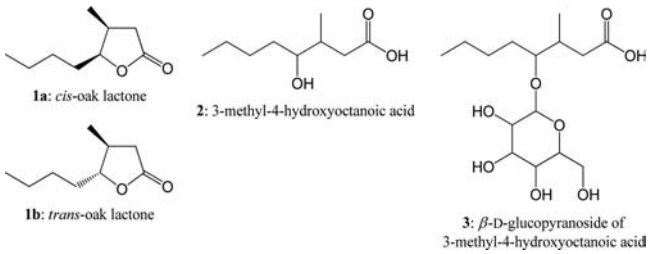

Figure 1. Chemical structures of *cis*- and *trans*-oak lactone **1a** and **1b**, 3-methyl-4-hydroxyoctanoic acid **2**, and the glucoside of 3-methyl-4-hydroxyoctanoic acid **3**.

important oak-derived volatile compound that typically imparts "coconut" and "vanilla" attributes to wine, following its extraction from oak chips or oak barrels.[15,16] Oak lactone occurs in green (i.e., unseasoned) oak wood,[16] but glycoconjugates of 3-methyl-4-hydroxyoctanoic acid (i.e., the ring-opened form of oak lactone **2**, Figure 1) have been identified in extracts of French and American oak wood,[17−20] including the β-D-glucopyranoside **3** (Figure 1). Oak lactone has also been detected in wines made with fruit from grapevines treated with oak extract or oak lactone,[7,8,21] and although increased glucosyl-glucose (G-G) levels were observed in grapes, suggesting glycosylation of oak derived volatiles,[21] it is not clear if glycoconjugate precursors of oak lactone accumulated, because this would necessitate a ring-opening step to generate the hydroxyl group required for glycosylation. The aim of this study was therefore to determine whether or not glycoconjugates of 3-methyl-4-hydroxyoctanoic acid accumulate in the fruits, leaves, and shoots of Monastrell grapevines following foliar applications of either oak extract or oak lactone, using qualitative and quantitative liquid chromatography−tandem mass spectrometry analysis.

MATERIALS AND METHODS

Chemicals. Chemicals were purchased from Sigma-Aldrich. Solvents were of HPLC grade from Merck (Darmstadt, Germany). Reference compounds included racemic *cis*- and *trans*-oak lactone and γ-hexalactone. [$^2H_4$]-(3*S*,4*S* and 3*R*,4*R*)-3-methyl-4-*O*-β-D-glucopyranosyloctanoic acid was synthesized in-house as previously reported.[19]

Grapevine Treatments. Field trials were conducted during the 2012 growing season and involved the application of oak lactone or oak extracts to grapevines (*Vitis vinifera* cv. Monastrell) grown in the experimental vineyard of the BSI winery, located in Jumilla, Spain (latitude, 38°28′ N; longitude, 1°18′ W). The plot covered an area of 1.09 ha and comprised loam soil. Vines were planted in 2002, with 2.8 m row and 1.5 m vine spacing, and were trained on a cordon trellis system and drip irrigated. The mean annual temperature was 16 °C, with a minimum temperature of −15 °C (in January) and a maximum temperature of 40 °C (in August).

Treatments were imposed on grapevines located in edaphologically homogeneous parts of the vineyard (excluding those located on vineyard edges), with buffer rows between treated and control vines to avoid contamination. Treatments comprised (i) the application of an aqueous solution of commercial toasted oak extract (Protea France S.A.S., Gensac la Pallue, France; comprising 231 μg/L *cis*-oak lactone and 247 μg/L *trans*-oak lactone) to grapevines (300 mL/vine, 16 vines per treatment) with and without bunches covered with plastic bags; and (ii) the application of a 0.6% aqueous solution of oak lactone (Sigma-Aldrich, Sydney, Australia) to grapevines (300 mL/vine, 16 vines per treatment) with and without bunches covered with plastic bags with 0.05% (v/v) adjuvant Fluvius (BASF, Germany) added to each solution as a wetting agent. All treatments were applied from a portable backpack sprayer. The placement of bunches in plastic bags was intended to prevent direct contact of fruit with oak lactone or oak extract solutions, but bags were removed immediately after solutions had evaporated (i.e., when droplets were no longer visible on leaves), typically 1 h after treatments were applied. Sixteen untreated grapevines were also selected as the control. Treatments were imposed in the early morning when ambient temperatures were <20 °C, at approximately 7 days postveraison.

Berry, leaf, and shoot samples were then collected from control and treated vines at three time points, designated as $t = 1$, being 10 days after foliar applications were applied; $t = 2$, being 20 days after application; and $t = 3$, being 36 days after foliar applications were applied (i.e., at maturity). For berry samples, approximately 15−20 grapes were randomly sampled from four clusters per vine per treatment (ensuring bunches from different locations within a vine were sampled). For leaf samples, four leaves per vine per treatment were randomly selected (ensuring different locations within a vine were sampled). For shoot samples, four shoots per treatment were randomly selected at $t = 1$ and $t = 2$, with one shoot per vine per treatment collected at $t = 3$. Samples were combined (within each treatment and at each time point) and then stored at −20 °C prior to analysis.

Quantitation of Oak Lactone by Gas Chromatography−Mass Spectrometry (GC-MS). Whole berries (50 g, in triplicate) were homogenized (T18 Ultra Turrax, IKA, Staufen, Germany), and the resulting homogenate was macerated for 2 h prior to centrifugation (3000*g* for 5 min). The resulting juice was then analyzed by stir bar sorptive extraction (SBSE)-GC-MS to determine *cis*- and *trans*-oak lactones according to previously reported methodology.[7] The SBSE analysis was performed using an automated thermal desorption unit (TDU, Gerstel, Mülheim and der Ruhr, Germany) mounted on an Agilent 7890A gas chromatograph (GC) coupled to a quadrupole Agilent 5975C mass spectrometry detector (Agilent Technologies, Palo Alto, CA, USA) operated in electron ionization mode. Separation was achieved with a fused silica capillary column (BP21 stationary phase, 30 m × 0.25 mm i.d. × 0.25 μm film thickness, SGE, Ringwood, Australia). The carrier gas was helium with a constant column pressure of 20.75 psi. The stir bars, coated with PDMS (Gerstel), were thermally desorbed in a stream of helium carrier gas at a flow rate of 75 mL/min with the TDU programmed from 40 to 295 °C at a rate of 60 °C/min (held for 5 min). The analytes were focused in a programmed temperature vaporising injector (PTV) (CIS-4, Gerstel), containing a packed liner (20 mg of tenax TA), held at 25 °C with Peltier cooling prior to injection. After desorption and focusing, the CIS-4 was programmed from 25 to 260 °C at 12 °C/s (held for 5 min) to transfer the trapped volatiles onto the head of the analytical column. The TDU was operated in the splitless desorption mode, whereas the CIS-4 was operated in the PTV solvent vent mode (purge flow to split vent of 80 mL/min, vent of 75 mL/min, and pressure of 20.85 psi). The initial GC oven temperature was 40 °C (held for 2 min); this was raised to 150 °C (at 10 °C/min, held for 5 min) and then to 230 °C (at 10 °C/min, held for 2 min). The MS was operated in scan mode (27−300 amu) with an ionization energy of 70 eV. The temperature of the MS transfer line was maintained at 230 °C. Identification of the *cis*- and *trans*-oak lactones was confirmed using the NIST library and by comparison of mass spectra and retention indices with oak lactone standards (Sigma-Aldrich, Steinheim, Germany). To avoid matrix interferences, MS quantitation was performed in single ion monitoring (SIM) mode using m/z 99 and was based on a five-point calibration curve of the oak lactone standards, using 200 μL of internal standard γ-hexalactone (Sigma-Aldrich, Steinheim, Germany) solution at 1 μL/mL in absolute ethanol (Merck, Damstadt, Germany).

Quantitation of Oak Lactone Glucoside by Liquid Chromatography−Tandem Mass Spectrometry (UHPLC-MS/MS). Extracts of fruits, leaves, and shoots sampled from control and treated

DOI: 10.1021/acs.jafc.5b01043
J. Agric. Food Chem. 2015, 63, 4533−4538

grapevines were analyzed by UHPLC-MS/MS to identify or determine oak lactone glycoconjugates.

Preparation of Fruit Extracts. Grape extracts were prepared according to methodology described previously.[22] Briefly, aliquots (2 mL) of juice (prepared as above) were loaded onto C18-HF solid phase extraction (SPE) cartridges (Grace, Australia), and each cartridge was washed with 10 mL of Milli-Q water. The retaining compounds were eluted with 2 mL of methanol and concentrated to semidryness under nitrogen at 40 °C. The resulting residue was reconstituted with 500 μL of 50% aqueous methanol and deuterated oak lactone glucoside, that is, [$^2H_4$]-**3** added (10 μg/mL) as an internal standard; the preparation of both glucoside **3** and its isotopically labeled derivative [$^2H_4$]-**3** is described elsewhere.[19,23] Samples were then filtered through a 0.45 μm GHP membrane (Acrodisc, PALL Life Sciences) prior to analysis.

Preparation of Leaf and Shoot Extracts. Extracts of leaves and shoots were also prepared according to previously described methodology.[13] Frozen plant material (cut in small pieces) was ground in a small grinder, and then a subsample (1 g, in triplicate) was extracted in 5 mL of Milli-Q water with shaking for 1 min and ultrasonication for 10 min. The resulting mixture was centrifuged (3000*g* for 5 min) and the supernatant collected. The remaining pellet was further extracted in another 5 mL of Milli-Q water as above. The supernatants were then combined and aliquots (5 mL) taken for SPE (as per the preparation of fruit extracts)

Instrument Analysis. An Agilent 1290 Infinity UHPLC combined with the 6490 QQQ LC/MS with iFunnel technology was used for identification and/or quantitation of oak lactone glycoconjugates. Data acquisition and processing were performed using MassHunter software version B.06.00 (Agilent, Palo Alto, CA, USA). Aliquots (10 μL) of each fruit, leaf, and shoot extract were injected and the components separated using a 150 mm × 2 mm i.d., 4 μm, Synergi Hydro-RP 80 Å column with a 4 mm × 2 mm i.d. guard column packed with the same material (Phenomenex, Lane Cove, NSW, Australia). The column temperature was maintained at 25 °C. A binary gradient was used with the mobile phases comprising 0.1% acetic acid in water (v/v) (eluent A) and 0.1% acetic acid in acetonitrile (v/v) (eluent B). Using a flow rate of 0.3 mL/min, the elution gradient was as follows: 0−10 min, 10% B; from 10 to 70% B in 1 min; then held at 70% B for 5 min (total runtime was 16 min). The column was re-equilibrated for 10 min prior to the next injection. The mass spectrometric analysis was performed using APCI in negative mode. The following source conditions were used: gas temperature, 290 °C; vaporizer, 370 °C; gas flow, 12 L/min; nebulizer pressure, 35 psi; and capillary voltage, 2500 V. Nitrogen was used as the nebulizer and collision cell gas. Quantitative analysis was performed in multiple reaction monitoring (MRM) mode, and the following mass transitions were monitored: *m*/*z* 335 → 119, 89, for unlabeled glucoside **3** and *m*/*z* 339 → 119, 89, for the internal standard, that is, [$^2H_4$]-**3**. The underlined ions were used as the quantifier ion, whereas the other ions were used as qualifiers. The transitions were monitored using a dwell time of 50 ms, a collision energy of 20 V, and a cell accelerator voltage of 4 V. The linear calibration range (LNR) was from 10 to 1000 μg/L in matrix-matched standards. The limit of detection (LOD) was 1 μg/L with a signal/noise ratio of 3, and the limit of quantitation (LOQ) was 10 μg/L with a signal/noise ratio of 10. Qualitative analyses of selected control and treated leaf samples were also performed, using full scan and selective ion monitoring (SIM) modes. Full scans ranged from *m*/*z* 50 to 600, with a step size of 0.1 amu. In SIM mode, the parent ion and acetate adducts of gallateglucoside, glucosylglucoside, and rutinoside glycoconjugates were monitored, with dwell times of 200 ms.

RESULTS AND DISCUSSION

Fruits, leaves, and shoots were collected for chemical analysis at three different time points, including at maturity and following treatment of grapevines with foliar applications of either oak extract or oak lactone. The oak lactone content of fruit was determined by GC-MS (Table 1), whereas the concentrations of a β-D-glucopyranoside of 3-methyl-4-hydroxyoctanoic acid in fruits, leaves, and shoots were determined by UHPLC-MS/MS (Table 2).

Table 1. Concentrations of *cis*- and *trans*-Oak Lactone (1a and 1b) in Fruit from Grapevines Treated with Oak Extract or Oak Lactone

		concentration[a] (μg/L)	
		cis-oak lactone	*trans*-oak lactone
control	*t* = 1	nd	nd
	t = 2	nd	nd
	t = 3	nd	nd
bunches uncovered			
oak extract	*t* = 1	nd	nd
	t = 2	nd	nd
	t = 3	nd	nd
oak lactone	*t* = 1	85 ± 9c	83 ± 12c
	t = 2	26 ± 2b	30 ± 5b
	t = 3	9 ± 1a	11 ± 1a
bunches covered			
oak extract	*t* = 1	nd	nd
	t = 2	nd	nd
	t = 3	nd	nd
oak lactone	*t* = 1	nd	nd
	t = 2	nd	nd
	t = 3	nd	nd

[a]Values are means (±standard error) of three replicates (*n* = 3). Values followed by a different letter are significantly different ($P < 0.05$). nd, not detected (i.e., <1 μg/L juice).

Table 2. Concentrations of Glucoside of 3-Methyl-4-hydroxyoctanoic Acid (3) in Fruits, Leaves, and Shoots from Grapevines Treated with Oak Extract or Oak Lactone

		concentration[a]		
		in fruits (μg/L)	in leaves (μg/kg)	in shoots (μg/kg)
control	*t* = 1	nd	nd	nd
	t = 2	nd	nd	nd
	t = 3	nd	tr	12 ± 1
bunches uncovered				
oak extract	*t* = 1	4 ± 0.3	261 ± 13	nd
	t = 2	5 ± 0.8	155 ± 5	nd
	t = 3	nd	nd	nd
oak lactone	*t* = 1	349 ± 13	16776 ± 6559	269 ± 27
	t = 2	292 ± 4	13109 ± 3921	124 ± 9
	t = 3	217[b] ± 9	2075 ± 360	259 ± 3
bunches covered				
oak extract	*t* = 1	nd	205 ± 63	nd
	t = 2	nd	139 ± 7	nd
	t = 3	nd	nd	nd
oak lactone	*t* = 1	22 ± 1	13111 ± 1754	66 ± 2
	t = 2	40 ± 3	10923 ± 2193	102 ± 26
	t = 3	37 ± 1	2699 ± 187	126 ± 8

[a]Values are means (±standard error) of three replicates (*n* = 3) unless otherwise indicated. nd, not detected (i.e., <2.5 μg/L juice or <5 μg/kg leaves and shoots); tr, trace (i.e., <10 μg/kg). [b]Mean (±standard error) of two replicates (i.e., *n* = 2; glucoside **3** not detected in one replicate).

DOI: 10.1021/acs.jafc.5b01043
J. Agric. Food Chem. 2015, 63, 4533−4538

Neither of the oak lactone isomers was detected in fruit sampled from control grapevines, as expected. Similarly, oak lactone could not be detected in fruit from grapevines treated with oak extract, but this most likely reflected the relatively low application rate, being equivalent to approximately 70 μg of oak lactone per vine. In contrast, the dose rate for the treatment comprising the direct application of oak lactone to grapevines was several orders of magnitude higher, at approximately 1500 mg of oak lactone per vine. Similar concentrations of *cis*- and *trans*-oak lactones were detected in fruit corresponding to this treatment, albeit only when bunches were exposed. A decline in oak lactone concentrations was observed as fruit ripened, which could in part be explained by increasing berry volume and water content[24] and possibly also volatilization (evaporation), but would also be expected if oak lactone were indeed being absorbed and assimilated by the grapevine in glycoconjugate precursor forms.

The earlier development of a quantitative method for the determination of the β-D-glucopyranoside of 3-methyl-4-hydroxyoctanoic acid **3**,[19] hereafter referred to as "glucoside", enabled the accumulation of glycoconjugate forms of oak lactone in different parts of the grapevine, that is, fruits, leaves, and shoots, to be investigated (Table 2). The oak lactone glucoside was not detected in fruit harvested from control grapevines, again as expected, albeit trace levels, that is, approximately 10 μg/kg, were detected in control leaves and shoots collected at maturity. In contrast, treatments involving foliar applications of either oak extract or oak lactone yielded glucoside **3** in fruits, leaves, and some shoot samples, with the highest concentrations being observed in leaves sampled at t = 1 from grapevines treated with oak lactone. The marked differences observed between the glucoside **3** content of samples derived from grapevines treated with oak extract versus oak lactone can again be explained by the different oak lactone dose rates associated with these treatments. Moderate glucoside levels, up to 261 μg/kg, were observed in leaves from grapevines treated with oak extract, whereas low levels, $\leq$5 μg/L, were observed in fruit, but only where bunches were uncovered and thus also exposed to the treatment. Glucoside **3** was not detected in the shoots of grapevines treated with oak extract.

Extremely high levels of glucoside **3** were observed in leaves from grapevines treated with oak lactone. Indeed, the concentrations far exceeded the working range (1−1000 μg/L) for which the stable isotope dilution assay used for quantitation was originally developed.[19] As such, the values reported for these samples are considered to be approximations, rather than absolute concentrations. Nonetheless, these results clearly demonstrate the accumulation of large quantities of glucoside **3** in the leaves of grapevines treated with oak lactone. The oak lactone glucoside was also observed in both the fruits and shoots of these grapevines, albeit at much lower levels than for leaves, that is, at levels up to 349 μg/L and 269 μg/kg (for fruits and shoots, respectively). When fruit was placed in plastic bags to prevent direct exposure to the oak lactone solution, glucoside **3** was still detected, but at concentrations approximately 1 order of magnitude lower than for fruit that remained exposed, at between 20 and 40 μg/L. The differences observed in glucoside **3** concentrations between covered and uncovered bunches might be explained by translocation of either oak lactone or the glucoside from leaves to fruit, but the higher amounts observed in uncovered grapes indicate oak lactone was directly absorbed by grapes, albeit to a lesser extent than by leaves.

An authentic sample of **3** was analyzed by UHPLC-MS/MS in MRM mode as a reference compound, and its retention time (Figure 2a) and product ion spectrum (Figure 3a) compared

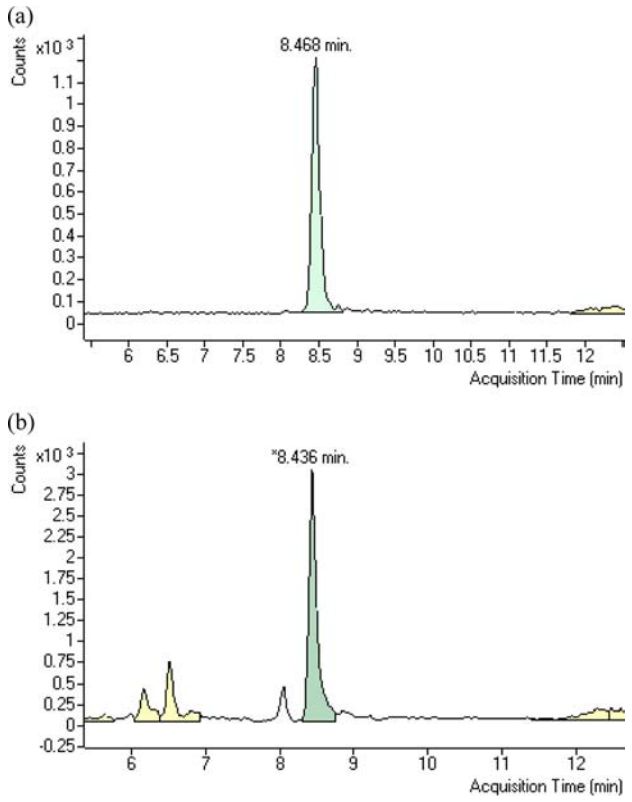

Figure 2. UHPLC-MRM chromatograms of (a) the glucoside reference compound **3** and (b) an extract of fruit taken from grapevines treated with oak lactone.

with those obtained for an extract of fruit corresponding to grapevines treated with oak lactone (Figures 2b and 3b). The reference compound eluted at a retention time of 8.47 min, which was close to that of the predominant peak present in the fruit extract, being 8.44 min. Furthermore, the mass transitions

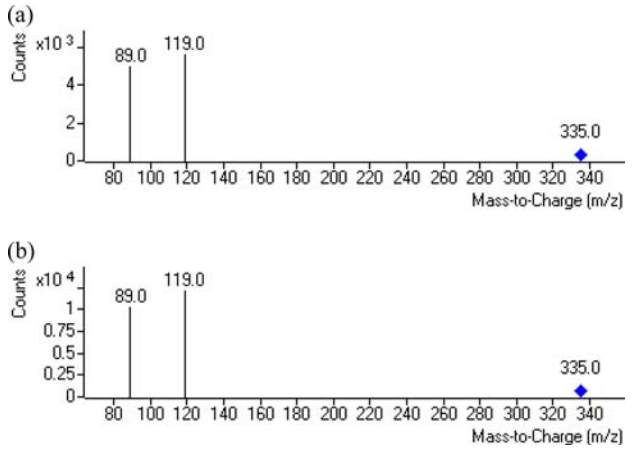

Figure 3. Product ion spectra of m/z 335 obtained by UHPLC-MS/MS of (a) the glucoside reference compound **3** and (b) an extract of fruit taken from grapevines treated with oak lactone.

DOI: 10.1021/acs.jafc.5b01043
J. Agric. Food Chem. 2015, 63, 4533−4538

m/z 336 → 119 and 89 obtained for the reference compound also matched those of the peak observed in the fruit extract. Together, these results validate the presence of glucoside **3** as a component of fruits and leaves of grapevines treated with oak extract and of fruits, leaves, and shoots of grapevines treated with oak lactone. This was in fact a somewhat unexpected result, because for glycosylation to occur, oak lactone must first undergo a ring-opening step to form 3-methyl-4-hydroxyoctanoic acid **2**, that is, an intermediate possessing the free hydroxyl function group required for glycosylation. Although the presence of glucoside **3** in fruits and leaves of grapevines treated with oak extract could conceivably be attributed to its presence as a constituent of the original oak extract (which was not measured), the accumulation of such large quantities of **3** in samples, leaves especially, derived from grapevines treated with oak lactone can only be explained by ring-opening and glycosylation of oak lactone post-treatment. Besides, in oak wood, the predominant oak lactone glycoconjugate precursor is the gallateglucoside, (3*S*,4*S*)-3-methyl-4-*O*-(6′-*O*-galloyl)-*β*-D-glucopyranosyloctanoic acid.[20] Leaf samples taken from grapevines treated with oak lactone (and from control grapevines) were analyzed by UHPLC-MS/MS in scan and SIM modes, in an attempt to identify mass transitions corresponding to the gallateglucoside, but there was no evidence to suggest its presence in the samples analyzed. The gallateglucoside derivative of **2** may therefore be a precursor that is unique to oak wood. In contrast, mass transitions corresponding to a glucose-glucose disaccharide, that is, m/z 557 → 497, were identified in extracts of leaves collected at t = 3 from grapevines treated with oak lactone, but not in extracts of leaves from control grapevines (Figure 4), suggesting further derivatization of glucoside **3** occurred. Without authentic reference compounds, the exact nature of this disaccharide cannot be confirmed; that is, it was not clear if the second sugar moiety was bound as a glucosylglucoside or as an ester via glycosylation of the carboxylic acid functionality. However, semiquantitation of the disaccharide using the standard curve for glucoside **3** suggested it accumulated at several-fold higher concentrations than the glucoside, which provides a plausible explanation for the declining concentrations of glucoside **3** observed in extracts of leaves with ripening (Table 2), that is, between t = 1 and t = 3 (maturity).

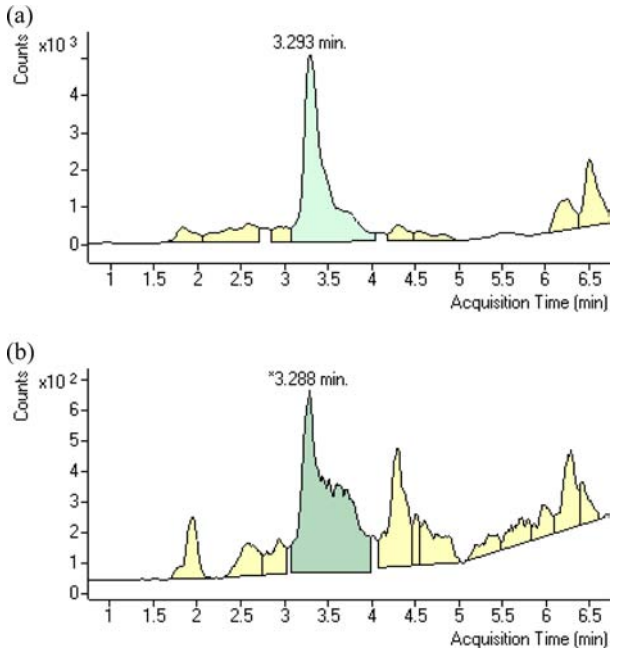

Figure 4. UHPLC-SIM chromatograms obtained for mass transitions corresponding to a glucose-glucose disaccharide, that is, m/z 557 → 497, in extracts of leaves taken from (a) grapevines treated with oak lactone and (b) control grapevines.

The rates of lactonization of the *threo*- and *erythro*-isomers of 3-methyl-4-hydroxyoctanoic acid **2** have been shown to be distinctly different, with lactonization of the *erythro*-isomer (to form *trans*-oak lactone **1b**) occurring at higher rates than lactonization of the *threo*-isomer (to form *cis*-oak lactone **1a**).[25] In the current study, the depletion of *cis*- and *trans*-oak lactones observed in fruit with ripening (Table 1) occurred at similar rates, suggesting stereochemistry did not influence the biochemical pathway responsible for the ring-opening step.

These results demonstrated the presence of oak lactone glycoconjugates in fruits, leaves, and shoots of Monastrell grapevines following foliar applications of either a commercial oak extract or an oak lactone solution, with both ring-opening and glycosylation occurring after oak lactone was absorbed by grapevines from the surrounding environment. This explains why in previous studies oak lactone could be detected in wine made from fruit from grapevines that were treated with oak extract or oak lactone, but not in the fruit itself; that is, the oak lactone was likely present in one or more glycoconjugate forms.

AUTHOR INFORMATION

Corresponding Author

*(M.R.S.) Phone: +34 967 599310. Fax: +34 967 599238. E-mail: Rosario.Salinas@uclm.es.

Funding

We thank the Ministerio de Ciencia e Innovación of the Spanish government for financial support given to Project AGL2009-08950), including an FPI scholarship (BES-2010-038613) and internship funding (EEBB-I-13-06899) awarded to A.I.P.-G.

Notes

The authors declare no competing financial interest.

REFERENCES

(1) Capone, D. L.; Jeffery, D. W.; Sefton, M. A. Vineyard and fermentation studies to elucidate the origin of 1,8-cineole in Australian red wine. *J. Agric. Food Chem.* **2012**, *60*, 2281−2287.

(2) Kennison, K. R.; Wilkinson, K. L.; Williams, H. G.; Smith, J. H.; Gibberd, M. R. Smoke-derived taint in wine: effect of postharvest smoke exposure of grapes on the chemical composition and sensory characteristics of wine. *J. Agric. Food Chem.* **2007**, *55* (26), 10897−10901.

(3) Kennison, K. R.; Wilkinson, K. L.; Pollnitz, A. P.; Williams, H. G.; Gibberd, M. R. Effect of smoke application to field-grown Merlot grapevines at key phenological growth stages on wine sensory and chemical properties. *Aust. J. Grape Wine Res.* **2011**, *17*, S5−S12.

(4) Ristic, R.; Pinchbeck, K. A.; Fudge, A. L.; Hayasaka, Y.; Wilkinson, K. L. Effect of leaf removal and grapevine smoke exposure on colour, chemical composition and sensory properties of Chardonnay wines. *Aust. J. Grape Wine Res.* **2013**, *19*, 230−237.

(5) Hayasaka, Y.; Parker, M.; Baldock, G. A.; Pardon, K. H.; Black, C. A.; Jeffery, D. W.; Herderich, M. J. Assessing the impact of smoke exposure in grapes: development and validation of a HPLC-MS/MS method for the quantitative analysis of smoke-derived phenolic glycosides in grapes and wine. *J. Agric. Food Chem.* **2013**, *61*, 25−33.

(6) Martínez-Gil, A. M.; Pardo-García, A. I.; Zalacain, A.; Alonso, G. L.; Salinas, M. R. Lavandin hydrolat applications to Petit Verdot

DOI: 10.1021/acs.jafc.5b01043
J. Agric. Food Chem. 2015, 63, 4533−4538

vineyards and their impact on their wine aroma compounds. *Food Res. Int.* **2013**, *53*, 391−402.
(7) Martínez-Gil, A. M.; Garde-Cerdán, T.; Martínez, L.; Alonso, G. L.; Salinas, M. R. Effect of oak extract application to Verdejo grapevines on grape and wine aroma. *J. Agric. Food Chem.* **2011**, *59*, 3253−3263.
(8) Martínez-Gil, A. M.; Garde-Cerdán, T.; Zalacain, A.; Pardo-García, A. I.; Salinas, M. R. Applications of an oak extract on Petit Verdot grapevines. Influence on grape and wine volatile compounds. *Food Chem.* **2012**, *132*, 1836−1845.
(9) Martínez-Gil, A. M.; Angenieux, M.; Pardo-García, A. I.; Alonso, G. L.; Ojeda, H.; Rosario Salinas, M. Glycosidic aroma precursors of Syrah and Chardonnay grapes after an oak extract application to the grapevines. *Food Chem.* **2013**, *138*, 956−965.
(10) Günata, Y. Z.; Bayonove, C. L.; Baumes, R. L.; Cordonnier, R. E. The aroma of grapes I. Extraction and determination of free and glycosidically bound fractions of some grape aroma components. *J. Chromatogr., A* **1985**, *331*, 83−90.
(11) Wirth, J.; Guo, W.; Baumes, R.; Günata, Z. Volatile compounds released by enzymatic hydrolysis of glycoconjugates of leaves and grape berries from *Vitis vinifera* must of Alexandria and Shiraz cultivars. *J. Agric. Food Chem.* **2001**, *49*, 2917−2923.
(12) Winterhalter, P.; Skouroumounis, G. K. Glycoconjugated aroma compounds: occurrence, role and biotechnological transformation. *Adv. Biochem. Eng. Biotechnol.* **1997**, *55*, 73−105.
(13) Hayasaka, Y.; Baldock, G. A.; Pardon, K. H.; Jeffrey, D. W.; Herderich, M. J. Investigation into the formation of guaiacol conjugates in berries and leaves of grapevine *Vitis vinifera* L. cv. Cabernet Sauvignon using stable isotope tracers combined with HPLC-MS and MS/MS analysis. *J. Agric. Food Chem.* **2010**, *58*, 2076−2081.
(14) Ristic, R.; Osidacz, P.; Pinchbeck, K. A.; Hayasaka, Y.; Fudge, A. L.; Wilkinson, K. L. The effect of winemaking techniques on the intensity of smoke taint in wine. *Aust. J. Grape Wine Res.* **2011**, *17*, S29−S40.
(15) Maga, J. A. Oak lactones in alcoholic beverages. *Food Rev. Int.* **1996**, *12*, 105−130.
(16) Pollnitz, A. P.; Jones, G. P.; Sefton, M. A. Determination of oak lactones in barrel-aged wines and in oak extracts by stable isotope dilution analysis. *J. Chromatogr., A* **1999**, *857*, 239−246.
(17) Masson, E.; Baumes, R.; Le Guernevé, C.; Puech, J.-L. Identification of a precursor of β-methyl-γ-octalactone in the wood of sessile oak (*Quercus petraea* (Matt.) Liebl. *J. Agric. Food Chem.* **2000**, *48*, 4306−4309.
(18) Hayasaka, Y.; Wilkinson, K. L.; Elsey, G. M.; Raunkjær, M.; Sefton, M. A. Identification of natural oak lactone precursors in extracts of American and French oak woods by liquid chromatography-tandem mass spectrometry. *J. Agric. Food Chem.* **2007**, *55*, 9195−9201.
(19) Fudge, A. L.; Elsey, G. M.; Hayasaka, Y.; Wilkinson, K. L. Quantitative analysis of β-D-glucopyranoside of 3-methyl-4-hydroxyoctanoic acid, a potential precursor to *cis*-oak lactone, in oak extracts using liquid chromatography-tandem mass spectrometry based stable isotope dilution analysis. *J. Chromatogr., A* **2008**, *1215*, 51−56.
(20) Wilkinson, K. L.; Prida, A.; Hayasaka, Y. Role of glycoconjugates of 3-methyl-4-hydroxyoctanoic acid in the evolution of oak lactone in wine during oak maturation. *J. Agric. Food Chem.* **2013**, *61*, 4411−4416.
(21) Pardo-Garcia, A. I.; De La Hoz, K. S.; Zalacain, A.; Alonso, G. L.; Salinas, M. R. Effect of vine foliar treatments on the varietal aroma of Monastrell wines. *Food Chem.* **2014**, *163*, 258−266.
(22) Dungey, K. A.; Hayasaka, Y.; Wilkinson, K. L. Quantitative analysis of glycoconjugate precursors of guaiacol in smoke-affected grapes using liquid chromatography−tandem mass spectrometry based stable isotope dilution analysis. *Food Chem.* **2011**, *126*, 801−806.
(23) Wilkinson, K. L.; Elsey, G. M.; Prager, R. H.; Tanaka, T.; Sefton, M. A. Precursors to oak lactone. Part 2: Synthesis, separation and cleavage of several β-D-glucopyranosides. *Tetrahedron* **2004**, *60*, 6091−6100.
(24) Coombe, B. G. Development and maturation of the grape berry. *Aust. Grapegrower Winemaker* **1975**, *136*, 60−66.
(25) Wilkinson, K. L.; Elsey, G. M.; Prager, R. H.; Pollnitz, A. P.; Sefton, M. A. Rates of formation of *cis*- and *trans*-oak lactone from 3-methyl-4-hydroxyoctanoic acid. *J. Agric. Food Chem.* **2004**, *52*, 4213−4218.

DOI: 10.1021/acs.jafc.5b01043
J. Agric. Food Chem. 2015, 63, 4533−4538

Table 1. Cocoa Samples Used in This Study

leaf samples		
type	sample name	source
CCN-51	C1	Farms, Naranjal, Ecuador
	C2	Farms, Naranjal, Ecuador
	C3	Farms, Naranjal, Ecuador
	C4	ICGD, University of Reading, England
	C5	Botanical Garden, Hamburg, Germany
	C6	Botanical Garden, Hamburg, Germany
	C7	CATIE, Cartago, Costa Rica
	C8	CATIE, Cartago, Costa Rica
EET-19 (Arriba)	A1	INIAP, Guayaquil, Ecuador
EET-48 (Arriba)	A2	INIAP, Guayaquil, Ecuador
Criollo	Cr1	INIAP, Guayaquil, Ecuador
	Cr2	INIAP, Guayaquil, Ecuador
bean samples		
type	sample name	source
CCN-51	C15	CATIE, Cartago, Costa Rica
	C16	CATIE, Cartago, Costa Rica

several authors.[20−24] First introduced by Lanaud et al. working at CIRAD (Centre de Coopération Internationale en Recherche Agronomique pour le Développement), most of the microsatellites are designated as "mTcCIR" (microsatellite *Theobroma cacao* CIRAD plus continuous numbering. All 10 SSR markers originated from this microsatellite collection database.

If numerous variations at microsatellite loci are detectable within CCN-51, it can be assumed that it is no pure clone that is propagated exclusively vegetatively. In this case, it is most likely that cross-breeding occurred during cultivation of CCN-51.

MATERIALS AND METHODS

Plant Material. Solely authentic leaf material from CCN-51, Arriba, Criollo, and two samples of beans removed from fresh fruits of CCN-51 (C15 and C16) were used (Table 1). Plant materials were obtained from the INIAP (Instituto Nacional de Investigaciones Agropecuarias, Guayaquil, Ecuador), Botanical Garden Hamburg (Hamburg, Germany), CATIE (Centro Agronómico Tropical de Investigación y Enseñanza, International Cocoa Collection, Cartago, Costa Rica), and from the ICGD (International Cocoa Germplasm Database, University of Reading, England). A total of 14 samples were picked freshly and stored at −20 °C.

DNA Extraction, Purity, and Concentration. The DNA was extracted using DNeasy Plant Mini/Maxi Kit (Qiagen, Hilden, Germany) following the manufacturer's instructions. The purity and concentration of DNA extracts were determined by spectrophotometry (260/280 nm; NanoDrop, Thermo Fisher Scientific Oy, Finland).

Qualitative PCR. A panel of 10 microsatellite markers (mTcCIR1, mTcCIR6, mTcCIR8, mTcCIR11, mTcCIR12, mTcCIR15, mTcCIR18, mTcCIR24, mTcCIR25, and mTcCIR60) was employed (Table 2).[20,23,25] Only primer pairs were chosen that were supposed to produce clearly discriminable PCR product lengths for Arriba EET and CCN-51 clones according to SSR profiles deposited by ICGD (http://www.icgd.rdg.ac.uk/). Forward primers were fluorescence labeled with 6-FAM (Sigma Life Science, Hamburg, Germany).

The SSR analysis was carried out four times with each primer pair to ensure reproducibility. The PCR conditions previously published by Cryer et al.,[23] Lanaud et al.,[20] Saunders et al.,[26] and Irish et al.[25] had to be adjusted to the sample set. For successful amplification, both template concentration and annealing temperatures had to be increased over those previously published.

The optimized PCR conditions were as follows: For qualitative PCR, 20 ng of the extracted DNA was used. The PCR reaction mix consisted of 1× buffer (10× buffer: 1 mM $MgCl_2$, 5 mM Tris, 25 mM KCl, 1% Triton X-100 (m/v)), 0.8 mM dNTPs (Bioline GmbH, Luckenwalde, Germany)), 1 μM of each Primer (Invitrogen, Darmstadt, Germany), 0.3 U Taq polymerase, and 2 μg BSA (10 mg/mL, New England Biolabs GmbH, Frankfurt am Main, Germany) in a final volume of 20 μL. The PCR started with a 5 min denaturation step at 94 °C, followed by 35 cycles of 94 °C for 40 s, an annealing at 50 °C (for primer pair mTcCIR11)/55 °C (all other primer pairs) for 40 s, 72 °C for 40 s, and a final elongation step at 72 °C for 1 min.

Fragment Analysis. Amplified PCR products were diluted (1:20) with ddH_2O, and 1 μL of the diluted fragments was mixed with 1 μL of GeneScan-500-LIZ size standard (Life Technologies, Darmstadt, Germany) and 10 μL of Super-Di formamide (Nimagen, Nijmegen, Netherlands). The amplicons were denatured at 97 °C for 5 min and

Table 2. Primer Sequences Used in This Study[a]

marker	primer sequence (5′-3′)	T_m (°C)	repeat motif	estimated allele range	published allel range (Irish et al.[25])
mTcCIR1	F: [6-FAM]GCAGGGCAGGCTCAGTGAAGCA R: TGGGCAACCAGAAAACGAT	55	$(CT)_{14}$	128−140	127−144
mTcCIR6	F: [6-FAM]TTCCCTCTAAACTACCCTAAAT R: TAAAGCAAAGCAATCTAACATA	55	$(TG)_7(GA)_{13}$	230−248	222−247
mTcCIR8	F: [6-FAM]CTAGTTTCCCATTTACCA R: TCCTCAGCATTTTCTTTC	55	$(TC)_5TT(TC)_{17}TTT(CT)_4$	288−304	288−304
mTcCIR11	F: [6-FAM]TTTGGTGATTATTAGCAG R: GATTCGATTTGATGTGAG	50	$(TC)_{13}$	302−315	288−317
mTcCIR12	F: [6-FAM]TCTGACCCCAAACCTGTA R: ATTCCAGTTAAAGCACAT	55	$(CATA)_4N_{18}(TG)_6$	188−212	188−251
mTcCIR15	F: [6-FAM]CAGCCGCCTCTTGTTAG R: TATTTGGGATTCTTGATG	55	$(TC)_{19}$	234−252	232−256
mTcCIR18	F: [6-FAM]GATAGCTAAGGGGATTGAGGA R: GGTAATTCAATCATTTGAGGATA	55	$(GA)_{12}$	331−345	331−355
mTcCIR24	F: [6-FAM]TTTGGGGTGATTTCTTCTGA R: TCTGTCTCGTCTTTTGGTGA	55	$(AG)_{13}$	185−201	185−203
mTcCIR25	F: [6-FAM]CTTCGTAGTGAATGTAGGAG R: TTAGGTAGGTAGGGTTATCT	55	$(CT)_{21}$	135−153	−
mTcCIR60	F: [6-FAM]CGCTACTAACAAACATCAAA R: AGAGCAACCATCACTAATCA	55	$(CT)_7(CA)_{20}$	194−212	187−223

[a]The forward primer is 6-FAM-labeled. F, forward primer; R, reverse primer; −, no data.

DOI: 10.1021/acs.jafc.5b01462
J. Agric. Food Chem. 2015, 63, 4539−4544

Table 3. Microsatellite Patterns Obtained with the 10 Primer Pairs[a]

Sample	mTcCIR																			
	1			6				8			11				12					
	A	B	C	A	B	C	D	A	B	C	A	B	C	D	A	B	C	D	E	
	128	138	140	230	236	240	248	288	292	304	288	292	302	315	188	200	204	210	212	
C1 (Ecuador)	+	-	+	-	-	+	+	+	-	+	-	-	+	+	+	+	-	-	-	
C2 (Ecuador)	+	-	+	-	-	+	+	+	-	+	-	-	+	+	+	+	-	-	-	
C3 (Ecuador)	+	-	+	-	-	+	+	+	-	+	-	-	+	+	+	+	-	-	-	
C4 (ICGD)	+	-	+	+	-	+	-	+	-	-	-	+	+	-	+	-	-	+	-	
C5 (HH)	+	-	+	-	-	+	-	+	-	+	-	-	+	+	-	+	-	-	-	
C6 (HH)	+	-	+	-	-	+	+	-	-	+	-	-	+	+	+	-	-	-	-	
C7 (CATIE,CR)	+	-	+	-	-	+	+	+	-	+	-	-	+	+	+	+	-	-	-	
C8 (CATIE,CR)	+	-	+	-	-	-	+	+	-	+	+	-	+	-	-	-	-	-	-	
C15 (CATIE,CR)	-	-	-	-	-	+	+	+	-	+	-	-	-	+	+	+	-	-	-	
C16 (CATIE,CR)	+	-	-	-	-	-	+	+	-	+	+	-	-	-	-	-	+	-	-	
A1 (EET-19)	+	-	+	+	+	-	-	+	+	-	-	-	-	-	-	-	+	-	+	
A2 (EET-48)	+	-	+	+	+	-	-	+	+	-	-	-	-	-	-	-	-	-	-	
Cr1	-	+	+	-	-	-	+	+	+	-	-	-	-	+	-	-	-	-	+	
Cr2	-	-	+	-	-	-	+	+	+	-	-	-	-	+	-	-	-	-	+	

Sample	mTcCIR																			
	15				18					24			25					60		
	A	B	C	D	A	B	C	D	E	A	B	C	A	B	C	D	E	A	B	
	234	248	250	252	331	333	335	343	345	185	193	201	135	141	141	148	153	194	212	
C1 (Ecuador)	+	-	-	-	+	+	-	-	-	+	-	-	+	-	+	-	-	+	+	
C2 (Ecuador)	+	-	-	-	+	+	-	-	-	+	-	-	+	-	+	-	-	+	+	
C3 (Ecuador)	+	-	-	-	+	+	-	-	-	+	-	-	+	-	+	-	-	+	+	
C4 (ICGD)	+	+	-	-	+	-	-	+	-	+	+	-	-	-	+	-	+	+	-	
C5 (HH)	+	-	-	-	+	+	-	-	-	+	-	-	+	-	-	-	-	+	+	
C6 (HH)	+	-	-	-	+	+	-	-	-	+	-	-	+	-	+	-	-	+	+	
C7 (CATIE,CR)	+	-	-	-	+	+	-	-	-	-	-	-	+	-	+	-	-	+	+	
C8 (CATIE,CR)	+	-	-	+	+	-	+	-	-	+	-	-	-	-	+	-	-	-	+	
C15 (CATIE,CR)	-	-	-	-	+	+	-	-	-	+	-	-	-	-	+	-	-	+	-	
C16 (CATIE,CR)	+	-	-	-	+	+	-	-	-	+	-	-	-	-	+	-	-	-	+	
A1 (EET-19)	-	+	-	+	-	-	+	-	+	+	-	+	-	+	+	-	-	+	+	
A2 (EET-48)	-	+	-	+	-	-	+	-	+	+	-	+	-	+	+	-	-	+	+	
Cr1	-	-	+	+	-	-	+	-	+	+	-	-	-	+	-	+	-	+	+	
Cr2	-	-	+	+	-	-	+	-	-	+	-	-	-	+	-	+	-	+	+	

[a]For each microsatellite, the up to five observed different alleles are individually designated by letters (A−E). Allele size (bp) is given below each letter, "+" = allele present; "−" = allele absent. Differences within CCN-51 are highlighted. In most cases, two fragment lengths are representing the two alleles (heterozygote). In some cases, both alleles show the same fragment length (homozygote).

immediately quenched on ice. For the separation and visualization of the PCR products, the eight-capillary sequencer 3500 Genetic Analyzer (Life Technologies, Darmstadt, Germany) was used with Nano POP 7 (Nimagen, Nijmegen, Netherlands) as a gel matrix. Default running conditions for fragment analysis were used according to the manufacturer's instructions. The allele sizes were estimated with GeneMapper Software 5 (Applied Biosystems/Life Technologies, Carlsbad, Germany). The correct base calling of the PCR products was checked manually. After obtaining the amplicons by the gene-mapper, a 1−0-matrix (1: amplicon present; 0: amplicon absent) in Excel-file format was created. The further statistical analysis was carried out by PAST. Within the cluster analysis, the neighbor joinings of Simpson, Jacard, Jukes, and Euclidean were used for the evaluation. The results for all four methods were identical. For the presentation, the evaluation by Simpson is shown.[27]

RESULTS AND DISCUSSION

In the present study, 14 cocoa samples, including 10 CCN-51, two Arriba, and two Criollo plants were analyzed with a set of 10 SSR markers. The estimated sizes of the PCR products correspond to the published allele sizes for these markers (Table 2).[20,23,25] In the following, amplicons with identical lengths of basepairs were expected and named as one homologue allele in a microsatellite locus.

Within this sampling set, the 10 microsatellites exhibited two to five alleles (A−E) per locus (Table 3). As expected, most microsatellite loci of CCN-51 and Arriba samples differed in allele sizes (e.g., mTcCIR8: CCN-51 with the alleles A and C, Arriba with alleles A and B) allowing a discrimination between the two cocoa types. However, the microsatellite patterns of the 10 CCN-51 samples also showed differences in allele sizes, which would not be expected for pure clones.

All samples from Ecuador (C1−C3) showed an identical microsatellite pattern. In these samples, eight SSR loci were heterozygote, showing two alleles of different fragment lengths; only two microsatellites (mTcCIR15 and mTcCIR 24) were homozygotes. In most cases, the same alleles were detected for C5, C6, C7, and C15, though in some cases only one of the two allels is present (e.g., C5 mTcCIR6, mTcCIR12, and

DOI: 10.1021/acs.jafc.5b01462
J. Agric. Food Chem. 2015, 63, 4539−4544

Table 4. Detailed Results of the Chloroplast Analysis Performed in the Recently Published Study of Herrmann et al.[11] [a]

Sample	Repeat $(TAAAG)_n$	SNPs				
		8	17	21	43	44
C1 (Ecuador)	14	C	C	C	C	C
C2 (Ecuador)	14	C	C	C	C	C
C3 (Ecuador)	14	C	C	C	C	C
C4 (ICGD)	12	C	A	C	C	C
C5 (HH)	14	C	C	C	C	C
C6 (HH)	14	C	C	C	C	C
C7 (CATIE,CR)	14*	C	C	C	C	C
C8 (CATIE,CR)	6*	A	A	A	A	A
C15 (CATIE,CR)	14*	C	C	C	C	C
C16 (CATIE,CR)	6*	A	A	A	A	A

[a]Differences in the number *n* of the TAAAG-repeat and 5 SNPs. SNP numbering according to Herrmann et al.[11] Differences are highlighted. C, CCN-51 typical SNP; A, Arriba typical SNP; *, this study.

mTcCIR25), showing a loss of heterozygosity in this locus. For some microsatellite loci, no amplicons were detected (e.g., C15 mTcCIR1, mTcCIR11, and mTcCIR15). These observations of differences in allele pattern might be explained by the occurrence of somaclonal variation, a common phenomenon in trees, observed among others in coffea or Populus trees.[28−30] The slight genetic variability also is well in line with the results from the previous published chloroplast analyses, where the samples C1−C3, C5−C7, and C15 showed identical results for the $(TAAAG)_n$ repeat (all $n = 14$) and for the restriction analysis (all CCN-51 typical).[11] A detailed summary of the chloroplast differences is given in Table 4.

But, the samples C4, C8, and C16 exhibit diverse different genetic patterns. These samples revealed both a reduced number of alleles but also the presence of complete different alleles in several SSR loci (Table 4). Whereas C8 and C16 showed three, respectively two different amplicons, the ICGD sample (C4), showed the most distinct differences among the CCN-51 samples. For example, for the microsatellites mTcCIR6, mTcCIR11, mTcCIR12, mTcCIR15, mTcCIR18, and mTcCIR24, one allele differs from the Ecuadorian CCN-51 pattern, whereas for mTcCIR8, mTcCIR25, and mTcCIR60, only one allele is present, indicating a loss of heterozygosity as demonstrated above.

It should be noted that for these three samples, the results from the chloroplast analyses also showed a different picture (Table 4). Whereas the results for C8 and C16 were completely identical to classical Arriba samples ($(TAAAG)_6$ and Arriba typical restriction pattern), for C4 only a slightly shortened $(TAAAG)_n$ repeat was detected ($n = 12$). Furthermore, the restriction pattern of this sample only differed at one restriction site from the Ecuadorian CCN-51 pattern.

According to the microsatellite results (Table 3), a manual scoring shows that samples can be divided into four types: C1, C2, and C3 (type I); C5, C6, C7, and C15 (type II); C8 and C16 (type III); and C4 (type IV). This grouping seems to reflect the geographical origin of the cocoa. Type I originates from Ecuador; samples of types II (C15) and III (C16) originate from Costa Rica, where they are already traded as CCN-51 type I (C15) and CCN-51 type II (C16). The ICGD sample behaves as fourth type. Comparing this presumption with the dendrogram of the cluster analysis (Figure 1), it was observed that samples from types I and II form one cluster (group I). The samples of type III, C8 and C16 from Costa Rica, form a second group (group II) basically separated from group I. Again, the ICGD sample C4 (type IV) is situated at the basis of all other investigated CCN-51 individuals and forms a

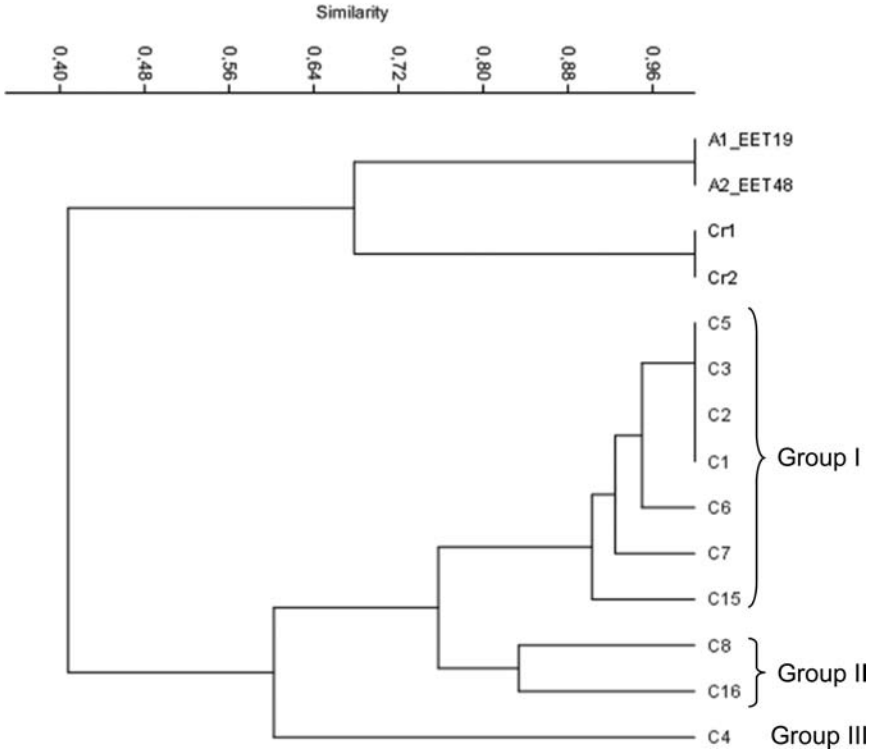

Figure 1. Dendrogram of the cluster analysis of the CCN-51, Arriba, and Criollo samples. Similarity measure by Simpson's index. The grouping of the CCN-51 samples suggests that there are three groups within this cocoa type.

DOI: 10.1021/acs.jafc.5b01462
J. Agric. Food Chem. 2015, 63, 4539−4544

distinct branch (group III). This individual shows different allele patterns in eight out of 10 SSR loci.

This grouping is well in line with the recent observations based on the chloroplast analysis ($(TAAAG)_n$ repeat and SNP analysis).[11] Taking these results into account, the same samples would be similarly grouped together: C1−C3, C5−C7, and C15 as one group; C8 and C16 as a second group; and C4 as a third group (Table 4).

Besides the CCN-51 samples, two Arriba and two Criollo were analyzed to classify the results in comparison to other cocoa types. The analysis of the microsatellite patterns of the two Arriba samples demonstrated a relatively high level of similarity. An apparent difference in Arriba was observed in the SSR locus mTcCIR12 (Table 3), which can be explained by sexual reproduction of the plant. The two Criollo samples showed nearly identical results but differed compared to the Arriba sample. This could be demonstrated by the microsatellites mTcCIR1, mTcCIR6, mTcCIR11, mTcCIR24, and mTcCIR25.

The previously published results of chloroplast marker analysis already gave reason to suggest that CCN-51 is not a pure clone. The present SSR analysis confirmed this by additional variations in the nuclear genome. This hypothesis is verified by different marker systems in two different genomes.

A possible explanation for these genetic variations within CCN-51 could be mistakes during propagation, including the growth of a seedling rootstock rather than the scion clone after grafting. Furthermore, in some cases, seed propagation rather than clonal propagation cannot be excluded. Moreover, mislabeling and misidentification in plant collections and arboreta cannot be ruled out. Misidentification of cocoa samples in germplasm collections was already observed earlier by other research groups.[31,32]

But, regarding the eight different SSRs of sample C4 in detail, it is striking that one of each microsatellite allele is a typical CCN-51 allele, whereas the second one is differing (Table 3). So, for C4 it is most likely that two different genomes were combined by a recent outbreeding event.

In the present study, various differences in the microsatellite pattern of CCN-51 could be detected. These genetic differences vary from slight differences in one to three SSR loci and a loss of heterozygosity up to complete different allele patterns in eight out of 10 microsatellite loci (CCN-51 sample C4 in Table 3). According to the statistical cluster analysis (Figure 1), the samples originating from Ecuador and some of those delivered from Costa Rica form one group, the two samples delivered from Costa Rica form a second group, and the ICGD sample forms an individual group. Hence, the suspicion is confirmed that one can differentiate between various types of CCN-51. Some of this genomic variation might be explained by somaclonal variation, but in other samples—especially in C4—outcrossing events probably occurred. The samples C4, C8, and C16 should be analyzed in more detail to clarify the doubtful classification into the CCN-51 type identified by different SSR patterns in the nuclear genome.

AUTHOR INFORMATION

Corresponding Author

*Tel: +49-40-428384357. Fax: +49-40-428384342. E-mail: markus.fischer@chemie.uni-hamburg.de.

Author Contributions

§Equally contributing authors.

Funding

This research project was supported by the German Ministry of Economics and Technology (via AiF) and the FEI (Forschungskreis der Ernährungsindustrie e. V., Bonn, Germany), Project AiF 16796 N.

Notes

The authors declare no competing financial interest.

ACKNOWLEDGMENTS

Cocoa sample material was obtained from the INIAP, Guayaquil, Ecuador, from the CATIE, Cartage, Costa Rica, from the Botanical Garden, Hamburg, Germany, and from the ICGD, University of Reading, England. We thank Dr. Rainer Schubbert (Eurofins Genomics, Ebersberg, Germany) for his skillful help with the data evaluation of the microsatellites.

ABBREVIATIONS USED

CCN, Colección Castro Naranjal; DNA, desoxyribonucleic acid; IRR, inverted repeat region; PCR, polymerase chain reaction; RFLP, restriction fragment length polymorphism; SNP, single nucleotide polymorphism; INIAP, Instituto Nacional de Investigaciones Agropecuarias; CATIE, Centro Agronómico Tropical de Investigación y Enseñanza; ICGD, International Cocoa Germplasm Database; CIRAD, Centre de Coopération Internationale en Recherche Agronomique pour le Développement; mTcCir, microsatellite *Theobroma cacao* CIRAD

REFERENCES

(1) Cook, L. R. *Chocolate Production and Use*, 1st ed.; Harcourt: Boston, MA, 1982.

(2) *Geschäftsbericht 2011/2012*; Kakaoverein: Hamburg, 2012.

(3) Lieberei, R. *Die Vielfalt des Kakaos*; Moderne Ernährung, Relations, Gesellschaft für Kommunikation GmbH: 2006; pp 6−12.

(4) Boza, E. J.; Motamayor, J. C.; Amores, F. M.; Cedeño-Amador, S.; Tondo, C. L.; Livingstone, D. S.; Schnell, R. J.; Gutiérrez, O. A. Genetic characterization of the cacao cultivar CCN 51: Its impact and significance on global cacao improvement and production. *J. Am. Soc. Hortic. Sci.* **2014**, *139*, 219−229.

(5) Stern, J. G. The History of CCN-51 in Ecuador. www.jeffreygstern.com.

(6) Turnbull, C. J.; Hadley, P. International Cocoa Germplasm Database: CCN 51. www.icgd.rdg.ac.uk.

(7) Sütterlin, S. Eine Frage des Geschmacks. *Berliner Zeitung*, December 21, 2006.

(8) Afoakwa, E. O.; Paterson, A.; Fowler, M.; Ryan, A. Flavor Formation and Character in Cocoa and Chocolate: A Critical Review. *Crit. Rev. Food Sci. Nutr.* **2008**, *48*, 840−857.

(9) Crouzillat, D.; Bellanger, L.; Rigoreau, M.; Bucheli, P.; Pétiard, V. *Genetic structure, characterisation and selection of Nacional cocoa compared to other genetic groups*; International Workshop on New Technologies and Cocoa Breeding, 2001; Ingenic: 2001; p 30.

(10) Kane, N.; Sveinsson, S.; Dempewolf, H.; Yang, J. Y.; Zhang, D.; Engels, J. M. M.; Cronk, Q. Ultra-Barcoding in cacao (*Theobroma* spp.; *Malvaceae*) using whole chloroplast genomes and nuclear ribosomal DNA. *Am. J. Bot.* **2012**, *99*, 320−329.

(11) Herrmann, L.; Haase, I.; Blauhut, M.; Barz, N.; Fischer, M. DNA-Based Differentiation of the Ecuadorian Cocoa Types CCN-51 and Arriba Based on Sequence Differences in the Chloroplast Genome. *J. Agric. Food Chem.* **2014**, *62*, 12118−12127.

(12) Dhingra, A.; Folta, K. M. ASAP: Amplification, sequencing & annotation of plastomes. *BMC Genomics* **2005**, *6*, 176.

(13) Botstein, D.; White, R. L.; Skolnick, M.; Davis, R. W. Construction of a Genetic Linkage Map in Man Using Restriction Fragment Length Polymorphisms. *Am. J. Hum. Genet.* **1980**, *32*, 314−331.

DOI: 10.1021/acs.jafc.5b01462
J. Agric. Food Chem. 2015, 63, 4539−4544

(14) Williams, P. E.; Marino, M. A.; Del Rio, S. A.; Turni, L. A.; Devaney, J. M. Analysis of DNA restriction fragments and polymerase chain reaction products by capillary electrophoresis. *J. Chromatogr.* **1994**, *680*, 525−540.
(15) Löffler, G. *Basiswissen Biochemie*, 7th ed.; Springer Verlag: Heidelberg, 2008.
(16) Tautz, D.; Renz, M. Simple sequences are ubiquitous repetitive components of eukaryotic genomes. *Nucleic Acids Res.* **1984**, *12*, 4127−4138.
(17) Allegre, M.; Argout, X.; Boccara, M.; Fouet, O.; Roguet, Y.; Bérard, A.; Thévenin, J. M.; Chauveau, A.; Rivallan, R.; Clement, D. Discovery and mapping of a new expressed sequence tag-single nucleotide polymorphism and simple sequence repeat panel for large-scale genetic studies and breeding of *Theobroma cacao* L. *DNA Res.* **2011**, 23.
(18) Litt, M.; Luty, J. A. A hypervariable microsatellite revealed by in vitro amplification of a dinucleotide repeat within the cardiac muscle actin gene. *Am. J. Hum. Genet.* **1989**, *44*, 397.
(19) Weber, J. L.; May, P. E. Abundant class of human DNA polymorphisms which can be typed using the polymerase chain reaction. *Am. J. Hum. Genet.* **1989**, *44*, 388.
(20) Lanaud, C.; Risterucci, A. M.; Pieretti, I.; Falque, M.; Bouet, A.; Lagoda, P. J. L. Isolation and characterization of microsatellites in *Theobroma cacao* L. *Mol. Ecol.* **1999**, *8*, 2141−2152.
(21) Pugh, T.; Fouet, O.; Risterucci, A.; Brottier, P.; Abouladze, M.; Deletrez, C.; Courtois, B.; Clement, D.; Larmande, P.; N'goran, J. A new cacao linkage map based on codominant markers: development and integration of 201 new microsatellite markers. *Theor. Appl. Genet.* **2004**, *108*, 1151−1161.
(22) Brown, J. S.; Schnell, R.; Motamayor, J.; Lopes, U.; Kuhn, D. N.; Borrone, J. W. Resistance gene mapping for witches' broom disease in *Theobroma cacao* L. in an F2 population using SSR markers and candidate genes. *J. Am. Soc. Hort. Sci.* **2005**, *130*, 366−373.
(23) Cryer, N. C.; Fenn, M. G. E.; Turnbull, C. J.; Wilkinson, M. J. Allelic size standards and reference genotypes to unify international cocoa (*Theobroma cacao* L.) microsatellite data. *Genet. Resour. Crop Evol.* **2005**, *53*, 1643−1652.
(24) Efombagn, I.; Motamayor, J.; Sounigo, O.; Eskes, A.; Nyassé, S.; Cilas, C.; Schnell, R.; Manzanares-Dauleux, M.; Kolesnikova-Allen, M. Genetic diversity and structure of farm and GenBank accessions of cacao (*Theobroma cacao* L.) in Cameroon revealed by microsatellite markers. *Tree Genetics & Genomes* **2008**, *4*, 821−831.
(25) Irish, B. M.; Goenaga, R.; Zhang, D.; Schnell, R.; Brown, J. S.; Motamayor, J. C. Microsatellite Fingerprinting of the USDA-ARS Tropical Agriculture Research Station Cacao (L.) Germplasm Collection. *Crop Sci.* **2010**, *50*, 656−667.
(26) Saunders, J.; Mischke, S.; Leamy, E. A.; Hemeida, A. A. Selection of international molecular standards for DNA fingerprinting of *Theobroma cacao*. *Theor. Appl. Genet.* **2004**, *110*, 41−47.
(27) Hammer, Ø.; Harper, D.; Ryan, P. PAST-Palaeontological statistics. *Palaeo-Electronica* **2001**, *25*, 2009.
(28) Etienne, H.; Bertrand, B. Somaclonal variation in Coffea arabica: effects of genotype and embryogenic cell suspension age on frequency and phenotype of variants. *Tree Physiol.* **2003**, *23*, 419−426.
(29) Rahman, M.; Rajora, O. Microsatellite DNA somaclonal variation in micropropagated trembling aspen (*Populus tremuloides*). *Plant Cell Rep.* **2001**, *20*, 531−536.
(30) Ostry, M.; Ward, K. Field performance of Populus expressing somaclonal variation in resistance to *Septoria musiva*. *Plant Sci.* **2003**, *164*, 1−8.
(31) Motamayor, J. C.; Lachenaud, P.; e Mota, J. W. d. S.; Loor, R.; Kuhn, D. N.; Brown, J. S.; Schnell, R. J. Geographic and genetic population differentiation of the Amazonian chocolate tree (*Theobroma cacao* L). *PLoS One* **2008**, *3*, e3311.
(32) Motilal, L.; Butler, D. Verification of identities in global cacao germplasm collections. *Genet. Resour. Crop Evol.* **2003**, *50*, 799−807.

DOI: 10.1021/acs.jafc.5b01462
J. Agric. Food Chem. 2015, 63, 4539−4544

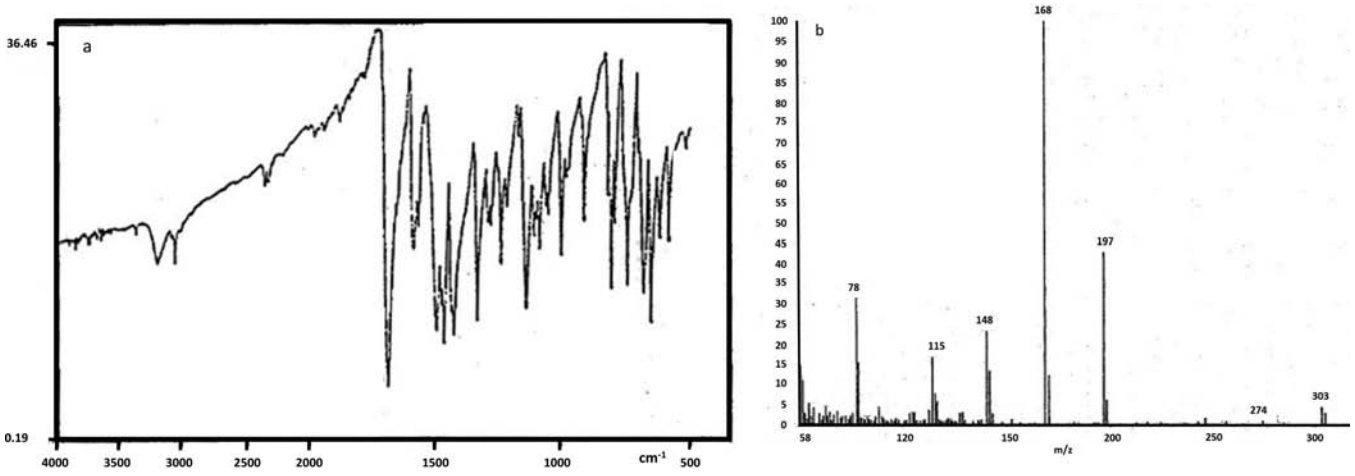

Figure 1. (a) Mass spectrum of DPKPH (electronic impact ionization); (b) IR spectrum of DPKPH.

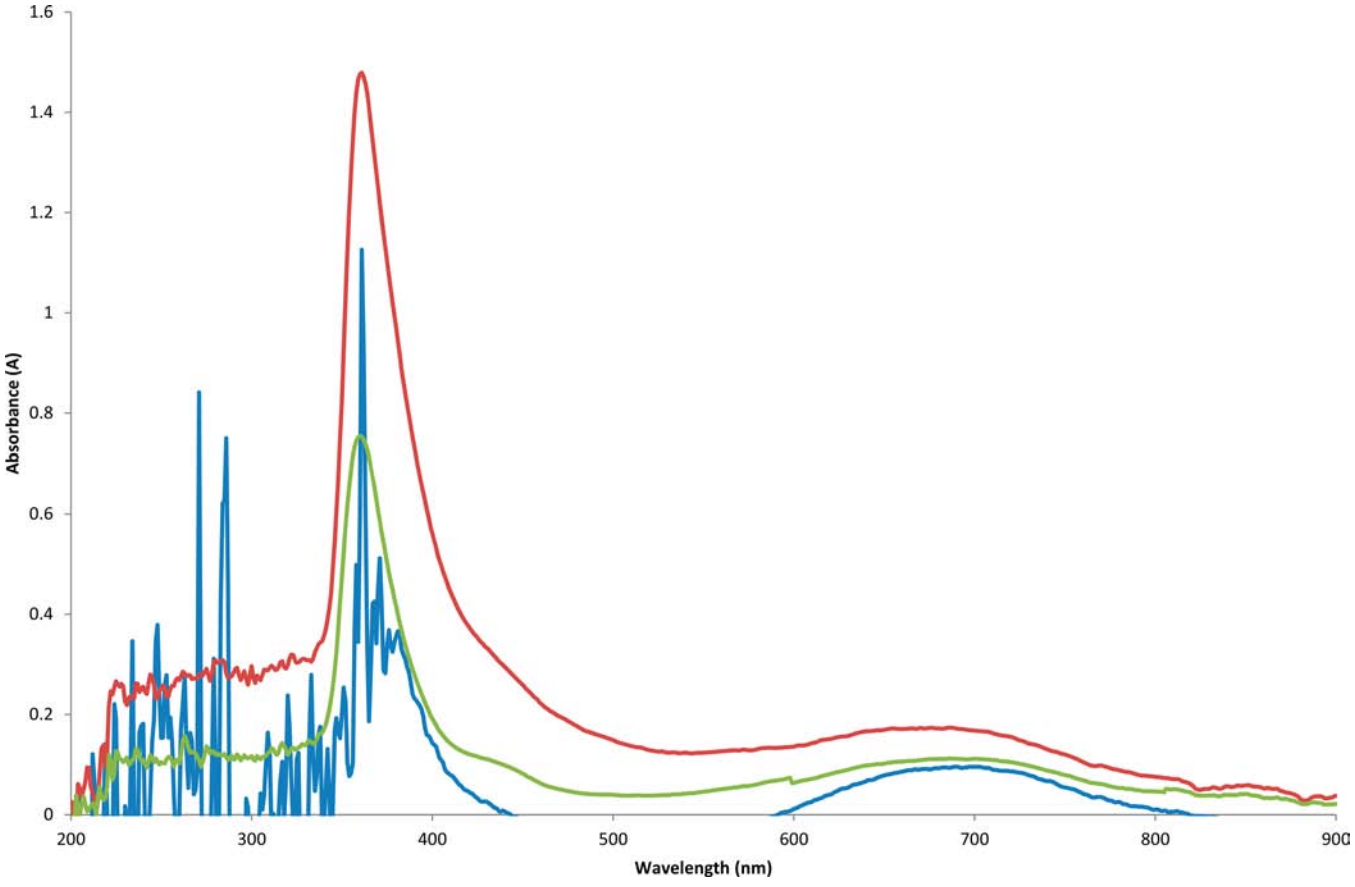

Figure 2. UV−vis spectra of Fe−DPKPH complex in water solution (spike of 1 mg L^{-1}), white wine (spike of 0.5 mg L^{-1}), and red wine (spike of 0.5 mg L^{-1}) samples. [DPKPH] = 1.25×10^{-4} mol L^{-1}.

EXPERIMENTAL PROCEDURES

Reagents and Solutions. Unless otherwise noted, all reagents were of analytical reagent grade. Picolinic acid ethyl ester (99.0%), 2,2′-dipyridylketone (97.0%), hydrazine (98.0%), NaOH (99.0%), ethanol absolute (96.0% v/v), acetic acid (97.0%), sodium acetate (98.5%), Br-ADAP, and ascorbic acid (99.0%) were purchased from Merck (Darmstadt, Germany). Solutions were prepared using high-purity deionized water with resistivity <18.2 MΩ cm (Milli Q, Millipore, Bedford, MA, USA). Standards of Fe(II) for calibration and to spike samples were prepared daily, by dissolving $FeSO_4 \cdot 7H_2O$ in 2% HCl from Merck.

Solutions of ascorbic acid dissolved in deionized water were prepared fresh daily. Finally, acetic acid/acetate buffer was used to control the pH in the sample during analysis. Buffer solution was prepared by dissolving equimolar proportions of acetic acid and sodium acetate in distilled water.

Wine Samples. Wine samples used in this study were purchased from the manufacturers. White wines with designation of origin (D.O.) *Jerez-Xéréz-Sherry* produced from Palomino fino grapes, Tio Pepe (Tío Pepe, Spain, 2008), and Romate (Sánchez Romate, Spain, 2009), as well as other white wines such as Casón Histórico, Don García, Don Simón (García Carrión, Spain), and Elegido (Viña Tridado, Spain) were analyzed. Rose wines Mateus Rose (Sogrape, Portugal, 2009)

DOI: 10.1021/acs.jafc.5b01571
J. Agric. Food Chem. 2015, 63, 4545−4550

with *D.O. Portugal* produced from a mixture of Portuguese red grapes Braga, Rufete, Tinta Barroca, and Touriga Franca, and, additionally, Carrefour (López Morenas, Spain), and Don Simón (García Carrión, Spain) were selected. Finally, the method was applied for the analysis of iron in the following red wines: Rincón (Marqués de Griñón, Spain, 2008) with *D.O. Dominio de Valdepusa* produced from Syrah and Garnacha grapes; Beronia Crianza (Spain, 2008) *D.O. Rioja* made from Tempranillo, Garnacha, And Mazuelo Grapes; and Río Mayor (Valero Winemakers, Spain, 2008) *D.O. Cariñena* produced from Garnacha, Tempranillo, And Cariñena grapes. Additionally, red wines Elegido (Viña Tridado, Spain) and Carrefour (García Carrión, Spain) were analyzed.

Synthesis of 2,2′-Dipyridyl Ketone Picolinoylhydrazone (DPKPH). The spectrophotometric reagent DPKPH was synthesized by condensation of equimolar amounts of the 2,2′-dipyridylketone and picolinoylhydrazide (PH) dissolved in ethanol, as reported by Mánuel-Vez and García-Vargas.[18] Reaction was quantitative, and the product was filtered and dried overnight at 80 °C to be stored dried. A purity of 99% was determined by elemental analysis. The product, DPKPH, was identified by mass spectrometry, and the following fragments were obtained: 303/197/168/148/115/78. The following bands were observed in an infrared spectrum for a sample supported on a KBr disk: 3200−300 cm^{-1} (ν_{N-H}), intramolecular hydrogen bond; 3050−3010 cm^{-1} ($\nu_{=C-H}$); 1690 cm^{-1} (amide I); 1490 cm^{-1} (amide II) (Figure 1). Finally, when dissolved in ethanol, the product presented maximum absorbance at 321 nm. The product was stored dry, and it was shown to be stable for up to 1 month in ethanolic solution at 4 °C.[19]

Apparatus. A pH-meter Jenway model 4330 was used during sample preparation, and spectrophotometric determination of Fe(II) was carried out in a Jenway 6300 spectrophotometer (Jenway, Stone, UK) using plastic cuvettes. Solaar series (UNICAM, UK) flame atomic absorption spectrometer (FAAS) was used for analysis of total Fe in validation studies as a reference method Commission Regulation (ECC) No. 2676/90 of September 1990 determining European Community methods for the analysis of wines for Fe analysis.[20] Identification of DPKPH was carried out using an IR spectrophotometer PerkinElmer 1600 FT-IR Series (PerkinElmer, Boston, MA, USA) and a VG 12250 mass spectrometer (VG Analytical Ltd., Wythenshaw, UK) using electronic impact as a source of mass fragments.

Procedure. The complexation of iron with DPKPH presents maximum yield at pH 4.9;[19] for this reason sample pH was adjusted prior to analysis using a small volume of 2 M NaOH that depended on the wine sample, so dilution of the sample was negligible. Maximum absorbance was observed at λ = 380 nm ($\varepsilon = 3.24 \times 10^4$ L mol^{-1} cm^{-1});[19] however, some interferences can also be detected at 380 nm associated with wine matrix components.[21] Consequently, a secondary maximum at 700 nm ($\varepsilon = 6.7 \times 10^3$ L mol^{-1} cm^{-1}) was selected for measuring $Fe(DPKPH)_2$ due to its better selectivity (Figure 2). Fe determination was in all cases carried out at room temperature after the samples had been filtered through a 0.45 μm pore sized nylon filter.

Formation of the green-blue complex $Fe(DPKPH)_2$ was directly conducted in a volumetric flask. This reaction takes place immediately after shaking the flask to homogenize the mixture. Conditions for application of the method were as follows in the case of total Fe analysis: 5 mL of sample or standard was placed into a 10 mL volumetric flask, 2 mL of 1 mol L^{-1} acetic acid/acetate buffer was added, followed by 1 mL of ascorbic acid 2×10^{-3} mol L^{-1} ascorbic acid and 2 mL of 6.24×10^{-4} mol L^{-1} DPKPH. Absorbance was measured at 700 nm. In the case of Fe(II) analysis, ascorbic acid was substituted by ultrapure water.

In the case of total Fe analysis, ascorbic acid was also added to ensure that Fe is in the form of Fe(II); the sample and all reagents were added in the following order: 5 mL of sample, 1 mL of ascorbic acid, 2 mL of acetic acid/acetate buffer, and 2 mL of DPKPH dissolved in ethanol. The signal was again measured at 700 nm.

To enhance the analytical signal due to Fe complexation, univariate optimization of DPKPH concentration and concentration of acetate buffer were carried. Furthermore, addition of ascorbic acid for analysis of total Fe was also studied.

Statistics. The extent of matrix effects on Fe determination was evaluated by comparing the slope of calibration curves and the analyzed total Fe concentration obtained by direct calibration using aqueous standards and by the standard additions method (SAM). In the case of direct calibration blank samples were prepared using an ultrapure water solution containing the reagents, and the standards were prepared by addition of a known concentration of Fe by dilution of a 1000 mg L^{-1} standard of Fe(II). SAM was applied by the addition of known spiked concentrations of Fe to the samples to build a calibration curve in which the blank was the sample itself without any spike. Concentration of Fe in the sample is estimated, by the standard additions method, as the intercept of the curve in the x axis. If the slope of the calibration curve using aqueous standards is comparable with that obtained by the SAM method, the method can be considered free of interferences.[22] Results were compared by a t test after three replicates of each sample were analyzed (t_c = 2.78). In the cases that t value was smaller than t_c, the null hypothesis that there is no evidence of significant difference between the results of the two methods was accepted with a 95% level of confidence.[22]

The limit of detection was calculated as the concentration that offered a response equal to the average of 10 independent blank samples plus 3 times its standard deviation. The limit of quantification was calculated as the concentration that offered a response equal to the average of 10 independent blank samples plus 10 times its standard deviation. The linearity of the method was evaluated using the criterion that the addition of a new standard of higher concentration resulted in a deviation of 5% between the measured and the theoretical concentration.[22]

To evaluate the accuracy of the method, three replicates of every sample were analyzed In the case of total Fe analysis, results were compared with those obtained by the reference method of Commission Regulation (ECC) No. 2676/90 of September 1990 determining Community methods for the analysis of wines for Fe analysis. For Fe(II) analysis results were compared with those obtained by the spectrophotometric determination of Fe(II) with Br-ADAP.[17] Comparisons were carried out by a t test for comparison of average experimental data (n = 4, α = 0.05, t_c = 2.78).

RESULTS AND DISCUSSION

Optimization of Fe(II) Complexation by DPKPH and Spectrophotometric Determination. Univariate optimization of the method was carried out using the analytical signal at 700 nm as a response factor. Fe(II) analysis was optimized by studying the effect of DPKPH and acetic acid/acetate buffer concentration in the presence of ascorbic acid to ensure that Fe was as Fe(II). The effect of ascorbic acid on the signal for total Fe was also evaluated.

Formation of the Fe(II)−DPKPH complex presents maximum yield at pH 4.9, in aqueous solutions containing up to 15% v/v ethanol.[21] For this reason the pH in the samples was buffered at pH 4.9 using acetic acid/acetate buffer during the whole study. All experiments were carried out using a 10 mL flask in which 5 mL of sample was placed. Concentrations of reagents are referred to the volume of the flask.

First of all, the effect of DPKPH concentration on the instrumental signal was studied. This study was conducted using water samples with an Fe concentration of 1 mg L^{-1} prepared by dilution of a standard of 1000 mg L^{-1} prepared by solution of $FeSO_4$. Ascorbic acid was added at a concentration of 30×10^{-4} mol L^{-1} during DPKPH optimization, and 0.5 mol L^{-1} acetic acid/acetate pH buffer was used. As can be observed in Figure 3, the absorbance due to the formation of the $Fe(DPKPH)_2$ complex was enhanced by an increase of the ligand concentration until it stabilizes at 1.25×10^{-4} mol L^{-1}. This concentration was used for further experiments.

DOI: 10.1021/acs.jafc.5b01571
J. Agric. Food Chem. 2015, 63, 4545−4550

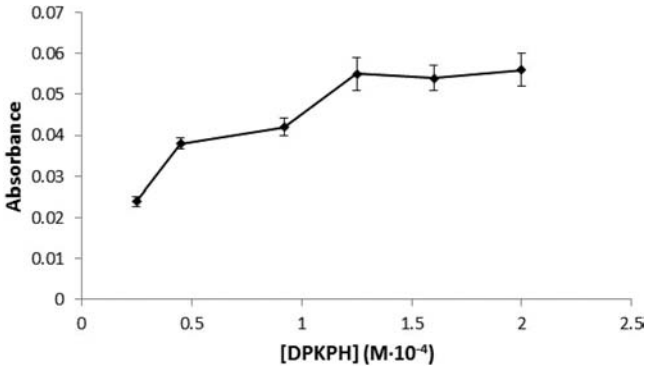

Figure 3. Optimization of DPKPH in 15% v/v ethanolic solution dissolved in water. Sample pH, 4.9; Fe concentration, 1 mg L^{-1}. Error bars represent the standard deviation of the average.

Thus, acetic acid/acetate buffer concentration to keep pH 4.9 in the sample was optimized. Figure 4 shows that absorbance

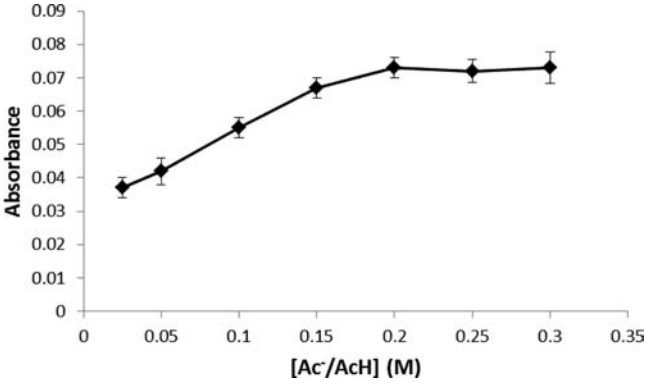

Figure 4. Optimization of acetic acid−acetate buffer (pH 4.9) for Fe concentration 1 mg L^{-1} and 1.25 × 10^{-4} mol L^{-1} DPKPH concentration. Error bars represent the standard deviation of the average.

was increased from buffer concentration 0.025 mol L^{-1} to 0.2 mol L^{-1}, being constant for higher concentrations. For this reason, 0.2 mol L^{-1} was selected as optimum concentration.

Finally, ascorbic acid concentration was optimized by keeping constant the optimized value of DPKPH and buffer concentration. Results showed that the analytical signal was increased with the addition of ascorbic acid up to 20 × 10^{-5} mol L^{-1} (Figure 5). This way the total concentration of Fe could be analyzed.

Effects of Wine Matrix on the Spectrophotometric Determination. Due to the complexity of the wine samples matrix, the effect of interferences that may appear in the samples affecting the Fe(II) complexation by DPKPH has been evaluated (Figure 2). This study has been performed for analysis of total iron. First, the effect of the presence of foreign ions that could compete in $Fe(DPKPH)_2$ formation was studied in white wine Tío Pepe (D.O. Jerez-Xéréz-Sherry, Spain, 2008) and red wine Río Mayor (D.O. Cariñena, Spain, 2008). For this study, wine samples were spiked with 1 mg L^{-1} of Fe(II). Cationic interferences were added as their chloride, nitrate, or acetate salt, and anionic interferences were added as sodium or potassium salts. Interference concentration was considered to have a negative effect on the method response if a variation of the analytical signal >4% was observed. As can be seen in Table 1, most anionic species are tolerated at relatively

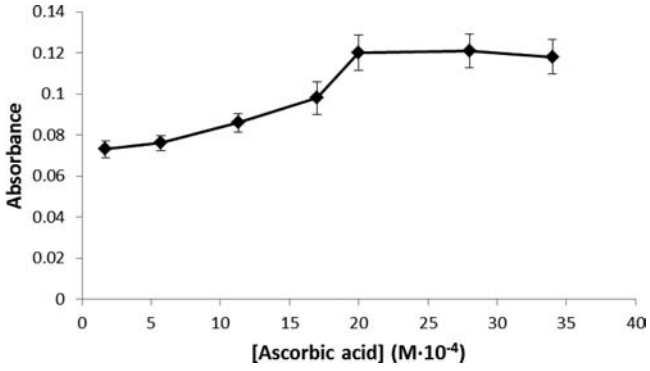

Figure 5. Effect of ascorbic acid concentration on the analytical signal. Fe concentration, 1 mg L^{-1}; sample pH, 4.9; buffer concentration, 0.2 mol L^{-1}; DPKPH concentration, 1.25 × 10^{-4} mol L^{-1}. Error bars represent the standard deviation of the average.

Table 1. Tolerance Limits of Chemical Interferences on Fe(II) Determination in White and Red Wine Samples

interference	concentration tolerated (mg L^{-1})
Cl^-, NO_3^-	10000[a]
CO_3^{2-}, Ca(II), Mg(II), Al(III)	950
Be(II)	700
citrate, NO_2^-, S^{2-}, SO_4^{2-}, BO_3^-, As(III), As(V)	120
F^-, Br^-, I^-, SeO_4^{2-}, SO_3^{2-}, SO_4^{2-}, $S_2O_3^{2-}$	100
Mn(II), Sn(II), Sr(II)	90
$PO_4H_2^-$, IO_3^-, BrO_3^-, Cu(II), Ni(II), Pb(II)	10
oxalate, Zn(II), Sb^3(III), Pd(II)	5

[a]Maximum concentration added.

high concentration. Furthermore, the main cationic species that coexist with Fe in wine, Ca(II), Mg(II), K(I), Na(I), Zn(II), Cu(II), Mn(II), and Se(II), do not affect signal due to Fe(II) in the concentrations at which they are normally found. This fact proves that the proposed method is highly selective for measuring Fe in wines.

However, the complexity of the wine matrix is not restricted to the aforementioned interferences. To contrast the robustness of the method against wine matrix, including ethanol concentration, results obtained by direct calibration and by the standard additions method were compared.[22] In particular, the slope of calibration curves and the analyzed total Fe concentrations using both methods were compared. This study was carried out on wine samples of different nature and ethanolic concentration, after the addition of 1 mg L^{-1} Fe: one white wine, Tío Pepe (D.O. Jerez-Xéréz-Sherry, Spain, 2008), and one red wine, Río Mayor (D.O. Cariñena, Spain, 2008). Slopes of direct calibration and standard additions method were compared by a t test. As shown in Table 2, there were no significant differences between the slopes for the direct calibration and the standard additions method (n = 4, α = 0.05). Finally, results of total Fe concentration analysis using both methods were compared, showing that there were no significant differences between the results due to matrix sample (Table 2). Thus, direct calibration could be used for analysis of Fe in white, rose, and red wines free of interferences of sample matrix, including ethanol concentration up to 15% v/v ethanol.

Analytical Features. Prior to application of the method to commercial wine samples, analytical features were evaluated. Limits of detection and quantification were calculated after

DOI: 10.1021/acs.jafc.5b01571
J. Agric. Food Chem. 2015, 63, 4545−4550

Table 2. Comparison between Results Obtained by Direct Calibration and the Standard Additions Method

		slope of calibration curve (L mg^{-1})			Fe (mg L^{-1})		
wine type	ethanol (% v/v)	direct calibration	standard additions method	t^a	direct calibration	standard additions method	t^a
white[b]	15.0	0.1182 ± 0.014	0.1195 ± 0.012	−0.17	2.47 ± 0.19	2.63 ± 0.24	−1.36
red[c]	12.5	0.1167 ± 0.008	0.1175 ± 0.011	−0.14	2.87 ± 0.18	2.93 ± 0.31	1.50

[a] t = 2.78, 95% confidence level. Uncertainty measured as RSD (%) for three replicates. [b] Tío Pepe (D.O. Jerez-Xéréz-Sherry, Spain, 2008). [c] Río Mayor (D.O. Cariñena, Spain, 2008).

Table 3. Determination of Fe(II) and Total Iron (Fe) in Commercial Wine Samples

wine type	designation	$Fe(II)_{DPKPH}$ (mg L^{-1})	$Fe(II)_{Br\text{-}ADAP}$ (mg L^{-1})	t^a	Fe_{DPKPH} (mg L^{-1})	Fe_{FAAS}[b] (mg L^{-1})	t^a
white	Tío Pepe (D.O. Jerez-Xéréz-Sherry, Spain, 2008)				1.43 ± 0.15	1.46 ± 0.02	−0.48
	Sánchez Romate (D.O. Jerez-Xéréz-Sherry, Spain, 2009)	2.43 ± 0.18	2.23 ± 0.17	2.25	2.29 ± 0.09	2.31 ± 0.08	0.36
	Casón Histórico	2.18 ± 0.13	2.59 ± 0.18	2.71	3.44 ± 0.29	3.21 ± 0.08	−2.15
	Don García	1.24 ± 0.11	1.99 ± 0.15	2.74	1.99 ± 0.19	1.92 ± 0.11	−0.89
	Don Simón	1.24 ± 0.11	1.31 ± 0.07	−1.62	1.26 ± 0.28	1.03 ± 0.09	−2.25
	Elegido	2.15 ± 0.19	2.32 ± 0.15	−2.00	2.52 ± 0.11	2.72 ± 0.18	2.62
rose	Mateus Rose (D.O. Portugal, Portugal, 2009)				5.35 ± 0.32	5.31 ± 0.08	0.33
	Don Simón	2.55 ± 0.12	2.73 ± 0.20	−2.24	3.68 ± 0.21	3.96 ± 0.19	2.75
	Carrefour	2.49 ± 0.23	2.21 ± 0.18	2.73	2.51 ± 0.11	2.67 ± 0.13	2.76
red	Rincón (D.O. Rioja, Spain, 2008)				2.00 ± 0.14	1.97 ± 0.11	1.19
	Beronia Crianza (D.O. Rioja, Spain, 2008)				1.58 ± 0.12	1.62 ± 0.12	−0.94
	Río Mayor (D.O. Cariñena, Spain, 2008)	5.31 ± 0.12	5.51 ± 0.27	−1.97	9.55 ± 0.45	9.12 ± 0.32	−2.22
	Carrefour	4.07 ± 0.31	3.86 ± 0.17	1.69	5.42 ± 0.25	5.89 ± 0.28	−2.75
	Elegido	2.93 ± 0.21	2.81 ± 0.09	1.51	3.99 ± 0.37	3.56 ± 0.24	−2.22

[a] $t_{(4,\ 0.05)}$ = 2.78, 95% confidence level. Uncertainty measured as RSD (%) for three replicates. [b] Method (CEE) no. 2676/90 of European Commission.

measurement of 10 reagent blank samples containing ultrapure water and the optimized concentrations of DPKPH, ascorbic acid, and acetate buffer. In these conditions, the method offered a limit of detection of 0.005 mg L^{-1}, a limit of quantification of 0.017 mg L^{-1}, and a linear response of up to 6 mg L^{-1}; for this reason samples containing higher concentrations were diluted before analysis. These analytical features allowed the use of this method in the analysis of Fe at the concentration level in which it normally appears in wine samples.

Application to Commercial Wine Samples. Finally, the capability of this method to selectively determine Fe(II) in wines was evaluated using different wine samples. In particular, five red wines, six white wines, and three rose wine were analyzed. In this section, results for Fe(II) and total Fe are discussed.

In the case of total iron concentration results were compared with those obtained by the reference method Commission Regulation (ECC) No. 2676/90 of September 1990 determining Community methods for the analysis of wines for Fe analysis.[20] Comparisons were carried out using a t test for three independent replicates of each sample. Results for total concentration of Fe by both methods were in good agreement in the two types of wine used (Table 3). This confirms the applicability of the spectrophotometric analysis of Fe in wine samples using DPKPH as a ligand, free of sample matrix effects for white, rose, and red wines.

Although some Fe(III) could be measured as Fe(II), the broadly accepted method of spectrophotometric determination by complexation of Fe(II) with Br-ADAP has been used as a reference method for selective analysis of Fe(II).[17] Results obtained by DPKPH complexation were compared with the reference method using a t test for three independent replicates of each sample (Table 3). Results confirmed the suitability of DPKPH for selective analysis of Fe(II) in wine samples.

In all cases the concentration of Fe(III) was smaller than the Fe(II) concentration. This can be explained by the reductive conditions of wine samples that prevents oxidative damage. Similar distribution of Fe ions has been observed for other wines such as sweet wines from Brazil, which could be explained by reductive characteristics of the wines.[17] Additionally, higher levels of Fe(III) were observed in the case of red wines if compared with rose and white wines.

For these reasons, spectrophotometric determination of Fe(II) and Fe using DPKPH as a colorimetric reagent appears as a simple and fast alternative to existing analytical methods for iron speciation in wine samples.

AUTHOR INFORMATION

Corresponding Author

*(J.A.L.-L.) Phone: +34956016165. E-mail: joseantonio.lopezlopez@uca.es.

Notes

The authors declare no competing financial interest.

This study was supported by Plan Nacional de I+D (CICYT) Project CTM2004-05718 and in part by Junta de Andalucía (PAI group RNM345).

REFERENCES

(1) Moreno Arribas, V.; Polo, M. C. *Wine Chemistry and Biochemistry*; Springer: New York, 2009.

DOI: 10.1021/acs.jafc.5b01571
J. Agric. Food Chem. 2015, 63, 4545−4550

(2) Riganakos, K. A.; Veltsistas, P. G. Comparative spectrophotometric determination of the total iron content in various white and red wines. *Food Chem.* **2003**, *82*, 637−643.
(3) Esparza, I.; Santamaría, C.; Fernández, J. M. Chromatic characterisation of three consecutive vintages of *Vitis vinifera* red wine − effect of dilution and iron addition. *Anal. Chim. Acta* **2006**, *56*, 331−337.
(4) Waterhouse, A. L.; Laurie, V. F. Oxidation of wine phenolics: a critical evaluation and hypothesis. *Am. J. Enol. Vitic.* **2006**, *57*, 306−313.
(5) Viviers, M. Z.; Smith, M. E.; Wilkes, E.; Smith, P. Effects of five metals on the evolution of hydrogen sulphide, methanethiol, and dimethyl sulphide during anaerobic storage of Chardonnay and Shiraz wines. *J. Agric. Food Chem.* **2013**, *61*, 12385−12396.
(6) Danielwicz, J. C. Mechanism of autoxidation of polyphenols and participation of sulphite: key role of iron. *Am. J. Enol. Vitic.* **2011**, *62*, 319−328.
(7) Jackson, R. S. *Wine Science. Principle and Application*; Academic Press: San Diego, CA, USA, 1994.
(8) Iland, P.; Bruer, N.; Wilkes, E. *Chemical Analysis of Grapes and Wine: Techniques and Concepts*, 2nd ed.; Patrick Iland Wine Promotions: Campbeltown, Australia, 2004.
(9) Kreitman, G.; Cantu, A.; Waterhouse, A. L.; Elias, R. J. Effect of metal chelators on the oxidative stability of model wine. *J. Agric. Food Chem.* **2013**, *61*, 9480−9487.
(10) Boonchiangma, S.; Kukusamude, C.; Ngeontae, W.; Srijarani, S. In-capillary derivatization and preconcentration for CE of metal ions as their phenanthroline complexes. *Chromatographia* **2014**, *77*, 277−286.
(11) Vidigal, S.; Toth, I.; Rangel, A. Exploiting the bed injection LOV approach to carry out spectrophotometric assays in wine: application to the determination of iron. *Talanta* **2011**, *84*, 1298−1303.
(12) Chanthai, S.; Suwamart, N.; Ruangiviriyachai, C. Solid-phase extraction with diethyldithiocarbamate as a chelating agent or preconcentration and trace determination of copper, iron, and lead in fruit wine and distilled spirit by flame atomic absorption spectrometry. *E-J. Chem.* **2011**, *8*, 1280−1292.
(13) Yildiz, O.; Demirhan, C.; Tuzen, M.; Soylak, M. Determination of copper, lead and iron in water and food samples after column solid phase extraction using 1-phenylthiosemicarbazide on Dowex Optipore L-493 resin. *Food Chem. Toxicol.* **2011**, *49*, 458−463.
(14) Pohl, P.; Prusisz, B. Application of tandem column solid phase extraction and flame atomic absorption spectrometry for the determination of inorganic and organically bound forms of iron in wine. *Talanta* **2009**, *77*, 1732−1738.
(15) Tašev, K.; Karadjova, I.; Arpadjan, S.; Cvetković, J.; Stafilov, T. Liquid/liquid extraction and column solid extraction procedures iron species determination in wines. *Food Control* **2006**, *17*, 484−488.
(16) Paleologos, E. K.; Giokas, D. L.; Tzouwara-Karayanni, S. M.; Karayanni, M. I. Micelle mediated methodology for the determination of free and bound iron in wines by flame atomic absorption spectrometry. *Anal. Chim. Acta* **2002**, *458*, 241−248.
(17) Ferreira, S. L. C.; Ferreira, H. S.; de Jesus, R. M.; Santos, J. V. S.; Brandao, G. C.; Souza, A. S. Development of method for the speciation of inorganic iron in wine samples. *Anal. Chim. Acta* **2007**, *602*, 89−93.
(18) Mánuel-Vez, M. P.; García-Vargas, M. Determinación espectrofotométrica de hierro con dPKPH y aplicación al contenido de hierro total en suelos agrícolas. *An. Quim.* **1993**, *89*, 218.
(19) Manuel-Vez, M.; Mora, M.; García-Vargas, M. Simultaneous determination of iron, cobalt, and nickel with 2,2′-dipyridylketone picolinoylhydrazone. *An. Quim.* **1994**, *90*, 353−358.
(20) Regulation (CEE) no. 2676/90 of Commission. 17/09/1990. Analysis Methods (section wine).
(21) Moreno, C.; Mánuel-Vez, M. P.; Gómez, I.; García-Vargas, M. Multicomponent analysis by flow injection using a partial least-squares calibration method. Simultaneous spectrophotometric determination of iron, cobalt and nickel at sub-ppm levels. *Analyst* **1996**, *121*, 1609.
(22) Miller, J. C.; Miller, J. N. *Statistics for Analytical Chemistry*, 4th ed.; Prentice Hall: London, UK, 2004.

DOI: 10.1021/acs.jafc.5b01571
J. Agric. Food Chem. 2015, 63, 4545−4550

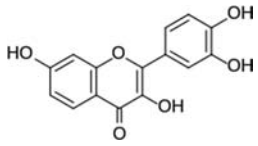

Figure 1. Structure of fisetin (3,7,3′,4′-tetrahydroxyflavone).

and facilitate the reparation of wrinkles in the skin.[24] Development of MMP inhibitors is a potential strategy for photoaging therapy.[5,25,26] In the literature, it had been reported that fisetin inhibited UV-induced ROS and activation of NF-κB and MAP kinase in lens epithelial cells.[27] However, few studies exist on the effect of fisetin against UV-induced photodamage in human skin and the related mechanisms. Therefore, this study investigates the potential mechanisms by which fisetin counteracts UVB-induced overexpression of MMPs/MAP kinases, COX-2, AP-1, and MMPs, the degradation of IκB and translocation of NF-κB, and the reduction in type I procollagen levels in human skin fibroblasts.

MATERIALS AND METHODS

Materials. Fisetin, DL-dithiothreitol, phenylmethylsulfonyl fluoride (PMSF), and Triton X-100 were purchased from Sigma-Aldrich Chemicals Corporation (St. Louis, MO). Collagenase was purchased from Calbiochem, Merck (Darmstadt, Germany). Dulbecco's modified Eagle's medium (DMEM), fetal bovine serum (FBS), penicillin−streptomycin, and trypsin−ethylenediaminetetraacetic acid (EDTA) were purchased from Gibco, Invitrogen (Carlsbad, CA). Coomassie Blue R-250, dibasic sodium phosphate, lgepal CA-630, 3-(4,5-dimethylthiazol-2-yl)-2,5-diphenyltetrazolium bromide (MTT), tris-(hydroxymethyl)aminomethane (Tris), and sodium dodecyl sulfate (SDS) were purchased from USB Corporation (Cleveland, OH). c-Jun, phosphor-c-Jun, NF-κB p65, and IκB antibodies were purchased from Cell Signaling Technology (Beverly, MA). Donkey anti-goat p38, p-p38, IgG-HRP, cAMP response element-binding protein (CREB), phosphor-CREB, ERK1, p-ERK 1/2, JNK1, p-JNK, MMP-1, MMP-3, and MMP-9 antibodies were purchased from Santa Cruz Biotechnology, Inc. (Santa Cruz, CA).

Cell Culture. Human foreskin fibroblasts (Hs68) were purchased from the Bioresources Collection and Research Center, Food Industry Research and Development Institute, Hsinchu, Taiwan. The cells were cultured in DMEM, which contained 10% FBS, 100 units/mL penicillin, and 100 units/mL streptomycin and were maintained at 37 °C in a humidified, 5% CO_2 incubator.

UVB Irradiation Dose. Cells were washed with phosphate-buffered saline (PBS) and covered with PBS for UV irradiation using a UV lighter (302 nm, CL-1000M, UVP, Upland, CA). The UVB irradiation dose was 40 mJ/cm^2 (exposure time was 15 s) according to the previous studies.[6,28] This dose equates to about 23 s exposure at the noontime on July in the middle of Taiwan measured by a UV meter (UVP, Upland, CA). At this UV dose, the cell viability does not reduce considerably, whereas the protein expression is induced. After UVB irradiation, PBS was replaced with a serum-free medium and then incubated for 24 h for the MTT and various assays.

Cell Viability Test. A MTT assay was performed to examine the viability of the cells as previous studies described.[25,29] After being irradiated with UVB, the cells were incubated with various concentrations of fisetin for 24 h and the culture medium was replaced with MTT solution (0.5 mg/mL) and incubated. The MTT solution was then removed, and 10% SDS−HCl was added. The absorbance of the dissolved formazan crystals was then determined at 570 nm using a spectrophotometer (Tecan, Grodig, Austria).

Measuring Intracellular ROS. Intracellular ROS generation was measured using a 2′,7′-dichlorodihydro fluorescein diacetate (DCFH-DA) fluorescence dye assay as a previous study described, with slight modification.[6,30] Fibroblasts were seeded into 24-well plates and irradiated with UVB. Subsequently, various concentrations of fisetin (5, 10, and 25 μM) were added and then incubated for 2 h. The cells were incubated with 10 μM DCFH-DA for 30 min. The fluorescence intensity was determined at 488 nm excitation and 520 nm emission using a fluorescence microplate reader (Thermo Electron Corporation, Ratastie, Vantaa, Finland), and images were observed under a fluorescence microscope (Leica DMIL, Wetzla, Germany).

Measurement of Total Collagen Synthesis. Total collagen synthesis in fibroblasts after UVB exposure was measured using the Sircol soluble collagen assay kit and modified on the basis of a previous study.[6,25] Briefly, a cell culture medium was collected and mixed with Sircol dye reagent and incubated. After centrifugation, ice-cold acid−salt washing reagent was added to the precipitate and then the mixture was centrifuged. The precipitate was dissolved using alkali reagent, and the absorbance was determined at 555 nm using an enzyme-linked immunosorbent assay (ELISA) reader (Tecan, Grodig, Austria).

Western Blot Analysis. The cells were harvested at the indicated time and washed twice with ice-cold PBS for western blot analysis. The cells were lysed in a cold lysis buffer; the lysates were centrifuged; and an aliquot of the lysate was used to determine the protein content by conducting a Bradford assay (Bio-Rad Laboratories, Hercules, CA). Equal amounts of proteins (30 μg) were separated using SDS−polyacrylamide gel electrophoresis (SDS−PAGE) and blotted onto polyvinyl difluoride membranes. The membranes were blocked with non-fat milk in a Tris-buffered saline and Tween 20 (TBST) buffer and then incubated overnight with specific antibodies. These were goat polyclonal antibodies, which are used against MMP-1 and type I procollagen, and mouse polyclonal antibodies, which are used against phosphor-CREB, CREB, MMP-3, MMP-9, ERK, p-ERK, JNK, p-JNK, p38, p-p38, c-Jun, phosphor-c-Jun, and NF-κB p65. The membranes were incubated with the corresponding horseradish-peroxidase-conjugated secondary antibody after washing with PBS buffer. Immunoreactive proteins were detected using the ECL western blotting detection system (Fujifilm, LAS-4000, Tokyo, Japan), and the signal intensity of each band was quantified using a densitometer system (Multi Gauge V2.2) and then normalized with the internal control (actin).

Immunofluorescence Staining. For immunofluorescence staining, 1 × 10^5 cells were cultivated on glass coverslips overnight. The medium was removed, and the cells were washed twice with a PBS buffer. The cells were fixed with 4% paraformaldehyde in PBS for 30 min. The fixed cells were blocked with 5% non-fat milk with 0.3% Triton X-100/PBS buffer for 40 min and incubated overnight, separately, with the primary antibody. After washing, cells were incubated with the Alexa Fluor 488 anti-rabbit IgG secondary antibody for 2 h (Invitrogen, Carlsbad, CA). The unbound secondary antibody was removed by washing the cells 3 times with a PBS buffer. Thereafter, the samples were counterstained with ProLong Gold antifade reagent with DAPI and observed using a microscope.

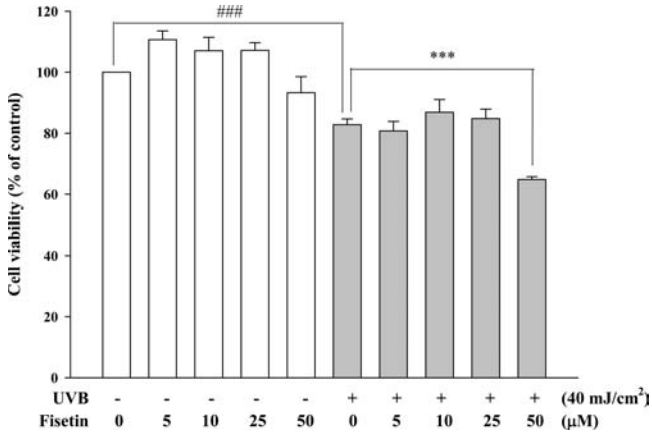

Figure 2. Cell viability of fisetin with or without UVB exposure on human fibroblasts. Significant difference versus control: (###) $p < 0.001$. Significant difference versus UV-exposed control: (***) $p < 0.001$.

DOI: 10.1021/jf502500t
J. Agric. Food Chem. 2015, 63, 4551−4560

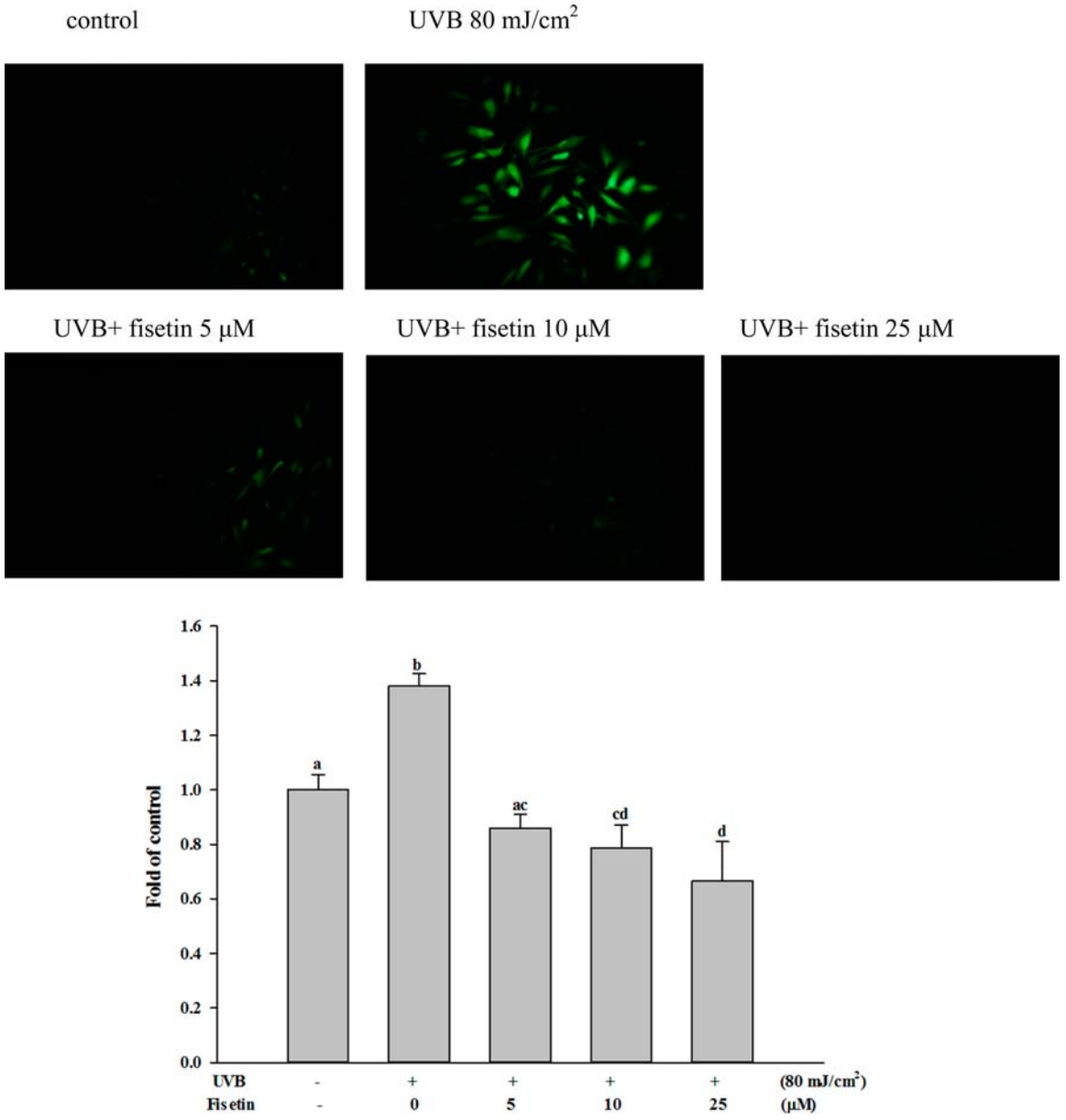

Figure 3. Repressive effect of fisetin on UVB-induced intracellular oxidative stress in human fibroblasts. Groups sharing the same letter are not significantly different ($p > 0.05$) as revealed by LSD post-hoc tests.

NO Measurement. The measurement of NO generation in human skin fibroblasts was by a previous study, with slight modification.[25] Cells were grown in a 6 well plate for 24 h before treatment. After UVB irradiation, cells were treated with different concentrations of fisetin for 24 h. Cell culture medium was then collected and mixed with Griess reagent (Promega, Madison, WI), and the absorbance of azo compound was determined at 540 nm using a spectrophotometer (Tecan, Grodig, Austria).

Quantitation of Prostaglandin E_2 (PGE_2). PGE_2 levels in cultured medium were determined using the protocol provided by the manufacturer of the kit (Cayman, Ann Arbor, MI). The cell culture and treatments were as described for the NO measurement.

Statistical Analysis. All measurements in the present study were obtained as averages of experiments that were at least three independent experiments performed in triplicate and are expressed as means ± standard deviation (SD). Differences between groups in experiments were analyzed for statistical significance using analysis of variation (ANOVA) with least significant difference (LSD) post-hoc tests or the Student's t test. $p < 0.05$ was considered statistically significant.

RESULTS AND DISCUSSION

Effect of Fisetin on the Cell Viability and UVB-Induced Phototoxicity. Safety is the primary criterion for skin-care products. Hs68 cells were treated with various concentrations of fisetin, and cell viability was measured using the MTT assay. The resulting survival curve indicated that fisetin (5−50 μM) did not exhibit cytotoxic effects on the proliferation of cells (Figure 2). After UVB irradiation (40 mJ/cm^2), the cell viability was significantly decreased to 82.7 ± 1.9% ($p < 0.001$). At 15−25 μM, fisetin did not significantly influence the cell viability of fibroblasts after UVB irradiation but decreased the cell viability to 64.8 ± 0.9% at 50 μM (Figure 2). Fisetin does not recover UVB-induced fibroblast mortality; indeed, the highest dose of fisetin (50 μM) even increases UVB damage. Therefore, 5−25 μM fisetin was used in the study of its anti-photoaging activity and mechanism.

Fisetin Reduced UVB-Induced Intracellular ROS. DCFH-DA staining and fluorescence microscopy were used

DOI: 10.1021/jf502500t
J. Agric. Food Chem. 2015, 63, 4551−4560

to qualitatively characterize the degree of ROS generation. ROS are potential inducers of skin-photoaging-related proteins and cause intracellular oxidative damage in human skin fibroblasts. Fibroblasts were exposed to UVB and then treated with various concentrations of fisetin for 2 h in a 24 well plate. After the fisetin-containing medium was removed, the cells were washed with PBS and incubated with 10 μM dichlorofluorescin diacetate (DCFDA) for 30 min. In this study, treatment with UVB significantly increased ROS generation 1.4-fold compared to control cells, whereas treatment with 5, 10, and 25 μM fisetin reduced UVB-induced ROS generation to 0.9-, 0.8-, and 0.7-fold, respectively (Figure 3). The results of fluorescence and immunofluorence staining indicate that fisetin protected Hs68 cells from the damage of UVB-induced ROS.

UV irradiation induced ROS generation in living organisms, causing oxidative stress, especially when ROS is not scavenged by an antioxidant defense system. Antioxidants, such as *N*-acetyl cysteine, scavenged ROS to protect skin from UVB-induced oxidative stress and cell death.[31,32] In this study, fisetin suppressed UV-induced intracellular ROS formation, protecting skin cells from oxidative damage and related diseases. In a previous study, fisetin exhibited 1,1-diphenyl-2-picrylhydrazyl radical scavenging activity.[33] It has been reported that the presence of a catechol group in the C-2 position and the number of hydroxyl substituents and their location in the molecule (especially at C-3, C-5, and/or C-7) are determinant structural factors for their ability to scavenge free radicals.[33,34] Fisetin, which has C-2 catechol and hydroxyl groups at C-3 and C-7, is an excellent free-radical scavenger. Therefore, its protective effect on skin against UV damage may contribute to its ability to scavenge UV-induced radical generation.

Anti-inflammatory Effect of Fisetin. *Fisetin on UVB-Induced COX-2 Expression.* The levels of COX-2 were 8.31-fold higher in fibroblasts exposed to UVB (40 mJ/cm^2) than in control cells (Figure 4a). In addition, fisetin (5, 10, and 25 μM) exhibited a dose-dependent reduction in UVB-induced COX-2 expression and a reduction of the UVB-induced expression of COX-2, which were 3.57-, 2.94-, and 1.06-fold compared to the control, respectively. The effect was significant when the dose was higher than 5 μM (Figure 4a). Epigallocatechin gallate (EGCG, 1 μM; positive control) significantly suppressed UVB-induced COX-2 expression (from 8.31- to 2.66-fold of the control).

Fisetin on UVB-Induced iNOS Expression. The result of fisetin on iNOS expression in fibroblasts is shown in Figure 4b. iNOS expression was increased to 1.6-fold after exposure to UVB; however, fisetin treatment (5, 10, and 25 μM) did not considerably reduce the levels of iNOS.

Effect of Fisetin on NO and PGE$_2$ Generation. As shown in Figure 5a, UVB exposure induced NO to 3-fold of the control and fisetin treatment reduced UVB-induced NO generation in human skin fibroblasts. UVB elevated PGE$_2$ in human skin fibroblasts, and fisetin at 10 and 25 μM would significant reduce PGE$_2$ production induced by UVB (Figure 5b).

UV irradiation leads to direct or indirect DNA damage and the formation of ROS, which induces an inflammatory response (induced COX-2 and iNOS) and damages the integrity of the extracellular matrix.[35] Our studies have shown that fisetin possesses anti-inflammatory activities by inhibiting UVB-induced PGE$_2$ and NO. The results of this study indicated that fisetin reduced UVB-induced COX-2 expression but not iNOS. The suppressive effect on COX-2 induction might be an independent process or an indirect phenomenon via reduced NO production. In addition, NO was controversially reported

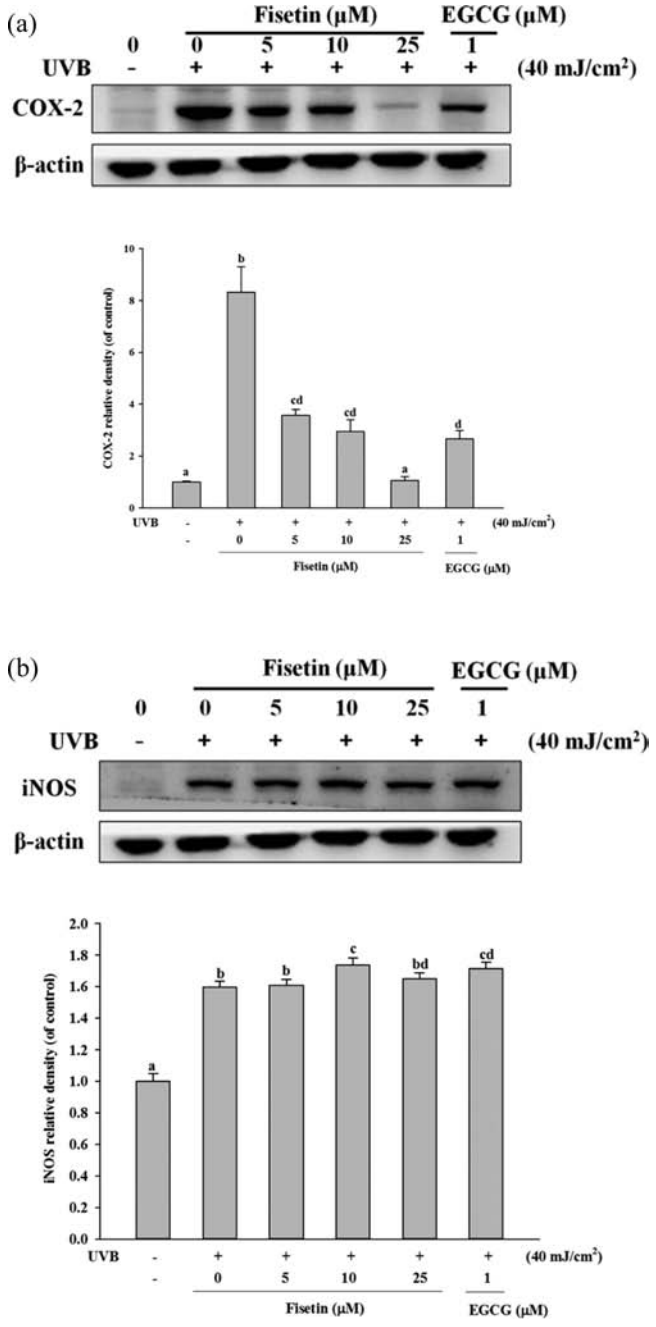

Figure 4. (a) Effect of fisetin on the UV-induced expression of COX-2 in human fibroblasts. (b) Effect of fisetin on the UVB-induced expression of iNOS in human fibroblasts. Groups sharing the same letter are not significantly different ($p > 0.05$) as revealed by LSD post-hoc tests.

to affect the level of COX activity and/or COX-2 expression.[36] It had been reported that flavonoids might directly affect COX-2 activity and/or expression, for example, wogonin, which was a direct COX-2 inhibitor but not an iNOS inhibitor.[37] Therefore, fisetin might directly inhibit COX-2 but not iNOS. The effect mechanism of fisetin on iNOS and COX-2 needs further study.

Effects of Fisetin on UVB-Induced Photodamage and Photodamage-Related Protein Expression. *Fisetin Attenuated UVB-Induced Reduction in Total Collagen Synthesis.* Fibroblasts were pretreated with fisetin (5−25 μM) for 1 h, exposed to UVB, and then treated with fisetin for 24 h. As shown in Figure 6a, fisetin treatment resulted in a dose-dependent

DOI: 10.1021/jf502500t
J. Agric. Food Chem. 2015, 63, 4551−4560

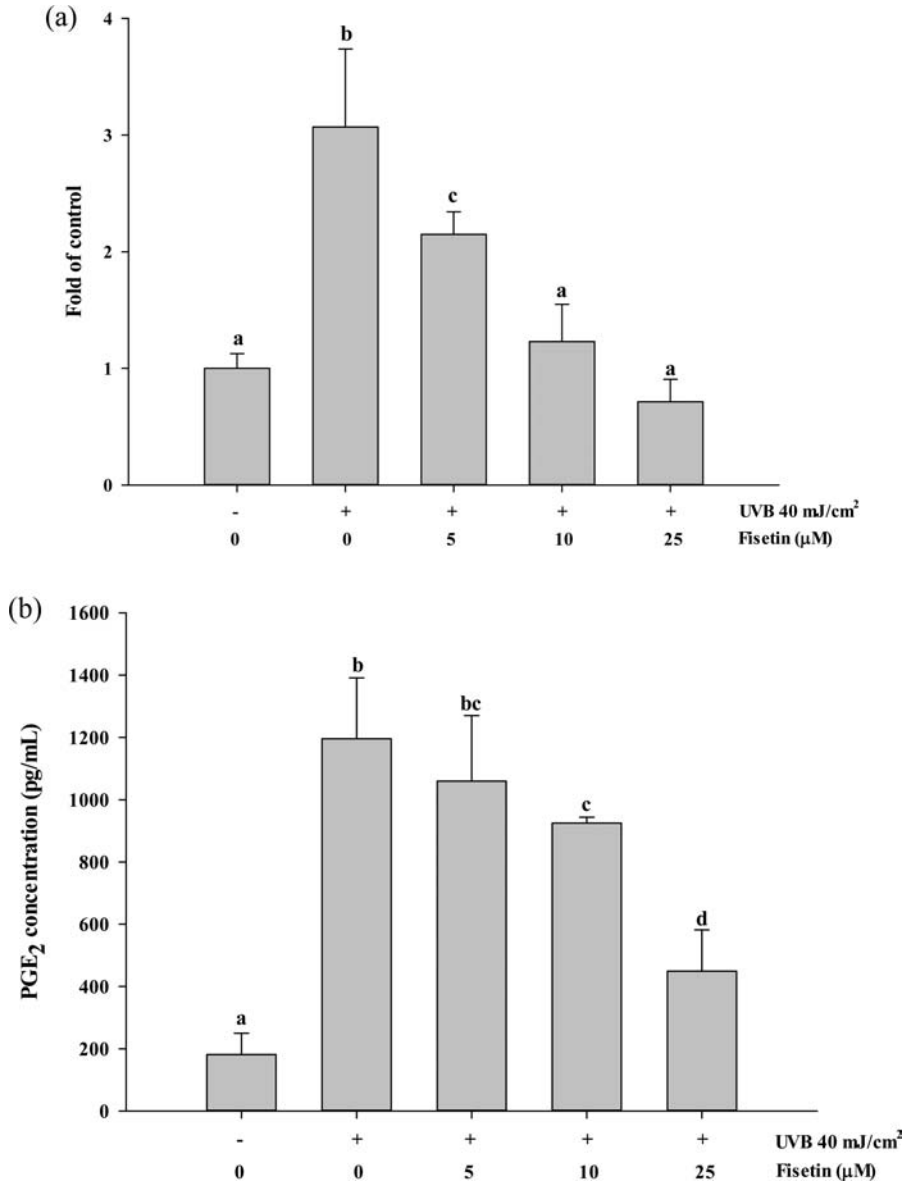

Figure 5. (a) Effect of fisetin on NO generation in human skin fibroblasts. Human fibroblasts were treated with/without UVB of 40 mJ/cm^2 and fisetin of 5, 10, and 25 μM. Groups sharing the same letter are not significantly different ($p > 0.05$) as revealed by LSD post-hoc tests. (b) Effect of fisetin on PGE_2 generation in human skin fibroblasts. Human fibroblasts were treated with/without UVB of 40 mJ/cm^2 and fisetin of 5, 10, and 25 μM. Groups sharing the same letter are not significantly different ($p > 0.05$) as revealed by LSD post-hoc tests.

restoration of collagen and fisetin at 25 μM would significantly increase total collagen synthesis.

Effect of Fisetin on MMP Expression. To examine the anti-damage effects of fisetin on UVB-irradiated human skin fibroblasts, we measured cellular MMP-1, MMP-3, and MMP-9 protein expressions. As shown in Figure 6b, UVB caused significant elevation of MMP-1, MMP-3, and MMP-9 protein expression (1.33-, 1.42-, and 1.53-fold compared to the control, respectively), whereas fisetin attenuated MMP expression. As shown in Figure 6b, the UVB-induced MMP-1 expression was reduced to 0.64-, 0.51-, and 0.42-fold when using 5, 10, and 25 μM fisetin, respectively, and 1 μM EGCG reduced MMP-1 0.54-fold compared to the control. Fisetin (5, 10, and 25 μM) suppressed UVB-induced MMP-3 expression 1.22-, 1.19-, and 0.92-fold compared to the control, respectively, and EGCG decreased 0.93-fold (Figure 6b). Furthermore, fisetin (5, 10, and 25 μM) inhibited UVB-induced MMP-9 expression 1.41-, 1.38-, and 1.43-fold, respectively, and EGCG decreased 0.8-fold compared to the control (Figure 6b). These results provide evidence that fisetin prevents the UVB-induced elevation of MMP-1, MMP-3, and MMP-9 levels, thus protecting UVB-induced skin damage and photoaging.

Effect of Fisetin on MAP Kinase Phosphorylation. In Figure 6c, the phosphorylation of ERK was increased after UVB irradiation, pretreatment with a high dose (25 μM) of fisetin diminished the effect (from 2.2- to 1.7-fold compared to the control), but pretreatment with lower doses (5 and 10 μM) did not. The results of the phosphorylation of JNK resembled those of the phosphorylation of ERK, whereas fisetin (10 and 25 μM) significantly reduced the phosphorylation of p-38 expression (Figure 6c).

Effect of Fisetin on c-Jun and p-c-Jun Expression. As Figure 7a shows, UV induced p-c-Jun expression (3.28-fold compared to the control), whereas fisetin treatment reduced

DOI: 10.1021/jf502500t
J. Agric. Food Chem. 2015, 63, 4551−4560

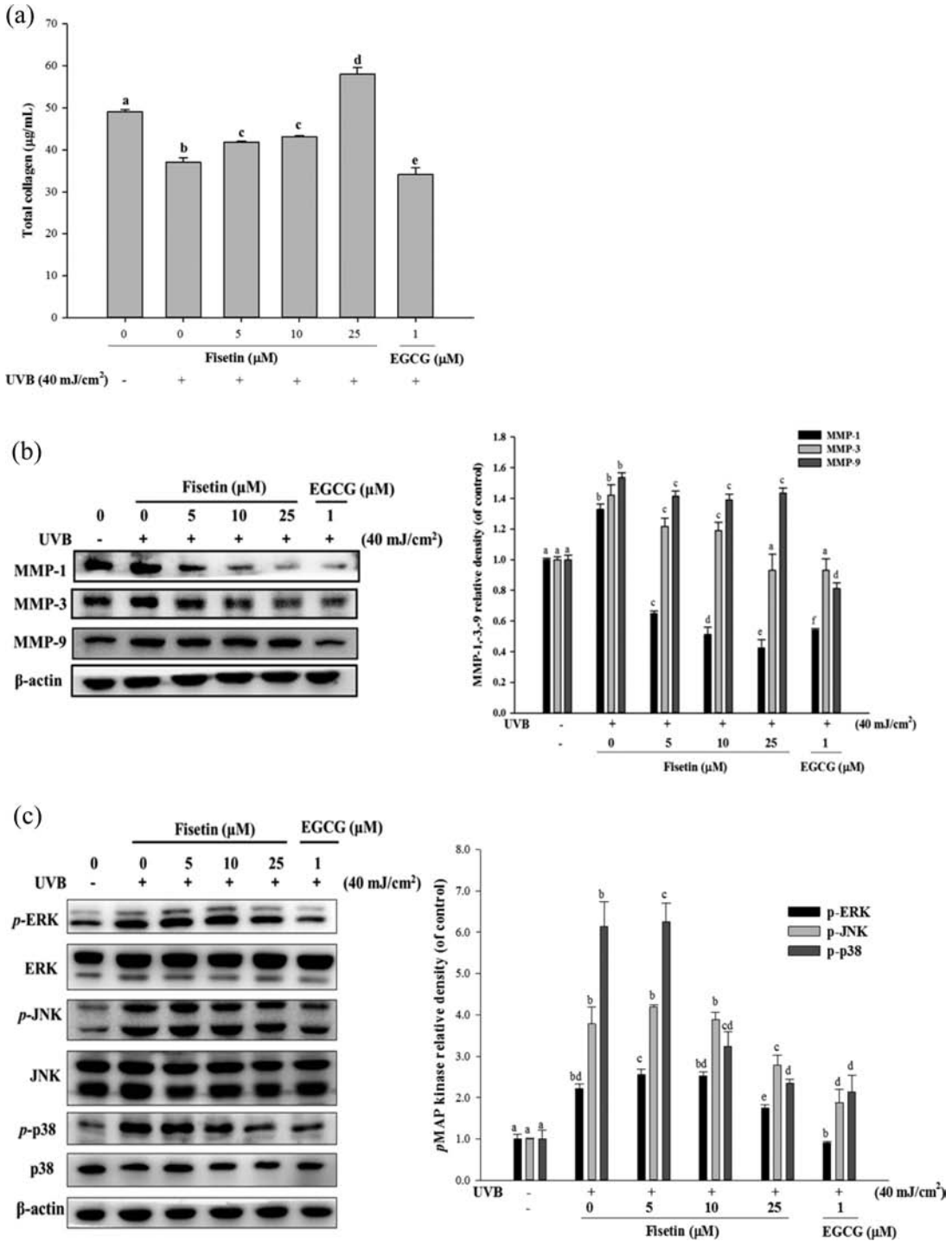

Figure 6. (a) Effect of fisetin on the UV-suppressed total collagen synthesis in human fibroblasts. (b) Effect of fisetin on the UVB-induced expression of MMP-1, MMP-3, and MMP-9 in human fibroblasts. (c) Effect of fisetin on the UVB-induced ERK, JNK, and p38 phosphorylation in human fibroblasts. Groups sharing the same letter are not significantly different ($p > 0.05$) as revealed by LSD post-hoc tests.

the c-Jun phosphorylation level in a dose-dependent manner. c-Jun expression was increased after UV irradiation, whereas fisetin inhibited the effect at 25 μM but not at 5 and 10 μM.

Effect of Fisetin on the IκB/NF-κB Pathway. Western blot analysis revealed that the protein levels of IκB were inhibited after the cells were treated with UVB irradiation, whereas fisetin significantly increased IκB expression in a dose-dependent manner (Figure 7b). In addition, the level of the NF-κB subunit, p65, was reduced 0.66-fold compared to the control in cytoplasma, whereas fisetin treatment significantly increased the expression of p65 in a dose-dependent manner (Figure 7b).

Immunohistochemistry Assay of NF-κB. The immunohistochemistry staining assay of NF-κB was conducted in fibroblast cells to determine the degree of NF-κB activation. As shown in Figure 7c, UVB induced the translocation of NF-κB to the nucleus, whereas fisetin suppressed the translocation of NF-κB induced by UVB.

Effect of Fisetin on the PI3K/AKT/CREB Pathway. Treatment of skin fibroblasts with UVB irradiation resulted in a

DOI: 10.1021/jf502500t
J. Agric. Food Chem. 2015, 63, 4551−4560

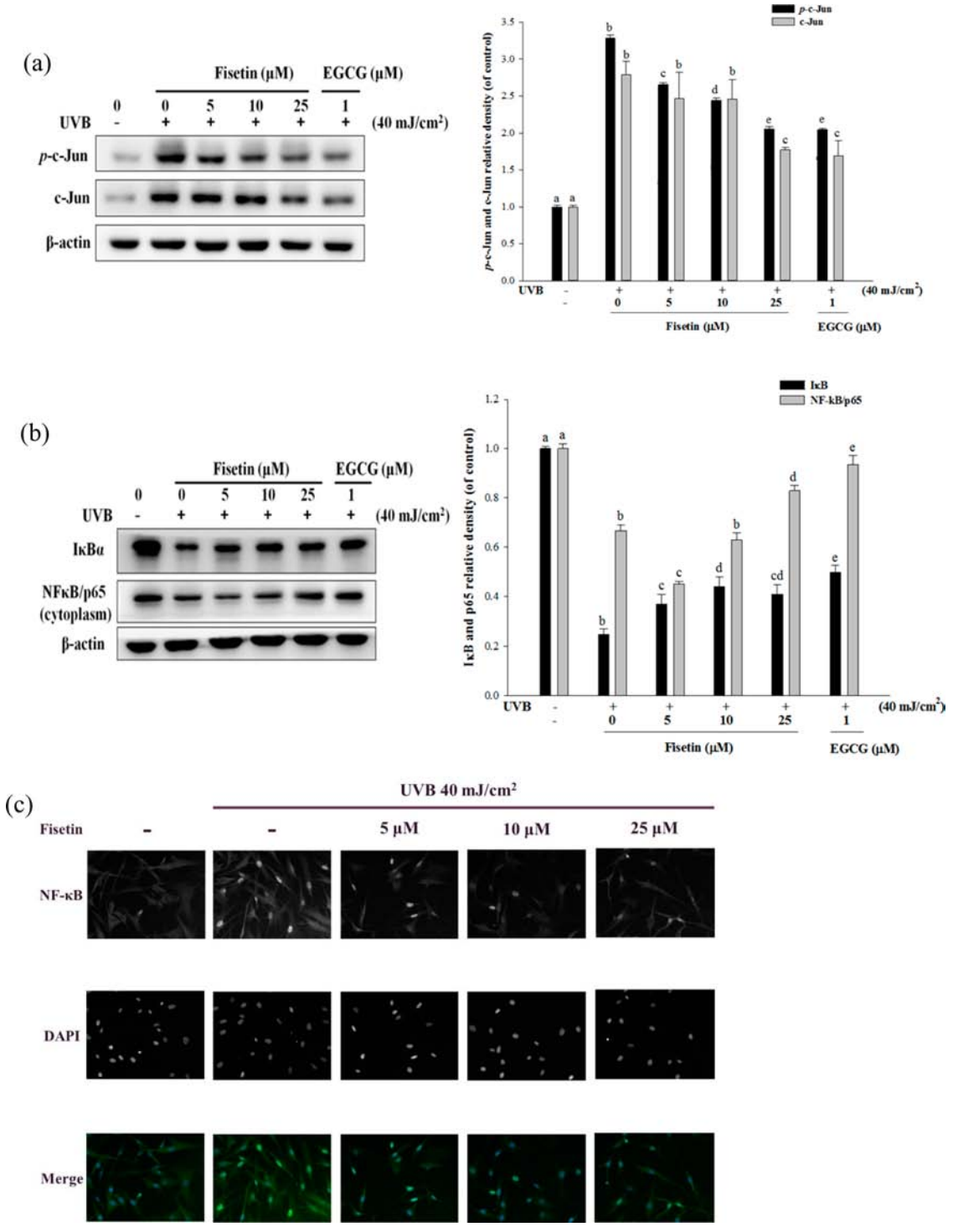

Figure 7. (a) Effect of fisetin on the UVB-induced c-Jun and c-Jun phosphorylation in human fibroblasts. (b) Effect of fisetin on the UVB-induced IκB degradation and the amount of NF-κB/p65 in cytoplasm. Groups sharing the same letter are not significantly different ($p > 0.05$) as revealed by LSD post-hoc tests. (c) Fisetin inhibits UVB-induced NF-κB activation by fluorescein isothiocyanate (FITC) immunofluorescence labeling.

2.21-fold increase in p-CREB Ser-133 levels (Figure 8). This showed the intense effect of UVB irradiation on the content of p-CREB Ser-133 in skin fibroblasts. This increase in p-CREB Ser-133 expression was significantly suppressed by fisetin treatment at 25 μM ($p < 0.001$). CREB expression was unchanged after either UVB or fisetin treatment and, similarly, was obtained after co-treatment of these two factors.

UV irradiation has been shown to upregulate the expression of iNOS, producing NO, and to react with superoxide, resulting in peroxynitrite and other ROS formations.[11] These ROS then induce an MAP kinase transcription factor, AP-1, phosphorylation of IκB, and then degradation, subsequently activating NF-κB and inducing COX-2 expression.[38,39] Furthermore, UV exposure activates MAP kinase and PI3K/AKT pathways, leading to upregulation of CREB Ser-133 and the subsequent transcriptional activation of the COX-2 gene.[40] In previous studies, the activation of p-38 resulted in AP-1 transcription, NF-κB expression and activation in the cytoplasma, and

DOI: 10.1021/jf502500t
J. Agric. Food Chem. 2015, 63, 4551−4560

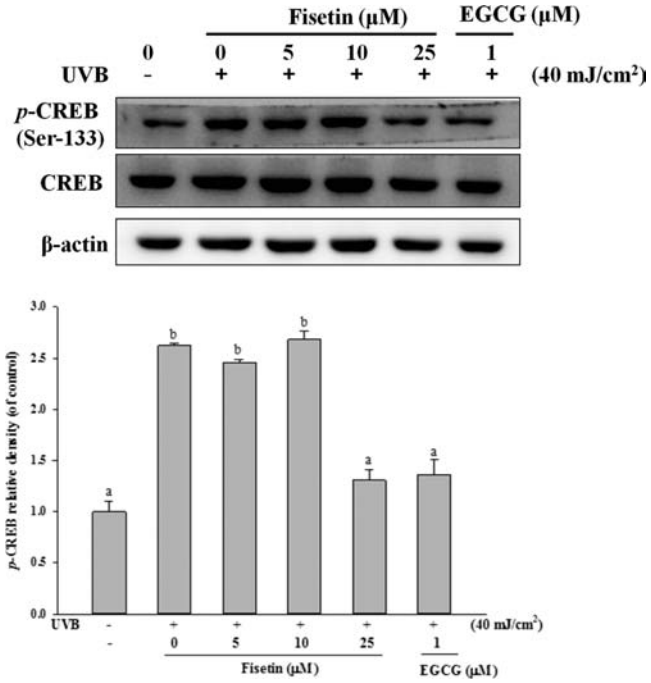

Figure 8. Effect of fisetin on the UVB-induced CREB phosphorylation at Ser-133. Groups sharing the same letter are not significantly different ($p > 0.05$) as revealed by LSD post-hoc tests.

p-CREB Ser-133 expression.[41] Results from this study indicated that fisetin attenuated the UV-induced overexpression of COX-2, p-CREB Ser-133, and MAP kinases and restored UV-induced IκB degradation, resulting in NF-κB down-regulation. In addition, fisetin inhibited UVB-induced NF-κB activation by inhibiting the translocation of NF-κB into the nucleus. Fisetin also inhibited UVB-induced NO and PGE_2 production. The inhibition of the phosphorylation of p-38, NF-κB transcription, and reduction of p-CREB Ser-133 by fisetin may contribute to the suppression of COX-2 expression. Inhibition of the MAP kinase pathway, therefore, prevents the phosphorylation of ERK, thereby enhancing the expression of type I procollagen.

The scavenging of ROS by fisetin may lead to a blockage of the MAP kinase pathway, which, in turn, may inhibit the activation of NF-κB and AP-1 and, therefore, inhibit the expression of MMP-1, MMP-3, MMP-9, and COX-2. MMPs play a vital role in UV-induced skin aging and degrade ECM in the dermis, resulting in the structural dysfunction of the skin. MMP-1 is a major enzyme that degrades collagen; MMP-3 activates proMMP-1; and MMP-9 degrades collagen fragments already degraded by MMP-1.[3] It has been shown that MMP-1 is expressed when the skin is exposed to UV, which induces a decrease of collagen and wrinkle formation.[5,6,42,43] Therefore, fisetin-inhibited MMP-1, MMP-3, and MMP-9 attenuated collagen degradation, thereby protecting skin from aging and photoaging. With regard to MMP expression, MAP kinase signaling cascades activate AP-1, a transcription factor and a complex containing c-Fos and c-Jun, and activate AP-1-dependent gene expression. The results indicate that fisetin suppressed the overexpression of UVB-induced MAP kinase/AP-1/MMPs and increased collagen content in human fibroblasts.

In summary, our results demonstrate that fisetin attenuated UVB-induced oxidative stress, photodamage, and inflammation

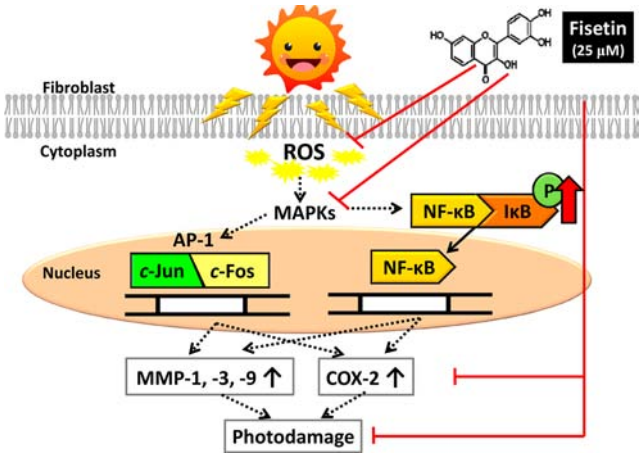

Figure 9. Schematic diagram showing inhibitory effects of fisetin in UVB-induced skin damage.

by modulating the expression of MMPs, MAP kinases, AP-1, COX-2, and p-CREB Ser-133 (Figure 9). In addition, fisetin effectively restored UV-induced IκB degradation, resulting in NF-κB inhibition. Therefore, fisetin is a potential agent used on UV-induced skin damage.

AUTHOR INFORMATION

Corresponding Authors

*Telephone: 886-4-22053366, ext. 5302. Fax: 886-4-22078083. E-mail: hmchiang@mail.cmu.edu.tw.

*Telephone: 886-4-22053366, ext. 5302. Fax: 886-4-22078083. E-mail: kcwen0520@mail.cmu.edu.tw.

Funding

This study was sponsored by the National Science Council (NSC99-2320-B-039-012-MY3 and NSC99-2622-B-039-001-CC3), Taipei, Taiwan, and the China Medical University (CMU99-S-39), Taichung, Taiwan.

Notes

The authors declare no competing financial interest.

ABBREVIATIONS USED

AP-1, activator protein-1; COX-2, cyclooxygenase-2; CREB, cAMP response element-binding protein; ECM, extracellular matrix; IκB, inhibitor κB; iNOS, inducible nitrite oxide synthase; MMP, matrix metalloproteinase; MAP kinase, mitogen-activated protein kinase; NO, nitric oxide; PG, prostaglandin; UV, ultraviolet

REFERENCES

(1) Halliday, G. M. Inflammation, gene mutation and photoimmunosuppression in response to UVR-induced oxidative damage contributes to photocarcinogenesis. *Mutat. Res., Fundam. Mol. Mech. Mutagen.* **2005**, *571*, 107−120.

(2) Rijken, F.; Bruijnzeel-Koomen, C. A. Photoaged skin: The role of neutrophils, preventive measures, and potential pharmacological targets. *Clin. Pharmacol. Ther.* **2011**, *89*, 120−124.

(3) Rittie, L.; Fisher, G. J. UV-light-induced signal cascades and skin aging. *Ageing Res. Rev.* **2002**, *1*, 705−720.

(4) Scharffetter-Kochanek, K.; Brenneisen, P.; Wenk, J.; Herrmann, G.; Ma, W.; Kuhr, L.; Meewes, C.; Wlaschek, M. Photoaging of the skin from phenotype to mechanisms. *Exp. Gerontol.* **2000**, *35*, 307−316.

(5) Chiang, H. M.; Chen, H. C.; Lin, T. J.; Shih, I. C.; Wen, K. C. *Michelia alba* extract attenuates UVB-induced expression of matrix

DOI: 10.1021/jf502500t
J. Agric. Food Chem. 2015, 63, 4551−4560

metalloproteinases via MAP kinase pathway in human dermal fibroblasts. *Food Chem. Toxicol.* **2012**, *50*, 4260−4269.
(6) Chiang, H. M.; Chen, H. C.; Chiu, H. H.; Chen, C. W.; Wang, S. M.; Wen, K. C. *Neonauclea reticulata* (Havil.) Merr stimulates skin regeneration after UVB exposure via ROS scavenging and modulation of the MAPK/MMPs/collagen pathway. *Evidence-Based Complementary Altern. Med.* **2013**, *2013*, No. 324864.
(7) Wu, N. L.; Fang, J. Y.; Chen, M.; Wu, C. J.; Huang, C. C.; Hung, C. F. Chrysin protects epidermal keratinocytes from UVA- and UVB-induced damage. *J. Agric. Food Chem.* **2011**, *59*, 8391−8400.
(8) Tsoyi, K.; Park, H. B.; Kim, Y. M.; Chung, J. I.; Shin, S. C.; Lee, W. S.; Seo, H. G.; Lee, J. H.; Chang, K. C.; Kim, H. J. Anthocyanins from black soybean seed coats inhibit UVB-induced inflammatory cylooxygenase-2 gene expression and PGE2 production through regulation of the nuclear factor-κB and phosphatidylinositol 3-kinase/Akt pathway. *J. Agric. Food Chem.* **2008**, *56*, 8969−8974.
(9) Deliconstantinos, G.; Villiotou, V.; Stavrides, J. C. Increase of particulate nitric oxide synthase activity and peroxynitrite synthesis in UVB-irradiated keratinocyte membranes. *Biochem. J.* **1996**, *320* (Part 3), 997−1003.
(10) Rhodes, L. E.; Gledhill, K.; Masoodi, M.; Haylett, A. K.; Brownrigg, M.; Thody, A. J.; Tobin, D. J.; Nicolaou, A. The sunburn response in human skin is characterized by sequential eicosanoid profiles that may mediate its early and late phases. *FASEB J.* **2009**, *23*, 3947−3956.
(11) Bickers, D. R.; Athar, M. Oxidative stress in the pathogenesis of skin disease. *J. Invest. Dermatol.* **2006**, *126*, 2565−2575.
(12) Su, Y. W.; Chiou, W. F.; Chao, S. H.; Lee, M. H.; Chen, C. C.; Tsai, Y. C. Ligustilide prevents LPS-induced iNOS expression in RAW 264.7 macrophages by preventing ROS production and down-regulating the MAPK, NF-κB and AP-1 signaling pathways. *Int. Immunopharmacol.* **2011**, *11*, 1166−1172.
(13) Chen, X.; Tang, S. A.; Lee, E.; Qiu, Y.; Wang, R.; Duan, H. Q.; Dan, S.; Jin, M.; Kong, D. IVSE, isolated from *Inula japonica*, suppresses LPS-induced NO production via NF-κB and MAPK inactivation in RAW264.7 cells. *Life Sci.* **2015**, *124*, 8−15.
(14) Bond, M.; Baker, A. H.; Newby, A. C. Nuclear factor κB activity is essential for matrix metalloproteinase-1 and -3 upregulation in rabbit dermal fibroblasts. *Biochem. Biophys. Res. Commun.* **1999**, *264*, 561−567.
(15) Xia, Q.; Chiang, H. M.; Yin, J. J.; Chen, S.; Cai, L.; Yu, H.; Fu, P. UVA photoirradiation of benzo[*a*]pyrene metabolites: Induction of cytotoxicity, reactive oxygen species, and lipid peroxidation. *Toxicol. Ind. Health* **2013**.
(16) Arai, Y.; Watanabe, S.; Kimira, M.; Shimoi, K.; Mochizuki, R.; Kinae, N. Dietary intakes of flavonols, flavones and isoflavones by Japanese women and the inverse correlation between quercetin intake and plasma LDL cholesterol concentration. *J. Nutr.* **2000**, *130*, 2243−2250.
(17) Suh, Y.; Afaq, F.; Johnson, J. J.; Mukhtar, H. A plant flavonoid fisetin induces apoptosis in colon cancer cells by inhibition of COX2 and Wnt/EGFR/NF-κB-signaling pathways. *Carcinogenesis* **2009**, *30*, 300−307.
(18) Sung, B.; Pandey, M. K.; Aggarwal, B. B. Fisetin, an inhibitor of cyclin-dependent kinase 6, down-regulates nuclear factor-κB-regulated cell proliferation, antiapoptotic and metastatic gene products through the suppression of TAK-1 and receptor-interacting protein-regulated IκBα kinase activation. *Mol. Pharmacol.* **2007**, *71*, 1703−1714.
(19) Hanneken, A.; Lin, F. F.; Johnson, J.; Maher, P. Flavonoids protect human retinal pigment epithelial cells from oxidative-stress-induced death. *Invest. Ophthalmol. Vis. Sci.* **2006**, *47*, 3164−3177.
(20) Geraets, L.; Haegens, A.; Brauers, K.; Haydock, J. A.; Vernooy, J. H.; Wouters, E. F.; Bast, A.; Hageman, G. J. Inhibition of LPS-induced pulmonary inflammation by specific flavonoids. *Biochem. Biophys. Res. Commun.* **2009**, *382*, 598−603.
(21) Lee, J. D.; Huh, J. E.; Jeon, G.; Yang, H. R.; Woo, H. S.; Choi, D. Y.; Park, D. S. Flavonol-rich RVHxR from *Rhus verniciflua* Stokes and its major compound fisetin inhibits inflammation-related cytokines and angiogenic factor in rheumatoid arthritic fibroblast-like synovial cells and in vivo models. *Int. Immunopharmacol.* **2009**, *9*, 268−276.
(22) Kim, H. J.; Kim, S. H.; Yun, J. M. Fisetin inhibits hyperglycemia-induced proinflammatory cytokine production by epigenetic mechanisms. *Evidence-Based Complementary Altern. Med.* **2012**, *2012*, No. 639469.
(23) Pal, H. C.; Sharma, S.; Elmets, C. A.; Athar, M.; Afaq, F. Fisetin inhibits growth, induces G_2/M arrest and apoptosis of human epidermoid carcinoma A431 cells: Role of mitochondrial membrane potential disruption and consequent caspases activation. *Exp. Dermatol.* **2013**, *22*, 470−475.
(24) Mukherjee, P. K.; Maity, N.; Nema, N. K.; Sarkar, B. K. Bioactive compounds from natural resources against skin aging. *Phytomedicine* **2011**, *19*, 64−73.
(25) Wen, K. C.; Fan, P. C.; Tsai, S. Y.; Shih, I. C.; Chiang, H. M. *Ixora parviflora* protects against UVB-induced photoaging by inhibiting the expression of MMPs, MAP kinases, and COX-2 and by promoting type I procollagen synthesis. *Evidence-Based Complementary Altern. Med.* **2012**, *2012*, No. 417346.
(26) Adil, M. D.; Kaiser, P.; Satti, N. K.; Zargar, A. M.; Vishwakarma, R. A.; Tasduq, S. A. Effect of *Emblica officinalis* (fruit) against UVB-induced photo-aging in human skin fibroblasts. *J. Ethnopharmacol.* **2010**, *132*, 109−114.
(27) Yao, K.; Zhang, L.; Zhang, Y.; Ye, P.; Zhu, N. The flavonoid, fisetin, inhibits UV radiation-induced oxidative stress and the activation of NF-κB and MAPK signaling in human lens epithelial cells. *Mol. Vis.* **2008**, *14*, 1865−1871.
(28) Chiang, H. M.; Chiu, H. H.; Liao, S. T.; Chen, Y. T.; Chang, H. C.; Wen, K. C. Isoflavonoid-rich *Flemingia macrophylla* extract attenuates UVB-induced skin damage by scavenging reactive oxygen species and inhibiting MAP kinase and MMP expression. *Evidence-Based Complementary Altern. Med.* **2013**, *2013*, No. 696879.
(29) Wen, K. C.; Shih, I. C.; Hu, J. C.; Liao, S. T.; Su, T. W.; Chiang, H. M. Inhibitory effects of *Terminalia catappa* on UVB-induced photodamage in fibroblast cell line. *Evidence-Based Complementary Altern. Med.* **2011**, *2011*, 904532.
(30) Wen, K. C.; Chiu, H. H.; Fan, P. C.; Chen, C. W.; Wu, S. M.; Chang, J. H.; Chiang, H. M. Antioxidant activity of *Ixora parviflora* in a cell/cell-free system and in UV-exposed human fibroblasts. *Molecules* **2011**, *16*, 5735−5752.
(31) Morley, N.; Curnow, A.; Salter, L.; Campbell, S.; Gould, D. *N*-Acetyl-L-cysteine prevents DNA damage induced by UVA, UVB and visible radiation in human fibroblasts. *J. Photochem. Photobiol., B* **2003**, *72*, 55−60.
(32) Rijnkels, J. M.; Moison, R. M.; Podda, E.; van Henegouwen, G. M. Photoprotection by antioxidants against UVB-radiation-induced damage in pig skin organ culture. *Radiat. Res.* **2003**, *159*, 210−217.
(33) Hyun, J.; Woo, Y.; Hwang, D. S.; Jo, G.; Eom, S.; Lee, Y.; Park, J. C.; Lim, Y. Relationships between structures of hydroxyflavones and their antioxidative effects. *Bioorg. Med. Chem. Lett.* **2010**, *20*, 5510−5513.
(34) Dias, M. M.; Machado, N. F.; Marques, M. P. Dietary chromones as antioxidant agents—The structural variable. *Food Funct.* **2011**, *2*, 595−602.
(35) Nichols, J. A.; Katiyar, S. K. Skin photoprotection by natural polyphenols: Anti-inflammatory, antioxidant and DNA repair mechanisms. *Arch. Dermatol. Res.* **2010**, *302*, 71−83.
(36) Goodwin, D. C.; Landino, L. M.; Marnett, L. J. Effects of nitric oxide and nitric oxide-derived species on prostaglandin endoperoxide synthase and prostaglandin biosynthesis. *FASEB J.* **1999**, *13*, 1121−1136.
(37) Chi, Y. S.; Cheon, B. S.; Kim, H. P. Effect of wogonin, a plant flavone from *Scutellaria radix*, on the suppression of cyclooxygenase-2 and the induction of inducible nitric oxide synthase in lipopolysaccharide-treated RAW 264.7 cells. *Biochem. Pharmacol.* **2001**, *61*, 1195−1203.
(38) Ashida, M.; Bito, T.; Budiyanto, A.; Ichihashi, M.; Ueda, M. Involvement of EGF receptor activation in the induction of

DOI: 10.1021/jf502500t
J. Agric. Food Chem. 2015, 63, 4551−4560

cyclooxygenase-2 in HaCaT keratinocytes after UVB. *Exp. Dermatol.* **2003**, *12*, 445−452.
(39) Cooper, S. J.; Bowden, G. T. Ultraviolet B regulation of transcription factor families: Roles of nuclear factor-κB (NF-κB) and activator protein-1 (AP-1) in UVB-induced skin carcinogenesis. *Curr. Cancer Drug Targets* **2007**, *7*, 325−334.
(40) Rundhaug, J. E.; Fischer, S. M. Cyclo-oxygenase-2 plays a critical role in UV-induced skin carcinogenesis. *Photochem. Photobiol.* **2008**, *84*, 322−329.
(41) Terazawa, S.; Nakajima, H.; Shingo, M.; Niwano, T.; Imokawa, G. Astaxanthin attenuates the UVB-induced secretion of prostaglandin E2 and interleukin-8 in human keratinocytes by interrupting MSK1 phosphorylation in a ROS depletion-independent manner. *Exp. Dermatol.* **2012**, *21* (Supplement 1), 11−17.
(42) Kim, S.; Chung, J. H. Berberine prevents UV-induced MMP-1 and reduction of type I procollagen expression in human dermal fibroblasts. *Phytomedicine* **2008**, *15*, 749−753.
(43) Chiang, H. M.; Lin, T. J.; Chiu, C. Y.; Chang, C. W.; Hsu, K. C.; Fan, P. C.; Wen, K. C. *Coffea arabica* extract and its constituents prevent photoaging by suppressing MMPs expression and MAP kinase pathway. *Food Chem. Toxicol.* **2011**, *49*, 309−318.

DOI: 10.1021/jf502500t
J. Agric. Food Chem. 2015, 63, 4551−4560

extracellular matrix. Therefore, the MMPs play an important role in the invasion process.[6]

Integrins are receptors located between the cell surface and adhesion. They are not only involved in adhesion of cell and extracellular matrix but also active in the downstream cell signaling transduction pathways. They are heterodimers constituted of α- and β-subunits by noncovalent bonds; the α-subunit has 18 types, and the β-subunit has 8 types.[7,8] In addition, integrin $\alpha v\beta 3$ has been shown to be overexpressed in multiple cancer cell metastasis processes. Some studies demonstrate that integrin $\alpha v\beta 3$ can bind with urokinase plasminogen activator (uPA) receptor and transfer plasminogen into plasmin that will then activate pro-MMPs and lead to the degradation of extracellular matrix by MMPs. Integrin $\alpha v\beta 3$ can directly bind to MMP-2 as well and help the degradation of MMP-2.[9]

FAK is the main controller of integrin-mediated cancer cell signaling transduction pathway. When FAK and integrin mix together to form a focal adhesion complex, the whole structure will be changed. The steroid receptor coactivator (Src) will phosphorylate FAK; the activated p-FAK will in turn activate the signaling transduction pathway of PI3K/AKT, MEK/ERK, and JNK and regulates the adhesion, migration, and invasion of cancer cells. Therefore, the protein expression and phosphorylation of FAK are usually recognized as one of the biomarkers of cancer metastasis.[9]

MATERIALS AND METHODS

Chemicals and Reagents. Basswood-cultivated *A. cinnamomea* (BCRC930103) mycelial powder was provided by PO-ZO Co., Ltd. (Taipei, Taiwan). Ethyl acetate (EA) was added to 500 g of *A. cinnamomea* dry powder to a total volume of 4 L and stirred for 3 days. The extract was then decanted and solvent removed by a rotary evaporator at 50 °C. The extraction was repeated. A silica gel column was used to fractionate the extracted sample and consecutively eluted with 10, 15, 20, 30, 50, 70, and 100% EA/hexane. The fraction with 100% EA/hexane contained the highest amount of antcin K. The purity of antcin K was >90% as determined by an HPLC analysis. The yield of antcin K from *A. cinnamomea* is about 0.5% in dry weight.

Bromophenol blue and sodium dodecyl sulfate were purchased from Bio-Rad Laboratories (Hercules, CA, USA). Antibiotic−antimycotic, Dulbecco's modified Eagle's medium, fetal bovine serum, and nonessential amino acids were purchased from Invitrogen (Carlsbad, CA, USA). Immobilon-P membrane (PVDF transfer membranes for Western blotting), Immobilon Western chemiluminescent HRP substrate (ECL), Millicell hanging cell culture insert (transwell), and dimethyl sulfoxide (DMSO) were obtained from Merck Millipore (Billerica, MA, USA). BD Matrigel Matrix High Concentration was purchased from BD Biosciences (San Jose, CA, USA). 3-(4,5-Dimethylthiazol-2-yl)-2,5-diphenyltetrazolium bromide (MTT), Brij 35, gelatin, bovine serum albumin (BSA), HEPES sodium salt, TritonTM X-100, trypan blue, Tween 20, crystal violet, and other analytical grade reagents were purchased from Sigma-Aldrich (St. Louis, MO, USA). Forty percent acrylamide/bis (29:1) solution, dithiothreitol (DTT), ammonium persulfate (APS), Coomassie brilliant blue R-250, glycerol, Tris base, and prestained protein ladder were purchased from Bioman (Taipei, Taiwan). Culture inserts (for wound-healing assay) were obtained from ibidi (Munchen, Germany). PRO-PREP protein extraction solution was purchased from Boca Scientific (Boca Raton, FL, USA). Trypsin−EDTA was obtained from Caisson Laboratories (North Logan, UT, USA). Acetic acid and methanol were purchased from Macron Chemicals (Center Valley, PA, USA). Phosphatase inhibitor cocktail tablet and protease inhibitor cocktail tablet were purchased from Roche (Basel, Switzerland). An SDS-PAGE kit was purchased from Bionovas Biotechnology (Toronto, ON, Canada). Anti-β-actin antibody and other secondary antibodies were obtained from Cell Signaling Technology, Inc. (St. Louis, MO, USA).

Cell Culture. Hep 3B cells were cultured in Dulbecco's modified Eagle's medium with 10% FBS, 1.5 g/L sodium bicarbonate, 2.38 g/L HEPES, 1% nonessential amino acids, and 1% antibiotic−antimycotic (100 units/mL penicillin, 0.1 μg/mL streptomycin, and 0.25 μg/mL amphotericin B) at 37 °C in a 5% CO_2 incubator.[10]

Determination of Cell Viability MTT Assay. Liver cancer cells at a concentration of 5×10^3 cells/well were seeded in 96-well plates and incubated for 24 h, followed by treatment with 0 (0.02% DMSO), 5, 10, 15, 20, and 40 μM antcin K and incubated for a further 24 h. At the end of the stipulated period, 100 μL of MTT solution (0.5 mg/mL) was added and incubated at 37 °C for 4 h. The resulting MTT formazan was dissolved in 100 μL of DMSO and the absorbance recorded at 570 nm using a PowerWave HT Bio-Tek microplate spectrophotometer (Winooski, VT, USA).[11]

Detections of Cell−Matrigel Adhesion Assay. Hep 3B cells with 5×10^4 cells/mL were seeded into 6-well plates and incubated for 24 h, and the medium was then removed. After two washings, the medium was changed to 2 mL of 0, 5, 10, 15, and 20 μM antcin K with 2% FBS and incubated in 5% CO_2 at 37 °C for 24 h. At the same time, matrigel (10 μg/30 μL) was coated into 96-well plates, 20 μL of BSA (2%) was added, and the mixture was incubated in 5% CO_2 at 37 °C for 1 h. Next, Hep 3B cells with 5×10^4 cells/mL were put into 96-well plates with 0, 5, 10, 15, and 20 μM antcin K in 2% FBS medium for 1 h. After removal of medium and two washings with PBS, 100 μL of 0.5 mg/mL MTT in 2% FBS medium was added. The following steps are the same as described in the cell viability MTT assay.[12]

Wound-Healing Assay. Putting ibidi culture-insert on the battle of 24-well plates, and Hep 3B cells with 3.5×10^4 cells/70 μL/well were seeded into other space and incubated in 37 °C at 5% CO_2 for 24 h. The next step was taking of fthe culture insert and adding 500 μL/well 0, 5, 10, 15, 20 μM antcin K in non-FBS medium incubation. Three pictures were taken by 100× microscopy at 0, 24, and 48 h randomly. Data were analyzed by ImageJ software to show the cell migration percentage compared with the control group.[13]

Cell Migration Assay. One transwell was set into 1 mL of PBS in 24-well plates and the unleakage transwell chosen after 30 min. To open the permeability of the transwell, 200 μL of PBS was added into the transwell and incubated for 18 h. PBS was removed next, and 1 mL of 10% FBS was added into the bottle of a 24-well plate seeded with Hep 3B cells (2.5×10^4 cells/100 μL/well, non-FBS medium) into the transwell. Then it was treated with 100 μL/well 0, 5, 10, 15, and 20 μM antcin K within non-FBS medium. After incubating in 37 °C at 5% CO_2 for 24 h, the cells were fixed by methanol in 15 min, dyed for 45 min by 2% crystal violet, and washed out by PBS. Finally, five pictures were taken by microscopy (200×), and cell number was analyzed by ImageJ software to demonstrate the ability of cell migration (cell migration percent of control).[14]

Matrigel Invasion Assay. Most steps were similar to the cell migration assay; the only different step was we would coat 4 μg/μL matrigel into the transwell to avoid bubble formation.[15]

Gelatin Zymography. Hep 3B cells (5×10^4 cells/mL) were seeded into 24-well plates at 37 °C in 5% CO_2 and incubated for 24 h, and the medium was removed and washed out with PBS twice. After treatment with various doses of antcin K, the upper medium was taken and mixed with 2× sample buffer (0.125 M Tris-HCl, 20% glycerol, 10% SDS, and 0.32% bromophenol blue). It was then loaded into 0.1% gelatin and 10% SDS-PAGE, run 100 V within 2 h, and 1× renaturing buffer (2.5% Triton X-100) was used to wash the gel twice; the gel was put in developing buffer (50 mM Tris-base, 200 mM NaCl, 5 mM $CaCl_2$, 0.02% Brij 35, pH 7.5) fpr incubation at 37 °C in 24 h. It was then dyed with Coomassie blue solution (2.5% Coomassie blue, 10% acetic acid, and 50% methanol) in 20 min. Finally, the destaining solution (10% acetic acid and 30% methanol) was used to remove color. After the gel had dried, it was analyzed by ImageJ.[16]

Western Blotting. For Western blotting, the cells (5×10^4 cells/10 mL/dish) were seeded in 10 cm^2 dishes for 24 h. After 24 h of incubation, the cells were treated with 10 mL of medium containing 0, 5, 10, 15, and 20 μM antcin K for 24 h. After 24 h of treatment, total

DOI: 10.1021/jf5059304
J. Agric. Food Chem. 2015, 63, 4561−4569

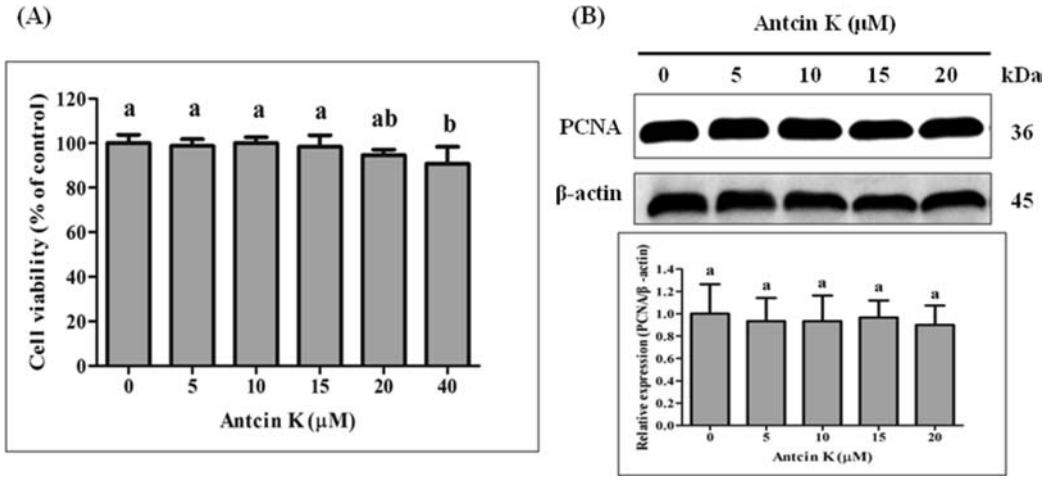

Figure 1. Effects of antcin K on cell viability and proliferation in Hep 3B cells. (A) Effect of antcin K on the cell viability in Hep 3B cells was determined by MTT assay. Data are expressed as the relative percentage to control (0.02% DMSO) and mean ± SD from three independent experiments (n = 3). (B) Effect of antcin K on the expression of proliferating cell nuclear antigen in Hep 3B cells was assessed by Western blotting. Protein levels are expressed as multiple of control (0.02% DMSO) by β-actin-normalized densitometry. Columns represent the mean ± SD from three independent experiments (n = 3).

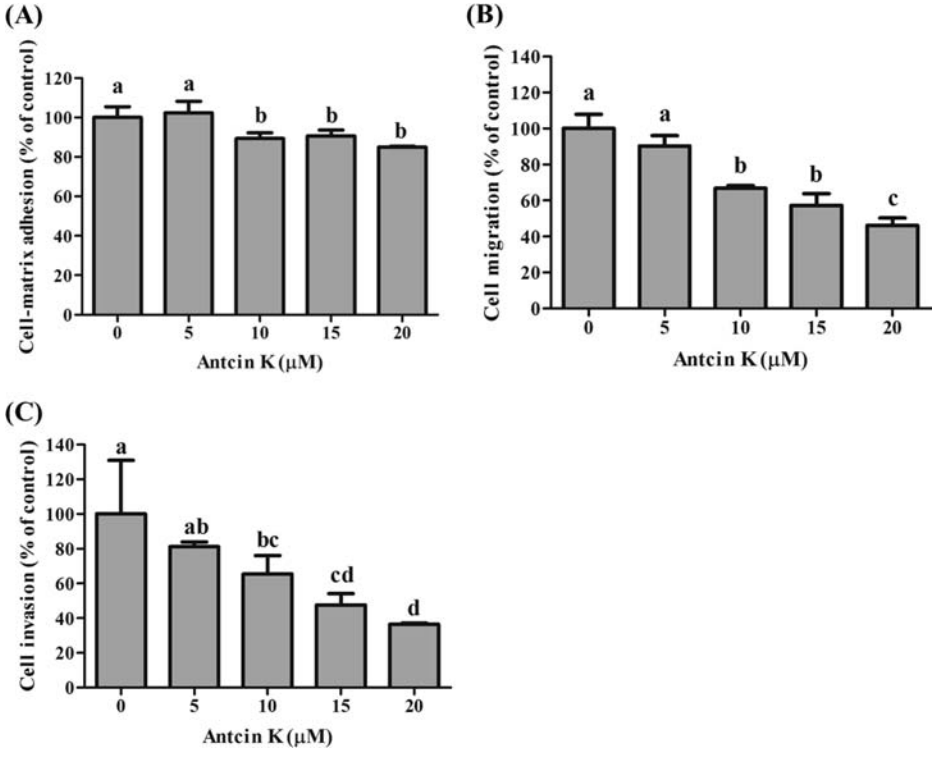

Figure 2. Changes by antcin K on the cell−matrix adhesion, migration, and invasion in Hep 3B cells. (A) Effect of antcin K on the cell−matrix adhesion in Hep 3B cells was determined by MTT assay. Data are expressed as the relative percentage to control (0.02% DMSO) and mean ± SD from three independent experiments (n = 3). (B) Effect of antcin K on the cell migration in Hep 3B cells was measured by Boyden chamber assay. The cells that migrated to the lower surface of the filter were stained with crystal violet and were photographed under a light microscope at 200×. Columns represent the mean ± SD from three independent experiments (n = 3). (C) Effect of antcin K on the cell invasion in Hep 3B cells was measured by Matrigel invasion assay. The cells that penetrated through the Matrigel to the lower surface of the filter were stained with crystal violet and were photographed under a light microscope at 200×. Columns represent the mean ± SD from three independent experiments (n = 3).

cell extracts were prepared in protein extraction solution, which contains 1 mM phenylmethanesulfonyl fluoride, 1 mM ethylenediaminetetraacetic acid, 1 μM pepstatin A, 1 μM leupeptin, and 0.1 μM aprotinin. The cell lysates were sonicated and cleared by centrifugation, and the protein concentration in the lysates was measured according to Lowry's method.[17] Fifty micrograms of proteins was loaded over 8% SDS-PAGE gels, transferred to polyvinylidene fluoride membranes, blotted with specific primary antibodies, and then labeled by horseradish peroxidase-conjugated secondary antibody according to the manufacturer's instructions. The membranes were performed using the enhanced chemiluminescence and EC3300 Corning UVP biospectrum AC system (Corning, NY, USA), and the relative density of each band after normalization for β-actin was analyzed using ImageJ 1.45 software.[18]

DOI: 10.1021/jf5059304
J. Agric. Food Chem. 2015, 63, 4561−4569

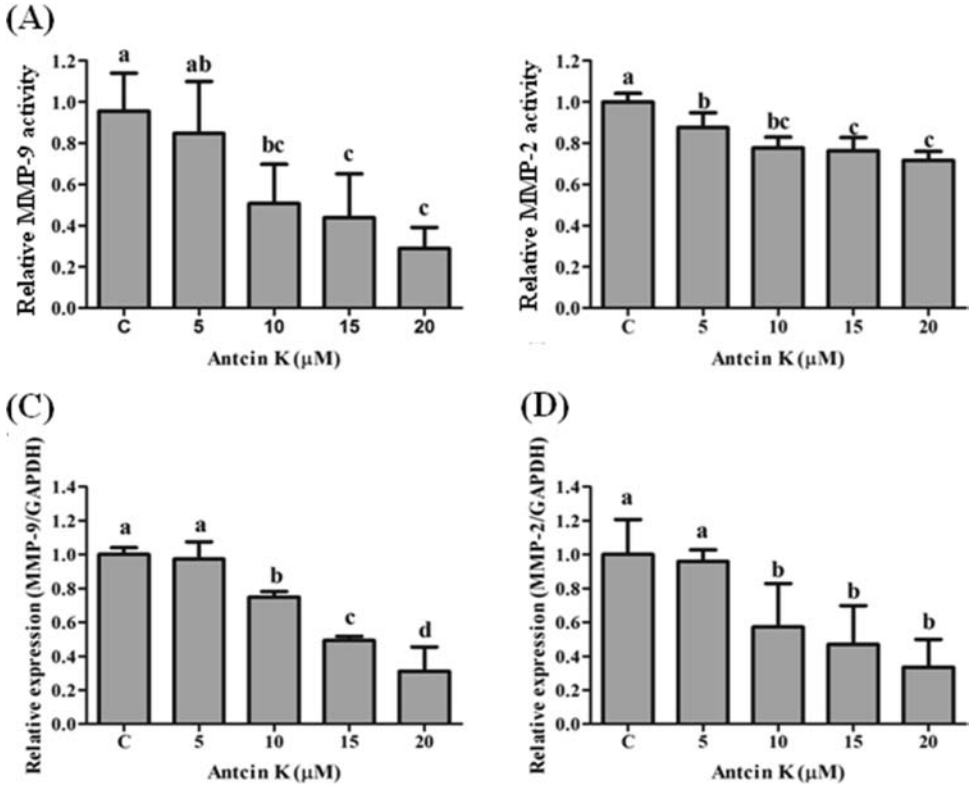

Figure 3. Effects of antcin K on the activity and protein expressions of MMP-2 and MMP-9 in Hep 3B cells. (A, B) Changes by antcin K on the activity of MMP-2 and MMP-9 in Hep 3B cells were assessed by gelatin zymography. Columns represent the mean ± SD from three independent experiments (n = 3). (C, D) Changes by antcin K on the expression of MMP-9 and MMP-2 in Hep 3B cells were assessed by Western blotting. Protein levels are expressed as multiple of control (0.02% DMSO). Columns represent the mean ± SD from three independent experiments (n = 3).

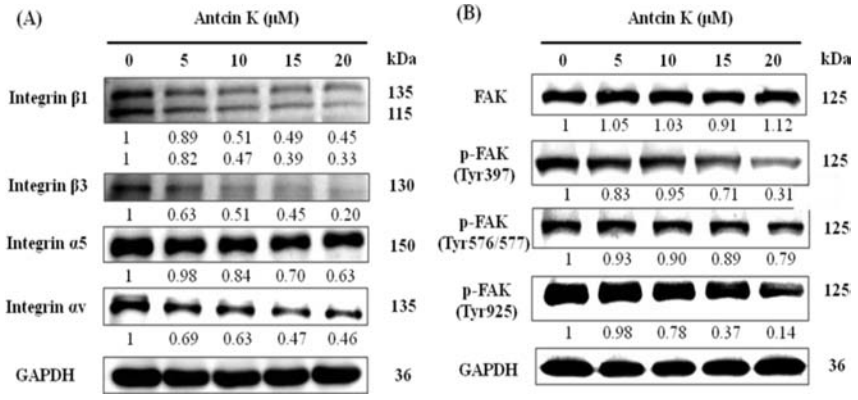

Figure 4. Effects of antcin K on the protein expression of integrin family and FAK-related protein in Hep 3B cells. (A) Effects of antcin K on the expression of integrin β1, integrin β3, integrin α5, and integrin αv in Hep 3B cells were assessed by Western blotting. The experiments were repeated at least three times with similar results (n = 3). Protein levels are expressed as multiple of control (0.02% DMSO) by GAPDH-normalized densitometry. (B) Effects of antcin K on the expression of FAK, p-FAK (Tyr397), p-FAK (Tyr576/577), and p-FAK (Tyr925) in Hep 3B cells were assessed by Western blotting. The experiments were repeated at least three times with similar results (n = 3). Protein levels are expressed as multiple of control (0.02% DMSO) by GAPDH-normalized densitometry.

Statistical Analysis. All results are reported as the mean ± SD, and the differences between the antcin K-treated and control groups were analyzed by one-way analysis of variance ANOVA and Duncan's multiple-comparison tests (SAS Institute Inc., Cary, NC, USA) to determine significant differences among treatments, $p < 0.05$.

RESULTS AND DISCUSSION

Effects of Antcin K on Cell Viability in Hep 3B Cells Measured by MTT Assay. The MTT assay was used to assess the nontoxic dose of antcin K in Hep 3B cells. Treatment with 0, 5, 10, 15, 20, and 40 μM antcin K for 24 h in Hep 3B cells showed that, except for the 40 μM antcin K treatment, there was no significant difference of antcin K treatment in Hep 3B cells compared with the vehicle control group (0.02% DMSO, viable cells = 100%, $p < 0.05$) (Figure 1A).

Protein Expression of PCNA on Antcin K in Hep 3B Cells. After treatment with 0, 5, 10, 15, 20, and 40 μM antcin K for 24 h in Hep 3B cells, the protein expression of proliferating cell nuclear antigen (PCNA) was not significantly different from the control group ($p < 0.05$). Therefore, 0−20 μM antcin

DOI: 10.1021/jf5059304
J. Agric. Food Chem. 2015, 63, 4561−4569

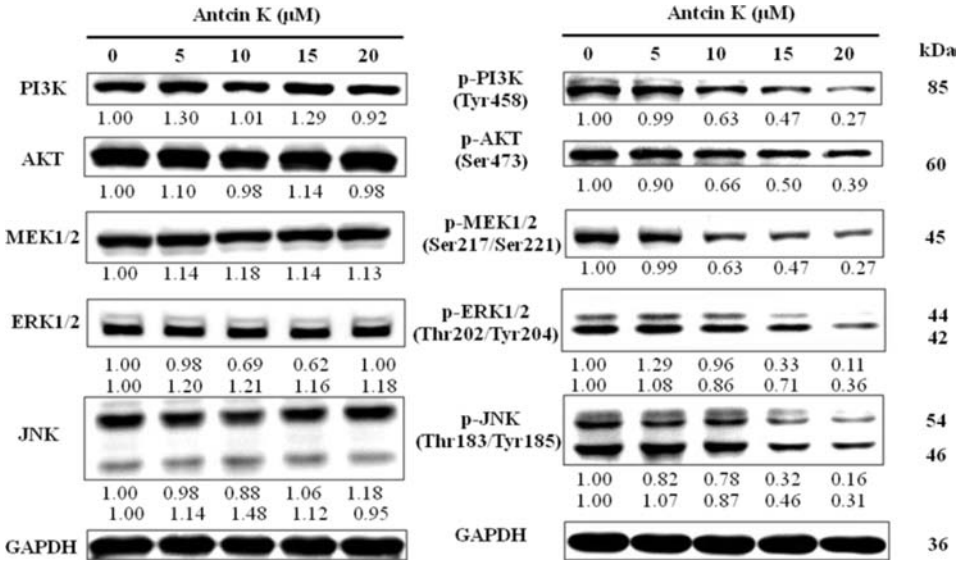

Figure 5. Total and phosphorylated protein expression of FAK's three downstream signaling transduction pathways, PI3K/AKT, MEK/ERK, and JNK. After incubation of the cells with 0−20 μM antcin K for 24 h, the expressed proteins were assessed by Western blotting. The experiments were repeated at least three times with similar results (n = 3), and GAPDH was used as loading control. Protein levels are expressed as multiple of control (0.02% DMSO) by GAPDH-normalized densitometry and shown on the bottom of each band.

K would not affect the cell proliferation (Figure 1B) or the cell viability of Hep 3B cells (Figure 1A).

Effects of Antcin K on Cell Adhesion in Hep 3B Cells. Hep 3B cells were pretreated with antcin K for 24 h and then seeded on 96-well microplates with matrigel. After 1 h, the medium was taken off, and the cells unattached on matrix were removed. The MTT assay was used to analyze the viable cells attached on matrigel to determine whether antcin K could inhibit the adhesion ability of Hep 3B cells. From Figure 2A, treatment of Hep 3B cells with 10 μM antcin K for 24 h could significantly inhibit Hep 3B cells' attaching on matrigel compared with the control group (0.02% DMSO, adhesion rate = 100%). Furthermore, the inhibition rates of 10, 15, and 20 μM antcin K were 10.9 ± 2.9, 9.3 ± 3.0, and 15.0 ± 0.5%, respectively.

Effects of Antcin K on Cell Migration in Hep 3B Cells. As shown in Figure 2B and Supplementary data 2, a Boyden chamber assay was used to analyze the migration effect of antcin K in Hep 3B cells. It showed that Hep 3B cells treated with 10, 15, and 20 μM antcin K for 24 h inhibited the migration of Hep 3B cells (p < 0.05), and the situation was similar to that in Supplementary data 1. It demonstrated that antcin K has significant migration inhibitory ability in human liver cancer cells.

Changes by Antcin K on Cell Invasion in Hep 3B Cells. Invasion is an important step of metastasis processing. Matrigel invasion assay was used to assess the effect of antcin K on invasion of Hep 3B cells in 24 h (Figure 2C and Supplementary data 3). It was found that 10 μM antcin K treatment significantly decreased Hep 3B cells invasion compared with control group (0.02% DMSO, invasion rate = 100%, p < 0.05), and the inhibitory rates of 10, 15, and 20 μM antcin K in Hep 3B cells were 34.7 ± 10.7, 52.4 ± 6.4, and 63.5 ± 0.7%, respectively. From the data of cell adhesion, wound-healing assay, and migration and invasion assays, antcin K not only decreased the adhesion of extracellular matrix but also inhibited the migration and invasion of Hep 3B cells in 24 h (Figure 2). Therefore, antcin K could be considered to decrease the activity of metastasis in human liver cancer cells. However, there are many reasons for metastasis, so additional experiments were designed to clarify the detailed mechanism of antcin K inhibiting Hep 3B cell metastasis.

Effects of Antcin K on the Activity and Protein Expressions of MMP-2 and MMP-9 in Hep 3B Cells. MMPs belong to a large family of proteases, which are calcium-dependent and zinc-containing endopeptidases. They are capable of degrading the composition of extracellular matrix and basal membrane such as collagens, laminin, fibronectin, and proteoglycans.[19] There are at least 20 types of MMPs known. MMP-2 and MMP-9 are considered the most related to the invasion of cancer cells.[9,10]

The activities of MMP-2 and MMP-9 were analyzed by gelatin zymography as shown in Figure 3A,B.[20] It was found that 10, 15, and 20 μM antcin K could inhibit the activity of Hep 3B cells (p < 0.05). The protein expressions of MMP-2 and MMP-9 had the same trends as activity (Figure 3C,D and Supplementary data 4). The data showed that antcin K could inhibit the protein hydrolysis of extracellular matrix and metastasis ability in Hep 3B cells. In addition, some researchers have shown that EMT-related proteins have a close relationship with MMP-2 and MMP-9.[21,22] Therefore, we inferred that antcin K might inhibit the metastasis ability of Hep 3B cells via decreasing MMP-2 and MMP-9 protein expressions. Then the EMT-related proteins were also regulated by MMP-2 and MMP-9.

EMT-Related Protein Expression of Antcin K in Hep 3B Cells. From Figure 6A, Western blotting was used to investigate the protein expression of E-cadherin and vimentin. Compared with the control group (0.02% DMSO), Hep 3B cells treated with 10−20 μM antcin K for 24 h, the protein expression of E-cadherin increased but the protein expression of vimentin decreased significantly (p < 0.05). These data supported our hypothesis about EMT-related proteins regulating metastasis ability after antcin K treatment in Hep 3B cells.

DOI: 10.1021/jf5059304
J. Agric. Food Chem. 2015, 63, 4561−4569

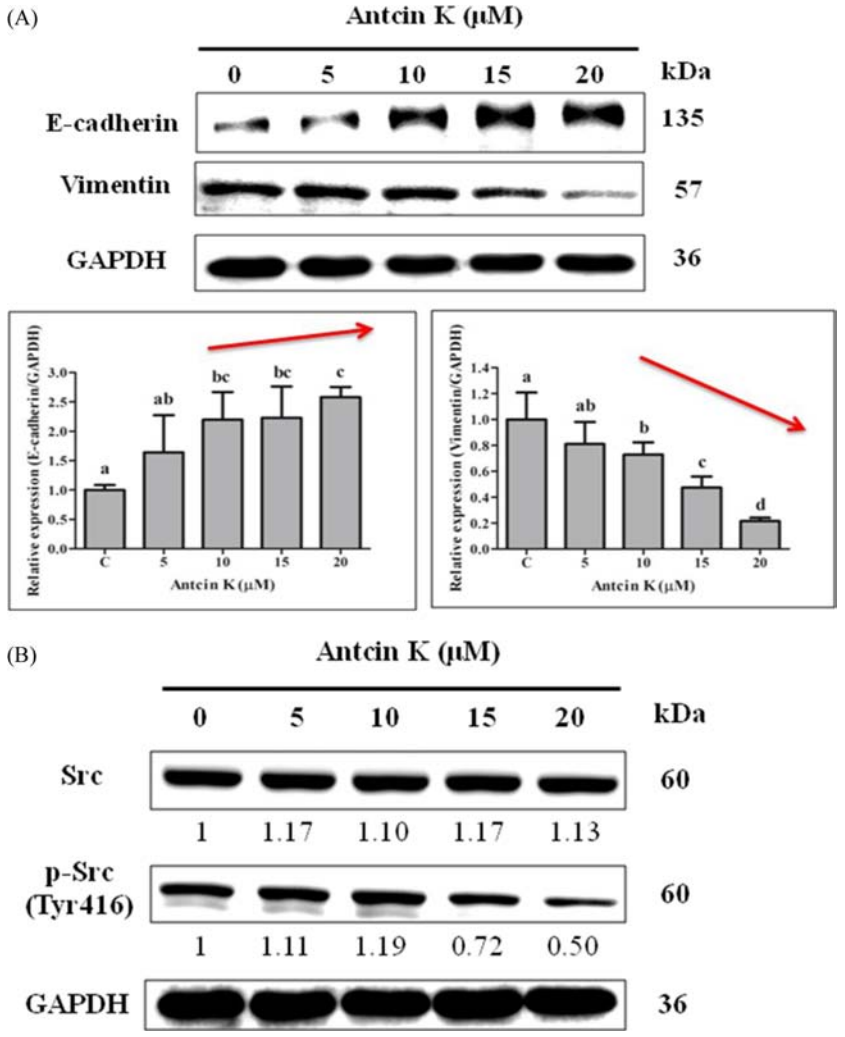

Figure 6. Effects of antcin K on the expression of E-cadherin, Src, and vimentin in Hep 3B cells were assessed by Western blotting: (A) effects of antcin K on the expression of E-cadherin and vimentin in Hep 3B cells; (B) effects of antcin K on the expression of Src and p-Src (Tyr416) in Hep 3B cells. The experiments were repeated at least three times with similar results (n = 3). Protein levels are expressed as multiple of control (0.02% DMSO) by GAPDH-normalized densitometry.

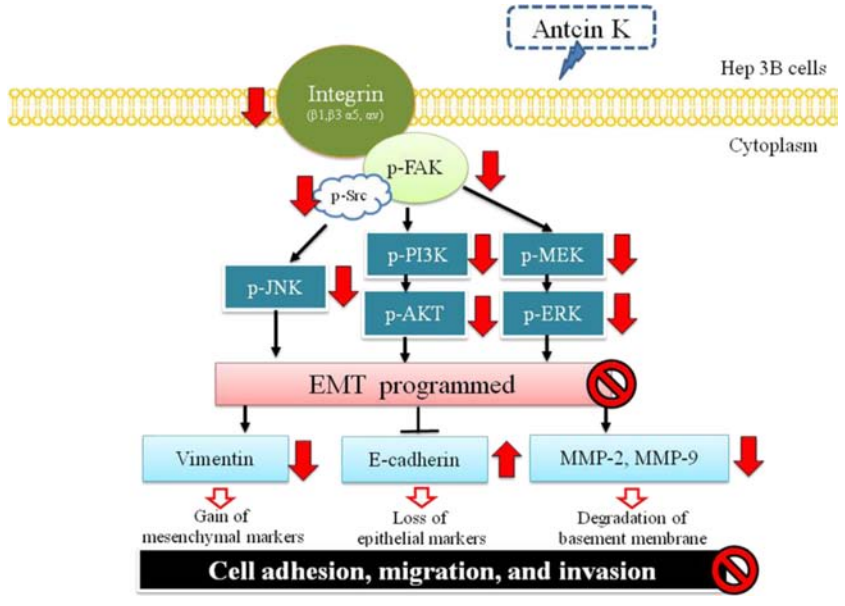

Figure 7. Potential mechanism of antimetastasis effect of antcin K in human liver cancer Hep 3B cells.

DOI: 10.1021/jf5059304
J. Agric. Food Chem. 2015, 63, 4561−4569

Protein Expression of Integrin of Antcin K in Hep 3B Cells. Integrin is the receptor protein that mediates cell adhesion, involving the interaction of extracellular matrix and regular migration and invasion of cancer cells. Previous studies have shown that some integrin subunits such as β1, β3, α1, α2, α3, α4, α5, and αv have been detected in Hep 3B cells.[23,24] However, various expressions of integrin are related to basal membrane, extracellular matrix-remodeling, adhesion, migration, invasion, and growth of cancer cells, and it is involved in the metastasis of multiple cancers.[24] In 2002, integrins β1, β3, α5 and αv were found in different liver tumors from liver cancer patients. In 80 cases of liver cancer patients, 77 patients had overexpression of integrin β1, 44 patients had overexpression of integrin αv, 15 patients had β3 overexpression, and 70 patients had overexpression of integrin α5. These findings demonstrate that integrin β1, β3, α5, and αv are indeed involved in the development and metastasis of liver cancer.[23]

In addition, Ly et al. showed that the expression of integrin $\alpha5\beta1$ could regulate integrin $\alpha v\beta3$-mediated adhesion or migration.[25] For specific and functional property, integrin $\alpha5\beta1$ only binds with fibronectin (F_n) of the extracellular matrix, which is the major component of the vascular wall. Fransvea et al. indicated that the expression of integrin $\alpha5\beta1$ could regulate the migration of the vascular wall.[26] To determine whether antcin K inhibiting metastasis was linked with the integrin family in Hep 3B cells, Western blotting was used to assess the integrin expression on antcin K treatment in Hep 3B cells. From the results, 10 μM antcin K could significantly decrease the protein expression of integrin β1, β3, α5, and αv in Hep 3B cells (Figure 4A). The data could explain that the antimetastasis ability of antcin K might be through the regulation of integrin receptor proteins in Hep 3B cells.

Protein Expression of FAK and Src of Antcin K in Hep 3B Cells. FAK is one of the major controlling proteins of adhesion. Migration and invasion are partially mediated by integrin and FAK regulation. Compared with the control group, the total protein expression of FAK after treatment with antcin K did not change in Hep 3B cells (Figure 4B), but the protein expression and phosphorylation of FAK of 15 and 20 μM antcin K treatment decreased significantly within FAK (Tyr^{397}), FAK ($Tyr^{576/577}$), and FAK (Tyr^{925}). In addition, the phosphorylated protein expression of Src decreased after antcin K treatment, but the total protein expression of Src did not change (Figure 6B). These data indicated that p-Src and p-FAK could mediate the antimetastasis mechanism of antcin K in Hep 3B cells.

Protein Expression of PI3K/AKT, MEK/ERK, and JNK of Antcin K in Hep 3B Cells. To confirm whether the expression of FAK downstream was changed like FAK and Src, the signaling transduction proteins PI3K/AKT, MEK/ERK, and JNK were investigated. As shown in Figure 5, when Hep 3B was treated with various concentrations of antcin K for 24 h, the total protein expressions of PI3K, AKT, MEK, ERK, and JNK were not changed compared with the control group, but the phosphorylated protein expressions decreased in dose-dependent manners. This demonstrated that antcin K treatment could decrease the phosphorylation of protein expression of FAK's three downstream signaling transduction pathways such as PI3K/AKT, MEK/ERK, and JNK. Our data proved that antimetastasis of antcin K was truly via the activation of PI3K/AKT, MEK/ERK, and JNK. Those results were agreeable to our data of viability and PCNA (Figure 1). For example, PI3K/AKT also controls the survival pathway.[27] Antcin K treatment changed only the phosphorylation protein expression of PI3K/AKT, which meant that 20 μM antcin K indeed inhibited the metastasis of Hep 3B cells and had no toxicity effect in Hep 3B cells.

From our results, the integrin family could interact with cellular molecular, transfer the extracellular signaling into cytosol, and then affect the expression of nuclei DNA and cytoskeleton. Moreover, the receptor tyrosine kinases (RTKs), β1 integrin cytoplasmic domains, integrin-linked kinase (ILK), and other adaptor proteins such as focal adhesion kinase (FAK) of cell membrane might interact with integrin, forming a focal adhesion complex. In addition, the Ras/Raf/MEK/MAPK signaling pathway could be involved in multiple functions such as cell proliferation, invasion, angiogenesis, extracellular matrix remodeling, and anti-apoptosis, which was regulated by the integrin−actin−RTK network.[28]

Antcin K is the most abundant triterpenoid from the fruiting bodies of basswood-cultivated *A. cinnamomea*. Most studies use the ethanol extracts of *A. cinnamomea* as material,[29−32] and previous study showed that the ethanol extracts of *A. cinnamomea* could inhibit the metastasis of human lung cancer CL1-0 cells through decreasing the phosphorylated protein expression of FAK, PI3K/AKT, JNK, and p38.[33] Our data demonstrated that antcin K acted through a similar mechanism as ethanol extracts of *A. cinnamomea* in antimetastasis of cancer treatment; it is therefore reasonable to assume that antcin K plays a major role in ethanol extracts of *A. cinnamomea*.

In conclusion, antcin K might inhibit the activation of PI3K/AKT, MEK/ERK, and JNK by decreasing the protein expression of integrind β1, β3, α5, and αv and activating FAK. Then antcin K decreased protein expression and activation of MMP-2 and MMP-9 to affect EMT (Figure 7) and inhibited the metastasis in human liver cancer Hep 3B cells.

■ ASSOCIATED CONTENT

Supporting Information

Supplementary data 1−4. The Supporting Information is available free of charge on the ACS Publications website at DOI: 10.1021/jf5059304

■ AUTHOR INFORMATION

Corresponding Authors

*(Y.-H.K.) Mail: China Medical University, Hsueh-Shih Road, Taichung, 404, Taiwan, Republic of China. E-mail: kuoyh@mail.cmu.edu.tw.

*(L.-Y.S.) Mail: No. 1, Sec. 4, Roosevelt Road, Taipei 106, Taiwan. Phone: 886-2-33664129. Fax: 886-2-23620849. E-mail: lysheen@ntu.edu.tw.

Author Contributions

Ω(Y.-L.C.) International Master's Degree Program in Food Science, International College, National Pingtung University of Science and Technology, 1 Shuefu Road, Neipu, Pingtung 91201, Taiwan. With equal contribution to first author.

Funding

The technical work was supported by the Joint Center for Instruments and Researches, College of Bioresources and Agriculture, National Taiwan University. In addition, the research work was partially funded by the National Science Council (NSC 100-2313-B-002-036) and CMU under the Aim for Top University Plan of the Ministry of Education, Taiwan, and Taiwan Ministry of Health and Welfare Clinical Trial and

DOI: 10.1021/jf5059304
J. Agric. Food Chem. 2015, 63, 4561−4569

Research Center of Excellence (MOHW104-TDU-B-212-113002).

Notes

The authors declare no competing financial interest.

■ ABBREVIATIONS USED

EMT, epithelial mesenchymal transition; MMPs, matrix metalloproteinases; uPA, urokinase plasminogen activator; ECM, extracellular matrix; PI3K, phosphatidylinositol 3-kinase; Src, steroid receptor coactivator; FAK, focal adhesion kinase; JNKs, c-Jun N-terminal kinases; ERKs, extracellular signal-regulated kinases; MEK, mitogen-activated protein kinase/ERK kinase; PKB, protein kinase B; PCNA, proliferating cell nuclear antigen

■ REFERENCES

(1) Jemal, A.; Bray, F.; Center, M. M.; Ferlay, J.; Ward, E.; Forman, D. Global cancer statistics. *Ca-Cancer J. Clin.* **2011**, *61* (2), 69−90.

(2) Siegel, R.; Ward, E.; Brawley, O.; Jemal, A. Cancer statistics, 2011: the impact of eliminating socioeconomic and racial disparities on premature cancer deaths. *Ca-Cancer J. Clin.* **2011**, *61* (4), 212−236.

(3) Ao, Z. H.; Xu, Z. H.; Lu, Z. M.; Xu, H. Y.; Zhang, X. M.; Dou, W. F. Niuchangchih (*Antrodia camphorata*) and its potential in treating liver diseases. *J. Ethnopharmacol.* **2009**, *121* (2), 194−212.

(4) Geethangili, M.; Tzeng, Y. M. Review of pharmacological effects of *Antrodia camphorata* and its bioactive compounds. *Evidence-Based Complement. Altern. Med.: eCAM* **2011**, *2011*, 212641.

(5) Gupta, G. P.; Massague, J. Cancer metastasis: building a framework. *Cell* **2006**, *127* (4), 679−695.

(6) Chu, Y. W.; Yang, P. C.; Yang, S. C.; Shyu, Y. C.; Hendrix, M. J.; Wu, R.; Wu, C. W. Selection of invasive and metastatic subpopulations from a human lung adenocarcinoma cell line. *Am. J. Respir. Cell Mol. Biol.* **1997**, *17* (3), 353−360.

(7) Zeng, J.; Sun, Y.; Wu, K.; Li, L.; Zhang, G.; Yang, Z.; Wang, Z.; Zhang, D.; Xue, Y.; Chen, Y.; Zhu, G.; Wang, X.; He, D. Chemopreventive and chemotherapeutic effects of intravesical silibinin against bladder cancer by acting on mitochondria. *Mol. Cancer Ther.* **2011**, *10* (1), 104−116.

(8) Arnaout, M. A.; Goodman, S. L.; Xiong, J. P. Structure and mechanics of integrin-based cell adhesion. *Curr. Opin. Cell Biol.* **2007**, *19* (5), 495−507.

(9) Guo, W.; Giancotti, F. G. Integrin signalling during tumour progression. *Nat. Rev. Mol. Cell Biol.* **2004**, *5* (10), 816−826.

(10) Chu, Y. L.; Ho, C. T.; Chung, J. G.; Rajasekaran, R.; Lo, Y. C.; Sheen, L. Y. Allicin induces anti-human liver cancer cells through p53 gene modulating apoptosis and autophagy. *J. Agric. Food Chem.* **2013**, *61*, 9839−9848.

(11) Mosmann, T. Rapid colorimetric assay for cellular growth and survival: application to proliferation and cytotoxicity assays. *J. Immunol. Methods* **1983**, *65*, 55−63.

(12) Liu, X. Y.; Fang, H.; Yang, Z. G.; Wang, X. Y.; Ruan, L. M.; Fang, D. R.; Ding, Y. G.; Wang, Y. N.; Zhang, Y.; Jiang, X. L.; Chen, H. C. Matrine inhibits invasiveness and metastasis of human malignant melanoma cell line A375 in vitro. *Int. J. Dermatol.* **2008**, *47* (5), 448−456.

(13) Behrens, J.; Kameritsch, P.; Wallner, S.; Pohl, U.; Pogoda, K. The carboxyl tail of Cx43 augments p38 mediated cell migration in a gap junction-independent manner. *Eur. J. Cell Biol.* **2010**, *89* (11), 828−838.

(14) Park, S.; Minai-Tehrani, A.; Xu, C. X.; Chang, S. H.; Woo, M. A.; Noh, M. S.; Lee, E. S.; Lim, H. T.; An, G. H.; Lee, K. H.; Sung, H. J.; Beck, G. R.; Cho, M. H. Suppression of A549 lung cancer cell migration by precursor let-7g microRNA. *Molecular Medicine Reports* **2010**, *3* (6), 1007−1013.

(15) Huang, Y. T.; Hwang, J. J.; Lee, L. T.; Liebow, C.; Lee, P. P.; Ke, F. C.; Lo, T. B.; Schally, A. V.; Lee, M. T. Inhibitory effects of a luteinizing hormone-releasing hormone agonist on basal and epidermal growth factor-induced cell proliferation and metastasis-associated properties in human epidermoid carcinoma A431 cells. *Int. J. Cancer* **2002**, *99* (4), 505−513.

(16) Liu, K. C.; Huang, A. C.; Wu, P. P.; Lin, H. Y.; Chueh, F. S.; Yang, J. S.; Lu, C. C.; Chiang, J. H.; Meng, M.; Chung, J. G. Gallic acid suppresses the migration and invasion of PC-3 human prostate cancer cells via inhibition of matrix metalloproteinase-2 and -9 signaling pathways. *Oncol. Rep.* **2011**, *26* (1), 177−184.

(17) Bradford, M. M. A rapid and sensitive method for the quantitation of microgram quantities of protein ultilizing the principle of protein-dye binding. *Anal. Biochem.* **1976**, *72*, 248−254.

(18) Wu, C. C.; Chung, J. G.; Tsai, S. J.; Yang, J. H.; Sheen, L. Y. Differential effects of allyl sulfides from garlic essential oil on cell cycle regulation in human liver tumor cells. *Food Chem. Toxicol.* **2004**, *42*, 1937−1947.

(19) Hiller, O.; Lichte, A.; Oberpichler, A.; Kocourek, A.; Tschesche, H. Matrix metalloproteinases collagenase-2, macrophage elastase, collagenase-3, and membrane type 1-matrix metalloproteinase impair clotting by degradation of fibrinogen and factor XII. *J. Biol. Chem.* **2000**, *275* (42), 33008−33013.

(20) Stamenkovic, I. Matrix metalloproteinases in tumor invasion and metastasis. *Semin. Cancer Biol.* **2000**, *10* (6), 415−433.

(21) Yoo, Y. A.; Kang, M. H.; Lee, H. J.; Kim, B. H.; Park, J. K.; Kim, H. K.; Kim, J. S.; Oh, S. C. Sonic hedgehog pathway promotes metastasis and lymphangiogenesis via activation of Akt, EMT, and MMP-9 pathway in gastric cancer. *Cancer Res.* **2011**, *71* (22), 7061−7070.

(22) Robichaud, N.; Del Rincon, S. V.; Huor, B.; Alain, T.; Petruccelli, L. A.; Hearnden, J.; Goncalves, C.; Grotegut, S.; Spruck, C. H.; Furic, L.; Larsson, O.; Muller, W. J.; Miller, W. H.; Sonenberg, N. Phosphorylation of eIF4E promotes EMT and metastasis via translational control of SNAIL and MMP-3. *Oncogene* **2015**, *34*, 2032 10.1038/onc.2014.146

(23) Nejjari, M.; Hafdi, Z.; Gouysse, G.; Fiorentino, M.; Beatrix, O.; Dumortier, J.; Pourreyron, C.; Barozzi, C.; D'Errico, A.; Grigioni, W. F.; Scoazec, J. Y. Expression, regulation, and function of alpha V integrins in hepatocellular carcinoma: an in vivo and in vitro study. *Hepatology* **2002**, *36* (2), 418−426.

(24) Desgrosellier, J. S.; Cheresh, D. A. Integrins in cancer: biological implications and therapeutic opportunities. *Nat. Rev. Cancer* **2010**, *10* (1), 9−22.

(25) Ly, D. P.; Zazzali, K. M.; Corbett, S. A. De novo expression of the integrin alpha5beta1 regulates alphavbeta3-mediated adhesion and migration on fibrinogen. *J. Biol. Chem.* **2003**, *278* (24), 21878−21885.

(26) Fransvea, E.; Mazzocca, A.; Antonaci, S.; Giannelli, G. Targeting transforming growth factor (TGF)-betaRI inhibits activation of beta1 integrin and blocks vascular invasion in hepatocellular carcinoma. *Hepatology* **2009**, *49* (3), 839−850.

(27) Hambardzumyan, D.; Becher, O. J.; Rosenblum, M. K.; Pandolfi, P. P.; Manova-Todorova, K.; Holland, E. C. PI3K pathway regulates survival of cancer stem cells residing in the perivascular niche following radiation in medulloblastoma in vivo. *Genes Dev.* **2008**, *22* (4), 436−448.

(28) Brown, M. C.; Turner, C. E. Roles for the tubulin- and PTP-PEST-binding paxillin LIM domains in cell adhesion and motility. *Int. J. Biochem. Cell Biol.* **2002**, *34* (7), 855−863.

(29) Hsu, Y. L.; Kuo, P. L.; Cho, C. Y.; Ni, W. C.; Tzeng, T. F.; Ng, L. T.; Kuo, Y. H.; Lin, C. C. *Antrodia cinnamomea* fruiting bodies extract suppresses the invasive potential of human liver cancer cell line PLC/PRF/5 through inhibition of nuclear factor kappaB pathway. *Food Chem. Toxicol.* **2007**, *45* (7), 1249−1257.

(30) Yang, H. L.; Kuo, Y. H.; Tsai, C. T.; Huang, Y. T.; Chen, S. C.; Chang, H. W.; Lin, E.; Lin, W. H.; Hseu, Y. C. Anti-metastatic activities of *Antrodia camphorata* against human breast cancer cells mediated through suppression of the MAPK signaling pathway. *Food Chem. Toxicol.* **2011**, *49* (1), 290−298.

(31) Chang, C. H.; Wang, H. E.; Liaw, P. Y.; Peng, C. C.; Peng, R. Y. *Antrodia cinnamomea* exhibits a potent neuroprotective effect in the PC12 Cell-Abeta25−35 model − pharmacologically through adeno-

DOI: 10.1021/jf5059304
J. Agric. Food Chem. 2015, 63, 4561−4569

sine receptors and mitochondrial pathway. *Planta Med.* **2012**, *78* (17), 1813−1823.
(32) Lu, M. K.; Cheng, J. J.; Lai, W. L.; Lin, Y. J.; Huang, N. K. Fermented *Antrodia cinnamomea* extract protects rat PC12 cells from serum deprivation-induced apoptosis: the role of the MAPK family. *J. Agric. Food Chem.* **2008**, *56* (3), 865−874.
(33) Chen, Y. Y.; Chou, P. Y.; Chien, Y. C.; Wu, C. H.; Wu, T. S.; Sheu, M. J. Ethanol extracts of fruiting bodies of *Antrodia cinnamomea* exhibit anti-migration action in human adenocarcinoma CL1-0 cells through the MAPK and PI3K/AKT signaling pathways. *Phytomedicine* **2012**, *19* (8−9), 768−778.

DOI: 10.1021/jf5059304
J. Agric. Food Chem. 2015, 63, 4561−4569

phenols in the olive oil process without the impact of different plant material, different sample preparation/extraction procedures, and chromatographic conditions which can hamper such phenol studies. To our best knowledge, this work is the most comprehensive study on the quantitative behavior of olive fruit phenols entailed in olive oil production, providing insight into the origin, degradation, and evolution of each throughout the processing, with novel transfer/partition calculations and transformative relationships established.

MATERIALS AND METHODS

Reagents and standards. All reagents and standards were obtained and prepared as described.[13]

Sampling and samples pretreatment. Olive fruits of Istrska belica *cv.* were harvested in Gradno (Goriška Brda, Slovenia), stored overnight and processed to olive oil the next day using a laboratory-scale Abencor olive mill (Seville, Spain). Prior to that, a lot of fruits were randomly chosen as a representative starting fruit material, weighed and frozen with liquid nitrogen before subjected to freeze-drying. Then, fruits were manually destoned and rebalanced in order to obtain the pulp/stone average mass ratio, ground separately into homogeneous powder with a liquid nitrogen and stored at −25 °C until analysis. Other olive oil process-derived matrices (pomace, wastewater and oil) were sampled at the end of processing with an exception of paste, which was collected immediately after fruits crushing. The samples were prepared as previously described,[14−16] where destoned fruits, stones, paste and pomace were frozen with liquid nitrogen, freeze-dried, homogenized and stored at −25 °C until analysis, while the wastewater was primarily acidified (HCl, pH = 2.0) and defatted with *n*-hexane prior to freeze-drying and storage at −25 °C. The olive oil sample was solely stored in the dark at room temperature until extracted. The dry matter measurements of freeze-dried samples were performed gravimetrically,[17] providing the basis for phenols transfer/partition calculations.

Olive oil processing. A laboratory-scale olive oil processing trial was carried out as described elsewhere.[13] First, olives were ground to a paste by the hammer mill and homogenized in order to reduce the potential differences in the starting fruit material. Then, the paste (∼700 g) was put into a metallic pitcher and 100 mL of water (25 °C) added to improve its rheology. Afterword, the paste was malaxed in thermo-malaxer (30 min, 25 °C) and centrifuged (1400 g, 1 min) in order to obtain the three final products, i.e. oil and two wastes (wastewater and pomace). While the yield of pomace, which remained in a centrifuge was calculated, the masses of two liquid phases (oil + wastewater) separated by decantation process were balanced in order to assess the mass balance of the process trail. All the procedure was performed in duplicate.

Phenols extraction. *Destoned fruits, stones, paste, pomace and wastewater.* Phenols were extracted at room temperature according to a previously published ultrasound-assisted solid liquid extraction (USLE) method,[14,15] where a freeze-dried sample (1.5 g) was sonicated (3 × 20 min) with 25 mL of methanol. The homogenates of each extraction step were centrifuged (2515 *g*, 5 min) and combined supernatants diluted with methanol to 100 mL.

Olive oil. Extraction (at room temperature) was carried using ultrasound-assisted liquid liquid extraction (US-LLE) method previously described,[16] where a 10 g of olive oil was dissolved in *n*-hexane (10 mL) and sonicated (3 × 10 min) with pure methanol (5 mL). The homogenates of each extraction step were centrifuged (2515 *g*, 2 min), combined and defatted with a freeze-based fat precipitation (for 20 min at −80 °C). Afterward, the remaining extract was reconstituted to 25 mL with methanol and stored in the screw-capped dark glass containers at −25 °C until analysis.

U(H)PLC-DAD analysis. Prior to analysis, the aliquots of extracts were rotary concentrated 10-fold and the dry-residue redissolved in a mixture of U(H)PLC eluents A (water: acetic acid =95:5, v/v) and B (methanol) (A:B = 90:10; v/v). The extracts were filtered through 0.22 μm/13 mm PVDF filters from Carl Roth GmbH+Co. (Düren, Germany) and immediately analyzed by U(H)PLC-DAD analysis.

A Dionex Ultimate 3000 U(H)PLC liquid chromatograph (Thermoscientific, CA, USA) equipped with UV−vis diode-array (DAD) detector was used for the quantification. The extracts of 10 μL (except for oil; 20 μL) were injected and the DAD signals were recorded at 280, 320, and 365 nm, presenting a compromise for individual phenolic class detection. Chromatographic separation was achieved by using gradient elution on Kinetex PFP column (2.6 μm, 100 mm × 4.6 mm) attached to a PFP security guard (2.1 mm × 4.6 mm) both from Phenomenex (Sydney, Australia) under the analysis conditions previously described.[13]

Flavonols were quantified at 365 nm, while simple phenols and secoiridoids at 280 nm with an exception of unknown A, uknowns 408 MW, caffeoyl-6′-secologanoside and comselogoside quantified at 320 nm along with the group of cinnamic acids and flavonoids. When authentic standards were available, phenols were quantified based on their calibration curves, whereas others were expressed as equivalents; hydroxytyrosol glucosides and hydroxytyrosol acetate as hydroxytyrosol, tyrosol glucoside as tyrosol, all verbascoside derivatives as verbascoside, luteolin rutinosides as luteolin-7-*O*-glucoside, luteolin-3′-*O*-glucoside and luteolin-4′,7-*O*-diglucoside as luteolin-4′-*O*-glucoside, and all secoiridoids as oleuropein with an exception of caffeoyl-6′-secologanoside expressed as caffeic acid, and unknown A, unknowns 408 MW and comselogoside, which were expressed as *p*-coumaric acid equivalents. The identification strategy of all is in depth described elsewhere.[13]

U(H)PLC method validation. Prior to quantification, the suitability of U(H)PLC-DAD system was checked in terms of injector's reproducibility and linearity using commercially available standards.

The linearity of method was evaluated by serial dilution of standard stock solutions over broad concentration ranges using ten-point calibration curves.

The LODs and LOQs were calculated from y-intercept standard deviations (S_b) and slopes (a) of calibration curves using signal-to-noise ratio criteria of 3.3 (LOD = 3.3 x Sb/a) and 10 (LOQ = 10 × Sb/a) in the concentration ranges close to LOQs expected for each phenolic compound in prepared extracts (μg/mL): 0.33−1.67 (vanillin), 0.35−1.73 (vanillic acid), 0.33−1.65 (*p*-coumaric acid), 1.24−7.44 (caffeic acid), 1.44−5.76 (hydroxytyrosol), 1.40−3.93 (tyrosol), 1.00−2.99 (oleuropein), 0.39−0.97 (verbascoside), 0.24−1.20 (rutin), 0.23−1.17 (quercitrin), 0.25−1.23 (luteolin-4′-*O*-glucoside), 1.62−5.85 (apigenin), 0.48−2.87 (apigenin-7-*O*-glucoside), 0.56−4.49 (luteolin), 1.26−3.78 (luteolin-7-*O*-glucoside) and 0.79−4.76 (pinoresinol).

Extraction efficiencies of USLE and US-LLE methods were checked prior to application to olive matrices in terms of phenol yield recoveries obtained via consecutive five-step extraction. The extracts of destoned fruits, stone, paste, pomace and wastewater were submitted to a complete USLE method (3 × 20 min) using 25 mL of pure methanol. Then, the remaining solid residue was re-extracted twice and analyzed by U(H)PLC for a potential phenols presence in the fourth and fifth extraction step, where the summation of phenol yields from a five-step extraction was considered as 100%. Analogously, the efficiency of US-LLE method (3 × 10 min, 5 mL 100% meOH) has been checked for the oil sample.

Phenols partition and transfer percentages. The phenols partition and transfer percentages from fruits to paste and to final products (pomace, wastewater, oil) were calculated considering the mass balance according to eq 1:

$$\%P_{matrix} = (P_{matrix}/P_{fruit}) \times (m_{matrix}/m_{fruit}) \times 100 \quad (1)$$

where P is the concentration of individual phenolic compound in particular matrix expressed in mg/kg per fruit FW and m the mass of selected matrix and fruit FW (g) in press experiment.

Additionally, the percentages of their increases/decreases during crushing and malaxation were calculated using eqs 2 and 3:

Increase/decrease during crushing is presented with parameter c_c (in %):

DOI: 10.1021/jf506353z
J. Agric. Food Chem. 2015, 63, 4570−4579

Table 1. Fate of the Olive Fruit Phenols during Olive Oil Processing at 30 min/25 °C Malaxation Conditions

		Olive matrix										
		Input			Intermediate			Output				
						Crushing[c]					*Malaxation*[d]	
No.[f]	Class/Phenolic compound	**Destoned fruit**[a]	**Stone**[a]	**Σ**[a]	**Paste** (t = 0)[a]	*Sign t*	c_c (%)	**Pomace**[a]	**Wastewater**[a]	**Oil**[b]	*Sign t*	c_m (%)
	Simple phenols											
1[f]	Hydroxytyrosol glucoside	51.8 ± 1.0	4.8 ± 0.3	56.6 ± 1.0	40.1 ± 1.3	***	−29	34.9 ± 3.8	7.1 ± 0.4	1.4 ± 0.1	ns	–
2	Hydroxytyrosol-1-β-glucoside	18.7 ± 1.3	9.9 ± 0.5	28.6 ± 1.6	48.5 ± 1.0	***	70	54.5 ± 0.9	5.5 ± 0.6	7.5 ± 0.6	***	24
3	Hydroxytyrosol	26.0 ± 1.0	6.3 ± 0.3	32.3 ± 1.2	87 ± 3.3	***	170	86.7 ± 3.0	21.6 ± 3.0	27.0 ± 5.6	***	25
6	Tyrosol glucoside	10.2 ± 1.1	6.1 ± 0.3	16.3 ± 1.3	37.8 ± 1.7	***	134	38.3 ± 1.8	10.9 ± 1.4	6.7 ± 0.4	***	30
8	Tyrosol	8.1 ± 0.3	2.3 ± 0.1	10.4 ± 0.4	21.4 ± 1.1	***	107	22.7 ± 1.5	5.2 ± 0.5	24.7 ± 3.9	**	32
19	Hydroxytyrosol acetate	26.6 ± 0.5	nd[e]	26.6 ± 0.5	nq (co)[e]	–	–	nq (co)	nq (co)	17.9 ± 1.3	–	–
	Total	*141.3 ± 4.9*	*29.4 ± 1.6*	*170.7 ± 5.7*	*235.0 ± 7.3*	***	38	*237.1 ± 10.1*	*50.3 ± 6.0*	*85.2 ± 11.7*	**	23
	Benzoic acids											
13	Vanillic acid	nd	nd	–	10.0 ± 0.3	***	100	7.9 ± 0.5	1.5 ± 0.1	6.4 ± 0.5	ns	–
15	Vanillin	nd	1.5 ± 0.1	1.5 ± 0.1	nd	***	*−100*	nd	nd	4.7 ± 0.3	***	100
	Total	–	*1.5 ± 0.1*	*1.5 ± 0.1*	*10.0 ± 0.3*	***	567	*7.9 ± 0.5*	*1.5 ± 0.1*	*11.1 ± 0.8*	***	*−6*
	Cinnamic acids											
16	*p*-Coumaric acid	nq (co)	nd	–	8.3 ± 1.0	–	–	6.4 ± 0.4	0.8 ± 0.1	5.5 ± 0.4	ns	–
17	β-OH-verbascoside isomer 1	6.0 ± 0.3	0.5 ± 0.0	6.6 ± 0.2	16.9 ± 1.2	***	157	21.6 ± 1.3	4.7 ± 0.4	nd	***	56
18	β-OH-verbascoside isomer 2	3.2 ± 0.2	0.4 ± 0.0	3.7 ± 0.2	15.4 ± 1.3	***	320	20.3 ± 1.4	4.6 ± 0.4	nd	***	64
24	β-OH-methyl-verbascoside isomer 1	8.3 ± 0.9	nq (tr)[e]	8.3 ± 0.9	24.1 ± 2.2	***	194	26.7 ± 0.5	1.8 ± 0.1	nd	***	19
25	β-OH-methyl-verbascoside isomer 2	5.8 ± 0.7	nq (tr)	5.8 ± 0.7	26.1 ± 2.5	***	357	30.2 ± 0.5	2.0 ± 0.1	nd	***	24
26	Verbascoside	358.5 ± 10.8	13.3 ± 0.7	371.7 ± 11.0	258.0 ± 19.6	***	*−31*	202.4 ± 22.1	20.3 ± 0.6	nd	*	*−13*
	Total	*381.8 ± 12.1*	*14.2 ± 0.7*	*396.0 ± 12.2*	*348.7 ± 27.4*	**	*−12*	*307.6 ± 26*	*34.3 ± 1.5*	*5.5 ± 0.4*	ns	–
	Flavonoids											
22	Luteolin-4′,7-*O*-diglucoside	19.5 ± 0.1	nd	19.5 ± 0.1	nq (ins)[e]	–	–	nd	nd	nd	–	–
37	Rutin	290.1 ± 6.8	nq (tr)	290.1 ± 6.8	181.9 ± 11.9	***	*−37*	119.1 ± 3.1	3.5 ± 0.3	nq (tr)	***	*−32*
41	Luteolin-7-*O*-glucoside	315.5 ± 9.9	nd	315.5 ± 9.9	41.8 ± 9.5	***	*−87*	32.5 ± 3.0	1.7 ± 0.1	nd	ns	–
42	Luteolin rutinoside isomer 1	42.7 ± 1.3	nd	42.7 ± 1.3	29.5 ± 0.7	***	*−31*	30.2 ± 2.3	4.3 ± 0.3	nd	*	17
44	Luteolin rutinoside isomer 2	15.0 ± 0.6	nd	15.0 ± 0.6	12.2 ± 0.3	***	*−19*	11.5 ± 0.9	1.4 ± 0.0	nd	ns	–
45	Quercitrin	50.1 ± 0.9	nd	50.1 ± 0.9	35.0 ± 2.1	***	*−30*	27.4 ± 0.7	1.2 ± 0.1	nd	***	*−18*
51	Apigenin-7-*O*-glucoside	79.9 ± 2.9	nd	79.9 ± 2.9	39.3 ± 2	***	*−51*	34.3 ± 2.8	4.1 ± 0.3	nd	ns	–
59	Luteolin-4′-*O*-glucoside	93.8 ± 2.3	nd	93.8 ± 2.3	29.7 ± 3.4	***	*−68*	24.7 ± 1.7	nq (ins)	nd	–	–
61	Luteolin-3′-*O*-glucoside	29.4 ± 0.7	nd	29.4 ± 0.7	30.1 ± 0.7	ns	–	27.7 ± 2	2.3 ± 0.1	nd	ns	–
66	Luteolin	nd	nd	–	123.5 ± 10.3	***	100	133.5 ± 16.2	5.1 ± 0.4	37.1 ± 2.8 d	ns	–
69	Apigenin	nd	nd	–	28.0 ± 1.9	***	100	28.0 ± 3.6	1.8 ± 0.1	31.6 ± 2.3 cd	ns	–
	Total	*936.1 ± 24.7*	–	*936.1 ± 24.7*	*551.1 ± 26.8*	***	*−41*	*469.0 ± 35.7*	*25.2 ± 1.6*	*68.7 ± 5.0*	*	*−10*
	Lignans											
55	Pinoresinol	nd	nd	–	nd	–	–	nd	nd	69.4 ± 4.8	***	100
58	Acetoxypinoresinol	nd	nd	–	nd	–	–	nd	nd	266.6 ± 18.3	***	100
	Total	–	–	–	–	–	–	–	–	*336.0 ± 23.0*	***	100

J. Agric. Food Chem. 2015, 63, 4570−4579
DOI: 10.1021/jf506353z

Table 1. continued

		Olive matrix										
		Input			Intermediate			Output				
						Crushing[c]					*Malaxation*[d]	
No.[f]	Class/Phenolic compound	**Destoned fruit**[a]	**Stone**[a]	**Σ**[a]	**Paste** (*t* = 0)[a]	*Sign t*	c_c (%)	**Pomace**[a]	**Wastewater**[a]	**Oil**[b]	*Sign t*	c_m (%)
	Simple phenols											
	Secoiridoids											
4	Unknown A	12.0 ± 0.4	nq (tr)	12.0 ± 0.4	10.6 ± 0.3	***	*−12*	8.9 ± 0.8	2.1 ± 0.1	0.5 ± 0.0	ns	–
5	Unknown 408 MW compound 1	2.0 ± 0.1	nq (ins)[e]	2.0 ± 0.1	2.0 ± 0.1	–	–	1.7 ± 0.2	0.3 ± 0.0	0.1 ± 0 0.0	ns	–
7	Unknown 408 MW compound 2	3.1 ± 0.2	nq (ins)	3.1 ± 0.2	3.5 ± 0.1	–	–	2.9 ± 0.3	0.6 ± 0.0	nd	ns	–
9	Unknown B	309.8 ± 10.8	nd	309.8 ± 10.8	284.9 ± 5	**	*−8*	261.9 ± 22.8	54.3 ± 3.5	nd	ns	–
10	Elenolic acid glucoside isomer 1	35.2 ± 1.3	5.4 ± 0.3	40.6 ± 1.4	50.1 ± 1.3	***	24	nd	nd	nd	***	*−100*
11	Secologanoside	54.1 ± 2.6	nq (tr)	54.1 ± 2.6	67.0 ± 1.2	***	24	56.1 ± 4.0	12.1 ± 2.5	9.4 ± 1.5	ns	–
12	Elenolic acid glucoside isomer 2	64.0 ± 4.1	5.2 ± 0.3	69.2 ± 4.3	nq (co)	–	–	nq (co)	nq (co)	11.4 ± 1.0	–	–
14	Elenolic acid glucoside isomer 3	151.4 ± 5.7	12.7 ± 0.6	164.1 ± 5.9	nd	***	*−100*	nd	nd	nd	–	–
20	Demethyloleuropein	3470.1 ± 99.2	nq (ins)	3470.1 ± 99.2	nq (tr)	–	–	nq (tr)	nq (tr)	nd	–	–
21	Dihydro-oleuropein isomer 1	118.5 ± 3.3	nd	118.5 ± 3.3	194.2 ± 6.8	***	64	189.9 ± 15.4	21.1 ± 1.2	nd	ns	–
23	3,4-DHPEA-EDA isomer 1	nd	nd	–	168.6 ± 6.7	***	100	118.9 ± 19.4	nd	nd	**	*−29*
27	Dihydro-oleuropein isomer 2	348.0 ± 10.9	34.4 ± 1.9	382.4 ± 11.9	275.1 ± 7.2	***	*−28*	105.3 ± 8.5	nq (tr)	nd	***	*−62*
28	Unknown 484 MW isomer 1	nd	nd	–	nd	–	–	nd	51.3 ± 2.6	nd	***	100
29	Unknown 484 MW isomer 2	nd	nd	–	nd	–	–	nd	38.9 ± 4.1	nd	***	100
30	Oleuropein diglucoside isomer 1	110.8 ± 8	30.0 ± 1.8	140.8 ± 8.9	230.8 ± 22.7	***	64	nq (ins)	nq (ins)	nd	–	–
31	Unknown 484 MW isomer 3	nd	nd	–	nd	–	–	nd	37.1 ± 2.9	nd	***	100
32	Nüzhenide isomer 2	57.0 ± 1.8	92.3 ± 4.9	149.3 ± 5.0	180.3 ± 2.7	***	21	143.8 ± 8.3	22.2 ± 1.6	nd	*	*−8*
33	Oleuropein diglucoside isomer 2	143.1 ± 4.7	nd	143.1 ± 4.7	nd	***	*−100*	nd	nd	nd	–	–
34	3,4-DHPEA-EDA isomer 2	nd	nd	–	1828.6 ± 188.9	***	100	3039.4 ± 382.9	241.6 ± 6.7	1925.8 ± 126.8	***	81
35	Nüzhenide isomer 3	nd	17.0 ± 1.2	17.0 ± 1.2	nd	***	*−100*	nd	nd	nd	–	–
36	Methoxynüzhenide	nd	34.0 ± 2.1	34.0 ± 2.1	nd[e]	***	*−100*	nd	nd	nd	–	–
38	Oleuropein aglycone isomer 1	nd	nd	–	4729.6 ± 167.5	***	100	3406.7 ± 198.3	331.4 ± 12.9[f]	3321.6 ± 238.6	***	*−20*
39	Nüzhenide isomer 4	nd	12.7 ± 0.8	12.7 ± 0.8	nd	***	*−100*	nd	nd	nd	–	–
40	Oleuropein	12222.0 ± 360.6	427.9 ± 25.0	12649.8 ± 369.0	698.5 ± 156.5	***	*−94*	377.6 ± 15.9	nd	nd	***	*−44*
43	Caffeoyl-6′-secologanoside	14.7 ± 0.6	nd	14.7 ± 0.6	14.7 ± 0.3	ns	–	13.2 ± 1.1	1.8 ± 0.1	nd	ns	–
46	*p-HPEA-EDA*	nd	nd	–	nd	***	–	nd	nd	1303.6 ± 90.0	***	100
47	Oleuroside	152.7 ± 5.0	16.6 ± 1.5	169.2 ± 5.0	nd	***	*−100*	nd	nd	nd	–	–
48 + 49	Ligstroside + Oleuropein aglycone sum	nd	nd	–	nd	–	–	nd	nd	1879.4 ± 109.0	***	100
50	Unknown C	227.5 ± 4.2	16.5 ± 1.3	243.9 ± 3.3	nq (co)	–	–	nq (co)	nq (co)	nd	–	–
52	Ligstroside	575.2 ± 17.2	52.0 ± 3.8	627.2 ± 18.1	nd	***	*−100*	nd	nd	nd	–	–
53	Comselogoside	33.7 ± 1	nd	33.7 ± 1.0	34.7 ± 2.0	ns		30.7 ± 2.5	3.9 ± 0.2	nd	ns	–
54	Nüzhenide 11-methyl oleoside isomer 1	nd	18.2 ± 1.7	18.2 ± 1.7	nd	***	*−100*	nd	nd	nd	–	–
56	Nüzhenide 11-methyl oleoside isomer 2	nd	18.3 ± 2.6	18.3 ± 2.6	nd	***	*−100*	nd	nd	nd	–	–
57	Acetal of 3,4-DHPEA-EDA	nd	nd	–	nd	–	–	nd	142.6 ± 9.5	nd	***	100

J. Agric. Food Chem. 2015, 63, 4570−4579
DOI: 10.1021/jf506353z

Table 1. continued

		Olive matrix										
		Input			Intermediate			Output				
						Crushing[c]					*Malaxation*[d]	
No.[f]	Class/Phenolic compound	**Destoned fruit**[a]	**Stone**[a]	**Σ**[a]	**Paste** (t = 0)[a]	*Sign t*	c_c (%)	**Pomace**[a]	**Wastewater**[a]	**Oil**[b]	*Sign t*	c_m (%)
	Simple phenols											
	Secoiridoids											
60	Oleuropein aglycone isomer 2	nd	nd	–	693.6 ± 17.4	***	100	661.7 ± 44.1	89.9 ± 3.8	1194.6 ± 78.8	*	10
62	Nüzhenide 11-methyl oleoside isomer 4	nd	31.9 ± 3.6	31.9 ± 3.6	112.4 ± 2.5	***	258	88.7 ± 4.0	nd	nd	***	*−21*
63	Methoxynüzhenide 11-methyl oleoside	nd	10.3 ± 2.3	10.3 ± 2.3	nd	***	*−100*	nd	nd	nd	–	–
64	Ligstroside aglycone isomer 2	nd	nd	–	nd	–	–	nd	nd	167.3 ± 4.4	***	100
65	Oleuropein aglycone isomer 3	nd	nd	–	347.0 ± 3.5	***	100	306.3 ± 9.2	46.2 ± 2.1	515.7 ± 40.4	ns	–
67	Nüzhenide di(11-methyl oleoside) isomer 1	nd	8.6 ± 2.5	8.6 ± 2.5	nd	***	*−100*	nd	nd	nd	–	–
68	Nüzhenide di(11-methyl oleoside) isomer 2	nd	15.0 ± 3.6	15 ± 3.6	nd	***	*−100*	nd	nd	nd	–	–
	Total	*18104.9 ± 536.6*	*859.1 ± 58.3*	*18964 ± 547.9*	*9926.1 ± 321.5*	***	*−48*	*8813.7 ± 711.3*	*1097.4 ± 34.4*	*10329.3 ± 686.0*	ns	–
	Σ TP[g]	19564.1 ± 577.7	904.2 ± 60.6	20468.3 ± 589.5	11070.9 ± 346.1	***	*−46*	9835.3 ± 783.3	1208.8 ± 42.1	10835.8 ± 725.5	ns	–

[a]Expressed as mean ± SD (mg/kg fruits FW); Σ = total initial fruit content (destoned fruit + stone); t = 0, paste obtained immediately after crushing. [b]Expressed as mean ± SD (mg/kg fruits FW × e^{-2}). [c]Crushing; Sign t: total initial fruit and paste means separated by t-test (***, $P \leq 0.001$; **, $P \leq 0.01$; *, $P \leq 0.05$; ns, not significant, $P \geq 0.05$), c_c = % of increase/decrease with respect to fruits (eq 2); (−) value could not be calculated. [d]Malaxation Sign t; paste and total output means separated by t-test (***, $P \leq 0.001$; **, $P \leq 0.01$; *, $P \leq 0.05$; ns, not significant, $P \geq 0.05$); c_m = % of increase/decrease with respect to paste (eq 3); (−) value could not be calculated. [e]Compound is described as not detected (nd), not quantified (nq) due to trace amount (tr), inconsistent UV−vis spectrum (ins), coelution problems (co). [f]Numbers of peaks are referring to Figures S1−S6 in the Supporting Information. [g]Σ TP = sum of U(H)PLC-DAD quantified phenols.

J. Agric. Food Chem. 2015, 63, 4570−4579
DOI: 10.1021/jf506353z

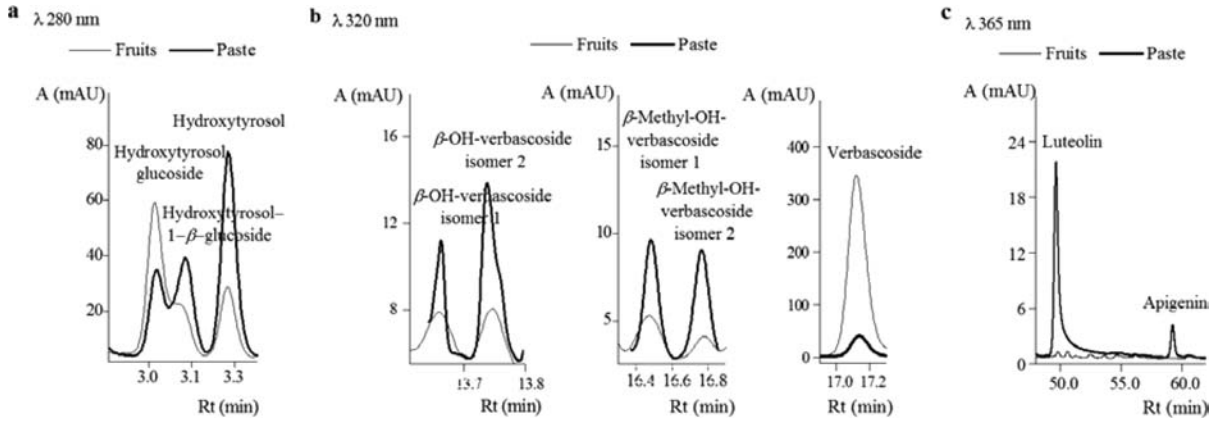

Figure 1. U(H)PLC-DAD phenolic profiles of olive fruits and olive paste.

$$c_c = (P_{paste} \times 100/P_{fruit}) - 100 \quad (2)$$

Increase/decrease during malaxation is presented with parameter c_m (in %):

$$c_m = ((P_{pomace} + P_{wastewater} + P_{oil}) \times 100/P_{paste}) - 100 \quad (3)$$

The initial fruit phenolic content was considered as the available (100%) pool derived from destoned fruit and stone marked as input (Table 1), while the term TP (total phenols) refers to a sum of U(H)PLC-DAD quantified phenols.

Statistical analysis. All results were expressed as means ± SD obtained from at least triplicate analyses and tested by ANOVA or *t* test (*, $P < 0.05$; **, $P < 0.01$; ***, $P < 0.001$; n.s., not significant) using Costat Statistics Software 6.4 (CoHort Software, CA, USA). When ANOVA was significant, means were separated using Tukey's HSD test ($P < 0.05$).

RESULTS AND DISCUSSION

Method validation. The suitability of the U(H)PLC-DAD system was satisfactory, where the linearity of the injector was always above 99% and the reproducibility of ten replicates has never exceeded 0.5% of RSD, respectively.

The linearity of the method was excellent with high correlation coefficients (R^2) obtained for all standards over their broad concentration ranges (μg/mL) tested as follows; vanillin (y = 0.6348x; R^2 = 0.9933; 0.33−64.83), vanillic acid (y = 0.2899x; R^2 = 0.9957; 0.35−67.26), *p*-coumaric acid (y = 0.7863x; R^2 = 0.9946; 0.33−64.21), caffeic acid (y = 0.6081x; R^2 = 0.9982; 1.24−99.19), hydroxytyrosol (y = 0.1488x; R^2 = 0.9970; 1.44−524.19), tyrosol (y = 0.0993x; R^2 = 0.9937; 1.40−219.00), oleuropein (y = 0.0359x; R^2 = 0.9963; 1.00−7953.12), verbascoside (y = 0.2403x; R^2 = 0.9991; 0.39−1013.12), rutin (y = 0.2368x; R^2 = 0.9952; 0.24−312.40), quercitrin (y = 0.2329x; R^2 = 0.9925; 0.23−121.44), luteolin-4′-*O*-glucoside (y = 0.1775x; R^2 = 0.9976; 0.25−896.56), apigenin (y = 0.2293x; R^2 = 0.9988; 1.62−232.80), apigenin-7-*O*-glucoside (y = 0.3362x; R^2 = 0.9999; 0.48−274.56), luteolin (y = 0.2684x; R^2 = 0.9928; 0.56−483.12), luteolin-7-*O*-glucoside (y = 0.2487x; R^2 = 0.9962; 1.26−765.24), pinoresinol (y = 0.1429x; R^2 = 0.9975; 0.79−285.76).

The sensitivities of the DAD detector were determined by calculating the LODs/LOQs for each standard expressed in μg/mL and were as follows: 0.36/1.09 (vanillin), 0.23/0.69 (vanillic acid), 0.22/0.67 (*p*-coumaric acid), 2.46/7.44 (caffeic acid), 2.55/7.74 (hydroxytyrosol), 1.75/5.29 (tyrosol), 1.57/4.76 (oleuropein), 0.19/0.58 (verbascoside), 0.03/0.01 × e^{-1} (rutin), 0.01/0.04 (quercitrin), 0.12/0.36 (luteolin-4′-*O*-glucoside), 1.20/3.87 (apigenin), 0.17/0.52 (apigenin-7-*O*-glucoside), 0.53/1.60 (luteolin), 0.16/0.49 (luteolin-7-*O*-glucoside), and 0.04/0.11 (pinoresinol).

The extraction methods for the phenol isolation from olive matrices entailed in the olive oil processing trial were adopted from our earlier reports performed as a preliminary step toward a high-yielding TP analysis in fruits, wastewater, and olive oil.[14−16] However, prior to application in this experiment and evaluation with U(HPLC)-DAD, their efficiencies had to be rechecked, owing to introduction of new olive matrices of richer quali- and quantitative profiles and novel ones for which the recovery optimizations have not yet been performed (paste, pomace, and stone). Even so, our results confirmed that both USLE and US-LLE extractions are efficient for the quantitative phenol analysis, where a three-step extraction provided recoveries superior to 98% on average for all six matrices (US-LLE for the oil and USLE for others), again testifying to high powerful US extracting abilities

Quantification results. Table 1 presents detailed insight into olive fruit phenols transfer, transformation, and partition trail behavior during olive oil processing as affected by two operational steps, i.e. crushing and malaxation (30 min/25 °C). The process itself has two inputs, i.e. destoned fruit and stone, one middle/intermediate product (paste), and three outputs, i.e. pomace, wastewater, and oil, allowing us to follow the origin, evolution, and disappearance of each phenolic compound throughout the processing. The identification of all compounds presented in this study is described elsewhere.[13]

Impact of crushing. The relative contribution of the crushing step to a phenols reduction during olive oil processing has been rarely quantified in the existing literature. Similarly, little scientific information is available regarding its role in their transformative process, as the range of phenols analyzed so far has been limited.[6−9,18] A direct comparison of olive fruits initial phenolic composition (destoned fruit + stone) with the corresponding paste obtained directly after crushing (t = 0) is the first approach to such an estimation. Looking quantitatively, a significant TP drop was observed immediately after crushing (46%), confirming the previous postulation of being the most critical step in the overall process.[4] A similar TP loss (50−60%) has already been reported before for industrial-scale trials.[6,9] Although brief, this technological operation has also induced several transformative changes arriving from the mechanical mixing action, chemical and/or biochemical reactions, i.e. enzymatic and nonenzymatic hydrolyses, and oxidations.[19] As seen from results, crushing implied a rise of

DOI: 10.1021/jf506353z
J. Agric. Food Chem. 2015, 63, 4570−4579

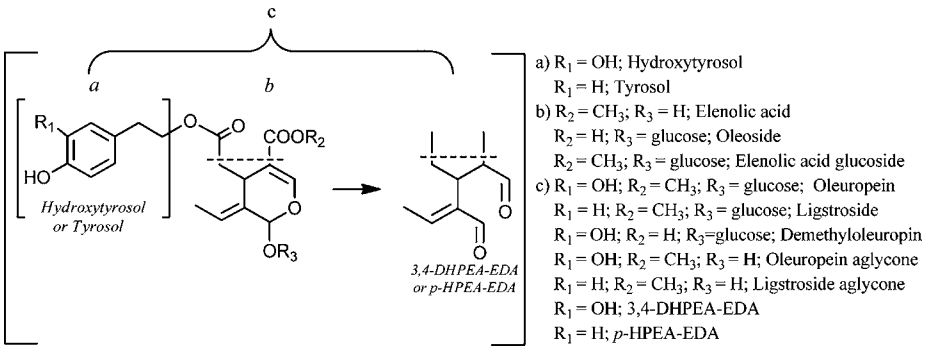

Figure 2. Possible interconversions of selected secoiridoids containing tyrosol and hydroxytyrosol in their structures.

simple phenols and benzoic acids, but decreased the yields of other classes with an exception of lignans, which were not involved/affected by the milling process. At the level of individual phenols, 13 out of 51 initially quantified fruit phenols have irrevocably disappeared after crushing (mainly those from stone) and eight newly appeared in the paste, indicating their technologically induced formation and/or release. The phenol profile of olive paste thus seems to be a result of all the transfer, liberation, and transformation phenomena with none, partial, or total hydrolysis/degradation of olive fruits native phenols, leading to a formation of new respective derivatives. A visual comparison of fruits' and paste's phenolic profiles (Figure 1) reflects some of the potential interconversion changes discussed below.

The highest decrease was observed for the main olive fruit secoiridoid glucosides, i.e. oleuropein, demethyloleuropein, and ligstroside, which is in line with previous reports.[6−9] While the content of oleuropein decreased for 94%, its demethylated form was almost completely degraded (traces of demethyloleuropein), whereas ligstroside could not be detected by DAD anymore. According to the mechanism of Servili et al.,[4] these glucosides can be transformed into their respective aglycones, primarily to oleuropein or ligstroside aglycones and further to their decarboxymethylated forms, i.e. 3,4-DHPEA-EDA or *p*-HPEA-EDA. Indeed, both of the potential (demethyl)-oleuropein transformants were found in olive paste after crushing; their first interconversion product eluted as three (oleuropein aglycone isomers), while the second as two peaks (3,4-DHPEA-EDA isomers), together accounting for 35 and 12% of fruits initial demethyloleuropein + oleuropein content together. This could indicate that crushing accelerated an enzymatic degradation of both glucosides, which already began in the fruit and would likely progress during maturation. Such an assumption is supported by the previous MS trace detection of oleuropein aglycones in destoned fruits[13] and the fact that 3,4-DHPEA-EDA has already been found in the fruits before.[20] Analogously, these transformants could also arrive from oleuropein diglucoside isomer 2, whose complete degradation was observed after crushing, while the rise of its isomer 1 (+64%) is thus far unexplained and warrants further investigation. Nevertheless, the transformation of these native fruit secoiridoid glucosides could also yield some other oleuropein structurally correlated phenols whose yields have increased after crushing, such as dihydro-oleuropein isomer 1 or others of lower molecular weight (MW) phenols. Indeed, there are many cleavage products possible upon the degradation of oleuropein, demethyloleuropein, and ligstroside, of which some are illustrated in Figure 2.

By contrast, the degradative mechanism of ligstroside was more ambiguous, as none of its two potential transformants (ligstroside aglycones and *p*-HPEA-EDA) could be detected in paste by DAD, but instead could easily be quantified in the oil at the end of the processing. The relationship that quantitatively explains such vague interconversion remains unclear and may indicate that (i) ligstroside was completely transformed into both, but the complexity of the paste's structure restricted their detection in paste, as its composition immediately after crushing is known to strongly differ from that after malaxation,[21] or (ii) these two transformants could have formed the complexes with polysaccharides released only after malaxation,[22] or (less likely) (iii) ligstroside was completely oxidized and/or transformed into other products, while its respected aglycones found in olive oil are the hydrolysis products of others, but structurally related compounds.

However, beyond the knowledge of fruits' prime secoiridoid glucosides behavior, the degradative mechanism of stone's main secoiridoid glucosides, *i.e.* nüzheonide and its esterified forms with methoxy group and 11-methyl oleoside, has not yet been established. Interestingly, only two out of ten quantified representatives were increased upon olives crushing (nüzhenide isomer 2 for 21% and nüzhenide 11-methyl oleoside isomer 4 for 258%), most likely due to improved release and/or the mill prompted hydrolysis of higher MW phenols such as nüzhenide (di)esters giving rise to their formation. All the other nüzhenide representatives have totally diminished throughout the milling operation due to either low oxidation resistance and/or crushing-induced degradation. Nevertheless, based on their chemical structures they could all yield a tyrosol glucoside, whose significant rise in paste (134%) should be marked after crushing.

Crushing also implied a rise of other simple phenols (Figure 1a, Figure 2a); hydroxytyrosol has increased for 170%, owing to degradation of hydroxytyrosol-containing compounds, while tyrosol for 107% due to the hydrolysis of tyrosol-containing phenols. This could have occurred via cleavage of the ester bond by the action of endogenous esterases splitting secoiridoid glucosides or their aglycones (Figure 2c), giving rise to elenolic acid glucoside, oleoside, or elenolic acid (Figure 2b). Until now, the release of simple phenols from aglycones was considered to ensue only during oil storage[23] and never during the course of its production. Alternatively, hydroxytyrosol could also be released from the fruits native hydroxytyrosol glucoside (−29%) and/or verbascoside (−31%) by the activity of glucosidases, analogously as tyrosol from nüzhenide and its esters. Owing to such complexity, it was not possible to assign their exact origin, as no obvious increase of the corresponding

DOI: 10.1021/jf506353z
J. Agric. Food Chem. 2015, 63, 4570−4579

cleavage compounds could be observed in olive paste. Another remarkable fact is also a distinct behavior of the two hydroxytyrosol glucosides displaying a rise (70%, hydroxytyrosol glucoside-1-β-glucoside) and a drop (29%, hydroxytyrosol glucoside) after olives crushing. Such a discrepancy clearly indicates their different chemical structure and for the first time experimentally supports (during the course of olive oil production) what has only been proposed before;[1] hydroxytyrosol glucoside-1-β-glucoside is a hydrolysis product of verbascoside enhanced by both the crushing and malaxation, while the formation of hydroxytyrosol glucoside appears not to be technologically prompted; instead it rather contributes to its degradation.

The appearance of vanillic acid in olive paste after crushing raises an issue of its origin. The fact that it was absent in both input matrices but present in all olive oil process-derived products suggests that is a formation product of the technological process. Possible explanations include a crushing-induced hydrolysis of lignin from stone once already proved to yield vanillic acid under acid stem explosion,[24] although there is always a possibility that a lab-milling of stone in a sample preparation was not efficient as the mill crushers of the Abencor system, hampering its expected detection in this fruit compartment. Interestingly, its quantitative yield was further unaffected by the malaxing conditions, which seems to only be facilitated its full distribution among the final products. By contrast, vanillin was detected in olive stone, but not in the corresponding paste, which could be attributed to a brief duration of crushing step, suffering less tissue damage, and hence a limited release immediately after it. The subsequent malaxation apparently induced its extractability, which allowed its quantification in olive oil, though in a much lower amount with respect to its original content in stone (3%).

Among cinnamic acids, only verbascoside has diminished after fruits crushing (−31%), whereas all of its derivatives have considerably increased (>150%, Figure 1b). It is of interest to add that their accumulation has further proceeded also during malaxation; thus, it is very likely that verbascoside derivatives had originated from any of the fruits' native unknown compound(s) hydrolyzed upon crushing and malaxation. Moreover, their initial presence in olive fruits suggests that the technology has only hastened the biosynthetic interconversion that would likely occur also at the fruit level; however, such a hypothesis undoubtedly warrants further investigation and is beyond the scope of the present study.

Crushing also contributed to a loss of glycosylated flavonoids with an exception of luteolin 3′-*O*-glucoside, which seemed to be resistant to any or all enzymatic and/or nonenzymatic degradations, transformations, or oxidations. The appearance of two new flavonoidal aglycones in olive paste, i.e. luteolin and apigenin (Figure 1c), indicates that some of them were hydrolyzed by the endogenous glucosidases, released, and/or activated by crushing, but a firm relationship could only be established for apigenin, whose formation in olive paste was collaborated with a drop of apigenin-7-*O*-glucoside. Luteolin, on the other hand, may have arisen from any or all of the six luteolin glycosides, rutin, and/or quercitrin.

In spite of several quali- and quantitative induced changes by crushing, a small portion of phenols remained unaffected, including luteolin-3′-*O*-glucoside, comselogoside, and caffeoyl-6′-secologanoside. A remarkable fact is that all of their yields have further remained constant also during malaxation, indicating their high technological resistance, which could have a wide potential in a forward design of TP enriched food products.

Impact of malaxation. Although phenols yield behavior during the course of malaxation has not been separately monitored, their levels in the output matrices yet permitted reliable insight into their further transformation/partition trail from paste to the final products, especially if it is considered that the time of the paste's span in the centrifuge is too short to allow important modifications to happen.

In general, the behavior of phenols during malaxation continued the trend initiated by the crushing, though quantitatively to a lower extend; a positive yield rise kept an increasing trend due to improved releases and/or transformative reactions, while the yield losses were followed by a further drop owing to enzymatic and/or nonenzymatic hydrolyses and oxidations. However, there were also a few exceptions; for example, luteolin rutinoside isomer 1 showed a rise after initial drop, while some of the potential transformants have decreased, i.e. elenolic acid glucoside isomer 1, 3,4-DHPEA-EDA isomer 1, nüzhenide isomer 2, oleuropein aglycone isomer 1, and nüzhenide 11-methyl oleoside isomer 4. This could indicate that the hydrolysis of their parent compounds has finished and their oxidative degradation prevailed due to operative conditions and/or enzymatic activities. By contrast, some other potential transformants (dihydro-oleuropein isomer 1 and oleuropein aglycone isomer 3) remained rather unaffected, similarly as most of the flavonoidal representatives. Moreover, the evolution of some new phenols could be evidenced in the final products; both representatives of lignans and some of secoiridoids (all unknown 484 MW isomers, *p*-HPEA-EDA, ligstroside aglycones, and the acetal of 3,4-DHPEA-EDA) have appeared in the oil or in the wastewater, while not in pomace, though some traces could still be previously detected by MS as well.[13] It is thus possible to deduce that only malaxation conditions were efficient enough to induce their formation and/or release due to prolonged mixing and/or enzymatic actions. However, there is always a possibility that the extraction method for these compounds was not equally efficient for all matrices, owing to structural specifics, requiring other approaches as previously demonstrated for lignans in fruits.[25]

Looking from a TP yield perspective, no losses could be observed during malaxation at 30 min/25 °C conditions, indicating a balanced degradation/formation equilibrium of the phenolic compounds quantified. In other words, the available pool of phenols detected in olive paste after crushing could also be quantified at the end of the process via a TP sum of output products (∼54%). This is somewhat in line with previous reports,[9] demonstrating no significant losses of phenol constituents during the malaxation process, though this operation has often been associated with major quantitative loss.[8] However, as further evident from results, only 0.53% of the available fruit phenols have ended up in olive oil and nearly 6% in the wastewater, while others have remained entrapped in the solid (48.12%). Such a partition distribution is rather different from our earlier industrial-scale results[6] (0.3−1.2% oil; 38.2−46.2% wastewater; 4.5−47.4% pomace), but not surprising as the latter is govern by the quantity of final products formed. In a present lab-scale study, pomace was clearly the predominant byproduct formed (82.3%), while the yielding indexes of liquid matrices were much lower, i.e. 8.9% for oil and 8.8% for the wastewater, most likely due to a less efficient

DOI: 10.1021/jf506353z
J. Agric. Food Chem. 2015, 63, 4570−4579

phases separation system in the Abencor mill. A similar components' yield distribution has been observed elsewhere.[11]

A high retention of phenols in pomace further suggests that the process conditions applied (30 min/25 °C) have not fully induced their transfer to liquid phases, yet constituting a challenge for some potential improvements. Our results also confirmed that a major proportion of fruit phenols is indeed lost with wastes, but some also owing to their technological destruction. This, however, is not in full agreement with the available results in the literature,[5] showing no TP losses during olive oil processing, but rather their unsuited yield distribution among the final products, i.e. 1−2% oil, 53% wastewater, and 45% pomace. However, it is rather uncommon that processing would quantitatively yield all the phenols confined in the initial fruit material (100% TP pool), especially not due to a well-known phenomenon of their oxidative catabolism.[4]

Partitioning model. The majority of phenols have originated from the pulp and/or peel, together accounting for 95% of the fruits initial TP content, while stone confined only a minor fraction (∼5%). Secoiridoids were the predominant class in both input matrices and maintained their prominent role also in the process-derived matrices, though represented by different individuals. With the exception of olive stone, the class distribution in solid matrices has decreased in the order secoiridoids > flavonoids > cinnamic acids > simple phenols. By contrast, in the wastewater, simple phenols constituted the second largest class, evidencing their hydrophilic nature, analogous to lignans in olive oil showing high tendency for the oily matrix. Interestingly, none of the fruit flavonoid glycosides were transferred to the oil above their trace amounts, but instead were largely confined in both of the waste matrices. Similarly, all cinnamic acids from fruits were lost with the byproducts, though one has scarcely been transferred to the oil as well, *i.e. p*-coumaric acid. The partition behavior of secoiridoids was rather similar to flavonoids, where apart from the two known glucosides (secologanoside and elenolic acid glucoside isomer 2), only aglycones were partitioned to the oil, while the other glucosides have ended up in the wastes (e.g., comselogoside and caffeoyl-6′-secologanoside). Such a partitioning model is quite similar to one previously reported at the industrial-scale level using different starting fruit materials,[6] which indicates that their qualitative distribution pattern among the final products is rather more common than unique.

The research interest in redesigning current technological approaches to provide higher extractability of olive oils with richer phenol yields and with lower ecological footprints has been great in recent years and is still significant due to increasing demands for functionally and sustainability in the olive oil industry. The results of the present study have provided us a deeper insight into phenols quantitative behavior during laboratory-scale olive oil processing, their tendency for individual matrices, and resistance to the technologically induced modifications, which are important in the recognition of their quality and value to mankind. Moreover, they provided us a better understanding of the relationship between the initial and final products, which could benefit any further industrial-scale trials.

■ ASSOCIATED CONTENT

Ⓢ Supporting Information

U(H)PLC-DAD phenolic profile of olive destoned fruit, olive stone, olive paste, olive pomace, olive mill wastewater, and olive oil extracts monitored at 280, 320, and 365 nm and results of additional statistical evaluation of the olive oil process; ANOVA analyses of the Input (Fruit + Stone), Intermediate (Paste), and Output (OMWW + Pomace + Olive Oil) Phenol Contents (mg/kg of Fruit FW) and Tukey's HSD separation of means ($p < 0.05$). The Supporting Information is available free of charge on the ACS Publications website at DOI: 10.1021/jf506353z.

■ AUTHOR INFORMATION

Corresponding Author

*Tel.: + 38659099701, e-mail: branka.mozetic@ung.si.

Funding

This work was financially supported by the Slovenian Research Agency (ARRS), the World Federation of Scientists (WFS), and the Slovenian L'OREAL-UNESCO program for 'Women in Science', and partially performed within the Creative Core program (AHA-MOMENT) with contract no. 3330-13-500031, cosupported by RS-MIZS and the European Regional Development Fund.

Notes

The authors declare no competing financial interest.

■ REFERENCES

(1) Obied, H. K.; Bedgood, D. R., Jr; Prenzier, P. D.; Robards, K. Chemical screening of olive biophenol extracts by hyphenated liquid chromatography. *Anal. Chim. Acta* **2007**, *603*, 176−189.

(2) Obied, H. K.; Allen, M. S.; Bedgood, D. R.; Prenzler, P. D.; Robards, K.; Stockmann, R. Bioactivity and analysis of biophenols recovered from olive mill waste. *J. Agric. Food Chem.* **2005**, *53*, 823−837.

(3) Obied, H. K.; Bedgood, D. R., Jr; Prenzler, P. D.; Robards, K. Bioscreening of Australian olive mill waste extracts: biophenol content, antioxidant, antimicrobial and molluscicidal activities. *Food Chem. Toxicol.* **2007**, *45*, 1238−1248.

(4) Servili, M.; Selvaggini, R.; Esposto, S.; Taticchi, A.; Montedoro, G.; Morozzi, G. Health and sensory properties of virgin olive oil hydrophilic phenols: agronomic and technological aspects of production that affect their occurrence in oil. *J. Chromatogr. A* **2004**, *1054*, 113−127.

(5) Rodis, P. S.; Karathanos, V. T.; Mantzavinou, A. Partitioning of olive oil antioxidants between oil and water phases. *J. Agric. Food Chem.* **2002**, *50*, 596−601.

(6) Jerman Klen, T.; Mozetič Vodopivec, B. The fate of olive fruit phenols during commercial olive oil processing: traditional press versus continuous two- and three-phase centrifuge. *LWT—Food Sci. Technol.* **2012**, *49*, 267−274.

(7) Servili, M.; Baldioli, M.; Mariotti, F.; Montedoro, G. Phenolic composition of olive fruit and virgin olive oil: distribution in the constitutive parts of fruit and evolution during the oil mechanical extraction process. *Acta Hortic.* **1999**, *474*, 609−613.

(8) Gómez-Rico, A.; Inarejos-García, A. M.; Desamparados Salvador, M.; Fregapane, G. Effect of malaxation conditions on phenol and volatile profiles in olive paste and the corresponding virgin olive oils (Olea europaea L. Cv. Cornicabra). *J. Agric. Food Chem.* **2009**, *57*, 3578−3595.

(9) Goldsmith, C. D.; Stathopoulos, C. E.; Golding, J. B.; Roach, P. D. Fate of the phenolic compounds during olive oil production with the traditional press method. *Int. Food Res. J.* **2014**, *21*, 101−109.

(10) Artajo, L. S.; Romero, M. P.; Tovar, M. J.; Motilva, M. J. Effect of irrigation applied to olive trees (*Olea europaea* L.) on phenolic compound transfer during olive oil extraction. *Eur. J. Lipid Sci. Technol.* **2006**, *108*, 19−27.

(11) Artajo, L. S.; Romero, M. P.; Motilva, M. J. Transfer of phenolic compounds during olive oil extraction in relation to ripening stage of the fruit. *J. Sci. Food Agric.* **2006**, *86*, 518−527.

DOI: 10.1021/jf506353z
J. Agric. Food Chem. 2015, 63, 4570−4579

(12) Artajo, L. S.; Romero, M. P.; Suárez, M.; Motilva, M. J. Partition of phenolic compounds during the virgin olive oil industrial extraction process. *Eur. Food Res. Technol.* **2007**, *225*, 617−625.
(13) Jerman Klen, T.; Golc Wondra, A.; Vrhovšek, U.; Mozetič Vodopivec, B. Phenolic profiling of olives and their olive oil process-derived matrices by UPLC-DAD-ESI-QTOF-HRMS analysis. *J. Agric. Food Chem.* **2015**, *63*, 3859.
(14) Jerman, T.; Trebše, P.; Mozetič Vodopivec, B. Ultrasound-assisted solid liquid extraction (USLE) of olive fruit (*Olea europaea*) phenolic compounds. *Food Chem.* **2010**, *123*, 175−182.
(15) Jerman Klen, T.; Mozetič Vodopivec, B. Ultrasonic extraction of phenols from olive mill wastewater: comparison with conventional methods. *J. Agric. Food Chem.* **2011**, *59*, 12725−12731.
(16) Jerman Klen, T.; Mozetič Vodopivec, B. Optimisation of olive oil phenol extraction conditions using a high-power probe ultra-sonication. *Food Chem.* **2012**, *134*, 2481−2488.
(17) Lesage-Meessen, L.; Navarro, D.; Maunier, S.; Sigoillot, J.-C.; Lorquin, J.; Delattre, M.; Simon, J.-L.; Asther, M.; Labat, M. Simple phenolic content in olive oil residues as a function of extraction systems. *Food Chem.* **2001**, *75*, 501−507.
(18) Inarejos-García, A. M.; Fregapane, G.; Desamparados Salvador, M. Effect of crushing on olive paste and virgin olive oil minor components. *Eur. Food Res. Technol.* **2011**, *232*, 441−451.
(19) Parenti, A.; Spugnoli, P.; Masella, P.; Calamai, L. The effect of malaxation temperature on the virgin olive oil phenolic profile under laboratory-scale conditions. *Eur. J. Lipid Sci. Technol.* **2008**, *110*, 735−741.
(20) Ryan, D.; Prenzler, P.; Lavee, S.; Antolovich, M.; Robards, K. Quantitative changes in phenolic content during physiological development of the olive (Olea europaea) cultivar Hardy's Mammoth. *J. Agric. Food Chem.* **2003**, *51*, 2532−2538.
(21) Herrera, C. G. Matter transfer during virgin olive oil elaboration. *Grasas Aceites* **2007**, *58*, 194−205.
(22) Vierhuis, E.; Servili, M.; Baldioli, M.; Schols, H. A.; Voragen, A. G. J.; Montedoro, G. Effect of enzyme treatment during mechanical extraction of olive oil phenolic compounds and polysaccharides. *J. Agric. Food Chem.* **2001**, *49*, 1218−1223.
(23) Boselli, E.; Di Lecce, G.; Strabbioli, R.; Pieralisi, G.; Frega, N. G. Are virgin olive oils obtained below 27 °C better than those produced at higher temperatures? *LWT—Food Sci. Technol.* **2009**, *42*, 748−757.
(24) Fernández-Bolaños, J.; Felizón, B.; Brenes, M.; Guillén, R.; Heredia, A. Hydroxytyrosol and tyrosol as the main compounds found in the phenolic fraction of steam-exploded olive stones. *J. Am. Oil Chem. Soc.* **1998**, *75*, 1643−1649.
(25) López, O. J. M.; Innocenti, M.; Ieri, F.; Giaccherini, C.; Romani, A.; Mulinacci, N. HPLC/DAD/ESI/MS detection of lignans from Spanish and Italian Olea europeaea L. fruits. *J. Food Compos. Anal.* **2008**, *21*, 62−70.

DOI: 10.1021/jf506353z
J. Agric. Food Chem. 2015, 63, 4570−4579

Previous reports have revealed that flavanone had better antioxidant ability than flavone because the single bond between C2 and C3 in flavanone had more flexibility than the double bond in flavones, which allowed cells to easily take up the compound.[20] Therefore, this study further focuses on their antioxidant activity as affected by the hydroxyl group found on the B-ring of flavanone structures. In this study, macrophage cell (RAW264.7), the main producer of superoxide, was used as cell model. Phorbol ester, phorbol 12-myristate 13-acetate (PMA), was used to stimulate superoxide production. Pinocembrin, naringenin, and eriodictyol, containing no, one, and two hydroxyl groups on their B-ring (Figure 1), respectively, were investigated for their antioxidant activity

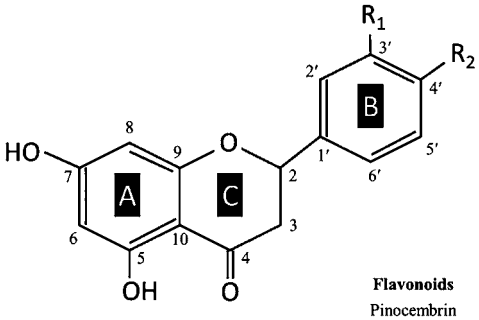

Flavonoids	R_1	R_2
Pinocembrin	H	H
Naringenin	H	OH
Eriodictyol	OH	OH

Figure 1. General molecular structure of flavanone. Numbers reflect position of carbon skeleton. A, B, and C indicate the name of carbon rings of flavonoid molecular structure. Pinocembrin, naringenin, and eriodictyol have different numbers of substituting hydroxyl groups to R_1 and R_2 position on the B-ring.

by various in vitro assays including scavenging activity, reactive oxygen species (ROS) inhibition, and protein immunoblotting. Finally, in silico analysis was introduced to this research to simulate interaction between the flavonoids and PKCδ phorbol ester binding site. Altogether, the results would indicate the influence of flavonoid structure on antioxidant activity at the molecular level and serve as a further guide on how to improve the efficiency of flavonoids.

MATERIALS AND METHODS

Chemicals. Pinocembrin, naringenin, eriodictyol, PMA, 2′,7′-dichlorodihydrofluorescein diacetate (DCFH-DA), dimethyl sulfoxide (DMSO), 2,2-diphenyl-1-picrylhydrazyl (DPPH), and butylated hydroxyanisole (BHA) were purchased from Sigma-Aldrich (St. Louis, MO, USA). Fetal bovine serum (FBS) and antibiotics were obtained from Biological Industries (Haemek, Israel). Dulbecco's modified Eagle's medium (DMEM) and 3-(4,5-dimethylthiazol-2-yl)-2,5-diphenyltetrazolium bromide (MTT) were bought from Gibco BRL (Grand Island, NY, USA) and AppliChem (Saxony-Anhalt, Germany), respectively.

Cell Culture and Treatments. Macrophage RAW264.7 cells were purchased from Bioresource Collection and Research Center, Taiwan. DMEM, supplemented with 10% FBS and 0.5% antibiotics (v/v), was used to culture the cells in a 10 cm Petri dish (Corning, New York, USA). The cells were incubated in a humidified incubator at 37 °C under 5% CO_2 and 95% air and subcultured every 2 days. Cell culture preparation before treatments was done by seeding cells at 1×10^6 cells/well into 96-well plates for cell viability assay or into 6-well plates for other assays. The seeded cell culture was allowed to acclimate for 12 h at 37 °C under 5% CO_2 before the flavonoid treatments.

Cell Viability Assay. MTT assay was used to investigate cytotoxicity effects of the flavonoids. RAW264.7 cell culture was prepared in 96-well plates as described under Cell Culture and Treatments. Each flavonoid at final concentrations of 10, 50, 100, and 200 μM in an appropriate amount of DMSO was added to the cell culture. After 24 h of the flavonoid treatments, the medium was discarded and MTT solution was added into each well. The plate was placed in the dark at room temperature for 3 h. Finally, DMSO was added to dissolve the purple formazan compound for 30 min, and the optical density (OD) was observed at 570 nm by ELISA reader (VersaMax microplate reader, Molecular Devices, San Francisco, CQA, USA). Ten replicates from each experiment were measured for the OD, and each experiment was repeated three times.

Measurement of DPPH Radical Scavenging Activity. The method to determine the scavenging activities of the flavonoids was adapted from that of Chao et al.[21] Briefly, 250 μL of 1 mM DPPH solution in methanol was added to 2 mL of 10 μM flavonoid solution. The mixture was shaken vigorously, allowing the reaction to proceed for 30 min in the dark, after which the absorbance was measured at 517 nm. The calculation of the scavenging activity was done by using the following formula where A_B and A_S are the absorbance of blank and sample, respectively. BHA was used as standard in this assay. The DPPH scavenging activity of each flavonoid was determined in triplicate.

$$\text{radical scavenging activity (\%)} = \left(\frac{A_B - A_S}{A_B}\right) \times 100$$

Reactive Oxygen Species (ROS) and IC_{50} Determination. Flow cytometer (FACSCaliburTM, BD Biosciences, Canada) was used to analyze ROS inhibition by the flavonoids. After 12 h of cell culture acclimation in 6-well plates, each flavonoid was added into each well (final concentration = 10 μM) for 24 h. PMA (final concentration = 100 ng/mL) was added at the last 30 min of the flavonoid treatment to induce the ROS production. Cells were washed twice by phosphate buffer saline (PBS) and harvested by using a cell scraper. Cell suspension was centrifuged at 500g (4 °C) for 5 min to obtain cell pellet. Cell pellet was incubated with 10 μM DCFH-DA at 37 °C in the dark for 30 min. After that, fluorescent intensity of dichlorodihydrofluorescein (DCF) was observed under FL-1 mode of the flow cytometer. Area gating was done in dot plot under E-1 mode, where >90% of cells were located inside the gated area. Data were collected from 10000 gated cells. The definition of IC_{50} is the flavonoid concentration required to inhibit half or 50% of PMA-induced ROS production. The IC_{50} was calculated using linear regression of ROS inhibition (%) from three different concentrations of each flavonoid. This assay was repeated five times for each experiment.

Proteins Immunoblotting Assay. RAW264.7 cells were treated with the flavonoids as described under Reactive Oxygen Species (ROS) and IC_{50} Determination. The cells were harvested and membrane proteins were collected and quantified using Mem-PER Plus Membrane Protein extraction kit and BCA protein assay kit (Thermo Scientific, Rockford, IL, USA), respectively, with bovine serum albumin as standard. Equal amounts of protein (30 μg) were loaded into each lane of 8% SDS–polyacrylamide gel, and protein separation was done by applying 110 V for 110 min. Polyvinylidene-fluoride (PVDF) membrane (PerkinElmer, Boston, MA, USA) was used to embed proteins from the gel through transfer process at 250 mA for 1 h. The membrane was blocked with blocking buffer and subjected to primary target antibodies (1:1000), phosphor-PKCδ Thr505, β-actin, (Cell Signaling, Beverly, MA, USA), and phosphor-p47 (Assay Biotech, San Diego, CA, USA), for 16–18 h at 4 °C. After that, the membranes were washed by TBST buffer for 1 h and subjected to diluted 1:5000 secondary antibodies (Merck Millipore, Bedford, MA, USA) for 1 h at room temperature. The membranes were washed again by TBST buffer for 1 h, and the protein bands were revealed with enhanced chemiluminescence reagent (ECL, Advansta, Menlo Park, CA, USA).

Molecular Docking. Docking study was performed in Accelrys Discovery Studio Visualizer version 3.0. Phorbol binding site, C1B domain, of PKCδ at 1.95 Å resolution and ligands were downloaded from RCSB Protein Data Bank (PDB code 1PTQ) and National

DOI: 10.1021/acs.jafc.5b00312
J. Agric. Food Chem. 2015, 63, 4580–4586

Center for Biotechnology Information (NCBI), respectively. All small molecules surrounding PKCδ structure including water molecules and phorbol ester ligand were removed for docking preparation. Molecules' energy was minimized by CHARMm program. Binding site of C1B domain was defined by using glycine 253 coordinate (*x*, 7.104; *y*, 24.326; and *z*, 27.682). The docking process was done by using the docking optimization CDOCKER tool in the software. The best 10 poses based on -CDOCKER_energy were obtained from docking, and hydrogen bond interactions between the ligands and amino acids in the receptor were sequentially visualized.

Statistical Analysis. Experimental results were used for analysis of variance using the Statistical Package for the Social Sciences (SPSS) computer program version 19. Significant differences between means were determined by Duncan's multiple-range test or Student's *t* test ($p < 0.05$).

RESULTS AND DISCUSSION

Cytotoxicity of Pinocembrin, Naringenin, and Eriodictyol in RAW264.7 Cells. Macrophages are well-known for their involvement in the immunological responses by producing superoxide compounds. Besides, it was reported that macrophages are targeted for oxidative stress therapeutic approaches.[22] Thus, murine macrophage RAW264.7 cells were used as cell model to evaluate oxidative stress level in this study. The influence of three flavonoids, pinocembrin, naringenin, and eriodictyol, on RAW264.7 cell viability was evaluated (Figure 2). After 24 h of exposure to the test compounds, it was found

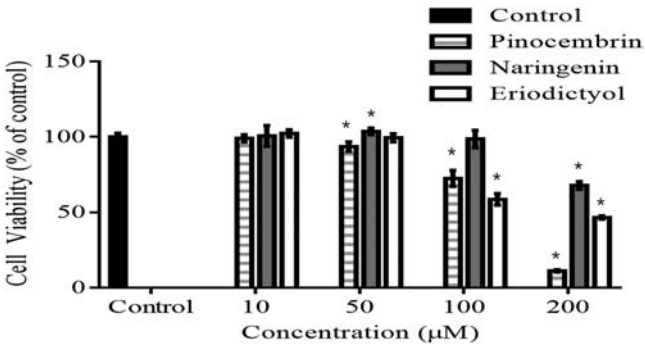

Figure 2. Cytotoxicity of pinocembrin, naringenin, and eriodictyol in RAW264.7 macrophage cells. RAW264.7 cells were treated with 0−200 μM of the flavonoids for 24 h. MTT was used to determine the viability of the cells after treatments. Optical density was measured at 570 nm. The experiments were performed with 10 replicates and were repeated three times. The values are expressed as mean ± standard deviation, and asterisks (∗) mark significant difference between each treatment and control group by Student's *t* test ($p < 0.05$).

that the highest concentrations of pinocembrin, naringenin, and eriodictyol, which did not significantly affect cell viability of in RAW264.7 cells, were 10, 100, and 50 μM, respectively. Previous literature reported similar results with different cell lines in which the highest concentrations of pinocembrin, naringenin, and eriodictyol were 10, 100, and 50 μM, in Y-79, microglia, and U937 cells, respectively.[23−25] In addition, it was also found that naringenin was the least toxic compound to RAW264.7 cells. Naringenin exhibited higher numbers of live cells than other flavonoids at concentrations between 50 and 200 μM, especially at 100 μM where the other two flavonoids significantly ($p < 0.05$) caused cell death. Finally, it was found that all flavonoids at 10 μM did not significantly affect cell viability. Therefore, the other assays in this research were conducted with flavonoid concentration at 10 μM.

Radical Scavenging of the Flavonoids. Pinocembrin, naringenin, and eriodictyol at 10 μM were tested for their scavenging activity. As shown in Figure 3, naringenin performed slightly higher scavenging activity than pinocembrin, but significantly higher activity ($p < 0.05$) was exhibited by eriodictyol over both pinocembrin and naringenin. The results from this assay were similar to those of Ye et al.,[26] where the number of hydroxyl groups on the B-ring was increased through the hydroxylation of naringin by *Trichoderma harzianum*. Adding one hydroxyl group to the B-ring of naringin could reduce the concentration of the compound by 40 times, whereas the DPPH scavenging activity remained at the same level.[26] Moreover, when two hydroxyl groups were added to the naringin, the scavenging activity was higher than when only one hydroxyl group was added.[26] Besides, the positions of hydroxyl groups on the B-ring also greatly contributed to the scavenging activity. Thavasi et al.[27] and Zhang et al.[28] illustrated that the addition of a hydroxyl group to the ortho position of phenol reduced O−H bond dissociation enthalpy (BDE) by 17.5 and 30.1 kJ/mol, respectively. On the other hand, addition to the meta position did not reduce the BDE.[27] Therefore, the greater number of hydroxyl groups and their ortho arrangement on the B-ring both made eriodictyol superior over pinocembrin and naringenin with regard to their scavenging ability.

Flavonoids Reduced ROS Production in PMA-Activated RAW264.7 Cells. Inhibition of ROS production in RAW264.7 was determined on the basis of the DCFH-DA principle. In brief, deacetylated DCFH-DA reacts with ROS compounds resulting in DCF, which can be detected by the FL-1 channel of flow cytometer. From this experiment, activated cells, treated with eriodictyol, had the lowest ROS level, followed by naringenin and pinocembrin, respectively (Figure 3). Furthermore, statistical analysis indicated that the three flavonoids could significantly reduce ($p < 0.05$) the ROS production compared with PMA-induced RAW264.7 cell (positive control). In addition, comparing the inhibition activity of each flavonoid, pinocembrin and naringenin showed similar ROS reduction. On the other hand, the inhibitory efficiency of eriodictyol was significantly higher ($p < 0.05$) than that of pinocembrin and naringenin. This implied that the two hydroxyl groups on the B-ring of eriodictyol had remarkable effects on the ROS reduction when compared to the lower number of hydroxyl groups on pinocembrin and naringenin. The reason was because the hydroxyl group on the B-ring acts as a hydrogen donor to stabilize radical species;[29] however, the presence of one hydroxyl group on the B-ring provides only little benefit to the antioxidant activity.[30] Thus, one hydroxyl group on the B-ring of naringenin could not importantly enhance ROS inhibition compared to pinocembrin. IC_{50} values of pinocembrin, naringenin, and eriodictyol were 44.9 ± 0.57, 30.2 ± 0.61, and 17.4 ± 0.40 μM, respectively (Supporting Information).

Flavonoids Reduced Oxidative Stress by Inhibiting Phosphorylation of PKC-δ and p47 in RAW264.7 Cells. From this assay, phosphor-PKCδ and phosphor-p47 expression at lipid raft were observed. PKCδ, a member of novel PKCs group originally located in cytoplasm, was found to be heavily phosphorylated compared to other PKC isoforms[31] and translocated to cell membrane when RAW264.7 cells were activated by PMA.[32] In addition, NADPH oxidase regulatory subunit, $p47^{phox}$, was found to be activated by phosphorylated PKC isoforms.[33] Overactivation of NADPH oxidase is one of

DOI: 10.1021/acs.jafc.5b00312
J. Agric. Food Chem. 2015, 63, 4580−4586

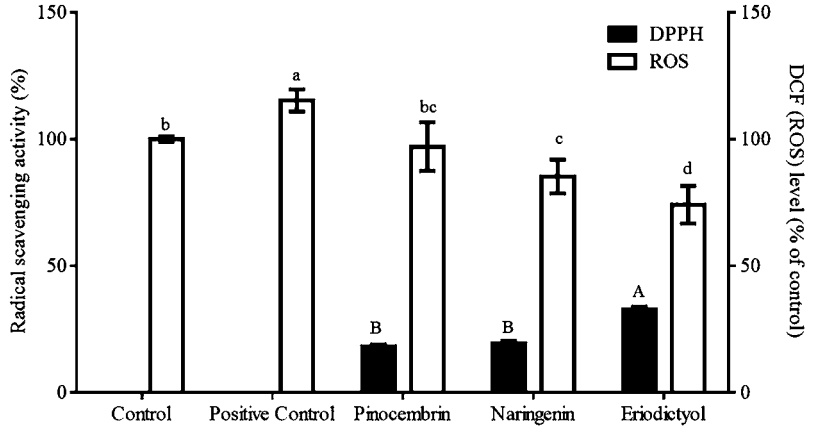

Figure 3. Radical scavenging activity of pinocembrin, naringenin, and eriodictyol at 10 μM concentration (black bars) and their reduction of ROS production in PMA-activated RAW264.7 cell (white bars). Cells were treated with the flavonoids for 24 h prior to 30 min of PMA activation. Cells without flavonoid treatment prior to PMA activation were named as positive control. The values were expressed as mean ± standard deviation from at least three individual experiments. Different letters indicate the significant difference in each group with other treatments ($p < 0.05$, Duncan test).

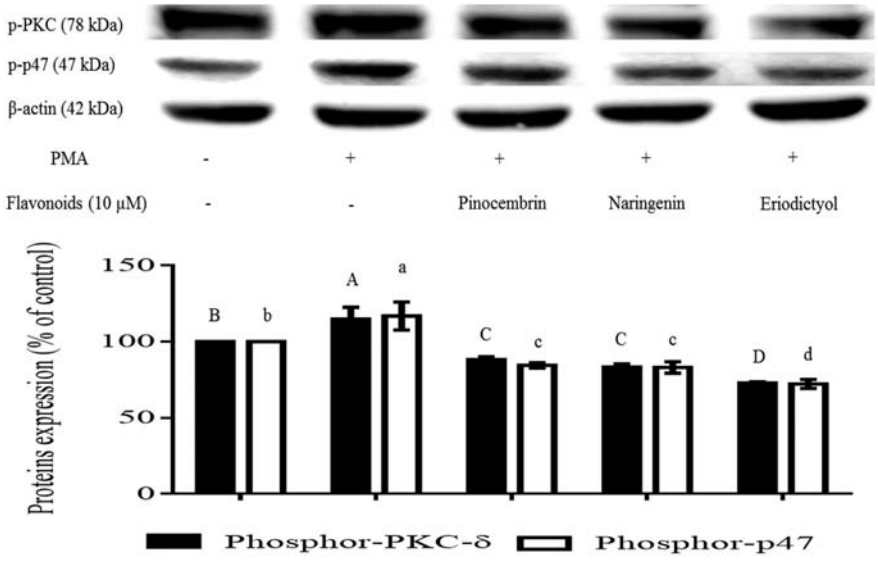

Figure 4. Flavonoids inhibited PKCδ activation to cell membrane. Pinocembrin, naringenin, and eriodictyol at 10 μM concentration were treated to 1×10^6 cells RAW264.7 macrophage cells for 24 h prior to 30 min of PMA activation. The values were expressed as mean ± standard deviation. Three replicates were done for each treatment. Different letters indicate the significant difference in each group with other treatments ($p < 0.05$, Duncan test).

the oxidative stress sources,[34] so the expression of phosphor-p47^{phox} at cell membrane is useful to determine the oxidative stress level. The results showed that all three flavonoids could significantly reduce ($p < 0.05$) phosphor-PKCδ and phosphor-p47^{phox} expressions in PMA-activated RAW264.7 cell membrane (Figure 4). Pinocembrin and naringenin inhibited the phosphorylation of both proteins at similar efficiencies, whereas eriodictyol performed significantly higher ($p < 0.05$) inhibition activity than pinocembrin and naringenin. The PKC inhibition activity of two hydroxyl groups on the B-ring over one hydroxyl group was similar to previous studies in which luteolin and quercetin showed higher PKC inhibition levels than apigenin and kaempferol for flavones and flavonols, respectively.[35]

Binding Mechanisms of the Flavonoids to PKCδ Phorbol Ester Binding Site. The phorbol ester binding site of PKCδ was well-defined at Tyr-238, Met-239, Ser-240, Pro-241, Thr-242, Phe-243, Leu-250, Leu-251, Trp-252, Gly-253, Leu-254, and Gln-257 of the C1B domain.[36] Phorbol esters bind and activate PKCδ function by forming three hydrogen bonds between C3 oxygen and hydrogen atom of Gly-253, between C4 hydroxyl group and the oxygen atom of Gly-253, and between the C20 hydroxyl group and Thr-242 and Leu 251.[36,37] Gly-253 is a key amino acid for phorbol ligand,[37] so Gly-253's coordinate was set up to be used as binding site for docking with ligands in this study. After the computational calculation, the best poses of pinocembrin, naringenin, and eriodictyol docking with the binding site had -CDOCKER_-energy values of 15.22, 16.95, and 21.49, respectively (Table 1). From the results, all flavonoids could bind with the phorbol ester binding site of PKCδ in which eriodictyol was the most favorable flavonoid in this study, and pinocembrin, on the other hand, had the poorest interaction. As shown in Table 1, all three flavonoids had different hydrogen bonding characteristics with the PKCδ C1B domain. Pinocembrin could form a hydrogen bond only between the hydrogen atom of the hydroxyl group at C7 and the oxygen atom of Ser-240.

DOI: 10.1021/acs.jafc.5b00312
J. Agric. Food Chem. 2015, 63, 4580−4586

Table 1. Hydrogen Bonding Characteristics from Docking Simulation between Phorbol Ester or the Best Pose of Each Flavonoid with C1B Domain of PKCδ at Phorbol Ester Binding Site

		hydrogen bonding	
ligand	-CDOCKER_energy	amino acid residue	distance (Å)
phorbol ester[a]	N/M[b]	Gly-253	N/M
		Leu-251	N/M
		Thr-242	N/M
pinocembrin	15.22	Ser-240	2.22
naringenin	16.95	Gly-253	2.21
		Leu-251	1.84
eriodictyol	21.49	Gly-253	2.1
		Leu-251	1.92
		Ser-240	2.24

[a]Reported by Majhi et al.[36] and Zhang et al.[37] [b]N/M, not measured.

Naringenin had a similar interaction by forming two hydrogen bonds between the oxygen atom in the carbon backbone of the C-ring and Gly-253 and between the C7 hydroxyl group and Leu-251. The single hydroxyl group on the B-ring of naringenin did not form any interaction with PKCδ. For eriodictyol, three hydrogen bonding bridges were built. The first bridge was the same as the first hydrogen bond in naringenin. The second and the third bridges were created between hydrogen atoms from two hydroxyl groups on the B-ring with Leu-251 and Ser-240 (Figure 5A). Interestingly, when two hydroxyl groups were available on the B-ring, the ligand (eriodictyol) turned the B-ring side to bind with the binding site (Figure 5D) rather than the A-ring as occurred with pinocembrin and naringenin (Figure 5B,C). This allowed the two hydroxyl groups to form hydrogen bonds with the kinase and strengthened the interaction. Although the catechol structure (B-ring) was reported to have lower hydrogen-bonding donor parameter than resorcinol ring (A-ring),[38] it was probably the distance between two hydroxyl groups of the resorcinol ring that did not

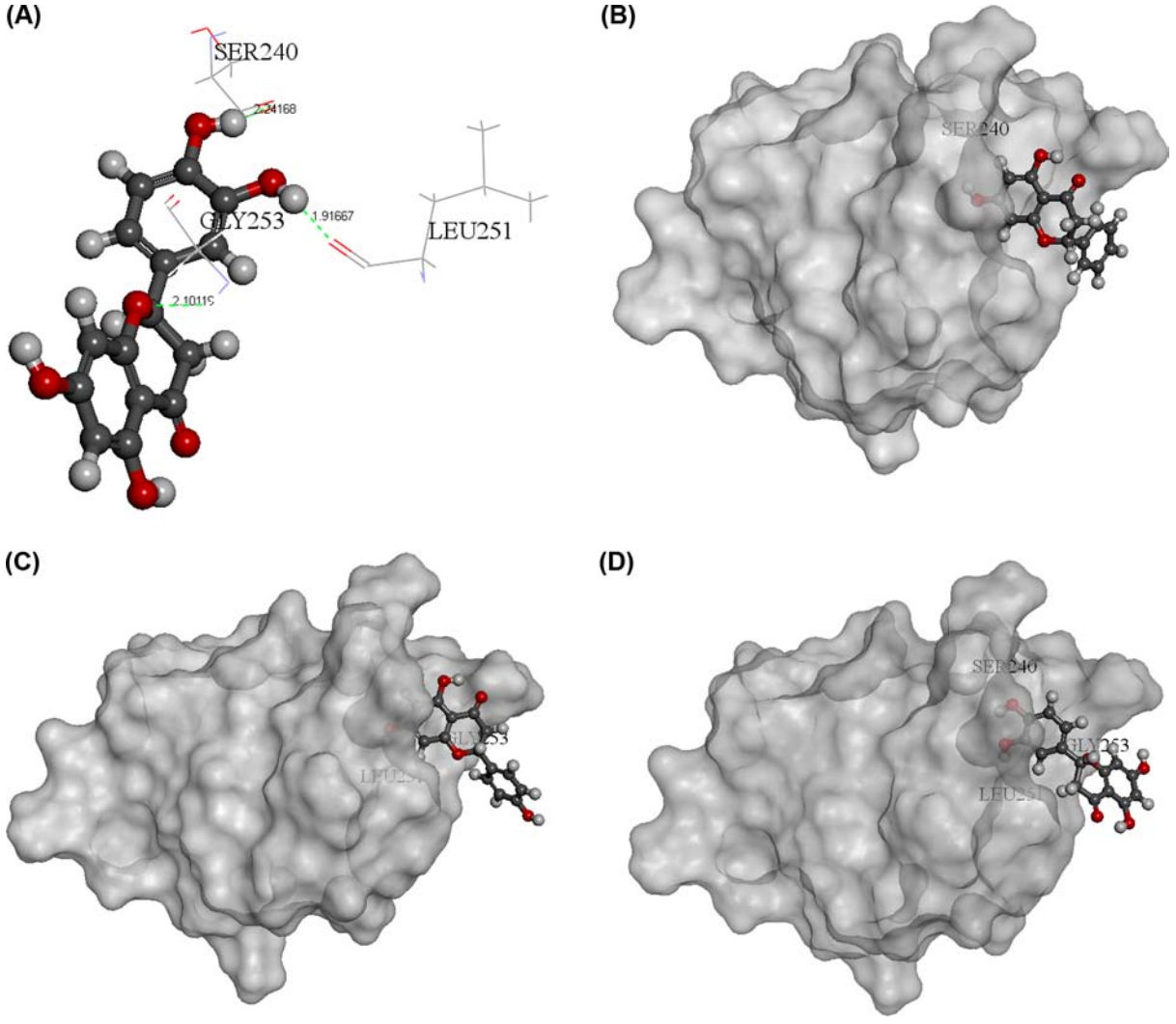

Figure 5. Docking simulation between flavonoids; pinocembrin, naringenin, and eriodictyol and C1B domain of PKCδ at phorbol ester binding site by Accelrys Discovery Studio Visualizer software. All flavonoid structures are represented in ball and stick type. Carbon, oxygen, and hydrogen atoms are colored in dark gray, red, and light gray, respectively. (A) Hydrogen-bonding interaction (green dashed lines) between the best pose of eriodictyol and PKCδ C1B domain amino acids (light gray lines). Numbers indicate hydrogen bonding lengths. (B, C, D) Illustrations of the best pose of pinocembrin, naringenin, and eriodictyol, respectively, docking with surface of PKCδ C1B phorbol ester binding site (painted with transparent gray) from -CDOCKER_energy values.

DOI: 10.1021/acs.jafc.5b00312
J. Agric. Food Chem. 2015, 63, 4580−4586

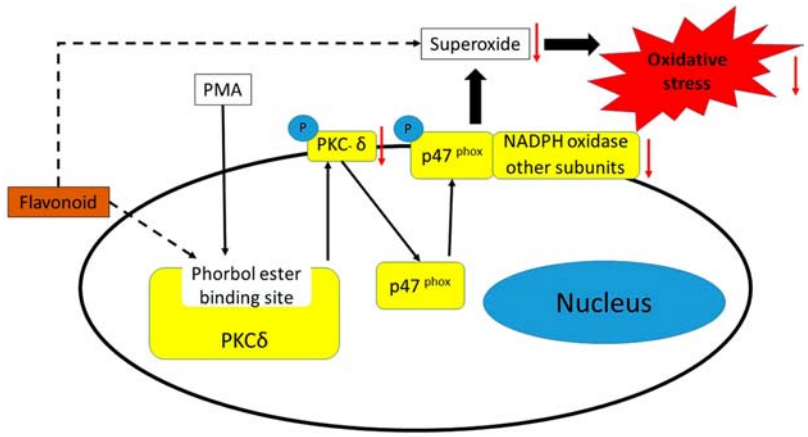

Figure 6. Flavonoid reduced oxidative stress in PMA-activated RAW264.7 by two approaches (dashed lines): neutralizing superoxide molecules and occupying PKCδ phorbol ester binding site.

fit with the amino acid residue arrangement at the binding site. Moreover, results also showed that the the C5 hydroxyl group of pinocembrin and naringenin could not form any hydrogen bond with the site. Thus, two ortho hydroxyl groups on the B-ring played a crucial role in forming a strong interaction with the binding site. The docking results correlated with the protein immunoblotting assays in which eriodictyol inhibited PKCδ activation better than pinocembrin and naringenin. Therefore, all three flavonoids could reduce oxidative stress by two ways (Figure 6, dashed lines). First, flavonoids directly neutralized the superoxide molecules. Second, the flavonoids could reduce the activation of PKCδ by phorbol esters by blocking the phorbol ester binding site. On the basis of both approaches, the number of substituted hydroxyl groups on the B-ring positively affects the antioxidant activity of the flavonoids.

■ ASSOCIATED CONTENT

Ⓢ Supporting Information

Supplementary figure of ROS inhibition activity of pinocembrin, naringenin, and eriodictyol from PMA-activated RAW264.7. The Supporting Information is available free of charge on the ACS Publications website at DOI: 10.1021/acs.jafc.5b00312.

■ AUTHOR INFORMATION

Corresponding Author

*(T.-C.H.) Phone: 886-8-7703202, ext. 5196. Fax: 886-8-7740594. E-mail: tchuang@mail.npust.edu.tw.

Funding

This work was financially supported by Taiwan National Science Council (NSC) grant (NSC 102-2923-B-020-001-MY2) and Taiwan ICDF.

Notes

The authors declare no competing financial interest.

■ REFERENCES

(1) Rahman, M. M.; Ichiyanagi, T.; Komiyama, T.; Sato, S.; Konishi, T. Effect of anthocyanins on psychological stress-induced oxidative stress and neurotransmitter status. *J. Agric. Food Chem.* **2008**, *56*, 7545−7550.

(2) Dinstel, R. R.; Casico, J.; Koukel, S. The antioxidant level of Alaska's wild berries: high, higher and highest. *Int. J. Circumpolar Health* **2013**, *72*, 796−802.

(3) Rajendran, P.; Nandakumar, N.; Rengarajan, T.; Palaniswami, R.; Gnanadhas, E. N.; Lakshminarasaiah, U.; Gopas, J.; Nishigaki, I. Antioxidants and human diseases. *Clin. Chim. Acta* **2014**, *436*, 332−347.

(4) Rochette, L.; Zeller, M.; Cottin, Y.; Vergely, C. Diabetes, oxidative stress and therapeutic strategies. *Biochim. Biophys. Acta, Gen. Subj.* **2014**, *1840*, 2709−2729.

(5) Butterfield, D. A.; Domenico, F. D.; Barone, E. Elevated risk of type 2 diabetes for development of Alzheimer disease: a key role for oxidative stress in brain. *Biochim. Biophys. Acta, Mol. Basis Dis.* **2014**, *1842*, 1693−1706.

(6) Marri, V.; Richner, H. Immune response, oxidative stress and dietary antioxidants in great tit nestlings. *Comp. Biochem. Physiol., Part A: Mol. Integr. Physiol.* **2015**, *179*, 192−196.

(7) Kazanietz, M. G. Novel "nonkinase" phorbol ester receptors: the C1 domain connection. *Mol. Pharmacol.* **2002**, *61*, 759−767.

(8) Kazanietz, M. G.; Caloca, M. J.; Eroles, P.; Fujii, T.; García-Bermejo, M. L.; Reilly, M.; Wang, H. B. Pharmacology of the receptors for the phorbol ester tumor promoters; multiple receptors with different biochemical properties. *Biochem. Pharmacol.* **2000**, *60*, 1417−1424.

(9) Fukahori, H.; Chida, N.; Maeda, M.; Tasaki, M.; Kawashima, T.; Matsuoka, H.; Suzuki, K.; Ishikawa, T.; Tanaka, A.; Higashi, Y. Effect of AS2521780, a novel PKC selective inhibitor, on T cell-mediated immunity. *Eur. J. Pharmacol.* **2014**, *745*, 217−222.

(10) Kikkawa, U.; Matsuzaki, H.; Yamamoto, T. Protein kinase Cδ: activation mechanisms and functions. *J. Biochem.* **2002**, *132*, 831−839.

(11) Hurley, J. H.; Newton, A. C.; Parker, P. J.; Blumberg, P. M.; Nishizuka, Y. Taxonomy and function of C1 protein kinase C homology domains. *Protein Sci.* **1997**, *6*, 477−480.

(12) Magiera, S.; Baranowska, I.; Lautenszleger, A. UHPLC-UV method for the determination of flavonoids in dietary supplements and for evaluation of their antioxidant activities. *J. Pharm. Biomed. Anal.* **2015**, *102*, 468−475.

(13) Akhavan, M.; Jahangiri, S.; Shafaghat, A. Studies on the antioxidant and antimicrobial activity and flavonoid derivatives from the fruit of *Trigonosciadium brachytaenium* (Boiss.) Alava. *Ind. Crops Prod.* **2015**, *63*, 114−118.

(14) Ravisshankar, D.; Rajora, A. K.; Greco, F.; Osborn, H. M. I. Flavonoids as prospective compounds for anti-cancer therapy. *Int. J. Biochem. Cell Biol.* **2013**, *45*, 2821−2831.

(15) Babu, P. V. A.; Liu, D.; Gilbert, E. R. Recent advances in understanding the anti-diabetic actions of dietary flavonoids. *J. Nutr. Biochem.* **2013**, *24*, 1777−1789.

(16) Geraets, L.; Haegens, A.; Brauers, K.; Haydock, J. A.; Vernooy, J. H. J.; Wouters, E. F. M.; Bast, A.; Hageman, G. J. Inhibition of LPS-induced pulmonary inflammation by specific flavonoids. *Biochem. Biophys. Res. Commun.* **2009**, *382*, 598−603.

(17) Zhou, H.; Lutterodt, H.; Cheng, Z.; Yu, L. Anti-inflammatory and antiproliferative activities of trifolirhizin, a flavonoid from *Sophora flavescens* roots. *J. Agric. Food Chem.* **2009**, *57*, 4580−4585.

DOI: 10.1021/acs.jafc.5b00312
J. Agric. Food Chem. 2015, 63, 4580−4586

(18) Scalbert, A.; Williamson, G. Dietary intake and bioavailability of polyphenols. *J. Nutr.* **2000**, *130*, 20735−20855.
(19) Ulrich-Merzenich, G.; Zeitler, H.; Vetter, H.; Kraft, K. Synergy research: Vitamins and secondary plant components in the maintenance of the redox-homeostasis and in cell signaling. *Phytomedicine* **2009**, *16*, 2−16.
(20) Huang, T. C.; Chang, J. Y.; Liu, H. J.; Tsai, S. S.; Chang, T. C.; Ho, C. T.; Chuang, K. P. Eriodictyol decreases reactive oxygen species (ROS) production and inhibits $p47^{phox}$ clustering and translocation in monocytes. *J. Food Biochem.* **2013**, *37*, 418−424.
(21) Chao, J. J.; Lo, D.; Panboon, N.; Wu, M. C. In vitro antioxidant capacity and antiproliferative effects of different parts and extractions from *Ajuga bracteosa* on HepG2 cell line. *Int. Res. J. Pharm. Pharmacol.* **2012**, *2*, 110−117.
(22) Matsebatlela, T. M.; Anderson, A. L.; Gallicchio, V. S.; Elford, H.; Rice, C. D. 3,4-Dihydroxy-benzohydroxamic acid (Didox) suppresses pro-inflammatory profiles and oxidative stress in TLR4-activated RAW264.7 murine macrophages. *Chem.−Biol. Interact.* **2015**, *233*, 95−105.
(23) Chen, K. S.; Shi, M. D.; Chien, C. S.; Shih, Y. W. Pinocembrin suppresses TGF-β1-induced epithelialmesenchymal transition and metastasis of human Y-79 retinoblastoma cells through inactivating $\alpha v\beta 3$ integrin/FAK/p38α signaling pathway. *Cell Biosci.* **2014**, *4*, 41−53.
(24) Chao, C. J.; Weng, C. S.; Chang, N. C.; Lin, J. S.; Kao, S. T.; Ho, F. M. Naringenin more effectively inhibits inducible nitric oxide synthase and cyclooxygenase-2 expression in macrophages than in microglia. *Nutr. Res. (N. Y., NY, U. S.)* **2010**, *30*, 858−864.
(25) Huang, T. C.; Tseng, K. Y.; Tsai, S. S.; Liu, H. J.; Ho, C. T.; Lin, H. Y.; Cheng, L. T.; Chuang, K. P. Eriodictyol decreases very late antigen-4 (VLA-4) expression, cellular adhesion, and migration through an NFκB-dependent pathway in monocytes. *J. Funct. Foods* **2010**, *2*, 263−270.
(26) Ye, H.; Xu, H.; Yu, C.; Dai, Y.; Liu, G.; Xu, W.; Yuan, S. Hydroxylation of naringin by *Trichoderma harzianum* to dramatically improve its antioxidative activity. *Enzyme Microb. Technol.* **2009**, *45*, 282−287.
(27) Thavasi, V.; Leong, L. P.; Bettens, R. P. A. Investigation of the influence of hydroxyl groups on the radical scavenging ability of polyphenols. *J. Phys. Chem. A* **2006**, *110*, 4918−4923.
(28) Zhang, H. Y.; Wang, X. L.; Sun, Y. M. Substituent effects on O-H proton dissociation enthalpies of catecholic cation radicals: a DFT study. *Internet Electron. J. Mol. Des.* **2003**, *2*, 262−273.
(29) Williams, R. J.; Spencer, J. P. E.; Rice-Evans, C. Serial review: Flavonoids and isoflavones (phytoestrogens): absorption, metabolism, and bioactivity. *Free Radical Biol. Med.* **2004**, *36*, 838−849.
(30) Rice-Evans, C. A.; Miller, N. J.; Paganga, G. Structure-antioxidant activity relationships of flavonoids and phenolic acids. *Free Radical Biol. Med.* **1996**, *20*, 933−956.
(31) Rajanbabu, V.; Chen, J. Y. The antimicrobial peptide, tilapia hepcidin 2-3, and PMA differentially regulate the protein kinase C isoforms, TNF-α and COX-2, in mouse RAW264.7 macrophages. *Peptides* **2011**, *32*, 333−341.
(32) Lin, W. W.; Chen, B. C. Distinct PKC isoforms mediate the activation of cPLA2 and adenylyl cyclase by phorbol ester in RAW264.7 macrophages. *Br. J. Pharmacol.* **1998**, *125*, 1601−1609.
(33) Zhao, K.; Huang, Z.; Lu, H.; Zhou, J.; Wei, T. Induction of inducible nitric oxide synthase increases the production of reactive oxygen species in RAW264.7 macrophages. *Biosci. Rep.* **2010**, *30*, 233−241.
(34) Silva, V.; Genta, G.; Möller, M. N.; Masner, M.; Thomson, L.; Romero, N.; Radi, R.; Fernandes, D. C.; Laurindo, F. R. M.; Heinzen, H.; Fierro, W.; Denicola, A. Antioxidant activity of Uruguayan propolis. In vitro and cellular assays. *J. Agric. Food Chem.* **2011**, *59*, 6430−6437.
(35) Gamet-Payrastre, L.; Manenti, S.; Gratacap, M. P.; Tulliez, J.; Chap, H.; Payrastre, B. Flavonoids and the inhibition of PKC and PI 3-kinase. *Gen. Pharmacol.* **1999**, *32*, 279−286.
(36) Majhi, A.; Rahman, G. M.; Panchal, S.; Das, J. Binding of curcumin and its long chain derivatives to the activator binding domain of novel protein kinase C. *Bioorg. Med. Chem.* **2010**, *18*, 1591−1598.
(37) Zhang, G.; Kazanietz, M. G.; Blumberg, P. M.; Hurley, J. H. Crystal structure of the Cys2 activator-binding domain of protein kinase Cδ in complex with phorbol ester. *Cell* **1995**, *81*, 917−924.
(38) Suresh, S.; Srivastava, V. M.; Mishra, I. M. Adsorption of catechol, resorcinol, hydroquinone, and their derivatives; a review. *Int. J. Energy Environ. Eng.* **2012**, *3*, 3−32.

DOI: 10.1021/acs.jafc.5b00312
J. Agric. Food Chem. 2015, 63, 4580−4586

study showed that SWE reduced oliec acid (OA)-induced hepatic lipid accumulation in HepG2 cells.[23] Therefore, in this study, we further investigated the anti-obesity effect of SWE in rats fed a high-fat diet (HFD). Adding caffeic acid (CA) and hesperetin (HPT), which are the main ingredients of SWE, also inhibit OA-induced lipid accumulation. In addition, animals fed with a HFD could serve as a model to attenuate hepatic lipid accumulation and evaluate the methods for healthcare foods for prevention of a fatty liver. The lipogenesis inhibitors could promote catabolism by downregulation of the activity of key enzymes of metabolism that account for the effect of healthcare foods.

MATERIALS AND METHODS

Materials. Fresh *S. edule* shoots and leaves were collected in Nantou county, located in central Taiwan. GPx, SOD, SREBP-1, SREBP-2, HMGCoR, PPARα, and carnitine palmitoyltransferase-1 (CPT-I) antibodies were obtained from Santa Cruz Biotechnology (Santa Cruz, CA). Anti-pThr172-AMPK, anti-AMPK, and FAS antibodies were purchased from Cell Signaling Technology (Beverly, MA). Anti-β-actin and anti-catalase antibodies were purchased from Sigma-Aldrich.

Preparation of SWE and Functional Polyphenol Extract from SWE. The fresh leaves were minced, air-dried under shade, and powdered for used. The extract prepared from 20 g of powder immersed in 1000 mL of distilled water under 4 °C for 24 h was filtered and lyophilized as the SWE with a yield of 17.24%. A total of 100 g of dried SWE powder was drenched with 300 mL of 50 °C methanol for 3 h. After refining 3 times, the extract was filtered and the solvent was removed from the combined extract using a vacuum rotary evaporator. The residue was dissolved in 500 mL of distilled water, removed the pigment with 200 mL of hexane, purified with 180 mL of ethyl acetate 3 times, and removed the solvent by a vacuum rotary evaporator. The residue was redissolved with distilled water and lyophilized to yield the powder as the polyphenol extracts of SWE (SWPE). The SWPE were analyzed for the presence and proportion of functional compounds by high-performance liquid chromatography (HPLC).

HPLC Analysis. HPLC was performed with a Hitachi HPLC system (Hitachi, Danbury, CT), which consisted of a pump (L-6200A), an ultraviolet detector (L-4250), and a Hitachi D-7000 HPLC system manager program. A systemic procedure for analyzing the phenolic acids contained a Mightysil RP-18 GP 250 column (Kanto, Tokyo, Japan), mobile phase solvent A [acetic acid/water (2:98, v/v)], and solvent B [0.5% acetic acid in water/acetonitrile (50:50, v/v)]. The flow rate was 1 mL/min. The gradient for the separation was 100% solvent A at 0 min, 70% solvent A and 30% solvent B at 5 min, 65% solvent A and 35% solvent B at 50 min, 60% solvent A and 40% solvent B at 55 min, and 0% solvent A and 100% solvent B at 60 min, followed by a 5 min post-run with HPLC-grade water. Phenolic acids were detected at 260 nm.

Animals and Treatment. The male Wistar rats (weight of 150 ± 10 g) obtained from the National Laboratory Animal Breeding and Research Center (Taipei, Taiwan) were housed and acclimated in laboratory conditions (23 ± 2 °C, 60 ± 5% relative humidity, and 12 h light/dark cycle) for at least 1 week before study. Different treatments of rats were divided into four groups (n = 10 per group) as follows: (A) normal meals (control), (B) HFD, (C) HFD + 0.5% SWE, and (D) HFD + 1.0% SWE. The composition of the HFD was 40% beef tallow, 26% casein, 15% corn starch, 9% sucrose, 5% cellulose, 4% mineral mixture, and 1% vitamin mixture.[24−28] The ratio of mineral and vitamin mixtures was according to AIN-93.[29] The metabolized energy of the control and HFD-fed rats, with or without SWE supplement, was 3.85 and 5.60 kcal/g, respectively. All rats, except the control group, were fed with the HFD for 12 weeks. The food intake of each rat was controlled as equal as possible. All rats were weighed every week. After the end of the experiment, animals were sacrificed to collect the blood sample and liver tissue. Serum was prepared and stored at −80 °C for further investigations, which were completed within 2 weeks. All animal experimental protocols used in this study were approved by the Institutional Animal Care and Use Committee of the Chung Shan Medical University (IACUC, CSMU), Taichung, Taiwan (IACUC Approval Number 885).

Hepatic Pathological Analysis. Liver tissues were fixed in 4% buffered paraformaldehyde overnight and embedded in paraffin. Consecutive paraffin sections were examined by hematoxylin and eosin (H&E) staining. Frozen sections were stained with Oil Red O and Sudan III reagents.[30,31] Then, the samples were analyzed by light microscopy (Nikon Eclipse, Nikon, Japan).

Blood Sample Analysis. Blood samples were collected into heparin tubes and immediately centrifuged at 3000g for 5 min at 4 °C. The serum was decanted and stored at 4 °C. Serum levels of total cholesterol, TGs, aspartate transaminase (AST), and alanine transaminase (ALT) were measured using clinical chemistry reagent kits (Randox Laboratories, Ltd., Antrim, U.K.). A free fatty acid (FFA) quantification kit (BioVision, Inc., Mountain View, CA) was performed to detect the FFA level of serum according to the protocol of the manufacturer.

Determination of Total Cholesterol and TGs in Liver. Fresh liver was collected for the extraction of liver lipids. Liver lipids were refined as described previously. Briefly, liver was homogenized with chloroform/methanol (1:2, v/v), and then chloroform and distilled water (1:1, v/v) were added to the homogenate and mixed well. The lipid extract was centrifuged at 1500g for 10 min, and the lower clear organic phase solution was transferred into a glass tube and then lyophilized. The lyophilized powder was dissolved in chloroform/methanol (1:2, v/v) as the liver lipid extract and stored at −20 °C. TGs and cholesterol in the lipid extracts were measured by enzymatic colorimetric methods using commercial kits (Human, Wiesbaden, Germany).

Preparation of the Protein Extract. The protein extracts of cultured cells or liver tissues were harvested in a cold RIPA buffer [1% NP-40, 50 mM Tris−base, 0.1% sodium dodecyl sulfate (SDS), 0.5% deoxycholic acid, and 150 mM NaCl at pH 7.5] containing proteinase inhibitor (17 μg/mL leupeptin and 10 μg/mL sodium orthovanadate). The cell lysates were vortexed at 4 °C for 4 h, and the liver tissues were homogenized on ice for 3 min. All protein extracts were then centrifuged at 10 000 rpm at 4 °C for 20 min. The protein concentration was measured with Coomassie blue (Kenlor Industries, Inc., Santa Ana, CA) using bovine serum albumin as a standard.

Western Blot Analysis. Protein samples (80 μg) were subjected to SDS−polyacrylamide gel electrophoresis and electrotransferred to nitrocellulose membranes (Millipore, Bedford, MA). Membranes were blocked with 5% non-fat milk powder/0.1% Tween-20 in Tris-buffered saline (TBS) and then hybridized with the primary antibody at 4 °C overnight. After washing with TBS 3 times, the secondary antibody was hybridized and conjugated to anti-mouse horseradish peroxidase (HRP) (GE Healthcare, Little Chalfont, U.K.) at room temperature for 1 h. HRP was activated by enhanced chemiluminescence (ECL) using ECL western blotting detection reagents and exposed ECL hyperfilm in Fujfilm LAS-3000 (Tokyo, Japan). Protein quantity was determined by densitometry using Fujfilm MultiGauge, version 2.2, software.

Cytotoxicity Assay. HepG2 cells were seeded at a density of 5 × 10^5 cells/mL in 24 well plates and incubated with OA, SWE, CA, or HPT at various concentrations. After 24 h, the medium containing (3-(4,5-dimethylthiazol-2-yl)-2,5-diphenyltetrazolium bromide) (MTT) reagent (0.5 mg/mL) was replaced and incubated for 4 h. Formazan was produced by viable cells, which was dissolved with isopropanol. The absorbance was read at 563 nm by a spectrophotometer (Beckman DU640).

Nile Red Stain. HepG2 cells were seeded in 6 well plates (2 × 10^6 cells/mL) and treated with 600 μM OA and the indicated concentration of SWE, CA, or HPT for 24 h. The cells were washed twice with phosphate-buffered saline (PBS) and fixed with 4% formaldehyde for 30 min. Cell were stained with 40 μg/mL Nile red at room temperature for 30 min. Lipid-bound Nile red fluorescence was

DOI: 10.1021/acs.jafc.5b00346
J. Agric. Food Chem. 2015, 63, 4587−4596

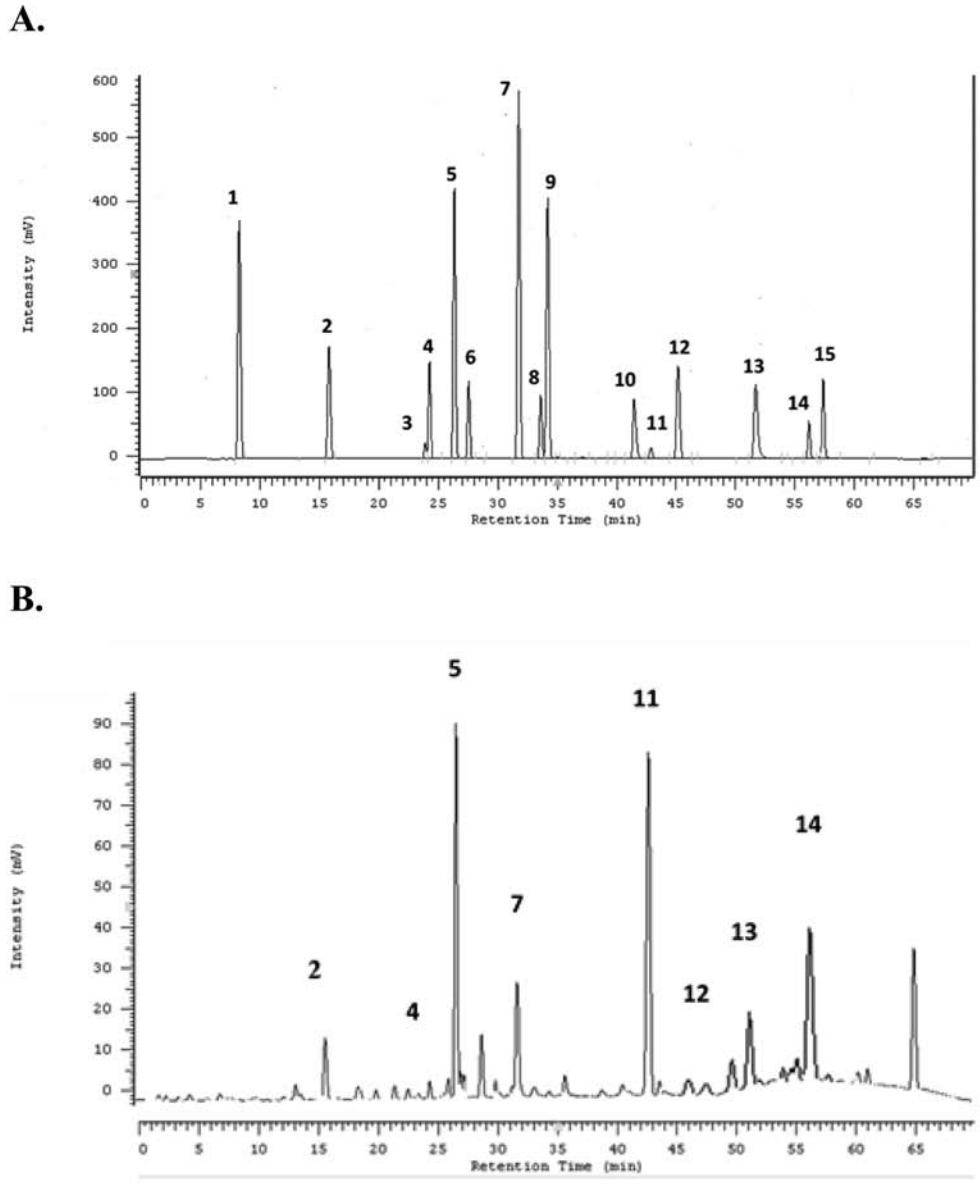

Composition of the phenolic compounds of SWPE by HPLC analysis

Peak no.	Assigned identity	Retention time (min)	Percentage (%)	Content in Sechium edule Shoot (mg/g dry weight)
2	PCA	15.87	3.56 ± 0.11	6.14
4	GCG	24.32	1.18 ± 0.12	2.03
5	CA	26.51	26.53 ± 0.28	45.74
7	p-CA	31.87	7.32 ± 0.24	12.61
11	HPT	42.69	23.44 ± 0.18	40.41
12	RV	45.17	0.61 ± 0.04	1.05
13	Q	51.97	4.18 ± 0.09	7.21
14	N	56.28	13.72 ± 0.14	23.65

Figure 1. (A) HPLC chromatogram of SWPE. HPLC chromatogram of 15 kinds of standard polyphenols. Peaks: 1, gallic acid (GA); 2, protocatechuic acid (PCA); 3, catechin (C); 4, gallocatechin gallate (GCG); 5, caffeic acid (CA); 6, epicatechin (EC); 7, *p*-coumaric acid (*p*-CA); 8, rutin (R); 9, ferulic acid (FA); 10, gossypin (G); 11, hesperetin (HPT); 12, resveratrol (RV); 13, quercetin (Q); 14, naringenin (N); and 15, hydroxyflavin (FlOH). (B) HPLC chromatogram of free polyphenols from SWPE.

DOI: 10.1021/acs.jafc.5b00346
J. Agric. Food Chem. 2015, 63, 4587−4596

Table 1. Effects of SWE on the Relative Body Weight Change of Rats with Obesity Induced by a HFD

		ND[a]	HFD	HFD + 0.5% SWE	HFD + 1.0% SWE
week	0	271.2 ± 24.43	274.1 ± 13.73	269.9 ± 13.25	266.0 ± 25.28
	4	358.8 ± 36.63[b] (32.80%)	448.6 ± 36.42[c] (63.58%)	441.2 ± 38.43 (63.96%)	433.5 ± 20.83 (64.70%)
	5	362.4 ± 35.93 (34.17%)	459.3 ± 38.62[c] (67.47%)	446.0 ± 22.96 (65.73%)	435.6 ± 35.12 (65.38%)
	6	365.9 ± 41.21 (35.53%)	470.1 ± 51.35[c] (71.34%)	450.8 ± 37.81 (67.50%)	437.6 ± 61.42 (66.05%)
	7	379.1 ± 28.48 (40.16%)	491.7 ± 41.66[c] (79.11%)	470.4 ± 36.62 (75.65%)	455.6 ± 40.47 (74.83%)
	8	392.2 ± 40.14 (44.78%)	511.1 ± 59.21[c] (86.88%)	493.9 ± 66.31 (83.79%)	481.5 ± 39.97 (83.60%)
	9	424.9 ± 23.90 (57.39%)	518.2 ± 22.32[c] (89.02%)	503.3 ± 34.97 (87.34%)	486.9 ± 34.97 (85.33%)
	10	457.0 ± 42.10 (69.98%)	523.3 ± 45.63[c] (91.15%)	512.7 ± 71.23 (90.898%)	492.2 ± 56.73 (87.04%)
	11	457.3 ± 31.81 (70.04%)	537.2 ± 37.50[c] (96.19%)	507.6 ± 45.57[d] (88.56%)	485.6 ± 44.11[d] (84.32%)
	12	457.5 ± 41.64 (70.10%)	551.0 ± 51.73[c] (101.23%)	502.5 ± 49.84[d] (86.22%)	479.0 ± 55.86[d] (81.59%)

[a]ND, normal diet group; HFD, rats fed a HFD-induced group; HFD + 0.5% SWE, rats fed a HFD with 0.5% SWE group; and HFD + 1.0% SWE, rats fed a HFD with 1.0% SWE group. [b]Data = [(week x − week 0)/week 0] × 100%. Each value is expressed as the mean ± standard deviation (SD) (n = 10/group). Results were statistically analyzed with a one-way ANOVA. [c]$p < 0.05$ compared to the ND group. [d]$p < 0.05$ compared to the HFD group.

measured and quantified the lipid content in cells by flow cytometry (Becton Dickinson, Mountain View, CA).

Statistical Analysis. Overall differences among groups were analyzed by one-way analysis of variance (ANOVA). When overall analysis demonstrated the presence of significant differences among all of the different groups studied, the differences between specific groups were tested using Duncan's multiple range test. All statistical analyses were performed using SigmaStat software (SPSS, Chicago, IL). $p < 0.05$ was considered statistically significant.

RESULTS

Functional Components of SWE. The presence and proportion of the main functional constituents of SWE were analyzed by HPLC. The HPLC results revealed that SWPE contained the presence of protocatechuic acid (PCA, 3.56 ± 0.11%), gallocatechin gallate (GCG, 1.18 ± 0.12%), caffeic acid (CA, 26.53 ± 0.28%), *p*-coumaric acid (*p*-CA, 7.32 ± 0.24%), hesperetin (HPT, 23.44 ± 0.18%), resveratrol (RV, 0.61 ± 0.04%), quercetin (Q, 4.18 ± 0.09%), and naringenin (N, 13.72 ± 0.14%) (Figure 1).

Effect of SWE on Body Weight of Rats Fed with a HFD. The effect of SWE on lipid homeostasis was examined. By feeding rats with HFD and the indicated concentration of SWE for 12 weeks, we compared relative body weight changes. In Table 1 and Figure 2, the rats fed with a HFD increased in weight in the entire experimental duration. In the termination of this experiment, the weight increased to 101.23%. Rats fed with 0.5 or 1.0% SWE decelerated the weight gain significantly at weeks 11 and 12. The results showed that feeding with SWE decreased weight gain in HFD-fed rats.

Effect of SWE on Body Fat Deposition. We further detected the lipid content of the liver in rats fed with a HFD or SWE (Table 2). First of all, we compared the weight of liver differences among different groups. The liver weight of rats fed a normal diet was 24.22 ± 3.08 g, and the liver weight of rats in the HFD group increased to 27.07 ± 2.09 g. After treating with 0.5 and 1.0% SWE, it was reduced to 23.54 ± 2.05 and 23.55 ± 3.21 g, respectively. Supplement of SWE significantly reversed the liver weight gain. The study also conducted weight variation of adipose tissue to evaluate whether SWE affected fat deposition. In Table 2, the results reveal that a HFD caused a significant increase in epididymal fat (23.27 ± 6.17 g), perirenal fat (40.01 ± 10.62 g), retroperitoneal fat (29.00 ± 10.70 g), and mesenteric fat (9.24 ± 2.53 g) in surrounding accumulation of adipose tissue compared to a ND, which means an increase in adipose tissue. However, 0.5 and 1.0% SWE showed a significant decrease in adipose tissue. The relative total fat was increased, while SWE reduced it even lower than the control. These results indicate that SWE inhibited adipose tissue fat deposition and obesity (Table 2).

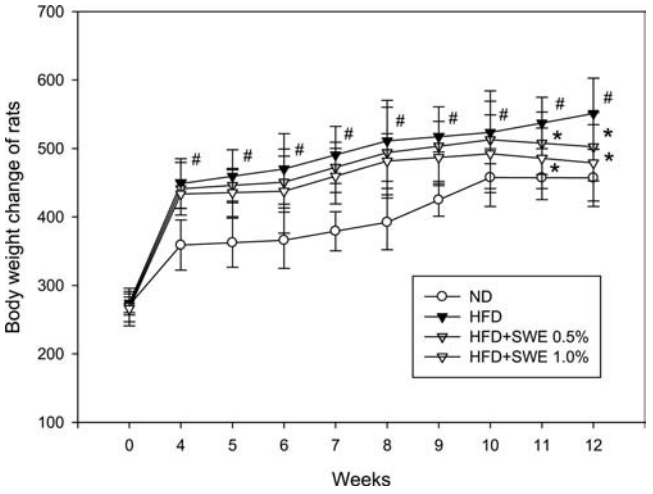

Figure 2. Effects of SWE on the body weight change of rats with obesity induced by a HFD. Body weight change versus time in rats fed various diets. All values are the means ± SD (n = 10). ND, normal group (rats fed normal chow); HFD, rats fed with 40% beef tallow. (#) $p < 0.05$ compared to the ND group. (∗) $p < 0.05$ compared to the HFD group.

Effects of SWE on the Serum Lipid and Hepatic Lipids of Rat Induced by a HFD. Because liver plays a critical role in metabolic regulations, we analyzed the hepatic content of cholesterol and TGs. After feeding SWE with both a HFD and 0.5 and 1.0% SWE for 12 weeks, animals were sacrificed and then the serum content of cholesterol, TG, and FFA were analyzed. As shown in Table 3, serum glucose, cholesterol, and FFA levels were elevated by a HFD. SWE reversed the serum levels of glucose and lipids, especially FFA. Merely 0.5% SWE exerted a profound effect of lowering of FFAs elevated by a HFD. A HFD increased low-density lipoprotein-cholesterol (LDL-C) and decreased high-density lipoprotein-cholesterol (HDL-C) and, thus, enhanced the LDL-C/HDL-C ratio. Supplementation of SWE effectively reversed the lipoprotein profiles. Noticeably, the analysis of AST, ALT, blood urea nitrogen (BUN), creatinine (CRE), electrolyte, and ketone

DOI: 10.1021/acs.jafc.5b00346
J. Agric. Food Chem. 2015, 63, 4587−4596

Table 2. Effects of SWE on the Weights of Organs and Adipose Tissue of Rats with Obesity Induced by a HFD

relative tissue weights (mg/g of rat)	ND	HFD	HFD + 0.5% SWE	HFD + 1.0% SWE
liver weight	24.22 ± 3.08[a]	27.07 ± 2.09[b]	23.54 ± 2.05[c]	23.55 ± 3.21[c]
epididymal fat	10.92 ± 1.84	23.27 ± 6.17[b]	17.90 ± 4.08[c]	17.49 ± 4.35[c]
perirenal fat	15.32 ± 6.29	40.01 ± 10.62[b]	24.55 ± 6.86[c]	23.06 ± 5.67[c]
retroperitoneal fat	15.45 ± 7.02	29.00 ± 10.70[b]	25.56 ± 9.63	25.06 ± 11.88
mesenteric fat	3.19 ± 1.35	9.24 ± 2.53[b]	5.73 ± 1.08[c]	5.29 ± 2.27[c]
total fat	44.90 ± 14.21	101.54 ± 25.75[b]	73.76 ± 17.81[c]	71.14 ± 13.91[c]

[a]Each value is expressed as the mean ± SD (n = 10/group). Results were statistically analyzed with a one-way ANOVA. [b]$p < 0.05$ compared to the ND group. [c]$p < 0.05$ compared to the HFD group.

Table 3. Effects of SWE on the Serum Biochemical Parameters and Hepatic Lipids of Rats with Obesity Induced by a HFD

	ND	HFD	HFD + 0.5% SWE	HFD + 1% SWE
total cholesterol (mg/dL)	48.80 ± 9.97[a]	63.40 ± 12.73[b]	59.40 ± 10.61	56.80 ± 12.52
total TG (mg/dL)	35.30 ± 12.45	85.80 ± 29.08[b]	55.30 ± 14.64[c]	45.00 ± 11.01[c]
HDL-C (mg/dL)	35.60 ± 6.34	29.41 ± 6.83	29.78 ± 6.43	32.09 ± 7.11
LDL-C (mg/dL)	12.50 ± 6.46	18.80 ± 6.35[b]	13.80 ± 5.32	12.60 ± 6.00[c]
LDL-C/HDL-C	0.37 ± 0.25	0.68 ± 0.37[b]	0.46 ± 0.14	0.41 ± 0.24
glucose (mg/dL)	104.00 ± 10.08	132.60 ± 15.95[b]	115.30 ± 2.64[c]	107.50 ± 12.96[c]
AST (U/L)	107.50 ± 17.86	131.70 ± 24.91[b]	115.70 ± 18.48	107.50 ± 19.68[c]
ALT (U/L)	58.70 ± 10.30	60.50 ± 13.68	53.30 ± 8.05	47.10 ± 6.10[c]
BUN (mg/dL)	13.96 ± 1.18	12.06 ± 1.45	13.52 ± 1.62	13.60 ± 1.15
CRE (mg/dL)	0.65 ± 0.05	0.62 ± 0.06	0.62 ± 0.06	0.63 ± 0.04
sodium (mmol/L)	152.20 ± 4.95	155.80 ± 9.07	150.60 ± 2.79	155.30 ± 6.78
potassium (mmol/L)	6.65 ± 0.32	6.47 ± 0.59	5.56 ± 0.34	5.47 ± 0.34
FFA (mmol/L)	1.30 ± 0.26	1.64 ± 0.45	1.33 ± 0.29	1.30 ± 0.17[c]
insulin (ng/mL)	0.90 ± 0.03	0.99 ± 0.13	0.98 ± 0.10	0.98 ± 0.14
leptin (pg/mL)	1.82 ± 0.26	1.90 ± 0.23	1.87 ± 0.18	1.83 ± 0.33
liver cholesterol (mg/dL)	223.60 ± 18.10	661.24 ± 90.81[b]	544.04 ± 77.07[c]	471.48 ± 54.19[c]
liver TG (mg/dL)	229.29 ± 23.04	622.86 ± 18..97[b]	444.18 ± 20.01[c]	429.27 ± 51.74[c]

[a]Each value is expressed as the mean ± SD (n = 10/group). Results were statistically analyzed with a one-way ANOVA. [b]$p < 0.05$ compared to the ND group. [c]$p < 0.05$ compared to the HFD group.

body showed that SWE did not burden the liver or affect kidney functions.

Next, we analyzed the cholesterol content of liver tissues. The results (Table 3) showed that the cholesterol content of rats fed with a normal diet was 223.60 ± 18.10 mg/dL. The cholesterol content of rats fed with a HFD alone was 661.24 ± 90.81 mg/dL. The cholesterol content of rats fed with 0.5 and 1.0% SWE was 544.04 ± 77.07 and 471.48 ± 54.19 mg/dL, respectively. As shown in Table 3, the TG and cholesterol contents of liver in rats fed with SWE were lower than the TG and cholesterol contents of liver in rats fed with a HFD alone. We also observed the TG content in liver tissues. The results showed that the TG content of rats fed with a normal diet was 229.29 ± 23.04 mg/dL. The TG content of rats fed with a HFD alone was 622.86 ± 18.97 mg/dL, while the TG content of rats fed with 0.5 and 1.0% SWE was 444.18 ± 20.01 and 429.27 ± 51.74 mg/dL, respectively. It showed the reduction of fatty metamorphosis in livers of SWE-supplemented rats (Figure 3 and Table 3). SWE reduced the contents of cholesterol, TG, and FFA to inhibit lipid accumulation.

Effect of SWE on the Hepatic-Lipid-Metabolism-Related Protein in HFD-Fed Rats. Previous studies showed that activation of AMPK-p could inhibit lipid accumulation and the activation of FAS and acetyl-CoA carboxylase (ACC).[32,33] In an animal model, we examined the protein level in lipid metabolism. In panels A and B of Figure 4, the results showed that the rats fed with 0.5 or 1.0% SWE had lower lipid accumulation.

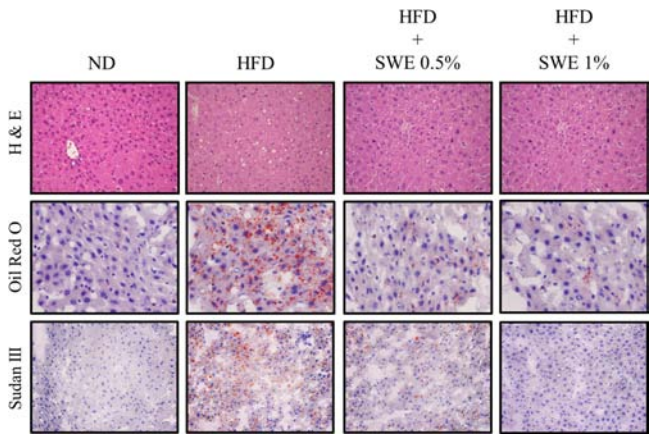

Figure 3. Histopathological examination of liver tissue in rats fed a control diet and HFD. Animals were fed a normal diet (control group), HFD, or HFD pair feeding with a 0.5 or 1% SWE diet for 12 weeks *ad libitum* (n = 10). Rats in all groups were sacrificed after 12 weeks of experiments. Liver tissues were obtained immediately after sacrifice and stained with H&E (100×, top), Oil Red O stain (400×, middle), and Sudan III stain (100×, bottom).

Effect of SWE on the Hepatic-Lipid-Oxidation-Related Protein in HFD-Fed Rats. In addition to the lipid synthesis, the hepatic lipid oxidation was also analyzed. PPARα was decreased in the HFD group, while SWE dose-dependently increased the PPARα (Figure 4C). SWE also increased the

DOI: 10.1021/acs.jafc.5b00346
J. Agric. Food Chem. 2015, 63, 4587−4596

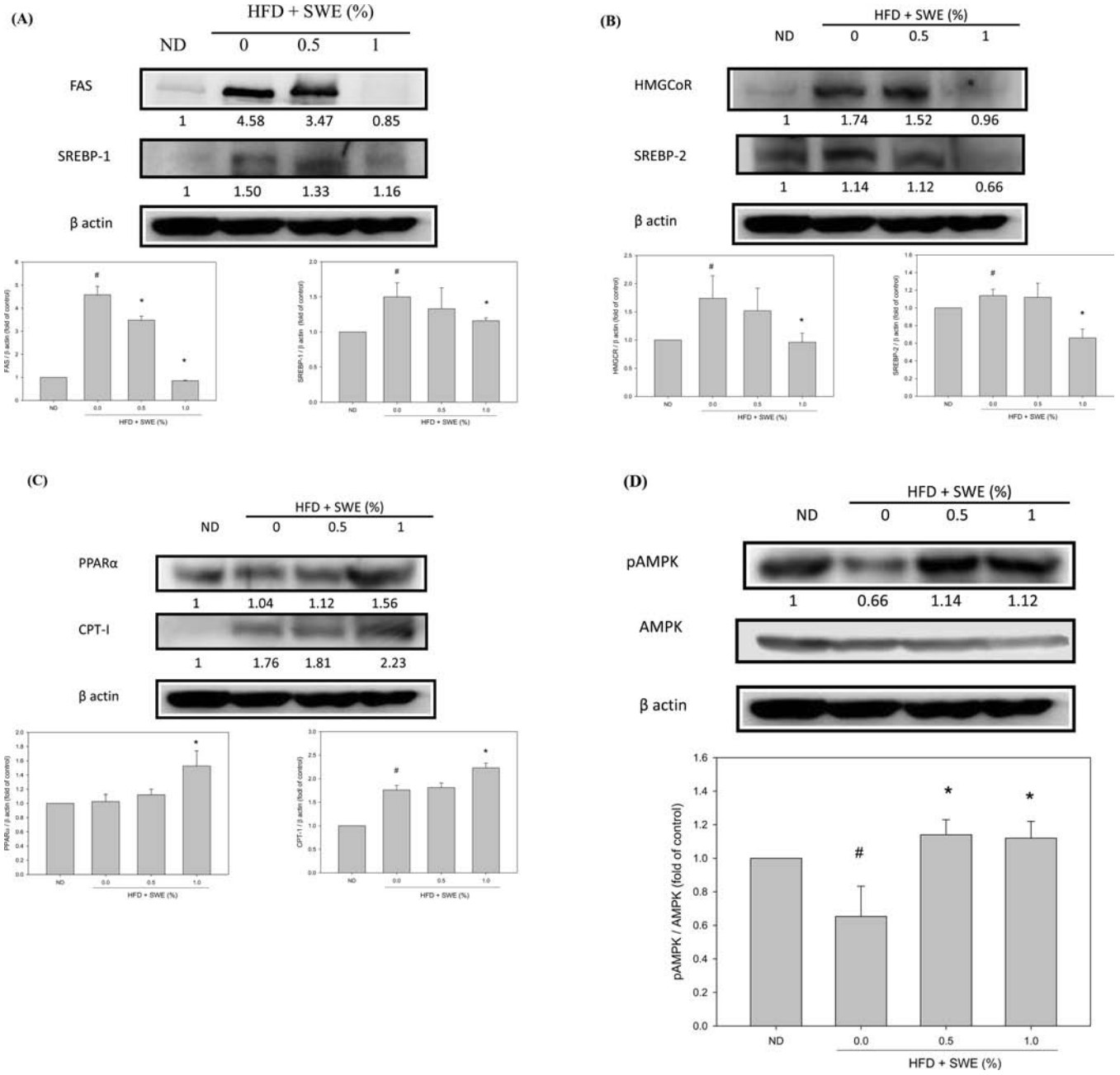

Figure 4. SWE treatment reduced fatty-acid-synthesis-related protein expression in rats fed a HFD. Animals were fed a normal diet, HFD, or HFD pair feeding with a 0.5 or 1% SWE diet for 12 weeks *ad libitum* (n = 10). Protein extracts from rat liver were subjected to western blotting to detect FAS, SREBP-1, HMGCoR, SREBP-2, PPARα, CPT-I, phosphorylated AMPK, and AMPK. β-actin was used as a loading control. The numbers below the panels represent quantification of the immunoblot by densitometry. Data are presented as means ± SD from three independent experiments. (#) $p < 0.05$ compared to the ND group. (∗) $p < 0.05$ compared to the HFD group.

expression of CPT-I and the activation of AMPK. In comparison to the control, 0.5 or 1.0% SWE significantly increased the AMPK phosphorylation (Figure 4D). Neither CPT-I nor AMPK was altered by a HFD. Hence, it was demonstrated that SWE inhibited lipid synthesis, stimulated lipid oxidation, and lowered hepatic lipid content.

Effect of CA and HPT on the OA-Induced Lipid Accumulation by SWE in HepG2 Cells. The main polyphenols of SWE are CA and HPT. The effects of CA and HPT on the intracellular lipid accumulation of HepG2 cells were conducted by OA. This experiment was focused on the change of intracellular lipid accumulation but did not cause cytotoxicity in HepG2 cells.[34,35] The cell cytotoxicity was not found under 4 mg/mL SWE, 200 μM CA, or HPT treatment (Figure 5A). SWE (1−2 mg/mL), CA (100−150 μM), and HPT (100−150 μM) can indeed reduce OA-induced lipid accumulation in HepG2 cells (panels B and C of Figure 5). Taken above, they showed that SWE, CA, and HPT have the ability to reduce the lipid accumulation in the liver.

DISCUSSION

The liver plays an important role in lipid homeostasis via regulation of lipogenesis and oxidative stress.[36] Recent studies on obesity in the field of food science have focused on the

DOI: 10.1021/acs.jafc.5b00346
J. Agric. Food Chem. 2015, 63, 4587−4596

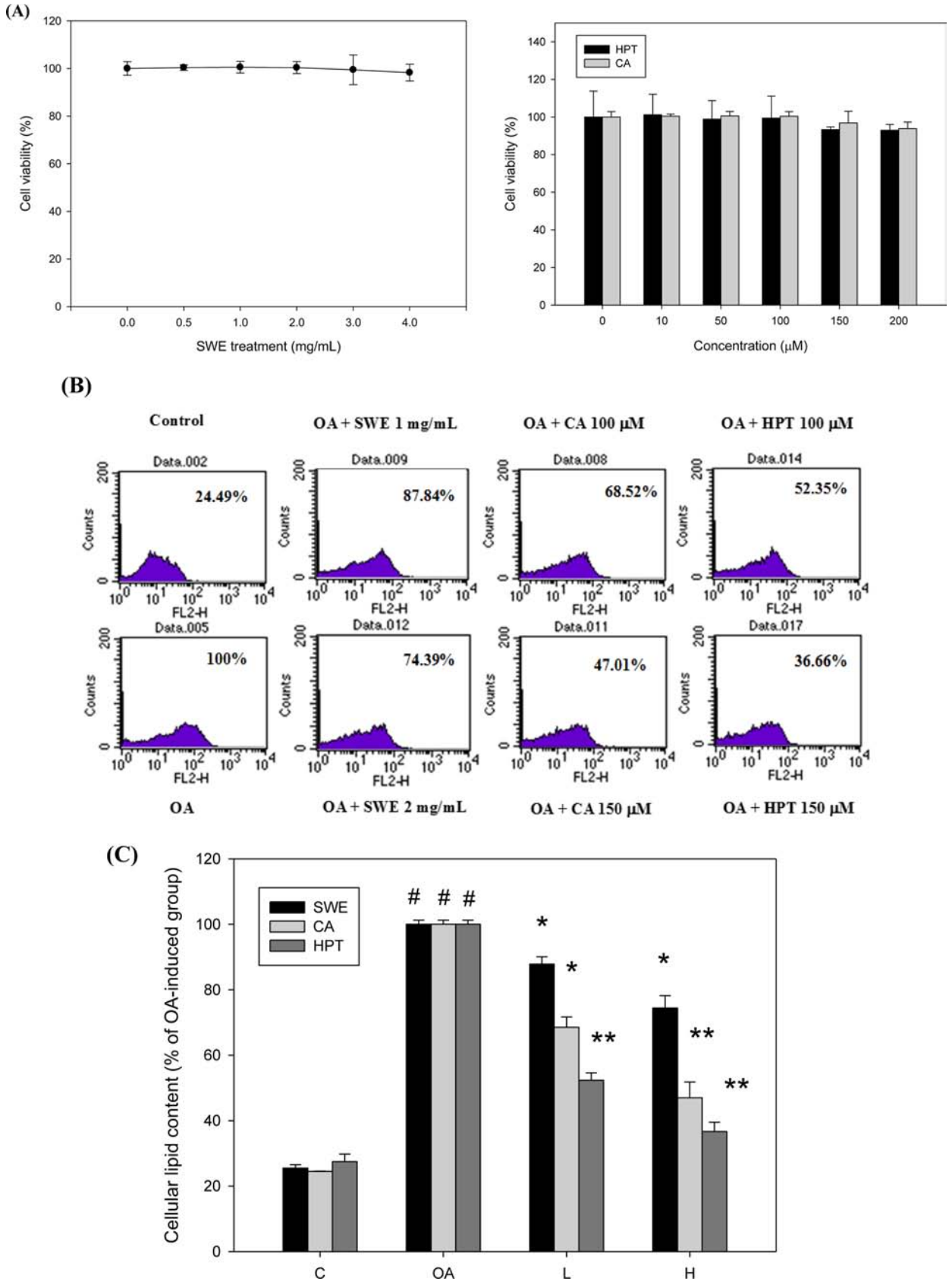

Figure 5. SWE, CA, and HPT attenuated OA-induced lipid accumulation in HepG2 cell. (A) SWE, CA, and HPT had no cytotoxicity effect on HepG2 cells. (B and C) Lipid accumulation was induced by 0.6 mM OA. Cells were co-treated with OA and the indicated concentrations of SWE, CA, or HPT for 24 h. Lipid-bound Nile red fluorescence was detected, and quantification of lipid in cells was immediately analyzed by flow cytometry. SWE-L, cells were treated with 1 mg/mL SWE as a low-dose SWE; SWE-H, cells were treated with 2 mg/mL SWE as a high-dose SWE; CA-L, 100 μM caffeic acid; CA-H, 150 μM caffeic acid; HPT-L, 100 μM hesperetin; and HPT-H, 150 μM hesperetin.

DOI: 10.1021/acs.jafc.5b00346
J. Agric. Food Chem. 2015, 63, 4587−4596

search for functional food ingredients or herbal extracts that can mend the body weight and body fat.[3,37−39] SWE suppressed OA-mediated lipid accumulation via regulating lipogenesis and lipolysis in an *in vitro* study.[23] The present investigation verified that SWE improved HFD-induced obesity by decreasing cellular lipid accumulation and increasing lipolysis via activation of AMPK in rats.

We first examined the effects of SWE on total cholesterol and TG contents in HFD-fed rats with respect to weight decrease (Figure 1) and serum cholesterol and TG reduction (Table 3). Our observations agree with other reports, which showed that polyphenols could significantly reduce the levels of total cholesterol and also availably diminish body weight in animals with a HFD.[39] In addition, there are other polyphenols, such as PCA, *p*-CA, and naringenin, existing in SWE. In 2010, Liu et al. pointed out that CA and *p*-CA possess the potential to reduce TGs.[40] Yoshida et al. showed that the administration of HPT and naringenin can reduce the FFA secretion in mouse adipocyte and improve lipolysis.[41] The previous study also showed that naringenin can effectively decrease body fat.[42] Hsu et al. revealed that PCA, *p*-CA, and CA have the potential to inhibit the differentiation of adipocytes.[43] In a previous report, Hsu et al. also showed that the flavonoid and polyphenol can reduce body weight and fatty liver formation in beef-tallow-induced rat obesity. In our result, we found that the rat body weight increases under a similar induction and SWE decelerates the weight gain and a fatty liver via reducing the accumulation of liver fat and increasing the fatty acid oxidation.[28] A previous study showed that CA (0.08%, w/w) or HPT (0.02%, w/w) exhibited the potential as an anti-obesity agent in an animal model.[44,45] After the analysis of HPLC, SWE contained 26% CA and 23% HPT. Accordingly, it was evaluated that the usage of SWE in 0.5 or 1% would be efficacious to improve obesity and fatty liver formation in our model. The present results showed that SWE has the potential role to reduce obesity in rats. Actually, the duration of 12 weeks is not long enough to confirm the efficacy. In a future study, we will extend the experimental duration to observe the results.

The synthesis of fatty acids and reduction of fatty acid oxidation are important events in regulating lipid accumulation of NAFLD.[46,47] We suggested that SWE may inhibit the synthesis of fatty acid and cholesterol. FAS is the primary enzyme involved in lipogenesis and serves as a marker of the treatment effect in obesity.[32] In the results, we found that SWE inhibited the expressions of FAS and HMGCoR in rats (panels A and B of Figure 4).

AMPK has high attention-getting importance to modulate the homeostasis of fatty acids in the research of lipometabolism.[48] Previous research indicated that polyphenolic components from many plants can activate AMPK.[49] In fact, our previous *in vitro* study and other research works showed that AMPK can be activated by polyphenol extracts.[23] We also investigated the effect of SWE on AMPK activity and the protein expression of SREBP-1. In this study, we found that SWE increased the activation of the AMPK pathway to regulate the lipid accumulation *in vivo* (Figure 4D). It is consistent that there are several reports demonstrating that AMPK plays an important role in regulating carbohydrate and lipid metabolism, serving as a metabolic master switch responsible for alterations in liver energy homeostasis.[50] It also agrees with previous studies that polyphenol extracts from plenty of plants can activate AMPK.[33] Activation of AMPK suppressed FAS expression because it prevents SREBP-1 translocation from the nuclei[49] and inhibits SREBP-2 activity to attenuate hepatic steatosis,[50] whereas SREBP-2 primarily controls cholesterol homeostasis by activating genes required for cholesterol synthesis and uptake.[51] In this study, we found that SWE can activate AMPK, reduce SREBP-1 expression (Figure 4), and lead to inhibition of hepatic lipogenesis, along with the other studies. Similarly, AMPK inhibits *in vitro* lipogenesis in hepatocytes through the downregulation of the cleavage processing and transcriptional activity of SREBP.[50] In another study, the protein levels of CPT-I and PPARα were ascertainable participating in the process of lipolysis.[52] In this study, we found that SWE had the same ability to activate PPARα and CPT-I expressions (Figure 4C). Others have also reported that activation of AMPK reduced fat storage while also increasing fatty acid oxidation.[53]

In our previous study, polyphenols were found in SWE at the level of about 7.73%.[23] SWE and CA augmented AMPK activation and mediated a decrease in SREBP-1, FAS, and HMGCoR in HepG2 cells.[23,34] In this study, we further demonstrated that SWE effectively improved various lipid-related parameters (body weight, adipocyte tissue, and serum-related parameters) in the HFD-induced rat model. It agrees with our previous study that CA exhibited potential as an anti-obesity agent by suppressing lipogenesis enzymes[44] or enhancing adipocyte glucose uptake, insulin secretion, and antioxidant capacity.[54] HPT intake alone at a dietary level of 0.02% showed a decrease in the plasma level cholesterol and TGs and reduced the activity of relative lipogenesis enzymes in high-cholesterol-diet-fed rats.[45] Meanwhile, in this study, we used CA and HPT, which are main ingredients of SWE, to show the effectiveness of reducing lipid accumulation in cells. Results in Figure 5 show that CA and HPT reduced the lipid accumulation in the liver. This is consistent with the CA-enhanced activity of AMPK to accelerate lipolysis.[34] In addition, CA inhibited OA-induced hepatic lipid accumulation and promoted the lipolysis via upregulation of AMPK. In conclusion, we showed that SWE can reduce lipid accumulation and elicit the fatty acid oxidation in the liver of HFD-induced rats. SWE would be developed as a potential therapeutic treatment to reduce the progression of a fatty liver and obesity.

AUTHOR INFORMATION

Corresponding Authors

*Telephone: +886-4-22053366, ext. 2113. Fax: +886-4-22038766. E-mail: chsunwu@mail.cmu.edu.tw.

*Telephone: +886-4-24730022, ext. 11670. Fax: +886-4-2324-8167. E-mail: wcj@csmu.edu.tw.

Funding

This work was supported by the National Science Council Grant NSC99-2321-B-040-001 (Taiwan).

Notes

The authors declare no competing financial interest.

REFERENCES

(1) Spiegelman, B. M.; Flier, J. S. Obesity and the regulation of energy balance. *Cell* **2001**, *104*, 531−543.

(2) Fabbrini, E.; Sullivan, S.; Klein, S. Obesity and nonalcoholic fatty liver disease: Biochemical, metabolic, and clinical implications. *Hepatology* **2010**, *51*, 679−689.

(3) Evans, R. M.; Barish, G. D.; Wang, Y. X. PPARs and the complex journey to obesity. *Nat. Med.* **2004**, *10*, 355−361.

(4) Wellen, K. E.; Hotamisligil, G. S. Inflammation, stress, and diabetes. *J. Clin. Invest.* **2005**, *115*, 1111−1119.

DOI: 10.1021/acs.jafc.5b00346
J. Agric. Food Chem. 2015, 63, 4587−4596

(5) Tilg, H.; Moschen, A. R. Adipocytokines: Mediators linking adipose tissue, inflammation and immunity. *Nat. Rev. Immunol.* **2006**, *6*, 772−783.
(6) Weissman, C. Nutrition in the intensive care unit. *Crit. Care* **1999**, *3*, R67−R75.
(7) Duval, C.; Muller, M.; Kersten, S. PPARα and dyslipidemia. *Biochim. Biophys. Acta, Mol. Cell Biol. Lipids* **2007**, *1771*, 961−971.
(8) Muller, H.; Lindman, A. S.; Brantsaeter, A. L.; Pedersen, J. I. The serum LDL/HDL cholesterol ratio is influenced more favorably by exchanging saturated with unsaturated fat than by reducing saturated fat in the diet of women. *J. Nutr.* **2003**, *133*, 78−83.
(9) Chan, D. C.; Watts, G. F.; Ng, T. W.; Hua, J.; Song, S.; Barrett, P. H. Measurement of liver fat by magnetic resonance imaging: Relationships with body fat distribution, insulin sensitivity and plasma lipids in healthy men. *Diabetes, Obes. Metab.* **2006**, *8*, 698−702.
(10) Reddy, J. K.; Rao, M. S. Lipid metabolism and liver inflammation. II. Fatty liver disease and fatty acid oxidation. *Am. J. Physiol.: Gastrointest. Liver Physiol.* **2006**, *290*, G852−G858.
(11) Heemers, H.; Maes, B.; Foufelle, F.; Heyns, W.; Verhoeven, G.; Swinnen, J. V. Androgens stimulate lipogenic gene expression in prostate cancer cells by activation of the sterol regulatory element-binding protein cleavage activating protein/sterol regulatory element-binding protein pathway. *Mol. Endocrinol.* **2001**, *15*, 1817−1828.
(12) Magana, M. M.; Koo, S. H.; Towle, H. C.; Osborne, T. F. Different sterol regulatory element-binding protein-1 isoformsutilize distinct co-regulatory factors to activate the promoter for fatty acid synthase. *J. Biol. Chem.* **2000**, *275*, 4726−4733.
(13) Magana, M. M.; Osborne, T. F. Two tandem binding sites for sterol regulatory element binding proteins are required for sterol regulation of fatty-acid synthase promoter. *J. Biol. Chem.* **1996**, *271*, 32689−32694.
(14) Browning, J. D.; Horton, J. D. Molecular mediators of hepatic steatosis and liver injury. *J. Clin. Invest.* **2004**, *114*, 147−152.
(15) Bugianesi, E.; Leone, N.; Vanni, E.; Marchesini, G.; Brunello, F.; Carucci, P.; Musso, A.; De Palolis, P.; Capussotti, L.; Salizzoni, M.; Rizzetto, M. Expanding the natural history of nonalcoholic steatohepatitis: From cryptogenic cirrhosis to hepatocelllar carcinoma. *Gastroenterology* **2002**, *123*, 134−140.
(16) Zhou, G.; Myers, R.; Li, Y.; Chen, Y.; Shen, X.; Fenyk-Melody, J.; Wu, M.; Ventre, J.; Doebber, T.; Fujii, N.; Musi, N.; Hirshman, M. F.; Goodyear, L. J.; Moller, D. E. Role of AMP-activated protein kinase in mechanism of metformin action. *J. Clin. Invest.* **2001**, *108*, 1167−1174.
(17) Oliaro-Bosso, S.; Calcio Gaudino, E.; Mantegna, S.; Giraudo, E.; Meda, C.; Viola, F.; Cravotto, G. Regulation of HMGCoA reductase activity by Policosanol and octacosadienol, a new synthetic analogue of octacosanol. *Lipids* **2009**, *44*, 907−916.
(18) Carling, D. The AMP-activated protein kinase cascade—A unifying system for energy control. *Trends Biochem. Sci.* **2004**, *29*, 18−24.
(19) Hardie, D. G.; Hawley, S. A.; Scott, J. W. AMP-activated protein kinase- development of the energy sensor concept. *J. Physiol.* **2006**, *574*, 7−15.
(20) Wu, C. H.; Yang, M. Y.; Chan, K. C.; Chung, P. J.; Ou, T. T.; Wang, C. J. Improvement in high-fat diet-induced obesity and body fat accumulation by a *Nelumbo nucifera* leaf flavonoid-rich extract in mice. *J. Agric. Food Chem.* **2010**, *58*, 7075−7081.
(21) Wu, C. H.; Lin, M. C.; Wang, H. C.; Yang, M. Y.; Jou, M. J.; Wang, C. J. Rutin inhibits oleic acid induced lipid accumulation via reducing lipogenesis and oxidative stress in hepatocarcinoma cells. *J. Food Sci.* **2011**, *76*, T65−T72.
(22) Chandrasekaran, C. V.; Vijayalakshmi, M. A.; Prakash, K.; Bansal, V. S.; Meenakshi, J.; Amit, A. Review article: Herbal approach for obesity management. *Am. J. Plant Sci.* **2012**, *3*, 1003−1014.
(23) Wu, C. H.; Ou, T. T.; Chang, C. H.; Chang, X. Z.; Yang, M. Y.; Wang, C. J. The polyphenol extract from *Sechium edule* shoots inhibits lipogenesis and stimulates lipolysis via activation of AMPK signals in HepG2 cells. *J. Agric. Food Chem.* **2014**, *62*, 750−759.
(24) Han, L. K.; Kimura, Y.; Kawashima, M.; Takaku, T.; Taniyama, T.; Hayashi, T.; Zheng, Y. N.; Okuda, H. Anti-obesity effects in rodents of dietary teasaponin, a lipase inhibitor. *Int. J. Obes.* **2001**, *25*, 1459−1464.
(25) Han, L. K.; Xu, B. J.; Kimura, Y.; Zheng, Yn.; Okuda, H. Platycodi radix affects lipid metabolism in mice with high fat diet-induced obesity. *J. Nutr.* **2000**, *130*, 2760−2764.
(26) Kwon, C. S.; Sohn, H. Y.; Kim, S. H.; Kim, J. H.; Son, K. H.; Lee, J. S.; Lim, J. K.; Kim, J. S. Anti-obesity effect of *Dioscorea nipponica* Makino with lipase-inhibitory activity in rodents. *Biosci., Biotechnol., Biochem.* **2003**, *67*, 1451−1456.
(27) Liu, W.; Zheng, Y.; Han, L.; Wang, H.; Saito, M.; Ling, M.; Kimura, Y.; Feng, Y. Saponins (Ginsenosides) from stems and leaves of *Panax quinquefolium* prevented high-fat diet-induced obesity in mice. *Phytomedicine* **2008**, *15*, 1140−1145.
(28) Hsu, C. L.; Wu, C. H.; Huang, S. L.; Yen, G. C. Phenolic compounds rutin and *o*-coumaric acid ameliorate obesity induced by high-fat diet in rats. *J. Agric. Food Chem.* **2009**, *57*, 425−431.
(29) Reeves, P. G. Components of the AIN-93 diets as improvements in the AIN-76A diet. *J. Nutr.* **1997**, *127*, 838S−841S.
(30) Xu, L.; Wei, Y.; Dong, D.; Yin, L.; Qi, Y.; Han, X.; Xu, Y.; Zhao, Y.; Peng, J. iTRAQ-based proteomics for studying the effects of dioscin against nonalcoholic fatty liver disease in rats. *RSC Adv.* **2014**, *4*, 30704−30712.
(31) Liu, M.; Xu, L.; Yin, L.; Qi, Y.; Xu, Y.; Han, X.; Zhao, Y.; Sun, H.; Yao, J.; Lin, Y.; Liu, K.; Peng, J. Potent effects of dioscin against obesity in mice. *Sci. Rep.* **2015**, *5*, 7973−7983.
(32) Kemp, B. E.; Stapleton, D.; Campbell, D. J.; Chen, Z. P.; Murthy, S.; Walter, M.; Gupta, A.; Adams, J. J.; Katsis, F.; van Denderen, B.; Jennings, I. G.; Iseli, T.; Michell, B. J.; Witters, L. A. AMP-activated protein kinase, super metabolic regulator. *Biochem. Soc. Trans.* **2003**, *31*, 162−168.
(33) Hwang, J. T.; Park, I. J.; Shin, J. I.; Lee, Y. K.; Lee, S. K.; Baik, H. W.; Ha, J.; Park, O. J. Genistein, EGCG, and capsaicin inhibit adipocyte differentiation process via activating AMP-activated protein kinase. *Biochem. Biophys. Res. Commun.* **2005**, *338*, 694−699.
(34) Liao, C. C.; Ou, T. T.; Huang, H. P.; Wang, C. J. The inhibition of oleic acid induced hepatic lipogenesis and the promotion of lipolysis by caffeic acid via up-regulation of AMP-activated kinase. *J. Sci. Food Agric.* **2014**, *94*, 1154−1162.
(35) Hsu, C. L.; Yen, G. C. Effects of flavonoids and phenolic acids on the inhibition of adipogenesis in 3T3-L1 adipocytes. *J. Agric. Food Chem.* **2007**, *55*, 8404−8410.
(36) Madan, K.; Bhardwaj, P.; Thareja, S.; Gupta, S. D.; Saraya, A. Oxidant stress and antioxidant status among patients with non-alcoholic fatty liver disease (NAFLD). *J. Clin. Gastroenterol.* **2006**, *40*, 930−935.
(37) Kopelman, P. G. Obesity as a medical problem. *Nature* **2000**, *404*, 635−643.
(38) Shapiro, H.; Halpern, Z.; Bruck, R. Polyphenols in the treatment of inflammatory bowel disease and acute pancreatitis. *Gut* **2007**, *56*, 426−435.
(39) Ziaee, A.; Zamansoltani, F.; Nassiri-Asl, M.; Abbasi, E. Effects of rutin on lipid profile in hypercholesterolaemic rats. *Basic Clin. Pharmacol. Toxicol.* **2009**, *104*, 253−258.
(40) Liu, Y.; Wang, D.; Zhang, D.; Lv, Y.; Wei, Y.; Wu, W.; Zhou, F.; Tang, M.; Mao, T.; Li, M.; Ji, B. Inhibitory effect of blueberry polyphenolic compounds on oleic acid-induced hepatic steatosis in vitro. *J. Agric. Food Chem.* **2011**, *59*, 12254−12263.
(41) Yoshida, H.; Takamura, N.; Shuto, T.; Ogata, K.; Tokunaga, J.; Kawai, K.; Kai, H. The citrus flavonoids hesperetin and naringenin block the lipolytic actions of TNF-α in mouse adipocytes. *Biochem. Biophys. Res. Commun.* **2010**, *394*, 728−732.
(42) Cho, K. W.; Kim, Y. O.; Andrade, J. E.; Burgess, J. R.; Kim, Y. C. Dietary naringenin increases hepatic peroxisome proliferators-activated receptor α protein expression and decreases plasma triglyceride and adiposity in rats. *Eur. J. Nutr.* **2011**, *50*, 81−88.

DOI: 10.1021/acs.jafc.5b00346
J. Agric. Food Chem. 2015, 63, 4587−4596

(43) Hsu, C. L.; Huang, S. L.; Yen, G. C. Inhibitory effect of phenolic acids on the proliferation of 3T3-L1 preadipocytes in relation to their antioxidant activity. *J. Agric. Food Chem.* **2006**, *54*, 4191−4197.
(44) Liao, C. C.; Ou, T. T.; Huang, H. P.; Wang, C. J. Prevention of diet-induced hyperlipidemia and obesity by caffeic acid in C57BL/6 mice through regulation of hepatic lipogenesis gene expression. *J. Agric. Food Chem.* **2013**, *61*, 11082−11088.
(45) Cha, J. Y.; Cho, Y. S.; Kim, I.; Anno, T.; Rahman, S. M.; Yanagita, T. Effect of hesperetin, a citrus flavonoid, on the liver triacylglycerol content and phosphatidate phosphohydrolase activity in orotic acid-fed rats. *Plant Foods Hum. Nutr.* **2001**, *56*, 349−358.
(46) Duval, C.; Muller, M.; Kersten, S. PPARα and dyslipidemia. *Biochim. Biophys. Acta, Mol. Cell Biol. Lipids* **2007**, *1771*, 961−971.
(47) Zhang, S.; Zheng, L.; Dong, D.; Xu, L.; Yin, L.; Qi, Y.; Han, X.; Lin, Y.; Liu, K.; Peng, J. Effects of flavonoids from *Rosa laevigata* Michx fruit against high-fat diet-induced non-alcoholic fatty liver disease in rats. *Food Chem.* **2013**, *141*, 2108−2116.
(48) Winder, W. W.; Hardie, D. G. AMP-activated protein kinase, a metabolic master switch: Possible roles in type 2 diabetes. *Am. J. Physiol.* **1999**, *277*, E1−E10.
(49) Weng, M. S.; Ho, C. T.; Ho, Y. S.; Lin, J. K. Theanaphthoquinone inhibits fatty acid synthase expression in EGF-stimulated human breast cancer cells via the regulation of EGFR/ErbB-2 signaling. *Toxicol. Appl. Pharmacol.* **2007**, *218*, 107−118.
(50) Li, Y.; Xu, S.; Mihaylova, M. M.; Zheng, B.; Hou, X.; Jiang, B.; Park, O.; Luo, Z.; Lefai, E.; Shyy, J. Y.; Gao, B.; Wierzbicki, M.; Verbeuren, T. J.; Shaw, R. J.; Cohen, R. A.; Zang, M. AMPK phosphorylates and inhibits SREBP activity to attenuate hepatic steatosis and atherosclerosis in diet-induced insulin-resistant mice. *Cell Metab.* **2011**, *13*, 376−388.
(51) Jung, E. J.; Kwon, S. W.; Jung, B. H.; Oh, S. H.; Lee, B. H. Role of the AMPK/SREBP-1 pathway in the development of orotic acid-induced fatty liver. *J. Lipid Res.* **2011**, *52*, 1617−1625.
(52) Yang, M. Y.; Peng, C. H.; Chan, K. C.; Yang, Y. S.; Huang, C. N.; Wang, C. J. The hypolipidemic effect of *Hibiscus sabdariffa* polyphenols via inhibiting lipogenesis and promoting hepatic lipid clearance. *J. Agric. Food Chem.* **2010**, *58*, 850−859.
(53) Puljak, L.; Parameswara, V.; Dolovcak, S.; Waldrop, S. L.; Emmett, D.; Esser, V.; Fitz, J. G.; Kilic, G. Evidence for AMPK dependent regulation of exocytosis of lipoproteins in a model liver cell line. *Exp. Cell Res.* **2008**, *314*, 2100−2109.
(54) Jung, U. J.; Lee, M. K.; Park, Y. B.; Jeon, S. M.; Choi, M. S. Antihyperglycemic and antioxidant properties of caffeic acid in db/db mice. *J. Pharmacol. Exp. Ther.* **2006**, *318*, 476−483.

DOI: 10.1021/acs.jafc.5b00346
J. Agric. Food Chem. 2015, 63, 4587−4596

chemical reagents were of analytical grade and manufactured by Sinopharm Chemical Reagent Co., Ltd. Methanol and acetonitrile were of HPLC grade and purchased from Shanghai Lingfeng Chemical Reagent Co., Ltd. The extraction procedure was conducted in an apparatus of USCCE that was designed by our laboratory to be suitable for industrial production, and its operation is clarified in Figure 1. The model of ultrasound probe is JY92-IIDN, purchased

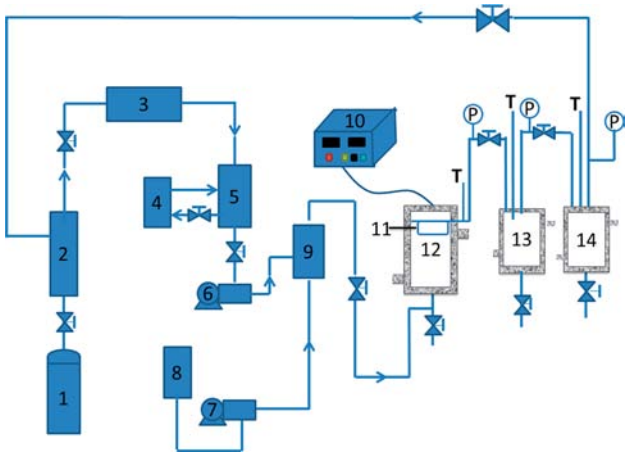

Figure 1. Scheme of ultrasound-enhanced subcritical CO_2 apparatus: 1, CO_2 cylinder; 2, bus-bar; 3, purifier; 4, refrigerator; 5, condenser; 6, main pump; 7, auxiliary pump; 8, cosolvent cylinder; 9, mixer; 10, ultrasonic generator; 11, ultrasonic transducer; 12, extraction kettle; 13, separation kettle I; 14, separation kettle II; T, temperature probe; P, pressure gauge.

from Ningbo Xinke Instrument Co., and its main technical parameters are operating frequency of 20−24 kHz and ultrasonic power of 20−900 W (adjustable), and the ultrasonic system is composed of a piezoelectric transducer (ultrasonic intensity range of 0−19 W cm^{-2}) and an ultrasonic generator. The generator comprises a power piezoelectric impedance-matching box and a power generator unit. The power generator unit consists of two parts: a power amplifier and a resonant frequency control system to maintain constant power to the transducer during the USCCE process. The transducer was placed in the extractor of the USCCE equipment, whereas the generator was located outside to control the ultrasonic intensity.

The operation of the apparatus of USCCE is as follows: CO_2 goes from the cylinder to the purifier to filter out possible liquid and particulate impurities in the gas, and then goes into the condenser and is cooled; after that, it is pumped into the mixer by a high-pressure pump and mixed with cosolvent pumped by the auxiliary pump; the mixture is pumped into the 5 L extraction kettle; under ultrasound, the mixture makes full contact with the material inside the extraction kettle; the extracted substances dissolve in supercritical CO_2 and flow into separation kettles I and II, in which case CO_2 goes back into the gaseous state and extracted substances sink to the bottom of separation kettle. Collected with plastic bottles, CO_2 flows out to the purifier and recycles again. During the extraction process, the pressure of the extraction kettle and separation kettle is controlled by the valves; the temperature is adjusted by the water bath outside the reactor.

Ultrasound-Enhanced Subcritical CO_2 Extraction. Extraction was carried out in the self-designed apparatus shown in Figure 1. *C. pyrenoidosa* (100.00 g) in the size of 4.5−5.5 μm was dried by spray-drying and then soaked in absolute ethanol and extracted at the designated extraction temperature, extraction pressure, CO_2 flow cosolvent, extraction time, and ultrasonic power conditions. Every experiment was in triplicate; 100.00 g was charged into the extract holder every time. The single-factor experiment can, on the one hand, investigate the effects of various factors on the law of USCCE and, on the other hand, lay the foundation for optimization design. The lutein dissolved in the subcritical CO_2 was separated from the carbon dioxide and collected in the separator. For the determination of lutein, chromatographic conditions used a Dionex HPLC system determination, Dikma C-18 (250 × 4.6 × 5 μm) separation column; the mobile phase was methanol/acetonitrile (90:10 by volume), the column temperature was 30 °C, the flow rate was 0.8 mL/min, the injection volume was 20 μL, and the detection wavelength was 450 nm. The lutein yield was determined gravimetrically as displayed in

$$\text{TLY}\ (\%) = \frac{E}{\text{FM}} \times 100\% \quad (1)$$

where TLY represents total lutein yield, E represents extracts (mg), and FM represents feed materials (g). Factors that affect ultrasound-enhanced subcritical CO_2 extraction methods are mainly extraction temperature, extraction pressure, CO_2 flow, cosolvent, extraction time, and ultrasonic power. To study the impact of various factors on the extraction yield of lutein, a single-factor experiment was designed, and then significant factors were chosen; orthogonal experiments were designed to optimize the extraction process parameters. The independent variables were pretreatment (absolute ethanol soaking and enzymatic pretreatment), temperature (18, 21, 24, 27, and 30 °C), pressure (9, 13, 17, 21, 25, and 29 MPa), flow rate (20, 25, 30, 35, and 40 kg/h), amount of cosolvent (0, 0.5, 1.0, 1.5, and 2.0 mL/g absolute ethanol), extraction time (0, 0.5, 1, 1.5, 2.0, 2.5, 3.0, 3.5, 4.0, 4.5, and 5.0 h), and ultrasound power levels (0, 250, 500, 750, and 1000 W). Three pretreatment methods were investigated: no treatment, cosolvent was 2.0 mL/g absolute ethanol; ethanol soak, 100 mL of absolute ethanol was added, and soaked for 18 h, cosolvent was 1.0 mL/g absolute ethanol; enzymatic broken, 150 mL of absolute ethanol was added, 5% citric acid solution was used to adjust the pH value of the enzyme solution to 5.0, 2.0 g of cellulose was added to the enzyme solution and stirred for 3 h at 50 °C, and after completion of enzymatic hydrolysis, *C. pyrenoidosa* together with enzyme solution put into the kettle, cosolvent was 0.5 mL/g absolute ethanol. On the basis of single-factor results, four factors that had a significant impact on the lutein yield were determined: extraction pressure, temperature, amount of cosolvent ethanol, and ultrasonic power, L9 (3^3); orthogonal experimental design was used to determine their influence on the extraction of USCCE process of lutein *C. pyrenoidosa* experiments.

Comparison with Other Extraction Methods. In Soxhlet extraction (SE), *C. pyrenoidosa* powder was wrapped with a paper tube and then added to the Soxhlet extractor; 100 mL of petroleum ether was added, extraction was at 43 °C reflux for 18 h, petroleum ether was removed by rotary evaporation, and the concentrated solution was dissolved with ethanol and then transferred to a brown volumetric flask and stored in a cold and no-light environment. The whole process is under weak light. In subcritical water extraction (SWE), 100.00 g of dried *C. pyrenoidosa* was extracted by deionized water in the extraction tank, the same as in USCCE; extraction at pressure 5 MPa and temperature of 150 °C for 20 min, collected when cooled to room temperature, and NaCl as emulsification. Dichloromethane was added to the extract at a 1:1 ratio and mixed thoroughly; the separated liquid was allowed to stand for 1 h and stratified. The dichloromethane part was added to anhydrous sodium sulfate and then filtered, and the filtrate was collected. In supercritical CO_2 extraction (SCE), 100.0 g of dried *C. pyrenoidosa* was extracted in the extraction apparatus the same as in USCCE; extraction at pressure 25 MPa, flow of CO_2 30 kg/h, temperature of 50 °C for 4 h, cosolvent dosage of 1.5 mL/g ethanol; separation kettle I temperature of 35 °C and pressure of 6.5 MPa; separation kettle II temperature of 30 °C and pressure of 5 MPa.

In subcritical CO_2 extraction (SCCE), 100.00 g of dried *C. pyrenoidosa* was extracted in the extraction apparatus the same as in USCCE. SCCE involved an extraction pressure of 21 MPa, a CO_2 flow of 30 kg/h, a temperature 27 °C for 4 h, and a cosolvent dosage of 1.5 mL/g ethanol; separation kettle I temperature of 35 °C and pressure of 6.5 MPa; separation kettle II temperature of 30 °C and pressure 5 MPa. In the SCCE with pretreatment, the ultrasonic process was not used and the other conditions were in accordance with the optimal

DOI: 10.1021/acs.jafc.5b00461
J. Agric. Food Chem. 2015, 63, 4597−4605

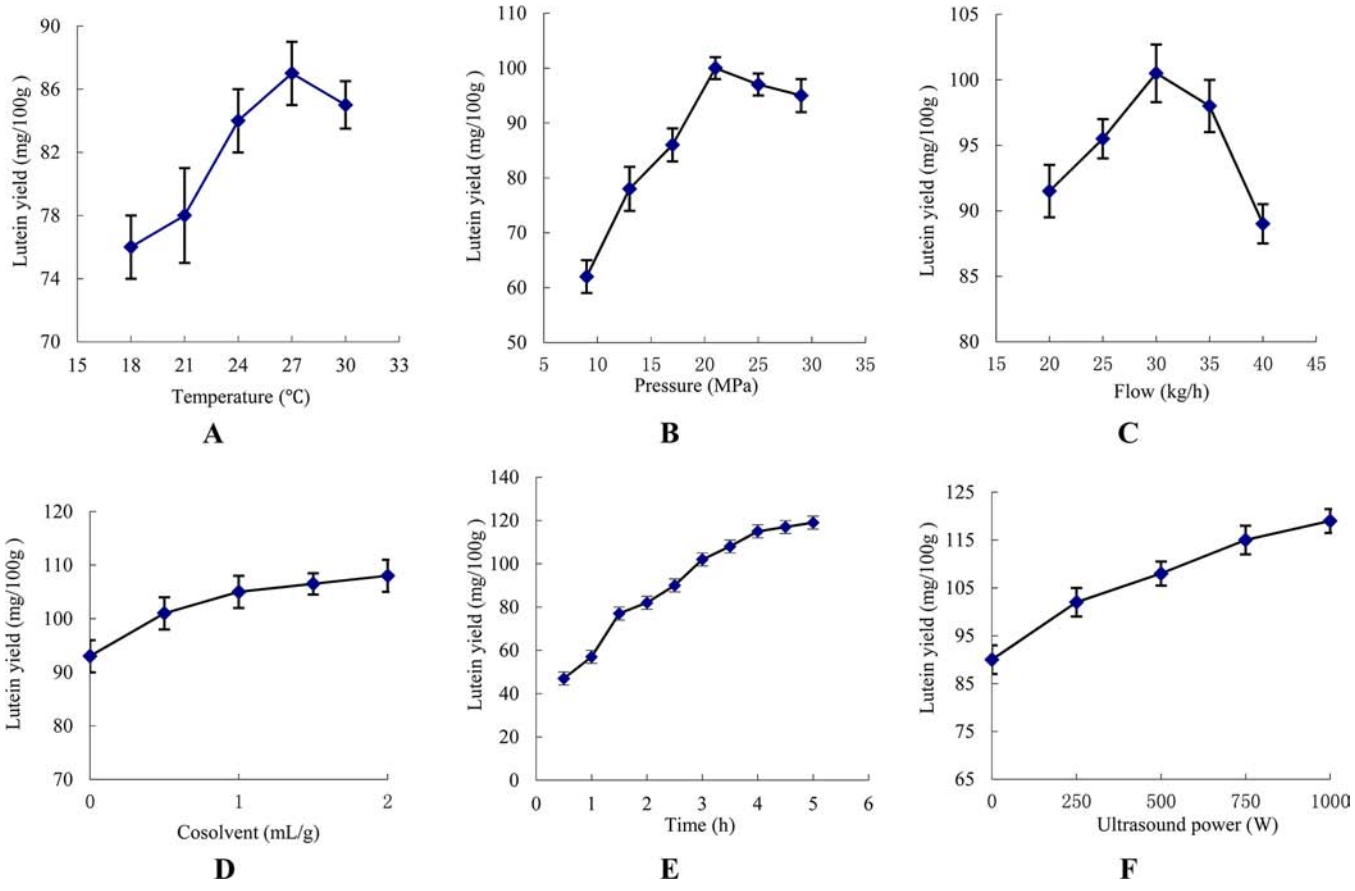

Figure 2. Effects of different factors on the ultrasound-enhanced subcritical CO_2 extraction of lutein: (A) effect of temperature on extraction yield of lutein; (B) effect of pressure on extraction yield of lutein; (C) effect of CO_2 flow rate on extraction yield of lutein; (D) effect of cosolvent amount on extraction yield of lutein; (E) effect of extraction time on extraction yield of lutein; (F) effect of ultrasound power on extraction yield of lutein.

Table 1. Orthogonal Experiment Results of Lutein Extraction Yield by USCCE

no.	temperature, *A* (°C)	pressure, *B* (MPa)	cosolvent, *C*(mL /g)	ultrasonic power, *D* (W)	yield (mg/100 g *Chlorella*)
1	24	17	0.5	500	87.89
2	24	21	1.0	750	114.86
3	24	25	1.5	1000	117.75
4	27	17	1.0	750	106.42
5	27	21	1.5	500	111.87
6	27	25	0.5	750	110.78
7	30	17	1.5	750	105.01
8	30	21	0.5	1000	115.59
9	30	25	1.0	500	107.73
k_1	106.833	99.773	104.753	102.497	
k_2	109.690	114.107	109.670	110.217	
k_3	109.443	112.087	111.543	113.253	
Δ^a	2.857	14.334	6.790	10.756	

[a] Δ, max−min values for each column.

process of orthogonal experiment. USCCE with pretreatment was based on the optimal process of the orthogonal experiment.

Kinetic Model Validation. The kinetic model can not only help us explore the subcritical fluid extraction process and predict the experimental results but also help budget before the investment, therefore effectively reducing the investment risk. However, studies on the kinetic model are complex; to reduce the load of work, only the extraction kinetic model established by our group was studied.[25] The ultrasound-enhanced subcritical CO_2 extraction kinetics equation for *C. pyrenoidosa* lutein is established as

$$E = E_\infty(1 - e^{-kt}) \quad (2)$$

wherein E_∞ is the lutein extraction yield when time tends to infinity, mg/100 g *C. pyrenoidosa*; k is the ratio of the solute concentration gradient descending rate; t is the extraction time, h; and E is lutein yield when the extraction time is t, mg/100 g *C. pyrenoidosa*.

For different extraction conditions, values of E_∞ are different, because the ultrasound, pretreatment, and entrainment agents will make a difference in equilibrium of the active component in solid particles.[26] For example, adding of cosolvent will increase the solubility of polar substances in subcritical CO_2, and ultrasound and pretreatment will destroy the cell structure and affect the absorption−desorption equilibrium in the solid particles. To obtain E_∞ and k values with and without ultrasound conditions, appropriate experi-

DOI: 10.1021/acs.jafc.5b00461
J. Agric. Food Chem. 2015, 63, 4597−4605

ments were needed. The experimental data were simulated in order that the yields calculated from the mathematical model have the smallest deviation with the lutein yields obtained under different experimental conditions.

The analysis of variance (ANOVA) was performed using origin 7.0, release 10 (OriginLab Corp., Northampton, MA, USA). Multiple-range tests were used to compare means of the estimated kinetic parameters. Evaluations were based on the $p < 0.05$ significance level.

Scanning Electron Micrographs (SEM). To further reveal the mechanism of USCCE, the present study investigated the effects of various extraction methods on *C. pyrenoidosa* powder microstructure. *C. pyrenoidosa* powders obtained with different extraction methods (Soxhlet extraction, subcritical CO_2 extraction, USCCE without pretreatment, USCCE with pretreatment) were observed by SEM. The control was dried in a vacuum oven at 45 °C for 12 h. The surface characteristics of dried cell were observed and recorded by using a Japanese Electronics Corp. JSM-6490LV scanning electron microscope. The samples were placed in a preparation chamber, and the morphology of the samples was magnified and digitally recorded.

RESULTS AND DISCUSSION

Effect of Pretreatment on Lutein Yield. The parameters remained constant as the effects of the different factors on the "ultrasound enhanced subcritical CO_2 extraction" of lutein were investigated. After enzymatic and soaking treatments of the *C. pyrenoidosa*, the yields of lutein were 85.05 and 69.02 mg/100 g *C. pyrenoidosa*, respectively. The better pretreatment method was enzymatic treatment; therefore, in subsequent experiments enzymatic treatment was adopted as the pretreatment method of *C. pyrenoidosa*.

Table 2. Variance Analysis between Factors Levels of Extraction Yield

factor	dev sq	degrees of freedom (DOF)	*F* ratio (*F*)	critical value ($\alpha = 0.05$)	significance
A	15.033	2			
B	361.143	2	24.023	19.000	*
C	73.787	2	4.908	19.000	
D	184.526	2	12.275	19.000	
error	15.03	2			

C. pyrenoidosa has a tough cellulose layer cell wall; it is not conducive for the solvent to penetrate into the cells to extract intracellular substances, so without any pretreatment, the extraction effect of lutein is poor. After soaking in high concentrations of polar solvents, its cells swelled, the structure loosened, and ingredients were released; the extraction became more conducive, so after soaking treatment the yield of lutein significantly increased. This effect has also been reported by the study conducted by Fang and others;[27] they studied the supercritical CO_2 extraction technology on the extraction of the colchicine roots. After enzymatic treatment, the cell wall of *C. pyrenoidosa* was degraded by cellulose, and the material in the cell can be better exposed to the solvent, thereby accelerating the release and extraction of the active ingredients and improving the yield of lutein.

Effect of Temperature on Lutein Yield. The results are shown in Figure 2A, when the extraction pressure was 17 MPa and the optimum temperature 27 °C. When the temperature was <27 °C, with the increase of extraction temperature, the yield increased; when the temperature was >27 °C, the yield began to decrease.

The effect of temperature on the extraction efficiency was mainly reflected in two aspects. On the one hand, when the temperature rises, the pressure of solute vapor increases, and the thermal motion of molecules becomes faster, the chance of colliding with each other increases, and the opportunity of subcritical fluid associating with lutein increases. On the other hand, an elevated temperature under a certain pressure will decrease the density of the CO_2 and the ability to dissolve, resulting in the lutein yield reducing. This phenomenon has been reported elsewhere when some natural components were extracted by supercritical CO_2.[28,29] Lutein having the highest yield at 27 °C is a combined effect of these two aspects.

Effect of Pressure on Lutein Yield. The results are shown in Figure 2B: with the extraction pressure increasing, lutein yield increases, and when the pressure exceeds 21 MPa, increasing the extraction pressure makes the yields decline, so the best extraction pressure is 21 MPa.

The ability of subcritical CO_2 to dissolve a substance is closely related to its density; changing the extraction pressure can make the subcritical CO_2 density change, thereby increasing or reducing its ability to dissolve lutein. When the temperature remains constant, extraction pressure rising leads to an increase in density, so there will be two opposite effects: increasing the ability of CO_2 to dissolve a substance, but reducing the diffusion of the substance.[30] At relatively low temperature, the ability of CO_2 to dissolve a substance is the dominant factor, so with pressure increasing, lutein yield increases; however, when the pressure exceeds 21 MPa, the diffusion of lutein was assumed to be inhibited, and this effect is greater than the positive effects brought about by the increased ability of CO_2 to dissolve the substance, and therefore yields begin to decline.

Effect of Flow Rate of CO_2 on Lutein Yield. The CO_2 flow rate also has some influence on the extraction capacity. It works mainly in two ways: when the fluid flow increases, CO_2 goes through the material layer more quickly, the agitation and contact with the material are enhanced, and the mass transfer coefficient and contact area are increased accordingly and promote the solubility of the fluid, thereby increasing the extraction speed. On the contrary, excessive flow decreases the relative retention time of the fluid in the extractor, so the solute and fluid cannot work sufficiently and the yield is limited. In addition, excessive velocity will also lead to subcritical fluid

Table 3. Comparison between Different Extraction Technologies of Lutein

extraction method	temperature (°C)	pressure (MPa)	ultrasound power (W)	time (h)	lutein yield (mg 100 g^{-1})
SE	43	0.1	0	18	54.64
SWE	150	5	0	1/3	0
SCE	50	25	0	4	39.33
SCCE	27	21	0	4	42.29
SCCE with pretreatment	27	21	0	4 (+3 h pretreatment)	92.15
USCCE with pretreatment	27	21	1000	4 (+3 h pretreatment)	124.01

DOI: 10.1021/acs.jafc.5b00461
J. Agric. Food Chem. 2015, 63, 4597−4605

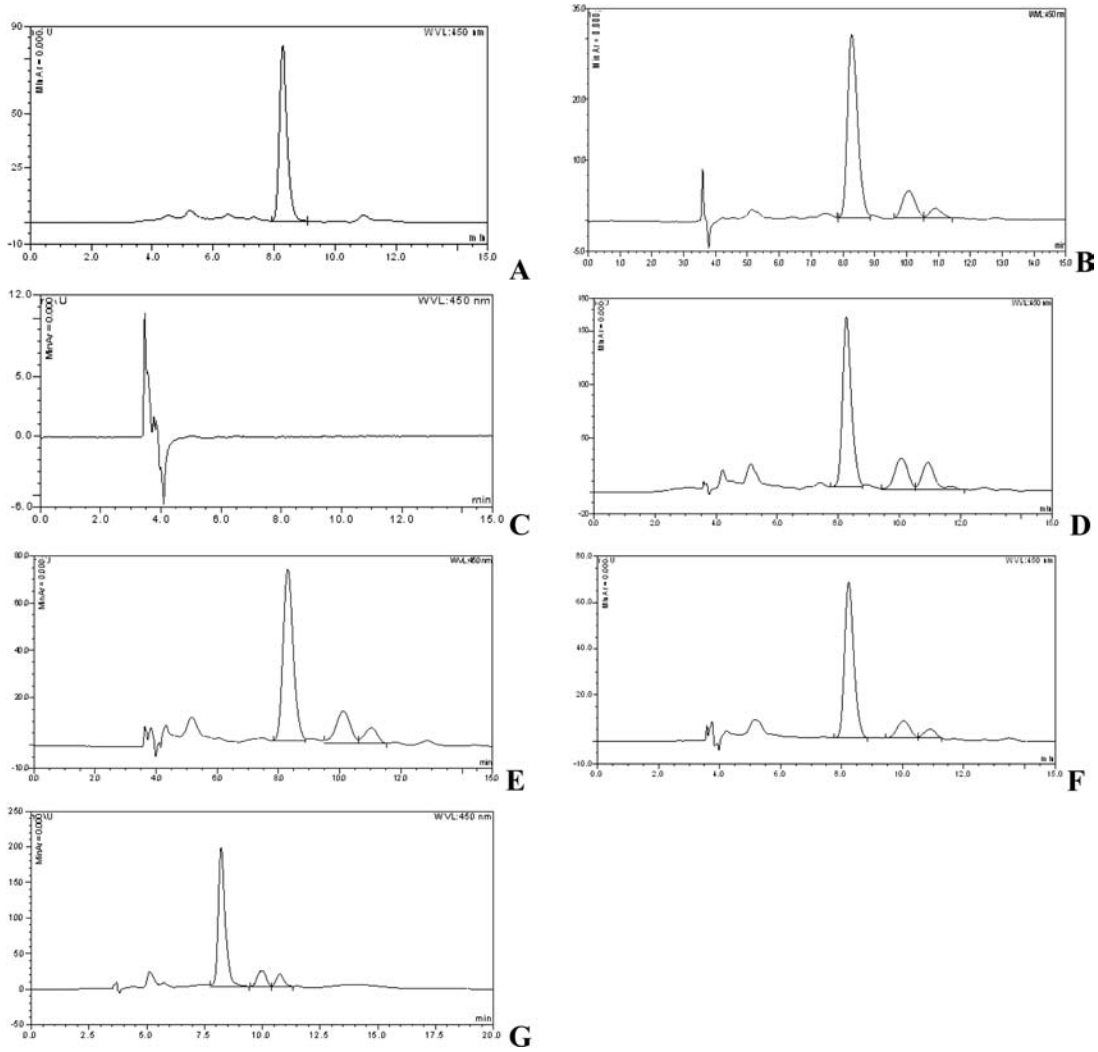

Figure 3. HPLC of extraction by different methods: (A) lutein standard; (B) SE; (C) SWE; (D) SCE; (E) SCCE; (F) SCCE with pretreatment; (G) USCCE with pretreatment.

carrying the solute into the circulation system before complete separation in the separation kettle, thus reducing the yield rate. Experimental results are shown in Figure 2C: with the increase of the fluid flow, lutein yield first increased and then decreased. The optimum fluid flow rate was 30 kg/h.

Effect of Cosolvent on Lutein Yield. Adding an appropriate amount of suitable cosolvent can significantly improve the solubility of certain extracted components in subcritical fluid and the selectivity of subcritical fluid. CO_2 is a nonpolar substance, whereas lutein is a polar material, its dipole moment being 1.863.[31] High pressure can increase lutein's solubility in subcritical carbon dioxide, but this effect is limited. Ethanol is the only organic reagent that is permitted for use in functional food and pharmaceutical processing.[32] As a cosolvent, ethanol can increase the density of a subcritical fluid, and its penetration ability is strong in the matrix diffusion, so after the addition of a cosolvent, the yield of lutein greatly improved. However, the positive effect of cosolvent on the extraction of lutein is limited; besides increasing the subcritical fluid solubility, it would also weaken the selective ability of an extraction system, resulting in an increase of total extracts. This phenomenon has been reported in a study by Wu;[23] before the addition of ethanol, lutein and other substances could be well separated in separation kettles I and II, respectively, but after the addition of ethanol, most of the extracts were brought into separation vessel II, resulting in lutein not being separated out. Experimental results are shown in Figure 2D: the yield of lutein increases as cosolvent increases rapidly in the range of 0−1.0 mL/g, but when the amount is >1.0 mL/g, the effect of cosolvent started to slow; considering the cost, the amount of cosolvent was chosen as 1.0 mL/g.

Effect of Extraction Time on Lutein Yield. The results are shown in Figure 2E: with the extension of the extraction time, yield also has a corresponding increase, but the slope of the yield curve is gradually reduced and eventually levels off. A similar result was presented in research by Deenu et al.,[11] in which when the temperature was fixed, the lutein yield increased until a certain amount of time (approximately 5 h) and then decreased. This could be explained as the chemical decomposition of the bioactive compound present in the extract may occur as the extraction time prolongs, resulting in a decrease in the extraction yield. Considering the technology and production cost, the preferred time for the extraction of lutein is 4 h.

Effect of Ultrasound Power on Lutein Yield. The results are shown in Figure 2F: with the introduction of ultrasound,

DOI: 10.1021/acs.jafc.5b00461
J. Agric. Food Chem. 2015, 63, 4597−4605

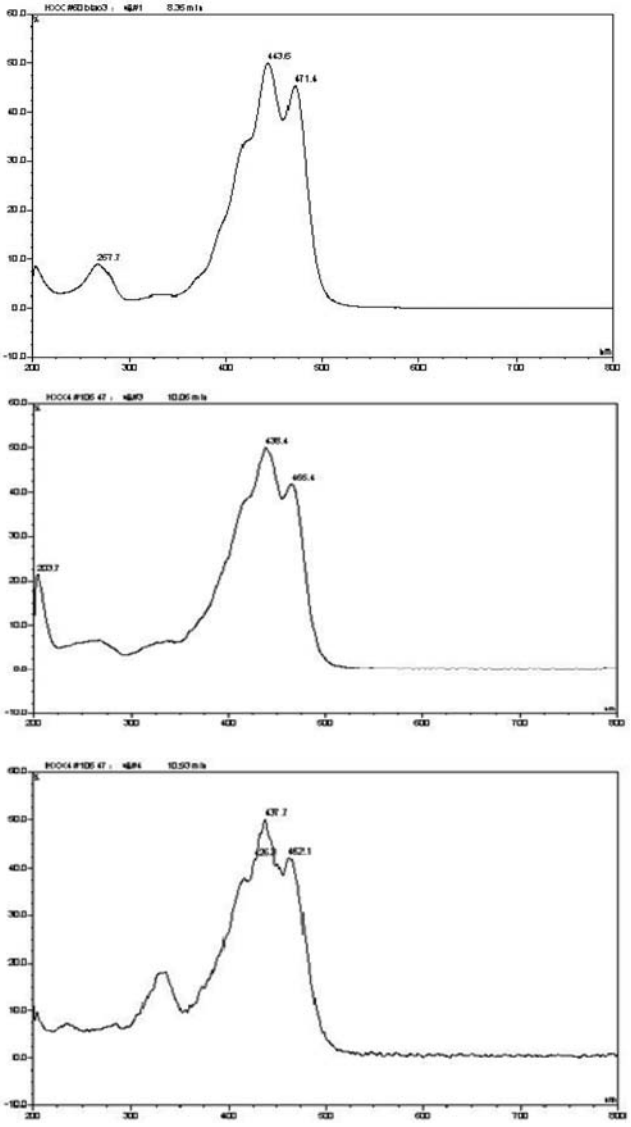

Figure 4. Absorption spectrum of different components: (A, top) lutein standard (retention time, 8.35); (B, middle) substance retains at 10.06 min; (C, bottom) substance retains at 10.93 min.

Table 4. Extraction Yield of Lutein from *Chlorella pyrenoidosa* by SCCE and USCCE

	yield (mglutein/100g*Chlorella*)			yield (mglutein/100g*Chlorella*)	
time (h)	USCCE	SCCE	time (h)	USCCE	SCCE
0	0	0	3.5	117.21	90.36
0.5	50.23	31.12	4	124.01	92.15
1	62.46	46.91	4.5	125.62	95.37
1.5	80.1	56.6	5	126.73	96.45
2	89.98	64.29	5.5	127.44	97.01
2.5	102.06	74.36	6	127.77	97.39
3	113.01	83.85			

lutein yield rises rapidly. Because of the increase in sound power, sound intensity and the effect of ultrasonic vibration increases, leading to accelerated movement of solute molecules and the enhancement of the mass transfer inside the material, thereby improving the yield of lutein. This result is consistent

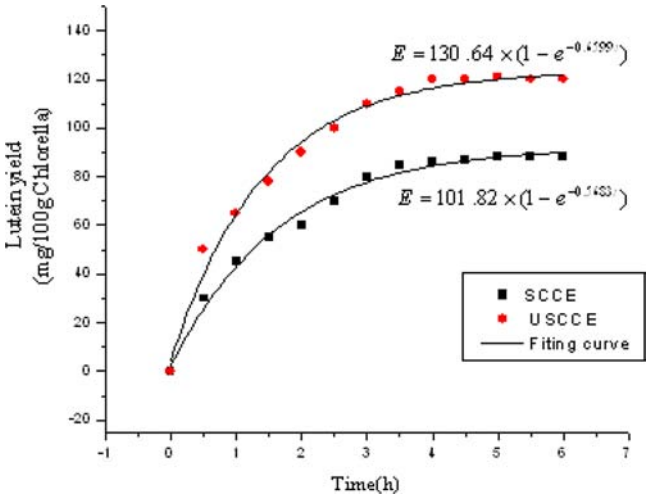

Figure 5. Model fitting curve of lutein extraction yield for USCCE and SCCE. The k value of USCCE was 0.6599, and the k value of SCCE was 0.5683.

with the findings of many other researchers on natural product extraction.[11,14,33−35] In research conducted by Riera et al.,[33] mass transfer enhancement in supercritical fluids extraction (SFE) by means of power ultrasound was calculated; at the end of the extraction time (8.5 h), the yield of the oil was significantly increased when the SFE was ultrasonically assisted. The improvement was about 20%. At the same time the process was accelerated by using ultrasound. Similar extraction yields were obtained in about 30% shorter time.

Optimization of Extraction Conditions of Lutein. Experiments were performed to determine the importance order of the factors influencing ultrasound-enhanced subcritical CO_2 extraction of lutein and calculate the optimum process parameters; according to the result of the orthogonal test, range analysis and variance analysis of factors are made. The orthogonal experiment results and the analysis results are shown in Tables 1 and 2, respectively.

Table 1 shows that in the four factors, extraction pressure had the maximum effect; extraction temperature had the minimum effect. According to Table 1, the importance order of each factor on lutein yield was $B > D > C > A$, and the optimization of process parameters of USCCE was $A2B2C3D3$ in which extraction temperature was 27 °C, extraction pressure was 21 MPa, dosage of ethanol was 1.5 mL/g, and ultrasonic power was 1000 W. Experiments were performed under the optimal conditions to verify the credibility of the best level combination, and results showed that the yield of lutein, 124.01 mg/100 g *C. pyrenoidosa*, was even higher than the highest yield in the orthogonal experiment, 117.75 mg/100 g *C. pyrenoidosa* (Table 1), so the best conditions were determined as $A2B2C3D3$.

As can be seen from the results of the analysis variance in Table 2, when $\alpha = 0.05$, the effects of extraction pressure (factor B) on the yield of lutein in broken *C. pyrenoidosa* reached a significant level, whereas the effects of the ultrasonic power (factor D) and cosolvent dosage (factor C) were not significant. The effect of ultrasonic power, by contrast, is more significant than that of cosolvent dosage, and with the increase of ultrasonic power, lutein yield increases. The extraction temperature (factor A) has a smaller effect on extraction; in the horizontal range of the experiments, the significance of factor A was the least, considering the production cost, and compared

DOI: 10.1021/acs.jafc.5b00461
J. Agric. Food Chem. 2015, 63, 4597−4605

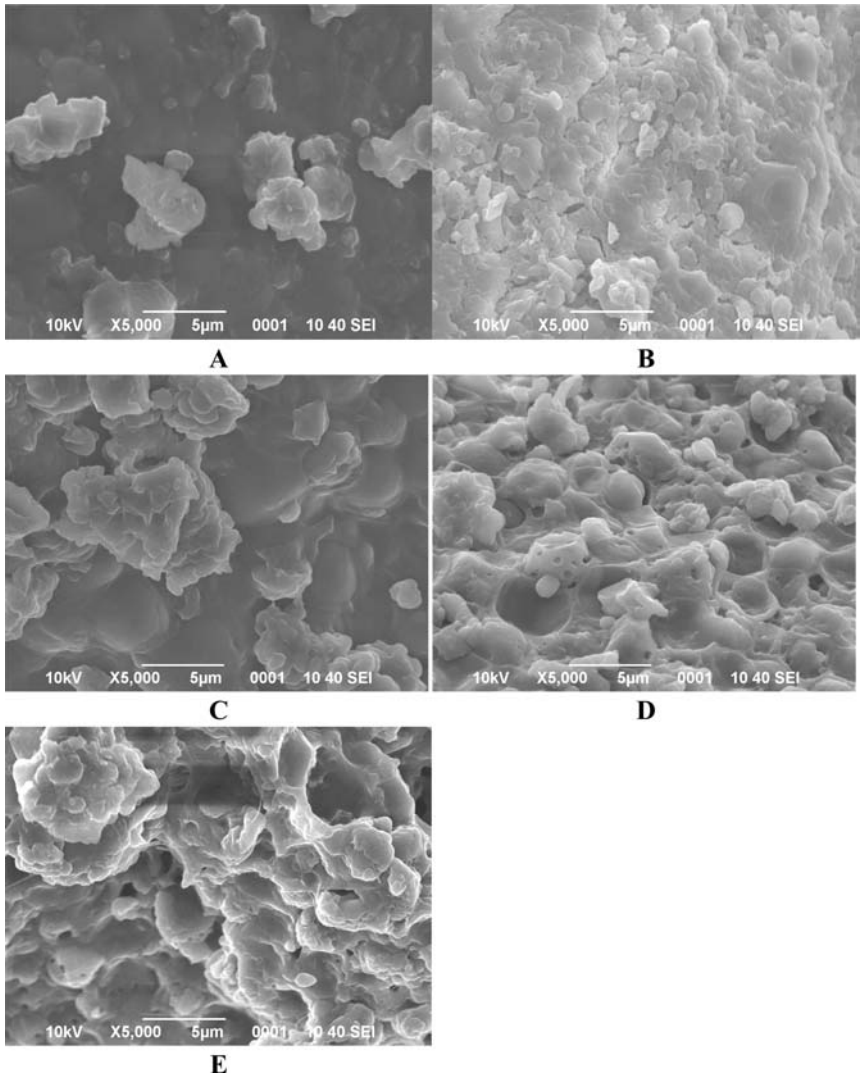

Figure 6. Scanning electron micrographs of seed powder from treatments of (A) control, (B) Soxhlet extraction (SD), (C) subcritical CO_2 extraction (SCCE), (D) USCCE without pretreatment, and (E) USCCE with pretreatment.

with other research, the temperature could be chosen as room temperature.[11]

Comparison of USCCE with Other Extraction Methods. It can be seen from Table 3, in terms of the extraction temperature, the temperature of USCCE and SCCE with or without pretreatment was room temperature, which was lower than the other three methods. In terms of the extraction pressure, the pressure of USCCE and SCCE is lower than that of SCE; therefore, the former two methods have a relatively low requirement for the equipment. In terms of extraction time, supercritical and subcritical CO_2 extraction needed at most 7 h, compared with 18 h for Soxhlet extraction. We assume efficiency as extraction rate per unit time; the least efficiency of supercritical and subcritical CO_2 extraction was 9.8, whereas the efficiency of Soxhlet was 3.04. Extraction time could be greatly reduced and still achieve higher efficiency.

Compared with SCCE without pretreatment, the extraction yield of lutein after pretreatment is greatly improved, pretreatment being more conducive to the extraction of effective constituents in *C. pyrenoidosa*. Because of the introduction of ultrasound and pretreatment, USCCE with pretreatment had a much higher yield than the other four methods; yield had a 100−200% increase. Compared with the SCCE with pretreatment, the yield also had a 34.5% increase. To sum up, the USCCE with pretreatment is the best to extract lutein; the yield of SCCE was slightly higher than the SCE; Soxhlet extraction yield is medium, but it was so time-consuming that its efficiency is not high.

The HPLC conditions achieved baseline separation of lutein from the total extract, the retention time of lutein was in the vicinity of 8.35 min, and in Figure 3A lutein typical strong shoulder peak can be seen at 445 and 474 nm. Except for the subcritical water extracts, the other five extracts have the other two substances detected at retention times of 10.06 and 10.93 min; the two substances were full wavelength scanned, and the results are shown in Figure 4B,C. The main absorption band profile of these two substances was in the 400−500 nm range and has a shoulder peak or even three absorption peaks of typical carotenoid,[36] so these two substances were inferred as carotenoids, too, but their specific structure needs more analysis.

Extraction Kinetics. The results of USCCE and SCCE are shown in Table 4. According to the experimental data, we used the nonlinear fitting method to get the E_∞ and k values in Origin7.0 software. As is shown in Figure 5 and Table 4, the kinetic model and experimental data have a rather good fitting

DOI: 10.1021/acs.jafc.5b00461
J. Agric. Food Chem. 2015, 63, 4597−4605

degree. The k value of USCCE was 0.6599, larger than that of SCCE 0.5683, suggesting that ultrasound can increase the diffusion coefficient of internal solute and material; E_∞ increased significantly after using ultrasound, suggesting that ultrasound had an effect on the adsorption/desorption balance of solute between the interface of solid and liquid phases, and it made the balance tilt in the desorption direction. This conclusion is consistent with research conducted by Romdhane.[30] Overall, E_∞ and k increase at the same time, suggesting that ultrasound can enhance subcritical CO_2 extraction.

Microstructure of *C. pyrenoidosa* Powder. The images of *C. pyrenoidosa* treated by ultrasound with or without enzymatic pretreatment and conventional extraction are shown in Figure 6. The microstructure of the microalgal cell by SD (Figure 6B) had a lot of holes and interspaces because of a long time soaking (18 h). Part of the microalgal cell surface by SCCE (Figure 6C) floated up and had stepped lamella, which was because 4 h is not enough for CO_2 to penetrate into the interior. The microstructure of the microalgal cell by USCCE (Figure 6D) had more interspaces and holes than the microalgal cell by SCCE. This was the same as the results of Li et al.[37] and Zhao et al.,[38] in which ultrasound treatment disrupted tissues and cell walls. Moreover, the physical disruption of *C. pyrenoidosa* cells by ultrasound, together with enzymatic pretreatment, was the most efficient method to destroy microalgal cell walls (Figure 6E). Enzymatic pretreatment has recently been shown to be another alternative method, which opens up cell walls through biodegradation and releases bioactive compounds from microalga.[39] The cell walls were damaged by the application of ultrasound and enzymatic pretreatment, which resulted in the greater penetration of solvent into the sample matrix and increased the contact surface area between the solid and liquid phase, and, as a result, the solute quickly diffused from the solid phase to the solvent. Hence, USCCE with pretreatment is much more efficient and rapid for the extraction of the bioactive compound. Therefore, the sonication played an important role in breaking up the microalgal cell walls to enhance the extraction yield.

The extraction conditions for USCCE with enzyme pretreatment of lutein were evaluated and optimized with regard to the extraction efficiency. Results indicate that lutein was successfully extracted using USCCE with enzyme pretreatment due to its high efficiency, especially compared to other extraction methods. Among the four significant factors that affect USCCE with enzyme pretreatment (extraction temperature, extraction pressure, cosolvent dosage, and ultrasonic power), extraction pressure has maximum effect and extraction temperature has minimum effect. The optimal parameters of USCCE with enzyme pretreatment are extraction temperature of 27 °C, extraction pressure of 21 MPa, ethanol dosage of 1.5 mL/g, and ultrasonic power of 1000 W. Experiments performed under the optimal conditions reached 124.01 mg/100 g *C. pyrenoidosa*. Kinetic models of USCCE and SCCE in *C. pyrenoidosa* were established; different E_∞ and k values illustrate that ultrasound could strengthen the subcritical CO_2 extraction, and the model can also be a significant guide to the study of the amplification of the extraction process.

AUTHOR INFORMATION

Corresponding Authors

*(T.-Q.Q.) E-mail: tqqiu@scut.edu.cn. Phone: +86-20-87113849. Fax: +86-20-87113843.

*(J.-G.J.) E-mail: jgjiang@scut.edu.cn. Phone: +86-20-87113849. Fax: +86-20-87113843.

Funding

This project was supported by the National Natural Foundation of China (Grant 21406074), Guangdong Province Science and Technology plan project (2013B020311006), and Guangdong Provincial Bureau of Ocean and Fishery Science and Technology to promote a special (A201301B04).

Notes

The authors declare no competing financial interest.

REFERENCES

(1) Domingos, L. D.; Xavier, A. A. O.; Mercadante, A. Z.; Petenate, A. J.; Jorge, R. A.; Viotto, W. H. Oxidative stability of yogurt with added lutein dye. *J. Dairy Sci.* **2014**, *97*, 616−623.

(2) Caseli, L.; Sousa-Martins, D.; Maia, M.; Lima-Filho, A. A. S.; Rodrigues, E. B.; Belfort, R., , Jr. An intraocular dye solution based on lutein and zeaxanthin in a surrogate internal limiting membrane model: a Langmuir monolayer study. *Colloids Surf., B* **2013**, *107*, 124−129.

(3) Bone, R. A.; Landrum, J. T.; Tarsis, S. L. Preliminary identification of the human macular pigment. *Vision Res.* **1985**, *25*, 1531−5.

(4) Sun, Z.; Liu, J.; Zeng, X.; Huangfu, J.; Jiang, Y.; Wang, M.; Chen, F. Protective actions of microalgae against endogenous and exogenous advanced glycation endproducts (AGEs) in human retinal pigment epithelial cells. *Food Funct.* **2011**, *2*, 251−258.

(5) Chew, B. P.; Wong, M. W.; Wong, T. S. Effects of lutein from marigold extract on immunity and growth of mammary tumors in mice. *Anticancer Res.* **1996**, *16*, 3689−3694.

(6) Slattery, M. L.; Benson, J.; Curtin, K.; Ma, K.-N.; Schaeffer, D.; Potter, J. D. Carotenoids and colon cancer. *Am. J. Clin. Nutr.* **2000**, *71*, 575−582.

(7) Zhu, H.; Zheng, J. Lutein structure, distribution, physical and chemical properties and physiological function. *Chinese Food Addit.* **2005**, 48−55.

(8) Hadden, W. L.; Watkins, R. H.; Levy, L. W.; Regalado, E.; Rivadeneira, D. M.; van Breemen, R. B.; Schwartz, S. J. Carotenoid composition of marigold (*Tagetes erecta*) flower extract used as nutritional supplement. *J. Agric. Food Chem.* **1999**, *47*, 4189−4194.

(9) Zhang, J.; Sun, Z.; Sun, P.; Chen, T.; Chen, F. Microalgal carotenoids: beneficial effects and potential in human health. *Food Funct.* **2014**, *5*, 413−425.

(10) Sowbhagya, H. B.; Sushma, S. B.; Rastogi, N. K.; Naidu, M. M. Effect of pretreatments on extraction of pigment from marigold flower. *J. Food Sci. Technol.* **2013**, *50*, 122−128.

(11) Deenu, A.; Naruenartwongsakul, S.; Kim, S. M. Optimization and economic evaluation of ultrasound extraction of lutein from *Chlorella vulgaris*. *Biotechnol. Bioprocess Eng.* **2013**, *18*, 1151−1162.

(12) Valderrama, J. O.; Perrut, M.; Majewski, W. Extraction of astaxantine and phycocyanine from microalgae with supercritical carbon dioxide. *J. Chem. Eng. Data* **2003**, *48*, 827−830.

(13) Kalampoukas, G.; Dervakos, G. A. Process optimization for clean manufacturing: supercritical fluid extraction for β-carotene production. *Comput. Chem. Eng.* **1996**, *20*, S1383−S1388.

(14) Mandal, V.; Dewanjee, S.; Sahu, R.; Mandal, S. C. Design and optimization of ultrasound assisted extraction of curcumin as an effective alternative for conventional solid liquid extraction of natural products. *Nat. Prod. Commun.* **2009**, *4*, 95−100.

(15) Shirsath, S. R.; Sonawane, S. H.; Gogate, P. R. Intensification of extraction of natural products using ultrasonic irradiations. A review of current status. *Chem. Eng. Process.* **2012**, *53*, 10−23.

(16) Zhang, Y.; Yu, Z.; Wu, X. [A new technique of extracting effective components from Chinese herb and natural plant–microwave assisted extraction, MAE]. *China J. Chinese Mater. Med.* **2004**, *29*, 104−108.

DOI: 10.1021/acs.jafc.5b00461
J. Agric. Food Chem. 2015, 63, 4597−4605

(17) Brunner, G. Supercritical fluids: technology and application to food processing. *J. Food Eng.* **2005**, *67*, 21−33.
(18) Herrero, M.; Cifuentes, A.; Ibanez, E. Sub- and supercritical fluid extraction of functional ingredients from different natural sources: plants, food-by-products, algae and microalgae − a review. *Food Chem.* **2006**, *98*, 136−148.
(19) Hawthorne, S. B.; Krieger, M. S.; Miller, D. J. Analysis of flavor and fragrance compounds using supercritical fluid extraction coupled with gas chromatography. *Anal. Chem.* **1988**, *60*, 472−477.
(20) Bleve, M.; Ciurlia, L.; Erroi, E.; Lionetto, M. G.; Longo, L.; Rescio, L.; Schettino, T.; Vasapollo, G. An innovative method for the purification of anthocyanins from grape skin extracts by using liquid and sub-critical carbon dioxide. *Sep. Purif. Technol.* **2008**, *64*, 192−197.
(21) Vilkhu, K.; Mawson, R.; Simons, L.; Bates, D. Applications and opportunities for ultrasound assisted extraction in the food industry − a review. *Innovative Food Sci. Emerging Technol.* **2008**, *9*, 161−169.
(22) Hu, Q.; Pan, B.; Xu, J.; Sheng, J.; Shi, Y. Effects of supercritical carbon dioxide extraction conditions on yields and antioxidant activity of *Chlorella pyrenoidosa* extracts. *J. Food Eng.* **2007**, *80*, 997−1001.
(23) Wu, Z.; Wu, S.; Shi, X. Supercritical fluid extraction and determination of lutein in heterotrophically cultivated *Chlorella pyrenoidosa*. *J. Food Process Eng.* **2007**, *30*, 174−185.
(24) Kitada, K.; Machmudah, S.; Sasaki, M.; Goto, M.; Nakashima, Y.; Kumamoto, S.; Hasegawa, T. Supercritical CO2 extraction of pigment components with pharmaceutical importance from Chlorella vulgaris. *J. Chem. Technol. Biotechnol.* **2009**, *84*, 657−661.
(25) Li, C.; Qiu, T.; Wang, W.; Gao, Z.; Cheng, Z. Mechanism of ultrasound-enhanced near-critical CO_2 fluid extraction. *J. Jiangsu Univ. Nat. Sci. Ed.* **2009**, *30*, 450−453.
(26) Jeong, M. L.; Chesney, D. J. Investigation of modifier effects in supercritical CO_2 extraction from various solid matrices. *J. Supercrit. Fluids* **1999**, *16*, 33−42.
(27) Fang, R.; Zhang, S. Supercritical fluid CO_2 extraction of colchicine from colchicine *Autumnele liliaceae*. *Chinese J. Chromatogr.* **1999**, *17*, 249−252.
(28) Lu, J.; Feng, X.; Han, Y.; Xue, C. Optimization of subcritical fluid extraction of carotenoids and chlorophyll *a* from *Laminaria japonica* Aresch by response surface methodology. *J. Sci. Food Agric.* **2014**, *94*, 139−145.
(29) Liu, J.; Lin, S.; Wang, Z.; Wang, C.; Wang, E.; Zhang, Y.; Liu, J. Supercritical fluid extraction of flavonoids from Maydis stigma and its nitrite-scavenging ability. *Food Bioprod. Process.* **2011**, *89*, 333−339.
(30) Romdhane, M.; Tizaoui, C. The kinetic modelling of a steam distillation unit for the extraction of aniseed (*Pimpinelia anisum*) essential oil. *J. Chem. Technol. Biotechnol.* **2005**, *80*, 759−766.
(31) Sun, Z.; Yao, H. Y. Study on the correlation of antioxidation activity of carotenoids with quantum chemical parameters. *Food Machinery* **2007**, *23*, 4.
(32) Macias-Sanchez, M. D.; Mantell Serrano, C.; Rodriguez Rodriguez, M.; de la Ossa, E. M.; Lubian, L. M.; Montero, O. Extraction of carotenoids and chlorophyll from microalgae with supercritical carbon dioxide and ethanol as cosolvent. *J. Sep. Sci.* **2008**, *31*, 1352−1362.
(33) Riera, E.; Golas, Y.; Blanco, A.; Gallego, J. A.; Blasco, M.; Mulet, A. Mass transfer enhancement in supercritical fluids extraction by means of power ultrasound. *Ultrason. Sonochem.* **2004**, *11*, 241−244.
(34) Cenci, S. M.; Cox, L. R.; Leeke, G. A. Ultrasound-induced emulsification of subcritical carbon dioxide/water with and without surfactant as a strategy for enhanced mass transport. *Ultrason. Sonochem.* **2014**, *21*, 401−408.
(35) Daneshvand, B.; Ara, K. M.; Raofie, F. Comparison of supercritical fluid extraction and ultrasound-assisted extraction of fatty acids from quince (*Cydonia oblonga* Miller) seed using response surface methodology and central composite design. *J. Chromatogr., A* **2012**, *1252*, 1−7.
(36) Valdivielso, I.; Bustamante, M. A.; Ruiz de Gordoa, J. C.; Najera, A. I.; de Renobales, M.; Barron, L. J. R. Simultaneous analysis of carotenoids and tocopherols in botanical species using one step solid-liquid extraction followed by high performance liquid chromatography. *Food Chem.* **2015**, *173*, 709−717.
(37) Li, T.; Qu, X.-y.; Zhang, Q.-a.; Wang, Z.-Z. Ultrasound-assisted extraction and profile characteristics of seed oil from *Isatis indigotica* Fort. *Ind. Crops Prod.* **2012**, *35*, 98−104.
(38) Zhao, S.; Baik, O. D. Application of ultrasound as pretreatment for extraction of podophyllotoxin from rhizomes of *Podophyllum peltatum*. *Ultrason. Sonochem.* **2012**, *19*, 22−31.
(39) Li, F.; Yang, L.; Zhao, T.; Zhao, J.; Zou, Y.; Zou, Y.; Wu, X. Optimization of enzymatic pretreatment for n-hexane extraction of oil from *Silybum marianum* seeds using response surface methodology. *Food Bioprod. Process.* **2012**, *90*, 87−94.

DOI: 10.1021/acs.jafc.5b00461
J. Agric. Food Chem. 2015, 63, 4597−4605